Q
1
S3
v.80-83
1977-80
SUB.
INDEX
MAS-PER
N/C
SCI

Physics Abstracts

Volumes 80-83 1977-1980

Cumulative Subject Index

Mas—Per

28 July 1982

inspec
The Institution of Electrical Engineers

© 1981 The Institution of Electrical Engineers

CUMULATIVE SUBJECT INDEX 1977-80

Coverage

The present index provides a subject key to all papers abstracted in *Physics Abstracts* for the years 1977–80. It therefore comprises all relevant entries included in the six monthly subject indexes for the same period.

Subject Headings

In the course of the four years covered by this index the list of subject headings has been revised and new headings have been added. The present index uses the latest (i.e. 1980) version of the list. Entries for articles abstracted in the 1977, 1978 and 1979 volumes have been examined and, where appropriate, re-indexed under the new headings.

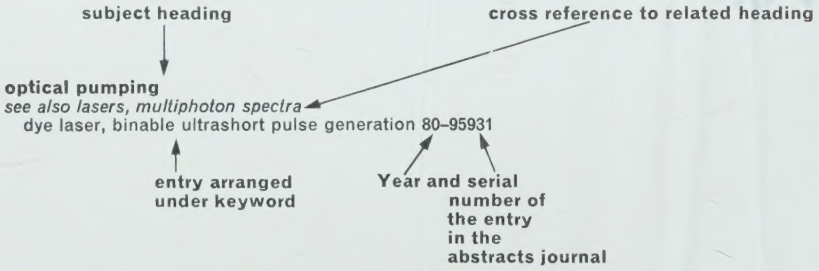
Arrangement

The subject headings are arranged in alphabetical order. The entries under each are prepared so that the most significant or 'key' words appear first and thus determine the position and grouping of entries in the alphabetical sequence under each heading.

Where the names of specific inorganic substances are significant under a given heading, the entries relating to them are found as a second alphabetical listing arranged by the chemical formulae of the particular elements or compounds.

Form of entry

The information contained in the subject index may be illustrated by an example.



How to use the index

The Subject index provides an alphabetical subject key to the articles included in the abstracts journal. Some general guidance on its use is given below:

1. Look in the index for the name of the specific subject in which you are interested. In most cases this name will be a heading in the index and you will find relevant articles listed under it. The majority of the subject headings fall into the following categories: property, phenomena, substance or named objects, instrument, device, theory, method, process, application, event.
2. Occasionally you will be directed from the subject heading chosen to a different heading under which the relevant or additional articles are listed.
3. If you do not find the subject heading you first chose, try a more general heading.
4. Each entry under the heading relates to an article appearing in the abstracts journal and gives the serial number of that article in the journal preceded by the last two digits of the current year, e.g. 78–12345; i.e. Abstract number 12345 in the abstracts journal for 1978.

   The language of the article, if it is not in English, is also indicated, e.g. optical fibre, three-wave stimulated Raman scattering (French) 0–78902.

   Each entry starts with a Keyword or Keyphrase considered to be most relevant to the heading. On sorting these Keywords, the qualifying prefixes are usually ignored (e.g. n-Ge is sorted under Ge).

   There are three main keyword lists; arabic numerals, alphabetical A–Z, and chemical symbols (organic substances are written and not given as chemical formula). More than one Keyword list may be present under each subject heading.

   For document on, say 'photoemission of silicon' at least two access points 'photoemission' and 'elemental semiconductors' are provided. Under the heading 'photoemission' the Keyword will be 'Si' and under 'elemental semiconductors' the Keyword will also be 'Si'.

   In a case like this, it is advisable and quicker to use the heading 'photoemission' and go straight to the chemical symbol list for 'Si' because there are few entries listed under 'photoemission'.

Printed by Unwin Brothers Limited, The Gresham Press, Old Woking, Surrey

Abbreviations and Acronyms

Abbreviations and acronyms are used in the modifiers in all INSPEC Cumulative Subject Indexes. Individual terms should be readily understood in the context of the subject headings. **Inorganic substances** are usually given by their chemical formulae. Iron aluminium garnets appear in the formulae lists as MIG and MAG (where M is metal element, e.g. YIG and $Y_3(Pb,La)(Zr,Ti)O_3$ and $Ce_2Mg_3(NO_3)_{12}$ appear as PLZT and CMN respectively. **Organic substances** including **liquystals** are not given as formulae but common abbreviations are used.

ABS resin	acrylonitrutadiene-styrene
AC	alternatinrent
ACV	air cushioicle
A/D	analogue-ital
ADP	administrdata processing
AES	Auger ele spectra(oscopy)
AF	audio fre-y
AFC	automatiuency control
AFL	abstract f of languages
AGC	automati control
AGR	advancedooled reactor
AM	amplitudulation
ANS	AstronorNetherlands Satellite
APACHE	accelerat physics and chemistry of heavy elements
APR	acoustic agnetic resonance
APS	appearantential spectra(oscopy)
APW	augmentne wave
ATR	attenuatal reflection
ATS	applicatichnology satellite
ATWS	anticipatnsients without scram
AVC	automatime control
BARITT	barrier in transit time
BBEA	4-butoxil-4'-ethylaniline
BCC	body ce ubic
BCD	binary-ccimal
BFO	beat-fre oscillator
BWO	backwa oscillator
BWR	boiling eactor
BWT	backwar tube
CAD	comput design
CAI	computted instruction
CARS	coherentokes Raman scattering (spectra
CATV	commutenna TV
CB	citizen
CBOOA	cyanobene octyloxyaniline
C-CD	charge- device
CDI	collectsion isolation
CDM	code dnultiplexing
CDW	charge-wave
CEM	channon multiplier
CEPA	couplon pair approximation
CERN	Conseilen pour la Recherche Nucléaire
CESR	conductron spin resonance
CGTO	contraussian-type orbital
CHF	couplee-Fock
CI	configinteraction
CIEH	charge extended Huckel
CIHY	configinteraction Hylleras
CNDO	complect of differential overlap
COC	cholesyl carbonate
COM	compout to microform (fiche or film)
COOB	4,4'-cyloxy-biphenyl
CP	charge
CPA	cohential approximation
CPSK	coher shift keying
CPT	charg time
CRO	cathode ray oscilloscope
CRT	cathode ray tube
CS	coupled states
CSM	continuous slowing down models
CTR	controlled thermonuclear reactor
CVD	chemical vapour deposition
CW	continuous wave
D/A	digital-to-analogue
DBR	distributed Bragg reflector
DC	direct current
DDC	direct digital control
DDL	diode-diode logic
DECENT	distribution of exact classical energy transfer
DESY	Deutsches Electron Synchrotron
DF	Dirac-Fock
DFB	distributed feedback
DH	double heterostructure
DIL	dual-in-line
DITE	divertor in torus experiment
DLTS	deep level transient spectra(oscopy)
DM	delta modulation
DMSO	dimethyl sulphoxide
DMSS	Defence Meteorological Satellite System
DOBAMBC	p-decyloxybenzylidene p'-amino 2-methyl butyl cinnamate
DODS	different orbitals for different spins
DORIS	Dopple-ring-Speicher
DOVETT	double velocity transit time
DP	data processing
DPCM	differential pulse code modulation
DPPH	diphenylpicrylhydrazyl
DPSK	differential phase shift keying
DSC	differential scanning calorimetry
DTA	differential thermal analysis
DV-Xα	discrete variational Xα method
E1,E2	electric dipole, quadrupole
EAS	extensive air shower
EB	exponential Born
EBBA	4-ethoxybenzylidene-4'n-butylaniline
EBR	experimental breeder reactor
EBT	Elmo Bumpy Torus
ECC	emergency core cooling
ECETR	epithermal critical experiment laboratory reactor
ECG	electrocardiography (-gram)
EDA	ethylene diamine
EDP	electronic data processing
EDTA	ethylene diamine tetra-acetic acid
EEBAC	ethyl-4-(4'ethoxy-benzylidene-amino) cinnamate
EEG	electroencephalography (-gram)
EELS	electron energy loss spectra
EFM	extended Flygare method
EHD	electrohydrodynamics
EHF	extremely high frequency
EHP	electron-hole potential method
EHT	extended Huckel theory
EHV	extra high voltage
ELDOR	electron electron double resonance

ELF	extremely low frequency
EM	electromagnetic
EMC	electromagnetic compatibility
EMF	electromotive force
EMG	electromyography(-gram)
ENDOR	electron nuclear double resonance
EOS	earth observatory satellite
EPEN	empirical potential energy function based on interactions of electrons and nuclei
EPMA	electron probe microanalysis
EPR	electron paramagnetic resonance
ERG	electroretinography(-gram)
ERPS	extramolecular relaxation polarisation shift
ERTS	earth resources technology satellite
ESCA	electron spectroscopy for chemical analysis
ESCAR	experimental superconducting accelerating ring
ESFI	epitaxial silicon film on insulator
ESS	electronic switching system
EUV	extreme ultraviolet
EXAFS	extended X-ray absorption fine structure
FBR	fast breeder reactor
FCC	face centred cubic
FDM	frequency division multiplex(ing)
FDNC	frequency dependent negative conductance
FDNR	frequency dependent negative resistance
FEM	field emission microscopy
FET	field effect transistor
FFHR	fusion-fission hybrid reactor
FFT	fast Fourier transform
FFTF	fast flux test facilities
FIM	field ion microscopy
FM	frequency modulation
FPT	finite perturbation theory
FSK	frequency-shift keying
FSGO	floating spherical Gaussian orbitals
FTR	fast test reactor
GAMBIT	gate modulated bipolar transistor
GANIL	grand accelerateur national a ions Lourds
GARP	global atmospheric research programme
GATE	GARP Atlantic tropical experiment
GCFR	gas-cooled fast breeder reactor
GCM	generator coordinate method
GHF-NO-CI	generalised Hartree-Fock/natural orbital/ configuration interactions
GIAO	gauge-invariant atomic orbitals
GO	Gaussian orbitals
GOO	generalised Overhauser orbitals
GPM	ground potential model
GSO	general spin orbitals
GTO	Gaussian-type orbitals
GVB	generalised valence bond
HAM	hydrogenic atoms in molecules
HBAB	hexyloxybenzylidene-p' aminobenzonitrile
HBT	N-(p-hexyloxybenzylidene)-p-toluidene
HCDA	hypothetical core disruptive accident
HCP	hexagonal close packed
HEED	high energy electron diffraction
HF	high frequency or Hartree-Fock
HFB	Hartree-Fock-Bogoliubov
HFER	hot fuel examination facility
HFIR	high flux isotope reactor
HFO	Hartree-Fock-Overhauser
HFS	hyperfine structure
HLW	high level waste (radioactive)
HMO	Huckel molecular orbitals
HOAB	heptyloxyazoxybenzene
HOBHA	p-n-heptyloxy-benzylidene-p-n heptylaniline
HOMO	highest occupied molecular orbitals
HORM	hybrid orbital rehybridisation method
HTGR	high temperature gas-cooled reactor
HV	high voltage
HVEM	high voltage electron microscopy
HWR	heavy water reactor
IAEA	International Atomic Energy Authority Agency
IBPBAC	isobutyl-4-(4'-phenylbenzylideneamino) cinnamate
IC	integrated circuit
ICDF	intermediate coupling Dirac-Fock
IDT	interdigital transducer
IEPA	independent electron pair approximation
IF	intermediate frequency
IGFET	insulated gate field effect transistor
IKO	Institute v. Kernph Ouder Amsterdam
I^2L	integrated injection logic
I^3L	isoplanar I^2L
ILS	instrument landing system
IMPATT	impact avalanche transit time
INDO	intermediate neglect of differential overlap
INDOR	internuclear double resonance
ING	intense neutron generator
INO	iterative natural orbital
INTELSAT	international telecommunications satellite consortium
I/O	input/output
IOC-ω	inclusion of the overlap charges in the omega
IR	infrared
IRDO	intermediate retention of differential overlap
ISABELLE	intersecting storage and acceleration
ISR	intersecting storage ring
ISX	impurity study experiment
ITEP	Institute of Theoretical and Experimental Physics
IU	Indiana University
IVO	improved virtual orbitals
JET	Joint European torus
JAERI	Japan Atomic Energy Research Institute
JINR	Joint Institute for Nuclear Research
KEK	Japan National Laboratory for High Energy Physics
KKR	Korringa-Kohn-Rostoker
LAMPF	Los Alamos meson physics facility
LC	inductance-capacitance
LCAO	linear combination of atomic orbitals
LCBO	linear combinations of (semi-localised) band orbitals
LCGO	linear combination of Gaussian orbitals
LCP	large coil program
LCRO	linear combination of Rydberg orbitals
LEC	liquid encapsulated Czochralski
LED	light emitting diode
LEED	low energy electron diffraction
LEP	large electron positron
LET	linear energy transfer
LF	low frequency
LMC	Large Magellanic Cloud
LMFBR	liquid metal fast breeder reactor
LMTO	linear combination of muffin tin orbitals
LOCA	loss of coolant accident
LOCE	loss of coolant experiment
LOFT	loss of flow test facility
LPE	liquid phase epitaxy
LSA	limited space charge accumulation

LSD	local spin density
LSI	large-scale integration
LTE	local thermodynamic equilibrium
LUMO	lowest unoccupied molecular orbitals
LV	low voltage
LWR	light water reactor
MADO	Mulliken approximation for differential overlap
M1,M2	magnetic dipole, quadrupole
MBBA	4-methoxybenzylidine-4'-n-butyl-aniline
MBE	molecular beam epiaxy
MBPT	many body perturbation theory
MCD	magnetic circular dichroism
MCPESCF	multiconfiguration paired excitation SCF
MCZDO	multi-centre zero differential overlap
MEDO	multipole expansion of diatomic overlap
MESFET	metal-semiconductor field effect transistor
MF	medium frequency
MFP	mean free path
MHD	magnetohydrodynamics
MIC	microwave integrated circuit
MIEHM	modified iterative extended Huckel method
MIM	metal-insulator-metal
MIS	metal-insulator-semiconductor or management information system
MIT	Massachusetts Institute of Technology
MMF	magnetomotive force
MNOS	metal-nitride-oxide-semiconductor
MO	molecular orbitals
MOCIC	molecular orbital constraint of interaction coordinates
MODPOT	model potential
MOS	metal-oxide-semiconductor
MOSFET	metal-oxide-semiconductor field effect transistor
MOST	metal-oxide-semiconductor transistor
MRD	multi-reference double excitation
MRINDO	modified Rydberg INDO
MSI	medium scale integration
MSR	molten salt reactor
MSU	Michigan State University
MTBF	mean-time between failures
MTF	modulation transfer function
MTXα	muffin-tin Xα
MUF	maximum usable frequency
MWH	Mulliken-Wolfsberg-Helmholz-semi-empirical method
NAL	National Accelerator Laboratory
NAND	not-and(logic)
NC	numerical control
NCMET	non-closed shell many electron theory
NDDO	neglect of diatomic differential overlap
NDT	nondestructive testing
NEMO	non-empirical molecular orbitals
NEVE	non-empirical valence-electron
NIC	negative impedance convertor
NMR	nuclear magnetic resonance
NNNDO	neglect of non-neighbour differential overlap
NOR	not-or(logic)
NPOST	non-perturbative open-shell theory
NPSO	non-paired spatial orbitals
NQR	nuclear quadrupole resonance
NRC	nuclear regulatory committee
NRM	natural remanent magnetisation
NTO	natural transition orbitals
OAO	orbiting astronomical observatory
OCR	optical character recognition
ODMR	optical detection of magnetic resonance
OER	oxygen enhancement ratio
OGO	orbiting geophysical observatory
OPHF	orbital polarised Hartree-Fock
OPW	orthogonal plane wave
OR	operations research
ORELA	Oak Ridge electron linear accelerator
ORNL	Oak Ridge National Laboratory
OSO	orbiting solar observatory
OTF	optical transfer function
PAA	paraazoxyanisole
PABX	private automatic branch exchange
PAC	perturbed angular correlation
PAHR	post accident heat removal
PAM	pulse amplitude modulation
PAMPUS	photons for atomic and molecular processes and universal studies
PAP	paraazoxyphenetole
PBF	power bursts facility
PBR	pebble bed reactor
PBX	private branch exchange
PC	printed circuit
PCAC	partially conserved axial currents
PCB	printed circuit board
PCGVB	pairwise correlated generalised valence bond
PCILOCC	perturbative configuration interaction using localised orbitals for crystal calculation
PCM	pulse code modulation
PCX	plasma confinement experiment
PDX	poloidal divertor experiment
PEP	positron electron proton
PETRA	positron electron tandem ringbeschle-uniger anlage
PF	power factor
PFM	pulse frequency modulation
PHWR	pressurised heavy water reactor
PID(PI,PD)	proportional+integral+differential (derivative)
PLA	phase locked arrays
PLC	programmable logic control
PLL	phase locked loops
PLT	Princeton Large Torus
PM	pulse modulation
PMMA	polmethylmethacrylate
PMDR	phosphorescence microwave double resonance
PNDO	partial neglect of differential overlap
PNO-CI	pair natural orbital configuration interaction
POL	pair orthogonalised Lowdin
POPAE	protons on protons and electrons
POPOP	phenyl-oxazolyl-phenyl-oxazolyl-phenyl
POS	point of sale
PPDP/S	Pariser-Parr-Del Bene-Pople/Segal calculations
PPI	plan position indicator
PPM	pulse position modulation or parts per million
PPP	Pariser-Parr-Pople
PRDDO	partial retention of diatomic differential overlap
PRF	pulse recurrence (repetition) frequency
PROM	programmable read-only-memory or Pockels readout optical modulator
PS	proton synchrotron (CERN)
PSK	phase shift keying
PTFE	polytetrafluoroethylene
PTM	pulse time modulation
PVC	polyvinyl chloride
PWM	pulse width modulation
PWR	pressurised water reactor

QCD	quantum chromodynamics
QDMBPT	quasi-degenerate many-body perturbation theory
QED	quantum electrodynamics
QPSK	quaternary phase shift keying
RAM	random access memory
RBE	relative biological effectiveness
RC	resistance-capacitance
RCNDO	Rydberg CNDO
R & D	research and development
RF	radio frequency
RFI	radio frequency interference
RHEED	reflection high energy electron diffraction
RINDO	Rydberg INDO
RKKY	Rudermann-Kittel Kasuya-Yosida
RLC	resistance-inductance-capacitance
RMS	root-mean-square
ROM	read-only memory
RPA	random phase approximation
RPM	relaxation potential model
SAMO	simulated ab initio molecular orbitals
SAS	small astronomy satellite
SAW	surface acoustic waves
SCF	self consistent field
SCL	space charge limited
SCPT	self consistent perturbation theory
SCR	silicon controlled rectifier
SDM	space division multiplexing
SDO	shielded diatomic orbitals
SEHF	spin extended Hartree-Fock
SEM	scanning electron microscope
SFE	solar-flare effect
SGHWR	steam generating heavy water reactor
SHF	superhigh frequency
SHG	second harmonic generation
SIMS	secondary ion mass spectrometer
SIN	Swiss Institute of Nuclear Research
SINDO	scaled INDO
SISAM	spectrometer with interference selective amplitude modulation
SMC	Small Magellanic Cloud
SMS	synchronous meteorological satellite
S/N	signal-to-noise
SOG	strongly orthogonal geminal
SOS	silicon on sapphire
SPA	separated pair approximation
SPC	stored program control
SPEAR	Stanford positron electron asymmetric ring
SPHF	spin polarised Hartree-Fock
SPIN-CIPSI	spin symmetry adapted generalisation of CIPSI
SPS	super proton synchroton (CERN)
SQUID	superconducting quantum interference device
SRMCASE	symmetry-restricted-multiconfiguration annihiliation of single excitations
SSB	single sideband
SSC	sudden storm commencement
SSI	supersonic transport
STD	salinity-temperature-depth or subscriber trunk dialling
STEM	scanning transmission electron microscopy
STO	Slater-type orbitals
STOL	short take-off and landing
STP	Slater-transfer Preuss
SUHFC	spin unrestricted Hartree-Fock with local approximation for correlations
SW	short wave
SWR	standing wave ratio
SXAPS	soft X-ray appearance potential spectrum
TBBA	terephthal-butylaniline
TCNE	tetracyanoethylene
TCNQ	tetracyanoquinodimethane
TCR	tempenture coefficient of resistance
TDHF	time dependent Hartree-Fock
TDM	time division multiplex(ing)
TDMA	time division multiple access
TDPAC	time differential perturbed angular correlation
TE	transverse electric
TEA	transversely excited atmospheric
TEM	transverse electromagnetic or transmission electron microscopy
TEXT	Texas Experimental Tokamak
TFTR	Tokamak fusion test reactor
TGFB	triglycine fluoroberyllate
TGS	triglycine sulphate
TGSe	triglycine selenate
TJS	transverse junction stripe
TLD	thermoluminescent dosimeter(-ry)
TM	transverse magnetic
TMMC	tetramethylammonium manganese chloride
TOP	transient overpower accident
TNS	The next step
TRAPATT	trapped plasma avalanche triggered transit
TREAT	transien reactor test facility
TRM	thermoremanent magnetisation
TSC	thermally stimulated currents
TSEE	thermally stimulated exo-electron emission
TTF	tetrathiofulvalinium
TTL	transistor transistor logic
TTT	tetrathiotetracene
TUCA	transient undercooling accident
TV	television
TW	travelling wave
TWT	travelling wave tube
UCHF	uncoupled Hartree-Fock
UHF	ultra high frequency unrestricted Hartree-Fock
UHV	ultra high voltage
UKAEA	United Kingdom Atomic Energy Authority
ULF	ultra low frequency
UMD	unitised microwave devices
UPS	ultraviolet photoelectron spectra
US	ultrasonic
UV	ultraviolet
VB	valence bond
VCR	video cassette recorder
VDM	vector dominance model
VDU	visual display unit
VHF	very high frequency
VLBI	very long base line interferometry
VLF	very low frequency
VLSI	very large scale integration
VOR	VHF omnidirectional range
VPE	vapour phase epitaxy
VRC	visual record computer
VRDDO	variable retention of diatomic differential
VSB	vestigial sideband
VSEPR	valence shell electron pair repulsion
VSWR	voltage standing wave ratio
VTOL	vertical take-off and landing
VTR	voltage transformation ratio or video tape recorder
VUV	vacuum ultraviolet
VVER	water moderated water cooled reactors
WWER	water moderated water cooled reactors
XPS	X-ray photoelectron spectra
ZEBRA	zero energy breeder reactor assembly
ZGS	zero gradient synchrotron
ZPPR	zero power plutonium reactor

masks continued
one-dimensional linear coherent processing b single optical element 79−94165
optical lens system, for photolithographic puposes 79−36976
optical microscope, large field, for use in semconductor manufacture 80−82812
optical transform masks, manufacture, mod drawing programs 79−40334
photoprojection method of image formation f submicron patterns 78−71180
sapphire, etching of arrays of orifices using t-Cr composite layer mask 80−3216
SAW device, interdigital transducer finger attern, modification of aperture 78−13883
selective epitaxial growth and morphology ontrol 77−77378
semiconductor, μP control systems for photcopying equipment *(Spanish)* 79−17529
semiconductor, distrib. of implemented ionsnear arbitrarily shaped mask edges 77−31689
semiconductor laser epitaxial growth with roulded reflectors 78−42347
semiconductor mask, emulsion processing emical and plastic factors 78−16872
surface grating relief pattern pofile alterin oblique shadow deposition technique 79−68451
surface topography, high-resolution polyme replication 78−10264
vacuum deposited thin films, specific thickess profiles 78−95697
vacuum deposition masks, using rib-suppored structures, solving stencil problem 78−23615
Al film ion plating, through mask hole, thikness nonuniformity *(Japanese)* 79−19999
AlAs-GaAs heterostructure, fabrication byselective liq.-phase epitaxy 79−15618
Cr film, pattern generation by laser-induced oxidation 80−61009
Cr film, reversal etching in gas plasma, rection mechanism, AES and XPS obs. 80−16564
Cr films, photoresist film on reverse gas plasma etching 80−97634
Cr plates, for photomasks, prep. by vacuum deposition, characts. *(Russian)* 79−33203
Fe_2O_3 films, DC reactively sputtered, for electively semitransparent photomasks, struct., mech. and chem. props. 80−59835
Fe_2O_3 films, DC reactively sputtered, for electively semitransparent photomasks, deposition conditions and optical props. 80−60782
GaAs, facet formation by preferential etching in $1NH_4OH$-$2H_2O_2$ *(Japanese)* 78−44242
GaAs film optical components, prep. by NBE using Si shadow masking technique 80−28358
Nb-Nb Josephson junctions, submicron, thermally recyclable, fabrication and characts. 80−100566
Si shadow mask etching for ion implantaton 78−6086
Si:As, ion implanted layers in device structures, boundary effects in laser annealing 79−73188
Si:B_2As selective area simultaneous doping 80−34015
Si:B^+, TEM of lateral implantation effects near mask edges in wafers 79−37724
Si:P^+, ions implanted through SiO_2 mask window, lateral spread 79−77627
Si-C films, plasma deposition with neutralisation 78−88429
Si_3N_4, appl. in selective oxidation of Si in high press. steam 79−38997
Si_3N_4:Ge films, intrinsic stress rel. to deposition conditions, use as Si oxidation mask 80−39467
SiO_2 diffusion mask, As diffusion O_2 effects 78−43180
SiO_2 diffusion mask, stress enhanced diffusion of B in Si, photodiode fabrication 78−67865
SiO_2, masking film in alkaline etching 80−71771

masonry dams *see dams*

mass
see also atomic mass; elementary particle mass; molecular weight
Abell 399/Abell 401, X-ray binary galaxy cluster, mass 80−90546
atmospheric, review 78−32377
3C 303b, N-galaxy, gravit. lens effect on 3C 303a rel. to core mass 77−78878
charged particle mass, confidence density method for parameter estimation *(Chinese)* 78−81811
charm particles mass spectra, SU(4) and SU(3)×SU(3)′ theories comparison *(Chinese)* 78−82127
clusters of galaxies, effect of subclustering on virial mass and stability 79−44624
Coma galaxy cluster, mass segregation and missing mass 80−98730
compact X-ray sources, masses 78−12430
conformal relativity, kinematic theory of mass 78−77706
conformal relativity, special, theory of mass 78−77707
cosmologies with varying mass, theory 78−57705
cosmology, expanding universe model with continuous mass creation 79−44647
disc galaxies, masses and mass-luminosity ratios 77−78871
double galaxies, data anal. and galaxian mass (M/L) determ. 80−4428
dynamical symmetry breaking and mass generation massless field theory, renormalisation group 77−6027
Earth, mass and moment of inertia 77−86735
electrons, rest mass, continuous increase hypothesis *(Chinese)* 77−71209
finite spectrum relativistic wave eqn. models of quark and lepton masses 78−74130
galaxies, elliptical, vel. dispersions rel. to mass to light ratios 80−98707
galaxies, masses and ang. momenta anal. rel. to morphological types *(Chinese)* 79−17097
galaxies nonflat components (halo), mass limits 80−62291
galaxies nuclei, vel. dispersions and mass/light ratios 77−57083
galaxy clusters, missing mass in relativistic spherically-symmetric inhomogeneities model 77−71147
galaxy groups, mass to light ratios and virial props. 79−9010
galaxy groups, mass-to-light ratios and crossing times 77−45572
galaxy mass determination from binary galaxies, anal. of Turner's (1976) sample 80−67849
galaxy systems, virial mass estimation 80−17678
globular clusters mass function, effects of tidal disruption by Galaxy 80−105294
hadron mass, instanton effects on light quark spectroscopy, MIT bag model 78−62372
heavy leptons, hadronic decay, production, mass, e^+e^- annihilation inclusive hadron spectrum 77−18304

mass continued
induced, equilateral triangular cylinder moving in an incompressible irrotational fluid 80−64237
inertia explained as reaction between mag. moments of negative and positive energy electrons *(German)* 79−88842
inertial induction of mass in general relativity 78−111
interstellar giant molecular clouds, gravit. field probing rel. to mass upper limits 80−62242
ion scattering spectrometer for surface studies 80−98995
K-dwarf stars, mass estimation for 12 objects 77−29837
leptons, $SU(3)_L \times SU(3)_R$ as gauge groups of weak and associated charges, symm. breaking 78−74175
linear dependence in Newton's laws *(Italian)* 79−12706
M87, elliptical galaxy, enormous mass rel. to extended X-ray source model 78−28775
meteoroids, mass distrib. determ. from occurrence of brilliant fireballs 77−45366
neutrino mass and Pontecorvo oscills. using chronon concept in electron theory 78−36879
neutron stars, nonrotating, eqn. of state and bounds on mass 77−45477
neutron stars, nonuniform rotating struct. and mass *(Russian)* 77−91559
NGC 1055, 681, 4594, galaxies, rot. curves and mass distribs. *(Russian)* 80−90541
NGC 2997, late-type galaxy, rot. and mass 79−21409
NGC 3115, S0 galaxy, rotation and mass of inner 5 kiloparsecs 80−105326
NGC 4378, anaemic spiral galaxy, extended rot. curve and mass 79−8990
NGC 5195, M51 companion galaxy, rot. and relative mass 77−22306
NGC 935-IC 1801, close pair of spiral galaxies, rot. curves and mass distribs. 77−45556
orthomuon mass lower limit from neutrino data anal. 78−62388
particle rest mass variability, theory and constraints from solar system expts. 77−45781
photon, rest mass, as cosmic test of Maxwell's eqns. 77−45708
photon rest mass upper limits from astrophysical data 77−34200
planets, mass distrib. rel. to conservation laws in form. process 78−81565
Pluto+Charon system, mass and density from speckle obs. 80−109394
proton/electron mass ratio, limits to past variability from quasar absorpt. line redshifts 77−61338
quark-potential-model mass formulae for hadrons 78−70349
Sculptor dwarf irregular galaxy, H I mass from 21 cm obs. 77−64843
shell, cylindrical, composite with viscoelastic filler, optimisation w.r.t. long-term stability 79−18760
shell of rotation exposed to vibrs., optimum shape and reinforcing struct. 79−18792
special relativity, mass and momentum density transform. 77−30005
spectral function sum rules for quark and baryon fields, using lightlike charges 78−93822
spiral galaxies, local mass-to-light ratio radial var. 80−31361
spontaneous generation of renormalisation invariant mass in IR stable theories 78−86411
spontaneously generated mass self-consistant computation anal., renormalisation group method, mass invariance 78−86412
standards for industry 80−42198
statistical bootstrap model, hadronic mass spectrum, pion condensation, boson gas 78−70345
SU(8) broken symmetry, baryon masses 79−290
superheavy Higgs particles, proportional renormalisation corrections to W and Z mass, Weinberg-Salam model 79−276
variation in Newtonian physics, rel. to gravit. const. var. 78−69675
AI Velorum, dwarf Cepheid, mass from uvbyβ photometry 77−78801
visual binary stars, parallaxes, mass ratios and masses for six pairs 77−64795
e, finite self-mass in nonperturbative iterative scheme of QED 78−89641
e mass calc. in terms of meas. quantities 78−66180
$\bar{\nu}_e$ rest mass, upper limit refining using ^3H β-spectrum meas. 78−17144
ν mass, four component Dirac particles, perturbation theory model for massless ν 79−435
Z^0 production and mass in left-right symmetric gauge models, $SU(2)_L \times SU(2)_R \times U(1)_L \times U(1)_R$, weak currents, Z^0 prod. and mass 79−253

mass analyzers *see mass spectrometer components and accessories*

mass differences
see also baryon mass; lepton mass; mass formulae; meson mass
atomic, for wide doublets, determ. with Manitoba II mass spectrometer 77−42432
atomic mass evaluation 1977: mass table, mass excesses, total BEs, β-decay energies 78−4894
b-mesons, mass splitting, SU_3 nonet of SU_6 80−47288
baryon 70, 1^- multiplet, transition mixing, mass splitting, degenerate perturbation theory model 77−2832
baryon EM mass differences in charmed quark model 77−82741
Born-term contribs. to EM mass splittings 78−78181
charm $m(D^+)-m(D^0)$ calc., EM effects 77−2833
charmed, baryon spectrum due to chromomagnetic and electromagnetic hyperfine interaction 79−13123
charmed and old meson EM mass differences 77−2834
charmed baryon, EM mass differences in charmed-quark model 77−71515
charmed baryon EM mass differences 77−65155
charmed baryons, SU(4) symmetric 20-plet representation, mass, EM splitting 78−54615
charmed hadron masses and EM mass differences in broken-SU(8) quark model 77−61256
charmed mesons, props. determ. from two-step pot. model 77−74682
chiral symmetry breaking, Dashen mass formula, baryon mass differences, $\eta \rightarrow 3\pi$ 79−289
colour model, mass splittings of heavy mesons and baryons *(Chinese)* 78−78146
Cottingham formula renormalisation, hadron mass EM contrib., np mass difference in QCD 79−36053
decomposition of mass operators, regional mass tables 77−22864
dynamical masses and p-n mass difference problem 78−12912
EM mass differences, one gluon exchange contrib. 79−3024
EM mass differences in MIT bag model calcs., charm particles 77−49965

mass differences continued
EM properties of charmed hadrons, $SU_6 \times U_c$ calcs., mag. moments, mass differences 78−70368
Gelfand pattern, charmed hadrons and magnetic moment 80−398
grand unified model, Yukawa coupling radiative corrections, lepton and quark masses 79−97555
hadron causality and EM mass shifts, remarks 80−73705
hadron EM mass differences, quark behaviour 79−58941
hadron EM mass differences and struct. 80−27502
hadron EM mass splittings in quark model 77−18285
hadron mass, instanton effects on light quark spectroscopy, MIT bag model 78−62372
isospin violating mass differences and mixing angles, quark mass and QCD 80−52505
isospin-violating mixing in meson nonets, $d\bar{d}$-$u\bar{u}$($s\bar{s}$) mass differences 80−32096
isotopic multiplets, microcausality condition *(Russian)* 77−38168
K_L and K_S mass difference in asymptotically free gradient theory *(Russian)* 77−30333
$K^0 \rightarrow \bar{K}^0$ transition in the standard SU(3)⊗SU(2)⊗U(1) scheme *(Russian)* 80−82951
meson mass spectrum, planar bootstrap, and Regge approach 80−22581
neutron-proton mass difference, classical electrodynamic model 77−6123
nonlocal quark model in $SU(3) \times SU^c(3) \times U(1)$, meson decay and mass correction *(German)* 80−27456
nonrelativistic colour quark model, meson and baryon masses 78−50014
nuclear family of mass relations based on residual n-p interactions 77−54141
nuclear mass formulae considering spin and compressibility effects 77−22865
octet baryons in SU_3, EM mass difference, u, d and c quark sectors 78−29334
pions, electromagnetic mass differences and radial excitations of ρ-A_1-π system 79−40775
proton-neutron mass difference, Cottingham formula simplification with causality conditions 77−61286
proton-neutron mass difference, higher intermediate hadronic states 78−45920
pseudoscalar mesons, EM mass shifts, quark-parton model, SU_3 quark triplet 80−42459
QCD, asymptotic freedom, energy levels J/ψ and Υ mass difference *(Chinese)* 80−52480
quark mass differences, magnetic moments and radiative decay widths 79−71724
quark mass differences in high energy collisions 78−45868
quark mass splitting bag model 78−45921
quark-gluon field coupling const., meson mass differences *(Russian)* 80−105898
quark-quark interactions, Bjorken scaling law violation 80−9160
quarkonium systems, binding energy effect on mass spectra 80−37229
quarks, EM form factors in instanton fields 80−99102
quarks, mass differences of up and down quarks, grand unification 80−62978
quarks, third and fourth generation, mass prediction using quantised magnetic self-energy 80−18133
shell model calcs. A=24, mass, spectra and β decay 78−4903
$SU(2)_L \times SU(2)_R \times U(1)$ gauge model for weak/EM interactions, u-d quarks mass difference 78−12850
$SU(2) \times U(1)$, $K^0 \leftrightarrows \bar{K}^0$ transition amplitude in MIT bag model 79−63450
unitarity and hadron self-energy, mass shifts, and SU_6 symmetry breaking in meson spectrum 79−17687
Weinberg model, upper limit on mass differences determ. 77−61245
B^0−B^-, EM mass difference, some phenomenological estimates about heavy quark (b,t) bound states 80−47262
C-quark, mass difference to be quark 80−78022
c-u quark mass difference, baryon mag. moments 80−37240
D, EM mass differences, quark behaviour 79−58941
D(1.87) isomultiplet, mass differences, effect of EM mixing on mass splitting *(Russian)* 78−89714
D meson EM mass differences, bag model calcs 77−6124
D mesons, e.m. props. 78−8668
D-meson EM mass difference in quark model, quark mass difference 77−71516
D^0, $\bar{D}^0$, decays, charm changing neutral current limits, QCD depend., mass differences 80−32062
D^+ D^0 in chiral SU(4)×SU(4) model 79−93311
D^+-D^0, Coulomb and tadpole contributions to EM mass differences 78−89713
D^+-D^0, D^{*+}-D^{*0} mass differences using modified nonrelativistic Schrodinger eqn. 78−58186
D^+-D^0 charmed mesons EM mass difference estimate, quark pair creation model 77−10250
D^+-D^0 mass difference, Bethe-Salpeter eqn. calc. 77−26525
D^+-D^0 mass difference, broken isospin symmetry in chiral SU(4)⊗SU(4) 78−89691
D^+-D^0 mass difference, form factors, SU(4) coupling, vector meson dominance model 79−391
D^+-D^0 mass differences, chiral SU(4)×SU(4) model, broken isospin symm. 77−87917
D^+-D^0 mass splitting and and forbidden decays $\psi' \rightarrow \eta\psi$, $\psi' \rightarrow \pi^0\psi$ 78−66114
$D^\pm$-D^0 mass difference, vac. isospin violations 77−26526
D*(2.01) isomultiplet, mass differences, effect of EM mixing on mass splitting *(Russian)* 78−89714
D*-D, mass difference calcs., scalar-exchange model 79−13124
D^{*+}, photoprod., D^0 mass difference 80−73720
D^{*+}-D^{*0}, QCD relation between EM mass differences 79−71750
D^{*+}-d^{*0} mass difference using form factors and vector meson interactions 78−21427
$D^*\bar{D}^*$ bound state, isospin mixing 78−41613
Δ mass splitting in $\pi^\pm p$ elastic scatt., charge exchange, partial wave anal., P_{33} resonance 78−29348
Δ^+-Δ^0, charge symmetry breaking mechanism in $np \rightarrow d\pi^0$ 79−85313
$\Delta^{++}-\Delta^0$ pole parameter determ. 80−13303
e/μ mass ratio, extended Weinberg model with heavy leptons, discrete symm. appls. 77−57482
e-ν, finite QED 80−47222
e^+e^- →hadrons, Υ, Υ', Υ'' states, mass differences, leptonic width ratio 80−68466
e^+e^- →vector mesons, colour quark model for new reson. above 4 GeV 78−17033
η_c and η_c', mass prediction using QCD 80−22590
F*-F, D*-D, pseudoscalar-vector mass differences, QCD nonrelativistic quark model 79−6339
F*-F, mass difference calc., scalar-exchange model 79−13124
K, EM mass differences, quark behaviour 79−58941
K, up quark mass effect on Dashen's formula 79−63461
$K^\pm$-K^0, Coulomb and tadpole contributions to EM mass differences 78−89713
K_L-K_S, quantum field theory with chiral Lagrangian 77−65110
K_L-K_S, weak-current angle of six quark model, constraints, from K^0-$\bar{K}^0$ system 79−71685
K_L-K_S mass difference, $K_L \rightarrow 2\mu$, strong interaction effects from short-dist. gluons 77−82737
K_L-K_S mass difference, restrictions on quark masses 77−57491
K_L-K_S mass differences, charged Higgs boson couplings 80−62917
K_L-K_S mass difference, SU3) gauge theory 78−58153
K_L−K_S, Kobayashi-Maskawa six quark model, mixing angles, mass matrix and CP violation 80−13284
K*, EM mass splitting determ. 79−3046
K*, EM mass splitting determ. 79−22138
K* (890), EM mass difference determ. from $\bar{p}p \rightarrow K_S^0 K^\pm \pi^\mp$ 79−390
μe, mass difference, lepton number and symmetry conservation, forbidden transitions *(Chinese)* 79−13121
N, EM mass differences, quark behaviour 79−58941
N EM mass shifts, asymptoic bounds and causality conditions 80−73704
n-p, charge symmetry breakng mechanism in $np \rightarrow d\pi^0$ 79−85313
n-p, finite QED 80−47222
N-π, EM mass difference in Nambu-Jona-Lasinio model 79−93415
NΔ mass difference, n charge distrib., quark model anal. 77−67653
np mass difference in gauge models 77−61285
$\nu p \rightarrow \mu^- p D^{*+}$, D^0(1863) and inclusive D^{*+} (2009) prod., mass difference 79−93396
$P \rightarrow \gamma\gamma$, relativistic quark pair creation model for reduced decays and enhanced EM tadpoles 79−67555
p-n mass difference, anal. of expt. data, scaling violation and renormalised struct. functions 79−97623
p-n mass difference, quark-parton model anal. 78−93859
p-n mass difference from scaing violation patterns in eN scatt. 77−57536
p-$\bar{p}$ symmetry, mass difference, Dirac and CPT theory test 78−82125
pn mass difference, effects of EM mixing, $\Lambda \rightleftharpoons \Sigma^0$, $\eta \rightleftharpoons \pi^0$, $\omega \rightleftharpoons \rho^0$ *(Russian)* 78−74255
π, EM mass differences, quark behaviour 79−58941
π, EM mass shifts, asymptotic bounds and causality conditions 80−73704
π, up quark mass effect on Dashen's formula 79−63461
π EM mass difference, finite temp. calc. 77−67591
π inertial mass, quaternion field theory of matter 78−24702
π mass difference, Bars-Halpern-Yoshimura unified gauge model, perturbative calc. 77−10251
π phenomenological form factor, EM mass difference, appl. to pionic ats. *(Korean)* 79−9372
π radius and EM mass difference from phenomenological form factor 77−65156
$\pi^+\pi^0$, isospin violating effects from nonvanishing quark mass difference 79−63385
Q_1-Q_2 mass difference and mixing, A_1-B mass difference, predictions 79−13122
ρ-ω mixing, quark mass differences 80−37243
Σ, EM mass differences, quark behaviour 79−58941
$\Sigma_c^{++}-\Lambda_c^+$, confirmation of Σ_c^{++}, Λ_c baryon and obs. of Λ_c^{++} two body decay modes 79−75770
Σ^{*-}-Σ^{*+}, QCD relation between EM mass differences 79−71750
Υ, EM mass splitting in nonrelativistic quark model 79−89152
Υ and charmonium spectra, common pot. fit, Υ''-Υ mass difference 80−86712
Υ resonances, mass splitting, bound states of exotic quarks 78−70338
Υ'-Υ mass difference from QCD $q\bar{q}$ β-function 79−343
Υ'-Υ mass splitting, data fit using quarkonium pot. 78−89666
$V \rightarrow P\gamma$, relativistic quark pair creation model for reduced decays and enhanced EM tadpoles 79−67555
Ξ, EM mass differences, quark behaviour 79−58941
^{37}Cl-^{35}Cl mass differences, for wide doublets, determ. with Manitoba II mass spectrometer 77−42432
Δ(1236)-N(939) mass difference from deep inelastic scatt. quark wave functions, hyperon masses 80−47289
^{2}H neutron binding energy and n mass excess from ^{1}H(n,γ) 80−47362
^{3}H-^{3}He charge asymm., neutron-proton mass difference 78−70464
^{3}He-^{3}H mass difference, separation of EM contribs. 77−23014

mass filters *see mass spectrometer components and accessories*

mass formulae
see also baryon mass; lepton mass; mass differences; meson mass
0^--mesons in broken SU(4), improved mass formula 77−30352
27-plet mesons, mass sum rules using SU_4 dynamical-group scheme 77−26505
ϕ^4 (rubber bag) model, hadron mass spectra and J/ψ family *(Chinese)* 79−80812
asymmetric systems described by a pair of local covariant wave equations 79−75391
b-mesons, mass splitting, SU_3 nonet of SU_6 80−47288
bag model, multibaryon states, SU(6) mass formulae 78−45848
bag model, string like solns., baryon-antibaryon states mass formulae *(Russian)* 79−93369
baryan spectroscopy, three body phenomenology for elementary particle systems 79−80846
baryon mass relations in internal SU(6) symmetry 80−82962
baryon mass splitting by the 'strong hyperfine interaction and SU(3) breaking 78−82184
baryon spectrum and the forces between quarks 80−102004
baryon SU_3 dynamical model, gravit. bound linear rotator 77−49904
baryonium, narrow states, mass formula, selection rule, quark model 78−66089
baryonium spectrum, SU(4) mass formulae, degenerate clustering 79−93393
baryons, formulae based on coloured quark model 78−12876

mass formulae continued
baryons, SU(1,4) dynamical group, anal. of discrete representations, mass formulae 77−45982
Bose quark model, mass spectrum of exotic particles 78−62358
bottom hadrons, masses and allowed decays, SU(5) quark model 80−62954
broken supersymmetry, general mass formulae 79−97535
charged leptons, mass formulae from EM self energy *(Chinese)* 79−93416
charm production, mass scales, in deep inelastic processes, parton model, generalised VDM 77−13930
charmed 0^- meson mass from SU(4,1) symmetry anal. *(Russian)* 78−74237
charmed baryon mass and F/D ratio, colour magnetic interaction 80−62957
charmed baryon mass formulae via SU(4) Regge trajectory anal. 77−79257
charmed baryons, one-parameter mass formula 77−10232
charmed baryons, tensorial mass operators, SU(8) model mass formulae 77−54091
charmed hadron masses, five-quark model of ψ particles *(Russian)* 77−61263
charmed hadron masses, unified approach *(Russian)* 77−61258
charmed hadron masses and EM mass differences in broken-SU(8) quark model 77−61256
charmed hadrons, SU(4) mass-breaking, mass sum rules 80−62959
charmed meson mass, effect of u and d quark differences calc. 77−46019
charmed meson masses, effects of fifth flavour 78−66098
charmed mesons, dynamic SU(4,1) symmetry, mass spectra, anal. *(Russian)* 78−70350
chiral SU(4)×SU(4) symmetry, broken chiral, mass spectrum of D, F and η mesons 79−93312
chiral symmetry breaking, Dashen mass formula, baryon mass differences, $\eta \rightarrow 3\pi$ 79−289
Cottingham formula renormalisation, hadron mass EM contrib., np mass difference in QCD 79−36053
covariant n^2-plet mass formulas 79−63460
distribution of masses of leptons and hadrons 80−99093
electron theory, chronon, charged-lepton mass formula 80−47224
electron-muon mass ratio, SU(2)×U(1)×D_4 symmetry model 79−89090
empirical formula for particles stable against strong decay 77−41833
exotic meson ($Q^2\bar{Q}^2$) spectroscopy, instanton effects 79−89140
exotic meson mass formulae in $SU_{1,3}$ 77−65147
fixed sphere MIT bag model, b-quark mass, zero-point energy, gs b-flavoured hadron masses 79−63429
fourth generation of quarks and leptons, mass formula 80−105876
fundamental fermions, mass eigenvalues, rate of increase 80−105871
generation in a normal product formulation 78−25027
hadron building blocks, pionic mass intervals in narrow and S-state resonances 80−105875
hadron empirical mass formulae *(Chinese)* 79−80816
hadron mass relns. in two six quark models with broken SU(12) symmetry 77−22693
hadron mass spectrum in lattice gauge theory 78−74139
hadron masses and current algebra quark masses 80−42436
hadron masses in bag model with surface tension 78−70337
hadron multiplets, realisations in SU(3) from stable particles 80−9159
hadronic lepton pair prod., hadronic mass corrections to Drell-Yan formulae 79−89139
hadronic matter exponential mass spectrum, incompatibility with weakly interacting quark phase 80−37219
hard QCD processes, relations through mass singularity universality 79−22054
heavy meson spectroscopy, centrifugal and harmonic oscill. pot. 79−17699
heavy mesons, polynomials approximating sequence of masses *(Russian)* 80−407
heavy quark-antiquark spectra in e^+e^- annihilation 77−26494
heavy vector mesons associated with $\Upsilon(9.4)$ and the nature of $\Upsilon'(10)$ 78−82187
Higgs bosons, masses, gauge hierarchies, SU_5 model 80−47236
J-dependence of statistical bootstrap mass spectrum, S-matrix and semi-classical formalism comparison 78−86448
lattice QCD, hadron mass spectrum, effective Hamiltonians, degenerate perturbation theory 80−102003
lepton mass in vector-like gauge theory with Majorana particles 77−18366
leptons, charged, mass ratios *(Russian)* 79−93478
leptons, charged, new quantum number n 80−13244
Lie group framework for composite particles and mass spectrum 79−97608
light hadronic spectroscopy, expt. and quark model interpretations, review, book contrib. 80−68438
meson and baryon mass formula, chromodynamics consideration *(Russian)* 80−91071
meson isosinglets, mixing angles, non-relativistic quark model, Schwinger-type mass relations for SU_4 and SU_5 80−18125
meson isosinglets, mixing angles, non-relativistic quark model, SU_5 and SU_n 80−22591
meson logarithmic mass formulae and new quantum number 78−82183
meson mass formula, quark line rule in u-, d-, and c-quark sector 78−8596
meson mass formula, SU(4) algebraic realisation *(Russian)* 78−45895
meson mass formula broken SU_N 77−6043
meson mass formulae in broken $SU(8)_w$ symmetry 78−37191
meson mass spectrum and unitarity in quark model 80−18115
meson masses calc. using harmonic oscillator pot. in Klein-Gordon eqn. 79−93392
meson resonances, empirical relation for masses 78−29323
meson spectroscopy, review of SU_3 quark model, quark confinement and bound states 78−74228
meson spectroscopy, spin struct., effective scale quark confinement in QCD 79−17684
meson spectroscopy, three body phenomenology for elementary particle systems 79−80846
meson spectroscopy based on nonlinear field proper oscills., equivalence theorem 78−89689
meson spectrum, quark-antiquark relativistic two-body wave eqn. bound states 77−30328
mass formulae continued
meson states, representation mixing, SU(4), mass formula, EM mass shifts 78−12890
mesons, vector and pseudoscalar, linear and quadratic formulae, charm 77−49935
mixing models, mass formulas and OZI rule isolation 77−71498
neutron star matter, mass formula rel. to comp. during decompression 77−33544
nonet formulae, vector-tensor-Pomeron couplings 77−49883
nonet mixing and gluon effects in current quark framework 79−80799
Okubo formula and $\psi \rightarrow \eta'\gamma(\eta\gamma)$, $c\bar{c}$ component of η 77−6116
planar bootstrap model calcs., $Q\bar{Q}$ and QQQ mass spectra 78−89685
positive parity excited baryons in quark model with hyperfine interactions 78−82161
pseudoscalar meson masses and sum rules, 4 quark model 77−10233
pseudoscalar mesons, chiral $SU_4 \times SU_4$ nonlinear Lagrangian symmetry breaking 77−57513
Q^6 dibaryon resonances, orbitally excited mass spectrum, decays 80−73670
QCD hadronic spectrum, α-expansion method extraction, harmonic oscillator test 79−3009
QCD spectrum calcs. in lattice gauge theory using Wilson's fermion method 79−367
quark shell model, meson spectroscopy 79−6328
quark-antiquark systems combined by Coulomb type attractive force 78−89677
Regge trajectory intercepts and mass formulae relation *(Russian)* 79−85283
relativistic oscillator formalism for hadron struct. and props. 80−9144
relativistic quark models, $c\bar{c}$ and $b\bar{b}$ singlet triplet splitting, mass formulae *(Russian)* 80−37232
semiempirical mass formula for hadrons in quark model and QCD 78−74236
SL(2,R) and SL(2,Z), mass group associated with hadronic mass spectrum 79−63459
soliton, two-dimens. scalar field theory 77−204
solitons with quantised charge, mass formula 79−93282
spectrum deformation of hadronic system, in coherent production on d *(Russian)* 79−93394
strong gravity and particle mass spectrum 77−30351
strong interaction models in 6-ε dimens., corrections to Gell-Mann Okubo mass formula 77−10182
SU_4 charmed-hadron multiplets 78−37192
$SU(2)_L \times U(1)$, mass hierarchies and Cabibbo angle formula 79−63420
$SU(2)_L \times U(1)$ with four flavours, relation between Cabibbo angle and quark masses 80−105872
SU(2)×U(1)×U(1) model, neutral current, quark mass reactors, spontaneous broken Lagrangian 79−97563
SU(3)×U(1) modified model, quark and lepton mass hierarchy 78−89653
SU(3) 27-plet mesons masses, existence of low-mass long lived exotics in quark model 78−33032
$SU(4)^4$, determ. of unifying mass scale 78−45830
SU(4)×SU(4) symmetry breaking, Cabibbo angle, nonlinear hadronic Lagrangian, PCAC *(Russian)* 80−42360
SU(4) 16-plet boson mass formulas, flavour symmetry breaking 80−37250
SU(4) breaking mass formulae for $^1/_2{}^+$, $^3/_2{}^+$ baryons and 1^-, 0^- mesons *(Russian)* 78−89692
SU(4) framework for higher order hadronic mass formulae 79−366
SU(4) framework for meson nonet struct., mass relations, mass splittings 79−288
SU(4) meson mass formula from generalisation of SU(3) Schwinger mass formulae 78−37190
SU(4) mixing angles and quark-loop anomalies 77−34104
SU(4) symmetry breaking pattern and baryon masses 78−89690
SU(5), broken, meson mass formulae 80−47267
SU(5) mass formulae, $b\bar{b}$ states masses, mass differences and splitting 79−17691
SU(5) symmetry with beauty quark, baryon and meson mass spectra 79−45079
SU(6) based renormalisable unified gauge model with calculable masses 78−89647
SU(8), $SU_W(8)$ symmetries, mass formulae, mixing *(Russian)* 78−66097
SU(8) mass relations among $J^P = 1^{12+}$ and $3/2^+$ baryons 77−71499
three quark oscillator model for baryon spectrum 77−22698
twistor struct. of hadrons, classification and masses 77−22695
unified gauge model with a nonlinear chiral hadron Lagrangian, SU_4 hadron multiplets 80−42378
vector mesons, unitarity corrections to masses and mixing angles 79−49487
A_1 meson, mass formulas and selection rules in large SU(3) mixing 80−86700
B meson, mass formulas and selection rules in large SU(3) mixing 80−86700
D(1.87) isomultiplet, mass differences, effect of EM mixing on mass splitting *(Russian)* 78−89714
D-meson masses and leptonic decay consts. 78−66087
$D^*(2.01)$ isomultiplet, mass differences, effect of EM mixing on mass splitting *(Russian)* 78−89714
$\Delta_{D35}(1925)$ baryonic degrees of freedom, nonrelativistic, harmonic oscillator quark model mass formula 80−91066
F-meson masses and leptonic decay consts. 78−66087
F^* meson and anomalous $e\mu$ events 78−66108
μ-e mass quotient, modified Weinberg-Salam model calcs. *(French)* 80−82926
ω-meson series mass formula 77−22714
pp and $\bar{p}p$ evidence for inclusive cross section ratio effective mass relationship 78−82185
π, K and baryon linear mass relations 78−41520
ψ and ψ' charmonium spectroscopy anal. using square root pot., decay widths 78−82182
$Q_1(1280)$, mass formulas and selection rules in large SU(3) mixing 80−86700
$Q_2(1400)$, mass formulas and selection rules in large SU(3) mixing 80−86700
$q\bar{q}(q^2\bar{q}^2)$ mesons, mass formula 80−62958
$Q\bar{Q}$ relativistic bound states, mass formula, unification of linear Regge trajectories 79−89141
Υ, SU(4) mass relation anal. *(Chinese)* 79−58934

mass formulae continued
ϒ(9.4 GeV), mass formulae and splittings 78−33107
ϒ(9.4) family, gauge theory mass anal., harmonic oscillator pot. 78−82186

mass measurement
see also weighing
absolute mass detection limits using laser microprobe anal. with cross excitation 78−7297
acceleration compensation of force transducers and weighing systems *(German)* 79−35733
accurate method for mass meas. using analytical balances with built in weights *(German)* 78−45596
aerosol, single droplet, size and mass meas. using electrodynamic balance 80−89535
air density effects, calc. from atm. variables 80−105615
astronomy, tracking data processing and mass determ. *(Russian)* 78−49297
beam balance, deviation from mutual disposition of working edge of prisms 78−4594
biological sections, mass thickness determ. from electron micrographs 77−70573
bone, using Xe-filled multiwire proportional counter as detector 78−15884
calibrations of multiples of the unit of mass, systematic search for orthogonal systems 80−82747
conference, Braunschweig, W.Germany (Sept. 1978) 79−35725
digital mass-measuring device, automatic, 0 to 9.99 g 79−71417
electromechanical balance type-test results *(German)* 77−79059
gravimetric standards, best fit calibration curve parameters, error estimates 79−87931
high-accuracy (0.01%), developed for spacecraft appl. 80−73324
impact ejecta parameters depend. on primary vel. 78−59291
kilogram as standard mass unit *(German)* 77−22532
left ventricular volume rel. to QRS voltage and Frank vectorcardiogram 79−44029
liquid N monitor for Li drifted Ge detectors 78−29122
mass standard error limits and accuracy class determ. *(German)* 77−74364
mass standards (1000 kg) for electromech. balance testing *(German)* 77−79060
measurement methods in Yugoslavia *(Croatian)* 80−105616
microweighing in vacuum and controlled environments and use of beam microbalance, book 80−62401
moulding materials and mixtures, exam. of gases released 79−52817
particle mass determination using STEM 78−21294
periodic mass variations obs., using electromechanical vibrating system 80−47020
quartz crystal with electrode-tab config., simultaneous mass and temp. determ. 78−54353
quartz mass/thickness detector using ICs, principle, design 79−17393
quartz microbalance, influence of tabs thickness on resonating props. of quartz cryst. 78−18140
resistive transducers, normalisation *(Rumanian)* 80−4699
respirable aerosol mass conc. meas., using piezoelec. microbalance 78−69518
secondary standards of 1 kg unit, stability, USSR 78−4595
SI units fundamentals *(French)* 80−95059
simultaneous mass and temperature determ. using single quartz wafer, optimized cryst. cut 79−49205
standards, calibration by sets of weights intercomparison 78−54342
STEM, mass thickness recording 77−71300
STEM methods and associated errors 80−73537
substance amount, precise meas. and dosage 80−90819
thin films, vac. deposited, mass change, optical transmittance, and reflectance, simultaneous meas. apparatus 79−75501
time measurement experiment in phys. education, mass and charge meas. using electronic time counter *(Japanese)* 78−41127
tissue samples, for energy-dispersive X-ray fluoresc. anal., use of X-ray scatt. 77−48971
two-phase flow, nonequil., true mass steam content meas. by diffusion indicator method 79−86538
two-string balance microprocessor operation *(German)* 78−57936
vectorcardiogram and ECG correlation with angiocardiographic left ventricular mass 79−44027
weighing value and mass comparison, w.r.t. air buoyancy corrections *(German)* 77−53863
$K^{\pm}$, average mass meas. in $e^+e^- \rightarrow \phi \rightarrow K^+K^-$ 79−30742
Cr film, vacuum-deposited, quantitative mass anal. by colorimetry 77−69998
Fe dust particles, respirable, meas. of mass and thickness by SEM backscattered electron imaging 79−21707

mass spectra
see also mass spectrometers; mass spectroscopic chemical analysis; mass spectroscopy; secondary ion mass spectra; time of flight mass spectra
acetaldehyde, multiphoton ionisation mass spectra 80−83436
acetaldehyde-d_1(-d_3), fragmentation processes, H scrambling, photoionis. mass spectra 78−42139
acetone ions, fragmentation, kinetic energy release, mass spectra 77−79192
acetylene cation+methane, reaction, vibr. and translational energy depend., mass spectrosc. obs. 79−47908
acetylenic iron carbonyls, mass spectra *(Italian)* 79−18313
adhesive bonds breaking under high vacuum, light and electron emission, spectral comp. obs. 80−55190
alcohols, chemical ionisation mass spectra 77−75273
alkali metal heteronuclear diat. mols., appearance pot., dissoc. energy, ionis. pot., mass spectra obs. 78−25750
alkanes, collisional dissoc., time of flight mass spectrometric obs. 77−74545
amine, chemisorbed on metal or oxidised metal, surface ionisation, mass spectra expts. 78−2360
atmospheric negative ions, photodissoc. and photodetachment 80−69199
atmospheric positive ions, photodissoc., 5300 to 6700 Å, mass spectroscopic obs. 78−16095
automatic recording, microphotometer modification 77−12845
azulene, multiphoton ionisation, mass spectra 80−63717
benzaldehyde, photoionisation mass spectra formation by UV laser radiation *(Russian)* 80−93781
benzaldehyde, proton affinity, MINDO/3 results compared to ICR obs. 78−1103

mass spectra continued
benzene, ^{13}C substituted, mass selective two-photon ionis., mass spectroscopy obs. 80−9651
benzene, mass spectra following reson. enhanced multiphoton ionisation 80−106362
benzene, mol. beam, fragmentation by reson. enhanced multiphoton ionisation 79−54213
benzene, multiphoton ionisation fragmentation patterns, statistical theory 80−95693
benzene, photoionisation mass spectra formation by UV laser radiation *(Russian)* 80−93781
benzene, trifluoromethyl derivatives, first ionis. pots., CF_3 group nature 79−27110
benzene, visible and UV photoionisation and fragmentation 80−69195
benzene+$O(^3P)$, reaction product identification by mass spectrometer 78−7185
benzene cation+benzene, trapped ion mass spectra 80−89470
borazine, triplet state, ICR trapped electron spectra obs. 79−6884
boroxines, trioxadiborolanes, evidence for aromaticity from mass spectral and NMR meas. 78−9172
bromobenzene ion fragmentation, photoelectron-photoion coincidence spectra 80−95682
butene, cations, photodissoc., branching ratio meas., unimolecular decay theory 77−6873
2-butene ion, fragmentation, angular momentum in ion-mol. reacts., RRKM calc. 80−66773
carbon tetrachloride, charge exchange mass spectra 80−43177
chloroethane molecular ion, laser induced photodissoc. in gas phase 79−94048
chlorofluoromethanes, negative ion form. by 0.10 eV near-monoenergetic electron impact 79−41245
chloroform, charge exchange mass spectra 80−43177
chloromethane, charge exchange mass spectra 80−43177
chlorophyll-a, hydration, field desorpt. mass spectral obs. 80−71936
classification, ion series-related index, fast library searching appls. 77−12837
coagulating system, disintegrating particles, steady-state distribution 79−57296
computer identification systems 78−86966
cycloalkane, mol. ion struct., photodissoc., charge transfer, ICR obs. 79−45774
n-decane-n-decane-d_{22}, γ-irrad., H_2/D_2 product ratio mass spectra, mechanism 77−40558
dibromoalkanes, energy partitioning in mass spectrometric displacement reactions 80−89471
dichlorodifluoromethane, IR multiple-photon laser-induced decomposition, Cl and Cl_2 form. 78−40066
dichloromethane, charge exchange mass spectra 80−43177
dictionary for library searching 79−89031
dimethyl sulphoxide, form. of $(CH_3SOCH_3)_2H^+$ and $CH_3.CH_3SOCH_3^+$ in ICR mass spectrometry, proton affinity 78−3319
dimethyl tartrate, chirality detection with chem. ionis. mass spectroscopy, meso ion obs. 77−68139
dioxirane, decomposition products, mass spectrometric obs. 78−11504
doubly charged negative ions, electron impact 77−31006
elastomers, vacuum compatible, chem. character correl. with physical charact., review 78−24804
electrolyte, aq. soln., field-induced ion evap. from liq. surface at atm. press. 80−29859
ethane, mass spectrometric ionis., dissociation 77−3488
ethanethiol, rare gas sensitised radiolysis and charge exchange mass spectra 77−48664
ethanol, ion internal energy selection by angle-resolved mass spectrometry 80−53164
ethyl chloride-NH_3 positive ion molecule reaction, high press. mass spectra 79−24729
ethylene, chemistry in RF discharge, mass spectrometric obs. 77−9084
ethylene, ion ejection mass resolution test of wideband freq.-swept marginal oscillator detector for ion cyclotron reson. spectrometer 80−9069
ethylene, line selective excitation with CO_2 laser light and vibr. relax. 80−9705
ethylene, mol. ion, mass spectra ion intensity internal energy depend., quasi equilibrium theory calcs. 80−53163
ethylene+$Ar^+(Kr^+)(Ne^+)(Xe^+)$, 2-stage ion beam mass spectrometric obs. 77−9061
ethylene oxide-d_0, -d_4, ion chemistry, photoionisation and ion cyclotron reson. obs. 77−21373
ethylenimine, gas phase photolysis and γ radiolysis fragments 77−29022
fluorocarbonyl compounds, triplet state, trapped electron ICR spectrosc. 79−59373
formic acid ions, fragmentation, energy selected, photoelectron-photoion spectra 80−95676
formyl fluorides, gas phase ion-mol. reactions, comparison with H_2CO+F_2CO, H_2CO+Cl_2CO 77−63900
fragmentation processes, dispersion relation 77−79704
furan, resonantly enhanced multiphoton ionisation 80−106362
furan, trifluoromethyl derivatives, first ionis. pots., CF_3 group nature 79−27110
halocarbons, multiphoton dissociation, product identification 78−37694
haloethylenes+$Ar^+(Kr^+)(Ne^+)(Xe^+)$, 2-stage ion beam mass spectrometric obs. 77−9061
heavy nuclei, Z=68-72, nucleon separation, pairing and decay energies and mass defect 77−79301
n-heptane, mass spectra, using QUISTOR, phase-synchronised ion ejection from quadrupole ion storage mass spectrometer 79−44975
1-heptene, field ionisation mass spectra, surface processes 79−11503
hexafluoro ethyl cation fragmentation, mass spectrometry 80−53070
n-hexane, mass selective storage mass spectra by quadrupole ion storage mass spectrometer 80−52351
hydrocarbon ions, mass spectra, H atom scrambling, delocalisation 80−58135
hydrocarbons and organic halides, fragment ion kinetic energy determ. by mass spectra 77−6958
ice, electron-irrad., cluster-ion prod., lattice and fragmentation energies 77−4911
ICR spectra, line shapes, linear response theory appls. 79−2874
inert gas ion-atom collisons, momentum transfer rate consts., energy depend., polarisation pots. 77−75260
inert gas Van der Waals dimers, electron impact ionis. 80−58400
inert gas-halogen mixture, ion form., ion-mole. reactions, mass spectra 77−61841

mass spectra continued
iodomethane+Rb reaction cross section, translational energy depend. min. 77−66753
iodomethane cation, photodissoc., mass spectrometric obs., isotope effects 77−75241
ion+molecule reaction, equilib. consts., ion cyclotron reson. spectrometer meas. 77−56218
ion + molecule, elastic collision frequency, determ. by Fourier transform ICR spectroscopy 79−50105
ion cyclotron motion coupling to ion internal degrees of freedom 79−18314
ion cyclotron resonance, nonlinear effects 77−34782
ion formation and relative yields from laser prod. plasma, mass spectra, appls. *(Russian)* 78−59631
ion microprobe trace element anal., high resolution 77−21445
ion photodissociation, kinetics meas. using time of flight mass spectrometer 77−75240
isotope separation, plasma ion cyclotron reson. 77−10787
ketene-d_0-d_2, mol. ion reactivity, vibr. energy effects, mass spectrometric obs. 77−44470
low capacity codes, based on statistical moments 78−255
metal, DC reactive sputtering, glow discharge mass spectrometry and X-ray diffr. 79−38701
metal, thermal ion energy distrib. by retarding field modulation method *(Japanese)* 79−78822
metal layer growth by sputtering, corpuscular diagnostics of hollow cathode discharge 80−16180
metastable atoms, charge permutation, appl. of reversed geometry mass spectrometers 80−37118
metastable ion decomposition, mass spectra peak shapes 77−44475
metastable ion decomposition, mass spectra peak shapes 77−44476
metastable negative ion, electron impact decomp., kinetic energy release 77−6944
metastable peak shapes, Monte Carlo calc. method 78−70968
metastable unimolecular transition, collision-induced transition, energetic analysis by static mass spectrometers *(Rumanian)* 78−46460
methane, ion internal energy selection by angle-resolved mass spectrometry 80−53164
methane ions, fragmentation, kinetic energy release, mass spectra 77−79192
methanol, and deuterates, dissoc. ionisation mechanisms, photoionisation mass spectra, ionic struct., interstellar formation 79−3503
methanol, ion internal energy selection by angle-resolved mass spectrometry 80−53164
methanol, ionic dissoc., photoelectron-photoion coincidence spectroscopy 80−66774
methanol-O_2 flame, combustion and ionisation 79−20357
methyl chloride-NH_3 positive ion molecule reaction, high press. mass spectra 79−24729
methyl halide ions, unimol. dissoc. and internal conversions, coincidence meas. 77−6869
methylchloride, CH_3Cl^+, photofragmentation at 366 nm 78−58752
4-methylene-cyclohexadiene-2,6-one-1, proton affinity, MINDO/3 results compared to ICR obs. 78−1103
MO-models and simulation of fragmentation 77−417
molecules, mol. wt. from 186-273, EPA/NIH mass spectral data base vol. 79−68329
molecules, mol. wt. from 273-381, EPA/NIH mass spectral data base vol. 79−64120
molecules, mol. wt. from 30 to 186, EPA/NIH mass spectral data base, vol.I 79−64119
molecules, mol. wt. from 381-1674, EPA/NIH mass spectral data base, vol.IV 79−64121
MSDC/EPA/NIH mass spectral search system 78−65912
naphthalene, multiphoton ionisation, mass spectra 80−63717
naphthalene, trifluoromethyl derivatives, first ionis. pots., CF_3 group nature 79−27110
negative ion unimolecular gas-phase decomposition, field ionis., technique for 10^{-11}-10^{-5} s lifetime 79−92046
nucleotide base stacking interactions in vacuum, field mass spectrometry 80−81526
organic ion, excited electronic state correlation with mass-spectral fragmentation pattern 80−45482
organic ion struct. determ. from collisional activation spectrometry *(Japanese)* 79−76531
organonitrogen derivatives of Si, Ge and Sn, prep. and props. 78−60456
peptide sequencing by DADI mass spectra 79−57573
perchloro-[4]-radialene, IR and Raman spectra 77−77198
perfluorobenzene, electron attachment, radiative and dissoc., negative ion lifetimes, ion cyclotron reson. spectra 80−74251
perfluorocyclobutane, electron attachment, radiative and dissoc., negative ion lifetimes, ion cyclotron reson. spectra 80−74251
perfluoromethylcyclohexane, electron attachment, radiative and dissoc., negative ion lifetimes, ion cyclotron reson. spectra 80−74251
perfluorotoluene, electron attachment, radiative and dissoc., negative ion lifetimes, ion cyclotron reson. spectra 80−74251
photosynthetic carboxylation reactions, ^{13}C kinetic isotope effect 79−57566
polyacetylene:AsF_5, thermal decomp. kinetics, elec. cond., ESCA and mass spectra 80−50830
polyatomic ions, energy deposition on high-energy collision, angle-resolved mass spectrometry obs. 80−32825
polyatomic molecules, structure recognition, from IR, UV, NMR and mass spectra, computer method 78−25737
polyatomic molecules, visible and UV photoionisation and fragmentation 80−69195
positive ions+H_2O, reaction rate consts., product distrib., ICR obs. 79−8428
propan-1-ol, ion internal energy selection by angle-resolved mass spectrometry 80−53164
propane, ion internal energy selection by angle-resolved mass spectrometry 80−53164
propane, mol. ion, mass spectra ion intensity internal energy depend., quasi equilibrium theory calcs. 80−53163
propane and deuteropropane, fragmentation, threshold photoelectron photoion coincidence mass spectra 77−14505
propane mol. ion, competing slow metastable processes, tunnelling mechanism, tandem-ICR obs. 77−28976
propion-aldehyde ion, fragment/mol. ion current ratio, field ionis. mass spectrum, CNDO/BW calc. 77−65544
mass spectra continued
propyl compounds, photolysis, photofragment free radicals, mass spectra *(Japanese)* 78−7220
propynyl cation+propyne, reactant structure effects 80−89469
pulsed microwave inert gas discharge, ion composition, mass spectra 79−14616
pyridine, on hot W filament, mass spectrometric obs. 79−81302
pyrrole, resonantly enhanced multiphoton ionisation 80−106362
rare earth hydrides, form. by rare earth reaction with H_2O vapour 80−76504
rare earth oxides, polyatomic gaseous, atomisation energies and stand. ht. of formation determ. 77−54622
reactive gas flow through porous barrier, exit flux, composition depend. 77−31383
spark source, photographical analysis 79−43658
sputtered neutral particle flux props., ion bombardment of polycryst. targets, review 77−44110
sputtered particles, energy and mass distribs. 80−84822
steel, volatile products from reaction with H_2O-CO_2, high temp. 80−81233
steroids, mass spectra, computer-aided interpretation by pattern recognition, preprocessing effects 78−15733
1,1,2,2-tetrafluorocyclobutane, ion-mol. reactions, reaction pathways, mass spectra 77−21368
sym-tetrazine, isotope selective mol. spectroscopy and isotopically pure mols. prod. with dye laser 80−11926
thermal desorption mass spectra, activation energy, rate coeff., analytic expressions 78−60022
thermal desorption mass spectra, effect of heating rate and pumping speed, quantitative anal. 78−60023
1,2,4-thiadiazolidine derivatives, isomers, negative ion mass spectrometry *(Japanese)* 78−5367
toluene+$O(^3P)$, reaction product identification by mass spectrometer 78−7185
transition metal tricarbides, atomisation energy, stability, mass spectrometric determ. 79−7037
tribromomethane-methane, mass spectra, vel. distrib. effects 77−54627
trichlorofluoromethane, IR multiple-photon laser-induced decomposition, Cl and Cl_2 form. 78−40066
trifluoroformamide, photodissoc., obs. of NO (v=1) 78−74712
trifluoromethoxide gas phase ion reactions with carboxylic acids, ion cyclotron reson. obs. of competitive solvation 79−79227
trimethylbenzene+$O(^3P)$, reaction product identification by mass spectrometer 78−7185
tropone, proton affinity, MINDO/3 results compared to ICR obs. 78−1103
TSeF salts, mol. props., one-dimens. cond. salts form. 78−6363
TTF-TCNQ, vaporisation. mass spectroscopy 77−1224
two photon absorptivity, ion cyclotron reson. photodissoc. spectra, CNDO/S-CI-perturbation theory 80−74123
vapour with different degrees of polymerization, mass spectra, line overlap coeff. calc. 79−96392
velocity distribution effects, mol. beam inlet method 77−54627
vinyl fluoride, vibr. excitation effects on ion-molecule reaction pathways, photoionisation mass spectra 77−16804
pp→$\Delta^{++}p\pi^-$, 4 GeV/c, mass spectra, ang. distribs. and momentum transfer *(Russian)* 80−42489
pp interaction, 52 GeV, two-photon mass spectra, X(2830) prod. 78−21470
pp→$pn\pi^+$, mass spectra at 28.5 GeV/c 77−22801
pp→$pp\pi^0$, mass spectra at 28.5 GeV/c 77−22801
Ag island films, on W, growth and desorption kinetics, mass spectra obs. *(German)* 79−46978
Ag, vaporization, thermodynamic props. determ. by mass spectroscopy 78−22841
Ag-Ge alloys, liq., thermodynamics and short range order, mass spectra meas. 79−52740
AgF(Br), sputtering processes during 6 keV Xe ion bombard. 78−68590
$Ag_2S(Se)(Te)$, solid and liquid, mass spectrometric obs. of VP, heats of form., comp. 79−42266
Al, industrial, depth profiling by ion microprobe with high mass resolution 79−46894
Al, thermal desorption of oxide film, influence of grain boundaries and recrystn. 80−61023
Al-B, enthalpies and free energies, effusion and mass spectra, phase diagram 78−23665
Al_2O_3 anodic film, gas emission, mass spectrometer study *(Polish)* 77−9157
Ar, collision processes, photoionisation mass spectra obs. 79−31479
Ar^+, conversion to mol. ions, three body association coeffs. determ. using drift-tube mass spectrometer 80−108699
$2Ar+Ar_2^+=Ar+Ar_3^+$, equilib. consts., mass spectrometric determ. 79−100347
$Ar^++CO(CO_2)(N_2)(N_2O)(NO)(O_2)$, charge transfer, thermal energy, product distrib. obs. 78−25656
Ar_2, electron impact ionisation, relative cross-sections, mass spectrometric meas. 79−86078
Ar_2^+, photodissoc., pot. curves and photofragment spectra 77−88514
Ar_2^+, photodissoc. cross sections at 3.0 and 3.5 eV 78−62861
Ar_2^+, photodissoc. mass spectrometric obs. 77−6867
ArKr, electron impact ionisation, relative cross-sections, mass spectrometric meas. 79−86078
As_2S_3, thermodynamic of evaporation 77−47568
As_2S_3, vaporisation, mass spectrometric analysis 78−22843
Au, energy and mass spectra of scattered 8 keV Ar^+ ions and desorbed species 77−32487
Au-Fe, liq., thermodynamic mixing effects, mass spectrometric meas. eval. *(German)* 77−59123
AuV, gas, bond dissoc. energy, from high-temp. mass spectra of V-Nb-Mo-Au 79−45860
BaBr, BaCl gas equilib. mass spectra, dissoc. energy 77−65543
Bi film, on Si(111) substrate, MBE deposition kinetics 80−10817
Br, diffusion in Ar at 298K, time resolved mass spectrometric determ. 79−90365
Br+F_2, reaction kinetics, mass spectroscopic obs. 77−77743
Br+O_3→BrO+O_2, rate consts., mass spectrometric obs. 77−63897
Br_2, diffusion in NO at 298K, time-resolved mass spectrometric determ. 79−90365
Br_2, dissoc. attachment by 0-8 eV electrons 78−74776
C foil, plasma production by laser irrad., study of mol. ion 79−90429
C thin foil, transmission of fast H_3^+ mols. 79−76484

mass spectra continued
$C^+ + H_2 \rightarrow H + CH^+$, energy spectrum and prod. vibr. excitation 77−77745
CF_3 radical, dipole moment from beam mass spectrometric anal. 79−59596
CH_3^+, CD_3^+, reactions with acetic acid methyl acetate, dimethyl ether and ethylene oxide 77−63901
$CH_4^+ + CH_4(CH_2D_2)$, dissoc. charge transfer reactions, H and D atoms elimination 78−85141
CLi_3, desorption from graphite expt., ionis. pot. 79−34392
CO, chemisorption on AgNa mordenite 80−2752
CO, chemisorption on Ti, flash desorption mass spectrometry obs. 77−89646
CO laser, mass spectra of positive ions in discharge plasma 77−89315
$CO^+ + H_2$, ion-molecule reaction detection of laser-induced ion spectrum, rot. components 78−74671
$^{13}CO^+ + CO$, charge-exchange detection of $^{13}CO^+$ electronic absorption spectrum, hyperfine consts. calc. 78−70822
CO_2, negative ion form., photodissoc., mass spectrometric obs. 78−13558
CO_2, positive and negative ion reactions 77−40540
CO_2^-, hydrated anion stable gas phase heteronuclear clusters, mass spectra, autodetachment rates 80−14266
CO_2-H_2O-O_2, gas mixture, photodetachment and photodissoc., mass spectra meas. 77−500
CO_2-O_2, negative ion form., photodissoc., mass spectrometric obs. 78−13558
$(CO_2)_2^+$, photodissoc., mass spectrometric obs. 77−6867
COS, dissoc. photoionisation, mass spectrometric obs. 79−72366
$CS + O \rightarrow CO + S$, rate const. temp. depend., ESR-mass spectrometer obs. 78−20013
CS_2, dissoc. photoionisation, mass spectrometric obs. 79−72366
CS_2, liq., vap. press., isotope effects, mass spectrometric determ. 77−24412
CS_2, photoionisation and dissociative ionisation due to 60-129 nm light, mass spectra study 79−94044
CS_2^+, and $(CS_2)_2^+$, photoionis. in supersonic mol. beam 79−98165
CS_2^+, dissociation mechanism 79−59601
CS_2+inert gas, translational excitation, energy transfer, cross spectra 77−50559
CSH_3^+ ions, structs. and relative energies 78−82861
CSe_2, photoionis. mass spectrum, Rydberg states props., heat of form., CSe dissoc. energy and ionis. pot. 77−46604
^{12}C+alkane (alkene), thermal energy reaction, mass spectra 77−9067
^{13}C+alkane (alkene), thermal energy reaction, mass spectra 77−9067
CaBr, gas equilib. mass spectra, dissoc. energy meas. 77−65543
$CdCr_2Se_4$, evap., mass spectra 78−53238
CdI_2, sputtering processes during 6 keV Xe ion bombard. 78−68590
CdS, cryst. growth from vapour in sealed silica tubes, emission and mass spectra 79−43117
CdTe, undoped, high-resist.- characterisation, impurity level investig. 77−39801
Cl^- hydration complexes, gas phase, electrostatic calcs. 80−100055
Cl^--Ne(Ar)(Kr)(Xe), longitudinal diffusion coeff., generalised Einstein relation 79−86552
$Cl^+ + CO \rightarrow O + CCl^+$, reaction cross section, heat of form., mass spectrometric obs. 79−61843
Cl_2, dissoc. attachment by 0-8 eV electrons 78−74776
Co complex, S_4N_4 with $CoCl_2$, mass and IR spectra, config. 78−13494
Co, pure surfaces, adsorpt. of water and decomp. *(German)* 80−26054
$Cr_pC_n^+$, p=1 to 4, CrC_n^-, clusters, electronic props., mass spectra obs. *(French)* 79−45877
Cs-N_2 discharge, Cs_2^+ form. rate, mass spectra obs., N_2 press. depend. 79−27853
$Cs + D_2O$, ion-pair form., energy, angle and mass anal. of products 78−70970
Cs_2CO_3 and Cs_2SO_4, ionic equil., mass spectra obs., heats of reaction and form. of ions 79−87867
Cu mirror, surface defect layer form. on mech. polishing 80−33122
Cu, vaporization, thermodynamic props. determ. by mass spectroscopy 78−22841
CuO, desorpt. of ions by low power laser beam 80−80092
D I, ionisation pot. photoionisation mass spectra 78−25632
$D + D_2^+(CO_2^+)(CO^+)(N_2^+)(HCN^+)$, reaction, ion cyclotron reson. mass spectrometric obs. 79−64098
Er, vaporisation, heat of sublimation, meas. 80−103471
ErD_2 thin film, degradation during film processing, investigation 80−101047
EuO(g), thermochem. props. 77−14604
EuS, vaporisation thermodynamics, Knudsen cell mass spectra 77−47569
F_2, dissoc. attachment by 0-8 eV electrons 78−74776
$Fe_pC_n^+$, p=1 to 4, clusters, electronic props., mass spectra obs. *(French)* 79−45877
$Fe_2(CO)_6(HC_2R)_2$, R=H, Bu^t, Ph, binuclear complexes, isomer identification and stability *(Italian)* 77−54620
Ga, atomic weight from solid-source mass spectra 77−541
GaAs, semi-insulating, elec. characts., correl. with mass spectra anal. 78−39104
$GeCl_2$, combined electron diffr. and mass spectra mol. struct. determ. 79−89783
GeTe, high temp. mass spectrometric obs. of vaporis. 77−76542
H I, ionisation pot. photoionisation mass spectra 78−25632
$H + H_2^+(HeH^+)(CO_2^+)$, reaction, ion cyclotron reson. mass spectrometric obs. 79−64098
$H + O_2$, singlet state O_2 form., reaction mechanism, mass spectrometric obs. 78−53204
H^++graphite, 10 keV, chemical sputtering coeff. temp. depend., methane form. *(Russian)* 77−4707
H_2, chemisorption on AgNa mordenite 80−2752
H_2, chemisorption on Ti, flash desorption mass spectrometry obs. 77−89646
H_2, solid, electron-irrad., cluster-ion prod., lattice and fragmentation energies 77−4911
H_2^+, 400 keV beam dissoc. collisions in air, ang. distribs., vibr. state effects 79−10197
H_2^+, photodissoc., mass spectra 80−86489
H_2+D(O)(Cl)(Br), relax. and chem. reaction, time resolved IR fluoresc. and mass spectrometry obs. 80−69177
H_3^+, ion density decay in He-H_2 plasma, mass spectral obs. 77−3987
$H_n^+ + N_2$, (n=2 to 27), 250-900 eV collisions, fragmentation 77−88525
HCl, charge exchange mass spectra 80−43177
HCl, dissoc. electron attachment kinetics in flame, mass spectra obs. 78−68872
HCl-N_2 mixture, electron swarm, Cl^-.HCl cluster formation, dissoc. attachment, drift tube mass spectra 78−68884
HCl+D(O)(Cl)(Br), relax. and chem. reaction, time resolved IR fluoresc. and mass spectrometry obs. 80−69177
HF, fragmentation, enhanced vibr. excitation effect, mass spectra 78−20004
HF, highly excited, ionis. pot., mass spectrometric meas. 78−58603
HF-ClF complex, and isotopic forms., mol. beam elec. reson. spectra, config., bonding, spectroscopic consts. 77−30860
HF+D, vibr. threshold energies, reagent energy effects 78−85145
$H_2^+(H_3^+) + He$, Hadamard mass spectroscopy, mass spectra 79−30601
$H^+(H_2O)_c$ ion-induced water clusters, mass spectra, IR continuum absorpt. 80−87257
$H^+(H_2O)_n$, secondary electron emission from charged clusters on 2.4 keV Ar bombarded surfaces 79−15580
HNC^+, radical cation, charge exchange mass spectrometry, HNC^+ ion recombination and ionisation pot. 78−76838
$H^+(NH_3)_n$, secondary electron emission from charged clusters on 2.4 keV Ar bombarded surfaces 79−15580
$HNO_2 + O_3$ reaction kinetics under stratospheric conditions 78−11499
H_2O, D_2O, fragment ion formation on photoionisation, energetics and mechanism 77−501
H_2O^++diatomic (polyatomic) molecule, reaction, ICR obs. 79−8429
$H_2O^+ + H_2$, ion-molecule reaction detection of laser-induced ion spectrum, rot. components 78−74671
$H_3O^+(H_2O)_n$ formation in vacuum spark, mass spectrometer expt. 79−32844
$H_3O^+.nH_2O$ cluster ions, stability, assoc. and dissoc. 77−60055
$H_3S^+.H_2O$ cluster ions, stability, assoc. and dissoc. 77−60055
$H_3S^+.nH_2S$ cluster ions, stability, assoc. and dissoc. 77−60055
He, field-ion appearance pot., theory 77−545
He^+, conversion to mol. ions, three body association coeffs. determ. using drift-tube mass spectrometer 80−108699
He-Cd, afterglow, Cd^+ excited state prod. by Penning and charge exchange reactions 77−15252
$He^+ + CO(CO_2)(N_2)(N_2O)(NO)(O_2)$, charge transfer, thermal energy, product distrib. obs. 78−25656
$He^+ + H_2(D_2)$, dissociative charge transfer, 78-330K 80−61079
He_2^+ form. in pulsed afterglow, mass spectroscopic obs. 80−54046
Hf-H, diffusion in hydride phase, exam. 80−29204
$Hg_{1-x}Cd_xTe$, vaporisation under Knudsen effusion conditions 80−2154
I^- hydration complexes, gas phase, electrostatic calcs. 80−100055
I_2, dissoc. attachment by 0-8 eV electrons 78−74776
I_2^+, impact dissoc. cross-section, excitation energy, mass spectral obs. 77−3489
InSb, undoped and Te-doped, anomalous impurity segregation, Hall and mass spectrum meas. *(Chinese)* 80−59501
Ir (110), chemisorption of O_2, sorption and dissoc. kinetics 79−33186
K+HCl, ion pair form., energy loss spectra 79−34286
K+halogenated methane, negative ion form., electron affinities, bond dissoc. energies 78−82827
K_2, beam, multiphoton ionisation mass selective laser spectroscopy, vibronic, gyrovibronic states, clusters 78−21985
K_2CO_3 and K_2SO_4, ionic equil., mass spectra obs., heats of reaction and form. of ions 79−87867
KCl, beam, surface ionisation on W ribbon, mass spectra 77−27173
KCl-CsCl solid soln., SIMS, clustering distance critical to metal dimer form. 79−72379
K_xO_y, mass spectrometric investigation 78−64873
K_2SO_4, mass spectrum obs. of vaporisation, vapour comp. and press., transition and form. heats 80−19933
K*+molecule, assoc. ionisation, mass spectra *(Russian)* 77−42393
Kr^+, and isotopes, trajectory in const. mag. field plus orthogonal sinusoidal elec. field 78−50687
$Kr + H_2S^+(CS_2^+)(CH_3I^+)(CF_3I^+)$, collision induced molecular ion dissociation, mass spectra *(Russian)* 77−88549
Kr_2, electron impact ionisation, relative cross-sections, mass spectrometric meas. 79−86078
Kr_2^+, photodissoc. cross sections at 3.0 and 3.5 eV 78−62861
KrXe, electron impact ionisation, relative cross-sections, mass spectrometric meas. 79−86078
Li atomic clusters, studied by quadrupole mass analyser 77−71900
Li-Pb, thermodynamic study using Knudsen effusion mass spectrometry 80−24578
Li_2Cl^+, mass spectra, struct., stability, expt. and theory 77−554
LiF, deformed in liquid He, penetration of He, dislocation effects 77−20131
Li_2F^+, mass spectra, struct., stability, expt. and theory 77−554
Li_2H, Li_2H^+, binding energies, ionisation pot., mass spectrometric determ. 77−65546
$LiReO_4$, thermodynamic activity in $LiReO_4$-$CsReO_4$ system, mass spectra meas. 80−2174
$^6Li^* + ^7Li^*$, laser-induced Penning and associative ionis., $^{13}Li_2^+$ enrichment 78−58796
$Li_2(g)$, thermochem. props. 77−21410
Mg, sputtering by He^+, isotope fractionation 79−87542
MoNb, mol. dissoc. energy, mass spectrometric obs. 79−10229
Mo_xSi_y films, magnetron DC reactive sputtering, struct. and props. 80−80966
N^-, appearance pot., form. by electron impact ionisation, mass spectra 77−75320
$N^+ + CO(CO_2)$ (methane)(NO), product distribs., rate consts., ion cyclotron reson. obs. 77−52618
N^++methane, charge transfer reaction, dissoc., isotope effects, mass spectra 77−21382
$N^+ + O_2$, drift tube mass spectra, rate coeffs. and prod. distrib. 77−77746
$N_2 + N^+$, collision, isotope exchange, ion cyclotron reson. obs. 77−52618
$N_2^+ + O_2$, drift tube mass spectra, rate coeffs. and prod. distrib. 77−77746
NH_2 radical, heat of form., a diabatic electron affinity, from proton affinity meas. 79−91987
NH_3, cluster-ion prod. in electron-irrad. solid, lattice, and fragmentation energies 77−4911
NH_3, electron impact ionisation, threshold to 180 eV, mass spectrometric obs. 78−13615
NH_3-ND_3, electron impact ionisation, threshold to 180 eV, mass spectrometric obs. 78−13615

mass spectra continued
$NH_3+C^+(CH_n^+)$, rate coeffs., ionised product distribs. 77−40522
NH_4^+, in afterglow, electron recomb. coeffs. mass spectrometric meas. 77−6927
N_2H_4, heat of form. determ. by electron impact dissoc. 78−61040
$(NH_3)_nH^+$, n=1-9, detected in photoionisation of supersonic mol. beam mass spectra, H-bonding 79−74356
$NH_4^+.(NH_3)_n$, in afterglow, electron recomb. coeffs. mass spectrometric meas. 77−6927
NO^+-N_2, temp.-dependent ion mobilities 79−86553
$NO+O_3 \rightarrow NO_2+O_2$, rate const., 203-361K, fast flow method 77−33143
NO_2^-, $NO_2^-.H_2O$, and peroxy isomers, photodissoc. and photodetachment 3500-8250 Å, rel. to ionosphere 80−35554
NO_3^-, $NO_3^-.H_2O$, and peroxy isomers, photodissoc. and photodetachment 3500-8250 Å, rel. to ionosphere 80−35554
NO_x^--HNO_x-H_2O clusters, gas phase, thermodynamic quantities, mass spectra obs. 80−50875
N_2O laser, mass spectra of positive ions in discharge plasma 77−89315
N_2O, photoionisation and ion dissoc., isotope effects, mass spectra 78−9203
N_2O^+, photodissociation 77−34705
$(N_2O)_2$, photo-induced vibr. predissoc. of van der Waals mol. 78−90242
$NO^+.H_2O$, photodissoc. cross sections, mass spectrometric determ. 78−1038
$NO^+.NO$, photodissoc. cross sections, mass spectrometric determ. 78−1038
$N(^4S)$ recombination rate in Lewis-Rayleigh afterglow 79−68968
^{15}N, isotopic anal., collector sensitivity error source 77−42441
Na (111) surface, epitaxial film, electron induced dissociation 80−6646
Na_2, beam, multiphoton ionisation mass selective laser spectroscopy, vibronic, gyrovibronic states, clusters 78−21985
Na_x, matrix-isolated, formed in supersonic nozzle beam, 400-800 nm absorption and mass spectra obs. 79−76439
$2NaBO_2$-B_2O_3 melt, thermodynamic props., mass spectra 80−65252
Na_2Cl^+, mass spectra, struct., stability, expt. and theory 77−554
NaF-ScF_3 system, ionic equilib., mass spectra 78−7222
Na_2F^+, mass spectra, struct., stability, expt. and theory 77−554
Na_2O-B_2O_3-GeO_2 vitreous melts, thermodynamic props. from mass spectra 80−65253
Nb, heat of sublimation, $Nb_2(g)$ form., dissoc. energy, Knudsen effusion mass spectrometric determ. 79−81297
$(NbF_5)_4$ mass spectra, vel. distrib. effects, mol. beam inlet method, mol. dissoc. 77−54627
Ne, photoionization mass spectroscopy using synchrotron radiation, reson. width meas. 79−31478
Ne^+, conversion to mol. ions, three body association coeffs. determ. using drift-tube mass spectrometer 80−108699
Ne-Ar mixture, cataphoretic segregation, mass spectra obs. 77−52649
Ne-N_2 mixture, cataphoretic segregation in DC discharge, mass spectral anal. 77−32799
$Ne^+ + CO(CO_2)(N_2)(N_2O)(NO)(O_2)$, charge transfer, thermal energy, product distrib. obs. 78−25656
Ne_2^+, photodissoc. mass spectrometric obs. 77−6867
Ni complex, S_4N_4 with $NiCl_2$, mass and IR spectra, config. 78−13494
NiAl, vapour phase mass spectra, correl. between bond strengths in liq. and gas phases 77−35466
O, autoionis., radiative emission, competition in excited state decay 77−75109
O desorption from W, electron-stimulated 77−31908
O_2, ionisation, photodissoc. of positive and negative ions, mass spectrometric obs. 78−13559
O_2^+-N_2, temp.-dependent ion mobilities 79−86553
$O_2+F^-(Cl^-)(Br^-)(I^-)$, 0.2-100 eV, reaction differential cross sections energy depend., exoergicity 77−63902
$O_2^+ + NO \rightarrow NO_2^+ + O$, photoionis. mass spectra, photoionis. efficiency 77−40537
O_3, photoionisation, O_4^+ and O_5^+ form., mass spectra 77−50477
O_4^+, form., in O_3 photoionisation, mass spectra 77−50477
O_5^+, form., in O_3 photoionisation, mass spectra 77−50477
$O(^1D_2)+N_2O$, chemical-ionisation mass spectrometry branching ratio measurements in N_2O/He mixtures 79−47905
P_4, photoionisation, mass spectra 77−30935
PH_3, electron impact dissoc. ionisation, mass spectrometric obs. 78−9264
PH_3-PD_3, electron impact dissoc. ionisation, mass spectrometric obs. 78−9264
Pb-Ar films, atomic arrangements, high energy electron energy diffractogram study, Ar conc. depend. 79−99444
PbI_2, sputtering processes during 6 keV Xe ion bombard. 78−68590
PbS vapour, mass spectroscopic study *(Russian)* 77−65545
Pd complex, 1,1,1-trifluoro-2,4-pentanedionate, struct., chem. ionisation mass spectra 78−61079
Pd complex, S_4N_4 with $PdCl_2$, mass and IR spectra, config. 78−13494
Pd, isotopic comp. and at. wt., using solid source mass spectrometry 79−864
Pd-Ti liquid alloy, mass spectrometric study of high temp. thermodynamic stability 78−15369
PrO, D_0^0-state struct., dissoc. energy, mass spectrometric obs., 79−10228
Pt (111), adsorbed H_2 and O_2 interaction investig. 77−55461
Pt, adsorption and desorption of O_2 on (110) surface, thermal desorpt., LEED/AES obs. 77−72788
Pt, adsorption of H_2 and CO, AES and flash desorpt. mass spectrometry 77−28078
Pt complex, 1,1,1-trifluoro-2,4-pentanedionate, struct., chem. ionisation mass spectra 78−61079
Re, atomic masses and mass differences, mass spectrometric obs. 77−42433
Rh (111), chemisorption of acetylene and ethylene, EELS, LEED and thermal desorption mass spectrometry 80−80057
Rh (111), co-adsorption of H_2 and CO segregation of co-adsorbed species 80−65361
Rh, coadsorption of CO and H_2, thermal desorption mass spectroscopy meas. 79−46948
Rh^+, Rh^{2+}, field evaporation, field ion mass spectra and field ion appearance spectra study 80−7479
RhTh, mol. vapour above Th-U-Rh-graphite, dissoc. energy, mass spectra 78−78832
RhU, mol. vapour above Th-U-Rh-graphite, dissoc. energy, mass spectra 78−78832
Ru complex, tris-1,1,1-trifluoro-2,4-pentanedionate, struct., chem. ionisation mass spectra 78−61079

mass spectra continued
SF^+_5, ion-mols. in beam, IR multiple-photon dissociation, mass spectroscopic detect. 79−89720
SF_6, equilib. electron-transfer reactions in gas phase involving long-lived neg. ion radicals 78−58807
SF_6, isotopically selective collisionless laser induced dissoc. 78−1037
SF_6, multiphoton dissoc., producing SF_5+F, ang. and vel. distribs. 77−27130
SF_6+He(Ar), mol. vibrational-translational energy transfer, mass spectrometric meas. 79−36739
$(SN)_x$ polymer, vaporised, mass spectra 79−98249
$(SN)_x$, vaporisation, mass spectroscopy 77−1224
$(SN)_x$, vapour phase species, mass spectra 77−61873
$(SNBr_{0.43})_x$, vap., electron impact and field ionisation mass spectra 78−44422
SO_2^+, state selected vibr. levels, fragmentation, photoelectron-photion coincidence spectroscopy 79−89707
SO_3, electron impact mass spectrometry, proton affinity, ion-mol. reactions 78−3415
S_2O, photoionis. mass spectrum, heat of form., dissoc. energy 77−46605
SO_2XY, (X,Y=Cl,F), positive and negative ion chemistry 78−85140
ScI_3, mass spectra and vapour press., and thermochemistry for dimerisation 78−27809
$ScPO_4$, $Sc(PO_3)_3$, mass spectra 77−47567
Sc_xS, high temp. vaporisation, enthalpy, atomisation, dissoc. energies 77−1223
Si (111) surface, heating effects on ellipsometric parameters 77−72764
Si film, amorphous, plasma-deposited, H_2 evolution, mass spectrometry and RHEED obs. 78−72050
Si, vapour species rel. to amorphous film deposition 78−14641
Si:P, implantation depth distrib. meas. by neutron activation anal., SIMS, junction depth method 77−31693
$Si_xC_yH_z$ films, reactive plasma deposited, comp., IR anal., and optical props. 79−95945
$SiCl_4$, electron bombardment and thermal dissoc., thermochem. stability 77−58185
SiCl(g), heat of formation, mass spectrometric determ. 78−15694
$SiCl_2$(g), heat of formation, mass spectrometric determ. 78−15694
$SiCl_3$(g), heat of formation, mass spectrometric determ. 78−15694
SiF_4+H_2, SiF_xH_{4-x} heats of form., mass spectrometric determ. 78−7221
SiH_4-He, reaction mechanisms of RF glow discharge deposition process 79−95944
SmO, dissoc. energy, mass spectrometric determ., rel. to EuO 77−58199
Sr, associative ionisation of laser-excited Rydberg states, mass spectrometry obs. 78−94303
SrBr, gas equilib. mass spectra, dissoc. energy meas. 77−65543
Ta, electron-stimulated desorption of O_2 bound state obs., 300K 77−85082
$Ta+F_2$, reaction, 690-930K modulated mol. beam mass spectrometry expts. 77−70341
TaF_x, x=1-5, reaction of SF_6 admitted to Ta effusion cell, thermochem. props. 79−100424
Te isotopic composition in meteoritic and terrestrial materials 78−82856
$TeO_{11}Cl_2$ thermal decomposition, matrix isolation IR and mass spectra 80−81306
Ti-H, diffusion in hydride phase, exam. 80−29204
Ti-Ir system, high temp. thermodynamic investig. of Ir-rich portion by Knudsen cell mass spectrometry 77−12595
TiO, high temp. vaporisation and thermodynamics, stoichiometry, mass spectra 77−59109
$TiO_{(g)}$, $TiO_{2(g)}$, thermochemistry, mass spectrometry 77−16857
TiO_x, surface film on plasma anodised Ti, comp. determ. 77−48591
$^{47,48}Ti$, precise atomic mass determ. 79−31718
V surface interaction with O_2, H_2, H_2+O_2 and H_2O, SIMS, EID 77−62753
W (100), adsorpt. of acetylene, room temp., electron spectroscopy obs. 79−7749
W, adsorption and desorption of Ag, mass spectra obs. *(German)* 79−46951
W, atomic masses and mass differences, mass spectrometric obs. 77−42433
WF_5, dissoc. electron capture, electron impact mass spectra, electron affinities 77−88579
WF_6, dissoc. electron capture, electron impact mass spectra, electron affinities 77−88579
WF_6, electron and fluoride affinities, ICR spectra 79−39130
WF_6, electron impact, negative ion form., mass spectra *(German)* 77−88586
WOF_4, dissoc. electron capture, electron impact mass spectra, electron affinities 77−88579
$Xe^+ + O_2 \rightarrow O_2^+ + Xe$, $O_2^+ + Xe \rightarrow Xe^+ + O_2$, charge transfer, photoionisation mass spectra 77−16793
Xe_2, electron impact ionisation, relative cross-sections, mass spectrometric meas. 79−86078
Xe_2^+, photodissoc. cross sections at 3.0 and 3.5 eV 78−62861
XeF_6, monomeric charact., electron ionisation mass spectra 77−75322
XeF_6 seeded mol. beam, transverse ionisation, space charge, mass spectra and vel. 80−78725
YC_{n+}(n=2, 3, 4, 5, 6), atomisation energies, Knudsen cell mass spectrometric obs. 80−58409
$Y_2O_3.2SiO_2.Al_2O_3$ glass, thermal stability 77−44502
ZnO powders, electron-beam-induced desorption, phase-sensitive detection 80−54502
Zr, isotopic composition, at. wt., rock standards, chondrite composition 79−3591
Zr-H, diffusion in hydride phase, exam. 80−29204
ZrO_2-HfO_2(Y_2O_3) solid soln. complex refractories, sublimation *(Russian)* 78−47513

mass spectrometer applications
see also isotope separation; mass spectroscopic chemical analysis
biomedical continuous in vivo meas. *(Japanese)* 80−94309
electronic component package, H_2O content determ., plasma chromatograph-mass spectrometer applic. 78−86379
fission products nuclear data from on-line mass spectrometer 77−22616
heavy ion interactions with gases, measurement apparatus 79−31741
hollow cathode discharge, particle diagnostics with mass spectrometer 79−46476
injected ion drift tube mass spectrometer ionic mobility data in non-parent gas 78−87428

mass spectrometer applications continued
ion-molecule reactions (thermal), emission spectra obs. using pulsed ICR cell 77−19108
ionosphere, positive ion detection with rocket-borne mass spectrometer 80−8459
isobar nuclei, separation of alkali and alkaline earth elements using surface ion source 80−37688
isotope composition determ. using RMO-4S omegatron mass spectrometer 78−5368
isotope fractionation, controllable, in thermal-ionis. mass spectrometry, SRM 987 standard test *(German)* 80−42299
isotope ratios by mass spectroscopy, δ values calc. method 79−10234
laser microprobe mass analyser (LAMMA) appl. 80−18041
leak detection, microleaks with He mass spectrometry *(French)* 77−10131
leak detection, probe with He-permeable membrane, domestic heating systems 80−98994
leak detector range extension 80−73375
Mattauch-Herzog, small, improved, planetary atmosphere study appl. 79−8795
medical applications in respiratory physiology 79−62383
metal clusters research, electronic time-of-flight mass spectrometer with separator 80−77907
molecular and atomic beams, vel., intensity and particle density, using mass spectrometer 79−67428
multisource deposition rate control using mass spectrometer as sensing element 78−72730
negative surface ionisation, mass spectrometer-energy analyser obs. 77−9149
planetary atmosphere investigation by mass spectrometer-molecular beam expt. 78−49327
planetary atmospheric composition determ. 80−8518
plasma stream ion component studies with monopole spectrometer 78−5926
polyethylene terephthalate, joint prosthesis fragment dispersal meas. *(German)* 79−8566
pyrocarbon coatings, mass spectrom. determ. of fission gas permeabilities 78−12785
quadrupole, applics. in at. and mol. physics 77−23581
quadrupole, control of mol. beam epitaxy apparatus *(French)* 78−15315
radioactive dating, evaluation of double-spiking procedure for K-Ar dating 77−60473
recoil mass spectrometer for fission fragments, HIAWATHA, thermal neutron fission of U, Pu 78−16892
RF, industrial furnace flue gas anal., features 77−71403
semiconductor packages, hermetically sealed, calibration and anal. of moisture by gas mass spectrometry 80−90928
space plasmas, mass and energy anal. over energy range 0.1 to 10 keV 77−53401
thin film sputter deposition, closed loop control using glow discharge mass spectroscopy 80−80973
UNILAC heavy ion accelerator, on-line separator facility 77−14299
upper atmosphere research applics., of quadrupole mass spectrometer, book contrib. 77−25911
vacuum gap electrode surface sorption, mass spectroscopic obs. 78−75466
AlAs, gas phase dissoc. energy, mass spectrometric determ. 79−81301
^{13}C, mass spectromatic calibration of mass and neutron separation energy 78−70434
^{14}C dating, high energy mass spectrometer appls. 80−101917
D_2-DT-T_2 system, quadrupole mass filter sensitivities and β-particle induced exchange kinetics 78−58090
H_2-HT-T_2 system, quadrupole mass filter sensitivities and β-particle induced exchange kinetics 78−58090
He mass spectrometer for leak detection *(French)* 77−37901
$LiCrO_2$, evaporation, as a corrosion product in compatability experiment of Li_2O pellets with Fe-Ni-Cr alloys, mass spectrometric study 79−73301
O_2 inhalation automatic control for patients with respiratory failure 80−17181
Rn isotopes, A=205, 206, 207, in flight mass separation of fusion recoils 78−25381
Se isotopic anal. in INS separator 77−38056
Si:O, comparision of depth profiling techniques 80−29048
SiF, heat of form. mass spectrometric determ. 78−76900
SiF_2, heat of form. mass spectrometric determ. 78−76900
SiF_3, heat of form. mass spectrometric determ. 78−76900
$^{112}Sn+^{32}S$ fusion, 160 MeV, mass, velocity, angular and charge state distribs. 78−82405
UO_2-Mg reactor fuel, U potentiometric and mass spectrometric determ. 79−97811

mass spectrometer components and accessories
see also ion sources
A/D conversion system of wide dynamic range, gas chromatography mass spectrometry 80−62788
accelerating voltage device, for metastable negative ion decomposition obs. 77−6944
achromatic ion prism, two-dimens. 77−54015
alkali ion source, duofilament, for undergraduate laboratory 79−40329
analyser, sector type, uncoupled, image props. 78−70218
apparatus for energy, angle, and mass analysis of products from alkali-molecule reactions 78−70970
autoionisation gun, 3-electrode, for ion field source in MKh1303 mass spectrometer 77−38055
automatic inlet system with pneumatic changeover valves for isotope ratio mass spectrometer 79−49333
automatic multiplier for ion detector circuit *(Japanese)* 79−97468
bakeable hollow cathode, ion-molecule reaction study in discharge gas mixtures 80−37117
bicylinder mirror aberrations, effects on multipassage mag. mass spectrometer props. *(French)* 79−75651
bicylinder mirrors for appl. in multichannel mag. mass spectrometer *(French)* 78−54494
capillary device construction for liquid introduction into analytic mass spectrometer 80−4805
channel electron multipliers, characts. and operating principles 79−93248
channel plate, for secondary ion images obs. *(French)* 79−58840
charcoal trap for rare gas mass spectrometry 78−54496
circuit for double suppression of parasitic signal in quadrupole mass spectrometer 77−74546
collector slit system, mag. deflection spectrometer for at. wt. determ. 78−8463
collision chamber for negative ion formation in CeI_3 vapour by electron impact 77−27190
computer-assisted retarding pot. difference system for ionis. efficiency meas. 77−41724
computerized GCMS solid state magnet control 79−12879
control block for 3-dimens. quadrupole spectrometer 77−13812
cylindrical condenser, finite length, elec. field distrib. calcs. 77−5957
cylindrical RF mass analyser, using axisymmetric high freq. optical dispersion element 79−80718
data system, continuous scan employing computer time sharing 77−18127
dense gas chromatograph/mass spectrometer, interface design 79−34378
digital, synchronously timed control system for pulsed ion cyclotron resonance spectrometer 79−71560
digital device for determination of the ratio of two numbers *(Bulgarian)* 79−85199
digital mass read-out system 79−67422
digital recording system for automated isotopic analysis 78−12783
display device, for ion beam profile 77−5960
double inlet system with viscous gas flow, C and O isotopic ratios 77−18131
double-pass cylindrical mirror analyser, for ion scattering spectroscopy, resolution factors 79−16078
drift tube, diatomic positive ion energy distrib. 78−21257
duoplasmatron ion source for secondary ion mass spectrometry 79−85196
dynamic mass analysers, charged particle motion in alternating elec. fields, scaling conditions 80−63903
effusion cell for high-temp. gas thermodynamic props. determ., surface evaporation effects and elimination 77−184
effusive beam source, heterogeneous reaction type, chem. equilib. 80−52362
electric quadrupole field production, electrode system 77−54012
electric sector modifications, on Mattauch-Herzog mass. spectrometer, for ion kinetic energy meas. 80−62791
electro-optical detector for spark source mass spectrometry, quantitative meas. 80−101868
electrodynamic trap., energetic props. of stored ions, elastic collision effects *(French)* 78−9306
electron cyclotron resonance type ion source *(Japanese)* 79−97467
electron gun for three dimens. quadrupole, poisoning resistant 78−54493
electron movable dynode multiplier for radioactive ion detector 79−716
electron multiplier, high gain, mass spectrometric positive ion detect. 78−74095
electron multiplier gains determ. for various ions by pulse counting method 80−57418
electron multiplier scintillator detector for positive/negative ions pulse counting 78−89583
electron multiplier three-state time delay switch 80−37116
electronic aperture, for depth profiling by rastered beam 77−18137
electrostatic accelerator, appl. to ^{36}Cl anal. in environmental water samples 79−20895
electrostatic analyser, electrode geometry tolerance calcs. 77−23611
electrostatic analyser attachment 78−86377
electrostatic prism, dihedral, for spectrometer aberration coeff. 79−26178
EM analyser control, automatic registration of the back-scattered ions 80−18042
emission current regulator for ion cyclotron resonance spectrometers using optical coupler 78−45749
energy analyzer, two-stage with cylindrical mirrors, aberration reduction 79−40640
field desorption ion source for gas chromatograph-mass spectrometer *(Japanese)* 78−32920
field ion emitters, high rate dendrite growth 79−2873
field ion source construction and recording systems modification for field mass spectrometry 77−49803
field ionisation source, preactivated, appl. to organic compounds anal. 77−5959
field ionisation/field desorpt./electron impact ion source for AEI MS9 spectrometer 78−70213
filter, overall transmission of quadrupole spectrom. *(French)* 80−101877
filter for RF spectrometer, background current elimination, expt. results *(Japanese)* 80−82844
focusing lens system, quadrupolar, for beam of mass-separator 80−47801
fourfold monopole spectrometer, analysing electrode optimum radius of curvature, simulation 79−93250
full ion current recorder 79−97466
gas chromatography/mass spectrometry system with complete microprocessor control 77−44533
gas inlet beam system, for stratospheric comp. meas. appls. 78−7808
gas mass spectrometer, ion source numerical simulation *(German)* 80−47141
glow discharge source combined with quadrupole mass filter for solids anal. 78−61075
graphic display, dynamically refreshable controller with vertical line generator 78−314
Hall probe temp. compensation for spark source mass spectrometer 77−12846
head, for helium mass spectrometer leak detector 79−63247
HF generator for supplying quadrupole mass spectrometer *(Rumanian)* 77−29628
high aperture ion source with surface ionization 79−93251
high-speed vacuum lock 79−67421
high-yield laser ion source with plasma focusing for mass spectrometric analysis 78−61097
hollow cathode discharge, with quadrupole mass filter, ion form. and handling 79−12878
injection system for high boiling point liqs. 79−85197
instrumentation, design and construction for analytical mass spectrometry, review 78−322
integration TIM for GC-CI-MS system *(Japanese)* 77−90697
ion analyser enhancement based on MI-1305 mass spectrometer 80−105745
ion beam, electrical adjustment in MSKh-4 mass spectrometer 78−24884

mass spectrometer components and accessories continued
ion beams in self-triggered mode of damped discharges 78−70214
ion cyclotron resonance cell, elec. pot. improvement 79−2875
ion cyclotron resonance cell, quantum theory of ion motion 78−317
ion cyclotron resonance cell for 80-450K range 78−56943
ion cyclotron resonance detector-oscillator 80−86492
ion detector, Be-Cu surface secondary electron yield 78−74094
ion detector, electro-optical, for spark source mass spectrometry 80−42246
ion detector, electro-optical, using fibre optics 77−45915
ion detectors for contamination reduction in EM isotope separators or spectrometers 79−67420
ion microanalyser, neutral particle beam separation, characts., anal. appl. *(Japanese)* 78−85248
ion microanalyzer, positive ion electron yield factors 78−73100
ion microprobe, element distributions, images quantification 78−73101
ion multiplier noise filter based on analogue delay device, anal. appl. 78−92541
ion sampling system, characts. and calibr., atm. press. flame 77−56270
ion source, cold cathode 80−42293
ion source, electron bombardment type, for use with mass spectrom. 80−77909
ion source, high sensitivity for quadrupole mass spectrometers 80−52353
ion source, laser, for MI-1309 spectrometer 79−21849
ion source, TOF spectrometer, electron beam collimation, rel. to resolution and sensitivity 80−42294
ion source, two-photon ionis. of mol. beam 79−27118
ion source and focusing optics, high-luminosity 79−44979
ion source cooling attachment using liquid M_2 for NI-1305 mass spectrometer 80−105744
ion source for MI-1309 mass spectrometer in high-temp. metallurgical studies 78−24885
ion source for spark source mass spectrograph, modification to reduce residual gas effects 80−98996
ion storage in a radio-frequency trap with semi-spherical electrodes 80−101869
ion trap, RF, cylindrical geometry, comparison with 3D quadrupole 77−61153
ion trap, RF quadrupole type, ion path length and stability calcs. 77−41722
ion-cyclotron reson. meas spectrometer emission current regulator, optically coupled feedback 77−61150
ion-field source emitter, influence of laser irradiation on ion current 80−101874
ionisation chamber acceptance characts. distortion by ion source mag. field 79−21852
ionisation detector, using new ionis. method for organic liqs. *(Japanese)* 79−93255
ionisation methods, review 78−323
Knudsen cell quadrupole mass spectrometer, high temp., control and data acquisition, system 79−26171
Knudsen effusion cell, high temp. mass spectroscopy, thermodynamic and physicochemical behaviour, review 80−52354
Knudsen evaporator for MI 1305 type, mass spectrometer, operational principles *(Hungarian)* 78−37101
laser ionisation source for ICR spectroscopy, metal at. ion chem. appl. 80−45597
laser microprobe mass analyser, development for biological specimens 79−17554
leak detector, increasing sensitivity by selective gas accumulation 79−6215
Leuven isotope separator on-line at CYCLONE cyclotron 78−70682
liquid He cryopump and opening device for balloon borne mass spectrometer 78−77370
magnet design for high-current implanters or small isotope separators 80−68222
magnet power supply, programmable, to allow rapid scanning with min. reset time 80−37121
magnetic analyser, sector type, with fringing field, geometric image aberration *(Japanese)* 78−8465
magnetic analyser constant current solid-state power unit 80−86499
magnetic analyser with inhomogeneous field and electrostatic lens, for ion beam radical focusing 78−78895
magnetic field stability control, solid-state device 77−26423
marginal oscillator detector instantaneous voltage, rot. elec. monopole theory 78−41371
marginal oscillator sensitivity calibration for ion cyclotron resonance mass spectrometry 77−67529
Mars Viking surface sampler subsystem, acquisition assembly 79−12380
mass analyser, two-stage, with vel. filter, using sector mag. 80−4808
mass analyzer using electron-beam-guiding type ion source 80−31933
mass filter performance, quadrupolar field distortion effects 79−35887
mass separator with low stray fields 77−10133
mass spectrometer, digital recording system for automated isotopic analysis 78−12783
MI-1305 spectrometer ion output slit 78−4729
microchannel plate technology and applications 79−23075
microcomputer scanning system for respiratory mass spectrometer 78−88756
microcomputer-based controller, for temp. programming direct inlet probe of high-resolution mass spectrometer 78−16893
mirror type ion electron convertor, for axially symmetric SIMS 79−5232
MIS integrated stepped-sawtooth waveform generator 78−86376
molecular beam nozzle, for sampling, gas dynamics 79−49330
multichannel Cerenkov mass spectrometer, automatic meas. of electronic apparatus characts. 79−26173
multichannel Cerenkov mass spectrometer, electronic recording apparatus 79−26174
multiemitter field source of ions 77−54013
multipeak residual gas analysis monitoring system 79−79342
multiple ion detection system, for mag. sector mass spectrometer 77−70348
multistage cylindrical analyzer for simultaneous detection of several beams with different energies 79−22891
needle electron source, for chemical ionisation 77−75273
negative ion detection system 77−29062
particle multiplier gain factors for singly charged alkali ions 77−30215
peak detector extremator, cct. 78−74096
peak height intensity normalizer, pocket size device, for teaching 79−35498

mass spectrometer components and accessories continued
pH interface, variable, use with mass spectrometer for measurement of dissolved volatile compounds 79−61930
plasma chromatograph/mass spectrometer column overload prevention valve 80−16748
plasma chromatograph/mass spectrometer sample overload protection 79−39237
plasma chromatograph/mass spectrometer simultaneous electron impact/chem. ionisation carrier gas mixture 79−30600
plasma-optical mass separator, double focusing, 'nontransitive' cylindrical model 79−67423
power supply polarity changing cct. for ion source 77−45914
pulse counting techniques, in organic mass spectroscopy-gas chromatography 78−31720
pulse discriminator, high-speed nonoverloading 77−401
pulse-counting detector systems, effective deadtime, theory 78−41369
pulse-forming circuit, double step, for ion extraction in mass spectrometer 77−18124
pump, orbitron ion-getter, small non-cooled and low power consumption 80−52352
quadrupole, RF-only, high efficency collision-induced mol. dissoc. 79−67419
quadrupole analyser, automatic operation using microprocessor systems *(French)* 79−54212
quadrupole electric field, 3-dimens., ion motion and charge exchange calcs. 77−9060
quadrupole filter design, appln. of fundamental props. of Hill equation 80−95186
quadrupole gas analyser with integral microprocessor 78−73109
quadrupole ion microprobe for secondary ion emission investigs., ion optics 79−35892
quadrupole ion storage mass spectrometer, cylindrical geometry and operational characts., QUISTOR comparison 80−52351
quadrupole ion storage trap, ion withdrawal studies 79−54216
quadrupole ion storage trap (quistor), relative confinement efficiencies of Ar^+ and Ar^{2+} 79−2869
quadrupole ion storage trap chemical ionisation source, for mag. sector mass spectrometer 79−12877
quadrupole ion store, of mass spectrometer, ion ejection expts. 79−89033
quadrupole ion store, of mass spectrometer, phase synchronised ion ejection study 79−89034
quadrupole ion store, QUISTOR, new mode of operation 78−29204
quadrupole ion store, simultaneous positive-negative ion mass spectrometry, scanning techniques and systems description 80−52350
quadrupole ion store, spatial distribution of ions derived by phase space anal. 80−95185
quadrupole ion store, three-dimensional, ion motion, charge exchange reactions effect, two-ion model 80−55738
quadrupole ion trap, three operating modes, field eqns., stability parameters 77−41723
quadrupole mass analyzer, performance meas. 77−186
quadrupole mass filter, acceptance 78−29203
quadrupole mass filter, appl. to charge spectrometer *(Japanese)* 77−57420
quadrupole mass filter, computer simulation of ion trajectories in quadrupole field 80−52349
quadrupole mass filter, operation and theory 80−52348
quadrupole mass filter, operation with only RF voltage applied to rod system 77−5955
quadrupole mass filter, peak shape and resolution calcs. 77−187
quadrupole mass filter, separated RF and DC fringing fields 78−8461
quadrupole mass filter operating with no DC component on rods 78−29206
quadrupole mass filter specification and calibration *(Japanese)* 78−12784
quadrupole mass filter spectrum control, using PWM 77−61152
quadrupole mass filter transmission 79−21851
quadrupole mass filter with flat electrodes, computer simulation 78−54492
quadrupole mass filters, ion transmission factors 77−54011
quadrupole mass spectrometer, transmission of narrow ion beam, for SIMS studies *(French)* 80−105747
reactive ion etching RF discharge plasma deceleration filter 78−41370
registration system for digital recording 79−93252
retarding field analyser-quadrupole mass filter for thermal ion energy distribution meas. *(Japanese)* 77−18130
RF quadrupole trap field, 3-dimens., external source injected ion trapping 79−44978
rotating electrode, for improved reproducibility in spark source mass spectrometry 78−93781
sample supply technique, for field desorption method 77−56279
sampling system, for liquid samples and thermoanal. 77−36816
secondary ion emission, conf., Stanford, USA (Aug. 1979) 80−105419
selected-ion flow tube (SIFT), applic. to ion-molecule reactions 77−188
separator for metal clusters research, electronic time-of-flight mass spectrometer 80−77907
seven decade reversing counter circuit, digital display, for quadrupole mass spectrometer 77−18129
shock tube, coupled to time-of-flight spectrometer via molecular beam sampling system 79−80717
SIMS, recording, optimisation 79−43683
SIMS detector sensitivity improvement 79−26172
six-channel MOSFET commutator, monopolar mass spectrometer appls. *(Russian)* 78−74099
slit, angle-resolving, for double focusing spectrometer, energy loss meas. 78−44426
small-scale device for moving solid specimens in vacuum chamber 78−315
sources, field ionisation and desorption, experimental techniques, review 79−26176
spark ion source, ion energy distrib. of late stages 79−55596
spark source (RF), of mass spectrometer, analysis of hard X-ray emission 79−90480
spark-source mass spectrometry; elemental sensitivity rel. to sparking conditions 79−57314
specimen heating and cooling installation, programmed, for MKh 1303 spectrometer 79−93253
system for He assay in fission reactor constructional materials 77−34397
tandem mass spectrometer with intermediate image, simultaneous angle and energy focusing 80−62793
Thomson parabola ion analyzer for laser-plasma studies 79−1343

mass spectrometer components and accessories continued
three-electrode emission lens, appl. for secondary ion microscopy 79−41324
time of flight spectrometer, electronic cct. 79−54997
transfer optics, for secondary ion emission microanal. *(French)* 79−58838
trapped ion analyser cell, for pulsed ICR spectroscopy 79−2876
turbomolecular pump, miniaturized for space appl. 80−52254
uncoupled S systems, axial aberration free, general conditions for existance 80−62794
vacuum envelope for high press. mass spectrometer 78−61077
vacuum value for gas chromatograph/mass spectrometer system 79−39245
voltage scanning system for sector field mass spectrometers 77−10132
voltage supply, variable freq., for monopole mass spectrometer 78−29205
wideband freq.-swept marginal oscillator detector for ion cyclotron reson. spectrometer 80−9069
Wien filter, cluster ion beam mass anal. appl. 80−86493
Co_3 electrochemically prod. emitters, field ionis. props. 77−90254
Cs^+ primary ion source for ion microprobe mass spectrometer 78−4732
Li ion source for mass spectrometer calibration 77−41727
Ni, electrochemically prod. emitters, field ionis. props. 77−90254
^{242}Pu preparation by EM isotope separation, for use as α-spectrometry and mass spectrometry tracer 78−9011
Si, emitter for field desorpt. mass spectrometry 79−79323
W, multiple field ion emitters, props., ionisation efficiency improvement 78−76588

mass spectrometers
see also ion optics; mass spectra; mass spectroscopy
additional memory effect in BF_3 spectrometry *(Japanese)* 79−29432
AEI MS702 mass spectrometer, setting-up and commissioning 79−63323
axially symmetric quadrupole SIMS, using mirror type ion-electron convertor 79−5232
background-line displacement factors 79−49332
balloon-born system with sputter ion pump for stratospheric comp. meas. 77−33200
balloon-borne ion sampling package 78−69497
Bennett ion mass spectrometers, on Pioneer Venus Bus and Orbiter 80−67499
Buechner magnet/PSD system, mass spectrom. of unslowed fission products, feasibility 78−29702
calibration by nonstationary flow method 78−4730
calibration for van der Waals dimers 78−89585
charged particle localisation in quadrupole spectrometer 79−67424
Cherenkov, ninety channel, high energy electrons and gamma photons 80−91362
computer controlled photoionisation mass spectrometer 80−77905
computerised, features, book 79−26179
computerised data acquisition and processing system, gas chromatograph input 80−13181
computerised system for collisional activation spectra 77−23576
computerized, technical aspects including data reduction and analysis 80−57417
computerized mass spectrometer for isotopic analyses of solids 78−78026
counter-flow mass spectrometer leak detector 79−63248
cryo mass spectrometer, for upper atmosphere neutral comp. meas. during winter anomaly 78−45192
cyclotron, as high-energy mass spectrometer, appl. to chem. anal., radioactive dating and quark detection *(Czech)* 78−86375
cylindrical electrostatic mirror analyser, image line aberrational expansion, nonplanar trajectories 79−41327
direct-molecular-beam method for mass selective outgassing rate measurement 79−85146
double collecting, device for automatic digital measurement of isotopic ratios 80−31932
double focusing, new design, investigation of focusing props. 78−37100
double focusing, portable, for gas analysis 78−21261
double focusing, reversed Nier-Johnson geometry, interfacing metastable signal 77−18126
double focusing MM-ZAB-2F mass spectrometer and MIKE spectrometer, characts. 79−2871
double focusing spectrum, second order image aberration correction by electrostatic hexapole lens 78−70216
double-focusing spectrometer, median planes imperfect alignment effect 77−87867
Du Pont DP-1, gas chromatograph/mass spectrometer, sub-picogram detection, wide dynamic range and automatic source rejuvenation 78−93782
electron impact, using axial magnetic field for collimation 79−49334
electronics appl. in chemical technology *(German)* 77−77841
electrostatic, cylindrical, num. comput. of design parameters 77−13815
electrostatic prism spectrometer, with finite source width aberrations 79−26178
EM ion separators and related ion accelerators 77−14276
EM sector separators, variable geom. multipocket collector 77−14611
energetic ion mass anal. using RF quadrupole filter 78−74100
field ionisation and desorption sources, for quadrupole and double focusing spectrometers 78−74092
field ionisation-ion kinetic energy spectrometer, for multicomponent mixture anal. 77−56272
fissile materials accounting, behaviour of the quadrupole mass-spectrometer towards various noble gases 80−63300
fission fragment recoil mass spectrometer HIAWATHA 79−9940
fourfold monopole mass spectrometer, performance and appls. 78−74093
fragment ion kinetic energies, modified ion source and mass spectrometer 77−6958
gas chromatograph-mass spectrometer computer system, GCMS PAC-500 series *(Japanese)* 78−32918
gas chromatograph/mass spectrometer/calculator, low-cost bench-top system 77−4972
gas chromatography/mass spectroscopy system, computer-controlled, DP-102 80−22470
gas chromatography/photoionisation mass spectrometry, organic compds. anal. appl. 78−92531
gas ion probe, instrument for gas conc. profile meas. in solids 79−39238
He-jet fed online mass separator for recoil atom mass spectroscopic anal. 80−98998
heavy element mass spectroscopy with the Berkeley 88-inch cyclotron 78−70217
heavy ion separation velocity selector 77−88324
mass spectrometers continued
heavy-ion energy-mass spectrograph 77−87869
heavy-ion separator SIS, at GSI, velocity filter 77−26425
helium mass spectrometer leak detector, design and appl. to industrial leak detection 79−63247
HIAWATHA, fission fragment mass spectrom., $^{235}U(n,f)$ meas. 77−26929
high energy molecular beam apparatus for solid and surface anal. 77−21443
high resolution, for isotopic anal. of H_2-He mixtures 77−77844
high-pressure spectrometer and gas-phase ion-mol. reactions, review *(Japanese)* 78−64830
high-resolution high-pressure, for gas anal. of ionosphere 79−87906
INS separator, high sensitivity anal. of Se isotopes 77−38056
instrumentation for chemists and biologists 80−42297
interface module for multichannel analyser ADC input 80−27916
International Sun-Earth Explorer A, ion mass spectrometers in plasma comp. expt. 78−85810
ion counting with CEM on double focusing mass spectrometer 77−79194
ion cyclotron reson. mass spectrometer, mass meas. accuracy 77−18128
ion cyclotron resonance spectrometer, positive ion trapping in electron beam 78−21254
ion detecting and measuring system with wide dynamic range, appl. to airborne particles 79−2870
ion energy and momentum spectrometer with high resolution 80−86495
ion injection into three-dimensional quadrupole spectrometer 79−58842
ion mass spectrometer, satellite-borne, 0-16 keV energy range, magnetosphere appl. 77−13207
ion optical props., aberration, crossed toroidal elec., mag. fields as mass spectrometer *(Chinese)* 80−82843
with ion probe and energy analyser, MI-1305, for solid anal. 78−74097
ion registration, stepwise selective photoionisation technique *(Russian)* 78−21262
ion source for twin mass spectrometer, charge exchange of metal atoms 80−106215
ion spectrograph, for mass and energy anal. of space plasmas over energy range 0.1 to 10 keV 77−53401
ion-impact spectrometer, 2-100 keV, for ion-solid interaction studies 79−49338
ion-kinetic energy spectrometer, high resolution mass analysed, design and performance 80−101872
ion-scattering and secondary-ion combined, ultrahigh vacuum, mag. anal. 78−21259
ionisation and analysis methods, review 78−323
ionisation mass spectrometer, with dedicated minicomputer, biological appls. 78−53586
ISOCELE high-current on line separator development 77−26922
isotope ratio and mass spectrometer, for $^6Li/^7Li$ anal. 77−88601
isotope separation, throughput limit in mass spectrograph type separators 78−65995
JOSEF gas filled separator, focusing and dispersive props. 77−26426
laser microprobe mass analyser, achievements and appls. 80−73536
leak detector ion source heating up to 550°C, sensitivity improvement 78−78028
linear mass-reflectron, non-magnetic time of flight mass spectrometer *(Russian)* 79−75652
Los Alamos on-line mass anal. facility, source modification for noble gases 77−14301
magnetic analyser, wide-range reaction products of heavy ion beams 80−86491
magnetic analysis of charged particles, α-, β- and mass spectrometers *(Russian)* 80−87011
magnetic field measurement using improved Hall probe 79−88987
magnetic scanning type, ion current meas., computer controlled electronics 78−8464
magnetic vector man analyser, stigmatic focusing condition 78−70215
magnetron, inverse, with ion source on outside 80−57416
mass spectrometer, blood gas anal., silicone rubber catheter operating mechanism *(Japanese)* 78−61273
Mattauch-Herzog, modification for ion kinetic energy meas. 80−62791
Mattauch-Herzog, small, improved, planetary atmosphere study appl. 79−8795
Mattauch-Herzog mass spectrometer, charge exchange 80−86486
medical, for recording respiratory, blood and tissue gas partial press. *(Japanese)* 77−70566
MI9302, for anal. of microscopic amounts of inert and chemically active gases 80−101873
MI9302, static mode of operation 80−105743
MI-1309 with high-aperture ratio ion source 77−13811
MKh1303, modification for operation in chem. ionisation regime 77−38054
MKh1303, small-scale device for moving solid specimens in vacuum chamber 78−315
molecular beam mass spectrometric detector for surface ionis. 77−2710
monopole, design and performance, book contrib. 77−26430
monopole, expt. meas. of transmission characts. *(Japanese)* 79−93249
monopole mass spectrometer, performance, phase space calcs. 77−5956
monopole mass spectrometer, simulation, rel. to determining operating parameter tolerances 78−21260
multiplexed exit slits and field scan, improved sensitivity, speed and S/N ratio 80−31930
neutral gas mass spectrometer expt., on Pioneer Venus Orbiter 80−67502
Nier-Johnson geometry, metastable transitions obs., using linked elec.-mag. fields scan 78−45747
Nier-Johnson geometry, reversed, high-resolution mass, collisional activation and metastable ion spectra meas. *(Japanese)* 79−27115
NODUS, ion scatt. spectrometer for surface composition anal. 78−76968
omegatron, characts. dependences *(Czech)* 79−41049
on-line, progress in targets and ion sources 77−14300
on-line mass separator for fission-produced alkali isotopes 80−98997
on-line system employing cooled and NaCl loaded He-jet methods 77−14288
on-line time-of-flight mass identification system, meas. on T=1/2 mirror nuclei 77−22951
online with 1 GeV proton accelerators, meas. of nuclear reaction yields *(Russian)* 77−10409
OSIRIS, target/ion source system for isotope separation in on-line mass separator, mol. ion prod. 80−99366
OSTIS, on-line mass separator for thermically ionisable fission products 79−714

mass spectrometers continued
parallel detection system 80−86489
partial pressure measurement and gauges for ultrahigh vacuum meas. 80−57323
photoionisation mass spectrometer, balloon-borne for stratospheric gas meas. 78−85732
photoionisation mass spectrometer for threshold photoelectron spectroscopy 77−87868
Pioneer Venus Bus neutral gas mass spectrometer 80−67513
Pioneer Venus large probe neutral mass spectrometer for measurement of composition and abundance of atmospheric gases 79−88563
Pioneer Venus Sounder Probe neutral gas mass spectrometer 80−67506
position sensitive proportional detector system for focal planes of multigap mag. spectrograph 77−54454
prism mass spectrometer with two dimens. deflecting system 77−54015
programmable quadrupole mass spectrometer *(Japanese)* 77−86415
pulse-counting mass spectrometer for noble gas anal. 80−95187
pulsed ion cyclotron resonance, digital, synchronously timed control system 79−71560
pulsed ion cyclotron resonance mass spectrometer for ion-molecule reaction studies 78−41372
quadrupole, 3-dim., with elliptical electrodes 80−31931
quadrupole, 3-dimens. theory 80−4806
quadrupole, attachment to EG-100 A electronograph for vapour composition monitoring 79−94108
quadrupole, design and operation 79−63322
quadrupole, design and performance, book contrib. 77−22613
quadrupole, for recording beams of light atomic particles 79−2872
quadrupole, nonlinear distortion in RF voltage 78−4731
quadrupole, on 'Vertical-7' geophysical rocket 80−31935
quadrupole, three-dimens. double suppression of parasitic signal 77−74546
quadrupole, transmission of narrow ion beam, for SIMS studies *(French)* 80−105747
quadrupole, using new ionis. method for organic liqs. *(Japanese)* 79−93255
quadrupole ion storage mass spectrometer, cylindrical geometry and operational characts., QUISTOR comparison 80−52351
quadrupole ion traps, book contrib. 77−22614
quadrupole mass analyser-field ionis. source interfacing, ferrite insert, repeller electrode 77−18125
quadrupole mass filter, for middle atmosphere plasma and neutral gas comp. and struct. anal. 78−45191
quadrupole mass spectrometers, charged particle selection 77−5961
quadrupole mass spectrometers, intrinsic background 78−21258
quadrupole RF field, ion storage *(Rumanian)* 77−41726
quadrupole RF trap, temporal invariance and energetic and spatial statistical properties of confined ions *(French)* 80−22471
quadrupole spectrometer, validity of meas. at press. exceeding 10^{-4} mbar 79−85198
quadrupole spectrometer with hyperboloid electrodes 79−54214
quadrupole spectrometers, design, approx. method 79−9256
quadrupole-focusing time-of-flight spectrometer 78−21804
quartz tube orifice leaks for local, fast-response gas sampling 80−35609
QUISTOR, phase synchronised ion ejection, ejection phase width and detection pulse delay effects 79−44976
QUISTOR, phase-synchronised ion ejection from quadrupole ion storage mass spectrometer 79−44975
QUISTOR, space charge and ion stability 80−86487
QUISTOR, total press. mode operation with phase-synchronised ion ejection 79−44977
recoil mass spectrometer for fission fragments, HIAWATHA, thermal neutron fission of U, Pu 78−16892
recoil separator, Lohengrin, ion optics, nuclear fission product spectroscopy 77−22607
recoil spectroms., determ. of thermal fission yields, analysing features 77−26424
residual gas analyser, microprocessor-based 79−26175
residual gas analyser *(Japanese)* 79−79349
resonance mass spectrometer with a coaxial helical undulator 80−9071
respiration, delay and response time measurement *(Hungarian)* 77−73617
respiratory mass-spectrometer model QGA-11 79−62382
reversed geometry mass spectrometer for organic compound identification 80−50913
reversed geometry mass spectrometers, charge permutation 80−37118
review of recent work *(Japanese)* 77−58247
RF, background current elimination, using energy filter *(Japanese)* 80−82844
RF, MKh 6202, for respiratory gas anal. 78−7468
RF mass spectrometer, numerical study of the AUREOLE 2 satellite spectrom. 79−2470
RMO-4S omegatron for isotopic comp. determ. 78−5368
scanning laser excitation in ion source, milliprobe appls. 79−35882
secondary electron energy analysis in 6 to 150 eV range *(German)* 79−75649
secondary ion emission, conf., Stanford, USA (Aug. 1979) 80−105419
secondary ion quadrupole mass spectrometer for depth profiling 78−54495
secondary ions, mass and energy spectrometer 77−13814
selected ion-monitoring mass spectrometers; dynamic characts. obs. 78−58087
SILYA-4 light nucleus isotope spectrometer for cosmic ray obs. above atmosphere 79−80111
SIMS, description, and cluster formation obs. in alkali halide sputtering 79−19959
SIMS, for surface anal. 79−12883
SIMS, high resolution Si wafer anal. 78−56929
SIMS, instrumental discrimination effects, evaluation 79−35888
SIMS high performance system 77−41725
simultaneous ion detect. with variable mass dispersion 78−78027
single particle trajectories, through ionising regions 79−6218
solar wind ion comp. expt. on International Sun-Earth Explorer C spacecraft 78−85793
solid-source, appl. to Rb-Sr dating of rocks 77−70840
space-borne, in-flight calibration device 78−93115
space-borne neutral mass spectrometers, fly-through mode theory 79−58274
spark source, AEI MS702, transistorised power supply 79−12881
spark source mass spectrograph, image plane, exptl. and math. determ. 77−5958
mass spectrometers continued
spark source quadrupole mass spectrometry, development, appls. 80−62789
spark-ion source electrode voltage, measured- and estimated-values discrepancy 78−74098
SSMS ion source modification, residual gas effects 80−98996
static field spectrograph for laser induced plasma expts. 77−26427
stigmatic second order double focusing mass spectrometer 78−21256
stratospheric composition investigation using gas expansion and mass spectrometer beam system 80−31934
surface analysis instrument for vacuum electronics *(Czech)* 77−18145
symmetric prism high resolution type, energy and spatial focusing, characts. 77−54014
synchrocyclotron, in line, electrostatic filter 80−86490
tandem, collisional activation mass spectrometry, resolution and transmission improvement 77−38053
tandem, for collision-induced dissoc. obs. 80−62790
tandem double focusing mass analyser, uncoupled E+M system 80−18043
tandem high-resolution system, sensitivity, mass range 80−90925
tandem mass spectrometer energy analyser, for negative surface ionisation and electron affinity obs. 77−9149
tandem quadrupole spectrometer with computer controlled data collection 78−82071
teaching, mobile spectroscopy, chem. anal. laboratory 78−93502
three-dimensional quadrupole type, ion beam struct. 80−9070
threshold photoelectron-photoion coincidence mass spectrometer for meas. ion kinetic energy release on fragmentation 77−79192
time of flight spectrom., for He-jet produced α-source recoil particle obs. 78−86717
time of flight spectrometer, 3-dimens., asymmetric quadrupole lens 80−4807
time of flight spectrometer using ^{241}Am source for triggering pulses *(Japanese)* 80−90926
time of flight tandem mass spectrometer, modified, for collision-induced dissoc. obs. 77−74545
time-of-flight, comparison of TOF and stripping cell low-energy ion scattering methods 80−73522
time-of-flight, inhomogeneous oscillatory elec. field spectrometer 77−13813
time-of-flight, recording unit 80−73520
time-of-flight, separator for metal clusters 80−77907
time-of-flight spectrometer, for studying dynamics of fast chemical transforms. 77−74547
time-of-flight spectrometer, with magnetic energy filter 79−44980
TOF radionuclei mass identification system, on-line experimental results 79−6785
triple focusing mass separator using Wien filter 78−45748
triple quadrupole mass spectrometer and technique, direct mixture analysis and struct. elucidation 80−35583
TRISTAN facility, target developments 77−23353
UNISOR integrated target-ion source 77−14302
vacuum dependent scientific instruments, hydrocarbon contamination 79−63259
vacuum extraction device, with mass spectrum analyser, gas-forming admixture in metals determ. 80−22371
vacuum materials, set up for meas. released gas 80−105746
vacuum technology, medium, high and ultrahigh, conf., Oxford, England (Apr. 1978) 79−63242
vacuum tightness monitoring in components with unclosed cavities, automatic mass spectrometer 79−52592
van de Graaff accelerator, appl. to ^{14}C detect. 79−11844
Viking lander gas chromatograph-mass spectrometer 78−77460
volcano field ion quadrupole mass spectrometer, performance characts. 77−87866
wide energy range mass spectrograph for diagnostics of fast pulsed sources 79−37549
Wien filter mass spectrometer, expt. results 79−45510
Wien filter mass spectrometer with inhomogeneous fields, resolution 77−79193
ZGS, Effective Mass Spectrometer 80−91310
H ion analyzing 180° magnetic deflection mass spectrometer 79−89039
H_2 in fused quartz tube diffusion coeffs., permeabilities and solubilities meas. *(Japanese)* 77−58832
He desorption spectrometer, clustering of Kr in W (100) obs. 80−77908
He-jet online mass separator, improvements in total yield 80−98999
Si, whisker, amorphous, growth method for field desorption mass spectrometry 79−28262

mass spectrometry *see mass spectroscopy*

mass spectroscopic chemical analysis
see also atom probe field ion microscopy; ion microanalysis; ion microprobe analysis; isotope separation; mass spectra; secondary ion mass spectra; secondary ion mass spectroscopy
acetic acid vapours, clustering, effect of supersonic mol. beam sampling, mass spectrometric study 80−104481
airborne particles, surface toxic elements, ion microprobe and Auger electron spectrometric anal. 78−7753
aliphatic perfluorocarbons, electron attachment, fragmentation 0-12 eV 80−5618
alkali halides, cluster ions and mol. ions in salt field desorption 80−40238
amino acids, ^{15}N-labelled, nanomole isotopic assay by collision induced dissoc. MS 78−20095
amino acids, isotopic enrichment determ. by chem. ionis. mass spectra 79−79694
α-amino acids, mass spectrometers study of evaporation 77−86402
amphetamine derivatives, detect. by GC/MS selected ion monitoring 79−43643
analytical physico-chem. methods, characts. *(French)* 79−48033
apatite, secondary ion mass spectra 78−68965
aromatic heterocyclics, (N- and S-), electron attachment, mass spectroscopic obs. *(German)* 77−64001
aromatic hydrocarbons, electron attachment, mass spectroscopic obs. *(German)* 77−64001
aromatic hydrocarbons, in airborne particulates, gas chromatography/mass spectrometric, NMR analyses 77−13116
artificial circulation system with gas enrichment using membrane oxygenators *(German)* 78−73294
atmospheric pressure ionisation mass spectrometry, cluster form. elimination using collisional dissoc. 77−90696

mass spectroscopic chemical analysis continued
atmospherical pressure ionisation by corona discharge, ionisation charcts. 77−60156
atomically clean surfaces, instruments for anal. and imaging 80−105749
automated isotopic analysis using digital recording system 78−12783
automatic evaluation of isotope anal. of nuclear fuels, isotope dilution, mass and α spectrometry 78−55120
benzene+molecular ion, fragmentation and electron transfer collisions 79−79229
benzo(a)-pyrene, separation and struct. resolution by thin layer chromatography-mass spectrometric meas. 78−7270
benzophenone, laser spectroscopy by cascade photoionisation method in mass spectrometer 80−99496
benzoyl ions, collisional activation mass spectra, energy depend. 80−104482
bio-organic molecules, polar, nonvolatile, anal. by laser desorpt.-mass spectrometry 78−92534
bioanalytical systems using mass spectrometry with atmospheric press. ionisation 78−88680
biological specimens, SIMS anal. appl. 79−44074
biomedical application of laser microprobe mass analyser 79−39630
biomedical laser microprobe mass analyser 80−98060
blood serum, rapid anal. by mass spectrometry/mass spectrometry 80−61173
book 78−318
trans-2-butene, charge transfer mass spectra and photoelectron spectra 80−40778
butene, isomers, ion-mol. reactions, photoionisation mass spectra 80−81298
cerebral blood flow, tissue pO_2 and pCO_2, continuous and simultaneous meas. 79−57829
charge spectrometer, appl. of quadrupole mass filter *(Japanese)* 77−57420
chemical ionisation mass spectrometry, simultaneous positive and negative ion form. technique 77−36806
chemical ionisation mass spectrometry, survey of instrumental techniques 79−57313
chemical ionisation mass spectrometry using drift tube ion source 78−7260
chemical ionization mass spectrum *(Japanese)* 79−43669
chondrite Kirin H, inert gas content interpretation *(German)* 80−46505
chondrite Yamato-74191, inert gas composition and neutron capture effects 80−46504
chromatography and mass spectrometry, conference, Carlsbad, Czechoslovakia (April 79) 80−73097
collisional activation mass spectra 80−48106
combined retrieval system for IR, ^{13}C NMR and mass spectral data 78−31717
comet fly-by mission, impact mass spectrometer for chemical analysis 78−93112
complex mixtures, GC/MS profiles, HISLIB comparison method 78−7268
complex mixtures, mass separation mass spectral identification system 78−44418
complex mixtures, rapid analysis by mass spectrometry/mass spectrometry 80−61173
computer controlled photoionisation mass spectrometer 80−77905
computer data search system, based on catalogue of compressed mass spectra *(Russian)* 80−30292
computer search system of MSDC/EPA/NIH 77−4947
computer-aided classification of mass spectra, pattern recognition techniques, decision-tree approach 80−40774
computerized data acquisition and interpretation, review 78−321
Conference, nuclear materials, safeguards and accountability meas., Williamsburg, USA (May 1978) 79−81045
constructional materials, electron bombarded, gas evaluation obs. *(Russian)* 79−1460
conversational data processing system for instrumental analysis *(Japanese)* 77−82496
corrins, field-desorption mass spectrosc. 78−80821
cortisol, gas phase fragmentation, high voltage scanning field desorption obs. 78−3320
crude oil classification via computerised gas chromatograph mass spectrometry 77−81456
cyclohexane, rapid anal. by mass spectrometry/mass spectrometry 80−61173
cyclotron, as high-energy mass spectrometer, appl. to chem. anal., radioactive dating and quark detection *(Czech)* 78−86375
data bases, information content of retrieval procedures calc. 80−30297
data identification, text search system based on Boolean logic 79−20480
dense gas chromatograph/mass spectrometer, interface design 79−34378
depth profiles obtained by ion-beam sputtering, edge-effects correction 80−55757
depth profiling by ion microprobe with high mass resolution 79−46894
diamond, powders, oxidised surfaces, thermal desorpt. spectra 78−47661
dichlorofluoromethane in atmosphere, gas chromatography-mass fragmentography anal. 79−62565
diffusion processes in spectrometer sample line 78−64907
digital isotope ratio meas. system, using programmable calculator with double collector mass spectrometer 80−63845
diphenylmercury, mol. photoionisation, up to 13.5 eV, formation of $HgPh^+$ 78−25633
dithiocarbamate complexes of Cr, Mn, Sn and Pb IR, electronic and mass spectra, mag. susceptibility, cond. meas. 80−97270
DNA, intact, modified bases characterisation by mass-analysed ion kinetic energy spectrometry 80−3591
dopamine derivatives, detect. by GC/MS selected ion monitoring 79−43643
double focusing MM-ZAB-2F mass spectrometer and MIKE spectrometer, characts. 79−2871
double inlet system with viscous gas flow, C and O isotopic ratios 77−18131
double-pass cylindrical mirror analyser, for ion scattering spectroscopy, resolution factors 79−16078
drift tube studies, buffer gas mixture choice, for ion-neutral reactions 79−57232
drug analysis, by chemical ionisation and electron impact mass spectrometry 79−57316
drugs in blood, anal. by chem. ionis. mass spectrometry 79−57317

mass spectroscopic chemical analysis continued
Du Pont DP-1, gas chromatograph/mass spectrometer, sub-picogram detection, wide dynamic range and automatic source rejuvenation 78−93782
EBR, dissolver soln. fission product determ. by spark source mass spectroscopy 80−32422
EHD ionisation mass spectrometry, instrumentation, mechanisms and appls., review 78−86378
electric arc, horizontal, in inhomogeneous mag. field, mass spectrometric anal. 80−79620
electron capture detector measurement of ions using atm. press. ionis. mass spectrometry 79−92017
electron capture negative ion chemical ionization mass spectrometry 79−43643
electron impact ionisation mass spectrometry using field desorption activated emitters as solid sample probes 77−90657
electron impact spectrometer, using axial magnetic field for collimation 79−49334
elemental compositions, computer assignment from isotopic abundance 78−20085
energy loss spectra using double focusing spectrometer with ang.-resolving slit 78−44426
environmental air samples, gas chromatography-mass spectrometry anal. *(Japanese)* 79−79424
environmental sampling, gas chromatograph/mass spectrometer/data system and spectral search 77−77834
ESCA-ion scatt. spectroscopy-SIMS, review, chem. appls. 79−43701
ethanol, H-bonding investigated with supersonic mol. beam using photoionisation quadrupole mass spectrometer 80−102543
F+dichloromethane, reaction products, modulated mol. beam mass spectrosc. obs. 80−97742
factor analysis of spectra 77−44534
fast reactor fuel consumption determ., automated techniques *(German)* 77−14236
field desorption mass spectrometry, analytical chem. uses 79−92015
field desorption mass spectrometry, appl. to biochemistry, medicine, and environmental science 80−35592
field desorption mass spectrometry of salts, emitter characts. and production 77−63980
field desorption mass spectroscopy, new sample supply technique 77−56279
field dispersed ion analysis, comparison with conventional technique for O^+, CO^+, and CO_2^+ 78−85234
field ionisation and field desorption mass spectrometry *(Japanese)* 79−66384
fissile materials accounting, behaviour of the quadrupole mass-spectrometer towards various noble gases 80−63300
fission product separation using Lohengrin mass separator, high flux reactor in Grenoble 78−17436
fission products of ^{252}Cf, masses, β decay energies, halflives, He jet TOF mass spectrometer 77−23355
flame, atm. press., ion sampling, aerodynamic disturbance by sampling system 77−60142
flame, atm. press., supersonic sampling, bounary layer cooling 77−60143
fluorocarbon glow discharges, plasma polymerising and etching, mass spectrometric obs. 77−32790
fly ash and trace organic compounds anal., from municipal incinerators 80−45584
Fourier transform ion cyclotron double resonance, complicated ion-molecule reactions 78−80808
Fourier transform ion reson. spectroscopy of ions undergoing collisions with mols. 80−35598
Freon 123, deuterium separation at high press. by ns CO_2 laser multiple-photon dissoc. 80−91616
fusion reactor, DITE-II, neutral beam ion source particle beam identification 80−99397
gas, quantitative analysis, non-constant cracking patterns, press. depend. 80−61218
gas analysis, combined photoemission/mass spectrometry technique *(German)* 77−40603
gas analysis, dynamic error determ., transfer function 80−61194
gas analysis, portable double focusing instrument 78−21261
gas analysis of ionosphere, high-resolution high-pressure, mass spectrometer 79−87906
gas atmosphere quantitative analysis adsorption chamber 80−85234
gas chromatograph-mass spectrometer, dual EI/CI ion source *(Japanese)* 78−32919
gas chromatograph-mass spectrometer computer system, GCMS PAC-500 series *(Japanese)* 78−32918
gas chromatograph-mass spectrometer system, gas proportional counter detector 77−36815
gas chromatograph/mass spectrometer/calculator, low-cost bench-top system 77−4972
gas chromatography, mass spectroscopy and mass spectrometry, current developments *(Japanese)* 78−35766
gas chromatography−mass spectrometry, sample anal., review 78−3437
gas chromatography applics. of quadrupole mass spectrometer, book contrib. 77−25350
gas chromatography mass spectrometry technique 80−26094
gas chromatography-mass spectrometry, computer-based library system 77−44523
gas chromatography-mass spectrometry, integrated analytical systems, applics. in biomed. and related sciences, review 80−36200
gas chromatography-mass spectrometry, isotope labelled internal standard, isotopic distrib. calc. 77−56265
gas chromatography-mass spectrometry data system, research-oriented, principles and applics. 80−40770
gas chromatography-mass spectrometry integrated anal. systems, review 79−1972
gas chromatography-mass-spectrometry, ion counting operational charcts. *(Japanese)* 77−60157
gas chromatography/chem. ionisation mass spectrometry, reactant ion monitoring detection technique 77−77821
gas chromatography/mass spectrometer detector system 77−77817
gas chromatography/mass spectrometry system with complete microprocessor control 77−44533
gas chromatography/mass spectroscopy analysis of volatile organic compounds in water supplies 79−12151
gas chromatography/photoionisation mass spectrometry, organic compds. anal. appl. 78−92531

mass spectroscopic chemical analysis continued
gas mixture of air and propane, mixing ratio determ., using quadrupole mass spectrometer *(Japanese)* 80−81391
gas mixtures, high-temp. reacting, using shock tube coupled to time-of-flight mass spectrometer 79−80717
gas-phase reactions, anal. using computer interfaced time-of-flight mass spectrometer 80−71967
gaseous impurities atm. press. ionisation mass spectrometric anal. technique 77−56263
gaseous impurity microconcentrations, nonconducting materials 80−73518
gaseous ion thermochemistry, metastable ion kinetic energy spectrometry, review 77−44537
GC/MS integrated systems, review of current techniques 80−68289
GC/MS system for isotope ratio monitoring 79−22855
geochemical appl. of spark source mass spectrography, element sensitivity, precision and accuracy 78−20544
geological and extraterrestrial sample element anal., laser mass spectra 79−16717
glass, excavation type, layers and profiles of SiOH, CaOH, and KOH polyatomic ion groups special corrosion effect 80−81387
glass, gas content determ. by dynamic extraction method 80−61219
glow discharge source combined with quadrupole mass filter for solids anal. 78−61075
granite, extraction of fission Xe, anomalous fission yields 78−96216
He-jet fed online mass separator for recoil atom mass spectroscopic anal. 80−98998
heterogeneous chemical kinetics by modulated mol. beam mass spectrometry 77−25305
1-5hexadiyne ion+neutral 1,5-hexadiyne, trapped-ion mass spectrometry 80−97694
hexamethyldisiloxane, polymer film, struct. determ., IR spectra, elemental anal. *(German)* 77−59224
1-hexene-water(-D_2O), field-induced surface reactions, field ionis. mass spectra obs. 78−95949
high temperature, Knudsen effusion cell, thermodynamic and physicochemical behaviour, review 80−52354
high temperature gas phase species, IR spectral meas., mol. beam mass spectrometry 80−52235
high temperature molecules, high pressure molecular beam mass spectrometric sampling, review 80−52355
high temperature vapour, charact. by angular distrib. mass spectrometry 80−55769
high temperature vapours, photoionisation mass spectrometry 80−52238
high-purity substances, analysis methods 79−39241
high-yield laser ion source with plasma focusing 78−61097
histological section, high mass resolution by ionic analyser *(French)* 80−109069
Holbrook chondrite, vapour phase comp. from mass spectrometry 78−65568
HTR individual coated fuel particles, gas anal., optimum heating and crushing 77−56294
HTR individual coated fuel particles, mass spectrum. determ. of Xe, Co and Kr gases 77−56293
human disease study using mass spectrometry and metabolite profiling 80−51289
human serum, definitive meas. of constituents 80−93818
hydrocarbons, normal, mass-spectrometric fragmentation processes, quantum field theory 80−40782
hydrocarbons, volatile, detection and meas. in atm. review 77−64492
hydrocarbons chemisorbed on SiO_2-supported Ni, chem. composition *(German)* 79−92002
hydroxonium complexes, produced by collisional dissoc. method, mass spectrometric study, dissoc. energies determ. 80−95707
hypersonic flow, in shock tunnel 77−31328
imaging atom probe mass spectroscopy, appl. to surface struct. anal. 79−23818
implanted ion depth distrib., secondary ion mass spectra 80−79829
impurities, conc. of C, O, Si 78−59832
Inconel 617, mass spectrometric study, high temp. reactor system appl. 79−43663
inert gas atoms, desorbing from solid surface apparatus for detection 78−32915
inert gas halide ions, form., mass spectrosc. obs. 79−29346
inorganic compounds, field ionisation mass spectrometry, review 78−35764
instrumental discrimination effects, evaluation 79−35888
instrumentation, design and construction for analytical mass spectrometry, review 78−322
integration TIM for GC-CI-MS system *(Japanese)* 77−90697
interface composition determ. methods 79−70396
involatile molecule thin films, electrospray deposition for ^{252}Cf plasma desorption obs. 80−35584
ion+molecule reactions, state selected, threshold electron-secondary ion coincidence method obs. 79−5190
ion cyclotron resonance spectroscopy, interpretive expt. 80−36814
ion extraction from continuum plasma, flowing (nonflowing) mass discrimination effects 77−63979
ion kinetic energy spectra, dish topped metastable peaks, rel. to field-free fragmentation regions 80−101871
ion kinetic energy spectrometry using negative chem. ionis., direct mixture analysis 79−34397
ion kinetic energy spectrum peaks, collision gas sensitive 80−40679
ion microprobe, appl. to natural silicates *(French)* 77−52710
ion microprobe anal., secondary ion mass spectrometry at close to single-atom concentration using DC accelerators 79−48004
ion multiplier noise filter based on analogue delay device 78−92541
ion reactivity arising from different region of translational energy release distribution, need for ang. collimation 80−104483
ion sampling, across small diameter hole, mass discrimination errors 77−56273
ion sampling system, characts. and calibr., atm. press. flame 77−56270
ion scattering double spectroscopy, isotope effects 77−59658
ion source, low energy (100-500 eV), high efficiency 78−62261
ion source active sites, effect on mass spectral fragmentation patterns 78−89581
ion-molecule equilibria in solvolysis, secondary β ^2H isotope effects, hyperconjugation 80−50874
ion-molecule reactions, bakeable hollow cathode for sampling 80−37117
ion-molecule reactions, gas-phase, and high-press. mass spectrometer, review *(Japanese)* 78−64830

mass spectroscopic chemical analysis continued
ion-molecule reactions, kinetics, spectrometer with selective introduction drift tube *(French)* 79−11839
ionisation in flames, mass spectrometric and mobility analyses for flame ionisation detector 78−40050
ionisation mass spectrometer, with dedicated minicomputer, biological appls. 78−53586
ions, multiple dissoc. probabilities 80−40678
ions with excess kinetic energy, simple mass spectra method 78−62262
isotope detection in terrestrial and extraterrestrial samples, tandem accelerator appl. 80−61923
isotope dilution anal. by spark source mass spectrometry using electro-optical detector 80−101868
LAMMA mass analyser, laser microprobe *(German)* 79−29419
laser ion source, appl. in mass spectrometry 80−89564
laser ionisation source for ICR spectroscopy, metal at. ion chem. appl. 80−45597
laser mass-spectroscopic method, elementary comp. of solids 79−83532
laser microprobe mass analyser, development for biological specimens 79−17554
laser microprobe mass analyser for organic samples 79−57315
laser-probe mass spectrometry, analytical capabilities, review 78−64902
liquid chromatography/mass spectrometry combined analysis, appls. 78−31735
liquid samples, inlet system design and appls. 77−36816
Lohengrin mass separator, techniques for fission product mass and charge distribs. *(German, English)* 78−16891
low energy ion scattering for composition and struct. anal. of outer surface 79−4458
low-resolution spectra identification using combined forward-reverse library search system 80−30296
LPE, molecular beam mass spectrometry, in situ anal. of minor gaseous species 80−52357
LSI surface analytical techniques applied to electronic components [Si LSI chip inspection] 80−81392
lubrication, spectroscopic methods for surface anal. *(French)* 80−26095
LWR, dissolver soln. fission product determ. by spark source mass spectroscopy 80−32422
MACS mass and charge analysis technique appl. 80−73521
many component sample GC-MS anal. *(Japanese)* 78−35767
margaric acid, evaporated film, X-ray diffr. anal. and mass-spectrography 77−15718
marine sample petroleum analysis by gas chromatography and mass spectrometry 77−4977
Mars Viking surface sampler subsystem, acquisition assembly 79−12380
mass analysed ion kinetic energy spectrometry, appl. to mixtures 78−44413
mass fragmentography with glass capillary columns, trace anal. of pesticides in biological extracts 77−9312
mass peaks identification in SIMS using computer program 80−101867
mass-analysed ion kinetic energy spectra, automated fast scanning method 79−35885
medical, respiratory, blood and tissue gas press. meas. *(Japanese)* 77−70566
medical and environmental applics. of quadrupole mass spectrometry, book contrib. 77−25622
metal, spark-source mass spectrometry, relative sensitivity coeffs. 79−92045
metal surfaces, characterisation by SIMS and XPS 79−16054
metal surfaces, clean, AES anal., contamination effects obs. 78−53293
metastable decomposition, kinetic energy release distrib., mass spectroscopic determ. 77−44538
metastable scanning, using double focusing mass spectrometer and laboratory data system 77−44522
meteorite Springfield specimens, mass spectroscopic element and isotope anal. 77−60731
meteorites, iron, elements distrib. between metal and phosphide phases 80−46508
methanol, dissoc. ionisation mechanism, correlation diagram approach, mass spectra obs., metastable processes 80−95728
methanol (-d), H-bonding investigated with supersonic mol. beam using photoionisation quadrupole mass spectrometer 80−102543
methyl radical+O_2 (NO), mass spectra, absence of reaction in combustion system 78−53195
MHD plasma, coal-fired, molecular beam mass spectrometric sampling system 80−52358
microanalysis, principles, practice 79−39259
microdot standards, ion implanted, SIMS anal., detection limits 79−39264
microlocal analysis using laser mass spectrometer *(Russian)* 77−12862
Microprobe Mole/plasma chromatograph system, for anal. of compounds on micron scale 80−101049
middle atmosphere, plasma and neutral gas comp. and struct. anal. via mass spectrometer probe 78−45191
mixture analysis, integrated MS/MS technique 79−34389
mixture analysis by mass analysed ion kinetic energy spectrometry 77−36807
mixtures, component determ. by target transform. factor anal. of mass spectra 77−52679
mixtures, negative chem. ionisation mass analysed ion kinetic energy spectrometric anal. 78−92550
modulated molecular beam mass spectrometry, anal., appl. to nonlinear systems 78−56944
modulated-field linked-scan studies of metastable ions 80−77904
molecular beam mass spectrometry, appl. to coupled diffusion and chem. reaction 77−73497
molecular ion formation on molecular cryst. surface UV laser irrad. *(Russian)* 80−71521
molecular spectroscopic laboratory strategies, queueing theory and digital simulation use 80−30299
molecular substructures, identification and retrieval, K-nearest neighbour methods 78−20084
monoterpene hydrocarbons in rural atmospheres, gas chromatography/mass spectrometric anal. 80−17336
MSDC/EPA/NIH mass spectral search system 78−65912
multicomponent deposition processes, monitoring and controlling techniques, review 78−11113
multicomponent mixture analysis by field ionisation-ion kinetic energy spectrometer 77−56272
multipeak residual gas analysis monitoring system 79−79342

mass spectroscopic chemical analysis continued
multiple ion detection system, for mag. sector mass spectrometer 77−70348
multiple reactions, Cl isotope effects, mass spectrometric monitoring 79−39135
natural products mass spectroscopy, conf., Rehovot, Israel, (Aug.-Sept. 1977) 78−88681
natural waters of Mt. Everest, mass spectrometric chem. anal. of D, ^{17}O and ^{18}O *(Chinese)* 80−77016
Nimonic PE 13, mass spectrometric study, high temp. reactor system appl. 79−43663
N-nitrosodimethylamine, trapping for GC/MS analysis 78−20094
NODUS, ion scatt. spectrometer for surface composition anal. 78−76968
non-crystalline solid, surface and thin film chem. anal. techniques *(French)* 77−73495
nonvolatile materials, in-situ sampling system for thermal volatilisation anal. by GC/MS 77−77828
nuclear fuel materials, chemical and isotopic anal. of U, Pu, and Th 79−81046
nuclear material accountability, analytical methods and laboratories, present and future 79−81047
nuclear materials analysis using plasma desorption mass spectrometry isotope ratio determ. using TOF mass spectrometry 80−78375
nuclear reactor pressure vessel/cladding interface, residual gas analysis *(German)* 77−40603
oligomers, polymer-derived, mass spectral charact. 80−37916
on-line literature search system 78−15734
on-stream analysers development, w.r.t. speed and reliability 77−66778
organic cations, extraction from acid soln. by elec. field, mass spectrometric anal. 79−66390
organic compound identification using reversed geometry mass spectrometer 80−50913
organic compounds, field ionisation mass spectrometry, review 78−35763
organic compounds in environmental samples, capillary GC/MC/computer techniques 78−80799
organic liquids, electrohydrodynamic ionisation, solvated ion mass spectroscopy, anal. appl. 78−73102
organic mass spectroscopy, techniques and appls. 79−43667
organic mixture analysis by high-resolution mass spectrometry/mass spectrometry 80−104476
organic mixtures, multiple reaction monitoring and direct anal. 79−74437
organic molecules, multiphoton ionisation mass spectra by ArF excimer laser 80−81381
organic non-volatile compounds ionisation by fast heavy ions, separation by TOF mass spectrom. 77−27170
organic solids, neat and Ar-diluted, secondary ion mass spectrometry 79−74441
organic solids, photoproduced in simulated Jovian atmosphere, mol. anal. 78−69740
organic surface contaminants, anal. by plasma chromatography-mass spectroscopy, and Raman microprobe technique 80−108773
organometallic compounds, secondary-electron capture negative-ion mass spectrometry 77−16892
organophosphorus pesticides, trace analysis by mass spectroscopy, ionisation methods 78−76939
palmitic acid, evaporated film, X-ray diffr. anal. and mass-spectrography 77−15718
pattern recognition, low resolution, super-modified simplex evaluation 79−52795
pattern recognition, mathematical programming techniques 78−92523
pattern recognition 79−52796
pattern recognition applications to mass spectra classification 78−48722
PDX vacuum vessel, glow discharge conditioning 80−79607
peak matching for known mass difference ion unit mass determ. 80−77906
pentafluoromethyl iodide, ion-molecule reactions, amongst radiolysis products, reaction rates, mechanisms, mass spectra 79−5136
peptide analysis by field desorption mass spectrometry using pretreated Si emitter 80−55751
phenyl cation, struct., ion-molecule reactions studied by trapped ion mass spectroscopy 80−102586
phosphonium cations, quaternary, produced by field desorption, collisional activation spectra 78−56946
photographically recorded spectra, semi-automatic interpretation, mass, at. spectra appls. 77−48708
Pioneer Venus large probe neutral mass spectrometer for measurement of composition and abundance of atmospheric gases 79−88563
plasma chromatograph/mass spectrometer sample overload protection 79−39237
plasma chromatograph/mass spectrometer simultaneous electron impact/chem. ionisation carrier gas mixture 79−30600
plasma etching, process development and monitoring via mass spectrometry 78−35546
PLT Tokamak vacuum vessel, residual gas and surface comp. changes with H_2 discharge cleaning 79−80631
polyacetylene, halogen doped, mass spectrometric anal. 80−108771
polymer, volatile constituents anal. by thermal desorpt., gas chromatography and mass spectrometry 79−43664
polymer breakdown plasma analysis, mass-spectrometric installation 78−88670
polymer matrix composites, component interaction mass spectrometry investigation *(Russian)* 80−35511
polymers, pyrolysis, inlet system design and appls. 77−36816
polymers degradation reactions, polyethylene and polyvinylchloride *(Dutch)* 79−87893
polystyrene, mech. degradation, mass spectroscopic investig. 77−16668
programmable quadrupole mass spectrometer *(Japanese)* 77−86415
propyl halides, photoionisation mass spectrometry 80−40779
propylene, electron impact ionisation and dissoc. 80−37894
PTFE film, reactive sputtering in Ar-CF_4 mixture, MSCA 78−92191
pulse counting detection, high precision, limitations, optical conditions 77−54463
pulse counting techniques, in organic mass spectroscopy-gas chromatography 78−31720
pulse-counting detector systems, effective deadtime, theory 78−41369
pyridine, deuterium substituted, Raman and IR vibr. spectra 80−84739
Quadmagnova, GC/MS system, computer scanning and control 78−76946
quadrupole gas analyser with integral microprocessor 78−73109
quadrupole ion microprobe for secondary ion emission investigs., ion optics 79−35892
quadrupole mass spectrometer, to study secondary and sputtered ions 79−83072
quadrupole-type SIMS development and applications *(Japanese)* 77−86414
quartz, synthetic and natural, water content determ. 77−86401
radioactive waste solidification products, radiolysis gases generation, mass spectrometric anal. 79−85626
radioisotope detection using tandem electrostatic accelerators 79−52806
rare earth oxides, determ. by mass spectrometric complexometric method 80−3442
rare-earth oxides, determ. using ion microanalyzer *(Japanese)* 78−23987
reactive gas mass spectrometric analysis with free-jet expansion sampling 80−89566
refractory metal-Al_2O_3 systems, vaporis. at elevated temp., mass spectrometric obs. 79−29388
relative sensitivity factors in mass spectroscopy 80−86497
residual gas anal., mass spectrometer *(Japanese)* 79−79349
resin bead mass spectroscopy for safeguarding Pu and U 80−73984
resonance ionization source for mass spectroscopy appl. isotope anal. and time of flight spectrometer 80−81380
review of literature, 1975-1977 78−85226
RF mass spectrometer, MKh 6202, for respiratory gas anal. 78−7468
RF spark ion source, multiply-charged species rel. abundance distribs. 77−61151
scanning electron stimulated desorption, appl. to surface anal. 78−34700
scanning laser mass spectrometer milliprobe 79−35882
scirpene toxins, in animal feeds, chem. anal. 78−48707
search system, one-dimensional, for GC and MS anal. 78−23977
second-generation ion microanalyser description and performance *(French)* 80−101055
secondary ion emission, conf., Stanford, USA (Aug. 1979) 80−105419
secondary-ion mass spectrometry, doping profiles meas. appl. *(German)* 78−95978
selected fragment scans in direct mixture analysis, active computer monitoring and control 80−35597
semiconductor materials, quantitative anal. 80−101052
sensitivity to microimpurities, algorithm of detection 77−64000
simplex pattern recognition 77−21429
SIMS, appl. to determ. of provenance of archaeological objects 80−61197
SIMS, depth profiling, automatic sequential mass analysis 80−108764
SIMS, one fitting parameter approach 80−108762
SIMS, quantitative, one fitting parameter method 79−39263
SIMS, quantitative, review 80−61195
SIMS, recording, optimisation 79−43683
SIMS, solid surface investig. applications *(Rumanian)* 80−49510
SIMS, specimen current integration, appl. 79−43685
SIMS data quantification, theoretical model and sensitivity factor calcs. 78−21255
SIMS for single-atom concentration, using DC accelerator 79−92042
SIMS primary ion sources, selection 79−39267
SIMS quantitative analysis, accuracy 79−39266
SISCOM, library search system for compound identification 79−49329
small particle identification, review 78−48739
soda-lime glass to Fe-Cr seal, field-assisted bonding, SIMS anal. 79−34399
solid and surface analysis using high energy molecular beam sample bombardment 77−21443
solid material, laser probe mass spectrometry 77−21427
solid microvolume mass spectrometric isotopic analysis 78−58088
solid substance qualitative analysis, spectrometer with laser ion source *(Russian)* 78−23990
solid surface monolayers, anal. by mass and energy spectrometry methods 77−56248
solids, elemental anal. by SIMS 80−97748
solids, quantitative anal., using laser plasma ion source 77−32863
space plasma, mass discrimination effects in mass spectrometers ion and neutral extraction 80−4230
spark ion source, ion energy distrib. of late stages 79−55596
spark plasma ion source effects on mass spectroscopic quantitative anal. 79−14631
spark source (RF), of mass spectrometer, analysis of hard X-ray emission 79−90480
spark source and sputter-ion mass spectrometric analyses *(Japanese)* 77−86413
spark source quadrupole mass spectrometry, development, appls. 80−62789
spark source sensitivity factors for elements in graphite matrix 80−16760
spark-source mass spectrometry; elemental sensitivity rel. to sparking conditions 79−57314
specimen charging control for SIMS and AES of insulators 80−101875
specimen heating and cooling installation, programmed, for MKh 1303 spectrometer 79−93253
spectra, computer identification systems 78−86966
spent fuel burnup determ., U, Pu, Nd, isotopic comp. and conc. determ. by mass-spectrometric isotope dilution 79−89373
spent reactor fuel, nondestructive burnup determ. calibration using destructive radiochem. anal. 79−89372
spent reactor fuel burnup determ. using anal. chem. [conf. Piestany, Czechoslovakia (Sept. 1978)] 79−89371
sputtered neutral mass spectrometry, for surface analysis and depth profiling 77−77833
sputtered products, thermal ionisation, method of solid microanalysis *(French)* 79−61924
sputtering, RF reactive, reaction mechanism analysis *(Japanese)* 78−19665
sputtering system, gas sampling 77−69989
stainless steel, in $MgCl_2$ solutions, Cl distrib. in oxide films, SIMS obs. *(French)* 80−108765
stainless steel, neutron dose determ., from isotope abundance ratio, mass spectra obs. 80−61220
steel, atom probe microanalytical expts., review 78−35622
steel, Cr-plated, H_2 distrib., laser-mass spectrometer investig. 78−61113
steel, He assay following irrad., mass spectrometer system 77−34397
steel, impurity element determ. by spark source mass spectrometry using powdered salt 78−7304

mass spectroscopic chemical analysis continued
steel, mass spectrometric analysis of S content by remote meas. technique 78−23994
steel, pearlitic atom probe microanal., computer controlled 77−66781
steroids, mass spectra, computer-aided interpretation by pattern recognition, preprocessing effects 78−15733
steroids, mass spectra, computer-aided interpretation by pattern recognition methods 78−64898
stratosphere, appl. of mass spectrometer beam system 78−7808
stratosphere, atmospheric constituents mass spectrometric obs. *(Japanese)* 79−79920
stratosphere, positive ion comp., balloon-borne mass spectrometric meas. 78−32194
stratospheric composition meas. 77−33200
sulphonium cations, tertiary, produced by field desorption, collisional activation spectra 78−56946
surface anal. by photon-induced field ionisation mass spectroscopy 80−40780
surface analysis, advantages and disadvantages of SIMS rel. to ion scattering spectrometry 79−12883
surface analysis, by secondary ion mass spectrometry, review 78−68949
surface analysis, combining secondary ion mass spectrometry and ion scatt. spectrometry 77−60158
surface analysis, spectroscopic methods, review *(Chinese)* 79−34414
surface analysis, system, modular combined ESCA, UPS, AES, and SIMS 78−73107
surface analysis by ion scattering and secondary ion mass spectrometry 77−40621
surface analysis instruments for vacuum electronics *(Czech)* 77−18145
surface analysis techniques 79−70411
surface and thin film, chemical analysis, comparative survey of methods, book contrib. 79−66393
surface characterisation, multiple technique instrument, ESCA, scanning Auger, UPS and SIMS 78−73108
surface charact., combined ion scattering spectrocopy, SIMS, SEM, energy dispersive X-ray techniques 79−43702
surface chemical analysis, low energy ISS compared with SIMS 78−64908
surface chemical ionisation mass spectroscopy, appls. 78−92547
surface contaminants analysis by plasma mass secspectroscopy 78−3433
surface contamination, anal. using mass spectrometer system with laser heating 79−87903
surface ionisation, elemental anal. of sputtering products *(French)* 80−50905
surface ionisation meas. after ion sputtering *(French)* 80−27374
surfaces and thin film studies by combined system of SIMS, AES and XPS 80−86536
teaching, mobile spectroscopy, chem. anal. laboratory 78−93502
tetrachlorodibenzo-p-dioxin determ. by low resolution gas chromatography-mass spectrometry 80−66893
tetrafluoromethane gas, total dissociation, in reactive ion etching system, reactant supply 79−83349
Δ^9-tetrahydrocannabinol, detect. by GC/MS selected ion monitoring 79−43643
thermal analysis, mass spectroscopy techniques, comparison 78−31742
thermal desorption mass spectroscopy, computer control, data acquisition, appls. 80−61181
thermoanalysis, inlet system design and appls. 77−36816
thin film surface anal. and depth profiling by spark-source mass spectrography, discharge model 80−40781
thin films and surfaces, ultra-high vacuum system for preparation and anal. 79−69986
thin layer chromatography-mass spectrometry, direct on-line coupling system 78−7270
time of flight atom probe, quantitative microanal., metallurgical appl. 80−86498
trace contaminants in substrates, laser-probe pyrolysis technique 78−92553
transition metal nitride formation by N_2^+ ion+metal reaction 79−96363
transpiration mass spectrometry, of high temp. vapours 80−52356
trapped-ion cyclotron reson. spectra, intensity oscills. characterisation 78−48716
Trichel corona, negative ion mass spectra 78−87537
trifluoroethanol, H-bonding investigated with supersonic mol. beam using photoionisation quadrupole mass spectrometer 80−102543
trifluoroiodomethane, IR multiphoton dissoc. yields, new technique, nonlinear pumping effects 79−100406
trifluoromethyl iodide, ion-molecule reactions, amongst radiolysis products, reaction rates, mechanisms, mass spectra 79−5136
1,3,5-trinitrohexahydro-1,3,5-triazine, thermal decomposition, mass spectra obs. 79−79340
tripeptides, synethetic, hormone models, field desorption mass spectrometry using needleless emitters 79−34398
triple quadrupole mass spectrometer and technique, direct mixture analysis and struct. elucidation 80−35583
turbogenerators, H_2 cooled, heating-up detect. by gas stream chromatography and mass spectrography *(French)* 79−48024
unstable compound analysis, surface reaction elimination, chem. ionisation method 78−61074
upper atmosphere neutral composition, cryo mass spectrometer meas. in winter anomaly campaign 78−45192
vacuum analysis, design and operation of small mass spectrometers 79−63322
vacuum deposits as calibration standards for X-ray fluoresc. anal., mass spectroscopic anal. 77−60177
vacuum extraction device, with mass spectrum analyser, gas-forming admixture in metals determ. 80−22371
vacuum gas chromatography-mass spectrometry, using short gas capillary columns 78−95968
vacuum technology, medium, high and ultrahigh, conf., Oxford, England (Apr. 1978) 79−63242
vacuum vibrator arc ion source, multiply-charged species rel. abundance distribs. 77−61151
vapour with different degrees of polymerization, mass spectra, line overlap coeff. calc. 79−96392
Venus atmosphere, Pioneer Venus Orbiter neutral gas mass spectrometer expt. 80−67502
Venus ionosphere composition, meas. by ion mass spectrometers on Pioneer Venus Bus and Orbiter 80−67499
vinyl chloride, trace determ. in water by direct injection GC/MS 78−35739

mass spectroscopic chemical analysis continued
vitamin B_{12} field-desorption mass spectrosc. 78−80821
volatile compounds, dissolved, measurement using variable pH interface mass spectrometer 79−61930
volatiles in submarine volcanic rocks from the Mariana Island arc and trough 79−92535
water clusters around alkali metal ions produced by ion bombardment, secondary emission obs. 77−63518
water pollution, analytical methods comparison 77−90685
Wien-Thompson modern mass spectrometer review 80−45613
Ag beams for MBE, modulated beam mass spectrometric anal. 79−43156
$Ag_2S(Se)(Te)$, solid and liquid, mass spectrometric obs. of VP, heats of form., comp. 79−42266
Al alloys, determ. by spark-source mass spectroscopic anal., sensitivity calibration 78−68962
Al anodic film, H profile meas. by SIMS 78−27847
Al, barrier film growth in soln. of film promoting and aggressive ions 77−8975
Al beams for MBE, modulated beam mass spectrometric anal. 79−43156
Al, condensed film, phase and struct. nonuniformity *(Russian)* 80−54536
Al, determ. by spark-source mass spectroscopic anal., sensitivity calibration 78−68962
Al, surface, pure, oxidised element determ. by SIMS 78−85247
Al, surface ionisation, elemental anal. of sputtering products *(French)* 80−50905
Al-Mg-Si, Mg loss, mass spectrometry/thermogravimetry 77−16620
Al_4C_3, vaporis. thermodynamics, 1321-1607K 80−66859
AlF_3-MF(M=Li, Na, K, Rb or Cs), ion-molecule equilibria studied by mass spectrometric method, heats of dissoc. and form. calc. 80−104479
AlN, cpd. form. reaction in reactive evaporation, quadrupole mass analysis *(Japanese)* 78−23628
AlO_2 molecule, mass spectrometric study 80−89563
Al_2O_3 anodic film, gas emission, mass spectrometer study *(Polish)* 77−9157
Al_2O_3, high temp. gas phase equilib. formation enthalpy, dissoc., mass spectra 78−23925
Al_2O_3, mass spectroscopic investig. of chem. reactions between adsorbed species 77−40600
$Al_xO_y^+$, spark source mass spectrometric study of species 79−29423
$Al_2(SO_4)_3$, decomposition, charact. of gaseous and solid products 78−44374
$^{26}Al/^{26}Mg$ isobars, separation via negative ion mass spectroscopy 80−31146
Ar-hexamethyldisiloxane, glow discharge positive column ion mass spectra identification 80−38834
Au beams for MBE, modulated beam mass spectrometric anal. 79−43156
Au contact films, dissociation of GaAs and $Ga_{0.7}Al_{0.3}As$ during alloying 79−79357
B, β-rhombohedral, purification by electron beam melting and CVD 80−20781
B, determ. in Al, spark-source mass spectrometric method 79−74479
β-B, rhombohedral, sublimation, 1823 to 2253K, torsion-effusion and mass spectroscopic meas. 77−39673
BF_2 radical, thermomechanical studies by mass spectrometry, enthalpy of form. and ionisation pot. determ., chem. bonds 80−81382
BF_3, additional memory effect *(Japanese)* 79−29432
$BaBr_2$-$BaCl_2$, vap. mixture, ion-mol. equilib., heat of form. of ions 80−26039
$BaCl_2$-$BaBr_2$, vap. mixture, ion-mol. equilib., heat of form. of ions 80−26039
BeO, heated on W, thermal anal. using mass spectrometric, technique, vaporisation behaviour 80−79932
^{10}Be, mass spectrometric meas. with cyclotron, geochronological appl. 79−57338
$^{10}Be/^9Be$ ratio meas. using electrostatic tandem accelerator 80−76579
CLi_3, desorption from graphite expt., ionis. pot. 79−34392
CO, decomposition in corona discharge, qualitative chemical anal. of reaction products 78−60992
CO, rapid anal. by mass spectrometry/mass spectrometry 80−61173
CO-He-O_2 gas discharge laser plasma, positive ion generation mechanism *(Russian)* 79−99005
$CO+CO_2$, exchange rates behind reflected shock waves for $C^{18}O$ and ^{13}CO 79−29363
CO_2, ion drift velocities and mobilities 80−43834
CO_2, proton affinity, cluster ion stability, mass spectrometer obs., appl. Martian ionosphere 77−77760
CO_2+N_2+He, glow discharge positive ion species identification *(Russian)* 80−84014
$(CO_2)_2^+$, ion-mol. reaction product distribs. and rate coeffs. 80−50852
CS_2, ionisation and fragmentation by monoenergetic electron impact, mass spectrometric study 80−102581
CS_2, proton affinity, cluster ion stability, mass spectrometer obs., appl. Martian ionosphere 77−77760
$^{13}C/^{12}C$, ratio analysis in carbonates by mass spectrometry *(Portuguese)* 80−7875
^{14}C dating using electrostatic accelerators and negative ions 78−32917
^{14}C, detect. via small van de Graaff accelerator 79−11844
^{14}C direct detection at natural concs. by mass spectrometry, for dating 78−32916
$CaCl_2$, cluster ions and mol. ions in salt field desorption 80−40238
CaO, heated on W, thermal anal. using mass spectrometric, technique, vaporisation behaviour 80−79932
Ca_2O:Bi, positive ion nonequilibrium emission in heterogeneous chemical reaction, mass spectra 80−55277
$12CaO.7Al_2O_3$, composition of gases released on heating, crystallisation *(Russian)* 80−93820
CdTe, gas, identification by high-temp. mass spectrometry 80−45593
CdTe, trace anal. by heavy ion induced X-ray emission and SIMS 80−55755
Ce oxidised surface, comparative sputtered neutral mass spectrometry and SIMS studies 79−90856
CeO_2, plasma deposition of crysts. and their characterisation 80−20800
$ClONO_2$, photolysis products, very-low press. meas. 79−29376
^{36}Cl in environmental water samples, anal. using electrostatic accelerator 79−20895
Cr, vapour deposition by hollow cathode discharge,mass and energy anal. for incident ions on substrate 78−23630

mass spectroscopic chemical analysis continued
Cr-N(C), vapour deposition by hollow cathode discharge, mass and energy anal. for incident ions on substrate 78−23630
Cs-SiO_2-Al_2O_3 system interactions, getter development for radiocaesium 80−83208
$CsAlSiO_4$, and $CsAlSi_5O_{12}$, cryst. evap., mass spectral investig. 80−49353
Cu film deposition, reactive sputtering in RF discharge, glow discharge mass spectrometry 77−44155
Cu film oxidised in ^{18}O, ion scatt. anal. 77−40463
Cu, surface ionisation, elemental anal. of sputtering products *(French)* 80−50905
Cu-Al, surface ionisation, elemental anal. of sputtering products *(French)* 80−50905
Cu-Al (0.5-17.6 at.%), mol. ions in spark source mass spectra 78−44427
Cu-Al alloys, spark-source mass spectrosc. chem. anal., using mol. ions 79−92031
D abundance, Indian radioactive thermal spring water D content, mass spectrometric anal. 79−39765
Er, film, reaction with H_2O vapour, spectroscopic and X-ray diffr. obs. 77−40575
ErD_2, thin film, reaction with H_2O vapour, spectroscopic and X-ray diffr. obs. 77−40575
Eu-W-O, reaction system, thermodynamics, mass spectrometric obs. 77−77748
Eu_2O_3, monoclinic, growth from molten NaF solvent 78−19653
$EuPO_2$, $EuPO_3$, gases, thermochem. props. 79−66334
Fe (110) surface, adsorption and decomposition of NH_3, identification of surface species using SIMS 79−90862
Fe, cast, graphite nodule form., ion microprobe mass anal. appl. 79−43295
Fe, purification, recrystn. temp. and elec. resistivity *(Japanese)* 80−100780
Fe-Al oxide system, depth profile anal. by secondary ion mass spectra *(Japanese)* 78−7290
Fe-TiB_2, phase composition, secondary ion-ion emission study *(Russian)* 80−20896
$Fe(CO)_5$, electron impact appearance pots. for ion fragments, mass spectra obs. 79−34281
$Fe_{1-x}O$, wustite, vaporisation, mass spectrometric analysis of gaseous phase 78−48652
Fe_3O_4, magnetite, vaporisation, mass spectrometric analysis of gaseous phase 78−48652
G_2-B_2O_3 melt, thermodynamic props. from mass spectroscopy 80−39318
GaAs anodic oxide, analysis using low-energy ion scattering spectrometry *(French)* 79−52845
GaAs epitaxial layer, Be, O, Si, S, Zn and Sn impurity concentrations 80−49260
GaAs oxide, passivated layers, quantitative in-depth profile, AES-SIMS thermal, anodic and plasma oxidations 78−84087
GaAs, SIMS, energy distrib. of sputtered ions 79−38706
$GaAs_{1-x}P_x$, SIMS, energy distrib. of sputtered ions 79−38706
GaN, film, secondary ion mass spectrometric qualitative anal. 78−7265
Ga_2Se_3-FeSe, phase diagram, elec. cond., mag. susceptibility 80−88301
Gd oxidised surface, comparative sputtered neutral mass spectrometry and SIMS studies 79−90856
$Gd_{0.27}Co_{0.64}Kr_{0.09}$, amorphous film, thermal release of Kr and H, meas. using UHV mass spectrometric technique 80−3439
GeO_2-SiO_2, glass, evaporation by high temp. mass spectrometry 80−79927
H isotope separation in DC-arc plasma, mass spectrometric anal. 79−90457
H+HCl, reaction kinetics, ESR and mass spectrometric obs. 77−21357
H+O_3, reaction mechanism studied using photoionisation mass spectrometer, form. of $O_2(a'\Delta g)$ 80−85168
H_2-He mixtures, isotopic anal. using high resolution mass spectrometer 77−77844
H_n^+ clusters with odd and even mass number 79−92840
HCl+Ba, beam-gas reaction, multiphoton ionisation, product identification 78−23946
$H(H_2O)_n^+$, macromol. clusters, detect. by SIMS 79−39239
HO_2+ClO, free radical reaction rate consts. and products at 298K, discharge flow mass spectra 80−67391
H_2O, determ. in gases, mass spectroscopic method, prep. techniques 77−40587
He desorption spectrometer, clustering of Kr in W (100) obs. 80−77908
He, extremely pure, preparation and purity meas. 79−20496
He-jet online mass separator, improvements in total yield 80−98999
He^++$H_2(D_2)$, dissociative charge transfer, 78-330K 80−61079
^3He, for environmental ^3H anal. 77−9447
HfO_2, plasma deposition of crysts. and their characterisation 80−20800
Hg_2Cl_2, surface composition, electron impact, mass spectrometry, AES and LEED meas. 79−60607
HgSe, gas, identification by high-temp. mass spectrometry 80−45593
Ir, chemisorption of H_2, adsorption and desorption kinetics, struct. of overlayer 80−84367
Kr anomalous isotope composition at Oklo natural reactor deposit 77−56630
Kr+Cl_2, $KrCl^+$ form., mass spectrosc. obs. 79−29346
LaB_6 crystals, zone refined, chem. characterisation 80−93821
LaIr(g), thermodynamic stability, high-temp. mass spectra obs. 80−7781
LiCl, Li isotopic comp. determ. by mass spectrometry 80−66899
$LiCrO_2$, evaporation, as a corrosion product in compatability experiment of Li_2O pellets with Fe-Ni-Cr alloys, mass spectrometric study 79−73301
Li_5FeO_4, compatibility of Fe-Ni-Cr alloy with Li_2O pellets, mass spectrometric study of Li_5FeO_4 evaporation 79−8385
LiH, form. on polycryst. Mo membrane, from diffusing gases, mass spectrometric obs. 77−66771
Li_2O-SiO_2 glasses, Li self-diffusion, mass spectrometric method 80−79982
Li_2O_2, gas, thermochem. props., mass spectra study 79−47957
Li_3O, gas, thermochem. props., mass spectra study 79−47957
MgO, atomic C anal. by laserflash induced mass spectrometry 80−108767
MgO, heated on W, thermal anal. using mass spectrometric, technique, vaporisation behaviour 80−79932
Mn, vaporization, thermodynamic study by Knudsen-cell mass spectrometry 79−10937
^{51}Mn, preparation in cyclotron by target bombard., extraction, anal. 77−61441

mass spectroscopic chemical analysis continued
$MoSe_2$, evaporation, mass spectroscopic investigation 77−76530
N in upper thermosphere, impact of gas-surface reactions on mass spectrometric meas. 79−66849
NH_3, gas phase proton solvation energetics, mol. beam-photoionis. obs. 79−29345
NO, state selective step-wise photoionis. with mass spectroscopic ion detect. 80−43119
NO_2, laser spectroscopy by cascade photoionisation method in mass spectrometer 80−99496
$NO_3^-.(HNO_3)_n$ clusters, form. studied by mass spectrometer, thermodynamic functions, sol. struct., 80−95754
$N(^4S)$ recombination rate in Lewis-Rayleigh afterglow 79−68968
NaAu(Ag), mol. dissoc. energy, third law enthalpy and heat of formation, mass spectra 78−40033
NaCl, thermodynamic equilib. vapourisation, transpiration mass spectrometry 80−52356
Na_2O-B_2O_3-GeO_2 glass-forming melts, thermodynamic props. and vaporisation processes, mass spectrometric study 80−79926
Na_2O-CaO-SiO_2 glass, SIMS anal. of aq. corrosion profile 79−66182
Na_2O-SiO_2 glass, evaporation by high temp. mass spectrometry 80−79927
Na_2SO_4, thermodynamic equilib. vapourisation, transpiration mass spectrometry 80−52356
Nb, impurity conc. monitoring during single cryst. production 78−31337
Nb wire interaction with stationary gases in high vacuum, HF fields effects *(Polish)* 79−34394
$NbSe_2$, thermal dissociation 78−44370
Nd isotopes, determ. in nuclear fuels as burnup indicator, separation, mass spectrometric method 77−44553
Ni (100), chemisorption of O_2, SIMS and XPS 79−15019
Ni, clean, chemisorpt. of S-containing alkanes, XPS and thermal desorpt. with mass spectrometric anal. 78−14595
Ni, electrolytic, O, H, N liberation during vacuum heating, Mossbauer spectra *(Russian)* 80−35594
Ni films, adsorption and decomp. of ethylene, coverage depend. meas. 80−96743
Ni, trapping and release of inert gases, thermal evolution mass spectrometry 78−95077
Ni-Cr(Fe)(Cu) alloy, matrix effect in SIMS anal. using O_2^+ primary beam 80−76576
$Ni_{1-x}S$, oxidation, TG/DTA/MS obs. 78−31745
NiZn ferrites, comp., X-ray diffr. and saturation magnetisation obs. 78−18617
O, anomalously heavy isotope, mass spectrometric search 79−81290
O atom production and removal in DC glow discharge 79−77432
O_3+ethylene, dioxirane form., decomp. products, mass spectrometric obs. 78−11504
O_3+U(Th), assoc. ionis. cross sections, in crossed beams, mass spectra obs. 78−94317
$^{18}OH+CO_2(CO)$, evidence for at. exchange 79−47910
$O_4^+(O_5^+)(O_6^+)(O_2^+H_2O)$ 80−95707
^{18}O tracer diffusion coeff. determ. in Ti_nO_{2n-1}, continuous mass spectrometry 77−20124
$^{18}O/^{16}O$ ratio analysis in carbonates by mass spectrometry *(Portuguese)* 80−7875
Os, isotopic anomalies from different ore deposits, LAMMA determ. 80−61800
Pb multicomponent glasses, alkali evaporation, mass spectrometry study, thermal anal. 79−74464
Pb surface, oxidation, XPS and SIMS study 79−15873
PbO_2, thermal decomposition, heating rate effect, kinetics, mechanism, struct. 78−92473
^{205}Pb in Tl minerals, for solar neutrino flux determ., proposed expt. 77−5447
Pt, reactive sputtering in Ar-O_2 mixtures, glow discharge mass spectrometric meas. 79−91552
Pu, isotopic analysis by resin-bead mass spectrometry for materials safeguards 80−78392
Pu, remote contamination and total inventory from Rocky Flats, mass spectroscopic anal. 77−73739
^{238}Pu, alpha spectrometric determ. 80−81404
^{241}Pu half-live determ. by mass spectrometry 80−78232
Re compounds formed from Re filament, in gas-chromatography vaporisation 79−74465
Ru, determ. in automobile exhaust-emission, by chem. ionisation mass spectrometry 78−61079
Ru, fission product, isotope anal., U and Pu fission investig. *(German)* 77−63996
S, orthorhombic-monoclinic heat of transition, by mass spectral determination of sublimation heat 79−73302
SF_6, photon-enhanced dissociative electron attachment, isotope selectivity 80−18939
$(SN)_x$, brominated, vapour species identification, mass spectrometric methods 78−44422
S_4N_4, pyrolysis products, mass spectrometric obs. 78−60994
SO_2, 193 nm photodissoc., photofragment translational energy distrib. 79−74402
SO_3, electron impact mass spectrometry, proton affinity, ion-mol. reactions 78−3415
$^{33}S/^{32}S$ ratio in ocean water SO_4^{2-} 78−65340
$^{34}S/^{32}S$ ratio meas. using SO_2 and SF_6 methods, discrepancies 78−65405
Sb_xSe_y (x=0 to 4; y=1 to 4) molecular species formed in vaporisation of solid $SbSe_3$, thermodynamic props. 80−11943
SeS gas, thermodynamic props., quadrupole mass filter study 80−16716
Si, emitter for field desorpt. mass spectrometry 79−79323
Si, etching by CF_4, plasma deposition reactor gas phase characts., mass spectra 80−70566
Si etching in fluorocarbon glow discharge, chemical aspects 79−86631
Si, etching in He-F_2 plasma, etch rates, mass spectra, direct ion sampling study 80−79510
Si film, epitaxial growth by partially ionised vapour deposition, RHEED-AES-QMS study 79−83136
Si, surface, pure, oxidised element determ. by SIMS 78−85247
Si wafer, high resolution SIMS 78−56929
Si wafer surface sputtering, secondary postive ion mass and kinetic energy anal. 78−88391
Si whisker field desorption ion source, Cu, Sn, Ag, Te, Cd and Sb isotope abundance ratios 80−11975
Si:As, SIMS, energy distrib. of sputtered ions 79−38706

mass spectroscopic chemical analysis continued
Si:As sputter rate meas. SIMS combination with Rutherford backscatter 80−21334
Si:B(As)(Sb) device, anal. using SEM-AES-IMA combination with SIM spectrometer *(Japanese)* 78−85249
Si:Na, quantitative analysis of residual impurities with SIMS 78−87688
Si-SiO_2 interface, chem. struct. of transitional region 78−95824
Si_3N_4, CVD from $SiCl_4$ and NH_3, mass spectroscopic anal. of intermediates 79−43149
Si_3N_4, intermediates in CVD, mass spectrometric detect. 78−27411
SiO_2 etching in fluorocarbon glow discharge, chemical aspects 79−86631
SiO_2, etching in He-F_2 plasma, etch rates, mass spectra, direct ion sampling study 80−79510
SiO_2 prepared in O_2-HCl and H_2O-HCl ambients, Cl conc. profiles using SIMS 79−65110
SiO_2-Si interface, detection of SiO_2^- ions by SIMS 77−77848
Sn film, reactively sputtered, discharge produce evaluation, mass spectrometer obs. 80−6668
SnNi electroplate, anal. by SIMS, ion scatt. spectrometry, and Rutherford backscatt. 78−95979
$SnSe_2$, sublimation, temp. depend. of equilib. constants 80−88312
Sr^+, hydration, gas phase clustering mass spectra, thermodynamics, bonding 77−16814
SrO, heated on W, vaporisation behaviour, mass spectrometric thermal anal. 77−56277
Ta+F_2 reaction, modulated molecular beam mass spectrometry 78−15678
TaO_n, combined SIMS, AES and XPS investigation 79−33199
$TaSe_2$, evaporation, mass spectroscopic anal. 77−76530
(Th, U) fuel, burnup determ., using ^{148}Nd 78−82459
ThO_2, plasma deposition of crysts. and their characterisation 80−20800
Ti (1011), of CO, XPS, UPS, flash desorption mass spectra, and active ion bombard. obs. 79−11822
Ti anode, surface deposit from NaCl electrolysis, elemental anal. 78−73117
Ti-Ir alloys, Ti-rich, thermodynamic study at high temp. using Knudsen cell mass spectrometry 80−45539
TiC, cpd. form. reaction in reactive evaporation, quadrupole mass analysis *(Japanese)* 78−23628
TiO_2(-Cr_2O_3), rutile, Cr_2O_3 effects on O_2 tracer diffusivity, depth profile meas. by SIMS 80−24651
U fuel, burnup determ., using ^{148}Nd 78−82459
U, isotopic analysis by resin-bead mass spectrometry for materials safeguards 80−78392
U, isotopic composition, determ. using thermal ionisation spectrometry with automatic data eval. 80−66913
U, isotopic compostion, determ. using thermal ionisation mass spectrometry 80−66914
U, mass analysis for accountability in nucl. fuel processing 79−16112
$U(BH_{4-x})_y^+$, identified in vap. above $U(BH_4)_4$, IR spectra 79−36639
UF_4-MF (M=Na or K), ion-molecule equilibria, heat of form. and dissoc. and electron affinities determ. 80−104480
^{235}U burn-up determ. by mass spectrochemical anal. 80−71989
$^{235}U/^{238}U$ isotope ratio determ. in UF_6 samples using gas quadrupole mass spectroscopy 80−78376
Uf_6, mass spectrometric determ. of ^{235}U content 80−68961
VO_2, chemical transport, mass spectrometric study 79−24860
V_2O_5, water in noncryst. solid, quenching of molten V_2O_5 *(French)* 78−42912
W (100), clustering of Kr, He desorption spectrometry 80−77908
W, zonal electronic purification, mass spectra of contaminants *(Polish)* 80−25552
W_bBr_b, enthalpy determ. by mass spectroscopy 78−11584
WO_bBr_b, enthalpy determ. by mass spectroscopy 78−11584
Xe anomalous isotope composition at Oklo natural reactor deposit 77−56630
ZnS, gas, identification by high-temp. mass spectrometry 80−45593
ZnTe, adsorpt. of CO_2, H_2, CO_2-H_2, manometric and mass-spectroscopic investig. 77−35808
ZnTe, gas, identification by high-temp. mass spectrometry 80−45593
Zr iodides, gaseous, generated by HI+Zr reaction, enthalpies of formation, Knudsen cell mass spectroscopy 79−20458
ZrO_2, plasma deposition of crysts. and their characterisation 80−20800
ZrO_2-Nd_2O_3 system, solid solns., evaporation, mass spectroscopy investig., thermodynamics 79−10938

mass spectroscopy
see also atom probe field ion microscopy; mass spectra; mass spectrometers; secondary ion mass spectroscopy
^{81}Br isotope enrichment by laser photodissociation of HBr 80−1075
acetic acid, ionised, pot. energy profiles for unimol. reactions 80−43210
alkali metal fluoroaluminates, dissoc. enthalpies, mass spectrometric determ., heat of form. 80−97720
angle resolved mass spectrometry, ion internal energy selection 80−53164
angle resolved technique, appls. 80−304
angular distribution, charact. of high temp. vapours 80−55769
application to in situ atmospheric measurements 80−17388
artificial intelligence for chem. inference, automatic rule formation in mass spectroscopy, meta-DENDRAL 77−18775
atomic weight determination, collector slit system 78−8463
atomically clean surfaces, instruments for anal. and imaging 80−105749
background-line displacement factors 79−49332
benzene, multiphoton ionisation mass spectra 80−57420
bioactive compound structural studies 80−51305
book 78−318
charged particle identification, magnetic analyser system, high resolution 78−66451
charged particle track reconstruction, fitting procedures, multiple scatt. effects *(German)* 78−74091
chemical ionisation, simultaneous positive and negative in form. technique 77−36806
chemical ionisation mass spectrometry, survey of instrumental techniques 79−57313
cluster ion beams, mass anal. by Wien filter 80−86493
collimating slit, edge effect on ion scatt. 79−27160
collisional activation mass spectra 80−48106
collisional activation technique, appls. 79−43667
combined with gas chromatography, forensic laboratory appl. 78−92556
computer acquisition and analysis of metastable transition data using electric sector voltage variation 78−70102

mass spectroscopy continued
computer search system of MSDC/EPA/NIH 77−4947
computerized, technical aspects including data reduction and analysis 80−57417
computerized data acquisition and interpretation, review 78−321
conference on nuclear physics, Mikolajki, Poland (2-14 Sept. 1979) 80−101662
contaminant identification by energetic beams 79−39250
convolution Fourier transform ion cyclotron resonance spectroscopy 79−75648
correlated events, in TOF spectrometry, appl. to fission fragment induced desorption 78−58089
cylindrical radiofrequency mass analyser, low resolution mass filter 80−73519
data bases, information content of retrieval procedures calc. 80−30297
data system, continuous scan employing computer time sharing 77−18127
diffusion processes in spectrometer sample line 78−64907
digital isotope ratio meas. system, using programmable calculator with double collector mass spectrometer 80−63845
digital system for cancer research 80−22469
direct-molecular-beam method for mass selective outgassing rate measurement 79−85146
double focusing spectrometer, automatic acquisition and shape anal. of metastable peaks 79−89036
eductation, advanced undergraduate expts. in vacuum physics and mass spectrometry 80−73153
EHD ionisation mass spectrometry, instrumentation, mechanisms and appls., review 78−86378
electron capture negative ion chemical ionization mass spectrometry 79−43643
electronic component hermetic package water content anal. 78−21263
electrostatic analyser with parabolic electrodes, particle energy distribution after traversing spectrometer 80−99000
elemental composition determination low resolution magnetic mass spectrometers 80−42296
energetics and theory, application of techniques, review 78−319
epitaxy, growth modes, exp. techniques, book contrib. 80−49558
error theory, target factor, appls. 79−49263
field emission source preparation, metallic multi-point source 80−100758
field ionis. spectrometry, field desorption and field ionis. kinetics, review 78−324
field-desorption mass spectrometry, principle and technique, appl. to corrins and vitamin B_{12} 78−80821
fission yields, meas. techniques and data status 79−9649
Fourier transform ICR spectrometry, error estimates 80−37061
Fourier transform ion cyclotron double resonance, complicated ion-molecule reactions 78−80808
Fourier transform ion cyclotron reson. mass spectroscopy, freq. sweep excitation 80−101810
Fourier transform ion cyclotron resonance spectroscopy 79−2877
fragmentation process, threshold conditions *(Rumanian)* 78−45750
fragmentation processes in mass spectroscopy, rate constant *(Rumanian)* 77−26429
gas chromatography−mass spectrometry, sample anal., review 78−3437
gas chromatography-mass spectrometry, computerised, data-blocking cross-correlation peak detection 80−62725
gas chromatography-mass spectroscopy technique in environmental study *(Japanese)* 79−29496
gas ion source, ion extraction and energy discrimination 78−70226
gas source stable isotope mass spectrometry, press. effect, peak broadening 77−88600
gas-surface interactions, mol. beam apparatus 78−72675
GC/MS integrated systems, review of current techniques 80−68289
GC/MS/computer techniques for environmental anal. 79−57554
Hadamard beam spectroscopy, computer simulation 79−93254
Hadamard mass spectroscopy, H ion-He mass spectra 79−30601
Hadamard transform appl. to beam spectroscopy 80−62741
heavy element quantitative sample preparation 79−9936
high temperature, Knudsen effusion cell, thermodynamic and physicochemical behaviour, review 80−52354
high-resolution mass, collisional activation and metastable ion spectra meas. on reversed Nier-Johnson spectrometer *(Japanese)* 79−27115
high-temp. thermodynamic anal., spectra interpretation, spectrometer sensitivity determ. 77−71402
history of development 78−56928
HTGR fuel element preparation, effluent monitoring using mass spectrometry 77−46376
inert gas extraction system incorporating ultra-high vac. furnace 78−77918
integrated MS/MS technique, mixture anal. appl. 79−34389
ion anal. based on periodic motion along closed trajectories 78−78029
ion cyclotron double resonance expts., oscillator coupling elimination 77−67530
ion cyclotron motion, Coriolis coupling of ion internal degrees of freedom 80−87246
ion cyclotron reson. cell, trapping efficiency, ionic photofragment ang. and energy distribs. meas. 77−31026
ion cyclotron resonance, appl. to meas. rate consts. of ion-molecule collisions 77−86287
ion cyclotron resonance, collision-dominated, quantum mech. description 79−2666
ion cyclotron resonance, molecular ionisation cross sections determ. 77−67527
ion cyclotron resonance, rapid scan spectroscopy, conceptual and exptl. basis 77−74544
ion cyclotron resonance, rot. elec. monopole signal model 79−12880
ion cyclotron resonance, sensitivity calibration of marginal oscillators as function of freq. 78−21177
ion cyclotron resonance phenomena, detection theory 80−95184
ion cyclotron resonance signal, broadband detection 80−62792
ion cyclotron resonance spectrometry, collisionally damped ion motion 80−57419
ion cyclotron resonance spectrometry 79−227
ion cyclotron resonance spectroscopy, interpretive expt. 80−36814
ion extraction from plasma, stagnation point, mass discrimination effects 79−35886
ion kinetic energy spectra, dish topped metastable peaks, rel. to field-free fragmentation regions 80−101871
ion lifetime distribution, following interaction with collision gas, determ. method 79−36732

mass spectroscopy continued
ion peaks, method of meas. mass numbers 77−82639
ion probe mass spectrometry microanalysis, basic physics *(Chinese)* 80−42311
ion reflection, by rough surfaces, contrib. to mass spec. peaks 78−8466
ion separation, method using plane elec. fields *(Russian)* 77−61154
ion space charge neutralisation, influence on mass separator transmission 78−82073
ion-kinetic energy spectrometer, high resolution mass analysed, design and performance 80−101872
ion-sensitive photographic plate evaluation using optical wedge microdensitometer *(German)* 80−42298
ions with excess kinetic energy, simple mass spectra method 78−62262
laser fusion target pellets, mass spectrometer determ. of AR contents 80−32442
laser ion source, appl. in mass spectrometry 80−89564
laser ionisation mass spectroscopy, appl. to fragmentation obs. via. multiphoton ionisation 79−54213
liquid organic compound ionisation under atm. press. 80−86488
low-resolution spectra identification using combined forward-reverse library search system 80−30296
magnetic analyser, sector type, with fringing field, geometric image aberration *(Japanese)* 78−8465
magnetic mass analyser ion motion in rot. reference system 77−61155
mass separator, plasma-optical model, optical props. optimisation 78−16894
mass-analysed ion kinetic energy spectra, automated fast scanning method 79−35885
mass-analysed ion kinetic energy spectrometer, computer-controlled system 79−35884
Mathieu eqn., transition matrix 78−82070
mechanism and struct., mol. orbitals calc. and isotopic labelling, review 78−320
mechanistic studies 80−47142
modulated mol. beam mass spectrometry, reaction prod. vector, surface reaction 77−63952
modulated-field linked-scan studies of metastable ions 80−77904
molecular beam, in inhomogeneous mag. field, electron impact detect. 77−6963
molecular beam mass spectrometic sampling, high press., high temp. mols., review 80−52355
molecular beam mass spectrometry, in situ anal. in crystal growth ambients 80−52357
molecular beam mass spetrometric sampling system, ion concs. in coal-fired MHD plasmas 80−52358
molecular density directional detector 79−80626
molecular geometry, mass spectrometric investigation, using mol. rearrangement 78−86972
molecular photoionisation in mass spectrometer, using H_2 vac. UV laser 77−88606
molecular photoionisation mass spectroscopy, reson. peak shapes 80−42295
molecular spectroscopic laboratory strategies, queueing theory and digital simulation use 80−30299
molecule+negative ion, thermochemical data, gas phase acidity scale, mass spectroscopic techniques 80−30234
monitoring chemicals, description of technique 80−4803
monoenergetic ion beam production, sequential pulsing technique using tandem mass spectrometer 77−74548
natural products mass spectroscopy, conf., Rehovot, Israel, (Aug.-Sept. 1977) 78−88681
negative chemical ionis. mass spectrometry, ionis. techniques, review 78−325
negative ions 80−43211
nucleation and molecular clustering about ions, energetics and structure 79−41260
nuclei far from line of beta stability, mass spectroscopic anal. techniques, book contrib. 80−69014
on-line literature search system 78−15734
on-line spectrom. of short lived nuclei using new target ion source system 78−66449
organic ion, excited electronic state correlation with mass-spectral fragmentation pattern 80−45482
organic ions, pot. energy profiles for unimol. reactions 80−43210
organic mass spectroscopy, techniques and appls. 79−43667
pattern recognition, mathematical programming techniques 78−92523
peak height intensity normalizer, pocket size device, for teaching 79−35498
peptide and glycopeptide research methods 80−51307
photoelectron spectroscopy in strong mag. field, trapped ions, with ion cyclotron reson. 78−50666
photoionisation, of high temp. vapours 80−52238
photoionisation mass spectrometry, applic. of vacuum UV lasers 77−87865
photoplate processing, microcomputer based system 80−62787
polyatomic molecules, new method, laser photoionisation in a mass spectrometer 78−78840
polyperfluoropropylene oxide, mass spectroscopic reference standard appls. 78−89582
porphyrins and related tetrapyrroles 80−51306
propane, vapour-liquid and vapour-solid equilib. data, mass spectroscopic tracer pulse chromatography 80−37115
pulsed ICR, with one-region trapped ion analyser cell 79−2876
quadrupole, analytical theory, book contrib. 77−22610
quadrupole, book 77−22608
quadrupole, fringing fields and other imperfections, book contrib. 77−22612
quadrupole, history, book contrib. 77−22363
quadrupole, numerical calcs., book contrib. 77−22611
quadrupole, principle and operation 79−21848
quadrupole, principles of operation, book contrib. 77−22609
quadrupole analyser, automatic operation using microprocessor systems *(French)* 79−54212
quadrupole ion store, simultaneous positive-negative ion mass spectrometry, scanning techniques and systems description 80−52350
quadrupole mass filters, ion transmission factors 77−54011
quadrupole spectrometer, validity of meas. at press. exceeding 10^{-4} mbar 79−85198
radioisotope dating using cyclotron as mass spectrometer 77−64489
rapid scan ion cyclotron resonance type, principle, appls. 78−54491
relative sensitivity factors in mass spectroscopy 80−86497

mass spectroscopy continued
resonance ionization source for mass spectroscopy appl. isotope anal. and time of flight spectrometer 80−81380
resonance mass spectrometer, ion mass at exit slit and polyharmonic technique 78−316
review, applications *(Japanese)* 80−27373
review of current status 80−55665
review of developments over last 25 years 77−67528
review of literature, 1975-1977 78−85226
sampling of rapidly reacting gases, mol. vel. distrib. effect on time resolved spectra 77−63888
secondary ion emission from solid surface, meas. apparatus, spherical condenser *(German)* 77−44103
SEM microanalysis techniques, review 80−71995
signal-to-noise ratio, improvement by eliminating scattered particles 79−89035
SISAK 2, chemical separation method for short lived fission products in spectroscopic studies 80−74068
SISCOM, library search system for compound identification 79−49329
smoothing of experimental ion kinetic energy data by digital computer 79−93112
solid, surface, modulated mol. beam scatt., pulse testing method 79−89032
spark source mass spectra, on photoplate, conversational data processing by computer *(Japanese)* 78−8468
spark source quadrupole mass spectrometry, development, appls. 80−62789
spectrometer sources, field ionisation and desorption, experimental techniques, review 79−26176
sputtered neutral mass spectrometry using post-ionisation in microwave plasma 78−92579
steady-state rotating plasma, for mass separation of elements *(Russian)* 78−25732
steroid research 80−51308
surface chemical ionisation mass spectroscopy, appls. 78−92547
surface sensitive analytical techniques, eval. 78−27876
tandem mass spectrometer, for collision-induced dissoc. obs. 80−62790
tetrachlorodibenzo-p-dioxin determ. by low resolution gas chromatography-mass spectrometry 80−66893
tetrafluoromethane, plasma oxidation in presence and absence of Si in tubular-alumina fast-flow reactor 79−96297
thermal ionisation spectroscopy data, statistical data evaluation program 79−89037
thermistor bolometer failure anal. appl. 78−24795
transition metal complexes, dimethylglyoxymate films, prep. and physical props. 79−90923
transition metal-O bond energy in O_2 glow discharge, mass spectrometry obs. 80−64808
transpiration mass spectrometry, of high temp. vapours 80−52356
ultrasensitive mass spectrometry with tandem electrostatic accelerators 80−101876
vacuum system N_2 pressure determ. 78−70133
water vapour, H-D isotope exchange, mass spectroscopic sensitivities and equilib. const. 77−42434
Wien-Thompson modern mass spectrometer review 80−45613
Ar^+ ions, mobilities in He gas at 82K 80−75023
$Ar^+ + O_2 \rightarrow Ar + O_2^+$, thermal energy charge transfer, energy disposal determ. 79−64099
Au-Ni, liquid alloy system, determ. of thermodynamic props. using Knudson effusion method, phase diagram calc. *(German)* 78−51707
Au-O bond energy glow discharge, mass spectrometry obs. 80−64808
BaOH, (BaCl), mol. dissoc. energies calc. by high temp. mass spectrometer 80−83514
BiLi, gas phase thermodynamics, Knudsen effusion mass spectrosc. 80−100057
$Br + NO \rightarrow Br + NO_2$, reaction rate const., mass spectrometric determ. 79−34288
$CH_4^+ + CH_4 \rightarrow CH_5^+ + CH_3$, ion cylcotron resonance technique for absolute rate constants determ. 79−8462
CO_2, vapour-liquid and vapour-solid equilib. data, mass spectroscopic tracer pulse chromatography 80−37115
CO_3^-, laser photodissociation, tandem quadrupole study 80−81343
CdI_2 crystals, photolysis obs. *(Russian)* 80−7833
Ce, gettering of H, mass spectrometry and microgravimetry study, rel. to HTGR gas purification 80−73374
$nC(graphite) + U(g) \rightarrow UC_n$ (n=1 to 6), enthalpy changes obs. 80−7842
$^{35}Cl^-$, ion mobility in inert gas, drift tube mass spectrometric obs. 79−68896
Cs^+, in mol. gases, ion mobility, drift tube mass spectrometer meas. 77−89228
Cu electrodeposition on Su, reliability anal. 78−24901
Cu-Ge, liq. alloy, thermodynamic activity meas. by Knudsen-cell mass spectrometry *(French)* 80−10684
Cu-H, evolution of gas during heating, mass spectroscopic exam. 80−30221
D_2, sticking and accommodation on low-temp. substrate, mol. beam expts. 80−84368
F^- ions in Kr and Xe; mobilities and diffusion determ. 80−100048
Fe-Al alloy, C saturated, at 1873K, activity meas. with Knudsen cell-mass spectrometer 78−39745
Fe-Ge, liquid alloy, thermodynamic mixing function determ. by mass spectrometric meas. 79−29025
Fe-Ni, solid and liquid, determ. of activities for temp. range 1500-1900K, using mass spectroscopy 79−11558
FeO, gas, thermochem. props., mass spectrosc. meas. 80−101034
FeOH, gas, thermochem. props., mass spectrosc. meas. 80−101034
H anomalous isotopes, including quarks of unit charge, search using cyclotron 77−61879
H/D, abundance ratio, mass spectrometric method 78−8462
H_2, sticking and accommodation on low-temp. substrate, mol. beam expts. 80−84368
He mass spectrometer leak detection, review 77−67447
He-Ar mixture, mass separation during molecular beam sampling process 80−31937
He-F(O)(N)(Ar) mixtures, RF discharge, mass spectroscopy, floating double probe meas. 80−84016
I^- beam, duoplasmatron ion source for SIMS, Ar-I_2 medium 77−18123
^{129}I, tandem accelerator mass spectrometry 80−86494
Ir (110), desorption of H, thermal desorption mass spectrometry, order plots 80−44409
Ir, chemisorption of CO on clean and oxidised (110) surfaces 79−11015

mass spectroscopy continued
K^+ mobilities in gases *(Japanese)* 79−60101
KrF_2, photoionisation study 79−45772
Li^+ mobilities in gases *(Japanese)* 79−60101
LiF, electron impact fragmentation, in mass spectrometer, porous barrier obs. 77−75313
Li_xO_y gaseous, mass-spectrometric study of thermochemistry 79−10940
MgOH (MgCl), mol. dissoc. energies calc. by high temp. mass spectrometer 80−83514
Na^+ mobilities in gases *(Japanese)* 79−60101
Na^+, mobility and longit. diffusion coeffs. in Kr and Xe 80−106866
^{92}Nb, half life determ. by gamma spectroscopy, comparison of ^{92}Nb, ^{94}Nb activities and abundances 78−29423
Ne, atomic wt. determ., collector slit system 78−8463
Ne^+ ions, mobilities in He gas at 82K 80−75023
$Ne^+ + O_2 \rightarrow O^+ + O + Ne$, thermal energy charge transfer, energy disposal determ. 79−64099
Ni-Ge, liq. alloy, thermodynamic activity, mass spectrometric determ. *(German)* 78−20052
Ni-Mo-W, type N55M20V25, quenched at various cooling rates, phase transformations *(Russian)* 79−66052
$O_2 + He^+$, thermal energy charge transfer, O^+ product ion obs. 79−64100
O_3^-, $(O_3^-.H_2O)$, photodetachment and photodissoc. cross-sections meas. 79−98170
O_3+thiirane+olefin+SO_2, excited neutral metastable SO_2 form. mass spectrometric study 80−83300
PbLi, gas phase thermodynamics, Knudsen effusion mass spectrosc. 80−100057
^{239}Pu, half life determ. by isotope dilution mass spectroscopy of ^{235}U 79−26409
^{239}Pu, half-life determ. specific activity meas., mass spectroscopy of ^{235}U daughter growth 79−26408
^{239}Pu, half-life determ. using isotope dilution mass spectroscopy and α-specific activity meas. 79−26410
RbI, vaporisation thermodynamics, mass-loss Knudsen effusion, mass spectrometry 79−28093
Rh, adsorpt. of CO and H_2, on (111) surface, 2-dimens. phase separation 80−107634
SF_6 with gaseous contaminants, arc decomposition kinetics investigation by combined gas chromatograph-mass spectrometry methods 80−92250
SO_2+active N_2, excited neutral metastable SO_2 form. mass spectrometric study 80−83300
Sb_xSe_y (x=0 to 4; y=1 to 4) molecular species formed in vaporisation of solid $SbSe_3$, thermodynamic props. 80−11943
ScP, thermodynamics and high temp. vaporisation 80−88310
ScRh, gaseous, dissociation energies, high temp. mass spectrometric determ. 80−93790
Si:B, polycrystalline, depth profiles of implanted B atoms, meas. by secondary ion mass spec. *(Japanese)* 78−67734
$SiBr_n$, (n=1,2,3) heats of formation, mass spectrometric determ. 80−89511
Si_nH_{4-n}, enthalpies of formation, effusion mass spectrometric meas. 80−26043
Te, atomisation energy, mass spectrometric determ. 79−70361
ThC_n(n=1 to 6), Knudsen effusion mass spectrometric investigations, enthalpies and heat of formation calcs. 80−66858
Ti, gettering of H, mass spectrometry and microgravimetry study, rel. to HTGR gas purification 80−73374
TiO_2, photodesorption of H_2O, pulsed-laser-dynamic-mass-spectrometer study 80−35568
U isotope spearation, throughput limit in mass spectrographs 79−21850
UO_2 pellets, retention and release of water 79−67923
YRh, gaseous, dissociation energies, high temp. mass spectrometric determ: 80−93790
ZnO, photodesorption of CO_2, pulsed-laser-dynamic-mass-spectrometer study 80−35568
Zr, gettering of H, mass spectrometry and microgravimetry study, rel. to HTGR gas purification 80−73374
ZrO_{2-x}(cubic)-ZrO_{2-x}(cubic+tetragonal), phase boundary 80−81038

mass standards *see measurement standards*

mass transfer
2A0311−227, AM Herculis star, IR photometry and polarimetry rel. to mass accretion 80−77517
A-type supergiant stars, mass loss rates from UV reson. line profiles 80−90424
ablation, statistical characteristics of mass lost in thermal destruction, zero gas dynamic press. 78−83429
accelerated flow, at permeable graphite burning surface, turbulent heat/mass transfer 78−38417
accreting main sequence stars, radii 77−17623
accreting neutron stars, He burning shell evolution 80−85968
accretion, spherical, buoyancy effect 80−109349
accretion disks, optically thick, pulsational instability to axially symm. oscills. 80−82190
accretion disks, theoretical review *(Polish)* 80−26739
accretion disks round neutron stars and white dwarfs, flux distrib. and colours 80−94778
accretion flow of pulsating X-ray sources from X-ray timing obs. 79−5917
accretion of gas onto intergalactic collapsed objects, source of cosmic X-ray background 80−90581
accretion onto binary stars, numerical simulation 79−21358
accretion onto compact gravitating object, hydrodynamic calcs. 80−67551
accretion onto compact X-ray sources 79−21462
accretion onto magnetised neutron stars, normal mode anal. of interchange instability at magnetopause 77−13376
accretion onto rapidly moving gravitating centre, self-similar soln. 80−17609
acoustic excitation effects on mass transfer from cylinders to air stream 79−32127
actinides in English Channel, transfer into S.North Sea 79−48519
adiabatic accretion onto Schwarzschild black hole 80−77445
advection-diffusion simulations, finite-element and finite-difference methods comparison 77−22424
aerosol, simultaneous diffusion and sedimentation in rectang. tube 77−11266
agitated vessel, flow behaviour and transport phenomena, correlation eqns. *(Japanese)* 78−38300

mass transfer continued
air cooling and dehumidifying coil, heat, mass and momentum transfer 79−192
air flow, with slot-injected He, vel. profiles, mass fractions and densities meas. 77−42808
air-sea interface, gas transfer 77−91154
air-stream mixture, direct contact dondensation on single droplet 77−68370
air-water fogs, mass, momentum and energy transfer rel. to audible sound propag. 78−1473
air-water interface, combined heat and mass transfer coeff. 78−30166
air-water interface, turbulent heat and mass transfer 79−68551
air-water mist flows, uniform heat flux wedge, heat transfer 79−23352
air-water surfaces, turbulence characts., mass transfer and eddies 80−14665
Algol type star, accretion and chem. struct., evolutionary calcs. 80−109481
Algol type stars, H I α obs. evidence for mass loss 80−109484
Algol type stars, mass loss and transfer 80−109480
alkali metal vapour condensation from gas flow (He,Ar,N_2) heat and mass transfer 78−75192
analog solution of free convection mass transfer from downward-facing horizontal plates 80−43706
annulus with non-Newtonian fluids, mass transfer to inner wall, Leveque soln. adaptation 80−10267
approximation method for solution of nonlinear integral equation with error estimation for problems in heat or mass transfer *(Russian)* 78−57879
AE Aquarii, cataclysmic variable, rapid light oscills. obs. rel. to mass transfer rate 80−36634
R Aquarii (M7+pec), primary star mass loss rate from IUE obs. of circumstellar emission 80−82370
aquifers, pollution transfer charact. evaluation using tracers *(French)* 77−41104
V603 Aquilae (Nova 1918), accretion disc eclipse model for periodic light vars. 80−82391
Arctic ice pack heat and mass balance 79−39750
Ariel 0620−00, transient X-ray source, spherical model 78−12415
arteries with longit. ridges, flow field and mass transport anal. 77−44702
artificial kidney, evaluation using systems anal. 78−36074
artificial kidney, tubular haemodialyser anal., ultrafiltration and dialysate concentration effects 78−7544
artificial lung, oscillating helix membrane design employing O_2 perfused inner capillaries 78−44712
artificial membrane lung, fluid vortices and mass transfer 77−52919
artificially disturbed strata, temp. distrib. during air filtration *(Russian)* 77−25667
astrophysics, nearly collisionless spherical accretion 78−12090
N.Atlantic central water, vertical mixing due to salt fingers 78−85571
atmosphere, bulk transfer velocity to and from natural and artificial surfaces 79−25302
atmosphere, turbulent mass transfer in boundary layer, plume dispersion *(French)* 80−61850
atmosphere global scale transport processes *(Dutch)* 78−3889
atmospheric aerosols, particle size distribs. evolution via Brownian coagulation, num. simulation 80−41513
SX Aurigae, early-type semidetached binary star, case A mass transfer 79−44521
T Aurigae (Nova 1891), old nova, cataclysmic binary model from photometric and spectroscopic obs. 80−90446
axisymmetric accretion discs and flows, thickening 78−40989
axisymmetric accretion in astronomy, energy considerations 77−33335
axisymmetric impinging jet, transfer characteristics at conical surfaces 77−3889
B 1 Ia-0 supergiants, mass loss meas. 79−16948
BD+33°2642, galactic halo blue star, mass loss determ. from IUE obs. 80−72947
Be and shell stars, mass loss from Copernicus UV data 77−56986
Be-star duplicity and mass exchange 77−60780
Be-stars, mass-exchange binary evidence from periodic spectral var. 77−60781
benzoic acid, dissolution, mass transfer at vibr. spheres 80−57220
bibliography, heat and mass transfer, Polish works (1977-78) 80−57020
bibliography, heat and mass transfer, Soviet works 78−22343
bibliography, Polish works, (1975-1976) 78−38320
bibliography, Soviet work on heat and mass transfer 79−86430
bibliography, Soviet works, 1976 78−34126
bibliography, Soviet works 79−32180
bibliography, Soviet works 80−94938
bibliography of Soviet work 77−39288
bibliography of Soviet works on heat and mass transfer 78−75027
bibliography of Soviet works on heat and mass transfer 80−41972
binary alloy, numerical calc. and simulation of nonsteady mass transfer by moving phase boundaries *(German)* 77−8811
binary gas mixtures, mass transfer analysis using model of convective diffusion for turbulent flow in tube 77−7454
binary gaseous mixtures, transient heat conduction 80−64670
binary mist flow, heat and mass transfer anal. *(Japanese)* 79−14467
binary mixture, thin shear flow layer, momentum, heat and mass transfer *(German)* 77−39293
binary mixture flow in vertical channel, film condensation 78−75139
binary neutron stars, evolution, gravit. radiation and mass transfer 77−78821
binary star, close low-mass, evolution with mass exchange and gravit. radiation losses 77−53631
binary star HD 101584, effective viscosity in accretion disc 77−64804
binary stars, β Persei-type, mass transfer rates from period changes 77−57040
binary stars, accretion onto ZAMS stars rel. to β Lyrae and X-ray binaries evolution 79−66994
binary stars, ang. momentum loss and mass exchange instability 77−49433
binary stars, close low-mass systems, evolution into contact 77−33557
binary stars, detached, evolution to contact binaries involving mass flow 80−109477
binary stars, disc accretion onto magnetised compact objects *(Russian)* 79−44467
binary stars, eqns. of steady accretion disc with mag. field 79−40179
binary stars, equipotential surfaces, modification due to pressure of radiation of component *(French)* 80−56880

mass transfer continued
binary stars, mass transfer and accretion disc flow, numerical simulation 77−57035
binary stars, mass transfer rel. to mass-radius relation 78−12290
binary stars, radiative tides in accretion disks 79−48853
binary stars, rapid mass accretion on to white dwarfs and extended envelope form. 80−67723
binary stars, semidetached, gas flow hydrodynamic calc. 77−57037
binary stars, semidetached, mass transfer and impact-driven accretion discs 77−57036
binary stars, semidetached, mass transfer instability 78−8047
binary stars with mass transfer, particle motion 77−5545
binary system, close, with mass and ang. momentum loss, period changes 80−72998
binary systems, radiation pressure force influence on critical surfaces 78−96505
binary vapour mixture, condensation in presence of inert gas 77−80051
binary vapour mixtures, simulation of unsteady state behaviour of dephlegmation 79−7285
binary X-ray systems, accretion flows 78−12432
Bingham fluids, single bubble motion and mass transfer 79−50758
black hole, charged rotating, accretion disc mag. torque effects 79−17010
black hole, disc accretion at subcritical luminosity 77−64791
black hole, massive, accretion of gas debris of tidally disrupted star rel. to radiation spectrum 80−90467
black hole, spherical, with thin accretion disc, image 79−67049
black hole accretion, photon pair prod. in transrelativistic plasma 78−20632
black hole accretion disc models, boundary condition modification and vel. matching at inner edge 77−13380
black hole accretion discs, boundary-layer behaviour of flow at disc inner edge 80−46598
black hole in radiation-dominated non-relativistic gas, Bondi accretion problem 78−77575
black hole X-ray sources in galactic bulge, disk model 80−17691
black holes, electron-positron pair production in hot unsaturated Compton accretion models 80−36658
black holes, nonsymmetric disc accretion *(Russian)* 80−36661
black holes, supercritical accretion discs models 80−105272
black holes in binary stellar systems, gamma emission during spherically symmetric accretion 80−17608
blackholes, accretion contrib. to background radiation density 80−4461
blood oxygenation using coiled tubes 78−40422
blood oxygenator, convective-diffusion model 78−44711
blunt-body boundary layers, three dimensional, surface curvature effects 80−1520
bodies in granular bed, heat and mass transfer 78−9701
body submerged in granular layer, heat and mass transfer 78−94536
boiling, bubble growth at superheated horizontal wall, pure liq. and binary mixtures 79−41719
boiling, in circuit system, effect of intense electric field *(Russian)* 78−46887
boiling in capillary gaps, heat and mass transfer 78−46885
boiling point drying by volumetric abs. of RF and MW EM energy, heat and mass transfer characts. 80−79130
Bondi accretion, linear stability problem 79−44359
i Bootis, light curve and period vars. of W Ursae Majoris type star 80−4398
boundary layer, calc. on spinning and curved surfaces 77−65737
boundary layer, conservation relations with heat/mass transfer and vel. slip 77−62246
boundary layer, improvement of heat transfer coeffs. using turbulence promoter 77−72297
boundary layer flow, unsteady, compressible, 3-D, near axisymmetric stagnation point 80−103011
boundary layer on porous plate, wall shear stress with mass transfer 78−47032
boundary layer turbulence, differential methods and finite-difference methods comparison 78−18279
boundary layer with mass transfer, blockage effects 78−26096
boundary value problems, mixed and oblique derivative boundary conditions 80−69820
bubble, single rising, internal mass transfer coeffs. 79−86487
bubble chain, diffusion of dissolved substance at large Peclet nos. 79−86489
bubble growth, noncondensing gas-vap. injected into liquid 78−55553
bubble in power-law liq., convective heat and mass exchange, $Pe \leq 1000$ 78−55683
bubble swarm behaviour and gas absorption in non-Newtonian fluids in sparged columns 79−4061
bubbles in fluidised bed, interphase mass transfer 79−7405
Z Camelopardalis, dwarf nova, mass transfer rates at standstill and in eruption 80−82366
UW Canis Majoris, eclipsing binary, mass flow anal. from UV spectrum 80−109429
29 Canis Majoris, massive hot binary star, spectrograms, mass loss 78−12299
RS Canum Venaticorum binaries, effects of tides and flares 79−71068
RS Canum Venaticorum-type binaries, evolutionary status 77−33570
capillary mass transfer of porous solids based on pore distrib. curves 77−7443
capillary porous body, drying, X-ray absorption obs., radiometry, temp. control 78−67023
capillary-porous bodies, internal mass transfer, influence of inhomogeneous elec. and mag. fields 80−6138
capillary-porous body, nonlinear heat/mass transfer problem, soln. using invariant groups 78−55688
ζ Capricorni, Ba star, white dwarf+giant, circumstellar gas mass transfer, UV obs. 80−105284
carbon tetrachloride-I_2-water system, mass transfer in pulsed perforated plate column 78−71385
carboxy methyl cellulose solns., mass transfer from cylinders to power law fluids 80−83826
carboxy methyl cellulose solns., mass transfer from spheres to power law fluids 80−83825
carboxymethyl cellulose, aqueous soln., diffusion and mass transfer from rotating disc 80−83827
OY Carinae, white dwarf cataclysmic, eclipsing binary, parameter determ. 80−82385
carrier mediated transport theory, survey of applications 77−89113
mass transfer continued
carrier-mediated extraction, development 80−66870
RZ Cassiopeiae, Algol-type binary, period vars. 77−13394
TV Cassiopeiae, eclipsing binary, mass transfer from period vars. 79−84818
AZ Cassiopeiae, interacting eclipsing binary, mass loss of cool supergiant component 78−32522
cataclysmic binaries, circumstellar material geometrical and photometric parameters 80−109492
cataclysmic binaries, mass transfer rel. to evolution and origin 80−56885
cataclysmic binaries accretion discs, convection as viscosity source 78−93307
cataclysmic variable stars, accretion disc models H line blocking of UBV colours 79−101155
cataclysmic variables, accretion discs models rel. to emission line spectra 80−51774
cataclysmic variables, period change due to mass transfer 80−82425
catalyst granular bed, static, flow transfer processes 80−45554
catalytic reactors, runaway inhibition 79−47983
cell with vibr. mixing for liq.-liq. systems 79−37425
SV Centauri, early-type contact binary, evolutionary models and mass exchange rate 80−4403
V748 Centauri (Centaurus X-4), eclipsing binary, VBLUW photometry rel. to mass transfer 79−44529
Centaurus X-3, neutron star accretion rel. to spin-up, and X-ray luminosity 80−101648
centrifugal extractor for mass transfer examination by single drop method, fission reactor fuel reprocessing 77−67848
U Cephei, accretion discs obs. 80−82412
U Cephei, eclipsing binary, gas stream effects in UV spectrum, IUE obs. 80−26898
U Cephei, mass transfer from light vars. outside primary eclipse, obs. and anal. 78−36636
U Cephei, UV excess, mass transfer in eclipsing binary system 77−33555
VW Cephei, W Ursae Majoris star, primary to secondary mass flow rel. to physical status 80−109495
9 Cephei (B2 Ib), circumstellar CO obs. and mass loss rate 80−94795
β Cephei stars, effects of mass loss on instability strip 80−90436
VW Cephei W Ursae Majoris system, period and colour change mass transfer model 80−77453
Cepheids, anomalous, in dwarf spheroidal galaxies, binary system model 77−45451
o Ceti (Mira), mass loss rate determ. 79−48831
Z Chamaeleontis, cataclysmic binary, mass exchange due to gravit. radiation 80−4386
Z Chamaeleontis, eruptive binary, accretion disc struct. rel. to photometric behaviour 80−72961
channel, corrugated wall 77−80157
channel with porous walls, convective diffusion and mass transfer *(French)* 80−79305
charged liquid, turbulent flow, transverse charge distrib. calc. 77−84334
chemical reaction at wall, turbulent mass transfer at $Pr \gg 1$, first order 78−18357
chemical reaction in both liq. phases 78−5825
chemical reactor, packed-bed type, diffusion controlled mass transfer coeff. 79−43555
chemical reactors, annular, cylindrical, mass transfer in laminar flow 78−22429
chemically peculiar A-type stars, accretion of grains 79−67017
chemically reacting nonequilibrium turbulent shear flow, prediction model *(German)* 79−18973
chemically reacting system, coupled heat and mass transfer, finite element soln. 80−68153
chemically reactive flow, heat and mass transfer, approximate theory 79−68821
chemically reactive flow characts., simultaneous heat-mass transfer *(Japanese)* 78−22431
chemically reactive flow in porous catalyst, conc. and temp. profiles, computation method 79−86523
Circinus X-1, binary star model with mass transfer and expanding shock fronts 79−75296
circular hollow porous cylinder with mass transfer through reflecting walls *(Russian)* 79−14220
classical and dwarf novae, energy sources and systematics 79−67041
close binaries, intermediate mass, mass transfer for different stars within evolutionary scheme 80−109476
close binaries, mass loss and parameters 77−13397
close binary stars, components periodic collisions induced by collisions with isolated stars 78−8061
close binary stars, mass accretion rel. to components oblique rot. axes problem 78−96509
close binary stars, mass flow 77−57039
close binary stars, orbital ang. momentum loss by gravit. radiation, mass transfer rates 78−40991
close binary stars accretion processes rel. to binary X-ray sources 77−57034
close binary stars props. before and after mass transfer, obs. and theory comparison 80−62187
close binary stars with black hole circumstellar gas motion 77−17628
close binary systems, tidal torques on accretion discs 78−12296
close low-mass binary systems, evolution, unsteady mass loss, contracting secondary star 77−17617
cnoidal wave, mass transport, in boundary layer second approx. 77−15049
co-current flow liquid-liquid binary mass transfer in ejectors 78−75185
coated cement stone heat and mass transfer obs. *(Russian)* 79−14219
cocurrent gas-liq. stratified flow, mass transfer obs. 79−18931
coefficients, concentration dependent diffusivities effect 80−98864
collocation finite element method for potential problems in irregular domains 79−54072
colloidal capillary-porous body, mass transfer parameters, adsorpt., osmotic moisture 78−11563
combined effects in mass transfer to planar electrode 78−23949
combined heat and mass exchange processes, model eqns. and techniques *(German)* 80−27236
compact stars, axisymmetric accretion theory 77−33334
compressible fluid flow through annular orifices, computer-aided numerical anal. 80−87806
concrete, effect of liner on heat and mass transfer characts. 78−17388

mass transfer continued
condensable rarefied gas flow through porous media, heat and mass transfer 78−59473
condensation, flow of vap. over cylinder, two-phase boundary layer eqns. 79−46306
condensation heat transfer, nonequilib. temp. profiles, mass transfer engineering calc. 80−63227
condensation of binary vapour in inert gas, heat and mass transfer 79−59916
condenser efficiency and performance enhancement, evaporative cooling *(German)* 79−72781
condensing mixed vapors, suction effects heat and mass transfer *(German)* 80−33609
cone, convective mass transfer, in nonlinear viscous field, rel. to heterogeneous reaction kinetics 77−55103
conical nozzle and diffuser, laminar compressible boundary layer swirling flow 80−48768
conservation equation, numerical soln. by variational approach, mass transfer problem appl. *(French)* 80−19317
contact binary star, mass loss rel. to dynamical evolution, idealised model *(French)* 80−62199
contact binary stars, gas circulation 77−57017
contact binary stars, particle motion from L_2 Lagrangian point, elliptic orbits 77−91579
contact binary stars, solar type, ang. momentum controlled evolution and mass transfer 80−36670
contact binary stars, transport processes in envelopes 78−4279
contact binary stars, unstable mass outflow 77−57018
contact sorption moisture exchange in vacuum, mass exchange kinetics *(Russian)* 79−19468
convection, free, unsteady, flow past vertical plate with const. suction and mass transfer 78−18290
convection, free, unsteady, flow past vertical plate with variable suction and mass transfer 78−18291
convective, stationary, inside drop, influence of chemical volume reaction at large peclet numbers *(Russian)* 80−28508
convective heat and moisture transfers with const. heat flux *(French)* 80−33582
convective ionic mass transport, at inclined circular disc electrode 78−26117
convective mass transfer measurement methods, review *(German)* 78−46959
cool giant stars, chromosphere mass loss determ. from Mg II UV line obs. 80−85935
cool stars, mass loss, review *(German)* 79−16957
cool stars, supersonic stellar winds and rapid mass loss 79−21268
coolant flow rates through porous media, heat and mass transfer *(Russian)* 78−59479
correlations for flow between fluidised spheres and liquid 80−14805
corrosion pit, convective diffusion 80−40601
counter current extraction column, efficiency, using nonlinear PD model *(Russian)* 79−64808
coupled heat and mass transfer, stability, inertial wave effects calcs. 80−105593
creeping flow mass transfer in size distrib. cloud drops, high Schmidt number 80−14783
critical sound pressure level in mass transfer processes, analytic expressions 78−90633
cryogenic heat pipe, heat and mass transfer 77−13758
crystal growth, one-dimensional Stefan problem, expansions in time 80−64354
crystallisation, activation energies of mass transfer at phase boundaries, quantum theoret. calcs. *(German)* 78−67671
crystallisation, activation energies of mass transfer at phase boundaries, quantum theoret. calcs. *(German)* 78−67673
curtain cooling, behind permeable surface section, effect of injected gas flow distrib. 78−42657
SS Cygni, dwarf nova, spectrophotometry rel. to accretion disc models in erruption and at min. light 80−36635
P Cygni, H Balmer line profiles, accel.-decel. envelope, mass loss 79−40205
ss Cygni, hard X-ray source, obs., accretion onto white dwarf 79−30078
32 Cygni, IUE obs. rel. to late-type supergiant mass loss rate 80−22036
α Cygni, mass loss from mid UV spectrum obs. 78−93217
CH Cygni, symbiotic star, mass transferring binary model 80−62158
59=V832 Cygni, variable mass flux from spectroscopic obs. 80−41840
V444 Cygni, Wolf-Rayet star mass loss rel. to orbital period var. *(Russian)* 79−101178
V1329 Cygni (HBV 475), symbiotic variable, accreting binary star model 80−62148
Cygnus X-1, model of neutron star surrounded by massive disc 80−36736
Cygnus X-1 (HDE 226868), accretion disc struct. rel. to long-term circular polarisation vars. 79−9031
Cygnus X-3, 4.8 hour modulation period meas. rel. to high mass loss binary models 80−8713
cylinder, and rising two-phase flow, electrochem. method 77−55076
cylinder array, convective mass transfer with surface reaction 78−79369
cylinder in developed region of two-dimens. jet 77−31352
cylindrical capillary, mass transfer kinetics during evaporation, BGK eqn. basis 77−47044
cylindrical channel with evaporation and condensation at walls, model kinetic eqn. 80−6101
Czochralski crystal growth, heat, mass and fluid flow, computer simulation 80−104055
data, book 78−154
deformational instability of plane interface with transfer of matter 77−46994
degenerate stars, slow deflagration mechanism for mass ablation 79−35248
HR Delphini (Nova 1967), premaximum mass loss rate, H line anal. 80−82378
dielectric drop in electric field, low Peclet number heat and mass transfer 80−6050
diethylphtalate layer, heated by radiant heat source, heat and mass transfer 80−74717
differential eqns. of heat and mass transfer, chessboard difference soln. method 77−82471
differential transfer equations for multiphase, multicomponent media 80−14794

mass transfer continued
diffusion boundary layers, with surface reactions, laminar or turbulent regimes, thermal simulation method 77−75912
diffusion in nonuniform multicomponent system with multidimensional regions *(Russian)* 79−12743
dilute alloys solidification, numerical soln. model 79−69228
dimers, dissociating, in nonisothermal ideal gas phase, stationary state anal. 78−76848
disc accretion by mag. neutron stars, model 78−93294
disc accretion in soft potential well, excess surface density ring form. 80−8532
disc accretion onto magnetised neutron star, fate of matter and ang. momentum 78−28715
discontinuity surface, nonequilib. thermodynamics, appl. to n-component viscoelastic mixture 78−93638
disperse annular flow, crit. heat transfer, liq. distrib. 79−32209
dispersed flow, heat and mass transfer, phase transition effect 78−67252
dispersed flow, heat and mass transport eqns. derivation, closure problem 77−89188
dispersed solids, kinetic methods for mass transfer props. 77−86387
dissociating gas in pipes, heat and mass transfer 80−24105
dissociating turbulent gas flow around triangular rod bundle, heat and mass transfer *(Russian)* 79−68822
dissolved species, advection-diffusion eqn. in pulsating crack 80−96312
dissolving sphere, mass exchange with elec. current carrying liq. 77−11274
S Doradus, LMC star, evidence for circumstellar envelope and mass loss from IUE and optical obs. 80−101595
double boundary layers in standing interfacial waves, mass transport velocity 77−3835
double boundary-layer model of mass transport in progressive interfacial waves 79−10573
double-diffusive system between infinite horizontal planes, heat and salt transfer 77−39298
CX Draconis, binary Be star, UBV obs. 80−82388
drop, drying of solute skin-covered soln. drop *(Russian)* 79−68561
drop, in electric field, transient heat and mass transfer 77−80226
drop, mass transfer, surface-active agents effect 79−77218
drop, mass transfer accompanied by chem. reaction at surface 79−77290
drop formation, mass transfer and internal circulation 77−35198
drop in ambient liq., mass transfer, combination of resistances 78−83458
drop in uniform (shear) stream, convective heat and mass exchange, $Pe \leq 1000$ 78−55683
drop in viscous fluid stream nonstationary mass transfer *(Russian)* 79−10561
droplet evaporation, modelled by wet porous sphere, heat-transfer meas. 78−59268
droplet evaporation from surface, theory 79−59909
droplet-vapour flow, burning, conservation eqns., mass transfer 77−39363
droplets in gas, heat and mass transfer rel. to high-intensity sound attenuation 77−62082
droplets in turbulent flow, heat and mass transfer 78−22410
droplets of concentrated cloud, approx. eqn. for mass and heat flux in constrained flow 77−47073
droplets of soln. dispersed in gas flow, heat and mass transfer during evaporation 78−90998
drops, diffusion of dissolved substance at large Peclet nos. 79−86489
drops, evaporating in vert. hot air tunnel, heat radiation effect 79−46400
drops and films, heat and mass transfer during vapour absorpt. 78−63427
drops in liquid, diffusional interaction 79−81947
drying, heat and mass transfer, optimal control 78−67006
drying, temperature coeff. depend. on heat and mass transfer similarity criteria 78−83214
drying, various conditions, heat and mass transfer formulae 77−84123
drying intensification, thermolabile porous material in contact with sorbent, in vac. 77−89641
duct flow, with transverse plate blockage, surface heat and mass transfer coeffs. 78−75138
ducts, spanwise-periodic and corrrugated, heat transfer and laminar flow 80−64547
dust transport on lunar surface 80−8558
dusty-gas equation modification to predict mass transfer in porous media 79−46377
dwarf novae, accretion disc struct. rel. to soft X-ray emission 77−45457
dwarf novae, outbursts, accretion model 79−88680
dwarf novae binaries, theory 77−56962
dynamic two-phase layer, heat exchange and mass transfer coeffs. of flat element 77−7439
early-type stars, mass loss from radio obs. at 6 cm 80−82347
eccentric spherical fluid shell, heat and mass transfer at large Peclet number 77−27520
eclipsing binary stars, near IR photometry rel. to mass transfer rates 80−67784
EHV transmission cable, in backfill, heat and mass transfer, physical props. effects 78−94543
elastic viscoplastic body, differential rheological eqn. *(Ukrainian)* 78−55617
electrically conducting fluid, laminar flow mass transfer at high Peclet numbers 80−43784
electrically conducting fluid, MHD natural convection flows, buoyancy effects 78−18351
electrochemical, reactors, dimensioning, with three-dimensional electrodes *(French)* 80−71921
electrochemical electrode, particulate-bed, H_2-evolving, mass transfer rate obs. 79−57243
electrochemical mass transfer, drag-reducing polymers, effects, comparative study 80−76528
electrochemical mass transfer between rough surfaces and solutions containing drag-reducing polymers 80−19447
electrochemical measurement of mass transfer, turbulent pipe flow 78−5830
electrochemical measurements, semi-cylindrical hollows 79−23365
electrochemical phase formation 80−55309
electrochemical reaction mass exchange in flat channel 79−74394
electrochemical reactions, in conc. solns., ionic mass transport rates calc. method 79−70352
electrochemical reactions, ionic mass transport, cathodic gas evolution influence 79−34323

mass transfer continued
electrodes, sheet, mass transfer to continuous moving surface 80−69821
electrodes on vibrating sphere, mass transfer 80−61106
electrogenerated chromophores, electrochemical conc. profiles, mass transfer, charge transfer, laser absorpt. spectroelectrochem. obs. 80−40765
electrolysing cell, free convective mass transfer, hydrodynamic model 77−81407
electrolysis, annulus flow, solenoidal mag. field effect on ionic mass transport 80−26021
electrolysis, mass transfer to stacked net electrode 80−11896
electrolysis, solid-liquid mass transfer, meas. by holographic interferometry 79−87852
electrolyte, ionic mass transfer in narrow rectangular conduits 80−61105
electrolytic method of mass transfer meas., advantages and disadvantages 79−68827
electrolytic method of mass transfer meas., appl. in oscill. and pulsating tube flows 79−68828
electropolishing of horizontal surfaces kinetics, role of natural convection mass transfer 79−57143
entrainment from body surface under convective aerodynamic heating, numerical soln. 79−81949
enzyme particle, encapsulated, reactor systems, effects of mass transfer resistances 79−96522
ethyl alcohol, free convection on turbulent horizontal layer, effect of thermocapillary forces 79−98722
evaporation, quasisteady half-space problem, gas kinetics theory and expt. 80−6106
evaporation, quasisteady one-dimens. problem, entropy-balance relation 80−6168
evaporation and condensation, BGK eqn., kinetic anal. 77−11683
evaporation by air jets, hydrocarbons on surface 79−72919
evaporation of drop, in EM field, theory 79−72787
evaporation with natural convection, simultaneous heat and mass transfer in laminar boundary layer, numerical anal. *(French)* 80−53778
evaporation-condensation two-surface problem, in presence of noncondensable gas 80−6169
evaporation-effusion problem, rarefied regime, nonlinear numerical soln. 80−6167
expanding vapour bubble, anal. of reactive forces exerted by evaporating molecules 78−1548
experimental data acquisition system operational analysis models *(Russian)* 79−80588
external flow, mass transfer to region of separation, visualisation using laser-induced fluoresc. 77−35283
fast nova model evolution from pre-explosion to decline 79−35273
film cooling with density difference between mainstream and secondary fluid, heat-mass transfer analogy 78−30293
filtration, plane, of underground waters, convective mass transfer, boundary problems *(Russian)* 80−83793
first-order Cosserat fluid kinetic energy decay with heat and mass transfer 78−94524
fission reactor fuel expansion, nonequilibrium evaporation and condensation 77−42021
fission reactor HCDA, debris transport in horizontal piping 79−93784
fixed-bed electrodes, three-dimensional, mass and charge transfer *(French)* 80−71920
flame, atm. press., heat and mass transfer meas. using Ir/Ir-Rh alloy thermocouple 77−86314
flame, mass streamline, vel. and density fluctuations correlation *(Japanese)* 80−6164
flame, round jet type, mass exchange between recirculation zone and outer flows, stabilisation 80−14842
flames, convective mass transfer, appl. to air pollutants distrib. *(German)* 79−52662
flare stars, large-scale winds driven by mass loss, effects on interstellar matter 78−32464
flat conduit, mass transport, asymmetrical boundary and starting conditions *(German)* 77−35236
flow, fully-developed, in non-circ. passages, prediction method 79−1254
flow, one-dimens., mass continuity eqn., change of variable soln. 79−27613
flow around rotating cones and discs, momentum, heat and mass transfer 79−1203
flow measurement, electrolyte soln., transducer-electrode freq.-ampl. charcts. 77−76001
flow on flat plate with chem. surface reaction, mass transfer *(German)* 79−72961
flow round a sphere immersed in a fluidised bed *(French)* 80−92214
flow with axial diffusion and chem. reaction 79−23376
fluctuating flow, mass transfer near front stagnation point of axisymmetric body 80−48675
fluid flow, use of dispersion model 80−48784
fluid interfaces, isothermal and deformable, mass transfer and surface tension, review 80−33564
fluid interfaces, Marangoni instability, dissipative structures and nonlinear kinetics 80−33565
fluid interfaces dynamics and instability, conf., Lyngby, Denmark (May 1978) 80−31423
fluid-fluid interface mass transfer, thermodynamic non-idealities 77−80683
fluidised bed, axial heat transport and solid phase displacement 79−14473
fluidised bed, boiling layer, axial mixing of solid phase *(Russian)* 78−47035
fluidised bed, heat and mass transfer, flow anal., separated flow model 78−9700
fluidised bed, heat and mass transfer, jet channelling theory 78−9702
fluidised bed, large scale, gas backmixing, solids movement, bubble activities 78−30349
fluidised bed, polydisperse particle entrainment in gas flow 77−65791
fluidised bed, random pulsations 80−24089
fluidised bed, wall to liq. mass transfer 78−1736
fluidised bed in oscill. mode, heat and mass transfer 78−22417
fluidised bed wall-to-liquid mass transfer, local particle influence 79−94713
fluidised bed with vibro-rotational motion, heat and mass transfer 78−9709
fluidised beds of ion exchange resins, mass transfer at low Reynolds numbers 77−68684
fluidised or fixed bed, high Peclet number mass transfer to sphere 77−35226
mass transfer continued
fluids, transport processes, space environment 79−46825
fog-containing vapour-gas mixture, mass transfer in vapour condensation 77−58772
forced and free convective heat and mass transfer *(French)* 80−48689
forced convection, at rough surfaces in annuli, rate meas. 77−27532
forced convection, from gases and liquids to circular cylinder in crossflow, correlating equation 77−80160
forced convection in two-phase flow from jets, mass transfer near interface *(German)* 80−53782
forced convection with chemical reactions, turbulent shear flow mixing, numerical modelling 79−1272
forced convective flow from spheres 79−1189
fractured medium, transient 2-D diffusion 80−106841
free binding liquid film, mean velocity distrib. meas. by laser Doppler velocimeter 80−38508
free convection heat and mass transfer on finned tubes 77−39284
free convection in Stokes' problem for infinite vertical limiting surface, mass transfer effects 80−28501
free convection mass transfer from horizontal surface, electrochemical and holographic interferometric obs. 78−87344
free interface film hydrodynamic and heat transfer characteristics 80−92140
free molecular vapour flow, mass transfer during condensation in channel 78−51198
free moving drop in pulsating liquid, mass transfer *(French)* 77−27588
freeze-drying of food models, heat and mass transfer 79−1098
freeze-drying techniques; mass transfer, appl. of calorimetric instrumentation 77−25628
freezing in finite domains not initially at fusion temp., singular perturbation theory 77−66014
Freon-12, annular mist flow in tube, wall film mass flow rate 80−69905
frost formation, under forced convection, heat transfer and mass transfer *(Japanese)* 77−58533
fuel cell reactor-condenser systems, thermal operating regimes selection 79−87987
fundamentals of momentum, heat and mass transfer, book 77−39294
fundamentals of transport props. of flows, book contrib. 77−84345
furnace heat transfer, 3-dimens, computer model predictions test 78−59504
galactic disc, primordial gas inflow problem rel. to chemical evolution 80−62279
galaxies, gas to stars mass transfer rel. to density waves overstability in disc 78−73752
galaxies close pairs, mass transfer rel. to excess radio emission 78−57658
galaxies early-type, accretion phenomena, role of gas-rich dwarfs 80−31349
Galaxy, mass infall rel. to cosmic ray accel. 77−78583
gas, dilute, reacting, mass and momentum transport, DIPR model extension 78−35666
gas, rot. in mass-transfer equipment, eddy contact element radial press. distrib. 78−26126
gas absorption, into accelerating thin falling liq. film on inclined surface 78−93632
gas absorption, plastic packed column, mass transfer characteristics, proposal of packed column blood oxygenator 80−74968
gas bubble motion in power-law fluid, heat and mass transfer with chemical reaction 79−77227
gas cloud, accretion onto point gravit. source, rel. to Jupiter formation 78−20630
gas diffusion through surfactant films, interfacial resistance 80−39385
gas evolving electrodes, data correlation model 79−79258
gas evolving electrodes, mass transfer mechanism 78−48659
gas flow, recirculating, in packed columns, mass transfer and mixing, cell model 80−69913
gas flow to liquid jet mass transfer 80−53827
gas mixture, multicomponent, transport equations near catalytic surfaces 80−43821
gas mixtures, removal of condensing component by suction through porous walls 79−98787
gas transfer into liq. interface bombarded by liq. pulses 77−7434
gas-dust clouds, rotation, mass transport processes rel. to solar system origin 80−8556
gas-evolving electrodes, mass transfer, superposition of hydrodynamic flow 78−73047
gas-fluidised bed, conc. profile for mass transfer, appl. Kunii-Levenspiel model 77−11256
gas-liquid cocurrent flow through packed beds, radial effective thermal conductivity 78−1723
gas-liquid dispersion, molar current changes in gas phase. fluid dynamical props. *(German)* 77−35200
gas-liquid flow, mass transfer in upflow and downflow 79−41738
gas-liquid interface, mass transfer, ultramicroprobe method obs. 78−63901
gas-liquid moving interface diffusion 78−22404
gas-liquid reacting flow, interfacial area and liq.-side mass transfer 79−37420
gas-liquid system, unsteady state determination of mass transfer coefficients 78−14106
gas-liquid upward flow, effect of tube size on liq. side mass transfer 78−9682
gas-side mass transfer coeff., diffusivity effect 79−18684
gas-solid reactive flow near stagnation point, transient heat and mass exchange 79−77104
gases, dense multicomponent, diffusion eqn., approx. mass transfer description 77−47609
gases, mass transfer, mag. field effects 78−63535
geostrophic flow, recycling over bottom topography, in rot. annulus 78−90916
geothermal energy resources of Kamchatka, unsteady heat and mass transfer model 77−64234
geothermal reservoir, effect of magma dike intrusion on free convection 78−7599
giant stars, mass loss before envelope ejection due to pulsational instability 80−72935
giant stars, Population I, mass loss during early evolution rel. to theoretical surface abundances 80−94796
glacial ice, melting in sea water, heat and mass transfer *(German)* 80−33606

mass transfer continued
glass melting process model, for flameheated tank furnace melting *(Polish)* 80−70380
glassy polymers, films and spheres, transport props., film thickness and sample history effects 78−76917
granular materials, heat and mass transfer with low Peclet number flow *(German)* 78−42656
ground to atmosphere *(French)* 79−84403
hard spheres permeation through hard disc monolayers, interfacial mass transfer 80−107460
HD 152667 (V861 Scorpii), phys. props. and orbital parameters, supergiant star with black hole companion model 79−71067
HD 153919 (=4U 1700−37), supergiant-neutron star, optical variability 80−82419
HD 174237, periodic radial vel. changes, interacting binary with var. mass transfer 79−53818
HD 192163, Wolf-Rayet star, mass loss rate 80−82386
HD 206267, exciting star in H II region IC 1396, stellar wind, role in cloud struct. 80−105316
HD 4174, symbiotic star, mass loss rel. to spectroscopic obs. 80−85945
HD 44179 (Red Rectangle), precessing jets model 80−4422
HD 49798, H-deficient subdwarf O-type binary, non-LTE anal. and non-conservative mass transfer 79−16978
HD 77581 (=Vela X-1), supergiant+neutron star, stellar wind mass transfer, spectral obs. 80−94892
HDE 232078, variable mass loss in metal deficient red giant 79−67010
heat and mass transfer, book contrib. 77−58693
heat and mass transfer and friction under complex thermogasdynamic conditions 79−1209
heat and mass transfer between turbulent flowing fluid and solid wavy surface 80−14681
heat and mass transfer bibliography−Soviet works 79−23318
heat and mass transfer bibliograpphy−Soviet works 80−90618
heat and mass transfer development in USSR 79−14201
heat and mass transfer in a suspension of matter in gas with capillary-porous particles 79−87885
heat and mass transfer in capillary-porous body, kinetic eqns. 78−5796
heat and mass transfer in domains with variable and fixed boundaries 78−33995
heat and salt transfer across diffusive interface, grid generated turbulence 77−7381
heat pipe, 2-component, heat and mass transfer 80−24021
heat pipe, low-temp., evaporator-condenser interrelation effect on thermal resistance 77−89003
heat pipe, wickless, low-temp., crit. heat/mass transfer 78−42517
heat pipes, flow with injection 79−1065
heat pipes, heat and mass transfer, one-dimens. model 79−1064
heat storage, periodic, heat-carrying fluid and storage material transport kinetics 79−3901
heat transfer bibliography, Japanese works 79−23317
heat transfer conference, Aug. 78, Toronto, Canada 78−90624
heated body in perfect incompressible fluid, convective heat and mass transfer 80−43698
heating surfaces, furring, mass transfer, convective heat transfer, mathematical model *(German)* 77−23854
heavy ion deep inelastic collisions, relax. phenomena anal. 78−13156
Helmholtz layer model diffuse layer, discreteness of charge effect calcs. 80−26030
Hercules X-1, neutron star in eclipsing binary, accretion, X-ray obs. 80−90580
Hercules X-1 (HZ Herculis), periodic mass transfer rel. to X-ray light curve 80−51911
Hercules X-1/HZ Herculis, evaporative winds 77−78888
AM Herculis, accretion onto highly magnetised white dwarf 79−92764
AM Herculis, highly magnetised, accreting white dwarf 77−49396
AM Herculis, photoelectric obs. rel. to accretion struct. around degenerate star *(Russian)* 78−77565
AM Herculis (3U 1809+50), single accretion column model 78−57578
DQ Herculis (Nova 1934), high time resolution spectrophotometry rel. to mass transfer rate 80−22017
DQ Herculis (Nova 1934), short-period oscills. modulation and pulsed emission lines asymmetry interpretation 80−22044
AM Herculis objects, accreting mag. white dwarf model for linear polarisation 78−16460
heterogeneous chem. reactions under action of turbulent jet, modelling 78−64885
high temperature boundary layer mass transfer, nonequilib. ionisation effects 78−93634
high-vacuum systems, eqns. of mass exchange 77−11222
hollow fibre dialyser, mass transfer 80−66873
hot astrophysical bodies, mass ejection, energy conversion process 77−68800
hot massive stars, stellar wind mass loss, evolution study 80−17578
hot stars, evidence for mass loss 78−69786
hot stars, mass loss, review *(German)* 79−16958
HR 2142 and 7084, mass loss from UV spectra obs. 80−109485
HTGR reprocessing plant off-gas streams, ^{85}Kr removal 79−30972
Hubble-Sandage variables, mass accretion model 80−26877
HV evaporation, mass transfer in evaporating space *(Japanese)* 80−50558
EX Hydrae, dwarf nova, accretion disc dimensions from IR and optical light curves 80−67747
VW Hydri, cataclysmic variable, mass transfer modulation rel. to light curve superhumps model 80−4381
VW Hydri, dwarf nova, accretion disc dimensions from IR light curves 80−67747
VW Hydri, dwarf nova, accretion disc inhomogeneities rel. to short period light oscills. 78−20837
hydrodynamic crisis, in two-phase channel flow 78−14066
hydrology, C mass transfer and isotope evolution in natural water systems 79−20882
hydrothermal systems, transport phenomena assoc. with cooling plutons 78−36206
hypersonic laminar boundary layer at stagnation pt., slip, mass transfer 77−19625
hypersonic laminar near wake of blunted cone, convective heat and mass transfer 79−98752
ice, heat and mass transfer during sublimation, thermal shock method 77−50864
immiscible incompressible fluids, interfacial convective instability, diffusional exchanges, adsorption-desorption processes 80−70504
mass transfer continued
impulse plasma centrifuge with circulation, theory *(Russian)* 80−38553
impulsively started vertical plate, mass transfer and free convection currents 80−64567
incompressible flow including heat and mass transfer, vel.-press. coupling treatment 80−69832
Indian rivers, chemical and sediment load input into world oceans 79−34870
infinite porous plate, heat and mass transfer 78−30352
integral transforms for boundary value calcs. *(French)* 77−13711
interfacial cellular convection, effect on mass transfer enhancement 80 14690
interfacial instability, mass transfer, Marangoni effect and interfacial longit. waves 79−46890
interfacial stability with heat and mass transfer, appl. to Rayleigh-Taylor and Kelvin-Helmholtz cases 78−67253
internal flows with initial swirl, generated heat and mass transfer law 80−24025
interstellar medium, mass accretion by stars from dense gas clouds *(German)* 80−109500
intraparticle ion exchange mass transfer, accompanied by instantaneous irreversible reaction 78−9722
ionic, in open channels, electrolyte probe determ. 80−59110
IRC+30219, C star, mass loss interaction with extensive circumstellar envelope, visible spectra var. 80−90569
irradiated stars in active galactic nuclei, mass loss and evolution 80−56949
irreversible chemical process, in elec. field, heat and mass transfer 78−11545
irreversible transport processes, noncoupled, nonstationary, classical variational principles 78−4567
isobutane-air, in packed bed, heat and mass transfer, axial mass dispersion 78−75200
isothermal flat plate, boundary layer flow with transpiration, heat and mass transfer 79−94613
isothermal incompressible gas jets, mass transfer eqns., nonlinear thermodynamic anal. *(Russian)* 79−18925
isotropic porous media, heat and mass transfer, physical props. effects 78−94543
isotropic turbulent flowfield, smoke downstream diffusion, mass transfer characts. 80−14668
IV-VI compound vapour growth and transport in microgravity 77−77400
jet, axisymmetric turbulent impinging 77−42887
jet, free, heated, turbulent, high temp., eddy diffusion, methane combustion obs. 78−30329
jet, laminar rectangular, mass transfer due to impinging on flat surface 77−68651
jet entering fluidised bed, aerodynamics and mass transfer 80−14809
jet flow with vectored surface mass transfer, heat transfer 78−26174
jet impinging on surface, transfer coeff. for slot jet 79−32606
jets, drop formation, continuous phase mass transfer, perforated plate extractor column design 79−90299
jets undergoing mass transfer, break-up effect of nonlinear concentration profiles 80−79371
Jovian atmospheric probe, mass loss, shape change, real-gas aerodynamic effects 78−4055
Krogh tissue cylinder, transient convective mass transfer 80−3598
Lake Ontario, evaporation during IFYGL 79−2318
Lake Superior, transports using depth integrated model 77−37252
lamina, porous, generalised boundary conditions, heat and moisture transfer Prudnikov problem soln. 78−1551
laminar boundary layer, heat transfer, mass transfer and friction coeffs. *(German)* 80−74881
laminar boundary layer flow along vaporising liq. layer *(German)* 78−83403
laminar boundary layer swirling flow with heat and mass transfer in conical nozzles and diffusers 79−81842
laminar channel flow, mass transfer electrochem. meas. 77−58794
laminar chemically nonequilibrium mixture flow, characts. of combined heat and mass transfer *(Russian)* 79−59965
laminar compressible boundary layer, with vectored mass transfer 77−23974
laminar compressible boundary layer flow at stagnation pt., vectored mass transfer 79−27661
laminar condensation heat and mass transfer at stagnation point of droplet in ternary mixture 79−14227
laminar dispersion in circular tubes, approx. anal. 77−46986
laminar falling liquid films, mass transfer with heat transfer and interfacial shear 80−80033
laminar film, mass transfer with dissolution 78−26098
laminar flow, coupled heat and mass transfer, around flat plate with uniform heat flux 78−1631
laminar flow, linear wall resist. entrance region solns. 78−67168
laminar flow between two plane parallel plates, mass transfer 79−37321
laminar flow in channel with mass transfer across porous walls 79−41759
laminar flow mass transfer with axial diffusion in pipe with chem. reaction 77−55101
laminar flow past sphere, unsteady mass transfer, heterogeneous chemical reaction 77−55102
laminar gas streams in wetted-wall columns, cocurrent gas-liquid flow with circulation in gas phase 79−94698
laminar impinging jets, heat and mass transfer 78−94777
laminar pipe gas flow, fluid-wall mass transfer, sonic oscills. enhancement 77−910
laminar-vacuum insulation, nonstationary heat and mass transfer 78−59279
laminar-vacuum insulation, nonstationary heat and mass transfer 78−59280
laser beam materials processing, thermophys. and hydrodynamic effects 78−19957
laser-beam induced heat and mass transfer 78−93635
late-type stars, Ca II emission V/R ratio rel. to mass loss 78−93208
late-type stars mass loss 80−67755
layered porous medium transient 2-D diffusion 80−106841
η Leonis, mass loss from mid UV spectrum obs. 78−93217
Lewis number, heat and mass transfer coeff. derivation 80−14698
limiting relative law of heat and mass transfer and friction, permeability parameter effect 80−23999
liquid axisymmetric jet on baffle, heat and mass transfer 79−98775

mass transfer continued
liquid drop coalescence, effect on disperse-phase-controlled mass transfer rates 78−26185
liquid evaporation in circulating gas, porous channel temp. determ., obs. 79−72943
liquid film, falling, theory of mass transfer 79−65309
liquid film, flow over horiz smooth tubes 78−38273
liquid film, in vertical tube with turbulent gas flow, friction coeff., press. losses 77−89189
liquid film, influence of waves on mass transfer *(Russian)* 79−64677
liquid film, laminar, stability, mass exchange and heterogeneous chem. reaction effects 77−75990
liquid film condensation on vertical wall, linearised stability anal. 79−55381
liquid film hydrodynamics and heat transfer expts. *(German)* 78−18305
liquid film vapour absorption, combined heat and mass transfer 79−19430
liquid flow in narrow channel, mass and momentum transfer, turbulence promoter effects 78−9631
liquid fluidisation, mass transfer models *(French)* 79−37390
liquid fluidisation, study of mass transfer between a liquid and a mobile object in a bed *(French)* 78−83465
liquid fluidised bed, mass transfer at low Reynolds number 78−9698
liquid fluidised bed, mass transfer time fluctuations 80−79380
liquid fuel film, combustion behind shock wave, heat and mass transfer in turbulent boundary layer *(Russian)* 78−71401
liquid interfacial instability, mass transfer under high press. 79−94601
liquid jet, axisymmetric, impingement onto horizontal plane, hydrodynamics and mass transfer 78−94780
liquid layer on rot. Archimedes spiral, mass transfer 79−14413
liquid metal motion, with azimuthal and axial forces, in EM trough *(Russian)* 79−1259
liquid phase mass transfer coeffs. at natural air-water interfaces 79−20922
liquid-gas interface, heat and mass transfer 78−30338
liquid-liquid mass transfer in systems agitated by submerged jets 78−22393
liquid-liquid ternary mass transfer in ejectors with cocurrent flow 79−46368
liquid-vapour transformations, statistical kinetic theory 77−20044
liquids, laminal flowing, concurrent, in horizontal cylindrical channel, mass transfer across interface of liquids 80−79397
liquids, multicomponent, diffusion eqn., approx. mass transfer description 77−47609
LMFBR, computer model for ^3H transport and release 79−36371
LMFBR hypothetical core disruptive accident, simplified multicomponent phase transition model 79−31016
LMFBR steam generators, steel props. test *(Japanese)* 77−348
local mass/heat transfer distribution on surfaces roughened with small square ribs 80−19506
long period variable stars atmospheres shock wave periodicity rel. to mass loss 79−44487
low mass close binary evolution, catastrophic mass loss 77−33554
luminous stars, stellar winds effect on evolution 79−12467
β Lyrae, high time-resolution Hα spectroscopy rel. to mass transfer 77−13388
β Lyrae, mass transfer characts. rel. to light curve and peculiarities of system *(Russian)* 79−97036
macromolecular solution, gel conc. and diffusivity at gelling determ. by ultrafiltration 80−21325
magnetic fluids, heat and mass transfer 80−59123
magnetite particles, deposition from high velocity water onto isothermal tubes 77−67801
magnetoelectrolysis in steady Hartmann flow cells, hydrodynamics, mass transport 77−36759
magnetoelectrolytic convection, accuracy of estimation method 80−14691
main sequence stars in close binary systems, rapid mass accretion effect 77−91578
mass flow measurements of single-phase and multi-phase flows using radionuclide methods *(German)* 79−86532
mass transfer inside drops in continuous fluid, effect of pulsation *(French)* 78−55686
massive binary stars, effects of mass transfer on heavy elements prod. 80−46534
massive single stars, main sequence evolution with and without stellar wind 79−16936
massive stars, mass loss and convective overshooting influence on evolution 79−84789
massive stars, single and binaries, evolution review 80−82343
massive stars ($M \gtrsim 50\ M\odot$), binary star mass transfer model rel. to evolutionary status *(Russian)* 80−109425
massive stars evolution, critical mass loss rates for Wolf-Rayet stars prod. 79−101138
massive X-ray binaries, OB stars, evolutionary influence of stellar wind 79−101172
mathematical model, stochastic perturbation effect 78−94546
measurement of local mass-transfer coefficients by holographic interferometry, vortex instability effect 78−75234
measurement using pulse gas chromatography of mass transfer coeffs. in packed bed 79−48002
melt reacting with gas jet, heat and mass transfer, mathematical modeling 80−87819
melt solidification, heat and mass transfer 79−14236
melt surface boundary, mass transfer, influence on crystal habit during growth 79−14712
melting in finite domains not initially at fusion temp., singular perturbation theory 77−66014
membrane transport, monosubstrate inhibited enzymes, conc. response, multiplicity and memory 80−30679
membranes, cellulose acetate, vector mass transport obs. and appl. 79−96360
membranes, tubular of dissolved gases 77−35225
membranes with low porosity, diffusional boundary layer resistance 77−58778
l-menthol, vap., homogeneous nucleation, high-temp. Becker-Doering theory predictions 78−67820
metallic membrane interface, mass transfer 80−81366
metals, anodic dissolution, ionic mass exchange effects on hydrodynamic conditions 78−3349
metals, atomic mobility under pulsed loading conditions *(Russian)* 80−96684
mass transfer continued
metals in molten salts, mass and electron transfer meas. via recording coulometer 78−3344
methane-H_2, in packed bed, heat and mass transfer, axial mass dispersion 78−75200
methane-hydrogen mixture, flow through glass bead bed, axial dispersion coefficients 79−46378
methanol-H_2O mixture, evaporating droplets in air, temp. modelling *(German)* 80−2243
MHD convective viscous flow past porous plate with suction, mass transfer effects 78−87398
MHD Stokes problem for vertical plate, mass transfer and free convection current effects 79−90347
microconvective heat, mass transfer processes 79−86435
microwave heating with mass transfer using Luikov's system equations 80−106715
Mira variable stars, supersonic mass ejection 77−53605
Mira variables, envelope instability and mass loss rel. to planetary nebula form. 80−26928
mixture, binary, nucleate boiling heat transfer, conc. depend. 78−87249
modelling of eigenvalues and eigenfunctions of heat and mass transfer systems 77−14872
moist dispersed solid, local Rebinder criterion determ. 77−89199
moist materials, drying kinetics calc. method, heat (moisture) transfer 78−55555
moist porous material subject to sudden heating, mass transfer, press. rise 77−58787
moisture transfer in annular vertical channels 77−15119
molar molecule heat and mass transfer phenomena, generalised variational principle 80−79104
momentum, heat and mass transfer during flow around a sphere, free stream turbulence effects, mathematical model *(German)* 79−41678
momentum, heat and mass transfer during flow around a sphere, free stream turbulence effects *(German)* 79−41677
momentum and mass transfer in moving-wall channel 77−39344
Moon of fission origin, volatile elements loss and transfer to Earth 79−30000
moving boundary domains, heat and mass transfer with phase transition 79−81695
moving boundary problems, mass transfer rate, Stefan-Nusselt effect 78−93633
moving layer, heat exchange, numerical-anal. soln. 77−7291
multicomponent condensation, simplified mass transfer anal. 80−10675
multicomponent mass transfer in turbulent flow 79−32477
multicomponent mixtures, approx. methods comparison 78−65887
multicomponent mixtures, mass transfer, penetration depths 79−42286
multicomponent solid soln., diffusion mass transfer *(Russian)* 77−41552
multilayer insulation, heat and mass transfer during evacuation 77−30167
multiperforate laminae, mass transfer of chem. species by diffusion, plate and associated boundary layer case 80−40736
multiphase flow through porous media, local vol. averaging and distrib. function 77−58780
MXB 1730−333, rapid X-ray burster, accreting rot. magnetised neutron star model 79−84866
N51D, giant filamentary shell in LMC, stellar wind driven 80−105343
naphthalene, sublimation, mass transfer at vibr. spheres 80−57220
natural convection, heat and mass transfer interaction, around vertical flat plate 77−58669
natural convection mass transfer along porous vertical plate 78−90876
natural fluid circulation, horizontal pipe, closed at one end 77−47091
neutron star, accreting, magnetopause struct. 78−65647
neutron star, interaction between accretion disc and mag. field *(Russian)* 80−51799
neutron star accretion, photon pair prod. in transrelativistic plasma 78−20632
neutron stars, accreting, nuclear burning and X-ray bursts 78−36724
neutron stars, accreting, thermonuclear bursts assoc. with chromosphere flares 80−98684
neutron stars, accreting magnetic, cyclotron line form. 80−90463
neutron stars, accretion disc interaction with rot. mag. field 80−62173
neutron stars, disk accretion, transition zone radial and vertical structure 80−4393
neutron stars, Eddington luminosity limit and supercritical accretion, time-independ. calcs. 80−67768
neutron stars, H rich material accretion rel. to thermonuclear runaways 80−22032
neutron stars, magnetised, accretion, fate of sinking filaments 80−51798
neutron stars, rotating, magnetic, accretion torques rel. to pulsating X-ray sources period changes 80−31320
neutron stars, supercritical time-dependent accretion 80−85967
neutron stars plasma accretion, interaction with mag. field and accretion flow hydrodynamics 80−109452
neutron stars supersonic accretion, radiative effects 78−40978
non Newtonian fluid, mass transfer due to rot. disc 79−41717
non-Newtonian fluid, free convection, heat and mass transfer 79−68765
non-Newtonian fluid, pipe flow, heat and mass transfer 79−46309
non-Newtonian fluid, unsteady laminar incompressible boundary layer eqns., flow, heat and mass transfer, similarity solns. 79−32590
non-Newtonian fluids, literature review 77−23999
non-Newtonian fluids, mass transfer from cylinders to power law fluids 80−83826
non-Newtonian fluids, mass transfer from spheres to power law fluids 80−83825
non-Newtonian laminar boundary layer flow, mass transfer 77−27562
non-Newtonian turbulent boundary layer flow of power law fluid, mass transfer 77−31339
non-Newtonian turbulent transport in circular tube 77−39313
non-stationary heat and mass transfer, coupled, with convective motion and relaxation, variational principle 80−106797
nonconducting drop motion and dissolution in current-carrying liquid 77−11275
nonequilibrium reactive flow over solid body, conjugate heat and mass exchange 77−42931
nonideal fluid mixtures, generalised film model for mass transfer across interfaces 77−67387
noninertial particle transfer to rotating in laminar flow under external force field 80−10250
nonisothermal fixed bed adsorpt. column with nonlinear equilib., heat and mass transfer 77−80209

mass transfer continued
nonisothermal sorption within adsorbent particle, heat and mass balance 79−19452
nonisothermal turbulent suction-controlled boundary layer, heat and mass transfer coeffs. at chemically-reactive surface 79−77102
nonlinear anisotropic simultaneous transport processes, variational principle *(Russian)* 79−88893
nonlinear direct and inverse heat and mass transfer, analogue and hybrid simulation 77−53767
nonlinear heat and mass transfer in porous media 80−1577
nonlinear interdependent heat and mass transfer, variational solution *(Russian)* 79−88894
nonlinear mass and energy transfer, variational soln. 79−12740
nonlinear Rayleigh-Taylor stability with mass and heat transfer 79−90224
nonlinear simultaneous transport processes, complimentary form of variational principle *(Russian)* 79−54076
nonlinear simultaneous transport processes, variational principle *(Russian)* 79−58653
nonstationary heat conduction problem in presence of mass exchange, finite element anal. *(Russian)* 79−27492
novae, accretion belts on white dwarfs 78−36582
nozzle, two phase, efficiency at high rates of heat and mass transfer 80−48767
nozzle expansion in turbulent flow, downstream heat and mass transfer 80−1669
nuclear collisions mass transport, nucleon exchange, drift and diffusion coeffs. 79−563
nuclear materials safeguards, computerised chemical modelling of deviations, from mass transfer equilib. 80−83171
nuclear power station spray cooling, heat and mass atmospheric transfer 78−94078
nuclear reactor, interfacial mass and momentum transfer in two-phase flow 80−27725
numerical solution of transfer theory problems by the direct reduction method 80−22309
O-type binaries, anomalous mass ratios, evidence for mass loss 80−109478
O-type star, wind, effect on H II region evolution in mol. clouds 80−94846
O-type stars, He I 10830 Å to spectral line, rel. to mass loss 79−80304
O-type stars, mass loss rate from UV spectra 80−82346
OB stars, stellar wind mass loss determ., UV spectra obs. 80−94789
ocean, double boundary layers in standing surface waves rel. to mass transport 77−25694
ocean, mass and momentum diffusion by internal gravity waves 77−13086
ocean, mass conservation calculations in natural coordinates with example from Baltic Sea 80−51433
ocean, Mn mass transfer model rel. to deep-sea nodules growth 79−2212
ocean gravity waves, air-water interface effects on mass transport vel. 79−57947
ocean microstructure, transport processes and mixing 77−60420
Of and O stars, reasons for difference in mass loss 80−90413
one dimensional heat and mass transfer, Stefan flow and Lewis number influence *(German)* 80−1590
open cavity, modelling 78−55640
β Orionis, mass loss from mid UV spectrum obs. 78−93217
α Orionis, supergiant variable, mass loss, visible spectra obs. 80−67755
ovalbumin aqueous soln., macromol. gel layer formed on ultrafiltration tubular membrane, charact. 80−14260
packed bed, appl. of limiting current method to mass transfer at very low Reynolds number 77−39337
packed bed, gas flow, mass transfer factors 77−39340
packed bed, interphase mass transfer at very low Reynolds no. 77−80208
packed bed, mass transfer coeff. at low Peclet no. 79−4077
packed bed, mass transfer time domain evaluation from chromatograph peaks 80−19496
packed bed, optimal control of heat and mass transfer *(Ukrainian)* 79−32655
packed bed, particle to fluid mass transfer, dispersion coeffs. 79−18940
packed bed reactor, creeping flow, mass transfer 77−80227
packed beds, low Peclet number particle-to-fluid heat and mass transfer 78−94799
packed beds, particle-to-fluid transfer coeffs., fluid diffusivities 77−31378
packed beds with gas-liquid concurrent upflow mass transport phenomena and hydrodynamics 79−50784
parallel streams with interfacial mass transfer, laminar boundary-layer anal. 77−31272
particle, spherical, transient heat-mass exchange 79−7276
particle impacting wall diffusion layer, enhancement of mass transfer *(French)* 79−60050
particle in fluid with steady linear ambient vel. distrib., mass and heat transfer 80−19385
particle transport in laminar stream *(Russian)* 77−58768
particles, spherical, interacting, different sizes and compositions transfer rate calc. by method of images 80−77729
particles in a fluid, convective diffusion and mass transfer, wakes, chemical reactions 80−38394
particles moving in reactive, dispersive system, mass transfer interaction 79−64738
particulate beds, sheared, mass transport kinetics, Markov chains appl. 79−60057
perforated flat plate over porous medium, turbulence penetration, eddies, mass transfer 80−64528
perforated plate composite cooling in turbulent gas flow 79−98716
permeable surface, injection, laminar to turbulent transition, heat and mass transfer 78−83361
RY Persei, eclipsing binary, effect of gas streams and envelope on spectrum 80−101618
GK Persei, X-ray outburst detect. from old nova 79−67033
β Persei (Algol), gas stream producing absorpt. features in red wings of Mg II reson. lines 78−24524
β Persei (Algol), orbital period, 1964 to 1978, rel. to mass transfer event 79−58377
β Persei (Algol) eclipsing binaries, mass loss and mass transfer theory 80−62191
β Persei type systems, orbital period changes and evolutionary status 80−4396
mass transfer continued
perspiration mass transfer coefficients and clothing models 79−92158
pipe, porous, uniform air outflow, turbulent momentum flow and friction coeffs. formula 78−1737
pipe inlets, turbulent local mass and heat transfer, swirling effects 80−64542
pipe outflow, turbulent, with wall suction, dynamic and thermal fields *(French)* 79−4082
plane channel of arbitrary shape, occupied by grid, heat and mass transfer, comput. method 77−7453
plane membrane in way of flowing stream, concentration effects *(German)* 79−41557
planetary satellite ejecta, effect of proximity to Roche limit on dynamics 80−98592
plastics, thermolabile, drying, heat and mass exchange in vibro-rotational bed *(Russian)* 77−68377
plate, flat, with uniformly distributed vectored surface mass transfer, flow and heat transfer analysis 77−42838
plate, simultaneous heat and mass transfer to flat plate in humid air stream under frosting conditions 79−7284
plate, thick, parallel flow, with separation and reattachment, local and average mass transfer *(German)* 78−22339
plate columns with dual flow, mass transfer modelling 78−51219
plates, vertical and inclined, mixed convection combined, heat and mass transfer 80−64552
plume, buoyant, turbulent, issuing vertically into stratified or uniform ambients 77−58756
PMMA, spreading of two-phase film of melt, heat and mass exchange, ignition and combustion *(Russian)* 78−76861
pneumatic gauging appl. to mass and heat transfer coeff. meas. 78−58329
polydisperse filter bed, immobile, heat and mass transfer eqns. soln. 77−7446
polymer melting, during extrusion, integral energy-balance model 77−46899
polymer sheet, stretching, with suction and blowing, heat and mass transfer 78−34033
polymer solns., mass transfer and drag reduction near wall, electrochemical methods 79−77138
polymer solution, mass transfer between solid surfaces and drag-reducing fluids 78−79339
polymer solution, turbulent mass transfer to pipe flow 78−1695
polymer solutions, aqueous, diffusion and mass transfer from rotating disc 80−83827
polymer solutions, turbulent, mass transfer rate, frictional force *(French)* 79−37357
polyolefine, deep drying, internal mass transfer 79−14239
polystyrene suspension, laminar flow, augmentation of heat and mass transfer, correl. of data 80−53840
polyvinylalcohol, macromol. gel layer formed on ultrafiltration tubular membrane, charact. 80−14260
pool flames, heat and mass transfer *(German)* 78−94677
porous bed with permeable boundary, natural convection 79−77238
porous bodies, drying, internal mass transfer coeffs. calc. 78−67011
porous bodies, stresses induced by drying, elastoviscoplastic model, finite element anal. 80−23904
porous body, heat and mass transfer, two-dimensional isoparametric finite element method 77−42708
porous body, sublimation, heat, mass transfer from parallel capillaries 79−37395
porous cylindrical bodies, heat and mass transfer, boundary layer method 77−2625
porous ducts, fully developed laminar flow 78−47038
porous electrode diffusion controlled operation, mass transport with memory 80−21298
porous media, heat and mass transfer, numerical soln. 77−7441
porous media, heat and mass transfer during phase and chemical transformations 77−42917
porous media, nonisothermal mass transport, thermal energy flux and radiation pressure theory 78−76916
porous media, nonisothermal multicomponent sorption dynamics 77−65793
porous media, simultaneous heat and mass transfer governing eqns., soil heating appl. 78−94562
porous media, thermomigration, capillary diffusion coeffs. *(French)* 77−89006
porous medium, deep evaporation characterisation, of water *(French)* 78−59468
porous medium during gas blow through, exothermal reaction wave propagation 79−79222
porous moist body, contact heating moulding, temp. distrib. heat/mass transfer 77−75784
porous oxide pellet, spherical, reduction by gas flow *(French)* 79−27713
porous structures for cooling laser reflectors, theoretical study 80−91809
power law fluid, swarm of bubbles motion, mass transfer 79−50759
power law fluids, mass transfer into boundary layers 79−32588
power law fluids, single bubble motion and mass transfer 79−50758
power law fluids in fluidised beds 80−100032
pressure-induced diversion cross flow for rod bundle subchannel interconnection geometry 78−13215
progressive gravity waves, transport velocity, double boundary layer model 77−78217
propulsion systems for use in space colonisation 77−87232
pseudocontinuum mass transfer in media with spatially periodic boundaries 79−86500
pseudoplastic fluid crossflow around circular cylinder, heat and mass transfer 80−19370
pulsating fluid, mass transfer to moving drops, renewal penetration model 77−31369
pulsating X-ray sources, secular period changes 77−45613
pulsed extraction column, with perforated plates, efficiency 79−64809
VV Puppis, AM Herculis type binary, accretion column absorpt. spectrum obs. 79−101176
VV Puppis, AM Herculis type binary, mag. pole accretion model 79−5860
VV Puppis, circular polarimetry in active state and evidence for two accreting poles 79−48854
ζ Puppis, of supergiant, mass flow var., visible and UV obs. 80−90431
ζ Puppis, Of type star, stellar wind model from UV line fit 80−72965
PWR, superheated containment atmosphere heat/mass transfer to passive heat sinks, analytical model 79−49658

mass transfer continued
PWR LOCA, generalized model for predicting mass effluence during reflooding 79−31056
pyrolysis, of single solid particle accompanied by consecutive reactions, vol. reaction model 79−47896
QSOs, accretion disc model 77−64872
qualitative analysis of unsteady heat and mass transfer modes in a boundary layer with chemical reactions and intensive injections 80−69819
radiative accretion flow onto giant galaxies in clusters 78−93433
radiative viscous-shock-layer analysis for equilib. flow about blunt axisymm. body, effect of coupled ablation injection 77−24033
radioactive waste, low-level, radionuclide migration in soil 79−54610
radioactive waste, solidified, assessment of loss of isotopes 79−54541
rate in diffusion controlled electrochemical processes, drag reducing additives effects 79−43593
reacting binary mixture, turbulent flow, Reynolds eqns. and heat and mass transfer *(German)* 77−11281
reacting particle in fluid, convective diffusion, nonlinear surface reaction kinetics 80−106854
reattaching laminar and turbulent separated flow, three-dimens. heat and mass transfer 77−65759
regenerators with hygrostatic materials, combined heat and mass transfer 79−81689
renal medulla, multinephron models, canonical mass balance eqn. 77−12941
river to atmosphere heat and mass transfer data 78−96253
Roche lobe formation in highly eccentric X-ray binary systems 80−41858
rotating bubbling beds, heat and mass transfer 78−30351
rotating cylinders in laminar and turbulent flows 78−42613
rotating disc, convective mass transfer 80−43707
rotating disc at high swirl rates 79−14405
rotating disc electrode mass transfer, appl. of pulsed voltage and pulsed current 80−21292
rotating disc system 77−15041
rotating disk, in Ostwald fluid, nonstationary mass transfer 79−23328
rotating metal disc electrode, mass transfer under turbulent conditions, suspended particle effects 78−27772
rotating rods and plates, mass transfer and flow regimes 80−79326
rotating wedge-shaped blades 78−30305
rough surface turbulent flow heat and mass transfer, Reynolds analogy deviations 78−83380
WZ Sagittae, cataclysmic variable, mass transfer modulation rel. to light curve superhumps model 80−4381
WZ Sagittae, eruptive binary, accretion disc radius from hot spot eclipses anal. 80−72962
WZ Sagittae, recurrent nova, accretion disc brightening during 1978 outburst, spectroscopic obs. 80−26862
WZ Sagittae, recurrent nova, accretion disc models comparison with IUE obs. during outburst 80−109448
WZ Sagittae, recurrent nova, photometric study and mass transfer model 78−24513
XZ Sagittarii, Algol system, UBV photometry rel. to circumstellar matter 80−22041
V356 Sagittarii, eclipsing binary, opaque circumstellar ring model 78−49477
salt solutions, freezing in cells, heat and mass transfer with phase change 80−6493
salt-brine interface, natural convection mass transport 78−30291
sand tracer dispersion under progressive water waves, laboratory and field obs. 80−46170
saturated porous medium, free convection boundary layers, lateral mass flux effects 77−27592
saturated porous wedge with impermeable boundaries, heat and mass transfer 80−19375
Schwarzchild black hole, gas accretion 80−56871
Schwarzschild black hole, $\gamma>5/3$ gas accretion 79−17011
Schwarzschild black hole stationary spherical accretion, stability 80−51800
τ Scorpii, expanding envelope, mass loss rate 78−65613
V861 Scorpii (HD 152667), X-ray binary, Hα obs. rel. to mass transfer and mass loss 79−101171
Scorpius X-1, linear X-ray polarisation upper limit rel. to accretion-disc model 78−49557
sea bottom, mass transfer, horizontally 2D bodies effect 78−11909
secondary vorticity in internal waves 79−72899
sediment transport by rivers rel. to denudation, fallacy of stream equilib. assumption 77−78236
semiinfinite porous media, heat cond., phase transitions effects 78−94523
separated flow with laminar mixing region, heat and mass transfer, math. simulation 78−59397
W Serpentis stars, long period eclipsing binaries, new class, accretion onto nondegenerate stars 80−109483
shear flow, linear, heat or mass transfer rate from freely suspended particle 80−79313
shearing flow over wavy boundary, heat, mass, momentum transfer, turbulence model 78−87335
short crested waves, boundary layer vels. and mass transport 80−92169
sieve plate column without downcomers, anal. and NH_3 stripping expt. 78−22430
silica gel regeneration by adiabatic desorption mathematical model 79−1967
sine-Gordon chain, mass diffusion, soliton solns. 79−85102
sintered composite-liq. metal interaction, mass transfer eqn. approx. soln. 78−67262
sintering, reduction in specific surface area for two mass transport mechanisms 79−100074
sinusoidally oscillating cylinder in Newtonian fluid, mass transfer *(French)* 77−57287
slow novae and symbiotic stars, mass transfer from late-type components 80−94813
slug in fluidised bed, mass transfer, wall effect 79−4079
small particles suspended in turbulent fluid, convection, mass transfer 80−87793
SMC X-1, mass accretion rel. to spin-up rate of X-ray pulsar 77−29956
soil, heat and mass transfer with phase change 79−1093
soil, mass exchange in filter medium, hydrodynamics *(Russian)* 79−37292
soil plasma lateral translocation in small valley basin in Hertfordshire 77−45026

mass transfer continued
solar convective envelope, meridional circulation and heat redistrib. 79−40150
solar corona, mass ejection into interplanetary space 78−49417
solar flare heated filament, mass motions 77−29770
solar prominence condensation, horizontal temp. gradient meas. 80−26832
solar regenerator, transient response for varying insolation and flow 79−62025
solar regenerator of hygroscopic solutions, for air dehumidification 79−57464
solid+liquid reactions, heat and mass transfer, with gas evolution 79−83443
solid disperse systems, electro-osmotic mass transfer, surface cond. influence *(Russian)* 80−76546
solid particle pnuematic conveyance, flow characts. 79−37380
solid particle systems, high Reynolds numbers, mass transfer, Karman-Pohlhausen method 80−79378
solid reacting particles, ordered system at high Peclet numbers, mass transfer, convection 80−69830
solid soluble phase extraction from mixture of polydisperse porous particles 79−14475
solid solutions, multicomponent, diffusion processes *(Russian)* 78−47552
solid spheres, reacting, in periodic array, convective mass transfer in liq. laminar flow 80−96176
solid spheres in oscill. fluids, mass transfer review 77−42902
solid-fluid turbulent mass transfer with instantaneous chem. react., appls. 77−3888
solid-liquid extraction, diffusion processes, general soln. 78−20136
solid-liquid mass transfer in concurrent two-phase flow through packed beds 79−4066
solidifying melt thermal gravitational convection, impurity distrib. and transfer processes 80−19367
solloidal solution droplets, solid, particle form., heat and mass transfer 78−95967
soluble flat surface stability in turbulent flow 80−14676
solution droplets vaporisation, in high-temp. gas flow, heat and mass transfer 78−75191
Soret driven convective instability, mass diffusion and boundary effects 80−53776
sorption processes, formation of new crystalline phases 80−6625
southern peculiar emission-line stars, observational data rel. to mass ejection 80−41843
Soviet bibliography, heat and mass transfer 79−68701
Soviet bibliography 80−77557
spark machining, heat and mass transfer 79−1369
sphere in current carrying liq., convection mass transfer, num. anal. 80−83851
sphere-packed beds, limiting Sherwood and Nusselt nos. 78−18339
spherical accretion onto compact X-ray sources, luminosity thermal limit 80−82546
spherical cap bubble, mass transfer coeff. 80−79383
spherical drop, mass transfer and chemical reaction at transitional Reynolds number zone *(Russian)* 79−50814
spherical drop combustion, asymptotic, drop shrinkage and flame movement, heat and mass transfer 77−81405
spherical droplet, evaporation and condensational growth, mass transport calcs. 80−97736
spherical droplets in vapour environment, time evolution, physical-mathematical model 79−68789
spherical particle in flow at high Peclet numbers and $Re\leq100$ 77−54988
spherical particle in free-fall, time-to-complete-dissolution prediction 80−15245
spontaneous condensation processes, classification 80−6500
spray drying, of highly viscous conc. solns., heat and mass transport *(Russian)* 78−83230
spray nozzle, transfer processes in droplet plume during counterdirectional atomisation in gas flow 77−24014
SS 433, accreting mag. neutron star model *(Russian)* 80−36647
SS 433, early-type star plus neutron star model 80−56843
SS 433, mass accel. and collimation mechanisms 80−4368
SS 433, relativistic beam interaction with interstellar matter, mass loss rate, visible obs. 80−101629
SS 433, ultra-close black hole-degenerate dwarf binary system model 80−4384
staggered tube bundle, pressure and friction drag, mass transfer effects 80−38388
stars, adiabatic mass loss, spin evolution 79−75201
stars, ang. momentum transfer during steady disc accretion 78−65609
stars, asymptotic giant branch evolution with steady mass loss 80−26846
stars, constraints on mass loss rates from white dwarf data 80−46548
stars, dwarf novae, mass transfer instabilities and accretion disk structure 77−82243
stars, early type, mass loss 78−69796
stars, evolution of massive (20-100 M$\odot$) objects with mass loss 78−36554
stars, luminosity vars, rel. to particle orbital motion, stochastic scatt., accretion and ejection 79−44338
stars, mass flux fluctuation theory 80−72923
stars, massive, effect of mass loss on chemical yields 80−36614
stars, massive, evolution with mass loss by stellar wind 78−4197
stars, massive, He burning, mass loss by stellar wind rel. to evolution and Wolf-Rayet binaries 80−36615
stars, massive, mass loss rates rel. to evolution 80−90416
stars, Mira type variables, mass outflow vel. rel. to luminosity 78−93270
stars, Mira variables, pulsation and mass loss 79−25608
stars, pre-main-sequence mass loss constraint 79−58335
stars, self-accreting winds 80−101588
stars in close binaries, mass transportation *(German)* 79−58383
stars in close binary systems, mass transfer and accretion disk flow 77−82280
stars in massive close binaries with OB components, evolution 80−90474
stars of galactic halo, mass loss during evolution from planetary nebulae nuclei props. 80−82344
stars of high mass, stellar wind effects on evolution 80−21982
stars of O and Of type, masses and mass loss 80−94793
steam condensation in moving two-phase film, heat transfer, volumetric coefficient 80−48696

mass transfer continued
steam-generating channels with cosine law heat liberation, mass exchange conditions 79−81710
steam-generating pipe, containing porous deposits, mass transfer (impurities) 78−38398
steam-water annular flow, moisture exchange, salt method 80−24078
steam-water mixture, upward flow in tube, liq. film-core mass transfer, liq. distrib. 78−75189
steel:Si alloy formation kinetics at solid cathodes, metal electrodeposition from molten salt electrolytes 80−26028
steel, carburisation, calc. of mass transfer in diffusional saturation 80−24676
steel, stainless 304, metallurgical factors on the corrosion and mass transfer in liq. Na *(Japanese)* 80−71804
steel St3 plates, mass transfer of C under influence of shock waves *(Russian)* 78−91380
stellar, winds, steady state transonic wind model, radiative cooling effects 80−77391
stellar accretion discs, steady, optically thick, convective vertical energy transport 80−62112
stellar accretion discs, viscosity determ. for Hercules X-1 and (SS 433) 80−62110
stellar accretion discs theoretical photometric and spectroscopic props., cataclysmic variables appl. 79−80312
stellar coronae, min. flux concept rel. to energy balance and mass loss 78−81611
stellar gas accretion, thermodynamics and hydrodynamics 80−67696
stellar line accretion theory, gas press. effect 78−32525
stellar mass flow models for cool, luminous objects 79−5813
stellar mass fluxes, fluctuation theory 79−53804
stellar models in gravit. contraction phase, mass outflow mechanisms 77−53579
stellar surfaces, accretion of interstellar matter 80−51734
stellar systems, effect of mass loss on dynamical evolution, analytic approximations 80−51815
stellar wind flow past compact object, hydrodynamic eqns. and X-ray intensities 80−22116
Stokes' problem, mass transfer effects of MHD free convective flow 80−62003
stratified atmosphere, nonadiabatic heat dynamics with mass exchange and water phase transitions 79−58004
stream transport of solids, magnitude and freq. in Mississippi basin 77−78235
strip in shear flow, heat and mass transfer 78−51163
sublimation-condensation in annular gap, heat and mass transfer 77−35141
submerged jets impinging on baffle, flow and mass transfer, polymer additive effects 80−92194
subsea permafrost heat and mass transport processes, mol. diffusion and consequences anal. 79−2302
Sun, convection zone mass rel. to diffusion time scales and accretion 77−33454
Sun, mass loss rel. to meteoroid swarm evolution 80−8592
Sun, non-spherical flow of matter in solar wind 77−56880
sunspot, Evershed flow in complex region 80−51732
supercritical accretion discs winds struct. and appearance, numerical models 80−21984
supergiant stars, sporadic mass ejection 79−40186
supernova explosion from shock heating, collapse of massive star cores 80−56863
supernovae, explosive core overturn and mass ejection 80−72988
supersaturated gas mixture-small liquid droplets, energy and mass transfer anal. 77−62135
supersaturation during heat and mass exchange in stationary gas medium 79−94480
supersonic gas particle flows over wedge *(German)* 80−43731
supersonic jet, thermogasdynamic interaction with inclined permeable baffle 79−98773
supersonic near wake, mass transfer 78−9650
surface reactions and mass transport, in Leveque's approx. 78−76907
swirling one- and two-phase liq.-gas flow in tube, heat and mass transfer 78−30339
symbiotic stars, accretion rates rel. to subclasses 80−62144
symbiotic stars, binary model with super-critical accretion 77−45458
symbiotic stars, mass loss and mass exchange processes *(Russian)* 77−17616
symbiotic stars and recurrent novae, high speed photometry 77−60799
symbiotic stars and slow novae, mass transfer from late-type components 80−94813
λ Tauri, eclipsing binary star, mass loss from UV spectra obs. 80−109485
DR Tauri, T Tauri star, evidence for simultaneous mass infall and outflow from Balmer line profiles 80−101591
DR Tauri, T Tauri star, mass flow var. in envelope, visible spectra 80−85939
T Tauri star formation, stellar wind as dynamic input into dark mol. clouds 80−85980
T Tauri stars in dust cloud Lynds 134, mass loss causing cloud turbulence 80−94845
Taylor vortex flow, heat and mass transfer with const. axial flow rates 77−15035
ternary gas mixture, natural convection, naphthalene sublimation appl. 80−6511
ternary mass transfer, comparison of predictive transport models 79−30392
thermal plasma, heat and mass transfer 78−1805
thermal plasma transport phenomena, conf., Odeillo-Font-Romeu, France (Sept. 1975) 78−1798
thermal regenerator, with variable mass flow rate, computer model 78−75047
thermodialysis of nonideal aq. solns. across non-isothermal partitions 79−96366
thermogravimetric method for recording mass transport of materials under action of radiant fluxes 80−17944
thermohydrodynamic equations for two-phase polydisperse medium with phase transformations and size distrib. 79−41743
thermomagnetophoresis of particles in magnetic suspensions 80−35581
thermophoretic and diffusiophoretic particle deposition estimation 77−90644
thermostatic control, rot. conical (spherical) jacket radiatively heated from side 77−42710
mass transfer continued
thermosyphon, two-phase, heat and mass transfer in evaporation zone 79−1048
thin liquid films, break-up due to mass transfer intensity in absorption 80−80032
three-component system transport coefficient determ. 78−21082
transfer rates at spheres, moving on circular path 77−3890
transient flow boiling in duct, dynamics 78−94528
transitional mass-transfer behavior from packed-bed conditions to onset of fluidization 79−86505
transonic normal shock-turbulent boundary layer interaction, Reynolds no. and mass transfer effects 79−37353
transportation flows in pipes, energy comparison for steady, unsteady flow 78−91017
true mass flow meas. theory and systems 77−11284
tube, circ., entrance region, mass transfer, asymptotic expansion soln. 78−87392
tube, cylindrical, coaxial, effect of array of spheres on mass transfer rate to tube wall 80−74884
tube, vert., uniformly-heated, crit. heat flux prediction, generalised graphical method 79−46313
tubular reactor, model calc. with longitudinal transfer and heat losses through sides *(Russian)* 78−73043
tubular reactor with non-Newtonian laminar flow, diffusion and raction analysis 77−68703
turbulence, book 78−90839
turbulence, isotropic, spectral space, comparison between kinematic and scalar fields *(French)* 78−87334
turbulence structure and mechanisms, conference, Berlin, Germany (Aug. 1977) 78−94647
turbulent air-water mass transfer under varied stratification conditions 79−84389
turbulent boundary layer, diffusion model and rel. to heat transfer 78−94544
turbulent boundary layer, mass transfer in viscous sublayer, statistical method *(Russian)* 80−87764
turbulent boundary layer, transport processes model 77−58663
turbulent boundary layer with suction under nonisothermal conditions, heat and mass transfer 80−92125
turbulent falling film with or without chem. reaction 79−41766
turbulent falling liq. film, gas absorpt. 79−50714
turbulent flow, coupled transport of heat, momentum, mass, numerical method *(German)* 77−11193
turbulent flow in annulus 79−14388
turbulent forced convection, heat and mass transfer, analogeous relationship *(Japanese)* 79−14396
turbulent heat and mass transfer 78−1639
turbulent heat and mass transfer from wall with roughness ridges 77−39286
turbulent heat and mass transfer in abruptly changing wall boundary conditions 78−94545
turbulent heat and mass transfer rates at high Pr, electrochemical modelling 78−83383
turbulent liquid, coherent struct.-caused mass transfer at wall, numerical computation 78−59379
turbulent liquid film, gas absorpt. accompanied by first order reactions 79−69327
turbulent mass transfer in viscous sublayer by electrochemical method, expt. 78−83368
turbulent mass transfer to wall, fluctuations, Schmidt no. effect 77−58659
turbulent nonisotropic scalar field, dynamic eqn. for concentration correl., energy spectra 77−14992
turbulent nonuniform boundary layer with condensation, analysis 77−89124
turbulent pipe flow, large Schmidt number mass transfer 79−90230
turbulent pipe flow, wall region mass transfer 78−1638
turbulent pipe flow with suction or injection, high Prandtl no. heat and mass transfer 80−74857
turbulent Prandtl and Schmidt numbers from modelled transport eqns. 80−19373
turbulent transport, large scale struct. of turbulence 78−90847
turbulent transport coefficients, derivation from turbulent parameters in isotropic turbulence 78−46948
turbulent two-phase isobaric jet, anal. *(Russian)* 77−27586
two immiscible liquids, mass transfer into laminar fluid stream from moving interface 78−1717
two-phase counterflow with freely-falling dispersed material, heat and mass transfer 78−30340
two-phase flow, one-dimens., heat and mass transfer, approx. math. model 79−86495
two-phase flow, transient, interfacial heat and mass transfer, surface renewal model 79−27683
two-phase flow, unstratified, in permeable tube, hydraulic resistance 77−35205
two-phase flow in pipe, effect of mass transfer on heat transfer 78−91003
two-phase flow through packing, with longit. dispersion 79−68796
two-phase gas-liquid mass transfer in packed beds, review 77−31381
two-phase multicomponent system interface, mass transfer relations *(German)* 80−74966
two-phase rising flow in channels, heat and mass transfer 77−62295
two-phase upflow, vertical cocurrent, interfacial areas determ. for mass transfer 79−86528
4U 0115+63, hard X-ray transient, orbital elements rel. to mass transfer 78−93470
4U 1626−67, X-ray pulsar, X-ray and optical obs. rel. to accretion disc optical emission 80−51914
4U 1700−37 (HD 15319), high-energy X-ray obs. rel. to neutron stars accretion 80−86014
unsaturated porous media, heat and mass transfer, expt. and simulation *(French)* 78−94542
unsaturated porous media, moisture transfer due to small temp. gradients *(French)* 78−150
unsteady mass loss in close binary stars 77−57049
unsteady state heat transfer through the interface of spherical particles *(German)* 80−1412
unsteady-state gas absorption/desorption, mass transfer product 80−79381
W Ursae Majoris stars, mass transfer rel. to struct. and evolution 77−45488

mass transfer continued
vaporisation of particles in high temp. gas, Sherman eqn. calcs. *(Russian)* 80−39270
vapour dispersion, near surface of evaporation 77−51487
vapour-gas mixture, condensation, effect of thermal resist. of drops on heat and mass transfer 77−15015
vapour-gas phase, heat and mass transfer during evaporation of fluid 77−55354
vapour-noncondensible gas mixture, body force convection condensation *(Japanese)* 79−50574
variable stars, long-period, mass loss and circumnebular shells form. 78−8014
variational irreversible thermodynamics of heat and mass transfer in porous solids 79−4081
variational thermodynamics of viscous compressible heat conducting fluids 77−50868
vertical cylinder, combined heat and mass transfer in natural convection 80−59027
vibrating cylinders, mass transfer 77−62100
vibrating spheres appls. 80−57220
viscoelastic reacting fluids flowing over flat plate, boundary layer anal. of surface deposition 78−42675
viscous fluid, incompressible, hydromagnetic free convective flow past vertical porous wall, mass transfer 80−64645
vorticity eqn., three-dimensions, conservative form, numerical soln. 77−55011
wall region heat and mass transfer in turbulent Newtonian and viscoelastic flow 80−14680
water, annular mist flow in tube, wall film mass flow rate 80−69905
water, vertical boundary layer convection, salinity and press. depends. 79−37316
water adjacent to vertical uniform flux surface, buoyancy driven flow, transition and transport 79−27631
water droplet forced convection and heat transfer rel. to vapour conc. *(Chinese)* 79−23185
water evaporative cooling, convection and mass transfer, fog formation in boundary layers 80−79293
water evaporative cooling, heat and mass transfer coeffs., fog formation effects 80−79294
water layer, heated by radiant heat source, heat and mass transfer 80−74717
water vapour, condensation from moist air in curved channels, mass and heat transfer 79−90251
water vapour, desublimation in vacuum, heat and mass transfer and duration 77−11687
wave equation for simultaneous heat and mass transfer in moving media 79−44747
wear, entropy production model 80−74815
wet granular material, heating rate during drying 77−89009
white dwarf in binary system, outer layer C and O enrichment from companion 80−109465
white dwarf with mass accretion, H shell flashes rel. to symbiotic stars vars. 78−57550
white dwarfs, highly magnetised, accretion theory 79−92764
white dwarfs, mass accreting, evolution 80−77281
white dwarfs undergoing spherically symmetric steady-state accretion, stability 80−77402
wind-induced heat and mass transfer over large bodies of water 77−11186
Wolf-Rayet stars, Roche lobe overflow and stellar wind mass loss 80−105250
X-ray, burst sources, thermonuclear flashes in envelope of accreting neutron star 80−109455
X-ray binaries, evolutionary history 78−12431
X-ray binaries, mass transfer rel. to radio emission 80−62317
X-ray binaries, matter supply mechanisms 77−9813
X-ray binaries, stellar parameters of early type companions and mass transfer processes 78−36564
X-ray binaries, transient accretion model rel. to spin-up and spin-down timescales 80−109565
X-ray binaries progenitors, mass transfer and evolution 77−29954
X-ray binary sources, pulsating, accretion from Keplerian disc rel. to spin-up 80−67904
X-ray binary sources with OB supergiant companions, possible mass transfer mechanism 77−9809
X-ray binary stars, Roche-lobe overflow model 78−32601
X-ray binary systems, evaporative winds 77−78888
X-ray binary systems, massive, gas streams and accretion discs 78−93464
X-ray burst sources, accreting neutron star thermonuclear flashes model 78−12417
X-ray burst sources, effects of thermal limit for spherical accretion 78−45430
X-ray bursters 80−4460
X-ray pulsars, relativistic accretion 79−9032
X-ray source Scorpius X-1, mass-exchange binary characts. 77−57046
X-ray sources, pulsating, accretion disc interaction with stellar mag. field 78−93461
X-ray sources, steady accretion discs general struct. with mag. field 80−8714
young stars with mass accretion, evolution 80−101592
AgBr(Cl) precipitates, phase boundary processes, quantum mech. law in mass transfer processes *(German)* 79−27937
Al-Cu (4.8 wt.%), homogenization, temp. gradient driver process 77−52362
Al-Cu alloy, nonstationary mass transfer in front of moving phase boundaries in mormal freezing *(German)* 77−44238
Au-Si-Al structure electrode mass transfer and switching with memory 78−95389
CO_2 laser amplifiers, porous tube generated flow field, heat and mass diffusion 80−63969
Cs, vapour in Ar, fog condensation in MHD generator, heat and mass transfer 80−1410
Cu, corrosion inhibition through decreasing rate of mass transfer by drag reducing agents 78−19920
Cu electrodeposition at vertical electrode, current distrib., H_2 evolution effect 80−35543
Cu:Be, alloy formation kinetics at solid cathodes, metal electrodeposition from molten salt electrolytes 80−26028
D_2O+H_2, isotope exchange and separation with Pt hydrophobic catalyst *(Japanese)* 80−37901

mass transfer continued
Fe anode in H_2SO_4, passivation, dissolution model 80−35545
Fe grain boundary grooving by N contaminated liquid Li, corrosion mech. 77−6522
Fe-Co, compositional diffusionally bonded alloy, mass transfer investigation *(Russian)* 80−39342
Fe-S system, solubilities in aqueous H_2S and mass transport role in girdler-sulphide heavy water plants 78−83963
$Fe(CN)_6^{4-}-Fe(CN)_6^{3-}$, redox reactions, mass transfer at vibr. spheres 80−57220
Fe_2O_3, hematite, reduction, exam. of role of convective mass transfer 78−52724
GaAs, bulk purification by chemical vapour transport 79−24437
H-O electrochemical matrix-type cells, transport effects study 80−26027
H_2O, sessile drop impinging on heated surface, heat and mass transfer mechanism 78−90908
He strong stars, mag. fields and mass loss rel. to rot. 79−44486
^{3}He-^{3}He normal solution, size effect influence on capillary mass transport *(Russian)* 80−70497
^{3}He-^{4}He liquid mixtures, holographic obs. of diffusion waves 79−60595
^{4}He, superfluid, combined axial mass and heat transport 78−63894
K_2CO_3 melt in combustion prods. medium, vaporisation of drops 79−57290
KNO_3 pellet, dissolution in KNO_3 soln., mass transfer coeff. in crossed electric and mag. fields 78−48741
$LaMnO_3$, solid phase synthesis mechanism 80−21268
NH_3, flow in steel tubes, wall heat transfer with catalytic dissoc. 78−14099
N_2O_4, dissoc. laminar gas flow, heat exchange with triangular bundle of rods 77−42930
N_2O_4, dissociating, turbulent pipe flow, heat transfer, resistance 78−91026
N_2O_4 flowing in axisymmetric channels, mass and heat transfer calcs. 80−1570
N_2O_4, heat and mass transfer in turbulent stream in axisymmetric channel *(Russian)* 79−18960
N_2O_4, reactive turbulent flow, heat and mass transfer anal. *(Russian)* 77−42932
$(NO_2)_2 \rightleftarrows 2NO+O_2$, chemically unstable mixture laminar flow in channel, heat and mass transfer *(Russian)* 77−68707
$(NO_2)_2 \rightleftarrows 2NO_2+O_2$, nonequilibrium mixture laminar flow in channel, zone method anal. of heat and mass transfer *(Russian)* 77−72370
NiO, grain boundary thermal grooving, mass transport, self-diffusion coeffs. 80−44217
NiO single crystals, growth by material transfer in DC arc, and X-ray anal. 79−52113
O_2 bubbles, rising in water, dissolution mass transfer coeffs. 79−41737
O_2-N_2, gas mixtures, mass transfer, mag. field effects 78−63535
rotating Ni cylinder electrodes, investigation 79−43589
Si-Ge-Br system, diffusion mass transfer 80−33911
$SiBr_x$, x=1,2,4, diffusive mass transfer of Si, calc. for closed system 77−44169
$SrSO_4$, activation energies for mass transfer during crystallisation, surface active agent effects *(German)* 78−63689
$SrSO_4$, mass transfer in precip. from mixed solvents *(German)* 78−67674
Ti, heat- mass- and charge-transfer in high temp. oxidation 79−83369
W-O-Br system, appl. of mass transfer model of halogen doped incandescent lamps 77−32832
Xe, gas, diffusion enhanced by radioactivity 79−60094
$YMnO_3$, solid phase synthesis mechanism 80−21268
ZnSe-HCl-H_2, vapour phase chemical kinetics in open tube horizontal furnace *(French)* 77−63909
Zr, heat- mass- and charge-transfer in high temp. oxidation 79−83369

master equation
asymptotic behaviour of Markov process, general master eqn. 78−62152
atom, in strong reson. field, fluoresc. props. 78−940
atom+vibrator, stochastic theory, master or Fokker-Planck eqn. numerical solns. 77−30965
atomic system in perturber gas in radiation field, master eqn. for density matrix 77−30834
atoms, superfluorescence initiation, master equation study, microscopic description 80−63577
autocatalytic reaction system, sustained oscills., deterministic and stochastic theories 78−95922
binary mixtures, diffusion processes master eqns., kinetic eqns. 79−75446
biological multistate systems, freq. of cyclic processes 80−108834
Boltzmann gas, stochastic theory of hydrodynamic systems 79−75476
Brusselator, dynamic correl. functions, Mori-Zwanzig formalism 80−25988
cell membrane nuclear hydrodynamic shear, non-equil. Ising model, master eqn. 78−61146
characteristic function eqn. of Markov process, Langevin process applications 80−57192
chemical master eqns., Poisson representation 78−35638
chemical metastable and unstable states relax., analytical theory of extrema 80−50829
chemical mixture in closed vessel, equilib. distrib. 77−21413
chemical reaction, conc. fluctuations, use of master and Langevin eqns., diffusion effect 78−3313
chemical reaction, unimolecular, Lindemann fall-off by master eqn. 79−20342
chemical reaction diffusion systems, Chapman-Enskog development of multivariable master eqn. 80−81283
chemical reaction with complex form., stochastic reduction for dynamics 78−3315
chemical reaction with spatial and temporal structures, stochastic analysis 78−35639
chemical reactions, lattice model, coupling of translational and reactive dynamics 78−55696
chemical systems, non-equilib., mol. dynamics studies of long range and short range fluctuations 80−21318
chemical systems, single variable, master eqn. approximation by Fokker-Planck type eqns. 80−77702
chemically oscillatory systems, critical fluctuation universality, soluble master eqn. 79−75454
collision processes, reduced phase space approach calcs. 80−83438
composite stochastic processes 79−80514

master equation continued
construction of different forms of exact and asymptotic master equations 78−65859
convolutionless master equation, perturbation expansion 78−70047
coupled system, time depend. projection operator anal., classical gas and quantum systems 78−16720
coupled systems, deriv. from Liouville eqn. 79−85060
coupled systems, dynamic correls. 77−13697
coupled systems, dynamic correls. 77−13698
coupling master equation for N-subsystems *(Chinese)* 79−93038
critical behaviour of first order transition, mean-field theory, master eqn. and nonlinear Fokker-Planck eqn. 78−8375
crystal growth, multi-component, master equations in lattice model 80−75194
crystallisation theory, master equations for two-component system *(Russian)* 78−47258
1,1-cyclopropane(-d_2), isomerisation in He bath, vibr. transfer, temp. depend. 79−24723
derivation and expansion of master eqn. 77−5785
deterministic eqn. of motion, master eqn. and steady-state probability distrib. 78−36925
diatomic molecule, bulk rot. or vibr. relax. processes, information theoretic approach 77−58132
diatomic molecule, dissoc. and recombination involving two states interacting via at. species, soln. 77−23535
diatomic molecule, gaseous, dissociation rate const. eqn. 77−32769
diatomics, master eqn. theory, dissoc. rate consts. 77−77742
diffusion constants, Kawasaki inequality generalisation 78−70076
dilute atomic gas, weak at.-at. interaction pot. from master eqn. for coupled radiation 80−23484
discrete, approx. methods for stationary solns. 77−22480
discrete, continued fraction solns. not obeying detailed balance 80−101758
discrete, struct. of exact solns. 78−77821
discrete, transition factor method, appl. to chem. reactions 78−36952
disordered systems, electronic energy transfer 80−57221
dissociation, unimolecular, master eqns., analytic theory of extrema 80−50841
distributive processes in discrete systems 79−80504
dynamical renormalisation group transform., Ginzburg-Landau model, kinetic Ising model 80−42170
electric power conversion in circuits, power from energy fluctuations 79−100536
electrical circuit, power conversion of energy fluctuations, rel. to 2nd law of thermodynamics 80−17911
energy quanta, dissipation, linearly damped harmonic oscillator 80−68074
EPR and saturation transfer EPR, fast computation, master supermatrix eqn. soln. 78−62213
EPR and saturation transfer EPR, fast computation, perturbation approach 78−62212
evolution systems, meas., rel. to master eqn., Bayesian anal. 80−90782
exact derivation of a generalized master equation for the motion of excitons 78−87911
exact solutions in terms of continued fractions 79−88882
exciton model, master eqn. conversion for mean lifetime algebraic eqns. for nuclear reactions 79−518
exciton motion, coupled coherent and incoherent, kernel of generalized master eqn. determ. 79−51497
exciton motion in molecular crystals, Nakajima-Zwanzig generalised master eqn. 80−65462
exciton transport in mol. cryst., generalised master eqns. under delocalised initial conditions 79−26003
excitonic annihilation phenomena in low dimensionality finite lattice, master eqn. 80−92821
excitons, coupled coherent-incoherent motion, rel. to mean square displacement 79−19519
expansions in terms of jump size 77−82472
Fermi golden rule and Markov master eqns. 78−36935
finite fluctuations, Monte Carlo simulation 77−87693
finite open systems, appl. to nuclear reaction theory *(Russian)* 77−34274
Fokker Planck equation, non-linear, asymptotic representation of master equation 77−74325
Fokker-Planck eqn. expansion, weak diffusion, critical point 80−57228
Forster migration of electronic excitation, randomly oriented system 78−48211
Friedrichs model, soln. through exact Markovian master eqn. 78−81913
gases, weakly ionised, electron motion, stochastic theory of homogeneous systems, review 80−77735
Gaussian model, kinetic, formulation from master eqn., diffusive and relax. behaviour 77−9966
generalised, generalised Langevin eqn. equivalence 77−13699
generalised (non-Markovian) Langevin eqns., correl. functions and master equations 79−21653
Glauber master equation, Ising spins, relaxation, 1-D Glauber model, effect of disorder 80−65761
H-space fluctuations, Boltzmann eqn., master eqn. for drift motion 79−146
Hamiltonian, thermodynamic, stochastic props. central limit theorem soln. 79−6069
hard chemical instabilities, stationary distribs., unimodality 79−5129
harmonic oscillator system spontaneous emission, master eqn. 79−17277
heat conduction, stochastic theory of atomic chain coupled to two reservoirs 78−54319
heavy ion collisions, generalised master eqn., drift and diffusion coeffs. 80−106075
Heisenberg model, validity of Fokker-Planck equation 77−89920
hopping conduction, master eqn. approach in presence of mag. field 80−103697
hopping transport kinetic theory, localised state separation, Pauli master eqn. 80−80276
hopping transport theory, master eqn. approach *(German)* 80−27237
hot electron quantum energy distribution function in crossed elec. and mag. fields 77−32019
hyper-Raman effect, master eqn. approach, quantum statistical treatment 78−82736
inhomogeneous systems, stochastic version of Boltzmann eqn. 79−55442
instability point, relax., fluctuation 77−13681
intermicellar kinetics theory, stochastic approach, master equation for, irreversible reactions 80−76561
master equation continued
irreversible processes, time evolution for large quantum systems in superspace 78−62172
Ising model, nonequilib., intensive parameters and detailed balance, theoretical estimate 78−76209
Ising models, stochastic dynamics 77−49690
Killing vectors in plane HH spaces 78−54104
kinetic eqn. for particle in field of randomly varying scatterers 79−58634
kinetic Ising chain, renormalisation group transform. for master eqn. 80−11214
kinetic theory of gases, stochastic approach 78−9744
Langevin equation with multi-Poissonian noise, appl. to birth and death process, Boltzmann-Langevin equation 79−25978
laser fluctuations, semiclassical stochastic master eqn. theory, and Scully-Lamb theory 79−27236
laserlike systems, stochastic master equation description 80−53243
limit cycle fluctutions near bifurcation point, Fokker Planck, Langevin eqn. calcs. 80−77709
linear response theory, master eqn. approach 80−31663
local fluctuations in chemical reactions, nonlinear master eqn., dimensionality expansions, augmented mean field theory 78−73019
macroscopic cell representation by density matrix eqn. 79−63130
macroscopic non-Markovian systems, microdynamics, time evolution 77−41541
macroscopic non-Markovian systems, microdynamics, time evolution 78−41236
Malthus-Verhulst process, crit. point calcs. 80−42176
Markov and nonMarkov process, derivation and solution of master equations and asymptotic representations 78−57881
Markov process time evolution, network theory 77−5642
Markov processes, exact solutions for energy transfer from molecule in heat bath 79−88875
Markovian, for unstable particles, weak coupling limit 77−45794
Markovian integro-differential master eqns., Langevin description 80−31676
Markovian master equation, inverse super operator construction 78−57864
memory kernel for generalised master eqn. 79−93044
molecular collisions, stochastic theory in perturbation limit 78−1042
molecular crystal, multicomponent, energy migration master eqn. 80−16075
molecular dissociation, RRKM formula correction by non Boltzmann character factors, Markov eqns. 80−71891
molecular dissociation-recombination, collision induced, exactly soluble model 78−7191
molecular energy transfer collisions, master eqn. transition probabilities and moments, stochastic theory 79−3533
molecular solid, fading memory as insufficient condition for exciton diffusion 79−19520
molecular vibrational relaxation and dephasing in condensed phases, non-Markovian theory 79−41224
molecules, luminescence-vibrational relaxation interaction, master eqn. calcs., theory 78−42123
multilevel system, laser excitation, Wilcox-Lamb rate eqn. approx. 79−27028
multiphoton excitation, collisionless, of large mol. kinetic eqns. 79−54914
multivariate master eqn. diffusion operator, reaction diffusion system eigenfunctions 78−29077
multivariate master equation for reaction-diffusion system 80−95045
Nakajima-Zwanzig's generalised master equation, evaluation of kernel of integro-differential equation 78−86123
Nakajima-Zwanzig generalised master eqn. for coupled coherent and incoherent exciton motion, Born approx. 79−60723
NMR spin-lattice relax., periodically-irrad. system, master eqn. predictions 78−43664
non equilibrium systems, stochastic model, master eqns. *(Chinese)* 80−68126
non-equilibrium systems, statistical mechanics of steady states 79−54038
non-Markov processes, time evolution, correls., linear response 77−13587
nonequilibrium phase transition, exact results, stochastic anal. 78−29076
nonequilibrium phase transitions in chemical systems 78−54325
nonequilibrium statistical thermodynamics, covariant formulation 77−41542
nonequilibrium steady states of open systems, 2nd order type transitions and fluctuations 77−49680
nonequilibrium systems, cluster expansions with contraction for homogeneous systems 80−46964
nonequilibrium systems, statistical mechanical theory from generalised phase space and damping theory 79−75481
nonequilibrium thermodynamic Hamiltonian, contact transformations 79−17371
nonequilibrium transition, stationary solns. 80−89466
nonisothermal system, equilib. distribs. and detailed balance relations 79−36737
nonlinear, asymptotic expansion 77−49682
nonlinear birth and death processes, relaxation mode anal. 77−49681
nonlinear chemical rate processes with multiple stationary states, stochastic theory 77−90582
nonlinear chemical reaction systems, dynamical correlations near instabilities 78−80715
nonlinear Fokker-Planck eqns., master eqns. 79−40503
nonlinear Langevin eqns., and time-convolutionless master eqn. 79−40502
nonlinear oscillator with fluctuating parameters, dynamics, thermal noise 80−101729
nonlinear system, equivalence to Langevin eqn. 77−71273
nonMarkovian Pauli type, rel. to adiabatic following soln. of Bloch eqn. 79−13940
nonuniform nonequilibrium systems, approx. scheme for fluctuations study 79−58637
nuclear double resonance, theory of double spin flips 80−66076
nucleation in early stage, stochastic process 79−80521
nucleon-induced preequilibrium reactions, ang. distrib. in exciton and hybrid models 79−40899
Onsager relations from Markov system master eqn., symmetry props. 77−22482
open systems, dynamics 78−36951
open systems, generalised master eqn. struct. 77−9972

master equation continued
open systems, generalised regression theorem for multitime correl. functions 77−9973
open systems theory, appl. to unstable particles 79−17281
operators, with extremal entropy prod. 79−2714
optical, bistability, cooperative effects and fluctuations 78−17885
optical bistability, Fokker-Planck eqn. from master eqn. 79−13935
optical bistability dispersion effect, master eqn. generalisation 79−31845
optical bistability in gas filled Fabry-Perot cavity, elec. field excited 79−76652
optical harmonic generation, second harmonic and subharmonic, master eqn. approach 78−33773
oscillatory superfluorescence, Markovian master eqn. model 79−27222
particle motion in stochastic force fields 78−73928
parton distribution, master eqns. 79−80792
path integral solution 79−12715
Pauli master equation, derivation 78−89397
phase transition probability, system size depend., consequences for stochastic eqns. 78−41258
phase transitions, kinetic theory, master equations *(Russian)* 78−47498
photon statistics, unsaturated k-photon absorption, exact soln. of master eqn. 80−37984
photosynthetic membranes, anal. of laser-induced fluorescence with Pauli master eqn. 79−39350
polyatomic gas, laser-induced rate processes, intermol. and intramol. relax. formalism 79−27070
quantal master equation for any time scale, Brownian motion 78−24725
quantum damped oscillator, master equation and pure state representations 80−8823
quantum diffusion, particle in fluctuating medium, memory effects 79−49180
quantum harmonic oscillator, driven and stochastically modulated, reduced eq. of motion 78−77764
quantum K-systems, kinetic description, stochasticity condition 79−85080
quantum Markovian master eqns. 79−144
quantum stochastic processes, thermodynamic limit 77−37814
quantum system under stochastic perturbation, time correlation functions 79−49154
quantum systems with strong interactions *(Chinese)* 78−86229
quantum two-level system, damped and stochastically modulated, reduced eq. of motion 78−77764
quenched-in vacancies, stochastic theory for clustering, general mathematical props. 79−65073
Raman scattering, resonant, intense optical waves, quantum mechanical theory 79−89958
random walk, with arbitrary pausing time distrib. 78−16736
rate processes in condensed media, master eqns. 80−77687
reacting gas system, master eqn. derivation by method of projection operators 78−1780
reacting reversible small bimolecular systems, numerical anal. of statistical functions 78−64831
relaxation phenomena, general treatment 78−44398
relaxation processes, initial slips and transient effects, theory 78−24729
semiconductor, hot electron fluctuations with displaced Maxwellian distrib. 80−29418
semiconductor, hot electrons, photoexcited in quantizing mag. field, energy distrib. calcs. 79−42586
soft pion theorem, appl. to currents in nuclear forces and matter. 79−26377
solution, electronic excited state transport, Green function soln. 79−68994
spatially extended systems, stochastic Liouville eqn. rel. to generalized master eqn. 78−45581
spin glasses, time translation, spatial scaling and nonexponential relaxation 80−97110
stationary Markov process, path integral solns. 78−86233
statistical mechanics, foundations 80−22271
statistical mechanics, stochastic master eqn. representation 77−33935
statistical mechanics, validity for finite closed systems 78−65864
steady state solns. without detailed balance, chem. react., two-photon laser appls. 77−9945
Sterman-Weinberg formula for quark jets and gluon jets, leading log version, master equation 80−22552
stochastic, metastability in macrosystems, eigenvalue problem 77−9977
stochastic Liouville equation, generalised, nonMarkovian and memoryless master eqns. 78−24737
stochastic phase spaces and master Liouville spaces in quantum statistical mechanics 79−85076
stochastic processes introduction for physicists 79−25988
superfluorescence, oscill., quantum statistics 79−917
superradiance, exact solution for complete initial excitation 77−68200
thermodynamic properties, of interacting particle ensemble, by simulation of stochastic disordering 77−87697
thermodynamics, nonequilib., with crit. fluctuations, master eqn. derivation of Keizer's theory 79−67240
three two-level atoms system, continuously incoherently-pumped, radiation rate, spectrum 80−5716
time convolution Master equation and generalised Langevin equation equivalence 78−93610
transition operator for Markov and non-Markov processes, interpolation model 80−8910
two time correlation functions for Poisson representation, nonequilib. and equilib. chemical reactions 79−1936
two-atom system, continuously pumped, radiation props., master eqn. 78−86828
unimolecular reaction theory, master eqn. basis 77−44457
unimolecular reactions, master eqn. for rate coeff. Nesbet's algorithm 78−48612
unimolecular reactions, master eqn. solns. 77−70291
unimolecular reactions, nonequil. time-depend., model calc., single collision approx. 80−25987
unimolecular reactions, strong collision rate consts. 77−73446
unimolecular reactions induced by monochromatic IR radiation, intensity and laser energy fluence influence 80−11903
van Hove master equation, derivation 78−89397
AgI, conductivity, hopping system, master equation 80−39348
CO, nonequilib. dissoc. induced by electron-vibr. and IR laser pumping 79−86016
$^{12}C^{16}O$, in Ar matrix, vibr. population time evolution temp. depend., master eqn. 78−9180
Cl_2+HI, pulsed chem. laser, rot. distrib. time evolution, kinetic master eq. calc. 77−65593
H, dense plasma, ionisation, master eqn. analytical soln. 78−59544
H, recombining atomic plasmas, population inversion 80−32679
H_2, diffusion in interstitials, master equation equivalence 78−79794
H_2+Ar, 4500K shock wave expt. simulation, vibr. state changes and dissoc. 79−61850
H_2+inert gas, vibr. relax. mechanism, master eqn. anal., density changes 79−76493
^{3}He, solid, phase separation of dil. ^{4}He impurities 80−88393
N, recombining atomic plasmas, population inversion 80−32679
O, recombining atomic plasmas, population inversion 80−32679

matched filters
debubbling filters, for marine seismograms source signatures 79−16692
electronically tunable, realisation using SAW technique *(Russian)* 79−98538
narrowband matched SAW filters realisation *(Russian)* 80−23850
optical, pattern recognition by means of holography *(Japanese)* 80−5699
phase-matched, application to study of Love waves 79−92602
SAW and semiconductor ccts., monolithic integration on Si 79−32164
SAW slanted device technology for radar system appl. 80−19181
SAW/CCD programmable matched filter 80−5896
target discrimination methodology in remote sensing 80−58470
visual perception, adaptive filters and eye movements 79−53153
weather radar matched filter criteria and range weighting 79−25341
$LiTaO_3$-SiO_3, temp. compensated SAW device fabrication 79−76923

materials
see also individual materials, e.g. ceramics
aerosols with organic constituents, effect on fog and clouds 78−73465
asphalt products for final disposal of radioactive wastes, safety evaluation *(Japanese)* 77−50254
bitumen, diffusion of ^{137}Cs and ^{90}Sr, radioactive waste treatment *(Russian)* 80−52771
bitumen, phys. props. and constitution, effect of air blowing 77−44384
bitumen, rheological model of Maxwell-Norton type *(French)* 79−64614
bitumen constitution, struct., and rheological props. *(French)* 79−18853
bitumen salt mixtures for rad. waste containment, thermogravimetric anal. *(German)* 79−89391
bitumens, oil sand, rheological props. 80−64506
bituminous surfaces, review of aggregate selection critera for improved wear and skid resist. 80−7689
book 78−11089
calorimetric sheath temp. distrib. for material selection criterion 78−77917
classification by brittleness and stress/deform. relationship 78−15528
conservation ethic 79−44700
conservation ethics, for material resources 79−43111
dental, uses and props., review 78−53548
dimensional stability for precision machine parts, review *(Japanese)* 79−39116
elbor, friction in contact with W, temp. depend. *(Russian)* 77−73350
electronic, optical, magnetic and thermal props., rel. to energy technology 78−88412
enamelling by electrostatic frit powder spraying 80−97428
engineering and materials science, as a multidiscipline 79−38726
engineering materials, physics, chemistry 78−88413
fluorine materials review *(Japanese)* 79−96282
granulated slag as road banking material *(Japanese)* 78−31612
handbook of industrial materials 78−56571
historical development, of interdependence between man and materials 79−38725
layered materials, prep. and growth, book 78−19646
molluscan shells, IR spectral anal. 78−3413
moulding materials and mixtures, exam. of gases released 79−52817
noise and vibr. control materials, review 78−13854
orchard leaf, multielement anal. by sequential instrumental and radiochem. neutron activation 78−7798
orchard leaves, metals, determ., in water and organic materials, flameless atomic absorpt. spectrometry with wire loop atomiser 80−45586
petroleum industry, plant, service failure modes gen. review 78−95904
physical properties, book 77−16476
pitch and bitumen, viscosity, temp. depend. up to 500°C 80−92698
plaster, fracture mode criterion, combined, disk test study *(Japanese)* 79−66153
processing, convection control, future fluid flow research, space environment possibilities 79−47622
processing, expt. capabilities in Space Shuttle/Spacelab 79−47883
proficiency for national progress 77−87624
radiographic image quality assessment using standardized step/hole type IQIs 77−66724
research and processing programme for Spacelab by German Federal Republic 78−88620
review of mech., corrosion, thermal, elec. props., appl., economics, design considerations 79−1818
safety, materials science contribution *(German)* 78−58352
schist containing clay and sand, integrated normal emissivity with low heat conductivity coeffs. 80−103504
schist dust, integrated normal emissivity with low heat conductivity coeffs. 80−103504
science and design, review *(Japanese)* 77−69974
science and technology, space flight appl., conf., Gaithersburg, USA (April 1977) 79−47881
semiconductor, diffusion length and lifetime meas. and assessment by SEM 80−96902
Shroud of Turin, IR reflectance spectrosc. and thermographic investigations 80−87578
Shroud of Turin, scientific investigation 80−87576
Shroud of Turin, spectral props. 80−87577
Shroud of Turin, UV-visible reflectance and fluoresc. spectra 80−87579
Skylab mission, materials sciences in space, review 77−36377
space environment, materials processing expt. capabilities 79−47882
space materials processing experiments 79−1817
space research impact, 1981 Spacelab era influence forecasting 79−19981
spacecraft materials in space environment, conf., Noordwijk, Netherlands (Oct. 1979) 80−67933
system concept in materials science 80−101003
technology, review 77−8733

materials continued
tissue substitute material formulation using basic interaction data 77−86640
tissue substitute materials formulation, effective atomic numbers 80−17169
tobacco shreds, filling capacity, effect of temp., moisture content, shred length, stalk position *(Japanese)* 79−43549
tobacco shreds, fragility, filling capacity, equilibrium moisture content, glycerol addition effects *(Japanese)* 77−77727
tobacco shreds, fragility, filling capacity and equilibrium moisture content, effect of sucrose and sorbitol additions *(Japanese)* 78−56876
tooth enamel, human cryst. struct. refinement, Rietveld method 80−51040
tyres, used, pyrolysis to produce organic raw materials *(German)* 80−3307
unconventional energy systems, exam. of material requirements 78−50255
undergraduate creative project in materials sci. 78−86082
vacuum system construction material selection and degassing 80−82783

materials handling
see also computerised materials handling; conveyors; crushing; fission reactor fuel preparation and reprocessing; fluidised beds; grinding; transportation; winding (process)
acoustic levitation devices of processing materials, limitations 80−74694
ampules for handling graphite specimens for irrad. in reactor core and reflector channels 77−50220
automated nondestructive assay system for Pu samples 77−61512
biological microspecimen holder for processing and critical point drying 79−74822
biomedical target, water-cooled pion-production, remote exam. and disassembly 80−25975
breeder reactor spent-fuel shipping cask design 79−9834
buried transuranic waste, equipment system for retrieval handling 79−89415
BWR spent fuel cask handling problems and solns. 79−9799
CANDU irradiated fuel, monitoring for sheath defects in shipments 78−54864
chemically reactive liquids, container construction for neutron diffr. studies 77−35443
Clinch River Breeder Reactor Project ex-vessel transfer machine design and development 79−9787
commercial LMFBR fuel handling and storage system 79−9845
compact servo master-slave manipulator 79−9214
computer system for automatic inspection of fuel pellets 80−68795
conference on nuclear engineering remote systems technology, San Francisco, USA (Nov.-Dec. 1977) 79−45438
CRBRP ex-vessel transfer machine 78−8943
cutting laser beam appl. in material-cutting, processing optimisation *(German)* 80−43384
dewatered pipeline coal dust pollution model 77−37401
electron beam radiation processing on commercial scale 77−73281
electron beam treatment facility 77−59795
environmental protection, radioactive waste from power plants in USSR 79−26601
fast reactor fuel, handling system for inspection of fuel pellets 79−49824
FBR, atternative fuel recycling technology search 80−5303
FFTF fuels and materials exam. facility and materials handling systems design 80−18421
FFTF interim examination and maintenance cell, equipment testing program 79−45451
fissile materials, reactivity enhancement in transportation and storage arrays from density reductions 77−57756
fission reactor fuel, mixed oxide, suitability of spent fuel shipping casks 80−27757
fission reactor fuel safeguards and transportation 77−34400
fission reactor irradiated cladding, in-cell facility for mechanical testing 80−21244
fuel defect test loop, remote handling system design 79−45395
fuel defect test loop remote handling system design 79−9730
fuel recycling remote manipulation systems design and performance 77−67854
Fuels and Materials Examination Facility, equipment design and development 79−45449
fusion power reactor waste management 78−21766
gamma irradiation plant, commercial, Japan 77−59794
glove box for sealed manipulator maintenance 80−18684
glove boxes, Pu-contaminated, size reduction and waste packaging 80−18469
granular material flow from parallel sided bins, thickness of shear zone 80−81279
HFEF/N, equipment repair room modifications 79−45439
HFEF/N, handling equipment for neutron radiography facility 79−45443
HFEF/S air cell, decontamination and refurbishment 79−45445
high-speed slitter for irradiated stainless-steel tubing 79−45450
hot cell, rigid hoist articulated grapple system development for enhanced remote maintenance 80−68968
hot cell for reprocessing of spent nuclear fuel samples 78−58364
hot cell liners, removable, design 80−18685
hot cell manipulator remote decontamination facility and repair station 79−9911
hot fuel examination facility, auxiliary equipment for remote handling systems 80−18686
hot fuel examination facility/north, equipment repair room modifications 79−9723
hot fuel examination facility/north, wall feedthrough removal, portable glove box system 79−9724
hydraulic coal trunk pipeline transport systems, methods of improving economic effectiveness 80−106837
hydrogen fuels, safety aspects of a future hydrogen technology 79−74551
hygroscopic materials, method for drying and cooling chamber 77−61054
ignition test reactor, remote maintenance system requirements 79−45420
inertial confinement from reactors, remote system needs 79−45421
irradiated fuel rods, storage options, comparisons 79−45383
irradiated fuel sipping, inspection, and repair at Point Beach Nuclear Plant 79−45384
irradiated nuclear fuel, transport, packaging, UK experience 79−26782
irradiated nuclear fuel transport, European experience 79−31235

materials handling continued
irradiated nuclear fuel transport and handling, French nuclear power plants *(French)* 79−31233
isotope induction at LAMPF, fabrication, cladding, handling of irrad. targets 80−23231
liquefied natural gas, nonsteady-state flow calculations in horizontal pipeline systems 80−106838
liquefied natural gas, safe handling, measurement system, prediction of roll-over 80−27269
liquid nitrogen filling system, automatic 77−41620
LMFBR, fuel handling and storage system 79−45394
LMFBR, spent fuel shipping system 79−45385
LMFBR fuel elements, remote exam. of shroud tubes 80−18470
LMFBR spent fuel shipping cask designs, subcriticality guidelines, Monte Carlo calcs. 78−82470
LNG, transport and storage hazards 80−45620
loop disposal system of sodium loop safety facility 80−18467
LWR, alternative fuel recycling technology search 80−5303
LWR fuel reprocessing, liquid waste handling facilities 79−36390
LWR spent fuel, head-end part of fuel reprocessing facility, unloading installations, handling and transfer techniques *(German)* 80−57939
magnetic separation of minerals using supercond. mags. *(Czech)* 78−88923
manipulator purposeful motion kinematics and dynamics modelling 77−78969
manipulator vehicles of Nuclear Emergency Brigade in Federal Republic of Germany 77−50315
master slave manipulator SM-229, compact servo system 79−45454
master-slave manipulator power-assisted grip system 79−9212
metal surface radioactive waste chemical decontamination 80−37530
mine large particle size photometric sorting machine, DATAC system 78−32853
mixed-oxide fuel pellets, remote encapsulation for transient testing 80−18422
moderation controlled low-enrichment uranium systems, regulatory perspective 77−65317
neutron radiography facility handling equipment 79−9726
nuclear, reprocessing and disposal, ecological problems nuclear plant fuel cycle closing, ecological problems solution *(German)* 77−54344
nuclear criticality safety analysis using solid-angle method and Monte Carlo program 77−65294
nuclear fuel centre, fuel and waste facilities, safety, protection and socioeconomic aspects 78−58395
nuclear fuel cycle material, computerised transportation model shipment 79−85743
nuclear fuel pin profilometry adaptation, cutoff saw 79−45452
nuclear fuel preparation, moderation control in large-capacity process unit 77−65316
nuclear fuel removal from irrad. cladding, eval. of methods 77−54306
nuclear fuel reprocessing hot cell facilities and techniques, Karlsruhe 79−45458
nuclear fuel transport by air, feasibility and economics 78−94154
nuclear material control with VACOSS variable coding seal system 78−82491
nuclear material transport, West Germany, status future aspects 79−31234
nuclear material transportation, ORNL Nuclear Legislative Data Base program 80−37539
nuclear materials, safeguards against theft or diversion 77−23213
nuclear power stations, fuel circuit review, radioactive conditioned waste final storage *(German)* 80−799
nuclear safeguards for control and accounting, NRC program 79−85619
nuclear spent fuel shipping cask licensing 80−37545
nuclear waste transportation, DOE transportation technology centre 80−37537
offshore disposal of dredged material, sediment props. as tracers 77−5245
photographic emulsion spreading, electric drive operational principles *(Russian)* 77−79172
plastics testing, automation 80−76443
pneumatic system for transferring radioactive samples at Savannah River Laboratory 80−68794
pneumatic transport of granular material 79−72927
portable glove box system, HFEF/N 79−45440
postirradiation examination facility 80−18682
power, charged, electrostatic spark hazard identification and control 80−69291
pulsed neutron physics facility, remote operation and maintenance 79−45465
PWR assemblies, pool-site fuel inspection and exam. techniques 80−18567
PWR fuel dissolution, Idaho processing plant remote systems 79−45455
radiation process control 77−67903
radiation processing, conf., Dorado Beach, Puerto Rico (May 1976) 77−67902
radioactive contact-handled transuranic waste transportation 80−37538
radioactive fuel and waste, review of treatment handling, storage and disposal *(Italian)* 79−63753
radioactive fuel storage, air-cooled, Canadian canister program 80−5253
radioactive fuel storage, dry, with air cooling 80−675
radioactive high level waste, retrieval system design, Hanford 79−45380
radioactive material transport, statistical anal. of low-radiation packages 77−88286
radioactive material transport, USA experience 79−31236
radioactive materials, reactor fuel transport requirements, Poland 79−31232
radioactive materials, remote handling, history at Los Alamos 80−78417
radioactive materials, transportation, safety aspects 79−67968
radioactive materials transportation, safety anal. 79−63814
radioactive sources, dry storage pit design 78−13248
radioactive waste, conditioning and storage costs estimation *(Italian)* 78−25303
radioactive waste, packaging containers, a survey 80−23097
radioactive waste, treatment and disposal methods *(German)* 80−57868
radioactive waste calcining facility, process filters, remote handling system 79−45382
radioactive waste calcining facility, remote maintenance equipment 78−13263
radioactive waste isolation repository, material control and accountability 79−85682
radioactive waste management, dismantling of PWR 80−27756

materials handling continued
reactor fuel reprocessing, remote handling experience, Windscale 79 45456
remote decontamination facility and repair station for hot-cell manipulators, Whiteshell, Canada 79−45453
remote manipulation in reactors by MA-23 bilateral servomanipulator system 77−50314
remote systems and maintenance, Japanese nuclear fuel reprocessing plant 79−45457
safety, use of electronic self-monitoring seal 79−85690
security, near-real-time accounting of strategic nuclear materials during reprocessing 79−85755
seismic response of flexible cylindrical liquid storage tanks 79−31241
slab tanks for criticality control, neutron multiplication calc. 80−13606
SOLASE, tritium pathways and handling problems in a laser fusion reactor 79−36411
solid neutron shield development, materials eval. for spent fuel shipping cask 80−13939
solids in mass flow bins, pressure prediction using minimum strain energy 77−35221
spent fuel storage, remote underwater rack removal and installation 78 21729
spent fuel storage expansion, planning, site preparation, installation considerations 79−45381
spent nuclear fuel shipping casks, R and D sea going vessel requirements 79−31083
spent nuclear fuel transport problems *(Russian)* 79−31084
temporary confinement structures, design criteria and guidelines 80−18683
Tokamak experimental power reactor, remote maintenance considerations 79−45418
Tokamak fusion test reactor, in-vessel maintenance remote manipulator system 80−18611
Tokamak fusion test reactor remote maintenance 79−45419
Tokamak next generation reactors, remote servicing considerations 79−45422
Tokamak power reactors, remote system requirements 79−45423
transport of nuclear material, especially nuclear fuel *(German)* 78−25314
tree form energy plantations, woodchip transport and handling 80−30327
two-phase servo master-slave manipulators, triac output control system 79−9213
UK reactor fuel reprocessing plant remote handling experience 79−9839
ultrahigh vacuum sample transfer system, for Auger analysis 79−80628
underground solidified high-level radioactive waste retrieval system development 79−9818
vacuum furnace, regulated particle-delivery system 78−21139
vacuum multistage sluice-gate loading devices 78−60576
weighing, automatic, application in ceramics industry 80−95074
weight handler, for piston gauge 78−8399
Zircaloy-UO_2 fuel rods, eddy-current testing of claddings using encircling and probe coils 80−21245
H, cryogenic storage and refuelling for automobiles 80−30604
H_2 fuel, safety anal. 79−74552
^3H, austenitic stainless steel embrittlement by He 80−102285
He liquid, safety aspects for cryostats and storage containers 79−58730
^{85}Kr, pressurised cylinder storage tests 80−5269
N_2, liq., decanting siphon using self-opening valve 80−57310
Na, contaminated, packaging and storage 80−18468
Pu fuel research facility for advanced LMFBR fuel *(Japanese)* 78−29624
Pu, high burnup fuels, shielding and handling problems 80−27833
Pu, transportation, effect on environment, evaluation study *(French)* 80−27785
$Pu(NO_3)_4$ solution concentrator equipment for criticality safety 80−18432
PuO_2 air transportable package PAT-1, dose rate and criticality calcs. 80−13938
^{238}Pu fuel form facility, Savannah River 79−45396
SF_6 purification in const. temp. adsorption process, appl. to electrostatic accelerators 78−29672
T facility at Lawrence Livermore Laboratory, quality assurance of systems 77−50297
T, handling facilities in US and Europe *(Japanese)* 79−9895
T handling systems, Monsanto-Mound Laboratory eng. development 77−50295
T transport, storage and disposal, charact. of metal tritides 77−54343
$(U,Th)O_2$ fuel rods, analytical stressing in hot cell 80−18566
U refining and decay processes, radioactive waste *(Dutch)* 80−21418
U-Al, storage of unirradiated fuel in borated concrete, criticality safety anal. 80−13608
UF_6, ^{235}U enriched, moderation control 77−65315
$UO_2(NO_3)_4$, secondary criticality control, use of chlorinated PVC piping 80−13607
$^AUO_2(NO_3)_2$, a=233, 235, slab tanks for criticality control, neutron multiplication calc. 80−13606
^{127}Xe, handling and dispensing technique 78−85378

materials preparation
see also crystal growth; hot pressing; powder metallurgy; powder technology; sintering; vulcanisation
actinide metals and their refractory cpds., synthesis from oxides and single cryst. growth 80−16229
γ− active pellet fuels, conceptual design of remotely operated plant for fabrication 80−32340
alkali metal indates and thioindates, prep. and physicodem. props. 80−35517
alloy colour and colour stability as alloy design criteria 80−101005
amorphous alloys, prep. by high rate sputter deposition *(Japanese)* 79−95971
amorphous materials, prep. techniques *(Japanese)* 79−43169
amorphous thin films, prep. from melt using roller-plate technique 80−71607
anatase fibres, synthesis from K_2TiO_3 fibres under hydrothermal leaching 79−56949
book, annual review of materials science 79−65985
ceramic, quartz glass based, organosilicon binder, spalling-resistant, prod. 80−40313
ceramics, development from organosilicon polymers by heat treatment 80−81014
ceramics, manufacture using waste glass fibres 80−40304
ceramics, prep. from metal-organic compounds 77−55922
ceramics, rare earth elements use as dopants *(Polish)* 80−97455
chaoite, a new allotropic form of carbon, produced by shock compression 80−80997
chlorination of Cu and Zn in Cu converter slag 80−20840
clay sample preparation for X-ray diffr. anal. 80−97647
composite materials preparation under microgravity conditions, stability during melting, thermal soak, solidification *(German)* 80−7521
composites, advanced, design, applications and test methods 80−77550
condensation of highly conc. dispersions, to give strong materials 80−40274
corundum refractories, production and performance 80−20866
crossed fields nitriding in air atm. 80−84867
diamond, synthesis *(Japanese)* 80−80994
diamond, synthesis and characterisation 80−50580
diamond production by C shock compression 80−11613
dispersion hardened metallic materials, production *(German)* 80−50646
dispersion-hardened materials, production *(German)* 80−45316
droplets in oxidizing slag, decarburization, rate limiting step 79−56944
dynamic stabilization of multiphase media subjected to vibrations under low gravitation conditions 80−7511
emulsions, dielec. and mag., prep. 78−3376
Eu-Ag alloy, amorphous, formation and mag. props. 79−91216
ferrites, soft, production and props. 80−88801
ferromagnetic thin film magnetometer, development and performance 80−31808
fibre growth, flow induced form. of long fibres, engineering model 79−78927
fibre reinforced composites with high work of fracture 80−81029
fibre reinforced plastics, preparation by pultrusion 79−95995
GFRP sheet moulding compound, influence of cure time restrictions, on minimum weight design of double layer panels 80−11623
glass, rare earth elements use as dopants *(Polish)* 80−97455
glass ceramic slag, white Cl containing, synthesis 78−52748
glass fibre, preparation, appl. in Portland cement reinforcement, alkali resistance 80−81019
glass fibre reinforced plastic, radial orientation of reinforcement for high strength shell 79−95994
glass fibre reinforced plastics, automated production methods 80−25651
glass fibres, and spheres, production and characterisation for microanalysts 79−24487
glass fibres, strength, forming conditions influence 80−20882
glass raw materials, and batch prep. 78−3085
glasses, prep. from metal-organic compounds 77−55922
glassy C bodies, prep. from phenolformaldehyde resin 79−83145
granulation, by dehydration of solns. and suspensions in a fluidised bed 80−81373
graphite fibre epoxy laminates, low thermal expansivity, design considerations 80−81031
graphite fibre filled phthalocyanine composites, cure cycle investigation 80−81030
graphite intercalation cpds. with AsF_5 and SbF_5, synthesis and elec. props. 80−70781
PAN graphite-Al composites, liquid metal infiltration process and interface barrier coatings 80−11779
graphite-alkali metal lamellar cpd., reversible intercalation of tetrahydrofuran 80−16211
graphite-Li compounds, prep. *(French)* 80−2970
Hayes alloy no.716, Fe-Cr-Ni-Co-W-Mo-Si-C-B (26, 22, 12, 3.5, 3, 1.2, 1.1, 0.4 wt.%), hardfacing alloy 80−100802
heated porous body, impregnation with viscous liquid 80−79392
high pressure technology in materials development *(Japanese)* 80−84863
intercalation compounds, synthesis, review *(French)* 78−27429
laminar compounds, prep. *(French)* 78−27445
latex solids, agglomerating and dewatering 80−104470
liquid crystals, prep. and phys. props., book 80−105444
metal composites, powder filled, production in space 78−52726
metal particles, small, characterisation and props., book contrib. 80−84417
metal refining by fractional melting 79−61537
metal refining by fractional solidification 79−61536
metallic filament production, by molten Pb ejection *(Japanese)* 78−52719
metallic filaments, prep. from birttle high-strength materials *(Russian)* 77−59712
metallic glass manufacture, struct. and stability 79−14687
metals, prep. by electromagnetic levitation in ultrahigh vac. 80−29899
metastable alloy formation 79−14828
methanol derivation from lignite, fuel appl. 80−61223
mineral fibres, production method *(German)* 78−19678
Nb, pure, production by carbothermic reduction-electron beam melting combination method 80−89177
niobate based ceramics, synthesis, struct., elec. cond., mag. props. *(Czech)* 80−45259
opal glass, chemically toughened, prep. and mech. strength *(German)* 80−89191
parylene polymers, synthesis, props., significance *(German)* 78−64521
periclase, fused, and periclase-chromite blocks, produced from beneficiated starting meterials, struct. and props. 79−87600
plasma chemistry of heterogeneous systems 80−61100
plasmochemical synthesis, powdered infusible compounds, props. 80−55330
plastic track detechns, proton-sensitive CR-39 thin sheets, production method 80−35155
PMMA, cross-linked positive electron resist, synthesis and props. 80−76221
polyaluminates of alkali metals, synthesis using solar-high temp. installation 78−84746
polydifluoroacetylene, electronic struct., tight-binding LCAO-SCF-MO calcs., prep. 80−70591
polyester resin, cross-linked unsaturated, synthesis and fracture toughness 80−93634
polyethylene fibre prod. by surface growth method, mech. props. 80−104108
polyethylene filaments, ultrahigh-strength, from soln. spinning and hot drawing 80−45268
polyfluoroacetylene, electronic struct., tight-binding LCAO-SCF-MO calcs., prep. 80−70591

materials preparation continued
polyfluorocarbon, synthesis and props. 78−23657
polymer, and polymer composite high temp. materials, production and props., pt. II *(Russian)* 79−8269
polymer, and polymer composites high temp. materials, production and props., pt. I *(Russian)* 79−8268
polymeric biomedical materials 79−83998
polypropylene fibrillated film reinforced cement matrix for low cost sheeting 80−80996
polypropylene rods, prep. by die-drawing 80−45327
polyurethane, quick;hardening, possible use in endoprosthetics, synthesis 78−6887
radiation processing, conf., Miami, FL, USA (Oct. 1978) 80−36772
rare earth metals, preparation methods and properties, review 79−69969
rare earth oxyphosphates, x Ln_2O_3.y P_2O_5, synthesis, characterisation and thermal stability 80−16256
rare earth perovskites and garnets, prep. and props. book contrib. 80−44193
rare earth pyrochlores, $R_2(V_{4/3}W_{3/3})O_7$ (R=Gd, Tb, Dy, Ho, Er, Tm, Xb, Lu), synthesis and elec. props. 80−29914
(rare-earth)$_2$ MoO_5, prep. *(French)* 78−76618
rare-earth-SbO_4, low temp. forms, production 78−47300
raw material acceptance testing for dielectric applications 80−97646
refractory borides, carbides, nitrides, manufacture and appl. in electronic and electrotechnic field *(French)* 80−40311
refractory compound fibre reinforced cpd. materials, diffusional reaction, effect of alloying calc. 80−20851
refractory compounds, refinement processes occuring during prep., by self propag. high temp. synthesis 78−60634
refractory filaments, viscous-sheath, production 78−3077
resin matrices and their contribution to composite properties 80−81028
rocket borne low-gravity programmes, conf., Bournemouth, England (Aug. 1980) 80−105433
serandite, synthesis and physicochem. props. 79−43187
sheet moulding compound, material, process and performance 80−81032
silicates, layered, not containing Al, synthesis and cryst.-chem. props. 78−51495
sitalls, synthesis based on elec. power plant residues 80−40314
skutterudite related compounds, prep. and charact. 78−52700
steel, austeritic (08KH18N10T), heat treatment and heavy plate prod. for fission reactor appls. 80−66454
steel, bar, and wire rod, small sample prep. and spectrometric anal. *(German)* 80−93704
superconductors, technical, development and manufacture *(English, German)* 79−19707
target preparation of aqueous samples for XFA and PIXE 79−87915
TCNQ salts with heterocyclic amines and hydroquinone form. via redox reaction 80−26013
tetraphenyldithiadipyranylidene-iodine, synthesis and cond. props. 80−24910
thermoplastic films, high modulus, prep. 79−100105
transition metal hydrides, synthesis and physicochemical props., conf., Moscow, USSR (Jan. 1978) 80−27032
transition metal silicides, self-propagating high temp. synthesis 80−2988
transition metals processing and appl., using vacuum technology *(Hungarian)* 80−55318
transuranic chalcogenides and pnictides, prep. and cryst. chem. 80−16255
Vycor glass, manufacture, struct., physical and chem. props. 80−7527
zero gravity material properties and preparation, cryst. growth, prod., and rare earth synthetic mag. materials *(French)* 79−83111
β-2CaO-SiO_2, hydration mechanism and rate, SEM and chem. anal. 79−79218
3CaO.SiO_2, hydration in presence of lignosulphonates, glucose, Na gluconate 79−100330
3CaO.SiO_2 pastes, structural props., curing temp. effect 79−100332
Ag_2TeO_3 chem. prep. and cryst. struct. *(French)* 80−79755
Al alloy, high strength, multicomponent, development *(Bulgarian)* 79−15628
Al alloy-mica particle composite, cast prep. and mech. props., bearing appl. 80−71613
Al-Pb alloy, production under microgravity hodes *(German)* 79−38766
Al-steel composites, prep. and props. 78−3075
AlN powders, synthesis and impurities 80−55329
Al_2O_3 ceramics, with thermoplastic bond, prep. 80−45254
Al_2O_3 compounds, shrink free, prod. method using slips made from clay, orthophospheric acid 80−66460
β Al_2O_3, fabrication methods 79−78916
α-Al_2O_3 fibre FP, manufacture, strength and modulus 80−81013
α-Al_2O_3 fibre FP reinforced Al and Mg composites, fabrication and props. 80−81004
Al_2O_3 porous refractories, production 80−35149
Al_2O_3, prep. from purification of technical gibbsite *(German)* 79−100091
Al_2O_3, transparent polycrystn., produced by sol-gel method *(Japanese)* 78−19698
β-Al_2O_3-D_2O, anhydrous, prep. and struct. of $DAl_{11}O_{17}$ 80−107187
β''-Al_2O_3-Na_2O tubes, fabrication from cast ceramic tape 80−60819
Al_2O_3-Ni cermets *(French)* 80−20877
$Al_2O_3.SiO_2.H_2O$, new materials from pianlinite minerals *(Chinese)* 79−95982
$3Al_2O_3.2SiO_2$, mullite, synthesis by freeze drying 80−16252
B fibre, prep. in closed CVD system 79−83129
B fibre reinforced Al VKA-1 composite, fibre/matrix interface reaction during prep. 80−25619
B fibres, prep. techniques 79−28983
B-Si compounds, thermoelec. material, prep. by pyrolysis of BBr_3-$SiBr_4$ mixture 80−20862
B_4C, synthesis in HF EM field 80−20864
BN composites, polymer impregnated 80−7526
BN, cubic, high pressure synthesis using water, urea and H_3BO_3 acid catalysts 79−83160
BN, hexagonal, production technique from CaB_6 *(German)* 79−74121
BN, hexagonal, survey of production, props. and uses *(German)* 79−74120
B_2O_3-containing ceramic glaze, neutron probe anal. for control of prep. process *(Polish)* 80−97751
$BaCa_2Mg(SiO_4)_2$, synthesis and X-ray characterisation 78−22698
$BaCuO_2$, prep. and study *(French)* 77−43201
$BaGeO_3$-(0.25$MgF_2$0.75YF_3)-Ga_2O_3 system, synthesis and props. 80−25648

materials preparation continued
$BaPO_3F$, prep. and props. 79−52147
$BaTiO_3$, prep. from coprecipitated $BaCo_xBaF_2$-TiO(OH) 77−24996
BeF_2, water-free vitreous, prep. and props. 79−66033
$Be_4Ti_2O_{12}$ grain oriented ferroelectric ceramic, prep. by molten salt synthesis-tape casting method 80−40296
Bi_2Te_3-Bi_2Se_3 thermoelectric alloys, diffusion and evaporation of volatile component during prep. 80−35118
Bi_2WO_6 grain oriented ferroelectric ceramic, prep. by molten salt synthesis-tape casting method 80−40296
C fibre composite, aligned, prep. and theoretical strength agreement 80−84906
C fibre reinforced composites for spacecraft use, prep., props. and struct. 80−71625
C fibres, engineering applications, production requirements and mech. props. 80−89168
C fibres, production from coal tar pitch *(German)* 78−44033
C molecular sieves, prep. by pore blocking 78−15324
$CaCeAl_3O_7$, melilite struct., prep. and props. 80−93524
CaO-SiO_2 glass prep. by gel method 80−100824
CaO.SiO_2 pastes, structural props., hydrating cmpd. effect 79−100331
$Ca_5(PO_4)_3OH$, prep. from sulphate, X-ray diffr. and IR spectrosc. 80−29893
β-Ca_2SiO_4-CaO-SiO_2 paste, hydration, compression strength and composition 80−50584
Ca_3SiO_5, formation by solid state reactions 78−56602
$CaTiO_3$, prep. from film forming soln. 80−60811
CdO-P_2O_5 glasses, prep., density, elec. and optical props. 79−70033
CdO-ZnO-P_2O_5 glasses, prep., density, elec. and optical props. 79−70033
CdS, rock-salt type high-press. phase synthesis using metal sulphide additives 80−104084
CeO, high press. synthesis, struct. and lattice consts. *(French)* 80−29913
CeO_2-Y_2O_3 solid soln. phases, synthesis 80−104132
Co, leaching, system geometry effects, mass transfer controlling case 79−61535
Co_xZrS_2, ($0<x\leq0.50$), intercalation compounds, ordered phases obs. 80−33962
Cr, high-purity, production by bis(ethylbenzene) chromium thermal degradation *(Russian)* 80−35128
Cr-Fe-C (28.4, 9.1 wt.%) prep. from $FeCr_2O_4$ chromite 80−100804
$Cr_{1-x}Fe_xOOH$, $0\leq x\leq10$, prep., Mossbauer effect, Neel temp. 80 108134
CrO_2, oxidative prep. method, mag. props. 80−44863
$Cr_{1-x}Rh_xO_2$, oxidative prep. method, mag. props. 80−44863
$Cs_3R_2X_9$ (=Sc,Y,Ho-Lu, X=Cl and R=Sc,Sm-Lu, X=Br), prep. and Guinier-Simon X-ray study 80−49204
Cu production, and developments in extractive metallurgy in 1978, review 80−20821
Cu, selective recovery from Ca-Ni sulphides by segregation technology 79−61534
Cu, suspension electrolysis 79−61542
Cu-Ga porous solid formed by shock compression 80−29905
Cu-Mg-Fe-O system, solid solns. spinel, synthesis, struct. and mag. props. 79−52142
$CuF_2.2H_2O$, synthesis, appl. for carrier-distillation emission spectroscopy 80−89164
Cu_xMS_2, ($0<x\leq0.50$) (M=Zr, Hf), intercalation compounds, ordered phases obs. 80−33962
$Cu(Mo_2Re_2)S_8$, synthesis and electrical props. of mixed tetrahedral cluster phases 80−2971
CuO-CdO-Fe_2O_3, sintered ferrite, preparation, mag. susceptibility, DC resistivity 80−34598
CuO-ZnO-Fe_2O_3, sintered ferrite, preparation, mag. susceptibility, DC resistivity 80−34598
$CuRTe_2$ compounds, synthesis and investigation 78−26529
Dy chalcochromites, prep. and props. 78−43390
Dy_xB_y, prep. and props., DTA study 80−20859
$3Er_2O_3$-Ta_2O_5, refractories 77−48384
$EuBr_{1.5}Cl_{0.5}$, preparation and characterisation 79−77571
Eu_2O_3-Y_2O_3 solid soln. phases, synthesis 80−104132
$Eu_5(PO_4)_3OH$, prep. from sulphate, X-ray diffr. and IR spectrosc. 80−29893
$Eu_3VTa_2O_9$, perovskite, prep., characterisation and mag. props. 78−26535
Fe complex, $FeOCl\{(ethyltetramethylcyclopentadienyl)_2Fe\}_{0.16}$ synthesis and struct. 80−44176
Fe, white cast, lamellar, prep. and morphological study *(French)* 79−43168
Fe-B(-Si) alloy filaments produced by glass-coated melt spinning 80−76213
Fe-Si-Al, Sendust, ribbon-form, prep. by rapid quenching, mech. and mag. props. 80−71611
$Fe(Mo_2Re_2)S_8$, synthesis and electrical props. of mixed tetrahedral cluster phases 80−2971
Fe_2O_3, powders, prep. conditions effect on morphology 77−8777
Fe_3O_4 aqueous mag. fluids, dilution-stable, prep. by extended peptization techniques 80−60373
Fe_3O_4, Co modified, synthesis with autoclave in H_2 atm. 80−35117
Fe_3O_4 precipitated with urea, prep. and props. 80−20854
γ−Fe_2O_3 small particle composites, low optical density, superparamag., prep. and charact. 78−60315
δ-FeO(OH) and its solid solns. synthesis, X-ray diffr. and TEM studies 80−29891
$FeTiO_3$, ilmenite, prep. at focus of solar furnace *(French)* 80−29908
Fe_xZrS_2, ($0<x\leq0.50$), intercalation compounds, ordered phases obs. 80−33962
$Ga(Mo_2Re_2)S_8$, synthesis and electrical props. of mixed tetrahedral cluster phases 80−2971
GdB_{12} high pressure synthesis 78−18608
Ge compounds, with gehlenite struct., synthesis 79−43181
Ge-S-Cu, phase separation in melt centrifugal quenching 80−25701
n-$Ge_{20}Bi_{10}Se_{70}$ glass, preparation and elec. props. 79−74126
GeO_2, amorphous, obtained by hydrolysis of $GeCl_4$, exam. of props. 79−95956
HfF_4-BaF_2-LaF_3 glass system, IR transmitting, synthesis and props. 80−71623
HfF_4-BaF_2-ThF_4-(ZrF_4) glass system, IR transmitting, synthesis and props. 80−71623
$K_2Cr_2V_6O_{16}$, hollandite type, synthesis 79−11543

materials preparation continued
$KHgC_4$, and $KHgC_8$, intercalation cpds., synthesis and struct. 80−44183
K_2O-Fe_2O_3 phosphates, condensed, synthesis in phosphoric acid melts 79−1837
$K_2Ti_4O_9$ fibres, synthesis by kneading-drying-calcination process *(Japanese)* 79−38779
$K_2V_8O_{16}$, hollandite type, synthesis 79−11543
La-Si-As ternary cpd., synthesis, stoichiometry 80−104083
$La_{2-x}A_{1+x}Cu_2O_{6-x/2}$ (A=Ca, Sr), synthesis and characterisation *(French)* 80−104085
$La_{76}Au_{24}$, disordered ribbons, quenched samples production using arc furnace 80−71612
LaB_6, synthesis by heating BN with lanthanum citrate hydrate 80−100819
$LaCrO_3$-W(Mo)(Cr) eutectics, prep. and microstruct. 80−108380
$La_{70}Cu_{30}$, disordered ribbons, quenched samples production using arc furnace 80−71612
$LaLi_{0.5}Ir_{0.5}O_3$, perovskite, prep. and mag. study 80−80486
La_2S_3-Ag_2S-Ga_2S_3 glass system, prep., thermal and elec. props. *(French)* 80−89192
La_3Sn, cubic phase, synthesis at high pressures and temps. 78−19687
Li-graphite intercalation compounds, synthesis and props. 79−74108
Li-pyrographite intercalation cpds., synthesis and elec. resist. 79−91601
$LiAlO_2$, fine particle size, heat treatment synthesis, molten carbonate fuel cell appl. 80−21395
$Li_2O.2SiO_2$, prep. from film forming soln. 80−60811
LiSiON, tetrahedral bianionic, allotropic forms, prep. *(French)* 78−63726
$LiTi_2O_4$, single-phase, prep., crystal struct. and superconducting transition characts. 80−50583
$MgAl_2O_4$, formation from amorphous substance prepared by homogeneous precipitation method *(Japanese)* 79−56950
$MgCaH_{3.72}$, synthesis *(Japanese)* 78−84751
MgF_2, synthesis for optical ceramic 78−52729
MgO-ZnO-Fe_2O_3, sintered ferrite, preparation, mag. susceptibility, DC resistivity 80−34598
Mo cluster compounds (Chevrel phases), synthesis and supercond. *(German)* 80−2503
Mo-Re, prep. from reduction in Mo-Re-O system *(Russian)* 80−16225
$MoCr_2O_6$, prep. in hydrothermal environment under high pressure *(French)* 78−35342
MoS_2, prep. and mag. props. *(French)* 80−93072
MoS_3, prep., use as Li battery cathode 80−29892
Mo_6S_8 Chevrel phases with group IIIa metals, Nb, Hg, Pb and Cu, synthesis, stability and characts. 80−71608
$MoSCl_4$, prep. and characterisation 77−59705
$Na_{5-x}Li_xErSi_4O_{12}$, solid electrolytes for Na/TiS_2 cells, synthesis, characts. and utilisation 80−107518
Na_2O-CaO glass, abrasion-resistant, high strength 80−76369
Na_2O-SiO_2 glass, fusion process study, EMF meas. *(French)* 80−89190
$Na_2O.SiO_2$, prep. from film forming soln. 80−60811
$Na_4R(WNb_2)O_9F_5$, (R=Y, Nd, Eu, Gd, Dy, Lu), synthesis, cryst.-chem. and dielec. study *(French)* 80−108164
Na_2TeO_3, chem. prep. and cryst. struct. *(French)* 80−79755
Nb, fabrication by carbothermic reduction-electron beam melting combination *(Japanese)* 79−100075
Nb-Mo, prod. by simultaneous carbothermic reduction of oxides/electron beam melting method *(Japanese)* 80−11590
Nb-N(O)(C) system, specimen prep. for metallography *(German, English)* 80−89439
Nb_3-Sn-Cu composites, superconducting fabrication 80−11602
Nb_3Au diffusion layers, superconducting, prep. 79−1834
$NbSCl_4$, prep. and characterisation 77−59705
Nb_3Si A15 struct., high press. synthesis *(Chinese)* 80−70917
Nb_3Si, metastable A-15 struct. synthesis by ion implantation, supercond. transition temp. 80−55319
Nb_3Sn superconductors, multifilament, produced by ECN method 79−33975
Nd_3PO_7, prep. and luminesc. props. 80−34964
$Ni(Mo_2Re_2)S_8$, synthesis and electrical props. of mixed tetrahedral cluster phases 80−2971
$Ni_{0.38}Zn_{0.62}Fe_2O_4$, preparation, Mossbauer study 80−50231
Ni_xZrS_2, ($0<x\leq0.50$), intercalation compounds, ordered phases obs. 80−33962
Pb bullion production, elec. smelting of $PbSO_4$ residues 80−11592
Pb-Se-As-Ge, phase separation in melt centrifugal quenching 80−25701
PbF_2-AlF_3 glass, optical props., crystn. and thermal expansion 80−48367
Pb_2MoO_5, form. conditions 80−20853
$Pb_5(PO_4)_3OH$, prep. from sulphate, X-ray diffr. and IR spectrosc. 80−29893
$Pb_{1-x}Sn_xTe$, polycryst. powder, low temp. prep. in PbI_2 flux 79−61524
Pb_2TaMnO_6, reaction of form. from oxides, ferroder. props. 80−55326
$Pb(Zn_{1/3})O_3$, perovskite type, high temp. high pressure synthesis *(Chinese)* 78−68654
PrO, high press. synthesis, struct. and lattice consts. *(French)* 80−29913
$Rb_2Cr_8O_{16}$, hollandite type, synthesis 79−11543
$RbHgC_4$, and $RbHgC_8$, intercalation cpds., synthesis and struct. 80−44183
ReS_2, prep. 79−38774
RuS_2 amorphous, prep. at ambient temp., magnetic structure 80−35119
$Sb_2O_5.nH_2O$ acid membranes, synthesis and characterisation 80−81027
Si, hyperpure, large scale production 78−95704
Si solar cells, production process effect on fracture strength 80−93656
Si, solar grade, prod., using Dow Corning process 80−29894
Si-Na-B-O-N glass, synthesis and characterisation 80−108381
SiAlON powder, prod. by reaction clay+C+N_2 80−40295
SiC fibre, development from organosilicon polymers by heat treatment 80−81014
SiC fibre, with high tensile strength, synthesis of polycarbosilane as precursor 79−15633
SiC fibre reinforced Al, synthesis by liquid pressing method 80−100816
SiC fibres obtained from polycarbosilane fibre 80−50582
Si_3N_4, finely dispersed, high-temp. synthesis 80−55331
Si_3N_4, pyrolytic, prep. by CVD, bulk and coatings, exam. of electrical, optical and physical props. 79−95935
Si_3N_4, reaction-bonded, strength, effect of Si purity in production 80−100902
Si_3N_4, synthesis in Cl_2 system 80−40308
SiO_2 glass, formation by hydrolysis of $Si(OC_2H_5)_4$ with NH_4OH and HCl soln., and characterisation 80−71622

materials preparation continued
SiO_2:Al_2O_3, ultrafine and ultrapure powder prep., SEM study 79−70025
SiO_2-$NaAlSiO_4$ glasses and devitrificates, prep. and vibr. spectroscopy study *(Polish)* 80−93530
Sm, high purity production *(Russian)* 79−70012
SmB_2, high pressure synthesis 78−18608
SmS-based alloys, prep. and props. 78−44034
Sn-Pb, refining by fractional solidification 79−61536
$Sr_5(PO_4)_3OH$, prep. from sulphate, X-ray diffr. and IR spectrosc. 80−29893
$SrFe_{12}O_{19}$, high coercivity micropowders, prep. and mag. props. 77−8776
$Sr_xPb_{1-x}(Zr_{0.545}Ti_{0.455})O_3$, piezoelec. resonator, preparation and props. *(Rumanian)* 80−28402
$Sr_2Sb_2O_{12}$, prep. *(French)* 79−32967
$SrTeO_3$, ferroelec. phase, synthesis at ambient temp. *(French)* 79−43190
$SrTiO_3$, prep. from film forming soln. 80−60811
$Sr_3VTa_2O_9$, perovskite, prep., characterisation and mag. props. 78−26535
Ta-N(O)(C) system, specimen prep. for metallography *(German, English)* 80−89439
TaN, cubic, formations by heating TaN in N-Ar plasma jets 78−84726
$TaSCl_4$, prep. and characterisation 77−59705
Tb chalcochromites, prep. and props. 78−43390
Ti complex, $TiOCl[Co(cyclopentdienyl)_2]_{0.16}$, synthesis and struct. 80−44176
Ti-Cr-B system, self-propagating high temp. synthesis, crystallochemical and mech. props. 80−20861
Ti-H, deposited on carriers, synthesis, structure and catalytic props. 80−29890
Ti_2AlN, prep. and props. 77−28745
TiB_2, electric arc melting prep. and oxidation props. 80−20860
TiB_2, preparation method rel. to compressive strength 80−55327
TiN formation, from TiO_2/Si_3N_4 reaction in N_2 atmosphere 80−71617
TiN, self-propag. high-temp. synthesis under high N_2 pressures 80−25630
TiN_2, ultrafine synthesis in RF plasma, X-ray diffr. chem. and electron microscopy anal. 79−70026
Ti_2O_3, prep. method *(French)* 79−10095
TiP, TiP_2, iodide synthesis, and catalytic props. of TiP 80−55316
$Tl_2Cr_2O_7$, $Tl_2Mn_2O_7$, pyrochlore type, synthesis and physical props. 80−33963
$(U,Pu)O_2$, FBR fuel pellets, gel-supported precipitation conversion and prep. 80−813
UCr_2O_6, prep. in hydrothermal environment under high pressure *(French)* 78−35342
UFe_2O_6, prep. in hydrothermal environment under high pressure *(French)* 78−35342
UI_6-alkali metal halide system, prep. 80−50568
UMn_2O_6, prep. in hydrothermal environment under high pressure *(French)* 78−35342
$U_2O_2Cl_5$, prep. and cryst. struct. *(French)* 80−84150
V complex, VOCL $[Co(cyclopentadienyl)_2]_{0.16}$, synthesis and struct. 80−44176
V-N(O)(C) system, specimen prep. for metallography *(German, English)* 80−89439
$V_2O_{3-x}F_x$ ($O<X<0.3$), prep. and some phys. props. 78−76619
$VSCl_4$, prep. and characterisation 77−59705
$VSe_{2-x}S_x$ ($0<x<2$) solid solutions, characterisation 80−88730
$V_{1x}Ti_xO_{1.75}$(x=0-0.1), synthesis and mag. props. 78−23243
W powder, prep. by WO_3 reduction in H plasma jet *(Russian)* 80−76211
W-PVC composites, fabrication rel. to performance 80−76218
W-Ti(Zr)(Hf)-C system, cubic solid solns., formation and props. 78−48348
Y-Si-Al-O-N glasses, prep. and props. 80−25647
Y-subgroup rare-earth sesquisetneides, powders, prep. conditions and optical characts. 77−28771
$YCrO_3$-W(Mo)(Cr) eutectics, prep. and microstruct. 80−108380
$Y_2Cr_2O_7$, $Y_2Mn_2O_7$, pyrochlore type, synthesis and physical props. 80−33963
Y_2O_3, transparent ceramic, manufacture 79−20013
$Y_2(V_{4/3}W_{2/3})O_7$ pyrochlore, synthesis and elec. props. 80−29914
Yb sulphides, synthesis and mag. props. 78−23242
$Zn(Mo_2Re_2)S_8$, synthesis and electrical props. of mixed tetrahedral cluster phases 80−2971
ZnS, high purity, prep. from ZnO *(Rumanian)* 80−76206
ZnS-Na_2O-K_2O-SiO_2, form. using electric furnace, furnace design 80−11620
Zr-Cr-B system, self-propagating high temp. synthesis, crystallochemical and mech. props. 80−20861
Zr-H, deposited on carriers, synthesis, structure and catalytic props. 80−29890
ZrB_2, electric arc melting prep. and oxidation props. 80−20860
ZrB_2 powders, synthesis and impurities 80−55329
ZrC powders, synthesis and impurities 80−55329
ZrF_4-BaF_2-NdF_3 glasses, prep. and optical props. 78−27304
ZrF_4-THF_4-BaF_2 glass, IR-transparent, synthesis using reactive atm. processing technique 80−100826
ZrH_x, synthesis and electron struct., X-ray anal. 80−29889
ZrN_xHy, synthesis and electron struct., X-ray anal. 80−29889
ZrO_2, Y_2O_3 stabilized, heat-resistant granular artifacts, procedure for making 80−35148
ZrO_2-SiO_2 glass fibres, prep. 78−6886
ZrO_2-SiO_2(-Na_2O) glass fibres, prep. from metal alkoxides, resistance to NaOH soln. 80−97454
$ZrSiO_4$, zircon yellow pigment, synthesis *(Polish)* 80−66466

materials properties
this heading is restricted to those properties which are not covered by other specific headings
see also dielectric properties of substances; electrical properties of substances; magnetic properties of substances; mechanical properties of substances; optical properties of substances; thermal properties of substances; thermodynamic properties
annual review of materials science, book 80−46740
book, annual review of materials science 79−65985
book 77−16476
data sources for materials scientists and engineers, book contrib. 79−65986
microstructure depend., book 78−88470

materials properties continued
practicing scientist's handbook 80−2
rare earth compounds, handbook 80−41957
rare earth non-metallic compounds, handbook 80−51972
review of material research for advanced energy technology 79−96429
unknowables in the essence of materials science and engineering 77−4721
USSR standard reference data for metrological services 79−97340
zero gravity material properties and preparation, cryst. growth, prod., and rare earth synthetic mag. materials *(French)* 79−83111
Cu_2S, mats. props. rel. to CdS/Cu_2S solar cells 77−77426

materials testing
see also acoustic applications; corrosion testing; creep testing; dynamic testing; electron beam applications; fatigue testing; fracture toughness testing; hardness testing; insulation testing; mechanical testing; nondestructive testing; notch testing; ultrasonic materials testing
abrasion testing, automatic device for discrete batching small amounts of abrasive suspension 79−87782
abrasive surface quantitative charact. profile meas. system, on-line computer controlled 77−52603
AC test dust, particle size distrib. for filter media testing 78−53060
accelerated method for developing and investig. engineering mats. *(Russian)* 78−53046
acoustic emission, amplitude distrib. anal. 80−66713
acoustic emission, unit for recording and reproduction of signals 80−79039
acoustic emission analysis for vibration and shock testing of industrially produced substances *(German)* 80−3279
acrylic, denture base, tensile testing 80−16621
acute fish toxicity and absorption tests of an experimental detergent builder, trisodium carboxymethyloxysuccinate 79−57184
adhesion measurement, locus of failure, bond failure in adhesive joints 80−50801
adhesion measurement, of thin films, thick films and bulk coatings, conf. Philadelphia, USA (Nov. 1976) 80−46729
adhesion measurement, of thin films, thick films and coatings 80−50817
adhesion strength determ. apparatus for gunite coating on refractory masonry, breakaway tests 78−35618
adhesive bonded joint, new test method for prediction of environmental resistance 78−7102
adhesive bonded surface durability, wedge test 78−31591
aerodynamic tests on thin assemblies, via two-component Si strain-gauge device 78−3263
aggregate particles, concept and test method for unified charact. of geometric irregularity 77−28954
aggregate phase contents, sampling in quantitative image analysis *(French)* 77−28961
airframe material defectometry, quantitative test specifications *(German)* 80−89427
alloy testing for use in heat treatment furnace, disc tribometer with high temp. pin 78−95900
alloys for coal gasifiers, susceptibility to stress corrosion cracking determ. 80−7726
alloys thermal expansion coefficient, and volume effect anomalies during transformations, review of differential dilatometric error sources *(Russian)* 79−34223
ampule for inside fission reactor exam. of materials, examining creep, long term strength in plane stress state 78−85098
animal soft tissue in vitro testing, apparatus review 78−31985
anisotropic materials, determ. of mutual influence coeffs. 77−75862
anodic, and free anodic film on Al substrate, deform.-strength props. *(Russian)* 77−69203
anodic oxide coatings on Al, quality testing *(German)* 77−28943
antifriction materials, device for wear testing 80−21223
apparatus for meas. mech. strength of glazes 78−85067
aramid fibre reinforced epoxy resin, shear props. 77−81354
automatic data processing from static tests on constructional materials 77−4885
automatic experimental control system, exam. of mech. props. under complex stress conditions 78−64802
automatic inspection of materials using lasers 80−66734
automatic test equipment for material props. determ. and quality control 77−86236
autoradiography on thin foils, high resolution, anal. of technique charcts. *(French)* 80−55598
Bauschinger effect, temp. influence, combined tension-torsion testing machine, appl. to Al 80−45453
bending, three point, at large deflections as elastic moduli meas. method 78−27699
bending test apparatus for high press., high temp. 80−85126
bending tests, four-point loading design instrument 77−40498
bias, testing and reduction 79−52541
biaxial flexure test, exam. of loading factors 78−80695
biaxial residual stress distrib., meas. method for determ. throughout workpiece height *(German)* 78−35596
biaxial testing machine, for flat specimens, study of specimen shape *(Japanese)* 77−70268
biocompatibility testing, cell culture and animal test correlation 77−81655
biomaterial evaluation considering species-related haematological differences 77−60291
bituminous mixture, aggregate surface area determ. 77−77689
blind hole method with off centre hole, for residual stress meas. 79−20300
bonded joints, device for automatically recording internal stresses 80−25963
brass, condenser tubes of steam turbine, multipositional apparatus of durability determ. *(Russian)* 77−70247
brass, corrosion and dezincification in water 77−16740
brass (37%Zn), workhardened thin specimens, fracture, anisotropy coeff. role *(French)* 80−104276
bricks, extensometer for meas. of linear expansion due to freezing 78−53062
brittle fracture under biaxial normal stress 78−68869
brittle material, tensile strength determ., based on radial and compression tests 78−7156
brittle materials, load-transmitting medium to measure strength 80−40652
brittle materials, normal elasticity modulus, strain gauge meas. 80−55601

materials testing continued
brittle rod, optimum specimen shape for compression tests, gluing technique effects 80−50797
brittle rod, optimum specimen shape for compression tests, struct. and technological parameters 80−50798
bubble materials characterisation using spatial filtering 77−12175
building product, nonmetallic, first crack determ. device, during load test *(Czech)* 80−45471
building stones, characterizing weathering processes *(German)* 77−86270
bulk material rigidity determ. using capacitive transducer 78−19977
BWR containment vessels of prestressed concrete, pressure tests 80−81254
calorimeter for differential thermal analysis, in temp. range 100-800°C, exam. of design 79−52514
capacitive stress transducer optimum dielectric selection 77−73428
casting method for epoxy tensile coupons for tensile testing 78−72957
casting-pit refractories, quality control, specific non-standardized test development *(French)* 77−90297
castings, economic testing by mag. powder method *(German)* 80−3277
catastrophe theory considerations *(German)* 78−64797
cathode temp. distrib., apparatus for meas. 79−15940
cement mortar, cured by 28-day standard and accelerated methods, strength correlation 77−16762
ceramic, automatic structure analyser, EPIQUANT, quant. microscopic meas. 79−83409
ceramic, proof testing 80−108654
ceramic, thermal shock resistance determ., new heat flux method *(Japanese)* 79−39075
ceramic building materials, high-temp. microscopy interpretation *(Polish)* 80−66743
ceramic components, design criteria and structural testing 79−39083
ceramic composition rheological meas. device for 20° to 90°C and constant moisture content 78−85079
ceramic layers on metallic substrates, mech. props. meas. *(French)* 80−104375
ceramic materials, SEM and anal. techniques *(German)* 78−56832
ceramic mineral, exam. by X-ray diff. at high temp. *(French)* 79−96234
ceramics, bending test results processing 80−97672
ceramics, cracking characterisation by double torsion test *(French)* 80−104369
ceramics, mech. props. meas., apparatus for up to 1700°C *(French)* 80−104374
ceramics, mech. test apparatus for up to 2200°C *(French)* 80−104372
ceramics, strength and deformation testing, wide temp. range, universal apparatus 79−57177
ceramics, surface cracks, acoustic surface wave meas. 80−61055
ceramics, thermal stress and thermal shock, review of test methods, thermal stress theory industrial problems 77−63805
charcoal filters, NDT of residual adsorption capacity 80−89523
cladding layers on metal, tear resistance, method of determ. 77−25211
clays and ceramics, plasticity determ. using drying process and shrinkage 79−20307
coating thickness gauges 77−63839
coherent-optical materials testing for vibration pattern and defect discrimination *(German)* 80−30181
coke, metallurgical, microstruct., using refl. light microscopy and image anal. 80−66732
COMECON standard reference-data system 80−45469
compact gas gun for materials testing 79−15909
complex dielec. and mag. props., modified von Hippel least square fit determ. 78−21179
complex dielectric constant meas. of thin foils in mm-wave region, method *(German)* 79−58755
composite, component bonding strength, apparatus, results 77−4887
composite flat-belt-drive materials, testing of birefringent coatings 77−77652
composite insulating materials, fatigue behaviour, influence of superposition of elec., mech. and environmental stresses 80−97590
composite laminates, proof test and fatigue study 80−93643
composite material, ring under one sided heating, strength testing assembly 79−96260
composite materials, laser beam determination, of elasticity-compressibility modulus, during compaction 79−43542
composite materials, universal chamber for high temp. strength testing up to 2000°C 77−63858
composite materials under complex stress-state conditions, mech. props., method for studying 80−50799
composite structures, fracture initiation prediction 80−11870
composites, thermal stresses investigation, using polymer models 80−40639
composition and structure of engineering and industrial materials, instrumentation 77−4882
computer based data acquisition and control, model 77−63844
concrete, accelerated curing procedures adoption 79−5091
concrete, core strength, effect of length to diameter ratio 77−63861
concrete, heat resisting, exam. of deform. behaviour, description of testing rig and operation *(French)* 79−15720
concrete, ionic conductance meas. by automatic instrument 77−77659
concrete, tensile strength determ. under impulse loading *(German)* 79−15919
concrete, tensile testing apparatus 79−96241
concrete, tensile testing device, axial 80−61054
concrete bearing with steel inserts in precast column to beam connections, load capacity determ. 77−73427
concretes, further development of 2 point test for workability and extension of its range 80−66728
condensation chamber, for flame photometric analysis, exam. of design 80−21342
controlled regenerated inhibited solvent processes, review 78−76799
crack measurement, recording instrument 80−100984
crack propag., continuous meas. of stress, description of method 78−73009
crack tip strain and stress, experimental investigation 79−68669
creep information, meas. device for in-reactor tests 79−83427
creep tests, machine, conditions of plane state of stress 80−21232
CRISP-E, use in a phase-in mode 80−40654
cryogenic structural materials 77−17989
CTR first-wall irradiation environment, appl. of dual-ion accelerator 78−13325

materials testing continued
cutting fluids testing rel. to tool wear, thin layer activation technique 80−55619
cutting oil performance, test machine 80−11848
cyclotrons, small, applications *(Hungarian)* 78−70656
defectoscope, multichannel, spectrometric method of recording γ-radiation in scintillation counter 78−53099
defectoscopy of gamma-active objects in their natural radiation *(Bulgarian)* 80−71867
deformation localisation in tension, determ. 79−87790
deformed boundary determ. by method of caustics 77−89077
deposit-substrate systems, adhesion testing 80−50814
depth profiling by ion microprobe with high mass resolution 79−46894
destructive, advances in servo-hydraulic test machines 80−35453
destructive materials testing anal. by nondestructive electromagnetic methods *(German)* 77−86267
diamond, absolute pressure meas., strength anal. 79−91888
diamond, high press. appl. by spherical diamond indentor, plastic deform. obs. method 78−35619
diamond laser beam use *(Russian)* 78−31595
differential scanning dilatometer, low temp., exam. of design, appl. to stainless steel, V_3Si *(Russian)* 79−34224
digital automatic thermodynamic enthalpy and specific heat determ. equipment 78−57951
disperse system, plastoviscous, cone plastometer for strength props. determ. 80−76426
droplet impact, high-speed, effect of gas medium on dimensions of contact area 77−28942
ductile fracture initiation, strain gauge method for detecting 78−85085
dynamic stress strain relations in combined tension and torsion, testing device 80−21197
E-glass fibre, pore size distrib. anal. method 79−87805
eddy-current transducers, double-ended, signal calc. for nonferromag. cylindrical products 80−89443
elastic characteristics of materials, determination from phase shift in sinusoidal stress, strain, device for measuring 79−52518
elastomer, long-term oscillatory testing arrangement, flexometer *(German)* 79−52552
elastometric materials, friction testing using reciprocating friction and wear tester 80−76451
electrical donductivity meas., standard models 80−86343
electro-optics/laser international conference, Brighton (1976) 77−38800
electrodeposit, on metallic substrate, peel test for determ. adhesion 80−50815
electrodeposits, multilayer, thicknesses meas., instrument based on destructive coulombmetric method *(Czech)* 80−8980
electrolytically polished surface evaluation 78−35627
electron accelerator irradiation facility, shielding system, industrial research appl. *(German)* 77−70244
electron microscope examination, feasibility and methodology of in situ experimentation *(French)* 80−68301
electron microscopy techniques, review, 1976-77 78−82077
electronics materials, possible applications of laser microanalysers *(Polish)* 80−33008
electroplated coatings *(German)* 80−2967
electroplated coatings thickness test standards 79−8405
elongation, dynamic, of material, stress/strain curve up to scabbing, meas. method 79−7348
EM shear stress gauge for large amplitude shear waves 78−70113
enamel, rapid method for determining thermal expansion coefficient 79−20308
environmental simulation *(German)* 79−20314
epoxide resin, tensile, compressive and shear yield strengths, pyramidal criteria 77−8884
epoxy polymers, high temp./press. materials test for undersea environment 78−3213
epoxy resin adhesives, capillary flow and bond strength 80−71883
epoxy-resin join with Teflon-glass fabric double layer material, adhesion strength determ. method 77−77681
ethylene vinyl acetate copolymer, torsional rigidity testing *(German)* 77−52596
extrusion rheometer, for characterisation of thixotropic materials 77−63876
facilities available at Altrincham Laboratories 80−35454
fatigue strength, of materials under acoustic loading, installation for meas. 79−83426
fatigue tests, improving accuracy with axial loading, specimen fixing 79−83428
FBR fuel pin safety expts. at SLSF, centerline fuel thermocouple performance 80−102283
FCC metal, origin of dislocations during microdeformation tests, X-ray topography 79−82226
femoral cortical bone tensile props. instrumentation system 77−60025
ferromagnet, Rayleigh const. determ. method 78−12732
ferromagnetic, higher harmonic signal analysis for eddy current transducers 78−70109
ferromagnetic metals and alloys, coercive force, automatic meas. by remote means 79−24690
ferromagnetic object inspection, method of higher harmonics, difference schemes 80−89444
FFTF, instrumented fuel test at the fuels open test assembly 80−102247
FFTF Fuels & Materials Examination Facility design features and objectives 79−9746
fibre, inorganic, refractory behaviour testing 77−25204
fibre composites, impetus of composite mechanics on test methods 80−11868
fibre mechanical tensile test machine 77−40484
fibre reinforced composite, shear props., test method eval. 77−81353
fibre reinforced composite, stiffness and strength investig. 77−63874
fibre reinforced composite, using burn-test apparatus 80−76441
fibre reinforced composite, viscoelasticity measurement using mech. drive viscoelastic tester *(Japanese)* 79−34232
fibre reinforced materials, prod. of uniform plane stress states 78−85064
fibre reinforced organic matrix composite, use of unidirectional flexural tests, to assess environmental behaviour 79−20301
fibre reinforced plastics *(Japanese)* 78−39974
fibreglass laminates, thermal NDT using liq. crysts. 80−93709
fibreglass plastics, fatigue lifetime prediction based on cumulative damage 80−11776
fibreglasses, long-term strength evaluation, parametric methods efficiency 80−40662

materials testing continued
fibres, reinforcing, strength eval. by dry bundle method 79−100312
fibrous materials, low-density, centrifugal method of studying mech. props. 80−71823
filaments, elastic, tensile test method, and treatment of expt. data 80−85111
film, adhesion measurement 80−50819
film permeability meas. using β-emitting vapours 77−56173
filmed structures, hardness and adhesion meas., scratch technique 80−50805
films and tissues multiple bending testing device 80−21225
filtration deposits, basic indices of structural-mechanical strength 77−40496
fission reactor materials testing, General Electric Test Reactor appls. 80−565
fission reactor vessels, methods, instruments and technology of periodic inspection 78−72984
fission reactors, LOCA simulation, armature testing *(German)* 80−42785
flame-sprayed coatings, adhesion testing 80−50812
flammability testing, problems, language and scientific basis 79−5092
floors, friction coeff. meas. method 79−52540
fluorescent penetrant inspection, heat assisted 80−45466
foil, push-pull straining device for h.v. electron microscope in-situ deform. 77−4875
foil strain gauges, use on materials with heat constraints during heat treatment 80−25938
fracture data, influence of edge failures, method of correcting 78−83346
fragile materials, mech. props. meas. using disc-shaped specimens *(French)* 80−104367
friction machine SMTs-2, broadening of test capabilities by modification 78−60919
friction test machine SMTs-2, automatic loading device 79−70257
fuel defect test loop remote handling system design 79−9730
fuel pin rupture detection system using meas. of time differential of acoustic emissions 80−102282
furnace, high-temp. processing and testing 77−49730
Fusion Materials Irradiation Test facility initial target design 80−95410
fusion reactor first-wall performance under ion bombardment and cyclic stresses, in-reactor materials testing 80−104407
galvanic coatings, adhesion after strain hardening, test device 80−71837
galvanic coatings, tensile testing device 80−100988
gamma-ray backscattering from media interface, calc. 78−85106
gas lubricated bearings, test equipment to examine friction and wear, exam. of design 79−52522
gas-abrasive wear tests, methods and apparatus, neutral gas flow 77−25209
gasdynamic stand for heat transfer and combustion product testing 79−39085
gels, swelling kinetics device 80−21210
geological materials, stress relaxation testing method for mechanical behaviour studies 78−96309
glass, compressive testing 77−16773
glass, elastic moduli, device for temp. depend. meas. at low pressures 80−30183
glass, homeogeneity measurement by improved Shelyubskii method using press. 79−29302
glass, molten design of level measuring gauge 79−29304
glass, stress in working zone under biaxial compression, Moire-band method 77−81369
glass, surface treatment effect, on chemical polishing time of crystal products 78−92436
glass, thermal stresses, temporary and residual, monitoring by semiautomatic heating polariscope-polarimeter 78−16833
glass and brittle materials, fracture energy meas. by modified double cantilever method 77−73387
glass and glass-to-metal seal, meas. device 77−63845
glass fibre, tensile strength meas. using chain-loading fibre tensometer *(Japanese)* 80−55610
glass fibre composite, shell, carrying capacity, heating effects 77−4865
glass fibre reinforced composites, glass fibre volume fraction determ., using photodiode scanning technique 78−48578
glass fibre reinforced plastic, fatigue fracture kinetics studied by diffusion scatt. of luminous fluxes 80−76446
glass fibre reinforced plastics, design criteria 80−25970
glass fibre reinforced plastics, shear characteristics of tubular specimens, strain gauge and clamp 80−85114
glass fibre reinforced plastics, stress/strain conc. round hole, Moire fringe study 77−28964
glass fibre reinforced plastics, winding device for mech. test specimens prep. 78−7138
glass fibre reinforced plastics mechanical properties measurement, use of electrical resistance strain gauges, effects on props. 79−43541
glass fibre reinforced resin, shear strength determ., comparison of methods 77−90527
glass inorganic, shell, stress/strain state investigation under external hydrostatic press. 77−81370
glass plastic coating, thick-walled, compressive strength evaluation method 79−15897
glass reinforced epoxy resin laminator, strength tests *(Polish)* 77−12772
glass reinforced plastic, thermal activity, prediction of struct. charact. and physicomech. props. 77−63872
glass textolite cylindrical shells, parallel wound, feasibility of diagnosing strength 78−67157
glasses and fragile materials, fracture energy, direct meas. *(French)* 80−104376
grain orientation nonuniformity across wire specimen sections, anal. of X-ray patterns 78−23886
granular material, simultaneous moisture content/thermal cond. meas. apparatus 78−53064
granular materials shear deformation, simulation by Al rods *(Japanese)* 80−11691
graphite, bending strength testing, quality improvement 79−52581
graphite, creep rig, high temp. 77−44423
graphite, failure in lab. tests, fracture mech. approach, finite element stress anal. 77−4149
graphite, thermal shock resistance and fracture toughness during graphitising heat treatment *(Japanese)* 80−71843
graphite reinforced epoxy, accelerated characterisation procedure 79−34263

materials testing continued
graphite/epoxy laminate, T300/5208, proof testing under cyclic tension-tension fatigue 80−81249
graphite/epoxy thermal deformation characts. test, mirror telescope appl. 77−78636
graphitic materials deformation, crack and fracture behaviour, SEM exam 80−11706
greases, use of torsional balance rheometer to measure normal and shear stresses 77−63877
H isotope penetrability through metallic membranes, apparatus for meas. *(Russian)* 77−70248
hard magnetic material, testing by permeameter with elec. analog. of standard demagnetisation curve *(Polish)* 79−5099
heat insulating material under uniform of one sided heating, installation for deform. props. study 79−66232
heterogeneous materials, conc. inhomogeneities control, electron and ion probe testing 79−43505
high alumina cement concrete, quality, thermal anal. investig. 79−15912
high flux reactor for materials testing, expt. facilities 79−63749
high irradiance solar simulator for thermal absorptive material evaluation 79−62063
high strain rate material behaviour and testing techniques, J.D. Campbell memorial lecture 80−82627
high strain rates, conf., Oxford, England (Mar. 79) 80−82575
high temp. inner press.-tensile test device *(Japanese)* 80−25972
high temp.-high flux material testing, solar power station appls. 80−40668
high-temperature, conf., Helsinki, Finland (June 1975) 77−52295
historical development, Instron Ltd., product range since 1946 80−35452
hydration kinetics, microwave obs. 79−34255
hydraulic loading system for testing under irradiation 78−31609
hydraulic materials-testing system with 10-nm positional accuracy 78−85065
hydrostatic installation for testing solids and tubes under liquid press., axial forces, torsion 78−31608
identification of materials, review of available methods 78−95876
immersion viscometer, exam. of design 79−52544
impact testing, machining for laminated thermoplastics 78−3272
implanted prosthesis failure analysis techniques and results 80−89906
in plane strain displacement near crack tip at high temp., optical meas. 79−32412
Inconel, steam generator tubing, mag. probe inspection 80−85119
Inconel 718, environment effect on high temp. fatigue crack growth 80−30090
indentation tester, vertical displacement, for compacted powders, plastics and foodstuffs 80−58988
inorganic nonmetallic building material with rough surface, abrasion test using pneumatic apparatus for thickness meas. *(German)* 79−52553
inspection penetrants, evaluation 80−61056
instrumentation for impact, erosion and fracture studies 77−81383
insulating replacement gases for SF_6 80−59313
interactive graphics system developed for NDT 80−66729
interphase boundary analysis using TV 77−40483
ion exchange resins, macroporous rapid method of rating total void volume 80−21208
IR determ. of temp. increase in tension tests *(German)* 79−61806
joint prosthesis materials, wear meas., test machine design 79−20716
laminate, simple shear charact., comparison of test methods 78−44283
lap shear test specimen comparison 77−40501
laser heating system, for meas. of high-temp. props. of materials over wide press. range 77−77699
laser microemission spectroscopy for local determ. of impurities in graphite reactor material *(German)* 78−7161
laser microprobe mass analyser (LAMMA) appl. 80−18041
light and water exposure apparatus 79−15914
liquid penetrant testing, continuum fluid mechanics aspects 80−43818
LMFBR, Na test of bellows expansion joints, metallographic study *(Japanese)* 79−67850
LMFBR fuel channels, measurement of irradiation creep in bending 80−104406
LMFBR fuel pin bundles in flowing Na, design and operation of SLSF test trains for safety tests 80−102281
LMFBR steam generators, mass transfer props. of steel, test *(Japanese)* 77−348
LMFBR structural materials, development of an instrumented materials irradiation test for FFTF 80−57858
LMFBR structural materials, development of an instrumented materials irradiation test for FFTF 80−68797
load cell design and development 80−105628
low temp. testing machines of IMASh-5S-65 type, new cooling techniques, exam. of machine design 79−52520
low-alloy heat resisting steel pipe tensile and impact strength micromechanical tests *(Polish)* 77−70246
lubricant evaluation, using four ball friction machine 80−25951
lubricant testing, test machine 80−76452
lubricants, ester-type, thin-film test for meas. of oxidation and evaporation 80−40626
lubrication of compliant bearing, study by optical interf. method 77−36711
LWR irradiated fuel assemblies, nondestructive exam. using γ-ray and neutron techniques 80−66760
magnetic particle inspection oxides, evaluation 80−40657
magnetically hard, instruments, classification *(Russian)* 77−67479
magnetically hard materials testing instrument, pulse magnetiser design *(Russian)* 77−67481
magnetostrictive hysteresis determ. by inductive method *(Russian)* 77−56171
measuring energy dissipation during cyclic loading of materials 79−100310
mechanical oscillation damping characts., apparatus for examining, based on amplitude-frequency relationship resonant trough 78−64803
medium-range data transmission optical cables 77−39096
metal, blackness rel. to heat treatment, measuring apparatus 79−57165
metal, ductile, jet-impingement solid-particle erosion testing, halo effect 80−76376
metal, effect of environment, lab. investigs. *(Russian)* 78−11458
metal, electronic work function under tension, 20 to 1200°C 80−76448
metal, hot deformability test methods, comparative evaluation *(German)* 77−36713
metal, plastic props. investig. at elevated temps. by torsional method, review 79−43509
materials testing continued
metal, thermoelec. temp. meas., error anal. 78−19975
metal, thin walled, cold deformed sheet methods and eval. of test results in Sweden 78−39980
metal, wear characts., mechanisms 77−32697
metal base+hard electrolytic Fe, adhesion strengths, quantitative determ. method 77−77680
metal coating stability, thermoelectric method of assessment *(Russian)* 78−11459
metal fatigue tests for plastic deformation *(Hungarian)* 80−97665
metal fibre stress/strain curves determ. using X-ray goniometer *(German)* 78−92413
metal films, ductility tester 77−63864
metal powder, hot swaging test method for tensile testing 77−25235
metal specimen, tensile, semi-automatic universal test machine *(German)* 77−81346
metal surface flaw, microwave ferromag. resonance probe for eddy current detection 79−34254
metal surfaces, radioactive contamination 80−68771
metallic and non-metallic surface defects, optical method 77−28973
metallic glasses, dynamic mechanical analysis appl. to materials testing 79−15911
metallic wear debris, morphological anal. 80−76453
metallurgical coke, mech. behaviour charact. *(French)* 80−104371
metallurgical slags, phase diagram, determ. by hot wire microscopy, exam. of technique 79−8413
metals, deformed, apparatus for determining gas penetration 77−86240
metals, gas saturation, apparatus 80−61039
metals, hydrogen brittleness measurement 80−104291
metals, ionised gas effects 79−70252
metals, positron annihilation, localised probe of lattice defects 80−55224
metals, test device for thermal cycling conditions 79−87778
metals, wear resistance, method for rapid determ. 77−25210
metals, working, method of applying fusion thermal indicators to surfaces, including heated surfaces 80−17937
metals and alloys, abrasion wear testing 77−40493
metals and alloys, cyclic strength in nonisothermal loading, exam. of method and equipment 78−85096
metals and alloys, emissivity determ. using low-inertia opt. dilatometry 80−59684
metrology use in material inspection 78−95899
MHD air heater, directly fired, using cored brick matrix 79−52949
microcomputer appl., comparison of automatic and conventionally obtained data *(German)* 77−73398
microcomputer applications *(German)* 77−32744
microprocessor application for destructive examination of materials with data processing *(German)* 80−93714
microscope 79−49280
microscope photometry appls. 80−21236
microscopy appl., modulation contrast 79−35818
microstructure observation apparatus, observation during heating, stressing, under vacuum, photography facility 77−73403
microwave, Intern. Microwave Power Symposium, Minneapolis, Minn., USA May 1977 77−70492
mineral crystallisation, barometric investigation autoclave 77−86241
mineral dispersed macromolecular matrix, holographic interferometric meas. of displacement vectors on boundaries 79−79015
mortar and concrete internal meas. using elect. resist. strain gauge 77−44446
Mossbauer effect appl., conference, Kyoto, Japan (Aug.-Sept. 78) 80−7199
mould material deformation meas. at high temp., apparatus 78−3266
moulding mixtures, consolidated residual stress meas. 79−87791
multilayer components, thermal quality control 78−85107
multispeed tool life tests with radioactive tools 78−44338
natural rubber vulcanisate, network changes during physical testing 80−60936
nematic liquid crystal material analysis in production quantities 77−76309
noncontact material testing using laser energy deposition and interferometry 79−34258
nonmetallic material, mech. props., testing installation, +600 to −190°C 78−15633
nozzle erosion, ion implantation effects, ion beam anal. 79−48011
nuclear materials, nondestructive neutron assay for accountability and criticality control 80−66759
nuclear plant, seismic testing of structures and components using two axial shaking table 78−44300
nuclear reactor, structural shock tests, prototype FBR MONJU scale models, computer code verification 77−3131
nuclear reactor materials, apparatus to meas. thermophysical props. at high temps. 80−37458
nuclear reactor materials, thermal properties at elevated temps., determ. method 77−73402
nuclear steam generator tubes testing and evaluation, using CIS/DASIO system *(Czech)* 80−63301
oils, antiwear props. determ. method in tests on friction machines 78−60915
opposed-anvil high-press. devices, material strength effect 80−47068
optical fibres and cables, tensile testing machine 77−3687
optical glass, K8, bending strength, sample dimension effects 80−9975
optical glass windows in hydrostatic press. vessels 79−90016
optical heterodyne interferometer, appl. to surface inspection 77−90529
optical material, photoelastic investigation of freezing and defreezing of temperature stresses 77−66733
optical waveguide materials, radioisotope methods and neutron activation anal. appls. 78−7286
organic electrical insulating materials, thermal lifetime prediction, thermal anal. appl. 79−15913
oxide systems, exam. of techniques used to determine phase diagrams and equilibria, and effects on equilibria 79−8415
petroleum products, reliability of multiple testing result analysis 79−87804
phase change materials, thermal energy storage, cycle life tester 80−72090
phase composition examination by tritiation system 79−39068
phase diagrams, construction, use of NMR, Mossbauer effect, and gamma ray perturbed angular correlation 79−8417
phase diagrams, electron microprobe and STEM determ. exam. of techniques 79−6241

materials testing continued
phase diagrams, ion beam determination of phase boundaries, exam. of techniques 79−8418
phase transformation apparatus, for glassy materials in thermal gradients, design and fabrication 78−84767
photoelastic coating method of meas. stress and strain 78−1614
photoelastic load meas. and testing *(German)* 80−19297
photographic development and materials sensitometry *(Italian)* 79−93241
piezoelectric materials and cells, method of measuring parameters 78−72989
planning and evaluation by statistical methods *(German)* 80−93725
plastic, arc resistance test *(Japanese)* 78−27697
plastic, static relaxation behaviour, test rig design *(German)* 79−39081
plastic, torsional rigidity testing instrument, used with strength testing instrument *(German)* 77−52596
plastic, Vicat softening temp., meas. instrument *(German)* 77−63871
plastic building components, material testing, for use as building component *(German)* 78−39984
plastic film tear test, fracture mechanical analysis *(Japanese)* 77−81351
plastic materials, process computers for control and meas. of laboratory testing *(German)* 79−61821
plastic tubular specimen, clamping device for complex stressing 78−23912
plastics, accelerated life testing, by thermal analysis 77−70261
plastics, auxiliary device for testing of property changes at high temps. *(German)* 80−66741
plastics, materials testing, application-oriented test standardisation *(French)* 78−85061
plastics, radio and light polarisation stress analysis 78−68857
plastics, short-time testing using process computers *(German)* 79−61822
plastics, stress-cracking test 79−74311
plastics, tensile and flexural testing device, incorporating an impacter *(German)* 80−3276
plastics, testing, attachment to MI machine 79−87784
plastics, wear meas., attachment to MI machine 79−87784
plastics *(German)* 78−27716
plastics *(Japanese)* 78−39974
plastics testing, automation 80−76443
plastometer, electronically controlled, for tensile and compression tests *(German)* 80−3273
plexiglas plates, static and dynamic stress intensity factor meas. by method of optical transmitted caustics 77−66740
polarisation resistance meas., technique and instrumentation 78−15609
polarographic sensor with microwire indicator electrode, exam. of design 80−21340
polyamide, torsional rigidity testing *(German)* 77−52596
polybutadienes, use of high modulus inclusion gauge, in stress analysis 80−21254
polycarbonate, bisphenol A, birefringent plates, cracks, stress intensity factors, refl. caustics method 80−93718
polychromatic X-ray stress meas. *(Japanese)* 78−7143
polycrystalline bodies, tensile test, uniaxial, for plastic deform. *(Hungarian)* 80−97657
polyester, practical testing methods for sheet and bulk moulding compounds *(German)* 79−70262
polyethylene, ageing prediction by isothermal differential scanning calorimetry 78−11485
polyethylene, expanded, dynamic model rel. to drop impact 78−7160
polyethylene, mixing of high and low density, mixing ratio determ. by thermo-optical anal. *(German)* 78−53070
polyethylene, torsional rigidity testing *(German)* 77−52596
polyethylene film, minimum running thickness, biaxial extensional flow study 80−100993
polyethylene pipe butt welding, tensile tests rel. to melt flow index 77−73389
polyethylene terephthalate, shear compliances meas. of oriented sheet 80−104363
polymer, accelerated ageing data processing using linear regression analysis 78−39815
polymer, bioabsorbable, standards for in vitro and in vivo comparison and qualification 78−3677
polymer, loaded, mech. of macrocrack generation and propag., photometric and X-ray meas. 77−4886
polymer, rubber-like manipulator for placing ring shaped testpiece in cold chamber of tensile testing machine 77−63859
polymer, viscofluid, extensional vibrorheometer 77−70257
polymer based composites, mechanical test unit, with intense high-temp. heating 80−100987
polymer elastic deform. meas., occurring under reversible slippage, friction method 77−52598
polymer films, instrument for studying sorption and diffusion of low-molecular liqs. 79−100305
polymer films elastic anisotropy based on thermal shrinkage strains 77−86245
polymer material bending strain, strain gauge to meas. reliably 80−25948
polymer materials, photodegradation tests, problems *(Japanese)* 77−55245
polymer melts, quasistatic bulk strength meas., specially built apparatus 80−7737
polymer orientation measurement methods, review 78−48589
polymer solutions, resistance to aggressive liquid media, accelerated determ. using periodic-action method 79−52533
polymer tensile testing method 79−39073
polymer viscoelasticity and strength characterisation, advanced light scatt. techniques 80−11857
polymeric adhesive layer, interlaminar stresses, direct determ. 77−86237
polymers, automatic recording device for thermomechanical and linear dilatometric testing 80−11858
polymers, corrugated surface, Rayleigh wave excitation, modified wedge method 79−37261
polymers, deform., device for testing under hydrostatic pressure and anisotropic conditions 79−87783
polymers, deformation under combined action of shear stress and hydrostatic pressure, testing equipment 77−56184
polymers, in situ EPR tensile testing apparatus 78−85086
polymers, microtoming for structure analysis 80−40665
polymers, photoresistor dilatometer design, with high stability and sensitivity 80−81251

materials testing continued
polymers, quality control method based on solid surface wetting 79−52534
polymers, stress-state meas. using chemiluminesc. system 80−40628
polymers, thermal anal. methods, appls. 78−68845
polymers, thermomechanical curves, automatic unit for recording 77−25217
polymers for artificial joints, wear testing 78−31981
polypropylene, oriented, microcracks diagnostics by paramag. probe method 80−66736
polystyrene, ref. std. material testing, evaluation, glass transition temps., instrumental effects 79−4404
polyurethane, high temp./press. materials test for undersea environment 78−3213
porcelain, equipment for translucency testing *(Polish)* 78−19985
pore size determ. from charged particle energy loss meas. 77−71730
porosity meas. device for fluidised beds, exam. 78−60911
porous ceramic, eval. of frost resistance by holography *(Japanese)* 78−19987
porous material, gas diffusion technique for pore struct. investigation 80−30185
porous materials, interpretation of structure by combinational method 79−29303
porous metal heat transfer coeff. determ. 77−66738
porous sintered materials, mech. testing device for hydrostatic pressure conditions 80−40645
porous solid, blind porosity and capillary press. meas. 77−90545
porous solid with below-freezing pt. adsorbate, isothermal adsorption and dimensional changes obs. 78−75925
positron measurements, for NDT of metals and alloys 80−55222
powder, triaxial test procedure and num. calc. method for flow props. 77−60028
powder and particle charact., review of current instruments 77−66735
powder cohesive strength and internal friction determination for small quantities of material 77−40495
powder dustiness, determ. method 80−45455
powder spraying guns, electrostatic, frictionally charged, exam. 78−80708
powders, brittle, shock wave disintegration test method 80−66744
powders, tensile testing, modification of split plate tester 77−70255
powders, unit for meas. strength charact. 77−25216
pressmold materials, stand for high-temp. mech.-props. test 77−56183
pressure vessel, proof testing, British standard 79−70269
programmed loading unit for test machines 78−23900
PTFE-C black composite form. monitoring by electrochem. method 77−36446
PVC cases for Pb-acid batteries, pneumatic shock test *(German)* 78−85093
PVC film gelling, auxiliary testing device, for prop. changes at high temps. *(German)* 80−66741
Pyrex glass, sedimentation pot. meas. device and ζ pot. determ. *(Spanish)* 77−70236
pyroceramic, stress in working zone under biaxial compression, Moire-band method 77−81369
radioactive materials, package design, construction and testing for safe transportation 80−63412
radioactive waste packages, developments and studies for marine disposal 77−61578
radiography, effect of stress on crack detection 80−40653
radionuclide methods, in West Germany, industrial use impetus *(German)* 79−96231
radiostereoscopic systems, anal. of conditions ensuring three dimensionality 78−76806
random signal analysis, conf., London (April 1977) 77−44822
raw material acceptance testing for dielectric applications 80−97646
reactor fuel cladding tube mech. props., ring compression test, finite element anal. 77−83037
reference materials for COMECON member countries 80−45468
refractories, hot-wire test, critical review and comparison with BS 1902 panel test 80−104409
refractories, sintered, X-ray diffraction method for assessing local stress levels 79−96265
refractories, strength and thermal properties, automated test system 80−100986
refractory, testing for casting bay appl. 77−25239
refractory abrasion test machine for use at high temp. 79−52505
refractory ceramic, deform. test apparatus and method *(Russian)* 78−35613
refractory concrete fracture strength, test apparatus simulating usage conditions 80−71824
refractory metal, strength charact., effect of thermal test conditions 78−39994
refractory metal, strength charact., error evaluation 77−16771
refractory metals and alloys, safe-life testing *(Russian)* 79−52476
refractory oxide, solar furnace for high temp. studies *(French)* 79−70268
regression of results by restraint consideration *(German)* 78−76802
reinforced composite pull-out forces, effect of matrix stresses 77−21334
remelting process, X-ray fluorescence and optical spectrum anal. appl. 78−23560
residual stress effects in failure from flaws 79−66228
residual stress measuring equipment for polymer materials based on cured synthetic resins 77−77675
resilient, impact testing machine and expt. results 77−25223
review of nondestructive and destructive testing, vibr. anal. and stress anal. 78−3298
rheological props., rotational viscometer use in calc., programme *(German)* 77−60026
ring test, evaluation for strain rate sensitive materials 78−39991
role of materials tester and methods used *(German)* 78−44290
rubber, crystallising, tensile test specimen prep. 80−71838
rubber, swollen, stretch testing, attachment to strength testing machine 79−15905
rubber, thermal defectoscopy study 80−89445
rubber *(German)* 77−73399
rubber mixtures, device for determining wear 80−21226
rubber testing, statistical anal., method variance *(Polish)* 77−28962
rust prevention in lubricants 78−15635
sandstone, determination of Biot parameters using static tests exam. of procedure 79−20299
scanning electron microscope appl., ISI Model (7) 79−89044

materials testing continued
scanning electron microscope appl. *(German)* 77−5965
science and technology, importance of safety and reliability, in materials testing 78−39982
seals elastoplastic behaviour obs., for high pressure chemical apparatus *(German)* 78−21160
secondary ion-ion emission, appl. to anal. of metal and alloy surfaces 77−56200
self-excited electromagnetic oscillations *(German)* 79−83417
SEM, combined deformation/heating stage, acoustic emission rate meas. 80−101892
SEM analysis of object microrelief, metallurgy appls. 80−73319
semiconductor defect birefringence detection by polarisation IR microscopy 79−83405
semiconductor domain instability and resistivity profile meas., universal capacitive probe 80−31796
semiconductor film X-ray and electrical characteristics meas. chamber 78−86396
semiconductor materials resistivity, thickness and permittivity meas., using EM methods, computer-aided results evaluation 79−80647
semiconductor probe point characterisation by footprint in porous Si 79−96243
semiconductors, cryst. growth and defects, appl. of analytical techniques for observation 80−73546
servocontrolled hydraulic hot-torsion machine for hot working studies 78−27698
shear modulus, static, determ. method 78−7111
shear resistance of finely dispersed bulk material 80−21224
sheet material, radioisotope method for measurement of average value, and dispersion in surface density 78−76811
sheet materials, heat stability, small automatic device for rapid testing 77−77672
sheet metals, shearing test using pressure sensitive pin *(Japanese)* 77−48602
simulative testing, systems analysis data sheet for friction and wear tests 77−28967
simulative wear study critically reviewed 77−28968
single-phase structure, nonuniform, grain size quantitative rating, exam. of system used 78−85072
soil, chemical grout for stabilization, simultaneous tests for engng. props. *(Japanese)* 78−31596
soil mechanics, triaxial test, limit analysis theory *(French)* 78−32073
solar collector material selection and blending guidelines 79−62060
solar energy concentrators, optical coatings, accelerated tests, using reliability principle 79−96419
solar flat plate collector coatings, NBS standard 74-635 testing 80−61426
solar thermal absorptive materials, high irradiance solar simulator solar thermal absorptive materials, high irradiance solar simulator *(Japanese)* 79−79185
soldered thick-film conductor, adhesion meas. technique 80−50811
solid dielectric props. meas. with superconducting resonators 78−21180
space environment, materials processing expt. capabilities 79−47882
space frame transient analysis in large displacement 77−14955
standard sample homogeneity evaluation, optimal obs. planning 80−93721
standard tests, precision, statistical anal. of data 79−74315
standards, USSR reference materials state service 79−96259
steam turbine lubricating oil, filter separators and centrifuges eval. for effects on props. 78−3283
steel, 3-cam plastometer determ. of deform. resist. 79−87792
steel, α to γ phase transform., during rapid resistance heating, apparatus for investigation *(Slovak)* 78−19742
steel, alloy, 37KhGSTF and 44KhGSTF, quenched X-ray diffr. testing of heat treatment 78−56834
steel, alloy, dynamic stress intensity factor meas., possibilities and limits *(German)* 80−93719
steel, alloy, rolling wear study of misaligned cylindrical contacts 80−108590
steel, alloy, temp. profile, IR obs. during pull tests 77−44427
steel, austenitic, decomposition, exam. of phase transformation kinetics, using new method 79−52509
steel, austenitic, intergranular defectiveness determ. using inductive instruments 78−53075
steel, austenitic, thermocyclic strength, cold working and subsequent heat treatment influence 77−66737
steel, austenitic grain size rating methods, comparison 78−85074
steel, C, cementation process testing, foil samples method 79−70238
steel, C, hardened by HF current, mech. testing method 80−61053
steel, C, hot plastic deform., vac. colour etching investigation 80−61036
steel, C, rolling wear study of misaligned cylindrical contacts 80−108590
steel, C, X-ray line fitting by Gram-Charlier distrib., appl. to tension test *(French)* 79−15689
steel, cast, equipment for thermal shock resistance determ. 80−55614
steel, cold-rolled sheet, St10 kp, St10 sp, mag. inspection of ferroprobe coercimeters 80−21234
steel, Cr-Mo, cold working influence on properties 77−70270
steel, Cr-Ni-Mo-Cu-Nb, martensitic precipitation hardenable, corrosion resistant, heat treatment, structure and props. 79−74169
steel, Cr-Ni-Ti, thermal expansion experimental investigation 77−66739
steel, data reduction for samples under high ambient press. and axial tension 78−3181
steel, deformed and welded mild, potential distrib. meas. technique, appl. to corrosion study, apparatus *(Japanese)* 78−53049
steel, double-layer, adhesion strength determ. method 77−63857
steel, elect., mag. props. determ. with Epstein hysteresis tester 80−60364
steel, fatigue limit assessment, progressive load methods *(German)* 80−61058
steel, Fe-Si coated grain oriented sheet, grain detection 78−11470
steel, friction measuring test for use under conditions of high normal interfacial force 80−76454
steel, heat treated, test specifications changes *(German)* 77−9019
steel, high strength low alloy, acoustic emission meas. from crack opening displacements 80−7732
steel, high tensile, H embrittlement estimation from viscous failure 77−73335
steel, hydrogen embrittlement, standard qualification tests 79−74259
steel, low C, dynamic stress intensity factor meas., possibilities and limits *(German)* 80−93719
steel, low C, nil ductility transition temp. 80−100896
steel, low C, welds, residual stresses, evaluation by Barkhausen noise meas. 80−76436
steel, magnetic inductive method appl. *(German)* 78−48581
steel, martensitic-ageing, etching technique, for revealing struct. inhomogeneities 80−61035
steel, medium C resulphurised, compressive strength at high strain rates, short load cells 79−29305
steel, microplastic deform. meas. in grains of polycryst. substances 77−77665
steel, mild, 1019 AISI, acoustic emission generated during deform. 80−60921
steel, mild, dynamic plastic loading of frames 79−20117
steel, mild, fatigue crack propag. study using servohydraulic test system 80−76431
steel, non-metallic inclusions changes due to heating obs., influence on ductile fracture *(Spanish)* 80−25744
steel, pressing die X45 CrNiWMoVCo 9.9, test results *(German)* 80−50785
steel, punch, for blanking tools, method of wear resist. determ. 80−55600
steel, quenched and low-annealed, X-ray determ. of macroscopic stresses 77−77660
steel, rolled, used of statistically justified methods in determining heterogeneity and mech. props. 79−52516
steel, sheet, effects of strain rate and deformation heating in tensile testing 78−85089
steel, sheet, rapid test for props. assessment 80−40650
steel, stainless, 18Cr-2Mo-Ti, atmospheric corrosion 80−85078
steel, stainless, pipes, electro-thermal method for NDT of welds 80−35447
steel, stainless, two phase, X-ray stress meas., by monochromator method *(Japanese)* 78−64792
steel, stainless, type 304, viscoplastic behaviour, strain rate sensitivity, creep, relaxation, tensile tests 80−66727
steel, stainless 304, explosive loading technique for uniform plastic expansion at high strain rates 80−81273
steel, stainless type SUS 304, diffusion welded joints, sound emission during tensile testing *(German)* 80−61062
steel, strength determ. from dynamic hysteresis loop EMF spectral content of coil, expt. 77−73414
steel, thermal props. meas. *(French)* 80−25977
steel, thin sheets, C and N contents determ. by internal friction *(German)* 78−27715
steel, tool, chipping resistance testing method for blanking punches *(Japanese)* 79−100308
steel, tufftrided, type S15CK, fatigue strength, estimation of size effect *(Japanese)* 80−81166
steel, wear charact. of burnished machined surfaces 80−108595
steel, wear meas. by ^{56}Co activity reduction 79−57166
steel, wear resistance, determ. using MI-1M machine 80−25943
steel, wear testing in oils containing organosulphur cpds., XPS obs. of surface comp. rel. to wear 77−36668
steel, welding residual stresses, sources, X-ray meas. *(German)* 77−86265
steel, welds obs. at high temperature, by moire photography 79−74336
steel fire simulation, determ. method of critical value in case of nonstationary heating *(German)* 77−86268
steel for nuclear reactor pressure vessels, irrad. and post-irrad. examination equip. and techniques *(German)* 77−36696
steel grain size spread, quantitative rating method 78−85073
steel H_2, embrittlement resist., selection of test conditions *(Russian)* 79−15883
steel H-beams, tensile samples shape influence on results of mech. props. determ. 77−52569
steel mild, acoustic emission during magnetisation, stress effects 79−82854
steel pressure vessel plates, destructive examination, PISC trial 80−52745
steel sheet, hot and cold rolled, cold formability, notched tensile test and stretch bend test *(German)* 80−61031
steel stress/deformation response meas. device *(German)* 78−3261
steel tearing rate determ. by elec. resist. meas. method *(German)* 78−15619
steel welding, development and results of an instrumented restrained cracking (IRC) test *(German)* 78−85060
steels, 45, Kh18N10T, and 30KhGSA, determining the relative elongation from a machine tensile curve 79−15927
steels, C and alloy, quality, effect of methodic factors on quality of S replicas 79−24691
steels, contact resist. in working media in static, dynamic loading, testing unit 79−15900
steels, hydrogen cracking under long-term strength tests 77−86243
steels, stainless, accelerated test for susceptibility to Cl_2 stress corrosion cracking 80−21199
strain and damage electrical measurement method *(French)* 80−71854
strain gauge measurements on plastic models, instrumentation, accuracy 80−21255
strain gauge protection, sealants suitability determ. 78−4610
stress analysis, expt., conf., Munich, Germany (Sept. 1978) 79−34256
stress-intensity factor determ. by strain-gauge method 80−76445
stress/strain curves using constant-rate-of-extension instrumentation 77−4883
stress/strain diagram, instrument for displaying on TV screen 80−21222
structural elements testing, methods and eval. of test results in Sweden 78−39980
structural reliability and safety, probabilistic methods 78−39978
structural vibration testing, using electromag. forcing device, use of feedback to reduce harmonics 79−20298
subsurface defects in metals, detection using gamma rays 78−85104
subsurface stress meas. 80−21252
surface potentials visualisation and meas., using SEM 80−68307
Swedish materials science expt. in Texus 1 and 2 sounding rockets 80−104362
tensile strength, statistical study, using small number of data *(Japanese)* 77−32736
tensile test, regulated, strength and deform. characteristic values, consistency *(German)* 80−93712
tensile test equipment and procedures for charact. value determ. *(German)* 80−93713

materials testing continued
tensile testing, control of test cycles, data logging and data processing *(German)* 80−97648
tensile testing, microcomputer for automatic meas. and data treatment *(German)* 77−44433
tensile testing cryostat for 200 kN tensions 79−96235
tensile tests, standardization from metal physics viewpoint *(German)* 80−93711
tension test with neck triaxiality reduction 78−7159
testing machines, contact area for nonuniformly distributed load, calc. 78−67155
testing procedure changes *(German)* 77−48604
texture goniometer alignment of Schulz reflection technique, method for testing 80−81272
texture meas., expt. methods, review 79−87815
textures materials, residual stress evaluation by X-rays *(German)* 80−40670
thermal analysis, symposium, Trondheim, Norway (Jun. 1977) 79−16079
thermal analysis, using complementary data, thermodynamic and kinetic parameters determ. 79−16080
thermal analysis system, Du Pont 1090, microcomputer-controlled 80−16613
thermal insulating materials, radioisotope thermoelectric generator appl. 79−48145
thermionic diodes materials, flame-heated, ceramic and alloy materials suitability evaluation 79−48157
thermo-optical measurements at six European laboratories compared *(French)* 78−29107
thermoelastic phenomena in epoxy resin and glass microcircuitry elements *(Polish)* 80−93724
thermoelectrode emissivity, test method 77−89556
thermography, NDI method for damage detection 80−35445
thermoplastic materials, flexure testing 77−86087
thermoplastic pipes, apparatus for time-to-failure determ. *(Polish)* 79−74328
thermoplastic plates, strength meas. when supported by annular ring 80−81257
thermoplastic polymers, dynamic mechanical analysis appl. to materials testing 79−15911
thermoplastic-based sheet materials, flexural anisotropy and stiffness assessment 80−76442
thermosetting polymers, dynamic mechanical analysis appl. to materials testing 79−15911
thick film, adhesion to ceramic, destructive and nondestructive meas. 80−50809
thick film terminations on chip components, adhesion meas. methods 80−50810
thin films, adhesion determination, electron and laser beam appls. 80−71833
three-point bend test optimisation for fracture energy determ. 77−21333
transducer, force measuring, EM, design and appl. *(Russian)* 78−16784
transducer, surface mounting, reliability test system for accelerated tests 78−49820
transducers, magnetically anisotropic force, optimisation of mechanical and electric operating conditions 79−17412
transtropic bodies, simplified method for plastic anisotropy determ. 78−3270
tree trunk, modified hole drilling technique for determining residual stresses *(Japanese)* 77−77683
trident seal, thermal expansion differential test 79−61815
TV analyzer for material structure studies 78−27696
US equipment, selection of material for concentrator-instrument section 80−21242
vacuum extraction device, with mass spectrum analyser, gas-forming admixture in metals determ. 80−22371
vibration damping materials, testing and development 77−84059
vitreous enamel coating, method of quantitatively assessing blistered structure 78−53108
volume compressibility of polymer materials, meas. equipment 77−77674
washing machines *(German)* 77−48605
Washington degradation test, aggregate behaviour 77−28955
wear, three-body abrasive, design of new tester 80−108682
wear evaluation, ferrography *(Polish)* 79−79197
wear loss from steel surface using $^{56}Fe(p,n)^{56}Co$ reaction 77−4881
wear resistance, effect of compressive stress, methods of investigation 77−25208
wear study using replica technique 79−20329
wear tests with plastic lubricants, friction machine attachment 78−3273
welded joints, strain concentration zone detection by holographic interferometry 77−40512
wires, thin, fatigue testing 80−25834
wood, load bearing capacity, and deformability, evaluation of timber structure safety *(German)* 78−39983
wood particle board, method of mech. testing, elastic deform. meas. 78−56837
wool fibre, diameter meas. for grade determ., truncated sequential sampling 79−87802
work of adhesion, technique for eval. 78−19969
wrought metals, plastic deform. testing, X-ray line profile anal. *(Hungarian)* 80−97663
X-ray microbeam meas. of local stress, appl. to fatigue crack growth *(Japanese)* 78−64793
X-ray stereoscopic image formation, exam. of charact. 78−85105
X-ray stress meas. of C steels, appl. of position sensitive proportional counter *(Japanese)* 78−64791
X-ray stress measurement method, appl. to practical materials *(Japanese)* 80−52379
zircaloy cladding tubes of irrad. fuel, flattening test *(Japanese)* 77−42054
Zircaloy-2, reactor cladding, delta-wrinkly zone near crack edge obs. 79−3203
Zircaloy-UO_2 fuel rods, eddy-current testing of claddings using encircling and probe coils 80−21245
Ag-Cu-Pb coin chem. anal. by low energy γ-rays and neutron transmission meas. 80−35591
Al alloy 7075-T6, stress intensity factor specimen design, constant factor for crack length range 77−73380
Al alloys, stress-strain state after treatment by pressure, moire strip method appl. *(Russian)* 80−40648
Al alloys, types 1100 and 5454, long-time rupture tests 80−76434

materials testing continued
Al, anodic oxide layers, meas. of growth by photoluminescence, description of equipment 79−52511
Al sheet, critical stress intensity factor determ., antibuckling constraint effect 77−40502
Al, thin film on fused quartz, threshold adhesion failure, meas. by stylus method 80−50806
Al, workhardened thin specimens, fracture, anisotropy coeff. role *(French)* 80−104276
Al-Cu, type 1100, synchrotron radiation microradiography 80−85121
Al-Cu-Mn, type 2219, synchrotron radiation microradiography 80−85121
Al-Cu-Si-Mg, deform. simulation using torsional test, elastoplastic constitutive eqn. 80−93594
Al-Zn eutectoid alloy, sensitivity analysis of torsion method in evaluating superplasticity indicators 77−56179
Al-Zn-Mg, acoustic emission meas. during tensile testing, reproducibility of results 80−50782
Al-Zn-Mg-Cu (6, 2.5, 1.5 wt.%), deform. simulation using torsional test, elastoplastic constitutive eqn. 80−93594
$Al_xGa_{1-x}As$ DH laser, rake-line form. in LPE growth, scanning photocurrent technique 80−2287
Al_2O_3, compressive stress state strength determ. in brittle material 77−16757
B fibre reinforced Al, strength determ. procedure in annular specimens *(Russian)* 78−95864
C and low-alloy steel inherent austenitic grain size determ., exam. of methods used 78−85071
C, baked mix, optimum binder content estimation 77−73253
C fibres in tension, testing equipment 77−40497
C materials, bend strength testing, bench assembly with strain recording 79−57176
Co enamel, vitreous, objective colour evaluation, rel. to firing parameters *(Czech)* 80−42252
Cu, activation vol. and dislocation density determ. from relaxation tests 78−3264
Cu conductors in reinforced concrete, radiographic method of inspection 79−15936
Cu, life testing 79−70256
Cu, metallic adhesion, use of fracture mechanics and contact resistance meas. 77−70271
Fe and alloys, softening effect, tensile test at low temps. *(French)* 77−63875
Fe, cast with spherical graphite, SiC-Q apparatus for tensile strength meas. *(German)* 80−76450
Fe, grey cast, tensile testing of mechanical props., from room temp. to liquidus *(Japanese)* 80−7728
Fe, metallic adhesion, use of fracture mechanics and contact resistance meas. 77−70271
Fe, pig, white, mech. props. meas. *(French)* 80−104370
Fe plastic strain, thermoactivation anal. exam. of method *(Russian)* 79−57164
Fe polycrystalline, two ferromag. methods for eval. of fatigue limit 80−89438
n-GaAs, and Te doped, homogeneity, IR introscopy investig. 79−15446
Ge, high press. appl. by spherical diamond indentor, plastic deform. obs. method 78−35619
Mg-Al single crystal growth, specimen for tensile testing in corrosive medium *(Russian)* 80−20774
$MgCO_3$ powder, high speed method of porosity determ. 77−90543
MnMgZn ferrites, accurate chemical comp. determ. by instrument-aided neutron activation anal. 79−29438
Mo, sintered, gas evolution and degassing 80−100814
Na_2O-CaO-SiO_2, proof testing 80−108654
Nb-Ga, superconductor, phase diagram determ. using various methods up to temp. of 2200°C 79−8414
Ni *(Japanese)* 78−15617
Ni, acoustic emission during magnetisation, stress effects 79−82854
Ni alloy, oxide film isolation and obs. method 77−52563
Ni electroplating method for high-temp. stress meas., fundamentals *(Japanese)* 78−15616
Ni-In alloy, deposited on Kovar, vacuum seal for borosilicate glass appl. *(Italian)* 80−40621
Ni-Zr-C (1, 0.1 wt.%), safe-life testing strengthening phases evolution and influence on heat resist. *(Russian)* 79−52476
Pb, life testing 79−70256
$Pd_{80}Si_{20}$ amorphous alloy, skip deform. and crit. shear stress, using tensile testing machine 80−89321
Pt-Au, thick film, adherence meas. and evaluation 80−50813
Pu, elastic constants at elevated temps., noncontact meas. tech. 80−104405
Si, high press. appl. by spherical diamond indentor, plastic deform. obs. method 78−35619
Si, near (111), fracture by painted indenter, SEM study 80−71734
Si semiconductor plates, control of quality of surface treatment, using Al spraying technique 80−60989
Si slices dislocation density determ., using ellipsometer *(Hungarian)* 79−99198
SiC heat-exchanger tubing, IR techniques for evaluation 80−76435
Si_3N_4, cracking characterisation by double torsion test *(French)* 80−104369
Si_3N_4, hot-pressed, proof-testing 78−80693
Sn plate, quality evaluation method using elasticity charact. 77−52582
Sn plate, rapid test for props. assessment 80−40650
Ti alloys, metallurgical characterisation using thermoelec. power meas. *(French)* 80−45462
Ti, dynamic plastic loading of frames 79−20117
UO_2 ceramic fuel fabrication, simulation of thermal processes by emanation thermal anal. 80−811
V_3Ga composite prep. and testing for high-field supercond. magnet 79−30513
W wire reinforced Ni alloy, heat resist. testing, specimen gripping arrangement 79−15895
WC-Co based cutting tools, temperature meas. method based on amount of W in binder 79−96264
$ZnCl_2$-oil system, simulation of steel-slag, macrophotographic method of diagnosing disperse system 80−25952
ZnO fibre reinforced elastomer, X-ray diffr. exam. of filamentary crystal distrib. 80−7738

mathematical analysis
see also approximation theory; Bessel functions; calculus; catastrophe theory; differential equations; eigenvalues and eigenfunctions; Fourier analysis; integral equations; numerical analysis; series (mathematics); spectral analysis; transforms
absorbing-scattering semitransparent planar layer, flat temp. waves 78−90683
acoustic wave propagation, review of techniques for soln. of problems 80−53514
air pollution effects, indicators mathematical model and provisional map 78−81387
annuli, spherical rot., stratified convection of viscous Boussinesq fluid 79−27635
annulus, spherical, rot., forced thermal convection of viscous fluid 79−27634
arc welding, molten pool solidification and bead formation 80−75341
asteroids orbital perturbations, analytical integration using regular proximities concept 80−72843
asymptotic methods use in fluid mechanics, review *(French)* 77−87653
asymptotic techniques for stress conc. regions in plane problems 78−28953
biology, medicine and ecology mathematical foundations of compartmental analysis 78−68978
boiling, forced convection type, in uniformly heated vert. tube, generalised crit. heat flux correlation 79−27498
book, mathematical methods for physics 77−45670
catastrophe theory, appl. to eqn. of state for gas-liq. transition 77−59092
catastrophe theory, claims and accomplishments 78−29
catastrophe theory, violation of certain conservation laws at crit. values of parameters 78−4575
catastrophe theory as tool for physical scientists 78−41136
catastrophe theory in chem. reactions, study and classification of propagating phenomena 78−7170
catastrophy theory appls., book 78−32665
category detecting nerve cells formation, mathematical theory 78−80859
celestial mechanics, analytical method for determ. of perturbations of orbital motion 78−24455
classical equilibrium statistical mechanics, mathematical struct., book 79−26017
global climate, mathematical model appl. to CO_2-climate sensitivity study 80−31117
cluster analysis, appl. to stellar spectral classification errors detect. 78−20819
complex pot. eqns., appl. to general relativity 77−13655
complex variable anal., appl. to elasticity theory 78−5660
conference, Tokyo, Japan (June 1979) 80−31412
convection driven by non-uniform surface tension 80−10116
cosmology, relativistic, hierarchical, mathematical formalism and Einstein eqns. 80−82555
critical heat fluxes in internally heated annular channels 78−31637
cumulative sum technique, appl. to peristimulus time histograms 79−34536
D-optimal design for quadratic regression on a hypercube 79−92921
decomposed partial peeling and limit bundler 77−60919
differential forms in mathematical physics, book 78−81810
diffraction catastrophe patterns, two dimens., caustics anal. 77−17827
dimensional anal., mathematical model of process 78−54171
earthquake occurrence as stochastic event, theoretical models 78−40491
EM fields about horizontal electric wire source of arbitrary length, analytical derivation 79−27130
falling film gas-liquid reactor anal. 79−86526
ferrofluid, helical flow with heat cond. between coaxial porous tubes 79−23371
ferromagnetic systems, crit. experiments, field theory, Borel transform. 80−80541
flow, transient, two-phase, flow reversal prediction LOCA conditions 78−94811
flows with vibrational relaxation, sudden-freezing analysis 77−58806
gel-chromatogram processing technique allowing for spreading, Friedholm eqn. soln. *(Russian)* 79−24880
geodesy, statistical, mathematical struct. and appls. 79−29696
geodesy, three-dimensional, rank defect anal. of datum problem 78−61310
geomagnetic declination field near Earth surface, error in analytic representation 78−73307
geomagnetic S_q-field, seasonal and latit. vars. deduced via natural nonorthogonal functions method 78−36359
geophysical fields configurations, analytical description in terms of different geometry *(Russian)* 79−74986
geophysical fluid dynamics, use of similarity theory in Soviet work *(Russian)* 78−16174
geophysics, analytic construction for two-dimensional gravimetric and magnetometric problem 80−21846
geophysics, analytic continuation of function for Earth surface *(Russian)* 79−35008
geothermal power plants flash cycle optimisation, analytical expression in terms of temp. only 80−40894
gravitational field, external. of three-dimensional body, analytic continuation into interior *(Russian)* 79−34731
heat conduction, elliptic cylinder, interior value problem 79−37123
heat conduction in adjacent regions, approx. analytic solns. *(Russian)* 78−83212
heat conduction problems, extended domain solns. 80−19209
heat exchange, conjugate problems soln. method *(Russian)* 79−64483
heat exchanging bodies, inverse heat cond. problem, boundary conditions identification methods 79−37115
holonomic formulation of boundary layer eqns., use of tensors 79−1153
Hopf bifurcation and applications, book 77−22365
imperfection sensitivity of semisymm. branching, rel. to catastrophe theory, stiffened plate appl. 77−84170
infiltration analysis and perturbation methods, absorpt. with exponential diffusivity 77−66944
integral inequalities and separation for Schrodinger type operators in $L_2(R^n)$ 78−77680
integral inequality 77−82373
interstellar shocks, analytical results for post-shock gas temp., density, vel. and comp. 80−56911
inverse problems, soln. via component ranking method using information on region with possible solns. *(Russian)* 77−13131
inverse theory, appl. to geostrophic ocean currents determ. independently of reference level 80−51574

mathematical analysis continued
isoperimetric monotonic property containing some classical theorems *(French)* 77−67203
isothermal melt spinning, Lagrangian and Eulerian viewpoint 79−7357
lakes, winter season energy balance *(Polish)* 78−24315
Laplace-Hankel transformation of generalised functions 78−54156
linear inverse problems solution, positivity constraints, appls. 77−45178
linear inverse problems solution, positivity constraints, theory 77−45177
linear regression analysis, steroids, mass spectra, computer-aided interpretation 78−64898
low and high pressure discharges, aspects *(French)* 78−14240
low and high turbulence flows, hot wire measurement based analysis 78−59511
magnetic anomaly field vertical intensity, autocovariance function analytic derivation for sources statistical distrib. *(German)* 79−34746
meteorology, isentropic objective anals. *(Polish)* 80−51546
minimum Entropy Deconvolution with an exponential transformation 80−17407
modal analysis, general introduction for managers 80−91955
mountain basin morphology, river branches and sides, models *(Italian)* 78−3829
multilayer cylindrical shells with fillers, analysis of stability 80−7643
multiple time scaling anal. of third order nonlinear differential eqns. 77−82369
musical texts, math. model for anal. and structuring 78−90608
N complex random variables, sum, statistical anal., atm. laser beam propag. appl. *(Italian)* 77−45796
non-standard anal. methods appl. to elasticity 77−47
non-standard analysis, approach to elasticity 77−46
nonlinear inverse Compton radiation spectrum, deepest descents method 78−85840
nuclear dense matter phase transitions, cusp catastrophe theory 77−22920
nuclear power station with VVER, for semi-peak load generation, mathematical model 80−68936
orbit computation, semi-analytical method *(Chinese)* 79−8798
path-integral functionals for randomly-stirred fluid vel. correlations, variational principle 78−81846
phase transitions with several order parameters, catastrophe and renormalisation theories 78−32782
pipe flow, turbulent, temp.-depend. viscosity effect on convective heat transfer 78−90884
planetary orbits, analytical method for asteroid belt effects 79−75082
pollutant dispersion during calm wind situations, analytical modelling 78−81385
porous medium being dried, heat transfer and moisture flow, generalised model *(Hungarian)* 80−83839
porous oxide pellet, spherical, reduction by gas flow *(French)* 79−27713
potential theory inverse problem, soln. uniqueness *(Ukrainian)* 77−71183
radiant-convective heat exchange problems, nonstationary, analytical soln. method 80−33432
radiating laminar boundary flow over flat plate at large free stream Mach no. 79−1270
radionuclide distribution, selective determ., mathematical modelling *(Rumanian)* 79−81098
radiowave propagation over curved anisotropic surfaces *(Japanese)* 78−42266
recycling flow over bottom topography in a rotating annulus 78−90916
singular Cauchy problems in symmetric spaces 77−5632
soft spring, dynamic behaviour, mathematical anal. 78−12491
solution generating theorem, appl. to general relativity 78−21027
space vehicle, motion in vicinity of collinear libration point, semianalytical method 78−4066
spacecraft, flexible, eigenvalues and eigenvectors for hybrid coordinate eqns. of motion 79−75085
spatial flow field determination, hot wire anemometry based analysis 78−59512
steam-water mixtures, reversible adiabaticity equations 79−12751
Steinbuch's Lernmatrix appl. in assessment of airborne Pb effects on children 77−44878
strain energy of elastic prismatic bar, theorems *(German)* 80−79142
strain meas. by holographic interferometry, mathematical formulation *(German)* 80−78815
strange attractors, analytic form 78−8227
sugarcane, evaluation of mathematical methods for optimum γ-dose prediction 79−29630
surface waves excitation near cut off freq. 77−68607
temp. meas. by thermal noise, appl. *(German)* 78−4615
thermal-ignition analysis in boundary-layer flows 79−64800
transonic flow, two- and three-dimens., perturbation soln. method 79−1208
two phase flow pressure drop measurement variations, analysis *(German)* 78−59445
undergraduate text, simple approach 77−71190
unsteady forced convection heat transfer from impulsively started circ. cylinder 79−27633
US atomization, cavitation-induced capillary waves 80−33328
visual pigment system kinetics 78−92623
Voronoi polyhedra 79−9073
wave transmission through pressure duct *(Italian)* 78−36838
waves, unsteady, from initial, periodic and travelling disturbances, asymptotic anal. *(Russian)* 78−77254
welding arcs, gas velocity fields modelling 80−75039
wind velocity gust factors, analytical approach 78−88897
X-ray analysis of partially disintegrated martensite, appl. of method of moments 79−52223

mathematical linguistics *see computational linguistics*

mathematical logic *see formal logic*

mathematical programming
see also dynamic programming; geometric programming; linear programming; nonlinear programming; stochastic programming
BWR control rod programming, heuristic and mathematical approaches 79−9779
deformation analysis at plastic collapse, math. programming methods 78−1572
elastoplastic structures, stresses and strains during loading, mathematical programming, pivoting procedure 80−53641
environmental pollution control system methodological approach problems 77−21899

mathematical programming continued
Faraday-type MHD generator optimisation, using a computer method *(Polish)* 78−79476
groundwater flow model using finite element method 78−92874
mixed integer programming and other optimisation techniques, DEMOS-E program library appl. *(Japanese)* 79−2615
nuclear radiation characteristics, mathematical programming methods to obtain internal estimates 78−5105
nulcear reactors, PWR core control, multistage mathematical programming 80−91227
reservoir operation, multigoal anal. 79−96768
spatial reactor control methods 77−83056
string, stretched, appl. of optimisation methods to vibr. control 78−83305
structural wt. optimisation, optimality criteria and mathematical programming 78−26029
water pollution model, Streeter-Phelps type, parameter estimation 79−5539
water resource problem with multiple objectives, interactive optimisation, Yodo River basin, Japan appl. 79−57516
water resources problems of Kakogawa River basin, multiobjective optimisation 79−57993

mathematics
see also algebra; combinatorial mathematics; convergence; digital arithmetic; duality (mathematics); equations; formal logic; functions; geometry; mathematical analysis; number theory; probability; statistics; topology
applied mathematics, conf., Delft, Netherlands, Jan. 1978 79−2617
applied mathematics and mechanics, conf., Giaz, Austria, Apr. 1976 *(German, English, French)* 77−67284
Aryabhata, 5th century Indian astronomer and mathematician, life and works 78−65741
Ball, Sir Robert Stawell, Victorian astronomer and mathematician 79−88783
celestial mechanics, applied modern mathematical techniques *(German)* 78−45211
course for engineering students, student and teacher perceptions of degree of difficulty 78−57712
education, Age of Newton workshops in optics, mechanics and mathematics 77−87586
education, physical sciences at Lanchester Polytechnic 79−44658
education, physics joint honours degree course at Manchester University 79−35456
education, university science course for talented secondary-school students 78−89282
educational course for undergraduates, self-study programme with unusual topics 79−80383
exponential law, concepts prior to 1900, review 78−86052
factoring 111...11, applications, teaching approach for pre-calculus students 78−57714
Glasgow University, computer-aided learning project in maths 77−71168
Lambert, Johann Heinrich, 1728-1777, biography *(German)* 79−17174
Laplace, P.S., chronology and citations of early work, 1770-1773 period 78−93505
learning, effect of specially constructed advance and post-organisers 79−35452
mathematical geophysics, 11th International Symposium (Seeheim, Germany, 18-27 August 1976) 77−73622
mechanics, limitations in description of physical phenomena 77−67263
modelling and appls., book 77−5617
module, description and evaluation 80−86056
M.Sc. course, mathematical education development, for teachers 79−80384
nature and foundations, Grassmann's Ausdehnungslehre and Schleiermacher's Dialektik 77−57143
philosophy of mathematics, renaissance of empiricism 77−1
physics course, success rate, rel. to math. skills, testing 77−60860
physics students, mathematics ability 80−77591
quantitative relations between infinite sets, philosophical arguments 77−57145
Regiomontanus, Johannes, 15th century astronomer, life and works 78−20929
remedial work for university students in engineering courses 80−86054
special relativity, arithmetic basis, numerical eqns. computer solvable 77−57185
Stokes Theorem, surface of mixed physical properties, mathematical method *(Italian)* 77−50589
student courses, effect of class evaluation method on learning 78−57719
teaching, general applied maths and statistics development for appl. to all sciences secondary level 78−57716
teaching, heuristic model evaluation appl. to geometrical problem 79−80385
teaching by computer, long division practice program 80−98775
teaching by computer-assisted learning 79−80401
teaching new naturalistic style 77−60867
undergraduate mathematical methods course for mixed discipline classes 79−80382
verbal computation problem-solving, hierarchical struct. of learner abilities rel. to material strength 79−35453

matrices *see matrix algebra*

matrix algebra
see also S-matrix theory
2-D polynomial matrices, factorisation and coprimeness 77−64915
3-j symbols, general set of relns. 78−41183
acoustic reflection from layered elastic absorptive cylinders, matrix methods 77−46826
acoustic signals, matrix formulation of multiple and partial coherence 77−46831
acoustic wave propag., product of matrices and random transfer *(French)* 78−5596
active electrooptic and magnetooptic media, matrix theory fundamentals *(Russian)* 78−63005
angular momentum expressions reduction by matrix arithmetic, computer method, perturbation calcs. 77−26126
anisotropic media, partially polarised light propag., differential 4×4 matrix calculus 79−41330
arbitrary molecular point groups, fractional parentage concept 79−10225
arbitrary pseudo-Euclidean space, real and complex boosts 78−113
arbitrary square matrix with multiple eigenvalues, analytical function evaluation 77−74188

matrix algebra continued
array algebra appls. 79−44702
astrometry, accuracy of star positions obtained by block adjustment 78−20623
astrometry, overlapping plate method appls. 80−36479
atom, unitary group generators representation matrices calcs. 78−78610
atomic quantities, algebraic expressions for matrix elements for operators 77−6664
automatic lens design, pseudo-second-derivative matrix computation 79−14077
beam bending and mass-spring system problem methods *(Dutch)* 77−41451
beam formulation, w.r.t. eccentricity 77−89028
bending and nonuniform torsion of prismatic bar, matrix analysis 80−83736
binary correlations in random matrix spectra 79−44851
binary reaction amplitudes for particles with spin 77−74273
birefringent retardation plate matrix representation 79−22894
Block-Stodola eigensoln. technique for large algebraic systems with nonsymmetrical matrices 77−26163
boost matrix elements of the homogeneous Lorentz group 79−92975
Born's discovery of the quantum-mechanical matrix calculus 80−82615
canonical pseudoscalar-meson matrices, chiral SU(n)×SU(n) symm. of strong interactions 78−29266
canonical transformation of the Hamiltonians quadratic in coordinate and momentum operators 79−84991
Casimir invariants and characteristic identities for generators of graded Lie algebras 80−13227
catadioptric systems, matrix optics 79−94167
Cholesky factorization of band matrix, method for updating, appl. to a stiffness matrix 78−16623
Clebsch-Gordan coeffs. for S_n, generation programs 78−86172
Clebsch-Gordan coeffs. program for finding functions on tableaux and frames of the symmetric group S_n 78−86173
closed linear operators, matrix representation, extension of Von Neumann's theory 79−40396
cluster approximation for an infinite-dimensional determinant 79−80503
coefficients of potential of two-dimensional regions with rotational antisymmetry 77−33830
coincidence site lattice rotation matrices, permissible angles 79−32932
colorimetry, appl. of matrix techniques 80−105690
combined transfer matrix and finite element techniques, analysis of static and dynamic structural problems 80−53619
compact Gaussian relations for n-component optical systems 79−14082
compact storage for iterative soln. of large sparse linear systems of eqns. 78−57713
computation methods and applics., book 77−37721
configuration space basis state generation, U(n) matrix elements 80−86120
congruent numbers note 78−54147
continued fraction solutions to systems of linear eqns. 77−2506
coupling coeff., general theory 79−88829
crack-tip problems and quarter-point triangular elements 78−83333
criterion matrices, appl. to design of homogeneous isotropic geodetic networks *(German)* 79−100983
crystal vacancy modelling, topological approach 80−10543
crystallographic orientation, distribution function generalisation using rotation matrix 80−11665
current transformers, oil insulated, parameters influencing heating assessment using sensibility matrix *(Hungarian)* 80−87708
curved beam with viscous damping forced vibrations 79−50622
cylindrical lenses, rotation of parallel fan of light, matrix representation 80−38089
damped linear systems, vibr. 79−18790
Davidson's algorithm with and without perturbation ocrrections 80−27570
decaying systems with degenerate livsic matrix 80−82629
decomposing a projection, Householder-Fox algorithm 78−77663
density matrices convergence and entropy 77−30046
density matrix geometry, definitions, N matrices and I matrices 78−65816
density matrix geometry, reduced density matrix and N-representability 78−65817
density matrix in QED and the Hawking effect *(Russian)* 78−89644
differential equation, rotations as solns., for teachers 78−62021
Dirac matrices, compact evaluation of traces 77−17750
direct methods, matrix formulation for finding strongest starting set of reflections 79−73065
discrete Gauss transform, inversion of $\{\rho^{(r-s)2}\}$ matrix 80−4505
discrete multiplicative processes in Markovian environments, long run growth rates 79−75453
dynamic system, two representations of sensitivity and error analysis 77−60900
education, Dirac γ matrices 77−45637
education, rotation matrix formalism for rots. 77−82349
eigenproblem developments for numerical weather simulation 77−25760
eigenvalue determination by continued fraction 80−105490
eigenvalue spectrum of large symmetric random matrix with finite mean 78−32646
eigenvalues of matrix operator $S.\pi$ for spins 1/2, 1, 3/2, const. mag. field 78−32712
eigenvector derivatives, banded eqn. soln. algorithms 77−22367
eigenvectors location methods 78−36790
electron interaction, trace evaluation in strong mag. fields, REDUCE based program 79−7480
electron storage ring, beam distrib. parameters using transport matrices 79−54725
ellipsometry, Mueller-Stokes calculus, conventions and formulas 80−102618
elliptic polarisation, Stokes parameters, vector trihedron, optical element evaluation 80−53209
elliptical tunnel with contained axial conductor, radio transmission 79−55030
EM propagation, birefringent layered media 79−76582
environmental assessment, graph-matrix method 79−57502
equations of state, search procedure, based on step-wise least-squares technique 80−19900
even-even deformed nuclei, multiphonon $K^{\pi}=0^{+}$ states, matrix elements of general Hamiltonian 78−41621
exceptional gauge theories in 3×3 matrix formalism 78−70248
exponential quadratic phonon operators, ensemble averages 78−54293

matrix algebra continued
extreme eigensolution calculation method for high order real symmetric matrix 80−90703
fermion reduced density matrices 78−16731
finite chemical graphs, characterisation by isomorphism invariant 79−13623
finite cylindrical scatterer near imperfectly conducting ground 78−71003
finite decomposition of tr e^{-A} as function of diagonal of A determ. from Laplace transform *(French)* 79−25824
finite element discretisation, two-dimens. stationary heat cond. using successive overrelaxation and conjugate gradients 78−83206
flat galaxies dynamics, integral eqn. for normal modes in matrix form 77−33637
flexibility matrix for skew-curved beams 79−98620
four subshells of equivalent electrons, matrix elements of relativistic energy operator 78−33407
Fourier and Walsh spectra relationship, physiological data processing appl. *(Russian)* 78−26
fractional-parentage coefficients, reduced in quasi-spin space, submatrix elements of tensor operators 80−4578
frame structs., large deflection anal. by fictitious forces 78−83249
frameworks calc., composed of thin-walled open sections, with aid of computer 78−51059
free particle Green's function, Gaussian matrix elements 79−2667
frequency anal. of unsupported structures 79−32333
full unsymmetric matrices, out of core eqn. solver 78−45477
G, F and Σ matrices for XY_8 molecules of D_{2d} symmetry *(French)* 80−970
gamma-ray spectral anal. using FFT *(Japanese)* 78−90047
Gell-Mann's matrix algebra for SU_3 group *(Russian)* 79−9308
geodesy, parameter accuracy improvement by choice and quality of obs. 79−44078
geodesy, sequential solns. with bandtype system of obs. eqns. 78−65169
geometrical optics teaching to engineers, numerical calc. methods 80−62415
gradient formula for the group U(2l+1) in nuclear collective model theory 78−37300
graphical method for matrix determinant and inverse, generating functions for harmonic oscillator integrals 78−57732
gyroscopic systems eigenvalue problems solution, with real symmetric matrix of same dimension 80−12895
H-matrix calculations, incorporation of linear constraints 79−30394
Hadamard and M-sequence transforms are permutationally similar 80−32921
harmonic chain with random masses, transmission coeff. and heat conduction 79−80547
heat transfer finite element and finite difference methods iterative substructuring 79−10564
Hermite polynomials, matrix eigenvectors 79−49013
Hermitian matrix, disorder effect on spectrum 80−31547
hermitian matrix, large, eigenvectors determ., new approach 77−37717
Hermitian matrix, low lying eigenvectors, pseudo-convergence in iterative method 79−92970
HF approximations, thermodynamic Fermi systems 80−4642
hologram interferometry, use of projection matrices 80−37965
homogeneous Lorentz group SO(3,1), boost matrix elements and Clebsch-Gordan coeff. 78−4505
Huckel matrix reduction, graphical method 80−14085
hypergeometric functions, partial differential matrix eqns. 77−37730
image restoration, pseudo-inverse, singular value matrix decomposition algorithm *(Russian)* 78−37810
incoherent optical system, improving the accuracy of matrix calcs. 78−78924
inequalities for fermion density matrices 79−6044
intelligent states, computation of Clebsch Gordan coeff. 78−62101
intelligent states, group-theoretic study and computation of matrix elements 78−62100
inverse matrices componentwise error estimates 78−32645
inverse matrix diagonal and off diagonal elements, self energy perturbation theory 78−82607
inverse of quasi-tridiagonal matrix, explicit formula 79−88793
inverse polynomial matrix calc. after changing elements in initial matrix *(Ukrainian)* 77−67185
inverse problems, soln. via component ranking method using information on region with possible solns. *(Russian)* 77−13131
inversionlike integral eqn. in multidimensional case 78−62054
invertible matrices, with Lie- and symplectic-admissibility, struct. and classification 79−40348
inviscid fluid conservation law eqns., coeff. matrices for implicit finite difference soln. 78−42580
isomorphous group representation appl. *(Portuguese)* 77−37724
isospectral matrices, finite transforms 80−105529
isotropic media, linear dynamical equations of state 80−22314
IU(n) group, matrix elements of irreducible representations *(Russian)* 78−54149
Jacobi matrices, rational, asymptotical eigenvalue density 78−81794
jj-coupling, submatrix elements of operators derived from unit tensors 77−422
Jost function treated by the F-matrix phase integral method 79−25884
K-matrix, off-shell 2-body scatt. with Woods-Saxon pot. 78−21002
Kalamboukis tests of Davidson algorithm, comments, nuclear structure 80−86822
Karle-Hauptman determinants, use for small struct. determ. 79−7513
Keplerian transition matrices for elliptical orbits 78−36442
kinetic theory differential operator, matrix representation 80−14867
Lanczos method, method of moments, tri-diagonalisation of a matrix 78−58240
large mol. reaction with intermediate complex, vibr. distrib., R-matrix, hybrid quantum statistical mechanics 77−52611
large real symmetric matrices, generalised eigenvalue problem, group coord. relax. method 78−16622
large symmetric matrices, ensemble averaged eigenvalue spectrum 78−132
large systems of linear eqns., computer soln. *(Russian)* 77−53764
Lie groups, compact, relations between quantities in representation theory 77−2512
Lie groups, semisimple, representation matrix elements and Clebsch-Gordan coeff. 79−97230
light transmission and reflection, in cholesteric liquid crystal incident angle dependence calc. 78−43834
linear eqns. integral soln. using integer arithmetic 78−69960
linear equations systems solution, unsymmetric, sparse, computer program 77−80210
linear transport relaxation equations, matrices, variational principle 80−17785
Lorentz group, linear representations and matrix element computation formulas 79−58571
Lorentz group linear representations and their matrix elements 79−93306
M-matrices, differential eqns. soln. *(German)* 77−82377
M-matrix theory *(Japanese)* 77−53737
magnetic spectrometers, momentum determ. using non diagonal weight matrix 79−59296
magnetotelluric analysis for layered Earth, matrix relation 78−32008
magnetotelluric anisotropic data, inversion technique 77−60475
many-electron atoms, determination of matrix elements of operators describing hyperfine structure 77−46505
many-electron atoms, generalised spherical functions 77−46483
many-electron spin degeneracy, recursive formula for Young's orthogonal representation 77−38596
matrix diagonalisations via involutional transforms. 80−17827
matrix diagonalisations via reduced characteristic eqns., appl. to ang. mom. coupling 80−17828
matrix eigenvalues sensitivity 78−89295
matrix eqn. soln. 78−45478
matrix function approximate factorisation algorithm 80−68022
matrix products with application to classical statistical mechanics 79−71351
matrix representation of unbounded operators 79−97231
matrix Riccati equation, numerical soln. method *(Russian)* 79−25822
Matrix variational Pade approximants and multi-step square-well potentials 79−71283
matrix-scaling technique, transient struct. response anal. 77−72148
membrane transport matrix, relation between conc. depend., matrix transformation and flux representation 78−20069
metric tensors, in Hilbert space, geometrical approach to solving cryst. structs. 79−32846
mode-coupled multimode fibre transfer function 79−10409
molecular graphs, matrix descriptions 77−38737
molecular rotation and vibration calcs., real symm. coords., groups having complex representations 78−82715
molecular vibration, non-rigid mol., FORTRAN FORMAC products of non-numerical matrices 78−50540
molecule, method of calc. from fragments 79−63905
multidimensional dimer problem, upper bound improvement 78−78607
multidimensional nonlinear partial differential eqns., integration by inverse scatt. problem method 77−60905
multidimensional reactor dynamics equation, fast factorization and exponential transform. procedures 78−17303
multielectron configuration, evaluation of matrix elements of energy operator 79−63895
multilayer thin film, optical scatt., matrix formulation 79−31804
multilink spatial mechanism structure and analysis *(German)* 79−21544
multiple parameter system vibrations and stability, book 78−93532
multiplying optical system resolution calc. *(Russian)* 79−98456
multivariate approximants with branch points, practical evaluation 78−54161
multivariate autoregressive feature extraction and the recognition of multichannel waveforms 79−39878
neutron spin-echo integral transform spectroscopy 80−4748
non-conservative systems, dynamics 77−2538
non-negative matrix, random evolutions and spectral radius 79−93042
non-numerical matrix products using FORMAC 78−50540
nonlinear laser spectroscopy, density matrix methods, review 78−74071
nonlinear rate equations, soln. by matrix inversion 78−93520
nonnegative at spectral radius, eigenprojection computation 77−53735
nonsymmetrical optical system, matrix representation 80−64130
normal mode calcs. of crystals and molecules, coordinates and force matrices generation, computer program 78−91393
nuclear fission, Sommerfeld-Watson transformation *(Rumanian)* 78−86526
nuclear two-particle density matrix, for U(3(n−1)) states with $E_{min}+1$ in nuclei with n≤16 78−41624
nucleon-nucleon interaction matrix, irreducible basis of representations of group O(n-1) 77−6271
nucleus, model density matrix, $U_{3(n-1)}$-irreducible decomposition 79−67692
octahedral group, symmetry-adapted functions, calc. of rotation matrices using recursion relation 80−31482
octonion, pseudo-alternative, and Lie-admissible algebras 79−40347
one dimensional Ising system with random long-ranged interaction, density of eigenvalues of random matrix PV 79−12733
one-dimensional oscillator, matrix elements of position coord., upper and lower bounds 79−35578
Onsager-Casimir symmetry, geom. of roots of matrices 79−100
operators for viscoelasticity with ageing *(French)* 79−18729
optical bare resonator eigenvalue analysis, matrix methods 80−78927
optical data cross-correlation matrix processing 79−13910
optical matrix multiplication, two-dimens. 79−59647
optical techniques for matrix multiplication 77−71936
optical thin film, Smith chart and charact. matrix for reflectance computation 79−45904
optics of anisotropic layered media, 4×4 matrix algebra 80−106445
orthogonalization of random variables, weather forecasting appl. 77−74203
oscillations by matrix theory, for teachers 78−61986
oxygen-type atoms, subdivision of 2p-shell 78−82609
P1 subgroups, mathematical tools, automorphism and matrix factorisation *(French)* 79−51037
Pauli algebraic formalism in polarisation optical studies 78−87010
Pauli spin matrices, generalised, commutation rules 79−17597
Pauli spin matrices, higher dimensional extensions 79−92969
permutation matrices using graphical methods of spin algebras, Serber coupling 79−6833
perturbation theory, many-body, arbitrary point group symmetry, wave operator matrix elements 80−23311
phase values reconstruction from phase differences, matrix formulation 79−59642
photoelasticity, matrix theory, book 79−64612
planar approximation for coupling N×N matrices 80−62872
Pn3n, Clebsch-Gordan coupling coefficients 79−90585

matrix algebra continued
point of refraction, analysis and theorem *(Japanese)* 77−79743
Poisson brackets, on extension 79−63080
polar semiconductor, nonlinear transport, field-dependent relaxation time 80−6866
polarised light impulse response matrix formalism, appl. to holography 78−63045
polarized waveform dectors, matrix and Stokes vector representations, teleseismic waves appl. 78−12008
polyatomic molecule anharmonic pot. theory, spatial matrix method 78−55161
precession theory, vector-matrix notation 80−51642
preconditioning of indefinite problems by regularization 79−46214
proper functions of two-dimens. field, air pollution appl. 79−21002
quadratic boson Hamiltonian, diagonalisation 78−93600
quantal matrix elements between unbound states, for radial Schrodinger eqn. 79−97240
quantum mechanics, EPR paradox, reduced density matrix method, review 78−77766
quantum mechanics two-centre problem, discrete and continuous spectra, nonadiabatic matrix elements 77−45726
quasi-degenerate Rayleigh-Schrodinger perturbation theory, calc. of effective Hamiltonians 79−71284
quasi-linearisation of matrix Riccati eqn., iterative approx. 78−57871
p-quaterphenyl, mol., charge density and bond orders, polynomial matrix method 78−74808
R-matrix theory, threshold cusp 79−58893
radiation transport, appl. matrix methods 78−13198
random matrix, asymptotic eigenvalue-distrib. 77−5618
random matrix ensembles, joint eigenvalue distrib. 80−101748
random sparse matrix block triangularisation 79−44703
ray transfer matrix, for 90 degree reflector 80−33184
rectangular matrix pseudoinverse using column approx., inconsistence systems of linear eqns. solns. 78−62061
reduced tensor matrix elements program, AAKP, adaptation for tensor product evaluation 78−17587
relativistic electron-transition operators, matrix elements 78−82789
renal counterflow systems differential equation, soln. by numerical method 78−24082
renormalized plane wave-projected and Coulomb-projected T-matrices 79−17267
residual spectra, general matrix approach 80−94947
residual spectra treatment appl. 80−68132
resolvent operator expansion 77−49551
Riccati equation, matrix differential, steady-state soln. calc., iterative algorithm *(Russian)* 77−49585
rotation formalism, coordinate-free 77−22366
rotations, nonlinear vector products calc. methods. 77−71201
roto-translations, method of conditioned observations 78−12531
rotor blades, dynamic characts. via transmission matrix method 77−39251
scale and conformal invariance, scalar currents, theory with continous mass spectrum 78−62335
Schrodinger equation, generalisations of finite element and R-matrix methods 78−24676
seismic fields, decomposition algorithm from charact. numbers and vectors of spectral matrices 77−9370
seismology, matrix methods for generally stratified media 77−2116
shells with internally attached structures, transient response 79−3941
Siegel matrix for triple rectilinear collision, eigenvectors *(French)* 77−70988
siesmic sources, gravitating Earth flattening approximations to Green matrices 77−33002
Singer polymals, evaluation of matrix elements 79−6813
single eigenvalue distrib. for non-zero mean matrix ensembles, correct form 80−73198
singular capacitance matrix equations. conjugate gradient method convergence 78−36791
skew plate, soln. of infinite matrix 78−75064
SO(n-1,1) representation matrix elements, computation formulas 79−43
space groups, coupling coeff. 79−90584
sparse symmetric matrices profile reduction 77−48989
sparse system of linear equations, solution 80−23
spectral anal. of linear systems with multiple inputs and outputs, comment 79−17344
spectral density matrix, consequences of non-negative definiteness 79−80511
spectral multiplication, props. as viewed in physical space, meteorological appls. 80−94607
spectral radiation detectors, calibration and error anal. 78−46177
spin system, ABC type, matrix elements of tensor operators calc., transition probability matrix 80−25182
spin wavefunction matrix element expansion 78−41185
spinor norm, new formula 78−62048
steady-state response of difference eqns., digital computation schemes 78−57718
steam-water-ice system, two-dimens. triangular lattice model, matrix calc., props. 77−27975
stiffness factor formulation, explicitly or using numerical integration 77−65676
structural analysis, combined finite element-transfer matrix method 77−62201
structural dynamics, system identification by pseudoinverse 77−72232
structural stiffness matrix eqn., algorithms for direct access Gaussian soln. 78−57766
SU_4 group, transformation matrices between canonical basis and basis of supermultiplet model 79−67693
SU(3) in SO(3) basis, sum rules for matrices of generators 80−13226
$SU(4) \supset SU(2) \otimes SU(2)$ chain, matrices of generators 78−37152
super Clifford algebra 79−98
surface potentials of stratified spheroidal volume conductors excited by electric dipole source 80−32867
T-matrix, perturbation formalism for complex poles and widths, appl. to intermediate struct. 78−66255
teaching model using stored water, discrete transforms 79−23
theory, book 78−12532
time-dependant generalised cost matrix solution *(German)* 77−49552
tops and d-functions in even spaces *(Russian)* 80−4508
transient electrical transport, general and unified treatment 80−59977
transition matrix approach to soln. of Bateman equations of radioactive decay 77−57632
matrix algebra continued
translationally invariant nonrelativistic Hamiltonian, for atom 77−5700
transport theory, analytic continuation of Wiener Hopf factorisation matrices 77−96
triangular finite element universal matrices construction 78−36805
two body scatt., non-relativistic, variational matrix Pade approximants *(German)* 78−54247
two-dimens. structs., finite dynamic element for free vibr. anal. 78−83287
$U(2)\sigma C^{2\times2}$, representation theory, generalised Bessel functions 80−98818
U(p,q), matrix elements and Casimir operators of discrete series representations 79−97238
U(p+q) and U(p,q) in U(p)×U(q) basis, matrix elements for infinitesimal operators 80−12928
U(p+q) and U(p,q) in U(p)×U(q) basis, matrix elements of infinitesimal operators 80−12929
Unimoment method, simplified matrix element representation 77−74207
variational bounds to excited states from generalised Brillouin-Wigner eqn. 78−45507
variational [1/1] matrix Pade approx. in pot. scatt., exact solns. 77−22447
vector-matrix differential eqn., convergence of assoc. eigenfunction expansions 78−69965
vibrating bars, transverse-mode, equivalent electrical networks and appls. 79−68469
vibrating beam, multiplicity of solns. of inverse problem 80−28462
virtual photon spectra calc. by matrix differential eqn. 77−88115
water network anal. using node recording algorithms and admittance matrix 78−85613
water network anal. using sparse matrix and successive linearisation methods 78−85614
wave propagation in piecewise continuous stratified non absorbing media 79−75355
wave propagation in stratified media, matrix anal. 79−12618
WKB method improvement 79−75383
X-ray diffractometry, of superimposed twins and clusters, establishing UB matrices of single cryst. individuals 79−37586
XY_9 molecules, D_{3h} symm., U-, G-, F- and Σ-matrix determ. *(French)* 80−78599
Yukawa pot., s-wave off shell T and K matrices by Ecker-Weizel approx. 79−63074
$Z_2 \oplus Z_2$ graded Lie algebras and superalgebras, sequences 79−5962
NN forces matrix elements in hyperspherical basis *(Russian)* 78−46009
H_2, expressions for calc. Coulomb repulsion between electrons using adiabatic basis 80−91427
H_2^+, exponentially small part of wave function *(Russian)* 80−9497
^{16}O, binding energy, wave function of ground state, orthogonal schema model 79−63582
^{16}O, Hamiltonian matrix analysis, base model of orthogonal scheme for 0^+ state 79−63610

matrix isolation spectra
see also Shpolskii spectra
acenaphthene in n-alkane matrices, Shpolskii spectra fluorescence 78−9190
acetaldehyde, matrix isolation spectra using tunable diode laser 78−45739
5-acetyl-5H-benzo[b]carbazole-5H-benzp[b]carbazole, singlet-singlet energy transfer *(German)* 80−93402
acetylene ($-d_2$), fluoresc., in matrix-isolated acetylene and ethylene photolysis 79−59505
acridine, Ar matrix-isolated, lowest triplet state IR and visible absorption spectra 79−68228
acridine in fluorene matrix, RF induced mag, reson. transitions, triplet state, optical nucl. polarisation 79−31561
acrolein, s-trans and s-cis, trapping from thermal mol. beams and UV-induced isomerisation in Ar matrices, enthalpy determ. 80−97688
alkali atom, in inert-gas solid, at level struct. calc. pseudopot. method 80−9532
alkali disulphide species, $M^+S_2^-$, laser photoluminescence spectra in solid Ar at 12K 79−5148
alkali tetrafluoroaluminates, matrix isolated IR spectra 80−985
alkaline earth dimens., heteronuclear, matrix-isolated, laser photoluminesc., van der Waals ground state 79−41192
alkene-halogen, matrix isolation vibr. spectroscopy, complex form. studies 78−62952
alkene-halogen compounds, assoc., matrix isolation vibrational spectra, appls. 78−46416
γ-aminobutyric acid, cryst., film, matrix IR spectra, low temp., neutral and zwitterion forms. 77−18920
dAMP.dTMP costacking complexes, γ-irrad., charge migration, computer-assisted EPR 77−86446
anharmonic molecules in low temp. matrices, vibronic dephasing 80−6469
anthracene, in stretched polyethylene film, UV-visible and fluoresc. spectral shifts 78−62852
anthracene, matrix isolated, vibr. relax., hot luminesc. obs. 79−85986
anthracene, orientated in nematic liq. cryst., UV-visible dichroism meas. *(German)* 77−34668
anthraquinone, in Shpolskii matrices, triplet state spin-lattice relax. rates 78−21952
9,10anthraquinone, lower triplet states, interactions and position, matrix isolation spectra 80−63634
aromatic compounds, in n-paraffin cryst., luminesc. characts. 79−3480
aromatic compounds, oriented in stretched polyethylene film, phosphoresc. polarisation 79−6961
aromatic esters, phosphoresc. and fluoresc. spectra in organic matrices 80−32756
aromatic hydrocarbons, Shpolskii systems, key and hole rule test, fluoresc. 77−42347
aromatic molecules in O_2 matrices, singlet-triplet absorpt. spectra 78−17683
atmospheric free radicals, meas. by matrix isolation EPR 78−46374
atomic clusters, matrix isolation spectra 78−46287
atoms, matrix influence, theory 78−46288
atoms, matrix influence, theory 78−46290
p-azoxyanisole, orientated in nematic liq. crysts., UV-visible dichroism meas. *(German)* 77−34668
bacteriochlorophyll absorption polarisation, in liq. cryst. cell 79−24950

matrix isolation spectra continued
benzaldehyde, and deuterated forms, in p-xylene, 4.2K, $n\pi^*$ phosphoresc. assignments 78−9197
benzaldehyde in methylcyclohexane, $n^3\pi^*$ spectra 80−63627
1,2-benzanthracene in polystyrene films, delayed luminesc. decay kinetics 80−43088
benzene, Ar and Kr matrix isolated, IR spectra, vibr. freqs. and intensities 78−50548
benzene, excited state props., by electrochromism in polymer matrix 79−22737
benzene, luminesc. yield spectra in VUV 79−36685
benzene, matrix fluoresc. spectra, rel. intensities of multiplet components 79−54882
benzene, photoluminesc. at 5K, N_2 and inert gas matrices 77−6838
benzene, solid and isolated in rare-gas matrices, spectroscopic study 79−3455
benzene($-d_6$), in Ar-Kr matrices, phosphorescence decay, external heavy atom effect 79−10132
benzene in rare gas matrices, photoelectron energy distrib. 79−10147
benzene in solid rare gas matrix, effect of surface on phosphorescent state 77−88489
benzene radical cation in solid Ar, fluorescence spectra obs. 80−83382
benzene-d_0, -d_6, in glass matrix, phosphoresc. lifetime and polarisation, rot. relax. time meas. 77−79648
benzene-d_1, ($-d_2$)($-d_3$), oriented, order, D nucl. quadrupole coupling, mag. reson. spectra 78−74683
benzil, excited electronic states; conformational relax., time resolved matrix isolation spectral obs. 80−32701
benzil, in PMMA glass, luminesc. temp. depend. matrix controlled photorotamerism 79−22743
1,12-benzoperylene, in n-paraffin solns., quasiline spectra, press. effects *(Russian)* 77−68053
1,12-benzoperylene, phosphoresc. in solid matrix, electronic transition multiplets 77−3413
benzophenone, and d_{10}, ODMR and phosphorescence spectra in organic matrix 79−36671
benzophenone, in DDE at 2K, vibr. overtone characterisation and local modes by emission spectroscopy 79−89682
benzophenones, in host crysts., triplet state PMDR, phosphoresc. spectra, transitions mechanisms 77−46585
5,6- and 7,8-benzoquinoline trapped in n-paraffins at 77K, quasilinear absorption spectra 78−90179
p-benzoquinone($-d_4$), $n\text{-}\pi^*$ excited states, distant intramol. interaction between identical chromophores 78−90203
3,4-benzphenanthrene cation radical, in boric acid glass, spectrum 200-1400 nm, MO calcs., assignments 77−75174
benzyl radical, in solid Ar, absorption and photodissociation spectra 80−69156
benzyl radical, IR absorpt. spectra, matrix isolated at 77K 79−22706
binaphthyl anion radicals, photoisomerisation, local heating effects 78−85179
biphenyl in Ar matrix, mol. struct., IR spectra 77−30875
biphenyl in Ne or Ar matrix, biphenyl ring torsion by vibronically resolved spectra 79−81228
2,2′-bipyrimidine, in nematic solvent, conformation, ab initio and PMR determ. 80−47869
bromodifluoromethyl radical, IR matrix isolation spectrum, stretching fundamentals 78−27788
bromofluoromethane cations in solid Ar, absorpt. spectra and photochem. 79−96339
bromoform and Cl substitutes, VUV photoionis. during condensation with Ar, IR spectra of (CHX_2^+)X and X^--HCX_2 ions 79−13773
bromotrifluoromethane-^{12}C, -^{13}C, matrix IR spectra and harmonic force fields *(German)* 79−76431
1,3-butadiene, matrix isolation, trapping from thermal mol. beam, IR spectra 78−46330
trans-2-butene, Ar matrix, TEA CO_2 laser irrad. photoisomerisation study 80−21303
cis-butene, ozonolysis, radical form., matrix ESR spectrosc. 80−16653
t-butyl alcohol, and deuterates, gaseous and matrix IR spectra, liq. Raman spectra, vibr. assignment 79−10113
n-butyl radical, matrix isolation IR spectrum 78−33510
β-carotene, orientated in nematic liq. crysts., UV-visible dichroism meas. *(German)* 77−34668
CF_3X^+ cations, (X=Cl, Br, I, H), IR spectra in Ar matrix 78−74710
p-chlorobenzene, and deuterated forms, in p-dibromobenzene and p-dimethoxybenzene, 4.2K, $\pi\pi^*$ phosphoresc. assignments 78−9197
chlorodifluoromethyl cation, transient species, matrix isolation spectra 78−48635
2-chloroethanol, IR and Raman spectra, normal coord. anal., isomerism 78−74661
chlorofluoromethane cations in solid Ar, absorpt. spectra and photochem. 79−96339
chlorophyll, and related mols., in solid solns., fine-structured vibronic spectra under tunable dye laser excitation *(Russian)* 80−74164
chlorophyll-a, mols. and complexes in PMMA and MTHF matrices, optical spectra 79−3433
chlorophyll-b, mols. and complexes in PMMA and MTHF matrices, optical spectra 79−3433
chlorotrifluoromethane, matrix IR spectra and harmonic force fields *(German)* 79−76431
chromophores, $^1O_2$, annihilation luminesc., in polymer matrices 77−88488
circular polarisation of emission, magnetically induced, appl. to inorganic complexes 78−78005
ClF_6, EPR of matrix, isolated radical 79−85977
coronene, in n-paraffin solns., quasiline spectra, press. effects *(Russian)* 77−68053
coronene, n-alkane matrix, up to 1.8 kbar emission multiplet struct. shift 77−34677
coronene, triplet mol. in n-heptane Shpol'skii sites, distortion and orientation meas. by MIDP 78−37668
cyanomethane, matrix-isolated, VUV photolysis, CNC radical vibr. and electronic spectra 78−85180
cyclohexane, IR absorption in Ar matrices and perdeutero-cyclohexane, vibrational anal. *(French)* 77−6769
cyclooctatetraene, anions, in condensed media, electronic spectra 79−22723
deca-2,4,6,8-tetraene, fluoresc. and absorpt. spectra, forbidden transition 78−82764

matrix isolation spectra continued
diacetylene radical cation, and deuterated forms, electronic spectrum in solid inert gases 79−94026
diatomic molecules, in inert gas matrix, cage size anal. 78−47397
diatomic molecules, matrix isolated, vibr. relax., rot.-translational coupling 80−53102
diatomic molecules, matrix isolated, vibr. spectrosc., IR line shape calcs. 79−72307
diatomic molecules in monatomic matrix, vibr. relax. 79−18263
diatomic mols. in Ar matrix, vibr. level energy cascades 77−79598
diatomics in rare gas matrices, vibr. modulation effects 77−23496
1,3-diazaazulene, vibronic coupling, Duschinsky effect, mixed cryst. spectra 77−79622
1,3-diazaazulene-azulene, Stark spectra, vibronic perturbations in mixed cryst. 77−79623
4,10-diazachrysene, absorpt. spectra and luminesc. in cryst. and glassy matrices, 77K 78−37650
4,4′-dibromobenzophenone, ODMR and phosphorescence spectra in organic matrix 79−36671
1,2-dichloroethane, conformer equilibrium by effusive beam-matrix IR spectroscopy 80−48100
2,2-dichloroethanol, vibr. spectra, normal coordinate anal. 79−22694
trans-1,2-dichloroethylene, Ar matrix, TEA CO_2 laser irrad. photoisomerisation study 80−21303
dichloromethylene, radical, emission and excitation spectra, in Ar matrix 77−34657
dichloronaphthalenes, heavy atom effects on subrates of lowest triplet states, MIDP obs. 80−91594
1,3- difluorobenzene radical cation, and deuterated forms, laser-induced fluoresc. matrix. study 79−98138
1,2-difluoroethane, in Ar matrix film, interference enhanced IR ATR spectra 79−9248
1,2-difluoroethane, internal rotation temp. frozen in supersonic jet, matrix IR spectroscopy 80−9594
1,2-difluoroethane, matrix isolation, trapping from thermal mol. beam, IR spectra 78−46330
1,2-difluoroethane in Ar matrix, IR hole burning and lineshape, vibr. transition 79−76425
2,2-difluoroethanol, vibr. spectra, normal coordinate anal. 79−22694
difluoromethane cation, in solid Ar, IR spectra, vibr. modes 79−68231
difluoromethyl cation, in solid Ar, IR spectra, vibr. modes 79−68231
dihydrophenazine derivatives, in 3-methylpentane (ethanol) (PMMA), radiationless processes, temp. depend. 80−43087
dimethyl-diacetylene, radical cation, fluoresc. spectra, matrix isolated 79−45752
dimethylbenzaldehydes in durene matrix, phosphoresc., $^3n\pi^*$ and $^3\pi\pi^*$ states vibronic coupling 79−22746
trans-dimethyldiazene-1, 1, 1-d_3, IR and Raman spectra, vibr. assignments and pot. functions 78−33507
dimethylether-HCl(I)(Br) mixture in N_2 matrix, IR induced proton transfer isotope effects, bond strengths 79−29335
2:3dimethylnaphthalene, in polystyrene matrix, singlet O_2 induced excimer fluoresc. 77−6832
2,10-dimethylundecapentaene, optical spectra, vibr. anal., rel. to visual chromophore 77−29102
diphenylene, n-paraffin soln., quasiline sensitised phosphoresc. spectra at 4.2K 77−68071
diphenylhexatriene, low-energy ^1A_g state obs., by two-photon matrix spectroscopy 78−74715
1,6-diphenylhexatrienes, electronic and fluoresc. spectra, solvent effects, 77K 78−21959
diphenylketyl radical, fluoresc. lifetime and quantum yield, organic matrix, 77-130K 78−42110
duryal radical in durene matrix, optical coherent transient spectra 79−76764
dye in polymer matrices, electrochromic props. and use as probe of matrix softening around T_g 80−84724
ethylene, IR spectra, solid and matrix isolated, dimer config. 79−36638
ethylene, ozonolysis, radical form., matrix ESR spectrosc. 80−16653
ethylene glycol, IR spectra, ab initio calcs., vibr. anal., conformations of isotopic modifications 78−5210
exciplex emission, effect of polymeric matrix and temp. 77−61785
excited state props., by electrochromism in polymer matrix 79−22737
fluorene, in polystyrene matrix, singlet O_2 induced excimer fluoresc. 77−6832
fluorene, n-paraffin soln., quasiline sensitised phosphoresc. spectra at 4.2K 77−68071
2-fluoro ethanol, Ar matrix, induced conformational isomerisation by IR irrad. 80−101010
fluorobenzene radical cations, matrix laser fluoresc. spectra 80−1009
fluorobenzene radical cations in solid Ne, laser-induced fluoresc. spectra, vibr. struct. of excited and ground states 80−95671
fluorobromomethanes, matrix photoionisation and radiolysis, IR spectra of free radicals 79−24765
2-fluoroethanol-d_0,-d_1, IR spectra in Ar, N_2 and Ar-N_2 matrices, normal coordinate anal. 78−25538
fluoromethane, in Kr matrix, vibr. relax., IR double reson. 77−79635
fluoromethane+HCl, IR spectra, intermol. interactions 80−9605
fluoromethane-d_0, -d_1, vibr. relax. in matrix, rot. effects, double reson. obs. 78−46375
fluoromethane-d_2, matrix isolated, vibr. energy transfer at low temps. 80−37860
fluoromethane-d_3, vibr. energy transfer at low temps., inert gas and N_2 matrix obs. 80−9706
fluoromethylene cation, in solid Ar, IR spectra, vibr. modes 79−68231
formaldehyde, low-temp. matrix photolysis, hydroxymethylene intermediacy, IR obs. 78−76877
formaldehyde, photolysis in Ar matrix, role of cage dimer 79−91973
formaldehyde, solid soln. in Xe, precipitation, IR spectra obs. 80−45059
formaldehyde dimers, matrix isolated, struct., IR spectra 80−99504
formaldehyde-d_0($-d_1$)($-d_2$), matrix isolated, IR spectra, monomer absorpt. 80−99503
formaldehyde-d_2, inert gas and N_2 matrix fluoresc. spectra, radiationless transitions and lifetimes 79−3469
formaldehydes, (deuterated), A^1A_2 state, photoluminesc. in low temp. matrices, vibr. relaxation 79−50070
formic acid anhydrides, valence force consts., IR spectra, isotope effects 79−93997
formic acid monomer, vib. spectra and normal coordinate analysis 77−58003
free radicals and molecular ions, formed in collision with AR 79−50008

matrix isolation spectra continued
free-base porphin, S_2-S_0 transition vibronic bands, photochem. hole-burning 79−36631
free-base porphin, Zeeman shift meas. by photochem. hole-burning 80−83416
frozen solution spectra, inhomogeneous broadening and phonon effects 79−33725
group IV tetrahalides, isotope shifts, Coriolis coupling and force consts., isotope substitution and matrix isolation 77−42322
haloalkanes, ^{19}F chem. shielding, temp. depend., FT NMR obs. 78−86888
α-heptacyclene, in solid matrix, photodissoc. quantum yields, fluoresc. temp. depend., phosphoresc. IR spectra 77−25292
hexafluorobenzene, γ-radiolysis, matrix isolation spectra of radical anions 79−52704
hexafluorobenzene cation, laser fluoresc. in solid Ar 79−18229
1,3,5-hexatriene radical cation, in Ne matrix, laser induced fluoresc. and emission spectra 80−87163
homogeneous IR line shape, Debye approx., space time phonon correl. functions 79−823
homonuclear diatomics, in zeolite matrices, induced IR spectra 78−46333
hydracids, monatomic matrix-trapped, assoc. forms, struct. and spectral response, intermol. pot. calcs. 79−93996
hydronaphthyl radicals embedded in naphthalene cryst., optical transition energies and ionisation energies 80−78595
hydroxyquinones, H-bonded, zero-phonon photochem., hole burning obs. 79−11802
ice, H_2O:D_2O, I_c phase cryst., IR spectra, H exchange activation energy 79−99866
indole, in PMMA matrix, high press. luminesc. 78−84629
inert gas, freq. shift anal. 79−91472
inert gas crystal, lattice vibrs. and radiative transitions of implanted ions *(Russian)* 80−69098
inorganic and coordinated cpds., IR and Raman spectra, book 79−807
intermolecular interactions, matrix isolation vibrational spectra, appls. 78−46416
interstellar molecules, matrix isolation spectra, review 78−46340
IR laser photochemistry of matrix-isolated mols. 79−34329
isolated molecules, IR spectral line broadening, theory 78−46332
isopropyl radical, Ar matrix isolated, IR spectra and UV photolysis 80−66827
ketones, triplet-triplet absorption carbonyl group role 77−83641
mesitylene, luminesc. excitation spectra in rare gas matrices 78−66575
metal atom reactions, cryogenic techniques and matrix isolation spectroscopy 77−9080
metal atoms, matrix isolation spectra 78−46287
methane, and methane-d_4, rotational transition in condensed Xe, 6K, optical excitation 78−60494
methane, matrix isolation spectra using tunable diode laser 78−45739
methane, solid, phase II and in Kr, Ar matrices, IR spectra quantum rot. 77−28562
methane in condensed inert gas matrices, optical excitation of rotational transition, far IR absorption spectra 80−37808
methyl nitrite, internal rotation temp. frozen in supersonic jet, matrix IR spectroscopy 80−9594
methylene-d_0, -d_2, in Xe matrix, EPR, temp. depend. 78−5255
5-methylindole, in PMMA matrix, high press. luminesc. 78−84629
5-methylpyrimidine, singlet-triplet intersystem crossing, ODMR and MIDP in matrix at 1.6K 79−50055
molecular aggregates, triplet, ESR line shape in solid matrix, fine and HFS 78−58878
molecules, high temp., appl. of matrix isolation studies 80−57399
molecules, IR isotope frequency and intensity patterns 78−46338
2(4)-monooxopyrimidines, gaseous, matrix, soln., tautomeric equilib., IR and UV absorpt. spectra 80−58256
sym-N_2O_3, mol. vibr. in N_2 matrix, normal coord. anal. 79−59432
naphthalene, absorption spectrum in rare-gas matrices 79−3454
naphthalene, matrix fluoresc. spectra, rel. intensities of multiplet components 79−54882
naphthalene, phosphorescence spectra in rare gas matrices, multiplet struct. and pot. energy functions 80−106341
naphthalene in Ar matrix, geometry changes and multiplet struct., mol. fluoresc. and phosphoresc. obs. 80−95663
naphthalene in durene matrix, spin-lattice relax. of phosphoresc. triplet state, PMDR study 79−27012
naphthalene radical cation, in organic glass, 77K, reson. Raman spectra 78−78704
naphthyl, excited electronic states; conformational relax., time resolved matrix isolation spectral obs. 80−32701
nitrocyclopropane, vibr. spectra struct. and bonding 80−102520
2-nitrofluorene, $^1A \rightarrow {}^1L_a$ transition, electronic absorpt. spectra, solvent effects 77−58028
nitroxide radicals, g- and A-tensor components, rot. mobility 2 mm EPR spectrosc. determ. 80−102530
noble metal, matrix-isolated, matrix-induced changes in opt. spectra 77−57913
octafluorotoluene, γ-radiolysis, matrix isolation spectra of radical anions 79−52704
1,3,5,7-octatetraene, lowest excited singlet state, dipole forbidden character 79−27024
organic molecule complex mixtures in solid-state matrices, dip shape saturation effects on nonuniformly broadened spectra 79−95799
oxalic acid, monomeric, IR matrix-isolation spectra, vibr. anal. 78−66550
palladiumporphin in n-octane cryst., lowest triplet state, ESR-optical detect. 77−58050
pentacene, intersystem crossing and internal conversion rates, fluoresc. transient and optical FID spectrosc. 79−81229
pentacene, laser fluoresc. of mol., excitation bandwidth and optical dephasing 79−36679
pentacene in naphthalene, intersystem crossing rates following single-mode laser excitation 80−43085
pentacene in naphthalene, triplet state, EPR study by electron spin-echo and laser flash excitation 80−58172
perdeuterobenzophenone, in 4,4'-dibromodiphenylether, cross-relax., microwave pulse obs. 80−53031
perfluorocyclobutane, matrix isolation Raman and IR spectra, pot. function 77−3352
perfluorocyclobutanone, IR and Raman spectra, vibr. anal. 77−38661
matrix isolation spectra continued
peroxyacetic acid, and isotopic forms, matrix IR spectra, force spectrum, force const., thermodynamic props. calc. 77−14427
perylene in n-heptane cryst., polarised fluoresc. 80−1017
perylene-tetracene in liquid crystal, absorption, fluorescence and polarisation, temp. depend. study *(German)* 80−18887
[2.2]phanes in glass matrices, transanular π-electron interaction, emission spectra 79−36682
phenanthrenequinone, in n-paraffin matrix, electronic-vibr. interaction in phosphoresc. 79−27027
photochemistry in solid state, IR lasers appl. 80−11929
photoexcited triplet state molecules, in cryst., cross-relax., variable freq. ODMR obs. 80−53031
phthalocyanine, in n-alcanes and polyethylene, absorpt. and fluoresc. spectra, 4.2 and 77K 78−976
picene, EPR in p-terphenyl cryst., triplet state 79−36668
polyatomic molecules, radiationless transitions, Fermi resons. and quasidiscrete spectrum 80−95665
polyatomic molecules in solid matrices, ODMR in triplet states, appl. of spin echoes 79−18217
polycyclic aromatic hydrocarbons, matrix isolated, quasilinear Shpol'skii fluoresc. spectra 78−9189
porphine-d_4, vibronic transitions, polaris. determ. 80−63614
n-propyl radical, matrix isolation IR spectrum 78−33510
pyrazine, pyrazine-Kr, ground and n-π* excited state struct. 79−68241
pyrazine.$(H_2O)_n$, n=1,2, ground and n-π* excited state struct. 79−68241
pyrene, in polystyrene, excimer fluorescence 79−68249
pyrene, in polystyrene matrix, singlet O_2 induced excimer fluoresc. 77−6832
pyrene, orientated in nematic liq. crysts., UV-visible dichroism meas. *(German)* 77−34668
pyridine cation radical in trichlorofluoromethane matrix, gamma irrad., EPR and optical obs. 80−23442
pyridine in rare gas matrices, absorpt. spectra, 1700-2900 Å, progressions 77−3376
pyridine-d_0-d_5, nπ* excited state vibronic coupling, vis. and Raman spectra 77−14438
pyrimidine, singlet-triplet intersystem crossing, ODMR and MIDP in matrix at 1.6K 79−50055
pyrometallic dianhydride radical anion, MTHF glass, 77K, reson. Raman spectra 78−78704
pyronine, reson. Raman scatt., normal and excited mol. struct. determ. 77−58024
quantitiative IR Fourier transform spectrosc., microsampling procedure 79−100460
quinoxaline, in naphthalene-d_8, sublevel phosphorescence spectra, radiative mechanisms 77−75203
quinoxaline, in p-dibromobenzene, triplet state NQR, nucl. spin polarisation effects 79−18208
rhodamine 3B solutions in polyvinyl alcohol matrix, spectrum-luminesc. characts. 79−13761
rhodamine 6G, aggregation, modulation Stark spectrosc. obs. 79−27030
rhodamine 6G, in rigid matrix, conc. effects in spectra 80−83347
rhodamines, reson. Raman scatt., normal and excited mol. struct. determ. 77−58024
scandium octaethylporphyrin, μ-oxo bridged dimer, triplet states and geometrys, ODMR obs. 80−9625
scandium octaethylporphyrin, triplet states and geometrys, ODMR obs. 80−9625
small molecules, spectroscopic techniques, review 77−54554
styrene, anions, in condensed media, electronic spectra 79−22723
p-terphenyl anion radicals, photoisomerisation, local heating effects 78−85179
tetracene in liquid crystal, absorption, fluorescence and polarisation, temp. depend. study *(German)* 80−18887
tetrafluoroethylene anion, EPR spectra in organic matrix 79−76453
tetrafluoromethane, bond length and chemical shielding, NMR lineshape anal. of multispin system 80−32741
tetramethylpyrazine-d_{12}, in durene matrix, intersystem crossing of 859.5 MHz transition 79−27015
tetraphenylporphyrin, free base in PVC matrix, excited state props., electrochromism obs. 80−37815
thiirene and deuteroderivatives, Fourier transform IR spectra using Ar matrix isolation, vibr. band assignments 80−14142
thiocarbonyl bromide, IR spectra, gas, liq. and matrix isolated, mol. force consts. *(German)* 79−36640
thioindigo, vibronic fluoresc. spectrum, vibr. struct. 77−54571
thiophosgene, IR spectra, gas, liq. and matrix isolated, mol. force consts. *(German)* 79−36640
toluene, luminesc. excitation spectra in rare gas matrices 78−66575
toluene cation in solid Ar, absorption and photodissociation spectra 80−69156
transition metal, bimetallic cluster, photoselective bimetallic aggregation, review 80−53182
trapped electrons in glassy hydrocarbons, gamma ray irrad., relax., spectral obs. 80−23416
1,3,5-trichloro,2,4,6-trifluorobenzene radical cation, $B^2A_2' \rightarrow X^2E''$ laser-induced fluoresc. spectra 80−14172
trichlorobenzene radical cation, gas and matrix isolated vibr. resolved electronic spectrum 79−68252
trichlorobenzene radical cation, symm. substituted, fluoresc. and emission spectra in Ne matrix 79−89702
2,2,2-trichloroethanol(-d_2), vibr. spectra and normal coord. anal. 79−72319
trichlorofluoromethane, matrix radiolysis and photoionis. at 15K,IR spectrochem. anal. 78−76893
trichloromethane, matrix isolation IR spectra, $^{35/37}Cl$ and $^{12/13}C$ isotope shifts 78−977
trichloromethane glass:O_3, ^{17}O, NQR by proton double reson., broad reson. assignments 80−53014
trifluorobenzene radical cation, symm. substituted, fluoresc. and emission spectra in Ne matrix 79−89702
2,2,2-trifluoroethanol(-d_2), vibr. spectra and normal coord. anal. 79−72319
trifluoromethylperoxy radical, in Ar:O_2 matrix, IR spectra 80−50845
2,4,6-trimethyl pyridine-N-oxide, linear dichroism in liq. cryst. matrix, out-of-plane components 78−17701
triphenylene, in n-heptane cryst., 2-photon excitation spectrum 78−82760

matrix isolation spectra continued
triphenylene, in n-heptane cryst., polarised fluoresc. spectrum, mol. deformation 79−10135
triphenylene, in PMMA matrix, two-photon phosphoresc. spectra 77−42366
triphenylene, triplet state, MIDP and T-S excitation spectrosc. 79−81233
tropolone, π-π^* singlet state, H^+ tunnelling dynamics and equilib. geometry 80−102539
tropolone vibr. spectra and proton tunneling 80−28014
trypaflavine solutions in polyvinyl alcohol matrix, spectrum-luminesc. charcts. 79−13761
unstable conformations, matrix isolation, trapping from thermal mol. beam, IR spectra 78−46330
vinyl chloride+O_3 reaction, IR matrix and microwave spectroscopy 77−90587
xanthione, large zero-field splitting of lowest triplet state 80−58171
xanthone, in n-pentane, heat pulse induced delayed phosphorescence 80−83404
xanthone in host crysts., triplet state PMDR, phosphoresc. spectra, transition mechanisms 77−46585
xanthone in n-hexane, 77 and 4.2K, phosphoresc. spectra, triplet lifetime 78−21957
XY_2 bent symmetrical systems in different environments, force consts. and mean amplitudes 79−18170
zeolites, matrix isolation of homonuclear diatomics, induced IR spectra 78−46333
Ag aggregates, matrix isolation spectra 78−46476
Ag, cluster and microcrystal, matrix isolated, optical absorpt. spectra, photolysis and plasmon absorpt. 79−89820
Ag, in Kr matrix, isolation and aggregation 78−45723
Ag, isolated in mol. matrix, absorption spectra 79−22724
Ag, matrix isolated, fluoresc. spectra. excimeric bond effects 78−50498
Ag microcrystals, matrix isolation spectra 78−46476
Ag_2, Raman spectra, matrix isolated in Kr 78−46347
Ag_3, Raman spectra, matrix isolated in Kr, linear config. 78−46347
Ag_n, (n<10), uv-visible absorpt. spectra in Kr matrices 79−13858
AgM (M=Mg, Ca, Sr, Ba, Zn, Hg) intermetallic mols., Ar matrix isolated, ESR investig. 79−811
AgO, electronic spectra in rare gas matrix 78−996
$AlBr_2$, IR spectra in Ar matrix, struct. 79−31520
$AlBrCl_2$, matrix isolated, vibr. spectrum, struct., vibr. freqs. 78−46339
$AlBr_2Cl$, matrix isolated, vibr. spectrum, struct., vibr. freqs. 78−46339
$AlCl_3$, matrix isolated, vibr. spectrum, struct., vibr. freqs. 78−46339
Al_2Cl_6, matrix isolated, vibr. spectra, isotopic fine struct. and valence force field calcs. 80−58258
AlClBr, IR spectra in Ar matrix, struct. 79−31520
$AlCl_2Br$, IR spectra in Ar matrix, struct. 79−31520
AlH^+ radical cation, EPR matrix isolation obs., hyperfine components calcs. 80−14158
Ar:H_2, nuclear spin relax. of H_2, crystal field meas. 79−51875
Ar:$N_2O(CO)(CO_2)$, fluoresc. and thermoluminesc. after photolysis 79−89700
ArO, in doped inert gas matrix, photoluminesc. 79−31579
ArS, photoluminesc. in rare gas matrices 80−5568
As_4O_6, matrix isolated, IR isotope freq. and intensity patterns 78−46338
Au, D matrix, spectroscopy using sputtering apparatus 77−26407
Au, isolated in mol. matrix, absorption spectra 79−22724
AuLi, vibr. freq. determ., IR spectra, matrix depend. 77−75146
AuO, electronic spectra in rare gas matrix 78−996
BCl_3, high-resolution IR Ar matrix-isolation spectra, 10K 80−32708
BCl_3, in solid Ar, Kr, high resolution IR absorpt. spectra, isotopic splitting 80−87109
BCl_2F, in solid Ar, Kr, high resolution IR absorpt. spectra, isotopic splitting 80−87109
BH_3CO, vibrational spectra in Ne matrices, pot. consts., bond strengths 79−45696
BaO_3, visible absorpt. and reson. Raman spectra in Ar and N_2 matrices 77−65487
Bi_2, in Ar matrix, electronic states, vis. and near IR absorption spectra 78−5213
Bi_n molecular clusters, laser fluoresc. spectrosc. 80−95755
BiN, form., IR matrix spectra, comparison with group V nitrenes 80−18853
Br matrix isolation ESR 80−106336
Br_2, Ar matrix reson. Raman excitation profile, red shift rel. absorption spectrum 77−14440
Br_2 in Ar matrix, reson. Raman scattering amplitude damping in discrete reson. limit 80−58262
BrF_6, EPR of matrix, isolated radical 79−85977
BrO, free radical, Ar matrix absorpt. spectra, mol. vibronic states obs., spectroscopic const. determ. 80−83387
BrO free radicals, IR spectra in Ar matrix at 10K 79−89669
BrOBr and BrBrO mols., IR sepctra in Ar matrix at 10K 79−89669
1-bromo-1-chloro-1-fluoroethane(-2-d_1), IR and Raman spectra, vibr. assignments, normal coord. anal. 78−42053
C_2, Swan transitions, relax. dynamics and two-photon excitation, in inert gas matrix 77−505
C_2^-, matrix isolated, vibr. relax., absorpt. spectra 77−75172
C_2^+, matrix isolated, vibr. energy transfer, fluoresc. 78−46382
C_3, matrix isolated, vibr. relax. 78−66637
CBr_2 emission in solid Ar, laser excitation spectra and lifetimes 80−48034
CBrCl emission in solid Ar, laser excitation spectra and lifetimes 80−48034
CCN radical in solid Ar, emission and excitation spectra 78−70868
CF_2, matrix-isolated, vibr. unrelaxed fluoresc., lattice mode coupling 77−14485
CF_3^+ cations, IR spectra in Ar matrix 78−74710
CF_2Br^+, CF_2Cl^+, IR spectra, C-F stretching fundamentals 78−37632
CF_2Cl^+, and parent cations, IR spectra in matrix radiolysis and photoionis. of Freons 78−80767
$CF_2Cl_2^+$, CF_3Cl^+, IR spectra, in matrix radiolysis and photoionis. of Freons 78−80767
CF_3X^+ cations, (X=Cl, Br, I, H), IR spectra in Ar matrix 78−74710
CH_3-d_n, matrix isolation IR spectra, rot. and vibr. struct. 77−83589
CN, matrix isolated, interstate cascading radiationless transitions 77−46594
CN, radical, nonradiative transition rates, matrix isolated molecule 78−78740
CN in solid Ne, internal conversions and relax. dynamics 77−34678
matrix isolation spectra continued
CNN, matrix isolation spectrum, 2600-1900 Å 78−86880
CNN, matrix-isolated, $^3\Pi$-$^3\Sigma$ system, laser-induced temporal and wavelength resolved spectra 77−83637
CNN radical, matrix isolation spectra, 23.5-25.6×10^3 cm^{-1}, vibr. relax. and Renner splitting 77−83612
CO, in Ar matrix, vibr. line shape, vibr.-phonon interaction 79−3493
CO isotopes in Ar matrix, vibr. energy accumulation 78−13485
CO, istopically enriched, Ar matrix isolation, laser-included vibr. fluoresc. 80−9707
CO, matrix-isolated, librational relax., IR line broadening 80−978
CO, solid and matrix isolated, IR and Raman spectra 78−48156
CO, Xe matrix-isolated and solid, UPES obs. 79−45762
$^{12}C^{16}O$, in Ar matrix, vibr. population time evolution temp. depend., master eqn. 78−9180
CO-NO mixtures, Ar matrix isolation, laser-included vibr. fluoresc. 80−9707
CO_2 dimers in rare gas matrices, struct. determ. from IR spectra 79−10101
CO_2, in alkali halide cryst., field induced vibr. splitting, IR spectra 78−46334
CO_2 lowest triplet state, Ar matrix isolation spectra 80−91569
CO_2, matrix isolated Raman and IR spectra, fundamental freqs., isotope effects 77−88457
CS, nonexponential decay of $a^3\Pi$-$X^1\Sigma^+$ luminesc., Π sublevel radiative lifetimes, matrix isolated spin-orbit 79−89699
CS_2, matrix isolated Raman and IR spectra, fundamental freqs., isotope effects 77−88457
CS_2^+, laser induced fluorescence spectrum 79−50068
$^{12}C^{16}O$ in Ar matrix, vibr. level energy cascades 77−79598
Ca, in Ar matrix, multiphonon relax. processes, emission spectra 78−37583
Ca_2, in solid Kr, discrete reson. Raman scatt. and vibr. relax. 79−18188
Ca_2, laser-excited fluorescence in inert gas matrices 78−94273
Ca_2, matrix isolated, vis. and near IR spectra 78−5214
Ca_2, optical spectra, inert matrices 78−58712
Ca_2, transient species, matrix isolation spectra 78−48635
Ca_2, van der Waals mol., in Kr matrix, absorpt. and emission spectra 77−83611
Ca_2, vibr. relax. in rare gas matrices 78−58711
Ca^+NO^-, Ca^+NO_2 in solid Ar, IR spectra at 15K 77−57996
CaO_3, visible and absorpt, and reson. Raman spectra in Ar and N_2 matrices 77−65487
^{44}Ca substituted oxides, matrix isolated, IR spectra 78−9151
Cd_2, in Ar and Kr matrices, 10K, UV spectrum, vibr. assignments 77−58038
Cd_2, matrix isolated, Raman spectra 79−50024
CdF, mol., ESR spectra in inert gas matrix 79−76455
CdFCl, CdFBr, existence and vibr. characterisation, IR and Raman matrix isolation obs. 78−78706
$CdF_2(FCl)(FBr)$, matrix isolated IR and Raman spectra, assignments, force consts., isotope effects and thermodynamic props. 80−63631
CdHg(Mg), Ar matrix absorpt. spectra, vibronic spacing and bonding 79−3453
CdX_2, CdXY, (X,Y=Cl,Br,I), matrix isolated vibr. spectra, isotopic effects, force consts. 77−3358
CdX_2, CdXY, (X,Y=Cl,Br,I), matrix isolated, far IR spectra, thermodynamic props. 78−86869
Cl+NO_2, matrix reactions, IR absorpt. obs. 78−15667
Cl_2, Ar matrix, vibronic dephasing 80−6469
Cl_2 in Ar matrix, MCD, emission spectrum at 13600 cm^{-1}, Zeeman anisotropy 78−82057
Cl_2, matrix isolated, Zeeman effect and magnetically polarised luminesc. 78−46379
ClCF, radical in Ar matrix, vibr. relax., multiphonon processes, fluoresc. 77−65430
ClCF radical in solid Ar, emission and excitation spectra, vibr. anal. 78−9164
ClO, free radical, Ar matrix absorpt. spectra, mol. vibronic states obs., spectroscopic const. determ. 80−83387
ClO_3^-, in $MClO_3$ and $MClO_4$ matrix, vibr. spectra, anion site asymmetry 77−27062
CoO, matrix isolated IR spectra, ground state vibr. freqs. 80−28015
$Cr(CO)_6$, solid and matrix isolated, Raman spectra 79−28755
CrH(CrD), molecular vibration, IR spectra electron spin resonance, 4K 79−98084
CrO_2Cl_2, inert gas matrices, IR spectra, emission spectra, photoselection 77−14443
CrO_2Cl_2, matrix isolation IR spectrum and force constants 79−3445
CsBr, far IR spectra, matrix isolated, monomers, dimers, trimers 78−66545
CsCl, far IR spectra, matrix isolated, monomers, dimers, trimers 78−66545
$Cs^+Cl_2^-$, transient species, matrix isolation spectra 78−48635
CsF, far IR spectra, matrix isolated, monomers, dimers, trimers 78−66545
CsI, far IR spectra, matrix isolated, monomers, dimers, trimers 78−66545
$Cs_{11}O_3$, ionic clusters in alkali metal suboxide cryst., struct., vibr. freqs., Raman spectra 79−37772
$CsReO_4$, IR matrix-isolation spectra 80−87108
Cs_2SO_4 molecules isolated in inert gas matrices, low freq. IR spectra 78−50547
Cu clusters, visible and near-UV spectra 78−19503
Cu complex, bis-acetylacetonatocopper II, in stretched PVA film, ESR 79−51847
Cu complex, bis-salycylal-1,2-ethylenediiminatocopper II, in stretched PVA film, ESR 79−51847
Cu complex, Cu(II) bis(dithiocarbamate), ^1H ENDOR 80−87154
Cu complex, with acetylene, Ar matrix-isolated EPR obs., bonding 78−50564
Cu complex (acetylacetonate), in vitreous liq. cryst. matrix, ang. depend. of EPR spectrum 78−9175
Cu, isolated in mol. matrix, absorption spectra 79−22724
Cu_nCO, interaction of Cu small particles with CO, IR spectra obs. 77−20195
CuO, electronic spectra in rare gas matrix 78−996
CuO, fluoresc., matrix isolation spectra 78−46381
D_2 IR spectra, mol. rot. and vibr. const. determ. 80−78617
D_2, in zeolitic matrix, IR active fundamentals obs. 77−71800
D_2, matrix rot. and vibr.-rot. spectra, free and hindered rot. 77−83607

matrix isolation spectra continued
DCN, self-assoc. in matrices, IR vibr. spectra of multimers 78−86858
DCl and $(DCl)_2$, matrix isolated Raman spectra 78−42063
DCl, IR matrix isolation spectra, N_2 matrix effects 79−36634
DCl, matrix isolated, vibr. relax., IR fluoresc. obs. 79−45749
D_2O, $(D_2O)_2$, isotopic forms, Ar matrix isolated IR spectra, assignments, config. 77−6779
D_2O, matrix isolation spectra, vibr.-rot. lines, nucl. spin interconversion 78−46336
$(D_2O)_2$, and isotopic species, Ar isolation IR spectra, band assignments, struct. 77−3364
$(D_2O)_2$, and isotopic species, Ar matrix IR spectra, Xe, HCl, $(CH_3)_2O$ doping, struct. 77−3365
$(D_2O)_2$, isotopic forms, Ar matrix isolated IR spectra, assignments, config. 77−6780
2,12-dimethyltridecahexaene, optical spectra, vibr. anal., rel. to visual chromophore 77−29102
Eu, Ar matrix, obs. of Stokes and anti-Stokes vibrational sidebands in emission spectra 77−73164
Eu, in inert gas matrix, pseudolocalised vibr. modes, UV/vis. spectra 78−46289
$EuCl_2$, matrix isolated, Mossbauer effect, isomer shift and quadrupole splittings obs. 78−46377
F+methane, reaction in Ar matrix, IR spectra obs. 79−96293
FCO, form. in Ar matrix, vibr. and electronic spectra, valence force potential determ., mol. photodissoc. obs. 80−85170
Fe complex, $FeCl_3$-tetraphenylporphyrin in PVC matrix, excited state props., electrochromism obs. 80−37815
Fe monomers and dimens. in solid Ar, EXADS study 80−97381
Fe-Co(Ni)(Cu), bimetallic molecule, matrix isolated, Mossbauer spectrum 78−68425
Fe-Co(Ni)(Cu), bimetallic molecule, matrix isolated, Mossbauer spectrum 78−88233
$^{57}FeBr_2$, matrix isolation Mossbauer spectra, isomer shift, quadrupole splitting 78−42104
$Fe(CO)_4$, IR spectra and laser photochem., matrix isolated at 20K 78−74651
$Fe(CO)_5$, matrix isolated species, MCD spectrosc. appls. 78−46378
$^{57}FeCl_2$, matrix isolation Mossbauer spectra, isomer shift, quadrupole splitting 78−42104
$FeCl_3$, Fe_2Cl_6, matrix isolation Raman spectra, assignments 77−65480
$FeCl_3$, matrix isolation Raman spectra, mol. config., thermodynamic props. 78−46346
Fe_2Cl_6, matrix isolated, Mossbauer effect, isomer shift and quadrupole splittings obs. 78−46377
Fe_2Cl_6, matrix isolation Raman spectra, mol. config., thermodynamic props. 78−46346
$^{57}Fe_2Cl_6$, matrix isolation Mossbauer spectra, isomer shift, quadrupole splitting 78−42104
FeCo molecules, matrix-isolation Mossbauer spectra 80−23448
FeH, FeD, matrix isolated IR spectra, mol. vibr. 79−93992
FeMn, matrix isolated Mossbauer spectra, ground state determ. 79−45740
FeO, matrix isolated IR spectra, ground state vibr. freqs. 80−28015
FeO_2, matrix isolated IR spectra, cyclic complex struct. 77−88449
$^{57}FeX_2$, (X=Cl,Br), matrix isolated, Mossbauer effect, isomer shift and quadrupole splittings obs. 78−46377
^{57}Fe, hyperfine fields in Xe matrix, Mossbauer spectroscopy, Hartree-Fock calcs. 78−43749
Ge, matrix isolated cluster, optical absorpt. 80−16045
GeF_4, $\nu_3(F_2)$ IR band contour, isotopically pure cpds., mol. consts. 77−61746
Ge_3O_3, isotopically substituted, IR freq. and intensity patterns 78−21926
Ge_3O_3, matrix isolated, IR isotope freq. and intensity patterns 78−46338
GeTe, matrix isolated absorpt. and emission visible spectra, electronic states 80−28026
H bonding molecules, self assoc., intermolecular interactions, matrix isolation vibr. spectra obs. Raman and IR spectra 80−52995
H^-, fluoresc. in γ- and UV-irrad. solvent matrices at 77K 78−70779
$H+CF_2$, IR matrix isolation spectra 80−97706
H_2, IR spectra, mol. rot. and vibr. const. determ. 80−78617
H_2 matrix shift, CoM freq., in solid Ar, Kr and Xe 79−6969
$HAlCl_2$, IR matrix spectrum, vibrs. and force consts. *(German)* 79−11786
HBr, and DBr, in monatomic matrices, near IR spectra and aggregate structs. 79−89667
HBr, far IR Ar matrix isolated spectra, 4.2K, press. and conc. effects 78−62801
HBr, IR matrix isolation spectra, N_2 matrix effects 79−36634
HBr-nN_2 aggregates, near IR spectra in monatomic matrix 78−21921
$(HBr)_2$, IR matrix isolation spectra, N_2 matrix effects 79−36634
$(HBr)_2$, intermol. distances, dipole moments, MINDO/3 and IR intensities and shifts calcs. 78−46335
HCCN, free radical, matrix isolation spectra and ab initio calcs. 78−46329
HCCN, matrix isolation IR and UV spectra, vibr. anal., struct. 77−65457
HCN, self-assoc., matrix isolation vibrational spectra, appls. 78−46416
HCN, self-assoc., matrix isolation vibr. spectroscopy, complex form. studies 78−62952
HCN, self-assoc. in matrices, IR vibr. spectra of multimers 78−86858
$(HCN)_2$, IR spectra in Ar matrix, vibr. bands, H-bonds 78−29782
HCO, UV matrix isolation spectra, 14K, 210-260 nm, C-X transition 78−62819
HCl and $(HCl)_2$, matrix isolated Raman spectra 78−42063
HCl and $(HCl)_2$, matrix isolated, pulsed NMR 79−22730
HCl, and DCl, in monatomic matrices, near IR spectra and aggregate structs. 79−89667
HCl, far IR Ar matrix isolated spectra, 4.2K, press. and conc. effects 78−62801
HCl, IR matrix isolation spectra, N_2 matrix effects 79−36634
HCl, matrix isolated, vibr. relax., IR fluoresc. obs. 79−45749
HCl-nN_2 aggregates, near IR spectra in monatomic matrix 78−21921
HCl-X, matrix isolation vibr. spectroscopy, complex form. studies 78−62952
$(HCl)_2$, IR matrix isolation spectra, N_2 matrix effects 79−36634
$(HCl)_2$, intermol. distances, dipole moments, MINDO/3 and IR intensities and shifts calcs. 78−46335
HClF, neutral free radicals, in Ar matrix, IR spectrosc. evidence 78−66546

matrix isolation spectra continued
HF-fluoromethylene anion, in solid Ar, IR spectra, vibr. modes 79−68231
HF_2, neutral free radicals, in Ar matrix, IR spectrosc. evidence 78−66546
HF_2^-, IR spectra and mol. struct. 79−63996
HF_2^-, matrix isolated, IR spectra and struct. 78−74655
$H_2(HD)(D_2)$, matrix rot. and vibr.-rot. spectra, free and hindered rot. 77−83607
$H_2O.(H_2O)_2$, isotopic forms, Ar matrix isolated IR spectra, assignments config. 77−6779
H_2O, dimers, IR spectra in N_2 matrix, assignments and force consts., isotope effects 77−61744
H_2O dimers, IR spectra in N_2 matrix, temp. and IR irrad. effects 77−61745
H_2O, in D_2O ice I_c, decoupled vibr. spectra 80−52984
H_2O, matrix isolation spectra, vibr.-rot. lines, nucl. spin interconversion 78−46336
H_2O, Pt catalytic oxidation of H_2 and D_2, matrix isolation and laser fluoresc. obs. of prods. 80−66865
H_2O:D_2O, ice Ic, vibr, decoupling, IR spectrum 79−13706
H_2O-formaldehyde complex, IR spectrum in solid Ar, N_2 matrix 80−43042
H_2O-HCl(HBr)(DBr) complexes, IR matrix isolation spectra, struct. 78−29781
$(H_2O)_2$, and isotopic species, Ar isolation IR spectra, band assignments, struct. 77−3364
$(H_2O)_2$, and isotopic species, Ar matrix IR spectra, Xe, HCl, $(CH_3)_2O$ doping, struct. 77−3365
$(H_2O)_2$, isotopic forms, Ar matrix isolated IR spectra, assignments config. 77−6780
HOI, $O_3(O)+HI$ matrix reaction, IR spectra, isotope shifts and band assignments 78−80737
$H_2O.H_2S$, IR spectra of complex in solid nitrogen, 20K 79−10102
HPO, in Ar matrix, IR and UV absorpt. spectra 80−47985
HgFCl, HgFBr, HgFI, existence and vibr. characterisation, IR and Raman matrix isolation obs. 78−78706
$HgF_2(FCl)(FBr)$, matrix isolated IR and Raman spectra, assignments, force consts., isotope effects and thermodynamic props. 80−63631
$HgX_2(HgXY)$, (X,Y=Cl, Br, I), IR and Raman matrix isolation spectra, bending force consts. 77−465
HgZn(Cd), Ar matrix absorpt. spectra, vibronic spacing and bonding 79−3453
I_2, matrix samples, laser spectroscopy, evidence for $(I_2)_2$ species 78−58735
I_2, N_2 and Ar matrix isolated, magnetic circular dichroism spectrum 80−5567
$^{129}I_2$, frozen soln. in o- or p-xylene, Mossbauer effect obs. 80−78637
I_2-benzene, N_2 and Ar matrix isolated, magnetic circular dichroism spectrum 80−5567
IF, in solid Ar, emission and excitation visible spectra at 12K 80−87137
IO, free radical, Ar matrix absorpt. and emission spectra, mol. vibronic states obs., spectroscopic const. determ. 80−83387
^{127}I atoms in Xe matrices, ESR spectrum 80−1005
$InCl_3$ in Kr lattice, Raman and IR spectra, vibr. assignments, force consts., isotope shift and config. 79−89671
$InCl_3$, planar D_{3h} struct., IR matrix isolated spectra 77−75148
IrO, ground state, matrix isolation spectra 78−46352
K, emission and absorpt. spectra in inert gas matrix 79−54800
$KReO_4$, matrix isolated, IR spectra 80−28012
K_2SO_4, IR and Raman spectra of vap. over heated matrices 78−25525
K_2SO_4 molecules isolated in inert gas matrices, low freq. IR spectra 78−50547
^{41}K, optical absorpt. isolated in Ar matrix 77−10619
Kr:Mg_n, matrix isolated Raman spectra 78−90170
KrF, matrix isolated, absorpt. and emission spectra 77−14446
KrF, matrix isolated, mag. circ. dichroism, UV and vis. absorpt. and saturation 78−46379
KrO, in doped inert gas matrix, photoluminesc. 79−31579
KrS, photoluminesc. in rare gas matrices 80−5568
Li, cluster and microcrystal, matrix isolated, optical absorpt. spectra, photolysis and plasmon absorpt. 79−89820
LiF microcrysts. in Ar, IR absorpt. by aggregated and isolated samples 77−55782
Li_3F_3, isotopically substituted, IR freq. and intensity patterns 78−21926
$Li^{129}I$, Ar matrix isolated and cryst., Mossbauer verification of distortion overlap 77−63325
$Li^+NO_3^-$ ion pairs and hydrated ion pairs, MO calcs., matrix isolation data 78−46267
$LiReO_4$, IR matrix-isolation spectra 80−87108
Mg, matrix isolated, ^1S-^1P transition, mag. circ. dichroism obs. 79−68248
Mg_2, Ar matrix isolated laser photoluminescence spectra, electronic absorpt., emission, vibronic and vibr. relax. 78−82744
Mg_2 matrix isolated, vis. and near IR spectra 78−5214
MgO_3, visible absorpt. and reson. Raman spectra in Ar and N_2 matrices 77−65487
MgZn(Cd), Ar matrix absorpt. spectra, vibronic spacing and bonding 79−3453
MnF, MnF_2, EPR, in inert gas matrices, high spin mag. parameters, level diagrams 78−66565
MnF_2 in Ar matr-x, X-band ESR spectra, extra line assignment 79−81218
MnH_2 in Ar matr-x, X-band ESR spectra, extra line assignment 79−81218
MnO, ESR spectra, matrix isolated at 4K 78−33531
MnO_2, ESR spectra, matrix isolated at 4K 78−33531
MnO_3, ESR spectra, matrix isolated at 4K 78−33531
MnO_4, ESR spectra, matrix isolated at 4K 78−33531
MnO_4^- ion, ^{18}O enriched, matrix isolated IR spectra, force consts. 80−52985
MnO_3Cl, matrix isolated species, MCD spectrosc. appls. 78−46378
Mo, in Ar matrix spectroscopy using sputtering apparatus 77−26407
Mo_2, matrix isolated visible absorpt. spectra, electronic, vibronic and vibr. states 80−28027
MoN, matrix isolated visible absorpt. spectra, electronic, vibronic and vibr. states 80−28027
MoO, matrix isolated visible absorpt. spectra, electronic, vibronic and vibr. states 80−28027
N_2 in Ar matrix, luminesc. lifetime 79−36690
N_2, in zeolite matrix, IR active fundamentals obs. 77−71800

matrix isolation spectra continued
N_2, matrix isolated, fundamental vibr. Raman spectra 80−272
N_2, mol. spectra, 500-1300 Å, matrix isolated 79−33724
N_2, molecular centre, in Ar matrix, vacuum UV luminesc., 8K 78−10958
N_2, solid and matrix isolated mol., triplet state spectra *(Russian)* 80−5574
N_2 solid matrix, ^{57}Fe Mossbauer spectra, Fe_xN mol. form., IR spectra confirmation 77−59496
N_2, Xe matrix-isolated and solid, UPES obs. 79−45762
N_2:N, dynamically induced electronic transitions of matrix isolated atom 78−63825
N_2+N_2(CO), in matrix, vibr. energy transfer and relax. 78−46426
NBr, in solid Ar, $b^1\Sigma^+ \rightleftarrows X^3\Sigma^-$ transitions 80−32702
NCO, $A^2\Sigma$ state, Fermi resonance and vibr. relax. in solid Ar 78−5212
NCl, in solid Ar, $b^1\Sigma^+ \rightleftarrows X^3\Sigma^-$ transitions 80−32702
NH, ND, $X^3\sigma^-$ state vibr. relax. Ar matrix, energy gap law breakdown 77−30963
NH_3, and -d_n IR matrix isolation spectra, rotation and inversion 78−5218
NH_3, self-assoc., matrix isolation vibrational spectra, appls. 78−46416
NH_3-CO_2 complex, matrix isolation IR spectrum, struct., ab initio SCF calcs. 78−5209
NH_3-HCl, assoc., matrix isolation vibrational spectra, appls. 78−46416
NI, in solid Ar, $b^1\Sigma^+ \rightleftarrows X^3\Sigma^-$ transitions 80−32702
NO, $3s\sigma(A^2\Sigma^+)$, in Ar Kr Xe matrices, Rydberg state 'bubbles', reson. fluoresc. obs. 77−83636
NO ($a^4\Pi$), condensed phase vibr. relax., isotope effect, time resolved obs. 78−94233
NO, fluoresc. spectra, $3s\sigma(A^2\Sigma^+)$ Rydberg state, vibr. relax. 79−13759
NO, IR spectra in O_2 matrix, vibr. freqs. 78−23936
NO in rare gas matrix, radiationless processes in luminesc. spectra 79−36689
NO_2, high-press. Raman matrix isolation spectra 78−45721
$(NO)_2$, IR spectra in O_2 matrix, vibr. freqs. 78−23936
NO_2, in Ar matrix, Raman spectra, high press., low temp. effects 78−52479
NO_2, Ne matrix isolated, 6K, B←X band system 78−993
NO_2^-, in KI matrix, Raman spectra, high press., low temp. effects 78−52479
NO_3^-, in $MClO_3$ and $MClO_4$ matrix, vibr. spectra, anion site asymmetry 77−27062
N_2O_4, IR spectra in O_2 matrix, vibr. freqs. 78−23936
N_2O_5, IR spectra in O_2 matrix, vibr. freqs. 78−23936
NO_2Br, formation and IR spectrum 79−98097
NO_2I, formation and IR spectrum 79−98097
NSF_3, IR spectra, matrix isolated, force const. calc. 78−62802
Na, cluster and microcrystal, matrix isolated, optical absorpt. spectra, photolysis and plasmon absorpt. 79−89820
Na, in Xe matrix, 3s excitation, UV and vis. spectra 78−46291
Na, matrix isolated in Ne, absorpt. and emission spectra 80−99465
Na, spectra, emission and absorpt., inert gas matrix 78−90106
Na_3, EPR spectrum, Ar matrix, bonding models 77−14462
Na_x, matrix-isolated, formed in supersonic nozzle beam, 400-800 nm absorption and mass spectra obs. 79−76439
NaBr, far IR spectra, matrix isolated, monomers, dimers, trimers 78−66545
NaCl, far IR spectra, matrix isolated, monomers, dimers, trimers 78−66545
NaF, far IR spectra, matrix isolated, monomers, dimers, trimers 78−66545
NaI, far IR spectra, matrix isolated, monomers, dimers, trimers 78−66545
$NaReO_4$, matrix isolated, IR spectra 80−28012
Na_2SO_4, IR and Raman spectra of vap. over heated matrices 78−25525
Ni atoms, Xe matrix isolation, photoemission 80−27987
Ni, UV matrix freq. shifts, ionis., pot., assignments, appl. to Ni_2, Ni_3 77−75178
Ni_2, A→X system, Ar matrix isolation fluoresc. spectrosc. obs. 80−9628
Ni_2, UV Ar matrix spectra theory 77−75178
Ni_3, in solid Ar, reson. Raman spectra 80−63638
Ni_3, UV Ar matrix spectra theory 77−75178
Ni_n clusters, Ar matrix, UV-visible spectra pot. energy curves 77−65552
NiO, matrix isolated IR spectra, ground state vibr. freqs. 80−28015
O+H_2S, matrix reactions, IR spectra of products, chemiluminesc. 77−60057
O_2, $A^3\Sigma_u^+$, $C^3\Delta_u$ and $C^1\Sigma_u^-$ states in van der Waals solids, electronic spectra, dynamics 78−1000
O_2, in zeolite matrix, IR active fundamentals obs. 77−71800
O_2, inert gas matrix, visible emission spectra, $c^1\Sigma_u^- \rightarrow a^1\Delta g$ and $C^3\Delta u \rightarrow X^3\Sigma_g^-$ transitions 77−14444
$(O_2)_2$, struct., energy transfer, high resolution electronic spectra 78−25550
$(O_2)_2$, struct., vibr. relax., local modes, isotope effects 78−25669
OAlCl and OAlF, IR matrix spectra, vibr. freqs. *(German)* 79−11785
OBrO free radicals, IR spectra in Ar matrix at 10K 79−89669
$OCBr_2$, IR spectra in Ar matrix, force consts. *(German)* 79−36641
O_2F radicals, preparation, EPR spectra rel. to phase, temp. 77−51954
$O_2F(Cl)(Br)$ radicals, matrix IR spectra, bonding 78−90160
OGaF, matrix IR spectrum, vibrs. and force consts. 79−11787
OH, Pt catalytic oxidation of H_2 and D_2, matrix isolation and laser fluoresc. obs. of prods. 80−66865
OH radical, matrix-isolated, from H_2 oxidation on Pt, laser diagnostics 80−5572
ONI, IR matrix isolated spectra, force consts. 79−10111
$O_2(c^1\Sigma_u^-)$, in Ar(Kr)(Ar-Kr) matrices, multiphonon vibr. relax. time-resolved emission obs. 80−18861
OsO_3F_2, OsO_4 matrix-isolated IR and Raman spectra 77−75166
PN, matrix IR spectra, aggregation to P_3N_3 77−83599
P_3N_3, matrix isolated, IR isotope freq. and intensity patterns 78−46338
PO, in Ar matrix, IR and UV absorpt. spectra 80−47985
Pb_2, in Ar matrix, excitation and emission spectra, vibr. freq. 78−13507
PbS, molecule, Ne matrix environment effects on vibronic emission systems 77−58070
Pr^{3+} aquo ion spectra, MCD of $^3P_0 \leftarrow {}^3H_4$ transition 80−7331
Pt porphin in n-alkane single cryst. ^3E_u-$^1A_{1g}$ transition, Zeeman expts. at 4.2K 80−78645
PtO, ground state, matrix isolation spectra 78−46352
PuN, in Ar matrix, IR spectra, stretching freq. and isotope shifts 78−78690
matrix isolation spectra continued
PuN_2, in Ar matrix, IR spectra, stretching freq. and isotope shifts 78−78690
PuO, in Ar and Kr matrices, IR absorption spectra, normal coord. anal., assignments, force consts. 78−78681
PuO, matrix isolation studies with Fourier transform IR 78−45740
PuO_2, in Ar and Kr matrices, IR absorption spectra, normal coord. anal., assignments, force consts. 78−78681
PuO_2, matrix isolation studies with Fourier transform IR 78−45740
Rb_9O_2, ionic clusters in alkali metal suboxide cryst., struct., vibr. freqs., Raman spectra 79−37772
$RbReO_4$, IR matrix-isolation spectra 80−87108
Rb_2SO_4 molecules isolated in inert gas matrices, low freq. IR spectra 78−50547
ReO_4^- molecules in alkali halide matrices, CO_2 laser saturation of internal vibr. modes 78−86922
Ru(II) complex, carbonyl(pyridine)-phthalocyaninatoruthenium(II), optical hole burning, matrix effects 80−102522
RuO_4, $\nu_3(F_2)$ IR band contour, isotopically pure cpds., mol. consts. 77−61746
S_2 and S_3, absorpt. spectra in Ar matrix 79−5149
S_2, chemilum. in solid Ar 79−47529
S_2, in Ar and Kr van der Waals solids, absorption spectra 77−52139
S_2, in Ar matrix, fluoresc. and excitation spectra 78−94271
S_2, matrix-isolated, $B^3\Sigma_u^-$ predissoc., relax. processes 80−58329
SBr_2, SI_2, matrix isolated, IR spectra 80−58254
SCF_2, IR, Raman and matrix isolation spectra, isotopic shifts, anharmonicity consts. *(German)* 77−83600
S_2Cl, blue absorpt. in Ar matrix 79−5149
SCl(Br), unstable radicals, matrix-isolated, IR spectra force const. *(German)* 80−43053
$^{32}SF_2$, $^{34}Sf_2$, matrix IR spectra, vibr. and force fields, bond angle *(German)* 78−74662
SF_6, high-resolution IR Ar matrix-isolation spectra, 10K 80−32708
SF_6, IR laser isotopic enrichment in low temp. matrices 78−90318
SF_6, matrix photolysis, vac. UV, using windowless discharge, IR spectra 77−71798
SF_6 molecule, matrix isolated, CO_2 laser irrad., photodissoc., IR absorpt. spectra obs. *(Russian)* 77−6877
SF_6^-, matrix isolated, IR spectra, evidence for form. 77−68037
S_2F_{10} 77−6775
SF_5Br, Ar matrix and solid phase Raman and IR spectra, vibr. assignments 77−6775
SF_5Cl AR matrix and solid phase Raman and IR spectra, vibr. assignments 77−6775
SF_4O, vibr. spectra, struct. and thermodynamic props. 77−63416
SO_2, chemiluminescence at ($c^1\Sigma^- \rightarrow a^1\Delta$) in Ar matrix, photolysis prod. and thermoluminesc. 79−5158
SO_2, matrix isolated, ν_3 vibr. spectrum, diode laser spectroscopy, temp. depend. 77−50433
SO_2, matrix isolation spectra using tunable diode laser 78−45739
SO_2 phosphorescence, in Xe, Kr, Ar, N_2 matrices, environmental perturbation effects *(French)* 77−3407
SPF_3, IR spectra, matrix isolated, force const. calc. 78−62802
SPF_3, isotopic forms, microwave spectra, centrifugal distortion consts., vibr. and rot. states, IR matrix spectra 77−10665
SPF_3 vibr. spectrum, assignment using matrix isolation and isotope substitution *(German)* 78−13498
$SSBr_2$, IR matrix isolation spectra in Ar matrix at 9K 79−93995
SSF_2, FSSF, and ^{34}S isotropic forms, matrix IR and Raman spectra *(German)* 79−89674
ScF_2, ESR spectra of radical in Ar matrix, 12K, hyperfine splitting 79−98122
Se_2, laser induced fluoresc. in inert gas matrix 80−87161
$SeCF_2$, IR, Raman and matrix isolation spectra, isotopic shifts, anharmonicity consts. *(German)* 77−83600
SeF_6, IR vibr. band contours, isotope substitution, force consts. 78−17670
SeF_6, in Kr matrix, temp. reversible IR spectral changes, site struct. dynamics 80−102505
Si, matrix isolated cluster, otpical absorpt. extended Huckel calcs., electron energy levels 80−16045
$SiCl_4^-$, ESR of radical in adamantane matrix, γ-irrad. of $SiCl_4$ in adamantane matrix 79−27011
$(SiCl_3)_2O$, IR matrix isolation spectrum, Raman spectrum 78−82730
SiF_4, $\nu_3(F_2)$ IR band contour, isotopically pure cpds., mol. consts. 77−61746
SiF_3Cl^-, radical anion struct. and ESR spectrum 78−25571
SiGe, matrix isolated cluster, optical absorpt. 80−16045
SiH_3 radical, in Ar(Kr)(N_2) matrix, anisotropic ESR spectroscopic parameters 80−63687
SiH_3D, in polycryst. SiH_4, mol. motions and symmetries, IR obs. 78−48163
SiO in Ar matrix, vac. UV spectrum, vibr. progression 80−23432
Si_3O_3, isotopically substituted, IR freq. and intensity patterns 78−21926
Si_3O_3, matrix isolated, IR isotope freq. and intensity patterns 78−46338
SiS, matrix IR spectra, aggregation to Si_2S_2 77−83599
Sm, in inert gas matrix, pseudolocalised vibr. modes, UV/vis. spectra 78−46289
Sn_2, in Ar matrix, absorpt., fluoresc. and reson. Raman spectra 80−95640
Sn_2, matrix isolation Raman spectrum, overtone bands breadth 78−33515
$SnBr_4$, matrix-isolation and $^{79/81}Br$ and $^{116/124}Sn$ isotope shifts in IR spectra 77−46561
Sn(IV)-, Sn(II) halide mols., rare gas matrix-isolated ^{119} Sn spectra 77−48097
SnX_2, (X=Br,Cl,F,I), matrix isolated, Mossbauer effect, isomer shift and quadrupole splittings obs. 78−46377
SnX_4, (X=Br,Cl,I), matrix isolated, Mossbauer effect, isomer shift and quadrupole splittings obs. 78−46377
^{119}Sn resonance from inert gas matrix, Mossbauer isomer shift calibration 77−46530
Sr_2, matrix isolated, vis. and near IR spectra 78−5214
Sr_2, Van der Waals dimer, inert gas matrix-isolated, laser excited emission spectra 78−78744
SrO_3, visible absorpt. and reson. Raman spectra in Ar and N_2 matrices 77−65487
TaN, matrix isolated, electronic and vibr. absorpt. spectra 79−64014
Te monomer in Ar matrix, formed by H_2Te photodissoc., Mossbauer spectra 77−20769

matrix isolation spectra continued
Fe_3, laser induced fluoresc. in inert gas matrix 80−87161
FeO_2Cl, thermal decomposition, matrix isolation IR and mass spectra 80−81306
$Th^{14}N$, $Th^{15}N$, matrix isolated IR spectra 79−59457
$Th(N_2)$ complex, IR matrix isolation spectrum 79−59457
Ti, and TiO, from sputtered Ti, sputtered ion fraction meas. using matrix isolation spectroscopy 80−60738
$TiF_2(TiF_3)$, ESR spectra in rare-gas matrices at 4K 77−88474
Tl, absorpt. and emission spectra, in inert gas matrix 77−57909
$Tl_2F_2(Cl_2)$, assignment of vibr. Raman and IR spectra bands 80−58268
$TlNO_3$, ion pair, in Ar matrix, solvation effects, IR spectra 77−46563
$TlReO_4$, IR matrix-isolation spectra 80−87108
U, matrix isolation studies with Fourier transform IR 78−45740
$U(BH_4)_4$, and d-16, IR specra, gas, matrix, isolated and film 79−36639
UF_4, matrix isolated, IR spectra, interactions with frozen gas 78−9148
$UF_4+F_2 \rightarrow UF_5$, UF_6, IR matrix isolation spectra 77−12787
UF_5, monomer struct. and pot. consts., IR and Raman spectra in inert gas matrices 78−5215
UF_6 in Ar matrices, fluoresc. and Raman spectra, vibr. anal. 78−66585
UF_6, matrix isolated, laser fluoresc. spectrosc. at 12K 79−68253
UF_6, matrix isolated, vibronic fine struct. in fluoresc. spectrum 80−83406
UF_6, matrix isolation spectra and photolysis 79−50043
UN, identification in AR matrix, IR spectra, vibr. freqs. 77−9066
UN, matrix isolation studies with Fourier transform IR 78−45740
UN_2, matrix isolation studies with Fourier transform IR 78−45740
UO, matrix isolation studies with Fourier transform IR 78−45740
UO_n (n=2,3), matrix isolation studies with Fourier transform IR 78−45740
V_2, formation, spectra, electronic struct. 77−54642
$V(CO)_6$, paramag. matrix isolated species, MCD spectrosc. appls. 78−46378
$W(CO)_6$ dissolved in oriented compensated nematic mixture, distortion of cubic mol., linear dichroism obs. 79−95797
Xe: ^{57}Co, solid, ion implantation for rare gas matrix isolation, Mossbauer spectroscopy study 80−54271
$XeF_2(Cl)(Br)$ matrix isolated, absorpt. and emission spectra 77−14446
XeF, in Ar and Ne matrices, reson. fluoresc., ground $X^2\Sigma^+$ state pot. well 77−14482
XeF, transient species, matrix isolation spectra 78−48635
XeF_2, photodissoc. yield in solid Xe and Kr, time-resolved photolum. excitation obs. 80−3372
XeO, Ar-matrix-isolated, UV absorpt. spectra 77−3375
XeO, excited state spectra, subpicosec. predissoc., solvation, in solid rare gas hosts 77−68050
XeS, photoluminesc. in rare gas matrices 80−5568
XeX, (X=F,Cl,Br,I), Ar matrix isolated, MCD, low temp. depend., spectroscopic parameters calc. 77−38682
$YbF(^2\Sigma^+)$, matrix isolated ESR spectra 78−86890
YbH(YbD), and isotopic forms, optical and EPR matrix isolated spectra, HFS, bonding 77−83613
$Zn+O_3$ matrix reactions, IR, Raman and visible spectra in Ar and N_2 matrices 80−87110
Zn_2, in Ar and Kr matrices, 10K, UV spectrum, vibr. assignments 77−58038
Zn_2, matrix isolated, Raman spectra 79−50024
ZnF, mol., ESR spectra in inert gas matrix 79−76455
ZnFCl, existence and vibr. characterisation, IR and Raman matrix isolation obs. 78−78706
$ZnF_2(FCl)(FBr)$, matrix isolated IR and Raman spectra, assignments, force consts., isotope effects and thermodynamic props. 80−63631
ZnHg(Mg), Ar matrix absorpt. spectra, vibronic spacing and bonding 79−3453
ZnX_2, ZnXY, X and Y=halogen, matrix isolation IR and Raman spectra 78−55171
ZnXY, (X,Y=Cl,Br or I), matrix isolation, vibr. spectra, isotope effects, force consts. and geometry 78−46337
Zr, and ZrO, from sputtered Zr, sputtered ion fraction meas. using matrix isolation spectroscopy 80−60738
Zr, in (Ar, Kr, Xe) matrices absorption spectra 78−78652
ZrN, in (Ar, Kr, Xe) matrices, absorption spectra 78−78652
ZrO, in Ne matrix, laser photoluminesc. 77−14481

matrix isolation spectroscopy
cluster formation in rare gas matrices, aggregation process 77−62630
complexation studies from vibr. spectra 78−62952
conference, Berlin, Germany, June 1977 78−46319
cryophotoaggregation, bimetallic cluster, transition metal atom nucleation, review 80−53182
ethylene, matrix isolated, shielding tensor anisotropy, ^{13}C NMR meas. 79−59491
fluorobenzenes in Ne matrices, molecular cation electronic absorption spectra, new photolytic technique 80−58415
Fourier transform IR, appls. 78−45740
free radical meas. by matrix isolation and EPR 78−73535
free radicals, matrix isolation spectrosc. 79−80688
frozen gas matrix, refr. index determ. by emission spectrosc. 80−90884
high pressure cell for matrix isolation Raman spectroscopy 80−272
high-pressure Raman matrix isolation spectroscopy 78−45721
high-temperature diatomic molecules, production optimisation appls. 78−46462
high-temperature molecules, matrix isolation spectra, review 78−46340
inert gas matrices, photoelectron energy distrib. meas. 78−48271
IR ATR-matrix spectroscopy, interference-enhanced, appl. to 1,2-difluoroethane in Ar matrix film 79−9248
IR interference enhanced attenuated total reflection spectroscopy, new technique 79−21823
laser-heated miniature oven, for prop. of matrix isolation samples for Raman studies 78−45737
metal atoms, in inert gas matrices, isolation and aggregation 78−45723
molecular ions, matrix isolation spectrosc. 79−80688
molecular spectroscopy book 80−27052
molecules high temp. appl. of IR isolation technique 80−57399
Mossbauer spectroscopy, matrix isolation techniques appls., review 78−46376
Mossbauer spectroscopy, rare gas matrix isolation system 77−12285
NMR spectroscopy, high resolution, using nematic liq. crysts. with negative anisotropy 79−40596
paramagnetic matrix isolated species, MCD spectrosc. appls. 78−46378

matrix isolation spectroscopy continued
pulsed condensation of matrix mixture for spectroscopic investigations 79−36799
Raman, toxic organic substances detection in water 80−30616
Raman spectroscopy, water pollution detect. appl. 80−108829
sputtered ion fraction meas. using matrix isolation spectroscopy 80−60738
sputtered products, spectroscopic apparatus 77−26407
stable molecules, matrix isolation spectroscopy obs., appls. 78−46320
synchronized flash photolysis and pulse deposition in matrix isolation experiments 78−73120
transient species, matrix isolation spectrosc. 79−80688
tunable diode laser, for high resolution matrix IR spectroscopy 78−45739
two coupled oscillators, decaying in the same bath, absorpt. line shape 79−10088
vibrational relaxation in matrices 78−46425
windowless AR discharge VUV lamp, for matrix isolation spectroscopy, spectrosc. evaluation 78−45730
Ar matrix deposition apparatus for magneto-optical obs. 78−82057
$^{40}Ar:^{41}K$, matrix isolation model system 78−45722
Au, sputtering yields of D^+ and Ar^+ ions using matrix isolation spectroscopy 79−78809
CF_2, in Ar matrix, conc. determ. by intensity calcs. 78−68941
CF_3, in Ar matrix, conc. determ. by intensity calcs. 78−68941
N_2 matrix N-N stretching vibr., IR activation, guest mol. depend. 80−60570
$NaPO_2$, mol. identification by matrix isolation IR spectrosc. 80−104485
$NaPO_3$, mol. identification by matrix isolation IR spectrosc. 80−104485
SF_6, matrix isolated, IR spectrosc., temp. reversible site structural changes 80−95613
Ti, sputtering yields of D^+ and Ar^+ ions using matrix isolation spectroscopy 79−78809
TiO_2:$TeCl_4$ system, chem. vapour transport, matrix isolation IR studies 80−93755

Matteucci effect
$Fe_{40}Ni_{40}P_{14}B_6$, amorhpous ribbon, influence of torsion on mag. props. 80−7138
Ni, tubular sample, basic EM theory 78−43620

maximum principle
see also dynamic programming
aeroelastic vibr. elimination, optimal control method 80−33514
capillary surface problems with prescribed contact angle, max. and min. principles 79−37907
Dirac operator, essential self adjointness anal. 80−18794
elastically supported membrane eigenfunctions 79−14341
multipoint boundary-value problem, maximisation of Green's function 77−37733
multizone reactor neutron flux profile optimisation program *(Russian)* 79−13412
nerve membrane, steady-state finite cable model, complementary variational principles 79−34545
neutron flux optimum control during nuclear station load following 79−9761
nonholonomic Chetaev systems, Lagrange eqns. derivation from modified Pontryagin maximum principle 78−12557
nonlinear parabolic differential eqns. 77−29996
optimum control theory, Hamilton-Jacobi theorem, canonical transforms 78−20962
processes governed by mildly nonlinear parabolic differential eqns. *(German)* 77−22416
shells of revolution, max. principles and pointwise error estimates for torsion 78−18180
solar heating system optimal controllers 80−45739
torsional creep problem, appl. of maximum principle 78−71284

maxmin technique *see minimax techniques*

Maxwell-Boltzmann distribution *see statistical mechanics*

Maxwell effect *see flow birefringence*

Maxwell equations *see electromagnetism*

MBE *see molecular beam epitaxial growth*

Mealy Moore machines *see finite automata*

mean free path, carrier *see carrier mean free path*

measurement
see also specific measurements, e.g. frequency measurement
see also instruments; measurement by laser beam; recording; testing; units (measurement)
accuracy, evaluation 79−17380
atomic science and engineering, measuring informational basis, nuclear instrument making 79−684
automatic process-control measurement systems, meas. of charact., compound and element-by-element methods 80−62612
basic metrological operations, validation and optimisation 78−41264
basic metrological operations and methods 78−41263
data processing, automation of meas. equipment state-inspection results, USSR Krasnodar territory 80−52152
diffusion coefficient of gases in liquids, bubble evolution method using crit. size concept. 80−4828
dimensions of physical quantities, use in metrology 80−77740
dust control, measurement methods *(Hungarian)* 80−35810
dynamic, problems and methods of overcoming them, reference standards 80−62613
education, measurement oriented basic physics laboratory 79−25790
electronic measurements, book 80−31805
fast processes, review of present methods in USSR, future prospects 80−57271
history of sensing apparatus and techniques, source guide 78−4457
hydrometeorological meas. equipment, USSR state testing 79−70897
international activity of USSR VNIIFTRI 78−41261
international metrological cooperation, legal aspects 78−89422
International Organisation for Legal Meterology, OIML, tasks and organisation *(German)* 77−87720
laser techniques, state of art in Poland 77−5790
logical structure of meas. science *(Japanese)* 80−73299
long-range metrological plans, USSR Comprehensive Production Efficiency Improvement System, Kuban region 80−52150
magnetic meas., terms and concepts 79−97334
matter under very high pressure *(French)* 80−90811
metrological certification of measurement techniques 79−67243

measurement continued
metrological collaboration among COMECON member countries, legal foundation 78−4582
metrological provision regulations in USSR 78−89421
metrological standardisation with Comecon framework 78−89426
metrology, scope and relationship with physics 80−52153
metrology in industry and government, seminar, Daeduk, Korea (Sept. 1978) 80−27259
National Bureau of Standards time code relay to western hemisphere by satellite 80−47039
NBS National Measurement System 79−21688
nomenclature, uniformity for testing-equipment 79−6109
oceanography system of metrological provisions for hydroaero-physical measurements 79−16709
oscilloscope measuring techniques, trends *(German)* 78−74020
photoelectric setting microscopes, recent developments 77−41681
photometric, facilities at National Measurement Laboratory, Australia 78−82019
plan programs for instrument development in the Ministry of Instrumentation 80−183
pollution, environmental, by means of light scatt. characts. 79−21061
precision measuring techniques, instrumentation, progress in manufacturing 77−9978
quality control management, metrological support 80−184
radiogauging, use of ionising radiation 79−41086
sample chamber for ultrasonic vels. and elastic consts. meas. *(German)* 78−46868
scientific advance, objectivity vs. relevance techniques 79−58520
SI units, introduction in Hungary, ionising radiation aspects *(Hungarian)* 78−8379
SI units, introduction in Hungary, practical aspects *(Hungarian)* 78−8380
solar technology, conf., Winnipeg, Canada, Aug. 1976 77−29412
Soviet-American collaboration 77−87719
state control of measuring equipment in the USSR 80−52151
superconducting materials, metrological problems 79−73650
technical term translation problems *(German)* 80−36965
units in measurement *(German)* 79−6076
water vapour adsorption isotherm, improved measurement method *(Japanese)* 78−6220
wet steam, high speed flows, drop dimensions meas. method 80−90817
He-Ne laser, I_2 stabilised, realisation of length unit 78−87068

measurement by laser beam
see also laser velocimeters; plasma diagnostics by laser beam
absolute acceleration due to gravity, meas. using laser ballistic gravimeter 80−12569
absolute interferometric dilatometer 77−45832
absorption calorimetry, automation 78−74084
absorption coefficients at 632.8 nm intracavity laser meas. 78−8454
absorption coefficients of film coatings, laser calorimetric meas. 78−25905
acoustic and acousto-optic properties, appl. of laser light diffraction *(Polish)* 78−76425
acoustic emissions, meas. at high temp. and press. by wide-band optical-mechanical system 78−1525
acousto-optical modulator, metrological certification of photodetection devices 80−23727
adiabatic laser calorimeter design for window and mirror evaluation 79−13971
advances in optical metrology, conf., San Diego, USA, Aug. 1978 79−80565
aerosol detector, in cryogenic systems 78−81986
aerosol meas. by lidar, error analysis and simulation 80−26617
aerosol particle sizing by laser beam Mie scatt., computer program 77−37457
aerospace simulation facilities, conf., Shrivenham, England, (Sept. 1977) 77−80251
air pollutant gas detection by dye laser and Fourier transform method 79−57558
air pollution detection, optical methods *(Czech)* 78−69444
air pollution detection, signal processor charact. *(Japanese)* 77−78449
air pollution meas. by incoherent optical heterodyne detection 79−48203
air pollution monitoring, spectrophone measurement of absorpt. coeffs. at CO_2 laser wavelengths 80−26193
air pollution monitoring by pulsed dye laser 79−48204
air pollution monitoring by pulsed lasers, numerical filters *(Japanese)* 79−43801
airborne bathymetric charting using pulsed blue-green lasers 77−29447
airborne laser scanner, modulation techniques 80−5770
airborne particle distributions, inertial sizing using laser velocimeter method 80−53901
airflow through cascade of turbine blades, laser anemometry 80−59146
alignment using He-Ne laser/polarimeter system 77−37967
alloy steel welds, distrib. of Cr, Ni, Mn, Si, Ti, laser emission microanal. method 78−61110
anemometers, operating principles *(Polish)* 79−4096
angle meas. using ring laser, principle 78−16777
angle measurement using ring laser *(Japanese)* 79−71408
angular displacement recording, using He-Ne laser and photodiode system 77−49712
angular measurement, errors 80−42196
angular velocity measurement, ring laser beat regime with nonlinear absorbed *(Russian)* 78−1273
astronomical laser ranging equipment, computer system *(Japanese)* 78−89080
astronomical laser ranging equipment, photoelectric circuit *(Japanese)* 78−89075
astronomical laser ranging equipment, range gate *(Japanese)* 78−89076
astronomical laser ranging equipment, system controller *(Japanese)* 78−89079
astronomical laser ranging equipment, telescope drive *(Japanese)* 78−89078
astronomical laser ranging equipment, timing system *(Japanese)* 78−89077
AT-cut quartz plate vibration anal. using light modulated oscillator 78−71255
atmospheric monitoring, laser systems appl. 78−69520
atmospheric structure parameter, altitude depend. 77−37316
atmospheric temp., surface to orbit gas laser, absorpt. of vibr.-rot. band 78−12015

measurement by laser beam continued
atmospheric turbulence structural characts., meas. using spatially limited laser beam 80−98413
atmospheric visibility meas. using long-path laser transmissometer 78−85751
atmospheric-turbulence-structure parameter meas. using space-limited laser beam 80−46285
atomic lifetime technique, laser ablation and selective excitation spectroscopy 78−17824
attenuation coefficients of deionised filtered water, split-pulse laser method in visible region 79−17505
autocollimator, photo-electric, calibration with laser interferometer system and microcomputer 80−1304
automation of real-time optical meas. of small structures 79−85115
autoradiography and soft laser scanning in radioisotope work, appl. to metabolic studies 78−3576
axon diameter changes concurrent with action pot., crayfish, laser interferometer meas. 77−64029
backswept centrifugal impeller, laser-Doppler investigation of flow 79−77304
ballistic expt. using diffraction interferometer 80−47093
beam polarisation in e^+e^- PETRA storage ring, backscattered Ar^+ laser meas. 79−63839
biaxial laser-based displacement transducer 78−73967
bidirection laser rod gauge, development program *(Chinese)* 79−64239
biological cell analysis, high speed light scattering system 79−12042
biological cells laser Doppler meas., scattering characts. of intersecting beams *(Russian)* 80−3874
biological isotope, distrib. meas. after sedimentation 79−44066
biological material, laser stereometry light-scatt. technique, cardiac images 80−56310
biological objects, electronic speckle pattern interferometry in vivo 80−109083
biomedical laser microprobe mass analyser 80−98060
biomedical measurements, review *(Japanese)* 80−94311
blood, O_2 saturation meas. in nonhaemolized sample *(German)* 77−44735
blood, stored, microaggregation direct meas., effects of micro-filtration *(German)* 79−2168
blood red cell shape monitoring, laser differential scatt. system 77−90873
body motion, quantitative meas. by Schottky barrier Si photodiode and laser beam 80−12207
boiling layer, laser radiation probe of bed space 77−15115
bonded interface defect testing by differential interferometric Stoneley wave meas. 80−76444
Brewster angle determ. by dithered laser beam synchronous detection 80−73422
bulk materials, low optical absorpt. coeffs. meas., adiabatic laser calorimetry with long rod samples 79−2804
calibration and measurement standard, high precision *(German)* 80−78862
calorimeter for absorpt. coeff. determ. of IR windows and mirrors 78−49838
calorimetric absorption coefficient measurements using pulsed CO_2 lasers 80−9918
calorimetric data analysis for surface and bulk absorpt. determ. 78−25904
CANDU type 19 rod bundle, velocity distrib. in peripheral subchannel 80−32328
cavitation meter, design and testing 77−68715
cavitation nuclei in liquid flows, size distrib. determ. technique 77−68716
cavitation shock wave, investigation by coherent optical methods 78−38431
CdSe two-photon absorption, laser calorimetric obs. 80−33076
ceilometer using low-power laser radar 78−24390
celestial bodies range measurements, atmospheric correction determ. *(Russian)* 80−12674
cell high-speed analysis, laser absorpt. and scatt. meas. *(German)* 78−92687
cell structure and function investigation by laser microirradiation 79−66599
cell type recognition by multiangle laser beam scattering flow system 77−21595
cell voltage measurement using voltage sensitive dyes 79−57833
circular surface trueness testing by laser speckle photography 79−86266
clock comparison by laser in the nanosecond range 80−47035
clocks, for psec. meas., review 78−12676
coating thickness on small cylindrical samples, laser diffraction method 79−35674
coherence implications for laser appls. 77−75599
combustion, turbulent, averaging of pulsed laser Raman signals 78−70839
combustion diagnostics, laser Raman and fluoresc. techniques 78−88635
composite materials, laser beam determination, of elasticity-compressibility modulus, during compaction 79−43542
conference, appls. of low power lasers, San Diego, Calif., USA (Aug. 1976) 77−75536
conference, laser and electro-optical systems, San Diego, CA, USA (Feb. 1980) 80−62392
conference, laser and electrooptical systems, San Diego, CA, USA (Feb. 1978) 78−42340
conference, lasers and applications, Erice, Italy (May-Jun. 1970) 77−38906
contactless laser interferometer sweep gauge for diamond-turned surfaces 80−73441
correlator, Malvern, based on photon correlation and laser scattering spectroscopy, development and appl. 80−5741
crystalline clouds meas., light scatt. matrices *(Russian)* 77−5317
crystalline material optical absorption meas. 80−105718
cutaneous blood flow, laser beam Doppler shift method, instrument 78−28030
CW dye laser spectroscopy, detectable limit of Na atoms *(Japanese)* 78−44435
dark-field surface inspection using total internal reflection 80−74519
deformable mirror figure sensor control 77−19384
densitometry using pulsed dye laser and optical delay 77−61104
diameter measurement of hot or cold objects, laser bar gauge system 80−105605

measurement by laser beam continued
diameter of circular cylindrical wires using He-Ne laser interferometric and diffraction methods 79−21703
diameter of linear configurations, using light diffraction and moire fringes *(Czech)* 79−40530
diameter of transparent fibres meas. with He-Ne laser 79−97352
diatomic gas, transient flow, temp. and conc. profiles, by rot. Raman scatt. 77−75995
diffraction grating, sinusoidal groove depth determ. using laser 77−83949
diffuse object real-time velocity meas. using laser speckle zero-crossings 80−77760
diffuse reflectance rel. to partial coherence and IR laser photogoniometric meas. 80−14283
diffusely reflecting objects, deformation meas. by lasers, appl. of holography and speckle, review *(Japanese)* 80−9832
dilatometer for small linear expansion temp. coeffs. 78−77957
dimension meas. and control in-process using laser sensors and microprocessor 79−80577
dimensional gauging using scanning laser beam 78−57898
dimensional metrology, light diffraction patterns, technical structures *(German)* 79−30415
dimensional stability of fused quartz tube in a test facility, measurement using modified Michelson interferometer 79−58779
displacement, small, using three-mode laser, geodesic problems solution 80−77748
displacement and vibration measurement by laser interferometry 79−6094
distance meas. using laser interferometer, principles and performance 78−89442
dithered-beam metrology 79−30408
Doppler blood velocimetry *(Japanese)* 80−94310
Doppler velocimeter for surface velocity measurement 79−63193
Doppler vibr. meas. system using bispectral anal. 80−38357
dot matrix space-coded surface topographical mapping 80−98885
double-beam interferometer for amplitude-phase transmission meas. in optical components 77−87815
dust content of gas meas. by laser *(French)* 77−64486
dye laser, CW freq. stabilised, spectroscopic and metrological appl. 78−9395
dye laser, for metrological interference measurements 80−28250
dye laser, interference metrological applications, spectral kinetic charact. *(Russian)* 79−27253
dye laser appl., CW, technology developments influence 80−43383
Earth's rotation and Earth's crust movement by laser geodynamic satellite 77−41206
Earth crust deformation determ. using underground optical waveguides 77−53230
Earth strain meas. with laser interferometer *(Japanese)* 77−81783
Earth strain measurement, He-Ne I_2 stabilised laser reliability as interferometer source 80−106545
Earth strain measurements with laser interferometer *(Japanese)* 79−25346
Earth surface deformation detect., 500-m base laser interferometer 80−105087
Earth-Moon system laser ranging meas. 80−21933
elastooptical constants and refractive index, thermo-optical method for meas. 80−7327
electric and magnetic field sensing in power transmission, polarisation modulated system 77−45870
electro-optics, conference, Utrecht, Netherlands (Oct. 1978) 80−31420
electro-optics, systems aspects, seminar, Huntsville, AL, USA (May 1979) 80−94921
electrolyte concentration meas. instrum. using laser diode, optimisation of parameters 79−20488
electron beam impact on materials, measurement of dynamic response using laser interferometer 79−42102
electronic pupillometer, especially suitable for anesthetised cats 79−48317
electronic speckle pattern interferometry, vibrating object meas., use of chopped laser light 79−85165
electrophoretic mobility, measurement using wide-angle, crossed-beam laser Doppler scattering configuration 80−33011
electrostatic precipitator, particle velocity, laser Doppler anemometry study 80−59144
ellipsometric charact. of optical surfaces, determ. using nanosecond laser pulses 80−101822
ellipsometric technique using stabilised two-frequency laser 80−101820
end-standards and ruled scales using laser sources *(German)* 80−86251
erythrocyte distribution profiles during sedimentation as determ. by HeNe laser light 80−81563
etching monitoring using grating test pattern, appl. to SiO_2 and Si_3N_4 78−76775
Euglena gracilis, motion parameters meas. by laser light scatt. 79−16173
extensometer, comparative anal. with rod extensometers 77−64452
eye, human, pupil diameter and depth-of-field as meas. by laser speckle 78−15826
eye movement measurement, laser Doppler technique 79−92322
eye optic disc topography, by laser contour angiography, error model 77−60236
Fabry-Perot interferometer length stabilisation using He-Ne laser radiation 77−79141
fatigue damage, development rate by exoelectron meas. 80−25835
FFTF element measuring system 79−9729
fibre dispersion meas. with Nd:YAG laser at 1.06 to 1.6 μm 80−87555
fibre-optic rotation sensor construction and laboratory test 79−98497
film, thickness meas. using laser based fluorescence technique 79−49201
fine particles in gas flow, Doppler laser velocimeter meas. of motion 77−27583
fission reactor fuel element in-cell laser profilometer 80−22955
flavins, meas. of sub ns fluoresc. decay by time-correl. photon counting and Ar laser 80−94429
flow, random, statistics analysed by photon correlation anemometry 80−64522
flow meas., laser Doppler anemometry, practical considerations 79−27725
flow visualisation techniques eval. for liquids 77−58817
flow-birefringence, meas. using circularly polarised laser beam 79−35813
flowfield diagnostics using lasers 80−14853
flowing aerosol, particle size distrib. *(German)* 78−20076
measurement by laser beam continued
fluid dynamics, measurement of vel. correlation function using Erdmann-Gellert rate correlation technique 79−27728
fluid dynamics, sinusoidally perturbed flow meas., photon correlation technique 77−42945
fluid meas. in mechanical engineering, conf., Johannesburg, South Africa, (Feb. 1979) 80−75016
fluid props. meas., by laser interferometry 80−75018
fluorescence lifetime measuring system with picosecond resolution CW laser and AM radio 78−41357
fluorescence temperature measurement of Na in flames 80−11893
fluorescence temperature measurements in flames 80−11892
fog, artificial, size distrib. meas. by extinction-sedimentation inversion technique 78−37042
frequency shift laser meas. of water and wind velocities 77−39385
gain probing by intracavity dye laser spectroscopy 77−7092
gas analysis, laser optical-acoustic spectroscopic method 79−66383
gas complex analysis method, resonance absorption with pulsed laser light *(Japanese)* 80−36421
gas concentration meas. using Raman intensity depend. on giant pulse laser polarization 80−98986
gas detector, all-electric, using Stark cell 80−74417
gas lasers, frequency stabilised by saturated absorpt., synthesis and measurement of optical frequencies, review *(French)* 79−31966
gas trace anal. by laser-induced Schlieren technique 80−9929
gasdynamic flow diagnostics by laser interferometry 77−51137
general relativity test, precision ring laser interferometry technique 80−52117
geodesic interference distance meas. using semicond. lasers 80−77175
geodesy, accuracy with transportable lunar laser ranging station 77−48988
geophysical distance measurement, multi-wavelength instrument 77−29484
glass thickness automatic measurement by laser beam 80−82744
graphite, impurity analysis, laser emission spectroscopy, material evaporation, auxiliary spark gap effects 79−87924
gravitational radiation, detection using Ar laser interferometer 79−101076
gravitational radiation detection, laser displacement sensor 80−101747
gravitational wave detector *(Russian)* 78−77794
gravitational wave recording possibility using laser detector 79−40442
gyromagnetic ratio of proton and fine-structure constant redeterm., by meas. distance between wires 80−74253
gyrometer, accuracy increase by automatic output signal correction *(Russian)* 80−215
heat capacities of $La_{1-x}Sr_xCoO_3$, at 80 to 950K, phase transitions obs. *(Japanese)* 80−54898
helical motion of rigid body, meas. by double exposure speckle method 78−16775
heterodyne interferometry real-time digital broad-beam, for measurements of deforming surfaces 79−85173
heterodyne laser beam position sensor 78−46705
HF SAW phase/amplitude meas. using phase sensitive laser probe 79−14171
high accuracy distance measurement by two-wavelength pulsed laser sources 80−192
holographic interference microscope, MGI-1 80−5706
holographic NDT system application of laser speckles 77−75457
hydrazine rocket fuel in ambient air, CO_2 laser absorption spectra and photoacoustic detection 80−104540
hydrometeor backscattering cross sections, meas. at 6328 Å 78−49135
hypersonic ballistics experiment, application of laser light source 78−38433
immunological reaction monitor using laser light scatt. 80−85463
in-process dimension, position and quality meas. appls. 77−54716
industrial, review *(German)* 77−14734
interferometer, for accurate positioning, built-in system for machine tools *(German)* 80−9022
interferometer, for phase changes $<10^{-5}$Å 77−18087
interferometer, NBS system designed for seismology appl. 80−13125
interferometer, two-frequency, small displacement meas. in LF range 79−30533
interferometer application to length meas. in production *(German)* 80−18007
interferometer for measuring beam oscill. in balance scales, construction *(German)* 77−79090
interferometer for precision linear displacement meas. 80−27285
interferometer length meas. by tunable laser 79−35817
interferometer system for creep measurement in pressurised tubes, in-reactor creep, reference fuel cladding appl. *(German)* 77−74925
interferometer systems, theory and application 80−73435
interferometers, AM and FM operation and applications *(German)* 80−86389
interferometric angle meas., 30°-60° range, calibration, accuracy *(German)* 77−79051
interferometric displacement meas. system for positioning of sphere and meas. roundness 79−97416
interferometric manometer with 8 mPa resolution 78−24808
interferometric system, double-freq., with automatic compensation *(Chinese)* 80−27340
interferometry measurement system 79−6171
interferometry seminar, San Diego, CA, USA (Aug. 1979) 80−73096
interlocked solid-state lasers, radiation intensity modulation for precision meas. 80−1250
intra-ocular pressure measurement using sonics and coherent optics 77−81548
IR astronomy, laser heterodyne techniques appl. to interstellar submillimetric lines detect. 79−44377
IR laser interferometer, length measuring, alignment using laser feedback 80−37075
IR laser interferometer operation and testing 80−73433
IR optical components and aspherics, 10.6 μm interferometric testing 80−74523
IR spectrophotometer spectral slit width determ., method comparison 80−86472
LAMBDA laser distance and thickness meas. system *(German)* 78−32792
LAMMA (laser microprobe mass analyser) appl., materials testing and thin film microprocessing 80−18041
laser Doppler anemometery digital data acquisition system 77−80253

measurement by laser beam continued
laser Doppler anemometry principles and status survey *(German)* 78−9738
laser extensometer with scanning beam modulation, improved gauging precision 78−57896
laser frequency meas. using diode laser, appl. to CO_2 weak transitions 77−88693
laser interferometer for meas. linear vibration report 78−86243
laser interferometry by induced modulation of cavity field 78−49888
laser Raman optical multichannel analyser, for gas conc. profile and temp. determ. 78−73098
laser rangefinder using pulsed CO_2 TEA laser 78−46760
laser shearing interferometer appl. to supersonic flow field meas. *(Chinese)* 79−32715
laser-flash calorimetry for small sample thermal capacity meas. *(Japanese)* 77−49725
length meas., development and appl. *(German)* 77−27297
length meas. error factor *(Japanese)* 78−8384
length meas. techniques using laser interferometry, problems with environmental influences *(German)* 79−30411
length measurement with heterodyne interferometry *(German)* 80−68181
levelling of railway track, practical experience *(German)* 79−98432
lidar for atm. meas. 77−37436
light beating spectroscopic instrument for continuous meas. of tissue blood flow 80−41160
light scattering in aqueous polymer solutions meas., apparatus 78−74058
light velocity and wavelength determ. 80−42190
line standard meas. using He-Ne laser photoelectric microscope 77−82599
linear dimensions, measured on production line by optical techniques 80−82746
liquid, extinction coefficient meas. using coaxial dual channel laser system 80−73425
liquid flow *(Italian)* 78−14107
liquid level meas., non-contact, laser interferometric method *(German)* 79−12769
long distance reference length, laser interferometer meas. 79−75497
lunar laser ranging, polishing and Foucault test of receiving telescope mirror *(Japanese)* 78−89065
lunar laser-ranging, review 77−5459
lunar ranging telescope 78−93106
machine part, rotating, surface finish, laser method for determ. 80−89454
machine tool geometry inspection using interferometry 77−9997
machine tool position feedback by laser interferometer 80−73438
macromolecular rapid circular dichroism meas. with small gas lasers 77−37968
magnetic angle convertor accuracy test method 78−77948
marine aerosol using laser scattering spectrometer system 78−36316
marine hydrosol scattering meas. by submerged laser nephelometer *(Russian)* 77−60418
Mars rover laser rangefinder accuracy estimate 78−24437
material and structure evaluation by laser methods 77−21345
mechanical vibration meas., using fibre optic laser Doppler probe 78−30248
mechanical vibration meas. by laser interferometry *(French)* 78−67156
mechanical vibration meas. optical heterodyne systems 77−13746
mechanical vibrations of small amplitude using multiple-beam interferometer 80−4759
membrane transport coeff. meas., laser interferrometric technique 78−15936
metal plate high-gradient transverse deformation interferometry 78−82024
metal surface, rough, hemispherical emittance 80−70434
metal ultrathin foils, laser monitored electrothinner *(German)* 79−34219
methane-air flames, meas. of temp. and OH conc. 80−16687
metrology, review 77−694
Michelson interferometer length meas. error rel. to illuminating beam form 77−26267
microcomputer based laser interferometer for angular displacement meas. *(Polish)* 80−90816
microellipsometer, for film thickness and optical parameters meas. *(Czech)* 77−61109
microemulsions, heat transfer meas. by laser-induced thermal blooming 80−91833
microfluorometer for fluorescence decay meas. of biological samples 79−66449
microinterferometer limiting sensitivity and accuracy characteristics 77−79142
microinterferometer transducer, air-bearing, for use with universal inspection machines 78−57899
microphotometry with laminar hydrodynamic focusing 77−37965
microstrain gauge principle and technique 77−68541
modular multi-axis laser distance measuring system of high accuracy *(German)* 78−77856
Moire contouring of large objects by scanning technique 78−32791
molecular models, semiautomatic coordinate meas. device using laser beams 79−37573
monomode fibre dispersion and bandwidth meas. by mode-locked Q-switched Nd:YAG laser 80−91933
Moon and satellite distance meas. by laser 77−9673
Mossbauer data calibration using laser interferometer 77−88326
multichannel device structure and testing, for pulsed energies *(German)* 80−95933
muscle sarcomere length, laser on-line meas. systems 79−48383
myxomycetes plasmodium protoplasmic flow, laser Doppler anemometry obs. 79−57681
natural water U content meas. 78−85705
NDT appl. *(German)* 78−39975
neutron flux energy spectrum meas. from luminesc. line freq. change 80−23272
non-isothermal flow, turbulence measurement, laser Doppler velocimetry appl. 79−41776
noncontact gauging systems, advantages and appl. 79−2745
noncontact material testing using laser energy deposition and interferometry 79−34258
noninterferometric optical probe for position and displacement meas. 77−74362
measurement by laser beam continued
nuclear track detectors, glass and plastic laser diffr. appl. to determ. of etched track parameters 80−95499
object deformation, determ. of components from 1 double-exposure hologram 79−94193
object dimension meas. by computer-controlled laser beam scanning 79−98431
object dimension meas. by computer-controlled laser beams 80−31715
ocean surface phenomena measurement *(Japanese)* 79−16716
ocean wave slope meter, fast response instrument, wind-wave moments meas. 78−45012
ocular tonometry through sonic excitation and laser Doppler velocimetry 80−56152
oil, Newtonian viscosity meas. by two optical methods 77−89214
oil detection, in water, using combined GaAlAs laser and fibre optic bundles 78−96301
opaque optical components' parallelism meas. 79−81549
ophthalmology and vision research, appl. of lasers, holography 80−12210
optical, thermal and mech. props. of materials, laser meas. techniques 77−74513
optical cables attenuation and dispersion, faults location *(German)* 79−14097
optical coating absorption meas. by 1.06 μm laser calorimeter calorimeter 80−33066
optical fibre, index profile meas., nondestructive 78−13796
optical fibre, PCVD, dispersion measurement by mode-locked synchronously-pumped dye laser 80−64191
optical fibre birefringence measurement system, computer-controlled 79−64352
optical fibre meas. using first positive system N_2 laser 78−59020
optical fibres, baseband freq. response meas. by modulated InGaAsP laser beam, dispersion charcts. 80−1308
optical fibres, sandwich ribbon, measurement of polarisation props. using He-Ne laser 79−64353
optical glass, thermally tempered, surface stress meas. by crit. ray method 80−106766
optical picosecond spectroscopy using mode-locked lasers 78−58065
optical precision physical expts., review 78−42246
optical radar ceilometer measures cloud base height using laser beam 77−29441
optical surface, scratch classifier for inspection of scratch severity 77−75722
optical surfaces, concave and convex, radii of curvature meas. 80−83654
opticophysical and physicochemical meas. instrum. 80−13121
oscillating quartz crystal stress distribution meas. by laser probe 77−20803
oxides produced during Al anodisation, thickness meas. by ellipsometry 78−171
parabolic mirror testing by vibration-insensitive laser unequal path interferometer 80−74537
parabolic mirror testing during fabrication by long-wavelength interferometer 80−74536
particle and spray sizing, using laser diffraction 80−17925
particle motion 3D sensing via multibeam laser system 80−83722
particle motion detection in transparent liquids, Fourier transform acoustooptical system performance 80−87680
particle size analyser, size estimated from diffraction pattern 79−6091
particle size analyser, using diffraction of light by particles 79−6090
particle size analysis using an ultramicroscope 79−44902
particle size and velocity simultaneous meas., laser technique 78−70096
particle size meas., digital control of expt. 78−70098
particle size meas., laser flowthrough microphotometer, double-beam technique, internal calibrated 79−17391
particle size meter using laser light scatt. spectroscopy 80−77754
particle size spectrometry, use of low power gas lasers 77−78485
particle sizing counter for in situ meas. 79−75489
particle sizing counter for in situ meas. 79−75490
particle sizing using laser photography 78−81946
particles, airborne, quantitative meas. *(Japanese)* 77−29426
particulate analysis, multiple ratio single particle counter 78−35732
pathological samples, mol. microanal. in situ with laser-Raman microprobe 80−81683
photoelastic method of thermal stress determ. circumferentially grooved cylinder 80−38363
photoelasticity in 3-D, optical slicing method 78−26093
photoelectric aerosol counter, use of laser light sources *(Russian)* 79−100969
photographic pulp quality control using He-Ne laser scanning system *(German)* 80−3272
phototachymeter, pulsed phase, distance meas. accuracy, semicond. laser temporal charcts. effect 78−70097
photothermoplastic film in holography *(German)* 78−22097
picosecond spectroscopy, appl. to chem. and biological reactions 79−80697
piezoelectric constant measurement, at frequencies up to 50 kHz 79−63270
piezoelectric material length changes laser interferometry appl., for sub-nano-meter range *(Slovak)* 78−77861
plane mixing layer, two-point LDV meas., vorticity distrib. 80−38506
planetary atmospheres, light scatt. process meas. via laser beam *(Russian)* 79−44365
planoconvex AT-cut quartz resonator vibration displacement meas. by laser interferometry 77−37976
PMMA Doppler scatt. optical determ. of US radiation patterns 79−76930
polarimeter for e^+ e^- beam polarisation meas. in storage ring 80−14019
polymer molecular weight distrib. determ., low angle light scatt. 78−92230
power system current and voltage meas. using electro-optical effects *(Japanese)* 80−86342
precision measurements using stabilized lasers 79−55151
radiograph densitometric anal., scanner for 79−70619
rain impact and erosion recording, laser techniques 79−62610
Raman microprobe, microscopic samples molecular analysis, particle charcts. determ. 80−57391
Raman microprobe analysis, principles and appl. 80−57390
Raman microprobe-microscope, molecular optical laser examiner appl. 80−62737
range finding and other appl. *(German)* 78−5522
rangefinder, AN/GVS-5 hand-held laser, production engineering techniques 78−59018

measurement by laser beam continued
rangefinder, with improved accuracy 79−17384
rangefinder and 3D object recognition algorithm 80−96016
rangefinder operating frequency selection 79−72691
rangefinder radiometric efficiency, optomechanical tolerance analysis 79−21705
rangefinder technology, present and future 77−34957
rangefinder using pulsed CO_2 TEA laser 77−88926
ranging equipment, range meas. system *(Japanese)* 78−89074
ranging laser atmospheric transmissometer with retroreflector 77−21905
ranging system, single and two colour, effects of random path fluctuations 77−7094
ranging system using non-Gaussian laser pulse shapes 77−10929
ranging systems, ground based and space based 77−88925
ranging systems, NASA applications 78−81527
rate calorimetry analysis with coating absorption 80−33050
rectilinearity measurement, laser transit prototype parameter optimisation 79−76745
red blood cell diameter meas. from He-Ne laser beam diffr. pattern 77−86582
reflectance of diffuse surfaces, in situ laser meas. 78−82022
reflective object displacement and vibration meas. *(Russian)* 79−21695
reflectivity measurement of highly reflective mirrors 78−54444
refractive index of liquids as function of temp. using laser beam interferometer 79−58780
refractometer laser detector for anal. of liquids 80−101830
remote atomic clocks synchronisation using injection laser diodes 77−82493
retinal resolving power meas. by laser interferometry 80−36066
retroreflector alignment, simple interferometric technique 80−95125
reversible fringe counter in laser interferometry 77−87816
review *(Japanese)* 78−4674
rhodopsin visual pigment, photochemical transformations, laser flash photolysis 79−66472
rotating shafts, torsional vibration meas., laser Doppler system 79−50685
rough surface interferometry at 10.6 μm 80−86385
roughness measurement of polished surfaces, using laser heterodyne apparatus 79−21696
roughness measurement using laser scanning analyser 80−36992
roughness of periodically shred surfaces, on-line meas. technique using He-Ne laser *(German)* 80−33014
satellite laser ranging system, 2cm accuracy, for geodetic research 77−21932
satellite laser tracking data, ray tracing evaluation of refraction errors 79−8588
satellite ranging, picosec. pulse freq. doubled Nd:YAG laser system 77−21933
scanning laser acoustic microscope applications *(German)* 80−3271
scanning laser acoustic microscopy, ceramic components nondestructive testing, comparison with SEM and optical microscopy results 80−58875
scattered light intensity, recurrence rate correl. 78−66760
scattering and depolarisation meas. in liquids 79−93198
Seebeck coefficient, AC method of meas. using laser beam, for semicond. 78−76096
seismic microvibration frequency analysis by 50 m interferometer 80−109276
semiconductor materials and devices *(Rumanian)* 78−52035
shock wave effects, laser interferometry 77−79145
shock wave vel. determ. by laser schlieren method 77−39370
sickle cell anaemia sickling kinetics, multiangle laser scatt. spectrophotometer 79−79494
single atom detection in particle tracks 80−9475
single pulse formation from measurement laser 80−23734
skin friction meter using viscosity balance principle for metal surfaces 77−35266
small angle meas. using laser interferometer *(Chinese)* 77−49768
small angle scattering meas. from streaming particles, laser heterodyne apparatus 80−1261
small linear dimension meas., contactless laser beam diffraction method 77−22525
small mechanical oscillations or vibrations 79−77032
solar cell carrier lifetime meas. from transient photoresponses of pulsed laser *(French)* 79−24898
solar radiation concentrator accuracy assessment, using laser radiator and sectioned photoreceiver 79−23038
solid laser, measurement, radiation pulses formation and stabilisation 80−23735
solid-state measurement laser, radiation pulse width meas. , 80−23736
solid-state measurement lasers, single-pulse with uniform distribution of energy density, correction equipment 80−23703
sonic laser radiation detector *(Polish)* 79−85113
Special Theory of Relativity, expt. 80−27118
speckle, appl. to vibrational charact. 79−94569
speckle pattern TV interferometer, principle and appl. 78−58014
speckle photography, review *(Chinese)* 79−35880
specklegram technique, strain, small displacement measurement appl. *(German)* 78−1616
spectrophone, low-noise, using continuous laser beam 80−74418
spectroscopic light sources, far-IR, using tunable diode lasers, optical coupling arrangement 80−73481
spectroscopy using lasers, summer school, Les Houches, France (June 1975) 78−301
spermatozoa mobility meas. by laser light scatt. *(French)* 78−36083
spermatozoa motility meas. by laser light scatt. *(German)* 79−12056
spermatozoa motility meas. by light scatt., appl. to reproduction immunology *(French)* 79−34628
spherical particle velocity and size meas., crossed-beam light scatt. interferometry 80−47011
sputtered particles, vel. meas. by Doppler-shift laser spectrometer 80−62638
stereometry using range-dependent time delay in reflected light 77−10127
stethoscope, non-contact high sensitivity, using interferometer technique *(German)* 78−69176
straight line meas., LINOMETER *(German)* 77−87727
straightness meas. using laser beam as reference line *(German)* 77−87726
strain distribution in plane opaque surfaces, laser grating meas. method 79−32407
measurement by laser beam continued
strain evaluation by specimen-grating photograph electro-optical processing 77−39266
strain tide spectroscopy, interaction Earth mantle, liquid core appl. 79−5440
Streptococcus mutans 10449, size determ. by laser light scatt. 80−109062
stress meas., absolute retardation patterns, laser diametrically compressed photoelastic disc 77−27496
submarine periscope optical design for laser rangefinding compatibility 80−78987
submillimetric waveguide laser for gas spectroscopy 80−33022
subnanosecond time-correlated photon counting with tunable lasers 78−45701
subpicosecond relax. time meas. using pulsed lasers *(Czech)* 78−78838
subpicosecond spectroscopy by passively modelocked continuously operated dye lasers 78−58066
supersonic chemical laser flowfield, laser induced I_2 fluorescence meas. 80−38008
supersonic flow, meas. turbulence parameters, in rocket exhaust, crossed beam correl. method 79−86541
surface displacement and vibration meas. using laser speckle *(French)* 78−4686
surface finish of machined surfaces, laser reflectance patterns 79−85126
surface mapping, interferometric method with variable sensitivity, IC manufacturing appl. 78−45592
surface oscillations meas. by 1.06 μm laser heterodyne method 79−50339
surface planarity, by interference pattern assessment 80−31711
surface profile meas. and ang. deflection monitoring, noncontact method using scanning laser beam 79−9203
surface profile meas. and angular deflection monitoring, noncontact method 79−85125
surface roughness estimation by the laser-section method *(German)* 79−49198
surface structure influence on image speckle pattern contrast 80−17985
surface tension and viscosity, meas. at liquid-gas interfaces, contactless method 79−1277
surface topography, meas. via laser profilograph 77−74356
survey of laser appls. in metrology *(German)* 77−698
surveying, precise direction measurement by laser, techniques and instruments *(Czech)* 79−30414
temperature gradients in liquid, using laser microrefractometer 80−57362
temperature measurement of high-temp. gases, using IR tunable diode laser 78−86268
terrain profiler, pulsed GaAs laser system 77−91297
terrain profiler, pulsed GaAs laser system 78−49145
thermal cond. of liquids, laser flash method 78−89476
thermal expansion at high temps., meas. via laser interferometry of two fibres 77−26270
thermal receiver with temp. readout by laser beam 77−82605
thermal turbulence in plane airstream, temp. fluctuation meas., interferometric method 79−7432
thin layer absorption loss meas. by CW dye laser intra-cavity technique *(German)* 80−16113
thread grinder, high precision, laser interferometric auto-correcting system 80−90830
thread parameters meas., Fraunhofer diffr. coherent optics method 78−89439
three-dimensional topographic mensuration, laser electro-optic system 80−99784
time and frequency, conf., Helsinki, Finland (Aug. 1978) 80−46728
time-of-flight ranging at very low signal levels, accuracy analysis 77−111
tissue fluorochrome meas. with He-Cd UV laser 77−77962
Tokamak, poloidal field meas. by far IR polarimetry 79−32794
torsional vibration meas. with laser Doppler system 78−45612
tracheal ciliary beat, improved device for freq. recording 80−109070
transcutaneous O_2 and skin blood flow, laser system for simultaneous meas. 80−26321
transient chemical events measurement using laser-based methods 80−40801
transparency optical thickness irregularity processing by laser heterodyne correlation 79−14119
transparent fibre, geometrical and optical parameter meas. 77−18062
transverse dimensions of extended objects, semiautomatic photoelec. laser 78−36966
truss joint strain meas. by modified Michelson interferometer 80−74821
tunable IR solid-state laser characteristics and principles 80−87406
tunable laser interferometry, oscillator strength meas. 80−105697
turbulence, pulse luminescence method using N pulse laser 77−24041
turbulence diagnostics, using multiple laser beam probe system 77−27630
turbulent convection in liquid 79−98831
turbulent flow field investigation techniques 78−34224
turbulent flow props., localised, crossed beam correlation method 78−34223
turbulent jet temperature fluctuations *(French)* 77−24038
turbulent mixing flow, velocity biasing resulting from non-uniform seeding 80−59143
turbulent mixing meas., laser light scatt. technique 77−11285
two objects movement rate, by laser interferometers *(Russian)* 77−26392
two-colour length measurement scheme using CO_2 laser 80−99747
two-dimensional structure in-plane vibr., stress analysis by laser speckle method 80−103006
underground optical cable transmission meas. 78−50942
unequal path interferometer with electro-optical camera and minicomputer, fabrication/test appl. 80−77847
US surface wave velocity measurement using reflections from laser scribed grooves 78−90614
US vel. in acoustooptically active solids, laser beam probing of standing wave 78−33965
US velocity meas. of mammalian collagen threads using scanning laser acoustic microscope 79−43972
vacuum breakdown, microparticles detection by laser scatt. 77−19787
vacuum evaporation, substrate temp. meas. 80−20794
vapour pressure, high temperature vapours, phase transitions, equations of state, appl. of laser pulse heating 80−52230

measurement by laser beam continued
velocimeter, non-contact, using laser produced speckle patterns *(Japanese)* 78−178
velocity, extremely low, using interf. effects of pair of two-freq. laser beams 77−79071
velocity gradients and laminar and turbulent diffusion, direct optical meas. 80−59132
velocity measurement application using laser beam, operation *(German)* 77−9991
velocity of liquid, meas. by coherent diffusion using triggered ruby laser *(French)* 77−68711
velocity-time history recording, by laser interferometer system 78−45602
very-small-angle light scatt. apparatus design and performance 77−10082
vibration analysis of plate and shell by laser speckle interferometry 77−10008
vibration and small mechanical displacements measurement, heterodyning two laser beams 80−73309
vibration and surface structure and dimensions, using Selcom System 1000 *(Swedish)* 78−63402
vibration measurement of reflecting surfaces, laser Doppler vibrometer 79−6117
vibration measurement using a frequency biased laser velocity meter 79−98675
vibration meter, Doppler, 100 Å to 10 cm *(French)* 78−30250
vibration meter, high sensitivity, laser type using a fibre-optic probe 79−7351
vibration probes, for remote surface 77−87756
vibration-insensitive He-Ne laser interferometer for plasma electron density meas. 79−14610
vibrations, periodic, nonsinusoidal, meas. by laser speckle interferometry 77−41673
vibrations, small vertical, interferometric method, using LF phase modulation 77−37970
vibrations, stroboscopic holographic interferometry, beam modulation methods *(Polish)* 79−3649
vibrations of very small amplitude in US transducers using laser probe 80−73443
vibrations testing, in precision units, by real-time holography *(German)* 80−38366
video disk pit geometry, control, optical techniques 80−5775
visibility, contrib. of particulate pollution 77−73852
water in multiphase flow systems, diagnostics, laser induced Raman scatt. 77−31373
water waves, oscillatory boundary layer meas. using laser Doppler anemometry 79−27719
wave-slope spectra in capillary-gravity range, increasing wind, laser beam meas. 77−3836
wideband laser-interferometer gravit. radiation expt. 78−41223
wind-tunnel laser anemometer photon correlation techniques 77−80256
e^+e^- beam polarisation meas., backscattered laser method, SPEAR storage rings 79−63838
Al foil, deformation, laser optical scanning obs. 80−100995
Al plate, thermal strain meas. by one-beam laser speckle interferometry 80−103005
As_2S_3 film, vacuum deposited, selective etching characts. obs. *(Russian)* 80−3207
As_2Se_3 film on CaF_2, interface and bulk absorption meas. 80−35001
BN thermal diffusivity meas. using ruby laser beam *(Spanish)* 79−90835
C particulate, airborne, photacoustic and absorption spectrum using tunable dye laser 80−4102
CO_2 laser multiwavelength interferometry, absolute distance meas. 79−31974
$CO_2/^{192}OsO_4$ laser, absolute light oscill. freq., universal const. variation meas. possibilities *(Russian)* 80−5723
CO_2-laser long-path absorption system for air pollution monitoring, error anal. 79−25340
CdTe two-photon absorption, laser calorimetric obs. 80−33076
GaAlAs DH pump laser for photoluminescence lifetime meas. 78−74085
GaInPAs, narrow-band tunable injection laser, 1.06 μm, description and appls. 79−76713
H, Doppler free laser expt., elementary particle props. from atomic expts. 77−34578
HO, detection by laser excited fluoresc., press. depend. of fluoresc. and photolytic interferences 80−95666
He-Ne 3.39 μm laser interferometer, length and refr. index meas. 80−68172
He-Ne laser for original equipment manufacturer, aligning, recording and meas. appls. 77−75597
He-Ne laser IR applications 79−94275
He-Ne laser interferometer for US displacement meas. 77−37972
He-Ne laser stabilisation and performance for dimensional meas. 80−19049
He-Ne laser wavelength stability, calibration and traceability 80−19050
He-Ne lasers, Original Equipment Manufacturer applics. 78−33765
InP substrates, HCl etching speed and polarity obs. *(Slovak)* 78−56575
KCl, bulk and surface absorption comparison, 9.2 to 10.85 μm 80−33051
$LiNbO_3$ waveguide absorption losses, laser calorimetric meas. 79−64311
$^6Li^+$, confined ions, density distrib., laser scanning meas. 79−81303
NaCl, bulk and surface absorption comparison, 9.2 to 10.85 μm 80−33051
NaF film on CaF_2, interface and bulk absorption meas. 80−35001
Nz pulsed laser stroboscopic fluorimeter 80−35593
Si, CVD, underlying oxide layer thickness effect on in-process thickness monitoring 80−6679
Si textured solar cell, hairline crack detect. using focused laser scanner 79−48123
UO_2, liquid, reactor safety research *(German)* 80−42787
ZnO monocrystal and RF sputtered heteroepitaxial film, SAW attenuation comparison 79−56063

measurement errors
3-dimensional probes *(German)* 79−80574
23rd International Aerospace Instrumentation Symposium tutorial, Las Vegas (1977) 78−12074
90° elbow flow meter, effect of inaccuracy of curvature *(Japanese)* 77−89215
Aanderaa Ni-coated current meter, pressure-induced direction error 80−4121

measurement errors continued
Abel integral eqn. solution by orthogonal polynomials 78−67436
aberrant values, recognition and elimination *(Rumanian)* 80−22316
aberrant values elimination, from series of repeated meas. *(Rumanian)* 80−47008
absolute radiation meas., receiver-coating thermal resist. effect on accuracy 77−87836
absorbent surface thickness meas. in differential digital radioisotope system, anal. *(Polish)* 77−53860
acceleration measurement during translational motion, errors associated with apparatus for standards 79−30432
accelerometer, piezoelectric impact, effect of damping on dynamic error 79−30435
accelerometer testing on standard vibratory testers, systematic-error correction 79−71423
accelerometer testing using apparatus for exact production of accelerations less than g 79−71424
accelerometer with centrifuge, linear, methods of eliminating systematic errors in calibration 79−71399
accuracy improvement by two-parameter meas. method 77−82480
accuracy influence factor grouping and correlation 78−41262
acid-base titrations, logarithmic diagrams for pH value and error estimation 80−35619
acoustic flowmeters, multiple and single path, sources of error, accuracy, appls. 79−94749
acoustic noise meas. of elec. machines, errors *(Hungarian)* 80−96102
acoustic reflection coeff. in liquid layer, error of interference methods 77−14865
acoustic reflex threshold, variability of measurements 77−16938
activated samples, simultaneous two-sample meas. immune to detector intercalibration 77−57835
aerosol, stratospheric, in S hemisphere, impactor and in situ detector errors 78−73437
aerosols, atmospheric, X-ray fluoresc. anal., filter attenuation corrections 78−35740
AGK3 declinations, random errors determ. by Sanders-Raimond method 77−53404
air, ultrapure, molar density at 298.15K for mass transfer buoyancy corrections 79−88917
air jet/piston dynamical interaction pressure transducer errors 77−80245
air pollution impurities, sampling method improvements *(Dutch)* 77−70827
aircraft noise, effect of small vars. in height of microphone above ground surface 77−23813
aircraft tracking system based on acoustic refr. scatt., timing errors effects 77−46840
ampere, realization by means of current balance at NPL 80−105678
analogue-digital measurement systems, errors in derivative determ. 79−80567
analytical correction in meas. results, probabilistic method 80−13030
anemograph data quality control 80−56642
anemometer, constant resistance hot wire, flow average temp. variations effect on reading *(Russian)* 78−88925
angle meas., photodetector freq. doubler nonlinear distortions effect 78−36968
angle measurement with sine-bar devices, error anal. 78−81944
angular meas., testing instrument for errors 80−42186
angular measurement, digital method using photoelectric angular transducer with unstable datum, increasing accuracy 80−17920
angular measurement using laser interferometer 80−42196
Ap stars, mag. fields photographic meas., errors rel. to surface field distrib. 77−26015
apparatus inspection, confidence and productivity improvement 78−77840
approximate treatment of experimental errors 77−12
aquatic eyes, retinoscopy, refractive error considerations 80−61750
artificial satellites, effective isotropic radiated power, error anal. using calibrated radio star 78−93070
astrolabe instrumental errors and transversal scale, work of Levi ben Gerson 78−21
astrometry, astroclimatic influences on precision of photographic star positions obtained with wide-angle astrographs *(Russian)* 80−72748
astrometry, daytime obs., anomalous refr. and personal errors meas. 78−24441
astrometry, tropospheric limitations of coordinate measurements using phase and fringe freq. 79−44375
astronomical atmospheric extinction data, time trend and internal errors 77−49161
astronomical azimuth determ., accuracy, geodetic networks orientation control appl. 78−92774
astronomical image tube spectrophotometry of weak emission lines, precision *(French)* 79−88601
astronomical observations errors, optimum linear estimation of mathematical expectation and standard deviation *(Russian)* 80−12673
astronomical optics testing by Hartmann method, estimation of reliability of results 80−67564
astronomical standard stars for uvby photoelectric photometry south of declination +10°, obs. 77−2347
astronomical time-modulated measurements with image-tube systems, effects of phosphor decay 79−88602
atmosphere 500 mb height, anal. error development, (1946 to 1969) 80−72615
atmosphere entrainment, overestimates from aircraft temp. sensors in cloud 79−53483
atmosphere measurements by double theodolite technique, control of inherent uncertainties 80−77160
atmosphere O_3 profile determ. from outgoing thermal radiation, disturbing factors effects 78−92945
atmosphere submicron aerosols, losses in aluminised Mylar bags 79−58114
atmosphere temperature determination by remote sounding, aerosol attenuation effects on accuracy *(Russian)* 78−81430
atmosphere temperature profiles, satellite retrieved, error due to aerosol particles effects 80−98449
atmosphere temperature sensors, humidity effects and sea salt contamination 80−82095
atmospheric O_3 depletion, supersonic gas sampling error 77−33193
atmospheric precipitation acidity measurement, error anal. applied to indirect methods 80−72108
atmospheric sampling of particulate nitrate with glass fibre filters 78−16169

measurement errors continued
atmospheric temp. and humidity anomalous profiles remote determ., errors *(Russian)* 77−17266
atmospheric testing instrums., standardisation and determ. of dynamic errors 79−8714
atmospheric turbulence measurement in marine environment, salt deposits effects on hot wires 77−33214
atomic absorption spectrometry, background-corrected, factors affecting accuracy 77−36819
atomic emission spectroscopy, quantometric meas. of spectra of controlled arc, spark generators, correls. 79−66382
atomic lifetime determinations, errors using pulsed dye lasers 77−42281
attitude determ. of uncontrolled satellite, correlated meas. error effect 78−16262
auroral ionosphere, large parallel elec. fields obs. 77−9595
autocollimating telescopes, instrumental and other errors *(German)* 78−77956
autocollimation goniometer, reading error 78−16829
autodensitometer, flatbed, for biophys. appl., error analysis 77−52937
automated variable pressure controller design and error analysis 77−57315
automatic gas analyser, meas. errors due to gas-water interaction *(German)* 78−44438
automatic network analyser, calibration, EM reflection coeff. meas. appl. 78−89463
average value voltage transducer for AC meas., anal. *(Russian)* 78−45649
balance indicators, using conventional galvanometers *(Polish)* 77−10064
beam-foil lifetime measurement, cascading problem, ANDC method use and error limits 80−14249
biochemical samples mag. susceptibility meas., sample holder contrib. elimination 77−26367
biological specimen complex permittivity meas. bench for 2-10 GHz at 77-300K *(Russian)* 77−32966
biomedical ECG recording, correction of timing errors due to tape speed variation 80−72354
biomedical pulse echo US, intensity meas. errors assess. when using miniature hydrophones 80−3743
blood flow and cardiac output, using indocyanine green and microspheres 77−77925
blood perfusion rate estimation from diffusible indicator meas., sensitivity anal. 80−104803
blood pressure, cuff method errors, Korotkov and impedance plethysmography techniques 77−40886
blood pressure measurement with portable systems using Korotkov sounds, meas. accuracy 80−76855
blood pressure recording, simple method for fidelity improvement, Korotkoff sounds 80−76811
body anelastic hysteresis determ. and error formula *(German)* 77−80123
body joints, centres and angles of rotation meas., errors and optimisation study 80−61604
body organ volume meas. in vivo using computer-based u.s. echography 77−2033
boiling point, uncertainty in thermistor ebullioscopes sensitivity 78−12695
bone, inclusions as source of error in radiocarbon dating 78−346
bone biopsy, automatic image anal., var. in rib architecture 78−61253
bridge circuit errors due to changes in resistance thermometer conductor resistance 79−30473
bridge circuits with thermistors and pulsed supplies, unbalanced, anal. 79−30474
buoy wave data analyses noise correction functions and error sources 80−46302
calibration of digital voltmeter, using potentiometer 77−10059
calorimetric props. changes meas. via direct difference technique 77−33988
camera objectives, quality testing by semiautomatic modulation transfer coeff. meas. 79−14124
capacitance displacement transducers, effect of tilt and surface damage 78−54356
capacitance meter operation with 10 kV Bias Isolation Unit 77−57364
capacitive hygrometers for measuring grain moisture content 79−75538
capacitive transducers, manufacturing error effect on accuracy 78−89467
capillary permeability determ. from multiple indicator data, effects of finite red cell permeab. 78−44483
capillary viscometry, systematic error source identification 79−18982
cardiac left ventricular ejection fraction meas., scintigraphic count-volume and geometric methods compared 79−83896
cardiac output measurement error due to nonuniform dye distrib. 77−36979
Carr-Purcell-Meiboom Gill pulsed NMR sequence, errors in T_2 values 77−85604
carrier distribution in Si:B(P) ion implanted layers, meas. precision 77−43603
cartography, point transfer error determ. 80−17227
catheter pressure meas., transducer smearing correction using microprocessor based discrete deconvolution 80−67275
cavity perturbation measurements, elimination of influence of non-ideal microwave circuit 79−88979
ceramics creep measurement, samples with initially nonlinear axis creep, expt. errors *(Russian)* 77−25224
cerebral blood flow meas. by radioisotope clearance, radiation scattering effect 78−3600
charcoal tube sampling technique, meas. accuracy 78−69508
charge distrib. determ., thermal pulse technique, meas. accuracy 78−80287
chemical anal. by counting meas. calibration determs., statistical uncertainties of anals. 78−92533
chemical analysis, systematic analytical errors of multicomponent materials, exposing and calc. methods 78−7274
chemical analysis methods, accuracy and lower determ. limit 79−52818
chemical composition, error analysis of analytical results 80−21341
chemical measurement representativity errors *(German)* 79−71400
chromatograph conversion factor, accuracy 79−74475
cigarette, density changes during burning as obs. by β-source attenuation 78−11792
cineroentgenography, quantitative biplane method, error propag. 78−73224
measurement errors continued
circular electron accelerator, with strong mag. field, errors introduced by synchrotron electron radiation 79−6779
circular magnetoelectric convertors, angle-of-rotation conversion errors 77−17968
clock synchronisation cct., error monitoring correction appl. 78−73970
cloud base height meas., with Mk3 CBR, potential accuracy limitation 78−45024
cloud droplet size meas., comparison of electrostatic disdrometer with impactor slides 77−2278
cloudy atmospheric parameter determination using microwave radiometric method 80−67435
coating thickness inspection, mounted eddy-current transducer error correction 80−77775
coating thickness meas., beta backscatter method, meas. uncertainty prediction 77−56206
coherence functions and input/output quantities, statistical errors in meas. 79−3965
colorimeter, Technicon Autoanalyzer II, systematic absorbance errors 79−21802
colour difference meas., spectrophotometric random errors effect 78−12741
colour thermochromism, Gardner standards behaviour obs. *(Hungarian)* 78−24842
combined meas. evaluating error in establishing relationship between quantities 77−71286
cometary orbits, reciprocal semimajor axes accuracy 80−62074
complex meas. system error correlation matrix *(Russian)* 77−9979
composition of several error distribution functions, determ. method 77−13731
computerised instrumentation, errors sources and reduction *(German)* 77−5791
computerised tomography, gantry geometry rel. to aliasing and other geometry dependent errors 80−81695
concentricity, round parts, profile determ. *(German)* 80−57249
contact lens, soft, in-office meas. 78−7339
contact-type flowmeter working in thermal boundary layer, temp. error determination 80−103093
control rod reactivity meas. error analysis 79−9783
convective heat transfer coefficient measurement using heat-flux sensor, error anal. 79−94463
conversion function of meas. facility, optimal value determ. 78−73958
convertor, linear, integrated parameters determination, experimental 77−74385
coordinate information processing, integer method 77−22518
coordinate meas. uncertainty computation program *(German)* 80−86256
coordinate measuring apparatus calibration problems *(German)* 78−77854
core physics parameter meas. uncertainty 79−9801
corrected measurement result, error description and confidence limit calc. *(German)* 80−27262
cosmic rays ultraheavy nuclei, errors due to geomagnetically forbidden light nuclei 77−37489
Couette viscometer, correction for non-Newtonian liquids *(German)* 78−94868
Coulter counter technique, errors in meas. of particle size distrib. in high-impact polystyrene 77−56257
cross-correlation flow meas. error estimation and reduction 79−3194
cross-section data adjustment iteration procedure 79−9696
cryo current comparator, toroidal, as DC ratio standard 79−88977
cup anemometer, rain-induced errors in mean wind speed meas. at sea 78−61485
cup anemometer overspeeding rel. to wind turbulence intensities 77−53241
current-to-frequency transducer systematic error and sensitivity threshold 77−79117
CW Doppler bloodflow meas., perivascular transducer effect on accuracy 77−90825
D-region, improved Faraday rotation expt. for electron conc. rocket meas. 77−9543
Danjon astrolabe, errors rel. to planetary obs. 77−64651
data acquisition systems, in steady and unsteady states, error determ. 80−95056
data processing system error analysis 78−41288
data processing system error expressions 78−41287
DC bridges, high-resistance wide range 79−75548
decay time meas., photomultiplier wavelength depend. errors, correction method 79−30558
deformation, resistance strain gauges 79−75521
denudation measurement by sediment transport fallacy of stream equilib. assumption 77−78236
determination techniques, meas. of mass 80−57237
deviation and error, concepts and definitions *(German)* 79−49188
device information-theoretic characts. estimation via radiation absorption *(German)* 78−65900
dielectric constant meas. by cavity method, freq. and mode errors 80−13103
dielectric parameters, using E_{010} cylindrical resonator, perturbation theory *(Russian)* 77−18051
dielectrics, very low losses meas. at 9 and 29 GHz, multireflection errors 77−8503
dielectrophoretic measurement of permittivity, effects of sample size 80−13094
differential pressure flowmeters, errors due to pressure fluctuations 79−68862
differential refractometer, effect of light scattering in double-prism cuvette on error 79−75573
differential-capacity transducers, improving metrological characts. for displacement measurements 79−75493
diffusion furnace temp. profile meas. systematic errors, theoretical model *(German)* 80−8989
diffusion furnaces, temp. profile meas., systematic errors *(German)* 80−37030
diffusion in gases, meas. depend. on cell geometry 77−3911
digital automatic system RMS, calc. *(Russian)* 79−97336
digital multimeter, resolution and sensing accuracy 77−74428
digital phasemeter, tracking, quantisation error reduction *(Russian)* 77−61079
digital velocity meas. meter *(Russian)* 80−86266
digital voltmeter, automatic checking method 80−57240
digital voltmeter, instrumental error estimation technique 80−57239

measurement errors continued
digital weighing systems, error estimation *(German)* 77−74365
digitization of mechanical meas. values by automatic calibration *(German)* 79−67247
dilatometric measurements, high-temp., systematic and fiducial error estimation 80−101796
direct loading, equipment used in standard force measuring machine 80−17934
Dobson O_3 spectrophotometer calcs., generalized treatment of particulate scatt. 79−12267
Doppler broadened laser amplification line frequency characteristics meas. 78−59060
dosimeters 79−93835
dosimetry calibration, estimation of confidence levels 79−3247
double stars, effects of erroneous positions on rectilinear trajectories calc., (appl. to h 5094) *(French)* 78−20857
double stars, rectilinear trajectory errors *(French)* 78−89223
dual-Doppler radar, meteorological, coverage area as function of meas. accuracy and spatial resolution 80−82093
dust trajectory photography for compressible flow velocity meas. 79−82008
dynamic, determ. and normalisation of meas. equipment characts. 80−62617
dynamic, in linear conversion, approximate calc. 77−5796
dynamic, of devices meas. turbulent temp. fluctuations, with detector dynamic response correction 80−77781
dynamic, of linear meas. facilities, analysis 77−74345
dynamic component, evaluation in terms of rate of change of measured quantity 79−17381
dynamic error definitions *(German)* 79−97337
dynamic properties of meas. device, standardisation 77−5797
Earth crust density logging, influence of standard material comp. on readings *(Russian)* 79−74989
Earth crust stress meas. by overcoring, error detect. by diagnostic stress-relief curves 79−29886
Earth electrical conductivity model parameters, resolution of deep magnetovariation sounding curves 79−53300
Earth induced polarisation (IP) sounding, effects of EM coupling in electrode arrays over uniform half-space 80−101324
Earth multifrequency EM sounding, topographic and misorientation effects study 80−101451
Earth optical horizon, errors in height determ. by (Soyuz 9) 77−53186
Earth structure, influence of lateral vars. on seismic refr. interpretation 77−21686
Earth tide meas., correction for M_2 freq. oceanic tides 77−9316
Earth transient EM sounding, meas. errors anal. in computer processing *(Russian)* 79−44269
earthquake epicentre and origin time determ. accuracy, Turkey 77−41002
earthquake records, digitization errors and base line corrections 80−98245
echolocation, bat, accuracy of meas. of target angular coords. using equi-signal zone 78−77071
elastic element characteristic vibrational-frequency meas. errors 77−74391
electrical capacitance, resistance, inductance, group storage errors, statistical analysis 77−53853
electrical meas. devices, drift and additional errors, algorithms *(Russian)* 80−62615
electrical resistivity four-point probe meas. error factors, SEM obs. on Si 79−71484
electrochemical measurement transducers, actual distribution of errors 80−45605
electromagnetic meas., precision, conf., Braunschweig, Germany (Jun. 1980) 80−98903
electromechanical balances, evaluation of limits of resolution using characteristic values of load cells *(German)* 79−71445
electron brightness meas. by 2-limiter method, accuracy calc. 79−6234
electron probe analysis, ZAF-correction procedures for biological bulk specimens 79−44073
electron-photon cascade energy determ., effects of optical density and energy spectrum meas. errors 79−84613
electronic micrometer error specification *(German)* 77−74354
electrostatic kilovoltmeter errors in unearthed circuits 77−13773
ellipsometric thickness meas. error estimation for water thin film on slightly rough quartz surface 78−32856
EM flowmeters with large-area electrodes, performance anal. of three models 80−1706
EM water current nonlinearity and sensitivity 77−5383
emissometers, refl. errors elimination by use of alternate instruments 77−10089
epithermal neutron activation anal., comparator technique, errors 77−81441
EPR of free radicals, simulated spectra, compensation for integerisation errors 79−33537
error separation processes, roundness meas. appl. *(German)* 80−31701
estimation, use of quartiles in undergraduate physics 77−60868
evaluation, tendencies in the USSR 80−95052
experimental measurement, review of error statements 79−85110
exponential statistical distribution and aberrant values elimination *(Rumanian)* 80−68163
exposure meter errors during colour photographic printing 80−101818
exposure meter with photoresistor, semi-automatic, bridge circuit error calc. *(Russian)* 77−54008
extragalactic distance scale, tertiary distance indicators errors 79−25708
eye optic disc topography, by laser contour angiography, error model 77−60236
faradmeters, errors checking with aid of tables 80−52271
fast reactor integral meas. consistency, cross-section adjustment 79−9867
fatigue testing of wire, error reduction 79−52493
feedback monitoring, normal conditions for linear and angular measurements 79−75492
feeler instrument meas. errors, effects of probing system dynamics 78−73965
ferrite rods in mode E_{010} resonators, measurement of dielectric constant 79−71483
ferrites, disaccommodation meas., errors analysis *(Bulgarian)* 78−21181
ferromagnetic suspension, magnetorheological characts. meas., errors 80−33550
ferromagnetic-resonance linewidth meas. method and apparatus 80−22411
measurement errors continued
ferromodulation meas. transducers, with increased temp. stability 80−52281
field galaxies luminosity function, anal. of errors 78−16526
film photon and electron absorbed-dose detector 80−91379
film thickness meter for dielectric material thickness meas. *(Russian)* 77−41566
FK4 catalogue stars, declinations systematic errors determ. from vertical circle obs. *(Russian)* 79−96888
FK4 catalogue stars, systematic errors from San Juan astrolabe obs. 77−13253
FKSZ stars, astrometric obs. and systematic differences spherical harmonic anal. *(Russian)* 79−44336
flame atomic absorption spectrometry, literature interpolation as possible source of error 77−70366
floated density meter contactless electromagnetic transformer *(Russian)* 79−54099
flow, errors due to plate buckling in orifice meter 77−84371
flow cytometry, fluoresc. polarisation meas., appl. to fluorescein in mammalian cells 77−52942
flow meas. by orifice meters, relative error in nonstandard approach conditions 78−79398
flow meas. in chemical industry, VDI and DIN specifications *(German)* 77−42946
flow measurement by dilution method with incomplete mixing 79−50821
flow rate measurement, using pitot static tube 79−68886
flow rate measurement reproducibility conditions, theory and expt. 77−80240
flow sensor using annular-averaging, error in discharge coeff. 80−38509
flowmeter, EM type, optimal mag. system design *(Russian)* 79−1275
flowmeter, flumes and weir, construction error compensation, computer anal. 78−30387
flowmeter, linear and nonlinear specific gravity digital compensation 78−34242
flowmeter, MHD type, with circ. cross section, inhomogeneous mag. field effect on signal 80−33709
flowmeter, MHD type, with circ. cross section, symmetry conditions effect on signal, arbitrary vel. profile 80−33708
flowmeter, open channel acoustic flowmeter, error sources and calibration 78−30389
flowmeter converging devices, effect of aeration on error 80−10327
flowmeters, effect of hydrodynamic factors 80−96322
flowmeters, mobile weighing system 80−96326
flowmeters, Price and Pygmy current meter traverses, error sources 78−30385
fluid flow meas. with pressure difference devices, accuracy limitations *(German)* 79−98841
fluid tube tiltmeters, thermally induced errors 78−36303
fluorescent tracers in hydrology, conc. meas., synchronous excitation method *(French)* 77−77840
fluxgate magnetometer, orientation error in inclination meas. *(Chinese)* 79−88477
fluxmeter measurement range extension 78−57993
force and strain meas., spring-mass-damping system, dynamic errors *(German)* 79−12794
force and weight meas. in vac., sensitivity limitations 78−65908
four-terminal meas. circuit stray-impedance errors 78−77940
Fourier spectrometer, mirror oscills., mathematical error corrections *(Russian)* 77−87849
Fourier spectroscopy, interferometer drive nonlinearities effect 77−61127
Fourier transform IR spectrometry, absorbance subtract, wedging errors diagnosis and correction 80−11967
Fourier transform IR spectrometry, focal shift photometric errors 78−86358
freely sinking probe horizontal velocity meas. interpretation 80−46321
frequency, probability anal. *(Russian)* 80−90823
frequency meter, digital, accuracy and noise rejection increase, weighting method *(Russian)* 80−27281
frequency pulse train standard deviation determ. *(Russian)* 79−30405
frequency standard, precision oscillator freq. stability meas. *(Japanese)* 78−4596
frequency thermoconvertor electrical correction *(Russian)* 80−57242
furnace temperature meas. with pyrometer and thermocouple 77−5845
galactic radio background emission, linear polarisation, spurious radiation effects 77−2500
galaxies, bright, in Virgo cluster area, standard total magnitudes and mean errors 78−65685
galaxies mass/luminosity ratios, errors from binary galaxies meas. 77−33644
galaxies radial velocities meas., distortion by night sky spectrum 77−41406
galaxies velocity dispersions and redshifts meas. 77−29916
galaxy counts, errors rel. to derived space distrib. and evolution 79−40261
galaxy redshifts, uncertainty cross correl. data reduction techniques 80−22074
gamma dosimeters, energy relationship of effectiveness and error estimation 79−31225
gamma radioactive source measurement, in dynamic condition, error sources *(Rumanian)* 78−46243
gamma-ray flaw detector with analogue data processing, design and error calc. 77−73406
gamma-ray spectrometry, error in total absorpt. peak location by linearization method 79−68125
gas absorption analyser, anal. by mean risk criterion *(Russian)* 78−70088
gas analysis, by mass spectrometer, dynamic error determ., transfer function 80−61194
gas chromatography, quantitative, errors, efficiency 78−92538
gas chromatography, unrecognised systematic errors 78−92537
gas microconcentrations in air determ., metrological certification of meas. methods 80−55972
gas volume counter and flowmeter calibration, gravimetric standard method *(German)* 77−55112
gastric emptying measurement by scintigraphy, techniques and errors 78−73206
gauge block measurements of interferometry, sources of uncertainty 79−26029
gauge blocks, errors associated with checking by interferometric methods 80−105613

measurement errors continued
geochemical analysis, element sensitivity, precision and accuracy of spark source mass spectrography 78−20544
geodesy, accuracy with transportable lunar laser ranging station 77−48988
geodesy, gravimetric geoids comparision with Geos 3 altimetric geoid 80−3898
geodesy, influence of temp on Talyvel electronic level *(German)* 78−45037
geodesy, parameter accuracy improvement by choice and quality of obs. 79−44078
geodesy, systematic errors detect. by hypothesis tests using adjustment in sections *(German)* 79−44083
geodetic levels with compensators, systematic errors, new instrumental development *(German)* 77−2289
geodetic measuring instruments, periodic errors determ. via spectral anal. *(German)* 77−87131
geodetic observations goodness, concept restatement rel. to recent crustal movements studies 79−57840
geodetic solutions based on NAVSTAR Global Positioning System satellites Doppler meas., accuracy 79−100803
geomagnetic AE index, influence of substorms appearing N of Cambridge Bay 79−75054
geomagnetic field, effect of obs. errors on models based on total intensity meas. 77−9335
geomagnetic field intensity vector components, determ. from magnitude, error estimate 78−73308
geophysical acoustic logging, signals limited spectrum rel. to time interval and damping determ. accuracy *(Russian)* 79−39971
Geos 3 altimeter data, bias due to ephemeris error rel. to sea surface topography 80−3908
Geos 3 altimetry, orbited bias error rel. to NW.Atlantic oceanic geoid and tides determ. 80−3901
Geos 3 tracking systems, intercomparison for meas. and time biases determ. 80−4227
Geos-3 altimeter data, long-wavelength errors rel. to geoid undulation and anomaly estimation 77−64178
geostrophic ocean currents, relative press. topography and relative vel., calc. accuracy 79−39758
Gor'kii latitude observations, half-year nutation wave terms errors 79−62728
Gorky latitude, relativistic var. *(Russian)* 78−40462
graduated circles, horizontal and vertical, determ. of micrometer errors and short period errors *(German)* 78−45038
graduated circles, short-period, error determ. *(German)* 78−88791
graphite ionisation chamber, ionisation error due to porosity 80−52829
grating type monochromators, spectrophotometry and colorimetry errors caused by polarisation of meas. system *(Japanese)* 80−101815
gravimeter, LaCoste and Romberg, vibr. errors *(Japanese)* 78−65400
gravimetric measurement of sorption isotherms, errors 78−67905
gravimetric networks, adjustment and errors *(German)* 79−44084
gravitational wave interferometer, quantum mechanical radiation press. fluctuations 80−90770
gravity, borehole data accuracy 79−5632
gravity data, allowance for errors rel. to approximation of Stokes and Vening-Meinesz eqns. 80−101459
gravity gradients, vertical and horizontal, measured by gravimeter, relative precision 79−84500
gravity measurement from aeroplane, error of aerogravimetric apparatus *(Russian)* 78−40704
gravity meters, quartz, terrestrial, microseisms influence on reading, mechanism *(Russian)* 79−39967
gravity vector and geodetic position survey, errors rel. to inertial navigation system 79−29914
groundwater ^{14}C dating, errors from ^{14}C subsurface prod. 80−85690
gyromagnetic ratio of proton in weak mag. field at NPL 80−105678
gyrooptical compass, signal measurement time *(Russian)* 80−33007
gyroscope, analyzing errors in measuring platform drifting rate by means of fixed-angle method 79−80609
gyroscope, with shock absorber, errors due to spatial vibr. *(Russian)* 78−13892
halfsecond levels, tilt meas. errors investigation *(Russian)* 78−40675
HF time signal bilateral transmission propagation time error anal. 77−87740
high intensity local heat flow, anal. *(Russian)* 80−74865
high precision voltage meas. automatic error correction using iterative method *(Russian)* 78−70089
high-energy physics magnet meas. 79−31353
high-performance telescope aspheric mirror test error budget 80−48386
hip joint geometry, human, three-legged micrometer spherometric errors 79−83832
hole diameter meas. with universal microscope and electronic contact indicator 77−79055
holographic image luminance determ. 79−81394
holographic interferometry, errors in small vector displacements meas., statistical anal. 78−78953
hot-plate thermal conductivity meas., errors associated with imperfect surfaces 80−95098
hot-wire anemometer temp. compensation errors estimation *(Russian)* 78−57345
hot-wire measurements in the wall vicinity, anal. of errors 78−34220
humidity meas. by psychrometer, Lewis factor effect on accuracy *(German)* 79−12808
hydrometeorological meas. equipment, USSR state testing 79−70897
hydrometeors in clouds, size, conc. and struct. meas. with impactor and replicating devices 77−41218
hydrophones and passive ranging, errors due to receiving position uncertainty 79−41522
illuminance meter error sources *(Hungarian)* 79−88995
illuminance meters accuracy test *(Hungarian)* 79−88996
image analyser comparative tests 79−14106
images aberrated by turbulence, undersampling errors in moments meas. 80−1137
impact torsional test accuracy determ. using simulation *(Japanese)* 77−56198
impedance measurement, accuracy of electrode props. determ. 80−61108
improvements by means of microcomputers *(German)* 78−24773
indentation hardness number conversion table analysis 79−11736
indicating measuring instruments, error estimation *(Croatian)* 78−57886
measurement errors continued
indication errors, Hilbert space and Fourier anal. *(Rumanian)* 79−40523
indicator, quadrature, current and voltage, errors components determination 77−74442
indicators accuracy categories *(Croatian)* 80−13063
indirect meas. error calc. method *(Polish)* 78−70091
individual realisation laser anemometry, sampling bias evaluation 77−58810
inductive transducer summing circuit errors 77−18046
inertial meas. systems, basic eqns. and error models *(German)* 80−56655
Information Measuring System error computation considering communication channel characts. 78−73957
information test for uniform quantisation 77−79048
information-meas. system accuracy, influence of residual voltages 78−77828
instantaneous linear velocity meas. by scanistor 79−67261
instrument accuracy and repeatability 78−21090
instrument block optimal precision synthesis *(Russian)* 78−70092
instrument inspection, optimal error correction signal 78−77829
instrument operation speed increase, additive-iterative correction method *(Russian)* 78−89423
instrument total error estimate, approx. methods 78−16769
integrated probability distribution for sum of two or more constituents 77−17940
integrating float, lag effects on water flow vels. integration 78−93012
internal friction apparatus for freqs. up to 200 Hz, automatic control and error sources 78−22308
International Latitude Service obs. 77−45324
interplanetary low energy charged particle measurements, Compton-Getting effect complications 78−49269
interval eval. of errors for process testing 79−71398
intracellular potential amplifier input capacitance determ. errors 77−60320
intraocular pressure measurement, for glaucoma, comparison of Schiotz standard tonometer and applanation tonometer 78−48915
ionosphere, ground refl. effects on ATS-6 radio beacon expts. 77−53144
ionosphere attenuation, errors in determ. for signals with small arrival angles 79−58155
ionosphere electron density profile parameters estimation from VLF propag. data, effectiveness 79−53614
ionosphere radar measurement incoherent scatter, systematic error due to noise contamination 78−49225
IR goniometric refractometer, construction and test results 79−71513
IR laser wavelength meas. by radiation conversion method, error anal. 79−7175
IR radiation brightness unit reproduction error anal., USSR standard 78−45699
IR sensor, long wavelength, uncertainties in calibration 77−170
IR spectrophotometers, meas. errors of polarising objects 80−86471
IR spectroradiometer systematic error calc. 79−75629
IR thermography, reflectance errors 80−62661
Kelvin double bridge, precison, for capacitance meas. up to 1 F, ratio arm adjustment 79−21776
klirr-factor unit dimension, error in digital meas. 80−98873
lake sediments, E_h meas. reliability conditions 79−48528
LANDSAT imagery, operator variation in lineament anal. 77−64467
laser bathymetry for near-shore charting appl., vertical accuracy from field tests 79−5679
laser Doppler anemometer measurement, effect of finite-size probe vol. 77−24036
laser Doppler anemometry, velocity and photomultiplier bias effects 80−59140
laser Doppler velocimeter, spatial resolution and accuracy 77−24043
laser interferometer appl. to positioning, built-in system for machine tools *(German)* 80−9022
laser interferometer application to length meas. in production *(German)* 80−18007
laser interferometer system, Doppler, error sources analysis, meas. volume structure *(Russian)* 80−27336
laser interferometry in linear measuring techniques, problems with environmental influences *(German)* 79−30411
laser Michelson interferometer length meas. error rel. to illuminating beam form 77−26267
laser power meas., scale comparison for calorimeter and radiometer systems 79−76729
laser radiation spatial distribution determ., mode parameters 80−95055
laser Raman signals, pulsed, from turbulent combustion media, averaging considerations 78−70839
laser range measurements, atmospheric correction determ. *(Russian)* 80−12674
laser sounding method and equipment for water absorpt. and attenuation coeffs. meas. *(Russian)* 79−34998
laser wavelength determ., random/systematic errors statistical estimation 78−17996
least squares fits, normalisation parameters and linear constraints 77−67405
least squares method, limit of applicability, modification for large errors in independent variable 80−73301
lecture demonstration for chem. course 80−17773
leg long bone growth meas. in children from radiogram, error reduction using computer processing 78−77103
length meas. by laser interferometer *(Japanese)* 78−8384
length meas. international standards compared *(German)* 80−36977
length measuring equipment, optical methods of elimination *(German)* 78−70094
lens focal length meas. error, student expt. 77−45653
level of material arranged in arbitrary fashion in tank, measurement using acoustic methods 80−17921
lever balance error calc. with adjustability consideration 77−30131
lever balance errors caused by knife edge height displacement 79−35680
light beam energy indirect meas. accuracy *(Russian)* 78−74046
limb 'diameter' setting errors 79−71416
limits of reducibility of random measurement errors through statistical evaluation under consideration of input signal signal *(German)* 80−95057
linear dimension meas. means choice in terms of error levels 79−6082
linear displacement meas. accuracy meas. accuracy improvement under vibration 80−90815
linear instrument mechanism analysis *(Hungarian)* 78−49823

measurement errors continued
linewidth measurement using optical microscope 77−79147
low currents, instantaneous capacitor discharge, errors and nonlinearity 79−6142
low energy cosmic rays, neutral particle background in Si solid state detector telescopes 78−28472
low speed rotating table of gear hobbing machine *(Japanese)* 77−53867
low temperature measurement in high mag. fields, instrumentation and methods, review 78−37003
low temperature specific heat measurement, dynamic differential calorimetry 77−74405
low-temperature measurement, mag. field effects on Krion 1-2 instrument errors 78−222
lunar magnetic fields, magnetometer data errors and EM induction studies 79−96932
lunar occultations of point-like X-ray sources, time meas. accuracy 79−88567
magnetic defectoscopes, nonsinusoidal periodic currents meas. 80−104386
magnetic flow meas. devices, mains supplied, elimination of transformer strayvoltage *(German)* 79−82018
magnetic losses, form factor influence *(Rumanian)* 80−68226
magnetometers, vibrating sample, operation and appls. *(German)* 79−93172
magnetoresistance measurements, influence of supercond. contacts 78−21184
magnetosphere outer zone electrons, wall scatt. effects on pitch angle diffusion meas. 78−28399
magnetosphere plasma density and temp. determ., multi-expt. results cross calibration 79−35074
magnets testing, permanent, test parameters selection 80−52280
manufactured part rejection validity, influence of random meas. errors 77−17947
marine air temp. sensor error analysis 77−78437
marine hydrocarbon pollution detection, caution on use of Niskin sampling bottles 78−45039
Mars, ephemeris errors from position meas., (1975-1976) *(French)* 78−45252
mass spectrometry and NMR spectrometry 79−49263
mass standard error limits and accuracy class determ. *(German)* 77−74364
maximum likelihood test in estimation of exptl. inaccuracies, applic. to equilib. data 77−9867
measurement and transmission system, relative error of analogue signal with bend for freq. band cut-off *(German)* 80−86242
measurement techniques regarded as a subset of information techniques, error correction by computer programs and by networks *(German)* 80−68164
measuring instruments, test reliability 79−75514
mechanical quantities, electrical meas. systems *(German)* 79−97382
medical US echoscopic meas., random error sources *(Croatian)* 78−44569
medium loss with time meas., optimal planning *(Polish)* 78−93642
meridian circles pivot errors, new determ. method 78−53822
metal, electron irrad., selfinterstitial atomic defect interaction radii, recovery expts. and error sources 80−65049
metal foil gauge, long-term stability of strain meas. 79−17417
metallic substrate, temp. meas. during evap. 77−69997
meteor trails, atmospheric ambipolar diffusion coeff. meas. errors 78−88952
meteorite dropping fireballs, accuracy of radiants 79−71006
meteorological pilot balloon position meas., error anal. of double-theodolite data 79−21051
meteors, magnitude errors and magnitude scales of observers in Sweden and Czechoslovakia 78−36533
methodic and instrumental, examples 80−57238
Michelson interferometer misalignment nonlinear phase errors 79−30535
microbalance, Cahn-RG, mass artifacts in water vap. 78−65909
microearthquake research, methods and meas. errors 79−39987
microgravimetric network for secular gravity studies in Scotland 78−36298
micrometer performance evaluation, aspects *(Japanese)* 79−97347
microvascular pressure, using micropipet, capacitive modulation of impedance 77−37080
microwave reflection coeff. meas., calibration error evaluation 79−21768
microwave systems phase measurement, error anal. due to reflections *(Bulgarian)* 79−88975
minerals optical constants, derivation from measured reflectances, errors in two-media method 79−58100
mixtures of compounds, statistical analysis 77−52697
Moire projection topography accuracy and sensitivity 78−45677
Moire strain measurement method using diffraction beams, compensation of errors 80−13068
moire topography, meas. accuracy evaluation 79−40528
moisture meters, representation as two series transducers, total error estimation 80−77792
monochrome photographic film densitometry errors and standards *(German)* 80−37102
MPP-1 stationary precision proton magnetometer, errors and calibration 79−53535
multichannel high resolution time analyser scale instability *(Russian)* 80−73326
multidimensional measuring block, parameter tolerance estimation *(Polish)* 78−29079
multiplicative comparator of spectral radiances, systematic errors *(Japanese)* 78−29139
multiscale measurement devices, max. likelihood estimate generating, synthesis and quality charact. calc. 79−40525
near-field radiation hazard and EMI meas. 77−44757
neutron activation analysis, parametric analysis of samples generating complex γ-ray spectra 79−92016
neutron activation analysis as applied to U prospecting at exploratory borehole 78−7817
neutron activation analysis at 14 MeV for determ. of O_2 conc. in reactive metals 78−11602
neutron activation analysis in archaeology, comparison of results from Lawrence Berkeley Lab. and Hebrew University 78−70245
NGC 2403, galaxy, distance determ. from Cepheids, systematic errors 77−2471
NGC 3532, stellar cluster, errors in V-magnitudes of photoelectric sequences 77−45502

measurement errors continued
NMR, rot. frame, ^{13}C spin-lattice relax. using proton decoupled Fourier transform spectra, errors origin 80−18945
NMR absorption peak voltmeter cct. error analysis *(Russian)* 79−26079
NMR fast inversion-recovery spin-lattice relax. time meas., systematic errors elimination 79−30516
non-Gaussian distribution laws for statistical error theory generalisation *(German)* 80−22315
nonelectric variables meas., current transformer error level calc. 77−13743
nonGaussian error limits, distribution and probability curves *(German)* 80−36967
nonplanarity of surface plates using optical planarity meter 80−17919
nonsinusoidal periodic current meas. using standard DC shunt with magnetic powder monitoring, frequency errors 80−104398
nonstationary Poisson train intensity meas. error analysis 79−67246
nuclear decay data, need for uncertainties 80−87023
nuclear materials safeguarding, measurement errors 80−73935
nuclear measurements, errors of parameters in least squares fitting procedure 78−16768
object dimension meas. by computer-controlled laser beam scanning 79−98431
object geometric param. single meas. in image linear space quantification, random error calc. *(Russian)* 77−37838
object spatial location, TV meas. system accuracy 79−49200
oblique and vertical joints, strike and dip determ. 77−64280
ocean geoid near Blake Escarpment, undulation values errors from Geos 3 satellite altimetry data 80−3902
ocean palaeosalinity implications of B loss from shells during weathering 77−78204
ocean random hydrophysical processes quantification, reconstruction error *(Russian)* 78−77359
ocean remote sounding, instruments quasi-optimum operating functions for min. meas. errors *(Russian)* 78−77362
ocean temperature determination by remote sounding, aerosol attenuation effects on accuracy *(Russian)* 78−81430
ocean temperature measurements with Aanderaa thermistor chains, solar radiation effects *(French)* 79−62611
ocean vertical temperature gradients, moored instrument accuracy 80−12561
ohmmeter, relative-error determination in checking 80−17961
open channel acoustic flowmeters, design, meas. errors and operation 78−63516
open channel flow meas. instrument errors 78−30384
optical attenuator metrological certification methods 80−91941
optical coating requirements in United States military specifications 80−48365
optical constants, ATR meas., 2-polarisation method, accuracy, optimisation 78−45673
optical constants meas. method using polarised light refl. coeffs., accuracy 80−73423
optical density, normalisation of meas. error 79−54091
optical density measurement accuracy by means of optical wedge 80−73416
optical fibre attenuation meas. by backscattering method, effect of noise 80−102824
optical fibre refractive index profile meas., nondestructive transverse interference method 78−38024
optical goniometer accuracy effect of atm. turbulence 78−55461
optical image centre of gravity coordinates, analysis of measurement accuracy 79−36850
optical instrument, target position meas., statistical model 80−101778
optical planimeter metrological characteristic test results 78−79148
optical power spectrum meas., error sources in diffr. pattern sampling 78−63030
optical rate sensor, discrete component Sagnac effect, error sources 80−1342
optical rotation sensor, passive ring cavity, drift performance 80−1343
optical system aperture, effect on measurements in thermophysical research 80−17992
opticomechanical anemometer for flow vel. meas. of optically transparent material 77−68718
optimal trajectory-meas. program and meas. error effects 77−53409
opto-electronic meas. system, with raster analysers, illumination distribution law effect on accuracy 77−79047
optoelectronic angular meas. devices, anal. method *(Russian)* 80−95066
optoelectronic devices 79−6073
optoelectronic scanning device accuracy, raster distortion and instability effects 79−72697
optoelectronic system threshold sensitivity calc., background spatial charact. determ. errors 79−26134
orbits determination, method for study of error propag. 77−25914
organic semiconductor film, optical consts. by refl. and transmission, errors 77−16414
palaeomagnetic meas., mag. declination and inclination errors in experimentally deposited specularite-bearing sand 80−90075
palaeomagnetic measurements, origin and stability of drilling induced remanence 77−33059
particle size distributions, statistical reliability 77−53858
particle sizing by forward lobe scatt. intensity ratio, diffr. theory errors 78−71031
particle sizing by forward-scattered lobe methods, error contour charts 77−79752
passive sonar, range and bearing estimation, errors 80−79030
passive value parameter transducer, correction method *(Russian)* 78−49819
path difference measurement on anisotropic materials 80−4758
pendulums, random interactions *(Russian)* 80−73313
periodic variables meas., multi-scale cyclical meas. analysis *(Russian)* 80−187
permanent magnets in instruments with partially closed mag. ccts., meas. errors *(Russian)* 77−67480
personal dosimeters, comparative evaluation 79−41042
personal noise dosimeter responses to impulsive noise 79−18646
phase cyclic meas. ambiguity elimination *(Russian)* 79−6072
phase meter system expt. error evaluation algorithm *(Russian)* 77−41636
phase tracking meteor radar ambiguity elimination algorithm *(Russian)* 77−41311

measurement errors continued
photochromic flow visualisation, effect of turbulence on precision of vel. and vel. fluctuation data 77−68714
photodetector relative spectral sensitivity meas. method using two tandem monochromators *(Japanese)* 80−101840
photoelectric apparatus, absolute calibration method errors 79−96919
photoelectric astrolabe type II, accuracy, time and latit. obs. *(Chinese)* 77−22063
photoelectric concentration meter, acceptable error determ. for automatic biochemical anal. 79−92435
photoelectric transducers with astatic characteristics, statistical error determ. 78−93760
photographic astrolabe at Turku observatory, errors 80−36499
Photographic Zenith Tube at Tokyo Astron. Observatory, observational errors anal. 80−98547
photographic zenith tube obs. for time and latit. determ., meas. errors estimation 77−56816
photographically recorded spectral lines, of nonuniform half-width, microphotometric errors 78−86337
photometer FM-89 conversion to measuring instrument, reflection coefficient meas. 79−71507
photometers drift errors due to ageing and preheating, evaluation method *(German)* 77−10087
photometry of retroreflectors and retroreflective materials, luminous intensity determ. *(Dutch)* 79−85159
photometry radiation energy units reproduction, error anal. 78−45670
photomulitplier meas. of threshold optical radiation fluxes, errors 78−12760
photomultiplier, ITT FW-130, linearity test 79−58255
photoresistor errors in exposure meter accuracy calc. 77−49773
Pitot tube meas. in large pipe flow, uncertainties 78−34228
planar angle meas. using rotating ring laser *(Russian)* 77−38942
plasma chromatography, baseline corrector for boxcar integrator instruments 77−52717
plasma differential emission measure solutions, errors 79−12397
plasma temperature, from measured particle vel. distrib. 79−77419
pneumatic feedback-monitoring instruments, pressure variation effects 80−77743
pneumatic press. transducer for corrosive media, error and sensitivity 80−22345
polarimeter, near IR, of Hatfield Polytechnic Observatory, instrumental polarisation 79−2482
polarimeter error quadratic mean value determ., statistical method *(Russian)* 77−41668
polarisation resistance method, using 2 and 3 electrodes, error anal. in corrosion rates 80−100930
polarisation torque-measuring system *(Russian)* 80−52191
polycrystalline materials, lattice parameter meas., systematic errors 79−10749
polyhedral prisms checking instrument, unit of plane angle transmission 77−7221
position-sensitive detector, influence of discrete struct. on accuracy of coordinates determination 80−58076
positron lifetime spectra for metals 78−19591
power and energy meas., digital, errors sources and suppression *(Rumanian)* 80−47078
power transmission spectrometry, systematic error in calc. value of power absorpt. coeff. 80−98982
precession, lunisolar, determ. via extragalactic radiosources obs., errors 77−5129
precision comparator, Zeiss PK-1, accuracy, appls. *(German)* 79−97359
precision comparator, Zeiss PK-1, astrometric plate meas. appl. *(German)* 79−97360
pressure gauge, gas-operated, effect of piston-cylinder relative rot. on meas. 77−41631
pressure meas. by crusher method, dynamic error calc. 78−57974
pressure transducer measurements, thermal transient effects 80−31700
primary meas. transducer error twin-circuit correction *(Russian)* 79−71404
primary T-wave determ., spatial ventricular gradient change factors 79−43850
prismatic astrolabe, Wollaston prism micrometer screw errors *(Russian)* 78−89066
probability distribution function determ. feasibility for various sample sizes 80−90806
proton polarisation measurement, symmetry errors *(Rumanian)* 79−59322
Pulkovo large transit instrument, orientation parameters determ. from 1953 to 1961 obs. *(Russian)* 79−96910
pulmonary mechanics vector scope meas., error anal. 78−40358
pulmonary resistance measurement by forced oscill. technique 77−40877
pulmonary volume meas. by closed-cct. He mixing method, reproducibility 77−48904
pulse counting, high precision, limitations, optimal conditions 77−54463
pulsed neutron source on multiplying media, anal. and interpretation of experimental data *(Rumanian)* 78−46203
pycnometry, determ. density of liquid metals 80−73321
pyrometer, reduction of errors using sighting device 79−71455
pyrometer operating principles survey and error sources *(German)* 78−49841
pyrometers, two-colour, modification of emissivity response 79−93142
pyrometric system, precision, residual aberration effect calc. 79−71456
pyrometric system image quality in temp. meas. of nonisothermal objects 78−41312
Q-factor measurement by damped oscillation method *(Japanese)* 78−89492
quantitative IR spectral analysis, background and overlapping of absorpt. bands influence on accuracy 80−55748
quantum freq. standards, output signal sidebands/resonator detuning effects on accuracy 77−87743
quantum magnetometer with alternating polarity modulating pulses *(Russian)* 80−90871
quartz transducer, multimodality influence on US vel. and attenuation meas. 77−11100
rack and pinion type instruments, indication error reduction *(Polish)* 78−49818
Radcliffe Cassegrain telescope, d-camera vel. system 78−73645
radial velocity spectrometer at McDonald Observatory, meas. uncertainty 80−51667
radiation, environmental meas. made with integrating detectors, error anal. 77−38428
measurement errors continued
radiation absorption measuring instrument characts. evaluation with reference to information theory *(German)* 78−86753
radiation pyrometers for temp. meas., error sources *(German)* 78−32819
radio astrometry, influence of troposphere on radio-interferometric meas. of coordinates 80−67581
radio astrometry, sources optical positions in FK 4 system, internal mean errors 78−65709
radio sources, measured ang. dias. errors 79−12534
radio-meteors, under-dense, influence of recomb. on data 79−80279
radioactive effluent monitoring problems, loss and error reduction procedures 78−89987
radioactivity measurements in radiopharmaceutical industry, Atomic Industrial Forum-NBS quality assurance programme 77−40769
radiochemical and chemical trace analysis, in environmental materials, reliability aspects 78−40106
radioheliograph phase error meas. and correction 77−87269
radiointerferometric frequency and coordinate meas. accuracy, tropospheric fluctuation constraints 79−8848
radioisotopic thickness gauges, errors due to fluctuation of source-detector spacing 79−67251
radiometers, spherical-cavity, computation of errors 79−35829
radiosources, resolved, errors in aperture synthesis obs. of circular polarisation 77−29656
rain and hail parameters, sampling errors 78−28279
rainfall rate meas. from weighing raingauge records 77−49126
raingauges, influence of cleaning on collection and chemistry of rainwater 77−2282
random, of instruments under transient conditions, analysis based on instantaneous frequency response 80−77741
random, simulation (Monte Carlo) method, teaching appl. 78−86062
random signal mean power meas. error *(Polish)* 78−89425
rangefinder with fluctuating phase shift, systematic averaging error elimination 77−67469
Rankine-type capillary viscometer, for gases *(Japanese)* 80−14859
rare earth metals, neutron activation anal., interference by neutron induced 2nd order nuclear reacts. 77−81444
ratemeters, with variable time const., error determ. 80−95507
reaction rate constants, temperature coefficients, evaluation of mean values, and standard errors 79−74346
reactive power, three-phase two wattmeters, meas. errors *(Croatian)* 80−105677
reactor coolant, automated system for radioiodine anal. 78−35768
Recent vertical crustal movements in N.Carolina and Georgia, possible systematic levelling error 79−79794
red dwarf stars, photometric errors rel. to space density 77−5524
reduction using microprocessors *(Czech)* 78−8398
reference standard US flowmeter error component estimation 77−80248
reflectance spectrophotometers, old geometry problems *(German)* 78−54431
reflection dispersive Fourier interferometer window eliminating backlash error 80−57402
refractive index of liquids, determ. with cell differential refractometer, prism wedge angle effect on meas. error 80−62715
refractometer, objective detection of light contrast limit, errors 77−74490
relative humidity of air, control, error comparison for various sensors, accuracy 77−10034
representativity error definition *(German)* 77−17941
resistance bridge type thermometer, operational principles *(Polish)* 78−49834
resistance meas. of tenso-resistors, closed Wheatstone bridge method *(Russian)* 79−12821
resistance thermometers, drift correct cct. 80−98912
resistance thermometers, meteorological, according to Baumbach and Frankenberger, comparison *(German)* 78−65433
resistance thermometry review, error sources 80−52206
respirometric open systems, error anal. *(German)* 80−104782
retroreflecting material metrology, errors in luminous refl., chromaticity meas. 80−68235
retroreflector photometric and goniometric accuracy 80−86375
retroreflector photometry, meas. error rel. to aperture size 80−73409
reverberation chamber LF sound power injection analysis and response averaging 78−42496
reverberation room ANS qualification error sources and effects 77−58514
review of error sources, internal and external *(German)* 79−67245
RF accurate voltage meas., review 77−18043
rheograph linear-distortion estimation 80−85502
rhino-manometry measurements, theory of some systematic errors *(German)* 79−83957
rivers suspended sediment rating curves, accuracy assessment for small basin 77−91170
RMS measurement errors quantified 80−57274
road traffic noise monitoring, errors between sampled data and continuous data 79−81618
rocks modal analysis, error assoc. with point-counting 78−32232
rotary gas flowmeter error anal. *(Russian)* 78−71407
rotary viscometer, error anal. *(Russian)* 78−91039
rotational anemometers, wind tunnel tests 77−29454
roughness measurement, electrical stylus tip instrums. 80−90818
rounding error uncertainty anal. *(German)* 77−87721
rubber testing, statistical anal., method variance *(Polish)* 77−28962
salinity determ. from sound vel. 77−70679
sampling error investigation, expt. 79−75613
sampling instrum. for recording/meas. instantaneous values of periodic events, oscilloscope appl. *(German)* 77−53876
satellite attitude determ. 79−88561
satellite cameras, sidereally driven, numerical corrections 78−40678
satellite temp. determ. in troposphere, sensitivity due to water vapour estimates 78−3874
sea gravimeter trials on Halifax Test Range, NW.Atlantic 77−2267
sea surface temperature meas. by Noaa 4 satellite, comparison with Aries airborne radiometer meas. 79−62517
sea temperature gradient meas., errors in stepwise stratified ocean 80−31149
sea wave space and time structure measurement from Doppler frequency shift 77−29482
sea-surface temperatures, satellite-determined, in tropical Pacific, climatological usefulness 80−31044

measurement errors continued
SEASAT radar altimeter, resolution capability preliminary estimates 80−72645
seawater conductivity/temperature/pressure profiler errors 77−5377
sediment analysis using vibration-frequency method 79−49202
sediment transport by rivers, errors from assumption of fine sediment uniform vertical distrib. 79−84313
seismic refractor velocity determ., cause and nature of errors 80−56621
seismic surface waves, group vel. meas., error estimation 77−86805
seismic surveys, mis-ties and zero time errors 77−21916
seismic wave travel times, errors of method of seismically conjugate points 77−9368
seismograms, noise effects on meas. accuracy 77−45181
semi-automatic measuring machine for plates taken with photographic vertical circle, errors *(Russian)* 79−96920
semiconductor, capacitive profilometry, accuracy 80−9005
semiconductor, complex dielectric permittivity meas., in H_{01n} cylindrical cavity 79−93160
semiconductor slice resistivity distrib., contactless meas. results *(Polish)* 77−89756
semiconductor volume and contact parameter determ. from V-I characteristic *(Russian)* 80−49912
sharp-lip capillary nozzle production and meas. precision 77−80246
shear flow direction meas., anal. of errors 78−22436
shearing interferometer inaccuracies due to a misaligned test section 78−93755
shock tube measurements of elem. gas reaction rate coeffs., review 80−3299
signal form distortion, in absorptive medium *(Russian)* 78−46856
signal peak recorded profile, influence of integration time const., appl. to crystallography *(French)* 77−5798
SIMS quantitative evaluation using Saha-Eggert type eqns. 77−60164
single interrelation equation on arbitrary number of factors subjected to meas. errors, statistical estimation 77−53848
single photon decay spectrometers with pile up correction, performance 77−61126
single-mode obs. distributions, invalid data rejection algorithm *(Russian)* 79−21690
size meas. of drops by holography 79−67252
skin-friction balance measurement, error sources 77−65828
snow, accuracy of water equivalent meas. with standard densitometer 79−29796
soil gas fluxes determination, chamber methods numerical evaluation 79−16700
solar constant, accurate determs. by cavity pyrheliometers and errors 79−2341
solar double-pass monochromator with automatic data processing, spectral lines recording error *(Russian)* 80−72777
solar hectometric and kilometric emission in August 1972, magnetospheric noise effects 77−25994
solar magnetic fields, ang. resolution effects in Mt. Wilson magnetograph meas. 77−22082
solar magnetic fields, errors from Fourier transforms of saturated and blended lines 77−22165
solar neutrino radiochemical detectors, internal contamination backgrounds 79−16827
solar spectrometer, reson. scatt., apparatus and instrumental errors 78−96393
solar spectrum, convective correction to measured wavelengths 78−93181
solar spectrum, photospheric lines damping const. determ. methods errors *(Russian)* 80−72899
sonar, deterministic and random error model of multibeam hydrographic system 79−3873
sound level meter meas. accuracy 78−59211
sound power estimation in free field above refl. plane 77−39154
sound velocity measuring instrument, digital electronic, comments 80−14528
sound-power level meas. of industrial machinery, environmental aspects 77−39153
space plasma, mass discrimination effects in mass spectrometers ion and neutral extraction 80−4230
spacecraft trajectory meas. errors, motion parameters estimation 77−29633
spacecraft trajectory meas. process optimisation, visibility limitations 77−29632
speckle interferometry, ang. depends of atmospheric turbulence and anisoplanatism errors 79−101080
spectrometer, millimetre-wave astronomical, intensity calibration error evaluation 78−53821
spectrophotometer, double-beam, measurement reproducibility 77−49792
spectrophotometer, double-pass, with digital registration, spectrum registration precision *(Russian)* 79−96917
spectrophotometer, single-beam UVI, multiple reflections as source of errors 77−49788
spectrophotometer, Zeiss DMC 25 automatic recording instrument errors 78−54430
spectrophotometer optical parameters, measurement errors, normalisation *(Russian)* 78−70198
spectrophotometric measurement, dual wavelength, precision optimisation 79−92019
spectrophotometry, errors and calibration procedures 77−53988
spectrophotometry, errors and calibration procedures 78−32849
spectroscopic measurement, convergence of iterative deconvolution technique, effect of errors 77−53849
spherical specimen glossiness meas. 79−54175
spinning analyser ellipsometer, meas. magneto-optic rotation and ellipticity *(Japanese)* 80−73419
spur-gear, combined length, angle measuring procedure *(German)* 78−77855
standards comparison, time and frequency, improved accuracy 80−95062
star positions obtained by block adjustment, accuracy 78−20623
star positions obtained from overlapping plates, accuracy of average 78−20622
star proper motions rel. to galaxies, systematic errors in photographic obs. *(Russian)* 79−16941
statistical conversion of instrument signals, optimal, with aid of computers 77−5795
steel sheet internal friction, errors of meas. apparatus 77−32752
stellar absolute spectrophotometry and UBV photometry, comparison of results 78−96476

measurement errors continued
stellar Balmer-index photometry, quantitative anal. of influencing factors 78−96404
stellar photographic equivalent widths, calibration against solar photoelectric equivalent widths, accuracy 78−73658
stellar right ascensions obs. with large transit instrument, accuracy of absolute chain method of equalisation *(Russian)* 79−96887
stellar spectra, Fe lines equivalent widths in cool standard stars, systematic errors 77−78771
stellar spectra, line equivalent width errors due to photon statistics, calc. formalism 80−8625
stellar spectral classification, errors detect. by cluster anal. 78−20819
stellar spectrophotometric accuracy, anal. 79−21193
stellar spectrophotometry, random and systematic errors 77−9737
stellar trigonometric parallaxes, freq. distribs. and systematic effects 80−94785
stellar trigonometric parallaxes, internal and external errors 77−91523
stellar trigonometric parallaxes, statistical anal. and systematic errors 77−64743
stellar trigonometric parallaxes, statistical use 77−45315
stellar trigonometric parallaxes, systematic differences 77−78776
STEM methods for mass measurement 80−73537
step-height measurement, stylus-type surface texture measuring instrument calibration appl. 78−77862
stochastic processes, mean values and standard deviations fundamentals *(German)* 80−13031
strain gauge, reduction in Wheatstone bridge cct. 77−10004
strain meas. of hip joint prosthesis, by built-in gauge *(French)* 78−44705
strain-gauge measurements in heat-resistance tests, error estimation 80−4703
strain-gauge transducer sensitivity to directional thermal gradient error 77−74382
stratosphere NO and ClO concs., effects of vars. at twilight on interpretation of solar occultation meas. 80−85756
streamflow changes after reclamation, errors of estimates 79−29794
strip lines meas, dielectric, small standing wave ratio and losses meas. 80−77811
stylus tip instrums. for surface roughness meas. *(German)* 80−101782
submarine basalts K-Ar ages, errors due to sea water weathering 77−86830
superconducting solenoid, in persistent mode, magnetothermodynamic meas. error anal. 79−17454
superfluous, meas. elimination, precision evaluation 80−90805
supernova remnants, diam. errors rel. to surface brightness-diam. correl. 77−29899
supersonic thin turbulent layer, hot-wire anemometry, error reduction 78−34235
surface potential distribution meas. by vibrating electrode 79−67340
surface roughness meas. using feeler probes 78−169
surface temperature meas., using radiation pyrometer, accuracy increase *(German)* 77−82522
surface waves meas., using resistance wave gauge, accuracy and calibration 80−24110
surveying, reduced three rosettes meas. method for ang. deviations determ. *(German)* 77−60497
swirling flow hydrodynamic parameters in flow transducer input, expt. 77−72390
systematic duplicative, algorithm *(Russian)* 80−86245
systematic uncertainties, randomisation and quantitative assessment 80−98869
teaching methods for undergraduate laboratory 79−35474
teaching statistical concepts in physics 79−35501
temperature error of some low-temp. thermometers magnetic field effects 79−12802
temperature field distortion by thermocouple seal-in 78−81968
temperature influence on meas. accuracy *(Polish)* 78−12664
temperature meas. accuracy, additive and multiplicative meas. errors influence *(German)* 80−8985
temperature measurement, error due to time varying mag. fields effects on thermocouples 78−4617
temperature measurement by photoemission method, systematic error 79−93140
temperature measurement by thermocouple, avoiding errors 80−62664
temperature measurement via pyrometry, effect of scattered light 77−26301
tenso-resistive strain gauge output error anal. *(Russian)* 78−89474
theodolite, reduction of influence of vertical axis error on horizontal angle meas. *(German)* 79−44278
thermal conductivity measurement of soil by probe method, minimisation of errors 77−17259
thermal convertor AC-DC transfer errors determ., absolute method 78−93643
thermal EMF of semiconductors, thermal cell and copper blocks method, more accurate treatment of results 80−77812
thermal measurements, optimal estimates, Kalman filter appl. to accuracy improvement 77−10013
thermal radiation sources, high-temp., for calibrating radiometers 80−17946
thermo-optical measurements at six European laboratories compared *(French)* 78−29107
thermocouple, 3-channel corrector of dynamic errors 80−17939
thermocouple, differential, effect of electrodes thermoelectric nonuniformity limitation 77−74398
thermocouple, differential, temp. drop meas. error determ. 79−21742
thermocouple errors due to Nernst effect 77−67434
thermocouples and resistance thermometers meas. uncertainty estimation *(German)* 77−53909
thermocouples principle, errors, due to windings heating *(German)* 80−95096
thermoelectric convertor error due to crystallographic misorientation anisotropy 78−77904
thermoelectric temp. meas. in metal testing, anal. 78−19975
thermoelectricity, errors in absolute scale between 10 and 350K 77−28162
thermogravimetric system for investigating gas-metal reactions at elevated temps. 80−229
thermogravimetry, balance inclination and specimen temp. error sources 80−98887
thermometer, resistance, meas. current standardisation 77−74399

measurement errors continued
thermometer thermoelectric, Pt-Rh, 1300 to 1700°C, errors obs. and analysis 80-77783
thermometers, low-temp., magnetic-field-induced temp. error 79-80618
thermophysical properties, standardisation of meas. methods 80-52197
thermosphere N mass spectrometric meas., gas-surface reactions impact 79-66849
thermostat metals, influence of specimen curvature on thermal sensitivity *(German)* 80-27291
thick planar films, transmission method for index meas., modal effects 80-102862
three-layer dielectric reflectivity standard error analysis 77-79727
three-phase two-element VAr meter inaccuracies 77-13774
three-term error-normalising instruments, optimum range and information capacity determ. 77-13732
time and latitude, astronomical refr. general theory *(Russian)* 78-89045
time meas. from star transit obs., external medium effect on accuracy 77-87746
time measurement, errors, accuracy of watches and clocks, time standard 80-90821
time signal from Loran-S station, propagation path effect on locking error 77-87742
time-domain measurement, mm-wave circular waveguide 77-18020
tornado, simulated, flow-pattern errors in meas. by three-dimensional anemometers 77-17244
torquemeters, calibration using rack with mobile primary transducer 79-80610
total dynamic characteristics of meas. facilities, limit error estimation 78-77841
trace metal analysis in water, accuracy in AAS and AES using graphite furnace 78-69510
transducer, pulsed frequency, continuous random signals errors evaluation, by means of computer simulation 77-74386
transducer nonlinearity error minimisation method *(Polish)* 78-41298
transducer precision model, angle-digital quantities conversion error evaluation 77-82498
transducers, dynamic, analysis using conversion factor 80-77770
transmission spectrophotometry, standardisation in UV and visible regions 78-32850
transonic flow with pressure gradients static pressure hole meas. errors 79-94645
trigonometric parallaxes, systematic errors 77-74042
triple point determination, of O_2 at low temp. *(Japanese)* 80-31749
turbine flowmeter, universal viscosity curve, errors 78-34243
turbine meter uncertainty, uncertainty pattern statistical anal. 78-30381
two instruments precision error estimation methods 78-89424
two objects movement rate, by laser interferometers *(Russian)* 77-26392
two phase flow, indirect meas., methodological error anal. and reduction 78-34241
two-beam mirror interferometer, accuracy, emission beam divergence effects 79-26115
two-phase flow meas., real-time, digital signal processor 77-80235
Tycho Brahe's astronomical instruments, errors 78-32642
UK 1.2-m Schmidt telescope, alignment, pointing accuracy and field rot. 80-4252
universal horizontal metroscope, rational determ. of composite error on small micrometers 80-82742
upper atmosphere wind meas. errors from meteor trails 77-49202
US flaw detector UDM-3 79-8409
US flowmeter, propagation time of acoustic signal 80-6175
US phase flowmeter, pulsating flow rate meas. error evaluation 77-72388
US phase vel. and absorpt. coeff. meas. incorporating exact. diffr. corrections 78-26010
US standard probe transducers, calibration uncertainty 77-840
US true pulse velocity meas. methods, review 77-84094
US vel. meter using sing-around technique, IC 80-38198
US vibrations, propag. time meas., accuracy increase with UK-10P instrument 79-96277
USSR All-Union State Standard for linear and angular meas. 77-17946
UTR-2 radiotelescope, expt. techniques, data processing, for decametric survey of discrete northern sources 78-57461
UV spectrophotometry, $K_2Cr_2O_7$ in H_2SO_4, nicotinic acid in HCl as standards 77-77819
vacuum press. meas. considerations *(French)* 78-49846
Vaisala-Brunt frequency vertical fine struct. meas. in Mediterranean Sea 80-26537
vapour pressure measurement, static method 77-74378
variational simulation of measuring equipment, machine-oriented description of the error determination and control process 80-95053
vector aeromagnetometer instrument set, geomag. field components errors in bench tests 78-45016
velocity measurement, by He-Ne laser velocimeter *(German)* 77-33977
ventricular ectopic beat detect. in rapid Holter scanners, prematurity and height as criteria 79-66575
Venus, positional obs. at Ukrainian Academy during 1972, errors *(Russian)* 79-44390
Venus atmosphere profile from Mariner 10 radio occultation, statistical and computational uncertainties 79-96938
Venus wind velocities, errors of vector determ. by radio interferometry 79-48722
vibration meas., errors evaluation due to pulse signals 80-23972
vibration measurement, using logarithmic instrument, estimation *(Russian)* 77-2648
vibration transducer, surface compliance of vibrating body *(Japanese)* 80-79046
vibrational, using analogue photoelectric velocimeters, systematic errors determ. 80-79246
Vickers hardness meas. of curved-surface components 78-80699
viscometer, capillary, Ubbelohde-type, surface tension effects for spherical fluid reservoir case *(German)* 79-86534
viscosimeter, capillary, Ubbelohde-type and types with different reservoir bulbous form, surface tension effects calc. *(German)* 79-86535
visual binary stars, observational selection in orbital eccentricities distrib. 77-74098
volt-ampere meters, pointer-type, automatic testing cct. 77-53937
voltage divider calibration, inductive, between 10 kHz and 100 kHz, international comparison of calibration methods 80-13100
voltmeter, digital, error determination algorithm 77-53938
measurement errors continued
voltmeter, digital, errors evaluation, causes and prevention *(Czech)* 77-57361
voltmeter frequency error reduction using eccentric and elastic transducer *(Bulgarian)* 77-61082
voltmeters, error estimation 80-22381
voltmeters and milliammeters, installation for determining freq. error over side range 80-4734
vowel duration meas., reliability study 78-65052
wall impedance in Kundt's tube by means of FM transmitter signal *(German)* 80-102878
water content meas. capacitance transducer systematic error reduction 77-79082
water turbines, characteristic parameters, using laboratory models 79-63186
wavefront distortion sensing for adaptive optics system control 77-19293
waveguides, coaxial, analyzing errors of standard measures when calculating step discontinuities, 1 to 2 GHz 79-80643
weighing, balances accuracy class increase, using several standard weights of equivalent mass *(Rumanian)* 80-47022
whistler extrapolation, comparison of systematic errors in different methods 77-53334
whistler extrapolation via linear-Q anal. and extrapolation factor, systematic errors 77-53333
wind determ. by airborne Doppler radar bias error 78-3879
wind error predictions for Omega stations, smoothing improvement factor 78-7719
wind fields derived from dual-Doppler radar meas., error estimation 77-17171
wind measurements, using OMEGA radiosonde, error estimation 79-29916
wind velocity spectra, determ. from cup anemometer meas., inertia errors *(Russian)* 77-13102
wire strain gauge in heat cycling condition, systematic error estimation *(Russian)* 78-65916
X-ray analysis of heterogeneous materials, expt. geom. effect on local analysis results 79-52819
X-ray binary stars, distortion of absorpt. line vel. curves due to X-ray heating 77-29878
X-ray crystallography, struct. factors, accuracy assessment 78-71636
X-ray diffr. residual strain meas., elastic const. meas., material errors 78-5714
X-ray stress meas. by counter method, statistical anal. 78-27694
X-ray stress measurement, error caused by side declining angle of counter scanning plane *(Chinese)* 80-52373
X-ray thickness gauge, factors affecting measurement errors 79-88911
X-ray tubes, focal spot size meas., systematic error in pinhole camera system 79-75666
Zeiss Eldi 2 electro-optical rangefinder, accuracy and range *(German)* 77-68274
ZTL-180 zenith telescope, objective distortion determ. from visual obs. of star pairs *(Russian)* 78-89068
$^{40}Ar/^{39}Ar$ age spectra of Mesozoic tholeiites from Antarctica, interpretation of discordances 77-49047
B, inorganic, content in St. Lawrence Estuary, analytical error *(French)* 78-77274
Cs beam frequency standard errors due to excitation asymmetries 77-5816
Cs clock, environmental effects on rate in astronomical observatories 79-16833
Cs clocks made by Oscilloquartz Company, investigation of metrological characts. 80-101787
Cs freq. standard, error due to second order Doppler shift 77-87745
Cu alloys, molten, gas content meas., reduced pressure test *(Chinese)* 80-81390
Cu Laue X-ray back reflection pattern solving, algorithm and statistical error analysis 79-99030
^{3}H in water, low-level meas., inter-laboratory comparison 78-44888
He metastable atoms beam, error source in time of flight expts. 77-14609
He-Ne laser two-beam interferometer phase errors *(Russian)* 79-6166
K-Ar radioactive dating, excess ^{40}Ar identification by $^{40}Ar/^{39}Ar$ age spectrum technique 77-5152
NO concentration meas. in gas mixtures, chemiluminescence method *(Russian)* 79-16094
Na, fission reactor coolant, meas. accuracy of plugging indicators 78-54813
O_2 partial pressure on blood sample, polarographic method, error reduction 78-7470
O_3, atmospheric, Umkehr vertical profile errors caused by presence of stratospheric aerosols 79-70849
^{18}O, palaeotemperature determs., effects of post-depositional alteration of rocks 77-29455
Pt resist. thermometers, 0-850°C range, principles and practice *(German)* 77-82512
Pt resistance thermometer, temp. meas. errors, 0 to 600°C 77-41605
Pt resistance thermometer, errors due to measuring-current heating in still air 79-30472
Pt resistance thermometers, effect of Pt oxidation 80-101794
Pt-Rh thermocouple, Ta-sheathed, Al_2O_3-insulated, large decalibrations above 1330°C 78-24790
^{87}Rb half life, errors in absolute counting and scintillator meas. 77-26943
^{222}Rn scintillation counting, standard deviation estimation 77-79519
SO_2 air pollution, daily volumetric meas., PVC tubing acid release effects 77-29449

measurement standards
see also atomic clocks; temperature scales
1 GΩ resistance standard, meas. process 77-82568
30th Annual Frequency Control Symposium, Atlantic City (1976) 77-37852
31st Annual Frequency Control Symposium, Atlantic City (1977) 78-57905
77.5 kHz transmitter signal, derivation of standard frequencies *(German)* 77-53928
600 MHz to 1 GHz coaxial thermal noise standard 80-98875
absolute ampere determ. using servo-controlled balance 78-82003
absolute luminescence quantum yields, actinometric meas. 77-41691
absolute ohm of ETL, determ. using calculable capacitance standard *(Japanese)* 79-6137

measurement standards continued
absolute radiometers, instrumental corrections, spatial responsivity variations 79−97434
absolute wavelength, ^{127}I stabilised He-Ne laser 78−73971
absorbed-dose standards comparison for ^{60}Co gamma rays 78−74512
AC high voltage meas., confirmation of voltage ratios up to 200 kV 78−74018
AC power, at 120 V, 5 A, 60 Hz, international comparison 78−93735
AC power in coaxial channels at HF, comparisons among COMECON countries 79−93166
AC unit, 40 Hz to 100 kHz, USSR special standard 77−30179
AC voltage, 20 Hz to 1500 MHz, standard apparatus using thermoelectric convertors 77−18036
AC voltage standard GK-10A 77−10055
AC voltage unit standard, USSR, 20 Hz to 30 MHz range 78−93734
AC voltages, small, combined meter checking 80−13057
acceleration during translational motion, errors associated with apparatus for standards 79−30432
acceleration unit, linear, 10^{-3} to 2×10 m/sec^2, Soviet primary standard 77−79070
accelerometer base strain sensitivity test device 80−52173
acoustic noise 77−35001
acoustic noise control, USSR basic state standard 79−23142
acoustic power, American National Standard S1.21-1972 qualification procedures 77−62120
acoustic scanning microscopy, Gray scale 78−94494
acoustics, USA National Measurement System 78−38102
adsorption vacuum measurements, standard devices 79−71464
aeronomical reference spectrum for solar UV below 2000 Å 79−25379
air density equation and mass unit transfer 79−88918
air quality standards derivation on basis of risk considerations 79−79429
air-bath enclosure for standard cell group monitoring by AC Josephson effect 77−82556
alternating voltage unit, 20 Hz to 30 MHz, USSR special standard 77−30180
ampere absolute value improved realisation 78−93737
ampere as standard electric current unit *(German)* 77−22574
ampere determination from levitation of supercond. mass 77−30178
angle measuring standards reproduction, autocollimating telescope appl. *(German)* 78−77851
angular drift rate standard, aircraft gyroscope accuracy increase 79−71421
angular velocity meas., USSR State Standard 1976-77 79−30429
antenna calibration, radioastronomical methods, standard sources *(Russian)* 78−4103
arbitrary nature of meas. standards, struct. of physical knowledge 77−74347
asbestos, airborne, X-ray diffr. anal., calibration standards 78−69517
assay-activation analysis of rock, use of Au and Ag standards based on phenolformaldehyde resin 78−3419
astronomical photometry, Cousins VRI system, temp. and absolute flux calibration, appls. 80−26750
astronomical standard stars for uvby photoelectric photometry south of declination +10°, obs. 77−2347
astronomical standard stars for VRI photometry with S25 response photocathodes 77−2422
ATA standard time broadcast, synchronisation methods 80−47024
atmosphere O_3 concentrations meas., UV photometric standards interagency comparison 79−35000
atmospheric pollution, systems for observing and checking 79−8684
atmospheric trace analysis, selection of calibration gas standards 77−91255
atomic frequency standard prediction error analysis 78−57906
atomic time and frequency standards development at Shanghai observatory, China 80−105617
atomic time scale instability, contrib. of computation algorithm 80−98890
atomic/molecular beam interrogation in Ramsey cavity, two freq. separated oscillating fields technique 78−89596
attenuator monitoring, computational tables and computers for efficiency improvement 77−79073
attesting weights of different classes of accuracy 79−49206
automated time keeping system of Van Swinden Lab. 80−98891
automatic information and control systems 79−71394
beta decay primary standard *(Rumanian)* 80−68603
beta dosimetry, comparison of laboratory standards 77−66858
blackbody radiators, effect of surface roughness 80−52228
botanic reference materials, candidate standards, homogeneity testing, anal. methods 78−11594
bremsstrahlung energy flux unit, 0.8 to 8 pJ, USSR special standard 77−30730
British Calibration Service 80−22319
British trade weights and measures activities 80−27267
building heat loss diagnostics, IR image evaluation requirements 80−86424
calibration, sealed metal freezing point cell 78−12696
calibration devices, made more accurate by improved basic standards 77−33980
calibration methods for primary and secondary standards, in Hungary 80−5357
calibrations of multiples of the unit of mass, systematic search for orthogonal systems 80−82747
calorimetry, organometallic compounds, standard for quantity-of-heat unit 79−17421
Candela as standard light intensity unit *(German)* 77−22521
capacitance, appl. of sensitivity criterion to Lampared-type electrostatic system 80−98942
capacitance, high, four terminal device with auto transformers for scaling 77−18025
capacitance, meas., capacitor with spherical caps calc. *(Slovak)* 77−87783
capacitance, primary standard capacitor design 77−53944
capacitance, secondary standards *(German)* 79−71402
capacitance unit reproduction, theoretical study 77−53943
capacitive grain moisture meter Standard Specimens 77−82481
capacitive Q standard, calculable 78−21176
capacitor, simple calibration method 77−82571
capillary discharge mode selection for IR brightness standard *(Russian)* 79−55198
cells, development of reference group with microcomputer-controlled intercomparisons 80−22384
measurement standards continued
cells, electric, saturated, use of air thermostat 77−10058
chemical data, reliability improvements using approx. methods 79−53966
clocks, standard-freq. controlled, for high precision time meas. *(German)* 78−77871
coaxial mutual-inductance, computation of parameters 80−4735
coaxial waveguide wave impedance, USSR special standards 77−30182
colorimetric data for samples of OSA uniform colour scales 78−65952
colorimetric educational laboratory, calibration of set of surface colour standards 78−49625
colour contrast math. determ., uniform chromaticity scale construction 78−49881
colour reproduction, of images obtainable by two-primary colour projections 80−12125
colour standards, prep. of OSA Uniform Colour Scales Committee samples 79−2807
colour thermochromism, Gardner standards behaviour obs. *(Hungarian)* 78−24842
colour TV burst signal, used for secondary frequency standard 78−24826
COMECON standard ST SEV 1052-78 for establishing units of physical quantities 80−42189
complex permittivity of low-to-medium loss standard liqs., meas. at 285 GHz 78−15083
conference on metrology and fundamental constants, Varenna, Italy (July 1976) 80−105603
constant angular acceleration unit, USSR standard, metrological charcts. 79−30430
convergent nozzles incorporated into gas flowmeter, comparison with standard 80−6126
correlated colour temperature and colour-difference formula 78−54424
cresyl violet, luminesc. quantum yield standard for red, calorimetric obs. 80−190
cryoelectrics, computerised measurement instrumentation 80−98920
cryogenic current standard based on AC Josephson effect 77−82557
cryogenic flow measurement, transfer standards 79−68888
cryogenic fluids, density reference system 78−54344
V1500 Cygni (Nova 1975), stellar magnitude sequence and nova brightness meas. 78−36618
D lamp calibration for transfer standards using synchrotron radiation 78−65954
DC ratio, toroidal cryo current comparator 79−88977
DC standard materials, physical and technological props. *(German)* 78−54400
DC voltage monitor for standard cell using AC Josephson effect 77−82552
DCF 77 standard time and frequency receiver, display ccts. *(German)* 77−13737
definitions, of units, standards and measurement methods *(French)* 80−27264
densitometers standardized density scale for photographic photometry *(Japanese)* 79−101075
density logging standard materials, influence of comp. on readings *(Russian)* 79−74989
development trends, length, press., mass, electrical and photometric standards 80−191
didymium glass filters for spectrophotometer wavelength scale calibration 80−43417
dielectric constant, class 1 standard specimens, certification methods 80−13036
differential EPR susceptance unit, USSR primary standard 77−30190
diffuse reflectance spectroscopy, applics., standards and calibration 78−32848
diffuse reflectance spectroscopy, calibration of reflectance standards, review 78−32860
dilatometer, absolute interference, for high-temp., high-precision testing installation 79−35677
dilatometry 78−26699
DIN 45 635 Part 1, envelope meas. method for sound power level, multi-position machines *(German)* 80−43523
directional-hemispheric reflectance factor scale establishment, Van den Akker method 78−77967
dose rate meter, use as X- and γ-ray secondary protection-level standard 77 81579
dosimetric primary and secondary standardization within the European Communities 80−9415
dosimetry, calibration and meas. standards at Austrian Dosimetry Laboratory 80−5362
dosimetry, primary standard for determination of absorbed dose in water for X-rays generated at potentials of 7.5 to 30 kV 80−5354
dosimetry, primary standards for industrial radiation processing 80−5356
dosimetry, Regional Calibration Laboratory, Cleveland, USA 80−5364
dosimetry, secondary standard laboratory organisation in India 80−5366
dosimetry, secondary standards laboratory, role in a nuclear power utility 80−5365
dosimetry calibration problems in connection with radiation protection around nuclear facilities 80−9422
dosimetry of electrons and photons, standardisation in Germany 80−5353
dosimetry standardisation in Japan, review 80−5359
dosimetry standardisation in UK, review 80−5358
dosimetry standards labs., international network 77−67898
double constant current source for cryogenic current comparators, standard resistor calibration appl. 78−93731
dynamic force meas. device comparison *(German)* 77−79089
dynamic measurement, time and measured-variable standards, problems and methods of overcoming them 80−62613
earphones, reference equivalent threshold sound pressure levels, audiometric zero 79−3872
eddy current testing of tubes, rods and wires *(German)* 80−25971
EELS, standard for TEM, implanted Si 80−99017
electric field intensity unit, 30 MHz to 1 GHz, USSR special standard 77−30181
electric primary standards, curved stabilisation, superconducting quantum interferometer design 77−53945
electrical, US system, brief description 77−37840
electrical and electronic parameters, echelon-I standards 78−24812
electrical capacitance, resistance, inductance, group storage errors, statistical analysis 77−53853
electrical capacitance, resistance, inductance standard transmission techniques 77−53854

measurement standards continued
electrical measurements engineering, standardised work importance, in International Organisation of Legal Metrology *(German)* 79−75486
electrical measuring instruments, new CEI standards *(Italian)* 80−31789
electrical standardising laboratory for developing countries 80−101774
electrical standards progress and fund. consts. role *(Japanese)* 78−24760
electrical unit realisation progress *(German)* 78−160
electrodynamic percussion unit, mode selection method 79−30448
electromagnetic meas., precision, conf., Braunschweig, Germany (Jun. 1980) 80−98903
electromagnetic units, atomic fine structure control determination accuracy, atomic metastable beam method 77−68105
electron and energy fluxes units, 5 to 50 MeV, Soviet primary standard 77−75031
electron probe X-ray microanalysis, P standards for ultrathin tissue sections 80−98193
electron-atom-bremsstrahlung standard radiometric source improvement 78−67484
electroplated coatings thickness test standards 79−8405
electrostatic-ion pumps in a vacuum calibration system 78−57971
EM flowmeter type ERO-1, calibration use 80−43812
EM meas. and instrumentation, conf., Ottawa, Canada, 1978 79−21731
EM precision meas., conf., Ottawa, Canada 1978 78−89462
end gauges, fused silica and pyroceramic, high-precision stability 79−76778
end-standards and ruled scales using laser sources *(German)* 80−86251
ends standards of length for calibration, alignment using autocollimator 79−54094
environmental measurement, conf., Gaithersburg, Maryland, USA (Sept. 76) 78−69504
environmental noise rating and standardisation 77−58508
EPR intensity standard, description and use 79−54164
EPR standard, Picein 80 cement, for g-factor and spin conc. determination 79−80658
EPR standard samples, precision meas. of g-factor 77−26370
equipment calibration using standard frequency broadcasts 79−67258
ethylene, supercritical, mass-flow meter inaccuracy 79−68842
exoelectron dosimeters, reference dosimeter bank, storage, exposure and reading 80−5360
exposure rate and absorbed dose meas. for 6-7 MeV 79−26766
exposure standards for U mining 80−46055
extragalactic reference frame, for stellar absolute proper motion catalogue *(Russian)* 80−51747
faint stars, spectral-type standards for objective prism plates 80−46539
fast reactors, impact of ENDF standards 79−9734
fatigue test standards, terms and symbols definitions, statistical methods *(French)* 79−91862
fiber-optic measurements, using standards and instruments 80−74488
fission cross sections and product yields, integral meas. in standard neutron fields 79−13364
fission reaction rate standards and applications 79−9650
flow, gas, measurement techniques, rel. to significance and treatment of phys. quantities *(German)* 78−1775
flow, volumetric and mass, development of COMECON standard 80−43809
flow measurement, international standards, adequacy of supportive data base 78−34247
flow measurement, international standards organisations, review 78−34246
flow measurement, transfer standards 79−68892
flow of liquid and gas, mass and volume, Soviet primary standards 77−76002
flow rate and quantity meas., economic evaluation of metrological services 77−80239
flow rate equipment calibration and testing with load ring equipment, noncorrosive gases appl. 80−43813
flow rate meas., in open channels, standardisation in Soviet Union 77−80241
flow rate meas., of gas-liquid mixtures, standard system design principles 77−76005
flow rate meas. of liquid and gas, in petroleum-gas industry, Soviet standardisation 77−76004
flowmeter, throttle-type, standardisation in Soviet Union 77−76003
flowmeter checking, gas, using standard throttle system 77−80242
flowmeter generators for calibration and checking of standard flowmeters 80−43814
flowmeter testing and calibration 77−76007
flowmeters, transfer-standard, calibration in water test rigs for comparison of laboratories 79−23389
fluid radioactive waste monitoring equipment, USSR standards *(Russian)* 78−89998
fluorescence efficiency of laser dyes 78−35205
fluorescence measurements of opaque samples, proposed indices of degree of fluoresc. 78−54425
fluorescence quantum yield measurements, real, observed and mol. parameters, ref. soln. standards 78−32898
fluorescence reference soln. standards for quantum yield meas. 77−42442
fluorescent measuring equipment, selection of standard testing substances 80−7882
fluorocarbon measurements, interlaboratory comparison 79−70483
force, 250 kN ONERA force standard machine, precision improvements 79−35728
force, compression, 0.5 to 30 MN, standardisation using hydraulic force machine 79−35727
force and meas. measurement, conf., Braunschweig, W.Germany (Sept. 1978) 79−35725
force standard machines, 100 kN, investigation of parasitic effects 79−35731
force standard machines, calibration using mass standards *(German)* 79−35735
force standard machines of national institutes for metrology, technical specifications 79−26022
force standards and measuring apparatus, Hungarian *(German)* 79−35730
force standards for industry 80−42198
force transducers, strain-gauge, normalization of AC characts. 79−35705
forces, large, metrological provisions in COMECON member countries 79−75523
measurement standards continued
four-terminal high capacitance standard 77−5869
free air chamber for X-ray exposure standardisation at high quantum energies 80−14053
frequency, atomic standards, transfer of freq. stability to quartz-crystal resonator 80−17927
frequency, clock error with a Wiener predictor and by numerical calculation 80−82748
frequency, crystal ovens using temp. gradient-free change of state for quartz cryst. standard *(Polish)* 79−30481
frequency, Cs beam clock, Millman effect origin and expt. determination 77−5810
frequency, electrically tuned far infrared lasers appl. 78−174
frequency, extension using digital clock CADM 79−67288
frequency, H_2 maser appl. stability improvements and cavity tuning 78−21099
frequency, HCN laser translator of standard freq. to submm. range 78−17973
frequency, NBS-4, 5 and 6 standards, clock calibration appl. 77−45825
frequency, passive quantum standard, static AFC system parameter optimisation 77−9989
frequency, phase automatic freq. control parameters optimal values *(Russian)* 80−77814
frequency, radio receiver XKE 2, 10 to 200 kHz, for regulating crystal and atomic freq. references 79−67259
frequency, Rb resonance cell XSRM 78−41281
frequency, relativistic Doppler shift in satellite tracking 80−46951
frequency, visible region, absolute freq. meas. using ^{20}Ne laser 79−93104
frequency reference derived from 22.3 KHz signal 77−61049
frequency secondary standard, source for BBC 200 KHz signal 78−24766
frequency sources for time meas., hydrogen maser *(French)* 77−53865
frequency standard, precision oscillator freq. stability meas. *(Japanese)* 78−4596
frequency standard in 17 μm spectral region, use of N_2O ν_2 band 79−63991
frequency standards using divergent beams, stability limits 79−26037
Fricke dosimetry, determ. of molar extinction coeffs. of Fe^{3+} 80−13949
fundamental ohm determ. by ASMW standardising office, status *(German)* 79−9221
future prospects *(Japanese)* 80−73303
galaxies, bright, in Virgo cluster area, standard total magnitudes and mean errors 78−65685
galaxies, bright, southern, photoelectric photometry for photographic photometry standards 79−21436
galaxies, small, 21 cm H I spectra and appl. as line calibrators 79−35382
galaxies photometry, reduction of magnitudes of Virgo area galaxies to standard B_T system 79−92852
gamma mixed-radionuclide sources for calibration of Ge(Li) detectors for environmental assay 77−38541
gamma radiation detector, reference material, based on silicate glass 80−78454
gamma radiation nationwide calibration system 77−38583
gamma sources, secondary standard preparation for low activity gamma spectrometry 80−18701
gamma-ray intensity standard using $^{27}Al(p,\gamma)^{28}Si$, E_p=992 keV resonance 78−17472
gamma-ray standard sources using complex decay schemes 80−9081
gas analysers for air-pollution control, metrological warranty 79−21005
gas flow rate, critical flow nozzle characts. *(Japanese)* 77−39375
gas laser wavelength standard development, ^{3}He-Ne laser *(German)* 78−79034
gas microwave absorption Fourier spectrometer for 300 GHz to 1.2 THz 77−5935
gas mixtures, standard, SMES-2 system for metrological support 79−20487
gas thermometer, 273.15 to 1337.58K range 80−77782
gauge blocks, profiling method for determining phase correction, interferometric methods appl. 78−73986
gauge pressure meas. up to 1 kPa, NPL primary standard instruments 79−63265
GDR atomic time scale 80−98892
gear tooth profile, portable meas. instrum. for large gears, interchangeable standard profiles 80−57259
geochemical $\delta^{18}O$ scales, proportional vars., interlaboratory comparison 78−69326
geochronology and cosmochronology, convention on use of decay consts. 78−28189
German Standards Institute, 50 years of standardisation in surveying *(German)* 78−45591
glass, white-surface, spectral reflection coeffs. and colour coordinate comparison 77−71358
glasses for fluorescence standards in radiophotoluminesc. detector reading device 77−67944
global coordinate time scale, practical implications of relativity 80−47030
goniometer verification prism manufacture and recertification 77−27392
graphite, Poco AXM-5Q1, thermal and elec. transport props., 4-3000K 78−6375
gravimetric standards, best fit calibration curve parameters, error estimates 79−87931
gravity base at Newcastle upon Tyne University, England 79−29693
gravity new system, changes in international gravity base values and anomaly values 80−51317
gravity surveying, modern standards 77−17016
gravity surveys modern standards 77−48990
gyro instruments, standards for metrological support 79−67262
gyromagnetic ratio of proton in strong mag. field, meas. 79−40527
hazemeter, NBS reference, development and testing 79−75565
HD 14969, IAU radial-velocity standard star, orbit from photoelectric radial vels. 80−56884
hearing protectors, meas. of real-ear attenuation by standardised test methods 78−1508
HF current intensity unit, USSR state standard 78−36979
hierarchical systems, calibration errors influence on end item performance 80−98788
high speed photometer of Asiago Observatory, time and freq. standard 79−25505
high-accuracy AC voltage standard 77−13771

measurement standards continued
high-pressure gas flow test facilities, EEC intercomparison campaign, transfer standards 79−72979
high-pressure meas., evaluation of effective area, deadweight testers 79−88973
high-temperature measurements, instrumental complexes developed as metrological guarantee 78−212
high-temperature thermal transport props., work of CODATA task group 77−45818
humidity and dew point, standards and calibration 79−49240
humidity test chamber, convectively mixed, calibration appl. 78−54379
HV standard, principle and appl. 78−240
hydrometeorological meas. equipment, USSR state testing 79−70897
IAU Radial Velocity Standard stars, radial vels. meas. *(French)* 80−51743
image assessment, review of German standards 78−50724
imaging system assessment, conference, London, England (Nov. 1976) 78−50718
immunochemical analysis, standardisation of light scatt. meas. 78−36081
impedance of coaxial waveguide, analyzing errors of standard measures when calculating step discontinuities, 1 to 2 GHz 79−80643
improvement by International Bureau of Weights and Measures 78−41272
Indian Secondary Standards Dosimetry Laboratory, development and functions 80−41244
inductance, calibration of permeability meters, short-cct. coaxial lines 80−77816
inductance and capacitance standards comparison with transformer ratio bridge *(Polish)* 79−80645
inductive voltage divider, calibration between 10 kHz and 100 kHz, international comparison of calibration methods 80−13100
industrial pollutant source emission meas. needs 77−41165
intense photon flux absorbed dose meas. 78−41387
intensity meter calibration for 20 kHz to 300 MHz range 79−2786
interferometer, two-beam, wavelength comparison to French primary standard 79−6173
intermediate-energy secondary spectrum system, determ. of neutron characteristics, ΣΣ-ITN *(Rumanian)* 79−22355
intermediate-energy standard neutron field, neutron transport calcs. 79−13588
internal diameter reference standard, caliper type, accuracy determination 77−71296
International Atomic Time, role of primary standards 78−89459
International Atomic Time Scale, problems of generation, quality and availability 80−98889
International Bureau of Weights and Measures, 1978 activities and news 80−188
international organisation of legal metrology tasks 78−73961
international radiation standards, role of ICRU 80−9414
international standard reference radiations and their application to the type testing of dosimetric apparatus 80−9416
international time standard coordination *(German)* 80−52171
intrinsic inductance, equipment description *(Czech)* 78−32837
ion backscattering analysis standards 79−2883
ion implantation, quantitative, current practice and appls. 79−69141
ion implantation, quantitative theoretical aspects 79−69140
ion laser, $^{127}I_2$ stabilised, beat freq. intercomparisons at 514.5 nm 80−74338
ion selective electrodes, review 78−85165
ionisation chambers, radiation exposure intercomparison 80−5363
ionising radiation, metrology and calibration, French system *(French)* 80−5351
ionising radiation, primary standards and transfer methods in France, review *(French)* 80−5352
ionising radiation, traceability in meas. systems 80−5355
ionising radiation, USA national standards 77−38588
ionising radiation calibration, meas. standards, CNEN, Italy 80−12273
ionising radiation meas. system and standards lab., US 77−38581
ionizing radiations, comparison of standards within COMECON framework 80−42899
ionosphere HF radiowave propag., freq. standard utilisation 78−93027
IPTS 68, for low temp. 77−26296
IPTS-68 values of secondary ref. pts. above 2000K 77−45819
IR and millimetric waves and applications, conf., Miami Beach, USA (Dec. 1979) 80−57009
IR and MM wave calibration standards requirements survey 80−57248
IR and optical frequency standards 80−47027
IR and UV temperature units, USSR special standards 77−30148
IR file searching, ASTM, algorithm using peak intensity data 80−30295
IR plasma temperature unit, 10000 to 15000K, USSR special standard 77−31519
IR radiation brightness unit reproduction error anal., USSR standard 78−45699
IR reference spectra, for GC-IR, presentation specifications 80−31908
IR spectrometer performance testing using CO line parameters 77−91275
IR thermometer and pyrometer calibration methods and standards 79−88958
isotope fractionation, controllable, in thermal-ionis. mass spectrometry, SRM 987 standard test *(German)* 80−42299
Josephson, voltage standard, resistive divides *(Japanese)* 79−63266
Josephson devices, voltage standard *(Japanese)* 77−51851
Josephson effect voltage standard, BIPM, France 77−82484
Josephson effect voltage standard, commercial prototype 79−26068
Josephson effects applications, review 77−8243
Josephson multiple junction generated higher voltage standard 79−26069
Josephson voltage standard maintenance using standard cells combination with low temp. coeff. 80−101788
Josephson voltage standard system, influence of voltage divider 78−74027
Josephson voltage standards, future of superconducting instruments in metrology 79−26020
Josephson voltage standards, recent advances 77−18023
Josephson-effect voltage standards, BIPM-and NLP-standard comparison 79−21778
Josephson-effect voltage-standard instrument, features 78−93729
kilogram as standard mass unit *(German)* 77−22532
kilogram mass standard, air buoyancy correction for different materials *(German)* 77−82483
kilovoltmeters and HV scale convertors, certification using highly accurate test apparatus 79−80606
measurement standards continued
klirr-factor unit dimension, error in digital meas. 80−98873
Krasnodar Centre of Standardisation and Metrology, regularisation of DP 80−52152
laboratory discharge lamp source, for O I 5577 and 6300 Å lines of known width 80−4148
Landolt celestial equatorial UBV standard stars, spectral classifications 79−75199
laser beam applications 77−694
laser. calibration and measurement standard, high precision *(German)* 80−78862
laser dyes, fluorescence efficiency 77−42531
laser energy standards inequivalence simplification 77−79876
laser freq. meas., review and extension to 197 THz 78−81952
laser frequency, precision of interferometric meas. based on Doppler shift 77−165
laser frequency and spectral parameter check system 77−79880
laser frequency stabilisation, atomic beam nonorthogonal to laser light 78−74940
laser low-level pulse meas. system at 1.064, transfer standards 80−86253
laser power and energy meters, calorimeter system for calibration 80−38024
laser power meas., radiometric and calorimetric scales' equivalence 77−7115
laser power meas. at 633 nm, international intercomparison 78−37930
laser power meter calibration for the range 5-1000 W using electrically calibrated calorimeters and beam splitters 78−1241
laser radiation fluctuation-spectrum recording for USSR state standard 78−45696
laser radiation pulse meas., based on semiconductor radiators 80−23710
laser radiation pulse-length monitor testing, precision test system 78−45697
laser wavelength, comparison of 2 beams, two-wave interference, book contrib. 78−9408
laser wavelength comparison with standard using interferometric digital wavemeter 77−162
laser wavelengths comparison, interference circuits analysis 80−23737
length, line standards 77−53855
length, plane-parallel gauges and spheres comparison *(Rumanian)* 78−21098
length, temperature meas. using thermocouples and Pt resistance thermometer *(Slovak)* 78−77907
length and time standards 77−13734
length comparator, ceramic base *(Hungarian)* 79−80570
length meas. 80−194
length meas. by holographic interferometry with phase heterodynage 79−6095
length meas. international standards compared *(German)* 80−36977
length measurement using Ar^+ laser, wavelength stabilisation 78−33766
length metrology, I_2 stabilised He-Ne lasers *(French)* 78−87074
length standard meas. procedures of GDR Bureau of Standards *(German)* 80−57246
lens, standard reference, for MTF equipment testing in IR 78−50898
lenses, standard reference, for assessment of OTF meas. equipment 78−50897
light scattering standards in immunochemical analysis 77−56548
light source, compact, for 0.95-1.1 μm 77−72041
light source, pulsed, as reference for photon counting systems 77−3640
light sources, suitability of W strip lamps as secondary sources below 1064 degrees C 80−27297
light sources props. meas., photometric laboratory equipment *(Slovak)* 80−17990
light velocity, feedback, optical transients and metre bar 77−109
line standard meas. using He-Ne laser photoelectric microscope 77−82599
linear accel. meas. instrument metrological support 78−45601
linear dimension meas. means choice in terms of error levels 79−6082
linear thermal expansion coeff. unit, 4.2 to 90K, USSR state standard 78−37001
liquid flowmeter calibration automated secondary standard 77−37841
liquid scintillation counting sealed standard production 79−68145
LORAN-C type standard freq. signal, time and freq. calibration standard comparison *(Rumanian)* 79−40542
loss-angle absolute meas. using toroidal cross capacitor 78−93736
low flow generator and calibrator development 77−30125
low level radiation monitors, calibration accuracy and precision 80−9428
low vel. airflow facility for calibration of wind-speed measuring instrums. 80−1718
low-temp. thermometry reference points based on H_2 and He 78−206
luminance standard using W halogen lamp *(German)* 79−89980
luminescence quantum and radiant efficiency meas. methods, standard materials 78−32899
luminescence quantum yields, absolute, chem. actinometric meas. 78−32892
LV deuterium lamp. stabilised, as secondary radiation standard in 220-360 nm 78−77998
machinery acoustic noise meas. standards and reference sources *(French)* 78−83185
magnetic, representation, transmission methods 77−67408
magnetic field induction meters, constants determ. using nutation teslameter 80−98946
magnetic field measurement methods, formulae, EM effect on living organisms appl. *(Polish)* 79−39450
magnetic flux absolute standard *(Polish)* 77−67482
magnetic induction unit, 2 to 10 T, USSR special standard 77−30191
magnetic permeability, HF standard samples 79−35801
magnetooptical rotation, InSb and Ge, use in polarimeters 80−60551
mass, air density effects, calc. from atm. variables 80−105615
mass, force and weight 80−27273
mass standard error limits and accuracy class determ. *(German)* 77−74364
mass standards, calibration by sets of weights intercomparison 78−54342
mass standards (1000 kg) for electromech. balance testing *(German)* 77−79060
mass unit of 1 kg, secondary standards, stability, USSR 78−4595
materials, USSR reference state service 79−96259
materials testing, COMECON standard reference-data system 80−45469
Measurement Standards Laboratory, capability improvement 78−54332
measuring system for use with Josephson device in maintaining voltage standard 78−93730

measurement standards continued
medical dosimetry standards programme of the National Bureau of Standards, USA, review 80−8187
Megalithic yard at Avebury, geometry and metrology of ring, new accurate survey results 77−33359
melting point standards, secondary, for temp. range 2000-3000°C, chemical aspects of choice 80−52226
metal fixed points, limitations caused by trace impurities 80−105644
meteorology, review 79−21032
meteorology 79−66746
methane triple point sealed cells using stainless steel envelope 80−95099
metre, Canadian standard 79−12768
metre, new definition proposal using 88 THz stabilized He-Ne laser 80−73304
metre, use of methane stabilised He-Ne laser 77−31113
metre as standard length unit *(German)* 77−22528
metrological activity of Gosstandart territorial agencies 79−93092
metrological certification of measurement techniques 79−67243
metrological Cs frequency standard MTs-1, description 77−79063
metrological reliability, standardization 79−80568
metrology standards and measurements laboratory, used by Matsushita Communication Industrial Co. Ltd. *(Japanese)* 80−82738
micromanometer test scheme and standard instruments 77−79049
micromanometers, type-MMN, simplified processing of results 79−35692
microwave hot/cryogenic noise standards, preliminary design 77−82563
microwave meas. advances reviewed 78−57984
microwave noise meas., Japanese national standards, 10 GHz system *(Japanese)* 78−57985
microwave radiation hazard monitors, calibration 80−26374
microwave radiometer calibration standard with Brewster angle impedance matching 77−5918
microwave thermal noise source, temp. of liq. N_2 in cryostat dewars 79−58700
microwave time and frequency standards 80−47026
moisture measurements using NMR, reference materials 79−34403
mole as standard molecular weight unit *(German)* 77−17943
molecular force constants, definition and symbolism 79−49192
monitored parameters for quality control in instrument production 80−186
monochromators for light scatt. and fluoresc. standard in colloid 80−57247
monochrome photographic film densitometry errors and standards *(German)* 80−37102
monoenergetic fast neutron flux density, international intercomparisons *(Japanese)* 78−29521
monoenergetic fast neutron flux density measurements, international comparison 80−83138
Mossbauer isomer shift reference scales, book contrib. 79−87368
motion parameters, measurement by comparison with motion of standard 79−30434
MTF measurement in France, ACOFAM and ACOMAT instruments 78−50727
MTF measurement of standard lenses in Japan, interlaboratory comparison 78−50720
multijunction thermal convectors for AC-DC transfer standards 80−98874
multijunction thermal convertor AC/DC transfer, Thomson effect error reduction 80−103679
National Bureau of Standards, calibration and related measurement services 79−168
national time and frequency standards of Finland 80−47031
NDT, by EM coating thickness meter 77−90561
neutron, intermediate energy, standard field, neutronics anal. 80−27692
neutron activation analysis, 14 MeV, nonidentical samples and standards 79−11858
neutron activation analysis, 14 MeV, screening effect of sample on standard calc. 77−56282
neutron activation analysis, 14 MeV, standards, nonidentical samples, formalism 80−71980
neutron activation analysis, multielement standards 79−57332
neutron beams at NBS reactor, prod. for calibration standards using reson. scatt. and filters 77−38539
neutron capture cross section standards, review, status of Au(n,γ) standard 79−9589
neutron cross section, energy and spectrum standards, status report 77−23017
neutron cross section standards, detection techniques 79−9970
neutron dosimeter and monitoring instrumentation calibration using ^{252}Cf and ^{238}PuBe sources 80−13946
neutron dosimetry, above 10 MeV, standards 79−13544
neutron dosimetry, fast pulse reactor, standardisation 79−13543
neutron dosimetry, international intercomparisons 79−12014
neutron dosimetry, meas. standardisation for biological and biomedical appl. 80−12271
neutron dosimetry, standardization, 0.001-14 MeV, description of sources 79−9919
neutron dosimetry, standardized techniques for appl. beyond reactor core 79−9920
neutron energy standards, accuracy 79−13587
neutron equivalent dose and dose rate units, USSR primary standards 77−32955
neutron personnel dosimetry, need for improved standards 79−12012
neutron production total cross sections, secondary standard detector 77−23381
neutron spectrum field *(Japanese)* 79−9562
neutron standard cross section expts., flux monitor, source, data acquisition and anal. 78−90039
neutron standards and appl., conference, Gaithersburg, MD, USA (March 1977) 79−9581
NGC 3379, elliptical galaxy as luminosity distrib. standard 80−22073
NGC 3532, stellar cluster, UBV photoelectric sequences 77−45502
NISUS facility, sensitivity anal. for secondary intermediate energy standard neutron field 79−36451
noise, Fourier transform as perturbation criterion, appl. to NMR intensity 78−65948
noise, max. acceptable levels in quiet rooms *(German)* 77−68307
noise, OSHA regulation at 29 CFR 1910.95 (b) (1), review 79−14157
noise emission measurements for computer and business equipment 80−53589
noise evaluation of portable air tools 80−23855
noise standard, OSHA regulation, effectiveness 79−14158

measurement standards continued
NPL standard voltage monitoring system based on AC Josephson effect 77−82554
NPL voltage standard based on Weston cells, computer control meas. 77−82572
nuclear fuel standard materials, analytic chemistry of trace impurities, and standard sample preparation 79−26521
nuclear gamma transition energy standard value and accurate determ. *(Czech)* 80−22755
nuclear materials safeguard, role of standard reference materials in achieving measurement traceability 80−78371
nuclear materials safeguarding, measurement standardisation 80−68812
nuclear materials safeguards, prototype, reference materials for nondestructive assay 80−78372
nuclear materials safeguards, reference materials and meas. traceability 80−78370
nuclear materials safeguards and materials control, meas. tech. conf. Charleston, SC, USA (November 1979) 80−77544
nuclear materials safeguards reference measurement system utilizing resonance neutron radiography for nondestructive assay meas. 80−78377
nuclear medicine and metrology of ionising radiations *(French)* 80−17057
ocean dynamics investigation, realisation of four dimensional topographic reference system 78−77176
oceanographic instrumentation, international standards 78−45043
ohm, absolute determ. based on standard capacitors 77−82565
ohm and volt representation, January 1977, France *(French)* 79−26077
optical density, NBS development of inverse fourth power photometric calibrator 80−73412
optical device performance assessment, British standards 78−50729
optical emission and X-ray spectrometry, synthetic calibration standards 79−24850
optical fibre attenuation measurement comparison among USA manufacturers 80−58747
optical frequency, ring laser power resonances shape 77−58355
optical frequency generators, for submillimetre IR, and visible light regions *(French)* 79−40602
optical frequency standard, collision shift and broadening *(Russian)* 79−59783
optical frequency standard, Doppler-free stimulated-emission technique 78−93765
optical frequency standard, highly stable, utilising an atomic beam 79−35685
optical frequency standards, use of lasers *(Chinese)* 79−173
optical measuring instrument standardisation 77−71357
optical radiation power photometry, USSR system of standards 77−30194
optical surface quality standards based on total integrated scatt. 80−48391
opticophysical measurements, metrological provisions 80−8953
OTF standardisation activities in Netherlands 78−50728
OTF standardisation in Japan 78−50726
OTF testing, USA standards 78−50725
Penning discharge as photoelec. UV spectroscopy source 120-300 Å 77−75637
pepperbush powder, a new standard reference material 79−39227
periodic inspection of meas. facilities, probabilistic confidence characteristic selection 78−77839
permittivity reference materials, dm wavelength appl. 79−6143
personnel dosimeter calibration, US NBS standard reference neutron fields 80−9417
personnel dosimeter design and use, physical requirements for dose meas. 80−9424
personnel dosimetry, criteria for testing of performance 80−23169
personnel dosimetry performance, testing standard 80−9421
personnel dosimetry photon calibrations, use of phantom 80−9425
pH meters, laboratory, revised British Standard BS3145 77−70371
phase and frequency instabilities in precision frequency sources, characterisation and mathematical models 79−2750
phenoxybenzene triple point cells, preparation and realization 80−105643
photocell specifications, for USSR state standards of radiation sources 78−45695
photodetector spectral response determ. using calibrated lamp and interference filters 79−71528
photodetector spectral response measurement 79−21812
photometric SI units proposition 78−93644
photometric standard lamp gas flow visualisation using holographic interferometry 79−12835
photometric standards and coatings, retrofefl. meas. 78−25940
photometric working standard establishment using photoreceptors *(Japanese)* 80−98964
photometry and colorimetry, colour matching and adaptation exam., using Japanese observers *(Japanese)* 79−6163
physical measurement and standardisation requirements *(Italian)* 79−93845
physical quantities, unit unification trends 78−41267
platforms, rotational and turning, kinematics 79−30220
pneumatic measuring/calibration system for strain meas. at up to 300°C 78−45610
polarimeter, precision, systematic errors, quartz plates standards *(German)* 78−16832
pollution, trace amounts of toxic substances, meas. techniques and standards 80−26188
pollution monitors, environmental, metrological support, pesticide control 79−21060
polychromatic MTF measurement reproducibility 78−50719
polyethylene, standard reference material, limiting viscosity numbers 79−14952
polyethylene, standard reference material, number average mol. wt. 79−13854
polyethylene, standard reference material, preparation 79−15641
polyethylene, standard reference material, weight average mol. wt. 79−13855
polyperfluoropropylene oxide, mass spectroscopic reference standard appls. 78−89582
portable radiation meters, accuracy checking facility at Berkeley Laboratories, UK 78−74507
portable voltage source, ultrastable 79−67351
potentiometric displacement transducers, standards for specification and tests, book 79−2763

measurement standards continued
powder diffraction data, American Crystallographic Association recommendations *(Czech)* 80−24306
power and energy units reproduction for optical, elec. and mech. quantities 77−71287
power illuminance unit, USSR state standard for continuous spectral radiation in range 0.2 to 4.5 micron 78−89524
power luminance spectral density unit, USSR state standard, 0.05 to 0.25 micron wavelength range, synchrotron radiation principle 79−2819
power luminescence spectral density unit of continium spectral radiation, 0.25 to 2.5 micron, USSR state standard 78−93752
power meas. in mm. wave region 79−26083
precise γ-ray standards 80−36973
precise elec. meas., conf., Brighton, UK (Sep. 1977) 77−82551
precise time dissemination via OMA-50 kHz 80−47032
precision thermostat and capacitor enclose, maintaining the unit of capacitance 80−95063
pressure, intercomparison for oil-operated pressure balances between NPL and LNE 80−98877
pressure, state standard and All Union test scheme, in 2.7×10^2-4000×10^2 Pa 78−73962
pressure balance standard for the pascal SI unit 77−87725
pressure balance standards, international comparison over 1 to 10 MPa range 80−105671
pressure balance standards of NPL and PTB, intercomparison expts. 79−21764
pressure gauges, secondary standard, for measurement up to 1 GPa 80−27289
pressure meas., primary standards comparison, mercury barometer vs. gas-operated pressure balance 80−13090
pressure scale representation by ASMW, Germany *(German)* 77−74348
pressure transducer long-term performance characterisation programme 78−12712
primary Cs atomic clock, time standards and scales generation 78−41283
primary dosimetric standards at the Memorial Sloan-Kettering Cancer Center, NY, USA 80−8190
primary high-pressure standard, USSR 78−49855
PVC, in chlorinated aromatic solvents, mol. wt. characteris., ref. materials, soln. props. 79−7045
pyrometer, low-temp. total radiation, for 50°C to 150°C range 79−30471
quantum freq., output signal sidebands/resonator detuning effects on accuracy 77−87743
quantum frequency standard with pulsed optical pumping of Rb^{87} vapours, performance factor 80−78823
quartz crystal oscillator checking against standard frequencies in LF/VLF ranges 77−74372
quick calibration checks, devices to calibrate commonly used meas. instruments 80−47010
radial-velocity standard stars; list of 200 stars 80−26849
radiance transfer, magnesium fluoride windowed deuterium discharge lamps, 115 nm to 370 nm 80−87451
radiation, test site suitability assessment for radiation measurements 80−82737
radiation calibration, mobile laboratory design 77−38582
radiation dosimetry standardisation, conf., Atlanta, GA, USA, Dec. (1977) 80−4469
radiation energy standards *(Japanese)* 80−62620
radiation irradiance scales intercomparison, 90 to 250 nm wavelength range 80−98963
radiation measurement, calibration program using NPL secondary standard ionisation chamber dosimetry system 77−38584
radiation measurements, for safe use, conf., Gaithersburg, USA (Mar. 1976) 77−40794
radiation protection instrumentation test and calibration 80−9420
radiation sources for USSR state standards, 0.4-10.6 μ range 78−46739
radiation standard, continuous bremsstrahlung emission from inert gas HF discharge 80−1856
radiation standards for source spectral emission and detector spectral sensitivity 77−39007
radiation therapy, calibration and meas. standards in USA 80−8188
radioactive, ^{14}C and ^{3}H, miniature, liquid scintillation counter appl. to colorimetric analysis 80−21346
radioactive pharmaceutical preparations, standardization of control of physical characts. 79−81139
radioactive release monitoring equipment test gas standard production *(French)* 79−3252
radioactive waste management, US NBS proposals for measurement standards 80−102276
radioactivity, American National Standards Institute quality assurance programme 77−38585
radioactivity, environmental standards, USA 77−38431
radioactivity measurements in radiopharmaceutical industry, Atomic Industrial Forum-NBS quality assurance programme 77−40769
radioactivity standards programme of the National Bureau of Standards, USA 80−18700
radioastronomy, flux density meas. of calibration sources at 2295 MHz 77−37663
radioisotope thickness gauge standard sample certification 79−35672
radiological instrumentation calibration by British Calibration Service 80−8186
radioluminescent emitter, continuous action, reference source for stellar simulator 77−10993
radiometric exploration meas. standardisation advantages and methods 78−28325
radiometric transfer standards calibration in UV and VUV by electron synchrotron radiation 79−12847
radiometry, development trends 77−61105
radiometry, far UV standards comparison 77−5912
radiometry and photometry advancements, calibration 79−6161
Ramsey separated oscillatory field method, two-freq. excitation, appl. to freq. standards 78−36974
reactor core dosimetry standards 79−9824
reference material certification 78−41269
reference materials, statistics 78−41268
reference materials for COMECON member countries 80−45468
reference materials for vapour pressure, critical temp. and critical press. meas. 77−71289
reference radiations for radiation protection dose meter calibration *(French)* 80−57998

measurement standards continued
reference ring gauge, precision improvement in meas. internal dia. 79−17388
reference sound sources, charact., and calibration 78−9515
reference standard for internal diameter meas. 78−29090
reference standard US flowmeter error component estimation 77 80248
reference temperature, 0.015 to 0.21K, based on superconducting phase transitions 80−17948
reflectance standards, calibration of 77−53983
reflection coefficient, waveguide standard 77−41644
reflective glass colour standards 80−90878
reflectivity, reference materials 79−49190
refractometric standards, Comecon, selection criteria 79−30531
refractory products, thermal conductivity, determ. standardisation 79−82397
relative dielectric constant, USSR state standard for 0.2-1 GHz range 80−9004
relative dielectric constant for insulators in range 1-10 GHz, State Special Standard 80−13037
remote atomic clocks synchronisation using injection laser diodes 77−82493
remote site timescale intercomparison technology 77−37855
reproducing unit of thermal neutron flux density, standard installation improvement 78−74524
resistive ratio standard, for DC voltage meas. to 10 kV 77−18028
resistive voltage-ratio standard for 10 kV DC meas. 77 -5873
retail equity, NBS Standard Reference Materials 80−86249
retroreflectance measurements, unified coordinate system 80−73408
retroreflectometer, NBS reference 80−73410
review, the measures of man 77−9981
RF frequency standard transmission, phase instability due to effect of ionosphere 78−41279
RF standard magnetic field generator, with loop antenna, freq. charact. improvement 77−26348
RF voltage standard, precision, using thermistor bridge, HF-UHF range 78−89504
RF voltage standard, precision, using thermistor bridge, HF-UHF range 79−21772
RF voltage standard system for voltages from microvolt to 1 V *(Japanese)* 78−89491
rock deformability, determ. by in situ methods 80−17411
Rockwell diamond indenters, meas. method rel. to standards 79−66251
role of metrology in solving national economic problems 79−93091
ruled steel grating system for length meas. 80−13039
Rutherford backscatt. standard for ion beam expts. 80−50496
Rutherford backscattering microanalysis, precision absolute thin film standard reference targets 79−2882
saturated water vapour pressure standardization 80−26596
scintillation counters, use of miniature glass vials in multi-functional standards 77−70370
scintillation counting using polyethylene mini-vials, construction of permanent standards 77−38550
scintillation techniques for calibration light sources 77−71720
Sculptor dwarf galaxy, photoelectric sequence and preliminary colour-magnitude diagram 77−53429
seawater, history of standards development 79−79871
seawater as elec. cond. standard, reliability 79−29779
seawater salinity standard, definition and calc. 78−40687
seawater standard, preparation and chlorinity calibration 79−74898
second as standard time unit *(German)* 77−22534
Secondary Standards Dosimetry Laboratory, review of role 80−5361
SEM magnification standard reissue 80−27375
shielded field coil as mag. induction meas. standard 77−74466
SI system, need for periodic recalibration of laboratory equipment 80−31705
SI system, Swiss legislation *(French)* 80−13032
SI-system, physical standards and units 80−17915
SIMS quantitative evaluation using Saha-Eggert type eqns. 77−60164
socialist economic integration, COMECON standardization 80−42188
solar constants, radiometric scales 77−78737
solar radiation meas., field instrument calibration standard 78−88946
solar radiation measurement requirements for energy conversion 79−57400
solar standards and testing activities in developed and developing countries 80−55819
solid density, liquid density meas., single-pan analytical balances *(German)* 80−52167
solid density measurement, hydrostatic weighing 80−77758
solution of calorimetry, standard substances 77−73462
sorption-gravimetric hygrometer, description 77−87770
sound insulation between buildings, standard procedure 80−96108
sound level meter meas. accuracy 78−59211
sound transmission loss, in noise meas. 77−19486
South African standard SABS 572 1973, meas. real-ear attenuation of hearing protectors 80−53581
southern standard stars, monochromatic flux from 3200 Å to 8800 Å 80−51742
southern standard stars for CMT_1T_2 photometric system 77−37507
Soviet, for linear and angular quantities meas., exhibition survey 80−52161
Soviet-American collaboration 77−87719
special nuclear materials, control and accounting, role of certified reference materials 80−68815
specific heat meas., modulation method with SOTS-2 standard specimen 80−8988
specific heat of solids, 4.2 to 90K, USSR special standard 77−31207
specific heat of solids, 90 to 273.15K, USSR special standard 77−31206
specific heat standards choice and certification, for liquids and vapours in 90 to 273.15K range 80−23877
spectral analysis, correlation of signals, internal standardisation 80−55749
spectral energy standard, for stellar absolute spectrophotometry *(Russian)* 79−44372
spectral irradiance scale, 1973 NBS standard 77−83942
spectral irradiance scales, international comparison 77−106
spectral luminous efficacy maximum, definition *(German)* 78−54333
spectral radiance, Ar mini-arc as secondary standard 77−34921
spectral reflectance, of ore minerals, establishment of international standards *(French)* 79−5627
spectral transmission and reflection coeffs., USSR special standard 77−30195

measurement standards continued
spectrochemical anal., line pair intensity ratio stability, internal standard variability 79−39247
spectrochemical analysis, standard samples, metrology *(Russian)* 77−70380
spectrochemical analysis, standards, for instrumental methods 77−70346
spectrochemical analysis of metallurgical substances, standard specimens, review 78−7273
spectrometric source conversion peak half-width determ. 77−79499
spectrophotometer, photometric scale calibration using fluorite 1200-800 cm^{-1} transmission 79−12837
spectrophotometric standard transmission materials, use in visible and UV 77−53989
spectrophotometric standards, glass filter SRM 930 by NBS, clinical laboratory appl. 78−54331
spectrophotometry, accuracy, linearity and Beer's law 77−38015
spectrophotometry, semi-transparent metallic thin films as transmittance standards 77−53991
spectrophotometry, UV absorpt. and fluoresc., practical standards 77−49783
spectrophotometry and luminescence meas., conf., Gaithersburg, USA (Nov. 1975) 78−32846
spectrophotometry standardisation to ensure original calibration 77−38020
spectroscopic reference frequencies in OCS 9.5 μm band, heterodyne freq. meas. 80−18850
specular gloss of paint, calibration of reference standards 80−95061
specular reflection coefficient comparison, sample materials 79−71512
specular reflectometer-spectrophotometer, NBS reference, mirror refl. meas. 80−68236
specular sphere scatt. radiance matrix, refl. standard for polarised beam scatt. meas. 80−74299
stable frequency standards comparison by TV carrier beat note transmission 78−57909
stable isotope abundances in natural compounds, meas. standards 78−32246
standard cell, combination type, composite amalgam electrodes, low temp. coeff. 77−18026
standard cell, temp. controlled enclosure with 25 μK stability 77−18027
standard cell calibration, using supercond. junction device 77−18029
standard cell calibration against Josephson voltage reference 77−5874
standard cell EMF stability testing, thin-film tunnel Josephson function method 77−67468
standard cells with low temp. coeff., characts. 80−101090
standard gas mixtures at high pressures 78−93718
standard neutron fields, integral meas. 79−13363
standard sound sources, sound isolation tests of residential buildings, correlation with subjective privacy opinions 80−64323
standard time/freq. service in East Germany *(German)* 78−93658
standards room, in factory air-raid bunker, general description 78−93646
standing-wave tube, use as an absolute sound power source in reverberation chambers 79−81674
stars, Harvard magnitude scale 77−71109
stars, UBV photoelectric magnitude sequence for AA Aurigae 77−74073
stars, zero polarisation standards list 79−40187
stars defining new two-colour photometric system for near IR, obs. 79−62759
stars in Magellanic Clouds, photoelectric (B, V) magnitude sequences 77−53592
stars of intermediate brightness, spectral energy distribs. 78−28651
stars within 25 pc of Sun as polarimetric standards, polarisation obs. 78−12202
stellar absolute luminosity calibrations, consistency 80−62111
stellar BVRI photometry, secondary standards 79−70962
stellar photoelectric UBV sequences, in fields of eight low-red shift quasars *(French)* 80−51904
stellar photometry, new UBV photoelectric sequences in Puppis (l=250°, b=0°) 77−45426
stellar photometry, secondary standards spectrophotometric obs. rel. to Ap stars HD 10783 and CU Virginis 80−98663
stellar photometry, UBV standards *(Polish)* 78−89082
stellar photometry, UBVR sequences around globular clusters (NGC 5946, 6440 and 6624) 79−88702
stellar secondary spectrophotometric standards, obs. in 5840-10800 Å range 79−29995
stellar spectra, Fe lines equivalent widths in cool standard stars for spectral anal. 77−78771
stellar spectral energy distribution in 3500 to 7500 Å region, absolute calibration 80−67710
stellar spectrophotometric standards, spectral energy distrib. determ. of eight stars 79−35147
stellar spectrophotometric standards calibration against α Lyrae 79−62760
stellar spectrophotometry, secondary flux standards 77−9737
stellar standard sequence in Coma cluster of galaxies 78−93436
strain gauge transducers in testing machine and as force standards 80−42215
streamflow, max. expectation levels, standards improvement 78−7674
stretched wires as standards of straightness *(German)* 80−36976
Sub-microsecond intercontinental time comparisons by satellite 77−82494
substrate uniformity, Kr vapour press. isotherms at 77K as standardized meas. 80−107657
superconducting critical current standard 77−28322
superconducting resonators, high stability oscillators, appl. to fundamental physics, metrology 79−26034
superconductive device to provide reference temps. below 0.5K 79−63220
superconductive fixed points for temperatures above 0.5K 79−63221
superconductor, techniques for determination of props. 79−69622
surface characterisation, state-of-the art and need for standards 78−38916
surface profile monitors for thin film thickness meas., calibration standards 80−17918
surface roughness, rel. to size tolerance 80−62634
surface roughness, standards and methods *(German)* 79−17398
surface roughness parameters meas., Soviet development, All-Union test scheme 80−22328
surface roughness standards for calibrating stylus tip instrums. *(German)* 80−101782
measurement standards continued
surface tables, maintenance, positioning, and possible sources of error 78−93651
surface transportation vehicles, sound meas. standards 80−14531
Swedish measurements establishment for time and freq. standards *(Swedish)* 79−75503
synchrotron orbit radiation characts. in visible spectrum, rel. to use as radiometric standard 78−9008
synchrotron radiation as an absolute standard source for radiometry 80−90879
system dynamic properties and standard-size series grouping 77−79046
technique, congress, Moscow (1979) *(German)* 80−36964
TEM cell for electromag. interference investigations, large 80−238
temperature, lamps with W ribbon filaments 80−95102
temperature calibration standard, melting point of pure Ga 77−41611
temperature reference standard for use below 0.5K, SRM 768 80−27303
temperature scale, 10000 to 15000K, construction using plasma spectral density measurements 79−30470
temperature-calibrated W filament lamp, characts. 78−218
temperature-stabilised enclosure for 54 standard cells 77−5872
temperatures, triple points of Kr, Ar, N_2 and Ne 78−73997
tensile force measurement instruments developed as first order reference standards *(German)* 80−105635
terrestrial solar spectral irradiance distrib. variations, sensitivity of solar transmittance, reflectance and absorptance 80−82739
test gas atmospheres, calibration standards, generated by gas phase titration 78−69507
thermal conductivity, use of graphite as standard reference material 79−27496
thermal conductivity and expansion, appl. of fluorite 80−96704
thermal conductivity of solids, 60 to 300K, USSR special standard 77−31205
thermal expansion coeff. of steel gauge blocks *(German)* 80−68171
thermal expansion reference data: 1-1000K 80−96669
thermal neutron flux density, working standard based on F-1 reactor 78−82410
thermal neutron standard field with Maxwellian distrib. using KUR heavy water facility 78−33342
thermo-optical measurements at six European laboratories compared *(French)* 78−29107
thermocouple calibrations, comparison, fixed point and melting wire methods 80−86252
thermocouple reference tables, standard, polynomial representation 77−74402
thermocouple reference tables, standard, polynomial representations, report 78−81973
thermocouples, IR thermometers and optical pyrometers, calibration 79−85141
thermocouples and meas. line inspection, using computer-controlled capacitor discharging method *(German)* 80−13079
thermocouples and resistance thermometers, testing GDR standards *(German)* 80−90842
thermodynamic standards for single substances and mixtures 78−14481
thermodynamic temperature in range 0 to 1064°C, International Practical Temperature Scale revision 80−62669
thermoelectric power, absolute scale 77−71288
thermoelectricity, absolute scale between 10 and 350K, meas. on Pb 77−28162
thermoelectrode wire classification standard samples 77−5865
thermometric reference materials, purification and certification 77−67436
thermometry, N_2 α-β transition applicability 80−13076
thermometry, review 80−86305
thermophysical properties, conf., Dubrovnik, Yugoslavia (June 1978) 80−51944
thermophysical properties, standardisation of meas. methods 80−52197
thin film permittivity standard certification 77−74444
thread gauges standardisation, w.r.t. inner-pitch error 77−79053
three-layer dielectric reflectivity standard error analysis 77−79727
time, electrically tuned far infrared lasers appl. 78−174
time, freq. and physical measurement, unified standard 79−26038
time, South African measuring standard, national and international role 80−36971
time and freq. meas., users' manual 80−94934
time and freq. transmission, OMA 50 kHz Czechoslovak station *(Czech)* 79−30425
time and frequency, conf., Helsinki, Finland (Aug. 1978) 80−46728
time and frequency, establishing common scale for COMECON member countries 80−42200
time and frequency errors in long-distance comparisons 80−95062
time and frequency meas. standard signals and applications *(German)* 77−71301
time measurement, errors, accuracy of watches and clocks, time standard 80−90821
time scale generation by international organizations 80−47028
time signals transmission times meas., dynamics of seasonal variations obs., in SW and VLW ranges 77−79061
time standard, precision and application *(Japanese)* 78−41282
time standard differences and celestial mechanics *(Italian)* 78−93087
time-freq. secondary standard comparison, based on LF/VLF radio link synchronisation 77−87737
time-freq. secondary standards, VLF radio station phase reception/processing convertor 77−87739
time-freq. secondary standards automatic recording/processing system 77−87738
timing systems, electonically based 79−85129
titrimeters, reference materials for metrological certification using chromatometric reactions 79−34402
TLD, calibration procedures in the Studsvik standardized personnel dosimetry system, Sweden 80−9418
TLD, dose intercomparison for orthovoltage X-ray therapy 80−12272
total luminous flux scale using precision goniophotometer 80−42250
trace analysis standard reference materials, suppliers 79−49191
trace element standards, for neutron activation anal., prod. by doping of SiO_2 matrix 78−7289
transducers, alternating-voltage, analogue, checking and calibration methods in USSR 80−98872
transfer standard radiometric sources and detectors, calibration using synchrotron radiation 78−65967
transmission spectrophotometry, standardisation in UV and visible regions 78−32850

measurement standards continued
transmittance standards in spectrophotometry, semi-transparent metallic thin films use 78−32852
transportable 1000 pF capacitance standard 77−5870
tribometry metrological provisions, Soviet installations and instruments development 80−23974
triple points cells, Ar, O_2, comparison 78−73996
triple-point cell, diphenyl ether, for calibration of thermometers and thermistors 79−21750
tris(hyroxymethyl)aminomethane, water solution calorimeter, determination of energy equivalent 78−23961
UBVRI standard stars, faint, photometric obs. 80−51813
ultraviolet radiation standards and meas. for health and safety 78−74056
underwater sound pressure unit, 0.01 to 1 Hz, USSR state standard 78−38160
uniform colour scales, space lattice used to sample colour space 79−26100
unit mag. moment primary USSR state standard 79−2753
unit of specific heat of solids, 1800-2800K, USSR 78−12665
unit power standard for 53.57 to 78.33 GHz 80−90808
units of physical quantities, standard for unification within COMECON framework 80−42187
US Naval Observatory clock time scale 78−89460
US reference block calibration procedures 77−62126
US thickness gauges calibration, thickness standards 79−35669
US transducer characterization standards, tissue equivalent testing for hospital use 79−29651
USA National Bureau of Standards reactor utilisation 79−9693
USSR acoustic noise metrological improvement 78−42502
USSR All-Union State Standard for linear and angular meas. 77−17946
USSR and E.German time scale comparison by transportable atomic clocks and TV signals 77−79067
USSR flowmeter testing aggregate as basis for single metrological testing system 79−94752
USSR physical-standards base, development 79−93093
USSR reference data for metrological services on physical constants and material props. 79−97340
USSR State Bureau of Standards, metrological resource programmes 80−90809
USSR State Standard of time and frequency 77−79062
USSR state testing of measuring equipment 79−93125
USSR state time and frequency standards *(Russian)* 78−161
USSR State Time and Frequency System data collection and processing automation 77−79074
USSR time and freq. state service 79−93103
Utrecht photometric system and adopted standard stars 80−62202
UV, at Australian Nat. Meas. Lab. 80−31704
UV absorbance standards, $K_2Cr_2O_7$ in perchloric acid soln. 78−32851
UV absorbance standards using $K_2Cr_2O_7$ acid solns. 77−53990
UV and VUV high-temp. luminance standard, plasma source 80−19084
UV and X-ray spectroscopy, synchrotron radiation as intensity reference 79−75619
UV measurement, accurate techniques 80−47103
UV radiation standard sources *(French)* 77−61142
UV radiometric standards, gas discharges, plasma diagnostics appls. 80−47088
UV radiometric standards 79−49193
UV radiometric standards at NBS 77−38011
UV range assessment of artificial sources, for best fit to D65 standard 77−58407
UV spectral radiance calibration using H_2 plasma *(French)* 78−12774
UV spectrophotometry, $K_2Cr_2O_7$ in H_2SO_4, nicotinic acid in HCl as standards 77−77819
vacuum, interferometric oil micromanometers 79−88970
vacuum press. meas. considerations *(French)* 78−49846
vacuum standardisation international 77−87774
vacuum standards intercomparison, 8×10^{-5}-8×10^{-2} Pa 80−86333
vacuum UV Cherenkov source as radiation standard *(Russian)* 78−63164
vacuum UV energy brightness spectral standard source, 0.05-0.25 μm range 77−79909
vacuum UV radiation scales, plasma blackbody lines and synchrotron radiation 78−1309
vacuum UV radiation scales 77−30124
VLBI, improvement of freq. stability of local oscillators *(Japanese)* 80−17504
volt, by BIPM since 1932 77−82566
volt dissemination method and standard cell enclosure design 80−98876
volt realization, method and equipment based on fundamental physical consts. and superconductivity phenomenon 80−98943
voltage, comparison with working standards, Josephson effect 77−53941
voltage, cryogenic comparator for Josephson standard 77−18030
voltage, inverse AC Josephson effect standard 78−16808
voltage, Josephson effect appls. 77−20503
voltage, Josephson-effect, at zero current bias 80−57245
voltage, Pb-Pb_xO_y-Pb Josephson junction stability at liq. N_2 temp. 77−72945
voltage, portable transfer standard digital voltmeter SM 215 78−41325
voltage, realization by means of Josephson effect *(German)* 79−71401
voltage, reference, on signal generators, testing with B3-24 compensation valve voltmeter *(German)* 79−54155
voltage, standard cell group enclosure monitored by AC Josephson effect 79−26076
voltage cell using Josephson junction, computer simulation 79−93089
voltage reference cct. with adjustable temp. coeff. 79−30407
voltage reference system description of system and principles *(French)* 77−67470
voltage standards, using Si reference diodes 80−62619
voltage standards for testing AC voltage calibrators 79−35786
voltage transfer standard based on AC Josephson effect, standard cell calibration appl. 77−82553
voltage transfer standard SDET01, battery powered instrum., specification and appls. *(French)* 78−236
voltage using Josephson effect *(German)* 78−93722
VUV light source, transfer standard, low-current AR arc with MgF_2 window 79−35856
Washington Photometric System, props. and standard stars 80−31213
wattmeter calibration, (3+3)-phase voltage and current source of high stability 77−18038
waveguide impedance meter verification scheme 78−37035
waveguide wattmeters, ponderomotive and bolometric types, comparison 77−71345
wavelength meas., use of He-Ne laser, with Ne or iodine cell 77−7124
weighbridge and heavy-goods weighing machines, changes in standards 79−6096
weighing, balances accuracy class increase, using several standard weights of equivalent mass *(Rumanian)* 80−47022
weights and measures, conference, Washington (1978) 80−27260
West German nuclear power plant airborne radioactive release control 79 13549
X-band frequency standard, high Q cavity resonator *(Polish)* 77−26342
X-ray absorbed dose unit, 1 to 5 J/kg, USSR special standard 77−32956
X-ray and γ-ray spectra, National Bureau of Standards (USA) 80−90807
X-ray fluorescence, analysis, energy-dispersive, external reference signal 77−21433
X-ray fluorescence spectrometry with incoherent scattered radiation as internal standard trace elements determ. 80−11970
X-ray fluorescence thin film calibration standards 80−22496
X-ray powder diffr. anal., reference intensity ratios determ. methods, errors 77−70385
X-ray powder diffractometer, APD3600, file searching techniques 80−24319
X-ray sources, monoenergetic, development and appl. 77−38078
n absorpt. power and equivalent dose 80−102351
Ag beam mag. resonance apparatus as freq. standard, features 78−89458
Ag, development of standard specimen 77−90680
Ag-beam mag. resonance apparatus as freq. standard, features 79−21712
α-Al_2O_3, synthetic sapphire, enthalpy determ., 900-1900K, use as calorimetry reference standard 79−42275
$Al_2O_3:Cr^{3+}$, standard reference material for EPR 79−12757
^{241}Am-Be thermal neutron flux standard density variation obs. 77−83409
Ar arc, new cathode shape for UV spectral radiance transfer standard *(French)* 80−38082
Ar plasma, wall stabilised arc, spectroscopic temp. and radiation standard 77−76199
Ar triple point sealed cells using stainless steel envelope 80−95099
Au films, thickness meas. standards for Rutherford backscatt. 79−40529
^{198}Au, redetermination of γ-ray standards between 0.1 and 1.0 MeV 78−37472
$BaSO_4$, pressed powder Eastman White reflectance standard, absolute refl. meas. 78−25939
$BaSO_4$ white reflectance standard, Kubelka-Munk optical props. 77−42581
$BaSO_4$ white reflectance standard, Kubelka-Munk optical props. 78−4675
C, natural, total and elastic scatt. cross sections for neutron energy <5 MeV, 8.5-15 MeV, use as standard 79−9588
C with Au and Al implants, Rutherford backscatt. standard 80−50496
CH_4 triplet point temp. meas. at 90.6861K 79−26060
CO, and isotopic forms, fundamental bands, absolute wavenumbers, mol. consts. 79−59458
CO_2, freq. stabilised laser with OsO_4 absorber, output freq. reproducibility 78−50800
CO_2 laser transition absolute freqs. by multiplication of difference-freqs. 78−90445
CO_2 laser transitions, absolute freq. meas. by multiplication of CO_2 difference freq. 80−105618
CO_2 laser wavelength standards 77−17945
Ca 657.3 nm line saturated absorption spectroscopy, photon-recoil component resolution 80−86457
Cd-Sn-Pb composite amalgam electrode standard cells and combinations 77−5871
^{141}Ce standard, measured by dose calibrators, simulated $^{99}Tc^m$ standard 78−61261
^{56}Co, relative intensities of γ-transitions meas. 79−97930
^{60}Co external source on liq. scintillation system for ^{32}P Cherenkov effect detect. efficiency meas. 78−25387
^{60}Co radiation therapy, eval. of dosimetric accuracy and uniformity 80−12269
Cs atomic time standard data combination 77−5814
Cs beam atomic freq. standards, Millman effect on freq. shift 78−32797
Cs beam deflection system for time and freq. primary standard 78−89453
Cs beam freq. standard, servo-control system anal. 80−42201
Cs beam freq. standard research at PTB, beam optics, Majorana transitions 79−21709
Cs beam freq. standards, freq. offset due to spectral impurities 78−89455
Cs beam freq. standards, freq. offset due to spectral impurities 79−21710
Cs beam frequency standard, frequency stability *(Japanese)* 77−108
Cs beam frequency standards, quadrupole and hexapole magnet combination 77−5813
Cs beam frequency standard errors due to excitation asymmetries 77−5816
Cs beam frequency standard design for satellites 78−57911
Cs beam frequency standard drift and noise performance rel. to velocity distributions 78−57912
Cs beam standard, Ramsey cavity and beam optics design, expt. 78−89456
Cs beam standard at Radio Research Lab., Japan 79−21714
Cs beam time/freq. standard, future prospects 77−74371
Cs clock, laser synchronisation between observatories of Paris and San Fernando *(French)* 78−89461
Cs freq. standard, angular distribution of atomic flux diffusing from rectangular channels 77−87744
Cs freq. standard, error due to second order Doppler shift 77−87745
Cs freq. standard, time scale unit duration estimation 77−74368
Cs frequency standard, construction of improved system (NRLM-II) 78−45599
Cs frequency standard, NRLM-I, improvement of freq. stability 78−62184
Cs long beam primary clock, accuracy, reliability 78−89454
Cs maser freq. standard, stability determ. method 77−83842

measurement standards continued
Cs primary freq. standard, mag. shielding case for screening terrestrial mag. field *(Japanese)* 77−22582
Cs primary frequency standard, recent progress of PTB 77−17942
Cs primary standard, limitations in operation 77−17951
Cs primary standard, TAI freq. estimation 77−17952
Cs primary standard operation limitations 77−5812
Cs standard frequency line, for receiver-controlled references 79−6099
Cs time/freq. standard of PTB, charcts. 77−74369
CsV clock, long-beam, primary standard, continuous operation, concept 79−21711
CsV frequency standard, operation as primary clock 77−107
CsV primary clock performance of NRC 77−74370
^{134}Cs, 1977 AECL 78−25371
^{137}Cs standardisation by 4π(PC)-γ efficiency tracing method 79−13577
Cu II spectral lines, vacuum UV wavelength standards 77−82619
Cu, thermal expansion, 300-700K 78−43152
D_2 lamp, spectral irradiance standard for UV, calibration 78−42397
D_2O laser phase locking to freq. standard, CO_2-OsO_4 laser freq. meas. 80−95080
^{56}Fe(n, p), 14-19 MeV, cross section meas., neutron flux, secondary standard 79−13291
Ga melting-point standard, near 30°C, clinical chemistry appl. 78−80997
Ge single cryst. prism, refr. index meas., interlaboratory comparison 78−54443
H bulk standards, appl. to calibration of ion beam surface anal. 80−7884
H frequency standard undisturbed transition evaluation 77−79066
H high power arc, standard source of continuum radiation, 53-92 nm 80−44054
H high-power arc as continuum radiation standard source, 53 to 92 nm, VUV radiometry 79−94311
H maser, atomic resonance effects on long-term freq. stability 77−75465
H maser freq. standard, time-dependent freq. shift obs. 78−89457
H profiling in Si, calibration standard, from anal. of H profiling methods using ion beams 79−5197
H time and frequency standards with redundancy 77−79065
H_2 maser, time-dependent freq. shifts obs. 79−21713
H_2O, vapour pressure meas. at triple point 77−43338
^{3}H in water, low-level meas., inter-laboratory comparison 78−44888
He vapour pressure scale determ. using paramag. salt thermometer and NPL-75 gas thermometer scale 80−95060
He-Ne, freq. stabilised, use as freq. and length standards *(French)* 79−31935
He-Ne complex resonator laser, stabilisation 78−55374
He-Ne laser, $^{127}I_2$ stabilised, length or freq. standard 80−106544
He-Ne laser, methane-stabilized at 88 THz 80−73304
He-Ne laser, optical freq. standard, freq. stabilised by warm walled I_2 cell *(French)* 78−42343
He-Ne laser, stabilised by $^{127}I_2$ saturated absorpt., wavelength international comparisons 80−95872
He-Ne laser freq. determ., interferometric comparison with upconverted CO_2 laser radiation 78−55395
He-Ne laser IR applications 79−94275
He-Ne laser reference IR frequency meas. installation 77−79068
He-Ne laser stabilised by methane E-component saturated absorpt., quantum freq. standard 80−9901
He-Ne laser stabilised by methane E-component, reference source freq. reproducibility 80−106507
He-Ne laser wavelength stabilisation on I_2 *(Czech)* 78−87061
He-Ne laser with methane absorpt. cell, hyperfine struct. influence on freq. reproducibility 78−50864
He-Ne lasers, freq. stabilised by ref. to I and methane absorption transitions 77−83913
He-Ne lasers, standard wavelength sources 78−74957
He-Ne ring laser, freq. shift of 3.39 μm methane transition 79−27298
Hg melting point at 0°C at high press. 77−37903
Hg-melting pressure scale determ. at temp. below 0°C 79−12813
$HgCo(NCS)_4$ calibration standard, low temp. molar mag. suscepts. meas. 78−65947
^{198}Hg electrodeless lamp, Ar lines 531 to 561 nm 78−42396
I_2, absolute absorption spectrum measured by Fourier transform spectroscopy 79−75622
I_2, absorpt. spectrum, visible region, wavenumber meas. by Fourier transform spectroscopy *(French)* 77−57407
IR frequency for diode-laser spectroscopy, using NH_3 78−5230
^{115m}In specific activity determination, for nuclear accident dosimetry 79−3248
^{192}Ir, redetermination of γ-ray standards between 0.1 and 1.0 MeV 78−37472
KCl, water solution calorimeter, determination of energy equivalent 78−23961
$K_2Cr_2O_7$, acidic soln., UV absorbance standard verification 78−21092
^{85}Kr, laboratory calibration standards preparation *(Czech)* 79−6782
^{6}Li(n,α)^{3}H reaction, as standard in neutron flux meas., instruments review 79−9969
Mo, standard ref. material, enthalpy and heat capacity 78−18792
Mo, temperature standard reference material, USA National Bureau of Standards 80−47009
N_3^-, 2 eV resonance as energy standard in low energy electron scatt. 77−71872
^{14}N NMR chemical shift, external neat nitromethane scale 78−24834
^{14}N(n,γ), γ-ray energies, calibration standards 80−52613
^{15}N NMR chem. shift references evaluation 78−24835
$^{15}NH_3$ frequency standard, 22.79 GHz, feasibility study 79−71418
NaCl high press. standard, eqn. of state to 32 kbar and 500°C, length change meas. 80−70361
^{237}Np(n,f), fission cross sections, use as standards in MeV region 79−13362
O_3 calibration methods, accuracy 78−69506
O_3 calibration using UV photometer 78−69505
O_3, reference methods, international comparative programme 79−88038
^{16}O standards, precision absolute thin film standard reference targets for nuclear reaction microanal. 79−2880
^{17}O, precision absolute thin film standard reference targets for nuclear reaction microanal. 79−2881
^{18}O, precision absolute thin film standard reference targets for nuclear reaction microanal. 79−2881
Pt resistance standard low-temp. thermometer checking methods 78−37006
Pt-alloy thermocouples, reference-standard testing apparatus 80−13077
^{195}Pt NMR shifts, referencing convention 79−33547
Rb atomic frequency standard, optical pumping phenomenon and techniques, review 77−65022
Rb frequency standard, Rb lamp stability and reliability factors, expt. 77−17955
Rb optically pumped at. beam clock, theory 77−34866
Rb, portable clock for transcontinental and intercontinental time comparison 78−57908
Rb portable clock transcontinental/intercontinental comparison 78−54345
Rb time standards, study review *(French)* 79−174
^{87}Rb, freq. displacement meas. by passing pumping light through ^{85}Rb filter cell 77−41702
^{87}Rb optically pumped freq. standard, buffer mixtures for gas cell 78−82938
^{87}Rb resonant frequency change, due to spectral profile of pumping light 78−45590
S powdered pressings proposed near IR reflectance standard 78−90464
Si microdot standards, ion implanted, SIMS anal., detection limits 79−39264
Si photodetector, shallow junction type, internal quantum efficiency meas. model fits, visible quantum yield 80−267
Si photodiode internal quantum efficiency basis for absolute radiometric standard 80−86410
SiO_2 gel, meso-porous, SCI/IUPAC/NPL surface area standard, pore meas. 77−4941
^{170}Tm, precise γ-ray energies from radioactive decay 79−45525
U, emission spectrum, visible region, wavenumber meas. by Fourier transform spectroscopy *(French)* 77−57407
U II, oscillator strengths for calibration 77−42280
$UO_2(NO_3)_2$, establishing traceability to standard reference material 79−81052
$UO_2(NO_3)_2$, preparation of uranium nitrate standards for X-ray fluoresc. anal. 79−81053
U_3O_8 enrichment standards, gamma-ray spectra 80−78378
^{235}U(n,f) fission cross section standard, propagation of uncertainties, critical benchmark meas. 79−13361
^{238}U(n,f), fission cross sections, use as standards in MeV region 79−13362
W incandescent lamp, thermostatic control 79−36970
W, Kα_1 X-ray line wavelength determ. 79−41132
W, Standard Reference Materials, electrical resist. and thermal props. at high temps. 78−89427
W, thermal conductivity and elec. resist., 4-3000K 77−45820
X-ray dosimetry, intercomparison and standardisation 80−12270
Xe I, 147 nm resonance line, wavelength stability 77−17948
Y_2O_3, secondary ref. stand., MP 77−45821
Y_2O_3, secondary standard investigation *(French)* 78−41271
^{169}Yb, precise γ-ray energies from radioactive decay 79−45525
Zr, standard cylindrical calibration sample for long wavelength neutron scatt. meas., proposal 78−29722

measurement systems
air quality meas. system design and operation 77−78414
analogue versus digital measuring instruments *(Italian)* 80−37015
analogue-digital measurement systems, errors in derivative determ. 79−80567
attenuation measurement, swept-frequency technique for attenuator calibration 77−18021
automated, general purpose, based on synchronous waveform digitisation under computer control, applications *(Portuguese)* 80−82753
automated dielec. meas., microwave, using resonance substitution techniques 77−82573
automated multichannel data and meas. system type MIIS-1, for transducer data 79−2754
automatic capacity/dissipation meas. device for LV/HV capacitors *(German)* 77−74459
automatic centring system for bubble chamber film measuring and premeasuring tables 77−83455
automatic differential variometer type equipment feasibility and preliminary design for big structure displacements remote measurements *(Italian)* 80−62623
automatic error correction methods 79−80566
automatic for optical fibre for total loss spectra precision meas. 80−64169
automatic gas/gaseous mixture thermal cond. analyser *(Spanish)* 78−76972
automatic measuring-limit selecting devices in multi-channel systems 79−71397
automatic power-spectrum density meter for pulsed laser beam 78−45698
automatic sun sighting system, for incident solar radiation meas. *(Italian)* 77−22062
bidirection laser rod gauge, development program *(Chinese)* 79−64239
capacitance-voltage profiling tech. 78−38749
capacitance/inductance measuring device 77−30186
centrifugal-pendulum system parameters selection *(Russian)* 79−97364
cine objectives quality evaluation, frequency transfer function *(Russian)* 77−41718
complex meas. system error correlation matrix *(Russian)* 77−9979
complex permittivity, real part meas. apparatus *(German)* 79−67338
contact resistance analyser system 79−99605
contactless precision micrometer using optical interferometer with capacitance frequency analogue *(German)* 77−30126
contactless speed meas., laser Doppler difference system *(German)* 77−17957
control of mechanical guides displacement, using speckle interferometry *(Czech)* 80−31852
coordinate measuring technique for plane, prismatic workpieces, computerised, mating simulation *(German)* 78−77846
Corning Model 135 pH/ion meter 79−100464
data processing system vector optimization 78−41289
design, systematic 80−95094
DIA analogue processing system *(Russian)* 77−12849
dielectric properties of solid and liquid dielectrics meas. automatic solid/liquid dielec. props. meas. set *(Polish)* 78−32836
differential digital radioisotope system for absorbent surface thickness meas. *(Polish)* 77−53860
diode forward slope resistance, small resist. value meas. cct. 77−37941

measurement systems continued
distributed parameters' correlation effect on meas. system output *(Russian)* 77−9980
disturbed, estimation of signal parameters, autoregressive linear models *(German)* 80−68165
dragline bucket angular inclination system *(Russian)* 80−22325
dust measurement 79−39331
dynamic properties and standard-size series grouping 77−79046
dynamics of meas., rel. to system and information theory 78−8377
ECG signal shape parameter automatic meas. *(Russian)* 79−25134
electronic, systematic error anal. *(Polish)* 79−88902
electronic measurements, book 80−31805
electronic measuring instruments, recent developments *(Japanese)* 78−77895
electronic system for ferroelectric thin film hysteresis, investigation 78−89496
error charact. improvements, using microprocessors *(German)* 78−24773
errors reduction, using microprocessors *(Czech)* 78−8398
evaporation rate monitor with quartz sensor 79−28921
ferrite materials and components, laboratory meas. automation *(Polish)* 80−101789
flow meter for liquids *(Spanish)* 80−6181
fluidic, principles and appls. *(German)* 77−53886
fluidic frequency-analogue measurement system for extreme conditions *(German)* 79−97396
frequency-fluctuation charact. 80−22333
gas turbine rotor vibration contactless system *(Russian)* 80−8982
heat exchanger measurement systems, one and two loop measurement systems *(Hungarian)* 80−31702
HF random process statistical characteristics meas. 77−18045
history from ancient to SI *(Norwegian)* 77−33972
hole position measurement, optoelectronic alignment technique 78−93650
holography, significance in measuring techniques *(German)* 78−90395
human step length measurement apparatus 80−67271
incoherent electro-optical, with arbitrary stops and misfocusing *(German)* 78−1366
industrial, thermography appl. *(German)* 80−13072
industrial plant and machines, radioactive tracer techniques *(German)* 77−70522
Information Measuring System error computation considering communication channel charact. 78−73957
information theory, construction using concept of entropy 79−93088
information-meas. system accuracy, influence of residual voltages 78−77828
insolation meas., Si-cell based sunstation system 79−5582
instrumentation techniques 78−8391
interference coordinate, of photogrammetric automaton 'Zenit', program-control module *(Russian)* 78−21103
interferometric profile scanning, automatic, contactless *(German)* 77−87729
ionising radiation metrological work automation 77−75033
isochronous cyclotron mag. field automatic meas. system 78−82547
LAMBDA laser distance and thickness meas. system *(German)* 78−32792
laser, multichannel device structure and testing, for pulsed energies *(German)* 80−95933
laser energy meas., pulsed 79−27301
laser picosecond pulse meas., Nd:YAG mode-locked laser 77−19271
light beam oscillographs, construction and performance *(German)* 79−93119
magnetoresistance and Hall EMF meas., of low-resistance materials, using AM method 80−52278
measuring instruments as tools of knowledge and control, book 80−41968
microwave Q-factor meas. system 78−54396
molten salt density meas., automated float method 78−12674
multi-point, transducer average meas. time reduction anal. *(Russian)* 78−159
multichannel biotelemetry, quality criteria 77−48887
multichannel system, MIK-48, for laser pulse energy meas. 79−17497
multiple electrochemical analyser for flowing liquids and gases, features *(German)* 78−27846
multiple measuring systems 79−26049
NBS automatic pulse measurement system, present capabilities 77−18018
nondestructive evaluation transducer figure of merit 77−27457
nucleonic and other meas. methods compared 77−38594
optical fibre impulse response measurement system time domain technique 77−19406
oscillating ball device measures ultra low flows 80−6171
oscilloscopes, multimeters, function generators and frequency counters, technology trends *(German)* 79−71437
ozone analysers, for industrial plant monitoring and control *(Japanese)* 78−57308
parallel-connected transducer systems, integral parameters determ. 77−17939
penetration depth, automatic measurement by 8 bit microprocessor device *(French)* 79−28440
permanent magnets in instruments with partially closed mag. ccts., meas. errors *(Russian)* 77−67480
pneumatic measuring/calibration system for strain meas. at up to 300°C 78−45610
porosimeter−volumetric apparatus *(Hungarian)* 79−40531
precisional requirements, on scientific instruments *(German)* 78−90535
Pseudemys scripta hemibladder $^{36}Cl^-$ transport meas. system 79−96529
pulse counter, high-speed DC coupled, sensitivity and performance 79−89524
pulse counting measurement systems, optimum parameters determ. 79−89523
pyranometer for total hourly horizontal solar radiation data, USA 77−25765
radio-controlled meas. system for oceanographic research in shallow water 78−77354
ratio/detection system, flexible, for comparing DC voltage developed by AC Josephson effect 79−21774
recorder waveform distortion anal. due to recording and playback speed instability 78−73981
reliability, activities at National Institute for Metrology (INMB), Bucharest *(Rumanian)* 79−40522
reverberation time meas. using digital freq. analyser 77−80033
rotary-vane attenuator, automatic calibration on modulated subcarrier system 77−18022
seafloor instrumentation, multifunctional, USA's offshore instrumentation program 79−53584
semiautomatic, for single-mode optical fibre index profile meas. 78−66935
semiconductor-insulator interface, microcomputer-aided interface-state analysis 80−80383
Shubnikov de Haas effect meas. system set-up, expt. *(Polish)* 77−72873
solar collector-heat pump installations, meas. of efficiency under operational conditions *(German)* 80−101077
solar-radiation meter, automatic 80−89592
standardised metrological characteristics of meas. methods and systems 78−41273
structure complexity and props. anal. *(German)* 77−74344
structures and functions *(Japanese)* 80−73300
superconducting instruments, future development in metrology 79−26020
surface tables, maintenance, positioning, and possible sources of error 78−93651
surface temp. meas. using automated zero-derivative method *(Japanese)* 78−210
test reliability 79−75514
thermovision flaw detector 'Stator-1', meas. channel 80−76449
throwing distance, for the Olympic Games, Moscow 80−82743
time-domain reflectometer, high-sensitivity, picosecond 77−18016
torsional pendulum oscillation damping meas. *(Polish)* 77−71314
total dynamic characteristics of meas. facilities, limit error estimation 78−77841
transducers, hyperbolic, with piecewise-linear-approx. and memory capacity 79−6110
transient-flow parameter meas. and computing set, features 77−72389
ultrasonic flow transmitter 80−1710
US beam scanner, automatic, features *(Dutch)* 79−27473
US heating process parameter meas. *(Polish)* 79−12798
US materials testing, SARD-1 automatic system with digital recording 77−77712
for use with Josephson device in maintaining voltage standard 78−93730
UV radiation meas. in agricultural production, instrument *(Russian)* 78−65969
voltage meas. from high impedance sources, precision 78−54402
weighing machine for loose and pulverised materials in motion, design and operation *(Polish)* 78−12673
welding stresses on component surfaces, semi-automatic measuring device 80−68194
wind velocity meas. system, computerised 77−56742
Cu alloys, molten, gas content meas., reduced pressure test *(Chinese)* 80−81390

measurement theory
aberrant values, recognition and elimination *(Rumanian)* 80−22316
aberrant values elimination, from series of repeated meas. *(Rumanian)* 80−47008
absolute radiometer instrumental correction theory improvement 77−82585
accuracy improvement by two-parameter meas. method 77−82480
accuracy increase, by optimal statistical conversion of instrument signals, with aid of computers 77−5795
ambiguous correlated measurements, regression problem 79−88903
angular reflectance variations of rough surfaces, near IR, correction method 77−75424
automatic measuring-limit selecting devices in multi-channel systems 79−71397
balance meas. instruments, system accuracy *(Slovak)* 78−49798
balances accuracy class increase, using several standard weights of equivalent mass *(Rumanian)* 80−47022
basic concepts *(Italian)* 78−21091
Bell's inequality, hidden parameters and probabilities, meas. theory 78−54244
bivariate point process connected with electronic counters 77−67406
capacitance meas. accuracy improvement by variable coeff. elimination *(Russian)* 78−49789
causality, macroscopic, Einstein correlation, CPT symmetry, decreasing probabilities, advanced waves, antiparticles 80−68073
clock random perturbations, absolute continuity theorem *(French)* 78−62150
colorimeters metrological qualification *(Hungarian)* 78−24841
combined meas. evaluating error in establishing relationship between quantities 77−71286
complex system characteristic derivative meas. by input deep modulation *(Russian)* 78−45588
concentration meas. kinetic reaction equation parameter determ. *(German)* 77−66782
conference Wroclaw, Poland, Sept. 1978 *(Hungarian)* 80−86247
contribution to measuring process intensification *(German)* 80−36966
coordinate information processing, integer method 77−22518
coordinate transformations and theory of meas. 78−36960
correlation function determination problem 79−71396
cyclical meas. ambiguity elimination, alphabetic soln. rule selection *(Russian)* 79−21689
data evaluation by probability calc., computer appl. *(Hungarian)* 78−8376
data volume determ., based on risk for arbitrary volume of a priori data 80−95054
deconvolution, Fourier analysis of methods, pitfalls 78−24638
deparalleling method for cyclic calculation processes *(Russian)* 80−86246
deviation and error, concepts and definitions *(German)* 79−49188
dimensional analysis 80−27263
dimensionally invariant numerical laws correspond to meaningful qualitative relations 79−12561
dosimetry calibration, estimation of confidence levels 79−3247
double connecting channel model *(Russian)* 80−90804
dynamic meas., fundamental concepts 77−5793
dynamic meas. concepts, analogy with static meas. 77−5794
dynamical interactions, empirical method for identifying observables involved 77−56326
dynamics of meas. instruments, averaging time as equivalent dynamic parameter *(Polish)* 78−29081
dynamics of measurement, rel. to system and information theory 78−8377

measurement theory continued
Einstein, quantum mechanics, conceptual problems 80−46783
electrical RMS value meas. devices and theory *(Dutch)* 77−87791
engineering development trends *(German)* 80−86243
entropy of density matrix, definition with respect to observable 78−45886
equal accuracy verification correlation anal. 78−8378
evolution systems, meas., rel. to master eqn., Bayesian anal. 80−90782
experiment planning for metrological reliability *(Rumanian)* 79−6075
experimental data, anal. function optimisation meas. theory, appl. to spectrometry 80−62614
experimental distribution function approx. determ. 79−35659
experimental measurement, review of error statements 79−85110
exponential processes, amplitudes and time constant calc. *(Russian)* 78−77831
expt. data analysis, normal distribution verification algorithm *(Bulgarian)* 80−27261
extreme measurements and null experiments *(Japanese)* 78−77830
Feynman path, trajectories in Hilbert space connecting any two states, dense measurements 80−82678
flowmeter reliability, overview 78−30382
foundations of quantum mechanics and uncertainty principle, book 78−29000
function segmentation from discrete readouts *(Russian)* 80−42185
fundamental constants, precise measurement, significance in physical science and metrology *(Chinese)* 79−75487
general performance parameter for meas. facilities, engineering formula 77−67404
generalised quantum meas., uncertainty relations, efficient meas. 77−37781
Gleason's theorem generalisation 80−36889
hidden variables, algebraic constraints 78−65797
ideal experiments connected with uncertainty principle 77−5679
indicating measuring instruments, error estimation *(Croatian)* 78−57886
indirect meas. definition and methods 77−71285
indirect meas. error calc. method *(Polish)* 78−70091
information amount determ. approach 80−8949
information propagation in a quantum-mechanical system between 2 physical parts 80−17832
information relationship 79−71395
information test for uniform quantisation, meas. error determ. 77−79048
information theory of quantum measurement 78−36863
instrument performance unified representation *(Japanese)* 78−70090
instrumental functions, asymmetric, generalised Lloyd's graphical deconvolution methods 79−84905
joint distributions of observables on quantum logics 79−71270
linear measuring instrument dynamics simplified model *(Polish)* 78−41265
linear state estimator design, updating budget 80−95058
local theories, probabilistic and deterministic, inequalities of Einstein locality 80−82656
magnetic field meas., precision, using Ampere's law 79−21720
Mason topological formula *(Russian)* 80−13029
mathematical models of instruments, fundamental principles 78−93641
maximising information, optimal initial state for indirect expts. 80−77744
measurement system structure complexity and props. anal. *(German)* 77−74344
measuring cycle improvement, correction of measurement path *(Polish)* 80−22318
measuring data determ. and appl. *(Rumanian)* 79−6074
medium loss with time meas., optimal planning *(Polish)* 78−93642
multi-point meas. system average meas. time reduction anal. *(Russian)* 78−159
multidimensional measuring block, parameter tolerance estimation *(Polish)* 78−29079
multiple measuring systems 79−26049
multiscale measurement devices, max. likelihood estimate generating, synthesis and quality charact. calc. 79−40525
nonlinear dynamic systems, observability criteria for multidimensional meas. *(Russian)* 78−49790
nonlinear experimental design, information measures 80−62616
nonlinear recursive estimation procedure, convergence and hybrid simulation 77−53850
nonmetrical method for paired comparisons *(Japanese)* 78−77833
nonstationary, stochastic processes, probability charact. of mass flow rate meas. 80−73302
nuclear decay, γ-decay of coherent rotational states, random quantum meas. 80−73855
null circuit balancing by Radischev draft procedure *(Russian)* 80−13028
open channel flow, monitoring or metering 78−30383
opto-electronic meas. system, with raster analysers, illumination distribution law effect on accuracy 77−79047
oscillator in coherent state, quantum nondemolition meas. 78−54228
periodic variables meas., multi-scale cyclical meas. analysis *(Russian)* 80−187
physical quantities, terminology and definition 79−75485
physical quantity definition ambiguity limiting meas. precision 78−36961
point-surface distance meas. adjustment, geometrical aspects *(German)* 80−86255
positron annihilation, pulsed distrib. from expt. data, parameter reconstruction 78−41290
probabilistic representation of instruments 78−49788
probability, theoretical structure, measuring techniques, ensemble concept 77−9868
profile deviation from circular, invariant props. determ. 80−22326
propositional systems and meas., quasi-tensor-products of certain orthomodular lattices 78−81871
pulse spectra, dynamic props. *(Russian)* 79−97335
quantum and classical correlations 78−73866
quantum logics and ideal measurement 78−54237
quantum mechanical measurement process, argument against superluminal transmission 80−52055
quantum mechanical one-system formalism, locality and joint probabilities 78−54238
quantum mechanics, consequences of more general theory of symmetries, isolated system 78−49718
quantum mechanics, meas. problem 80−12948
measurement theory continued
quantum mechanics and relativity, interrelations between truth space and time space, holistic analysis of theory of measurement 80−27177
quantum observables, relative compatibility and joint distributions 80−105524
quantum radiation from a point source, angular coords. determ. 77−65050
quantum system decay and reduction laws, repeated measurement perturbations 80−62496
quantum theory, experimental verification, hidden variables 78−54245
quantum theory, initial correl. and observables with continuous spectra 77−33885
quantum theory, Newman's theorem, Bell's hypothesis *(Hungarian)* 77−71226
quantum theory, noncommutative analogues of Cramer-Rao inequality 77−26209
quantum theory and gravitation inter-relation 78−54235
quantum theory of perception 78−49689
radiointerferometric phase meas. ambiguity detection, recurrence relationship *(Russian)* 79−25513
reliability aspects in metrology, appl. to Weibull distrib. *(Rumanian)* 79−40524
reliability in metrology, statistical approach *(Russian)* 80−22317
resistance thermometer transmission function approximation by Laplace transforms and Taylor series *(Russian)* 78−62197
retroactive influence, EPR paradox, quantum theory of spin meas. 78−70000
roundness, reference criteria 80−62628
scales marking determination *(Russian)* 80−86244
selection of observables, general criteria 77−71735
signal peak recorded profile, influence of integration time const., appl. to crystallography *(French)* 77−5798
simultaneous measurement and joint probability distributions in quantum mechanics 79−30278
single process integral parameter meas. method 77−5792
snowfall intensity photometer theory *(Japanese)* 78−85736
spectral anal. of randomly sampled records by direct transform 77−30134
spontaneous state reduction criterion, meas. problem in quantum mechanics 77−26205
spontaneous symmetry breaking and metastable state blocking, various appls. 78−45510
standard deviation of obs. in meas., statistical estimation 78−16770
standardisation of dynamic properties 77−5797
Stark effect in Gaussian noise field, three-level system 78−41266
statistical error prediction in measurement of probability densities *(French)* 78−57885
statistical parameter estimation methods, application to physical measurements 77−67237
statistical parameter estimation methods, physical meas. appls. 78−49786
statistical treatment of experimental data, book 78−77834
stochastic processes, mean values and standard deviations fundamentals *(German)* 80−13031
student physics laboratory courses, university level, mathematical statistics of measurement 78−24601
synchronised detection system, elimination of influence of low-freq. perturbations 78−45589
system theory in metrology, survey 79−85111
technique, congress, Moscow (1979) *(German)* 80−36964
time averaged magnitude fluctuations during measuring process *(Russian)* 78−73923
transient input processes reconstruction, from output and dynamic props. 80−77742
transient quantity meter repeatability, test procedure 78−30379
two-scale meter, max. likelihood param. estimation, probability density function 77−61047
unbiased clock variance calc. in uncalibrated atomic scale algorithms 80−105620
unstable systems, repeated measurements effects, homogeneous chamber and general case 77−41563
unstable systems, repeated measurements effects, primary decay law in spark chamber 77−41562
unstable systems, repeated measurements effects, theory 77−22517
von Neumann entropy and entropies of meas. 78−54229
von Neumann theorem extension to unreproducible meas. in quantum field theory *(Ukrainian)* 77−71415
Wheatstone bridge, optimisation of sensitivity 78−86298

mechanical birefringence
see also photoelasticity
block copolymers, morphology rel. to stress/strain props., deform. hardening effect, birefringence meas. 77−48501
constitutive relations in photomechanics 80−43251
defect images produced by piezobirefringence, simulation 78−30521
discs, doubly-connected, noncircular, full yielding at collapse, photoplastic verification 80−74756
elasto-optical birefringence modulator construction method *(Japanese)* 77−54809
epoxies and polyurethane rubbers, material and optical props. in complete photoelastic analysis 77−42734
epoxy, elastic and rubbery strain optic coeff., birefringence effect depend., room temp. 77−32348
fibre, single-mode, pressure sensitivity meas. and limitation 80−106605
fibre optic devices, single-mode, fractional wave devices and polarisation controllers 80−106606
fibre optical polarisation transformer, in-line 79−72667
filter, single mode fibre birefringent 80−58713
filter mechanical tuning techniques 80−102834
fluorophosphate laser glasses, Nd doped, piezooptic coeffs. meas. 80−99815
germanosilicate optical fibres, single polarisation, strain birefringence 80−1314
glass, birefringence dispersion, meas. with Babinet compensator using white light 78−27177
glass, blanks, stresses and birefr. changes with dimensions 78−30100
glass, optical anisotropy due to laser-induced electrostriction *(Russian)* 79−99846
glass, tempered, stress analysis, oblique incidence light scattering, birefringence *(Polish)* 80−71374

mechanical birefringence continued
glass, thermally tempered sheet and plate, surface stress meas. using optical waveguide effect 80−25967
glass fibre reinforced epoxy composite, mech. and photoelastic props. at high temps. 78−19799
glass multimode fibres, signal transfer props., stress birefr. effect *(German)* 77−62044
hydrostatic stress and deformation meas., photoelasticimetry and holographic interferometry appl. 79−7353
III-V heterojunctions, misfit dislocation banding, stress-induced birefr. 77−28542
Large Azimuthal Telescope primary mirror, glass blank quality 79−29991
laser glasses, figures of merit and physical/optical property correlations 79−13970
laser single crystal windows, stress-induced birefr. elimination 77−88818
laser window and rod critical orientations for stress-induced depolarisation elimination 79−14054
laser window materials stress birefr. elimination 77−58362
measurement using photoelastic modulator 80−31838
nonlinear photomechanics, birefringence in polymers, stress anal. appl. 80−33545
opaque material, stress-induced birefr., Raman meas. 78−65951
opaque region, piezobirefringence anal. 80−60541
optical fibre, elliptically clad borosilicate single-mode, strain birefringence 80−33148
optical fibre, single mode, bending induced birefringence 80−87537
optical fibre, single mode, stress birefringence 77−68263
optical fibre, single-mode, for current meas. system, birefr. induced by bends and twists 80−99832
optical fibre, single-polarisation single-mode, exposed cladding fabrication 80−58725
optical fibres, single-mode, tension-coiled, high birefr. 80−99858
optical fibres, single-mode exhibiting extremely low polarisation birefringence, fabrication 79−64318
optical fibres, single-polarisation, slab model, strain birefr. 79−50381
optical glass, thermally tempered, surface stress meas. by crit. ray method 80−106766
optical single mode CVD fibre, bend-induced birefringence obs. 80−58723
path difference measurement in birefringent plates, Senarmont compensation method, photoelectric polarimeter *(German)* 77−10091
phosphate laser glass, Nd doped, piezooptic coeffs. meas. 80−99815
photoelastic birefringent material stress determ. in single hologram exposure 80−106770
plane slice optically isolated in three dimens. photoelasticity, plane and circular anal. 77−68540
plastics, anisotropic reinforced, stress-strain state, theoretical principles of nonvisible exam. 78−68745
PMMA, glassy, photoelasticity 80−45034
PMMA, piezobirefringence, optical and mech. relaxations, temp. depend. 80−34885
PMMA, stimulated backscatt. under mech. stress 78−1304
poly-n-benzamide, mols. in soln., dynamic birefringence and rigidity *(Russian)* 77−32349
1,2-polybutadiene crosslinked in strain states; entanglement networks, stress-birefr. relations 80−66590
polycarbonate, glassy, IR dichroism at small strains 78−56475
polycarbonate, secondary flow and stress birefringence patterns in pressure hole 80−64590
polyester, stress-optic law, photoplasticity, RPE transition temp. 78−10120
polyethylene terephthalate, film, two-stage orientation in monoaxial extension *(Russian)* 77−62488
polyisobutylene, relax. of birefringence and stress, extension ratio depend. 77−43962
polymer, brittle photoelastic, use of gelatin gels in prep. for optical polarization stress study 80−40325
polymer, viscoelastic-plastic, birefr. relation 77−31266
polymer birefringence, hereditary depend. of optical propag. difference on strain 78−48142
polymer film, pressed, light-scattering, effect of birefringence *(Russian)* 77−44007
polymer film between two rigid or quasirigid bodies, memorised mechanical birefringence *(French)* 80−43677
polymer network, crosslinks and trapped entanglements, two-network model 80−38962
polypropylene drawn film, rheo-optical studies 78−15440
polystyrene, crazed, orientation and struct., optical meas. 80−30121
polystyrene, stress birefringence under nonisothermal conditions 78−15468
PVC, uniaxially stretched, mol. orientation, birefringence, effect of plasticizers, draw ratio 77−48500
quartz, α and β phases coexistence state, elastic light scatt., birefringence 79−47412
quartz, plate and fibre, internal stress and birefringence microanal. using optical phase microscope interference-polarisation 79−39109
rotating birefringent and achromatic quarter wave plates, appl. to ellipsometry and photoelasticimetry *(French)* 80−14278
rubber, filled, birefringence 78−68472
rubber under biaxial strain, nonGaussian theory, optical props. 80−16367
sapphire, shock compressed, refractive index, density, and polarisability behaviour 80−50295
silica windows in liquid He cryostat, unwanted birefringence 78−66926
single mode fibre analysis and fabrication for low polarisation birefringence 80−58722
single mode optical fibre polarisation stabilisation 80−33154
small retardation meas. using uniform-field Babinet compensator 79−93208
split birefringent coating on birefringent material, determ. of dynamic stress intensity factors 79−50684
stimulated Brillouin scattering in media with induced anisotropy 78−1304
stress measurement in birefringent medium by fast three-dimens. ellipsometry 80−101821
surface films and bulk material, optical props. meas. using ellipsometry, review 79−44926
surface stress meas. by optical waveguide effect 80−43681
tempered glass discs, meas. of nonuniform distribution of residual stresses 78−95865
thermal stresses in photoelastic cylinder, fringe order due to integrated relative retardation 77−62219
time-depend. principal strain directions, photoelectric meas. 77−2647
transition temp. and assoc. mechanical props. determ., simple test method 78−56454
visco-elastoplastic medium mechanical birefringence in loading and unloading processes 78−59314
viscoelastic dielectric under combined stresses 78−68470
AgCl, surface layer stress distrib. after mech. treatment, polarisation-optical obs. 78−18887
BaF_2, single cryst. windows for high power lasers, stress-induced birefr. elimination 77−88818
C fibres, optical anisotropy caused by strain birefringence 79−56760
CdS, wavelength dependence of pressure coefficients 77−20820
CdSe, wavelength dependence of pressure coefficients 77−20820
CsCl type crystals, piezo-optic birefr. 78−39523
CuCl, electrooptic props. below absorpt. edge 77−28548
GaAs, birefringence, photoelastic consts. dispersion 80−11361
GaAs, resonant Brillouin scattering 79−78695
GaP, birefringence, photoelastic consts. dispersion 80−11361
GaP, birefringence observations of strain and plastic deform. 80−50678
GaP, piezobirefringence above direct gap 79−51929
Ge, photoelastic consts. determ. 78−68474
InP, piezobirefringence above direct gap 79−51929
KBr, residual birefr., 3000-7000 Å, rel. to intrinsic piezooptical behaviour 78−60416
KCl laser window, thermal lensing, effective optical distortion parameter 77−83916
KCl, photoelastic consts. at 10.6 μm, interferometric and polarimetric meas. 78−25934
KCl single cryst., stress birefr. 80−60542
KCl single crystals, piezobirefringence and plastic deform., stress-strain curves 77−69798
KCl-KBr mixed crystal, piezo-optic birefringence 78−31169
KH_2PO_4, optical props., plastic deform. effect 77−59552
$MgO:Cr^{3+}(V^{2+})$, $^4A_{2g}\rightarrow{}^4T_{2g}$ spectra, new expt. results 80−11441
NaCl, rock salt, quenched, residual stresses, optical study 80−55061
NaCl single cryst., stress birefr. 80−60542
Nd doped (fluoro) phosphate laser glass piezo-optic coeffs. meas. at 0.6328 and 1.15 μm 80−34888
Nd:YAG high performance laser system efficiency and beam uniformity 77−19327
PLZT ceramics, elastooptic effect, stress induced birefr. 80−60543
Si, piezobirefringence above fundamental edge, Raman scatt. meas. 79−42941
Si, piezobirefringence in opaque region 80−60541
SiO_2, fused, shock compressed, refractive index, density, and polarisability behaviour 80−50295
SiO_2-Na_2O-CaO-MgO, glass, fibre and plate, internal stress and birefringence microanal. using optical phase microscope interference-polarisation 79−39109
$Y_3(Al,Fe)_5O_{12}$, optical anisotropy and stress birefringence assoc. with growth striations 79−42940
ZnS, heterogeneous birefringence 79−95728
ZnS, natural and stress induced birefringence dispersion 78−6651
ZnS, reson. Brillouin scatt. and piezobirefringence 80−93348
ZnSe, piezobirefringence in opaque region 80−60541
ZnSe, reson. Brillouin scatt., dispersion curves, piezobirefringence anal., electronic state lifetime broadening effects 79−61390

mechanical contact
see also abrasion; friction; lubrication; wear
abraded surfaces, topography rel. to contact area and abrasion mechanism 80−58986
abrasive wear of soft surface against rough hard surface 79−33034
activation volume determination by change in hardness 79−18836
adherends shaping in bonded joints 79−27599
adhesion of elastic particles to a solid surface 77−42787
adhesive bond stresses and strains at discontinuities, cracks in bonded structures 78−90793
adhesive fracture of bonded plate or membrane strips 78−59342
adhesive joint under normal and shear stresses, stress distrib. 79−18837
adhesive joints, effect of structural parameters on stressed state 79−41630
adhesive layers effect on fracture of laminated structures 78−90791
adhesively bonded graphite composite/steel scarf joint, failure anal. 78−92350
anisotropic elastic half-space; crack and contact problems 79−10480
annulus, circular, elastic contact problems, approx. soln. 80−38349
apparent friction paradox 77−31263
appl. to reversible and irreversible contact between rough surfaces 78−13976
approximate load-deflection relation for a long half-cylindrical tybe compressed between parallel plates 77−50999
automorphic functions in plane elasticity theory *(Russian)* 79−35563
axisymmetric butt joints loaded in torsion and tension, stress anal. 78−63397
axisymmetric contact problems for elastic orthotropic cylindrical shells of reinforced plastics 78−1569
axisymmetric deformation of Winkler layer by internally loaded elastic halfspaces 78−26044
bar, stability against self excited frictional oscillations *(German)* 77−54916
bar with concentrated masses under longitudinal impact *(Russian)* 79−50627
Barber boundary conditions for thermoelastic contact, heat flows 80−69745
beam, cracked, transverse loading by stamp, stress and fracture anal. 80−10187
beam bending on Pasternak foundation, reciprocal variational inequalities 80−92091
bearing viscous plastic lubricant motion *(Russian)* 79−50672
Bergman operator method and anti-plane contact problems 79−14353
bimaterial full-plane with a crack at any angle to the interface 77−14965
bimaterial interface, wave propagation in non-uniform motion of displacement discontinuities 80−19264
bimetallic adhesive force at small separation 77−35823
bodies with wavy surfaces, thermoelastic contact, heat conduction 80−64492

mechanical contact continued
bonded anisotropic wedges, plane problem *(Russian)* 79−23284
bonded wedge shaped stamp apex singularity, Green's functions for elastic half space 80−64489
bouncing of cantilever beam chattering against a stop, Bernoulli-Euler beam theory treatment 80−83752
Boussinesq problem for a flat-ended cylinder with elliptical cross-section 79−68663
circular plate on elastic foundation, bending and contact problems 80−96235
circular sliding contact on transversely isotropic spheres, stress field 79−18833
coaxial cylinders, contact problem, iterative soln. technique *(Russian)* 80−23963
coefficient of friction of rolling disks 79−14360
coefficient of sliding friction at high contact speeds 78−87308
colloids, linear elasticity, soft contact problems 80−48653
component-support impact dynamics, elastic anal. 79−45343
consolidation in compressible mixtures 79−46271
contact adhesion between solids in vacuum, deformation and interfacial energy 78−22306
contact adhesion between solids in vacuum, single-asperity experiments 77−11149
contact area under a nonuniformly distributed load 78−67155
contact between spheres and rough planes for nondirectional surface roughness *(Japanese)* 77−19575
contact compression of circular cylinders with rough surfaces *(Ukrainian)* 79−50671
contact film absorption on plastic deform. of contacting bodies *(Russian)* 80−93596
contact force interactions between deformed solids *(Ukrainian)* 80−10214
contact of rough surfaces, computer simulation 79−19470
contact on a transversely isotropic half-space, or between two transversely isotropic bodies 80−64488
contact problems with slip and cohesion, variational anal. 78−63398
contact stress minimization by contour design 78−63396
contact stress of a rigit, circular cylinder insertion with play in an undefined plate *(French)* 79−72862
contact stress solutions using computer techniques 78−34096
contact stresses on cylindrical vessels, anal. method 78−63395
contact surfaces with nonspherical asperities, friction coeff. 79−20200
contact visco-elastic stress analysis using finite element method *(Japanese)* 78−54817
cooled punch, contact problems 79−32390
Coulomb bearing friction films 79−64601
Coulomb friction, elastic theory 80−33539
Coulomb friction forces during rotation *(Polish)* 79−64597
counterformal contact stress problems, numerical method and computer program 79−41632
crack propagation mechanics in delamination wear 78−3231
cylindrical non-axisymetric contact problem 77−19574
cylindrical shell, contact problem with ribbed cylinder under axisymmetric loads 80−99974
cylindrical shell and belt, interaction contact stresses, elastic layer model 80−33543
cylindrical tubes or shells, mild steel, quasi-static piercing 80−45351
deflection stability of work-hardening structures 79−27528
delamination theory of wear 78−3229
disc and coaxial ring, partial contact, loaded by external pressure *(Russian)* 80−74814
disc inclusion, rigid, embedded in with transversely isotropic elastic medium 80−83763
discs, photoelastic obs. of static and dynamic contact conditions *(Japanese)* 80−23970
dislocation generation beneath static and rolling contact with sphere 78−87671
drag reduction of an oscillating flat plate with an interface film 80−10268
dynamic contact of elastic bodies, direct connection and feedback *(Russian)* 79−50670
dynamic contact stresses by impact on nonlinear elastic half space by axisymmetrical projectile 78−42573
dynamic indentation of elastic half-space by rigid punch 78−1612
dynamic rigid indentation induced by sliding frictionless contact 78−75107
dynamical contact problem, shock waves in elastic layer after impact *(Russian)* 80−23964
elastic contact and friction mechanisms between rough surfaces 78−87309
elastic contact between flexible plate and isotropic halfspace 80−43679
elastic contact of two disks by method of caustics end 79−59948
elastic contact problem of half-space pressed onto rigid base with cylindrical protrusion or pit 79−37249
elastic contact problems in fracture mechanics 78−67142
elastic contact problems of an elliptical punch 78−9613
elastic contact problems soln. by the finite element displacement method 77−31261
elastic contact problems with friction soln. using suitable nodal parameters *(French)* 78−63401
elastic contact problems with friction using suitable nodal parameters *(French)* 79−10475
elastic cylinders, approx. soln. of Shtaerman's eqn. 80−38355
elastic half space, rectangular cylinder penetration, contact problem, stress fields 80−64490
elastic half space, ring shaped punch contact stress determ. 80−38356
elastic incompressible body, contact problems involving forces and moments, rigid punch problems 80−53719
elastic interface waves and sliding between two solids 79−18800
elastic layer on substrate, frictional slip caused by normal load 80−33541
elastic ring indentation by rigid roller system 80−36854
elastic spheres, oblique conpression 79−27564
elastic strain of transversely isotropic half space caused by rigit punch 79−59947
elastic strip pressed against elastic half plane by steadily moving force 79−7345
elastic surface waves on interface of pre-stressed elastic bodies *(Ukrainian)* 80−10176
elasticity plane problems in terms of dislocation layers 79−64507
mechanical contact continued
elasticity theory, orthogonal polynomial solus. to mixed boundary value problems 77−75857
elasticity theory for space with spherical hollow *(Ukrainian)* 79−50669
elasto-plastic contact problem 78−46917
elastohydrodynamic contacts, optimisation 78−79288
elastohydrodynamic contacts, traction prediction technique 78−63394
elastohydrodynamic films formed between a rubber cylinder and glass plate, comparison of theory and experiment 77−28910
elastohydrodynamic lubrication at high pressures 78−34094
elastomers, tackiness, fracture mechanics theory *(French)* 80−38344
elliptical-contact deformation between two elastic solids 78−55616
end-values of distributed loads in half planes by caustics 79−18851
erosion of ductile metals by solid particles at low angles of incidence, vel. depend. 78−87311
failure criteria for adhesive joints under complex loading 78−92344
fatigue, rolling contact, fracture mech. approach 80−23961
fatique crack approaching and growing beneath an adhesively bonded doubler 78−92348
fatique crack growth behaviour in adhesively bonded metallic structures, parametric study 78−92347
fatique crack growth of bondline cracks in structural bonded joints 78−92346
fatique life dispersion in rolling contact, model 78−59349
ferrite and ceramic joining, bulk interaction *(Russian)* 80−40277
fission reactor, FEM anal. of pellet-clad bonding 80−42765
fission reactor fuel performance anal. by finite element method 80−42750
fission reactor fuel rod deformation code FEMAXI-II and its application 80−37446
fluid-coupled concentric cylindrical vessels, normal mode soln. 79−37157
forced azisymmetric membrane vibrations *(Russian)* 79−32368
fracture analysis of adhesively bonded cracked panels 78−90792
fracture mechanics and the adherence of viscoelastic bodies 78−83336
frequency-independent internal friction, linear models *(Russian)* 79−18834
friction, Coulomb, elast. solid with one-sided contact *(French)* 80−64485
friction and wear, gaps in knowledge 77−8955
friction as a thermomechanical phenomenon *(Ukrainian)* 77−68537
friction problem of structures with convex strain energy density 79−27601
friction transients, role in friction failures 77−35096
frictional shear effect on dynamic stresses produced by reciprocating load 79−10537
frictional unloading problem, variational soln. 78−59350
frictionless contact problem for an elastic layer under axisymmetric loading 78−83341
frictionless indentation and plane crack extension 79−18835
frictionless indentation by elastic punch 79−32389
frictionless indentation by rigid wedge; effect of tangential displacements in contact zone 79−37250
frictionless stamp impression in elastic half space, contact problem with semiunknown boundary of the contact region 80−69744
glass particulates removal from solid surface 79−50676
glass segment, resting on elastic ring, structural strength 80−14630
glass-to-metal foil seals, stress aval. 79−29197
glue joints with optimal shearing stress distrb. within the glue layer *(Polish)* 79−66256
granular layer lying over an elastic foundation, contact problem 79−27600
granular materials, packing parameters, calc. from particle size anal. results 80−19294
Griffith crack, stress distrib. at interface of elastic layer bonded to half plane 80−23955
ground surface profile, crest and trough height distrib. *(Japanese)* 79−34180
ground surface profile, power spectrum *(Japanese)* 79−34179
guillotining materials, mechanics, fracture and burr formation 80−14619
harshness numbers conversions between various types of indentation hardness 79−11736
Hertz problem for finite linear and nonlinear elastic bodies 77−54938
hitches, theory 77−33769
hydrodynamic lubracation 79−59946
hysteresis of tension and bend-loaded screw connections *(German)* 78−87312
hysteretic friction in small velocity approx. 79−37252
hysteretic friction of a plane punch on a half-plane with arbitrary viscoelastic behaviour 77−68450
impact abrasion *(German)* 78−88536
impact backling of thin bar via Monte Carlo method 79−32317
impact vibrations, steady, of body having hysteresis collision characteristics 80−14602
impact viscosity resolution into components by Otani method 79−50657
impulse load effects, EPIC-3 code anal. 80−19293
incremental contact analysis with various frictional conditions 79−32388
indentation of a consolidation half-space, effect of Poisson's ratio 78−83340
indentation of elastic support, numerical applications *(French)* 79−50673
indenter moving on anisotropic elastic half-space 79−37248
inequality conditions in contact and crack problems 79−37242
interface separation for elastic layer loaded by rigid stamp 78−87307
interfacial waves in pre strained neo-Hookian body, biaxial strain states 80−48630
interfacial waves in pre-strained neo-Hookian body, triaxial strain states 80−48631
internal friction and modulus measurements 77−42789
joints, double adhesive bonded, loaded in shear tension *(French)* 80−23968
journal motion on oil film, partition method 79−68662
junction growth during friction, anal. *(Japanese)* 79−32391
kinematic examination of constraint systems realized on pairs of surfaces in contact *(German)* 77−31262
Lame polynomial solutions to elliptic crack and punch problems 78−75069
lamination, hydrodynamic analogy, utilisation of current function *(French)* 80−19292
linear elastic half space, frictional unloading problem 80−33542
linearly deformable base reinforced with finitely large cover plates 80−14631

mechanical contact continued
localized dynamic contact on structures anal. using matched asymptotic expansions 79−7342
lubrication flow of particle fluid mixture 79−64600
lubrication for rough surfaces 79−14355
lubrication of high loaded contacts *(German)* 77−46974
magnetic flexible disc/head interface interaction analysis 80−92093
mechanical and temperature contact in fuel rod and cladding 78−66341
mechanics in delamination wear 78−3230
membrane indentation on an elastic half space 79−20522
metal surfaces, factors influencing contact behaviour 80−92092
metal-to-metal bonds in hostile environment, stress anal. 79−20338
metallic adhesion, utilisation of fracture mechanics and contact resistance meas. 77−70271
microcontinuum theory for the elastohydrodynamic inlet zone 77−50998
microparticle impact, strain rate effects 77−80577
microscopic damage, reln. between inhomogeneity and dispersion of strength param. *(Russian)* 77−86122
mirror/flaw-size relations, residual contact stresses effect 80−107363
moving load on elastic strip on elastic half plane, steady soln. 80−10215
moving rigid punch on an unlubricated viscoelastic half-plane 79−64598
multilayered packet, contact elastic-plastic problem 80−5997
non-linear friction element with stockastic input 79−50674
nonlinear props. of solid systems in presence of dry friction *(French)* 77−54937
nonplanar stamps, contact area determ., variational aspects 80−36855
nonuniform friction as a physical basis for earthquake mechanics 79−20766
parametric resonance of 4th order in a nonlinear vibrating system under the influence of frictions 77−58620
peel mechanics of adhesive strips with constraints 79−23285
peel mechanics with large bending 77−80122
penetrating an obstacle by a cylinder *(Russian)* 78−30246
penny-shaped crack in elastic cylinder bonded to elastic surrounding material 80−19285
percussive impact wear 78−94623
photoelastic investigation of impact stresses in discs 79−37182
planar thermoelastic contact problems, Green's function for exterior contact 80−38350
planar thermoelastic contact problems, Green's function for interior contact 80−38351
plane symmetric contact problem for dissimilar elastic semi-infinite strips 78−55615
plate, rectangular with asymmetrically reinforcing beams, contact interaction 80−99975
plates with pressed in solid discs, contact stresses *(Russian)* 80−43678
point contact problem using finite element method 78−1613
point contacts lubracation, elasticity effects 79−52379
polymer film between two rigid or quasirigid bodies, memorised mechanical birefringence *(French)* 80−43677
polymer materials, device and methods of NDT *(Russian)* 77−48601
Prandtl punch problem for case with eccentric forces *(Russian)* 80−23965
Prandtl-Reuss plastic material with kinematic work hardening, constitutive equs. *(Japanese)* 77−77502
Prandtl-Reuss plastic material with kinematic work hardening *(Japanese)* 77−77503
pressure between elastic bodies having a slender area of contact and arbitrary profiles 79−64596
pressure on vertical screen by massive noncoherent powder *(French)* 78−42572
punch, axisymmetric, contact with semi-infinite transversely isotropic elastic body *(French)* 80−23969
punch adherence on foundation plane of viscoelastic solid *(French)* 78−42535
punch indentation problem with an isolated slip line 78−79286
quick connection behaviour under a blow *(Russian)* 79−32289
rapid interface flaw extension with friction 79−18810
rigid circular punch on an elastic halfspace and a Mindlin force, interaction 79−18716
rigid disc inclusion embedded in isotropic elastic medium, displacements for external force 80−48652
rigid indentor and elastic halfspace, dynamic contact with perfect adhesion and frictional slip 80−58980
rigid indentor sliding over a power-law viscoelastic half-space 79−27602
rigid perfectly plastic strip, plane strain compression between parallel dies with slipping friction 80−48603
rigid punch bonded to elastic half plane, stress singularities 80−64491
rigid punch problems, forces and moments by reciprocal variational techniques 80−23967
rigid stamp, elastic layer indentation under complete adhesion conditions 80−58979
rigid-plastic continua adaption under dynamic loadings 79−27548
rock penetrator, initial response 79−32392
Rockwell diamond indenters, meas. method 79−66251
rolling, critical line nature in multiple-roll passes *(Russian)* 80−38347
rolling, determ. of stress distrib. in rolled material 80−48651
rolling, inhomogeneous deformation model 80−48650
rolling contact fatique life, traction and microgeometry effects 79−20205
rolling of rigid cylinder on rigid/perfectly plastic half-space 79−41629
rotational firction coefficient of permeable cylinder in a viscous fluid 79−46385
rough curved surfaces, elastic contact stresses calc. 80−10213
rough elastic bodies, plane and axisymmetric contact problems 80−74812
rough materials, stressed state on contact 80−38352
rough spheres, elastic contact, anal. approx. 80−79240
rough surface, plastic deformation in mechanical contact 80−14583
rough surface contact, review of expt. work 80−76377
rubber covered rolls, contact and deformation nonlinear elastic problem, stress anal. 80−79239
ruled three-layer shell, stressed-strained state 79−14354
rupture and particle velocity during frictional sliding 79−20820
sensitive instrument to measure the friction between single fibres in various media 77−27498
shear contacting displacements of mating surfaces *(Russian)* 80−23962
shear loaded interface crack, friction effects, contact zones, stress fields 80−79225
shear modulus and void ratio in granular media *(Japanese)* 79−32401
sheet metal stamping by a finite-element anal. 79−7344
mechanical contact continued
shell, cylindrical, liquid and gas, breakaway from solid lodgement *(Russian)* 80−87744
shell, high-shallow, with rib of equal resistance, contact interaction, tangential stress distrib. *(Russian)* 80−87745
shell, supported cylindrical, interaction pressure variation 80−38354
shell wall on fluid, impact problems *(Ukrainian)* 80−38345
singularity at the corner of a wedge-shaped punch or crack 78−83252
sliding contact, friction, wear, temp. anal. 80−93659
sliding contact, mixed boundary value problems, variational soln. 78−83331
sliding fit, stick-slip phenomena 80−5996
sliding friction, dynamic loading effects 79−50675
sliding interfaces and impact 79−41631
sliding of rigid indentor over power law viscoelastic layer 79−7346
sliding rules in constant friction problems 79−14351
slip friction characteristics in nonstationary motion *(Russian)* 80−43652
smooth circular plates, axisymmetric elastic contacts 80−19291
soldered layer on half-plane, rigid stamp impression 80−38353
solid friction damping of mechanical vibrations 77−42764
spectrum crack growth in adhesively bonded structure 78−92349
sphere sliding on plane, transient thermoelastic contact 80−83765
spot weld between elastic plates, near field stress anal. 77−11160
steadily moving load on elastic strip resting on rigid foundation 78−87264
steady-state vibration elastic contact problem for the half-space 78−18219
steel, austenitic stainless, friction in vac. at elevated temps. 80−55542
steel, C and Ni-Cr surface hardened, rolling contact fatigue failure 80−16608
steel, mild, ground/sandblasted interfaces, tangential displacement, contact press. and lubricating film distrib. effect 80−16484
steel, mild, two sandblasted interfaces, tangential displacement, contact press. and lubricating film distrib. effect 80−16484
stick-slip motion and surface deformation 79−37253
stress determination in axially-symmetric glued joint loaded by torque *(Polish)* 78−79287
stress singularities at vertices of composite plates with smooth or rough interfaces 77−7348
stressed state in contact zone of plyurethane with a solid indentor 78−1624
stressed state of compound rotor taking into account interference stresses 78−83342
stresses and spreading resistance at contacts between spheres 78−71296
strip rolling, kinetostatics *(Russian)* 80−38348
superposition principle in contact friction stress problems 79−32394
superposition principle in problems taking friction forces into account *(Russian)* 79−7343
superseismic stage of dynamic contact between punch and elastic body, exact soln. 78−55614
surface analysis, appl. to lubrication problems, review *(French)* 80−45616
surface curvature effect on the friction coefficient 78−87310
surface deformation in point contact elastohydrodynamic lubrication 78−18255
surface deformation of elastic solids subjected to a hertzian contact stress 77−35097
surface friction measurements 79−68668
surface irregularities, deformation under static loads 80−58985
surface layer bonded to a half space, fracture 79−27586
surface strength in friction, structural and energy conditions *(Russian)* 77−56111
surface waves as nonlinear phenomena arising in collision of elastic bodies *(Ukrainian)* 79−32331
symmetrical indentation over a uniformly expanding contact region, perfect adhesion 77−23919
tensionless contact without friction between elastic layer and elastic foundation 80−64487
thermoelastic contact involving a sharp corner 80−83766
thermoelastic instabilities in sliding contact 78−18257
thermoelastic punch problem for an elastic layer overlying an elastic half-space 77−42742
thermoelastic transition from line to point contact 80−83768
thin elastic layer, bending by rigid die 80−14627
three-part contact problem, Chebyshev polynomials and elliptic integrals 80−33540
tops rising by friction, problem, exact soln. 78−83343
toroidal wheel, contact phenomena during curvilinear rolling, tangental stresses *(Russian)* 80−58983
transversally isotropic plate, bending by smooth stamp, contact problem *(Ukrainian)* 80−38346
transverse impact method for studying the viscoelastic prop. *(Russian)* 79−32398
transverse impact of ideal fibre-reinforced rigid-plastic plates 78−38211
transverse impact of load on approximate models *(Russian)* 79−37251
transversely isotropic half space, indentation anal. 80−92090
transversely isotropic half-space idented by flat annular rigid stamp 79−55347
tribology' science and practice 77−59066
tribology of rough surfaces 78−95106
two thick walled pipes, axisymmetric contact allowing for fitting surface roughness *(Russian)* 80−58982
ultrasonic reflection from interfaces experiencing state versud dynamic friction 77−27494
uniformly loaded plate, interaction with isotropic elastic halfspace 80−23966
unilateral contact problem in linear elasticity 80−79238
unilateral contact problem integral eqn. approach 80−8798
variation approach to calc. of elastic and elastoplastic contact of medium-thickness shell 79−64599
vibrating string motion subject to solid friction *(French)* 79−32326
visco-plasticity problem approximation *(French)* 79−46222
viscoelastic contact, aging 80−64486
viscoelastic lubricants in reference to human joints 79−39430
viscoelastic solids, kinetics of crack propagation and adhesion *(French)* 77−89065
viscoelastic substrates, deformational contact and friction 79−50677
viscoplastic medium and solid surface under pressure 79−69320
viscous-plastic lubricant, nonlinear effects on bearing tenon movement *(Russian)* 79−32393
wear and its measurement for joint prosthesis materials 79−20716

mechanical contact continued
wear as an energy transformation process 79−18838
wear initiation of boundary lubricated surfaces 79−34157
wear of spherical bearings with stone pillow blocks *(French)* 79−18832
work-hardening due to residual stresses constitutive equations for the rates *(French)* 77−70068
Cu, virgin surface, contact formation and cohesion, influence of multiple contacting *(Russian)* 80−40548
Fe, Armco, friction in vac. at elevated temps. 80−55542
Fe, cast, contact deformation, reverse slipping effect *(Russian)* 80−97591
LiF crystal, contact damage obs. by cathodoluminesc. 80−71728
MgO crystal, contact damage obs. by cathodoluminesc. 80−71728
Pb, virgin surface, contact formation and cohesion, influence of multiple contacting *(Russian)* 80−40548
SiC single crystal, friction and fracture in contact with itself and Ti 80−11780
W brittle alloy rolling, contact stresses *(Russian)* 80−93576

mechanical control equipment
see also hydraulic control equipment; pneumatic control equipment
fatigue test machine, automatic control 77−56181
manual control operator performance, gain and vibration effects interaction 78−44756

mechanical engineering
arches with flexibly supported ends, freqs. and critical loads 78−30218
automotive struct. analysis using hybrid stress finite elements 78−30176
beam, 2-span, transverse vibr. under moving conc. load *(Russian)* 78−34063
Beck's column, influence of tip mass offset on stability 79−72842
bladed discs, finite element dynamic anal. 79−37230
bridges, buffeting due to wind action 79−14321
bridges, flutter due to wind action 79−14320
caliper gauges for meas. outside dia. 79−12766
cantilever minimum weight design with plural torsional frequency constraints 79−68629
cantilevered column with stretching follower force, vibration 79−37233
Cholesky factorization of stiffness matrix, method for updating factorization 78−16623
circular arches, curved finite elements 78−5652
circular plate on floating central collar, moving load stability theory 77−46863
column design, optimisation of support conditions and segmentation 78−51062
conference, Haifa, Israel (July 1978) 79−75304
crack anal., three-dimens., finite element method 78−83332
cultivator, relative movement under random stationary ergodic load *(Rumanian)* 78−34003
curved box girders, coupled free vibrations 78−30217
discs, varying radial thickness, finite element dynamic anal. 79−37229
expansion bellows, elastic flexibility of axially loaded omega and toroidal bellows, review 79−32266
expansion bellows, flexibility of axially loaded toroidal bellows in creep 79−32299
fluid flow, upstream differences critical evaluation 77−900
fusion reactor, ISX-B, with bundle divertor, structural anal. 80−91254
fusion reactor, ISX-B toroidal field coil finger joints, fatigue life, structural evaluation 80−91253
fusion reactor, TFTR, neutron spectrometer mech. design 80−95498
fusion reactors, Large Coil Program, superconducting mag. coil struct. design status 80−106189
gauge blocks, WC, determ. of thermal expansivity using interferometric dilatometer 79−12767
gyrostabilized platform, nonlinear response to transient input 78−30219
heat exchanger tube bank, cross-flow induced vibrations 79−3957
helical marking of cylindrical specimens, device for holding and scratching 79−58679
high speed cine photography, in industrial engineering environment 78−37099
hypervelocity impact initial stages finite element analysis 77−41
IR pyrometer performance parameters and applications *(German)* 80−86315
irregularly shaped clamped plates, free vibration 79−37231
LMFBR concrete containment struct., exptl. anal. of dynamic loading 78−41867
machine noise transmission, device for meas. and comparison with computation 80−28380
machinery vibration control, resilient mounting on platelike and modified platelike substructs. 77−50818
nuclear power station, full scale tornado-missile impact tests 78−41876
nuclear reactor building, soil-struct. interaction behaviour, damping effects, expt. anal. 77−38434
nuclear reactor structural mechanics, conf. 78−41874
O-ring compounds, resistance to heat and ionizing radiation 78−29584
orthotropic composite circular plates, axisymmetric vibrations 79−37228
orthotropic shallow spherical shells under concentrated central load, nonlinear flexural oscillations 79−37234
plane four-bar linkages, synthesis *(German)* 78−42524
pressure vessel, reinforced concrete, stress anal. of cracked shell 78−44213
pump-induced acoustic pressure distribution in an annular cavity bounded by rigid walls [pressurised water reactor] 79−72848
reinforced concrete deep beams, optimal force transmission 78−34009
rigid rotor in elastic ball bearings, free oscillations *(Russian)* 79−18773
rigid shaft in short journal bearings, aperiodic behaviour 78−46905
rotary structural joints, energy dissipation 78−30245
screw connections, bend and tension loaded, hysteresis *(German)* 78−87312
shear joint, discontinuous, holonomic elastoplastic anal. *(German)* 79−1117
Shiva mechanical systems 78−63135
spur-gear measurement errors, combined length, angle measuring procedure *(German)* 78−77855
thermoplastic beams, constant stress, design 80−38248
thick flexible ring rotating at high speed, vibration anal. 79−37227
threaded article parameter measurement by spatial spectra analysis 79−30409
three-support bearing shaft system, flexural amplitude determ. and reduction method 78−46890
time domain finite element solns., accuracy and stability 79−37232

mechanical engineering continued
Tokamak Mk. II reactor, remote separation and rejoining of coolant pipes 78−29650
two-dimens. structs., finite dynamic element for free vibr. anal. 78−83287
two-way continuous rectangular plate free vibration theory 79−68631
undamped linear elastic systems, stability under follower forces, perturbation study 79−1110
US rod systems, excitation and stabilisation of reson. modes 77−14839
vibration isolation of industrial machinery 79−72868
Viking lander radar system mechanical design 78−57427

mechanical engineering computing
see also computerised control
acoustic emission signal sorting by computerised pattern recognition 77−40516
acoustic problems modal anal. techniques 79−18651
aerodynamic surface structural tests, systems approach to analysis and design 77−16760
alloy design by automatic modelling, CAD system *(Japanese)* 77−52607
anisotropic shells symmetry considerations 77−11123
ANTRAS program system for structural anal. of shells of revolution *(German)* 79−46192
applied mechanics computing, conference, New York (1976) 77−67285
arbitrary elastic structure in infinite inviscid fluid, acoustic radiation and scatt. 79−7318
automatic data processing from static tests on constructional materials 77−4885
axisymmetric solids under nonsymmetric loads, structural analysis programme *(German)* 78−13896
bar with two natural freqs., minimum mass design 79−46246
beam design, HIFIX performative method 78−26064
beam vibration frequencies by Schelkunoff iteration with HP-65 calculator 78−1592
beams, finite element soln. using element averaging technique 78−26079
beams, nonlinear bending, finite element anal. 78−26068
bending circular plates nonuniform, finite element analysis 77−7316
bimetallic tube, residual stress after thermal cycling 77−90465
boundary-integral equation method, stress anal. fracture mechs., computer calcs. 77−80111
bronze 905, partially solid, die thermal behaviour in machine casting 78−6917
building structs., eigenvalue routines 78−26078
cable dynamics, nonlinear finite segment approach 77−2532
cantilever beam axial vibration, min. mass structures determ. 78−63278
cantilever columns, spring hinged, post-buckling anal. 79−46235
cold-rolling mill, Sn plate use of roll-force model 77−4788
composites, dynamic anal., review and computer programmes 77−50946
concrete reactor pressure vessels, finite element creep anal. 78−41813
conference, computational methods in nonlinear problems in mechanics and engineering, Austin, Texas, USA (March 1979) 80−51945
convective heat transfer anal. by finite element method 78−18148
cooling tower supporting columns and reinforcing rings, displacement analyses 78−38187
crack simulation computer program for plate structures *(Japanese)* 80−79218
cross-spring hinge problem, 2-D, use of minimization methods in solving 78−18163
curved beam with viscous damping forced vibrations 79−50622
cylinder based bodies, turbulent boundary layers, three dimens., soln. method 79−1167
cylinders, stiffened, subjected to pure torsion, min. weight design 78−1582
data processing of metal fatigue test results *(Japanese)* 77−9013
deformation analysis at plastic collapse, math. programming methods 78−1572
dielectric parts, stress patterns and deformation characts., computer anal. 80−17787
diesel engine pistons, simulation of slap at TDC 77−72222
dislocation groups, of opposite sign emitted from a stressed source, computer simulation of dynamic behaviour 80−6406
dynamic buckling of axisymmetric spherical caps with initial imperfections 79−3934
EBR-II, dynamic response of ducts to press. pulse, finite element calcs. using STRAW 77−3124
elastic deformation of continuous flexible member, shooting method with Newton-type iteration 80−48575
elastic lateral torsional buckling of unbraced and braced planar frames 79−46236
elastic quadrilateral plates 79−46201
elastic structures, computer automated synthesis for minimum struct. weight 78−34015
elasto-plastic material, crack tip stress and strain fields and fracture behaviour, work hardening 78−22304
elastoplastic fracture mechanics, finite element analysis *(German)* 77−54935
fatigue crack growth testing, computer-controlled stress intensity gradient technique 80−76432
fatigue cracks, computer simulation of propag., model based on Elber's eqn. *(Japanese)* 78−7030
fatigue cracks, computer simulation of propag. based on BCS model *(Japanese)* 78−7029
fatigue design, rain-flow calcs. for wide band random stress process 78−11332
fatigue testing, computer controlled system, simulated service loading 79−15885
fatigue testing, digital simulation of environmental processes 77−40499
fatigue tests, short-term, methodological problem of automating data computer processing 79−15931
finite element discretisation, two-dimens. stationary heat cond. using successive overrelaxation and conjugate gradients 78−83206
finite element linear constraint eqns., soln. algorithm 78−24654
finite element method, critical features rel. to simulation 77−50882
finite element method, reduced integration, appl. to elastostatics 78−75066
fission reactor pressure vessels, high temperature design system *(Japanese)* 78−673
flawed elastoplastic structure, method of lines applied to crack problem 79−46259

mechanical engineering computing continued
flow meas. using spherical probe, pressure and velocity gradients influence *(Polish)* 78−34222
flow rate meas., based on velocity distribution curves *(Polish)* 78−34221
fluid dynamics, transient blast loading on three-dimensional structures 77−68624
fluid dynamics, unsteady leading edge separation bubble calc., numerical solution using finite difference procedure 77−72317
fluid flow prlblems, incompressible, free surfaces 80−106774
fluid flow problems skew upstream differencing schemes 77−3822
frame structs., large deflection anal. by fictitious forces 78−83249
fusion reactor, compact toroidal ignition experiment, support struct. anal. by numerical code 80−106167
fusion reactor, SLPX TF coil, stress anal. using COSMIC-NASTRAN 80−106168
gas turbine material behaviour simulation 78−34041
general heat transfer anal. using CSMP package 78−75145
heat exchanger optimisation 79−3895
heat treatment, prediction of large component response 78−31435
HF heated cylindrical component temperature field computation for quench control 78−90632
inelastic structural behaviour, finite element computational aspects 78−42546
initially stressed Mindlin plates, finite strip method, buckling anal. 78−26067
internal stresses, calc. with integration methods, X-ray stress meas. 79−32415
isochoric const. strain finite elements, modification of TRIM 3, TET 4, and TRIAX 3 elements 78−41144
isoparametric nine-noded finite elements, accuracy 78−26039
large deflection anal. of tail-wheel struct. of light aircraft 78−83272
large reflector antenna structural design for gravity and wind loading 78−57448
liquid cavitation and droplet impact erosion, predictability of prototype machine from lab. tests 78−64723
LMFBR, HCDA, Eulerian computer code anal., primary system response 77−3127
LMFBR, HCDA, structural response calcs., methods, codes development 77−3126
LMFBR, nonlinear structural dynamics of fuel elements, press. pulses, struct. models, expt. verification 77−3125
LMFBR shell structures, finite element elastic-plastic anal. 78−41804
locally modified structs., derivatives of eigenvectors 78−5651
machine fault diagnosis, vibr. anal., bispectrum method 79−8404
material fatigue under random complex state of stress, simulation 77−42786
mechanical impulse testing techniques, computer evaluation, high-speed film recording 78−44343
mechanical vibrations, two-dimensional, layer potentials *(French)* 78−59337
metal, bulk deform. process 78−31459
metal extrusion process, stress and deform. distribs., elastic-plastic anal. 77−48364
metal sheeting, profiled, shear deformation, stressed-skin anal. 79−1121
metal structures, collapse load and energy absorpt., matrix anal. methods 77−35050
metal working by pressure, full scale adaptive simulation applied to computer aided management 79−79055
metals, dynamic compression testing, mech. behaviour 80−40464
Mindlin plate elements, free vibration anal. 79−46244
motorcycle carrier stress anal. 79−43545
multilayer shells, stress-strain state and stability at high temps. 77−54903
noise environment modelling at General Motors Corporation 80−43542
non-ferrous, recycling, system study, computer simulation 78−35278
non-uniform pipe gas flow simulation model 80−33682
nonlinear anal. of deep arches, using mixed curved-beam finite elements 78−18161
nonlinear structures, progressively changing equilib. eqns. soln. 78−1581
nonstationary stochastic process, computer programme for statistical characts. 80−22283
nuclear containment vessel, dynamic response to fluid pressure pulses 78−26077
nuclear fuel rod anal. program CYGRO-4 78−41805
nuclear piping systems, pipe rupture and steam/water hammer design loads for dynamic anal. 78−41868
nuclear reactor, LOCA, thermal shock, reinforced containment wall safety anal. 77−3135
nuclear reactor nonlinear dynamic response of containment, seismic analysis 77−3180
nuclear reactor structural mechanics, conf. 78−41874
numerical modelling of fatigue, crack, creep and corrosion test results, review 78−30243
optical system surfaces CAD *(Russian)* 78−74963
optimal design of dynamically loaded continuous structs. 78−38185
orientation angle calc. using image matrix transformation *(Russian)* 80−73314
pendulum random interactions anal. *(Russian)* 80−73313
plastic instability during tensile deform., numerical calc. 78−30203
plastic zone ahead of crack, development under creep conditions, computer simulation 78−34091
plate, rectangular, variable thickness, stability and vibr. anal., finite element method 77−54918
plate structures, two-dimensional, stress intensity factors calc. *(Japanese)* 78−51123
plates, thin rectangular elastic, bending, finite difference anal. 79−46181
plates design, circular, rigid-plastic, w.r.t minimum-cost variational formulation 77−68440
plates on elastic foundation, simplified finite element soln. 78−26041
pressure vessel, programs and appls. *(Japanese)* 79−21555
pressure vessels, axisymmetric, with structural discontinuities, elastic stress analysis *(Japanese)* 80−38265
Princeton Large Torus, coil stress and deflection analysis, ANSYS computer code appls. 78−50356
random vibrations, statistical data digital processing method *(Japanese)* 80−64430
rectangular laminated plate, free vibrs., freq. and shape determ., complex boundary conditions 80−79203
rectangular orthotropic plates with nonlinear stress-strain relns., large deflections 78−26040
mechanical engineering computing continued
reflector illumination estimation calc. by coordinate systems transformation theory *(Croatian)* 78−16835
refractory, thermal shock resistance by resonant frequency expt., computer program *(German)* 77−9009
ribbed plate single-panel buckling detection, computational procedure *(German)* 78−13941
rock fracture in uniaxial compression, computer modelling *(Japanese)* 80−12379
rolling process, math. model based on plasticity theory *(Russian)* 80−16335
rolling texture control, theoretical and practical study 79−87656
rotating systems, steady motions, computational anal. 80−53618
rough surfaces computer simulation of contact 79−19470
round notch tension test, computer simulation 79−24705
seismic structure yielding rate approx. 77−2522
shell element, triangular facet, linear and nonlinear equilibrium and elastic stability appl. 77−68460
shell wall anal., circular tanks under axisymmetrical pressure 79−46202
shells, paraboloid, elliptic, stress analysis 78−59294
shells of revolution, computer program for linear and geometrically nonlinear static analysis *(Japanese)* 80−64500
ship structure, stress fields hybrid simulation 79−41637
shock waves in bubbly liquids *(French)* 78−26183
slab, semi-infinte, stress amplitudes and fatigue damage resulting from cyclic Hertzian compression 77−19567
solid transient dynamic problems, finite element formulations using explicit time integration 78−18162
steam hammer noise, scale model and on-line computer investigation 79−23137
steel, alloy, tension test, computer simulation of deform. to fracture 79−11667
steel, stainless 304, cyclic plasticity, exponential stress-strain law 77−25157
steel bridges, higher order horizontally curved beam finite element 78−26028
stiffened cylinders under torsion with axial compression 78−26065
stiffened plates, constraint method anal. 78−26066
stiffness factor formulation, explicitly or using numerical integration 77−65676
stiffness matrix for sandwich beams with thick anisotropic laminated faces 79−46182
strength of axisymmetric body, optimum shape calc., finite element technique 78−51060
strength of materials and mechanical systems dynamics, based on three-dimensional models and finite element analysis *(German)* 80−58976
stress analysis, artificial softening of finite elements 77−80067
stress analysis, improved equilibrium finite elements 78−75067
stress distribution of frictional bonds, w.r.t. elastic deformation *(Hungarian)* 79−14275
stress state of structural elements of vessels under external hydrostatic press. 77−14908
stress wave propagation, nonlinear, in perfectly flexible string 78−5670
stresses analysis in non-circular shafts, analogue simulation *(German)* 77−68551
structural anal., axisymmetric solid of revolution elements based on assumed stress hybrid model 79−3917
structural design, role of expt. stress anal. 79−32418
structural design, using 'moment schema' of finite elements, convergence *(German)* 80−14563
structural dynamics analyser development, microcomputer-based 80−53733
structural dynamics problem soln., generalised Euler method 79−46245
structural stiffness matrix eqn., algorithms for direct access Gaussian soln. 78−57766
structural wt. optimisation, optimality criteria and mathematical programming 78−26029
structures dynamic problems, eigenvalue economisation, program *(Italian)* 79−35544
tensile testing, microcomputer for automatic meas. and data treatment *(German)* 77−44433
tension test, computer simulation, effect of testing conditions 80−7729
thermal stress simulation in continuous casting, finite element method 78−30170
thermal stresses rel. to uncoupled thermoelasticity, finite element method appl. *(Italian)* 79−18719
thermoelectric coolers, numerical anal. of transient behaviour 78−21140
torispherical vessel heads, internally pressurised, elastic-plastic buckling 78−79241
transonic potential flow, finite element method programme 80−24045
transverse isotropic inelastic work hardening constitutive model, numerical implementation 78−42547
turbine cascade flow, surface-oriented coords. in num. simulation 77−55018
two-phase recirculating flow, num. calc. procedure 77−55081
u.s. automatic inspection system, computer aided *(German)* 77−4877
US nondestructive inspection system, microprocessor utilization 80−71845
vibration installations certification results processing 80−22336
vibration modal anal. *(French)* 80−42216
vibrational anal., iterative methods, accelerated automatic root search algorithm 78−59321
virtual crack extension method, nonlinear material behaviour 78−18230
water resource finite element anal., conf. at London, England 1978 78−92867
weldbonded joint deform., finite element simulation 78−35636
welding, thermal stresses and metal movement, computer simulation 78−34002

mechanical impact *see impact (mechanical)*

mechanical interfaces *see mechanical contact*

mechanical organs *see artificial organs*

mechanical permeability *see permeability*

mechanical properties of liquids
see also elasticity of liquids
excess Gruneisen parameter in binary liq. mixtures, rel. to intermolecular interactions 77−20082
internal tension, transparent recording Berthelot tensiometer 79−35723
interpenetrating EM structured continua, thermodynamic and mech. props. calcs. *(Russian)* 77−47580

mechanical properties of liquids continued
liquids, response to dynamic tension, conf., Ispra, Italy (Sept. 1977) 79–69178
octyloxycyanobiphenyl, smectic-A phase, dislocation effects on viscoelastic props. 77–84633
polyacrylamide solutions, dil., static and dynamic breaking tensions 79–23346
polymer melts, quasistatic bulk strength meas., specially built apparatus 80–77377
polymethylsiloxane liquids, complex shear modulus determ. from shear wavelength meas. 79–14871
rupture, Berthelot tube method, theory for tension before breaking 77–24341
tap water, tension pulse propag. in column 79–69176
tension pulse propagation in a liquid column 79–69176
viscoelastic fluid theory, entropy effects 77–14971
viscoelastic props. meas. using torsion resonator, 20-1200 KHz *(Russian)* 80–52196
water, estimate of ultimate tensile strength 77–7779
water, free surface, metastable effects associated with press. pulse refl. 80–6463
water, tension pulse transmission 79–68750
water under tension monitoring, Berthelot-Bourdon tube method 80–88238

mechanical properties of solids *see mechanical properties of substances*

mechanical properties of substances
see also anelasticity; bending; brittleness; creep; deformation; elastic aftereffect; elastic moduli; elasticity; fracture; hardness; internal stresses; mechanical properties of liquids; mechanical strength; photoelasticity; photoplasticity; plasticity; slip; stress relaxation; stress/strain relations; tribology; viscoelasticity
acrylate adhesive coating on glass substrate, mech. props. determ. using transfer functions of US oscillations *(Russian)* 79–87644
acrylic moulding formulations, optical and mech. props. 80–106582
acrylonitrile-methylacrylate-acrylamide latexes graft copolymerised onto PVA,for haemodialysis membranes *(Japanese)* 80–12297
aorta, canine, mech. props. following hypercholesterolemia 80–104620
bone, rel. to US surface wave vel. 77–32937
bone mechanical properties and functional adaptation *(Japanese)* 77–25479
brass, free cutting, machinability and mech. props., cooling rate effects *(Korean)* 77–63695
ε-caprolactone-γ-(tert-butyl)-ε-caprolactone copolymers, dynamic mech. props., glass transitions 77–25086
ceramic, mech. engng. props. and applic., conf., London, England (Dec. 1977) 79–38840
ceramics, engineering materials, nature and props., book 78–72707
ceramics, mech. props. meas., apparatus for up to 1700°C *(French)* 80–104374
chitin (poly-N-acetyl-D-glucosamine), dynamic mech. behaviour, effect of water 80–97522
chitosan (poly-D-glucosamine), dynamic mech. behaviour, effect of water 80–97522
clay, mech. props. at high-press. 80–76966
clay layer, non-homogeneous, consolidation estimation method 79–58110
concrete, refractory, high temp. mech. props. *(French)* 77–56019
cracked material, elasticity parameters calc. 79–55346
N,N-diethylacrylamide, cross-linked copolymer, improved mech. props. 80–61091
elastomer, adhesive 77–16638
elements, monotonous series based on atomic bond energy, for mech. and phys. props. calc. *(Russian)* 80–19740
epoxy, filled, adhesive, mech. props. 77–16638
epoxy resin cross linked with aliphatic polyamines, struct. and dynamic mech. props. *(Japanese)* 80–38956
Estrodur 31s, polyester moulding material *(Polish)* 80–66523
ethylene vinyl alcohol copolymer, prep., props. and appls. *(German)* 80–89194
fibre reinforced plastics, mech. props. stabilisation by PVA fibres modification 79–20022
fluorinated copolymers, mech. and elec. props., processing and appls. 78–84760
fragile materials, mech. props. and fracture mech. *(French)* 80–104274
fragile materials, mech. props. meas. using disc-shaped specimens *(French)* 80–104367
glass, engineering materials, nature and props., book 78–72707
glass characteristics, electromagnetic, mechanical and thermal props. 80–106587
glass composition and props. for structural material 80–84944
glass reinforced plastic, microwave determ. of mech. strains, anisotropic props. in millimeter range 77–9023
glass-C fibre composite, mech. props. and residual stresses in wound components 77–52436
gradient index material models and exptl. verification 80–16002
high polymer physics, conf., Washington, USA (March 1978) 79–11633
high strain rates, conf., Oxford, England (Mar. 79) 80–82575
high strength Al-Zn-Mg-Cu alloys, mechanical props. *(Japanese)* 79–91654
inhomogeneity of materials, statistical considerations 78–67033
injection-moulded article mech. props. rel. to process parameters 79–78929
Kayenta sandstone, influence of pore press. on mechanical props. 78–81150
low-temperature materials props. and appl. *(German)* 80–3081
magnetostrictive ferrites, magnetising field influence on amplitude depend. of mechanical props. 78–2723
mass produced parts, appl. of statistical algorithms for optimisation of mech. props. 77–68550
materials science, phys. and mech. props. 80–25538
medical polymers, chem. problems, conf., Prague, Czechoslovakia (Aug. 1977) 80–56996
metal fibre filled polymer, mech. and cond. props. 79–91808
metal-glass mats. alloyed with Cu, powder prep. and props. inc. running-in ability 78–72912
metallic glasses, atomic struct., mech. and mag. props., prod. methods, uses 77–1081
metallic glasses, prep., characterization, review struct., formation, electronic, mag. and mechanical props., review 78–3074
metallic glasses, production and properties, technological appl. 80–71105

mechanical properties of substances continued
metallic glasses, structure, stability and prod., elec., mag. and mech. props., review 80–44134
metallic glasses props., developments and appl. 80–19710
metals, effect of H_2 on mech. prop., methodological approach to study *(Russian)* 78–31507
metals, engineering materials, nature and props., book 78–72707
metals, high temperature testing, MEITP-1 indentation system (USSR) 80–74820
microballoon reinforced plastics, acoustic and mech. props. rel. to hydrophone applic. *(Japanese)* 77–7793
microstructure influence 77–7302
microstructure-property relations in materials 77–36378
nuclear fuel rod structural anal. criticism 78–82441
optical material physical props., seminar, San Diego, CA, USA (Aug. 79) 80–105423
oxide, solid electrolytes, thermal and mech. props. at steelmaking temps., review *(German)* 78–15418
phosphate bonded synthetic mica ceramics, form., physical props., texture 77–21063
piezoelectric transducer with current in semiconducting boundary layer, mech. response 78–18139
plastic ligaments and tendons, dynamic motion simulator for testing *(German)* 78–81070
poly-N-vinylcarbazole, polymerisation, struct., props., elec. characts., review 79–41972
polyacrylic acid film, structurisation and mech. props., EM obs. *(Russian)* 80–59406
polyether-urethane elastomers, crosslinked, three dimensional polymerisation, kinetics, gel. form., mech. props. *(Russian)* 80–7792
polyethylene fibre prod. by surface growth method, mech. props. 80–104108
polyethylene films, fibres, radiation initiated graft polymerisation of acrylonitrile, initiation rate rel. to props. *(Russian)* 80–7531
polyhexamethylene terephthalate/polyoxytetramethylene block copolymers, thermal and mech. props. 78–91260
polyimides, oriented cycloaliphatic, thermomech. props., synthesis *(Russian)* 80–55443
polymer, interstructural filling, effect on props. 77–63622
polymer orientation measurement, in solid, by spectroscopic techniques, mech. anisotropy 78–75558
polymer structure and optical behaviour 80–106583
polymers, engineering materials, nature and props., book 78–72707
polymers, solid, orientation effects, conf., Budapest, Hungary (April 1976) 78–75557
polymethylsiloxane-polyarylate block copolymer, soln., viscosity, rel. to film mech. props. and microstruct. *(Russian)* 79–23762
polyurethane, adhesive, mech. props. 77–16638
polyurethane, elastic fibres, cross link density effect on mech. props. 77–70023
polyurethane, heat treatment, physical and chemical structure mutual effects *(German)* 79–57229
powdered minerals, adsorbed films influence on cohesion and angle of internal friction 77–25084
products for nuclear power stations, research and development *(Russian)* 79–34080
prosthetic material mech. props., effects of physiological environment, cardiovascular appls. 80–8212
PTFE, mech. and elec. props., processing and appls. 78–84760
PVC, chlorinated, fibres, radiation initiated graft polymerisation of acrylonitrile, initiation rate rel. to props. *(Russian)* 80–7531
PVC, influence of thermal history on physical props. 79–4984
PVC, rigid asbestos reinforced, stabilization and dynamic thermal stability 79–8270
PVC, technological obs. and methods 79–7349
PVC physics symposium, Lyon-Villeurbanne, France (July 1976) 79–7554
PZT, ferroelec. ceramic, mechanical props. determ. by acoustic techniques 79–28685
reactor fuel pin tubes 79–47755
refractory metals, mech. props. and diffusion figures *(Russian)* 80–40436
rock salt from New Mexico Salado formation, mech. props. at high-press. 80–72492
rocks, mechanical characts. rel. to terrestrial heat flux in vertical orogenetic profile *(German)* 78–81123
rocks, mechanical heterogeneities rel. to flow cleavage form. 79–57934
rocks, metamorphic, thermomechanical expts. using shear machine *(French)* 79–5474
rubber latex, natural, mechanical and chemical stability enhancement, by potassium fatty-acid soaps 79–96034
sea ice, in-situ meas. of mech. props. using flatjack methods 80–69751
sediments of United States Atlantic continental shelf, engineering props. 80–72511
sheet metals, strain-induced changes in mech. props. and press formabilities 78–19781
sheet moulding compound, material, process and performance 80–81032
skin, X-ray effects, mouse 77–12960
soil, consolidation due to shear loads distributed over rectangular area 79–57936
soil, mechanical properties rel. to viscoplasticity under dynamic loads 78–96197
spinel single crystals, mech. props., 1350-1650°C *(French)* 80–104374
stainless steel aged by discontinuous precipitation mechanism ultrafine grain and mech. props. *(Russian)* 77–70053
steel, bainitic, low C and alloy, quenched microstruct. effect on mech. props. *(French)* 79–79003
steel, C, texture effect on mech. props./magnetic props. relationship, NDT appl. 79–96274
steel, case carburised, residual stress effect in mech. performance 79–24659
steel, complex alloy, Cr (12-18 wt.%), transformation behaviour *(German)* 80–40349
steel, corrosion resistant, review of heat treatment, mech. and corrosion resist. characts. *(Korean)* 79–24653
steel, Cr-Mo-V, cast, creep resistant, rare earth addition effect on deoxidation, nonmetallic inclusions and mech. props. *(German)* 79–66067
steel, Cr-W-Mo-Co, high-speed, from atomised powders, mech. and cutting props. 80–66556
steel, hot-rolled high quality sheet use of stat. maths. for NDT determ. of mech. props. 79–11749

mechanical properties of substances continued
steel, low C, quench-hardened, plastic deform. effect on mech. props. and struct. *(Russian)* 77−70102
steel, maraging, hot work die use, mech. props., heat resistance 77−70081
steel, mech. props., temp. effects *(French)* 77−56017
steel, Mn-Si, 17G2S, VN and NbV dispersion hardening effect on mech. props. 78−3137
steel, Ni-Mo-C (2.0, 0.2, 0.4 wt.%) sintered, struct. transforms. and mech. props. after quenching 80−66557
steel, prestressed, use as pressure vessels for nuclear reactors *(German)* 79−3196
steel, rare earth metal additions effects on mech. props. 78−52829
steel, rolled, used of statistically justified methods in determining heterogeneity and mech. props. 79−52516
steel, rolled sections, continuous rolling process considerations *(Rumanian)* 79−29097
steel, tube, mech. prop. testing by harmonic method using instrument type KAP with feedthrough transducer 78−53154
steels, constructional and tool, heat treatment effects on elec., mag. and mech. props. expt. 77−77719
structural materials, radiation effects, review 80−49267
UV and IR instrument material mech. and thermal props. 80−106584
variational principle in general dissipative materials *(Japanese)* 77−23896
weathered Athenian schist, basic geotechnical and mineralogical props. 78−61408
AgMgO for LV switchgear contacts *(Slovak)* 78−56603
Al-Mg-Zn, granulated, degassing atm. effect on mech. props. of semifinished products 80−7720
Al-Si, thermal control of interphase microstresses and mech. props. 77−12654
Al-Ti alloy for use in aircraft, work hardening *(French)* 80−97502
Ar, solid state props., statistical thermodynamic calc. using gas phase intermol. pair pot. *(German)* 77−20083
Au-Cu-Ag, phase transform. effect on mech. props. *(Russian)* 78−3122
BN/BN composites, prep., mech. props. 77−21080
C fibre reinforced C, fibre-matrix interactions 78−84725
C fibre reinforced composite, space appls. rel. mech. and thermal props. 78−7016
C fibres, engineering applications, production requirements and mech. props. 80−89168
C film, sputtered glassy, prep., mech. and struct. props. 77−66588
C-C composite, reinforcement scheme effect on mech. props. 77−66620
Ca aluminophosphate foam glasses, for prosthetic appl., porosity and mech. props. 79−74128
CdTe, physical props., review 77−39833
Co, review 79−95909
Cr pyrolytic coating, effect of support metal mech. props. on formation *(Russian)* 80−7713
Cr_2O_3-Mo_2O_3, catalyst, effect of Al_2O_3 additives on catalytic activity, in oxidation of methanol to formaldehyde *(Russian)* 79−66346
Cu, electrodeposited, struct, physical and mech. props. *(Russian)* 79−56939
Cu-Al, gamma-2 phase intermetallic cpd., mech. props., effect of inversion domains 79−61599
Fe and Fe alloys, fast neutron irradiated at high temps., mech. props. 79−51157
Fe, Armco, flat-rolled and annealed, dislocation struct. and mech. props. *(Russian)* 79−20062
Fe based alloy, amorphous, liq. quenched, struct., thermal stability and mech. props. 80−88059
Fe, cast, rare earth-Mg, metallurgical and technological features, appl. in China *(Chinese)* 78−84851
Fe powder sintered compacts, mech. props. effect of powder type and processing conditions *(Czech)* 77−59830
Fe-Al (16 wt.%), prop. improvement *(Chinese)* 77−73280
Fe-Cu-glass ternary multiphase composite, microstruct. and props. *(German)* 77−90314
Fe-Ni-Al-Co-Cu-Sn alloy YuNDK35T5, Sn addition effects on physicomechanical and magnetic props. and workability *(Russian)* 77−70101
Fe-VN(NbN)-(C), dispersion hardening effect on mech. props. 78−3137
Mg-Y-Zn-Nd-Cd alloys, influence of Zr addition on struct. and mech. props. *(Russian)* 80−40370
MgO, polycrystalline, ductile, porous, model 79−47653
MgO polycrystals, mech. props., 900-1150°C *(French)* 80−104374
MgO, single crystal, effect of heat treatment on mechanical props. 77−70070
Mn-Al-C alloy, anisotropic, permanent magnet appl., properties and production *(German)* 79−8309
Mo, impurity interactions with C, N, and O, struct., mech. props. and purification 79−52277
Mo-Zr-B, porosity and mech. props. after neutron bombard., 780-1080°C *(Russian)* 80−24502
Nb, vacuum heat treatment effects on gas content and elec. and mech. props. *(Russian)* 79−43281
Nb-Mo-Zr-Ti, Zr and Ti effects on struct. and mech. props. 77−70061
Nb-Mo(Zr) alloys, vacuum heat treatment effects on gas content and elec. and mech. props. *(Russian)* 79−43281
Ni based alloy, amorphous, liq. quenched, struct., thermal stability and mech. props. 80−88059
Ni-based superalloys, mechanical integrities of surface oxides, oxidation 78−95844
Ni-based superalloys, mechanical integrities of surface scales, contaminant corrosion 78−95845
Ni-Cr-Ti-Al-Mo-Nb-Fe (13-16, 2.35-2.75, 1.3-1.7, 2.8-3.2, 1.8-2.2, 2.0 wt%), heat resistant props, mech props. struct., stepwise ageing effects *(Russian)* 78−76666
$Pb(Zr, Ti)O_3$ ceramics, low temp. sintering, elec. and mech. props. 80−71616
Pu and other actinides, conf., Baden-Baden, Germany (Sept. 1975) 77−19807
Si_3N_4 reaction bonded, microstructure, formation, properties, phase composition 79−56947
SiO_2-Al_2O_3-MgO-TiO_2 devitrificates, microstruct. and props. *(Polish)* 80−70141
T, metal and alloys, mechanical props., electrochemistry, oxidation and corrosion resist., conference, Nantes, France (Nov. 1978) 80−41932
Ta-C-B system, mech. and physical props. 77−59731
ThO_2-UO_2 solid solns., props. of importance for use as nuclear fuels 79−54506

mechanical properties of substances continued
α-Ti alloy, crystallographic texture, importance in characterization 77−28821
Ti alloy VT9L, cast, welded joint mech. props., filler material and heat treatment effects 79−87671
Ti, implant surgery appl. 77−73615
Ti, TiN, TiC, CVD layers on Fe substrate *(Japanese)* 78−27415
Ti-Al-Cr-Mo (6, 2.0, 2.5 wt.%), microstructural changes and mech. props. 77−25080
Ti-Al-O, V effect on thermal stability and mech. props. 77−21171
UO_2, nuclear fuel, mechanical response to transient heating, accident conditions 77−14237
W, impurity interactions with C, N, and O, struct., mech. props. and purification 79−52277
WC-Co, TiC coated, TiC stoichiometry effects on mech. props. 77−66715
WC-Co (5wt.%) hardmetal, η-phase precipitation effect on struct. and mech. props. 79−47696
Zr alloys, thermal neutron capture cross-section var. with time, calc., and mech. props. var. 77−61505

mechanical relaxation *see anelastic relaxation*

mechanical strength
for fatigue strength, see fatigue; for creep strength see creep fracture see also bending strength; compressive strength; fracture toughness; impact strength; notch strength; shear strength; tensile strength; yield strength
acrylic bone cement spinal fixation, mech. props. 78−81072
adhesion testing, use of fracture mechanics concepts 80−50802
adhesive bond testing, US trapped modes in layered media 77−32761
agglomerate characterisation methods, review *(German)* 79−100443
alloy, austenitic, mechanical changes after electrolytic quenching *(Russian)* 80−50653
alloy, heat-resistant, alloying and heat treatment effects on struct. and strength 78−95758
alloy, production process strength *(Russian)* 77−21152
alloy, spinodally decomposed, interfacial energy effect on mech. strength, theoretical estimation 79−38790
alloy parts, heat treatment, chem., principles and practical procedures *(Russian)* 79−52260
alloys, magnetic, amorphous, magnetic strip appl. *(German)* 77−16700
aluminoborosilicate glass fibre reinforced epoxyphenol and phenolformaldehyde, strength props., binder effects 79−5028
ampule for inside fission reactor exam. of materials, examining creep, long term strength in plane stress state 78−85098
anisotropic materials, strength-surface tensor components, determ. 79−98603
anodic, and free anodic film on Al substrate, deform.-strength props. *(Russian)* 77−69203
austempered reinforcing wire, tempering under stress, effect on mech. props. and relaxation resistance 80−100861
austenitic steel, hardened by thermomechanical treatment with ageing, influence of stabilisation on mech. props. *(Russian)* 77−52356
bimetal, obtained by facing, static and fatigue strength, obtained by facing 77−90457
bonded Al-CFRP single lap joint strength 79−29328
bone, compact, deform. and strength 78−24087
bone, deform. and strength, change dynamics at early stages of form. 78−7383
bone, demineralised dense human, strength props. nonuniformity 80−104611
brittle fibre reinforced composite, static strength depend. on component separation boundaries *(Russian)* 80−76304
brittle material, strain rate depend. effect of specimen vol. on strength 78−90726
brittle material, strain rate dependent effect of specimen vol. on strength 77−56085
brittle materials specimen prep. for strength determ. 80−40632
brittle model mats., porous and nonporous, strength and struct. 77−4849
brittle plate containing stochastically distributed rigid rod like inclusions, strength *(Russian)* 77−23917
and brittleness estimation in low-deform. inorg. mats. 77−86131
butt welded joint dynamic strength, partial penetration and slag inclusion effects 79−83288
cable design and testing, optical fibre 80−69551
carbon steels isotropic-kinematic strengthening during plastic deform. *(Russian)* 77−20007
cavitation mechanical strength, US assessment of materials in various media 77−16772
cellulose, nitrated, strength, deform. and disintegration, influence of stable free nitroxyl radicals 80−11717
cellulose acetate fibre and film, stabilisation, post UV-irrad. mech. strength *(Russian)* 79−24778
cellulose hydrate, nondestructive control of mech. props. anisotropy, appl. of capacitance method 77−86277
cement and mortar, strength, fracture mode, statistical props. *(Japanese)* 78−31520
cement based materials, fatigue hardening 79−29086
cement mortar, cured by 28-day standard and accelerated methods, strength correlation 77−16762
ceramic, compaction during pressing, green strength, effect of adsorbed layers *(German)* 78−6880
ceramic, strength recovery by diffusive crack healing 77−77555
ceramic composite, mech. props. *(Polish)* 78−31481
ceramics, fracture mech. appl. 79−43426
ceramics, microstructure and microcrack processes, applicability of fracture mechanical methods *(German)* 78−31500
ceramics, polycrystn., strength-grain size relations 79−79081
ceramics, US investigation, porosity, mech. and dielectric strengths *(Polish)* 79−52565
chain of bundles probability model for fibrous material strength 78−67095
chemical apparatus, expt. strength anal. *(German)* 79−32427
cladding layers on metal, tear resistance, method of determ. 77−25211
coated specimens, bearing capacity, testing under external and internal pressure 79−70254
cohesive strength of constructional components with crack-type defects, stress intensity coeff. *(Russian)* 78−30234
coke, metallurgical, microstruct., using refl. light microscopy and image anal. 80−66732

mechanical strength continued
composite, multilayer cylindrical shell, elastic filler, strength and stability under combined loading, mass minimising 77−65699
composite glasses, high strength, prod. by overlayering 80−89193
composite laminates, proof test and fatigue study 80−93643
composite material, mechanical behaviour, book 80−94935
composite material strength criteria 80−10208
composite materials, bearing capacity of designs, subject to intense surface heating 78−67057
composite materials, density depend. of strength *(German)* 78−94592
composite materials, internal stress depend. on density gradients *(German)* 79−1105
composite materials, laser beam determination, of elasticity-compressibility modulus, during compaction 79−43542
composite materials, mech. props., theory, review 80−64392
composite materials, reliability, exam. of mech. strengths and fatigue charcts., review 80−11762
composite materials, stochastic fracture models, and strength test results statistical anal. 80−64470
composite materials, universal chamber for high temp. strength testing up to 2000°C 77−63858
composite materials *(Japanese)* 77−9039
composite T-beams, repeated loading effects 77−86253
composites, reinforced in two directions, strength 80−19288
composites, review *(Japanese)* 78−39850
composites, strength criteria, stress anal. *(Russian)* 80−1482
composites, three-dimensional structure, mech. charcts. 80−38266
computing, based on three-dimensional models and finite element analysis *(German)* 80−58976
concrete, bamboo-reinforced columns, behaviour when subjected to eccentric loads 79−52320
concrete, beam, unbonded partially prestress reinforced, ultimate moment of resistance 77−25107
concrete, core strength, effect of length to diameter ratio 77−63861
concrete, fatigue strength rel. to static strength *(Japanese)* 78−11329
concrete, polymer impregnated, polymerised by accelerated electrons, fabrication and strength *(Japanese)* 77−77456
concrete, pressure vessels, multicavity PCRV, design and anal. for ultimate strength calc. 78−44182
concrete, strength, NDT standardization 79−91902
concrete, US assessment, of strength at early ages 77−25225
concrete and mortars, containing S, durability study in temp. cycles and water resistance 78−27613
concrete cylinders, fracture, fluid pressure testing using H_2O and N_2 gas 78−60750
concrete quality assessment, US pulse vel. meas. practical use 80−100991
concrete testing, accelerated curing procedures adoption 79−5091
continuous bodies under gravity load, centrifugal force, optimum strength shape 79−98665
conveyor belts with steel reinforcing cables, computer-aided magnetic defectoscopy 77−73417
corundum, grinding material, review *(Polish)* 80−29917
corundum, mech. strength rel. to tension intensity factor *(Polish)* 80−11725
corundum ceramic, high-temp. treatment, powder medium effect on microstruct., comp., strength and dielec. props. 79−33984
creep, influence of strength for given strain *(Russian)* 79−55815
creep analysis of thin wall structures, subject to transient heating and loading 80−33486
defective material, with strength, anisotropy induced by pretreatment, limiting state probability calc. 77−86123
diamond, mechanical strength depend. on thermal working parameters, microcracks *(Russian)* 80−55501
diamond, synthetic, N impurity effect on strength charcts. and thermal stability 80−11726
diamond-metal strip, strength props. 79−61678
die steels for cold plastic working, powder metallurgy, charcts. 78−68649
dispersion hardened alloys, strengthening theories 80−97498
dispersion-hardened single crystals, theory of high-temp. strength 77−48445
elastic structures, computer automated synthesis for minimum struct. weight 78−34015
elastic-liquid systems, dynamical strength *(Russian)* 78−51085
electromagnets, high field, historical review of development, mech. strength, performance limits 77−10073
electromagnets for nuclear fusion and high energy research, insulation systems, aspects 78−89506
epoxides, dielectric relax. and deform props., cross-link density effect *(Russian)* 80−60942
epoxy resins, alteration by reactive elastomers *(German)* 79−100106
epoxy type adhesives, solidification temp. conditions rel. to strength *(Russian)* 79−56972
epoxy-based crosslinked polymers, deform. and strength charcts., temp. effects *(Russian)* 79−65139
ethylene vinyl acetate copolymer, torsional rigidity testing *(German)* 77−52596
failure criterion considering stress state at crack apex 79−57113
fatigue crack growth dependence on loading parameters, phenomenological model 80−38340
Fe, Armco, long-term strength, H effect 80−55581
α-Fe, long-time strength *(Russian)* 77−44330
femoral cement-free implant, mechanical strength tests *(German)* 79−8570
femur with proximal prosthesis, 3-dimens. anisotropic stress anal. and failure prediction 78−40424
ferrite core, strength improvement method, SiO_2 and Bi_2O_3 additions, mag. charcts. 79−24484
ferrites, 2000NM and 2BA, effect of temp. 80−7753
ferrites, sintering, strength and mag. props., vacuum effects 79−70028
fibre reinforced composite, mech. behaviour, axial residual stress effect 77−36573
fibre reinforced composite, stiffness and strength investig. 77−63874
fibre reinforced composite aircraft materials, design allowables 80−81204
fibre reinforced composites, conf. Moscow, USSR (Nov. 1978) 80−8733
fibre reinforced composites, failure, probability bounds 79−87716
fibre reinforced composites, materials properties, unsolved problems, review 77−4843
fibre reinforced composites, mech. props. 79−52329

mechanical strength continued
fibre reinforced composites, micro- and macrocracks 80−65148
fibre reinforced composites, US method for evaluating strength props. 78−76796
fibre reinforced composites, zonal winding pattern analysis, thin spherical shells 80−38253
fibre reinforced concrete, strength calc. 78−11286
fibre reinforced polyester composite, interface strength *(Japanese)* 78−15646
fibre reinforced polymer matrix composites, space environmental effects 80−71721
fibre reinforced thermoplastic, mechanical strength, depend. on fibre morphology *(German)* 80−30043
fibreboard, made from Asplund pulp-PMMA composite, props. *(Japanese)* 80−7664
fibres, reinforcing, strength eval. by dry bundle method 79−100312
fibrous materials, chain of bundles probability model for strength, numerical study of convergence 78−88496
fibrous materials, NDT determ. of mech. strength anisotropy using radiowave method 80−25969
filament, thin, technical strength rel. to diameter environmental effects *(German)* 79−27529
filament reinforced hypoeutectoid C steel, strength charcts. after deform. and quenching 80−35271
filled system, vibrational thinning, visoelasticity and strength 77−8795
filtration deposits, basic indices of structural-mechanical strength 77−40496
fracture mechanics, stability of mech. strength 79−57117
fusion reactor, TFTR, vacuum vessel bellows, strength and fatigue anal. 80−95455
fusion reactor first wall materials, mechanical, corrosion and irrad. behaviour requirements 77−67875
girder, circ-arc bow type, ultimate strength, plasticity *(Japanese)* 80−43631
glass, co-acting (synergistic) flaws and strength 77−20168
glass, devitrified opaque technical, microstrength and hardness 80−89312
glass, mechanical destruction role of relaxation processes 80−89282
glass, mechanical properties, review 78−3162
glass, rupture behaviour, long-term strength, thermofluctuation theory *(Russian)* 80−40536
glass, silicate, ultimate strength, and max. breaking rate 80−25863
glass, strength test, biaxial, use of Weibull statistics 78−68798
glass, surface damage by abrasive contact, effect on strength 80−85066
glass, surface treatment, improvement in mech. and optical props. recent progress *(Japanese)* 79−79141
glass and glass fibres, microbrittleness and strength depend. on chem. comp. 79−38937
glass fabric, effect of phosphate binders on properties 78−44075
glass fibre reinforced composite, thick-walled shell, crack prevention during heat treatment 77−52376
glass fibre reinforced epoxy, short aligned fibres, mech. charact., SEM and optical obs. 78−72761
glass fibre reinforced epoxy, unidirectional, strength distrib. 78−68735
glass fibre reinforced epoxy resin, local defect effect on strength 77−90317
glass fibre reinforced epoxy/Al bonded joint, mean strength, moisture effects 79−20106
glass fibre reinforced plastic, laminate, comparison of single and multihole bolted joint strength 79−91739
glass fibre reinforced plastic, monolithism and reliability conditions 78−48364
glass fibre reinforced plastic, NDT of strength after immersion in hot water 77−90530
glass fibre reinforced plastic, pin-bearing strength, stacking sequence effect 77−70105
glass fibre reinforced plastic, radial orientation of reinforcement for high strength shell 79−95994
glass fibre reinforced plastic, reliability determ. 78−1568
glass fibre reinforced plastic, residual strength, hygrothermal history effect 77−77513
glass fibre reinforced plastic, ring, exposed to press., transverse prop. effect on bearing capacity 77−86177
glass fibre reinforced plastic, strength dispersion, statistical anal. *(Japanese)* 79−61655
glass fibre reinforced plastic, strength geometry 77−70123
glass fibre reinforced plastic, structural inhomogeneity and strength 79−43358
glass fibre reinforced plastic laminate in plane-stress state, strength depend. on reinforcement struct. 78−23796
glass fibre reinforced plastic laminates, strength and deformability, artificial ageing effect 80−60893
glass fibre reinforced plastic panels, design for strength and stiffness 79−61601
glass fibre reinforced plastic stiffened shells, residual stress formation 79−100108
glass fibre reinforced plastic wound struct., scale factor rel. to strength 80−3135
glass fibre reinforced plastics, coupling agent/matrix interface investigation by Fourier transform IR spectroscopy 80−20884
glass fibre reinforced plastics, dielectric const./mechanical strain relation, microwave study 77−32650
glass fibre reinforced polyester and epoxy resin, vacuum hardened shell, strength and deform. charact. eval. 78−48528
glass fibres, forming conditions influence 80−20882
glass laser rod, mech. strength and heat resistance obs. 79−76776
glass plastics, strength criteria 80−10208
glass segment, resting on elastic ring, structural strength 80−14630
glass surfaces, cracked layer thickness determ., chemical method 80−64226
glass textolite cylindrical shells, parallel wound, feasibility of diagnosing strength 78−67157
glass workability rel. to melting history, microstruct., apparent liquidus temp., mechanical props. 80−11633
glass-carbon fibre-reinforced composite disc, rot. strength 79−74198
glass-ceramic/bone histological and mechanical bonding *(German)* 79−8569
glass-ceramics, transparent, microstruct. and props. 78−59960
glass-textolite shell, NDT 78−11471
glass/C reinforced epoxy resin, hybrid effects, conditions for positive or negative effects vs. rule of mixtures, mech. props. 78−68769

mechanical strength continued
granular materials, abrasive, failure and strength charact. in US field, test unit 80−85112
graphite, porosity effect on strength variation 78−31369
graphite fibre reinforced epoxy matrix laminates, microscopical anal. 78−3288
graphites, strength and struct., conf., Bath, London, England (Apr. 1979) 80−82566
heat resistant material, long term loss of strength 80−71751
heterogeneous materials, linear analysis 78−5664
high temperature materials, classification and long-term strength charact. prediction 77−44324
high-strength metal development theory and technology *(French)* 77−21057
high-temperature materials for space power systems, mech. props. 79−57045
hydroxylapatite, sintered bioceramic, prep. and props. 79−43174
ideal strength of solids, computer calc. 78−30697
Incoloy, evaluation for use in nuclear process heat appl. 78−13234
inorganic glass, effect of liq. medium on process of mechanical destruction 80−89283
IR transparent materials and components 77−19374
joint, glued permanent in spherical shell of brittle material, structural strength 80−3293
joint strength, effect of change in surface morphology of adherend 77−36672
laminate cylindrical shells, prepared by continuous filament winding calc. of strength and reliability 80−10194
laminated composites, effective length of reinforcing component 80−25797
laminated plates, anisotropic strength optimisation, within supercritical range 79−59934
laminates, thin, optimal struct. and strength in two-dimens. stress state 80−64395
large optical component antireflection and protective coatings 79−72660
laser glasses, figures of merit and physical/optical property correlations 79−13970
layered thin composites, optimum design and strength 80−10210
leucosapphire, unique polishing features of hard crystals 80−64225
lightguide fibre, ensuring mechanical reliability 80−79001
load-bearing structures, behaviour prediction of materials degradation 79−34133
long-term strength, accelerated method 77−40494
long-term strength prediction by stepwise loading based on theory of damage accumulation 80−48644
long-term tests, automatic temperature regulation system 77−63853
low C steel, explosive-thermal treatment, sulphide cracking decrease, hydrogen embrittlement *(Russian)* 80−108477
Mersilene mesh, herniorrhaphic reinforcing prosthetic, mech. and struct. props., SEM study 79−74789
metal, computer prediction of long term strength by generalised diagram method 77−70133
metal, deformed, dispersion-hardening, theory of strength *(Russian)* 78−35424
metal, microstructure and strength *(German)* 77−70138
metal, pure, with max. of cryst. lattice distortion, struct. and strength props. *(Russian)* 80−89234
metal, strength, long-term charact. interpolation calc. using generalized curves and computer 77−86121
metal heat resistant power installation elements, estimating strength, ductility, heat resistance diagrams 80−25770
metal-dielectric interference mirror coatings, high mech. strength 78−30043
metal-polymer joint, meas. of temp. dependence of joint strength 80−50824
metallic glass, composition, mech. props., simulation 80−49117
metallic two-phase coating, ductility maximum, weakening and strengthening 79−11681
metals, crack resistance, high temp., during creep due to stress relaxation *(Russian)* 79−52348
metals, creep limit and long-term strength, parametric eval. method 80−100996
metals, determ. with pulsation attachment for TsDMU-30t test machine 79−52538
metals, high temp. stress anal. by finite element method 80−96203
metals, monovalent, mechanical ideal strength, pseudopot. model calcs. 79−77670
metals, strength and corrosion tests, NDT, electromagnetic methods, use in anal. of destructive materials testing *(German)* 77−73396
metals, strength and corrosion tests, quantitative noncontact meas. of physical and geometric props. *(German)* 78−23909
metals, time to rupture and accumulation of damage under load *(Russian)* 79−5029
metals and alloys, polycryst., strength differential effect, temp. and strain rate sensitivity in saturation cycling 79−66094
metals radiation damaged long term strength curve forecasting *(Russian)* 80−34040
microinhomogeneous brittle bodies *(Russian)* 77−58608
monocarbide, cubic, calc. of surface energy, rupture energy, and theoretical strength 77−11775
montmorillonite, mech. props. at high press., rel. to fault behaviour 79−84234
mullite-corundum ceramics, thread-like crystals reinforced, props. 80−108525
multilayer cylindrical shell, theory in inhomogeneous temp. field 80−1434
mylonites, grainsize reduction and grain boundary sliding rel. to flow strength 80−21721
Ni powder 2JJ, porous, effect of sintering conditions in struct. and strength 80−20823
Nichrome wire, porous, strength charact. 78−6997
Nichrome/steel, porous metal-thread sheet materials, filteration, permeability and strength props. *(Russian)* 79−78915
nuclear reactor structural materials assessment, AISI 316 and 9Cr-1Mo steels, for UK LMFBR 78−86581
nuclear reactor valve bellows, effect of service parameters on fatigue life and fracture 78−58348
opal glass, chemically toughened, prep. and mech. strength *(German)* 80−89191
opposed-anvil high-press. devices, material strength effect 80−47068
optical element, antireflection or protective film effect 78−1318

mechanical strength continued
optical fibre, mechanical strength, fractographical analysis, review *(Japanese)* 80−35319
optical fibre cable transmission and strength improvement technology 80−28347
optical fibre waveguide cables, reinforcement, mech. props. *(German)* 78−33861
optical fibres, investigated using fracture mechanics *(Japanese)* 79−59817
optical fibres, mechanical strength reinforcing and reliability improvement methods of fabrication *(Japanese)* 80−87568
optical fibres for communication, fibre technology and props. *(German)* 79−81564
optical glass strength limit rel. to Knoop microhardness 79−72641
optical high-strength fibre production and prooftesting 80−64204
optical waveguide performance before and after storage 79−27392
optimum machine element shape finite element technique 77−62152
optimum strength shape, axisymmetric body, finite element technique 78−51060
ordered alloys *(Czech)* 77−1854
organic fibre reinforced plastics, failure 80−11774
organic textolite, long-term strength in plane stressed state 80−60930
organicfibre reinforced epoxy, temp. dependence of strength under plane stress state 80−7642
orthodontic adhesive joints, adherend topography effects 77−52916
para-polyamide based fibres, struct. deform. props. 80−60928
parabolic lens, mag. field limited, mech. strength and dynamic loading 79−18341
particles, abrasive, mech. strength determ. 79−87781
phase transformation, $\alpha \rightleftarrows \beta$, influence on mech. props. *(Russian)* 78−68681
phosphate bonded refractory plastics, hot modulus of rupture, 1500 to 2500°F 78−19855
piezoelectric ceramic, TsTBS-3, mech. strength, effect of glass powder addition 78−31370
plasma coating, fused, strength of adhesion to base by gas flame soldering 78−23894
plasma sprayed materials, control of mech. props. 80−11560
plastic, elastic filler reinforced, cylindrical shell, design optimisation under dynamic loading 79−59935
plastic, torsional rigidity testing instrument, used with strength testing instrument *(German)* 77−52596
plastic, with wide range of moisture content, mech. props. determ. with conic plastometer 78−11270
plastic deforms ands rupture mechanisms, depend on B additives *(Russian)* 79−61650
plastics reinforcement theory, functional model *(German)* 77−58564
plate, transversely isotropic with elliptical notch, in a steady temp. field, calc. of strength 78−63330
plexiglas shell, orthotropic, cylindrical, interacting under straight angle, manufacture and strength 77−90417
plexiglass composite, long term strength and durability 80−75294
plywood, strength geometry 77−70123
PMMA, defect build up in service, effect on notch sensitivity 77−66694
PMMA moist surface mech. strength reduced by electric charge *(Russian)* 80−60486
poly(p-benzamide), highly oriented, ultimate mech. props. 79−91751
poly(p-phenyleneterephthalamide), highly oriented, ultimate mech. props. 79−91751
poly(vinyl alcohol)-acrylonitrile copolymer membrane, water permeability increase *(Japanese)* 79−70375
polyamide, torsional rigidity testing *(German)* 77−52596
p-polyamide based organic fibres, effect of temp. and deform. time, on deform. strength props. 80−11720
polyamide mixtures, thermodynamically incompatible, composition-prop. relationship *(Russian)* 80−7872
polyamide-6, surface defects and mech. strength, oriented polymer *(Russian)* 78−51451
polycaprolactam, fibre, struct. change when used as resin reinforcement *(German)* 77−21091
polycarbonate, effect of thermal treatment on strength, TSC meas. 77−52368
polyethylene, effect of Se on electrical and mechanical strength, after mechanical and electrical ageing *(Russian)* 79−52396
polyethylene, high density, biaxial tension, long-time strength 77−66696
polyethylene, high density, inorganic filler, calendered sheets, anisotropy of tear strength and crystalline texture *(Japanese)* 77−70110
polyethylene, high-density unorientated, damage buildup kinetics under creep conditions, during prolonged loading 80−60932
polyethylene, influence of Se on mechanical and electrical strength *(Russian)* 79−11662
polyethylene, torsional rigidity testing *(German)* 77−52596
polyethylene structural transformations under fast electron irradiation *(Russian)* 79−94987
polyethylene terephthalate, mech. props., influence of cryst. arrangement and noncryst. region struct. 78−76707
polyethyleneterephthallate, sorption of low MW solvents on struct. and mech. props. *(Russian)* 78−11358
polyimide substrate foils for nuclear targets 80−18739
polymer, brittle, in vitreous state, resistance to brittleness and fracture kinetics *(German)* 77−32688
polymer, deformation, failure, kinetic model *(Russian)* 78−72832
polymer, high, material behaviour under influence of stress and aggressive media *(German)* 79−39009
polymer, nonoriented partially crystalline, elasticity and strength 77−52386
polymer, rubbery state, correl. between strength and relaxation props. 77−28848
polymer, strength, activation energy eval. from temp.-rate depend. 77−86103
polymer, vibrational thinning, viscoelasticity and strength 77−8795
polymer blends, viscoelastic props. *(Russian)* 78−72808
polymer blends and composites, behaviour, review 78−76626
polymer viscoelasticity and strength characterisation, advanced light scatt. techniques 80−11857
polymers, amorphous, semi-cryst., mech. motions, review 77−32616
polymers, crosslinked, specific charact. *(German)* 78−75585
polymers, long-term strength prediction, review 80−104226
polypropylene, glass-fibre-reinforced, design stress data, w.r.t. time, temperature and composition effects 79−96098

mechanical strength continued
polypropylene fibrillated film reinforced cement, loading capacity, cracking 78−72759
polystyrene, oriented high-molecular, physicocomech. props. *(Russian)* 79−33028
polystyrene monofilaments, uniaxial extension, strengthening 79−8334
porcelain, strength eval. after grinding 77−52518
porcine skin, herniorrhaphic reinforcing prosthetic, mech. and struct. props., SEM study 79−74789
porous material, strength, elastic modulus, exponential porosity depend. 77−36563
Portland cement, containing Cr, superhigh-early-strength, early hydration 77−21072
powder cohesive strength and internal friction determination for small quantities of material 77−40495
powder metal sprayed coatings, bond strength, influence of surface preparation 78−11150
powders, unit for meas. characts. 77−25216
PTFE, crystalline, subject to simple plane loading, limiting resistant, time and temp. factors 78−23794
PTFE, struct. effects in stress-strain relations at elev. temps. 78−31484
PVA-fibre-reinforced composites, thermal fluctuation dimensional effect on strength 80−16476
pyrocarbon, fuel particle coating, strength and Young's modulus meas., brittle ring test 77−8868
quartz, hydrolytic weakening of natural and synthetic crystals, mech. and IR study 78−61410
refractory, strength determ., taking account of stress/deform. relation 77−28965
refractory concrete fracture strength, test apparatus simulating usage conditions 80−71824
refractory masses, subsidence, high temp., without load exam. using deform. during continuous heating *(French)* 79−15721
refractory metal, strength charact., effect of thermal test conditions 78−39994
refractory metal, strength charact., error evaluation 77−16771
refractory multiphase systems, infusible, some novel effects, rel. to practical appls. 80−55460
refractory wear-resistant coatings, composite struct. develop., props. 77−63618
reinforced composites, strength and deformation anisotropy, numerical characts. 80−38285
reinforced concrete, cracking strength and max. rack width *(Chinese)* 80−5988
reinforced concrete, lower bound anal. for torsion 78−35436
reinforced plastics, equations of state, taking account of mech. damage 80−97553
reinforced plastics, load-bearing capacity, effect of one-sided heating 80−81135
reinforced polymer, strength, statistical struct. parameter effects *(German)* 77−56095
reinforced shell, in plane stressed state, strength characts. 79−14264
remaining creep life for components under stress at elevated temperatures 80−59566
resins, glass fibre reinforced, selection for marine appl. 79−96035
rocks, dynamic and static strength rel. to criteria for impulsive fracture 80−85646
rubber, effect of Se on electrical and mechanical strength, after mechanical and electrical ageing *(Russian)* 79−52396
rubber-like polymer, molecular relaxation process effect on strength *(German)* 78−31440
ruby, unique polishing features of hard crystals 80−64225
scale factor, kinetic approach to strength scale factor problem 78−79665
semiconductor-insulator system, mech. of contact interaction, mech. and optical props. 78−88375
shaft, operating under torque, structural strength evaluation 79−83280
sharp contact cracking, residual stress effects 79−100245
shell, cylindrical, inelastic with initial shape imperfections and residual stresses, buckling and carrying capacity *(Ukrainian)* 77−50937
shell carrying capacity, statistical eval. 77−89075
silicone resin clad fibre technology, optical and mech. props. 80−28349
sintered mats., complex diffusion alloying 78−68650
soil, cohesionless, strength, influence of high pore-water press. 77−25678
spheroplastics, mech. characts. calc. 80−60931
stainles steel, type 316, irrad. in simulated environment, tensile props. 80−34076
stainless steel, ferritic SUS 410 type, coated with organometallic complexes and Ti alkoxides 80−34078
stator end winding under short circuit, dynamic deform. and strength *(Japanese)* 78−11465
Steatit ceramic strength determination by measuring US dynamic elastic modulus *(German)* 79−43301
steatite, ceramic, exam. of thermal damage by strength meas. 78−84997
steel, 12 MKh, strength, ductility rel. to H_2 corrosion at 1000 kg/cm^2 press., 450°C *(Russian)* 79−15723
steel, 12Kh1MF, influence of preferrred dislocation orientation on high-temp. strength *(Russian)* 79−4999
steel, 15Kh1M1F, thermal cycling and cyclic stress effects on strength and creep resist. *(Russian)* 79−52341
steel, 30N9K4, effects of Mo, V, and N on grain growth, tempering, hardenability, strength and toughness 78−44202
steel, 35Kh3MFS, strengthening involving austenite fine grain processing *(Russian)* 77−52358
steel, 35KhN3MFA, 25KhN3MFA, bainite transform. kinetics and mech. props. *(Russian)* 78−80539
steel, 50 and 1Kh18N9T, strength, effect of H_2 78−3197
steel, alloy, Cr-Mo-V, fatigue, failure probability based on residual strength 78−68797
steel, alloy, Ni-Cr-Mo, SNCM8, mech. stre-ngth under combined alternating strength 78−64690
steel, alloy cast, optimal alloying, carburising effect 80−50771
steel, alloy high-C, amorphous, mech. props. and thermal stability 80−76361
steel, alloy X8CrNiNb1613, creep limit and long-term strength, parametric eval. method 80−100996
steel, and alloy, fatigue strength improvement, by subcritical quenching 78−44153
steel, austenitic, 33N25Yu3F, hardening, effect of quenching and ageing temps. *(Russian)* 77−81267
steel, austenitic, ageing and plastic deform. effect on struct. and mech. props. of N15Kh5G3T3 *(Russian)* 80−71691
mechanical strength continued
steel, austenitic, Cr-Mn, Kh4G18F, microstruct. and mech. props. during tensile deform. *(Russian)* 79−20114
steel, austenitic, explosive-thermal treatment, sulphide cracking decrease, hydrogen embrittlement *(Russian)* 80−108477
steel, austenitic, mechanical strength, effect of mech. and heat treatment 77−12659
steel, austenitic Mn-Ni ageing , alloying element influence on struct. and mechanical props. *(Russian)* 80−35256
steel, austenitic stainless, fast neutron irrad., effect on mech. props. 78−92309
steel, austenitic stainless, grain size effect on softening *(Russian)* 78−23731
steel, austenitic stainless, Mn-Cr, austenite decomposition by deform., rel. to mech. props. *(Russian)* 78−27515
steel, austenitic-martensitic, phase comp., struct. and mech. props. 80−29974
steel, C, corrosion carcking by sulphide, effect on props. 80−55587
steel, C, developments, properties and fabrication processes *(Dutch)* 77−70021
steel, C, hardened by HF current, mech. testing method 80−61053
steel, C, hypo-eutectoid naturally fibrous composites, strength analysis 78−3190
steel, C, isoforming and warm rolling, effect of mech. props. 80−11673
steel, C, natural reinforced composite 80−30039
steel, C content effect on annealing texture, plastic anisotropy and mechanical props. 80−29976
steel, C type 45, martensitic needle size, effect on mech. props. after induction hardening 80−11672
steel, carburised, alloying effect on props., mathematical-statistical determ. 78−19794
steel, cast, effect of non-uniform struct. on props. 78−84850
steel, cast, type 20, exam. of strain characts. in premelting temp. range *(Russian)* 79−29140
steel, cast 18OSKhNM, fractographic investigation 77−21266
steel, Cr, tempering resist., mech. props., Cu addition effect 79−79012
steel, Cr (12 wt.%), thermomechanical treatment, high temperature, effect on props. and struct. *(Czechoslovakian)* 77−32603
steel, Cr-Al (12, 6 wt.%), ferritic stainless, high temp. treated, strengthening mechanisms 80−3106
steel, Cr-Mo-(Nb)-(Ni)(Ti), low-alloy selection for nuclear steam generator tubes 78−54834
steel, Cr-Mo-(V), microstruct. effect on high-temp. props. *(Czech)* 80−89300
steel, Cr-Mo-V, strength and ductility in creep, purity influence 80−66598
steel, Cr-Ni (14, 5 wt.%), tempering resist., mech. props., Cu addition effect 79−79012
steel, Cr-Ni-Mo-Cu-Nb, martensitic precipitation hardenable, corrosion resistant, heat treatment, structure and props. 79−74169
steel, Cr-Ni-Mo-V-Nb (12,8,1,1.5,0.4 wt.%) Ce addition effects on strength and hardness *(Russian)* 78−15454
steel, Cr-W-V-Mo (3.9 to 4.5, 1.5 to 2, 0.9 to 1.2, 3.9 to 4.4 wt.%), heat resistant, type 8Kh4M4V2F1-Sh, mech. props. 80−16464
steel, determ. from dynamic hysteresis loop EMF spectral content of coil, expt. 77−73414
steel, electric field effect on strength, hardness 80−50714
steel, heat resisting, type 15Kh1M1F, exam. of structural stability and props. *(Russian)* 79−29104
steel, heat treatment with induction heating, 78−92285
steel, high strength, low alloy, low cycle fatigue, composition, thickness effects 79−57100
steel, high strength, treatment effect on ductility and strength 80−60880
steel, high-strength, 30KhGSA and Kh12M, low cycle fatigue 79−87724
steel, high-temp. isothermic combined heat treatment and mech. working influence on struct. and mech. props. of 60S2 *(Russian)* 80−20969
steel, induction hardened sheet, inhomogeneity and distrib. of residual stresses effect on fatigue *(Japanese)* 78−31518
steel, interrelation between static and dynamic strength 79−15725
steel, law-C, hot deform., austenite strengthening and weakening 80−76282
steel, long-term strength, H effect 80−55581
steel, long-term strength prediction, nature of temperature-time parameter 77−21275
steel, low alloy, brittle fracture, quenched and tempered 80−11677
steel, low alloy, high strength, HSLA metallurgy in Europe, review 77−48614
steel, low C Mn-V, VC effects on strength and brittleness 77−70055
steel, low Si, martensite struct. and mech. props. *(Korean)* 80−93614
steel, low-alloy sheet, welded hydraulic turbine volute chamber, strength and toughness 78−68820
steel, low-C, phosphorus effect on annealing texture, plastic anisotropy and mech. props. 77−25069
steel, low-C, preliminary thermomech. treatment, cold deform. effect on struct. and props. 79−38847
steel, low-temperature tempered, shock wave loading effects on mech. props. *(Russian)* 77−59857
steel, maraging, effect of thermal cycling (γ to and from α) on props. 80−20986
steel, maraging, inert gas atomised, hot isostatic pressing temp. effect 79−24460
steel, martensitic, corrosion resistant type 07Kh16N4B, long time strength and ductility, 340 to 450°C 79−100233
steel, martensitic, high C, Co addition effect on strength *(Korean)* 78−68736
steel, martensitic transform. critical temp. determ. 77−90349
steel, mech. strength, effect of H_2 sorption and Al and N_2 surface treatment *(Russian)* 78−31570
steel, medium alloy, constructional, strength-toughness relationship 77−70137
steel, medium C resulphurised, compressive strength at high strain rates, short load cells 79−29305
steel, microalloy V-Nb, V, Nb effects on strength and formability of cold rolled sheets 77−55979
steel, Mn-Mo-Nb, high strength, ductile, acicular ferrite struct. 77−21191
steel, Mn-Si, for springs, metallographic study, present phases rel. to mech. props. *(French)* 80−21090
steel, Nb-V, cold rolled, HSLA, prod. by precipitation hardening, annealing 78−88471

mechanical strength continued
steel, Ni, sintered, relation between microstruct., microchemistry and mech. props. 78−64504
steel, Ni (9 and 5 wt.%), for liquefied natural gas appls., material and weld props. 79−61736
steel, Ni (9 wt.%), mech. props., effect of alloying 77−48462
steel, Ni-Co-Cr, high-strength medium C, Cr effect on props. 80−76339
steel, Ni-Co-Mo-Ti, hot formed, recrystallization and grain boundary precipitation effect on mech. props. *(German)* 79−66073
steel, Ni-Cu-Mo-C, powdered, influence of cooling rate after sintering on preps. 79−95969
steel, pearlitic, brittle fracture of structures 78−72869
steel, pearlitic, Cr-Mo, Cr-Mo-V and Mo-V, heat resist., Mo content rel. to mech. props. 79−20134
steel, pearlitic, strength, fracture, microstructure effect 77−40449
steel, rail, AE use for mech. tests 80−35467
steel, Rheocast, struct. and props. 77−28804
steel, rotor, Ni-Cr-Mo-V, reversible temper embrittlement 77−36656
steel, Si-Mn-Cr-C (1.1, 0.9, 1.0, 0.29 wt.%) 30KhGSA, heat treatment effect on strength and toughness 78−15437
steel, sintered, maraging, N14K7M5T, mech. props., effect of Ti additions 77−25081
steel, sintered, mech. props., effect of small cold reduction 79−39048
steel, sintered, mech. props. 77−40439
steel, St3 and KhVG, strength variation under influence of shock waves *(Russian)* 78−92299
steel, stainless, 08Kh18N10T, long-term strength in He atm. containing impurities 79−24662
steel, stainless, 304, thermal fatigue and strength estimation, creep fatigue interaction 79−11708
steel, stainless, Cr-Ni (18, 10 wt.%), long-term strength in H at high pressure 80−55485
steel, stainless, durability in H_2 up to 500°C 80−30170
steel, stainless, electrohydraulic effect and struct. changes *(Russian)* 78−23783
steel, stainless, ferritic, Cr-Mo-Ni (29,4,2 wt.%) 77−44276
steel, stainless, fibre reinforced wustite, strength and toughness 78−27602
steel, stainless, fixing pins for fractured bones, strength, ultrasound effect 80−71710
steel, stainless, Kh18N10T, long-term strength under in-pile irrad. conditions 78−6940
steel, stainless, martensitic, ageing, strength/structural charact. relationship 77−90426
steel, stainless, Ni-Cr-Mo-W (29, 13, 3, 2 wt.%), long-term strength in H at high pressure 80−55485
steel, stainless, nickelless, low cycle fatigue 80−35326
steel, stainless, type 304, BWR coolant pipe, critical strength under stress corrosion cracking 80−52743
steel, stainless, type Kh17N13M2T, strengthening by plastic deformation and cold working *(Russian)* 78−52839
steel, stainless 12kh18N9T, wire, mechanical and heat treatment effect on static and cyclical strength *(Russian)* 78−35410
steel, structural, with elevated and high strength, damping capacity 77−21205
steel, tapered beam, collapse behaviour 78−87287
steel, tempering effect on struct. and mech. props. of types 70, U8, and U12 *(Russian)* 80−50655
steel, TRIP, strength and plasticity rel. to thermomech. treatments 77−44281
steel, type 12Kh1MF, dislocation struct. changes after thermomechanical treatment *(Russian)* 80−66545
steel, type 12X18H10T, strengthening based on intensifying heat exchange processes in martensitic transformation region *(Russian)* 79−70065
steel, type Kh13N9D2MT martensitic aged, struct. and mech. props. *(Russian)* 80−93600
steel, type Kh18N9T and 15Kh1M1F, study of long term cyclic strength under soft asymmetric and rigid loading 79−57076
steel, type Kh8CrNiNb1613, approach to numerical soln. of problem of predicting long-term strength by summary diagrams 79−56988
steel, type KVK, deform. strengthening of bayanite phase *(Russian)* 80−100851
steel, ultra high strength, historical 80−7609
steel, ultra-high strength, strengthening, props. and charact. *(Korean)* 79−24607
steel, US testing of strength 79−39104
steel, V-Nb and Cr-Mo-V-Nb, supercooled austenite isothermal decomp., struct., strength and fracture charact. 80−60966
steel, white layers forming at high rates of friction, struct. props. *(Russian)* 79−15800
steel 12Kh1MF, fine struct., effect of isothermal transform. temp. 77−21137
steel 18 Gps, chemical composition effect on strength, statistical treatment of test data 79−57081
steel 2Kh13, anisotropy of strength and ductility, elevated temp. effect 77−4825
steel butt weld structure and mech. props., explosive treatment effects 79−24541
steel Co-Ni three layer composite, high strength with increased damping capacity 77−1850
steel composite vessels, martensitic welded, glass fibre reinforced plastic wound, struct. strength 80−97552
steel Cr-Mn (13, 19 wt.%), for liquefied natural gas appls., material and weld props. 79−61736
steel fibre reinforced Al_2O_3-Al, production and mech. props. 80−11619
steel fibre reinforced Al, vacuum hot pressing, strength *(Czechoslovakian)* 77−32543
steel fibre reinforced concrete, strength problems 77−4844
steel mesh, herniorrhaphic reinforcing prosthetic, mech. and struct. props., SEM study 79−74789
steel reinforced concrete beams, mech. strength determ. under combined bending and tension 78−60749
steel vessels, internal pulsed loads, effect of scale, geometry and filler on strength 78−21659
steel-aluminium plates, exam. of adhesion strength by impulse loading 78−84943
steel-Babbitt bimetal, exam. of structure of transition layer 79−100293
steels, die, mech. props. high temp. thermomech. treatment 79−20086
steels, strength reduction by adsorpt., stress corrosion *(Russian)* 79−29265

mechanical strength continued
steels, ultrahigh C, superplastic, mech. behaviour at elevated temps 80−21028
strength parameter dispersion/inhomogeneity of microscopic damage relation 77−86122
structural materials in complex stress state, criterion for strength at low temp. 78−71292
synthetic high strength material structures, mechanical strength, microstress levels *(Russian)* 80−76334
technological strength and nondestructive methods of testing during heat treatment 78−85090
temperature-time depend., phys. principles, for solids 79−28040
test system, long term strength meas. 79−70253
testing allowing for stress form *(Russian)* 77−60008
Textolite, mech. props. in elastic symmetry planes 77−21211
thermomechanical treatment on struct. and props. 79−29109
thermoplastic plates, strength meas. when supported by annular ring 80−81257
thin skin structures, residual strength prediction, using crack resistance curves 78−90795
thin-wall tubing expansion, scale factor, limiting edge deform. 77−23900
Thornel reinforced epoxy laminates, strength and biaxial stress-strain response, analytical expt. correlation 79−29131
thumb functions in normal and pathological state, biomech. eval. 77−40708
Ticonal strength, effect of thermal stresses and phase transforms. 79−87721
vegetable fibre reinforced cement sheets, strength 80−21024
vertebrae, human, mech. props. 80−72206
vinyl fluoride based polymer stabilisers, thermal degradation, post UV-irrad. mech. strength *(Russian)* 79−24778
viscoelastic body containing cracks, durability calcs. 80−79227
viscoelastic material, strength long term, generalize criterion 77−27477
viscoelastic structures, strength and stability, a method of solving integral eqns. used 80−10167
wind generator, vertical axis, 1 kW, using steel reinforced fibreglass blades 79−61940
window, composite vacuum-tight, for IR and visible observations, strength and IR transmission 80−48406
wire reinforced Al, stress-deformed state, elastic, strength props. *(Russian)* 80−76303
Zircaloy, effect of dispersion and spheroidisation treatment of δ ZrH 79−76073
Ag, dispersion strengthened with MgO particles, electrical contacts appl. *(Slovak)* 78−31544
Ag-CdO cermets, coprecipitated carbonates and hydroxides, physicomech. props. 80−25706
Al alloy, multicomponent, optimum composition for high-strength *(Bulgarian)* 79−15628
Al alloy AL22, influence of ultrasonics application on creep during multistage ageing *(Russian)* 79−91708
Al alloys, effect of melt treatment with granules *(Russian)* 77−44190
Al alloys, electric field effect on strength, hardness 80−50714
Al alloys, laser generated stress waves, effect on microstruct., hardness and strength 79−69192
Al alloys, microstruct. effects on strength, fracture toughness, fatigue cracks 79−43434
Al conductor alloys, subgrain-strength relationship, effect of alloying and processing 77−32606
Al, dispersion hardened, mech. props., effect of strain rate *(Czech)* 77−59865
Al, dynamic strength and logarithmic modulus of plasticity 77−16655
Al, recrystallised, substructure strengthened, long-term strength 77−21173
Al, stability and strength of FCC metal using Morse pot. 80−59430
Al substitutional solid solution alloys, volumetric effect and props. *(Russian)* 80−39293
Al, surface strengthening of single crysts. on coating with evaporated films 77−8972
Al, vacuum condensate, struct. and mech. props. depend. on deposition conditons 80−15417
Al, wire, appl. of subgrain control 77−86060
Al wire, hot and cold deformation drawing strengthened, thermal EMF study *(Russian)* 80−54674
Al-Al_3Ni eutectic composite, substructural matrix hardening *(Russian)* 77−21162
Al-B fibre-D16 alloy welded composites, structure, strength and fracture props. *(Russian)* 80−108524
Al-Be, two-layer foils, mech. props. *(Russian)* 78−51858
Al-Cu-Mn, long term strength and creep 80−60925
Al-Mg, AMg6 alloys, effect of chem. comp. on strength and ductility at low temps. 80−3148
Al-Mg (4.4 and 6 wt.%), for liquefied natural gas appls., material and weld props. 79−61736
Al-Mg alloys, relationship between props. and nonequilib. phase diagram 79−96000
Al-Mg(Zn-Mg), long term strength and creep 80−60925
Al-Ni mixed-powder-based plasma-sprayed coatings, strength charact. 77−12548
Al-polymer joint, temp. depend. meas. of joint strength 80−50824
Al-Si (35 wt.%), Cr, Co, Si addition effects on strength of powder 77−24983
Al-Si alloys, eutectics and hypoeutectics, mech. props. and thermal cond., P impurity effect 79−83271
Al-Si-Cu casting alloy, optimum selection of chem. contents for optimum strength *(Czech)* 79−15625
Al-W(Mo)(Nb), struct. and props. of alloys obtained from granules 80−50717
Al-Zn-Mg alloy, thermomech. treatment, precipitation and strengthening 79−24527
Al-Zn-Mg and Al alloy 7050, age hardenable, microstruct., effect of monotonic and cyclic straining 77−36633
Al-Zn-Mg-Cu alloy, type 7050 and AZ 74.61, engineering props. 79−70219
Al-Zn-Mg-Cu-Cr-Zr, high strength Cr and Zr addition effects 77−59820
Al-Zn-Mg-Li alloys, effect of Li on thermal props. 79−24515
AlN filamentary crystal reinforced mullite-corundum ceramics, filaments strength, eval. 80−104230
AlN whiskers, strength rel. to growth conditions using vapour-liquid-solid method 79−11052

mechanical strength continued
Al_2O_3, anodic film on Al, strain to failure, failure characts. 77−12734
Al_2O_3 bioceramic synthesis, for orthopedic purposes, props. *(Polish)* 80−66465
Al_2O_3, creep and long term strength 78−23802
Al_2O_3, effect of quenching hardening on mech. strength, for various quenching mediums *(German)* 78−35403
α-Al_2O_3 filamentary crystal reinforced mullite-corundum ceramics, filaments strength, eval. 80−104230
Al_2O_3, high-purity, modulus of rupture, expt. test of Weibull scaling theory 77−21258
β-Al_2O_3, hot isostatic press. 80−108377
Al_2O_3 porcelain for high voltage insulators, increased mech. strength 78−11269
Al_2O_3 rods, quenched, exam. of contact induced strength degradation 78−76731
Al_2O_3 sintered, and hard metal alloys, comparison of stress intensity factor depend. on notch base dia. *(German)* 78−35470
Al_2O_3, sintering in reducing atmosphere, Na effect on density and strength 77−63613
Al_2O_3 strength-size relation 77−21255
Al_2O_3, thermally shocked, strengthening kinetics 77−8920
Al_2O_3-Mo cermets, effect of processing factors on props. 79−100103
Al_2O_3-$MoSi_2$, for use as heating element, fabrication method and prop. *(Japanese)* 79−95989
β-Al_2O_3-Na_2O, AC impedance, microstruct. and strength 80−100349
β-Al_2O_3-Na_2O electrolyte development for Na-S battery 79−29461
Al_2O_3-TiC, multiphase ceramics, mech. strengthening due to dispersion of non-metallic particles *(German)* 78−60674
Al_2O_3-ZrO_2, multiphase ceramics, mech. strengthening due to dispersion of non-metallic particles *(German)* 78−60674
Al_2TiO_5, grain size pseudobrookite oxide, microcracking relations 79−29194
B fibre reinforced Al, strength determ. procedure in annular specimens *(Russian)* 78−95864
B fibre reinforced Al-Zn-Mg, packet rolling, thermodeform. process parameters *(Russian)* 80−55433
B fibre reinforced AlB_2 and TiB_2 fibre coating effect on strength *(Russian)* 80−40426
BN ceramic with organosilicon polymer additions, strength and oxidation resistance 80−20880
$BaTiO_3$, ferroelectric ceramic, internal stress and strength, failure mechanism 80−66128
$BaTiO_3$, ferroic materials, fracture processes 80−79869
Be, fracture and strength properties, dynamic ageing effects 80−81202
C and graphite, mechanical props., high temp., review 79−38897
C, baked mixes, use of coal tar and petroleum pitches as binders 78−80483
C fibre, mech. prop. determ. from C fibre reinforced plastics 77−81287
C fibre, metallic coated, increased temp. effect on strength *(Russian)* 78−35429
C fibre, thermal treatment temp. effect on struct. and props. 78−23743
C fibre composite, oxidation and mech. strength at intermediate temps. 77−81330
C fibre reinforced Al, interaction between components and compatibility, mech. props. effect 80−11761
C fibre reinforced composites, mech. props., rel. to aircraft appl. 77−81289
C fibre reinforced Cu, mech. props. *(Japanese)* 77−63723
C fibre reinforced Ni, hot pressed and electrodeposited, strength 79−38898
C fibre reinforced Ni, struct. and strength change at high annealing temp. *(Russian)* 79−66076
C fibre reinforced plastic, specimen size effect, statistical anal. 78−68724
C fibre reinforced polyphenylsiloxane composites, long-time strength, and influence of protective coatings 80−3133
C fibres, mech. props., thermal stability up to 2000°C 80−60929
C fibres coated with SiC *(Polish)* 79−52408
C materials, conf., Baden-Baden, Germany (June 1976) 78−43990
C, ribbon, high modulus, strength, prep. 77−21062
C steel joints, with interference, increasing supporting capacity, by electrophysical methods, exam. 78−85055
C, strength and struct., conf., Bath, London, England (Apr. 1979) 80−82566
CC TaC based hard metal, non-stoichiometric sintering, mech. props. 80−25616
β-$CaSiO_3$ fibre, continuous unidirectional crystallisation from melt 78−95739
$CaTiO_3$-TiO_2, ceramic, phys. props. 78−43784
Cd-Zn (1.5 wt.%), warm worked, effect of grain size, texture, on mech. props. 79−4988
Co alloys, binary, and MAR-M322 type, influence of phase transform. on diffusion and mech. props. *(Russian)* 79−5000
Co-Si, directionally solidified eutectic composite alloy, form. and strength 77−90294
Cr-AlN, dispersion hardened, erosion resistance 77−12637
Cr-La-V-Nb-Ta, La, V, Nb Ta effect on hardness and strength *(Russian)* 79−34050
Cu, compacted powder, thermal agglomeration, green strength 77−36417
Cu, dynamic strength and logarithmic modulus of plasticity 77−16655
Cu film, vacuum deposited, thickness depend. *(Russian)* 77−59238
Cu, microalloyed with B, elec. cond. and strength props. *(Polish)* 80−89285
Cu, strip, formed by high deform., mech. props. charact. *(Russian)* 78−27534
Cu, vacuum condensate, struct. and mech. props. depend. on deposition conditons 80−15417
Cu/Ni double layer evaporated film, misfit dislocation effect on strength *(Japanese)* 79−42425
Cu-Al, directionally solidified eutectic composite alloy, form. and strength 77−90294
Cu-Al, vacuum condensate, struct. and mech. props. depend. on deposition conditons 80−15417
Cu-Al_2O_3 dispersion hardened wires, drawn, substruct. and strength 78−35405
Cu-Au (50 at.%), ordered, influence of elastic stresses on mech. props. *(Russian)* 78−92298
Cu-Ce(Y)(In), effect of alloying additions on electrical cond., and mech. strength 78−44233
Cu-Cu_6Y eutectic alloy, cast and directionally solidified, struct. and props. *(Russian)* 80−104138
Cu-Ni, cast, strength and hot ductility, alloying and residual elements effect 80−66595
Cu-Ni-Zn-Mn fine grained precipitation-hardenable alloy, high strength and ductility 80−100805
Cu-Ni(Al), strength and substruct., strain point influence *(Russian)* 79−52233
Cu-plated C fabric, plasma sputtering influence on strength and elec. cond. *(Russian)* 80−21008
Cu-Sn, graphite dispersed, wear, effect of graphite content *(Japanese)* 77−56114
Cu-Sn-Ni alloys, mech. props. after thermomech. treatment 79−79009
Cu-Ti (4 wt.%), combined recrystallization and precipitation 79−29072
Cu_2O-Al_2O_3-SiO_2 glasses, strengthening by alkali-Cu ions exchange 80−55467
$Cu_{60}Zr_{40}$, metallic glass, composition, mech. props., simulation 80−49117
D_2-DT-T_2 mixture, solid and liq., props. for fusion reactor applications 78−66415
Eu_2O_3, mech. and physical props. rel. to reactor control rod appl. 78−21641
Fe, Armco, grain size and strength depend. on nonmetallic inclusions *(Russian)* 80−100894
Fe, Armco, sleeve, deformed by cold drawing, exam. of surface and texture *(Russian)* 79−34057
Fe, cast, high-strength bainitic with spheroidal graphite, mech. props., isothermal transform. 79−96023
Fe, cast, homogenization of property difference due to mass effect by repeated heat treatment *(Japanese)* 79−38857
Fe, cast, malleable, with divorced pearlite, structural strength improvement by annealing 79−96049
Fe, cast, Mg, Pb impurity effect on struct. and mech. props. 79−96089
Fe, cast, quantitative metallography, study by image anal. 78−31492
Fe casting in metal mould, strength before, after heat treatment *(Japanese)* 77−48461
Fe, fatigue fracture strength and failure, at 77K after cyclic loading at room temp. 78−84996
Fe, powder, atomised, processing props., particle size distrib. effect, with and without Zn stearate additions 79−100077
Fe powders, cold-pressed, props., effect of air 80−100810
Fe, sintered and pressed, props., effect of atomised Fe powder particle size distrib. 80−11601
Fe solid solution, substitution strengthening by Cr and Mo *(Czech)* 80−30080
Fe-containing glass-ceramics, effect of Mn_2O_3 on strength 77−48380
Fe-Cu, sintered compacts, cooling effect on strength 77−73293
Fe-glass-Cu sintered material, Cu effects on strength 77−77443
Fe-Mn, struct. and props., effect of Nb, C and Si alloying *(Russian)* 77−90360
Fe-Mn-Ni, age hardenable, struct. and strength 77−52339
Fe-Mn-Ni-C, age hardenable, struct. and strength 77−8844
Fe-Ni (32 wt.%), electrohydraulic effect and struct. changes *(Russian)* 78−23783
Fe-Ni-C, single crystal, form. and strength of strain-induced martensite 79−100225
Fe-refractory compound, dispersion strengthened, thick vacuum condensate, control of struct. and mech. props. 80−16324
Fe-TiC pseudofused composite magnetoabrasive powders, props. 80−100926
Fe-VC alloys, struct. and mech. props. 79−52171
Fe_2TiO_5, grain size pseudobrookite oxide, microcracking relations 79−29194
p-GaSe, monocrystal, temp. depend. of mechanical strength *(Russian)* 79−10892
Ge mechanical strength in brittle fracture region, influence of Si and O impurities 79−87682
Ge transparent IR window design for uniform pressure loading 79−23088
K, mechanical ideal strength, pseudopot. model calcs. 79−77670
KCl:Eu, flow stress 77−36577
KCl:KOH, influence of anion impurities on mech. props. of alkali halide crystals 78−87736
KCl:RbCl, $SrCl_2$, laser window material, prep., grain boundary stability 77−46774
KCl:S, influence of anion impurities on mech. props. of alkali halide crystals 78−87736
$La_{0.003}Ba_{0.66}Sr_{0.34}TiO_3$, water absorpt., mech. strength, stability, TCR *(Russian)* 80−16511
Li, mechanical ideal strength, pseudopot. model calcs. 79−77670
Mg-Er (<25%) alloys, struct. and props. 79−96001
Mg-Tb, (up to 45 wt.%), phase diagram, and mech. preps. 80−16277
Mg-Y-Al alloys, phase equilib. *(Russian)* 80−20890
MgO, thermally shocked, strengthening kinetics 77−8920
MgO-Al_2O_3-SiO_2, glass ceramic, structure and props. *(German)* 80−38927
MgO-Al_2O_3-SiO_2 based cordierite glass-ceramic, strength and thermal shock, surface treatment effect 80−25884
$MgTi_2O_5$, grain size pseudobrookite oxide, microcracking relations 79−29194
Mo alloys, fusion reactor first-wall and blanket material, mech. props. 80−34074
Mo and Mo superalloys high temperature properties 78−44173
Mo fibre reinforced Al and Al alloys, SEM study *(Slovenian)* 78−84923
Mo, single crystals, high temp. creep and strength depend. on thermomechanical treatment *(Russian)* 79−79034
Mo, strength, temp. depend. 78−3193
Mo, strength and internal friction 77−63711
Mo-AlN, dispersion hardened, erosion resistance 77−12637
Mo-Hf (0.3 wt.%), strength, plasticity and microhardness, internal nitriding effect *(Russian)* 80−40433
Mo-Re, cold worked, strength 78−31426
Mo-Re(Os)(Ru), recovery after deform. and annealing, destrengthening mechanism *(Russian)* 80−97546
Mo_2B_5, monocryst., grain size, abrasive and strength props. 80−11787
Mo_2B_5-based alloys, mech. props., rel. to appl. as electrodes in electrospark machining 80−21174
$NH_4H_2PO_4$, surface effects on strength of whiskers and microcrysts. *(Russian)* 78−51864

mechanical strength continued
Na borosilicate glass microsphere material, sintering, struct., strength props. *(Russian)* 80−108383
Na, mechanical ideal strength, pseudopot. model calcs. 79−77670
NaCl, optical strength, effect of irrad. in mechanically stressed state 80−80695
NaF powder, porous, of skeleton struct., grain size effect on strength *(Russian)* 77−24991
Nb alloys, fusion reactor first-wall and blanket material, mech. props. 80−34074
Nb, and alloys, interstitial impurity effects on strength 78−3194
Nb base alloy, high temp. creep estimation and long term strength charact. 78−3195
Nb-Mo-Al-(Cr) eutectic directionally crystallised alloy, heat resistance, alloy struct. *(Russian)* 80−40481
Nb-O(N), dislocation pinning, impurity interactions, strengthening *(Russian)* 80−92532
Nb-W-Mo-Zr, long-term strength props., vac. level effect 80−55484
Nb-W-Mo-Zr-C, strength and ductility, prolonged high-temp. soaking effect 80−55483
Nb-W-Zr-Ta, long-term strength props., vac. level effect 80−55484
Nb-Zr-C alloy, effect of ageing on high temp. strength *(Ukrainian)* 79−52249
NbC, and NbC-ZrC solid soln., prep. by impregnation, strength, surface submicrocracks 77−16661
NbC, NbC-ArC, right-through sat. prep., strength and plasticity, temp. depend. 77−40432
NbC, physicomechanical props. within the homogeneity range 77−1848
Ni alloy, heat resistant, high temp. plasticity at different strain rates 77−21233
Ni alloy, KhN55VMTFKYu, produced by powder metallurgy, hot worked, short- and long-time strength 77−28752
Ni alloy EI867, heat resistant, mech. props., effect of prolonged elevated temp. 77−21194
Ni alloy IN-738, Y_2O_3 (1.5 wt.%) addition, mechanical alloying 77−40427
Ni, dynamic strength and logarithmic modulus of plasticity 77−16655
Ni, EP742 type alloys, optimum struct. for strength, heat resist. and ductility *(Russian)* 79−52250
Ni, powder charact. effects on sintering 77−1828
Ni-Al_2O_3(ZrO_2), dispersion strengthened, thick vacuum condensate, control of struct. and mech. props. 80−16324
Ni-Al-Cr-Mo-Ti-W-(Co) alloys EhI 826 and EhI 929, reverse elastic after effect under loading 78−39829
Ni-Al-Cr-Ti-W-Mo, US vibration applied during solidification, improved strength, corrosion resistance *(Russian)* 78−15382
Ni-Al-Ti(Nb), heat-resisting dispersion-hardening alloys, props. and struct., γ'-phase comp. influence *(Russian)* 80−20943
Ni-base, heat resistant alloy KhN60MKBYuT, plasticity, precipitation 77−70120
Ni-base alloy computer prediction of long term strength by generalised diagram method 77−70133
Ni-base alloys, US vibration during crystallisation, effect on mech. props. *(Russian)* 78−19827
Ni-based eutectic alloys, struct. and props. *(Russian)* 77−21129
Ni-Ce-Fe-Ti (77, 20, 4, 2.5 wt.%), long-term strength in H at high pressure 80−55485
Ni-Cr Nimonic alloys, mech. props., high-temp. irrad. effects 80 100885
Ni-Cr-Co-Al-W-Mo-Ti-Ta, heat resist. and struct., Ta effect 80−76312
Ni-Cr-Fe-Ti alloy KhN77TYuR, long-term strength under in-pile irrad. conditions 78−6940
Ni-Cr-Mo (74, 20, 4 wt.%), long-term strength in H at high pressure 80−55485
Ni-Mo (14.4 wt.%) single crystals, ordered phase precipitates influence on deformation character, mechanical props. *(Russian)* 79−74155
Ni-Mo (5.8-24 at.%) solid soln. struct. and strength charact. *(German)* 79−4975
Ni_3Al-Ni_3Nb composite, long term annealing effect on impact strength and long-term strength *(Russian)* 79−74182
Pb, strength loss during upsetting 77−90430
Pb, strength loss in supercond. state, size factor effect *(Russian)* 80−88677
Pb-Sn(Bi)(Ni), strength loss in supercond. transition, nonmag. and paramag. impurities influence *(Russian)* 80−70875
PbIn films strengthening, by preventing formation of misfit dislocations 80−84858
PbO glass, strength, effect of HNO_3 etching 77−56124
Pb(Zr,Ti)O_3, effect of spherical pores on strength 77−70103
Pb(Zr,Ti)O_3, ferroic materials, fracture processes 80−79869
Pb(Zr,Ti)O_3, polarisation effect on deform. and strength, Curie pt. region 79−42902
Pd alloys, controllable hydrogen phase naklep, hardening and phase-strengthening 80−16323
$Pd_{80}Si_{20}$, metallic glass, composition, mech. props., simulation 80−49117
PtRh5 alloy, phosphate glass addition effect on high temp. strength *(German)* 80−25807
Si, failure in strong melt grown single crysts. 78−3205
Si, mechanical strength, origin of difference in Czochralski grown and float-zone-grown cryst. 80−44212
Si whiskers as basis for strain resistors 79−5094
Si-SiC composite, high temp. time depend. strength 77−56083
SiC, chem. stability, mech. and thermal props. rel. to appls. 80−21103
SiC fibre reinforced Al interaction between components and compatibility, mech. props. effect 80−11761
SiC, fuel particle, coating meas. of strength and Young's modulus, brittle ring test 77−8868
SiC, pyrolitic coating for nuclear fuel particles 77−79465
SiC, REFEL, strength parameters 77−1830
SiC, self bonded, exam. of fracture 79−20149
SiC, self-bonded, fracture charact. and rupture strength, temp. effects 79−96136
SiC, strength assessment by Young's modulus meas. up to 1400°C *(German)* 78−11253
SiC, strength-grain size relation, surface finish effects 77−81333
Si_3N_0 reaction bonded, strength parameters 77−1830
Si_3N_4, effect of oxide impurities on physicomechanical props. 80−16396
Si_3N_4, hot pressed, crack healing *(German)* 79−24599
Si_3N_4, hot pressed, effect of powder composition and sintering temp., on phase transformation kinetics, microstructure and mech. strength *(German)* 79−4939

mechanical strength continued
Si_3N_4, hot pressed, strength and life prediction 80−3173
Si_3N_4, hot-pressed, proof-testing 78−80693
Si_3N_4, porous, reaction sintered, organosilicon infiltrated, decomposition, strength, density 79−29000
Si_3N_4, reaction bonded, exam. of strength as function of nitrided density, microstruct. design 78−68731
Si_3N_4, reaction bonded, fracture mech. pararucters, microstmet. amd temp. effect 79−24598
Si_3N_4, reaction bonded, post-sintering, injection moulding applications 80−60807
Si_3N_4, reaction sintered, α- and β-phase form., effect on strength 77−21075
Si_3N_4, reaction sintered, H_2 in nitriding gas, effect on strength, struct., and composition 79−24478
Si_3N_4, reaction-sintered, strength/nitrided density relationship 77−28891
Si_3N_4, synthesis and props. of shapes 79−47650
Si_3N_4 with Y_2O_3 and Al_2O_3 additions, hot pressed, exam. of mech. props., grain boundary crystallization 79−20009
Si_3N_4, Y_2O_3 doped, hot pressed, improved high temp. strength 79−61613
Si_3N_4-SiO_2-MgO, phase relations and interrelation with mech. strength, and oxidation 78−48386
SiO_2-Al_2O_3-B_2O_3 glass mech. strength increased by etching 80−97609
SiO_2-Li_2O-K_2O-ZnO glass ceramic, prep., phase transformations and physical props. 80−45299
Ta-O(N), dislocation pinning, impurity interactions, strengthening *(Russian)* 80−92532
Ta_2O_5, anodic film on Al, strain to failure, failure charact. 77−12734
Ti alloy, cyclic creep 77−81323
Ti alloy, disc, rotating notched, strength in quasibrittle fracture 80−55533
Ti alloy, VT22, thermomechanical treatment, effects on struct. and props. *(Russian)* 78−19785
Ti alloy substrate, Ni-Cr plasma spray coated, interface interaction 77−21323
Ti alloy VT16, strengthening heat treatment in vacuum 79−79013
Ti alloy VT22, hardening during thermomechanical treatment, precipitate particle internal struct. *(Russian)* 79−91657
Ti alloys, corrosion resistance in H_2S and NaCl, cracking tendency, strength *(Russian)* 78−31568
Ti alloys, fusion reactor first-wall and blanket material, mech. props. 80−34074
Ti and Ti alloys, mechanical, thermal and elec. props., data sheet 79−43317
Ti, integral composite joints, finite element and expt. eval. 79−11670
Ti, laser generated stress waves, effect on microstruct. hardness and strength 79−69192
Ti, long-term strength criterion 77−44323
Ti-Al alloy, VT5-1, strength variation under influence of shock waves *(Russian)* 78−92299
Ti-Al-Mo(Cr)(Fe), thermomechanical treatment effect on mech. props., strengthening mechanisms 80−55441
Ti-Al-V-Sn-Zr alloy TS5, annealing effect on ductility and strength *(Russian)* 78−35427
Ti-Mo (Zr) (Nb), sintered, manufacture and exam. of props. 79−95975
Ti-Mo-Fe-Cr-Al, alloy VT3-1, influence of constitution on fracture toughness *(Russian)* 77−77559
Ti-W(-Al), mech. props. and heat treatment 80−35274
TiC-Ni-Mo sintered hard alloy TN-20, fracture surfaces 80−7684
TiN-AlN composites, struct. and props. 77−40413
TiN-Nb(Ta)N, microcomposite film prod. for radio resistors 78−3052
U/(Zr-Cu-Mo alloy) welded joints, mech. charcts. determ. 20 to 750°C 79−29113
U/Ti welded joints, mech. charcts. determ. 20 to 750°C 79−29113
U-V (0.2 wt.%), mech. and struct. props., effect of internal H *(French)* 77−21253
V alloys, fusion reactor first-wall and blanket material, mech. props. 80−34074
V, plasticity and strength change in temp. range 20 to 1000°C impurity effects 80−35235
V-O, dislocation pinning, impurity interactions, strengthening *(Russian)* 80−92532
W fibre reinforced, Co powder alloys, reactions and recryst. 80−11603
W fibre reinforced Cu composite, hardening in two-phase material 77−52448
W fibre reinforced Ni composite, prep. by hot isotactic pressing, mech. props. *(Slovak)* 78−19694
W, fibre reinforced powder metal and alloy based composites, high temp. strength of W wire 79−70021
W, single crystals, high temp. creep and strength depend. on thermomechanical treatment *(Russian)* 79−79034
W-Cu, porous material, skeletal type, produced by liquid phase sintering, exam. of mech. strength, determ. resistance 80−16245
W-Cu-(Ti)(Zr), exam. of mech. props. as function of temp., composition, and oxidation props. 80−16472
W-Mo, vapour deposited, long-term strength and thermocyclic creep 80−16405
W-Re fibre-reinforced Ni-base refractory alloy, struct. and props. *(Russian)* 77−59721
W_2B_5, monocryst., grain size, abrasive and strength props. 80−11787
W_2B_5-based alloys, mech. props., rel. to appl. as electrodes in electrospark machining 80−21174
WC-Co, developments, properties and fabrication processes *(Dutch)* 77−70021
WC-Co, VK type hard alloy, influence of residual stresses on static strength 77−1862
WC-Co cemented carbide, carbide grain size effect on strength rel. to structural defects 77−32689
WC-Co hard alloy composite, calc. of weakest link in struct. 80−11730
Y, polycrystn., plastic deform. at different deform. speeds, dislocation glide *(Russian)* 80−93598
YAG, interrelationship between mech. props. and elec. relief on surface layer 79−23821
$YCrO_3$-$MgCr_2O_4$ sintered ceramics, elec. cond. 80−24927
ZnO-$Al_2O_3SiO_2$, transparent glass-ceramic, microstruct., physical props., crystallisation ht. treatment depend. 78−80506
Zr, martensite, furnace cooled and water quenched, strength and deform. 79−20101
Zr-Al (4.6 wt.%), microstruct. effect on mech. props. 79−20080

mechanical strength continued
Zr-Ti martensites, furnace cooled and water quenched, strengh and deform. 79 - 20101
ZrC, and ZrC-NbC solid soln., prep. by impregnation, strength, surface submicrocracks 77−16661
ZrC, NbC-ZrC, right-through sat. prep., strength and plasticity, temp. depend. 77−40432
$ZrC_{0.91}$, sintered, strength charact. effect of struct. and substruct. 80−16260
ZrN, physicomechanical props. with the homogeneity range 77−1848
ZrN-Al_2O_3 composites, strength rel. to solid-, liquid-phase sintering 80−100823
ZrN-AlN composites, struct. and props. 77−40413
ZrO_2, containing metastable tetragonal phase, stress induced phase transform. effect on props. 78−68683
ZrO_2, metastable, tetragonal, strengthening by surface grinding 80−71777
ZrO_2, partially stabilised, high temp. effect on strength *(German)* 79−43316
ZrO_2, porous, sintered stabilised microspheres, strength and fracture studies 80−85019
ZrO_2, stabilised microspheres, sintered, temp. depend. of strength, 20 to 1700°C *(Russian)* 78−23766
ZrO_2-CaO-SiO_2, relationship between texture parameters, and sintering, elec. cond. and mech. strength props. *(German)* 79−24474
ZrO_2-CaO(Y_2O_3) ceramics with grainy structure, props., effect of heating to 2000°C 80−104194
ZrO_2-ZrO_2, multiphase ceramics, mech. strengthening due to dispersion of non-metallic particles *(German)* 78−60674

mechanical testing
see also creep testing; dynamic testing; fatigue testing; fracture toughness testing; hardness testing; materials testing; mechanical variables measurement; notch testing
abrasive and impact abrasive wear testing equipment for materials at elevated temps. 78−7136
abrasive impact wear test system 79−43513
accelerated characterisation procedure for composite materials, appl. to graphite-epoxy laminates 79−34263
acoustic emission, amplitude distrib. anal. 80−66713
acoustic microscopy, with microwave freq., determ. of mech. props. of materials 80−48535
acrylic, denture base, tensile testing 80−16621
adhesion measurement, locus of failure, bond failure in adhesive joints 80−50801
adhesion measurement, of thin films, thick films and bulk coatings, conf. Philadelphia, USA (Nov. 1976) 80−46729
adhesion measurement, of thin films, thick films and coatings 80−50817
adhesion testing, use of fracture mechanics concepts 80−50802
adhesion testing of coating to substrate, specimen prep. device 79−43518
adhesive joint strength testing under normal rupture and shear stresses 79−52500
adhesive strength measurement of electroplates device 78−56843
aerodynamic surface structural tests, systems approach to analysis and design 77−16760
alkali silicate glass, isothermal mech. loss spectrum, appl. of Rheovibron 80−88260
alumina ceramic artificial hip joint wear tests *(German)* 79−8567
apparatus for creep and long-term strength tests, with cyclic temp. var. 80−61046
apparatus review of testing mech. props. of soft animal tissue in vitro 78−31985
artificial hip joint biomechanical test procedures *(German)* 79−8577
Aryabhata satellite structure, static and dynamic loading tests 79−84634
asbestos-rubber plates compressibility and resilience *(Polish)* 79−75500
automated systems, rating quality for investigating mech. props. of materials and structural members 79−15928
automatic test equipment for material props. determ. and quality control 77−86236
automatic unit for mech. testing of materials in complex stressed conditions 79−15898
bend testing unit for sheet materials 77−25214
bending, four point, large deflections of slender beams 77−27487
bending crack test, for fatigue crack propag. laws determ. *(French)* 77−51007
bending test apparatus under high press. and high temp. *(Japanese)* 78−76795
biaxial residual stress distrib., meas. method for determ. throughout workpiece height *(German)* 78−35596
biaxial testing machine, for flat specimens, study of specimen shape *(Japanese)* 77−70268
bimetallic plates, deflection meas. during high-temp. heating 78−7134
blood vessels, medium sized, mech. charcts. 80−41101
brittle coating, ductility meas., four point bend test 78−48577
brittle cracks, propagation velocity determ., expt. eval. 79−70236
brittle material, tensile strength determ., based on radial and compression tests 78−7156
brittle materials, load-transmitting medium to measure strength 80−40652
capacitance type AC dilatometer for piezoelectric and electrostriction const. meas. 80−77747
ceramic artificial hip joint, wear and friction tests *(German)* 79−8568
ceramic components, design criteria and structural testing 79−39083
ceramic rods, arrangement type 2037/ZT-10 for testing flexural resistance *(Polish)* 80−35455
ceramics, impact toughness testing device 80−25941
ceramics, strength and deformation testing, wide temp. range, universal apparatus 79−57177
cervical mucus spinability automatic meas. device 78−31928
coated specimens, bearing capacity, testing under external and internal pressure 79−70254
coatings, adhesion strength, meas. using microindentation method 80−40640
coke, metallurgical, industrial strength meas. methods, critique 80−85117
composite, fatigue life and static strength testing, sample size estimation 79−91867
composite laminates, proof test and fatigue study 80−93643
composite material, ring under one sided heating, strength testing assembly 79−96260

mechanical testing continued
composite materials under complex stress-state conditions, mech. props., method for studying 80−50799
compression, biaxial, machine for testing brittle, plastic materials 79−15899
compression, elastic, uniaxial, of single crysts. at low temps., device 78−49809
compression tests, device for centering specimens 80−61033
concrete, prestressed reinforced rods, tension testing, comparison of instruments 79−8410
concrete, tensile testing apparatus 79−96241
concretes, further development of 2 point test for workability and extension of its range 80−66728
creep tests, machine, conditions of plane state of stress 80−21232
cupping, sheet material, automation of standard testing 79−57172
curved sandwich beam, five point loading test, bending and shear stiffness determ. *(German)* 77−16765
curved specimens, elastic and strength charcts., universal clamping device 80−25960
cylindrical surface linearity testing device 77−30129
cylindrical testpieces, axial residual stresses determ. problem 78−7115
deformation meas., interferometric method, appl. to sheet metal and transparent plastic sheets 78−75108
deformation processes in complex profile shells, installation UDM-1 80−81261
deposit-substrate systems, adhesion testing 80−50814
device for determining the compressive stress-strain curves in small specimens. Application to the study of antimony single crystals *(French)* 79−47852
dislocation dynamic props., investigation by impact loading *(Russian)* 78−85069
disperse system, plastoviscous, cone plastometer for strength props. determ. 80−76426
double ligament tensile test in deformation processing 77−32753
droplet impact, high-speed, effect of gas medium on dimensions of contact area 77−28942
dry strength determinations, testing conditions influence *(German)* 80−25928
ductility meas. under tension or compression at high press., apparatus *(Japanese)* 78−35617
elastic contact problems, mixed approach using finite element methods *(Chinese)* 80−5995
elastometric materials, friction testing using reciprocating friction and wear tester 80−76451
electrodeposit, on metallic substrate, peel test for determ. adhesion 80−50815
electronic tensile/compressive strength test machine calibration *(German)* 77−77654
EM tensile adhesion test method 80−50804
fatigue crack growth investigation, testing equipment 80−81247
fatigue test data, statistical anal. *(Japanese)* 80−62452
fatigue test results, numerical expressions *(Japanese)* 80−62455
fatigue testing, in situ, devices for automatic emergency protecting of mill stands *(Russian)* 80−93717
fatigue testing, of thin wires 80−25834
fatigue tests, improving accuracy with axial loading, specimen fixing 79−83428
fibre reinforced composite, viscoelasticity measurement using mech. drive viscoelastic tester *(Japanese)* 79−34232
fibre reinforced composites, unidirectional, tensile testing 80−40664
fibre reinforced organic matrix composite, use of unidirectional flexural tests, to assess environmental behaviour 79−20301
fibreglass, structural, compression testing method 78−23895
fibrous structure, low-density, centrifugal method for mech. prop. obs. 80−71823
filamentary crystals, complex stressed state, method of investigating mech. props. 80−3264
film, adhesion measurement 80−50819
filmed structures, hardness and adhesion meas., scratch technique 80−50805
films and foils, mechanical testing methods, review 80−40637
flame-sprayed coatings, adhesion testing 80−50812
foam plastic, device for compression tests at different temps. 80−25947
four ball test re-examination for lubricants 78−60964
fracture monitoring with simultaneous recording of acoustic emission signals 80−55599
friction machine, residual stresses meas., appl. to wear resist., surface wear 78−60906
friction machine, type SMTs-2, exam. of electronic loading cycle counter 79−52527
friction machine SMTs-2, self adjusting fixture for block specimens 80−25944
friction surfaces, wear meas. using profilograph, mould producing material quality factors 78−7116
friction test simulation in lubricated condition *(French)* 79−57189
friction tester, variable speed 80−100990
furnace, heating specimens to 1400°C 80−3265
fusion reactor Large Coil Segment test, struct. anal., mag. force loadings 78−50373
gas lubricated bearings, test equipment to examine friction and wear, exam. of design 79−52522
geological materials, stress relaxation testing method for mechanical behaviour studies 78−96309
glass fibre, tensile strength meas. using chain-loading fibre tensometer *(Japanese)* 80−55610
glass fibre reinforced epoxy resin composites, fatigue behaviour, influence of superposition of elec., mech. and environmental stresses 80−97590
glass fibre reinforced plastics, winding device for mech. test specimens prep. 78−7138
glass-fibre reinforced plastic specimens, prep. of three-layer cylindrical with syntactic foam base 80−3267
glazed surface, abrasion resistance testing *(German)* 77−32728
graphite, stress/strain behaviour, exam. with high temp. short time testing facility 78−53051
graphite fibre reinforced epoxy, US attenuation as an indicator of fatigue life 80−85118
grid method for residual deforms. meas. 77−52572
gripping attachment for wire and strip specimens on dividing machine type PTA 80−40647
hard tension/compression tester, high temp. microscope and metallurgical appl. 79−100320

mechanical testing continued
hard tension/compression tester developed for high temp. microscope, metallurgical appl., functional features *(Japanese)* 79−70259
heat energy relaxed due to deform., thermocouples obs. 80−21214
heat-resistant alloys, installation for mech. tests under superplasticity conditions 80−55603
heater, for static testing of riveted samples for short-term high-temp. strength determ. 79−87793
high and cryogenic temperature range mech. testing devices 78−7137
high strain rate material behaviour and testing techniques, J.D. Campbell memorial lecture 80−82627
high strain rates, conf., Oxford, England (Mar. 79) 80−82575
high temp. exam. facility 78−53051
holographic interferometry, review 79−87788
hot pressing, apparatus for laboratory investigation 77−10038
hydraulic loading system for testing under irradiation 78−31609
hydrodynamic testing equipment with gravitational channel for reactor core meas. *(Slovak)* 78−21625
hydrogen, embrittlement resist., selection of test conditions, steel testing appl. *(Russian)* 79−15883
hydrostatic installation for testing solids and tubes under liquid press., axial forces, torsion 78−31608
hydrostatic pressure testing device, tensile, upsetting tests 80−25959
ice, Antarctic deep core, mech. tests under hydrostatic pressure *(Japanese)* 79−79890
ice strength meas., in situ tests 77−37423
impact force meas. by elastic stress wave obs. 79−34215
impact tester attachment, for bending impact tests, method of obtaining asymmetric cycles 80−16628
impact torsional test by means of dropped bar, appl. to low C steel 79−100304
impression fatigue test 80−25861
inorganic nonmetallic building material with rough surface, abrasion test using pneumatic apparatus for thickness meas. *(German)* 79−52553
instrumented restrained cracking (IRC) test, development and applic. *(German)* 78−85060
interferometry, two-wavelength investigation of deform. and vibration of objects 77−46976
internal friction test device for thin-walled tubular specimens 80−71836
J integral and its components, determ. method 80−45458
lap shear test specimen comparison 77−40501
large scale for material in tension and compression 79−43530
low temperature, temp. control for tests in liquid coolant vapours 80−81260
machine for cold rolling, deformed contrete reinforcing bars for model tests 78−60924
machine for uniform applied load flat plate testing, report 77−1908
machine stiffness, activation volume 77−28966
magnetic loss during polarity reversal, stress determ., mech. props. determ. 77−59879
masonry units, splitting tensile test 78−53061
mechanical oscillations amplifier 80−13069
mechanicochemical testing of metals, electrochemical cell for mechanico-chem. behaviour determ. 78−60905
mechanotron unit for structural strength determ. 77−77658
medial collateral ligament substitute specification and design 78−36060
medical equipment, standardisation of mechanical action resistance testing methods 79−92403
membrane with radial slots, expt. study of structural strength 77−81372
metal, effect of environment, lab. investigs. *(Russian)* 78−11458
metal, plastic props. investig. at elevated temps. by torsional method, review 79−43509
metal electroplastic deformation meas. pulse generator *(Russian)* 80−25931
metal fatigue, eddy current sensors, tuning method 80−21231
metal foil bulge-test samples, shape meas. by optical contouring 77−63843
metal hot sprayed deposit adhesion quality factors 79−83365
metals, high temperature testing, MEITP-1 indentation system (USSR) 80−74820
metals, test device for thermal cycling conditions 79−87778
metals and alloys, mech. props. electric current effect, test device for 4.2-300K 80−66719
microprocessor application for destructive examination of materials with data processing *(German)* 80−93714
microprocessor applications in deformation processes *(German)* 80−40627
modal test methods and applications 78−79252
Moire strip attainment at specified pt. on contour of stress concentrator 77−52573
Monel, Ni-Cu-Fe-Mn, resistance spot weld quality evaluation, using stress wave emission technique 78−53066
multistage force measuring equipment, design, operation 77−77673
nuclear pressure vessel surveillance capsule remote dismantling and testing 79−9817
oceanographic two-stage mooring design and performance test 77−5365
optical coating adhesion characterisation pull-off tests 79−14128
optical fibre, mechanical performance characterisation methods *(German)* 78−33870
optical fibres and cables 80−3285
optical glass, K8, bending strength, sample dimension effects 80−9975
optical multifilm manufacturing, large scale, function stress testing 79−81576
orthodontic appliance mechanical behaviour determ., computer-controlled device 78−44727
orthopaedic implants and biomaterials, mech. testing 78−36057
orthotic material characterisation by mech. impedance method 78−36066
perforating rods, length reduction at high impact velocities, X-ray studies 78−40016
plastic, static relaxation behaviour, test rig design *(German)* 79−39081
plastic deformation, compression test method *(Hungarian)* 80−97658
plastic deformation, fatigue test method *(Hungarian)* 80−97665
plastic deformation, Griffith fracture test method *(Hungarian)* 80−97666
plastic deformation, hardness meas. test method *(Hungarian)* 80−97664
plastic deformation, internal friction test method *(Hungarian)* 80−97662
plastic deformation, stress relax. test method *(Hungarian)* 80−97661
plastic deformation, torsion test method *(Hungarian)* 80−97659
plastic deformation, uniaxial tensile test method *(Hungarian)* 80−97657

mechanical testing continued
plastic deformation, X-ray line profile test method *(Hungarian)* 80−97663
plastic tubular specimen, clamping device for complex stressing 78−23912
plasticity diagram plotting by testing cylindrical samples in combined tensile tension 77−63879
plastics, for transmission media, thermomech. reliability 80−40666
plastics, tensile and flexural testing device, incorporating an impacter *(German)* 80−3276
plastometer, electronically controlled, for tensile and compression tests *(German)* 80−3273
Poisson ratio of nearly incompressible elastomers, dilatometric method 79−11733
polychromatic X-ray stress meas. *(Japanese)* 78−7143
polyethylene film, minimum running thickness, biaxial extensional flow study 80−100993
polymer, relaxation properties investigation method and instrument 78−39967
polymer tensile testing method 79−39073
polymer testing by dynamic mech. anal. 80−16626
polymers, automatic recording device for thermomechanical and linear dilatometric testing 80−11858
polymers, in situ EPR tensile testing apparatus 78−85086
polymers, relaxation props., photometric transducer method of meas. 80−3268
polymers, torsional shear testing using electromech. high-press. apparatus 77−51005
powder, high-pressure triaxial testing cell 79−74329
powder-cushion gripping to promote good alignment in tensile testing 78−92418
power transmission cables, pipe-type, low-cycle fatigue tests 80−7731
pressure vessel for tensile testing in high-pressure gases at high temps. 78−44303
prismatic specimens, method for plotting deformation fields 77−63851
proof-testing in strength-distrib. truncation of Si_3N_4 78−80693
prosthesis mechanical efficacy determ. by holographic strain meas. *(German)* 79−8573
PTFE, transfer layers produced by rubbing, apparatus for study 79−47861
radioactive materials, package design, construction and testing for safe transportation 80−63412
reactor pressure vessel brittle fracture, safeguards, American and German ductility requirements *(German)* 79−41017
refractories, high-temp. installation for thermomech. testing 79−83425
refractories, microsamples, high-temp. mech. testing, unit 78−60904
refractory abrasion test machine for use at high temp. 79−52505
relative elongation determ. from machine tensile curve 79−15927
relaxation processes activation energy determ. method, sample and holder design 78−39966
relocation profilometer stage, three dimensional 77−77725
residual stresses, methods of detecting, review *(German)* 78−44291
review of mechanical test methods and strength of structures 79−43507
ring samples in tension 77−25215
rock beam, laterally-constrained, ultimate strength investigation with constrained beam test apparatus 79−29299
rocks tensile strength indirect measurements, new theoretical aspects 79−29883
rolled stock, stat. quality control w.r.t. mech. props. 79−43510
round specimen, tensile testing, at const. true strain rate simple beam diameter transducer 78−7162
rubber, angle tearing testing appliance 78−7140
rubber, swollen, stretch testing, attachment to strength testing machine 79−15905
scale effect, rel. to kinetic theory of material strength 79−15930
sea ice, in-situ meas. of mech. props. using flatjack methods 80−69751
SEM attachment to record stress-strain diagram 80−25961
shear modulus, static, determ. method 78−7111
shear press apparatus with roller bearing 77−41592
shear tests on single crysts., stress equipment 77−81367
sheet galling, development of quantitative test 78−92433
sheet material, method for strength meas. under biaxial tension 80−66717
shock-test stand for repeated impact acceleration effect 79−80611
SiC-Q apparatus, for tensile strength meas. of cast Fe *(German)* 80−76450
simple shear generation *(German)* 77−44432
simple tension test, appl. of hyperbolic theory of plasticity 77−39235
sliding contact, friction, wear, temp. anal. 80−93659
slippage in crystals, photogrammetric obs. method 80−100975
soil, cohesionless, strength, influence of high pore-water press. 77−25678
solar cell welds, NDT for mechanical strength evaluation 78−35630
soldered thick-film conductor, adhesion meas. technique 80−50811
space shuttle insulation coating, combined load testing at 1100°C 79−34261
space-shuttle thermal-protection coating, testing techniques at 870°C 78−35604
static bending testing device for samples at different temps. in aggressive media 78−39972
static strength testing at low, high temps., appl. to reinforcement steel 79−15902
static tensile-compressive testing, smooth tubular specimens, grip for 80−66724
steel, 3-cam plastometer determ. of deform. resist. 79−87792
steel, Cr-Mo-Ni-V, dynamic stress intensity factor meas., possibilities and limits *(German)* 80−93719
steel, Cr-Ni-Mo-V, ductile fracture during tensile loading 80−45381
steel, high strength low alloy, acoustic emission meas. from crack opening displacements 80−7732
steel, hot rolled strip formability, mech. testing and mech. props. *(German)* 79−66089
steel, industrial tests for determining lamellar tearing susceptibility *(French)* 80−21250
steel, low alloy, elastoplastic strain evaluation in crack weakened cross sections by fracture mechanics 80−45380
steel, low C, dynamic stress intensity factor meas., possibilities and limits *(German)* 80−93719
steel, low C, mech. characts., specimen size and shape effects 80−66715
steel, Ni-Co-Mo, dynamic stress intensity factor meas., possibilities and limits *(German)* 80−93719

mechanical testing continued
steel, Ni-Mn-C, austenitic, proof stress change meas. by internal friction with martensitic transform. 78−56638
steel, pressing die X45 CrNiWMoVCo 9.9, test results *(German)* 80−50785
steel, sheet, rapid test for props. assessment 80−40650
steel, stainless, stress/strain behaviour, exam. with high temp. short time testing facility 78−53051
steel, stainless type SUS 304, diffusion welded joints, sound emission during tensile testing *(German)* 80−61062
steel, structural, wide plate tensile testing eval. *(German)* 80−100969
steel, testing in moist H_2S 78−23901
steel, tufftrided, type S15CK, fatigue strength, estimation of size effect *(Japanese)* 80−81166
steel, wear resistance, determ. using MI-1M machine 80−25943
steel bar deformation meas. by holographic interferometry using four point bending machine 78−60721
steel bimetallic tube with internal Cu coating segmental specimens, tensile testing 79−70255
steel wire rope, tensile testing, fastening method 79−87779
steels, dynamic material props. for FBR safety anal., testing devices 78−60966
stiffened panels with rectangular cut outs, stresses and deform. *(Japanese)* 79−3977
strain diagram plotting from data obtained during elastoplastic bending or torsion 77−81371
strain gauge, resistance device for calibration at low temps. 79−17413
strain gauge application on compact bone 80−3883
strain rate sensitivity parameter measurement, from expt. load vs. time curves 79−8406
strength, long term, test system 79−70253
strength of materials, empirical determ., cleavage fracture in plane waves 80−96225
strength of metals, ionised gas effects, test apparatus for 20-900°C 79−70252
strength testing allowing for stress form *(Russian)* 77−60008
strength testing machine for use in mobile laboratories 79−15908
stress corrosion testing device, lab. and autoclave testing 79−52502
stress intensity factor specimen design, constant factor for crack length range 77−73380
stress intensity factors, photoelastic meas. correlation, for various specimen and defect geometries *(German)* 80−53727
stress relaxation test device, for variable temp. 80−85113
stress-strain diagram, automatic plotting during mech. testing 78−27724
stress/strain, of fragile materials, at high temperatures, improved clamp for transducer attachment 80−73351
structural failure detection by vibration detector 78−15641
supersonic gas jet, penetration into the ground *(Russian)* 80−28544
surface measurements in manufacturing processes, precise mechanical test method *(German)* 80−62624
T-10 M tokamak toroidal field coil shape struct. anal. 78−50374
tactical rugged lightweight fibre-optic cable performance 79−37025
tensile, effects of strain rate and deform. heating 78−85089
tensile, plotting device for stress-strain diagrams 80−3269
tensile and flexural testing device, incorporating an impacter *(German)* 80−3276
tensile deformation of flat samples, meas. equipment using exoelectron emission 77−77679
tensile machines, temperature control of suspended electric furnaces 77−82523
tensile specimen preparation, stress distrib., for TEM 78−73973
tensile strength of optical fibre waveguide, extrapolation of short length test results 78−9456
tensile test, regulated, strength and deform. characteristic values, consistency *(German)* 80−93712
tensile test diagram remote recording device 78−7139
tensile test equipment and procedures for charact. value determ. *(German)* 80−93713
tensile test specimens, cylindrical, area reduction determ. 79−100306
tensile testing, control of test cycles, data logging and data processing *(German)* 80−97648
tensile testing, low-temp. strain gauge for testpiece deform. meas. 78−7118
tensile testing, methods of measuring stored energy by calorimetry 79−29325
tensile testing, methods of measuring stored energy by calorimetry 79−29326
tensile testing, microcomputer for automatic meas. and data treatment *(German)* 77−44433
tensile testing, strain meas., device 79−43515
tensile testing at high temp., self-locating grips design 79−52507
tensile testing machine by up to 3000°C 79−87776
tensile tests, standardization from metal physics viewpoint *(German)* 80−93711
tension, torsion and compression testing under hydrostatic press. 78−11482
tension test, computer simulation, effect of testing conditions 80−7729
tension test instability *(German)* 77−52555
tension test with neck triaxiality reduction 78−7159
tension-torsion impact testing apparatus, instantaneous plastic property 79−52474
test machines, elastic yielding determ. 79−70251
thermal insulating materials, radioisotope thermoelectric generator appl. 79−48145
thermally sprayed coating adhesive strength testing method 79−83432
thermoplastic pipes, apparatus for time-to-failure determ. *(Polish)* 79−74328
thermoplastic plates, strength meas. when supported by annular ring 80−81257
thermoplastic-based sheet materials, flexural anisotropy and stiffness assessment 80−76442
thermostatic glass-float adhesiometer 79−43519
thick film, adhesion to ceramic, destructive and nondestructive meas. 80−50809
thick film conductor, adhesion meas. 80−50808
thick film terminations on chip components, adhesion meas. methods 80−50810
thin film adhesion meas., semiautomatic installation 79−96245
thin films, adhesion, meas. device 80−66720
thin walled pipes, device for gripping in tests with complex stress state 80−25945
thin walled tubular specimens, plotting hardening curves based on torsion tests 77−56180
thin-walled tubes accelerated rate test system for two-dimensional stress states 79−43514
three-point bend test optimisation for fracture energy determ. 77−21333
thyristor controlled drive for machines 77−25213
tissue, human, in vitro uniaxial testing apparatus 78−61295
torsion machine for simulation of multistage deformation 77−40492
torsion rig, testpieces testing during variable torsion 79−52494
torsional strain curves plotting 80−40638
triaxial testing large specimens, machine for dynamic and static testing 79−83407
tube, spirally welded, pressure-test apparatus 77−52583
tubular sample testing unit with axial force, internal and external press. and torsional moment 78−39969
universal interference and polarisation apparatus 78−19986
US plate testing equipment, computer controlled, working experience *(German)* 80−93720
volume stressed material under static or low-cycle load, testing device 80−71834
wear, specimen loading device 79−43516
wear due to impulse friction, device 80−25957
wear meas. by ^{56}Co activity reduction 79−57166
wear of specimens on friction machine, device for continuous recording 80−55604
wear test friction machine, exam. of design 79−52526
wear test system, low temp., exam. of design 79−52523
wear testing device, cyclic load and temp. var., to 800°C 80−66718
welded pressure vessels, residual stresses determination 78−40014
wind generator, vertical axis, 1 kW, using steel reinforced fibreglass blades 79−61940
wing pump wear when using flash-resistant hydraulic fluids *(German)* 79−83331
wire in torsion, installation for automated determination of yield strength 80−21221
wood particle board, method of mech. testing, elastic deform. meas. 78−56837
Young's modulus determ. from microimpression tests 77−86281
Al alloys, types 1100 and 5454, long-time rupture tests 80−76434
Al, Bauschinger effect, temp. influence, combined tension-torsion testing machine 80−45453
Al, thin film on fused quartz, threshold adhesion failure, meas. by stylus method 80−50806
Al-Si alloy, rod, tensile loaded, internal friction and Young's modulus measuring equipment, inelastic phenomena exam. *(Hungarian)* 79−52546
Al-Zn eutectoid, superplasticity, test machine rigidity effect 79−70250
Al-Zn-Mg, acoustic emission meas. during tensile testing, reproducibility of results 80−50782
Au, rod, tensile loaded, internal friction and Young's modulus measuring equipment, inelastic phenomena exam. *(Hungarian)* 79−52546
B fibre reinforced Al. strength determ. procedure in annular specimens *(Russian)* 78−95864
C materials, bend strength testing, bench assembly with strain recording 79−57176
Cu, activation vol. and dislocation density determ. from relaxation tests 78−3264
Cu alloy, ductile fracture during tensile testing 80−45381
Cu, rod, tensile loaded, internal friction and Young's modulus measuring equipment, inelastic phenomena exam. *(Hungarian)* 79−52546
Cu-Ni-Sn (4,4 wt.%) resistance spot weld quality evaluation, using stress wave emission technique 78−53066
Fe, grey cast, tensile testing of mechanical props., from room temp. to liquidus *(Japanese)* 80−7728
Fe plastic strain, thermoactivation anal. exam. of method *(Russian)* 79−57164
Fe polycrystalline, two ferromag. methods for eval. of fatigue limit 80−89438
Fe-Si, stress and plastic deform. effect on Barkhausen effect, instrumentation 78−52313
Ni coatings on Al alloy substrates, adhesion strength, meas. using microindentation method 80−40640
$Pb(ZrTi)O_3$ ceramic transducer for generation and detection of unipolar stress pulses 80−64328
$Pd_{80}Si_{20}$ amorphous alloy, skip deform. and crit. shear stress, using tensile testing machine 80−89321
Pt-Au, thick film, adherence meas. and evaluation 80−50813
Si based ceramics, stepped temperature stress rupture testing 79−61804
Si, near (111), fracture by painted indenter, SEM study 80−71734
Sn plate, rapid test for props. assessment 80−40650

mechanical variables control
this heading is restricted to those variables which are not covered by other specific headings. See also, for example, force control; thickness control; velocity control; vibration control
crystal diameter system design and operation 77−1797
crystal growth, Czochralski and related methods, diameter control, review 78−31328
Czochralski growth of alkali halides, dynamical aspects, use of optical diameter controller 78−31332
gyrostatic bodies, control of motion by means of gyroscopes *(Italian)* 78−12549
handwriting a Japanese letter to investigate the patternization of motion 78−12555
optical fibre drawing process, diameter control 78−13794
radio reflector surface of radiotelescope antennae, surface contour control 79−80221
Si, Czochralski growth with automatic diam. control 78−52658

mechanical variables measurement
see also elastic moduli measurement; force measurement; pressure measurement; shock measurement; strain measurement; stress measurement; torque measurement; vibration measurement
200 kW Gedser windmill in Denmark, structural response meas. 80−61431
acoustic holographic techniques, NDT appl. 79−86300
adhesion, locus of failure, bond failure in adhesive joints, experimental methods 80−50801
adhesion, locus of failure 80−50818
adhesion, of evaporated thin films 80−50822
adhesion, of preformed film to solid 80−50819

mechanical variables measurement continued
adhesion, of thin films, adhesive failure, rel. to interfacial structure 80−50820
adhesion, of thin films, thick films and coatings 80−50817
adhesion measurement, of thin films, thick films and bulk coatings, conf. Philadelphia, USA (Nov. 1976) 80−46729
adhesive energy, meas. techniques, in metal/ceramic systems 80−50803
anelastic relaxations and magnetic aftereffects in solids, conf., Katowice, Poland (Jan. 1978) *(Polish)* 79−96072
angular rate of vehicle, meas. by vortex rate gyro 78−21125
articular cartilage in uniaxial tension, nonhomogeneous directional mech. props. meas. 77−29167
automatic internal friction and modulus meas. apparatus using phase-locked loop 78−13981
bimetallic plates, deflection meas. during high-temp. heating 78−7134
capillary piezometer with opticomech. readout, for compressibility meas. 77−39264
compressibility of solids, optical method *(Slovak)* 80−37023
cone and plate rheometer, press. distrib. in gap for viscoelastic fluid with high shear rate *(German)* 77−51143
damping characteristics of pendulums, digital, using amplitude-time convertor *(Czech)* 77−71310
deformation analysis, holographic image motion due to reconstruction source movement 77−10866
deformation measurement, expt. using transmitted light 77−86860
deformation of mech. struct., accuracy and reproducibility of heterodyne holographic interferometry 78−37843
deposit-substrate systems, adhesion testing 80−50814
double ligament tensile test in deformation processing 77−32753
elastic-wave ellipsometer for meas. of material property variations 79−46143
elasticity of supports, in dynamic regime 77−75864
electrical meas., using strain gauges or inductive transducers 77−33981
electrical meas. systems, errors *(German)* 79−97382
electrodeposit, on metallic substrate, peel test for determ. adhesion 80−50815
electronic, using capacitive transducers, frequency superposition principle appl. *(German)* 77−53955
EM tensile adhesion test method 80−50804
end standards, phase correction by profiling technique, interferometric methods appl. 78−73986
film-substrate bond strength, meas. by laser spallation 80−50821
filmed structures, hardness and adhesion meas., scratch technique 80−50805
flame-sprayed coatings, adhesion testing 80−50812
framed particles, automatic selection of polymer shells for laser targets 77−80336
friction, meas. at lubricated sliding surfaces *(German)* 79−81826
friction, small mobile apparatus for meas. of floors 80−69747
friction measuring instrument for single fibres in various media 77−27498
friction measuring test for use under conditions of high normal interfacial force 80−76454
friction surfaces, wear meas. using profilograph, mould producing material quality factors 78−7116
gases PVT study, weight handler for piston gauge 78−8399
geological materials, mechanical behaviour studies via stress relaxation testing method 78−96309
holographic interferometry, appl. to machine tool framework rigidity *(German)* 77−7040
holographic interferometry, deformation analysis of opaque bodies, book 80−27050
holographic photoelasticity, technique for calibration of isochromatic and isopachic fringe pattern *(Rumanian)* 79−86388
ice strength meas., in situ tests 77−37423
impact machines, pendulum, energy meas. using optical system 80−69746
impulse technique for mechanical structure investigations *(German)* 79−68667
internal friction, determ. from dynamic hysteresis loop area and specimen cross section in deform. 78−23897
internal friction, measurement using automated Marx's composite oscillator method 80−37151
internal friction, RIM-3 relaxator *(Polish)* 79−94572
internal friction, torsion pendulum oscillations recording equipment 78−36998
internal friction apparatus for freqs. up to 200 Hz, automated control 78−22308
internal friction meas. instrument for use at high temps. 78−13977
internal friction meas. using torsional pendulum 78−13980
internal friction measurement *(Spanish)* 80−6002
internal friction measurement of metals using sound emission during vibration 77−77715
internal friction Q-factors, meas. apparatus for brittle materials 77−27499
internal tension, transparent recording Berthelot tensiometer 79−35723
laser beam applications, survey *(German)* 77−698
layered media, asymptotic analysis of nonlinear effects in acoustic diagnostics 77−84090
magnetostriction, device for meas. at high temps. 77−26365
mechanical oscillating distribution, measurement techniques *(Japanese)* 78−41300
metal-polymer joint, meas. of temp. dependence of joint strength 80−50824
metals, determ. of yield strength 80−25937
optical fibres, breaking strain estimation for long lengths of fibres 78−30060
plastic deformation measurement, moire method *(Polish)* 80−69749
polymer solution, viscoelastic properties, direct meas. method using channel flow 79−37265
polymer solutions, dynamic compressibility study via press. transient technique 77−86256
polymethylmethacrylate, rheological meas. with new rotational rheometer *(German)* 77−51006
porosimeter, continuous scan mercury type, pore pot. contrib. to hysteresis 80−77928
porosimetry technique for up to 6 kbar, Hg porosimeters design 79−21761
prebending measurement methods, plate, compression osteosynthesis appl. *(German)* 77−40895
mechanical variables measurement continued
pulse electromagnetic mechanical characts. meas. method *(Polish)* 77−67478
reactor coated fuel particles, automatic size anal. 77−79460
resonant electromagnetic fatigue tester, features *(French)* 78−56870
Rheovibron viscoelastomer, Massa correction for loss tangent meas. 78−83349
rock joints roughness determination, new laboratory method 78−96315
rock materials, strength determ. in triaxial compression, suggested methods 78−81432
rock materials tensile strength determination, suggested methods 78−96314
rocks, petrographic description rel. to mechanical behaviour, suggested method 78−81431
rocks hardness and abrasiveness determ., suggested methods 78−96313
rocks tensile strength indirect measurements, new theoretical aspects 79−29883
sapphire fibres, meas. of bending strength 80−25964
SAW amplitude measurement, optical probe 79−28185
skin friction, meas. by viscosity balance method, appls. to three dimensional flow 77−19645
soldered thick-film conductor, adhesion meas. technique 80−50811
Steatit ceramic strength determination by measuring US dynamic elastic modulus *(German)* 79−43301
steel, cold-formed, NDT of mech. props., coercimeter results 79−34240
steel sheet internal friction, mechanical anal. of meas. apparatus 77−32752
stretch measurement of ribbons in industrial processes, digital instrument *(Polish)* 80−42194
structuring dispersions, struct. determ. using dynamic dielectric behaviour meas. device 78−31710
superconductors, test facility for dynamic stress effects 77−77698
surface measurements in manufacturing processes, precise mechanical test method *(German)* 80−62624
tension testing of reinforcement rods for prestressed concrete structures, comparison of instruments 79−8410
thick film, adhesion to ceramic, destructive and nondestructive meas. 80−50809
thick film conductor, adhesion meas. 80−50808
thick film terminations on chip components, adhesion meas. methods 80−50810
thin film, internal friction meas. during plastic deformation, 4.2 to 300K 79−71442
thixotropic materials, characterisation via extrusion rheometer 77−63876
threadlike crystals, precision method of internal friction investig. 78−36997
torsion pendulum, automatically driven, for continuous meas. of amplitude and amplitude-independent damping 77−35099
tribometry development, friction reduction and meas. 80−23973
tribometry metrological provisions, Soviet installations and instruments development 80−23974
viscoelastic properties of liqs. meas. using torsion resonator, 20-1200 KHz *(Russian)* 80−52196
volume compressibility of polymer materials, meas. equipment 77−77674
volume compression sensors, sensitivity under cyclic load 79−29315
wristwatch balance period/oscill. amplitude meas., photoelec. method *(German)* 77−87755
Ag, granular thin film, adhesion measurement 80−50807
Al, thin film on fused quartz, threshold adhesion failure, meas. by stylus method 80−50806
Cu, on thermally oxidised Si, EM tensile adhesion test method 80−50804
Pt-Au, thick film, adherence meas. and evaluation 80−50813
mechanical waves *see elastic waves*
mechanics
see also bending; biomechanics; celestial mechanics; classical mechanics; damping; density; dynamics; fluid mechanics; intermolecular mechanics; kinematics; momentum; relativistic mechanics; statics; statistical mechanics; wave mechanics
applied mathematics and mechanics, conf., Giaz, Austria, Apr. 1976 *(German, English, French)* 77−67284
biomechanics, living tissue mechanical props., boundary value problems 77−70491
computational techniques in interface problems, conference, San Francisco, CA, USA (Dec. 1978) 79−41655
dimensional analysis in electricity and mechanics, teaching 79−97165
dynamic interaction of moving vehicles and structures 80−64357
education, Age of Newton workshops in optics, mechanics and mathematics 77−87586
evolutive mechanics, relativistic analytic mechanics 77−17800
frontal method for structural mechanics, algorithm for excluding unknowns 80−79157
inertia, origin, experimental approach to understanding 77−17799
Jourdains variational principle, use in nonlinear mechanics and transport phenomena 79−9093
limitations in description of physical phenomena 77−67263
long span bridges, rational design and struct. safety *(Japanese)* 77−7303
negative energies, teaching approach 77−13553
non-standard formulation 78−36812
Polish mechanics, history before 1918 *(Polish)* 78−20930
sliding interfaces and impact, numerical treatment 79−41631
soil, triaxial test, limit analysis theory *(French)* 78−32073
static loads in bins containing granular material, classical formula for pressure 78−38264
system theoretic representation of mechanical systems 79−17342
teaching approach starting with dynamics *(Hungarian)* 79−17157
teaching in Britain to undergrad. students, eval. of standard 77−53722
teaching in Italy 79−17160
theoretical and applied, conference, Delft, Netherlands (August-September 1976) 77−67262
unbounded contact problems analysis by quadratic programming 77−2533
work, teaching of mechanics 79−21493
mechanics of fluids *see fluid mechanics*
mechanoception
acceleration effects, +Gz influence on semicircular canal function, aircraft appl. 80−94245
acoustics and hydrodynamics of certain marine animals 77−36963
active hearing in dolphins, critical interval 77−40682

mechanoception continued
afferent nerves from muscle spindles, signal interpretation method 80−101188
amplitude spectrum representation in auditory cortex of mustache bat 77−52810
arm movements controlled by peripheral feedback, human, simulation 78−80891
auditory impedance changes elicited by tactile and electrocutaneous stimulation 80−56066
auditory/vibratory perception of syllabic struct. in words by profoundly hearing impaired children 78−27962
balance, flow of endolymph in the semicircular canals 79−92258
balance in standing position on a mobile platform *(French)* 80−94244
baroreceptor activation reactivity to noxious stimulation reduction, hypertension implications 80−61596
baroreceptor Na sensitivity, mediation of reflex changes of blood press. and urine flow 77−48818
bat, moustache, target range sensitive neurons in auditory cortex 79−83808
bats, echolocation, pursuit of prey 79−83807
blind aid, image conversion to a tactile presentation 80−94414
cercal system, cricket, constant representation of sound source position 77−25475
cerebral laterilisation of haptic perception, interaction of responses to braille and music obs. 78−7374
CLONUS, simplistic model of a complex system 77−48786
cortex, human, no-stimulus, no-response, event-related pot., motosensory system obs. 80−108923
cortical evoked potentials, math. model for source localisation, somatosensory stimulation 80−89774
cricothyroid muscles, response to FM sounds in FM bats, myotis lucifigus 77−21540
cutaneous cross-model interactions, punctuate press. sensitivity rel. to skin surface temp. 78−3527
cutaneous receptors, multiple unit correl. anal. 79−100638
cutaneous receptors, on-line receptive field mapping technique 79−74797
D_2O effects on mechano-sensory receptor 77−44696
digit-wrist sensory compound nerve action pot. obs. in patients with focal nerve injuries 80−3655
disproportionate tonotopic representation for processing CF-FM sonar signals, mustache bat 77−12940
dolphins and pinnipeds, echolocation system acoustics and hydrodynamics 77−36963
Doppler echolocator of the horseshoe bat, use in surroundings ob. 77−70483
Doppler-shifted-CF processing area of Mustache bat auditory cortex, aural representation 78−80892
echo-detecting characteristics of neurons in inferior colliculus of unanesthetised bats 77−70484
echo-locating animals, model of the neurocorrelometer 78−96059
echo-locator of bat, precise determ. of target direction 77−36962
echolocation in bats and auditory system 80−108906
echolocation signals propagation, atlantic bottlenose dolphin 78−88721
echolocation systems in nature, a theory of optimum insensitivity to motion for bats 79−53163
echolocator, bat, calcs. of pot. accuracy of target angular coordinates meas. 78−77071
electrocutaneous tracking, a methodology for evaluating sensory feedback codes 79−25004
electrophysiological responses of Didinium nasutum to Paramecium capture and mechanical stimulation 80−56001
electrotactile two point discrimination rel. to freq., pulse width and pulse time delay 79−43975
energy dependence in the human cutaneous system, conditions of simultaneous, residual and reverse masking 78−20196
equilibration, physiopathology in aerospace medicine 79−11950
equilibrium reception in an insect, mediation by giant interneurons 80−45925
escape responses of the queen scallop Chlamys opercularis after mech. stimulation 78−53430
evoked giant sensory nerve pots., EMG in quadriparetics and quadriplegics 80−3653
evoked potentials, use in monitoring residual function of injured spinal cords 80−81747
habituation of gill withdrawal reflex, Aplysia californica, synaptic depression 79−83806
hair cells, vertebrate, response to controlled mech. stimuli 78−15852
harmonic-sensitive neurons in the auditory cortex of the mustache bat 79−43933
insects, sound radiating cuticular motion, measurement by irradiance modulation technique 79−84057
intramuscular nerve action pot. derived from sensory fibres 80−56071
ionic channel, model of reception and macromolecular rearrangement, effect of deform. 79−79564
ipsilateral vibrissae in adult rodents, projections on cortical somatic I barrel subfield 80−8074
irritant receptors and afferent C-fibres in the lungs, stimulation by prostaglandins 77−12939
joint receptors, role in mammalian limb control in locomotor activity *(Russian)* 79−43938
labyrinth, estimating the stimulus produced during caloric test 78−40210
lateral line, onset of neural function in South African clawed frog 80−21480
LF sonar signals of the dolphin, Phocoena phocoena, some props. *(French)* 77−52809
lingual tactile sensory system, automated instrumentation for research 80−8205
locator signal, horseshoe bat, echo freq. stabilisation system model 78−20195
lumbo-sacral motoneuron pools, human, response patterns to distant somatosensory stimuli 80−108924
lumbosacral spinal cord and cauda equina, evoked pots. recording 80−17147
matching information to brain, problems 80−51114
maxillary gum trigeminal evoked pots. in humans 80−97948
mechanical and chemical sensitivity at the mantle edge of the file clam Lima scabra 78−53429
mechanostimulator, new, simple, rel. to physiological appls. 78−92762
median nerve, transient responses to elec. stimulation, SQUID appl. to somatically evoked field meas. 80−104706

mechanoception continued
midbrain, similarities between overlapping visual and tactile maps in mammals and reptiles 80−61550
millipore-DOPH model membrane showing an excitation phenomena with a press. stimulus *(Japanese)* 78−3526
moment of inertia, human sensitivity, psychophysical study 80−72180
multisensory orientation stimuli, integration of semicircular canal and otolith information 78−20199
myoelectrically controlled hand with a sense of touch, experience in fitting 79−12035
nerve cell impulse flows, determ. of quantity of useful information 78−69038
nerve evoked pots., sensory and mixed conduction vel. obs. 79−74693
nervous responses from mechanosensory hairs on the antennal flaggelum in the lobster 78−27974
neural conduction times, central and peripheral, in multiple sclerosis, somatosensory obs. 80−89773
optical-to-tactile convertor 80−57041
oral mucosa, EMG registration of sensory thresholds *(Croatian)* 80−108925
otolith sensitivity associated with habituation to linear accels. capable of inducing motion sickness, meas. 78−44621
peripheral nervous system multichannel data anal., frog sartorius muscle mechanoreceptor transducer characts. *(Japanese)* 80−3656
proprioception, input to horizontal oculomotor system of crayfish, expt. obs. 80−72181
proprioceptors with central cell bodies, in locust 80−51132
prosthetic hand pinch force, sensory-feedback system compatible with myoelectric control 80−41324
receptor hair motion in fluid environments, mathematical model 79−88092
receptor-activated ciliary motor responses, mediation considerations 79−11916
receptors, energy transformation problem 78−96058
receptors sensitive to muscle length in the horseshoe crab 80−12167
semi-circular canal, frog, determ. of impulse weight functions of primary afferents 78−69116
semicircular canal afferent responses, system identification 78−27927
semicircular canal units spontaneous activity, anesthetized pigeon, point process anal. 78−24079
sensory evoked pots. at the wrist, infants and children 79−79566
sensory feedback for artificial limbs 79−84012
sensory nerve conduct. vel. of medial antebrachial cutaneous nerve 80−3654
sensory neuron, second order, summation of excitation and inhibition by computer simulation 80−76769
sensory transduction in an insect mechanoreceptor, nonlinear anal. 77−64061
sharks, open-ocean, rapid withdrawal from a sound source 79−16224
skin surface temperature, effect on localisation error and 2-point threshold 78−77072
skin vibroctactile sense study for artificial visual machine *(Korean)* 79−66583
somatosensory decision tasks in man cerebral pots. evoked by finger stimulation 78−11628
somatosensory evoked potential, extended sources assessment method 80−26244
somatosensory evoked potentials, abnormalities due to brainstem lesions 80−56070
somatosensory evoked potentials, in man, cerebral, subcortical, spinal and peripheral nerve pots. 80−16961
somatosensory evoked potentials, reduction during movement, cat extralemniscal pathways recordings 80−85421
somatosensory evoked potentials, review of acquisition and anal. 80−101281
somatosensory evoked potentials, short latency, in man following median nerve stimulation 80−94243
somatosensory evoked potentials, short latency, stimulus intensity effect 80−35924
somatosensory pathways, assessment of central conduction 80−97949
somatosensory potentials following electroconvulsive therapy 80−97947
somatosensory short latency pots. in humans 80−67099
sonar, bat, perception of echo phase information 79−83800
sonar, bats, object advoidance obs. 79−2086
sonar signals of bats, phase-locked loop device for fine freq. anal. 77−56392
sonar signals of mustache bat, information-bearing elements, cortical neurons 79−11943
sound production and air recycling mechanism in Delphinids, cineradiographic evidence 79−48275
spatial orientation of animals, role of auditory mechanisms *(Russian)* 80−45915
speech reading, Tadoma method, untrained observers' discrimination ability, tactile sensitivity 79−96587
spider, web vibr. sensed by Argyrodes elavatus kleptoparasite 80−61595
stretch receptor, crayfish, nonlinear systems anal. of repetitive firing behaviour 78−80853
stretch receptor neuron, crayfish, excitation and inhibition summation 77−2015
stretch receptor neurons, rel. between trains of action pots. across an inhibitory synapse 77−9185
stretch receptor organs, crayfish, recurrent inhibition 79−100636
stretch receptor organs, slowly adapting, periodic stimulation with and without perturbations 79−92242
stretch receptors, dog. intrapulmonary and extrapulmonary, dynamic response obs. 78−20194
stretch receptors array, enhanced contrast arising from reflex inhibition 77−2016
stretch-receptor organs, crayfish effects of length-steps with and without perturbations 79−25003
tactile hearing aid, portable with microprocessor control 79−84029
tactile information transfer between hemispheres in normal young children 79−83809
tactile receptor response on stepped and sinusoidal vibrations of a hair 77−70481
tactile sensation, mechanoreception physiology and psychophysics *(Japanese)* 80−16962
tactile stimuli, rostral-candal, simultaneously applied, physiological mechanism 78−20198
tactual sound localiser for the deaf, basic studies *(Japanese)* 77−86707

mechanoception continued
tactual vocoder, max. information transmission, time-invariant stimulation *(Japanese)* 80−41317
thermal fluctuations in membranes and the problem of mechanoreception 79−53057
time integration for visual pattern preception and a comparison with the tactile mode 79−53143
vestibular mechanisms, rel. to eye movement control, book contrib. 79−96588
vestibular nuclei neurons, goldfish, time constants model with ocular proprioception 78−40142
vestibular nuclei visual-vestibular convergence in cat 80−85420
vestibular research, rotating room acceleration and damping 79−84048
vestibulo-ocular reflex in monkey at high rotational freqs. gain obs. 78−56973
vestibuloocular reflex, model of quick phase generation 78−56971
vibration sensibility threshold meas., pallaesthesiometer automatic signalling and signal fixation unit 79−57784
vibrotactile frequency for encoding a speech parameter 78−11772
vibrotactile speech reading, analytic study of the Tadoma method 78−28127
vibrotactile stimulation by using both elec. and mech. stimuli 77−5109
vibrotactile vocoder display identification of speech sounds 77−78055
visual prosthesis, processing and tactile stimulation of images *(French)* 79−100788
visual-vestibular interaction during body rotation in man, nonlinear model 80−76735
visual-vestibular interactions, model of cerebellar influence 78−40156
voltage noise from hair cells during mechanic stimulation 77−90817
Ca-dependent responses in paramecium mechanoreceptor, loss by artificial deciliation 77−2017

medical administrative data processing
see also medical computing
automated TLD processing and dose record keeping service 80−12267
cardiac catheterisation, automated processing and storage system 79−70694
cardiac catheterisation computer system 79−70695
cardiac cellular electrophysiologic-clinical correlations using a relational data base 80−89890
cardiac computing conf., Geneva, Switzerland, (Sept. 1979) 80−82582
cardiology, conf., Rotterdam, Netherlands, (Sep.-Oct. 1977) 78−81013
cardiology applications, conf., Stanford, USA, (Sept. 1978) 79−62387
cardiology data processing system 80−56236
cardiovascular regional information system including computer-assisted ECG anal. system 78−81049
direct reading pen dosimeters, radiation exposure recording aspects *(German)* 78−5050
documented patient file concept and implementation 78−7498
health care deliverty data processing course 79−80394
hospital integral picture processing and communication system 78−57104
intracavity radiotherapy, interactive treatment planning using CT 80−8145
King Faisal Specialist Hospital (Saudi Arabia) information system 78−57105
microprocessor systems for data acquisition, image processing, RIA anal., patient data retrieval 80−61670
myocardial infarction diagnostic data anal. database 79−70693
nuclear medicine computers 79−25096
obstetric computer system for intensive care of mother and foetus during labour *(German)* 80−3857
oncology, radiation, use of computers review 79−25098
pacemaker computerised data management systems 77−81698
radiation therapy, comprehensive computer system, design and development 79−25078
radiology, introduction to computer systems 79−34663
radiotherapy, tumour registration system 80−81710
radiotherapy treatment planning using microcomputer 80−8191
radiotherapy treatment verification and recording using small computer 77−81554
review, computer applications in biomedical engineering *(Japanese)* 80−12289
skin resistance measurements, collection and off-line processing *(German)* 80−67273
thermoluminescent dosemeter, NRPB's new record keeping service 77−81577
treatment planning, three dimensional model for CT radiotherapy 80−8192

medical computing
see also medical administrative data processing; medical diagnostic computing
absorbed-dose computations for inhomogeneous media in radiation-treatment planning using differential scatter-air ratios 79−25115
ambulatory EKG recording using several computers in parallel 79−62389
anaesthesia administration automation, use of dynamic programming model 77−5107
anatomy, 3D display for radiotherapy treatment planning 80−3773
Anger camera image digital filtering 77−9256
angiographic images of left ventricle, system for off-line anal. using minicomputer 78−80964
angiography, computerised, anal. and visualisation of blood dynamics and motion of organs 80−8170
angiography, effects of asymm. focal spots 77−21617
angiography, validity of computer simulation of blood vessel imaging 78−3594
anti-HBs determination by AUSAB procedure 77−13036
aortic stenoses modelling 79−79581
aortic valve replacement, computerised simultaneous press./vol. anal. before and after 80−85531
arterial blood pressure, indirect noninvasive automatic meas. device 77−44771
arterial pathology discrimination from angiograms 79−16274
artifical vision machine for blind people *(Korean)* 79−66583
assay data automatic treatment by competitive protein binding and radioimmunoassay 77−13037
atherosclerosis detection, computerised electronic radiographs appl. 80−8169
atrial pacing stress test quantification, normal, abnormal values, coronary artery disease in man 78−85449
auditory frequency measurement based on neural timing 77−5011

medical computing continued
auditory nonlinear distortion in sound perception 77−5010
bacterial proteins, quantitation of electrophoretic profiles 79−70331
bioelectronics symposium, Ahmedabad, India, (Dec 1975) 77−40808
bioengineering and medical instrumentation, symposium, Laramie, USA, (May '76) 77−25571
Biomedical Computing Technology Information Centre, for technology transfer 77−40824
biomedical engineering conference, Boston, USA (Nov., 1976) 77−25573
biomedical pictures, digital processing and enchancement techniques 77−40815
biomedical R&D programmes in Norway *(Norwegian)* 78−48909
biomedical surface mapping, interpolation methods, in FORTRAN 80−81750
biophysics, physiology, pharmacology CAI 77−25
biosignals processing, seminary, Brno, Czechoslovakia (Sept. 1976) *(Czech)* 77−17001
blood pressure continuous recording system for ambulant hypertensives 79−62390
blood pulse measuring by computer *(German)* 80−104823
body control mechanism, human, investigation using analysis of body's period signals 79−66576
body radioactivity, SABRE computer system for assessment 77−77998
bone Ca activation anal., prod. of uniform ^{38}K yield using range modulator 77−40735
bone imaging radiopharmaceutical local accumulation model 78−24127
brachytherapy program used with the Philips Treatment Planning System 80−81738
breath by breath anal. of ventilation and pulmonary gas exchange, minicomputer system 79−62393
breathing, vars. in total respiratory impedance 77−52835
cancer therapy treatment planning 79−57754
cardiac arrhythmia detect. and classification using atrial electrogram 77−40867
cardiac arrhythmia monitoring, Aztec replacement by correl. for VPB detect. 79−62388
cardiac arrhythmia monitoring, joint interval histogram and correlation coeff. scatter diagram techniques 77−25572
cardiac arrhythmias, computerised quantitative evaluation of cardiac arrhythmias 78−85435
cardiac assessment using microprocessor 79−83962
cardiac assistance, in-series, by intra-aortic balloon pumping, haemodynamic responses, computer model 79−96711
cardiac catheterisation data analysis via remotely located hybrid computer system 77−40869
cardiac catheterisation data on-line analysis by remote access computer system 77−40870
cardiac cellular electrophysiologic-clinical correlations using a relational data base 80−89890
cardiac computing conf., Geneva, Switzerland, (Sept. 1979) 80−82582
cardiac disc mitral valve in left ventricle, computer model of motion 80−8214
cardiac EM field computation, method of secondary sources 79−39391
cardiac left ventricle blood flow field off-line computation from Doppler US velocimetry 79−62324
cardiac left ventricular efficiency evaluation using pot. energy distrib. 77−40757
cardiac output and shunts, automatic computation from indicator dilution curves 79−48359
cardiac output determ. using Stewart-Hamilton method, algorithm 77−86691
cardiac output estimation during exercise by rebreathing technique, automated system 77−37090
cardiac pacing, symposium, Tokyo, Japan (Mar., 1976) 77−81666
cardiac scintigraphic cineangiography with ECG gating 77−9255
cardiac surgical patient postoperative computerised meas., analysis, and treatment 78−36044
cardiac US data, moving heart surfaces extraction 80−8114
cardiac V_{max} determination from intraventricular press., on-line digital computation 77−40866
cardiograms, image processing, cardiac function meas. *(Japanese)* 80−94354
cardiology, conf., Rotterdam, Netherlands, (Sep.-Oct. 1977) 78−81013
cardiology applications, conf., Stanford, USA, (Sept. 1978) 79−62387
cardiology data processing system 80−56236
cardiopulmonary analysis 77−44814
cardiovascular computerised modelling, pressure regulation in hypertension 79−88098
cardiovascular desease, mass medical examination, automatic system, USSR 77−25576
cardiovascular flow disturbance detection by pulsed US Doppler velocimeter autocorrelograms 77−25526
cardiovascular nuclear medicine, instrumentation and data processing, ventricular function evaluation 80−85481
cell lethality model for radiation therapy population kinetic parameter derivation 79−43965
cerebellothalamocortical signals influencing factors anal. 79−16191
cerebral blood flow, atraumatic meas. by ^{133}Xe *(French)* 77−37039
cerebral blood flow meas., regional, computer program description 77−5098
cerebral blood flow parameterisation, scintiangiography meas. 79−25025
cineangiocardiograms, automatic anal. using TV system on line with minicomputer 78−92699
circadian rhythm related to human body temp. 79−70525
clinical nuclear cardiology computer system 79−25094
collective radioactive dose distribution anal. using census data, graphical method 77−6567
colonic contractile activity meas., pharmacological tests in dogs appl. 80−109068
computerised tomography workshop, conf., Newport Beach, USA (Jan 1979) 79−66507
conditioning EEG activity, computerised laboratory 80−30912
conference, Washington, USA (Nov. 1978) 79−25132
conference on medicine and techniques, Zagreb, Yugoslavia, 1979 80−101667
constant value curve tracing technique, nuclear medicine, EEG appl. 77−70510
contour map production for electrophysiology 80−72340
control signals and transducers for the control of upper extremities in plegic patients, computer controlled experiment *(Slovak)* 80−109061

medical computing continued
coronary haemodynamic parameter estimation using elec. analogue [illegible] 37092
coronary intensive care unit, computerised monitoring system 77−21656
cortical bone diameter meas., manual and computer-aided methods comparison 78−85376
counterpulsation, external, computer anal. using nonlinear math. model of cardiovascular system 77−2069
cross section imaging for treatment planning, using radiotherapy simulator 77−13030
curvelinear view generation from CAT scanned data 80−8149
data evaluation system, for use with gamma cameras in nuclear medicine 78−92732
data processing, radioimmunoassay and bioassay, logistic curve fitting routine adapted to desk top computer 77−37059
deaf people, computer generated speech training patterns 80−51290
defibrillator ground-loop current elec. skin burn computer simulation 77−78039
defibrillators, ultrahigh energy, programming to deliver optimal quality rectangular wave shocks 77−37102
desmodontal gap evaluation with data-processing system, mandible X-ray image changes 79−62337
dialysis therapy, single compartment model appl. to urea and creatinine kinetics 78−48931
digestive tract electrical rhythms simulation 78−64970
direct reading pen dosimeters, radiation exposure recording aspects *(German)* 78−5050
discrete-time Doppler frequency meter for blood flow imaging 79−57704
dosage selectivity by planning 3-D radiation treatment using computer 80−41178
dose and LET distributions due to neutron and photons from stopped pion [illegible] 77−52878
dosimetry, automated data acquisition and anal. system at LAMPF pion therapy facility 78−53506
dosimetry, cylinders irrad. by pion [illegible] beams, effects of tissue inhomogeneities 77−9266
dosimetry, isotropic and cloud source irrad. by monoenergetic neutrons and photons 78−24138
dosimetry, programs for internal absorbed dose determ. 78−15895
dosimetry calcs., linear accelerator electron beam parametrisation 79−83945
dosimetry of embryo in nucl. medicine procedures 77−5083
drug elimination interactions, physiological flow model in rat 80−81628
ECG, A/D conversion, meas. changes caused by precision level 77−40865
ECG, computerised technique to record new components of His-Purkinje ECT 77−44801
ECG, models solving direct and inverse problems, systems approach 78−28121
ECG, surface potential distributions, equiv. dipole recovery in presence of noise 79−70671
ECG 22 78−81027
ECG activity models for computer simulation *(Spanish)* 78−11758
ECG analogue and digital transmission 79−39564
ECG analysis program capable of serial comparison, 1976 IBM program description and performance 78−57086
ECG analysis program testing 79−25146
ECG body surface potential mapping data acquisition system 77−40861
ECG data analysis for data compression 77−40862
ECG data analysis for data compression 79−100766
ECG data compression and transmission 79−83989
ECG data reduction using a microcomputer *(German)* 80−81748
ECG fault-tolerant anal. systems 77−44811
ECG lead CAD 80−85526
ECG map reconstruction computer system 79−39561
ECG measurement, evaluation of results *(Japanese)* 78−24165
ECG parameter correlation with constitutional variables in infants and children 79−39406
ECG telephone transmission, analogue and digital, errors and noise 80−94398
ECG theory computer application programs *(Spanish)* 78−20165
ECG/VCG minicomputer digitising and preprocessing system 77−40863
ECGs, left ventricular hypertrophy study in borderline hypertensive young men 80−109050
echocardigram, automatic anal. and VTR recording 80−8112
echocardiograms, left ventricular anal. *(German)* 80−81667
echocardiograms, M-mode, microcomputer editing for semiautomatic anal. 80−94299
echocardiography and pulsed Doppler, off-line data processing of left ventricle performance 79−62323
EEG, automated monitoring of long-term implanted electrodes *(Russian)* 80−76857
EEG, automatic interpretation, background activity anal. 80−85503
EEG, cable telemetry computer seizure monitoring system 77−5090
EEG, quantification of computer analysed serial EEGs from stroke patients 77−5096
EEG, real-time detection using two-component wave model 80−104788
EEG, simple computer-generated dot-density topogram 80−94407
EEG, syntactic anal. software system 80−104787
EEG alpha-detection system, feedback stimulation and data analysis system 79−29642
EEG alternations, power spectral analysis 80−30924
EEG and electrooculograms, sleep research anal. 79−62377
EEG biofeedback conditioning, signal detection methodologies 79−29656
EEG bispectra computation computer program, in FORTRAN 78−92727
EEG data acquisition and data processing system, peripheral equipment 80−41270
EEG data compression via computer-generated evoked response to sensory stimuli 78−36016
EEG data processing, discrete Fourier transformation 80−26385
EEG eye movement artefact removal, by correlation methods 77−44826
EEG frequency-domain numerical analysis 77−9292
EEG photic flash response, quantitative approach 80−30923
EEG power spectra, parameter estimation using Gaussian functions 77−21635
EEG spectral parameter analysis operating system 77−9291
EEG wave duration anal., microcomputer implementation 80−21558
ejection fraction rel. to ventricular vol., computer anal. 80−104599
electrocardiogram, computer anal. *(Chinese)* 79−57787
electrocardiograms computer anal. 78−48917

medical computing continued
electrocardiology 4th International Congress, Balatonfured, Hungary (Sept. 1977) 79−39384
electromyography, clinical, computer anal. 78−80985
electromyography, computerised, software support in clinical dentistry 79−74780
electron beam treatment planning, symposium, Cincinnati, USA (July 1977) 79−100730
electron beam treatment planning algorithms 79−100733
electron beam treatment planning system, absorption equivalent thickness factor 79−100734
electronic radiography 80−8162
electroretinogram signals computer anal. 79−8559
electrosurgical dispersive electrode site temp. and current density distrib. model 79−92424
EM dominant reson. freqs. of human body 78−31857
EMG, interactive minicomputer system for anal. of twitch waveforms of human motor units *(Japanese)* 78−28103
EMG, single fibre, microcomputer-based jittermeter 80−46078
EMG, single motor unit action pots. identification 80−72343
EMG power spectrum analysis, in neuromotor speech disorders 77−29161
EMG processing for sleep research 80−67267
EMG recording computer editing 78−80999
EMG single motor unit potential parameter analysis 77−9290
epicardial mapping of ventricular arrhythmia onset by digital computer 79−70672
epileptic spike pattern determ. by point spectrum 77−9294
epithelial tissue pattern recognition 79−25145
ERG recording, computer assisted standardised quantitative method 80−109048
evoked potential analysis, on-line signal optimisation using minicomputer 77−5112
EVOQ: a system configurable for automatic simulation and recording of mean evoked potentials on a minicomputer *(French)* 80−85507
exercise ECG automated anal., clinical experience 78−81050
exercise ECG computer-assisted anal., implementation and clinical anal. 78−81051
external beam radiation dose distribution calculation, radiation therapy planning 79−62364
external beam radiotherapy, isodose planning, new suite of programs 80−41243
external beam radiotherapy optimisation, relative radiation effect and isoeffect pattern computer study 79−62368
extraocular muscle system mechs. model for clinical ophthalmology 78−40155
eye, detached retinal tears computer localisation for scleral buckling procedure 78−7529
eye motion kinetics in moving target pursuit, oculomotor abnormalities in neurological disorders detect. 80−108888
eye movement, minicomputer processing of dual Purkinje image eye-tracker data 79−29645
fluid management records system 79−25150
foetal breathing movement computer anal., from real-time US images 78−40375
force distribution under human foot, online meas. system 78−96110
Fresnel zone plate aperture for γ-ray imaging system, digital modelling 78−7442
gait analysis subsystem for smoothing and differentiation of human motion data 80−35953
gait patterns, normalised, using computer anal. of EMG and fast-fall patterns 77−40819
gamma camera image processing *(French)* 77−37038
gastrointestinal signals, quantitative analysis 80−41339
haemodialysis by extra corporeal ultrafiltration method, parameter estimation of vascular bed 79−84015
haemodynamics, coronary, analysis by circulation model, use of hybrid simulator *(Japanese)* 77−5021
head and neck 3-D mapping derived from computed tomographic serial scans 80−8148
heart fourth sound studied by FFT 80−94397
heart left ventricle, finite element stress analysis 77−86518
heart rate on-line statistical anal., using special-purpose computer 78−35984
heart relaxation parameters, digital anal. of isovolumic press. fall, dogs 80−94276
heart shunt diagnostics by radioisotope angiography, anal. by PASD computer program 78−20250
intact heart stress and strain three dimensional finite element anal. 77−66821
heart vibration quantitative characterisation by multipolar acoustic heart model, minicomputer method 78−85429
high speed biological cell sorter, data acquisition and display 78−44622
His bundle ECG pattern recognition program for drug evaluation 78−35999
human body model, health, disease and treatment use 79−48205
human body tomography using computerised pattern recnogition *(Japanese)* 78−3603
human disease study using mass spectrometry and metabolite profiling 80−51289
human respiratory system, role of the Van der Pol oscillator 78−65073
IEEE 7th Northeast Bioengineering Conference, Troy (1979) 79−79672
image processing, introduction *(Japanese)* 80−81699
image processing microprogrammed video display 80−72366
image reconstruction formulae, computer implementation 80−52179
image reconstruction from projections, book 80−51961
image reconstruction from projections 80−52178
insulin delivery to diabetics, by computer controlled pulsed insulin infusion 77−37099
interactive verification of clinical trials data 77−48893
intestinal myoelectrical activity model 79−70537
intra-aortic balloon pumping efficacy evaluated by nonlinear cardiovascular system model 78−44732
intra-uterine pressure data, on-line computerised quantification 78−85424
intracranial pressure dynamics modelling 79−25026
isolated heart preparation computer control for biomedical research 78−53603
kidney membrane conformational changes anal. after renal ischemia 78−73142
laboratory test interpretation using computer 79−74770

medical computing continued
labour monitoring, Montevideo units computation algorithms 77−40896
laryngeal films, ultra high-speed, automated anal. 79−57746
left ventricle ejection fraction meas., scintillation camera deadtime 79−62355
left ventricular regional function anal. from cineangiogram, computer system appl. 78−80963
left ventricular wall motion assessment from computer-processed fluoroscopy 79−62358
left-heart haemodynamics, mathematical model 78−65074
lidocaine infusion regimes, computer assisted planning, clinical studies 77−40919
ligand distribution among multiple binding sites on different proteins in plasma 77−12877
limbs motion analysis using goniometers, prosthesis microcomputer control appl. 80−51138
liver scintigraphy, intercomparison of computerised image processing and display methods 79−53234
long bone mechanics study under microprocessor control 80−76851
lung, mag. field meas., comparison between two methods 80−104712
lung tissue micrograph computer processing approach 80−8123
magnetoencephalogram and electroencephalogram, comparison of spatial response 80−26245
magnetopneumography, analytic methods 80−104713
mammacarcinoma conservative radiotherapy, computer assisted dosimetric soln. *(Dutch)* 80−36139
mammary lymphoscintigraphy in radiation treatment planning, minicomputer technique 80−12223
mechanical heart computer simulation 79−70709
medical physics conference, Ottawa, Canada (Jul. 1976) 77−16897
microcomputer, use in ventilatory function testing 80−41291
microcomputer based digital filter for electroencephalogram processing 78−73278
microcomputer-based data acquisition and analysis system for CO_2 rebreathing studies 80−36161
microprocessor appl. developments 80−51285
microprocessor-controlled cardiac output meter 80−36162
microprocessors in bioscience, review 80−21557
mitral valve replacement, prediction of postoperative systolic left ventricular wall stress 78−40427
mobile gamma camera with remote image processing computer system, for nuclear medicine 78−92700
moire contourography, computer-aided replication of human anatomy 80−67189
Monte Carlo computer code for calc. of radiation dose from syringes 80−41246
MORPHOQUANT automatic microscope image analyser, universal program system 80−56160
movement dynamics, human, investigation using a computer 80−51284
MTF calculation, modified FORTRAN program 78−25807
MTF calculation in radioisotope scanning, improved FORTRAN II program 77−21612
multichannel analyser, microprocessor-controlled, transfer of blood pressures and neural activities for computer anal. 80−72356
multicompartment diffusion and reaction modeling system applied to transmitter-mediated photoreception 79−70547
myocardial perfusion imaging using ^{201}Tl, algorithm for background activity calc. 80−56195
myocardial perfusion index calculator for prediction of subendocardial ischaemia in cardiac surgery 77−40915
myocardial regional blood flow from dynamic anal. of ^{201}Tl 79−70627
myocardium of human left ventricle, stiffness distrib. rel. to shape change in diastole 80−41095
nerve cell unitary discharge automatic recognition *(French)* 77−37072
neural spikes amplitude discrimination appl. 77−52778
neuron electric potential field evaluation, with time-dependent surface potential, using hybrid computer 77−86478
neuronal ensemble principle and epileptic oscillation 79−83739
neuronal interspike intervals, meas., teleprocessing, anal. 80−85375
neuronal structure, three-dimensional reconstruction and display 78−11624
nuclear angiocardiogram anal. program for radiology trainees 80−8143
nuclear images, computer definition of regions of interest, double-cursor method 79−29612
nuclear medicine, appl. of computers, review *(German)* 80−41214
nuclear medicine, appl. of midi-maxi computer interaction to renographic data 78−7476
nuclear medicine, buyer's guide to current performance and future promise 78−48883
nuclear medicine, computer appls. in image and data processing 79−16294
nuclear medicine, computer software package for internal dose calc. 80−98139
nuclear medicine, computers and quality control 79−16295
nuclear medicine, history of computer appls. 80−42037
nuclear medicine, image processing system 80−41174
nuclear medicine, Janus III, computer system for acquisition, processing of diagnostic units data 78−80948
nuclear medicine, microprocessor systems for data acquisition, image processing, RIA anal., patient data retrieval 80−61670
nuclear medicine computers 79−25096
nuclear medicine images greyshade scale improvement 77−21609
nuclear medicine imaging, computer display system 78−61275
nuclear medicine monitoring appl. 78−7466
nuclear medicine studies, automated interpretation 80−8164
nystagmographic data analysis *(German)* 77−40663
obstetric computer system for intensive care of mother and foetus during labour *(German)* 80−3857
ocular motility test in strabismus and amblyopia evaluation, computer administration and analysis via PAL8 program 78−48784
oculomotor function analysis 80−46092
olfactory bulb, 55 counts/sec rhythm anal. and simulation 80−85422
oncology, radiation, use of computers review 79−25098
online real-time data acquisition system design 78−35994
orthodontic adhesive joints, adherend topography effects 77−52916
oxyhaemoglobin dissociation curve direct obs. in man in vivo, computer investigation 78−85433
paediatric EEG reactivity, spectral and temporal analysis 77−9293
patient contour drawing using US compound B-scanner 79−83865
patient-contouring, electronic device, for radiotherapy treatment planning 77−13029
medical computing continued
pattern classification, for identification of irradiated chromosomes 77−37114
perimetry standards 80−46084
personnel monitoring for radiological protection, current status and developments, review 79−22490
photosynthetic systems, computer assisted scanning and kinetic spectrophotometry 78−68963
pion radiation, uniform depth-dose distrib. technique and cell survival obs. 80−17139
pneumoconiosis, small lesions, computer aided identification 80−30887
positron camera, 3-dimens. imaging using Fourier techniques 77−32951
positron image reconstruction in nuclear medicine, three-dimens., fast iterative method 78−7443
preventive examination population, automatic systems, static, mobile, specialist groups 77−25578
prosthesis, hand, electromyograph controlled aid development *(Spanish)* 78−15924
prosthetic aortic heart valve dysfunction computer-assisted detection 77−40922
prosthetic aortic valve stress analysis using finite element compute program 78−48930
prosthetic heart and mock circulatory system, math. model 78−81080
prosthetic heart valves, rigid leaflet and caged-ball types, diastolic ventricular mechs. 78−81079
prosthetic ventricle and valve evaluation, flow visualisation data anal. 78−40425
protein-ligand binding parameters estimation from continuous ultrafiltration results 77−12878
psychogalvanic reflex curve automatic anal. 78−7332
pulmonary artery press. estimation using pulse wave velocity 80−12203
pulmonary oedema detect. by quantitative elec. impedance plethysmography 78−31951
pulmonary resistance measurement by forced oscill. technique 77−40877
pupil, human, normal and diseased, model for computer simulation 77−77895
radiation dose deposition calcs. in human marrow 80−26365
radiation therapy, comprehensive computer system, design and development 79−25078
radiation therapy, computer program for negative pion beam calcs. 80−46061
radiation therapy, external beam, planning using the Edinburgh algorithm 80−94316
radiation therapy, external beam, three-dimensional dose distribs. 79−25064
radiation therapy, scatter dose distribs. for 6 MV photon beams 79−62370
radiation therapy optimisation 77−86593
radiation therapy planning programs development for SIN pion applicator 80−26339
radiation therapy simulator and linear accelerator meas. and control by microprocessor 77−40902
radiation therapy treatment planning, computer algorithm 79−62351
radiation treatment planning, accuracy 80−72328
radiation treatment planning 77−9268
radiation treatment planning interactive computer/ultrasound system 77−9269
radioactive seed implants, computation of dose distrib. 80−101265
radioactive tracer, compartmental models short parameter-fitting routine 77−82378
radiographic equipment, computer-assisted quality assurance 80−89838
radiographic image computer-controlled subtraction procedures 80−109014
radiographic pictures, digital encoding, redundancy reduction 77−40850
radiographs filing and retrieval system 79−16289
radiography, photon path visualisation by Monte Carlo simulation 77−66848
radiography, tomographic scanning, general principles, review 77−16973
radiography, tomography, present state and technical perspective, review *(French)* 77−16974
radioimmunoassay data processing, semiautomated polylinear system 79−70614
radioimmunoassays in clinical chemistry laboratory, statistical quality control 77−90878
radiological images, conf. Newport Beach, CA, USA (June 1979) 80−8141
radionuclide cardiac output determination, automated computer program 80−56196
radionuclide concentrations in food products, FOOD II interactive code calc. 79−48348
radionuclide intake by man through terrestrial pathways, TERMOD II interactive code analysis 79−48349
radiotherapy, computational anal. and dosimetric evaluation of commercial irregular-fields computer program 78−24147
radiotherapy, computer assistance in planning seed implants 79−100711
radiotherapy, external beam, optimisation using computer 77−86632
radiotherapy, freq. of occurrence of nucl. reactions due to neutrons in tissue-equiv. material, HETC code 77−9243
radiotherapy beam-flattening filter calcs. for high-energy X-ray machines 78−65126
radiotherapy cervical intracavitary applicators, computer program for optimisation of source loading 77−13005
radiotherapy photon beam, 10 MV, dosimetry characts. and computerised treatment planning 77−48875
radiotherapy planning, ^{60}Co beam model 77−66857
radiotherapy treatment planning, correction for inhomogeneities, appl. of ACTA scanner 77−60259
radiotherapy treatment planning, FORTRAN program for optimisation using complication probability factor 80−81686
radiotherapy treatment planning, inter-hospital interactive computerised system 80−36068
radiotherapy treatment planning, phys. charact. of 45 MV photon beams 77−48873
radiotherapy treatment planning and follow-up of superficial tumours, US B-scan appl. 78−11721
radiotherapy treatment planning for irregular fields 80−81739
radiotherapy treatment planning system, clinical experience *(German)* 77−77991
radiotherapy treatment planning system implemented in FORTRAN on interactive computer 77−5080

medical computing continued
radiotherapy treatment planning system utilising interactive colour graphics 79−62336
radiotherapy with fast electrons, computerised treatment planning, dose distrib. calc. 80−81740
rapid eye movements, computer analysis 78−48900
regional myocardial function quantitative parameters 79−25095
remote medical care technology 77−48895
renal dialysis, improved patient management by computer simulation 79−70703
renovascular hypertension, computer-assisted static/dynamic imaging evaluation as screening test 79−79635
repetitive muscular contraction, localised fatigue evaluation from EMG power spectrum 78−57103
respiration, computer-assisted PaO_2 management during veno-arterial bypass and mech. ventilation 77−44838
respiration, two-stage ladder network model for detect. of small airway disease 78−31846
respiratory tracer gas nonlinear computer anal., non-invasive meas. method 79−62395
review, computer applications in biomedical engineering *(Japanese)* 80−12289
scan-rescan process anal. using dynamic programming *(Japanese)* 78−3602
scintigraphic camera systems and their assessment by computer 78−57063
scintigraphic joint imaging, technical aspects 80−56197
scintigraphy, computerised image processing and display methods, multicentre comparison 79−53233
scintigraphy, real-time system for multi-image gated cardiac studies 77−21611
scintigraphy of human organs, digital image anal. 78−20251
scintillation camera interface to scintigraphic data and computer 77−21613
scintillation detector MTF calc. on programmable pocket calculator 77−66844
shape differences comparison, between two-dimensional irregular forms, computer program 77−87639
signal analysis and simulation program 79−79678
simulation of ventricle, sac-type, in mock circulation 78−11780
skeletal muscle motor unit contractile characts. determ. through twitch characts. 80−17159
skin resistance measurements, collection and off-line processing *(German)* 80−67273
sleep research, microprocessor appl. 79−96693
spatial image processing, research projects at IROE Institute (Firenze) *(Italian)* 80−56668
spectral estimates of auditory brainstem responses 80−30913
speech disorder evaluation using basilar membrane electronic model 78−40206
speech training aid, SIRENE 79−70701
spinal radiograph standardisation for scoliosis assessment 78−57066
spirometric parameters, interactive on-line computerised computation 78−44656
SQUID fluxgate magnetometers, magnetopneumographic meas. 80−104711
surface EMG, computer anal. during isometric exercise, muscle tension quantification 80−85505
symposium, Toulouse (1977) 78−36003
systolic time interval, off-line processing of exercise data 77−40868
systolic time intervals from surgical patients, continuous real-time computation and display 77−37098
TC-chromatograms online analysis by scanning system 77−40599
teletherapy, implementation of Philips treatment planning system 78−73244
television data compression interface, for cytology and chromosome anal. 77−86683
thorax impedance finite element model for cardiovascular and respiration meas. 77−40887
thyroid function radioimmunoassay, quality control, computer program *(French)* 80−94348
thyroid junction assay digital simulation 77−44778
thyroid radiation protection during radioiodine-labelled pharmaceutical administration 78−44616
tomography, computerised, using video recorded fluoroscopic images 77−37082
tomography, high speed convolving kernels, for CT with triangular spectra and/or binary values 79−66515
tomography, resource sharing computer hierarchy for 3D image reconstruct. 80−26345
tomography, rigorous error bounds 79−66514
tomography, stochastic filter for transverse section reconstruction 79−66513
tomography depth-dose distribution, effect of slice thickness 80−46038
tooth, artificial-denture base joint, adhesion, fracture mech. 79−16350
total artificial heart haemodynamic study 79−84018
treatment planning in ^{60}Co radiotherapy using computerised tomography techniques 78−35964
tumour detection, computer processing of microwave enhanced thermographic images 80−8125
tumour growth simulation, in vitro 77−86464
tumour registry system 77−44805
upper extremity prosthesis online control based on EMG signal identification using microprocessor hardware 79−2166
US computerised tomography, improvements in data acquisition and pre-processing 80−26309
US data compression 78−77093
US Doppler flowmeter spectra for asymm. transducers 78−31880
US flowmeter data processing, transfer function modelling of arteries 78−61225
US two-dimensional images, extraction of cardiac parameters 77−25533
vectorcardiogram, human, computer dialog modelling 79−39389
vectorcardiogram computer system for anal., display and storage 78−85437
vectorcardiographic systems compared, Akulinitchev and McFee 79−44039
vectorcardiography, computerised meas. and display system 77−40864
ventilation inhomogeneity identification using minicomputer data processing 77−44816
ventilation-perfusion ratio intraregional maldistribution simulation 78−31834
medical computing continued
ventilation-perfusion ratio recovery from inert gas data 77−40829
ventricle, left, human, 3-D time-varying reconstruct error sources and magnitude estimation 80−85454
ventricle excitation spread, simulation *(Japanese)* 80−3847
ventricular arrhythmias, intraoperative mapping system 80−56242
ventricular excitation, digital simulation, computer model evaluation 78−85302
ventricular pressure and ECG continuous monitoring during angina attacks, computer anal. 78−85436
ventriculography, algorithm for automatic selection of end diastolic and end systolic cine frames 78−88757
versional eye movement control 80−46090
vertebrate retinal horizontal cells, spatial integration, computer analysis 77−36920
vestibular nystagmus, computer anal. of irregularities indicating central vestibular disorders 78−81036
video output signal, composite, from GAMMA-11 computing system 79−29610
video processor for computer calc. of press.-vol. indices from left ventriculograms 78−53495
video-sync mixer for cassette videotape recording of computer images 79−29604
visual and nervous systems simulation, straight line recognition algorithm 79−34562
visual fields, computer appls. 80−45892
visual perception, computer-based testing system for expts. 79−74769
vocal cord vibration, computer simulation of pathological conditions 77−16940
vocal tract, computer representation of geometrical configuration *(Russian)* 80−46111
volume measurement in vivo using computer-based u.s. echography, errors 77−2033
X-ray imaging using holography or electronics, tomosynthesis 77−40847
CO_2 expiratory concentration analysis by computer 78−57106
^{137}Cs gynecologic insertions, expt. derived algorithm for computer calc. dose rates 80−101264
O_2-CO_2 transport real-time and interactive control in mechanically ventilated patients in ICU 79−62404
Ra needle implants, computer program for reconstruction and dose-rate calc. 77−40770

medical diagnostic computing
see also computerised signal processing
21-channel EEG monitor with real-time result colour display 80−72364
A-scan quantitative analysis of normal and cirrhotic livers 77−64109
abdominal and pelvic diagnosis, US and computed tomography evaluation 78−61228
angiography, new tool for X-ray functional diagnostics 79−79640
aqueous humor flow rate determination by fluorescein tracer model 79−43943
arrhythmia data base of American Heart Association 79−62391
arrhythmia sorting, oesophageal electrode for atrial electrogram 79−39574
atrial overload ECG computer analysis 78−7504
atrial septal defect differential diagnosis by vectorcardiogram and computer 79−44040
audiometric tests, automatic operation using a programmable system, hardware *(Italian)* 77−5006
automated patient testing 80−46088
automatic comparative program for ECG analysis 78−7488
average evoked potentials, localising technique in aphasia diagnosis appl. 78−31950
axial tomography, abdominal area appl. 77−44782
bioelectric signal waveform analysis, computerized method for electronystagmogram anal. *(Croatian)* 79−20697
blood flow plethysmograph microprocessor control 79−62402
blood gas and acid-base calculations 79−25139
blood white cells classification 78−3663
bone, disease diagnosis, automatic texture anal. methods 80−8156
breast thermographic interpreter, comparison with human interpretation 77−81547
cancer thermograms analysis, breast cancer diagnosis *(Japanese)* 77−5099
cardiac catheterisation data analysis programs 78−36017
cardiac potential distribution, human body surface, digital simulation 77−29221
cardiological data processing in real time by hybrid computer, optical link 77−86677
cardiology, computer graphic techniques for heart damage quantification 79−29654
cardiology data processing system 80−56236
cell type recognition by multiangle laser beam scattering flow system 77−21595
cephalometric tracing processing system, software development *(Japanese)* 80−94409
cervical smear screening with coherent optical processing 77−21653
chaotization based diagnostic algorithm for handling small samples 79−39568
chest photofluorograms, recognition of vessel shadows for automated meas. and classification 77−81566
chest photofluorograms automated interpretation using AISCR-V3 software system 79−88183
chest radiograph nodule detection system 80−8140
chest radiographs, computed detection of nodules 80−8172
chest X-ray automated anal. 80−98098
chest X-ray images computer-aided anal. 78−40400
chest X-rays, coal miners, small opacities computer anal. 78−40324
chest X-rays automated screening, image segmentation and cardiac silhouette anal. 79−88178
clinical decision support systems, automated medical signal anal. 79−34685
clinical ECG interpretation system experience 78−7486
clinical ECG laboratory methods and difficulties 78−7482
clinician and computer ECG diagnostic accuracy 78−7494
complex ECG and triaxicardiometric recording and analogue processing 79−44023
computer graphics for red cell anal. 80−21597
computer-processed ECG trends, conference, Amsterdam (1976) 78−7477

medical diagnostic computing continued
congenital cardiac disease VCG processing, right ventricular hypertrophy criteria 79−39575
coronary artery disease diagnosis, exercise ECG, VCG and body surface mapping 79−44046
Cytocomputer biomedical image analysis 79−92419
data terminal with voice indication for general practitioner use, ECG analysis via telephone network appl. 77−81613
Delta Scan, computerised entire body transverse scanner, technical description 77−44781
dichotic tape generation, computerised method 78−92740
digital image processing applications, conference, San Diego (1977) 78−81528
distributed microprocessor system for cardiac arrhythmias detection and diagnostic 79−25142
documented patient file concept and implementation 78−7498
dyslexia, detect. by computerised brain mapping 80−36185
ECG, program performance in separating normals from non-normals 78−81046
ECG analysis, myocardial infarction diagnosis 77−25577
ECG analysis, state of art 78−11767
ECG analysis automation, advantages 78−7493
ECG analysis program modification allowing for correlated constitutional variables 78−40385
ECG analysis programs, diagnostic statement reproducibility 78−7495
ECG and EEG analysis, special purpose hybrid computers 77−40842
ECG and vectorcardiogram interpretation, modular software system 77−9288
ECG classification by linear multiple regression analysis 77−13027
ECG computer programs, differences in meas. results 78−81048
ECG computer-assisted interpretation, routine automated quality control 78−40394
ECG diagnosis, variation in probability levels 78−44664
ECG diagnosis improvement by nonlinear feature extraction methods 80−85530
ECG diagnostic information from HF notches 79−39570
ECG diagnostic interactive minicomputer system 78−36022
ECG diagnostic system validity experiences 79−39571
ECG interpretation, automatic protection against diagnostic errors due to wrong electrode placement 78−81052
ECG interpretation system evaluation results 78−7497
ECG interpretation sytems, user's experiences 78−7496
ECG monitoring and premature ventricular contraction detection in heart beats 77−78022
ECG optimum data processing and storage design 78−57118
ECG pattern classification from complete computer descriptions 80−56265
ECG serial changes in hypertensive cardiovascular disease, computer display 78−81047
ECG signals, diagnostical functions, effect of random noise *(Croatian)* 80−98169
ECG/vector cardiogram interpretation modular system 78−7484
echocardiographic left-ventricular diameter time curve automated analysis 77−21578
echocardiography, high-resolution, computerised US signal processing 80−76814
echohepatograms in children, computer analysis 79−57728
EEG, interictal epileptic activity, comparison of traditional reading and automatic recognition 78−48913
EEG computer display system, brain lesion localisation *(Japanese)* 77−5100
EEG computerised analytical method *(Slovenian)* 78−28113
EEG isolated events identification, automatic system 79−5400
electrocardiological diagnostics automation problems 79−39577
electrophoretic waveform analysis for blood serum protein composition determ. 78−64928
EMG envelope spectral anal., Parkinson's disease diagnosis and treatment appl. 79−5390
epidemiological use of rest ECG 78−7505
evaluation using expected outcome loss 77−25587
exercise ECG analysis, noise-impervious pattern recognition approach 78−7515
exercise ECG analysis methods and requirements 78−7509
exercise ECG computer analysis 78−7516
exercise ECG computer processing expts. 78−7510
exercise ECG processing, influence of heart rate and coronary artery disease 78−7512
exercise ECG processing, value of orthogonal lead system 78−7514
exercise ECG processing principles and multivariate analysis results 78−7511
exercise ECG processing reproducibility rel. to waveform recognition and lead system 78−7513
exercise ECG quantitative analysis system *(Japanese)* 79−29652
eye, computer assisted examination, Refractor III system 79−29650
Frank ECG correlates of left ventricular ejection fraction 79−39405
fuzzy diagnostics from ECG/VCG analysis programs 78−7499
gamma-ray imaging 77−56452
gastric Ba-filled X-ray films, computer screening *(Japanese)* 78−73211
Glasgow Royal Infirmary ECG interpretation program 78−7483
gradient pattern coding−an application to the measurement of pneumoconiosis in chest X-rays 79−34632
haemodynamic data processing in intensive care unit *(French)* 77−40903
Hannover EKG system HES, description 78−7485
heavy particle computed tomography 80−8146
hepatocellular disease diagnosis, computer quantification of spleen/liver ratio 79−83909
Hewlett-Packard ECG analysis program 78−7490
hierarchical computer networks for processing data base generated by X-ray CT scanner 80−81732
hybrid optical-digital radiography system for lung disease detection 78−11753
hypertensive left ventricular hypertrophy, orthogonal ECG multivariate analysis 79−39579
hyperthyroidism, in vitro and radioisotope uptake tests compared 77−9252
hypertrophy criteria in VCG of children with Fallot's tetralogy 78−7503
IBM program for ECG analysis 78−11769
imaging system, new, in computed radiography 80−8147
interval data presentation, graphical method, bioelectric measurement appl. 78−31949
medical diagnostic computing continued
intracranial disorder diagnosis by cerebral sequence scintigraphy 79−92335
IR pattern recognition for breast cancer screening 77−21652
ischaemic cardiac disease determ., heartbeat interval analysis and questionnaire evaluation 79−39580
ischaemic episode, computerised continuous beat by beat anal. and rational plots 79−62394
ischaemic heart disease determ. by heart beat interval anal. and medical questionnaire evaluation 78−65145
ischaemic heart disease diagnosis using respiratory sinus arrhythmia 78−65147
karyotyping automatic image processor *(French)* 77−40953
laboratory medicine trends, automated procedures and equipment development *(Japanese)* 77−44766
left ventricular cineangiograms, numerical information extraction, wall movement 77−90891
left ventricular hypertrophy and bundle branch block, vectorcardiogram interpretation 79−44028
leucocyte classification by parametric and nonparametric analysis 77−78016
liver disease, diffuse, hepatic scintigram pattern characterisation 79−83926
liver disease diagnosis using nonlinear stochastic modelling techniques 78−36024
liver gamma camera scans, clinical evaluation of computer processing 79−29579
lung ventilation and perfusion scintigrams, automated diagnosis 79−88181
Lyon ECG interpretation program 78−7487
mammogram densitometric distinction between cancer and fibrocystic lesions 77−25551
mandibular movements diagnosis, system for meas. and processing *(Japanese)* 80−101249
microprocessor based cardiac probe for gated equilib. and beat-by-beat left ventricle function 79−62396
microprocessor-based blood gas analyser computational algorithms 79−57805
microscope image histological specimens traced on optical mark recognition computer cards, quantitative analysis appl. 77−81612
minicomputer-aided ECG diagnostic system 79−44024
Minnesota code ECG classification program 78−7506
Minnesota code ECG program validation 78−7507
monitoring systems, automatic diagnosis systems 77−40841
multiterminal ECG processing system experiences 79−39573
multivariate and conventional ECG analysis programs compared 78−7492
noisy blood flow meas. pulsed US spectral analysis 79−57705
nuclear medicine display algorithms evaluations 80−8144
nuclear medicine display systems 79−16298
obstetrics, foetal biophysical signal and ultrasound image analysis 77−77999
oncological clinical research, data storage and retrieval system 79−48321
oncology, project development *(Swedish)* 77−44763
online vectorcardiographic analysis microprocessors and instrumentation 78−36020
ophthalmic tissue signature characterisation by US frequency-domain analysis 77−40857
ophthalmology diagnosis, computer assisted 78−92739
optimal 9-lead ECG system design 78−7500
orthogonal transforms program for medical scintigrams 80−72365
pancreatic diseases, expt. approach to clinical decision problem *(Japanese)* 79−57793
pattern recognition for lesion detectability in medical scintigraphic images 79−62354
phase invariant signature algorithm (PISA) processing of ECG and phonocardiogram for cardiac anomaly detect. 78−40395
phased array US imaging, real-time digital scan conversion and multidimensional processing 79−48363
photomotogram evaluation Achilles tendon reflex, analogue computer technique *(German)* 78−7465
physical activity determination, analogue/digital data output equipment appl. 77−70560
physics of computer assisted tomography 78−24173
physiological curves peak detection algorithm 78−96107
physiopathological mechanisms study by computer 77−70562
piecewise-linear approximated ECG waveform recognition 78−57119
problems of computer applications *(German)* 79−20696
pulmonary oedema, quantitative diagnosis from chest X-rays using computer controlled optical system 77−77981
pulmonary vascularity automated diagnosis from chest roentgenograms 77−60248
radiocardiogram parameter identification *(Slovene)* 78−44586
radiographic image analogue processing by photographic spatial filtering 78−57070
radiographic image smoothing and edge enhancement 80−109015
radioisotope image correction and computer-aided processing 77−9253
radioisotope lung scan automatic classification 77−29201
radioisotope scanning system control 77−9254
radiological digital image processing facility 80−36127
radiology, introduction to computer systems 79−34663
radiology reporting system based on individualised list of diagnostic possibilities 79−83860
renal histopathological section image dissection and analysis 79−79679
rest ECG computer interpretation 78−7508
review, computer applications in biomedical engineering *(Japanese)* 80−12289
sequential ECG comparison system design 78−7501
serial ECG processing computer techniques 78−7502
Siemens program for ECG analysis 78−7489
sinus rhythm, diagnosis by IBM ECG anal. program *(Japanese)* 80−67278
skeletal muscle disease, Fourier optical evaluation of histopathologic findings 77−37091
sleep EEG data classification by autoregressive model 79−57628
speech, hypernasality quantitative evaluation using acoustic perception computer method 78−27971
statistical pattern recognition for early diagnosis of heart attacks 77−25584
statistical thermogram classifiers using coherent and incoherent light 79−96644

medical diagnostic computing continued
stenosis densitometric analysis from remote terminal 79−83900
stomach radiograms image anal. 79−88176
strabismus and amblyopia, eye movement analysis by computerised ocular motility test system 80−41299
TELEMED system user support organisation and program library 78−7491
thermography of breast, automated diagnosis of abnormality using minicomputer 77−21593
thyroid functional state, interdependence of symptoms and signs 79−8560
tibia fractures, ^{99m}Tc-pyrophosphate scans, algorithm for automatic computer anal. 79−88171
tissue US parameters, quantitative cross-sectional imaging 79−53277
tomographic image processing 78−35950
tomographic thermography, numerical simulation 79−83889
tomography, radiation protection requirements for patients and accompanying parent 77−70524
tomography machine uses radioisotopes for patient diagnosis 77−56464
tomography principles, realisations and results interpretation *(Czech)* 80−36085
tomosynthesis, flashing system, using simultaneously 25 X-ray tubes 80−81768
trauma indices 77−25588
trauma prognostic indices 77−25589
triaxicardiometry, clinical use 79−39584
tumour detection by microwave enhanced thermography and computer-aided image analysis 79−70604
US lateral and range resolution improvement by optical computer 79−53203
US system, real-time, for dynamic and still images 79−92309
USA Veterans Administration ECH computer analysis system 78−11768
vectocardiogram analysis program for children, with multivariate diagnostic classification 78−81045
vectorcardiogram diagnostic algorithm improvement by outlier elimination 79−39572
vectorcardiogram parameter sensitivity to digital filtering 79−39576
vectorcardiographic discrimination of left bundle branch block, descriptive statistical methods 79−44026
ventricular hypertrophy diagnosis, three-orthogonal-lead ECG criteria 79−44034
ventricular septal defect, prediction by non-invasive examination using interactive terminals 78−31954
weighted entropy method for clinical data reduction 78−92742
Woodward polarcardiographic service for ECG diagnosis improvement 79−39583
X-ray reporting in German language 78−73284
^{59}Fe tracer data analysis program and kinetics model *(German)* 79−5342

medical effects of radiation *see biological effects of radiation*

medical electronics *see biomedical electronics*

medical information processing *see medical administrative data processing; medical computing*

medical sciences *see medicine*

medicine
see also biomedical engineering; cardiology; health hazards; patient diagnosis; patient monitoring; patient treatment; physiology
aeronautical and space medicine, conf., Brussels, Belgium (Jan. 1979) 80−41944
aerospace medicine, prospective medicine opportunities, conf., London, England (Oct. 1977) 79−39532
air flow patterns in the operating theatre 80−94439
air flow patterns in the operating theatre 80−94440
arm, lower part, statics and equilib., for 1st yr. medics 79−35505
aviation medicine, visual, auditory and vestibular fitness standards (report) 79−11920
Beclere, Antoine, pioneer of radiation therapy techniques, biography 79−62982
Berson, Solomon A., biography, achievements in nuclear medicine 80−42028
bioengineering curriculum enhancement through collaboration in rehabilitation medicine 77−81596
biopolymers, electronic struct. and possible chem. carcinogenesis mechanisms 79−22874
cathodoluminescence, bibliography of papers till 1977 79−21482
compartmental analysis in biology, medicine and ecology, mathematical foundations 78−68978
conference, Jerusalem, Israel (Aug. 1979) 80−98758
conference, South Africa (Mar. 1979) 80−62366
conference, Stockholm, Sweden (Dec. 1979) 80−31410
cyclotron, compact, clinical appl., isotope production *(Japanese)* 80−104757
diagnostic aids, Japanese developments 78−24164
education, physical sciences in medicine diploma 80−31444
electronic communications systems and biomedical equipment, maintenance programme 79−5385
engineering in medicine and biology, conf. Atlanta, USA (Oct. 1978) 79−39332
flying fitness assessment, cardiology and pulmonary function findings, conf., London, England (Oct. 1977) 79−39531
griseofulvin tablets, tensile strength and disintegration times 77−60027
helicopter aviation medicine, conf., Fort Rucher, USA (May 1978) 79−79664
intensive care, instrumentation and control, conf., London, England (May 1979) 79−70702
laser applications in medicine and biology, bibliography, 1963-74 77−25539
laser beam appls. *(French)* 80−41165
Linus Pauling, publications, 1968-78, bibliography 79−24932
low-temperature biology, appls. to medicine *(Japanese)* 77−44870
master's level graduate training in medical physics at the Univeristy of Colarado Health Sciences Center 80−82603
materials chemical resistance medical laboratory techniques 79−88926
Medical College Admission Test, 1977, America, physics content evaluation 79−35462
medical physicists, training, survey of program directors 79−17159
microwave radiometry, natural emission detection, experimental results 77−32949
nuclear, spallation cross sections for medical radioisotope preparation 77−23052
nuclear and atomic data sources 79−25081
nuclear medicine department, radiation safety 80−89868
nuclear medicine in the UK, history 80−42039
nuclear medicine laboratory, radiation safety 80−104772
ophthalmology, research and training, TV appl. *(German)* 78−24157
optical instrumentation, conference, San Diego, California (1976) 77−44829
optical instrumentation in medicine, conf., Toronto, Canada, (Mar. '79) 80−36777
optics in medicine and biology, conf., San Diego, California (1977) 77−44876
pancreatic diseases, expt. approach to clinical decision problem *(Japanese)* 79−57793
photographic department, appls. and organization at large hospital 79−17514
photography, medical, problems encountered in hospitals 79−12875
physics and its methods in medicine *(Polish)* 80−12048
pulmonary function, SI unit system 77−21541
quality health care and cost containment, conf., Washington, USA (Mar.-Apr. 1978) 79−39333
quantum biology and pharmacology, conf., Florida, USA (1978) 79−24934
radioactivity standards for medical use 80−67232
radioisotope applications in agriculture, hydrology, medicine industry etc., booklet 78−35947
Spacelab, biological and medical appls. 77−45281
systems theory, importance and motivations *(Spanish)* 80−104549
technological advances, rigorous assessments of benefits and costs 80−17163
telemedicine, development of medical treatment system for first deep sea mining ship 78−77147
^{75}Br, excitation functions for production, pot. nuclear medicine appls. 80−98135
^{18}F, prep. with an electron linear accelerator, medical and biological appls. 80−98136
^{123}I, prep. from gaseous TeF_6, nuclear medicine appl. *(French)* 80−98137
^{99m}Tc generators, operational assessment by performance indices 80−94332

Meissner effect
composite superconductor, flux jump nucleation theory, critical state stability 77−28290
core radius of current-carrying supercond. cylinder in intermediate state 80−11134
gauge field theory, phase transition anal. 78−29250
Ginzburg-Landau parameter crit. value 78−10597
hard superconductor, flux jump nucleation theory, critical state stability 77−28290
London equations in Riemann space 77−15989
magnetic flux structures in superconductors, book 79−91199
magnetic surface states in supercond. 79−33389
metals, triplet supercond. transition in strong mag. field 80−25040
quasi-one dimensional system, supercond. props. *(Russian)* 77−51840
registering superconducting transitions under high pressure by contactless methods 78−23191
semiconductor, laser induced superconducting props. 77−72960
semimetal, mixed superconducting-excitonic insulator phase, diamagnetism, virtual intraband transitions 80−2520
solders, superconducting transition temp. determ. 77−28281
SQUID, operating principles *(Hungarian)* 80−75686
superconductor Faraday effect obs. in polarising microscope 80−70892
teaching, cryostats for laboratory course in supercond. 79−58494
$(TMTSF)_2PF_6$, quasi-dimens. cond., diamagnetic AC susceptibility 80−103781
triplet superconductivity, incomplete Meissner effect 79−15255
type II annular superconductor, field replication and flux shielding 77−28286
Ag brazing alloy, type BAg-3, props. 79−1639
CdS, flux exclusion, superconductivity at high temp. 80−97058
$CeCu_2Si_2$, collective phenomena 80−65933
CuCl, anomalous diamagnetism, high temp. Meissner effect *(Russian)* 78−34955
$Hg_{2.86}AsF_6$, linear-chain cpd., anisotropic Meissner effect, magnetisation meas. 77−85387
$Hg_{3-\delta}AsF_6$, linear chain compound, mag. field induced residual resist., anisotropic supercond. 80−24897
$Hg_{3-x}AsF_6$, supercond., absence of surface Hg 80−20350
In-Bi, single spheres, supercond. props. 79−73617
Nb wire, Cu clad, proximity effect, Meissner screening length meas. 79−60996
Nb wire, Cu clad, supercond., Meissner effect in Cu meas. 78−64166
Nb-Ti superconducting wire, Cu clad, Meissner effect in Cu meas. 78−64166
Nb-Ti-Zr, supercond. wire, anomalous increments of AC losses due to flux jumps 77−28289
Nb-Ti-Zr superconductor wires, flux jumping 79−60965
$Nb-V_3Ga$ mixed state, Meissner effect investigation by muon method *(Russian)* 80−107954
$NbSe_3$, CDW form., supercond. and Fermi surface determ., press. study 80−70891
NbTi, superconducting, orientation effects on magnetisation 77−28287
NbTi superconducting wire, Cu clad, proximity effect, Meissner screening length meas. 79−60996
Pb intermediate state, Meissner effect investigation by muon technique *(Russian)* 80−107954
Pb shell, mag. vacuum prod. by supercond. transition 78−8427
Pb-In alloys, supercond., AC losses of EM energy, critical current densities 79−33423
$Pb_{0.84}In_{0.16}$, barriers to flux entry and exit, magnetisation meas. 79−60963
$(SN)_x$, Meissner effect, mag. susceptibility meas. 80−20351
$(SN)_x$, supercond., obs. of Meissner effect 78−6478
TiN, superconductivity 78−2605
V, small particles, crystal structure, magnetic and superconducting props. 80−97121
$(Y,La)B_6$, superconducting transition temps., impurity effects 80−20341

Meissner-Ochsenfeld effect *see Meissner effect*

melting
see also melting point; zone melting
ablation, transient, with time-depend. heat flux, integral solns. 79−60088
acetic acid, solid, structural features during melting process 79−7596
4-acetyl-4′-n-alkanoyloxy-azobenzenes, type A, B smectic, nematic phase, solid state polymorphism, preparation, melting behaviour 78−59745
adenine-uracil polynucleotides, alternating, premelting, melting, postmelting transitions 79−57574
adsorbed film monolayer melting, dual symm. systems, periodic struct. *(Russian)* 80−107405
adsorbed monolayer of orientable molecules, lattice fluid model, real-space renormalisation group method 80−17882
aerodynamic ablation of melting bodies, effect of temp.-depend. heat capacity 79−37431
alkali alkanoates, phase relationships and thermal behaviour branching effects 78−43111
alkali halide, melting, mechanical instability 77−89524
alkali halide, melting mechanism, vol. and enthalpy changes 79−55866
alkali halides, mol. dynamics study 80−15220
alkali halides, premelting elec. cond., heat capacity 78−91445
alkali metal,thermodynamics of melting *(Russian)* 78−71840
alkali metal nitrates, melting pressure curves up to 5 kbar 77−15547
alkali nitrites, combination scatt. spectra, freq. shifts, jumps at melting, line widths *(Russian)* 77−40241
alkali-$PbSiO_3$ optical fibres, high aperture, double-crucible preparation 78−1450
alkaline earth nitrites, combination scatt. spectra, freq. shifts, jumps at melting, line widths *(Russian)* 77−40241
n-alkane binary mixtures, melting and solid-state transition 77−72685
n-alkanes, orientational phase transitions with mol. config. change 78−14444
α,ω-alkoxypolyethylene oxide, low mol. wt., crystallinity and fusion 78−51448
alloy, laser surface melted, heat transfer props. and microstructs. 79−70085
alloy, surface segregation prediction from bulk melting curve shape 77−12597
alloy systems assessment of accuracy of cryoscopic calcs. from fusibility diagrams 77−25010
alloys, melting line slope 77−15553
aluminophosphate glass:Mn:Mg(Sr), optical props. H_2O effects 77−28600
annular region, perturbation soln. for melting/freezing interface 78−59286
Antarctic iceberg melting 78−88863
approx. soln. for damage by pulsed discharge 77−39500
atomic aggregates, small, melting transition characts., random walk Monte Carlo calc. 77−75355
atomic and plastic crystals, melting transitions, thermodynamic props. 80−96452
basaltic achondrite meteorites, rare earth element abundance patterns rel. to origin 80−36581
behaviour induced by horizontal row of heating cylinders 80−33442
benzene, phase transform. process, energy-dispersive X-ray diffractometry 80−96631
benzene, thermal expansion at high press., near melting 79−77777
benzene adsorbed on graphite, melting and orientation, NMR study 80−100403
biological cells, mechanism of dehydration on thawing 77−81478
biomembrane phase transition studied by positron annihilation energy spectrometry 80−35854
bisphenol-A polycarbonate, plasticized, melting and equilib. melting temp. 78−2234
butadiene iron tricarbonyl, adsorbed on graphite, diffusion and melting, Mossbauer meas. 79−61270
butanethiol, volume change on melting and reduced Lindemann's relation 80−29151
caesium alkanoates, phase transitions, differential scanning calorimetry 77−43315
caesium propanoate, solid state transitions and melting process, diffr. and conductometric meas. 80−10670
calorimeter, AC, high-resolution, for organic- and biological-material melting study 79−6127
calorimeter, adiabatic heat capacity small sample low temp., with automatic data acquisition system 78−12697
carbon tetrachloride, dual melting curves and metastability 80−92647
carbon tetrachloride, freezing and melting of stable and metastable phases 77−27984
carbon tetrachloride, phase transform. process, energy-dispersive X-ray diffractometry 80−96631
carbon tetrafluoride, liq. and plastic crystn., Raman spectra 77−59565
cathode arc spot crater form. model 77−62414
cell water permeability during freezing and thawing, cryomicroscope multiple nonlinear regression analysis 79−92197
cells, volumetric changes during freezing and thawing, thermodynamic model 80−108863
Chainpur meteorite chondrules, rapid melting form. model rel. to volatile elements concs. 79−101121
cholesteryl acetate, phase transitions and solid polymorphs 78−2255
chondritic meteorities, L-group, incipient melting rel. to shock classification 79−88629
chondrules origin, primordial melting mechanism 80−4310
chromatin structure and thermal denaturation profiles 77−12881
classical one-component plasma, melting parameter 78−47092
closed form solution to problem with heat generation by viscous friction *(Japanese)* 80−19225
comet interiors, primordial radiogenic melting 80−67659
commensurate-incommensurate transition and melting in two-dimensions 80−75339
computer simulation, using array processor 80−54353
computer simulation using two species soft core model, melting curve max. phenomenon 78−6146
contact fusion in complex metallic systems 78−26664
convection, natural role in solid melting 78−71275
convective boundary condition problem, surface temp. rel. to time 79−76960
copolyester, melting temperature changes due to heat treatment *(Japanese)* 79−70096
Coulomb vector gas in two-dimens. 79−69449

melting continued
crystal-melt interfaces, kinetics of motion 79−69040
crystal-met interface of Lennard-Jones substance, Monte Carlo simulation 79−60622
crystal-smectic and smectic-nematic transitions, Lennard-Jones and Devonshire model extension 79−94883
crystalline material, melting criterion based on dilatation depend. of shear moduli 77−35673
crystalline solid, pre-melting near cryst. dislocations 77−76524
crystalline species, melting mechanism 77−35674
cubic crystal, self-diffusion and melting 77−31803
cubic metals, anisotropic relation between work function and melting temp. 79−37813
cyclohexane, plastic cryst., NMR determ. of phase diagram 77−12210
cyclohexanone, solid, phase behaviour, at press. up to 3 kbar, DTA 78−43108
cyclopentanol, solid, phase behaviour, at press. up to 3 kbar, DTA 78−43108
cyclopentanone, solid, phase behaviour, at press. up to 3 kbar, DTA 78−43108
cylinder, heated, melting around it, photographic appl. 79−23195
cylinder, stable conditions for phase change problem with internal heat generation 80−10130
density changes during melting by X-ray absorption 80−103462
dialkylammonium cupric chloride, calorimetric study of phase transitions 78−75804
diamond, 'melting' to solid metallic C phase above graphite triple point 80−15236
dibenzyl, diphenyl, US velocity and absorption near melting point 78−6127
1,2-dibromoethane, volume change on melting and reduced Lindemann's relation 80−29151
p-dichlorobenzene, expansivity, determ. by calorimetric compression from 0 to 400 MPa 80−44339
1,2-dichloroethane, volume change on melting and reduced Lindemann's relation 80−29151
differential scanning calorimetry, theoretical melting curves anal. 78−16799
diffusion/melting, linear correlation 77−20108
2,2-dinitropropane, specific heat meas., adiabatic calorimetric method 78−71854
dislocation generation, anharmonicity and solitons 78−79746
dislocation model, appl. to FCC cryst. 78−26658
dislocation model, theory 78−83923
dislocation model 78−26657
dislocation theory, Clausius-Clapeyron eqn. and press. depend. 78−18744
dislocation theory, cooperative effects 78−59934
dislocation theory 79−99298
dislocation theory of melting 80−65198
dislocation-mediated melting in two dimensions 79−73287
dislocations and melting in two and three dimensions 80−103454
disordering processes, in relation to molecular shape 79−37810
distillation deoxidation during electron beam melting *(Russian)* 79−70306
DNA, double helix, breathing modes and induced resonant melting 79−62180
DNA, local stability correl. with environmental conditions 79−88048
DNA and polydeoxyribonucleotides, thermal properties in wide range of concs. of ions of neutral salts and of polymer 78−80833
DNA derivate melting curves, automatic recorder using real time processing *(French)* 80−104833
DNA water salt solns., microcalorimetric investigation of phase transition and eutectic fusion 79−79448
DNA-type macromolecule, melting, low mol. wt. impurity effect 80−12050
Earth, primitive, melting due to primordial dense atmosphere blanketing effect 79−57935
Earth core, Gruneisen parameter reevaluation 79−39685
Earth crust, Panafrican thrusting and melting within Brazilian Continental Margin 77−21769
Earth interior, melting low and thermal model 78−15982
Earth interior shear heating rel. to melting and lithosphere-mantle decoupling 79−20790
Earth Mantle, partial melting, effect on elec. cond. 80−76936
EBBA, crystallisation and melting of metastable solid crystalline phases 78−2240
education, Brownian motion, melting, surface tension and rubber networks, thermodynamic anal. 80−73132
elastic solid, variational principle in ablation 78−90698
elastic-solid, variational principle 77−84894
electron solid, two-dimens., defects and implications for melting 80−39076
electron solid, two-dimens., shear modulus and melting, temp. depends. 80−158
electroslag refining, mathematical formulation for EMF, fluid flow, and heat transfer 78−52722
electroslag remelting, steady state segregation and heat flow 79−11629
element, melting, vol. change, simple model 79−55865
elements, anomalous entropies of fusion, deviations from Richard's rule 77−47601
embedded heater in solid, melting and natural convection 78−90646
entropy change on melting of simple substances, thermal expansion, configurational entropy 80−59630
entropy of melting for simple compounds and elements 77−59101
erythrocytes, human, effect of hydration on water content 77−16921
ethane submonolayer on graphite, struct. and melting, elastic neutron scatt. 80−29266
ethylene-CO copolymer, highly alternating, melting and internal motion 77−51474
ethyleneterephthalate-ethylene glycol copolyester/15% polyglycol, semicryst. melting and glass transitions 80−49346
eutectic alloy directionally solidified, contact melting kinetics, mass transfer during solidification *(Russian)* 77−52310
fast reactor ceramic fuel-steel system, freezing of flowing liquid in melting tube, simulation expt. 79−30981
FBR LOF accident, role of fission gas and fuel melting on transient fuel response 79−59191
feldpsar in porcelain, melting behaviour *(German)* 79−90758
Fermi quantum crystals, melting curves low temp. anomalies rel. to neutron stars 78−24757

melting continued
ferrous alloy melting, chromatogravimetric equipment for redox studies 78−40097
ferrous metallurgy, surface purification using laser and N_2 jet 78−92392
fine particles, model, surface phonon softening effect 79−99297
finite domains not initially at fusion temp., singular perturbation theory 77−66014
finite medium freezing (melting), variational anal., radiation and convection effects 80−38244
finite steel slabs, melting by flowing fast reactor fuel 79−54494
first order melting transition in the incommensurate phase 79−85094
fixed boundary condition modal, phase interface velocity *(Russian)* 78−15390
flexible chain polymer, topomorphism and phase dualism 78−14265
flexible structures, physical props. 79−19331
fluoride-oxide-SiO_2 system, containing Mg^{2+}, Ca^{2+}, Ba^{2+}, Pb^{2+}, cryoscopy 77−28798
fluoride-oxide-SiO_2 system, containing Na^+, K^+, Li^+, cryoscopy 77−28797
fluorides of alkaline earths and transition metals, high-press. melting systematics 77−51475
fluorophosphate optical glass development 80−106588
formulated as heat conduction problem with moving heat source 78−91420
free convection melting, Prandtl no. power exponent 77−89116
fusion curve, p vs. T equation, comparison exp. results for 39 substances 77−55345
fusion thermal tracers, thermophys. characts. investig. 77−5837
gelatin, aq., crystn. and melting 79−61914
geothermal well logging, temp. meas. utilising melting props. of materials 80−56659
glacial ice, melting in sea water, heat and mass transfer *(German)* 80−33606
glacial ice free convection melting in saline water 78−3835
glacial ice melting effects on Antarctic surface water 79−34866
glass, heat transfer, review 78−3084
glass, K-8, radiation coloured, msec laser pulse effects 77−16435
glass, kinetic equation for interaction between grain material and liq. 80−84901
glass, melting in fire-heated tanks, modelling *(Polish)* 80−96633
glass, new aspects, review 78−3087
glass, rare earth elements use as dopants *(Polish)* 80−97455
glass, related to chem. comp., for glass manufacturing industry *(Czech)* 78−80505
glass, TV monitoring, equipment potection 79−58756
glass, ultrapure, prep. for optical waveguides, review 78−3086
glass devitrification, heat treatment parameters determ. from viscosity changes *(Polish)* 80−40404
glass melting furnaces, development and prospectives, review 78−3088
glass melting process model, for flameheated tank furnace melting *(Polish)* 80−70380
glass workability rel. to melting history, microstruct., apparent liquidus temp., mechanical props. 80−11633
glass-melting furnaces, resist. between electrodes calc. 79−58690
glass-metal bonding, review of physical properties *(German)* 79−83167
glass-metal composite, heat conduction, memory switching 80−96703
glasses and solids, melting eqn. 78−87772
glassy alloy prod. using low temp. melt spinning device 80−100825
grain-boundary melting transition, in two-dimensional lattice-gas model 80−59634
graphite, Cs-intercalated, melting and staging, X-ray scatt. obs. 79−19180
graphite, interfacial tension determ. between C saturated liquid Fe by buoyancy meas. *(German)* 80−34273
graphite melting point rel. to press. 78−24811
group VI-A elements, thermodynamic basis for generalisation of melting curves 78−2236
hard sphere crystal, thermoelasticity in relation to melting 80−107353
hard sphere melting law 77−47359
hard-disc system, expt. model for melting transition 78−43100
heat balance integral method, refinement 79−14229
heat conduction, at freezing/melting boundary, model for approx. calcs. 78−5630
heat transfer, melting of substrate into different miscible liq. layer, hydodynamic instability 78−90695
heat transfer in steady laminar flow over flat plate 77−15027
heterogeneous system, US appl. to increase melting rate 80−74723
heteropolymers, melting theory, correlated chains 79−25996
heteropolymers, melting theory, random chains 79−25995
hexamethyldisilane, plastic cryst., NMR determ. of phase diagram 77−12210
high melting particle heating, melting and vaporisation in hot gas 80−6201
high-speed friction, intensity calc. 80−103416
highly absorbing media melting by laser radiation, liq.-phase surface shape 79−28082
HOAB, liq. cryst. phase transitions, specific ht. meas. 79−33075
horizontal boundary, steady-state convection, interface corrugations 78−26118
horizontal surface, flowing vapour laminar film condensation 77−15661
hydrometeor precipitation from anvil clouds, melting and evaporation 80−17323
ice, cloudy layers, back-melting by radiative heating 79−76961
ice, crystallisation and melting rate in laminar stream of liquid 80−100770
ice, heated water jet impingement melting, cavity formation, expt. and simulation 78−95133
ice, horizontal clear layer, radiative melting, rel. to atm. icing *(German)* 79−18679
ice, melting, in porous solid, NMR and differential scanning calorimetry obs. 77−62621
ice, one-phase Stefan problem, continuity of soln. in n space dimensions 78−95130
ice, pressure melting within glacier, indicated by regelation ice chem. comp. 78−61447
ice, upwelling in stratified ocean due to melting of glacier ice 80−81897
ice, vitreous, sp. ht., entropy and 'glass transition' 77−51520
ice block with impinging water jet, heat transfer 77−935
ice cubes, melting time, water film thickness, interface temp., weight var. 80−29153
melting continued
ice layer, heated, free convection onset criterion, density anomaly effect *(German)* 78−22351
ice layer, onset of free convection criterion 77−58685
ice melting model, appl. to Antarctic ice shelf and icebergs 80−4036
ice on Great Lakes, formation, freeze-up, breakup predictions 77−45038
ice surface, jet impingement 78−22394
icebergs, in Weddell Sea, melting rel. to upwelling 77−56647
icebergs, melting in environment with salinity gradient, rel. to fresh water supply 78−24305
induction melting, fluid velocity, large scale meas. and predictions 77−46985
inert gases, melting curves, quantum corrections, effective pair pot. calcs. 77−55347
initial subcooling problems, heat balance integral appl. 80−96627
internal friction temp. depend. in region of solid-liquid transition 79−23675
Invar, Fe-Ni (36 wt.%), alloy 36N, effect of melting conditions on thermal expansion coeff. 80−65256
ion impact induced shock processes in solids 80−89104
ionic crystals, structurally modulated, elasticity and its limits, yielding and melting 80−49295
ionic salts, melting transition statistical model, dielectric const., surface tension 80−70378
ionic systems, microscopic melting theory 78−79748
ionic systems, simple, stability and melting 78−71839
IV-VI compounds, interaction of internal s states 79−10826
IV-VI compounds, interaction of outer s states 79−10825
Josephine Peridotite, effect of partial melting on mineral comp. rel. to geothermometry and geobarometry 77−81880
lake ice cover, dissipation, effect of surface meltwater accumulation, heat flow 80−8364
Landau melting problem, numerical soln. of bedding eqns. 79−14233
laser annealing mechanisms, continuous and pulsed laser impact, melting 80−84964
latent heat storage materials, high temp. corrosion resistance and thermodynamic stability 80−30582
latent heat-of-fusion energy storage: experiments on heat transfer from cylinders during melting 80−6492
latent-heat thermal energy storage materials, energy density and materials cost *(Japanese)* 80−26168
latex, monodisperse, phase transition pressure determ. from sedimentation equil., Alder transition model 77−70344
latex, monodisperse, reflectivity obs. of phase separation into ordered and disordered phases 77−70345
latex colloidal crystal, melting, particle packing fraction depend. 77−73475
lattice-gas model, modified, for gas-liquid-solid phase diagram 80−62591
Lennard-Jones system, two-dimens., appl. to Xe adsorbed monolayer 79−28071
Lennard-Jones two-dimensional system, Monte Carlo study 80−49338
leucosapphire, supercooling and crystn. temp. determ. 79−51237
levitation melting process control *(Russian)* 78−80531
Lindemann's criterion and necessary condition for melting curve maximum 80−2145
Lindemann's melting law, derivation from Clausius-Clapeyron relation 78−18743
Lindemann's melting law, exptl. test 77−89522
Lindmann's melting law and the size dependence of melting temperature 78−59929
liquid phase nuclei form. during bulk melting 80−88304
liquids, simple, corresponding states correls. and triple point solid vol. 80−92649
liquids with spherical- and linear-like mols., fusion 79−82318
liquidus line curvature and estimation of degree of dissociation 78−22828
living cell volumetric changes in freezing and thawing, thermodynamic model and expt. 79−92192
lunar crust melting and differentiation evidence from trace element abundances 77−60651
Manicouagan impact crater, Quebec, impact melting 78−81163
Manicouagan impact melt, Quebec, chemical interrelationships with basement rel. to form. processes 78−81165
Manicouagan impact melt, Quebec, stratigraphy, petrology and chemistry 78−81164
Manicouagan impact melt sheet, Quebec, thermal history 78−81167
Manicouagan impact structure, Quebec, melt rocks petrogenesis 78−81166
Manicouagan melt sheet, Quebec, Canada, Rb-Sr isotopic data rel. to crustal rocks melting 78−81168
Mars, core and mantle melting during thermal evolution 78−65533
Mars mantle, partial melts comp. rel. to surface lavas props. 78−65532
Martin steel, thermoelectric determination of C content during melting 77−56276
MBBA liquid crystal, premelting detected by spin probes, effect of spin probe size 79−46563
mercury carboxylates, phase transitions, DTA 79−90759
mesogen compounds, melting behaviour, proton NMR spectra 78−15044
metal, crystal melt interfacial free energy calc. from exptl. radial distrib. function data 79−10926
metal, Debye charact. temp. and fusion transitions 78−63864
metal, effect of fusible-metal deform. on contact-melting kinetics 80−49339
metal, entropy/free energy relation 78−15368
metal, fusion and evacuation after elec. contact treatment *(Russian)* 77−73365
metal, HCP to BCC phase transition and melting 78−14463
metal, laser irrad., evidence of melt using Nomarski microscopy 79−69819
metal, plasma-arc refining remelting calc. *(Russian)* 78−18463
metal, spallation on emergence of shock wave on free surface, pulse X-ray photography exam. 77−51439
metal, thermal cond. changes at melting point, vacancy model 79−33279
metal, thermal expansion and melting 77−69103
metal and alloy surfaces, highly reflecting, pulsed laser stress phenomena 79−14015
metal cone, vaporisation, solution by wave front method 78−5640
metal film, laser hole melting for real-time, high density digital data storage 78−71135
metal melting by laser emission, laws governing fluid phase spattering *(Russian)* 77−20963

melting continued
metal melting in suspended state, large vol. and mass samples *(Russian)* 78−44036
metal mirrors, for high-power appls., multithreshold damage analysis 77−88884
metal powders, sintering at 1 to 10 MPa *(German)* 80−35122
metal refining by fractional melting 79−61537
metal sample preparation furnace for remelting prior to spectrochem. analysis 77−44556
metal subjected to intense heat source, plastic deformation 77−86085
metal surface, flash mechanism caused by monochromatic laser radiation 79−95878
metal transfer during vacuum consumable arc remelting 79−82317
metallic fine particles, anharmonic lattice vibr. theory, Einstein model appl. 78−18714
metallic fine particles, melting and size depend. on melting temp. 79−73294
metallic fine particles, theory of melting in the Percus-Yevick limit, appl. to particles on SiO_2 and C substrates 80−20060
metallic fine particles Percus-Yevick limit 79−42222
metallic heat carrier in loops, phase transition process, temp. field 79−55867
metallic mirrors, laser damage, temp. depend. of absorptance, melting 79−81470
metallic surface, heat treating and melting with scanning laser or electron beam 78−11406
metallic surface rippling induced by surface tension during laser melting 78−11405
metals, contact melting, state of cryst.-liq. boundaries, influence of impurities and hydrostatic pressure *(Russian)* 79−37812
metals, contact melting process kinetics, investigation method 80−39259
metals, dislocations and shock compression, thermodynamics 80−100235
metals, electron beam sweeping device for heating 78−6889
metals, EM levitation for melting without crucible *(Polish)* 80−89130
metals, enthalpy and average mass temp. on plasma-arc melting *(Russian)* 80−54405
metals, entropy of fusion and allotropic behaviour, exam. of correlation and modification of Richard's rule 78−71838
metals, heat capacity near melting point, vacancy mechanism of melting 80−10641
metals, melting temp., press. depend., vacancy mechanism 80−103460
metals, melting theory for small particles, Helmholtz free energy 80−59629
metals, pressure depend. 78−85517
methane, melting curve investig. by blocked capillary method 77−35672
methane adsorbed on graphite basal plane, first order melting transition, triple point 80−2269
methane adsorbed submonolayer on graphite, structural transitions between epitaxially ordered phases 80−96740
methylcyclohexane, dense liq., self-diffusion and viscosity 80−15278
microcrystal, temp. gradient, mol. dynamics model calc. *(German)* 77−76527
minerals, dislocations and shock compression, thermodynamics 80−100235
minerals (petrurgy) *(Czech)* 80−44298
minor planets, melting by EM heating in early solar system 80−36555
model, two-dimens., renormalisation group anal. 79−42218
molecular crystal, action of external forces on mesogenic struct. form. 80−2147
molecular dynamics calc. of melting curve extrema from repulsive step potential 77−59102
molecular dynamics simulation, Gaussian core model 78−67811
molecular solids, melting curves, Lennard-Jones Devonshire theory 80−65201
monolayers, Lennard-Jones system, melting in external field 80−65362
Moon, primaeval melting by superheavy elements 78−24478
multimode optical fibres, fusion splicing using gas flame heat source, development of splicing machine 80−102866
naphthalene, melting of rotational degrees of freedom near cryst.-liq. transition 80−54352
natural convection, in melted region around heated horizontal cylinder 79−46165
natural convection in melt region 78−30156
Nb, pure, production by carbothermic reduction-electron beam melting combination method 80−89177
nematic eutectic-forming binary system, melting behaviour 77−89526
nematic liquid crystals, coherent neutron scatt. studies, review 79−41956
non-Newtonian model for melting in single screw extruders 79−32589
nonFourier melting, semiinfinite solid, temp. distrib., interface location, small times 77−58542
nonisothermal devitrification kinetics 80−92465
nuclear reactor mixed-oxide fuel, two-component gas transport within interconnected porosity 79−617
nylon 6, drawn yarn, origin of double melting peaks 78−3118
oceanic basalts, press. depend. of solidus temps. and elec. cond. 77−91109
octaphenylcyclotetrasiloxane, phase behaviour and nucleation kinetics 80−29168
optical glass, K-8, laser pulse heating, softening and hardening points obs. 78−33794
optical glass, K-8 type, laser irradiated, transient thermal self-focusing and melting 77−50733
optical glass, melting, fining, surface tension, diffusion, nucleation in microgravity 80−81016
optical glass melting in Pt crucibles, thyristor freq. convertor-fed power supply 77−50780
organic compounds, high-press. expansivity determ. by piezo-thermal anal. 77−72705
orientationally ordered two-dimensional fluid phase, existence, mol. dynamics calcs. 79−73095
n-paraffin, crystals, phase transitions, statistical theory 80−44290
paraffin, solid-liq. interface motion during melting, convection effects, photographic obs. 79−18890
paraffin plate heat storage element, fusion, periodic solidification, heat transfer kinetics *(French)* 80−40913
paraffin wax, two-phase Stefan problem solns. 80−43594
particles in nonisothermal plasma jet, trajectory and temp. calcs. *(Russian)* 80−7514
peridotite, from upper mantle, rare earth fractionation patterns in partial melts 77−37198
melting continued
permafrost, approx. calc. of thawing zone boundaries under heat sources 77−25706
permafrost soil in Yakutia (USSR), long-term studies of thaw dynamics 77−78240
permanent magnet alloys manufacture, Co-mishmetal alloys *(Polish)* 80−35132
PET, densification, cryst. perfection, mechanism 79−66082
PET, thermodynamic equilib. melting parameters, effect of annealing 78−71837
phase diagrams, step pot. particles, 2- and 3-dimens., mol. dynamics 79−28072
phospholipid bilayer melting transition, thermodynamic fluctuations, ion permeability, statistical mechanics model 78−73140
physisorbed monolayer on graphite, neutron scatt. studies 80−107655
plagioclase, flotation and remelting in Kalka Intrusion, central Australia, rel. to anorthosite genesis 77−60371
plagiogranites of Iceland oceanic layer, partial melting rel. to rhyolites generation 77−86885
planar melting front stability in two-phase thermal Stefan prob. 80−43600
plasma arc refining melting, allowing two phase region and plotting distrib. functions *(Russian)* 78−31358
plasma furnace for steel industry, development in GDR *(German)* 78−22522
plasma furnaces, mineralogy and extractive metallurgy appls. *(French)* 80−28849
plastic crystal, anomalous high resoln. of NMR linewidths 77−12218
plastic crystals, phase transition and melting, dynamical model 77−84677
plate, melting, inverse heat cond. problem soln. 79−37112
plate melting in free convection flow 78−94531
plate with internal continuously-active source, influence of absorpt. coeff. *(Russian)* 79−37811
PMMA-PVC mixtures, dielec. relax. and struct. rel. to formation *(Russian)* 77−20073
polar ice sheets, basal temps. and melting 77−78250
poly(1-butene), melting and annealing behaviour, X-ray diffr. and DTA 79−28083
poly(ethylene-oxide), isothermal growth, thickening, melting, bilayer crysts. and chain end effects 80−38939
poly(trioxane), γ-irrad. effects on melting behaviour 77−62620
poly(vinylidene fluoride), melting and crystn. temps., press. depend., DTA meas. 79−90568
poly (trioxane), melting behaviour, simultaneous thermogravimetric and differential scanning calorimetric meas. 77−76529
poly-1-butene, annealing and melting behaviour 79−38871
poly-ε-caprolactum, semicryst. melting and glass transitions 80−49346
polyamide-Cu(Ni) oxalate, oxalate decomposition kinetics, in polymeric medium, thermogravimetry and DTA 78−52749
1,4-cis-polybutadiene, stereoregular, recrystn. in partial melting temp. region *(Russian)* 80−6495
polycaprolactam film, subjected to 9 kV elec. discharge, X-ray obs. *(Russian)* 79−23536
polydioxolan, crystallisation, morphology and melting props. 78−14297
polyethylene, drawn, ultrahigh modulus, linear, melting behaviour 80−19916
polyethylene, extended-chain cryst., high-press. crystallisation and melting obs. 77−27985
polyethylene, flow-induced fibril form. from soln. 80−59402
polyethylene, high-density fibres, extrusion conditions influence on thermal props. and morphology 79−61617
polyethylene, linear, single cryst., surface melting, X-ray diffr. 77−31755
polyethylene, low density, γ irrad. effect on elec. cond. and temp. charcts. 77−85221
polyethylene, low density, melting and crystallisation, DSC characterisation 80−64927
polyethylene, low density, UV and heat treatment effects, DSC obs. 79−14915
polyethylene, melt-crystallised fractions, surface and full-strand melting, small-angle X-ray scatt. obs. 80−84279
polyethylene, melting against Al, XPS meas. 78−15556
polyethylene, melting against Al, XPS obs. 77−32700
polyethylene, relax. phenomena, −30 to 200°C, premelting and glass transition 78−51440
polyethylene, sp. ht. after annealing at low temps., cryst.-melting phenomenon interpret. 77−39679
polyethylene, ultra-high-strength filaments, soln. spun/drawn, mech. and thermal props. 80−40440
polyethylene crystal, longitudinal growth in flowing soln., melting of continuous fibrillar crystal 80−19917
polyethylene fractions, quasi-binary systems, solidification and crystn. 80−84108
polyethylene melt, cryst. kinetics during cooling, nucleation density effect 80−100181
polyethylene oxide, melt grown single crystal, isothermal growth, thickening and melting 78−51432
polyethylene oxide, relax. phenomena, −30 to 200°C, premelting and glass transition 78−51440
polyethylene oxide-polystyrene-polyethylene oxide triblock copolymer, surface and full-strand melting, small-angle X-ray scatt. obs. 80−84279
polyethylene terephthalate, differential scanning calorimetry of melting, mosaic block struct. of cryst. layers 78−26452
polyethylene terephthalate, effects of preliminary ht. treatment on crystallisation *(German)* 78−75593
polyethylene terephthalate, fibre, melting in crystn., intermediate and amorphous phases 77−84898
polyethylene terephthalate-p-oxybenzoate, nematic→isotropic transition loss 80−44300
polyethylene-isostatic polypropylene mixture, melting anal. 80−29150
polyhexamethylene terephthalate/polyoxytetramethylene block copolymers, melting and crystallisation 78−91260
polymer crystal growth, during annealing 78−14300
polymer crystallisation and fusion, conf., Louvain-la-Neuve, Belgium (1976) 78−51429
polymer crystals, melting, intramol. and intermol. interactions effects 78−18745
polymer melting, during extrusion, integral energy-balance model 77−46899
polymer melting, theoretical aspects 80−59633
polymer transitions, domain size effects 79−69232

melting continued
polymeric cryoprotectants in preservation of biological ultrastruct., aq. soln. low temp. states 78−65157
polymers, melt transition, theory 77−76325
polymers, melting theory, phonon anharmonicity effects 78−67659
polymers, model equivalent to Ising model 80−37914
polymethylene, melt transition, theory 77−76325
polymethylpentene, press. effects on melting 78−56625
polymorphous material, Stefan problem, melting or freezing, interfacial boundaries 80−64350
polyoxyethylene-glutaric acid eutectic, melting and crystn. 80−28924
polyoxymethylene, relax. phenomena, −30 to 200°C, premelting and glass transition 78−51440
polyoxymethylene diacetate, bulk cryst. and melting, polyoxyethylene additive effects 79−32921
polypentenamer, thermodynamics *(Russian)* 77−21386
polypropylene, Halen and Daplen, semicryst. melting and glass transitions 80−49346
polystyrene, isotactic and static cold-crystallised blends, thermal transitions 80−24381
polystyrene, solution grown isotactic crystal, thermal change kinetics study by X-ray diffr. 78−9965
polystyrene+poly(2,6,-dimethyl phenylene oxide), isotactic, crystallisation and melting 78−18554
polyvinyl fluoride, relax. phenomena, −30 to 200°C, premelting and glass transitions 78−51439
polyvinylidene fluoride, high-press. melting and crystallisation 78−91422
polyvinylidene fluoride, relax. phenomena, −30 to 200°C, premelting and glass transitions 78−51439
polyvinylidene fluoride-PMMA blends, differential scanning calorimetry of cryst. melting 78−26454
polyvinylidenefluoride, melting and freezing, effect of structural factors *(German)* 78−15389
pool heated volumetrically, reactor accident condition, phase change, free surface, thermal instability 78−89960
potassium alkanoates, phase transitions, differential scanning calorimetry 77−43319
powder grains, melting, in plasma flame 79−60200
power overdistribution to AC and DC arcs for melting metals *(Russian)* 80−54055
process anal., X-ray fluorescence and optical spectrum anal. appl. 78−23560
PTFE, annealing effect on melting and crystallisation *(Japanese)* 80−20980
PTFE, melt transition, theory 77−76325
pure material, two-phase solid-liq. melt regime, thermodynamic props., eqns. 77−55342
PVC, enthalpy determ. of order 79−7556
PVC, rheology, viscoelasticity, panel discussion 79−3984
PVC, rheology, viscoelasticity 79−3982
quartz glass, effect of fusion temp. and time 77−36441
radiative ablation of melting solid 78−94564
radiative ablation of melting solids, Biot's variational method 77−31203
radiative melting of ice layer adhering to a vertical surface *(German)* 79−76956
radioactive low level contaminated metal waste volume reduction by melting 79−89412
radioactive waste, high-level liquid, vitrification, full scale in-can melting 79−59213
radioactive waste, vitrification using in-can melting process 80−83204
radioactive waste immobilisation using continuous glass melter 80−83199
radioactive waste immobilization, continuous glass melter 79−59214
rapid melting of metals including alloy effects 79−23701
rare earth metals, heat capacity near melting pt., vacancy mechanism of melting 80−15221
rare earth RNb_3O_9, synthesis and physicochem. props. 77−90304
rare gas solids, Debye Waller factors from unpaired elastic force model, Lindemann's melting criterion 80−19896
refractory oxide, high temp. props. conf., Odeillo, France (June/July 1977) 79−100125
repulsive interatomic potential, shouldered, melting curve maxima 77−43313
restoration, evaporation and melting of materials in high temp. gas flow *(Russian)* 80−39271
tRNA, conformation and intensity fluctuation spectroscopy, melting curves 78−35798
rock melting drills, thermal analysis 77−17258
rocks, partially melted, struct.-sensitive physical props. 79−12116
rubber, natural, oriented, crystallisation kinetics and melting 78−75554
rubidium propanoate, solid state transitions and melting process, diffr. and conductometric meas. 80−10670
self-consistent field theory 79−42221
semi-infinite solid, laser surface melting and subsequent solidification, computer heat flow models 79−69916
semi-transparent medium, melting rate, radiative transfer effects 78−94590
semiconductor, dynamics of surface melting and resolidification during laser annealing 79−69918
semiconductor, entropy of fusion allowing for dissociation at melting point 77−55348
semiconductor, surface melting during laser annealing 79−74023
semiconductor electronic component of entropy of fusion 78−47503
semiconductor melts, estimate of positional component of entropy of fusion, cluster model 77−55349
semitransparent material, approx. temp. profile calc. method 77−75787
p-sexiphenyl, solid-smectic and smectic-nematic transitions 79−82322
shells, creation of finite perturbations by use of laser beam 79−18849
silicate slag melt, physicochemical optimisation 78−85112
simple body melting time with convection boundary condition 80−99914
simultaneous melting and evaporation due to area heat source *(German)* 78−59282
single crystal growth, techniques 80−108341
single sphere, mathematical model of melting *(German)* 77−89521
slab, melting in contact with fluid, heat cond. prob. *(Japanese)* 80−53612
slab, zeroth order variable eigenvalue approach to melting or solidification 77−67392
slab with heat generation by friction, approx. anal. *(Japanese)* 80−14555
smectic B, liq. cryst., positional short-range order 79−10790
melting continued
snow, deposition and melting with altitude on Mt. Teine, Hokkaido *(Japanese)* 80−36346
snow, melting of prairie snowpack, energy budget approach 79−84310
snow, melting prediction via radiometry in 3 to 60 mm wavelength region 80−72561
snow, stream temps. during melt *(Japanese)* 78−88860
snow in river drainage basins, estimated water equivalents and melting characts. determ. 78−96249
snow melting rate, urban/rural area comparison in Sapporo, Hokkaido *(Japanese)* 80−36342
snow on slopes of Mt. Asahidake, Hokkaido *(Japanese)* 80−36343
snowpack, two-dimens. turbulent diffusion model 77−78277
soft discs, two-dimens. melting, phase transition boundary 80−96629
soft-sphere melting transition, phase coexistence props., mol. dynamics calcs. 79−10909
soil, moisture change-of-state front advancement in freezing and thawing 77−91163
soil, seasonal freezing or thawing depth calc., eqns. eval. 77−78243
soil, struct. changes during freezing and thawing 77−25707
soil thawing under polar conditions using synthetic film covers, thermal balance meas. on polymeric film covered surfaces 77−78244
solar concentrator, paraboloidal, flat receiver melting temp. calc. 77−45843
solar furnace, materials melting process dynamics rel. to automatic control 79−39317
solder melting point, US exam., equipment design 79−15937
solid bounded by curved interfaces, melting point 79−7678
solid surfaces, ablation in impingement region of water jet 80−14766
solid-liquid interface free energy anisotropy clustering influence 80−80054
solid-liquid transition, optical reflectance spectra 80−24569
soliton lattice melting, functional integral method 80−17883
solution droplets vaporisation, in high-temp. gas flow, heat and mass transfer 78−75191
sphene in high-pressure partial melting of hydrous mafic compositions 79−44174
spherical end faced coupling fibre fabrication by selective etching/melting 80−53492
spherical solids melting in turbulent carrier fluid, deformation and breakup 80−92646
sputtered particles-substrate, temp. overaging *(Russian)* 80−40385
stainless steel, laser surface melting for corrosion protection 80−93698
steel, alloy, electroslag remelting effect, an impact-abrasive wear resistance 80−55541
steel, austenitic stainless, high N, plasma arc remelting, processing parameters and props. 80−16336
steel, C, plasma melting, N_2 absorpt., CO form. influence *(Russian)* 79−39193
steel, Cr, high C, ingot, macrostruct., effect of diffusion annealing, solidification condition *(Chinese)* 78−15429
steel, diffusion melting in Fe-C melts, heat transfer correl. 80−54348
steel, effects of laser light focusing conditions *(Russian)* 77−59823
steel, hardness, effect of laser irrad. in inert gas atm. *(Russian)* 79−38935
steel, high alloy, instrumental anal., use of HF induction melting and centrifugal casting *(Japanese)* 77−56280
steel, high alloy, preparation for instrumented anal., HF induction melting, casting 78−48607
steel, high speed, props. after electroslag remelting 80−104139
steel, high speed tool, laser surface melting 79−24654
steel, high-strength tool steel D7KhFN, remelting effect on mech. props. 80−76284
steel, laser beam melting kinetics *(Russian)* 77−56121
steel, low C, alloy, nonmagnetic 40KhNM, corrosion resistance, melting procedure effects 77−70226
steel, low C, HF oscillations during electron beam welding *(Russian)* 80−76273
steel, low C, rapidly solidified laser surface alloyed, electron microprobe obs. 79−70201
steel, melting and solidification *(French)* 77−66635
steel, stainless, deoxidation in melting with Si *(Korean)* 78−19947
steel, stainless, oxidation in melting *(Korean)* 78−19946
steel, stainless, type 304, laser surface melted, topographical characts. 79−70200
steel, tool, type M2, laser melting and heat treatment, microstruct. charact. 79−100188
steel, tool and high speed samples, high frequency induction melting and centrifugal casting method for prep. in instrumental anal. *(Japanese)* 79−43232
steel, tool and high-speed, high freq. induction melting and centrifugal casting in instrumental anal. 80−84886
steel, tool type M2, surface hardening and microstruct. refinement by laser melting, electron beam melting, heat treatment *(Korean)* 79−70093
steel, W-Mo-Cr-V tool, laser surface melted, struct., heat treatment effect 80−76424
steel, W-Mo-V-Cr(6,5,2,4 wt.%), 56-5-2, microstruct. produced by melting and powder metallurgy *(German, English)* 77−63591
steel 1018, laser surface melted, topographical characts. 79−70200
steel ShKh15, austenite, grain growth, melting procedure effects 77−12650
Stefan and dam problems, free boundary convexity 78−83356
Stefan problem of melting in annular duct with nonlinear outer boundary conditions 79−86329
Stefan problem of plane or cylindrical interface, joining of solns. 78−83233
Stefan problems, particle model 78−32779
Stefan-like problems, soln. improvements 79−23181
subcooling effect on cylindrical melting 79−32214
superionic conductor, sublattice melting, phenomenological model 77−35663
surface, air bubble evolution effect on boundary layer separation 78−67015
surface dynamics, phase boundary configuration calcs., moving heat source *(Russian)* 80−54342
surface melting, molecular dynamics exam. 78−75807
surface theory 80−10644
surface velocity, expt. meas. and prediction in 30000 lb inductively stirred melt 78−11139
surface vibration and melting, self-consistent Einstein theory 79−33171

melting continued
temperature distribution of melting fission reactor fuel clad, Pekeris-Slichter series expansion method 77−88238
temperature meas., theoretical aspects, thermometric reference materials 77−67436
terrestrial planets, melting rel. to core formation 80−17514
tetrabrommethane, surface melting, transition from atomically smooth to rough struct. 77−76648
thermal energy storage material cylinders, heat transfer during melting 79−3894
thermal plasma engineering in metallurgy, inorganic materials technology 78−3070
thermal problems, one-dimens., with phase change, efficient numerical technique 78−59270
thermoelectric materials, B_4C_x and $(B,Si)_4C_x$ P-type LaS_x N-type alloys, fabrication and thermoelectric props. 80−107771
thin absorbing films, laser-induced removal, two-phase mechanism 80−97384
three-dimensional single-phase Stefan problem 77−7300
Tilting Harbour igneous complex, Fogo Island, Newfoundland, magma melting rel. to petrology 78−77230
Tokamak fusion test reactor, thermal response of first wall limiters 80−79585
toluene, melting curve up to 9 kbar and down to LNT *(French)* 77−15551
transition metal, fusion entropy, electronic contrib. 79−42217
s-triazine, sp.ht. 130-380K, melting enthalpy and solid-state transition 79−46812
tube flow, heat transfer problem of flowing liquid solidification onto a melting wall 78−94585
tunnel theory for melting, expt. test 78−10173
two dimensional system, melting and condensation theory 80−57231
two dimensions, Kosterlitz-Thouless dislocation model 79−7677
two-dimensional, dislocation-mediated theory predictions and consequences, light scatt. use as probe 80−92651
two-dimensional crystal, theory 78−51645
two-dimensional electron solid, melting 78−83921
two-dimensional Lennard-Jones system, phase transitions, calc. 80−59621
two-dimensional triangular lattice, melting theory 78−71833
Tysnes Island meteorite, melting rel. to origin of unusual Fe+FeS and silicate clast 79−2526
Udimet 700 superalloy, laser melt quenching and alloying 79−69919
universality of melting and freezing indicators, additivity of melting curves 77−1214
vacancy cell model and BGY integral eqn. 80−38887
vacancy mechanism 78−38814
vacancy mechanism 78−38815
vacancy model theory, melting temperature-av. energy of interaction correl. 79−28080
vacancy theory, cell model calcs. 77−55224
vacuum extraction system for vacuum stoving and sample melting 78−21146
vacuum melting furnaces and casting techniques 78−84727
Van der Waals film adsorbed on graphite, two-dimensional phase transitions 80−107653
vertical surface melting, heat transfer interferometric meas., convection effects 80−64339
Vredefort structure, S.Africa, spherules prod. on shatter cone surfaces 79−29773
water emulsions, dielec. props. obtained after crystallisation/melting cycle 77−86381
water in capillary, freezing and melting behaviour, dilatometry, elec. cond. meas. 78−75908
welding, ultra pulse type, heat transfer characts. 79−1047
Wigner electron crystal, melting curve 79−19531
Wigner lattice, two-dimens., melting temperature calc., dislocation theory 78−43207
Wurm glacier of Val Tresa, melting rel. to Quaternary glaciolacustrine sediments dislocations *(Italian)* 79−8647
Ag-Cu (6.6% at.wt.), laser melt quenching and alloying 79−69919
Ag-Cu surface alloyed films, laser melt quenched, microstruct. 80−76423
α-AgI, superionic conductor, Raman scattering evidence for sublattice melting 78−80350
$AgSbSe_2(Te_2)$, exam. of kinematic viscosity of melts, and short range ordering 79−1383
Ag_3Sn, dental alloy, prod. by melt extraction technique, exam. of mech. props. 78−48349
Al alloy, 2024 T-351, laser surface melted, topographical characts. 79−70200
Al alloys, laser surface melted, porosity form. 78−44279
Al, cutting, temp. effect on built-up edge behaviour *(Japanese)* 78−7083
Al, dislocation behaviour at melting, HV electron microscope in-situ obs. *(Japanese)* 77−43216
Al, existence of before and after effects, neutron scatt. 77−84895
Al film, vacuum deposited, structural changes during annealing at temp. near melting point 78−84096
Al, melting curve and Gruneisen coeff. at high press. 80−65200
Al, melting transition, TEM 77−80603
Al, powder, fission under weightlessness conditions *(Russian)* 78−31357
Al powder, liq.-solid phase transforms. *(French)* 80−45294
Al, rapid melting and solidification of surface layer, exam. using computer heat flow model 78−83228
Al sputtered coating development, porosity, durability temp. depend., electric arc metallisation regime *(Russian)* 80−39402
Al, structure sensitive props., temp. hysteresis after melting and crystallisation *(Russian)* 79−29036
Al-Cu, isothermal coarsening of liquid inclusions 77−21166
Al-Cu (4.8 wt.%), homogenization, temp. gradient driver process 77−52362
Al-Cu alloy, vacuum deposited thin film, abnormal grain growth before melting transition and subsequent struct. change 79−60663
Al-Mg alloys, overheating effects on microstruct. and props. 77−63698
Al-Zn-Mg-Li alloys, effect of Li on thermal props. 79−24515
$Al_xGa_{1-x}As$ DH laser material, Ar laser induced catastrophic damage 79−86178
Al_2O_3, melting speed, effect of struct. and grain shape *(Polish)* 79−29002
Al_2O_3, powder grains, melting, in plasma flame 79−60200
melting continued
Al_2O_3:Zr ceramic, elec. props., additives effect, and interaction with steel melt 80−104305
Al_2O_3-B_2O_3-P_2O_5 system, glass formation by laser melting 78−44074
Al_2O_3-CaF_2, phase relns. 78−23700
Al_2O_3-Dy_2O_3, phase diagram at high temps. *(Japanese)* 80−50619
Al_2O_3-Nd_2O_3, phase-diagram at 1100°C *(Japanese)* 78−79747
Al_2O_3-Y_2O_3, melting behaviour and metastability determ. by optical DTA 80−92648
Ar, lattice parameter determ. at melting, X-ray diffr. 78−10174
Ar, solid, density at melting and isochoric equations of state 78−83915
Ar, solid, vol. depend. lattice dynamics, pseudo-harmonic approach 79−99260
Ar, solid-liq. transition and mech. props., modified cell theory 79−23703
As_2Se_3, struct. determ. in amorphous and liq. state using EXAFS meas. 77−89366
As_2Se_3-As_2Te_3, liquid, mixture enthalpies *(German)* 79−77770
$(AsSe)_{1-x}Te_x$ glasses, thermal props. and viscosity, temp. and conc. depend. 77−76324
Au, vacancy size effect, surface energy in small particles and bulk specimens 80−75223
B, β-rhombohedral, purification by electron beam melting and CVD 80−20781
B modifications, exam. of physical props. and electron structure 79−94954
B_4C, melting and phase homogeneity range 80−20911
Ba I-Ba II phase boundary, Ba I fusion curve peak at high press. *(Russian)* 80−2165
BaF_2-xBaO.ySiO_2 freezing point depression meas., effect of SiO_2 compound additions 77−28798
$BaTiO_3$-PbO-B_2O_3, liquid phase sintering, effect on props. *(German)* 79−33980
Be casting produced in zero gravity environment, BeO particles uniform distrib. 78−72753
Be, containerless grain refinement using BeO in space environment, melting and solidification 79−47673
BeF_2, melting curves at high press., rel. to SiO_2 extended phase diagram 77−11672
Bi, effects of asymmetrical friction in piston-cylinder device on melting curve 80−86292
Bi, optical phonon anharmonicity and melting, light scatt. study 80−60621
Bi, shock loading and unloading effects, 473K 77−84840
Bi solid and liquid, positron annihilation temp. depend. 80−108296
Bi-Cd eutectic alloy, directionally solidified, contact melting kinetics, mass transfer during solidification *(Russian)* 77−52310
Bi-Cd(Sn), eutectic, contact melting kinetics *(Russian)* 80−70377
$BiH(PO_3)_4$, condensed, thermal behaviour and IR spectra 80−19912
Bi_2O_3-$ZnO(CdO)$, elec. cond., dielec. const., mag. susceptibility meas., effect of melting transition 77−7849
BiP_5O_{14}, condensed, thermal behaviour and IR spectra 80−19912
Bi_2Se_3-Bi_2Te_3, liquid, mixture enthalpies *(German)* 79−77770
$Bi_2W_2O_9$, struct., dielec. props., melting character and thermal stability 79−23572
$C_6Eu(Yb)(Ba)$ intercalation compounds, three dimensional continuous melting 80−59631
CO, press. depend. of melting and α-β phase transition temp. 77−69075
Ca, acoustic effect in crystallisation and melting *(Russian)* 79−51238
$CaCl_2$, fused, exam. of hydrolysis at high temp. 79−11791
$CaCl_2.6H_2O$ heat of fusion system for solar energy storage 80−16846
CaF_2, fluorite, phase relations, to 60 kbar and 1800°C 78−84785
CaF_2-xCaO.ySiO_2, freezing point depression meas., effect of SiO_2 compound additions 77−28798
$Ca(NO_3)_2.4H_2O$, high press. phase behaviour, dehydration and congruent melting 79−78947
CaO-Al_2O_3-SiO_2 melt, at 1723 to 1823K, determ. of inter diffusivities matrix 78−43161
CaO-Fe_2O_3-SiO_2 glass, struct. behaviour at melting, Mossbauer exam. 79−10802
$CaYAl_3O_7$, type of melting, crystallisation from melt 77−12515
Cd, atomic vibr. and fermion behaviour of HCP metals 80−6474
Cd, Lindemann's rule and X-ray Debye temp., anisotropic single crysts. 79−28076
(Cd-Bi)-Sn, eutectic alloy, directionally solidified, contact melting kinetics, mass transfer during solidification *(Russian)* 77−52310
CdI_2-PbI_2-NaI, fusion diag. and thermodynamic calc. *(Russian)* 77−48417
$Cd(NO_3)_2.4H_2O$, high press. phase behaviour, dehydration and congruent melting 79−78947
Cd_3P_2, high press. phase relns. and cryst. structs. 78−59792
CdSb single crystals, surface layer melting and recrystallisation due to laser irradiation *(Ukrainian)* 79−46699
CdTe, mag. susceptibility at 20-1400°C 77−12085
$CdTl_2Se_4(Te_4)$:Au, elec. cond., density, dielectric const., changes on fusion 80−88553
$CdTl_2Te_4$, Hall and thermo-EMF coeffs., in solid, liquid states 80−54704
Co melt, struct. charact. time depend. in X-ray studies *(Russian)* 80−24350
Co-H, system, melting temp., effect of H_2 *(Ukrainian)* 79−52153
$CoCl_2$, vapour pressure meas. 77−89534
$CoCl_2$-KCl-NaCl system, melting diagram investigation by thermographic anal. *(Russian)* 78−3111
CoO, plasma reduction melting *(Russian)* 78−31359
Cr, volt ampere characteristics during electron melting process *(Russian)* 80−75336
Cs, high press. melting curve maximum 80−75337
$CsPO_3$-$Sr(PO_3)_2$ system, physicochem. investigation 77−35666
Cu, defects at thermal equilib. and melting, positron annihilation meas. 77−76391
Cu, impurity distribution between crude Cu, white metal and SiO_2 saturated slag 78−44055
Cu, molten surface layer thickness, emissivity and AES meas. 80−39261
Cu, spherically shaped crysts., surface melting, IR emission obs. 77−20050
Cu surface melt of spherical crysts., microscopic obs. 78−34599
Cu-Ag (Pb)(Bi), evaporation of Ag, Pb, Bi in vacuum induction melting 77−28742
Cu-Ag(Bi)-O, evaporation of Ag, Bi in vacuum induction melting 77−28742
Cu-Al, fission under weightlessness conditions *(Russian)* 78−31357

melting continued
Cu-Al-Mn, Heusler alloy, magnetic prop. investig. of struct. transitions *(German)* 77−8289
Cu-Fe, metastable solid solutions, production by explosive plasma compressor *(Russian)* 77−90289
Cu-M, M=Al,Cd,In,Ga,Zn, magnetic susceptibility, comp. and temp. depend., melting effects 78−52202
$CuGaTe_2$, exam. of kinematic viscosity of melts, and short range ordering 79−1383
$CuInTe_2$, exam. of kinematic viscosity of melts, and short range ordering 79−1383
$Cu_2S(Se)(Te)$, thermal cond. changes on melting 77−7848
D_2, solid, melting curve, meas. of P, V, T and longitudinal sound velocity 79−37814
Eu, electrical resistivity of solid and liquid phases, thermopower, melting temp. 80−59955
Fe and steel, centrifugal casting method and high frequency induction melting, sample prep., emission spectral anal. 77−48367
Fe, diffusion melting in Fe-C melts, heat transfer correl. 80−54348
Fe, EM levitation for melting without crucible *(Polish)* 80−89130
Fe, electrolytic, oxidation in melting *(Korean)* 78−19946
Fe melting and adiabatic temp. distribs. in outer Earth core 77−70626
Fe meteorites of groups IAB and IIICD, origin by impact melting 80−109404
Fe, pure and alloyed, density and thermal expansion in liq. and solid states 80−96668
Fe, rapid melting and solidification of surface layer, exam. using computer heat flow model 78−83228
Fe, spreading behaviour of Al-Si melts 80−84345
Fe-base samples, for working curves, HF induction melting and centrifugal casting 80−22340
Fe-Cr-Co-Mo, melted in open induction furnace, microstruct. and magnetic props. 79−61626
Fe-Cr-Ni, Fe-rich, melting equilibria *(German)* 77−52282
Fe-Cr-Ni, melting and solidification *(French)* 77−66635
Fe-Cu (30 wt.%) alloy, dendrite remelting during isothermal holding, microspin obs. *(Japanese)* 78−71836
Fe-N system, spattering phenomenon during arc melting 79−39053
Fe-Ni-Co base alloys, composition changes during electron radiation melting *(Russian)* 78−19718
Fe-Si, spreading behaviour of liq. Al 80−84345
Fe-Si system, melting equilibria study *(German)* 80−66473
Fe_3Pt:Sn Invar alloy, Mossbauer shift temp. depend. 80−100626
Fr, properties from melting point to 7500K, prediction *(Russian)* 80−44296
Ga, dislocation structure on melting of nearly perfect crysts., Borrmann topography 77−31663
Ga, melting point as temp. calibration standard 77−41611
Ga metastable phases, melting curve under atm. and high press. by microcalorimetry *(French)* 77−43314
Ga solid and liquid, positron annihilation temp. depend. 80−108296
Ga-Te system cpds., degree of dissoc. from curvature of liquidus line 78−22828
GaAs, electrical conductivity and thermoelectric power charge due to melting 80−100490
GaAs(Sb), high-temp. thermodynamic data and quantitative fits to liquidus line 77−63637
Ge, amorphous, first order transition to metallic liquid, calc. of transition temp., enthalpy and entropy 79−69227
Ge, ion-implanted amorphous layers, melting model for pulsing-laser annealing 79−56080
Ge, laser irradiation, photoacoustic detection 80−2901
Ge-FeS, GeS-FeS, density of alloys, volume changes on melting 77−51473
Ge-Si, phase diagrams near melting point, Helmholtz free energy, heat of solution 80−70379
Ge-Si:Sb, prepared in Universal Furnace expt. in Soyuz-Apollo programme, melting and crystn. 80−19737
Ge-Si-S system, glass formation, transition temp., crystallisation and melting 80−100178
Ge-Si-Sb solid soln., struct. peculiarities and mech. props. under weightlessness *(Russian)* 78−23693
GeO_2 glass, nonisothermal devitrification kinetics 80−92465
GeO_2, melting curves at high press., rel. to SiO_2 extended phase diagram 77−11672
GeO_2-CdO system, phase diagram anal. by differential thermal, X-ray anal. 77−8805
$GeSe_2$-As_2Se_3-Sb_2Se_3, elec. cond. over wide range of temp. 80−88564
GeTe, enthalpy and specific heat, 0 to 860°C, polymorphic transitions obs. 77−43350
GeTe-As_2Te_3 system, phase diagram, eutectic comp., thermographic and X-ray anal. *(Russian)* 77−63646
H, solid polarised spin system of H atoms metastable in mag. field 78−30812
H_2, melting curve up to 10 kbar *(Russian)* 77−27987
H_2, melting curves, quantum corrections, effective pair pot. calcs. 77−55347
H_2, solid, melting curve, meas. of P, V, T and longitudinal sound velocity 79−37814
He, room temp. melting at high-press. 80−80025
He, sound transmission at liq. solid interface, probe of melting kinetics 80−92734
^{3}He, liq., spin polarisation, rapid melting of polarised solid 79−46872
^{3}He demountable melting curve thermometer 78−54369
^{3}He, liq., polarisation effect on mag. ordering, melting curve 80−80021
^{3}He, melting, specific heat, entropy, latent heat 78−75904
^{3}He melting curve obs. by Pomeranchuk cooling 79−7731
^{3}He, melting curves, quantum corrections, effective pair pot. calcs. 77−55347
^{3}He monolayer film, adsorbed on Grafoil, phase determ. by sp. ht. meas. 77−11764
^{3}He, solid, low temp. thermal cond., structural crystalline defects 80−2240
^{3}He, solid, mag. phases *(Russian)* 77−72743
^{3}He, solid, melting, formal treatment of low temp. props. 79−69315
^{3}He, solid, melting curve shifts due to pore condensation 80−54469
^{3}He, solid, ordering obs. at melting press. in high mag. fields 80−84341
^{3}He, solid, spin ordered, melting press. and entropy 80−84340
^{3}He, solid, strongly magnetised, low-temp. melting props. 77−11765
^{3}He, solid, susceptibility along melting curve, 20 mK to nucl. ordering temp. 77−31837
melting continued
^{3}He, two-dimens. solid, melting mechanism 80−10643
^{4}He, at ambient temp. under high pressure *(French)* 79−73373
^{4}He, crystallisation wave detection, solid-liquid boundary oscillation spectra *(Russian)* 79−90844
^{4}He, Lennard-Jones model at 0K, props. using Monte Carlo method 79−82401
^{4}He, liq., phase transitions, positive and negative ion mobilities meas. 78−87833
^{4}He, liq. and solid, dielec. const. meas. 77−20143
^{4}He, melting curve from fourth sound meas. 78−2322
^{4}He, melting curves, quantum corrections, effective pair pot. calcs. 77−55347
^{4}He, melting obs. at 297K and 115 kbar 79−82413
^{4}He monolayer film, adsorbed on Grafoil, phase determ. by sp. ht. meas. 77−11764
^{4}He, solid, nucleation in Vycor under press., superfluid oscills. near melting press. 79−51388
^{4}He, solid-fluid, eqn. of state, melting props. under press. 80−96721
^{4}He, solid-superfluid interface, struct., surface tension 80−88380
^{4}He, viscosity and positive ion mobility in liq. phase, near melting transition 78−10240
HfC, pressing regime influence on high-temp. creep *(Russian)* 80−100852
Hg film, melting and crystallisation kinetics, electron microscopy 77−15725
Hg, melting line determ., latent heat method, high press. 77−37903
Hg, melting line determ., pressures up to 1200 MPa 80−84281
Hg on metal surfaces, flow kinetics in temp. grad. *(Russian)* 78−6198
In, effects of asymmetrical friction in piston-cylinder device on melting curve 80−86292
In film, thermal hysteresis of phase transitions and mechanism of crystallisation 77−89679
In, island film, melting and crystn. kinetics, dark field electron microscopy 79−11026
In surface, impurity precipitation and resolution at melting point 78−14553
In, vacancy size effect, surface energy in small particles and bulk specimens 80−75223
In-In-P-GaP, liquidus surface obs. 78−22829
In-Te system cpds., degree of dissoc. from curvature of liquidus line 78−22828
In-Tl liquid alloy, thermodynamic props. and struct. *(German)* 77−48400
InAs, electrical conductivity and thermoelectric power charge due to melting 80−100490
InAs, heat and entropy of melting, assessment by quantitative thermography 77−15550
InAs(Sb), high temp. thermodynamic data, quantitative fits to liquidus line 77−63637
In_2Bi, pre-melting absorption of sound 80−88277
InP, electrial props. at high temp. and in liquid state 77−11888
InSb, thin film prep. with remelting, elec. props. 77−52255
K, thermodynamics of melting at high pressures 78−91426
$KAlSi_3O_8$, feldspar microwedge, melting by CO_2 laser, deform. of IR absorpt. spectra 77−19984
KCl microcrystal, computer simulation of melting and glass form. 79−65173
KCl, premelting due to thermal form. of dislocations 77−11671
KCl, thermal expansion, compressibility and melting calcs. 79−33069
KD_2PO_4, transparent dielec., thermal analysis of laser-induced damage 80−66336
KF_2-$3K_2O.2SiO_2$ freezing point depression meas., effect of silica compound additions 77−28797
$KMg_2(AlSi_3O_{10})F_2$-$KMg_{2.5}Si_4O_{10}F_2$, solid soln., melting and crystn., quenching and DTA study 80−39263
$KMg_2LiSi_4O_{10}F_2$-$NaMg_2LiSi_4O_{10}F_2$, solid soln., solid solubility and swelling characts. 80−59660
KNO_2, melting pressure curves up 5 kbar 77−15547
K_2O-PbO-SnO_2, glass, effect of DC on corrosion of SnO_2 electrodes 80−85075
K_2SO_4-Cs_2SO_4-MoO_3 system, fusibility diagram 79−87619
Kr, solid, density at melting and isochoric equations of state 78−83915
Kr, submonolayer, adsorbed on graphite, melting, X-ray scatt. obs. 78−95234
Kr, thermodynamic props., behaviour near m.p. *(French)* 77−1212
Li bearing metasediments, melting rel. to Li rich pegmatites petrogenesis 79−57918
Li, thermodynamics of melting at high pressures 78−91426
Li-Pb, thermodynamic study using Knudsen effusion mass spectrometry 80−24578
Li-Sn, phase relationships between Li_7Sn_2 and LiSn 79−78933
Li_2BeF_4, melting systematics at high press. 77−51475
LiCl, microcrystal, melting, mol. dynamics simulation 80−65199
LiF-$Li_2O.SiO_2$, activities rel. to liquidus comp. 77−28797
$Li_{0.5}Fe_{2.5}O_4$-LiNb(Ta)O_3, in situ composite growth, phase diag., melting relns. 77−21132
$LiNO_3.3H_2O(D_2O)$, crysts. and melts, density, mol. vol., thermal coeff. of expansion, rel. to struct. 80−15270
$Li_2W_2O_7$ 77−48407
$LiY_{1-x}Er_xF_4$, structure, constitution and melting behaviour 77−39665
Mg, atomic vibr. and fermion behaviour of HCP metals 80−6474
Mg-Cd melts, atomic struct., short range order and melting *(German)* 78−14273
MgF_2-xMgO.ySiO_2, freezing point depression meas., effect of SiO_2 compound additions 77−28798
Mn-Bi alloy, melting and solidification under microgravity, mag. props. *(German)* 80−45296
Mn-Ni-C system, pressure effect on melting diagram *(Russian)* 77−55943
Mo, vaporisation, influence of inert gases on losses *(Russian)* 79−55878
Mo, volt ampere characteristics during electron melting process *(Russian)* 80−75336
Mo wire, laser shock induced microstructural changes, rel. to explosive shock induced phenomena 78−67768
Mo-Al-Ge, phase equilibria, X-ray and microstructural anal. 80−93536
Mo-Cr, fusibility diagram *(Russian)* 80−20897
Mo_3C_2, pressing regime influence on high-temp. creep *(Russian)* 80−100852
NO, adsorbed monolayer on graphite, melting and polymorphism 78−84063

melting continued
Na, solid and liquid eqns. of state melting curve 80−103448
Na_3AlF_6 *(French)* 77−51297
Na_2BeF_4, melting systematics at high press. 77−51475
NaCl, interpolational eqn. of state with allowance for melting, vaporis., dissoc. and ionis. processes 80−24566
NaCl, premelting due to thermal form. of dislocations 77−11671
NaCl, thermal expansion, compressibility and melting calcs. 79−33069
NaCl-CsCl-$CrCl_3$ system, phase struct. anal. by X-ray method *(Russian)* 78−3112
NaCl-CsCl-$CrGl_3$, thermography *(Russian)* 77−63645
NaCl-KCl-CuCl system diagram investig. *(Russian)* 79−96015
$NaClO_2$, molten electrolytic cond. at pressures up to 6 kbar, rel. to melting model 77−15609
$NaClO_3$, melting pressure curves up to 5 kbar 77−15547
NaF, anharmonicity of lattice vibrations, neutron scatt. study, rel. to melting 77−84862
NaF-$3Na_2O.2SiO_2$, freezing point depression meas., effect of silica compound additions 77−28797
NaF-SrF_2-CrF_3, glass transition, crystn. and melting temps., optical transmission *(French)* 80−64910
NaF-YF_3 system, fusibility diagram, quasibinary section of NaF-YF_3-YOF system characts. 80−55371
NaI, transport processes, test of validity of Arrhenius law *(French)* 79−77808
$NaNO_2$, melting curve maximum 77−43311
$NaNO_2$, melting pressure curves up to 5 kbar 77−15547
$NaNO_3$-$CsNO_3$-$Pb(NO_3)_2$, fusion diag. *(Russian)* 77−48418
$NaNbO_3$-$SrNb_2O_6$, phase diagram, props. meas. 79−11576
NaO-CaO glass, melting speed, effect of struct. and grain shape *(Polish)* 79−29002
Na_2O-CaO-SiO_2 glass, redox phenomena evaluation in melting-fining process, SO_2 evolution 80−84900
Na_2O-PbO-B_2O_3-SiO_2, homogeneous melt formation rate, exam. 78−64520
Na_2O-SiO_2 glass, bubble gas comp. change 80−79946
Na_2O-SiO_2 glass, fusion process study, EMF meas. *(French)* 80−89190
Nb, vaporisation, influence of inert gases on losses *(Russian)* 79−55878
Nb, volt ampere characteristics during electron melting process *(Russian)* 80−75336
Nb-Ge, thermal anal. of levitation-heated samples 79−2772
Nb-Mo, prod. by simultaneous carbothermic reduction of oxides/electron beam melting method *(Japanese)* 80−11590
Nb-Si diagram of state, melting temp., polymorphic transform. temp. *(Russian)* 80−50594
NbC, pressing regime influence on high-temp. creep *(Russian)* 80−100852
Ni base superalloy, instrumental anal., use of HF induction melting and centrifugal casting *(Japanese)* 77−56280
Ni base superalloy, preparation for instrumented anal., HF induction melting, casting 78−48607
Ni based powders, determination of entrapped Ar content, using vacuum fusion tech. 79−5193
Ni, defects at thermal equilib., positron annihilation meas. 77−76391
Ni melt, struct. charact. time depend. in X-ray studies *(Russian)* 80−24350
Ni, optical constants at high temp. 79−24281
Ni, rapid melting and solidification of surface layer, exam. using computer heat flow model 78−83228
Ni, spreading kinetics of Al 80−24717
Ni-Al (51 to 55 at.%), vacancy defective, TEM exam. of structure 78−76677
Ni-H, system, melting temp., effect of H_2 *(Ukrainian)* 79−52153
$NiFe_2O_4$-$BuTiO_3$, in situ composite growth, phase diag., melting relns. 77−21132
NiO, plasma reduction melting *(Russian)* 78−31359
Os, atomic vibr. and fermion behaviour of HCP metals 80−6474
Pb, changes in electron image contrast 80−100147
Pb crystal glass melting, elec. furnace 79−58691
Pb, diffusion and saturation solubility of Pt, melting curve, conc. profiles 80−88365
Pb melting curve, high press. effect, and Pb diffusion in Cu 80−49337
Pb, melting curve, use for press. determ. in girdle apparatus 77−65043
Pb, melting studies by temperature wave anal. method 80−15217
Pb, structure sensitive props., temp. hysteresis after melting and crystallisation *(Russian)* 79−29036
Pb-Sn(20 wt.%), partially remelted interdendritic fluid flow 77−4771
Pb-Tl-Te, liquidus of ternary system 79−8285
PbF_2, superionic, F^- motion and F sublattice melting, NMR obs. 77−43374
PbF_2-x$PbO.ySiO_2$, freezing point depression meas., effect of SiO_2 compound additions 77−28798
$Pb_{1-x}Mn_xTe$ (x=0.005, 0.001, 0.05), solid solns., exam. of electrical and thermal props. 79−1599
$PbNb_2O_6$-$NaNbO_3$, DTA *(French)* 77−44234
PbO-Bi_2O_3-GeO_2, exam. of glass forming and liquid phase separation regions, and optical props. 78−88453
Pd-Cu-Si, laser melting and splat quenching to form foils for TEM obs. 80−29986
Pd-Si, amorphous thin films, laser irrad., metastable phases 80−96622
Pt ribbon, melting temp. determ. from continual melting and freezing 77−51476
Pt-Si, amorphous thin films, laser irrad., metastable phases 80−96622
Pu-Zr alloys, BCC, self-diffusion activation volumes, melting-diffusion correl. validity 77−20122
$R_{1-x}Co_x$, rare earth amorphous alloys, thermal stability, elec. cond. enthalpy 80−100172
Rb, thermodynamics of melting at high pressures 78−91426
Re, atomic vibr. and fermion behaviour of HCP metals 80−6474
Re, thin film preparation, by laser melting *(Japanese)* 79−78909
Ru, atomic vibr. and fermion behaviour of HCP metals 80−6474
α-S, monoclinic allotrope, thermal behaviour 78−67813
S_xSe_y, s=6-3, y=2-5, thermal behaviour 78−67813
Sb, optical phonon anharmonicity and melting, light scatt. study 80−60621
Sb-Bi, melting kinetics of solid soln. during high heating rates, superheating *(Russian)* 78−15358
Sb_2Se_3-Sb_2Te_3, liquid, mixture enthalpies *(German)* 79−77770
Sc_2O_3, fission and phase transition enthalpies 79−99299
Sc_2O_3, solid, enthalpy investig. at high temp. 80−103498
α-Se, monoclinic allotrope, thermal behaviour 78−67813

melting continued
Se, monoclinic to trigonal conversion, thermodynamic stability and associated investigs. 80−24592
$(Se)_x$, crystn. and melting 80−40241
Si, amorphous, small dia. laser beam annealed, temp. distrib. and microstructure 79−73098
Si, amorphous and crystalline, heating by Q-switched laser radiation 80−84963
Si, amorphous-implanted, surface melting related to laser pulse 79−69123
Si, defect annihilation depth by pulse laser annealing 80−16128
Si, dislocation growth during laser melting and solidification 80−2022
Si, growth and melting processes, origin of swirl defects 77−76407
Si, impurity solubility limit after laser induced melting 80−107426
Si, ion implanted, extent of annealed or melted regions as function of pulsed laser irrad. energy 79−74025
Si, ion implanted, self implanted, self annealing using high ion current density treatment 80−89254
Si, ion-implanted amorphous layers, melting model for pulsing-laser annealing 79−56080
Si, laser annealed ion implanted, elec. props., melting threshold 80−10969
Si, laser annealing mechanisms, disordered overlayers, crystalln. 80−84967
Si laser annealing of SiO_2 layers 80−97505
Si, laser irrad., anisotropic melting and epitaxial regrowth, surface struct. 79−33163
Si, laser pulse induced amorphous to cryst. transition, thickness depend. 78−47678
Si, melting and resolidification, laser-induced, surface morphology 79−87529
Si monocrystal peripheral fusion channelling under HF heating *(Russian)* 80−59627
Si on sapphire, laser annealing dynamics epitaxial regrowth, optical reflectivity 80−29285
Si:As, melting by high power ns laser pulsing, As diffusion 78−79789
Si:Cu, segregation effects after laser pulse melting 79−1843
Si:P, depth of melting produced by pulsed-laser irrad. 79−55756
Si:Sb vacuum deposited coating, p-n junction, pulsed electron beam annealing doping, diffusion 80−75480
Si:Te, laser melting, surface Te atom accumulation, profiles 80−100258
Si_3N_4-Si_2N_2O-Mg_2SiO_4, melting and eutectic studies 80−45285
SiO_2, melting curves at high press. 77−11672
SiO_2, molten, struct., X-ray radial distrib. anal. 78−67651
SiO_2-Al_2O_3-CaO-BaO-SrO-ZnO-Na_2O-K_2O-B_2O_3, glaze effect of P_2O_5 additions 80−60824
SiO_2-Al_2O_3-Fe_2O_3-CaO-MgO-Na_2O-B_2O_3-SO_3, exam. of white flaky inclusions, causes and formation time 79−29237
SiO_2-Na_2O-CaO (13, 11 wt.%) glass, phase separation, SiO_2 purity effect 80−44144
SiO_2-Na_2O-CaO glass, phase separation characts., melting atmosphere effect 80−44141
SiO_2(-TiO_2) glass prep., melting *(Polish)* 80−40316
Sn, extremely fine crysts., surface melting 77−62622
Sn film, melting and crystallisation kinetics, electron microscopy 77−15725
Sn film, thermal hysteresis of phase transitions and mechanism of crystallisation 77−89679
Sn, melting studies by temperature wave anal. method 80−15217
SnS-GeS_2, exam. of phase diagram using DTA *(German)* 79−11585
SnSe-Tl_2Se, phase diagram, DTA and X-ray diffr. peritectic decomposition *(French)* 77−51471
$SrAg(PO_3)_3$, physicochem. characts. 77−52302
SrSn, Sr_2Sn, prep. by melting, characterisation *(French)* 77−70017
Ta, vaporisation, influence of inert gases on losses *(Russian)* 79−55878
Ta(C,N)-Ni-VC, sintering behaviour, VC effect 80−93520
TaC, pressing regime influence on high-temp. creep *(Russian)* 80−100852
Te alloy, intermetallic, melting entropy and molar specific heat 79−29024
$Te_{80}Ge_{20-x}Sb_x(Bi_x)$, DSC studies of struct. phase transformation 80−66505
$ThCl_4$, thermodynamics of vaporisation and melting 79−60492
ThO_2, simultaneous freezing and melting in finite media 80−620
Ti, melting point, normal spectral emittance and elec. resistivity, pulse heating method 78−91423
Ti-Al (27.3 wt.%), arc melted, microstruct. 79−61577
Ti-Al-V (6,4 wt.%), laser surface melted, topographical characts. 79−70200
Ti-Al-V (6.4 wt.%), electron beam melting for scrap recycling 77−66604
Ti-Ni, laser melting and splat quenching to form foils for TEM obs. 80−29986
TlCl, Raman spectra in melting region 78−27224
TlS_x, struct. from radial electron density distrib. curves, entropies of melting and crystallisation 79−23527
Tl_2Te_3, exam. of electrical props., in solid, liquid state 80−54686
Tl_5Te_3-Tl_4SnTe_3-Tl_4PbTe_3, phase equilib., DTA, SPA and microhardness meas. 80−96628
UO_2, molten pool, heat transfer to concrete slab following LMFBR HCDA 78−8930
UO_2, nuclear fuel, mechanical response to transient heating, accident conditions 77−14237
UO_2, simultaneous freezing and melting in finite media 80−620
V slag enrichment by oxide reduction during plasma melting *(Russian)* 78−52716
V, volt ampere characteristics during electron melting process *(Russian)* 80−75336
V-Ni-Mo, structure in alloy crystallisation region, peritectic equilibria *(Russian)* 80−50622
V-Os system, equilib. phase fields, X-ray diffr., elec. resist., DTA, and EPMA meas. 79−47661
W, heat resistant particles in low temp. Ar plasma, heating, melting, vaporisation *(Russian)* 80−40384
W reinforced Al, melting under weightlessness *(Russian)* 78−23691
W, vaporisation, influence of inert gases on losses *(Russian)* 79−55878
W, volt ampere characteristics during electron melting process *(Russian)* 80−75336
W wire, laser shock induced microstructural changes, rel. to explosive shock induced phenomena 78−67768
W-complex, $WOCl_4.Ph_3PO$, prep. and characterisation 78−30592

melting continued
Y, electrical resistivity of solid and liquid phases, thermopower, melting temp. 80−59955
$YAlO_3$, melting behaviour and metastability determ. by optical DTA 80−92648
Y_2O_3, fission and phase transition enthalpies 79−99299
Zn, atomic vibr. and fermion behaviour of HCP metals 80−6474
Zn, Lindemann's rule and X-ray Debye temp., anisotropic single crysts. 79−28076
Zn, optical phonon anharmonicity and melting, light scatt. study 80−60621
Zn, structure sensitive props., temp. hysteresis after melting and crystallisation *(Russian)* 79−29036
Zn, vacancy conc., lattice parameters meas. 78−10040
Zn-S system, Zn-rich liquidus, 1000-1300°C 78−18747
Zn-Sn-Hg, diagram of state, melting temp., peritectic and eutectic phases *(Russian)* 80−55350
α-$ZnCl_2$, sp. ht., melting, heat of fusion determ. 77−66029
$Zn(NO_3)_2.4H_2O$, high press. phase behaviour, dehydration and congruent melting 79−78947
$Zn(NO_3)_2.6H_2O$, high press. phase behaviour, dehydration and congruent melting 79−78947
ZrC-W (75 wt.%) eutectic refractory alloys, smelting in suspended states, components distrib. *(Russian)* 80−19913
ZrO_2 glass, melting depend. on minute components, surface crystallisation 80−84278

melting point
alkali halide, migration enthalpy of cation vacancy correl. with MP 77−76606
alkali halide, pressure effect on melting temp. 77−84896
alkali halides, boiling, melting points rel. to mol. wt. 79−46785
alkali halides, crit. consts., dense gas formulation 79−23700
alkali halides, melting and boiling points vs. Coulomb pot., parabolic behaviour 80−70375
alkali halides, melting temperatures, press. depend. 79−77726
alkali halides, Schottky defect correl. of form. enthalpy and melting point 78−43015
alkali halides, thermal expansion, rapid increase near melting point 77−51521
alkyl-cyano-biphenyls (and p-terphenyls) and related cmpds., chiral, synthesis and liq. cryst. props. 77−27820
alloys, heterogeneous nucleation activity, and melting point ratio correlation 78−92255
aromatic hydrocarbons, melting behavior and role of free radicals and molecular site in producing mesophase pitch 79−90523
aryl esters, cyano-substituted, liq. cryst. props. 77−27822
benzene, melting temp. and latent heat 79−55869
n-benzoates, Raleigh and Raman spectra *(Russian)* 77−69074
binary solid-liquid equilibria, student experiment, phase diagram computer program 78−89285
biphenyl, melting temp. and latent heat 79−55869
bisphenol-A polycarbonate, plasticized, melting and equilib. melting temp. 78−2234
capillary-syringe method for prep. of air-sensitive samples for MP determ. 77−67419
Ω-caprolactam-ε-caprolactam polymers, vitrification, fusion, crystallisation *(Russian)* 77−47561
ceramics, lattice and grain boundary diffusion consts., correls. 80−96679
cholesteric liquid crystal, stabilisation, multicomponent mixtures, refl. spectra, clarification temp. and melting point meas. 78−9951
cholesteryl esters, liq. crysts., P-T diagrams up to 5000 kg/cm^2 78−2003
classical quadrupole solids, correl. effects 80−10628
COC, prep., cryst. state, and mesophases 79−95143
crystalline sample fusion temp. meas. automatic instrument 78−57945
cyclohexane derivatives, low melting nematic cpds., characterisation 79−10798
decrease in solids 79−73295
diamond-like solids, laser irrad. effect on cohesion 80−50470
dimethylacetylene, NMR linewidth at melting point 78−6583
9,10-cis-endo-dimethyltricyclo[4,2,2,$0^{2,5}$]dec-7-ene, substituted, crystal and molecular struct. 79−86785
disperse systems, solubility increase, phase composition, size effect calcs. 80−70418
Earth mantle, Uffen method, remarks 78−20367
EBBA, fusion of metastable solid cryst. forms 79−14678
ethane, solid, PMR line shape, band width and second moment, phase transition 77−85584
extruded, glass transition temp., melting pt., DTA 78−2235
glass, melting in fire-heated tanks, modelling *(Polish)* 80−96633
glass, photochromic, thermo-optic transitions 80−50307
halobenzenes, aqueous molar solubilities and partitioning, 25°C obs., rel. to melting pts. 80−40803
high-pressure liquid MP determ. centrifuge cell 80−31783
ice, Ih, thermal resist. near melting point meas. 80−44375
ice, intrinsic surface order near melting point 79−14986
ice VII, melting curve up to 150 kbar 78−67812
impurity distribution on growing crysts. from melt 78−52656
inorganic compounds, Lindemann's theory 79−23702
inorganic crystals, glasses, thermal expansion coeff. rel. to phys. props. 80−49389
interstitial compounds, electronic structure and useful phys. props. 77−89683
intertransition metal compounds, hardness and oxidation resist. 77−63773
ionic salts, melting transition statistical model, dielectric const., surface tension 80−70378
Lindemann hypothesis and size depend. 80−15222
lipid bilayer membrane, melting point rel. to electrostatic field 78−92602
liquid crystal phase transformations, size and surface effects 77−15555
liquid metal droplets, oxide coated, negative pressures and melting point depression 79−60485
melting-pressure curves, press.-temp. analysis 79−23697
metal, cubic, melting anisotropy 78−91425
metal, positron-vacancy interactions, equilib. temp. depend. of positron annihilation 78−76547
metal, surface free energy of solid, at MP, estimated from liq. surface tension data 77−31866
metal, vacancies and change of surface free energy at melting point 79−42219

melting point continued
metal, vacancy formation parameters and Gruneisen constant 78−22709
metal borides and carbides, thermal stability 79−8286
metal cluster, 9 Å, in zeolite matrix 77−59103
metal fixed points, limitations caused by trace impurities 80−105644
metallic alloy, prediction of glass-forming ability from melting point 79−23524
metallic fine particles, melting and size depend. on melting temp. 79−73294
metallic thin films, surface and grain boundary diffusion, charact. temp/melting point ratio 79−90919
metals, cubic, relationship between defect resist. and bulk resist. at melting temp. 78−6344
metals, entropies and heats of fusion 80−103458
metals, heat capacity near melting point, vacancy mechanism of melting 80−10641
metals, lattice and grain boundary diffusion consts., correls. 80−96679
metals, particle size depend. of melting temp., thermodynamic theory 77−89523
migration and formation energies rel. to Debye temp. and melting point 78−22710
molten metal, relation between surface energy melting temp. and Fermi wavelength 77−51571
nylon-11, folded-chain crystal, pressure-induced crystallisation from melt, annealing 77−84671
nylon-12, folded-chain crystal, pressure-induced crystallisation from melt, annealing 77−84672
nylon-6 pressure-crystallised, annealing under pressure 77−84670
nylons 6, 66, 610, change in cryst. struct. with temp. 77−15324
paraffin waxes, melting point determ., automatic analyser, based on dilatometry 79−14223
particle, 9 Å, in zeolite matrix, melting point 77−59103
phase form. and relations, phys. props. 79−43218
PMMA isotactic, syndiotactic stereocomplex formation in soln., composition, struct. 79−66292
poly-m-phenylene isophthalamide-ε-caprolactam, complex polymer cryst. 78−9967
poly-tetramethyl-p-silphenylene-dimethylsiloxane block copolymers, crystn., morphology, kinetics 79−14695
polyamide chain, conformational freedom above MP 77−55344
polyaryloxyphosphazene copolymers, thermal, morphological and rheological props. 80−103265
polybromoprene, crystn., morphology, kinetics *(Russian)* 79−4256
polydiphenylsiloxane, thermodynamics of fusion 80−84280
polyether-polyester elastomers, differential scanning calorimetry, crit. points *(Japanese)* 80−75344
polyethylene, extended chain, prep. and study of separated single crystals 78−42924
polyethylene, melting, equilib. temp., confomational modifications *(Russian)* 79−51240
polyethylene, melting point, heating rate depend. 79−99296
polyethylene, MP, heat of fusion, degree of crystn. determ. by differential scanning calorimetry *(Russian)* 77−62489
polyethylene, single, polycryst., ^{60}Co-γ irrad., effect on melting behaviour 77−15548
polyethylene, solid-state extruded, exam. of props. 80−11669
polyethylene, stress crystallised, melting behaviour 77−47554
polyethylene, structure formation, near and below melting point 79−65003
polyethylene, ultraoriented high-density, MP variation on annealing 77−8852
polyethylene fibres, high density, ultra oriented, physical, mech. props. 80−25649
polyethylene melt, lightly crosslinked, crystn. under uniaxial compression, stretching 80−38957
polyethylene oxide, low mol. wt., effect of end-group on crystallinity and fusion 77−84897
polyethylene oxide, peculiarities of struct. form. near below the melting point 80−54150
polyethylene oxide blends, thermal and mechanical props. 79−11679
polyethylene ribbons, flow-induced crystn. from melt, in dies fed by single screw extruder 80−84110
trans-1,4-polyisoprene crystals, press. effect on growth rate 80−88064
trans-1,4-polyisoprene crystals, press. effect on melting temp. and lamellar thickness, press. crystn. 80−88302
polymer crystal and melt, stat. thermodynamics using Midha-Nanda cryst. state theory 79−41979
polymer films, Brillouin scatt. at transitions 80−70312
polypropylene, flow-induced crystn. from melt, in dies fed by single screw extruder 80−84110
polyvinylidene fluoride, crystallisation, α-polymorph equilib. melting point, heat of fusion determ. 77−4054
pressure dependence appl. of Tait eqn. for inorganic solids 77−24381
PTFE, rheological props. below m.p. with certain low molecular smectic states 79−87675
PTFE copolymer, melting point, cryst. struct., modification *(Russian)* 77−31607
p-quaterphenyl, melting temp. and latent heat 79−55869
p-quinquephenyl, melting data and liq. cryst. transitions 79−55869
rare earth and transition metal oxides and fluorides, thermal expansion and MP correl. 77−47605
rare earth borides, higher types, phys. props. and electronic struct., group orbitals-LCAO calcs. 80−20077
rare earth compounds, binary, regression eqns., for calc. props. from electron struct. 80−39498
rare earth germanates, R_2O_3-GeO_2 system cpds., physicochem. charact. 80−97469
rare earth metal nitrides, m.p. N_2 press. depend., Pirani-Alterthum meas. 78−43103
rare earth metals, elastic props., connection with electron struct. *(Russian)* 80−19895
rare earth oxyorthotitanates, crystallochem. classification 80−107142
rare earth RNb_3O_9, synthesis and physicochem. props. 77−90304
rare earth titanoniobates, $RTiNbO_6$, physicochem. investig. 77−47422
rigorous bounds, quantum anharmonic phonon model 77−15541
secondary ref. stand., MP of Y_2O_3 77−45821
semiconductor, tetrahedral, lattice thermal cond., ionicity depend. 79−37884
semiconductor, tetrahedral, thermal expansion and MP, ionicity and bond length effects 77−47606
semiconductors, isoelectronic series and trends in band struct. 77−89696

melting point continued
simple liquid, self-diffusion and viscosity near MP, hard sphere model *(Russian)* 77−66035
solid bounded by curved interfaces 79−82319
sputtered particles-substrate, temp. overaging *(Russian)* 80−40385
standards, secondary, for temp. range 2000-3000°C, chemical aspects of choice 80−52226
steel, continuously cast, ductility near melting pt., hot tearing 79−83314
sulphonyl compounds, H-bonding by methyl groups, Raman spectra obs. 79−24320
terephthalate copolyester, heat treatment effect on melting point *(Japanese)* 80−40400
p-terphenyl, melting temp. and latent heat 79−55869
tetraethylammonium iodide-Ag_nI_{n+1}, ionic conductors, electrochem., props. 77−31808
thermal expansion correl. with MP 77−47604
transition metal borides, higher types, phys. props. and electronic struct., group orbitals-LCAO calcs. 80−20077
transition metalloids, t-matrix theory of thermal and nonstoichiometric softening 79−86788
transition metals, thermophysical data at high temps., submicrosecond-pulse-heating method 80−103459
tungstates, hexagonal bronze type struct., cryst. struct. and props. 77−39574
vaporisation entropy/surface tension relation near melting point *(Japanese)* 79−99397
Wigner solid, two-dimens., melting temp., quantum effects 80−88491
Wigner solid, two-dimens., melting temp. in strong mag. fields, quantum effects 80−88492
Ag, melting curve to 60 kbar press., reinvestigation 80−39260
Ag_2CO_3, high press. phase relations, DTA 77−43329
$Ag_5Rb(PO_4)_2$, struct., density and elec. cond. 80−33952
$Ag_2S(Se)(Te)$, changes in elec. cond. and thermoelec. power at melting point 79−15147
$AgSbS_2$, synthetic crystals, melting point and cryst. struct. *(German)* 78−42943
Al, Fermi momentum, for solid and liq. phases, temp. variation, Compton scatt. obs. 80−50451
Al, time-to-rupture and character of fracture, near MP *(Russian)* 77−21245
Al-Bi(Cd)(Pb)-Ti, containing low-melting pt. inclusions, mech. props. 80−93632
Al_2O_3-SiO_2-MgO-CaO, blast furnace slag, viscosity, MP *(Russian)* 77−25039
Am metal, dilatometry and thermal anal., melting point, transformation regions 79−43241
Au, melting curve to 60 kbar press., reinvestigation 80−39260
Au_2P_3, melting temp., Au_2P_3-Au eutectic temp. 80−59628
B, liq., thermoelastic props. near melting point 80−19862
Ba, phase transitions under high press. 80−96641
Ba_2ZnS_3, prep. by solid state reaction and melt growth, X-ray anal. 77−73226
Bi, equilib. vacancy conc., at MP, thermal expansion meas. 77−59007
Bi, Young's modulus and internal friction, 20°C to melting point *(Russian)* 80−89278
Bi_2Se_3, high-temp. calorimetric determ. *(French)* 77−44501
$CaCeAl_3O_7$, melilite struct., prep. and props. 80−93524
$CaEuAl_3O_7$, mechanism of solid-phase reactions of formation and physicochem. props. 77−52622
$CaTaRO_6$, (R=La, Nd, Gd, Sm, Er, Lu), synthesis and physicochem. props. 79−52139
$CaZrO_3$-$CaHfO_3$, solid soln. formation obs. 77−86003
Cd, Young's modulus and internal friction, 20°C to melting point *(Russian)* 80−89278
$CdLn(TiNb)O_7$, Ln=La-Lu, synthesis physicochem. props. 77−43186
CdS(Se), reaction with Sn chalcogenides, thermodynamic anal. 80−40728
Ce-In, phase equilibrium and cryst. struct. 80−66483
Ce-Tl, phase equilibrium and cryst. struct. 80−66483
Co-Al-Cr(Nb)(Ta), eutectic alloys, charact. by melting, oxidation resistance and composition 78−52768
Co-Cr-Mo (Zr)(Nb)(Ta), eutectic alloys, charact. by melting, oxidation resistance and composition 78−52768
Co-Si-Nb(Zr), eutectic alloys, charact. by melting, oxidation resistance and composition 78−52768
CoB, thermophysical props., 296-2000K 78−14477
Cr-Ge system, phase anal. and physical props. 79−24160
CrB_2 77−86001
$CsSbF_6$, high press. phase relations, vibr. spectra, and cryst. chemistry 80−108200
Cu, melting curve to 60 kbar press., reinvestigation 80−39260
Cu, time-to-rupture and character of fracture, near MP *(Russian)* 77−21245
Cu-Ni-Ti system, reactions with melt in Cu-rich region *(Japanese)* 80−89202
CuTlS, melting heat and melting entropy *(Russian)* 80−70374
D_2 80−86338
D_2, room temp. melting point, press. depend. calcs. 80−103463
$Dy_2(MoO_4)_3$, cryst. growth and props. 79−55727
Dy_2O_3-based ceramic, preparation, mech. props. 77−24998
EuB_6 77−86001
Fe, melting temps. depend. on interatomic pots. choice 79−74863
FeB, thermophysical props., 296-2000K 78−14477
$Fe_{40}Ni_{40}P_{14}B_6$ glass, viscosity near T_g, using rapid heating, and fusion characts. 80−70438
Fe_3O_4-$FeAl_2O_4$-$FeTiO_3$ titaniferous magnetite, chlorination, 1273 to 2273K 80−55752
Ga, for thermometer calibration, enzymologic appl. 78−85460
Ga, liq., effective pair pot. and thermodynamical props. 77−47600
Ga, magnetic susceptibility near melting point 80−60186
Ga, measurement standard for clinical chemistry appl. 78−80997
Ga melting point, thermometric standard 77−82516
Ge alloy, amorphous film, formation and stability criteria 79−10799
Ge-FeS, GeS-FeS, density of alloys, volume changes on melting 77−51473
H_2, room temp. melting point, press. depend. calcs. 80−103463
^4He, room temp. melting point, press. depend. calcs. 80−103463
^3He, melting pressure temperature scale 77−22557
^4He, meas. using diamond-anvil cell 80−86338
Hf, 0.3 wt.% Zr, melting pt. and radiance temp. meas. by pulse heating method 77−53914
Hf, liquid, viscosity at melting point, free energy *(Russian)* 80−92699
HfC-HfB_2, reactions, cpd. formation and props. 78−23685
HfN_n, effect of equilib. N_2 press., 10^{-2} to 100 atm, on MP 77−36465
HfO_2-La_2O_3 system, phase form. and relations, phys. props. 79−43218
Hg-In (3, 15, 30, 45 at.%) amalgam, viscosity meas. near melting point 80−70441
HgS, melting point and vapour pressure 77−15549
HgS(Se), reaction with Sn chalcogenides, thermodynamic anal. 80−40728
I_2 liq., static structure factor, neutron diffraction 80−103236
K, liquid, interionic interaction theory, pseudopotential calcs. *(Russian)* 80−79675
KCl-CuCl eutectic fused salt, potential as intermediate temp. solar heat transfer and storage medium 80−101135
KF-YbF_3, KF-LuF_3, phase analysis 78−44101
$K_2M(MoO_4)_3$, M=Zr, Hf, synthesis and struct. 77−36386
$Li,K/PO_3,F$ system, low melting point comp., solvent for InP electrodeposition 79−28079
$Li,Na/PO_3,F$ and $Li,K/PO_3,F$ systems, low melting-point comps. for electrodeposition appl. 79−43662
$Li,Na/PO_3,F$ system, low melting point comp., solvent for InP electrodeposition 79−28079
Li-LiH, evaporation diagram at high liq. phase hydride concs. 77−35681
LiO_2, melting point determ. for single crystal synthesis using vacuum fusion technique 80−71585
$Li_{x+2}P_xO_{3x+1}$, polyphosphate, melting and crystallisation 80−70376
$Li_{1+y}Ta_{1.5y}Ti_{6y}O_3$ ($0 \le y \le 0.028$), non-stoichiometric phase, crystallographic and dielec. props. 80−75212
Mg, melting temp. under shock loading 77−47553
Mo complex, $MoOCl_3.2Ph_2SO$, prep. and characterisation 78−30592
Mo, specific heat near melting point, rapid pulsed heating method 77−35704
MoF_5, prep., melting temp., vapour density, press., enthalpy of fusion, meas., assoc. 78−38813
$Na,K/PO_3F$ system, low melting-point comps. for electrodeposition appl. 79−43662
Na alloys, very dilute, sp. ht. meas. close to melting point 78−47501
Na liquid, interionic interaction theory, pseudopotential calcs. *(Russian)* 80−79675
$NaCaPO_4$-$Ca_3MgSi_2O_8$(CaO) systems, phase diagrams of partial system 78−35369
$NaCaPO_4$-$CaMgSiO_4$ system, phase diagram 78−35370
Na_2SO_4, melting point determ., DTA method 80−218
Na_2WO_4-$CsWO_4$-WO_3, system form., melting point 79−43222
Na_2WO_4-Pb_2WO_4-WO_3 system investigation, crystn. from melt, coordination compounds form. 79−52189
Nb complex, $NbOCl_3.2L$ (L=Ph_2SO, Ph_3PO and $(Me_2N)_3PO$), prep. and characterisation 78−30592
Nb complex, prep. by halide reaction with tetramethylurea and tetramethylthiourea, and characterisation 79−15972
Nb, elastic constants up to melting point, US meas. 77−86081
$Nb(OR)_2Cl_3.L$, halo-alkoxide complex, prep. and props. 78−18605
$Nd_2Zr_2O_7$-$Nd_2Hf_2O_7$, struct., elec. cond. and melting point 80−54197
Ni-Al-Ti, eutectic alloy charact. by melting temp., composition and oxidation resistance 78−52771
Ni-Cr-Ti(Nb)(Zr), eutectic alloy charact. by melting temp., composition and oxidation resistance 78−52771
Pb, ion bombardment-induced photon emission near melting point 80−100699
Pb, Young's modulus and internal friction, 20°C to melting point *(Russian)* 80−89278
Pb_2WMO_6, M=Cd, Mg, synthesis, struct., phase transitions 77−84715
Pd, effect of surrounding O_2 80−27299
Pd, radiance temperature at 653 nm, at melting point 79−90805
Pt freezing point determ. 77−26288
Pt ribbon, melting temp. determ. from continual melting and freezing 77−51476
RbI-CrI_2 system, phase diagram, melting point *(French)* 79−46632
Rh, melting pt. determ. 79−1491
S, effect of high pressure system configuration 78−43104
Sb_2S_3 crystals, X-ray and DTA methods melting point variation *(German)* 78−43119
$SbSbO_4$ 77−84714
$(Se)_x$, crystn. and melting 80−40241
Si, laser annealing, threshold energy density, amorphous-liquid-crystalline transitions 79−60390
SiO_2-P_2O_5 binary glass, fibre fusion temp. rel. to composition 78−95131
Sm_2O_3-Ga_2O_3 system, garnet-perovskite transform., phase diagram relationships 80−97460
Sm_2O_3-Ga_2O_3 system, phase diagram relationships of garnet-perovskite transform. 80−97460
Sn, ion bombardment-induced photon emission near melting point 80−100699
Sn, Young's modulus and internal friction, 20°C to melting point *(Russian)* 80−89278
Sn-Te, molten, elec. cond. and phase diagram 80−84454
SnF_2, phase transitions, X-ray diffr., elec. cond. and thermal analysis 80−100329
SrF_2, vaporisation and sublimation thermodynamics *(German)* 80−81355
Ta complex, prep. by halide reaction with tetramethylurea and tetramethylthiourea, and characterisation 79−15972
Ta, radiance temp. at melting point 77−15603
TaC-TaB_2, phase diag., solubilities, reactions 77−63643
$Ta(OR)_2Cl_3.L$, halo-alkoxide complex, prep. and props. 78−18605
TcF_6, heat capacity, entropy Gibbs energy, 2.23-350K 78−38852
Th-based metal alloy fuels for FBRs, determ. of solidus temperature 80−104124
Ti, liquid, viscosity at melting point, free energy *(Russian)* 80−92699
Ti-Al-V alloy, thermophysical meas. above 1450K, using subsecond transient technique 78−95161
Ti-ZrO_2(HfO_2), eutectic system metallographic investigation *(Russian)* 77−66629
TiN_n, effect of equilib. N_2 press, 10^{-2} to 100 atm, on MP 77−36465
TiN_zO_y, cubic, thermal expansion coeffs., Ti-Ti bond screening 79−10970
Tl-B-Se system, vitrification region, primary crystalli[illegible]fields 77−15321
Tl_2CuI_3, melting point, cryst. struct., DTA, X-ray diffr[illegible]*ch)* 77−84710

melting point continued
$TlNO_3$, boiling and melting pts., heats of transformation, solid-solid transformation 78−91441
$Tl_2Te(Se)(S)$, mag. susceptibility at melting point 79−24128
UF_4, vaporisation behaviour 80−84283
US-UC-UC_2 system, potential nuclear fuels, phase solid soln. studies, prep. and props. exam. 79−40996
V, radiance temperature at melting point, surface roughness depend. 80−59683
V-ZrO_2(HfO_2), eutectic system, metallographic investigation *(Russian)* 77−66629
W, specific heat near melting point, rapid pulsed heating method 77−35704
W-Hf-C, phase equilib. 80−55348
WC, depend. on press. up to 80 kbar, optical meas. *(Russian)* 77−80604
Xe, suitability as temperature fixed point 78−77838
YAG, melting behaviour and metastability determ. by optical DTA 80−92648
Y_2O_3, laser heated pellet, melting point determ., secondary melting point standard 78−37011
Y_2O_3, secondary standard investigation *(French)* 78−41271
Yb_2O_3-based ceramic, preparation, mech. props. 77−24998
$ZnGa_2Te_4$, cryst. struct., melting point 78−35360
ZnS(Se), reaction with Sn chalcogenides, thermodynamic anal. 80−40728
Zr, liquid, viscosity at melting point, free energy *(Russian)* 80−92699
ZrC-NbC-MoC_{1-x} alloys, physicomech. props., comp. depend. 79−66097
ZrN_x, MP N press. depend. 77−35669
ZrO_2-Y_2O_3-Nd_2O_3, high-temp. thermophys. props. 78−26663

membranes
see also biomembranes; lipid bilayers; osmosis
acoustic radiation, due to a fluid loading discontinuity on an infinite membrane 78−90579
acrylonitrile-dimethylaminoethyl methacrylate membrane, as burn wound covering 78−44676
adsorbed, use of Si-SiO_2 as electrode for elec. and ellipsometric meas. 80−15366
aggregation in membranes, fluctuation-induced interactions in liquid crystals 77−90732
amperometric membrane probes for residual Cl determ. in saline cooling waters 80−82112
anion, cation exchange, electrodialysis polarisation, rotating disc studies 79−47933
anisotropic fluid, diffusion, EPR spin exchange and nuclear spin relax., theory 80−34753
annular elastic membranes, large deflections, theoretical and expt. exam. 78−30186
arbitrarily shaped, vibrs. and dynamic response 79−7334
artificial, light-driven carrier-mediated electron transfer 77−29110
artificial kidney dialysis exchange model reliability tests *(German)* 79−2165
artificial kidney microporous membrane plasma filtration efficiency 78−48926
artificial lung, oscillating helix membrane design employing O_2 perfused inner capillaries 78−44712
artificial lungs, membrane design and application 77−25601
artificial membrane lung, fluid vortices and mass transfer 77−52919
asymmetric, diffusion eqn. soln. for gas flux 78−56918
asymmetric dense polymeric membrane, gaseous mixture separation 78−9696
asymmetric skinned synthetic polymeric membranes struct. 79−29417
ballistic impact on thin plates, membrane model 78−30193
barrier plastics, high nitride polymers, liq. transport, temp. effects 78−76921
bilayer lipid membranes, flexoelectric polarisation at blocked flip-flop 79−100582
bilayer membrane dynamics, combination of Rouse model and Marcelja liq. cryst. theory 79−100581
bilayer membranes, elec. surface props., asymm. charge effects 77−32805
bile salt micelles as liquid membranes 80−21327
biological and synthetic, 1/f noise, empirical relations and theories 79−24969
biological microspecimen holder for processing and critical point drying 79−74822
BKZ fluid tubular membrane, simultaneous elongation and inflation 79−90294
blood filtrating, with pore-size 0.6 μ, artificial kidney and liver appl., expts. with dog 79−44051
blood membrane oxygenator effectiveness 79−48365
blood oxygenator, artificial membrane lung 77−78051
blood oxygenator, CO_2 transfer 79−25154
blood oxygenator, stationary membrane type, O_2 and CO_2 diffusion process 77−78046
blood oxygenator design, data on diffusion of O_2 and CO_2 through blood flowing in channel 77−60303
blood plasma filtration from whole blood, effect of various parameters 78−48826
blood pO_2 meas. polarographic technique 79−100782
blood ultrafilter design analysis 77−64152
bubble dynamics, motion of relativistic membrane, relevance to quark confinement 79−2989
cable-band membrane, axisymmetric, interdependence between geometry and forces 80−96185
capillary, for blood diafiltration *(German)* 77−48921
capillary membrane oxygenator semiautomatic fabrication 79−20711
carrier mediated transport theory, survey of applications 77−89113
carrier-mediated photodiffusion membranes 78−23965
catheter tip device incorporating CO_2 and O_2 sensors 79−100783
cation binding to membranes, modified Gouy-Chapman equation 80−55998
cation exchange membrane, counterion interdiffusion 80−26044
cation exchange membrane, transport parameters for KOH aqueous solution 78−64883
cation exchange membranes, voltage against current curves 79−96365
cation-exchange membranes, electrochem. props. rel. to interfacial polarization in electrodialysis 79−16038
cellophane membrane, polarised, electret transport props., permeability coeff. 77−760
cellulose, diffusion, friction coeffs. for polystyrenes in toluene soln. 78−73085
cellulose acetate, granulocyte growth enhancement on peritoneal cell-coated membranes following irradiation 80−21504
cellulose acetate, reverse osmosis membranes, ion mobility, diffusion coeff., elec. resist. obs. 80−45550
cellulose acetate, vector mass transport obs. and appl. 79−96360
cellulose acetate freeze-dried membrane, gas permeation rates 79−79295
cellulose acetate membrane, asymmetric, elec. and electroosmotic transport behaviour in dialysis-osmosis expts. 80−108745
cellulose acetate membrane, asymmetric, elec. and electroosmotic transport behaviour in hyperfiltration expts. 80−108746
cellulose acetate membrane, thermoosmosis of H_2O 79−52768
cellulose acetate membrane water permeab. at low press., nature of flow 77−73467
cellulose acetate membrane water permeab. at low press., temp. var. 77−73466
cellulose acetate membranes, modified, tensile props., desalination performance 79−11818
cellulose acetate-g-polyacrylamide, radiation grafted, appl. in water desalination by reverse osmosis 80−45548
cellulose diacetate, for reverse osmosis, transport phenomena analysis, pressure effects on permeability characts. 79−96361
cellulose diacetate membrane, diffusive permeability 80−104460
cellulose diacetate membranes, press. depend. of permeabilities *(French)* 79−52756
cellulose diacetate membranes, unilayer, transport phenomena, hydration and dialysis coeffs. 80−76556
cellulose membrane, methanol(formamide)-water soln. permeabilities 78−11557
cellulose membrane, nonstationary diffusion of glycerol trioctadecanoate soln. in toluene 79−52767
chalcogenide ceramic membrane, Cu-selective electrode *(Chinese)* 80−81357
choline phosphate calcium chloride tetrahydrate, struct., conformation, metal coordination, model for membrane surface interactions 80−15085
circulation system with gas enrichment using membrane oxygenators, mass spectrometer inlet system study *(German)* 78−73294
coated Hg electrode, continuous voltammetric anal., appls. 77−25341
compliant, in turbulent boundary layers, appl. of tension 77−31287
composite, relaxation time, network thermodynamics formalism 78−68926
composite circular membrane fastened at circumference, symmetrical vibr. 79−37216
composite membrane, anion exchanger-urease, coupling of transport and enzymic reaction 79−83510
composite rectangular membrane consisting of strips, free vibr. anal. 77−39252
compressor for inert gas and mixtures 78−86286
conference, Ravello, Italy (May 77) 78−76911
corrugated, with rigid centre, free axisymmetric oscillations *(Russian)* 80−38302
coupled fluxes, concentration distributions near electrodialysis membranes 79−47974
coupled transport of electrons and metal cations 80−3403
DECHEMA symposium, Tutzing, Germany, (Mar. 1978) 80−62373
diafiltration process, technical aspects *(German)* 77−48920
diffusion, through permeable barriers, applied to NMR with pulsed field grad. 78−91986
diffusion of $^{241}Am^{3+}$ ions in ion-exchange membrane, autoradiographic method 78−35721
diffusional boundary layer resistance for low porosity membranes 77−58778
diffusive flow, frictional coeff. formalism and mech. equilib., mol. scale 77−90638
dimethylpolysiloxane rubber reinforced film in membrane oxygenator 79−48373
dipalmitoyl phosphatidylcholine, gel and liquid crystalline phases, deuterium mag. resonance obs. 79−91308
directional time-lag asymmetry in media with position-dependent sorption and diffusion props. 78−3372
dissolved gas mass transfer through tubular membranes 77−35225
Donnan systems displaced from equilib., transient press. changes 77−52749
drug delivery osmotic pump, design and operating principles 77−56544
dynamic loading of prestressed membrane 78−51068
dynamic response of a membrane with both curved and straight line boundaries 80−64440
elastic, rigid centre, press. gradient, large deflections *(Russian)* 78−5662
elastic, slack circular, under point load, deformation and stresses 77−46911
elastic and isotropic, universal solns. 77−84139
elastic cylindrical membrane, non-uniform inflation, direct determ. of strain energy function 77−75805
elastic membrane deformations, constitutive relation effects 79−14269
elastic membrane dynamic response to expanding ring load 77−46957
elastic membranes, universal deforms. 78−67048
elastic membranes and cords as slender bodies, dynamics 77−50878
elastic support, mixed boundary-value problems, variational principles and hypercircle 78−57749
elastically supported membrane eigenfunctions 79−14341
electrode, rotated disc, for membrane mass transport evaluation 80−26069
electrodes, antibody-selective 79−84058
electrolytic cell, nonaqueous medium, heat transfer through diaphragm 78−73049
electroosmotic pump for regulated release of medicaments *(German)* 78−7518
elliptic ring membrane, fundamental frequencies 77−50978
enzyme particle, encapsulated, reactor systems, effects of mass transfer resistances 79−96522
ethyl cellulose membrane, sorption and transport of hydrocarbon gas 78−76913
ethylene-vinyl alcohol copolymer, O_2 permeability *(Japanese)* 78−31702
ethylene-vinyl alcohol copolymer membranes for haemodialysis, prep. conditions and props. *(Japanese)* 80−12299
excitable, nonlinear anal. for shaping threshold action 77−12871
excitable, statistical theory, nonlinear force-flux reln. and fluctuation 77−9179

membranes continued
filters as selective electrodes for synthetic penetrating ions 80−104821
filters used in air analysis, review 79−79316
filtration device for aerosols and liq. suspensions, filter mounts and quick-change device 77−53873
finite elasticity theory, research directions 77−68416
flat elliptic paraboloid shells subjected to uniformly distrib. horizontal load at edges *(German)* 79−27518
flexible membrane, acoustic wave scatt. near reson., panel deflection and vel. pot. field 77−42657
flexing, appl. of displacement meas. by holographic interferometry 80−8962
Fourier transform IR transmission spectroscopy, appl. to natural and model membrane study 80−17218
Galerkin's method, non-uniform convergence 78−83304
galvanic dissolved O_2 sensor, improved, activated sludge aeration appl. 77−70364
gas mixture separation by membranes *(Japanese)* 78−48691
gas permselective membranes, irrad. effects on permeation and separation performances 78−29591
gas separation performance of tapered cascade with membrane 79−22478
gas transport, in synthetic polymer membranes, history 78−76912
glass, transient diffusion of sucrose, mannitol, pentaerythritol stirred aq. solns., thermodynamics 78−92507
glassy polymers, films and spheres, transport props., film thickness and sample history effects 78−76917
graphite charged polyethylene membrane electrode, electron transfer *(French)* 78−27778
gravity waves, propag. in two liquids separated by membrane *(French)* 78−87355
haemodialyser, permeability of Cuprophane and polyacrylonitrile *(Japanese)* 77−66873
haemodialysis and haemoperfusion, joint system, evaluation of novel sorbent systems 78−7542
haemodialysis cellulosic films and hollow fibres, diffusive and hydraulic permeabilities 78−28128
haemodialysis membranes, for disposable dialysers, comparison of cuprophane and cellophane 77−78049
haemodialysis membranes, permeability and rejection coeffs. 80−26207
haemodialysis membranes prepared from acrylonitrile-methylacrylate-acrylamide latexes graft copolymerised onto PVA *(Japanese)* 80−12297
haemodialysis technique with dialysate regeneration by absorpt. and ion exchange *(German)* 77−48919
haemodialysis with hollow fibre membranes, flow maldistribution effect on performance 80−26248
hollow fibre dialyser, mass transfer 80−66873
holographic interferometry, stroboscopic analysis of asymmetric membrane vibrs. 78−66786
hydrocarbon chain ordering in model membrane, D quadrupole splitting 78−64947
hydrostatic pressure loaded membrane of revolution 80−64363
N-hydroxyethyl acrylamide-styrene(methyl methacrylate) copolymers, synthesis, anion active membrane transport appl. 80−61142
hyperfiltration, outer phases composition 79−92003
inflated, thin walled elastic circular cylinder under axial loading, bifurcations, membrane theory 80−19246
inhomogeneous, diffusion, theory 78−76914
inorganic membrane electrolyte 79−74396
inviscid shear flow over flexible membranes, stability 80−14658
ion exchange, appl. to electrolytic ion separation 78−53247
ion exchange, unstirred layer effects on pot. difference calcs. 77−48680
ion exchange filter membranes, water preconcentration appls. for X-ray fluoresc. anal. 78−7228
ion exchange membrane, equilib. props. calcs. *(German)* 77−12830
ion exchange membrane, nonequilib. props., steady flow in const. elec. field 78−23966
ion exchange membrane detector for liquid chromatography, characterisation appls. 79−16055
ion exchange membrane electrode, for ionic activities in aq. soln. meas 79−74392
ion exchange membrane selectivity w.r.t. dialysis prospects 80−45560
ion exchange membranes, electric and electrokinetic transport props. 79−57293
ion exchange membranes, ion and water transport eqns. 78−68930
ion exchange membranes, ion diffusion studied by autoradiography 77−90637
ion exchange membranes, production by electron irrad., cross linking, graft polymerisation *(Japanese)* 77−81403
ion flow, effect of chem. reaction on time depend., binding of mobile ion 78−95954
ion flow, step pot. change, conc., current responses 79−5177
ion selective membrane, polarisation at high current densities, Nernst model 79−91962
ion specificity, determ. criterion 79−57597
ion transport, in reversible electrostatic channel 79−96356
ion-exchange membrane, all-round electrochem. investig. equipment 79−91970
ion-exchange membrane, electroosmotic energy conversion efficiency 80−61430
ion-exchanger membranes, coarse-grained, oscillatory phenomena 79−34356
ion-selective, neutral complexing agents basis, limiting step of ionic transport using conc. cells method *(Russian)* 79−96367
ion-selective electrodes, Ag^+ and F^- based ceramic materials appl. *(Japanese)* 80−61203
ion-selective electrodes, liq. membrane, free and supported, ion transport, bulk elec. props. 79−83534
ion-selective electrodes, liq. membrane, free and supported, ion transport, interfacial kinetics, time depend. phenomena 79−83535
ion-selective electrodes, solid-state, for potentiometric determ. of phosphate 79−92044
ion-selective liquid chloride electrodes, solvent effects *(Russian)* 79−91972
ion-selective membrane, flicker noise and turbulent convection in depleted layer 78−48692
ion-selective membrane electrodes, selectivity, statistical calcs. 78−92549
iosperimetric inequality for first eigenvalue of boundary value problem 77−67220
membranes continued
isotope separation, by semipermeable membrane, secondary-stage processes, photoexcitation effects *(Russian)* 77−6962
isotropic elastic, large deform., static solns. 78−13903
kaolinite membranes, anion permeation 80−11952
leaching from model porous bodies by reflection spectroscopy 80−100031
light optical imaging, of focused US field *(German)* 80−3275
linear laminated media, permeation, sorpt. 79−1966
lipid bilayer stabilisation by polymer resins 79−57288
lipid bilayers, voltage transients from photo-isomerising azo dye 79−92166
liquid, facilitated, transport for separation of liq. mixtures 78−76920
liquid, three-dimensional gravitationally-elastic, gravitationally-capillary surface waves *(Russian)* 79−32537
liquid crystals, textures, deform. and struct. order, review 77−43135
liquid membrane permeation technique applic. to separation of styrene-ethylbenzne system 79−87871
liquid membranes, emulsion-type, pertraction appls., comparison with double liq.-liq. extraction 80−66869
liquid membranes, separation and reaction appls. 80−66871
liquids, permeability inlet press. effect *(German)* 79−100438
macrocyclic receptor mols., chem. reactivity, mol. catalysis, transport processes 80−21280
macromolecules, epitaxial crystallisation, review 79−42409
mass or heat transfer across plane membrane in the way of a flowing stream *(German)* 79−41557
membrane surfaces, antibody association kinetics with spin-label haptens 80−66787
membrane-solution interface, phase jump of osmotic press., theory 79−11825
metallic, lifetime prediction and design 80−71752
metallic membrane interface, mass transfer 80−81366
microcapillary system, staged, tortuous, for haemodialysis and ultrafiltration 77−37107
microporous, for blood plasma filtration 77−48947
Millipore-dioleylphosphate model membrane, elec. current stimulus effects 80−67046
miniature pH-sensitive polymer membrane electrode 79−100781
model using millipore-DOPH membrane, increase in elec. resist. with Ca^{2+} ions and its oscill. 80−40745
molecular seive, permeability rel. to Br_2 mols., laser-induced changes *(Russian)* 79−91999
mosaic, charged, thermal membrane pot. 79−34358
Nafion cation exchange membranes, IR spectrum assignment 79−89818
Nafion per fluorosulphonic acid ion exchange membranes, Mossbauer spectroscopy 80−80659
negative resist., current controlled, model 79−34357
Newtonian viscous fluid, flow through thin pipe, with thin linear elastic wall 78−42664
non-univariate automodel problem, of membrane dynamics *(Russian)* 78−42529
nonhomogeneous, isoperimetric inequality connecting fundamental frequency with equilib. energy of Poisson problem *(French)* 77−7327
nonlinear elastic membranes, large finite strain effects, asymptotic solns. 79−50597
nonlinear wrinkling of nonlinear membranes of revolution 79−32242
Nucleopore membrane, pore struct., determ. by electron microscopy and Hg penetration 78−43165
nylon 12 membranes, permeation characts. *(Japanese)* 78−31692
optimised dishes, strength and stability *(German)* 78−87256
organic liquid, active transport of picrate anion 78−11556
organised molecular systems, monomolecular layers, micellar and bilayer membranes, conf., Elmau, W.Germany (April 1978) 79−39188
osmo-hydro power system, using aqueous saline solutions, technical and economic feasibility 79−52916
osmometry, mol. wt. determ. 77−88593
osmosis, pressure-retarded, two-coeff. water transport eqn. 79−83509
osmosis, reverse, using sulphonated aromatic polysulphone, expt. results 77−44508
oxygenator, membrane envelope type, capacity improvement *(German)* 79−2157
oxygenator membrane blood compatibility, correl. of IR spectroscopy with platelet morphology 79−53279
oxygenator using microchannel membrane, transport and flow phenomena 78−69253
paper membrane sound generation by impulsive tension 78−90581
parchment-supported $AgPO_3$, determ. of thermodynamics of ionic diffusion processes 78−20068
partially disordered, X-ray scatt., anal. method 78−91196
particle diffusion, through small pores, latex particles in ionic soln. 79−43622
passive transport through open membrane, multicomponent system, statistical-mech. theory 78−67261
Payne-Rayner isoperimetric inequality, extension to N dimensions *(French)* 78−54323
percolation problem for lattices of bonds, sites, perforation points, graphical technique 77−63954
percolation problem for lattices of bonds, sites, perforation points, graphical technique 77−63955
percussion instrument acoustics, multidimens. vibrs., review for teaching 77−57128
pH measurements using polarizable electrodes 80−76514
phosphatidylcholine bilayers, artificial, interaction with C-reactive protein 80−3579
phosphatidylcholine multilayers, alignment and defect structs. 79−92167
phospholipid vesicle walls, photosensitised electron transport 78−80787
photochemical H prod. from H_2O using sunlight and asymmetric membranes 80−45776
physico-chemical aspects of transport 77−29107
piezoresistive semiconductor, vibrating membrane, current amplification 78−75025
plasma filtration, stagnant 77−48948
plate, thin elastic, with line constraints acoustic scattering 78−90554
PMMA, diffusion-controlled penetration by monohydric normal alcohols 78−76918
PMMA, sheets, in methanol, case II swelling and transport kinetics 78−76922
PMMA, water swollen membrane, permeability *(Japanese)* 78−31704
poly(2-hydroxyethyl methacrylate), crosslinked, solute transport 79−43630

membranes continued
poly(vinyl alcohol)-acrylonitrile copolymer membrane, water permeability increase *(Japanese)* 79−70375
poly(vinyl alcohol)-based membranes for haemodialysis *(Japanese)* 78−96115
poly-n-hexyl L-glutanate, sorption and permeation mechanism 80−26048
poly-N-vinylpyrrolidone-containing nonionisable membranes, equilib. props. struct. *(French)* 80−61138
polyamide 6 and 12 films, permeability to H_2O vap. *(Russian)* 78−53255
polycarbonate membrane, porous, gas permeability *(Japanese)* 78−31698
polycarbonate porous membrane, pore size effect on gas permeability *(Japanese)* 78−31699
polydimethylsiloxane membrane, permeability of triethylamine vapour *(Japanese)* 78−31697
polyelectrolyte solution, thermodynamic props. determ. from Donnon equil. obs. 80−7846
polyester-hydrazide, aromatic, fibres and films, synthesis and props. *(Japanese)* 80−108387
polyethylene, permeation of hydrocarbons 80−30281
polyleucine membrane, water and water vapour permeation and solute separation *(Japanese)* 78−31701
polymer, O_2 permeability, determ. with Zircon gas analyser 79−39195
polymer, self-supporting, 2-3 μm, dip-coating technique, props., appls. 79−1838
polymer, transport of organic liqs., review 80−16720
polymer, use of McInnes glass electrode for determ. of CO_2 diffusion coeffs. 78−20067
polymer membrane, penetrant sorption kinetics, transverse differential swelling stresses 78−76923
polymer membrane gas permeation, pore size distrib. *(Japanese)* 78−79372
polymeric film, variable-shape solar energy concentrator appl. 80−76645
polymeric membrane, porous, gas permeability *(Japanese)* 79−24825
polymers, diffusion coeffs. of gases, sorption, permeation investigs., review 78−67868
polyphenylquinoxaline-cellulose acetate, battery separator membrane, diffusion meas. 80−35574
polystyrene sulphonic acid, charged membrane, electroosmosis and streaming potential *(Japanese)* 78−31696
polysulphone membrane, prep. and performance for ultrafiltration *(Japanese)* 78−31695
polytetrahydropyran 2,6 diyliminocarbonyl, water permeation and solute rejection props. 79−74419
polyvinylbutyrolactonecoacrylonitrile membrane, selective and counter transport of Na^+ and K^+ *(Japanese)* 78−31700
polyvinylidene fluoride and poly-1-vinyl-3-methylimidazolium iodide interpolymer ultrafiltration membranes 79−15639
porous, filtration characts., pore and particle size distribs. correl. *(Japanese)* 80−3418
porous, H_2O, double tagged, self-diffusion, struct. props. 79−52765
porous cellulose acetate membranes for mixed uni-valent electrolytes in aqueous solns. reverse osmosis predictability 78−53250
porous electrode type cells, electrochem. and capillary characts. 79−91967
porous hydrophobic membrane, anomalous gas mixture flow into liqs. 80−40744
porous media, nonisothermal mass transport, thermal energy flux and radiation pressure theory 78−76916
potassium palmitate-water bilayer, lamellar liq. cryst. polymorphism, NMR and birefringence 79−60270
potentials, meas. in ionic environment, biological membrane simulation 80−3412
potentials measurements 80−3411
preparative scale thin-film dialysis apparatus 80−101296
pressure meas., nonlinear characts. calc. *(Czech)* 79−26021
pressurised spherical, necking 77−68448
protein membranes, immobilised, H^+ ion transport, assoc.-dissoc. time-scale factor 79−34529
protein-membrane interactions probing using laser flash spectroscopy of indoles in presence of nitroxide radicals 79−87855
PTFE grafted membranes, struct.-properties relationships, bifunctionality *(French)* 80−61137
PTFE grafted membranes, struct.-properties relationships *(French)* 80−61136
PTFE grafted membranes, struct.-properties relationships for poly-N-vinylpyrrolidone-containing membranes *(French)* 80−61138
PVA, hollow fibre membrane for industrial scale dialyser *(Japanese)* 78−31693
PVC, struct. and performance of porous membranes prepared from soln. *(Japanese)* 79−24823
PVC film, permeability to H_2O vap. *(Russian)* 78−53255
quantum model for transport through membranes 80−93796
radioactive rare gas separation, using cell with two membranse of differing permeability 78−29590
rectangular under uniform pressure, large deflections 78−55560
regenerated cellulose-activated charcoal membrane adsorpt. characts. for haemoperfusion *(Japanese)* 80−12298
reinforced cellulose acetate membrane water and salt permeability, complementary direct osmosis test 79−96359
renal dialysis membrane leak detector 77−60294
reverse osmosis, mechanisms, membranes, transport and appls. 79−29396
reverse osmosis salt rejection, membrane pore size 77−9122
reverse osmosis separations of inorganic ions in aqueous solns., free energy parameters 77−32831
reverse osmosis transport processes *(German)* 78−95946
reverse separations of ions and ion pairs in aqueous solns. free energy parameters 78−53251
rigid plastic axisymmetric, shape and thickness distrib. under impulsive loading 77−23897
ring, polymer, physical props, meas. and control appl. *(Slovak)* 80−61141
rotating circular cylindrical elastic membranes bifurcation 80−33494
second order symm. tensors in compact Riemannian manifold, compatibility and orthogonal decomp. 77−57161
secondary cell appl. review *(French)* 78−3374
selectivity, influence of particle/pore size ratio 80−11946
semi-permeable, for species-selective electrochem. sensor, in book, for teachers 78−8200
membranes continued
semipermeable, for KCl separation from Dead Sea brine, theory 78−31673
separation method, flow field-flow fractionation 77−960
separation processes, principles, practice and prospects 78−92505
shell, forced axisymmetric vibrs., including inner friction effects *(Russian)* 79−32368
silicon rubber tubular membrane oxygenator appl. 77−48930
silicone membrane progesterone release rate control by plasma polymerisation 77−60285
silicone rubber, inert gas separation appl. 77−36791
skin impedance change, equivalent cct., exptl. results 77−81773
smectic lipid bilayer, in cryst. matrix, phase transition 80−21453
solid, superpermeability, gas evacuation 79−74422
solute molecules, diffusive and convective transport models 77−32841
sorption and desorption time lag meas. apparatus 78−38428
spatial light modulator with CCD address 80−48445
spherical rubber balloon, aspherical deform. under inflation 77−46914
spiropyran, membrane, lipid effect on photoinduced potential change *(Japanese)* 78−31703
stability of nonlinear oscillations from Liapunov method 80−96212
star shaped membranes, new bounds of Poincare const. *(French)* 79−25860
steady nonionic countergradient transport through membranes by coupled diffusion [dialysis application] 80−16718
steel, bimetal, alloy with austenitic stainless, H permeability 80−107572
stress-equilibrium membrane elements with holes 77−78980
strong acid types, with enhanced hydrophilicity 80−66872
supersonic flow past conical parawings with small camber, trailing edge slope and membrane weight effect *(German)* 77−31331
surface water continuous analysis by NH_4^+-sensitive plastic membrane electrode 80−89701
synergetics, chemical processes far from equilib., conf. Bordeaux, France (Sept. 78) 80−3334
synthetic, transport props., rel. to biological membranes 78−77030
synthetic membrane cells, elec. relax., time-independ. rectification 77−90731
thermodialysis of nonideal aq. solns. across non-isothermal partitions 79−96366
thermoosmotic concentration difference meas. for gaseous mixtures across membranes 79−83508
thick film hybrid fabrication of pH-sensitive implantable bioelectrode *(German)* 78−40369
thick membrane strip, effect of shearing prestress, static case 80−10137
thick membrane strip, effect of shearing prestress on response, dynamic case 80−10138
thickness, statistical distrib. determ. by lineal analysis, biomembrane appls. 79−5253
thin circular membrane, forced symmetric vibrs. 80−10181
thin stretched foils, membrane wave excit. 78−90578
thoria effusion membrane, production techniques based on that of incandescent gas mantles 78−39724
transport, chemical reaction augmented, facilitation factors, prediction, appl. 79−91992
transport coeff. meas., laser interferrometric technique 78−15936
transport matrix, relation between conc. depend., matrix transformation and flux representation 78−20069
transport processes, phenomenological coeffs., frames of reference, isothermal systems 78−38862
transport processes, phenomenological coeffs., frames of reference, nonisothermal systems 78−38884
turbulence formation during flow round elastic membrane *(Russian)* 79−41666
turbulent flow, meas. in vicinity of cation-selective membrane using scatt. laser radiation Doppler shift 79−46301
turbulent heat transfer across membrane between two liquids *(Russian)* 78−38180
ultrafiltration, hybrid reverse osmosis, water treatment appl. 77−44507
ultrafiltration, using membrane surface, slip vel. effects in channel flow system 79−60054
ultrafiltration, using membrane surface, slip vel. effects in tube flow system 79−60055
ultrafiltration apparatus, biopolymer appl. 78−7547
vanadate polystyrene based membranes, parameters, biionic pot. 79−57294
vibrating, fixed, on the first eigenfunction 77−50980
vibrating membrane speckle pattern analysis 80−106769
vibrating wedge-like, isoperimetric norm bounds for first eigenfunction 77−14950
vibration, functionals method for lateral vibr. freqs. determ. *(Japanese)* 80−12918
vinylbenzyl gluconate acrylonitrile copolymer, for heavy metal ions separation 79−74418
4-vinylpyridine acrylonitrile copolymer membrane, reverse osmosis charact. *(Japanese)* 78−31694
N-vinylpyrrolidone-methyl methacrylate copolymer water swollen membrane, permeability *(Japanese)* 78−31704
viscoelastic properties dynamic evaluation for use in cardiac prosthetics 78−40405
viscoelastic spherical membrane, nonlinear, quasistatic inflation, bifurcation of response 78−46897
viscoelasticity, nonlinear, for axisymm. deform. 78−90808
water swollen membrane, rapid prep. technique, obs. using SEM with cryo-unit 79−89047
webs, stress state under uniform partial edge loading 79−77028
wedge stroke blow, along membrane at surface of incompressible liquid *(Russian)* 78−55561
wrinkled membranes with anisotropic and nonlinear elastic props., tension field theory 77−31220
Ag membrane filters for sample collection for X-ray diffr. chem. anal. 77−63972
Al, life testing 79−70256
Al membranes, circular, plastic deform. under impulsive loading by underwater wire explosion 79−100208
Au thin films, with nm-sized pores, prep. from Au-Ge eutectic films by etching 80−16227
C membrane, graphitised, adsorption meas. in situ using steady state flows and time lags 79−33183
Ca-selective membrane electrodes, asymmetric, potentiometric meas. 77−77785

membranes continued
CrFeCN epoxy resin-based membrane studies, Ag sensitive electrode 80−16726
Cu, kinetics of permeation of H_2 79−99371
Cu, life testing 79−70256
$Cu_3(PO_4)_2$, polystyrene based membranes, parameters, biionic pot. 79−57294
Fe, Armco, membrane, superpermeability to D 79−24830
Fe, membranes, effect of electrodeposited metals on H permeation, proposed catalytic mechanism 78−53252
H production, electrolytic, using inorganic ion exchange membrane 80−45804
H_2O in model membrane systems, structural element, structural changes in lecithin-water system 78−96023
Mo, membrane, polycryst. LiH form. on surface from diffusing Li+H_2 77−66771
Na_2O-P_2O_5 and Li_2O-Na_2O-P_2O_5 glasses with oxide additions, eval. as membranes for chem. sources of current *(Russian)* 79−96338
Nb, membrane, H permeation *(Japanese)* 80−100363
Pb, life testing 79−70256
Pd alloy membrane pump, for thermonuclear fusion devices 78−89980
Pd, D beam interaction, permeability 77−51538
Pd, diffusion-cell for separation H_2 containing mixtures, solar furnace appl. 80−92245
Pd, gaseous H quasiequilib. processes, 100-500°C, 10 $^{-4}$-10^{-2} torr 77−29047
Pd membrane, H atom interaction, superpermeability 80−81365
Pd membrane, H penetrability reduction by C coating *(Russian)* 77−77808
Pd, sorption of H_2, adhesion and penetration probabilities, extreme values 80−101040
Pd, superpermeability, of atomised H_2, under different gas and membrane boundary conditions 79−71469
Pd-H, solid soln., excess entropies, variation of H solubility with pressure 79−46846
Pt membranes, H_2 diffusion at high press. and temps. 78−55984
$Sb_2O_5.nH_2O$ acid membranes, synthesis and characterisation 80−81027
Ti, high strength unsupported membrane fabrication 77−66589
Zn^{2+}, transport in cation-exchange membranes 78−96033
$Zr(HPO_4)_2.H_2O$-Kynar membranes, struct., ion mobility 78−76915

memories *see digital storage*

memory devices *see storage devices*

mendelevium
see also nuclei with .....
No entries

mendelevium compounds
No entries

mercury (metal)
see also nuclei with .....
acoustic streaming meas. 79−64380
adsorbed monolayers, on W (100), fractional and zero order desorption kinetics 79−60634
adsorbed on W, thermal desorption kinetics, theory 80−59792
adsorption of water vapour, critical anal. of expt. data *(Spanish)* 79−82435
adsorption on Au, Ag, Mo, and Re, work function change 77−7966
adsorption on metals, alloys, effect on mech. strength *(Russian)* 79−29267
Aegean Sea, Cu, As and Hg conc. determ. 79−2292
air and water pollution from wastes stored near Cl manufacturing plant 77−66938
air jet injected horizontally, physical behaviour 77−3857
air-Hg flow, stratified, co-current, in rectangular channel, interfacial wave structure 80−74955
alkali halide:Hg, EPR and optical props. 78−91933
arc, continuum radiation meas. 77−62416
arc, high press., convection 78−59701
arc plasma, azimuthal RF cond. meas. by eddy current effect, expt. 77−1029
atmosphere quantitative analysis of aerosols 79−12179
atmospheric dispersion, expt. meas. 79−92565
atom, 1849 Å absorption line broadening and shift in inert gases *(French)* 77−30825
atom, 2537 Å line satellites, Kr broadening 77−83523
atom, 435.8 nm spectral line, stigmatic imaging with spherical concave grating 77−38808
atom, 5.2 eV resonance in electron impact excitation 79−10208
atom, 5d level open shell interactions, 304 Å photoelectron spectrum 80−87087
atom, 5d spin-orbit X-ray excitation, 21-2700 eV, by ESCA sources 78−53301
atom, $6^3P_{0,2}$-state, electron impact excitation, optical detect. 77−50546
atom, 6^3P_0 and 6^1P_1 states, relax. effects 78−5272
atom, 6^3P_2 state, stepwise excitation by slow electrons, effective cross-section *(Russian)* 78−5348
atom, 6D levels excited by dye laser, lifetimes 80−42996
atom, 8^3S_1 level, Lande factor *(French)* 77−430
atom, ^1S, ^3P, ^1P states, dipole polarisabilities from compact variational trial functions 80−63568
atom, $^3P_0$ quenching rates, laser fluoresc. meas. 77−46522
atom, Breit-Margenau correction, relativistic calcs. 77−3281
atom, bright field image, on C support film, signal-to-noise enhancement by incoherent superposition 80−101906
atom, doubly K ionised, energy shift between K_α X-ray and its hypersatellite line 78−9107
atom, effective core potentials calcs. rel. to bond lengths and energies 78−66464
atom, electron elastic scatt., 4-6 eV, reson., scatt. ang. and spin polaris. spectra 78−25702
atom, electron elastic scattering, 8 to 18 eV, electron spin polaris. 80−91669
atom, electron impact excitation in visible and UV; cross sections 78−17801
atom, electron impact excitation of $^3D^0_3$ metastable state 78−5350
atom, electron impact ionisation cross-sections for excited states 80−9742
atom, electron impact spectra, intermediate energy 78−82842
atom, electron resonant elastic and inelastic scatt. *(Russian)* 80−78710
atom, electron scatt., absolute total cross section 79−59570
atom, ESCA spectra from 132.3 eV YMζ radiation source 77−4958

mercury continued
atom, four-photon resonant ionis. 77−42289
atom, Hanle resonance in radio-frequency fields 80−91508
atom, hyperfine effect on polarisation of 6^3P_1-6^1S_0 intercombination line excited by electron impact 78−37750
atom, IR arc spectrum, fine struct., HFS and isotope shifts 77−79559
atom, IR arc spectrum, fine struct., HFS and isotope shifts 77−79560
atom, isotope shift by on-line laser spectroscopy 77−34589
atom, L-shell X-ray photoelectric cross sections, fluorescence spectra 78−58636
atom, Lande factor of 6^3P_0 metastable level of odd isotopes *(French)* 78−5162
atom, laser stepwise excitation of $6s6d^3D_1$ level, transition probabilities and collisional excitation transfer 78−55146
atom, lifetimes and cross sections of depolaris. collisions of laser working levels 79−76387
atom, line crossing obs. in 2537 Å line from Hg lamp 78−9129
atom, low energy electron scatt., shape resonances, electron affinity 77−14581
atom, metastable and excited states, pulsed dye laser absorption spectroscopy 79−26924
atom, $N_{6,7}O_{4,5}O_{4,5}$ Auger electron spectrum, electron impact excitation 77−57958
atom, partial photoionis. cross section 78−42022
atom, photoelectron angular distrib. resonance 79−13687
atom, photon-bound-electron scatt. meas. 77−14394
atom, polarised electron excitation, electron depolarisation depend. on coupling type *(Russian)* 79−89792
atom, positron scatt. at low energy 80−91670
atom, relativistic effective core pots., appl. to HgH and $HgCl_2$ ab initio calcs. 78−86767
atom, short-lived isotopes, HFS and isotope shift 78−37594
atom, spectral transition probabilities, 238-1530 nm 78−13455
atom, spontaneous emission, fluctuation spectroscopy 77−434
atom, transition probability of valence shells, relativistic pseudopot. calc. 78−86803
atom, two photon excitation, time resolved spectroscopy 80−87075
atom, two-photon excitation by photodissoc. of Hg halide 78−90114
atom, UV photoelectron spectra, wavelength depend. of satellite struct. 77−34597
atom ionisation in plasma of magnetron ion source, Penning phenomena effects 79−18069
atom-atom potential, relativistic effects on interactions 77−75252
atomic absorption determination, background absorpt. calc. *(Russian)* 79−52860
atomic electron elastic scatt., electron spin polarisation, detector, experimental exam. 78−32927
atomic electron impact excitation, spin polaris. and differential cross section 78−17800
atomic line profile and shift at 546.1 nm, high-press. discharge *(French)* 79−785
atomic multiphoton inoisation probability, Green's function model pot. 78−25498
atoms, elastic electron scatt., relativistic effects 80−102568
atoms, electron binding energy and shift, core level XPS 80−87088
atoms, electronically excited, form. by electron impact dissoc. of Hg halides 79−18296
atoms, gaseous, collection by electrostatic precipitators 78−95964
atoms, in aq. soln., transient spectra 79−6899
atoms, metastable, diffusion coeffs. temp. depend. in Ne and Ar 77−68731
background levels in air over S.Norway 79−12239
biological material analysis, As and Hg determ. by neutron activation anal. 80−36216
boiling heat transfer, surface roughness effect 78−9534
bubble motion with and without mag. field 78−91021
cataphoretic laser, transverse separation dynamics 77−38865
cathode, H^+ (D^+) discharge activation energies in H_2O(D_2O) 80−40707
cathode, motion of cathode spot of vacuum arc 80−54069
cell, capillary-Hg electrolyte, elec. characts. rel. to mag. field, gravity 77−1937
chelation with aspartic acid, US study 77−44464
chemisorption on W (100), AES, LEED, work function and thermal desorption expts. 78−34709
clusters in NaA neolyte, transition to paramagnetic state due to mag. field *(Russian)* 80−60183
concentration determ. in Arabian Sea waters 79−25268
concentration determ. in troposphere *(German)* 79−53406
concentration meas. in Lake Windermere catchment area 79−24924
concentration meas. in South Atlantic Bight 80−4046
concentration meas. in urban runoff 79−24923
condensation, dropwise, at Cu surface, heat-transfer meas. 77−75781
condensation, two-dimensional, on W 80−107666
contact potential and charge exchange meas., at Hg-polymer interface 80−75642
coulostatic deposition at underpot., pot. relax., chem. effects 78−48335
critical exponent β, for liq.-vapour coexistence curve 77−76538
DC vacuum arc anchored cathode spot current density obs. 78−75467
de Haas-van Alphen effect, electron-phonon interaction effects in single cryst. 78−84130
de Haas-van Alphen effect, electron-phonon scatt. calc., appl. to Hg 79−65360
de Haas-van Alphen effect, influence of electron-phonon interaction 79−65361
Debye temperature, temp. and press. depend. 77−1202
dense vapour, electron injection 77−47138
dense weakly ionised plasma, molecular dynamics 78−71456
density, −20° to 300°C International Practical Temperature Scale of 1968 77−4139
detection by forward scatt. of reson. radiation in mag. field and Voigt effect *(Japanese)* 77−60155
determination, cold vapour atomic absorption method, sorption effects *(Russian)* 78−73122
determination, in fresh and saline waters, automated UV digestion-AAS method 78−44414
determination by at. emission, cold vapour method, allowance for nonatomic absorpt. *(Russian)* 77−36853
determination by at. emission from static induction plasma, anal. curves, detection limits 79−87919
determination by cold vapour at. absorpt. spectroscopy, effect of sorption on sensitivity 79−52829

mercury continued
determination in drinking water, surface water and sewage effluent 79−92103
determination in environmental samples, neutron activation anal. methods, review 77−56284
determination in food by neutron activation anal. 77−36848
determination in sea and fresh waters, interlaboratory comparison 78−81209
determination in sea and inland waters, differential pulse anodic stripping voltametry method 77−70361
determination in water samples, error anal. 78−69519
diffusion in Al *(Japanese)* 79−19403
diffusion in liq. Te 77−84955
diffusion in Pb at high press. 77−72721
diffusion of Al, diffusion coeff. meas. 80−24627
discharge, high-pressure, NaI and TlI additives, line broadening and radiative transport 80−74199
discharge, low-freq. oscillation spectrum in weakly ionised plasma 80−87885
discharge, radial distrib. of low-freq. oscills. *(Russian)* 78−1928
distribution in Gulf Stream waters 80−7965
drop, optical consts. meas. from Hg-air interface, ellipsometry at spherical object 79−61326
drop electrode in MOS struct., Na-induced work function shift 79−42652
drop fall detector, circuit, design appls. 77−63924
droplets, film boiling 78−14453
dropping electrode, for square wave voltammetry, exptl. appls. 78−35734
dropping electrode, for square wave voltammetry, theory 78−35733
dropping electrode, photoemission into electrolyte solns. 77−24620
dropping electrodes, double layer capacity measurements 77−53933
dropping electrodes, polyethylene capillary type for corrosive media, prop. 78−61090
dropping Hg electrode, synchronisation in natural drop expts., high speed device 80−37049
dropwise condensation of Hg, heat transfer meas. 78−94560
electric field gradients at different Be lattice sites, gamma-spectral study 80−80224
electrical and thermodynamic props. in metal-semicond. transition range 80−20144
electrical conductivity of supercritical vap., semiconductor model 77−51154
electrical discharges, electron-collisional excited-state kinetics 77−24226
electrode, adsorption of n-butanol, diffusion layer theory, exptl. test 78−35701
electrode, electroreflection spectra calc., electromodulation mechanisms 77−1658
electrode, membrane coated, continuous voltammetric anal., appls. 77−25341
electrode metal-solvent interaction rel. to elec. double layer struct., adsorpt. 78−61023
electrodes, thin film, staircase voltammetric stripping anal. 77−12843
electron density of states at 20 and 200°C 77−15754
electron density of states of expanded liquid Hg, using effective medium approx. 79−99468
embrittlement of Cu-Al alloys under cyclic load 77−86225
emissions from geothermal power plants 77−73838
epitaxial layer resistivity meas. using Hg−n-GaAs barrier contact 79−60945
excimer fluorescence, electron beam and optically produced systems 77−27107
expanded, Knight shift interpretation in terms of electronic struct. and transport 77−43895
expanded fluid, optical props. 79−19902
expanded fluid, thermoelec. power near crit. point 79−23951
expanded liquid, simultaneous investigation of eqn. of state and elec. cond. 77−55337
extrusion from $Hg_{2.86}AsF_6$ and $Hg_{2.91}SbF_6$, on cooling below 200K, DTA 78−55953
fallout in Hawaii 78−61551
Faraday effect for reversible depolarisation, optical communication scrambling appl. 77−42596
ferromagnetic liquid, Fe particles in Hg, mag. props., ageing effects 77−12154
filament, crit. mag. field and supercond. transition temp. 77−16013
filament, ultrathin, influence of fluctuations on supercond. transition 77−8234
film, melting and crystallisation kinetics, electron microscopy 77−15725
flow, unsteady stagnation heat transfer through laminar, incompressible boundary layer 80−1584
flow in annuli, turbulence, heat transfer eddy diffusivity 77−19602
flow in curved channels under transverse mag. field, transition and turbulent flows 80−79396
flow of liquid metals in curved channels laminar, transversely applied mag. field 80−14829
flow transition, in mag. field, 2-dimens. to 3-dimens. turbulence *(Russian)* 77−7471
fluid, expanded, optical absorpt., excitonic and continuum states 79−95801
fluid layer with rot. and mag. field, cell sizes at thermal convection onset 77−54991
gas discharge positive column, elec. probe for diagnostics, teaching appl. 79−62979
grain boundary fracture of Al bicrystal 77−36690
gravity fed heat pipe for production of high purity fixed density of Hg atoms 80−69627
Greenland Ice Sheet, Hg contents 78−65349
HF discharge mode two-valued depend. on arcing voltage, geometric reson. *(Russian)* 77−47283
high vacuum technology appls. 78−81998
high-pressure discharge, temp. and electron density meas. *(French)* 78−59705
Iceland, Hg natural conc. 77−64244
inductively stirred, convective flow rate controlled by Lorentz's number rel. to solidified struct. 79−10444
interatomic potential, Gordon-Kim theory variants, appl. to inert gases and Hg_2 79−76478
intercalation with graphite and alkali metal 80−44183
interface with aqueous KCl film, secondary electrocapillary effects 77−55420
mercury continued
interface with electrolyte, polarizable, dynamics of double layer 79−24756
ion-laser discharges, high-power, stability limits 78−37872
irradiation by protons and deuterons, Tl yield determ. 78−2174
island film, melting and crystn. kinetics, dark field electron microscopy 79−11026
Laccadive Sea waters, total Hg concs. 80−104996
laser, optically pumped, saturable absorber overlap of ^{127}I 77−83932
light sources, high press., spectral distribution of irradiance, 240 to 600 nm *(German)* 77−79910
liquid, and dil. liq., amalgams, elec. cond. and thermoelec. power 77−55511
liquid, Brillouin scatt. obs. 77−24858
liquid, Brillouin scattering from reflections of surface ripples 78−48188
liquid, elec. cond. and thermoelec. power meas. 77−59273
liquid, electron energy states calc. *(Russian)* 79−4506
liquid, eqn. of state parameters rel. to Earth core energetics 77−15536
liquid, expanded, band model for electronic struct. 77−89690
liquid, expanded, thermodynamic and electron transport props. 79−23938
liquid, expanded electronic props. 77−55477
liquid, ferromagnetic, containing Fe particles, time depend. magnetisation 80−44877
liquid, flow in transverse mag. field, laminar and transition, channel wall effects 78−63500
liquid, nucl. spin relax. and quadrupolar relax. mech. 78−64292
liquid, P-V-T relations for temperatures of 40 to 240°C and press. up to 1400 kg cm^{-2} 78−6140
liquid, quadrupole relaxation rate temp. depend 80−88884
liquid, soft-sphere equation of state 79−55863
liquid, sound vel. near metal-nonmetal transition, up to 1600°C and 2000 kg/cm^2 80−39222
liquid, struct., X-ray diffr. obs. 77−84619
liquid, structure factors, higher order distrib. functions 77−51299
liquid, surface plasmon dispersion 77−62978
liquid, surface tension temp. depend. 77−4248
liquid, T_c, P_c, V_c, from eqn. of state 78−2228
liquid, thermoelectric power, pseudopotential calc. 80−59959
liquid, X-ray diffraction analysis 79−4232
liquid metal, electronic density of states, pseudopotential calcs. 80−70578
liquid metal, flow and energetic characts. in linear induction MHD pump *(Russian)* 77−3882
liquid structure, X-ray diffr. obs., 173-473K 80−14997
liquid-vapour interface, density profile near triple point, X-ray refl. 78−75821
long wavelength limit, triplet and higher correls., Percus-Yevick eqn., perturbative anal. 79−37613
loss rate from contaminated estuarine sediments 80−85310
low-pressure pulse-modulated discharge optical and electrical parameters 78−67491
luminescence photosensitisation in $NH_3(ND_3)$, at low press. 78−13542
manometer, automatic press. recording by capacitive sensor 77−37871
marine pollution conc. in coastal waters of North and South Lebanon 79−12146
marine pollution in Kuwait, meas. 79−5510
melting line, pressures up to 1200 MPa 80−84281
melting line determ., latent heat method, high press. 77−37903
on metal surface, flow kinetics in temp. grad. *(Russian)* 78−6198
methyl Hg in River Mersey estuary sediments, H_2S effect 79−2295
3-methylpentane, glassy soln., Hg sensitised UV photolysis, radical production 79−52720
MHD duct flow, hot-film probe vel. meas. 80−75009
MHD flow, shear turbulence with transverse mag. field 79−32695
MHD laminar flow, longitudinal dynamic effects determination for Hg *(Rumanian)* 80−64792
MHD shear flow, energy transfer from turbulent to mean motion 77−35252
molecule, pseudopot. theory calcs. of electronic struct. 77−42230
monitoring, personal piezoelec. cryst. dosimeter 77−21672
natural convection in mag. field parallel to the gravity vector 79−81990
natural waters, radiotracer methods for speciation study 79−88490
neutron activation anal. for low levels in water 79−70503
neutron activation anal. in Bi 79−57336
neutron activation analysis of human thumbnails 77−64130
S.New England coastal rain, Hg flux 80−41508
NQR, relax. rate, temp. depend. 77−48084
nuclear magnetic moment ratio of odd isotopes *(French)* 77−75081
nuclear quadrupole relax. rate for ^{201}Hg, −35 to 80°C 77−36151
ocean model, for geomag. vars. induced by waves 77−49003
optical gap of expanded fluid, KKR band calcs. 77−1354
optical properties by spectroscopic ellipsometry, review 80−103929
optical tilt gauge, based on Hg pool 78−88931
partial vapour pressure, determ. for volatile component by static method 80−37150
penetration, in porous materials, pore size determ. 78−43165
photodissociation laser, optically pumped 77−68206
photoemission, into electrolyte soln., five-halves law 77−44132
photoemission, transition from ordered solid to disordered liquid 80−45217
photoionisation cross sections, Hartree-Slater and Hartree-Fock calc. 79−89653
plasma, dense weakly ionised, thermo EMF, calc. 80−64686
plasma, emission spectra near photorecomb. threshold, high press. effects *(Russian)* 78−38545
plasma, molecular dynamics model for atom-electron interactions 78−42708
plasma, optically pumped positive column, E-I characts. 80−44035
plasma, spectral line strength, charge density effect 79−73040
plasma continuous spectra at series limit $6p^2\,^3P_2$ *(French)* 77−88413
plasma flow, electron temp. determ. from partial LTE populations 80−24248
plasma formation by strong Hg line irrad., mechanism 78−83585
plasma under HF voltage, frequency depend. of Langmuir probe *(Russian)* 77−11407
plastic deform. and fracture obs. by acoustic emission of Zn single crysts. in metal melt *(Russian)* 78−56737
pollution, conc. in fish and waters of United Kingdom fishing grounds 78−36204
pollution, detect. in sediments in semienclosed bay, Norway 78−81220

mercury continued
pollution, future average Hg content of oceans and European air, soil, and river sediments 79−8687
pollution of Mediterranean sediments around Alexandria, Egypt 80−3538
pool boiling heat transfer in mag. field 80−33584
positive column, electron energy distrib., numerical soln. of Boltzmann eqn. 80−87982
positive column, high press., excimer densities and destruction mechanisms 78−5967
positive column of discharge, alignment of Hg levels 78−83639
positron annihilation, ang. correl. data analysis for solid and liq. phases 78−52592
positron annihilation rates, electron-electron and electron-positron correl. effects 78−76548
powders, rapidly solidified, nucleation, undercooling and homogeneous structs. 78−52708
probe for quality control of Si-SiO_2 interface *(Chinese)* 77−89857
quadrupole interactions in Zn, lattice location, gamma spectral study 80−80227
quadrupole relaxation of ^{202}Tl impurities 77−16215
radiochemical neutron activation anal. of environmental matrices for Hg and noble metals 80−16889
reduced density, screening, struct. and elec. resist. 78−19016
reflection spectra, electronic density of states, calc. 80−66229
relaxation time constants meas. of optically pumped stored Hg ions 80−106287
rhombohedral crystals, slip dislocations and slip systems 79−23617
river Hg dispersal from lode sources in Kuskokwim River drainage, Alaska 78−40600
sediment pollution by Hg and As, instrumental neutron activation and atomic abs. spectrometric anal. 80−16890
self-diffusion coeffs. by radioactive tracer technique 80−49392
slow atoms, inverse scatt., semiclassical approx. calcs. 78−17747
soil and water in Israel and Sinai, Hg levels 77−29337
solid, phonon dispersion curves, neutron inelastic scatt. 78−14410
solid, resistivity ratio, 1.65 to 234K 80−59952
solidification, optical and elec. effects 78−47502
solubility of CdTe and $Cd_xHg_{1-x}Te$, rel. to LPE 78−35359
spectroscopic light source, Hg linewidth meas. *(Russian)* 78−4708
static charge generation, evidence of electron transfer as mechanism, contact with nylon 6 79−47153
static drop electrode, voltammetry appls. 80−97740
structure, −30 to 290°C, X-ray diffr., and appl. to electron transport props. 79−46551
superconducting crit. temp., functional derivative with electronic density of states, Eliashberg eqns. 79−56368
superconducting film, far IR and electrodynamic prop. meas. 80−103957
superconducting transition temp., perturbative corrections, direct and indirect ladder diagrams 80−49979
superconducting transition temp. from Eliashberg eqns. 79−51709
superconductor, law of corresponding states, Eliashberg eqn. *(Russian)* 79−87183
superconductor, strong coupling, finite-freq. US attenuation 77−51846
supercritical, elec. cond., four electrode method 80−62685
superheated liquid, growth of spherical bubbles, anal., numerical calcs. 77−24399
surface, reflectance, use in surface temp. meas. 77−2653
surface plasmons at inhomogeneous liq. metal/dielec. interface, second dispersion branch 77−32059
surface props. rel. to adsorbed O_2, H_2O vapour, work function determ. 78−60187
surface tension, in Rankine-type capillary viscometer *(Japanese)* 80−14859
surface tension and width, density functional theory 80−103537
targets for nucl. physics., thick target preparation 79−63851
thermal switching at solid-liquid transition 77−8154
thermophysical properties rel. to clustering in liqs. 77−1065
Townsend discharge, electron swarm props. Boltzmann eqn. anal. 80−19648
transport coeffs., temp. and press. depend., Enskog theory 78−6170
triboelectrification of insulation surface 79−78157
turbulent channel flow, in mag. field, spatial correl. and vorticity *(Russian)* 77−3876
turbulent flow on stabilising thermal section, temp. fields and heat transfer 80−19366
two photon photoelectric emission, photocurrent vectorial depend. 79−95906
ultrathin metallic filaments, appearance of dielec. instability, coexistence with supercond. 80−103784
unsteady channel flow with transversely applied mag. field 77−84328
US velocity meas. depend. on liquid density 78−43073
vacuum arc, vapour-cone angles of neutrals and ions emanating from cathode 77−4007
valence band spectra by PES study 80−4822
vapour, electron drift vel., expt. 78−30403
vapour, electron drift vel., momentum cross-section, theory 78−30404
vapour, electron drift velocity at 573K 80−103103
vapour, electron momentum transfer cross section, from 0.1-5 eV 80−103104
vapour, gas analysers testing using Zarzma equipment 78−76962
vapour, high density, optical absorpt. edge, density depend. 79−72985
vapour, line splitting on Tonks-Dattner reson. 80−59317
vapour, low pressure gases, dielectric breakdown model 78−9883
vapour, resonance line shape in presence of $Hg(6^3P_1)$-$Hg(6^1S_0)$ interactions 80−78572
vapour, thermal cond. coeff. meas., 600 to 2500K 77−35303
vapour, two photon reson. tripling of Nd laser fourth harmonic 78−30014
vapour, viscosity and thermal cond. meas., data anal., 694-1054K 80−19545
vapour conc. meter, construction and performance 79−2759
vapour discharges, high-press., e-beam initiated, laser absorpt. meas. 80−92412
vapour drag effect, McLeod gauge, capillary depression phenomena 80−98923
vapour excimer lasers, theory, review 79−59684
vapour laser, optically pumped, gain and output power 78−66843
vapour plasma, RF, probe diagnosis *(Russian)* 78−75423
vapour-gas mixture, Hg diffusion, data correlation 78−79403
vapours, viscosity meas. by vibr. disc method, 620-800K 80−19530
mercury continued
volatilisation losses during neutron irradiation in a reactor 80−13596
volatility, in NAA from samples and standards *(Russian)* 80−41128
wetted reed switch, heat treatment variations effects on Fe-Ni alloys surface conditions and on switch behaviour 80−66547
wetting of GaAs surface, doping degree influence 80−92762
work function, temp. coeff. from electrochem. data 78−60186
X-ray microanalysis, quantification of losses 80−85261
Al, sacrificial anode dissolution, Hg effect study using ion implantation 79−39016
Al-lead stearate-Hg, transient and alternating electric currents 78−84311
Al|chlorophyll-a|Hg/In, sandwich cell, photovoltaic, rectifying and tunnelling effects 79−1628
Ar-Hg, gas mixture, diffusion coeffs. and electron temps. 77−62327
Ar-Hg-Cl_2, elec. discharge, electron inelastic collision props. 80−79617
atom, resonance line, 253.7 nm for atomic absorpt. meas. 80−78556
Au/Hg probe for C-V meas., work function difference between probe and Si 80−2450
Bi_2Se_3:Hg point defects in crystal lattice, Hall coefficient and IR spectra determ. 80−55129
Cd UV subshell photoionisation cross section, expt. and GIPM theory 78−21887
Cd(Hg)/$CdSO_4$, aq. electrochem. system, kinetics, impedance *(German)* 77−32807
$Cd_xHg_{1-x}Te$, inhomogeneous composition effect on carrier lifetime and photosensitivity *(Russian)* 79−73526
CsI-Hg-Ar discharge, high-press., temp. and plasma comp. determ. 79−10709
DyI_3/CsI/Hg arc, oscillations induced by external mag. field, arc constriction 79−60205
DyI_3-Hg arc discharge plasma, spectroscopic study 80−54033
Ge:Hg, anomalous photocond. with 10.6 μm laser light *(Russian)* 77−47861
Ge:Hg, anomalous room-temp. impurity photocond. 78−39159
Ge:Hg, impurity characterisation from thermal carrier meas. 80−65595
Ge:Hg, S-type diode, elec. props. 80−20299
Ge:Hg, Sb, photoelec. props., 70 to 300K 80−65621
p-Ge:Hg,Au,Sb, radiation-defect form., Au influence 80−92911
Ge:Hg photoconductive detector, laser damage thresholds calc. 78−90443
Ge:Hg S-type diodes, photoelec. props. 80−6964
p-Ge:Hg^-, deep levels, optical-phonon-assisted capture of carriers 79−51597
He-Hg afterglow plasma, time resolved double probe study 78−18444
He-Hg direct nuclear pumped laser, optimum conditions for lasing 77−50655
He-Hg laser, Hg II direct nuclear pumped gain at 7945 Å 78−5467
He-Hg nuclear pumped laser, charge exchange pumping 80−63996
He-Hg plasma, prod. by nucl. radiation, charge exchange effects 77−24103
He-Hg RF discharge, atomic ionis. and excitation, spectral line intensities 78−26334
He+Hg, metastable He, collision rate consts. in pulsed discharge afterflow 78−50627
$He^+ + Hg_0 \rightarrow He_0 + (Hg^+)^* + \Delta E$, cross sections, rate consts. 78−17785
^{3}He-Hg (−Kr)+^{3}He(n,p)T, high press. plasma excitation, luminesc. spectra 80−38719
$He(2^3S_1) + Hg_0 \rightarrow He_0 + Hg^+ + e$, in afterglow, rate const. meas. 78−17785
Hg $6\ ^1S_0$-Hg $6\ ^1P_1$, Van der Waals term in interaction, blue satellite line *(French)* 80−37848
Hg 6^3P_1 collisional transfer rate between m-sublevels mag. field depend. 80−32802
Hg 6^3P_1 states, detection impact excitation cross section meas., using self calibrating apparatus 79−50135
Hg, determ., cold vapour atomic absorption method, sorption effects *(Russian)* 78−73122
Hg, determ., in Pb, radioactivation and other methods 78−76952
Hg, electron inelastic scatt., spin-polarisation, differential cross-section, DWBA 78−50644
Hg emission rel. to Hg-sensitised UV photoreactions in abiogenetic organic synthesis on primitive Earth 77−37173
Hg, ground state correl., photoelectron spectra, multiconfig. Hartree-Fock calcs. 77−50471
Hg I, II, electron impact excitation, absolute emission cross sections, 284.7 and 479.7 nm 77−19086
Hg II, $6p^2P$ and $6p^2D$ levels, radiative lifetimes meas. 80−78576
Hg II, excitation cross sections, transition probabilities, by electron impact 79−3580
Hg II, hyperfine struct. of 194.2 line, $^2S_{1/2}$-$^2P_{1/2}$ transition *(French)* 77−27009
Hg II, pulse excitation in discharge *(Russian)* 77−54704
Hg II, relativistic oscill. strengths 77−14388
Hg II line oscillator strength determ. in Ap-type stars, diffusion model implications 80−72966
Hg III, quasi c.w. laser action, low press. discharge 77−664
Hg, thermodynamical Gruneisen parameter, press. depend. 78−14479
Hg vapour, absorpt. spectrum, 1849 Å line, self-broadening, interatomic interaction *(French)* 80−32661
^{199}Hg, 6^1S_0-6^3P_0 forbidden transition absorpt. at 265.6 nm, A coeff. and self-press. broadening determ. 80−95562
Hg^{2+} selective liquid-state electrode, construction and basic charact. 77−90705
Hg/aqueous solution interface, elec. double layer in presence of adsorbed ions 79−83469
Hg/electrolyte contacts, adsorption model for double layer capacitance 80−44706
Hg/$Na_2B_4O_7$.$10H_2O$ contacts, double-layer capacitance, temp. depend. 80−44707
Hg/Xe films, optical study of metal-insulator transition 79−65947
Hg-A positive column discharges, scaling towards display cells 77−84565
Hg-Al_2O_3-Al structure, I-V charact. at room temp. for different thicknesses 79−47172
Hg-aqueous electrolyte interface, double layer charge relax., thermal jump meas. 78−53216
Hg-Ar, HF discharge, electron energy distrib. and atom ionisation processes 80−44048
Hg-Ar, low press. discharge positive column ionisation processes 78−75445

mercury continued
Hg-Ar, low-pressure discharge, energy balance and Coulomb relax. 77−43098
Hg-Ar, two phase flow in vertical tube, transverse mag. field, bubbles and slug flow 77−84303
Hg-Ar mixture, RF discharge, frequency characts. investig. 80−38761
Hg-Ar quench condensed system, annealing effects on elec. cond. 79−60880
Hg-Ar(Kr)(Xe) mixtures, prebreakdown discharges, discharge current depend. on electron mobility 79−77433
Hg-Au, minigrid optically transparent thin-layer electrode 77−70305
Hg-C optically transparent electrodes, prep., props. 78−7210
Hg-Cd, sensitised fluoresc., anomalous Hanle effect 79−81186
Hg-Cd cell, EMF rel. to temp., thermodynamics 77−12805
Hg-Cl_2-Ar, photochem. reaction producing $HgCl(B^2\Sigma^+)$, chemiluminesc. 79−39154
Hg-Cs, vac. UV laser, charge exchange pumping 77−31095
Hg-electrolyte capillary cell, capacitative control of interelectrode gap 77−90610
Hg-electrolyte interface, with imposed temporal and spatial periodicity, double-layer transduction 78−88639
Hg-gas interface, electrocapillary effects, CH_2Cl_2 adsorption in CF_4 77−32798
Hg-He(Ar), modulated discharge, elec. and optical props. 77−7627
Hg-I ANL-4 cycle for thermochem. H prod. 80−35785
Hg-in-glass thermostat 80−22359
Hg-InP Schottky-barrier diode, contact times, I-V characts. 80−96971
Hg-KI solution interface, specific adsorption of I ions, electrical double layer, interface excess activity coeff. 80−49523
Hg-N_2, optical pumping, vibr. excitation, laser theory 78−66517
Hg-N_2, optically pumped pulsed 546.1 nm laser emission 79−13952
Hg-polyvinylcarbazole interface, contact electrification, internal photoemission study 78−60191
Hg-sensitised fluorescence, in Tl+N_2, quenching 79−22643
Hg-Tl, vap., Tl sensitised fluoresc., spectral line Doppler broadening 77−3314
Hg-Tl-I discharges, 50 H_2, Tl atoms axial segregation 80−38781
Hg-Tl-I discharges, 50 Hz, axial segregation effect on elec. field strength 80−59320
Hg-Xe film, random mixtures, superconducting transition temp. and metal-nonmetal transition 80−29498
Hg-Xe solid films, optical absorpt., localised states 79−61452
Hg-Xe solid mixture, optical criterion for Mott transition 78−75996
Hg-Xe system, metal-insulator transition temp.-coeff. of cond. 77−66188
Hg-Xe vapour deposited films, cond. transitions, effect of disorder on supercond. 80−88659
Hg-Xe(Kr)(Ar), fluoresc. emission, high press., electron beam excitation, laser appl. 77−34676
Hg+2NH_3→$HgNH_3$+NH_3, photosensitised, $HgNH_3$ complex lifetime 78−53193
Hg+Ar, spectral line broadening of Hg in UV, interaction pot. 79−26937
Hg+benzene electronically excited, mol. fluoresc., vibr. relax. cross sections and equilibration rates determ. 80−87205
Hg+Cd, quantum beats under transfer of orientation 79−98206
Hg+Cl_2+$\hbar\omega$→HgCl*+Cl, laser-induced harpooning reactions 80−83458
Hg+Cl_2→$(HgCl_2)_n$, surface catalysed reaction 79−100430
Hg+Cs(K)(Na)(Rb), scatt. cross-sections, pseudopot. calcs. 78−9225
Hg+H, differential cross sections, orbiting contribution 79−41221
Hg+H_2(CO)(NH_3)(ethylene), quenching rate constants determ. with nanosecond light pulser with Hg vapour 80−100111
Hg+H_2(HD)(D_2), intramultiplet transitions 77−54597
Hg+H^+, L-subshell ionisation cross-sections, X-ray meas. 77−46520
Hg+H^+, L-subshell X-ray prod., cross-section meas. 77−46575
Hg+H(H_2), resonance scatt., HgH potential determ. 77−61830
Hg+halomethane, $^3P_1$-state total quenching 80−52927
Hg+He, afterglow, $Hg^+(7^2P_{1/2}, 7^2P_{3/2})$, excitation processes, rate consts. *(Russian)* 78−29848
Hg+He^+, thermal energy charge transfer reaction, ion states, relative yields 79−45840
Hg+He^{2+}, autoionisation, 5-20 eV, electron and ion ang. distrib. 78−78795
Hg+He*, Penning and assoc. ionisation, correl. diagrams calcs. 77−50521
Hg+He(Xe), collisionally induced coherence, orientation and alignment, transfer among 6s6d levels 78−74747
Hg+Hg, depolarising collisions in positive column of discharge 78−83639
Hg+Hg, gas discharge plasma, collision cross section anal. 80−33735
Hg+Hg*, combination into ungerade dimer states 80−55633
Hg+I_2 reaction, adiabatic pot. energy surface 78−15666
Hg+I_2→HgI+I, endoergic reaction, prod. ang. distrib. 78−15665
Hg+inert gas interaction potential *(French)* 78−25647
Hg+K, electronic excitation, integral cross-section, 50-1500 eV 78−62888
Hg+N_2, $6(^3P_0)$→$6(^3P_1)$ excitation, double modulation obs. 79−27072
Hg+N_2, inelastic collision, 6^3D_1 population transfer to other 6s6d Hg levels, fluoresc. obs. 78−78791
Hg+NH_3, excited UV luminesc., low press., $HgNH_3$* form. 77−21388
Hg+Na(K)(Rb), 15-1400 eV, electronic excitation, integral cross sections 80−43159
Hg+Ne(Na)(K)(Rb), elastic scatt., interatomic pots. 77−58122
Hg+Tl, excitation energy transfer, excitation rate consts. 80−37772
Hg+Tl, Tl sensitised fluorescence 78−70778
Hg+Tl vap., sensitised fluoresc. 77−88423
Hg+water systems, drop fragmentation rel. to thermal explosion detonation requirements 78−71368
Hg+Xe, pressure broadened absorption profiles *(French)* 79−98033
Hg+Xe^{x+}, single and multiple collisions, charact. and quasimolecular X-rays 77−83713
Hg+Zn(Cd), sensitized fluoresc., orientation and alignment transfers *(French)* 79−13808
Hg^++2Hg→Hg_2^++Hg, gas phase reaction rate const. calc. 78−92457
Hg^++Cl^-, in Ar, high press. ion-ion recomb. rate calcs. 78−31621
Hg_2, absorpt., fluoresc. and two-photon spectroscopy 78−998
Hg_2 and Hg_3 metastable states in flash photolysis of Hg vapour, electronic absorpt. spectra 79−76438
Hg_2 as energy storage medium, energy extraction from metastable excimers 79−59677

mercury continued
Hg_2, dissociative recomb. and optical transmissions meas. in high press. discharge 80−37816
Hg_2, emission and form. kinetics, sequential two-photon absorpt. expt. 80−32767
Hg_2, emission bands, pot. energy surface calcs. 77−10601
Hg_2 excimer states, energy transfer kinetics 78−63090
Hg_2 excimers, photoassoc., spectroscopy and kinetic processes of high-lying vibronic states, laser applics. 80−9649
Hg_2 excimers in constricted positive column, radial intensity distrib. meas. 78−63091
Hg_2, fluoresc. and absorpt. spectra anal., pot. energy curves 78−999
Hg_2, fluoresc. decay, 335 and 485 nm 78−46387
Hg_2, fluoresc. decay of 1_u state 78−70864
Hg_2 laser, high press. transverse discharge for high efficiency, elec. and optical props. 78−63092
Hg_2, model calc. of electronic struct. and spectroscopy 79−3352
Hg_2, optical pumping, continuous emission obs. 78−5296
Hg_2, photoassoc., 0_u^+→0_g^+ fluoresc., Condon internal diffraction 78−78747
Hg_2, photoassociated, collision-induced predissoc. with Hg 79−31626
Hg_2, quenching and predissociation, possible excimer laser 80−32770
Hg_2 vapour, high-press., selective refl. meas. up to 700 bar 80−28031
Hg_2^+, electronic struct. and photoabsorpt. calcs. 80−27932
$Hg_{99}As$, struct. reinterpretation 78−38660
$Hg_{1-x}Cd_xTe$:Hg, ion implanted, damage and lattice location study 80−103381
$Hg_{1-x}Cd_xTe$:Hg, p-n junction photovoltaic diode, appl. as IR detector 78−86330
HgH+NO→HNO+Hg, Hg photosensitised reaction in H_2-NO gas mixtures 77−36757
$Hg_2(Hg_3)$, violet emission, formation and decay kinetics, luminesc. time resolved spectra 79−76464
HgMn stars, evidence for Hg in thin atmospheric layer rel. to diffusion model 80−105243
$HgNH_3$ complex, fluoresc., lifetime meas. 78−53193
$Hg(^3P_0)$+Br_2→HgBr(B)+Br, crossed mol. beam chemiluminesc., cross section 78−31622
$Hg(^3P_0)$+N_2 fluorescence decay following pulsed laser excitation 77−30817
$Hg(^1P_1)$+CO, $Hg(^3P_1)$ production mechanisms 78−29847
$Hg(^1S)$, dipole polarisability, relativistic effective core pot. calc. 79−76362
$Hg_2(X^1\Sigma_g^+)$ potential, intra-atomic correl. in HF calcs. 78−5314
^{A}Hg, A=198-202,204, muonic X-ray transitions, nuclear state quadrupole moments and charge distrib. 79−41253
^{190}Hg ($T_{1/2}$=20 m) isotope, IS in 2537 Å line, on-line laser spectroscopy 77−61712
^{191}Hg^m, and $^{190m-185m}$Hg, nucl. spins, on-line quantum beat spectrosc. determ. 80−9562
^{197}Hg fixation test, new kidney physiopathology concepts *(French)* 77−70518
^{197}Hg, kidney function studies following radiation therapy of spleen 79−20615
^{197}Hg, labelling of human albumin microspheres 80−51251
^{197}Hg source for Mossbauer studies 79−26796
^{197}Hg use in lung tumour diagnosis *(French)* 77−70519
^{199}Hg, atom-surface interaction, nucl. relax., temp. depend. 80−88886
^{199}Hg optically oriented atom interaction with cell wall paramag. centres 80−37762
$^{199}Hg^+$, hyperfine separation of ground-state, optical double-reson. 78−78828
$^{199}Hg^+$ isolated ions, mag. hyperfine spectrum 78−29760
$^{199}Hg^+$ trapped ion frequency standard 78−57914
^{201}Hg, NMR line shape, effect of static and alternating field inhomogeneities 78−50491
^{202}Hg/^{196}Hg anomalous ratios in meteorites, interrelations, cosmological inferences 77−2375
^{202}Hg/^{196}Hg ratio anomalies in meteorites, possible prod. by extinct radioactive nucleus ^{202}Pb 77−49343
^{203}Hg nuclei, optically pumped, anharmonic mag. resonance phenomena 79−94015
^{203}Hg separation from chlormerodrin-203, electrophoretic method 77−56283
^{203}Hg, tracer for Hg conc. in seawater expts. ^{75}Se tracer 80−21420
^{203}Hg, tumour tracer accumulation, autoradiographic study, experimental infectious lesions 79−5348
Hg*+Ar(Ne), 6^3P_0 and 6^3P_2 metastable states, interaction pot. parameters 77−79670
Hg*+NH_3, UV emission at low press., pulsed excitation, relax. meas. 77−79570
^{199m}Hg radioisotope preparation at variable energy cyclotron of Frederic Joliot Hospital Service *(French)* 77−65361
$Hg(6^3P)$+O_2, photosensitised reaction, excited intermediates, energy transfer detect. 78−73030
$Hg(6^3P_0)$, $^3P_1$-$^3P_0$ fine struct. obs., CO_2 laser mag. res. 77−61696
$Hg(6^3P_0)$+Cl_2 reaction, reactive quenching metastable states 79−57208
$Hg(6^3P_0)$+$Hg(6^3P_2)$, line excitation and population decay in afterglow 80−74242
$Hg(6^3P_0)$+Na, energy transfer, rate consts. *(Russian)* 79−54952
$Hg(6^3P_0)$+t-butylamine, attachment mechanism, kinetics, dimer emission, luminesc. spectra 77−73442
$Hg(6^3P_1)$ resonance level population, in vap. and inert gas modulated discharges 77−83532
$Hg(6^3P_1)$, slow electron scatt. stepwise excitation function to 6^3P_2 state 79−858
$Hg(6^3P_1)$+$Hg(6^1S_0)$, collisional excitation transfer in high mag. fields, fluoresc. obs. 80−9689
$Hg(6^3P_1)$+Li^+(Na^+)(K^+), excitation, optical polarisation fractions and mag. sublevels obs. 78−50619
$Hg(6^3P_{2,0})$+inert gas, diffusion in low-current discharge 78−63618
$Hg(6^3P_2)$, Pt surface impact, in $Hg(6^3P_1)$ stepwise electron excitation function meas. 79−858
$Hg(6^3P_2)$+$Cd(5^1S_0)$, spectral width of $Cd(5^3P_1)$ line *(French)* 77−50397
$Hg(6^3P_2)$+Hg, aligned metastable ats., longitudinal and transverse relax. times, simultaneous meas. 78−13585
$Hg(6^3P_1)(6^3P_0)$+CO(NO), electronic-vibr. energy transfer collision, IR obs. 79−45716
n-InP-Hg, Schottky barrier height and stability characterisation 80−54786

mercury continued
KCl:Hg^+, X-irradiated, ESR meas. 77−1588
KF:Hg^{2+}, electrolytic colouration 78−75665
LiF:Hg^{2+}, electrolytic colouration 78−75665
liquid, polyvalent, electrical resistivity by harmonic model potential 80−54668
NH_3, photosensitisation by Hg, fluoresc. spectrum 78−90198
$NH_3(ND_3)$+Hg, photosensitised luminesc., phase shift anal. 79−15966
NO+Hg, vibr. relax. of states v=2-10 79−89752
Na-Hg high-press. discharge, Na reson. radiation, self-reversed maxima shifts 80−92411
Na-Hg-Xe cylindrical high pressure arc discharge, acoustic resonance 78−67454
Na^++Hg, low-energy collision, quantum mech. phase interference and optical polarisation 77−42385
NaCl:Hg^+, X-irradiated, ESR meas. 77−1588
NaF:Hg^{2+}, electrolytic colouration 78−75665
Na(^2P)+Hg, differential cross section, orbiting backward peak, obs. 79−76482
Na($^2P_{3/2}$)+Hg, differential scatt. cross sections 78−66644
Na($^2P_{3/2}$)+Hg, laser excited atoms, differential cross sections 78−62905
Ne-Hg RF discharge, atomic ionis. and excitation, spectral line intensities 78−26334
Sb-Hg, quadrupole interaction, time differential perturbed ang. correl. and nucl. orientation 79−24250
Se, Hg activated amorphous film, anomalous photocond. 77−43658
Se:Hg amorphous film, photocond. anomaly due to HgSe layer form. 77−66183
Se:Hg film, amorphous, anomalous photocond. and residual interelectrode photo-EMF 77−69376
Si:Hg, photomag. effect 77−4401
TiO_2 electrode, illuminated, Hg deposit from Hg(II) solns. *(French)* 79−52696
Tl-Hg, excimer band emission from electron beam initiated discharge in TlI-Hg 80−78841
Tl-Hg, UV preionised discharge, possible excimer laser 79−55119
Tl-Hg excimer, emission pressure and temp. depend., blue band gain, RF excited discharge 79−22941
Tl(Hg)/$TlClO_4$, aq. electrochem. system, kinetics, impedance *(German)* 77−32807
Xe ion+Hg vapour collisions, quasimol. M-radiation 77−14566
Zn-Hg, metal/liquid metal, exam. of crack propag. in liquid metal environment 78−60766

Mercury (planet)
airglow, Mariner 10 UV spectrometer expt. 77−64611
albedo features, IAU nomenclature 78−53848
albedo features, longits. and nomenclature 78−53849
atmosphere, comp. from Mariner 10 data 77−9684
atmosphere, occultation expt. by Mariner 10 UV spectrometer 77−67023
basalts, redox state 78−77217
bow shock location compared with Venus Mars and Earth 78−28560
bright patches in several large craters, possible physico-chemical alteration process 78−32375
Caloris basin, comparison with lunar Orientale basin 78−12121
Caloris Basin, tectonic implications of gravity struct. 78−28561
capture into resonance rotation, tidal friction 77−78620
charged particle fluxes, electron calibration of Mariner 10 instrumentation 80−12628
cometary collision, origin of swirl patterns on surface 80−51675
convection in interior, evidence from gravity field 78−12127
core, effect of obliquity on spin-orbit constraints 77−87300
core, formation, history and energetics 79−84694
crater doublets expected frequency 78−61777
crater saturation and equilibrium, Monte Carlo simulation 77−71038
crater size-shape profiles, terrain effects, interplanetary comparisons 79−66936
cratered surface entropy 80−101541
craters, discovery from Earth (in 1901) 78−53847
craters and plains, comparative studies of Moon, Mars and Mercury 77−53439
crustal evolution in silicate planets, review 78−61774
crustal tectonics, relation to internal evolution 78−12116
development and structure, Earth and Moon comparison *(German)* 77−67055
dipole displacement 79−80252
diurnal motion of Sun seen from Mercury, computer aided soln., teaching aspects 78−61969
dynamo theory for mag. field generation *(German)* 78−40852
EM heating, EM heating in early solar system 80−36555
EUV albedo, comparison with Moon 77−33378
exosphere, Monte Carlo modelling 78−96416
exosphere simulation, Monte Carlo methods 80−67588
exosphere simulation, Monte Carlo methods 80−67589
expansion and gravit. constant changes, limits 78−28155
geologic evolution of terrestrial planets 77−53442
global fracture patterns of despun planet 79−66941
global tectonics, consequence of tidal despinning 78−85874
global tectonics, following tidal despinning 77−60698
global tectonics, of Mercury and the Moon 78−12128
impact craters, endogenic modification 78−12129
intercrater plains, Mariner 10 obs. 77−9685
intercrater plains on Moon and Mercury, origin and relative ages 78−12117
interior, solid-state convection, obs. evidence 79−84692
interior structure, rel. to mag. field origin 78−12115
internal structure evolution, calc. 77−82137
landform degradation evidence from crater depth/diameter relations 77−37536
large impact structures, numbers and isostasy rel. to average crustal viscosity 78−12120
late heavy bombardment in inner solar system 77−71019
liquid core viscosity spin-orbit constraint 77−33377
lithosphere global TRM in presence of central dipole field, theory 80−31223
magnetic field, characts. and origin 78−12131
magnetic field, dimensional anal., simple model 79−58286
magnetic field, dynamo origin 77−29675
magnetic field, fit to scaled down geomagnetic field 77−87299
magnetic field, spacecraft meas. 79−2503
magnetic field and interior, review 78−65524

Mercury continued
magnetic field and magnetosphere, Mariner 10 obs. and theory 80−36530
magnetic field apparent source depth, rel. to planet interior struct. 78−57478
magnetic fields in early solar system, recorded in lunar rocks, meteorites and planets 79−5765
magnetic moment, deduction methods using limited data 80−36532
magnetosphere, compression by solar wind 79−96936
magnetosphere model 80−36531
magnetospheric magnetic field, model 77−45336
Mariner 10 2nd and 3rd encounters 77−73989
Mariner 10 expedition stages *(Norwegian)* 78−49291
Mariner 10 images, digital processing 77−78647
Mariner 10 UV spectrometry results 77−45337
Mercury and the Moon, conference, Houston, Texas (15-17 November 1976) 78−12126
meteorite impact ejecta, depend. of mass and energy lost on planetary escape vel. 78−45295
micrometeorite impact, ion emission 80−77362
morphological features of crust from Mariner 10 obs. 80−67603
morphology of fresh crater landforms, form. and modification 78−40847
natural satellites, theory of escape 78−16323
natural satellites escape rel. to planet's slow rot. 79−25529
optical characteristics, interpretation rel. to surface material props. 78−12130
orbital motion, Lorentz-covariant model of the system of two gravitating particles 80−8865
orbiter missions, new concepts 79−80197
perihelion precession, determ. by relativistic force equation *(Afrikaans)* 79−97270
perihelion precession, nonrelativistic contrib. 79−71184
perihelion shift, gravitation, modified theory with regular solns. *(German)* 79−88844
plain formation, tectonic implications 80−101542
plasma electron experiment, Mariner 10, bow shock and magnetosphere obs. 77−60700
position in relation to Jupiter, coincidence with Red Spot 90 day oscill. 77−82158
radio emission in H_2O 1.35 cm line 78−20664
radius and atmosphere data from Mariner 10 occultation obs. 77−37535
rayed craters on Moon and Mercury, interpretation 78−12119
reflectance meas. in thermal emission region, thermal component removal 80−17497
regolith containing Fe^{2+}, refl. spectra, 0.65-2.5 μm 80−56736
right ascension determ. from radio obs. *(Russian)* 79−21213
ring structures, rock mechanics theory 77−64675
rotation and solar tidal torques 79−66940
rotational motion theory *(Russian)* 78−93134
Schrodinger-Kepler eqn., perihelion precession rate in system of two charged masses 78−73897
secondary craters preservation states, comparison with Moon 78−12118
silicate mantle, nonhydrostatic stresses *(Russian)* 79−35162
solar wind interaction with surface of Mercury, planetary conductivity effects 79−101039
solar wind stand-off distance, erosion effects 79−80251
spin-orbit resonance, mathematical aspects 79−12389
surface, interaction with exospheric atmosphere 78−49351
surface, simple mols. prod. 78−16324
surface, structure, atmosphere, magnetic field, development *(Hungarian)* 77−73987
surface compressional features, rel. to gravit. const. secular decrease and Earth expansion 77−32972
surface evolution *(Italian)* 79−21212
surface features and internal structure, post-Mariner 10 assessment 80−12697
surface history from Mariner 10, review 77−37537
surface layer structure prediction *(Russian)* 77−41342
surface structure forecast, based on thermal conditions 78−77502
swirl patterns produced by comet collision 80−51675
tectonic and volcanic history, inferred from scarps, ridges, troughs and other lineaments 79−16855
tectonic processes rel. to photographs of surface relief *(Russian)* 77−73988
thermal evolution, calc. 79−2501
topographic changes on airless bodies, meteorite impact and ejecta deposition 78−65523
transit, 1973, November 10, photographic obs. *(German)* 77−22127
transit, 1973 November 10, photographic obs. at Pulkovo *(Russian)* 78−28562
transits in 1677-1973 period, collected obs. of internal contacts 77−25964
translational-rotational resonance motion in sphere gravit. field, intermediate theory 79−96899
volcanism and thermal tectonics on one-plate planets 78−77507
Fe/silicate fractionation and planet origin 78−85873
He exosphere model based on Mariner 10 UV spectrometer data 78−77509
Hg II 3984 Å, variation during eclipse in eclipsing binary Hg star AR Aurigae 80−98679

mercury alloys
see also mercury compounds
amalgam, dental, corrosion, immersion conditions 79−12037
amalgam, dental, corrosion behaviour, market survey 79−12038
dental amalgam, exam. of fracture toughness and critical strain energy release rate 78−48933
Dispersalloy, Sn-Hg amalgam, γ_2 precip. suppression and gettering kinetics 80−71651
liquid amalgams, dil., elec. cond. and thermoelec. power 77−55511
liquid amalgams mixing, excess entropy, vibr. contrib. *(Russian)* 79−51263
rare earth-Hg alloys, cryst. struct. determ. 79−77555
Wood's alloy, liq. enthalpy effects when solute is added 80−39314
Ag-Hg alloys, thermopower, thermal cond., elec. resistivity 79−65439
Ag-Hg amalgam, lattice const., temp. depend., explained in terms of Hg evaporation 78−26704
Ag-Hg-Sn dental amalgams, non-γ_2 phase, transmission electron metallography 79−74162
Ag-Pb-Hg system, DTA of phase diagram 77−12594

mercury alloys continued
Ag-Sn-Cu-Hg, constitution of quaternary amalgam at 37°C *(German)* 77−81250
Ag_2Hg_3, grain-boundary and volume diffusion coeffs. of Hg 77−55385
Ag_3Sn-Hg, metallic powder-liquid system, correlation between hardness and evolution and sintering states 80−25614
Al-Zn-Hg alloy, cathodic protection characts., surface free energy, lattice struct. 79−29281
$BaHg_{11}$ type structure, role of elongated rhombic dodecahedron in alloy structs. 79−32946
Ba_2Hg, cryst. struct. 77−11505
Be-Hg, dil., quadrupole interaction and lattice location for Hg 78−48086
Bi-Pb-Hg, liquid, surface tension and density *(Russian)* 77−55418
Cd-Hg, and Cd-Mg-Hg, magnetic susceptibility behaviour *(Russian)* 77−80912
Cd-Hg, dil., anomalously high elec. field gradients below 0.05K 78−72442
Cd-Hg, ω-phase, mag. susceptibility *(Russian)* 79−87231
ω-Cd-Hg alloy, melt-growth, morphology of single crysts. 78−64464
Cd-Zn-Hg, liq., comp. and temp. depend. of Hg VP, activity, free energy and enthalpy *(Russian)* 77−20087
CdHg, electric field gradient temp. depend., TDPAD meas. 79−56647
CdHg, ω phase, mag. susceptibility anisotropy w.r.t. uniform compression *(Russian)* 80−71143
$Cd_{55}Hg_{45}$, X-ray study of cryst. struct. and thermal expansion 80−24405
$Cd_{65}Hg_{35}$, X-ray study of cryst. struct. and thermal expansion 80−24405
CdHg*, metal vapour exciplex laser, stability criteria 78−66802
Cs-Hg, liq., elec. resist. meas. 77−51717
Cu-Hg, dil., pool electrodes, passivation in alkaline soln. 79−70214
Cu-Hg amalgam electrode, standard pot. 78−76874
Gd-Hg, dil., mag. hyperfine field, TDPAC meas. 78−52414
Ge:Hg, Sb, influence of electron irradiation on elec. props. 77−20318
Hg-Ag-Sn, dental amalgams, corrosion penetration in crevices 80−3238
Hg-Au(Tl)(Bi), liquid dilute amalgams, elec. cond. and thermoelec. power 78−51976
Hg-Cd, behaviour of Cd d-bands, comparison with Au and Ag alloys 79−37972
Hg-Cd liq. amalgam, elec. cond. and thermoelec. power meas. 77−59273
Hg-Cd(-Te), partial vapour pressure, determ. for volatile component by static method 80−37150
Hg-In, liq., positron annihilation meas. 78−43955
Hg-In, liq., positron studies, trapping at solute-vacancy complexes 78−31271
Hg-In, liq. alloy, chem. diff. coeff. determ. 77−1249
Hg-In (3, 15, 30, 45 at.%) amalgam, viscosity meas. near melting point 80−70441
Hg-In (3 at.%), amalgam, thermodynamic and electron transport props. 79−23938
Hg-In-Bi, liquid alloy, elec. resist. *(Russian)* 79−51544
Hg-In(Tl)-Zn, liquid alloys, thermodynamic props., 25 to 75°C *(German)* 77−73259
Hg-K, liquid, structure factors, X-ray scatt. *(Japanese)* 80−54122
Hg-Na, liquid, structure factors, X-ray scatt. *(Japanese)* 80−54122
Hg-Na (3 at.%), amalgam, thermodynamic and electron transport props. 79−23938
Hg-Tl, liq., positron annihilation meas. 78−43955
Hg-Tl, liq. alloys, struct. from thermodynamic props. *(German)* 77−1066
Hg-Tl, liq. alloys, struct. from elec. cond. 77−1067
Hg-Tl, metastable system, prep. by quenching, phase struct. 78−52762
Hg-Tl, phase limits, determ. by enthalpy functions along liquidus *(French)* 80−84911
Hg-Tl alloys, compositional depend. of positron annihilation 79−99973
Hg-Tl amalgam, viscosity meas. 80−88349
Hg-U system, thermodynamic props., vap. press. and EMF expts. 79−91625
Hg-Zn(In)(Pb), dil. liq. amalgams, expanded, cond. at high temps. and press. 77−20287
Hg_2-Pt, ^{199}Hg Mossbauer meas., isomer shift and quadrupole splitting calcs. 80−28039
$Hg_{99}As$, struct. reinterpretation 78−38660
β-$Hg_{0.80}In_{0.20}$, cryst. struct. from powder patterns 79−51052
$Hg_{1-x}Zn_xCr_2Se_4$, magnetic struct., neutrongraphic and mag. investigation *(Russian)* 80−88726
In-Hg, liq., Knight shift of ^{115}In, temp. and conc. depend. 79−47343
In-Hg amalgam, EMF meas. of In/$InCl_3$/amalgam cell and thermodynamic quantities 79−33999
In-Hg amalgam, thermal and electric cond., temp.-conc. depend. 78−43349
In-Hg liquid alloy, activities meas. 77−86351
Li-Hg, liq. semicond., electronic struct., resist. and thermoelec. power meas. 77−47712
MgHg, de Haas-van Alphen effect obs. 77−24512
β'-MgHg, energy bands and Fermi surface calc. 77−43481
Na amalgam-Na conductive glass interface, electrochem. obs. 78−76870
Ni amalgam, anodic polarisation in alkaline soln. 80−11823
Pb-Sn-Hg amalgam, liq., thermodynamic props. *(Russian)* 77−66624
PdHg-Rh, dil., quadrupole interaction of ^{100}Rh 79−99520
Rb-Hg liquid amalgams, thermodynamic props. determ. from conc. cell EMFs 77−1246
Re-Hg, dil., anomalously high elec. field gradients below 0.05K 78−72442
Sn-Hg dilute alloys, thermo EMF *(Russian)* 79−33285
Tl-Bi-Hg alloys, phase diagrams and equilib. *(Russian)* 79−52166
Tl-Pb-Hg system, thermodynamic props. *(Russian)* 77−25018
U-Hg system, phase relations determ. 79−91624
UHg prep. from uranyl ion using two-compartment electrolyser 80−802
Zn-Hg, dil., anomalously high elec. field gradients below 0.05K 78−72442
Zn-Sn-Hg, diagram of state, melting temp., peritectic and eutectic phases *(Russian)* 80−55350
Zn-Sn-Hg amalgam, liq., thermodynamic props. *(Russian)* 77−66624

mercury arc rectifiers
ignitrons, high current, for plasma physics expt. equipment *(German)* 78−75435

mercury compounds
see also mercury alloys
benzyl mercury chloride, cryst. struct. and absorpt. calcs. 80−84166
carboxylates, DTA study of phase transitions 79−90759

mercury compounds continued
$Cd_xHg_{1-x}Te$, vertically grown crysts., effects of growth speed on comp. variations 79−55684
chalcogenides, electrical charact. of pressure-induced phase transitions 77−84921
dimethyl mercury, coupling consts., solvent depend., ^{1}H, ^{13}C and ^{199}NMR 78−76334
dioxane-$HgCl_2$ complexes, IR and Raman vibr. spectra, inter- and intramol. forces 77−66489
diphenylmercury, cryst. struct. refinement 77−24310
eutectics, HgTe-PbTe and Au-PbTe, prep. and thermoelectric behaviour characts. 80−107774
halide electrically excited dissociation laser, kinetic processes 80−38013
halide electronic transition laser, quantum chem. 80−32971
halides, acoustic props., cryst. lattice bonds 78−30700
halides, HgX_2, positron annihilation ang. correl., bonding depend. 77−20951
halides in aq. soln., pulse radiolysis, emission species 79−24764
hexaphenylene mercury, bright-field imaging of single heavy atoms in an electron microscope with superconducting lens system 80−10472
HgCdTe/CdTe, limited diffusion volume photodiode, characterisation 80−75627
α-HgS, cryst. growth from soln. at low temps. 80−7487
mercuric halide dissociation lasers, discharge pumping 78−79009
performance at large bias currents *(Russian)* 78−76105
plasmon refl., 86 to 320K 80−50346
silicones, fungicidal protection of optical components made of chem. unstable glass 78−59107
tetrohydrofuran-$HgBr_2$ complexes, IR and Raman vibr. spectra, inter- and intramol. forces 77−66489
titration, amperometric, using thioxanthate 79−57326
zinc blende semiconductors, small-gap, electron scatt. and transport props. 78−95295
$AgHg_2AsO_4$, cryst. struct. by X-ray diffr. *(French)* 78−34490
Ag_2HgI_4, disordered multicomponent solid solutions conc. fluctuation waves, microscopic theory 80−44327
$AgHg_2PO_4$, cryst. struct. by X-ray diffr. *(French)* 78−34490
$Ag_xHg_ySI_z$, prep. of mixed sulphide iodides, photochromism 77−36385
AgI-HgI_2, solid electrolyte, ionic and electronic cond., phase composition determ. 78−2296
$AgPO_3$-HgI_2 glass, elec. cond. and Raman. spectra rel. to struct. *(French)* 79−10979
$Ag_2S.HgI_2$ and $Ag_2Se.HgI_2$ thin films, transmission spectra and photochromism 79−52032
As_2S_3-HgS, phase diag., IR spectra 77−36479
As_2Se_3-HgSe double-layer system detector for temp. meas. 79−88952
$As_2Se_3Hg_x$, semicond. glassy system, struct. 77−35489
(Cd,Hg)Te epitaxial structures, comp. profile depend. on deposition parameters 80−100795
(Cd,Hg)Te, photoconductive detector, uncooled, for 8-14 μm region 80−31868
Cd-Hg-Te, phase diagram, computer estimation 80−20903
Cd_x-$Hg_{1-x}Te$, cyclotron magneto-optical resons., photoconductivity meas. *(Russian)* 78−23133
CdHg, excimer kinetics and transmission meas. 80−37832
CdHg, fluoresc. kinetics, optical excitation, energy spacings and equilib. consts. 80−43090
CdHg, positive gain measurements or 470 nm continuum band 78−66805
Cd_xHg_{1-x} Te, elec. characts., impurity effects 80−92890
Cd_xHg_{1-x} Te, photodetectors, recomb. processes, photoconductive decay obs. 79−38129
Cd_xHg_{1-x}, x=0.2 and 0.26, photomagnetoelectric effect in strongly excited samples 79−47124
$Cd_{1-x}Hg_xCr_2Se_4$, ferromag. semicond. surface magnetism, magneto-optical meas. 77−20831
$Cd_{1-x}Hg_xCr_2Se_4$, photoferromag. effect and photocond. obs. 79−28376
$Cd_{1-x}Hg_xGa_2S_4$ solid solns., band struct. behaviour w.r.t. comp. *(French)* 80−107699
$Cd_{0.2}Hg_{0.8}Se$, longitudinal Nernst-Ettingshausen effect, effect of disorder scatt. 78−84240
$Cd_xHg_{1-x}Se$, carrier mobility, 4.2 to 300K, scatt. mechanisms 79−4561
$Cd_xHg_{1-x}Se$, elec. props., 77-400K *(Russian)* 78−2485
$Cd_xHg_{1-x}Se$, Hall coeff. and electron mobility, band parameters 79−73506
$Cd_xHg_{1-x}Se$ mixed cryst., electron mobility and electron scatt. 78−95296
$Cd_xHg_{1-x}Se$, narrow band gap semicond., electron scatt., and transport phenomena 80−49706
$Cd_xHg_{1-x}Se$, phase transition and elastic consts., US vel. study 80−75354
$Cd_xHg_{1-x}Se$ type semiconductor, small-gap, electron scatt. and transport props. 78−95294
$Cd_xHg_{1-x}Se$ type semiconductor, small-gap, electron scatt. and transport props. 78−95295
CdHgTe, anomalous avalanche breakdown 80−80284
CdHgTe detectors, high-performance, for thermal imaging 79−40616
CdHgTe detectors for CO_2 laser appls. 79−40615
CdHgTe, far IR cyclotron emission 79−61226
(CdHg)Te, ion implanted graded gap photodiodes 78−39192
(CdHg)Te photoconductive detector, thermal figure of merit limit 78−89540
(CdHg)Te photoconductive IR detectors, ultimate detectivity 79−58788
CdHgTe photoelectromagnetic detector for 10.6 μm radiation, non-cooled, performance 80−82818
$Cd_{0.1}Hg_{0.9}Te$, polycrystalline thin film, correlation between structure and 1/f noise 78−39234
$Cd_{0.175}Hg_{0.825}Te$-Au(In) contacts, photo-effect in the 77-300K range, barrier height estimation 80−107850
$Cd_{0.2}Hg_{0.8}Te$, annealing in saturated Hg vapour *(German)* 79−43447
n-$Cd_{0.2}Hg_{0.8}Te$, fundamental absorption edge, influence of temp. 80−20640
$Cd_{0.2}Hg_{0.8}Te$ IR photoresistors/detectors, lateral geometry requirements *(German)* 79−93213
$Cd_{0.2}Hg_{0.8}Te$, ion implantation doping for realisation of IR detectors, responsivity meas., ion range straggling 80−73452
$Cd_{0.2}Hg_{0.8}Te$ recrystallisation for supercooled IR detector production *(German)* 80−86403
n-$Cd_{0.21}Hg_{0.79}Te$, excess generation-recombination noise 80−107880
$Cd_{0.24}Hg_{0.76}Te$, mag. quantum oscills. in photovoltaic effect 79−19619

mercury compounds continued
n-$Cd_{0.245}Hg_{0.755}Te$, magnetophonon reson. and quantum oscillations 77−39902
n-$Cd_{0.3}Hg_{0.7}Te$, photoelec. props. at 78K, relax. time, minority carrier extraction 80−107864
n-$Cd_{0.3}Hg_{0.7}Te$, recomb. levels 79−91076
$Cd_{1-x}Hg_xTe$, lattice dynamics of low conc. of Hg atoms, perturbation model impurity description 79−55853
$Cd_xHg_{1-x}Te$ film, vacuum departed, struct. and elec. props. 77−59344
n-$Cd_xHg_{1-x}Te$, action of laser pulses, elec. charact. 79−11212
n-$Cd_xHg_{1-x}Te$ alloys, x=0.19 to 0.21, electron optical heating influence on photoelec. effects 79−11183
$Cd_xHg_{1-x}Te$, Auger effect, temp. depend. of Auger lifetime 79−38097
$Cd_xHg_{1-x}Te$, band struct. and optical props. 80−15450
$Cd_xHg_{1-x}Te$, carrier lifetime, effect of comp. fluctuations and second-phase inclusions 80−80294
$Cd_xHg_{1-x}Te$, cast-recrystallise-anneal growth 79−91578
$Cd_xHg_{1-x}Te$, charact. of low temp. transport props. 78−39160
$Cd_xHg_{1-x}Te$, comp. determ. by electroreflection method 77−52708
$Cd_xHg_{1-x}Te$, comp. in successive layers determ. by chem. polishing etching of surface 77−7868
$Cd_xHg_{1-x}Te$ compressed sintered slabs, Hall coeff. and microstructure obs. *(Russian)* 78−10475
n-$Cd_xHg_{1-x}Te$, conduction band struct., IR refl. spectra obs. 80−39502
n-$Cd_xHg_{1-x}Te$, conductivity inversion under laser radiation *(Russian)* 79−15198
$Cd_xHg_{1-x}Te$, correlation between structural and chemical inhomogeneity *(Russian)* 80−49484
$Cd_xHg_{1-x}Te$, crystal growth by zone passing techniques 77−40360
$Cd_xHg_{1-x}Te$, crystallisation from solution in Hg 77−19883
n-$Cd_xHg_{1-x}Te$ crystals, carrier recomb. in extrinsic conduction range 80−70722
$Cd_xHg_{1-x}Te$ crystals, donor compensation, low temp. cond. study 80−75571
$Cd_xHg_{1-x}Te$, current-voltage charact., pinch effect, mag. field effects 80−6858
$Cd_xHg_{1-x}Te$, determ. of slip planes by dislocation etching 79−82220
$Cd_xHg_{1-x}Te$, diffusion and struct. of defects 77−84775
$Cd_xHg_{1-x}Te$, dislocation motion, effect of lattice defects on microhardness *(Russian)* 80−70220
$Cd_xHg_{1-x}Te$, disorder scatt. 78−39137
$Cd_xHg_{1-x}Te$, effects of electron heating at low temps. 80−49823
$Cd_xHg_{1-x}Te$, electron irradiated, elec. and recomb. charact. 78−39113
$Cd_xHg_{1-x}Te$, electron mobility and conc. near gapless state, influence of hydrostatic press. 79−65486
$Cd_xHg_{1-x}Te$, epitaxial graded-gap layers, elec. transport props. 77−85358
$Cd_xHg_{1-x}Te$ epitaxial graded gap layers, plasma reflection and magnetoreflection 80−71391
$Cd_xHg_{1-x}Te$, epitaxial growth from stoichiometric melt, crystn. and diffusion 80−75475
$Cd_xHg_{1-x}Te$, epitaxial layer p-n junction, current-voltage characteristics of photovoltaic detectors, 1 to 15 μm 80−86407
$Cd_xHg_{1-x}Te$, film, optical props., struct. depend. 77−1751
$Cd_xHg_{1-x}Te$ films, epitaxial growth, optical, elec., and photoelec. props. 79−11512
$Cd_xHg_{1-x}Te$ films, growth by cathodic sputtering in Hg vapour plasma 80−97431
$Cd_xHg_{1-x}Te$, fine-graded gap struct., electrophysical props. *(Russian)* 78−60144
$Cd_xHg_{1-x}Te$, gap width temp. depend., absorpt. band edge meas. 78−72521
$Cd_xHg_{1-x}Te$, graded gap epitaxial layers, elec. and photoelec. props. 77−85362
$Cd_xHg_{1-x}Te$, graded gap epitaxial layers, spectral charact. of photoelectromagnetic effect 80−60022
$Cd_xHg_{1-x}Te$ graded-gap epitaxial layers, photocond. meas. 0.5 to 6 μm, detector appl. 79−60869
$Cd_xHg_{1-x}Te$, graded-gap layers, galvanomag. props. at low temp. and in weak mag. field 80−75664
p-$Cd_xHg_{1-x}Te$, Hall const. variation with comp. after annealing in Hg vapour 77−15868
$Cd_xHg_{1-x}Te$, homogeneous mixed crysts. with large segregation tendency, Bridgman growth *(German)* 79−33923
$Cd_xHg_{1-x}Te$, IR detector appls., prep., elec. props. *(German)* 78−86332
n-$Cd_xHg_{1-x}Te$, in strong mag. field, current-voltage charact., current instabilities 78−87980
$Cd_xHg_{1-x}Te$, influence of nonparabolicity on transverse magnetoresist. near transition to zero gap 80−20228
$Cd_xHg_{1-x}Te$ inhomogeneous p-n junctions, elec. props. at high hydrostatic press. *(Russian)* 77−80835
$Cd_xHg_{1-x}Te$, intrinsic carriers, Fermi level calc. rel. to conc. 77−55481
$Cd_xHg_{1-x}Te$, isothermal growth of epitaxial layers 78−60577
$Cd_xHg_{1-x}Te$ layers, epitaxial graded-gap, nonlinear elec. effects 80−100468
$Cd_xHg_{1-x}Te$ layers, photoelectromagnetic effect 78−43445
$Cd_xHg_{1-x}Te$, long term stability at 300K, rel. to device appl. 80−59978
$Cd_xHg_{1-x}Te$, low temp. piezoresistance, Hall effect, elec. cond., plastic flow 80−6844
n-$Cd_xHg_{1-x}Te$, magnetophonon oscills. of transverse magnetoresist. 78−72177
$Cd_xHg_{1-x}Te$, magnetoresist. near gapless state, 77-370K 78−2503
$Cd_xHg_{1-x}Te$ magnetoresistor prep. and props. 79−7844
$Cd_xHg_{1-x}Te$, magnetoresistance in range 4.2 to 300K 79−11156
$Cd_xHg_{1-x}Te$ narrow gap semiconductor, charge transfer device for IR detection appl. *(French)* 79−30563
$Cd_xHg_{1-x}Te$, photoconductivity under uniaxial compression, band gap 77−43657
$Cd_xHg_{1-x}Te$ photoconductive detectors, 77 to 300K, normalised thermal figure of merit 80−31878
$Cd_xHg_{1-x}Te$ photodiode, high efficiency, energy level diagram 77−15891
$Cd_xHg_{1-x}Te$ photodiode, IR responsivity and detectivity 78−19139
$Cd_xHg_{1-x}Te$, photoelectric props. at high temp. 77−4403
$Cd_xHg_{1-x}Te$, photomag. and photothermomag. effects *(Russian)* 79−78137
n-$Cd_xHg_{1-x}Te$, photomagnetic effect in the quantum limit under electron heating conditions 79−69553
$Cd_xHg_{1-x}Te$, photomagnetic and galvanomagnetic effects in quantising mag. fields 80−20223

mercury compounds continued
$Cd_xHg_{1-x}Te$, photothermomag. effect and photocond. in millimetre wavelength range 80−44657
$Cd_xHg_{1-x}Te$ polycrystalline films, electrical props., rel. to struct. *(Polish)* 78−31002
$Cd_xHg_{1-x}Te$, precip. 77−90352
n-$Cd_xHg_{1-x}Te$, quantum oscills. of transverse photocond., fields up to 30 kOe, 1.5-4.2K *(Russian)* 77−72885
n-$Cd_xHg_{1-x}Te$, recombination due to surface excitation, photoconductivity, impurity states *(Russian)* 80−60042
$Cd_xHg_{1-x}Te$, resistivity, Hall effect and magnetoresist. in strong elec. field 77−28199
n-$Cd_xHg_{1-x}Te$, semicond. current carrier recombination heating in photoelectric effects *(Russian)* 79−78138
$Cd_xHg_{1-x}Te$, single cryst. homogeneity and molar conc. determ. with electron microprobe *(German)* 78−2109
$Cd_xHg_{1-x}Te$ single crystal, photoconductivity spectral distrib. rel. to surface condition 79−78136
n-$Cd_xHg_{1-x}Te$, single crystal, scattering mechanism on intensity of 1/f noise 80−39642
p-$Cd_xHg_{1-x}Te$ solid soln., thermoelec. effects 79−73538
$Cd_xHg_{1-x}Te$, solid soln., pure and Ag(In) doped, defect struct. model, Hg self-diffusion coeff. 79−95213
$Cd_xHg_{1-x}Te$ solid solns., epitaxial growth under isothermal conditions 77−16504
$Cd_xHg_{1-x}Te$, solid solns., role of stoichiometry defects 77−47813
$Cd_xHg_{1-x}Te$ solid solns., dimensional resonances of HF helicons, band struct. and electron mobility 77−47846
$Cd_xHg_{1-x}Te$, solid solns., solubility in Hg 78−35359
$Cd_xHg_{1-x}Te$, strong elec. field effect on galvanomagnetic effects 79 11159
$Cd_xHg_{1-x}Te$, surface microhardness depend. on surface treatment method 78−15560
$Cd_xHg_{1-x}Te$, temp. shift of energy gap 77−51658
$Cd_xHg_{1-x}Te$, temp. shift of energy gap, contrib. of lattice dilatation 78−51892
$Cd_xHg_{1-x}Te$, thermal cond. in mag. field, thermopower, and Nernst-Ettingshausen effect 77−31814
n-$Cd_xHg_{1-x}Te$, thermal EMF, in transverse quantised EM field *(Russian)* 79−23993
$Cd_xHg_{1-x}Te$, thermally activated slip, microhardness temp. depend. *(Russian)* 78−34567
$Cd_xHg_{1-x}Te$, tunnelling effect in p-n junctions 80−75630
$Cd_xHg_{1-x}Te$, uniaxially compressed, deform. effects, elec. resist. 78−39114
$Cd_xHg_{1-x}Te$, VPE on CdTe *(Russian)* 78−11129
$Cd_xHg_{1-x}Te$, vac. evap. film struct. rel. to carrier scatt. 77−85116
$Cd_xHg_{1-x}Te$, vacancy electron states, acceptor behaviour, electron mobility 80−70193
$Cd_xHg_{1-x}Te$, variable-gap struct., additional p-n junction in epitaxial film, photosensitivity 77−24588
$Cd_xHg_{1-x}Te$, variable-gap structures, galvanomagnetic effects 80−11014
$Cd_xHg_{1-x}Te$, X-ray topographic assessment 79−37716
$Cd_xHg_{1-x}Te$, x=0, x=1, effective mass of heavy holes, 4.2 to 300K 77−1353
$Cd_xHg_{1-x}Te$, zero gap semiconductor, interband optical-phonon scattering 80−6846
p-$Cd_xHg_{1-x}Te$-metal contact, negative resist. effects, impact ionisation 77−4440
$Cd_xHg_{1-x}Te$-metal contact, transport mechanism, thermionic and field emission processes 77−20425
$Cd_xHg_{x-1}Te$, Auger and radiative recombination of acceptor bound excitons 79−47023
$Cd_xHg_{1-x}Te$(:Ag), impurity diffusion, gamma-ray effects 80−54441
CdHg* excimer, kinetic model of sustained discharge excitation 78−66804
CdTe/$Hg_{1-x}Cd_xTe$ multilayers, LPE growth 80−80104
CdTe/HgTe superlattice, new IR material 79−72634
CdTe-HgTe, neutron irrad. rel. to elec. props. 79−15141
CdTe-HgTe, semicond. solid solns., effect of reactor irrad. on electrophys. props. 77−51744
CdTe-HgTe superlattice on CdTE layers, evanescent states, tight binding calcs. 80−70611
CuHgSBr, cryst. struct. *(French)* 79−90620
CuHgSCl, cryst. struct. *(French)* 79−90620
$Cu_{3.75}Hg_{1.75}S_2S_8$, velikite, cryst. struct. determ. 78−2097
H_2I_2, crysts., growth, optical props. *(German)* 77−77167
HbBr($B^2\Sigma^+_{1/2}$), rate coeffs. for collisional quenching, time resolved emission obs. 79−89705
p-(Hg,Cd)Te, carrier lifetime, dominant Auger transitions comparison 80−49768
(Hg,Cd)Te IR detector array, 72-element, 8-12 micron, performance, FLIR system appl. 79−2829
(Hg,Cd)Te n^+-p photodiodes, 8 to 12 μm IR imaging appls. 80−9044
(Hg,Cd)Te photodiode for 2 μm IR detection 77−82603
(Hg,Cd)Te photodiode IR detectors, planar technology 80−9043
(Hg,Cd)Te photodiodes, wide-bandwidth 10.6 μm IR heterodyne detect. 80−9042
Hg complex, aspartic and chelation, US obs. 77−44464
Hg complex, DNA-Hg (II) in soln., theoret. interpret. of elec. dichroism obs. 80−85347
Hg complex, methylethynylmercury(II)(-d_1,-d_3,-d_4), vibr. spectra and normal coord. calcs. 80−58259
Hg complex, trihalogenomercurate II ions in amide solvents, config. equilib. 79−26997
Hg complexes, tertiary phosphines, NMR, ^{199}Hg-^{31}P spin-spin coupling, temp. depend. 78−62825
Hg halide lasers, efficiency of different pumping methods 79−36886
Hg II halides, electron impact dissoc., excited fragment emission 79−18296
Hg-As-S chalcogenide glass system, prod. and acoustooptic props. *(Russian)* 78−63158
Hg-As-S modulating glasses, optical parameters and struct. *(Russian)* 78−63159
Hg-As-S-I system, glasses, optical and acousto-optical props. 78−83053
Hg-B system, interactions, product chem., phase, struct. anal., book contrib. 78−47305
Hg-HgTe-CdTe system, equilib. phases comp. by dew point method 79−78941
Hg-S binary system, phase relations, bulk resist. meas. 79−66040

mercury compounds continued
$Hg_{2.86}AsF_6$, anisotropic linear-chain conductor, optical reflectance meas. [illegible]
$Hg_{2.86}AsF_6$, anisotropic supercond. caused by Hg extrusion, DTA 78−55953
$Hg_{2.86}AsF_6$, elec. cond., pseudo-one dimens. 77−20304
$Hg_{2.86}AsF_6$, linear chain, anomalous low temp. sp. ht. 78−14476
$Hg_{2.86}AsF_6$, linear chain compound NMR exam. 78−19359
$Hg_{2.86}AsF_6$, linear-chain cpd., anisotropic Meissner effect, magnetisation meas. 77−85387
$Hg_{2.86}AsF_6$, one-dimens. conductor, thermopower, temp. depend. 79−65465
$Hg_{2.86}AsF_6$, thermoelectric power 78−34852
$Hg_{2.91}AsF_6$, elec. cond., pseudo-one dimens. 77−20304
Hg_3AsF_6, one dimensional conductor *(Japanese)* 79−73499
$Hg_{3-\delta}AsF_6$, dynamical props., Hg chain behaviour, neutron scatt. study 79−95103
$Hg_{3-\delta}AsF_6$, Fermi-surface of incommensurate Hg-chain compounds 79−56115
$Hg_{3-\delta}AsF_6$, incommensurate crystal phases symmetry, incommensurate basic struct., superspace group approach 80−79727
$Hg_{3-\delta}AsF_6$, linear chain compound, mag. field induced residual resist., anisotropic supercond. 80−24897
$Hg_{3-\delta}AsF_6$, low-temp. sp. ht., lattice dynamics, 1- to 3-dimens. crossover 79−86864
$Hg_{3-\delta}AsF_6$, one dimens. fluctuations and chain ordering transform 80−24593
$Hg_{3-\delta}AsF_6$, one dimensional phonons and chain ordering 80−24544
$Hg_{3-\delta}AsF_6$, one-dimens. phonons and phase-ordering phase transition, neutron scatt. expts. 78−26644
$Hg_{3-\delta}AsF_6$, one-dimens. fluctuations and chain ordering transform., neutron scatt. calc. 78−59923
$Hg_{3-\delta}AsF_6$, one-dimens. liq., fluctuations and freezing in order-disorder transitions 79−82301
$Hg_{3-\delta}AsF_6$, quasi one-dimensional, anomalous magnetoresistance 80−24884
$Hg_{3-\delta}AsF_6$, quasi-one-dimens., mag. field induced residual resistivity 79−1596
$Hg_{3-\delta}AsF_6$, space group symmetry and phase ordering 80−6396
$Hg_{3-\delta}AsF_6$, theory of phase transitions 80−6486
$Hg_{3-x}AsF_6$, energy gap in phonon dispersion of linear Hg chains 79−42172
$Hg_{3-x}AsF_6$, incommensurate chain compound, anisotropic Knight shift, spin-spin interactions 78−80233
$Hg_{3-x}AsF_6$, linear chain metallic cpd., square Fermi surface model for conduction 80−6822
$Hg_{3-x}AsF_6$, linear chain cpd., open orbits, induced torque meas. 80−29309
$Hg_{3-x}AsF_6$, one-dimens. conductor, thermopower, phonon drag 79−65466
$Hg_{3-x}AsF_6$, one-dimens. lattice dynamics, X-ray scatt. study 80−75317
$Hg_{3-x}AsF_6$, phase-ordering phase transition, elastic neutron scatt. obs. 79−33087
$Hg_{3-x}AsF_6$, supercond., absence of surface Hg 80−20350
$HgBi_2S_4$, X-ray cryst. struct. determ., rel. with pavonite homologous series 80−92487
HgBr, 502 nm stimulated emission, prolonged optical pumping of $HgBr_2$ 79−18414
HgBr, ab initio CI calcs., spectroscopic parameters 79−72245
HgBr, $B^2\Sigma_{1/2}^+ \rightarrow X^2\Sigma_{1/2}^+$ band at 5018 Å, lasing action 77−83856
HgBr $B^2\Sigma_{1/2}^+ \rightarrow X^2\Sigma_{1/2}^+$ laser, sustained discharge excitation 78−42342
HgBr, B-state radiative lifetime, determ. by photolysis of $HgBr_2$ 79−10130
HgBr, B→X transition radiative lifetime, charge transfer model 78−17719
HgBr dissociation laser is elec. discharge 78−50768
HgBr electrically excited dissociation laser, kinetic processes 80−38013
HgBr emission intensity, $HgBr_2$ dissociative excitation by inert gas and N_2 metastables 80−40687
HgBr, laser action on B→X bands, 5018 Å 77−88709
HgBr, laser photolysis prep., laser induced fluoresc., collisional quenching processes 80−38014
HgBr laser using dissociative excitation of $HgBr_2$, extraction efficiency increased by N_2 addition 80−38012
HgBr, polarised photofluoresc. spectroscopy, $HgBr_2$ photodissociation by ArF laser 80−37841
HgBr radical, laser action by $HgBr_2$ photodissociation, ArF excimer laser pumping 78−13695
HgBr vapour, nanosecond excitation using photopreionisation-stabilised discharge scheme 79−98982
HgBr, visible laser action due to $HgBr_2$ photodissociation 77−88710
HgBr, visible laser transitions at 5018 Å and 4984 Å 79−939
HgBr+O_2(N_2)(H_2)(He)(Ne)(Ar)(Kr)(Xe), vibr. relax., rate coeffs., fluoresc. obs. 80−63697
$HgBr_2$ dissociation laser, elec. excited, kinetic processes 80−48231
$HgBr_2$, dissociative excitation for HgBr laser, extraction efficiency increased by N_2 addition 80−38012
$HgBr_2$ dissociative excitation by inert gas and N_2 metastables, HgBr emission intensity 80−40687
$HgBr_2$, electronic struct. and photodissoc., effective core pots. and POL(1) CI wave function 80−63560
$HgBr_2$, photodissoc., two-photon excitation of Hg atom 78−90114
$HgBr_2$ photodissociation by ArF laser, characterisation of transition prod. HgBr($B^2\Sigma^+$) 80−37841
$HgBr_2$, photofragment fluoresc. polarisation, press. depend. 80−63720
$HgBr_2$, prolonged optical pumping, photodissociation producing stimulated emission from HgBr 79−18414
$HgBr_2$, UV absorpt. cross-sections of vapour 78−25554
$HgBr_2$, vac. UV absorpt. cross section 80−91574
$HgBr_2$, vapour, excited by photodissociation, fluoresc. yields 78−55138
$HgBr_2$/HgBr dissociation laser, oscillator and oscillator-amplifier expts. 80−48232
$HgBr_2$-$BiBr_3$, molten, elec. cond., 500-870K, composition depend. 78−55965
$HgBr_2$+ inert gas metastable atom ($N_2(A^3\Sigma_u^+)$), dissoc. excitation 80−63774
$HgBr_2$+AgI, solid state reaction, kinetics and mechanisms 77−16790
$HgBr_2$+K, laser irrad., HgBr* form., chemiluminescence 80−55658
$HgBr_2$+N_2*, dissociative excitation, mol. fluoresc. obs. 80−91634
Hg_2Br_2, crysts., growth, optical props. *(German)* 77−77167
Hg_2Br_2, ferroelastic, Brillouin and Raman scatt. spectra 79−95770
mercury compounds continued
Hg_2Br_2, ferroelastic phase, softening of acoustic and optical modes 79−33064
Hg_2Br_2, improper ferroelastic, soft mode props. in Raman spectra 77−36246
Hg_2Br_2, nonintrinsic ferroelastic, thermal expansion and thermodynamic potential 80−88344
Hg_2Br_2, powder, Raman spectra, press. effects 78−2837
Hg_2Br_2, sp. ht. near phase transition region meas. 78−38855
HgBr(B→X) radiative lifetime, laser induced fluorescence 77−30900
$Hg_2Br(Cl_2)$, paraphase, Raman scatt. spectra, soft mode from Brillouin zone boundary *(Russian)* 78−2851
$Hg_2(BrO_3)_2$, Raman and IR spectra, vibr. anal. 77−66492
HgBr*, collisional quenching by inert gas (molecule) 80−42986
HgBr*, collisional quenching by inert gas (molecules) 80−43091
HgBr* form. from laser irrad. K+$HgBr_2$, chemiluminescence 80−55658
$Hg(CN)_2$, phonon freq. anomalous press. depend., mol. struct. distortion 80−88981
$Hg(CN)_2$, solvation by NH_3 and ND_3, Raman spectroscopic study 78−90172
$Hg(CN)_3^-$ ion, CN and HgC stretching vibrations and HgCN bending vibration assignments 80−69140
$Hg(CNS)_2$, solvation by NH_3 and ND_3, Raman spectroscopic study 78−90172
$Hg_{1-x}Cd_xGe$, quantum oscillations of magnetoresistivity *(Russian)* 80−11007
HgCdSe MIS junction, phonon-assisted tunnelling 79−47170
$Hg_{0.985}Cd_{0.015}Se$, interband $\Gamma_6 \rightarrow \Gamma_8$ magnetoabsorption and band parameters 79−82960
$Hg_{1-x}Cd_xSe$, (x=0 to 0.15), Shubnikov-de Haas oscillations, influence of level broadening 79−11155
$Hg_{1-x}Cd_xSe$, IR absorpt. spectra, band struct., refr. index 80−50337
$Hg_{1-x}Cd_xSe$, zinc blende structure, optical and electronic properties 80−6723
HgCdTe, 0.1 eV photodetector performance background dependence 77−32038
HgCdTe, 0.1 eV photodetector performance 77−32039
HgCdTe, 0.1 eV photodetector performance, geometrical enhancement 77−32040
HgCdTe, crystal and photodiode, imperfections and surface conditions using electron induced current technique 79−67385
HgCdTe, electron irradiated, high temp. defects 79−78122
HgCdTe IR photovoltaic detectors for 8-14 μm range, review *(Italian)* 78−54451
HgCdTe, interband magnetoabsorption and band struct. 79−82959
HgCdTe, ion implantation, junction form. 80−100260
HgCdTe MIS junction, phonon-assisted tunnelling 79−47170
HgCdTe MIS structure, modelling and appl. to CCD IR imagery 78−80058
HgCdTe, Magneto transport anomalies at low carrier densities, Wigner crystallisation 80−20222
HgCdTe, narrow band gap semiconductor IR devices, advances 80−48464
n-HgCdTe, photocond., Hall mobility and resist. 80−34478
HgCdTe photodiode IR detector, selection 79−58791
HgCdTe photodiodes formed by double-layer LPE 80−104078
HgCdTe, radiation effects on low-temp. carrier recombination lifetimes, photocond. meas. 78−6400
HgCdTe, recomb. effects, mag. quantum oscills. in Auger transition rate 79−82610
HgCdTe reverse-biased photodiodes for wideband appls., excess noise 80−107876
HgCdTe Schottky barrier diode and n-p diffused junction IR detectors, comparison 80−9039
HgCdTe solid solution photodiode for CO_2 laser active medium study 80−95868
HgCdTe, zero gap, unusual high electron mobility and related phenomena 79−82601
HgCdTe-CdTe IR detector arrays, 3 to 11 μm, fabrication techniques 80−9041
HgCdTe-CdTe photodiode, 1.33 μm, grown by LPE, phys. props. 80−107892
$Hg_{0.60}Cd_{0.40}Te$, LPE growth from Te-rich soln. 80−7508
$Hg_{0.6}Cd_{0.4}Te$, annealing temp. effect on carrier conc. 78−72167
$Hg_{0.6}Cd_{0.4}Te$ LPE layer growth from Te-, Hg-, and HgTe-rich solns., comparison 80−76199
$(Hg_{0.6}Cd_{0.4})_{1-x}Te_x$, defect anal., intrinsic material parameters 80−75519
n-$Hg_{0.61}Cd_{0.39}Te$ single crystals, flicker noise due to grain boundaries, meas. 79−1611
$Hg_{0.68}Cd_{0.32}Te$ photodiode, minority carrier lifetime determ. 79−38084
$Hg_{0.7}Cd_{0.3}Te$, 17 to 77K, photo- and cathodoluminesc. 78−52569
$Hg_{0.72}Cd_{0.28}Te$ semiconductor, two-mode reson. polaron 79−15105
$Hg_{0.74}Cd_{0.25}Te$ thin film deposition on Si substrates by RF triode-sputtering, large-area photodetector arrays 80−80965
$Hg_{0.75}Cd_{0.25}Te$, single crystal, reflection spectra 80−40140
$Hg_{0.75}Cd_{0.25}Te$, thermorefl. spectra, effect of excitons on E_1 and $E_1+\Delta_1$ structs. 80−16057
$Hg_{0.77}Cd_{0.23}Te$, near reson. spin-flip Raman scatt. 79−82983
$Hg_{0.77}Cd_{0.23}Te$ nonlinear optical IR generation 80−58642
$Hg_{0.77}Cd_{0.23}Te$, resonant four-photon and higher order mixing 79−41415
$Hg_{0.77}Cd_{0.23}Te$, spin-flip Raman laser, high conversion efficiency 77−79832
n-$Hg_{0.785}Cd_{0.215}Te$, slightly compensated, transport props. of photo-excited carriers 78−47832
$Hg_{0.79}Cd_{0.21}Te$, ion implanted, elec. props. 80−20184
n-$Hg_{0.8}Cd_{0.2}Te$, microwave bolometer heterodyne receiver based on magnetic field induced phase transition 80−13135
$Hg_{0.8}Cd_{0.2}Te$ surface, sputter cleaning and dry oxidation, XPS and LEED study 80−108618
$Hg_{0.8}Cd_{0.2}Te$-ZnS MIS struct., nonparabolic bond semicond., surface state studies, capacitance measurements 79−78190
$Hg_{0.82}Cd_{0.18}Te$, electronic anomalous mass near reson. acceptor level, Shubnikov-de Haas meas. 80−80163
$Hg_{0.85}Cd_{0.15}Te$, acceptor states, galvanomagnetic effects study 79−82560
$Hg_{0.86}Cd_{0.14}Te$, spin-flip electron scatt., longit. magnetoresist. obs. 77−43622
$Hg_{1-x}Cd_xTe$ 0.1 eV, thermal conductivity meas. 77−24578
$Hg_{1-x}Cd_xTe$, acceptor bound exciton Auger and radiative transition rates, radiative recomb. 80−6733
$Hg_{1-x}Cd_xTe$, acceptor impurity band form. 80−20119
$Hg_{1-x}Cd_xTe$, acceptor levels due to local impurity potential 79−11084

mercury compounds continued
$Hg_{1-x}Cd_xTe$ and $Pb_{1-x}Sn_xTe$ quantum detector selection for 8 to 14 μm 79−80681
$Hg_{1-x}Cd_xTe$, anodic oxide films, formation and props. 80−3212
$Hg_{1-x}Cd_xTe$, avalanche formation, high intensity IR transmission limit 79−78684
$Hg_{1-x}Cd_xTe$ breakdown-limited MIS device, increased charge capacity using ramped gate voltage 80−103751
$Hg_{1-x}Cd_xTe$, CESR *(Russian)* 78−23344
$Hg_{1-x}Cd_xTe$, CESR meas., four-photon mixing via spin-flip Raman scatt. 79−82873
$Hg_{1-x}Cd_xTe$, carrier conc., Hall effect, photocond., IR spectra meas. 80−49771
$Hg_{1-x}Cd_xTe$, cyclotron resonance, in zinc blende struct. semiconductor *(German)* 78−10337
$Hg_{1-x}Cd_xTe$, cyclotron reson., 337 μm transmission expts., 77 to 150K 78−34750
$Hg_{1-x}Cd_xTe$, degenerate four-wave mixing of 10.6 μm radiation 80−95943
$Hg_{1-x}Cd_xTe$, doping props. of selected impurities, diffusion behaviour 77−72632
$Hg_{1-x}Cd_xTe$, Einstein relation for inversion layers 80−103706
$Hg_{1-x}Cd_xTe$, epitaxial layer, vapour phase growth 79−1829
$Hg_{1-x}Cd_xTe$, epitaxial layers, elec. properties in the range 4.2 to 300K *(French)* 80−65721
$Hg_{1-x}Cd_xTe$ epitaxial layers, elec. props. 80−96910
$Hg_{1-x}Cd_xTe$, far IR cyclotron resonance in inversion layer 77−69396
$Hg_{1-x}Cd_xTe$, far IR cyclotron reson., band edge effective mass and relax. time 79−19781
n-$Hg_{1-x}Cd_xTe$, far IR recomb. radiation in elec. field, acceptor states 77−16399
n-$Hg_{1-x}Cd_xTe$, far IR recomb. radiation with applied elec. field 78−27324
$Hg_{1-x}Cd_xTe$, Faraday effect at CO_2 laser freq. 78−64348
$Hg_{1-x}Cd_xTe$ films, Tamm surface states, Kane model 79−28395
$Hg_{1-x}Cd_xTe$, for appl. in IR detector arrays, comp. control 80−31872
$Hg_{1-x}Cd_xTe$, grown from melt, Kirkendall and Frenkel effects 80−100365
$Hg_{1-x}Cd_xTe$, high intensity IR transmission limit 78−79074
$Hg_{1-x}Cd_xTe$, high-pressure reflex growth technique, IR detector appl. 77−40347
$Hg_{1-x}Cd_xTe$, homogeneous single cryst., growth by modified Bridgman technique 78−39682
$Hg_{1-x}Cd_xTe$, Hooge's flicker noise MIS expt. 78−56233
$Hg_{1-x}Cd_xTe$ hot-electron photoconductive detection of near mm wave radiation 80−57377
$Hg_{1-x}Cd_xTe$ IR detector technology 78−77989
$Hg_{1-x}Cd_xTe$ IR focal plane status and performance 78−77987
$Hg_{1-x}Cd_xTe$, IR optical absorpt. and refr. index, 80 to 300K 79−91418
$Hg_{1-x}Cd_xTe$ IR photodetectors for night vision appl. 80−22429
$Hg_{1-x}Cd_xTe$ implanted detector 8 to 14 μm, performance, p-n junction characts. 77−15941
$Hg_{1-x}Cd_xTe$, implanted with Hg, Al, damage and lattice location study 80−103381
$Hg_{1-x}Cd_xTe$, interband magnetoreflectance 78−19448
$Hg_{1-x}Cd_xTe$ interface with native oxide, elec. props. 80−20318
$Hg_{1-x}Cd_xTe$, ionized intrinsic pt. defects, effect on carrier density 77−47835
$Hg_{1-x}Cd_xTe$, LPE current controlled 80−40272
$Hg_{1-x}Cd_xTe$, LPE growth and characterisation 80−50565
$Hg_{1-x}Cd_xTe$, LPE-grown and optically pumped crystal, continuous lasing at 2.79 μm 79−68397
$Hg_{1-x}Cd_xTe$, long-term Hall-type conversion by vacancy diffusion at room temp. 79−65498
$Hg_{1-x}Cd_xTe$, magnetooptical and impurity effects 80−6721
$Hg_{1-x}Cd_xTe$, magnetoreflection studies 79−82963
$Hg_{1-x}Cd_xTe$, material capabilities for 1 to 1.3 μm room temp. photodiodes 78−24859
$Hg_{1-x}Cd_xTe$, mixed crysts., band struct. and optical transitions, distorted atomic orbitals 77−69224
$Hg_{1-x}Cd_xTe$ mixed crysts., magneto-opt. obs., semicond. config., semimetal-semicond. transition 77−73131
$Hg_{1-x}Cd_xTe$, mixed crystals, crystn. by chemical transport 80−20775
$Hg_{1-x}Cd_xTe$, n-surface inversion layers study 80−25017
$Hg_{1-x}Cd_xTe$, narrow-gap semiconductor, high intensity IR transmission limit 80−7361
$Hg_{1-x}Cd_xTe$, near band-gap photoluminesc., bound exciton luminesc. obs. 80−103973
$Hg_{1-x}Cd_xTe$, nonlinear absorption and saturation, 10.6 μm 77−746
$Hg_{1-x}Cd_xTe$, nonlinear optical effects 80−14389
$Hg_{1-x}Cd_xTe$, optical absorpt., quasilocal acceptor level effects, theory 80−92853
n-$Hg_{1-x}Cd_xTe$, optical phase conjugation 80−83644
$Hg_{1-x}Cd_xTe$, p-T diagrams, p⇌n intrinsic-extrinsic lines 77−36481
n-$Hg_{1-x}Cd_xTe$, photoconductor, contact noise at 77K 78−88028
$Hg_{1-x}Cd_xTe$ photoconductors, gamma ray effects on surface props. and detector props. 79−17489
$Hg_{1-x}Cd_xTe$ photoconductive IR detector, optimum bias attainment with batteries 79−58789
$Hg_{1-x}Cd_xTe$ photodiodes, for IR detection 80−13144
$Hg_{1-x}Cd_xTe$ photodiodes, implanted n^+-p, improved performance using insulated field plates 80−52309
$Hg_{1-x}Cd_xTe$ photodiodes, long cutoff wavelength, effect of trap tunnelling on IR detector performance 80−73451
$Hg_{1-x}Cd_xTe$, photolum. and optical pumping 80−50424
$Hg_{1-x}Cd_xTe$, props. and appl. book 77−36250
$Hg_{1-x}Cd_xTe$, props. and appls., book contrib. 77−39834
$Hg_{1-x}Cd_xTe$, quasi-local acceptor levels and electron mobility 78−67974
$Hg_{1-x}Cd_xTe$, recombination processes using impact ionization capture cross sections 80−75577
$Hg_{1-x}Cd_xTe$, resonant acceptor level, single and multiple scatt. effect 77−47767
$Hg_{1-x}Cd_xTe$, segregation, compositional characterisation 80−107434
$Hg_{1-x}Cd_xTe$, semiconducting phase, acceptor states and galvanomagnetic effects 80−11017
$Hg_{1-x}Cd_xTe$, semimetallic state, magneto-optical investig. of Landau levels and band parameters 77−63410
$Hg_{1-x}Cd_xTe$, semimetallic and semicond., Hall coeff., anomalous temp. depend., 4.2 to 70K 80−65604
$Hg_{1-x}Cd_xTe$, shallow acceptor contribution to near-resonance spin-flip Raman scatt. 79−95754

mercury compounds continued
n$Hg_{1-x}Cd_xTe$, single-phonon and plasmon recomb. lifetime effect, with magnetically tuned bandgap 79−38098
$Hg_{1-x}Cd_xTe$, surface topographic stoichiometry variations, electrolyte electrorefl. obs. 78−27249
$Hg_{1-x}Cd_xTe$, Tamm surface states 77−55595
$Hg_{1-x}Cd_xTe$, theory of optical absorpt., contribution by quasilocal acceptor levels *(Russian)* 80−71451
$Hg_{1-x}Cd_xTe$, transverse magnetoresist. in extreme quantum limit 77−39885
$Hg_{1-x}Cd_xTe$, two-photon absorption coefficient, 3-band model 79−78679
$Hg_{1-x}Cd_xTe$, two-photon absorpt. spectra 80−20660
$Hg_{1-x}Cd_xTe$, vaporisation under Knudsen effusion conditions 80−2154
$Hg_{1-x}Cd_xTe$, zero-bandgap state induced by press., galvanomag. props. 77−47725
$Hg_{1-x}Cd_xTe$, zero-gap semicond. with nonparabolic band struct., hot electron mobility and conc. 78−76080
$Hg_{1-x}Cd_xTe$, zero-gap semicond., reson. states 79−82558
$Hg_{1-x}Cd_xTe$:Hg, p-n junction photovoltaic diode, appl. as IR detector 78−86330
$Hg_{1-x}Cd_xTe$-CdTe photodiodes, backside-illum., LPE growth and thermal noise characts. 79−40610
$Hg_{1-x}Cd_xTe$-In contact, diffusion of In 80−103520
$Hg_{1-x}Cd_xTe$-oxide interfaces, MIS capacitance characts. 80−49926
$Hg_{1-x}Cd_xTe$-type semimetals, kinetic props., local acceptor level effects 80−65557
$Hg_{a-x}Cd_xTe$, ($x<0.16$), semimetallic phase, acceptor states and galvanomagnetic effects 80−6882
$Hg_{a-x}Cd_xTe$, single-LO-phonon and -plasmon recombination channels narrow-bandgaps 78−91728
$Hg_xCd_{1-x}Te$, Hall effect and elec. cond., carrier density and mobility temp. depend. 77−4341
n-$Hg_xCd_{1-x}Te$, narrow band gap, Auger effect under high mag. fields 79−82609
$Hg_xCd_{1-x}Te$, photodiode, anomalous noise behaviour in heterodyne and background limited operation 79−69568
$Hg_xCd_{1-x}Te$, zero-gap props. correlated to Γ_8 symmetry, review 80−6717
HgCl, ab initio CI calcs., spectroscopic parameters 79−72245
HgCl $B^2\Sigma_{1/2}^+ \rightarrow X^2\Sigma_{1/2}^+$ laser, sustained discharge excitation 78−42342
HgCl, B→X transition radiative lifetime, charge transfer model 78−17719
HgCl, chemiluminesc. of $B^2\Sigma^+$ state produced by photochem. of $Hg/Cl_2/Ar$ 79−39154
HgCl discharge laser, electron beam sustained, operation, appls. 78−59043
HgCl, HgBr, HgI, $B^2\Sigma$-$X^2\Sigma$ systems, Franck-Condon factors and r-centroids 79−64051
HgCl laser, $B^2\Sigma^+ \rightarrow X^2\Sigma^+$ band, electron beam excited $Ar/Xe/Hg/CCl_4(CCl_3Br)$ mixtures 78−13683
HgCl laser, HgCl(B) state radiative lifetime meas. 78−94390
HgCl, laser action obs. at 5576 Å 77−83855
HgCl, laser action on B→X bands, 5576 Å 77−88709
HgCl, photodissociation cross section, laser extraction efficiency 80−32972
HgCl, photodissociation calcs., laser efficiency 80−48047
HgCl photolytically pumped laser system, quantum chem. 80−32971
HgCl, visible laser transition at 5576 Å 79−939
$HgCl_2$, ^{35}Cl powder Zeeman NQR, injection and phase locked NQR spectrometer 80−54979
$HgCl_2$, ab initio effective core potential studies, relativistic effects 79−93933
$HgCl_2$, deformation densities, relativistic effect 80−42928
$HgCl_2$, effective core potentials calcs. rel. to bond lengths and energies 78−66464
$HgCl_2$, electronic struct. and photodissoc., effective core pots. and POL(1) CI wave function 80−63560
$HgCl_2$, intensity changes between He(I) and He(III) photoelectron spectra 78−21969
$HgCl_2$, liquid, partial struct. factors in mol. fluid model 78−22628
$HgCl_2$, NQR freq., intermol. force effect 80−66065
$HgCl_2$, NQR press. depend. 77−12225
$HgCl_2$, non-resonant impurity atom substitution effect on ^{35}Cl NQR reson. 78−5252
$HgCl_2$, photodissoc., two-photon excitation of Hg atom 78−90114
$HgCl_2$, reaction on metallic Cu, reaction velocities, effect of neutral salt addition 78−64887
$HgCl_2$, second order phase transition, elastic consts. meas., Brillouin scatt. 78−10908
$HgCl_2$, solid and molten state, elec. conductance, relative behaviour 79−33113
$HgCl_2$, vac. UV absorpt. cross section 80−91574
$HgCl_2$, X-ray cryst. struct. redeterm. and refinement 80−107140
$HgCl_2$, Zeeman NQR spectra obs. asymmetry parameters 80−80634
$HgCl_2$-PCl_5, Raman spectra, solid and melt, species identification *(German)* 80−45083
$HgCl_2 + AgI \rightarrow AgHgCII_2(AgHgCl_2I)$, solid state diffusion controlled reaction at 100°C 78−34659
Hg_2Cl_2, calomel, birefractive cryst., light spreading *(German)* 77−77168
Hg_2Cl_2, calomel, press. depend. optical soft mode 79−55859
Hg_2Cl_2, calomel cryst., symmetry of low temp. phase 78−26544
Hg_2Cl_2, cryst., birefringence and dichroism, 200-500 nm and far IR 78−27257
Hg_2Cl_2, elec., dielec., and thermophysical props. 79−10989
Hg_2Cl_2, ferroelastic, sp. ht., 100-273K 77−59064
Hg_2Cl_2, ferroelastic transition, refr. index, 80 to 300K 79−82941
Hg_2Cl_2, high pressure induced phase transitions 79−69242
Hg_2Cl_2, improper ferroelastic, soft mode props. in Raman spectra 77−36246
Hg_2Cl_2, low temp. phase transition, X-ray diffr., Raman spectra 78−22849
Hg_2Cl_2, neutron and Raman scatt. studies, ferroelastic transitions 80−76015
Hg_2Cl_2, p-T phase diagram, pressure effect on phase transition 80−107370
Hg_2Cl_2, powder, Raman spectra, press. effects 78−2837
Hg_2Cl_2 prototype phase, soft mode, inelastic neutron scattering, Raman effect 78−91411
Hg_2Cl_2, single cryst., luminesc. 397 nm band props. 77−66529
Hg_2Cl_2 single crysts., IR refl. spectra and ferroelasticity 79−99889

mercury compounds continued
Hg_2Cl_2, surface composition, electron impact, mass spectrometry, AES and LEED meas. 79−60607
Hg_2Cl_2, thermal expansion and ferroelastic $D^{17}_{4h} \rightarrow D^{17}_{2h}$ transition 79−99337
HgCl*, collisional quenching by inert gas (N_2) 80−42986
HgCl*, laser action using electron-beam-controlled discharge pumping 78−42325
HgCl*, metal vapour excimer laser, stability criteria 78−66802
HgCl*(B1/2), fluoresc., collisional quenching kinetics 78−94269
$HgCo(NCS)_4$ calibration standard, low temp. molar mag. suscepts. meas. 78−65947
$HgCr_{2-x}Al_xSe_4$ and $HgCr_{2-x}Ga_xSe_4$, temp. depend. of ESR linewidth, 105-300K 80−71161
$HgCrO_4$, cryst. struct. determ. 78−63712
$HgCr_2O_4(S_4)(Se_4)$, magnetic exchange interactions 77−24690
$HgCr_2S_4$, cooling efficiency near 60Kas mag. refrigerant 80−71034
$HgCr_2S_4$, spinel, mag. struct., symmetry anal. in neutron diffr. studies 80−25091
$HgCr_2S_4$, thermal stability, thermochemical, thermodynamic and crystallochemical props. of chalcogenide spinels 77−51519
$HgCr_2Sd_{4-x}Te_x$, ferromag. semicond., zero bandgap transition 80−96783
$HgCr_2Se_4$, crit. behaviour near Curie point 78−31068
$HgCr_2Se_4$, cryst., preparation, elec. cond., thermo EMF 77−8125
$HgCr_2Se_4$, ESR line intensity near Curie point 78−64269
$HgCr_2Se_4$, electronic props. rel. to departure from stoichiometry 80−100472
$HgCr_2Se_4$, ferromag. semicond., surface magnetism, magneto-optical meas. 77−20831
$HgCr_2Se_4$, ferromag. semicond., Raman spectra 78−52496
$HgCr_2Se_4$, ferromag. semicond., transport props. 78−68039
$HgCr_2Se_4$, influence of Co ions on anisotropy and magnetostriction, ferromag. reson. meas. 77−69659
$HgCr_2Se_4$, initial mag. permeability freq. depend. near Curie temp. 78−10729
$HgCr_2Se_4$, initial mag. permeab., 77 to 300K, domain wall motion and damped ferromag. reson. 79−28562
$HgCr_2Se_4$, n-type ferromag. semicond., galvanomagnetic props. 80−70727
$HgCr_2Se_4$, optical and magneto-optical surface effects 79−82953
$HgCr_2Se_4$, prep., thermal cond., temp. depend., 100 to 500K 77−24451
$HgCr_2Se_4$, Raman scattering, as function of temp. and incident photon energy 79−95781
$HgCr_2Se_4$, spontaneous magnetisation temp. depend., nuclear resonance freq. depend. *(French)* 80−80483
$HgCr_2Se_4$, thermorefl. near ferro- to paramagnetic transition 79−78660
$HgCr_2Se_4$, thermoreflectance, photoconductance, Raman scattering near magnetic phase transition 80−97298
$HgCr_2Se_4$, vapour growth using $AlCl_3+Cl_2$ as transport components 78−35282
$HgCr_2Se_4$:Cd, precipitations during growth by chem. transport method 80−55409
$HgCr_2Se_4$-$CdIn_2S_4$ heterojunction, prep. and photovoltaic prop. *(Japanese)* 78−34889
$HgCr_2Se_4$-$CdIn_2S_4$ heterojunctions, prep. and photovoltaic prop. 78−34892
$HgCr_2Se_{4-x}S_x$, EPR linewidth, 100-300K, spin-lattice relax. 77−51942
$HgCr_2Se_{4-x}S_x$, temp. depend. of EPR line intensity 78−27074
HgD, $A^2\Pi$ state radiative lifetime, pulsed dye laser excitation meas. 78−94288
HgF_2, electronic structure of outermost levels, UPS study 80−7468
Hg_2F_2, ^{199}Hg Mossbauer meas., isomer shift and quadrupole splitting calcs. 80−28039
HgFCl, HgFBr, HgFI, existence and vibr. characterisation, IR and Raman matrix isolation obs. 78−78706
HgF_2(FCl)(FBr), matrix isolated IR and Raman spectra, assignments, force consts., isotope effects and thermodynamic props. 80−63631
HgF(OH), X-ray cryst. struct. refinement 79−46611
$HgFe(CO)_4$, IR and Raman spectra, vibr. anal. 78−66553
$Hg_{1-x}Fe_xTe$ mixed crystals, zero gap, magneto-optical evidence of exchange interactions 80−45045
$Hg_{1-x}Fe_xTe$, struct. invest. using X-ray diffr. and electron microscopy 80−75365
$HgGa_2S_4$, melt growth, optical props. and SHG, HgS-$HgGa_2S_4$ phase diagram 80−50548
$HgGa_2S_4$, energy band struct. calc., empirical pseudopot. method 80−24793
$HgGa_2Se_4$, anisotropic photocond., pleochroism, and band struct. 78−19094
$HgGa_2Se_4$, energy band struct. calc., empirical pseudopot. method 80−24793
$HgGa_2X_4$, X=S,Se, Fourier IR and Raman spectra, cryst. struct. and symm. *(German)* 79−24313
HgH, $A^2\Pi$ state radiative lifetime, pulsed dye laser excitation meas. 78−94288
HgH, $HgCl_2$, relativistic effective core potentials, ab initio calcs. 78−86767
HgH, potential curve determ. from Hg+H resonance scatt. 77−61830
HgH, predissoc. by rot., continuous rot.-vibr. spectrum, Weyl's theory 77−18996
HgH, predissoc. by rot., continuous rot.-vibr. spectrum, resons. and eigenvalues, Weyl's theory 77−18997
HgH, pseudopot. theory calcs. of electronic struct. 77−42230
HgH, rot. predissociation, Weyl's theory and Jeffreys' approx., resons. 78−926
HgH, two-level laser system, discharge simulations 80−74351
HgH^+, HgH_2, relativistic (non-relativistic) HF one-centre expansion calcs. 80−52908
$HgH+M \rightarrow Hg+H+M$, reaction rate temp. depend., chemiluminescence 78−68885
$HgH+NO \rightarrow HNO+Hg$, reaction rate temp. depend., chemiluminescence 78−68885
HgI, B→X transition radiative lifetime, charge transfer model 78−17719
HgI_2, and photomagnetoelectric and photocond. meas., carrier lifetimes 77−55562
HgI_2, aq. soln., luminesc. after high energy electron pulse radiolysis 77−32793
HgI_2, cooperative fluoresc. by excitonic reson. pumping 79−33732
HgI_2, cryst. growth by multiple vacuum sublimation 80−7485
HgI_2, cryst. growth from soln., doping rel. to elec. cond., phase transitions 77−55880
mercury compounds continued
HgI_2 crystals, native defect compensation, doping, mobility-lifetime and TSC meas. 77−55492
HgI_2 detectors, recent improvements 78−37507
HgI_2 detectors, room temp. X-ray spectra of Na and Mg 78−78049
HgI_2 detectors, state-of-art crystal growth and nucl. spectroscopic evaluation 78−41895
HgI_2 detectors for X-ray 80−89837
HgI_2, dielectric const., up to 500 bar, press. depend. 78−27153
HgI_2, doped, vap. growth by temp. oscill. method 78−39674
HgI_2, electrons and holes cyclotron reson. 78−72061
HgI_2, emission spectra in highly excited state 77−52167
HgI_2, exciton study by wave length modulated reflectivity, band parameters 77−51667
HgI_2, excitons, spectral obs. 78−23492
HgI_2, high energy gamma spectrometers, room temp., appl. to ^{60}Co 77−65378
HgI_2, IR lattice vibr. and dielec. dispersion 80−76018
HgI_2, imperfections determ. by thermally stimulated currents method 77−54413
α-HgI_2, inelastic neutron scatt. selection rules 78−79503
HgI_2, layered, photoelectromag. effect meas. of transport parameters 77−59301
HgI_2, low temp. luminesc. spectra by holographic spectroscopy 79−33820
HgI_2, mobility anisotropy determ. by photoelectromag. effect and photocond. 79−38126
HgI_2, mol., gas-phase electron diffr. for geom. struct. 79−97368
HgI_2, mol. struct. and vibr. pot. function, gas-phase electron diffr. obs. 79−31689
HgI_2, NQR spectra of ^{127}I and cryst. struct. 77−12230
HgI_2, nuclear detectors, high X-ray fluence irrad., DC currents 77−54415
HgI_2, nuclear radiation detector, status *(Japanese)* 78−33398
HgI_2, phonon struct. in wavelength modulated refl. spectra and mag. circular dichroism 79−8125
HgI_2, phonon-assisted recomb. of free electron-hole pair 78−23521
HgI_2, photo-EM effect and photocond., trapping effects 77−32042
HgI_2, photodissoc., quantum yield for $I(5^2P_{1/2})$ 79−11805
HgI_2, photodissoc., two photon excitation of Hg atom 78−90114
HgI_2, photoelectronic props. 78−41897
HgI_2, photoexcited, Hall effect, magnetocond., and cyclotron reson., carrier mobility and effective mass 77−59294
HgI_2, photomagnetoelectric effect anisotropy, photocond. 77−15897
α-HgI_2, Raman scatt. at room temp., improved polarisation spectra 80−25368
HgI_2, Raman spectra, in high-temp. $CsNO_3$, metaterphenyl, and paraterphenyl solns. 78−86876
HgI_2, Raman spectra in $CsNO_3$, meta-terphenyl, para-terphenyl at 703K, 508K, 513K 78−29796
HgI_2, Raman spectrum 114 cm^{-1} line, differential analysis using covalence bonds modulation 79−24315
HgI_2, red, liminesc. and Raman scatt., biexcitons and exciton-phonon interactions 79−61424
HgI_2, red, luminesc., excitation spectra on M-band 79−28822
α-HgI_2, red, normal modes vibrations, use of group of neutral elements of crystalline sites 79−37774
HgI_2, red, phonon dispersion, inelastic neutron scatt. obs. 78−75756
HgI_2, red, reson. Raman scatt. and luminesc. 78−84579
HgI_2, red, resonant Raman scatt. in B-exciton and band to band transition regions 79−61381
HgI_2, red anisotropic polariton dispersion, reson. Brillouin scatt. 80−7366
HgI_2, relativistic effects, photoelectron spectra, Hartree-Fock-Slater method, perturbation theory approach 80−27962
HgI_2, single cryst. elec. and thermal props. 79−11111
α-HgI_2, single cryst. growth from iodomercurate complexes 80−35069
α-HgI_2, single cryst. growth from dimethylsulfoxide complexes 80−35070
HgI_2, single crystal growth in small opened ampoules using dynamic sublimation technique 79−4904
HgI_2, soft γ-ray detector fabrication and props. 77−3208
HgI_2, solid and molten state, elec. conductance, relative behaviour 79−33113
HgI_2, soln. grown crystals, low-energy gamma-ray cond. type detectors 80−97418
HgI_2, stimulated emission and optical gain, 80K 78−33738
HgI_2, stimulated emission at high exciton density, temp. depend. 78−84608
HgI_2, stimulated photoluminesc. excitons role 77−48201
HgI_2, thermally stimulated current meas. 78−41896
HgI_2 thin sections with Peltier-cooled preamplification for X-ray spectrosc. 80−324
HgI_2, UV absorpt. cross-sections of vapour 78−25554
HgI_2, vac. UV absorpt. cross section 80−91574
HgI_2, vap. growth by temp. oscill. method in horizontal furnace 78−39675
HgI_2, vapour, excited by photodissociation, fluoresc. yields 78−55138
HgI_2 X-ray luminesc., emission band characts., use as X-ray detectors 77−55815
HgI_2:Ag, trapping effects, TSC, photocond. and photolum. meas. 77−32023
HgI_2:CdS, photodielectric effect 77−11955
HgI_2:CdS binder layer photoreceptor, surface charge characts. thickness depend. 80−57409
HgI_2-BiI_3, molten, elec. cond., temp. depend. 77−89562
HgI_2-CdS binder layers, surface charge characts. for electrophotography 77−10123
HgI_2-CdS mixed system, photocond. depend. on composition and binder content 79−51625
HgI_2-CdS photoconducting binder layers, surface charge decay characts. 77−43642
Hg_2I_2, cryst. growth by multiple vacuum sublimation 80−7485
Hg_2I_2, large single crystal far IR spectra 78−92057
Hg_2I_2, thermal softening of mode on Brillouin zone boundary in Raman scatt. spectra 79−73948
$Hg_2{}^{129}I_2$, Mossbauer effect, bonding, quadrupole coupling const., comparison with $Hg^{129}I_2$ 78−2774
HgI*, collisional quenching by inert gas (N_2) 80−43091
$HgIn_2Se_4$, IR refl. spectra and cryst. struct. 79−56777

mercury compounds continued
$Hg_3In_2Te_6$, complex ordered-vacancy cpd., struct. and lattice dynamics 78−34496
$HgIn_2X_4$, X=S,Se, Fourier IR and Raman spectra, cryst. struct. and symm. *(German)* 79−24313
$HgLi_2(PO_3)_4$, cryst. struct. determ. *(French)* 77−4069
$Hg_{1-x}Mn_xS$, EPR, order-disorder transition temp. 80−50176
$Hg_{1-x}Mn_xS$, phase studies and hydrothermal synthesis 77−48333
$Hg_{1-x}Mn_xS(Se)$ solid solution, magnetic props. 79−51758
$Hg_{1-x}Mn_xSe$, band struct. from anomalous Shubnikov-de Haas effect 80−20080
$Hg_{1-x}Mn_xSe$, EPR, order-disorder transition temp. 80−50176
$Hg_{1-x}Mn_xSe$, spin-orbit coupled bands, indirect exchange interaction via electrons 80−34407
HgMnTe, interband magnetoabsorption and band struct. 79−82959
HgMnTe, semimagnetic semiconductor, band structure, transport phenomena 79−95331
$Hg_{0.98}Mn_{0.02}Te$, resonance acceptor level 78−23048
$Hg_{1-x}Mn_xTe$, impurity magnetoabsorpt. 79−91473
$Hg_{1-x}Mn_xTe$, 1.7 to 3.5 eV, reflectivity spectra 78−43899
$Hg_{1-x}Mn_xTe$, acceptor reson., states in high mag. field 80−49668
$Hg_{1-x}Mn_xTe$, EPR, order-disorder transition temp. 80−50176
$Hg_{1-x}Mn_xTe$, EPR investigation of ordering effects 79−47330
$Hg_{1-x}Mn_xTe$, energy levels at Γ-point in intense mag. fields, Shubnikov-de Haas effect meas. 80−24951
$Hg_{1-x}Mn_xTe$, exchange interaction effect on $\Gamma_8 \rightarrow \Gamma_8$ magnetoabsorption 79−61351
$Hg_{1-x}Mn_xTe$, far IR interband absorption obs. 79−33696
$Hg_{1-x}Mn_xTe$, far IR studies of lattice and free carrier effects 78−39544
$Hg_{1-x}Mn_xTe$, helicon-excited ESR 79−95437
$Hg_{1-x}Mn_xTe$, indirect exchange interaction 79−61094
$Hg_{1-x}Mn_xTe$, indirect exchange interaction 80−97087
$Hg_{1-x}Mn_xTe$, mag. field induced microwave transparency 80−49797
$Hg_{1-x}Mn_xTe$, mag. props., 4.2-300K 77−4508
$Hg_{1-x}Mn_xTe$, mag. props., self-consistent two spin cluster model 80−54874
$Hg_{1-x}Mn_xTe$, mag. susceptibility, 2.3-300K 77−63074
$Hg_{1-x}Mn_xTe$, mag. susceptibility, 2.4 to 300K 80−20379
$Hg_{1-x}Mn_xTe$, magnetic behaviour of Mn 78−14938
$Hg_{1-x}Mn_xTe$, magnetooptical and impurity effects 80−6721
$Hg_{1-x}Mn_xTe$, microwave helicon propag. and helicon excited EPR 77−43637
$Hg_{1-x}Mn_xTe$ mixed crystals, zero gap, effect of exchange on interband magneto-absorption 78−23443
$Hg_{1-x}Mn_xTe$, non-parabolic zero-gap semicond., indirect exchange interaction 80−80498
n-$Hg_{1-x}Mn_xTe$, quantum transport phenomena, exchange interaction influence 78−76093
$Hg_{1-x}Mn_xTe$, semimagnetic, exchange interactions between localised and delocalised electrons 80−97245
$Hg_{1-x}Mn_xTe$, semimetallic, giant spin splitting induced by exchange interactions 77−28150
$Hg_{1-x}Mn_xTe$, Shubnikov de Haas effect and quantum oscills. of thermoelec. power 80−49781
$Hg_{1-x}Mn_xTe$, spin-orbit coupled bands, indirect exchange interaction via electrons 80−34407
$Hg_{1-x}Mn_xTe$, thermo-oscills. of magnetoresist. 79−56249
$Hg_{1-x}Mn_xTe$, transverse magnetoresistance in quantised mag. fields 80−96922
$Hg_{1-x}Mn_xTe$, zero-gap semicond., indirect-exchange interactions 80−29370
$HgMoO_4$, luminesc. efficiency, temp. and high-press. 78−23507
$Hg_xMo_6S_8$ Chevrel phase, synthesis, stability and charact. 80−71608
$Hg(NH_3)_2Br_2$, $Hg(NH_3)_2Cl_2$, thermodynamic study of disorder 79−28109
$HgNH_3$*, excited complex photosensitised luminesc. and fluoresc. phase shifts 78−33535
$Hg(NO_3)_2$, solvation by NH_3 and ND_3, Raman spectroscopic study 78−90172
$Hg_2(NO_3)_2.2H_2O$, Raman and IR spectra, vibr. anal. 77−66492
β-$Hg_3O_2Cl_2$, cryst. struct. 77−31647
$Hg_6O_4Cl_4$, cryst. struct. determ. 78−26516
$Hg(ReO_4)_2$, solid state synthesis, thermal and X-ray anal. *(French)* 79−66281
$Hg_2(ReO_4)_2$, solid state synthesis, therm. and X-ray anal. *(French)* 79−66281
$Hg_3Re_2O_{10}$, solid state synthesis, therm. and X-ray anal. *(French)* 79−66281
$Hg_4Re_2O_{10}$, solid state synthesis, therm. and X-ray anal. *(French)* 79−66281
$Hg_6Re_2O_{10}$, solid state synthesis, therm. and X-ray anal. *(French)* 79−66281
α-HgS, band gap shrinkage, cathodolum. under very strong excitation 77−85146
HgS, cathodoluminescence, evidence of donor-acceptor type transition 77−24902
HgS, cinnabar, chem. vapour growth in closed system 78−35283
α-HgS, cinnabar, donor-acceptor transitions, cathodolum. meas. *(French)* 77−48250
HgS, cinnabar, photoelectron X-ray spectroscopy study 80−29858
α-HgS, cinnabar, photolum. meas. 79−19929
α-HgS, cinnabar, reson. Raman effect and luminesc. meas. 80−50338
HgS, cinnabar powder, 1.65 eV pair recomb., thermal quenching and total light decay 78−27330
α-HgS, crystn. in NaHs solutions 77−8740
HgS, electrodeposition, using nonaqueous solvents 80−76200
α-HgS, electronic energy level calcs. 80−6718
HgS film, deposition from colloidal solns. 78−92209
HgS film, RF sputtered, effect of K on cryst. modification 77−62773
α-HgS films, sputter-deposited in Hg vapour, growth and props. 80−75467
α-HgS, gas-phase and solid-state Hg 5d photoionisation processes, direct comparison 80−76149
α-HgS, green cathodoluminesc., impurity effects 78−2924
HgS, habit variation of crystals of the $C3_12$-$C3_22$ space group 80−107090
α-HgS, hydrothermal synthesis 77−48333
HgS, melting point and vapour pressure 77−15549
α-HgS, natural, yellow emission 78−68567
HgS, photo-stable semicond. in electrolyte soln., photo-EMF and photocurrent obs. 79−42637

mercury compounds continued
α-HgS, polarised reflectance spectra, 2-5 eV, 77 and 293K 77−77243
HgS, RF sputtering on NaCl, growth and struct., electron diffr. and TEM obs. 77−90271
α-HgS, synthetic cinnabar, morphological, optical and X-ray studies *(French)* 77−43223
α-HgS, trapping parameters determ. by TSC meas. 80−59997
γ-$Hg_3S_2Cl_2$ order-disorder structures, desymmetrisation 80−38986
Hg_2SO_4, Raman and IR spectra, vibr. anal. 77−66492
$HgSO_4.H_2O$, X-ray and neutron diffr. study of struct. 80−33936
HgS(Se), reaction with Sn chalcogenides, thermodynamic anal. 80−40728
$Hg_{2.91}SbF_6$, anisotropic visible and IR refl. rel. to metallic cond. 77−8602
$Hg_{2.91}SbF_6$, anisotropic supercond. caused by Hg extrusion, DTA 78−55953
$HgSb_4S_8$, photosensitive semiconductors with high permittivity, elec. props. 79−65518
HgSe,, Fermi surface anisotropy parameters, magneto-optical effect 80−25350
HgSe, band struct. and spin splitting Shubnikov de Haas study 80−65445
HgSe, Bridgman growth at hydrostatic press. to 3 kbar, free electron conc. and mobility 77−52245
HgSe, CVD crysts., electrophys. characts. 77−85910
HgSe, dielec. function at 2, 95, and 300K, reflectivity spectra meas. 79−15458
HgSe, Dingle temp. exam. 79−65358
HgSe, elec. resist., high press. phase transform., band gap 80−70707
HgSe, epitaxial growth on CdSe, struct. and electrophysical props. 77−12540
HgSe film, anomalous photocond., electron microscope study 80−65623
HgSe, film form. in amorphous Se:Hg, photocond. anomaly 77−66183
HgSe film on Se, dark relax. of anomalous photocond., photofield model 77−51776
HgSe, gas, identification by high-temp. mass spectrometry 80−45593
HgSe, highly-electronegative stable metallic contact for semicond. devices 77−24617
HgSe, interband absorpt. and Γ-point band structure parameters 79−47010
HgSe, interband $\Gamma_6 \rightarrow \Gamma_8$ magnetoabsorption and band parameters 79−82960
HgSe, interband $\Gamma_6 \rightarrow \Gamma_8$ magnetoabsorption, temp. study 80−76032
HgSe, magnetooptical and impurity effects 80−6721
HgSe, NMR, chemical shift and linewidth determ. 79−19792
HgSe, narrow band gap semicond., electron scatt., and transport phenomena 80−49706
HgSe, optical determ. of Γ-point band struct. parameters 79−82523
HgSe, point defect model rel. to elec. props. and phase diagram 77−4339
HgSe, press. induced phase transitions, nucleation, resistance discontinuity 77−27996
HgSe, quantum oscills. in Seebeck effect in high mag. fields 77−72875
HgSe, Schottky barrier to II-VI and III-V semiconds., barrier height, compared with Au 77−85312
HgSe, Shubnikov-de Haas oscills. in pulsed mag. field, Fermi energy var. 77−15873
HgSe, Shubnikov-de Haas oscills., electron conc., g-factor and Dingle temp. 77−69354
HgSe, Shubnikov-de Haas effect 78−6402
HgSe, Shubnikov-de Haas determ. of electron g factors 80−6704
HgSe, thermoelec. power, spin split quantum oscills. 77−11948
HgSe, two-phonon resonant effect, far-infrared reflectivity 80−108203
HgSe, zero-gap props. correlated to Γ_8 symmetry, review 80−6717
HgSe, zero-gap semicond., impurity states model 79−60758
HgSe:In, enrichment of doping substances at pseudo phase boundaries *(German)* 80−29036
HgSe:Mn^{2+}, temp. depend. of EPR of ^6S state ions 80−80593
HgSe/CdSe lattice-matched heterostructs. as Schottky barriers, CVD epitaxial growth and elec. props. 80−49877
HgSe-As_2S_3 structure, anomalous photocond., relax., curves 77−55567
HgSe-CdSe pseudobinary alloy, phase diagram and cryst. growth 78−68620
HgSe-MnSe system, phase exam., solubility limit 77−36488
HgSe-Se, photo-field model, rel. to anomalous photocond. in Se:Hg 77−43658
$Hg_3Se_2I_2$ film, holographic characts. *(Russian)* 77−79786
$HgSeO_4.H_2O$, cryst. struct. determ. by neutron diffr. 78−55838
HgSe(Te), dynamic dielectric function, IR absorpt. meas. 78−68508
HgSe(Te), zero-gap semicond., reson. two phonon absorpt. 79−55847
HgTe, 1.5 to 30K, thermal expansion and heat capacity meas. 80−59681
HgTe, acceptor reson., states in high mag. field 80−49668
HgTe, and ternary compounds, mag. field induced microwave transparency 80−49797
HgTe, contrib. of resonant states to conductivity 79−51577
HgTe, creep activation energy and velocity *(Russian)* 78−56716
HgTe, diamond-like semicond., Mossbauer isomer shift meas. 77−16233
HgTe, electron conc. temp. depend., 1.6 to 32K, Hall effect and cond. meas. 80−24952
HgTe, energy bands and optical props. calcs., tight-bonding model with spin-orbit interaction 80−65448
p-HgTe, experimental and theoretical study of the dynamic dielectric function 78−92069
n-HgTe, far IR magnetoabsorption involving resonant acceptor states 79−69813
HgTe film, vac. deposited, elec. props, 78-420K 80−11119
HgTe, freq. tripling and self-interaction of strong EM wave in zero-gap semicond. 79−10355
HgTe, gapless, nonlinear effects in transverse quantising mag. fields 77−69353
HgTe, gapless semicond., magnetophonon conc. oscills. *(Russian)* 77−11943
HgTe, gapless semicond., effect of nonlocal pot. on hole energy spectrum in mag. field 78−39017
HgTe, growth of epitaxial layers, activation by UV and IR radiation 80−71598
HgTe, Γ_8 symm. acceptor centre hole mag. props. *(Russian)* 80−88733
HgTe, heteroepitaxial growth by close-spaced technique of confined type *(Japanese)* 77−24967
HgTe, high purity cryst. grown from soln. by travelling heater method 77−52243

mercury compounds continued
p-HgTe, inverted band struct., negative energy gap from IR absorpt. meas. 77−62820
HgTe, long-wavelength magneto-absorptions 80−11397
HgTe, mag. sub-band struct. under uniaxial stress 77−11883
HgTe, magnetooptical study of Γ_8 bands anisotropy 79−82984
HgTe, magnetophonon oscills. of thermoelec. power 80−49789
HgTe, mobility of electrons and holes, 4 to 100K 80−107821
HgTe, NMR, chemical shift and linewidth determ. 79−19792
HgTe, narrow band gap semicond., electron scatt., and transport phenomena 80−49706
HgTe, optical absorption 77−28572
HgTe, p-T diagrams, p⇌n intrinsic-extrinsic lines 77−36481
HgTe, phonon dispersion relations, neutron study 80−70340
HgTe, photocond. and magnetoabsorption, 1.4-20K 78−34859
HgTe, pressure-induced polymorphic transition 80−10667
HgTe, quantum galvanomag. effects 80−49782
HgTe, resonance states in scatt., variational methods 79−60754
HgTe, self diffusion of Hg and defect struct. 79−23775
HgTe, self-diffusion of Te, layer stripping technique 79−37873
HgTe, single crystal, diffusion of transition metals 79−77818
HgTe single crystals, crystn. from vapour phase, thermodynamical conditions 79−33908
HgTe surface, sputter cleaning and dry oxidation, XPS and LEED study 80−108618
HgTe, temp. depend. of energy gap, oscillatory magnetotransmission meas. 79−15441
HgTe thin film Hall sensor fabrication 80−2951
HgTe type semiconductor, small-gap, electron scatt. and transport props. 78−95294
HgTe type semiconductor, small-gap, electron scatt. and transport props. 78−95295
HgTe type semiconductors, spin-flip transitions in magneto-optics and magneto-transport 80−50306
HgTe, uniaxial stress effect on magneto-optical props. 77−59558
HgTe, uniaxially compressed, anomalous magnetoresist. and band crossing 79−65501
HgTe, VPE growth control by EM irrad. *(Russian)* 80−34338
HgTe, vacancy doping, effect on elec. characts. 79−82595
HgTe, vacancy doping by off-stoichiometry, influence on transport props. 78−55862
HgTe, vacancy electron states, acceptor behaviour, electron mobility 80−70193
HgTe, vacancy mech. of resorption of Hg droplets 80−39070
HgTe, vapour phase epitaxial growth, conditions for oriented crystn. 79−52124
HgTe, zero gap semiconductor, review 77−31944
HgTe, zero gap semiconductors, Coulombic resonance states 79−38020
HgTe, zero gap semiconductor, resonant acceptor states 80−6772
HgTe, zero-gap props. correlated to Γ_8 symmetry, review 80−6717
HgTe, zero-gap semicond., impurity states model 79−60758
HgTe, zero-gap semicond., reson. states 79−82558
HgTe, zero-gap semicond., absorpt. spectrum in mag. field 80−11370
HgTe, zero-gap semiconductor, variational approach to resonances 79−82559
HgTe:Cu, effect of prep. conditions on impurity distrib., hole conc. 77−8743
HgTe:Cu(In), dopant interactions 77−47834
HgTe:In, enrichment of doping substances at pseudo phase boundaries *(German)* 80−29036
HgTe:Mn, impurity scatt. contrib. to electron mobility and thermoelec. power 77−15852
HgTe-CdTe, distrib. ratios of components during crystn. of melt 77−16485
HgTe-CdTe, epitaxy by evap. and interdiffusion under isothermal conditions book contrib. 77−12549
HgTe-CdTe, high intensity US effects on synthesis and growth 77−819
HgTe-CdTe, mixed semiconductor with comp. fluctuation, kinetics of intraband absorpt. and magnetoabsorption coeff. 79−19865
HgTe-CdTe, mixing energy and short-range order, diffuse X-ray scatt. 77−28006
HgTe-CdTe ideal superlattice, electronic props. calc. 80−49885
HgTe-CdTe(ZnTe) solid solns. form., equil. vacancy conc. changes 77−43208
HgTe-HgSe film, optical spectra in fundamental absorption edge 79−74012
HgTe-InAs, phase diags. 77−52299
HgTe-InSb system solid solutions, elec. cond. and thermo-EMF 79−51570
HgTe-MnTe, growth from two-phase melts, crystallisation characts. 77−36393
HgTe-type crystals, inverted band structure, influence of interband scattering on cond. *(Russian)* 79−51563
$(HgTe)_x$-$(CdTe)_{1-x}$, diamond-type semiconductor, Mossbauer spectra, quadrupole interaction of ^{125}Te 80−44992
HgTe(:Ag), impurity diffusion, gamma-ray effects 80−54441
$HgTe_xSe_{1-x}$, solid soln., intrinsic carrier density and energy band struct. 78−39134
HgTl excimer laser, kinetics, optical excitation obs. 80−58527
HgTl optically excited excimers, upper state kinetics 80−37831
HgX (X=Br, I), B-state quenching rate consts. from radiative decay of photodissociated mols. 79−54877
HgX (X=F, Cl, Br, I), three-body ion-ion recombination rates 78−63068
HgX, (X=I, Br, Cl), ground state dissoc. 77−6755
HgX_2, (X=Cl, Br), spectroscopic parameters of mols. from vibr. isotopic effects 78−74798
HgX_2 (X=Cl,Br), aprotic donor solns., Raman spectra, mol. vibr. and solvent strength 78−29788
HgX_2+N_2, $A^3\Sigma_u^+$-state quenching obs. 80−108693
HgX_3^- (X=Cl,Br), aprotic donor solns., Raman spectra, mol. vibr. and solvent strength 78−29788
HgX_4^{--} (X=Cl,Br), aprotic donor solns., Raman spectra, mol. vibr. and solvent strength 78−29788
Hg_2X_2 (X=Cl, Br, I), calomel family, single crysts., microhardness using Vickers method 80−25848
HgX_2(HgXY), (X,Y=Cl, Br, I), IR and Raman matrix isolation spectra, bending force consts. 77−465
HgX_4^{--} (IO_4^-), (X=Cl,Br,I), force consts., compliance and Coriolis consts. calc. 78−42242
mercury compounds continued
HgXY, (X, Y=Cl, Br, I), spectroscopic parameters of mols. from vibr. isotopic effects 78−74798
HgXe, excited molecule formation 77−23519
HgXe, fluoresc. spectra, pot. curves and binding energy 78−66581
HgZn(Cd), Ar matrix absorpt. spectra, vibronic spacing and bonding 79−3453
$Hg_xZn_{1-x}Cr_2Se_4$, absorption spectra near the absorption edge 78−80340
$^{197}HgCl_2$, renal uptake meas., single tracer method for background subtraction 80−67217
$Hy_{2.86}AsF_6$ linear chain cpd., metallic, anomalous elec. props. 77−51731
$(In_2Te_3)_x$-$(Hg_3Te_3)_{1-x}$, photoelec. and luminesc. props. 77−39889
$(In_2Te_3)_x(Hg_3Te_3)_{1-x}$, characts. of photocond. in strong absorption region 77−66184
$(In_2Te_3)x$-$(Hg_3Te_3)_{1-x}$, $0.15 \leq x \leq 0.37$, E_g-comp. depend., spectral photo EMF meas. 77−47851
$K_2Hg(CN)_4$, third order elastic consts. 80−84231
$K_2HgCl_4.H_2O$, cryst., IR spectra, water mol. struct., H-bonding 77−81089
$Mn_xHg_{1-x}Te$, long wavelength optical phonons, IR refl. obs., 50-300 cm^{-1}, x 90 and 295K 77−36243
NH_4HgCl_3, high resolution heat capacity meas. *(Japanese)* 80−52218
αNH_4HgCl_3 quasione dimensional type cryst., phase transition statistics, molecular field approx. calcs. 80−34190
α-NH_4HgCl_3, Raman study of phase transition *(French)* 80−11378
Pb-Al_2O_3-HgSe junction, asymmetry of tunnelling characts. 79−47169
$Pb_{1-x}Hg_xS$, electroless film deposition with variable comp. and polymorphic structs. 79−95952
$Pb_{1-x}Hg_xS$ electroless-deposited films, optical and elec. props. 80−7011
$Pb_{1-x}Hg_xS$ epitaxial films, electroless deposition and struct. props. 79−90915
$Pb_{1-x}Hg_xS$ film, IR detector material, struct. and IR props. 78−26775
$Pb_{1-x}Hg_xS$ film, solution-grown, struct., lattice parameters and optical band gap var. 77−69201
$Pb_{1-x}Hg_xS$, soln. growth, variable gap film for i.r. detector 77−1796
$Pb_{1-x}Hg_xS$-Si heterojunctions, elect. props. 80−100513
$Pb_{0.97}Hg_{0.03}Te$ photovoltaic detector produced by Sb^+ ion implantation 80−82821
Re-Hg-O system, solid state synthesis of 5 crystn. compounds, thermal and X-ray anal. *(French)* 79−66281
Tl_2Te-HgTe(HgSe) systems, phase diagrams 79−87620
(Zn, Cd, Hg)S:Cu,In, electroluminesc. temp. depend. 77−1732
(Zn,Cd,Hg)S:Cu,In, electroluminesc., brightness waves 77−59616
(Zn, Hg)S:Cu, Cl, effect of superposition of two sinusoidal fields and freq. on electroluminesc. 78−39606
Zn-HgO, primary battery, self-discharge rates using microcalorimeter 79−61963
$(Zn_{0.877}Hg_{0.116}Fe_{0.002})_{0.995}S$, unit cell dimensions *(Chinese)* 79−90616
$Zn_{0.1}Hg_{0.9}Se$ type alloy, dispersion law of cond. band *(Russian)* 77−1366
$Zn_xHg_{1-x}Se$, band struct. and scattering mechanism, determ. from transport coeffs. 77−59254
$Zn_xHg_{1-x}Se$, band struct. from Shubnikov de Haas effect and hydrostatic press. meas. 80−49599
$Zn_xHg_{1-x}Se$, current carrier scattering mechanism 80−65546
$Zn_xHg_{1-x}Se$, galvanomagnetic effects, Shubnikov-de Haas oscill. determ. of band struct. 80−6884
$Zn_xHg_{1-x}Se$ semimetal-semicond. transition, thermo-EMF in mag. field and Hall expts. *(Russian)* 77−15881
$Zn_xHg_{1-x}Se$(Te,S) film preparation and props. *(Russian)* 78−11122
$Zn_xHg_{1-x}Te$, impurity influence on thermomagnetic effects and elec. cond. 79−60856
$Zn_xHg_{1-x}Te$, vacancy electron states, acceptor behaviour, electron mobility 80−70193
ZnSe-HgSe, solid soln., defect distrib., elec. props., Hagemark's theory 78−64040
mercury lamps *see mercury vapour lamps*
mercury vapour lamps
546.1 nm line transition probability and Stark constant determ. 78−67471
dark film anal. in RF-excited lamps 80−92789
DRT-220 lamp temp. and Hg 253.7 line intensity relationship 79−2836
electrodeless ^{198}Hg lamp, Ar lines 531 to 561 nm 78−42396
Grimm lamp structure and use in emission spectrochem. analysis of metals *(Japanese)* 78−27867
high-pressure lamps with Sn halide additives, chemical transport obs. 78−71576
illumination systems using DRSh-1000 and PRK-7 Hg-quartz lamps, γ-ray effects 77−88879
light output increase by use of fine quartz or glass fibres *(Dutch)* 77−62028
low pressure lamp, pump for high efficiency I laser 79−31929
low-power UV source, with electronic chopper 78−79087
luminous colour control methods in pulsed arc discharges in Ne-Hg lamps *(Japanese)* 80−103214
nanosecond light pulser with Hg vapour, quenching rate constants determ. 80−100111
plasma props. meas. by untuned cavity calorimeter 77−82520
rapid-scan polarising Michelson interferometer and InSb detector calibration 80−59305
spectral power, appl. of microprocessor-controlled apparatus for pulsed spectra meas. 80−68261
UV sources for curing 78−88443
Hg discharge, high-pressure, NaI and TlI additives, line broadening and radiative transport 80−74199
Hg I 4047 Å night sky contamination and Simkin effect 78−41032
Hg-Sn halide arc, molecular optical absorption obs. 78−75457
Hg-TlI, lamp, chem. comp., temporal and spatial evolution 78−87532
In amalgam lamp, Hg vapour partial pressure meas. 78−67488
mercury vapour rectifiers *see mercury arc rectifiers*
merging
liquid jet breakup, second perturbation soln. for one-dimensional Cosserat theory 79−86478
m.e.s.f.e.t. *see Schottky gate field effect transistors*
mesic atoms
atomic capture, mesic and muonic X-ray intensities effect, allotropic effect, relative capture rates 80−69277
atomic negative meson capture, nuclear giant resonance excitation *(Russian)* 80−42623

mesic atoms continued
conference on high energy physics and nuclear struct. Vancouver, Canada (Aug. 1979) 80−41936
Coulomb de-excitation of neutral exotic atoms, μ^-p and π^-p H atoms 78−25757
deformed nuclei, absorption of slow π^-, mesic atoms 80−78321
dynamic electron screening in mesonic atom and nuclear E1 transitions 78−55260
energy levels, widths and nucleon distribs. in nuclei *(Russian)* 77−88608
exotic atoms, conf., Erice, Sicily, (1979) 80−67939
Fermi-Teller fuzzy model, atomic capture and cascade 77−58209
Fermi-Teller model, formation and de-excitation 77−58208
formation in mixtures of lightest elements 80−87252
interfaces of nuclear and chemical physics, elementary particles and biochemistry 77−6284
kaon-nucleus reactions, low energy, nuclear density shape optical pot. kaonic atom level shifts 80−63213
kaonic, black sphere model for line widths, WKB approx. 77−14618
kaonic, coherent nucleus approx. 79−86086
kaonic, effects of Λ(1405) 77−14056
kaonic, particle and nuclear physics aspects 77−14619
kaonic, radiationless mixing, Er even-even isotope X-ray yield *(Russian)* 77−61880
kaonic, strong shifts, atomic level widths, decay modes 79−86083
kaonic ^{12}C, coupled channel formalism, role of Λ(1405), binding effect, Pauli blocking 78−55261
kaonic atoms, atomic cascade calcs. 77−54633
kaonic atoms, quadrupole hyperfine structure 80−78726
kaonic H atom X-rays obs. 79−86088
kaonic level shifts, multiple scatt. formalism 77−10788
kaonic level shifts, potl. approach 77−14617
kaonic X-rays from Li, LiH, Be 77−10796
light mesic atoms, effect off reson. EM radiation in charact. *(Russian)* 77−79713
mesoatoms in static electromagnetic fields, excited state lifetimes and population, nuclear moments *(Russian)* 80−53170
meson transfer reactions, role of electron distrib. 79−55007
negative mesons in H, atomic capture 80−69276
nuclear bound states of k−, $\bar{p}$ and Σ 80−13399
pion radiative capture on light nuclei, partial transitions, shell model calc. 77−57693
pion s-wave absorpt., optical potl. calc. 77−10439
pionic, invariant impulse approx. 77−10789
pionic, particle and nuclear physics aspects 77−14619
pionic, X-ray transitions, π^- rest mass determ. 77−268
pionic atom, X-ray intensity, at. no. variation, Z=5-90 80−43212
pionic atom broadened X-ray lines, appl. of absorpt. edge technique 78−70976
pionic atom transitions for m_π determ. 77−10297
pionic atoms, Auger electron emission from C, N, O, Ag, Br *(Russian)* 80−69271
pionic atoms, E2 nuclear resonance effects 79−76534
pionic atoms, electron screening and inner shell refilling, X-ray 80−78729
pionic atoms, energy level shifts *(Korean)* 79−9372
pionic atoms, nuclear and atomic research review 80−43216
pionic atoms, quadrupole hyperfine structure 80−78726
pionic atoms, strong interaction effect, pionic X-rays 79−76535
pionic atoms and strongly bound states 79−86084
pionic atoms nuclear density oscills. due to pion condensation 78−70476
pionic Ti, Klein-Gordon eqn., relativistic fine struct. term, verification 79−22868
prompt fission internal γ-ray conversion, fragment radiative transitions *(Russian)* 80−86944
quadrupole moment and relax. of muonium and mesoatom spins 78−19404
quantum defect method, rel. to phase shifts for Klein-Gordon and Dirac eqns. *(Russian)* 77−79207
radius perturbation theory, appl. to NN system and pionic atoms 78−21007
relativistic π-mesic atom, eigenfunctions and eigenenergies, N-space dimensions calcs. 80−41988
spectra, interaction with external quantised EM field, H-like atom 79−68332
stimulated production, photoassociation, induced, in field of strong EM wave *(Russian)* 80−1091
strongly bound π^- nuclear states, vel. depend. pot. binding, pionic atoms 80−37331
weak neutral interaction between muons and nuclei, effects impeding obs. *(Russian)* 77−31031
X-ray radiation anisotropy, suppression coeffs. *(Russian)* 78−22058
Z=8-50 kaonic atoms, X-rays, strong interaction effects 80−9763
Z-dependence of the intensity of $|\Delta n| \geq 2$ pionic X-rays 79−94111
(K,X) optical pot. from KN scatt. and kaonic atom pot. models 79−97731
K mesonic atom, impulse approx. in peripheral region 79−507
K̄-nucleus optical pot. at low energy 78−94032
K^- nucleus, optical model pots. 77−2962
K^--nucleus optical pot. for kaonic atoms 79−98255
K^-p atom and Λ(1405), K̄N interaction model 80−68479
Λ(1405) resonance behavior in nucl. matter 77−18466
π-atomic states in A=12-52, nuclear structure influence, doorway processes 80−99588
π-μ atom prod. in $K_L^0 \rightarrow \pi\mu\bar{\nu}$ *(Russian)* 78−54629
$\pi^-\mu$ Coulomb bound states detection, track correlator as fast trigger 79−45574
π^--mesonic atom, π^--nucleus optical pot. information 79−85559
π^3He, liquid, K X-ray transition energies and Lorentzian widths 80−78727
$\pi^+\pi^-$ atomic bound states and ππ scatt. lengths in H_2 gas target, X-ray spectra 77−27206
$(\pi^+\pi^-)$s atoms, relativistic covariant B-S wave-function *(Chinese)* 79−81308
Al, pionic atom, 2p level shifts and widths 78−46469
^{27}Al, pionic, energy and width of 3d-2p transitions *(Russian)* 78−25760
^{27}Al, pionic, Lorentz-Lorenz quadrupote term, P-wave optical pot. 79−22252
^{27}Al, strongly bound π-nuclear states, criticality condition, optical pot. 78−90325
Ar, pionic, X-ray ang. distrib. meas. 77−3496
As, pionic, s-wave contrib. to 2p-level shifts 77−61881
Be, kaonic X-ray meas., strong interaction widths, shifts, yields 77−58210
Bi, pionic 4f→3d X-ray transition 79−86085
^{209}Bi, pionic 4f→3d transition, pionic 3d state strong interaction level shift and width 79−98251
C, pionic X-ray intensities in graphite 80−32858
^{12}C kaonic atom, level shifts and widths, Λ(1405) dynamics in nucleus 77−3495
Ca, pionic atom, 2p level shifts and widths 78−46469
^{A}Ca, A=40, 42-44, 48, pionic X-rays, strong interaction and isotope shifts, π-nuclear optical pot. 80−53169
^{A}Ca, A=40, 44, pionic X-rays and neutron radius 79−36802
^{40}Ca, pionic, Lorentz-Lorenz quadrupote term, P-wave optical pot. 79−22252
^{48}Ca, strongly bound π-nuclear states, criticality condition, optical pot. 78−90325
Cd+Te, π^- capture, radioactivity meas. 80−47831
^{111}Cd, pionic, E2 nuclear resonance effects 78−29868
^{112}Cd, pionic, E2 nuclear resonance effects 78−29868
^{112}Cd, pionic atoms, dynamical nuclear polarisation, nuclear structure effects 79−94113
Cd(π^-, X), 0 MeV, A=111, 112, E2 nuclear resonance effects, γ and X-ray meas. 78−41774
Cu, pionic atom, 2p level shifts and widths 78−46469
F, pionic X-ray transitions, strong interaction line widths and shifts 77−23586
^{19}F, pionic 2p-1s X-ray transitions 79−18319
Fe, pionic atom, 2p level shifts and widths 78−46469
Ge, pionic, s-wave contrib. to level shifts 77−61881
H, atomic X-ray yields 1s and 2p level shifts and widths, cascades, calc. 80−78730
H, kaonic, strong interaction effects, K^-p scatt. length Coulomb corrections 80−14257
H kaonic atom X-ray observation, energy shift 79−55008
H, mesonic primary population, formation cross section by Born approx. 80−43214
H_2-D_2-T_2 mixtures, mesic at. and mol. processes 80−23580
^{1}H, pionic, pion mass high accuracy meas. from transitions 80−106406
^{2}H pionic atom, energy shift off-shell contribs., zero energy approx. validity 79−76537
^{2}H+$\pi^-\rightarrow\pi^0$nn, rest capture branching ratio, impulse approx. 78−62957
^{3}He, liquid, pionic atoms, X-ray energies, Lorentzian widths, relative intensities 78−46470
^{3}He, pionic, X-ray transitions obs. 77−65549
^{3}He+π^-, strong interaction shift, multiple scatt. and absorptive effects, calc. 78−62958
^{4}He, kaonic and pionic X-rays, strong interaction widths and shifts 79−98253
^{4}He pionic atom, invariant impulse approx. 77−10789
^{A}He, A=3,4, pionic, scatt. lengths and 1s width charge exchange contribs. calcs. 79−17934
^{A}He, A=3,4, pionic 1s state energy shift and line broadening *(German)* 80−48107
Heπ^-, mol. ion formation in liq. He, X-ray intensities, Auger and Stark transitions 78−94338
^{165}Ho, pionic atom, quadrupole hyperfine interactions, nucl. moment 78−37772
^{165}Ho(π^-,X), 175 MeV/c, monopole and quadrupole strong interaction effects in pionic atoms 78−41777
Li, kaonic X-rays meas., strong interaction widths, shifts, yields 77−58210
^{6}Li, radiative π capture from 1s level, partial rates 79−3180
^{175}Lu(π^-,X), 230 MeV/c, monopole and quadrupole strong interaction effects in pionic atoms 78−41777
Mg isotopes, pionic, energy and width of 3d-2p transitions *(Russian)* 78−25760
Mg, pionic X-ray transitions, strong interaction line widths and shifts 77−23586
Na, pionic X-ray transition strong interaction line widths and shifts 77−23586
^{23}Na, pionic 2p-1s X-ray transitions 79−18319
Nd, A=148, 150, pionic X-rays in 4f→3d transition, neutron isotope shift 77−75347
O, in oxides, ang. distrib. of muon decay electrons *(Russian)* 78−48105
^{A}O, A=16,18, pionic 1s state energy shift and line broadening *(German)* 80−48107
^{110}Pd, pionic atoms, dynamical nuclear polarisation, nuclear structure effects 79−94113
Re, pionic 4f→3d transition, pionic 3d state strong interaction level shift and width 79−98251
Re, pionic 4f→3d X-ray transition 79−86085
^{104}Ru, pionic atoms, dynamical nuclear polarisation, nuclear structure effects 79−94113
S isotopes, pionic, energy and width of 3d-2p transitions *(Russian)* 78−25760
S, pionic atom, 2p level shifts and widths 78−46469
^{32}S, kaonic, Y* resonance nonlocal effects, kaonic shifts and widths 79−7039
^{32}S kaonic atom, level shifts and widths, Λ(1405) dynamics in nucleus 77−3495
Si isotopes, pionic, energy and width of 3d-2p transitions *(Russian)* 78−25760
Si, pionic atom, 2p level shifts and widths 78−46469
^{150}Sm, pionic atoms, dynamical nuclear polarisation, nuclear structure effects 79−94113
^{122}Sn, kaonic, E2 nuclear resonance effects 78−29868
^{122}Sn(K^-, X), 0 MeV, E2 nuclear resonance effects, γ and X-ray meas. 78−41774
Ta, pionic 4f→3d X-ray transition 79−86085
^{181}Ta, pionic 4f→3d transition, pionic 3d state strong interaction level shift and width 79−98251
^{181}Ta, pionic atom, quadrupole hyperfine interactions, nucl. moment 78−37772
^{181}Ta, pionic X-rays, effective quadrupole moment determ. 78−66200
Ti, pionic, pion mass high accuracy meas. from transitions 80−106406
Ti, pionic, relativistic fine struct. splitting obs. 79−10237
^{A}Ti, A=46, 48, 50, pionic X-rays, strong interaction and isotope shifts, π-nuclear optical pot. 80−53169

mesic atoms continued
^{48}Ti, pionic atoms, dynamical nuclear polarisation, nuclear structure effects 79−94113
^{140}Xe, μ-mesic conversion of γ-rays 77−82865
Zn, pionic, s-wave contrib. to 2p-level shifts 77−61881
Zn, pionic atom, 2p level shifts and widths 78−46469
Zn+Se, π^- capture, radioactivity meas. 80−47831

mesic molecules
binding energy, using Schrodinger perturbation theory in adiabatic rep. *(Russian)* 77−60976
exotic atoms, conf., Erice, Sicily, (1979) 80−67939
hydrogenic mesomolecules and muon catalysed fusion 80−68719
interfaces of nuclear and chemical physics, elementary particles and biochemistry 77−6284
kaonic hydrides (deuterides), Z=3, 6, 8, 11, 20, X-ray intensities, comparison with the atoms 77−58212
mixtures, atomic capture prediction model 80−69277
stimulated production, photoassociation, induced, in field of strong EM wave *(Russian)* 80−1091
three-body system in mesoatomic physics, adiabatic two level approx. *(Russian)* 79−22870
ddμ mesic mol. form. in gas D_2, reson. depend. *(Russian)* 79−50171
H_2 μ-mesic molecules resonance formation *(Russian)* 78−46471
H_2-D_2-T_2 mixtures, mesic at. and mol. processes 80−23580
$He_2\pi^-$, mol. ion formation in liq. He, X-ray intensities, Auger and Stark transitions 78−94338
LiH, kaonic X-ray spectra, strong interaction widths 77−10796
LiH, kaonic X-rays meas., strong interaction widths, shifts, yields 77−58210
$(LiH)^+$+meson system, ground and 1st excited state pot. surfaces, quantum mech. calc. 78−5377

mesomorphic state *see liquid crystals*

meson absorption
photoemulsion nuclei, π^+ absorption, up to 114 MeV, nuclear scaling *(Russian)* 78−25247
total pion absorption cross section, A depend., proton yields 80−106081
K^- absorption at rest in C nuclei, study of final states containing Λ-hyperon 77−41997
K^- absorption cross section on nuclei, 60-280 GeV/c 79−22293
($\pi^\pm$, X), absorption cross section in range 20 to 280 MeV for Al, Ti, Cu, Sn, Au nuclei 80−78327
π energy dependent mean free path length for star formation 77−23393
π s-wave absorption, sensitivity to off-shell props. of πN scatt. 77−50158
π^+ absorption cross section on nuclei, 60-280 GeV/c 79−22293
^{197}Au(π^-,X), X=d,t, ^{3}He, ^{4}He, particle emission following stopped pion absorption 80−91196
C, absorpt. of stopped π^-, charged particle energy spectra meas. 78−33224
Cd+Te, π^- capture, radioactivity meas. 80−47831
^{59}Co(π^-,X), X=d,t, ^{3}He, ^{4}He, particle emission following stopped pion absorption 80−91196
^{7}Li+π^-→^{4}He+^{3}n (or ^{3}He+^{4}n), search for neutron nuclei *(Russian)* 77−74889
Zn+Se, π^- capture, radioactivity meas. 80−47831

meson-baryon interactions
see also kaon-baryon interactions; meson-baryon scattering; pion-baryon interactions
additive diquark spectator model for meson-baryon quasi-two-body reactions, addendum 79−89114
additive diquark spectator model test in meson-baryon quasi-two-body reactions 79−40742
background scattering 77−22753
Brayshaw and Peierls mechanisms for generating hadron peaks, N*(1470), 0(1020) and charm 79−404
coupling strength of meson-baryon interactions in u-, d- and c-quark sector 78−25011
crossing invariant solution of baryon exchange degeneracy, reggeon F/D ratios in SU(4) 77−2766
diquark and quark jet fragmentation model, lepton pair triggered meson-nucleon events 79−2979
extended baryon fields and meson-baryon interaction 77−41751
four-body reaction amplitudes in exact SU(4) 77−18192
isoscalar meson-nucleon couplings, finite energy sum rules, duality determ. 77−13940
JINR experiments using Serpukhov accelerator, present and proposed *(Russian)* 79−63545
massive lepton pair production in meson-nucleon collisions 79−63532
meson+proton→3 mesons+proton, partial wave anal., Ascoli anal., fireball dimens. 78−17054
meson production by charge exchange reactions, production cross section 78−58200
meson spectra in forward jets, hadron cascade model anal. 80−32103
meson-meson, pion spectra forward-backward asymmetry, fragmentation effects, meson reson. decay 78−86457
meson-nucleon, meson spectra in meson fragmentation region, quark cascade model 77−67689
meson-nucleon cross sections in topological bootstrap model 77−22708
meson-nucleon inclusive prod. of non-zero charm mesons in central region, quark model *(Russian)* 77−14008
meson-proton multiplicity data, two-component fireball model applications 79−63453
peripheral scattering dominance, possible interpretation 77−18241
quark fragmentation distribs., meson, baryon and photon reactions 77−74655
resonance-nucleon and particle beam-nucleon scatt. cross sections *(Russian)* 80−32115
SU(4) broken symm., duality, baryon+baryon and baryon+antibaryon exotic mesons prod. 78−89629
total cross sections, semiempirical formulae, three component model with SU(3) components 78−41600
unitarity restrictions on meson-nucleon helicity-flip amplitudes and slope of the diffraction peak 79−54348
unitary analytic isobar model, N-meson to N-meson-meson process 78−78114
vector meson-nucleon interaction, SU(3) symm., coupling consts., form factors 77−13886
ηN, 414 to 682 MeV, total cross section determ. *(Russian)* 79−22122
fN, <500 MeV, total cross section determ. *(Russian)* 79−22122
MB→l^+l^-X, meson quark struct. functions, and Drell-Yan process 79−63551

meson-baryon interactions continued
N+vector meson, polarised deep inelastic collisions in nuclei *(Russian)* 80−102209
ωN, <500 MeV, total cross section determ. *(Russian)* 79−22122
ϕN, cross sections and quark multiple scatt. model 79−54350
ψN total cross section, photon and hadron interactions of radially excited states 78−82170
ψp total cross-section in SU(4) 77−46089
ψN, soliton model *(Russian)* 77−46071

meson-baryon scattering
see also kaon-baryon scattering; meson-baryon interactions; pion-baryon scattering
bag model $Q^4\bar{Q}$ states, meson-nucleon low-energy S-wave scatt., P-matrix formalism 80−13271
charmed particles, hadronic props., superconvergence sum rules 80−78043
chiral invariance for asymptotic momenta, elastic scatt. of hadrons, helicity amplitudes 78−4800
chiral Lagrangian model, scatt. lengths, πN coupling const. 77−88001
data amalgamation technique 80−37293
differential cross section ang. depend., constituent interchange model 77−255
diffractive scatt., field theoretic model with quark field operators 79−26318
elastic partial wave amplitude construction from knowledge of Barrelet zeros 77−22777
exotic states, expt. test for absence 77−13987
extended PCAC hypothesis, soft-meson chiral symm. breaking, meson+-nucleon scatt. 78−21353
gauge-dual-topological approach to soft hadronic reactions, trajectory slopes 80−18142
hadronic total cross sections, model, using covariant harmonic oscillator pot. wave functions 79−26306
large angle elastic scatt. calcs. 80−83002
meson-proton, high energy, review 77−257
QCD, heavy-vector meson-nucleon scatt., cross section suppression, Υ and ψ 80−22564
Regge spectra of charmed baryons in dual resonance amplitudes 79−13088
resonance vertex functions and scatt. amplitudes resonance-nucleon scatt. ρ rescatt. *(Russian)* 80−105918
$K^\pm$N, 70, 125, 175 GeV/c in Be, C, Al, Cu, Sn, Pb nuclei 80−83128
ωN elastic scatt., and meson size, in quark multiple scatt. model 79−54349
$\pi^\mp$N, 70, 125, 175 GeV/c in Be, C, Al, Cu, Sn, Pb nuclei 80−83128
ρN elastic scatt., and meson size, in quark multiple scatt. model 79−54349

meson capture
see also mesic atoms; mesic molecules; radioactivity
atomic capture, mesic and muonic X-ray intensities effect, allotropic effect, relative capture rates 80−69277
Coulomb capture in inhomogeneous matter 78−55116
exotic atoms, conf., Erice, Sicily, (1979) 80−67939
giant dipole resonance, as nuclear collective state *(Slovak)* 77−61395
(π^-,X), n and charged particle emission following π^- capture 80−73867
(π^+,X), 85 to 245 MeV, capture cross sections for Li, C, Al, Fe, Nb, Bi 80−73869
π radiative catpure, current algebra model with hard pions *(Russian)* 77−74890
π^- capture by H in $TiH_{1.65}$ and $PdH_{0.67}$ *(Russian)* 78−13167
Au(π^-,X), stopped π^- capture, product nuclei distribs., isomeric yield ratios, neutron multiplicity 77−18625
C+K^- at rest, absorpt. branching fractions determ. 77−67771
$CH_2(CD_2)$, pionic X-ray intensities in polyethylene($-d_n$) 80−32858
^{3}He, threshold pion photoproduction and radiative capture, π-^{3}He-^{3}H coupling constant 79−40962
Hg(π^-,X), stopped π^- capture, product nuclei distribs., isomeric yield ratios, neutron multiplicity 77−18625
^{7}Li+π^-→^{4}He+^{3}n (or ^{3}He+^{4}n), search for neutron nuclei *(Russian)* 77−74889
^{16}O(π,γn), direct and resonance reaction unified shell model, n, γ spectra 80−52696
Pt(π^-,X), stopped π^- capture, product nuclei distribs., isomeric yield ratio, neutron multiplicity 77−18625

meson decay
see also kaon decay; meson hadronic decay; meson leptonic decay; pion decay
σ SU(3) model, quark-loop contrib., low-energy meson dynamics 78−12869
Bethe Salpeter model for strong, EM, and weak meson decays effective quark mass 78−70336
bottom mesons, weak decays, strong correction meas. 80−82970
charm particles, sum rules for four-body semi-leptonic decays 79−36067
charmed decay and asymptotic scale factors 77−38202
charmed meson, non-leptonic decay in SU(3) Bose quark model 79−85278
charmed meson, possible semileptonic decay to K's in ν interactions 77−2819
charmed meson decay props. anal. 77−71507
charmed meson pair semileptonic decay obs. in pp→$e^\pm\mu^\mp$X 78−89759
charmed meson semileptonic decay, effective chiral Lagrangian method 78−74254
charmed meson semileptonic decay effects of hadron multiplicity on distribs. 78−4856
charmed meson semileptonic decay inequalities for decay rates and lepton polarisations 79−89147
charmed mesons, lifetime measurement 80−73693
charmed mesons, semileptonic decays, charged weak current struct. 80−102042
charmed mesons, weak decay mechanism 79−93405
charmed particle semileptonic decay to K_s^0e in e^+e^- 77−2853
charmed particle weak semileptonic decays, free parton model 79−75766
charmed particles, masses and decay consts. in SU(4)×SU(4) broken chiral symmetry 79−40686
charmonium, $^1P_1$ state, mass, branching ratios, decay rates 78−62370
charmonium decay, effective strong coupling constant for timelike Q^2 80−99091
charmonium electromagnetic decay, relativistic eval. 80−68459
charmonium states, multimesonic decays, statistical quark model 78−82171

meson decay continued
EM decay, contact terms 79−63481
gluon and quark jets in a recursive model motivated by quantum chromodynamics, ϒ decay 80−62936
hadron resonance decay, intermediate vector boson and high energy weak interaction detect. 79−22012
hadronic charmed particle decays, quark and particle helicities, charm changing current chirality 80−37256
heavy 1^{--} quark-antiquark bound state decays, fast gluons 79−85297
heavy charged quark system decays, CP noninvariance, six-quark model/QCD anal. 79−80826
heavy flavoured meson decays, charged Higgs bosons 79−22014
heavy meson inclusive semileptonic decays, lifetime estimates, quark-parton model difficulties 80−86704
heavy meson weak decays, heavy quark decay, QCD corrections, real gluon role 80−57586
heavy quark semileptonic decay, gluon radiative corrections 79−75743
heavy quarkonium, energy-energy correlations, testing of gluons in QCD 79−71690
heavy quarkonium decay in the presence of instantons 79−85296
heavy quarkonium states, decay rate to lepton pairs, gluonic corrections 80−102043
heavy vector mesons, decay into Higgs particles 78−12908
lifetimes and branching fractions of mesons with heavy-quark constituents 79−93404
light meson radiative decay, Zweig law *(Russian)* 80−102051
M1 radiative meson decays, QCD corrections 79−17718
meson spectroscopy, a review using quark models 78−25010
multi-channel baryonium and some peculiarities of its decays *(Russian)* 80−105857
neutral charmed particle decay, direct observation in ν-emulsion interactions 80−9165
neutral pseudoscalar meson radiative decays, K_{l4} decay in chiral quark model *(Russian)* 80−105900
nonlocal quark model in SU(3)×SU^c(3)×U(1), meson decay and mass correction *(German)* 80−27456
nonrelativistic quark model, $\eta\eta'$ and $\omega\phi$ mixing in meson decay 78−21423
orthoquarkonium decay, Dalitz plot population and thrust ang. distrib., scalar gluon nonexistence 80−27470
OZI rule violation model due to spinless bosons 79−89107
P→2γ, EM decays of vector and pseudoscalar mesons, dispersion theoretic approach 79−93423
P-wave radial mixing, effect on E1 radiative decays, charmonium mass 80−37271
perturbative QCD, renormalisation improvement, charmonium decay and scaling violations 80−101993
photocoupling in quark model 80−82954
prompt electron yield from hadron interactions anal. 77−26517
pseudoscalar decay in three quark oscillator model for baryon spectrum 77−22698
pseudoscalar meson decay, symm. breaking in chiral SU(4)×SU(4) model 78−21424
pseudoscalar-meson decay constants, Goldberger-Treiman relations, and chiral SU(4)×SU(4) symmetry breaking 79−293
QCD low energy tests, gluon non-zero effective mass, ψ decays 80−91054
$Q\bar{Q}$ bound states, hadronic decay, azimuthal correlations 79−93442
$Q\bar{Q}$ states, P wave decays, jet ang. distrib. and kinematics 79−75737
radially excited states, photon and hadron interactions 78−82170
radiative decay, SU(3) octet-broken VMD anal. 77−71517
radiative decay rates for V→Pγ, P→PPγ, P→γγ and V→PPP, symmetry, angle mixing 77−49969
radiative decays, higher order effects 79−13131
radiative transitions and gluon-exchange contributions in QCD 79−45074
Regge spectra, symm. breaking effects, decay rates of mesons in dual resonance amplitudes 77−82715
resonances, high spin, natural parity, dual reson. model with nondegenerate Regge trajectories 79−359
resonances, strong and EM decays, particle mixing and meson pole dominance 80−18127
semileptonic decay, effect of symmetry breakdown *(Russian)* 79−6337
spin zero charm mesons, in broken chiral SU(4)×SU(4) symmetry 79−58900
strange baryonium, spectrum, decay, production 78−93854
SU(3) rules for semileptonic weak decay of charmed and strange mesons 78−45916
SU(4)×SU(4) current two point functions, meson decay consts. and bare quark masses from duality 78−8598
SU(4) symm., appl. to meson decays 78−12835
tensor meson radiative decay in SU(6)×O(3) broken symmetry quark model 80−73710
top mesons, weak decays, strong correction meas. 80−82970
two-body amplitudes calc. in lattice gauge theory 77−34126
V→Pγ, effect of SU(3) admixture in VMD model 77−49970
vector meson mass spectrum, radiative decay, QCD nonrelativistic potential model 79−36046
vector meson radiative decay evaluation in spectrum generating SU_4 scheme 79−54342
vector meson radiative decays, SU(3) symmetry viewpoint 80−95273
vector meson radiative width determ. from Primakoff effect meas. 79−89157
vector mesons, EM decay in broken SU(3) 80−82976
vector mesons, in SU(4) σ model with massive gauge fields 77−10184
vector mesons, neutral, P-odd effects in decay *(Russian)* 78−54628
vector mesons, radiative decay, single parameter scheme 80−86720
B meson, cascade decays, CP nonconservation 80−105811
b-quark meson, decay, weak mass mixing, CP violation 80−32086
$b\bar{b}$ meson state lifetimes, R predictions above bottom threshold, quark model 80−99097
$B^0\bar{B}^0$ mixing in six quark model, decay, mass mixing and CP nonconservation 80−42406
$c\bar{c}$ and $b\bar{b}$ states, spectra and strong decays 80−52502
$c\bar{c}$ meson radiative decays, generalised VMD mechanism 78−8606
$\bar{c}c$ $\bar{q}q$ states, decay, hadronic and photo-prod., e^+e^- annihilation prod. 80−99092
χ→2γ, invariant mass spectrum in π^-p interactions *(Russian)* 78−45963
χ→γγ, decays of 0^{++} scalar mesons 77−13963
χ→γγ, radiative width calc. 77−71508
χ→ψγ, charmonium E1 radiative transitions and quark mag. moments 80−86721
D, CP violation effects, predictions of six-quark model *(Russian)* 79−93379
D, decay constants from Weinberg type sum rules 79−54336
D(1865), charmed meson semileptonic decays 78−4854
D(1865)→eνK*(890), right handed current, eK* ang. correl., energy spectra 78−74248
D(1.87) mesons semileptonic decay, multiplicity effects 77−49953
D→$\bar{K}$+l^++ν, semileptonic decay of charmed particles, formalism using helicity amplitudes 78−4852
D→Klν, D meson weak decay const. determ. 79−93407
D→Kπ and semileptonic decay in massive quark model 79−93376
D→Kπlν, charm-changing weak hadronic current, models 80−57585
D-meson, charged Higgs boson couplings 80−62917
D-meson decay mechs., weak and leptonic two-body decays 78−41535
D-meson semi-leptonic decay, current algebra treatment, rel. to charmed current quark mass 79−97577
D-meson semileptonic decays, K-e correl. anal. 78−78179
D^0, $\bar{D}^0$, decays, charm changing neutral current limits, QCD depend., mass differences 80−32062
D^0, lifetime difference from D^+ 80−91084
D^0−D^+ lifetime difference, possible mechanism D^0→s+$\bar{d}$+gluon 80−37255
D^+D^0 decays and lifetimes assuming sextet dominance and colour clustering 80−32094
δ(980)→γγ decay rate implying δ is four-quark state 79−93422
e^+e^-→3γ, 3.6 GeV and ψ′ reson., comparison with QED 77−46066
e^+e^- annihilation, CP violating effects, D^0, G^0 and H^0 meson decays 79−80769
e^+e^-→γγ, 9.4-31.6 GeV, differential cross section, ϒ→γγ decay limits 80−91073
e^+e^- initiated γγ processes, charged pair prod., f^0→γγ width 80−91123
e^+e^-→O particle, decay, mass, prod. from Zweig rule intermediate vector particle model *(Chinese)* 80−73697
e^+e^- resonance decay modes in Han-Nambu colour model 77−18307
ε→γγ, decays of 0^{++} scalar mesons 77−13963
ε→γγ, sum rules for γγ scatt. 77−6128
η, η′ and η_c, mixing and decays in nonrelativistic quark model for QCD idea 78−82166
η, mesonic octet decays, chiral QFT description using one loop approx. *(Russian)* 79−63471
η, vacuum symmetry, decay consts., mixing consts. in SU(3)×SU(1) QCD 80−27483
η→2γ, η-problem of meson masses, quark charges, colour model 77−57542
η(η′)→γγ, quark model tests 80−78067
η→π^0γγ decay width and processes in chiral QFT *(Russian)* 80−32099
η→$\pi^0\nu\bar{\nu}$, presence of second class neutral currents 79−26284
η^0→2γ decay rates from γN amplitudes, N EM polarisabilities 77−18289
η_c, decay constants from Weinberg type sum rules 79−54336
η_c, production cross sections in e^+e^- colliding beams, two-photon processes 79−36089
ηγ decays of ρ^0, ω and φ, widths 77−22736
F, decay constants from Weinberg type sum rules 79−54336
F(0⁻), F*(1⁻), charmed strange mesons, weak decays 78−74249
f→γγ, sum rules for γγ scatt. 77−6128
F→φ+l+ν, semileptonic decay of charmed particles, formalism using helicity amplitudes 78−4852
F-meson, decay mechs., weak and leptonic two-body decays 78−41535
F-meson semileptonic decay modes, explanation of inclusive electron spectra 78−37202
f^0→γγ, covariant polarisation density matrix analysis *(Russian)* 78−454
F^+ lifetime, 6 dominance and W^+ exchange dominance 80−37254
γ radiative decays, unified mechanism, form factors *(Chinese)* 77−57540
J particle, tensor meson decays in SU_4 model *(Chinese)* 79−75767
K_{l3}, struct. constants of mesons in quark diagram model *(Russian)* 79−30717
K^0_L+Cu, 4-20 GeV/c, $\mu^+\mu^-$ prod. from vector meson decay 78−45951
ω→$\pi^0\mu^+\mu^-$, branching ratio determ., dis. in π^-p collisions 79−67556
ω radiative decay, contrib. to pp bremsstrahlung field theoretic calc. 78−62451
Ω radiative decay effect on pp bremsstrahlung at 158-400 MeV 77−74706
pp bremsstrahlung, ω radiative decay contrib. 78−70386
φ decay modes following p+Be→φ+X at 400 GeV/c 78−599
π^-p→η(η′)n, 8.45 GeV/c, differential cross section ratio, η′ decay branching 80−78094
ψ, ψ′, DASP results on e^+e^- annihilation 80−42483
ψ→2γ(3γ), charmonium model calcs. 77−30387
ψ(3684) radiative decays, energy correlation 80−13307
ψ→3γ, dispersion sum rule charmonium theory, decay probability lower bound *(Russian)* 78−89716
ψ→3γ, dispersion theory of charmonium, self consistency test, decay probability *(Russian)* 78−89717
ψ→η(η′)γ, quark model tests 80−78067
Ψ family, EM decays, relativistic corrections in potential model 79−49522
ψ→fγ, f′γ, πππγ, KKγ, meas. using DASP detector at DORIS 78−45922
ψ→fγ, form factor depend. in relativistic harmonic oscill. model 79−89156
ψ→gravitino+antiphotino, gravitino mass lower limit, light gravitino weak interactions 79−75698
ψ hadronic and photonic decays, pseudoscalar mixing effects, cylinder dominated model 77−6120
ψ mass spectra and radiative decay in light-quark model 77−18258
ψ meson, radiative decays, charmonium model 77−38174
Ψ meson decay rate in charmonium models 79−22061
ψ neutral decays, identification of ψ→γη→3γ and ψ→γη′→3γ modes 77−49968
ψ radiative decay obs. in e^+e^-→3γ 77−46065
ψ resonances neutral and radiative decay modes 77−57530
ψ→X(3410)+γ, means of J^P determ. of X(3410) *(Chinese)* 77−57581
ψ/J (3100) and ψ′ (3700) decays results from DASP collaboration/DORIS 77−61282
ψ′→χγ, charmonium E1 radiative transitions and quark mag. moments 80−86721
ψ′→χγ, decays of 0^{++} scalar mesons 77−13963

meson decay continued
$\Psi''(4.4)\rightarrow\Omega'\bar{\Omega}'$, $\Omega'\rightarrow\Xi^0 e\ \nu_e$ or $\Xi^0\mu\ \nu_\mu$, explanation of anomalous lepton prod. in e^+e^- annihilation 77−41834
Q mesons, sum rule for decay widths 78−449
$q\bar{q}$ states, decay with large mass in 2-D QCD, appl. to meson decay anal. 79−89126
$\rho\rightarrow\pi\gamma$, chiral SU(3)×SU(3) representation, spontaneous symm. breaking, VDM, PCAC 77−57512
$\rho\rightarrow\pi\gamma$ decay width, explanation using SU(3)-scalar term in the EM current operator 78−82206
$\sigma\rightarrow 2\gamma$, tensor-trace and triangle anomalies 80−73709
Υ, EM decays, relativistic corrections in potential model 79−49522
Υ, production and decay in quark fusion model 80−102018
$\Upsilon\rightarrow 3\gamma_{,,}$ IR and collinear divergences, cancellation in one-loop corrections to QCD cross sections 79−40730
$\Upsilon(9.5,b\bar{b})$, decay into Higgs scalar and photon 79−36082
$\Upsilon(9.5)$, nature of heavy particle anal. *(Chinese)* 78−86443
$\upsilon(9.5)$, prod. in e^+e^- annihilation, photoprod., decay modes, quark model 78−12877
Υ decay, implications from heavy quark content of light hadrons 78−93853
Υ decay, photon spectrum, branching ratios, leptonic-, hadronic widths, quarkonium model 79−3020
$X(2.85)\rightarrow 2\gamma$, obs. in charge-exchange reaction $\pi^- p\rightarrow Xn$ 78−25047
$X(2.8)\rightarrow 2\gamma$ decay width, possible determ. by Coulomb photoprod. *(Chinese)* 77−57541
x-boson, mass and asymmetric decay rel. to cosmological baryon asymmetry 80−4464
$X^0\rightarrow\gamma\gamma$, prod. in $\pi^- p\rightarrow X^0 n$, four-momentum transfer region 0.38-0.79 $(GeV/c)^2$ 77−67656
$D\rightarrow K\pi l\nu$, hadronic current form factors, $(\bar{c},s)$ weak current and symmetry props. 79−67545
$\eta\rightarrow\pi^0 e^+e^-$, presence of second class neutral currents 79−26284
pN, 350 GeV in Ne, $D^\pm$ prod. cross section and lifetime 80−68494

meson detection and measurement
binary encoded position-sensitive scintillation hodoscope with reduced photomultiplier, pion detection 78−17506
dosimetry, automated data acquisition and anal. system at LAMPF pion therapy facility 78−53506
drift chamber system for K+e elastic scatt. expt. at Fermilab, efficiency, accuracy 77−57809
high LET radiation therapy beams, expt. microdosimetry 80−12280
liquid Ar calorimeters, props. of EM and hadronic showers 79−45599
multilayer gas proportional counter system, CM CERN external particle identifier 79−45530
pion, simulated treatment planning for Stanford Medical Pion Generator 77−86634
pions, two-dimens. visualisation of stopping pion distribs., for therapy 77−12999
proportional wire chambers system for particle coords. meas. in π^- beam 78−9025
scintillation spectrometers based on flight time 79−26818
scintillator Pb-acrylic shower detector, meas. of electron and pion cascades 79−81124
Vekton-1 double arm spectrom. for ρ^- meson photoproduction 78−33362
K^- tracks, 1.5 GeV/C, fast stable particles from light emulsion nuclei, emission probabilities 78−17245
(π^+,π^-) reactions on light nuclei, micron spectrometer for meas. with energy resolution of 1 MeV for 400 MeV/c momentum 78−13368
π polarisation measurement using multiwire proportional chamber with analogue data plotting 78−78566
π^-, sensitivity of personnel monitoring film 78−28079
π^- and π^+, stopping density distribs. in 1 and 2 dimensions 80−26340
π^- broad therapeutic beams, microdosimetric characterisation 80−12277
π^- capture at rest, exptl. method for pion discrimination and absolute counting 80−5432
π^- radiotherapy, biological effect prdiction, star distrib. for high LET dose determ. 80−12248
π^0 high resolution spectrometer for nucl. struct. anal. 78−37500
π^-p elastic interactions, methodics of identification in bubble chamber *(Rumanian)* 79−63520
$\pi^+ p\rightarrow n\pi^+\pi^+\pi^+\pi^-$, reaction, extraction from background 78−880
$\pi^0\pi^0$ correlations determ. in $pp\rightarrow\pi^0\pi^0$ 80−5011
Si semiconductor counters, response to relativistic pions, electrons and protons 79−13597
Si surface barrier telescope, for low energy π detection 79−13591

meson-deuteron interactions
see also meson-deuteron scattering
K^-d, low-energy interaction, generalised final state interaction model 77−65175
K^-d, two and three body reactions around 1660 MeV 77−22788
K^-d$\rightarrow K^-\pi^+\pi^-$d or $K^0\pi^-\pi^0$d, 12 GeV/c coherent interactions, cross sections, resonance signals 77−50016
K^-d$\rightarrow\Lambda p\pi^-$, 680 to 840 MeV/c, Λp enhancement near ΣN threshold 77−67672
K^-d$\rightarrow\Lambda p\pi^-$, Λp invariant mass distrib., ΣN bound state 77−30428
K^-d$\rightarrow\Lambda p\pi^+\pi^-\pi^-$, 1.45, 1.65 GeV/c, Λp mass enhancement 79−416
K^-d$\rightarrow\pi^-\Lambda$p, anal. of Λp enhancement at 2.129 GeV in cross section meas. 79−22141
K^-d$\rightarrow\pi^-\Lambda$p, pole in $^3S_1$ hyperon-nucleon scattering amplitudes 80−102068
K^-d$\rightarrow\pi\Lambda$p, ΣN bound state and Λp enhancement 80−47326
K^-d$\rightarrow\Xi^- K^0$p, 1.45, 1.65 GeV/c, Ξ^-p invariant mass enhancement 80−57639
K^0d interaction, 10 to 50 GeV/c, transmission regeneration *(Russian)* 78−41590
K^+d experiments below 2 GeV/c and status of Z^* resonances 77−22794
K^+d inclusive reactions, 4.6 GeV/c, topological cross sections, π^-, K^0, Λ prod. 77−50004
K^+d$\rightarrow K^{0*}$pp, exotic final state interaction, intermediate Δ, ΔN threshold parameters 78−50043
πd, bound states, scatt. in light front field theory dynamics 80−68477
πd, nonadiabatic effects in inelastic scatt., Green's function technique *(Russian)* 79−9402
πd, scatt. length, binding corrections 78−17046
πd$\rightarrow A_1$d, double scatt. at high energy, unstable particle scatt. amplitude 78−45929
πd interactions at large momentum transfers 77−13972
πd$\rightarrow$NN, near threshold, effect of nucleon small components, nucleon pole diag. 77−30423
πd system, resonances near ΔN threshold, Argand diagrams 78−62582
π^-d, 15 MeV, charged multiplicity distribs. and rescatter probabilities 80−52545
π^-d, inclusive neutral particle prod., 205 GeV 77−67686
π^-d$\rightarrow 2n+\gamma$, n-n scatt. length from γ spectrum 78−62576
π^-d$\rightarrow(n_s)p\bar{p}n$, 13.2 GeV/c, $p\bar{p}$ forward low mass enhancement 80−86761
π^-d$\rightarrow(p_s)X^{--}$p, 13.2 GeV, search for charge −2 mesons 78−66167
π^-d$\rightarrow(p_s)p\bar{p}\pi^-$, 13.2 GeV/c, $p\bar{p}$ forward low mass enhancement 80−86761
π^-d$\rightarrow$d$\pi^-\pi^-\pi^+$ at 9 GeV/c, $\pi^-\pi^-\pi^+$ system decay 77−22766
π^-d$\rightarrow\gamma$nn, capture rate calc. in impulse approx. 77−82763
π^-d$\rightarrow$nn, nnγ, nnπ^0, neutral reactions, 224 MeV cross-sections 78−54651
π^-d$\rightarrow\pi^-$pn, 438 GeV/c, break up process, kinematic variables, np final state interaction *(Russian)* 80−52701
π^-d$\rightarrow\pi^-$pn final state interactions and d breakup for 438 MeV/c π^- impulse *(Russian)* 80−18145
π^-d$\rightarrow\pi^0$nn, expt. and theory, π^-d$\rightarrow$all branching ratio 77−41858
π^-d$\rightarrow\pi^0$nn, transition rate of charge exchange process 80−435
π^-d$\rightarrow\pi^+$X, screening effect of protons in deuterons *(Russian)* 77−267
π^-d$\rightarrow\rho^0\pi^-$d, 9 Gev exchange Deck model anal. 80−47322
π^+d, 15 GeV, high-mass even-g states, broad dipion states beyond g(1680) 80−68487
π^+d, 15 GeV, neutral three pion resonance prod., pure I=1 exchange 80−57644
π^+d, 15 GeV/c, many-pion prod. and resonant prod. cross sections 80−22642
π^+d, 4 GeV/c, cross sections for strange particle prod. 79−17753
π^+d, neutron fragmentation and inclusive charge exchange, 195 GeV/c 77−22814
π^+d interactions, strange-particle cross-sections at 4 GeV/c 78−89734
π^+d$\rightarrow K^+$Yp, E>1 GeV, Glauber correction and final state interaction *(Russian)* 77−6161
π^+d$\rightarrow$p(N^*,Δ^+), 1-5 GeV, inclusive cross-sections 77−6157
π^+d$\rightarrow$pp, 40-60 MeV, ang. distribs., D-state admixture 77−2864
π^+d$\rightarrow$pp, calc. including form factor at absorption and scatt. vertex 77−6155
π^+d$\rightarrow$pp, review, medium energy pion-nucleus absorption and scattering, pion condensation 78−8858
π^+d$\rightarrow$pp', effect of form factors on disintegration 77−6156
$\pi^\pm$d collisions, double scattering hadron struct. probe 77−74732

meson-deuteron scattering
see also meson-deuteron interactions
πd scatt., and NN covariant dynamics 77−6449
Faddeev πD calcs. 77−18622
high-energy elastic data, effect on πN amplitudes in Glauber model 77−30442
K_L^0-K_S^0 transmission regeneration on deuterons and neutrons, 10 to 50 GeV/c 80−4985
$K^\pm$+d, high energy cross section calc., complex ang. momentum theory *(Russian)* 78−46067
Kd study, $K^\pm$n elastic scattering, 10 GeV/c, real part of forward amplitude, dispersion relation 78−45950
K^-d, 1.2 to 2.2 GeV, cross sections for K^-n and K^-p scatt. 78−29353
K^-d$\rightarrow K^-$d or K^-n(p_s), 4.5 GeV/c, Glauber formalism, amplitudes, cross section 77−88004
K^+d elastic scatt., low energy, diagram formalism anal. *(Russian)* 77−26543
K^+d low momentum scatt., 250-600 MeV/c, cross sections, phase shift anal. 77−50006
π^+-d 100 GeV/c, rescattering 77−50011
π+d, high energy cross section calc., complex ang. momentum theory *(Russian)* 78−46067
π+d scatt. length 78−58306
πd, 142, 180 MeV, covariant three-body calc. 77−6450
πd, impulse approx. calc. of scatt. in resonance region 77−6452
πd, microscopic theory, review 80−47511
πd, multiple scatt. formalism 77−6451
πd, relativistic effects in deuteron alignment 78−25068
πd, relativistic Faddeev calc. 80−102066
πd elastic scatt., 142-256 MeV, dibaryon resonance interference with Faddeev amplitudes 80−32123
πD elastic scatt., 47.5-256 MeV, single scatt. contrib. 77−67671
πd elastic scatt., multiple scatt. calcs. 77−18623
πd elastic scatt., relativistic three-body calc. 77−74715
πD elastic scatt. constrained phase anal. from NNπ system relativistic 3-body theory 77−61457
πd elastic scatt. in (3,3) resonance region, relativistic description 80−105923
πd multiple scatt., kinematical ambiguities anal. 77−22764
πd quasielastic and inelastic rescattering as cumulative particle prod. source *(Russian)* 79−22340
πd scatt., 142 MeV, polarisation observables 78−78210
πd scatt., effect of genuine π absorpt. and emission 79−17939
πd scatt. in (3,3) reson. region, relativistic description 77−57558
πd scatt. length, pion absorpt. contrib., simple dispersion theoretic approach 77−13976
π^-d, 552 MeV/c, elastic differential cross section Glauber theory anal. *(Russian)* 80−52700
π^-d 1.57, 1.66 and 1.76 GeV/c elastic back scatt. cross section energetic shape struct. *(Russian)* 80−47510
π^-d$\rightarrow\pi^-$pn, 1 GeV/c, reaction 77−57559
πd, pion absorption effect from threshold to resonance 80−99193

meson effects
biological effects of π^-, depend. on intrinsic props. of reaction systems, RBE 78−3562
biomedical experiences with π^-, conf., Brugg-Windisch, Switzerland (Dec. 1978) 80−22138
cell survival, OER and RBE, comparison of heavy particles for therapy 78−85337
cell survival as function of depth, modulated negative pion beams 79−43966
cell survival vs. depth, comparison of heavy particles for radiotherapy 78−85336
corneas, canine, γ and negative pion irradiation of microvasculature 79−43964

meson effects continued
Ehrlich ascites carcinoma cells, effects of pions$^-$ rel. to electrons and X-rays 80−26267
K-electron ionisation in solids by relativistic heavy particles 80−84824
lymphocyte chromosome aberrations, pion$^-$ peak expansion to range of depths useful in radiotherapy 78−20243
mammalian cells irrad. with π^- and Co γ-rays, cell cycle progression 78−40269
pig, usefulness for assessing π^- damage in locally treated pelvis and abdomen 78−3554
pion$^-$, OER and RBE for beams of different peak widths, Chinese hamster cells 79−62301
pion$^-$ long-term effects on mice, partial body irrad. 77−81537
pion$^-$ radiation, uniform depth-dose distrib. technique and cell survival obs. 80−17139
pion radiotherapy facility at TRIUMF, dosimetry and radiobiology 77−70526
radiosensitivity of CHO cells, negative pions rel. to X-rays at various cell stages 80−17021
RBE of mouse skin damage, pions$^-$ rel. to X-rays 80−26272
Vicia faba bean root growth, effects of π^- and neutrons 78−28003
π^-, cell survival over the depth profile after irradiation 80−26268
π^-, chromatid breaks induced in Chinese hamster cells, rel. to X-irradiation 80−26270
π^-, effect on brain vascular permeability of neonatal rats 80−26275
π^-, effects on monolayers and spheroids of Chinese hamster cells 80−26269
π^-, effects on mouse embryo pronuclear zygote stage 80−26274
π^-, long-term effects on female mice rel. to X-rays 80−26273
π^-, pre-clinical studies at TRIUMF 80−26264
π^-, RBE and OER values from Vicia Faba root growth inhibition obs. 80−26271
π^-, radiobiological data for clinical dosimetry in pion tumour therapy 80−26266
π^-, suitability for use in radiotherapy, radiobiological obs. 80−26338
π^- irradiation of Chinese hamster cells, OER 79−88126
π^--meson channelling in crystals 78−6115

meson field theory
see also nuclear forces
ρ-exchange isovector parity-violating potential 79−93525
σ model, $SU_2 \times SU_2$, modified Goldberger-Treiman relation, pseudoscalar form factor 80−27421
σ model relativistic, finite temp., renormalisation, many body problem, interacting nucleons 77−18178
σ-propagator, summation of two-pion inserts 77−10186
A=16 to 40, mag. moments, shell model calcs, mesonic exchange current effects, book contrib. 80−479
a giant resonance theory in the 1p1h+2p2h+continuum approximation 79−67628
alternating layer spin structure, one-dimensional, localised, in nuclear system, and π^0 condensation 78−4902
asymptotic particle states, local definition in flat space-time 79−21906
axial currents in nuclei, one-pion exchange diagram 78−46008
baryon interactions through scalar meson field viar Yukawa-like interaction 79−67225
baryon matter struct. and pion condensation *(Russian)* 79−22222
baryonium dual S-matrix approach 80−52526
bilocal fields, quark confinement and conservation laws 78−74120
Bose-Einstein correl. expt., coherence of hadronic fields 77−87909
boson fields, massless, spontaneous symmetry breaking, and Goldstone theorem *(Chinese)* 80−62861
boson scattering, variational method 79−255
bound states in baryon-antibaryon systems, NN, NN̄, dispersion method *(Russian)* 78−16933
charge dependent nuclear forces, meson theory, book contrib. 79−97671
charmed particle-antiparticle system, bound states near charm threshold 78−45857
chiral nonlinear field eqns., exact solns. 78−54527
chiral symmetry and pion condensation, review book contrib. 80−437
chiral symmetry and the NN interaction, book contrib. 79−97669
classical fields in meson correlations 78−78082
cold matter at super-nuclear densities including pion condensates 78−17128
collective excitations of nuclei in a relativistic mean-field theory 80−95300
collective mode of nucleon system with π^0 condensate 78−41660
conference on interacting bosons in nuclear physics, Erice, Italy (June '78) 80−27042
conference on mesonic interface in nuclear struct. Erice, Italy (Sept. 1976) 79−26374
consistent S-matrix with nonlocal Yukawa interaction and relativistic form factor 79−93300
current algebra, representation on ultralocal quantum field theory model 79−6288
dense matter, U(1) symm. gauge model, eqn. of state 78−62500
deuteron wave functions, relativistic, π-NN coupling 80−22595
direct energy minimisation methods in self-consistent nuclear fields, ground state props. 80−22702
doorway isobar theory 77−10327
education, Schrodinger eqn. solns. using approximate nucleon-nucleon and Λ-nucleon pots. 80−62429
Einstein equations with zero-rest-mass scalar meson field 78−70021
elementary particle method for nuclei in weak and EM processes, book contrib. 79−97663
energy-momentum tensor, effect of motions, meson field and perfect fluid 78−73903
energy-momentum tensor in the fermion-pairing model 80−62857
exchange effects in nuclei, introduction 79−26375
extended meson fields as alternative to quark confinement 77−22642
extended meson model, Euler-Lagrange eqn. bilocal field theory conservation laws 79−21938
extended phase space, unified meson fields 80−86551
f-meson-other field strong gravitational coupling, effect on nuclear force in nucleon-nucleon interactions 78−514
fermion-fermion scattering in supersymm. field theory, high energy behaviour 77−13887
few nucleon systems, 3N and 4N calcs., review 78−50094
four fermion field theory, renormalisation in mean field expansion, Yukawa coupling 79−21939
free relativistic field in curved space, quantisation *(French)* 79−30639

meson field theory continued
generalised Low eqn. approach to reaction matrix 79−85491
generalised Takeno space-time, coupled EM and zero-rest-mass scalar meson fields 78−70020
generating functionals in current formulation of quantum meson field 78−16947
gravitational bubbles, radiative corrections to covariant massless quartically self-interacting meson theory 80−62826
Green's function method for many-body problem for relativistic meson field theory, book contrib. 80−357
hadrons, extended, second-quantisation of strongly interacting fields 80−13270
Hamiltonian field theory for systems of nucleons and mesons 79−75860
Hartree eqn., quasiclassical soliton soln., Newtonian interaction with screening 80−68569
Hartree-Fock anal. of nucl. many-body problem 77−18457
heuristic Hamiltonian for fermions interacting via meson fields 77−6022
high density nuclear Mach shock waves, central heavy ion collisions, compressed nuclear matter, meson condensation 78−46089
high-energy collisions, two-component model 79−323
hydrodynamic model, nonlinear pion+pion chiral Lagrangian, e^-+e and p+p collisions 78−32966
instantons, generation of meson mass spectrum, current algebra, mixing angles 80−86567
isotopic spin, possible origin from extended conformal symmetry, Yukawa interaction 79−40684
isotopic spin and coherent states 80−4843
isotopic symmetry group in strong interactions, possible geom. origin 79−17628
isovector scalar meson interaction, static source, variational method, coherent states 78−16921
Kerr-Newman background space, nonstatic nuclear forces, meson field at black hole event horizon 78−61880
Kerr-Schild's gravitational fields, quantisation 80−31653
Klein-Gordon equation for massive scalar meson field, Kerr-Newman metric 77−22262
l-forbidden M1 transitions, single pion exchange effects 77−6286
large maplitude collective motion, field theory, excitation energies 80−22665
liquid neutron matter, pion condensation and the linear σ-model 79−59027
long range NN interaction, axial polarisability, two pion exchange 78−29397
low-energy meson physics in theory with chiral Lagrangian 77−65110
magnetic moments of light nuclei, configuration mixing and meson exchange 78−17100
many-body forces in nuclear physics, review, book contrib. 79−97670
many-phonon monopole pairing vibrs. interaction in nuclear field theory, IBM 80−27578
massless boson, unified nonlinear theory 80−376
meson condensation and two photon emission in hadron capture by nuclei and heavy-ion collisions 79−3109
meson exchange, relativistic corrections, book contrib. 80−475
meson exchange currents, configuration mixing, role in nucl. mag. moment, beta decay, review, book contrib. 80−478
meson exchange currents, conservation principles, symmetries, book contrib. 80−473
meson exchange currents, effect in electron inelastic scatt., book contrib. 80−480
meson theory of nuclear vector and axial vecotr exchange currents, review, book contrib. 80−474
mesonic effects in photonuclear sum rules, book contrib. 80−476
mesonic exchange effect on nuclear mag. moment, expt. study, book contrib. 80−477
mesonic processes and quarks in nuclei 80−42564
mesonic test fields and spacetime cohomology 78−78065
mesonic wakes, appl. to meson prod. in nuclear collisions 77−6280
mesons in nuclei, and introduction, book contrib. 79−97662
mesons in nuclei, exchange current effects on nuclear mag. moments, book 80−471
mesons in nuclei, field theoretical aspects, book 80−481
mesons in nuclei, nuclear forces, baryon reson. effects, book 79−97661
micrononcausal Euclidean wave functions for hadrons, virtual mesons in deuterons 78−41408
microscopic dynamics of nuclei, meson exchange currents 78−12980
minimal three body scatt. effective interaction, Yukawa pot. 79−17820
multilocal field theory description of hadron struct. 80−9148
nonlinear chiral fields *(Russian)* 78−28968
nonlinear SU(2)×SU(2) and SU(2)×SU(1,1) chiral theories, exact finite energy solns. 79−54253
nonrelativistic wave eqn., second order in time, EM interaction 79−80774
nuclear, Compton scattering, diffractive behaviour, meson exchange effects 78−33165
nuclear critical opalescence, percursor to pion condensation 78−62498
nuclear critical opalescence, pion field and condensation 80−42559
nuclear currents, elementary particle description, microscopic anal., book contrib. 79−97664
nuclear Dirac phenomenology, consistency with meson-nucleon interactions 80−9272
nuclear Dirac phenomenology and the Λ-nucleus potential, anomalous mag. moment 80−37344
nuclear exchange mag. moments, meson exchange currents, field theoretical approach 80−52574
nuclear field theory, Dyson boson expansion and Faddeev-Watson resummation technique 80−13385
nuclear field theory, path integral techniques, Fermi systems with two body force interactions 78−50096
nuclear field theory, phonon renormalisation, eigeneqns. and sum rules *(Chinese)* 80−102127
nuclear field theory, renormalisation of single particle states 78−24926
nuclear field theory, schematic model functional approach, diagram rules 80−102128
nuclear field theory and structureless particle inelastic scatt. by nuclei 78−78332
nuclear field theory foundation, schematic model, many-body problem 79−85378
nuclear field theory treatment of the interacting boson model 80−27577
nuclear forces and isobar configs. in nuclei, review 78−50093
nuclear matter, π condensed, eqn. of state of finite temp. 79−3110
nuclear matter, mean field theory, correlation corrections 79−6467

meson field theory continued
nuclear matter, symm. and asymm., simple effective interaction for props. 78−25141
nuclear matter theory, one pion exchange processes, condensate effects 77−6276
nuclear pion field struct., book contrib. 80−482
nuclear potential energy surfaces, folded Yukawa-plus-exponential model 80−86816
nuclei, description in relativistic field theory, book contrib. 80−358
nucleon self-energy in finite nuclei; renormalisation, nucleon-meson interaction, ^{16}O calcs. 78−17110
nucleon-nucleon interaction and nuclear forces, meson exchange 80−32195
one pion exchange currents, relativistic corrections 77−18400
one pion exchange effects on 0 level positions 77−6232
one-pion exchange current, conservation and form factors 77−38098
pairing correlations in finite nuclei including virtual mesons 77−41899
Paris nucleon-nucleon potential, book contrib. 79−97665
parity violating nucl. force, unified treatment 80−47400
partially conserved axial-vector current and model chiral field theories in nuclear physics 79−67698
path integral representation for U- and S-matrix, scalar meson model renormalised S-matrix elements 78−78103
path integral representation of QFT for S-matrix, meson field-nucleon field interaction 79−2947
Pauli principle effect in nuclear matter, exchange of interacting two pions 78−12983
phenomenological Lagrangian construction 79−63356
pion condensates, supercond. props., σ model anal. with nucleons 79−59029
pion condensation, field theoretic many-body system 80−22703
pion condensation and the pion-nuclear interaction, book contrib. 80−485
pion condensation in nuclear matter, book contrib. 80−484
pion condensation threshold in finite nuclei 80−18218
pion exchange current operators, their construction and effect on nuclear props. and reactions 78−86490
pion excitations and phase transitions in nuclear matter, review, book contrib. 80−483
pion field and weak interactions in nuclei 79−26376
pion nucleus physics, field theoretic aspects 77−10325
pion scattering by nuclear pion cloud 79−85372
pion-nucleon field interactions, covariant perturbative expansion in SU(2)×SU(2) model 77−5983
pionic degrees of freedom in nuclei 77−10326
progenitor sum rules, nuclear theory appl., meson+nucleon interaction, inelastic form factors 78−54690
proton magnetic moment and EM struct. 78−54633
QED, hamiltonian formulation in generalized linear electrodynamics 79−97543
quantised gravitational interaction with meson field 80−31652
quark bag model, description of nucleons and isobars 79−49452
quark effective-bare mass distinction 78−12866
Reggeon field theory, meson trajectories, Markoffian approach 79−45037
relativistic dense matter, statistical mechanics using phenomenological quantum field model 78−89814
relativistic quantum field theory of finite nuclei 79−6466
relativistic two-body forces in many-body systems, Weinberg and Yukawa interactions 80−32203
ring diagrams, Landau parameters, pion condensation, binding energy, of nuclear matter 78−74321
S-matrix for interaction of gravitational and Yang-Mills fields 80−42315
scalar meson field and many-body forces, book contrib. 80−359
scalar meson fields in conformally flat space 78−8278
scalar mesonic fields on a curved space, quantisation *(French)* 79−30640
scalar Yukawa$_2$ field theory, vacuum energy density in large order perturbation theory 79−17620
Schwinger model, Ward identity, fermion axial vector current divergence, chiral invariant regulator field 80−57524
second quantisation, meson field interaction with nucleons 77−22633
soft pion theorem, appl. to currents in nuclear forces and matter. 79−26377
solidification of π^0 condensation in nucl. matter 78−89813
solidification of nucleon system, π^0 condensation, πN P-wave interaction 78−54715
solitary wave exchange in NN pots. 78−70457
solitary wave exchange potential in pseudoscalar and scalar meson fields 79−71617
static meson potentials 80−95219
static nuclear Laplacian force *(Bulgarian)* 78−54688
statistical bootstrap model, hadronic mass spectrum, pion condensation, boson gas 78−70345
strong gravity, field equations, strong interactions, de Sitter microsphere idea of hadrons 80−68111
strong gravity const. determ. from pion mass difference 77−22715
SU(2)×U(1) gauge models, CP violation origin, Yukawa interaction 79−40712
SU(2)×U(1) unified model, universal Yukawa coupling 80−91032
SU(2) nonlinear σ model, kink solns., form factor interpretation 78−24964
superconducting props. of π condensates 78−32993
superposed Yukawa and inverse square potentials, eigenenergy expansion 79−30281
Thomas-Fermi model of finite nuclei 78−8747
three body systems in nuclear physics, review 78−517
three nucleon clusters in nuclear matter, intermediate Δ-states, exchange diagrams calc. 78−17112
three-nucleon potentials due to π, S and ω, binding energy in nuclear matter 78−62486
two pion exchange charge density in static approx. ^3He, ^3H form factors 78−66222
two-dimens. SU(N) gauge theory for mesons 77−49840
vector meson covariant redefinition, $SL_{3,c}$ chiral symmetry 77−54045
virtual mesons effect on hadron-nucleus reactions, book contrib. 80−472
virtual particle interactions *(Polish)* 79−40802
virtual pions, Yukawa field and effects on μ-capture, β-decay, mag. moment etc. 79−26379
wave functions, spinor struct., inter-straton potentials 79−12969

meson field theory continued
weak axial coupling constants in nuclei, polarizability, pionic field, PCAC 77−6055
weak interaction symmetry struct. and $K\to\pi\pi$, $\pi\pi\pi$ *(Russian)* 79−22016
weak interactions in nuclei, axial polarisability 77−22924
Yang Mills theories, high-energy gauge meson exchange reactions, factorisation, Reggeisation 77−18172
Yukawa$_2$ model, Schwinger functions, analyticity and Borel type summability *(French)* 80−73570
Yukawa$_2$ QFT, Lorentz invariance of CPT invariant states 80−52381
Yukawa, mass divergences of wide angle scatt. amplitudes 79−49402
Yukawa model with anomalous dimensionalities in four-dimensional space 80−101934
Yukawa pot. problem, S-matrix exact evaluation from transformed Schrodinger eqn. 78−82120
Yukawa potential function, determ. of phase shifts 78−58237
Yukawa potentials, finite sum S-matrix 80−101940
Yukawa quantum field theory, Matthews-Salam integral representations 80−327
Yukawa quantum field theory in 2D space-time, linear N_τ bound, locally Fock property 80−326
Yukawa spherical diffuse massless sources in relativity 77−87931
ed→ed, nucleon forces, meson exchange current effects, impulse approx., review 80−57603
$K_{l4}\to\pi\pi\gamma$, form factors in chiral quantum field theory *(Russian)* 79−67550
N form factor, isovector, meson field theory, pseudoscalar πN interaction 80−62986
NN generalised one-boson-exchange pot. meson field theory 78−66096
NN $\bar{I}=1$ scattering with one boson exchange, Bethe Salpeter eqn. 77−57455
NN̄ interaction, low energy, meson exchange forces, one boson exchange potential, dual quark models 78−62444
NN interaction, meson field theory, one-boson-exchange model 78−66216
NN interactions, conf., Vancouver, Canada (July 1977) 78−62418
NN→NNπ, anal. via nonrelativistic field theory with HBE 79−85317
NN nonrelativistic 1-boson exchange potentials based on generalised meson field theory 78−70459
NN P-violating interaction in Bars-Halpern-Yoshimura gauge model 77−22758
NN potential, meson field theory two-pion exchange anal. 77−208
NN potentials repulsive part, mesonic theory *(Russian)* 79−30792
NN scatt., small angle, appl. of eikonal vector meson exchange theory 78−17052
NN scattering, attractive retarded effect of one boson exchange pot. 77−2859
NN̄ system, single γ and π emission rates, meson quantum number assignments 78−78208
ω meson contrib. to nucl. forces, field theory model 77−74772
$\bar{p}N\to\bar{N}(N\pi)_{I=1/2}$, 5.7 GeV.c ρ exchange contrib., cross channel isospin amplitude anal. 78−45938
pp, bremsstrahlung, field theoretic calc., treatment of OBE external emission processes 78−62451
(π,π') many body QFT framework anal., final state particle-hole correlations 80−13508
π bound states in finite nuclei, π-nuclear optical pot. 78−46013
π compositeness from wave function renormalisation constant 80−101997
π condensation, vacuum instability in external fields 78−50114
π condensation effects in degenerate matter, appl. to theory of superdense celestial bodies *(Russian)* 79−96907
π condensation in finite nuclei 78−78299
π condensation in neutron matter, N-N interaction, critical density 80−57711
π condensation in nuclear matter, Hartree-Fock and generator coord. methods 78−17129
π condensation induced density oscillations, infinite nuclear matter and pions atoms calcs. 78−70476
π condensed phase, σ-model, alternating-layer-spin struct. 80−83057
π double charge exchange in heavy nuclei, pion condensation 77−79402
π field, nonlinear chiral models, many dimensional solitons 78−4792
Π field in nuclei, μ absorpt. and doubly radiative Π absorpt. as probes 77−88063
π field relaxation in nuclear materials *(Russian)* 78−8764
π fields in nucl. matter 78−58246
π form factor, expt. behaviour, influence of left-hand cut on second Riemann sheet 80−13304
π multiple scattering, higher order effects, NN correls., self-consistency 78−89799
π multiple scattering theories, in nuclear matter, NN correls., self consistency 78−89800
π prod. and absorpt. in nucl. reactions, vertex function anal. 78−12989
π resonances, Peierls-Yoccoz projection applied to satellite meson coherent state 79−26345
π-condensate phase transition at finite temp. *(Russian)* 79−3111
π-nucleon coupled field, progenitor sum rules, ρ-mesonic effects 78−17111
π^- condensation, nonrelativisitc treatment, mean field method 77−30500
π^- condensation in electric field of supercharged nucleus *(Russian)* 78−54717
π^0 condensation in finite system, extended Thomas-Fermi model 78−41645
π+d scatt. length 78−58306
π+nucleus absorption and scattering, pion condensation 78−8858
π+nucleus scatt. field theoretic treatment 78−29505
πN low energy interaction, field theoretic approach 79−67602
πN P-wave interaction, effect of non-condensed pions in nuclear medium 79−13237
πN scatt., special coherent states and scatt. phase shifts, meson field theory 79−67601
πN scattering amplitude in nuclear matter, quantum field theory approach 80−42570
πNN form factor, $\Delta(1236)$ contrib., calc. 80−22609
$\pi\omega$ meson exchange contribution to NN interaction 77−18401
$\pi\pi\to\pi\pi$, self-interactions, nonperturbative, scatt. amplitudes containing only convergent integrals 80−68480
σ model, pion condensation, use of chiral symmetries 79−296
A=12, nuclear axial dipole transition moment in the sigma model for 1^+, $T=0\to0^+$, T=0 transition 79−45184

meson field theory continued
^{12}C M1 (15.11 MeV) form factor, evidence for nuclear pion field critical opalescence 80−32232
^{12}C, pion-exchange contribs. to charge densities, HF calcs. 78−46001
^{12}C(π,π), nonlinear meson dynamics and binding corrections, optical pots. 80−106080
^{40}Ca, pion-exchange contribs. to charge densities, HF calcs. 78−46001
^{48}Ca, pion-exchange contribs. to charge densities, HF calcs. 78−46001
^{3}H, EM form factors, 3-nucleon wave function calc. 80−95302
^{3}H$_{\Lambda}$, binding energy, Fadeev equation in coord. space, Lambda-nucleon potential 80−63120
^{3}H(e,e), many-body exchange effects, charge form factors calc. 78−33169
^{3}He, EM form factors, 3-nucleon wave function calc. 80−95302
^{3}He, nuclear charge form factor, two-boson exchange charge density π, ρ, ω exchanges 80−63073
He(e,e), A=3,4, many-body exchange effects, charge form factors calc. 78−33169
^{93}Nb B(Eλ) transitions, quasiparticle-phonon multiplet, nuclear field theory for superfluid nuclei 80−47427
^{16}O, pion-exchange contribs. to charge densities, HF calcs. 78−46001
^{16}O(π,π), nonlinear meson dynamics and binding corrections, optical pots. 80−106080
^{17}O, mag. form factor, core polarisation and exchange current effects 78−46003
^{206}Pb, pion-exchange contribs. to charge densities, HF calcs. 78−46001
^{90}Zr, pion-exchange contribs. to charge densities, HF calcs. 78−46001

meson hadronic decay
see also kaon hadronic decay
1.87 GeV/c^2 states, evidence for parity nonconservation in decays 77−10245
$\Gamma(\psi\rightarrow\phi\pi^+\pi^-)/\Gamma(\psi\rightarrow\omega\pi^+\pi^-)$ and Okubo-Zweig-Iizuka rule 77−6119
$\eta\rightarrow\pi^+\pi^-\gamma$, one-loop approx. in quantum chiral theory 78−25041
ψ decay, multiplicity decrease due to charm prod. suppression 79−49518
ψ meson, hadronic decay, generalised Veneziano model 78−58182
ψ production and decay, book contrib. 78−82208
axial vector mesons, three body decays, rel. between D(1285) and $A_1(J^P=1^{++})$ 78−78176
baryonium muliquark system model of fireball, high energy pion production 79−97603
bottom hadrons, masses and allowed decays, SU(5) quark model 80−62954
bottom meson nonleptonic decay, many body final states, isospin-statistical models 80−62975
bottom meson weak hadronic decays, Kobayashi-Maskawa weak current model 80−42456
broken-SU(4) model of meson decays $1^-\rightarrow0^-\gamma$, $0^-\rightarrow1^-\gamma$ 78−70361
Cabibbo-suppressed nonleptonic D decays, $\Delta I=1/2$ rule 80−52501
charm particle $\rightarrow\pi^+\pi^-\pi^+\bar{K}^0$ 79−26426
charm particle $\rightarrow\pi^+\pi^-p\bar{K}^0$, lifetime determ. 79−26426
charmed hadronic decay branching, $\bar{p}p\rightarrow n\pi$'s multiplicity 77−10288
charmed hadrons $\Delta C=\Delta S$ decays, sum rules, internal symm. props. 77−30376
charmed meson decay, interference effects, 2nd order suppressed amplitudes 80−4987
charmed meson decay, simple symm. breaking 78−21418
charmed meson decay, SU(4) symm. breaking 77−26518
charmed meson decays, soft hadron interaction effects on nonleptonic weak decays 80−86705
charmed meson decays and right handed currents 78−8662
charmed meson hadronic decay, D^0, D^+, F^+ branching ratios 78−45913
charmed meson non-leptonic decay, resonant struct., phenomenological calc. 77−49960
charmed meson radiative decay, quark loop model, SU(3) splitting of quark masses 80−62990
charmed meson weak nonleptonic decay, SU(2) and SU(6) models 77−26521
charmed mesons, Cabibbo-suppressed nonleptonic decays 77−71509
charmed mesons, nonleptonic decays, dual model current algebra relations and amplitudes 79−89132
charmed mesons, nonleptonic decays of charmed mesons and chiral Lagrangians *(Russian)* 79−30732
charmed mesons, props. determ. from two-step pot. model 77−74682
charmed mesons, three body decay, Dalitz plots quark line diagrams 79−30731
charmed-meson decay, massive quark model 78−33067
charmonium, radially excited states, small Q-value channel dominance in decay 79−54335
charmonium narrow states, hadronic and EM decays 78−70343
CP noninvariance test in nonleptonic decay of mesons containing one 6-quark 79−71654
D-meson decay at ψ(3772), inclusive props. 78−93876
dipion cascade decays, current algebra techniques, pole plus remainder model, chiral symmetry breaking and QCD 80−62972
extended PCAC+Veneziano type model, Goldberger Treiman relations, $\eta\rightarrow\gamma\gamma$or $\pi^+\pi^-\gamma$ 78−21354
Gell-Mann-Nishijima formula for EM current operator generalised 78−78109
gluon observation in P-wave quarkonium decay 80−32068
gluonic decay of heavy quarkonium states, QCD test, three jet struct. 78−62365
hadronic decay and evidence for $(\bar{c}s)_R$ current 78−58167
hadronic gauge couplings in meson decays 80−102037
heavy meson hadroproduction, QCD effect on scale breaking 80−37239
heavy meson nonleptonic and inclusive semileptonic decay, lepton spectrum calc. 79−3018
heavy quarkonium decays, renormalisation group approach, exclusive two meson and inclusive decays 80−82972
heavy quarkonium states, hadronic transitions, QCD anomalies for Υ'' and ψ' 80−105888
M1 radiative meson decays, QCD corrections 79−17718
meson strong decay, 2 quark-antiquark pair model 80−52496
multimesonic decays of charmonium states in a constant matrix element quark model 79−26298
narrow resonances by strong coupling 77−30370
new meson radiative decay and heavy quarks 77−2798
nonrelativistic pot. models for heavy quark systems, Υ and ψ hadronic decay 78−89688
OZI rule, pseudo-dimension rule and ψ(3770) decay 79−40724

meson hadronic decay continued
partially conserved axial vector currents, corrections, light-plane commutators, sum rules, meson decay 79−304
penguins in $\Delta S=1$ nonleptonic weak decays 80−91086
pseudoscalar and vector meson decays, triangular quark diagram anomalies, ψ, η and η' appl. *(Russian)* 80−42455
pseudoscalar mesons, in spectrum-generating SU(3), beta-decay 78−4858
QCD, 2-dimens., nonleptonic weak decays of charmed and storage mesons 79−40773
QCD, inclusive hadronic annihilation of heavy quark-antiquark bound states, Υ, ψ decays 78−45866
QCD, quark and gluon fragmentation functions, quarkonium decay inclusive hadron spectrum 79−97584
quark mass effects as isospin and SU(3) violations in radiative decays of vector mesons 79−22091
quarkonia, S- and P-wave, gluon jets, perturbative QCD anal. 80−32070
quarkonia states, heavy, strong decay into other heavy flavours, and triple-gluon vertex 80−47279
radiative, consistency with SU(3), vector dominance, quark models 77−79265
radiative decay, decay widths, relativistic quark models anal. 79−13118
radiative decay of vector mesons into pseudoscalar mesons, relativistic harmonic oscillator model *(Russian)* 78−453
radiative decays, SU(4) and OZI violations 77−74688
radiative decays 78−21419
radiative transition, symm. and duality constraints 78−78178
radiative transitions of low-lying positive-parity mesons, VMD and single-quark selection rules 77−18279
Reggeon-photon coupling analogy, estimates of various meson decay rates 78−78204
relativistic quark model, vector meson strong decay widths 77−57529
resonances, binary decays, centrifugal effects *(Russian)* 78−17012
scalar meson decay width, meson-meson sigma terms and phenomenology 77−74680
single quark transition model, parity violating charmed hadron decays, current-current interaction 78−12907
spectral function sum rule and onium 79−26329
strange particle nonleptonic decay, asymptotic freedom, light quarks and $\Delta T=1/2$ rule 77−38164
SU(3)′×SU(3)″ scheme of three triplet model, colour symm. ψ-mesons descript. 78−78151
SU(3) rules for nonleptonic weak decay of charmed and strange mesons 78−45916
SU(3) symmetry violation models for interactions with vector mesons, tests *(Russian)* 77−10196
SU(3)-breaking models, meson radiative decays, VDM 77−18282
suppressed decays of ρ', ω2N, ψ'(4.03) and particle degeneracies 77−74684
tensor and vector meson decay, relativistic confined quark model anal. 79−13116
tensor meson decay, current algebra approach, symmetry-breaking Hamiltonian, chiral SU(3)×SU(3) or SU(4)×SU(4) 80−68450
tensor meson dominance for γ decays of new particles 78−66112
V→Pγ, EM decays of vector and pseudoscalar mesons, dispersion theoretic approach 79−93423
vector and pseudoscalar two-body decays in broken SU(4) 77−67648
vector and scalar mesons, linear and quadratic mass formulae 77−49935
vector and tensor meson decays in relativistic confined quark model 77−79256
vector meson radiative decay, off-shell factors in vector dominance model 79−22084
vector meson Zweig rule violations in sequential pole model, glueball possible identification 77−26520
vector mesons, two body photonic decays, SU(4) scheme, ideal mixing angles, amplitudes, quark sectors 78−54630
vector mesons, two-body photonic decays, 16-plet mixings in SU(4) quark symm. 78−33062
Zweig rule in two-dimensional QCD, ψ and Υ decays 80−52479
Zweig suppressed decay of heavy 1^{--} vector mesons, two gluon exchange 78−54616
$0^-\rightarrow\pi\gamma$ or $\eta\Gamma$, SU_3 symm. breaking schemes, radiative widths 77−6114
A_1 decay, rescattering effects in 3π system 77−13957
$A_2\rightarrow\pi\gamma$, suppression factors for VMD couplings calc., duality constraints anal. 77−13960
$A_2^-\rightarrow\eta\pi^-$ obs. in $\pi^-p\rightarrow\pi^-\pi^-\pi^+\pi^0p$ at 11.2 GeV/c 77−22806
B(1235)→$\omega\pi$, many pion correlations from nonstrange mesonic resonances *(Russian)* 80−86708
B(1235)→ϕ(1020)π, Okubo Zweig Iizuka rule violation 78−21425
B→B′$\pi\gamma$, contribs. of B→B′γ process 80−78066
B(f′(1520))→$\pi^+\pi^-$, Zweig forbidden decay 79−17687
B→J/ψ+hadrons, branching ratio, b quark decay calcs. 80−32095
B→ψX, weak decay for B mass and other props. determ. 79−97621
B→ψX, weak decay predictions, B identification in hadronic collisions 79−93408
B→ψpK$^-$, search for b flavoured baryons 80−42450
b quark→$\psi(\eta_c)$+X, B branching ratios assuring colour suppression 80−37259
B-meson decays, Cabibbo patterns, QCD effects, Kobayashi-Maskawa model 80−42451
B^0, B^- hadronic decay modes, W boson exchange model clean test 80−57592
$B^0\rightarrow D^+X(F^+X)$, W-exchange dominance, decay rates 80−86706
C→$\Lambda(K^0)$+hadrons, charm prod. cross section, new particle search *(Russian)* 78−89711
$c\bar{c}g(c\bar{c}q\bar{q})$, exotic mesons, masses, decay widths, mixing matrix elements 80−62943
χ, charmed particles, particle multiplicity distribs. in hadronic decays 77−46044
$\chi(3.45)\rightarrow\pi^+\pi^-X(2.83)$, test of $c\bar{c}$ dynamics 77−74685
χ particles, radiative decay widths calc., broken SU(4) model 78−62395
$\chi/\bar{c}c\rightarrow\psi\gamma$, scalar and tensor meson dominance 79−3019
$\chi_{1,2}\rightarrow\gamma J/\psi$, radiative decays of 2^{++}, 1^{++} mesons 78−21420
$\chi_J\rightarrow\gamma\psi$, upper and lower bounds using dipole sum rules 77−13958
$\chi_J\rightarrow\psi\gamma$, radiative decay widths of charmonium states, superconvergent sum rules 78−21422
D, mass and mean life from high energy cosmic ray data *(Chinese)* 80−102045
D, two-body hadronic decays, six-quark model mixing angle constraints 79−97618

meson hadronic decay continued
D(1285) from $\bar{p}p \rightarrow K\bar{K}\pi\pi\pi$, 700-760 MeV/c, spin-parity assignment, dominant decay mode 78−54646
D(1285)→δ(975)π D meson spin parity determ. 79−3052
D(1285)→δ(975)π D meson spin parity determ. 79−9410
D(1285)→ρππ or δπ, δ(970)→ηπ or KK̄, branching ratio 77−46084
D charm decay, 20-dominance model validity from QCD 79−71747
D→ηππ, D meson spin parity determ. by partial wave analysis 79−3052
D→K ππ, branching ratios, isospin anal. 78−70363
D→KKπ, D meson spin parity determ. 79−3052
D→K*lν, A(c,s) vector current 77−87976
D→K̄π, branching ratios, charged and neutral D-meson lifetimes 78−62396
D→Kπ, effective Hamiltonian in Kobayashi-Maskawa model 80−105887
D→K̄π(K̄ππ), nonleptonic decay rates, quark diagrams and pole approx. 80−86707
D→Kπ(π), current algebra relations and dual model amplitudes 80−82969
D meson, charm particle nonleptonic weak decays, pole dominance model 79−63475
D meson, nonleptonic decay, matrix element computation and iteration 79−384
D meson decay, SU_4 20-plet dominance model, inclusive branching ratios 80−13299
D meson parity violating nonleptonic decays, vector meson dominance model 80−78058
D meson prod. and decay in e^+e^- at 4.03 , 4.41 c.m. energy 77−87989
D mesons, anomalous Cabibbo suppressed decay ratios, simple model 80−42452
D mesons, charmed, MIT bag model calcs. 78−82207
D nonleptonic decay rates and branching ratios, lifetimes 80−102047
D→ππππ, S_3 permutation group approach, charm model test 79−17723
D two body nonleptonic decays, quark model predictions 80−9164
D-meson decay, hadronic, six-quark model, quark-mass dependence, final state interactions, mixing angle effects 80−62973
D-meson prod. model, charmed particles 77−38124
D^0,D^+ decays, gluon enhancements in charmed-meson decays 80−95265
D^0 Cabibbo suppressed hadronic decays, Cabibbo universality fake violation, RH currents 80−73699
D^0 decay enhancement mechanism, quark diagram with gluon prod. 80−105891
D^0 decay following $\pi^-p \rightarrow D^0\bar{D}^0n$, 40 GeV, search for associated prod. of charmed particles 77−13990
D^0 hadronic decay modes, W boson exchange model clean test 80−57592
$D^0 \rightarrow K_S^0\pi^+\pi^-$ following charmed-D-meson prod. by neutrinos 78−70354
$D^0 \rightarrow K^-K^+$, Cabibbo suppressed decay obs., partial decay widths 79−89149
$D^0 \rightarrow K^-p^+$ signals, evidence for$(\bar{c}s)_R$ current 79−71745
$D^0 \rightarrow K^-\pi^+$, Cabibbo suppressed decay compatibility with weak interaction mixing angles, branching ratios 79−97620
$D^0 \rightarrow K^-\pi^+$, quark total number conservation, D^+ lifetime longer than D^0 80−57590
$D^0 \rightarrow K^-\pi^+$, role of free-quark pairs 80−78059
$D^0 \rightarrow K^-\pi^+(K^-K^+)(\pi^-\pi^+)$, charmed meson nonleptonic decays and weak interaction mixing angles 79−85294
$D^0 \rightarrow K^-\pi^+\pi^-$, obs. in 3.77 GeV e^+e^- annihilation 78−37206
$D^0 \rightarrow K^-\pi^+\pi^0$, nonleptonic charm decay, branching ratio 78−70364
$D^0 \rightarrow K^-\rho^+$ strong signal, $(\bar{c}s)_R$ current implications 79−36070
$D^0 \rightarrow \bar{K}^0\pi^0$, branching ratio from final state soft gluon exchange 80−52498
$D^0 \rightarrow \bar{K}^0\pi^0$, ΔT=1 constraints and final state interactions 80−95267
$D^0 \rightarrow \bar{K}^0\pi^0$, quark total number conservation, D^+ lifetime longer than D^0 80−57590
$D^0 \rightarrow \bar{K}^0\pi^0$, role of free-quark pairs 80−78059
$D^0 \rightarrow \bar{K}^0\pi^0(K^-\pi^+)$, weak interaction effects, Kπ scatt. phase shifts 80−57591
$D^0 \rightarrow \bar{K}^0\pi^0(\pi^+\pi^-)(K^+K^-)$, phenomenological model for inclusive and exclusive decays 80−99098
$D^0 \rightarrow K^0\pi^+\pi^-$, prod. and decay from νN interaction 78−89700
$D^0 \rightarrow K^+K^-$, Cabibbo suppressed decays, Penguin diagram contribution, mixing angles 80−22604
$D^0 \rightarrow K^+K^-$, $\pi^+\pi^-$, branching ratio, $\Delta I = {}^1/_2$ rule violation, colour radius interactions calc. 79−93412
$D^0 \rightarrow K^{*-}\pi^+(K^-\pi^+)$, heavy quark weak isospin, constraints from nonleptonic transitions 79−85257
$D^0 \rightarrow \bar{K}^{*0}\pi^-$ signals, evidence for$(\bar{c}s)_R$ current 79−71745
D^0 lifetime from ν and ν̄ interactions 80−105890
D^0 nonleptonic decay, quark annihilation hypothesis test 80−102044
D^0 nonleptonic exclusive and semi-inclusive decays, pole model test 80−37258
D^0 prod. and decay in high energy photon interaction, mass and decay time 80−42478
$D^0 \rightarrow \pi^+\pi^-$, Cabibbo suppressed decay obs., partial decay widths 79−89149
$D^0 \rightarrow \pi^+\pi^-$, Cabibbo suppressed decays, Penguin diagram contribution, mixing angles 80−22604
$D^0 \rightarrow \pi^+\pi^-$ 79−97620
D^+, D^0, weak nonleptonic decays, SU(3) symmetry and quark diagrams *(Russian)* 79−93411
D^+, D^0 nonleptonic decays, vectorial colour octet qq̄ annihilation 80−52500
D^+ decay, Cabibbo suppression, strong 20-plet dominance and W exchange 80−42453
$D^+ \rightarrow \bar{K}^0\pi^+$, $D^0 \rightarrow K^-\pi^+$, two body decays of charmed mesons, quark recombination scheme 78−37207
$D^+ \rightarrow \bar{K}^0\pi^+$, quark total number conservation, D^+ lifetime longer than D^0 80−57590
$D^+ \rightarrow \bar{K}^0\pi^+$, role of free-quark pairs 80−78059
D^+ nonleptonic decays, uniformly populated Dalitz plot, soft π theorem appl. 80−52503
$D^+ \rightarrow \pi^+\pi^+K^-$, contradiction in uniformly populated Dalitz plot 79−17724
$D^\pm(1870) \rightarrow \Lambda(K^0)$+hadrons, charm prod. cross section upper bounds *(Russian)* 78−89711
$D^\pm$ nonleptonic and semileptonic decays, isospin selection rule tests 80−73700
D^0,D^+, SU(3) predictions for decay using new weak mixing angles 79−97619
D^*, pion and photon couplings, SU(4) violations, decay rates calc. 78−45914
meson hadronic decay continued
D^* widths, using finite energy sum rules for pion and photon couplings 77−67649
$D^{0*} \rightarrow D^0\gamma$, SU(4) theory, suppression factor in radiative decay amplitude 77−30372
$D^{*+} \rightarrow D^0\pi^+$ observations in e^+e^- annihilation, decay width, Q value 77−57531
D^{**}, charmed tensor meson, strong and EM decay modes 80−68451
$D^0\bar{D}^0$, mixed spinless charmed mesons from e^+e^- annihilation, decay, CP violation tests 77−46067
$D\bar{D}^*$ production and decay, VDM, dual amplitude anal., e^+e^- annihilation 77−49992
D_1O^*, $D_1{}^+{}^*$, weak decay modes, annihilation contribs. 79−93410
δ(970)→ηπ or KK̄, branching ratio 77−46084
δ(980) scalar meson, prod. and decay props. 77−87975
δ(980)→ωγ, radiative decay width using a vector dominance model 78−82205
δ(980)→πγγ, radiative decay width using a vector dominance model 78−82205
δ(980)→ργ, radiative decay width using a vector dominance model 78−82205
$\delta^- \rightarrow \pi^+\pi^-\pi^-$ decay mode, nonobs. in missing mass counter expt. 79−13113
E(1420)→K*K̄, correlation between A_1 parameters and Q data 80−82968
E(1420)→ηππ, correlation between A_1 parameters and Q data 80−82968
$e^+e^- \rightarrow x\pi$, even G parity hadronic cross section, ρ′(1600) 2π branching ratio 78−12921
η→3π, nonet mixing and gluon effects in current quark framework 79−80799
η→3π chiral symmetry breaking, Dashen mass formula, baryon mass differences 79−289
η→3π width, quark pair creation model 77−41841
$\eta \rightarrow 3\pi^0$, decay rate, up quark masslessness 79−40761
η→3π°, chiral SU(4)×SU(4) breaking and tadpole term 80−22532
η decays of ψ's, VMD and colour model coupling const. calcs. 77−26516
$\eta \rightarrow \pi^0\gamma\gamma$, $\pi^+\pi^-\pi^0\gamma$, $\pi^+\pi^-\gamma\gamma$, scalar meson dominance model 78−4860
$\eta \rightarrow \pi^+\pi^-\gamma$, quantum chiral theory, decay width determ. *(Russian)* 78−41544
$\eta \rightarrow \pi^+\pi^-\pi^0$, decay width 78−70362
$\eta \rightarrow \pi^+\pi^-\pi^0$, on-mass-shell current algebra, SU(3)×SU(3) σ model 77−34151
η→ππγ, quark loop model, SU(3) splitting of quark masses 80−62990
η→ργ(γγ), C-even meson radiative decay, SU(3), and VDM anals. *(Russian)* 80−68460
$\eta^0 \rightarrow \gamma\gamma(\pi^0\gamma\gamma)(\pi^0\pi^0\pi^0)$, neutral decay channels, possible $3\pi^0$ system *(Russian)* 80−42454
η_C, coherent prod. and baryon-antibaryon pair decay 78−21421
$\eta_c \rightarrow \gamma$+anything, OZI rule violating decay in QCD 78−89709
η_c meson hadronic decay 78−8664
η′→3π, isospin violating effects from nonvanishing quark mass difference 79−63385
η′(958), spin-parity test from collinear prod. and decay 78−41543
η′(958)→4π, decay mode in broken $SU_6 \times O(3)$ quark model 79−36071
η′→ηππ, amplitude satisfying Adler conditions, relativistic quark pair creation model 80−95262
η′→ηππ, current algebra calcs. with symmetry breaking, inconsistency with expt. 79−13114
η′→ηππ, finite dispersion relation calc. of decay rate 78−41542
η′→ωγ, decay rate obs. in $\pi^-p \rightarrow \pi^+\pi^-3\gamma n$ 77−74683
$\eta' \rightarrow \pi^-\pi^-\gamma\gamma(\pi^+\pi^-\pi^+\pi^-\gamma\gamma)$, rare decay modes near production threshold from $\pi^-p \rightarrow \eta' n$ reaction 80−9171
η′→ππη, δη′ and δηπ coupling constant ratio, δ(980) quark content 80−82955
$\eta' \rightarrow \pi\pi\eta(\pi^+\pi^-\gamma)$, quark model description 80−62970
η″(2.8) radiative decay, charmed quark content of ω and φ mesons 77−71511
F, nonleptonic decay rates and branching ratios, lifetimes 80−102047
f(1270)→4π, many pion correlations from nonstrange mesonic resonances *(Russian)* 80−86708
F→Dπ enhancement and the ΔI=1/2 rule 79−36069
F meson nonleptonic weak decay modes 77−49961
F mesons, charm particle nonleptonic weak decays, pole dominance model 79−63475
F parity violating nonleptonic decays, vector meson dominance model 80−78058
F→ππππ, S_3 permutation group approach, charm model test 79−17723
F-meson decay, hadronic, role of free-quark pairs 80−78059
F^+, weak nonleptonic decays, SU(3) symmetry and quark diagrams *(Russian)* 79−93411
F^+ decay, SU_4 20-plet dominance model, inclusive branching ratios 80−13299
F^+ decay widths and branching ratios, quark recombination widths, free quark model 80−27500
F^+ nonleptonic decay, quark annihilation hypothesis test 80−102044
$F^+ \rightarrow p\bar{n}$, decay mode meas. for PCAC test 80−91018
$F^+ \rightarrow \phi\pi^+(\eta\pi^+)$, heavy quark weak isospin, constraints from nonleptonic transitions 79−85257
$F^\pm \rightarrow 3\pi$ or $K^+K_S{}^0$, charmed pseudoscalar meson nonleptonic decays, right handed c+λ quark doublet 77−49958
f′→ππ analytic S-matrix theory, Zweig Iisuka rule compatibility with unitarity 77−41782
f′(1514)→2π, decay amplitudes, OZI rule, dispersion relations, intermediate states contribs. 79−383
$^3F_3 \rightarrow \pi d$, branching ratio in Faddeev πNN dynamics 80−105886
F^{**}, charmed tensor meson, strong and EM decay modes 80−68451
g(1680)→ρρ, many pion correlations from nonstrange mesonic resonances *(Russian)* 80−86708
γ(10.0), two-body hadronic and radiative decays, pseudo-dimension rule, ππ and KK̄ suppression, SV_3 singlet 80−52495
J/ψ decay, gluon source, search for scalar gluonium, QCD 80−47296
J/ψ decay, via ω, φ, ρ^0 poles and cascade decays, vector meson pole dominance 79−85295
J/ψ hadronic decay, energy crisis interpretation, anomalous neutral component 78−41540
$J/\psi \rightarrow K_SK^-\pi^+$, low lying resonance saturation 79−54338
J/ψ→3π, low lying resonance saturation 79−54338
J/ψ→η(η′)γ decay rate, QCD sum rules 80−52497
K*→Kγ, quark loop model, SU(3) splitting of quark masses 80−62990
$K^-p \rightarrow \Lambda D$, 4.2 GeV/c, D(1285) prod. and decay props. 79−49517

meson hadronic decay continued
$\nu_\mu N$, $F^+(2030)$ prod. and hadronic decay $F^+ \rightarrow \pi^+\pi^+\pi^-\pi^0$, mass 80−91085
$\omega(1670) \rightarrow B\pi$, decay mode cross section from K^-p backward prod. 80−37257
$\omega \rightarrow 2\pi$, nonet mixing and gluon effects in current quark framework 79−80799
$\omega \rightarrow 3\pi$, decay width for $V \rightarrow 3=$ in Bethe Salpeter model 79−58955
$\omega \rightarrow \eta\gamma$, decay rates calc. SU(3) theory 78−58181
$\omega \rightarrow \eta\gamma$, radiative decay width determ. 78−467
$\omega \rightarrow \pi^0\gamma$ in reaction $\pi^- p \rightarrow \omega n$, $\omega \rightarrow \pi^0\gamma$, $\pi^0 \rightarrow 2\gamma$, differential cross sections 79−93464
$\omega \rightarrow \pi + \gamma$, radiative decay in the MIT bag model 78−66110
$\omega \rightarrow \pi\gamma$, radiative decays, final state interaction, π rescatt. *(Russian)* 78−89710
$\omega \rightarrow \pi\gamma$, suppression factors for VMD couplings calc., duality constraint anal. 77−13960
$\omega'(1.78)$ vector meson props., quark model, VDM 77−54103
pp, polarised p, W prod. estimates for hadron jet decay detection, parity violating asymmetries 79−40821
$\bar{p}p \rightarrow F_1\omega$, F_1 spin-parity anal., boson spin tests from sequential decays 78−29345
pp interactions, charmed D^+ prod., total cross section, $D^+ \rightarrow K^{*0}\pi^+$ observation 79−36102
$\phi(1020) \rightarrow 3\pi$, decay amplitudes, OZI rule, dispersion relations, intermediate states contribs. 79−383
$\phi \rightarrow 2\pi$ decay probability *(Russian)* 79−45086
$\phi(3100)$ two-body decays and SU(3) breaking 77−18277
$\phi \rightarrow 3\pi$, decay width for $V \rightarrow 3=$ in Bethe Salpeter model 79−58955
$\phi \rightarrow 3\pi$, Zweig forbidden decay 79−17687
ϕ decays, hadronic, asymptotic freedom, one-photon or three-gluon exchange 80−62971
$\phi \rightarrow \eta\gamma$, quark loop model, SU(3) splitting of quark masses 80−62990
$\phi \rightarrow K^+K^-$, average mass meas. of $K^\pm$ 79−30742
ϕ meson, two-body hadronic decay, quark model 78−25040
$\phi \rightarrow \pi^+\pi^-$, π form factor, ϕ peak, unitarity and gluonic corrections 80−22615
$\phi \rightarrow \pi^+\pi^-$, search in $e^+e^- \rightarrow \pi^+\pi^-$ reaction *(Russian)* 78−45915
$\phi \rightarrow \pi\gamma$, SU(3) algebra, appl. to ground state mesons, coupling constraints and decay rate 78−58183
$\phi \rightarrow \pi\gamma$, suppression factors for VMD couplings calc., duality constraints anal. 77−13960
$\phi \rightarrow \rho\pi$, dynamical calc., energy depend. of Zweig-rule violating couplings 78−33063
π production, direct and by meson resonance decay in π^+p interactions 78−29365
$\pi^- p \rightarrow nk_s^0K_s^0$, 6, 7 GeV/c, cross section, decay ang. distribs. and S-wave amplitude 79−49539
ψ, charmonium state, decay modes, prod. mechs. 77−10247
ψ, OZI rule breaking in decays 79−97597
Ψ, one photon intermediate state 79−54337
ψ, ψ' hadronic decays from DORIS, DASP expts. 77−243
ψ, $\psi' \rightarrow \pi^+\pi^-$, K^+K^-, decay suppression, dimensionality based selection rule 78−33061
ψ, radiative decay, gluonic bound state O width 80−37272
Ψ, radiative decay rate calc. in spectrum-generating SU(4) 77−34152
ψ, stiff quark line hypothesis, strong interaction suppression, Zweig Izuke rule origin 77−2792
ψ, strong and radiative decays, SU(3)′×SU(3)″ scheme of three triplet model 77−30371
$\psi, \psi' \rightarrow \eta_c\gamma$ rates, suppression in SU(4) multiplet mixing 77−18195
$\psi(3095)$ mesonic decay branching ratios, two-, quasi-two- and three-body decays 77−49959
$\psi(3095) \rightarrow p\bar{p}$ or $\Lambda\bar{\Lambda}$, branching ratios, quantum numbers, final state resonances 78−74252
$\psi(3684)$, radiative decay into high-mass states 78−66113
$\psi(3684) \rightarrow D\bar{D}$ decay width from $e^+e^- \rightarrow$hadrons multistate approach anal. 77−71521
$\psi(3772) \rightarrow D\bar{D}$, $D^{0,?}$ masses, branching fractions 78−17009
$\psi(3.1) \rightarrow f\omega$, $\psi(3.1) \rightarrow B\pi$, branching ratios meas. 78−17011
$\psi \rightarrow 3\pi$, generalised Veneziano model, 3π Dalitz plot 79−381
$\psi \rightarrow 3\pi$, ρ recurrences, quantitative study 77−79266
ψ(4.0 to 4.5 Gev) decay to D, F charmed mesons 79−17719
$\psi(4.03) \rightarrow D\bar{D}$, suppression problems, model-independent approach 80−52494
$\psi(4.03) \rightarrow D\bar{D}(D^*\bar{D}, D\bar{D}^*, D^*\bar{D}^*)$, vector state strong decay 80−78057
$\psi(4.1) \rightarrow \psi(3.1) + \pi + \pi$, coloron model, quark composite struct. 78−29332
$\psi(4.414)$, width anal. in quark model 78−17010
$\psi(4.42) \rightarrow D\bar{D}$, suppression problems, model-independent approach 80−52494
$\psi(4.42) \rightarrow F\bar{F}$, suppression problems, model-independent approach 80−52494
ψ (3095) and ψ (3684) radiative decays, possible intermediate states from inclusive photon spectra 77−10246
ψ (3100) decay, inclusive γ and π^0 momentum spectra, direct γ prod. at large x 80−42466
ψ and ψ', decays and intermediate states from SPEAR, LBL-SLAC expts. 77−242
ψ and ψ' charmonium spectroscopy anal. using square root pot., decay widths 78−82182
ψ and ψ' decays violating Zweig Iizuka rule, asymptotic freedom phenomenology 78−451
ψ and ψ' hadronic decays and soft pion theorems in charmonium model 77−6117
ψ and related particle decay, data anal. using quark model and VMD 77−54101
$\psi \rightarrow \chi\gamma$, radiative width calc. 77−71508
$\psi \rightarrow D\bar{D}$ radial excitations of charmonium 80−102046
ψ decay, charmonium model, $^1D_2$ level at 3.5 GeV 77−2826
ψ decay, high energy direct photons, γ, π^0 momentum distribs., QCD calcs. 80−32098
ψ decay into baryon-antibaryon pairs 77−71510
ψ decays, hadronic, asymptotic freedom, one-photon or three-gluon exchange 80−62971
$\psi \rightarrow \eta_c\gamma$, η_c hadronic decay, charmonium model 78−41502
$\psi \rightarrow \eta_c\gamma$, quark-string model anal. 78−33065
$\psi \rightarrow \eta'(958) + \gamma$, width upper limit 77−38173
$\Psi \rightarrow \eta'\gamma$, QCD, width, exclusive OZI violating radiative decay 80−68458
$\psi \rightarrow \eta'\gamma(\eta\gamma)$, Okubo mass formula, $\eta(c\bar{c})$ component 77−6116
$\psi \rightarrow \eta(\eta')\gamma$, SU_3 violation, symmetry breaking and decay amplitudes 80−52499
meson hadronic decay continued
$\psi \rightarrow \eta(\eta')\gamma$, Ward identity anal., η,η' quark-glue struct. 80−42449
$\psi \rightarrow \eta\gamma$, pseudoscalar meson mixing and M1 radiative decays 77−30329
$\psi \rightarrow f^0\gamma$, meas. of $f^0(1270)$ polarisation 78−74251
$\psi \rightarrow f^0\gamma$, $\psi \rightarrow \rho\pi$, branching ratios meas. 78−25043
$\psi \rightarrow f^0\gamma$, prod. and decay distribs. 78−89765
ψ family, suppression factor 79−13112
$\psi \rightarrow f\gamma$, intermediate one photon state description 78−62397
$\psi \rightarrow K\bar{K}\pi$, Veneziano model anal., $K\bar{K}\pi$ Dalitz-plot density calc. 79−26331
ψ meson, two-body hadronic decay, quark model 78−25040
$\psi \rightarrow n\bar{n}$, $p\bar{p}$, simultaneous meas. of decay channels at J/ψ resonance 78−93893
$\psi \rightarrow \omega\pi\pi$, local derivative coupling model 78−58184
$\psi \rightarrow \phi\pi\pi$, local derivative coupling model 78−58184
$\psi \rightarrow \pi\pi\gamma$, local derivative coupling model 78−58184
$\psi(\psi') \rightarrow B_8\bar{B}_8$ and $B_{10}\bar{B}_{10}$ modes, decay widths 77−6118
$\psi(\psi') \rightarrow$vector meson + pion + pion, disconnected quark diagram, decay widths 77−2824
ψ radiative decay, radial excitations and q^2 depend. in VDM 78−452
ψ radiative decays, generalised quark line rule, SU_4 symm. scheme 78−54614
$\psi \rightarrow \rho\pi$, $\psi \rightarrow \gamma\eta'$, branching ratios meas. 77−2827
$\psi \rightarrow X(2830) + \gamma$, E1 amd M1 radiative decays using the geometrodynamical approach 78−86452
ψ/J, charmed particles, particle multiplicity, distribs. in hadronic decays 77−46044
ψ/J and ψ' decay properties, intermediate states, Iizuka model 77−2825
ψ/J and ψ' production in hadronic collisions, quark-antiquark annihilation, cascade process 78−25013
ψ/J hadronic decays, dynamics, SU(3) violation, dispersion relations, mass splitting 79−382
$\psi/J(3100) \rightarrow \eta'(958)\gamma$, e^+e^- storage rings expt., upper limit on partial decay width 77−49956
ψ-family hadronic decays and non-charmed meson spectroscopy 77−26519
ψ', ψ decay branching ratios, isospin and flavour symmetry breaking 80−95264
$\psi'(3684) \rightarrow \chi\gamma$, $\chi \rightarrow \psi(3095)\gamma$, inclusive γ spectra in e^+e^- colliding beam expts. 77−57549
$\psi'(3684) \rightarrow \gamma\gamma J/\psi(3093)$, cascade decays, evidence for new C=+ intermediate state 79−13115
$\psi'(3685) \rightarrow \gamma P_c/\chi \rightarrow \gamma\gamma J/\psi(\pi^+\pi^-)(\gamma K^+K^-)$, investig. of $\gamma\gamma\mu^+\mu^-$ final state 80−18132
$\psi'(3.7) \rightarrow \psi\pi^0$, isospin violating decays 78−37205
ψ' and ψ decay ratios, composite particle matrix elements 80−95266
$\psi' \rightarrow \chi_J\gamma$, radiative decay widths of charmonium states, superconvergent sum rules 78−21422
$\psi' \rightarrow \chi/ec\gamma$, scalar and tensor meson dominance 79−3019
$\psi' \rightarrow \chi(3455) + \gamma$, E1 amd M1 radiative decays using the geometrodynamical approach 78−86452
ψ' decay, Higgs bosons, five-quark model, P and T nonconservation 77−74686
$\psi' \rightarrow \eta J/\psi(\pi^0 J/\psi)$, investig. of $\gamma\gamma\mu^+\mu^-$ final state 80−18132
$\psi' \rightarrow \eta\gamma$, $\psi \rightarrow \eta'\gamma$ and η-$c\bar{c}$, η'-$c\bar{c}$ coupling consts. *(Russian)* 77−49962
$\psi' \rightarrow \eta\psi$, $\psi' \rightarrow \pi^0\psi$, forbidden decays anal. 78−66114
$\psi' \rightarrow \gamma\chi_{1,2}$, radiative decays of 2^{++}, 1^{++} mesons 78−21420
$\psi' \rightarrow \gamma\chi \rightarrow \gamma\gamma\psi$, radiative decay width in charmonium model 77−18283
$\psi' \rightarrow \pi^0\psi$, isospin isolating decay, branching ratio 80−57601
$\psi' \rightarrow \psi + 2\pi$, decay width dynamical calc. 77−18278
$\psi' \rightarrow \psi + \eta$, two gluon mechanism, T dynamics test 78−89665
$\psi' \rightarrow \psi\eta$, Ward identity anal., η,η' quark-glue struct. 80−42449
$\psi' \rightarrow \psi\eta(\pi^0)$, decay branching ratios 80−105889
$\psi' \rightarrow \psi\gamma\gamma$, $\psi\gamma\gamma$ final state meas., $\psi' \rightarrow \gamma\chi$, $\chi \rightarrow \gamma\psi$ branching ratios 80−57601
$\psi' \rightarrow \psi\pi^0(\eta)$, SU_2 violation, symmetry breaking and decay amplitudes 80−52499
$\psi' \rightarrow \psi\pi^+\pi^-$, local derivative coupling model 78−58184
$\psi' \rightarrow \psi\pi\pi$, charm model 78−74250
$\psi' \rightarrow \psi\pi\pi$ mass spectrum, hadronic cascades between $Q\bar{Q}$ bound states, QCD anal. 79−85261
$\psi''(4.414)$ GeV, third radial excitation of $c\bar{c}\,^3S_1$, unorthodox branching ratios 79−17720
$\psi''(4.42) \rightarrow D\bar{D}$, $F\bar{F}$, decay suppression, pseudo-dimension selection rule 80−9163
$\psi''(4.028) \rightarrow D\bar{D}$, or $\bar{D}D^* + \bar{D}D^*$ or $D^*\bar{D}D^*$, strong decay theory, radial excitation of charmonium 78−12909
$\psi' \rightarrow \psi\eta$, OZI rule violating transition, unitary corrections using dual model 79−26330
Q mesons, decay amplitudes, partial widths, Lorentz and SU(3) invariant coupling constants 79−26328
$Q_1(1289)$ decay, SU(3) octet mixing 77−18281
$Q_1(1290)$, $Q_2(1400)$ vector-pseudoscalar decay rates and SU(3) implications 77−61283
$Q_2(1404)$ decay, SU(3) octet mixing 77−18281
Q_A-Q_B mixing angle, axial vector meson decay, A_1 and C obs., SU(3) implications 79−89148
$(\bar{q}q) \rightarrow (\bar{q}'q')\gamma$, width, exclusive OZI violating radiative decay 80−68458
$q\bar{q}$ p-wave systems, fast decay anal. 78−50030
ρ, decay width, chiral $SU_2 \times SU_2$ representation 77−30369
$\rho \rightarrow \eta\gamma$ radiative decay width determ. 78−467
$\rho \rightarrow \pi + \gamma$, radiative decay in the MIT bag model 78−66110
$\rho \rightarrow \pi\gamma$, EM decay rates, spectrum generating SU(4) approach 79−26334
$\rho \rightarrow \pi\gamma$, quark anomalous mag. moments 79−17693
$\rho \rightarrow \pi\gamma$, radiative decays, final state interaction, π rescatt. *(Russian)* 78−89710
$\rho \rightarrow \pi\gamma$, SU_3 symm. breaking schemes, radiative widths 77−6114
$\rho \rightarrow \pi\gamma$ decay width, explanation using SU(3)-scalar term in the EM current operator 78−82206
$\rho(\rho') \rightarrow \pi\gamma$, obs. in $A(\pi^\pm, \pi^\pm\pi^0)A$ *(Russian)* 79−9639
$\rho^- \rightarrow \pi^- + \gamma$ decay width, comments 77−13959
$\rho_0^- \rightarrow \pi^-\gamma$, radiative decay width from pion excitation anal. 80−57599
$\rho^0 \rightarrow \eta\gamma$, decay rates calc. SU(3) theory 78−58181
$\rho^0 \rightarrow \pi^0\gamma$, decay rates calc. SU(3) theory 78−58181
$\rho^+ \rightarrow \pi^+\pi^0$, decay widths calc. in MIT bag model 77−74681
$\rho^\pm \rightarrow \pi^\pm\gamma$, parity nonconservation effects in $np \rightarrow d\gamma$, short dist. contrib. to γ circular polarisation 77−41855
$\rho'(1275)$ vector meson nonet, main decay channels 77−79267
$\rho'(1600) \rightarrow \pi\pi$ decay mode suppression, Veneziano model 77−46031
$S^* \rightarrow K^+K^-$ cross section, S-P waves interference in $\gamma p \rightarrow K^+K^-p$ 79−6343

meson hadronic decay continued
ss̄ vector mesons, hadronic decays and props., nonrelativistic quark model 80−105892
t-quarkonium decay props. *(Russian)* 80−105856
Υ(10), decay modes and pseudoscalar partner 79−13179
Υ(9.46) decay into charged hadrons, jet anal. 79−49519
Υ(9.46) orthoquarkonium decay, jet profiles, three gluon structure 80−73698
Υ(9.46)→hadrons, gluon spin and colour, QCD nontrivial test 80−82971
Υ(9.4), decay modes and pseudoscalar partner 79−13179
Υ(9.4)→charmonium, quarkonium prod. via one gluon mechanism 80−95263
Υ(9.5) decay modes from Zweig rule intermediate vector particle model *(Chinese)* 80−73697
Υ (9.5) props., SU(4)×$S_3^{(1)}$ scheme in straton model *(Chinese)* 79−9347
Υ decay, multiplicity decrease due to charm prod. suppression 79−49518
υ decays, hadronic, asymptotic freedom, one-photon or three-gluon exchange 80−62971
Υ→ηγ or η′γ, other hadronic and two body charmed and strange modes 78−78175
Υ family, leptonic, hadronic, two-body decay widths, suppression factor 79−49514
Υ′ decay and 10 GeV reson. struct. 78−66115
Υ′→Υ+η, two gluon mechanism, Υ dynamics test 78−89665
V→γh, use of QCD in OZI-violating radiative decays 79−26302
X(2.8)→$\pi^+\pi^-\gamma$, OZI rule violating decay in QCD 78−89709
X→φφ→$(K^+K^-)(K^+K^-)$, new spin-0 mesons, Yang's parity test 78−66111
X^0(958)→ηππ, ηX^0 mixing angle, broken SU(6)×O(3) quark model 79−17721
$X^0\to\pi^+\pi^-$ decay, 1 GeV/c^2, prod. in $\pi^-p\to X^0n$ 77−67670
D^0, D^+ decay widths and branching ratios, quark recombination widths, free quark model 80−27500
η_c(2830), OZI rule breaking in decays 79−97597
F^+, SU(3) predictions for decay using new weak mixing angles 79−97619
$F_t{}^+{}^*{}_b$ weak decay modes, annihilation contribs. 79−93410
ψ→ρ°π, meas. of ρ°(770) polarisation 78−74251
$X^-\to\bar{p}n$, search for narrow state mass enhancement 78−89708
$X^-\to\pi^-K^+K^-$, search for narrow state mass enhancement 78−89708
$X^-\to\pi^-\bar{p}p$, search for narrow state mass enhancement 78−89708
$X^-\to\pi^-\pi^+\pi^-$, search for narrow state mass enhancement 78−89708

meson interactions *see lepton-hadron interactions; meson-baryon interactions; meson-deuteron interactions; meson-meson interactions; meson-nucleus reactions; photon-hadron interactions*

meson leptonic decay
see also kaon leptonic decay
bottom mesons, weak decay struct., multilepton production 79−54319
charged pseudoscalar mesons, radiative corrections 77−38162
charm meson decay, inclusive electron spectrum 77−13970
charmed meson→l^+l^-X, model for charm fragmentation function 80−37237
decay widths, relativistic formula, quark-pair creation effect estimate 80−105883
heavy lepton production via decay of heavy vector mesons 77−87974
heavy quark states, weak decays and prod., jet like distrib. in SU(2)×U(1) model 79−75746
heavy vector meson annihilation to lepton pairs, hadronic corrections 80−68424
lepton pair width regularity of vector mesons, ρ, ω, φ, ψ and γ 79−63472
mass spectrum and Regge trajectories from relativistic quasipot. eqn. *(Russian)* 80−73690
meson weak and EM decays, relativistic confined quarks, MIT bag model 80−47277
meson-antimeson hadronic molecules, spectrum, leptonic and radiative decays *(Russian)* 80−57602
multilepton configurations in b and t decays from tt̄ and bb̄ 80−18130
parent-child relationship for prompt leptons and neutrinos produced in the forward direction 79−80824
pseudoscalar Dalitz decays, form factor slopes, VDM with subtracted dispersion relation 78−58181
pseudoscalar direct lepton production mechanism *(Russian)* 77−82738
pseudoscalar heavy meson decay by t and b quarks 79−380
quark bag model with finite potential barrier, S-wave mass spectra of QQ̄ and leptonic widths 80−47242
quark spinors in bound quark system, small component effects 80−73694
quarkonium leptonic decay rates for 1S and 2S states, constraints 80−37252
resonance decay, quark confinement potential 78−41536
V→e^+e^-, EM decays of vector and pseudoscalar mesons, dispersion theoretic approach 79−93423
vector meson→e^+e^-, standard leptonic decay width correction, effecting pot. model predictions 78−89707
vector meson decays to eē, constituent quark spinors, small component effects 79−85279
vector meson leptonic width, duality between vector mesons and perturbative QCD 80−57589
vector meson widths in quark confining two-step pot. 77−26492
vector mesons, gluon condensate *(Russian)* 78−33060
vector mesons, leptonic and radiative decays, Schwinger model with U(3) symm. breaking 79−379
vector mesons, leptonic decays, six-quark sequental model 80−52490
wave functions at zero point, decay processes π→μμ, K→μμ, $1^-\to e^+e^-$ *(Chinese)* 77−10242
cc̄ bound states, e^+e^- decay processes, relativistic harmonic oscillator model 78−62393
D(1.87) leptonic decay branching and $pp\to e^\pm\mu^\mp X$ upper limits 77−65186
D→e^- branching ratio from e^+e^- annihilation multiprong data 78−78200
D meson decay, semileptonic and leptonic modes, electron momentum spectrum 78−8657
D-meson masses and leptonic decay consts. 78−66087
$D^-\to\tau^-\bar{\nu}_\tau$, charmed mesons, heavy lepton decays, ν_τ neutrino mass depend. *(Russian)* 78−62394
$D^\pm$, weak decay constant from bag model extension 80−62967
$^1D_1$-charmonium decay into eē and relativistic effects of constituent quarks 79−3017

meson leptonic decay continued
DD̄ production in large p_T hadronic collisions, eμ and eK correlation study 79−40772
$e^+e^-\to e^+e^-$, Υ(9.46) electronic branching ratio and total width 80−86702
$e^+e^-\to F\bar{F}(B\bar{B})$, τν decay signature for $F^\pm$ and $B^\pm$ detection 80−91099
$e^+e^-\to\gamma V\to\gamma\nu\bar{\nu}$, neutral vector meson radiative prod. and decay *(Russian)* 80−52492
$e^+e^-\to$hadrons, Υ″ observation at CESR, mass and leptonic width 80−86738
$e^+e^-\to$hadrons ($\mu^+\mu^-$), Υ(9.46) muonic branching ratio, total and leptonic width 80−86703
$e^+e^-\to\psi$(3770), cross section, ψ mass, total width and e^+e^- partial width 80−73696
η, neutral weak current effect on decay mode Weinberg-Salam model, P-violation contrib. 78−86450
η(η′)→2γ, nonet mixing and gluon effects in current quark framework 79−80799
η→γe^+e^-, form factor slope calc., VDM 78−58181
η→γ$\mu^+\mu^-$, vector dominance model *(Russian)* 79−58954
η→$\mu^+\mu^-\gamma$, branching ratio and η EM form factor 80−105899
η→$\mu^+\mu^-\gamma$, mass spectrum 79−9367
η→$\mu^+\mu^-\gamma$, obs. in π^-p collisions at 25 GeV/c *(Russian)* 79−22090
$\eta^0\to\gamma+(e^+e^-)$, EM bound states, approx. Bethe-Salpeter wave function *(Chinese)* 80−42448
$\eta^0\to\gamma+(\mu^+\mu^-)$, EM bound states, approx. Bethe-Salpeter wave function *(Chinese)* 80−42448
η_c pseudoscalar decay const., linear potential model 77−74679
η′→$\mu^+\mu^-\gamma$, in π^-p interactions at 25 and 33 GeV/c, form factors *(Russian)* 80−4984
F-meson masses and leptonic decay consts. 78−66087
$F^-\to\tau^-\bar{\nu}_\tau$, charmed mesons, heavy lepton decays, ν_τ neutrino mass depend. *(Russian)* 78−62394
$F^+\to\tau^+\nu$, gluon enhancements in charmed-meson decays 80−95265
F^+, weak decay constant from bag model extension 80−62967
$F^+\to\tau^\pm\nu_\tau(\bar{\nu}_\tau)$ beam-dump experiment, observation of ν_τ interactions 80−22601
F* meson and anomalous eμ events 78−66108
from π p mass spectrum 80−27498
$K^0\to\mu e$, flavour changing neutral current search 80−105836
$\mu^+\mu^-$ pair system, meson reson., leptonic decay *(Russian)* 77−67646
μN, 209 GeV, ψ diffractive prod. cross section, ψ→$\mu^+\mu^-$ decays 80−102054
μN→μΥX, 209 GeV, Υ muoprod. limits from trimuon final states 80−105909
ν production, prompt sources, and axion decays and interactions, pN beam-dump experiment 80−63028
$\omega^0\to e^+e^-$, in π^+p 4.0 GeV/c 77−26542
$\omega^0\to e^+e^-$, obs. in 4.0 GeV/c π^+p interactions 77−38199
P→γl^+l^-, EM characts. for pseudoscalar meson decay in nonlocal quark model *(Russian)* 80−102050
pp, 53, 63 GeV, massive electron pair prod., Υ ang. decay, scaling function 80−68495
pp, 53, 63 GeV, Υ and ψ prod., dielectron decay angles 80−68496
φ→e^+e^-, decay widths from QCD *(Russian)* 78−45812
π, modified quark loop model, form factors, struct. functions, radiative decay 80−91088
π→eμ and possible violation of e-μ universality 77−2739
π→eνγ, branching ratio, axial vector form factor determ. 78−74247
π→eνγ, isospin violation in form factor, induced by current quark mass 80−32069
π→eνγ, modified quark loop model, form factors, struct. functions, radiative decay 80−91088
π→eνγ, vector form factor, quark masses and isospin breaking 79−13111
π→eνγ and SU(3)×SU(3) σ-model 80−78054
π lifetimes, ratio of neutral to charged π in general relativity 79−49513
π→$l\nu_e\gamma(l\nu_e l'^+l'^-)$ in review of weak-EM decays *(Russian)* 77−2818
π→lνγ, struct. constants of mesons in quark diagram model *(Russian)* 79−30717
π→μμ, mesonic wave functions at zero point *(Chinese)* 77−10242
π^0, neutral weak current effect on decay mode Weinberg-Salam model, P-violation contrib. 78−86450
$\pi^0\to e^+e^-$, branching ratio meas. 78−41538
$\pi^0\to e^+e^-$, form factor slope meas. 78−41537
$\pi^+\to\mu^+\nu_\mu$, at rest, μ^+ momentum meas. 78−45911
$\pi^+\to\mu^+\nu_\mu$, muon momentum meas. 80−37253
$\pi^\pm$ decay, gauge theory, radiative corrections to μ-e universality 77−10244
π^-p, 70 GeV/c, direct electron prod. from charm particle pair decay, e/π ratio 80−105928
π^-p, 70 GeV/c, directly produced electrons from charmed D particle decay, cross sections 80−73755
ψ, production and decays, probability calcs. *(Chinese)* 77−65153
ψ, wave functions and partial decays in SU_4 model *(Chinese)* 77−65152
ψ(3,1)→e^+e^-, radiational effects *(Russian)* 77−46060
ψ(3100) decay into muon pairs, $e^+e^-\to\mu^p\mu^-$ study at J/ψ energy, ang. distrib. 77−2846
ψ(3.1)→νν̄, neutral current decays, possibility of expt. obs. 77−18276
ψ and ψ′ charmonium spectroscopy anal. using square root pot., decay widths 78−82182
ψ decay width calc. in one parameter pot. 80−13279
ψ→e^+e^-, quarkonium, quantum mechanical applications, masses and leptonic widths of ψ and Υ 80−27484
ψ family, charmed triplet and leptonic decays 77−67622
ψ family, suppression factor 79−13112
ψ→l^+l^-, radiational effects *(Russian)* 77−46060
ψ leptonic decays, spectral-function sum rules 78−4857
ψ meson, phenomenology and quark confinement 78−29308
ψ→$\mu^+\mu^-$, Drell-Yan mechanism in colour quark model 77−6181
ψ→$\mu^+\mu^-$, search for extra μ in (π^-, ψ CC̄), 225 GeV/c 80−82967
Ψ′, neutral radiative decay, possible intermediate states 77−241
qq̄ resonance energy spectrum, leptonic and radiative decay widths, QCD pot. calcs. 80−52491
ρ, ω, coherent interference patterns, vector dominance model, book contrib. 78−82335
ρ→e^+e^-; decay widths from QCD *(Russian)* 78−45812
$\rho^0\to e^+e^-$, in π^+p 4.0 GeV/c 77−26542
$\rho^0\to e^+e^-$, obs. in 4.0 GeV/c π^+p interactions 77−38199
ρ′(1250) leptonic decay, observations in γp→pe^+e^- 900 to 1500 MeV expts. 79−30738

meson leptonic decay continued
- Υ, evidence for b quark, weak interactions and multilepton final states 79−49516
- Υ, interpretation as coloured particle, masses and leptonic decay widths 79−54322
- Υ, leptonic decay width, mass depend. in QCD 79−49488
- Υ, vibrational states in string picture, mass and leptonic width 80−62949
- Υ(10), decay modes and pseudoscalar partner 79−13179
- Υ(9.46), leptonic branching ratio, from electronic width and muonic branching ratios 80−57588
- $\Upsilon(9.46)\rightarrow\mu\mu$, branching ratio determ. 79−26339
- Υ(9.4), decay modes and pseudoscalar partner 79−13179
- Υ (9.5) props., $SU(4)\times S_3^{\alpha}$ scheme in straton model *(Chinese)* 79−9347
- Υ (9.6) constituents, heavy quarks as colour sextets, possible weak decay 79−2998
- Υ decay width calc. in one parameter pot. 80−13279
- $\Upsilon\rightarrow e^+e^-$, harmonic oscillator model, QCD gluon-bottom quark coupling 79−3016
- $\Upsilon\rightarrow e^+e^-$, quarkonium, quantum mechanical applications, masses and leptonic widths of ψ and Υ 80−27484
- $\Upsilon\rightarrow e^+e^-$, widths and b-quark interpretation of peaks 79−63435
- $\Upsilon\rightarrow e^+e^-(\mu^+\mu^-)$, charge asymmetry in lepton pair decay of polarised resonances 79−17716
- Υ energy spectra using quark model, leptonic decay widths, spin depend. forces 79−13109
- Υ family, leptonic, hadronic, two-body decay widths, suppression factor 79−49514
- Υ leptonic decay widths, determ. of new quark 78−50029
- Υ leptonic width, test of quarkonium pot. 78−89666
- Υ′, lepton heavy width QCD radiative corrections 79−49515
- $\Upsilon'\rightarrow\gamma 2^{++}(\bar{b}b)$, photonic decay widths in tensor meson dominance 79−75754
- Υ″ leptonic width, some phenomenological estimates about heavy quark (b,t) bound states 80−47262
- Z^0, weak-EM interference effects, LEP studies 79−97614
- $Z^{0\prime}\rightarrow\mu^+\mu^-\gamma$, Weinberg model anal. of Z^0 decay ang. distrib. 80−47275
- ζ energy spectra using quark model, leptonic decay widths, spin depend. forces 79−13109
- $\bar{b}b2^{++}\rightarrow\gamma\Upsilon$, photonic decay widths in tensor meson dominance 79−75754

meson magnetic moment
- charmed hadrons, mag. and transition moments, radiative decay widths 79−71724
- composite models, mag. moments of quarks, leptons and hadrons 80−32081
- hadron mag. moments, colour mag. moments and transition M1-moments, quark mass parameter 79−97596
- pion magnetic polarizability relation to electric and magnetic proton polarizabilities *(Russian)* 79−93420
- relativistic quark model with instantaneous interaction, spectra and mag. moments 77−61255
- SU(10) symmetry, charmed vector bosons mag. moments 78−17018
- topped and bottomed hadrons, mag. moments in additive quark model 80−52478
- truthful hadrons, mag. moments, transition moment, using state vectors and quark additivity principles 79−71723
- $\gamma N\rightarrow\Delta\pi$, mag. dipole photoexcitation, singular integral eqns., polynomial ambiguity 80−57608

meson mass
- η′ meson as pseudoscalar gluon, current sum rule saturation in QCD *(Russian)* 79−71718
- axial vector multiplets, mass spectrum, mixing angles, pseudoscalar mesons, decay consts. 77−13892
- axion, astrophysical limitations on mass *(Russian)* 78−61835
- b-mesons, mass splitting, SU_3 nonet of SU_6 80−47288
- baryonium mass spectrum in planar bootstrap model 78−25020
- baryonium masses in a quark model 80−37241
- bilinear symmetry-breaking in σ-model, meson mass and decay const. 77−49877
- bootstrap, QCD, meson mass spectrum 80−22581
- bottom hadrons, masses and allowed decays, SU(5) quark model 80−62954
- broken SU_N symm., meson mass formula 77−6043
- Cabibbo angle universality and association with K, π and D meson mass 79−12974
- charm $m(D^+)-m(D^0)$ calc., EM effects 77−2833
- charmed, dynamics SU(4,1) symmetry, mass spectra, anal. *(Russian)* 78−70350
- charmed 0 meson mass from SU(4,1) symmetry anal. *(Russian)* 78−74237
- charmed and old meson EM mass differences 77−2834
- charmed hadron masses, from effective quark masses, sum rules 80−4965
- charmed hadrons, SU(4) mass-breaking, mass sum rules 80−62959
- charmed meson mass, effect of u and d quark differences calc. 77−46019
- charmed meson mass calc. 77−10231
- charmed meson mass spectrum, quark model calc. 77−26491
- charmed meson mass splitting in universal confining potential model 80−4967
- charmed meson mass via duality calc. 77−22697
- charmed meson masses, effects of fifth flavour 78−66098
- charmed meson spectra from effective quark-quark interaction, D^0 mass 79−36018
- charmed mesons and charmoniums, masses and mixing, OZI rule breaking 78−12889
- charmed particles, duality constraints on spectroscopy 78−21398
- charmed particles, masses and decay consts. in $SU(4)\times SU(4)$ broken chiral symmetry 79−40686
- charmed states with high spin, unified calc. *(Russian)* 77−61258
- charmonium, $^1P_1$ state, mass, branching ratios, decay rates 78−62370
- charmonium, mass in QCD 80−105867
- charmonium mass spectrum using oscillator pot., Υ and Υ′ masses 79−97595
- charmonium psion states, confining pots. and inverse scatt. problem, Υ mass 80−4946
- chiral $SU(4)\otimes SU(4)$, broken model, F, L_s, F_s mesons 78−12836
- chiral $SU(4)\otimes SU(4)$ symmetry breaking parameter, meson mass 78−12838

meson mass continued
- composite model of mesons in relativistic space, masses, leptonic widths *(Russian)* 77−74658
- dynamically broken chiral symmetry and the gauge technique for Ward identities 80−47211
- EM mass differences, one gluon exchange contrib. 79−3024
- empirical formula for particles stable against strong decay 77−41833
- exotic meson $(Q^2\bar{Q}^2)$ spectroscopy, instanton effects 79−89140
- exotic meson mass formulae in $SU_{1,3}$ 77−65147
- exotic mesons, qq̄g states in bag model, energy, spin, parity, mass spectrum *(French)* 79−80807
- gauge theory with harmonic oscillator pot., coloured quark-gluon model 79−350
- generation by instantons in coloured gauge field theory 79−54321
- generation in chiral flavour $U(3)\times U(3)$ symmetry by instantons 79−89121
- gluon model of meson, MIT bag model *(Russian)* 77−74657
- gluonium concept, mass calc. *(Russian)* 78−45879
- grand unified theories, vector meson mass restrictions 80−32058
- hadron building blocks, pionic mass intervals in narrow and S-state resonances 80−105875
- hadron spectroscopy with covariant Coulomb and confining interactions 80−32090
- heavy meson spectroscopy, centrifugal and harmonic oscill. pot. 79−17699
- heavy mesons, polynomials approximating sequence of masses *(Russian)* 80−407
- heavy vector mesons associated with Υ(9.4) and the nature of Υ′(10) 78−82187
- Higgs boson mass, perturbation constraint 79−67493
- hyperfine splittings and asymptotic freedom 77−79252
- instantons, generation of meson mass spectrum, current algebra, mixing angles 80−86567
- Klein-Gordon eqn., meson masses calc. using harmonic oscillator pot. 79−93392
- L=1 meson spectrum, SU(6)×O(1) quark shell model anal. 78−89678
- light quark meson spectroscopy, recent results 78−78134
- light vector mesons, mass spectra and Regge trajectories in relativistic quark model *(Russian)* 78−93864
- linear SU(4) meson σ-model, one-loop approx., spin zero mass spectrum and leptonic-decay 80−47278
- logarithmic mass formulae and new quantum number 78−82183
- $m_{\eta c}^2=m_{\psi}^2-(m_{\rho}^2-m_{\pi}^2)=(3000\pm 20\ \mathrm{MeV})^2$ after all 79−85288
- $M_{\psi}-M_{\eta(c)}$ and $M_{\Upsilon}-M_{\eta(b)}$ lower bounds, concave and convex pots. 80−91057
- mass differences in relativistic quark model 77−26489
- mass formulae in broken $SU(8)_w$ symmetry 78−37191
- mass spectrum and Regge trajectories from relativistic quasipot. eqn. *(Russian)* 80−73690
- meson and baryon mass formula, chromodynamics consideration *(Russian)* 80−91071
- meson spectroscopy, quark mixing and quantum chromodynamics *(Russian)* 79−54329
- MIT bag model, coloured quark and gluon constituents of mesons 80−4929
- MIT bag model, PCAC effects, pion field exchange energy, η mass 79−93378
- mixing angles, non-relativistic quark model, Schwinger-type mass relations for SU_4 and SU_5 80−18125
- mixing angles, non-relativistic quark model, SU_5 and SU_n 80−22591
- multi π systems, mass distrib. using information theory method 78−82250
- naive quark model predictions for meson mass and baryon mass and mag. moment 80−78036
- narrow resonances, dynamical model, mass mixing and splitting in degenerate multiplet states 78−93813
- non-charmed spectroscopy in narrow ψ-family decays 77−26519
- nonet formulae, vector-tensor-Pomeron couplings 77−49883
- nonperturbative QCD, large N_c, QCD bag model, instantons and η′ mass 80−57559
- P-wave radial mixing, effect on E1 radiative decays, charmonium mass 80−37271
- potential model of meson mass 78−45874
- pseudoscalar meson masses and sum rules, 4 quark model 77−10233
- pseudoscalar mesons, chiral $SU_4\times SU_4$ nonlinear Lagrangian symmetry breaking 77−57513
- pseudoscalar mesons, EM mass shifts, quark-parton model, SU_3 quark triplet 80−42459
- pseudoscalar mesons, $SU_4\times SU_4$ chiral symm. 77−67583
- pseudoscalar mesons, sum rule, symm. breaking of chiral SU(4)×SU(4), decay const., masses 78−33000
- QCD, hadron masses, behaviour of constituent quarks 80−57557
- QCD, multicolour, series expansion for meson masses 78−21315
- quantum chromodynamics psi-spectroscopy model *(Hungarian)* 79−13068
- quark, harmonic confinement, hard gluon exchange corrections, meson mass spectrum 78−86440
- quark model and hadron spectroscopy, review 79−80808
- quark model with 4 quarks pseudoscalar meson masses 77−46021
- quark shell model, meson spectroscopy 79−6328
- quark-antiquark relativistic two-body eqn. bound states 77−30328
- quark-string model, meson mass spectra 78−33065
- quarkonium mass spectra, one gluon exchange corrections, gauge invariance and choice 80−52483
- quarkonium systems, binding energy effect on mass spectra 80−37229
- Regge spectra, symm. breaking effects, decay rates of mesons in dual resonance amplitudes 77−82715
- reggeisation in theories with broken global symmetries, nondegeneracy of vector meson masses, non-trivial mixing 80−13236
- relativistic quark model for mesons, symm. breaking via quark mass differences 77−79253
- resonances, empirical relation for masses 78−29323
- semilocal duality constraints for mesons, on-shell particles, masses, couplings 78−58174
- spectra based on bilocal model 79−67521
- spectral function sum rule and onium 79−26329
- spectroscopy, review of SU_3 quark model, quark confinement and bound states 78−74228
- spectroscopy based on nonlinear field proper oscills., equivalence theorem 78−89689

meson mass continued
spin struct. in meson spectroscopy with effective scalar quark confinement 79−17684
strong gravity and particle mass spectrum 77−30351
strong interaction theory, development from the Fermi-Yang model to the quark model *(Chinese)* 79−30711
strong-coupling calcs. of hadron spectrum in QCD, lattice Hamiltonian 77−41819
$SU_{1,4}$ as dynamical group, discrete representations anal. 77−74642
SU(3) 27-plet mesons masses, existence of low-mass long lived exotics in quark model 78−33032
SU(4) 16-plet boson mass formulas, flavour symmetry breaking 80−37250
SU(4) algebraic realisation, meson mass formula *(Russian)* 78−45895
SU(4) broken symm., duality, baryon+baryon and baryon+antibaryon exotic mesons prod. 78−89629
SU(4) framework for meson nonet struct., mass relations, mass splittings 79−288
SU(4) meson mass formula from generalisation of SU(3) Schwinger mass formulae 78−37190
SU(4) six-quark models, meson masses and EM decays 77−38129
SU(5), broken, meson mass formulae 80−47267
SU(5) symmetry with beauty quark, baryon and meson mass spectra 79−45079
SU(8), $SU_W(8)$ symmetries, mass formulae, mixing *(Russian)* 78−66097
symmetry-breaking, current algebra quark masses 80−42436
tensor mesons mass, model Lagrangian, SU(3) Yang-Mills fields, tensor fields 77−13874
trajectory slope parameters on basis of two-body model 77−67634
unitarity and hadron self-energy, mass shifts, and SU_6 symmetry breaking in meson spectrum 79−17687
unitarity and spectrum in quark model 80−18115
vector and pseudoscalar, linear and quadratic formulae, charm 77−49935
vector meson mass predictions, SU(3) formalism of S quark model 78−37177
vector meson spectroscopy in quark confining two-step pot. 77−26492
vector mesons, unitarity corrections to masses and mixing angles 79−49487
Weinberg sum rules, derivation of meson spectrum, duality unification with chiral symm. 78−29272
$B\rightarrow\psi X$, weak decay for B mass and other props. determ. 79−97621
b-quark meson, decay, weak mass mixing, CP violation 80−32086
b-quark mesons, mass, quark model predictions 80−95256
$B^0\bar{B}^0$ mixing in six quark model, decay, mass mixing and CP nonconservation 80−42406
$c\bar{c}g(c\bar{c}q\bar{q})$, exotic mesons, masses, decay widths, mixing matrix elements 80−62943
D, mass and mean life from high energy cosmic ray data *(Chinese)* 80−102045
D(1.87) isomultiplet, mass differences, effect of EM mixing on mass splitting *(Russian)* 78−89714
D and F meson spectra, electromagnetic interactions effect 80−47293
D meson EM mass differences, bag model calcs 77−6124
D mesons, decay const. using current algebra with Lagrangian model 78−58176
D-meson, gauge theoretic formulation of $SU_2\times U$, model, mass limit 78−70316
D-meson masses and leptonic decay consts. 78−66087
D^0 and D^+, 3.772 GeV, mass and decay branching ratios 78−78199
D^0 prod. and decay in high energy photon interaction, mass and decay time 80−42478
D^+-D^0, D^{*+}-D^{*0} mass differences using modified nonrelativistic Schrodinger eqn. 78−58186
D^+-D^0 charmed mesons EM mass difference estimate, quark pair creation model 77−10250
D^+-D^0 mass difference, broken isospin symmetry in chiral SU(4)⊗SU(4) 78−89691
D*(2.01) isomultiplet, mass differences, effect of EM mixing on mass splitting *(Russian)* 78−89714
D^{*+}, photoprod., D^0 mass difference 80−73720
D^{*+}-d^{*0} mass difference using form factors and vector meson interactions 78−21427
E(1420) assignment of η' in broken SU(3) plus SU(2) 77−38144
$e^+e^-\rightarrow$hadrons, Υ'' observation at CESR, mass and leptonic width 80−86738
$e^+e^-\rightarrow$O particle, decay, mass, prod. from Zweig rule intermediate vector particle model *(Chinese)* 80−73697
$e^+e^-\rightarrow\psi(3770)$, cross section, ψ mass, total width and e^+e^- partial width 80−73696
$ep\rightarrow ep\pi^0$ or $en\pi^+$, threshold cross section slope, form factors, π axial mass and radius 78−62411
η, instanton effects on light quark spectroscopy, MIT bag model, hadron mass 78−62372
η meson large mass, quark-gluon model, virtual annihilation mech. 79−351
η or η' meson, tunnelling effects, phase coherence and mass in non-Abelian gauge theory 79−93287
η_c, mass and other props, review from theoretical models 80−102025
η_c and η_c', mass prediction using QCD 80−22590
η_c mass determ. from QCD sum rules 78−74223
η_c mass from dispersion sum rules in QCD, identification with X(2.83) *(Russian)* 78−89681
η', QCD sum rules for mass, possible pseudoscalar gluonium, instanton effects 80−388
F mesons, mass and decay const. using current algebra with Lagrangian model 78−58176
F-meson masses and leptonic decay consts. 78−66087
f'-f mass mixing sign from gluonic annihilation model, OZI rule violation 79−71722
J/Ψ meson mass spectra, quasipotential calcs. *(Russian)* 80−47268
K_L mass shift 78−45920
K^+ mass meas. in $e^+e^-\rightarrow\phi\rightarrow K^+K^-$ 79−30742
K_L and K_S mass difference in asymptotically free gradient theory *(Russian)* 77−30333
K_L-K_S mass differences, charged Higgs boson couplings 80−62917
K_L-K_S mass difference, SU(3) gauge theory 78−58153
K_L-K_S mass difference, Kobayashi-Maskawa six quark model, mixing angles, mass matrix and CP violation 80−13284

meson mass continued
K^{0*}, Klein paradox and the mass spectra of the neutral vector mesons 79−26299
K^-p, 10 and 16 GeV/c, diffractive dissociation, multiplicity structure 79−89197
$\nu_\mu N$, F^+(2030) prod. and hadronic decay $F^+\rightarrow\pi^+\pi^+\pi^-\pi^0$, mass 80−91085
ω, Klein paradox and the mass spectra of the neutral vector mesons 79−26299
Ω meson, compilation study of unused data 77−65188
ω/N, mass ratio in QCD lattice gauge theory 80−4928
ω-meson, mass of radial excitation, quark confinement potential calcs. 78−93860
ω-meson series mass formula 77−22714
ω'(1.78) vector meson props., quark model, VDM 77−54103
Φ, Klein paradox and the mass spectra of the neutral vector mesons 79−26299
ϕ, mass compilation study 80−52552
ϕ meson mass determ. in $e^+e^-\rightarrow\pi^+\pi^-\pi^0$ and $e^+e^-\rightarrow K_S^0K_L^0$ *(Russian)* 78−45935
ϕ-meson, mass of radial excitation, quark confinement potential calcs. 78−93860
ϕ-ω mass mixing sign from gluonic annihilation model, OZI rule violation 79−71722
π, field theory, chiral symmetry and pion-nucleus interactions 79−80961
π, instanton effects on light quark spectroscopy, MIT bag model, hadron mass 78−62372
π, K and baryon linear mass relations 78−41520
π, mass shift 78−45920
π EM form factor, dispersion theoretic study, mass, charge radius 77−67652
π inertial mass, quaternion field theory of matter 78−24702
π mass determ., 2-level vac. polarisation concept 79−40766
π mass in improved static bag model 80−73667
π mass via pionic-atom transitions 77−10297
π/N, mass ratio in QCD lattice gauge theory 80−4928
π^- rest mass determ., from pionic atoms X-ray transitions 77−268
$\pi^+p\rightarrow(\pi^+\pi^-\pi^0)\Delta^{++}$, 16 GeV/c, partial wave anal., ω^* and A_2^0 80−63033
ψ, Klein paradox and the mass spectra of the neutral vector mesons 79−26299
ψ, quarkonium, quantum mechanical applications, masses and leptonic widths of ψ and Υ 80−27484
ψ(3772)→DD̄, $D^{0,?}$ masses, branching fractions 78−17009
$\psi\rightarrow\eta'\gamma(\eta\gamma)$, Okubo mass formula, $\eta(c\bar{c})$ component 77−6116
ψ mass spectra and radiative decay in light-quark model 77−18258
ψ/J hadronic decays, dynamics, SU(3) violation, dispersion relations, mass splitting 79−382
ψ''(3770), mass width from quark model 80−73723
QQ̄ mass, approx. scheme is QCD 80−42398
$q\bar{q}$ potential, asymptotic freedom, linear confinement 80−13279
$q\bar{q}(q^2\bar{q}^2)$ mesons, mass formula 80−62958
QQ̄ relativistic bound states, mass formula, unification of linear Regge trajectories 79−89141
$q\bar{q}$ spectra, heavy systems, equaltime relativistic wave eqn. with confining potential 80−77977
$q\bar{q}$ systems, nonperturbative potential model 80−78040
ρ/N, mass ratio in QCD lattice gauge theory 80−4928
ρ-meson, mass of radial excitation, quark confimement potential calcs. 78−93860
ρ^0, Klein paradox and the mass spectra of the neutral vector mesons 79−26299
t-quark mesons, mass, quark model predictions 80−95256
tt vector meson, proposed 40 GeV mass 80−62942
Υ, EM mass splitting in nonrelativistic quark model 79−89152
Υ, interpretation as coloured particle, masses and leptonic decay widths 79−54322
Υ, quarkonium, quantum mechanical applications, masses and leptonic widths of ψ and Υ 80−27484
Υ, vibrational states in string picture, mass and leptonic width 80−62949
Υ(9.4) family, gauge theory mass anal., harmonic oscillator pot. 78−82186
Υ mesons, level struct., masses, new quarkonium state 78−33031
υ p-wave ground state, mass scaling inequalities for quarkonium levels 80−32071
Υ-meson mass spectra, quasipotential calcs. *(Russian)* 80−47268
Υ' at $M(\Upsilon')=10.02$ GeV in e^+e^- annihils. using NaI lead-glass det. 78−93894
Υ' obs. at $M(\Upsilon')=10.01$ GeV in e^+e^- annihils. using DASP det. 78−93895
w-meson mass determ., 2-level vac. polarisation concept 79−40766
x-boson, mass and asymmetric decay rel. to cosmological baryon asymmetry 80−4464
X^0 meson mass determ. in chiral symmetry at infinite momentum 79−40685
^{1}H, pionic, pion mass high accuracy meas. from transitions 80−106406
Ti, pionic, pion mass high accuracy meas. from transitions 80−106406

meson-meson interactions
see also meson-meson scattering; pion-pion interactions
Brayshaw and Peierls mechanisms for generating hadron peaks, N*(1470), 0(1020) and charm 79−404
cross sections in QCD *(Russian)* 80−4968
effective potls. of quartic interaction and large NO(N) σ-model, dynamical symmetry restoration 77−5989
inelastic collisions, Glauber multiple-quark scatt. model, quark-quark scatt. amplitudes 78−21459
QCD, two dimens., hadron scatt., leading order calcs., meson-meson scatt. 78−4831
quark fragmentation distribs., meson, baryon and photon reactions 77−74655
scalar meson decay width, meson-meson sigma terms and phenomenology 77−74680
SU(4) broken symm., duality, baryon+baryon and baryon+antibaryon exotic mesons prod. 78−89629
virtual particle interactions *(Polish)* 79−40802
Zweig-superconvergence relations in meson collisions 78−21397
$B\bar{B}$ annihilation process, simple geometrical picture 80−95291
η-η', pseudoscalar meson mixing, phenomenological model with radial excitations in mass matrix 79−54316
$K\bar{K}$ off shell annihilations from $K^-p\rightarrow\lambda+$pions at 4.2 GeV/c 79−45101

meson-meson interactions continued
$K\bar{K}\rightarrow\pi\pi$, analytic S-matrix theory, Zweig Iisuka rule compatibility with unitarity 77−41782
πK scattering, chiral dynamics and asymptotical restrictions, sum rules *(Russian)* 78−17047
$\pi\omega\rightarrow\pi\pi$, operator dual model for bound relativistic quark based mesons *(Russian)* 79−9408
$\pi\rho$ scatt. amplitude asymptotic limit, sum rules, predicted resonance with A_1 meson quantum numbers *(Russian)* 78−78214
$Q\bar{Q}$ annihilations in QCD, strong radiative corrections 79−80809

meson-meson scattering
see also meson-meson interactions; pion-pion scattering
asymptotic energy scale factors for pseudoscalar meson scatt. and charmed meson couplings 78−8620
charmed particles, hadronic props., superconvergence sum rules 80−78043
chiral invariance for asymptotic momenta, elastic scatt. of hadrons, helicity amplitudes 78−4800
compilation of coupling constants and low-energy parameters 79−22159
crossing symmetric, unitary Regge theory for meson-meson scatt. 79−63458
gauge-dual-topological approach to soft hadronic reactions, trajectory slopes 80−18142
hadronic total cross sections, model, using covariant harmonic oscillator pot. wave functions 79−26306
high energy meson elastic scatt. amplitude, leading term approx. in SU(2) Yang-Mills theory 80−5017
$K\pi$ scatt. at complex energies 78−21458
pseudoscalar meson S-wave scatt., anal. of internal quark-gluon eigenstates, Wigner-Eisenbud formalism 79−63525
pseudoscalar scatt. and asymptotic scale factors 77−38202
quantum chromodynamic two-dimens. anal., high-energy behaviour 77−65140
quark model asymptotic completeness for meson scatt. 80−73738
Regge theory, crossing symmetric representation of dynamical eqns. 78−4841
Regge theory with crossing symmetry and unitarity, strong coupling 77−65177
Regge theory with crossing symmetry and unitarity, weak coupling 77−67676
resonating group calcs., low energy limit 78−424
supersymmetry, field theory, fermion (meson)-meson scatt., high energy behaviour 79−295
two-particle resonance+particle interactions, scatt. amplitude, arbitrary spins *(Russian)* 77−74621
vector meson scatt., two to three body, high energy, in Yang-Mills theory 78−17051
$K^*\pi\rightarrow K^*\pi$, analytic quasi-unitary isobar model anal. 79−36099
$K\bar{K}\rightarrow K\bar{K}$, dispersion model, matrix N/D method *(Russian)* 78−45954
$K\pi$, geometrical scaling, possible low energy phenomena 77−22797
$K\pi$, geometrical scaling at inelastic threshold 77−18323
$K\pi$ asymptotic scattering amplitudes, positivity anal. 79−45102
$K\pi$ elastic scatt., asymptotic total cross sections and positivity 80−13334
$K^+\pi$, QCD, one-gluon-exchange, resonating group method, soft-core approx. 80−63025
$\phi\pi\rightarrow\rho\pi$, analytic quasi-unitary isobar model anal. 79−36099
πK, low energy cross sections *(Chinese)* 80−52535
πK low energy scatt., dispersion relation anal. 78−33088
πK low energy scatt., solvable realistic model 78−33089
πK phase shifts, perturbation expansion about $SU(3)\times SU(3)$ symm. limit 79−58975
πK phase shifts and two-variable analyticity 79−13156
$\pi K\rightarrow\pi K$, modified K-matrix formalism for meson-meson scatt. amplitudes 77−82774
πK scatt. and related processes *(German)* 79−30750
πK scattering amplitude, analytic continuation, chiral symmetry breaking 80−63027
πK scattering length, dispersion relation anal. of phase-shift 80−63026
$\pi\omega\rightarrow\pi\omega$, $\rho'(1250)$ meson and two channel $\pi\pi$, $\pi\omega$ problem, N/D method *(Russian)* 80−37297
$\rho\pi$ scatt. in Bardakci-Halpern model 1^+ channel, N/D anal., A_1 status 79−40688
$\rho K\rightarrow\rho K$, analytic quasi-unitary isobar model anal. 79−36099

meson-nucleus reactions
for inelastic meson-nucleus scattering, see "meson-nucleus scattering"
see also kaon-nucleus reactions; meson-baryon interactions; meson capture; pion-nucleus reactions
bremsstrahlung of vector mesons induced by nuclei *(Russian)* 78−78424
CERN School of Physics, Austerlitz-Zeist, Holland (June 1978) 79−30857
conference, Les Houches, France (July-August 1977) 79−71864
emulsion nuclei, 20 TeV, balloon-borne chamber, Monte Carlo simulation 80−9309
hadron+nucleus cross-section, energy depend., multiplicity, scaling violation model *(Russian)* 79−22350
hadron+nucleus high energy collisions modified cascade model, multiplicities energy depend. 79−59064
hadron multiproduction on nuclei, nature of pomeron 77−87955
hadron-nucleus collisions at high energies, simple collective effects model *(Russian)* 78−89809
hadron-nucleus high energy collisions, two-particle correlations, cluster cascade model 79−49615
hadron-nucleus interactions, existence of slowly moving sources, vel. depend. frictional sources 79−6690
hadron-nucleus reactions, multiple production, expt. results, review *(Russian)* 79−3118
heavy nuclei meson induced fission, statistical relaxation process 79−59098
high energy particle-nucleus interactions, discussion 79−30858
intermediate energy reactions as struct. probes with $p,\pi K,\gamma,e$ projectiles 77−88107
internuclear cascade mechanism, meson(nucleon)-nucleus high energy reactions *(Russian)* 79−80903
intranuclear cascade model reply to criticism 77−71501
isobars and nuclei, N* components in meson-nucleus reactions and scatt. 79−85522
momentum space method for hadronic atoms including relativistic hadron-nucleus reactions 79−872

meson-nucleus reactions continued
momentum wave function determ. in atomic, molecular and nuclear systems 77−88556
multi-chain model for high energy hadron nucleus collisions 79−59042
multiplicity of particles produced in hadron-nucleus high-energy interactions 78−4933
nuclear structure determination method 79−85351
nucleon knockout, off-shell effects, momentum-space wavefunctions 77−88122
optical model, for total cross-section, 180-1600 MeV 79−6538
pion cumulative production in hadron-nucleus collisions *(Russian)* 78−607
pion production, intranuclear-cascade model, criticism 77−71500
pion radiative capture, effective Hamiltonian *(Russian)* 77−74887
relativistic hadron+nucleus reactions, degree of collectivisation 79−40956
$(\pi,\pi N)$ quasi-free scatt. in reson. region, (p,2p) comparison 77−88173
$(\pi^-,xnyp)$, E=0, medium nuclei in $Z\simeq 50$ region, isomer yield ratios 77−71624
π^- ^{12}C, 40 GeV/c, Λ and K_1^0 inclusive distribs. *(Russian)* 77−34196
$^{197}Au(\pi^-,X)$, X=d,t, ^3He, ^4He, particle emission following stopped pion absorption 80−91196
Be+π^-, 43 GeV/c, J/ψ prod. A depend. 78−25089
$^{40}Ca(K^-,\pi^-)\,^{40}_{\Lambda}Ca$, possible strange giant reson. 77−82969
$^{59}Co(\pi^-,X)$, X=d,t, ^3He, ^4He, particle emission following stopped pion absorption 80−91196
$C(\pi^-,\Lambda^0)$, 2.9 GeV, production cross section of cumulative λ^0 hyperons *(Russian)* 78−78419
$C(\pi^+,\pi^0p)$, 2.9 GeV, determ. of π^0N interaction cross-section *(Russian)* 77−14199
$C(\pi^+,\pi^0p)$, 2.9 GeV charge exchange *(Russian)* 77−339
Cu+π^-, 43 GeV/c, J/ψ prod. A depend. 78−25089
$^2H(t\mu,n\mu^-)^4He$, fusion reaction, 2 GeV energy release 78−17250
$^3He(\pi^-,\pi^0)^3H$, 100 to 260 MeV optical-model calcs. 77−79403
$^3He(\pi^-,\pi^0)^3H$, Glauber theory calc. in (3,3)-reson. region 77−82968
$^{16}O(\pi^+,p)^{15}O$, 66 MeV, $(p_{3/2})^{-1}$ and $(p_{1/2})^{-1}$ hole state excit. 77−74886
W+π^-, 43 GeV/c, J/ψ prod. A depend. 78−25089
$Xe(\pi^-,\Lambda^0)$ 2.9 GeV, production cross section of cumulative Λ^0 hyperons *(Russian)* 78−78419
$Xe(\pi^+,\pi^0p)$ 2.9 GeV, determ. of π^0N interaction cross-section *(Russian)* 77−14199
$Xe(\pi^+,\pi^0p)$, 2.9 GeV charge exchange *(Russian)* 77−339

meson-nucleus scattering
see also kaon-nucleus scattering; meson-baryon scattering; pion-nucleus scattering
conference, Les Houches, France (July-August 1977) 79−71864
hadron-nucleus scatt., optical treatment in terms of scatt. amplitudes 78−89838
hadronic atoms, low-energy hadron-nucleus interaction theory 78−70977
inelastic scattering, evidence for giant resonances 79−17883
isobars and nuclei, N* components in meson-nucleus reactions and scatt. 79−85522
optical model, for total cross-section, 180-1600 MeV 79−6538
two-channel optical model of high energy hadron-nucleus collisions 79−36210
$^2H(\pi,\pi)$, relativistic three-body calc. 77−74715
$\pi^\pm+Z\rightarrow Z+W^\mp+\pi^0$, high energy total cross sections calcs. *(Russian)* 77−46086
$^3He(\pi,\pi)^3He$, Glauber theory calc. in (3,3)-reson. region 77−82968
$^3He(\pi^\pm,\pi^\pm)$, 100-260 MeV, optical model calc. 77−79403
^4He $(\pi^\pm,\pi^\pm)$, 100-260 MeV, optical-model calc. 77−79403

meson photoproduction
amplitudes in resonance region, polarised nucleon targets 77−34162
charm particles photoproduction, asymptotically free field theories 77−13934
charmed hadrons, assoc. prod. by 9.3 GeV photons 77−18301
charmed meson productions in hadronic and EM hadron interactions 79−13143
charmonium photoprod., ψ_c, η_c ang. distribs., non-Abelian gauge gluon exchange 77−57546
charmonium photoprod., gluon-exchange model 78−74214
Conference on meson-nuclear physics, Houston, USA (Mar. 1979) 79−85489
core valence quark model, vector meson dominance total photoproduction cross section 79−49497
current algebra with unitarity corrections, vector-meson exchange 78−41557
double pion photoprod., correction to Chew-Low model amplitude 77−2844
heavy quark bound states, peripheral and VMD models 78−33074
heavy vector meson photoprod., vector meson dominance model anal., Regge trajectories 78−78195
high energy production, review 80−73719
impulse approx. for partial reaction amplitudes *(Russian)* 78−41698
pair production in two-photon processes 77−2809
phenomenological analysis of single pion photoproduction in the first resonance region 78−89721
photoproduction of negative pions, 510 to 750 MeV 78−74347
photoproduction processes of charm particles with charm nonconservation *(Russian)* 78−74201
pion photoproduction, weak interaction induced parity violating assymetries 79−71758
pion photoproduction and radiative capture 78−50213
pion photoproduction on nuclei in $\Delta(1236)$ region, nonrelativistic operator 77−41949
pion prod., role of $\Delta(3,3)$ resonance 77−6146
pion prod. on polarised nucleons above 3 GeV 77−34164
pion threshold prod., research at Saclay 77−82917
QCD, charm photoprod., ψ, D, F etc. prod., sum rules, cross sections 78−58169
resonance photoproduction, small amplitude lower bounds 77−54109
single pion photoproduction between threshold and 16 GeV, multipole and amplitude anals. 79−3031
tensor meson production in photon-photon collisions 79−93414
VDM, generalised, electroprod. and photoprod. of vector mesons 78−41519
vector meson photoprod., Carlitz-Green-Zee mechanism and vector meson dominance model 79−13137
vector meson photoprod. from nucleus, invariant amplitudes 79−63488

meson photoproduction continued
vector meson photoproduction and Compton scatt. by nucleons 79 – 22114
vector meson photoproduction from nucleons, quark rescatt. effects *(Russian)* 77 – 65160
vector-meson production, pomeron-photon analogy, current-current model 77 – 87984
Vekton-1 double arm spectrom. for ρ meson photoproduction 78 – 33362
$D^0(\bar{D}^0)$ high energy photoprod. in zero total visible strangeness events, cross section 79 – 80831
D^{*+}, photoprod., D^0 mass difference 80 – 73720
$\delta d \rightarrow \pi^+ nn$, final state interaction effects *(Russian)* 78 – 41558
$e^+e^- \rightarrow e^+e^-\rho$, bremsstrahlung production of neutral vector mesons 80 – 5006
η meson production in $^6Li(\gamma,\eta)^6Li$, partial cross section meas. 77 – 65220
η_C, coherent prod. and baryon-antibaryon pair decay 78 – 21421
$(\gamma,p\pi^-)$ reaction on nuclei, investigation using 2-arm spectrometric arrangement 79 – 711
$(\gamma,\pi^- p)$, detector system and ccts. 78 – 877
(γ,ρ^-), forward photoprod. on Al, Be, C, Cu up to 4.5 GeV *(Russian)* 77 – 50113
$\gamma \rightarrow \eta d$, differential cross-section calc. using resonance model 79 – 93432
$\gamma + N \rightarrow N + \pi$, spatial parity nonconservation in π-meson photoproduction *(Russian)* 77 – 61301
$\gamma d \rightarrow d\omega$ or $pn\omega$, 3.9 GeV, cross sections, A_2 exchange amplitude 77 – 34168
$\gamma d \rightarrow \eta d$, coherent photoproduction impulse approximation 77 – 82749
$\gamma d \rightarrow \pi^0 d$, 450 MeV cross section asymmetry *(Russian)* 79 – 89171
$\gamma d \rightarrow \pi^0 d$, meson-exchange currents in photomesic reactions, relativistic many-body theory 80 – 422
$\gamma d \rightarrow \pi^\pm NN$, off-energy shell photoprod. amplitudes for reactions on bound neutrons 80 – 421
γN, $\pi^\pm$ photoprod., low energy, emission ang. depend. *(Russian)* 80 – 57769
$\gamma N \rightarrow \pi^\pm$ + anything, 9-18 GeV, forward hemisphere 77 – 6134
$\gamma N \rightarrow \Delta\pi$, mag. dipole photoexcitation, singular integral eqns., polynomial ambiguity 80 – 57608
$\gamma N \rightarrow K^+\Sigma$, meas. of asymmetries and cross sections using 16 GeV linearly polarised photons 80 – 13318
$\gamma N \rightarrow K^\pm$ + anything, 9-18 GeV, forward hemisphere 77 – 6134
$\gamma N \rightarrow NX(2.8)$ as possible means of $X \rightarrow 2\gamma$ width determ. *(Chinese)* 77 – 57541
$\gamma N \rightarrow N\pi$, P-odd multipole amplitude, dispersion relations *(Russian)* 79 – 93435
$\gamma n \rightarrow n\pi^+\pi^-$, threshold to 1 GeV, Δ production 77 – 26532
$\gamma N \rightarrow \omega\Delta$, pion exchange mechanism anal. 77 – 82750
$\gamma n \rightarrow p\pi^-$, to 500 MeV, multipole anal. near P_{33} reson. *(Russian)* 77 – 74695
$\gamma n \rightarrow p\pi^-\pi^0$, threshold to 1 GeV, Δ production 77 – 26532
$\gamma N \rightarrow \phi N$, pole-cut nature of Pomeron 77 – 6136
$\gamma N \rightarrow \phi N$, suitability of reaction for revealing pomerons pole-cut nature 79 – 13091
$\gamma n \rightarrow \pi^- p$, 0.9-1.65 GeV, pol. γ, cross section asymmetry *(Russian)* 80 – 86728
$\gamma n \rightarrow \pi^- p$, 250 to 500 MeV, multipole anal. *(Russian)* 77 – 10266
$\gamma n \rightarrow \pi^- p$, 700 MeV, polarised neutrons, target asymmetry meas. 77 – 13967
$\gamma n \rightarrow \pi^- p$, 700 to 1200 MeV, recoil proton polarisation 80 – 78075
$\gamma n \rightarrow \pi^- p$, 850 MeV, target asymmetry meas. 78 – 21438
$\gamma n \rightarrow \pi^- p$, cross section determ. from 20-100 MeV meas. on $\pi^- p \rightarrow \gamma n$ reaction *(French)* 79 – 411
$\gamma n \rightarrow \pi^- p_0$ proton polarisation in $^2H(\gamma,np)$ *(Russian)* 78 – 41700
$\gamma n \rightarrow \pi^- p$, Chew-Low amplitude correction 77 – 2844
$\gamma N \rightarrow \pi^+ X$, QCD cross sections 80 – 73715
$\gamma N \rightarrow \pi^+ n$, meas. of asymmetries and cross sections using 16 GeV linearly polarised photons 80 – 13318
$\gamma n \rightarrow \pi^+ p$, $\pi^+ n$, $\pi^- p$, $K^+\Lambda$, $K^+\Sigma^0$ final state comparisons above resonance region 80 – 105906
$\gamma N \rightarrow \pi\Delta$, low energy prod. and Δ-N axial transition vertex 77 – 49981
$\gamma N \rightarrow \pi\Delta$, meas. of asymmetries and cross sections using 16 GeV linearly polarised photons 80 – 13318
$\gamma N \rightarrow \pi N$, backward π prod., effective pole model phenomenological study 79 – 3030
$\gamma N \rightarrow \pi N$, fixed Regge singularities 77 – 74694
$\gamma N \rightarrow \pi N$, P-odd partial amplitudes, dispersion relns. *(Russian)* 79 – 85304
$\gamma N \rightarrow \pi N$, resonance region photoprod., dispersion model, M1 and E2 photoexcit. $N \rightarrow \Delta(1236)$ 78 – 70377
$\gamma N \rightarrow \psi N$, spin and mass depend. of constituent and phenomenological models 77 – 61304
$\gamma N \rightarrow \psi(3.1)$ + anything, cross section and N charmed quark composition 80 – 423
$\gamma n \rightarrow \rho^0(p\pi^-)$, 7.5 GeV, cross channel isospin amplitude meas. and anal. 77 – 18299
γp, heavy quark particle photoprod., QCD model, vector dominance implications 80 – 86730
γp, π^0 prod. in resonance region, asymm. *(Russian)* 78 – 17031
$\gamma p \rightarrow (p\bar{p})p$, inclusive and exclusive $p\bar{p}$ photoprod. S(1936) prod. 80 – 86729
$\gamma p \rightarrow$ charmed mesons, photoprod. at CERN SPS and search for charmed mesons 79 – 26336
$\gamma p \rightarrow \eta^0 p$, phtotproduction cross-section asymm. for 1.39 to 1.78 GeV polarised photons *(Russian)* 77 – 79273
$\gamma p \rightarrow K^+K^-\pi^+\pi^-$, photoprod. at CERN SPS and search for charmed mesons 79 – 26336
$\gamma p \rightarrow K^+\Lambda$, meas. of asymmetries and cross sections using 16 GeV linearly polarised photons 80 – 13318
$\gamma p \rightarrow N\pi$, 250-500 MeV, multipole anal. *(Russian)* 77 – 246
$\gamma p \rightarrow N\pi$, position and residue of the pole in the $M_{1+}^{(3/2)}$ amplitude *(Russian)* 79 – 22112
$\gamma p \rightarrow n\pi^+$, differential cross sections meas., 500-930 MeV 77 – 79271
$\gamma p \rightarrow n\pi^+$, multipole anal. in region of first reson. 80 – 22622
$\gamma p \rightarrow n\pi^+$, pion photoprod. using coherent bremsstrahlung beam and polarised proton target *(Russian)* 79 – 80830
$\gamma p \rightarrow n\pi^+$ 340 MeV, cross section asymmetry *(Russian)* 79 – 63487
$\gamma p \rightarrow n\pi^+$, 340 MeV, pol. p, first resonance region, π^+ photoprod., T-asymmetry *(Russian)* 80 – 62997
$\gamma p \rightarrow p$ + vector meson, total cross section *(Russian)* 78 – 8674
$\gamma p \rightarrow pe^+e^-$, prod. of ρ, ω, ϕ anal. 78 – 50037
$\gamma p \rightarrow p\phi$, 3.0 to 6.7 GeV, elastic and inelastic ϕ photoprod. 79 – 9380

meson photoproduction continued
$\gamma p \rightarrow p\pi^0$, multipole anal. in region of first reson. 80 – 22622
$\gamma p \rightarrow p\pi^0$, pion photoprod. using coherent bremsstrahlung beam and polarised proton target *(Russian)* 79 – 80830
$\gamma p \rightarrow p\pi^0$, quantum chromodynamics and P-odd effects *(Russian)* 79 – 89172
$\gamma p \rightarrow p\pi^0(n\pi^+)$, to 500 MeV, multipole anal. near P_{33} reson. *(Russian)* 77 – 74695
$\gamma p \rightarrow p\pi^0\pi^0$, 710 to 950 MeV, cross section determ. from momentum spectrum of recoil protons 79 – 22108
$\gamma p \rightarrow p\pi^+\pi^-$, 710 to 950 MeV, cross section determ. from momentum spectrum of recoil protons 79 – 22108
$\gamma p \rightarrow p\pi^0$, differential cross sections meas., 500-930 MeV 77 – 79271
$\gamma p \rightarrow \phi p$ photoprod. at CERN SPS and search for charmed mesons 79 – 26336
$\gamma p \rightarrow \pi^0 p$, 0.6 to 1.8 GeV, backward angles, η-cusp 80 – 57609
$\gamma p \rightarrow \pi^0 p$, 1.0 and 1.1 GeV, forward prod. on polarised protons 77 – 74692
$\gamma p \rightarrow \pi^0 p$, 1.4 GeV, differential cross section meas. 80 – 42476
$\gamma p \rightarrow \pi^0 p$, 2 to 6 GeV, differential cross section meas., parton model anal. of energy depend. 79 – 63485
$\gamma p \rightarrow \pi^0 p$, 250 to 500 MeV, multipole anal. *(Russian)* 77 – 10266
$\gamma p \rightarrow \pi^0 p$, 360-500 MeV, secondary proton polarisation meas. *(Russian)* 78 – 54637
$\gamma p \rightarrow \pi^0 p$, 390-975 MeV, differential cross section 80 – 86725
$\gamma p \rightarrow \pi^0 p$, 400 to 1142 MeV, recoil proton polarisation 80 – 82981
$\gamma p \rightarrow \pi^0 p$, 450 to 800 MeV, proton polarisation, Walker-type anal., $P_{11}(1470)$, $D_{13}(1470)$, $S_{11}(1535)$ resonances 80 – 73721
$\gamma p \rightarrow \pi^0 p$, differential cross sections at large angles, 2-6 GeV 78 – 37214
$\gamma p \rightarrow \pi^0 p$, $E_\gamma = 1.3$ to 2.1 GeV polarisation parameter meas. 79 – 80829
$\gamma p \rightarrow \pi^0 p$, high energies, semiempirical amplitude anal. dispersion relations and Regge poles 80 – 86726
$\gamma p \rightarrow \pi^+ n$, 0.5-0.8 GeV, ang. distrib. of polarised target asymmetry 77 – 34165
$\gamma p \rightarrow \pi^+ n$, 1.35-1.65 GeV, pol. γ, resonance energy region, cross section asymmetry *(Russian)* 80 – 86727
$\gamma p \rightarrow \pi^+ n$, 250 to 500 MeV, multipole anal. *(Russian)* 77 – 10266
$\gamma p \rightarrow \pi^+ n$, 520 to 2250 MeV, meas. of Σ, T, and P polarisation parameters 79 – 75778
$\gamma p \rightarrow \pi^+ n$, 850 MeV, target asymmetry meas. 78 – 21438
$\gamma p \rightarrow \pi^+ n$, π^+ form. asymm. near first πn resonance *(Russian)* 78 – 66124
$\gamma p \rightarrow \pi^+ n$, $\pi^+ n$, $\pi^- p$, $K^+\Lambda$, $K^+\Sigma^0$ final state comparisons above resonance region 80 – 105906
$\gamma p \rightarrow \pi^+\pi^- p$, Chew-Low amplitude correction 77 – 2844
$\gamma p \rightarrow \pi^+\pi^-\pi^0 p$, $\rho'(1.6)$ production 80 – 102056
$\gamma p \rightarrow \pi^+\pi^-\pi^+\pi^-\pi^+\pi^- p$, diffractive production, jet-like structure 80 – 57606
$\gamma p \rightarrow \pi^+\pi^+\pi^-\pi^- p$, $\rho'(1.2)$ production 80 – 102056
$\gamma p \rightarrow \pi^\pm X$, comparison with $\bar{p}p \rightarrow p\pi^\pm X$, quark parton model anal. 79 – 63512
$\gamma p \rightarrow \pi\pi N$, 710-950 MeV 79 – 63484
$\gamma p \rightarrow \rho^-\Delta^{++}$, 2.8 to 4.8 GeV, cross-sections, ρ spin density matrices 80 – 62999
$\gamma p \rightarrow \rho^-\Delta^{++}$, 9.7 GeV, pion exchange mechanism anal. 77 – 82750
$\gamma p \rightarrow \rho^+ n$, 2.8 to 4.8 GeV, cross-sections, ρ spin density matrices 80 – 62999
$\gamma p \rightarrow \rho^+ n$, 9.7 GeV, pion exchange mechanism anal. 77 – 82750
$\gamma p \rightarrow \rho'(1500)p$, $\rho'(1500) \rightarrow \pi^+\pi^-\pi^+\pi^-$, photoprod. at CERN SPS and search for charmed mesons 79 – 26336
$\gamma p \rightarrow V^0 p$, one-pion exchange contrib., vertex corrections 78 – 50039
$\gamma_V p \rightarrow \pi^0 p$, phase shift anal., shrinking photon, geometrical duality 77 – 87983
$\gamma\rho$-Pomeron-Regge vertex function, spin depend. calc., multiperipheral model 78 – 82223
$^2H(\gamma,\pi^0)$, near threshold, total and differential cross-sections 77 – 14106
J/ψ mesons, prod. on nucleon, peripheral model of diffraction mechanism *(Russian)* 77 – 38180
K^+K^- high mass pairs, 1.4 to 2.4 GeV mass range, in H 79 – 22110
$^6Li(\gamma,\pi^+)^6He$, cross-section determ. 77 – 14100
$\nu p \rightarrow \pi$, threshold to 450 MeV, energy depend. multipole anal. 80 – 32110
ω, inelastic photoprod., 7.5-10.5 GeV, with $\Delta(1236)$ and higher masses 78 – 45930
ω photoproduction on D, Be, C, Al, Cu, Ag, Au, cross sections 78 – 58261
$p\alpha$, 1300 to 2300 MeV, π^0 photoproduction, double polarisation parameters 80 – 13317
$p\gamma$, one-gluon exchange, quark loop contrib. to photon total cross sections 80 – 4999
$\phi(1019)$ photoproduction on proton, 2.8-4.8 GeV 79 – 9381
ϕ photoproduction, quark multiple scatt. model anal. under vector meson dominance 79 – 54350
$\phi\pi$ prod. in e^+e^- annihilation and diffractive photoprod., 4 quark state signature 79 – 6324
π, photoproduction in E<450 MeV region, dispersion relations, CT invariance, review, book contrib 80 – 47311
π photoprod., final state theorem extension, anal. of accurate low energy expts. 77 – 65172
π photoprod. at intermediate energy, review 78 – 50061
π photoproduction $\leq$450 MeV, one-particle exchange model 79 – 13135
π photoproduction amplitudes, Pade approximants and dispersion relation solns. 80 – 91096
π photoproduction in first resonance region, one particle exchange model 78 – 4864
π photoproduction in large cosmic-ray showers 80 – 4214
π photoproduction on N, multipole $E_{1+}^{(3/2)}$ and its double zero at reson. $\Delta(1232)$ 79 – 40790
π photoproduction on nuclei, current algebra model with hard pions *(Russian)* 77 – 74890
π photoproduction reacts. on few body systems and Δ-N interaction 79 – 71842
π prod., double polarisation meas. up to 2.5 GeV 77 – 34163
π prod. in $\gamma^3He \rightarrow \pi^+\pi^-{}^3He$, gauge-invariant one-pion-exchange model 77 – 18298
π production, multichannel N/D model fit, Δ^+ pole parameters 77 – 10265
π production, theoretical anal., fixed-t dispersion relations 77 – 22743
π production near threshold, interior dispersion relations appls. 78 – 93889
π threshold photoprod., exchange currents, equivalence theorem 77 – 79321

meson photoproduction continued
π^0, in $^{12}C(\gamma, \pi^0 p)$ at 0.7-1.65 GeV, cross section asymmetry meas. *(Russian)* 80−63164
π^0 coherent photoprod. on ^{4}He, screening corrections and rescatt. *(Russian)* 78−41697
π^0 inclusive photoprod. and quark-parton model 78−78189
π^0 photoprod. from complex nucl. targets 77−82905
π^0 photoproduction, Regge poles and cuts 78−66127
π^0 photoproduction and nonhadronic duality 77−67661
π^0 photoproduction from protons, 0.7-1.45 GeV, polarised target asymmetry 77−46054
π^0 photoproduction on H, 300 and 310 MeV 79−527
π^0 photoproduction on H at 320 MeV 77−22742
π^+, π^-, from protons and neutrons, 250 to 790 MeV, cross section features 77−46053
π^- photoprod. cross sections calc. 77−82762
$\pi p \rightarrow p\pi^0\pi^0$, medium energy, cross section *(Japanese)* 77−41847
$\pi p \rightarrow \pi^0 p$, 650 and 700 MeV, angular depend. of secondary p polarisation *(Russian)* 78−78191
$\pi^+\pi^-$ pairs, vector dominance model, book contrib 78−82335
$\psi(3100)$ N total cross section from modulus dispersion relation anal. of photoprod. 77−18300
$\psi(3.1)$ photoproduction, vector dominance model 77−18302
ψ meson photoprod., direct peripheral mechanism *(Russian)* 77−46056
ψ photoprod. and helicity conservation from $\psi \rightarrow l^+l^-$ ang. distrib. 77−18297
ψ photoprod. from Be and Ta targets, mass no. depend. of cross-section meas. 77−26668
ψ photoproduction, two-gluon exchange model 78−21437
ψ photoproduction by nucleons and nuclei, soliton model *(Russian)* 77−46071
$q\bar{q}$ prod., quark-mass effects, ψ and Υ mesons 78−66130
ρ^0 and ρ^- photoprod. at 3 GeV 77−30390
ρ^0-mesons, vector dominance model, book contrib 78−82335
ρ^+ inelastic photoprod., 7.5-10.5 GeV, with $\Delta(1236)$ and higher masses 78−45930
$\rho'(1600)$ diffractive photoprod. in two pion final state 80−22624
$\Upsilon(9.4)$, photoprod. cross section estimation 78−78195
^{27}Al, π^+ high energy photoproduction and electroproduction 78−21543
^{27}Al(e,e'π^+), energy and ang. distribs. of πs, low lying residual states 78−54740
$^{11}B(\gamma,\pi^-)^{11}C$, 142.0-169 MeV, cross-section near threshold 77−6348
^{9}Be(e,e'π^+), energy and ang. distribs. of πs, low lying residual states 78−54740
^{12}C(e,e'π^+), energy and ang. distribs. of πs, low lying residual states 78−54740
$^{12}C(\gamma,\pi^-)^{12}N_{gs}$, threshold prod., 15.11 MeV M1 form factor 78−62519
$^{12}C(\gamma,\pi^0 p)$, 450 MeV, pion^0 photoproduction with proton ejection 79−80921
$^{12}C(\gamma,\pi^-)$, model yield calc. 77−14107
$^{12}C(\gamma,\pi^-)$, near (3,3) resonance, differential cross-section meas. 77−10385
$^{12}C(\gamma,\pi^-)^{12}N$, near threshold, total cross section 77−14104
$^{12}C(\gamma,\pi^-)^{12}N$, total cross-section anal. 77−14102
$^{12}C(\gamma,\pi^-)^{12}N$, total cross section calc., $\Delta(1232)$ contrib. 80−91175
$^{12}C(\gamma,\pi^-)^{12}N_{g.s.}$, near threshold, total cross section calc. 78−50152
$^{12}C(\gamma,\pi^+)^{12}B$, nuclear critical opalescence study 80−105988
$^{12}C(\gamma,\pi^+)^{12}B$, spin flip transition strength 77−14103
$^{12}C(\gamma,\pi^\pm)$, 300 to 850 MeV, charged pion momentum spectra 78−93987
$^{12}C(\gamma,\pi^\pm)$, PWIA anal. 77−14108
$\gamma N \rightarrow \eta X$, 9.7 GeV, inclusive η photoprod. on H- and ^{2}H-targets, ρ^0-dominance model anal. 79−63486
$\gamma p \rightarrow K^+\Lambda(\Sigma^0)$, $\pi^+ n$, $\pi^- p$, $K^+\Lambda$, $K^+\Sigma^0$ final state comparisons above resonance region 80−105906
$^2H(\gamma,\pi^+)nn$, excitation function, cross-section, threshold π^+ prod. 77−26670
$^2H(\gamma,\eta)^2H$, impulse approx. calc. of elastic η photoproduction 77−14110
$^2H(\gamma,\pi^- p)^1H$, π^--p coincidence obs., mechanism and rescatt. effects *(French)* 79−3133
$^2H(\gamma,\pi^0)$, 450 MeV cross section asymmetry *(Russian)* 79−89171
$^2H(\gamma,\pi^0)$, impulse approx. calc. of differential cross-section 77−18524
$^2H(\gamma,\pi^+)$, 1-4 MeV, cross-section meas. 78−21544
$^2H(\gamma,\pi^+)$, threshold prod., excitation function 77−14105
$^2H(\gamma,\pi^+)nn$, photoprod. near threshold, nucleus axial props. rel. to nucleon spin-fip *(French)* 79−522
$^2H(\gamma,\pi^+)nn$, threshold cross-section, impulse approx. 77−38256
$^2H(\gamma,\pi^-)$, photprod. on neutrons effect of Fermi motion 78−74349
$^2H(\gamma,\pi)$, impulse approx. and π rescattering effects 77−6346
$^3H(\gamma,\pi^0)$, polarisation effects 180 to 700 MeV, impulse approx. calcs. *(Russian)* 80−37368
$^3H(\gamma,\pi^0)^3H$, polarisation effects 180 to 700 MeV, impulse approx. calcs. *(Russian)* 80−37368
^{3}He, threshold pion photoproduction and radiative capture, π-^{3}He-^{3}H coupling constant 79−40962
$^3He(\gamma,\pi^0)$, polarisation effects 180 to 700 MeV, impulse approx. calcs. *(Russian)* 80−37368
$^3He(\gamma,\pi^0)^3He$, polarisation effects 180 to 700 MeV, impulse approx. calcs. *(Russian)* 80−37368
$^4He(\gamma,p\pi^-)$, π^--p coincidence obs., mechanism and rescatt. effects *(French)* 79−3133
$^4He(\gamma,\pi^0)$, impulse approx. for differential cross sections in resonance region *(Russian)* 78−41698
$^4He(\gamma,\pi^0)$, polarisation effects 180 to 700 MeV, impulse approx. calcs. *(Russian)* 80−37368
$^4He(\gamma,\pi^0)$, reaction cross section meas. equipment 78−29694
$^4He(\gamma,\pi^0)$, relative cross section depend. on pion parity *(Russian)* 78−66129
$^4He(\gamma,\rho^0)^4He$, eikonal and quasi-eikonal models in complex ang. momentum plane *(Russian)* 77−50160
$H(\phi,\pi^0)$, 350 MeV, differential cross sections 78−86527
$^6Li(\alpha,\pi^-)^6He$, threshold prod. in α-d cluster model 77−79356
$^6Li(\gamma,\eta)$, partial photoprod. cross-section calc. 77−14111
$^6Li(\gamma,\eta)^6Li$, E_γ=3.56 MeV, partial photoproduction cross-section calc. *(Russian)* 79−9547
$^6Li(\gamma,\eta)^6Li^*$(3.56 MeV), partial photoproduction reactions, large momentum transfer anal., form factor choice 80−22808
$^6Li(\gamma,\pi^-)^6He$, analysis using current algebra model with rigid π-mesons *(Russian)* 77−14112
$^6Li(\gamma,\pi^+)^6He$, photoprod. near threshold, nucleus axial props. rel. to nucleon spin-fip *(French)* 79−522
meson photoproduction continued
$^6Li(\gamma,\pi^+)^6He$, threshold to 7 MeV, cross sections rel. to proton target 77−54207
$^6Li(\gamma,\pi^0)^6Li^*$(3.56 MeV), partial photoproduction reactions, large momentum transfer anal., form factor choice 80−22808
Li(e,e'π^-), A=6,7, energy and ang. distribs. of πs, low lying residual states 78−54740
$^{14}N(\gamma,\pi^-)^{14}C$, threshold, impulse approx. anal. 77−14109
^{16}O, pion photoproduction and radiative capture 78−50213
^{16}O(e,e'π^+), energy and ang. distribs. of πs, low lying residual states 78−54740
$\pi d \rightarrow \pi^0 d$, 350-500 MeV, differential cross section asymm., impulse approx. with pion rescatt. terms 77−30389
^{51}V π^P high energy photoproduction and electroproduction 78−21543
^{89}Y(e,e'π^+), energy and ang. distribs. of πs, low lying residual states 78−54740

meson production
see also kaon production; meson photoproduction; pion production
$\pi^+ p \rightarrow \pi^+ p\phi$, 3.75 GeV/c, ϕ production angular distrib. and derived cross sections 78−58201
$\pi^- p \rightarrow \delta^- p$, $\pi^+\pi^-\pi^-\gamma\gamma$ backgrounds produced near the δ^- mass region 80−9182
ψ production and decay, book contrib. 78−82208
angular distribution in hadron + hadron collisions, semi-empirical formulae 79−54362
axion production, astrophys. implications of new light Higgs boson 79−22007
bag model, meson and massive photon production 80−105850
beauty and charm photoprod. in QCD, $q\bar{q} \rightarrow b\bar{b}$ or $c\bar{c}$ mechanism 80−32079
channel coupling effects and resonance phenomena in pp interactions, N/D eqn. study 79−71765
charge correlations from residual hadrons using electroprod. data 79−3032
charged scalar pair prod. by two virtual photons *(Russian)* 77−6069
charm particle, production in high energy ν-induced reaction, lifetime determ. 79−26426
charm particles, inclusive production cross sections, correlating quark rearrangement model 79−54320
charm production of pseudoscalar and vector mesons in e^+e^- annihilation 77−2855
charmed axial vector meson prod. in e^+e^- at $\sqrt{S} \simeq 4.1$ GeV 77−13969
charmed meson prod. at SPEAR 78−4865
charmed meson prod. in e^+e^- annihilation, quark model 78−8680
charmed meson prod. in quark exchange model 78−8600
charmed meson produced in e^+e^- annihilation 80−91106
charmed meson productions in hadronic and EM hadron interactions 79−13143
charmed particle prod. and subsequent decay, complete ang. correl. calc. 77−49986
charmed vector mesons, ν inclusive prod. 77−18273
coherent π^0,p^0 meson prod., test for neutral weak currents of exotic space-time struct. 79−75715
cosmic ray heavy nuclei + emulsion nuclei, meson generation 77−61446
cosmic ray induced nuclear interactions, multiple meson production, total $E_\gamma > 2\times10^{13}$eV 79−58989
cosmic ray-nuclear emulsion collisions, ~20 GeV/nucleon, mean meson multiplicity and ang. distribs. 79−58988
cumulative hadron production, statistical bootstrap model with strangeness *(Russian)* 80−62948
cumulative production processes, phenomenological model for mechanism 78−58266
diffractive meson prod. 78−21416
diquark and quark jet fragmentation model, meson and baryon production 79−2979
e^+e^- → hadrons, 9.4-10.4 GeV, three Υ states, mass spacings, lepton pair widths 80−68465
electroproduction in correlating quark rearrangement model 80−86666
exclusive meson electroprod. on nucleon, cross section asymptotics, scaling functions *(Russian)* 79−22111
extended PCAC hypothesis, soft-meson chiral symm. breaking, pseudoscalar meson photoprod. 78−21353
fast mesons as dressed quark fragmentation products, Kuti-Weisskopf model 80−91061
fireball coplanar decay, 24 GeV/c proton-nucleus interaction 78−50157
hadron + hadron → meson + X, quark elastic scatt. as high transverse momentum meson source 77−57575
hadron collisions, high transverse momentum, nonscaling parton model 77−71483
hadron-hadron inclusive interactions, charmed particle production, η_c, ψ and other $c\bar{c}$ bound states 80−63036
hadron-hadron interactions, QCD appl. to meson and jet prod. 79−45076
hadron-nucleus collisions, relation between low mass dimuon and meson prods., quark-antiquark interactions 78−41477
hadronic charm prod. cross section and particle lifetimes, Monte Carlo anal. 78−89679
hadronic collisions, production of D- and ψ-mesons, QCD calc. *(Russian)* 79−9348
hadronic production of heavy quark bound states, quark fusion, fluon processes, for J/ψ, Υ prod. 79−349
hard scattering models comparison for large transverse momentum meson prod. 78−41498
heavy flavour prod. in e^+e^- annihilation, QCD contrib., inclusive quarkonium prod. 79−85267
heavy meson hadroproduction, QCD effect on scale breaking 80−37239
heavy quark prod., nonperturbative gluoprod. versus perturbative QCD fusion models, B and ψ 80−91058
heavy quark states, weak decays and prod., jet like distrib. in SU(2)×U(1) model 79−75746
Higgs meson prod., muon-number violation 78−41422
Higgs scalars, decay into vector mesons and photons 79−49442
high energy collisions, cumulative particle prod., parton recombination and quark-parton models 80−82956
high-transverse-momentum symmetric-particle-pair spectra and correlations 80−95250
hydrodynamic theory of multiple hadron production, new approach *(Russian)* 79−6332
inclusive coherent interference phenomena between pions in S-matrix theory 77−61206

meson production continued
inclusive J/ψ production in 43 GeV/c π⁻ on Be, Cu, W, A-depend. '78−62581
inclusive prod. in quark cascade model in pp, πp and e⁺e⁻ 77−50025
inclusive vector and tensor meson prod. in beam fragmentation region, Mueller-Regge formalism 78−17057
inclusive vector meson production in fragmentation regions of meson at small P_T 80−105931
inclusive vector meson production in triple Regge region, absorpt. corrections 78−93867
interference effects in identical high-energy prod. *(Russian)* 77−49938
isoscalar vector meson production in heavy lepton decay *(Russian)* 79−85349
I/Ψ production in NN interactions, failure of Drell-Yan parton model 79−89106
jets from quark fragmentation, flavour, power counting rules at x→1 78−37185
LAMPF, polarised ion facility 77−83377
large p_T, interrelation between πp and pp collisions 77−50030
large transverse momentum particle and jet prod., QCD approach 79−17761
meson-nucleon collisions, meson fragmentation region, meson spectra, quark cascade model 77−67689
missing mass counter experiment, non-reproducibility of data 77−22762
multiparticle production meson ratios, statistical quark model *(Chinese)* 79−49558
multiplicity prod. at large p_T, quark rearrangement model 77−61259
multipole moments for the study of mixed spin reactions 79−97611
non-zero charm mesons, inclusive prod. in meson-nucleon and nucleon-nucleon interactions *(Russian)* 77−14008
nonperturbative gluon jet model, gluon fragments, meson prod. 80−68420
nonstrange exotic meson production via baryon exchange, cross section upper limit meas. 77−50015
nuclear collisions, appl. of mesonic wakes in nuclear matter 77−6280
particle and antiparticle prod. by 200 GeV/c p is CERN SPS charged hyperon beam 79−71768
Pomeron-f identity scheme, vector meson prod. 78−12887
pseudoscalar meson prod. in triple Regge region, absorpt. corrections 78−78228
QCD, high transverse momentum meson prod. hadron-hadron collisions 78−45861
quark cascade model, appl. to meson spectra in e⁺e⁻ annihilation 78−41482
quark fragmentation functions in inclusive hadron muoproduction 79−67565
quark fragmentation into mesons, statistical model, vector meson contrib. 78−54639
quark generated meson jet, parametrisation of props. 78−58168
quark jet fragmentation, large momentum transfer reactions, implication of large vector meson prod. 79−345
quark model of heavy mesonic resonance prod. *(Russian)* 78−45881
quark model predictions of η and η′ prod. in multiparticle reactions 78−423
quark recombination model, meson and baryon prod. sum rules 80−4922
review of three years e⁺e⁻ research at SPEAR 79−63490
soft meson inclusive multiple prod., density matrix *(Russian)* 77−49929
strange axial vector meson non-diffracture prod. in Kp and πp interactions 80−32122
subnuclear structure concept via dilepton prod. in hadronic collisions, historical review 79−93365
t-flavoured meson production in photonuclear and pp collision 80−22623
TRIUMF meson factory, basic and applied research 78−21792
ultrapressure generation of mesons and neutrinos in plasmas and ion beams *(Russian)* 78−93920
VDM, radial excitations and q^2 depend., appl. to ψ radiative decay 78−452
vector boson pair photoprod., theoretical cross sections 80−57610
vector meson diffr. neutrino prod. calc., VMD model 77−61277
vector meson diffr. prod. in l+N reactions 77−34167
vector meson dominant prod. in pp inclusive interactions, 53 GeV 77−67685
vector meson emission, quark scatt., non-Abelian gauge theory *(Russian)* 78−45883
vector meson inclusive prod. cross section in hadron-nucleon collisions, parton transversal motion *(Russian)* 79−67617
vector meson production, 6 GeV, anomalous interaction mediator, e⁺e prod. data anal. *(Chinese)* 77−67664
vector meson production in pp interactions, constituent-interchange model 80−22579
A_1 diffractive prod. in νN→μN(πρ) 79−89143
A_1 meson in quark model and chiral symm. 78−12834
A_2^-, in π⁻p interactions, 9.8 and 18.8 GeV, decay ang. distribs. and differential cross sections 79−17754
C+p, 24 GeV, J/ψ prod. cross section 78−46055
c̄c q̄q states, decay, hadronic and photo-prod., e⁺e⁻ annihilation prod. 80−99092
$χ_c$ radiative decay, ψ and ψ′ prod., straton coupling constants *(Chinese)* 80−42467
D(1285)→δ(975)π D meson spin parity determ. 79−3052
D(1285)→δ(975)π D meson spin parity determ. 79−9410
D(1865) charmed meson hadronic prod., cross section limits from pN 79−89211
D and D* prod. from e⁺e⁻ annihilation, form factors and free quark model 78−37222
D charmed meson prod. from ψ(4.0 to 4.5 GeV) decay 79−17719
D meson prod. and decay in e⁺e⁻ at 4.03 , 4.41 c.m. energy 77−87989
D meson production by neutrinos, and $D^0 \to K_S^0 \pi^+ \pi^-$ 78−70354
D meson production in e⁺e⁻ annihilation, c quark fragmentation function *(Russian)* 79−85312
D mesons, prod. rates in e⁺e⁻ annihilation calc. 78−8668
D^0(1865) prod. anal. *(Chinese)* 78−487
D^0(1865) prod. from neutron interactions at 300 GeV/c 78−37244
D^0(1.865) production in proton-nucleus collisions at 400 GeV/c 78−13099
DD̄:DD̄*:D*D̄* prod. ratio in e⁺e⁻ collisions 77−6140
DD̄* production and decay, VDM, dual amplitude anal., e⁺e⁻ annihilation 77−49992
δ(980) scalar meson, prod. and decay props. 77−87975
e(μ)N, deep inelast. scatt. from polarised targets 78−25053

meson production continued
e⁻e⁺ annihilation, >2 GeV, production of charmed particles and charged τ lepton, review 78−17006
e⁺e⁻ → hadrons, quark existence and theory 80−37234
e⁺e⁻ → 1^{++} resonance states, direct production through neutral currents 78−93891
e⁺e⁻ annihilation, CM energies 29.90-31.46 GeV, narrow resonance search upper limit 80−63003
e⁺e⁻ annihilation, charmed axial vector meson prod., nonrelativistic quark model 78−25055
e⁺e⁻ annihilation, charmed meson pair prod., quark model of broken SU(8) symm. 77−38182
e⁺e⁻ annihilation, gluon jets, multiplicity and ang. distribs. asymmetries 80−91105
e⁺e⁻ annihilation, heavy vector meson prod., quark model estimations 77−18306
e⁺e⁻ annihilation, meson pair prod., multichannel formalism 77−22747
e⁺e⁻ annihilation, narrow resonance search upper limit at PETRA, 29.90-31.46 GeV 80−57618
e⁺e⁻ annihilation, prod. of orbitally charmed hadrons, free quark model anal. 79−22120
e⁺e⁻ annihilation, ratio of secondary baryon and meson yields and quark combinatorics *(Russian)* 79−49532
e⁺e⁻ annihilation at SPEAR, total hadron cross section, ψ prod., μe events 77−57548
e⁺e⁻ annihilation in upsilon region, quark model predictions 78−54640
e⁺e⁻ →charmed hadrons, quark mass effect on fragmentation functions 80−91098
e⁺e⁻ →charmed mesons, decoupling of highly excited vector mesons 77−87986
e⁺e⁻ → D^0, SPEAR expt. results 79−93444
e⁺e⁻ → $D^0\bar{D}^0 + x\pi^0 + y\gamma$, mixing of neutral spinless charmed mesons, decay, CP, violation tests 77−46067
e⁺e⁻ → D^+, SPEAR expt. results 79−93444
e⁺e⁻ → D̄D, above charm threshold at energy corresponding to ψ″(3770) 80−73723
e⁺e⁻ → e⁺e⁻ BB̄, cross-section from equivalent photon approx. 80−68467
e⁺e⁻ → e⁺e⁻ $χ_b$, cross-section from equivalent photon approx. 80−68467
e⁺e⁻ → e⁺e⁻ $η_b$, cross-section from equivalent photon approx. 80−68467
e⁺e⁻ → e⁺e⁻ $η_c$, two photon process, numerical distrib. studies 79−13142
e⁺e⁻ → e⁺μ± + anything by Ψ″(4.4)→Ω′Ω̄′, Ω′→Ξ⁰e⁻$\bar{ν}_e$ or Ξμ⁻$\bar{ν}_μ$, anomalous lepton prod. explanation 77−41834
e⁺e⁻ → η′(X^0)γ, generalised VMD theory 77−10268
e⁺e⁻ → F*, SPEAR expt. results 79−93444
e⁺e⁻ → FF̄(BB̄), τν decay signature for F± and B± detection 80−91099
e⁺e⁻ → F*F̄* → Fγ₁F̄γ₂, photon ang. correlations and prod. amplitudes 80−47319
e⁺e⁻ → γX, obs. at DORIS 80−102058
e⁺e⁻ → hadrons, fourth ϒ state observation in annihilation events 80−86737
e⁺e⁻ → hadrons, narrow resonance at 9.46 GeV 78−62415
e⁺e⁻ → hadrons, search for narrow resonances in mass region 1.42-1.92 GeV/c^2 79−17740
e⁺e⁻ → hadrons, ϒ, ϒ′, ϒ″ states, mass differences, leptonic width ratio 80−68466
e⁺e⁻ → hadrons, ϒ‴ observation at CESR, mass and leptonic width 80−86738
e⁺e⁻ → J/ψX, 4.0-5.0 GeV, Zweig rule violation 77−61305
e⁺e⁻ pair production, two photon processes at high energy 77−71524
e⁺e⁻ → π⁺π⁻, 4π, dispersion anal., ρ°(1250), ρ″(1600) prod. 78−8677
e⁺e⁻ → ψX, EM corrections, low energy theorem, unitarity, dispersion relations *(Russian)* 77−49982
e⁺e⁻ → ψX, estimate of inclusive ψ and $ψη_c$ prod., QCD anal. of cross section 79−85308
e⁺e⁻ → ψππ, radiative corrections, model estimates 77−10271
e⁺e⁻ →quarkonium state, D,F, ϒ mesons, importance as experimental tool in new particle searches 80−42425
e⁺e⁻ → $ρ^0$X, 1.45 to 1.61 GeV 79−63489
e⁺e⁻ → ρe, transition form factors, dispersion theory 79−63495
e⁺e⁻ → ρππ, radiative corrections, model estimates 77−10271
e⁺e⁻ → ϒ(9.46), electronic width determ., energy spectra for hadron inclusive production 79−26339
e⁺e⁻ → VX, parton model, polarisation effects *(Russian)* 80−63002
e⁺e⁻ → VX, polarisation states and differential cross sections for $πA_1$ and $ρ^+ρ^-$ *(Russian)* 80−102059
e⁺e⁻ → Vπ→π⁺π⁻π⁰, EM mixing effects, dynamics of vector meson prod. *(Russian)* 78−58191
eN→e meson boson, nature of gluons, spin, helicity struct. of amplitudes 77−18293
ep→epK⁺π⁺K⁻π⁻, 1.8, 2.1, 2.5 GeV/c^2, meson resonance observ. 80−82982
ep→epη, meas. in S_{11} (1535) reson. region 78−50038
ep→epη at S_{11}(1535) resonance, longit. to transverse cross sections ratio 78−78194
ep→epω, prod. by virtual photons, ω prod. to $ρ^0$ prod. ratio 79−6344
ep→epπ⁺π⁺π⁻π⁻, 1.8 GeV/c^2, meson resonance observ. 80−82982
ep→ep$ρ^0$ or eX, polarised beam and target, cross section asymm., vector-meson dominance model 77−6135
ep→ωp, ω prod. by virtual photon, ang. distrib., cross section 77−61302
η prod., 4-5.2 GeV, F, F* masses determ. 77−87988
η-η′ complex, quark-line rule in π⁺p→ηΔ⁺⁺, π⁻p→ηn, pp̄→π⁺π⁻η 77−30330
$η^0$, backward $ω^0$ and $η^0$ prod. in π⁻p interactions at 9 and 12 GeV/c 79−45100
$η_c$, production cross sections in e⁺e⁻ colliding beams, two-photon processes 79−36089
$η_c$ associated with gluon, hadronic prod. 80−105846
η′(958), spin-parity test from collinear prod. and decay 78−41543
f, in K⁻p at 32 GeV/c, vector and tensor meson prod., with quark model anal. 79−80854
f, multiparticle production in multiperipheral resonance model complemented by duality 79−36050
F charmed meson prod. from ψ(4.0 to 4.5 GeV) decay 79−17719
F-meson production, F⁻ → τ⁻$ν_τ(\bar{ν}_τ)$, beam-dump experiment, observation of $ν_τ$ interactions 80−22601
F-meson production suppresion relative to D-meson 79−36100
F-meson semileptonic decay modes, explanation of inclusive electron spectra 78−37202
f^0(1270) production in π⁻p→π⁺π⁻n, cross sections, decay density matrix elements 78−33095
γ*N→ψN, gluon momentum, spin, parity and coupling 80−42395

meson production continued
- $\gamma N \rightarrow \pi^+\pi^-\Delta$, EM mixing effects, dynamics of vector meson prod. *(Russian)* 78−58191
- γp, 30-180 GeV, ρ and ϕ elastic photoprod. cross sections 80−95278
- γp, 40-70 GeV, inclusive $\bar{D}^0$ photoprod. cross sections, pair and associated prod. 80−91097
- $\gamma p \rightarrow K^+K^-p$, 20-36 GeV, $\Phi(1019)$ prod., cross sections 80−105907
- $\gamma p \rightarrow \rho$+anything, 2.8, 4.7, 9.3 GeV, cross section, multiplicity, energy depend. 77−61303
- H+p, 24 GeV, J/ψ prod. cross section 78−46055
- J/4, in hadronic collisions, appl. of quark parton model 79−30715
- J/ψ, inclusive production cross sections, correlating quark rearrangement model 79−54320
- J/ψ hadronic prod. *(Chinese)* 78−8696
- J/ψ meson hadronic prod., role of ^{3}P charmonium states 77−22744
- J/Ψ prod., valence- and sea-quark distribs., deep inelastic scatt. and Drell-Yan processes 79−13069
- $KN \rightarrow K^*\Delta$, positivity conditions in joint vector-meson Δ prod. 77−13975
- K^-n reactions, quasi two-body final states at 8.25 GeV/c 79−22139
- $Kp \rightarrow Qp$, diffractive production, unitary analytic coupled channel model 79−36051
- K^-p, 32 GeV/c, exclusive reaction anal. in terms of multiparticle variables *(Russian)* 80−86757
- K^-p, η and ω prod. at 10 and 16 GeV/c 77−34191
- $K^-p \rightarrow 1^-3/2^\pm$, 4.2 GeV/c, hypercharge exchange, cross sections, momentum transfer depend. 77−71531
- $K^-p \rightarrow A_1$, 4.15 GeV/c, nondiffractive production, double-Regge model 80−78097
- $K^-p \rightarrow B^-Y^{*+}(1385)$, 8,25 GeV/c, quasi-two-body channel data 80−63023
- $K^-p \rightarrow f'(1514)\Lambda$, 4.15 GeV/c, cross sections, Λ polarisation, tensor meson density matrix elements 77−46077
- $K^-p \rightarrow \Delta D$, 4.2 GeV/c, D(1285) prod. and decay props. 79−49517
- $K^-p \rightarrow \Lambda\rho(760)$, transversity amplitude analysis 79−80847
- $K^-p \rightarrow \phi\Lambda$, $\omega\Lambda$, $\rho\Lambda$, $\phi\Sigma^0$, or $\rho\Sigma^0$, 4.2 GeV/c, cross sections, density matrix elements, hyperon polarisation 78−41580
- $K^-p \rightarrow \pi^+\Sigma^-$ 78−82239
- $K^-p \rightarrow \rho^-Y^+$, $Y^+ = \Sigma^+$ or $Y^{*+}(1385)$, 7 and 11.5 GeV/c, hyperon polarisation, vector meson decay angular distribs. 80−82997
- $K^-p \rightarrow \rho^-(760) + \Sigma^+(1385)$, amplitude anal. 79−97635
- $K^-p \rightarrow \rho^0$+anything, or f+anything, 10, 16 GeV/c, central and fragmentation contribs., quark model predictions 78−62467
- $K^-p \rightarrow \Sigma^-\pi^+\omega$, 4.2 GeV/c, B (1235) backward prod., $\pi^+\omega$ mass enhancement 78−89736
- $Kp^- \rightarrow X^0\Lambda$ anal. and $X^0(958)$ spin determ. 77−14010
- $K_L^0p \rightarrow K_S^0p(\pi^+\Lambda)(\pi^+\Sigma^0)(\pi^+\pi^0\Lambda)$, differential and polarisation cross sections near 550 MeV/c 79−17757
- $K_L^0p \rightarrow Q^0(\bar{Q}^0)p$, differential cross section slope, further Deck model anal. 80−73737
- μN, 209 GeV, ψ diffractive prod. cross section, $\psi \rightarrow \mu^+\mu^-$ decays 80−102054
- $\mu N \rightarrow \mu\Upsilon X$, 209 GeV, Υ muoprod. limits from trimuon final states 80−105909
- μ^+N, 280 GeV/c in Fe, Ψ virtual photoprod. 80−37279
- (N,N′X), shower proton and meson transverse momenta, intranuclear cascade model 80−102185
- $\bar{N}N \rightarrow (\pi, \rho, \omega, f)$, statistical model 80−102028
- $\nu(\bar{\nu})$-induced prod. of vector mesons and Higgs boson, muon prod. 78−82198
- νH_2, possible new meson or baryon reson. decay 77−240
- $\bar{\nu}H_2$-Ne, possible new meson or baryon reson. decay 77−240
- $\nu N \rightarrow e^-N\phi^+$, phi meson as light scalar boson in unified weak and EM interactions 79−17706
- $\bar{\nu}N \rightarrow \mu^+$+anything, Tanikawa-Watanabe meson prod. anal. 77−61274
- $\nu N \rightarrow \mu\mu X$, dimuon events, D prod., lifetime and fragmentation function 79−93397
- $\nu_\mu N$, $F^+(2030)$ prod. and hadronic decay $F^+ \rightarrow \pi^+\pi^+\pi^-\pi^0$, mass 80−91085
- νp high energy interactions, vector meson diffr. prod., charged and neutral current 78−54625
- νp interactions, charmed meson prod., Regge pole model, cross sections 78−33052
- $\nu p \rightarrow \mu^-D^+X$ or $\mu^-D^{*+}p$, cross sections estimation using V+A form of charm current 77−41839
- $\nu p \rightarrow \nu$+vector meson + X, neutral currents, generalised VDM, Regge pole anal. 78−41532
- ω, in K^-p at 32 GeV/c, vector and tensor meson prod., with quark model anal. 79−80854
- ω, prod. cross section in $pp \rightarrow e^+e^-X$ at 53 and 63 GeV 79−54365
- ω, production in $\bar{p}p$ annihilations, 0.70 to 0.76 GeV, effect on OZI rule 79−22124
- ω^0, backward ω^0 and η^0 prod. in π^-p interactions at 9 and 12 GeV/c 79−45100
- ω^0, production by charge exchange reactions, production cross section 78−58200
- p-nucleus, high energy reaction temp., kinematic props. of nuclear fragments 78−54761
- $p+Be \rightarrow e^+e^-X$, 30 GeV, J/ψ prod. and decay into e^+e^- 77−57570
- $p+Be \rightarrow \phi+X$, 400 GeV/c, ϕ decay modes, OZI rule 78−599
- $\bar{p}d$, 355-1066 MeV/c, total and annihilation cross sections, S meson search 80−68473
- pD, phenomenological relations between large-p_T meson spectra 79−26349
- $\bar{p}n$ annihilation, 5.55 GeV/c, meson resonance prod. and transverse spectra 79−93450
- pN in Fe, 400 GeV/c, bottom meson prod. search in multimuon final states 80−47334
- $pN \rightarrow NNf^0$, 7-24 GeV, isospin anal. 77−46083
- $pN \rightarrow NN\rho$, 7-24 GeV, isospin anal. 77−46083
- $\bar{p}p$, 100 GeV/c, inclusive meson and strange particle prod., energy partition 80−95289
- $\bar{p}p$, 355-1066 MeV/c, total and annihilation cross sections, S meson search 80−68473
- pp, 405 GeV/c, ρ^0, f, g^0, h meson prod., cross sections 80−105930
- $\bar{p}p$, azimuthal correlations at 22.4 GeV, ρ^0, Δ^{++} reson. prod. 79−67611
- pp, ISR energies, inclusive high p_T ω^0 and η' prod. 80−42504
- pp, phenomenological relations between large-p_T meson spectra 79−26349
- $\bar{p}p$, pp, 12-405 GeV, low p_T meson prod., quark-antiquark formation model 80−63056

meson production continued
- $\bar{p}p$, pp, 540 GeV, Υ and ψ transverse momenta from QCD 2→3 processes, gluon subprocesses 80−52546
- pp, probabilistic quark-model approach to p fragmentation 80−63049
- pp, secondary hadron absolute yield, L=1 meson prod., quark model *(Chinese)* 80−99113
- pp, total inclusive cross sections for δ^0, g^0, K^{*0} and $\bar{K}^{*0}$ at 53 GeV 79−17771
- pp, Υ production cross sections, colour excited states in Han-Nambu model *(Chinese)* 79−49480
- $\bar{p}p$ 12 GeV/c search for D, D* and λ_c charmed particles, charmed pair prod. 79−426
- $\bar{p}p \rightarrow 2\pi^+2\pi^-$, 5.7 GeV/c, pion ang. distribs., ρ^0, f^0, prod. rates 77−2857
- $pp \rightarrow (\pi^\pm$ or $K^\pm) + X$, fast-meson production and the recombination model, proton multiquark structure functions 79−89208
- pp collisions, azimuthal correl. of high $\rho_T\pi^0$ and η with second π^0 79−85347
- $pp \rightarrow D\bar{D}+X$, upper limit for $D\bar{D}$ prod. at 55 GeV 78−89758
- $pp \rightarrow D$+anything, parameter free exchange model 77−10293
- $\bar{p}p \rightarrow F_1\omega$, F_1 spin-parity anal., boson spin tests from sequential decays 78−29345
- pp inclusive interaction, 30 to 50 GeV η meson prod. 80−5023
- pp inclusive interactions, narrow vector meson hadroprod., ϕ, J, ψ, charmoniumlike states 77−57573
- $\bar{p}p$ inclusive prod. of π^-,η,ρ^0,ω,f, mesons at 0.7 GeV/c 77−65170
- pp interactions, charged secondaries, 69 GeV/c ^{1}, transverse momentum and rapidity distribs. 79−9409
- pp interactions, charmed D^+ prod., total cross section, $D^+ \rightarrow K^{*0}\pi^+$ observation 79−36102
- pp interactions, effects of hard gluon bremsstrahlung in dimuon and Υ prod., QCD anal. 79−13058
- $pp \rightarrow J/\psi X$, OZI rule violation 79−58929
- $\bar{p}p \rightarrow K\bar{K}\pi\pi\pi$, 700-760 MeV/c, D(1285) an E(1420) resonance prod. 78−54646
- $\bar{p}p \rightarrow K^*(890)X$, S^* (993)X, 12 GeV/c, prod. cross sections 78−93911
- $pp \rightarrow$meson+lepton pair, transverse momentum distrib. and branching ratios, proton gluon distribution 80−52537
- $pp \rightarrow$mesons, multimeson inclusive spectra and recombination model, multiquark structure functions 80−73751
- $pp \rightarrow \mu^+\mu^-X$, 62 GeV, ψ and γ cross sections, scaling function 80−105932
- $\bar{p}p \rightarrow$neutral meson+$\pi^+\pi^-$, or neutral meson+$\bar{p}p$, 7.2 GeV/c, quark model anal. 78−41561
- $pp \rightarrow p\pi^+n$, 800 MeV, Δ^{++} prod. and cross sections 79−22294
- $pp \rightarrow \phi X$, OZI rule violation 79−58929
- $pp \rightarrow \pi^+\pi^-X$, 405 GeV/c, indictive ρ^0 and f meson prod. 79−45111
- $\bar{p}p \rightarrow \pi^+\rho$, 6 GeV/c, differential cross sections, line reversal symmetry test for baryon exchange 78−78202
- $\bar{p}p \rightarrow \pi^+\rho^-$, 6 GeV/c, line reversed reaction, Δ exchange, ρ decay 78−12926
- $pp \rightarrow \psi X$ 70 GeV to ISR energies, pion exchange model anal. *(Russian)* 79−40823
- $pp \rightarrow \psi X$ or $\bar{p}p \rightarrow \psi X$, J/$\psi$ prod. mech., p gluon distrib. determ. 79−430
- $pp \rightarrow \psi$+anything, parameter free exchange model 77−10293
- $pp \rightarrow \psi\gamma$, inclusive prod. anal. 78−25091
- $pp \rightarrow \rho^0X$, OZI rule violation 79−58929
- $pp \rightarrow \rho^0X$, study of ρ^0 prod. using Heisenberg uncertainty relation *(Russian)* 79−49560
- $\bar{p}p \rightarrow \rho^0$+X, 22.4 GeV/c, cross section, average transverse momentum 78−62468
- $pp \rightarrow \rho^0$+X, $S^{1/2}$=23.6 to 63.0 GeV, inclusive cross section meas. 79−75805
- $pp \rightarrow \rho^0$+n charged, 300 GeV/c, high multiplicity search 77−22807
- $\bar{p}p \rightarrow \rho^0\rho^0,\omega\rho^0,\rho^0f$, or ωf, T(2200) region, partial wave anal. 77−34171
- $\bar{p}p \rightarrow V^0\pi^0 \rightarrow e^+e^-\pi^0$, annihilation at rest, heavy vector meason prod., ρ' (1250), ρ'' (1600) existence 77−13971
- ϕ, in K^-p at 32 GeV/c, vector and tensor meson prod., with quark model anal. 79−80854
- ϕ, prod. cross section in $pp \rightarrow e^+e^-X$ at 53 to 63 GeV 79−54365
- ϕ, production in $\bar{p}p$ annihilations, 0.70 to 0.76 GeV, effect on OZI rule 79−22124
- ϕ inclusive and semi-inclusive prod. in thermodynamic model 77−18238
- ϕ prod., Zweig suppression and statistical factors 77−46025
- (π^-, ψ $C\bar{C}$), $\psi \rightarrow \mu^+\mu^-$, $C\bar{C} \rightarrow \mu^\pm\nu X$, 225 GeV/c, search for extra μ 80−82967
- π-Be, associative production of D^0 mesons, with muons 55 GeV/c *(Russian)* 79−3060
- π^0/η prod. ratio at high transverse momenta 78−41602
- π^+ N 200, 280 GeV on Pt target, γ resonance prod. 79−93460
- π^-+C(Al)(Cu)(Pb)(H), 3.7 Gev/c, incoherent prod. of ρ^0 mesons *(Russian)* 78−33084
- π^- +nucleus→$\pi^+\pi^-\pi^-$+nucleus, 8.9, 12.9, 15.1 GeV/c, resonance behaviour of coherently prod. A_1, A_3 mesons 78−50047
- $\pi^\mp U$ interaction at 55 GeV/c, search for long lived heavy mesons *(Russian)* 80−5029
- $\pi^-Be \rightarrow D^0\bar{D}^0X$, pair production at 55 GeV/c *(Russian)* 79−3059
- $\pi N \rightarrow A_2N$, ρ and f Regge exchanges, an interpretation 79−63531
- π^-N, 40 GeV/c, leading and conserved mesons *(Russian)* 78−45987
- $\pi^-n \rightarrow p\pi^-\pi^-\pi^0$ or $\rho^-\pi^-p$, 5, 9 GeV/c, model independ. anal. of final states 78−25071
- $\pi^-N \rightarrow \psi X$, 225 GeV, bottom meson pair production limit 80−73750
- $\pi^-N \rightarrow \rho^0(\omega)X$ at 40 GeV/c, cross sections 77−18359
- $\pi^\pm N \rightarrow \omega(N,\Delta)$, EM mixing effects, dynamics of vector meson prod. *(Russian)* 78−58191
- $\pi^\pm N \rightarrow \rho^\pm\gamma N$, bremsstrahlung in vector meson prod. at high energy *(Russian)* 79−80851
- $\pi p \rightarrow (\rho\pi)p$, A_2 diffractive prod., Deck model and Pomerons 79−71733
- $\pi p \rightarrow \psi X$, 70 GeV to ISR energies, pion exchange model anal. *(Russian)* 79−40823
- π^-p, 100 GeV/c, inclusive meson and strange particle prod., energy partition 80−95289
- π^-p, 150 GeV/c, leading particles and diffraction dissociation, 2-, 4- and 6-prong events 80−68486
- $\pi^-p \rightarrow (\pi^+\pi^-\pi^0)n$, 12, 15 GeV/c, partial wave anal. of neutral 3π system, A-meson prod. 78−58207
- $\pi^-p \rightarrow \chi n$, 40 GeV/c, prod. of $\chi(2.85)$ particles *(Russian)* 78−45963
- $\pi^-p \rightarrow D^0\bar{D}^0n$, 40 GeV, D^0 hadronic decay search for associated prod. of charmed particles 77−13990
- $\pi^-p \rightarrow D^0\bar{D}^0n$, 40 GeV/c, search for associative prod. of charmed hadrons *(Russian)* 77−6178

meson production continued
$\pi^- p \to \eta^0 n$, 3.3 GeV/c, differential cross section, helicity-flip amplitude *(Russian)* 78−45945
$\pi^- p \to \eta' n$, cross-section over momentum range 15 to 40 GeV/c *(Russian)* 79−89194
$\pi^- p \to \eta' n$, Regge pole model with phenomenological residue functions 80−102077
$\pi^- p \to \eta\eta n$, 40 GeV/c, production cross sections and $\eta\eta$ angular distribs. *(Russian)* 78−78223
$\pi^- p \to \eta\eta n$, 1171 to 2267 MeV/c polarised cross section meas., partial wave anal. in resonance region 79−89182
$\pi^- p \to \eta n$, 15 to 40 GeV/c, study of $\eta \to 2\gamma$ 79−58978
$\pi^- p \to f^0 X$, tensor meson prod. in triple Regge region, cut corrections 77−46087
$\pi^- p \to \gamma\gamma n$, search for η_c 79−22150
$\pi^- p$ inclusive interactions, ρ^0, ω, f-mesons prod. cross section *(Russian)* 78−33098
$\pi^- p$ interaction, Δ exchange, 4 GeV/c 78−74275
$\pi^- p \to K_S^0 K^- p$, 10 GeV/c, spin 4 meson reson. prod. 78−50050
$\pi^- p \to K^- K_S^0 p$, 10 GeV/c, isospin 1 meson reson. prod. 78−50051
$\pi^- p \to K^- K^0 p$, 10 GeV/c, A_2 and g reson. prod. 78−82230
$\pi^- p \to K^+ K^- n$, 10 GeV/c, obs. of new structure in K^+K^- system at 2.20 GeV, width approx. 200 MeV 79−80843
$\pi^- p \to$meson pair + X, 11.2 GeV, longit. and azimuthal correls. 77−6180
$\pi^- p \to n\epsilon^0$, 1.3 to 3.8 GeV/c, differential and total cross-sections 80−83000
$\pi^- p \to n\pi^- \pi^- \pi^+ \pi^+$, 12 GeV/c, Δ^-, ρ and f prod., baryon exchange 79−423
$\pi^- p \to n\pi^- \pi^+$, 12 GeV/c, ρ and f prod., differential cross section, baryon exchange 79−423
$\pi^- p \to n\pi^- \pi^+ \pi^0$, 12 GeV/c, ω prod., differential cross section, baryon exchange 79−423
$\pi^- p \to \omega n$, 20-200 GeV/c, prod. cross section, Regge formalism test 77−26546
$\pi^- p \to \omega n$, c.m. momentum 40 to 200 MeV/c, cross section meas. 79−75789
$\pi^- p \to \omega n$, Reggeon cuts and reaction description *(Russian)* 78−45947
$\pi^- p \to \omega\pi^- p$, 11.2 GeV/c, partial wave anal. of g-meson prod. 78−78220
$\pi^- p \to p_{fast}\pi^+\pi^-\pi^-$, 9, 12 GeV/c, backward meson prod., quasi two body processes, A_1, A_2 prod. 79−413
$\pi^- p \to p\pi^- \pi^0$, 9 and 12 GeV/c, backward e^- prod. 78−8704
$\pi^- p \to p\rho^-$, 6 GeV/c, line reversed reaction, Δ exchange, ρ^- decay 78−12926
$\pi^- p \to \phi n$, 1.6-2.0 GeV/c, total cross-section 77−87998
$\pi^- p \to \phi n$, quark line rule, violations 80−52530
$\pi^- p \to \phi\phi n$, 22.6 GeV/c, cross section meas. 78−37242
$\pi^- p \to \pi^- \phi p$, 10 GeV/c, prod. cross section meas. 77−65174
$\pi^- p \to \pi^- \pi^- \pi^+ \pi^0 p$, 11.2 GeV/c, anal. of $\omega\pi^-$ system prod. 77−88012
$\pi^- p \to \pi^+ \pi^- \pi^0 n$, 12, 15 GeV/c, prod. of A_2^0 (1310) and ω^* (1675) 78−74283
$\pi^- p \to \psi n$, 8.2-9.8 GeV/c, upper limit on prod. cross-section determ. 78−41578
$\pi^- p \to \rho^0 + X$, 100-360 GeV, cross sections 79−40816
$\pi^- p \to \rho^0 n$, 17 GeV, polarised target, partial wave analysis 79−45106
$\pi^- p \to \rho^0 n$, Reggeon cuts and reaction description *(Russian)* 78−45947
$\pi^- p \to X^- p$, background produced near δ meson mass region 79−36096
$\pi^- p \to X^0 n$, $X^0 \to \gamma\gamma$, 15 and 40 GeV/c, cross sections *(Russian)* 77−34183
$\pi^- p \to Xn$, 40 GeV/c, X(2.85)$\to 2\gamma$ obs. 78−25047
$\pi^+ p$, inclusive yields, transverse spectra, of nonstrange mesons, quark model 78−4886
$\pi^+ p \to (\rho^0, \omega)\Delta^{++}(1238)$, q_L=7.1 GeV/c, role of new exchanges *(Russian)* 79−54355
$\pi^+ p \to f + X^{++}$ 8 GeV/c, reaction anal. 79−93457
$\pi^+ p \to K^+ \Sigma^+$, exchange degeneracy in hypercharge exchange reacts. 78−41581
$\pi^+ p \to K^+ \Sigma^+$, exchange degeneracy in hypercharge exchange reacts. 78−82239
$\pi^+ p \to$meson resonances, 15 GeV/c, SLAC bubble-chamber expt. 78−41595
$\pi^+ p \to \pi^+ p\pi^0$, p diffractive dissociation, ρ^+ prod., one-pion-exchange model 78−21451
$\pi^+ p \to \rho^0 \Delta^{++}$ or $\omega\Delta^{++}$, positivity conditions in joint vector-meson Δ prod. 77−13975
$\pi^+ p \to \rho^0 \Delta^{++}(1236)$ or $\omega\Delta^{++}(1236)$, 10.3 GeV/c, cross-section meas. 78−82248
$\pi^+ p \to \rho^0 X^{++}$, 8 GeV/c, reaction anal. 79−93457
$\pi^+ p$, 16 GeV/c, $\delta(970)$ and D(1285) prod. and decay, branching ratios 77−46084
$\pi^+ p$, η and ω prod. at 10 and 16 GeV/c 77−34191
$\pi^+ p$, inclusive meson prod. with large transverse momentum, effective gluon model 78−8717
$\pi\pi \to \pi\pi$, p-resonance production, quasipotential approach, linear σ-model 80−86755
$\pi\rho$ scatt. amplitude asymptotic limit, sum rules, predicted resonance with A_1 meson quantum numbers *(Russian)* 78−78214
ψ, production and decays, probability calcs. *(Chinese)* 77−65153
$\psi(4.03) \to D\bar{D}$, suppression problems, model-independent approach 80−52494
$\psi(4.42) \to D\bar{D}$, suppression problems, model-independent approach 80−52494
$\psi(4.42) \to F\bar{F}$, suppression problems, model-independent approach 80−52494
ψ associated with gluon, hadronic prod. 80−105846
$\psi \to \eta\gamma$, conflict with single parameter scheme for radiative decays of vector mesons 80−86720
$\psi \to \gamma f$, tensor dominance for γ decays of new particles 78−66112
ψ hadronic prod., lepton pair ang. distribs., cross section χ contribution from πN, pN, $\bar{p}N$ 80−42487
ψ hadronic production, gluon contrib. in QCD framework 78−78139
ψ hadronic production of heavy quark bound states 79−63435
ψ meson hadronic prod., P-state dominance 77−46024
ψ prod., multimuon events in $\pi(p)$+nucleus reactions 77−30460
ψ prod., Zweig suppression and statistical factors 77−46025
ψ prod. cross-sections in pp collisions at E_{cm}=23-63 GeV 77−57572
ψ prod. in pp and πp inclusive interactions, quark energy distrib. 77−22813
ψ production, gluon-gluon fusion model, gluon distrib. x-depend. 80−62922
ψ production cross-sections by $\pi^\pm$, $K^\pm$, p, and $\bar{p}$ beams at 39.5 GeV/c 77−57571
ψ to charm particles, 1975 and 1976, e^+e^- colliding beam technique *(Polish)* 78−74297
ψ/J and ψ' production in hadronic collisions, quark-antiquark annihilation, cascade process 78−25013
$\psi''(4.028) \to D\bar{D}$, or $\bar{D}D^* + \bar{D}D^*$ or $D^*\bar{D}D^*$, strong decay theory, radial excitation of charmonium 78−12909
$\psi\psi$ prod., correl. effects in large p_T pion events 77−26549
Q production in $\pi^- p$ and $\bar{p}p$, Breit-Wigner parameters, decay modes 77−57560
$q\bar{q}$ recombination model with resonance prod. 79−75740
ρ, prod. cross section in $pp \to e^+e^-X$ at 53 to 63 GeV 79−54365
ρ diffractive muoproduction in μp reactions at 147 GeV 77−30391
ρ reson. prod., N/D calc. 77−71461
ρ-meson production and charged-neutral correlations in high energy pp interactions 79−17760
ρ^0, in $K^- p$ at 32 GeV/c, vector and tensor meson prod., with quark model anal. 79−80854
ρ^0, multiparticle production in multiperipheral resonance model complemented by duality 79−36050
ρ^0, production by charge exchange reactions, production cross section 78−58200
ρ^0-electroproduction, parity violating effects 80−9178
ρ^+, ρ^-, ρ^0 inclusive prod., cross sections, quark model, $\pi^+ p$, pp interactions 78−93912
$\rho'(1600)$ meson resonance from 2- and 4-pion distribs. in photoproduction data 80−95279
$\Sigma^\pm(1385)$, masses and width determ. from partial wave anal. of $K^- p \to \pi^- \Sigma^\pm$ 78−54653
Υ, hadron production of heavy quark bound states 79−63435
Υ, narrow high mass resonance formation in e^+e^- annihilation at 9.46 GeV, heavy $q\bar{q}$ bound state 78−62414
Υ, production and decay in quark fusion model 80−102018
$\Upsilon(9.46)$, prod. in e^+e^- interaction at DORIS, quark parton model agreement 79−93443
$\upsilon(9.5)$, prod. in e^+e^- annihilation, photoprod., decay modes, quark model 78−12877
$\Upsilon(9.5)$ hadronic prod., parton distrib. and QCD 78−78142
Υ flavoured vector mesons, production in e^+e^- annihilation at DORIS energies 78−93890
Υ production, photon-gluon fusion model, gluon distrib. x-depend. 80−62922
$\Upsilon'(10.02)$, prod. in e^+e^- interaction at DORIS, quark parton model agreement 79−93443
$W^\pm$ production in π, p scattering in nuclear Coulomb field, cross section calcs. *(Russian)* 77−46086
W+p, 24 GeV, J/ψ prod. cross section 78−46055
Be+p, high transverse momentum scatt., two particle correlations and ϕ prod., jet trigger 78−78225
Be(π^-, Ψ), 43 GeV, A dependence of inclusive distrib. *(Russian)* 78−45983
C+p, C+$\pi^\pm$, 225 GeV/c, J/ψ and $\psi'(3.7)$ prod. study using muon pair meas. 77−57694
$^{12}C + \pi^-$, 40 GeV/c, leading and conserved mesons *(Russian)* 78−45987
Cu(π^-, Ψ), 43 GeV, A dependence of inclusive distrib. *(Russian)* 78−45983
Cu(π^-, ψ' (3700)), 50 GeV, formation cross-sections *(Russian)* 80−106082
$^1H(p,p\pi^+)n$, 800 MeV, Δ^{++} prod. and cross sections 79−22294
$pp \to D^+ X$, 53 GeV, $D^+ \to K^- \pi^+ \pi^+$ *(Polish)* 80−9187
Sn+p, Sn+$\pi^\pm$, 225 GeV/c, J/ψ and $\psi'(3.7)$ prod. study using muon pair meas. 77−57694
W(π^-, Ψ), 43 GeV, A dependence of inclusive distrib. *(Russian)* 78−45983
Xe+π^-, 3.2 GeV/c, π^0, η, ω, f meson prod. determ. of meson-N total cross sections *(Russian)* 79−22122

meson resonances
see also D mesons; eta meson resonances; omega mesons; phi mesons; psi mesons; rho mesons
0^- meson, EM form factor in straton model *(Chinese)* 80−22616
0^--mesons in broken SU(4), improved mass formula 77−30352
1.87 GeV/c^2 states, evidence for parity nonconservation in decays 77−10245
3^{--}, 4^{++}, 5^{--} mesons, 2.0 to 2.6 GeV/c^2, evidence from $\bar{p}p$ elastic scatt. 77−74712
27-plet mesons, mass sum rules using SU_4 dynamical-group scheme 77−26505
$\pi^- p \to \delta^- p$, $\pi^+\pi^-\pi^-\gamma\gamma$ backgrounds produced near the δ^- mass region 80−9182
additive quark model with six flavours 80−27455
asymptotic SU_5 and a new mass constraint for the ω, ϕ, ψ and Υ mesons 79−36001
axial vector meson model, quasi-renormalisation using BPHZl approach 80−13208
axial vector mesons, three body decays, rel. between D(1285) and $A_1(J^P = 1^{++})$ 78−78176
axion, appearance in $k \to \pi^+$ + axion 78−33064
axion, implied by U(1) symm. 78−33037
bag model, string like solns., baryon-antibaryon states mass formulae *(Russian)* 79−93369
baryonium, broad resonance states, S(1963), T(2190), U(2350), expt. evidence review 78−89764
baryonium, connection between exchange-degeneracy breaking and multi-quark states 79−93387
baryonium, empirical evidence and theoretical interpretation review 80−42394
baryonium, exotic nuclear state or four quark boson resonance? 79−325
baryonium, geometrical approach 80−91065
baryonium, ground state hyperfine splitting, harmonic oscillator potential anal. 80−68422
baryonium, mass and selection rule, string model 78−29319
baryonium, molecular model, quark-diquark picture of baryon 80−27462
baryonium, narrow states, mass formula, selection rule, quark model 78−66089
baryonium, nuclear and quark confinement forces 80−68431
baryonium, quasinuclear, annihilation level widths in coupled-channel problem *(Russian)* 79−93476

meson resonances continued
baryonium, review of QCD, duality, string models and bag models 78−78135
baryonium, S-matrix representation 80−399
baryonium, Schwinger partial symmetry, quark flavour EM interaction 79−93335
baryonium, SO_4 symmetry for classification 79−97531
baryonium and exotic baryons, SU(4) Clebsch-Gordan coeff. 79−75739
baryonium and nonexotic hadron trajectories from a color-dependent potential 80−13286
baryonium dual S-matrix approach 80−52526
baryonium exchange, evidence from pp and $p\bar{p}$ reactions, total cross section differences 78−66171
baryonium four body problem, Schrodinger eqn. soln. by stochastic variational method 79−36008
baryonium interaction, dual amplitudes 78−25022
baryonium interactions, string model, dual amplitudes *(Russian)* 78−54620
baryonium mass spectrum in planar bootstrap model 78−25020
baryonium masses in a quark model 80−37241
baryonium model, spectrum of $qq\bar{q}\bar{q}$ hadrons 78−62363
baryonium model from $qq\bar{q}\bar{q}$ hadron spectrum, T- and M-diquonium 78−58172
baryonium muliquark system model of fireball, high energy pion production 79−97603
baryonium Regge trajectories exchange in medium and high energy scatt., expt. evidence 78−50022
baryonium spectroscopy based on duality and unitarity 79−58947
baryonium states in QCD, review 80−102001
baryonium width, string-junction model 79−58928
beauty and charm photoprod. in QCD, $q\bar{q}\rightarrow b\bar{b}$ or $c\bar{c}$ mechanism 80−32079
beautyonium bound states, Υ, Υ', Υ'', dispersion sum rules *(Russian)* 80−13235
binary decays, centrifugal effects *(Russian)* 78−17012
bottom meson nonleptonic decay, many body final states, isospin-statistical models 80−62975
bottomium, potential models, non-relativistic description 80−68426
Brayshaw and Peierls mechanisms for generating hadron peaks, N*(1470), 0(1020) and charm 79−404
bremsstrahlung of vector mesons induced by nuclei *(Russian)* 78−78424
C-exotic mesons, molecular charmonium 77−71487
channel coupling effects and resonance phenomena in pp interactions, N/D eqn. study 79−71765
charged vector meson electrodynamics *(Russian)* 78−66057
charged vector mesons, Compton scatt. cross section meas. 79−22102
charm particle, production in high energy ν-induced reaction, lifetime determ. 79−26426
charm particle spectroscopy 80−73680
charmed axial vector meson prod. in e^+e^- at $\sqrt{S}\simeq 4.1$ GeV 77−13969
charmed baryons, Regge spectroscopy 77−38148
charmed mag. moments determ., SU(8) symm. 78−4794
charmed meson mass calc. 77−10231
charmed meson weak nonleptonic decay, SU(2) and SU(6) models 77−26521
charmed mesons, dynamic SU(4,1) symmetry, mass spectra, anal. *(Russian)* 78−70350
charmed mesons, props. determ. from two-step pot. model 77−74682
charmed mesons and charmoniums, masses and mixing, OZI rule breaking 78−12889
charmed particle production from two-gluon annihilation in proton-proton collisions 79−347
charmed particle semileptonic decays 79−63473
charmed particles lifetime, semileptonic decay rate calc. 79−9366
charmed-strange exotic mesons, quark model 77−87946
charmonium, $^1P_1$ state, mass, branching ratios, decay rates 78−62370
charmonium, ψ and χ states, hyperfine struct. 78−12878
charmonium, mass in QCD 80−105867
charmonium, potential models, non-relativistic description 80−68426
charmonium, radially excited states, small Q-value channel dominance in decay 79−54335
charmonium decay, effective strong coupling constant for timelike Q^2 80−99091
charmonium mass spectrum using oscillator pot., Υ and Υ' masses 79−97595
charmonium model, tensor force affects on ψ' and χ 77−87943
charmonium model and the ψ and Υ families 80−47253
charmonium narrow states, hadronic and EM decays 78−70343
charmonium quark-antiquark pots., flavour independ., γ, γ', ψ and ψ' appls. 80−47254
charmonium resonances above open charm threshold, nonrelativistic quark model 80−78039
charmonium states with small hyperfine splitting, coupling constants 79−97599
chiral SU(4)×SU(4) breaking scheme, vector mesons radiative decays 79−22099
colour confining forces and effects saturation 80−73672
colour model, mass splittings of heavy mesons and baryons *(Chinese)* 78−78146
composite heavy quarks, Υ and Υ' structure 79−36020
Coulombic $q\bar{q}$ bound states, short range behaviour, quark mass 80−78033
coupling strengths and renormalization scale parameter in QCD by dimensional transmutation 79−6316
cryptoexotic states of the four-quark system 79−40762
current induced reactions, conf. 77−34106
DC K^+p, 32 GeV/c, resonance inclusive prod. cross sections, quark model comparison 78−93913
decay constants, smoothness and spin-zero charm mesons in broken chiral SU(4)×SU(4) symmetry 79−58900
decay of heavy vector mesons, heavy lepton prod. 77−87974
Deck model, rescattering effects for diffr. dissociation of hadrons 78−4844
dibaryon resonances, pp phase shifts 79−63540
dibaryon resonances in πNN and $\pi\pi$NN dynamics 79−75862
dibaryon resonances in NN scatt. 80−57605
dibaryon resonances in pp system, Pure spin total cross sections 79−63539
diffractive neutrino prod. of charged vector mesons, VMD model 77−61277
meson resonances continued
diffractive scatt., pomeron and f exchange in elastic and inelastic scattering 79−36049
dihadron mass continuum and narrow resonance prod. in p-Be, 400 GeV interaction 78−33178
dimuon enhancement at 9.5 GeV, vector meson family with hidden 'beauty' *(Russian)* 78−33030
diquark constituents of baryons and baryonium 79−93383
diquark model and baryonium, location of mesons with exotic quantum numbers 79−63436
discrete charm of new resonances 77−34129
dual spectrum elasticities, multipion channel coupling 77−38136
dual unitarisation scheme for baryon and baryonium states with string junctions 78−25021
dyonium Hamiltonian on S^3 sphere, gauge invariant formalism 80−27460
$e^+e^-\rightarrow$hadrons, 9.4-10.4 GeV, three Υ states, mass spacings, lepton pair widths 80−68465
eight quark model, modified left-handed currents, ν reactions and e^+e^- annihilations 78−16982
elementary length and time in the strong interaction, meson reson. width data 78−82189
EM decays and props. of stratons *(Chinese)* 78−29336
energetic delayed hadrons in air showers, possible new massive particle 79−75065
exotic meson ($Q^2\bar{Q}^2$) spectroscopy, instanton effects 79−89140
exotic mesons and p-$\bar{p}$(e^+-e^-) annihilation 78−21393
exotic NN resonances, joined spring model, Bose quark model anal. 79−89120
extended Regge trajectories, modified Chew-Frautschi plot for meson and baryon resonances 78−82176
f^0(1270) prod. cross section in 53 GeV pp inclusive interactions 77−30462
f-mesons, spin 2 coupled with other field, effect on nuclear force in nucleon-nucleon interactions 78−514
finite nuclei, constrained variational calcs. for binding energy and RMS radii, N*(1234) allowance 79−3074
flavour independence of forces between quarks, ψ and Υ spectra 80−22569
four quark mesons, recoupled wave functions, phase inconsistency 80−68425
ghost-pole subtraction and the σ-exchange NN potential 80−86819
gluon and quark jets in a recursive model motivated by quantum chromodynamics, Υ decay 80−62936
gluonic bound states, masses and decay widths, X(2.8) as possible candidate, $\gamma\gamma$ decay 79−93364
gluonic resonances in hadronic spectrum, scalar mesons, pomerons 78−21394
hadron induced multiparticle reactions, S-1500 GeV, resonance prod. correlations, jet model *(German)* 80−91118
hadron lepton model interpretation of particle resonance states 80−4957
hadron resonance decay, intermediate vector boson and high energy weak interaction detect. 79−22012
hadronic and electromagnetic widths of mesons in the style schemes, Sp(8) and SO(8) schemes 79−45051
hadronic coupling constants and the nonrelativistic quark model with charmonium potential 80−37207
hadronic production of heavy quark bound states, quark fusion, fluon processes, for J/ψ, Υ prod. 79−349
hadronic resonance props., consideration as compound of bradyons and tachyons 78−58163
harmonically confined $q\bar{q}$ system, relativistic wave eqn. 80−95247
heavy 1^{--} quark-antiquark bound state decays, fast gluons 79−85297
heavy 1^{--}-onia, two-jet cross section in perturbative QCD 79−93357
heavy charged quark system decays, CP noninvariance, six-quark model/QCD anal. 79−80826
heavy flavour prod. in e^+e annihilation, QCD contrib., inclusive quarkonium prod. 79−85267
heavy flavoured meson decays, charged Higgs bosons 79−22014
heavy Higgs scalars, in $SU(2)_L\times SU(2)_R\times U(1)$ gauge theory, no decoupling at low energy 79−13018
heavy meson inclusive semileptonic decays, lifetime estimates, quark-parton model difficulties 80−86704
heavy neutral mesons, parity determ. 80−37264
heavy quark bound states of top quark and antiquark pairs, QCD test 80−68430
heavy quark mesons, inclusive hadronic prod. *(Russian)* 80−86770
heavy quark prod., nonperturbative gluoprod. versus perturbative QCD fusion models, B and ψ 80−91058
heavy quark states, weak decays and prod., jet like distrib. in SU(2)×U(1) model 79−75746
heavy quark system prod. in QCD, duality predictions 79−13074
heavy quark-antiquark bound states, short distance anal., appl. to ψ and Υ 79−93345
heavy quark-antiquark bound states, short distance anal., diagrammatics 79−89103
heavy quarkonium decay in the presence of instantons 79−85296
heavy quarkonium decays, renormalisation group approach, exclusive two meson and inclusive decays 80−82972
heavy quarkonium states, hadronic transitions, QCD anomalies for Υ'' and ψ' 80−105888
heavy quarks, widths of neutral vector mesons 78−8602
heavy quarks and new particles 80−73661
heavy vector meson annihilation rate to lepton pairs, hadronic corrections 80−4943
heavy vector meson annihilation to lepton pairs, hadronic corrections 80−68424
heavy vector meson photoprod., vector meson dominance model anal., Regge trajectories 78−78195
heavy vector meson weak decays 79−13110
heavy vector mesons, decay into Higgs particles 78−12908
heavy vector mesons associated with Υ(9.4) and the nature of Υ'(10) 78−82187
heavy-quark content of light hadrons, implications for Υ-family 78−93853
Higgs bosons in SU(2)×SU(2)×U(1) left-right gauge field, coupling strength 79−13017
Higgs scalars, decay into vector mesons and photons 79−49442
high energy meson elastic scatt. amplitude, leading term approx. in SU(2) Yang-Mills theory 80−5017

meson resonances continued
high energy vector meson scatt., two to three body, in Yang-Mills theory 78−17051
high spin, natural parity, dual reson. model with nondegenerate Regge trajectories 79−359
high-mass resonance enhancement by large transverse momenta selection 77−28?1
inclusive vector and tensor meson prod. in beam fragmentation region, Mueller-Regge formalism 78−17057
inclusive vector meson production in fragmentation regions of meson at small P_T 80−105931
inclusive vector meson production in triple Regge region, absorpt. corrections 78−93867
inverted charmed meson multiplets as a test for scalar quark confinement 78−70325
isoscalar vector meson production in heavy lepton decay *(Russian)* 79−85349
isospin-violating mixing in meson nonets, $d\bar{d}$-$u\bar{u}$($s\bar{s}$) mass differences 80−32096
$J^P=0^-$, 1^- and 2^+ multiplets, level shifts and chain mass, test of asymptotic planarity 77−38130
$K\rho$ resonance, spin-parity 1^+ backward prod. at 1.28 GeV 78−70409
Klein Gordon equations superposition, meson model, ϕ, f', F, K spectrum 78−58121
left-handed quarks, phenomenology 78−21383
leptonic and radiative vector meson decays Schwinger model with U(3) symm. breaking 79−379
leptonic decay, quark confinement potential 78−41536
leptonic decays, six-quark sequental model 80−52490
light quark meson spectroscopy, recent results 78−78134
light vector mesons, mass spectra and Regge trajectories in relativistic quark model *(Russian)* 78−93864
long-lived heavy particles, 4 to 10 GeV/c^2 78−78380
Lorentz structure of confining quark-quark interaction, asymptotic freedom, new particle spectroscopy 78−66077
low quark scheme and narrow resonances 77−34130
$M_\psi - M_{\eta(c)}$ and $M_\Upsilon - M_{\eta(b)}$ lower bounds, concave and convex pots. 80−91057
mass formulae and mixing in SU(8) and $SU_W(8)$ symmetries *(Russian)* 78−66097
mass spectrum, planar bootstrap and Regge approach 80−22581
masses, empirical relation 78−29323
masses of new mesons and effects of the fifth flavour 78−66098
meson spectroscopy, a review using quark models 78−25010
meson-antimeson hadronic molecules, spectrum, leptonic and radiative decays *(Russian)* 80−57602
meson-nucleon collisions, pion spectra forward-backward asymmetry, fragmentation effects, meson reson. decay 78−86457
metastable exotic mesons, explained by diquark-antidiquark model 79−17692
mixing angles, non-relativistic quark model, Schwinger-type mass relations for SU_4 and SU_5 80−18125
mixing angles, non-relativistic quark model, SU_5 and SU_n 80−22591
molecular charmonium prod. in e^+e^- annihilation into hadrons 77−30394
multi-channel baryonium and some peculiarities of its decays *(Russian)* 80−105857
multilepton configurations in b and t decays from $t\bar{t}$ and $b\bar{b}$ 80−18130
multiplicative processes, ρ^0 meson formation cross section, pion prod., multiperipheral cluster model *(Russian)* 78−17067
multiquark states, obs. in $p\bar{p}$ formation and prod. expts. 80−9153
narrow reson., low energy 78−29341
narrow resonance, 2.5-3.0 GeV/c^2 mass region in e^+e^- 77−2852
narrow resonance in an open channel 78−66099
narrow resonance search in 2.5-3.0 GeV mass range in e^+e^- 77−2851
narrow resonances, dynamical model, mass mixing and splitting in degenerate multiplet states 78−93813
narrow resonances, search in 2520-2990 MeV mass region in e^+e^- 77−2850
narrow states in $\bar{p}p$, $qq\bar{q}\bar{q}$ mesons, $\bar{B}B$ bound states, duality, expt. 78−62378
new particle discoveries since J/ψ, review 80−57018
new particle searches in e^+e^- interactions at LEP energies 79−97617
new particles and weak interactions, models *(Chinese)* 79−93334
non-Abelian gauge theory with many flavours, high energy processes, asymptotical behaviour *(Russian)* 80−101935
nonrelativistic pot. models for heavy quark systems, Υ and ψ hadronic decay 78−89688
nucleon-nucleon interaction and nuclear forces, meson exchange 80−32195
orthoquarkonium decay, Dalitz plot population and thrust ang. distrib., scalar gluon nonexistence 80−27470
OZI relations for SU(4) coupling constants with applications to tensor mesons 79−80793
P-wave radial mixing, effect on E1 radiative decays, charmonium mass 80−37271
paracharmonium states, corrections to two-gluon annihilation rates 78−33039
particle correlations in multiperipheral resonance prod. model, broken SU_3 theory 78−45891
photoproduction, high energy review 80−73719
photoproduction, small amplitude lower bounds 77−54109
pion prod. in resonant decay, correl. *(Russian)* 77−228
pomeron-f identity 79−22077
Pomeron-f identity scheme, vector meson prod. 78−12887
protonium formation in flight, $\bar{p}p$, antiproton+neutral and negatively ionised hydrogen atoms 79−85319
pseudomesoniums, spectroscopy, prod. and decay props. 79−45058
pseudoresonance Argand loops *(Russian)* 79−9354
pseudoresonances, nonresonant Argand loops 77−61264
pseudoscalar heavy meson decay by t and b quarks 79−380
pseudoscalar mesons in the c-$\bar{c}$ and b-$\bar{b}$ systems 79−93359
pseudoscalar transitions between high-spin reson. 78−8666
$Q^2\bar{Q}^2$ resonances in baryon-antibaryon systems, $N\bar{N}$ scattering and $N\bar{N}\to\pi^+\pi^-$ 78−58171
q meson mixing and SU(3) breaking 79−282
QCD_2, $q\bar{q}$ bound state spectrum in leading 1/N approx. 80−78031
QCD, asymptotic freedom, energy levels J/ψ and Υ mass difference *(Chinese)* 80−52480
QCD, heavy-vector meson-nucleon scatt., cross section suppression, Υ and ψ 80−22564
QCD, lifetime of $Q\bar{Q}$ states, pseudoscalar charmonium and upsilon states 80−68429
QCD, quark and gluon fragmentation functions, quarkonium decay inclusive hadron spectrum 79−97584
QCD, resonance props. from sum rules 79−26301
QCD, spin-dependent forces in heavy-quark systems 80−4937
QCD, string constant, Regge slope and Λ parameter, empirical quarkonium approach 80−91053
QCD, strong interaction gauge theory, SU(3) colour gauge vector mesons, confinement 78−78136
QCD, two-dimens. extrapolation to four-dimens. 78−78081
QCD and dual resonance model vertices, string prod. operators, singlet colour states *(Russian)* 80−42410
quark bag model with finite potential barrier, S-wave mass spectra of $Q\bar{Q}$ and leptonic widths 80−47242
quark cluster, model of ordinary and exotic hadrons 79−40759
quark fusion model, strange and charmed quark numbers, vector meson description 78−58158
quark jet, $q\bar{q}$ pair production mechanism, average transverse momenta 80−18118
quark jet fragmentation, large momentum transfer reactions, implication of large vector meson prod. 79−345
quark model of heavy mesonic resonance prod. *(Russian)* 78−45881
quark model of resonances, $SU_6\times O_3$, form factors, review 77−67624
quark models, axial vector mesons decoupling from local currents 77−87938
quark recombination model, vector meson prod., effect on $\pi^\pm$ and $K^\pm$ fragments from proton 78−82160
quark string model, hadron spectrum, semiclassical approach, baryons and exotic hadrons 79−40747
quarkonia, S- and P-wave, gluon jets, perturbative QCD anal. 80−32070
quarkonia states, heavy, strong decay into other heavy flavours, and triple-gluon vertex 80−47279
quarkonium, leptonic decay, quark spinors in bound quark system, small component effects 80−73694
quarkonium decays into heavy quarks 79−58943
quarkonium leptonic decay rates for 1S and 2S states, constraints 80−37252
quarkonium level spacings 78−8604
quarkonium level splittings, scaling behaviour, semiclassical methods 79−75742
quarkonium mass spectra, one gluon exchange corrections, gauge invariance and choice 80−52483
quarkonium pot., ψ data and Υ'-Υ mass splitting fit, Υ leptonic widths 78−89666
quarkonium radiative transition amplitudes, QCD dispersion sum rules 80−52511
quarkonium systems, sum rules 80−68423
radial excitations in a dynamical quark model, spectra, decays 78−93840
radially excited, total widths calc. in relativistic harmonic oscillator model 77−38126
radially excited states, photon and hadron interactions 78−82170
radiative decay of vector mesons into pseudoscalar mesons, relativistic harmonic oscillator model *(Russian)* 78−453
radiative decay rates for $V\to P\gamma$, $P\to PP\gamma$, $P\to\gamma\gamma$ and $V\to PPP$, symmetry, angle mixing 77−49969
radiative decays 78−21419
radiative decays of vector mesons, single parameter scheme 80−86720
radiative widths of vector mesons, EM characteristics, bag model *(Russian)* 79−93380
Regge trajectories for narrow meson resons. 78−82178
Regge-pole approach to charmonium and bottonium 80−86697
reggeisation in theories with broken global symmetries, nondegeneracy of vector meson masses, non-trivial mixing 80−13236
Reggeization of gauge vector mesons and unified theories 79−97562
reggiezation of vector mesons for non-Abelian theories with arbitrary symmetry 77−2740
relativistic hadron couplings, unified framework, symms., quark models *(German)* 78−50012
relativistic quark model, vector meson strong decay widths 77−57529
relativistic quark models, $c\bar{c}$ and $b\bar{b}$ singlet triplet splitting, mass formulae *(Russian)* 80−37232
resonance vertex functions and scatt. amplitudes resonance-nucleon scatt. ρ rescatt. *(Russian)* 80−105918
s-channel resonance model based on peripheral resonances, exotic peaks 80−91069
s-wave pion-nucleon phase shifts in Pade approximation using ε, ρ, f, N, Δ 79−67603
scalar mesons, $J^{PC}=0^{++}$ partial waves self-consistent anal. 79−71711
Schrodinger eqn. with logarithmic pot., soln. for quark model particle spectroscopy 80−32065
simultaneous pion and meson resonance production, correl. jet model 78−86456
spectroscopy in quartz confining two-step pot. 77−26492
spontaneously broken symmetry restoration in mag. field, massive charged vector meson effects *(Russian)* 78−74178
strange axial vector meson non-diffracture prod. in Kp and πp interactions 80−32122
strange baryonium, spectrum, decay, production 78−93854
strange exotic meson resonances of quasinuclear type, masses near 2 GeV *(Russian)* 77−79295
straton model theory, extension to SU_5 *(Chinese)* 78−24996
strong and EM decays, particle mixing and meson pole dominance 80−18127
SU_3 couplings of scalar mesons to two pseudoscalars, S^* to $\pi\pi$ and ε to $K\bar{K}$ 80−22580
SU(10) symmetry, charmed vector bosons mag. moments 78−17018
SU(3) symmetry violation models for interactions with vector mesons, tests *(Russian)* 77−10196
$SU(4)\times S_3^n$, straton model, meson classification *(Chinese)* 78−78145
$SU(4)\otimes SU(3)'$ model, Υ particles and SU(3)' colour space *(Chinese)* 80−42409
SU(4) broken symm., duality, baryon+baryon and baryon+antibaryon exotic mesons prod. 78−89629
SU(4) symmetry, meson-quark interactions, mag. moments *(Russian)* 78−45804
SU(5), Clebsch-Gordan series, quark model appl. 80−47256
$SU(5)\times SU(5)$ chiral symm. breaking, Cabibbo angle, meson mass spectrum 77−74614

meson resonances continued
SU(S) based grand unified theory, monopoles and vector bosons, symmetry breaking 80−99079
subnuclear structure concept via dilepton prod. in hadronic collisions, historical review 79−93365
T′ (10040) as an I=1 vector meson resonance 80−47241
T-baryonium system, four-body potential in multiquark states 80−101996
t-flavoured meson production in photonuclear and pp collision 80−22623
tensor and vector meson decay, relativistic confined quark model anal. 79−13116
tensor meson production in photon-photon collisions 79−93414
tensor meson radiative decay in SU(6)×O(3) broken symmetry quark model 80−73710
tensor mesons, EM decay possible source of photons and leptons 79−13130
three particle systems, diffractive prod. and relativistic rescatt. 79−12988
three-body mechanism for narrow resonances 77−74654
twenty-plet of vector mesons *(Russian)* 78−58220
two body photonic decays, SU(4) scheme, ideal mixing angles, amplitudes, quark sectors 78−54630
two-body photonic decays, 16-plet mixings in SU(4) quark symm. 78−33062
two-dimensional gauge model perturbation theory, Schwinger and massive vector meson models 79−6269
two-particle resonance+particle interactions, scatt. amplitude, arbitrary spins *(Russian)* 77−74621
ultrarelativistic nuclear collisions, asymptotic hadron spectrum, hot hadronic matter 80−63118
unitary symmetry in baryon-antibaryon systems *(Chinese)* 80−102000
V→Pγ, effect of SU(3) admixture in VMD model 77−49970
VDM, radial excitations and q^2 depend., appl. to ψ radiative decay 78−452
vector and tensor meson decays in relativistic confined quark model 77−79256
vector boson pair photoprod., theoretical cross sections 80−57610
vector meson, in quantised monochromatic EM plane wave field, exact solns. 78−89638
vector meson→e^+e^-, standard leptonic decay width correction, effecting pot. model predictions 78−89707
vector meson covariant redefinition, $SL_{3,c}$ chiral symmetry 77−54045
vector meson decay in SU(4) σ model with massive gauge fields 77−10184
vector meson decays to eē, constituent quark spinors, small component effects 79−85279
vector meson dominant prod. in pp inclusive interactions, 53 GeV 77−67685
vector meson electroprod. in deep inelastic e and μ scatt. 78−78184
vector meson in a quantized electromagnetic field 79−40705
vector meson inclusive prod. cross section in hadron-nucleon collisions, parton transversal motion *(Russian)* 79−67617
vector meson leptonic decay and gluon condensate *(Russian)* 78−33060
vector meson leptonic width, duality between vector mesons and perturbative QCD 80−57589
vector meson mass predictions, SU(3) formalism of S quark model 78−37177
vector meson mass spectrum, radiative decay, QCD nonrelativistic potential model 79−36046
vector meson masses, possible bounds on their ratios in gauge hierarchies 78−93791
vector meson photoprod., Carlitz-Green-Zee mechanism and vector meson dominance model 79−13137
vector meson photoprod. from nucleus, invariant amplitudes 79−63488
vector meson photoproduction and Compton scatt. by nucleons 79−22114
vector meson photoproduction from nucleons, quark rescatt. effects *(Russian)* 77−65160
vector meson prod. by high energy photons, review *(German)* 79−40779
vector meson production in pp interactions, constituent-interchange model 80−22579
vector meson radiative decay, δ(980) scalar meson contributions 79−36083
vector meson radiative decay, off-shell factors in vector dominance model 79−22084
vector meson radiative decays, SU(3) symmetry viewpoint 80−95273
vector meson radiative decays, vector dominance model in broken SU(3) 80−73711
vector meson radiative width determ. from Primakoff effect meas. 79−89157
vector meson search in 0.9-2.2 GeV mass region in γp→pe^+e^- 7.2 GeV reaction 77−54110
vector mesons, EM decay in broken SU(3) 80−82976
vector mesons, neutral, P-odd effects in decay *(Russian)* 78−54628
vector mesons, unitarity corrections to masses and mixing angles 79−49487
vector-tensor-Pomeron couplings, nonet mass formulas 77−49883
very high energy cosmic ray-nuclear interactions, new particle search, X particles 80−8508
Wilson loop critical point behaviour in gauge and lattice guage theories 80−90993
Yang-Mills theory, IR divergences and zero mass limit 80−32025
Zweig forbidden processes, intermediate vector particle model, neutral vector mesons *(Chinese)* 80−62918
Zweig rule in two-dimensional QCD, ψ and ϒ decays 80−52479
Zweig rule violations in sequential pole model, glueball possible identification 77−26520
Zweig-superconvergence relations in meson collisions 78−21397
A_1, A_2, A_3, prod., $\pi^\pm$p reactions, polarisation anal. 78−41577
A_1, A_3 and A_4 prod. in π^+p interactions at 15 GeV/c 77−82780
A_1, chiral $SU_2 \times SU_2$ mixing and decay width with ρ 77−30369
A_1, Dalitz arrays from $K^-p \to \pi^+\pi^-\pi^-\Sigma$ 80−105924
A_1, in $\tau^- \to \nu_\tau \rho^0 \pi^-$, current algebra anal. 79−13176
A_1, mass and width determ. by unitary, analytic isobar parametrisation 77−61339
A_1, resonance characts., isobar models 77−22680
A_1, spectral function sum rules and A_1-W coupling const. 80−27429
A_1, unitary isobar model, appl. to partial wave anal. of three π and K*K̄ data 79−40721
A_1,A_2, prod. in K^-n reactions to quasi two body final states 79−22139
A_1 decay, rescattering effects in 3π system 77−13957

meson resonances continued
A_1 diffractive prod. in $\nu N \to \mu N(\pi\rho)$ 79−89143
A_1 meson, mass formulas and selection rules in large SU(3) mixing 80−86700
A_1 meson in quark model and chiral symm. 78−12834
A_1 reson. diffr. prod., $\pi p \to (\pi\rho)p$, unitary coupled-channel anal. 78−8687
A_1 resonance, chiral symmetry scheme fit 79−284
A_1 resonance in $\tau \to \nu_\tau \rho\pi$, ρπ mass distrib. 78−45902
A_1^+, upper limits on prod. in high energy νp interactions 78−54625
A_2, Dalitz arrays from $K^-p \to \pi^+\pi^-\pi^0\Lambda$ 80−105924
A_2 meson, inclusive prod. in p̄p interactions in 9.1 GeV/c 79−6355
$A_2 \to \pi\gamma$, suppression factors for VMD couplings calc., duality constraints anal. 77−13960
A_2^-, in π^-p interactions, 9.8 and 18.8 GeV, decay ang. distribs. and differential cross sections 79−17754
A_2^+, forward production in $\pi^+p \to K^+\bar{K}_S^0 p$ at 12.7 GeV/c 79−22149
B, structure of hadrons containing heavy quark, MIT bag model 80−86672
B(1235)→ωπ, many pion correlations from nonstrange mesonic resonances *(Russian)* 80−86708
B→B′πγ, contribs. of B→B′γ process 80−78066
B(f′(1520))→$\pi^+\pi^-$, Zweig forbidden decay 79−17687
B meson, cascade decays, CP nonconservation 80−105811
B meson, mass formulas and selection rules in large SU(3) mixing 80−86700
B→ψX, weak decay for B mass and other props. determ. 79−97621
B→ψX, weak decay predictions, B identification in hadronic collisions 79−93408
B→ψ(ηc)+X, branching ratio 80−37259
B-meson decay, partial unification of strong, weak and EM interactions 80−18106
b-quark mesons, mass, quark model predictions 80−95256
B^0, B hadronic decay modes, W boson exchange model clean test 80−57592
$B^0 \to D^+X(F^+X)$, W-exchange dominance, decay rates 80−86706
B^+, upper limits on prod. in high energy νp interactions 78−54625
$B^0-\bar{B}^0$, EM mass difference, some phenomenological estimates about heavy quark (b,t) bound states 80−47262
BB̄ channel narrow widths, use of 'mock' diquoniums, quark-pair-creation model 79−75734
b̄b meson state lifetimes, R predictions above bottom threshold, quark model 80−99097
BB̄ production in e^+e^- annihilation 80−68467
$B^0\bar{B}^0$ mixing in six quark model, decay, mass mixing and CP nonconservation 80−42406
cc̄ and bb̄ states, spectra and strong decays 80−52502
cc̄ meson radiative decays, generalised VMD mechanism 78−8606
$C\bar{C} \to \mu^+\nu X$, search for extra μ in (π, ψ CC̄), 225 GeV/c 80−82967
c̄c q̄q states, decay, hadronic and photo-prod., e^+e^- annihilation prod. 80−99092
cc̄ spectrum, equaltime relativistic wave eqn. with confining potential 80−77977
cc̄g(cc̄qq̄), exotic mesons, masses, decay widths, mixing matrix elements 80−62943
χ, suggested J^P values, is χ(3505) a vector boson? 78−62473
χ(3415)(3510)(3555), spin assignments, consistency checks 79−80765
χ(3.45), γ-transitions in charmonium system 78−78138
χ(3.45), radiative M1 transitions with charmonium model 79−13132
χ(3.45) resonance, time-like cc̄ excitation 78−8599
χ(3.45)→$\pi^+\pi^-$X(2.83), test of cc̄ dynamics 77−74685
χ mesons, radiative transitions anal. in nonrelativistic quark model 78−8607
χ particles, radiative decay widths calc., broken SU(4) model 78−62395
χ production properties from inclusive electron pair and J/ψ prod. at CERN ISR 79−36113
χ→ψγ, charmonium E1 radiative transitions and quark mag. moments 80−86721
χ→ψγ, limits from pp→e^+e X 79 425
χ states, multimesonic decays, statistical quark model 78−82171
$\chi_{1,2} \to \gamma J/\psi$, radiative decays of 2^{++}, 1^{++} mesons 78−21420
χ_c radiative decay, ψ and ψ′ prod., straton coupling constants *(Chinese)* 80−42467
$\chi_J \to \gamma\psi$, charmonium states radiative and hadronic widths, gluon spin 80−4998
$\chi_J \to \gamma\psi$, upper and lower bounds using dipole sum rules 77−13958
χ_J P-wave charmonium states, hadronic prod. cross section in K p, p̄p, and π p 80−37292
$\chi_J \to \psi\gamma$, radiative decay widths of charmonium states, superconvergent sum rules 78−21422
D,D* mesons in algebraic approach to broken SU(4) 77−38097
D mesons, colour triplet diquark states 77−30325
D mesons, decay const. using current algebra with Lagrangian model 78−58176
D-meson decay mechs., weak and leptonic two-body decays 78−41535
D-mesons, semileptonic decay in spectrum generating SU(4) 77−54098
D^0 meson prod., search in 53 GeV pp inclusive interactions 77−30462
D^+-D^0, D^{*+}-D^{*0} mass differences using modified nonrelativistic Schrodinger eqn. 78−58186
D^+-D^0 mass difference, Bethe-Salpeter eqn. calc. 77−26525
$D^\pm$-D^0 mass difference, vac. isospin violations 77−26526
$D^{0*} \to D^0\gamma$, SU(4) theory, suppression factor in radiative decay amplitude 77−30372
$D^{*+} \to D^0\pi^+$ observations in e^+e annihilation, decay width, Q value 77−57531
DD̄, DD̄*, D*D̄*, charm molecules, dynamical model, light meson exchange 80−57572
DD̄ meson pair prod. in e^+e annihilation, quark model of broken SU(8) symm. 77−38182
δ(970), optical spark chamber expt., decay mode and $J^G J^P$ determ. 79−9428
δ(980) quark content from η′→ηππ 80−82955
δ(980) scalar meson, prod. and decay props. 77−87975
δ(980)→γγ decay rate implying δ is four-quark state 79−93422
δ-meson four quark nature *(Russian)* 80−101999
E(1420)→K*K̄, correlation between A_1 parameters and Q data 80−82968
E(1420)→ηππ, correlation between A_1 parameters and Q data 80−82968
e^+e^-→ hadrons, scaling and quark struct. 80−425
e^+e^-→ jets, in ϒ and ϒ′ region, sphericity and charged multiplicity 80−428

meson resonances continued
e^+e^- → 1^{--} resonance states, direct production through neutral currents 78−93891
e^+e^- annihilation, CM energies 29.90-31.46 GeV, narrow resonance search upper limit 80−63003
e^+e^- annihilation, CP violating effects, D^0, G^0 and H^0 meson decays 79−80769
e^+e^- annihilation, fine energy scan for narrow states between 29.9 and 31.46 GeV 80−22627
e^+e^- annihilation, gluon jets and heavy quarkonium prod., QCD test, ψ prod. 80−42479
e^+e^- annihilation, heavy vector meson prod., quark model estimations 77−18306
e^+e^- annihilation, narrow resonance search upper limit at PETRA, 29.90-31.46 GeV 80−57618
e^+e^- annihilation, search for narrow resonances in mass region 1.4 to 1.75 GeV/c^2 79−17743
e^+e^- annihilation, vector meson of mass 1.82 GeV obs. 77−65162
e^+e^- annihilation in upsilon region, quark model predictions 78−54640
e^+e^- annihilations, resonance states below 2.2 GeV 78−78197
e^+e^- →D^0, SPEAR expt. results 79−93444
e^+e^- →D^+, SPEAR expt. results 79−93444
e^+e^- →DD̄, bound state model of charmed meson prod. 77−10269
e^+e^- →e^+e^-, Υ(9.46) electronic branching ratio and total width 80−86702
e^+e^- →e^+e^- KK̄, δ and S* meson interf., S*-ε mixing angles, and K^+K^-, $K^0\bar{K}^0$ cross sections *(Russian)* 79−80832
e^+e^- EM annihilation into quarkonium states with even charge conjugation, vector dominance 79−93438
e^+e^- →F^+, SPEAR expt. results 79−93444
e^+e^- →FF̄(BB̄), τν decay signature for $F^\pm$ and $B^\pm$ detection 80−91099
e^+e^- →γV→γνν̄, neutral vector meson radiative prod. and decay *(Russian)* 80−52492
e^+e^- →γγ, 9.4-31.6 GeV, differential cross section, Υ→γγ decay limits 80−91073
e^+e^- →HX, associated production of gluonic jets and heavy mesons 78−93892
e^+e^- →hadron jet, 3 to 17 GeV, including charm threshold and upsilon resonances, review 80−47321
e^+e^- →hadrons, cross-section struct. in 0-8 GeV range, quark models and heavy leptons 77−30392
e^+e^- →hadrons, fourth Υ state observation in annihilation events 80−86737
e^+e^- →hadrons, narrow resonance at 9.46 GeV 78−62415
e^+e^- →hadrons, search for narrow resonances in mass region 1.42-1.92 GeV/c^2 79−17740
e^+e^- →hadrons, Υ, Υ′, Υ″ states, mass differences, leptonic width ratio 80−68466
e^+e^- →hadrons, Υ″ observation at CESR, mass and leptonic width 80−86738
e^+e^- →hadrons ($\mu^+\mu^-$), Υ(9.46) muonic branching ratio, total and leptonic width 80−86703
e^+e^- initiated γγ processes, charged pair prod., f^0→γγ width 80−91123
e^+e^- interactions, review 79−80833
e^+e^- →$\mu^+\mu^-$, Pauli type interaction, vector meson role 80−4974
e^+e^- →μ^+e^- + neutrinos, heavy vector meson intermediate state 77−30396
e^+e^- →O particle, decay, mass, prod. from Zweig rule intermediate vector particle model *(Chinese)* 80−73697
e^+e^- →$\pi^+\pi^-\pi^+\pi^-$, 890-1100 MeV, cross section, πA_1 prod., φ branching ratio 79−36087
e^+e^- →quarkonium state, D,F, Υ mesons, importance as experimental tool in new particle searches 80−42425
e^+e^- →Υ, suggested search for gluon hadronic states in collinear gluon jets 78−89663
e^+e^- →Υ(9.46), electronic width determ., energy spectra for hadron inclusive production 79−26339
e^+e^- →VX, parton model, polarisation effects *(Russian)* 80−63002
e^+e^- →VX, polarization states of produced vector meson *(Russian)* 78−25058
e^+e^- →vector mesons, colour quark model for new reson. above 4 GeV 78−17033
e^+e^- →Vπ→$\pi^+\pi^-\pi^0$, EM mixing effects, dynamics of vector meson prod. *(Russian)* 78−58191
ep→eppp̄, cross sections and possible resonances in final state pp̄ system 79−71756
ep→ep$\pi^+\pi^+\pi^-\pi^-$, 1.8 GeV/c^2, meson resonance observ. 80−82982
ep→$K^+\pi^+K^-\pi^-$, 1.8, 2.1, 2.5 GeV/c^2, meson resonance observ. 80−82982
ε-resonance model, ψ dipionic decays 78−58184
η_c mass from dispersion sum rules in QCD, identification with X(2.83) *(Russian)* 78−89681
F, decay constants from Weinberg type sum rules 79−54336
f, f′ and A_2^0 interference in πN→K^-K^+N at 6 GeV/c 77−253
F, F* masses determ., inclusive η prod. by e^+e^- annihilation 77−87988
f, in K^-p at 32 GeV/c, vector and tensor meson prod., with quark model anal. 79−80854
f, model independent partial wave anal. of $\pi^+\pi^-$ prod. in π^-p→$\pi^+\pi^-$n at 17.2 GeV/c 79−54363
f, multiparticle production in multiperipheral resonance model complemented by duality 79−36050
F, nonleptonic decay rates and branching ratios, lifetimes 80−102047
F, search in e^+e^- annihilation, preliminary results 78−78199
f,f′ mesons, high statistics π^-p→K^-K^+n, and π^+n→K^-K^+p studies 77−79279
f,f′ mesons, fueld unitarisation, renormalisation of trajectories with zero quantum numbers 78−21400
f(1270)→4π, many pion correlations from nonstrange mesonic resonances *(Russian)* 80−86708
f and A_2^0, source of low mass dimuons in $\pi^\pm$p, 16 GeV 78−70411
F and F* from e^+e^- annihilation 78−78198
F→Dπ enhancement and the ΔI=1/2 rule 79−36069
F meson discovery, review of exptl. results and theoretical advances *(German)* 78−66184
f meson inclusive prod. in pp→$\pi^+\pi^-$X 79−45111
F meson prod. characts. from e^+e^-→ηX, F→ηπ 79−26338
F mesons, mass and decay const. using current algebra with Lagrangian model 78−58176
F mesons, nonleptonic decays of charmed mesons and chiral Lagrangians *(Russian)* 79−30732
meson resonances continued
F mesons, semileptonic decay const., D and F decay const. ratio determ. 78−62392
F parity violating nonleptonic decays, vector meson dominance model 80−78058
f resonance pole position in ππ system 77−6096
F-meson, decay mechs., weak and leptonic two-body decays 78−41535
F-meson masses and leptonic decay consts. 78−66087
f-meson production cross section in π^-p inclusive interactions *(Russian)* 78−33098
F-meson semileptonic decay modes, explanation of inclusive electron spectra 78−37202
F-mesons, DASP results on e^+e^- annihilation 80−42483
f-mesons, strong spin-two interaction and general relativity, review 79−45046
f^0(1270), polarisation meas. in ψ→f^0γ 78−74251
f^0(1270) production in π^-p→$\pi^+\pi^-$n, cross sections, decay density matrix elements 78−33095
f^0 exchange, lepton-hadron relation and the nucleon-nucleon potential 79−22207
f^0→γγ, covariant polarisation density matrix analysis *(Russian)* 78−454
F^+ decay, SU_4 20-plet dominance model, inclusive branching ratios 80−13299
F^+ nonleptonic decay, quark annihilation hypothesis test 80−102044
F^+→φπ$^+$($\eta\pi^+$), heavy quark weak isospin, constraints from nonleptonic transitions 79−85257
F_1 meson from p̄p reactions, spin-parity anal., boson spin tests from sequential decays 78−29345
f′-f mass mixing sign from gluonic annihilation model, OZI rule violation 79−71722
f′-f mixing, Okubo-Zweig-Iizuka rule, unitary constraints on resonance mixing 79−22024
f′-meson prod. in 10 GeV/c K^-p interactions 78−4874
f′(1514)→2π, decay amplitudes, OZI rule, dispersion relations, intermediate states contribs. 79−383
$^3F_3$→πd, branching ratio in Faddeev πNN dynamics 80−105886
F* meson and anomalous eμ events 78−66108
g, model independent partial wave anal. of $\pi^+\pi^-$ prod. in π^-p→$\pi^+\pi^-$n at 17.2 GeV/c 79−54363
g(1680)→ρρ, many pion correlations from nonstrange mesonic resonances *(Russian)* 80−86708
g resonance pole position in ππ system 77−6096
g^0-meson enhancement by large transverse momenta selection 77−2871
γ(10.0), two-body hadronic and radiative decays, pseudo-dimension rule, ππ and KK suppression, SV_3 singlet 80−52495
γ′→γππ, current algebra techniques, pole plus remainder model, chiral symmetry breaking and QCD 80−62972
γd→np, 400-650 MeV, proton polarisation and possible dibaryon resonances 80−105908
γN, exclusive photoprod. reactions, Okubo-Zweig-Iizuka rule 80−95277
γN→$\pi^+\pi^-\Delta$, EM mixing effects, dynamics of vector meson prod. *(Russian)* 78−58191
γp→(pp̄)p, inclusive and exclusive pp̄ photoprod. S(1936) prod. 80−86729
γp→K^+K^-p, 20-36 GeV, Φ(1019) prod., cross sections 80−105907
γp→p+vector meson, total cross section *(Russian)* 78−8674
γp→pe^+e^-, 900 to 1500 MeV, 1100 MeV struct. confirmation, ρ′(1250) leptonic decay obs. 79−30738
γp→$\pi^+\pi^-$p, Lagrangian model, ε(700), ρ(770), f(1260), Δ(1236) resons. 78−17028
γp→V^0p, one-pion exchange contrib., vertex corrections 78−50039
γp→vector meson+p, elastic and total cross section using Reggeon-photon coupling analogy 78−78193
J/ψ→K,$K^-\pi^+$, low lying resonance saturation 79−54338
J/ψ→3π, low lying resonance saturation 79−54338
K, mixing of p-wave axial vector resonances 77−30374
K^+(892) resonances in K^+p→$K^0p\pi^+$ reaction at 5, 8.25 and 16 GeV/c 78−12931
K*, EM mass splitting determ. 79−3046
K*, EM mass splitting determ. 79−22138
K*(1420)→K*(890)ππ, possible evidence 77−2823
K*(1780) prod. in Kp^-→$K^-\pi^+$n at 6 GeV 78−33087
K*(890) and K*(1420) prod. in 405 GeV/c pp interactions 79−30757
K̄*(890)(1420), in K^-p at 32 GeV/c, vector and tensor meson prod., with quark model anal. 79−80854
K*(892) prod. in e^+e^- multihadron annihilation 78−66132
K*→K+γ, radiative decay in the MIT bag model 78−66110
K*→Kππ rate, vector meson pole dominance in coupling-constant models 77−30373
K* mass enhancement in K^-p→$K^-\pi^+$n at 10 and 16 GeV/c 77−74726
K^{*+}(890) produced in π^+p→K*Y^+, $Y^+=\Sigma^+$ or Y^{*+}(1385) 80−82997
$K^{*\pm}$(892) production in pp and π^+p inclusive interactions 80−86765
K^-d→$\pi^-\Lambda$p, three body Faddeev formalism, unstable dibaryon bound state search 80−32130
K^+K^- high mass pairs, 1.4 to 2.4 GeV mass range, in H 79−22110
KK̄* mass enhancement in π^+p→($K^+K^-\pi^+$)p 77−26547
K̄N, below 1 GeV/c, Y* states, SU(6)⊗O(3) quark model classification 80−27523
KN→K*Δ, positivity conditions in joint vector-meson Δ prod. 77−13975
K̄N two-body data multichannel anal. in resonance region 77−88006
Kp→Qp, diffractive production, unitary analytic coupled channel model 79−36051
K^-p, 32 GeV/c, exclusive reaction anal. in terms of multiparticle variables *(Russian)* 80−86757
K^-p, 4.2 GeV/c, backward axial vector meson prod., isospin and SU(3) struct. 79−93458
K^-p→($\bar{K}\pi\pi$)$^-$p, 4.2 GeV/c, partial wave anal. in Q region 80−13330
K^-p→A_1, 4.15 GeV/c, nondiffractive production, double-Regge model 80−78097
K^-p→B$^-$$Y^{*+}$(1385), 8,25 GeV/c, quasi-two-body channel data 80−63023
K^-p→f+anything, 10, 16 GeV/c, f(1270) yield, comparison with ρ^0(770) 78−62467
K^-p→$K_s^0\pi^+\pi^-$n, 6 GeV/c, K* and Q_2 signals, partial wave anal. 80−86754
K^-p→K* (890) Δ (1236), 10 GeV/c, multidimens. anal., reaction subchannel separation 80−32127
K^-p→K^{*-}(890)p, determ. of mass and width of K^{*-}(890) 79−3046
K^-p→K^{*-}(890)p, determ. of mass and width of K^{*-}(890) 79−22138
K^-p→$\bar{K}^{*0}$(890)n, determ. of mass and width of $\bar{K}^{*0}$(890) 79−3046
K^-p→$\bar{K}^{*0}$(890)n, determ. of mass and width of $\bar{K}^{*0}$(890) 79−22138

meson resonances continued
$K^-p \rightarrow \bar{K}^*(1420)X$, at 10 and 16 GeV/c 77−18338
$K^-p \rightarrow \bar{K}^*(890)X$, at 10 and 16 GeV/c 77−18338
$K^-\bar{p} \rightarrow \bar{K}\pi N$, 14.3 GeV/c, low-mass $K\pi$ system and $\bar{K}^*$ prod. mechanisms 77−74725
$K^-p \rightarrow \Lambda^0(\Sigma^0)$+vector mesons, 3.1-3.6 GeV/c, exchange model anal. 77−74718
$K^-p \rightarrow \phi\Lambda$, $\omega\Lambda$, $\rho\Lambda$, $\phi\Sigma^0$, or $\rho\Sigma^0$, 4.2 GeV/c, cross sections, density matrix elements, hyperon polarisation 78−41580
$K^-p \rightarrow \Sigma^+(1385)+X$, 16 GeV/c, spin density matrix of $\Sigma^+(1385)$ by statistical tensor method 78−37235
K^+p, 32 GeV/c, vector meson inclusive spectra 79−30703
$K^+p \rightarrow K^0p\pi^+$, 3 to 16 GeV/c, resonance production, cross sections and density matrix elements 78−17048
K^+p scatt. anal. to 2 GeV/c, coupled-channel K-matrix parametrization, resonance poles 79−17758
$K^\pm p$, 32 GeV/c, ρ, K^*, ϕ inclusive prod., quark fusion model 80−32135
$K^\pm p \rightarrow K_S^0\pi^\pm p$, 10 GeV/c, $K\pi$ prod., two arm spectrometer studies 78−50052
$K^+p \rightarrow K^-\pi^+\pi^-p$, 13 GeV/c, mass depend. of $1^+K^*\pi$ and ρK partial waves 78−8705
$K_L^0p \rightarrow K_S^0\pi^+\pi^-p$, up to 17 GeV/c, Q^0-$\bar{Q}^0$ prod., cross sections 80−32129
$K_L^0p \rightarrow Q^0(\bar{Q}^0)p$, differential cross section slope, further Deck model anal. 80−73737
$(\bar{K}^0\pi^+\pi^-)$ system, partial wave anal., prod. in $K^-p \rightarrow \bar{K}^0\pi^+\pi^-n$ 78−45969
$K_S^0\pi^\pm\pi^+\pi^-$ narrow peak at 2.6 GeV in 12 GeV/c $\bar{p}p$ interactions 77−30452
$K_S^0\pi^\pm\pi^+\pi^-$ resonance near 2.6 GeV/c, search in $\bar{p}p$ interactions 78−74289
L(1770), spectral function sum rule and onium 79−26329
$l+N \rightarrow l'+V+N$, diffr. prod. cross-section calc. 77−34167
M(1.86) as possible coloured kaons, Han-Nambu weak interaction theory 77−2799
$\mu N \rightarrow \mu\Upsilon X$, 209 GeV, Υ muoprod. limits from trimuon final states 80−105909
$\mu N \rightarrow x\mu X$, x=2 or 3, charm muoprod. with small angle veto 80−47306
NΔ system, theoretical investigation of bound states and resonances 79−75749
N$\bar{N}$, baryonium, internal struct. *(Norwegian)* 79−36032
N$\bar{N}$, resonances and bound states, multichannel N/D formulation 80−78087
$\bar{N}N \rightarrow (\pi, \rho, \omega, f)$, statistical model 80−102028
N$\bar{N}$ cross-sections and resonances in nonstatic OBEP 80−13386
$\bar{N}N$ narrow meson resonances near threshold, theoretical approaches 80−9157
$\bar{N}N$ potential, imaginary part 80−32118
$nN \rightarrow \bar{p}pX$, narrow struct. in $\bar{p}p$ mass spectrum, threshold to 2700 MeV/c^2 79−63511
N$\bar{N}$ quasinuclear states and the Bethe-Salpeter equation 79−13212
NN scatt., small angle, appl. of eikonal vector meson exchange theory 78−17052
$\bar{N}N$ spectrum in pot. models, meson exchange forces 80−9156
2 N$\bar{N}$ system, bound state energies, Faddeev method *(Russian)* 79−49407
N$\bar{N}$ system, effects of annihilation on resonances 79−58949
ν, charmonium and strangeonium, linear+Coulomb pot. study, high αs regime 80−62935
νH_2, possible new meson or baryon reson. decay 77−240
$\bar{\nu}H_2$-Ne, possible new meson or baryon reson. decay 77−240
$\nu_\mu N$, $F^+(2030)$ prod. and hadronic decay $F^+ \rightarrow \pi^+\pi^+\pi^-\pi^0$, mass 80−91085
ω, production in $\bar{p}p$ annihilations, 0.70 to 0.76 GeV, effect on OZI rule 79−22124
ω-f exchange degeneracy, anal. of Pomeron-f complex 78−483
$P \rightarrow \gamma\gamma$, relativistic quark pair creation model for reduced decays and enhanced EM tadpoles 79−67555
$\bar{p}d$, 355-1066 MeV/c, total and annihilation cross sections, S meson search 80−68473
$\bar{p}d \rightarrow \Lambda + X$, cross section calc. for quasinuclear $\bar{\Lambda}N$ meson generation *(Russian)* 79−9398
$\bar{p}d \rightarrow NX_s$, <500 MeV/c, narrow $\bar{N}N$ state search 80−57627
$\bar{p}d \rightarrow p_s\pi^-\pi^-\pi^0$, 0.4 to 0.9 GeV/c, meson resonance production 79−93447
$\bar{p}n$ annihilation, 5.55 GeV/c, meson resonance prod. and transverse spectra 79−93450
$pN \rightarrow$charm particles, obs. in high resolution streamer chamber 80−73742
pp, $^1D_2$ state, multichannel N/D formalism 79−63506
$\bar{p}p$, 100 GeV/c, inclusive ρ^0 and f^0 prod. 78−41605
$\bar{p}p$, 355-1066 MeV/c, total and annihilation cross sections, S meson search 80−68473
$\bar{p}p$, 373-734 MeV/c, total cross section enhancement, 1936 MeV narrow resonance 80−13324
$\bar{p}p$, 400-850 MeV/c, annihilation and elastic cross-sections meas. reson. obs. at 1939 MeV 77−46082
pp, 405 GeV/c, ρ^0, f, g^0, h meson prod., cross sections 80−105930
pp, 53, 63 GeV, massive electron pair prod., Υ ang. decay, scaling function 80−68495
pp, 53, 63 GeV, Υ and ψ prod., dielectron decay angles 80−68496
pp, 62.4 GeV, e^+e^- massive pair prod., continuum and Υ resonance cross sections 80−18153
pp, 93 GeV, $\bar{p}p$ narrow enhancement at 1940 MeV, S(1936) mass 80−52542
pp, D, B, K prod., QCD model for heavy flavour prod., two gluon annihilation 80−86744
$\bar{p}p$, pp, 12-405 GeV, low p_T meson prod., quark-antiquark formation model 80−63056
$\bar{p}p$, pp, 540 GeV, Υ and ψ transverse momenta from QCD 2→3 processes, gluon subprocesses 80−52546
pp, Υ production cross sections, colour excited states in Han-Nambu model *(Chinese)* 79−49480
$pp \rightarrow e^+e^-+X$, resonance prod. 77−34198
$pp \rightarrow cX$, $p\bar{c}$ exotic, triple-Regge formalism, Pomeron exchanges 80−63041
$p\bar{p}$ channel narrow resonances, baryonium degeneracy, $qq\bar{q}\bar{q}$ or N$\bar{N}$ existence 79−58971
$pp \rightarrow D+$anything, parameter free exchange model 77−10293
$pp \rightarrow e^+e^-X$, large p_T, reference to $\Upsilon(9.5)$, $\xi(3.5)$ and direct γ-prod. 78−89749
meson resonances continued
pp elastic C_{LL} scatt., interpretation of dibaryon resonances at 2140, 2260, and 2430 MeV 79−75781
$\bar{p}p$ elastic scatt., FESR constraint on baryonium resonances, S, T, U, contrib. 80−27520
pp inclusive interactions, narrow vector meson hadroprod., ϕ, J, ψ, charmoniumlike states 77−57573
pp interaction, 52 GeV, two-photon mass spectra, X(2830) prod. 78−21470
$\bar{p}p \rightarrow K^-K^+$, differential cross sections, evidence for meson reson. existence 2.1 and 2.5 GeV/c^2 78−93897
$\bar{p}p \rightarrow K^+K^-$, evidence for $J^P=3^-$ and 4^- meson resonances from differential cross section 78−70399
$\bar{p}p \rightarrow K\bar{K}\pi\pi\pi$, 700-760 MeV/c, D(1285) an E(1420) resonance prod. 78−54646
$\bar{p}p \rightarrow K^*(890)X$, S^* (993)X, 12 GeV/c, prod. cross sections 78−93911
$pp \rightarrow \mu^+\mu^-X$, 62 GeV, ψ and γ cross sections, scaling function 80−105932
$pp \rightarrow ppX$, cross sections at ISR energies, ρ, ω, A_2 and f meson prod. 79−40815
$pp \rightarrow pp\bar{p}_{forward}$+anything, observation of qq with $qq\bar{q}$ bound states, pseudobaryons and baryonium 78−58219
$pp \rightarrow p\pi^+n$, 800 MeV, Δ^{++} prod. and cross sections 79−22294
$\bar{p}p \rightarrow \pi_f^+X^-$, 6 GeV/c search for narrow states in X^- decay 78−89708
$\bar{p}p \rightarrow \pi^-\pi^+$, 2020-2580 MeV/c, differential cross section zeros 77−41854
$\bar{p}p \rightarrow \pi^-\pi^+$, amplitude anal., 2020 to 2580 MeV/c^2, spin 3, 4 and 5 mesons 77−41853
$\bar{p}p \rightarrow \pi^0\pi^0$, 2.12 to 2.43 GeV, 2.15 GeV resonance from partial wave amplitude anal. 79−9394
$\bar{p}p \rightarrow \pi\pi$, 1-2 GeV/c, Barrelet zero anal., resonant struct. 80−73735
$\bar{p}p \rightarrow \rho^0X$, 9.1 GeV/c, topological and channel cross-sections 77−30415
$\bar{p}p \rightarrow \rho^0\rho^0$, $\omega\rho^0$, ρ^0f, or ωf, T(2200) region, partial wave anal. 77−34171
$\bar{p}p \rightarrow S \rightarrow \bar{p}p$, S meson as baryonium state 80−62938
pp scatt., eikonal mechanisms at high energy 78−82256
pp scatt., exchange degeneracy violating A_1-Z Regge amplitude and dibaryon resonances 80−4971
pp scatt., natural and unnatural parity exchanges, exact separation, A, exchange 79−13144
$p\bar{p}$ system, possible evidence for narrow bound states below threshold, mesonic struct. 78−62443
pp total cross-section, dibaryon resonant states, narrow peaks 80−63016
$\bar{p}p \rightarrow V^0\pi^0 \rightarrow e^+e^-\pi^0$, annihilation at rest, heavy vector meason prod., ρ' (1250), ρ'' (1600) existence 77−13971
ϕ meson, two-body hadronic decay, quark model 78−25040
π form factor, analytic representation at all Q^2 accommodating higher vector meson states 78−58188
π-ρ system, bag model, quark-quark interaction anal. 78−33029
$\pi^\pm$ N 200, 280 GeV on Pt target, γ resonance prod. 79−93460
π^-+nucleus$\rightarrow\pi^+\pi^-\pi^-$+nucleus, 8.9, 12.9, 15.1 GeV/c, resonance behaviour of coherently prod. A_1, A_3 mesons 78−50047
πd elastic scatt., 142-256 MeV, dibaryon resonance interference with Faddeev amplitudes 80−32123
πd elastic scatt., dibaryon resonance effects on differential cross section, Glauber model 79−97634
πd polarised scatt., dibaryon resonance signals in excitation functions 80−9181
$\pi^-d \rightarrow (n_s)p\bar{p}n$, 13.2 GeV/c, $p\bar{p}$ forward low mass enhancement 80−86761
$\pi^-d \rightarrow (p_s)X^{--}p$, 13.2 GeV, search for charge −2 mesons 78−66167
$\pi^-d \rightarrow (p_s)p\bar{p}\pi^-$, 13.2 GeV/c, $p\bar{p}$ forward low mass enhancement 80−86761
π^+d, 15 GeV, neutral three pion resonance prod., pure I=1 exchange 80−57644
π^+d, 15 GeV/c, many-pion prod. and resonant prod. cross sections 80−22642
πK partial waves, resonance parameter determination for scatt. amplitude 79−40692
$\pi N \rightarrow A_2N$, ρ and f Regge exchanges, an interpretation 79−63531
πN interactions, N form factor, isovector, meson field theory, pseudoscalar πN interaction 80−62986
$\pi N \rightarrow \pi^+\pi^-N$, 4-17 GeV/c, ρ^0 and f prod. mech. 80−436
πN scattering, ρ trajectory, finite-energy sum rules, three component duality 80−82996
$\pi^\pm N \rightarrow \omega(N,\Delta)$, EM mixing effects, dynamics of vector meson prod. *(Russian)* 78−58191
$\pi p \rightarrow (\rho\pi)p$, A_2 diffractive prod., Deck model and Pomerons 79−71733
π^-p, 70 GeV/c, direct electron prod. from charm particle pair decay, e/π ratio 80−105928
$\pi^-p \rightarrow (\bar{p}p)X^0$, narrow $p\bar{p}$ state search 80−78102
$\pi^-p \rightarrow \eta^+\pi^-n$, D, E, and δ mesons obs. at 12 and 15 GeV/c 79−3052
$\pi^-p \rightarrow \eta\pi^+\pi^-n$, axial vector and pseudoscalar resonances near 1.275 GeV, D mesons 79−30747
π^-p interaction, Δ exchange, 4 GeV/c 78−74275
$\pi^-p \rightarrow J/\psi+n$ or $\chi+n$, 27-40 GeV/c, nuclear proton, upper limit on cross section *(Russian)* 78−78218
$\pi^-p \rightarrow K_S^0K^-p_s$, 10 GeV/c, spin 4 meson reson. prod. 78−50050
$\pi^-p \rightarrow K_s^0K^\pm\pi^+n$, 3.95 GeV/c, E(1420) quantum numbers and branching ratio 80−95286
$\pi^-p \rightarrow K^-K_S^0p$, 10 GeV/c, isospin 1 meson reson. prod. 78−50051
$\pi^-p \rightarrow K^-K^0p$, 10 GeV/c, A_2 and g reson. prod. 78−82230
$\pi^-p \rightarrow K^-K^+\pi^0n$, D, E, and δ mesons obs. at 12 and 15 GeV/c 79−3052
$\pi^-p \rightarrow K^0\Lambda^0$, up to 1334 MeV/c, cross sections and polarisation, energy depend. phase shift anal. 78−70404
$\pi^-p \rightarrow K^+K^-n$, 10 GeV/c, obs. of new structure in K^+K^- system at 2.20 GeV, width approx. 200 MeV 79−80843
$\pi^-p \rightarrow K^+K^-n$, 62 GeV, spin-5 boson resonance at 2300 MeV 80−102078
$\pi^-p \rightarrow \bar{K}KN$, S-wave anal., scalar mesons and branching ratios 80−13328
$\pi^-p \rightarrow n\pi^+\pi^-$, 8 GeV/c, backward meson and baryon reson. prod. 79−415
$\pi^-p \rightarrow p_{fast}\pi^+\pi^-\pi^-$, 9, 12 GeV/c, backward meson prod., quasi two body processes, A_1^-, A_2^- prod. 79−413
$\pi^-p \rightarrow p\pi^+\pi^-\pi^-$, 9 and 12 GeV/c, backward enhancement in A_1 region and A_2 prod. 78−45970
$\pi^-p \rightarrow pX$, 40-240 GeV, B^- boson missing mass search between 2 and 12.5 GeV 79−93473
$\pi^-p \rightarrow p\bar{p}n$, 18 GeV, $p\bar{p}$ resonant state partial wave anal. 80−32134
$\pi^-p \rightarrow \pi^-X$, 30-60 GeV/c, inclusive cross sections, resonance effects *(Russian)* 79−67615

meson resonances continued
$\pi^- p \to \pi^- \pi^- \pi^+ p$, 25 GeV/c, boson states 77−30451
$\pi^- p \to \pi^- \pi^- \pi^+ p$, 63, 94 GeV/c, A_2 meson prod. from partial wave anal. 80−37303
$\pi^- p \to \pi^- \pi^- \pi^+ p$, 63, 94 GeV/c, A_1 meson existence from partial wave anal. 80−37304
$\pi^- p \to \pi^- \pi^- \pi^+ p$, 63, 94 MeV/c, A_3 meson, 3π resonances in 2^- partial waves 80−37305
$\pi^- p \to \pi^+ \pi^- n$, amplitude anal. of $\pi\pi$ scatt. 1.0 to 2.08 GeV, f, g, h mesons 79−3042
$\pi^- p \to \pi^+ \pi^- n$, polarization measurements and a narrow $\varepsilon(750)$ 79−63514
$\pi^- p \to \pi^+ \pi^- n$, $\pi\pi$ scatt. partial wave anal. f, g and h mesons 80−5015
$\pi^- p \to \pi^+ \pi^- n$, 12, 15 GeV/c, prod. of A_2^0 (1310) and ω^* (1675) 78−74283
$\pi^- p \to \pi^+ \pi^- \pi^- n$, D, E, and δ mesons, obs. at 12 and 15 GeV/c 79−9410
$\pi^- p \to \pi^+ \pi^- \pi^- \pi^- n$, D, E, and δ mesons obs. at 12 and 15 GeV/c 79−3052
$\pi^+ p$, 11.46 GeV/c, search for new meson resonance prod. in μ channel 80−22641
$\pi^+ p$, 16 GeV/c, narrow mass enhancement at 1.36 GeV in diffractive (πN) systems 79−45109
$\pi^+ p$, 16 GeV/c, transverse energy spectra of hadrons 77−38209
$\pi^+ p$, 32 GeV/c, π and ρ^0 inclusive prod., f and η cross section estimates *(Russian)* 80−68499
$\pi^+ p$, angular correl. reson. prod. effect at 16 GeV/c 77−88014
$\pi^+ p \to (\pi^+ p\bar{p})p$ 50 GeV/c, narrow baryonium states, diffractive prod. cross sections 80−442
$\pi^+ p \to (\pi^+ \pi^- \pi^0)\Delta^{++}$, 16 GeV/c, partial wave anal., ω^* and A_2^0 80−63033
$\pi^+ p \to \Delta^{++} \bar{p}p$, 9.8 GeV/c, narrow $\bar{p}p$ state search 80−57636
$\pi^+ p \to f + X^{++}$ 8 GeV/c, reaction anal. 79−93457
$\pi^+ p \to$four prong final states, 10.3 GeV/c, resonance prod. cross-sections 78−74276
$\pi^+ p \to$meson resonances, 15 GeV/c, SLAC bubble-chamber expt. 78−41595
$\pi^+ p \to \pi^+ \pi^- \Delta^{++}$, polarization measurements and a narrow $\varepsilon(750)$ 79−63514
$\pi^+ p \to \rho^0 \Delta^{++}(1236)$ or $\omega\Delta^{++}(1236)$, 10.3 GeV/c, cross-section meas. 78−82248
$\pi^+ p \to \Sigma^+(1385) + X$, 16 GeV/c, spin density matrix of $\Sigma^+(1385)$ by statistical tensor method 78−37235
$\pi\pi$ partial waves, resonance parameter determination for scatt. amplitude 79−40692
$\pi\pi$ phase shift analysis, imposed analyticity effects 79−418
$\pi\pi$ S-wave phase shift, lower bounds, ε° and ρ poles 78−45953
$\pi^+ \pi^-$ from $\pi^+ d$, 15 GeV, high-mass even-g states 80−68487
ψ dipionic decays, local derivative coupling model 78−58184
ψ hadronic prod., lepton pair ang. distribs., cross section χ contribution from πN, pN, $\bar{p}N$ 80−42487
Q, axial vector mesons, dynamical mixing model 78−24973
Q decay amplitudes, partial widths, Lorentz and SU(3) invariant coupling constants 79−26328
Q($K\pi\pi$) prod., SLAC data anal., 1^+ strange meson prod. 77−54100
Q mesons, SU(3) anal. of mass, widths 78−4802
Q production in $\pi^- p$ and $\bar{p}p$, Breit-Wigner parameters, decay modes 77−57560
Q_1(1280), mass formulas and selection rules in large SU(3) mixing 80−86700
Q_1(1289) decay, SU(3) octet mixing 77−18281
Q_1(1290), Q_2(1400) vector-pseudoscalar decay rates and SU(3) implications 77−61283
Q_1-Q_2 mass difference and mixing, A_1-B mass difference, predictions 79−13122
Q_2(1400), mass formulas and selection rules in large SU(3) mixing 80−86700
Q_2(1404) decay, SU(3) octet mixing 77−18281
Q_A-Q_B mixing angle, axial vector meson decay, A_1 and C obs., SU(3) implications 79−89148
$\bar{Q}Q$, bound system, dynamics 80−73676
$q\bar{q}$ recombination model with resonance prod. 79−75740
$q\bar{q}$ resonance energy spectrum, leptonic and radiative decay widths, QCD pot. calcs. 80−52491
$q\bar{q}$ spectra, heavy systems, equaltime relativistic wave eqn. with confining potential 80−77977
$q\bar{q}$ systems, nonperturbative potential model 80−78040
$Q^2\bar{Q}^2$ states with relatively narrow widths 79−54300
$qq\bar{q}\bar{q}$ diquonium states, production in e^+e^- processes 80−57615
ρ-A_1-π system, radial excitations, and EM mass difference of pions 79−40775
ρ-A_2 exchange degeneracy breaking, s-channel discontinuities of torus insertion, dual unitarisation scheme 78−93866
ρ-A_2 exchange degeneracy breaking, estimate from Fermilab $\pi^- p$ ($d\sigma/dt$) data 79−13162
ρ^1(1250) resonance, chiral symmetry scheme fit 79−284
$\rho\pi$ scatt. in Bardakci-Halpern model 1^+ channel, N/D anal., A_1 status 79−40688
S(1935), reson. parameters determ., finite energy resolution effects, folding problem 80−32673
S(1936), evidence against existance from $\bar{p}p$ interaction 80−78089
S*, bias free pole search in S-wave $\pi\pi$ scatt. 79−58976
$S^* \to K^+K^-$ cross section, S-P waves interference in $\gamma p \to K^+K^-p$ 79−6343
S* scalar meson, four-quark nature *(Russian)* 80−68432
$s\bar{s}$ vector mesons, hadronic decays and props., nonrelativistic quark model 80−105892
SU(8)×SL(3,R) colour quark model, vector states in e^+e^- annihilation at 3.9-4.5 GeV 77−41850
$\sigma \to 2\gamma$, tensor-trace and triangle anomalies 80−73709
T(2150), $p\bar{p} \to \pi^+\pi^-(K^+K^-)$ cross-sections, structure 80−68485
T(tt) decay into Higgs scalar and photon 79−36082
t-quark mesons, mass, quark model predictions 80−95256
tt states, t threshold, potential model predictions 80−86682
tt vector meson, proposed 40 GeV mass 80−62942
$\tau \to \nu p\pi$ decay parameters from PCAC and current algebra, A_1 characts. 80−37314
U(2310), $p\bar{p} \to \pi^+\pi^-$ (K^+K^-) cross-sections, structure 80−68485
Υ, appl. of quarkonium system inverse scatt. formalism, interquark pot. 78−82154
meson resonances continued
Υ, bound state of unconfined integer charge spin-$^1/_2$ fermions, theory 79−93375
Υ, EM decays, relativistic corrections in potential model 79−49522
Υ, EM mass splitting in nonrelativistic quark model 79−89152
Υ, evidence for b quark, weak interactions and multilepton final states 79−49516
Υ, evidence for b-quark, $b\bar{b}$ states masses, decay widths 79−17691
Υ, hadron production of heavy quark bound states 79−63435
Υ, heavy quark bound states in potential model with relativistic corrections 80−37247
Υ, in pp interactions, effects of hard gluon bremsstrahlung in dimuon and Υ prod., QCD anal. 79−13058
Υ, interpretation as coloured particle, masses and leptonic decay widths 79−54322
Υ, leptonic decay width, mass depend. in QCD 79−49488
υ, masses and leptonic-decay widths, one-parameter potential 80−13279
Υ, narrow high mass resonance formation in e^+e^- annihilation at 9.46 GeV, heavy $q\bar{q}$ bound state 78−62414
Υ, obs. in muon pair prod. in pn and pp collisions *(Hungarian)* 79−13163
Υ, polarised, charge asymmetry in lepton pair decay of polarised resonances 79−17716
Υ, possible evidence for massive new quark 79−40753
Υ, pot. model, heavy quarks 78−45875
Υ, production and decay in quark fusion model 80−102018
Υ, QCD, three gluon jets as test 78−25001
Υ, quarkonium spectroscopy in a potential model with vacuum-polarization corrections 80−78038
Υ, quixotic interpretation as $Q\bar{Q}$ bound state 80−13280
Υ, SU(4) mass relation anal. *(Chinese)* 79−58934
υ, Schwinger partial symmetry, quark flavour EM interaction 79−93335
Υ, Schwinger phenomenological and dyon description 78−82109
Υ, sum rules for Υ-family formation in e^+e^- annihilation *(Russian)* 79−54347
Υ, vibrational states in string picture, mass and leptonic width 80−62949
Υ(10), decay modes and pseudoscalar partner 79−13179
Υ(9460), hadron mass spectra, MIT bag model formalism 79−63429
Υ(9.4 GeV), mass formulae and splittings 78−33107
Υ(9.46), $b\bar{b}$ bound state, bottom hadrons, masses and allowed decays, SU(5) quark model 80−62954
Υ(9.46), leptonic branching ratio, from electronic width and muonic branching ratios 80−57588
Υ(9.46), prod. in e^+e^- interaction at DORIS, quark parton model agreement 79−93443
Υ(9.46) decay into charged hadrons, jet anal. 79−49519
Υ(9.46) orthoquarkonium decay, jet profiles, three gluon structure 80−73698
$\Upsilon(9.46) \to \mu\mu$, branching ratio determ. 79−26339
Υ(9.4), decay modes and pseudoscalar partner 79−13179
Υ(9.4), photoprod. cross section estimation 78−78195
Υ(9.4) family, gauge theory mass anal., harmonic oscillator pot. 78−82186
$\Upsilon(9.4) \to$charmonium, quarkonium prod. via one gluon mechanism 80−95263
Υ(9.5,$b\bar{b}$), decay into Higgs scalar and photon 79−36082
Υ(9.5 GeV), prod. cross section at ISR energies in pp collisions 78−25085
Υ(9.54) and broken SU_3 in nonstrange quark sector, vector mesons 78−58166
Υ(9.5), cascade-gluon model, bound state of heavy quarks 78−4834
Υ(9.5), nature of heavy particle anal. *(Chinese)* 78−86443
υ(9.5), prod. in e^+e^- annihilation, photoprod., decay modes, quark model 78−12877
Υ(9.5) decay modes from Zweig rule intermediate vector particle model *(Chinese)* 80−73697
Υ(9.5) hadronic prod., parton distrib. and QCD 78−78142
Υ (9.5), heavy quark charge 78−37180
Υ (9.5), implications of Υ for ν interactions in weak gauge theories 78−70271
Υ (9.5), possible colour-excited states *(Chinese)* 78−82169
Υ (9.6) constituents, heavy quarks as colour sextets, possible weak decay 79−2998
Υ and charmonium spectra, common pot. fit, Υ''-Υ mass difference 80−86712
Υ decay, multiplicity decrease due to charm prod. suppression 79−49518
Υ decay, photon spectrum, branching ratios, leptonic-, hadronic widths, quarkonium model 79−3020
Υ decay, QCD, inclusive hadronic annihilation of heavy quark-antiquark bound states 78−45866
Υ decays, hadronic, asymptotic freedom, one-photon or three-gluon exchange 80−62971
$\Upsilon \to e^+e^-$, harmonic oscillator model, QCD gluon-bottom quark coupling 79−3016
$\Upsilon \to e^+e^-$, limits from $pp \to e^+e^-X$ 79−425
$\Upsilon \to e^+e^-$, widths and b-quark interpretation of peaks 79−63435
Υ energy spectra using quark model, leptonic decay widths, spin depend. forces 79−13109
$\Upsilon \to \eta\gamma$ or $\eta'\gamma$, other hadronic and two body charmed and strange modes 78−78175
Υ family, EM transition rates, geometrodynamical quark model 80−47295
Υ family, leptonic, hadronic, two-body decay widths, suppression factor 79−49514
Υ family, resonance fit parameters 78−78368
Υ flavoured vector mesons, production in e^+e^- annihilation at DORIS energies 78−93890
Υ leptonic decay widths, determ. of new quark 78−50029
Υ meson, asymptotic symm., new duality 78−21348
Υ meson, bottom quark mass inequality 79−9345
Υ mesons, level struct., masses, new quarkonium state 78−33031
Υ observation, charmonium, c-quark and new elementary particles *(Danish)* 79−45048
υ p-wave ground state, mass scaling inequalities for quarkonium levels 80−32071
Υ particle at 9.4 GeV, differential dispersion relations theory of 1^+1^- annihilation 78−86424
Υ particles near 9.5 GeV, straton model, SU(5) extension *(Chinese)* 78−82168
$\Upsilon \to$photons+gluons, QCD perturbation theory 78−33028
υ prod. from duality and new quark charge 78−74224

meson resonances continued
ϒ production, photon-gluon fusion model, gluon distrib. *x*-depend. 80−62922
ϒ resonances, mass splitting, bound states of exotic quarks 78−70338
ϒ signals in dimuon mass spectrum from W+p at 400 GeV/c 78−89857
ϒ spectroscopy, asymptotic freedom 78−45865
ϒ spectrum, equaltime relativistic wave eqn. with confining potential 80−77977
ϒ states with small hyperfine splitting, coupling constants 79−97599
ϒ structure, new heavy quark-antiquark system 78−78138
ϒ systems, heavy quark potentials, effect on triplet cc̄ charmonium and triplet bb̄ upsilonium systems 79−49456
ϒ-meson mass spectra, quasipotential calcs. *(Russian)* 80−47268
ϒ′, lepton heavy width QCD radiative corrections 79−49515
ϒ′(10.00), two gluon jets 78−29302
ϒ′(10.02), prod. in e^+e^- interaction at DORIS, quark parton model agreement 79−93443
ϒ′ at M(ϒ′)=10.02 GeV in e^+e^- annihils. using NaI lead-glass det. 78−93894
ϒ′ decay and 10 GeV reson. struct. 78−66115
ϒ′→γ2^{++}(bb̄), photonic decay widths in tensor meson dominance 79−75754
ϒ′ obs. at M(ϒ′)=10.01 GeV in e^+e^- annihils. using DASP det. 78−93895
ϒ′→ϒ+η, two gluon mechanism, ϒ dynamics test 78−89665
ϒ′-ϒ mass difference from QCD qq̄ β-function 79−343
ϒ″, prod. in Pt+p 4 to 18 GeV collisions, search for new narrow resons. 79−30833
ϒ″ leptonic and total width 79−40760
ϒ″ leptonic width, some phenomenological estimates about heavy quark (b,t) bound states 80−47262
ϒ9.5 GeV dimuon resonance, evidence for fifth quark of 4.7 GeV 78−29312
V→γh, use of QCD in OZI-violating radiative decays 79−26302
V→Pγ, relativistic quark pair creation model for reduced decays and enhanced EM tadpoles 79−67555
V→pμ$^+$μ$^-$, vector meson decay EM form factors in bag model *(Russian)* 80−62982
X(2.82), γ-transitions in charmonium system 78−78138
X(2.82) DASP results on e^+e^- annihilation 80−42483
X(2.83), radiative M1 transitions with charmonium model 79−13132
X(2.85)→2γ, obs. in charge-exchange reaction π$^-$p→Xn 78−25047
X(2.8)→π$^+$π$^-$γ, OZI rule violating decay in QCD 78−89709
X→φφ→(K$^+$K$^-$)(K$^+$K$^-$), new spin-0 mesons, Yang's parity test 78−66111
x-boson, mass and asymmetric decay rel. to cosmological baryon asymmetry 80−4464
X^0(958)→ηππ, ηX^0 mixing angle, broken SU(6)×O(3) quark model 79−17721
ξ(2800) as a four-quark 0^+ scalar meson, SU(5) dynamical group anal. 79−67497
ζ energy spectra using quark model, leptonic decay widths, spin depend. forces 79−13109
b̄b2^{++}→γϒ, photonic decay widths in tensor meson dominance 79−75754
F_1^{+*}, weak decay modes, annihilation contribs. 79−93410
γN→ηπ$^\pm$, 9.7 GeV, one-pion-exchange model 78−25054
^{1}H(p,pπ$^+$)n, 800 MeV, Δ^{++} prod. and cross sections 79−22294
^{2}H(π,π), polarised d, dibaryon resonance signals in excitation functions 80−9181
^{4}He(π,π), 75-260 MeV, dibaryon contrib. to πNN cluster 79−89328
KN(K̄N) scattering amplitudes, resonance region, t-channel couplings, hyperbolic dispersion relations 80−57643
pp̄→π$^+$π$^-$ (K$^+$K$^-$), T, U and V resonances 80−68485
S*-δ^0 scalar meson mixing as threshold phenomenon from coupling constants 80−27477
V(2480), pp̄→π$^+$π$^-$ (K$^+$K$^-$) cross sections, structure 80−68485

meson scattering *see lepton-hadron scattering; meson-baryon scattering; meson-deuteron scattering; meson-meson scattering; meson-nucleus scattering; photon-hadron scattering*

meson spin and parity
ψ production and decay, book contrib. 78−82208
charged pseudoscalar meson photoprod. from H and D with 16 GeV linearly polarised photons 80−13318
charmonium spectroscopy, spin forces, obs. in ψ′(3.68)-ψ″(3.77) struct. in e^+e^- annihilation 79−36047
charmonium spin structure, and possible origin of quark spin depend. forces 79−30707
exotic mesons, qq̄g states in bag model, energy, spin, parity, mass spectrum *(French)* 79−80807
field equation for arbitrary hadrons and parity operators 80−37263
heavy neutral mesons, parity determ. 80−37264
high spin mesons and unexplained multiphoton phenomena *(Chinese)* 79−22160
pion form factor, ω and φ effects G-parity violation 79−35963
Reggeon loop model, sign of unnatural-parity cylinder 77−57506
semiclassical model for rotational states of mesons containing massive quarks 79−36038
spin tests for charmed mesons produced in e^+e^- annihilation at √s=4.028 GeV 78−74269
straton model, meson wave functions, Bethe-Salpeter eqn., SU_6 symm. *(Chinese)* 77−34125
three pion states, permutation group S_3 irreducible representation 79−17635
two body reactions, spin system constraints, quark additivity, geometrical hypothesis 78−29309
unnatural parity mesons in dual unitarization scheme 77−87951
(3π)^0 system, from π$^+$p, 12 and 15 GeV 78−29359
χ, suggested J^P values, is χ(3505) a vector boson? 78−62473
χ(3415)(3510)(3555), spin assignments, consistency checks 79−80765
D(1285) from pp̄→KK̄ππ, 700-760 MeV/c, spin-parity assignment, dominant decay mode 78−54646
D→ηππ, D meson spin parity determ. by partial wave analysis 79−3052
D→ηππ, D meson spin parity determ. by partial wave anal. 79−9410
D→KK̄π, D meson spin parity determ. 79−3052
DD̄, DD̄*, D*D̄*, charm molecules, dynamical model, light meson exchange 80−57572
δ(970), optical spark chamber expt., decay mode and J^GJ^P determ. 79−9428

meson spin and parity continued
e^-e^+→ψ(z), spin correlations, spin 0, $^1/_2$, or $^3/_2$ pair prod. *(Russian)* 79−22117
η′(958), spin-parity test from collinear prod. and decay 78−41543
F_1 meson from p̄p reactions, spin-parity anal., boson spin tests from sequential decays 78−29345
K$^+$n→K$^+$π$^-$p, 4.6, 8.25, 12 GeV/c, spin-parity anal. of K$^+$π$^-$ system 77−82766
K$^-$p→K$^-$π$^+$π$^-$p, 10, 14.3, 16 GeV/c, partial wave anal. of (Kπ)$^-$ system in the L-region 79−17764
K$^\pm$π$^\pm$π$^\pm$ state in 1876 MeV/c^2 state decay, non-natural spin and parity assignment 77−10245
L(1770), spectral function sum rule and onium 79−26329
ω′(1675), prod. in π$^+$p→Δ^{++}π$^+$π$^-$π^0 78−37241
p̄n→π$^+$π$^-$π$^-$, 1.09 to 1.43 GeV, spin-parity function, Veneziano model anal. 79−13148
π^0, space parity, determ. from ^{4}He(γ,π^0) *(Russian)* 78−66129
π$^+$, negative parity assignment from pp→πd 80−32117
π$^+$p→(π$^+$π$^-$π^0)Δ^{++}, 16 GeV/c, partial wave anal., ω* and A_2^0 80−63033
ψ (4.03), isospin and G-parity, model independent prediction 80−86689
ψ″(3770) isospin and G-parity 79−63569
ρ^0-electroproduction, parity violating effects 80−9178
S(1936) J^{PC} assignment form p̄p→p̄p backward scatt. anal. 77−49998
V→γh, use of QCD in OZI-violating radiative decays 79−26302
X→φφ→(K$^+$K$^-$)(K$^+$K$^-$), new spin-0 mesons, Yang's parity test 78−66111
X^0(958), Kp$^-$→X^{0}Λ anal. and spin determ. 77−14010
X(3410), J^P possible expt. meas. from ψ→X+γ process *(Chinese)* 77−57581

mesonic atoms *see mesic atoms*

mesonic molecules *see mesic molecules*

mesons
for μ mesons see muons
see also cosmic ray mesons; eta mesons; kaons; meson resonances; pions
bound state wave function, probability interpretation, form factors, Bethe-Salpeter eqn. *(Chinese)* 80−101930
charmed, hadronic props., superconvergence sum rules 80−78043
Clebsch-Gordan coefficients for meson sector in SO(8) model of elementary particles 78−58135
collective model based on quantum chromodynamics 77−13926
composite model of mesons in relativistic space, masses, leptonic widths *(Russian)* 77−74658
duality, diagram topological expansions incorporating baryons and mesons 77−57505
electric and magnetic confinement schemes for mesons and baryons 80−4960
EM form factors and integral representation of wave function in straton model *(Chinese)* 77−34124
exotic mesons, qq̄g states in bag model, energy, spin, parity, mass spectrum *(French)* 79−80807
form factors, relativistic covariant quark model *(Russian)* 80−9140
gluonic resonances in hadronic spectrum, scalar mesons, pomerons 78−21394
gluonium type, solns. to scalar Higgs eqn. *(Russian)* 78−12829
Green function, rainbow approach of scalar model *(Russian)* 80−68436
high-spin meson possibility with mag. monopole and antimonopole *(Chinese)* 78−17068
isospin classification, same finite group for mesons and baryons *(Chinese)* 80−62887
Klein Gordon equations superposition, meson model, φ, f′, F, K spectrum 78−58121
light scalar, phion, in neutron struct. theory 80−18134
mass formula, quark line rule in u-, d-, and c-quark sector 78−8596
meson spectrum in simple planar bootstrap model 78−8618
MIT bag model, coloured quark and gluon constituents of mesons 80−4929
multicolour QCD as dual resonance theory, mesons on rising Regge trajectories 78−16987
neutral mesons, quark flavour mixing 78−426
pairing vibration model of meson states, supercond. model of hadrons *(Chinese)* 77−10217
parton distribs. consistent with naive quark model and QCD 80−62937
PCAC and dual resonance amplitudes, old and new mesons, charm 78−45885
pion spectrom. for meas. electro- and photo-pion spectra in high background environment 80−27868
properties, review from particle data group 80−67944
pseudoscalar, $SU(3)_E$-invariant form factor 77−61288
pseudoscalar meson mixing problem, SU(4) spectral function sum rules, chiral symm. 77−38143
pseudoscalar mesons, charge radii and PCAC without soft current limit 80−99070
pseudoscalar mesons, $SU_4×SU_4$ chiral symm. 77−67583
pseudoscalar nonet, chiral SU(3) breaking 77−6046
QCD, 1+1 dimens., meson wave functions 78−54559
QCD, 2-dimens., confinement effects on analyticity meson inelastic form factor, scatt. amplitude 79−333
QED of vector mesons, effective electric charge and asymptotic freedom *(Russian)* 78−45827
quark masses and structure functions, 0$^-$, 1$^-$ mesons 80−22585
quark model relativistic generalisation minimal boosting of SU(6) scheme, meson, baryon props. 77−41814
quark theory with internal coords., Dirac eqn., Bethe Salpeter eqn. 77−13937
quark-antiquark-gluon bound state 78−45877
representation mixing, SU(4), mass formula, EM mass shifts 78−12890
straton model, bound states of mesons, average radii, pion appl. *(Chinese)* 78−78150
straton model, meson wave functions, Bethe-Salpeter eqn., SU_6 symm. *(Chinese)* 77−34125
straton model, near-flat-bottom interaction pot., wave function of pseudoscalar meson *(Chinese)* 78−82167
string model with two massive quarks 77−10212
strong PCAC appls., axial vector current 4-divergence, meson fields *(Chinese)* 80−42364
structure function in covariant parton model context 80−78020
structure model with covariant oscillator potentials *(Chinese)* 78−82180
structure wave functions, harmonic oscillator model *(Chinese)* 77−34123

mesons continued
structure wave functions in relativistic straton model, Bethe-Salpeter eqn. *(Chinese)* 78−50011
structure wave functions of mesons, instantaneous interaction approx. straton+antistraton pair *(Chinese)* 77−10216
SU(3)×SU(3) model, meson spectrum, prod. and decay of new particles *(Chinese)* 77−49870
superconductivity phase transition in meson states, quark quasiparticle model *(Chinese)* 80−102021
superluminal antimesons in 1955 antiproton-discovering time-of-flight expt.? 79−67158
topological expansion for baryons and mesons, reaction diagrams using coloured quark lines 77−82700
topological expansion for baryons and mesons, Veneziano scheme 78−70335
two-nucleon pot. and meson physics, nucleon-nucleon interactions, review 78−89802
vector mesons in weak interactions, gauge model *(Russian)* 78−45838
wave eqn. from Bethe-Salpeter eqn., comments 77−65136
wave functions, SU_n representation transformations and phase *(Chinese)* 79−93313
Yang-Mills gauge theory, classical soln. in colour meson model 78−45780
D^+-D^0 charmed mesons EM mass difference estimate, quark pair creation model 77−10250
ϵ(700), four quark bag model, high statistics data anal. 78−82147
F-meson production suppresion relative to D-meson 79−36100
$q\bar{q}$ systems, nonperturbative potential model 80−78040
Υ (9.5) props., $SU(4)\times S_3$'' scheme in straton model *(Chinese)* 79−9347

mesosphere
quasi 2-day wave in S.Hemisphere mesosphere, obs. 80−109207
acoustic-gravity waves propagation 78−44912
aerosol, remote sensing techniques 80−109269
aerosol layer, contrib. to polar albedo 77−60467
aerosol meas. by solar occultation method 77−45090
airglow diurnal var. and seasonal depend. rel. to solar semidiurnal tidal wind 77−21965
airglow in upper mesosphere, seasonal and long-term vars. and dynamics 77−33237
Antarctica and equatorial India, atm. struct. during southern summer 77−53121
Arctic, vertical temp. and density patterns anal. as gravity waves 79−16622
autumn-winter transition in mid-mesosphere, ionospheric absorpt. at 25 kHz 79−62644
baroclinic instability in summer circulation 77−45111
chemical composition, importance of energetic particle precip. 80−109213
circulation, extensions of Leovy's linear model 78−32201
circulation and clouds, rel. to thermosphere semi-annual temp. vars. 78−45061
circulation over Antarctica, seasonal vars. 77−21829
cluster ion chemistry for Na and Na^+ layers 79−74934
composition, chemical response to changes in UV solar flux 77−33167
composition of middle atm., in situ meas. 80−17339
corpuscular radiation flux variations in daytime midlatit. mesosphere 77−29538
cosmic ray ion-pair production rate above 18 km altitude, parametrisation 78−65469
data and models 79−84553
daytime neutral winds trace constituents sounding rocket campaign results 78−45071
density variations and meteor rates correl. with solar activity 77−53485
diurnal and seasonal variations of O, H and N components 77−9586
dynamic model rel. to ALADDIN I program meas. 79−48592
dynamics, characteristics and processes, review 77−25734
dynamics of middle atmosphere, review 80−17338
eddy diffusion, models for mesosphere and lower thermosphere 80−109198
eddy diffusion coefficient, semi-theoretical global models based on satellite data 79−21086
electric field strength max. meas., 30-90 km altitude range 77−29358
electrical conductivity and ion mobility height var. 77−21837
electron density and drifts correl. with stratospheric temp. and wind 77−9470
electron precipitation at high latitude, X-ray bremsstrahlung obs. 80−77205
energetic charged particle precipitation, meas. during European Winter Anomaly Campaign (1975-76) 78−45001
energetics and thermal struct., theory 80−98412
equatorial, vertical vel. determ. from Diurnal Experiment 80−77047
equatorial circulation indices seasonal vars. at Thumba 78−85630
equatorial waves in upper stratosphere and mesosphere, rel. to zonal wind semiannual oscill. 79−5575
W.Europe, atmos. temp. 20-110 km altitude, 1975/6 winter anomaly 80−36356
W.Europe, ion production obs., 50-120 km altitude, 1975/6 winter anomaly 80−36439
W.Europe, mesosphere and lower thermosphere temp. and density, 1975/6 winter anomaly 80−36357
W.Europe, mesosphere and lower thermosphere trace constituents, 1975/6 winter anomaly 80−36433
general circulation, anal. of rocket soundings on Kerguelen Island (February-May, 1973) 78−20489
general circulation, radiative transfer, transport processes, review 78−49105
gravity waves component in partial refl. drift obs. 80−81993
gravity waves in inhomogeneous atmosphere, wave-field calc. 77−17186
gravity waves induced by Earth's diurnal rotation, heating effects 78−40613
heat budget of mesopause 78−28258
heating rate parameterization, 15-120 km altitude, due to O_2 and O_3 absorpt. of solar radiation 79−39798
horizontal eddy diffusivity in northern hemisphere 79−84439
ice clouds production by Earth encounter with interstellar cloud, climatic effects 78−57292
incoherent scatter spectrum, ion component meas. in 60 to 90 km region over Arecibo 79−16569
infrasound, refr. by winds 77−33229

mesosphere continued
internal gravity waves, at mid-latits. in mesosphere and lower thermosphere 77−5298
internal gravity waves, propag. range *(Russian)* 79−16575
internal gravity waves near mesopause rel. to OH emission 78−12031
ion bunching, model 78−73424
ion conductivity, concentration and measurement, meas. via payload B III instrument package 78−45194
ion mobility and concentration, and conductivity, 10-70 km altitude 80−36358
ionisation model of upper mesosphere, rel. to ionospheric reflecting layer below classical D-region 80−98508
ionisation of equatorial lower mesosphere, effect of galactic X-ray source 78−36233
IR nonthermal emissions from O_3, Spacelab obs. 77−21906
Joule heating at high-latitude 80−41500
Kelvin waves, struct. and behaviour from Nimbus 5 IR meas. 80−8394
LF radio wave absorpt. temp., seasonal variation 79−48602
LF radio wave absorpt. variations, press. and temp. depend. 79−44282
light scatt. coeff. correl. to atmos. stratification *(Russian)* 80−105049
long-perioc waves in upper mesosphere, radar obs. 80−77056
mass motions, mean meridional 79−88419
mean meridional circulations of stratosphere and mesosphere, monthly mean planetary wave fluxes 80−109219
mean zonal circulation in meteor zone above France and Sweden 79−75003
mesopause, energy characts. of internal gravity waves obs. by OH emission *(Russian)* 79−12324
mesopause, lidar meas. of Na conc. and neutral temp. 78−61613
mesopause, prevailing wind altitude-latit. struct., 80-100 km altitude 79−29829
mesopause, radiative cooling 80−26660
mesopause region, ion-clustering during winter anomaly, temp. and NO density vars. effect 79−21087
upper mesopause region, wind systems behaviour in winter and winter/summer conditions transition 79−44220
mesopause temperature, determ. from $[NO^+.H_2O]/[NO^+]$ ratios 79−96849
mesopause wind from ionospheric drift meas., geomagnetic storm effects 79−35025
meteor trail diffusion, radio refl. determination 80−46329
microwave limb sounding for composition and temp. determ. 77−21940
middle atmosphere, obs. from balloons, rockets and satellites, conference, London, England, (1978 December 12 to 13) 80−77540
minor constituents concentration profiles, Spacelab obs. 77−21967
minor constituents distrib. in thermal interface 78−3891
minor species and temp. meas. using cryogenic etalon-spectrometer on Space Shuttle 79−58232
motions in winter mesosphere using partial reflection drift obs. 77−64393
neutral temperature from nightglow OH emission obs. 80−82121
neutral winds, rocket determs. compared with partial refl. drifts 77−87019
nightglow near IR continuum, implications for upper mesosphere 77−78551
noctilucent cloud aerosol particles, temp. profiles *(Russian)* 78−16093
noctilucent cloud obs. over western Europe and Atlantic during 1976 77−78346
noctilucent cloud region, ion comp. 77−87011
noctilucent clouds, advances in space era, review 80−105095
noctilucent clouds, cine and television high-resolution obs. 79−39891
noctilucent clouds, circularly polarised light detect. 79−48568
noctilucent clouds, mesospheric structural parameters variations 77−49203
noctilucent clouds, obs. in Poland during 1974 77−21826
noctilucent clouds, photographic obs. on 1976 June 18-19, Scotland 77−81982
noctilucent clouds observed during 1976 in Poland 79−16559
noctilucent clouds over W.Europe (during 1979) 80−109289
particulate transport, downward to aerosol layers 77−78348
periodic temp. and wind fluctuations 77−78361
pitot pressure measurements for density determ. between 50 and 120 km, W.Europe Winter Anomaly Campaign 78−45193
planetary wave, radiatively damped, in middle atmosphere, interaction with zonally averaged circulation 80−109217
planetary waves, struct.-correction 80−8403
planetary waves at 20-80 km altitude rel. to ionospheric absorpt. winter anomaly 80−36359
planetary waves in winter, Nimbus 6 PMR preliminary results 77−87040
plasma and neutral gas composition and structure, anal. during winter anomaly 78−45191
positive in composition and chemistry of high-latitude mesopause 80−46224
radar echo mechanisms, returns from clear air 80−90181
radar facility, MST radar at Poker Flat, Alaska 80−90254
radar for observing middle and upper atmosphere, Yaggi antenna array design 80−90255
radar signal detection, VHF, complementary code and digital filtering 80−46274
radar studies at VHF and UHF freqs., review of obs. 80−90180
radar techniques (VHF and UHF) for dynamic struct. 80−105078
radiation belt energetic electron precip., natural depletion mechanism for stratospheric O_3 77−41134
radiative equilibrium temperatures, comparison for stellar occultation and BUV O_3 data 78−81280
radiative transfer in CO_2 4.3 μm band with non-LTE *(Russian)* 78−88914
radiative transfer in Doppler broadening atmospheres, stratosphere, mesosphere and thermosphere 77−78418
radiowave backscattering, depolarisation obs. at 50 MHz 80−85729
radiowave scattering of tropical latitude, VHF radar study 80−90193
radiowaves, medium and short, seasonal absorpt. courses, rel. to strato-mesosphere dynamics 79−58149
Sardinia (40°N), comp. and temp. during D-region winter anomaly 80−21871
satellite observations of middle atmosphere processes 80−21803
satellite solar occultation sounding of the middle atmosphere 80−105079
seasonal and latitudinal variations in temp. and composition 77−45207
semiannual oscillation in tropical middle atmosphere, review of observational evidence 80−109216

mesosphere continued
silver clouds, visible spectroscopic investig. from Salyut-4 orbit 80−82014
solar H Lyman-α radiation extinction, meas. rel. to O_2 density, press. and temp. profiles 78−44947
solar Lyman-α extinction, meas. during European Winter Anomaly Campaign (1975-76) 78−45001
solar Mesosphere Explorer mission description (1981-2), O_3 and related chemistry 80−105096
Solar Mesosphere Explorer optical-mechanical systems engineering 79−58230
solar UV radiation, absorpt. in mesosphere and stratosphere 80−109248
sonic booms from Concorde aircraft flight, atm. struct. information 79−66742
spectral absorption, Lyman-α extinction by O_2 80−77180
spectrally integrated transmittance in O_2 Schumann-Runge bands and O_2 column density, 76-102 km altitude 79−70902
spherical ice particles, equilibrium temps. rel. to noctilucent cloud formation 77−37302
stationary planetary waves and zonal wind, southern hemisphere 78−28276
strato-mesosphere, seasonal relation between winds and LF radiowave absorpt. 79−62645
structure, composition, temperature and motion, general review 79−39997
structure and thermal regime, average daily closed model 77−17264
structure at Thumba from in situ UV absorpt. photometry obs. 80−105051
structure in presence of noctilucent clouds 80−8412
structures diurnal vars. in different seasons, VHF radar meas. 79−84370
SURF storage ring calibrations for NASA stratosphere and climate programs 80−94721
temperature, day-night depend. of geomag. activity effects 77−21835
temperature, obs. by satellite IR limb scanning method 80−105086
temperature corrections for Menaka-II meteorological rocket payload 79−5558
temperature diurnal variation, 25-65 km altitude equator region 80−82022
temperature rel. to water cluster ions form. in D-region 77−21842
temperature vars. rel. to solar mag. sector struct. 79−34905
temperature waves of annual and semiannual period, radiometer obs. 80−51500
tidal energy distrib. with altitude, wind field influence *(Russian)* 78−69402
tides, thermal exciting energy, numerical anal. 79−70833
tides and gravity waves, at mid and low latits. 78−36231
tides and planetary waves in upper mesosphere *(French)* 77−21962
tides at meteor altitudes, CTOP radar obs. 80−77181
transport and chemical processes 77−25761
travelling neutral disturbances and minor constituent particle mass 78−49189
turbidity from twilight obs. 77−5318
turbulence characts. from D-region partial refl. method 78−49215
turbulence structures, high-resolution VHF radar obs. 79−100895
turbulent diffusion coefficient in mesosphere and lower thermosphere, seasonal vars. 79−53424
turbulent structure, spectral range *(Chinese)* 80−105092
UHF radar echoes, Arecibo expt., for wind and turbulence obs. 77−33135
Van der Waals molecules comp. of lower atmos. 80−85699
vertical velocities, first VHF radar meas. at temperate latits. 79−16572
VHF radar obs. of struct. and dynamics 80−105032
VLF absorpt. seasonal variations, geopot. field 79−66766
water vapour concs. above mesopause 77−73898
wave motions and daily neon winds, 52-110 km altitude, at midlatits. 79−5565
wavelike struct. seen in radar obs. of vertical velocity 59-95 km altitude 80−90117
waves and winds over Jicamarca, preliminary multiheight radar obs. 78−36230
waves rel. to dynamics of mesosphere and lower thermosphere 79−53464
wind and temp. diurnal and semidiurnal oscills., rocket meas. 79−5556
wind and thermal structure, W.Europe 1975/6 winter anomaly obs. 80−36438
wind determination by meteor track movement *(French)* 80−51589
wind diurnal variation, 25-65 km altitude equator region 80−82022
wind in upper mesopause, diurnal variation of zonal and meridional components 80−109284
wind measurement at 60-120 km, radiowave drifts technique 80−31137
wind structure over Antarctica 80−81992
wind systems behaviour during transition from summer to winter conditions 78−49097
winds, mid-latitudes, mag. storm effects 80−61970
winds and turbulence continuous meas. using VHF Doppler radar, preliminary results 80−8444
winds and waves over Jicamarca, 1974 May 23-24 VHF radar obs. 80−12497
winds at equatorial latits., observational aspects review 78−36229
winter processes, rel. to wind regime of lower thermosphere 78−4019
zonal mean circulation of middle atmosphere, numerical model 80−109218
zonally averaged circulation, 15-125 km altitude region 79−5564
CC Na layer, seasonal var. at low latits. 79−79964
CO mixing ratio from ground-based microwave meas. 79−58036
H distribution, UV dayglow obs. 80−109290
H_2O cluster ions at cold mesosphere, rocket borne expt. 80−17429
H_2O near mesopause, dissoc. during auroras rel. to ionosphere winter absorpt. anomaly 79−58152
H_2O rocketborne obs. in auroral zone 78−7688
H_2O vapour amount of rel. to particle sizes in noctilucent clouds 78−57248
H_2O vapour line at 22.2351 GHz, hyperfine structure 79−8666
H_2O vapour meas. from ground-based microwave obs. 77−33161
$H_3O^+(H_2O)_n$, photodissoc. meas. and calc., rel. to atmospheric stability 79−86017
N and NO density in polar regions under auroral perturbs. 77−73897
NO concentration geomag. control from simultaneous D and F regions ionisation meas. 79−8651
NO, density profile from airglow obs., 72-120 km altitude 80−105094
NO, photodissoc. in mesosphere and stratosphere, theory 80−41580
NO, photodissoc. rate, calc. 80−51498
mesosphere continued
NO predissociation, photochemistry 80−21802
NO vertical density profiles at midlatitudes 77−87012
Na I 5893 Å nightglow and Na atoms distrib. in mesosphere, simultaneous obs. 78−88961
Na, K, mesospheric abundances, simultaneous nighttime lidar meas. 78−36239
Na layer, extra-terrestrial source, evidence 79−12191
Na layer, mesosphere, meas. by efficient forced oscillator dye laser 80−41563
Na layer at 23°S, nocturnal and seasonal vars. 79−74932
O 2.53 mm line, Zeeman splitting rel. to geomagnetic field vars. 80−77124
O concentration, inference from positive ion comp. data 80−8405
O I 5577 Å, Na and OH nightglow emissions var. during stratospheric warmings 77−53270
O I 5577 Å nightglow obs., evidence for vertical transport latit. var. near mesopause 79−70903
O profile of mesosphere and lower thermosphere 80−72660
O remote sensing in mesosphere and lower thermosphere, two-photon lidar technique 79−39869
O-H atmospheric model rel. to OH emission problem 77−60503
O_2 and O distrib., effect of magnetospheric elec. fields 79−66850
O_2 densities, meas. from atmospheric absorpt. of solar Lyman α radiation 77−87010
O_2, photodissoc. and spectral absorpt. in stratosphere and mesosphere 80−51497
O_2, Schumann-Runge bands, atmospheric absorpt. model 79−96823
O_2, seasonal vars. in 70-90 km altitude range 79−100994
O_3, 9.6 μm band radiance calc., excitation processes 78−36350
O_3 abundance, meas. from ground-based millimetre wave obs. 77−29381
O_3 abundance from backscattered solar radiances 78−69414
O_3, Cl abundances, OAO 3 stellar occultation meas. 77−9580
O_3 conc. meas. at high latit. during twilight 77−41128
O_3 concentrations, meas. from 1.27 μm O_2 airglow at middle latit. 80−72606
O_3 content in tropics, during March-April 1976 stratospheric warming 80−12494
O_3 meas. during Aladdin 74 program above Wallops Island 78−57247
O_3 meas. from ground-based mm wave obs., comment 78−11967
O_3 measurement by satellite IR limb scanning method 80−105086
O_3, nighttime conc. from OH nightglow obs. 79−5698
O_3, nighttime concentration (15-68 km), Nimbus 6 obs. comparison with OAO-3 obs. 80−105016
O_3 number density profile of lower mesosphere 80−41579
O_3, obs. of shadow on D-region in ionosphere VLF guide over Atlantic Ocean 79−58161
O_3 seasonal var. from rocket-borne UV obs. 77−29402
OH emissive layer, waves, near IR photographic studies 80−51545
OH nightglow emission, intensity meas., and O-H comp. model 77−29529
OH radical, in Earth's atmosphere, pure rot. lines 79−92593
$O(^3P)$ translationally hot, energy distrib. function 80−21811
$^{18}O^{16}O$, photodissociation as source of atmospheric O_3 80−94559

metal castings *see castings*

metal clusters
amorphous metals, icosahedral microclusters as possible structural unit 78−34439
Be small metallic clusters size fluctuations of work function 78−14792
bicrystal, mech. behaviour, continuous theory of dislocations appl. 78−67717
bimetallic cluster, segregation and short range order props. at boundaries 79−29071
binary microcluster, struct. and thermodynamics, Monte Carlo simulation 79−7736
binding energy of aggregates 79−51464
boride coating, diffusion soaking effect on struct. 78−18846
chemisorption of H on 'cubium' clusters, size effects, embedding 77−59202
discrete variational Xα cluster calculations, applic. to metal clusters 78−90332
dispersed metal catalyst clusters, EXAFS obs. 79−91530
electronic time-of-flight mass spectrometer, separator for metal clusters research 80−77907
energy spread of cluster ion from molten metal, charge exchange 80−37922
epitaxial small islands, one-dimens. model of mobility, parabolic substrate pot. 79−95299
formation, by ion bombardment of single cryst. surface 78−92157
growth and props., appl. to catalysis and photographic processes, conf., Villeurbanne, France (Sep. '79) 80−105431
high molecular weight, on surfaces, characterisation by SIMS and XPS 79−16054
isomer shift of ^{57}Fe, nearest neighbour effect 80−44988
rel. to macrometals as possible excitonic superconductors 79−42688
matrix isolation of aggregated species, cluster form. 77−62630
melting of 9 Å particle in zeolite matrix 77−59103
metal-rich compounds, struct. and props. 78−95045
mixture, binary, off-critical, quenched, struct. functions and mobilities renormalisation 79−82343
molecular clusters, UPS 80−80940
molecular metal clusters rel. to chemisorpt. and catalysis 77−76668
moment development method, appl. to small metallic clusters *(French)* 77−31925
monovalent metal distortions induced by finite size in regular clusters 77−35507
nucleation and mass spectra, clusters from 2 to 500 atoms 80−102596
nucleation of metal vapour in inert atmosphere 78−63645
one dimensional motion, statistics 77−85050
SCF-Xα-MS calc. for H 78−47730
spinglass mean-field model, static props. 79−4689
structure and properties 80−39304
TC, internal conversion, scattered-wave cluster technique 80−107696
transition and noble metals, electronic struct. and mag. props., MO calc. 77−20219
transition metal, bimetallic cluster, photoselective bimetallic aggregation, review 80−53182
transition metal, cohesive energy and level statistics 78−95267
transition metal, higher-order isotropic exchange, Schrodinger exchange model 79−7955

metal clusters continued
transition metal, local densities of states and bonding props. 77−20401
transition metal cluster carbonyls. fluxionality, collective oscills. and low energy spectra 80−78738
transition metal clusters, bonding capabilities, MO calcs. 79−22589
transition metal clusters, chemisorption, alloying effects, model calc. 77−62751
transition metal clusters, particle size rel. to bulk metallic props 80−44490
transition metal surface clusters, Hartree-Fock-Slater model calcs. 77−72899
transition metal surface electronic struct., influence of size and roughness 78−14785
Wolfsberg-Helmholz relation analysis, reson. integral approx. 80−49566
X_α method of theory of multiple scattering, appl. to props. of metal clusters *(Russian)* 78−38996
Ag, chemisorption of I, UPS obs. 80−84830
Ag, cluster and microcrystal, matrix isolated, optical absorpt. spectra, photolysis and plasmon absorpt. 79−89820
Ag clusters, latent image particles, electronic effects 80−82840
Ag, on Si substrates, opt. spectra investig. of struct. *(German)* 80−25492
Ag-Au clusters, latent image particles, electronic effects 80−82840
Ag_n, ($n<10$), uv-visible absorpt. spectra in Kr matrices 79−13858
Ag_n, n=7,10,13,19, atom clusters, local density of states, $X\alpha$ scattered wave calcs. 78−18989
Al, chemisorption of O_2, orbital resons., $X\alpha$ cluster model calcs. 77−72774
Al, growth and composition on NaCl substrate 77−89677
Al-Cu complexes, in ZnS, localised vibrational modes 78−63827
Al_5, chemisorpt. of Na, Si and Cl, core hole induced electronic relax. 79−90874
Al(111), chemisorption of O_2, SCF X_α scatt. wave MO calc. 79−42374
Au, coalescence on NaCl substrates at room temp. 78−18935
Au crystallites, vacuum deposited on MgO (111) surface, in-situ TEM obs. of mobility 77−76686
Au, FCC cluster, 40 kV electron scatt. dynamic effects 77−79721
Au, pentagonal symmetry, icosahedral struct. *(French)* 80−79729
Au small particles, size effects studied by electron energy loss anal. 79−47567
Au small particles in glass, transition cluster-solid state 79−33593
Au-Fe spin glass, susceptibility cusp, influence of Fe clusters 79−61163
Be_4, Be_2, dissoc. energy, electron correlation effect, self-consistent electron pair calc. 77−30790
Be_n^- (n=2,3,4), electronic struct., ab initio calcs. 78−17560
Bi, 2 to 500 atoms, nucleation, mass spectra 80−102596
$Co(CO)_4^-$, extended CNDO calc. 80−918
$Co_2(CO)_8$, extended CNDO calc. 80−918
$Co_4(CO)_{12}$, extended CNDO calc. 80−918
Cu, and bulk, struct. and electronic props. 78−95592
Cu atom in bulk, local density of states 79−37947
Cu, atomic clusters, struct. and electronic props., Mulliken-Walsh diagrams, extended Huckel procedure 78−46479
Cu, clusters, size, geometric effects, catalysis implications 78−73131
Cu clusters, valence band and core binding energies, UPS meas. 79−38721
Cu clusters, visible and near-UV spectra 78−19503
Cu, film growth on graphite and amorphous C, electronic struct. by photoemission and Auger obs. 79−77947
Cu, interaction with CO, Cu_nCO form., chemisorpt. bond 78−31631
Cu metal cluster, adsorption of CO, mol. orbital calc. 78−18895
Cu, optical spectroscopy, atom to bulk 78−95591
Cu, resonance line, degree of coordination of clusters in metallic vapours *(French)* 77−58218
Cu small particles, CO interaction, IR spectra obs. 77−20195
Cu-Fe, Mossbauer studies of ageing and precip. 79−38415
Cu_3 Zn clusters, electronic structures, SCF-Xα-SW method 80−88468
Cu_4 clusters, electronic structures, SCF-Xα-SW method 80−88468
Cu_n, cluster formation, by ion bombardment of single cryst. surface 78−92157
Cu_3Au alloy, dynamics of ordering clusters in thermal non-equilib. state 79−51257
$Cu_{0.435}Ni_{0.565}$, clustering, temp. depend., diffuse neutron scatt. study 79−42013
Fe clusters, supported, Mossbauer spectra 80−7220
Fe, ferromagnetic, cluster method, environmental effects 78−95405
Fe-Cu clusters, mag. interaction, Mossbauer study 79−82895
Gd clusters in faujasite type zeolites, mag. suscept. temp. depend. 78−14925
Hg, thermophys. props. rel. to clustering in liqs. 77−1065
Ir, adsorption of H_2, influence of surface steps and clusters, field emission investig. 77−28698
K atom clusters, cluster beam Stern-Gerlach mag. deflection 78−54504
Kr:Mg_n, matrix isolated Raman spectra 78−90170
Li, chemisorption of H, ab initio HF calcs. 77−76670
Li cluster, density functional calcs. 77−8031
Li, cluster and microcrystal, matrix isolated, optical absorpt. spectra, photolysis and plasmon absorpt. 79−89820
Li, dissociative chemisorption of H_2, ab initio SCF-MO calcs. 79−77918
Li, thermophys. props. rel. to clustering in liqs. 77−1065
Li_2, and anion, electronic struct., spin-unrestricted, spin-restricted SCF HF calc. 78−90331
Li_2^-, electronic struct., ab initio calcs. 77−34553
Li_{2n}, (n=1, 2, 3), stable cluster configs., ionisation pots., binding energies, vibr. freqs., al initio SCF and CEPA calcs. 80−14265
Li_3, multibody and stability considerations, small clusters 78−90333
Li_4, plane configs., ab initio SCF calc., rel. to condensation *(French)* 77−4062
Li_n, equilibrium struct., effect of p-functions *(German)* 79−89823
LiNa, and anion, electronic struct., spin-unrestricted, spin-restricted SCF HF calc. 78−90331
$Mn_2(CO)_{10}$, extended CNDO calc. 80−918
Mo_{12}, one-dimens. condensation of Mo_6 octahedral clusters, prep. and struct. of $Tl_2Mo_9S_{11}$ and $K_2Mo_9S_{11}$ 80−107168
N_2+Fe (atomic), interaction mechanism via clusters 77−25263
Na cluster, density functional calcs. 77−8031
Na, cluster and microcrystal, matrix isolated, optical absorpt. spectra, photolysis and plasmon absorpt. 79−89820
Na clusters, electronic relaxation energies in $KL_{2,3}L_{2,3}$ Auger transitions, SCF-Xα-SW calcs. 78−90334
metal clusters continued
Na, metallic; Auger cross relaxation energy, SCF cluster model calc. 79−46945
Na, thermophys. props. rel. to clustering in liqs. 77−1065
Na_2, and anion, electronic struct., spin-unrestricted, spin-restricted SCF HF calc. 78−90331
Nb, scattered wave Xα calcs. 79−15068
Nb_6 clusters, electronic struct., scattered wave-Xα calc. 79−11053
Ni, adsorbed S(Se) surface bonding mechanism for ang. resolved photoemission 79−69360
Ni, adsorption of H_2, activation mechanism, extended Huckel calc. *(French)* 79−42379
Ni, chemisorptive binding of O, CNDO calc. of potential energy curves *(German)* 80−44431
Ni, cluster approach to single H atom in single crystal 78−47334
Ni cluster-H, electronic struct. calc., H-metal bonding 77−89823
Ni clusters, chemisorption of H, macroscopic props. 79−82445
Ni clusters, electronic props. and implications for chemisorption 79−23886
Ni clusters, FCC and icosahedral structs., relax. and stability, cohesive energy minimization 79−42479
Ni clusters, valence band and core binding energies, UPS meas. 79−38721
Ni clusters local densities of states 80−88466
Ni, dynamic rearrangement of atomics in large cluster using Frohlich-Raimes method 78−30586
Ni, film growth on graphite and amorphous C, electronic struct. by photoemission and Auger obs. 79−77947
Ni, highly dispersed K_β emission spectra, cluster effects 77−28650
Ni metal cluster, adsorption of CO, mol. orbital calc. 78−18895
Ni, metallic particles, stability and electronic struct. *(French)* 80−80155
Ni-Cu alloys, short-range atomic clustering, residual resist. meas. 80−29386
$Ni_{13}(O_h)$ cluster, electronic states and X-ray spectra in Xα approx. of multiple scatt. theory 77−28645
Pb, 2 to 500 atoms, nucleation, mass spectra 80−102596
Pb microclusters, mol. beam electron diffr., amorphous struct. 78−66703
Pb, thermophys. props. rel. to clustering in liqs. 77−1065
Pd, adsorption/desorption of CO, AES and thermal desorption meas. 80−75436
Pd, calculated structural stability 78−95268
Pd, catalyst, Z-contrast, in STEM 79−46530
Pd catalytic clusters, electronic structure, XPS obs. 77−77345
Pd cluster-H, electronic struct. calc., H-metal bonding 77−89823
Pd, clusters, size, geometric effects, catalysis implications 78−73131
Pd clusters, valence band and core binding energies, UPS meas. 79−38721
Pd, density of states profiles, Hartree-Fock-Slater model 77−31930
Pd, film growth on graphite and amorphous C, electronic struct. by photoemission and Auger obs. 79−77947
Pt, at. struct. 79−19186
Pt, catalyst, Z-contrast, in STEM 79−46530
Pt catalytic clusters, electronic structure, XPS obs. 77−77345
Pt cluster, conduction electron density oscills., NMR spin-echo meas., indirect exchange interaction 80−44954
Pt cluster-H, electronic struct. calc., H-metal bonding 77−89823
Pt clusters, supported on Y-zeolites, X-ray absorpt. spectrosc. obs. 79−24390
Pt small particles, on graphite substrate, crystallographic struct., electron microscopy study 79−99465
Pt, struct. sensitivity of O_2 reduction in acid electrolyte 79−70343
Re_2, dimer surface diffusion on W(211) atoms and dimers, surface diffusion 77−20183
Re_3Cl_9 metal cluster complexes, He(I) photoelectron spectrum, SCC DV Xα calcs., $Re_2Cl_8^{2-}$ comparison 80−28063
Ru-Cu clusters, EXAFS study 80−84804
Sb, 2 to 500 atoms, nucleation, mass spectra 80−102596
Sb discontinuous thin films, cluster shape models 80−100419
$Sm_{11}Cd_{45}$, cryst. struct. similarity with γ-brass and α-Mn clusters 78−75625
$TcCl_8^{3-}$, metal-cluster, EHT calcs. of electronic struct., metal-metal bonding *(Russian)* 77−61687
Ti-Fe, H storage material, Mossbauer surface studies, Fe clusters 80−97167
V_2, formation, spectra, electronic struct. 77−54642
Zn_4 clusters, electronic structures, SCF-Xα-SW method 80−88468

metal corrosion *see corrosion*

metal-insulator boundaries
see also metal-insulator-metal structures
aliphatic unsaturated poly(1,3,4)-oxadiazole films, electrode and bulk limited currents 77−69436
band gap closure in insulator near metal-insulator interface 80−11086
bulk states in semiconductors and insulators in contact with metals, charging 80−54781
catalytic reactions studied by work function meas. 80−55711
charge injection, dynamic, unidimensional numerical simulation of carrier and field distrib. *(French)* 77−32079
charging polymer surfaces, injection times obs. 80−70796
contacts, model of charge injection 78−68088
current injection in presence of space charge 79−1619
cyclohexane, liq., ion injection by metallic electrodes *(French)* 79−51289
dielectric space charge distrib., carrier mobility and interface injection mechanism identification 80−15974
dielectric-plasma like medium interface, image potential 78−14794
electrification of polymers by metals, contact time effect obs. 80−70829
electron states near interface, Hubbard model, possibility of insulator-metal transition 78−52084
electron tunnelling, its role in contact electrification 80−2453
electrostatic interaction of charges with metal-insulator interface 80−24996
energy barrier, self-consistent theory 80−60087
exciton quenching and excited state props. 77−4416
film-covered electrodes, electron transfer reactions, mechanisms, theory 78−20023
frictional electrification of PVC contrib. of polymer mol. motion 80−70798
hexafluoropropylene-tetrafluoroethylene copolymer, surface component of vac. absorpt. and resorpt. currents, source of dielec. loss 80−70792

metal-insulator boundaries continued
image charge pot. at interface of two semi-infinite media, Thomas-Fermi soln. 79−87155
interfacial photoemission at metal insulator contacts, book contrib. 78−95676
interfacial polarisation effect on dielectric props., sandwich capacitor model 80−15614
metal polymer contact, charge transfer and contact charge spectroscopy 80−65680
metal polymer contact, charge transfer and contact charge spectroscopy 80−65681
metal-air interface, far IR propag. distances of surface EM waves 79−42616
metal-dielectric interface, static point charge in dielec., pot. distrib. *(Russian)* 80−60088
metal-NaCl system, sliding and rolling electrification 78−14796
metal-oxide system characterisation by high-resolution electron spectroscopy 77−40624
metallic films, metal-dielectric boundary thermal resistance, nonlinear elec. resistance *(Russian)* 80−65530
metallic thin films, electric field distrib. and emission currents of island condensates 78−88047
multilayer, irradiated, model for calc. of electrical response 77−24607
noble metal-ceramic interface, effects of noble metal corrosion 78−53035
PET, ionic cond. current rel. to neutralisation at polymer-metal interface at elevated temps. 80−24664
phonon hydrodyhamics, boundary conditions *(Russian)* 77−80692
photon assisted tunnelling and internal photoemission 78−60202
poly-2-chloro-p-xylylene, photoinjection of holes using Au, Ag, Cu, Sn, Pb and Al electrodes 79−47161
poly-N-vinylcarbazole−metal electrode, photoemission of electrons, photocond. meas. 79−91142
polyethylene terephthalate charge transfer from metallic electrodes 80−15605
polymer, molecular charge states, contact charge exchange 78−14822
polymer-metal contact, material transfer in contact electrification 78−6432
polymers, surface component of vacuum absorpt. and resorpt. currents, surface charge accumulation 80−60063
polymers, surface component of vacuum absorpt. and resorpt. currents, origin and magnitude 80−70791
polymers, vacuum-UV irrad. photoelec. emission and contact charging 79−52075
polymonochloro-p-xylylene, γ-ray-induced cond., hole injection effects 80−34452
polystyrene, γ-ray-induced cond., hole injection effects 80−34452
polystyrene, pure and doped, metal contact effect on persistent internal polarisation 79−78617
polystyrene films on metal substrates, electrode effect on carrier injection, TSC, I-V characts. 80−34463
polystyrene-metal contact-charge-exchange expt., charge induced relaxation 77−4309
polyvinylidene fluoride film, piezoelectricity, importance of metal-polymer interface 78−76391
PVC-metal interface, ionic carriers behaviour 79−99622
PVF_2 charge injection from metallic electrode, obs. 80−15947
rubber-metal interface, adhesion mechanism, XPS study 80−65382
sapphire-Al interface barrier, transport and trapping obs. 77−76921
secondary electron emission near dielectric-metal interface 79−38697
solid electrolyte interface, low-amplitude AC passage 77−32080
solid electrolyte interface, small signal AC response 78−6444
surface barrier Rayleigh wave transducer 79−98578
thermal resistance, role of cond. electrons *(Russian)* 78−19149
Al electrodes charge effects, on PET and SiO_2 films 80−75625
Al-Al_2O_3, unoccupied interface states in oxide band gap 79−69595
Al-Al_2O_3 electron transport in very thin multilayers 79−4602
Al-Al_2O_3 thin film system, electrical conductivity and I-V characts. meas. *(Polish)* 79−56310
Al-Al_2O_3 triple-barrier structure, negative resist. caused by resonant tunnelling 78−14819
Al-Al_2O_3:Mn-electrolyte, yellow electrolum. during anodisation of Al-Mn (1 wt.%) 77−63464
Al-Al_2O_3-Al junctions, Dy doped at Al_2O_3-Al interface, electron transport mechanisms and barrier height 78−91778
Al-dimethyl terephthalate contacts, effect of elec. field on contact electrification 79−19660
Al-Plexiglas, double layer barrier, deform. of electron spectra *(Russian)* 78−84292
Al-polymer contacts, charge transfer and contact charge spectroscopy 79−56305
Al-SiO_2, film system, kinetics of interaction 77−44459
Al-SiO_2, internal photoemission, phonon scatt. effects 77−85315
Al-SiO_2, surface reactions and interdiffusion, photoemission study 80−49532
Al-SiO_2 film-substrate interface, obs. of Al_2O_3 and free Si 78−91571
Al-SiO_2 interface, chem. struct., deposition conditions depend. 78−72007
Al-SiO_2 interface, internal photoemission and photon-assisted tunnelling 80−6982
Al-SiO_2 interface, stress and microstruct. via TEM 78−26797
Al-SiO_2 interface in MOS capacitors, conductivity effects of oxidation temperatures 80−100518
Al_2O_3, metal layer interdiffusion, Rutherford backscatt. 77−85000
Al_2O_3, plasma-anodised, current efficiency 78−91797
Al_2O_3-Al interface, AES depth profiling, appl. of tailored modulation techniques 77−15702
Au-poly(N-carbazole), hole photoinjection from Au 78−76144
Au-polyethylene interface, algorithm for energy deposition of X-rays 77−28648
Au-sapphire interface, effect on shear strength of adsorbed species 80−49485
Bi-Bi_2S_3 superlattice, elec. props. 78−10558
Cr/polymer interface, electronic struct., XPS study 80−45204
Cu/polymer interface, electronic struct., XPS study 80−45204
Cu-Cu_xO film, numerical anal. of normal reflect. data 79−99457
Cu-dimethyl terephthalate contacts, effect of elec. field on contact electrification 79−19660
Cu-Plexiglas double layer barrier, deform. of electron spectra *(Russian)* 78−84292
Cu-sapphire interface, effect on shear strength of adsorbed species 80−49485

metal-insulator boundaries continued
Ge-Au-Ni(Pd)(Pt) trilayer film, on SiO_2, annealing behaviour, interdiffusion obs. 78−2308
Hg-polymer interface, contact potential and charge exchange meas. 80−75642
Mg-polymer contacts, charge transfer and contact charge spectroscopy 79−56305
MgF_2/In/MgF_2 struct. surface plasma wave optical excitation in In 79−91516
Mo-dimethyl terephthalate contacts, effect of elec. field on contact electrification 79−19660
Mo-Si, pelicular structures, struct. transitions during vacuum thermal treatment *(Russian)* 78−95238
Nb-epoxy, interface, Kapitza resist. in supercond. and normal states 77−66085
Ni/polymer interface, electronic struct., XPS study 80−45204
Ni-7070 pyrex glass boundary, 9 MHz Stoneley wave generation 79−82433
Ni-polymer contacts, charge transfer and contact charge spectroscopy 79−56305
Ni-sapphire interface, effect on shear strength of adsorbed species 80−49485
$Pb_5Ge_3O_{11}$, ferroelec., surface capacitance effect on dielec. props., DC cond. and dielec. const. meas. 79−91333
Pd-SiO_2, work function changes due to adsorbed H_2, surface and interface dipoles 80−96972
Pd-SiO_2 interface, H induced interfacial polarisation, internal photoemission meas. 77−1490
Pt tips, glass-coated, field emission microscopy Fowler-Nordheim emission regime and periodic current oscills. 79−95907
Pt-polymer contacts, charge transfer and contact charge spectroscopy 79−56305
$RbAg_4I_5$-metal interface, photocurrents, photoelectrochem. effects 78−34897
Se-Ni-Mylar multilayered struct., interfacial bonding effect on adhesion, ESCA obs. 79−95274
Si-SiO_2 inversion layer, n-channel, anomalous magnetoresist., model 80−96996
SiO-Al multilayer capacitors and inductors, heat treatment effect on elec. props. 77−32082
SiO_2 charge transfer from metallic electrodes 80−15605
SiO_x, metal layer interdiffusion Rutherford backscatt. 77−85000
Ti-sapphire interface, solid-state reaction 78−72008
V-SiO_2 interface reaction, identification of diffusion species 78−75890
W-dimethyl terephthalate contacts, effect of elec. field on contact electrification 79−19660

metal-insulator-metal devices
diodes, metal whisker point contact junctions, tunnelling and rectification characts. 80−6955
diodes, negative differential resistance, stimulated inelastic tunnelling theory 80−49951
discontinuous metal film, fast detector for MM-wave through optical freq. range 77−18092
discontinuous metal film millimetric-wave and IR detectors *(Japanese)* 77−49771
electrical hygrometer with thin layer of LiF *(Czech)* 80−231
far IR laser output detection by MOM point-contact diodes *(Japanese)* 79−21811
integrated MOM device, detect. expts. at 10.6, 3.39, 1.15 and 0.6328 μm 77−89878
metal-oxide-metal diode for IR detection, fabrication by positive photoresist process 77−67496
metal-oxide-metal photodetector, noise, ultimate sensitivity 77−5915
metal-oxide-metal wide band IR detector, long life 77−5916
millimetric and IR discontinuous-metal-film detector 78−289
MIMIM triodes, photoresponse 77−39963
MOM diodes fabrication, two-level e-beam resist process with 1000 Å resolution 80−49996
optical waveguide mode coupling to metal films and metal-barrier-metal devices 79−81567
photoemissive detector, picosec., using metal-oxide-metal junctions 79−44932
point contact diodes, freq. response, effect of d-electrons 77−47898
point-contact diode harmonic generators and mixers 80−60105
point-contact diodes, use as far IR detectors 79−6180
point-contact diodes for harmonic generation and mixing 78−88044
Raman laser freq. meas. with MIM diode, spectroscopy in 5.3 μm region 77−10935
Raman laser IR freq. synthesis with MIM diode 77−19277
SQUID, V-V_xO_y-Pb tunnel junctions, IV characts. 79−19704
thin film MIM cold cathode emission density improvement, pinhole and compound insulator methods *(German)* 78−39670
tunnel diode, US effect on tunnel current for normal and supercond. metals 77−16006
tunnelling diode, detector performance, IR and microwave freqs. 79−12844
Al-Al_2O_3-Al, thin film capacitors, dielec. losses 78−76382
Al-Al_2O_3-Au device in Cl_2 atmosphere, current-voltage characts., press. depend. 80−65704
Al-Al_2O_3-Au thin-film cathode anomalous electron emission 79−8232
Al-Si_3N_4-Al thin film cathode, pulsed emission obs. 77−8728
Ni-NiO-Ni, integrated MOM junctions, characts. at DC and optical freqs. 78−41349
Ni-Nichrome, MOM diode, breakdown effect in visible and near-IR regions 80−6999
Pt-Pd discontinuous film MIM point-contact diode detector 77−5917
Ti-TiO_2-Au diode, spectral photoresponse and I-V characts. 80−15617
Ti-TiO_2-Cr, switching, double injection mechanism 78−14771
W-Ni, MOM diode, breakdown effect in visible and near-IR regions 80−6999
W-Ni point contact diode, rectifying props. in CO_2 laser radiation 77−76942
W-Ni point contact diode detectors at 10.6 μm, mech. and props. 78−24861
W-Ni(Co) point-contact diodes as harmonic generators and mixers, DC bias dependence 80−75653

metal-insulator-metal structures
Al-SiO_x-Al structure, maxima of TSC obs. 78−23178
barium stearate film, between Al electrodes, intrinsic voltage 78−72277

metal-insulator-metal structures continued
barium stearate single-layer Langmuir films, elastic and inelastic tunnelling 80−80403
benzene, polymerised, barrier in MIM tunnel junction, zero-bias anomalies 77−43739
cadmium arachidate mixed with cyanine dyes, mol. layers, photoelec. props. 80−80401
cadmium behenate in Langmuir multilayer assembly system, single layer conductance 79−51701
calcium behenate monomolecular layers between Al electrodes, nonlinear dielec. props. 80−80405
cathode, hot electron emission 78−2997
cathode, local electron emission and electroluminescence patterns obs. 80−108327
cathode, radial temp. distrib. *(Russian)* 78−6833
charge measurement in MIM and MIS struct., MOS system appl. 78−2572
charge migration kinetics, nonstationary VI characts. anal. 77−76943
chlorophyll-a, microcryst., trapped-electron doping in photovoltaic sandwich cells 78−53334
CL Al_2O_3, film, dielec. const. and resist., thickness depend. 78−39502
coherent coupling of radiation by surface plasmons 77−89877
conduction properties in sandwich structures *(Japanese)* 78−43486
cyanine dye monolayer assemblies with Al and Ba electrodes, photovolt., dark cond. and photocond. 80−80400
DC conductivity and Shubnikov-de Haas effect 80−11012
defect film insulators, AC characteristics, theory and analysis 77−1492
defect film insulators, AC characts. 77−1493
device progress over past 10 years 78−72280
dielectric diode, Joule instability under space-charge-limited current conditions 80−15618
diodes, quantum noise at low temperature 80−103733
doped electrode junction, tunnelling, Kondo scatt., coherence distance 78−31001
edge metal-oxide-metal junction, coupling via evaporated long antenna 79−87161
edge MOM diode, integrated optical nonlinear device 77−88963
elastic tunnelling current, phenomenological theory 78−19159
elastic tunnelling spectroscopy of single-particle excitations 78−56260
electrical transport, influence of mech. modulation 80−2481
electroformed structures, current-voltage characts., rel. to distrib. of filament resist. 79−78204
electroluminescence, comparison with MIM struct. 78−23533
electron emission mechanism, and electron propag. in metal electrode *(French)* 77−76944
electron emission modelling *(Czech)* 80−2479
electron irradiation and space charge accumulation *(Russian)* 79−38450
electron source, non-heated, review 80−84516
electron tunnelling through insulating layer 79−24082
emission current density in second intermediate region of Christov 79−33360
ethyl cellulose films, secondary ion injection 79−24094
external doping of tunnel junctions 79−3510
fatty acid monolayers, electron tunnelling 77−69428
hexamethylcyclotrisilazane film, glow-discharge-polymerized, in MIM and MIS structs., elec. cond. mechanism 79−42680
hopping model of zero-bias tunnelling anomalies, mag. field effect 79−60936
inelastic electron tunnelling spectroscopy, vibr. spectra of organic mols. meas. 77−14510
injection current enhancement at metal insulator interface, theory 80−49953
ionic crystal, space charge polarisation involving electrode reaction with surface adsorption 77−12019
isothermal current-time characts. and trap parameters determ. 77−89879
layered metal structure, acoustic size effect, sound attenuation anisotropy *(Russian)* 79−46752
leakage currents and conduction channels on splits 79−42664
light absorpt. in insulator-metal multilayered structs. *(Japanese)* 79−38191
light emission, by inelastic electron tunnelling 77−1734
light emission from inelastic tunnelling spectroscopy, surface plasmon modes 79−3598
lysozyme, anomalous diamag. susceptibility and elec. cond. 79−29498
malononitrile, plasma-polymerised, in Ag-polymer-Ag struct., SCL currents and carrier trapping 79−51687
metal whisker diode, thermal field emission, nonlinearity, response time and polarity reversal 78−2579
metal-Al_2O_3-Au type uniformly emitting MIM thin film cathode with evaporated insulator *(German)* 79−19675
metal-barium stearate-metal structs., internal voltage work function meas. 79−82684
metal-polyethylene terephthalate metal system, electrochem. effects as source of EMF 79−87163
metal-polyethylene terephthalate-metal, electrochem. effects as source of EMF 78−72278
metal-polyethylene terephthalate-metal system, electrochem. effects as source of EMF 79−87162
metal-polymer-metal structure, elec. props., electrode-limited cond. 77−28256
metallic particle tunnel junctions, light emission 78−80066
metallic point contact diodes, tunnelling props., geometrical asymmetry effects 78−10576
MIM heterojunction, theory of reson. tunnelling through insulator cond. band. 77−59336
MIMIM, photostimulated tunnelling 77−8204
MIMOS structure, charge storage props., effect of Pt particles in dual SiO_2 interface 77−35992
MIMS tunnel triodes, hot electron transmission 78−6456
MNMOS, with Pt interposed at Si_3N_4-SiO_2 interface, charge storage props. 77−51821
MOS, n-type inversion layers, two-valley model low temp. phase study, CDW coupling consts. 78−72275
nonequilibrium states, kinetic eqns. *(Russian)* 80−11101
nonlinear properties, EM signals detect. appl. *(Russian)* 78−34912
organic molecular monolayer in MIM tunnel junction, anomalous surface 79−72324
oscillatory effects connected with electromagnetic radiation in inelastic electron tunnelling *(Russian)* 78−91777

metal-insulator-metal structures continued
oxide thin film electroforming, threshold switching and memory effects 77−76940
[p-]quinquaphenyl film between metal electrodes, memory switching 80−2484
paper cellulose sandwiched between metal electrodes, thermo-induced elec. current 80−25021
PET, in MIM struct., injection current enhancement at metal insulator interface, theory 80−49953
phenol, adsorbed layer, inelastic electron tunnelling spectral lineshapes below 100 mK 78−31000
photoemission, internal, effect of quantum mech. transmission coeff. on yield 77−1494
PMMA film, in Al-PMMA-Al struct. SCL currents and cond. mechanism 79−51686
PMMA film in small area lateral MIMS device, cond., switching 80−97003
polyethylene, electrical capacitance under high DC elec. field 80−54705
polyethylene, relation between electrostatic capacity and electronic space charges induced by high field 79−15154
polyethylene structure, TSC study 79−78201
polyethylene terephthalate, electret, TSC, due to injected charge 77−16242
polyethyleneterephthalate film, in m.i.m. struct., short-circuit current induced by temp. change 77−4450
polyferrocene, in MIM sandwich, I-V and I-d characts. 78−80064
polyferrocene film, plasma polymerised, dielec. props., 40 kHz to 50 MHz, 30-400°C 78−52439
polymer, charge carrier species determ. using interfacial phenomena 80−24978
polymer, predominant carrier species determ. using galvanic cell 77−69384
polymer films, electron irrad. controlled form., elec. props. 80−15635
polymeric capacitors, injection charging 77−76902
polyphenylene oxide thin films, electrochem. prep., impurity effects on cond., electroforming 80−88655
polypropylene film, in MIM struct., electroforming 80−25019
polypropylene film, vac. evaporated, electron trap depth, TSC meas. for MIM struct. 79−95535
polypropylene thin film conduction mechanism, expt. obs. 77−28271
polystyrene, atactic, bulk and surface elec. props., contact charging obs., dielec. const. 80−15615
polystyrene film, in MIM struct., elec. conduction and free radicals 80−20340
polystyrene structure, TSC study 79−78201
polytetrahydrofuran, AC characs. 80−40062
polytetrahydrofuran films, electrochemically prepared between metal electrodes, DC elec. props. 80−39695
polyvinylacetate film, in MIM struct., DC cond. phenomena 80−25020
PTFE structure, TSC study 79−78201
PVC film, soln.-grown, between Al electrodes, AC elec. props. 80−15619
PVC films, soln. grown, DC cond. mechanisms, field and temp. depend. 80−97021
PVC in metal sandwich struct., switching props., voltage- and current-controlled negative resist. 80−103767
PVC structure, TSC study 79−78201
quantum size effect, struct. at 0.8 eV 77−63000
resonant tunnelling, IV characteristics, comments 80−70847
review of sandwich structures with anomalous props. 77−59337
RF sputtered film, transient current meas. 78−52113
sandwich sputtered film, interfacial effects characterisation 79−82685
shellac, electrical cond. mechanisms, Schottky and Poole-Frenkel processes and work function 80−29402
slow leaky waves, supported by metal-insulator thin conductive plate 78−78863
space charge limited cond. in MIM struct., transport eqns. 80−97002
stearic acid, insulator in MIM struct., electric dipole moment internal voltage meas. 79−76532
stearic acid film, in MIM struct., AC cond. and dielec. props., freq. depend. 80−55030
stearic acid multilayers, dielec. props. 80−80404
styrene glow-polymer in MIM sandwich, tunnelling and interface barriers 77−63001
surface plasma oscillation, refl. coeff. and energy density repartition for p-polarised waves *(French)* 79−69606
surface plasmon excitation by electron tunnelling 78−91779
surface plasmons, stimulated emission by electron tunnelling 78−56236
switching effect of atmospheric pressure 78−80067
thermal dielectric relaxation 77−76941
thermal dielectric relaxation 79−11237
thin disordered film, electronic energy spectrum calcs. extended Halpern Green's function technique 80−20066
thin film complex permittivity in VLF range, meas. apparatus and method 79−21782
TSC, space-charge layer model 80−93009
tunnel currents, closed-form approximation, analytical expressions 80−60064
tunnel junction, conductance-voltage charact., analytic expression for zero-bias offset 78−52102
tunnel junction, direct calc. of resonance tunnelling 78−14837
tunnel junction, magnetically doped, hopping model of zero-bias tunnelling anomalies, comparison with expt. 80−65703
tunnel junction, plasma radiation in Ag layer, expt. interpretation 77−31966
tunnel junction, small-particle type, light emission, local plasmon modes 79−19676
tunnel junction, surface plasmon excitation 78−10578
tunnel junctions, enhancement of light emission 77−51824
tunnel junctions, instabilities, for inelastic electron tunnelling spectroscopy 78−56235
tunnel junctions, roughened, photon emission, calc. 80−44738
tunnel point-plane junction, nonlinear optical response 77−28259
tunnelling, elastic, in MIM structures, zero bias anomaly calc. 80−2483
tunnelling, quantum size effect 79−73601
tunnelling, tight-binding Green function calc., disorder effect 78−10577
tunnelling current vs. voltage characts. calc. 77−12020
tunnelling junction, open system normal tunnelling Hamiltonian, stationary state 78−39190
tunnelling spectroscopy, review *(German)* 78−91776
tunnelling structure, eqns. for potential barrier height determ. 77−47899

metal-insulator-metal structures continued
vinyl chloride-vinyl acetate copolymer film between metal electrodes, depolarisation current studies 80−2691
zero bias anomalies, inelastic electron tunnelling spectroscopy, review 79−4603
zero bias anomaly in tunnel resistance and electron-electron interaction 79−65539
zero-bias anomalies due to Kondo scatt., hopping model, mag. field effect 77−59334
Ag:Al_2O_3:Al tunnel-junction struct., surface polariton mean free path, roughness 80−93008
Ag-Al_2O_3-Al junction, internal photoemission 79−82683
Ag-Al_2O_3-Al photoinduced currents, UV detection characts., 325 nm 77−53979
Ag-Al_2O_3-Au structure, electrorefl. meas. *(French)* 80−50366
Ag-SiO-Ag sandwich structures, elec. props. and nonvolatile memory effect 79−87164
Al, tunnel junction, barrier layer structure, mol. adsorption mechanisms *(Russian)* 79−31634
Al/(Al_2O_3)-BaSt/Sn struct., internal voltage temp. variation 80−20326
Al/Al_2O_3/Al, dielec. props. 80−80404
Al/Al_2O_3/Al structures with organic monomolecular layer, cond. at high elec. fields 80−80402
Al/SiO-B_2O_3/Au *(French)* 80−39681
Al-absorbed monolayer-Pb junction, current-voltage charact. meas. 79−28482
Al-Al oxide-Pd tunnel junctions, exposed to H_2, inelastic electron tunnelling spectra 80−20327
Al-Al_2O_3-Ag, electron bombard, charge accumulation kinetics, exoelectron emission obs. 77−51825
Al-Al_2O_3-Ag tunnel junction, 4-pyridine carboxaldehyde-doped, surface enhanced Raman spectra, surface plasmons 79−98111
Al-Al_2O_3-Al, elec. props. of anodic Al_2O_3 films 79−99646
Al-Al_2O_3-Al, non-thermal switching in Al_2O_3 amorphous film *(Russian)* 78−80069
Al-Al_2O_3-Al, tunnelling junctions *(Russian)* 78−60232
Al-Al_2O_3-Al junctions, Dy doped at Al_2O_3-Al interface, electron transport mechanisms and barrier height 78−91778
Al-Al_2O_3-Al MIM struct., photocond. anal. *(French)* 77−72921
Al-Al_2O_3-Al MIM struct., elec. cond., island metal struct. 79−15231
Al-Al_2O_3-Al structure, elec. cond. 261 to 418K *(Russian)* 78−64144
Al-Al_2O_3-Al structure, tunnel I-V charact., transmission coeffs. 78−80068
Al-Al_2O_3-Al(Au), thin films, elec. props. *(Czech)* 78−76159
Al-Al_2O_3-Au, conduction props. in O_2 atmosphere 78−26971
Al-Al_2O_3-Au, electron trapping due to neutron irradiation 80−2505
Al-Al_2O_3-Au sandwich conduction props. 78−2580
Al-Al_2O_3-Au(Al), capacitance, water sorption effects 77−43738
Al-Al_2O_3-Dy junctions, steady state and nonsteady state behaviour 79−78205
Al-Al_2O_3-Dy thin junctions, Poole-Frenkel effect obs. and cause 80−80398
Al-Al_2O_3-Fe, spin polarised electron tunnelling results for Fe 79−28417
Al-Al_2O_3-Hg structure, I-V charact. at room temp. for different thicknesses 79−47172
Al-Al_2O_3-M, thin film sandwich, leakage current and dielec. relax., 80-500K 78−76158
Al-Al_2O_3-Pb, oxide-layer chemisorbed phenols, electron tunnelling spectra, 2K 77−62736
Al-Al_2O_3-Pb, traps in Al_2O_3 detected by tunnelling 77−8202
Al-Al_2O_3-Pb contacts, tunnelling spectroscopy, band struct. of Pb 80−80169
Al-Al_2O_3-Pb diode for electron tunnelling spectroscopy 77−72919
Al-Al_2O_3-Pb tunnel junction, depend. of conductance curves on chemisorbed ion conc. in barrier 79−15233
Al-Al_2O_3-Pb(Au), solid-state anodisation of Al by vapour infusion, oxide growth rate 80−11830
Al-Al_2O_3-Pd diodes, resonant tunnelling via localized inpurity states 79−28416
Al-Al_2O_3-$(SN)_x$ structure, tunnelling spectroscopy study of electronic struct. of $(SN)_x$ *(Japanese)* 80−49954
Al-Al_2O_3-metal capacitors, elec. props. interrelations 80−54801
Al-Al_2O_3-metal capacitor, capacitance and power factor rel. to voltage and temp. changes 80−54802
Al-Al_2O-Al tunnel junction, Fe doped, Kondo-type zero-bias conductance 78−56237
Al-Al_2O_3-Pb tunnel junction, thermal annealing effects 80−49952
Al-AlF_3-Al, dielec. props. temp. irreversibility *(Czech)* 80−15616
Al-AlF_3-Al thin film structures, dielec. and elec. props. *(Slovak)* 80−100536
Al-AlN-Au, voltage controlled negative resist., O_2 press. effect 78−72281
Al-BN-Au device, prep. of BN films and IV charact. *(Japanese)* 77−73230
Al-Ba stearate-Sn, internal voltage, thickness depend. 77−72920
Al-barium stearate-Al symmetric junction, internal voltage due to Al_2O_3 film on electrodes 79−78202
Al-barium stearate-Sn struct. diode charact. obs. 77−4449
Al-CeF_3-Al(Au), dielec. props. temp. irreversibility *(Czech)* 80−15616
Al-Formvar-Sn coupled films, Ginzburg's excitonic supercond. model 80−97039
Al-I-Al, conductance vs. voltage characteristics, tunnelling conductance of asymm. barrier 78−72279
Al-I-Pb tunnel junction, clean and doped, tunnelling conductance 79−15232
Al-insulator-Al(Au) diodes, elastic tunnelling current 79−42666
Al-insulator-Au tunnel junction, conductance peaks produced by Kondo scatt. from O_2 78−95387
Al-insulator-$In_{1-x}Mg_x$ film tunnel junction, resistance zero-bias anomalies 80−107925
Al-insulator-Pb tunnel junction doped with m-cresol, asymm. in tunnel spectra 77−6782
Al-lead stearate-Hg, transient and alternating electric currents 78−84311
Al-MoO_3-Al structure, current-voltage characts., 251K-301K 79−91156
Al-$NdAlO_3$-Al(Ta)(Nb), prep., electrophys. props. 77−24956
Al-octadecyl-trichlorosilane-Al, junction, elec. cond. mech. 78−95386
Al-oxide-Pb tunnel junction, clean and doped, cond. 77−59335
Al-oxidised Al-Pb tunnel junction, nature of oxide barrier for IETS 77−72922
Al-perfluoro fatty acid-Al junction, elec. cond. mech. 78−95386

metal-insulator-metal structures continued
Al-polyacrylonitrile-Al films, current-voltage characteristics 80−11125
Al-polymer-Au, short circuit current with temp. variation 77−32090
Al-saturated fatty acid-Al junction, elec. cond. mech. 78−95386
Al-Sb_2O_3-In films, negative resistance characts. 80−11103
Al-Si_3N_4-Al cathode, fluctuation noise 78−2998
Al-Si_3N_4-Al thin-film cold cathode, electrical forming, expt. 78−76160
Al-$Si_xN_yO_z$-Al structure, electron microscope obs. of irreversible changes *(Russian)* 77−85342
Al-$Si_xN_yO_z$-Al thin film cathode, physical model from expt. study 80−100535
Al-Si_xNyO_z-Al systems, mechanism of current transfer *(Russian)* 77−69427
Al-SiO_2-Au, thin layer struct., electroluminesc. *(French)* 78−76531
Al-SiO_x-Al evaporated film anomalous dielectric dispersion under high DC field 80−15620
Al-SiO_x-Al structure with evap. amorphous films, threshold and memory switching 77−76945
Al-SiO_x-Au, electroformed, struct. and elec. props., 4-300K 79−78206
Al-SiO_x-Au cathode, emitted electron energy distrib. 78−52645
Al-SiO_xN_y-Al, effect of fast neutrons on elec. strength *(Russian)* 77−85343
Al-SiO-Al, with amorphous SiO, VLF behavior 77−76946
Al-SiO-Al structure, tunnel I-V charact., transmission coeffs. 78−80068
Al-silicon oxynitride-Al cathode, LF noise sources and reduction 80−108328
Al-stearic acid-Al, low-loss thin film capacitor 80−71317
Al-Ta_2O_5-Al, healing of defects in dielec. film by anodisation 80−65406
Al-TbF_3-Al structure, AC conduction in TbF_3 film 80−70868
Al-tetracene-Au cell, depletion layer, LF capacitance meas. 79−56328
Al-Y_2O_3-Al(Ta)(Nb), prep., electrophys. props. 77−24956
Al-Y_2O_3-Au, electroforming props. in thin evaporated films 80−65705
AlN films, RF glow discharge deposited, current-voltage characts. 80−84515
Al_2O_3 film, dielec. props., AC and DC elec. characts. 78−68445
Al_2O_3 film, RF sputtered, transient currents 78−23184
Al_2O_3 plasma anodised films, dielec. props. and high-field cond. *(Japanese)* 78−23185
Au-Al_2O_3-Al system, influence of mech. modulation on elec. transport 80−2481
Au-Al_2O_3-Au structure, non-ohmic conduction behaviour in Al embedded Al_2O_3 film 78−64157
Au-AlF_3-Au structure, dielec. props. of RF sputtered AlF_3 film 77−36173
Au-dye-amorphous SiO_2-Au struct., dye-sensitised steady-state photocond. 80−107924
Au-SiO_x-Au diode and triode struct., angular distrib. of emitted electrons 77−69429
Au-SiO_x-Au evaporated thin film sandwich, circulating and emission currents 80−11102
Au-SiO-Au structure AC conductivity, bulk and interface effects 80−54798
Au-Y_2O_3-Y junctions, migration of Au rel. to voltage-controlled negative resist., SIMS obs. 79−91157
BaO-CaO, amorphous, Cu-electrodes, electrical props. 77−35997
Bi-NbO_2-Bi system, Schottky barrier effects in transport and dielec. props. 80−29486
Bi_2O_3, thermally-grown capacitor-film, dielec. props. 80−2480
Bi_2O_3, thin film capacitor elec. props. under reduced press. 80−80397
CaF_2 thin films, initial ionic thermocurrent meas. 80−97018
Cd-palmitate (arachidate) multilayer struct., hopping rate, direct evaluation 78−88045
$CeCu_2Si_2$, tunnelling anomalies due to intermediate valence phenomenon 77−62873
CeF_3 film, in MIM struct., dielec. props. *(Czech)* 80−25309
$CePd_3$, tunnelling anomalies due to intermediate valence phenomenon 77−62873
Cu upper electrode effect on MIM cathode emission 77−85344
Cu-GeO_2/BaO-Cu thin film, amorphous, effect of electroforming on conductance and capacitance 80−34537
Cu-polypropylene-Cu(Al) structure, elec. props. of evaporated polypropylene 78−84335
Cu-SiO/B_2O_3-Cu thin film, amorphous, conductance and capacitance, effect of electroforming 80−34537
ErO_x film, in MIM struct., nonstoichiometry effects on elec. cond. 79−1635
Eu_xO_y film, dielec. props. rel. to annealing 79−99636
FeF_3 film, localised electronic states effect on elec. cond., MIM struct. meas. 80−20328
GeO_2 films, memory switching phenomena 79−82650
GeS amorphous layers between Al electrodes, dielec. relax. currents, pot. distrib. 77−16250
GeS film, between Al(Zn)(Sn) electrodes, Schottky and Poole-Frenkel cond. mechanisms 80−54799
Li MIM struct., electron-phonon interaction function investigation by microcontact spectroscopy 79−95108
Mg-MgO-Ag, tunnel junction, potential barrier, equivalent rectangular shape 79−7906
Mg-MgO-Ag junction, stable room temp. light emission 78−31257
Na MIM struct., electron-phonon interaction function investigation by microcontact spectroscopy 79−95108
Na-NaO-Na struct., inelastic tunnel effect, spectra, potential barrier parameters 79−95511
Nb-Nb_2O_3-Al structures, oxide film space charge density obs. *(Russian)* 78−10579
Nb-Nb_2O_5-Au thin film, conduction phenomena, drift phenomena 78−2581
Nb-Nb_2O_5-Nb structure, Schottky barrier effects on capacitance and loss tangent 77−8203
Pb-I-Al, conductance vs. voltage characteristics, tunnelling conductance of asymm. barrier 78−72279
Pb-SiO_2-Au tunnel junction, obs. of conductance anomalies 78−26968
Pt film, quantum size effect, and its temp., tunnelling obs. 79−91160
Pt/polymer/metal capacitors, electroforming and elec. cond. 80−54800
Pt-polymer-Au capacitor, electroforming, negative resist., electron emission 80−80406
Si, polycryst. barrier layer, physical properties *(Slovak)* 78−92196
Si_3N_4 dielectric film, high-speed electron irradiation effect on charge storage 77−69430
Si_3N_4 film, on W-coated Si, photocond., 1.31-3.10 eV, mechanism 79−19679

metal-insulator-metal structures continued
Si_3N_4 films grown by pyrolytic reaction between silane and ammonia, DC cond. 79−15243
SiO, alumina surface deposited film, SiH bond form., inelastic electron tunnelling spectra 79−69375
SiO amorphous thin film capacitor, EPR, elec. cond. 78−68358
SiO film, electrode effects in TSC and capacitance meas. 79−78203
SiO_2 film, IR spectra and elec. props., influence of prep. conditions 79−87176
SiO_2, in MIM struct., dye sensitisation of photocond., steady state and pulse photoelectric props. 78−6408
SiO_2:Na film, RF sputtered, low elec. field Poole-Frenkel effects in MIM struct. 79−95536
SiO_x film, in MIM sandwich, elec. props. 77−72933
SiO_x thin film dielec., in MIM struct., interfacial props. rel. to non-stoichiometry 80−80399
Sn-I-Al, conductance vs. voltage characteristics, tunnelling conductance of asymm. barrier 78−72279
Sn-SnO_4-Sn junctions, oxide growth, tunnelling characts. 79−47173
Ta-Ta_2O_5-Ag junctions, polarity-depend. tunnelling cond. 80−70846
Ta-Ta_2O_5-Au capacitive system, freq. depend. of dissipation factor, dielectric const., conductance *(Spanish)* 77−69426
Ta_2O_5 anodic film with Au counterelectrodes, conduction process 78−84312
Ta_2O_5 films, Poole-Frenkel effect and cond., effect of heat treatment in oxygen and in vacuum 80−39693
Ti-anodic oxide-Au(Al), electronic cond. *(French)* 79−95512
TiO_2, rutile ceramic capacitor, elec. cond. meas., anomalous conduction, ageing effects 78−14836
Tm_2O_3, electron beam deposition, elec. props., and struct. 79−87580
Tm_2O_3 film, between Al electrodes, prep. and elec. props. 80−60103
V_2O_5-P_2O_5 glass, dielec. relax. mechanism, SDRC investigation, Schottky barrier formation in metal-glass-metal systems 78−60388
W-Ni, MBM diode, resist. depend. of detected signals 80−2482
W-oxide-Ni high speed submicron junction, electron tunnelling spectra 79−99635
Y-Y_2O_3-Au, electroforming props. in thin evaporated films 80−65705
Y-Y_2O_3-Au junction, defect struct. and local conduction 78−26970
Y-Y_2O_3-Au thin film capacitors, self-healing dielec. breakdown 80−11104
Y-Y_2O_3-metal junction, electroforming and conduction 78−26969
$YbCu_2Si_2$, tunnelling anomalies due to intermediate valence phenomenon 77−62873
Yb_2O_3 film, amorphous, electron beam deposited, dielec. props. 79−91339

metal-insulator-semiconductor devices
see also charge-coupled devices
$AlSiO_x$-Si photodiode, experimental verification of theoretical predictions 80−29485
capacitance measurements, method of separating hysteresis effects, interface state density estimation 77−85324
diode, abrupt depletion layer approximation 79−58473
diode, C-V curve used to examine trapping level in semiconductors 80−65697
diode, metal-dielectric-semiconductor structures, with sub-micron channels, photosensitivity *(Russian)* 77−89876
dosimetry unit development for use in space 79−22485
dual dielectric charge storage cells, writing and erasing, differential studies 78−80059
electron beam induced current technique appl. to semicond. device characts., review 78−21302
injection laser, single heterostruct. 78−59005
inversion layer solar cells, numerical modelling 80−81444
metal-nitride-oxide-semiconductor transistor as a radiation dosimeter detector 79−22486
MIS solar cell development for space applications 79−96453
MIS solar cells, interface-state Fermi level change from dark to illuminated conditions 79−66407
MNOS capacitor, HCl annealing of memory oxide, effect on memory window size and location 79−70079
MNOS devices, switching characts. at low fields 79−56311
MNOS diode, trap distribution, memory characteristics 77−85326
MNOS memory device, charge distrib. of nitride 78−2571
MNOS memory device, trapped charge behaviour, UV light effects 77−12014
MNOS thin-oxide devices, effects of Si-SiO_2 interface states on memory characts. 79−82681
MOS, charge build-up due to radiation, mathematical model 79−19667
MOS, doping profile and threshold voltage, of B isolation region, numerical estimation 77−80843
MOS, voltage ramp technique for meas. of lifetimes in damage gettered Si 80−75247
MOS capacitor, generation lifetimes from C-t transients 78−88036
MOS capacitor, interface state parameter determ. by DLTS 80−65642
MOS capacitor, pulsed, transient response calc. 77−85341
MOS devices, interfacial and bulk trap props., expt. characterization techniques 80−49950
MOS devices, inversion layer, pot. and carrier distrib., quantum mechanical determ. 80−29483
MOS devices, nonequilibrium response to linear voltage ramp under illumination 79−95500
MOS devices with 500 Å and 700 Å thick oxides, saturation radiation effects 78−60209
MOS diodes, Al-SiO_2-Si, defects due to electron beam lithography obs. *(Japanese)* 80−54787
MOS diodes, minority carrier lifetime determ. from photocurrent spectra 80−49920
MOS diodes, tunnel-assisted transport at room temp. 80−92975
MOS dosimeters, series configuration, sensitivity increase *(Czech)* 79−36425
MOS photodiode, low dark-current, using $GaAs_{0.6}P_{0.4}$ 77−32083
MoS processing-related interface state meas., transient capacitance method 78−10574
MOS solar cell operation, role of interface states 79−61979
MOS solar cells, IV characteristics obtained under dark and illuminated conditions 79−48126
MOS solar cells, theory 79−87993
multichannel analog memory, using MOS transistors for data transmission to M6000 computer 79−26043

metal-insulator-semiconductor devices continued
nuclear and space radiation effects, conf., Albuquerque, USA (Jul. 78) 79−19276
p-n-insulator (tunnel)-metal devices, switching theory; punchthrough mode 79−60926
p-n-insulator metal switching devices, avalanche mode operation 80−70838
phosphosilicate glass flow mechanism, and appl. in MOS devices 77−77393
photodetector, pulsed avalanche, MIS struct. based, with stable internal amplification feasibility 79−58794
piezoelectric double-diffused MOS transducer, detection of acoustic waves 77−80043
point-contact diodes, use as far IR detectors 79−6180
SAW convolver, in monolithic MIS struct., charact. 77−80027
Schottky barrier, optically biased tunnelling MIS device 77−85334
Schottky barrier and conducting diodes with interface traps, capacitance and conductance 78−10564
Schottky barrier solar cells, photovoltaic props. anal. 78−6448
solar cell, effects of pinholes, oxide traps and surface states 78−80055
solar cell, general theory, expt. on Si 77−8197
solar cell, interface props. and stability 79−61984
solar cell, MIS tunnel structures, theory of operation 77−39948
solar cell, on amorphous hydrogenated Si *(French)* 79−24897
solar cell, photocurrent depend. on thickness of Schottky barrier metals 79−34437
solar cell open-circuit photovoltage rel. to oxide thickness 79−61985
solar cells, automated surface states anal. 80−93966
solar cells, basic principles of operation theoretical characts. 80−50986
solar cells, computer simulation studies rel. to interface state meas. 80−72048
solar cells, ecliptic-align V-grooved hyperjunction thin film cell, MIS and SIS device appls. 80−94082
solar cells, effects of nonuniformity of insulating layer 80−104507
solar cells, electron beam evaporated Si films 80−93490
solar cells, etched slotted mask for direct deposition of metal contact pattern 80−97786
solar cells, fabrication and performance characts. 80−45707
solar cells, fundamental mechanisms affecting performance of MOS-inversion layer cells 80−61377
solar cells, grating minority carrier, design and expt. results 80−81445
solar cells, I-V characts. calc. 79−43766
solar cells, interface problems, AES, SIMS and XPS study 80−89627
solar cells, inversion layer, surface passivation 80−101098
solar cells, inversion layer, two-dimensional model 80−89641
solar cells, low-temp. CVD of SiO_2 to form inversion layer 80−12019
solar cells, optimal interface design using computer simulation and expt. meas. 80−16805
solar cells, review 79−39300
solar cells, Schottky barrier height change and current transport in presence of interfacial layer 80−61353
solar cells, spectral response characts. and meas. of effective diffusion lengths 80−16804
solar cells with diffused back surface field (BSF), and diffused junction solar cells with MIS BSF 80−94074
solid-state device conference, Tokyo, Japan (Sept. 1976) 77−76901
SOS, elec. characts., cryst. defects and residual stress effects 78−34906
SOS MOS devices, effects of planar defects near Si-SiO_2 interface on elec. props. 79−11231
SOS MOS devices, hole mobility under residual stress, Hall meas., valence band struct. 78−88039
spectrometer for low energy X-and γ-rays 79−36462
strain transducer, diffused MOS device 77−5825
switching voltage criteria for metal-insulator-Si(n)-Si(p^+) device 80−15610
tetrodes, effect of impurity concentration in substrate, analytical models *(Spanish)* 79−99624
thin-oxide MIS thyristor devices, interface state charge 79−38172
three-terminal charge-injection device image sensor 77−39084
transient radiation induced ionisation effects 77−80788
tunnel diode, minority-carrier, pot. barrier height 80−96998
tunnel MIS solar cells, grain boundary effect on performance 79−79394
tunnel solar cell, interface states, kinetic and electrostatic props. 79−52933
tunnel structure, injection and extraction effects, self-consistent model 80−92996
Ag-SiO_2 film, elect. and struct. props., ion beam sputtering 78−80071
Al-Si MIS solar cells, depth conc. profiles, elec. and optical props. of Al films 80−94076
Al-SiO_2-Si Schottky barrier solar cells, recomb. effects 79−39310
Al-SiO_2-pSi solar cells, comparison of majority- and minority-carrier Si MIS cells 80−85280
Al-SiO_x-Si MIS solar cells, short-wavelength response 79−57428
Al-SiO_x-Si MIS solar cells, I-V characts. temp. depend. 80−7935
Al-SiO_x-Si MOS solar cells, open-cct. voltage var. with oxide layer thickness 80−81434
Al-SiO_x-p-Si MIS solar cells with back surface fields 80−12006
Al-SiO_x-pSi solar cells, comparison between MIS and SIS 80−81443
Al-ZnO-SiO_2-Si monolithic MIS struct., charge-transfer device using SAW 79−11229
Au-SiO_2-n-Si solar cells, comparison of majority- and minority-carrier Si MIS cells 80−85280
Be-SiO-p-Si, MIS solar cell, performance figures 78−88030
CdS, Au deposition, Schottky diodes and MIS devices, surface treatment effects, SEM obs. 80−54794
CdTe, MIS contacted small portable detector head for X-ray spectrometry 77−61662
CdTe/Langmuir film photovoltaic structures for solar cells 80−49918
Co_3O_4, detection of CO 78−76908
Cr MIS solar cells on Si, proton radn. effects 79−92074
Cr-MIS solar cells, on polycryst. Si, grain boundary effect and conduction mech. 80−93894
Cr-MIS solar cells on p-type wacker poly-Si substrates, high efficiency design 80−93935
Cr-MIS solar cells on Si, revised process to increase active area efficiency and reproducibility 80−81462
Cr-SiO_x-Si MIS solar cell, current cond. 80−7936
Cr-SiO_x-Si MIS solar cells, photovoltaic performance and interface states, nucl. radiation effects 80−94004
Cu_2O MIS solar cell with SiO_2 interfacial layers, semi-transparent layers of Au, Cu, Ag and Al 80−93946

metal-insulator-semiconductor devices continued
GaAs antireflecting MOS solar cells, epitaxial and polycryst. using OM-CVD techniques 80−94072
GaAs diode, anodic oxidation and annealing effects on elec. props. 77−80845
GaAs MAOS diode, prep. by anodic oxidation, stable charge storage 77−15960
GaAs MIS diodes, interface states determ., by deep-level transient spectroscopy *(Japanese)* 80−49917
GaAs MIS solar cells, effects of thin oxide layers on characts. 80−89624
GaAs polycryst. tunnel MIS solar cells, grain boundary problem 80−16809
GaAs polycrystalline thin film solar cells, fabrication 80−94066
GaAs-$Al_xGa_{1-x}As$ MOS rib waveguide polariser, modulator and isolator 80−64217
GaAs-oxide-metal solar cell, field shaping and barrier height 77−20454
GaN:Zn LED, I-V characts., elec. cond. mechanism 77−55614
GaP diode, anodic oxidation and annealing effects on elec. props. 77−80845
GaP-anodic oxide devices, optoelectronic device, processing appl. 78−84304
Ge MIS photocapacitative IR detector 80−47106
InAs, single- and double-layer insulator MOS capacitors 78−14835
InP, MIS diode prep. by anodic oxidation 79−74270
n-InP, MOS solar cells, electrical and photovoltaic characteristics 80−85276
p-type InP/Langmuir film MIS diodes, characts. 80−80384
InP-Langmuir film, surface state distrib. obs. 77−89859
InP-SiO_2 interface, CVD problems, ESCA profiles 80−93497
InSb MIS diode, anodised, C-V characts., effect of high elec. field pulse 80−60092
Si, amorphous, MIS diode I-V characts. 78−43485
Si, amorphous, solar cell construction and performance *(German)* 79−61970
Si based MOS device irradiation with γ-rays, minority carrier generation, CV characts. 80−88637
n-typeSi breakdown heavy ion counters, physical props. determ. 79−732
n-Si channel ⟨100⟩ inversion layer MOSFET, valley splitting, conductivity 80−70840
Si MIS grating solar cells on minority carrier blocking back surface field substrates 80−94078
Si, MIS photocapacitive IR detector 78−62223
Si MIS phototransistors, photoelec. props. at high illum. intensities 80−60101
Si MIS solar cells, 655 mV open-circuit voltage 79−79391
Si MIS solar cells with Cr, Hf, Be, Sc and Y as barrier forming metals, expt. investigation 80−94077
Si MIS/inversion layer solar cells 80−94075
Si MOS back-surface-field solar cells, open-cct. voltage >700 mV, 20% conversion efficiencies 80−81435
Si MOS device, electron optical identification of precipitations 80−16309
Si MOS diodes, P^+ implanted, DLTS of bulk traps and interface states 79−33350
Si minority carrier MIS solar cells, AM1 efficiencies 80−93975
Si, polycrystalline Czochralski-grown, MIS solar cell characterisation using scanned laser response exam. 80−93884
Si Schottky barrier solar cell, V-I characts. and efficiency 78−14828
Si solar cell, I-V curves, open circuit voltage 77−8196
Si solar cells, interface states effects on performance 78−76153
Si:H amorphous MIS solar cell, loss mechanisms and photovoltaic parameters, overview 80−93923
Si-P, time dependence of depletion region formation at cryogenic temp. 80−34522
Si-SiO_2 in MOSFETs, inversion layer carrier mobility, theory 80−60094
Si-SiO_2 interface in MOS solar cells, operational characts. and struct. 80−93901
Si-SiO_2 MIS systems, dynamic props. of switching, appl. to charge transfer devices 80−92997
Si-SiO_2-Al MOS surface channel influence on channel-to-contact diode charact. 80−92994
Si-SiO_2-Au Schottky barrier solar cells, back-illuminated, theoretical performance 80−61345
Si-TiO_x-Ni, MIS amorphous solar cell, increase in open-circuit voltage and short-circuit current on addition of TiO_x layer 79−57425
SiO_2-Si, low-energy neutral particle bombardment of SiO_2 film, degradation 80−54790
SnO_2-Si solar cells, stability and degradation mechanisms 80−16806
Ti-TiO_2 gated MOS diode light sensor, scan freq. improvement 78−58037
ZnO Sezawa mode pn-diode array memory correlator 79−78178
ZnSe, electroluminescent MIS diodes, surface state density determ. 77−35993
ZnSe MIS diode, blue electrolum., heat treatment effects 78−19569
ZnSe MIS diode, forward-bias electrolum. 78−23532
ZnSe MOS diodes, injection luminesc., edge emission 79−28842

metal-insulator-semiconductor integrated circuits *see field effect integrated circuits*

metal-insulator-semiconductor structures
accumulation regime, C-V data anal., insulator capacitance determ., interface states effects 77−12016
AES depth profiles, factors affecting depth resolution 79−15567
amorphous insulator film, high-field cond. 79−56320
amorphous semiconductors, barrier controlled charge carrier transport in structures *(German)* 79−47162
Anderson localisation in Landau level tails, anal. of Shubnikov-de Haas cond. minima 77−76947
avalanche photodetector linear array 79−63308
breakdown voltage of thin insulating layers, rapid destruction-free determ. 78−84306
bulk dielectric charge calc., from C-V characts. 79−56326
buried channel MOS structures, charge-handling capacity under hot electron conditions 80−80381
buried layer MOS structure, surface and bulk charge transport 78−30990
capacitance, high- and low-freq. steady state 80−54796
capacitance meas. for Schottky barrier 80−39678
capacitance voltage characts., meas. by resistance-capacitance divider gauge 77−37923

metal-insulator-semiconductor structures continued
capacitance-voltage characts., built-in charge fluctuation effects, negative surface state density 80−6992
capacitor, flatband voltage shift time depend., injection of minority carrier from Si into SiO_2 79−42656
capacitor, freq. and temp. tests for lateral nonuniformities, C-V characts. 78−10563
capacitor, laterally nonuniform, flat-band voltage distrib., appl. to test for nonuniformities 79−42649
capacitor, light induced electron-hole pair generation 79−38167
capacitor, nonequilib. response to linearly varying voltages 78−52091
capacitor, thermally stimulated discharge in differential regime 79−15214
capacitor C-V characts. meas. by nondestructive method using Au ball probe 77−1491
capacitor capacitance-voltage characts., automatic computation method *(Polish)* 79−1624
capacitor with single-level traps in semicond. region, model 77−35991
capacitors, inversion mode stepped I-V characts. 79−78180
capacitors, theory of nonequilibrium props. including charge exchange of interface states 79−42659
carrier injection and extraction anomalies, theory *(French)* 77−69420
characterization of MOS structures with buried layers 79−33355
charge centres, removal by RF annealing 78−88035
charge current in MIS structures intended for IR detectors, band to band tunnelling *(French)* 77−1487
charge density on ultrathin dielec. layer in MIS struct. determ. *(Polish)* 79−51675
charge distrib., optoelectric determ. methods *(Polish)* 80−39675
chlorophyll a film, charge injection and storage 78−53317
compound semiconductor interfaces, conf., Los Angeles, USA (Jan. 1978) 78−91756
conductivity, measuring apparatus with automatic compensation for geometric capacitance, 1 Hz-100 kHz range 79−21780
conductor-insulator-semicond. (CIS) solar cells, noncrystalline (poly and amorphous), interface importance 80−81466
conference, Durham, England (July 1979) 80−90612
current-voltage characteristics, influence of positive ions 78−64117
cyclotron resonance ECR lineshape, quantum theory, two-dimens. electron-impurity system 78−48045
deep centres investigation using capacitance method 80−39677
deep level parameters determ. in surface layer of semiconductor of MIS struct. 80−15612
defects, SEM 79−23507
dielectric layer, transient processes during charge trapping for injecting contact 80−70844
dielectric polarisation effects on instability 77−69418
dielectric-semiconductor structures, surface ion migration, theoretical analysis 80−65700
dielectrics, charge centre removal, low press. RF annealing technique 78−56230
effective mass approximation, interface effect 78−64082
electric strength of dielec. films *(Slovak)* 78−56231
electrical behaviour and SIMS depth profiling 78−84308
electron beam induced charge carriers in MOS structs. *(German)* 77−12007
electron energy and potential evaluation 77−51819
electron gun evaporated, HF C-V characts. and surface state density 78−84310
electron transport in quantised inversion and accumulation layers 79−60935
electron-beam induced-current investigations, transient behaviour 79−99630
electron-beam irradiated, effect of RF annealing 79−91152
electron-impurity system in two dimensions, model for MIS struct., cyclotron reson. lineshape theory 78−19332
electronic processes *(Russian)* 79−56312
electronic properties of two-dimens. system, conf. Berchtesgaden, Germany (Sept., 1977) 78−60177
EMF origin in pulsed UHF field 77−4448
Faraday rotation, far IR, 2D electron gas, carrier effective mass determ. 80−80389
fast surface states density, photoelectric method of determ. 80−70835
film on GaAs, elec. props. 79−66189
flat-band capacitance, impurity concentration, approx. formulae 79−95497
flat-band volt. determ., photoelec. method 79−38168
free carrier profile measurement on thin-layers, fast current pulse MOS deep-depletion technique 78−80075
GaAs, Schottky barrier, effect of oxide composition on elec. behaviour, AES meas. 79−87141
gate electrode, using localisation effects 79−38171
generation lifetime, surface generation velocity determ., linear sweep MOS-CV method *(Chinese)* 80−107916
graded and stepped energy band-gap MIS structures 80−2473
grain boundary diffusion, chemical reactions, contamination, AES and SIMS 80−72066
hexamethylcyclotrisilazane film, glow-discharge-polymerized, in MIM and MIS structs., elec. cond. mechanism 79−42680
HF capacitance, minimum value and position 77−85338
high frequency capacitance, simplified formula 77−72918
holographic image scanning by SAW on monolithic MIS structure 77−23771
hot electron transport, expt. review 78−30994
hypersound resonant excitation by 2-dimens. plasmons *(Russian)* 79−78032
hysteresis measurement, second order equivalent ccts. 80−57332
I-V characteristic with insulator opaque to tunnelling 78−80061
III-V narrow bandgap compounds, C-V characts., interface state densities and storage times meas. 77−89861
III-V semiconductor based layered multielectronic systems, electronic process investig. survey *(Russian)* 80−107891
III-V semiconductor MIS structs., review 78−95372
III-V semiconductor n-channel inversion layers, subband struct. and gate-controlled Gunn effect 77−76929
III-V semiconductor-oxide interface states, photoemission obs. of energy levels induced by adsorpt. 80−93000
III-V semiconductors, MBE developments in device fabrication, high quality structures 79−78902
III-V semiconductors, MOS processing, review 78−10570

metal-insulator-semiconductor structures continued
inhomogeneous MOS transmission lines, analytical solutions for charge transport 79−91153
instantaneous characteristics determ., experimental method *(French)* 77−55616
insulating film, detection of self-drifting of ionic charges by surface potential decay method 78−72295
insulating films on Si, instability phenomena, review 77−12037
insulator charge centroid determ. by photoinjection or photodepopulation 77−85323
insulator trapped electron release by UV photoinjection 78−6453
interface between ordered and disordered material (SiO_2-Al and SiO_2-Si), electrochemical obs. 78−2381
interface states, capture cross-sections 78−64129
interface states, deep level transient spectroscopy 79−78183
interface states, evidence for multiphonon emission 78−39220
interface states, thermally stimulated surface pot. 78−68091
interface states and deep level impurities, DLTS, charge storage and charge release modes 80−49923
interface states induced by amorphous SiO_2 77−28254
internal electron photoemission phenomenon *(Polish)* 79−91144
inversion channel hole mobility rel. to field treatment in active media 78−91774
inversion layer, Einstein relation, modification 77−12015
inversion layer, hot electron effects in Landau levels 80−6998
inversion layer, transient response of hot electrons, calc. 80−49747
inversion layer in quantising mag. field, Einstein relation 78−19156
inversion layer near electrode edge, pot. and charge density distribution 80−88642
inversion layers, carrier effective mass, contribs. of electron-electron and electron-phonon interactions 78−64087
inversion layers, implications of coupled electron-phonon system in two dimensions 78−6425
inversion layers, mag. field induced Wigner transition 77−89869
inversion layers, many-body effects, excitation to higher subbands 77−62997
inversion layers on high-index surface of Si, valley-valley splitting 78−39219
inversion or accumulation layer, electron scatt. by polar optical phonons 78−72237
inversion quantum model 78−30961
ion implantation and annealing effect on surface and bulk generation currents 78−47883
ion implantation profiles of B, P, junction depth meas. *(Japanese)* 77−39606
ion instability, analytical and phys. model 78−23167
ionising radiation effects on mobile-ion density in MOS oxides 79−28411
irradiated MIS device positive space charge formation kinetics 78−76155
junction field effect structures, 2-D subbanding 78−64125
leakage currents and conduction channels on splits 79−42664
localised states, Frenkel effect in strong elec. field, kinetics of nonequilib. processes 77−66206
magnetodiode and magnetoconcentration effects, influence of field effect 80−107903
magnetooptic absorption by electron gas, optical phonon effects 80−97248
magnetooptic absorption with participation of optical phonons 79−99858
magnetooptic interband absorption by semicond. surface layer 80−93288
magnetoresistance in range of low temps. and high mag. fields *(Russian)* 77−66203
MAOS capacitor, cond. and charging behaviour 78−26963
MAOS structure, for memory appl., cond. and charge storage 78−52099
MAS capacitor, cond. and charging behaviour 78−26963
metal-gelatin-n-GaAs struct., C-V characts. and gelatin-semiconductor interaction rel. to photographic process *(Russian)* 80−49944
metal-polymer-Si structure, elec. props., tunnel current 77−28256
metal-TiO_2-SiO_2-Si structure, dielectric props. and charge storage characts. 78−52098
metal-tunnel oxide-Si junctions, processing condition depend. 80−80380
metal-ZnO-SiO_2-Si structure for SAW appl., fabrication related deterioration 78−14829
metal-ZnO-SiO_2-Si structures, charge injection 80−49919
metallisation via automatic S-gun planetary deposition system 78−72724
microelectronics, conf., Calcutta India (Jul. 79) 80−96755
MIMOS structure, charge storage props., effect of Pt particles in dual SiO_2 interface 77−35992
minority carrier, lifetime and generation determ., graphical technique 78−95378
minority carrier generation rate meas. using transient response of MOS capacitor with guard ring 78−2576
minority carrier generation time constant meas. 77−89873
minority carriers surface generation rate determ. using dynamic nonequilibrium I/V characts. 78−64139
minority-carrier lifetime and surface generation velocity determ., hysteresis pulsed C-V method 80−70839
MIOS memory structs., degradation 79−38179
MISIM, electron energy and potential evaluation 77−51819
MISIM, photoresponse in alternating elec. field 79−38189
MISIM struct. inversion layer, symmetrical, carrier conc. calc. 80−75651
MISIM structure, charge transport kinetics, nonequilibrium props. 79−38188
MISIM structure, Hall meas. of carrier mobilities and doping conc. in semicond. film 77−76975
MISIM structure impedance and equivalent cct. 77−62998
MM wave modification by surface carrier scatt., surface pot. depend. 80−44736
MNMOS, with Pt interposed at Si_3N_4-SiO_2 interface, charge storage props. 77−51821
MNOS, Au-diffused, with chem. oxidised (100) substrate Si-SiO_2 interface traps 77−62995
MNOS, Auger depth profiling and ion sputtering of interfaces 77−20200
MNOS, charge centroid, as function of charge injected 77−85328
MNOS, dharge distribs. in Si_3N_4 film exam. 79−38184
MNOS, diffusion of Al into Si_3N_4 films 78−51744
MNOS, flat-band voltage, effect of distrib. charge in nitride 77−15959
MNOS, mechanical stress and elec. props. as function of nitride deposition temp. 79−42651
metal-insulator-semiconductor structures continued
MNOS, non-biased, charge storage by irradiation with UV light 77−43735
MNOS, on GaAs substrate, as optically controlled memory element 77−35995
MNOS, pseudostable, characts. 78−19154
MNOS, Si-SiO_2 interface state density meas. 78−47873
MNOS, small-signal response of bulk traps 77−39959
MNOS capacitor, current transient response, effect of insulator surface conduction 78−34910
MNOS capacitors, 'write' characteristics, SiO_2 layer thickness effect 78−34904
MNOS capacitors, effect of 2 MeV electrons at 80K 79−19668
MNOS capacitors, retention and endurance characts., annealing and oxidation effects 79−74274
MNOS capacitors, simple technique for charge centroid meas. 80−34521
MNOS device, high temperature annealing, effect on Si_3N_4 stress, interface charge density and memory props. 79−87158
MNOS devices, transient charge and current distribs. calc. 77−55611
MNOS memory device, charge retention by Frenkel-Poole detrapping 78−47874
MNOS memory structure, Si_3N_4 layer, distrib. and role of N-H and Si-H bonds 79−33358
MNOS P-channel switch, accelerated reliability testing *(German)* 80−6988
MNOS struct., electronic anal. 79−99632
MNOS struct. with complementary tunnelling emitter bipolar transistors, current transport characterization 79−91146
MNOS structure, depth chem. profiling by AES 77−89875
MNOS structure, model for degradation mechanisms 80−29477
MNOS structure, state discharging 79−38166
MNOS structure, temp. depend. of flat band voltage 77−20456
MNOS structure, trap parameters determ., review of expt. techniques 77−55612
MNOS structure, V/I characts. determ. *(Russian)* 77−8201
MNOS structure conductivity instability caused by passed charge 80−80394
MNOS structure photoelectric writing operation 78−95382
MNOS structures, Auger depth profiling by Ar ion sputtering 77−55613
MNOS structures, charge pumping investigations 77−43729
MNOS structures, discharge behaviour 79−38174
MNOS structures, electron-beam-irrad., interface defects, high temp. H_2 anneal 80−96745
MNOS structures, high temp. H anneal, effects of fast surface states 79−38178
MNOS structures, new technique for determ. of charge centroid 80−6990
MNOS structures, transport processes of electrons 80−34523
MNOS structures with tunnelling-thickness SiO_2 films, charge trapping obs. 78−95379
MNOS system, interface states 78−84309
MNS struct., reactively sputtered hysteresis elimination 79−99633
mobile charges determ., using triangular voltage sweep methods *(German)* 80−4740
mobile ions, TSIC meas. 78−68090
MOS, C-V characts.,-temp. and Si dislocation density effects *(Russian)* 78−6447
MOS, capacitors, SEM investigs. using electron beam induced current technique 78−23177
MOS, charge motion, surface state effects 78−2573
MOS, charge transport in SiO_2 film, TSD obs. 77−89870
MOS, current-voltage characts. meas. by triangular voltage sweep method 77−8198
MOS, degradation after irrad. with low energy electrons *(French)* 77−55617
MOS, density of states mass for quantised accumulation layers from C-V characts. 78−26967
MOS, dynamic props. of interface states 78−95373
MOS, electron irrad. effects, pulsed CV charact. obs. 77−76935
MOS, electron traps in Al-implanted SiO_2 obs. 79−15226
MOS, electronic cond. mechanisms of SiO_2:Cs(B) films 77−15983
MOS, electronic ground state of inversion layers in many-valley semicond. 77−43731
MOS, flatband shift induced by electron beam radiation, Si dopant effects 77−32085
MOS, hole emission from interface states, transient capacitance meas. 78−14830
MOS, hot electron transport, review 78−60221
MOS, instability *(French)* 77−39960
MOS, insulator bulk trapped charge densities and centroids, photocurrent-voltage characts. meas. 77−1489
m.o.s., inversion layers, localised state wave functions 77−4417
MOS, inversion layers, optical props. of CDW ground states 77−43732
MOS, ion implanted, spatial position of deep levels near Si-SiO_2 interface 77−12008
MOS, minority carrier nonuniform generation, SEM obs. 78−72273
MOS, negative bias stress at high elec. field rel. to MNOS device degradation 77−62996
MOS, non-steady state, energy distribution of interface traps obs. *(Korean)* 78−64119
MOS, quenched-in bulk defects and interface states, transient capacitance spectroscopy 79−24081
MOS, SiO_2 implantation with Al, trapped charge location, using photo I-V technique 79−15227
MOS, thickness dependence of radiation charging, hole trapping model 77−20442
MOS, total dose effects on surface state density, carrier conc. and mobility 77−20443
MOS, use of mini-computer for rapid evaluation of C-V-plots *(Russian)* 79−28413
MOS, with ion implanted oxide layer, optically induced charge storage 77−35994
MOS C-V data in strong inversion, surface minority carrier redistrib. 78−72266
MOS capacitor, Au-doped, bulk and interfacial prop. determ. using quasiequilibrium and linear voltage ramp techniques 79−95501
MOS capacitor, carrier generation lifetime profiles meas. in diffused layers 78−47803
MOS capacitor, carrier lifetime profiles meas. in diffused layers 78−47811

metal-insulator-semiconductor structures continued
MOS capacitor, characterisation of surface states of HCl-grown oxides 80−65696
MOS capacitor, comparison of lifetime meas. techniques 78−56232
MOS capacitor, direct cap./surface-potential recording meas. method 79−91143
MOS capacitor, direct current/voltage relns. as function of oxide doping 80−88635
MOS capacitor, drift mobilities of Na^+ and K^+ ions in SiO_2 films 78−10213
MOS capacitor, filament-metallised, effect of K contamination of W 79−51679
MOS capacitor, generation lifetime determ. from non-equilib. linear sweep current and capacitance meas. 78−47881
MOS capacitor, high-field electron trapping in SiO_2 78−6449
MOS capacitor, ion-implanted, C-V and G-V charact., effect of geometrical struct. of implanted region 77−55615
MOS capacitor, ionising radiation effect on mobile Na^+ current peaks 78−47876
MOS capacitor, minority carrier generation time and surface generation rel. determ. from Q-t meas. 78−72265
MOS capacitor, minority carrier lifetime, effects of swirls and stacking faults 77−32088
MOS capacitor, neutralisation of Na^+ ions, TSIC method 79−38181
MOS capacitor, neutron damage mechanisms in CCDs 79−19672
MOS capacitor, polycryst. Si gate, surface state annealing 77−39946
MOS capacitor, pulsed capacitance meas. anal. 79−38185
MOS capacitor, SiO_2 precipitation in Si, effect on generation currents 79−78188
MOS capacitor, surface state distrib. determ. from transient capacitance plots 79−42658
MOS capacitor, threshold voltage instability due to defect states produced during e-beam metallisation 78−72264
MOS capacitor, TSC meas., suppression of meas. interferences from interface states and mobile ions 80−29479
MOS capacitor, with TA metallisation elec., props. as function of induced stress 79−24434
MOS capacitor breakdown voltage *(Rumanian)* 79−51677
MOS capacitor formed over p-on-n semiconductor structure, G-V charact. 80−100532
MOS capacitor photovoltage characterisation 78−10573
MOS capacitor relaxation time, effect of stacking faults 78−76157
MOS capacitor switched from inversion to accumulation, minority carrier lifetime meas. 77−39957
MOS capacitor with Si deformed surface, defect struct. rel. to elec. props. 78−72231
MOS capacitors, charge distribs. for large electron beam irrad. doses 80−34518
MOS capacitors, charge yield and dose effects, 80K, electron irrad. 77−20440
MOS capacitors, dynamic model for e-beam irrad. 79−91147
MOS capacitors, electron injection studies of radiation induced positive charge 77−20441
MOS capacitors, establishment of inversion layer in Si substrate under high oxide field conditions 77−66202
MOS capacitors, ion-implanted, temp. sensitivity 79−78181
MOS capacitors, irrad., interface state buildup depend. on hole generation and transport 77−20446
MOS capacitors, irradiated and avalanche injected, trapping effects 79−19669
MOS capacitors, numerical method for small-signal AC anal. 77−89860
MOS capacitors, p-type, substrate generation current effect on oxide I-V meas. 79−73594
MOS capacitors, pulsed relax. time meas., reln. to oxidation induced stacking faults 77−39943
MOS capacitors, radiation-induced increase of Na ions 78−26956
MOS capacitors, temp. and field depend. charge relax. in SiO_2 gate insulators 78−60206
MOS charge layer, strip transmission line spectroscopy of inter-subband transition 77−28257
MOS charge layer n-channel (001) surface induced valley splitting 79−28414
MOS deep levels in semicond. surface layer, pulsed C-V study method 79−7905
MOS devices, irradiated, low-temp. appl. 78−26961
MOS devices, radiation effects, rel. to multiple trapping model and hole transport for SiO_2 78−6394
MOS devices, SEM, electron beam induced currents, Si stacking fault investig. appl. 79−42665
MOS devices doped nonuniformly near surface, onset of heavy inversion 77−28252
MOS diode, impurity profile effect on density of interface states 79−33359
MOS electron inversion layers, temp. depend. of subthreshold currents 79−73596
MOS elements in depletion, interfacial tunnel interaction anal. 78−64121
MOS hardness characterisation, depend. on process and meas. variables 77−20444
MOS insulator, energy and spatial distrib. of electron traps, photocurrent response 77−39947
MOS interface states density, photoemission obs. using photocurrent and photocapacitance meas. 80−92990
MOS inversion layer, 2-dimens. disordered electron systems in strong mag. fields 77−76930
MOS inversion layer, hot electron effects in Landau levels 80−20315
MOS inversion layers, acoustic plasmons 78−18983
MOS inversion layers, electron-phonon interaction and cyclotron reson. 80−25014
MOS inversion layers, freq. response of charge transfer 80−88638
MOS inverted-channel carrier scatt., effect of oxidation in Cl media 78−76156
MOS layer structure, UV illumination effect on elec. props. 79−82676
MOS movable-gate-field-effect struct., use as electromech. transducer 79−1043
MOS p-channel transistors, ion implantation effect on threshold voltage 78−34903
MOS parameters, effect of oxidation expanded defects 78−19152
MOS plasma-oxidised nitride structures, charact. 79−65552
MOS pulsed capacitor, minority carrier lifetime meas. influence of Si-wafer surface state density 80−60098

metal-insulator-semiconductor structures continued
MOS radiation sensitivity, influence of Si surface defects 77−20445
MOS rectangular vol., distrib. function for ion track lengths 79−85872
MOS relaxation of nonequilibrium depletion layer 79−56325
MOS sandwich, itinerant electron ferromagnetism 77−24666
MOS self aligned structures, anomalous electrical gate conduction 77−43737
MOS solar cell, role of interface states 79−15228
MOS space charge layer physics 80−92980
MOS struct. with Hg drop electrode, Na-induced work function shift 79−42652
MOS struct. with nonuniformly doped semiconductors, depletion approx. anal. of differential C-V charact. 79−99625
MOS structs., gate biasing elec. field rel. to charge carriers in semicond. layer 78−52092
MOS structs., Schottky barrier characterisation by scanned internal photoemission 80−49915
MOS structs. formed on stain films on Si wafers, electrophysical props. *(Russian)* 78−52095
MOS structs. with chlorine oxides, high-temp. annealing in N *(Russian)* 77−89858
MOS structure, B ion implanted, form. and annealing of radiation damage 79−56321
MOS structure, bulk lifetime determ. by voltage step response method 78−47882
MOS structure, cathodolum. meas. on SiO_2 with O vacancy 77−24901
MOS structure, distrib. of interface states conc., method for determ. 80−44733
MOS structure, effect of pre-oxidative chemical treatment on quality of active oxide 79−42647
MOS structure, electron trapping region to improve performance 78−19150
MOS structure, electrophysical props. after B^+ ion bombardment 77−12013
MOS structure, irradiated, interface state effects 78−39218
MOS structure, leakage effects 79−91155
MOS structure, mobile ion density distrib. in dielectric 79−87159
MOS structure, model for ion-electron (configurational) interface states 80−29478
MOS structure, n-channel, evidence for impact ionised electron injection in substrate 78−88031
MOS structure, p-channel, effect of isotropic stress on Si valence band struct., press. transducer appl. 80−25011
MOS structure, piezoresist. in Si inversion layers 77−35935
MOS structure, quench-in defects and interface states exam. by transient capacitance techniques 78−39225
MOS structure, semiconductor conductance and capacitance, extended AC conductance−bias method 80−96995
MOS structure, slow-trapping instability, effect of high temp. H_2 annealing 78−47880
MOS structure, tail states of London subbands under strong mag. field 77−15962
MOS structure, with reverse biased p-n junction, impulse current behaviour *(German)* 79−82675
MOS structure concentration profile numerical evaluation *(Slovak)* 80−65690
MOS structure dynamic volt-capacitance characteristic meas. 78−60207
MOS structure implanted with B ions, radiation defects and impurity activation 80−103757
MOS structure Pt diffused, hysteresis and memory props. 80−96992
MOS structure semicond. surface potential, quasistatic meas. 79−56323
MOS structure switching and memory effects 79−78197
MOS structure under strong inversion conditions, freq. response of bulk traps. 77−39958
MOS structure with highly doped region, relaxation processes at high voltages 80−70843
MOS structure with nonuniformly doped semiconductors, heavy inversion, definition for onset 80−96994
MOS structures, interface state density evaluated from charge-voltage data 79−11234
MOS structures, quasi-2-dimens. system, review 79−33352
MOS structures, quasistatic and nonequilibrium phenomena with constant gate-current bias 80−80385
MOS structures, radiation-induced positive charge, thermal annealing 80−75648
MOS structures, static technique for differential capacitance meas. 77−65044
MOS structures obtained by etching of Si and SiO_2 surfaces, props. 80−93671
MOS structures of small-gap semicond., capacitance, effect of quantising mag. field 80−84513
MOS structures with external p-n junction, linear gate volt., impulse-current behaviour *(German)* 79−56319
MOS structures with semicond. layer under gate, C-V characteristic obs. 79−56322
MOS structures with superthin gate dielectric, hole mobility in inversion layers 80−29482
MOS surface states, DLTS spectra synthesis and anal. 80−11090
MOS system containing interface traps, equilibrium and nonequilibrium response to linear voltage ramp 79−38173
MOS system photocapacitance, influence of surface charge fluctuations *(Russian)* 78−43480
MOS system surface charge inhomogeneity modelling and analysis *(Russian)* 78−43479
MOS thin capacitors, electron-beam irrad., enhanced flatband voltage recovery 79−19670
MOS transmission line, distributed model computer anal. of free charge transport 78−76150
MOS transmission line, model, charge propagation 77−85325
MOS transmission line, resistive, free charge transport, simulation, distrib. model 78−68092
MOS transmission line, surface charge transport, bit-line appls. 77−39956
MOS transmission line, transient anal. of gate potential 78−76149
MOS transmission line models, differential eqn. solns. generalised to lossy cases 79−38182
MOS tunnel device, interface props. 78−34911
MOS tunnel diodes characterisation, solar cell appls. 77−32089
MOS tunnel structure, Si-SiO_2 barrier height, SiO_2 thickness depend. 78−14831

metal-insulator-semiconductor structures continued
MOS two-dimens. systems under strong mag. field, many-body effect on level broadening and cyclotron resonance 79−78195
MOS with resistive gate electrode, CV characts., losses and phase shifts 78−80057
MOS-structure, with adjoining reversed biased p-n junction, charge pumping current and reverse current *(German)* 80−88636
MOSFET structure, artificial superlattice near carriers 78−64130
MOST struct., gamma irrad., interface states and carrier mobility 79−73593
MOST structure, determ. of hole mobility in Si 77−66204
MOST structure modelling, using hybrid computer, Poisson partial differential equation solution *(Slovak)* 80−75643
MS'IS structure free carrier redistribution control 78−95384
n-type capacitors, optically active interface states study 80−60096
negative resistance, C-V characts. 79−11236
non-stationary processes, computer-aided analysis *(German)* 77−39952
nonequilibrium capacitance relax., Ar ion implantation effects 78−64140
nonequilibrium response to linear voltage ramp, bulk discrete traps 78−6450
nonuniformly doped MOS devices with lateral symmetry 80−15606
one-dimensional inversion (enrichment) layers in MOS structure semicond. surface, production method 79−42663
optical image recording, As_2Se_3 as photosensitive element 80−42286
optical phononelectron gas interaction, high freq. cond. 80−6888
p-n-p-I-M structure, tunnel cathode thyristor, theory of switching effect 77−39930
parametric amplification and generation of SAW 79−10438
passivation by phosphosilicate glass layer, flat-band voltage, effect of growth conditions 80−107913
photocurrent flow mechanism, carrier tunnelling 77−28258
photocurrent spectra investig. of fund. absorption edge 77−4397
photocurrent-voltage characts., insulator bulk trapped charge 78−30991
photosensitive high resolution struct., spatial light modulation with liq. cryst. 80−96026
photosensitive MIS structure in contact with nematic liq. cryst., light spatial modulation 80−48436
photovoltaic effects, pulsed 78−2577
photovoltaic effects *(Japanese)* 80−54737
photovoltaic efficiency, effect of insulating film and interface states *(French)* 77−1488
photovoltaic efficiency, interface states effect 77−80844
photovoltaic properties of MIS-Schottky barriers anal. 78−26966
photovoltaic technology, conf., San Diego, CA, USA (Jan. 1980) 80−86041
plasmon-acoustic wave interactions due to deformation potential *(Russian)* 80−15356
polar-optical phonon interaction with two-dimens. electron gas 79−82434
polarisation hysteresis, ion motion, on thermal SiO_2 *(Russian)* 80−54793
poly Si gate MOS capacitor post-irradiation flat-band shift expts. 77−76939
polymer, in MIS struct, charge movement study using capacitance-voltage characts. *(French)* 80−39575
polymethylsiloxane, in MIS struct., C-V characts. and charge movements 77−85340
ponderomotive force effect on dielec. breakdown 79−15230
potential barrier height determ. using photoelectric methods *(Polish)* 80−20317
processing, detection of trace Na in furnace 77−4955
production by neutralised ion beam sputtering 78−3046
pulsed MIS capacitor, non-steady-state bulk generation processes 77−12017
pulsed MOS capacitor, recombination lifetime meas. 80−25012
quantised inversion layer, hot carrier transport 78−30993
quantised inversion layers, hot electron microwave cond. calc. 77−43734
radiation induced charge storage 80−6997
random attractive electron-electron interactions in two-dimens. systems 78−60183
resistive gate MOS transmission line, charge propagation study *(Rumanian)* 79−11233
resistive gate MOS varicap with steplike C-V characts. 79−60924
resistive-gate MOS structure, in deep depletion, gate potential, transient anal. 78−43482
reverse biased MIS tunnelling Schottky barrier, appl. to photodetection 79−7904
review of applications, ion sensitive techniques 79−33353
RF annealing method for removing radiation damage 78−39224
SAW charge transfer theory 79−56327
SAW convolver, minority carrier response 77−80847
Schottky barriers, photocurrent suppression and interface state recomb. 78−39222
Schottky-barrier metal-thin oxide-semicond. structures, physical processes and microelectronics applications *(Russian)* 78−84307
SEM used for investigating MIS structures 78−95377
semiconductor interfaces, conf., San Diego, Calif., USA (Feb. 1976) 77−20377
with semiconductor layers of critical thickness, potential distrib. and capacitance calc. 78−95381
semiconductor submillimetric-wave spectroscopy 79−33221
semiconductor surface states, capacitance, admittance, freq. depend. 80−49940
sensitivity contamination with H^+, Na^+, and K^+ ions 79−24080
Si-Al_2O_3-SiO_2 in MIS struct., charge accumulation and spreading *(Russian)* 78−64116
solar cells, influence of interface states, efficiency improvements 78−39227
solar cells appl. minority carrier MIS diodes *(Slovak)* 80−97792
SOS films, carrier recomb. props., magnetosensitive method 79−38186
SOS films, surface recomb. profile and transport parameters 79−33357
SOS MOST, electronic props. at Si-sapphire interface 80−96993
SOS single crystal films, struct. and elec. props., review *(Japanese)* 77−63009
spectral characteristics of MIS struct. with variable-gap semicond. 80−44735
surface channel, quasitwo dimens. excitons and plasmons at different carrier conc. 78−60063
surface characterisation by C(V) curves 78−72276
surface charge, effect of process induced defects in Si 78−72274
surface depletion and inversion, arbitrary doping profile, theory 80−107912

metal-insulator-semiconductor structures continued
surface electron states in band gap, calc. by Green's function method 80−15611
surface inversion layers, energy relax. to acoustic phonons 78−26857
surface piezoacoustic waves, interaction with two-dimens. plasmons 79−28683
surface piezoelectric shear wave, two-dimens. electron plasma interaction *(Russian)* 79−19842
surface potential and interface disorder *(French)* 77−15966
surface potential distributions *(Russian)* 78−80065
surface properties, methods of influencing 77−15965
surface recombination and photoeffects within a quantum range *(Russian)* 78−39221
surface state density, determ. from surface saturation photo-EMF meas. 80−75652
surface state density determ., error caused by numerical differentiation of Q-V data 78−43483
surface state spectrum meas. by pulsed C-V method 80−88641
surface states, in presence of radiation, dielec. deposition temp. effect 77−89872
switching characts., theory, appls., expt. 78−68093
switching experiments on metal-semi-insulating-n-p^+ Si devices 78−26965
switching phenomena in thin-insulator MIS diodes, current-control-type negative resist. characts. 80−107915
switching theory for metal-semi-insulator-n-p^+ Si devices 78−26964
temperature distribution of struct. with several heat sources 77−43730
thermal generation of carriers through surface centres 79−69603
thermodepolarisation charge and change of effective charge in MIS struct. with two ohmic contacts *(Russian)* 78−52093
transient response of quasi-two-dimens. semicond. under hot electron conditions 78−60223
tunnel currents, closed-form approximation, analytical expressions 80−60064
tunnel diodes, photoionisation of states 80−11099
tunnel junction, light emission via inelastic tunnelling effect 79−24076
tunnel structure, injection and extraction effects, self-consistent model 80−92996
tunnelling MIS structures, photovoltaic energy conversion, band struct. 80−92995
tunnelling Schottky barrier, surface state effect on electrical characts. 78−47877
tunnelling spectra, interaction of holes with local modes and one and two optical phonons 77−20457
tunnelling spectroscopy *(Japanese)* 77−39953
two-dimensional electron system in strong mag. field, crystallisation 78−30966
unbalanced behaviour, external factors affecting *(German)* 78−43477
wideband admittance meas. by phase-selective rectifier *(German)* 77−61089
Wigner crystallisation in MOS struct. induced by strong mag. fields 77−28253
Ag-In_2S_3-Si layered struct., Hall effect, I-V characts., surface states *(Russian)* 80−97001
Al/Al_2O_3/CdS, junction characts. 79−82481
Al/SiO_x/p-Si contacts for IMS solar cells, high temp. lifetesting 79−87988
Al/SiO_x/pSi MIS solar cells, stability 80−85287
Al-Al_2O_3-Bi junction, electron tunnelling and band struct., mag. field effect 79−37979
Al-Al_2O_3-CdS diodes fabricated by MBE, junction characts. 79−65550
Al-Al_2O_3-GaAs backwall MIS Schottky barrier solar cell, anal. model 80−85289
Al-Al_2O_3-GaAs MOS struct., mol. beam reaction growth of Al_2O_3 film, C-V characts. 80−11095
Al-Al_2O_3-InP MIS struct., elec. props. 79−78184
Al-Al_2O_3-InSb structures, recomb. processes and carrier lifetimes 79−38177
Al-Al_2O_3-Si structure, study of charge trapping 80−60097
Al-Al_2O_3-SiO_2-Si capacitors, physical and elec. props. of RF plasma grown Al_2O_3 80−100530
Al-Al_2O_3-SnTe, junction, tunnelling, Fermi level depend. on carrier conc., influence of surface states 80−25016
Al-Al_2O_3-SnTe, tunnelling characts., model anal. 80−29480
Al-Al_2O_3-(a-Ge)-Al, electron tunnelling into a-Ge, press. effect 80−49938
Al-Al_2O_3-p-GaAs MOS diode, capacitance-voltage characts. 80−107914
Al-AlN-SiO_2-Si capacitors, physical and elec. props. of RF plasma grown AlN 80−100530
Al-anodic oxide-n-GaAs MOS struct., elec. instabilities and annealing effects 79−60928
Al-anodised Ta_2O_3/native oxide-n-GaAs MOS structure evaluation 80−84514
Al-gelatin-GaAs, C-V characts., irrad. effects *(Russian)* 77−51823
Al-gelatin-GaAs, capacitance-voltage characts. after and before incorporation of $AgNO_3$ 79−51684
Al-In_2S_3-Si layered struct., Hall effect, I-V characts., surface states *(Russian)* 80−97001
Al-oxide-Si(GaAs), plasma anodisation of Al film to exhaustion, MOS C-V meas. 79−83388
Al-Pd_2Si-Si junction thermal stability improvement 79−78186
Al-PtSi-Si junction thermal stability improvement 79−78186
Al-rare earth oxide-Si, elec. props. of oxide thin film, oxide-Si interface props. 80−7013
Al-sapphire-Si capacitor, effect of electron-beam aluminisation on Si-sapphire interface 77−89856
Al-Si_3N_4-Ge, thermally stimulated depolarisation current meas. 80−88643
Al-Si_3N_4-Si, electrical strength effect of struct. defects in Si_3N_4 *(Russian)* 78−26955
Al-Si_3N_4-Si, photocurrents 79−24092
Al-Si_3N_4-Si struct., surface energy bands under step function illumination 80−49840
Al-Si_3N_4-SiO_2-Ge structure, small signal HF photo EMF meas. 78−52097
Al-Si_3N_4-SiO_2-Si capacitors with optical data writing, relaxation obs. 78−76154
Al-Si_3N_4-SiO_2Si, MNOS structures degradation under UV irradiation effect 80−107923
Al-Si-SiO_2-Al structure switching and memory effects 78−95385
Al-SiO_2, Al-SiO_2(SiO)-Si, solid-state reaction mechanism 77−52623

metal-insulator-semiconductor structures continued
Al-SiO_2 interface in MOS capacitors, conductivity effects of oxidation temperatures 80−100518
Al-SiO_2-Ge, electroreflectance spectra of Ge meas. 77−1677
Al-SiO_2-Si, Auger depth profiling and ion sputtering of interfaces 77−20200
Al-SiO_2-Si, charge measurement in MIM and MIS struct., MOS system appl. 78−2572
Al-SiO_2-Si, effect of β-radiation on fast surface states and space charge 77−55610
Al-SiO_2-Si, interface states, thermally stimulated charge decay 77−12009
Al-SiO_2-Si, MIS diode, neutralisation of mobile ions in insulating film *(Japanese)* 79−73591
Al-SiO_2-Si, noncryst. SiO_2, Na ion impurities motion 78−10223
Al-SiO_2-Si, photoelectron-grain boundary scatt. in Al film 78−64120
Al-SiO_2-Si, photon-assisted tunnelling 77−89865
Al-SiO_2-Si, pyroelectricity 80−100524
Al-SiO_2-Si, SiO_2 film electric strength obs., under unidirectional, alternating and combined voltages *(Slovak)* 78−88034
Al-SiO_2-Si, TSC due to trapped electrons, rate-determining process 77−59290
Al-SiO_2-Si, void form. in Al interconnection lines at Si-SiO_2 boundaries 80−2476
Al-SiO_2-Si capacitor, current and C-V instabilities at high fields 77−80841
Al-SiO_2-Si capacitor, N_2 gas reaction, elec. and structural charact. 77−39950
Al-SiO_2-Si capacitor C-V characteristic determ. of surface minority carrier lifetime *(Polish)* 77−89855
Al-SiO_2-Si capacitors, transient capacitance temp. depend., −40 to 70°C 79−47167
Al-SiO_2-Si MOS structures, elec. strength meas. of SiO_2 *(Slovak)* 78−56231
Al-SiO_2-Si MOS structures, charge motion, TSC meas. 80−100534
Al-SiO_2-Si struct., mobile ion neutralisation in SiO_2 layer, TSC and C-V charact. meas. 79−95503
Al-SiO_2-Si structs., implanted B^+ ions, high-freq. CV charact. *(Russian)* 78−80056
Al-SiO_2-Si structure, ionic impurities motion in noncryst. SiO_2, trapping layers 78−30999
Al-SiO_2-Si structure, location of positive trapped charge by internal photoemission 77−51820
Al-SiO_2-Si structure, lateral photovoltaic effect 79−4601
Al-SiO_2-Si structure, photocurrents, 1.4 to 3.1 eV 79−65514
Al-SiO_2-Si structure, positive interface charge, exciton and H diffusion models 80−2471
Al-SiO_2-Si structure, small signal HF photo EMF meas. 78−52097
Al-SiO_2-Si structures, minority carrier lifetime investigation in Si:Zn and Si:Co 80−80292
Al-SiO_2-Si system with reactively sputtered SiO_2, work functions difference 80−6987
Al-SiO_2-Si:B ions, annealing effect on energy spectrum of radiation defects *(Russian)* 78−88488
Al-SiO_2-Si-Pb, MIS system, photocurrent, effect of supercond. to normal transition in Pb 78−72271
Al-SiO_2Si, mobile ion kinetic behaviour 79−56315
Al-SiO_x-GaAs, C-V characteristics 79−65553
Al-SiO_x-Si minority-carrier MIS photodiodes, elec. charact. 79−51676
Al-SiO_x-(p-)Si barrier structs., minority carrier injection ratio meas., MIS solar cell model 80−93007
Al-SiO_x(+SiO_2)-Si structures, I-V and C-V charact., current and capacitance kinetics 78−88043
Al-silicide-Si systems with $CoSi_2$, $Pt_xNi_{1-x}Si$, and $MoSi_2$ as silicide, diffusion, compound form., and microstructure 80−34253
Al-silicide-n-Si systems with $CoSi_2$, $MoSi_2$, and $Pt_xNi_{1-x}Si$ as silicide, Schottky-barrier height 80−34520
AlAs epilayers, MBE growth on GaAs, self-terminating thermal oxidation, MOS capacitor prep. 78−92374
$Al_xGa_{1-x}As$ native oxide, low leakage, MOS characterisation 78−91795
$Al_xGa_{1-x}As$:O, appl. as insulating layer in MIS struct. 78−64115
$Al_xGa_{1-x}As$:O-n-GaAs heterojunction for MIS device, capacitance voltage meas. 79−87157
$AlGe_3N_3$-GaAs structures and MISFETs based on them 79−60932
Al_2O_3 amorphous layers, prep. and physical props. *(Slovak)* 78−64122
Al_2O_3 film, MOS gate insulator, photoconductive processes 77−8216
Al_2O_3 gate insulator, low temp. radiation response 78−26960
Al_2O_3 insulation layer, DC reactively sputtered, effects of annealing on C-V charact. 77−51822
Al_2O_3, insulation layer, DC reactively sputtered, optical and elec. props. 79−19486
Al_2O_3 MIS Schottky structures, photovoltaic response 80−101115
Al_2O_3 plasma anodised film on Si, elec. resist. 80−7722
Al_2O_3, polycryst. on Si, anodisation, MAOS struct. form, and elec. props. 77−48563
Al_2O_3-$Al_xGa_{1-x}As$-GaAs heterostructure, MBE grown, MOS GaAs capacitor appl. 79−77943
Au/oxide/n-GaAs struct., photocurrent relax. 80−92978
Au/Se(As_2Se_3)(CdS)-liquid insulator interface, carrier injection 80−24970
Au-InP, MIS Schottky barriers, interfacial parameters determ. 79−95505
Au-oxide-GaAs, reverse bias influence on photocurrent 80−107921
Au-oxide-GaAs struct., steady-state and transient photocurrents 80−6994
Au-oxide-n-GaAs structs., reverse-bias depend. photocurrent, photoionisation of surface states 80−20323
Au-Si_3N_4-GaAs-GaP structures, as elec. controlled optical transparencies, optical processing use 77−85339
Au-SiO_2-Si, wetting of quartz by Au-Si eutectic melt rel. to degradation 77−31840
Au-SiO_2-Si structures, electron and ion emission from MOS field cathodes *(German)* 77−12499
Au-SiO_2-Si system, oxide film 16-36 Å thick, tunnel currents 80−70842
Au-SiO_x-Ge, sandwich structure, exam. of image structure using mirror electron microscopy *(German)* 79−11019
Au-Ti/SiO_2/p-Si MOS struct., interface state distrib., DC tunnelling spectra determ. 80−75611
$BaTiO_3$/SiO_2-Si charge storage memory films for IGFETs 80−11566
Bi film, quantum size effect and band struct. Bi-dielec.-metal system obs. 80−54811

metal-insulator-semiconductor structures continued
CdF_2, rare earth doped, multicoloured electroluminesc. in MIS struct. 79−78755
CdF_2:Mn,Y, in MIS struct., blue-green electrolum. 79−52025
$Cd_xHg_{1-x}Te$ narrow gap semiconductor, charge transfer device for IR detection appl. *(French)* 79−30563
CdS MIS devices surface states 78−72267
CdS_xSe_{1-x} multilayered struct., charge pattern formation during recharging 80−47129
CdSe, MIS thin film capacitance, theory 79−87156
CdSe MIS thin film solar cell 80−45688
CdSe thin film transistor and MISM struct., effect of annealing on electron mobility and conc. 79−78198
CdTe/Langmuir film photovoltaic structures for solar cells 80−49918
p-CdTe-Langmuir film interface, prep., characters. and MIS struct. 80−92998
CdTe-Langmuir film MIS structures 79−65551
Cr-SiO_2-Si, solid-phase interaction between Cr and SiO_2, X-ray spectral obs. 78−10560
Cr-SiO_2-n-Si tunnel diodes elec. charact. meas. and modelling 77−39955
GaAS(P)(Sb)-anodic oxide MOS struct. oxide and interface props. 79−60929
p-$Ga_{1-x}Al_xAs$ crystals, spectral charact. of photosensitivity, mechanism 80−44735
$Ga_xAl_{1-x}As$, Schottky barrier, effect of oxide composition on elec. behaviour, AES meas. 79−87141
GaAs, acoustic plasmons in MOS inversion layers 78−18983
GaAs anodic MIS system, dynamic props. of interface state bands 80−49933
GaAs anodic MOS structs., interface-state band model 80−11093
GaAs, anodic native oxides for MOS devices, quality assessment 79−61767
GaAs, anodic oxidation in nonaqueous electrolyte and MOS charact. 79−38183
GaAs, anodic oxidation using O plasma, and oxide layer evaluation 78−85015
GaAs anodic oxide, electrical props. 79−38170
GaAs, anodic oxide diode, elec. instabilities and field-induced hysteresis 79−61770
GaAs anodic oxide film prep. by plasma anodisation of O-sputtered surfaces, MOS device charact. 79−66176
n-GaAs anodised MOS, electrorefl. spectra 79−99901
GaAs based MIS structures as possible optical memory elements 79−65556
GaAs based MOS capacitors, scanning photovoltage investigation 80−80396
GaAs conducting MIS structures and metal-semicond. structures, effects of ultrathin oxides 79−1626
GaAs films for solar cells appl., deposition and characterisation 80−84853
GaAs, in MIS system, nature of surface carrier depletion layers 77−1469
GaAs, low temp. plasma oxidation and MIS struct. charact. 78−31546
GaAs MIS capacitor, transient capacitance and C-V charact. 78−95374
GaAs MIS devices, multidielectrics using composition-graded $Al_xGa_{1-x}As$ and oxidised AlAs 79−65333
GaAs MIS dynamic optically controlled transparencies 78−90523
GaAs MIS struct., elec. props., effect of interface As domains 78−88032
n-GaAs MIS structs., native oxide, effect on interface props. and removal by sputter etching 79−11228
GaAs MIS structs., nitride-based passivation for reduced surface state density 80−16537
n-GaAs, MIS structures, C-U curves, surface state densities 77−85335
GaAs, MIS structures, dielec. and interfacial charact. appl. to microwave MISFETs 79−60933
GaAs MOS and Schottky systems, electromodulated reabsorption of luminesc. 79−15524
GaAs MOS capacitor fabrication and transient response for minority carrier lifetime meas. 79−47103
In-GaAs, MOS capacitor struct., elec. props., annealing effects 80−34519
p-GaAs MOS capacitors, anodized, C-V charact., surface pot. 79−11227
GaAs MOS device, new method of fabrication 78−47872
GaAs MOS diodes, interface states, deep-level transient spectroscopy 80−44727
GaAs MOS solar cells by anodisation in active region 80−101107
GaAs MOS structure, props. of surface carriers 77−20453
GaAs MOS structure, small signal admittance study 80−2478
GaAs MOS structure, white light emission obs. 78−76148
GaAs MOS structures, props. of capacitance transient 80−25013
GaAs MOS structures, leakage current for anodic oxide layers, space charge trapping effects 80−60091
GaAs MOS system, elec. meas. interpretation 78−43484
GaAs, native oxide growth by wet anodisation 80−70832
GaAs, oxidation in multipole plasma, MOS elec. props. 80−44737
GaAs oxidation saturation and MOS diode equivalent cct. 78−47875
GaAs oxide film form., ion implantation effects 80−100266
GaAs, photocapacitive MIS IR detector, spectral response, noise charact. 80−75644
GaAs, plasma anodisation in DC discharge, AES and MIS diode expts. 78−95826
GaAs, surface passivation using composite Al_2O_3 and native oxide, MIS charact. 80−93004
GaAs, surface passivation using Si_3N_4, interface charact. 80−93005
GaAs, surface passivation using GaO_xN_y based multiple insulating layers 80−93006
GaAs, thermal oxide film growth and characterisation 80−11808
n-GaAs thin films carrier wave amplification, external medium stratification effects *(Russian)* 78−34905
GaAs, tunnel MIS structures, surface states 77−85336
GaAs, with anodic oxides, leakage currents 79−38169
GaAs, with natural anodic oxide elec. props. 79−99634
GaAs:Ar^+-metal, capacitor, capacitance-voltage and current-voltage meas., assuming intermediate dielec. layer 79−56316
GaAs:Cr, deep levels, wavelength-modulated photocapacitance spectroscopy 80−76055
GaAs-$Al_{0.5}Ga_{0.5}As$-Cr/Au MIS capacitors, charact. meas. 78−95371
GaAs-Al_2O_3 anodic oxide interface, elec. props., rel. to MESFET passivation 80−49934

metal-insulator-semiconductor structures continued
GaAs-Al_2O_3 MIS struct., interface props. and MISFET fabrication 79−65557
GaAs-Al_2O_3 MOS struct. capacitance-voltage and conductance-voltage characts. before and after annealing in H_2 79−60927
GaAs-$Al_xGa_{1-x}As$ MOS rib waveguide polarizers 80−64207
n-GaAs-anodic oxide MIS devices, inversion and accumulation layer form. at elevated temps. 79−60934
GaAs-anodic oxide MOS struct., interface state band 79−60930
GaAs-insulator interface, processes of electron emission from traps 79−73598
n-GaAs-SiO_2 interface, MOS capacitors, surface states from conductance and capacitance meas. 80−100533
GaAs-SiO_2 MIS structures, fabrication and elec. props. 79−47166
GaAs-Ta_2O_5, surface pot. variation, capacitance-voltage meas. 79−61769
n-$GaAs_{0.6}P_{0.4}$, anodic oxide diode, elec. instabilities and field-induced hysteresis 79−61770
$GaAs_{0.6}P_{0.4}$, anodic oxide, electronic props. 79−61771
$GaAs_{1-x}P_x$, thermal oxides, elemental composition and C-V characts. 79−61772
GaN, reactive sputtering, GaAs MIS struct. fabrication and props. 78−39686
Ga_2O_3 thin films, reactively evaporated, props. *(Japanese)* 79−99648
GaP anodic MOS structs., interface-state band model 80−11093
n-GaP, anodic oxide diode, elec. instabilities and field-induced hysteresis 79−61770
n-Ge accumulation layers, effect of low-energy Ar^+ ion bombardment on electron scatt. 77−66205
Ge, high purity, surface inversion layer electron and hole mobilities 77−76937
Ge, spectrum of photocapacitance current near fundamental absorpt. edge 77−28217
Ge-GeO_2, MIS struct., electrophysical characts. 79−82680
Ge-GeO_2 MIS structure, growth of GeO_2 from liq. phase *(Russian)* 80−40273
Ge-InAs based MIS struct., avalanche carrier multiplication 80−88566
Ge-SiO_2, MIS struct., electrophysical characts. 79−82680
Ge-SiO_2-Al, vacuum heating effect on stability 78−64143
Ge-SiO_2-Si_3N_4, MIS struct., electrophysical characts. 79−82680
Ge-SiO_2-Si_3N_4-Al, electrophysical props. 77−76934
Ge_3N_4 CVD film prod. and Al-Ge-Ge_3N_4-Al structure V-I and V-C characteristics *(Russian)* 78−47893
H_2 sensitive, Pd-gate MOS 78−2578
HgCdTe MIS structure, modelling and appl. to CCD IR imagery 78−80058
$Hg_{0.8}Cd_{0.2}Te$-ZnS MIS struct., nonparabolic bond semicond., surface state studies, capacitance measurements 79−78190
$Hg_{1-x}Cd_xTe$ breakdown-limited MIS device, increased charge capacity using ramped gate voltage 80−103751
$Hg_{1-x}Cd_xTe$, Hooge's flicker noise MIS expt. 78−56233
$Hg_{1-x}Cd_xTe$ photoconductors, gamma ray effects on surface props. and detector props. 79−17489
$Hg_{1-x}Cd_xTe$-oxide interfaces, MIS capacitance characts. 80−49926
HgCdTe(Se) MIS junction, phonon-assisted tunnelling 79−47170
InAs epilayers in MOS carrier transport coeffs. determ. by multilayer model 78−2575
InAs, heteroepitaxial, charge transport obs. by gate-voltage-controlled meas. on MOS struct. 77−47912
InAs surface accumulation layers, magneto-transconductance meas. 78−64137
InAs surface accumulation layers, magneto-transconductance study 80−49948
InAs surface layers, oscillatory transport coeffs. 78−64136
InAs(Sb), in MOS struct., electrorefl., band-population effects under heavy surface accumulation 77−48167
In_2O_3-InSb, with Al(Au) electrode interface state density and oxide charge meas. 77−8200
InP, and $In_xGa_{1-x}As_yP_{1-y}$ binary and quaternary cpds., surface and dielec.-semicond. interface props. 80−93001
InP, elec. characts. of InP surface meas. 77−20451
InP, MIS capacitor, transient capacitance and C-V characts. 78−95374
InP MIS capacitor surface states 80−49931
InP, MIS diode prep. by anodic oxidation 79−74270
InP, MIS structures, dielec. and interfacial characts. appl. to microwave MISFETs 79−60933
p-InP, oxidised, mercury probe, I-V characts., van der Pauw meas. 78−14745
InP, surface passivation using composite Al_2O_3 and native oxide, MIS characts. 80−93004
p-type InP/Langmuir film MIS diodes, characts. 80−80384
n-InP/SiO_2 capacitors, minority carrier generation 79−95496
InP-Al_2O_3 MIS struct., interface props. and MISFET fabrication 79−65557
InP-SiO_2, with reduced interface state density near cond. band 78−26954
n-InP-SiO_2 capacitor, carrier generation and trapping 80−49929
n-InP-SiO_2 system, interface and dielec. props. 80−49930
InSb based MIS structs., charge accumulation in insulator layers 80−6993
n-InSb based MIS struct., carrier generation under nonequilibrium conditions 80−88640
p-InSb diodes, metal-BSG-InSb oxide-p-InSb, C-V characts. 77−80848
n-InSb, in MIS struct., accumulation layer submillimetric cyclotron resonance obs. 77−39912
InSb, in MISIM struct., photovaractor effect and CV characs. obs. 77−8205
p-InSb inversion layer, magnetotransport 78−64138
InSb inversion layer, spectroscopy of electron subband levels 78−10569
InSb inversion layer, spectroscopy of electron subband levels 78−64364
InSb MIS capacitors, gamma-ray radiation effects at cryogenic temps. 80−34517
n-InSb MIS device interfaces, low-temp. CVD of SiO_2, characts. 80−16196
InSb MIS devices, large-amplitude hysteresis, model 79−19665
n-InSb, MIS diode, time-dependent photovoltaic effect 80−75601
InSb, MIS struct., background radiation effect on photoelec. processes 80−25015
p-InSb MIS struct., field effect studies 80−80386
InSb MIS structure, effect of room background on noise props. 80−103755
InSb, MIS thin film capacitance, theory 79−87156

metal-insulator-semiconductor structures continued
InSb, MISS struct., surface electron and hole mobility and conc. *(Russian)* 80−44701
InSb MOS capacitor, AC behaviour, semicond.-oxide interlayer effect 78−19151
InSb MOS struct., capacitance of n-channel inversion layers, elec. field effects 80−80393
InSb MOS structs., energy spectrum of traps in oxide layer 80−107922
InSb MOS structure, props. 80−49947
p-InSb, magnetoconductivity and cyclotron reson. in inversion layers 80−49946
InSb, n-type, anodic oxide film dielectric, MOS structure *(Russian)* 77−89874
n-InSb substrates, MIS struct. form. by reactive deposition of Si_3N_4, C/V meas. 80−103752
n-InSb, surface accumulation layer, sub mm electron cyclotron reson. 78−6576
n-InSb, surface quality improvement by low temp. CVD of SiO_2, and characterisation 80−49932
InSb-anodic oxide MIS struct., electrophys. props. *(Russian)* 77−39961
InSb-anodic oxide-Ni, energy band diagram, internal photoemission meas. 79−33356
InSb-SiO-Al, vacuum deposited, prep. and characts. *(Italian)* 78−84715
InSe MOS structs. 79−69605
InSe, photovoltaic energy conversion efficiencies 79−7854
LaF_3 insulators for MIS structs. 79−78182
LaF_3 superionic conductor insulating layer, used for photocapacitive detectors 80−92976
MOS capacitor, photoionisation cross section and interface state density 80−92974
MOS capacitor structure, cond. mech. in oxide grown on polycrystalline Si 77−76989
Mo, film, vacuum deposited, elec. cond., internal stresses, surface corrosion, MOS gate appl. *(Japanese)* 78−80073
Mo-SiO_2-Si, effect of heat treatment after deposition on internal stress in MO film 78−22973
Mo-SiO_2-Si, pelicular structure, struct. transitions during vacuum thermal treatment *(Russian)* 78−95238
Mo-SiO_2-Si, R/MOS struct., heat treatment effects 78−76683
Mo-SiO_2-Si, thermally stimulated ionic cond. 78−10565
Na^+ neutralisation characteristics of HCl oxides 78−10572
Pb/oxide/InAs structure, effective mass determ. by tunnelling spectroscopy *(Russian)* 80−44482
Pb-Al_2O_3-HgSe junction, asymmetry of tunnelling characts. 79−47169
Pb-SiO_2-$Pb_{1-x}Ge_xTe$, semicond. band struct., tunnelling obs. 80−54795
$Pb_{1-x}Sn_xTe$, in MIS struct., tunnelling investig. of band gap and phonon energies 77−43733
$Pb_{1-x}Sn_xTe$, in MOS junction, phonon-assisted tunnelling 77−76928
p-PbTe, MIS struct. inversion layer sub-bands, IR magnetoreflectance obs. 80−44731
PbTe substrate for MIS capacitor, C-V and G-V characts. 78−26962
PbTe surface space charge layers, far IR magnetoreflectance meas. 78−64349
p-PbTe with Al_2O_3 and MgO insulator layers, 5 μm IR detector appls. 78−52101
PbTe-oxide-Pb(Sn) junctions, quantum levels obs. 80−49945
PbTe-ZrO_2 (SiO_2), epitaxial MIS struct., fabrication and elec. props. 80−2472
Pd surface chemical reactions using MOS structure 77−73470
Pd/SiO_x/Si, Schottky-barrier type devices, chemical and polarisation characteristics, comparative study 79−78173
Pd-SiO_2-Si, H induced interfacial polarisation at Pd-SiO_2 interface, internal photoemission meas. 77−1490
n-Si (100) inversion layer mobility depend. on intersubband scatt. at low temps. 79−95506
Si (100) MOST, comparison of Shubnikov-de Haas effect and cyclotron reson. under uniaxial stress 80−20320
Si (100) surface accumulation layer, subband struct. and inter-subband absorption in strong mag. field 78−39177
Si (110), (111) surfaces, inter-subband spectroscopy in hole space charge layers 77−32064
n-Si (111) MOS charge layer, optical spectrum of inter-subband transition 78−64133
Si, (111) surface, electron inversion layers, obs. of sixfold valley degeneracy 79−38176
Si based MIS negative barrier contact for induced back surface field solar cell 80−101101
Si based MIS structure, photoelectric characts. carrier injection levels *(Russian)* 80−96946
Si based MOS capacitors, scanning photovoltage investigation 80−80396
n-Si, capture cross section and generation lifetime determ. of Au, MOS expts. 78−91772
Si, epitaxial layers, minority carrier lifetime and diffusion length meas., photocurrent technique 78−95302
Si high-resistivity structure, photoelec. props. 78−91730
Si inversion layer, elec. break-through, exactly solvable model 78−56234
Si inversion layer, elec. cond., freq. depend. 78−72270
Si inversion layer, high field drift vel., Monte Carlo calc. 77−32087
Si inversion layer, high freq. cond., Drude relax., 2D plasmons and minigaps in surface lattice 78−60230
Si inversion layer, IR spectrum, 10^5G effect on linewidth 78−946
Si inversion layer, in strong mag. fields, electron localisation 78−60219
Si inversion layer, negative differential resist. 78−60225
Si inversion layer, press. depend. of struct. of field effect mobility 78−60216
Si inversion layer, surface quantum oscillation under pressure 78−60228
n-Si inversion layer, thermal activation of two-dimens. Shubnikov de Haas cond. extrema 78−60218
Si inversion layer, transient response of hot electrons, calc. 80−49747
Si inversion layer, warm electrons 78−60222
Si inversion layer electronic transitions for voltage-tunable far IR emission 77−39962
Si, inversion layer electrons, temp. depend. cyclotron reson. lineshape 78−10568
Si inversion layer in MOS struct., carrier-phonon interaction, nonohmic transport 80−49943
Si inversion layer surface cyclotron resonance, temp. and stress effects 78−60229
Si inversion layers, cyclotron and subband emission 78−64128
Si inversion layers, discrepancies between absorption and photocond. meas. 78−6451

metal-insulator-semiconductor structures continued
Si inversion layers, far IR transmission spectra, two-dimensional plasmons 77−76931
Si, inversion layers, far IR emission from hot electrons 78−30995
Si inversion layers, far IR reson. magnetotransmission, temp. and band gap light depend. 78−64363
Si, inversion layers, intervalley transitions and subband splitting 77−20455
Si inversion layers, low density, far IR resonant magnetoabsorption 77−55789
Si inversion layers, magnetocond. in ground Landau level, defect diffusion in Wigner cryst. 77−39914
Si inversion layers, near threshold at low temps., cond. anomalies and electronic states 77−59333
Si inversion layers, review 77−80842
Si inversion layers, stress and intersubband correlation 78−60227
n-Si inversion layers, stress and temp. depend. of subband struct., plasmon-pole approx. 79−95461
Si, inversion layers, two-subband screening and transport 78−64126
Si ion damage critical gettering doses, elec. characts. 78−10085
Si, lattice scattering mechanism in quantised inversion layers 79−78187
Si MIS capacitors, C-V curves, outer oxide surface conditions effects 80−97000
Si MIS switch diode, charge storage effects, threshold depend. on driving voltage pulse freq. 80−49939
Si MIS-inversion layer solar cells 80−76632
Si MNOS structures with tunnelling-thickness SiO_2 films, surface channel hole mobility obs. 78−95380
Si MOS (111) inversion layers, angular dependent negative magnetoresist. 78−80062
Si MOS capacitor, carrier generation in depletion layer, effect of stacking faults 79−23983
Si, MOS capacitor, minority carrier lifetime determ. 77−85264
Si, MOS capacitor, nondestructive of P^+ and He^+ induced damage, doping profiles 80−34087
Si MOS capacitors, on Czochralski-grown wafers, lifetime improvement by two-step annealing 80−49916
Si MOS capacitors, pulse response anal., lateral depletion region around gate area 79−38187
Si, MOS device, subject to linear voltage ramp, non-steady-state studies 79−78189
Si MOS diode, bulk traps and interface states determ., deep-level transient spectroscopy appl. *(Japanese)* 79−42645
Si, MOS diode, dependence of minority carrier bulk generation on HCl concentration 80−88639
Si MOS diode characts. obs., electron irradiation damage effects *(Japanese)* 79−42646
Si MOS inversion layer, Anderson localisation and Wigner crystal form. *(Japanese)* 77−69425
Si MOS inversion layer, subband struct., many body effects 78−64131
Si, MOS inversion layers, Hall effect 78−64118
n-Si MOS inversion layers, Hall cond. meas. 80−39676
Si, MOS struct., electron-irrad., surface defect distrib., deep-level transient spectroscopy 79−1459
Si MOS struct., space-charge generation props. of Au 80−2475
Si MOS structure, electronic density of states of discharge produced amorphous Si 79−46992
Si MOS structure, low leakage, determ. of surface- and bulk-generation currents 79−24055
Si MOS structure two-layer dielectric interface In doping effect 79−56324
p-Si MOSFET, intersubband reson. photoresponse, mechanism 79−82677
Si n-channel (100) inversion layer, valley splitting, formulation by extended zone effective mass theory 77−85329
Si n-channel (100) inversion layer, theory of valley splitting, electric break through 77−85330
Si n-channel (100) inversion layer, valley splittings, enhancement by many-body effects 77−85331
Si, on sapphire, MOS inversion layer, magnetoconductance oscillations 80−20325
Si oxidation mechanism and kinetics 78−95833
Si oxides, grown in Cl-containing ambients, correl. between elec. and material props. 80−39479
Si p-channel MOS structure, stress effects on elec. props., press. transducer props. 80−100526
Si, p-n junctions in MIS struct., dislocation study by high voltage electron microscopy and SEM 79−82217
Si, photocapacitive MIS IR detector, spectral response, noise characts. 80−75644
Si, polycryst., energy distrib. of trapping states, from impedance of MOSS struct. 80−65691
Si polycrystalline film resistivity reduction by Nd:YAG laser annealing 80−100539
Si rich SiO_2-SiO_2-Si rich SiO_2 layers for dual electron injector struct. 80−96991
Si solar cells, interface states effects on performance 78−76153
Si solar cells, spectral response and diffusion length 79−92077
Si solar cells using minority carrier MISS 80−101103
n-Si, surface quantum oscills. in inversion layers under uniaxial press. 78−88041
Si surface space charge layers, cyclotron reson. of holes 77−76932
Si, thermal oxidation technology, improved using 1,1,1-trichloroethane as optimised additive 79−29239
Si, thermally oxidised surfaces, electron mobility in inversion and accumulation layers, MOS devices 80−103753
Si, under stress, density functional calc. of subband struct. 80−20321
Si:Ar, ion implant gettering of MOS capacitors using linear voltage ramp and N^+ backscattering 79−95502
Si:Au Ar ion implant gettering obs. by MOS and Rutherford backscatt. techniques 80−39119
Si:B MOS structures, implanted laser beam irrad. effects on interface electrophys. props. 79−1627
p-Si:B-SiO_2 interface in MOS structures, carrier mobility and impurity distrib. 78−34902
Si:H, amorphous, density of states determ. using field effect 80−49937
Si:H, amorphous, surface states distribution using MOS tunnel junctions 80−103735
Si:H, amorphous oxidised, Pt film growth AES and LEED study 80−88447

metal-insulator-semiconductor structures continued
Si:H,P, amorphous, in MOS tunnel junction, electron tunnelling characts. 79−73592
a-Si:H MIS junction, electronic struct. study by tunnelling 80−44729
Si:In, MIS structure, determ. of deep level parameters in surface layer of semiconductor 80−15612
Si:Na^+, variation of cond. in two-dimensional impurity band with Fermi level position 79−95510
Si/SiO_2 interface, slow-trapping instability, kinetics 78−76151
Si-Al_2O_3, capacitance-voltage and conductance-voltage characts. 79−60927
Si-Al_2O_3, from UV irradiation converted metalorganic compounds *(Russian)* 80−45245
Si-Al_2O_3, inversion layer subbands, magnetocond. oscills. 78−64124
Si-BN interface, elec. characts., expt. 77−20459
Si-Cr_2O_3-Al, current-voltage characts., oxide film effects 80−70841
Si-insulator interface, non-avalanche charge injection, expt. study, charge trapping effects 80−60099
Si-polymer interface states in MOS structure, capacitance and cond. meas. 77−20438
Si-Si_3N_4 interface in MNS capacitors, surface state density investigation 80−60100
Si-Si_3N_4-Al, photoexcitation of emission currents, I-V characts. *(Russian)* 77−72917
Si-Si_3N_4-SiO_2-Si multilayer structs., impurity distrib., activation anal., autoradiography techniques 77−16881
Si-SiO_2, Al-implanted, low-temp. annealing effect on charge and surface state density 77−85337
Si-SiO_2, effect of Cl incorporation during prep. 78−11378
Si-SiO_2, flat-band voltage due to fixed surface charge density, modified expression 79−56317
Si-SiO_2, intentionally contaminated interface, transient capacitance meas. 79−33349
Si-SiO_2, interface, hopping conduction, anal. in impurity bands in inversion layers 79−47171
Si-SiO_2, MOS interface states density, meas. techniques and model development 80−92988
n-Si-SiO_2, MOS structures, radiation states 80−103758
Si-SiO_2, Si oxidation, solubility and transport behaviour of water, dissolution 80−93801
Si-SiO_2, SiO_2 layer charging in UV irrad. of MISS struct., photoinjection currents *(Russian)* 80−39680
Si-SiO_2, specific memory effect, radiation defects 79−51680
Si-SiO_2, thermal growth mechanisms of vitreous oxide layers on Si 80−93675
Si-SiO_2 interface, Au conc., effective impurity doping 78−52094
Si-SiO_2 interface, barrier height in MOS tunnelling structures 80−88644
Si-SiO_2 interface, bias temp. treatment effect, stability, Cl oxides effect 77−69419
Si-SiO_2 interface, doping depend. of interface states and charges 80−92992
Si-SiO_2 interface, effect of hot electron injection on interface charge density 80−49921
Si-SiO_2 interface, γ-ray irradiated thin oxide, MOS struct. *(Russian)* 78−84302
Si-SiO_2 interface, in MOS struct., fast surface states density, electron irrad. effects 78−88042
Si-SiO_2 interface, interface-state parameters near band edge, MOS conductance meas. 79−11226
Si-SiO_2 interface, O_2 plasma effects on elec. props. 80−100523
Si-SiO_2 interface, quasistatic capacitance-voltage determ. of interface state density, sources of error 77−12011
Si-SiO_2 interface, rad. hardness, carrier localisation in inversion layer 77−85332
Si-SiO_2 interface, radiation damage coeffs. for fission neutron and gamma-ray irrad. 80−34058
Si-SiO_2 interface, radiation hardness eval. using elec. meas. technique 80−34516
Si-SiO_2 interface, relax. of injected charge, temp. depend. 78−72269
Si-SiO_2 interface, surface states characterization, expt. techniques review 80−49949
Si-SiO_2 interface, thermally grown, surface pot. inhomogeneities after stress ageing 80−92993
Si-SiO_2 interface charge inhomogeneities effect on surface state density meas. by MOS AC cond. technique 78−14833
Si-SiO_2 interface in MIS struct., B^+ ion implanted, elec. props. due to laser irrad. 78−72272
Si-SiO_2 interface in MIS structs., effects of crystal defects on generation process 80−65702
Si-SiO_2 interface in MOS structs. low-energy electron beam irrad., charge accumulation process anal. 80−65701
Si-SiO_2 interface in MOS capacitors, lateral diffusion of Na^+, neutralisation 80−92986
Si-SiO_2 interface of MIS structure, generation-recomb. characts., effect of γ-irradiation *(Russian)* 77−76938
Si-SiO_2 interface state spectrosocpy using MOS tunnelling strucures 80−6991
Si-SiO_2 interface states, deposition of H containing layers and annealing 80−92991
Si-SiO_2 MIS systems, dynamic props. of switching, appl. to charge transfer devices 80−92997
Si-SiO_2 MOS capacitors, two-dimens. calc. of avalanche breakdown voltage 80−11096
Si-SiO_2 MOS capacitors, relationship between trapped holes and interface states 80−70830
Si-SiO_2 MOS interface, surface-state density and minority carrier generation rate, meas. by DLTS, hot hole effect 80−100527
Si-SiO_2 MOS interface states density, transient capacitance meas. eval. 80−92989
Si-SiO_2 metal structure, ponderomotive force effect on dielec. breakdown 79−15230
Si-SiO_2 structures, electron trapping, donor state generation, photo I-V study 80−20210
Si-SiO_2 systems, spectral characts. *(Russian)* 79−42657
Si-SiO_2-Al, interface barrier energies for tunnel oxides, internal photoemission meas. 80−84512
Si-SiO_2-Al, internal photoemission, pot. barrier height determ. 80−65699
Si-SiO_2-Al structure, mechanical stress at Si(111) surface 78−63921
Si-SiO_2-Al structures, SiO_2 thin dielec. film elec. props. with DC voltage *(Slovak)* 80−88634
Si-SiO_2-Al with thick dielec. layer, photoelec. props. 80−92979

metal-insulator-semiconductor structures continued
Si-SiO_2-Mo-Si_3N_4-Al MNOS structures with metal grains, charge transport at SiO_2-Si_3N_4 interface 80−65693
Si-SiO_2-Si thin film MOS structures, elec. props. with applied DC voltage *(Slovak)* 80−92977
Si-SiO_2-Si_3N_4 MNOS structure, chem. comp. and electronic states, Auger and energy loss spectra obs. 80−92999
Si-SiO_2-Si_3N_4 system, internal photoelec. emission and residual photoelec. effects 79−73599
n-Si-SiO_2-ZnO-Al, SAW convolver in monolithic MIS struct. 77−23791
Si-SiO_2-metal, electron photoemission from Si, band struct. effects 79−19977
Si-SiO_2-metal structures, tunnelling probabilities for electrons and holes in ultrathin SiO_2 79−99631
Si-TiO_2-Al, current-voltage charact., oxide film effects 80−70841
Si-V_2O_5-Al, current-voltage charact., oxide film effects 80−70841
Si(111) inversion layers, CDW induced cyclotron reson. harmonics 78−64085
Si_3N_4, amorphous, in MIS struct., high field conductivity 78−23101
Si_3N_4, amorphous insulator film, high-field cond. 79−56320
Si_3N_4 CVD films, microstruct. and MNS struct. charact. 79−65339
Si_3N_4 CVD films on Si, dark currents 79−78240
Si_3N_4 degradation due to high-temp. processing 78−6454
Si_3N_4 film, CVD, high-field dark currents 80−54791
Si_3N_4 film, in MNOS struct., kinetics of irreversible changes in cond. 79−73600
Si_3N_4 film, in MNS structures, dark conduction and photoconduction phenomena 78−30989
Si_3N_4 film, pyrolytically deposited, AC cond. at low freq. 78−84334
Si_3N_4 films, CVD in MNOS and MNS structs., elec. resist. 80−97019
Si_3N_4 films grown by pyrolytic reaction between silane and ammonia, DC cond. 79−15243
Si_3N_4 MNS capacitors, elec. cond. 79−95499
Si_3N_4, unsteady cond. in high elec. fields 78−76152
Si_3N_4:Si amorphous insulator film, elec. props. obs. 77−76987
Si_3N_4-Si, thermally grown films for high performance MNS devices 78−48322
Si_3N_4-SiO_2, interface, electron and hole cond. at moderate elec. fields 78−95376
Si_3N_4-SiO_2:As, graded and stepped energy band-gap MIS struct. 80−2473
SiO_2, As-implanted, electron trapping and detrapping charact. 80−65692
SiO_2, avalanche injection of holes 78−26959
SiO_2 CVD layer, high current injection from Si rich SiO_2 film 80−80430
SiO_2, electron-beam irrad., electron trapping, MOS capacitor expts. 78−72268
SiO_2 film, in MIS struct., current-field charact. 79−99623
SiO_2 film, migration parameters of alkali ions, elec. meas. in MOS capacitor 80−39359
SiO_2 film, thermally grown or sputtered, electrostriction and piezoelectricity 77−12010
SiO_2 film deposition from SiH_2Cl_2 on Si 77−77407
SiO_2 film growth technology *(Japanese)* 77−40381
SiO_2 film on Si, negative bias instability 78−91773
SiO_2 films in poly-oxide poly Si structures, elec. cond. and charge distrib. 80−92984
SiO_2 gate insulator, mobile K ions 77−47623
SiO_2 gate insulator MOS capacitors, hole transport, recovery charact. following electron beam irrad. 77−20439
SiO_2 grown anodically over Si, optical and electrophys. props. 77−72934
SiO_2 in MOS struct., prep. by O_2 implantation into Si, elec. props. 77−80523
SiO_2 in MOS struct., exciton transport rel. to surface states 78−34901
SiO_2 in MOS struct., room temp. cond., mobile Na^+ location 78−39217
SiO_2 in MOS structure, Cl conc. effect on negative bias instability 77−59332
SiO_2 layer of MOS structs., centroid location of implanted ions by photo I-V technique 79−24079
SiO_2 layer used for MOSFETs, electron trapping behaviour 80−92981
SiO_2 layers, DC current-voltage behaviour 77−85333
SiO_2 layers, in MOS struct., hole trapping induced by ion implantation and annealing at room temp. 80−54792
SiO_2 layers, passivating, deposition by plasma decomp. in planar reactor, appl. in MOS struct. 78−88430
SiO_2 layers, thermally grown, undoped and ion implanted, elec. props. 78−23187
SiO_2 layers on Si, ionis. thresholds of electron traps 80−92983
SiO_2 MOS capacitor, defect current obs. 80−92987
SiO_2 MOS structure, Cl role in passivation 79−91150
SiO_2 MOS structures, removal of electron traps by RF annealing 80−44728
SiO_2 MOS system, current transport, T-D emission theory 79−91149
SiO_2, mobility and trapping of ions, Si-SiO_2 interface states 80−92985
SiO_2, pyrolytic, in MOS struct., C-V charact., non-equilib. lowering in inversion mode 77−55630
SiO_2, reactive ion etching damage, electron trapping charact. in MOS struct. 79−90704
SiO_2, sputter deposition onto GaAs, and MIS struct. charact. 77−89864
SiO_2, thin film, prep. from low-temp. oxidation of tetraisopropoxysilane, dielec. props. 77−8759
SiO_2 thin film capacitors using polycrystalline Si and Al electrodes, dielec. breakdown 79−69600
SiO_2 tunnelling barrier asymmetry to electrons and holes in MOS struct., photocurrent 80−75645
SiO_2:As^+ implanted layers in MOS struct., electron trapping and detrapping charact. 80−92982
SiO_2:F-ion implanted, mobile-ion drift compensation 79−19664
SiO_2:W film electron trapping charact., obs. by avalanche injection techniques 77−89862
SiO_2-InP, MIS struct., prod. by pyrolytic deposition resist., breakdown and interface states 77−15961
SiO_2-InP MOS struct., capacitance-voltage and surface photovoltage meas. 79−60931
SiO_2-Si, irradiated SiO_2 film electron and hole trapping 80−11098
SiO_2-Si interface of hardened MOS capacitors, radiation effects 78−26958
SiO_2-Si MOS capacitor, two-stage process for building up of radiation induced interface states 80−20313

metal-insulator-semiconductor structures continued
SiO_2-Si MOS system, ion irrad. effects on struct. and electrophysical props. 80−6995
Si(100) inversion layers, effects of uniaxial stress on cyclotron reson. 80−20322
Si(100) inversion layers, magnetoelec. and piezoresist. evidence for mobility domains 77−4447
Si(100) inversion layers, two-dimensional electron fluid, spin density, valley density waves 77−69400
n-Si(100) inversion layers on sapphire, surface quantum oscills. 78−19158
Si(100)-SiO_2 interface, mobility in Si inversion layers, screening and neutral impurity effects 79−28412
p-Si(111) surface inversion layer, Cs covered, negative magnetoresist. in 2D impurity band 78−64135
Su-SiO_2 interface states, exptl. study of charge model 79−65554
Ta-Ta_2O_5-InP thin refractory MIS struct. deposition 80−75647
Ta-Ta_2O_5-ZnS:RF_3-Au struct., electrolum. and cathodolum. meas. *(French)* 77−16398
Ta-Ta_2O_5-ZnS:TbF_3-Au thin films, MIS struct., DC electrolum. obs., Poole-Frenkel effect 78−88038
Ta_2O_5 film, for MIS device, CVD and characterisation 77−4742
Ta_2O_5, film on Al, Cu, Au, Ag electrode, electric strength of MIS system 80−96999
Ta_2O_5, sputter deposition onto GaAs, and MIS struct. charact. 77−89864
Te $(1\bar{1}00)$ surface, electron-hole cyclotron resonance freq. depend. 79−69724
Te in MIS structure, impurity photocond. 78−72203
Te inversion layers, surface quantum transport 78−64088
Te, MIS structure, photosensitivity spectrum 78−14834
Te, surface cyclotron resonance, freq. depend. 78−64084
Ti-Pt link on Si_3N_4-SiO_2-Si substrate, laser vaporisation, interference effects 77−69941
TiO_2/SiO_2-Si charge storage memory films for IGFETs 80−11566
TiO_2-Si, MIS capacitor, C-V charact. meas. 78−60208
TiO_2-Si struct., I-V charact. 78−80063
TiO_2-SiO_2-Si structure, SiO_2 growth under TiO_2 film during postdeposition high temp. annealing 80−15400
TiW-TiO_2-InP thin refractory MIS struct. deposition 80−75647
(W-Au)-SiO_2-Si:B MOS transistor, ion implantation effect on threshold voltage 78−34903
ZnO-Si structure, MIS and SAW propag. charact. 78−30988
ZnO-Ti transparent type MIS solar cells 80−45662
ZnSe MIS LED, donor density calc. from C-U meas. 78−47878
ZnSe MIS structure, photolum. and blue electrolum. obs. 77−20928
ZnSe MOS diodes, injection type electrolum. 77−59614

metal-insulator transition
see also electrical conductivity transitions; minimum metallic conductivity
adamantine ceramic, structural, thermophysical and electrophysical props. 80−6918
alkali metal film, inert gas impurities, metal-insulator transition, optical absorption and cond. 77−24598
alkali metal-ammonia solns., elec.-cond. and thermopower 77−1370
alkali metal-ammonia solns., metal-insulator transition, h.f. and u.s. props. 77−1369
alkali metal-NH_3 solution, Hall effect and cond. at metal-nonmetal transition 78−2530
alkali metal-NH_3 solutions, metal-nonmetal transition Hall mobility, electrodeless meas. 78−56194
alkali metal-V_2O_5 bronzes, single cryst., elec. cond., 300 to 900K 77−20369
alloys, amorphous, exhibiting Mossbauer spectra, elec. props. *(French)* 80−80244
alloys, binary, 50-50, singularities at metal-insulator transition, CPA calc. 80−84428
alloys, binary narrow-band, metal-dielectric transition, off-diagonal disorder *(Russian)* 79−4512
AMO method of calc. 78−63982
Anderson localisation problem, cond. numerical studies 80−49673
Anderson localisation problem, numerical results 78−23040
Anderson localised states, electron correlation effects 79−23919
Anderson localised states, negative magnetoresistance 79−28357
Anderson transition, electron localisation in disordered systems, review 80−29361
Anderson transition, electron-electron interaction effects 80−65453
Anderson transition, elementary approach 79−28279
Anderson transition in mag. field, weak field cond. and Hall effect 80−6726
Anderson transition in systems with purely off-diagonal disorder 79−19518
Anderson transition in three dimensions, crit. strength of disorder 77−59256
band calculation by tight-binding method, orbital effect 77−15736
chemical mechanism, thermodynamics, vacancies 80−103626
cluster model 78−10351
cold semiconductor, Mott transition 78−91616
commensurate-incommensurate phase transition in nearly half-filled band 79−65384
condensed media, universality aspects of metal-nonmetal transition 78−56075
conducting liquid, effect of metal-insulator transition on crit. state 80−20089
conduction electron behaviour and role of electron-ion and electron-electron interactions *(Japanese)* 77−66102
Coulomb gas, classical, two-dimens., screening props. from sine-Gordon eqn. low-temp. phase transition 79−4524
Coulomb gas in d-dimensions, roughening transition 77−89718
cubic arrays of spheres in dielectric matrix, permittivity 78−56415
density-functional theory 80−75507
diamond, 'melting' to solid metallic C phase above graphite triple point 80−15236
diamond type crystals, semicond.-metal transition 78−72072
dielectrics, transfer processes, theoretical model review 80−15529
disordered electronic systems, low-dimensionality, Anderson localisation, resist. 80−84491
disordered one-dimensional system, electron density of states and Peierls transition *(Russian)* 80−29304

metal-insulator transition continued
disordered system, Anderson localised states, intra- and inter-state interactions 80−44543
disordered system, conductivity and mobility edge, square and diamond lattice calc. 78−43347
disordered system, particle diffusion in Anderson model 79−33273
disordered system, two band model 77−51662
disordered systems, one dimensional, nonvanishing zero temp. static cond., Anderson transition 80−29396
doped semiconductor, density functional approach 79−11067
doped semiconductors, correlation effects on Anderson localised states 79−95337
doped semiconductors, metal-insulator transition pretransition range anal., screening model 80−6724
education, electrochromism in WO_3, advanced lab. expt., colour centres, proton diffusion 80−17738
electron correlation problems, lattice statistical aspects, Gutzwiller approx. 78−84160
electron gas, dielectric transition temp. in strong mag. field 80−24813
electron microscopy *(French)* 78−26815
electron-hole drops, mobility and US absorption near metal-insulator transition, effect of fluctuation pairing 78−2434
electron-hole system, two-dimens., phase diagram for plasma to liq. transition 79−95342
electron-phonon interaction, electronic transport props. 77−89702
electron-phonon interaction role in insulator-metal transition in narrow-energy-band solid 77−89701
electronic Peierls transition, gap eqns. 80−24801
energy bands, narrow, electron correlation, Gutzwiller variational method 80−84426
energy sub-bands in polar model of crystal *(Russian)* 80−80183
exciton insulators with spontaneous currents, impurity scatt. effect on phase transitions 80−80242
excitonic insulator, quasi-one-dimens. 79−90966
expanded fluid metals, review of continuous metal-nonmetal transition 77−51787
extrinsic semiconductors, impurity interaction and metal-nonmetal transition 80−29325
f-electron hybridisation and damping, valence change 77−24520
Falicov-Kimball model, intermediate soln. 79−47015
Fermi gas, one-dimens. model, metal-dielec. parametric transition 77−15780
Fermi surface topological transition, electron-phonon interaction contrib. calc. 80−6697
fermion gas moving in strong three-dimens. random pot., conductivity 79−56130
ferroelectric phase-transition, semimetal-insulator, due to interband electron-phonon interaction 77−8531
ferromagnet, insulator-metal transition, s-d exchange interaction effects 78−2421
ferromagnetic semiconductor with defects, exchange Hamiltonian 79−82777
ferromagnetic semiconductors with doubly charged donors, quasiphase transition 79−65684
filament surrounded by polarisable mols., metal-insulator transition, electron density waves 77−24519
granular metal, EM wave propag., self-consistent approach 78−51920
group velocity and minimum metallic cond. 78−23141
heavily doped semiconductor, impurity bands, review of expt. results 79−95367
heavily doped semiconductor, n-type, disordered mag. system, hierarchy of exchange interactions 80−80235
heavily doped semiconductor, n-type, Mott transition, dielec. enhancement and conduction electron screening, unified treatment 78−72073
high pressure effects, review 77−43278
homologous series of semiconductors, homeomorphous, polymorphous and morphotropic transitions 79−37988
Hubbard band, half-filled, in paramag. state 80−92817
Hubbard bands, interaction as mechanism in metallic phase transitions 77−85148
Hubbard model, anharmonism effects 78−56072
Hubbard model, appl. to TCNQ-NMP 78−18966
Hubbard model, cluster-variation method in two-site approx. at high temp. 80−7071
Hubbard model, dynamic elec. and mag. susceptibilities near metal-insulator transition, functional-integral method 77−28119
Hubbard model, electron correl., first order transition obs. 77−11854
Hubbard model, FCC lattice, mag. and elec. props. 78−56334
Hubbard model, mag. field effect on Mott transition 78−34748
Hubbard model, Mott metal-insulator transition, ten-fold spin-orbital degeneracy 78−52285
Hubbard model, off-diagonal long-range order 77−28118
Hubbard model, Poisson approx. to functional approach 80−96790
Hubbard model, random one-body approx., one-dimens. case 79−37944
Hubbard model, self-consistent approx. 77−28357
Hubbard model, two band, mag., orbital and charge ordered states 78−27012
Hubbard model with nearest and next nearest neighbour hopping in Hartree Fock approx. 78−52189
hybridization effect on phase transitions in the Falicov-Kimball model 78−91617
II-V semiconductor, electronic theory, covalent-metallic or covalent-ionic phase transition under pressure 78−72105
III-V semiconductor, electronic theory, covalent-metallic or covalent-ionic phase transition under pressure 78−72105
impurity conduction phenomena, review of exptl. work *(Japanese)* 80−49737
inhomogeneous materials, effective medium theory with dipole-dipole interactions 79−4544
inhomogeneous materials, electronic props., metal-nonmetal transitions, review 78−56073
inhomogeneous media, elec. transport, optical props., exact theory 78−56119
inhomogeneous medium, Hall coeff., computer simulation 77−24597
intermediate valence, phase diagram and Kondo behaviour 80−29366
intermediate valence compound, pressure-temperature phase diagram 79−28283
intermediate valency compounds, conduction processes, metal-insulator transition 80−96787
inversion layer, threshold conduction 78−43450
Ising model, for transition temp., Green's function calc. 79−15084
metal-insulator transition continued
Ising model, phase transition in 2-dimens. Coulomb gas, interfacial roughening transition 77−20394
itinerant electron system, cond. transition to antiferromag. metallic phase 77−72980
liquid binary semiconducting alloy, metal-insulator transition induced by density changes 78−2529
liquid metal, metal-insulator transition induced by expansion 78−2529
liquid metals, lattice model 77−69220
liquid metals and semiconductors, review 77−1367
liquid semiconductor, metal-insulator transition model 77−1368
liquid semiconductors, data and model densities of states 80−50364
liquid systems, book 78−51406
low-dimensional materials, cond. temp. depend., metal-insulator transition, supercond. and semicond. behaviour 79−95391
low-dimensional systems, infrared problems and phase transitions of continuous order 78−6286
magnetic field induced, impurity cond. 79−65383
magnetic semiconductor, with impurities, semicond.-metal transition and instability phenomena 77−59257
magnetites, cond. mechanisms *(Russian)* 79−42539
many-valley semiconductor, metal-insulator transition at finite temp., calc. 80−49603
maximum metallic resistivity, approx. expressions 78−14773
metal inhomogeneous granular, superconductivity 80−103795
metal pulse evaporation under laser irrad., metal-insulator transition 77−81181
metal-dielectric transition with lattice distortion, two-band model 77−8023
metal-insulator interface, Hubbard model, possibility of insulator-metal transition 78−52084
metal-NH_3 solutions, metal-nonmetal transition 77−51789
metal-semiconductor transition, i.r. detection model 77−1442
mixed valence states, excitation mechanism in tight-binding approx., metal-insulator transition 80−10925
mixed-valence compounds, dielectric-metal phase transition *(Russian)* 80−6788
mobility edge, classical solns. and crit. exponents 80−10936
mobility edge problem, continuous symmetry 80−10939
model, using macroscopic sphere mixture 77−87615
model Hamiltonian 80−34361
Mott insulator electronic struct. review 78−18963
Mott insulator susceptibility 79−78302
Mott transition, spin glass description 79−65386
Mott transition criterion within Hubbard model, mag. field effect *(Russian)* 77−28120
Mott transition in Hubbard long range model, isostructural instability, thermodynamic props. *(Russian)* 80−65454
Mott transition in the multidimensional Hubbard model *(Russian)* 79−28282
Mott transition in the presence of impurities, Hubbard model and SCF anal. 80−10878
Mott transitions, temperature induced, Hubbard model theory 80−29326
Mott-Hubbard transition, props. of metallic state near phase boundary 77−62853
narrow band electron systems, unified theory of magnetism 80−70928
narrow band gap semiconductor, antiferromag. in strong mag. field *(Russian)* 77−28387
neutral Hubbard model appl. of information theoretical model 79−47014
noncrystalline system, continuous and discontinuous metal insulator transitions 78−56076
one-dimensional disordered system, extended electronic states and Anderson transaction 79−51487
one-dimensional Fermi system, mag. susceptibility, and dielec. function of two-dimensional Coulomb gas 78−10387
one-dimensional organic semiconductors, resonant states, mag. excitations and impurities 80−24839
one-electron approximation, effect of correls. and defects 78−63960
optical criterion for Mott transition 78−75996
orientational metal-insulator phase transitions in quadrupolar strands with itinerant electrons 80−15455
Peierls phase transition, in one-dimens. conductor 79−60806
Peierls-Frohlich dielectric, metallic screening, with pinning to impurities at finite temps. *(Russian)* 79−56208
percolation problem, two-dimens., crit. indexes of cond. 77−62964
phenomenological theory of first- and second-order metal-insulator transitions at absolute zero 79−69420
plasma, three-component, weakly-ionised, ionis. equilib. instability 80−10877
polar crystal model, instabilities in electron energy spectrum, metallic state stability criterion 79−82524
poly(p-phenylene), AsF_5 doped, highly cond. charge transfer complexes, elec. and optical props. 80−70778
polyacetylene: Br(Cl)(I)(AsF_5) electrical conductivity, metal-to-insulator transition 78−10525
polyacetylene:AsF_5, mag. susceptibility, Fermi surface density of states, semicond.-metal transition 79−95566
polyacetylene:AsF_5, soliton doping mechanism, mag. susceptibility meas. 80−107979
polyacetylene:SbF_5, elec. cond. meas. 80−60055
polyacetylene, doped, elec. cond. and thermopower 80−96951
polyacetylene, doped, field theoretical model of insulator-metal transition 79−99483
polyacetylene films, doping investigation, insulator-metal transition, optical transmission meas. 80−103729
proximity effect at low temp. for exciton insulator 79−73643
quasi one-dimensional metal, crit. temp. for phase transition *(Russian)* 79−78253
quasi-one-dimensional conductor, chiral charge density waves form. 78−6302
quasi-one-dimensional conductor, high temp. struct. instability, tight-binding approx. and fluctuation model 78−6292
quasi-one-dimensional conductors, impurity effect on phase transitions 78−6297
quasi-one-dimensional conductors, thermopower studies 79−65463
quasi-one-dimensional metallic system, phase transitions problem, Gorkov-Dzyaloshinskii model 78−6296
quasi-one-dimensional metallic systems, crit. behaviour, Ginzburg-Landau theory 79−56147
quasi-one-dimensional system, first and second order phase transitions, qualitative theory 78−31086

metal-insulator transition continued
quasi-one-dimensional system with repulsion, three dimens. dielec. transition *(Russian)* 77−43499
quasione dimensional crystals, effect of band filling on features of struct. transition 78−2424
randomly shifted bands model for semiconductor-metal transition 78−79929
rare earth compounds, pseudospin model of valency transition 77−72819
rare earth compounds, virtual bound state, f-level broadening 77−47773
rare earth compounds electron-phonon interaction influence on electronic phase transitions *(Russian)* 78−47743
rare earth monochalcogenides, electronic transitions 77−43496
rare earth perovskites, prep. and props. book contrib. 80−44193
rare earth trihydrides, light, low-temp. sp. ht., mag., elec., and cryst. field splitting effects 80−49379
review 79−15082
s-f model with electron-hole reson., antiferromag. behaviour and phonon spectrum 78−47992
semiconductor, doped, anal. 80−88478
semiconductor, doped, coexistence of insulating and metallic electronic phases 79−65385
semiconductor, doped, Coulomb repulsion term in Hubbard model for impurities 79−42492
semiconductor, electric field induced nonequilib. phase transitions 80−10879
semiconductor, Falicov-Kimball model, intermediate valence states, metal-insulator transition 78−51897
semiconductor, impurity band props. 79−23888
semiconductor, layered, electron-hole liq. and metal-dielec. transition *(Russian)* 78−2425
semiconductor, liq., NMR and metal-nonmetal transition 77−51973
semiconductor, n-type, donor-polarizability enhancement as the insulator-metal transition is approached from the insulating side 80−80184
semiconductor, n-type, electronic phase diagram 77−8022
semiconductor melts, metallic cond. at high temp. 80−49832
semiconductor models for non-equilibrium phase transitions due to impact ionisation from traps 79−51520
semiconductor-metal phase transition, cryst. existence in intermediate mixed state *(Russian)* 79−90962
semiconductor-metal transition, electron-hole fluid 77−43500
semiconductor-metal transition, struct. changes 80−34360
semiconductor-metal transition, structural transformations 79−23897
semiconductors, doped, dielec. const. enhancement on insulating side 80−20087
semiconductors, doped, insulator-metal transition, dielec. constant enhancement on insulating side 80−20088
semiconductors, doped, local spin-density-functional method, appl. to metal-insulator transition 80−96789
semiconductors, homologous series, structural transitions associated with morphotrophy 77−39675
semimetal in strong mag. field, metal-dielectric transition of electron-hole fluid *(Russian)* 77−80731
semimetal-exciton phase transition, microwave cond. 80−29430
simple metal alloys, electronic theory for metal-non-metal transition 78−47702
spatially disordered systems, Anderson localisation and metal-insulator transition 80−59926
spin-density functional approach to metal-insulator transition and local moment-formation 80−65451
statistical mech. treatment of impurity states 78−64004
structurally disordered systems, with diagonal and off-diagonal disorder in non-orthogonal basis set, numerical study 79−69387
sulphide group minerals, elec. cond., four-point probe technique meas. 78−64045
superconductor, metal-insulator transition, electron pairing, effect on optical props. 80−60139
superconductors, effect of insulating pairing of electrons on mag. props. 80−15651
supercritical fluid metals, metal-insulator transition, quantal percolation method 79−56129
system with two parameters, Mott and ferromagnetic transitions, phase diagram of the extended Caron Pratt model 79−15083
TCNQ complexes with dipyranylidene and dithiadipyranylidene, high cond. investigs. and related props. 78−6368
TCNQ derivatives, substituted, org. cond. with low-symmetric acceptors, cond. behaviour rel. to cryst. struct. 78−6365
TCNQ ion radical salt, DECA$(TCNQ)_2$, IR absorpt. spectra obs. of first-order transition 80−71397
TCNQ salt, $(TMA^+)_3(I_3^-)(TCNQ^-)_2(TCNQ^0)$, struct., phys. props. and lattice distortion evidence 78−6305
TCNQ salt, DECA $(TCNQ)_2$, struct., phys. props. and irreversible phase transition 78−6273
TCNQ salt, HMTTF-TCNQ, quasi-one-dimensional organic conductor, mag. susceptibility meas. 78−6508
TCNQ salt, MEM$(TCNQ)_2$, phase transition electronic struct. interpretation 80−24781
TCNQ salt, tetramethylhexamethylenediammonium-TCNQ-iodine, elec. and mag. props., struct., specific heat 80−24898
TCNQ salt, TMTTF-TCNQ, mag. gaps, EPR meas. 77−8390
TCNQ salt, TSeF-TCNQ, doped with TTF-TCNQ, phase transitions 77−80732
TCNQ salt, TSeF-TCNQ, electrical conductivity, press. depend. 77−51729
TCNQ-HMTTF, metallic state stabilisation at low temp. under press. 78−30911
TCNQ-NMP, metal-insulator transition theory based on generalised Hubbard model 78−18966
TCNQ-TMTSF, conducting salt, cryst. and mol. struct., rel. to metal-insulator transition 77−24307
TCNQ-TSeF:TCNQ-M, thermopower determ. 78−47772
TCNQ-TSeF, model for phase transition and low-temp. phase 77−47734
tetramethylaminelithium(0), $Li(CH_3NH_2)_4$, existence, conduction- and localised-electron spin reson. 80−66035
thermochromic material, vanadium oxides mixture, appl. to laser beam indicator/visualiser 80−9976
thin wire, max. metallic resist. 78−14663
$(TMTSF)_2PF_6$, ESR g-factor, linewidth, spin susceptibility, metal-insulator transition 80−103887
$(TMTSF)_2X$, $(X=PF_6^-, AsF_6^-, SbF_6^-, BF_4^-, NO_3^-)$ highly conducting salts, props. 80−59969
TMTSF-DMTCNQ, metallic state, transport props. 80−24974

metal-insulator transition continued
transition metal chalcogenide, possible anionic clusters and mixed valence effects 78−43333
transition metal chalcogenides, Mott metal-insulator and mag. phase diagrams 78−10354
transition metal compounds, minimum conductivity and electron localisation near metal-insulator transition 78−30960
transition metal cpds., review 80−59874
transition metal oxides, sulphides, and selenides, Mott transition electronic and mag. phase diagrams 78−51894
3d-transition-metal dichalcogenides, mag. props. rel. to Hubbard model 79−78373
transport processes, isothermal method for static cond. of electrons 80−29373
$(TSeF)_x(TTF)_{1-x}(TCNQ)$, interstack hybridisation role in metal-insulator transition temp. determ. 78−6304
$(TSeF)_x(TTF)_{1-x}TCNQ$, struct., cond., phase transitions 78−47770
TSeF-TCNQ, Ginzburg-Landau model for metal-insulator transition 78−6301
$TTF(Br)_{0.7}$, EPR temp. depend., metal-insulator transition 77−43863
$TTF(I)_{0.71}$, EPR temp. depend., metal-insulator transition 77−43863
$TTF(I)_{0.71}$, physical props., Fermi energy scaling of metal-insulator transition temp. 77−8081
$TTF(SeCN)_{0.54}$ and $TTF(SCN)_{0.54}$, Fermi energy scaling of metal-insulator transition temp. 77−8081
$(TTF)_{12}(SCN)_7$ and $(TTF)_{12}(SeCN)_7$, charge-transfer salts, elec., mag. and optical props. 77−43575
TTF and derived cpds., intramolecular vibrs. and vibronic effects, IR and Raman spectra 80−25387
TTF and TTN derivatives, quasi-one-dimens. cond., phys. and electronic props. 78−6366
TTF-DETCNQ, heat capacity, elec. cond., cryst. struct., metal-insulator transition 77−8077
TTF-DETCNQ, struct. elec. cond. and sp. ht. expts. 78−14662
TTF-TCNQ:TCNQ-M, thermopower determ. 78−47772
TTF-TCNQ, 53 and 38K transitions, mag. and elec. props. meas., doping effect 77−66159
TTF-TCNQ, CDW transition with tripling of period along chains 80−96805
TTF-TCNQ, coupled Peierl's systems, model, phase transitions 77−69230
TTF-TCNQ, crit. behaviour near 53K phase transition, Ginzburg-Landau theory 79−33249
TTF-TCNQ, crit. behaviour near 53K transition, generalised Ginzburg-Landau theory 79−56147
TTF-TCNQ, electron-molecular distortion coupling near Peierls transition, IR spectra obs. 80−25390
TTF-TCNQ, impurity effects on CDW fluctuations 80−44576
TTF-TCNQ, intramol. coupling contrib. 77−15782
TTF-TCNQ, phase transitions, thermoelec. power meas. 79−65464
TTF-TCNQ, phase transitions and CDW state, controlled disorder effects 80−15507
TTF-TCNQ, phason and metal-insulator microdomain model, Young's modulus temp. depend. anal. 77−31964
TTF-TCNQ, physical props., Fermi energy scaling of metal-insulator transition temp. 77−8081
TTF-TCNQ, possible Lifshitz point, struct. transitions exam. 78−2423
TTF-TCNQ, symmetry changes and phase transitions 78−6299
TTF-TCNQ, Young's modulus, temp. depend., rel. to transition points 77−15475
TTF-TCNQ derivatives, transport props., reflectance spectra 78−91683
TTF-TCNQ salts, self-consistent continued-fraction theory of cond. 79−69482
TTF-TCNQ type crystals, Kolmogorov Arnold Moser theorems, appl. to struct. problems in condensed matter 80−59878
TTF-TCNQ type salt, trimethylene-TTF-TCNQ, unsymmetric cation, phys. props. 78−76059
$TTT_2I_{3+\delta}$, thermoelec. power and metal-semicond. transition 80−34431
$(TTT)_2I_3$, metal-insulator phase transition, elec. cond. and mag. susceptibility meas. 78−14719
two band model, dielec. transition in current state *(Russian)* 78−34770
two-band model, Coulomb interactions, self consistent calcs. *(Russian)* 80−80185
two-dimensional random potential, localisation of particles 79−60672
two-dimensional system, phase transitions and metal-insulator transitions 80−2143
V_2O, semicond.-metal transition, hysteresis effects, appl. in optical information storage 78−88006
valence transition, entropy and phase diagram 80−59877
Wannier-Mott excitons in layer structures and near interface of two media 77−66124
weakly coupled 1-D metallic chains, phase transition *(Russian)* 77−31946
Ag_2S, metal-nonmetal transition, crystallographic, optical, mag. and transport props. 78−6418
Ag_2Se, metal-nonmetal transition, crystallographic, optical, mag. and transport props. 78−6418
Al, film, bleaching possibility by laser pulse, liq. metal-insulator transition 77−43498
Al, granular supercond., normal state cond. 80−88529
Al-Al_2O_3-(a-Ge)-Al, electron tunnelling into a-Ge, press. effect 80−49938
Al-Ge film, random percolation, elec. resist. meas. 79−28418
Al-Ge thin film alloy, critical currents near metal-insulator transition 79−65626
AlSb film, laser-induced metal-semicond. transition in Al-Sb mixed film 80−6661
$(Al_xV_{1-x})_2O_3$, heat capacity anomalies, metal-insulator transition, phase diagram 77−11701
AsSe, molten semicond., pseudogap, elec. cond. and optical absorption meas. 77−8160
As_2Se_3, molten semicond., pseudogap, elec. cond. and optical absorption meas. 77−8160
As_2Te_3, amorphous, press.-induced semicond.-metal and supercond. transitions 77−43671
Au_xSi_{1-x} amorphous films, phys. studies 80−75476
B_xC_y, metal-insulator transition, elec. cond. and thermoelec. power, 80 to 700K 80−44673
$Ba_xLa_{1-x}CoO_3$, x=0 to 0.5, structural, elec. and mag. props., Zener double exchange and Goodenough's model 79−65663

metal-insulator transition continued
- $BaPb_{1-x}Bi_xO_3$, semiconductor-metal transition and supercond., IR absorpt. and struct. meas. 77−28278
- $BaSi_2$, semicond.-metal transition, high-press. and temp. 78−43299
- Bi, Shubnikov-de Haas effect in high mag. fields 80−2404
- Bi-$BiBr_3$ liquid system, miscibility gap, elec. cond. meas. 79−90790
- Bi-Sb, Shubnikov-de Haas effect and semimetal-semicond. transition in high mag. fields 80−44674
- β'-$Cu_xV_2O_5$, mag. and spectroscopic study, semiconductor to metal transition 80−2628
- C, anthracene char, density fluctuations effect on physical properties 78−51420
- C liquid, metal-non-metal transition 79−60712
- CaO, band struct. calc. rel. to high press. metallisation 80−84427
- $CdCr_2Se_4$:In(Ga), temp. driven metal-semiconductor transition, temp. and mag. field depend. *(Russian)* 78−88003
- $Cd_{1-x}In_xCr_2Se_4$, electric, photoelectric and mag. props., metal-semicond. transition *(Russian)* 80−54738
- CdS, doped, amorphous antiferromagnet model, susceptibility and spin-flip Raman scatt. meas. 80−97057
- CdS, press. quenched, mag. moment, semicond.-conducting transition 80−15683
- CdS:Cl, heavily doped, fluoresc. spectrum upper threshold calculated 78−52568
- CdSe, electrical cond. near metal-insulator transition 79−73550
- CdSe:Au impurity light absorpt. for current control in negative resistance region 80−11052
- $CeH_{2.70}$, low temp. phase transition, sp. ht. meas. 78−47535
- $CeH_{2.70}$, sp. ht., 2 to 260K, second-order phase transitions and cryst. field splitting 79−82355
- $Co_{0.83}[Pt(C_2O_4)_2].6H_2O$, quasi-one-dimens. conductor, Peierls distortion and superlattice, X-ray study 80−29397
- $Cr_{1-x}Fe_xS$, metal-dielec. transition, X-ray, thermal anal., elec. cond. temp. depend. 78−67942
- Cs alloys, charge transfer insulators, mechanism, resistivity 78−80070
- Cs, fluid, metal-nonmetal transition and mag. interactions 80−49602
- Cs fluid, metallic and nonmetallic, mag. props. 80−44799
- Cs-Au, liq. ionic alloy, elec. props. 79−99338
- Cs-Au, liquid, metal-insulator transition, mag. susceptibility, Knight shift, theory 80−44672
- Cs-Au(Sb), liq. alloys., mag. susceptibility and electronic struct. 77−1537
- Cs-NH_3, Cs-ND_3, solns., US absorption, metal-nonmetal transition 79−69194
- Cs-NH_3 solution, metal-nonmetal transition, cond. density and Hall coeff. meas. 77−51789
- Cs-Sb(Au) liq. alloys, metal-nonmetal transition and change in electronic and mag. props. 77−51790
- CsAu, band struct. and charge distrib., semicond. and metallic behaviour 77−20238
- $Cs_{1-x}Au_x$, liq., metal-nonmetal transition, electronic theory 78−79930
- Cu-Xe film, metal-nonmetal transition, optical and resist. meas. 77−89818
- CuCl, optical microscopic, X-ray diffr. and elec. resist. studies at high press. 80−11051
- CuCl, possibility of excitonic dielectric-supercond. phase transition 77−43797
- $Cu_{0.75}VS_2$, cryst. struct. and phys. props. *(French)* 78−14328
- donor polarisability, enhanced, below insulator-metal-transition, self-consistent calc. 80−7262
- $Eu_{1-x}^{2+}Eu_x^{3+}N_xO_{1-x}$, resist., pressure depend., semicond.-metal transition obs. 79−78104
- $Eu_{1-x}Gd_xO$, mag. props., transport meas. 80−97117
- $Eu_{1-x}^{2+}Nd_x^{3+}N_xO_{1-x}$, resist., pressure depend., semicond.-metal transition obs. 79−78104
- $Eu_{1-x}^{2+}Nd_x^{3+}O_{1-x}N_x$, lattice parameters, mag. and elec. props. 80−100578
- EuO, anomalies in transport props. under hydrostatic press. due to bound mag. polaron 77−20372
- EuO, degenerate ferromag. semiconductor, mechanism of transition to insulating state *(Russian)* 77−8024
- EuO, Eu doped, temp. depend. of carrier conc. and mag. susceptibility 77−69483
- EuO, Eu rich, model Hamiltonian with Coulomb repulsion 78−2422
- EuO, Eu-rich, IR absorpt. spectra, 4.2 to 300K, transitions assoc. with O vacancies 77−52142
- EuO, hydrostatic press. effects on elec. resist. in temp. range 3 to 300K 79−23968
- EuO, light-induced metal-insulator transition, mol. mag. polarons 77−4396
- EuO, reflectivity spectra near absorpt. edge 79−47471
- EuO, rotation of polarisation plane in very high mag. field 78−92054
- EuO:Eu, doped ferromag. semicond., carrier density and mag. susceptibility rel. to M-S transition 77−72820
- $Eu_{1-x}O$, optical absorpt. spectra at metal insulator transition 78−10928
- $EuO_{1-x}N_x$, ferromag. semicond., elec. and mag. props. *(French)* 78−79993
- EuTe, magnetic impurity states, mag. and transport props. 80−96913
- $Fe_{1-x}Co_xSi$ solid solution, semiconductor-metal transition 80−103627
- $Fe_{3-x}Cr_xO_4$, Mossbauer study above Verwey transition 78−43750
- $Fe_{1-x}Cu_xCr_2S_4$, Hall effect and magnetoresist. 79−78119
- $(Fe^{2+}Fe_{2-x}^{3+}M_x^{3+})O_4^{2-}$, ($M^{3+}$=$Cr^{3+}$ or Al^{3+}), elec. cond., Verwey transition temp. *(French)* 79−60878
- $Fe_{3-x}Mg_xO_4$, Verwey transition, Mossbauer study 80−39942
- $Fe_xNb_xV_{2-2x}O_4$ complex solid solns., synthesis and phase diagram, semicond.-metal transition temp. 79−43214
- $Fe_xNb_xV_{2-2x}O_4$, NMR analysis of semiconductor transitions 78−52367
- $Fe_{3-\delta}O_4$, mag. aftereffects near Verwey temp. 79−87294
- Fe_3O_4 and $Fe_{3-x}Ti_xO_4$, IR transmission spectra changes at Verwey temp. 77−85714
- Fe_3O_4, Coulomb gap and hopping cond., effects on thermopower and Verwey ordering 80−44583
- Fe_3O_4, doped, electron correls. above and below Verwey transition, Green function theory 77−51687
- Fe_3O_4, electron energy band theory, thermodynamic functions *(Korean)* 79−7785
- Fe_3O_4, electronic struct. and charge density oscills. near Verwey transition, Mossbauer expt. 78−27150
- Fe_3O_4, finely dispersed powder, volt-ampere characts. *(Russian)* 77−62967

metal-insulator transition continued
- Fe_3O_4, hyperfine field temp. depend., Mossbauer meas. near Verwey transition 77−69749
- Fe_3O_4, low temp. phase, effect of residual stresses on Verwey temp. 77−59308
- Fe_3O_4, magnetic after-effect by valency fluctuations assoc. with cond. transition 77−8365
- Fe_3O_4, magnetite, anomalous electrical conductivity, press. effects 79−56222
- Fe_3O_4, magnetite, charge order-disorder and metal-insulator transition 77−20241
- Fe_3O_4, magnetite, Compton profile, rel. to Verwey transition 78−35219
- Fe_3O_4, magnetite, ferrimag. reson. at 9.3 GHz near Verwey temp., g-factors *(French)* 78−91959
- Fe_3O_4, magnetite, low temp. phase transition, magneto-optical exam. 78−27193
- Fe_3O_4, magnetite, polarisation screening effect on charge ordering, pure ionic model 78−6272
- Fe_3O_4, magnetite, Verweg transition temp., isotope effect, elec. resist. and DTA meas. 80−24976
- Fe_3O_4, magnetite Mossbauer spectra, mag. dipolar and elec. quadrupole effects 80−20544
- Fe_3O_4, multistage phonon softening in Verwey transition region, Mossbauer spectra 77−72670
- Fe_3O_4, nuclear gamma reson. investig. of high temp. electronic struct. 77−20751
- Fe_3O_4, optical cond. anisotropy calcs. below Verwey transition 80−50289
- Fe_3O_4, Verwey transition, electron-phonon versus Coulomb interaction effects 80−39280
- Fe_3O_4, Verwey transition, cond. processes 80−96787
- Fe_3O_4, Verwey transition as potentially incommensurate but eventually commensurate phase transition 79−95120
- Fe_3O_4, XPS and UPS 79−91565
- Fe_3O_4:Sn, hyperfine field temp. depend., Mossbauer meas. near Verwey transition 77−69749
- $Fe_3O_{4-x}F_x$ substituted magnetite, low temp. resistivity, Seebeck coeff., thermopower 80−20234
- $Fe_3O_4F_x$ ($0 \le x \le 0.25$), Mossbauer spectra, Verwey transition suppression 78−15075
- $FeSi_2$ films, structural and Anderson transitions, cond. and IR reflectance meas. 79−15200
- $Fe_xTa_xV_{2-2x}O_4$ complex solid solns., synthesis and phase diagram, semicond.-metal transition temp. 79−43214
- $Fe_{3-x}Ti_xO_4$, elec. transport near Verwey transition, thermoelec. power and cond. meas. 79−95455
- $Fe_xV_{2-x}O_4$ solid solutions, specific heat near semiconductor-metal transition 80−24612
- Ga-NaX zeolite system, press. depend. of metal-insulator transition 78−88005
- Ga-Xe film, metal-nonmetal transition, optical and resist. meas. 77−89818
- n-GaAs, metal-insulator transition in impurity band induced by loss of dimension 77−47732
- n-GaAs, metal-insulator transition in impurity band induced by mag. field and loss of dimens. 78−52042
- GaAs(P), semiconductor-metal transition, press. calibration above 100 kbars fixed points 80−77808
- $Ga_{1-x}In_xSb$, press.-induced structural phase transition 78−30751
- GaP, electron-hole plasma luminesc. 79−38651
- GaP, first order Mott transition of exciton gas 78−76535
- GaSe, absorpt. spectra, electron-hole system at high densities 77−69854
- GaSe, press. induced metallic and supercond. state 80−75666
- $Ga_xV_{1-x}O_2$, resistivity, EPR, enthalpy and entropy meas., rel. to semicond.-metal transition 78−88004
- Gd_2S_3, antiferromag. to ferromag. and semiconductor to metal transitions *(Russian)* 79−33485
- $Gd_xSm_{1-x}S$ K X-rays chem. shifts, electronic phase transition, semicond.-metal transition 77−28116
- Ge, cold semiconductor, Mott transition 78−91616
- Ge, doped, Dingle's theory using modified screened impurity pot. 79−99500
- Ge, effect of pressure on the Raman shift 78−92064
- n- Ge, heavily doped, extrinsic sp. ht. in metallic regime 78−59956
- Ge, indentation hardness and semicond.-metal transition 78−35499
- Ge, metallic, eqns. of state under high press. 79−60475
- Ge, plastically deformed low temp. cond. *(Russian)* 80−6831
- Ge, stressed, metal-insulator transition, luminesc. 80−20695
- Ge, transmutation doped, high field magnetoresist. of hopping transport 78−10474
- Ge:As, NMR, conduction electrons in impurity band, metal-nonmetal transition 79−78544
- Ge:Sb, low-freq., low temp. dielec. behaviour below metal-insulator transition 80−50250
- Ge-Te, As-Te, Ge-As-Te molten systems, metal-semicond. transition, cond. obs. *(German)* 77−1457
- $Ge_{0.08}Se_{0.92}$, molten semicond., pseudogap, elec. cond. and optical absorption meas. 77−8160
- H_2, highly compressed, combined representation method for use in band struct. calc. 77−89685
- H_2, metallic and molecular, transition press. and eqns. of state calc. 78−26685
- H_xWO_3, amorphous, Anderson transition, disorder depend. and optical detection 78−47840
- H_xWO_3, amorphous film, electronic transport meas., insulator-metal transition 77−72923
- H_xWO_3 bronzes, Anderson transition, XPS 80−107705
- ^3He, solid, as mag. semicond., analogy to Mott insulator 80−96720
- hexamethylphosphoramide:Li glass, metallic condensation of Wannier-Mott impurity states 78−2420
- Hg, electrical and thermodynamic props. in metal-semicond. transition range 80−20144
- Hg, expanded fluid, optical cond., at low frequencies 79−19902
- Hg, expanded liq., band model for electronic struct., Knight shift and electronic transport 77−89690
- Hg, liq., sound vel. near metal-nonmetal transition, up to 1600°C and 2000 kg/cm^2 80−39222
- Hg, liquid, expanded, Knight shift interpretation in terms of electronic struct. and transport 77−43895
- Hg/Xe films, optical study of metal-insulator transition 79−65947
- Hg-Na (3 at.%), amalgam, decrease of cond. by Na near metal-insulator transition 79−23938

metal-insulator transition continued
Hg-Xe solid mixture, optical criterion for Mott transition 78−75996
Hg-Xe system, metal-insulator transition temp.-coeff. of cond. 77−66188
Hg-Xe vapour deposited films, cond. transitions, effect of disorder on supercond. 80−88659
$Hg_{2.86}AsF_6$, one-dimens. conductor, thermopower, temp. depend. 79−65465
$Hg_{1-x}Cd_xTe$ mixed crysts., magneto-opt. obs., semicond. config., semimetal-semicond. transition 77−73131
$HgCr_2Sd_{4-x}Te_x$, ferromag. semicond., zero bandgap transition 80−96783
I, metallic, mol. and monatomic phase, elec. resist. at high press. and low temp. 80−65638
I_2, solid, metallic, insulating-metal transition at high-press., exptl. and theoretical shock-compression curves 77−39781
I_2, solid, press.-induced struct. phase transition, X-ray obs., rel. to metallisation 79−65192
In-Ar mixture, resistivity meas. 77−76883
In-Ge film, random percolation, elec. resist. meas. 79−28418
n-InP, impurity and minimum metallic cond. in mag. field 80−103731
InSb, amorphous, pressure induced struct. transform., X-ray diffr. obs. 77−11690
p-InSb, deformed, giant negative magnetoresistance 78−87990
n-InSb, galvanomagnetic props. at low temp., mag. field induced metal-nonmetal transition 77−76845
InSb, high-purity, electron irradiation effects on transport props., evidence for semicond.-metal transition 79−23650
p-InSb, uniaxially deformed, mag. field induced semicond.-metal transition 79−95457
In_2Se_3, transitions of high temp. α form *(French)* 80−92473
$K_2Pt(CN)_4Br_{0.3}.3H_2O$, one-dimens. cond. transition, spin suscept. and DC cond. temp. depends. 78−84198
$K_2Pt(CN)_4Br_{0.3}.3.2H_2O$, motion of Br^- ions, NMR 77−90051
$La_{1-x}Ca_xVO_3$, struct., elec. and mag. props., temp. and conc. depend. *(French)* 77−4293
$LaH_{2.69}$, low temp. phase transition, sp. ht. meas. 78−14665
LaH_x, x=2.3 to 2.98, EPR investigation 79−78513
$La_{0.71}Pb_{0.29}MnO_3$, metal-semicond. transition at Curie point, transport props. obs. 79−73554
Li-methylamine soln., metal-nonmetal transition, electron and nucl. spin-lattice relax. 79−87306
Li-methylamine solution, NMR investig. of metal-nonmetal transition 77−40142
Li-NH_3 solution, metal-nonmetal transition, US absorption coeff. 77−51443
LiH, electronic struct., equation of state, insulator-metal phase transition 79−33234
LiH, electronic struct. and equation of state up to 100 Mbar 77−1361
LiH, insulator-metal transition press. calc. 78−34769
LiH, zero temp. phases, high density props. 78−75725
LiHLiH array, Mott transition mag. analog, Hamiltonian for paramagnetic-diamagnetic transition 79−95565
$Li_{1-x}Pb_x$, liq., metal-nonmetal transition, electronic theory 78−79930
$Mg_xFe_{3-x}O_4$, polycryst., Verwey type transition, resist., magnetisation, Mossbauer effect and permeability obs. 80−75764
MgO, compressed, SCF electronic struct. calcs., necy. press. for conversion to metallic state 78−43300
Mg_2Sn, Mossbauer effect exam. under press. up to 75 kbar 79−69759
Mn metallic perovskite, structural instability *(French)* 79−100123
Mo, field emission anomalies in mag. field *(Russian)* 80−93462
Na-Ar film, metal-nonmetal transition 77−62966
Na-NH_3, nonmetal-metal transition, thermodynamics 78−18964
Na-NH_3 film, quench-condensed, anomalous elec. cond. obs. 77−32057
Na-NH_3 film, vapour deposited, elec. resistivity, metal-nonmetal transition 78−84317
$Na_{1-x}Bi_x$ liq. alloys, metal-nonmetal transition, mag. susceptibility meas. 79−82525
$Na_{1.9}V_{13}O_{29.7}$, phase transitions, elec. cond., susceptibility and sp. ht. meas. 78−14776
Na_xWO_3, (0.22≤x≤0.84), ^{183}W NMR, electronic struct. near metal-semicond. transition, Knight shift 78−48063
Na_xWO_3, degenerate electron gas, Friedman effect, review 77−20242
Na_xWO_3, Knight shift, spin-lattice and spin-spin relax., high press. NMR obs. 80−50211
Na_xWO_3, metallic, transport props. near metal-insulator transitions 77−24596
Na_xWO_3 microscopic inhomogeneity rel. to electronic transport props. 77−24518
Nb, field emission anomalies in mag. field *(Russian)* 80−93462
NbI_3, metal-insulator transition 79−60830
NbI_4, metallic state, resistivity anomaly 79−15136
NbI_4, quasi-one dimens., press.-induced metal-insulator transition 78−43447
NbO_2, electronic band struct., optical props., generalised susceptibility, struct. transition 79−95328
NbO_2, structural phase transform., neutron scatt. obs. 78−14458
Nd-H, possibility of H ordering, DTA meas. 79−52174
$NdH_{2.70}$, low temp. phase transition, sp. ht. meas. 78−14665
$Nd_xSm_{1-x}S(Se)$, K X-rays chem. shifts, electronic phase transition, semicond.-metal transition 77−28116
$Nd_{1-x}Sr_xCoO_3$, Anderson transition, elec. cond. meas. 77−51786
Ni-S, defect control by heat-treatment in S atmos. 79−43293
Ni-Sn, electrical cond. and magnetic susceptibility of B 8_2-compounds *(German)* 79−42520
$Ni(As_xS_{1-x})_2$, mag. elec. and structural props. meas. 77−85447
$Ni_{1-x}Cr_xS$, elec. transport, mag. susceptibility and DTA meas. 80−96954
$NiFe_2O_4$, electronic phase transition 80−65640
$(Ni_{1-x}Fe_x)_{1-y}S$, anomalous thermal hysteresis in metal-semicond. transition 80−39640
$Ni_{1-x}Rh_xS$, nonvolume effect of Rh substitution on paramag. metal-antiferromag. nonmetal transition 79−28277
NiS, antiferromag., press. effect on metal-nonmetal transition 77−69229
NiS, metal-nonmetal transition under press. 77−69228
NiS, spin polarons exam. and metal-insulator transition 78−10377
NiS_2, high press. effect on mag. transition temps. 78−91866
$Ni_{1-x}S$, and $Ni_{1-x}S_{1-y}O_y(Se_y)$, mag. state in metal-semicond. transition region, neutrnon diffr. obs. *(Russian)* 77−89926
$Ni_{1-x}S$, metal-semimetal transition, lattice dynamics and thermodynamic props. 80−29324
$NiS_{2-x}Se_x$, electronic struct., UPS and XPS study 80−80935
$NiS_{2-x}Se_x$, mag. struct., ^{57}Fe Mossbauer study 78−56409
metal-insulator transition continued
NiS_yTe_{1-y}, mag. susceptibility, correl. with metal-insulator transition data 79−24145
P, red to black conversion in quasiisentropic compression 79−33036
Pb-Ar (Xe) film, struct., electron diffr. meas., rel. to metal-nonmetal transition 77−51626
Pb-Ge thin film alloy, critical currents near metal-insulator transition 79−65626
Pb-Xe mixture, resistivity meas. 77−76883
PbAr, resistivity meas. 78−80028
$Pb_{1-x}Sn_xGe$:In, press.-induced transition to gapless state, galvanomag. effects 78−19108
Po-Ge film, random percolation, elec. resist. meas. 79−28418
Pr_2NiO_4, elec. props., 300 to 1000°C 78−91694
$PrH_{2.65}$, sp. ht., 2 to 260K, second-order phase transitions and cryst. field splitting 79−82355
$Pr_{1-x}Sr_xCoO_3$, Anderson transition, elec. cond. meas. 77−51786
$Ru_{1-x}Ti_xO_2$ solid solns., metal-nonmetal transition 78−91735
S, dielectric to metal transition at ultrahigh dynamic press. *(Russian)* 79−60881
S, shock wave method observation of transition to highly conducting state 80−4738
S, transition to conducting phase 77−35972
SMS, band struct. and semicond. metal phase transition 80−80180
Sb amorphous film, elect. resist. 78−95390
Sb-Au amorphous film, elec. resist. 78−95390
$(Sc_xTi_{1-x})_2O_3$, semicond.-metal transition, sp. ht. meas., 300-600K 77−43347
Se, elec. cond., 0-500 kbar 79−99589
Se, electronic struct. of cryst. phases and hydrostatic press. effects 80−59865
Se, liq., electronic transport props. at sub- and supercritical conditions 77−51788
Se, liq., review of continuous metal-nonmetal transitions 77−51787
Se, metal-insulator transition induced by temperature 78−2529
Se, trigonal, electronic struct., near metal transition, press. depend. 78−34758
Si, doped, basis functions for studying intervalley effects 79−69442
n-Si, EPR linewidth, Orbach relax. process, conc. depend. 80−44901
Si, electronic structure at high press. near semicond.-metal transition 80−49586
Si, heavily doped, doping density striation effects in studies of metal-nonmetal transition 79−28383
n-Si, heavily doped, extrinsic sp. ht. in metallic regime 78−59956
n-Si, heavily-doped, EPR near metal-nonmetal transition 77−28446
Si, indentation hardness and semicond.-metal transition 78−35499
Si, metallic, eqns. of state under high press. 79−60475
Si, polymorphism under high press. *(Russian)* 78−59947
Si, static compression in [100] and [111] directions, elec. resist. obs. 80−65637
Si:I, obs. of donor exciton in far IR transmission meas., near metal-insulator transition 79−91477
Si:Li, electron-phonon scatt., in intermediate conc. region 80−65180
Si:P, dielec. susceptibility meas., polarisation catastrophe at metal-insulator transition 80−59873
Si:P, electronic states, NMR of metallic and intermediate samples 79−4511
Si:P, heavily doped, 100 GHz ESR of impurity band, near metal-nonmetal transition 79−95631
Si:P, heavily doped, degenerate electron gas, Friedman effect, review 77−20242
Si:P, heavily doped, electronic sp. ht. meas., rel. to metal-nonmetal transition 78−6162
Si:P, heavily doped, mag.-field depend. of sp. ht., rel. to metal-nonmetal transition 80−29183
Si:P, heavily doped, sp. ht. near metal-nonmetal transition, generalized Matsubara-Toyozawa theory 79−73321
Si:P, metal-nonmetal transition, Anderson localisation 79−95335
Si:P, submillimetre wave study of metal-insulator transition 79−95336
Si:P, thermal cond., electron-phonon interaction at low temps. 80−92730
Si-Au amorphous film, metal-nonmetal transition, elec. cond., thermoelectric power meas. 79−47132
Si-H, amorphous, struct. and press. induced transition 80−44131
$Si_{100-x}Au_x$, amorphous, dielec. anomaly, rel. to nonmetal-metal transition 78−2791
Sm chalcogenides, metal-dielectric phase transitions involving valence changes *(Russian)* 79−51489
Sm chalcogenides, semiconductor-metal transition, extended Felicov-Kimball model calcs. 80−70616
Sm monochalcogenides, semicond.-metal phase transition 79−47017
SmB_6, mixed valence cpd., EPR and heat capacity obs., metal-semicond. behaviour 80−20456
Sm_4Bi_3, press. induced valence instability, elec. resist. transition 78−95317
$Sm_{1-x}Ca_xS$, XPS, electronic struct. excitonic effects, insulator to metal transition 78−43988
$Sm_{0.8}Gd_{0.2}S$, low temp. phase transition, X-ray diffr. expts., 110-293K 77−59115
$Sm_{0.8}Gd_{0.2}S$, valence transition, positron annihilation study 80−15454
$Sm_{0.85}Gd_{0.15}S$, metal-semicond. transition, X-ray diffr. obs. 90-473K 79−95333
$Sm_{1-x}Gd_xS$ (x=0.15 to 0.18), magnetic susceptibility meas., phase transition 77−63071
$Sm_{1-x}Gd_xS$, calorimetric exam. of metal-semiconductor transition 78−18967
$Sm_{1-x}Gd_xS$, electron mechanism of high temp. phase transform., X-ray K-line shift obs. *(Russian)* 77−89704
$Sm_{1-x}Gd_xS$, metal-insulator transition, induced by temp. and press. *(Japanese)* 79−51488
$Sm_{1-x}Gd_xS$, metal-semicond. isomorphous transition curve, low temp. crit. point, lattice parameter changes 79−95334
$Sm_{1-x}Gd_xS$, phase transition temp. depression by mag. field, hybridisation 77−62828
$Sm_{1-x}Gd_xS$, press. induced electronic transitions 78−68058
$Sm_{1-x}Gd_xS$, resistivity investig. of metal-semicond. transition, press. effects 77−62829
$Sm_{1-x}Gd_xS$ system, equilib. of isomorphous phases and crit. point 78−34772
$Sm_{1-x}Gd_xS$ system, semicond. to metallic isomorphous phase transition mechanism 80−2338

metal-insulator transition continued
$Sm_{1-x}Gd_xS$, XPS, electronic struct. excitonic effects, insulator to metal transition 78−43988
$(Sm_{1-x}Gd_x)_3S_4$, mixed valence compound, elec. cond. transition 80−70777
$Sm_{1-x}La_xS$, magnetoresist. in semicond. and metallic phases 80−96914
$Sm_{1-x}La_xS$, press.-induced semicond.-metal transition, refl. and lattice compression meas. 77−62826
$Sm_{1-x}R_x^{3+}S$, (R is rare earth metal), semicond.-metal phase transition 79−47017
SmS (001) surface, mixed valency and phase transitions 80−39658
SmS, and $Sm_{0.8}Tb_{0.2}S$, resistivity and thermopower 80−20260
SmS, crit. point for isostructural black to metallic phase transition, thermoelec. power meas. 78−60174
SmS, defect struct., TEM obs., semicond.-metal transition in surface layer 80−44214
SmS, electron mechanism of high temp. phase transform., X-ray K-line shift obs. *(Russian)* 77−89704
SmS, electronic phase transition, mechanism, trivalent metal impurity effects 80−49604
SmS, energy of metal-semicond. transition, optical and DSC expts. 77−62830
SmS, energy of metal-semicond. phase transition and threshold recording energy density 79−28386
SmS, f-d hybridisation, valence fluctuation and phonon spectrum, Raman scatt. expts. 78−60464
SmS, film, laser generation of US using metal-insulator transition 79−90734
SmS film amplitude-phase hologram recording *(Russian)* 79−94192
SmS film for holographic storage, laser-induced semicond.-metal transition 77−88676
SmS, intermediate valence compound, pressure-temperature phase diagram 79−28283
SmS, LO phonon freq. softening in semicond. and metallic phases 80−96619
SmS, mechanical polishing, stabilisation mechanism for metallic phase on surface 78−60015
SmS, metallic phase, compressibility anomalous behaviour 80−29114
SmS, mixed valence states at surface 77−20398
SmS, nonorthogonal orbitals in intermediate valence 78−43323
SmS, phase diagram in p-T plane, theory 79−28278
SmS, semicond. and metallic phases, electronic struct., optical props. 0.03 to 12 eV 77−28594
SmS, semicond. phase, cond. band model, elec. and thermal cond. meas. 77−39854
SmS, semicond.-metal transition, cond. band type, deform. pot. determ. 79−69417
SmS, trivalent rare earth substituted, stability of Sm^{2+} 80−65508
SmS, valence fluctuation phenomena 80−24800
SmS, valence transition, positron annihilation study 80−15454
SmS, valence transition, two band model 80−65507
SmS, vol. changes at press. up to 20 kbar 78−71791
SmS-CdS system, T-p-X diagram, semicond.-metal transition 79−69421
SmS-GdS system, crit. effects and phase equilibria 79−7692
$SmS_{1-x}As_x$, magnetoresist. in semicond. and metallic phases 80−96914
$SmS_{1-x}P_x$, valence changes, XPS and UPS study 80−97402
$SmSb_xS_{1-x}$, intermediate valence, susceptibility and lattice parameter meas. 78−51943
$Sm_{1-x}Th_xS$, XPS, electronic struct. excitonic effects, insulator to metal transition 78−43988
$Sm_{1-x}Y_xS$, CPA calc. of rare-earth impurity, valence change 77−63096
$Sm_{1-x}Y_xS$, effect of valence fluctuations on lattice dynamics 78−47493
$Sm_{1-x}Y_xS$, magnetoresist. in semicond. and metallic phases 80−96914
$Sm_{1-x}Y_xS$, metal-semicond. isomorphous transition curve, low temp. crit. point, lattice parameter changes 79−05334
$Sm_{1-x}Y_xS$, press.-induced semicond.-metal transition, refl. and lattice compression meas. 77−62826
$Sm_{1-x}Y_xS$, XPS, electronic struct. excitonic effects, insulator to metal transition 78−43988
$Sm_{1-x}Yb_xS$, $Sm_{1-x}Tm_2S$ and $SmS_{1-x}As_x$, optical investig. of substitution effects on metal-semicond. transition 77−63427
$SrO.R_{1-x}Sr_xVO_{3-0.1x}$, R=Nd, Eu, Gd, solid solns., elec. and mag. props. 77−89819
$(TSeT)_2Cl$ complex, metal-semimetal transition, magnetoresist. and cond. *(Russian)* 79−38138
$(TSeT)_2Cl$, high press. metallic phase *(Russian)* 78−95316
$(TSeT)_2Cl$, one-dimens. conductor, metallic phases 80−20159
$TTT_2I_{3+\delta}$ complex, influence of press. on metal-dielectric phase transition *(Russian)* 80−92818
TaS_2, Peierls transit transition 77−66119
TaS_3, one-dimensional compound, phase anal., X-ray and elec. meas. 79−51086
TaS_3, phase transitions and elec. props. 80−20178
TaS_3, press. depend. of metal-semicond. transition 79−47016
TaS_3, transport props. 80−20175
TaS_2(1T) pure and doped, electrical, structural and mag. props. 79−78141
$Ta_{1-x}Ti_xS_2$ (1T), magnetoresistance in the Anderson localized states near the metal-nonmetal transition 80−88479
$Ta_{1-x}Ti_xS_2$ (1T), magnetoresist. near metal-nonmetal transition at ultra low temps. 80−88600
Te, elec. cond., 0-500 kbar 79−99589
Te, electronic struct. of cryst. phases and hydrostatic press. effects 80−59865
Te, high pressure metallic phase, cryst. struct. 80−49161
Te, liq., elec. cond. at high temps. and press. 77−55592
Te, Mossbauer spectra under press. up to 8000 MPa 80−80647
Te, trigonal, ^{129}I Mossbauer obs. at high press. 80−55005
Te, trigonal, electronic struct., near metal transition, press. depend. 78−34758
Te:Sb, impurity states and impurity conduction, hydrostatic pressure 80−39521
Te-Se liquid mixtures, sound vel. meas., adiabatic compressibility determ. 80−65161
Te-Se liquid semicond., resist. meas. under high press. 77−51791
Te-Se mixtures, liquid, semiconductor to metal transition, high temps. and pressures 80−39639
Ti-Ni, electron phase transition XPS, optical spectra and mag. susceptibility meas. 80−19943
$(Ti_{1-x}V_x)_2O_3$ spin glass, mag. props., metallic antiferromagnetism 79−82791

metal-insulator transition continued
TiO_2, metal-insulator transition meas. by microcalorimetry *(French)* 77−47733
TiO_3, semicond.-metal transition, positron annihilation study 78−15246
Ti_2O_3, $(Ti_{0.98}V_{0.02})_2O_3$, lattice parameters, temp. depend. 77−11855
Ti_2O_3, electronic structure from single crystal thermoreflectance spectroscopy 79−87420
Ti_2O_3, metal-semicond. transition, refl. spectra study 80−10880
Ti_2O_3, optical consts., polarisation dependent reflectivity 78−52531
Ti_2O_3, semiconductor-metal transitions, photoelectron spectra meas. 78−84144
Ti_2O_3, struct. changes at semicond.-metal transition 77−47397
Ti_2O_3, structural changes associated with semicond.-metal transition 77 15583
Ti_3O_5, semiconductor-metal transitions, photoelectron spectra meas. 78−84144
Ti_3O_5-V; semicond.-metal transition, resist., enthalpy and mag. susceptibility changes obs. 77−62965
Ti_4O_7 and $(Ti_{1-x}V_x)_4O_7$, metal-insulator transitions, EPR, elec. and mag. props. 80−2336
Ti_4O_7, optical absorpt. and metal-insulator transitions 78−15165
Ti_nO_{2n-1}, cryst. growth and characterisation 78−31311
TiS_2, layer cpd., energy gap calcs. 79−78009
$TiSe_2$ (IT), structurally induced semimetal-to-semicond. transition, ab initio LCAO calc. 78−51896
$TiSe_2$, layer cpd., energy gap calcs. 79−78009
$(Ti_{0.9975}V_{0.0025})_4O_7$, metal-insulator transition, struct. aspects 79−86752
$(Ti_{1-x}V_x)_4O_7$ order-disorder and metal-insulator transition theory 80−24802
$(Ti_{1-x}V_x)_2O_3$, crystal struct. determ., metal-metal distance, effect on electronic struct. 77−47431
$(Ti_{1-x}V_x)_2O_3$, semicond. to semimetal electrical transition, lattice parameter changes 79−60714
$(Ti_{1-x}V_x)_2O_3$, US velocities in high mag. field 78−84262
$(Ti_{1-x}V_x)_4O_7$, elec. cond. and phase diagram near metal-insulator transition 80−11054
$(Ti_{1-x}V_x)_4O_7$, mag. susceptibility calcs. 78−91850
$(Ti_{1-x}V_x)_4O_7$, metal-insulator transition investig. by resist., sp. ht. and X-ray diffr. 77−43497
$(Ti_{1-x}V_x)_4O_7$, metal-insulator transition and mag. behaviour 78−51895
$(Ti_{1-x}V_x)_4O_7$, order-disorder and metal-insulator transitions 80−39504
Tl-Te liquid semicond., resist. meas. under high press. 77−51791
Tl_2Te-Tl liquid system, conc. fluctuation, time-of-flight quasielastic neutron scatt. obs. 80−88324
$Tm_{1-x}Eu_xSe$, valence changes, semicond.-metal transition 80−20086
TmSe-TmTe(EuSe), semiconductor-metal transitions 80−96953
$TmSe_{1-x}Te_x$, valence changes, semicond.-metal transition 80−20086
UO_{2+x}, possible anionic clusters and mixed valence effects 78−43333
V oxides, change in phonon damping due to metal-insulator transition 80 103625
V oxides, XPS and AES study, electron correl. effects, semicond.-metal transition 80−7467
$V_{0.985}Al_{0.015}O_2$, insulating T-phase cation disproportionation and V-V pairing 77−62825
$V_{0.985}Al_{0.015}O_2$, struct. aspects of metal insulator transitions 78−18965
$(V_{1-x}Cr_x)_2O_3$, single cryst. obtained by chemical transport method, elec. cond. transition *(French)* 77−24940
$(V_{1-x}Cr_x)_2O_3$, thermal props., rel. to phase transition 77−35709
$(V_{1-x}Cr_x)_2O_{3+y}$, elec. props. and struct. 80−84494
$V_{0.986}Fe_{0.014}O_2$, metal-insulator phase transition, effect of hydrostatic press. 80−6725
$V_{1-x}Fe_xO_{2-x}F_x$, $0<x<0.2$, phase diagrams, ^{57}Fe-Mossbauer spectra, X-ray diffr. studies *(German)* 80−29663
$V_{1-x}Ga_xO_2$, phase transitions, semicond. metal transition, antiferromag. props. 77−11969
VO_2, amorphous thin films, phase transition, resistivity and opt. transmission discontinuities 77−47871
VO_2, change in optical props. at semicond.-metal transitions 77−28597
VO_2 clusters in metallic and semiconductor phases, electronic struct., $X\alpha$ calcs. 78−63977
VO_2, cylindrical specimen, thermal switching 80−44679
VO_2, diffuse X-ray scatt. due to lattice instability near metal-semiconductor transition 78−56074
VO_2, discontinuous metal insulator and spin dimerisation transition, Hubbard model 78−51893
VO_2, electronic struct., quadrupole coupling, Mulligen-Wolfsberg-Helmholtz calcs. 78−87948
VO_2, ferroelastic metal-insulator transition, electronically triggered crystallographic phase transition 80−70614
VO_2, film, IR induced metal-semicond. phase transition *(Russian)* 77−15769
VO_2 film, ion bombard. effect on metal-dielec. phase transition, optical props. meas. 79−90963
VO_2 film, metal-dielec. transition, refl. after 40 keV ion bombardment 79−23899
VO_2, film, metastable metallic phase due to laser and electron beam irrad., refl. spectra 79−19944
VO_2 film, optical and elec. props., 0.8 to 4.2 mm, near metal-semicond. transition 77−32473
VO_2 film, optical characts. of phase transition, ion bombardment effects 79−28281
VO_2 film, optical props. meas. near semicond.-metal transition 77−1742
VO_2 film, semicond.-metal transition, light absorption by metallic drops *(Russian)* 77−59579
VO_2, film, semiconductor-metal phase transition, fast laser kinetic studies 79−69419
VO_2, film, visualisation of microwave and IR radiation 80−5839
VO_2 film based recording medium, holographic characteristics calc. *(Russian)* 79−7092
VO_2 film sub-mm wave modulators and switchable polarisers 77−75664
VO_2 films, chemically deposited, chemical transition layers at interface with substrate, AES and SEM obs. 79−95533
VO_2 films, elec. cond. near metal-semicond. phase transition 77−1503
VO_2, first principles calc. of intra-atomic correlation energy 79−23920
VO_2, laser beam induced, thermal switching dynamics 77−76885
VO_2, lattice instability and metal-insulator transition 78−63834
VO_2, layer, resist. meas. 78−14770
VO_2, light scatt. near semicond.-metal phase transition 78−60414
VO_2, magnetic susceptibility in insulating and metallic phases, electron-electron and electron-lattice interactions 80−96788

metal-insulator transition continued
VO_2, metal-insulator transition meas. by microcalorimetry *(French)* 77−47733
VO_2, metal-insulator transition, electron correls. and spin dimerization, thermodynamical study 80−70615
VO_2, metal-insulator transition and electronic struct., ion bombard. effects 80−92948
VO_2, metal-semiconductor transition, effect of deviations from cryst. lattice periodicity 79−23898
VO_2, metallic, electronic struct., lattice instability 78−14664
VO_2, nonlinear wave generation in system with metal-semicond. transition, wave propagation velocity *(Russian)* 79−73549
VO_2, nonstoichiometry influence on electron struct. and metal-insulator phase transition 80−44507
VO_2 pyrolytic film, phase transition and electrical cond. 77−89890
VO_2, quasi-one-dimens. system, appl. of qualitative theory for phase transitions 78−31086
VO_2, semicond.-metal phase transition, fast laser excitation, kinetics obs. 79−47018
VO_2, semiconductor-metal transition LCAO cacl., cryst. distortions 77−4294
VO_2, semiconductor-metal transitions, photoelectron spectra meas. 78−84144
VO_2, semiconductor-metal transition, effect of ^{18}O substitution 78−84268
VO_2 single cryst., switching, visual obs. of metallic and semicond. domains 78−52041
VO_2 single cryst. film, ion-irrad., 'splitting' of semicond.-metal transition 80−11053
VO_2 single crystal, positron annihilation, metal-insulator transition obs. 77−85830
VO_2, single crystal and polycrystalline, synthesis and resist. near metal-semicond. phase-transition 80−44680
VO_2, technical appls. possibilities *(German)* 79−99587
VO_2, thermal cond. meas., metal-dielectric phase transition, phonon scatt. mechanism 78−87831
VO_2, thermochromic film, visualisation of microwave radiation using metal-semiconductor phase transition 79−65845
VO_2 thin film semiconductor-metal transition applications 80−49835
VO_2, thin films, doping by ions of Ar, B, P 77−84781
VO_2 thin films, light modulation appls., optical props. at metal-insulator transition 80−87547
VO_2 thin films, resist.-temp. characts. and structure at phase transition temp. *(German)* 77−28265
VO_2, $V_{1-x}Nb_xO_2$, crysts. and polycryst. films, metal-semicond. transition, polarised Raman scatt. 77−90151
VO_2, V_2O_3, film, absorption spectra, semicond.-semimetal transition 78−19512
VO_2, V_2O_3, V_3O_5, isotope effect on metal-dielectric phase transitions temp. *(Russian)* 78−34771
VO_2, V_2O_3 and V_3O_5, film prep. under equil. conditions, struct. and elec. props. 80−108352
VO_2, V_3O_5, V_2O_3, metal-insulator transitions, effect of isotopic substitution 80−2337
VO_2, X-ray determ. of lattice constants and thermal expansion coeffs. near transition temp. 79−86747
VO_2:Ga(Al)(Fe), phase transforms., influence of nonstoichiometry 77−85274
$VO_{(2n-1)/n}$, metal-semicond. transition temps. 80−59876
VO_x, minimum conductivity and electron localisation near metal-insulator transition 78−30960
V_2O_3, 500 to 530K, magnetic susceptibility meas., high temp. transition, interacting Hubbard bands 78−39325
V_2O_3, effect of metal-insulator transition on V K-absorption spectrum 79−19950
V_2O_3, high-temp. transition domain, small angle diffuse neutron-scatt., 400-600K 77−69231
V_2O_3, impurity doping effects, elec. props. obs. 80−75609
V_2O_3, insulating phase, mag. struct. 79−38305
V_2O_3 insulating phase, realistic Hartree-Fock calc. 79−38306
V_2O_3, lattice parameters and anomalous high temp. behaviour 78−87790
V_2O_3, phase transitions, Raman scatt. expts., 20-300K 78−39538
V_2O_3, polarised Raman scatt. in metallic and semicond. phases 77−90152
V_2O_3, pure and Cr doped, metal-insulator transition 79−37989
V_2O_3, semiconductor-metal transitions, photoelectron spectra meas. 78−84144
V_2O_3, semiconductor-metal transition, effect of ^{18}O substitution 78−84268
V_2O_3, single cryst. obtained by chemical transparent method, elec. cond. transition *(French)* 77−24940
V_2O_3, thermal cond. meas., metal-dielectric phase transition, phonon scatt. mechanism 78−87831
V_2O_3:Al, struct., props., rel. to V_2O_3:Cr, X-ray diffr. and elec. resist. obs. 78−2531
V_2O_3:Cr, anomalies in X-ray diffuse scatt. at high temp. metal-insulator transition 79−87042
V_2O_3:Cr, pure and doped, sound vels. and elastic consts. from phonon dispersion curves in insulating phase 79−55844
V_2O_3-M_2O_3, M=Ti, Cr, struct. and mag. props. 78−27041
V_2O_{3+x}, nonstoichiometric, microscopic mag. props., NMR and inelastic-spin-flip neutron scatt. 79−38323
V_2O_4 films, characterisation using XPS, metal-semiconductor transition 79−28900
V_2O_5-P_2O_5 glass, switching and memory behaviour, Pt point contact effects 77−11970
V_3O_5, dielec.-metal transition obs. and interpretation *(Russian)* 78−23023
V_3O_5, increase of X-ray refl. intensities and profile widths at phase transition temp. 79−69052
V_3O_5, insulator-metal phase trnasition at 450K, properties 78−39023
V_3O_5, metal-insulator transition, effect of doping *(German)* 78−30869
V_3O_5, Mo,Ti, and Ga doping effects on conductivity transition 77−11971
V_3O_5, phase transition temp., hydrostatic press. depend. 77−62827
V_3O_5, semiconductor metal transition, IR spectra obs. *(German)* 78−23456
V_3O_5, semiconductor-metal transition, effect of ^{18}O substitution 78−84268
V_3O_5, struct. and electronic aspects of cond. transition 78−15078
metal-insulator transition continued
V_3O_5, thermal cond. meas., metal-dielectric phase transition, phonon scatt. mechanism 78−87831
V_4O_7, metal-insulator phase transition temp. depend. on hydrostatic press., DTA meas. 79−73438
V_5O_9, metal-insulator phase transition temp. depend. on press. 80−29327
V_6O_{11}, metal-insulator phase transition temp. depend. on press. 80−29327
V_6O_{11}, metallic Magneli phase, electron state 79−94946
V_6O_{11} single crystals, heat capacity anomaly at 172K 78−10197
V_6O_{13}, optical props. in metallic and semicond. phase 80−40135
V_7O_{13}, metallic Magneli phase, electron state 79−94946
V_nO_{2n-1}, cryst. growth and characterisation 78−31311
V_nO_{2n-1} Magneli phases, elec. and mag. props. 79−37990
V_xO_y, film, preparation by calcining vanadium naphthenate, formation process exam. *(Japanese)* 78−30849
V_xO_y, metal-insulator transition, external mag. field effects 80−92819
V_xO_y, phase transformation interference reversible light reflector material, visualisation of CW EM radiation 79−71531
$V_{1-x}Re_xO_2$ ($0 \leq x \leq 0.15$), DTA, X-ray diffr., mag. susceptibility, elec. cond. meas. 78−10353
$V_{1-x}Ti_xO_{1.75}$, synthesis and mag. susceptibility obs. 78−23243
$V_{1-x}Ti_xO_2$ layer, resist. meas. 78−14770
$(V_{1-x}Ti_x)_2O_3$, solid solution, phase transition exam. 77−15590
W, field emission anomalies in mag. field *(Russian)* 80−93462
WO_3 films on Si, sapphire, glass and metal substrates, colour intensity dependence obs. *(Russian)* 80−2430
WO_3, metal-insulator transition meas. by microcalorimetry *(French)* 77−47733
Xe, condensed at high press., electron-band theory and fluid theory calcs. 80−59875
Xe, crystalline, lattice constant at insulator-metal transition 80−107706
Xe, metallic state transition under high press., supercond. *(Russian)* 79−60713
Yb, FCC phase, low temp. mag. props., impurity effects 80−20387
Yb, semimetal-semicond. transition at high press., Seebeck coeff. meas. 77−62956
$Zn_{0.005}Fe_{2.995}O_4$, phase transitions, neutron elastic scatt. and resist. meas. 77−28000
ZnS(Se)(Te), thermal expansion and lattice dynamics under press. 80−100316
ZnTe(S), semiconductor-metal transition, press. calibration above 100 kbars fixed points 80−77808
ZrC-C composite system, electrical resist. meas., percolation theory anal. 78−84269

metal-oxide-semiconductor devices *see metal-insulator-semiconductor devices*

metal-oxide-semiconductor field effect transistors *see insulated gate field effect transistors*

metal-oxide semiconductor structures *see metal-insulator-semiconductor structures*

metal-semiconductor boundaries *see semiconductor-metal boundaries*

metal semiconductor field effect transistors *see Schottky gate field effect transistors*

metal-semiconductor-metal structures
amorphous chalcogenide switching devices, reliability 79−11238
chromophore phospholipid Langmuir films, photoeffects 80−80409
copper phthalocyanine in MSM struct., electronic props. *(German)* 78−23089
electrogradient EMF, V-I characts. *(Russian)* 78−47852
magnesium phthalocyanine, depletion layer studies, temp. depend. of LF capacitance 80−65617
MBBA-EBBA mixtures and MBBA, thin and mol. films, between Hg electrodes, I-V characts. 79−11253
metal-chalcogenide glass-metal structure, freq. response characts. 77−76951
metal-chalcogenide glass-metal structures, elec. field influence on opt. parameters, electrostimulated chem. transforms. 77−76950
metal-GeS-metal system, current-voltage characts., band struct. effects in field emission region 79−42667
metal/PbI_2/metal struct. reson. and inelastic tunnelling 80−44739
MISM structure, photoresponse of residual conductivity 77−15968
molecular semiconductor/metal film junction, TEM method for cross-sectional exam. 78−95241
phthalocyanine layers, metal-free, between Ag and Al electrodes, switching effects 80−65706
polyacetylene films, AsF_5 doped, photocond. and junction props. 80−70770
polymer film, in MSM struct., thermionic field emission from metal 79−1629
p-quaterphenyl, polycryst. thin layer-metal sandwich, elec. cond. 80−34526
superconducting metal contacts, anal. of conductivity of Si. 80−15621
TCNQ salt, Cu-TCNQ thin film between Cu and Al electrodes, elec. switching and memory phenomena 79−65562
tetracene, depletion layer studies, temp. depend. of LF capacitance 80−65617
thermal switching and current-voltage characts., necessary conditions 77−4451
tunnelling phenomena in terms of exact method and WKBJ approximation 80−20329
zinc phthalocyanine film, between Au or Ag layers, microstruct. characterisation by TEM method 78−95241
Ag-BN-Si-Al sandwich, humidity sensitive threshold switching 78−88046
Ag-CdTe-Ag, negative differential resist. 78−19161
Ag-Cu_2O-Ag bistable switching devices, freq. distrib. of threshold voltage 77−32091
Ag_2Se, between metal electrodes, current-voltage characts *(French)* 80−97005
Ag_2Se thin film, switching and Ag movement, point contact technique 80−60107
Al/As_2SeTe_2/Sb structures, rectifying effects 80−75654
Al/copper phthalocyanine/Au cell, photoexcitation, doping, energy loss mechanisms 79−99573
Al/Ge/Al sandwich structs., interdiffusion effect on Ge film conductivity 79−23788
Al-amorphous GeSe-Al junctions, electrical contact effects on properties *(German)* 80−93010
Al-amorphous GeSe-Al structs., AC cond. and capacity, thickness depend. 79−65566

metal-semiconductor-metal structures continued
Al-amorphous Se-Al struct., capacitance variation with illumination 79−87165
Al-As_2Se_3-Al, photographic process based on electrochem. reactions *(Russian)* 79−6213
Al-As_2Se_3-Al layers, photoelectrochem. process 77−76953
Al-CdS-Au, interfacial phenomena, complex impedance meas. *(French)* 79−42668
Al-CdS-Au structures, asymm. Poole-Frenkel effect *(French)* 77−76949
Al-CdSe-Ag dry air stabilised struct., elec. cond. mechanism, breakdown phenomena 80−34527
Al-CdTe-Ag(Al) sandwich structures, switching obs. 77−43752
Al-CdTe-Al thin film VLF dielectric props. *(Slovak)* 79−7907
Al-copper phthalocyanine-Ag diode struct. with Schottky barrier 77−43740
Al-Fe_2O_3-Al, space charge limited current, current density as function of elect. field and temp. 79−51688
Al-fuchsin-SnO_2 MSM structure, field depend. of electroabsorption spectra 77−40263
Al-GaAs-Al sandwich-type sputtered film, elec. props. 78−91780
Al-GeS-Al structure, current-voltage characts., thermionic electron emission model 77−28260
Al-GeSe-Al(Mo)(Au)(C), effect of contact material on DC and AC behaviour of sputtered amorphous GeSe film 79−95513
Al-nSi-Al, p^+np^+ reach through structs., electronic cond. mechanism 78−64103
Al-Se-Ag switching element, diffusion and electrodiffusion of Ag and its role in switching effect 78−19163
Al-Si-Al contact current response to 100 keV neutron irrad. *(Russian)* 80−49956
Al-Si-Al(Mo), sputtered Si film, photovoltaic props. 77−24623
Al-TeAsSiGe-Al, amorphous film, AC performance *(German)* 77−63012
Al-TeO_2-Al, field-assisted cond. mechanism 80−11105
Al-ZnS-Au structure, coulombic centres, thermal ageing, cond. and photovoltaic characts. *(French)* 77−43741
An-TTT-Al sandwich dark injection current, sign inversion of low mag. field *(Russian)* 79−73602
As-Te-Ge-Si sandwich type amorphous films with metal electrodes, space-charge-limited switching, pre-breakdown characts. *(Japanese)* 77−69385
As_2Se_3 disordered films in flash evap. systems, nonsteady-state behaviour of interface states 77−76952
As_2Se_3, glassy, photostimulated changes in contact props. 78−19162
As_2Se_3, in evaporated layer systems, electric field forming and ageing processes 77−12021
a-As_2Se_3-Au contact sandwich, response to voltage step in dark and with illum. 77−69431
$AsSeI_{0.1}$, glassy, photostimulated changes in contact props. 78−19162
$As_{50}Te_{50}$, amorphous films, metal and semicond. contacts, threshold switching, IR emission 80−49831
Au/(Zn-)phthalocyanine/Al(In), photovoltaic effects, dark elec. props. of rectifying cells 79−4604
Au/(Zn-)phthalocyanine/Al(In), photovoltaic effects, illuminated thin-film cell props. 79−4605
Au-amorphous GeSe-Au junctions, electrical contact effects on properties *(German)* 80−93010
Au-amorphous GeSe-Au structs., AC cond. and capacity, thickness depend. 79−65566
Au-B-Au systems, elec. field effect on B film struct. 80−20050
Au-CdSe-Au capacitor, thermally stimulated and isothermal discharges, grain boundary barrier characts. 78−2582
Au-CdTe-Au structure, as spectrometric detector of nucl. radiation 77−54460
Au-CdTe-Au structure, current transport props. 80−80408
Au-Ge-Au, room temp. interdiffusion 78−76161
Au-$GeSe_2$- Al(Au) structures, photoconductance meas. in amorphous $GeSe_2$ layers 80−65632
Au-$Pb_xSn_{1-x}Te$-Au structure, third harmonic variations at 77K and 300K 78−84313
Au-PbTe-Au, semiconductor thin films, random noise measurements 80−15629
Au-Si-Al structure electrode mass transfer and switching with memory 78−95389
Au-TTT-Al sandwich, strong mag. field effects on dark cond. and photocond. at charge carrier injection *(Russian)* 79−69607
Au-tetrathiotetracene-Al systems, dark cond., photocond. mechanisms rel. to contact phenomena *(Russian)* 78−52103
Au-ZnO-In metal-semicond. diode, electrolum. spectra 79−99948
$BaTiO_3$:Nb, elec. props., contact material influence 80−70848
C film, amorphous, elec. transport props. 78−6457
CdTe, MSM detectors, charge collection 77−61660
CdTe metal-semiconductor-metal γ-ray detector characts. 80−57451
CdTe, sputtered film, electrode effects in AC characts. from equivalence impedance meas. of metal-CdTe-Al struct. 79−82686
Cr-phthalocyanine-Cr sandwich, I-V and C-V characts. 80−60106
Cu-CdP_2-Cu diode structure, switching effect obs. 77−4452
Cu_2O, cond. filament props. and bistable switching effect *(German)* 78−2532
GaAs, epitaxial layers, low freq. current noise between 4.4 and 300K 78−95388
GaAs:Cr, Se layers, ion implanted, ohmic contact form., contact resist. meas. 79−91158
GaSe film, charge transport models *(Russian)* 78−60233
GaSe MSM struct., inelastic tunnelling investigation of lattice dynamics, electron-phonon interaction 80−20330
Ge amorphous evaporated film, study of metal contact resistance and microstruct. 77−89880
Ge m-n-m structure, current-voltage characts. 77−1476
Ge-As-Te glass, between metal electrodes, contact props. determ. 79−7908
GeS film, between Al(Zn)(Sn) electrodes, Schottky and Poole-Frenkel cond. mechanisms 80−54799
In-CdS-In(Te) contacts, ohmic nature, monitoring method 77−39935
In-GaAs:Cu-In, phototrigger effect 78−56238
In-GaAs:Cu-In S-type diode, role of deep trapping levels in form. of current-volt. characts. 77−76948
In-PbTe-In semiconductor thin films, random noise measurements 80−15629
In-ZnO-Al metal-semicond. diode, electrolum. and photoluminesc. spectra 79−99948
In-ZnSe:Al-In, MSM structure, mechanism of current flow *(Russian)* 79−78208
InSb, in MISIM struct., photovaractor effect and CV characs. obs. 77−8205
Mo-amorphous GeSe-Mo junctions, electrical contact effects on properties *(German)* 80−93010
Mo-chalcogenide glass-Mo-Al struct., strong elec. field effects 80−97004
Mo-GeSi-Mo, amorphous film, AC performance *(German)* 77−63012
Mo-Si-Mo structure, non-volatile memory switching 80−54814
Pb-CdS-Pb junctions, Josephson effect through 80−100558
Pt-Cu_2O-Cu double injection diodes, I-V characts. and photomemory effects 77−47900
Pt-Cu_2O-Cu single carrier space charge limited diodes, I-V characts. 77−47901
Si amorphous films, switching, electrothermal model 80−80407
SiC, semi-insulating in struct. with injecting contacts, cond. in strong elec. field 78−19160
$Si_{12}Ge_{10}As_{30}Te_{48}$, conducting filaments and switching phenomena 79−87134
$Te_{43}Se_{30}Sn_7$ in MSM struct., switching effects 78−19164
Ti-Si-Ti sandwich, elec. cond. processes and threshold switching in amorphous Si layer 79−78207
$TlInS_2(Se_2)$, electrical cond. of single crysts. with symm. and asymm. Ag-In contacts 80−6835
V_2O_5-P_2O_5 (70-30), electrical cond. and thermoelectric meas., Au-glass-Au sandwich 80−29403
V_2O_5-P_2O_5 glass, in metal-semicond.-metal struct., TSC of dielec. relax. *(Russian)* 77−35998
V_2O_5-P_2O_5-CaO glass with metal electrodes, elec. characts., thermal conditions effect *(Russian)* 78−47884
Zn-GeS-Zn structure, current-voltage characts., thermionic electron emission model 77−28260
$Zn_{1-x}Cd_xS$ films, polycryst., reactively sputtered, MSM struct. obs. of dielec. props. and cond. mechanism *(French)* 78−14841
Zn_3P_2-Al(Mg)(Be), diode, spectra response meas. of minority carrier diffusion length 79−78131
ZnS, photocell, transient photoelec. phenomena 79−82687
ZnS:Ag film, photocapacitance IR quenching, hole photoionisation energy and spectral distrib. 79−87127
ZnS-metal interface in MIM struct., photoexcitation level assignment *(French)* 80−15622

metal theory
see also band structure of crystalline metals; electron gas; lattice dynamics of metallic crystals
1/f noise, temp. fluctuations as source, theory 80−11059
3d system, configuration based quasi-particles 78−91648
A15 compounds, self-consistent LMTO band calcs. 79−37954
AB alloy, equilib. props. by Markovian simulation 78−91302
acoustic wave propag., strong and weak waves nonlinear interaction *(Russian)* 78−60168
actinide metals and intermetallics, electronic energy band struct., 5f electrons role 77−28107
actinide metals and intermetallics, localised versus itinerant character of 5f electron states 77−28138
actinide metals and semimetallics, electronic structure *(Japanese)* 79−37941
actinides, electronic struct., Hubbard's alloy approx. 79−73665
actinides, electronic structure, role of 5f electrons, Dirac-Slater wave function structure 77−28108
actinides and alloys, metallurgical props. rel. to electronic struct., energies calc. method 77−20221
adsorption potential in hydrodynamical model 80−100396
aggregated system, optical props., interband transitions and optical cond. reson. 77−44016
alkali metal, Ashcroft pseudopotential, unified study of props. 80−39239
alkali metal, atomic props., accuracy of description depenxence on pseudopotentials *(Russian)* 78−38997
alkali metal, local Heine-Abarenkov-type model pot. 79−87031
alkali metal as classical one-component plasma, melting parameter 78−47092
alkali metal surface, electronic struct , mixed-representation method 77−20399
alloy, binary, ordered and disordered, transfer of charge 77−15785
alloy, nearly-free-electron, random, charge transfer rel. to stability 78−6316
alloy transfer matrix approx., dispersion relations and transport props. 79−42524
alloys, random binary, single-particle Hamiltonian and self-consistency 79−37953
amorphous, electronic states calc. 79−69399
amorphous metal, electronic density of states 78−51868
Animalu transition-metal model potentials, nonlocality 78−6250
anisotropic metal, with impurities, long-range interactions of spins 79−47092
anomalous microwave penetration for near-specular electron refl. *(Russian)* 77−89785
antiferromagnetic metal, thermoelec. power in mag. field 80−70686
APS, multiple scatt. approach using muffin-tin pot. 80−25490
atomic binding energy and surface energy rel. to prediction of physical props. 80−59434
atomic displacements around impurity and three body interaction 78−91406
atoms as structural components in metallurgy *(Dutch)* 80−96465
Auger spectrum, quasiatomic lineshapes in narrow-band metals and electron correl. effects 77−81183
band calculation by tight-binding method, orbital effect 77−15736
BCC divacancy binding energy, appl. stress effect, computer simulation 77−15408
BCC metals, stressed, computer simulation of vacancy and divacancy migration 78−47573
binary alloy, electron localisation, self-consistent theory *(French)* 78−60088
binary alloy, electron theory of short range order 78−10390
binary alloys, and intermetallic cpds., struct. and stability, ab initio pseudopot. calcs. 78−34460
binary alloys, form factors of pseudopot., OPW calc. *(Russian)* 79−19498
binary substitutional alloy, with long range order, electron energy spectrum *(Russian)* 78−84121

metal theory continued
Boltzmann equation for electrons, solns., energy depend. 80−88537
Boltzmann equation for electrons in metals, new method of solution 78−72127
bound electron gas, static semiclassical response 78−56089
CDW detection by angle-resolved photoemission 78−95658
charge perturbations around impurities, review 77−85582
charge screening and Friedel oscillations of electron density *(Russian)* 78−79951
charge-density-wave metal, mag. susceptibility of cond. electrons 80−44523
charged fermion system, in random external field, dielec. instability 77−85170
chemisorption, on metals, theoretical models, review *(Russian)* 78−84071
classical cleavage energy, layer summation method 77−85287
classical plasma frequency in long-wavelength limit, quantum correction 80−107728
close-packed metals, elec. field gradients, vol. and struct. depend. 78−64014
cluster, electronic spectrum fluctuations, appl. to Ni and Ti 79−19501
cluster model theory and its application to metal surface-adsorbate systems, book contrib. 80−24991
cohesion, local-density approx. to exchange and correlation effects 77−47749
cohesion energy of narrow band metals, intraatomic Coulomb correlations 78−43322
cohesive energy, pseudopot. calc., many electron correl. 77−51393
cohesive energy, simplified local-density theory 79−60749
cohesive properties, energy density functional-pseudopotential method 79−73462
compensated metal, with closed Fermi surface, Hall coeff. temp. depend. 77−8074
compressed atom model, energy level shifts for changed boundary conditions 77−43473
compressibility, local pseudopot. approach 80−65129
conduction band X-ray photoemission, intrinsic plasmons effects 78−39661
conduction electron behaviour and role of electron-ion and electron-electron interactions *(Japanese)* 77−66102
conduction electron distribution function and corrections to surface impedance for normal skin effect *(Russian)* 78−76100
conduction electron effects on dislocation mobility in metals and superconductors 79−7932
conduction electron photoemission spectrum, effect of recoil on shake-up spectra, infinite summation method 80−50526
conduction electron polarisation, magnetisation densities, neutron mag. form factors 77−72981
conduction electron spin echo modulation in small metal particles 80−39872
conduction electrons spin magnetisation kinetics, role of surface scatt. *(Russian)* 77−80989
core level binding energy shifts between free and condensed atoms 80−20136
core overlap interaction, interatomic forces 78−47724
core overlap interactions 77−47759
core-level binding-energy shifts 78−47740
cubic metals, anisotropic relation between work function and melting temp. 79−37813
cubic metals, intra-atomic correl. energies with canonical d bands, Hubbard interaction calc. 80−39518
cyclotron resonance and geometric oscills. of sound velocity 77−20230
cyclotron resonance line shape in inclined mag. field *(Russian)* 77−36136
cyclotron resonance on open electron orbits *(Russian)* 80−88878
cyclotron resonance with almost specular boundary *(Russian)* 78−10778
d-band metal force fields 79−33051
d-band metals and alloys, s-d hybridisation 78−91644
d-electrons, electron density model 78−91580
damping of excited molecules located above surface 78−92160
degenerate free electron metal, cyclotron wave propag., finite $\omega\tau$ effect 77−20228
density functional approach to electron and positron states 79−56107
density gradient expansion for kinetic energy 78−34794
density matrix, using Wannier functions 77−69210
dielectric function, degenerate electron gas at metallic densities, nonlocal interactions, compressibility and dispersion 80−107730
dielectric response of solids, approxs. for treatment of local field effects 79−47033
dilute binary alloy, residual resistivity 77−1406
dipole-nuclear acoustic resonance, electron band struct. influence, in cubic metal 79−19787
dislocation dipole and prismatic dislocation loop effects on thermodynamics of electrons *(Russian)* 79−56161
disorder systems, conduction electron surface scatt. *(Russian)* 80−24917
disordered alloy, Blackman-Esterling-Berk approximation, rederivation and proof of analyticity 78−10318
disordered alloy, bulk and surface density of states, effect of surface segregation 77−15729
disordered alloy, electron correl. in Hubbard model, and spin susceptibility 77−76762
disordered alloy, strongly correlated extended CPA anal. 77−20217
disordered alloys, electronic struct., CPA calcs., short-range order 78−63964
doubly occupied Wannier functions, constructive definition 80−75492
dynamic screening of core hole, semiclassical model 79−69445
dynamic screening of ions passing through solids 78−10379
education, deep one-dimens. periodic pot., zero energy gaps, Kronig-Penney model 80−62426
elastic constants of cubic metals, vol. depend. contrib., pseudo-pot. theory 77−72646
electric field gradient analysis, free electron approach 78−51950
electric field gradient press. and temp. depend., noncubic metals 77−8057
electric properties calc., book 79−28274
electrical resist., correction from non-Hermiticity of pseudopotential 79−7815
electrodynamics at boundary, including plasma waves 77−59317
electromigration, dielectric function approach using equivalence theorem 77−11733
electron correlation, Gutzwiller theory at finite temp. 77−43527
metal theory continued
electron correlations, ground state results in high density regime 78−72097
electron correlations due to Brewer-Engel and Samsonov-Pryadko-Pryadko 79−60737
electron densities at muons 79−56655
electron density behaviour near impurity charge 80−75518
electron fluid, adiabatic de Haas-van Alphen effect at low temp., Fermi fluid interaction and chem. pot. effects *(Russian)* 80−84442
electron fluid model, for lattice dynamics calc. 78−75738
electron gas, correlation effects on polarisation 80−54628
electron gas, degenerate, distrib. function in periodic field 79−23914
electron gas, exchange and correlation effects, self consistent theory 77−85161
electron gas, inhomogeneous, kinetic energy *(Russian)* 77−85160
electron gas, local density functional for kinetic energy near defect, metal surface 80−20105
electron gas, mean free path of low energy electrons, influence of damping 78−10385
electron gas, metallic densities, dynamical dielectric function and paramagnetic spin susceptibility 80−39514
electron gas, optical props. in generalised HF approx. 80−24825
electron gas, pair potential between two ions 78−47723
electron gas, paramag. susceptibility, RPA calc. 78−43559
electron gas, semi-infinite, nonlocal cond. tensor calc., effective optical surface region 80−20283
electron gas, spin polarised, model for conduction electrons of simple metal in mag. field and ferromag. Gd 77−8034
electron gas correlation function, high density expansion 77−1386
electron gas in metal, free energy virial expansions *(Russian)* 78−10380
electron liquid, excitation spectrum, memory-function approach 77−39791
electron liquid, excitations 79−4522
electron liquid, magnetic susceptibility quantum oscillations, low temp., mag. instabilities in electron liq. *(Russian)* 78−87928
electron liquid, static struct. factor, short-range correl. and Wigner crystn. 77−39795
electron momentum distrib., reconstruction from point-geometry positron-annihilation data 79−56883
electron resonance and energy spectrum, quasi-particle approach 79−61225
electron response to local fields, X-ray processes 78−23584
electron theory, contrib. of Sir Rudolf Peierls 1928-1935 80−57054
electron theory, work at Univeristy of Bristol, 1930-37 80−57068
electron theory of metals, contrib. of Felix Bloch 80−57053
electron theory of metals and geometry, review 80−103611
electron waves, tight-binding description, appl. to heterogeneous catalysis 79−60700
electron-electron interaction, self-consistent perturbation theory based on Hartree-Fock theory 79−95357
electron-lattice interaction effect on equilib. struct. form. *(Russian)* 80−34380
electron-phonon interaction, contrib. of John Bardeen 80−57057
electron-phonon interaction function of normal metal determ. by proximity effect *(Russian)* 77−89902
electronic Fermi fluid, instabilities in mag. field *(Russian)* 79−11073
electronic structure of H impurity in simple metals 78−67978
electrons around vacancies, electron density calc. 78−64003
elements, metallic, core-level binding-energy shifts 80−88502
ellipsometry, metallic films and surfaces, nonlocal effects, theory 80−104006
EM excitations in strong mag. fields, review 77−8130
EM properties, general lecture 78−26901
entropy production and choice of heat flux 77−15778
equation of state, from statistical electronic free energy 79−99495
equation of state of simple metals, non muffin-tin corrections *(French)* 80−59906
equations of state between 300-200000K for all press., numerical calcs. for Cu, Al *(French)* 77−72672
exchange enhancement of electron-phonon coupling 78−47968
FCC metal, covalent component of electron density and energy *(Russian)* 80−28945
FCC metal, phonon dispersion relations and Debye-Waller factor calcs. 78−51630
Fermi fluid, degenerate, spin correlations at metallic densities *(Russian)* 78−43321
Fermi liquid model, two-component, for nonferromag. d-metals *(Russian)* 77−51683
Fermi surface, electronic props., book 80−105445
Fermi surface geometry, effect on sound absorpt. and vel. 79−7775
Fermi surface local geometry effects on phonon spectrum, acoustic props. *(Russian)* 77−55333
Fermi surface mapping from one-dimens. Fourier transform of Compton profile 77−39764
Fermi surface topological transition, electron-phonon interaction contrib. calc. 80−6697
ferromagnet, antiresonance region, EM wave propag., Maxwells' eqns. soln. 80−66038
ferromagnet, electron transport with arbitrarily oriented ellipsoidal Fermi surfaces, cyclotron wave excitation 78−23006
ferromagnet, excitations in mag. field, theory *(Russian)* 77−8291
ferromagnetic metal, band struct. contribs. to shear consts., deform. pot. formalism and Stoner model 79−91280
ferromagnetic metal, exciton condensation effects on props., Hubbard model 80−60171
ferromagnetic metal, impurity resist., band model calcs. 77−39830
ferromagnetic metal, itinerant electron model, for US propagation and structural instabilities 78−95508
ferromagnetic metals, dislocation drag by conduction electrons 80−24451
field gradient, temp. depend., and antishielding effects 78−51951
film, electron Fermi liquid, microscopic theory *(Russian)* 77−35999
film, electron liquid oscills. *(Russian)* 78−43315
film, lattice sum, for use in self-consistent warped muffin tin pots. 77−15741
film, oscill. kinetic effects, boundary electron scatt. *(Russian)* 78−52104
film, size-quantised, energies and Fermi level of electrons 77−15749
film with magnetic impurities, electron Fermi liq. theory, collective excitation spectrum *(Russian)* 77−62846
forces due to cond. electrons in external fields *(Russian)* 78−79987

metal theory continued
free electron approx. and symm. Hermitian pseudopot. *(Russian)* 79−28263
free electron metal, electron-phonon interact., comparison with metallic hydrogen 77−66125
friction coeff. of atom near metal surface 77−59312
Friedel sum rule, high conc. extension, appl. to coherent pot. approx. 80−44462
Friedel sum rule in static mag. field, impurity-induced mixing between Landau levels 77−31976
Gantmakher-Kaner effect in strong mag. field *(Russian)* 78−80015
generalized pseudopotential theory, density functional formulation, d-band metals 78−10389
generator coordinate method and the theory of metals 79−28299
ground state energy, structural expansion, HF approx. 80−65420
ground state energy, structural expansion 80−88497
Gruneisen parameters, interatomic forces, pseudopot. calc. for simple metals 80−44165
heavy metal, relativistic one-particle equation for electron states 78−43280
Heine-Abarenkov type model potential, parameter determ. 78−6248
heterogeneous state form. due to long range interaction *(Russian)* 77−7842
Hubbard model, photoemission spectrum, effect of electron correlation 79−78828
hydrodynamic model, surface effects, review 79−78148
hydrogen-like impurities electron. struct. μ^+ probes 79−56653
impurities in metal cryst. with and without surfaces, asymptotic displaced charge 79−95364
impurity, surrounding electron density calc. using Wannier functions 77−20262
impurity effect on electric field gradient 78−23061
impurity effect on electronic struct. 78−47692
impurity induced shift in k-wave electron state energy level 77−39805
impurity interactions in pseudo-molecule form. 78−47735
impurity potential determ. 79−78039
incomplete shell metal, spin-depend. final-state interactions in core photoelectron spectra 77−20981
incomplete shell metal, spin-depend. final-state interactions in core photoelectron spectra 77−20982
independent electron metal, soln. of X-ray edge problem, recoil spectrum of suddenly perturbed Fermi sea 80−80932
indirect exchange interaction through narrow conduction zones *(Russian)* 79−4538
inhomogeneous electron gas, exchange energy *(Russian)* 77−72830
interacting metal half space, effect of retarded-surface-plasmon dispersion and Van der Waals interaction 79−69452
internal press. in electron theory of metals 80−92802
interstitials, quadrupole effect on dipolar field width 78−2457
ion pair potentials, asymptotic, contrib. to lattice energy, elastic consts., phonon dispersion 77−19898
IR absorption, contrib. of conduction electron scatt. 79−42971
isotropic metals, CDW, Fermi-surface instability 78−79947
jellium metal, bounded, linear response function in RPA 79−69444
jellium metal, surfaces props., statistical calc. 80−24987
jellium metal, work function changes on single crystal planes 79−99604
jellium metal surface, work function calc. 79−65536
jellium model, impurities and photoexcited ions in metal 80−39523
jellium model with finite discontinuity in potential, response function 77−1466
kinetic equation, iteration soln. 77−43564
lattice dynamics model, homogeneous electron liquid concept *(Hungarian)* 77−27952
lattice stability, comparison of BCC and FCC struct. in tight-binding calc. 77−51632
lattice stability, perturbation formalism for comparison of crysts. with different lattices 77−51631
lattice sums with screened potentials 78−43341
layer metal particles, surface plasmons 77−1465
Li, elec. resist., effects of core and correl. corrections 78−64026
Lifshitz transitions and tunnelling effect 78−91591
light impurities, electronic struct. 80−34394
liquid metal, electron momentum density, perturbed Green's function method 78−60052
liquid metals, d-band, electronic spectrum 77−51646
liquid metals, review of research, phys. aspects, Knight shift, elec. resist. *(Dutch)* 77−7657
liquid non-simple metals, electronic props. 77−47721
localised dynamic perturbations 80−73262
localised non-magnetic impurities, general theory 77−1392
long range metallic pair potentials, use in computer simulation 79−37942
low frequency surface impedance, temp. depend. 78−56207
magnetic metals, crit. transverse US attenuation, spin fluctuations 78−48022
magnetoresistance, intrinsic, for metal with open Fermi surface 77−11899
magnetoresistance of localized impurities, multiple scatt. theory 78−43360
many-band metals, elect. resistivity from force correlation function method 78−43357
many-electron theory, sp. ht. and electron energy states 79−46991
metal, acoustic breakdown, electron energy spectrum *(Russian)* 78−18948
metal, dislocation scattering and de Haas-van Alphen effect 79−77982
metal, dislocations rel. to electron gas thermodynamics at $2^1/_2$th order transition *(Russian)* 78−51910
metallic particles, effective interactions due to irregular surface 79−99470
metallic sphere, very small, surface plasmon dispersion, RPA 77−47886
metals, degenerate electron gas, collective props. using electron knock-out processes 80−6758
microwave transmission, time-of-flight effects in Fermi vel. determ., calc. 80−20238
model potential parameters 78−47731
model pseudopotential calcs., elastic consts., spin susceptibility, Fermi surface distortions 78−79922
Morse potential appl. in molecular-metallic framework 80−79742
muon screening spherical solid model 79−56654
narrow band metals, extra-atomic relax., X-ray spectra 77−36312
narrow-band metals, Auger line shape 80−60719
metal theory continued
nearly-free-electron metals, holelike Fermi surface, Hall coeff. and magnetocond. tensor 79−4547
nearly-free-electron metals, role of plasmon decay in secondary electron emission 77−81186
noble metal, electron-ion interaction, model pseudopot. 78−34785
noble metal, van der Waals forces and their contrib. to vacancy form. energy and phonon dispersion 78−91635
noble metals, Krasko-Gurskii model potential, test of validity for Cu 80−39485
noble metals, liq., muffin-tin pot. model, electronic density of states determ. 77−51645
noble metals, Van der Waals contribution to binding energy 78−2062
non-simple metals, dielectric matrix, analytic model 80−75512
noncubic metal, charge screening enhancement of quadrupole shielding factors 78−43342
noncubic metal, conduction-electron elec. field gradient, probe valence effects 78−47749
noncubic metal, possibility of isotopic mass effect on quadrupole coupling const. 78−43725
noncubic metals, conduction electron electric field gradient, effect of orthogonalisation 78−26832
noncubic metals, elec. field gradients, nuclear electric quadrupole interaction 79−65420
nonferromagnetic metal, two-component electron Fermi fluid, in mag. field *(Russian)* 77−20252
nonlinear cyclotron reson., anomalous skin effect *(Russian)* 77−28449
nonlinear electron density distribution around point defects, formulation 79−19548
nonlinear electron density distribution around point defects, applications 79−19549
nonlinear EM absorption of short-wave sound *(Russian)* 78−43446
nontransition metals, jellium approach to vacancy energetics 78−47347
nontransition metals, zone struct., fully OPW calc. *(Russian)* 79−46994
one- and two-dimens., periodic lattice distortion and CDWs 79−60678
one-dimensional metals and charge density wave effects in these materials, review 79−78085
optical surface plasmon modes, spheres 78−2539
optics of spatially dispersive solids 79−19858
oscillating dipole-metal surface interaction, jellium model and random phase approx. 80−92955
p-wave pairing, and superconductivity 77−39998
paramagnetic metal, band struct. contribs. to shear consts., deform. pot. formalism and Stoner model 79−91280
paramagnetic metals, nonphonon mechanism of supercond. and static screening *(Russian)* 79−78258
paramagnetism, closed-shell many-electron systems 77−20539
phenomenological theory of first- and second-order metal-insulator transitions at absolute zero 79−69420
phonon anomaly near Fermi surface topological transition 78−95120
phonon spectra pseudopot. calcs., exact normalization of single OPW conduction electron states 77−7803
phonon spectrum, nonadiabatic effects, in mag. field *(Russian)* 78−19106
photoemission, ultrasoft XPS, plasmon satellite intensity 80−35058
photoemission from metals, book contrib. 78−95670
physical props., correl. with outer electron density of state *(Chinese)* 79−51466
plasma and conduction resonance dispersion 78−79952
plasmon, long-wavelength, pseudopot. theory of full width at half max. 77−11864
plasmon dispersion, effect of band struct., dielec. function calc. 78−26825
plasmon dispersion at metal surface or metal-metal interface 78−52053
plasmon dispersion in simple metals 78−91629
plasmon frequencies of small metal spheres, calc. by hydrodynamic theory 78−43319
plasmon satellite struct. in (e,2e) process 80−96809
plasmon-plasmon interactions 78−30882
plasmons, APW dispersion relation 77−69265
plasticity at very low temperature, dislocation motion, rel. to supercond. and tunnelling *(Czech)* 77−32630
polar states and free electron gas *(Russian)* 80−84415
polycrystalline metals with open Fermi surface linear magnetoresist. calcs. 78−56129
positron thermalisation on cond. electrons *(Russian)* 79−19558
positron trapping at defects, positron-phonon scatt. effect 77−89736
positron trapping rate into vacancy clusters in metals 80−2890
positron-phonon interaction through cond. electrons *(Russian)* 80−29126
positron-phonon scatt. effect on positron trapping at monovacancies 78−26829
pressure equation derived, Hartree-Fock approx. 78−72103
proton in jellium, self-consistent screening 78−2441
pseudopotential for electron-ion interaction, appl. to K and Na props. 78−26486
pseudopotential method used to obtain binding energy, compressibility, interionic pot. and transition temp. of simple metals 79−46598
pseudopotential theory, completely OPW method and orthogonalised hole conception *(Russian)* 77−62792
quantum kinetic equation for electrons 78−91686
quantum mechanical electron theory develop., 1900-28 80−57065
quasi-one-dimensional, pair correl. function and plasmon dispersion curve 77−62851
quasiparticle bands, cond. electron mixing with impurity d(f) ions *(Russian)* 78−10409
quasiparticle props., density functional approx., electron gas calc. 80−96808
Raman scattering by adsorbed molecules on metal surface, intensity enhancement, theory 80−54518
random alloys, CPA calcs. cluster extensions, appraisal of applicability 79−15063
rare earth metal, lattice dynamics and scatt. reson. 78−59872
rare earth metal, screening effects on cryst. electric fields 79−78058
rare earth metals, 5s electron excitation energies 78−10408
rare earth metals, electronic struct., Hubbard's alloy approx. 79−73665
Rayleigh sound, reson. absorption by surface electrons 78−71924
recrystallisation, induced, in thin metal plates *(German)* 78−19783
residual resistivity for electrons scatt. by spin-depend. potentials 77−39829
resonant model potential of d band metal, total energy 77−69263

metal theory continued
resonant photoemission, mech. 80−50524
retarded Van der Waals' force near a metal surface 79−38146
review, free electron model *(Japanese)* 77−47710
s-d electron model, finite temp. diagram technique, perturbation theory 78−67932
screening energies in photoelectron spectroscopy of localised electron levels 77−1781
secondary electron emission, Monte Carlo calc. 79−69932
semistatistical calcs. 77−35879
short range atomic order, size effect in electron theory, static conc. waves approximation *(Russian)* 78−39049
simple, density functional theory of chemisorption, book contrib. 80−107647
simple metal, Knight shift, single-ion approach 80−44935
simple metal, optical properties, equivalence of local field corrections and dynamical screeening 79−33250
simple metals, compressibility, Harrison pot. calcs. 80−96460
simple metals, elastic moduli, chem. trends, pseudopot. method 80−107355
simple metals, model pseudopot. appl. to various props. 80−59845
simple metals, photoemission theory, book contrib. 80−16159
simple metals, plasmon dispersion anal. from electron gas dielectric response 80−6761
simple metals, X-ray absorpt. and emission edges, one-electron and many-body effects 80−25484
simple metals, X-ray threshold anomaly, exponents in theory 77−85838
single-particle density matrix, perturbation expansion 80−54635
size-quantised metal, dielec. response 77−31968
small metal particles, thermodynamic props. of electrons 80−59844
small-core approx. and structural phase stability 79−99498
solid state physics, 1925-33 80−57066
solid state physics, 1933-40, contrib. of Sir Nevill Mott 80−57055
solid state theory, 1926-33 80−57067
solidification of metals, variational formulation of stationary free boundary problem *(French)* 80−96626
spherical Fermi surface, cyclotron reson. line shape and cyclotron waves 78−95251
spherical solid model for muon and H in metals 79−78601
spin fluctuations, mag. field effect, electronic sp. ht. and elec. resist. 80−108026
spin scattering and spin-orbit coupling 80−29369
static dielectric permittivity sign *(Russian)* 78−76012
strained metals, interpolation functions for Fermi surface 80−65425
superconductivity, generalized jellium model, effect of ion core repulsion *(Russian)* 79−11260
superconductor and normal metal, Raman sound scattering *(Russian)* 78−23199
surface, adatom mobility, density functional approximation calc. 80−103577
surface, corrections to local density approx., gradient expansion vs. wave-vector analysis 77−51796
surface, density functional theory, review 80−44698
surface, dynamic image pot. for tunnelling electrons 80−49874
surface, effect on ground state of approaching H atom 77−35979
surface, electrodynamics, microscopic effects *(Russian)* 80−6936
surface, electron correl. in chemisorbed H atom, friction coeff. 78−60026
surface, electron-phonon coupling in image-potential bound states 80−54752
surface, electron-plasmon interaction 80−39649
surface, electronic density, variational calc. 79−15205
surface, exchange-correlation hole 78−80037
surface, excited molecules located above surface, theory of damping 79−15203
surface, force on moving charge, spatial dispersion effects 80−65646
surface, gradient approx. anal. appl. 80−96810
surface, gradient correction to electron exchange-correl. energy 77−43691
surface, influence of submonolayer films on props., calc. *(Russian)* 80−2273
surface, integro-differential eqn. for electron density and formula for surface tension of jellium 80−44689
surface, interaction with H_2 80−29259
surface, jellium model, nonlocal density based self consistent surface calc. 77−72898
surface, narrow-band, self consistent model calcs. of electronic states 77−85295
surface, Nonlinear mixing of oppositely travelling surface plasmons 79−95460
surface, positron-electron correlations, RPA calc. 80−40181
surface, self consistent electronic struct. effect on atomic positions, computer simulation 78−30969
surface, semiclassical infinite barrier model 78−64079
surface, step potential model, static semiclassical response of bounded electron gas 78−72221
surface, theory, book 80−36787
surface, tight-binding, dissociative chemisorption of molecule 78−2368
surface, virial theorem for jellium model 79−60892
surface, with substitutional disorder, density of states, Green's function theory 78−23145
surface, work function, pseudopot. calc. 80−96970
surface atom vibrations, self-consistent calc. in tight-binding model 80−103560
surface bonding, book contrib. 80−24990
surface correlation energy, plasmon contrib. 77−69397
surface dielectric response in local representation, microscopic theory 77−85289
surface dipole barrier, calc. 80−96958
surface dipole barrier, semi-empirical calc. 80−39659
surface electron density of states, random impurity distrib. 78−6424
surface electronic barrier, elec. field effect in presence of adsorbate, Thomas-Fermi model 80−49864
surface electrons, reson. and cyclotron waves *(Russian)* 77−73081
surface energy, barrier height and work function, jellium model calc. rel. to fracture model 77−72907
surface energy, exchange and correl. contrib., wave-vector decomp. 80−75615
surface energy, gradient corrections in interpolation formulae, surface plasmons 80−2441
surface energy, semi-empirical theory 77−76895

metal theory continued
surface energy 78−91528
surface energy calc., exchange contrib., convergence of gradient expansion 77−43684
surface energy calc. in model of discrete positive charge *(Russian)* 78−38911
surface energy of electron gas, virial theorem 77−69398
surface He implantation, lateral stress role in blister form. mech. 78−95068
surface impedance, extreme anomalous limit, diffuse refl. from boundary 80−29460
surface impedance in mag. field, cyclotron waves 77−89787
surface impedance in mag. field 77−89786
surface impedance near anomalous skin-effect limit, electron-electron N processes 80−100497
surface interaction with external mol. complex 79−47140
surface photoeffect, energy and angular energy distribs. 77−63535
surface plasmon dispersion 80−2440
surface plasmon polariton modes, struct. induced, using ATR, theory 79−60890
surface plasmons, on rough surfaces, dispersion relation changes 77−69394
surface plasmons *(Russian)* 79−33327
surface plasmons around cavity in semiinfinite metal *(French)* 78−56196
surface plasmons in thin film, circular cylinder and spherical void, RPA calcs. 77−80823
surface potential drop and contact pot. difference in terms of orbital electronegativity 78−2546
surface problems in microwave region, theory and meas. *(Chinese)* 80−44704
surface props. in square barrier and linear one electron potential model 79−19645
surface region, absorption of EM radiation 78−43456
surface region, electrostatic energy and screened charge interaction for different Fermi surface shape 80−70631
surface roughness effect on light absorptivity 78−80314
surface scattering of conduction electrons and kinetic phenomena *(Russian)* 79−56210
surface with substitutional disorder, electronic struct. 78−23144
surfaces, exchange and correlation energy, wave vector anal. 80−20273
surfaces, Van der Waals forces computation 79−15204
temperature dependent multi-ion interactions in simple metals 78−22691
thermal resistivity, role of electron diffusion over Fermi surface 77−62894
thermodynamic properties, outer electron contributions *(French)* 78−43091
third order perturbation theory self consistency 78−76014
Thomas-Fermi-pseudopotential approach to static props. of simple metals 80−75514
tight-binding metals, electronic struct. and kinetic props. at high temp. 80−59848
transition, rare earth, and normal metals, electronic struct. and magnetism, review 80−70573
transition metal, 2nd and 3rd long period, covalence of atoms 78−47274
transition metal, 3d, electron struct. 79−69455
transition metal, 3d, electron-electron interaction, X-ray excited Auger spectra 78−91631
transition metal, 3d, paramag., energy band calcs. 78−91608
transition metal, 3d, superatomic relax. and positions of inner levels 78−11069
transition metal, 3d and 4d, local density theory, mech. and mag. props. evaluation 78−91630
transition metal, 4d, rel. to systematic struct. in K-edge photoabsorpt. spectra 78−43960
transition metal, band theory, rel. to bulk props. and cryst. struct. trend 78−34757
transition metal, d-metals, electron Fermi liquid oscillations *(Russian)* 79−90979
transition metal, de Haas van Alphen signal anal. by linearly recursive approx. 78−91603
transition metal, Einstein temp. and vibr. entropy, semiquantitative calc. 78−2221
transition metal, electronic sp. ht. calc. 79−73323
transition metal, energy band structure and X-ray emission spectra, calc. *(Russian)* 77−1763
transition metal, eqn. of state, s- and d-contribs. 78−91633
transition metal, extraatomic relaxation energies *(Russian)* 78−31295
transition metal, Fermi surface, stress depend., from quantum oscill. effects 78−91597
transition metal, fusion entropy, electronic contrib. 79−42217
transition metal, inner shell photoelectron and photoabsorpt. spectra 79−43091
transition metal, itinerant-localised electron model for magnetism 78−14918
transition metal, lattice dynamics and scatt. reson. 78−59872
transition metal, Lorenz number and high-temp. interband transitions 78−26844
transition metal, model potential, generalised APW formulation 78−91579
transition metal, nonmag., possibility of mag. monolayer formation 78−15009
transition metal, one-electron theory, atomic sphere approx. to KKR and LMTO methods 78−91584
transition metal, X-ray and ESCA spectra, effect of correl. interaction of electrons with core holes 78−92178
transition metal alloys, d-band hybridisation, electronegativities, structural stability 79−42007
transition metal alloys, disordered, density of states, elec. cond., extended Hubbard model 79−37948
transition metal alloys, disordered, generalised perturbation theory, appl. to self-consistent calc. of ordering energies 78−75975
transition metal alloys, heats of formation, tight binding theory, moments approach 79−61891
transition metal cluster, local densities of states and bonding props. 77−20401
transition metals, conf., Toronto, Canada (Aug. 1977) 78−91577
transition metals, correlation effects, perturb. treatment within Hubbard model 80−70582
transition metals, liq., muffin-tin pot. model, electronic density of states determ. 77−51645

metal theory continued
transition metals, OPW and MOPW calcs. 79−90942
transition metals, partial resonance, Hubbard's theory of phase shifts 79−28264
transition metals and alloys, group IV, electronic basis for ω-phase stability 79−91616
transition metals and alloys, metallurgical props. rel. to electronic struct., energies calc. method 77−20221
transition metals and their alloys, liq., electronic struct. and elec. resist. 77−51647
transition models, and free-electron like metals, alkali metal adsorpt., valence electronic struct., wave-function matching calcs. 78−72235
two-metal systems, plasmon dispersion 79−82656
ultrasonic wave propagation by open-orbit electrons at reson. condition 78−51877
unidimensional metals, plasmon freq., effect of nonuniform electron density profile *(Russian)* 80−59896
US attenuation, quantum oscills. with dislocations under pressure *(Russian)* 80−88273
vacancy electron density distrib. using Thomas-Fermi eqns. 77−15791
vacancy formation energies and volumes, exam. of models 78−47349
vacancy formation volume, self consistent electron theory 77−89426
vacancy properties, semilinear approach 77−89425
vacancy type point defects, calc. of migration energies in pure metals and dilute alloys 78−47572
vacancy-dislocation interaction, tight-binding calc. 80−92554
van der Waals energy estimation 78−91634
vector potential calc., semi-infinite electron gas approximation 77−32063
voids, spherical, X-ray excitation of surface plasmons 77−11974
rel. to volume photoemission 78−2978
wavevector-dependent spin susceptibility, variational principle 78−91586
work function, free electron contrib. 78−56208
work function, nonideal terraced surface, calc. 80−6950
work function depend. on plasmon energy, for periods IV, V and VI 78−18986
X_α method of theory of multiple scattering, appl. to props. of metal clusters *(Russian)* 78−38996
x-ray edge singularities of relaxed-out bound states and relaxed-in band states 78−92173
X-ray emission spectra of light metals, renormalisation theory 78−52595
X-ray line shapes for core levels, phonon broadening 77−12464
X-ray spectra, finite lifetime of deep hole 77−85845
X-ray spectra, independent-electron metal calc. 79−83056
XPS lineshape asymmetries, free-electron-like metals 78−14681
Ag, empirical parametrisation of electronic structure 78−91585
Ag, mag. susceptibility, Animalu model pot. calc. 80−75711
Ag, resonant model potential, energy depend. 78−18952
Al, atomic structure factor calc. from band struct. eigenfunctions 78−6030
Al, dynamic susceptibility, model pot. theory 80−75710
Al, electron energy loss spectra 78−34560
Al, heat of soln. of H, electron charge distrib. calc. 78−51689
Al, liquid, electron momentum density, correlations and ionic potentials 78−60052
Al, liquid, momentum density of electron 78−6309
Al, struct. stability 77−8015
Au, lattice vibr., electron press., central pair pot. model calc. 78−75749
Au, mag. susceptibility, Animalu model pot. calc. 80−75711
Au, resonant model potential, energy depend. 78−18952
Au, self-consistent relativistic band struct. 80−75501
Au, thermal radiative props. at cryogenic temps., comparison with model predictions 77−15604
β′-Au-Mg, de Haas-van Alphen effect, relativistic LMTO bandstructure, Fermi surface 79−37959
Be, longitudinal dielec. function calc. 77−1358
Be, spin susceptibility, electronic effective mass, spin density functional calcs. 78−43291
Ca, FCC, ground-state props. 78−75989
Cd, inversion of cyclotron resonance data 78−91593
Cd, nonlinear cyclotron absorption of hole doppleron *(Russian)* 78−10779
β-Ce, electronic energy band calcs. by KKR method 79−95317
Cs, elec. and thermal resist. calc. using modified noncentral force model 79−91016
Cu atom in bulk, local density of states 79−37947
Cu, dynamic susceptibility, model pot. theory 80−75710
Cu, empirical parametrisation of electronic structure 78−91585
Cu film, electronic struct., self-consistent calc. 77−76959
Cu, Krasko-Gurskii model potential, test of validity 80−39485
Cu, mag. susceptibility, Animalu model pot. calc. 80−75711
Cu, resonant model potential, energy depend. 78−18952
α-Fe, BCC metals, stressed, computer simulation of vacancy and divacancy migration 78−47573
Fe, mag. breakdown and Hall resist., theory and model calcs. 80−75552
$Fe_{1-x}P_x$ dilute alloys, electronic struct., mag., elec. and struct. props. 79−37971
Ga, liquid, effective pair potential and entropy *(French)* 78−14267
Ga-M, liq. alloys, mag. susceptibility *(Russian)* 77−24671
Gd, self consistent relativistic ferromag. band struct. 78−91609
H storage, electronic struct., many electron theory 80−49667
H-impurity, energy and electron density of states 80−34398
Hg, expanded liq., electronic props. 77−55477
K, binding energy and equilib. struct., pseudopot. calc. *(Russian)* 79−47037
La, FCC, ground-state props. 78−75989
Li, binding energy and atomic radius calc., effect of nonlocalised charact. of pseudopot. *(Russian)* 78−18575
Li, binding energy and equilib. struct., pseudopot. calc. *(Russian)* 79−47037
Li, elec. and thermal resist. calc. using modified noncentral force model 79−91016
Li, impurity and conduction electron scatt. at 4.2K *(Russian)* 77−35931
Li, local orbital energy bands using Kohn-Sham and near Hartree-Fock exchange 78−30866
Li, potentials and wave functions of electrons *(Russian)* 78−47688
Li, struct. stability 77−8015
Lu, band structure, influence of relativistic effects 78−75991
Mg, heat of soln. of H, electron charge distrib. calc. 78−51689
Mg, spin susceptibility, electronic effective mass, spin density functional calcs. 78−43291

metal theory continued
$MgZn_2$, struct. exam. using Shaw's model potential calc. 77−19906
Mo, localised electronic states near dislocations 79−33257
Na, BCC, doubly occupied Wannier functions, constructive definition 80−75492
Na, binding energy and equilib. struct., pseudopot. calc. *(Russian)* 79−47037
Na, conduction electron spin props. 77−8036
Na, equilibrium struct. and phys. props., pseudopot. method 80−96778
Na, Fermi surface distortions, model pot. 80−80157
Na, liquid, entropy calc. using phonon theory of liquids 80−39310
Na, potentials and wave functions of electrons *(Russian)* 78−47688
Na(1s), X-ray photoelectron spectrum, binding energy, at. compared with metal 78−70800
Nb, band effective mass, Animalu TMMP theory 80−29312
$Nb_3Ge(Al)$, anomalous resistivity, insight from band theory 78−60106
Ni, de Haas van Alphen signal anal. by linearly recursive approx. 78−91603
Ni, dielectric matrix, analytic model 80−75512
Ni, metallic particles, stability and electronic struct. *(French)* 80−80155
Pb, ab initio band struct. calcs. 80−75502
Pd (111), electronic states calc. and adsorbate-induced photoemission struct. interpretation 78−60179
Pd, Kohn anomalies and phonon dispersion, model including exchange-correl. corrections 78−59886
Pd, liq., energy bands and electronic density of states, resistivity 78−34755
Rb, quasiparticle dynamics, density-functional approx. 79−60682
Sc, Kohn anomalies and phonon dispersion, model including exchange-correl. corrections 78−59886
Sc, mag. susceptibility, temp. depend., theoretical explanation 78−47944
Sm metal, XPS evidence for weak surface divalent component 77−39808
Tc, superconductivity and Fermi surface calcs. 80−70873
Th, FCC, ground-state props. 78−75989
Th, local model pseudopotential applic. to lattice dynamics 77−39646
Tl, relativistic Green's function theory 79−82512
V, band effective mass, Animalu TMMP theory 80−29312
V, dynamic susceptibility, model pot. theory 80−75710
V, energy bands, calcs. using LCGO method 78−91608
V, Kohn anomalies and phonon dispersion, model including exchange-correl. corrections 78−59886
W, de Haas van Alphen signal anal. by linearly recursive approx. 78−91603
W, Fermi velocity calc. 79−4504

metal vapour lamps
see also mercury vapour lamps
alkali metal vapour arc lamp, source for Nd^{3+}:YAG laser pumping 80−78924
far UV source, 1150-3100 Å, for spectrometer calibration 77−41696
film lighting appl. luminance fluctuations assessment 80−4796
halide, filler composition, physico-chemical studies *(Russian)* 80−48373
halide lamps, photometric charact. 79−9236
halogen metal vapour lamp, additive partial pressure determ. from self-reversed spectral line maxima 78−67476
heavily doped semiconductors as transparent heat reflectors *(German)* 78−79197
laser wavelength and bandwidth calibration using optogalvanic effect 78−5514
Cd, discharge lamp, electrodeless, microwave excited, SIMPLEX optimisation 78−83061
Cs vapour, nearly saturated, prebreakdown elec. cond. 80−48841
$MgO-NH_4F-GeO_2$:Mn phosphor, luminance. spectra due to UV irrad., 26-294°C 79−83005
Na, high-press. discharge lamp, theory and plasma diagnostics appl. 78−9829
Na lamp, high-press. advantages of use in interferometry 77−9837
Na, low press. depleted discharge, recomb. struct. 79−94837
Na vapour lamp reflector design *(Spanish)* 79−23042
Na-Ne-Ar AC discharge, positive column 77−39487
Rb spherical electrodeless lamp, spectral profile of D_1 line 77−50744
W halogen, as luminance standard *(German)* 79−89980

metallic epitaxial layers
growth on muscovite and fluophlogopite substrates, orientation rels. *(Russian)* 77−31910
interface modification during interdiffusion 78−71890
ionised-cluster beam deposition and epitaxy, for electronic device fabrication 78−11133
ionised-cluster beam epitaxy, film characts. 79−28230
islands, small, one-dimens. model of mobility, parabolic substrate pot. 79−95299
large misfit systems, epitaxy and misfit dislocations 80−24767
metal-InP contacts, metal beam epitaxy, struct. and elec. props. of films on ion bombarded InP 79−28922
nucleation, high resolution dark field electron microscopy 77−85111
TEM, high resolution topographical imaging method for small particles 77−43439
TEM obs. appls. *(Spanish)* 77−47308
VPE on sapphire, highly oriented film prod. 77−66097
Ag (100) and (111) epitaxial films, ang. depend. UPS 80−55270
Ag (111), epitaxially grown on mica, surface defect struct., LEED study 80−80038
Ag, adsorbed on Si (111), electronic and cryst. struct., Schottky barrier form. obs. 78−84091
Ag contacts on InP, TEM obs. of struct. 77−62765
Ag, cryst. orientation effect on EELS 78−80442
Ag, electron channeling pattern, large angle, generation and appl. 80−100296
Ag epitaxial films, grain boundary struct. evolution during recrystn., interface energy effect *(Russian)* 80−15387
Ag, epitaxial growth and reaction with SnTe substrates 78−14640
Ag, epitaxial growth on InP (001) by at. beam deposition in ultrahigh vac. 77−59691
Ag, epitaxial growth on Pd, AES and LEED obs. of growth modes and substrate influences *(French)* 80−84408
Ag, epitaxially grown, on (001) Fe substrate, interface struct. 77−55470
Ag film, elongated epitaxial (111) island growth on Cu(001), interface misfit, dislocations 79−82493
Ag film, epitaxial growth, effect of electron bombard. of NaCl substrate, TEM and AES obs. 79−90916

metallic epitaxial layers continued
Ag film, epitaxial growth on isolated Au patches covered with amorphous C layer 80−40270
Ag film, MBE deposited on InP(001), struct. using TEM and RHEED 79−82492
Ag film on Mo, epitaxial growth, exam. of S impurity segregation at interface 78−84076
Ag, form. simultaneously on (111) and (100) NaCl 77−11826
Ag, growth on electron bombard. NaCl(111) surfaces, RHEED and AES 80−15419
Ag, island film on Ni foil substrate, elec. props. 77−43745
Ag monolayer on (111)Si surface, Schottky barrier, interface electronic nature and epitaxy 79−77934
Ag, on mica, microstruct. changes 78−72013
Ag on W (001), geom. factors of FCC-BCC epitaxy 78−60041
Ag, oriented crystallisation on active amorphous C centres 79−7762
Ag, thin-film bicrystals, planar lattice defects and migrating grain boundaries interaction 80−79835
Ag, twin boundaries of recrystn. type, electron microscope obs. *(Russian)* 79−4484
Ag, twin form., LEED detection 80−88442
Ag, VPE on W (110), alignment of (111)FCC-(110)BCC epitaxial metal pairs 79−19488
Ag, vac. deposition of oriented coating on doped alkali halide substrate 80−2303
Ag, vacuum deposited on NaCl, microstructure and orientation, surface condition influence 79−82486
Ag-Au film system grain-boundary diffusion at low temp., meas. by surface accumulation method 79−77839
Ag-Dy, dil., thin films, ESR spectra, stress effects 80−39866
Al epitaxial films, grain boundary struct. evolution during recrystn., interface energy effect *(Russian)* 80−15387
Al, epitaxial growth on GaAs (001) 80−24757
Al epitaxial layers, elec. props. 79−42671
Al film, MBE and field emission deposition on III-V semiconductors, comparative study 79−87016
Al, film, single cryst., defects, residual gas effects, TEM obs. 77−39587
Al, resist. vs. grain diameter curves, theory and expt. 77−76961
Al-Cu, vacuum deposited on NaCl(001), orientation obs. *(French)* 79−95294
Al-GaAs interface, struct. study by X-ray total-external-refl.-Bragg diffr. 80−34321
Al-GaAs Schottky barrier diode, prep. by MBE on GaAs, and characts. 78−72257
Au bicrystalline film, lattice imaging of low angle tilt boundaries by TEM 78−79620
Au, contrast from epitaxially sandwiched macromolecules in TEM 80−85565
Au, electron channeling pattern, large angle, generation and appl. 80−100296
Au, epitaxial films, grain boundary struct. evolution during recrystn., interface energy effect *(Russian)* 80−15387
Au, epitaxial growth in NaCl with continuous C-intermediate film, electron microscope obs. 78−84102
Au epitaxial single-crystal film occluded DNA molecule electron-microscopic contrast 79−57568
Au, epitaxially grown bicrystal on (001) Fe substrate, interfacial dislocation behaviour 77−51622
Au film, epitaxial growth, whisker form. 77−76713
Au film, epitaxial growth, effect of electron bombard. of NaCl substrate, TEM and AES obs. 79−90916
Au film, MBE and field emission deposition on III-V semiconductors, comparative study 79−87016
Au film, on NaCl, preferential epitaxy induced by electron bombard. or elec. field 80−10824
Au, film, on sapphire substrate, nucleation, growth and postdeposition thermally induced epitaxy 79−77946
Au, grain boundaries, electron microscope obs. 79−11025
Au, growth and nucleation on NaCl during ion bombardment 79−11024
Au, growth on Ag(111) surface, LEED meas. 78−14632
Au, growth on clean and contaminated GaAs (001) surfaces 78−26785
Au, high resolution TEM topographical images 77−43439
Au island epitaxial films, on (111) surface of fluorite, discrimination of twin orientation 79−46983
Au, on corundum, with intermediate Cu and Cr layers, struct. obs. 77−28084
Au, on NaCl substrate, electrotransport inferred from void growth rate *(German)* 80−10699
Au, on Si, specific high-angle boundaries *(Russian)* 77−76678
Au, on vacuum deposited Fe, interfacial dislocations 78−30847
Au on W (001), geom. factors of FCC-BCC epitaxy 78−60041
Au on W (110), LEED and AES 77−69198
Au, sandwiching of biopolymers, electron microscopy specimen prep. 78−36080
Au, struct., LEED, AES, resist. and X-ray diffr. analysis 77−59223
Au, twinned crystals, epitaxial growth on KCl crystals, electron microscopic study of microstructure 78−91566
Au, VPE on W (110), alignment of (111)FCC-(110)BCC epitaxial metal pairs 79−19488
Au vacuum deposited layer on KI, nucleation and growth 79−61516
Au, vacuum evaporated particle coalescence behaviour on doped alkali halides 79−77961
Au, Volmer-Weber mode of epitaxy, deposition on KCl and MgO, post-nucleation phenomena 79−77955
Au/Cu, bilayers, interdiffusion phenomena, lattice dislocations, TEM obs. 80−59736
Au/Cu, initial epitaxial growth at room temp. 80−59829
Au-Pd alloy, on rock salt, epitaxial growth and struct. 77−20211
Au-Pt epitaxial film system, mismatch dislocations obs., electron microscopy 77−4268
Au_3Cd, sputtered epitaxial films, order-disorder reaction obs. 78−84092
AuMn alloy, ordered, vacuum deposited epitaxial films, orientation control by external stress 80−100426
$AuPb_2$, formation during Pb absorpt. on Au, LEED, AES study of $Au/AuPb_2$ interface 78−71988
Co vacuum deposited coatings on metal substrates, cryst. struct. and stability 80−75481
Co-Fe films, singularities of $\gamma \rightarrow \alpha$ transform., X-ray diffr. obs. *(Russian)* 79−52198
Co_3Pd epitaxial films, multiray dynamic theory of diffr. contrast to explain defects nature 79−64962

metallic epitaxial layers continued
Cr film, on NaCl, preferential epitaxy induced by electron bombard. or elec. field 80−10824
Cr film, on sapphire, epitaxial relations 79−60649
CrPt film, on sapphire, epitaxial relations 79−60649
Cu, bicrystalline, characterisation of [001] tilt boundaries 80−75473
Cu, epitaxial electrocrystallisation, substrate imperfections effect 78−18921
Cu film, on (001) Ag, FCC and BCC metal-on-metal epitaxy, geometric factors, electron microscopy 78−22980
Cu film, on W substrate, cementation, vac. deposition, and electroplating, growth characts. 79−95291
Cu film on Mo, epitaxial growth, exam. of S impurity segregation at interface 78−84076
Cu films on Ru (0001), growth, struct. and electronic props. 79−77958
Cu, on (111) Au, periodic arrays of misfit dislocations, electron diffr. 78−51857
Cu on Fe (001) substrate, orientation relationship 80−65415
Cu on W (001), geom. factors of FCC-BCC epitaxy 78−60041
Cu single crystal film, electrodeposited, fatigue cracks *(Japanese)* 78−84975
Cu, twin form., LEED detection 80−88442
Cu, VPE on W (110), alignment of (111)FCC-(110)BCC epitaxial metal pairs 79−19488
Cu/Ni double layer evaporated film, misfit dislocation effect on strength *(Japanese)* 79−42425
Cu-Ni bicrystal, misfit dislocation config., moire patterns, interdiffusion effects 78−84110
Cu-Ni bicrystals, epitaxial growth, chemical interdiffusion, X-ray diffr. line profile anal. 79−1527
Cu-Ni bimetallic film, Moire patterns, interdiffusion effects 77−51621
Cu-Ni bimetallic films, dislocation wall form. during interdiffusion, TEM obs. 78−51856
CuAu alloy, ordered, vacuum deposited epitaxial films, orientation control by external stress 80−100426
Fe, epitaxial film on Sb, ultrahigh vac. deposition 78−56572
Fe epitaxial growth on Au single crystals, substrate temp. effect on morphology 78−26798
Fe epitaxial layer on Au(111), misfit dislocation obs. 79−73415
Fe film, on NaCl, preferential epitaxy induced by electron bombard. or elec. field 80−10824
Fe, on Au, growth processes, ultra high vac. in situ electron microscopy 78−30842
Fe, VPE on W tip, depositing direction depend. 80−10812
Fe-Au (111) bicrystal films, misfit dislocations obs., for 500°C substrate temp. 77−51624
Fe-Au bimetal epitaxial films, examination of interaction at temps. ≥600°C 80−75482
Fe-Au interface, two types of dislocation dependent on deposit thickness *(French)* 77−85109
Gd films, electrical props. correlation with microstructure 80−97009
Gd, vacuum deposited and VPE, deposition parameters effects on struct. 79−90912
Hf, oxidation, microstructural study *(French)* 80−45436
In, epitaxial layer on imperfect FEM/FIM W emitter 78−60037
In, growth and desorption on W tips, high field microscopy 79−69380
Ir, epitaxial growth on (001)W and (001)Mo 79−99450
Mo, on sapphire, struct. rel. to prod. by electron beam deposition in vacuum *(Russian)* 77−59228
Mo, vacuum deposition on fluorophlogopite at 650 to 1050°C, orientation rels. *(Russian)* 77−48342
Nb, film, epitaxy, struct. and supercond. props., on (001) surface of fluorophlogopite *(Russian)* 80−80101
Nb heteroepitaxial layers on sapphire, residual mechanical stress and strain influence on superconductivity 80−15644
Nb on sapphire, highly oriented film prod. 77−66097
Nb_3Al film, electron-beam coevaporated, prep. and characts. 80−76187
Ni electrodeposition, surface-stress phenomena at start 80−35542
Ni epitaxial monocrystal structure rel. to externally applied stress 77−76708
Ni film, epitaxial growth on (001) diamond, TEM exam. 77−66098
Ni film, on (001) Ag, FCC and BCC metal-on-metal epitaxy, geometric factors, electron microscopy 78−22980
Ni island film, cond. of two-layer metal systems *(Russian)* 79−51693
Ni, on diamond 77−72758
Ni on Fe (001) substrate, orientation relationship 80−65415
Ni, on NaCl, struct. and purity 78−72047
Ni on W (001), geom. factors of FCC-BCC epitaxy 78−60041
Ni solar collector coating, microstruct., FIM and SEM obs. 80−26166
Ni, VPE on W (110), alignment of (111)FCC-(110)BCC epitaxial metal pairs 79−19488
Ni-Cu diffusion couple surface, epitaxial, chemisorption of CO and AES 77−31891
$NiSi_2$, epitaxial film on Si, ^4He ion channelling meas. and RHEED anal. 80−10834
Pb film, monocryst., heteroepitaxial growth, struct. defects, and elec. props. *(Russian)* 80−84403
Pb, underpotential adsorption, cathodic deposition, on Ag(111) and (100) *(German)* 80−108363
Pd, epitaxial growth on (001)W and (001)Mo 79−99450
Pd, on (111) Au, periodic arrays of misfit dislocations, electron diffr. 78−51857
Pd, on Au, misfit dislocation nucleation and growth 77−1338
Pd particles formed by evaporation on alkali halide crystals, orientation and struct. 78−84108
Pd, VPE growth on Au(111), interface struct. 79−95297
Pd-Ag (Cu) alloys, epitaxial growth and surface characterisation 78−14638
Pd_2Si, epitaxial film on Si, ^4He ion channelling meas. and RHEED anal. 80−10834
Pd_2Si films on Si, lattice imaging obs. of structural details 80−103604
Pt, epitaxial growth on (001)W and (001)Mo 79−99450
Pt film, on sapphire epitaxial relations 79−60649
Pt, on Au, crit. thickness of pseudomorphic film growth, substrate size depend. *(Russian)* 80−29286
Pt-Rh alloy, on rock salt, epitaxial growth and struct. 77−20211
PtSi, epitaxial film, cryst. perfection and thermal stability, channelling and backscatt. meas. 79−99255
PtSi, epitaxial film on Si, ^4He ion channelling meas. and RHEED anal. 80−10834
Rh, epitaxial growth on (001)W and (001)Mo 79−99450

metallic epitaxial layers continued
Rh, film, annealing effect on struct., TEM, electron diffr. study 78−76682
Sn film, on NaCl, preferential epitaxy induced by electron bombard. or elec. field 80−10824
Sn film epitaxially grown on KCl substrate 79−99441
Ta epitaxial layers, formation conditions influence on struct. *(Russian)* 80−20045
Te film, microstructure 80−103598
Tl, underpotential adsorption, cathodic deposition, on Ag(111) and (100) *(German)* 80−108363
V epitaxial films on sapphire by electron beam evaporation *(Russian)* 77−76701
W, CVD growth, inelastic light scatt. as in situ probe of chem. reaction 77−40383
W/α-Al_2O_3, heteroepitaxial structs., refined formulation of relative orientation criterias 80−44448
W/α-Al_2O_3 heteroepitaxy, orientation relationships, X-ray diffr. study 79−60661
W-Os system films, condensation temp., conc., and phase comp. effect on struct. and props. *(Russian)* 80−24749
Zn film deposition on Al, TEM and electron diffr. obs. 80−75460

metallic glasses
aged, atomic clustering exam. using positron annihilation methods 77−84655
aligned composites, in-situ growth by disproportionation of amorphous metal systems 78−72755
amorphism, rapid quenching, techniques for determ. very short room temp. lifetimes 80−84981
amorphous, ribbon samples, Young's modulus, using impulse induced resonance method 80−30008
amorphous alloys, thermal stability, crystn., DSC and elec. resist. study 80−107060
amorphous magnetic alloys, characts. and appls. *(French)* 80−39815
amorphous magnetic materials, props. *(Japanese)* 79−28561
amorphous magnetic materials, review 79−82839
amorphous magnetism, review 79−82818
amorphous Newtonian-quenched ribbons, formed by melt spinning and melt extraction, dimens. variations 79−56943
amorphous ribbon, fluid-flow-temp. model for casting by melt extraction 79−56942
analog, plastic flow in disordered bubble raft 79−91745
annealing, struct. relax. and crossover effect 79−86715
annealing behaviour, thermal stability and crystn. 80−75167
applications of glasses, review 78−3306
atomic position correlations, nearly free electron approx. 77−39529
atomic structure, mech. and mag. props., prod. methods, uses 77−1081
atomic transport behaviour, review *(Japanese)* 79−94907
bonding of glass and metal, review of physical properties *(German)* 79−83167
Bragg bubble glass, struct. and plastic flow 80−84091
Brillouin-Mandelstam scattering from thermal and excited magnons 80−70980
bulk and surface properties, review 80−44147
Cl $(Co_{100-x}Fe_x)_{83}B_{17}$, $1 \leq x \leq 30$, annealing embrittlement and crystn. 80−45329
Co-base metallic glasses, elastic const. 77−66671
conduction electron and tunnelling level interaction 79−60817
conduction electrons interacting with tunnelling states 79−15137
continuous cooling versus isothermal transformation diagrams, critical cooling rate 80−15012
continuous-biased sputter-deposited, Kr entrapment 80−24603
corrosion behaviour, metalloid elements influence 80−89421
corrosion characteristics, book contrib. 79−66225
crystallisation, appl. of Grange-Kiefer transform. method *(Hungarian)* 79−73105
crystallisation, thermosonimetric investigation 80−75180
crystallisation temperature, continuous-heating transform. diagram from isothermal time-temp. diagram 77−47558
deformation processes 77−4813
density and Young's modulus, struct. relax. effects 78−72804
development and magnetic props. *(German)* 79−51813
ductile-brittle transition of Fe, Co and Ni based metallic glasses 77−4847
education, metallic glasses, phase transition and mech., elec. and mag. props. 78−36765
electrical and thermal properties 78−72131
electrical conductivity, phenomenological theory 78−60102
electrical resistance min. at low temp., mixed conduction model 80−44560
electrical resistivity, anomaly in temp. depend., modified relax. time approx. 79−65424
electrical resistivity, press. depend. 80−96841
electrical resistivity, temp. depend. 78−14702
electrical resistivity calc. 78−60103
electrical transport 79−38040
electron physics of vitreous materials *(French)* 79−33225
electron transport theory, diffr. model applic. 80−80245
electronic lifetime, noncommutative two-level model 80−103663
electronic spectrum 77−51646
electronic structure, neutron scatt., elec. resist., Hall coeff., mag. susceptibility and XPS 78−23013
electronic structure rel. to elec. cond., supercond. and mag. props. 80−65429
electronic transport properties, review 79−4546
eutectic alloy prod. using low temp. melt spinning device 80−100825
$Fe_{40}Ni_{40}P_{14}B_{20}$, Metglas 2826, amorphous ferromag., resistivity down to 60 mK 79−60783
$Fe_{40}Ni_{40}P_{14}B_6$, amorphous, tape wound core, fluctuations of driving field 78−10726
Fermi level calc. 79−33217
ferromagnetic, hyperfine field and spin wave excitations, $T^{3/2}$ depend. 78−10672
ferromagnetic, quenched from melt, appl. as soft mag. materials *(German)* 78−10676
ferromagnetic, sputter-deposited, soft mag. props., magnetostriction 80−34696
ferromagnetic alloys, amorphous, domain struct. and mag. microstruct., review 80−15751
ferromagnetic alloys, form. and stability 77−16515

metallic glasses continued
ferromagnetic amorphous alloys, thermal expansion anomaly near Curie temp. *(Japanese)* 77−85542
ferromagnetic amorphous system, directional order and induced anisotropy energy, theory 78−95431
ferromagnetic metglas, elec. resist., temp. depend. 77−15815
ferromagnetic ribbon, HF mag. characts., magnetostriction role 77−66408
ferromagnetic thin films, fabrication by sputtering, and mag. props. 78−91881
ferromagnets, book contrib. 80−75743
ferromagnets, itinerant electron model 79−73664
ferromagnets, resist. and magnetoresist 77−66148
ferromagnets, structural instabilities and mag. permeability relax., 77 to 400K 80−80559
film, SAW device appls. 80−28389
flow behaviour, entropy model 77−24345
formation, generalised kinetic treatment 77−52315
formation, model based on nearly-free-electron approx. 77−52316
formation, stabilities, and props. 80−64912
formation, structure and thermal stability, review *(German)* 78−83747
formation and rapid quenching techniques 80−76214
formation kinetics, review 77−66606
formation prediction with bond parametric diagram *(Chinese)* 80−11587
friction coeff. determ. using sliding friction rig 80−89355
glass forming region of metal-metalloid systems predicted by Polk model 79−19158
glass transition, free vol. theories, and special case of metallic glasses 78−14284
glass transition temperature 79−99081
hardness, elastic moduli, density, cryst. temp., mech. props., for flywheel appl. *(Dutch)* 78−52878
heat of crystn. and viscous behaviour 80−75166
homogeneous and isotropic hard sphere model 78−83731
internal friction and relaxation in vitreous solids *(French)* 77−72651
ion implantation production 79−14686
load relaxation studies 78−48441
local structure exam. by EXAFS 80−108301
low temperature US props., supercond. state effects 79−87192
magnetic, indirect exchange interaction and paramag. Curie temp. 80−75752
magnetic, soft-magnetic properties *(German)* 80−71108
magnetic amorphous alloys, atomic struct., energy dispersive X-ray diffr. meas. 79−73100
magnetic and nonmag. amorphous alloys, thermoelec. power, 15 to 580K 80−80255
magnetic materials, prep. and appraisal *(Japanese)* 77−36420
magnetic properties, development trends *(Slovak)* 79−4694
magnetic properties, struct., and prep., book contrib. 79−65665
magnetic properties 77−16054
magnetic properties anal. *(German)* 77−89977
magnetic properties and appls. 78−95475
magnetic properties and appls. 79−8016
magnetoelastic effects, review 78−68352
magnetostrictive film, overlay for variable SAW delay line 78−63240
magnetostrictive metallic-glass ribbon, stress dependences of longitudinal wave velocity 80−75825
manufacture, struct. and stability *(Norwegian)* 79−14687
material testing by dynamic mechanical analysis appl. to materials testing 79−15911
mechanical characts., review *(Japanese)* 77−86109
metal metal system, glass formation 80−64921
metal-metalloid amorphous alloys produced by ion implantation, TEM 80−15128
metal-metalloid amorphous systems, thermal instability, crystn. characts. 77−4044
metallic glass, phonon transport below 100K 78−14422
metallic glasses, structure and formation, thermodynamic props., cluster relaxation approx. 80−54143
metastable, determination and representation of phase diagram features 79−11568
metastable phase formation, bond formation 77−1237
METGLAS™2826, load relaxation studies 78−48441
Metglas 2605, and 2605 A, transport props., resist. and magnetoresist. 79−1590
Metglas 2605 ribbon, saturation magnetostriction meas. by small-angle magnetisation rot. 80−60391
Metglas 2826 ribbon, saturation magnetostriction meas. by small-angle magnetisation rot. 80−60391
Metglas 2826 ribbon, voids formation during crystallisation 80−108428
Metglas 2826 ribbons, ferromagnetic resonance and SEM obs. 80−15804
Metglas 2826-A, anomalous magnetisation, critical effects, superparamagnetism 77−8328
Metglas 2826A, direct meas. of decomp. on crystn. by X-ray microanal. in STEM 79−48025
Metglas 2826A, Invar related system, high press. Mossbauer spectra 79−56642
metglas type system, structural and amorphous props. 78−84323
$Mg_{70}Zn_{30}$, amorphous alloy 77−27835
micromagnetic calculations and props. 80−80501
Mossbauer spectra, hyperfine field distrib. determ. 80−39965
Mossbauer studies 80−39917
moulding process 78−80536
packing models and structural specificity 79−37629
physical principles, manufacture, mech. and mag. props. *(French)* 78−83744
physics review *(German)* 79−41962
plastic deformation, theory below transition temp. of metallic glasses 79−29128
Polk model and struct. 78−42916
polymer model 80−6361
powder, filled polymers, mech. props *(Japanese)* 79−15742
preparation and phys. props. development 80−81003
production and properties, technological appl. 80−71105
properties and development review, scientific and industrial appl. 80−19710
rapidly quenched metals, conf., Brighton, England (July 1978) 80−67934
rare earth-iron alloy amorphous film, crystn., TEM obs. 79−87019

metallic glasses continued
rare earth-transition metal alloys, amorphous, electronic and mag. props. 80−93093
rare earth-transition metal alloys, amorphous, ferrimag., spin arrangements in large fields 80−75718
resistivity and magnetoresist. 79−69486
resistivity due to two-level systems 80−10941
review 77−4043
review 80−88051
review of prep., characterization, struct., formation, electronic, mag. and mechanical props. 78−3074
review of properties, current and potential applications 78−30539
ribbon form. by cylindrical jet on flat moving substrate, uniformity 78−52718
ribbons, manufacturing magnetic and physical props. 80−29898
ribbons, quenching stabiliser to improve geometrical uniformity and cross-section 80−55343
Sendust ribbon, mag. props. 80−15761
shear deformation, mechanism involving dislocation glide 78−15462
soft magnetic properties 79−73774
spin glass, spin wave theory 79−11306
spin waves in amorphous ferromagnets, asperomagnets and spin-glasses 80−75747
splat cooled, mag. props. 80−80491
splat cooling prep., new, transition-metal free *(German)* 79−28989
splat quenched metal, electron transparent area prod. 77−4754
splat quenched metal, electron transparent prod., comment 77−4755
splat-quenched, grain size, isothermal transform. 77−77463
sputtering deposition of bulk samples, magnetic props. *(Japanese)* 79−95971
stability, hole theory of liquids appl. 80−100174
stability, microscopic calcs. 79−32914
stability 80−75184
steady state inhomogeneous flow, microscopic mechanism 77−48476
steel, alloy, high C, amorphous, produced by rapid quenching from melt, hardness and strength 78−59764
steel, C-Cr(MO)(W), high-C, amorphous crystn. behaviour *(Japanese)* 79−94911
steel, C-Cr-Mo(Cr-W)(Mo-W)(Cr-Mo-W), high C, amorphous crystallisation behaviour *(Japanese)* 79−94911
steel, stainless, alloyed with C, magnetron-sputtered, microstruct., and cryst.-amorphous transition 80−19719
steel, stainless, amorphous film, sputtered, prep. and characterisation 78−43266
steel, W, high C, amorphous, rapidly quenched from melt, mech. and thermal props. 79−38874
strength and stiffness 77−8899
structural characteristics, preparation techniques, potential appls. *(Croatian)* 79−10800
structural imperfections, review of expt. evidence 79−37630
structural relax., compositional SRO 78−79538
structure, atomic-scale, direct methods for determ. 79−37623
structure, one- and two-component hard sphere models, integral eqn. approach 77−76312
structure, review of current exptl. data 80−88058
structure, stability, phys. charact., prod. principles *(Hungarian)* 77−84656
structure, stability and prod., elec., mag. and mech. props., review 80−44134
structure, transport props., magnetic behaviour, review 80−70138
structure and crystallisation, review 78−2008
structure and low temp. props. 79−37631
structure and properties, review 78−47245
structure change and kinetics during low temp. annealing, geometrical relax. model *(Japanese)* 79−94908
structure direct obs. by bright field TEM 80−10502
structure model, structural changes 80−92462
structure modelling 77−31596
structure of simple inorganic amorphous solids, review 80−15004
structures based on disclination-dislocation model 79−82159
superconducting metastable alloys, review of current work 80−81002
superconducting transition temps. of liq.-quenched amorphous alloys 79−38234
surface oxide film removal using US oscill. energy *(Russian)* 78−72935
Taylor wire prod. by rapid quenching 78−44045
thermal stability, validity of energy and entropy interfacial tension models 78−91255
transition metal, binary alloy with metalloids, glass forming ability 79−86714
transition metal alloyed with metalloids, glass transition temp. 80−24371
transition metal alloys, amorphous, mag. props., chem. short-range order 80−75739
transition metal alloys, amorphous, mag. props., structure and preparation 80−75737
transition metal based amorphous alloys, elec. resist., 20 mK to 300K 79−73483
transition metal based amorphous mag. alloys, elec. field gradient 78−39475
transition metal glasses and amorphous films, supercond. and electronic props. 79−73612
transition metal metalloid glasses, computer simulation of atomic struct. 77−31598
transition metal-boron alloy amorphous film, crystn., TEM obs. 79−87019
transition metal-metalloid, short-range order, hyperfine field distrib. determ. by Mossbauer spectroscopy 80−39962
transition metal-metalloid, struct. simulation 78−38624
3d-transition metal-metalloid cryst. and glassy alloys, electronic struct. from magnetisation and Mossbauer meas. 80−29363
transition metal-metalloid glass, mag. props., charge transfer model 78−39324
transition metal-metalloid glasses, short range order of dense-random-packing models 80−64907
transition metal-metalloid glasses, struct., compositional effects *(Japanese)* 80−84086
transition metal-metalloid glasses, struct., elec., supercond., and mech. props. 80−6365
transition metal-metalloid glasses, struct. end plastic flow, review 80−84090
transition metal-metalloid glasses, struct. model 79−64997
transition metal-metalloid glasses, structural model 79−14690
metallic glasses continued
transition metal-metalloid metallic glasses, deformed, mag. props., mag. screening 79−15287
transition metal-nonmetal glasses, with defined local coordination, struct. model 80−84092
transition metal-Si-B ternary and quaternary amorphous alloys, effect of comp. on crystn. *(Japanese)* 79−94910
transport properties, applicability of liq. metal theory 79−56179
transport properties and thermopower of amorphous alloys 80−34411
tunnelling states, struct. model 80−70137
tunnelling two-level system, Kondo-like state 80−88547
vapour quenching techniques, high-rate, use in amorphous phase prep. 80−80977
Wiedemann-Franz law in semiconductor and metal glasses 79−65422
Young's modulus meas. by impulse induced resonance technique 80−40411
Young's modulus/thermal props. correlation 78−6961
Ag-Mn, dilute spin glass, AC susceptibility and ESR meas. 79−7968
Al-Cr, rapidly solidified, crystalline and amorphous structures 77−44274
Al-Cu, splat quenched, amorphous regions 77−4047
Al-Cu, splat quenched, amorphous regions, comment 77−4048
Al-Cu, splat quenching, electron transparent area prod. 77−4754
Al-Cu, superconducting amorphous films of high stability 80−70889
Al-$Fe_{78}Mo_2B_{20}$ wire composite, mech. props. 80−40441
$Al_{20}Cu_{25}Zr_{55}$ metallic glass, inelastic deform., free energy spectra 80−71699
Au-Ge-Si, influence of struct. on elec. resist. of glass forming alloys 80−65518
$Au_{0.77}Ge_{0.136}Si_{0.094}$, undercooled metallic melt, viscous behaviour 77−66037
$Au_{77}Ge_{13.5}Si_{9.4}$, heat of crystn. and viscous behaviour 80−75166
$Au_{35}Si_{65}$, vacuum-deposited and liquid-quenched films, diffusion and crystn. 80−84094
$Au_{81.4}Si_{18.6}$, glass forming alloy, Gibbs free energy change on crystallisation 80−25676
Au_xSi_{1-x} amorphous films, phys. studies 80−75476
B-transition metal thin films, amorphous to cryst. transformation 80−7563
Be-Nb-Zr alloys, glassy and partially crystalline, supercond. T_c and struct. props. 78−60239
Be-Zr alloy, quenched from melt, supercond. props. 78−26983
$Be_{40}Ti_{50}Zr_{10}$, metallic glass, thermoelectric power and resist. 78−95289
Bi-Pb amorphous alloys, superconductivity and the very strong electron-phonon interaction *(Japanese)* 79−95552
Ca containing alloy systems, prep., glass form., thermal props. 79−24461
$Ca_{0.65}M_{0.35}$, glass transition temp., comp. depend. 80−79702
Cd-Co(-Mo), amorphous films, thermal stability of mag. props. *(Japanese)* 79−47307
CdGeAsMn, glass, recrystallisation 80−44133
$Ce_{30}Au_{20}$, amorphous, cryst. field effects and mag. interactions, magnetisation and transport props. meas. 78−68191
$Ce_{80}Au_{20}$, mag. ordering and cryst. field effects, speromagnetism 80−80531
$(Co,Fe,M)_{78}Si_8B_{14}$ amorphous alloys (M=V,Nb,Ta,Cr,Mo,W,Mn or Ni), zero magnetostriction and low field mag. props. 80−34741
$(Co,Fe)_{0.75}B_{0.25}$ metallic glasses, annealed, equilib. crystalline phases 80−3019
$(Co,Fe)_{80}B_{20}$, induced anisotropy and time changes of permeability 80−75815
Co alloys, amorphous, effects of metalloids on mag. props. 80−75738
Co base amorphous alloys, alloying elements influence on corrosion behaviour, XPS obs. 80−89422
Co based amorphous alloy, mag. ordered, hyperfine field distribs., NMR meas. 78−68409
Co based amorphous alloys, struct. and thermomag. meas. 77−16055
Co based metallic glass, B and P glass former additions, elastic consts., flow behaviour correlations 78−44154
Co-B, amorphous alloys, phase diagram 79−96002
Co-B, X-ray obs. of struct. 79−1399
Co-B-Mo-Cr, amorphous, Mo and Cr addition effect on corrosion behaviour 80−16568
Co-B-Si, mag. props. different in amorphous and cryst. phases 77−69617
Co-B-Si amorphous alloy, liq. quenched, elec. resist. and cyclic deform. 80−59949
Co-B(-Cr) thin film glasses, mag. props. and corrosion resist. 80−80576
Co-based amorphous alloys, effect of alloying additions on corrosion resistance *(Japanese)* 79−96215
Co-Fe amorphous alloys, high permeability props. *(Japanese)* 77−51927
Co-Fe amorphous alloys, worked, perminvar type mag. hysteresis loop, longit. Kerr effect obs. 80−65958
Co-Fe-B, amorphous, crystn. and thermal stability 80−107057
Co-Fe-Ni-Si-B, soft mag. props. 79−73774
Co-Fe-Si-B, decomp. of amorphous state during annealing below recryst. temp. *(Russian)* 80−75164
Co-Fe-Si-B, ferromag., magneto-optical spectra in amorphous and cryst. states *(Russian)* 80−84749
Co-Gd film, amorphous, prep. conditions influence on supernetwork struct. 77−76709
Co-Mn-Ni-Fe-Si-B amorphous alloys, mag. props., low magnetostriction 80−75832
Co-Mo-B metallic glass ribbons, tensile strength, crystn. temp. 80−89173
Co-Ni-Fe-Si(B), amorphous ribbon, magnetostriction meas. 80−15778
Co-Ni-Mo-C, amorphous alloys, med. props. and thermal stability *(Japanese)* 80−85049
Co-P, amorphous, ferromag. antireson. 24 GHz microwave transmission, mag. props. 80−34778
Co-P, amorphous, sound propagation 77−62586
Co-P, crystn. kinetics by differential scanning calorimetry 78−91257
Co-P, domain struct., mag. anisotropy origin 80−80554
Co-P, metallic glass, phonon propagation at low temp. 78−87756
Co-P alloys, geometric struct. models and diffraction exam. techniques 80−79700
Co-Si-B, amorphous ribbon, saturation magnetostriction meas. by small-angle magnetisation rot. 80−60391
Co-Si-B, embrittlement by crystallisation *(Japanese)* 78−48513
Co-Si-B amorphous alloys with metalloid elements, embrittlement/crystn. relationship *(Japanese)* 79−96134
Co-Zr, amorphous phase form. in Zr-poor region, hardness and fracture strength *(Japanese)* 80−84914

metallic glasses continued
$Co_{1-x}B_x$, polycrystalline and amorphous sputtered films, Brillouin spectra 80−2775
$Co_{100-x}B_x$, amorphous, mag. struct., mag. susceptibility meas. 80−80485
$Co_{100-x}B_x$, amorphous alloys, saturation magnetostriction and annealing behaviour 80−34739
$Co_{100-x}B_x$ glassy alloys, mag. props. 79−73689
Co_3B, hyperfine field distrib., ^{59}Co spin echo spectra 80−80635
$Co_{80}B_{20}$, amorphous metal ribbon, stresses, magnetoelastic anisotropy and zero-field mag. domain struct. 80−44896
$Co_{35}Dy_{65}$, metallic glass, internal friction peaks 80−25753
$Co_{67}Er_{33}$ amorphous alloy, sputtered, local order and amorphous struct. 80−88061
$Co_{74}Fe_6B_{20}$, zero magnetostriction, magnetisation charact. 77−12158
$Co_{79}Fe_{6.5}B_{14.5}$ amorphous thin films, zero magnetostriction, high magnetisation 80−34708
$(CoFeB)_{100-x}Cr_x$ thin films, magnetic props. and corrosion resist. 80−34709
$(Co_{0.93}Fe_{0.07})_{75-x}Cr_xSi_{15}B_{10}$ amorphous alloy, thermal stability, Cr conc. effects, DTA expts. 80−59395
$(Co_{0.89}Fe_{0.11})_{72}Mo_3Si_{15}B_{10}$, metallic glass, strain- and field-induced mag. anisotropy 80−108004
$Co_{57}Fe_5Ni_{10}(Si,B)_{28}$, amorphous, soft mag. props., switched-mode power supply appls. 80−88850
$(Co_{1-x}Fe_xNi_y)_{80}(Si_{1-z}B_z)_{20}$, amorphous films, spin wave spectra 80−34777
$Co_{70}Fe_5Si_{15}B_{10}$, amorphous, crystn. and thermal stability 80−107057
$Co_{70.4}Fe_{4.6}Si_{15}B_{10}$, amorphous, mag. aftereffect spectra and annealing props. 80−88831
$Co_{75-x}Fe_xSi_{15}B_{10}$, quenched ferromag. ribbon, Brillouin spectra 80−2776
$Co_{73}Mo_2Si_{15}B_{10}$, metallic glass, strain- and field-induced mag. anisotropy 80−108004
$Co_{40}Ni_{40}B_{20}$, magnetostriction, temp. depend. 78−91921
$Co_{40}Ni_{40}B_{20}$, spontaneous Hall effect and resistivity 79−19576
$Co_{50}Ni_{20}Fe_6Si_{12}B_{12}$, amorphous, mag. props., effects mech. deform. 80−39840
CoP amorphous alloy, heat treatments influence on opt. props., struct. and DC resist. obs. 80−80892
CoP, elec. and optical props., annealing effects 79−38565
$Co_{0.9}P_{0.1}$ noncrystalline ferromagnet, electroless deposited, struct. and microscopic mag. props. 80−88063
$Co_{1-x}P_x$ amorphous alloy film, elec. resistance, temp. depend. *(Russian)* 80−103660
$Co_{1-x}P_x$, crystn., spin wave reson. 79−73104
$Co_{80}P_{20}$, amorphous, sign and magnitude of ^{60}Co hyperfine field, nucl. orientation 78−48100
$Co_{80}P_{20}$, mag. props. 77−63125
$Co_{82}P_{18}$, amorphous alloys, electronic struct., γ-ray Compton scatt. study *(Japanese)* 80−84422
$Co_{85}P_{15}$, strip domains, anisotropy const. effects 80−29571
$Co_{78}P_{14}B_8$, amorphous, photoemission and electronic struct. 80−2926
$Co_xPd_{80-x}Si_{20}$, structural and mag. heterogeneities 80−80484
$Co_{74}Si_{10}B_{16}$ amorphous toroidal core, switching charact. and domain structs. 78−95477
$Co_{74}Si_{10}B_{16}$, amorphous ferromagnetic alloy, isothermal annealing effect on static magnetic props. *(Japanese)* 79−52398
$Co_{75}Si_{15}B_{10}$, amorphous, crystallisation study *(Japanese)* 78−9959
$Co_{75}Si_{15}B_{10}$, amorphous, crystn. and thermal stability 80−107057
$Co_{75}Si_{25-x}B_x$, mag. moment, Curie temp., and microhardness, metalloid comp. depend. 77−55665
$Co_{35}Y_{65}$, metallic glass, internal friction peaks 80−25753
$Co_{90}Zr_{10}$, ferromag. amorphous alloy, crystn. and domain struct. study 80−107056
$Cr_xPd_{82-x}Ge_{18}$, RF sputtered, elec. resist. and magnetoresist., Kondo type behaviour 78−76066
$Cs_{1-x}O_x$, metallic glass, prep., elec. props. and struct. 78−67652
Cu-Ag-Ge, Hume-Rothery glass form. 80−96449
Cu-Ag-P(6-14, 11-14 wt.%) amorphous, crystn. and elec. props., X-ray diffr., elec. resist. and DTA meas. *(Japanese)* 80−84088
$Cu\text{-}Fe_{78}Mo_2B_{20}$ wire composite, mech. props. 80−40441
Cu-Zn, amorphous, viscoelastic behaviour *(Japanese)* 77−86110
Cu-Zr, amorphous, viscoelastic behaviour *(Japanese)* 77−86110
Cu-Zr, metallic glasses, valence band struct. investigation 80−11533
Cu-Zr, vapour quenching prod. (thermal evaporation and r.f. sputtering), amorphous film for electron microscopy 78−6851
Cu-Zr (50 or 54 at.%), splat-quenched, glass transition and crystn. temps. determ. 78−22659
Cu-Zr amorphous alloy, splat cooled, local order and amorphous struct. 80−88061
Cu-Zr amorphous alloys, mech. props. *(Japanese)* 77−86179
Cu_xLa_{1-x}, splat-cooled, phase diagram and supercond. props. 80−70881
$Cu_{66}Ti_{34}$, metallic glass, neutron diffr. meas. of struct. factor 80−24367
$Cu_{40}Z4_{60}$, $Cu_{56}Zr_{44}$, and $Cu_{60}Zr_{40}$ metallic glass, inelastic deform., free energy spectra 80−71699
$Cu_{0.57}Zr_{0.43}$ amorphous alloy, neutron diffr. obs. of struct. 80−88060
$Cu_{40}Zr_{60}$, amorphous alloys, supercond. transition temp., press. depend. 80−84524
$Cu_{46}Zr_{54}$, devitrification effect on mech. props. 80−30082
$Cu_{46}Zr_{54}$, metallic glass, dynamical struct. factor and freq. distrib. meas. 80−54136
$Cu_{50}Zr_{50}$, metallic glass, internal friction peaks 80−25753
$Cu_{56}Zr_{44}$ metallic glass, devitrification and its effect on mech. props. 80−33893
$Cu_{60}Zr_{40}$, amorphous, ductility and stress relief, low-temp. annealing effects 80−76296
$Cu_{60}Zr_{40}$ glassy metal, photoemission and mag. susceptibility 79−28896
$Cu_{60}Zr_{40}$, stability, crystallisation, ductility meas. 78−47246
$Cu_{66}Zr_{34}$, amorphous metallic glass, differences caused by preparation technique *(French)* 80−103247
Er-Fe amorphous alloys, mag. props. 79−90557
$Er_{65}Co_{35}$, amorphous, amg. ordering, susceptibility, magnetisation and hysteresis meas. 78−68190
$(Er_{65}Fe_{35})_{100-x}B_x$, mag. props. 79−73693
Eu-Ag, formation and mag. props. 79−91216
(Fe,Co,Ni)-Si(B), amorphous mag. alloy, magnetostriction rel. to soft mag. props. 80−84633
(Fe,Co)PBAl, metallic glass, viscous flow, alloying effect 78−79793
$(Fe,Mo)_{80}B_{20}$, glassy alloy, Curie temp. and crystn. temp., Mo additions effect, Mossbauer spectra 78−68428
(Fe, Ni, Co)-Si-B, amorphous, compositional effect on struct. changes, after heating up to 700°C, exam. *(Japanese)* 78−48433

metallic glasses continued
$(Fe,Ni)_{80}(P,B)_{20}$, quenched alloy ribbon, mag. moments, Curie temp. 77−40041
Fe alloys, amorphous, effects of metalloids on mag. props. 80−75738
Fe alloys, amorphous, mag. saturation, spin wave stiffness, temp. depend. 80−75741
Fe, amorphous structure obtained by liq. state quenching 79−46573
Fe and Fe-Ni Metglas alloys, ohmic and Hall resist. 100-700K, mag. behaviour 80−80254
Fe base amorphous alloys, Invar and Elinvar charact. 80−29592
Fe based, B and P glass former additions, elastic consts., flow behaviour correlation 78−44154
Fe based, Curie temp., struct. relax. effect 77−8313
Fe based alloy, amorphous, liq. quenched, struct., thermal stability and mech. props. 80−88059
Fe based alloys, amorphous toroidal core, switching charact. and domain structs. 78−95477
Fe based amorphous alloy, mag. ordered, hyperfine field distribs., NMR meas. 78−68409
Fe based amorphous alloys, struct. and thermomag. meas. 77−16055
Fe based amorphous alloys, Invar effects, mag. and elastic props. *(Japanese)* 79−20100
Fe Based amorphous alloys, delayed fracture in atmosphere, effect of alloying additions *(Japanese)* 79−96212
Fe group transition metal metalloid binary alloys, metallic glass form., eutectic composition 79−74133
Fe, heat of crystn., and bulk modulus, calc. using struct. model 78−51428
Fe, realistic relaxed struct. model pair distrib. function 78−30544
Fe wire, shape, energy, eddy current loss and relax. damping of mag. domain walls 77−89975
Fe-(Co)-B and Fe-Ni-B(P), amorphous, crystn. 80−79704
Fe-Al alloys, rapidly quenched, mag. props. 80−29579
Fe-B, (16.3 at.%) amorphous, coercive force temp. depend. 80−25158
Fe-B, amorphous, crystn., metal or metalloid exchange influence 80−75172
Fe-B, amorphous, elec. resist., temp. depend. 80−44563
Fe-B, amorphous, high-temp. mag. anal. 78−91258
Fe-B, amorphous, induced anisotropy, development by mag. annealing and under applied mech. stress 80−65868
Fe-B, amorphous, induced anisotropy by heat treatment in mag. field and under applied mech. stress 80−75758
Fe-B, amorphous, Invar-type alloy, mag. moment and high field susceptibility 78−34965
Fe-B, amorphous, low-temp. resistivity in mag. field 78−91667
Fe-B, amorphous, mag. aftereffect, initial susceptibility time depend. 80−88829
Fe-B, amorphous, short-range order, Mossbauer meas. 80−44986
Fe-B, amorphous alloy, mag. props. 80−84618
Fe-B, amorphous alloys, phase diagram 79−96002
Fe-B, amorphous ferromag., temp. depend. of resist., appl. of extended Ziman theory 80−59950
Fe-B, amorphous paramag. alloys, hyperfine field distrib., Mossbauer study 80−39958
Fe-B, amorphous to cryst. transition 80−88048
Fe-B, compositional study on short-range struct. 80−84095
Fe-B, crystn. kinetics by differential scanning calorimetry 78−91257
Fe-B, metallic glass, theoretical studies on structural models 79−37633
Fe-B, Mossbauer investigation of electronic struct. 78−92009
Fe-B, rapidly quenched, metastable phases 80−76234
Fe-B, short range order 79−77528
Fe-B, sputtered amorphous film, strong stripe domains, Kerr effect obs. and theory 79−91265
Fe-B, X-ray obs. of struct. 79−1399
Fe-B (14-25 at.%), saturation magnetisation, temp. and comp. depend. 77−85430
Fe-B (15-25 at.%) glass, quasicryst. struct. Mossbauer expts. 79−4255
Fe-B amorphous, crystallisation, activation energy conc. depend., DTA calcs. 79−60284
Fe-B amorphous alloy, annealed, microstruct. and mag. domain changes 80−75790
Fe-B amorphous alloy, crystallisation kinetics 78−83736
Fe-B amorphous alloy, fast neutron and ^{235}U fission fragment irrad. 80−100288
Fe-B amorphous alloy, mag. anisotropy temp. depend. 80−15846
Fe-B amorphous alloys, mag. aftereffect 80−65970
Fe-B amorphous alloys, Mossbauer spectra, soft ferromag. props. 80−11302
Fe-B amorphous alloys, Mossbauer spectra, mag. moment conc. depend. 80−15847
Fe-B amorphous alloys, valence band spectrum, XPS study 80−50534
Fe-B amorphous ribbons formation, high-speed photography investigation 80−76216
Fe-B based alloys, amorphous, amorphous, thermopower meas., Nordheim-Gorter relations 79−99535
Fe-B glass, crystallisation kinetics, elec. resist. meas. 78−83741
Fe-B glass, crystallisation kinetics, elec. resist. meas. 79−4254
Fe-B metallic glass, hardness, elastic moduli, density, cryst. temp., mech. props., for flywheel appl. *(Dutch)* 78−52878
Fe-B metallic glass, role of Fe_3B in crystn., mag. and Mossbauer expts. 78−94997
Fe-B metallic glass, struct. and crystallisation, Mossbauer spectra, calorimetry and magnetisation meas. 79−23528
Fe-B metallic glass, X-ray diffr. meas., semi-empirical struct. model 80−107059
Fe-B metallic glasses, density, mech. and thermal props. 78−31432
Fe-B metallic glasses, diffusion coeffs. from primary crystn. data 80−100345
Fe-B metallic glasses, short-range orders 79−65002
Fe-B metallic glasses, struct., stability and crystn. 80−75173
Fe-B metallic ribbons, correl. between quenching temp. and mech. and mag. props. 80−89373
Fe-B metastable alloys, Mossbauer spectroscopy and electron microscopy 79−28653
Fe-B phase ferromag. amorphous alloys, stiffening below Curie temp., pole effect *(Japanese)* 80−84632
Fe-B ribbon, microhardness, and static coercive force, melt overheating effect 80−84978
Fe-B-C, formation, mag. props., thermal stability and density 80−75796
Fe-B-C alloys, temp. depend. of magnetisation 79−73690

metallic glasses continued
Fe-B-C amorphous alloys, atomic struct., energy dispersive X-ray diffr. meas. 79−73100
Fe-B-C amorphous alloys, effect of Si addition on mag. props. 80−34694
Fe-B-C amorphous alloys for use in power transformers 80−88808
Fe-B-C amorphous alloys with high saturation induction 80−84617
Fe-B-Cr(Mo), mag., struct., and elec. props. 80−88751
Fe-B-Cr(Si) thin film glasses, mag. props. and corrosion resist. 80−80576
Fe-B-Mo-Cr, amorphous, Mo and Cr addition effect on corrosion behaviour 80−16568
Fe-B-Si, amorphous ferromag. alloys, mag. struct., Mossbauer study 80−39746
Fe-B-Si amorphous alloy, liq. quenched, elec. resist. and cyclic deform. 80−59949
Fe-B-Si amorphous alloys, crystallisation temp., Curie temps., saturation magnetisation 79−82820
Fe-B-Si amorphous ribbons, effect of annealing conditions on magneto-mechanical props. 80−34740
Fe-B-Si ribbon, strain induced anisotropy, and toroid diam. effect on mag. props. 80−34623
Fe-B-Si-C amorphous alloys, prep. and props. 80−88748
Fe-B(-Co), two amorphous phases form. and crystallisation 79−27924
Fe-B(-Si), glassy, field-induced mag. anisotropy near eutectic comp. 80−93110
Fe-B(-Si) alloy filaments produced by glass-coated melt spinning 80−76213
Fe-B(-Si)(-Ni), amorphous alloy, anelastic relaxation 79−4997
Fe-B(C), amorphous phase form. by rapid quenching from melt *(Russian)* 77−66664
Fe-B(P) amorphous alloys, anomalous thermal expansion, ΔE effect, Invar and Elinvar charact., delay time 80−80589
Fe-B(Si) amorphous alloys, Mossbauer spectra, struct. 80−15840
Fe-B(−Ni), chemical ordering, crystallisation and glass transition temp. 79−90563
Fe-base metallic glasses, elastic const. 77−66671
Fe-based, effect of metalloidal elements on thermal stability, crystn. temp. *(Japanese)* 79−94909
Fe-based, Mossbauer effect at high press. 80−15858
Fe-based, Mossbauer spectroscopy, effect of neighbours on hyperfine field 80−39931
Fe-C (4.3 wt.%), splat cooled, amorphous phase form. and crystn. 77−15323
Fe-C amorphous alloys, corrosion resistance improvement by Cr and/or Mo addition 79−66211
Fe-C-B alloy, room-temp. saturation induction 78−95476
Fe-C-X, glasses and metastable cryst. phases, third element effect 80−75171
Fe-Co-B, Mossbauer investigation of electronic struct. 78−92009
Fe-Co-C-B alloy, room-temp. saturation induction 78−95476
Fe-Co-Mo-C, amorphous alloys, med. props. and thermal stability *(Japanese)* 80−85049
Fe-Co-Ni-Si-B amorphous alloy, magnetostriction and permeability, effect of annealing 79−1701
Fe-Co-Si-B, amorphous soft ferromagnet with high mag. induction 80−84619
Fe-Co-Si-B, zero magnetostrictive amorphous alloy with high saturation induction, mag. annealing 80−60362
Fe-Co-Si-B sputtered amorphous thin film, coercivity, galvanomagnetic props., resistivity 80−29578
Fe-Co-Si(B), amorphous ferromagnet, mag. after effect on soft mag. props. 80−84626
Fe-Cr, amorphous alloy, effect of metalloidal impurities on corrosion resistance and electrochem. behaviour 78−72925
Fe-Cr-B, amorphous, Elinvar and Invar charact. *(Japanese)* 80−11832
Fe-Cr-B amorphous alloys, corrosion resistance, Invar and Elinvar charcts. *(Japanese)* 79−96213
Fe-Cr-Mo and Fe-Cr-Mo-Si alloys, amorphous films, corrosion resist. and ion plating use 80−89423
Fe-Cr-Ni-P-C, amorphous, stress corrosion cracking 77−25123
Fe-Cr-P-C, corrosion resist. in 1N HCl 78−80678
Fe-Cu alloy, vapour-deposited, struct. and thermal stability 78−43265
Fe-Mn-P-B-Al, exchange anisotropy 77−16068
Fe-Mn-PBAl, amorphous mixed mag. system, resist. minima 79−60784
Fe-Mo-B metallic glass ribbons, tensile strength, crystn. temp. 80−89173
Fe-Mo-C amorphous alloys, Mo effect corrosion resistance in HCl *(Japanese)* 79−96214
Fe-Mo-P-C, amorphous, XPS study of passivity 79−96185
Fe-Mo-P-C, corrosion resist. in 1N HCl 78−80678
Fe-Ni base amorphous alloy, crystallisation 77−84660
Fe-Ni base metallic glass, annealing embrittlement 78−64635
Fe-Ni base metallic glasses, microhardness charact. of stability under annealing 79−57011
Fe-Ni based, hydrostatic press. effect on mag. props. 78−19300
Fe-Ni based alloys, amorphous, amorphous, thermopower meas., Nordheim-Gorter relations 79−99535
Fe-Ni based metallic glasses, nonisothermal crystallisation kinetics, DSC anal. 79−27927
Fe-Ni based metallic glasses, search for Invar-like magnetoelastic behaviour 79−56596
Fe-Ni based metallic glass, Metglas 2826 MB, Mossbauer study 80−75897
Fe-Ni film, amorphous, martensite form. time and struct. 80−104159
Fe-Ni metallic glass wide strips, low-field mag. props. 79−51822
Fe-Ni metallic glasses, crystallisation 77−43157
Fe-Ni-B, Mossbauer investigation of electronic struct. 78−92009
Fe-Ni-B glassy ribbons melt spinning, gas boundary layer effects 80−76217
Fe-Ni-B metallic glass, X-ray diffr. meas., semi-empirical struct. model 80−107059
Fe-Ni-B-Mo, crystn. temp. and elec. cond. correl., Mo effect 80−75179
Fe-Ni-B-Si, amorphous, mag. props., heat treatment effects 80−89370
Fe-Ni-B(-P), ferromag., magneto-optical spectra in amorphous and cryst. states *(Russian)* 80−84749
Fe-Ni-C-B alloy, room-temp. saturation induction 78−95476
Fe-Ni-Co-B-C-Si alloy, room-temp. saturation induction 78−95476
Fe-Ni-Co-B-P soft magnetic metallic glasses, status report 78−64226
Fe-Ni-Cr-P-B, Metglas 2826A, TEM of shear bands 78−48483
Fe-Ni-Cr-P-B, Metglas 2826A, hardness, elastic moduli, density, cryst. temp., mech. props., for flywheel appl. *(Dutch)* 78−52878

metallic glasses continued
Fe-Ni-Cr-P-B amorphous alloy, localized corrosion 80−16559
Fe-Ni-Mo-C, amorphous alloys, med. props. and thermal stability *(Japanese)* 80−85049
Fe-Ni-P-B, amorphous, crystn. and struct. 80−75175
Fe-Ni-P-B, amorphous ferromag. alloys, mag. struct., Mossbauer study 80−39746
Fe-Ni-P-B, amorphous paramag. alloys, hyperfine field distrib., Mossbauer study 80−39958
Fe-Ni-P-B, metallic glasses, fracture toughness, shear rupture failures, critical thickness 79−52365
Fe-Ni-P-B, metallic glasses, struct. relax., annealing effects on mag. props. 80−89261
Fe-Ni-P-B alloy, magnetically induced anisotropy 77−89948
Fe-Ni-P-B amorphous ribbons, form. by melt spin technique 80−76215
Fe-Ni-P-B metallic glass, crystallisation temperature values from isothermal transformation times 80−59397
Fe-Ni-P-B(C), amorphous alloy, anelastic relaxation 79−4997
Fe-Ni-Si-B, amorphous paramag. alloys, hyperfine field distrib., Mossbauer study 80−39958
Fe-P, metallic glass, theoretical studies on structural models 79−37633
Fe-P alloys, amorphous, Mossbauer spectra 79−51886
Fe-P alloys, X-ray exam. of amorphous structure *(Japanese)* 77−84661
Fe-P electrodeposited foil, amorphous, mag. domains 80−75821
Fe-P film, amorphous, ion implanted, struct. and domain struct. obs. 79−91272
Fe-P-Al(Si)(B), amorphous alloy, anelastic relaxation 79−4997
Fe-P-B, amorphous alloys, mag. props., conc. depend. 77−8314
Fe-P-B-Al, magnetostriction as function of glass formers 78−19299
Fe-P-C, amorphous, crystn. and struct. 80−75175
Fe-P-C, amorphous, internal friction and shear modulus 77−25085
Fe-P-C, amorphous, struct. and mag. props., Mossbauer, X-ray diffr. and elec. resist. meas. 78−2009
Fe-P-C, amorphous alloy, crystallisation 79−100112
Fe-P-C, embrittlement by crystallisation *(Japanese)* 78−48513
Fe-P-C, viscoelastic behaviour of amorphous alloys *(Japanese)* 77−86110
Fe-P-C amorphous alloy, small angle X-ray scattering study of struct. and crystallisation 79−50999
Fe-P-C amorphous alloys, corrosion resistance by alloying with metallic elements 79−66212
Fe-P-C amorphous alloys, Mossbauer spectra, struct. 80−15840
Fe-P-C amorphous alloys with metalloid elements, embrittlement/crystn. relationship *(Japanese)* 79−96134
Fe-Sb amorphous films, Mossbauer effect study 80−75896
Fe-Si amorphous film, struct. and crystallisation, Mossbauer study 80−11300
Fe-Si-B, crystn., differential scanning calorimetry obs. 79−82160
Fe-Si-B, embrittlement by crystallisation *(Japanese)* 78−48513
Fe-Si-B, mag. props. 80−84620
Fe-Si-B, magnetisation meas. 78−23252
Fe-Si-B amorphous alloys, Mossbauer spectroscopy *(French)* 80−80653
Fe-Si-B amorphous alloys with metalloid elements, embrittlement/crystn. relationship *(Japanese)* 79−96134
Fe-Si-B amorphous films, mag. props. 80−34710
Fe-Si-B ferromagnetic amorphous alloys, Young's modulus and delay time charcts. *(Japanese)* 77−85543
Fe-Si-B glassy alloys, mag. props., comp. effects 80−88752
Fe-Si-B metallic glasses, mag. props., depend. on metalloid content 77−85485
Fe-W-P-C, corrosion resist. in 1N HCl 78−80678
Fe-Zr, amorphous phase form. in Zr-poor region, hardness and fracture strength *(Japanese)* 80−84914
$(Fe\text{-}Ni\text{-}Mo)_{80}(P\text{-}B)_{20}$, amorphous, mag. aftereffects and struct. instabilities 80−88833
$Fe_{1-x}B_x$ alloys, struct. and cryst., Mossbauer spectra, DSC, and magnetisation meas. 79−94906
$Fe_{1-x}B_x$, amorphous, hyperfine fields and local mag. moments, Mossbauer study 80−75895
$Fe_{1-x}B_x$, polycrystalline and amorphous sputtered films, Brillouin spectra 80−2775
$Fe_{100-x}B_x$, amorphous, mag. struct., mag. susceptibility meas. 80−80485
$Fe_{100-x}B_x$ amorphous alloys, magnetostriction meas. 79−19760
$Fe_{100-x}B_x$, amorphous alloys, saturation magnetostriction and annealing behaviour 80−34739
$Fe_{100-x}B_x$, crystalline and glassy, low temp. magnetisation study 79−95608
$Fe_{100-x}B_x$, mag. and struct. props., comp. depend. 78−60314
$Fe_{100-x}B_x$ metallic glass, magnetisation meas. 78−80134
$Fe_{100-x}B_x$, quenched ferromag. ribbon, Brillouin spectra 80−2776
$Fe_{100-x}B_x$ ribbon, magnetostriction exam. 79−73794
$Fe_{75}B_{25}$, correlation between elastic consts. and flow behaviour 78−44154
$Fe_{75}B_{25}$ metallic glass, nonisothermal meas. evaluation, non-existence of dynamic correction term 80−107406
$Fe_{80}B_{20}$, absolute thermoelectric power between 300 and 1000K 79−19579
$Fe_{80}B_{20}$, amorphous, Brillouin scatt. from magnons, ferromag. reson. 80−65844
$Fe_{80}B_{20}$, amorphous, cold neutron scatt., local and extended defects 80−84089
$Fe_{80}B_{20}$, amorphous, crystallization 78−42917
$Fe_{80}B_{20}$, amorphous, crystn. temp. under press. 79−23523
$Fe_{80}B_{20}$, amorphous, crystn. 80−75187
$Fe_{80}B_{20}$, amorphous, deform. and annealing effects on mag. and mech. props. 77−12717
$Fe_{80}B_{20}$, amorphous, elec. and mag. hyperfine field distribs., Mossbauer study 80−39964
$Fe_{80}B_{20}$, amorphous, evaluation of complex Mossbauer spectra 78−43755
$Fe_{80}B_{20}$, amorphous, fast neutron and fission fragment irrad., effect on elec. resist. 80−19846
$Fe_{80}B_{20}$, amorphous, mag. permeability aftereffect during annealing 80−88834
$Fe_{80}B_{20}$, amorphous, transverse magnetoresist., stress effect 80−15501
$Fe_{80}B_{20}$ amorphous alloy, low field magnetic props. 77−55690
$Fe_{80}B_{20}$ amorphous alloys, domain struct. exam., magneto-optic Kerr effect 79−28550
$Fe_{80}B_{20}$, amorphous ferromag., temp. depend. of hyperfine field distrib. 78−43756
$Fe_{80}B_{20}$, amorphous ferromag., hyperfine field distrib., Mossbauer effect 78−60371

metallic glasses continued
- $Fe_{80}B_{20}$, amorphous ferromag. metallic glass, stress-induced rot. of magnetisation, Mossbauer study 80−20445
- $Fe_{80}B_{20}$, amorphous ferromagnet, Mossbauer hyperfine fields, mag. struct. 80−75894
- $Fe_{80}B_{20}$ amorphous ribbons, magnetomechanical coupling constant and Young's modulus, mag. annealing 79−15333
- $Fe_{80}B_{20}$, amorphous struct., Mossbauer spectroscopy investigation 80−84677
- $Fe_{80}B_{20}$ amorphous wire, crystn. by annealing at 780°C 80−100177
- $Fe_{80}B_{20}$, binary amorphous ferromagnet, Mossbauer spectra 79−4749
- $Fe_{80}B_{20}$, elastic, magnetoelastic and thermal props. 79−19759
- $Fe_{80}B_{20}$, electrical resist., 78 to 1000K, probe of crystn. process 77−76787
- $Fe_{80}B_{20}$, evaluation of complex Mossbauer spectra 78−60370
- $Fe_{80}B_{20}$, $Fe_{78}Mo_2B_{20}$ glasses, internal friction and shear modulus 79−52287
- $Fe_{80}B_{20}$, ferromag. props. 77−16107
- $Fe_{80}B_{20}$, ferromagnetic metallic glasses, Brillouin scattering 78−92085
- $Fe_{80}B_{20}$ film, amorphous metallic, standing spin waves, Brillouin scatt. obs. 80−97291
- $Fe_{80}B_{20}$ glass, low-field mag. props. 77−8380
- $Fe_{80}B_{20}$ glass, magnetisation reorientation, Mossbauer effect 80−66092
- $Fe_{80}B_{20}$ glass, temp. depend. of magnetostriction 77−59443
- $Fe_{80}B_{20}$, glassy, ferromag. anisotropy of resistivity 79−23939
- $Fe_{80}B_{20}$ hardness, elec. cond., photo emission, and mag. props. *(Norwegian)* 79−32909
- $Fe_{80}B_{20}$, high-resolution XPS study, electronic state struct. 80−29846
- $Fe_{80}B_{20}$, METGLAS 2605, mag. anisotropy and electronic struct., Mossbauer meas. 77−28384
- $Fe_{80}B_{20}$, magnetostriction, temp. depend. 78−91921
- $Fe_{80}B_{20}$, metallic glass, Mossbauer spectroscopy 78−60365
- $Fe_{80}B_{20}$ metallic glass, spin texture determ. 80−15842
- $Fe_{80}B_{20}$, metallic glass, low temp. specific heat, metalloid effects 80−34654
- $Fe_{80}B_{20}$, metallic glass, triplet correlation, field-ion microscopy study 80−38921
- $Fe_{80}B_{20}$, metallic glass, Doppler broadening of positron annihilation γ-radiation and elec. resist. 80−66321
- $Fe_{80}B_{20}$ metallic glass, crystn. and struct. relax., Mossbauer effect study 80−75182
- $Fe_{80}B_{20}$ metallic glass, crystn. kinetics 80−84083
- $Fe_{80}B_{20}$, metallic glass, optical and magneto-optical props. 80−84728
- $Fe_{80}B_{20}$ metallic glasses, stability and transforms. 80−75174
- $Fe_{80}B_{20}$, Metglas 2605, amorphous ferromag., resistivity down to 60 mK 79−60783
- $Fe_{80}B_{20}$, Metglas 2605, Young's modulus meas. using piezoelectric US composite oscillator technique 80−108656
- $Fe_{80}B_{20}$ Metglass, Mossbauer spectra line broadening 78−52400
- $Fe_{80}B_{20}$, sputter deposited amorphous, low field mag. props. 78−68335
- $Fe_{83}B_{17}$ metallic glass, struct. from neutron diffr. study 80−6363
- $Fe_{83.4}B_{16.6}$, amorphous, mag. props. and microstruct., cooling rate and melt overheating effects 80−65965
- $Fe_{83.4}B_{16.6}$ amorphous, mag. props., melt overheating and cooling rate effects 80−89371
- $Fe_{84}B_{16}$, amorphous, struct., X-ray diffr. meas. 79−4252
- $Fe_{84}B_{16}$, metallic glass, electrical resistivity and crystallisation 80−88526
- $Fe_{84}B_{16}$, metallic glass, ion implanted, UPS meas. 80−97411
- Fe_xB_{100-x}, amorphous, mag. props., ^{57}Fe Mossbauer spectra and magnetisation meas. 79−95693
- Fe_xB_{100-x}, amorphous, stress relax. after annealing 80−55447
- $Fe_{80}(B_yC_{1-y})_{20}$, saturation magnetostriction, comp. effects 80−34735
- $Fe_{84}B_{16-x}C_x$, amorphous alloys, short range order, Mossbauer and DSC study 80−39960
- $Fe_{84}B_{16-x}C_x$, hyperfine interaction and Curie temps., Mossbauer meas. 79−73858
- $FeB_5C_{15}SSi_{15}Cr_5$, amorphous, exam. of metalloid atom mobility by Auger spectroscopy 78−47575
- $Fe_{80}B_{20-x}M_x$ (X=Al, Si, Ge, C, P) and $(FeCo)_{80}B_{20}$ glass, magnetisation, Curie and crystn. temps. 79−87289
- $Fe_{80}B_{20-x}M_x$, M=C, Si, P, Ge, amorphous, effect of metalloids on mag. props. 79−11304
- $Fe_{80}(B_{1-z}P_z)_{20}$ amorphous alloys, isothermal crystallisation kinetics 80−33895
- $Fe_{40}B_{40}P_{14}B_6$ and $Fe_{80}B_{20}$, Metglas 2826 and 2605, amorphous ribbon, power loss variation with freq. and applied stress 80−88849
- $Fe_{78}B_{12}Si_{10}$, amorphous, Mossbauer study of hyperfine interaction and mag. anisotropy 80−40027
- $Fe_{78}B_{12}Si_{10}$, amorphous ferromagnet, long and short range exchange interactions, Mossbauer spectra and interpretation 79−56526
- $Fe_{80}B_{15}Si_5$ metallic glass, large uniaxial magnetostrictive anisotropy, magnetisation reversal 80−34736
- $Fe_{80}B_{20-x}Si_x$, metallic glass, mech. and mag. props., depend. on metalloid content 79−91213
- $Fe_{80}(B_ySi_{1-y})_{20}$, saturation magnetostriction, comp. effects 80−34735
- $Fe_{81.5}B_{14.5}Si_4$, amorphous metal ribbon, stresses, magnetoelastic anisotropy and zero-field mag. domain struct. 80−44896
- $Fe_{82}B_{14}Si_4$, chill block melt-spinning process, geometry depend. 80−97448
- $Fe_{82}B_{15}Si_3$, metallic glass, low temp. specific heat, metalloid effects 80−34654
- $Fe_{82}B_{18-x}Si_x$, soft mag. props. 79−73774
- $Fe_{83}B_{16.5}Si_{0.5}$, spin waves, inelastic neutron scatt. meas. 79−73701
- $Fe_{84}B_{13}Si_3$, metallic glass, electrical resistivity and crystallisation 80−88526
- $Fe_{100-x}Be_x$, amorphous ribbon, saturation magnetostriction, and electronically controllable delay line 79−1700
- $Fe_{80}(C_{1-x}B_x)_{20}$ amorphous alloy, α-Fe crystn., morphology 80−70129
- $(Fe_{0.06}Co_{0.94})$-B, amorphous, ferromag., mag. instability rel. to struct. 79−99729
- $(FeCo)_{80}B_{20}$, glass, elastic consts. 79−83249
- $(FeCo)_{80}B_{20}$, saturation moments and Curie temp. 77−1542
- $(Fe_{0.5}Co_{0.5})_{1-x}B_x$, amorphous, hyperfine fields and local mag. moments, Mossbauer study 80−75895
- $(Fe_{0.65}Co_{0.35})$B, crystalline disordered, evaluation of complex Mossbauer spectra 78−43755
- $Fe_5Co_{75}B_{20}$, amorphous, magnetisation reversal and domain boundary configs. 80−88809
- $Fe_{71}Co_9B_{20}$, glassy ribbon, magnetostatic effects 79−73790
- $Fe_{80-x}Co_xB_{20}$, ferromag., saturation magnetostriction meas. 77−36108
- $Fe_{80-x}Co_xB_{20}$, spontaneous Hall effect and resistivity 79−19576

metallic glasses continued
- $Fe_{35}Co_{32}B_{20}Si_{10}Al_3$, stress-induced variation in magnetisation and dynamic magnetostrictive charact. 80−88855
- $(FeCoNi)_8B_{20}$, evidence supporting split-band model from magnetostriction 78−95509
- $(Fe_{0.2}Co_{0.8})_{80}P_{17}Al_3$, Mossbauer spectra, isomer shift, mag. hyperfine field 80−11301
- $(Fe_{100-x}Co_x)_{79}P_{13}B_8$, amorphous, hyperfine field distrib., ^{59}Co NMR spin-echo meas. 80−34818
- $(Fe_{1-x}Co_x)_5$PBAl metallic glasses, influence of composition and ageing on Curie temps. 77−85445
- $(Fe_{1-x}Co_x)_{80}P_{13}C_7$ amorphous alloy, soft mag. material, props. 77−4533
- $(Fe_{0.9}Co_{0.1})_xSi_yB_2$, $(Fe_{1-x}Co_x)_{78}Si_8B_{14}$ amorphous ribbons, magnetomech. coupling and saturation magnetostriction 78−68353
- $(Fe_{1-x}Co_x)_{75}Si_{15}B_{10}$ amorphous alloy, soft mag. material, props. 77−4533
- $(Fe_{1-x}Co_x)_{77}Si_{10}B_{13}$, amorphous, mag. moments at 0K, Curie temp., mag. interactions 79−4670
- $(Fe_{1-x}Co_x)_{77}Si_{10}B_{13}$, amorphous magnetic alloys, density meas. 80−1934
- $(Fe_{1-x}Co_x)_{78}Si_{10}B_{12}$, amorphous alloys, magnetic anisotropy meas. 80−2570
- $(Fe_{1-x}Co_x)_{78}Si_{10}B_{12}$, amorphous, roll mag. anisotropy 80−75757
- $(Fe_{1-x}Co_x)_{78}Si_{10}B_{12}$, Hall effect and magnetoresist. *(Japanese)* 77−85199
- $(Fe_{1-x}Co_x)_{78}Si_8B_{14}$, amorphous ribbon, saturation magnetostriction, and electronically controllable delay line 79−1700
- $(Fe_{1-x}Co_x)_{78}Si_8B_{14}$ ribbon, magnetostriction exam. 79−73794
- $Fe_{4.7}Co_{70.3}Si_{15}B_{10}$, amorphous ferromag., roll mag. anisotropy 79−51773
- $Fe_5Co_{70}Si_{15}B_{10}$, amorphous ribbon, zero magnetostriction, low residual mag. loss 77−12157
- $Fe_5Co_{70}Si_{15}B_{10}$ amorphous ferromag. ribbons, change of permeability by heat treatment 77−85493
- $Fe_5Co_{70}Si_{15}B_{10}$, amorphous, change of mag. props. by low temp. annealing 78−27058
- $Fe_5Co_{70}Si_{15}B_{10}$, amorphous ferromagnetic alloy, isothermal annealing effect on static magnetic props. *(Japanese)* 79−52398
- $Fe_5Co_{70}Si_{15}B_{10}$, amorphous, crystn. effect on mag. props. *(Russian)* 80−44858
- $(Fe_xCo_{1-x})_{78}Si_8B_{14}$, amorphous, saturation magnetostriction, strain modulated FMR obs. 80−75863
- $(Fe_xCo_{100-x})_{100-(y+z)}Si_yB_z$ amorphous ribbon, mag. moment and Curie temp., comp. depend. 78−95421
- $Fe_{85-x}Cr_xB_{15}$, Curie temp., crystn. temp. and room temp. elec. resist., Cr content effect 79−91229
- $Fe_{36}Cr_{32}Ni_{14}B_{12}B_6$, amorphous X-ray absorpt. spectra, effective coordination charges 80−84805
- $(Fe_{98}Cr_2)_{79}P_{13}B_8$ and $(Fe_{96}Cr_4)_{79}P_{13}B_8$, amorphous, low temp. sp. ht., mag. contribs. 80−80552
- Fe_xGe_{1-x}, amorphous, conversion electron Mossbauer spectra down to 4.2K 80−7205
- $Fe_{83-x}M_xB_{17}$ and $Fe_{78-x}M_xSi_{10}B_{12}$ (M=refractory metal), glass form. and thermal stability 80−79703
- $(Fe_{1-x}Mn_x)_{75}P_{16}B_6Al_3$, amorphous, spin-glass-ferromag. multicritical point, AC susceptibility meas. 80−50117
- $(Fe_xMn_{1-x})_{75}P_{16}B_6Al_3$, amorphous, mag. ordering temp., hyperfine field distrib., elec. resist. 80−34633
- $(Fe_{1-x}Mn_x)_{75}P_{15}C_{10}$, amorphous, mag. ordering, Mossbauer study 80−39747
- $(Fe_{1-x}Mn_x)_{75}P_{15}C_{10}$, amorphous pair radial distrib. functions, neutron scatt. study 80−49128
- $Fe_{78}Mo_4B_{20}$, quenched ferromag. ribbon, Brillouin spectra 80−2776
- $Fe_{78}Mo_2B_{20}$, amorphous, transverse magnetoresist., stress effect 80−15501
- $Fe_{78}Mo_2B_{20}$, amorphous, fast neutron and fission fragment irrad., effect on elec. resist. 80−19846
- $Fe_{78}Mo_2B_{20}$, amorphous ferromag., $T^{3/2}$ depend. of hyperfine field 78−39474
- $Fe_{78}Mo_2B_{20}$, amorphous ferromag., mag. props. 79−38309
- $Fe_{78}Mo_2B_{20}$, electrical resist., 78 to 1000K, probe of crystn. process 77−76787
- $Fe_{78}Mo_2B_{20}$, Elinvar-type behaviour 79−66091
- $Fe_{78}Mo_2B_{20}$, exam. of mag. props. between 300 and 900K 78−85010
- $Fe_{78}Mo_2B_{20}$, glassy, ferromag. anisotropy of resistivity 79−23939
- $Fe_{78}Mo_2B_{20}$, metallic glass, triplet correlation, field-ion microscopy study 80−38921
- $Fe_{78}Mo_2B_{20}$, metallic glass, Doppler broadening of positron annihilation γ-radiation and elec. resist. 80−66321
- $Fe_{78}Mo_2B_{20}$, Metglas 2605 A, amorphous ferromag., resistivity down to 60 mK 79−60783
- $Fe_{78}Mo_2B_{20}$, thermal expansion, glass transform. and crystn. temps. 80−2183
- $Fe_{80-x}Mo_xB_{20}$, Curie temp., crystn. temp., elec. cond. as function of composition 79−60285
- $(Fe_xMo_{1-x})_{75}P_{16}B_6Al_3$, effects of Mo on mag. props., Mossbauer meas. 79−73859
- $Fe_{40}Ni_{38}Mo_4B_{18}$ amorphous alloys, compatibility of DC and AC mag. props. 80−34695
- Fe_xNi_{1-x} amorphous film, growth stress and structure factor, stabilisation by conduction electrons 80−38920
- FeNiB, amorphous alloy, high resolution imaging by electron microscopy 79−99039
- $(FeNi)_{80}B_{20}$, glass, elastic consts. 79−83249
- $(FeNi)_{80}B_{20}$, saturation moments and Curie temp. 77−1542
- $(Fe_{0.6}Ni_{0.4})_{100-x}B_x$ and $(Fe_{100-x}Ni_x)_{80}B_{20}$ amorphous alloys, X-ray diffr. struct. determ. 80−64906
- $(Fe_{1-x}Ni_x)_{75}B_{25}$, amorphous and cryst., short range order, Mossbauer study 80−39961
- $(Fe_{1-x}Ni_x)_{83}B_{17}$, amorphous alloys ferromagnetic resonance 80−108080
- $(Fe_{100-x}Ni_x)_{100-y}B_y$, metallic glass, embrittlement and crystn. 80−7685
- $(Fe_{100-x}Ni_x)_{83}B_{17}$, amorphous, crystn. 80−75176
- $(Fe_{100-x}Ni_x)_{83}B_{17}$ glassy alloys, Ni content influence on crystn., and bend ductility changes, during annealing 79−73103
- $Fe_{38}Ni_{38}B_{24}$, magnetisation and FMR expts. 79−95607
- $Fe_{40}Ni_{20}B_{20}$, metallic glassy ribbon, casting conditions *(Japanese)* 80−55386
- $Fe_{40}Ni_{40}B_{20}$, amorphous, induced mag. anisotropy, reorientation kinetics 77−43829
- $Fe_{40}Ni_{40}B_{20}$, amorphous, hyperfine field distrib., Mossbauer effect meas. 79−4755
- $Fe_{40}Ni_{40}B_{20}$, amorphous, hyperfine field distrib., Mossbauer study 79−28657

metallic glasses continued
$Fe_{40}Ni_{40}B_{20}$, amorphous, anomalous thermal dilatation 79−55668
$Fe_{40}Ni_{40}B_{20}$, amorphous, resist. min. disappearance on annealing 79−60786
$Fe_{40}Ni_{40}B_{20}$, amorphous, high-field magnetisation curve, spin wave spectrum and microstructural inhomogeneities 80−15702
$Fe_{40}Ni_{40}B_{20}$, amorphous, casting conditions effect on mag. props. *(Japanese)* 80−34698
$Fe_{40}Ni_{40}B_{20}$, amorphous, mag. props., effects mech. deform. 80−39840
$Fe_{40}Ni_{40}B_{20}$, amorphous, phase transforms., resistometric anal. 80−75538
$Fe_{40}Ni_{40}B_{20}$, amorphous, RF annealing effects 80−108037
$Fe_{40}Ni_{40}B_{20}$, amorphous and crystalline, resist. minimum 79−47079
$Fe_{40}Ni_{40}B_{20}$, amorphous ferromag., resistivity down to 60 mK 79−60783
$Fe_{40}Ni_{40}B_{20}$, amorphous ribbon, anal. of casting conditions 79−95965
$Fe_{40}Ni_{40}B_{20}$, amorphous ribbon, power loss variation with freq. and applied stress 80−88849
$Fe_{40}Ni_{40}B_{20}$ and $Fe_{40}Ni_{40}P_{14}B_6$, amorphous, mag. aftereffect spectra and annealing props. 80−88831
$Fe_{40}Ni_{40}B_{20}$, chill block melt-spinning process, geometry depend. 80−97448
$Fe_{40}Ni_{40}B_{20}$, embrittlement kinetics and crystn., quenching influence 78−68766
$Fe_{40}Ni_{40}B_{20}$ glass, ^{10}B self-diffusion, meas. by SIMS 80−49406
$Fe_{40}Ni_{40}B_{20}$ glass, phase transform. during isochronal annealing 78−14451
$Fe_{40}Ni_{40}B_{20}$, mag. loss meas. 79−73776
$Fe_{40}Ni_{40}B_{20}$, metallic glass, low temp. specific heat, metalloid effects 80−34654
$Fe_{40}Ni_{40}B_{20}$, molten, jet streaming, planar and cylindrical, instabilities rel. to glassy alloy casting 80−35129
$Fe_{40}Ni_{40}B_{20}$, processing conditions effect on mag. props. 79−73775
$Fe_{40}Ni_{40}B_{20}$, ribbon prod., apparatus parameters effect on dimens. 77−12570
$Fe_{50}Ni_{30}B_{20}$, crystallisation of amorphous alloys, TEM and X-ray diffr. exam. of struct., growth characts. 78−79539
$Fe_{80-x}Ni_xB_{20}$ and $Fe_{80-x}Ni_xP_{14}B_6$ amorphous alloys, microhardness correl. with mag. props. 80−88826
$Fe_{80-x}Ni_xB_{20}$, $Fe_{80-x}Ni_xP_{14}B_6$, amorphous, microhardness meas., dependence on mag. props. *(Croatian)* 79−11688
$Fe_{80-x}Ni_xB_{20}$, ferromag. saturation magnetostriction meas. 77−36108
$Fe_{80-x}Ni_xB_{20}$, spontaneous Hall effect and resistivity 79−19576
$(Fe_xNi_{1-x})_{80}B_{20}$, $(Fe_xNi_{1-x})_{80}P_{14}B_6$, new soft amorphous ferromagnetic glasses *(Croatian)* 79−11298
$(Fe_xNi_{1-x})_{80}B_{20}$, amorphous alloys, engineering mag. props. 79−51832
$(Fe_xNi_{1-x})_{80}B_{20}$, amorphous, Mossbauer spectra, mag. props. 80−15843
$(Fe_xNi_{100-x})_{80}B_{20}$, glassy, elec. resist. at elevated temp. 79−73484
$Fe_xNi_{80-x}B_{20}$, amorphous ferromag., low temp. resistivity 79−56181
$Fe_xNi_{80-x}B_{20}$ and $Fe_xNi_{80-x}P_{14}B_6$, low temp. resist. and galvanomag. effects, mag. state influence 80−84461
$Fe_xNi_{80-x}B_{20}$, $Fe_xNi_{80-x}P_{14}B_4$, amorphous Hall effect voltage meas. *(Croatian)* 79−11102
$Fe_xNi_{80-x}B_{20}$, $Fe_xNi_{80-x}P_{14}B_6$, amorphous ferromag., galvanomag. props. 79−56196
$Fe_xNi_{80-x}B_{20}$ glass, resist., magnetoresist., and thermoelec. power 80−70681
$Fe_xNi_{80-x}B_{20}$, quenched ferromag. ribbon, Brillouin spectra 80−2776
$(Fe_xNi_{1-x})_{80}B_{20}$, mag. anneal anisotropy in amorphous alloys 77−16069
$(Fe_{1-x}Ni_x)_{0.8}B_{0.2-x}P_x$, amorphous, hyperfine fields and local mag. moments, Mossbauer study 80−75895
$Fe_{16}Ni_{78.4}B_{10}P_{10}$, superparamag. behaviour, chem. inhomogeneities role 80−84625
$Fe_{20}Ni_{60}B_{19}P_1$, spin waves, inelastic neutron scatt. meas. 79−73701
$Fe_{40}Ni_{40}B_{20-x}P_x$, local struct. and dynamic disorder of Fe and Ni, EXAFS obs. 80−89088
$Fe_{80-x}Ni_xB_{20-y}P_y$, amorphous, Rayleigh region and coercive force 80−88806
$(FeNi)_{80}Bi_{17.5}Al_2Si_{0.5}$, stress-induced variation in magnetisation and dynamic magnetostrictive charact. 80−88855
$Fe_{40}Ni_{40}C_{14}P_6$ amorphous film, dislocation and mag. struct., neutron diffr. study 80−70956
$Fe_{32}Ni_{36}Cr_{14}P_{12}B_6$, metallic glass, changes in Curie temp., physical dimensions and mag. anisotropy during annealing 77−85446
$Fe_{32}Ni_{36}Cr_{14}P_{12}B_6$, shear band form. 78−68756
$Fe_{32}Ni_{36}Cr_{14}P_{12}B_6$ metallic glass, dynamic mechanical props. 79−10894
$Fe_{32}Ni_{36}Cr_{14}P_{12}B_6$, elastic, magnetoelastic and thermal props. 79−19759
$Fe_{32}Ni_{36}Cr_{14}P_{12}B_6$, METGLAS 2826A, metastable crystallization phases, TEM obs. 79−55671
$Fe_{32}Ni_{36}Cr_{14}P_{12}B_6$, amorphous ferromagnet, long and short range exchange interactions, Mossbauer spectra and interpretation 79−56526
$Fe_{32}Ni_{36}Cr_{14}P_{12}B_6$, amorphous mag. solids, Mossbauer exam. 79−61281
$Fe_{32}Ni_{36}Cr_{14}P_{12}B_6$, Metglass 2826A, mag. props. under high press., Mossbauer meas. 79−73860
$Fe_{32}Ni_{36}Cr_{14}P_{12}B_6$, Metglas 2826A elec. resist. during crystn. 79−91014
$Fe_{32}Ni_{36}Cr_{14}P_{12}B_6$, thermal expansion, glass transform. and crystn. temps. 80−2183
$Fe_{32}Ni_{36}Cr_{14}P_{12}B_6$, high-resolution XPS study, electronic state struct. 80−29846
$Fe_{32}Ni_{36}Cr_{14}P_{12}B_6$, metallic glass, Doppler broadening of positron annihilation γ-radiation and elec. resist. 80−66321
$Fe_{32}Ni_{36}Cr_{14}P_{12}B_6$ metallic glass, crystn. kinetics by TEM 80−75186
$Fe_{32}Ni_{36}Cr_{14}P_{12}B_6$, Metglas 2826A, EPR at 20 GHz 80−75848
$Fe_{32}Ni_{36}Cr_{14}P_{12}B_6$ Metglas, bending deform., shear band form., high-speed cinematographic obs. 80−89322
$Fe_{32}Ni_{36}Cr_{14}P_{12}B_6$, Metglas amorphous films, corrosion resist. and ion plating use 80−89423
$Fe_{32}Ni_{36}Cr_{14}P_{12}B_6$ metallic glass, effect of pre-ageing on glass transition temp. 80−100326
$Fe_{40}Ni_{40}(Mo,Si,B)_{20}$, amorphous, soft mag. props., switched-mode power supply appls. 80−88850
$Fe_{40}Ni_{38}Mo_4B_{18}$, amorphous, crystallization, heat treatment and irradiation effects *(French)* 79−90558
$Fe_{40}Ni_{38}Mo_4B_{18}$, amorphous, mag. anisotropy, Mossbauer study 80−65864
$Fe_{40}Ni_{38}Mo_4B_{18}$, amorphous, reversible enhancement of mag. directional ordering rate 80−103829
$Fe_{40}Ni_{38}Mo_4B_{18}$ and $Fe_{78}Mo_2B_{20}$ amorphous ribbons, magnetoelastic effects in as-quenched and stress-relieved states 80−80588
$Fe_{40}Ni_{38}Mo_4B_{18}$ glassy alloy, high permeability, low field mag. characts. 78−68301
$Fe_{40}Ni_{38}Mo_4B_{18}$, metallic glass, mag. and transport props. 80−39752
$Fe_{40}Ni_{38}Mo_4B_{18}$, reorientation kinetics of magnetization 79−24155

metallic glasses continued
$Fe_{40}Ni_{38}Mo_4B_{18}$ ribbon, magnetic characterisation 80−34680
$(Fe_{1-x}Ni_x)_{80}P_{20}$, amorphous, ferromagnetic alloys, mag. anomalies of Invar type *(Russian)* 80−93089
$Fe_{40}Ni_{40}P_{14}$, glass transition, viscous flow and differential scanning calorimetry meas. 80−96635
$(Fe_{1-x}Ni_x)_{80}P_{10}B_{10}$, amorphous, magnetostriction meas. by ferromag. reson., induced anisotropy 77−32232
$(Fe_{1-x}Ni_x)_{80}P_{10}B_{10}$, amorphous microwires, magnetisation reversal and anisotropy 78−91885
$Fe_{20}Ni_{60}P_{14}B_6$, $Fe_{30}Ni_{50}P_{14}B_6$, amorphous ferromags., thermoelec. power and resistivity near Curie temp. 79−56200
$Fe_{27}Ni_{53}P_{14}B_6$, amorphous, Hall resist. and mag. props., short range order effects 80−34422
$Fe_{27}Ni_{53}P_{14}B_6$, metallic glass, changes in Curie temp., physical dimensions and mag. anisotropy during annealing 77−85446
$Fe_{40}Ni_{40}P_{14}B_{06}$, strip domains, anisotropy const. effects 80−29571
$Fe_{40}Ni_{40}P_{14}B_6$, (Metglas 2826), ferromag. Curie temp. determ. 78−64206
$Fe_{40}Ni_{40}P_{14}B_6$, amorhpous ribbon, influence of torsion on mag. props. 80−7138
$Fe_{40}Ni_{40}P_{14}B_6$, amorphous ribbon, cold rolling, annealing mag. props. 77−8958
$Fe_{40}Ni_{40}P_{14}B_6$, amorphous, deform. and annealing effects on mag. and mech. props. 77−12717
$Fe_{40}Ni_{40}P_{14}B_6$, amorphous alloy, small angle X-ray scattering 77−65953
$Fe_{40}Ni_{40}P_{14}B_6$, amorphous, domain struct. 78−10719
$Fe_{40}Ni_{40}P_{14}B_6$, amorphous tape wound cores, mag. props. *(German)* 78−10727
$Fe_{40}Ni_{40}P_{14}B_6$, amorphous, mag. props. 78−10728
$Fe_{40}Ni_{40}P_{14}B_6$, amorphous alloy, structural relaxation kinetics, X-ray diffr. exam. 78−38627
$Fe_{40}Ni_{40}P_{14}B_6$ amorphous ribbon, mag. anisotropy distrib. near surface 78−95430
$Fe_{40}Ni_{40}P_{14}B_6$, amorphous, energy dispersive X-ray diffr. study of structural relaxation 79−14689
$Fe_{40}Ni_{40}P_{14}B_6$, amorphous alloy sheet, fabrication by gas melt spraying method 79−24466
$Fe_{40}Ni_{40}P_{14}B_6$, amorphous, annealed and unannealed, temp. depend. of flow stress and ductility 79−29119
$Fe_{40}Ni_{40}P_{14}B_6$, amorphous, stress-induced mag. easy axis 79−33516
$Fe_{40}Ni_{40}P_{14}B_6$, amorphous, transverse magnetoresist., stress effect 80−15501
$Fe_{40}Ni_{40}P_{14}B_6$, amorphous, mag. props., effects mech. deform. 80−39840
$Fe_{40}Ni_{40}P_{14}B_6$, amorphous, resistometric study of short-range ordering rel. to heat treatment 80−70140
$Fe_{40}Ni_{40}P_{14}B_6$, amorphous ferromagnet, Mossbauer hyperfine fields, mag. struct. 80−75894
$Fe_{40}Ni_{40}P_{14}B_6$ amorphous alloy, temper embrittlement 80−76295
$Fe_{40}Ni_{40}P_{14}B_6$, amorphous, steady-state creep rate, cryst. effect 80−81102
$Fe_{40}Ni_{40}P_{14}B_6$, amorphous, mag. permeability aftereffect during annealing 80−88834
$Fe_{40}Ni_{40}P_{14}B_6$ amorphous ribbon, mag. domains and anisotropy distrib. 80−108029
$Fe_{40}Ni_{40}P_{14}B_6$, and $Fe_{32}Ni_{36}Cr_{14}P_{12}B_6$, glassy, ferromag. anisotropy of resistivity 79−23939
$Fe_{40}Ni_{40}P_{14}B_6$, bending tests, evidence of ideal elastic-plastic deform. 80−97543
$Fe_{40}Ni_{40}P_{14}B_6$, crystn. kinetics, DSC expts. 78−26444
$Fe_{40}Ni_{40}P_{14}B_6$, elastic, magnetoelastic and thermal props. 79−19759
$Fe_{40}Ni_{40}P_{14}B_6$, fabric for mag. shield 77−8347
$Fe_{40}Ni_{40}P_{14}B_6$, $Fe_{29}Ni_{49}P_{14}B_6Si_2$ glasses, internal friction and shear modulus 79−52287
$Fe_{40}Ni_{40}P_{14}B_6$, $Fe_{32}Ni_{36}Cr_{14}P_{12}B_6$, Hall effect, press. and temp depends. 77−66155
$Fe_{40}Ni_{40}P_{14}B_6$, $Fe_{35}Ni_{32}Cr_{15}P_{12}B_6$, amorphous ferromagnets, Barkhausen noise and core losses 77−69618
$Fe_{40}Ni_{40}P_{14}B_6$, ferromagnetic, low temp. heat capacity meas., electronic, phonon contributions exam. 78−10689
$Fe_{40}Ni_{40}P_{14}B_6$, ferromagnetic metallic glasses, Brillouin scattering 78−92085
$Fe_{40}Ni_{40}P_{14}B_6$ glass, positron lifetimes in as-received, cold-rolled, embrittled and crystallized samples 79−74177
$Fe_{40}Ni_{40}P_{14}B_6$ glass, struct. relax., ferromag. reson. and X-ray scatt. 79−90566
$Fe_{40}Ni_{40}P_{14}B_6$ glass, viscosity near T_g, using rapid heating, and fusion characts. 80−70438
$Fe_{40}Ni_{40}P_{14}B_6$, hardness, elec. cond., photo emission, and mag. props. *(Norwegian)* 79−32909
$Fe_{40}Ni_{40}P_{14}B_6$, high-field suscept. and spin wave spectrum 78−10662
$Fe_{40}Ni_{40}P_{14}B_6$, high-resolution XPS study, electronic state struct. 80−29846
$Fe_{40}Ni_{40}P_{14}B_6$, induced anisotropy energy and saturation magnetisation temp. depend., torque magnetometer meas. 78−10680
$Fe_{40}Ni_{40}P_{14}B_6$, irradiation swelling 78−30682
$Fe_{40}Ni_{40}P_{14}B_6$, mag. props. and hyperfine interactions, Mossbauer obs., 4.2-1000K 78−10812
$Fe_{40}Ni_{40}P_{14}B_6$, mag. polarisation in approach to ferromag. saturation 80−80560
$Fe_{40}Ni_{40}P_{14}B_6$, magnetoelastic props. 77−16136
$Fe_{40}Ni_{40}P_{14}B_6$, metallic glass, acoustic emission generated during viscous flow 78−39853
$Fe_{40}Ni_{40}P_{14}B_6$, metallic glass, cryst., isothermal annealing behaviour 80−6367
$Fe_{40}Ni_{40}P_{14}B_6$ metallic glass, ferromag. reson., spin waves, thermal ageing and long-range order effects 80−25214
$Fe_{40}Ni_{40}P_{14}B_6$ metallic glass, isothermal viscosity and crystn. 80−49395
$Fe_{40}Ni_{40}P_{14}B_6$ metallic glass, crystn. 80−70127
$Fe_{40}Ni_{40}P_{14}B_6$, Metglas 2826, ferromag. antireson. transmission at 24 GHz, 26 to 270°C 77−69696
$Fe_{40}Ni_{40}P_{14}B_6$, Metglas 2826, magnetising processes 78−10725
$Fe_{40}Ni_{40}P_{14}B_6$, Metglas 2826, acoustic emission during viscous flow 78−42915
$Fe_{40}Ni_{40}P_{14}B_6$, Metglas 2826, stability, crystallisation, ductility meas. 78−47246
$Fe_{40}Ni_{40}P_{14}B_6$, Metglas 2826, amorphous ribbon core, appl. in force transducer 78−93669
$Fe_{40}Ni_{40}P_{14}B_6$, metglas 2826, amorphous, Hall resistivity, thermal cycling and annealing effects 79−38050

metallic glasses continued
$Fe_{40}Ni_{40}P_{14}B_6$ Metglass, spontaneous vibr. modes excited by reversible magnetostriction 79−56587
$Fe_{40}Ni_{40}P_{14}B_6$, Metglas 2826, hot forming 80−84980
$Fe_{40}Ni_{40}P_{14}B_6$, Metglas 2826, amorphous ribbon under tension, mag. domain walls and pulsed magnetisation reversal 80−88825
$Fe_{40}Ni_{40}P_{14}B_6$, quenched amorphous, high field susceptibility and microstructure 77−69506
$Fe_{40}Ni_{40}P_{14}B_6$, thermal stress effect on mag. easy axis 77−80928
$Fe_{40}Ni_{40}P_{14}B_6$, thermal expansion, glass transform. and crystn. temps. 80−2183
$Fe_{40}Ni_{40}P_{16}B_6$, amorphous, kinetics of induced mag. directional order 80−44824
$Fe_{40}Ni_{40}P_{20-x(B)}B_{x(B)}$, ferromagnetic metallic glass, thermal and mech. stability 77−66698
$Fe_{40}Ni_{40}P_xB_{20-y}$, amorphous, mag. props. effect of metalloid elements 79−28658
$Fe_{44}Ni_{40}P_{14}B_6$, homogeneous deformation effect on crystn. and Curie temp. 80−21045
$Fe_cNi_{80-c}P_{14}B_6$, amorphous, annealing effects on mag. props. 79−78383
$Fe_xNi_{1-x}P_{14}B_6$, amorphous, spin-glass regime, magnetoresist. meas. 80−34418
$(Fe_xNi_{1-x})_{80}P_{10}B_{10}$, amorphous, weak itinerant ferromag., Arrott plots 77−73007
$(Fe_xNi_{1-x})_{80}P_{10}B_{10}$, amorphous, magnetisation reversal and domain boundary configs. 80−88809
$(Fe_xNi_{1-x})_{80}P_{14}B_6$, Mossbauer spectroscopy, mag. hyperfine interaction, Curie temps. 78−6617
$Fe_xNi_{80-x}P_{14}B_6$ (x=0, 20, 40, 60, 80), metallic glass, low temp. sp. ht. 80−2588
$Fe_xNi_{80-x}P_{14}B_6$, amorphous, sp. ht. and susceptibility meas., spin glass and mictomag. props. 78−68274
$Fe_xNi_{80-x}P_{14}B_6$, amorphous ferromag., resistivity, mag. contrib., 1.5-50K 79−56182
$Fe_xNi_{80-x}P_{14}B_6$, amorphous ferromag., T^2 saturation in resist. below 0.3K 79−60785
$Fe_xNi_{80-x}P_{14}B_6$, and $Fe_xNi_{80-x}B_{20}$ glass, microhardness, correl. with mag. props. 79−57085
$Fe_xNi_{80-x}P_{14}B_6$ glass, resist., magnetoresist., and thermoelec. power 80−70681
$Fe_xNi_{80-x}P_{14}B_6$ metallic glasses, low temp. resistivities 78−91659
$Fe_xNi_{80-x}P_{14}B_6$, metallic glass, low temp. sp. ht. for spin-glass and spin-cluster-glass regime 80−71071
$(Fe_xNi_{100-y})_{79}P_{13}B_8$, metallic glass, low temp. sp. ht. for spin-glass and spin-cluster-glass regime 80−71071
$(Fe_{0.3}Ni_{0.7})_{0.75}P_{0.16}B_{0.06}Al_{0.03}$, amorphous, spin wave spectrum, neutron scatt. 77−16064
$(Fe_{0.5}Ni_{0.5})_{75}P_{16}B_6Al_3$ glass, struct. relax. as origin of Curie temp. ageing 78−84418
$(Fe_{1-x}Ni_x)_{75}P_{16}B_6Al_3$, amorphous, low temp. elec. resist. 79−56183
$(Fe_{1-x}Ni_x)_{75}P_{16}B_6Al_3$, saturation magnetisation, temp. depend., ferromag. reson. meas. 79−73818
$(Fe_{65}Ni_{35})_{75}P_{16}B_6Al_3$, amorphous, crystn. temp., press. and heating rate depend. 80−70132
$(Fe_xNi_{1-x})_{0.75}P_{0.16}B_{0.06}Al_{0.03}$, thermal expansion 78−43151
$(Fe_xNi_{1-x})_{75}P_{16}B_6Al_3$, spin wave excitations and low temp. magnetisation 79−33468
$(Fe_xNi_{1-x})_{75}P_{16}B_6Al_3$, magnetisation temp. depend., spin wave theory 80−44927
$Fe_xNi_yP_{14}B_6(S_2)$, coiled ribbons, stress relaxation 79−29120
$Fe_{29}Ni_{49}P_{14}B_6Si_{12}$, Metglas fibre reinforced mortar, fracture props. 79−70159
$Fe_{29}Ni_{49}P_{14}B_6Si_2$, crystn. kinetics, DSC expts. 78−26444
$Fe_{29}Ni_{49}P_{14}B_6Si_2$, metallic glass, changes in Curie temp., physical dimensions and mag. anisotropy during annealing 77−85446
$Fe_{29}Ni_{49}P_{14}B_6Si_2$, Metglas 2826B, Hall, elec. resist., magnetisation and heat capacity meas. 78−68019
$Fe_{29}Ni_{49}P_{14}B_6Si_2$, Metglass 2826B, saturation magnetisation, temp. depend., ferromag. reson. meas. 79−73818
$Fe_{72}Ni_8P_{13}C_7$, erosion craters produced by spark machining, scanning microscopy obs. 78−44268
$(Fe_{1-x}Ni_x)_{80}PyB_{20-y}$, local struct. disorder and crystallisation, Mossbauer exam. 79−1728
$(Fe_{1-x}Ni_x)_{77}Si_{10}B_{13}$, amorphous magnetic alloys, density meas. 80−1934
$(Fe_{1-x}Ni_x)_{77}Si_{10}B_{13}$, amorphous, Landau-Ginzburg theory, magnetisation and Curie temp. 80−75700
$(Fe_{1-x}Ni_x)_{78}Si_{10}B_{12}$ amorphous alloys, cold rolled and as-quenched, mag. anisotropy 80−97089
$(Fe_{1-x}Ni_x)_{78}Si_{10}B_{12}$, Hall effect and magnetoresist. *(Japanese)* 77−85199
$Fe_{62.4}Ni_{15.6}Si_7B_{15}$ amorphous ferromagnetic alloy, anomalous magnetisation possible reasons, Mossbauer spectra *(Russian)* 79−78441
$Fe_{1-x}(P,B)_x$, amorphous and crystalline, photoemission and band structure 80−60754
$Fe_{100-x}P_x$, structural analysis of models for amorphous metallic alloys 80−103249
$Fe_{75}P_{25}$ amorphous alloy, atomic struct., computer simulation 80−88043
$Fe_{76}P_{24}$, amorphous alloy, electronic struct., KKR calc. 80−96775
$Fe_{80}P_{20}$, binary amorphous ferromagnet, Mossbauer study 80−34829
$Fe_{80}P_{20}$, mag. props. 77−63125
$Fe_{79}P_{13}B_8$ amorphous alloys, splat cooled, Mn, Cr and V substituted, mag. and transport props. 80−84593
$Fe_{80}P_{14}B_6$, ferromagnetic, low temp. heat capacity meas., electronic, phonon contributions exam. 78−10689
$Fe_{83}P_{17-x(B)}B_{x(B)}$, ferromagnetic, metallic glass thermal and mech. stability 77−66698
$Fe_{75}P_{16}B_6Al_3$, aged metallic glass, Mossbauer effect 79−91318
$Fe_{80}P_{16}B_3C_3$, ferromag. metallic glass, Mossbauer spectra, crystn. 77−12276
$FeP_{13}C_7$, amorphous, exam. of metalloid atom mobility by Auger spectroscopy 78−47575
$Fe_{0.75}P_{0.15}C_{0.10}$, amorphous, mag. excitations and static struct., neutron scatt. obs. 78−68204
$Fe_{75}P_{15}C_{10}$, glassy ferromag., crit. sp. ht. meas. 78−10716
$Fe_{75}P_{15}C_{10}$, mag. excitations, inelastic neutron scatt. 78−10674
$Fe_{75}P_{15}C_{10}$, magnetoelastic props. 77−16136
$Fe_{75}P_{15}C_{10}$, spin echo NMR of ^{31}P 78−2770
$Fe_{80}P_{13}C_7$, amorphous, mag. anisotropy 79−65670
$Fe_{80}P_{13}C_7$, amorphous, rapidly quenched, magnetic props., effect of annealing 77−16701
$Fe_{80}P_{13}C_7$, amorphous ferromag. ribbons, US rel. meas. 77−80582

metallic glasses continued
$Fe_{80}P_{13}C_7$ amorphous ferromag. ribbons, change of permeability by heat treatment 77−85493
$Fe_{80}P_{13}C_7$, amorphous ferromagnetic alloy, isothermal annealing effect on static magnetic props. *(Japanese)* 79−52398
$Fe_{80}P_{13}C_7$, amorphous ribbon, giant ΔE effect, magnetomech. coupling factor 77−8379
$Fe_{80}P_{13}C_7$, metallic glass, crystallisation kinetics 77−66637
$Fe_{80}P_{16}C_3B_1$ amorphous filament, produced by glass coated melt spinning, mech. props. 78−15483
$Fe_{80}(P_{13}C_7)_{20-y}B_y(Si_y)$, density, microhardness, and crystn. temp., comp. depend. 80−84093
$Fe_{80}P_{20-x}C_x(Si_x)(Ge_x)$, amorphous, size effect of metalloids on mag. props. 80−84594
$Fe_xPd_{80-x}Si_{20}$, structural and mag. heterogeneities 80−80484
$Fe_xPd_{82-x}Si_{18}$, amorphous, magnetisation, magnetoresist., spin glass and ferromag. phases 80−34697
$Fe_xPd_{82-x}Si_{18}$ metallic glass, mag. phase diagram, weak ferromagnet-spin glass transition 80−54893
$Fe_xPd_{82-x}Si_{18}$ metallic glass, long range interaction and spin wave interactions 80−65949
$Fe_xPd_{82-x}Si_{18}$ metallic glass, mag. transitions, weak ferromagnetism 80−100583
$Fe_{75}Si_{15}B_{10}$, amorphous ferromag. ribbons, US rel. meas. 77−80582
$Fe_{75}Si_{15}B_{10}$, amorphous ferromagnetic alloy, isothermal annealing effect on static magnetic props. *(Japanese)* 79−52398
$Fe_{78}Si_{10}B_{12}$ amorphous ferromag. ribbons, change of permeability by heat treatment 77−85493
$Fe_{78}Si_{10}B_{12}$, amorphous alloy crystallisation study *(Japanese)* 78−9959
$Fe_{78}Si_{10}B_{12}$ amorphous ribbons, magnetomechanical coupling constant and Young's modulus, mag. annealing 79−15333
$Fe_{79.5}Si_{15}B_{19}$, evaluation of hyperfine parameter distribs. from overlapped Mossbauer spectra at room temp. 79−99804
$Fe_{80}Si_5B_{15}$, amorphous, soft mag. props. and potential uses 80−88807
$(Fe_{1-x}Si_x)_{1-y}By$, metallic glass, mag. props., crystallisation 80−65885
Fe_xSn_{1-x}, amorphous alloy stability, comp. and temp. depend. 79−19156
Fe_xSn_{1-x}, amorphous alloy, elec. resistivity, Ziman's formula 79−15130
Fe_xSn_{1-x}, amorphous alloy, Mossbauer spectra, charge transfer and atomic vol. effects 80−39959
Fe_xSn_{1-x}, amorphous film, struct. and mag. props. 80−65972
$Fe_{80}b_{20-x}C_x(Si_x)(Ge_x)$, amorphous, size effect of metalloids on mag. props. 80−84594
Ga-Mg(Al), metallic glasses, stability, microscopic calcs. 79−32914
Gd-Al(C)(Cu)(Ga)(Ni)(Pd)(Rh) alloys, mag. and elec. props. 80−80499
Gd-Fe amorphous alloys, mag. props. and crystn. 79−90557
Gd-Fe(Co), thin amorphous system, resistance and hardness, chemical comp. and temp. effect 80−15625
$Gd_{80}Au_{20}$, amorphous ferromag., critical phenomena and mag. props. 77−85469
$Gd_{65}Co_{35}$, amorphous, amg. ordering, susceptibility, magnetisation and hysteresis meas. 78−68190
GdFe, amorphous films, thermal stability of mag. props. *(Japanese)* 79−47307
$(Gd_{65}Fe_{35})_{100-x}B_x$, mag. props. 79−73693
$(Gd_{65}Fe_{35})_{90}B_{10}$, amorphous, mag. props., Mossbauer study 80−93093
GdFeBi, amorphous ferrimag. films, magneto-optical props., optical spectra 80−76008
Hf-Fe(Cu), amorphous, thermal stability, crystn., DSC and elec. resist. study 80−107060
Hf-Ni(Co), amorphous, formation, decomposition and elec. transport props. 80−20143
Hf-V foil, rapidly quenched and heat treated, supercond. props. 80−54852
$Hf_{1-x}Fe_x$ amorphous alloys, formation, crystallisation and electrical resistivity 80−96838
La-Al alloys, internal friction, relaxation process 80−92607
La-Au, splat-quenched, Mossbauer effect and elec. resist., amorphous struct. 80−84676
La-Fe, amorphous alloy film, spin reson. meas. 78−68389
La-Fe bulk amorphous alloys, mag. props. *(Japanese)* 79−95588
$La_{1-x}Au_x$, supercond. splat cooled amorphous alloy, sp. ht. 78−19182
$La_{0.8}Ga_{0.2}$, amorphous, Hall effect at 4.2, 78K and room temps. 79−60797
$La_{75}Ga_{25}$, amorphous, local symmetry around glass-former sites, elec. quadrupole effects, NMR 80−80618
$La_{80-x}Gd_xAu_{20}$, amorphous dil. alloy, RKKY interaction, magnetisation meas. 77−32207
$La_{80-x}Pr_xAu_{20}$, mag. and supercond. props. 80−75713
Lu-Fe, amorphous alloy film, spin reson. meas. 78−68389
Mg-Ga, metastable cryst. and glassy phases, X-ray struct. anal. and electron microscopy *(German)* 79−46601
Mg-Ga system, thermodynamic props. of metastable and glassy phases *(German)* 79−52743
Mg-Zn, metallic glass, stability, microscopic calcs. 79−32914
Mg-Zn metallic glass, hardness, elastic moduli, density, cryst. temp., mech. props., for flywheel appl. *(Dutch)* 78−52878
$Mg_{70}Zn_{30}$ metallic glass, struct. and dynamics 79−37632
$Mg_{74}Zn_{26}$, glass, exam. of crystallisation 78−71681
$Mn_{46}Co_{54}$, amorphous alloy prep. by high-rate sputtering, struct. and prop. characteris. 79−24462
$Mn_xPd_{82-x}Ge_{18}$ amorphous alloys, elec. resistivity and magnetoresistivity 79−51543
Mo-based metallic glass development 80−89172
Mo-Ru(-Si), amorphous superconductors, prep. by electron beam evaporation and liq. quenching, crit. temp. 80−103776
$Mo_{70}B_{30}$, amorphous, local symmetry around glass-former sites, elec. quadrupole effects, NMR 80−80618
$(Mo_{0.6}Ru_{0.4})_{82}B_{18}$, supercond. metallic glass, neutron irrad. effects 80−29060
$Mo_{48}Ru_{32}B_{20}$, amorphous, local symmetry around glass-former sites, elec. quadrupole effects, NMR 80−80618
$(Mo_{0.6}Ru_{0.4})_{0.8}G_{0.2}$-Fe (G=P,B), amorphous supercond., upper crit. field as function of temp. 79−73646
$(Mo_{1-x}Ru_x)_{80}P_{20}$, amorphous alloys, superconductivity, mag. susceptibility and electronic props., liq. quenching 78−88057
$(Mo_{1-x}Ru_x)_{80}P_{20}$, amorphous, liq. quenched, mag. susceptibility, supercond. and electronic props. 79−56376
$(Mo_{0.6}Ru_{0.4})_{80}Si_{10}B_{10}$, amorphous supercond. matrix, flux pinning by MoRu precips. 80−65756
$Mo_{70}Si_{20}B_{10}$, amorphous alloys obtained by liq. quenching, superconductivity 80−75670

metallic glasses continued
Nb-Ir(Rh) system glasses, form., crystn. and microhardness, resist. obs. 80 - 89178
Nb-Ni, amorphous, thermal stability, crystn., DSC and elec. resist. study 80 - 107060
Nb-Ni, amorphous thin film, vapour quenched, elec. resistivity and thermoelectric power 79-33275
Nb-Ni, glassy alloy, struct. anal. using X-ray diffr. 79-51004
Nb-Ni, synthesis by vapour quenching, and struct. 78-11111
Nb-Ni amorphous alloys, glass transition and ductility, O additions effect 80-75168
Nb-Ni glass, photoemission spectra meas. 77-55867
Nb-Ni glasses, struct. factor temp. depend. 80-28920
Nb-Ni metallic glass, hardness, elastic moduli, density, cryst. temp., mech. props., for flywheel appl. *(Dutch)* 78-52878
Nb-Ni metallic glass, temp. depend. of resistivity 78-47759
Nb-Si(-V)(Zr)(Mo)(Ta)(W)(C)(B)(Ge), ductile amorphous, superconductivity 80-60131
Nb_3(Al,Ge) and Nb_3(Al,Si), liq. quenched, supercond. props. 80-84580
$Nb_{40}Fe_{40}P_{14}B_6$, Metglas 2826, explosive compaction, mech. props. 80-89176
Nb_3Ge, metallic glass, internal friction peak obs. 78-79666
$Nb_3Ge(Si)$, amorphous films, thermally-activated internal friction peaks, structural obs. 80-80147
$Nb_{0.55}Ir_{0.45}$ metallic glass, Young's modulus meas. by impulse induced resonance technique 80-40411
$Nb_{0.4}Ni_{0.6}$, pair distrib. function, temp. depend., rel. to glass transition 80-24368
$Nb_{40}Ni_{60}$, 3 MeV Ni^+ ion implantation, electron microscope exam. of ion damage 78-91365
$Nb_{40}Ni_{60}$, amorphous, produced by Ni^+ implantation, damage distrib. 80-107062
$Nb_{60}Ni_{40}$, metallic glass, obs. of temp. depend. of struct. factor 78-87624
$Nb_{50}Ni_{50-x}Fe_x$, amorphous, mag. ordering and local random anisotropy 78-68273
$Nb_{50}Ni_{50-x}Fe_x$, magnetically dil. glass, 3d moments, mag. susceptibility and magnetisation meas. 79-95574
$Nd_{64}Co_{36}$, amorphous, amg. ordering, susceptibility, magnetisation and hysteresis meas. 78-68190
$Ni_{75}Si_8B_{17}$, amorphous alloy, crystallisation study *(Japanese)* 78-9959
Ni based alloy, amorphous, liq. quenched, struct., thermal stability and mech. props. 80-88059
Ni, splat quenched, gaseous impurities effect on struct. 77-4042
Ni-B, amorphous alloys, phase diagram 79-96002
Ni-B, X-ray obs. of struct. 79-1399
Ni-B thin film glasses, mag. props. and corrosion resist. 80-80576
Ni-base metallic glasses, elastic const. 77-66671
Ni-C-W-Cr(-Mo), Vickers hardness and crystallisation temp. 80-16361
Ni-Cr-P, amorphous, corrosion behaviour, immersion tests and electrochem. meas. *(Japanese)* 80-85085
Ni-Fe based, Curie pt. anomalies 80-60256
Ni-Fe metallic glass, METGLAS 2826, creep props. 79-15746
Ni-Mo-B metallic glass ribbons, tensile strength, crystn. temp. 80-89173
Ni-Mo-C(-Cr)(W), Vickers hardness and crystallisation temp. 80-16361
Ni-Nb amorphous alloy, transformation to crystalline state, ion emission microscope study *(Russian)* 79-82158
Ni-P, acoustic wave vel. log. temp. depend. *(French)* 77-72659
Ni-P, amorphous, reversible effects of temp. on struct. 78-34442
Ni-P, amorphous alloy, elec. resistivity 78-91654
Ni-P, amorphous electrodeposited alloys, phase-separation *(Japanese)* 80-54140
Ni-P, crystn. kinetics by differential scanning calorimetry 78-91257
Ni-P, electrodeposited film, thermal anal., occlusion of gases rel. to mag. props. 80-59823
Ni-P, NMR expts. and interpretation 79-8060
Ni-P, struct. obs. by X-ray diffr., low temp. annealing and deform. effects 79-56995
Ni-P alloy, electrodeposited, heat induced struct. changes *(Japanese)* 78-15433
Ni-P alloys, amorphous, electrical transport, appl. of extended Ziman theory 77-47787
Ni-P amorphous alloys, electrodeposited and melt-quenched atomic and electronic structures 80-88062
Ni-P film, amorphous, ion implanted, struct. and domain struct. obs. 79-91272
Ni-P metal metalloid glass forming alloys, gram atomic volumes 78-38628
Ni-P-B alloy, giant moments and short-range order 77-4499
Ni-Pd-P, electronic structure, pulsed NMR study 80-75869
Ni-Pd-P, Ni-Pt-P, amorphous and electronic structs., NMR Knight shifts and linewidths meas. 78-68400
Ni-Pd-P amorphous alloys, tensile deform. 77-32646
Ni-Pd-Si, amorphous, low-field mag. susceptibility meas., 4.2-580K 79-61057
Ni-Pt-P, electronic structure, pulsed NMR study 80-75869
Ni-Si-B, amorphous, thermal stability of ductility 80-76327
Ni-Si-B, embrittlement by crystallisation *(Japanese)* 78-48513
Ni-Si-B amorphous alloys with metalloid elements, embrittlement/crystn. relationship *(Japanese)* 79-96134
Ni-Ta (70, 30 wt.%) metallic glass, struct. and crystn. *(Russian)* 80-70136
Ni-Ti-P, amorphous, corrosion behaviour, immersion tests and electrochem. meas. *(Japanese)* 80-85085
Ni-Y, amorphous, resist. and magnetoresist. meas., weak itinerant ferromagnet 78-68018
Ni-Zr, amorphous phase form. in Zr-poor region, hardness and fracture strength *(Japanese)* 80-84914
$Ni_{100-x}B_x$, amorphous, mag. struct., mag. susceptibility meas. 80-80485
$Ni_{100-x}B_x$, rapidly quenched, mag. moment, temp. and comp. depend. 78-47957
$Ni_{50}Co_{40}P_{10}$ amorphous film, spin wave excitation, ferromagnetic resonance study 80-50198
$(Ni_{1-c}Co_c)_{0.78}P_{0.14}B_{0.08}$, amorphous, mag. props., local environment model 77-12119
$Ni_{40}Fe_{40}B_{20}$ glass alloy, rapidly quenched, explosive welding to A516-70 steel and to itself 78-39954
$Ni_{50}Fe_{30}B_{20}$, magnetostriction, temp. depend. 78-91921
$Ni_{35}Fe_{30}Cr_{15}P_{14}B_6$, amorphous, anodic polarisation and localised corrosion 77-21310
$Ni_{36}Fe_{32}Cr_{14}P_{12}B_6$, crystallisation 79-77520

metallic glasses continued
$Ni_{36}Fe_{32}Cr_{14}P_{12}B_6$, amorphous, electrochem. corrosion in chloride solns. 80-50763
$Ni_{36}Fe_{32}Cr_{14}P_{12}B_6$ metallic glass, mech. props. and thermal stability 80-76362
$(Ni_{100-x}Fe_x)_{79}P_{13}B_8$, amorphous dil. alloys, spin glasses, magnetisation meas. 79-61178
$Ni_{40}Fe_{40}P_{14}B_6$, amorphous alloy, microstruct. study of crystallisation 77-86062
$Ni_{40}Fe_{40}P_{14}B_6$ metallic glass alloy, US spot welding to Cu 79-21730
$Ni_{80-x}Fe_xP_{14}B_6$, amorphous alloy, resistivity variations near critical temp. 79-73488
$(Ni_{99}Fe_1)_{79}P_{13}B_8$, amorphous, low temp. sp. ht., mag. contribs. 80-80552
$(Ni_xFe_{1-x})_{80}P_{10}B_{10}$, Curie temp., press. effect 80-75833
$Ni_{49}Fe_{29}P_{14}B_6Si_2$ glass, flow and failure 80-40438
$Ni_{78-x}M_xSi_{10}B_{12}$ (M=refractory metal), glass form. and thermal stability 80-79703
$(Ni_{0.75}Mn_{0.25})_{82}Si_{10}B_8$, amorphous, exchange anisotropy, mag. susceptibility meas., 4.2K to room temp. 80-11186
$Ni_{60}Nb_{40}$, stability, crystallisation, ductility meas. 78-47246
$Ni_{62}Nb_{38}$, metallic glass, struct., neutron diffr. study 80-54148
NiP amorphous alloy, heat treatments influence on opt. props., struct. and DC resist. obs. 80-80892
$Ni_{76}P_{24}$, thermopower and resist. meas. 80-20145
$Ni_{77}P_{23}$, struct. relax., X-ray expts. 79-1400
$Ni_{78}P_{22}$, amorphous metallic alloy, US attenuation 78-75789
$Ni_{80}P_{20}$, amorphous, struct. factor temp. depend., X-ray diffr. study *(Japanese)* 79-51005
$Ni_{80}P_{20}$ amorphous alloy, liquid-quenched structure 77-1082
$Ni_{80}P_{20}$, mag. props. 77-63125
$Ni_{81}P_{19}$, amorphous alloys, electronic struct., γ-ray Compton scatt. study *(Japanese)* 80-84422
$Ni_{78}P_{14}B_8$, amorphous, local symmetry around glass-former sites, elec. quadrupole effects, NMR 80-80618
$Ni_{78}P_{14}B_8$, $Ni_{80}P_{12}B_8$, amorphous mag. clusters, sp. ht. meas. 78-68274
$Ni_{80}P_{14}B_6$, low temp. heat capacity meas., electronic, phonon contributions exam. 78-10689
NiPBAl, metallic glass, viscous flow, alloying effect 78-79793
$(Ni_{0.5}Pd_{0.5})_{82}P_{18}$ amorphous alloy, liquid-quenched, crystn. kinetics, effect of thermal history 80-100175
$(Ni_{0.5}Pd_{0.5})_{82}P_{18}$ amorphous alloy, liquid-quenched, crystn. kinetics, nucleation 80-100176
$(Ni_5Pd_5)_{82}P_{18}$, amorphous alloy, crystallisation 77-89382
$(Ni_5Pd_5)_{82}P_{18}$, phase separated, exam. of crystallisation by differential thermal analysis 78-87623
$(Ni_5Pd_5)_{82}P_{18}$ amorphous alloy, glass transition temp. 77-84909
$(Ni_xPt_{1-x})_{75}P_{25}$, ^{31}P and ^{195}Pt NMR 77-12211
$Ni_{78}Si_{10}B_{12}$, amorphous, struct. factor temp. depend., X-ray diffr. study *(Japanese)* 79-51005
$Ni_{40}Ti_{60}$, amorphous, chem. short-range-order, X-ray and neutron scatt. obs. 80-96447
$Ni_{100-x}Zr_x$, (x=34-40) metallic glass, cryst., isothermal annealing behaviour 80-6367
Ni_2Zr_{1-x}, crystallisation kinetics, elec. resist. and mag. susceptibility meas. 80-103659
$Ni_{64}Zr_{36}$ and $Ni_{62}Ti_{29}Zr_9$, H-sorption, X-ray and DSC obs. 80-49526
Pb, film, polycryst. or amorphous, thermal cond., 0.5-11K 78-39260
Pb-Ni-Si, metallic glass, electron irrad., positron annihilation radiation, angular correlation study 78-84678
Pb-Si-Sb amorphous alloys, electrical resistometric detection of relaxation 79-60278
$Pb_{0.9}Cu_{0.1}$, film, polycryst. or amorphous, thermal cond., 0.5-11K 78-39260
Pd-Ag-Si alloys, amorphous, crystn. kinetics, DSC meas. 80-1933
Pd-Au-Si, influence of struct. on elec. resist. of glass forming alloys 80-65518
Pd-Cu-Si, glass form., crit. cooling rate 80-75169
Pd-Cu-Si, metallic glass, miscibility limits, computer study 79-65198
Pd-Cu-Si glass, cold drawn, serrated plastic flow, optical and SEM study 79-79052
Pd-Cu-Si metallic glass, energy loss spectra and Auger spectra 78-23563
Pd-Ge, appl. of EXAFS methods for struct. determ. 79-37624
Pd-Ge, metallic glass, theoretical studies on structural models 79-37633
Pd-Ge, short range order obs. for $Pd_{80}Ge_{20}$ and $Pd_{78}Ge_{22}$, EXAFS expts. 78-55815
Pd-Ni-P, amorphous, elec. resistivity negative temp. coeff., CAP calcs. 79-42515
Pd-Ni-P, metallic glass, viscous flow, alloying effect 78-79793
Pd-Ni-P metallic glass, energy loss spectra and Auger spectra 78-23563
Pd-Si, amorphous, neutron irradiated, small angle X-ray scatt. study 79-14850
Pd-Si, amorphous, struct., crystn. and Hall effect meas. 80-75178
Pd-Si, amorphous, viscoelastic behaviour *(Japanese)* 77-86110
Pd-Si, amorphous alloys, elastic props. and temp. coeff. of delay time, appl. to US delay lines *(Japanese)* 79-96069
Pd-Si, amorphous metallic, sound propag. at low temps. 77-72656
Pd-Si, amorphous metallic glass, with defined local coordination, struct. model 80-84092
Pd-Si, amorphous $Pd_{0.8}Si_{0.2}$, struct. anal. by dense random packing model 79-51003
Pd-Si, amorphous thin films, laser irrad., metastable phases 80-96622
Pd-Si, compositional study on short-range struct. 80-84095
Pd-Si, internal friction, shear modulus 77-25085
Pd-Si, metallic glass, phonon propagation at low temp. 78-87756
Pd-Si, metallic glass, theoretical studies on structural models 79-37633
Pd-Si, struct. obs. by X-ray diffr., low temp. annealing and deform. effects 79-56995
Pd-Si, thermal cond. 0.1-30K 77-20286
Pd-Si, XPS and UPS studies 79-74062
Pd-Si alloys, metallic glass, structural model 79-14690
Pd-Si amorphous alloy, heat treated, low temp. lattice sp. ht. 80-75368
Pd-Si amorphous alloy, neutron irradiation effects *(Japanese)* 77-84806
Pd-Si amorphous alloys, anal. of crystallisation kinetics 79-32912
Pd-Si glasses, changes in density of states with alloys comp., UPS obs. 80-50531
Pd-Si metallic glass, high-resolution electron microscopy 80-84097
Pd-Si-Cu metallic glass tips, appl. as electron field emission source 79-8229

metallic glasses continued
Pd-Si-Fe amorphous alloy, Mossbauer spectra, struct. and bonding 80−7224
Pd-Si-Sb, amorphous, phase separation and crystallisation 79−51002
Pd-Si(-Cu), amorphous, Hall effect meas. and electronic struct. 80−75551
Pd-Si(-Cu) amorphous ribbons, low temp. sp. ht., density of states trends 80−79957
Pd-Si(−Cu), glassy, liq. and cryst., mag. and elec. props. 77−66249
Pd-Zr, metallic glasses, valence band struct. investigation 80−11533
$Pd_{78}Ag_4Si_{18}$, amorphous, crystallisation kinetics 77−35487
$Pd_{82-x}Ag_xSi_{18}$, amorphous, roller-quenching conditions determ. 77−21051
$(Pd_{80}Au_7Si_{13})/Fe_{30}$, compositionally modulated amorphous film, diffusion, struct. relax. 80−103518
$Pd_{0.775}Cu_{0.06}Si_{0.165}$ alloys, glassy and crystallised, low-temp. specific heat 79−60516
$Pd_{0.775}Cu_{0.06}Si_{0.165}$ glass, optical props. in energy range 0.67 to 5.6 eV 80−34872
$Pd_{0.775}Cu_{0.06}Si_{0.165}$, undercooled metallic melt, viscous behaviour 77−66037
$Pd_{68.5}Cu_{15}Si_{16.5}$ glass, elec. resist., struct. and mag. props. 79−65423
$Pd_{77.5}Cu_6Si_{16.5}$, cold drawn wires, surface markings, fracture stresses 79−56997
$Pd_{77.5}Cu_6Si_{16.5}$, heat of crystn. and viscous behaviour 80−75166
$Pd_{77.5}Cu_6Si_{16.5}$ metallic glass, diffusion of Au 78−55983
$Pd_{77.5}Cu_6Si_{16.5}$, metallic glass, composition, mech. props., simulation 80−49117
$Pd_{77.5}Cu_6Si_{16.5}$ metallic glass wire, cold drawing 80−50650
$Pd_{77.5}Cu_6Si_{16.5}$, ternary miscibility gap, simulation, dispersed phase composite form. 80−54379
$Pd_{77.5}Cu_{6.0}Si_{16.5}$ metallic glass, glass transition temp., cooling rate depend. 80−75181
$Pd_{77.6}Cu_6Si_{16.5}$, metallic glass, viscosity meas. from rates of thermal transformations 78−26713
$Pd_{781}Cu_{55}Si_{164}$, erosion craters produced by spark machining, scanning microscopy obs. 78−44268
$Pd_{781}Cu_{55}Si_{164}$, liquid quenched metallic glass, wear resistance 79−66079
$Pd_{48}Ni_{32}P_{20}$, metallic glass, viscosity meas. from rates of thermal transformations 78−26713
Pd_8Si_{19} and $Pd_{84}Si_{16}$, optical refl. spectra and optical consts. 79−87464
PdSi alloys, amorphous thermal behaviour and crystallisation kinetics 78−26446
PdSi, amorphous, crystn. kinetics 79−99078
PdSi, amorphous, structural relaxation enhancement following stress reduction 80−3118
$Pd_{0.8}Si_{0.2}$, amorphous ribbon, struct. factor anisotropy, pulsed neutron diffr. study 78−87619
$Pd_{0.8}Si_{0.2}$, liquid and amorphous states, short-range order comparison 77−1069
$Pd_{0.81}Si_{0.19}$, amorphous, partial densities of states, XPS, UPS and AES meas. 79−95315
$Pd_{80}Si_{20}$, amorphous, struct. factor temp. depend., X-ray diffr. study *(Japanese)* 79−51005
$Pd_{80}Si_{20}$, amorphous, structural changes with neutron irrad., X-ray scatt. obs. 80−33898
$Pd_{80}Si_{20}$, amorphous alloy crystn., high press. effect 78−95001
$Pd_{80}Si_{20}$, amorphous alloy, partial struct. functions, X-ray, electron and neutron diff. studies *(Japanese)* 80−88050
$Pd_{80}Si_{20}$ amorphous alloy, skip deform. and crit. shear stress, using tensile testing machine 80−89321
$Pd_{80}Si_{20}$, deform. localisation, plastic instabilities and fracture 80−89320
$Pd_{80}Si_{20}$, electronic struct. calcs. 79−87032
$Pd_{80}Si_{20}$, high-resolution XPS study, electronic state struct. 80−29846
$Pd_{80}Si_{20}$ metallic glass, vibrational spectrum, inelastic neutron scatt. meas. 79−60465
$Pd_{80}Si_{20}$, metallic glass, composition, mech. props., simulation 80−49117
$Pd_{80}Si_{20}$ metallic glass, inelastic deform., free energy spectra 80−71699
$Pd_{80}Si_{20}$, plastic flow, fracture, slanted necking and elongation at high temps. 79−57057
$Pd_{80}Si_{20}$, shear band form. 78−68756
$Pd_{80}Si_{20}$, struct. relax., X-ray expts. 79−1400
$Pd_{80}Si_{20}$, struct. simulation 78−38624
$Pd_{80}Si_{20}$, tensile deform., shear band form., high-speed cinematographic obs. 80−89322
$Pd_{82}Si_{18}$ glassy, long term creep tests, isoconfigurational viscosity rel. to annealing treatment 79−66122
$Pd_{82}Si_{18}$, stress/strain rate depend. of homogeneous flow 80−71687
$Pd_{82.5}Si_{17.5}$, struct. comparison with liq., X-ray diffr. 77−24275
$(Pd_{85}Si_{15})_{61}/(Fe_{85}B_{15})_{39}$, compositionally modulated amorphous film, diffusion, struct. relax. 80−103518
PdSiCu, amorphous, US attenuation and vel. studies 80−19881
PdSiCu, amorphous, US attenuation and vel. studies at low temps. 80−88278
$Pd_{0.775}Si_{0.165}Cu_{0.06}$, metallic glass, intensity-depend. US attenuation at low temps. 78−79671
$Pd_{0.775}Si_{0.165}Cu_{0.06}$, metallic glass, 0.01-10K, relax of tunnelling systems by conduction electrons, US expts. 79−14889
$Pd_{0.775}Si_{0.165}Cu_{0.06}$, resist. minimum associated with mag. impurities 79−56187
$Pd_{0.78}Si_{0.16}Cu_{0.06}$, phonon propagation below 1K 78−71824
$Pd_{1-x-y}Si_xCu_y$, glassy, low temp. specific heat 78−83969
$Pd_{18}Si_{14}Cu_6$, glass, changes in density of states with alloys comp. UPS obs. 80−50531
$Pd_{77}Si_{17}Cu_6$, amorphous, struct. changes due to cold rolling and low temp. annealing 79−66072
$Pd_{78}Si_{16}Cu_6$, hardness, elec. cond., photo emission, and mag. props. *(Norwegian)* 79−32909
$Pd_{80}Si_{17}Cu_3$, glass, changes in density of states with alloys comp., UPS obs. 80−50531
$Pd_{82-x}V_xSi_{18}$, amorphous, effect of structural relax. on elec. resist. 79−56186
$Pd_{82-x}V_xSi_{18}$, metallic glasses, effect of press. on elec. resist. 80−6805
$Pd_{30}Zr_{70}$, amorphous alloys, supercond. transition temp., press. depend. 80−84524
$Pd_{35}Zr_{65}$, mag. susceptibility meas. 80−75740
Pr-Ni, amorphous, thermal stability, crystn., DSC and elec. resist. study 80−107060
Pt-Ni-P, metallic glass, viscous flow, alloying effect 78−79793
Pt-Si, amorphous thin films, laser irrad., metastable phases 80−96622
metallic glasses continued
$Pt_{45}Ni_{30}P_{25}$, metallic glass, viscosity meas. from rates of thermal transformations 78−26713
$Rb_{1-x}O_x$, metallic glass, prep., elec. props. and struct. 78−67652
Sr containing alloy systems, prep., glass form., thermal props. 79−24461
Ta-Co(Ni)(N)(Ar), amorphous metal films, struct. and elec. characterisation 79−87017
Ta-Ir(Rh) system glasses, form., crystn. and microhardness, resist. obs. 80−89178
Te-Pb, amorphous, obtained by splat cooling, crystallisation, TEM obs. 77−66638
Te-Pb (20 at.%) alloy, amorphous, obtained by rapid cooling from liq. state, crystn. behaviour 78−26445
Th-Cu, amorphous, thermal stability, crystn., DSC and elec. resist. study 80−107060
Th-Fe (20 to 70 at.%), amorphous alloy, electrical resistivity and thermal stability 80−33901
Ti-Be, metallic glass form. and props. 80−16219
Ti-Be-Si glass ribbons, physical and mech. props. 78−95767
Ti-Be-Zr base, temp. depend. of resist., rel. to resist. thermometer appl. 77−82532
Ti-Nb-Si, amorphous alloy, supercond. props. and crystn. behaviour, TEM and DTA study *(Japanese)* 80−84536
Ti-Ni amorphous alloys, glass transition and ductility, O additions effect 80−75168
Ti-Ni-Si metallic glass, prep., thermal and mech. props. 78−64497
Ti-Si amorphous alloy, melt-quenched, transform. studies and mech. props. 80−100838
η-$Ti_3Be_3(O,N)_x$, formation and struct. 79−73151
$Ti_{50}Be_{40}Zr_{10}$, amorphous, thermopower meas., Nordheim-Gorter relations 79−99535
$Ti_{50}Be_{40}Zr_{10}$, amorphous, crystn. temp., press. and heating rate depend. 80−70132
$Ti_{50}Be_{40}Zr_{10}$ glass, mech. props., X-ray diffr. exam. 78−11292
$Ti_{50}Be_{40}Zr_{10}$, Metglas 2204, stability, crystallisation, ductility meas. 78−47246
$Ti_{70}Co_{20}B_{10}$, amorphous alloys, crystn. behaviour, TEM study *(Japanese)* 80−84087
$Ti_{70}Fe_{20}B_{10}$, amorphous alloys, crystn. behaviour, TEM study *(Japanese)* 80−84087
$Ti_{0.60}Ni_{0.40}$ metallic glass, Young's modulus meas. by impulse induced resonance technique 80−40411
$Ti_{70}Ni_{20}B_{10}$, amorphous alloys, crystn. behaviour, TEM study *(Japanese)* 80−84087
U-Co(Ce)(Fe)(Mn)(Ni)(V) metallic glasses, glass form. and thermal stability 80−75183
W, laser-irrad., plasma electron energy profile steepening, polarimetry obs. 78−34349
W-Cu(N) amorphous metal films, struct. and elec. characterisation 79−87017
W-Ru based refractory transition metal-metalloid glass, struct. 80−1938
$W_{50}Fe_{50}$ glassy alloy, refractory, triode sputtered 80−75185
$W_{70}Si_{20}B_{10}$, amorphous alloys obtained by liq. quenching, superconductivity 80−75670
Y-Co, amorphous alloy film, spin reson. meas., exchange stiffness 78−68389
Y-Fe(Co), amorphous, thermal stability, crystn., DSC and elec. resist. study 80−107060
Y-Ni amorphous alloy, spontaneous magnetisation, Curie temp. and paramag. susceptibility 78−68189
$(Y_{65}Fe_{35})_{100-x}B_x$, mag. props. 79−73693
Zr-Be, metallic glass form. and props. 80−16219
Zr-Co(Fe), amorphous alloy film, spin reson. meas. 78−68389
Zr-Cu, amorphous alloy, sheet production by plasma spray quenching 77−44193
Zr-Cu, glass transition temp., crystallisation temp., exothermal relaxation effect 79−52747
Zr-Cu, glassy alloy, struct. anal. using X-ray diffr. 79−51004
Zr-Cu amorphous alloys, glass transition and ductility, O additions effect 80−75168
Zr-Cu(Ni)(Co)(Fe) metallic glasses, glass form. and thermal stability 80−75177
Zr-Fe, amorphous alloy quenched by levitation method, crystallisation 79−55669
Zr-Pd, electronic props. and supercond. 79−73486
Zr-Ti-Be metallic glass, phase separation 80−97464
Zr-V foil, rapidly quenched and heat treated, supercond. props. 80−54852
$Zr_{70}Co_{30}$, low temp. resist., supercond. T_c 79−38235
$Zr_{70}Co_{30}$, $Zr_{70}Fe_{30}$, $Zr_{70}Ni_{30}$ and $Zr_{70}Pd_{30}$ amorphous alloys, struct. factors and radial distrib. functions 80−84096
$Zr_{0.35}Cu_{0.65}$ metallic glass, Young's modulus meas. by impulse induced resonance technique 80−40411
$Zr_{65}Cu_{35}$, low temp. resist., supercond. T_c 79−38235
$Zr_{40}Cu_{50}Fe_{10}$, magnetically dil. glass, 3d moments, mag. susceptibility and magnetisation meas. 79−95574
$Zr_{40}Cu_{60-x}Gd_x$, magnetically dil. glass, 4f moments, mag. susceptibility and magnetisation meas. 79−95575
$Zr_{0.475}Cu_{0.475}M_{0.05}$, glass transition temp., comp. depend. 80−79702
$Zr_{40}Cu_{60-x}M_x$ (M=Fe,Mn,Gd,Tb), amorphous, mag. ordering and local random anisotropy 78−68273
$Zr_{40}Cu_{50}Mn_{10}$, magnetically dil. glass, 3d moments, mag. susceptibility and magnetisation meas. 79−95574
$Zr_{40}Cu_{60-x}Tb_x$, magnetically dil. glass, 4f moments, mag. susceptibility and magnetisation meas. 79−95575
$Zr_{70}Ni_{30}$, low temp. resist., supercond. T_c 79−38235
$Zr_{0.7}Pd_{0.3}$, supercond., sp. ht. and thermal cond., 0.1-10K 78−26991

metallic thin films
see also discontinuous metallic thin films; electronic conduction in metallic thin films; metallic epitaxial layers; metallic glasses; metallisation
1/f fluctuations *(Japanese)* 78−43448
1/f noise, nonlinear mechanism 80−96955
1/f noise mechanism, review of experimental investigations 78−64076
1/f noise theory 78−34872
absolute work function meas. by field-emission retarding-pot. device 77−59322
adhesion, locus of failure, bond failure in adhesive joints, experimental methods 80−50801
adhesion determination, on polymer base, US test device 79−91865

metallic thin films continued
adhesive force at small separation 77−35823
adsorbed molecules, surface plasmon enhanced light absorption 80−40176
adsorption studies using modulated surface plasmon reson. method 79−82439
alkali metal, inert gas impurities, metal-insulator transition, optical absorption and cond. 77−24598
alkali metal, inert gas impurities, optical excitation spectra obs. 77−24876
alkali metal, inert gas impurities, optical spectar, rel. to inert gas solids 77−24878
alkali metal, inert gas impurities, sharp pair spectra and excited states 77−24877
alkali metal, inert gas impurities, X-ray edge and recoil problems in optical excitation spectra 77−24879
amorphous, structural and amorphous props. 78−84323
amorphous metal-metalloid alloys production by ion implantation, TEM study 80−15128
anomalous optical props., interpretation *(French)* 80−60692
antireflection coatings on metal layers for photolithographic purposes 79−76837
apodising and attenuating filters, phase shifts and aberrations 78−90514
atomic absorption analysis with laser atomisation 80−30308
attenuated total reflection minima, correlation with surface polariton modes, computational study 78−31265
Au film, diffusion of Ag along grain boundaries, scanning Auger microscopy obs. 78−22897
Au film growth on Si(100), LEED and X-ray texture anal. 79−99452
band structure, appl. of extended rigorous cellular method 78−52055
beam splitter phase coatings, for producing phase quadrature interferometer outputs 78−77974
bimetallic layers, positron diffusion, ang. distrib. of annihilation photons meas. 79−8207
binary alloy films, anal. by X-ray fluorescence *(Chinese)* 79−48035
carrier density, evaluation from transverse elec. field and cond. meas. *(French)* 80−39682
CESR, line width and shape, surface relax. contrib. *(Russian)* 77−32260
CESR line shape, strong surface relax. case *(Russian)* 78−56378
chemisorption, use of external mag. field 78−72003
chemisorptive luminescence systems for surface reaction obs. 78−7236
coated Mo tips characterised by atom probe FIM, atomic clusters, voids 80−33863
complex permittivity, microwave meas. 79−24253
condensate, anisotropy in electric field 80−15624
condensed, on supercond. film, effect on T_c and residual resist. 78−47900
condensed alloy film vaporisation method 77−85942
conduction electron surface scatt. process, magnetoacoustic oscillations *(Russian)* 80−15575
contact to Te film, time evolution of photovoltaic effect 80−65687
conversion electron scatt. processes anal. 80−45181
cyclotron resonance on open electron orbits *(Russian)* 80−88878
density response function and dynamic struct. factor, nonlocal effects 79−69447
deposition, positive particle beam technique 77−85948
deposition by ion beam sputtering, composition and stress state 77−89674
deposition by organometallic compound decomp. on surface 80−71599
deposition by plasma stream transport method, use of charge exchange plasma source 79−15613
deposition with periodically pulsed CO_2 laser, film characts. 79−28926
diffusion thermopower, boundary scatt. effect 80−6817
disordered and amorphous, quench-condensed, optical cond. and band struct. 77−1746
dispersed metallic film, I-V characts., struct. changes *(Russian)* 79−38195
electrical conductivity measurement, thickness dependence, quantum size effect *(German)* 80−86344
electrocrystallisation, soln. component interaction 80−20055
electromigration, book contrib. 79−1521
electromigration, generalized theory 77−24423
electromigration and diffusion, new examination technique 78−67852
electron backscattering, empirical study 80−108310
electron density and potential, variational calc. 79−78218
electron Fermi liquid, microscopic theory *(Russian)* 77−35999
electron Fermi liquid in films with mag. impurities, collective excitation spectrum *(Russian)* 77−62846
electron liquid oscills. *(Russian)* 78−43315
electron microscope investig., on SiO_2-based glass substrate 77−1285
electron penetration and energy transfer in solid metal targets, film bulk method 78−2963
electronic density of states, sp. ht. and spin susceptiblity 77−15730
electronic props. and elec. cond. 79−78228
electrostatic interaction of charges with metal surface in size-quantised film 80−24996
ellipsometry, metallic films and surfaces, nonlocal effects, theory 80−104006
EM excitation of sound, Mossbauer study *(Russian)* 79−99795
EM wave induced voltage 79−56330
EM wave transmission under resonance conditions *(Russian)* 80−54805
embossed metallic film absorber for solar energy 79−29451
energy dispersive X-ray meas. 77−52721
energy dispersive X-ray meas. 77−52722
epitaxial growth with ionised beams and surface imperfections 77−32529
etching by conical beam of Ar ions *(Russian)* 80−76383
evaporated metal nuclei on C, SiO_2 films, atm. contamination, AES meas. 77−4264
Everhart theory extension of backscattered electron energy spectra 80−108309
failure processes due to powerful light pulses *(Russian)* 80−7443
fast electron scattering with core electron excitation, plasmon satellite 79−33873
FCC, on NaCl, electron diffr. pattern interpretation, appl. to Ag 77−1332
ferromagnetic film in mag. field, pulsed laser beam induced EMF *(Russian)* 77−55564
film, evaporated, galvanomag. and mag. props., thickness depend. 78−23181
film, evaporated at oblique incidence, columnar grains inclination angle 80−75468
film characterisation technique, APFIM, time-of-flight spectroscopy 80−75138
film on Si substrate, eutectic point displacement on annealing *(Russian)* 80−100850
free-electron films, optical props., theory including electron surface scatt. 80−29817
growth, initial stages, ion bombardment effects 78−14639
growth by sputtering, corpuscular diagnostics of hollow cathode discharge 80−16180
Hall coeff., temp. depend. 79−95516
Hall coeff. in mean free path model 79−11240
heating by light pulse of linear intensity time dependence *(Russian)* 77−59827
holographic recording materials and devices, book contrib. 78−25838
hot electron distribution function, nonlinear elec. resistance *(Russian)* 80−65717
hypersound point excitation in millimetre microwave region *(Russian)* 78−2204
inhomogeneous, elec. cond. determ. 77−15973
interdiffusion and reactions, effect on Si device technology, book contrib. 79−1620
interdiffusion in metal-metal systems, book contrib. 79−1529
interference filters, metal-dielec., in transmitted light 80−96013
ion backscattering analysis standards 79−2883
ion beam milling, amomalous sputter yield behaviour 80−108624
ion sound velocity in mag. field *(Russian)* 78−18982
ion-plated metal film structure on plastic substrate 79−82501
ionised-cluster beam deposition and epitaxy, for electronic device fabrication 78−11133
IR metallic film reflectivity rel. to thickness less than penetration depth 77−39018
island surface coverage, determ. by optical interference 77−1810
laser hole melting, for real-time, high density digital data storage 78−71135
laser induced damage, surface effects 77−16436
laser induced transverse voltages, detector appl. 0.33 to 10.6 μm 77−39824
laser photodeposition 79−100061
laser-surface impact, on metal surface, atom vel. distrib. 80−5637
lattice sum, for use in self-consistent warped muffin tin pots 77−15741
layer thickness measurement using X-ray fluorescence principle *(German)* 80−93705
liquid, supercooling, electron diffraction study *(French)* 79−7676
magnetoresistance and Hall effect, gas sorption and polycrystalline structure influences *(Czech)* 77−51827
mass transport and assoc. failures 80−59694
metal film, laser damage determ. using quartz resonator 78−31286
metal-dielectric boundary thermal resistance, nonlinear elec. resistance *(Russian)* 80−65530
metallised coating on polyethylene terephthalate film, fracture under laser irrad. *(Russian)* 80−76333
microcontacting in thin metallic layers *(German)* 80−55624
mirror coatings, protected and unprotected specular reflectance 79−76792
multicomponent alloy films, struct. form. laws and elec. prop. changes obs. during vacuum condensation 78−6850
multilayer system, scaling law for interdiffusion 79−65262
multilayered, Auger depth profiling, improved depth resolution by reactive ion sputtering 79−91557
noble metal, electronic structure and d-holes of films and surfaces 78−39180
noble metal, modulated surface plasmon reson. in situ meas., O_2 adsorpt. 77−77311
noble metal contact, substrate material diffusion and corrosion film formation, model 80−2312
nonferromagnetic film sheet resistance meas., eddy-current method 78−45658
nucleation, controlled interaction with Si substrate, silicide form. 80−10711
nucleation and growth on alkali halide substrates, surface study techniques, review 80−10809
one-dimensional, electronic states 80−54758
optical absorption due to particle-hole excitations 80−45160
optical absorption measurement, by multiple attenuated total reflections *(Japanese)* 79−40603
optical and electrical props. in situ determ. during deposition 77−59341
optical characts., structure-related, in visible and UV 77−55841
optical coatings, algorithms for determ. of reflectance and transmittance 79−98271
optical consts., determ. from Abeles formulae for reflectance, transmittance 78−15240
optical frequency mixing and detect. by interaction of radiation 77−75614
optical properties, review 80−45106
optical properties as function of wavelength *(Russian)* 78−52591
optical props., effect of quench condensation 79−78773
optical waveguide mode coupling to metal films and metal-barrier-metal devices 79−81567
overlayers, on mol. monolayers, IR absorpt. enhancement, ATR technique 80−88995
Permalloy-Rh, film, influence of Rh on corrosion resist. and mag. props. 80−3235
phonon emission by metal heater film into insulating substrate, spectral distrib., model treatment 79−14896
phonon fluorescence stimulated by laser radn. 79−87504
PIXE, low energy mass absorpt. coeff., meas. technique 78−7309
planar magnetron sputtering 78−72725
polycrystalline, plastic flow, dislocation slip 79−82505
polycrystalline films, grain boundary reflection coeff. thermal expansion effect on resistivity temp. coeff. 79−91162
powders, SAW interactions, for various directions of propagation 80−49486
preheating as aid to laser recording 80−102753
pressure effects on intrinsic property meas., case for in-situ measurements 78−39228
pressure operated shutter for thickness control and monitoring 79−15607
pulse nonlinearity meas. 78−56242
quench-condensed, specific heat, 0.6 to 4.4K 78−41309

metallic thin films continued
rare earth films, Auger emission from excited atoms 77−20967
rare earth impurities and struct., general review 80−54556
rare earth metal, anomalous crystal structures 79−28222
rare earth metal silicide thin film formation on (100), (111)Si substrates, backscattering study 80−70542
rare earth metals, reactions with O_2 and water, XPS obs. 77−31888
rare earth metals, room temp. i.r. cond., free electron contrib. 77−1745
rare earth-transition metal amorphous alloy film, magneto-elastic tensors, pair model calcs. 78−80185
rare earths, optical cond., rel. to cryst. struct. and electronic config. 77−36303
reaction with compound semiconductor substrates, book contrib. 79−1622
reflecting coating for light filter, transmission coeff. zonal nonuniformity 79−32063
refractive index for X-rays, elec. current density influence *(Spanish)* 79−78784
refractory metal, electron beam evaporator for in situ deposition studies in UHV electron microscope 80−40264
refractory metals, vaporisation by electron bombardment in UVN-71R-3 installation 77−28722
resistance and magnetoresistance 79−61225
resistivity strain coeff. calcs. 80−100449
resistor, 1/f noise 79−38193
scanner laser marking 80−43385
segregation, microscopic electronic theory 77−85112
SEM specimen preparation thin film coating techniques 80−68308
silicide formation, book contrib. 79−1530
size effect conductivity in transverse mag. field, Hall coeff. *(French)* 78−91787
size effect in Landau diamagnetism, surface pot. effect *(Russian)* 80−93012
size-quantised, energies and Fermi level of electrons 77−15749
SmS film, metallic, interpretation of optical absorption spectrum 78−27344
soft, role in reducing friction between metal surfaces 80−55592
solid-liquid transition, optical reflectance spectra 80−24569
solid-state plasma, steady-state Langmuir turbulence spectrum and turbulent energy absorption 78−26899
spectrophotometry, semi-transparent metallic thin films as transmittance standards 77−53991
sputtered, deposited by cylindrical magnetron sputtering, internal stresses 80−24773
sputtered compressive stress transition 78−10310
stability and rupture using perturbation analysis 78−79911
strain coefficients of resist., size effect 79−42673
structure, on amorphous or crystalline substrate, effect of zero point EM oscills. *(French)* 78−22983
structure-related optical characteristics in visible and UV 78−35217
superconducting state realisation 80−49977
supported film, thickness determ. using ^{63}Ni radioactive source 78−22989
surface and grain boundary diffusion, charact. temp/melting point ratio 79−90919
surface appls. for adsorption and catalysis 78−75943
surface dielectric response in local representation, microscopic theory 77−85289
surface EM wave launching at edge of metal film 78−43945
surface impedance oscills. in perpendicular mag. field *(Russian)* 78−76165
surface plasmon light emission due to low energy electron irrad. 80−34997
surface plasmon light scatt. 79−87517
surface plasmons, coupled, in thin metallic layer structures 79−56873
surface plasmons, size effect, RPA calcs. 77−80823
surface polariton motion in thin surface layer, nonstationary phenomenological theory *(German)* 80−88608
surface potential of interacting metallic films 78−30968
surface region, electrostatic energy and screened charge interaction for different Fermi surface shape 80−70631
surface roughness, by ellipsometry and TEM 77−20205
surface vaporisation under conc. energy sources, thermal model development *(Russian)* 79−74091
surface wave attenuation due to electron-phonon interaction 79−55848
surfaces, catalytic reactions studied by work function meas. 80−55711
Ta, oxidation in ambient conditions, resist. and ellipsometric meas. 79−34209
target preparation for stopping power meas. of channelled ions in low energy region 80−63431
thermal conductivity and thermal diffusivity, determ. method *(German)* 78−19165
thermal strains, effect of support, theory 80−88647
thermoelectric power, thermal stress effects, theory 80−65714
thermoelectric power 79−78210
thermoelectric props. of conductor covered with electrolytic deposit, thermal flux meas. *(French)* 80−59961
thickness measurement, for single layer and mutlilayer systems, X-ray fluoresc. technique 80−68180
thickness measurement, methods and instruments *(German)* 78−32787
thickness measurement, using nondestructive radioisotopic technique 80−68179
thickness measurement by electron probe microanal. *(Czech)* 79−44899
thickness measurement using nuclear resonance methods 77−81334
transition metal, amorphous and liq. state, simulated model 79−14733
transition metal, anomalous crystal structures 79−28222
transition metal, calc. of tight-binding surface density of states 77−55594
transition metal, chemical compound formation by ion bombardment 78−30846
transition metal, electronic structure and d-holes of films and surfaces 78−39180
transition metal, one-electron theory, atomic sphere approx. to KKR and LMTO methods 78−91584
3d transition metal films, EELS, anomalous L_3/L_2 white-line ratios 80−93444
transition metals, 4d, optical absorption meas. using synchrotron radiation, 20-250 eK 77−12457
transition metals, BCC, films, vac. evaporated, optical cond. 80−76100
transition metals, BCC, optical props. 79−78781

metallic thin films continued
transition metals, energy band calc. by linear combination of muffin tin orbitals method 77−4283
transition metals, on Si, silicide form. at interface, interface marker technique obs. 80−59734
transmittance standards in spectrophotometry, semi-transparent metallic thin films use 78−32852
transparency, on semicond. substrates 77−16411
transparent conducting coatings, book contrib. 78−10587
transparent conductors, figure of merit 77−1741
transverse electric quantum wave spectrum *(Russian)* 80−84517
ultra-fine metal particle form., pulsed laser breakdown of carbonyl vapours 80−84881
ultrasound attenuation, size magnetoacoustic effect *(Russian)* 80−107869
ultrathin metal film mounting method on cylinders 79−35696
unlike surface properties, transport coeffs., diffuse surface scatt. 80−20331
vacuum deposited, appl. to brittle fracture growth dynamics obs. 78−83347
vacuum deposited, grain struct., influence of impurities and alloying elements *(Russian)* 78−56048
vacuum deposited, internal friction *(Japanese)* 78−47685
vacuum deposited, O^+ bombardment sputtering rates 78−88390
vacuum deposition, early stage obs. using microbalance technique and electron microscopy *(Japanese)* 80−54554
vacuum deposition, ultra-high vac. technique 80−100791
valve metal thin films, deposited on dielectric supports, exam. of anodisation kinetics *(Russian)* 80−7702
vaporisation by laser, vaporisation front relativistic velocities *(Russian)* 80−66337
vaporisation kinetics on absorbing laser radiation *(Russian)* 77−43423
vapour deposited, struct., resist. component manufacture appl. *(German)* 77−55467
vapour deposited coatings, mech. props. 78−6247
vapour deposited on polymer, ageing, adhesion, elec. cond., electrochem. pot. *(Russian)* 79−33362
voids, size and number prediction 79−28256
wet-chemical etching, galvanic effects 80−25915
X-ray interferences obs., energy dispersive method 78−79499
yield stress of film bonded to rigid substrate 79−99463
AP, RF sputtered, thermal ageing, thickness dependent effects 78−6462
Ag, 1/f noise, role of substrate 79−28388
Ag, (111) surface electron microscopy 80−103556
Ag, absolute work function meas. by field-emission retarding-pot. device 77−59322
Ag, adhesion meas. 80−50822
Ag, adsorbed CO, enhanced Raman scatt. mechanism in ultrahigh vacuum 80−107645
Ag, adsorbed on Si (111), electronic and cryst. struct., Schottky barrier form. obs. 78−84091
Ag, adsorption and desorption on W, mass spectra obs. *(German)* 79−46951
Ag, adsorption of O, dielec. perm., plasma surface vibr., modulation spectroscopy 77−48198
Ag, bounded by dielectric slabs, attenuated total refl. angular spectra 78−92135
Ag chemically deposited layer, reflectivity rel. to heat treatment 79−27366
Ag, cluster growth and nucleation on Mo (100), UHV-SEM, AES/(RHEED or LEED) obs. comparison 78−63956
Ag, condensate obtained in electric field, anisotropy of elec. props. 80−44743
Ag, condensation on glass, temp. depend. *(Russian)* 77−32525
Ag, conduction electron spin disorientation at surface 80−75855
Ag, contact material, contamination layer thickness, resist., ESCA study *(German)* 80−55561
Ag, continuous film, 1/f noise, temp. and substrate depend. 79−24086
Ag, damping and vel. of longit. elastic waves at 9.4 GHz 80−10596
Ag, defect density, thickness depend., elec. resist. obs. 80−70568
Ag, deposited by cathodic sputtering using high-resolution electron microscopy, voids obs. 80−49557
Ag, deposited on substrates at 10K and 293K, specific stacking charact. *(French)* 77−43459
Ag, dye monolayer effect on surface plasmons, ART obs. 79−87001
Ag, electrodeposited and vac. deposited, AES depth profiling anal. 77−59232
Ag, electrolyte deposition on semicond. substrates 77−77425
Ag, electron bombarded, transition radiation 77−85828
Ag, electroplated, stress meas. using holographic interferometry 80−20806
Ag, energy depend. of defect production in displacement cascades 77−31700
Ag, energy losses and straggling for H^+ and He^+ beams *(Russian)* 80−84226
Ag, energy transfer from excited dye mol. to surface plasmons 79−91119
Ag, enhancement of electron photoemission by excitation of surface plasmons *(French)* 77−63524
Ag, evaporated, chemisorption effects on reflectance and elec. resist. 80−11495
Ag, evaporated, sulphide formation 79−15874
Ag, evaporated film, density, adhesion, intrinsic stress, substrate temp. effects 77−15709
Ag, evaporated layer, secondary electron energy distrib. and work function *(French)* 79−99993
Ag film, 1/f noise and its temp. depend. 79−60939
Ag film, 1/f noise and its temp. depend. 79−60940
Ag film, adhesion changes on 10 MeV electron irrad. *(Russian)* 77−43460
Ag film, angular depend. UPS, surface electronic struct. 79−83095
Ag film, CESR linewidth exam., sample size effect 79−33536
Ag, film, chem. deposited, agglomeration, SEM and TEM obs. 80−59828
Ag film, chemisorption effects on optical reflectance and elec. resistance 79−33361
Ag, film, electron inelastic scatt. mean free paths, synchrotron radiation photoelectron spectra meas. 78−76587
Ag film, electronic stopping power on irrad. by He, Li, C ions, damage-rate measurements 79−77654
Ag film, electroreflectance effects 79−43055

metallic thin films continued
Ag film, ellipsometric response to CO adsorption 80−103571
Ag film, energy losses of 20-40 keV electrons 78−92153
Ag film, energy losses of electrons, microcalorimetric meas. 80−59543
Ag film, epitaxial growth on isolated Au patches covered with amorphous C layer 80−40270
Ag film, friction and fear in ultrahigh vacuum, effects of speed, film thickness and substrate surface roughness 79−20202
Ag film, He^+ ion bombardment, radiation damage, ion entrapment, gas release and bubble formation 78−30679
Ag film, in situ struct. determ. by internal stress meas. 80−54569
Ag film, intrinsic stress meas. 80−71696
Ag, film, ion deposition *(Japanese)* 77−36407
Ag film, on amorphous C and Si substrates, dispersion force contrib. to adhesion *(French)* 80−59842
Ag film, optical props., inverse problem of phenomenological theory 79−43053
Ag, film, plasma reson. radiation exam. *(German)* 79−69453
Ag film, polycrystalline with artificial surface roughness, electrical resistivity temp. coeff. *(Russian)* 79−82688
Ag film, reflection coeff. minima and surface plasma wave dispersion curve comparison *(French)* 78−80429
Ag, film, sputtering mechanism, SEM 80−29839
Ag film, surface roughness, light scatt. meas. 80−107624
Ag film, twin boundary faceted struct., struct. coarsening due to dislocations *(Russian)* 79−99215
Ag, film, vacuum deposited, Young's modulus determ. by differential technique 77−1340
Ag film, vacuum deposited onto SiO, C and mica, quantitative study of nucleation 79−77959
Ag film, vacuum deposition on Pb (111), substrate diffusion effects, RHEED, LEED, AES 80−65410
Ag film, void growth, TEM obs. 80−59833
Ag film coated with dye monolayer, anomalous dispersion of surface plasma oscills. 79−8203
Ag film deposition, thermal effects, influence on internal stress meas. 80−96767
Ag film for Ga liquid spreading, kinetic eqn. *(Russian)* 80−59376
Ag film growth on Pd substrate, interface cpd. form., AES study *(French)* 80−80131
Ag film on Cu(111), plasma reson. absorption in interfacial photoemission 78−15289
Ag film vacuum deposition and ion plating, effects on surface topography 79−82427
Ag films, effect of Ar- and N-ion bombardment on texture *(Russian)* 80−107338
Ag films, excess (1/f) voltage noise 79−42598
Ag films, hillock form. hole growth and agglomeration 80−44455
Ag films, underlayer effect on surface roughness, surface plasmon excitation meas. 79−51456
Ag foil, surface-plasmon resonance, roughness-induced wavelength corrections 80−108288
Ag, formation on salts of carboxylic acids by photolysis 77−75720
Ag, Ga spreading kinetics, influence of melt-support interaction *(Russian)* 79−37903
Ag granular film, plasma reson. absorpt. by incident light 79−28850
Ag grating, with LiF coating, p-polarised reflected light intensity, reson. anomalies 77−3665
Ag, growth on C replica stripped from pure and doped NaCl single crysts., elec. memory expts. 77−76691
Ag, growth on KCl, LEED, AES meas. 77−35834
Ag, high temp. stabilisation using SiO_2 78−1319
Ag, hole formation and hillock growth after heating in O_2 atmosphere 79−65345
Ag, in contact with dye, enhanced total refl. with surface plasmons 79−59694
Ag, inert gas ion refl., semiempirical analysis, compared with expt., 10-30 keV 78−6823
Ag, interaction with adsorbed dye mols., absorpt. and luminesc. 80−103981
Ag ion plated film on permalloy, Cu and Vicalloy substrate, AES, SEM and X-ray study *(Japanese)* 78−11128
Ag, ion plating on AT-cut quartz crystal, crystallographic structure obs. 80−2280
Ag, lifetimes of surface plasmons 79−47143
Ag, low energy electron irrad., visible and UV emission 78−2921
Ag, on Al splitting of surface plasmon dispersion curves 78−60178
Ag, on Au substrate, monolayer overgrowth, quantitative AES method 80−10813
Ag, on Cu, ion-induced intermixing 80−15420
Ag, on MgF_2 and SiO substrates, internal stresses correl. with struct. 79−87026
Ag, on mica, graphite, and Si, early growth by ion-beam sputtering 77−44158
Ag, on mica, microstruct. changes 78−72013
Ag, on Si, backscatt. spectrum edge determ., theory and expt. 77−8702
Ag, optical props. after thermal cycling, thickness and substrate temp. effects *(French)* 77−48263
Ag, optical props. as function of wavelength *(Russian)* 78−52591
Ag, optical props. in intermediate region between pure Drude and interband absorption 77−81170
Ag, photodissolution in amorphous As_2S_3 78−26737
Ag, Raman scatt. from adsorbed CO 79−78672
Ag rough film, multiple light scatt. of surface plasmons 77−48262
Ag, spike effects of heavy ion sputtering 80−35034
Ag, sputtered, hillock growth and agglomeration by annealing, SEM obs. 80−2309
Ag, sputtering, photon emission enhancement compared with sputtering rate 79−78815
Ag, sputtering yields for ions over 15-135 keV 79−56899
Ag, surface and volume plasmon light emission due to low energy electron scatt. 80−40177
Ag surface layers, reflectivity, contrib. of longit. polarisation waves 79−83046
Ag surface layers on Au and Al substrates, reflectance spectroscopy 79−78780
Ag, surface plasmon reson. interaction with dye monolayers 78−84674
Ag, surface plasmon wave excitation of dye mol. fluoresc. emission 79−89703
Ag, surface-plasmon modulated reson. for adsorption studies 79−83045
Ag, temp. depend. of 1/f noise meas. 77−85277

metallic thin films continued
Ag, thermal and elec. cond., Lorenz no. 78−43487
Ag thin evaporated films, rel. between microstruct. and excess free energy, TEM 80−70427
Ag, thin film, thickness meas., Hall effect and interferometric methods 77−5802
Ag thin film, X-ray fluoresc. spectroscopy of surface using RHEED-solid state detector method 80−108760
Ag, thin film deposited on Si, work function *(French)* 80−80353
Ag, thin layer on Al surface, surface plasmon ATR spectroscopy 79−78770
Ag thin layered structures, coupled surface plasmons 79−56873
Ag, thin sub-monolayer film, Auger emission coeffs. meas. 80−55236
Ag, thin targets, electron transmission below 3 keV *(French)* 80−60725
Ag, UV photostimulated oxidation, electron microscopy, study *(Russian)* 78−95850
Ag ultra-thin film, deposited on MgF_2 and SiO substrates, struct. and internal stress 78−91572
Ag, vac. deposited films, surface pot. and work function rel. to thickness 79−42672
Ag vacuum condensates, on Cu substrate, struct. and substruct *(Russian)* 79−73412
Ag, vacuum deposited, internal friction vibr. reed technique 78−43276
Ag, vacuum deposited, internal stress and its depend. on gas adsorption 80−6683
Ag, vacuum deposited, orientation axis tilt rel. to vapour angle of incidence 80−88456
Ag, vacuum deposited, thickness meas. using X-ray fluoresc. technique 79−90911
Ag, vacuum deposited coating on quartz resonator 78−11116
Ag vacuum deposited coating on glass, strength 80−55505
Ag, vacuum deposited film, surface struct., HEED meas. 78−6234
Ag, vacuum-condensed film, structural changes under glow discharge *(Russian)* 79−15852
Ag vacuum-condensed films, on glass substrate, X-ray texture study 79−83226
Ag, vacuum-deposited, removed from substrate, internal strain *(Japanese)* 78−22872
Ag, vapour deposited on Cu, defects and their effect on props. 80−39474
Ag, vapour-deposited on rotating substrate at oblique angle, X-ray struct. anal. 77−62775
Ag, with thin transparent and absorbing coatings, surface plasma oscills. 78−43951
Ag:Er(Dy), orbit-lattice coupling, nonuniform strain effects 78−88182
Ag:He, implanted films, solid solutions radiation induced polymorphism 79−86810
Ag/Au thin film couple, interdiffusion mechanism 77−20132
Ag/stearic acid layer periodic struct. prep. and optical props. 77−69199
Ag/Te double films, interdiffusion and struct. modifications *(French)* 77−62682
Ag-Al polycryst. thin-film couples, interaction process 79−51443
Ag-Au, interdiffusion, pore formations, stress effects, adhesive effects *(Russian)* 79−82502
Ag-Au thin film couples, polycrystalline, low temp. diffusion, resist. obs. 79−4435
Ag-Au-Ay thin films, diffusion induced grain boundary migration 79−77833
Ag-Cu, metastable alloy film, optical props. 77−12460
Ag-Cu couple, grain boundary diffusion of Ag through Cu film, Rutherford backscattering obs. 80−34252
Ag-Hf(Ta)(Pt) film, optical absorption spectra meas. 77−85823
Ag-InP interface, AgP_2 formation during sintering 80−65309
Ag-liquid Ga interface, γ-phase interlayer growth, two-dimens. electron diffr. 79−19487
Ag-metals thin film couples, room temp. interactions 80−2220
Ag-MgF_2-Ag layered system bounding dielec., ATR ang. spectra, assoc. reson. EM oscills. 79−15541
Ag-Ni, SO_2 adsorption on mixed metal films 79−87003
Ag-Sn, double, high-speed superconducting bolometer appl. 80−57368
Ag-Te, amorphous, effect of annealing on elec. resist., phase transitions 79−11241
Ag-Te, thin film system, stress-relief appearance conditions 80−65416
Al, 1/f noise depend. on internal mech. stresses 80−65711
Al, (e, 2e) reaction, ang. correlation functions, plasmon satellites 79−19955
Al, absolute work function meas. by field-emission retarding-pot. device 77−59322
Al, action of plasma in capacitive electrode HF discharge *(Russian)* 78−95818
Al, adhesion to substrate, meas. 80−50822
Al alloy-Cu alloy evaporated couples interdiffusion *(Russian)* 77−43389
Al and Al-alloy films, struct. induced electromigration failure, Monte Carlo calcs. 80−49405
Al, appl. of current noise technique for dislocation processes during plastic deform. 80−35442
Al bimetal film with Cu, Ti(V,Ni) and alloy MLT(RS-3710), struct. and macroscopic defects *(Russian)* 79−1555
Al, bleaching possibility by laser pulse, liq. insulator transition 77−43498
Al caesiated thin film, surface plasma wave excitation by polarised light, photoemission obs. 80−50518
Al clean films, O_2 interaction study using synchrotron-radiation-induced-photoemission 80−55709
Al cluster, growth and composition on NaCl substrate 77−89677
Al, colour anodised, selective surfaces for solar collectors *(Japanese)* 80−55893
Al, condensate, effect of growth conditions on critical thickness 79−69985
Al, condensate obtained in electric field, anisotropy of elec. props. 80−44743
Al, condensed and fused, on Ge, press. and residual gas comp. influence on struct. 77−16497
Al, condensed film, phase and struct. nonuniformity *(Russian)* 80−54536
Al, damage production rates of 5 MeV Al ions 78−47444
Al, deposited metallic thin films, H incorporation effects on stress and electromigration 80−80139
Al, deposition by cathode sputtering in enriched plasma *(Czech)* 77−63557
Al, deposition using pulsed ruby laser *(Czech)* 79−52126

metallic thin films continued
Al deposition using solar furnace 80−89148
Al, dispersion curve of surface plasma waves, rel. to refl. power minimum curve *(French)* 78−88372
Al, electron beam evaporation, on Kapton laminates, and characterisation 78−11373
Al, electron beam transmission, reflection, and absorp., $35 \leq E \leq 70$ keV 77−39754
Al, electron energy-loss spectrum, wavelength depend. fine struct. 77−11609
Al, electron transmission, 1-5 keV, electron MFP 77−15472
Al, electron transmission, ang. aspects *(French)* 80−49284
Al, energy losses and straggling for H^+ and He^+ beams *(Russian)* 80−84226
Al, enhanced mirror, high-rate sputtering, reflectance and dispersion 77−42636
Al, evaporated, corrosion in distilled water, ellipsometric obs. 77−48590
Al, evaporated layer, secondary electron energy distrib. and work function *(French)* 79−99993
Al evaporated on quartz substrate, surface irregularities 79−90920
Al, film, adsorption of O_2 and N_2 77−24486
Al film, caesiated, photoelectron escape length, 1.5-4 eV *(French)* 79−47585
Al film, deform. under He ion bombardment 80−65073
Al film, dislocation observation by electron microscope using convergent beam *(French)* 80−96532
Al film, electromigration, AC and DC studies 77−24424
Al film, electron transmission less than 3 keV *(French)* 78−10109
Al film, electron transmission, calc. 80−60724
Al film, electron transport, grain boundary scatt. 79−60937
Al film, energy losses of 20-40 keV electrons 78−92153
Al film, energy losses of electrons, microcalorimetric meas. 80−59543
Al film, etching in carbon tetrachloride plasmas 80−76407
Al, film, initial oxidation, AES, work function and gravimetric meas. 78−7087
Al film, initial oxidation, electron energy loss spectra 78−7088
Al film, internal stress, effect of residual gas press. 77−66100
Al film, intrinsic stress meas. 80−71696
Al film, ion plated, morphology exam. by SEM 79−28251
Al film, lattice and bulk heat capacity meas. for normal and supercond. states 80−92684
Al film, magnetron sputtered deposition, characts. 79−91587
Al film, mean free path for plasmon excitation, 1.5 to 10.9 keV 78−51915
Al film, nucleation and growth on C layers, adsorption energy and surface diffusion 79−99451
Al film, on amorphous C and Si substrates, dispersion force contrib. to adhesion *(French)* 80−59842
Al film, Pb^+ implanted, ion scatt. erosion rate, Rutherford backscatt. 79−74038
Al film, plasma anodisation to exhaustion on Si and GaAs substrates 79−83388
Al, film, reflection coeff., effects of plasma bursts prod. 78−56547
Al film, sputtered, physical props. 79−77938
Al film, strips, thermal emissivity, appl. of distant-focused IR radiometer system 77−169
Al film, struct. and props., effect of ion implantation 79−77936
Al, film, surface resist. freq. depend. in range 7.7 to 37 GHz 77−20468
Al film, thermomodulation of Al $L_{2,3}$ absorption edge 79−91533
Al, film, transport equation treatment of transmitted electrons *(French)* 77−80558
Al film, vacuum deposited, rate and press. depend. of contamination 78−72732
Al film, vacuum deposited, structural changes during annealing at temp. near melting point 78−84096
Al film, vacuum evaporation growth, impurity presence, effects *(Hungarian)* 80−7495
Al film, wave front reversal, holography applications *(Russian)* 80−58483
Al, film and polished bulk specimens, initial stages of oxidation obs. using SIMS 80−81239
Al film deposition on Kapton laminates by electron beam evaporation 78−76603
Al, film growth on C, conductance meas. 79−82495
Al, film integral radiation ability determ. by electron diffr. *(Russian)* 80−54413
Al, film on Si(111) substrate, struct., props. depend. on vapour flow, ionisation *(Russian)* 80−75453
Al film+vitreous silica substrate, reaction 77−86380
Al films, anodisation rate and augmentation factor, oxidation in ammonium tartrate 79−79152
Al films, deposited on calcite substrate, grain boundary scattering, elec. resistivity meas. 79−65096
Al films, N_2^+ and O_2^+ ion bombardment, structural and phase changes 80−2094
Al films, RF sputtered, resist. recovery obs. 77−8207
Al films, resistance changes due to bombardment by N, C, or Ar ions 80−103670
Al, He^+ irrad., overpressurised bubble obs. 79−51165
Al, ion plated through mask hole, thickness nonuniformity *(Japanese)* 79−19999
Al, ion plating deposition system using electron beam evaporation *(French)* 80−20802
Al, lattice and grain boundary diffusion of Cu 78−2303
Al, lattice dimens., difference between vacuum condensates and massive specimens *(Russian)* 77−31912
Al, meas. of stress gradients generated by electromigration, X-ray topography and SEM 77−51541
Al metallization of semiconductor devices by high rate magnetron/plasmatron sputtering 79−28919
Al, neutron irradiated, increase of elec. resist. 78−26973
Al, nucleation-grown, RF sputtered, Mayadas-Shatzkes cond. 77−1498
Al, on Au layer, stopping power and energy straggling meas., Li ion backscatt. anal. 79−3328
Al, on CdS, bonding and interdiffusion, XPS obs. 80−80000
Al, on GaAs and Si, surface phonon Brillouin spectra 79−78694
Al, on polyethylene terephthalate, thickness determ. using photometry 80−62626
Al, on Si substrates, electromigration and diffusion of Cu 79−77820
Al, optical cond., energy derivative spectrum 77−66551
Al, optical dielec. const. in visible region, 300 and 1.5K 77−90211

metallic thin films continued
Al overlay film on quartz for temp. compensation, SAW device appl. 80−79043
Al, photoelectron-grain boundary scatt. in Al-SiO_2-Si struct. 78−64120
Al, plasma etching, MOS processing appl. 80−40577
Al, polycryst., chemisorpt. of O_2, synchrotron radiation photoemission expts., 70-150 eV 78−95228
Al, polycryst. heat cond. depend. on thickness, block boundary density *(Russian)* 79−82689
Al, polycrystalline, trapping of ^3He and ^4He ions at room temp. 80−84221
Al, porous anodisation, initial stages of oxide growth and pore initiation, ellipsometry obs. 77−1888
Al, room temp. oxidation, scanning HEED expts. 78−91567
Al, simulation of transmission of 1 keV electrons 77−12475
Al, spontaneous destruction by atmospheric pressure, electron microscopy *(Croatian)* 77−76711
Al, sputtered and electron gun evaporated films, grain size and orientation obs. 78−10308
Al sputtered coating development, porosity, durability temp. depend., electric arc metallisation regime *(Russian)* 80−39402
Al sputtered film, effects of sputter etching and process technology on props. 79−83122
Al, supercond. film, quasiparticle injection, tunnel junction characts. 78−76193
Al surface, plasma cleaning and etching, removal of C 80−97645
Al, thickness measurement using Talbot effect 78−9321
Al thin conducting film, electromigration under superimposed DC and noise powers 80−107879
Al, thin film, K X-ray production due to ^{16}O ions, 0.25-2.25 MeV/amu 79−69906
Al, thin film, thermal cond. meas., size effect 80−65715
Al, thin film deposited on Si, work function *(French)* 80−80353
Al thin film stripes, electromigration lifetimes width depend. 80−92799
Al thin films, electromigration under pulsed current conditions, calc. 77−1495
Al thin films, HF induction plasma treatment, effect on phys. props. *(Russian)* 80−24961
Al thin films, vacuum deposited, crystal growth in presence of O_2 and Ni 80−15409
Al thin films evaporated on rough quartz substrates, surface irregularity, light scattering measurements *(Polish)* 80−88450
Al, threshold adhesion failure, meas. by stylus method 80−50806
Al, transparent, secondary electron emission of 10-100 keV electrons 77−32477
Al, two photon photoelectron effect in surface plasma reson. 77−69962
Al ultrafine particle film, size effects in optical absorption 79−99965
Al underlayer, effect of deposition parameters on mag. props. of Ni-Fe-Co film 77−77078
Al, vacuum deposited, 7 to 65 μ thick, morphology and purity determ. 77−76699
Al, vacuum deposited, influence of film thickness on internal stresses magnitude *(Russian)* 79−37938
Al, vacuum deposited, solar radiation props., grey-reflector appl. 77−20098
Al vacuum deposited coating on glass, strength 80−55505
Al, vacuum-condensed film, structural changes under glow discharge *(Russian)* 79−15852
Al, vapour deposited on NaCl, defects and their effect on props. 80−39474
Al:Er(Dy), orbit-lattice coupling, nonuniform strain effects 78−88182
Al:Si, film deposition by reactive sputtering 79−66005
Al/Cr thin films, interdiffusion meas. 79−82391
Al/Cu thin film couples, TEM study of intermetallic nucleation at interface 80−65305
Al/GaAlAs, film, epitaxial growth on (100) GaAs by hot vac. deposition and characterisation 79−56085
Al/Hf/Al structure, anomalous growth of $HfAl_3$ 77−43462
Al/Pd thin film couples, thermal reactions 80−59830
Al-Ag, struct. of two-layer film 79−23851
Al-Cr, thin film metal contact, sheet resistance changes 80−80356
Al-Cu, prep. by planar magnetron sputtering *(Japanese)* 80−16184
Al-Cu alloy, vacuum deposited thin film, abnormal grain growth before melting transition and subsequent struct. change 79−60663
Al-Cu alloy layer, photolithographically patterned, separation from substrate using plasma etching *(Slovak)* 80−45405
Al-Cu thin film couple, interdiffusion, AES obs. 80−6569
Al-Cu thin films, microstruct. rel. to electromigration 80−44355
Al-Li-Mg-Be alloys, phase composition of surface films, oxidation protection mechanism *(Russian)* 80−65417
Al-Pt film sandwich, interdiffusion and intermetallic form. 77−24448
Al-Sb, laser-induced metal-semicond. transition 80−6661
Al-SiO multilayer capacitors and inductors, heat treatment effect on elec. props. 77−32082
Al-SiO_2 film-substrate interface, obs. of Al_2O_3 and free Si 78−91571
Al-SiO_2 interface, stress and microstruct. via TEM 78−26797
Al-Xe film, ion implanted radiation enchanced Xe outdiffusion, Rutherford backscatt. 77−76609
Al-Zn thin film, prep. using Sn-Zn evaporant source 80−100789
Al-Zn-Mg-Cu alloy, X-ray microanalysis in scanning transmission electron microscope, limitations 78−20122
Au 79−77938
Au (001), surface struct., high resolution TEM 80−100383
Au, (001) surface atomic steps obs. using TEM 77−20173
Au (111) film, sputtered, surface struct., HV electron microscopy and theoretical model 78−22981
Au, (111) surface electron microscopy 80−103556
Au (111)/Ag (111) thin film system, diffusion processes 79−77843
Au, absolute work function meas. by field-emission retarding-pot. device 77−59322
Au, adsorbed CO, enhanced Raman scatt. mechanism in ultrahigh vacuum 80−107645
Au amorphous film, getter sputtering at 25K 79−38741
Au, angular-dependent studies on some prototype vertically and laterally inhomogeneous samples 78−95655
Au, annealing curves, size effect parameter determ. from Mayadas Shatzkes theory 77−76962
Au anodic electrodeposition from liq. NH_3 solns. 79−28957
Au, bicrystal, diffraction effects from inclined grain boundaries 80−103362

metallic thin films continued
Au, bicrystalline thin films, faceting of [001] grain boundaries 80−70222
Au, calc. of defect conc. 78−95052
Au, Co-hardened, characterisation by Mossbauer spectroscopy, Co precip. formation 80−80108
Au condensed films on NaCl, ion bombarded, film growth, thermally stimulated exoelectron emission 80−50537
Au, damping and vel. of longit. elastic waves at 9.4 GHz 80−10596
Au, deposition on polymer substrates, effects of glow discharge on nucleation characts. 79−77963
Au, deposition with sputter gun 77−44162
Au, diffusion barrier formation, at metal-semiconductor or metal-metal interface, using laser annealing 80−80373
Au, diffusion on atomically clean Si (111) surface 78−72037
Au, dynamic recoil implantation in Si 79−14833
Au, early growth stages on amorphous C, cluster migration obs. 79−77964
Au, effect of high DC density stressing on pre-existing voids 80−24770
Au, effect of intermittent deposition on nucleus formation and growth on alkali halide substrates 79−23853
Au, electrodeposit, Co-hardened, state of Co in as-deposited material, Mossbauer obs. 80−15397
Au, electron beam transmission, reflection, and absorp., $35 \leq E \leq 70$ keV 77−39754
Au, electron bombarded, transition radiation 77−85828
Au, electron transmission, 1-5 keV, electron MFP 77−15472
Au, electrotransport-induced failure site, minor constituents effects 79−23763
Au, ellipsometric obs. of optical props. 79−78776
Au, energy losses and straggling for H^+ and He^+ beams *(Russian)* 80−84226
Au, epitaxially grown bicrystalline thin films, preferred inclinations of ⟨100⟩ grain boundaries 80−103367
Au, evap., temp. change and gas adsorpt. effect on opt. consts., ellipsometric obs. *(German)* 80−89081
Au, evaporated, surface resistivity at 890 GHz rel. to waveguide applic. 77−34004
Au, evaporated layer, secondary electron energy distrib. and work function *(French)* 79−99993
Au film, angular depend. UPS, surface electronic struct. 79−83095
Au, film, contact reaction with amorphous Si 79−23846
Au film, Cr and Si low temp. diffusion, CO effect 80−100361
Au film, deposition on NaCl by ion beam sputtering, initial growth features 79−77962
Au film, detection of faceting on (h,k,0) surfaces by diffr. in electron microscope at 100 kV 78−43273
Au, film, electron inelastic scatt. mean free paths, synchrotron radiation photoelectron spectra meas. 78−76587
Au film, electron transmission, calc. 80−60724
Au film, electroreflectance effects 79−43055
Au film, energy losses of 20-40 keV electrons 78−92153
Au film, energy losses of electrons, microcalorimetric meas. 80−59543
Au, film, evaporated, DC elec. resist. 80−29487
Au film, excess vacancy diffusion to free surfaces and voids, resist, decay 79−65237
Au film, low temp. void growth and resistivity decay 78−10302
Au film, on amorphous C and Si substrates, dispersion force contrib. to adhesion *(French)* 80−59842
Au, film, on C/Ag system, epitaxial growth in ultra high vacuum 77−1336
Au film, on glass or quartz, laser-induced damage, determ. of surface fluctuation of slide 77−1279
Au film, on KCl, influence of coalescence on growth kinetics 79−46981
Au film, on Si, coincidence site phase boundaries 78−67927
Au film, on Si (100) substrate, growth and struct., LEED and AES obs. 79−51457
Au film, on W substrate, chemisorbed N_2 effect on crystallite growth, FEM obs. 79−46976
Au film, photoelectron emission, intershell interaction influence on 3d and 5d branching ratio 80−104038
Au film, polycrystalline, temp. depend. of Drude absorption 79−78779
Au film, threshold current density and incubation time to electromigration 78−14643
Au film, work function changes upon water contamination 80−44705
Au film (001) surface, computer modelling of high resolution TEM images 80−6330
Au film bicrystals, exam. of low energy planes for tilt grain boundaries 78−51551
Au film decoration, of individual Ag crysts. by ion bombardment *(German)* 79−69164
Au film deposition, thermal effects, influence on internal stress meas. 80−96767
Au film electrodeposition, substrate effects on film props. 80−81329
Au film growth on Mo (110) surface, AES, LEED, thermal desorption study 80−80130
Au, film on ⟨100⟩ Si, meas. of SAW dispersion and thickness using acoustic microscopy 80−53575
Au film on Cr adhesion layer, etching, SEM anal. of abnormal undercutting 79−5075
Au film on Si, SAW dispersion and film thickness meas. 80−10769
Au film room-temp. plasma chemical transport deposition 79−78894
Au film sandwiches, recovery kinetics and early stages of diffusion, DC resist. expts. 79−77971
Au, film with micron-size pinhole, low energy electron scatt. 79−81351
Au films, (111), sputtering in high voltage electron microscope 80−35027
Au films, excess (1/f) voltage noise 79−42598
Au, films, optical props. meas. rel. to electron surface scatt. theory 80−29818
Au films, thermal phonon radiation into α-quartz substrates 79−42363
Au films, thickness meas. standards for Rutherford backscatt. 79−40529
Au films, vac. condensed at oblique vapour incidence, oriented cryst. growth, electron diffr. study 80−97432
Au, films on barrier-layer photocells, spectral distrib. of transmission coeffs. 77−1744
Au films on Si substrate, solid-solid reactions 78−95369
Au fine particles, vacuum deposited, morphological features using TEM weak-beam dark-field technique 80−15410
Au, grain boundary electromigration, tracer meas. 77−31802
Au, grain boundary structure, high resolution HVEM 80−103360

metallic thin films continued
Au, growth, optical and elec. prop. meas. during depositon *(French)* 77−70007
Au, growth kinetics of icosahedral particles *(French)* 77−24494
Au, growth on C replica stripped from pure and doped NaCl single crysts., elec. memory expts. 77−76691
Au, heated thin film in liquid ^4He at 0.1K, temp. for large energy flux 79−55981
Au, in mag. field up to 40 kOe, microwave skin effect 77−12032
Au, in Si detector, electrical contact at He temp. 78−37019
Au, inert gas ion refl., semiempirical analysis, compared with expt., 10-30 keV 78−6823
Au, integrated condensation coeff. on NaCl cleavage faces, Rutherford ion backscatt. obs. 80−59827
Au, interaction with adsorbed dye mols., absorpt. and luminesc. 80−103981
Au, interface reaction with n-type $Ga_{0.7}Al_{0.3}As$ and GaAs 80−39482
Au, ion bombarded, surface craters induced by displacement cascades 80−107344
Au, ion implanted, ellipsometry, 1.8-5.5 eV, dielec. function 78−6697
Au, ion plated, defect growth structs., SEM obs. 80−24768
Au, ionic sputtering and AES anal. *(French)* 78−76959
Au, laser absorpt. vs. temp., calorimetric meas. 79−98423
Au, low energy electron irrad., visible and UV emission 78−2921
Au, material transport instabilities accompanying ageing *(German)* 80−7601
Au, metallised coating on polyethylene terephthalate film, fracture under laser irrad. *(Russian)* 80−76333
Au, migration in GaAs, ESCA study *(French)* 78−75885
Au, modifications of optical and elec. props. as function of struct. during deposition 79−78777
Au, nonohmic characts. and electron emission 80−60066
Au on Ag, optical constants, 4000-6000 Å using surface plasmon optical excitation 77−69925
Au, on Ag(111), thickness and optical consts. using surface plasmon excitation 79−47533
Au, on Al, Ni, EUV reflection efficiencies 79−14073
Au on anthracene, energy transfer 77−85775
Au, on α-quartz substrate, optical consts. evaluation from surface polariton dispersion 78−48249
Au, on CdS, bonding and interdiffusion, XPS obs. 80−80000
Au, on complementary cleavage planes of TGS, morphology, electron microscope obs. 79−15031
Au, on Cu, ion-induced intermixing 80−15420
Au on Cu, oxidation exam. by ion scatt. spectra 79−79153
Au, on MgF_2 and SiO substrates, internal stresses correl. with struct. 79−87026
Au, on Ni, AES anal., influence of ion bombardment on depth resolution 77−20210
Au, on Si, early growth by ion-beam sputtering 77−44158
Au, on Si, oriented crystn., formation of coincidence orientations on interphase boundary 79−90922
Au, on Si and CaF_2 substrates, interphase coincidence boundaries 79−1560
Au, on Si substrate, critical Au-film thickness obs. for room temp. interfacial reaction 80−75390
Au, on Si use of sputtering for layer removal 79−78813
Au, on W substrates, interface struct., FIM obs. 80−65384
Au, optical characterisation, inversion method 78−11008
Au, optical consts. meas., using automatic ellipsometer without phase plate 77−53970
Au, optical dielec. const. in visible region, 300 and 1.5K 77−90211
Au, optical props., dielec. function, void model, sample effects 80−76048
Au overlay film on quartz for temp. compensation, SAW device appl. 80−79043
Au overlayer, on GaP photoelectrode 78−14812
Au, pulsed potentiostatic deposition from Au(I) sulphite solns. 78−15321
Au, refr. index, obs. using automated Fourier-Stokes analyser ellipsometer system 78−49886
Au, self-supporting, thermotransmission meas. 1.8 to 3.5 eV 78−27343
Au, simulation of transmission of 1 keV electrons 77−12475
Au single cryst., thin films and bulk, anisotropic X-ray emission 80−108303
Au, spatial resolution of X-ray microanalysis 80−101065
Au, spike effects of heavy ion sputtering 80−35034
Au, sputtered, hardness and ductility 79−87025
Au, sputtering yields for ions over 15-135 keV 79−56899
Au, surface resistivity at 337 μm 77−39913
Au, surface step structure imaging by dark field electron microscopy 80−15346
Au, surface-plasmon modulated reson. for adsorption studies 79−83045
Au, thin film, anomalous stopping power effects 80−65102
Au thin film, electromigration, adhesion layer effects 80−96685
Au, thin film, self-sustaining, electron mean free path meas. 80−92883
Au thin films, cryst. ripening rel. to heat treatment *(German)* 80−3109
Au thin films, electron diffr. investigation of Debye temp. 80−88420
Au thin films, with nm-sized pores, prep. from Au-Ge eutectic films by etching 80−16227
Au thin layers, diffusion rate of H_2, N_2, Ar, CO_2, air, and O_2 80−100359
Au, transparent, secondary electron emission of 10-100 keV electrons 77−32477
Au, twin boundary struct. and migration, atomic scale electron microscopy obs. 80−107276
Au, unbacked, optical constants by transmission interferometry 79−78778
Au, unsupported, simultaneous meas. of refractive index and thickness *(French)* 77−55842
Au, vac. deposited thin film, Auger spectroscopy 80−2952
Au, vacuum condensation, on mica, saturation density of nuclei 78−18932
Au, vacuum deposited, internal stress and its depend. on gas adsorption 80−6683
Au vacuum deposited coating on glass, strength 80−55505
Au, vacuum deposited film, surface struct., HEED meas. 78−6234
Au, vacuum deposited on Cu, sputtering yield by substrate Auger meas. 79−95889
Au, van der Waals energy of interaction with heavy alkali atoms 77−11829
Au, vapour deposited coatings, mean thickness at which films reach continuity 79−51459

metallic thin films continued
Au, vapour deposited on Au with Cr interlayer 77−20202
Au very thin film on MgO (001) surface, AES obs. 79−33870
Au, void growth in early stages of ageing and electromigration 78−38991
Au, void size and number prediction 79−28256
Au, whisker growth due to high current densities 77−69191
Au/Al thin film, Al diffusion studied by attenuated total reflection method 80−92722
Au/Cu, double layer film, oxidation *(Japanese)* 80−61010
Au/In film structure, interdiffusion at room temp. 77−39703
Au/Pb thin film couple, room temp. interdiffusion study 79−28154
Au/Pt interface, diffr. studies of conc. variations 79−42322
Au/Pt/Cr films, diffusion of Si, depth anal., optical and Rutherford backscatt. meas. 79−10981
Au/Si films, laser-irrad., phase transform. study 80−49536
Au/Sn, evaporated, microstructure and texture, TEM obs. 80−39481
Au/Sn evaporated film, interdiffusion, X-ray diffr. and ion backscatt. obs. 79−33121
Au/Sn thin film couples, evaporated, TEM study 80−59832
Au/Ti thin films, effect of Cl_2 on elec. resistance, Ti atom migration and preferred orientation 80−34530
Au-Ag, thin film, double layer system electron beam effects during sputter profiling AES obs. 79−65347
Au-Be, contact form. for semicond. devices by ionised-cluster beam deposition 77−32528
Au-Cr bifilm, resistivity and struct. changes under heat treatment, diffusion effects 77−1497
Au-Er, stress-induced g-shift, ESR meas. on Er 77−51951
Au-Ge film, evaporated, for ohmic contacts to GaAs, compositional stratification, effect of source material impurities 79−77951
Au-Pd-Au sandwich, obs. of strongly enhanced mag. susceptibility 80−93076
Au-refractory film interdiffusion obs., by combination of scattering techniques 80−65308
Au-Si, elec. resist. decay and struct. change on exposure to air 77−72924
Au-Si, film-substrate system, relax. effects, internal friction meas., temp. range 20 to 900°C 78−18886
Au-Si, spatial origin of electrons in internal photoemission struct. *(French)* 78−91770
Au-Si thin film double layer, silicide form., electron diffr. study 80−80005
Au-Sn evaporated films, comp. and annealing behaviour, 20-400°C 77−76695
Au-Sn film, evaporated, interdiffusion and phase formation, in situ He ion backscattering meas. 78−22901
Au-Sn layer system, on glass, thin film interdiffusion 77−20134
Au-$Ti_{0.3}W_{0.7}$, thermal annealing study of metallisation on Si 80−80134
(Au-Ge)-Ni, for contacts to n-GaAs, metallurgical investigation using inert substrate 77−85313
(Au-Ge)-Pt, for contacts to n-GaAs, metallurigical investigation using inert substrate 77−85313
AuAl formation by thin film interactions, identification by X-ray diffraction 79−99442
AuCu-Al thin film bilayer system, phase formation, backscattering spectra 80−96728
Au_3Mn thin films, electron diffr. study 80−92793
$Au_{1-x}Si_x$, amorphous film, spectra 0.01-6.2 eV, $0.13 \leq x \leq 0.5$ 78−68574
Au(111)/Ag(111) thin film system, diffusion processes, diffused Ag composition profile 79−90832
B-transition metal thin films, amorphous to cryst. transformation 80−7563
Ba film, deposited on W (100), struct. determ. using LEED 79−90902
Ba film, on SiO_2, interfacial chemistry, AES obs. 80−44434
Ba films, chemisorptive luminescence systems for surface reaction obs. 78−7236
Ba getter, initial reaction probability with O_2, water, CO and CO_2, AES obs. 80−61153
Ba, multilayer and monolayer, on W substrate, AES and work function meas. 77−24921
Ba, oxidation, SXAPS 77−73189
Ba, semitransparent, opt. props. in 2-5.6 eV range, electronic transitions, thickness depend. *(French)* 80−108289
Ba, structure effects on work function, electron micrographs and photoemission meas. 79−83107
Ba, work function and struct. 78−80040
Be film, on W (110), growth mode, work function, thermal desorption, and struct. 80−75477
Be film, opt. filter in He discharge lamp for photoelectron spectroscopy 78−79115
Be film, vapour quneched, mech. stresses and elec. cond. 79−73414
Be, growth on W, FEM obs. 78−26799
Be, on Cu substrate, monolayer overgrowth, quantitative AES method 80−10813
Be, on Pt substrate range of primary electrons 77−4134
Be, RF sputtered film, props. rel. to deposition conditions 77−39965
Be, ultra-thin fabrication 79−33933
Bi, evaporated film, internal friction 77−7998
Bi, film, size effect of carrier heating, surface scatt. *(Russian)* 80−100474
Bi films, resistance changes due to bombardment by N, C, or Ar ions 80−103670
Bi, refractive index determ. using Rayleigh-Lowe refractometer 80−7427
Bi, thin film, resistivity, rel. to thickness 80−107928
$Bi_{1-x}Sb_x$, sputtered thin films, first order Raman scatt. 79−69831
Bs, laser beam hole machining 80−30207
Ca, film struct., mass-thickness depend. 78−80040
Ca, imaginary part of permittivity determ., 2-5.6 eV *(French)* 77−4694
Ca, optical absorption and plasma reson. 77−40296
Ca, optical consts. meas., 2 to 5.6 eV *(French)* 78−52586
Ca, oxidation, SXAPS 77−73189
Ca, structure effects on work function, electron micrographs and photoemission meas. 79−83107
Ca, vac. deposited, struct. and photoemission meas. 80−11538
Ca, vacuum deposited photoionisation coeff. from photoemission meas. 79−91569
Cd deposited layers on Ti (0001), LEED and AES determ. of struct. 77−72804
Cd deposited layers on Ti (0001), LEED and AES determ. of structure 77−76688
metallic thin films continued
Cd, deposition props. on specially prepared substrate, desorption energy and surface diffusion 79−90917
Cd, dry lubrication on C steel, tribological behaviour 80−89364
Cd epitaxial monolayer, nucleation and growth on Ge (111), RHEED and mol. beam study 77−43447
Cd films, struct. and props., X-ray diffr. spectra anal. 80−80119
Cd, freshly deposited, 77K, refl., annealing effect, thickness depend. 77−16413
Cd, HCP, crystal struct. changes on ion bombard. 77−69018
Cd, influence of source material and shape on sublimation props. 78−80474
Cd, nucleation and growth, props. 80−29878
Cd, thin film, vac.-deposited, X-ray diffr. struct. obs., props. 79−37937
Cd, vacuum deposited, microstruct. exam., X-ray diffr. profile anal. 79−46973
Cd, vacuum evaporated, HCP, microstruct., X-ray obs. 80−10827
CdSe, influence of source material and shape on sublimation props. 78−80474
$CeCoSi_2$ film, Hall effect and magnetoresist. *(Russian)* 80−11109
Co, evaporated, adsorption of H_2, surface pot. meas. 77−31890
Co evaporated film, X-ray diffr. study 80−6663
Co film, electromigration exam. from structural changes and resistance increases 77−20213
Co film, evaporated, columnar struct. depend. on degree of texture 80−54567
Co film, evaporated, texture and columnar struct. 80−54566
Co, film, Kerr magneto-optical consts. 78−76541
Co film, on Si substrate, laser irrad., cellular struct. and silicide form. 80−10710
Co film, optical props. by self-consistent photometric technique 80−55217
Co film, work function changes upon water contamination 80−44705
Co films, electromigration and Hall effect 77−62664
Co, HCP, crystal struct. changes on ion bombard. 77−69018
Co, reactive cathodic sputtering, X-ray diffr. exam. of chem. struct. *(French)* 77−63519
Co thin film, nuclear spin echo excitation on subharmonics, and multiple freq. *(Russian)* 80−60454
Co, thin films, optical and magneto-optical permittivities 80−66163
Co-Gd, amorphous, prep. conditions influence on supernetwork struct. 77−76709
Co-Mo, multilayer films, depth resolution determ. in Auger depth profiling meas. 79−78800
Co-Ni-P, film, props. independent of mag. hysteretic and anhysteretic remanences *(French)* 80−2604
$Co_{1-x}B_x$, polycrystalline and amorphous sputtered films, Brillouin spectra 80−2775
Co_5Ge_3 amorphous film, elec. resist., microstruct. and annealing 77−85188
Co_3Pd epitaxial films, multiray dynamic theory of diffr. contrast to explain defects nature 79−64962
Co_3Pd ordered, stacking fault obs. by TEM and interpret. using many-beam theory 80−107680
Cr, 1/f type noise, spatial correlation 79−38194
Cr black, coating on Cu substrate, selective solar energy absorpt., model calcs. 79−57440
Cr containing Cr_2O_3, film struct., oxide percentage determ. and temp. coeff. of resist. 80−103607
Cr, damping and vel. of longit. elastic waves at 9.4 GHz 80−10596
Cr, defects and mechanical stability, different deposition methods *(Bulgarian)* 80−44438
Cr, evaporated, black selective solar absorbers 77−34956
Cr, evaporated, on die-cast Zn, microstruct. and intrinsic stresses, substrate temp. effects 78−10304
Cr film, 3p-3d intershell interaction, photoemission 80−80934
Cr, film, contact reaction with amorphous Si 79−23846
Cr, film, deposition on glass surface heated between room temp. and 300°C 77−90277
Cr film, effect of substrate temp. on formation, electron microscope obs. 80−39469
Cr film, evaporated, concurrent ion bombard. effects 80−80142
Cr film, obtained by thermo ionic precipitation, phase composition, lattice parameters *(Russian)* 80−96756
Cr film, pattern generation by laser-induced oxidation 80−61009
Cr, film, prep. by evap. and ion plating, AES determ. of comp. profiles 77−89675
Cr film, residual stress meas. by X-ray diffr. using $\sin^2\psi$ method 79−15059
Cr, film, sputtering yields, proton-induced X-ray meas. 80−50488
Cr film, trivalent, cathodic deposition, as bonding interface between Cu and polyethylene 80−76201
Cr films, on Al_2O_3, quartz and glass, electron-beam deposition techniques improvement 80−7496
Cr films, photoresist film on reverse gas plasma etching 80−97634
Cr, fine particle solar absorber, effective medium theory 80−21396
Cr, lattice dimens., difference between vacuum condensates and massive specimens *(Russian)* 77−31912
Cr, on polycryst. CdS, thermal diffusion, 240-400°C 80−80001
Cr, on Si, ion implanted, inert-gas-bubble form., TEM and Rutherford backscatt. anal. 79−90682
Cr, overlayers on polymer, electronic struct., XPS study 80−45204
Cr, preparation by decomp. of bis-arene cpds., struct. and phys. props. 80−60785
Cr, reversal etching in gas plasma, reaction mechanism, AES and XPS obs. 80−16564
Cr, thin film, chemical cpd. form. by N_2^+ and Ar^+ ion bombardment *(Russian)* 79−73225
Cr, vacuum deposited coating on Zn substrate, cracking caused by intrinsic stresses 78−6238
Cr vacuum deposited coating on glass, strength 80−55505
Cr, vacuum-deposited, quantitative mass anal. by colorimetry 77−69998
Cr, vapour deposited on low temp. KCl substrates, struct. obs. 80−10826
Cr/Au layered films, microstruct. and interdiffusion during ageing, 423 to 573K 79−46965
Cr/Au metallisation system, corrosion inhibition using intermediary Pd layer 79−79155
Cr-Au film structure, on Si interdiffusion 77−39698
Cr-C, hard coating preparation by ion beam methods 80−25579
Cr-Pt thin film couple, diffusion, new Cr-Pt phases obs. 79−42319

metallic thin films continued
Cr_5Ge_3, amorphous film, short-range-order struct., electron diffr. meas 79−15047
CrTe, film, attenuated total refl., magneto-optical effects 77−52196
Cs, condensation on fused quartz meas. by torsion microbalance *(German)* 77−35839
Cs film, elec. props. *(Russian)* 77−47906
Cs film, work function theory, size effect 78−43460
Cs film on Mo substrate, ang. depend. XPS, depth profile determ. 78−88404
Cs-O film, metallic, on Ag substrate, photoemission, surface plasmon excitation 77−16461
Cu, 1/f noise, role of substrate 79−28388
Cu (001) monolayer, electronic struct., self-consistent LCAO calc. 79−4606
Cu (100), three-layer film, work function and density of states, self-consistent calc. 77−35978
Cu (100) film, chemisorbed N_2, electronic struct. 77−59315
Cu, (110), energy bands, tight binding calc. 77−15761
Cu (111) energy bands, tight binding calc. 77−15760
Cu, (111) surface electron microscopy 80−103556
Cu, absolute work function meas. by field-emission retarding-pot. device 77−59322
Cu, adhesion meas. 80−50822
Cu, adhesion to ABS polymers deposited in internal magnet magnetron sputtering system 79−83121
Cu, adsorption of CO, effect on resist., negative p-values 77−85083
Cu, adsorption of O, study of gravimetric uptake and work function 79−33179
Cu, aging effect of thermoelectric power 78−2584
Cu alloy, precipitation strengthened compositions with oxide particles, condensed, struct. criteria and thin layer possibilities *(Russian)* 80−89236
Cu alloy film, multicomponent secondary ion emission meas. of composition var. laws *(Russian)* 77−80704
Cu alloy-Al alloy evaporated couples, interdiffusion *(Russian)* 77−43389
Cu, bulk and (001) films, extended tight-binding calcs. 80−70592
Cu, condensates of different thicknesses, polycrystalline, mech. props. 79−65350
Cu, continuous film, 1/f noise, temp. and substrate depend. 79−24086
Cu, damping and vel. of longit. elastic waves at 9.4 GHz 80−10596
Cu, deposition with sputter gun 77−44162
Cu, EXAFS meas. by total refl. 80−55228
Cu, electrochem. overgrowths, role of substrate dislocations and grain boundaries in nucleation and growth 79−51454
Cu, electrodeposit on Al and Fe, defects and their effect on props. 80−39474
Cu, electrodeposited, work function, heating temp, influence 79−33331
Cu electrodeposition in cylindrical pores by pulse plating 80−81330
Cu, electron beam transmission, reflection, and absorp., $35 \leq E \leq 70$ keV 77−39754
Cu, electron transport props., struct. defects role 77−40117
Cu, electronic struct., self-consistent calc. 77−76959
Cu, electronic structure and d-holes of films and surfaces 78−39180
Cu, energy losses and straggling for H^+ and He^+ beams *(Russian)* 80−84226
Cu, evaporated, surface struct. 79−69381
Cu, evaporated layer, secondary electron energy distrib. and work function *(French)* 79−99993
Cu film, 1/f noise and its temp. depend. 79−60939
Cu film, 1/f noise and its temp. depend. 79−60940
Cu film, adhesion changes on 10 MeV electron irrad. *(Russian)* 77−43460
Cu film, angular depend. UPS, surface electronic struct. 79−83095
Cu film, annealing effect on grain size 78−72015
Cu film, band structure, appl. of extended rigorous cellular method 78−52055
Cu film, complex impedance, IR transmission and refl. meas. 79−78216
Cu film, diffuse optical scattering from variable roughness surfaces 80−100704
Cu film, effect of thermal strain on orientation 80−49294
Cu film, electrodeposited, recrystallisation kinetics, X-ray scatt. *(Russian)* 78−60045
Cu film, electron transmission, calc. 80−60724
Cu film, energy losses of 20-40 keV electrons 78−92153
Cu film, Gorsky effect, internal friction maxima, atom diffusional mobility *(Russian)* 80−70446
Cu film, in situ struct. determ. by internal stress meas. 80−54569
Cu film, internal stress determ. by stress relaxation method *(Russian)* 77−62787
Cu film, on amorphous C and Si substrates, dispersion force contrib. to adhesion *(French)* 80−59842
Cu film, on Au substrate, oxidation and interfacial behaviour, ion scatt. spectroscopy study 80−66691
Cu film, optical consts. deduced from surface EM wave propag. 80−60697
Cu film, photoelectron emission, intershell interaction influence on 3d and 5d branching ratio 80−104038
Cu film, pure and CO covered, optical consts., ellipsometry meas. 79−78645
Cu film, pure and CO covered, work functions 79−91570
Cu, film, sputtering mechanism, SEM 80−29839
Cu film, stability and rupture using perturbation analysis 78−79911
Cu film, struct., oxidation, and exoelectron emission rel. to bulk samples *(Russian)* 79−37927
Cu film, ultra thin, EXAFS 79−15559
Cu film, vacuum deposition on Pb (111), substrate diffusion effects, RHEED, LEED, AES 80−65410
Cu film, valence bands, XPS excited by Zr Mζ radiation 80−40236
Cu film, work function changes upon water contamination 80−44705
Cu film deposition, reactive sputtering in RF discharge, flow discharge mass spectrometry 77−44155
Cu film deposition, thermal effects, influence on internal stress meas. 80−96767
Cu, film growth on graphite and amorphous C, electronic struct. by photoemission and Auger obs. 79−77947
Cu film on Mo substrates, film stability on reinforced fibre substrates *(Russian)* 80−39462
Cu film on Ni substrate, EXAFS in photoelectron yield spectra 80−16123
Cu films, excess (1/f) voltage noise 79−42598

metallic thin films continued
Cu films, ion plated on polyethersulphone, structural and resistivity study 79−42411
Cu films, resistance changes due to bombardment by N, C, or Ar ions 80−103670
Cu films, thermal phonon radiation into α-quartz substrates 79−42363
Cu films, vac. condensed at oblique vapour incidence, oriented cryst. growth, electron diffr. study 80−97432
Cu free electrolytic films, tensile creep for various film thicknesses calcs. *(Russian)* 80−11697
Cu, growth by ionised-cluster beam deposition, adhesion to substrate 77−32527
Cu, growth on amorphous C, electronic props., UPS and XPS obs. 79−82476
Cu, inert gas refl., semiempirical analysis, cmpared with expt., 10-30 keV 78−6823
Cu, interaction with adsorbed dye mols., absorpt. and luminesc. 80−103981
Cu, ion bombardment induced preferential orientation 79−19293
Cu, ion plated, defect growth structs., SEM obs. 80−24768
Cu ion-plated coating, grain structure 79−28249
Cu, lattice dimens., difference between vacuum condensates and massive specimens *(Russian)* 77−31912
Cu, low energy electron irrad., visible and UV emission 78−2921
Cu, metallised coating on polyethylene terephthalate film, fracture under laser irrad. *(Russian)* 80−76333
Cu, Monte Carlo simulation of energy distrib. of low energy protons 77−15466
Cu on Ag (001), ultrathin film electronic states calc. 78−6318
Cu, on Ni, recrystallisation and interdiffusion, electron microscope obs., 450-600°C 80−39363
Cu, on Ni single cryst., diffusion coeff. using method of nets 78−22903
Cu, on Ni(111) surface, twinning 77−24495
Cu, on thermally oxidised Si, EM tensile adhesion test method 80−50804
Cu, optical props. in intermediate region between pure Drude and interband absorption 77−81170
Cu, overlayers on polymer, electronic struct., XPS study 80−45204
Cu, oxidation, RMEED/SEM studies 80−100968
Cu, partially oxidised, EXAFS studies on superficial regions 80−75474
Cu, partially oxidised, oxide removal and O_2 desorption on vac. annealing 77−12738
Cu, polycryst., nodule mechanism of diffusion-induced disintegration *(Russian)* 78−51829
Cu, quench-condensed thin film, annealing effect on resistivity 78−43488
Cu sandwiches, size effect 79−73604
Cu, simulation of transmission of 1 keV electrons 77−12475
Cu, sputtering yields due to Ar^+ milling, He^+ Rutherford backscattering and AES obs. 79−65969
Cu surface, plasma cleaning and etching, removal of C 80−97645
Cu, surface electronic struct. determ. by ab initio calc. 77−43679
Cu, surface-plasmon modulated reson. for adsorption studies 79−83045
Cu, temp. depend. of 1/f noise meas. 77−85277
Cu, thermoelec. power meas. 77−79092
Cu thin film, electromigration, adhesion layer effects 80−96685
Cu thin foils, intrinsic struct. in grain boundaries and boundary mobility 80−103368
Cu thin layers, thickness meas. by proton-induced X-ray emission 80−4690
Cu, thin single cryst. films, new technique for prep. employing two stages of evaporation 79−33932
Cu, thin targets, electron transmission below 3 keV *(French)* 80−60725
Cu, transport prop. investig. 80−13011
Cu, vac. deposited thin film, Auger spectroscopy 80−2952
Cu, vacuum deposited, breakdown stress, thickness depend. *(Russian)* 77−59238
Cu, vacuum deposited, thickness meas. using X-ray fluoresc. technique 79−90911
Cu, vacuum deposited film, surface struct., HEED meas. 78−6234
Cu, vacuum deposited layer, ion bombardment induced preferential orientation 80−100290
Cu, vacuum-condensed film, structural changes under glow discharge *(Russian)* 79−15852
Cu, vacuum-deposited, interrelation between dynamic and static distortions, X-ray diffr. meas. *(Russian)* 77−43305
Cu, vacuum-deposited, separation from leucosapphire substrate during annealing *(Russian)* 77−7997
Cu/Al film system, interdiffusion and phase growth kinetics 77−69122
Cu/Ni film counter, surface counting method for diffusion study 79−42321
Cu/Ni interface, diffr. studies of conc. variations 79−42322
Cu-Ag, preparation with const. comp. by diffusion-limited evaporation from liquid 77−21038
Cu-Al alloy, vacuum deposited, composition, structure, resistivity 78−6852
Cu-Al films, elec. cond. of vacuum condensates depend. on composition, annealing *(Russian)* 80−65709
Cu-Al thin film multistructure, Xe^+ ion beam cratering 80−66708
Cu-Au film, optical props. of ordered and disordered alloys 77−20945
Cu-Au thin film system, interdiffusion coeff. from cond. and Auger anal., 25 to 250°C 77−59154
Cu-Au thin films after accelerated ageing, failure by Kirkendall porosity 80−6675
Cu-Au-Cu, sandwich struct., bombarded by 3-15 keV Ar^+ at angle of incidence of 30°, sputtering yield coeff. 79−65968
Cu-Au-Cu thin film, diffusion induced grain boundary migration 79−77833
Cu-metal thin film couples, room temperature interactions 80−96699
Cu-Mn alloys, vacuum deposited, electrophys. props. 77−63006
Cu-Mn-Ni, thin film, vacuum deposited, struct., elec. cond. *(Russian)* 78−19668
Cu-Mn-Ti alloy, physical and electrical props. *(Russian)* 77−66208
Cu-Ni, bimetallic film, exam. of diffusion by electrical resistivity meas. *(Russian)* 79−14970
Cu-Ni, film, preferential sputtering due to altered layer struct., AES meas. 78−76573
Cu-Ni bimetallic thin film, effect of microstructre on interdiffusion 79−77840
Cu-Ni film system, time depend. diffusion coeffs., grain boundary and dislocation effects 77−80656

metallic thin films continued
Cu-Ni films, compositionally modulated, magnetic anisotropy, magnetisation curves 80−88840
Cu-Ni thin thin film couples, polycryst., interdiffusion singularities, Frenkel and Kirkendall effects *(Russian)* 77−24447
Cu-Pb thin film couple, interdiffusion and recrystallisation, grain size effects 77−76625
Cu_3Au thin films, fine-grained and disordered, low temp. ordering 80−97433
Dy, appl. of vaccum deposition system using liq. He cooled cryopumping panel 78−56581
Er film, work function, effects of O_2 sorption 78−19125
Er-H_2 system, work function changes correlated with phase changes, elec. resist. meas. 77−11828
Es film, preparation and characterisation 80−15405
Eu, film, optical cond. meas. 78−76112
Fe amorphous film, getter sputtering at 25K 79−38741
Fe, amorphous-polycrystalline resistivity transform. temp., of codeposited N_2 78−6461
Fe, and Fe-Cr, film, sputtering yields, proton-induced X-ray meas. 80−50488
Fe, atomic layers, Pauli paramagnetism to band ferromagnetism transition thickness depend. 78−72377
Fe, chemisorption of O_2 and water vapour, XPS obs. 77−48587
Fe, columnar grain struct. 77−11808
Fe, core electron polarisation measurement 79−4756
Fe deposited W tip, FIM obs., epitaxial growth 78−79904
Fe, epitaxial growth on Au platelets, dislocations 80−96760
Fe epitaxial growth on Cu(111), supersaturation and mode of growth, LEED and AES exam. 78−18929
Fe, evaporated, adsorbed acetylacetone, XPS study 80−76133
Fe, ferromag. film, surface states, surface magnetisation and electron spin polarisation 80−65648
α-Fe film, deform. in electron microscope, dislocation mechanism 79−82227
Fe film, evaporated at oblique incidence, columnar and textural struct. *(Japanese)* 77−62776
Fe film, implanted with C ions, HCP struct. formation, electron diffr. study *(Russian)* 79−82469
Fe film, nuclear spin system dynamics Mossbauer study in FMR conditions *(Russian)* 80−80651
Fe film, vacuum deposited, resist. minimum 80−44741
Fe film, work function changes upon water contamination 80−44705
γ-Fe film on Cu (111) mag. props. 78−31098
Fe films, evaporated at oblique incidence, columnar struct. and texture 79−77967
Fe, lattice dimens., difference between vacuum condensates and massive specimens *(Russian)* 77−31912
Fe multilayer films stability, Mossbauer spectra 80−29651
Fe, thermally evaporated, contamination effects obs. 80−49545
Fe, thickness variations in extraordinary and spontaneous Hall coeffs. 80−97013
Fe, thin foil, extrinsic grain boundary dislocations, low C content influence 80−107273
Fe thin layers, vacuum coated on PMMA, mag. behaviour during mech. stress cycles *(German)* 80−80581
Fe, vacuum deposited on Au (111), interaction layer formation mechanism 80−54559
Fe vacuum deposits on Ni(Cu)(Ag) (111) FCC substrates, orientation relationships 80−59836
Fe, vacuum-evaporated contamination, conversion electron Mossbauer spectroscopic obs. 78−23985
Fe-Co films, optical props. order-disorder transformation influence, absorpt. band existence *(Russian)* 79−65942
Fe-Ge, characteristic energy losses and optical props. 80−29834
Fe-Ni alloy, X-ray microanalysis in scanning transmission electron microscope, limitations 78−20122
Fe-Ni film, electrodeposited, struct. and mag. props. 80−107668
$Fe_{1-x}B_x$, polycrystalline and amorphous sputtered films, Brillouin spectra 80−2775
Fe_5Ge_3, amorphous film, elec. resist., microstruct. and annealing 77−85188
FeNi amorphous films, fast phase transition investigation by TEM method 80−107029
Fe_xNi_{1-x}, amorphous films, crystallisation, effect of codeposited O_2, N_2 or Kr gases 80−10807
Ga amorphous film, elec. field gradient 80−25264
Ga, amorphous film, X-ray diffr. 79−51451
Ga, amorphous metal films, crystallisation with and without mag. field 80−70570
Ga, freshly deposited, 77K, refl., annealing effect, thickness depend. 77−16413
Ga, optical props., 2-15 eV 77−77308
Ga, vacuum deposited film characterisation *(French)* 79−51447
Gd, appl. of vacuum deposition system using liq. He cooled cryopumping panel 78−56581
Gd, hydride form. under water vap. 79−91997
Gd, photoabsorpt. spectra, band structure at. ionisation mechanisms, electron energy loss spectra 77−24909
Gd, vacuum deposited and VPE, deposition parameters effects on struct. 79−90912
Gd-Co amorphous films, model calculations for anisotropy formation induced by resputtering processes 78−64242
Gd-Co amorphous films, uniaxial perp. anisotropy induced by resputtering effect, expt. *(Japanese)* 77−55885
Gd-Co thin films sputtered from mosaic target, thickness and composition distrib. 80−6676
Ge, inelastic mean free path, 700 to 1200 eV, bulk method 80−20763
Ge-Al, elec. resist. and IR transmission, comp. and substrate temp. depend. 78−52112
Ge-Au-Ni, interdiffusion obs., on annealing 78−2308
Ge-Au-Pd, interdiffusion obs., on annealing 78−2308
Ge-Au-Pt, interdiffusion obs., on annealing 78−2308
Ge-Cu (0, 23, 40 at.%), amorphous film struct. *(German)* 78−95391
Hf film on Si substrate, ion-beam induced silicide form. 79−46718
Hf, oxidation, microstructural study *(French)* 80−45436
Hf, RF sputter deposition, ion bombardment and ion implanation 80−25564
Hf, RF sputtered onto sapphire, high stress in graded interfacial layers, AES meas. 77−43446
$HfPt_3$, corrosion resist. and elec. cond., bulk and film samples 78−72285

metallic thin films continued
Hg, condensation, two-dimensional, on W 80−107666
Hg, rotating thin film electrodes, staircase voltammetric stripping anal. 77−12843
In, damping and vel. of longit. elastic waves at 9.4 GHz 80−10596
In film, friction and fear in ultrahigh vacuum, effects of speed, film thickness and substrate surface roughness 79−20202
In film, oxidation, XPS excited by Zr Mζ radiation 80−40236
In film, polycrystalline optical transitions from d core states 77−85827
In film, submonolayer superstructures on Si (111) isothermal desorption, RHEED meas. 79−86992
In, film, vac. deposited, influence of ion bombardment during condensation 79−82483
In film, vacuum evaporation growth, impurity presence, effects *(Hungarian)* 80−7495
In, freshly deposited, 77K, refl., annealing effect, thickness depend. 77−16413
In, RF plasma oxidised, surface analysis using ESCA 80−50742
In, recrystallisation of films prep. by vacuum evap. 79−4488
In sandwiches, size effect 79−73604
In, vacuum deposited, growth conditions effect on elec., optical, and structural props. 79−78215
In, vol. plasmon dispersion and damping, electron energy loss spectra 79−7797
In-PbTe contacts, fabrication and props. 80−60078
InP-Al interface struct., low temp. interaction, AES study 80−107661
insular metal films, influence on crystn. of continuous films 80−88454
Ir, evaporated, CO adsorption, IR refl.-absorpt. spectroscopy 80−34925
Ir, thin film, electrographic investigation of interaction with atmospheric O_2 *(Russian)* 77−25196
K film, adsorbed on Ni (100), plasmon losses in electron energy loss spectra 79−61480
K film, splitting of surface plasmon emission spectra 79−99954
Li, film, adsorption on Mo (112) surface, LEED and contact pot. method 80−10794
Li film band structure, appl. of extended rigorous cellular method 78−52055
Li, optical absorpt. spectra, rel. to phase struct. 77−4651
Li, temp. depend. of K X-ray emission edge 77−32472
$LiNbO_3$ SAW filter bulk wave suppression by triangular metal film overlay 77−23830
Mg clean films, O_2 interaction study using synchrotron-radiation-induced-photoemission 80−55709
Mg, deposition props. on specially prepared substrate, desorption energy and surface diffusion 79−90917
Mg, deposition using low-energy ion beam, Rutherford backscatt. and SEM anal. 77−59700
Mg, deposition using low-energy ion beam, Rutherford backscatt. and SEM anal. 77−70004
Mg, deposits of different roughness, refl. drops and surface plasmons 77−20392
Mg, film, electron inelastic scatt. mean free paths, synchrotron radiation photoelectron spectra meas. 78−76587
Mg films, chemisorptive luminescence systems for surface reaction obs. 78−7236
Mg films, struct. and props., X-ray diffr. spectra anal. 80−80119
Mg, optical cond., energy derivative spectrum 77−66551
Mg, polycryst., chemisorpt. of O_2, synchrotron radiation photoemission expts., 70-150 eV 78−95228
Mg, synchrotron radiation photoemission, plasmon loss struct. 79−28897
MgF_2/In/MgF_2 struct. surface plasma wave optical excitation in In 79−91516
Mn film, heat treated, lattice distortion energy, resist. meas. 79−19492
Mn film, resistivity-temperature variation 79−24085
Mn film, vacuum-evaporated, H(D) uptake kinetics and energetics 80−88430
Mn, optical, magneto-optical and struct. props. 77−1664
Mn, refractive index determ. using Rayleigh-Lowe refractometer 80−7427
Mn-Bi, negative transverse magnetoresist. in c-plane, domain wall effects 77−20465
Mn-Bi, perpendicular anisotropy film, galvanomag. props., hysteresis loops 77−20464
Mn-Ge, amorphous, short-range order, electron diffr. obs. 80−39473
Mn-Sb two layer film, cpd. formation kinetics, ion backscatt., X-ray diffr. and mag. meas. 77−72801
MnBi film for recording optical information, analogue characts. *(Russian)* 78−50716
$Mn_{46}Co_{54}$, amorphous alloy prep. by high-rate sputtering, struct. and prop. characteris. 79−24462
MnCuBi, optical and magneto-optical props. 77−4695
Mo, amorphous thin films, for photothermal conversion, CVD fabrication 80−7503
Mo, CVD, with high IR refl. and large solar absorpt., prep. and props. 80−26163
Mo, cc preparation by H_2 reactive sputtering *(Japanese)* 79−95929
Mo, condensed layers, restricted growth texture formation singularities *(Russian)* 77−7982
Mo, electron beam deposition on Si, X-ray obs. of silicide form., diffusion processes *(German)* 77−1341
Mo, energy loss function, Kramers-Kronig anal., reflectivity, optical props., EELS 80−40194
Mo film, CVD, passivating against IR reflectance losses caused by oxidation 79−3758
Mo film, carbonisation and oxidation, electron diffr. exam. *(Russian)* 77−44399
Mo film, characteristics of elastic reflection of slow electrons 79−14657
Mo film, constrained, 20 MHz thermoelastic wave generation 79−47880
Mo film, deform. in electron microscope, dislocation mechanism 79−82227
Mo film, on Si, X-ray line-shape anal., simplifications using Fourier series 79−82123
Mo film, on Si substrates, laser irrad., cellular struct. and silicide form. 80−10710
Mo film, sputtered on Si, annealing effect on uniform and nonuniform strains 79−82504
Mo film, vacuum deposited onto SiO_2-Si substrates, elec. resist. 78−76166
Mo film, work function, effects of O_2 sorption 78−19125
Mo films, sputtered from cylindrical-post magnetron with Ne, Ar, Kr and Xe, compressive stress and presence of inert-gas obs. 80−80140

metallic thin films continued
Mo, formation by reduction of $MoCl_5$, influence of electric field 80−93491
Mo, laser induced reactions with Si 79−70365
Mo, layer, grain size depend. on thickness *(Czech)* 77−47695
Mo, migration in GaAs, ESCA study *(French)* 78−75885
Mo, on Si, silicide form. 78−43261
Mo, on SiO_2/Si substrate, effect of heat treatment after deposition on internal stress 78−22973
Mo, thin film, chemical cpd. form. by N_2^+ and Ar^+ ion bombardment *(Russian)* 79−73225
Mo thin film fabrication for photothermal solar convertors using CVD 80−11573
Mo-Ni sputter deposited, amorphous and crystn., Ni^{++} ion irradiation effects, TEM study 79−65128
Mo-Ni thin film junction, phys. vap. deposition parameters effect on thermoelec. power 77−39922
Mo-Si diffusion couples, $MoSi_2$ or Mo_3Si/Mo_5Si_3 form. 79−77836
Mo-Si film-substrate interface, reaction on heat treatment, silicide formation 80−79999
Mo-W bilayer films on Si substrates, silicide formation 79−99376
Na film, adsorbed on Ni (100), plasmon losses in electron energy loss spectra 79−61480
Na film, slow electron bombarded, light radiation 80−40168
Na-NaO-Na struct., inelastic tunnel effect, spectra, potential barrier parameters 79−95511
Nb CVD coatings on graphite, grain struct. depend. on temp. 80−25574
Nb electron beam deposited on Si surface 80−66862
Nb, evaporated film, adsorpt. of CS_2 and H_2S, 195 to 473K 79−33197
Nb film, deform. in electron microscope, dislocation mechanism 79−82227
Nb film, thermal and elec. cond., 9-50K 79−87078
Nb film on Si, Ar ion bombard., $NbSi_2$ form. 80−10709
Nb, H absorption rate, metallic film effect 80−49525
Nb, ion bombardment with N_2^+, Ar^+, struct. changes, chemical compound formation *(Russian)* 78−95084
Nb, laser induced reactions with Si 79−70365
Nb, low temp. internal stresses *(Russian)* 79−11036
Nb, sputter-deposited on stainless steel, electron microscopy and ESCA 77−52554
Nb, surface oxide softening, anisotropy 78−60716
Nb thin films on Si substrate, intermixing, ion induced silicide formation 80−34101
Nb thin foils, surface segregation during sputtering at elevated temps., Auger study 80−54386
Nb, thin-film SQUID working at 4.2K, fabricationa and characterisation 80−100570
Nb/Cu layered ultrathin coherent struct. 80−80122
Nb-Ge film, phase transformations due to annealing, electron diffr. study 80−54551
NbTi films, effect of Ar- and N-ion bombardment on texture *(Russian)* 80−107338
Nd film, on W(100), struct., electronic and dynamic props. *(Russian)* 77−76702
Ni (001) film, electronic struct. by self-consistent numerical-basis-set LCAO discrete variational method 79−60938
Ni (100) films, spin density by self-consistent linear APW method 80−65710
Ni, adsorption of CO, effect on resist., negative p-values 77−85083
Ni alloy, precipitation strengthened compositions with oxide particles, condensed, struct. criteria and thin layer possibilities *(Russian)* 80−89236
Ni, amorphous film, getter sputtering at 25K 79−38741
Ni, amorphous layer covered, target prep. for channelled ion stopping power meas. 80−63431
Ni, atomic layers, Pauli paramagnetism to band ferromagnetism transition thickness depend. 78−72377
Ni coated Mo and W filaments, creep and recrystn. *(Russian)* 78−19822
Ni, damping and vel. of longit. elastic waves at 9.4 GHz 80−10596
Ni, electrochem. overgrowths, role of substrate dislocations and grain boundaries in nucleation and growth 79−51454
Ni, electrodeposit on Cu, defects and their effect on props. 80−39474
Ni electrodeposited film, appl. of stereomicroscopic method for obs. of organic molecule incorporation 80−2288
Ni electrodeposition on Cu (001), three-dimens. epitaxial crystallites, TEM image contrast 80−88457
Ni electrodeposits, influence of Ni sulphamate operating parameters on impurity content and props. 79−28971
Ni, electroless, on stainless steel, internal stress meas. by proximity method, features 79−64611
Ni, electrolessly deposited, structural comparison with electroplated films 79−23869
Ni, epitaxial growth, on NiO(100), by low pressure hydrogen reduction *(French)* 80−11578
Ni, evaporated, adsorbed acetylacetone, XPS study 80−76133
Ni, evaporated, effect of CO adsorption on galvanomag. and mag. props. 79−33364
Ni, evaporated, effect of CO adsorption on galvanomag. and mag. props. 79−33363
Ni, evaporated, galvanomag. props., oscill. due to CO adsorption 77−1496
Ni evaporated thin films, stress and relaxation effects meas. by Michelson interferometer 77−2650
Ni, ferromag. film, surface states, surface magnetisation and electron spin polarisation 80−65648
Ni film, adsorbed $H_2(CO)$, ferromag. reson. exam. 78−15028
Ni film, CO adsorption effect on galvanomagnetic and magnetic props. 78−43490
Ni film, electrodeposited, recrystallisation kinetics, X-ray scatt. *(Russian)* 78−60045
Ni film, epitaxial growth on (001) diamond, TEM exam. 77−66098
Ni film, evaporated, galvanomag. and mag. props. 78−23180
Ni film, evaporated hydrocarbon chemisorption, IR refl. study 79−69343
Ni film, ferromagnetic (100) and (110), energy bands 79−1630
Ni film, implanted with C ions, HCP struct. formation, electron diffr. study *(Russian)* 79−82469
Ni film, interaction with O_2, AES, EELS, work function, and gravimetric meas. 80−75433
Ni film, ion bombarded, porosity 77−66099
Ni film, laser-induced reaction with Si, surface struct. obs. 79−19471
metallic thin films continued
Ni film, struct., oxidation, and exoelectron emission rel. to bulk samples *(Russian)* 79−37927
Ni film, transition from Pauli paramagnetism to band ferromagnetism 79−61192
Ni film, two-dimens. (110) domain wall 77−69648
Ni film, vac. deposited, hexagonal phase *(French)* 78−63944
Ni film, work function changes upon water contamination 80−44705
Ni, film (111), ferromag., energy bands and planar densities of states, LCAO calc. 79−4509
Ni film coating of optical fibres, magnetron sputtering, mechanical props. improvement 79−72723
Ni film crystallisation on C fibres and sapphire crystals *(Russian)* 80−75455
Ni, film deposit on (001)Fe substrate, misfit twin crystals 77−4273
Ni, film growth on graphite and amorphous C, electronic struct. by photoemission and Auger obs. 79−77947
Ni film on Si substrate, ion-beam induced silicide form. 79−46718
Ni film presence effect on NiSi dissoc. 79−47892
Ni film-Fe thermocouple, fabrication and calibration 77−37885
Ni films, adhesion on graphite 80−80141
Ni films, CO-covered adsorpt. of H, isotherms, resist., work function changes 78−75926
Ni films, excess (1/f) voltage noise 79−42598
Ni films, self-supporting, electroplating method of prep. 80−66436
Ni foil, crystal struct. as function of substrate temp. during deposition 80−18742
Ni, growth on amorphous C, electronic props., UPS and XPS obs. 79−82476
Ni, growth on Au (001) substrates *(French)* 80−44446
Ni, HCP and amorphous, RF sputtered, O_2 incorporation, ESCA obs. 80−10832
Ni, hexagonal phase identification, electron microscopy *(Russian)* 77−15711
Ni, inelastic electron scattering 78−92155
Ni, inelastic electron scatt. 79−15570
Ni, kinetic electron emission when penetrated by H^+ ions with 0.3 to 30 keV energy 79−91554
Ni, laser CVD 79−78897
Ni, laser induced reactions with Si 79−70365
Ni, lattice dimens., difference between vacuum condensates and massive specimens *(Russian)* 77−31912
Ni layer, vol. composition of sharp filamentary textures, elec. cond. meas. *(German)* 78−22978
Ni, layer mode growth on Fe (001) surface, AES study 80−49540
Ni, metallised coating on polyethylene terephthalate film, fracture under laser irrad. *(Russian)* 80−76333
Ni monolayer and submonolayer films, on ZnO, UPS study 80−7472
Ni on Au substrate, interdiffusion, backscatt. study 80−79991
Ni, on Si, formation of Ni_xSi_y, effect of substrate nature 77−15703
Ni, on Si, ion implanted, inert-gas-bubble form., TEM and Rutherford backscatt. anal. 79−90682
Ni, overlayers on polymer, electronic struct., XPS study 80−45204
Ni, phonon transport into SrF_2 substrate, diffusive scatt. at impurities 80−49487
Ni, single-crystal films, spin wave reson. spectra 79−11350
Ni, size depend. electronic cond., annealing effects 79−47174
Ni solar collector coating, microstruct., FIM and SEM obs. 80−26166
Ni, sputter deposited on Cu, induced stresses 80−24774
Ni, sputtered, on Si, annealing effects on transmission electron diffr. patterns, silicide form. 78−91562
Ni sputtered films, hexagonal and amorphous, O incorporation, ESCA and electron diffr. meas. 79−11046
Ni, surface IR wave propag. distance 77−28641
Ni, surface properties and photoelectron spin polarisation 78−14782
Ni, thin film, chemical cpd. form. by N_2^+ and Ar^+ ion bombardment *(Russian)* 79−73225
Ni ultrafine particles for solar energy photothermal conversion 79−100538
Ni, vacuum deposited, ethylene adsorption and reactivity with adsorbed H, surface pot. meas. 79−86995
Ni, vacuum-condensed film, structural changes under glow discharge *(Russian)* 79−15852
Ni, work function change during water adsorpt. *(German)* 79−42365
Ni/Fe layers, interdiffusion, Auger sputter profiling obs. 79−46848
Ni/GaAs film contact system, alloying reaction 80−96747
Ni-Ag, thin-film, elec. cond. depend. on substrate film thickness and condensation temp. 79−7911
Ni-Au, amorphous, ferromagnetic, anomalous Hall resist. 77−15832
Ni-B, amorphous, electronic transport and crystn. activation energies *(French)* 80−6807
Ni-B, film crystallisation on C fibres and sapphire crystals *(Russian)* 80−75455
Ni-Cr, electrical props. rel. to AES conc. depth profile 77−32092
Ni-Cr films implanted with N ions, electric properties *(Russian)* 80−107927
Ni-Cr multilayer structs., sputter profiling, depth resolution and surface roughness effects, AES obs. 77−76694
Ni-Cr-P, deposited by electroless plating, resist. characts. 79−4607
Ni-Cr(Fe)(Cu) alloy, matrix effect in SIMS anal. using O_2^+ primary beam 80−76576
Ni-Fe, magnetisation reversal magnetoresistance meas. 77−16132
Ni-Mo, multilayer films, depth resolution determ. in Auger depth profiling meas. 79−78800
Ni-Si film struct., silicide form. He^+ back scatt. and X-ray diffr. obs. 79−51442
Ni-Si film-wafer interface, marker motion in Ni_2Si formation 77−89593
Ni-Ti thin film, phase growth kinetics due to diffusive processes *(Russian)* 77−72722
$Ni_{66}B_{34}$, morphological, structural and phys. props. *(French)* 80−44444
$Ni_{50}Co_{40}P_{10}$ amorphous film, spin wave excitation, ferromagnetic resonance study 80−50198
NiCr, electron beam deposition, evaporation gas phase analysis *(Polish)* 79−20492
Ni_5Ge_3, amorphous film, elec. resist., microstruct. and annealing 77−85188
Ni_5Ge_3, amorphous-crystalline transition, opt. and elec. characts. *(Russian)* 77−85191
$NiSi_2$ layer, on Si, struct. modelling, using axial and phase channelling techniques 79−4489

metallic thin films continued
Ni(001) surface states, surface magnetisation, electron spin polarisation 80−88612
Pb, atomic beam impinging on mica and SiO in vac. deposition, thermal accommodation 79−77960
Pb, deposition on Au, quantitative Auger electron spectroscopy, substrate and instrumental effects 80−71523
Pb, deposition props. on specially prepared substrate, desorption energy and surface diffusion 79−90917
Pb, deposition using low-energy ion beam, Rutherford backscatt. and TEM anal. 77−59699
Pb, deposition using low-energy ion beam, Rutherford backscatt. and TEM anal. 77−70003
Pb, electrolytic deposition on semicond. substrates 77−77425
Pb, film, deposited on Si substrate, residual strains 78−18915
Pb film, friction and fear in ultrahigh vacuum, effects of speed, film thickness and substrate surface roughness 79−20202
Pb film, polycrystalline, optical transitions from d core states 77−85827
Pb film, reactive ion beam sputtering 78−19666
Pb, film, sputtering mechanism, SEM 80−29839
Pb film, thermal strain, depend. on cryst. orientation 78−10311
Pb film, thermal strain, strain relax. mech. 79−42427
Pb, film, thermal strain, strain relax. above room temp. 80−59841
Pb, film, ultra-thin, hexagonal phase, struct. 78−38982
Pb film, vacuum deposited onto SiO, C and mica, quantitative study of nucleation 79−77959
Pb films, conduction electron surface scatt. phase shift, tunnelling meas. 79−51648
Pb, grain boundary self diffusion, microtome serial sectioning anal. 80−79975
Pb, hillock formation by grain boundary sliding 80−107673
Pb, hillock growth upon cycling to cryogenic temps. 80−88448
Pb, inelastic mean free path, 700 to 1200 eV, bulk method 80−20763
Pb, O ion irradiated, damage rate decrease 78−26604
Pb, on Ag electrode, anisotropy of optical props. 80−60534
Pb, on Au (100), initial stages of condensation 78−91569
Pb overlayers, on Cu substrate, oxidation, AES and XPS obs. 79−47833
Pb, oxide form. on (111) surface, orthorhombic PbO 77−63835
Pb, oxidised (111) surface, electron microscope anal. of oxides 78−23878
Pb, polycrystalline film, electron diffr. evidence by off coincidence grain boundaries 77−47469
Pb, single and polytextured thin films, band struct., tunnelling spectroscopy 80−80169
Pb, splat-cooled and vapour-deposited, metastable structs. 79−87018
Pb, thermal strain investigation multiple cycling to 4.2K effects 79−90918
Pb, ultra-thin, existence of double-hexagonal close packed phase 78−63952
Pb, vacuum deposited, reflectance spectra, structural rearrangement effects 77−24905
Pb, vacuum deposited, thermal strain depend. on thickness and grain size 79−90926
Pb, vapour deposited FCC, normal and oblique incidences, microstructure, X-ray diffr. study 80−20048
Pb:O, thin film, microstruct. and thermal stress, doping effects 80−88458
Pb/Ag-Pd, sequentially deposited, thin film reaction kinetics, X-ray diffr. expts. 77−89594
Pb-Bi film, amorphous and polycrystalline, specific heat meas. 77−80715
Pb-In films, atom redistrib., ion-ion emission obs. *(Russian)* 78−18926
Pb-Ni, SO_2 adsorption on mixed metal films 79−87003
Pd, (111) surface electron microscopy 80−103556
Pd, adsorption and absorption of H_2, kinetic analysis of models 77−47679
Pd, adsorption of H_2 or O_2, reciprocal titration of gases, film surface area determ. 77−1318
Pd, electrolytic deposition on semicond. substrates 77−77425
Pd, electron beam deposited on Si surface, silicide formation using scanning CW laser beam 80−66862
Pd film, band structure, appl. of extended rigorous cellular method 78−52055
Pd, film, contact reaction with amorphous Si 79−23846
Pd, film, electrical resist., influence of hydrogenation 77−85348
Pd film, evaporated, hydrocarbon chemisorption, IR refl. study 79−69343
Pd, film, growth on amorphous C, electronic props., UPS and XPS obs. 79−82476
Pd film, high dose Si^+ ion implantation, silicide phases, backscatter spectra 80−19820
Pd film, laser-induced reaction with Si, surface struct. obs. 79−19471
Pd film, on Si substrate, laser irrad., cellular struct. and silicide form. 80−10710
Pd, film, on ZnO, struct., elec. props., AES, UPS study 78−76168
Pd, film form. on Si surface by ion beam plating 77−90284
Pd, film growth on graphite and amorphous C, electronic struct. by photoemission and Auger obs. 79−77947
Pd film on Si, Xe ion beam induced form. of PdSi 80−10800
Pd film presence effect on PdGe dissoc. 79−47892
Pd, film with defects, field-induced resist. min. 80−11050
Pd films, catalytic reactions studied by work function meas. 80−55711
Pd, H-permeable, on V, Nb and Ta foils, Auger and secondary ion mass spectroscopy 79−52467
Pd, IR optical constants, determ. by surface plasmon excitation 78−76418
Pd, laser induced reactions with Si 79−70365
Pd on Ag (001), ultrathin film electronic states calc. 78−6318
Pd, on Si, ion implanted, inert-gas-bubble form., TEM and Rutherford backscatt. anal. 79−90682
Pd, on Si, ion-induced intermixing 80−15420
Pd on Si substrate, epitaxial silicide growth, LEED and AES study 80−103590
Pd, on Si substrate, Pd-Si layer form. by laser irrad. 79−99438
Pd, optical properties, 0.1 to 6 eV 78−92092
Pd overlayers, on Nb, form. of Pd (111) surface states and reson. d-levels, photoemission obs. 80−50523
Pd sandwiches, size effect 79−73604
Pd, surface IR wave propag. distance 77−28641
Pd, two-dimens. nucleus form. on Ag (111), UHV electron microscope obs. 80−10760

metallic thin films continued
Pd, vacuum deposited, ethylene adsorption and reactivity with adsorbed H, surface pot. meas. 79−86995
Pd, work function changes due to adsorbed H_2, surface and interface dipoles 80−96972
Pd-Ag(Au)(Cu) film on $BaTiO_3$ dielectric ceramic substrate, interaction between film and substrate during sintering 79−33958
Pd-amorphous Si thin film interaction, metal rich Pd-silicide formation 80−2284
Pd-H thin film system, phase diagrams using quartz crystal thickness monitor 80−7537
Pd-Ni, bilayers, on single cryst. Si, vacuum annealing, silicide form. 79−51444
Pd-Ni, SO_2 adsorption on mixed metal films 79−87003
Pd-Pt bilayers, on single cryst. Si, vacuum annealing, silicide form. 79−51444
Pd-Si film struct., silicide form. He^+ back scatt. and X-ray diffr. obs. 79−51442
Pd-Ti on Si substrate, silicide form. 80−80006
PdH_x layer, galvanostatic desorption of hydrogen, quantitative theory 80−40694
Pd_2Si layer 79−4489
Pt coatings on glass, quartz, ceramic or sitall, method 77−44376
Pt, electron beam deposited on Si surface, silicide formation using scanning CW laser beam 80−66862
Pt, electroplated, Schottky barrier metallisation, Au diffusion, AES obs. 79−14968
Pt film, growth on amorphous Si:H, AES and LEED study 80−88447
Pt film, laser-induced reaction with Si, surface struct. obs. 79−19471
Pt film, RF sputtered, thickness distribution function 78−11083
Pt film, work function changes upon water contamination 80−44705
Pt film on Si substrate, ion-beam induced silicide form. 79−46718
Pt film presence effect on PtSi dissoc. 79−47892
Pt films, high-purity, sputtered onto Si, PtSi and Pt_2Si form. 77−76676
Pt films, optical props. and radiation stability 80−34999
Pt foil, crystal struct. as function of substrate temp. during deposition 80−18742
Pt, laser induced reactions with Si 79−70365
Pt, nucleate and film boiling in travelling wave regime 80−19231
Pt, on Si, ion-induced intermixing 80−15420
Pt, on Si substrate, Pt-Si layer form. by laser irrad. 79−99438
Pt, polycrystalline, trapping of ^3He and ^4He ions at room temp. 80−84221
Pt, RF diode sputtered, thickness distrib., XPS determ. 77−39743
Pt, spike effects of heavy ion sputtering 80−35034
Pt, sputtered film, Al and Mg contamination, AES, SIMS 77−11822
Pt, sputtering yields for ions over 15-135 keV 79−56899
Pt, surface IR wave propag. distance 77−28641
Pt thin-film temp. sensor *(Japanese)* 80−105645
Pt, triode sputtering, for beam lead metallisation, reduction of contamination 78−72721
Pt, vacuum deposited, ethylene adsorption and reactivity with adsorbed H, surface pot. meas. 79−86995
Pt, vapour deposited on Ir and W, defects and their effect on props. 80−39474
Pt-Au film couple, diffusion of Au, depend. on annealing ambient, AES exam. 77−1261
Pt-Cr(Si) interface, low-temp. diffusion, ambient effects 80−100355
Pt-Ni bilayers, on single cryst. Si, vacuum annealing, silicide form. 79−51444
Pt-Pb fibre, CO adsorption and oxidation, AES and ESCA obs. 79−52469
Pt-Si film struct., silicide form. He^+ back scatt. and X-ray diffr. obs. 79−51442
Pt-Si system, formation of Si enriched metastable cpds. using ion bombardment and post annealing 79−69143
Pt-Si:As, silicide form. during laser irrad., p-n junctions and ohmic contacts 80−84397
PtSi, formation by ion sputtering and annealing, form. and exam. problems 80−100782
Rb film, adsorbed on Ni (100), plasmon losses in electron energy loss spectra 79−61480
Rb film, elec. props. *(Russian)* 77−47906
Re epitaxial film growth on sapphire *(Russian)* 78−35311
Re film, electrodeposition on Cu, packing defects, X-ray diffr. 77−1333
Re film, prep. by laser melting 80−84859
Re, prep. by laser melting *(Japanese)* 79−78909
Rh, evaporation onto single crystal Ag films and mica cleavages 77−40375
Rh, resistive film, electron diffr. structure obs., heat treatment effects 77−51620
Rh-Si thin film interaction, interdiffusion, temp. depend. 80−54443
Ru, thin film, electrographic investigation of interaction with atmospheric O_2 *(Russian)* 77−25196
Sb, epitaxial growth, of electrodeposits on oriented single cryst. surfaces of CU, electron diffr. study 79−66016
Sc, photoabsorpt. spectra, at. ionisation, band struct. mechanisms, electron energy loss investig. 77−24909
Sc thin films, obtained in vac. of 10^{-5}-10^{-6} Torr, struct. and elec. resist. 80−107931
Se, film, obliquely deposited, elec. resist. anisotropy 80−2486
Se, laser beam hole machining 80−30207
$Se_{5,6}$, influence of source material and shape on sublimation props. 78−80474
Sm, ion plating deposition system using electron beam evaporation *(French)* 80−20802
Sm, XPS, 50-250 eV, 4d→4f transition and surface mixed valence 79−15588
SmS, energy of metal-semicond. transition, optical expts. 77−62830
SmS, film, laser generation of US using metal-insulator transition 79−90734
SmS, metallic, transmission, refl. and absorpt. spectra 78−19587
Sn, anomalous transmittance of metal-insulator interface for thermally radiated phonons *(Russian)* 80−103664
Sn film, evaporated on cooled substrate, influence of annealing temp. on elec. resist. and struct. 79−65561
Sn film, polycrystalline, optical transitions from d core states 77−85827
Sn film, polycrystn., elec. props., internal size effect rel. to annealing temp. 79−65560
Sn film, thermoreflectance meas. 77−28640

metallic thin films continued
Sn, film, vac. deposited, influence of ion bombardment during condensation 79−82483
Sn film, vapour-deposited on NaCl single cryst., nucleation, growth, microstruct. 78−91561
Sn film, white, optical props. between 2-15 eV 78−19584
Sn, inelastic mean free path, 700 to 1200 eV, bulk method 80−20763
Sn, oxidation mechanism, depth selective Mossbauer spectroscopy method 78−35549
Sn polycrystalline films, elec. props. and crystallite size, 4.2K to room temp. *(Russian)* 80−93011
Sn, superconducting, paraconductivity 80−54845
Sn, thermoelec. power, 3.7-8K 78−39231
Sn, vacuum deposited, reflectance spectra, structural rearrangement effects 77−24905
Sn, vacuum deposited, substrate and substrate temp. effects on struct. 80−107677
Sn/Au thin film diffusion couples, Kirkendall void form. 80−96698
Sn/CU electroplated bimetallic films, interfacial reaction 80−96765
Sn-Cu(Au) films, amorphous and polycrystalline, thermopower meas. *(German)* 77−80857
SnO_2, optical and elec. props., rel. to stoichiometric deviation and struct. 77−47701
SnSb, metallic, defect density variation with deposition rate, annealing, elec. resist. meas. 77−21027
Sr, film struct., mass-thickness depend. 78−80040
Sr, oxidation, SXAPS 77−73189
Sr, photoemission, action of elec. field 77−48317
Sr, structure effects on work function, electron micrographs and photoemission meas. 79−83107
Ta, amorphous, UHV deposited, elec. and struct. props. obs. 78−6233
Ta, deposition by ion beam sputtering 77−73228
Ta, deposition by sputtering, influence of Ar plasma 77−69988
Ta, deposition parameters, struct., and elec. props. 77−81222
Ta, electron beam deposited, periodic chemical var. effect on mech. props. 79−91590
Ta, evaporated film, adsorpt. of CS_2 and H_2S, 195 to 473K 79−33197
Ta film, anodisation voltage relationship to oxide thickness *(German)* 78−11443
Ta film, photoemiss. from conduction band and core levels 77−16464
Ta, film, sputtered, physical props. 79−77938
Ta film, vacuum-deposited, gas adsorpt. effects on photoelec. props. 78−15298
Ta film on Corning glass, N and O content nondestructive determ. *(German)* 78−43272
Ta, H absorption rate, metallic film effect 80−49525
Ta, H^+ and D^+ sputtering in energy range 0.6 to 15 keV 79−78808
Ta, ion bombardment with N_2^+, Ar^+, struct. changes, chemical compound formation *(Russian)* 78−95084
Ta, nucleation of α or β phase, impurity effects 77−24493
Ta, on Si, film-substrate interaction obs. 77−1324
Ta, on SiO_2, struct. and mech. props. 77−24965
Ta, optical const. var. with struct., ellipsometric meas. 77−63478
Ta, planar-magnetron-sputtered, props. 79−82474
Ta, planar-magnetron-sputtered, phys. and elec. props. 80−6673
Ta, precision absolute thin film standard reference targets for Rutherford backscattering microanalysis 79−2882
Ta, RF sputtered, thermoelec. power, Hall coeff. and struct. props. 77−43743
Ta, reactively sputtered, N content determ. from Fourier anal. of X-ray diffr. profile 77−76693
β-Ta sputtered film, stabilisation by Ta-Si interlayer, SIMS depth profiling 80−54568
Ta sputtered films, difference between α-phase layers and β-phase layers 79−52116
β-Ta, Ta^{n+} transport number during anodic oxidation 79−39036
Ta-Ni alloy, amorphous, UHV deposited, elec. and struct. props. obs. 78−6233
Ta_2N film, high temp. nitriding kinetics depend. on press. *(Russian)* 80−50838
(Tb,Dy)-Fe amorphous films prep. by cosputtering, magnetoelastic props. 80−97429
Tb, nucl. echo signals, cryst. anisotropy *(Russian)* 79−99790
Te film, microstructure 80−103598
Te trilayer for high-performance optical recording 79−50382
Ti (0001) film, electronic struct., Fermi level, surface states, GO calcs. 80−6927
Ti, chemisorption of N_2, O_2, CO and CO_2, changes in work function 77−59221
Ti, deposition on Si wafers, backscattering anal., of layer structure, silicide formation 79−69377
Ti, depth profiles of D and T from gas emission during sputtering by Ar ions 77−35581
Ti, deuteriding inhibition by surface contamination rel. to Ti sublimation pump operation 77−57335
Ti, effect of surface and bulk oxidation on charact. electron energy loss spectra *(French)* 78−39641
Ti, electrochem. oxidation, AES, XPS and electrochem. characterisation 78−7086
Ti, evaporated film, adsorpt. of CS_2 and H_2S, 195 to 473K 79−33197
Ti, film, CO surface contamination effect on deuteriding 77−35814
Ti, film, elec. resist. Hall effect and absolute differential thermoEMF *(Russian)* 79−24083
Ti film, ion plated, morphology exam. by SEM 79−28251
Ti film, ion stimulated N_2 sorption, TiN_x form., sorption ratio, capture coeff. anal. 80−39411
Ti, film, pumping $H_2(D_2)$, isotope effect on pumping speed 78−51819
Ti, film, reactive ion beam sputtering 78−19666
Ti film, work function, effects of O_2 sorption 78−19125
Ti film on Si, induced interface interaction by ion implantation, AES exam. 79−77625
Ti, films, implanted inert gas desorption, reemission process 80−39453
Ti films on Al_2O_3, quartz and glass substrates, electron-beam deposition techniques improvement 80−7496
Ti, interaction with O_2, resist. and work function changes obs. 80−45431
Ti, interference enhanced Raman scatt. 80−40105
Ti, ion bombardment with N_2^+, Ar^+, struct. changes, chemical compound formation *(Russian)* 78−95084
Ti, on Be(AG) substrate, range of primary electrons 77−4134
Ti, on Si, ion implanted, inert-gas-bubble form., TEM and Rutherford backscatt. anal. 79−90682

metallic thin films continued
Ti, polycryst., adsorpt. of O at room temp., UPS and XPS 77−89645
Ti, RF sputter deposition, ion bombardment and ion implanation 80−25564
Ti, solid state reaction with Si or SiO_2 substrates backscatt. anal. 80−34257
Ti, sputtered film, energetic neutrals rel. to impurities 79−69980
Ti thin films, H absorption and desorption, Tokamak gettering, Auger electron spectrosc. 80−75092
Ti, triode sputtering, for beam lead metallisation, reduction of contamination 78−72721
Ti, ultra-thin, AES and XPS anal. 78−91573
Ti/Ag metallisation system, corrosion inhibition using intermediary Pd layer 79−79155
Ti-Al alloy, evaporated, anodisation, anodic voltage-time dependence obs. *(Polish)* 80−55574
$Ti-C_x(N_x)(O_x)$, solid soln. film prep. by reactive sputtering, solubility and effect on props. 79−28231
Ti-Cu thin films, oxidation kinetics in air at 100 to 300°C, meas. 80−40590
Ti-Pt link on Si_3N_4-SiO_2-Si substrate, laser vaporisation, interference effects 77−69941
TiN_x, film, non-stoichiometry rel. to optical charact. 77−12456
TiO_2, reactive DC sputtering deposited films with magnetron-plasmatron, mechanical elec., optical props. 80−25566
Tl, α and β-phase stability range and supercooling, electron diffr. obs. *(French)* 77−84924
U, for bombardment targets, prod. techniques 77−389
U/Te thin film junctions, combined electron, proton and X-ray beam obs. 77−85041
V, film, vac. deposited, influence of ion bombardment during condensation 79−82483
V film, vapour-deposited on Be substrate, diffusion anal. by ion backscatt. 77−35752
V, fluxural oscillations in longitudinal mag. field, sound attenuation, magnetoelasticity *(Russian)* 80−54844
V, on Si, ion implanted, inert-gas-bubble form., TEM and Rutherford backscatt. anal. 79−90682
V thin film-amorphous Si interface, V silicide formation, backscattering diffraction meas. 80−2285
V-Al thin film system, phase growth kinetics, electrochemical anode etching 77−72805
W, CVD by reaction of WF_6 and H_2, kinetics 79−19995
W. CVD on Si, properties and kinetic parameters for deposition 78−91570
W, electron beam deposition on Si, X-ray obs. of silicide form., diffusion processes *(German)* 77−1341
W, evaporated coatings, produced by carbonyl method, struct. *(Russian)* 77−43441
W film, adsorbed Th layer, work function, temp. depend. 77−28701
W film, band struct., appl. of extended rigorous cellular method 78−52055
W film, carbonisation and oxidation, electron diffr. exam. *(Russian)* 77−44399
W film, sputtered, physical props. 79−77938
W film production 77−21029
W films, (010), energy band calc. including spin-orbit interactions 80−20274
W, ion plating deposition system using electron beam evaporation *(French)* 80−20802
W, support film for electron microscopy, Fourier spectrum analysis of phase contrast 80−95199
W, surface IR wave propag. distance 77−28641
W, vapour deposited, dislocation struct., rel. to texture *(Russian)* 80−65394
W-Re, structure and props. of electron beam deposited film *(Russian)* 77−24490
Y, ion plating deposition system using electron beam evaporation *(French)* 80−20802
Y, photoabsorpt. spectra, at. ionisation, band struct. mechanisms, electron energy loss investig. 77−24909
Y, prepared in ultrahigh vac., optical meas. 6 to 14 eV 79−78767
Y, struct. and elec. resist., electron diffr. meas. 78−87888
Yb, amorphous metal films, crystallisation with and without mag. field 80−70570
Yb, film, energy-scanning X-ray diffr. technique, stacking faults and coherent domains *(French)* 78−43264
Zn, deposition props. on specially prepared substrate, desorption energy and surface diffusion 79−90917
Zn film, hexagonal struct., vacuum deposited, X-ray peak shift anal. 79−65335
Zn, film, sputtering mechanism, SEM 80−29839
Zn film, vac. deposited, X-ray diffr. study of microstruct. 78−26796
Zn, film, vac. deposited, X-ray diffr. study of microstruct. 78−75966
Zn film growth, HEED and projection microscope obs., surface orientation depend. on deposition parameters 77−32523
Zn, film growth on C, conductance meas. 79−82495
Zn, hexagonal, residual stress meas. from X-ray peak shift anal. 77−72807
Zn, on Cu_2O, effect of ion irradiation on form., struct. and props. 77−36408
Zn, RF and DC sputtered, thermal ageing, thickness dependent effects 78−6462
Zn, RF sputtered, electrical conduction 79−42674
Zn thin metal primer systems for steelwork 79−79148
Zn/Cu film system, UPS during atomic diffusion 79−43097
Zr film, reactive ion beam sputtering 78−19666
Zr, RF sputter deposition, ion bombardment and ion implanation 80−25564
Zr, TEM, sources of background X-radiation 80−101908
$ZrPt_3$, corrosion resist. and elec. cond., bulk and film samples 78−72285

metallisation
see also electrodeposition
ABS polymers, deposited in internal magnet magnetron sputtering system, adhesion of Cu films 79−83121
airborne particulate detection by metal-coated Nuclepore filters 77−37463
ceramic/metal layer adhesion mechanism for metallization of electronic ceramics, elec. props. *(German)* 80−76381
compound semiconductor-metal reactions, book contrib. 79−1622

metallisation continued
corrosion, IR microscopy failure anal. 80−98976
cracked stripe, temp. gradient and current crowding, electromigration 77−51828
defected stripe, current crowding and flux divergence 78−71885
delineating large metallisation patterns, technique using non-line-of-sight vacuum methods 78−23615
diamond powders, Mo coated, X-ray diffr. study 80−100936
electrets, metallised, mech. instabilities *(French)* 80−88906
electrically exploded foils, heating and burst phenomena 77−39488
electrode surface prep. for excimer lasers metallisation techniques 80−19048
electrolytic and electroless plating discrete microparticles for laser-fusion targets 79−15841
ferrite, surface metallisation installation 77−77626
glass fibre reinforced epoxy laminate, metallization by Cu and chem. treatment by H_2CrO_4 *(German)* 80−93670
III-V semiconductors, MBE developments in device fabrication 79−78902
injection laser mounting in single heat cycle 78−82982
MBE, device appls. 80−25570
metal oxides, chemical dissoc. under pressure as alternative to metallisation, feasibility study *(Russian)* 78−48553
metal-semiconductor junction, deposition and post-deposition treatment effects on electrical props. 77−89853
MIS solar cells, etched slotted mask for direct deposition of metal contact pattern 80−97786
MOS capacitor, filament-metallised, effect of K contamination of W 79−51679
MOS capacitor, threshold voltage instability due to defect states produced during e-beam metallisation 78−72264
MOS metallisation via automatic S-gun planetary deposition system 78−72724
PET film, metallized reflecting surface, ageing under natural conditions, destructive factors identification 79−83340
plastic-encapsulated IC, metallisation corrosion test 78−11486
quartz SAW resonator design with Al metallisation 77−39147
reliability physics, conference, Las Vegas (1977) 77−79086
SAW devices, use of Cu-doped Al 80−23856
solar cell metallisation using screen printing tech. 80−85291
solar cells, front- and back-surface metallisation patterns 80−93943
SOS structure, radiation dose at interface due to electron beam aluminisation 78−68089
sputtering, particle no. filling spot area, calcs. *(Russian)* 78−52668
steel, unalloyed, electric metallisation, corrosion resistance tests *(Russian)* 78−19935
substrate surface damage induced by RF-diode sputtering 77−90274
substrates, compensating work holder for coating two sides uniformly 80−22372
transition metal silicides, refractory for ICs, review 80−100820
vacuum seals, Cu-ceramic, metallisation process 80−37046
VLSI Al and Al alloy metallisation sputter deposition 80−66429
Ag-In-Ge alloyed contacts to GaAs 79−78174
Al, 1/f noise depend. on internal mech. stresses 80−65711
Al, and its alloys, reactive etching in RF plasma containing halogen species 78−72923
Al and its alloys, reactive ion etching, preferential lateral chemical etching 79−83371
Al, Cu electromigration, apparent effective charge, 325-500°C 77−39695
Al, film deposition from metal plasmas 78−6859
Al film on GaAs, interdiffusion, 250-450°C, AES meas. 77−1263
Al film on single cryst. Si slices, long-term tests 79−33346
Al, metallisation on (100)Si, Si epitaxial regrowth and grain struct. 78−79901
Al metallization of semiconductor devices by high rate magnetron/plasmatron sputtering 79−28919
Al, oxidation, in water, oxide growth rate and struct. 78−76783
Al, sputtered and electron gun evaporated films, grain size and orientation obs. 78−10308
Al sputtered coating development, porosity, durability temp. depend., electric arc metallisation regime *(Russian)* 80−39402
Al, step coverage optimisation by computer simulation and SEM 78−51838
Al thin films, electromigration under pulsed current conditions, calc. 77−1495
Al-Cu, evaporation, successive dilution method for reproducible control 77−69994
Al-Cu alloy, deposition from RF induction source, onto laminated polyimide substrates and characterisation 80−16535
Al-Cu film, anodic oxidation, corrosion props. 78−35581
Al-GaAs (110), XPS study of interface interaction, Al proximity effects and replacement reaction 79−100019
Al-GaAs Schottky barrier diode, prep. by MBE on GaAs, and characts. 78−72257
Al-n^+Si ohmic contacts, metallisation structs. for very shallow n^+/p junctions 80−60084
Al-Pt film sandwich, interdiffusion and intermetallic form. 77−24448
Al-Si alloy metallisation by rate controlled dual electron beam gun evaporator 79−11516
Al-SiO_2 interface, stress and microstruct. via TEM 78−26797
Al-SiO_2-Si, void form. in Al interconnection lines at Si-SiO_2 boundaries 80−2476
Al-Ta-poly-Si interdiffusion, Ta barrier effect, Auger anal. 78−71888
n-$Al_xGa_{1-x}As$, Au-based ohmic contacts TEM obs. 80−34509
Al_2O_3 *(Russian)* 80−50552
Au, Cu diffusion, 75-150°C, AES, device appls. 77−1262
Au electrodeposition, heavy metal ion induced depolarisation effects 77−16511
Au, electroless deposition, substrate structure influence 77−8771
Au electroplating, selective, on Pd-Ti conductor patterns, Si IC manufacturing appls. 79−95951
Au, electrotransport-induced failure site, minor constituents effects 79−23763
Au film, chem. deposition on Si, form., struct. 78−34723
Au film, threshold current density and incubation time to electromigration 78−14643
Au, growth on clean and contaminated GaAs (001) surfaces 78−26785
Au, layer growth and ageing in Pb-In solder joints 77−32764
Au, on corundum, with intermediate Cu and Cr layers, struct. obs. 77−28084

metallisation continued
Au on oxidised Si with metal adhesion layer, ageing props. 77−11820
Au, pulsed potentiostatic deposition from Au(I) sulphite solns. 78−15321
Au thick film surface, Cu and Ag contamination, AES obs. 80−24763
Au/Pt/Cr films, diffusion of Si, depth anal., optical and Rutherford backscatt. meas. 79−10981
Au/Ti thin films, effect of Cl_2 on elec. resistance, Ti atom migration and preferred orientation 80−34530
Au-Fe-Ni layer coating, Fe and Ni conc. meas. by X-ray diffr. *(German, English)* 80−34330
Au-Ge-Ni metallisation scheme used for alloyed contacts to GaAs 77−43726
Au-refractory film interdiffusion obs., by combination of scattering techniques 80−65308
Au-$Ti_{0.3}W_{0.7}$, thermal annealing study of metallisation on Si 80−80134
Au-Ti/n-GaAs contacts, interdiffusion and Schottky barrier height variations 77−89849
Au-W/n-GaAs contacts, interdiffusion and Schottky barrier height variations 77−89849
(Au-Ge)-Ni, for contacts to n-GaAs, metallurgical investigation using inert substrate 77−85313
(Au-Ge)-Pt, for contacts to n-GaAs, metallurigical investigation using inert substrate 77−85313
Be, RF sputtered film, props. rel. to deposition conditions 77−39965
Be-Au, ohmic contact to p-InP, low contact resist. 80−65677
Co film, electromigration exam. from structural changes and resistance increases 77−20213
Cr deposition as diffusion barrier layer, improved Cr-Zr source 80−76163
Cr films, on Al_2O_3, quartz and glass, electron-beam deposition techniques improvement 80−7496
Cr, on polycryst. CdS, thermal diffusion, 240-400°C 80−80001
Cr/Au metallisation system, corrosion inhibition using intermediary Pd layer 79−79155
Cr-(Pd_2Si)-Si, $CrSi_2$ form. kinetics 77−24492
Cr-Au film structure, on Si interdiffusion 77−39698
$CrSi_2$ formation on Pd_2Si and PtSi, radioactive Si tracer obs. 78−60578
Cu, film deposition from metal plasmas 78−6859
Cu-based metallisation systems, in 85°C 78% RH SO_2 contaminated environment, performance 79−74304
$Ga_{1-x}Al_xAs$, ohmic contacts, metallisation systems 80−25010
GaAs, alloying with Au and Au alloy ohmic contact metallisations, SEM and optical study 80−70820
GaAs conducting MIS structures and metal-semicond. structures, effects of ultrathin oxides 79−1626
GaAs, epitaxial and metallic thin-films, anodic oxidation anal. 78−80673
GaAs, review of ohmic contacts fabrication 80−49901
GaAs, shallow-homojunction solar cell by MBE, conversion efficiency 80−30476
GaAs thin Schottky barrier metallisation, thermal reactions 79−78176
GaAs, vacuum deposited Shottky barrier metallisation 79−78153
n-GaAs:Sn, heavily doped, nonalloyed ohmic contact form. by MBE and metallisation 79−7895
GaAs/metal contacts, metallisation of defined surfaces *(French)* 80−107909
$Ga_xIn_{1-x}Sb$ diode, with Au metallisation, interdiffusion effect of heat treatment 78−14820
Ge, vacuum deposition of Al, press. and residual gas comp. influence on film struct. 77−16497
Ge-Au-Ni(Pt)(Pd) trilayered films, annealing, interdiffusion 78−22902
InP-Ag contact system, evaluation of Auger depth profiling technique 79−56893
$LiNbO_3$ optical waveguide surface, acoustooptical interaction for TE modes, metallisation effect 80−69541
$LiNbO_3$ SAW resonator design with Al metallisation 77−39147
Mo film, vacuum deposited onto SiO_2-Si substrates, elec. resist. 78−76166
Mo-Si junctions, metallurgical boundary props. and elec. resistivity 78−2568
Ni/Au film on silicon vacuum deposited, electron impact mass spectrometric exam. of surface contaminants 78−75957
Ni-Cr/Au films, interdiffusion processes and oxidation phenomena 80−59735
Ni-Si film system, silicide first phase form., reaction kinetics 78−79821
NiFe, film deposition, sputter gun system, bubble device appls. 77−12532
Pt electroplated film, Schottky barrier metallisation, Au diffusion, AES obs. 79−14968
Pt film on Si, PtSi form. kinetics, AES, SIMS, EPMA 77−11800
Pt, sputtered film, Al and Mg contamination, AES, SIMS 77−11822
Pt, triode sputtering, for beam lead metallisation, reduction of contamination 78−72721
Pt-Au film couple, diffusion of Au, depend. on annealing ambient, AES exam. 77−1261
Pt-Si film system, silicide first phase form., reaction kinetics 78−79821
Si, (111) surface, Ag interaction, AES 78−14589
Si device metallisation, TiN and TaN as diffusion barriers 80−65304
Si device technology, thin film interaction effects, book contrib. 79−1620
Si, Pd-Al metallisation, Cr thin film used as barrier to interaction of Pd_2Si with Al 77−43724
Si, Pt_2Si and PtSi form. with high-purity Pt films 77−76676
Si Schottky barrier metallisation characteristics 77−76922
Si solar cells, low cost, Ni contacts 80−94017
Si solar cells, low cost processes for fabrication 80−94013
Si solar cells, Ni-Cu conductor system 80−93991
Si solar cells with screen printed diffusion and metallisation 80−94015
Si terrestrial solar cells, stress tested, contact integrity testing 80−94018
Si wafer, effects of sputter etching and process technology on props. of sputtered Al films 79−83122
Si/Al and Si/Al-Si(Cu), Si regrowth minimisation through overlying Al or Al alloy film 80−70569
p-Si-Al, ohmic contacts, Si dissoln. and recrystn. effects, computer calc. 80−103749
Si-Al interface in semiconductors, electronic parts, electromigration aspects 80−39355
Si-metal contacts, low temp. reactions 78−2567
Si-$Pd_{80}Si_{20}$, amorphous, Pd_2Si layer form., shallow contact 80−103586
SiO_2 substrate reaction with thin metal films obs. 78−51851
Sn-Ag ohmic contacts, for InP, thin film epitaxy 79−38159
Ta, sputtered deposition on Si, Si-SiO_2 interface, induced stress meas., X-ray transmission topography 79−24434

metallisation continued
Ta-Ta_2O_5-InP thin refractory MIS struct. deposition 80−75647
Ti films on Al_2O_3, quartz and glass substrates, electron-beam deposition techniques improvement 80−7496
Ti, triode sputtering, for beam lead metallisation, reduction of contamination 78−72721
Ti/Ag metallisation system, corrosion inhibition using intermediary Pd layer 79−79155
Ti/Cu/(Au) thin films thermocompression bonds degradation by thermal ageing 80−66546
Ti-Cu, evaporated adhesion after electroplating 79−82475
Ti-Cu thin films, oxidation kinetics in air at 100 to 300°C, meas. 80−40590
Ti-Pd-Au, patterning, by plasma etching of Ti 78−27677
Ti-Pt-Au, nonalloyed ohmic contacts to n-GaAs by pulse-electron beam annealed Se implants 80−2466
Ti-Si cosputtered films, silicide form., X-ray diffr. and resist. study 80−54546
Ti-Si film thin film interaction, metallisation, X-ray diffr. and sheet resist. 80−54442
Ti-W, bias-sputtered, resist. and comp. 80−25023
Ti-W magnetron sputtered films 80−45231
Ti-W/Au metallisation on Al, temp. stability, barrier props. 79−23868
TiW-TiO_2-InP thin refractory MIS struct. deposition 80−75647
V-SiO_2 interface reaction, identification of diffusion species 78−75890
W CVD for thin film passive components fabrication for high temp. instrumentation 80−40266
ZrO_2 particles, influence of ionic treatment on formation of Al coatings *(Russian)* 80−50552

metallising *see metallisation*

metallo-organic compounds *see organometallic compounds*

metallocenes *see organometallic compounds*

metallography
see also electron diffraction examination of materials; electron microscopy; optical microscopy
adhesion in metal cutting, direct SEM obs. of frictional sliding 80−104412
AES appl. 79−91883
alloy, lamellar multiphase, struct. and spatial comp. variation, analytical STEM 78−24011
alloy, two phase microstrct. revealed by selective sublimation 79−24698
alloy steels, microstructure characteristics, statistical processes *(German, English)* 78−95884
Alnico 5 alloy, S and Ti additions effect rel. to non-metallic inclusions, coercive force and grindability 80−89375
austenitic solid solution, chem. evaluation of B and its correlations with hardenability and hardness *(German)* 79−39230
automatic microstructure analyser, construction and operation, optical mechanical scanning advantages *(German, English)* 77−77697
automatic structure analyser, EPIQUANT, banded structure determination in ferrous metals 78−39973
autoradiography on thin foils, high resolution, anal. of technique charcts. *(French)* 80−55598
bainite, formed from deformed austenite, morphology and mech. props. 79−43345
Berg-Barrett single crystal substructure exam. using microfocus X-ray source 79−52495
bimetallic welded joints, heterogeneous, metallographic anal., etcharts and etching regimes 80−40635
biomedical target, water-cooled pion-production, remote exam. and disassembly 80−25975
blast furnace magnetic structure of ferromagnetic metals and alloys, metallographic study *(Bulgarian)* 78−73008
boride coatings, method of revealing structural components 80−21228
boride coatings on Ni alloy, thermal stability, exam. of coating 78−44271
brass, 70:30, rolled, nucleation and annealing texture development 80−45320
α-brass, Al bearing, high temp. relief cavitation, SEM, STEM, TEM, SIMS and EDX anal. 79−5039
brass, crystal structure and morphology of thin needle-like martensite 78−31425
brass, failure obs. with optical microscope 78−11472
α/β brass, grain boundary sliding and intergranular cavitation during superplastic deformation 79−5009
α-brass, metallographic and fractographic study of void formation during creep 80−16449
brass, plastically deformed, phase transforms. and diffusion phenomena *(Russian)* 79−20115
brass, shear band development during rolling, twinning, metallographic obs. *(Japanese)* 78−39849
brass formation by diffusion in multilayer Cu-Zn condensates 78−43186
bronzes, ancient, chem. polishing and etching for metallographic exam. 78−356
CANDU irrad. fuel bundles, sheathed in Zircaloy-4, long term stability investig. 80−13774
carbides, sintered, sample prep. for metallographic structural anal. 80−13048
case hardened and structural steel fracture obs. by SEM *(German)* 77−60032
cast iron, white, high Cr-Mo, fracture toughness 80−50726
cathodic device for electropolishing and etching in situ 79−39067
ceramic, polished section prep. using pedepin *(German)* 78−19983
ceramic material specimens, prep. with Pedemax-Planopol automatic grinder and polisher 79−74333
ceramic nuclear fuel, porosity characterization, optical and electron microscope exam. 78−44302
ceramics, and metal-ceramic mixtures, metallographic method for polishing specimens 78−56850
cleaning solution for metallographic mounts 79−87808
coal, polished section prep., structural anal. 79−15924
coherent optical defectoscopy, signal processing *(German)* 78−7110
composite structures, multipoint moments meas. by optical struct. anal. 79−15910
convergent beam electron microscopy for materials science 80−107028
corrosion failure, metallographic anal. 79−61836
crack tip, plastic deform., metallographic anal. by recrystn. 80−85029
crack tip strain distribution measurement by recrystn. *(German, English)* 77−56203
critical temperatures determination, elec. resist. method, IMASh-5S-69 installation 80−71827
crystal defect observation *(Japanese)* 79−82130
crystallite orientation distribution function, determ. from isolated axis density values 77−48612
Cunial MNA13-3, Mn addition effect on props. 80−21035
damage investigation on metallic parts *(German, English)* 79−70265
deformed crystal, optical method for quantitative evaluation of electron channelling patterns *(German, English)* 77−7777
deformed solids under tensile loads, automated installation of metallographic and exoemission obs. 80−50792
diamond grain configuration in high temp. creep and fatigue 77−21221
diffusion phenomena determ. between coated metal carbide and steel *(German)* 78−15623
disperse particles concentration and spacings between them in Poisson point field model 78−39963
EDTA uses 77−60014
electrolytic deep etching 78−31604
electrolytically polished surface evaluation 78−35627
electron beam microanalysis 77−60152
electron metallography of material wear using SEM, TEM 80−76455
electron microprobe analysis for oxide layer struct. and comp. determ. of secondary ion emission *(French)* 77−56286
electron microscope, 1000 kV, appl. to metallurgy 78−8472
electron microscope appl. transmission type, steel microstructure determ. *(German)* 80−15089
electron microscope examination, feasibility and methodology of in situ experimentation *(French)* 80−68301
electron microscope extraction replicas, X-ray microanalysis, appl. to steel separation estimation *(Bulgarian)* 78−40012
electron microscopy on etched thin foils, comparative SEM, STEM and TEM analysis 80−100144
electron probe microanalysis for high-temp. applic. *(French)* 77−29074
electron probe microanalysis use for microstruct. determ. of thin surface layers *(German, English)* 77−56204
electropolishing and etching sections in situ, cathodic device 79−39067
ellipsoidal flaw characterisation by US scatt. 79−47865
environmental cell for 3MV-class microscope, and its appl. to metallurgical problems 77−10141
EPIQUANT, assessment of post-hotforming recrystallization condition of 34Cr4 steel 80−84949
EPIQUANT, automatic structure analyser 80−85116
EPIQUANT automatic structure analyser for inclusion investigs. in free-cutting steel 80−55609
EPMA design, performance and applic. in materials research 78−35780
etching technique for revealing plastic zone in Al 78−72955
eutectic alloy, multiphase, metallography 79−61823
eutectic alloys, phase volume fraction determ. using manual point count practice 78−53052
failed steam accumulator anal., role of metallography 78−95877
failure analysis, fault tree technique and electron fractography 78−53071
failure analysis appl., conf., Houston, USA (July 1977) 79−61832
failure mechanisms and metallography, review 79−61833
fatigue crack tip displacement visualis. and meas. using stereo viewer 79−24700
fatigue damage examination using two-crystal X-ray spectrometer method 79−52481
fatigue failure origin areas, metallographic charact. 79−61835
Fe, ingot, cast, exam. of nonmetallic inclusions, size freq. distrib. 78−39989
ferrogarnet crystal, surface layer damage thickness meas. 79−5106
ferrographite, sintered, porous, electrolytic prep. 79−52530
ferrous material fractured surface exam., oxide scale removal 78−95886
fiducial grid for high resolution metallography 77−25230
FIM atom probe technique, suitability for continuous phase transforms. obs. 78−35621
FIM techniques, appl. to metallurgical problems, review 78−35620
fine fragmented crystals, complex struct. analysis by electron microscopy 80−104416
fission reactor fuel, metallographic cross sections after high temp. treatment *(German)* 78−29586
foil laser-monitored electrothinner *(German)* 79−34219
foil thickness measurement in TEM 78−35632
fracture, profilometric anal. 78−88600
fracture topography-microstruct. correlations in SEM 77−32687
gases in metals, trends in modern anal. *(Russian)* 80−15123
geikielite, solid soln., phase transform. during reduction *(Russian)* 78−44042
glass microbubbles, method for polishing bubbles into hemispheres 78−95869
goniometer, universally adjustable polishing device 79−2755
grain neighbourhood relationships *(French)* 77−77694
grain size meas., NDT, deep-drawing steel sheet and band, method and instrum. *(German)* 78−85059
grain volume meas. and topological parameters by serial section analysis 77−36705
graphite surface energy determ. using high temp. vacuum metallography *(Russian)* 77−15677
grinding and polishing apparatus for metallographic specimens 78−23889
ground surface, light interferometry appl. 79−34216
hard and brittle materials, microsection prep. technotron and polishing systems *(German, English)* 80−11859
hard tension/compression tester developed for high temp. microscope, metallurgical appl., functional features *(Japanese)* 79−70259
Hastelloy X, grain size effect. creep and creep-rupture *(Japanese)* 80−16382
Hastelloy-X, Ni-Cr-Fe-Mo, cyclic oxidation resist. improvement by high temp. etching treatment 80−97627
high temperature, attachment, appl. to graphite form. on supersaturated solid soln. surfaces 79−29306
high temperature, equipment improvement 77−40489
high-temperature, conf., Helsinki, Finland (June 1975) 77−52295
HV electron microscopy, recent progress, book contrib. 79−67442
HV electron microscopy appls. in phys. metallurgy, irrad. machine, struct. obs. 77−1891
ilmenite, solid soln., phase transform. during reduction *(Russian)* 78−44042

metallography continued
image analysis, semiautomatic quantitative system *(German, English)* 77−52602
Incoloy 800, creep and fatigue props. in high temp. gas cooled reactor He environment 79−47776
Incoloy 800, from KFA experimental duct at 700°C and 480 d in DRAGON reactor, mech. props. before and after contamination 79−47777
incomplete pole figures, calc. 79−87816
Inconel 617, creep, morphological changes of carbides, affect on creep props. 80−108509
Inconel 718, superalloy, wear of superhard tool during cutting, SEM and metallographic obs. 78−64720
interference microscopy, for colour development and phase separation 80−100976
interphase boundary analysis using TV 77−40483
inverted camera microscopes, IM 35 and ICM 405, for biology, medicine and metallography 79−30540
inverted incident light microscope, METAVAL, for metallographic examinations 79−49282
ion etching, adaption of simple sputtering apparatus 78−56849
ion-etching application, to metallography *(Japanese)* 80−93715
Kossel diffraction, in scanning electron microscopes, metallurgical appls. 79−20335
lamellar eutectic, specimen thinning for TEM *(German, English)* 78−95885
large parts, without taking specimens, portable grinding and polishing machine 80−61042
LMFBR, Na test of bellows expansion joints, metallographic study *(Japanese)* 79−67850
low temperature modified installation IMASh-5S-65 80−21229
macroscopic examination procedures for failure analysis 79−66254
metallic components, damage investigation 79−74330
metallic polycrystals, deform. during cooling, revealed by deposited graphite layer *(Polish)* 80−25755
metallographic specimens, automatic machine and procedure for prep. 80−13050
metalloids electromechanical polishing 79−61824
microanalysis of migration processes 77−36706
Microcell for polishing TEM specimens 79−96248
microfractographic charact., in determ. of failure stages in repeated loading 77−40490
microfractography *(Japanese)* 80−71841
microsection preparation by vibration polishing 79−87786
multiphase system, second phase vol. fraction determ. using incomplete pole figures 79−11741
NEOPHOT 2, assessment of post-hotforming recrystallization condition of 34Cr4 steel 80−84949
Ni-base wrought superalloy, creep and stress rupture behaviour in air and vacuum 80−60918
nuclear ceramics, quantitative image anal. using light and SEM obs. 79−12912
nuclear fuel, quantitative metallographic anal., computer program, QMA 79−15951
Oberhoffer etch, suitability for identifying surface defects 79−43525
orientation distribution determ. from incomplete pole figures, computer program 78−64804
pearlite spheroidization, quantitative meas. 77−44275
plasma-sprayed coating, process instability, effect on struct. and mech. props. of coatings 77−56131
plastics applications, advantages 77−60030
polarisation curves in polishing solns. 78−56851
pole figures, automatic determ., review 79−87819
polished section, contour amplifier appl. using TV camera and monitor *(German, English)* 79−96261
poly-phase microstructures, quantitative metallography, review 79−15925
polyethylene, electron microscopy with chlorosulphonation aid 77−89351
porous materials, effects of different methods of prep. on reproducing surface 80−60995
precious metals, Au, Ag, Pt, Ru, Os 78−3289
programmable semiautomatic instruments for quantitative struct. anal., geometric eval. in materials lab. *(German, English)* 78−64798
protective coatings, thermodiffusional, form. kinetics and struct. on iron, steel, and cast iron 77−56158
pyrocarbon coatings on HTGR fuel particles, Bacon anisotropy factors meas. technique 79−13418
quantitative, errors due to measuring masks *(French)* 78−15622
quantitative, with automated electron microscope-microprobe systems 78−35631
quantitative fractography review 79−39072
quartzite, naturally deformed, textural and microstructural development, metallurgical approach 79−83228
radiation damage, FIM and atom probe FIM expts., review 78−35623
radioisotope X-radiation sources in defectoscopy 77−56176
rapid heating attachment, for IMASh-5S installation 80−21230
recording apparatus, semiautomatic for quantitative metallographic anal. 79−87767
refractory technique for investigation of nonmetallic inclusions 77−52587
Rene 95, as hot isostatically pressed (HIP) and HIP+forged, low cycle fatigue 80−25854
replica technique for increased information from SEM 79−74334
review, quantitative metallography *(French)* 80−30205
rocks used as aggregate in pavement surfaces, exam. of polishing charcts. 78−53057
sample preparation, procedures 80−57272
scanning optical microscope as new metallographic tool 80−71852
secondary ion emission for oxide layer struct. and comp. determ. of electron microprobe analysis *(French)* 77−56286
SEM, in situ ion etching facility, description and appl. 77−54020
SEM appl. to fracture surfaces 79−34220
SEM channelling contrast technique for material deform. obs. 78−23917
SEM fractograph quantitative analysis, develop. and exptl. verification 77−60023
SEM microsection assessment for machine failure prevention *(German)* 79−8412
sheet material, ideal texture determ., rapid method using colour slides 77−25226
sheet material, texture determ. using one pole figure *(German)* 77−25242
sintered materials, porous, electrolytic preparation 79−52530
skeletonization in quantitative metallography 80−101002
metallography continued
spacecraft materials failure, metallurgical exam. 80−71868
spatial structure parameters estimation of basic material, instrument resolution power influence 79−52543
specimen prep. using micromilling device *(German)* 78−19980
specimen preparation for TEM, ultrasonic separation method 79−52561
spherical powder, particle deform. and sliding during compaction, metallographic study 79−66020
spinodal alloys characterisation techniques, props. and appls., review 80−50588
steel, 0.2 to 0.8% C, ferrite-pearlite transformation, tensile strength, cooling rate effect 80−7549
steel, 0.7% C, welded zone, fatigue strength and microstruct. *(Japanese)* 80−89339
steel, 35NiCr18, bainite transformation, study with aid of hot stage microscope 80−76253
steel, (0.36 wt.% C) Ni-Cr-Mo, electroslag refined, fracture toughness and fatigue behaviour 80−81171
steel, alloy, softening process in deformed type 15GYuT, metallographs *(Russian)* 78−52840
steel, alloy, type 11Kh18M, eutectic carbide composition change due to heating 80−16353
steel, alloy, type ST.5, structural and phase changes after high temp. heating *(Russian)* 80−55439
steel, alloy structural, anomalous grain growth 80−20984
steel, austenite grain size eval. technique 80−25933
steel, austenitic, 16H2NMB, struct., texture and mech. props. of product of transform. 78−92273
steel, austenitic, martensitic transform. effect on hardening kinetics and fracture resist. of friction surface of 45Kh12G8 and 110G13 *(Russian)* 80−50727
steel, austenitic, metallography study of high temp. decomposition 79−61559
steel, austenitic 30KhGSA, white phases structure after heat treatment 80−76281
steel, austenitic and austenitic ferritic, welds, rel. between solidification and microstructs. 79−61579
steel, austenitic stainless, 18-8, effect of H on martensitic transformation *(Chinese)* 80−55394
steel, austenitic stainless, cast struct., determination of origin using etching techniques 78−39985
steel, austenitic stainless, creep props., effect of high temp. ageing, SEM 80−97516
steel, austenitic stainless, deformation induced cavitation, exam. 79−43363
steel, austenitic stainless, deformed plate, X-ray line profile anal. *(Japanese)* 78−7144
steel, austenitic stainless, electron transmission microscopy, microstructural zones *(Spanish)* 79−39059
steel, austenitic stainless, grain boundary segregation studies, intergranular fracturing technique for stress corrosion cracking investigation 79−39057
steel, austenitic stainless, magnetic phase content determ. via permeability meas. using MF-10F probe 77−77648
steel, austenitic stainless, Ni-alloyed, Cr_2N precipitation, interface struct. and morphology 80−11644
steel, austenitic stainless, precipitates and grain orientation by non aqueous electrolyte potentiostatic etching method *(Japanese)* 80−15102
steel, austenitic stainless, SUS 304, stress corrosion cracking in various environments, fractography *(Japanese)* 80−93690
steel, austenitic stainless, tube carburised layer metallographic determ. 78−85077
steel, austenitic stainless, welded explosively, induced martensites morphology 80−104153
steel, austenitic stainless, X-ray line profile analysis 77−86048
steel, bainitic, habit plane determ., austenite orientation determ. 79−1926
steel, brittle fracture resist., fractography and grain refinement 77−60024
steel, C1020, dual phase, mech. behaviours and structs. *(Korean)* 80−25779
steel, C, cementite formation and properties 80−45313
steel, C, nonmetallic inclusions, improved metallographic technique for examining 78−72956
steel, carbide formation, microscopic exam. aided by rating charts *(German)* 79−61805
steel, carbide struct., quantitative analysis using Epiquant analyser *(German)* 80−3284
steel, carbonitrided, case struct. investigation by warm electrolytic etching 80−35414
steel, carbonitrided, nature of dark component, metallographic exam. 78−19978
steel, case-hardened and carbonitrided, determ. of degree of C saturation 77−86239
steel, cast, nonmetallic inclusion size frequency distrib. determ. 78−39989
steel, CC Cr-Mo-V, low alloy, creep fatigue interaction 78−64673
steel, chemical polishing for opt. microscopy 77−9021
steel, chemicothermal treatment quality control by fractographic method 79−39080
steel, cleaning corroded surfaces for electron microscope exam. by cathodic polarisation 79−70242
steel, cold rolled strip, surface defects, online automatic system, design study 79−34231
steel, constructional, austenite grain shape eval. method 78−35607
steel, continuously cast slabs, formation of longitudinal midface cracks 79−83315
steel, Cr, cold roll, frictional heating surface damage 80−76289
steel, Cr, exam. of surface layer after electrochemical treatment, effect on mech. props. *(Russian)* 80−7727
steel, Cr (25 wt.%) recrystallisation annealing, surface structure investigation in polarised light 77−28947
steel, Cr-Al (12, 6 wt.%), ferritic stainless, high temp. treated, strengthening mechanisms 80−3106
steel, Cr-Mn, metastable constitution diagram and phase transforms. *(Russian)* 80−50590
steel, Cr-Mn, non-metallic inclusions anal. with increased N content *(Bulgarian)* 79−82259
steel, Cr-Mo:P (2.25, 1 wt.%), stress relief cracking, effect of P segregation 80−89324

metallography continued
steel, Cr-Mo, crack decoration in oxides by electrodeposited metals *(German, English)* 79−70266
steel, Cr-Mo, oxidised, mechanism of crack decoration of oxides by electrodeposition 80−97560
steel, Cr-Mo (10-14, 2-6 wt.%), heat-resist., creep-rupture strengths 80−104271
steel, Cr-Mo (2.25, 1 wt.%), small changes effect in impurity elements, creep life 80−25790
steel, Cr-Mo-V type X 41 CrMoV 5 1, austenized, carbide detection by etching *(German, English)* 79−91884
steel, Cr-Ni, bainitic habit plane determ. 79−1927
steel, Cr-Ni, microstructural distrib. of cathodic H_2, autoradiography *(French)* 79−99234
steel, Cr-Ni-(Mo), austenitic, strengthening by modified ausforming 78−76665
steel, Cr-Ni-Mn, adiabatic shear band determ. by surface obs. 80−97579
steel, CrMoV, low alloy, quantitative stereological anal. of carbide phase, comparison of methods *(German, English)* 79−91886
steel, CrMoV, low alloy, quantitative stereological anal. of carbide phase, struct. stability during creep *(German, English)* 79−96262
steel, dual phase, improved etching technique for percent martensite determ. 80−16624
steel, electron microdiffr. determ. of orientational correls. between ferrite and cementite 77−52584
steel, En 24, Cr, V, deform. effect on decomp. of austenite, carbide precipitation 80−84938
steel, etchant for revealing austenite grain boundaries 80−85098
steel, Fe-Mn-C austenitic, deform. twinning and mech. props. 77−59868
steel, Fe-V-C (1, 0.2 wt.%), austenite formation 80−84927
steel, ferritic, base material for powder flame spraying process, intercrystn. corrosion *(Czech)* 80−30158
steel, ferritic and austenitic, microstruct. study by means of replicas taken from components at 100°C 80−81256
steel, ferritic Cr-Mo type, microanalysis of precipitates using TEM 80−108688
steel, fracture obs., shell-shaped fracture 77−25153
steel, fully killed, nonmetallic inclusions, microprobe and metallographic exam. 80−30196
steel, galvanised, identification of grains with (0001) orientation, chem. test 79−47853
steel, heat resisting, type 15Kh1M1F, exam. of structural stability and props. *(Russian)* 79−29104
steel, heat-resist., C replica method of investigating creep damage in TEM 80−21012
steel, high alloy, potentiostatic development of structures 78−95887
steel, high Si dual-phase, mech. props and microstruct. anal. 80−40444
steel, high speed, tempered, etching reagents for austenite grain boundaries 78−80704
steel, hot deformed austenite, transition from discontinuous to continuous formation of pearlite *(German)* 80−35214
steel, HSLA, V and N effect on recovery and recrystn. during and after hot working 80−84973
steel, inclusion behaviour investigations using SEM 78−23916
steel, inclusion content, sampling in quantitative image analysis *(French)* 77−28961
steel, inclusions, SiO_2 Al_2O_3, FeS, effect of high temp. heating on size, number and distrib. 78−44145
steel, locally deformed, Fry's reagent action 79−87806
steel, low alloy, exam. of microstructure, in type PZhK-1000 soldered joint by metallography 79−52257
steel, low alloy, rel. between over-heating embrittlement and behaviour of S, Auger spectroscopy anal. *(Japanese)* 79−79088
steel, low C, 10Kh2G3M, development of plastic deform., slip and dislocation struct. *(Russian)* 79−15722
steel, low C, hot rolling effects on struct. *(Russian)* 78−19793
steel, low C, type AISI 1018, microstruct. effects on fatigue crack growth 79−61718
steel, low C, type En3, high strain deform., struct. and props. 80−89301
steel, low C rimming, effect of addition of Al to Zn on phase composition and morphology *(Polish)* 78−53014
steel, low-C, ferritic, deform. microstruct., electron microscopy *(German)* 78−64589
steel, low-C sheet, texture anisotropy determ. using inverse pole figures *(German)* 77−44431
steel, low-C-Si, LS1.2, LS1.5, phase transformation 80−45302
steel, maraging, heated to high temperatures, γ to δ transformations 80−20930
steel, martensitic, dendritic structure assessment with Elypovist electropolisher 77−52565
steel, martensitic, tEM examination of microcracking in plate martensite *(German, English)* 79−91887
steel, medium C, Nb addition, effect on transformation and strength 80−7607
steel, microalloyed, types V1599, V1600, V1286, NbCN precipitation in undeformed austenite 80−89230
steel, mild, etching method for revealing plastic deformation 78−72825
steel, Mn (16 to 20 wt.%) metallographic analysis method 80−50791
steel, Mn-Si, for springs, metallographic study, present phases rel. to mech. props. *(French)* 80−21090
steel, N determ. by track autoradiography 80−100979
steel, Ni and W, recrystallisation mech. during laser treatment 80−50658
steel, Ni-C, martensitic, microstructural distrib. of cathodic H_2, autoradiography *(French)* 79−99234
steel, Ni-Mo, sintered, martensitic transformation due to cold working, metallographic study 78−44127
steel, non metallic inclusion eval. using Quantinet systems 79−15923
steel, pearlitic structural, austenite grains, growth rate during heating 80−100860
steel, plain C having ferrite-martensite mixed structs., microstructural parameters effect on fatigue strength *(Japanese)* 80−71735
steel, rail, fracture rough exam. of wear in rollers, subject to creep 79−15808
steel, rimmed, metallographic method of cleanliness eval. 77−52562
steel, rolled products, H flaking 80−50719
steel, Si, nonoriented elec. sheet, solute oxidation effect on mag. props. 79−83335
steel, spring leaf retainer with variable ductility, processing error, cold working error *(German, English)* 79−70267

metallography continued
steel, stainless, 0Kh12G14N4Yu2, effect of plastic deform. on biphase struct. 78−44176
steel, stainless, austenitic, microstructural distrib. of cathodic H_2, autoradiography *(French)* 79−99234
steel, stainless, austenitic type 304, martensite transform, acoustic emission identification, opt. microscopy obs. 80−81062
steel, stainless, cold worked, pitting corrosion in NaCl soln. 78−44257
steel, stainless, Cr-Ni-Ti, metallographic detection of $(Ti,Ni)_6C$ 80−66721
steel, stainless, ferritic, Ti stabilised, exam. of grain boundary structure *(Russian)* 79−15662
steel, stainless, fixing pins for fractured bones, strength, ultrasound effect 80−71710
steel, stainless, grain boundary ledges, contrast phenomena identification 78−51555
steel, stainless, high strength, influence of corrosive medium on low cycle fatigue, photography obs. *(Russian)* 79−34199
steel, stainless, martensite nucleation, in situ electron microscope obs. 80−7572
steel, stainless, martensitic new etchant to reveal prior austenite grain boundaries 78−3290
steel, stainless, martensitically ageing, techniques for revealing microstruct. characts. 79−70241
steel, stainless, metallographic technique for detection of ferromagnetic δ-ferrite to paramagnetic σ-phase 79−61816
steel, stainless, metastable, determ. of strain-deform. martensite content 78−3282
steel, stainless, type 304, piping cracks, metallurgical exam., failure anal. 79−67849
steel, stainless, Type 304, pitting corrosion in Na_2SO_4 soln. *(French)* 80−40581
steel, stainless, type 316, electron beam heating effect on extracted intermetallic precipitate 78−35394
steel, stainless, type 316, low cycle fatigue props. in vac., fracture mode 80−85021
steel, stainless, type 316, microstruct. changes in creep ductility, SEM, TEM, optical microscopy and X-ray diffr. study 79−38927
steel, stainless fracture character under tension, in S-H_2 atmosphere *(Russian)* 79−34198
steel, stainless type 304, evaluating tendency for sensitization using Jominy bar test 80−16337
steel, stainless type 316 welds, post weld heat treatments on struct., composition and ferrite amount 80−29992
steel, structural, macroscopic and microscopic features of fracture 80−81179
steel, structural recrystallisation, phase and struct. transformations during heating 77−55990
steel, surface state influence on etching effect 80−81235
steel, texture sheet, mechanical anisotropy estimation using quantitive metallography *(German, English)* 77−77696
steel, tool, low alloy, methods of revealing austenitic grain 80−25949
steel, tool, martensitic hardened, reagent for revealing austenitic grain size 80−21207
steel, tool, NC6, carbide lattice, kinetics of its destruction *(Polish)* 78−92280
steel, type 12Kh1Mf and 15Kh1M1F, damage accumulation during prolonged high-temp. creep, fractography study 79−57026
steel, type 1Kh17N2, white zone formation and props. during friction in vac. *(Russian)* 80−40542
steel, type 27KhGSNL, castings, exam. of cracks due to treatment 78−44205
steel, type 34Cr4, post-hotforming recrystallisation condition, use of NEOPHOT 2 and EPIQUANT 80−84949
steel, type 35L, heat treated, exam. of surface defects using fluorescent liquids 79−15933
steel, type A533B, fatigue crack propag., metallographic and fractographic anal. 79−83325
steel, types 45, 50, U8, U10, diffusion chromizing,, microscopic examination 79−43357
steel, unkilled deep drawing sheets, influence of N content on recrystn. *(German)* 80−40376
steel, use of impressions for fracture study under optical microscope 77−56185
steel, W-Mo, types R6M5 and R6M5K5, decarburising layer evaluation 80−21164
steel, wear mechanisms, metallographic data 77−59942
steel, Zi, high permeability grain-oriented, AlN precip. study 79−83337
steel ball bearing, fatigued, phase changes, nomenclature 80−89198
steel fibre reinforced Mg, fibre-matrix interfacial reactions 80−20043
steel medium C, type 45, electroerosion, white-layer structures detection method 79−52485
steel nitride phase hardening, precipitation and solution kinetics after heat treatment 78−95756
steels, 110G13 and 40Kh10G10, hardening and structural transformations during friction *(Russian)* 77−52527
steels, C and alloy, quality, effect of methodic factors on quality of S replicas 79−24691
steels, free-machining, fractography and X-ray photoelectron spectroscopy 80−7673
steels, high-purity and commercially based, containing 10 wt.%W or 5 wt.%Mo, tempering behaviour 80−7600
steels, obs. and anal. of sulphides, using non-aqueous electrolyte-potentiostatic etching method *(Japanese)* 80−89433
steels, structural St 37-2, cleavage fracture, report 80−25868
steels ShKh15 and 12KhN3A, white phases structure after heat treatment 80−76281
STEM, low resolution imaging problems and soln. 80−108685
STEM, metallurgical appl., review 77−44422
STEM microdiffraction use for misorientation between subgrains obs. 80−104415
subgrain imaging, in bulk specimens to study localised plasticity using SEM 80−66609
substructure exam. by astigmatic X-ray microbeam method 78−85076
superalloys, phase extraction, chemical and X-ray diffr. anal. 78−72951
surface deformation and wear track obs. using analytical electron microscope 80−108687
surface quality for difficult specimens *(German, English)* 78−60935
techniques improvement *(Rumanian)* 78−35603
Technotron system for specimen prep. *(German, English)* 80−30199
TEM specimen preparation by chemical etching 77−52589

metallography continued
TEM specimen preparation using photochem. etching *(German, English)* 77−56202
texture anal. by orientation distrib. functions 77−86282
texture anal. three dimensional, computer simulation of errors 78−64805
textured material, X-ray quantitative phase anal. *(Chinese)* 80−21195
textured sheet metals, X-ray diffr. anal. 80−6316
thin foil, energy dispersive X-ray microanal. 77−60153
thin metallic foil prep. for TEM obs. *(German, English)* 79−91885
Tishomingo Fe meteorite, microstructural study 79−16898
Tomkeieff eqn. applicability to truncated multiphase systems 77−44437
transition metals and compounds, electromechanical polishing method 78−53073
two-surface analysis, of polished sections in scanning electron microscope 80−77912
type 35L, heat treated, exam. of surface defects using fluorescent liquids 79−5101
Udimet 700, microstruct. of resolidified zones formed by laser melting single crysts. 79−78953
ultramicrotomy in corrosion and protection TEM 77−81358
wear resistant coatings, sprayed-on *(German)* 78−19981
wear test specimen, metallographic technique 80−35496
wear theory, metallography of worn surfaces 80−35346
weld, submerged arc, metallographic study of chevron cracking 78−56761
welded joint non-metallic inclusions, metallography method, and X-ray spectrum microanalysis appl. 77−76245
welding by grain struct. comparison *(German)* 77−86273
white cast Fe, abrasive wear 80−108587
white cast iron, plasticity in impact toughness, bending angle tests 77−56039
white Fe castings, morphology of eutectic M_3C and M_7C_3 80−108427
wire, device for uniform electrolytic removal of surface layers for residual stress determ. 78−60918
worn ball, metallographic micro prep. method 78−3274
worn surfaces, exptl. difficulties, delamination theory implications 79−34253
X-ray residual stress anal. theory 77−84200
X-ray stress anal., recent German activities 77−81359
X-ray synchrotron radiation topography for recrystallisation obs. 79−8411
X-ray tensometry *(Czechoslovakian)* 77−28958
Zircaloy-2, effect of simulated fission products on elongation fractography and metallography 80−649
Zircaloy-2, neutron irradiated, inhomogeneous deformation behaviour 80−50679
Zircaloy-4, ^{51}Cr bulk diffusion 79−73347
α-Zr, ω phase proportion during high press. deform. *(Russian)* 79−74147
Ag, (211)[$\bar{1}$11] single crysts., shear band effects on rolling deformation 80−50651
Ag, electropolishing, cyanide-free solution 78−88603
Ag thin evaporated films, rel. between microstruct. and excess free energy, TEM 80−70427
Ag-Cd (approx. 50 at.%), disordered hcp to ordered bcc transition, meas. of activation energy 78−72773
Ag-Cu (6.2 at.%), with discontinuous precipitates, quantitative struct. anal. using SEM 79−43527
Ag-Cu eutectic and off-eutectic alloys, thermal stability 77−25077
Ag-Hg-Sn dental amalgams, non-γ_2 phase, transmission electron metallography 79−74162
Ag-Sn alloys containing Au, splat cooled ribbons, electron microscope exam. 78−39987
Ag_3Mg, ordered alloy, projected pot. image of defect obs. 79−99176
Ag_2S-(As)(Sb)(Bi), temp.-comp. diagram 78−44105
Ag_2Se-(As)(Sb)(Bi), temp.-comp. diagram 78−44105
Ag_3Sn, containing Au, etching technique for alloys and amalgams 78−3291
Ag_2Te-(As)(Sb)(Bi), temp.-comp. diagram 78−44105
Al alloy, age-hardenable, extraction of precips., electrochem. method 77−32735
Al alloy, anodic finish exam. by SEM and electron probe micro anal. obs. 79−96278
Al alloy, FIM and microanalysis, developments 80−100155
Al alloy, sintering of powder metallurgy parts, metallographic exam. and hardness testing 77−4752
Al alloy, type 2024-T3, fatigue deformation and crack growth, holographic study 80−25836
Al alloy, type 2024-T4 and 2124-T4, fatigue crack initiation and microcrack growth 79−79100
Al alloys, inclusions, oriented distrib. metallography and effects on anisotropy *(Russian)* 78−80589
Al alloys, optical contrast enhancement by vacuum deposited ZnTe layers 78−44301
Al alloys aged, local plastic strain distrib. by selected areas channelling patterns 77−44349
Al, cold rolled, annealed, fatigue crack propag. rate, temp. effect 78−39904
Al, fracture mechanism 80−100903
Al, struct. changes in single cryst. under influence of static and dynamic stresses *(Russian)* 78−92300
Al-Ag, type-II superconductor, torque oscillations in mag. field *(Russian)* 80−103800
Al-Ag (7.27 wt.%), peculiarities exhibited during fatigue loading *(Chinese)* 80−71723
Al-Al_3Ni eutectic composite, structural response to shape variations 79−83190
Al-Al_3Ni two-phase matrix, Al electrolytic etching in $AlCl_3$ molten salts 78−3280
Al-alloy plates, type VAD23, thermomech. parameters effect on struct. and props. 80−20988
Al-Bi-(Fe), directionally solidified monotectic, growth parameters for aligned microstructs. 79−43236
Al-Bi(Cd)(Pb)-Ti, containing low-melting pt. inclusions, mech. props. 80−93632
Al-Cu, high strength, type 2024-T3, crack growth, fatigue induced surface deform., holographic detect. 80−85120
Al-Cu (4 wt.%) fractography *(German)* 78−19982
Al-Cu-Zn system, solid-phase reactions, phase diagram 80−50603
Al-Ge alloy, Ge particle size, determ. by small- and wide-angle X-ray scatt. 78−19966

metallography continued
Al-Mg-Si, type 6010, microstruct. characts. influence on formability, heat treatment 80−81090
Al-Ni (6 wt.%), fine-grained, deform. in tension and torsion 80−85008
Al-Ni(Cd)(Fe)(Si), cold worked, struct. and props. 80−71666
Al-Pd eutectic, microstruct. morphology 80−3018
Al-Si, inoculated with NaCl+KCl+NaF, effect on morphology of eutectic columns *(Russian)* 79−15684
Al-Si eutectic alloy, banded struct., SEM and optical microscopy 80−104144
Al-Si-Cu-Mg-Ni cast alloy, fractography *(German, English)* 79−87809
Al-Si-Li alloy system, Al-rich, phase comp., limits of solid solubility *(Russian)* 77−21097
Al-Ti alloys, growth crystallography and morphologies of Al_3Ti primary dendrites, metallography study 79−43230
Al-W(Mo)(Nb), struct. and props. of alloys obtained from granules 80−50717
Al-water vapour reaction, stress corrosion susceptibility STEM study, Mg addition effect 80−3247
Al-Zn alloys, interfacial stability of planar solid-liq. interface during solidification 80−104145
Al-Zn-Mg/Al-Mg filler welds, weld fusion boundary structure 80−39459
Al-ζ(AlAg) eutectic and off-eutectic alloys, thermal stability 77−25077
Al_2O_3-Cu composite, vapour deposition, microstruct., texture and surface topography 77−70001
Al_2O_3-glass mixture, microstructural changes and shrinkage during sintering 80−25640
Al_2O_3-TiC sinter products, grain size meas. by combination etching process 79−74331
Au, coherent twin boundary, electron microscopy obs. *(Japanese)* 79−82130
Au, electroplate, delineation of hard from soft by etching 78−3292
Au, thin disc prep. and electropolishing for TEM 78−88601
Au thin films, with nm-sized pores, prep. from Au-Ge eutectic films by etching 80−16227
Au-Ge-Te ternary system, solid soln. in vicinity of GeTe, phase diagram *(French)* 77−85994
Au-Ni-Cu-Zn, white gold, metallographic struct., heat treatment and plastic working effect 80−40403
Au-Pd-Zn system, quasibinary section phases investig. 77−12596
B fibre reinforced Mg, fibre-matrix interfacial reactions 80−20043
B films, prep. by H reduction of BCl_3, struct. and hardness 80−54543
B, zone-refined effect of Ni doping on conductivity type, microhardness and metallographic obs. 77−31682
B-C system, electron probe microanalysis and destructive chem. methods of study *(French)* 80−11982
B-C system, region of existence of B_4C phase 78−76636
B_4C, melting and phase homogeneity range 80−20911
B_4C, metallography and Knoop microhardness *(French)* 78−76730
Be, machining damage, SEM exam. 78−39990
Be polycrystalline, metallographic observation of cleaved grains 78−72824
Be-Co (0-50 at.%) alloys, thermal, metallographic and X-ray anal., phase diagram *(Russian)* 78−56611
$Bi_{24}CoO_{37}$, in Bi_2O_3-CoO system, X-ray diffr., thermal anal. and metallography obs. 80−24598
Bi_2O_3-CoO system, X-ray diffr., thermal anal. and metallography obs. 80−24598
C fibre reinforced Al composite, C-Al contact interaction kinetics 79−20007
cast Fe, grey and ductile, subsurface defects, SEM and EDAX study grey and ductile, subsurface defects, SEM and EDAX study 80−44400
Cd and Cd-Ag (3 wt.%), metallographic prep. at room temp. *(German, English)* 77−9026
Cd, polycrystn., annealed, effect of hydrostatic pressure on grain size, growth and boundary mobility 79−37717
Cd-Zn eutectic and off-eutectic alloys, stability 77−25077
Ce-Ga system, phase equilib. and cryst. struct. of phases 80−35159
Co, corrosion in Ar-SO_2 atmospheres, scale struct. obs. *(Japanese)* 80−55568
Co-CoAl, two phase, interaction between deform., fracture initiation and propag. 80−85006
Co-Cr-Ni-Ta-Al-Y (25, 10, 5, 3, 0.5 wt%), exam. of hot corrosion 79−20251
Co-Fe-Ti (12,6 wt.%), semihard permanent magnet, magnetic precipitation hardening 78−52830
Co-Ga-B, phase diagram, metallographic, X-ray and electron probe anal. 78−92241
Co-rare-earth permanent magnet, grain alignment determ., method using eutecoid transform. of Co_5R 77−9003
Co-Sm permanent magnet, grain alignment determ., method using eutectoid transform. of Co_5Sm 77−9003
Co_5Ge_3, phase and struct. characts. 77−36450
Cr, interaction with dense stream of N ions, metallography, microhardness, specific volume *(Russian)* 80−15169
Cr-V-Ce-N, (2.4 to 2.6, 1.7 to 2.3, 0.005 to 0.23 wt.%) V effect on hardness, and ductile to brittle transition temp. *(Russian)* 79−34138
Cu crystals, two-phase, recrystn. retardation, particle size, spacing effects 80−89242
Cu, fatigued specimens, 'etch pit slip', SEM obs. 79−100258
Cu, heterogeneous, new polishing technique *(German, English)* 79−20322
Cu ingot, cast, nonmetallic inclusion size frequency distrib. determ. 78−39989
Cu, polycrystn., strain localisation during hot deform. 80−104195
Cu, porous, sintering, cold working, recrystn. annealing, mech. props. and microstruct. 78−76660
Cu single cryst., drawing deform. band form., axial orientation force meas., X-ray pole figure determ. *(Japanese)* 78−76710
Cu single crystals, neutron irradiated, secondary slip 80−88161
Cu, single crysts., ⟨110⟩ oriented, tensile deformed, HVEM of recrystn., recrystallised state 80−89256
Cu single crysts., deformed, HVEM study of recrystn. texture 80−104179
Cu, sintered, residual voids, quantitative anal. of morphological changes by metallography 79−47854
Cu, struct. changes in single cryst. under influence of static and dynamic stresses *(Russian)* 78−92300
Cu-Al (15 at.%), rolled single crysts., metallographic study of deformation struct., orientational change, shear bonds *(Japanese)* 79−24582

metallography continued
Cu-Al-Fe-Mn (10,3,2 wt.%), phase comp. struct., continuous cooling from β-phase effect 79−24499
Cu-Al-Ni-Fe system, corrosion behaviour in sea water 80−45421
Cu-Al-Zn, period of periodic antiphases, quant. metallography *(French)* 79−100111
Cu-B(25 wt.%) *(Japanese)* 80−55402
Cu-Be (2 at.%), plastic deform. and dislocation substruct. 80−76307
Cu-Be (2 wt.%), alloying addition effects on grain boundary reaction *(Japanese)* 80−49236
Cu-Be-Co, cuboid (Co, Cu, Ni, Fe)Be inclusions, metallography, ageing effects 80−11645
Cu-Be-Co(0.1,0.2 wt.%), discontinuous precipitation *(Japanese)* 80−55402
Cu-Cr (0.75 wt.%), deformation charact., fully reversed cyclic strain with fatigue cracks and dislocation struct. 80−81148
β-Cu-In, directionally transformed eutectoid, morphology exam. by metallography *(German)* 78−92257
Cu-Ni-Be-(Al) (30,0.5,(0.2-2) wt.%), Al addition effect on grain boundary reaction *(Japanese)* 80−54254
Cu-Ni-Zn alloy, surface comp., outdoor exposure influence 80−59770
Cu-Si-Te, phase equilib., DTA and metallographic anal. *(French)* 79−52182
Cu-Sn alloy, surface comp., outdoor exposure influence 80−59770
Cu-Ti, liquid phase sintering, metallographic electron beam microanalytical investigation 78−95888
Cu-Zn alloys, surface comp., outdoor exposure influence 80−59770
$ErCo_6$, domain wall grooving due to mech. polishing 79−70232
Er_2Co_{17}, domain wall grooving due to mech. polishing 79−70232
ErZn, preferred mag. domain orientation, and microstructural defects, magnetostriction meas. 79−73769
Fe alloy, surface layers examination, X-ray method 78−35606
Fe, Armco, borided surface layers, Mossbauer and metallographic anal. 80−50769
Fe, Armco, sleeve, deformed by cold drawing, exam. of surface and texture *(Russian)* 79−34057
Fe, Armco low-cycle fatigue, electric field effects 77−1868
Fe, cast, austenitic grain size determ. 80−81255
Fe, cast, eutectic solidification, expt. study by quantitative metallography 79−24516
Fe, cast, graphite content determ. by X-ray diffr. method 80−100977
Fe, cast, grey, solidified in oscillatory and rotating moulds, metallographic study 80−89213
Fe, cast, inoculated with Ce, exam. of phase composition 78−56620
Fe, cast, Mg, despheroidising effect of Bi, Sn on graphite in alloy 78−56670
Fe, cast, Mg-modified, scale for shapes eval. of graphite inclusions 78−35609
Fe, cast, quantitative metallography, study by image anal. 78−31492
Fe, cast, rare-earth-Mg nodular, fracture toughness and fatigue *(Chinese)* 78−95791
Fe, cast, spatial dispersion of graphite particles, metallographic study 78−92419
Fe, cast, spheroidizing effect of Mg and Ce modifiers 80−35193
Fe, cast, wear mechanisms, metallographic obs. 77−59942
Fe, cast, white, high Cr, phase composition, B effect 80−104172
Fe, cast, with spheroidal graphite, crystn. *(German, English)* 80−97473
Fe, cold rolled, struct., transmission Kossel patterns obs. 77−48451
Fe, ductile, with different secondary struct., abrasive wear *(German)* 80−25871
Fe, high purity, boriding with cryst. B powder 80−84951
Fe, interaction with dense stream of N ions, metallography, microhardness, specific volume *(Russian)* 80−15169
Fe one raw material, sintered, ionic etching as new method of struct. investigation 77−52588
Fe pellets, re-oxidation at high temp., growth of needle-like haematite crystals 80−35431
Fe, pig, white, mech. props. meas. *(French)* 80−104370
Fe, pure, initial grain boundaries effect on cold-rolling and annealing textures *(Japanese)* 80−35205
Fe, sintered, influence of metallographic treatment on pore analysis 80−76417
Fe surface, laser doping with V *(Russian)* 78−95065
solid Fe/liquid Zn, interdiffusion reaction 79−77845
Fe/ZrB_2, metal-like cpd. form. in diffusion layer during solid phase saturation 80−19994
Fe-Al, sintered and worked alloy, nonmetallic inclusion identification by quantitative metallography 77−77701
Fe-Al (up to 7.2%), oxidation process 78−85022
Fe-Al(Cr)(V)(Ti), hardness after nitriding, metallographic, electron microscopic and microprobe anal. 78−51608
Fe-As (0.22 to 1.68 wt.%), martensitic transform., struct. features 77−36499
Fe-base amorphous alloys, embrittled by H and heat-treatment 80−55518
Fe-C (synthetic diamond) role of diffusion of graphitisation in phase interaction 77−36449
Fe-C-Ti (0.2 to 1.8, 0.1 to 1.7 wt.%), crystallisation and microstruct. *(Russian)* 77−66632
Fe-Co-Ti-Al alloy type YuNDK magnets, metallographic method of distinguishing cracks 80−85096
Fe-Co-V alloy, Remendur, heat treatment effects on mech. and struct. props. 77−8846
Fe-Cr, from ore reduction, metallographic investigation, optical miroscopy and SEM *(French)* 78−68648
Fe-Cr, surface segregation of impurities (C,N and S) *(French)* 77−56192
Fe-Cr-Co alloy, spinodally decomposed, micro-twinning 80−92537
Fe-Cr-Mo-Ti (13, 1.5, 3.5 wt.%), equilibrium studies on chi-phase strengthening 79−24496
Fe-Cr(W)-M, (M=Si,Mo,Ni,Mn,P,Cr), cellular growth of S-pearlite formed by carburisation 80−108486
Fe-Cu-Ti, improvement of irradiation-enhanced Cu embrittlement by Ti addition 79−43393
$Fe-Fe_2O_3$ composite films, structural props., microhardness, 250 to 700K 78−84095
Fe-Mg, Burgers vector determ., crystal defect observation by weak beam image *(Japanese)* 79−82130
Fe-Mn (15(24)(30)wt.%), high hydrostatic pressure influence on stress-strain curve 80−25805
metallography continued
Fe-Mn-C, variation of martensite morphology with Mn and C composition 80−50635
Fe-Mn-Ti alloys, austenitic, precipitation strengthened 80−25714
$Fe-MoS_2$, exam. of props., using differential thermal analysis, and metallography *(Russian)* 79−15653
Fe-Ni, interference microscopy, for colour development and phase separation 80−100976
Fe-Ni, oxidation, Mossbauer spectroscopy, metallography, SEM and X-ray diffr. anal. 78−15577
Fe-Ni (23 wt.%), struct., composition changes during α to γ transform., martensite plastic deformation influence *(Russian)* 80−11642
Fe-Ni (3 wt.%) alloys, embrittled, microanalysis of grain boundary segregation using STEM 78−35633
Fe-Ni (31 wt.%), thermoelastic martensite obs. 80−3052
Fe-Ni (32.86, 30.65 wt.%), charact. of quenched struct. formed in textured sheets, TEM and optical microscopy study 79−34084
Fe-Ni-Al system, multiphase diffusion at 1000°C, diffusion structs. and props. 80−19995
Fe-Ni-C (31.9, 0.02 wt.%), metallographic study of austenite grain size effect on martensite kinetics 79−1863
Fe-Ni-C (31.9, 0.02 wt.%) alloy, hardness of martensite-austenite mixtures 80−60959
Fe-Ni-Cr alloy, cast, etching methods for determ. of primary struct. 78−23888
Fe-Ni-Cr-Al-Y, oxidation mechanism, Y addition effect on kinetics and oxide adherence 80−97623
Fe-Ni-Mn (20, 5 wt.%), rel. orientation between adjacent martensite laths 80−76254
Fe-Ni-WC hard alloy, struct. and props. 79−79007
Fe-Ni-(Al) (Ti) (V)-(Cu), Cu addition strengthening at 77K, mech. props. 80−60875
Fe-Pt (24 at.%), colour metallographic technique, for studying microstructural reproducibility, in martensitic transformations 78−72954
Fe-Si, etch figure method appl. *(Chinese)* 80−21194
Fe-Si (3 wt.%), exam. of plastic deformation, slip band dislocation, under hydrostatic pressure 78−56695
Fe-Ti-C, rapidly quenched by splat-cooling 80−84923
Fe-X-C (X=Cr, Mo, W), quenched rapidly from melts, nonequilib. phases *(Japanese)* 80−71630
Fe-Zn, liquid-solid reaction in Zn bath, effect of Fe concentration, alloy layer growth, exam. *(Japanese)* 78−85037
$Fe_{80}B_{20}$, amorphous, crystallization 78−42917
FeTi, H storage alloy, prep. for TEM *(German, English)* 80−30197
GaSb, thin film prep. for TEM 77−9027
$GdCo_5$, domain wall grooving due to mech. polishing 79−70232
Ge-Sb, eutectic alloy, exam. of morphology during solidification *(Russian)* 79−34022
Ge-Te system, phase equil. diagram, $GeTe_{1\pm x}$ region analysis by metallography, microhardness and DTA *(French)* 77−70034
GeTe, nonstoichiometric, homogenisation 78−44004
Hf-V, superconductivity, X-ray and optical metallography 79−4610
HfB_2, oxidation in O_2 atmosphere, exam. 80−11814
n-InAs:Cr, Czochralski growth of high-resist. single crysts. 77−66587
InBi single crystal, deform. mode under dynamic indentation 80−88163
La-N-C system, metallographic investigation *(German, English)* 77−52600
$LaNi_{4.4}B_{0.6}$, H_2 absorpt. props. 80−88432
Li-Sn, phase relationships between Li_7Sn_2 and LiSn 79−78933
LiF crystal, dislocation movement study with new chem. polish 78−15614
$LiTi_2O_4$, prep., characterisation and supercond. props. 77−40010
Mg cast iron, effect of heating temp. on microstruct. and mech. props. 77−56005
Mg cast iron, effect of heat treatment on phase comp., microstruct., wear resistance 77−56006
Mg cast iron, microstruct. of spheroidal graphite, rel. to polishing and annealing treatments 77−56160
Mg-Al-Zn (3, 1 wt.%), alloy AZ31, mech. props. of extruded and welded pipe and sheet, optical microscopy exam. 79−34065
Mg-Nd-Zn dilute alloy, metallography and precip. kinetics 80−71655
Mg-Ni-S, electroforming, mech. props. rel. to heat treatment 80−35133
Mg-Zn-Zr-Cd-Nd, Lawes phase separation using acetate electrolyte, Cd and Nd effects 79−70237
MgO single crystals, chem. polishes for {100}, {110} and {111} surfaces, spectrochem. anal. for impurity content 79−29241
Mn-Ga, mag. and cryst. struct. in conc. region of gamma phase, temp. depend. *(Russian)* 79−65649
Mn-Pt (<29 at.%), eutectoid transform., antiferromag. struct. transform. *(French)* 78−92259
Mn-Si (62.5 to 63.8 wt.%), phase anal. and cryst. struct. *(Japanese)* 80−15049
Mn_xN, metallographic exam. *(Bulgarian)* 79−100319
MnSi-Si system, striations and cryst. struct. of matrix 80−103292
Mo, grain structure characteristics analysis using Quantimet-720 79−52496
Mo, macroscopic heterogeneity of plastic deform., metallographic examination *(Russian)* 79−100210
Mo powder, influence of powder reduction processes on props. 80−89175
Mo, structure of large single crystals produced by electron beam spot welding *(Russian)* 77−44136
Mo-(Zr+V+C) (1.1 wt.%) alloy, phase composition, carbide phase microhardness *(Russian)* 80−60834
Mo-low alloys, C enrichment mechanism of intercrystallite zones *(Russian)* 80−20963
Mo-Zr-C (0.12, 0.002 wt.%), prep. of diffusion metal coating on alloy, oxidation rates *(Russian)* 78−56816
Mo-Zr-Nb-C alloys, phase diagram and comp., Zr and Nb influence *(Russian)* 79−52167
N determinaiton by track autoradiography 80−100979
Nb alloys, non-metallic inclusion form. during quenching from liquid state 78−95766
Nb, defect struct. and torque anisotropy 77−20509
Nb, pure, reaction with gas residual in vacuum, physicomech. props. effect 80−16587
Nb-alloys, reaction with gas residual in vacuum, physicomech. props. effect 80−16587
Nb-Ga-Cu, phase diagram, metallographic and X-ray study, annealed and as-cast supercond. crit. temp. *(Russian)* 78−56617
Nb-Ge system, reaction diffusion, electron probe anal. 79−28152

metallography continued
Nb-N(O)(C) system, specimen prep. for metallography *(German, English)* 80−89439
Nb-Pd constitution diagram, metallographic and X-ray diffr. anal. 80−89204
NbC coating, vapour deposition, phys. and chem. props. 77−40456
NbC, deformation behaviour during rubbing in wide temp. range 80−16486
Ni alloy, STEM microanalytical techniques comparison for precip. comp. determ. 78−35790
Ni alloy 718, intermetallic second phase obs. using electrolytic extraction and SEM 79−34074
Ni alloy EhI698, new etchant for revealing microstructure 80−25934
Ni alloys, cast, interference microscopy, for colour development and phase separation 80−100976
Ni base superalloy, γ' precipitate size determ. technique 79−34221
Ni, C precipitation 80−29958
Ni, grain boundary ledges, contrast phenomena identification 78−51555
Ni, inner layer of high temp. oxide scale, metallographic obs. 80−3240
Ni, pure, anomalous grain growth 80−20984
Ni, single crysts., H and liq.-Hg embrittlement 80−25862
Ni, sintering kinetics, metallographic study 80−93519
Ni wire plasma sputtering with W particles, coagulation, struct. and particle size *(Russian)* 80−40260
Ni-(Co)-Cr, aluminide coating, microstruct. and chem. 80−76189
Ni-Ag alloy, metallographic struct. and formability *(German, English)* 80−30201
Ni-base superalloy, phase extraction *(German, English)* 77−52599
Ni-base superalloys, technique for replication of γ' 80−79648
Ni-C system, satellite structs. of intermed. phases in diamond synthesis using Ni catalyst *(German)* 77−32538
Ni-C-Ce, overmodification *(Russian)* 80−40432
Ni-Co-Cr-Ta-Al-W-Mo-Ti, cast, phase volume fraction determ. using manual point count practice 78−53052
Ni-Cr alloy, cast, etching methods for determ. of primary struct. 78−23888
Ni-Cr alloy, structural changes, during thermal stress cracking, X-ray and microhardness meas. *(Russian)* 78−35496
Ni-Cr alloys, method of etching in Br-methanol reagent 77−90516
Ni-Cr-Al-Ti alloy type ZhS6U, effects of heat treatment in high vel. gas streams on props. 79−57025
Ni-Cr-Fe-Mo-Co (21.41, 19.28, 8.64, 2.16 wt.%), Hastelloy alloy X, exam. of thermal stability 78−84865
Ni-Cr-NbC eutectic composite, unidirectional solidification, thermal cycling, temp. range effect on microstructural degradation 80−89272
Ni-Fe-Cr superalloy 718, heat treatment effect on room temp. and elevated temp. fracture toughness response 80−100922
Ni-Ta-Al system, phase equilibria and diagram, electron probe, X-ray diffr. anal. 80−29927
Ni-Ti (1.6, 7.64 wt.%), monophase high temp. scaling, metallography study 80−21159
Ni-W-Co-Cr, superalloy MAR 200, with Hf, cellular composite prod. by isothermal dendrite ripening 78−44150
Ni_3Al-Ni_3Nb eutectic, directionally solidified, high-temp. oxidation mechanism 80−16544
Ni_3Ge-Fe_3Ge solid soln., flow stress, transition from positive to negative temp. depend. 80−60906
NiH_x, formation and decomp. studies 80−71626
Pb, high purity microstructural investigation by etching with aqueous $HClO_4$ 77−56205
Pb, Pb alloys, metallographic preparation using pH controlled silica gel and superior microetchant 80−16623
Pd sponge powder, sintering shrinkage kinetics 80−29900
Pd-Ag-Cu (35,25 at.%), determ. of ageing transformations by resist. meas., metallography, TEM and X-ray diffr. 79−4967
Pd-Cu-Ga, cold work and annealing-induced hardening, X-ray diffr. anal. and metallographic exam. *(Russian)* 79−38844
Pu, $\beta \rightarrow \alpha$ and $\gamma \rightarrow \alpha$ transforms., microstructures and kinetics 77−25048
Pu-Pt(Rh)(Pt-Rh), exam. of phases and crystal structure 78−80518
Sc-Co(Ni)(Cu), phase diagram determination, using X-ray diffr., metallography and DTA techniques *(Russian)* 79−34004
Si polycrystalline films, texture formation study 79−87662
Si-B system, DTA, X-ray diffr. and metallographic study *(German)* 80−66484
SiC fibres reinforced Ni complex alloy, influence of TiN coating on fibre matrix interaction *(Russian)* 78−95820
B SiC, sintered, effect of Al trace amounts on specimen props. 79−83289
SiC-Ni based superalloy reaction, at elevated temps. 80−3287
Si_3N_4, phase content determ., using X-ray diffr. anal. 78−44281
Si_3N_4, reaction-bonded, microstructural analyses 77−8782
SiO_2 film, local defects detection by electrolytic decoration *(Bulgarian)* 78−60896
Sm-Co, decomp. kinetics when aged, X-ray mag. props. and metallography study *(Russian)* 78−56644
$Sm(Co_{1-x}Cu_x)_{7.8}$ alloys, coercive fields, domain wall energies, mag. and metallographic exam. 78−91897
Sn droplets, on Bi, Zn and Al, heterogeneous nucleation 80−44294
steel, 36NKhTYu, aged, rate of discontinuous precipitation of γ'-phase, short high-temp. treatments *(Russian)* 78−11226
strengthened by lattice transformations, mech. props. study *(Japanese)* 79−43332
Ta and Ta alloys, electrolytic polishing, use of pure FSO_4H 78−85094
Ta-N(O)(C) system, specimen prep. for metallography *(German, English)* 80−89439
Ta-O supersaturated solid solution, precipitation processes, hardness change meas. 80−25712
Ta-Pd system, phase diagram exam. of composition by X-ray diffr., electron microprobe anal., and metallography 78−76632
$(Ti,Ni)_6C$, metallographic detection in 12Kh18N10T steels 80−66721
Ti alloys, H_2 diffusion at room temp. 79−51312
Ti alloys, surface layers examination using vacuum UV spectrograph *(French)* 80−71987
Ti alloys VT23 and VT15, etching as a function of struct. *(Russian)* 78−15568
Ti, electron microscope specimen prep. technique for dynamic straining expt. 78−88602
Ti, metallographic specimen prep. for chem., mech. electrolytic polishing 78−80705
α-Ti, recrystallised commercial purity, Fe-rich precipitates obs. *(French)* 80−50637

metallography continued
Ti, surface layer, study using vac. UV spectrograph *(French)* 80−71987
Ti, Ti recrystallisation texture from neutron diffr., cf X-ray diffr. *(French)* 77−84593
Ti-Al alloy system, quenched from β-region, struct. obs. *(Russian)* 77−21146
Ti-Al alloys, α_2 phase obs. using microscopy and X-ray diffr. 79−52497
Ti-Al-H, H effect on mech. props. and lattice constants 80−21036
Ti-Al-Mo-Sn-Si (2.25, 4, 11, 0.25 wt.%), type IMI 680, internal friction study of martensitic transformations 80−7573
Ti-Al-Mo-Sn-Si (2.25, 4, 11, 0.25 wt.%), type IMI 680, stability of martensitic phases 80−7574
Ti-Al-Mo-Sn-Si (4, 4, 4, 1/2 wt.%), type IMI 551, internal friction study of martensitic transformations 80−7573
Ti-Al-Mo-Sn-Si (4, 4, 4, 1/2 wt.%), type IMI 551, stability of martensitic phases 80−7574
Ti-Al-Mo-(Cr), etching as a function of struct. *(Russian)* 78−15568
Ti-Al-Sn (5, 2.5 wt.%), annealing of near-basal hydrides 80−20989
Ti-Al-Sn-Zr-Mo (6,2,4,6 wt.%), α-β type 6246, fusion zone fracture behaviour in weldments 80−30093
Ti-Al-Sn-Zr-Mo (6,2,4,6 wt.%) fusion weldment, substruct. charact. 80−84183
Ti-Al-V (6, 4 wt.%), targets, metallographic features after ballistic tests 79−79046
Ti-Al-V (6, 4 wt.%), type IMI 318, internal friction study of martensitic transformations 80−7573
Ti-Al-V (6, 4 wt.%), type IMI 318, stability of martensitic phases 80−7574
Ti-Al-V (6,4 wt.%), α/β interface phase influence on tensile props. 80−30034
Ti-Al-V (6,4 wt.%), metallogaphically prepared, fracture surface, phase anal. by energy dispersive X-ray microanal. *(German, English)* 77−48606
Ti-Al-V (6,4 wt.%), to H effect on fracture props. and microstruct. 80−40512
Ti-Al-V-Sn (6,6,2 wt.%), α-β type 662, fusion zone fracture behaviour in weldments 80−30093
Ti-Al-V-Sn (6,6,2 wt.%) fusion weldment, substruct. charact. 80−84183
Ti-B-W(Mo), annealed at 1400°C, exam. of phase diagram, using X-ray phase and metallographic analysis 79−1847
Ti-Cu-Si alloy system, transforms. in Ti-Ti_3Si_3-TiCu region, 800-1600°C *(Russian)* 77−21099
β-Ti-Mo alloys, thinning transformation 77−44438
β-Ti-Mo-Zr-Sn(11.5, 6, 4.5 wt.%), metastable phase III, microstruct. and age hardening response 80−84945
Ti-V (15.5 wt.%), {332} deformation twins, optical microscopy study 79−79047
Ti-V-Ru alloy system, metastable phases form. *(Russian)* 77−21098
Ti-$ZrO_2(HfO_2)$, eutectic system metallographic investigation *(Russian)* 77−66629
TiB_2, erosion resistant boride coating on Ti and Ti alloys 79−20290
TiC, deformation behaviour during rubbing in wide temp. range 80−16486
TiC, sintering and grain growth, metallographic anal. 80−25642
TiC-Kh6V3M steel alloy, reaction during sintering and heat treatment 78−60617
TiC-Ni, particle growth quantitative anal. by metallography and stereology 77−77684
TiN, gaseous phase, crystallisation, effect of temp., vapour-gas mixture conc., and deposition time 79−33910
TiO-ZrO_2, pseudo binary system, effect of Ti addition on struct. and props. of zirconia 79−11583
$Tm_{1-x}Y_xTe$, $(0 \leq x \leq 1)$, single cryst. growth and charact. 78−23603
α-U, strain rate effect on flow and fracture 80−100887
α-U, strain rate effect on tensile flow and fracture 80−84992
U-Mo (10 wt.%), commercial alloys, influence of metallurgical factors on fracture processes *(French)* 78−60751
U-UNi_2-UCo_2, system, phase equilibria, lattice constants *(German)* 80−50598
UO_2, fine grained, low-stress creep study, metallographic obs. 79−43312
UO_{2+x}-ThO_2-MgO system, in air, phase rel., X-ray diffr., electron probe and metallography anal. 79−74137
(V,Ti)C+Ni cermet, binder grain size 80−44401
V, oxidation in low press. O_2 at high temp. *(Japanese)* 80−71807
V, structural changes in single crystal under single electric impulse discharge *(Russian)* 79−65086
V-D, exam. of phase diagram, using DTA and calorimetry, isotope effect 78−80527
V-Ga-Sc, phase diagram, metallographic and X-ray meas., solubility boundaries *(Russian)* 78−56618
V-H(D), metallographic and thermal differential anal., potential for H energy storage appls. 80−45281
V-N(O)(C) system, specimen prep. for metallography *(German, English)* 80−89439
V-Os system, equilib. phase fields, X-ray diffr., elec. resist., DTA, and EPMA meas. 79−47661
V-$ZrO_2(HfO_2)$, eutectic system, metallographic investigation *(Russian)* 77−66629
W, deformed, surface layer struct. effect on polygonisation and recryst., X-ray diffr. anal. and metallographic exam. *(Russian)* 80−84948
W fibre reinforced Cu, interface porosity formation, on thermal cycling 80−30092
W fibre reinforced Cu composites, correl. between thermal cycling-induced microstructural changes at interphase boundaries and tensile behaviour *(Japanese)* 80−71674
W fibre reinforced Ni-Cr alloys, Ni, Co, Co alloys, and Ni alloys, effect of alloying on structural stability, mech. props. 78−56600
W spheres, in liq. Ni, sintered, coalescing, crystallographic orientation, SEM study 80−45249
W-Ni sintered alloy, etching 79−29323
WC, deformation behaviour during rubbing in wide temp. range 80−16486
WC-Co, on-line computer anal. of SEM obs. 79−87807
WC-Co, rupture of bending specimens, use of quantitative metallography and stereology *(French)* 77−28899
$YFe_{1-x}Ga_xO_3$, zone refined, exam. of Curie point and magnetisation 79−4673
Yb-Ga system, phase diagram, cryst. structs. of phases 79−52169
Zn, dislocation etch pits on (0001) surface of single crystal *(Japanese)* 78−59811

metallography continued
Zn, stacking faults, plastic deformation, due to laser beam irrad., X-ray metallography study *(Russian)* 80−15121
Zn-Al, unidirectionally solidified eutectic, morphology and crystallography 77−48421
Zr alloys, H_2 diffusion at room temp. 79−51312
Zr, creep, optical and electron metallographic anal., 473 to 873K 78−39986
α-Zr, H terminal solid solubility, optical metallographic study 80−34195
Zr, microstructure exam. by electron microscopy, oxide film appl. 79−70243
Zr, pure, laser microprobe damage, metallographic exam. of craters formed 78−39988
Zr, terminal solid solubility of H, optical metallography, internal friction meas. 78−83962
Zr-H formation, of $\delta \rightarrow \gamma$ transformation 80−84929
Zr-H formation, the $\delta \rightarrow \varepsilon$ transformation 80−84930
Zr-H phase diagram, auto-radiographic and metallographic study of γ-phase *(Russian)* 78−56616
Zr-Nb (1 at.%), high-temp. nitriding, chemical and metallographic anal., disintegration test 79−24668
Zr-Nb (2.5 wt.%), seam welding tubing, microstruct. in weld region 79−61621
Zr-Nb (2.5 wt.%) alloys, microstruct investigation by electron microscopy using oxide films 79−70243
Zr-V, superconductivity, X-ray and optical metallography 79−4610
Zr_3Al, ordered, oxidation, weight gain and metallography 80−89398
ZrB_2, etching method using H_3PO_4 and H_2SO_4, effect of Pt 78−44339
ZrB_2, oxidation in O_2 atmosphere, exam. 80−11814
ZrB_2-Nb, reactions between components 80−100812
ZrC coating, vapour deposition, phys. and chem. props. 77−40456
ZrCu, constitutional and struct. studies, by mag. susceptibility, metallography and X-ray diffr. 80−70166
ZrH_x, laser irrad. effect on interstitial phases, metallographic obs. 79−37734
$Zr(V,Al)_2$, struct., supercond. props., elec. resist. and mag. susceptibility, 4.2 to 300K *(Russian)* 79−15246

metallurgical industries
see also forging; rolling mills
aluminium plants electrolytic baths, power consumption limitation method *(Russian)* 80−3366
analysis by atomic absorption spectrophotometry *(French)* 79−5241
arc furnaces, stabilisation methods *(German)* 78−75402
automated sintering and hot pressing system 79−33961
automatic barrel line type ATS closed system, small parts electroplating, after-treatment and drying *(German)* 80−84861
cast iron foundry, iron smelting, chemical composition and operation control using SiC-Q apparatus *(German)* 80−76450
coercimeters with EM attachments 77−12765
complex profiled surface alloying, automatic electrode feeding *(Russian)* 78−19936
electric furnaces, investig. of gas conditions, plasma production *(Russian)* 78−94921
electroplating, rack parts or bulk goods, in GTL-barrel units, Zn coating using acid electrolyte *(German)* 80−84862
electrorefining, recording coulometer for controlled atmosphere reactions of metals in molten salts 78−3344
electroslag refining, mathematical formulation for EMF, fluid flow, and heat transfer 78−52722
fluidised bed for heat treatment appl., development *(German)* 77−41596
fusion crystallisation device for refractory block production 77−63606
high speed steel, vacuum hardening *(German)* 79−100175
high-temperature materials, technological requirements, R and D, report 80−45222
high-temperature power-technological industrial processes use of nuclear power, reviews 79−26729
hydrometallurgical plant effluent waters, Mo and W determ. by activation analysis with low-power neutron sources 78−7279
ingot solidification and reheating, thermal model 77−73340
mathematical models appl. 77−70276
metallic ore processing, effect of ultrasonics and appl. 78−92214
methematical modelling appl. 77−73429
microwave appl., w.r.t. economics and safety 80−3754
ore dressing X-ray spectrometric analysis centre 80−86541
rare earth industry review 80−25537
steelmaking, heat transfer correl. during diffusion melting of Fe, steel in Fe-C melts 80−54348
surface properties improvements, using vacuum thermal process techniques 79−100283
tensile testing, automatic methods *(German)* 78−35598
tensoresistors, measuring force 80−17930
thermal plasma processing 77−42996
thermal regenerator, with variable mass flow rate, computer model 78−75047
thermoelectric MHD, appl. to fission and fusion reactors and metallurgy 79−50806
US soldering, industrial applications 77−58499
vacuum furnace developments, heat treatment, high speed steels *(German)* 79−100174
vacuum metallurgy, using electron beam techniques, technical problems *(German)* 80−84850
workplace lighting, vision problems, Swedish report *(Swedish)* 77−77896
Al smelting cathodes, comp. and props. 77−28740
Fe making industry, evolution, review 77−73431
N_2, liquid, use as cooling agent 79−58709
Ni, recovery from nickeliferous pyrrhotite, by thermal upgrading 77−60034
Si transfer from gas phase to molten Fe in blast furnace 77−4930

metallurgy
see also ageing; alloys; crystal microstructure; deformation; electrical properties of substances; hardening; heat treatment; magnetic properties of substances; materials testing; mechanical properties of substances; metallography; metallurgical industries; metals; metalworking; phase diagrams; phase transformations; physical chemistry; powder metallurgy; precipitation; recrystallisation; surface treatment; zone refining
actinide metal preparation and refining 78−84705
alloy design by automatic modelling, CAD system *(Japanese)* 77−52607

metallurgy continued
applications of XPS, AES, and SIMS *(French)* 80−81253
blast furnace reactions, review 78−85116
chalcopyrite, electrooxidation in ACl, stoichiometry and reaction mechanism, Cu extraction appl. *(French)* 80−16231
chlorination of Cu and Zn in Cu converter slag 80−20840
coal fired steam power plants, metallurgical problems 79−52089
coatings, metallurgical, conf., San Francisco (Apr. 1976) 77−40363
education, physical sciences at Lanchester Polytechnic 79−44658
electrochemical recovery of metal ions from dil. solns., design geometries for fixed flow-through packed beds 77−16833
electron beam for vacuum metallurgy *(Japanese)* 78−18465
electron microscopy, review 80−76458
electroslag smelting of large ingots, selection of slag system 79−20340
electrotransport refining of Sc 77−11738
extraction kinetics, from deep-sea Mn nodules, pore diffusion controlling case 77−28984
extraction kinetics, from deep-sea Mn nodules, pore diffusion with chemical reaction 77−28985
extraction of metals from ammoniacal soln. with low rank coals 79−11530
extractive, developments in basic principles and phys. chem., review 80−20819
extractive, fluidised bed electrode system appl. 79−57249
extractive metallurgical processes, thermodynamic evaluations 80−11591
fluid-solid reactions, law of additive reaction times 79−83452
furnace slags, effect of Cr_2O_3 and V_2O_5 desulphurising capacity 78−85119
furnace tapping operations, fluid flow, mathematical model 78−85117
high-strength metal development theory and technology *(French)* 77−21057
high-temperature materials, technological requirements, R and D, report 80−45222
high-temperature phenomena, conf., Helsinki, Finland, June 1975 77−52295
hydro-metallurgy, dispersed three-dimensional electrodes appl. *(French)* 80−71919
hydrometallurgy, developments, review 80−45252
inductive stirring, melt vel. 77−73250
inductive stirring of metal melts, surface velocity meas. on 30000 lb charge 78−11139
industrial metallurgical processes, alteration due to political considerations, and raw material availability, review 79−4901
ingot formed in EM crystalliser, control of metal melt circulation *(Russian)* 78−84790
international system of units *(German)* 77−22519
ion implantation, survey of developments 77−59027
ion microprobe mass analyzer appl. *(Japanese)* 77−25233
kaolinic clay chlorination in Al production 78−6878
magnetic materials, soft, magnetism and metallurgy, book 78−31029
metal electrowinning, energy consumption reduction via anodic coal reaction 79−91965
metallic oxides reduction, mechanism and intrinsic rates 79−83153
microanalysis, high resolution, using electron energy loss measurements, review 77−56190
micrometallurgy and microelectronics, review *(Russian)* 77−55874
microneutronographic and neutron-induced autoradiographic techniques, review of appl. in metallurgy 78−60892
neutron scattering techniques in applied research, medium-flux research reactors 79−13514
ore, flotation extraction, thermoelectric power, extraction yield depdnd. 78−19686
ore processing, US effects and appl. 78−92214
oxidizing slag-metal droplet reaction kinetics 78−11153
phase diagrams, non ferrous materials, use in sophisticating pyrometallurgical processes 79−11571
process and equipment developments in electrothermics and metallurgy over the last twenty-five years 78−92437
pyrometallurgy, industrial methods and research, review, book contrib. 77−40407
pyrometallurgy, process developments, review 80−25596
rare earth metal preparation and refining 78−84705
recycling of non-ferrous metals, system study, computer simulation 78−35278
refractory metal refining, at. absorpt. spectroscopy for continuous process control *(Russian)* 77−56302
sample preparation facility 79−180
SL/RN direct reduction process, mathematical model 78−6876
slag-metal interface determination using electrochem. conc. element 78−7114
smelting cell, C lining, nonfuming room temp. seam mix 78−11495
Spacelab, proposed French metallurgy programme 78−57423
Spacelab metallurgical experiments, possible influence on current procedures 78−88619
standard specimens for spectral analysis, review 78−7273
sulphide ores, phase equilibria in pyrometallurgy 79−11588
sulphides, direct leaching 77−29033
surface science in metallurgy, review 79−42388
thermal plasma engineering in metallurgy, inorganic materials technology 78−3070
thermophysical property research, metallurgical applications 80−97457
US applications, conference, Brighton (1977) 78−59223
vacuum metallurgy rel. to crit. resources 77−70011
vacuum processing of metallurgical melts, diffusion-limited condensation meas. for Zn and Pb vapours 77−8775
weightlessness expts., ERNO spcae research, with vertical Skylark rocket *(German)* 79−19980
Cu extraction, from aq. soln., hydroxyoxime and hydroxyquinoline derivative reagents 79−74115
Cu production and extractive metallurgy, developments, review 80−20821
Cu smelting, exam. of vacuum lift refining 78−60621
Cu_2S-Fe S mattes equilibration with Fe-O-SiO_2 slags under controlled partial pressures of SiO_2 79−83152
Fe, cast, Mg treated, fading behaviour *(Japanese)* 78−11152
Fe, phase diagrams, use in production 79−11572
$Fe_{0.925}O$, wustite, kinetics of reduction at moderate temps. 79−83154
Hf, calciothermic, electrorefining 78−68647
O_2 technology and conservation in metallurgical extraction 78−7169
Pb (II), solvent extraction by versatic acid 10 *(Japanese)* 79−4928

metallurgy continued
Pb blast furnace, gas composition, temp. and pressure meas., O_2 potential diagram, reduction mechanisms 78−85118
Pb, extractive metallurgy, developments, review 80−20820
Sn, extractive metallurgy, developments, review 80−20820
TiO_2 reaction with C/Cl_2, high temp. chlorination, volatile species 79−83451
V slag enrichment by oxide reduction during plasma melting *(Russian)* 78−52716
Zn, extractive metallurgy, developments, review 80−20820
Zn_2SiO_4 ore, processing review 77−48365
Zn_2SiO_4 ores, hydrometallurgical treatment for Zn recovery 77−52263
Zr_3Al, ordered, review of physical metallurgy 78−15419

metalorganic compounds *see organometallic compounds*

metals
see also actinides; alkali metals; alkaline earth metals; aluminium; bimetals; cadmium; gallium; indium; lattice dynamics of metallic crystals; lead; mercury (metal); metallic thin films; rare earth metals; thallium; thermoelectric effects in metals and alloys; tin; transition metals; zinc
abrasive finishing with refractory carbide micropowders surface struct. 80−11842
abrasive wear and impact and arc erosion, exam. of comparative tendencies of metal loss 79−15811
abrasive wear resistance, effects of microstruct. 78−92367
abrasive wear resistance rel. to physicomechanical props. 79−91804
abrasive wear testing under conditions of rolling friction 79−15894
abrasive wear theory based on shear effects 80−89363
absorption of H_2, determ. by mag. sound technique *(Russian)* 77−60009
AC anodic dissolution rate, effect of H^+ evolution *(Russian)* 80−16693
acoustic attentuation in collision regime, variational principle 79−82648
acoustic nuclear magnetic resonance, absorption and dispersion 77−36143
acoustic signal shape produced by high density electron fluxes 80−108674
acoustic wave attenuation, low-freq. longit. waves, viscous and induction mechanisms 77−8152
acoustoelectric current for conductivity electron arbitrary dispersion law *(Russian)* 80−49829
acoustoelectric effects, anisotropy *(Russian)* 78−91732
adatom pair, on metal surface, effective interaction, from FIM expts. 78−22953
adhesion, fundamental nature 79−52616
adhesion between two arbitrary metals, theory *(Russian)* 77−44455
adhesion experiment for Spacelab 78−88621
adhesion of two metals with lattices of different types, theory, incl. dislocations *(Russian)* 78−7165
adhesion theory for two surfaces 80−20270
adhesion to polymer, temp.-depend. determ., rapid method 77−51610
adhesive bonds with polymers, shear resist., polymer crystn. effect 80−89462
adiabatic shear in metals, explanation 77−14924
adsorbate vibrational excitation by inelastic electron scatt. 77−43428
adsorption, metal atoms on metallic substrate, enthalpy calc. 80−100406
adsorption mechanisms for H_2 79−69368
adsorption of atoms on metals, Green's function formalism for studying electronic struct., local density of states calc. 80−107884
adsorption of gases, review *(Japanese)* 79−46930
adsorption of gases 77−85078
adsorption of H_2, interaction between gas atoms on approach to surface 78−14609
adsorption of S, thermodynamics of two-dimen. and three-dimen. sulphides 80−20036
adsorption potential of He, HF calc. of repulsive contrib. 77−43434
adsorption systems, relationship between work function and degree of adsorption coverage 79−83092
AES anal. in adhesion, friction and wear 78−53179
air pollution control, activation analysis for 14 volatile heavy metals as constituents of aerosol particles 80−16891
alkali metals, electron-electron scatt., thermal and elec. resistivity 80−59956
allotropic transform., anharmonicity, effects due to thermal expansion and Gruneisen parameters 79−52207
ammonia-metal soln., ionis. equilib. instability of weakly-ionised 3-component plasma 80−10877
amorphous, electronic and vibr. props. 78−10151
amorphous, ferromagnetic, effective-field distributions and resistivity minima 79−73501
amorphous, icosahedral microclusters as possible structural unit 78−34439
amorphous, struct., simple computer modelling 79−19154
amorphous, struct. model and SRO characts. *(Japanese)* 77−84654
amorphous, superconducting properties rel. to ordering 80−65735
amorphous and liquid, harmonic approx. model 77−47331
analysis, quantitative, spectral appl. of microdensitometry *(Czech)* 79−30524
analysis of H ratios and profiling using nucl. techniques and Rutherford backscatt. 80−61202
Anderson model, local moments and localised states *(Czech)* 80−2353
anelastic study of intrinsic point defects, irradiation effects 78−47323
anharmonic parameter, $\gamma\beta T$, interpretation *(French)* 80−34160
anisotropic, continuum description of anomalous yielding 79−11677
anisotropic, description of history dependent plastic flow behaviour 80−11732
anisotropic, electrical resistivity meas. by eddy current method 77−67466
anisotropic, inelastic deformation, generalised strain rate dependent constitutive eqn., load relaxation tests 79−11655
anisotropic metals in perpendicular mag. field, surface impedance behaviour *(Russian)* 78−39145
anisotropic normal, linearised Boltzmann eqn. solved, magnetoconductivity calc. 79−1595
anisotropic normal metal, thermopower calc. 80−24879
annealing, struct. and grain boundary mobility 79−47728
annealing embrittlement, AES study *(Chinese)* 79−38982
annealing temp. for radiation damage field, correlation to melting point in DPAD expts. 78−43737
anodic activation of passive metals, theory 80−25918

metals continued
anodic dissolution, ionic mass exchange effects on hydrodynamic conditions 78−3349
anomalous crystal-field splitting of rare earth metal S-state 79−19563
antiferromagnetic, electron scatt. features, s-d exchange model 77−8085
antiferromagnetic, nesting type model, spin fluctuations 78−56329
antiwear action of Zn di-n-butyl phosphate 80−11782
Arrhenius plot of diffusion, curvature, disappearance under press. with single-vacancy model 79−10975
atomic absorption spectrometric analysis, of laser-vaporised solid samples 78−7252
atomic defect config. from X-ray and neutron scattering studies 78−47322
atomic defect configuration from high resolution TEM 78−47324
atomic defect props., conf., Argonne, IL, USA, (Oct. 1976) 78−47318
atomic displacements near impurities and many-particle interactions *(Russian)* 80−24553
atomic electron collision cross sections 77−42410
atomic heat capacity change during polymorphic transformations 79−29055
atomic interaction force characts., association with struct., mech. props. 80−49172
atomic mobility under pulsed loading conditions *(Russian)* 80−96684
atoms sputtered by light and heavy particles, velocity distrib. meas. by fluorescences spectroscopy 78−95626
Auger kinetic and relax. energies in atoms and solids 78−15297
axisymmetric drawing simulation, numerical method development 78−30206
Bauschinger effect, in metals, review 80−21025
Bauschinger effect and mutual restriction between grains 78−52895
BCC, coherent twin boundaries and interatomic pots. 78−51558
BCC, computer simulation of stacking faults 78−30653
BCC, computer simulation of twin boundary and twinning dislocation struct. 78−30644
BCC, cryst. lattice change during deform., influence of boundary dislocations with different Burgers vectors *(Russian)* 77−21219
BCC, D dynamic quadrupole nuclear spin relax., α or α' phases 77−48085
BCC, deform. 77−4815
BCC, deforming by {110} ⟨111⟩ and {112} ⟨111⟩ slip, lattice rotation calc. in axisymmetric flow *(Japanese)* 77−21225
BCC, diffusion of H_2 and its isotopes, phonon-assisted quantum-mechanical tunnelling of interstitials 80−59730
BCC, diffusion of heavy interstitial atoms 79−90829
BCC, dipole interactions and trapping effects of positive muons 78−47342
BCC, discrete-continuum hybrid method for dislocation-point defect interaction 77−89467
BCC, dislocation (100) stability, field stress effects *(Russian)* 80−10558
BCC, dislocation cores of screw and 71° dislocations, kinks and constrictions *(German)* 77−24316
BCC, dislocation processes, straining expts., electron microscope obs. 80−29025
BCC, dislocations, anisotropic elasticity theory *(Japanese)* 79−10853
BCC, effect of screw dislocations on mech. props. *(Russian)* 78−60704
BCC, effective valence, from phonon data, rel. to vacancy formation energies 80−79781
BCC, fine particles formed by gas-evap. technique, cryst. struct. and habit 79−27935
BCC, geometry of slip systems *(Hungarian)* 77−47463
BCC, glide and work hardening, review *(German)* 79−29089
BCC, glide and work hardening, review *(German)* 79−34067
BCC, grain boundary struct., and segregated impurity sites, computer simulation 79−73173
BCC, HF mech. relax. peak 78−91379
BCC, high temp. positron annihilation 78−47421
BCC, influence of screw dislocations on cryst. lattice rotations during deform. *(Russian)* 78−6966
BCC, intracrystalline fracture *(Russian)* 79−5031
BCC, lattice vibrs., axially symm. and ang. force models 78−26637
BCC, migration of vacancies near twin boundaries 78−51535
b.c.c., modified Cheveau model for lattice waves, phonon dispersion and Gruneisen parameter 77−1189
BCC, multi-layer faults on (112) planes and interatomic pots. 78−51563
BCC, neutron irradiated, spontaneous recomb. volumes of Frenkel defects, rel. to compressibility 78−71765
BCC, plastic deform., review 80−104213
BCC, plastically deformed, electron microscopy *(French)* 77−44299
BCC, polycrystalline aggregate, prediction of plastic props., deformation by ⟨111⟩ pencil glide 80−11731
BCC, predicted rolled textures, influence of slip system and deform. model *(French)* 79−43309
BCC, quantum diffusion model of light interstitial atoms 80−2212
BCC, relation between elastic energies of dislocations and choice of slip system *(Japanese)* 78−18656
BCC, rolling texture, effect of critical shear stress ratio of {112} and {110} 79−91673
BCC, screw and 71° dislocations, energies of kinks and constrictions *(German)* 77−19950
b.c.c., sessile-glissile transforms. of screw dislocation under stress 77−1126
BCC, small-polaronic diffusion of light interstitials 79−42315
BCC, solid solution hardening, crystal resolved shear stress depend. on dislocations 80−40373
BCC, solution hardening and softening 77−12635
BCC, sputtering processes, due to Ar^+ bombardment, computer modelling 79−19957
BCC, stacking fault and twin boundary energies 77−76420
BCC, strain depend. elastic dipole tensor for interstitial impurities, non-linear Snoek effect 79−8311
BCC, struct. of tilt grain boundaries 80−84184
BCC, struct. of twinning dislocations, computer simulation 78−2140
BCC, tensor of deform. of cryst. lattices by impurity atoms *(Russian)* 77−7711
BCC, twin boundary and stacking fault structs., computer simulation 80−59485
BCC, under elastic stress, Snoek peak height determ. 80−65153
BCC, vacancy-edge dislocation interactions, computer simulation 78−83845

metals continued
BCC, viscous-brittle transition during fracture, dislocation model 77−62582
BCC and FCC, dislocation dynamics method appl. to plastic flow 79−47745
BCC crystals, surface indentation pyramids, kinetics of shape changes 77−43417
BCC lattice, crit. embrittlement temp., struct. parameters effect *(Russian)* 80−66618
BCC metal crystallite, mechanisms of growth of vacancy complexes 78−14338
BCC metals, plastic deform., computer simulation 80−40456
BCC metals and alloys, review of plastic deformation and work hardening *(German)* 78−84946
BCC single crystals, plastic deformation localisation 80−54303
BCT, electron-ion interactions 80−10527
bending spring effects of stress, temp., thermal and mech. treatment on non-elasticity *(German)* 77−77531
bending springs at small mech. stress, non-elastic props. *(German)* 77−77532
bending test device for thin spring strip 80−61052
bicrystals, residual resistance theory, diffusivity, disorientation effects *(Russian)* 80−49875
bimetallic interface energies 78−2545
binding energy spectrum approach to grain boundary segregation 78−15409
biometallic interfaces, dynamic response of electrons and dispersion force fields 78−47845
blister formation due to the ion irrad. 80−65072
Bloch-Gruneisen formula validity for elec. resistivity, temp. depend 77−31991
Bloch-Simon struct. index, chem. bond geometry interpretation 77−35508
bond energy calcs. for metal-H system 78−51940
bond energy rel. to thermal expansion coeff. *(Chinese)* 79−14946
brittle, ductility improvement by plating *(German)* 77−8954
brittle and plastic, energetic strength theories *(Bulgarian)* 80−38296
brittle fracture, low temp. statistical strength criterion 77−73318
brittle intercrystalline fracture, impurities effect 80−100915
bulk deformation processes 78−31459
Cambay drinking water, metal contents 79−20899
carbonmetalplastic, heating rate effect on thermal deform. in various atmos. 79−65226
carburising, process parameters and gas conditions 79−96208
carburising, surface-gaseous medium interaction laws 80−76411
carburising in fluidised bed of C-graphite materials 79−20276
cast, nonmetallic inclusions, size frequency distrib. determ. 78−39989
cast, oxide particle dispersion, new method of introduction 77−73283
catalysts for C graphitisation 80−3401
cathodic protection using lightning conductors connected with diodes 79−52418
cavitation erosion 78−48538
cavitation erosion resist., increase by case hardening, possible mechanism 80−11845
cavity growth in irrad. sample under stress 79−73211
ceramic to metal joint, problems of characterizing the adherence 79−43552
ceramic-metal seal technology, history and trends 78−81992
ceramic/metal layer adhesion mechanism for metallization of electronic ceramics, elec. props. *(German)* 80−76381
CESR, cond. electron spin scatt. due to dislocations 80−75856
CESR, mm waves, surface effects 80−66036
CESR and inhomogeneous broadening due to local moments 79−99769
CESR line shape, strong surface relax. case *(Russian)* 78−56378
charge density perturbation around impurities 78−39058
chemicothermal treatment, mathematical modelling 80−100955
chemicothermal treatment, process kinetics 80−35415
chemiluminescent oxidation using laser vaporisation, kinetics 79−100385
chemisorbed atom investig. by angle resolved Auger surface spectroscopy 77−28694
chemisorbed gases on surfaces, replacement phenomena, review *(Japanese)* 77−72779
chemisorption, atom-jellium model 78−84066
chemisorption, intra-adsorbate Coulomb correl. and surface struct. roles 78−71979
chemisorption, intra-adsorbate Coulomb correl. and surface struct. roles 78−71980
chemisorption, intra-adsorbate Coulomb correl. surface structure 77−15685
chemisorption, review 79−42377
chemisorption at metal surface 77−11978
chemisorption energetics, book contrib. 80−24140
chemisorption exam., appl. of field emission techniques 78−35255
chemisorption of CO, electronic struct., vibr. spectra, and chem. 79−42390
chemisorption of diatomic mol., competition between adsorbate-substrate bond and mol. bond *(French)* 77−35810
chemisorption of gases, book 79−69370
chemisorption of metallic atoms, work function variations 79−46936
chemostress effect in ionic crysts. and metals 79−28193
clad fibre reinforced composites, debonding risk 80−3132
clean polycrystalline metal surfaces, ion-induced electron emission, review 80−35032
clean surface, H release rate 78−95187
cleaning surface to micron level cleanliness 78−72921
cleavage plane prediction, Ayres-Stein method 79−29214
cleavage plane prediction, Ayres-Stein method 79−29213
close-packed, temp. depend. of stacking, fault energy 79−19266
closed-orbit, uncompensated, elec. and thermal magnetoresist., quadratic field depend. 79−95388
coal gasification, demands made on materials used in process *(German)* 80−45438
coated, heat resistance assessment at varying temps. *(Russian)* 77−25189
coated, IR surface wave interferometry 80−63913
coated abrasive belt grinding, relation between wear of grain cutting edge and material removal 80−16507
coating, hot dip, on strip, analytical description of jet finishing 77−28935
coating, prep. by plasma arc spraying and characterisation 79−23873
coating with H-transparent Pd layers, spot welding technique 79−47816

metals continued
coatings, corrosion testing standardisation 78−11454
coatings, electric field atomisation from melt 80−76174
coatings for corrosion control, book 77−44413
cohesion and Cauchy discrepancy 80−54170
cold rolling, friction and slip 78−64707
cold worked, grain size depend. of dislocation density 79−7614
collective modes of void-surface coupled systems, surface plasmons 80−49642
combustion, laser initiated, time resolved spectroscopy 78−7207
combustion under CW CO_2 laser radiation action 80−30241
compensated, Gantmakher-Kaner effect in strong mag. fields 78−91595
compensated, transport of spatially inhomogeneous current under mag. fields, pot. and current distribs. 79−87081
compensated, transport of spatially inhomogeneous current under mag. fields, dynamical props. 79−87082
compensated and uncompensated effect of spherical voids on electrical magnetoresistivity 80−65531
complex, RF size effect, mean free path depend. of reson. strength 79−56202
composite shell, three-layer, stochastic formulation of optimisation using heuristic methods 80−38268
composite spherical pressure vessels with hardening metal liners 80−7655
composite with metal matrix, state of the art review, book 78−72706
compressibility in presence of anharmonic interaction *(Russian)* 78−23763
concentrations of metals in very small volumes of soil solution 79−34824
conduction band width calcs. 80−103619
conduction current and generalised Einstein rels., from Boltzmann transport eqn. 77−15810
conduction electron coupling with moments of 3d and 4f ions 78−60090
conduction electron focusing by nonuniform mag. field *(Russian)* 79−99533
conduction electron response, memory function 78−56096
conduction electron-magnetic ion Coulomb interactions, unitary transform., spin angular momentum operators 80−84451
conductivity, plasma model 80−80311
conference, condensed matter physics, Sarajevo, Yugoslavia (Oct. 1976) 77−51629
constitutive equations of continuum creep damage mechanics 78−67054
constitutive model at high strain-rate, shear modulus, yield strength 80−75292
contact, strain in microrelief ridge 77−44443
contact melting process kinetics, investigation method 80−39259
contamination of marine sediments, trace metals from wastewater 79−83643
corrosion, colloid chem. appls. 80−89541
corrosion, localized, apparatus for exam. 79−91863
corrosion, metallurgical viewpoint *(Japanese)* 78−39947
corrosion, use of XPS 78−15586
corrosion anal. using ion beam and nucl. techniques 79−52448
corrosion and passivation, ion selectivity effects 80−35377
corrosion conditions simulation in crack-like defects using electrochemical cell *(Russian)* 79−52445
corrosion fatigue, electrochemical aspects 79−79167
corrosion fatigue, role of mechanics 79−79168
corrosion in electrolytes, pit growth 80−21186
corrosion in ionising solvents, review 77−8973
corrosion in marine atm., potentiometric technique, appls. 79−24693
corrosion meas. specifications and quality assurance 77−12764
corrosion pit initiation and growth, salt film form. 80−16563
corrosion protection with plastics 79−96211
corrosion rate determ. by Faradaic rectification of metal/metal ion systems 78−80666
corrosion rate in soln., appl. of coulostatic method for rapid evaluation 79−20310
corrosion rate in soln., new rapid electrochem. eval. method 79−1931
corrosion stability under stress, test apparatus 79−70248
corrosion testing in boiling $MgCl_2$ 78−39962
corrosion testing under stress, unit for producing biaxial tensile stresses 79−57174
corrosion theory, rel. to protective coatings 78−19918
coulostatic deposition at underpot., pot. relax., chem. effects 78−48335
coulostatic deposition at underpot., pot. relax. 78−48334
crack depth meas. by potential probe method, principle *(German)* 77−86234
crack detection, holographic interferometry, double impulse method 77−9033
crack propag. mech. and fracture toughness, microstruct. effects 78−19859
crack propagation, model rel. to appl. of stress wave emission anal. 77−63837
crack resistance, aggressive environment influence *(Russian)* 79−52434
crack resistance, high-temp., during creep due to stress relaxation *(Russian)* 79−52348
crack resistance determination, cyclic loading, methodological instructions 80−108660
cracked, J-integral estimation 77−1876
crater deepening under action of laser emission *(Russian)* 77−20962
crater form. at tip of crack, under powerful local electromagnetic field *(Russian)* 77−70149
creep, high temp., influence of dislocation splitting width *(Russian)* 79−5004
creep, high temp. steady state, activation energy determ. *(Russian)* 77−50920
creep, point defects 78−48462
creep, power law representations, deviations at high strain rates 77−48504
creep anal. using boundary integral eqn. method 79−46231
creep and stress relaxation curves, phenomenological description 79−100231
creep characteristics, multi-axial 80−64398
creep conditions at high temp. 77−77550
creep damage and cavity growth, assessment using density meas. 80−104217
creep deterioration effect on structural performance, at elevated temps. 77−3787
creep limit and long-term strength, parametric eval. method 80−100996
creep loading, engineering approach for cumulative damage 80−58935

metals continued
creep movement of dislocations, effect of stress distrib. of grain boundaries *(Russian)* 78−27564
creep of metals and plastics under combined stresses. A review 80−59567
creep prediction using analytical tabular method *(Ukrainian)* 78−68725
creep state, small-angle boundary migration 77−39624
creep theory, nonlinear integral eqn., existence and approx. solns. 78−13931
creep-electron emission relation 78−6994
critical temperatures determination, elec. resist. method, IMASh-5S-69 installation 80−71827
crystal equilib. and Cauchy deficiency 79−19328
crystal growth, electrochem. Czochralski method, growth rate limitations 78−88433
crystallisation, apparatus for decanting solid and liquid phases 78−56597
crystallisation process, X-ray fluoroscopic obs. 80−50620
crystallites, characterisation by selected-zone and weak-beam dark field TEM 80−79654
crystallites, orientation and shape determ. by TEM 80−1907
crystallites, polyhedral, growth in inactive gas, review 79−27934
crystallites of supported catalysts, size distrib. from wide-angle X-ray meas. *(German)* 77−84566
crystallographic orientations distribution function, computer calc. for cubic metals 80−64827
cubic, Debye temp., elastic consts. averaging 80−54332
cubic, HCP, non-central, non-isotropic interactions, third-order elastic const. determ. 79−10474
cubic, heavily rolled, shear band occurrence 79−34058
cubic, ionic interaction in dynamical matrices 79−77693
cubic, lattice dynamics, central pair pot. vs. axially symm. pot. 78−87747
cubic, noncentral force model for lattice dynamics 79−69209
cubic, plastic strain ratio, strain effects 77−16651
cubic, press.-vol. relations calc., pseudopotential method 77−11662
cubic, relation between surface energy and Debye temp. 78−10271
cubic, relationship between defect resist. and bulk resist. at melting temp. 78−6344
cubic, vol. and temp. of phonon frequencies 77−15514
cubic lattice, inverse pole figures, calc. method on digital computer 80−20950
cubic structure, numerical simulation of cross-rolling textures *(French)* 79−20061
current pulse effects on structure at crack tip *(Russian)* 77−44332
cutting, appl. of Taylor eqn. for different cutting speeds *(German)* 78−72915
cutting, chip forming mechanisms, deform. diagrams 77−28854
cutting, with slowly varying system parameters, self vibrs. *(Ukrainian)* 77−68477
cutting rel. to plasticity theory 80−16610
cyclic and damage constitutive laws, calculation methods *(French)* 79−43408
cyclotron resonance, attenuation length 77−90038
cyclotron resonance depend. on surface, anomalous skin effect *(Russian)* 80−75860
cyclotron resonance in weak mag. fields surface impedance, current density asymptotic *(Russian)* 80−2641
cyclotron wave dispersion and obs. of many body effects 77−28097
cyclotron wave excitation, diffuse boundary scatt. *(Russian)* 80−54729
cylindrical magnetron sputtering sources, substrate heating 79−24435
damage by intense EM radiation, kinetic mechanism 77−20167
damageability determ. by meas. of elastic, inelastic, internal friction charact. 79−66133
damping capacity rel. to struct. defects *(Russian)* 77−44283
de Haas-van Alphen effect 79−99473
Debye charact. temp. and fusion transitions 78−63864
Debye temperature, determ. from elec. resist. meas. *(French)* 77−4322
defect annealing study by positron annihilation, and elec. resistivity meas. 78−51584
defects in structure of lattice 78−88617
deformability, quantitiative determ. in drawing 79−52229
deformation, elastic-plastic model *(Russian)* 77−48484
deformation, time-depend., continuum props. of constitutive relationships 77−35053
deformation broaching of difficult-to-form metals 80−108473
deformation heat during forming, eqn. *(German)* 79−66105
deformation in quantizing mag. field, dislocation loop formation *(Russian)* 80−103354
deformation process, stage-by-stage nature investigation using acoustic emission *(Russian)* 80−40434
deformation resistance, depend. on hot press. working speed *(Russian)* 80−65126
deformation resistance, rel. between uniaxial stress state and breaking stresses in shear 80−3147
deformation resistance determination, plastometer 78−7121
deformation strengthening and anisotropy prediction *(Russian)* 78−27533
deformation structure during cutting, investigation by TEM *(Japanese)* 80−70086
deformed, degree of deform. effect on thermophys. props. at high temps. 78−26694
deformed, dispersion-hardening, theory of strength *(Russian)* 78−35424
deformed, microcrack effect on elec. resist. temp. depend. 77−51726
deformed in pressing process, temp. field modelling *(Russian)* 80−53602
deformed struct. role in recrystallisation nucleation, review 79−34060
density measurement, using X-ray total external reflect. and double crystal spectrometer 80−64831
density measurements 0-2000°C automatic device using γ-ray transmission 79−87787
density of states and spin susceptibility, normal and giant surface effects 78−10322
deposition condition relationship with struct. and props. 78−11369
designing from abundant resources for more efficient utilisation 77−9035
destructive materials testing anal. by nondestructive electromagnetic methods *(German)* 77−86267
DHCP, second and third order elastic consts. 79−51189
diamagnetic, crit. point of diamag. transition of first kind, and DMR linewidth 77−59469
diamagnetic domains, helicon attenuation *(Russian)* 78−10721

metals continued
diamagnetic susceptibility, determ. from average internal pot. 77−28367
diamond grain configuration in high temp. creep and fatigue 77−21221
dielectric function, inverse RPA calcs. at metal-vacuum interface 78−14789
diffusion, coeff. determ. in system of one-dimens. eqns. 77−28035
diffusion, correlation with entropy of fusion 78−43109
diffusion, meas. of conc. profile by changes in polarisation current density 77−89584
diffusion, radiation effects 78−47555
diffusion bonding 77−62687
diffusion coefficient of H in metal with low adsorption activity, steady-state flow method 80−10795
diffusion coefficients of H, appl. of H and He quenching methods *(Japanese)* 80−7604
diffusion constants, melting pt. diffusivity activation energy and volume correls. 80−96679
diffusion controlled stress rupture 77−32681
diffusion in presence of high diffusivity paths, random walk model 80−24640
diffusion layers, effect of chemicothermal treatment on struct., surface energy, and bulk props. 79−96207
diffusion of H_2, neutron radiography meas. 77−24438
diffusion of H_2, neutron scatt. studies 79−42316
diffusion of H_2 at low temps. 79−55941
diffusion of H, complex jump diffusion model rel. to quasi-elastic neutron scatt. by H 80−24638
diffusion of H, correlated jump diffusion model, nonlinear eqns. 79−82386
diffusion of H, neutron spectra, book contrib. 77−89573
diffusion of H, random walk model with correlated jumps 80−24639
diffusion of H, theory, book contrib. 79−82389
diffusion of H(D), slow neutron scatt. obs., review 80−34248
diffusion of H isotopes, nonclassical processes 78−47591
diffusion of H isotopes, self-capture effect and activation energy *(Russian)* 78−75879
diffusion of interstitial atoms through crystal lattice interstices *(Russian)* 77−24425
diffusion of interstitial solute 77−62672
diffusion of O, new EMF method 77−84994
diffusion of protons 79−55933
diffusion rate in Al melts, meas. apparatus 79−86913
diffusion thermodynamics, kinetics and mechanism 78−95179
diffusion welding, migration of oriented intergranular boundary with pores *(Russian)* 80−84943
diffusional relaxation of stress conc. at second phase particles 79−1889
dilatation centres and grain boundaries, induced elastic interaction *(Russian)* 80−84205
dilatometric method for study of dimensional anomalies in metallic materials rel. to crystal struct. *(French)* 79−52563
dilatometric methods *(French)* 79−5100
Dingle temp. plot calc., dislocations perpendicular to orbit 77−59248
dislocation annihilation during tensile and cyclic deform. and limits of dislocation densities 80−34007
dislocation cell diameter rel. to free energy during creep 79−91756
dislocation density, positron annihilation method 77−85834
dislocation dynamics study by current noise measurements 79−14813
dislocation electrical resistivity and reson. scatt. 77−43550
dislocation kinetics of superplasticity and creep 77−76404
dislocation models of plastic deformation at elevated temps. 77−70139
dislocation motion depend. on electrons *(Russian)* 79−65260
dislocation movement, in volume dispersion of obstacles, stochastic model, low temp. anomalies rel. to yield stress 79−60367
dislocation multiplication, deformation conditions and initial defect struct. effects 78−30614
dislocation scatt. and de Haas-van Alphen amplitudes 78−63967
dislocation scattering of electrons, Fermi's 'golden rule' 77−62884
dislocation struct., X-ray diffr. exam. by vibrating crystal method *(Russian)* 78−34519
dislocation-core movement and frictional stress 80−92529
dislocation-impurity interactions, electrical and elastic interactions *(Russian)* 78−22758
dislocations, research at Birmingham, (1945-55) 80−62444
dislocations and shock compression, thermodynamics 80−100235
dislocations in metals, residual elec. resist., one-electron approx. *(German)* 80−39568
disordered, conductivity electrons and elastic scatt. by static inhomogeneities *(Russian)* 80−29375
disordered surface, multiple scatt. of cond. electrons 80−10959
dissolution of interstitial H_2 and D_2, diffusion coeffs., reverse isotope effect *(Russian)* 80−88368
dissolved species in cracks, linear differential eqn. problem 79−51316
Doppler broadening of positron annihilation line 79−43057
Doppler-shifted cyclotron reson., excitation of dopplerons and Gantmakher-Kaner waves *(Russian)* 77−32261
Drucker postulate verification at high temp. 80−30025
ductile, hard inclusion effect on plastic strain distrib., model meas. 77−59062
ductile, jet-impingement solid-particle erosion testing, halo effect 80−76376
ductile, spall damage accumulation theory 77−70153
ductile fracture, crack initiation at dislocation cell boundaries 77−66692
ductile fracture, void growth stress/strain relations *(French)* 80−19280
ductile fracture criterion 78−60817
ductile fracture mechanism, theoretical and expt. investigation *(German)* 77−70142
ductile fracture surfaces, statistical charcts. of microcracks *(Russian)* 78−23807
ductile metals, spontaneous void growth in elastic and elastic/plastic media 80−48567
ductile metals, velocity depend. of erosion by solid particles, at low incidence angles 78−87311
ductile-brittle transition temperature evaluation, as function of thickness 80−3261
ductility meas. technique at high strain rates 78−80694
ductility tester for films 77−63864
dynamic compression testing, mech. behaviour 80−40464
dynamic elastic moduli of finite temps. *(Russian)* 79−14873
dynamic hardness testing of metallic materials 80−21241
dynamic stability of dislocation sub-boundaries during straining, computer simulation 78−30635

metals continued
dynamic study of defect mobility using HVEM 78−47327
edge dislocation screening in metals and superconductors, metal softening *(Russian)* 80−64997
elastic constants, resonance method for determ. within 80-300K temp. range 78−46918
elastic constants and moduli of axial textures 80−75286
elastic constants determ. by resonant vibr. in thin disk, apparatus 77−56182
elastic constants of cubic metals, vol. depend. contrib., pseudo-pot. theory 77−72646
elastic moduli vol. depend., Born-Durand melting hypothesis 79−60420
elastic precursor wave model in shock loading, polycrystalline sample 78−1601
elastic-plastic vector props. at normal and low temps. 80−16406
elastically strained, elec. field gradients on nuclei, calc. *(Russian)* 78−60096
electric domains at low temp. 79−65368
electric field gradient at nucleus, antishielding theory 77−4316
electric field gradients in closed packed metals, vol. and struct. depend. 78−51947
electric resistance, temp. depend., qualitative anal. by audible demonstration 80−46775
electric-arc metal vaporizer with cathode spot magnetic confinement 77−77383
electrical and thermal resistance, influence of static atomic displacements 80−103674
electrical conductivity, Bloch theory agreement and limitations 79−28332
electrical conductivity, contactless measurement method, cylindrical sample motion in solenoid field *(Russian)* 79−214
electrical conductivity, high pressure effects 80−92879
electrical domains at low temps. *(Russian)* 78−91687
electrical pulsed discharge action under air environment *(Russian)* 77−43091
electrical resistance, exam. at high temp. using inductive heating 79−7816
electrical resistance at high temperature, $T^{3/2}$ depend. 77−43561
electrical resistance meas. at increased temp. under stress. 77−56147
electrical resistance variations due to defects, one and two interstitial model 80−88143
electrical resistivity, comparison between first principles form factor and empirical form factor 78−2463
electrical resistivity, temperature-depend., continuous contactless meas. method 78−21171
electrical resistivity changes during polymorphic transform. A1 to A2 and A3 to A2 77−48430
electrical resistivity of dislocations 77−69310
electrical transport measurements, kinetic effects at high anisotropic strains 78−54384
electrically conducting spherical specimens, electromagnetic control 78−53138
electrochemical nucleation, potentiostatic obs. 79−15038
electrochemical reaction on surface in aq. soln. 79−83387
electrochemical surface treatment, method for reducing H_2 absorption *(Russian)* 79−15858
electrodeposited from molten salts, faceting rel. to texture axis direction 79−28969
electrodeposition, chemical factors 80−16207
electrodeposition, ion mass transfer migration effect 79−61523
electrodeposition, using fluidised bed electrodes, math. model 79−100062
electrodeposition fundamentals 77−36413
electrodeposition protrusion growth and inhibitor action model and meas. 79−96314
electrolytic growth of dendrites, CCTV obs. 78−51863
electrolytic polishing, solution of problems rel. to current distrib. in narrow electrode space 79−91855
electrolytic polishing and etching to reveal the structures of high melting point metals *(German, English)* 80−89417
electromechanical forces, theory *(Russian)* 77−81063
electromigration, generalized theory 77−24423
electron absorpt. and transmission characts., 5 to 30 keV, film-massive block method 78−88387
electron anisotropic scatt. by dislocations, kinetic eqn. *(Russian)* 77−47802
electron bottleneck effect, impurity spin relax. and EPR linewidth 79−28589
electron drag od dislocations 80−10961
electron energy loss spectra, threshold potentials and X-ray absorption, band struct. determ. *(Russian)* 78−39009
electron energy spectra, of Ar ion or electron irrad. metals *(Russian)* 77−8706
electron field emission, energy distrib. 77−1788
electron field emission *(Polish)* 80−35063
electron impact, material removal by high power beam 77−81187
electron irradiated, elastic point defect-dislocation interactions, defect dragging model extension 80−65050
electron irradiated, selfinterstitial atomic defect interaction radii, recovery expts. and error sources 80−65049
electron irradiated, threshold energy for atomic displacement, bulk modulus and interatomic pot. 78−38754
electron mediated nucl. spin-phonon interaction 77−1604
electron momentum density, positron annihilation meas., book contrib. 79−99976
electron penetration and energy transfer in solid metal targets, film bulk method 78−2963
electron reflection from metal surfaces, surface roughness, IR absorpt. 80−71526
electron scattering, inelastic, plasma oscillations effect 80−100439
electron specific heat and effective mass, temp. depend. *(Russian)* 78−59958
electron spectroscopy of crystals, book 80−36786
electron state effect on mech. props. and electroplasticity 78−14725
electron transport properties 79−19565
electron-deformation interaction, lattice contraction, Hubbard model calcs. *(Russian)* 80−59592
electron-dislocation scatt. anisotropy effect on electron-electron scatt. contrib. to elec. resist. 80−29398
electron-electron scatt. 79−38045
electron-phonon and electron-impurity collision frequencies, Fermi surface, RF size effect method 77−20227
metals continued
electron-phonon drag and interaction of first and second sound 77−66009
electron-phonon interaction and lattice thermal conductivity 79−42189
electron-phonon interaction effects on spin susceptibility 80−93108
electronegativity scale 79−73129
electronic characts. from thermomodulation spectra 79−87421
electronic structure, optical absorption 79−38566
electronic structure, positron annihilation studies *(Japanese)* 78−18951
electronic surface reson. band struct. and lineshapes 79−82655
electronic transport eqns., optical cond., number conserving relaxation time approx. calcs. 80−49681
electronic work function under tension, 20 to 1200°C 80−76448
electroplastic deform. *(Russian)* 77−86108
electroplastic deform. 78−3200
electroplastic effect 79−24589
electroplating, for engineering components and structures 78−35587
electropolishing, holographic interferometry obs. of metal removal rate 77−8985
electroreflectance, electromodulation spectroscopy, developments, mechs. 77−66475
electroreflectance by deep field penetration 79−19864
electrothinning, laser-monitored, for preparing ultrathin metal foils 78−53074
electrowinning, energy consumption reduction via anodic coal reaction 79−91965
Elliott relation in pure metals 79−19780
EM acoustic reson. for elastic moduli meas. 80−15573
EM excitations in strong mag. fields, review 77−8130
EM generated ultrasound, position-depend. amplitude 79−37763
EM generation of ultrasound, theory 80−103727
EM levitation for melting without crucible *(Polish)* 80−89130
EM sound generation in cyclotron reson. regime *(Russian)* 77−69381
EM waves near cyclotron reson. in inclined mag. field *(Russian)* 80−29625
EM-acoustic oscills. during EM field emission by inductive convertor, nonferromag. polycryst. *(Russian)* 77−11638
embrittlement of He-containing metals, high temp. embrittlement model 79−83320
EMF appearance due to mag. field and laser pulse irrad. 77−76797
EMF production by shock compression 77−31719
emission spectrochemical analysis using glow discharge, Grimm lamp struct. and discharge characts. *(Japanese)* 78−27867
emissivity angular dependence, meas. in IR spectral region 80−34214
emissivity determination, using low-inertia opt. dilatometry 80−59684
emissivity measurement of small specimens at high temp., structural materials appl. 79−7281
energy gap determ. by optical methods *(Russian)* 78−30867
engineering materials, nature and props., book 78−72707
enthalpy and average mass temp. on plasma-arc melting *(Russian)* 80−54405
entropies and heats of fusion 80−103458
entropy and lattice parameter relation 77−36464
entropy of fusion and allotropic behaviour, exam. of correlation and modification of Richard's rule 78−71838
entropy/free energy relation 78−15368
epoxy-metal joints, environmental fracture and effects of shrinkage stresses 80−16635
epoxy/metal joint under combined stress, expt. study of strength 79−74339
equation of state, isentropic expansion method 78−91414
equation of state Gruneisen formulation 78−30733
equations of state based on free energy expressions, isothermal compression moduli *(Russian)* 79−90753
equilibrium vacancy conc. 78−38694
erosion accompanying simultaneous action of laser emission and ultrasound *(Russian)* 80−7442
erosion by high speed particles, temp. effects 80−40556
erosion damage, temp. effects 79−34156
erosion resistance, eval. of role of mech. props. 79−83328
erosive wear by impinging SiC particles, surface hardness and material props. effect 77−66705
evaporation, by laser pulse, numerical anal. *(Russian)* 77−40312
evaporation rate determ. by tip profile change meas. 77−24403
evaporation under laser irradiation *(German)* 78−52599
exchange interaction, hybrid, of localised moments 77−28381
exoelectron emission defectoscopy, metal fatigue strength prediction 78−76807
exoelectron emission from surface during fatigue damage 78−44217
exotic atoms, conf., Erice, Sicily, (1979) 80−67939
expansion, isentropic, vaporisation and condensation kinetics anal. 77−66623
extraction kinetics, from dee-sea Mn modules, pore diffusion with chemical reaction 77−28985
extraction kinetics, from deep-sea Mn nodules, pore diffusion controlling case 77−28984
facings, rubber-metal, vulcanisation degree determ., γ-ray method 80−61043
failures analysis, structural for industrial appl. 80−76429
far IR absorptivity, meas. via multireflection cell 77−18075
fatigue, crack initiation and propagation studies *(German)* 77−77587
fatigue, stochastic model under repeated stress or strain 77−56107
fatigue *(Japanese)* 77−8929
fatigue analysis, inversion of strain-life, and strain-stress relationships 80−16428
fatigue analysis, inversion of strain-life and strain-stress anal. 80−19289
fatigue and inelasticity testing apparatus in symmetrical bending mode, 36 to 330 Hz 78−27722
fatigue behaviour of metals and alloys, vacuum effect, review 80−35309
fatigue crack growth at low stress intensities 77−86167
fatigue crack growth calc. 78−27638
fatigue crack growth fracture toughness prediction *(Polish)* 79−34134
fatigue crack growth micromechanisms at high stress 80−108569
fatigue crack growth rate, expt. programme for determ. in thickness direction 79−57168
fatigue crack growth rate characts., fracture mechanics fatigue design methods 78−7034
fatigue crack propag. life, statistical study on distrib. characts. *(Japanese)* 80−25847
fatigue crack propagation and initiation, high frequency, US meas. 78−60978

metals continued
fatigue damage accumulated by combination of alternately applied over- and under-stresses *(Japanese)* 80−35306
fatigue damage examination using two-crystal X-ray spectrometer method 79−52481
fatigue failure, book 78−76747
fatigue failure, low cycle, adiabatic heating as cause 77−21339
fatigue failure, similarity eqns. in components with stress concentration factors, coeff. anal. 78−39907
fatigue failure, similarity eqns. in components with stress conc. factors, error estimation 78−39908
fatigue fracture-stacking fault energy correlation *(Russian)* 78−15499
fatigue life distrib. theoretical obs. near fatigue limit 80−59569
fatigue lives, eval. using crack initiation model *(Japanese)* 80−104258
Fatigue lives of metals up to crack initiation 78−7050
fatigue monitoring by US velocity and attenuation meas. 78−60970
fatigue resistance, processes leading to failure 80−94907
fatigue strength testing unit for metal in atomized NaCl solutions 77−77677
fatigue test method using EM pulsator 80−89440
fatigue test results data processing *(Japanese)* 77−9013
fatigue testing at US frequency, hardness change 77−44440
fatigued, relationship between stress and point defect cluster density 80−10592
FCC, 'brass to copper' transition in rolling textures 80−76246
FCC, (001) twist boundaries symmetry and struct. 79−82242
FCC, anisotropy of surface free energy, computer simulation *(Russian)* 78−87858
FCC, atomic defects, computed electron microscope images 78−26392
FCC, cavitation erosion 77−86191
FCC, climb model of extended dislocations 78−6059
FCC, coincidence-site lattice interfaces 80−15381
FCC, creep rate, stress depend. *(Russian)* 79−1896
FCC, Debye-Waller factor determ. from X-ray data 77−1205
FCC, deform. behaviour 77−8892
FCC, deformed single crysts., struct. evolution at heating 80−103337
FCC, diffusion of H_2, anomalous isotope effect 77−24444
FCC, dipole interactions and trapping effects of positive muons 78−47342
FCC, dislocation barriers at coherent twin boundaries, anisotropic elasticity solns. 80−96522
FCC, dislocation behaviour at high strain rates, US detection method, data analysis basis 80−85136
FCC, dislocation loops and voids, growth kinetics, role of divacancies 79−99196
FCC, epitaxial growth, role of lattice fitting 78−34728
FCC, fracture mechanism maps and construction 79−61693
FCC, Frenkel pair annihilation, discrete lattice model *(Russian)* 78−10042
FCC, grain boundary energy and self-diffusion, effect of solute segregation 78−15412
FCC, grain boundary struct., and segregated impurity sites, computer simulation 79−73173
FCC, H implantation, lattice location and trapping, ion beam anal. 79−55769
FCC, H isotope diffusion coeffs. calc. *(Russian)* 78−91483
FCC, hardened, plasticity review 79−11683
FCC, He ion irrad., He gas bubble lattices obs. 79−14858
FCC, homovalent impurity migration energies, fluctuation theory model 79−95219
FCC, interstitial diffusion, theory *(Russian)* 80−65296
FCC, investigation of stage-I_E interstitial nature by TEM 78−47329
FCC, low stacking fault energy, nucleation phenomena 79−90681
FCC, macroscopic shear band contrib. to rolling texture 77−86056
FCC, misfit defect and extended screw dislocation anisotropic elastic interaction 80−96563
FCC, model for form. of annealing twins 78−59818
FCC, modelling of growth from melt *(Russian)* 78−60664
FCC, muon diffusion, theory 78−22883
FCC, plastically deformed, electron microscopy *(French)* 77−44301
FCC, polycrystalline, computer simulation of rolling texture *(Japanese)* 77−63686
FCC, polycrystalline, quantitative anal. of cross-slip and twinning 79−90677
FCC, props. of vacancies and divacancies 80−10545
FCC, quenched, form. of prismatic loops 77−65979
FCC, self-diffusion calc. 78−10212
FCC, single and multiple interstitials 77−68964
FCC, single phase FCC, cyclic deform. long range stress changes 80−54308
FCC, slip dislocation reactions at coherent twin boundaries, effect on work-hardening 79−1431
FCC, small vacancy clusters, structures and energies, computer simulation 80−39073
FCC, sputtering processes, due to Ar^+ bombardment, computer modelling 79−19957
FCC, stacking faults, long-range oscillatory interactions and stability 80−65012
FCC, structure and dynamics of multiple interstitials 78−47330
FCC, tensile fracture mechanism, review of pressure effects 77−70155
FCC, texture changes in running surface as result of frictional stress 79−91699
FCC, transitional creep *(Russian)* 77−25101
FCC, under H_2 press., crit. phenomena and isomorphic transitions 80−49367
FCC, vacancy migration near twin boundaries and stacking faults 80−39075
FCC, very high dose reactor neutron irrad. at low temp. 78−71766
FCC, vibr. anharmonicity and Debye-Waller factors, Willis approach 77−51467
FCC, void volume, swelling, errors in determ. by TEM 80−84208
FCC, with fibre texture, X-ray method of twin fault probability determ. 79−87817
FCC, X-ray Debye-Waller factors, CGW vs. DAF models 79−37794
FCC, yield threshold at 4.2K, effect on strain-hardening curve *(Russian)* 80−50671
FCC and BCC polycrystalline, ang. distribs. of sputtered atoms 77−85879
FCC and CC metals, behaviour during rolling, numerical simulation study *(French)* 78−84891
metals continued
FCC anisotropic crystals, extended screw dislocation, ⟨110⟩ misfit defect elastic interactions 80−100232
FCC irrad., annealing, Frenkel pair annihilation in discrete lattice model 77−59009
FCC metal, ^{119}Sn implantation by isotope separator method, Mossbauer spectra 79−24240
FCC metal, dislocation dissociation 80−107235
FCC metal, origin of dislocations during microdeformation tests, X-ray topography 79−82226
FCC metal with cube orientation, texture variation during rolling 77−70065
FCC metals, plastic deform. mech., TEM appl. *(French)* 77−1853
FCC metals, polycrystn., fatigued, behaviour model during plastic deformation *(German)* 80−21023
FCC nonhomogeneous sheet, orientational distrib. function calc. of mean texture 80−11659
FCC polycrystalline metals, work hardening plastic deform. *(Hungarian)* 77−77504
FCC polycrystals, deform. during cooling, revealed by deposited graphite layer *(Polish)* 80−25755
FCC texture transitions, computer simulation 79−90666
FCT, electron-ion interactions 80−10527
Fermi surface, effect of nonlocal potential, phase shift parametrisation scheme 78−43289
Fermi surface local geometry ultrasonic absorpt. ang. depend., Pippard oscill. spectrum *(Russian)* 79−19507
ferromagnet, spin-polarised field emission, many-body and spin-dependent surface pot. effects 79−74065
ferromagnet, uniaxial, anisotropic spin fluctuations and anisotropic band struct. effects on resist. near T_c 80−65543
ferromagnetic, coercive force, automatic meas. by remote means 79−24690
ferromagnetic, dragging of domains by temp. gradient 80−34425
ferromagnetic, elec. cond. review 77−31993
ferromagnetic, electron spin polarised tunnelling from superconductors 79−78263
ferromagnetic, electron spin-lattice relaxation *(Russian)* 80−103823
ferromagnetic, electron-magnon mass enhancement 77−15748
ferromagnetic, freq. depend. elec. cond. 77−66181
ferromagnetic, magnetisation density in vacancies, μ^+ probe, theory 77−28504
ferromagnetic, magneto-volume effect and Invar phenomena 80−66007
ferromagnetic, max. in acoustic attenuation at low mag. fields 80−93158
ferromagnetic, mechanically stressed, magnetic-inductive method of discontinuous vibration detection, theory *(German)* 79−20315
ferromagnetic, Nernst-Ettingshausen effect, rel. to Hall effect and thermoelec. power 79−56199
ferromagnetic, nonmagnetic impurity hyperfine field temp. depend. 80−34402
ferromagnetic, point contact spectroscopy, electron-magnon interactions *(Russian)* 80−54766
ferromagnetic, thermal oxidation rate determ. using nanowebermeters 80−61045
ferromagnetic, thermodynamic props. 79−91245
ferromagnetic, transport props., crit. behaviour 80−65522
ferromagnetic 3d metals, many-electron direct exchange interaction 79−69667
ferromagnetic cubic, mechanisms for elec. field gradients 78−43340
ferromagnetic metal, magnon and cond. electron relax. processes *(Russian)* 80−7102
ferromagnetic metal, temp. depend. of hyperfine fields at impurities 79−15300
ferromagnetic metal, two-band model ordinary Hall effect and spin-depend. phenomena 79−19577
ferromagnetic metal polycrystals, model for EM generation of US guided waves 78−22236
ferromagnetic metals, itinerant electron, theory of crit. US propag. 77−69655
ferromagnetic metals, magneto-optical effects, electron scatt. 77−90133
ferromagnetic metals, simple theory of spin-wave relax. 78−19231
ferromagnetic resonance linewidth, interaction of spin waves with conduction electron current 80−25216
ferromagnetic slab, transmission of 24 GHz radiation, effect of diffuse surface scatt. of carriers, calc. 80−34780
ferromagnetic transmission resonance, nonlinear phenomena 77−85577
ferromagnetics, two-magnon scatt. on dislocations, resonance linewidth broadening 77−20708
ferromagnetism, disordered, in crystalline metals 78−19207
ferromagnetism quantitative criterion correlation calcs. *(Russian)* 80−2540
ferrous and non ferrous, exam. of abnormal deformations and transformations *(French)* 78−60714
ferrous and nonferrous, air-plasma cutting 79−8401
fibre knitted gauze permeable materials, mech. props. 80−66607
fibre materials, permeable, obliteration phenomenon 79−98799
fibre materials, permeable, porous struct. parameters 79−100083
fibre materials, thermal and elec. conductivities 78−10419
fibre mats., porous, struct., hydraulic characts., liq. permeability 78−67848
fibre permeable materials, struct. characts. 79−24464
fibre reinforced metals and alloys 77−21060
fibres, cubic struct., texture form. in uniaxial deform. theory 79−24532
fibres, stress-strain curves determ. using X-ray goniometer *(German)* 78−92413
field distribution under anomalous skin-effect conditions 77−15887
field evaporation, field desorption microscopy investigations 77−21010
filler metal, deformation mechanism at brazed joint 78−80616
fine particles, melting and size depend. on melting temp. 79−73294
finishing, use of ion implantation technique, affect on wear and corrosion props. 79−34204
finite element analysis of elastic-plastic materials displaying mixed hardening 79−27543
flat plate, electromagnetic-acoustic conversion 78−44320
flow during rolling *(Russian)* 78−27561
flow stress, subgrain size and subgrain stability of elev. temps. 77−86094
foam solidification in space environment, fluid flow effects 79−47674
foil, continuous electrochemical perforation *(Russian)* 78−20020
foil, surface temp. meas. during laser irradiation heating *(Russian)* 79−74030

metals continued
foil photoetching profile, quantitative obs. 78−39943
foil with thin film coating, failure by laser pulse *(Russian)* 78−23561
foils, electron irrad., loss of pt. defects 79−73215
foils, for X-ray filters, electrolytic production method 79−95947
foils, low energy heavy ion multiple scatt. in finite range potential 80−70283
foils on bobbins, thermal insulation, ARGAS apparatus, depressuriser, report *(German)* 77−130
forging of circular blank, stress-strain state *(Russian)* 79−52231
formation energy of spherical cavities 77−80499
forming, limit anal. appl., book contrib. 78−11140
forming limit curve for bending processes 80−7627
fracture, brittle in ductile metals, specimen dimensions influence *(Russian)* 79−52345
fracture, physicomechanical characts., review 79−52368
fracture and ductile deform., microprobabilistic approach 78−64665
fracture and tensile props., effect of strain rate and temp. 77−36662
fracture due to laser irrad. and shock compressed plasma *(Russian)* 80−55500
fracture during creep 78−68778
fracture during laser working, depend. on physico-chem. props., heat cond. *(Russian)* 80−55432
fracture mechanism maps for materials which cleave 79−91774
fracture processes, adsorption-sensitive, control and appl. 77−52468
fracture strain measurement at high strain rates, radial expansion technique 80−85134
fracture test methods applicability and interpretation 79−15950
fracture toughness, micromechanical modelling *(Russian)* 78−31504
fracture toughness and temp.-rate sensitivity of plastic flow stress 78−35501
fracture toughness charact. in fatigue 79−15790
fracture toughness determ. in conditions of similarity to local fracture *(Russian)* 78−31505
free atoms of metals [and their chemistry] *(French)* 80−21281
free electron, model-independent constraints on many-electron XPS asymmetries 77−52219
free-electron like metals, interface energy 77−62984
free-electron-like, electron struct. of single and interacting H impurities 79−95365
freezing at mean heat exchange intensity in irregular mode stage *(Russian)* 79−52193
friction and wear rel. to comp., struct. and props., review 80−25872
friction between wood and metal 77−1167
friction during working stresses and rheological charact. at high temps. *(Russian)* 77−66702
friction equation 77−16699
friction heating during cutting 79−39055
friction pair, seizure centres on contacting surface *(Russian)* 77−70185
friction pair with polymer, temp. calc. under severe friction 80−40550
frictional contact of rough hard surface, metal transfer 78−64739
frictional electrification between metal and polymer, depend. on temp. and friction speed, contrib. of mol. motion to electrification 80−6953
fusible-metal deformation, effect on contact-melting kinetics 80−49339
fusion and evacuation after elec. contact treatment *(Russian)* 77−73365
fusion reactor metals, He embrittlement, grain boundary cavity model 80−34075
galvanomagnetic phenomena, quantum theory, cond. rel. to migration of cyclotron orbit centres *(Russian)* 77−66153
gamma-ray irradiated, energy spectra of secondary electrons 78−84683
gas nitriding, automatic control of NH_3 dissociation 77−70223
gauze reinforced porous permeable mats. with prearranged struct., prep. 78−68652
giant heat pulse, temp. distrib., classical Fourier and wave heat cond. eqns. 78−94518
glass-metal material, relation between struct. and props., prod. by hot densification 78−11145
grain and phase boundary model *(German)* 79−99216
grain boundaries, low energy 77−27895
grain boundaries, low energy 77−84764
grain boundaries, struct. and props. recent developments 79−99217
grain boundary diffusion, temp. depend. and activation energy 78−95191
grain boundary elec. resist., dislocation model 77−76800
grain boundary elements, FIM *(German)* 77−27894
grain boundary groove migration at solid-liquid interface, simulation with camphene 78−52789
grain boundary migration obs. using FIM 78−79617
grain boundary relax., model *(Russian)* 80−39107
grain boundary structure, description of as polyhedra packing 79−10863
grain boundary structure model, polyhedra packing 78−47393
grain neighbourhood relationships *(French)* 77−77694
grain struct. form. during two-dimensional recrystallisation, simulation on electronic calc. machine *(Russian)* 79−87666
granular, dielec. const., Maxwell-Garnet and effective medium theories 77−47760
granular, supercond. transition, increased resistance rel. to quasi-particle tunnelling 80−88689
granular superconductivity, instability 80−103796
granules, electron work function interrelation with granule size 80−39660
graphite fibre reinforced metals, tribological behaviour, fibre origin effects 79−96158
grinding in oxidising medium, electromechanical processes *(Russian)* 79−79149
ground state of solids, spin density functional method, binding energy, compressibility 80−65477
growth in space, theoretical models, comparison with ground expts. 78−84786
Gruneisen coeff. rel. to press. depend. of Poisson ratio 77−47504
Gruneisen ratio, rel. to Poisson ratio press. depend. and shock data 77−11712
Gurney equations for multilayer metal fragments 79−86367
H system, permeation technique for electron transport studies 77−7904
halogen-metal vapour lasers, average lasing power 79−936
hard, brittle, correlation between wear, crack resistance and stress intensity factor *(German)* 77−36666
hard, comparison of stress intensity factor depend. on notch base dia. with alumina *(German)* 78−35470
hard, developments, properties and fabrication processes *(Dutch)* 77−70021
metals continued
hard, roll deform. effect on separating forces in cold strip rolling 80−35212
hard metal, tensile strength meas., bend test-piece geometry effect 80−30184
hard plated pit props., vacuum impregnation by immersion, secondary anticorrosion treatment *(German)* 79−79144
hardening and softening during adsorption fatigue in surface active medium, governing laws 77−86230
hardening due to increased subgrain boundary stability 78−52934
hardening response in small deform. 79−47719
hardness testing, review 79−87773
Hartree, static dielec. permeability, local potential screening *(Russian)* 77−51684
HCP, anisotropy of phsy. props. rel. to texture 79−91700
HCP, atom movement in twinning, $\{10\bar{1}1\}$, $\{10\bar{1}3\}$ twins $\{10\bar{1}1\}$ $\{10\bar{1}2\}$ double twinning, new model 80−100252
HCP, atomic struct. of defects 78−30611
HCP, development of Kronberg's model for $\{10\bar{1}2\}$ twins, extension to $\{11\bar{2}2\}$ twins 79−51119
HCP, electrostatic contrib. to second- and third-order inner elastic consts. for different axial ratios 79−51186
HCP, exam. of texture and Young's modulus anisotropy, developed during deformation *(Russian)* 79−15694
HCP, LCAO description of (0001) surface electron states 78−72232
HCP, long-range interstitial migration rel. to c/a ratio 79−28125
HCP, plastically deformed, electron microscopy *(French)* 77−44300
HCP, regular soln. model for interstitial soln. 77−15591
HCP, self-migration energies, elastic calc. 79−95205
HCP, stacking faults, long-range oscillatory interactions and stability 80−65012
HCP, systematic electron diffr., main beam transmission 78−63643
HCP, vacancy and interstitial config. 79−65071
HCP metals, mag. susceptibility near $2^1/_2$th order electron transition, non-linear magnetisation anal. *(Russian)* 80−44859
HCP metals, phonon dispersion 78−59883
HCP polycrystals, deform. during cooling, revealed by deposited graphite layer *(Polish)* 80−25755
HCP to BCC phase transition and melting 78−14463
He behaviour 79−17981
heat capacity, ultra-low temp., anomalies due to CDWs 79−42271
heat capacity near melting point, vacancy mechanism of melting 80−10641
heat conduction, thermal wave, steady-state soln. 78−9527
heat content correlation under fast heating *(Russian)* 80−70426
heat resistant charact. extrapolation by temp.-time methods, creep data 78−15477
heat resistant power installation elements, estimating strength, ductility, heat resistance diagrams 80−25770
heat treating and melting with scanning laser or electron beam 78−11406
heating by concentrated energy sources, simple analytical expressions *(Russian)* 80−38215
heating by electrolytic plasma, temperature distribution obs. *(Russian)* 79−1045
heating by laser emission, spatial nonlinear problems *(Russian)* 80−7440
heating by laser radiation, calc. allowing for thermal props. temp. depend. 78−30770
heating kinetics in oxidising medium, exam. using CO_2 continuous laser emission *(Russian)* 79−57135
heavily deformed recrystallisation 79−34062
heavy, ions separation using vinylbenzyl gluconate acrylonitrile copolymer membrane 79−74418
heavy, levels in air, related to wind direction, Belgian North Sea coast 79−83665
heavy ion bombard., high density collision emission cascades 80−71531
heavy ion implantation, site populations in case of immobile defects 79−23624
heavy ion implantation, stochastic formulation of site populations 79−19271
heavy irradiation damage at high temps., void swelling problems *(Japanese)* 77−59049
heavy metal pollution, use of lake sediments as indicators 77−25710
heavy metals, Belgian network meas. of atmospheric concs. 77−70833
heavy metals, distrib. and speciation in aquatic systems, analytical techniques 78−69390
heavy metals in aqueous solns., adsorption on inorganic minerals 78−49006
heavy metals pollution of mountain watershed, impact of ski basin 79−20903
helicon-phonon interaction for parallel wave propagation 78−64054
hexagonal, temp. depend. anisotropy of phonon scatt. resist. 78−51967
hexagonal, twin refl. indexing in four-axis hexagonal reciprocal lattice 80−14970
hexagonal compensated, chemical pot. shift due to coupled orbit conduction 79−28273
hexagonal crystal structure, anisotropy of elastic props. calc. *(Russian)* 78−23749
HF wave dispersion for complex wave numbers, ordinary waves 80−70740
high plasticity, fracture nature *(Russian)* 77−25149
high strain rate material behaviour and testing techniques, J.D. Campbell memorial lecture 80−82627
high temperature, remarks with respect to zero creep method 77−12671
high temperature oxidation, interference phenomena and integral emittance *(Russian)* 78−91458
high temperature radiative characteristics, EM theory of radiation 79−7704
high temperature species, absorpt. and fluoresc., high temp. fast flow reactor technique 80−42231
high-pressure effects, conf., Moscow, USSR (May 1975) 77−43279
higher sound harmonic generation in momentum nonlinearity regime *(Russian)* 78−38783
hot deformability test methods, comparitive evaluation *(German)* 77−36713
hot plastic deformation, stress/strain/time relations *(Russian)* 80−20968
hot surface, thermal ion energy distrib. by retarding field modulation method *(Japanese)* 79−78822
hot twisting, differential method of shear stress determ. 77−56026

metals continued
Hume-Rothery's class-I metals, Engel-Brewer theory and related phys. props. 78−2059
hydride forming phase hardening 78−52833
hydriding and dehydriding kinetics, H_2-diffusion-rate-limited 80−35764
hydroextrusion, effect of longitudinal US vibrs. 79−96046
hydrogen brittleness measurement 80−104291
hydrogen crack development 79−20189
hydrogen embrittlement, effect on props. 80−104290
hydrogen embrittlement review *(Russian)* 79−15762
hydrogen embrittling effects from acoustic emission meas. 80−11742
hydrostatic forming, novel industrial appls. 77−44191
impact abrasive wear, anal. 79−43443
implantation by heavy ions, site population model 77−80518
impure, elec. conductivity calc., effect of electron-electron correlation *(Russian)* 78−68010
impurities, H and He, electronic struct. 78−10402
impurity atoms, diffusion in region of dislocations *(Russian)* 80−24670
impurity conductivity at low temperatures, temp. depend. *(Russian)* 79−7817
impurity effects on cond. electrons, perturbation theory 79−60763
impurity origin in DIVA, ion sputtering, evaporation and arcing 79−656
individual atomic events on surfaces, quantitative examination 80−75409
indoor corrosion rates meas. 80−76404
inductional dislocation braking in mag. field *(Russian)* 80−79791
inelastic cyclic strain under nonuniform stress state conditions, residual stresses effect 80−81132
inelastic deform., time-depend. anal. using constitutive relations 77−39237
inelastic electron scattering, interaction effect in final state 79−69454
inelastic neutron scatt. cross-section, effect of cryst. field 79−65642
inelastic time-depend. deform., boundary integral eqn. 78−51090
ingot, continually cast, optimum conditions for variable drawing rate *(Russian)* 79−70056
ingots, controlled crystn. using Bridgman method, modernisation of OKB-8093 unit 79−24425
inhomogeneous, magnetoresist. and Hall coeff. 79−95387
inhomogeneous circular cylinders, non-radiative surface plasmon-polariton modes 80−29455
inhomogeneous dislocation struct., model 79−90655
inhomogeneous granular, superconductivity 80−103795
intense optical irradiation, behaviour of surface temp. and refl. coeff. 78−15260
interaction energies between point defects 78−47360
interaction with gases and C, conf., Stuttgart, Germany (Sept 1977) *(Russian)* 79−57134
interatomic potential determ. from phonon spectra 77−65962
interbubble fracture mech. of blister form., He irrad. 78−6109
interface with insulating liquids, meniscus rise, in presence and absence of applied elec. field 79−19429
interfaces, self-consistent electronic densities and adhesive energies 78−72005
interferometer for 90° reflecting angle meas. *(German)* 78−164
interion interaction and interion force constants, effective pots. in nonlocal pseudopot. method *(Russian)* 78−22684
intermediate valence metals, renormalisation of collective excitations, acoustic wave vel. near electronic transition 79−82539
internal friction, amplitude depend., for polycryst. specimens *(Russian)* 79−90726
internal friction meas. via torsional pendulum oscillation damping meas. *(Polish)* 77−71314
internal friction measurement of metals using sound emission during vibration 77−77715
internal stress meas. by decremental unloading technique 78−64576
internal stresses during rolling friction and their evaluation 77−28912
interstitial diffusion, cooperative nature 78−47556
interstitial loop growth, pulsed irrad. effects 80−88210
interstitial soln., conversion of thermodynamic functions from const. press. to const. vol. 77−7877
ion, fluoresc. quenching of organic excited singlet states, rate meas., mechanism 77−38685
ion adsorption, nucleation effects *(German)* 78−68635
ion beam analysis of light elements using nucl. reaction technique *(Japanese)* 78−31744
ion bombard., void conc., effect of implanted He *(Russian)* 80−88213
ion bombarded surface, using 1.05 keV inert gas ions, electron yields 78−52611
ion bombardment, excitation of plasmons 78−34793
ion etching, dispersion coeff. determ. *(German)* 80−40597
ion impact desorption cross section of H and O by light ion bombardment 78−95096
ion implantation, book contrib. 79−1835
ion implantation 79−28008
ion implantation damage, light element, review 80−88219
ion implanted H(D), interstitial positions and vibr. amplitudes, fast ion channelling study, review 80−79848
ion implanted with He, statistical model of low temp. blister formation 78−67754
ion irradiated, outer electronic shells contrib. to heavy ions stopping *(Russian)* 79−1474
ion lasers, hollow cathode 80−99708
ion plated soft film, friction and wear 78−15549
ion surface treatment 78−11415
ion-beam textured, adhesive bonding 79−87752
ion-implanted, friction and wear, review 80−40555
ion-metal atom processes, charge exchange cross sections, calcs. and computer program 78−55236
ionic interaction in axially symmetric and Bhatia models 79−37767
IR optical consts., meas. by self-radiation method 80−84710
IR window materials, diamond machinability 78−5586
irradiated, containing pre-existing dislocations, interstitial loop form. kinetics 80−65040
irradiated, containing self-interstitials and vacancies, electronic transport props. 78−60105
irradiated, determ. of true threshold energy for Frenkel pair creation 77−47444
irradiated, heavily, exam. of percolative mass transfer 78−79639
irradiated, mechanism of formation of vacancy dislocation loops *(Russian)* 80−65053
irradiated, multiple atom displacements 79−46701
irradiated, ordered arrangement of micropores on dislocations 77−19943
metals continued
irradiated, peak void swelling temp. 77−72608
irradiated, self-interstitial type defects, combined single-double alignment channelling backscatt. 78−34561
irradiated, solute segregation and annealing kinetics at sinks 79−23640
irradiated, solute segregation and precipitation effects on void swelling 78−67741
irradiated, triangular Frank loop dissociation 77−11599
irradiated, validity of rate theory, point defect diffusion eqns. 79−55777
irradiated, void growth, appl. of Langevin method 79−77632
irradiated, void nucleation theory 79−1464
irradiation creep and swelling, cascade damage effect 77−19991
irradiation-induced creep, transient stage, vacancy loop contrib. *(Russian)* 80−29115
isotope compounds, conversion to metals by reduction-distallation methods 80−23223
isotope enrichment, by combined elec. migration and zone melting 78−76600
isotope enrichment during zone refinement *(Russian)* 77−59686
isotropic, Brillouin scatt. 78−80367
itinerant ferromagnet, tight-binding metal, Einstein temp. 79−24126
Knight shift for ions with Z>83 77−12275
Kondo effect, Anderson hamiltonian 80−60187
laminated, laws governing development and retardation of fast cracks 78−15527
laminated composite, crack growth retardation *(Russian)* 77−70144
Larmor wave theory, Fermi-liquid interactions, Fermi surface, and g-tensor anisotropy 79−69397
laser, metal vap. type, upper and lower laser states population densities, simultaneous determ. method 78−87042
laser and nuclear radiation induced emission anomalies, current sources *(Russian)* 80−25536
laser beam optimal heating in oxidising medium 80−69445
laser drilling velocity and efficiency 77−24913
laser erosion, influence of metallic target temp. *(Russian)* 79−39028
laser heating kinetics, influence of oxide film interf. effects 80−11841
laser irradiated, optical and electronic emissions *(French)* 80−2919
laser irradiated, time-resolved specular reflectivity 79−69819
laser irradiation effects on struct. and props. *(Russian)* 78−30665
laser produced shocks rel. to material damage 78−31285
laser radiation absorption in craters on metal targets 80−97386
laser shock production rel. to material damage 77−90221
laser-assisted hot spot machining, advantages and potential 79−70199
laser-photoinduced etching, photodissociation of dissolved complexed halogens in soln. 80−100929
latent cold work heat release kinetics meas. using adiabatic elec. heating 77−52344
latent slip in FCC and CC metals, computer simulation *(French)* 79−32998
lattice decohesion, due to H_2 78−15533
lattice defects, positron annihilation study, book contrib. 79−99977
lattice dynamics, Krebs and Cheveau models, three-body forces inclusion and equilibrium condition 78−47480
lattice dynamics and three body interaction 78−10139
lattice dynamics of HCP metals 78−22795
lattice heating by radiation, plasma effects, degenerate electron gas calcs. 80−70742
lattice surface relaxation, electrostatic model 80−49488
LEED intensity and image pot. above beam threshold 80−44084
LEED intensity profiles, surface-reson. fine struct. surface-resonance fine struct. in LEED intensity profiles 77−39518
light absorption, multistage, vol. nonlinear photoeffect *(Russian)* 77−44129
light interstitial diffusion, quantum theory, motion of positive muon 79−56690
light interstitials, self-trapped, quantum diffusion 79−19405
light interstitials diffusion, multiphonon transition modes classification 80−70448
light metal, surface effects on X-ray level widths 79−47147
light reflection, adatom characts. depend. 78−10918
light scattering from surface acoustic phonons 78−76484
limiting elastic moduli, Morse pot. appl. 77−69025
liq. metal embrittlement, mechanism, Rebinder effect *(Russian)* 79−34186
liquid, contactless resistivity meas., impedance change of a coil 80−73388
liquid, density meas. by pycnometry, errors 80−73321
liquid metal embrittlement, review 80−3257
liquid metal embrittlement 79−52421
liquidus and solidus temperatures, determ. by γ-ray method 80−65193
load-bearing surfaces, secondary structures obs. by electron microscopy, specimen thinning method 79−52484
localised atomic states, resist. and free energy calc. 77−8069
localised magnetic moment magnitudes of transition or rare earth impurity, Anderson model 80−25086
localised moments, ESR 80−71153
longitudinal flow velocity distribution in rolling *(Russian)* 80−93575
longitudinal weakly damped EM waves near cyclotron resonance 80−103890
low temperature frictionless heat motion 79−69495
low temperature phonon resistivity 77−62888
luminescence, visible region emission associated with deformation and destruction *(Russian)* 77−12453
luminescence of electron irrad. surfaces 79−65934
magnetic, and SEM exam. of fatigue, dynamic strength problems *(German)* 77−86272
magnetic impurity-conduction electron interaction, g factor renormalisation 79−69652
magnetic localisation and charge oscillations 80−75781
magnetic oscillations, Fermi surfaces and high magnetic fields 79−73423
magnetic surface states induced linear magnetoresistance 79−60798
magnetisation densities and neutron mag. form factors; theoretical determ. 79−47243
magneto-quantum oscillations obs., new method 77−62946
martensitic memory mechanism *(Russian)* 77−21217
martensitic transitions accompanied by interactions between phases *(Russian)* 80−7568
mathematical model for unidirectional solidification, massive moulds 79−56971
mechanical behaviour under impulse loading, model 79−52332

metals continued
mechanical degradation of PMMA in presence of metals *(Russian)* 78−31422
mechanical properties, effect of H_2, methodological approach to study *(Russian)* 78−31507
mechanical properties, electric current effect, test device for 4.2-300K 80−66719
mechanical properties, meas. at high temperatures, MEITP-1 indentation system (USSR) 80−74820
mechanical props., testing and modelling 80−25811
mechanical props. and strain rate, low temperature effect 79−1911
mechanical stability, loss of physical model and neck formation *(Russian)* 78−6969
mechanical stability under HF vibrs. rel. to surface treatment *(Russian)* 77−52400
mechanical treatment in aq. salt soln., material transport rel. to wear 80−16506
mechanically stressed, lattice strain distrib., X-ray elastic const. calc. *(German)* 78−52884
melting, contact, state of cryst.-liq. boundaries, influence of impurities and hydrostatic pressure *(Russian)* 79−37812
melting by electron beam sweeping device 78−6889
melting by laser emission, laws governing fluid phase spattering *(Russian)* 77−20963
melting in suspended state, large vol. and mass samples *(Russian)* 78−44036
melting temp., press. depend., vacancy mechanism 80−103460
melting temperature depend. on particle size, thermodynamic theory 77−89523
melting theory for small particles, Helmholtz free energy 80−59629
membrane, lifetime prediction and design 80−71752
metal:magnetic ion, ESR, book 77−48037
metal:rare earth, effective exchange interaction model 80−25127
metal, inelastic scatt. of electrons by vibrating dislocations 78−26853
metal extrusion process, stress and deform. distribs., elastic-plastic anal. 77−48364
metal surface crater form., by laser pulse, frontal method, approx. soln. 77−77327
metal surface-ultrashort coherent IR pulse interaction, inertialess radiation *(Russian)* 79−95879
metal surfaces, abrasion mechanism rel. to groove sizes, shapes 79−20216
metal-electrolyte boundary, elec. refl. and photoemission relationship 80−45211
metal-electrolyte boundary, electrodynamics in visible and near UV range, microscopic effects 80−45521
metal-electrolyte boundary, photoemission effect on elec. refl. 80−45212
metal-gas interactions, kinetics and mechanisms, book contrib. 78−11558
metal-gas system, ignition conditions with account of radiative heat loss *(Russian)* 77−32789
metal-glass mats. alloyed with Cu, powder prep. and props. 78−72912
metal-H system, basic props., book 79−82349
metal-H system, elastic interaction and phase transition, book contrib. 79−83178
metal-H system, lattice strains, expt. methods, book contrib. 79−82202
metal-H system, long wavelength density modes 78−79745
metal-H system, NMR depend. on struct., H diffusion and electronic struct., book contrib. 79−82887
metal-H system, solubility, mobility, and phase transitions, book contrib. 79−82350
metal-H systems, appl. oriented props., book 80−22154
metal-H systems, heat transformer for energy cascading, book contrib. 80−26151
metal-H systems, temp. depend. of impurity resist. 80−65529
metal-H systems 79−82906
metal-metal contacts, use as prevention H escape from metals 80−24595
metal-metal interface, effect on adhesion and friction 77−24488
metal-NH_3 solutions, optical and microwave props. of microscopically inhomogeneous materials 77−77161
metal-polymer friction pairs, triboelec. effects 80−11784
metal-semimetal system, local and total density of states determ. *(Russian)* 80−54586
metallurgically bonded plates, structural integrity determ. by high energy impulse 79−39111
metals, cold forging, upset tests anal., stress-strain law determ. appl. *(French)* 79−20064
metals, cubic, heavily deform., development of lattice curvature 80−81136
metals, diffusion alloying conditions, deep chemical-heat treatment *(Russian)* 80−40393
metals, noble, dilute alloys, solute vacancy binding energy, Dingle temp. 80−49177
metals, radiation creep speed and swelling, self diffusion mechanisms *(Russian)* 80−92595
metals, rods with temp. gradient, apparatus for examining corrosion along surface 79−52513
meteorites, iron, elements distrib. between metal and phosphide phases 80−46508
microanalysis of migration processes 77−36706
microcrack, generated in oxides during high temp. oxidation, defection by slight sulphidisation 77−8999
microdetermination of C, purification of O_2 and flux selection *(Japanese)* 78−92571
microelectronics and microprocessor impact on metals prod. and NDT 79−74320
microinhomogeneous plastic deformation, rules 80−89307
microparticle impact, strain rate effect 77−80577
microplasma welding, heat propagation in parent metal *(Russian)* 78−15642
microstructural inhomogeneities resulting from high strain deformations 79−87705
microstructure, effect on bulk material props. 80−34004
microstructure and strength *(German)* 77−70138
mirror, diamond turned, optical figure inspection by interferometry 78−5545
mirror design and mounting specifications 80−48388
mirror substrates, manufacturing processes, review 78−5542
mirrors for CO_2 laser fusion systems, material constraints and fabrication 78−5476
monolayers, on metal cryst. surfaces, surface struct., review 80−80067
monovacancy form. enthalpy 79−90649
metals continued
monovalent, low temp. eqn. of state 78−22820
Morse parameter calc., elastic const. evaluation 77−7692
Mossbauer spectra of implanted ^{83}Kr, line widths, isomer shifts 80 39899
Mulliken electronegativities, rel. to work function 78−9096
multiaxial creep charact. exam. 79−43364
multilayer scale form. and parabolic oxidation, different rate const. 78−64758
multilayer scale form. and parabolic oxidation, temp. and press. depend. of rate const. 78−64759
multiplication photoemission in strong field 77−85891
muon$^+$ polarisation, anomalous temp. depend. of relax. rate *(Russian)* 78−92012
muon$^+$ relax., theory 77−59501
muon$^+$ spin relaxation, precession freq. and depolarisation *(Russian)* 77−69761
muon macroscopic diffusion 79−56698
muon spin rot. diffusion expts. 79−56680
muon trapping by defects and impurities 80−20573
narrow band, quasiatomic Auger spectra 78−60536
narrow-band, extra-atomic relax. and X-ray spectra 77−24928
narrow-band metals, magnetism and mag. excitations 77−69478
NDT using positron annihilation technique 78−3293
NDT using positron annihilation technique 78−3294
near surface microstructure effect on wear 78−64730
negative ion emission during microsecond laser pulse irrad. 78−2981
neutron activation anal. of O in non-ferrous metals 79−24865
neutron irradiation, low temp., dose depend. of recovery peaks 78−71767
neutron scattering by surface imperfection 77−51578
nitridation and oxidation, comparison of behaviour at high temp. 79−74288
NMR results, metals and alloys, brief survey 79−73830
noble-metal tubes, cold-weld sealing 80−41556
non-Arrhenius diffusion and NMR relax. relationship 78−47568
non-ferrous, recycling, effect on comp. 80−66455
non-ferrous, recycling, system study, computer simulation 78−35278
noncommensurate charge density wave dynamics in K-like metals 78−30913
noncubic s-p metals, influence of impurities on solute elec. field gradient 77−24770
nonferrous, unlubricated wear data interpretation 79−38989
nonferrous metals, unlubricated wear data 80−16510
nonfissile irradiation creep 77−42072
nonlinear anelasticity and the martensitic transformation 79−61634
nonlinear interaction of strong and weak sound waves 78−59865
nonlinear mechanical response, Swift effect 78−35433
nonlinear photoelectric emission from metals by high power layer radiation review 78−48288
nonmagnetic host metal, indirect mag. coupling between local moments 78−52207
nonsimple metals, calc. of elec. resist. and thermoelec. power 78−19019
nonstationary temperature fields due to moving heat sources, heat capacity, thermal cond. *(Russian)* 80−107448
normal and magnetic, temp. depend. of plasma freq. 78−56100
normal crystal growth, fluctuation theory, modelling of melt-growth interface motion 80−15025
notched, cyclic stress/strain behaviour, random fatigue life *(German)* 80−100907
notched, fatigue under alternately over- and under-stresses *(Japanese)* 80−35307
notched sheet, thickness effect on deform. and fracture under tension 79−70113
nuclear acoustic resonance, quantum theoretical treatment 79−42846
nucleation, oriented island growth on point defects 78−87889
ocean ridge sediments, metal accumulation rates, in Indian Ocean 77−33052
oceanic residence times of trace metals, river discharge effects 77−78228
optical constants determ., review 79−33655
optical constants meas., simple polarimetric method *(French)* 77−45880
optical erosion, interpretation of screening effects 77−66559
optical functions, effect of surface roughness 78−56447
optical materials, metallic and glass components compared 80−69473
optical properties by spectroscopic ellipsometry, review 80−103929
optical properties in radiative heating, O_2 diffusion and dissolution effects 79−65884
optical props., high-temp., from emissivity ang. depend. data 78−39519
optical reflector metal specifications 80−48387
optical SHG effects of electron band struct. 77−740
optoacoustic phase angle meas. for subsurface struct. 80−28388
orbital magnetic and spin paramag. susceptibilities, effect of strain 77−16137
orientation distribution function determ. using one pole figure *(German)* 77−25242
overbarrier states of H and D, subsystem heat capacity, equilibrium props. *(Russian)* 80−79998
oxidation, O Auger peak studies 77−1769
oxidation, oxide thickness and oxide transfer in wear 77−16755
oxidation, Rosenburg kinetic method applied to determ. of parabolic rate const. 78−64774
oxidation, standard free enthalpy *(French)* 79−61867
oxidation kinetics, effects of control of scale structure 77−16751
oxidation mech., exam. using autoradiography 79−20326
oxidation of high temp. material, lattice vacancy effect 77−70203
oxidation of metal with dispersed oxide phase, charged particle theory 78−19925
oxide film growing by cation diffusion, stress generation 78−60865
oxide thick film growth, fund. theory 80−89391
oxides, diffusion activation process, interatomic bonding energy *(Russian)* 80−54428
oxides, used as battery cathodes or electrocatalysts, electrochemical behaviour 80−45516
oxidising metal heating by periodically pulsed CO_2 laser 80−7445
oxidizable, laser heating in air by obliquely incident radiation 80−71815
pack rolling, bonding, deform. struct., small reduction before seizing 77−90503
packed powder, induction heating mechanism *(Japanese)* 79−59615
paramagnetic, CESR linewidth and g-shift in presence of spin-orbit perturbation, spin-phonon scatt. 77−63285
paramagnetic, EM excitation of sound, Mossbauer study *(Russian)* 79−99794

metals continued
paramagnetic, narrow band electron system, temp.-induced local mag. moment 78−76221
paramagnetic, temp. depend. of susceptibility, microscopic Fermi liq. theory 77−28364
paramagnetic and diamag. susceptibilities, density depend., ring diagram contrib. 79−95571
paramagnetic impurities, contrib. of collective excitations to mag. relax. 77−12190
paramagnetostriction anisotropy of metals and HCP struct. 77−32231
particle erosion meas. 77−66703
particle surface tension depend. on size, vaporisation time *(Russian)* 80−34290
particles, far IR absorption 79−61383
particulate matter, graphite furnace atomic absorption spectrometry appl. 80−94134
particulates, theory of melting in the Percus-Yevick limit, appl. to particles on SiO_2 and C substrates 80−20060
passivation, using in situ polymerisation by microwave plasma discharge 78−64762
passivation termination, ESCA study 79−20267
passivity, in metals and alloys 80−50750
Peierls transition in quantizing mag. field, possibility 80−103441
phase analysis by Mossbauer spectra 80−15922
phase growth kinetics, solid-liq. metal diffusion layer *(Russian)* 79−37882
phase stability and elastic const. 78−31387
phase transformations in metals and alloys, thermodynamic and mechanistic classification, review 80−2995
phonon drag direct obs. feasibility *(Russian)* 77−85187
phonon limited resistivity, anharmonicity, Debye Waller factors, multiphonon terms 80−49691
phonon point-contact spectroscopy 79−65152
phonon-phonon scatt. role in lattice thermal cond., phonon drag, elec. cond. 80−70483
photo-induced field emission, total energy distrib. meas. 79−74068
photodesorption, review 79−51424
photoelectrochemical cells, metal, electrodes in contact with fluoresent dye solns., photovoltage generation, comprehensive model 80−40871
photoelectron, nonlinear vol. effect, anal. 79−15593
photoelectron emission at high laser intensities, multiphoton phenomena 79−28886
photoelectron emission processes at high laser intensities, multiphoton phenomena 78−60550
photoelectron spectroscopy of surface states 79−56909
photoemission, effect of refraction of p-polarised light 78−72686
photoemission, influence of oxide films *(Russian)* 77−81194
photoemission, nonlinear, picosecond lightpulse, electron heating effects *(Russian)* 77−40331
photoemission from clean and adsorbate covered single cryst., appl. of simple selection rules 79−33896
photoemission in solids, book 80−12860
photofield emission, vol. effect 77−32494
photogalvanic effect for free carriers in crysts. without symmetry centre *(Russian)* 78−87999
photosensitivity of semicond.-metal system, theory *(Russian)* 78−3357
physical props., correl. with outer electron density of state *(Chinese)* 79−51466
pinch effect on plastic deform. *(Russian)* 78−35426
Pippard sound attenuation oscills., ang. depend. *(Russian)* 80−103613
plant deform. and recrystallisation textures 78−68708
plasma, TEA CO_2 laser prod. plasma, charge collection meas. 77−19739
plasma anodisation, model 79−28952
plasma arc refining melting, allowing two phase region and plotting distrib. functions *(Russian)* 78−31358
plasma cooling by metal snow, expt. evidence 78−71495
plasma cooling by metal snow, origin of effect and elimination 78−71494
plasma oscills. of cond. electrons localised near point defects, contrib. to charact. losses *(Russian)* 77−43525
plasma-arc refining remelting calc. *(Russian)* 78−18463
plasmon dispersion effect in (e,2e) process with atomic electron knockout 80−2904
plasmon struct. in X-ray absorpt. spectra 79−38692
plasmons, long-wavelength, interband damping 77−85165
plastic, anisotropic hardening pot., stress/strain relation under combined axial load/torsion 78−52896
plastic, work hardening, sintered, porous, irreversible deform. 78−19849
plastic clad, corrosion charact. by electrical resist. and capacitance meas. *(German)* 80−30171
plastic deform., constitutive relns. 78−42544
plastic deform., time depend., thermodynamics model 80−76309
plastic deform after pinch effect *(Russian)* 78−27563
plastic deform. and sliding friction 79−87743
plastic deform. generalised constitutive eqns. 80−104219
plastic deform. of anisotropic billets, energy method anal. *(Russian)* 79−98629
plastic deformation, deform. resist. *(Bulgarian)* 80−88248
plastic deformation, grain size and microstrain from X-ray diffr. data, moment method *(Czech)* 78−31593
plastic deformation, influence of mech. vibrations 78−60722
plastic deformation, stored energy determ., temp. recording method 79−87775
plastic deformation, volume charges *(Czech)* 77−63729
plastic deformation of metal subjected to intense heat source 77−86085
plastic deformation review *(Russian)* 78−19825
plastic deformation under pulse action 77−76486
plastic flow, during extrusion, computer simulation 78−31491
plastic flow, finite element approach to axisymmetric problems, METFLO 78−31490
plastic flow, role of osmotic forces in low cycle fatigue, vacancy generation *(Russian)* 79−60430
plastic flow at intermediate temps., athermal region 77−48497
plastic flow rate during rolling under two dimensional strain *(Russian)* 79−52264
plastic flow through ultrasonic vibrated die, mechanism *(Rumanian)* 77−70242
plastic impact, energy absorbed by elastic waves 80−5972
plastic properties investig. at elevated temps. by torsional method, review 79−43509

metals continued
plastic strain graph plotting at high strain rates by cutting method 77−90521
plastic yield criteria, interpolation scheme 80−64400
plastically deforming at high strain rates, distrib. of temp., strain rate and strain 79−19311
plasticity, dynamic, governing relations, elastic energy 79−43328
plasticity, influence of hydrostatic press. and stress state 78−52907
plasticity, theory extension to three dimens. and appl. to geophysics 80−104955
plasticity under hydrostatic pressure *(Russian)* 78−68726
plate, penetration by combined CW and pulsed laser radiation 79−89955
plate, radioelectric effect 80−70744
plate, subject to laser heating, nature of thermoelastic stresses *(Russian)* 77−21199
point contact, α^2F depend. of electrical impedance 78−47848
point defect and microstruct. behaviour during irrad., appl. to fusion reactors 79−23638
point defect clusters, TEM obs., review 78−26564
point defect diffusion controlled reaction theory, book contrib. 80−103318
point defect dynamic props. and diffusion controlled reactions, book 80−101674
point defect dynamical props., book contrib. 80−103317
point defect relaxation volumes, dipole tensors and Kanzaki forces 80−54222
point defect simultaneous clustering during irrad. 79−95000
point defect solute interactions 78−47410
point defects, μSR studies 79−56703
point defects, high-field magnetoresistance 79−7819
point defects, lattice theory 78−47321
point defects, review 77−7709
point defects, theory, book 78−71730
polishing, electrochemical, AC current influence obs. *(Russian)* 79−1922
pollution by heavy metals, sedimentary record, Lake Erie 79−83644
polycrystalline, elastic deform., free surface influence on mutual restriction between grains 77−51431
polycrystalline, elastic moduli rel. to those of single crysts. 79−23671
polycrystalline, electron or proton irrad., coherent acoustic emission *(Russian)* 77−81355
polycrystalline, LF viscosity meas. 78−80576
polycrystalline, plastic stress-strain relations computation 77−22419
polycrystalline, plateaus in cyclic stress-strain curves 79−79054
polycrystalline, relations between shear modulus, bulk modulus and Young's modulus 80−97540
polycrystalline, secondary ion energy spectra 79−24401
polycrystalline metals, stored energy and strain hardening 79−82276
polycrystals of anisotropic substances under hydrostatic press., microstresses 79−25231
polymer, films thickness determ. using profilograph-profilometer 79−70244
polymer coated, wear and friction 77−21328
polymer coated metal spheres, flow, degradation mechanism 77−9036
polymer coating, chemiphoretic deposition without electric current onto metal 78−64763
polymer-metal contacts, methods of decreasing wear 79−20209
polymer-metal pair adhesive interaction during friction 78−3227
polymer-metal sliding, wear eqn. in terms of fatigue and topography of sliding surfaces 80−108597
polyvalent, Matthiessen's rule deviation crit. resist. 80−6811
pore form. mech. investigation by directional solidification 77−28800
porous, mean principal stress in rolling without lateral expansion 80−25803
porous, shear stress enhancement of void compaction 79−69182
porous, shock compression calcs. using approx. eqn. of state 77−35657
porous, shock speed meas., continuous recording 78−5708
porous, stresses in deform. region during cold rolling 78−11241
porous, thermal conductivity meas. 78−18150
porous, yield stress variation during cold deformation 80−16395
porous gauze materials, struct. and hydraulic charact. 80−11729
porous gauzes, hydraulic resist. in laminar filtration 80−100034
porous homogeneous couple, vacancy migration and void form. 77−55401
porous strip, metal pressure in cold rolling in elastic aftereffect zone 80−40421
porous trip, elastic aftereffect in cold rolling 80−11689
positive muon diffusion 79−19388
positive muon diffusion studies, anal. of μSR linewidth 79−56691
positive muon interactions 80−71284
positive muon spin depolarisation, defect study 78−47314
positron annihilation, ang. correl. curves parametrization *(German)* 77−90214
positron annihilation, ang. correl. data analysis 78−52592
positron annihilation, localised proble of lattice defects 80−55224
positron annihilation, mag. field effects 77−62803
positron annihilation, real-space approach 79−95874
positron annihilation, theoretical and expt. techniques, book 79−99975
positron annihilation experiments, electronic struct. and Fermi surface studies 80−54594
positron annihilation line broadening, Ge detector 77−16418
positron annihilation technique in Fermiology 79−69902
positron density distribution, temp. effects 78−47739
positron lifetime spectra, anal. errors 78−19591
positron lifetime spectra, lifetimes and intensities 79−33858
positron lifetimes, phenomenological interpretation 77−73186
positron self trapping conditions 78−47338
positron thermalisation by non-equilibrium statistical operator method 79−15551
positron trapping at dislocations 78−10091
positron trapping by defects influence of positron-phonon and electron-phonon interactions *(Russian)* 80−93425
positron-defect interaction and annihilation charact., book contrib. 79−99978
positron-phonon interaction 77−15796
positron-vacancy interactions, equilib. temp. depend. of positron annihilation 78−76547
positronium in 'metallic' pore 78−35222
powder, method for TEM study 80−84038
powder coatings, in metal finishing, review 80−104330

metals continued
powder compact with polymer, cond. threshold, particle size ratio effect 80−80337
powder compacts, elec. resist., surface layer effect 80−34415
powder on piezoelec. substrate, dynamic SAW reflecting struct. 80−74565
powdered materials, nonlinear mechanism leading to polarisation echoes 78−87739
powders, echo effect at low temp. *(Russian)* 78−34853
powders, fundamentals of compaction 80−40279
powders, packed, complex mag. permeability calcs. 80−29583
power overdistribution to AC and DC arcs for melting metals *(Russian)* 80−54055
preparation by electromagnetic levitation in ultrahigh vac. 80−29899
proper EM radiation on inelastic electron tunnelling with photon emission, cond. *(Russian)* 80−54765
protective coating of metal on metals and alloys, anticorrosion mechanism *(Rumanian)* 78−23853
protective coatings, chemically vapour deposited 78−44261
proton energy losses, Bohr equipartition rule 77−15467
proton movement in FCC, BCC and HCP metals 79−69293
pseudopotential investigation of phys. props. 77−43526
PTFE+metal, fluoride prod., DSC and XPS anal., rel. to polymer wear 80−11889
PTFE-metal interaction, X-ray photoelectron spectroscopy obs. 80−11788
pulsed mechanical stressing equipment for dislocations motion study 79−52532
pulsed press. created by electron beam, effect on struct. and mech. props. *(Russian)* 78−34539
pure, friction stress for high temp. creep 78−11289
pure, oxidation in mixed atmosphere, simultaneous oxide/sulphide form. 79−61788
pure, vacancy injection during oxidation, reexamination of evidence 78−60864
pure, with max. of cryst. lattice distortion, struct. and strength props. *(Russian)* 80−89234
quantum magneto-dimensional effects, open Fermi surfaces, conduction electrons *(Russian)* 80−80487
quantum oscillation effects in weak mag. field *(Russian)* 79−11105
quenched, vacancy cluster form. process 80−92706
quenching, heat transfer between high temp. solid and boiling water *(French)* 77−62136
radiation blistering developments, review 80−44239
radiation characteristics estimation, classical electron theory *(Russian)* 78−38859
radiation damage, role of He migration, interaction with defects 77−28041
radiation damage and hyperfine fields 78−38752
radiation damage effects, neutrons and heavy ions, rel. to reactor technology, review 77−43255
radiation damage prediction and measurement 78−75693
radiation damage production in stage II, temp. and impurity effects 77−68997
radiation damaged long term strength curve forecasting *(Russian)* 80−34040
radiation defect treatment at annealing stages V and VI *(Russian)* 80−71676
radiation defects, localized deformation of electronic state *(Russian)* 79−87061
radiation effects, ion beam study, review 79−10883
radiation effects on elasticity and elastic moduli, yield stress 80−2078
radiation flux polarised components 78−94566
radiation induced creep, fundamental mechamisms *(Italian)* 80−55457
radiation induced damage, review 78−51580
radiation induced vaporisation, press. behaviour 80−84288
radiation stimulated diffusional flow, neutron irrad. *(Russian)* 79−29132
radiation-induced creep and swelling, radiation dose depend. *(Russian)* 80−29050
radiative electron capture by channelled ions, theory 78−30685
radioactive waste, decontamination by smelting 80−13741
Raman scattering from molecules adsorbed on metal surfaces, enhancement, theory 79−99882
Raman scattering of sound in quantising mag. field 78−60171
rare earth metal impurity in metallic host, exchange interaction, electrical resistivity 80−84453
Rayleigh waves, detect. via electrostatic transducer, NDT appls. 77−19498
reactive, trapping of energetic H^+ ions 78−10096
reactive plasma cleaning 77−44409
recovered dislocation substructure, prod. and utility, review 77−84749
recrystallisation during hot deform. 78−68714
recycling, residual and additive elements control by specifications 80−66522
refining by crystallisation and reflux, three component Raoultian behaviour 77−28799
refining by fractional melting 79−61537
refining in superhigh vacuum, condensation from vap. and zone recrystallization *(Russian)* 79−15604
reflectance changes during laser irrad. 80−93261
reflection of light, nonlinear thermo-optic effect at high intensity 80−93289
reflectivity anomalous behaviour after 10.6 μ pulsed laser irrad. 80−93260
refractory, BCC, free migration of self-interstitials 78−47574
refractory, Cl detect., spectrosc. method *(Russian)* 79−16095
refractory, evaporation in inert gas atmosphere *(German)* 79−55879
refractory, generalised model for prediction of periodic trends in sintering activation 78−64498
refractory, heat treatment and zone melting installation 80−20959
refractory, internal friction meas. from 20 to 2000°C in superhigh vac. 77−86249
refractory, mech. props. and diffusion figures *(Russian)* 80−40436
refractory, nitriding reactions and processing conditions, thermodynamic approach *(Russian)* 80−21169
refractory, safe-life testing *(Russian)* 79−52476
refractory, surface investigation by FIM and atom probe *(German)* 79−55623
refractory, water vapour attack, immersion heater appl. in vacuum radiation furnace *(German)* 80−21184
metals continued
refractory group VI metal, activated sintering mechanism 79−91605
refractory metal, disturbed layer depth on abrasive lapping with TiC, NbC, WC micropowders 77−44391
refractory metal, strength charact., effect of thermal test conditions 78−39994
refractory metal powder adhesion forces on metallic substrates, electrostatic eval. method 77−52564
refractory metal vapour-phase epitaxial growth *(Russian)* 77−59227
refractory metals, enhanced diffusion model for activated sintering 80−25612
refractory metals and alloys, processing by powder and vacuum melting techniques 79−33966
refractory oxide-metal eutectic system 77−36483
refractory single crystal growth by plasma heating *(Russian)* 78−35292
refractory strength charact., error evaluation 77−16771
relaxation, rel. to defect struct. *(Russian)* 78−19801
relaxation resistance testing using constantly loaded sample 78−39965
residual stress and deformation, due to quenching, elastic-plastic anal. *(Japanese)* 78−83268
residual stress on drawing calcs. by stress state changes variational principle *(Russian)* 80−65125
residual stresses, determ. using internal boring technique 80−3263
residual stresses determ., ground and lapped metal surfaces 79−34211
residuals, impurities and props. 80−66521
resistance welding apparatus for metals with high elec. and thermal cond. 77−79077
reversible H embrittlement 80−104292
RF size effect, electron scatt. by impurities diffuse layer boundary *(Russian)* 78−91717
RF size effect, line shape, exactly solvable models 78−43429
RF size effect, small-angle scatt., exactly solvable models 78−47821
RF size effect as tool for cond. electron scatt. investigations 79−23957
rheological interpretation of planar deformed state in extremal friction regime *(Russian)* 80−64385
road transportation, review 78−88622
rod, US heating to onset of plastic deform., temp. field calc. 77−69049
rods, static mech. props. rel. to impulse stress 78−95779
rods, stress state and fracture in pulsed mag. field 80−81201
rolling, critical line nature in multiple-roll passes *(Russian)* 80−38347
rolling, hot longitudinal, periodically charging sections with flash, pressures calc. *(Polish)* 80−89257
rolling moments, calc. for longit. rolling periodically changing sections *(Polish)* 80−89239
rolling of complex sections, unified anal. function of surface of strain focus *(Russian)* 80−21017
rolling theory, deformed and kinematic state eqns. using Gauss principle *(Russian)* 80−65124
rough dielectric and rough metallic surface discrimination, specular scatter depolarisation 80−32911
rough metal surface, depolarisation of scattered light 77−71919
s-p bonded surface, review of electronic struct. calcs. 77−28226
saturation with gas, apparatus for 80−61039
SAW absorption with and without external mag. field *(Russian)* 77−31936
SAW attenuation coeffs. and wave speeds 79−46903
SAW mode conversion by EM generation of ultrasound 80−84357
scaling, theory, electrochem. transport model 78−64761
scattering of conduction electrons with spin flip by dislocations 78−26852
scoring resistance under dry friction *(Russian)* 79−99267
secondary creep rate, comparison of sinh and effective stress creep 79−52321
secondary electron emission coefficient recorder 78−58094
secondary ion mass spectroscopic detect. of H content 77−32854
sediment enrichment and partitioning of metals, Ranafjord, N. Norway 79−83641
segregation, non-equilib., review 80−66516
segregation studies by imaging atom probe microscopy 80−66911
self- and impurity diffusion, connection between preexponential factor and activation enthalpy 77−69111
self-diffusion, atomic jump processes 78−47562
self-diffusion, review 78−47561
self-diffusion, vacancy migration energy 78−51723
self-diffusion acceleration by dissolved H_2 *(Russian)* 78−34647
self-diffusion along edge dislocations by vacancy mech. for FCC and BCC metals *(Russian)* 78−87810
self-interstitial atoms, review 78−47332
semi-infinite, nonlinear interaction of oppositely travelling surface plasmons 79−28393
semiautomatic bridge for high-precision DC resistance measurements on pure metals at low temperatures 79−35788
shaving, densification, effect of intermolecular and electrostatic cohesive forces 77−77445
shear and Young's moduli ratio 77−25088
shear waves, rotary activity under helicon-phonon interaction 80−2412
shearing, scissors type, slip-line analysis 78−23761
sheet, numerical anal. of tensile tests 77−86101
sheet, recovery strain during unloading in tensile test, roll-forming appl. *(Japanese)* 79−100182
sheet, roll bending on machine with elastic element, bending moment determ. 78−6948
sheet, sliding on dies under plane strain drawing, sliding surface damage obs. *(Japanese)* 77−44369
sheet, strain propag. under non-uniformly distributed load 77−16653
sheet for manufacture of scales and grids, one-sided etching 79−32102
sheet metal forming, strain hardening and strain rate sensitivity 78−7000
sheet metals, shearing test using pressure sensitive pin *(Japanese)* 77−48602
sheet parity, pressed, X-ray TV system for automatic analysis *(German)* 77−90536
sheet strength improvement by localised thermal shock 78−88483
sheets, theories of necking and limit strain calc. 79−29115
sheets, yield locus prediction using texture data 79−86347
shell, explosive expansion, rupture behaviour 80−85063
shell, fracture behaviour, forming severity and metal flow in deep drawing 79−38975
SHG by surface polaritons, theory 78−9416
shock wave effect on martensitic transform. *(Russian)* 80−96595
silicide-metal coating system, thermal stresses *(Russian)* 78−13891

metals continued
simple, isotropic Fermi surface, cond. tensor calc., cyclotron waves 79−42528
simple, monovacancy formation parameters, temp. depend. 78−75658
simple, vacancies and vacancy clusters, electronic struct. 79−11077
simple, vacancy and divacancy form. energies and divacancy binding energy 77−35554
simple metals, dynamical calcs. of X-ray absorption and emission spectra 80−55227
simple metals, effect of core hole on X-ray emission spectra 80−20737
simple metals, Fermi energy, density of states 77−76730
simple metals, mech. for transverse linear magnetoresist. 79−23949
simple metals, pseudopot. theory of k-depend. plasmon line width 77−85169
simple metals, solid and liq., electronic struct., mag. susceptibilities calc. 78−52204
simple single vacancy, relax. energy and form. vol. calcs. 78−38691
single crystals, plateaus in cyclic stress-strain curves 79−79054
single electron excitation damping, conduction electron scatt. *(Russian)* 80−15510
sintered compacts, residual pore effect on grain size distrib. 77−85961
sintered strip rolling, algorithm for force and geometric parameters calc. 80−11727
sintering analysis using sintering maps 80−93513
slag-metal equilibrium, thermodynamics 78−44108
sliding contact, glow discharge effect 79−83333
sliding wear, surface topography and integrity effects 78−3235
slow positron studies 80−55223
small metal particles, dielectric function and IR absorption 80−60607
small particles, characterisation and props., book contrib. 80−84417
small particles, far IR absorption cross-section calc. 78−10879
small particles, thermodynamics and paramag. props. of electrons 78−31051
Snoek-Koster relaxation, theory 80−16369
soft film, initial wear rate 80−11795
soft magnetic metals, ideal, AC response 78−64223
soft metal used as solid lubricant, compatibility effects 77−21291
solar water heating system, corrosion 80−30131
solid electrolyte-metal interface adsorption layer capacitance calc. *(Russian)* 80−59697
solid solution hardening theories, review *(Czech)* 80−3084
solid-liquid and solid-solid interfacial energy 79−42396
solidification interface in reduced gravity, bubble interactions 78−84787
solidification models for high cooling rates 79−91639
solidifying, heterogeneous nucleation 78−39754
solubility of H_2, deviations from Sievert law 77−76567
solute atom displacement in mixed dumbbell interstitials for FCC lattice 78−79631
solution, association 78−15373
sorption of H, multiplateau absorpt. isotherms, theory 80−103564
sound absorpt, coefficient at phase transition of order $2^1/_2$, effect of geometry of const. energy surfaces 77−39769
sound absorpt. and dispersion, Fermi surface flattening 78−91596
sound absorption and dispersion temp. depend. associated with Fermi surface plateaus *(Russian)* 80−65166
sound propagation, anomalous, by cond. electrons 80−11048
sound propagation, HF, nonlinear effects 80−88279
sound pulse spike like transport near acoustic cyclotron resonance *(Russian)* 80−100617
space environment, metallurgical studies in Skylab and Apollo-Soyuz 79−47700
space environment research, phenomena and priorities 79−47884
space lattice types A_1, A_2 and A_3, strain hardening function *(German)* 80−20955
spacecraft materials failure, metallurgical exam. 80−71868
spacecraft thermal control materials, low-energy proton effects 80−70288
spallation on emergence of shock wave on free surface, pulse X-ray photography exam. 77−51439
spalling produced by elastoplastic waves 77−80574
spark-source mass spectrometry, relative sensitivity coeffs. 79−92045
spatially dispersive, EM waves and plasmons, propagation 80−15549
specific heat meas. method at low temperatures and high pressures 80−52246
sphere, LF plasma reson., interband transitions effect 79−99906
spherical particles, CESR line shape 77−43886
spin and charge polarisation around mag. impurities 80−75714
spin-lattice relax. model, electron spin-transverse phonon interaction, spin lifetime perturbation calc. 77−12189
spin-orbit coupling enhancement of 3d ions 79−47069
spin-phonon interaction, dynamic screening by carriers, effect on paramag. relax. times 77−16150
spin-susceptibility, exchange-correlation enhanced, calc. 77−85415
splat-quenching device, refractories in magnetic levitation furnace *(Croatian)* 79−11639
spraying methods and appls. 79−66202
sputtered, atomic laser spectrosc. 79−87917
sputtering, cone form. 77−44389
sputtering, effects of adsorbed Cs on photon and secondary ion emission 80−35038
sputtering induced photon and ion emission similarities, O_2 adsorpt. effect 77−28674
sputtering yield, energy depend., semiempirical formula 80−100736
stacking fault energy meas. by electron microscopy *(French)* 79−42079
static and dynamic isothermal elasticity moduli *(Russian)* 80−24524
static electrification, surface charge density 78−14797
static skin effect in metals with open Fermi surfaces, galvanomag. effects *(Russian)* 80−29389
storage of H_2, review 79−10956
strain criteria for fatigue at high cycle loading 79−61712
strain hardening, creep, stress relaxation correlation with high temp. processes *(Russian)* 79−34053
strain hardening criteria eval. 77−55982
strain induced thermal signals, detection 79−1141
strain rate history, endochronic theory of viscoplasticity 80−65122
strength, ionised gas effects, test apparatus for 20-900°C 79−70252
strength, long-term charact., interpolation calc. using generalized curves and computer 77−86121
strength and corrosion tests, NDT, electromagnetic methods, use in anal. of destructive materials testing *(German)* 77−73396
metals continued
strength and corrosion tests, quantitative noncontact meas. of physical and geometric props. *(German)* 78−23909
strength and ductility determination pulsation attachment for TsDMU-30t test machine 79−52538
strength characteristics, high temp., prediction from creep processes 77−86119
strength/ductility relation *(Japanese)* 79−29145
strengthening by electroplastic strain, surfactant effect *(Russian)* 80−20953
stress analysis, at high temp. by finite element method 80−96203
stress and deform. conc. in plastic region during creep, approx. calc. 77−56045
stress conc. caused by grain boundary sliding under power law creep 78−60732
stress concentration sensitivity, scale factor effect on fatigue strength 79−39064
stress corrosion cracking, multisection plan for H_2 absorpt. of metals for tests under cathodic polarisation conditions 79−52504
stress corrosion cracking *(Japanese)* 78−56820
stress corrosion cracking avoidance, critical potential data appl. 79−74308
stress corrosion cracking testing apparatus in rapidly flowing liquid environment *(Russian)* 77−70249
stress relaxation, pre-exponential factor 79−18748
stress to rupture strength charact. at high temps. 77−81321
stress transients, at changes of electron drag during plastic deformation 79−61677
stress-induced EM effect, phys. model 78−55909
stress-strain time dependence based on nonlinear heredity, delayed yielding 78−48452
stress/strain diagram determ. by spherical punch *(German)* 78−76803
strip, high-speed compression, force parameters determ. *(Russian)* 80−21016
strip rolling, kinetostatics *(Russian)* 80−38348
strong, compressive stress/strain props. meas. at very high strain rates, modified Hopkinson bar system 80−85128
structural part, fatigue crack propag., new approach 78−56752
structural state and physical similarity criteria *(Russian)* 79−52298
structure and thermodynamic properties at high temperatures, microscopic theory *(Japanese)* 80−29191
submicron particle heating in hot gas, plasma metallurgy 80−81092
submicroscopic defects, influence on HVEM in-situ expts. 80−103392
submicroscopic surface relief after finishing 79−29276
submonolayer films on metallic surface, struct. and props. review 78−38972
substitutional impurities in solids, entropy and volume of solution 80−15253
substrate, plasma polymerisation, mech., effect of substrate and substrate topography 78−88633
subsurface imaging with photoacoustics 80−74648
sulphidation, high-temp., thermobalance for studying kinetics 78−23876
sulphidation mechanisms, review *(Polish)* 80−45413
superconducting and normal, attenuation, EM generation and detection of US shear waves 78−39261
superconducting properties of metals with $Z \leq 49$ 77−66221
superconducting props. as probe of mag. state of local moments 77−20491
superconducting transition, effect of change of electrostatic interaction of defects 78−10610
superconducting transition temp. of metallic elements and A-15 compounds *(Chinese)* 78−52116
superconductivity studied by electron-phonon and Coulombian e-e coupling strength and quasi particle mass 80−88666
superconductors, polyvalent Brillouin zone boundary influence on Coloumb interactions 80−24827
superpotential flow problems and application to metal forming processes with friction boundary conditions 79−66119
supported crystallites, wetting in sintering and redispersion 80−24751
surface, adsorbed atoms, XPS satellite spectra 77−20993
surface, adsorbed benzene, obs. of vibrational modes 80−6649
surface, adsorbed C^+ layer, removal by Ar^+ impact, 20-30 keV, in plasma 77−76103
surface, adsorbed mol. low energy electron scatt., appl. to Ni-CO 79−56896
surface, adsorbed molecule, IR spectra exam. by surface EM wave spectroscopy 78−71967
surface, adsorbed O and CO, sputtering effects, combined analytical techniques 80−35047
surface, adsorption of neutral molecules, excitation spectrum 79−23832
surface, anisotropic contrib. to optical pot., in electron spectroscopy, theory 80−44086
surface, approached by substrate, surface amplitude patterns 80−75620
surface, atomic and mol. beam scatt., review 80−40203
surface, band effects and dipole interaction between two adatoms 79−33323
surface, catalysed thermal desorption and dissoc. processes, microscopic theory 80−75439
surface, change in refl. on adsorption of molecular monolayer 79−65877
surface, chem. active sites 79−52757
surface, chemical conversion coatings for wear resist., review 78−72893
surface, chemisorption, vac. UV photoelectron spectrometer for study *(Japanese)* 78−62264
surface, clean and adsorbate covered, exptl. aspects of angle-resolved photoemission 78−15294
surface, clean or oxidised, chemisorbed amine, surface ionisation, mass spectra expts. 78−2360
surface, continuous emission spectra of particles ejected by ion beams *(Russian)* 78−55140
surface, dense metallic, diffr. intensities in He scatt., topographic curves 78−15274
surface, electrochemical exam. of multiple states of chemisorbed atoms 77−44512
surface, electrodynamics, optical refl. coeffs. and surface plasmon dispersion law 80−75619
surface, electron and photon stimulated desorption 80−75440
surface, electron beam impact, time-varying evaporation, metastable state lifetime 79−10943
surface, electron beam impact, time-varying evaporation 79−10942
surface, electron density depend. on modulation, adsorption, diffusion 80−54526

metals continued
surface, electron scatt., effect of surface on lattice defects, surface Landau level reson. 79−65534
surface, electron-surface-plasmon scatt. using parabolic nontouching trajectory 77−28228
surface, enhanced Raman scatt. by adsorbates, including nonlocal metal response, nonradiative modes excitation 80−88994
surface, fast ion scatt. by plasmons, theory 80−45190
surface, flash mechanism caused by monochromatic laser radiation 79−95878
surface, Friedel oscillations around adatom 78−30967
surface, giant Raman scatt. by adsorbed mols., review 80−93343
surface, giant Raman scatt. by adsorbed mols., theory 80−93345
surface, heat treatment, using W-inert gas arc 79−96209
surface, heterogeneous cluster ion bombardment, secondary electron emission 80−60742
surface, high-intensity laser beam interaction 80−19600
surface, image-potential-induced states, plasmon model 79−78147
surface, indirect long-range oscillatory interaction between adsorbed atoms 78−71997
surface, interaction with molecules and reactivity, theoretical description 80−39652
surface, interaction with neutron mol. 77−80701
surface, ion beam induced desorption of overlayers 80−59786
surface, ion bombarded evidence for recomb. mech. of cluster emission 79−100007
surface, keV neutrals energy determ. method 80−89100
surface, light refl. from dye molecule monolayer 78−48246
surface, linearised secondary electron cascades, surface and subsurface sources 78−11036
surface, linearised secondary electron cascades 78−11035
surface, linearized secondary-electron cascades, line-shape synthesis 79−74035
surface, low energy atom scatt., theory 78−39648
surface, luminesc. due to equilib. excitation of electrons by laser radiation 80−7399
surface, microalloy layer formation by ion implantation 80−16600
surface, mirror electron microscopy for total electron refl. coeff. determ. 78−5994
surface, mol. chemisorption, self-consistent calc. 79−95260
surface, mol. vibr. energy transfer, classical EM theory 80−96806
surface, $N_2^+(Ar^+)$ energy accommodation coeffs. meas. in rarefied plasma stream by thermoanemometric sounding 80−16722
surface, near point-defect, annealing, diffusion theory and Monte Carlo anal. 78−47646
surface, newly generated, occurrence of salt films during repassivation 79−15860
surface, nonlinear photoelectric effect, laser-induced electron emission 78−19638
surface, normal mode anal. of image pot. 79−33325
surface, optics by reflectance of p-polarised light 79−78706
surface, perturbative calc. of elec. field 80−45108
surface, photoionic emission 78−48287
surface, plasma cleaning and etching, removal of C 80−97645
surface, plasmon mechanism for energy loss, dissoc. and orientation of fast ions excited by grazing collisions 80−11523
surface, reflectivity, single laser pulses, plasma burst effect 78−19609
surface, reson. interaction with neutral mol. 77−80702
surface, resonance interaction with removal mol. 78−84279
surface, rough, anomalous low-freq. Raman scatt. from localised acoustic vibrs. 80−93307
surface, rough, hemispherical emittance 80−70434
surface, rough, reflection loss for s and p polarised waves near surface plasmon freq. *(French)* 80−97225
surface, SHG, hydrodynamic theory of electron gas 80−87437
surface, slow-positron emission 78−95079
surface, spectroanalytical investig. of friction processes and subst. transfer products *(Russian)* 79−34418
surface, sticking coeff. and transmission problem, quadratic phonon coupling effects 80−39424
surface, sticking probability, correl. with adsorbate-induced electron struct. 80−39425
surface, thermionic-field emission anal. 78−19642
surface, thermomechanical treatment by ionic bombardment *(French)* 78−11418
surface, van der Waals interaction with mol. effect of spatial dispersion 78−10534
surface, vibr. motion of adsorbed molecules, inelastic scatt. of electrons, model 78−34718
surface, with adsorbed at., XPS intrinsic plasmon satellites, dispersion and lifetime effects 79−56151
surface, work function, change-in-SCF theory 78−84282
surface, work function change on simultaneous adsorption of atoms of two different elements 78−60184
surface acoustoelectric H-waves, theory 77−69159
surface adatom pair interaction asymptotics, degenerate electron gas permittivity 80−29281
surface atom polarisation energy, effect of depolarisation 79−60620
surface characts., combined ion scattering spectrocopy, SIMS, SEM, energy dispersive X-ray techniques 79−43702
surface charge waves *(Russian)* 78−64077
surface chemisorbed H_2O molecule structure, interband angle 80−59787
surface chemisorption theory, electron localisation, surface interactions 80−84376
surface cleanness control by photoemission recording *(Russian)* 80−49839
surface contamination detection by nondestructive test, surface potential difference meas. method 79−83424
surface crack parameter determ. by diffr. method 79−66237
surface diffusion and atomic interactions, FIM obs. 78−34716
surface electrochemical smoothing, roughness, diffusional pre-electrode layer *(Russian)* 80−76401
surface EM wave enhancement of nonlinear optical effects 77−68240
surface energies, variational calc. 77−24603
surface energies and work function, simple analytic model 80−49862
surface energy, effect of lubricants, plasticity during cold working stresses *(Russian)* 77−55419
surface energy, semi-empirical theory 77−76895
surface energy, temp. depend. 77−72753
surface energy 79−23825
metals continued
surface energy meas. by zero creep method at extremely low O_2 partial press. *(Czech)* 78−63926
surface energy of cubic metals, theoretical eqn. 78−43234
surface finish after diamond turning, differential light scatt. meas. 78−5544
surface finish measurement, using backscattered electron intensity *(Japanese)* 79−4465
surface free energy for BCC, FCC and HCP structs. etch pit depend. 80−29258
surface free energy of solid phase, at MP, estimated from liq. surface tension data 77−31866
surface $H_2 \rightleftarrows H+H$ reaction rel. to catalysis, friction coeff. calc. 77−77807
surface hardening by plasma nitriding 79−8400
surface impedance in mag. field, theory *(Russian)* 78−6427
surface impedance of metal in mag. field normal to surface, reson. singularities 78−10495
surface investigation, IR spectroscopy *(Japanese)* 78−19470
surface laser beam irrad., effective absorpt. coeff., temp. field determ. *(Russian)* 80−76108
surface layer dissolution, effect of rate on softening during plastic strain 78−39957
surface layer transform. and failure, kinetic charact., under dry friction 77−52506
surface molecule enhanced Raman scatt., rough surface spheroidal model 80−84744
surface oxidation study, vacuum microbalance investigation 80−76552
surface oxide covered, primary electron beam effect on secondary emission coeff. *(French)* 79−47563
surface photoemission, spatially-varying photon field effects 80−2921
surface photoemission of model system, book contrib. 78−95665
surface physics, conf., Eindhoven, Netherlands (June 1976) 77−62708
surface plasmon dispersion relation, hydrodynamical model, spherical metal particles 78−84277
surface plasmon modes of voids in irradiated metals 79−60617
surface plasmons on spherical voids, excitation by fast electrons 77−11975
surface positronium formation, stopping distance, positron-phonon interactions 80−96582
surface properties improvements, using vacuum thermal process techniques 79−100283
surface reconstruction, physical realisation of two-dimensional Ising and X-Y model 80−15351
surface relax. from LEED, Fourier transform-convolution method 79−4459
surface relaxation, lattice statics calc. 78−63925
surface rippling induced by surface tension during laser melting and alloying 78−11405
surface roughness meas. using laser speckle 78−8383
surface self-diffusion of single atoms and diffusion of adatoms, activation energies calc. 80−24732
surface SHG, nonlinear response to optical fields 80−83645
surface sliding damage, no lubrication, materials depend. *(Japanese)* 78−56780
surface state angular resolved photoemission, refraction effects 79−38720
surface strain meas. by intensity of reflected light flux 77−17972
surface struct. and initial stages of reactivity, review 78−68837
surface transient heating by CO_2 laser pulses with air-plasma ignition 79−98942
surface treatment, evaluation by microdensitometry *(Czech)* 79−30524
surface treatment, ionic bombardment, new technique *(French)* 77−77643
surface-plasmon dispersion relation, reflectivity of parallel-polarised light 79−78030
surfaces, adhesion theory, electron distribution tail effective length *(Russian)* 79−99430
surfaces, adsorbate spectra, vac. UV differential reflectivity obs. 79−28783
surfaces, and interfaces, slow exchange processes study using SIMS 80−55653
surfaces, catalytic reactions studied by work function meas. 80−55711
surfaces, collective effects in physical adsorption of inert gas atoms 79−19456
surfaces, dipole barrier and work func. calc. 79−15208
surfaces, laser heat treatment, wear resist., corrosion protection, hardening, review 78−72939
surfaces, radioactive contamination 80−68771
surfaces, rough, characterisation by meas. of single roughness constant 80−86264
surfaces, shape and deformations, holographic contour immersion method *(Polish)* 80−62630
Swift effect, dynamic and static response to simple compression, tension and torsion 77−28858
Swift effect, in twisted tubes 77−28859
Swift effect, rel. to stress/strain behaviour in simple compression, tension and torsion 77−28860
synthetic, anisotropy of elec. props. rel. to chem. bond struct. 80−24888
Taylor wires, texture and metastable phases 77−8812
tenacity parameters 80−60973
tensile fracture, transient elec. and mag. field form. 77−4148
tensile strength and butt joint strength, rel. to cohesive energy density, surface tension 77−55431
test device, for thermal cycling conditions 79−87778
testing, thermoelec. temp. meas., error anal. 78−19975
textured cubic, residual stress evaluation 80−89435
textured specimens, with uniaxial symm. ellipsoidal model *(Russian)* 80−80100
textures and collective props. of lattice defects, external surfaces, grain boundaries 77−62543
thermal cond. changes at melting point, vacancy model 79−33279
thermal conductivity, and elec. resist., temp. depend., correl 77−8064
thermal conductivity, pseudoharmonic effects of phonons, high temp. region 80−70326
thermal conductivity model, during hot deseaming *(Russian)* 80−24869
thermal conductivity size effect in normal and supercond. state 78−60245
thermal coupling of 2.8-μm laser radiation to metal targets 80−76107
thermal desorption of adsorbed atoms, dislocation effects 78−47670
thermal diffusivity determ., thermoelastic method 79−23940

metals continued
thermal expansion, equivalence of Gruneisen and Brillouin theories *(French)* 79−77773
thermal expansion, positron response 80−84306
thermal expansion and melting 77−69103
thermal expansion characts. determ. using strain gauges 78−81942
thermal expansion coeff. of defect-entropy volume 78−26707
thermal expansion coeff. rel. to heat capacity 77−43354
thermal fatigue testing, installation for −180 to 1100°C 80−3266
thermal instabilities due to recomb. of radiation-induced Frenkel pairs 79−23597
thermal magnetoresistance, effects of voids 78−91658
thermal props, at high temp., acoustic method, apparatus 79−14222
thermal radiation from surface 79−28114
thermal vibration amplitude of atoms and fusion behaviour *(Korean)* 79−69218
thermal vision systems, theoretical basis of use to monitor boundary stratification in hot metals 80−7748
thermionic electron emission anisotropy 80−20757
thermionic emission during stretching 79−95897
thermodynamic equations of state, complete 80−24561
thermodynamic props., calc. for liq. and solid phases 77−43348
thermodynamic props. of grain and phase boundaries, review *(German)* 79−34012
thermodynamics of solutions, α-parameter approach 77−4207
thermodynamics of solutions, α-parameter approach 77−4208
thermoelastic coeff. meas. by strain gauges 78−56853
thermoelastic distortion in machining metals 80−5939
thermoelectric coefficients, influence of phonon drag *(German)* 77−80766
thermoelectric power, electron-phonon enhancement 77−72855
thermoelectricity, electron-phonon enhancement 78−56135
thermoelectromagnetic waves in conductors in a mag. field *(Russian)* 80−49695
thermoemission props. determ., meas. instrument based on scanning electron beam 78−74025
thermomechanical deformation, analytical description 80−49391
thermophysical charact., peculiarities of temp. depend., dimensional change meas. *(Russian)* 78−95868
thermophysical characteristics for metals with high thermal cond. 77−45833
thickness meas. by backscatt. γ radiation 80−101781
thin layer, impulsive and continuous heating with CO_2 laser 77−40311
thin metal conductors, surface impedance oscills. in RF range *(Russian)* 79−91090
thin metal disks, anomalous microwave transmission 79−60864
thin section fusion weld, US inspection 79−15916
thin sheet, crack growth, effect of strain rate 77−1869
thin sheet, tensile instability and limit strains, growth of surface roughness 77−86084
thin-walled cylinder, elongation upon torsion 80−64386
threshold energy displacement, depend. on bombarding particle energy *(Russian)* 79−90697
threshold energy displacement, depend. on energy of bombarding particles *(Russian)* 79−90698
tight binding metal, vibr. freq. of atom normal to surface, Einstein model 79−51412
time to rupture and accumulation of damage under load *(Russian)* 79−5029
Tokamak, DITE, time resolved metal impurity conc. using RBS anal. 79−1329
torsion pendulum for damping capacity meas. and related phenomena 77−77687
torsional creep under accelerator irradiation, meas. instrument 78−3262
trace analysis in jet engine oils by atomic emission/fluoresc. spectrometer system, computer controlled 80−45587
trace element detection by atom probe microanalysis 80−66910
transient heating by microsecond-duration CO_2 laser pulses with air plasma ignition 79−69915
transport coefficients in strong mag. field, Wiedemann-Franz law and Mott rule 77−69303
transport in hot seawater rel. to Cyprus sulphide ores 77−44997
transport reactions in molten salts, isothermal system *(German)* 77−63568
transport reactions in molten salts, isothermal system *(German)* 77−63569
transversely isotropic plastic props., yield charact. 78−60707
trapped positron, effect of vacancy migration on annihilation 77−48271
trapping of H, book contrib. 80−24491
triboemission from oxide covered metals, meas. apparatus 77−90260
triplet supercond. transition in strong mag. field 80−25040
TSEE, role of surface pot. 77−8732
twinning, HCP struct., relative orientation of cryst. lattices 80−84181
two atom surface coupling, double reson. at plasmon freq., collective effects 80−34934
two-bar struct., creep problems with variable temp. 77−50935
two-phase solid-liq. melt regime, thermodynamic props. eqns. 77−55342
two-phonon sound absorption in quantising mag. field 79−28382
two-way polishing, thermal stresses and surface quality *(Russian)* 80−30151
ultrafine particle, positron annihilation exam. 78−56542
ultrafine particles, eddy current nonlocal calc. 79−60744
ultrafine particles, retardation effects on optical props. 78−6677
uncompensated, interband transition, effect on Curie temp. of ferromagnetic phase transition 79−7994
unfilled f-shell, elec. resist. *(Russian)* 78−72141
uniaxial ferromagnetic, influence of anisotropic fluctuations on elec. resist. near T_c 79−91038
unidirectional solidification, heat flow model 80−79914
unidirectional solidification, in cooled mould, mathematical model 79−11600
unidirectionally reinforced metal composite, complex torsional and tensile loading 79−61669
US attenuation, apparent screening breakdown mechanism 77−27946
US excitation and detection in mag. polarised nonferromag. metals, elastic displacements 78−53091
US excitation and detection in mag. polarised nonferromagnetic metals., dispersion relations 78−56856
US flaw detection of ingots, struct. effect 80−66722
US generation by EM radiation, surface scatt. effects 80−24973
US heating *(Russian)* 77−44258

metals continued
US inspection, echo-mirror method with transform. of elastic waves 80−108663
US propag. factor rel. to fracture toughness props. 78−80698
US quality control standardisation 78−53142
US velocity, effects of deform. and high temps. 78−26626
UV/O_3 cleaning of surfaces, procedure and results 77−25168
vacancies, energy charact. *(Russian)* 77−24314
vacancies, formation entropy, anal. of exptl. data 78−75657
vacancies 77−27879
vacancies and change of surface free energy at melting point 79−42219
vacancies and interstitials, electronic struct. 78−47320
vacancies and lattice elec. cond. determ. method at high temp. 79−37695
vacancy concentration 78−47319
vacancy defect mobilities and binding energies obtained from annealing studies 78−47325
vacancy diffusion during plastic deform., possibility of stimulated electron emission obs. *(Russian)* 79−5007
vacancy entropy of formation due to anharmonic effects 77−62521
vacancy form. vol. from positron annihilation meas. 78−47339
vacancy formation energy, validity of lattice statics at all temps. 77−27877
vacancy formation parameters and Gruneisen constant 78−22709
vacancy porosity kinetics at high irradiation doses of fast neturons 79−28018
vacancy precipitation nucleation during quenching 77−72612
vacancy-solute interaction 78−47409
vacuum heat treatment, efficiency 80−81089
vacuum rolling at high temp. *(Russian)* 79−15708
vacuum-deposited nuclei, model for latent-image centre 79−39170
valence band Auger spectra, effect of edge anomaly 79−69908
valence conduction band transitions, appl. of modulation spectroscopy with synchrotron radiation 78−4710
vaporisation by laser beams, effect of delivery pressure time dependent behaviour *(Russian)* 79−55877
vaporisation by laser irrad., effect of plasma 79−1800
vaporization rate improvement in electron-beam vaporizers with water-cooled crucibles 78−21266
vapour, condensing ejector thermal design 77−61062
vapour, diffusion coefficients in gases, data correl. 79−77330
vapour, partial pressure meas. *(Japanese)* 80−34179
vapour arc, in vacuum, axial mag. field effects 78−87573
vapour columnar arc instability, mag. fields effect, up to 67 kA 78−9893
vessel with glass fibre reinforced plastic reinforcing layer, carrying capacity 78−39876
Vibration modes of split screw dislocations in BCC metals 78−22804
vibrational amplitudes of atoms near melting points, Lindemann's melting law 77−89522
viscoplastic behaviour, anal. 80−6457
viscoplastic constitutive eqns. for cyclic and anisotropic behaviour 77−62162
void growth and time-lag, statistical theory 80−88208
void growth in irrad. sample, fully dynamic rate theory 79−73212
void lattice, plasma oscill. 78−10382
void lattice form., spinodal decomp. of vacancies 78−92234
void surface topology 77−89424
void swelling, depth dependent, by self-ion irradiation, generalized model 79−14856
void swelling and dislocation loop growth on fast particle irrad. *(Russian)* 77−59047
void swelling under irradiation, theory 78−75692
volumetric plastic deform., kinematic and static parameter calcs. *(Russian)* 80−34124
wake potential of ion beams, 'surf-riding' electrons 77−80747
wave movement, resonance phenomena in deformation zone during rolling *(Russian)* 80−65123
wear, dimensional anal. 77−70193
wear, grinding and erosion, microsphere form. mechanism 79−79123
wear, steady state rate calc. from profilometric traces 77−77592
wear debris, morphological anal. 80−76453
wear energy balance under abrasive and boundary friction, expt. 78−85006
wear explanation empirical linear wear law 78−60851
wear mechanisms, review of metal-metal and metal-polymer sliding 79−70174
wear metals in lubricating oils, spectrographic anal. 78−20114
wear resistance, method for rapid determ. 77−25210
weld, submerged arc, metallographic study of chevron cracking 78−56761
weld pool solidification under EM agitation 79−24510
welded joints, pore formation mechanism evaluation, rel. to solidification 80−3017
wettability, using macroscopic theory of mol. forces *(Russian)* 77−66073
whisker, growth axes determ., rapid X-ray technique 77−11830
whisker thickness meas. using MII-4 microinterferometer 78−166
whiskers, quantum oscills. of mag. moment 79−15280
wire, influence of grain boundaries on high temp. creep *(German)* 78−72812
wire, plastic strain during extension, temp. gradient and high density elect. current *(Russian)* 79−57049
wire and bar NDT, electrical and EM methods 80−11865
wire reinforcing rolled glass 80−104107
wires, DC resistance, size effect correction 78−91679
work function, absolute determ. method for metals and semiconductors 77−28697
work hardening anal., appl. of parabolic curve 79−43264
work hardening curves, critical points 79−43263
work-hardening, plastic, sintered, porous, irreversible deform. 78−35459
work-hardening dislocation multiplication model 79−61608
X-ray absorption edges, exciton effects 80−108298
X-ray analysis of inhomogeneities, using STEM with field emission gun 80−59354
X-ray diffr. curves, centre of grav. determ. 77−51271
X-ray emission edges, effect of incomplete phonon relaxation 78−35227
X-ray emission spectra, renormalised first order theory 77−8688
X-ray fluorescence, near absorpt. threshold *(Russian)* 77−4704
X-ray K- and L-emission bandwidths from characteristic electron energy loss values 79−83057

metals continued
X-ray mass absorpt. coeffs. meas. by thin film technique 78−2942
X-ray photoelectron and absorpt. spectra, edge singularities in spin-depend. final-state interactions 78−6810
X-ray photoemission line shape, Fermi surface excitations, book contrib. 79−61499
X-ray Raman scattering, many-body suppression 77−20953
X-ray scattering, reson., theory 78−11017
X-ray self-absorption spectroscopy method for unoccupied valence states obs. *(Russian)* 77−81175
X-ray small-angle scattering, rel. to elec. resist. 79−19125
X-ray spectra, effects of correlation interaction of electrons with deep holes 78−31279
X-ray spectra, final state pot., one-electron theory 80−55230
X-ray spectra, method of effective non-Hermitian Hamiltonian in theory *(Russian)* 77−77323
X-ray spectroscopy 77−55849
X-ray threshold, role of ferromag. exchange interaction 77−90219
X-ray threshold anomaly of simple metals, exponents in theory 77−85838
XPS, anomalous, frequency dependence of exponents 80−71563
XPS, solid-state and adsorbate shifts, equivalent cores calc. 79−28888
XPS and X-ray absorption spectra, thermal broadening of core levels, many-electron effects 78−31284
XPS angular depend. *(Russian)* 79−38722
yield criterion, rheological interpretation *(Russian)* 80−21014
yield strength determ. 80−25937
Young's modulus anomalies under Shoenberg effect conditions *(Russian)* 78−35018
C content determ., isotope-spectral method *(Russian)* 80−55766
C fibre composite/metal joint, fatigue research 78−15497
C high sensitivy meas. using nuclear microprobe 80−50908
H chemisorption, surface sp-conduction electrons, spin-density functional formalism 79−33321
H determ. spectrochemical method *(Russian)* 78−31748
H diffusion, and solubility in solid metals 80−49422
H permeability, general transport eqn. 80−54426
H system, permeation technique for electrotransport studies 77−7903
H-He fluid, phase diagram and transport props., planetary appl. 78−28554
H^+ + metal ion, pot. curve, for exchange, Landau-Rosen and Rosen-Zinner model *(Russian)* 77−75287
H_2, embrittlement, mechanisms *(Russian)* 77−25128
He^3/He^4 high isotope ratio in technical-grade metals and semiconductors 79−86080
NaCl-metal system, sliding and rolling electrification 78−14796
O, determ. in metals, neutron activation anal., sensitivity 78−15742
O_2 covered metals, secondary ion yield, quantitative determ. *(German)* 79−48003
Si and N, simultaneous determ. by deuteron irrad., nucl. microprobe anal. 78−7285

metalworking
see also bending; cold working; forging; hot working
bounded metalworking process, iterative numerical anal. technique 79−83212
cutting tips, BN on Ti and WC-Co, contact reactions 80−61029
electro-optics, conference, Utrecht, Netherlands (Oct. 1978) 80−31420
extrusion apparatus for soft metal wires 78−68871
forging in closed dies, deformation parameters determ., theory and expt. comparison *(German)* 80−25745
fracture initiation mode 78−64662
friction, role in metalworking, and energy saving in deep drawing 80−76271
industrial process principles, book 77−59817
metal sheets, theories of necking and limit strain calc. 79−29115
plastic deformation analysis, plane strain 78−27586
press forming of sheet metal, frictional surface damage 78−76768
pressure, full scale adaptive simulation applied to computer aided management 79−79055
rectilinearity and planarity deviations meas. 79−97348
shearing process, basal section profile effect 79−47754
sheet metal, punch stretching, friction coeff. determ. method 78−27647
sheet metals, ductile, shearing process 78−84841
sheet metals, strain-induced changes in mech. props. and press formabilities 78−19781
steel, heat-resistant, 12Kh1MF, yield point rel. to dislocation density and cryst. lattice spacing *(Russian)* 77−44291
steel, low C, rimmed, structural damage in sheet metal forming 78−64614
steel, stainless/Al laminate, sandwich sheet material, plane strain compression and rolling 79−57062
steel 1Kh18N9T, physico-mech. props. after boring in metallic melts *(Russian)* 78−56736
steel 40Kh, surface working effects on crack resist. *(Russian)* 78−56734
steel 81B45, chevron fracture in tube reduction by spinning 78−64664
toolsetters, optimal adjustment parameters, one-way adjustment 79−97349
tribology, material aspects in manufacturing processes 80−81210
US tube expansion force reduction expts. 78−59186
Al alloy 5182-0, punch stretching, strain and strain rate hardening effects at elev. temps. 79−56998
Al alloys 7178 and M580, chevron fracture in tube reduction by spinning 78−64664
Fe, pig, liquid gas bubble form. at nozzles, acoustic exam. 78−52723
Fe, porous, volume strained, correlation between strength and acoustic props. 77−16770
Ti-Ni alloy, effect on $[Cu(NH_3)_4.(H_2O)]^{2+}$ solns. on drilling *(Russian)* 78−53017
W fibre, KAl, KSi, KSiAl and KSiGa, addition effects on workability *(German)* 78−64557
W-ThO_2 composite, struct., lamination tendency, effects of method of manuf. 78−68653

metamagnetism
antiferrodielectrics with antiferromag. intrasublattice exchange interaction 79−38352
antiferromagnet, one-magnon light scatt. from metamagnetic phase effect of anisotropy 79−33678
antiferromagnet, single-ion anisotropy, theory of metamag. phase transitions 78−39327

metamagnetism continued
antiferromagnetic cubic model, one-dimens., ground states and magnetization in mag. field 79−78372
antiferromagnetic garnets, review 77−80952
chain-like metamagnet, absence of first-order transitions 79−51794
collinear metamagnets, two-sub-lattice Ising model 78−95410
compressible metamagnet, renormalisation group theory of pseudocritical point 80−60337
cyclohexyl ammonium copper chloride, one dimensional spin $^1/_2$ ferromag., mag. props. 80−71000
dielectrics, at finite temp. *(Russian)* 78−88118
disordered metamagnets, random field effects 80−60318
four-ion anisotropy as source 79−47277
free energy calc. for metamagnetic model in field of arbitrary direction 79−95593
Heisenberg metamagnet, collinear, mag. phase diagram 80−71035
hysteresis of metamagnetic transitions 79−15305
insulating material behaviour in external mag. field, microscopic model *(Russian)* 77−43798
intermediate state, theory 78−72360
Ising metamagnet, dilute tricritical point calcs. 80−50099
Ising model, phase diagram and crit. points, const. coupling approx. 78−34991
layer systems, mag. polaritons 78−31060
manganese acetate tetrahydrate, susceptibility and magnetis. meas., crit. exponents and crossover behaviour 77−66309
multicritical points, fluctuation dynamics *(Russian)* 77−27977
nucleation of new phase, role of planar, linear and point defects 77−24695
phase diagram, determ. method 78−68254
phase transitions, temp. depend. anisotropy in classical approx. 79−33481
rare earth alloys, RM_2, (M=Fe, Co, Ni), magnetism, review 80−20365
rare earth compounds, RCo_2 metamagnetic transitions in internal fields 80−60272
rare earth intermetallics, RAu_3 (R=Gd, Tb, Dy, Ho, Er, Tm), mag. props. *(German)* 79−51761
rare earth intermetallics, RCo_2, itinerant metamagnetism, Van Vleck model 79−78297
rare earth-copper intermetallic cpds., RCu_2, metamag., mag. props. 79−87242
rare earth-copper intermetallic cpds., RCu_2, metamag., mag. props. 79−87243
rare earth-Cu intermetallic compds. single crysts., mag. props. 80−54892
rare earth-Ga_2 intermetallics, mag. structs. 78−84394
review of materials, theories and phys. props. 78−19248
semiconductor, metamagnetic, magnetostriction ferrons 78−88160
sublattice metamagnet, temp. dependent anisotropy, magnetisation curves, mag. transitions, classical approx. 80−39795
surface of magnetic systems, multicritical phenomena 77−32208
temperature induced, caused by mag. anisotropy 80−11195
transition, metamagnetic, in magnets with multi-sublattices *(Russian)* 78−23267
transition in absence of mag. field, model 80−97092
3d-transition-metal dichalcogenides, mag. props. rel. to Hubbard model 79−78373
transitions, theory 77−16076
transitions in crystals with low exchange fields *(Russian)* 77−32188
tricritical point, anisotropic Ising model high-field expansions 77−63198
tricritical point, effective exponent 80−71045
tricritical point variation of metamagnet with dilution 79−87266
trimethylammonium cobalt trichloride, AC susceptibility and exchange consts. 80−70961
two-dimensional, tricritical spinodal decomp., Monte Carlo study 80−93117
weak metamagnets, novel multicritical points 79−78398
$Ag_{1/2}In_{1/2}Cr_2S_4$, first order macro to microdomain transition 77−69562
Au-Mn-Cr(Pd) alloy, ferro- to non-mag. transform. 77−12117
$BaCo_2(AsO_4)_2$, planar X-Y model, mag. ordering 77−66256
$Ca_3Mn_2Ge_3O_{12}$ garnet, metamagnetic transition, high anisotropy peculiarities *(Russian)* 80−60274
$Ca_3Mn_2Ge_3O_{12}$, neutron diffr. in mag. field, metamagnetism, antiferromag. ordering 79−65651
$Ca_3Mn_2Ge_3O_{12}$, mag. field induced transition 80−50094
CeAl, mag. props. and mag. struct. 78−6517
Ce_3Al_{11}, competition between ferro- and antiferromag. interactions 80−60258
CeB_6, resist. anomaly and mag. ordering obs. 79−61110
$Ce_2Mg_3(NO_3)_{12}.24H_2O$, ground state with dipole-dipole and exchange interactions in external mag. field 80−84582
CeSb, mag. transition, effect of applied mag. field 78−43590
Co complex, dipyridine chloride, single crystal metamagnetism 78−72345
Co complex, dipyridyl chloride, metamag., mag. struct., NMR 77−85418
$CoBr_2(Cl_2).2H_2O$, linear chain metamag. system, phonon and magnon widths 77−36065
$CoBr_2.2H_2O$, metamagnetic, relax. phenomena at phase transitions 79−24164
$CoCl_2$, one-magnon Raman scatt. 78−43877
$CoCl_2.2H_2O$, metamagnetic transition, microscopic dynamics 77−16073
$CoCl_2.2H_2O$, metamagnetic, ^{55}Mn NMR of impurity spin 77−85613
CoMnP, ferromagnetism and metamagnetism, polarized neutron diffr. study 80−44809
$CoNb_2O_6$, ordered state, field induced mag. transitions 77−16074
$Co(S, Se)_2$, metamagnetic transitions in external fields 80−60272
$CoS_{2-x}Se$, magnetism and metamagnetic transition, neutron diffr. and NMR meas. 80−15717
$Co(S_xSe_{1-x})_2$, $(0 \leq x \leq 1)$, mag. props. and elec. resist. 79−65657
$Co(S_xSe_{1-x})_2$, high field magnetisation, metamag. 79−91253
$Co(S_xSe_{1-x})_2$, metamagnetic transition, ^{59}Co NMR 79−38322
$CrCl_3$, two-dimensional mag. insulator, cryst. field splitting, spectroscopic g-factors 79−47059
$CrCl_3$, two-dimensional mag. insulators, cryst. field spectra, mag. circular dichroism 79−47058
$Cr_{3\pm x}Se_4$, struct., elec. and mag. props. 80−107160
$CsCoCl_3.2H_2O$, pseudo one-dimens. Ising-like system, mag. heat capacity and metamag. transitions 77−66351
$CsCoCl_3.2D_2O$, crit. behaviour along metamag. phase transition 77−59409
$CsCoCl_3.2D_2O$, thermodynamic props. near multicrit. pt. 77−66305

metamagnetism continued
$CsNiF_3$, one-dimens. ferromag. far IR investig. of ferromag. reson., temp. and mag. field depend. 77−66427
DyAG, light scatt. from metamag. domains, crit. exponent determ. 77−66482
DyAG, magnetic tricriticality nonuniversality 79−78392
$Dy_3Al_5O_{12}$, antiferromag., optical birefringence in fields along [111] meas. 77−28540
$Dy_3Al_5O_{12}$, magneto-optical rotation in transverse field 79−73902
DyB_4, mag. behaviour, in strong mag. field *(Russian)* 78−88119
$Dy_2O_2SO_4$, antiferromag., mag. props. and Zeeman effect meas. 79−33464
$DyPO_4$, mag. phase diagram and crit. exponents, MCD obs. 77−66307
$DyPO_4$, mag. transitions under hydrostatic press., neutron diffr. study 80−71030
$DyPO_4$, metamagnet, mag. phase transitions, elastic neutron scatt. study 79−78371
$DyPO_4$, metamagnet, phase diagram, influence of internal strains 79−28544
DySb, magnetisation study, intermediate metamagnetic phase transitions 79−99698
ErB_4, mag. phase diagram, neutron diffr. study 80−50091
ErB_4, theory of metamagnetic transitions *(Russian)* 78−95436
$EuCd_2$, Mossbauer effect, mag. props. and lattice consts. 77−36164
EuSe, spin order and fluctuations, Raman scatt. study 80−97273
$Eu_5Sn_3S_{12}$, mag. and thermodynamic props., metamagnetism 80−60273
Fe complex, $Fe(1,2,4\text{-triazole})_2(NCS)_2$, quasi-2-dimens. $S=^1/_2$ antiferromag., mag. props., hidden canting 80−107986
$FeBr_2$, Faraday rot., optical absorption, multicrit. behaviour 77−4627
$FeBr_2$ metamagnet, unusual phase diagram, theory 80−93119
$FeBr_2$, metamagnetic, optical study of mag. phase diagram 78−56312
$FeCO_3$, metamagnetic insulator Neel temp. anal. by model including spin fluctuations *(Russian)* 80−15715
$FeCl_2$, collinear metamag., mag. phase diagram 80−71035
$FeCl_2$, light scatt., metamagnetic transition effects 77−4513
$FeCl_2$, logarithmic corrections to tricritical scaling 80−65940
$FeCl_2$, magnetic tricriticality nonuniversality 79−78392
$FeCl_2$, magnon-phonon hybridisation, inelastic neutron scatt. study 79−47272
$FeCl_2$, metamagnet, scaling props. of magnetisation and heat capacity, test of tricritical scaling 80−60336
$FeCl_2$, metamagnetic, sound propag. near tricritical point 78−48024
$FeCl_2$, metamagnetic hysteresis, magnetooptical rot. meas. 77−40057
$FeCl_2$, mixed antiferromag.-paramag. state, light scatt. in mag. field 77−40069
$FeCl_2$, one-magnon Raman scatt. 78−43877
$FeCl_2$, optical determ. of thermodynamic phase diagram 78−60285
$FeCl_2$:Cd, thermodynamic phase diagram determ., using pulsed dye laser, piezoelectric modulator, and gated amplifier 79−7991
$FeCl_2.2D_2O$, excitonic Davydov splitting in Raman spectrum 79−33704
$FeCl_2.2D_2O$, magnon-phonon coupling 78−72530
$FeCl_2.2H_2O$, and $FeCl_2.2D_2O$, Raman scatt. at metamagnetic phase transitions, mag. hysteresis 78−14958
$FeCl_2.2H_2O$, antiferromag. metastable state obs. in metamag. transition 77−66314
$FeCl_2.2H_2O$, linear chain metamag. system, phonon and magnon widths 77−36065
$FeCl_2.2H_2O$, metamagnetic, resonant magnon-optical phonon coupling 79−28773
$Fe_xCo_{1-x}Cl_2$, metamagnet, mag. phase diagram by mag. induced light scatt. 80−65883
FeI, magnon energies, phase transitions of eight sublattice model 77−59463
FeI_2, eight sublattices model, antiferromag. reson. uniform modes and metamag. behaviour 77−69498
$Fe_xMg_{1-x}Cl_2$, metamag. percolation, Ising model calc. 79−28542
$Fe_xMg_{1-x}Cl_2$, metamagnetic transition, magnetooptic exam. of mag. phase diagram 77−63175
$Fe_xMg_{1-x}Cl_2$, metamagnet, mag. phase diagram by mag. induced light scatt. 80−65883
$FePt_3$, metamagnetic transitions in external fields 80−60272
$Fe_6Si_4O_{10}(OH)_8$, greenalite, metamag. clay mineral, mag. props. *(French)* 78−88817
Gd_3Al, magnetic properties, 4.2 to 400K, metamagnetism 77−32193
Gd_2In, mag. props., 4.2 to 270K 79−56512
GdN, and $GdN_{1-x}O_x$, mag. interactions 80−60218
$GdN_{1-x}O_x$, magnetic interaction and carrier conc. 80−71005
$(Ho,Y)Co_2$, mag. props., elec. resist. and thermal expansion 78−76246
$HoCu_2$, resist. and magnetoresist., mag. ordering obs. 80−70677
$Ho_2O_2SO_4$, antiferromag., mag. props. and Zeeman effect meas. 79−33464
$HoPO_4$, metamagnet, mag. phase transitions, elastic neutron scatt. study 79−78371
$MnNiSi_{1-x}Ge_x$, mag. props. 77−12118
$NiBr_2$, low-temperature magnetic phase, incommensurate spin structure 80−93082
$Ni_xMg_{1-x}(OH)_2$, random magnet, magnetisation 79−24195
PrAl, annealed, mag. props. and mag. struct. 78−6517
$PrCu_2Ge_2$, magnetic props. 77−32180
$RbCoCl_3.2D_2O$, metamagnetic phase transition, crystallographic and mag. struct., neutron diffr. meas. 80−44174
$RbFeCl_3$, $2H_2O$, pseudo one-dimens. Ising-like system, mag. heat capacity and metamag. transitions 77−66351
$RbFeCl_3.2D_2O$, cryst. and mag. struct., neutron scatt. and NMR expts. 79−7969
Tb_2Au, mag. props., 4.2-300K 79−7972
$TbCo_2$, polarised neutron diffr. exam. of mag. struct. 79−73681
TbF_3, mag. phase diagram, crit. and tricrit. behaviour 78−14959
$TbFeO_3$, metamag. phase transitions, mag. struct. instability *(Russian)* 79−61107
$TbMnO_3$, mag. struct., ordering of Mn^{3+}, Tb^{3+} moments, neutron diffr. expt. 77−69500
$TbNi_{2-x}Cu_x$, elec. resist. and mag. props. 78−72348
$ThCo_5$ itinerant electron metamagnetism, polarised neutron study 80−39742
$ThCo_5$, mag. transition due to Co moment change, metamagnetism of 3d-band 77−63184
TmB_4, mag. behaviour, in strong mag. field *(Russian)* 78−88119
TmSe, mixed valence systems, spin dynamics and mag. ordering 78−68162
TmSe, mixed valency, field-depend. mag. phase transitions 78−10657
metamagnetism continued
TmSe, valence mixing, mag. props. obs. 80−70648
$Tm_xSe_yTe_{1-y}$, magnetic ordering studies *(German)* 80−54882
YCo_2, density of states, mag. props. 79−90936

meteor trails *see meteors*

meteorites
see also meteors; micrometeorites
Abee, C rich material with high volatile element content, implications 80−85908
Abee, enstatite chondrite, thermal history 79−30019
Abee, noble gases and gas-rich fractions, stepwise heating study 78−49403
Abee meteorites, mobile element transport in heated sample 80−36586
ablation model for large meteorite entry, theory and obs. 79−66967
ablation process, modelling, lab. expt. of supersonic plasma flow interaction 77−87351
abundance anomalies, rel. to explosive neutron processing of stellar He burning shells 79−58302
achondrite meteorites, mag. effects of brecciation and shock 80−8603
achondrite parent body, chemical history rel. to Earth and Moon 77−60639
achondrites, Mg-Cr relationship 80−51704
achondrites, petrogenetic model 80−4312
acoustic-gravity waves generated in atmosphere *(Russian)* 80−21795
Adelaide, member of new subgroup of carbonaceous chondrites 78−65573
Adelaide meteorite, carbonaceous chondrite description and chemical anal. 79−2532
aerolites from Moon, translation of 1808 dissertation 77−87622
Allan Hills, terrestrial ages, consequences for Antarctic ice 79−88631
Allan Hills 77005, achondrite petrological study 80−21949
Allan Hills 77005, new meteorite type found in Antarctica 80−26824
Allegan, size and shape meas. of near-spherical chondrules 78−65555
Allende, ^{26}Al and inert gas composition 80−98620
Allende, ^{33}S anomaly 78−49402
Allende, amoeboid olivine aggregates, trace element anal. 80−17553
Allende, Ba and Nd isotopic anomalies in Ca-Al-rich inclusions 78−32409
Allende, Ca, Mg isotopic comp. of individual crystals, direct loading technique 78−32417
Allende, Ca and Mg isotopic anomalies and lack of ^{26}Al in unusual inclusion 79−40142
Allende, Ca isotope anomalies in Ca-Al-rich inclusions 78−32410
Allende, chem. props. reveal condensation sequence in presolar nebula 80−26758
Allende, chondrite, occurrence of Fe-Ni-Cr-S-O compounds *(French)* 78−32411
Allende, CV3 carbonaceous chondrite, composition of metal particle 77−5510
Allende, element anal. using laser mass spectrometer 79−16717
Allende, evidence for ^{244}Pu in early solar system 77−29663
Allende, evidence for new cosmothermometer based on Ti^{3+}/Ti^{4+} ratio 79−12437
Allende, evidence for supernova trigger for solar system form., description 80−12683
Allende, excess ^{26}Mg in anorthite crystal, ion microprobe obs. 78−40882
Allende, I-Xe dating of inclusions 80−67666
Allende, isotopic anomalies, rel. to He-driven r-process in supernovae 78−57567
Allende, Mg isotope anomalies 77−78725
Allende, Mg isotopic anomalies rel. to ^{26}Al stellar nucleosynthesis 79−5809
Allende, mineralogy and petrology of isotopically unusual Ca-Al rich inclusion HAL 80−109399
Allende, molybdenite in Ca-Al-rich inclusions 78−12170
Allende, multielement neutron activation anal. scheme appl. 77−48739
Allende, Ne and Ar isotopes meas. 77−87344
Allende, neutron multiple emission, evidence for new fissioning nuclide *(Russian)* 77−87352
Allende, new fissioning nuclide, chemical conc. *(Russian)* 77−87353
Allende, noble gases and gas-rich fractions, stepwise heating study 78−49403
Allende, noble gases isotopic anomalies in separated minerals 77−33430
Allende, normal $^{39}K/^{40}K$ ratio for inclusions confirmed 80−26820
Allende, O isotope anomalies 77−78724
Allende, primordial refractory metal particles 80−85906
Allende, rhonite-bearing Ca-Al rich inclusion mineralogy 79−2530
Allende, S content, neutron capture gamma-ray spectroscopy 80−94728
Allende, search for ^{26}Al effects in FUN inclusion (Cl) 79−16896
Allende, search for ^{41}K anomaly prod. by proton-associated alpha-irradiation 78−49398
Allende, search for fission tracks from superheavy elements 78−32415
Allende, Sm isotope anomalies 78−89134
Allende, Sr isotope anomalies 78−89133
Allende, superheavy element search 80−21752
Allende, Te, Xe and Kr isotopes, record of nucleosynthesis 79−40147
Allende $^{238}U/^{235}U$ ratio, early Solar System ^{247}Cm evidence 80−90347
Allende (C3) thermal metamorphism, noble gases, C and S 79−92732
Allende C3 chondrite, search for Xe fission fragment recoil 80−62083
Allende chondrule magnetisation and solar nebula mag. field 80−36520
Allende inclusion, Sr anomalies and p-process odd-A abundances 78−93101
Allende inclusion EK1-04, Sm isotopic anomalies 79−35208
Allende inclusion HAL, member of FUN family, O isotopic study 80−105211
Allende meteorite, ^{40}Ar-^{39}Ar ages 80−98621
Allende meteorite, ^{40}Ar-^{39}Ar dating of pre-4550 Myr inclusions 79−35212
Allende meteorite, isotopic anomalies rel. to cosmochronology 80−4462
Allende meteorite, neutron activation anal., isotopically anomalous Xe and $^{184}Os/^{190}Os$ ratio 77−45368
Allende meteorite, Sr fractionation in Ca-Al inclusions 80−46503
Allende meteorite chondrules, primordial mag. field meas. 78−49399
Allende meteorite gas rich minerals chemical characterization 77−17449
Allende meteorite inclusions, trace element distrib. in mineral separates and genetic implications 78−49400
Allende meteorite trace elements, results from coarse-grained inclusions 78−49401
Allende mineral grain inclusion, excess ^{129}Xe meas., chronological information 80−67675

meteorites continued
Alta'ameem, hypersthene chondrite, mineralogy and chem. comp 79-25554
amphoterite chondrites, mag. effects of brecciation and shock 78-65565
analysis, neutron activation, using standard reference materials as multielement irrad. standards 78-80815
Angra dos Reis, ^{244}Pu distrib. and cooling history 77-82181
Angra dos Reis, chemical and microprobe study of Fe meteorite *(Italian)* 78-77523
Angra dos Reis, crystal field spectra of fassaite 77-78723
Angra dos Reis, crystal struct. and comp. variation of fassaite 77-82186
Angra dos Reis, isotopic and chemical investig. 77-82182
Angra dos Reis, O fugacities as function of temp. 77-82187
Angra dos Reis, origin and history 77-82183
Angra dos Reis, Sm-Nd-Pu timepieces 77-82180
Angra dos Reis, struct. and comp. of $Ca_3(PO_4)_2$ minerals 77-82185
Angra dos Reis and other achondrites, origin 77-82184
Antarctic C2 carbonaceous chondrite, meteoric origin, amino acid existance 80-67674
Antarctic meteorite Yamato 74123, new ureilite 79-35206
Antarctic meteorites, review of discoveries and significance 80-8597
Antarctic meteorites, trace element contents, weathering effect 80-56784
Antarctica, petrography, mineralogy and chem. of new meteorites 79-21240
asteroid IR spectral obs. indicative of achondrite parent body, 349 and Vesta 80-98595
astroblemes on Earth's surface, review 80-98324
astrons, cosmic impact features, role in geological evolution 77-56632
Atlantic, stone, inert gas content, isotopic composition 80-46506
atmospheric cosmogenic radioisotope flux variation due to cosmic dust and meteoritic matter 78-61634
atmospheric entry, expansion, decel. and intense shock wave emission 77-37584
Barwell preatmospheric size, cosmic ray track fusion crust and thermoluminesc. study 78-53893
basaltic achondrite meteorites, rare earth element abundance patterns rel. to origin 80-36581
basaltic achondrite parent body rel. to Rb-Sr meas. of eucrites 78-65561
Bench Crater, member of new subgroup of carbonaceous chondrites 78-65573
Bencubbin meteorite, metal clast origin, evolution model 80-8599
Bencubbin polymict meteoritic breccia, form. 78-96443
Bereba, ^{26}Al and inert gas composition 80-98620
Binda howardite, ^{87}Rb-^{87}Sr chronology 80-26819
Bjurbole, chondrule mass distrib. and Rosin and Weibull statistical functions 79-35201
Bjurbole, L4 chondrite, size and shape of chondrules 77-29734
Bjurbole and Chainpur, size and mass distrib. of chondrules 78-65556
Bjurbole chondrite, origin of fission fragment tracks in whitlockite 78-81595
bombardment of planetary surfaces, evidence *(Russian)* 79-101098
British Museum (National History) collection, chemical anals. 78-65569
Bruderheim, L6 chondrite, U-Pb age and 500 Ma shock event in L-group meteorites parent body 80-98616
Buenaventura (Mexico), new Fe meteorite find, discovery, classification and mass 78-65571
C1 carbonaceous chondrites, vein form. 79-2533
C1 chondrites, Earth and Moon origins, siderophile and volatile elements 78-7892
C2, C3 carbonaceous chondrites, grain size and petrography 79-2529
C2 chondrite meteorites, evidence for chemical fractionations 80-109400
C3 carbonaceous chrondrite (Ornans), noble gas component of minerals 80-51698
Canon City meteorite, ^{37}Ar and ^{39}Ar radioactivities 80-36582
Canyon Diablo, iron meteorite, shock effects in phosphide and carbide phases 77-56879
Cape York, Fe, Mossbauer and X-ray spectra of ordered Fe-Ni phase 77-78727
Cape York (III.A), Fe meteorite, Mossbauer study of taenite lamellae 78-65575
carbonaceous chondrite fission Xe, elimination of ^{248}Cm as possible progenitor 77-37581
carbonaceous chondrite groups, refractory elements fractionations obs. 80-36595
carbonaceous chondrite Kr and Xe isotopes, studies of ^{248}Cm and ^{250}Cf spontaneous fission products 80-63215
carbonaceous chondrite material on Deimos, spectral evidence 80-41754
carbonaceous chondrite matrix, new phyllosilicate types 79-80285
carbonaceous chondrite matrix composition 78-12168
carbonaceous chondrite mineralogies, remote spectroscopic identification in Ceres and Pallas 79-96946
carbonaceous chondrite origin and classification, review 80-56781
carbonaceous chondrites, amino acids 79-88632
carbonaceous chondrites, B concs. 79-16897
carbonaceous chondrites, Be and B abundances, interstellar grain synthesis 79-16894
carbonaceous chondrites, C2, formation chronology 77-5509
carbonaceous chondrites, C2, origin of isolated olivine crystals 78-53890
carbonaceous chondrites, C3V and C3O, chemical fractionations 77-9712
carbonaceous chondrites, comparison with solar Na/Ca and S/Ca ratios 77-29735
carbonaceous chondrites, constraints on origin of chondrules and inclusions 78-32421
carbonaceous chondrites, distrib. of pre-solar component 77-37582
carbonaceous chondrites, fission Kr and Xe origin 79-35199
carbonaceous chondrites, H/D ratio study 80-46497
carbonaceous chondrites, ion beam analysis 80-62089
carbonaceous chondrites, isotopically anomalous noble gases, comments on criticisms 79-75163
carbonaceous chondrites, Li, Be, B abundances rel. to cosmic-ray nucleosynthesis 79-17084
carbonaceous chondrites, nature and origin of isolated olivine grains 77-64711
carbonaceous chondrites, Ne in gas-rich samples 78-65559
carbonaceous chondrites, organic polymer anal. rel. to organic matter origin in early solar system 78-20767
carbonaceous chondrites, parent bodies form. 80-36580
meteorites continued
carbonaceous chondrites, primitive grain clumps and organic compounds 77-2374
carbonaceous chondrites, rare gas-rich separates 79-62796
carbonaceous chondrites, reduction kinetics, Mossbauer obs. 80-41777
carbonaceous chondrites, solar system B abundance determ. 77-49318
carbonaceous chondrites, superheavy element fission hypothesis for Xe origin 77-78726
carbonaceous chondrites, type 2, origin of isolated olivine grains 79-30020
carbonaceous chondrites, type III, chem. comp. *(Russian)* 77-9718
carbonaceous chondrites ^{15}N/^{14}N ratios, isotope fractionations in Fischer-Tropsch and Miller-Urey reactions 80-46496
carbonaceous chondrites of Ornans type, metamorphic sequence 77-87341
carbonacous chrondritic matrix material planet forming unit, occurrence, formation review 78-53892
Carlton, octahedrite, analytical electron microscopy of plessite struct. 78-32422
catalogue of 230 terrestrial impact structures 77-73741
Chainpur, D anomaly *(French)* 79-88628
Chainpur, LL3 chondrite, size and shape of chondrules 77-29734
Chainpur, volatile elements concs. in chondrules 79-101121
Chainpur LL3 chondrite, and H isotope study 80-36518
Charlevoix structure, Quebec, shock produced mosaicism in plagioclase 77-44988
Chassigny, achondrite, abundances rel. to ureilites and nakhlites 77-41363
Chassigny meteorite, cumulate dunite with hydrous amphibole-bearing melt inclusions 79-21235
Chenier Crater, on Moon, impacts rel. to lava-like material origin 78-81569
chondrite, fluid drop chondrule size freq. distrib. 80-36588
chondrite classification and metamorphism based on metal phase composition 80-98619
chondrite exposure ages study using spallogenic ^{53}Mn 79-53776
chondrite magnetisation meas. 80-36599
chondrites, ^{129}I/^{127}I early solar system chronometer 80-62043
chondrites, ^{40}Ar/^{39}Ar dating of collisional events in parent bodies 77-17452
chondrites, C3-type, trace element anal. 78-69756
chondrites, CI and CM, discordant, leaching experiments, Rb-Sr studies 79-84754
chondrites, cosmogenic isotope radioactivity, galactic cosmic ray solar latitude variations 80-101507
chondrites, crystallisation of chondrules 80-77361
chondrites, Fe-Ni superstructure in metal particles 80-12713
chondrites, H and C3, norm calcs., Fe_2O_3 content estimation 77-87350
chondrites, H- and LL-group, trace element content 78-12166
chondrites, kinetics of volatile loss 80-4311
chondrites, LL and C1, C, N and noble gases, origin and abundances rel. to terrestrial planets 78-28559
chondrites, microscopic obs. of Ni-Fe particles *(Russian)* 77-9724
chondrites, nebular condensation of moderately volatile elements 78-12163
chondrites, nebular condensation of moderately volatile elements, comments and reply 78-12164
chondrites, noble gases, exposure ages rel. to ^{26}Al ages 78-7949
chondrites, noble gases abundance in separated minerals 77-33429
chondrites, porosity estimation by image anal. of polished sections *(French)* 79-71009
chondrites, rare gases trapping during condensation of solids 79-66965
chondrites, remanent magnetisation rel. to shock and metamorphic history 80-36598
chondrites, severely reheated, metallic microstruct. and thermal history 78-12167
chondrites, slightly or not shocked, microscopic struct. *(French)* 77-29736
chondrites, thermoluminescence 80-51706
chondrites, trace elements in metal, silicate and sulphide phases 77-9711
chondrites, U isotopic comp. 78-4157
chondrites and 'mysterite' as late condensate in solar nebula 78-7946
chondrites and C1 carbonaceous chondrites origin, rel. to solar gases in meteorites 79-71008
chondrites of H-group, thermal history by orthopyroxene struct. 80-46499
chondrites primordial noble gases, abundance pattern established in solar nebula 78-32424
chondritic meteorites, chemistry, analytical scheme, appl. to Cocklebiddy 79-2483
chondritic meteorites, rare-earth abundances 79-21234
chondritic meteorites, search for U isotopic anomalies 80-85903
chondritic meteorites rel. to terrestrial rocks, meteoritic Earth model validity *(Italian)* 77-44982
chondrule anal. using PIXE 77-49344
chondrule formation, constraint on impact theories 77-82178
chondrules, origin 80-4310
chondrules origin, chemical energy in cold-cloud aggregates 80-105210
chondrules textures, experimental reproduction 80-94763
chromite grains in Fe formation from Early Precambrian Isua supracrustal belt, W. Greenland, probable cosmic origin 80-72508
CI carbonaceous meteorites, magnetite morphology and form. in parent body 80-51707
CI chondrites, origin of sulphide minerals 79-80282
CI meteorites, new sulphide phase, cubanite discovery 78-12173
classification systems *(Polish)* 79-101123
Clearwater Lake impact structures, Quebec, meterotic component and impact melt comp. 78-65314
CM, refractory-element-rich inclusions 79-30022
CM chondrite, aq. alteration inferred from matrix chem. 80-62084
Cold Bokkeveld, carbonaceous chondrite, Ne in gas-rich samples 78-65559
Collescipoli meteorite, H-5 type, fusion crust glass fragments, electron microprobe obs. 80-67669
collisions with planets, review 79-8884
composition, influence on solar system formation *(French)* 79-92687
conference, 42nd Annual Meeting of Meteoritical Society, Heidelberg, Germany (1979 September 3 to 7) 80-62374
Conquista, Minas Gerais, chondrite, mineralogy, petrology and chem. 79-25553

meteorites continued
cooling rates of group IVA iron meteorites determined from a ternary Fe-Ni-P model 79−66964
Copiapo group IA Fe meteorite, cooling history 80−36578
cosmic ray induced fission of heavy nuclides, influence on apparent ^{238}U fission track ages 79−40047
cosmic ray produced ^{53}Mn in meteorites, neutron activation anal. 79−30018
cosmic ray tracks to determine galactic cosmic nuclei time averaged abundance 80−101513
cosmic spherules from deep-sea sediments, surface features and origin 77−41361
crater field formation, effects of meteoroid atmospheric breakup 80−94760
crater formation modelling, meteorite impact effects 80−90088
crater structures, Kola Peninsula 79−70802
cratering by meteorite impact 79−21244
cratering processes, erosion of material layer which loses charact. props. during regolith reprocessing 80−62053
craters, geophysical and geomechanical aspects 80−17265
craters, Morasko, Poland 79−20837
craters probable number in USSR, calc. 77−66921
Darwin glass and crater, gravity survey 80−67365
deep-sea sediment magnetic spherules, $^{40}K/^{41}K$ ratio rel. to possible meteorite origin 78−11874
Dehesa, Fe meteorite chem. classification 80−109403
Del Rio ataxite, Ni content, mineral inclusions 77−74018
Denver City (Texas), anomalous Fe meteorite find, discovery and mass 78−65571
Dhajala, chondrite, cosmogenic radioisotopes rel. to interplanetary cosmic ray vars. 79−35207
Dhajala, H-group chondrite, strewn-field fragments spatial distrib. 78−32423
Dhajala, India, cosmic radiation effects, fossil track studies 80−72733
Dhajala, orbital elements determ. for meteoroid 78−36540
Dhajala, unequilibrated H3 chondrite, props. 78−32425
Dhajala H-group chondrite, cosmogenic and radiogenic noble gases 78−16360
Dhajala meteorite, ^{37}Ar and ^{39}Ar radioactivities 80−36582
Dhajala shower, atmospheric fragmentation and ablation based on cosmic ray track obs. 77−82188
diamond-containing meteorites, polished thin section preparation technique 78−65566
Djermaia (H) chondritic breccia, preirradiation history 80−36579
dynamic processes on Earth, extraterrestrial causes, rel. to extinction of life 78−92820
Eagle Station pallasite, cosmic ray tracks, ultraheavy (Z>52) nuclei abundances 77−9641
Earth impact, primitive ocean basins form. 79−20770
Earth surface large scale circular structures, possible impact craters 78−28237
East Anglia, England 1646 fall record 79−96978
East Anglian 'meteorite' of 1646, meteorological interpretation 80−68009
Efremovka, neutron multiple emission, evidence for new fissioning nuclide *(Russian)* 77−87352
El Quemado, stone found near Acapulco, preliminary report 80−82318
element analysis of geological and extraterrestrial samples, laser mass spectra 79−16717
Elgygytgyn meteorite impact crater, Siberia, probable source of Australasian tektites 77−91135
Emery mesosiderite, cooling rate rel. to schreibersite growth 79−35211
enstatite achondrites, origin, E-type asteroids as parent bodies 78−32384
enstatite chondrite, Bi and Pb microdistribution obs. 80−62085
enstatite chondrite, mineralogy and petrology rel. to solar nebula composition 80−51699
enstatite chondrites, ^{87}Rb-^{87}Sr chronology 80−8596
enstatite chondrites, siderophile element fractionation 80−98617
Estacado, thermoluminescence and 'terrestrial age' determ. 79−2535
Estherville, Nakhala and Odessa, fission track records 79−35209
Estherville meteorite, electron-optical obs. of ordered FeNi 80−62088
eucrite parent asteroid, bulk composition, planetary evolution bearing 80−56786
eucrite parent body, chemical comp. rel. to Earth and Moon 77−60636
eucrite parent body, chondritic comp., inference from trace elements 78−69755
eucrite parent body comp. and evolution, evidence from rare earth elements 78−20766
eucrites, expt. petrology 77−87343
eucrites, major and trace elements, preliminary modelling 80−51704
eucrites, parent body size from melt/solid segregation numerical treatment 79−40144
extinct radioactivities, as trapped residuals of presolar grains 77−49342
extinct radioactivities, trapped residuals of presolar grains 77−45367
fall observations anal. 80−62090
falls, science and social intelligence about anomalies 79−40346
falls and crater formation *(Polish)* 79−88630
falls and finds during 1966-74 period *(Japanese)* 78−57514
Farmington, last parent body remains undiscovered *(Russian)* 79−101124
Farmington chondrite, U-Pb abundances and Pb isotopic studies 80−56778
Faucett chondrite, Buchanan County, Missouri, petrography and chemistry 77−74019
fireballs photographed in central Europe, classification and relation to meteorite falls 78−36534
flux recent temporal changes, from lunar sample data 79−2534
Galatia, Kansas, chondrite, mineralogy, petrology and chem. comp. 79−21242
gas-rich meteorites, volatile element trends 80−51701
glass formation by meteorite impact, EPR study 80−85659
glass particles impacting on metal barriers, piercing, stony meteorite simulation 78−89043
Goat Paddock cryptoexplosion crater, W.Australia struct. and shocked rocks petrology 80−98322
Gorlovka chondrite, cosmogenic isotope concs., data on galactic cosmic ray anomalous behaviour (1971-4) 78−61695
Governador Valadares, Nakhlite achondrite, age determ., 1.3 aeons 77−33428
Gow Lake, N.Saskatchewan, terrestrial meteorite impact crater 78−7640
Grant, disintegration during Earth atmosphere entry 77−67080

meteorites continued
Grefsheim meteorite, Norway, mineralogy of L5 chondrite 80−36591
H chondrites, ^{87}Rb-^{87}Sr chronology rel. to parent body evolution 79−44421
H-type chondrites, noble gas-rich separates 80−85907
Happy Canyon, new type of enstatite achondrite 77−91492
Haviland meteorite crater site, location and photograph 80−51399
heavy-ion tracks, etchable ranges 77−30734
hexahedrites, cooling rates 78−57511
hexahedrites, platelike schreibersite habit planes 78−65572
hexahedrites, shock transformed, sensitivity to grain boundary corrosion 80−72894
history of meteoritics, early chemical and mineralogical work 77−71175
Hoba, ataxite, low temp. impact props. 79−80283
Holbrook chondrite, chem. alterations due to terrestrial weathering 79−71007
Holbrook chondrite, vapour phase comp. from mass spectrometry 78−65568
Homewood hypersthene chondrite, chemistry and mineralogy 80−51703
howardite, metal composition and origin 80−72888
howardite parent body, layered crust model 80−36554
howardites and mesosidrites petrography and neutron activation anal. 80−8598
hypersthene, fresh and fossil tracks, rel. to Fe abbundance in cosmic ray flux 77−41276
hypersthene chondrites from three French falls *(French)* 79−44417
IAB irons, ^{40}Ar-^{39}Ar date of inclusions 80−62086
Ibitira eucrite, mineralogy, comparison with other eucrites and lunar rocks 77−5512
igneous lithic clasts from mesosiderites and howardites, petrography and chemistry compared with eucrites and diogenites 80−72890
impact, craters, internal struct. model 78−44825
impact and ejecta depostion on airless planetary bodies, topographic effects 78−65523
impact and explosion craters on Earth and Moon 78−45296
impact and impact-explosive craters, destruction asymm. *(Russian)* 77−9726
impact blast, gasdynamical models and two-dimens. unsteady computs. 77−60565
impact crater, central Alaska, possible glacial origin 79−25249
impact crater discovered in central Alaska with LANDSAT imagery 77−91136
impact craters, diameter to depth ratio dependence 80−94765
impact craters, modification by fallback ejecta 80−82317
impact ejecta, depend. of mass and energy lost on planetary escape vel. 78−45295
impact erosion on moon and planets 78−57476
impact on glass, surface erosion 77−90445
impact structure, Gosses Bluff, Australia, gravity investigation 80−72520
Indarch enstatite chondrite, cathodoluminescence of clinoenstatites 80−36596
inert gas abundance patterns, Sudbury phenomenon *(Japanese)* 77−73735
inert gas content, solubility in serpentine 80−12712
inert gas isotope and element anomalies, He and Xe 80−56779
initial and terminal mass calc. 78−20769
Inman, McPherson County, Kansas, meteorite, mineralogy, petrology and comp. 79−2527
Innisfree, Canadian camera network record and orbit determ. 78−65563
Innisfree, fireball photograph, meteorite recovery on Earth 78−61821
Innisfree meteorite, description of fall and orbit 77−71070
IR (JHK) photometry, of meteorites and asteroids 79−2531
IR spectra, comparison with astrophysical IR features 80−26728
irons of group IA and IIA, phosphide morphology revealed by Cl_2 etching 80−36593
irradiation and accretion in space, evidence from obs. of lunar rocks and grains 77−60562
isotope abundance anomalies, astrophysical implications 80−46511
isotope abundance anomalies, cosmological implications 80−46510
isotope abundance ratios, determ. with Si whisker field desorption ion source 80−11975
isotope anomalies, rel. to supernova trigger for solar system formation 78−77499
isotope fractionation, expts. under simulated space conditions 78−73623
isotopic anomalies, injection into early solar nebula 79−101094
isotopic anomalies, presolar grains from supernova ejecta 78−20845
isotopic anomalies, rel. to explosive nucleosynthesis 79−62795
isotopic anomalies, rel. to supernovae and solar system origin 80−17509
isotopic anomalies, role of grains as carriers in early solar nebula 80−26757
isotopic anomalies from neutron reactions during stellar explosive C burning 80−12651
isovaline radioracemization, cosmochemical implications 80−62087
Italian chondritic meteorites, Cu, Ir, Pt and Au content by destructive neutron activation anal. 78−12172
Itapicuru Mirim chondrite, Brazilian meteorite, mineralogy, petrology, chemistry 78−81594
Ivory Coast microtektite strewnfield: new data 79−66697
Jilin, organic compounds 80−17557
Jilin, thermolumin. of IV-1 Nanlantum meteorite 80−90372
Jilin chrondrite magnetism *(Chinese)* 78−85917
Jilin meteorite swarm, trajectory calc. *(Chinese)* 79−35198
Jiling (Kirin) meteorite, description 78−85918
Jodzie howardite, CM xenoliths characterisation 80−62082
Juvinas, ^{26}Al and inert gas composition 80−98620
Kaalijarv, chem. comp. and struct. group IA Fe meteorite classification 77−67079
Kakangari, a unique chondrite 77−29738
Kakangari, unique chondrite, noble gases comp. 78−65570
Kamiomi olivine bronzite chondrite; mineralogy, petrography and chemistry 80−51702
Kapoeta howardite, $^{40}Ar/^{39}Ar$ chronology of lithic clasts 80−46501
Karoonda (C4) chondrite, volatile/mobile trace elements abundances 78−20768
Karoonda meteorite, classified as Vigarano type carbonaceous chondrite by chem. composition 80−36590
Kenna ureilite, C and S abundances 77−41365
Kenna ureilite, diminished ^{26}Al activity 77−41368
Kenna ureilite, evidence for igneous, metamorphic, and shock origin 77−41362
Kenna ureilite, O isotopic composition of minerals 77−41367

meteorites continued
Kenna ureilite, rare gases and fossil particle tracks 77−41366
Keyes, ^{21}Ne cones. rel. to Mg(n,α)Ne cross sections at 14.1 and 14.7 MeV 79−96874
Kinsella (Alberta), new Fe meteorite find, discovery, classification and mass 78−65571
Kirin, China, 1976 March 8, large scale shower obs. *(Chinese)* 78−24495
Kirin, China, 8th March 1976, large scale shower obs. *(Chinese)* 77−17453
Kirin, cosmogenic radionuclides study *(Chinese)* 79−21237
Kirin, fusion crust, microstruct. from SEM study *(Chinese)* 79−2525
Kirin chondrite, Rb-Sr age and Sr isotopes *(Chinese)* 78−89135
Kirin chondrite, remanent magnetisation, early interplanetary space mag. field *(Chinese)* 78−89136
Kirin H5 chondrite, ^{40}Ar/^{39}Ar age and thermal history 80−101567
Kirin H chondrite, inert gas content interpretation *(German)* 80−46505
Kirin meteorite, fissure anal. *(Chinese)* 79−80280
Kirin meteorite, temp. gradient prod. in atm. passages, thermolum. obs. 80−67672
Kirin meteorite shower, ^{18}O abundance *(Chinese)* 79−16900
Kirin meteorite shower, Mossbauer anal. *(Chinese)* 79−62797
Kirin meteorites, proton-induced X-ray emission anal. *(Chinese)* 79−40145
Kirin meteoritic chondrules, origin *(Chinese)* 79−40146
Kirin mineralogy and petrology, formation and evolution 79−44426
Kramer Creek, Colorado, L4 chondrite 77−91491
Krymka chondrite, heating to 400-1000°C, trace element anal. 77−64710
Krymka LL3 chondrite, mysterite inclusions, electron microprobe study 80−85905
Krymka LL-chondrite carbonaceous inclusion, noble gas and trace element anal. 80−17555
L chondrites, ^{87}Rb-^{87}Sr dating, shock and brecciation effects 80−51705
L-6 chondrite, perogenesis evidenced by mineral chemistry 80−41775
L-group chondrites, incipient melting rel. to shock classification 79−88629
L-group chrondrites, Sb, Ge and refractory siderophile element content 77−17450
Lance carbonaceous chondrite, basalts 80−56783
Landes group IA Fe meteorite, cooling history 80−36578
Lappajarvi impact melt crater projectile 80−56785
large impact craters, meteoritic material detect. and chemistry 78−57208
Late Cretaceous astroblemes in western Canada 77−44999
Leoville, type III carbonaceous chondrite, ^{57}Fe Mossbauer spectroscopy 78−49404
Libyan Desert Glass, redox form. conditions, EPR obs. of as-received and irrad. samples 78−28228
light noble gases in chondrites, achondrites and ureilites, anal. compilation 78−65574
LL-chondrite, noble gas isotope anomalies 80−51697
LL-group ordinary chondrites, metamorphic history 79−30017
Lonar Crater, India, chem. study of impact glasses and basalts 79−20836
Lost City, disintegration during Earth atmosphere entry 77−67080
Louisville, chondrite, Mossbauer anal. 79−21238
Luna 24 soil samples, meteoritic and submeteoritic metallic phases 78−32367
lunar and planetary science, ninth conference, Houston, Texas, (1978 March 13 to 17) 80−17711
lunar crater Giordano Bruno, AD 1778 impact obs. consistent with laser ranging results 78−69717
lunar highlands, effects of meteorite bombardment on primordial crust 80−109381
lunar impact, rel. to elements volatilisation from regolith solid particles 77−9680
Macau chondrite, Brazil, mineralogy, petrology, chemistry 78−93171
macroparticle impact with meteoritic vels., physical modelling principles, quasi-full laser modelling 79−52049
magnetic field, characts. of first order shock induced mag. transitions in Fe, discrimination from TRM 78−64205
magnetic field origin, conf., Nov. 1978, Texas USA 80−36234
magnetic fields in early solar system, recorded in lunar rocks, meteorites and planets 79−5765
magnetisation and early solar system 80−36597
Malvern howardite, petrological and chemical discussion 77−49346
Manicouagan impact crater, gravity study and upper crust density contrasts 78−81170
Manicouagan impact crater, Quebec, investigation 78−81163
Manicouagan impact melt, Quebec, chemical interrelationships with basement rel. to form. processes 78−81165
Manicouagan impact melt, Quebec, stratigraphy, petrology and chemistry 78−81164
Manicouagan impact melt sheet, Quebec, thermal history 78−81167
Manicouagan Impact Structure, Canada, formation *(French)* 79−88355
Manicouagan impact structure, Quebec, melt rocks petrogenesis 78−81166
Manicouagan melt sheet, Rb-Sr isochron age 78−81168
Manicouagan structure, Quebec, central mag. anomaly 78−81169
Manych, L-3 chondrite, droplet chondrules comp. and chondrules origin 79−30014
Manych chondrite, large microporphyritic chondrules 78−65562
Marjalahti, VVH cosmic ray nuclei abundance from tracks in olivine 78−36414
Marjalahti pallasite, cosmic ray induced ^{53}Mn production 80−72891
Marjalahti pallasite, cosmic ray tracks, ultraheavy (Z>52) nuclei abundances 77−9641
mass ablation, cosmic-ray track study 78−53894
mass distribution indices of chondrules and cometary meteoroids 77−17451
mass loss and shape change with radiative heating 80−31198
Mayfield chondrite, Cu alloy, Ni content determ. 80−67671
Mayo Belwa, enstatite achondrite, metal and schreibersite occurrence 79−21241
Melrose-b howardite, REE distrib. and pre-terrestrial Ce depletion 80−101566
mesosiderites, silicate fraction, Mg-Cr relationship 80−51704
metallic fragment, from Mare Foecunditatus, struct. and comp., meteoritic origin *(Russian)* 77−9682
meteorites continued
Meteoritical Society, 41st. annual meeting (Sudbury, Canada, 1978 Aug. 14-17) 79−101122
Meteoritical Society 39th annual meeting, Oct. 1976, Bethlehem, USA 77−64706
Mezo Madaras, L3 chondrite, ^{87}Rb-^{87}Sr dating, shock and brecciation effects 80−51705
microtektites, chemical comparison of bottle-green and normal microtektites and tektites 77−82179
Middle Ages, list of events from European mediaeval sources 78−86105
Mistastin Lake crater, Labrador, Sr isotopes and trace element geochem. of impact melt 78−32105
Mokoia, carbonaceous chondrite, Ne in gas-rich samples 78−65559
Moore County, eucrite, quench temp. and residence time on eucrite parent body 78−96444
Moore County meteorite, geochem. study and genesis 80−36587
Morasko, composition and origin 80−77359
Morasko, Poland, craters due to meteoritic shower 79−70801
Morasko, Poland, soil anal. near crater lakes 80−8605
Mt. Baldr (a,b), rel. to ten stone Antarctic meteorite inert gas contents 80−46506
Muchison, Si in metal grain from type 2 carbonaceous chondrite 80−77363
Mundrabilla, analysis of anomalous Fe meteorite specimen *(German)* 78−65576
Mundrabilla, octahedrite, chem. obs. by neutron activation 78−12171
Murchison, α-hydroxycarboxylic acids discovery 78−45294
Murchison, acid-labile amino acid precursors, chromatographic fractionation 77−64707
Murchison, acid-labile amino acid precursors, peptides and amino acylamides 77−64708
Murchison, anomalous Xe isotopic composition, reply 79−44425
Murchison, anomalous Xe isotopic composition 79−44424
Murchison, C2 carbonaceous chondrite, evidence for alcohols and carbonyl compounds 77−33433
Murchison, carbonaceous chondrite, Ne in gas-rich samples 78−65559
Murchison, Fe-Ni sulphides props. and rel. to phase Q1 79−58303
Murchison, Mg isotopic vars. in hibonite, ion microprobe study 79−58305
Murchison, organic polymer chem. composition of C2 chrondrite 80−98622
Murchison (C II), search for purines and pyrimidines 78−7948
Murchison (CZ), mineralogy-petrology of heated samples 79−53777
Murchison C2 chondrite, presolar gas components, isotopic anomalies 80−85904
Murchison carbonaceous chondrite, monocarboxylic acid isomer struct. 80−26823
Murchison carbonaceous chondrite, rel. to interstellar grain clumps and prebiotic molecules 77−26042
Murchison carbonaceous chondrite, spectroscopic evidence for interstellar grain clumps in inclusion 77−25987
Murchison chondrite, noble gases isotopic anomalies, evidence for stellar condensates 80−41772
Murchison chondrite, s-process Kr comp. rel. to s-process neutron capture time scale 80−73080
Murchison matrix, heating expt. rel. to evaporation metamorphism of solar nebula primitive dust 79−58279
Murchison meteorite, inert gases as possible relics of s-process nucleosynthesis 79−21243
Murray (C-2) carbonaceous chondrite, I-Xe age and trapped Xe components 80−98618
nakhlites, abundances rel. to ureilites 77−41363
Naragh, nondestructive neutron activation anal. 78−77522
Naragh olivine-bronzite chondrite, composition and petrographic features, chem. anal. and X-ray fluoresc. obs. 80−67668
natural nuclides from meteorites, spontaneous fission neutron multiplicity *(Russian)* 79−40977
Netschaevo, IIE iron, silicate inclusion age, I-Xe and Ar isotope ratios 80−77360
Netschaevo, new class of chondritic meteorite 77−91495
Niger (I) carbonaceous chondrite, origin of olivine grains in C2s 80−67667
noble gases, isotopic anomalies origin, comment 80−26818
Nogoya carbonaceous chondrite, IR spectrum comparison with 10 and 20 μm interstellar absorpt. bands 79−48741
Nordlinger Ries giant meteorite impact crater, K-Ar and fission track dating 78−28236
Norton County aubrite, shielding effects 77−87345
Norton County enstatite achondrite, ^{87}Rb-^{87}Sr history 77−5508
oceanic sediments, silicate spherules, trace element concentrations 79−84755
olivine and enstatite of meteoritic and terrestrial origin, porosity determ. *(Russian)* 77−9725
olivines, cosmic ray nuclei groups Z≥ abundances, fossil tracks 80−105139
orbits, chem. comp. and origin *(Swedish)* 77−71048
orbits of meteorites and parent bodies, perihelia distrib. *(Russian)* 77−49345
ordinary chondrite composition for Earth and Mars rel. to Viking rare gas abundances 77−45342
ordinary chondrites, condensation from gas phase 77−60732
ordinary chondrites, Ga, Ge, Cu, Sb, moderately volatile siderophiles content 80−8595
ordinary chondrites, trace element distrib. between mag. and nonmag. portions 79−35205
ordinary chondrites, W abundance and distrib. 78−32412
Orgueil, Ni and S abundances correl. in phyllosilicates 78−12169
Orgueil, type C-1, IR spectra, comparison with serpentine minerals 80−17556
Orgueil chondrite, ^{22}Ne anomalous abundance, evidence for presolar grains 80−41773
palaeomagnetic field intensity determ. from remanent magnetisation 77−37583
pallasite meteorites, olivine ion microprobe anal. for Ni 79−58304
pallasites, metal comp., classification, relationship with Fe meteorites 77−64709
pallasites, metallic and olivine phases equilib. conditions *(Russian)* 77−9720
pallasites, mineralogy and chemistry 78−7945
pallasites, olivine-metal texture formation 78−7944

meteorites continued
pallasites origin, role of minor planets EM heating in early solar system 80−36555
parent body era, evidence for primordial mag. field 78−45293
Pasamonte eucrite, formation age and history 78−32413
petrographic obs. and rare gases of six chondrites from Kansas 79−21239
Piancaldoli, chemistry, mineralogy and petrology 77−33431
pinon, Fe meteorite, isotopically anomalous Ag discovery 80−85902
in planetary science conference (Boston, MA, 28 October 1977) 79−53740
Poluyamki, Rakity and Markovka chondrites, composition *(Russian)* 77−9721
polymict brecciated meteorites, evidence for multiple parent bodies 78−57513
Pontlyfni, differential meteorite related to group IAB irons, chemical anal. 77−82177
Poplar Bay, Lac du Bonnet, Manitoba, possible meteorite impact crater 77−17150
preservation in Antarctic ice cap 78−36541
presolar grains, isotopic anomalies prediction in K and Ar 78−28761
presolar grains, prod. by supernovae 78−24520
presolar meteoritic sulphides, supernovae origin 77−29866
Pribram, disintegration during Earth atmosphere entry 77−67080
Pribram, pre-atmospheric size from spallation prods. and fossil cosmic ray tracks 80−82314
primitive meteorites thermal metamorphism, trace element loss from Allende heated to 1400°C 80−109401
primitive meteorites thermal metamorphism, trace element loss from Allende (C3V) heated to 1400°C 80−109402
primordial condensation of components, expt. evidence of source medium state 80−26816
primordial metal grains, thermal history 79−40097
Putinga, Rio Grande do Sul, chondrite, mineralogy, petrology and chem. 79−25552
pyroxenes from planetary basalt, silicate mineralogy study 80−72802
r-process nuclei, isotopic anomalies 79−5740
radiants of meteorite dropping fireballs, accuracy 79−71006
radioactivity, appl. to galactic cosmic ray solar modulation *(Bulgarian)* 80−72728
rare earth elements in solar nebula, fractionation 80−72796
rare gas concs. in Fe meteorites rel. to cosmic-ray-produced nuclides 78−65473
refractory lithophile elements, condensation and fractionation 80−36517
regmaglyptic relief index, meas. 80−56782
Renazzo type meteorites, rel. to evolution of Martian atmosphere, implications to Viking data 77−87307
review 79−96977
Rica Aventura Fe meteorite, petrology 80−36585
Richardton chondrite, U-Pb abundances and Pb isotopic studies 80−56778
Richardton H5 chondrite chondrules, chemical-petrological study 79−44418
Ries crater, nature of C metastable phases 77−89404
Ries impact crater, siderophile and volatile element anal. 80−17552
Ries impact crater, thermal events, age and intensity 79−79760
Rochechouart crater, France, projectile identification, IIA Fe meteorite 77−33025
Rochechouart crater, Massif Central, France, shock zoning study 77−81897
rocks destruction by meteorite impact 77−66910
s-process, Xe and Kr isotopic abundances 79−5739
Saint Mesmin chondrite, ^{87}Rb-^{87}Sr age, and dating of gas-rich polymict breccia 79−53778
Saint Severin amphoterite, U-Th-Pb and Rb-Sr studies 78−65560
San Juan Capistrano, cosmic ray record 78−57512
Santa Barbara, chondrite, mineralogy and petrology 79−25551
Santa Catharina, anomalous Fe, cloudy taenite origin, TEM examination 79−66968
Santa Catharina, Fe-Ni (50 wt.%) superstructure obs. 79−30024
Santa Catharina, FeNi superlattice formation 79−8885
Santa Catharina meteorite, Mossbauer spectra and X-ray diffr. of Fe-Ni phase 80−67673
Santa Clara, Fe meteorite, isotopically anomalous Ag discovery 80−85902
Santa-Catharina, Fe-Ni 50-50 wt.% alloy detection *(French)* 79−16895
Saratov, neutron multiple emission, evidence for new fissioning nuclide *(Russian)* 77−87352
scattering ellipse after original meteoroid break up in atm. 80−77356
Sena stone, bronzite chondrite formation conditions *(French)* 80−26817
Serra de Mage, pyroxene cooling history rel. to Moama and Moore County 79−66963
Serra de Mage meteorite, geochem. study and genesis 80−36587
Shaw, L-group chondrite, missing metal 77−5511
Shaw L-group chondrite, lithologies 79−92730
shergottite meteorites, petrology and origin 80−51700
shergottite meteorites, trace elements rel. to planetary origins 79−44420
Shergotty achondrite, $^{40}Ar/^{39}Ar$ age and post-shock thermal history 80−46502
Shergotty achondrite, mineralogy, petrography and minor elements 80−36592
Shergotty achondrite, Rb-Sr age and isochron age resetting 80−41774
Shibayama chondrite, chem. composition, petrography and mineralogy 80−72892
shower characteristics *(Japanese)* 78−89137
Shuang Yang meteorite shower, May 1972, preliminary study of debris *(Chinese)* 79−80281
Siberia, Outer Mongolia and Indochina Peninsula, geographical distrib. pattern *(Japanese)* 80−31263
Sikhote-Alin, chem. comp. *(Russian)* 77−9715
Sikhote-Alin, density, mag. and elastic props. *(Russian)* 77−9716
Sikhote-Alin, fragmentation *(Russian)* 77−9713
Sikhote-Alin, radiant improvement by square deviations calc. *(Russian)* 77−9717
Sikhote-Alin field craters, determ. of flight trajectory azimuth of original meteoroid 80−72893
Sikhote-Alin octahedrite, comp. and struct. *(Russian)* 77−9714
silicate spherules in deep-sea sediments, extraterrestrial origin 79−48743
Slate Island impact site, shock remanent magnetisation 80−30986
Slate Islands, Lake Superior, probable meteorite impact structure 77−9427

meteorites continued
Slate Islands structure, partially submerged meteorite impact crater in Lake Superior 77−78183
solar nebula, charged dust accretion rel. to Fe, stone and planetesimal formation 78−28548
solar system formation, re-evaporation of condensed matter, evidence from meteorite mineral content 78−85864
solar system formation, role of supernova, isotopes found in primitive meteorites 79−44380
solar system origin aspects 77−91490
space weathering effects, microprobe studies 77−60725
Springfield specimens, mass spectroscopic element and isotope anal. 77−60731
St. Mesmin brecciated chondrite, noble gases abundances rel. to irradiation history 78−28593
St. Severin, ^{21}Ne concs. rel. to $Mg(n,\alpha)Ne$ cross sections at 14.1 and 14.7 MeV 79−96874
St. Severin chondrite, ^{53}Mn production due to nucl. spallation, depth-depend. 80−82316
St. Severin chondrite, U and Pu distrib. 80−72889
St. Severin LL-chondrite, Fe-Ni ordered phase Llo superstruct., Mossbauer spectrum Debye-Scherrer pattern 80−50241
St. Severin meteorite, flux of low energy particles in solar system 77−82096
stone meteorite, laboratory simulation of impact *(Russian)* 77−91489
stones, U and Th microdistribs. 79−75162
stony, ^{53}Mn determ. by activation anal. for cosmic ray effects investig. 78−12018
stony, electron microscopy of mineral grain substructs. 77−87349
stony, gamma-ray induced thermoluminesc. gradients 77−74020
stony, mag. props. and remanent magnetization 79−16899
stony and Fe meteorites genetic relations 79−35204
stony meteorites, cosmogenic ^{26}Al and ^{22}Na *(Russian)* 77−9719
superheavy element composition of irons, fission track study 80−26821
superheavy element search in Earth samples, meteorites and cosmic rays *(Russian)* 79−84277
superheavy elements, detection by fission activity detect. *(Russian)* 79−13358
supersonic and hypersonic movement through atmosphere, ablation modelling 79−32780
Supuhee, chondrite, lithic clasts composition 77−91493
Supuhee H6 chondrite, chemistry of 'mysterite'-bearing clast 78−7947
Tacoma (Washington), new Fe meteorite find, discovery, classification and mass 78−65571
clear taenite, identification as ordered FeNi FeNi 80−8604
tektite, Lei-Gong-Mo, chronostratigraphic study *(Chinese)* 79−84756
tektite, Muong Nong-type indochinites, mineral inclusions 80−36301
tektite and impact glass Li abundance 80−61799
tektite origin, review 77−67078
tektite-like material in archaelogical remains, Indonesia 80−101365
tektites, fission-track plateau dating evidence of australites older than indochinites 80−56780
tektites, minute, from Central Java 79−5790
tektites, N.American strewn field assoc. with Earth ring system form. and Eocene terminal event 80−76890
tektites, origin problem 79−5791
tektites, Russian, water content 77−87346
tektites and natural glasses, Mossbauer anal. 80−21952
tektites and natural glasses, N concs. 80−41446
tektites from Australasia, possible origin in Zhamanshin impact struct. 80−51358
tektites of Australasia, possible origin crater in Cambodia 80−36302
Tenham, ringwoodite and majorite identification of cryst. dislocations 80−85909
Tenham chondrite, β-$(Mg, Fe)_2SiO_4$ high-press. spinel phase identification 79−80284
terrestrial circular structures in central Russia, possible impact craters *(Russian)* 77−9385
terrestrial cratering history, theory incorporating galactic modulation 80−31043
terrestrial impact, shock effects on rock magnetism 78−85538
terrestrial impact craters and astroblemes, morphology and struct. *(Russian)* 77−45000
terrestrial impact structs., so called, non-random geographical distrib., implications 79−34825
terrestrial meteorite craters, form., props. and catalogue 78−96411
thermobarometric chemistry of mineral inclusions *(Russian)* 80−104954
thermoluminescence, rel. to orbit, pre-impact history and Earth residence time 80−31262
thermoluminescence as measure of irrad. history, validity of method 80−36584
thermoluminescence measurement apparatus, lunar samples and meteorites appl. 77−13803
thermoluminescence of meteorites of known age 80−46498
Thiel Mountains pallasite, chem. comp. *(Russian)* 77−9722
Tieschitz, H3, chondritic meteorite, accretion temp. 79−75166
Tieschitz, H3 chondrite, Cd isotope fractionation in meteorite fractions 80−94764
Tieschitz, primitive H3 chondrite, effects of thermal metamorphism on trace elements 78−20765
Tieschitz unequilibrated chondrite, taenite petrogenesis 80−82315
Tillaberi, L_6 hyperthene chondrite with lithic inclusion *(French)* 77−33432
Tishomingo Fe meteorite, microstructural study 79−16898
Toluca octahedrite, Mossbauer spectra petrological study 80−36589
Tunguska, 1908, catastrophe, cosmochemical anomaly in silicate microspherules comp. 78−96430
Tunguska, and USA prairie network bolides, identical nature, low-density microcomet objects 77−67073
Tunguska, meteorite explosion, eyewitness account 79−30023
Tunguska, possible mechanism of event 77−78728
Tunguska catastrophe, computational modelling 80−41779
Tunguska catastrophe, motion of low-density gaseous bodies in the atmosphere 79−84554
Tunguska cosmic body, chemical comp. and nature 78−61810
Tunguska event, 1908, new egregious theory 79−21229
Tunguska event, comet collision with Earth 78−49390
Tunguska explosion, energy, atm. inhomogeneity, comment 78−20424
Tunguska explosion, shock wave propag. calc. 77−66973
Tunguska meteorite, collision between Earth and comet 78−32396

meteorites continued
Tunguska meteorite explosion, shock wave effects, model, computation 77−5507
Twin City (Georgia), place of origin from alloy struct. 78−65567
Tysnes Island, unusual clast composed of solidified immiscible Fe+FeS and silicate melts 79−2526
Uberaba H5 chondrite, mineralogy, petrology and chemistry 78−65554
unequilibrated ordinary chondrites, matrix textures 77−87340
Unter-Massing Fe-meteorite, cosmic-ray exposure age and preatmospheric size *(German)* 80−46507
uracil in carbonaceous chondrites, Murchison, Murray and Orguiel meteorites 80−31261
ureilite meteorites, mag. effects of brecciation and shock rel. to strong nebular mag. fields 80−8602
ureilites, abundances rel. to genesis 77−41363
ureilites, chemical fractionation 77−41369
ureilites, classification and elemental fractionation 77−41364
ureilites, fluorescent accessory phases in carbonaceous matrix 79−40143
ureilites, trapped noble gases in bulk samples and C-rich veins 78−40883
vaporisation of lithophile elements, vac. conditions 80−36583
velocity meas. by radar technique *(Spanish)* 79−5759
Verkhne-Chirsk stony meteorite, microscopic obs. *(Russian)* 77−9723
Vigarano-type carbonaceous chondrites, petrographic vars. 78−32420
volatiles in chondrites rel. to metamorphism or nebular fractionation 79−66966
volatiles source, abundance in Mars and Earth atm. 78−36482
Vredefort Dome, S.Africa, coesite and stishovite discovery 78−53653
weathered specimens on Earth's surface, recovery possibilities 77−87347
Weekeroo Station, IIE iron, silicate inclusion age, I-Xe and Ar isotope ratios 80−77360
Yamamato cabonaceous chondrite, amino acid content 80−26822
Yamato, constituent minerals determ. 78−77524
Yamato meteorites (j), (k), (l) and (m) from Antarctica, petrology 79−2528
Yamato Mountains, Antarctica, significance of stony meteorites 77−91494
Yamato-74191 chondrite, inert gas composition and neutron capture effects 80−46504
Yamato-74 chondrites, crystallisation of chondrules 80−77361
Zaisho, Japanese pallasite, mineralogical and petrographical study 80−46509
Zhamanshin crater, age determ. by different methods 80−101568
Zhamanshin impact structure, USSR, impact glass chemically similar to tektites 80−51358
Zhamanshin meteor crater, tektites-irgizites form. conditions from Fe ions states 78−61420
^{26}Al anomaly, relative yields of $^{26}Al^{g}$ and $^{26}Al^{m}$ from $^{25}Mg(p,\gamma)$ reaction 79−101058
^{26}Al, as planetoid heat source in early solar system 78−65511
^{26}Al content of Dalgety Downs meteorite 79−75167
^{26}Al content of stony meteorites with gas losses 78−32418
^{26}Al from meteorites, possible 'record' of solar wind action and luminosity variations 78−61830
^{26}Al from red giant stars and decay to anomalous ^{26}Mg 80−67712
^{26}Al in Fe meteorites and past cosmic ray intensity 79−44422
^{39}Ar concentrations, evidence for Maunder minimum in solar activity 78−57529
^{37,39}Ar content rel. to spatial cosmic ray gradient 77−17312
Ba conc. determ. in stony meteorites 78−65557
$BaTiO_3$ particulates coagulation in solar nebula 77−53434
CNO isotope importance in astrophysics 77−87263
CNO isotopes in astrophysics, conf. Grenoble, France, 1976, Aug. 77−87262
Ca, isotope fractionation on Earth and other solar system materials 79−20835
Ca-Al rich inclusions, origin rel. to cosmoradiogenic ghosts 78−12162
Cd isotopic abundances, survey of 28 objects 78−53891
^{36}Cl content of Antarctica meteorites, cosmic irrad. histories 80−21950
F conc. meas. using nuclear microprobe technique 77−87342
Fe group, thermodynamic model evidence for asteroid belt origin 80−36577
Fe, group IAB, silicate inclusions, rel. to anomalous stony meteorites 78−32416
Fe, group IV A, pre-terrestrial history 79−44419
Fe meteorites, Ar, Kr and Xe isotopic abundances 78−12165
Fe meteorites, chem. classification 80−109403
Fe meteorites, chem. comp. *(Russian)* 77−9722
Fe meteorites, chemical fractionations and cosmochemical history of metal phase 77−49347
Fe meteorites, composition from factor anal. 80−67670
Fe meteorites, condensation and comp. 79−30021
Fe meteorites, cosmic ray produced nuclides, $^{41}K/^{40}K$-$^{4}He/^{21}Ne$ exposure ages and age distribs. 79−30015
Fe meteorites, group IAB, silicate and troilite dating by Xe-I method 80−17554
Fe meteorites, group IC, comp., mineralogy and origin 78−32414
Fe meteorites, group IIICD, plessite struct., electron microscopy study 80−8600
Fe meteorites, group IVA, cooling rates 79−30016
Fe meteorites, group IVA, core origin 79−35203
Fe meteorites, group IVA, cooling rate vars. 79−35202
Fe meteorites, mineralogy, review 77−87348
Fe meteorites, nuclides formed by cosmic ray exposure 80−21951
Fe meteorites, primary fractionation of elements 79−35210
Fe meteorites, radial distrib. of spallogenic K, Ca, Ti, V, Mn and Cr isotopes 80−67488
Fe meteorites, superheavy elements possible existence 79−48742
Fe meteorites, thermoremanence hypothesis rel. to origin of magnetisation 78−65564
Fe meteorites, W concs. 79−35200
Fe meteorites chemical classification, role of Ga, Ge and Sb nebular condensation 80−36594
Fe meteorites of groups IAB and IIICD, origin 80−109404
Fe meteorites with low Ga and Ge concs., comp., struct. and genetic relationships 79−21236
Fe natural and artificial meteorites, fusion crusts and ablation debris 78−61819
Fe-meteorites, elements distrib. between metal and phosphide phases 80−46508
Fe-Ni, taenite, superstruct. in Fe meteorites 78−61820
meteorites continued
Fe-Ni (25 to 50%), FCC, meteorites and thermodynamic equilib., Mossbauer and X-ray diffr. study 80−88087
Fe-Ni meteorite, STEM/X-ray microanalysis across α/γ interface 80−105212
Fe-Ni ordered phase in meteorites, Mossbauer studies 80−41776
Hf, abundance in stones 79−92731
Hf, determ. in silicate rocks, meteorites and lunar samples by neutron activation 78−20547
Hg isotopic anomalies, possible prod. by extinct radioactive nucleus ^{202}Pb 77−49343
$^{202}Hg/^{196}Hg$ anomalous ratios, interrelations, cosmological inferences 77−2375
Li and halogens determ., rel. to cosmochemical processes 78−12111
Mg isotope anomalies explained by ^{26}Al form. in collapsing star *(Russian)* 80−77285
Mg isotopic anomalies, role of ^{26}Al synthesis in explosive H burning 80−85929
^{26}Mg negative anomalies and ^{26}Al, effects of proton irradiation on gas phase with condensation 79−13289
^{53}Mn meas. in chondrites, evidence for cosmic ray modulation absence during glacial period 79−80129
N abundance and isotopic comp. in stony meteorites 78−65558
Ne-E, anomalous meteoritic Ne component, thermonuclear origin, supernova models 78−45292
Ni-Fe primordial metal grains, with occluded Pt spherules, thermal history 79−40097
O isotope anomalies 77−87354
^{17}O-^{18}O, fractionation by chemical equilib. 80−89513
Pa abundance, mass spectroscopy 80−8601
^{107}Pd existence in early solar system, evidence from meteorites 79−40096
Re-Os, rel. abundance, rel. to nuclear chronometer reliability 78−85919
^{187}Re-^{187}Os systematics in meteorites, rel. to solar system early chronology and Galaxy age 80−41778
Te isotopic composition in meteoritic and terrestrial materials 78−82856
Ti, abundance in stones 79−92731
Ti isotopic anomaly from meteoritic materials study 79−53716
Xe anomaly, fission origin implications for astrophysical r-process 78−93204
Yb isotopic and elemental abundances 78−32419
Zr, abundance in stones 79−92731
Zr, determ. in silicate rocks, meteorites and lunar samples by neutron activation 78−20547
Zr, isotopic composition, at. wt., rock standards, chondrite composition 79−3591

meteoroids
see also meteorites; meteors
ablation in Jupiter upper atmosphere, rel. to CO source 78−93144
albedo and size distrib. in 0.3-4.8 AU range 78−36539
atmospheric breakup, effects on crater field form. 80−94760
attenuating shock waves, following meteoroidal impact on metals *(Russian)* 77−71068
bombardment of lunar rocks, Apollo samples obs. rel. to microcrater and accretionary grain populations 80−94732
bombardment of lunar rocks, microcrater and accretionary grain populations temporal development 80−94731
break up in Earth's atm. 80−77356
close encounters with Jupiter, mass distrib. throughout Solar System implications 80−77329
cosmic dust, book 78−57498
crater shapes formed by high-speed impact 77−33364
density distribution in vicinity of planet 78−20762
detector film penetration, lab. expts. on Al and parylene films 80−77292
Dhajala meteorite, orbital elements determ. for meteoroid 78−36540
disintegration during Earth atmosphere entry, appl. to Lost City, Grant and Pribram meteorites 77−67080
Earth grazing fireball, eqns. of motion, vel., orbit and mass determ. 80−67663
fireballs photographed in central Europe, trajectories, orbits and classification 78−36534
flight trajectory azimuth from Sikhote-Alin field craters 80−72893
Geminid meteor stream, orbital period 78−53889
geomagnetic disturbances prod. by ballistic shock waves and explosion 77−13139
high-velocity impact destruction of basaltic bodies, appl. to Martian satellites 77−64704
impact effect on spacecraft attitude 78−73608
impact on small solar system bodies, seismic effects, rel. to Phobos *(Russian)* 78−69754
impact on Space Shuttle Orbiter, hypervel. tests on RCC thermal protection material 79−16795
inner solar system micrometeroids, orbital and physical characts. 80−77355
interplanetary dust distrib. near terrestrial planets, methematical modelling 79−96976
interplanetary micrometeoroids, rel. to meteoric night-glow 77−91488
lunar surface, gardening process, by meteoroid impact cratering *(Japanese)* 77−91452
mass distrib. in 10^{1}-10^{7} g range 77−64705
mass distribution function for large meteoroids 78−49394
mass distribution indices of chondrules and cometary meteoroids 77−17451
mass scale and meteor emissions at max. brightness 78−20761
massive meteoroids, mass distrib. determ. from occurrence of brilliant fireballs 77−45366
material structure, determ. via fireball end heights 77−29732
micrometeoroid data from Helios 1 78−24485
micrometeoroid detection, acoustic method reliability 79−80232
micrometeoroid detection, ion comp. of plasma produced by fast impact on Au or W target 77−39438
micrometeoroid distrib. and flux at 1 AU from lunar crater obs. 77−60730
micrometeoroid hazard of Comet Halley probe, workshop proceedings (Noordwijk, Netherlands, 18-19 April 1979) 80−36782
micrometeoroid impact, laboratory simulation 78−57510
micrometeoroid orbits, Helios obs. 78−20731
micrometeoroids within 10 R_E, HEOS-2 dust expt. 79−48740
microparticle studies by space-borne instrumentation 78−57460

meteoroids continued
orbit determ., correl. with interplanetary dust, radio and photographic meteor obs. 80−101555
orbital angular momentum, effects on Earth's atmosphere 77−56877
orbital histories, rel. to relative crater prod. rates on planets 77−60699
orbits determination, accuracy of meteorite dropping fireballs radiants 79−71006
particle flux near Saturn, Pioneer 11 meteoroid obs. 80−82291
Periodic Comet d'Arrest (1976 XI), meteoroids characts. from tail photometry 78−53876
Perseid shower meteoroids, evidence for progressive fragmentation from television obs. 80−4309
properties and deionisation processes rel. to radio echo characteristics 80−17550
Quadrantid meteor shower, orbit 78−61815
Quadrantid meteor stream, effect of orbital evolution on meteoroids influx 80−56776
Quadrantid meteor stream, long-term orbital evolution 80−17551
Quadrantid meteor stream, orbital evolution between (AD 1830 and 2030) 80−21948
rotation effect on meteor train initial radius 79−16893
sampling techniques 78−57459
shock waves, causing geomag. disturbances 77−49231
solar flare activity large scale variations, evidence from meteoroid data 77−82190
solar wind sputtering rate 80−85835
spacecraft meteoroid shield, destructive effect and meteoroid vel. 78−53788
stream widths, rel. to zodiacal light interp. 78−4156
structure determ., atmosphere as obstacle 79−16891
surface shielding by vaporised and refl. mols., theory of first collisions 80−77357
swarm evolution, solar mass reduction link 80−8592
Tunguska event, thermal explosion of porous meteoroid, model 78−61813
upper atmosphere, odd N prod. by meteoroids 79−2404
Venus atmosphere, nightside ionosphere maintenance by meteors 77−2359
Mg(n,α)Ne reaction, cross sections at 14.1 and 14.7 MeV and implications for meteorites 79−96874

meteorological instruments
see also anemometers; barometers; hygrometers
acoustic Doppler and angle of arrival wind detect., comparison with direct meas. 79−39884
acoustic sounder for lower atm. remote probing 77−17243
acoustic-microwave Doppler radar system, wind and wind shear meas. at Dulles Airport 78−32233
air pollutant deposition research using rain gauges *(Dutch)* 78−81367
airborne particulate sampler, wind tunnel testing, using monodisperse particles 77−82053
aircraft dropwindsonde system 80−17393
aircraft meteorograph, design, appls., accuracy *(Chinese)* 80−17387
aircraft satellite data link, for operational reconnaissance data transmission 78−96299
aircraft-borne instruments for meas. monsoon clouds elec. parameters 78−7792
anemograph, digital, for wind direction and average speed meas. *(Czech)* 80−77174
anemometer, CSIRO liquid water probe, hot wire, freq. response 80−12562
anemometer and lidar meas. of wind vel., comparison 79−39885
anemometer for medium and high winds, Gill propeller instrument 80−26618
anemometers, three dimensional feasibility of use in simulated tornado flow meas. 77−17244
automatic mobile weather station, design, for microclimatic studies 78−61617
automatic sequential precipitation sampler, chem. anal., rel. to acid rain problem 79−83681
automatic sequential rain sampler 78−73545
automatic telemetering raingauge system 79−21038
automatic weather stations, use in United Kingdom observational network 79−80047
bead thermistors for temperature measurement *(German)* 77−21920
bidirectional vane, response characts. 79−66814
bolometer, for measurement channels of actinometric apparatus of Meteor Earth satellite 79−35828
boundary layer data acquisition and analysis system 77−60471
Cairngorm summit automatic weather station 77−53252
Campbell-Stokes sunshine recorder rel. to Dirmhirn global radiation recorder *(German)* 78−44953
capacitive dew-point sensor 78−81421
cloud condensation nuclei counters, comparison of two instruments 78−61598
cold-wire thermometers used for atmospheric turbulence meas. in marine environment, freq. response 80−56650
colour radar displays for weather detection and groundmapping 79−92608
data acquisition and processing, computerised data collection system *(German)* 80−37007
data acquisition system, microprogrammable microprocessor-based 77−64496
data acquisition systems for operators on continental shelf 79−70887
data buoy DB1, source of meteorological data for UK 79−21079
dew-point hygrometer, fast-response, calibration *(Russian)* 77−13761
Doppler sodar antenna configs. for horizontal wind meas. 78−65410
drifting buoy, development 79−5661
dual-Doppler radar, coverage area as function of meas. accuracy and spatial resolution 80−82093
electric rainfall intensity sensor 79−39888
electronic high-resolution rainfall intensity recorder and totaliser 78−7793
engineering developments 79−16702
European satellite system, Meteosat, weather forecast appl. *(Swedish)* 77−56769
evaporimeters, thermal insulation calc. 79−29803
Finnish developments, by Vaisala Oy manufacturer 79−12310
fog, quantitative meas. of precipitation onto surfaces 80−56654
gauge undercatch, meas. precipitation adjustment 77−45095
geostationary weather satellites, global network *(German)* 78−24389

meteorological instruments continued
Glaisher stand and Stevenson screen, max. summer temp. recording 77−81976
gust probe and hot-film anemometer meas., vel. spectra comparison 77−78339
hail-meas. instruments, review 77−33196
hailcube for hailstone kinetic energy meas. inc. wind effects 77−17173
hailpad calibration, comment 78−3986
hailpad calibration for Italian hail damage documentation 77−29488
hailpads calibration 78−93001
hair hygrometer, technique to linearise hair extension *(German)* 80−46284
HF radio acoustic sounder, atm. wind and temp. remote meas. 78−32235
hot-wire meas. of wind and temp. in atm. surface boundary layer, Denmark 77−9458
hydrometeorological meas. equipment, USSR state testing 79−70897
Hydrometeorological monitoring in weather modification programs 78−69544
hygrometer, Meteorological Office Mk3, frostpoint meas. systematic error 78−73538
hygrometer with a heated electrolytic sensor 80−109262
hygrometer with $LiNbO_3$ sensor *(Japanese)* 80−95103
information flow system *(Japanese)* 77−56754
interpretation device, for signals from meteorological radar equipment *(Russian)* 80−67432
IR Doppler wind-sensing system, spaceborne, atmospheric effects 79−96828
IR fluctuation hygrometer, design, calibration, field trial results 78−77368
Japanese weather satellite, on board equipment, geostationary orbit 78−4076
Joss-Waldvogel rainfall disdrometer, obs., comments and reply 77−64386
Keily probe, assessment for ground-based meas. of drop size distrib. in clouds 79−12317
laser photoelectric spectrometer for large condensation nuclei meas. *(Russian)* 78−65408
laser radar system, mobile computerised meteorological phenomena observation 80−56644
laser recorder of satellite signals, using dry-developed photosensitive paper *(French)* 78−92998
LASR-2 airborne maritime surveillance radar, medium range 77−29507
lightning flash counters, for ground flash density meas. 80−51552
liquid water content meas. of lab. supercooled clouds, instrument design 78−96316
liquid water content measuring device 79−88489
marine environment test range semi-automatic data recording and monitoring (SADRAM) system 79−39993
mast for tidal salt marsh study 79−66819
mean value data acquisition system *(German)* 78−16220
METEOSAT, Europe's first weather satellite 78−53785
Meteosat, weather and communications satellite 79−16790
Meteosat data collecting platform *(Danish)* 80−12637
METEOSAT data processing system *(Italian)* 80−109275
METEOSAT project, interactive image system 80−109330
Meteosat-I, observational history *(French)* 80−8513
microprogrammable integrated data acquisition system 78−77374
microwave ground-based radiometer, regional precipitation meas. *(Chinese)* 79−84547
microwave radar for wind meas. 77−33195
microwave radiometry for precipitable water vap. and liq., dual-channel method 80−51564
monostatic Doppler sodar system, meas. method, wind obs. appl. *(German)* 79−16710
multimoment Doppler display for severe storm identification 77−56756
ocean buoys, environmental data acquisition 78−36287
ocean data buoys, meas. of Hurricane Eloise (1975) 78−77302
ocean surface meteorological buoy and aircraft VHF link 80−46298
offshore oil industry, operation of sensors 79−70866
optical array precipitation probe, small-particle response 80−51577
optical radar ceilometer measures cloud base height using laser beam 77−29441
optical wind and precipitation sensors *(Japanese)* 78−16207
optimal raingauge densities and accumulation times, decision making precedure 77−29485
parachute dropsonde as vertical motion sensor 78−16185
picture facsimile machine, sample-and-hold detector and line dividers for weather satellite 77−17260
pilot balloon position meas., error anal. of double-theodolite data 79−21051
Portable Automated Mesonet, design, performance and operation, for meteorology 77−78426
pressure jump detector array, gust front detect. at Dulles Airport 78−32234
pressure probe, omnidirectional, for wind meas. *(French)* 79−25349
pressure-jump sensor design for thunderstorm gust front detect. 78−57357
psychrometer, microprocessor-based, for determ. of relative humidity and dew point *(German)* 79−29875
psychrometer, portable differential system construction and operation 80−105072
pulse height analyser for wind speed and direction meas., automatic distrib. meas. system 79−96839
pulse height analyser for wind speed intensity distrib. anal. 78−88937
pyrheliometers of the UK Meteorological Office, and radiation reference scales 80−109206
radar, at Spino d'Adda, performance as device for propagation studies 79−84342
radar, attenuating, rain-rate estimation 78−73540
radar data acquisition system at Spino d'Adda 78−69468
radar echo systems for upper midwestern U.S., analysis 78−16183
radar for mm wave propag. expt. *(Japanese)* 78−16208
radar network, contrib. to local precip. forecasting, case study 77−56692
radar rainfall meas. system, weather radar and real-time data processor combination 77−91326
radar system Doppler pulse, Ronsard, G-band 77−87086
radiometer, microwave, multichannel scanning, for Nimbus-G and SeaSat-A 77−29625
radiometers, hemispherical soft dome net type, recirculating purging system 78−3984

meteorological instruments continued
radiosonde Mark 3, brief introduction 79−84548
rain gauge, rapid response 77−87128
rain gauge, simplified optical path-averaged, based on scintillation detect. 78−40674
rain gauge, standards rel. to homogeneous record of monthly rainfall totals for Norwich (1836 to 1976) 78−3886
rain parameters meas. by optical scintillation 77−82015
rain rate and drop size distribution, with fast-response optical sensor 80−31135
rain sequential sampler, design, construction and operation 80−105090
rainfall instantaneous rate, meas. instrument and influence on high-voltage transmission lines 80−98471
raingauge corrections, mountain meas. accuracy 80−26597
raingauge dust excluder 78−73548
raingauges, high density meas. of convective mean rainfall over small areas 80−77157
raingauges, influence of cleaning on collection and chemistry of rainwater 77−2282
raingauges, tipping bucket type, digital recording system description and field testing 80−77161
range instrumentation for the measurement of the effects of a marine environment on electro-optical radiation 79−8726
resistance thermometers according to Baumbach and Frankenberger, comparison *(German)* 78−65433
review of recent developments 79−25313
rocket telemetry system *(German)* 77−64606
Ronsard radar for investigation of vertical rising winds *(Dutch)* 78−81447
S-band radar at Spino d'Adda 78−69467
satellite picture processor for TIROS-N series, visible and IR pictures 80−67439
satellite solid-state imaging for meteorology and astronomy 77−39074
satellite systems LEOS and GEOS, for global and regional remote imaging 79−5727
satellites, appls. in weather modification programmes 78−96259
satellites, future and present *(Japanese)* 77−87109
satellites, visible and IR instrumentation 77−22041
scatterometer, sea surface wind speed meas. using SeaSat-A 77−29626
sequential precipitation sampler, design and operation 77−70844
shipboard meteorological data system 80−46299
simple construction of amateur equipment 77−33218
snow balance used as rain gauge *(German)* 77−33207
snow depth recorder using optical fibres *(Japanese)* 77−87112
snow gauge, cosmic-ray, snowpile meas. *(Japanese)* 77−5347
snowfall detectors and automatic depth recorder *(Japanese)* 79−8700
snowfall intensity photometer theory *(Japanese)* 78−85736
solar data collection system using microprocessors 78−69542
spin scan camera system, on geostationary satellite, for global weather monitoring 78−61600
stratospheric balloons flight behaviour 77−13138
temperature recorder, long-term *(Japanese)* 77−82035
temperature sensors, humidity effects and sea salt contamination 80−82095
thermistor, microbead, as atm. temp. sensor, response between 0-80 km altitude 77−53234
thermometry in range 253-318K, resistance thermometer 80−46291
TIROS-N weather satellite, detection circuits and sync pulses for picture facsimile machine 79−53577
tri-Doppler radar, tetrahedral scan appls. 78−16184
triangulation direction finding network, for atmospherics sources fixing 79−100981
USSR Hydrometeorological Service, automation of data collection and processing 79−34994
visible IR spin-scan radiometer, on Japanese weather satellite 78−49290
vortex anemometers, second-generation 77−78436
weather displays and data acquisition systems, minicomputer appl. 77−78431
weather forecasting, electronics appl., developments 77−41108
weather radar, results of simultaneous surface precip. meas. at 3.2 cm and 5.4 cm *(German)* 77−82038
weather radar calibration, correl. with rain gauge data *(Japanese)* 78−85670
weather radar matched filter criteria and range weighting 79−25341
weather radar systems, receiver bandwidth effect on refl. and Doppler vel. estimates 79−53549
weather station, Butser Hill, Hampshire, England, 1972-76 period 79−58128
weather-satellite picture facsimile machine 77−9558
wind and turbulence meas. with propeller vane devices, dynamic props. 80−31138
wind data acquisition and processing for wind power site evaluation 79−66400
wind direction gauge based on pulse height analyser 79−25351
wind direction meas. by vane, graphic recording and averaging 80−82098
wind direction measurement, electronic method *(Croatian)* 77−41181
wind gust recorder, digital 77−56762
wind meter, with speed and direction indication 80−207
wind observation system, low latit., First GARP Global Expt. 79−39983
wind profile determ. X-band solid-state radar system 78−12028
wind vanes, wind direction meas. and motion 80−90264
windvane with optical transducer 79−39889
wire temperature sensors, frequency response meas. by internal and acoustic heating 80−31123

meteorological optics *see atmospheric optics*

meteorology
see also climatology; wind
50 mb geopotentials from SIRS soundings and analyzed charts 77−78345
Aberdeenshire, mesoclimate of Upper Don Basin 80−61889
acoustic forecasts production, method using digital computer 79−79960
acoustic study of the atmosphere, acoustic radar appl. *(Spanish)* 78−88944
Adriatic Sea, meteorology contrib. to high tides prediction 77−86906
advection equation, numerical study *(Chinese)* 80−46233
aeronautical meteorology, progress and challenges 78−53692
S.Africa, coastally trapped waves 77−91242
W.Africa, criterion for locating subtropical high, rel. to Sahelian drought 78−7718

meteorology continued
W. Africa, natural ice nuclei concs. and props. *(French)* 77−9474
Africa, rainfall over Sahel rel. to upper air circulation 77−87038
Africa, southern east coast rainfall rel. to southern oscill. and subtropical high press. belt 80−12518
S.Africa, unusual deep depression (1974, Feb.-March) 77−91247
agricultural weather service, New Jersey, user survey 80−4065
agrometeorological data, information flow organization and processing automation 77−78430
agrometeorological management, survey *(Italian)* 77−81989
air pollution episode, Greater Manchester 79−84464
air pollution episodes in Venetian region, real-time forecasting via advection-diffusion model 80−77096
air pollution episodes in Venetian region, real-time forecasting via Kalman predictor 80−82046
air pollution meteorology, rel to 1976 USA Clean Air Act amendments 78−11989
air pollution meteorology, use of sodar acoustic echo sounder, low level stability and wind velocity monitors 80−108828
air temperature, five-day average, forecasting, combined technique improvement 79−29817
air temperature, monthly mean anomalies, mathematical treatment and forecasting *(German)* 79−62557
air warming and cooling rates, urban and rural sites 79−88454
air-sea interaction at large scale, math. modeling 80−41535
airborne weather radar, return anal. 77−53108
aircraft accidents related to weather 79−84463
aircraft-to-satellite data relay system 80−17380
airline meteorology, early days 77−49544
airmasses over Asia in winter *(Japanese)* 79−66768
airport weather service, future trends 78−53694
airports, recurrence probabilities of weather events 80−51491
Amderma region, winter wind speed increase prediction *(Russian)* 77−21852
N.America, weather prospects for 1979, February 26, solar eclipse 79−2473
S.America and Antarctica, synoptic climatology and mountains 80−12532
American network and rocket systems in 1960s *(Russian)* 77−21927
Ampere Glacier, Kerguelen Is., heat balance in ablation area 77−64335
Ampere glacier (Kergueler Is.), surface boundary layer *(French)* 77−56666
AMS and industrial meteorology policy 77−53195
analogue prediction of short-term climate vars. using climate state vector 79−58019
analysis of flood freq., storm prediction techniques 78−11976
analysis of W.Europe network meteorology data, polynomial interpolation *(French)* 80−85710
Andhra Pradesh, aridity and its fluctuations 77−56661
annual rainfall records, comparison methods for climatology 80−51587
anomalous propagation, meteorological aspects 78−57277
Antarctic Ocean, interdisciplinary studies 78−11915
Antarctica, Franco-American collaboration, automated weather monitoring stations *(French)* 79−66786
Antarctica, geodetic and meteorological meas. of refraction 77−87073
Antarctica, polar desert pond dynamic chemical equilib., as sensitive index of meteorological cycles 80−12441
applied meteorology use in energy conservation 77−86958
approximation of meteorological fields by polynomials 79−29831
Arabian Gulf, 1977 June 78−69429
Arctic and Antarctic, Soviet meteorological research 79−34933
areal rainfall amount assessment, two techniques compared 79−62612
artificial clouds form. possibilities and methods 79−29823
artificial satellites, SMS-1, SMS-2, GMS-1, METEOSAT systems *(Polish)* 79−58219
artificial satellites development, new trends 79−29964
artificial satellites future role in meteorological obs. 79−79965
Ashkhabad 1975 dust storm *(Russian)* 77−29396
S.Asia, monsoon circulation, role of mountains 77−49121
Asian monsoon effects on ang. momentum and kinetic energy balances in tropics 78−40630
Asian summer monsoon, hemispheric simulation 78−40629
Asian summer monsoon, simulation by general circulation models 78−40637
Asiatic monsoon area, synoptic aspects of droughts 77−56703
asynchronous data from satellite, scheme for reduction to a common time 80−85735
asynchronous meteorological data interpretation 80−109271
asynoptic data continuous assimilation, dynamic-statistical approach 78−3901
central Atlantic, meteorology in mesoscale vortex area *(Russian)* 78−85658
N Atlantic, quasi-biennial cycles of water temp. fluctuations rel. to weather 79−53357
S.Atlantic anticyclonic gyre, hydrometeorological conditions *(Russian)* 79−100863
Atlantic Ocean, meteorological parameters changes and interaction with different-scale processes *(Russian)* 77−60447
tropical Atlantic surface atm. and oceanic circulation patterns assoc. with Subsaharan weather anomalies 79−5587
Atlantic tropical belt, rainfall field *(Russian)* 77−21851
N.Atlantic weather forecasting, multiday, for press. field 80−98417
atmosphere dynamics in quasistatic approximation, characterisation of approximation *(German)* 80−98383
atmosphere fronts dynamics, numerical modelling *(Russian)* 77−64370
atmosphere physics, book 80−51976
atmosphere Rn concs., influence of meteorological parameters *(Spanish)* 79−92562
atmosphere sound propagation, effects of meteorological phenomena, historical review 78−15
atmosphere surface layer parameterisation, influence of active soil layer *(Russian)* 78−44924
atmosphere turbulence characts. under convective conditions, meteorological meas. *(Russian)* 79−16577
atmosphere turbulent flows, nonlinear perturbation development and predictability problem *(Russian)* 77−62238
atmosphere vorticity area index, correl. with solar plages 78−73459
atmosphere water balance, over Bihar and neighbouring areas 77−56709
atmospheric fronts, numerical investigation of motion employing two-layer model *(Russian)* 77−53109
atmospheric numerical model *(French)* 80−21814

meteorology continued
atmospheric pollution modelling appls. *(German)* 80−51496
atmospheric propagation, remote sensing progress and implications for local weather services 77−81990
atmospheric research, introduction and current areas of interest 79−2351
atmospheric stability, rel. to S dry deposition vels. over E United States 80−56507
atmospheric surface pressure measured using microwave signals transmitted from orbiting satellite 80−94581
Atmospheric Variability Experiments, NASA programme results 77−70835
SE.Australia, meteorological conditions rel. to ground level gravity waves occurrence 78−73439
Australia, thunderstorm, wind gusts 77−86996
N.Australian coast, tropical cyclone guest speeds 77−86997
Australian region forecasts using Nimbus 6 temp. sounding 79−5550
Automated Meteorological Data Acquisition System 77−87077
automated meteorological data transmission from commercial aircraft via satellite 78−57327
automated ship routing, computer program for environmental surveillance 79−84390
automated weather service rocket sounding system, information theory effectiveness rating 79−58057
automatic observation for atm. refr. determ. *(Japanese)* 80−82110
automatic weather station for severe icing climates 79−74973
automatic weather stations, network in Switzerland, computerised monitoring appl. *(German)* 80−17356
AUTOPREP, met. office data prep. and telecommunication terminal 79−100923
available potential energy budget eqns., limited-area 79−53453
available potential energy in atm. in press coords. *(Russian)* 80−109187
available potential energy over uneven topography, theory 80−51514
average over W.India during summer monsoon from H_2O vapour continuity eqn. 79−79990
aviation, forecasting systems, TECAM '79 conf. 80−94569
aviation weather, automation in prediction procedures 78−49080
Baghdogra airport, India, probable thunder occurrence, climatological study 79−39802
balloon tethering system, for very low altitude meteorological obs. 80−36430
Baltic area, thunderstorm activity in October-March period *(Russian)* 77−21850
S.Baltic Region weather severity optimum *(Russian)* 78−7723
Baltic Sea region, aerological climatology rel. to atmospheric heat and moisture balance 77−87057
Baltic Sea region, evaporation-precipitation during IHP 78−44865
baric depressions formation near Alps 77−49099
baroclinic atmosphere, two layer model, Helmholtz term effect 79−79986
baroclinic instability of short-wavelength two-layer Eady model 80−72593
baroclinic instability of zonal flow, modified quasi-geostrophic eqns. 80−56574
baroclinic models, growth rate and vertical propag. of initial error 79−16620
baroclinic spatially growing waves finite amplitude dynamics on f-plane 79−79985
baroclinic wave amplitude, continuous model of the atmosphere 80−72592
baroclinity over India in winter, rel. to western disturbances and jet streams 79−20914
barotropic model for N.hemisphere spectral integration 80−82027
barotropic primitive equation model using splines for typhoon prediction *(Chinese)* 80−4063
W.Bay of Bengal, 1978 southwest monsoon effects. on wave characts. 80−109152
Bay of Bengal, forecasting tropical storm movements 80−41531
Bay of Bengal, tropospheric structure during Aug. 1977 active and break monsoon 80−56570
Bay of Bengal and Arabian Sea, cyclones and depressions during 1975 78−32148
beach atmosphere, microclimate of sandy shoreline 80−8417
Beaufort Sea, mesoscale weather conditions rel. to August ice cover vars. 80−101366
Beijing, China, weather conditions effect on pollution *(Chinese)* 80−108825
Belgium, 1975 Dec.-1976 Nov., analysis *(French)* 78−32198
Belgium, fog freq. *(French, Flemish)* 78−11978
Belgium, meteorological episodes increasing air pollution 78−81374
Belgium, meteorological events in 17th century in Namurois *(French)* 77−64391
Belgium, weather in 1975, review 77−25747
Belgium, weather in 1977 79−58049
Bergeron, Tor (1891-1977), meteorologist 79−2589
biography of James Glaisher (1809-1903) 79−36
biometeorology, plants, animals, human beings, weather change effects *(French)* 80−17360
Birmingham, England 1917/18-1976/7 winters, snow depth records 78−44890
blizzard, 1978 February 18 to 19, in SW.England and S.Wales 80−12507
blocking anticyclones, further remarks 79−20958
blocking anticyclones, prediction possibilities, comments 78−44974
blocking problem, role of wavegroup vel. 78−3892
blocking weather systems, atmosphere multiple flow equilibria theory 80−56536
Boston, air quality during fuel shortage 77−64424
boundary layer, normalization of second order moments of vertical air velocity and temperature *(French)* 79−88447
boundary layer, numerical calc. method for meteorlogical variable fields 78−7733
boundary layer, numerical modelling rel. to local weather forecasting 79−84396
boundary layer heat and pulse transport *(Dutch)* 78−3890
boundary layer interacting with free atmos. *(Russian)* 80−77037
S.Britain, 1978 warm dry autumn 80−4093
Britain, diurnal var. of heavy rainstorm occurrence 77−64402
Britain, max. rainfall in few hours 80−4091
Britain, N.Pennines, altitudinal temp. gradients 80−4094
British Isles, 1968 and 1977 summers, comparison 80−41538
British Isles, 1975-76 drought 77−17201

meteorology continued
British Isles, 1976 June 23-July 8 heat wave 78−20471
British Isles, freezing level during rainfall 77−29391
British Isles, hot spell of 1976 June-July, effective temperature and human comfort 77−53166
British Isles, meteorological parameters affecting climate 78−7745
British Isles, poor summers and assoc. atmospheric conditions 80−109241
British Isles, regular rainfall meas. since 1677, historical review 78−36248
British Isles, systematic rainfall recording since 1677, tercentenary 78−44950
British National Meteorological Library, MOLARS automation 80−82068
British spring weather of 1979, compared with average climate 80−98427
California, spring rains correl. with Pacific Ocean December sea surface temps. 80−77064
calm wind situations, pollutant dispersion analytical modelling 78−81385
Cambridge, England, sea-breeze front passages 78−44973
Campus Weather Service of Pennsylvania State Univ. 78−3849
Canada, chinook weather effects 78−61534
Canadian Middle North, surface heat and water budgets 77−29409
Canterbury, New Zealsnd, evapotranspiration, comparison of methods for estimating 77−53092
Cape Verde Islands, hurricane form., general circulation from Meteosat 80−105042
Carpathian meteorology, conference, Tatranska Lomnica, Czechoslovakia (1975 September 21 to 25) *(French, German, Russian)* 80−46739
Chandler wobble, excitation by earthquakes and meteorological sources 77−78083
Chicago Area Program, mesoscale meteorology 78−77294
chimney height for optimal air pollution reduction 80−26588
NE.China, persistently low summer temp., causative circulation pattern *(Chinese)* 80−109235
Chinese chronicles, 2187 BC-AD 3 meteorological record 80−46213
chronology of air pollution events (up to 1970) 80−7975
chronology of development 78−45452
circulation, by two-level quasi-geostrophic model 80−56546
circulation characts. forecasting rel. to autumn low temp. over Yangtze basin 80−12531
circulation models of atmosphere 77−37348
climate data archiving and quality control by computer 80−61907
cloud cover, forecasting from middle troposphere organised vertical vels. 78−92939
cloud dynamics and modelling, appl. to forecasting 80−8375
cloud motion wind data, meas. improvement 80−8386
cloud motions, automatic tracking system using weather satellite picture sequences 78−45022
cloud physics, course book 79−44239
cloud seeding, ice 80−12489
cloud seeding devices, AgI nuclei formation efficiency 80−41552
cloud seeding experimental results analysis 80−8389
cloud seeding experiments, statistics appl. 80−8438
cloud seeding with AgI and metaldehyde, Fujian province, China *(Chinese)* 80−46235
clouds and atm. phenomena, integrated automatic processing of obs. data 79−29907
cloudy atmosphere moisture content determ., long-range, by thermal radioemission meas. *(Russian)* 79−5637
coastal networks to monitor nuclear plant cooling systems 77−53103
Cochin Harbour mouth, India, monsoons rel. to hydrographic characts. and tidal prism 80−41452
coherent polarization-diversity radar techniques 79−58111
cold front, obs. of 3-D circulation, precipitation and wave motions 80−90142
cold front of midlatitude cyclone, cloud and precipitation struct. 80−109192
cold front passage, response to W.Florida continental shelf waters 77−37225
cold front passage in Southern Hemisphere near equator 77−53102
cold-frontal rainband, cellular struct. obs. 80−51512
Colorado winter storms snowcrystals and natural ice nuclei 77−9475
composite charts, experimental objective classification 78−3906
computer applications *(German)* 80−36363
computer weather prediction, 1950 ENIAC computations 80−42030
computer worded forecasts, description of input and useage 80−17310
conference, computing methods in applied sciences, Le Chesnay, France (Dec. 1975) 77−33846
conference, on climatology, hydrology, atmospheric research and meteorology from space, Ajaccio, Corsica (1979 November 12 to 16) 80−62397
conference on air pollution, New Orleans, USA (March 1980) 80−90603
conjugate equations use in calc. meteorological fields, inclusion of a priori information *(Russian)* 80−4136
convection, aspects relevant to astrophysics 78−88898
convective cloud activity, urban induced influences 77−78341
convective clouds, dry ice appls. for on-top seeding 78−73531
convective mixed-layer entrainment, for realistic capping inversion layer 80−12487
convective scale precipitation downdraughts in cumulus and synoptic scale interactions 77−33145
convective systems, life cycles, GATE data 79−53440
convective systems during Phase III of GATE 80−90153
convective vortex model, unsteady two-cell similarity soln. 79−16626
cooling towers, effects, review *(German)* 77−73800
N.Cornwall, record March rainfall in one day 78−44971
correlations of changes in geomag. field, climate and weather 79−39648
cosmic ray muons meas., meteorological coeffs. for scintillation supertelescope 77−13202
cosmic ray observations, meteorological conditions determ., spectrographic method 78−69627
cotton canopy aerodynamic features 77−45105
Cross Fell, England, severe low level turbulence occurrence and synoptic situation 79−79962
cumulus cloud statistics, satellite-derived, for W.Kansas 79−79955
cumulus parametrization for 10-level atm. model 77−70782
cyclogenesis, asymmetric jets instability theory 80−56537
cyclogenesis and anticyclogenesis, optimum modelling of Earth's topography 78−28256
cyclogenesis in lee of Alps 78−77305

meteorology continued
cyclone at temperature latitude, water vap. and energy budget 80−85731
cyclone development along weak thermal fronts, model soln. 80−81994
cyclone forecasting applications to typhoons 77−25801
cyclone formation, kinetic energy budget 78−16127
Cyclone Joan 1975, wind and rain meas. over W.Australia by satellite microwave sensing 80−98485
cyclone waves and front development, surface friction effects 77−86966
cyclones, dynamics, two-arm struct. and tracking 78−77299
cyclones, unstable baroclinic waves downstream and upstream development 80−56540
cyclonic storm, Arabian Sea, 1976 June, diurnal var. and secondary vortices form. 79−20915
cyclonic storm, Porbandar, India, 1975 Oct., features 79−48538
cyclonic storm, rainbands, precip. cores and generating cells 78−81307
cyclonic storms, mesoscale and microscale organization and struct. of clouds and precip. 79−74946
cyclonic storms and depressions during 1974, Bay of Bengal and Arabian Sea 77−53110
cyclonic systems in SW monsoon period moving towards lower latits. 79−96796
cyclonic weather conditions and short period oscills. in F-region 78−16234
daily precipitation stochastic models, estimation of Fourier coeffs. to describe parameters seasonal vars. 79−53481
daily temperatures, statistical forecasting using short records of previous temps. 79−58015
daily temps. and sunshine, spatial variability over uniform terrain 78−3887
dangerous weather phenomena prediction, research prospects 79−34932
data acquisition system for airborne meteorological research 79−66808
data collection and processing system at Leningrad TV tower 78−4004
data collection in North Sea *(Dutch)* 79−96827
data communication system, Africa, SIRIO 2 satellite system appl. 79−96806
data determination by weather satellites *(French)* 80−82019
data editing and validation using interactive graphics 78−77330
data flow program 79−70878
data processing of M-100 meteorological rocket system 77−53233
Denver air quality, effects of meteorological and climatological factors 79−84350
depression life-cycle as function of latitude, rel. to meridional transport 80−51508
E.Derbyshire, local temp. var. 77−64404
derivatives computation from equally spaced data, rainfall rate determ. 77−49125
dew duration forecasting, Pendleton, Oregon, using simple weather obs. 79−70857
diagnostic analysis in weather forecasting, appl. to storms *(Chinese)* 80−12467
diffusion props. over urban site, anal. using radioactive tracers, effect of meteorological variables 79−84348
digital data compositon for satellite and radar imagery 80−67413
digital image system for atmospheric research 79−39873
digital phasemeter optical threshold determ., meteorological Doppler radar station appl. *(Russian)* 78−20560
digital radar data computer processing for High Plains Coop. Program (HIPLEX) 78−92989
digital satellite imagery in industrial meteorology 77−91282
digital terrain data appl 79−84440
dimensional analysis and power laws limitations 79−25333
direct solar radiation and global radiation for 69 places in West Germany, solar power appls. *(German)* 79−70837
diurnal surface temp. range sensitivity to changes in physical parameters 78−3875
diurnal variation of rain and low cloud over Ozar airfield rel. to forecasting 79−100904
Doppler radar weather surveillance near airports 80−46272
Doppler weather radar, development of weather echo props. 80−26645
downslope severe windstorm and aircraft turbulence event induced by mountain wave 78−73431
drought, forecasting in subcontinent of India 77−56710
drought and weather modification in India, review 77−56715
drought definitions 80−105010
drought effects on agriculture in United Kingdom, 1975-76 period 78−57298
drought effects on hydrological independent mixed models 80−81954
drought in California and western Europe, 1976, atm. and oceanographic factors 79−48560
drought in England and Wales, 1975-6, development of water resources 78−88869
drought in England and Wales, 1975-6, effect on agriculture 78−88890
drought in England and Wales, 1975-6, effects on groundwater and aquifers 78−88866
drought in England and Wales, 1975-6, effects on the river systems 78−88867
drought in England and Wales, 1975-6, meteorological aspects and numerical expts. 78−88889
drought in England and Wales, 1975-6, pollution problems 78−88868
drought in streamflow series, statistical characts. 80−105009
drought years at Masulipatam (Andhra Pradesh), water balances 77−56663
droughts, diagnostic study by quasi-geostrophic diabatic four level model 77−56713
droughts, in Himalayan region of Uttar Pradesh, influence on ground water supplies 77−56708
droughts and floods, in India and other countries 77−56702
droughts in the Asiatic monsoon area, symposium, Poona, India (Dec. 1972) 77−56701
dry and wet days occurrences, Markov chain model 78−7698
dust haze of African Harmattan wind, 1962-1973 visibility obs. 80−61900
dust storms, freq. and diurnal var. in contiguous United States 77−29353
dynamic meteorology, atmospheric motions, spectrum analysis 79−20957
dynamic meteorology fundamentals, book contrib. *(French)* 77−87052
dynamical meteorology, 350 years of development 78−44970
dynamical meteorology, perspectives 79−100933
dynamical meteorology, trough-ridge systems as slantwise convection 79−79993
meteorology continued
dynamical meteorology, trough-ridge systems as slantwise convection 79−84456
dynamical meteorology topics, atmospheric energetics 79−66780
dynamical meteorology topics, vorticity and divergence 79−12226
early spring warm spells, case study for (1977 March 2) 79−79994
Earth annual wobble, affected by wind stressed sea level 80−36221
Earth observation programme of ESA 80−109250
Earth radiation budget data collection and interpretation model 77−37497
Earth rotation effects, contribution of space technology *(French)* 79−74827
Earth rotation variability, meteorological and oceanic causes and consequences 77−56571
earthquake prediction, rel. to temp. rainfall and soil tilt 77−91058
East Anglian 'meteorite' of 1646, meteorological interpretation 80−68009
easterly perturbation intensification under westerly trough influence, India, 1975 Feb. 79−48548
eddy fluxes of conserved quantities by small-amplitude waves 80−61858
edge detection for meteorological data 79−100989
education, textbook survey 78−16087
effects of solar thermal electric conversion plant, numerical modelling 80−35794
electrical coupling to upper atmosphere, quasi-static model 80−61865
element field adaptation, variational method *(Russian)* 77−29491
EM Waves refraction in atmospheric boundary layer, expt. investigation 80−36400
empirical orthogonal functions, stability 77−67224
empirical orthogonal functions of 500 mb height, truncation of series 80−56581
empirical orthogonal functions of 500 mb level, N.hemisphere 80−56580
energetics in dynamical meteorology 79−58064
energy budgets, Priestley-Taylor large scale evaporation, comments and reply 77−45039
energy transfer in tropical subcloud layer, aircraft meas. during GATE 79−79989
S.England, 1977 January 25 rapid pressure var. 78−44972
England, decreasing wetness in 1969-77 period 78−65377
England, hot spell of 1976 June-July 77−17203
E England, meteorological situation rel. to storm surge (1978 January 11 to 12) 80−12419
central England, monthly mean temps. for quintile distrib. 77−29418
central England, persistence and monthly mean temps. 78−73497
S.E.England, rainfall, medium term fluctuations 77−21861
England, summer max. temp. recorded in Glaishev stand and Stevenson screen 77−81976
SE.England, summer weather in 54 BC 77−49149
environmental assessment for air pollution abatement, diffusion model evaluation 79−57547
environmental impact assessment, air pollution problems 78−49124
environmental obs. from space based systems, present and future 79−5657
equatorial atmosphere zonal model, Coriolis force and stratification on stationary motions 80−77071
equatorial region, air and moisture transport during S.W. monsoon, MONEX-73 obs. 77−53112
equatorial stationary zonal circulation, numerical calcs. 80−85732
equatorial trough zone, heat balance 80−81977
equatorial trough zone occurrence and struct. in Venezuela 79−79974
equatorial vortices over South China Sea and Malaysia during winter monsoon 78−40633
equatorial wave mean-flow interaction, role of latitudinal shear 80−51461
equatorial wave resonant interaction, nonlinear dynamics 80−56550
Ethiopia, annual rainfall reliability 77−33172
Eurasian winter snow cover rel. to Indian summer monsoon rainfall 77−41076
W.Europe, 1976, summer drought 77−64401
Europe, exceptional weather in (1975) 77−25756
NW Europe, polar air outbreak, subsynoptic disturbance case study 80−101408
E.Europe, tropospheric wind variance spectrum 80−8397
European air temperature band-pass filtered series, correls. and phases 80−26579
European Grosswetterlagen, temporal vars. and possible causes 79−58081
European large scale weather pattern and N.Atlantic temp. fluctuations *(German)* 78−85660
European meteorological information system, network structure, facilities 77−70772
evaporating downdraught model comparison with obs. behind squall lines 78−92913
evapotranspiration est. from thermal scanner meas. of canopy temp. 77−5324
events between 1574 and 1609 from journals of Pierre de l'Estoile *(French)* 79−58510
Everglades Agricultural Area, USA, soil temp. obs. in winter nighttime 80−56559
exceptional weather in 1976 over Europe 78−36251
extratropical cyclone, enhancement after separation from polar front *(French)* 80−56517
fair weather condition concept in atm. elec. 78−61517
S.Far East, weather variability rel. to NW.Pacific currents 80−101417
FGGE, data acquisition and processing test 79−16674
FGGE, global weather expt. 79−16673
FGGE observing system, data system tests 80−56610
field data, objective anal. 79−12321
finite difference scheme solution of physical instability and weather prediction problems 77−53763
first GARP Experiment (FGGE), formation of data sets from obs. 80−101437
First GARP Global Experiment, data collection 79−58055
First GARP Global Experiment, introduction 80−12550
flash floods, American National Weather Service (NWS) warning and disaster preparedness program 79−25289
flood warning system, on-line, based on adaptive model, desk-top computer appl. 79−34977
floods of E.Australia catchments, freq. distribs. 80−105012
flow pattern forecasts, impact of synoptic observing and analysis systems 77−45061

meteorology continued
fluid dynamics conference, Aug. 1978, Strasbourg, France 80−36764
flux calculation methods, relative errors 79−79953
fog forecasting using point discharge current 77−70748
forced plume characteristics 78−18286
forced Rossby waves on a zonal shear flow, model 80−77072
forecast accuracy for rain, limit due to spatial variability of rainfall 80−56510
forecast model, with boundary layer vertical eddy flux representation 80−61844
forecast model with 10 levels, lower boundary condition 80−51494
forecasting, climate prediction, problems 79−92570
forecasting, complex statistical long-term method 78−16129
forecasting, evaluation of dynamical/statistical initialization 77−86970
forecasting, initialization methods for gravity wave generation in two-layer linearized model 77−86971
forecasting, moisture processes in quasi-geostrophic model 78−7696
forecasting, overview and future work 77−91196
forecasting, satellite technology development, (1960 to 1979) *(Dutch)* 80−12559
forecasting, stochastic-dynamic system, asymptotic behaviour 80−12474
forecasting, via baroclinic model using high accuracy horizontal discretisation 77−45065
forecasting dry thermals for gliding 78−49103
forecasting for Ninian Field drilling platform construction 80−41522
forecasting hail, thunderstorms, and showers, book 77−73821
forecasting in atmosphere-ocean models, max. attainable accuracy 80−82036
forecasting max. and min. temp., use of probabilities 80−82020
forecasting method for weather assoc. with western disturbances 79−100903
forecasting model to determine meteorological elements effect on geopotential field 80−82033
forecasting nocturnal temperature, short-rnage model 80−109200
forecasting NW.Europe winter weather, time-mean atmos. study 80−77040
forecasting of average air temp., underlying ocean surface influence 79−29827
forecasting of daily pressure by statistical method 80−56528
forecasting of daily var. of meteorological elements, ordered risk minimisation *(Russian)* 77−60451
forecasting of diurnal average air temp. in N.Vietnam 78−3903
forecasting of local weather, numerical prediction models 80−67398
forecasting of orographically enhanced rainfall accumulations using 10-level model 78−69420
forecasting of sea-level press. with allowance for surface press. tendency 80−85738
forecasting of surface winds, statistical method *(German)* 77−64475
forecasting precipitation, evaluation of real time operation 79−88443
forecasting procedures for aviation, development and improvement 78−92950
forecasting skill, daily precipitation and temp. 1966-78, Boston, USA 80−56509
forecasting solenoidal wind vel. component 80−82034
forecasting SW.monsoon onset over Kerala, India 78−32158
forecasting with non-hydrostatic mesoscale model including orography 80−51507
forecasting with topography, pressure gradient force and advection scheme 77−86977
forecasts for flat country using Ficker's rules *(German)* 78−45026
forecasts for limited areas, boundary conditions 79−16582
four-day forecast, influnece of sensible and latent heat fluxes over land 79−96805
four-dimens. analysis of meteorological information in GARP 78−7740
France, 1852-1956 cyclones, anticyclones and depressions *(French)* 77−45063
France, meteorological events at the end of the 14th century and the beginning of the 15th *(French)* 77−86960
freeze-thaw cycles causing road potholes in USA, 1977-8 obs. 80−56560
French contribution to First GARP Global Experiment *(French)* 78−77310
front formation over central Europe, internal processes 80−81979
front position, precise determination from temp. and press. field data 80−98426
frontal passage, VHF radar obs. 79−53482
frontal rainband, conditional symm. instability explanation 80−56584
frontal waves development, numerical simulation accounting for mountain ridges effect *(Russian)* 78−53701
frontogenesis, 3-dim. study using stream axis coords. 77−87001
frontogenesis, baroclinic instability of jet flow 80−61855
frontogenesis, Hoskins-Bretherton model and surface frontal zone anal. 80−94572
frontogenesis, semigeostrophic theories, energy spectra prediction 79−2338
frontogenesis and warm sector formation affected by boundary layer vertical motion *(Russian)* 80−105027
frontogenesis caused by cumulonimbus convection 77−21845
fronts, as source of mesosphere internal gravity waves *(Russian)* 79−16575
frozen precipitation forecasting, regression estimation of event probabilities method *(German)* 79−66770
frozen soil, prediction using weather records 79−88379
functional dependency recognition using meteorological data *(Russian)* 78−40609
funnel clouds, characts. from meteorological sounding and sailplane flights 78−69396
GARP Winter Monsoon Expt., Dec. 1978 field phase report 80−46262
GATE, 1974 field project 77−2247
GATE, introduction 77−2246
GATE, Meteorological Research Flight work 77−2248
GATE, Synoptic-scale Subprogram Data Centre 77−2250
GATE, telecommunication data, computer processing 77−2251
GATE aircraft measurements, their value 80−82071
GATE C-scale triangle, mass and energy budgets rel. to weather 79−16583
GATE ship surface meas. systems, anal. or drift 80−82070
general circulation, models with lower boundary condition and energy consistency 80−56547
general circulation at mid-latitude, fluctuations seen in rawinsonde data 80−81980
general circulation by GLAS model, cumulus friction and Jan. Hadly circulation 80−72588
general circulation model, Earth rot. increased or decreased 5 times 80−56545
general circulation model, extended range prediction expt. 77−86963
general circulation model, response time rel. to ocean surface temp. change 80−98422
general circulation model (NCAR), response to sea surface temp. change 80−98390
general circulation of midlatitude troposphere, NCAR and GFDL models 80−61856
general circulation of N.hemisphere in winter, horiz. transport by transient eddies 80−72589
general weather situation rel. to tropospheric O_3 concs. 80−101397
Genoa, 1833 to 1900 meteorological obs. *(Italian)* 79−34936
geopotential field numerical analysis using meteorological information 78−7814
geopotential height fluctuations, geographic variation of vertical struct. 80−90132
geopotential values retrieved by objective anal. methods 80−36386
NW.Georgia, monthly rainfall spatial correls. rel. to climatology and weather modification expts. 80−51479
GEOS, IUF, and METEOSAT ground stations, weather obs., Earth exploration *(German)* 77−56763
geostrophic four level model, predictability, effects of grid point numerical errors 78−40642
German Bight, meteorological parameters rel. to trilateration distance meas. *(German)* 80−8248
German weather, hydrometeors, extinction and scattering in 0.25-15 μm range 79−53501
Germany, 1851-1975 precipitation changes *(German)* 77−33164
SW.Germany, heavy rainfall from May 22 to 24 (1978) *(German)* 80−61869
S Germany, large scale weather conditions and flight conditions *(German)* 77−17178
Germany, weather forecast for New Year's Day 1978-9, moist baroclinic model *(German)* 80−77065
Ghaggar River catchment area, India, hydrometeorological study of rainfall trend 77−56660
glaze storms and wire icing in Ukraine 78−81329
global barotropic primitive eqns., Hough harmonics for spectral model 77−78442
global barotropic primitive eqns. with Hough harmonic expansions 79−79925
global divergent barotropic model, finite difference schemes for initial value problems 77−86986
global general circulation, 4th order model 78−11952
global problems of fluid dynamics 78−96173
global weather data, sunspots and geomag. activity, cross-spectral anal. 77−78313
Global Weather Experiment, communications and data management system 79−5620
Global Weather Experiment, objectives and observing systems 79−5619
Global Weather Experiment, observational phase through first special observing period 80−51543
Global Weather Experiment, role played by geostationary meteorological satellites 80−77256
Global Weather Experiment, Second Special Observing Period 80−77119
Global Weather Expt., roles played by METEOSAT and TIROS-N 80−26714
global weather model, thermodynamic, with turbulent transport *(Spanish)* 80−36372
Great Britain, global solar radiation distrib. on horizontal surface, monthly maps 79−79959
Great Britain, northerly gales of (1978 January 11 to 12) 80−12508
great frost of January 1776 77−56721
Great Lakes, ice formation, freeze-up, breakup predictions 77−45038
Greenland, summer aerosols and trace gases 80−72609
ground-based inversion decay, analysis by direct and indirect meas. methods *(German)* 77−37310
NE. Gulf of Alaska, development of synoptic climatology 80−98405
W.Gulf of Maine, meteorological data rel. to gulf winter circulation 80−51430
Haar series use in constructing difference schemes for meteorological appl. 79−58125
hail cell detection, for cloud seeding criteria, radar method 80−90170
hail probability rel. to radar echo heights, South African Highveld 79−20925
hail reports rel. to 45 dBZ contour level 77−56688
hail size sorting in three-dimens. updraught, rel. to hail suppression 79−20926
hail suppression, crop protection, involvement of society 79−8677
hail suppression, current status 77−64363
hail suppression expts., improvements 77−91218
hail suppression paradox, stratification approach to statistical expt. 77−37312
hail volume model extrapolation from surface meas. 77−21871
hail-prevention operations, cost effectiveness estimation methods anal. 78−93013
halo displays, meteorological conditions 78−36282
hang gliding and assoc. weather 80−105043
heat wave and cold wave days in Indian subcontinent 78−7699
heavy precipitation of Fergana Valley, short-term forecasting 78−92946
heavy rain, anal. by potential pseudoequivalent temp. field *(Chinese)* 79−48532
heavy rain, dynamical anal., potential pseudoequivalent temp. condition conservation *(Chinese)* 79−48533
Hebei Plain, summer drought and flood rel. to atm. circulation seasonal var. 80−90203
hedging and categorical and probabilistic forecasting 79−5548
helicopter icing problems, role of meteorology 78−85657
N.Hemisphere transient motions, RMS 1000 and 500 mb geopotential height 80−90163
N. hemisphere winter circulation, general circulation model, comparison with obs. 80−109189
Himalaya, summer weather and climate 80−72620
historical meteorological data, appl. to hourly mixing depths estimation 80−51482

meteorology continued
historical series spectral anal. using maximum entropy method *(Chinese)* 79−79958
Hohenpeissenberg Meteorological Observatory, precipitation duration *(German)* 77−56693
hot spells of 1976, micrometeorological charact. at Cardington 79−79961
S.Humberside, 1949-76 summer months, evaporation and rainfall 77−73819
Hunan and Zhejiang Provinces, rainy season, long range forecasting 80−90204
hurricane and typhoon forecasting appl. of Kalman filter 77−64409
hurricane Ava, Skylab scatterometer meas., anomalous data correction 79−29881
Hurricane Camille, evolution, Nimbus 3/ATS 3 obs. 78−92921
hurricane Camille, wind speed and direction, ocean wave height and barometric press. meas. 78−36254
Hurricane Eloise (1975), meteorological meas. by ocean data buoys 78−77302
hurricane modification expts. by cloud seeding, evaluation 78−85654
hurricane season activity analysis, N.Atlantic (1886-1974) 80−101427
hurricane-intensity extratropical storms, satellite forecasting, comments and reply 77−17249
hurricanes, forced secondary circulations 79−84387
hurricanes and tropical meteorology 79−39785
hurricanes temporal variability, rank order statistics appl. 78−92910
hydrodynamic equations appl. to dynamical meteorology 78−57286
hydrodynamic forecasting problem, coupling-moment atmospheric turbulence charact. 78−7734
hydrodynamic weather prediction 77−70801
hydrodynamic-type system, existence of anomalous modes, rel. to weather patterns *(Russian)* 78−65361
hydrodynamics, vertical eqn. of motion and wind eqns. 78−69428
hydrometeorologic elements in coastal zone, indicators of long-term vars. *(Russian)* 78−77258
hydrometeorological data, Weibull distrib. appl. 78−65415
hydrometeorological data acquisition, microprocessor appl. *(Italian)* 77−82067
hydrometeorological data for US, autocorrelation charact. 77−66939
hydrometeorological fields, probability algorithms for objective anal. *(Russian)* 77−78247
hydrometeorological information in USSR, economic effectiveness 79−29909
hydrometeorological process harmonic components, separation by least squares *(Russian)* 77−78246
hydrometeorological series stationary properties study, Oise river basin appl. *(French)* 78−36210
hydrometeorological time series, spectral analysis for United States 77−64341
hydrometeorology, new directions review 78−96240
hydrometeorology, USSR research vessels, information acquisition and processing *(Russian)* 77−21909
hydrometeorology rel. to water resources design engineering 79−70819
ice evolution within seeded and nonseeded Florida cumuli 79−100920
ice nucleation, on natural and man-made particles 79−48530
ice nucleation by fluid-breaking metaldehyde particles *(Chinese)* 80−12468
ice nucleation in atmosphere, natural nuclei origin 79−48531
image data processing in Geostationary Meteorological Satellite System *(Japanese)* 79−92627
India, moisture flux across west coast and rainfall during SW monsoon 77−70783
India, N.E. monsoon rainfall singularities over Tamil Nadu 77−70746
India, westerly upper air troughs rel. to western disturbances development 80−90173
Indian monsoon, spectrum anal. appl. 78−44957
Indian monsoon rel. to equatorial stratospheric westerlies 77−29370
Indian Ocean, sea levels in western equatorial region rel. to tides, meteorology and ocean circulation 80−4018
Indian region, primitive eqn. barotropic model for storm tracks prediction 78−85625
Indian sea areas, 1976 cyclonic storms and depressions 80−56533
Indian subcontinent summer monsoon, causes of 1899 drought 77−56705
Indian summer monsoon, Arabian Sea surface temp. anomaly effects 77−49120
Indian summer monsoon, effects of five-day oscill. in E.African low-level jet stream 78−53705
Indian summer monsoon, influence of Arabian Sea 78−81333
Indian summer monsoon cyclogenesis and variability 78−81319
Indian summer monsoon meteorology 79−74938
Indian summer monsoon rainfall rel. to Eurasian winter snow cover 77−41076
Indian summer monsoon rel. to tropospheric flow patterns over southern hemisphere 78−81334
Indian SW monsoon field mesoscale accentuations, very heavy rainfall 78−85629
Indiana tornado warning systems 79−5549
industrial meteorologists, trade assoc. and National Council 77−53193
industrial meteorology, AMS 56th annual meeting (Philadelphia, 20 January 1976) 77−53098
industrial meteorology, future 77−53100
industrial meteorology and American Meteorological Society, history 77−49543
industrial meteorology and weather modification, history 77−49542
industrial site, local weather effects on air pollution, field studies 77−53165
industrial weather service, starting difficulties 77−53099
information processing system, AOIPS 77−78519
information retrieval publications, comparative study hydrometeorology in USSR 80−36401
Institute of Meteorology and Climatology, Slovak Acad. Sci. (1964-74) *(Russian)* 78−88920
intertropical convergence zone cloud cluster, wind field behaviour 80−17322
inverse problems in meteorology, estimation theory appls. 79−35018
ionosphere F_2-region, meteorological perturbations due to gravity waves at sunspot minimum *(Italian)* 79−29922
IR satellite data automatic segmentation and classification 79−5638
irradiance, seminumerical method accounting for atmos. H_2O *(Spanish)* 80−36373
isentropic and sigma coord. hybrid numerical model 80−12485
meteorology continued
isentropic objective analyses, theory and appl. to meteorology *(Polish)* 80−51546
isoline printing, computer method *(Russian)* 77−53245
isotropic-distribution approximation validity, in solar energy estimations, exact procedure comparison 77−78358
Israel and Jordan, rainfall fields, cloud seeding effects 78−73452
Israeli rainfall stimulation expt., 1961-67 period, anal. 78−92926
Israeli rainfall stimulation expt., 1961-67 period, reply to criticisms 78−92927
NW.Italy, large-scale winds rel. to coastal waters oceanographic conditions during 1977 spring 79−34827
ITCZ over W. central Bay of Bengal, disturbances during 1974, October 77−45115
jet stream as source of medium scale thermospheric gravity waves, exptl. study 79−21088
jet stream-frontal systems, pot. vorticity, role or turbulence 80−77044
jet streams, low level SW over S.China April to June *(Chinese)* 79−66744
Kansas, storm and tornado watches compared to observed tornadoes, rel. to weather modification 80−12505
Kashmir region, vars. of aerosols and snow chemical components with weather conditions 80−94594
Kerala (S.India), weak monsoon rel. to satellite-determined cloudiness and large-scale flow 77−56706
Kew, monthly mean temp. and rainfall in August 1973-July 1976 period 77−73820
Kew, monthly potential evaporation totals for 1698-1976 period 78−7724
kinetic energy balance of large-scale motion over British Isles 80−56578
Kitt Peak National Observatory, probability of clear daytime skies 80−12512
Kropotkin, Pyotr Alekseevich (1842-1921), meteorologist *(Russian)* 79−97167
La Porte (Indiana) precipitation anomaly reexamined 78−49076
La Porte precipitation anomaly, relocation effects 78−49077
Lake Constance, heavy storms and wind strength and direction *(German)* 77−56695
land and sea surface temp. fields, seasonal vars., NOAA 5 satellite IR obs. 78−85676
Landsat 2 cloud imagery rel. to future meteorological obs. systems 78−40626
lapse rate regimes and parameterisation 80−12486
large scale atmospheric process simulation, conf., Hamburg (30 Aug.-4 Sept. 1976) 77−86961
large scale numerical forecasts at mid-latitudes, convection parameterisation 77−86967
large scale processes, temporal spectral density evaluation *(Russian)* 77−5337
Leningrad, air pollution forecasts *(Russian)* 77−53181
Liege, Belgium, sixteenth century weather record *(French)* 80−82029
Liege, Meteorological events in the 15th century *(French)* 79−2328
light refraction calc. in three-dimensional model atmosphere, meteorological data requirements 80−46260
lightning incidence prediction and effects in electrical systems, obs. 79−39789
Ligurian Sea, free oscill. correl. with meteorological perturbations 79−34826
limited area forecasting model, forward-backward integration scheme 77−87084
Limited Fine Mesh model and data from aerial reconnaissance of Atlantic storms 77−70731
line thermal numerical model, initial conditions influence 78−92932
linear prediction models, review 80−56590
liquid cooling towers, effects *(German)* 77−73799
local severe storms in summer, anal. and forecasting method *(Chinese)* 79−84450
local situations, statistics and pollution potentials *(Spanish)* 79−29813
local weather prediction, hydrodynamic methods 78−61521
London, 1976 June-July heat island 77−91248
London Weather Centre, urban influence on wind directions 77−73817
long-range numerical weather forecasting *(Chinese)* 77−87051
long-range prediction of averaged meteorological fields, theoretical scheme 78−3905
long-range weather forecasting, art and science 80−109184
long-term processes in atmosphere and hydrosphere, statistical predictability *(Russian)* 77−49105
Los Angeles, anal. of meteorological processes affecting oxidant and precursors in LARPP (operation 33) 80−61479
Los Angeles Basin, urban climate, model of aerosol effect 77−66978
SE.Louisiana, forecast model 80−46216
low vortex over S.E. Chinghai-Tibetan Plateau, annulus expt. simulation *(Chinese)* 77−70787
low-level jet, struct. rel. to synoptic evolution *(German)* 78−69422
lunar tide in atmosphere, influence of local weather on solar modulation 80−94593
macroprocess classification, statistical methods 78−16132
maize canopy, turbulent transport 77−33129
central Mali, rainfall comparison between Kabara and Tombouctou 80−4092
man-machine interface, weather forecaster console for satellite data handling system 80−90205
mapping of rainfall by radar 78−24397
marine fogs, charact. of air mass histories, Nova Scotia, 1975 August 79−70847
marine radiofacsimile weather chart receiver and recorder 80−46297
maritime boundary layer model for fog prediction 77−78293
Markov chain modelling of weather data 77−49124
Markov theory rel. to meteorological data for spacecraft launch planning 77−45091
Masirah Oman, September monsoon depression 79−8669
mathematical analysis of cloud seeding expts., physically meaningful covariates 80−56522
mathematical analysis of weather modification and meteorological data 80−56521
maximum likelihood estimates for parameters of mth extreme value distrib. 77−78332
maximum temp. forecast for cloudy or overcast days *(German)* 77−37311
measurement system noise spectra determ., simultaneous eqns. soln. method 78−57354

meteorology continued
medieval European climate reconstruction using weather compilations, reliability 79−74929
meso- and microscale phenomena study using superpressure balloon sounding technique 79−66815
mesometeorological processes development over inhomogeneous heated surface *(Russian)* 77−29365
mesometeorological stationary problem of flow around obstacle 78−81271
mesoscale convective systems, inertial instability 80−90131
mesoscale divergence of horizontal vel. field and press. gradient force, rel. to momentum transport 78−11954
mesoscale models, results in Alsace plain *(French)* 79−84411
mesoscale precipitation areas persistence and orographic modulation 79−79967
mesoscale precipitation forecasting over mountainous terrain 77−49143
mesoscale satellite system design 79−58224
mesoscale structure of line convection at surface cold fronts 80−12514
mesoscale weather, impact of large solar energy systems 78−81358
mesoscale winds aloft, numerical prediction models, verification 78−16110
mesosphere, meteorological fields rel. to eddy diffusion models 80−109198
meteoradiolocator echo signals, optical spectral processing *(Russian)* 79−100968
Meteorological Office 10-level prediction model (Dec. 1975 status) 77−91250
Meteosat, role in obs. 78−36219
Meteosat, single cabinet telecommunication equipment 78−36419
Meteosat 78−93072
METEOSAT 1 weather satellite pictures, amateur facsimile reception *(German)* 80−81982
METEOSAT appls., conf., Rome, Italy (Mar. 1978) 78−96384
Meteosat data-collection system, description and appl. 80−77122
Meteosat ground facilities, European/W.Indian network *(French)* 78−45183
Meteosat image processing 78−36297
Meteosat imaging payload, functional aspects 78−36424
Meteosat launch operations 78−36425
Meteosat programme organisation and management 78−36422
Meteosat project MISS IDA, interactive image system 80−36404
Meteosat remote sensing equipment for atm. general circulation obs. 80−94595
METEOSAT role in global observing system *(German)* 78−36437
Meteosat satellite in-orbit performance, results 78−88875
Meteosat spacecraft, elec./mech. configurations 78−36423
Meteosat system, missions and performances 78−36421
Meteosat system, organizational aspects *(French)* 79−29969
Meteosat system, wind vector calculation from cloud motion 80−46270
Meteosat-1, research uses of early data, review 80−77257
Mexico, sunshine hours and meteorological data rel. to total solar radiation 79−44237
microclimatic and mesoclimatic stability indices, statistical relation, rel. to pollutants diffusion *(Spanish)* 78−44964
micrometeorological measurement principles, book 77−9559
micrometeorological statistical tests 78−3866
micrometeorology, simulation of field crops and glass houses *(Dutch)* 77−64389
microwave radiometric determ. of wind speed at ocean surface, Bering sea expedition 77−17158
mid-ocean eddies and weathership records 77−64294
Middle East, monthly temps./rainfall relation appl. to palaeoclimates evaluation 80−31091
Middle Europe, 1708-54 precipitation record for Zurich *(German)* 78−85661
minor species meteorological control of lower stratosphere 79−12171
model grid length and orographic rainfall efficiency effects on surface rainfall calc. 77−70774
models, medium and small scale *(French)* 79−84406
modified quasi-geostrophic eqns. using geometric height as vertical coord. 77−87036
Mohliner Feld (east of Basle), topoclimate investigations *(German)* 80−61890
moist available energy, numerical procedure 80−46241
MONEX, monsoon experiment 1979, objectives 79−8665
monsoon, digital simulation of evaporation phase, development of moisture eqn. 77−56712
monsoon, model of large scale seasonal struct. 80−98393
SW.monsoon, orographic effects, review 78−44962
monsoon breaks, effects of surface press. 10 to 20-day westward propag. mode 80−94592
monsoon circulation and rainfall S.Asia 78−44958
monsoon circulation dynamics 79−5559
monsoon depression, Bay of Bengal, intensifying into cyclonic storm over land 79−20916
monsoon depression, Bay of Bengal, tropospheric vertical wind shear 79−8670
monsoon depression, composite structure 77−45117
monsoon depression formation, effect of wind shear 79−84461
monsoon depressions, life history, struct. and movements 78−44963
monsoon depressions and tropical cyclones, movement prediction 77−17167
monsoon depressions growth, combined CISK-barotropic-baroclinic instability 79−2337
monsoon depressions in Bay of Bengal, freq. of first occurrence, 10-day epochs, 1891-1970 period 78−81303
monsoon disturbances over India, quasi-geostrophic model 80−98394
monsoon driving mechanisms, model of seasonal struct. 80−98392
Monsoon Experiment, Monex, GARP subprogram 80−8428
monsoon in winter over warm ocean current, heat and moisture budgets 80−72590
monsoon monthly activity, Western Ghats region, major climatological discontinuities 79−96790
SW.monsoon over India, onset and northern limit 78−49102
monsoon rainfall rel. to summer solar radiation and temperature 78−32154
monsoon seasons at old Mangalore port, rel. to waters hydrographic conditions 80−41451
monsoon squalls over Goa, India 79−48546
monsoon system oscillations, spectral anal. of obs. records 77−33148

meteorology continued
monsoon trough typical config. at 850 mbar, assoc. rainfall patterns 79−96795
monsoonal quasistationary ultralong waves, real data numerical prediction over global tropical belt 78−40631
monsoons, symposium (New Delhi, 1977 March 7-12) 79−88410
monsoons and Indian Ocean equatorial currents variability, modelling *(Russian)* 78−44839
Monte Capellino, ice formation, meteorological conditions statistical analysis *(Italian)* 80−12471
monthly average insolation, incident on tilted surface 77−78357
monthly expected rainfall, confidence limits for Peninsular Malaysia 78−81300
monthly rainfall forecasting and synthetic generation, stochastic models 79−70861
Montreal, rain estimation using geostationary satellite data 80−90244
morphological method in research, appls. 79−71216
Mount Kenya, condensation nuclei and weather obs. 80−82012
Mount Kenya, daily weather cycle, obs. on Lewis Glacier 78−24346
mountain meteorology, work of H.-B. de Saussure 79−21513
moving frontal systems and quick weather change *(German)* 78−85659
multi-level spectral model, appl. to data assimilation 79−34906
multilevel and multilayer models, coincidence of eqns. and computations *(German)* 77−56696
Munster, minimum ground temperatures, var. *(German)* 80−4083
national inventory of weather stations 78−69462
National Weather Service information, external user survey 80−4064
natural orthogonal bases, construction method *(Russian)* 79−25305
natural orthogonal components of meteorological fields calc. *(Russian)* 80−4137
Navier-Stokes type eqns. for determ. wind vel. from press. field 77−78374
Navstar global positioning system, meteorological appl. 80−17396
NCAR objective analysis v. subjective analysis 77−86985
Negev rainfall diurnal variation, climatological and meteorological implications 80−17344
network design for estimation of areal mean of rainfall events 77−41082
network design for runoff prediction 77−41083
network stations optimum density 79−39825
New England, 1816, snow and frost in year without summer rel. to Tambora volcano eruption 80−4089
New Orleans, synoptic climatology for environmental baseline analysis 77−64410
New South Wales, Australia, fog devil, photographic obs. 77−81985
New York State, local climate trends in four cities 80−105044
New Zealand, thunderstorm freq. distrib. 77−53160
Nile valley, synoptic disturbances north of ITCZ 77−45116
NMC forecasting of record-breaking Feb. 1978 winter storm 79−16564
NOAA library and information services, description 80−109180
NOAA policy on industrial meteorology 77−53194
nonlinear least squares appls. 78−16182
E. North America, acid precipitation, 1920 onwards 77−37334
North Sea, wave and swell forecasting 78−7658
Norway Station/Sanae (Antarctica), surface temp. and sea-level press. 78−81324
notes from Charles Darwin's voyage on the Beagle 79−17173
numerical advection scheme with small phase speed errors 79−12211
numerical analysis of meteorological fields, math. technique *(Russian)* 78−81272
numerical and models of atmosphere, spectral-transform method 77−37342
numerical dynamic model atmosphere on a spherical Earth, used in forecasting 80−101416
numerical forecasting, adiabatic invariants conservation as criterion for barotropic schemes evaluation *(Russian)* 77−64369
numerical forecasting for summer monsoon conditions 77−78377
numerical modelling of atmosphere, applications to weather-forecasting 79−84459
numerical modelling of the atmosphere, review 79−44234
numerical models of dynamic processes, time integration step *(Russian)* 79−16573
numerical prediction, weather and climate, recent advances 78−96276
numerical weather computation, modified implicit scheme 78−11959
numerical weather forecasting, determ. of boundary layer orography and turbulence-induced vertical currents 78−96278
numerical weather forecasting, long-range, filtering method 79−84446
numerical weather prediction, appl. of telescoping method *(Polish)* 79−16557
numerical weather prediction, difference scheme for vorticity eqn. soln. *(Chinese)* 79−20951
numerical weather prediction, dynamical/statistical initialization 77−41118
numerical weather prediction, finite element method appl. 80−12526
numerical weather prediction, influence of two and three dimensional turbulent flow 78−69395
numerical weather prediction, initialization with data assimilation method 78−57282
numerical weather prediction, isentropic and σ coords. combination 77−86987
numerical weather prediction, modified forward- backward scheme for two-grid-interval noise 80−26575
numerical weather prediction, review 78−69393
numerical weather prediction, split explicit integration scheme 79−12210
numerical weather prediction model, limited area nested, for Australian region 78−49111
numerical weather prediction model, multimicroprocessor system SMS 201 programming example 79−53500
numerical weather prediction model with momentum boundary layer 80−51451
numerical weather prediction models updating by dynamical relaxation 77−70773
numerical weather prediction rel. to monsoon problem 78−40635
numerical weather prediction using GATE data 80−56586
numerical weather prediction using general balanced model 77−86964
numerically predicted synoptic fields, local energetic contribs. 77−86973
NWS National Meteorological Center, prediction capabilities 77−70834
objective analysis using aerological and satellite meas. system, accuracy determ. 79−39832
observation system using telephone switching network 79−80031
Observatorio Astronomico Nacional, Baja California, climatological and meteorological charcts. 78−20635

meteorology continued
occlusions, rolled-up and bent-back, development and structure 79−88451
ocean passive radiometry, radio meteorology colloquium, Victoria, British Columbia, Canada (1978 June 14 to 21) 80−46724
ocean thermal structure and current influence, NORPAX project 79−84517
ocean tide caused by meteorological conditions, energy transfer calc. *(Russian)* 80−76988
ocean topographic Rossby waves, meteorological generation rel. to kinetic energy on continental shelf 80−51425
oceanic wind fields, high resolution mapping using skywave radar 77−29480
oceanic wind speed meas. using HF skywave radar sea scatter 77−29481
Oklahoma hail falls and storms charcts. 80−12504
omega equation, rederivation, appl. to synoptic situations 78−49106
S.Ontario weather pattern rel. to suspended particulate nitrates 80−17365
operation reconnaissance data, transmission via aircraft satellite data link 78−96299
operational computer processing of synoptic information at USSR Hydrometeorological Centre 77−78366
operational forecasting using automated guidance 78−49147
operational numerical weather prediction, radiometric sounding data impact 78−53696
optimal sampling and anal. method 78−73530
optimum difference schemes, synthesis on sphere 78−93011
optimum interpolation analysis, role of obs. errors 80−8383
orthogonalization of random variables, weather forecasting appl. 77−74203
Oviedo, Spain, global solar radiation and air temp. *(Spanish)* 80−36377
Oxford, 1682 May 31, point deluge and tornado 80−51521
Oxford, cold winters (1767-8, 1776 and 1814) 80−51520
Oxford, England, private records of rainfall in 1767-1814 period 78−44948
Oxford max. temp. anomaly rel. to quasi-biennial oscill. strength in equatorial stratosphere 77−81975
tropical Pacific, ITCZ and atmospheric fronts 80−41509
Pacific and E.Asia, average vertical circulation in winter 80−90199
W.Pacific high long-term fluctuation, tropical ocean effects *(Chinese)* 78−16117
NW.Pacific Ocean, relation between atmospheric press. and sea level 80−101415
W.Pacific subtropical high, summer, form. and struct. simulation *(Chinese)* 80−109233
panoramic lightning recorder, operational use for aviation weather support 77−78482
parametric wave prediction model 77−60398
Paris region, events recorded in diary of Pierre Driart during 1522-35 period *(French)* 78−32199
particle collection efficiency of cylinder at aircraft speeds 77−17170
pattern recognition applic. using regression model 77−37404
pattern recognition theory methods, appl. to meteorological field anal. and forecasting 80−98421
Peak Terskol, climatic data, 1972-4 period *(Russian)* 77−70728
persistence, runs and recurrence charcts. of precip. 78−3865
persistent weather patterns, mechanisms 77−91246
Ph.D. meteorologists, training and distrib. 77−67179
photographic obs., cold front passage over Salt Lake Valley, Utah, obs. of orographic effects 80−98380
physics of atmospheres, book 79−62568
Planck blackbody radiation function integration 77−45059
planetary boundary layer processes, incorporation into numerical forecasting models 80−17312
planetary jet stream, hydrodynamical model and spatial fields of meteorological elements *(Russian)* 77−64371
planetary meteorology rel. to weather and climate on Earth 79−84697
planetary scale monsoon, mechanisms affecting structure and evolution 78−40639
planetary scale monsoons, theoretical problems 78−44956
Po Valley, circulation driven by diurnal heating 80−85716
point discharge current, effect of meteorological factors 79−88409
N.Poland, rotating camera obs. of lightning 77−91185
polar air outbreaks, cyclone-anticyclone couplet constuction, vorticity budget computation 80−8391
polar low as extratropical CISK disturbance 80−51502
polar lows, numerical model, shallow baroclinic waves struct. 77−70775
polar region, rawinsonde obs. from single station 80−81981
pollutants long-range transport, meteorological aspects 79−20969
pollutants long-range transport, meteorology 79−20966
pollution long-range transport modeling review 80−108823
Port Moresby, Papua New Guinea, rainfall trend, (1945 to 1976) 80−98430
potential evaporation, Priestley and Taylor α parameter for high latitudes 78−3833
Prague, Czechoslovakia, meteorological obs. since 1775 at Clementinum 78−49075
precip. time struct., daily precip. amounts modelling with Markov-I chain 80−101401
precipitation five-day forecasting using successive graphical regression *(Russian)* 77−29492
precipitation forecasting 0-6 hours ahead, radar and satellite imagery, FRONTIERS plan 80−12509
precipitation forecasting in Arizona, rel. to marine layer depth and moisture content at San Diego, California 80−101395
precipitation forecasts using a single radiosonde 79−88397
precipitation over Central Europe, large-scale field components extraction for forecasting purposes 78−92940
precipitation over ocean, quantity rel. to precipitation freq. 80−31105
precipitation probability forecasts, nonparametric technique based on pattern recognition algorithm 78−44946
predictability of thermally-forced and unforced flows, in nonlinear quasi-geostrophic eqn. 77−2191
prediction methods *(Japanese)* 80−31095
prediction of meteorological events, overview and recommendations 79−8703
prediction of weather, normalised variance anal. for meteorological time series, F-distribution *(Chinese)* 80−67388
Prestel, Post Office viewdata system, Met. Office participation 79−16675
meteorology continued
primitive eqn. model initialization, divergent wind in initial state 77−86974
primitive eqns., semi-implicit and filtered integration schemes 77−86976
primitive equation models initialisation for alternating grid 77−45119
primitive equations model for limited area forecasts 78−11956
probability characteristic function in stochastic dynamic modelling 79−16621
probability forecasts, nonexistence of ordinal relationships between measures of accuracy and value 78−61503
process computer appl., thermal balance recording methods 80−82044
prognostic models, automatic timestep control 77−86975
public forecasts at Louisville, Kentucky, skill trends 78−49073
pyrocumulus cloud over North Canterbury, New Zealand, effects of synoptic situation 80−109240
quasi-cycles in meteorology, anal. of evidence 80−109239
quasi-geostrophic flow over anisotropic mountain 80−61860
radar, differential reflectivity and differential phase shift 78−57270
radar applications in Polish meteorological service 78−92992
radar appls. in meteorology and atmospheric behaviour research, review 78−77371
radar echoes from distributed targets, averaging of time, angle and range 80−109264
radar measurement of clouds and precipitation, correl. and spectral anal. 80−12529
radar observation from aircraft, pulse Doppler method 80−85757
radar observation of lower atmos., VHF pulsed Doppler method 80−46277
radar remote sensing, optimal positions of multiple-Doppler system 80−31140
radar system appls. 80−26651
radar system synthesis, economical aspects 79−62543
radiation balance meas. as instrument design problem 77−41173
radiation balance of ocean-atmosphere system *(Russian)* 77−78200
radiation budget expt., Nimbus-6 obs. 77−41106
radiation climate of Thailand, calcs. from routine meteorological data 79−29814
radio meteorology in Switzerland *(French)* 79−25319
radio refractive index variations over Arabian Sea during MONEX 1973 77−2281
radio weather chart, facsimile machine 77−70878
radiometeorological characteristics, statistical structure *(Russian)* 79−84376
radiothermal sounding of press. and geopotential *(Russian)* 80−77038
rain measurement and forecasting in UK using radar as part of integrated system, progress and plans 80−98490
rain measurement by dual-polarisation radar, drop size and fall rate 80−72650
rain parameter diagram, methods and appls. 78−57349
rain rate distribution estimation technique *(Japanese)* 79−66827
rainband dynamics and cloud microphysics in occluded frontal system 77−33147
rainfall, annual, stochastic anal. rel. to effects of urbanisation 80−98407
rainfall, charcts. within 200 km of steel industry 77−56714
rainfall forecasting for N.E.Brazil using sea surface temp. data 77−29398
rainfall in England and Wales, long-period records spectral and filter anal. 80−4080
rainfall measurements on board ships using raingauges, comparison with weather reports 78−57258
rainfall prediction for attenuation prediction in Earth-space paths *(French)* 78−49062
rainfall prediction for short response time hydrological basins 80−98491
rainfall recording at Oxford, England, since 18th century 79−29810
rainfall variations near Neyveli thermal power station, India 77−37286
rapid morning boundary-layer transition, case study from Haswell, Colorado, expt. 80−81996
real-time data acquisition and anal. 78−69466
real-time vertical cross sections for forecasting 77−53101
remote sensing, review *(Japanese)* 77−2273
remote sensing *(Japanese)* 78−16205
remote sensing by two satellites, radio illumination method 80−51550
remote sensing of environment, automated digital data handling 78−3960
remote sensing of global phenomena by automatic satellites 77−64457
response to external forcing, pattern detection, S/N problem 79−88464
review of recent developments 79−25313
ridge regression-time extrapolation of short records of rainfall 80−51489
riming process, laboratory expts. 80−105037
Riso, Denmark, 1975 direction fluctuations 77−53148
river management operational system development using weather radar 78−40718
River Murray, Australia, air-sea-river interactions 77−45032
rivers runoff and sediment discharge model, response to meteorological input 77−91178
rocket launching, appl. to M-3C *(Japanese)* 79−25304
Rossby neutral mode, secular stability 80−81983
Royal Meteorological Society, history 79−2376
Rustavi, USSR, coordinated radiation and meteorology study, CENEX-72 77−78413
Sahel, long-range weather forecast values 77−70729
Sahel drought, Africa, 1967 to 1974, Earth surface albedo vars. investigation 80−76981
Sahel rainfall 1975-6, D, T and ^{18}O evidence and regional winds *(French)* 80−21809
Sahel region, general and regional circulation effects on climate *(French)* 79−20962
satellite, Russian weather, amateur reception signals 77−56808
satellite communication systems, weather sensitive economic activities appl. 80−46244
satellite data uses, ESA conf. (Lannion, France, 17-21 September 1979) 80−36783
satellite derived cloud imagery, optical Fourier transform anal. 78−85749
satellite imaging, A/D conversion for digital processing *(Japanese)* 78−7711
satellite NOAA, digital signal processing techniques *(Japanese)* 78−24424
satellite observations, their contribution to FGGE 80−36403
satellite picture transmission, automatic continuous, NOAA satellite series 77−60458

meteorology continued
satellite pictures and teledetection methods used for snow measurement and forecasting *(French)* 79−96770
satellite telemetering system, NOAA 80−56592
satellite visible and IR image data, computer processing 79−29864
satellites, operation and appls. 79−29967
satellites, S-band reception, monopulse aerials *(German)* 79−92628
S.E.Scotland, potential moisture deficit, 200-year series 78−7746
E.-central Scotland, snow and sleet freq. var. in 1708-1975 period 78−44951
Scotland, snow survival during 1976 summer 77−91168
sea breeze forecasting at Eskmeals 78−69418
sea ice, long range forecasting for north coast of Alaska 77−2174
sea level pressure anomalies predictability over N.Pacific Ocean 78−92905
seasonal climate model on global scale 80−41544
seasonal forecasts and northern hemisphere circulation anomalies 77−2237
seasonal forecasts based on pressure anomaly rules, accuracy 78−7744
SESAME '77 experiments and data availability 78−65355
severe cyclonic storm, 1975 October, over India 78−85626
severe local storm, Pennsylvania, predictibility of location and damage 77−66965
Severe Local Storm Warning and Disaster Preparedness Programs at NWS 77−86959
severe local storms, automated 12 to 36 hour probability forecasts 80−77062
severe local storms, St. Louis region, urban effects 79−12199
severe rainstorm in Honan province, China, 1975 August, case study *(Chinese)* 79−84448
severe storm warning using Doppler radar 78−49148
severe weather computerised forecasting system 78−20498
severe weather pattern classification and machine recognition 77−21879
Shanghai plum rains, mid-range forecasting *(Chinese)* 80−109232
Shetland weather during 1975 77−56718
shipboard automated information processing system, for hydrometeorological data 80−41553
shipboard sounding system for GWE 80−17394
short-range numerical forecasts intercomparison 77−86962
short-range numerical weather forecasting, effect of subjectively enhancing initial vorticity field 80−82008
short-range weather forecast, rel. to approx. of derivatives of thermohydrodynamic eqns. *(Russian)* 77−60450
showers and simultaneous floods in Alps, meteorological study *(French)* 79−66721
Siberian anticyclone, intensity rel. to annual motions of Earth rot. and excitation poles *(Russian)* 78−40461
S.Sicily coast, passage of fronts rel. to 'Marrubbio' phenomenon 77−53062
Sierra Leone, climatic regime rel. to surface and soil temps. seasonal vars. 80−109242
Sierra Leone, monsoon characts. 78−7693
Skagit Cloud Seeding Project, Washington, effects on river annual runoff 79−79949
slant meteorological visibility, definition, determ. and appl. 79−100954
snow cover at Munich, (October 1887 to April 1977) *(German)* 78−69421
snow prediction, using 10-level model 80−82025
snowfall systems induced by Lake Ontario, objective forecast method 80−51484
snowstorm avalanche forecasting in Khibins, model *(Russian)* 77−21812
snowstorms in Scotland, (1729 to 1830) 77−25757
sodar appl. to weather analysis and local forecasting 80−85713
solar activity effects on weather and climate 79−16644
solar activity rel. to weather and geomag. field vars., spectral anal. 77−5308
solar activity-weather correlation, anal. 78−40628
solar activity-weather relationship, study of temp. and rainfall at Oxford 78−85674
solar and wind power, meteorological aspects 78−36250
solar corpuscular radiation effects 79−79982
solar energy utilisation, participation of meteorology *(Czech)* 79−83567
solar equatorial rotation, rel. to climatic changes 78−7960
solar flares influencing lower atmos. phenomena 80−109230
solar global insolation, calc. model 79−16613
solar insolation, in India, daily total and diffuse, estimation from weather data 79−100926
solar radiation, numerical model based on standard meteorological observations 79−34929
solar radiation data, statistical correl. between daily and monthly averages 80−8409
solar wind, effect on terrestrial weather *(Swedish)* 79−79910
Somali coast, wind stress, spatial and temporal var. 78−49092
Somali jet, planetary boundary layer model 80−72591
South Africa, above and below normal rainfall periods estimation, 1972-2000 period 77−66980
South Polar Plateau, meteorological transport of particulate material 80−51481
Soviet Meteor satellite imagery, reception and processing in USA 79−39872
Soviet meteorological satellite development review 78−16266
Soviet progress 80−26598
spectral energetics, determ. via numerical filtering anal. 80−26577
spectral global models, var. fine mesh 77−86978
spectral transmittance sensitivity to line and meteorological parameters 80−26610
spectrum width estimtes for weather echoes 80−12477
spiral bands in linear model of cyclonic vortex 77−25736
splitting scheme for weather forecasting *(Russian)* 79−84366
squall forecasting from synoptic and thermodynamic condition anal. 77−78360
squall line, formation from boundary layer forcing and temp. gradient, model 80−8396
squall line at midlatitude, thermodynamic and kinematic struct. obs. 80−109191
squall line formation, nonlinear process 78−81323
Sri Lanka, weather during drought of December 1971 to April 1972 77−56704
St. Louis, Missouri, pollutant source strength-rainfall relationships investigation 80−77059
meteorology continued
St. Louis area, land use and cover correl. with meteorological anomalies 79−12201
St. Louis urban precip. anomaly rel. to synoptic weather factors 79−39806
stability evaluation of statistical couplings, meteorology appl. 77−74204
standards, review 79−21032
standards 79−66746
STAR-100 computer, experience 79−70879
stationary mesoscale fields, method of calc. from remotely sensed data 80−85734
statisical heresies in meteorological data reduction 78−57291
statistical analysis of weather modification projects 80−56520
statistical weather-forecasting model 78−92941
steam fog in Fenlands, obs. after heavy rain, (1979 May 1) 80−98431
steppe meteorology, boundary layer universal profiles in rainy season *(German)* 79−84420
stochastic weather algorithms for predictions of solar cooling performance 80−35642
storm detection and prediction by ionospheric Doppler sounding 79−2326
storm spotting, National Weather Service's training programme 80−8382
storm surges in Sea of Azov, two-dimensional numerical calc. 78−96231
storms, principal component anal., hail index *(French)* 78−96267
stratiform clouds, horizontal dimensions rel. to synoptic situation 78−20490
stratosphere, generalised Lagrangian-mean description of wave/mean flow interaction 80−109214
stratosphere, southern hemisphere, temp. and press. field spring transformation anal. 80−98420
stratosphere, zonal mean winds vars. rel. to planetary wave props. and links with troposphere 80−109225
stratosphere data compatibility used in meteorological analysis, empirical study 80−17308
stratospheric sudden warming, planetary-scale forcing of USA Jan. 77 weather 78−57279
strong gales in E.Atlantic region, jet stream effects in subtropical latits. *(Spanish)* 78−44966
subsynoptic analysis, time continuiuty incorporation using dynamic constraints 79−79987
subtropic and polar front jet confluence, rawinsonde obs. 80−81981
subtropical high in N.Pacific rel. to sea surface temp. anomaly *(Chinese)* 80−46237
summer monsoon, mid-tropospheric cyclones 78−40636
summer monsoon circulation aspects 80−8413
summer monsoon over S. Asia, break and active phases 78−3912
summer monsoon rel. to radiation budget 78−40664
summer monsoons over Africa and India, comparison 78−32149
summer rainfall, St. Louis region, urban, topographic and diurnal effects 79−12198
Sun-weather connections 80−51467
Sun-weather correlation, reality and nature 77−66956
Sun-weather long-term relationships, critical review 79−48558
Sun-weather relation, energetics study 78−81285
Sun-weather relation, vorticity area index to interplanetary mag. sector struct. 80−46222
Sun-weather relations, solar mag. sector crossings effect on troposphere 78−88876
Sun-weather relationship, possible implications of solar modulation of atmospheric electrification 78−57261
Sun-weather relationships, role of atmospheric water vapour of extraterrestrial origin 78−69416
sunlight intensity, data rehabilitation, SOLMET-2 procedures criticised 80−4071
Sunray tornado, photographs showing evolution 77−25731
sunshine, differences between morning and afternoon, in New Zealand, statistical anal. 77−29401
sunspots influence on weather, possible mechanism 77−91238
supersonic expansion method of ice nuclei generation for weather modification 77−29487
surface atmospheric pressure field, vars. in periods of high and low geomag. activity 78−36245
surface synoptic obs., automatic real-time quality control 78−92920
surface weather charts for wind speed over drifting pack ice 80−41476
Swiss randomized hail suppression expt., design of Grossversuch IV 79−84542
Switzerland, 1975 August rainfall at Vitznau on Lake Lucerne 78−7743
synoptic and mesoscale mechanisms for heavy rainfalls causing flash floods 80−8385
synoptic data rel. to air pollution statistical analysis 77−70816
synoptic features on satellite picture, anal. 79−8713
synoptic long-term weather forecasting methods, unified complex method development 79−34931
synoptic meteorology, use of automatic weather stations in United Kingdom observational network 79−80047
synoptic obs. for direct solar radiation and diffuse radiation calcs. *(German)* 79−34925
synoptic observation program in Sun-weather investigations 77−45088
synoptic prediction, modernization approach *(Chinese)* 79−84453
synoptic scale processes effects on equatorial surface air layer meteorological variables 77−70689
synoptic scale studies using Numbus 6 SCAMS 78−16114
synoptic weather maps and typical local conditions *(Spanish)* 78−88891
synoptic weather types prediction based on model output statistics 79−70856
synoptic windfinding, NCAR aircraft dropwindsonde system 80−17393
synoptic-scale vertical motion calcs. in Atmospheric Variability Experiment (AVE) IV 77−21831
synoptical eddy scales, rel. to Rossby waves stability *(Russian)* 78−44923
Taiwan, weather connected with typhoons 80−90200
Takoradi-khartoum air route, general synoptic climate 78−28300
Tamil Nadu, rainfall pattern during N.E. monsoon rel. to solar activity 77−70749
technical meteorology, technical and commercial appls. *(German)* 80−46231
technological implications of weather and climate 77−45101
Tel-Aviv during 1975, O_3 concs. rel. to meteorology 79−12172
telecommunications and meteorology, special relationships 77−2236

meteorology continued
temp. in central England, 1660-1977, air temp. variability study 80−98437
temperature, five-day average low and high temp. anomalies forecasting procedure 78−92938
temperature and pressure, forecasting from statistical struct. of air temp. fields *(Russian)* 77−64373
temperature anomalies forecasting using parametric linear discriminant anal. 79−58056
temperature anomaly over European USSR, monthly forecasting 79−39830
temperature forecasts, case for an operational programme 80−17311
thermal oscill. for nocturnal min. temp. prediction *(Spanish)* 77−9478
thermal pollution from fuel and energy consumption, effects on weather and climate 78−61539
thermal wind-field disturbances in sea coastal zone, statistical forecasting of frequency 80−36371
thermally driven flow in beta-plane channel, regime diagrams 80−56552
thermodynamics in dynamical meteorology, relevant eqns. 78−73496
thermosphere, lower, meteorological quantities fields rel. to eddy diffusion models 80−109198
thunderstorm activity index determ. technique, accuracy 78−61529
thunderstorm birth zone prediction by satellite surveying *(Italian)* 77−81988
thunderstorm forecasting at Srinagar, India 77−53128
thunderstorms, automated 12 to 36 hour probability forecasts 80−77062
thunderstorms, severe, nature and effects on society 79−5560
thunderstorms forecasting, simple method 78−81304
tidal motion on sphere, simulation by geodesic finite-difference method for curved domains 80−109153
tilt meter observations, S_1 diurnal meteorological wave influence *(Russian)* 78−88788
time extrapolated eigenvector prediction for time series analysis 77−56757
time series, running means appl. 78−65378
time variability of wind and temp. vertical profiles, uncorrelated standing waves *(Russian)* 77−91215
time-averaged data, variance by simple approx. 80−31139
TIROS satellite program 80−109328
Tiros-N environmental spacecraft series launching 79−29973
tornadic storms and hurricanes warning system, gravity waves ray tracing 78−73448
tornado, 1978 January 3, at Newmarket, England 79−39812
tornado, math. model, flow past axially uniform viscous vortex 78−59405
tornado frequency correl. with thunderstorm days, seasonal and regional vars. 79−79957
tornado over Punjab, 1975 March 10, synoptic situation and meteorological conditions 79−96793
tornado vortex simulation at Purdue University 78−40677
tornado-producing cumulonimbus, 1973 June 4, Oklahoma, USA 77−17202
tornadoes, multiple vortex phenomenon, inertial instability 79−53454
tornadogenesis, numerical model of vortex growth 78−49114
tornadogenesis, vertical stability effects 79−53442
tornadogenesis in rotating thunderstorm, numerical model 79−79970
Transcaucasia rainless periods, 1966-75 obs. 80−26603
transients eddies, synoptic-scale, observational study of upward sensible heat flux 80−94591
transmitting weather charts by facsimile for military appl. 80−90206
Trinidad, West Indies, funnel cloud obs. 78−73498
Tromso, Norway, intensive precip., 1965-73 period *(German)* 79−16609
TROPEX-72 near Equator, ocean surface wind and pressure fields 77−37320
TROPEX-74, USSR meteorology expedition, consistency of shipboard meas. with 'Meteor' buoy 80−36402
tropical, role of thermodynamic instability 77−25751
tropical air-sea interaction at large scale, numerical study 80−56549
tropical atmosphere, large-scale features 79−92584
tropical atmosphere, numerical prediction and simulation 79−88463
tropical atmosphere, Taifun-75 data from equatorial Pacific area, typhoons 79−58052
tropical boundary layer over ocean, turbulence closure model for BOMEX data 80−56583
tropical cloud cluster, struct. and evolution 80−12488
tropical coastal region, lower troposphere features during rainfall 78−81332
tropical cyclone development, latent heat release, numerical simulation 78−81309
tropical cyclone nested grid model, noise control 78−11957
tropical cyclone recurvature forecast from temperature wind-height data 77−64380
tropical cyclone statistical prediction models, Monte Carlo significance testing 78−44943
tropical cyclones, landfall numerical simulation 78−81308
tropical cyclones, photometric method for estimating cloud cover from satellite data 78−4007
tropical cyclones simultaneous occurrence on either side of equator, Indian Ocean area 78−81301
tropical E.Atlantic, press. and wind fields from TROPEX data 80−82040
tropical expts. 79−92583
tropical meteorology, review 77−64365
tropical middle atmosphere, observational evidence of semiannual oscillation 80−109216
tropical observing system, role of geostationary satellites 79−92651
tropical ocean meteorology, conference (London, 21-25 August 1978) 79−88458
tropical storm motion statistical prediction for Bay of Bengal and Arabian Sea 79−96789
tropical W.Africa, monsoon rain 77−37321
tropical weather prediction, multilevel primitive eqns. with press. wind adjustment 80−77070
Tropical Wind, Energy Conversion and Reference Level Experiment (TWERLE), results 78−40605
tropical zone, numerical modelling of atm. processes 78−61532
troposphere, temp. lapse rate effects on pilot balloons ascent rates 77−2204
troposphere dynamical indices, lack of response to solar mag. sector crossings 78−57244
troposphere response to solar mag. field daily changes 78−88888

meteorology continued
tropospheric temp. anomalies, conjugate functions appl. in anal. and forecasting 79−39829
tropospheric-stratospheric polar vortex breakdown 1977 January 77−53107
Tsimlyansk Reservoir, hydrometeorological studies 79−39784
Tsinghai-Tibetan high movement, annulus simulation, summer flow pattern forecast of high troposphere 78−32211
typhoon and hurricane areas, distrib. models of press. and wind over sea surface 79−62570
Typhoon Della, weather conditions in eye of storm 79−29828
typhoon havens research program at the Naval Environmental Prediction Research Facility 79−5616
typhoon movements expt. simulation *(Chinese)* 79−84449
typhoon Ora, form. in intertropical convergence zone under influence of midlevel jets 80−12527
typhoon track prediction, appl. of multiple-category discriminant anal. *(Chinese)* 77−66967
typhoon trajectories seasonal activity rel. to subarctic frontal zone position over NW.Pacific 78−61526
typhoons transformation, forecasting via extratropical circulation 78−3908
typical weather determination for solar energy simulations 79−16614
Uccle, Belgium, homogeneity and stability of meteorological elements *(French)* 79−74941
Uccle, vertical ozone distrib., during polar front passage 80−94582
UK, meteorological controls on ground level smoke and SO_2 concs. 79−12253
ultralong waves forced on cyclone scale, numerical expt. 80−61857
United Kingdom, 1975-6 drought, atmospheric circulation 77−70770
United Kingdom, 1975-6 drought, hydrometeorological aspects 77−70769
United Kingdom, 1975-6 drought, synoptic climatology 77−70802
United Kingdom, regional units, wet and dry periods defined 80−51522
United Kingdom Climatological Network, history and role of co-operating observers 79−5618
continental United States, 1976-7 winter and prediction of extreme weather 78−49078
E.United States, meteorological control of sulphates diurnal var. at rural sites 80−30621
United States, synoptic weather situations assoc. with major wildland fires 78−61499
unusual weather frequency variability over last century 78−73479
upper air meteorological data, rel. to regional evpotranspiration determ. 77−91171
Uppsala urban meteorology project 79−53419
urban air, meteorological conditions rel. to dimethyl-N-nitrosamine concs. 78−81378
urban atmosphere, roof level, long wave radiative flux divergence and nocturnal cooling 77−33123
urban atmosphere, urban canyon, long wave radiative flux divergence and radiative cooling 77−33124
urban effects on precipitation, appl. to severe storm in London during August (1975) 78−81339
urban effects on precipitation initiation in convective clouds, radar first echoes appl. 79−16601
urban environment, cold air drainage effects on temp. fields, case study of topographical influence on climate 80−94555
urban environment, meteorological obs. 79−25312
urban hydrology, US National Weather Service programme 77−37267
urban microclimate of Alma-Ata, significant factors 80−101418
urban valley micrometeorology of N.Saskatchwan river valley 80−61843
USA, National Severe Storms Forecast Centre, 1970-9, predictive success 80−46214
USA National Weather Service graphic display network 79−12320
USSR, air temp. and precipitation var., five-year changes 78−16130
USSR Hydrometeorological Service, objectives and prospects 78−7770
uw covariance in lower atmosphere, corrections 77−64381
Vancouver, urban canyon, energy balance 77−64379
variational adjustment of meteorological fields 79−39837
Venice, SO_2 pollution levels, meteorological factors 77−91253
vertical precipitation structure recording, meteorological radar appl. *(German)* 80−17358
N.Vietnam, cold intrusions forecasting 3 to 7 days in advance via discrimination anal. 78−3910
viscous forecast eqns., boundary conditions for limited-area integration 77−86979
visibility at ground level, two meas. methods 80−82078
visibility probed with lidar 80−31141
visual observation from space, by Salyut-5 astronauts *(Russian)* 78−40796
VLF radiometeorology for thunderstorm location *(German)* 77−17254
vorticity and divergence 78−88893
vorticity response to IMF sector boundary crossing (southern hemisphere) 80−109199
central Wales, large, summer storm 1971, June 77−56717
S.Wales floods of late December 1979, meteorological anal. 80−98429
warm frontal clouds in midlatitude cyclones, air motion and precipitation 80−109193
warm frontal region, wind and precipitation struct., Doppler radar study 80−81995
warning of ocean storms using meteorological satellites 78−69423
water vapour images from Meteosat, comparison to tropical streamline analyses 80−8384
waterspout frequencies along USA East and Gulf Coasts 77−78329
waterspout of 3 March 1977 at Iraklion, Crete *(German)* 78−16121
waterspout statistics for Nassau, Bahamas 78−92919
wave forecasting 79−66710
wave generation and frontal collapse 78−77300
wave motions in tropical spectral expt. 78−3893
weak monsoon, atmospheric energy conversions 77−56711
weather, severe convective event numerical simulation and prediction, Navier-Stokes eqns. initialisation 80−31111
weather analysis, charts with plotted parameters, meteorological support to low-level aircraft flights 79−66772
weather analysis and forecasting, phys. and math. aspects 79−39831
weather and climate, definitions 80−41540
weather and climate, solar-terrestrial influences, symposium/workshop proceedings (Columbus, Ohio, 1978 August 24-28) 80−27037
weather and crop spraying, N.Nigeria 77−81983

meteorology continued
weather changes and air pollution, meteorological meas., brief survey *(French)* 80−17359
weather charts, electronic conversion from a scanning radiometer to a stereographic projection geometry 79−21056
weather conditions for long gliding flights over England 79−58048
weather conditions occupying a line or area, probability model 80−56558
weather data reduction for building and solar energy system optimisation 79−57397
weather effects on sport 77−81984
weather event at two locations, joint probability estimation 79−53480
weather experimentation, statistical issues 80−8439
weather facsimile (WEFAX), expanded digital system 79−66817
weather forecast model, low-order spectral difference type 80−98415
weather forecast verification, pattern recognition techniques appl. 78−11958
weather forecasting, adaptive learning network approach 78−40643
weather forecasting, analysis method *(Chinese)* 80−46238
weather forecasting, aspects of satellite anal. at Central Forecasting Office 77−41123
weather forecasting, assessment of model initial conditions using satellite imagery 80−31084
weather forecasting, atmospheric prediction models, computing and numerical methods 80−77095
weather forecasting, balance eqn. soln. with min. correction of mass field 78−36246
weather forecasting, complexing of alternative forecasts 80−41530
weather forecasting, conditional probabilities prediction method *(Chinese)* 80−109238
weather forecasting, dynamic statistical model of complex stable processes 80−26599
weather forecasting, electronics appl., developments 77−41108
weather forecasting, optimization of atm. model 78−20494
weather forecasting, prospects and methods of improvement 78−69394
weather forecasting, satellite systems for local short-period forecasts 80−94558
weather forecasting, stochastic dynamic prediction appl. to real data 77−56669
weather forecasting, use of satellite imagery by the Meteorological Office (UK) 80−85714
weather forecasting and general circulation, finite element models 80−51504
weather forecasting as a problem in fluid dynamics 79−84359
weather forecasting by computer, Switzerland *(German)* 77−37317
weather forecasting for central Asia, for short-term press. field 80−98416
weather forecasting for N. hemisphere, six days ahead 80−82024
weather forecasting games at American Universities, survey 80−98770
weather forecasting impact of meteorological satellites 78−7861
weather forecasting in USSR, short-term predictions since 1920 80−41529
weather forecasting nonlinear evolutionary problems, finite element methods appl. 80−21865
weather forecasting numerical model, parameterisation of boundary layer 80−72572
weather forecasting on radio and TV, development in America 77−49549
weather forecasting processing of radar and satellite imagery data 80−109252
weather forecasting scheme, determ. of initial wind field 79−39833
weather forecasting skill, solar influences 79−88420
weather forecasting skill of beginners 80−4066
weather forecasting via oceanographic buoys, electronics and telemetry evolution 79−5659
weather forecasts, economical and optimal combination method *(Russian)* 80−21792
weather forecasts, impact of satellite temp. sounding data 80−77028
weather identification by laser forward scatt., feasibility study 79−70893
weather maps, for present weather, wind, and ceiling, examples, forecasting use *(German)* 80−4081
weather maps, structural description of contour maps 80−101419
weather modification, covariance anal. technique based on bivariate log-normal distrib. 77−70767
weather modification, economic context 79−20936
weather modification, insurance perspective 79−20937
weather modification, international liability 79−5617
weather modification, managerial and research aspects 79−20935
weather modification, national policy 79−20938
weather modification, operational aspects 79−20939
weather modification, physico-chemical agents *(French)* 78−3883
weather modification, prospects and problems, book 80−36790
weather modification, scientific and technological aspects 79−20934
weather modification, statistical anal. of cloud seeding expts. 80−56519
weather modification, three dimensional mesoscale models 77−25730
weather modification due to waste heat release from large dry cooling towers 79−84471
weather modification economics, review, future anal. 79−20927
weather modification expts., bibliography 80−56523
weather modification from cooling tower effluents at conceptual power parks 78−11951
weather modification in USSR 77−64362
weather modification programmes, meteorological satellites appls. 78−96259
weather modification projects, value assessment, hail suppression example 78−7713
weather modification single area expts., confidence limits for seeding effect 79−79948
weather modification technology, statistical approach, review 78−53706
weather perception, subtropical winter study 77−2238
weather predictability on various space- and time-scales 77−29400
weather prediction, development and status 77−82358
weather prediction, finite differencing and group vel. errors 77−86981
weather prediction, numerical modelling of baroclinic instability *(Russian)* 78−44922
weather prediction, objective methods, book contrib. 78−61535
weather prediction, probabilistic model 79−39835
weather prediction, short range numerical hemispheric model 80−81976
weather prediction, vertical vel. variations in soln. of complete atmospheric eqns. by decomposition method *(Russian)* 77−73806
meteorology continued
weather prediction and physics of atmosphere and ocean *(Russian)* 77−21774
weather prediction by finite difference scheme *(Chinese)* 80−46234
weather radar, Doppler, estimation of echo spectral moment 80−51563
weather radar, signal anal. *(French)* 80−36418
weather radar data transmission using VHF satellite links, expt. 78−20569
weather reconnaissance using Lockheed WC-130 aircraft 79−66816
weather rel. to solar and interplanetary mag. sector struct. 80−17340
weather review (1978) for Belgium *(French)* 80−77069
weather satellite, detection of 300 Hz pulses 78−36420
weather satellite data, complex demodulation 78−49177
weather satellite receiving terminal for continuous weather update 78−81452
weather simulation, matrix generalised eigenproblem developments 77−25760
weather station operation, management practices on USAF stations 80−46215
weather stochastic prediction, stochastic dynamic method, perturb. approx. 79−58060
weather variations, of forced or free nature 80−56596
weather-related aircraft accidents, analysis 78−53693
weather-satellite picture facsimile machine, constructional details 77−21870
weather-satellite picture facsimile machine 77−29629
weather-solar activity rel. to periodic vars. of solar radiation 79−34920
weather-solar activity relationships, possible mechanisms 80−17341
westerly trough unusual SE. movement over India, 1974 December 78−32161
western boundary currents and detached shear layers in rot. liq. 80−81984
western depression over N. India, mean model 77−53113
western disturbance intensification moving from central Iran to NW India 78−81302
Western Pacific subtropical high in summer, exptl. simulation *(Chinese)* 79−84415
wet bulb potential temperature charts, meteorological use 77−91232
wind, beaufort scale data, conversion to wind vel. study *(German)* 80−8407
wind, synoptic time scale vars. correl. with sea level changes on Scotian shelf 80−72531
wind and wave forecasting for offshore operations 79−2353
wind chill in lowland Britain, anal. 79−66782
wind measurement (absynoptic scale) using dual Doppler radar and vel. azimuth display 80−109263
wind obs., freq. isopleth diagram 77−73892
wind power, meteorological aspects, resource assessment, site selection, US R and D program 80−76593
wind shear detection radar, for airport use 80−51565
wind speed and direction prediction using empirical eigenvector method *(German)* 77−87030
wind speed at sea, climatic comparisons of estimated and measured winds from ships 80−105020
wind speed freq. distrib. determ. for lowest 200 m using routine meteorological data 79−21052
wind-field analysis methods 80−105038
windchill maps of lowland Britain, calc. from instantaneous data 80−61893
winter data for soil temp. prediction 77−37418
winter lower atmosphere, influence of interplanetary mag. field sector struct. 80−8510
winter of 1657-58, Denmark's frozen sea areas, invasion by Swedish army 79−88791
winter orogaphic cloud seeding project, predictor control for evaluation 78−92922
winter season temperature outlooks by objective methods 78−85641
winter weather in W.Fife in 18th century 77−29981
World Meteorological Organisation programme activity development 78−61531
yearly variations, effect on pollution zones definition and assessment 78−81383
Zambia, weather during rainy system rel. to upper westerly waves interaction with intertropical convergence zone 80−90175
zonal and meridional large scale flow over British Isles 80−56579
CO_2 and global warming, effect on regional climate 80−77099
H_2O dimer, meteorological implications 80−8418
H_2O dimer, props., influence on tropic meteorology 79−2349
O_3 photochemical production, W.Europe, rel. to meteorology 77−78292
Rn concentrations, influence of meteorological parameters *(Spanish)* 79−92562
Rn evolution in neutral atmospheres, correl. with meteorological parameters *(Spanish)* 80−4058
Rn meteorology, appl. to lower atmosphere vertical stability determ. *(Spanish)* 79−92560
SO_2 conc. decrease near Rotterdam rel. to meteorological parameters during 1961-74 winters 77−37359

meteors
see also meteorites; meteoroids
1178, June 18, interpretation of eye witnesses account of lunar crater form., meteor crossing Moon explanation 77−71174
acoustic gravity wave generation *(Russian)* 77−91340
atmospheric ionization rel. to LF radiowave absorpt. events 79−48608
atmospheric turbulent diffusion coeff. determ. from meteor trail photographs 78−45073
atoms, effective excitation cross-sections, var. with meteor vel. 80−101565
bolides, photographic patrol station network 77−87278
bolides of USA prairie network and Tunguska meteorite, identical nature, low-density microcomet objects 77−67073
bolides topocentric coordinates determination, use of photography 78−61818
bright sporadic meteor, spectrum obtained with Wampler scanner 78−57508
brightness, magnitude errors and magnitude scales of observers in Sweden and Czechoslovakia 78−36533
Brno fireball (1977 Sept. 14), photographic data 80−41771
bursts, forward scatt. technique, obs. over India 78−89132
α Capricornid meteors, anal. 79−71004
α Circinids, shower on June 4, Australian obs. 78−16359

meteors continued
collisional ionisation, thermalisation in atmosphere 78−36346
colour index and relation to magnitude distrib. 79−84752
comet debris studies, video techniques 79−80241
cosmic dust, book 78−57498
counts, test for registration independence 80−8594
dense trains deionisation rel. to HF radio echoes duration 79−5697
Draconid meteor shower, prediction for (1979 October 9) 79−92728
Draconids, number in (1972) 77−67077
drift due to tidal winds at 80-100 km altitude, poleward momentum transport 80−12581
E_2-layer production, statistical evidence for class 1 E_m 77−29572
E_s-layer, occurrence rel. to meteor metallic ions 80−46336
E_s-layer prod. by meteors 77−25837
E-region, ion production function from meteor particles 79−12336
E-region, nighttime ionization during meteor showers 77−29560
Earth grazing fireball, eqns. of motion, vel., orbit and mass determ. 80−67663
effective dynamic cross section 77−74015
effective field of view for line sources, theory and obs. 78−36535
evaporated meteoric matter, mass spectrum of particles formed in condensation 79−71005
faint trains, spectral line excitation 79−35197
fast sporadic meteor, spectrum 78−93170
fireball, over Japan 1977 May 10, sonic boom recorded on seismographs *(Japanese)* 79−66962
fireball end heights, diagnostic for meteoric material struct. 77−29732
fireball luminous efficiency, theory 80−21947
fireball meteors, satellite-borne IR obs. 79−35196
fireball networks, review of 12 years of operation 77−33427
fireball of 1977 September 14 over Czechoslovakia 78−32408
fireball of meteorite, deduction of props. from behav. in atoms 80−82311
fireballs, atmosphere as obstacle to struct. determ. 79−16891
fireballs photographed in central Europe, trajectories, orbits and classification 78−36534
Geminid meteor stream, orbital period 78−53889
Geminid shower, radar obs. statistical modelling 78−61816
Geminid shower characteristics 79−80277
Geminid stream, struct. from radar obs. 80−82310
Geminids, dispersion of orbital elements 79−21230
Geminids, flux in 1974, magnitude ratio and mass index 80−4307
Geminids, visible obs. over Waltair during 1961-66 period 78−40881
P/Griff-Skjellerup (1977b) assoc. meteors, Florida results 77−53484
head echoes, heights 78−36537
heights, results from decay rates of 18000 meteor echoes 77−82175
historical meteors, Latin terminology 80−62437
hollow trains, expanding cylinder model 78−16357
hypersonic flow past disintegrating blunt bodies, radiative heating in H_2-He atms. 80−69865
hypersonic free-molecular heating of micron size particulate 79−4058
influx rate of meteoric material at Earth from photographic obs. of bright meteors 79−21233
initial radius measurement, simultaneous radar observations, three wavelengths *(Russian)* 77−22108
Innisfree meteorite fireball Canadian camera network record and orbit determ. 78−65563
intense showers and cometary origin 78−16358
ion-ion recombination radiation 77−74016
ionisation columns of bright meteors, initial radii meas. 80−94762
ionisation effects on LF radio navigational signals, meteor rate determ. 80−82309
ionisation trails, charact. 77−71069
ionised meteor trails initial radius, height and time depend. investigation 79−58301
ionization curve length and vaporization altitude var. with speed 79−21232
ionosphere E_{s2}-layer, creation, effect of variable meteor particle sizes 80−105108
ionospheric ionization due to low level meteors, contrib. to LF propag., radio and optical obs. system 79−84514
Kitchener daylight fireball of November 4, 1977, no meteorites 79−16892
Leonids, spectral analysis 79−16890
Leonids, struct. and activity, 1971 Nov. 15-19 obs. 77−67075
Leonids, struct. and relative activity of radiants, 1972 November 78−45291
LF signals attenuation due to meteor trains 78−40726
long-lived meteor train, IR brightness obs. 80−94629
luminosity of meteor trains, lifetimes, Na catalytic cycle 80−12711
luminous efficiency coefficient, determ. from photographic obs. 78−96440
magnitudes and enduring trains 78−49396
mass scale and meteor emissions at max. brightness 78−20761
mesosphere, meteors rel. to Na seasonal var. 78−36239
metallic ions of meteor origin effect in VHF ionospheric forward scattering, contribution to sporadic-E formation 80−67461
meteor wind automatic meas. set, drift obs. accuracy *(Russian)* 77−41248
meteor wind automatic meas. set, programming and systems interaction *(Russian)* 77−41247
meteorite dropping fireballs, accuracy of radiants 79−71006
Middle Ages, list of events from European mediaeval sources 78−86105
modelling of influx of meteoric matter with radar observations *(Russian)* 80−67664
momentum analysis rel. to effects on Earth's atmosphere 77−56877
NASA-NMSU meteor observatory trajectories and orbits 77−22152
nature, techniques of obs. and general parameters 78−57509
New South Wales fireball, 7 April 1978, trajectory and ground track 80−82313
nightglow assoc. with meteor showers, origin 77−91488
nonequilibrium thermodynamic model 80−4308
observation methods in Poland, review *(Polish)* 78−61750
observing probability determ. from apparent luminosity function 79−21231
optical brightness rel. to ionised trail props. 80−77354
Orionid shower, simultaneous radar obs. at Ondrejov and Dushanbe 78−20760
Orionids 1975, radar echo rates, long-baseline obs. 80−36576
Orionids and η Aquarids, viewing conditions during 1986 return of Periodic Comet Halley 77−74011
meteors continued
overdense trails, determ. of diffusion coeff. and initial radius 77−13140
Perseid meteor shower, television obs. 80−4309
Perseid stream, orbital element dispersion 78−20757
Perseids, meteoritic aerosols, twilight optical charact. modification *(French)* 80−46255
phase tracking meteor radar ambiguity elimination algorithm *(Russian)* 77−41311
photographic altitudes, observational-theoretical comparison 80−8593
photographic spectra, identification of air radiation 77−29733
plasma diffusion, geomagnetic field effect expt. *(Russian)* 78−61814
Pons-Winnecke 1916 shower, possible age *(Russian)* 79−92729
Quadrantid meteor shower, orbit 78−61815
Quadrantid meteor stream, long-term orbital evolution 80−17551
Quadrantid meteor stream, orbital evolution between (AD 1830 and 2030) 80−21948
Quadrantid meteors influx, effect of meteoroid stream orbital evolution 80−56776
Quadrantids, overdense radio meteors, stream maxima position var. with meteor magnitude 78−12161
radar, A/D filter charact. *(Italian)* 79−80032
radar echo drift, deceleration 78−36538
radar echoes, atm. diffusion coeff. and height relation determ. 78−49187
radar facility in France 79−2386
radar meteor echo rates, correl. with zonal winds at 95 km altitude 80−56775
radar meteors rate depend. on geomag. activity and coronal activity 80−67662
radar obs. at Ondrejov and Dushanbe 78−20760
radar obs. during GRMWSP/CTOP periods 79−2412
radar obs. of neutral wind gradients 80−41575
radar observations at Illinois University, radar system description and results 77−41205
radar rates correl. with geomag. activity and solar wind sector struct. 78−65553
radar receiver design, logarithmic, operating at 37.5 MHz *(Czech)* 79−21188
radar research, growth and decline 77−78722
radio echo characteristics, rel. to deionisation processes and meteoroid props. 80−17550
radio echo data and atmospheric scale heights 79−84560
radio meteor rates observed with meteor wind radar during non-shower period 79−84753
radio meteor wind facility at Christchurch, New Zealand 79−2387
radio meteor wind meas. over Atlanta 79−2411
radio meteors, wind data anal. using finite element approximation 78−81475
radio waves scattering by meteor trails, trapping by ionospheric ducts 80−4172
radiometeors, forward scatter, amplitude distrib. index, D-region absorpt. effect 78−65552
radiometeors charact. assessment, statistical analysis of time-dependent series *(Russian)* 80−56777
radiowave reflection from meteor trail, ambipolar diffusion coeff. 80−46329
radiowave scatt. theory appl. to radio meteor obs. in upper atm. 79−5696
radiowave scattering from meteoric ionisation, theory 77−87337
rates and atm. density vars., correl. with solar activity 77−53485
real luminosity function determ. from apparent luminosity function, least squares method 79−80231
recording frequency, influence of form and orientation of antenna directivity diagram *(Russian)* 80−67665
red afterglow in meteor wakes, origin 78−36536
shower dates and N.E. monsoon in India 77−70746
shower from Periodic Comet Grigg-Skjellerup (1977b) in 1977, April, possibilities 77−33418
shower hypothesis for origin of ionospheric ringing irregularities 79−84581
shower radiant precise determ. by means of many photographs *(Japanese)* 79−101085
showers, LF radio absorpt. events rel. to meteoric constituents ionization 78−40736
Spacelab image intensifying TV obs. 77−21966
spectacular showers, possible assoc. nightglow 80−94761
sporadic, sunrise effect on persistent radar echoes 78−20759
sporadic background obs., 1974 November, by Ondrejov meteor radar 79−80278
sporadic radio-meteors, ionisation height meas., VHF obs. 80−82312
stratosphere, chem. of meteor trail metal ions 80−72580
stream disintegration, solar radiation and planetary perturbation effects *(Russian)* 80−46495
stream radiant determ. from single station obs. 78−20647
stream radiant distrib. using spherical harmonic analysis 78−20648
streams, statistical simulation of radar obs., algorithm 78−20763
streams detection in interplanetary space 77−87338
streams formation and evolution theory, matter ejection from cometary nuclei 77−67074
surface shielding by evaporating mols. 80−101564
surface shielding by vaporised and refl. mols., theory of first collisions 80−77357
Taurids, dispersion of orbital elements 79−21230
telescope performance for meteor obs. 78−49319
televised spectra of meteor trails, photometry 78−20764
television photographs, photometry technique 78−96441
television spectra, prod. and study 77−67076
terrestrial comets and theories of Thomas Clap 77−74017
theoretical light cuarves and meteoric mass scale 78−49397
thermal fracture, detached particles mean dia. 80−62081
thermosphere, winter motions radar in S.hemisphere meteor region 80−109287
trail, diffusion of weakly ionised plasma filament forming angle with mag. field 79−53610
trail, initial expansion 77−2373
trail ionization effects on ionospheric radio signals propag. 79−101001
trail maximum ionisation height, detect. method 80−8487
trails, atmospheric ambipolar diffusion coeff. meas. errors 78−88952
trails, causes of fluctuations in effective linear electron density 78−73687
trails, effect of thermal on measured drift speed 77−21955
trails, studies using large-aperture radio system 80−85870

meteors continued
train initial radius, rotation effect 79−16893
train luminosity decay 78−81593
trajectories and orbits, from NASA-NMSU Meteor Observatory 77−74014
trajectories and orbits, visible obs. 80−72887
tribo-induced discharge luminesc. 80−25471
Tunguska event, thermal explosion of porous meteoroid, model 78−61813
TV apparatus for meteor spectra photography 77−67047
TV observations 77−87339
twilight sky polarisation during meteor showers *(French)* 77−9578
under-dense radio-meteor data, influence of ion recomb. 79−80279
upper atmosphere, meteor wind obs. from Sheffield during January 1976 winter anomaly 78−45070
upper atmosphere, odd N prod. by meteoroids 79−2404
upper atmosphere Na^+ and Na layers, meteor ablation-cluster ion theory 79−58138
upper atmosphere tides and winds meas. from meteor radar obs. 79−66851
upper atmosphere wind meas. errors from meteor trails 77−49202
upper atmosphere winds at 95 km altitude, meteor obs. at 45°N 80−46330
upper atmosphere winds observed by radio meteor drift, 80-100 km altitude 80−46328
VHF duty cycle diurnal and seasonal vars. due to meteor forward scatt. 79−88534
VHF ionospheric forward scattering, effect of metallic ions caused by meteors *(Japanese)* 78−81504
video detection and analysis techniques 79−80239
visual data, rigorous method of normalization and analysis 79−88627
visual meteor shower radiants, statistical study 78−96442
wake spectra, excitation of ionic lines and mol. bands 79−29919
wind data for global comparisons 79−2413
wind height structure determination, statistical method *(French)* 80−51589
wind profile comparison with electron density obs. 77−9587
winds over Sheffield, radar obs. 79−2415
N_2^+ 4278 Å bands in spectra, quantitative anal. 78−45290
Na and minor constituents in atmosphere, meteoric origin 79−70835
Na enhancement in upper atmosphere possible meteoric origin, lidar obs. 80−101466
O I, 5577 Å emission, plasma column dynamic and reaction processes 77−82176
O I 5577 Å emission, vel. dependence 78−20758
O I 5577 Å forbidden line collisional quenching 77−17448
O I 5577 Å forbidden line in meteor trains, emission mechanism 78−49395
OH emission, UV photometric obs. 78−7943

metering
see also ammeters; electrometers; frequency meters; galvanometers; level meters; ohmmeters; phase meters; Q-meters; standing wave meters; volt-ampere meters; voltmeters; watthour meters; wattmeters; wavemeters
acoustic intensity meter for small machine in a room 78−33975
acoustic noise meas. systems and equipment 78−83189
amplitude-phase ratio meter for microwave signals *(Russian)* 78−62209
analogue meters, ballistic performance specification 78−41293
analogue or digital differences and basis for rational choice 80−52184
analogue versus digital, analogue meter advantages 80−13053
artificial pancreas programmed control technology *(German)* 79−16346
automatic single-channel power factor meters 77−79116
averaging meter, dual slope principle, nonelectric periodic quantities meas. appl. *(German)* 78−73983
capacitance meter, linear based on integrator 79−6146
capacitance meter, linear direct reading, cct. *(French)* 78−237
capacitance meters, direct reading using auto-ranging 78−32835
DC voltage instability meter 79−2790
dielectric constant meter, Tangens-2M, sensitivity and static charact. anal. 78−45651
digital capacitance meter *(Spanish)* 80−13062
digital impulse meter, 5 to 500 N range 78−191
digital meter for inductance coil parameters meas. 78−12718
digital panel meters, charact. and appls. 80−68190
direct reading capacitance meter 79−75513
E-field meter for electrostatic field strength meas. *(German)* 77−74425
electric exposure meters, photography appl. *(German)* 77−87856
film thickness meter for dielectric material thickness meas. *(Russian)* 77−41566
HF elec. conductivity meter, semicond.-based, principles and advantages *(Hungarian)* 78−16815
impedance meter, high-speed, for electrochem. system obs 79−30490
inductance meter, direct reading 79−2787
integrating sound level meters, response to impulsive sounds 79−50547
interchangeable-scale switchboard meters *(German)* 77−82497
isotropic RF electric/magnetic field strength meter, design 80−82751
meter, using ICs, 10 pF to 1 μF, design 79−6140
modulation meters, history of development, selection, special features, calibration *(French)* 77−53948
multifunctional digital instruments for school use 78−12504
pH meter, selection method 77−56271
pH meter construction for amateurs 77−57321
photosensor time charact. meas. meter 78−283
pointer instrument freq. response determ. by stroboscopic methods *(Polish)* 78−29102
precision acoustic meter *(French)* 78−71254
self-recording heat flux meter, mathematical model 78−93678
sound level meters, comparative listing 79−50546
sound-level meter, innovative high school teaching project 80−4495
time-interval series meter 78−176
tolerance gauging, Mercer electronic unit 79−12780
vibration meter, dynamics, sensitivity and accuracy aspects *(Dutch)* 78−36999

meters *see metering*
metrology *see measurement*
metrosils *see varistors*
MHD *see magnetohydrodynamics*
MHD convertors *see magnetohydrodynamic convertors*

mica
alpha-particle tracks, prompt process and post effect 78−43053
alpha-recoil tracks in archaeological ceramic dating 78−70237

mica continued
asbestiform chain silicates, new minerals and struct. groups 78−28227
biotite, anisotropy of Mossbauer absorpt. 78−80263
biotite, disordered mica struct. high resolution electron microscopy exam. 78−91344
biotite, elec. field gradient Mossbauer absorption 77−85629
biotite, Precambrian, Po-haloes 78−85556
biotite, temp. transformations, spinel formation 77−78163
biotite, thermal decomposition, stability of ferromag. products 78−57195
biotite pegmatite in Calicut area Fe ore, dating by fission track 77−13066
biotite stress corrosion cracking, seen in granodiorite 80−36299
biotites, X-ray photoelectron diffr., quantitative anal. 80−66912
Chinese name rel. to cloud formation and ice nucleation 77−91195
cleavage, emission of high-energy electrons 79−56917
composite, epoxy resin/mica, thermal depolarisation current, 20-190°C 77−90091
crystal chemistry, review 79−46612
defects effect on epitaxial film struct. 78−26794
deformed, syntectonic nucleation of new grains 79−65102
dislocation detection by divergent polychromatic beam method 77−35568
dispersed Al-Cu-Mg (4, 1.5 wt.%), wear charact. and bearing performance 80−108591
dosimeters for visualisation of electron isodose curves in a medium 80−99349
electrical conductivity change and EM radiation during weakly bound water separation *(Russian)* 77−31779
EM effects during liberation of water of constitution from cryst. lattice *(Russian)* 77−31778
epoxy mica generator insulation, dielectric stress conc. influence on voltage endurance 78−15094
EPR spectra using mag. field and US strain modulation 77−69688
fission fragment track registration development efficiencies, etchant (etching conditions) depend. 78−66454
fluorophlogopite, glass-ceramic, thermal diffusivity, crystallisation effects 78−6190
fluorophlogopite, substrate for vac. deposition of Mo at 650 to 1050°C *(Russian)* 77−48342
fluorophlogopite as ice nucleating agent 77−87007
fluorphlogopite, synthetic, luminesc. props. 78−19579
fluorphlogopite, synthetic, with excess Al, radiation-induced paramag. O^- centres 80−60417
fluorphlogopite, valence transition of Ti impurity, ESR and optical absorption data 77−16155
gaseous reduction and extraction of Ga from mica 78−92216
giant haloes, cleavage cracks enhancing radiation damage 78−7623
giant halos round α-emitting inclusions containing water, production 77−51420
glass ceramics, near perfect shape-memory solid 77−48492
glauconites, Mossbauer anal., Fe^{3+}/Fe^{2+} ratio 80−17252
layer deformation and cryst. energy, struct. models for 1M and $2M_1$ polytypes 79−19184
light scattering by flakes in water 78−40565
margarite, stability and compatibility relations as press.-temp. indicators 77−5183
mica, metamorphic white, surface microtopography 80−54493
Mossbauer spectra of Fe in mica 78−23380
muscovite, annealing of latent tracks of heavy ions *(French)* 79−19290
muscovite, crystalline track detector, etching charact. anisotropy 77−46465
muscovite, Fe^{3+} localisation determ. by EPR *(French)* 77−43196
muscovite, fission track etching and annealing anal., dating appl. 78−32036
muscovite, natural cryst., submicroblock struct., electron microscopy 79−14816
muscovite, pulse electric breakdown under pressure, lamination effects 80−66110
muscovite, thermal cond., 3-320K 77−43392
muscovite for high neutron fluence meas. using fission track technique 80−91395
muscovite in medium to high grade metapelites of NW.Maine, comp. var. 79−62493
muscovite mica, Pb diffusion rel. to Po haloes 79−44186
muscovite of regional metamorphic rocks in Xizhang, b_0 value and geological significance *(Chinese)* 79−74890
muscovites, Himalayan, fission track dating and U conc. estimation 78−40524
muskovite, disordered mica struct. high resolution electron microscopy exam. 78−91344
natural, high γ- and electron-irrad. doses effect on annealing behaviour, thermal decomp. resist. 80−60897
NMR, Fe^{2+} distrib. on octahedral sites, PMR investig. 78−15041
North American, electrical cond. rel. to chem. composition 77−29285
nuclear track microfilters, prod. and props. 80−96574
nuclear tracks, etched, statistical distrib. of quadratic holes on planar surface, computer simulation 80−37705
optical narrow-band interference filter with mica separating layer 77−7207
particle size measurement by monoparticulate film method *(Japanese)* 78−95874
particle track formation and minimal energy loss *(German)* 77−18757
phase retardation plate, cleaving and optical meas. method 79−64364
3T-phengite, existence in Xingyang metamorphic belt, tectonic significance *(Chinese)* 79−84264
phlogopite, cryst. struct. and compressibility at high press. 78−63717
phlogopite, Fe^{3+} localisation determ. by EPR *(French)* 77−43196
phlogopite, fission track etching and annealing, chronological application 79−84230
phlogopite, pulse electric breakdown under pressure, lamination effects 80−66110
phlogopite, solubility in basic aqueous solns. under hydrothermal conditions 78−43127
phlogopite, source of K and Rb in upper mantle 77−5165
phlogopite, thermal cond., 3-320K 77−43392
phlogopite in S.African kimberlites, $^{40}Ar/^{39}Ar$ anals. 79−34769
phlogopite mica, press. depend. of Ar diffusion 77−86861
phlogopites, mica, Fe^{2+}, F^-, and OH^- distrib. in octahedral sheet, NMR study 79−82183
phosphate bonded synthetic mica ceramics, form., physical props., texture 77−21063

mica continued
polystyrene composite with mica flakes, TDC meas., interfacial polarisation 78−64316
polytypism, phase and growth aspects 78−83764
reactor neutron detection, plastic with ^{65}Zn impurity used as nuclear track and activation detector 78−13346
scientific meeting (Orleans, France, 1978 February 9) 79−48457
soft X-ray spectra, photoelectric yield spectra 78−72640
solid state particle track detectors, fission fragment ranges rel. to cryst. orientation 80−91408
β-spodumene-mica glass ceramic, thermal expansion thermal shock and moduli of rupture and elasticity 78−60736
β-spodumene-mica glass ceramics, phase evolution and TiO_2, MgF_2 additive effects, exam. 78−44089
stress-induced K^+ ion migration, X-ray fluoresc. anal. 77−4221
substrate, $Pb_{1-x}Sn_xTe$-PbTe heterostructures produced by MBE 80−88629
substrate for Au thin film growth, surface defects on heterogeneous nucleation 78−47684
superheavy elements, proton-induced K- and L-shell ionis. cross sections, comparison with actinide fission prod. X-rays 77−50581
superheavy elements, X-ray anal. of monazite inclusions in mica 77−25685
surface, static SIMS anal. 78−38922
surface energy density by wedging method 77−75858
surface free energy dispersive component, to water and n-alkanes 77−55435
surface free energy nondispersive component, adhesion to polar liq. 77−55436
surface impurity levels by static SIMS, cleaning treatment effects 77−59190
surfaces, interaction forces at small separations in polar and non-polar liquids 80−39458
surfaces, van der Waals interactions 78−30973
surfaces in aq. poly(ethylene oxide) soln., forces meas. 79−23833
synthetic, polytypism and faulting, lattice imaging obs. *(French)* 78−79587
synthetic phlogopite, Fe content as function of growth rate 78−32089
tetraferriphlogopite, cryst. struct. refinement using least squares approx. 78−79594
tetrahedra, cation-apical O vibrs., IR spectra 79−47420
Van der Waals forces, direct meas. 78−43461
van der Waals forces for interacting mica and quartz plates, calcs. from complete dielectric data 77−32340
vermiculite, electric field gradient, Mossbauer absorption 79−73865
vermiculite, interlayer space struct. anal., by replacing exchange cations with NH_4^+ 77−7700
vermiculites, chem. treated, for liq. radioactive waste treatment by ion exchange 79−45370
windows for interferometric vessels 77−41675
Yugoslav biotites, search for giant halos assoc. with superheavy elements 78−16008
Al alloy-mica particle composite, cast prep. and mech. props., bearing appl. 80−71613
Al-Cu-Mg/mica particulate composite mech. props. 80−100919
Au ion tracklengths in mica 78−38767
Fe rich micas, X-ray absorpt., heat treatment effects, chem. and struct. interpretation 80−84806
I ion tracklengths in mica 78−38767
Mg rich micas and amphiboles, Mossbauer spectra 79−38412
Mn rich micas and amphiboles, Mossbauer spectra 79−38412
Na_2O-CaO glass phlogopite mica powders, composite fabrication, cellular struct. 80−84902
ZnSe-mica epitaxial heterostructure, growth and struct. 78−43257

Micelle systems *see colloids*

microcalorimeters *see calorimeters*

microchemical analysis *see chemical analysis*

microcircuits *see integrated circuits*

microcomputers
for microcomputer applications see under relevant applications e.g. computerised control; natural sciences computing
see also microprocessor chips; personal computing
A/D data acquisition module for microprocessor systems, high-speed, multiple channel 77−57304
aerosol particle size spectrometer, microcomputer-modified 79−39329
aerospace test meas. symposium, San Diego (1976) 77−41284
arrhythmia detection using a low-power, CMOS processor 78−73276
biomedical signal processing appl. 78−81012
bubble chamber pictures, SNOOP module CAMAC interface to 168/E microprocessor 80−58103
comparative eval. 79−30173
criteria for selecting and interconnecting micro-, mini-, midi- and maxicomputers 77−17961
Culham fusion expts., distributed control systems using microcomputers 80−13909
Culham fusion expts., integrated data network for microcomputer based diagnostics 80−13910
Culham fusion studies, appl. of microcomputer to data acquisition and control 80−13908
data acquisition for wind study, features 79−60087
didactic microcomputer *(German)* 79−80396
disturbed cell renewal systems, simulation by microprocessor system 80−35859
doubler tevatron microprocessor quench protection system 79−72088
education, micro-computer based test scoring system 78−81757
EOSCOR: A light weight, microprocessor controlled solar neutron detector 79−101063
flexible multi-scaler system with micro-processor control 78−90037
fusion experiments, microprocessor applications in data acquisition and control 80−13918
gamma-ray spectra, microprocessor system 79−9955
general purpose, use for hypothetical spectra synthesis in NMR undergrad. instruction 80−42009
IEEE computer standards 79−89544
illumination measurement using photoresistors, digital linearisation using microprocessors *(German)* 78−77961
industrial service, of microprocessor *(French)* 80−17729
Intel 8080 development system 77−83314
Intel 8080A for data evaluation of X-ray emission analyser *(Hungarian)* 79−43522

microcomputers continued
Intel MDS-800, DMA interface for Biomation 8100 recorder 80−203
interface/controller for desktop programmable calculator 79−35690
ion-selective electrode analysis use of microprocessor-based millivoltmeter 80−16752
ionising radiation effects on SBP9900 microprocessor 77−75002
laboratory data acquisition and control system based on Commodore PET microcomputer 80−204
liquid-scintillation counting, one-button, using microprocessor 77−14308
medical application, ventilatory function testing 80−41291
microcontroller, radiation tolerant, design, elec. and radiation tests, performance 77−18709
microelectronics and microprocessor impact on metals prod. and NDT 79−74320
microprocessor based beam loss monitor system for AGS 79−72070
microprocessor based control of RF linac cavities 79−71996
microprocessor based respiratory function analyser 79−25131
microprocessor control of He refrigerator system for Fermilab switchyard 79−68006
microprocessor equipment to analyse eye movements during radiograph scanning 79−25130
microprocessor multichannel analyzer laboratory project 80−101685
microprocessor technology, appl. to digital data recording in instrumentation cameras 77−79189
microprocessor-assisted flow-through anodic stripping voltammeter for oceanographic appls. 78−36324
microprocessor-based experiment controller/interface 79−80590
MIDCON conference, Dallas, USA, Dec. 1978 79−87939
minicomputer interface 77−54483
Mossbauer microprocessor controlled spectrom. 79−97931
multiple detector data acquisition system, microcomputer based 78−90049
nonvocal communication aid improvement by microprocessor technology 80−8217
nuclear diagnostic system, operating systems for microprocessor multiple arrays 79−49918
nuclear reactor guard line circuits dual microprocessor system, decision-making and self-testing 80−57901
nuclear reactor power monitor 79−85644
number oriented microprocessor appl. to real time data processing 79−49921
oceanography, Kiel multi-purpose sea probe microprocessor-based data acquisition system *(German)* 78−85701
online EEG data analysis system 78−73277
online vectorcardiographic analysis microprocessors and instrumentation 78−36020
PDP 11/03, data handling system for nucl. physics expts. 79−76319
physics teachers and students guide to calculator choice 80−4494
Picker FACS-I diffractometer, microprocessor-controlled optical incremental angle encoder system 80−18058
portable microcomputer system, associated movement study 80−51299
potentiometric analyser, automated, with selective electrodes, microcomputer control 80−40773
programmable, electrochemical calc. appl. 79−43592
pulsed NMR spectrometer incorporating microprocessor, operational, software and hardware details 78−45666
radiation therapy simulator and linear accelerator meas. and control by microprocessor 77−40902
rehabilitation of severely disabled, microcomputer environmental control and communication system 80−8216
scientific calculating system with number-oriented microprocessor 78−36983
selection for specific appl. *(German)* 77−32744
single-chip, architecture and operation, use in instruments design and meas. techniques *(German)* 80−27276
spectroscopy application techniques *(Japanese)* 78−16855
system, appl. to NMR experiments *(Japanese)* 79−75564
teaching, systems, appls. for chemistry CAI 80−57042
TFR Tokamak, microcomputer data acquisition system 80−13916
theodolite microprocessor selection, development, and programming 78−24218
visual stimuli generation for psychology experiments, Z-80 based system 80−41328
weighing system, microprocessor based electronic scale 77−74421
X-ray astronomy balloon, microprocessor-controlled payload 79−62716
X-ray double crystal spectrometer, microcomputer automatic control *(Polish)* 80−32563

microcopying *see microphotography*

microelectrodes
bioelectrode methods *(Japanese)* 80−30919
biological special purpose electrode *(Japanese)* 80−94426
bipolar suction electrode catheter for intracavitary ECG 79−44018
brain impedance scanner principles and exptl. results 79−57804
captured nerve fibre multiple single-unit recording by tubular electrode array 77−60321
catheter-tip electrode for continuous pO_2 and pCO_2 meas. 79−34693
circular interacting microelectrodes, collection factor calcs. *(French)* 77−27759
collagen fibre electrode for peripheral neural activity recording *(Japanese)* 77−66879
current and voltage clamp cct. for central nervous system neurons 78−24191
current injector for Coulomb titration of chloride 79−29684
double-barrel ion-sensitive microelectrodes, extra thin tip diameters, intracellular meas. appl. 80−101298
ECG manual electrode 79−57801
EM microelectrode holder for pulsating penetration of brain tissue 80−98199
EMG electrode array for single muscle fibre activity measurement *(Swedish)* 78−24193
endocardial electrode lead and pacemaker failure, actuarial analysis 80−30945
endogastric probe for telemetric pH meas. *(German)* 78−85452
extracellular action potential recording, interference suppression 78−61294
geometry determ., indirect method 77−40949
glass, open tip, influence of diffusion, double layer, and glass conduction on elec. resistance 80−67300
glass microelectrode, for pH meas. 80−21291

microelectrodes continued
glass microelectrode, piezoelectric drive appl., for cell membrane penetration 79−5420
glass microelectrode puller for reproducibility 77−48967
hearing aids, photolithographic fabrication and neurophysiological performance 79−12034
histological marking with multiple thin-film electrode probe for intracortical recording 80−67297
hydraulic microdrive for recording single nerve cell activity 79−70727
implantable 8-channel stimulation system for labyrinthine deafness *(German)* 79−16347
implantable cardiac pacemakers, non-polarizable stimulating electrode development 79−92428
implantable pair for recording from intact small nerves 80−36204
insulation, chronically stable, reproducible, using parylene 77−40942
integrated micro multi-ion sensor using IGFET 78−40439
intracardiac ECG trends 79−44031
intracellular measuring production method micropipettes of very low resistance 80−61738
intracellular recording from pulsating cerebral cortex 77−48960
intracortical recording of field pots., 16-fold semi-microelectrode 80−67298
intravascular O_2 measurement, current-to-voltage convertor 79−34684
intravascular O_2 sensors, Monopolar, in vitro evaluations 79−34683
ionic channel formation in living cell membrane, microelectrode obs. 78−53372
liquid-ion exchanger microelectrode estimates of epithelial cells Na^+ activity, resistive artifacts 80−89909
metal biomedical microelectrodes, noise characts. *(Japanese)* 80−3846
metal electrodes, impedance props., chronic recording from mammalian nerves 79−12043
metal-filled, reproducible manufacture 78−69263
MHD generator electrodes in arc regime of operation, math. model 79−86620
microcircuit electrodes, extracellular, recording of action pots. from cultured neurons 80−72382
miniature pH-sensitive polymer membrane electrode 79−100781
motion artifacts in surface applied bioelectrodes, quantification *(German)* 80−3829
motor unit recruitment and firing freq. control in elec. stimulated muscles of cat 78−81092
moving cell microelectrode puller 80−67309
moving-coil microelectrode puller 80−30964
multi-microelectrode system characts., neuron single-unit pots. recording appl. *(Japanese)* 80−21581
multi-microelectrode system for simultaneous recording of closely spaced neurons *(Japanese)* 78−61284
multi-microelectrode system with independent penetration and structural reinforcement by mag. coupling, characts. *(Japanese)* 79−66586
multi-unit neuronal spike train separation by improved time amplitude window discriminator 77−86726
multibarrel microelectrodes, 'piggy-back', simple technique for construction 80−85541
multiparameter clinical diagnostic miniature transducers, colloquium, London, England (May 1979) 79−100776
muscle surface pH meas., significance of impedance changes 77−52908
neurological, W-Re wire, CVD SiO_2 and Mo coatings, elec. cond. and bending props. 78−11752
neurological multichannel depth probe fabricated using electron-beam lithography 79−57822
neuromuscular miniature endplate potential online acquisition microcomputer system 78−36015
neuron single-unit pots., simultaneously recording system *(Japanese)* 79−57826
photoelectrode for recording intracerebral cellular Ca^{2+} transients 80−67307
photoetched Au multimicroelectrode surface for neural single unit activity recording 79−57824
pipette electrode tips, beveled, non-destructive electron microscopic exam. 80−89915
pipette electrodes, dry beveling 80−89914
potentiometric gas sensing probes, micro-size, for ammonia, CO_2 78−61071
puller with high temp. heating element 77−61059
reference electrodes for in vivo meas. 79−52687
reference microelectrode sterilizable with ethylene oxide 80−17153
stepping motor presettable digital control for neurophysiological microelectrode drive 78−36079
thick film hybrid fabrication of pH-sensitive implantable bioelectrode *(German)* 78−40369
tip fabrication method 77−81758
tissue measurements of local PO_2, local flow and local ion activity 80−51287
tissue microelectrode design for skin pH meas. 79−100780
tissue pH electrodes for clinical applications 80−36175
vibrating, excursion in tissue 80−104829
voltage clamp, single electrode, design for neuroresearch 80−72385
Al, micro-fabrication technique for SAW transducers 77−80042
C-fibre microelectrodes, neurophysiology appl. 80−67314
Ca^{2+} intracerebral transients, photoelectrode for recording 80−30961
KCl filled, boiled and not boiled, potential and resistance comparison 77−81760
Na liquid ion exchanger, appl. to meas. of large extracellular Na transients 77−52949
Na-selective liquid ion-exchanger, for intracellular meas. 80−3888
Ni-Fe microelectrode array probe for electrophysiology 79−84049
O_2 partial pressure and bioelectric potential simultaneous meas. in living tissue *(German)* 78−85453
Pt microelectrode potentials and small-signal impedances 79−34716
Sb-Sb_2O_3 pH electrode improvement 79−53270
Ta-Al_2O_3 microelectrode array, design and fabrication 80−76868
W microelectrode potential and small-signal impedances 79−34715

microelectronics *see integrated circuits*

microfarad meters *see capacitance measurement*

microfiche *see microforms*

microfilm *see microforms*

microfilming *see microphotography*

microforms
see also computer output to microfilm; publishing
biomechanics film data reduction and anal. using PLATO system 79−35873
development trends *(Czech)* 77−18114
electrophotographic process of contact copying of microfiches and microfilms 80−47127
holographic document miniaturisation system automation 79−72538
holographic document reduction system design *(Russian)* 79−98309
holographic document retrieval and conversion to photographic microforms 79−76643
holographic microfiche of picture like information 77−38833
information retrieval systems, colour reversal film evaluation, strip film appl. *(Japanese)* 79−97455
laser transfer printing 78−65994
microfilm laser transfer printing 77−18121
microfilm reader and projector 79−72648
patent information system, appl. of microfilm camera DA 5 DOKUMATOR 79−75632
personal reader, Izon system, using distributed optics 78−29098
reproduction and scale changes of recorded information using a scanning electron microscope 78−93775
spatial filter correlator, coherent optical matched, for microfilm data base word recognition 80−43279
surface-relief phase gratings for image recording and display 77−19429
text information micro-recording using laser beam *(Russian)* 77−54750
As_2S_3, amorphous film, light enhanced vaporisation, photolithographic process, photographic appls. 77−5949

microhardness *see hardness*

micromanometers *see manometers*

micrometeorites
ablation spheres in deep-sea sediments 80−46500
black magnetic spherules in marine sediments, origin 78−24494
cosmic dust, black spherules collected at Mt. Norikura, Japan, accretion rate 78−96445
cosmic dust, book 78−57498
element composition, neutron activation study, stratosphere collected particle 80−82319
extraterrestrial matter in fresh snow, preliminary results 79−84302
impact on atmosphereless planets, ion emission 80−77362
impact on Io, form. of Na clouds and regolith 80−77330
interplanetary micrometeoroids, rel. to meteoric night-glow 77−91488
ionospheric sublayers in lower thermosphere caused by micrometeorites 80−61956
Ivory Coast microtektite strewnfield: new data 79−66697
lunar microcraters, diameter to depth ratio dependence 80−94765
lunar regolith, solar wind and micrometeorite effects 77−60669
lunar rocks, microcrater and accretionary grain populations under meteoroid and solar wind bombardment 80−94731
lunar rocks, microcrater and accretionary grain populations from lunar surface and Apollo samples obs. 80−94732
lunar surface, micrometeorites and solar flare particles in and out of ecliptic 77−29737
magnetic spherules in marine sediments, K and Ca isotopic comps. 79−44423
micrometeoroid hazard of Comet Halley probe, workshop proceedings (Noordwijk, Netherlands, 18-19 April 1979) 80−36782
micrometeoroid impact, laboratory simulation 78−57510
particle flux rel. to deflection of orbital effects of direct solar and Earth albedo radiation pressure 79−88566
sampling techniques 78−57459
spacecraft measurements of meteorite material near Earth and in interplanetary space 77−53486
spherule identification, rel. to black magnetic spherule fallout in E. Gulf of Mexico 77−37242
stratosphere particles, detect. of ^4He rel. to extraterrestrial origin 77−56878
studies by space-borne instrumentation 78−57460

micrometeoroids *see meteoroids*

micrometers *see micrometry*

micrometry
see also interferometry; strain gauges
arterial diameter meas. using US transit-time micrometer 78−7410
caliper gauges for meas. outside dia. 79−12766
clamp, micrometer, for measuring electron microscope filaments 79−21700
coating thickness meas., 1979 status in USSR 80−77749
contactless laser beam diffraction method 77−22525
contactless precision using optical interferometer with capacitance frequency analogue *(German)* 77−30126
coplanar surface plane deviation meas. appl. *(German)* 78−163
differential thermocouple transducer for electrically insulating liquid level 77−17969
digital micrometer development and appl. 78−65902
digital micrometer/counter accuracy assessment *(Polish)* 78−45654
Ebert plates, wavelength determ. using microphotometer with micrometer attachment 78−16853
electronic micrometer error specification *(German)* 77−74354
electronic micrometers and their applications *(French)* 78−65903
EM position transducers, dynamic characs., contactless displacement meas. appl. 78−41277
external micrometers with transmission and counter type display *(German)* 77−26278
graticules, highly accurate calibration technique 78−24762
hip joint geometry, human, three-legged micrometer spherometric errors 79−83832
holographic interferometry appl. *(French)* 78−42305
linear and angular microdisplacement instrument *(Japanese)* 79−21728
micro-optics testing, width meas. of slit test objects 80−64223
microhole axis perpendicularity deviation meas. device 77−13739
micrometer performance evaluation method *(Japanese)* 79−97347
micrometer stiffness effects anal. *(Japanese)* 77−87731
optical ultramicrometer technique using composite diffr. grating 78−4589
photomicrometry with moire 78−4690
piezoelectric micrometer for precision movement in optical alignment applics. 77−65017

micrometry continued
pneumatic micrometer with positive feedback system *(Japanese)* 79−93101
reflection dispersive Fourier interferometer window eliminating backlash error 80−57402
reliability assessment method *(Rumanian)* 80−68175
scanning Fabry-Perot interferometer for far IR balloon astronomy 79−35093
sharp-lip capillary nozzle production and meas. precision 77−80246
slides, for linear meas. in range of 100 mm to 1 μm accuracy 77−5808
Talcott photoelectric micrometer for Bamberg zenith telescope latitude obs. *(Russian)* 78−4113
universal horizontal metroscope, rational determ. of composite error on small micrometers 80−82742
Vernier Calipers with partly digital value indicators, development *(German)* 77−87728
ZTL-180 zenith telescope, micrometer screw turn from declination arc. obs. *(Russian)* 78−89067

microphones
absolute calibration of laboratory standard microphones using laser-pistonphone 77−58519
AC voltage level measuring system for microphone sensitivity 79−50545
acoustically coupled rooms, reverberation time extension, directional microphone appl. *(German)* 79−41518
acoustically nonresonant optoacoustic signal depend. on pressure, buffer gases and microphone response 79−59862
air condenser microphone, environmental effects 77−84091
appliance acoustic emission determ. facility development 77−58507
array, constant beamwidth, for use in near-field, 300 to 3000 Hz 79−59900
array microphone, const. beamwidth, wideband, near field use 80−14535
arrays, cross-correlation analysis for noise source location in industry 79−18601
artificial heads with stereophonic intensity signals, directional effects *(German)* 80−106701
auditory training apparatus, individual for persons suffering from severe hearing loss 79−39590
calibration, industrial noise meas. appl. *(German)* 77−80039
calibration at depth in dry hyperbaric chambers 80−38205
calibration method for measurement of peak amplitude response and step-function decay 79−41548
cardioid microphones, transmission props. in LF region *(Czech)* 80−43584
coincident, for triphonic sound reproduction system 80−28405
condenser, arrangement for precision reciprocity calibration 80−19203
condenser, draft laboratory standard *(Japanese)* 80−79096
condenser, electronic circuits 79−98585
condenser, pressure calibration, note concerning the implementation of IEC 327:1971 80−74686
condenser microphone, freq. response and equivalent lumped elements 79−14190
condenser microphone as ionisation chamber for intense α fluxes 77−79506
condenser microphone using air gap as diaphragm control 77−27445
condenser microphones with flat freq., response up to 500 kHz 78−33968
coupler for noise source location, BOTSEAR 80−43576
coupler for reciprocity calibration of microphones 77−75754
development and calibration accuracy, review 80−96167
ear simulators, constants meas., for earphone calibration 78−27960
earphone shielding effectiveness for artifact control, auditory evoked pots. meas. 79−57790
earphones, comparison of DT 48, TDH 49, and TDH 39 types 79−94438
EL2 electret telephone transmitter, technology development 80−83723
electret, ceramic and condenser microphones, environmental effects on sensitivity 77−39180
electret condenser, design for meas. purposes 80−79086
electroacoustic transducers using piezoelectric polyvinylidenefluoride films for diaphragm material 80−10100
environmental effects on microphones and Type II sound level meters 77−62127
environmental effects on microphones of various constructions 78−13872
equipment and services, 1979 video yearbook 79−14197
fibre-optic microphones and hydrophones compared with conventional devices 79−72717
granule microphone using Se-Te alloy 79−3878
high-impedance low quality microphone using small 8 Ω loudspeaker *(Spanish)* 80−96173
high-temp. microphones for nuclear reactor acoustics 77−46361
history in America, rel. to acoustical meas. and instrumentation 77−45666
laser interference microphone for US and nonlinear acoustics 77−46874
line powered pre-amp 77−7274
low-impedance microphone calibrator for pressure transducers 78−59212
meas., with prepolarized cartridges (electrets) 80−74649
measurement microphones, comparison of performance and environmental charact. and applications, review 79−1038
miniature probe microphone using optical fibre 80−48534
monitoring shock waves in liquids, new developments *(German)* 79−82001
MOS movable-gate-field-effect struct. with foil electret 79−1043
noise cancelling microphone with piezoelectric plastic diaphragm, coupled oscillator theory 80−43581
nonlinear US fields in air, numerical representation, microphone signal example *(French)* 80−53521
outdoor noise monitoring microphone installation and calibration *(Japanese)* 78−42504
phonocardiographic microphones, air cavity characteristics, effect of vibrations, room noise 77−81611
photocardiogram contact microphone 77−21634
piezoelectric microphones with rigidly supported piezopolymer membranes 80−64330
piezoresistive, appl. of current amplification by vibrating membrane of piezoresistive semicond. 78−75025
polychlorotrifluoroethylene, electret, TSC 80−7266
pressure microphones, closely spaced, signals cross-spectral density for acoustic intensity meas. 78−9514
probe-tube, for press. fluctuation meas. in flowing combustion plasma 78−18443
microphones continued
probe-tube microphone, math. modelling 77−39179
pulsed acoustic sinusoids generated with phased-array speakers, transient free 77−54847
radio, receiver for parallel operation in film, TV studios, theatres *(German)* 80−4787
respiratory parameter meas. using 200 Hz acoustic pneumograph 77−48913
respiratory rate monitor using microphone pickup 79−79617
reverberation chamber array, use of standing-wave tube as calibration device 79−81674
reverberation room ANS qualification with microphone traverse and LF absorption 77−62123
reverberation room modifications for ANS qualification 77−58517
reverberation room sound pressure level spatial averaging by microphone array and traverse 77−58515
road vehicle microphone windscreens, acoustic sensitivity 78−38133
selection and use for engine and aircraft noise meas. 79−90104
semianechoic chamber sound power meas. by traversing microphone 77−62116
sound measurement in flames and inaccessible places, microphone probe design 77−62114
sound-controlled flashlamp trigger circuit *(Spanish)* 80−13175
sound-level meas. 78−83190
soundfield, design and development 79−98586
techniques for recording or broadcasting symphonic music 80−5885
turbine-generator sound level meas. using directional microphones 79−68520
vibration pick-up-type ear microphone and two way communication device 78−1535

microphonics *see microphones*

microphony
optical fibres as microphonic instrumentation transducers 77−17970

microphotography
see also microforms
35 mm camera control cct. for automated time-lapse photography 78−58076
AHU microfilm Kodak 5460 Recordak, 35 mm black/white 79−6204
bone polychrome fluorescence labelling and photomicrography 80−89821
chromosome autoradiograph analysis by computer 78−57071
chromosome-classification system based on banding technique 80−36199
cinemicrography time recording on 16 mm film 79−9252
Dancer microphotographic emulsion identification 79−17177
dark field magnification microphotographic illumination system 78−58025
development trends *(Czech)* 77−18114
electrophotographic process of contact copying of microfiches and microfilms 80−47127
epidermal imprinting by celloidine 79−25170
equipment to improve microscope photography 80−22460
exposure control, manual 80−98975
fundamentals and practical use 80−13166
holocamera for 3-D micrography of the alert human eye 80−98057
holographic document retrieval and conversion to photographic microforms 79−76643
holographic microfilms, expts. to improve recording density 78−82931
holographic reader-copier development and speckle suppression 79−81395
information storage and image retrieval, perforated film, mag. striped film, pocket microfilm reader 78−16779
inverted camera microscopes, IM 35 and ICM 405, for biology, medicine and metallography 79−30540
laser irradiated solid target, picosecond microphotography 78−42828
low-power, critical focusing, use of auxiliary telescope 80−13165
microfilm camera, DA 5 DOKUMATOR, appl. to patent information systems 79−75632
microfilm recording without after-treatment 78−21243
microslides for photomicrography 79−21833
modulation contrast optical microscope appl. 78−89533
neurosecretory cell IR photomicrography 80−30959
photomicroscopes with automatic exposure control 80−86475
photothermoplastic film, high resolution, meas. of sensitivity and transmissivity *(Russian)* 79−46022
pulsed laser stereophotography, of electrically exploded bridges 77−79190
relative legibility of text rel. to resolving power 79−21845
SEM and TEM temporal event representation by colour microphotography 79−17566
stroboscopic method for picosecond diagnostics of rapid processes 78−47159
TEM coma-free alignment using optical diffractograms 79−21860
transparent material, small particle impact, high speed photomicrographic recording of shock wave 78−44342
TV microscopy and cinephotomicrography with Zeiss Axiomat 80−27343
TV photomicrography using planimeter and trinocular microscope 79−71523
vesicular film, contact printing density determ. by densitometer meas. 77−53995
Vickers M85/M86 microdensitometer, film holder 79−21832
zero order diffraction microimage reproduction from surface relief gratings 79−17518
AgBr vacuum evaporated thin films, sensitometric obs. 78−78010
V foil, air-oxidised, reversible switching, mechanism determ. 79−28387

microphotometers *see densitometry; photometers*

microprobe analysis, electron *see electron probe analysis*

microprobe analysis, ion *see ion microprobe analysis*

microprocessor chips
4 bit, one-chip, charact. *(Slovenian)* 79−181
horological microprocessor, design and circuit architecture, functions *(French)* 80−90822
programmable fast logic unit 80−52842
speech synthesis microprocessor 80−91983
three-coordinate measuring machine, dynamic acquisition and automatic reduction of data 79−75507
US nondestructive inspection system, microprocessor utilization 80−71845

microprocessor systems *see microcomputers*
microprocessors *see microcomputers; microprocessor chips*
microprogramming
see also computer architecture
high energy physics and microcircuits 79−89572
microprocessor multichannel analyzer laboratory project 80−101685
Proteus, advanced signal processor system 77−65648
software for microcircuit systems 79−89573
micropulsations
0.005 to 0.5 Hz pulsations and concurrent precip. pulsations, obs. near College, Alaska 77−53307
5-50 mHz pulsations, correl. with interplanetary field 77−29590
1977, August to October, geomag. activity assoc. with solar McMath region 14943 79−48625
activity related to substorms and cosmic noise absorpt. 80−72727
artificial generation by heating of ionosphere with strong radiowave 77−29541
auroral and solar flare effects on long-period pulsations 78−28424
auroral luminosity rel. to geomag. field changes 80−77187
bounce resonances, nonlinear attenuation of pulsations 79−62681
boundary layer, hydromagnetic waves as origin of mag. pulsations 80−105133
complex demodulation for nonstationary data anal. *(French)* 79−70922
complex representation of polarised signal rel. to ULF wave anal. 77−53236
conductivity anomaly near Exeter, effect on micropulsations 79−53305
continuous (Pc 3,4) pulsations in European sector, high resolution study 80−21877
daylight hemisphere Pi at low latitude, coincident with Pi2 of local midnight sector 80−77232
Earth-ionosphere waveguide, geomag. disturbances propag. 77−17157
electron flux modulations rel. to geomagnetic pulsations 78−16247
EM variations propag. parameters determ., appl. to pearls 77−13183
evening magnetic pulsations in auroral zone during substorm 77−25884
frequency shift relative to modulated VLF emission 80−77229
geomagnetic field line forced oscills. due to ionospheric cond. change 79−48623
geomagnetic transfer functions at pulsation periods 80−72417
high latitude, time of flight calcs. 79−62688
high-latitude Pc1-2 in rel. to dayside polar cusp 80−51623
horizontal propagation, from EM obs. 78−49231
hydromagnetic oscillations coupling modes in non-uniform finite press. plasmas, rel. to geomag. pulsations 79−21108
hydromagnetic pulsations, rel. to mid-latit. modulation of ionosphere electron fluxes and VLF emission 79−12335
interplanetary medium affecting pulsations 80−77228
ion flux ULF oscillations during Pc 4, 5 80−72707
ionosphere, geomag. pulsations damping 78−49218
ionosphere control of micropulsations obs. at ground 80−77207
ionosphere propagation of Pc 1 pulsation signals 80−51604
ionospheric disturbances effects on mag. pulsations propag. 77−25819
ionospheric internal gravity wave effects 78−45143
ipc1 props rel. to location of dayside cusp 78−20586
IPDP field fluctuations and proton precipitation, simultaneous obs. 80−77238
IPDP pulsation polarisation, correl. with particle precipitation 80−51612
IPDP pulsations, assoc. source movements 79−25404
IPDP source regions and resonant proton energies 79−53673
latitude dependence of Pc pulsation periods 80−101502
latitude dependence of power spectra, ssc and si excited near L=4 80−51619
latitude-dependent waves and impulse-produced waves 77−49245
long period, magnetospheric magnetoacoustic waves generation by high-freq. turbulence 77−13187
long-period, correl. of ground-based and satellite obs. 78−28423
long-period, global electric circuit model 80−41646
long-period geomag. pulsations, synchronous obs. on ATS-6 satellite and at Earth surface 79−12345
long-period geomagnetic oscillations, magnetosphere energetic particle fluxes modulation 79−25407
long-period geomagnetic pulsations, appl. to magnetosphere day cusp dynamics tracking 79−53656
long-period hydromagnetic waves, substorm-associated, longit. extent meas. 78−40772
long-period pulsations at midlatit. rel. to interplanetary mag. field parameters 77−29583
low-frequency pulsations in polar cusp, possible generation mechanism 79−53657
low-frequency wave packet, passage across stand-off shock front 78−45138
magnetic ULF waves over auroral arc during substorm event 80−72722
magnetosphere, Alfven wave stimulation by trapped electrons, geomag. pulsation generation *(Russian)* 77−22003
magnetosphere, effect of bounce resons. on Alfven waves generation outside plasmasphere 79−12344
magnetosphere, geomag. pulsations reson. interaction with high-energy radiation-belt electrons 78−28422
magnetosphere, geostationary satellite mag. field records appl. to plasma condensations diagnostics 79−58189
magnetosphere, increasing freq. MHD wave generation in evening sector during substorms 79−62680
magnetosphere, MHD waves orientation 79−8783
magnetosphere, particles pitch angle diffusion by bounce reson. 78−36408
magnetosphere, trapped particles self-consistent diffusion on bounce-drift reson. with geomag. pulsations 79−58188
magnetosphere hydromagnetic oscills., VLF noise intensity modulation 78−45139
magnetosphere hydromagnetic pulsations, generation by Kelvin-Helmholtz instability 78−73584
magnetosphere ULF waves, cold plasma densities meas. comparison with VLF whistlers 78−28436
magnetospheric equator, Pc 3, 4, 5 pulsations obs. by synchronous satellite 80−41647
measurement using RF SQUID magnetometer *(Japanese)* 79−5641
midlatitude pulsations, 8-25 mHz band, east-west struct. 79−62686
morphology and physical processes 80−41638
multiple onset substorms, ground signatures of expansion phase 77−17299
nighttime Pi 1 and 2 obs. on E-W axis, propag. characts. 80−98519
micropulsations continued
nonlinear theory of low frequency geomagnetic pulsations 79−40027
numerical frequency-time anal. 79−39990
Pc1 ducted propagation in upper ionosphere 77−17292
Pc3, depend. of occurrence on AE index of mag. activity *(Russian)* 77−44914
Pc3, propag. obs. 77−22004
Pc3 magnetic pulsations at synchronous orbit, statistical study of ATS 6 obs. 77−45256
Pc5 pulsation theory, consequences of ionosphere Hall current 80−105129
Pc5 pulsation theory, consequences of N. and S. hemispheres ionosphere electricity 80−109316
Pc5 pulsations, model of magnetosphere and ionosphere elec. and mag. fields 80−77234
Pc, high speed spectrum analysis method appl. 77−73896
Pc 1, 0.2 to 5 Hz, cross-correlation and cross-spectral analyses *(French)* 79−70928
Pc 1, and ionospheric absorpt. following enhanced geomag. activity 77−53332
Pc 1, atm. elec. field vertical component pulsations correl. with mag. components 78−61687
PC 1, chevron freq. struct. obs. 77−33283
Pc 1, chevron struct. 79−58193
Pc 1, classification of pulsation occurrence, and pulsation prediction 80−109317
Pc 1, determination of number of sources using cross-spectral matrix *(French)* 79−70929
Pc 1, ducted propag. in F_2-layer 77−2299
Pc 1, generating energetic particle movement and distrib. 78−61680
Pc 1, generation at plasmapause 77−87200
Pc 1, generation region location, hot and cold plasma parameters estimation 79−35064
Pc 1, intensity modulation by ionospheric waveguide disturbances 77−49233
Pc 1, ionospheric dispersion 77−64541
Pc 1, ionospheric propag. characts. 77−2298
Pc 1, longitudinal survey 77−25882
Pc 1, propagation in off meridian directions 77−64540
Pc 1, simultaneous satellite and ground obs. rel. to IPDP generation 77−25883
Pc 1, source determination using ULF goniometer techniques *(French)* 79−70890
Pc 1, source regions using ionospheric waveguide propagation data 77−25881
Pc 1 (pearls), stability of waves in magnetosphere 78−12051
Pc 1 magnetic pulsations, statistical study at synchronous orbit 77−25875
Pc 1 pearl event correl. with 4278 Å nightglow, Antarctic obs. 80−72664
Pc 1 pearl pulsations in equatorial region of India, study 79−25405
Pc 1 propagation, five-station network obs. 78−40769
Pc 1 propagation paths and whistler obs. rel. to plasmapause location 77−9604
Pc 1 pulsation polarisation, correl. with particle precipitation 80−51612
Pc 1 pulsations, problems in appl. of spectral-temporal anal. 77−13188
Pc 1 pulsations, relation to interplanetary plasma flow struct. 78−45142
Pc 1 stimulation by controlled VLF transmissions 77−49239
Pc 1-2 wave obs. in outer magnetosphere 80−12618
Pc 1b, isolated bursts, at high latits. 79−53664
Pc 2-3, with modulated amplitude, depend. on solar activity 78−69620
Pc 2-4, Borok B-index as probe of interplanetary mag. field 77−29589
Pc 2-4, extramagnetospheric origin theory 77−13185
Pc 2-4, period rel. to magnetopause position 77−91375
Pc 2-4 pulsation excitation, numerical study 80−77227
Pc 3, 4 activity, correl. with interplanetary mag. field orientation 77−25870
Pc 3, 4 characteristics from digital dynamic spectra 77−64547
Pc 3, nonmagnetospheric origin theory 77−60548
Pc 3, obs. in conjugate areas around L=4 77−45260
Pc 3, space-time distrib. near plasmapause 77−49237
Pc 3 and 4, Dodge satellite and ground-based obs., correlated effects 80−12617
Pc 3 and 4, evidence for control of pulsations by solar wind vel. 78−7837
Pc 3 and 4 spectral analysis rel. to dayside plasmapause position 80−56681
Pc 3 and energetic electron precipitation 80−8493
Pc 3 and Pc 4 activity rel. to interplanetary mag. field orientation hourly distribs. 79−75046
Pc 3 magnetic pulsations, synchronous orbit obs. and assoc. interplanetary mag. field conditions 78−28438
Pc 3 micropulsations, theory with orthogonal curvilinear coordinates 79−80097
Pc 3 micropulsations observed by whistler-mode transmissions in VLF (6.6 kHz) 79−8781
Pc 3 obs. at synchronous orbit by ATS 1 77−87194
Pc 3 pulsations, characts. of spatial distrib. at Earth surface 79−53659
Pc 3 pulsations, modulation by solar surface oscills. 79−8777
Pc 3 pulsations in magnetosphere, obs. by new space-borne ring-core type magnetometer *(Japanese)* 80−94671
Pc 3 to 5 nightside pulsations origin, Alfven waves excitation by bouncing electron beams 80−4203
Pc 3-4, effect of doubling period in vertical elec. component meas. in air 77−41270
Pc 3-4, rel. to solar wind pulsations 78−65476
Pc 3-4 activity, interpretation of depend. on solar wind vel. 78−73585
Pc 3-4 and Pi 2, synchronous obs. at meridional and latitudinal stations 78−28425
Pc 3-4 pulsations, generation outside magnetosphere 77−33310
Pc 3-4 pulsations, geomag. conjugacy with quasi-periodic ELF-VLF emissions 80−67475
Pc 3-4 signals, correl. with interplanetary mag. field orientation and solar wind vel. joint distrib. 79−53672
Pc 4,5 geomagnetic pulsations generation, influence of bounce effects 80−4197
Pc 4, in plasmasphere, meridional characts. 79−5716
Pc 4, satellite meas. of Poynting vector of standing MHD waves 78−45162
Pc 4 compressional pulsation, obs. by three satellites in geostationary orbit near local midnight 79−80094

micropulsations continued
Pc 4 giant pulsations in morning sector, magnetometer obs. 80−26690
Pc 4-5, effects on Doppler shift of ducted whistler mode signals 78−4040
Pc 4-5, longit. phase vars. 78−88993
Pc 4-5, spatial characts. 77−49244
Pc 4-5 pulsation band, phase correl. of riometer and magnetometer data 80−82147
Pc 5, 180-300 s period range, characts. 77−78576
Pc 5, activity in morning sector rel. to auroral westward electrojet 78−61685
Pc 5, in morning sector, generation mechanism 78−61686
Pc 5, in outer magnetosphere, HEOS-1 data survey 77−2307
Pc 5, morphological features at Choutuppal, India 79−66885
Pc 5, quiet-time pulsation events (Spacequakes), origin in outer magnetosphere 79−40025
Pc 5, storm time, obs. at synchronous orbit, correl. with partial ring current 78−45163
Pc 5, substorms morphological features at high latits. 78−49232
Pc 5 event, 1972 Aug. 4, incoherent scatt. radar obs. of ionospheric response 77−33264
Pc 5 generation mechanism in morning sector, comments 79−84595
Pc 5 oscillations, storm-associated, prod. by Alfven and compressional waves coupling 78−89001
Pc 5 pulsation power depend. on cond. vars. in morning sector 79−62687
Pc 5 pulsations, characts. at Indian equatorial station, Trivandrum 77−91379
Pc 5 pulsations, features during solar cycle 78−36406
Pc 5 pulsations, Stare auroral radar obs. 79−96862
Pc 5 pulsations recorded in auroral regions, Earth induction effects on vertical polarisation 79−12355
Pc 5 waves, latitudinal struct. by satellite obs. 80−51621
Pc 5 waves, OGO-5 obs., ground-magnetosphere correl. 77−9623
Pc 5 waves in magnetosphere, particle flux modulations Ogo 5 obs. 77−87190
Pc 6, ground-based polar station obs. 77−73907
Pc micropulsations, reson. theory examination by anal. of mag. fluctuations in magnetosheath and magnetosphere 79−80092
Pc polarization states, detection 79−74966
Pc pulsations, connections with interplanetary mag. field 78−85773
Pc pulsations, effect of the interplanetary mag. field *(Hungarian)* 79−25544
pearl pulsations, stimulated excitation in near-Earth plasma by pulsed radio emission 79−58192
pearl type, analysis rel. to ion cyclotron waves in magnetospheric plasma *(Russian)* 79−55490
pearls, nonlinear evolution, role of proton injection processes 79−35065
peninsular method for ULF generation in iono- and magnetosphere 80−90247
perturbation magnetic fields and current systems associated with eastward drifting auroral structures 79−75009
Pg, obs. in northern auroral zone and lower latit. conjugate regions 79−29940
Pilc pulsations (auroral radiation), theory of generation 79−75051
Pi2, morphology of spectra 77−87209
Pi2 propagation at low latitude, longitudinal range 80−51624
Pi3, long-period irregular mag. pulsations, reviews 78−45164
Pi 1, Pi 2 pulsations rel. to fluctuations of auroral zone current system 77−87188
Pi 1 in mid-latitudes rel. to interplanetary geomagnetic field sector structure *(Russian)* 78−12066
Pi 1 to 2, appl. to geomag. induction study of seismically active fault along SW Japan Sea coast 80−26475
Pi 1-2 on dayside cleft field lines 77−87206
Pi 2, 1971 Dec. 24 and 1972 Jan. 4, high latit. obs. 78−28448
Pi 2, attenuation along meridional profile 78−28426
Pi 2, attenuation rel. to ionospheric conductivity 78−45101
Pi 2, coincident precipitating electron intensity modulation in auroral zone 77−60539
Pi 2, complex demodulation appl. 79−84588
Pi 2, during magnetosphere substorms rel. to plasma.sheet radial dynamics 77−25871
Pi 2, harmonics in power spectra assoc. with plasmapause 77−25885
Pi 2, latitudinal profile from five-station synchronous records 80−105125
Pi 2, low-latitude, use as sensitive indicator of magnetospheric substorm 77−9626
Pi 2, lower ionosphere total cond. vars. effect on propag. 78−40730
Pi 2, mid-latitude secondary resonance 79−35061
Pi 2, night time, seasonal vars. at Kodaikanal 78−85772
Pi 2, rel. to plasma sheet modes 79−66875
Pi 2, spectral components latit. var. in auroral zone 77−64546
Pi 2 and high-freq. enhancements, simultaneous ground and satellite obs. 80−105136
Pi 2 as indicators of magnetospheric substorms, onset and intensification 79−88552
Pi 2 event, long-period, assoc. with mini-substorm, 1978 December 11, Jikiken satellite obs. *(Japanese)* 80−94653
Pi 2 parameters vars. during substorm development 77−25864
Pi 2 pulsations, equatorial, fine struct. 80−72721
Pi 2 pulsations, initial movements arrival at conjugate stations 80−31173
Pi 2 pulsations, polarisation characts. and phase differences at conjugate stations 79−21107
Pi 2 pulsations, substorm-related, coincidence with kilometric radiation enhancement, JIKIKEN (EXOS-B) satellite obs. *(Japanese)* 80−94648
Pi 2 pulsations and magnetospheric substorms assoc. mechanism 77−22018
Pi 2 pulsations and simultaneous ionospheric oscills., hydromagnetic wave theory 77−9615
Pi pulsation at high latitude, rel. to plasma convection 80−77226
Pi pulsations, assoc. with VLF radio waves phase anomalies in midlatitudes 80−56671
Pi ULF waves generated by magnetosphere-ionosphere current system 80−85819
PiB magnetic pulsation during substorm 80−72723
planetary pulsation indices of geophys. activity 79−40041
plasmapause, correlated electron precipitation and magnetic IPDP events 78−28388
plasmapause afternoon sector, simultaneous ULF and strong riometer absorption events 77−25849
micropulsations continued
plasmapause electric field variation from pulsation-pearl method, effect of substorm phases 77−25848
plasmapause props. and struct. rel. to micropulsations 77−25846
plasmapause region pulsations, elec. field obs. 80−85814
plasmasphere, parameter determ. from geomagnetic pulsation amplitudes 77−25847
plasmasphere struct. from geomagnetic pulsation data 77−45257
power spectra and Stokes vector representations of LULF micropulsation states 80−51608
precipitating electron flux modulation by geomag. pulsations 77−49236
Ps 6, assoc. with magnetospheric substorm, obs. polarization, two-snake model 79−66887
Ps 6 magnetic disturbances, seasonal and diurnal var. 80−67477
Psc 6, 1972, August 4 obs. in dayside polar region 77−73908
pulsations of decreasing period, relation to D_{st} vars. field 79−53655
quasiperiodic, correl. with solar proton flares *(Russian)* 78−69291
quasiperiodic disturbances, effect on pulsations 78−73568
recording system for mag. pulsation obs., first results from Alibag 79−88488
resonance structure in magnetosphere, multiple satellite obs. 77−33289
self-excitation and particle flux instability in ionospheric elec. field 77−49232
short period pulsations, spectra rel. to topside ionosphere low-freq. emission pulsations 79−58157
simultaneous observations of three events by geostationary satellites 78−57401
solar wind controlled micropulsations, origination region 80−85823
solar wind speed correl. with Pc 3, 4 and 5 activity 80−41665
source induced vertical components in pulsation signals 78−93052
southern auroral zone, pulsations detect. using solenoid with ferrite core 78−24384
spectra, rel. to modulation of precipitating electrons and VLF emissions 77−64511
spectral characteristics of 0.3-300 s period vars. 77−9622
structure and propagation, ground obs., rel. to magnetotelluric sounding 78−49230
ULF activity in Pc 3-4 range, correl. with interplanetary mag. field radial orientation 78−28434
ULF plasma waves in magnetosphere, high latit. ground based obs. 78−49228
ULF pulsations, meas. using pairs of electrodes inserted into trees as receiving antennas 78−32249
ULF pulsations obs. at large longit. separations, rel. to interplanetary mag. field direction 77−87201
ULF wave propag., axisymmetric guided mode sources in magnetosphere model 80−77231
ULF waves analysis, techniques using spectral matrix 77−13137
variable period pulsations in polar cap, props. and generation mechanism 77−25863
VLF quasiperiodic emissions interaction with micropulsations, model 78−61682

microrecording *see microphotography*

microreduction *see microphotography*

microscopes
see also acoustic microscopes; electron microscopes; ion microscopes; optical microscopes
cryogenic scanning microscopy 80−79080
Doppler microscope for flow velocity meas. in areas $<10\ \mu$ dia., signal-analysing system *(Japanese)* 78−22441
grazing incidence optics, total transverse aberration function 78−45765
grazing incidence X-ray microscopy, of laser fusion targets 78−47178
high resolution X-ray optics, for astronomical and laboratory sources 78−45766
intelligent microscopes, recent and near-future advances 80−98166
introduction to microscopy by means of light, electrons, X-rays and ultrasound, book 79−49283
Kerr magneto-optic microscope and measuring system 78−58023
scanning, imaging theory for Gaussian pupil functions 79−35820
scanning acoustic, operation and appl. 77−84095
segmentation method of detecting cellular images using colour information *(Japanese)* 78−11783
single line CCD camera to improve positioning 78−41347
X-ray, aplanatic grazing incidence, design and performance 77−18147
X-ray, axisymmetric grazing incidence, for laser fusion diagnostics, imaging characts. 78−75422
X-ray holographic microscopy *(Russian)* 78−12799
X-ray imaging, conf., Reston, USA (Apr. 1977) 78−45762
X-ray imaging, MOS solid-state detector arrays 78−47180
X-ray microscope, with high time resolution X-ray streak camera *(French)* 78−42823
X-ray microscopy of biological specimens, flash X-ray method 80−51310

microscopy
see also electron microscopy; ion microscopy; optical microscopy
aggregate phase contents, sampling in quantitative image analysis *(French)* 77−28961
apodised condenser, effects on microscope imaging of extended objects, annular source 78−280
bibliography, equipment, methods, applications and related topics 80−73124
bibliography 80−90619
bibliography of equipment, methods, appls. and related topics 80−105450
bibliography of microscopic equipment, methods, appls. and related topics 80−94941
bibliography of publications on microscopic equipment, methods and appls. 80−62406
biological materials, unmodified, transmission microscopy radiation dose with electrons vs. ultrasoft X-rays 78−11788
biological sample microtoming, freezing technique for long specimens of small width/depth 78−3695
cell distributions topographical size analysis, TOGA interactive program *(German)* 77−40951
cell image scene segmentation technique 77−78073
ceramic building materials, high-temp. microscopy interpretation *(Polish)* 80−66743
chemical microscopy, review of literature 1976-1977 78−85221
clamp for holding and stretching fibrous sheet microscope specimens 77−26396

microscopy continued
edge effect in numerical density estimation of arbitrary profiles 78−58024
equipment, methods, appls. and related topics, publications 79−75566
Fourier transform, IR spectroscopy, microscopic technique for sub-ng level anal. 78−32901
grid handling, of semi-thin sections of GMA-Quetol 523 embedded tissue, with reference to O_3O_4 78−92766
holographic interferometric microscopy, appls. 77−34015
image analyser control, diode matrix replacement by PROMs 77−22539
introduction to microscopy by means of light, electrons, X-rays and ultrasound, book 79−49283
IR, NDT wire bonds on Si chips 78−95867
IR light scattering, and absorpt. microscopy study of dislocations in GaAs 80−107249
liquid crystal, optical characterisation apparatus 77−7222
lung tissue stereological parameter computer anal. 78−73280
membrane thickness distrib. determ. from orthogonal intercepts 79−74804
metal, laser irradiated, evidence of melt using Nomarski microscopy 79−69819
molecular microprobe using laser, MOLE 77−60141
NMR determination of phys. and biological struct. *(Rumanian)* 78−49874
particle size distributions, statistical reliability 77−53858
planar particle aggregates, sampling by quadrats 79−17485
polyethylene-polypropylene blend, size distribution determ. of spherical occlusions from photomicrographs *(Czech)* 80−89539
powders microscopic quantitative analysis 80−22475
projection microradiography, historical development and applications 80−37138
publications concerning microscopic equipment, methods, appls. and related topics 80−22167
quantitative, appl. of statistical methods, review 79−17484
scanning X-ray projection microscopy, using energy dispersive spectrometer 79−17593
soft X-ray microscopy and lithography using synchrotron radiation 78−66018
stereological method for estimating relative membrane surface area 77−64158
stereological method for rapid volume ratio estimation 79−80571
stereological methods in neurobiology, recognition and classification of struct. 77−64159
stereology, conf., Gaithersburg, USA, (Sept. 1975) 77−61055
stereology, estimation of linear functionals by max. likelihood 77−61056
teaching, course at North Carolina State University 80−95135
thermistor bolometer failure anal. appl. 78−24795
UV, with image intensification and TV image displays 77−5888
X-ray, high resolution, with synchrotron radiation, for chem. microanal. 80−81416
X-ray 10 nm resolution, development *(German)* 77−38077
X-ray microscopy, coded imaging techniques, of laser fusion plasmas 78−47177
X-ray microscopy, possibility of utilizing holographic schemes 79−36861
X-ray microscopy and X-ray lithography, techniques, appls. 77−34059
X-rays, ultrasoft, potential operating region for biological materials 77−90972

microstructure, crystal *see crystal microstructure*

microtext *see microforms*

microtomes *see laboratory apparatus and techniques*

microtrons
22 MeV, for radiation therapy, design, beam transport, gantry and depth doses 77−81552
30 MeV microtron, appl. to metals radioactivation anal. 77−66720
booster resonator in HF path 78−830
cascaded 800 MeV normal conducting CW race track microtron, design 77−6583
Catania 13.5 MeV microtron facility, photofission experiments 79−41050
cathode focusing and drift apertures, hybrid computer calc. 78−21796
electromagnet optimum shape, computer numerical anal. 77−18718
electron 60 MeV CW accelerator using conventional standing wave linac 77−38507
electron beam, extraction and transportation system 77−65061
electron CW 820 MeV normal conducting accelerator 77−38503
electron injection and capture processes, digital simulation 77−18717
electron orbit, correction scheme 77−65366
electron phase motion, accelerating field higher harmonics influence 80−106212
high-frequency path, simplification of construction 77−65367
Mainz microtron project, MAMI A status report 80−23197
modulator, thyristor, circuit and construction 80−63422
MUSL-2, second microtron using superconducting linac 77−83198
MUSL-Z, 6 pass microtron using superconducting linac, operating experience 80−23196
NDT application in industrial products inspection 80−81267
neutron flux distribution from microtron convertor in graphite moderator with water reflector *(Russian)* 77−82979
race track, beam blowup anal. 79−76217
race track, review of photonuclear research at Lund and future accelerator plans 77−82907
racetrack microtron, electron in line injection using annular cathode electron gun 77−3193
racetrack three cavity variable energy microtron with intra-sector beam focusing 77−65369
radial motion, inhomogeneity mag. field effects 79−45487
for radiographic testing, of thin-walled reactor vessels, sensitivity 78−70603
shuttle design, electron and X-ray therapy unit 77−83188
split 25 MeV microtron linear electron accelerator 77−23319
split microtron injector for Pakhra synchrotron 77−83136
stereomicrotron, construction and appls. 77−65064
thyristor modulator with periodically interrupted supply, microtron appl. 78−55061
tuning of coupled-cavity structs., nondimensional 80−32546
UHF microtron system with ferrite gate, frequency responses 77−46430
voltage control system using thyristor convertors 77−14280

microwave acoustic devices *see acoustic microwave devices*

microwave amplifiers
see also masers; microwave parametric amplifiers
cyclotron-resonance maser amplifier with freq. conversion 78−55329
gyrotrons for high power millimeter wave generation, fusion reactor appl. 78−62611
negative energy waves and anomalous Doppler effect, illustration of analogy 77−65881
preamplifier, for ESR/ENDOR spectrometer sensitivity enhancement 78−82014
superconductor-semiconductor contact amplification props. 79−7941
Very Large Array multiband low-noise receivers 77−41299
YIG-semiconductor coupled system, magnetostatic surface wave amplification, ferromag. loss 77−85434

microwave antenna arrays
array antennas, radiometric earth and atmospheric sensing systems for large structure 77−41281
miniature dipoles, probe for 0.2 to 12 GHz with fibre optic telemetry system, microwave radiation effects obs. appl. 78−15859
probe for subsurface soil moisture profiling 78−65939
satellite, power transmission system design for solar power system 79−52893
solar power satellite, appl. of solid state microwave technology 80−40870
solar power satellite ground station rectifying antenna, basic design concepts 80−16782
solar power satellites microwave power transmission system rectennas, Yagi-Uda receiving elements design, characteristics and economics 80−66938
tumour irradiation using focused array system 80−21521
Very Large Array multiband low-noise receivers 77−41299
Very Large Array waveguide transmission system for radiotelescope 77−5444
waveguide slot array with const. intensity for biological effects research 78−40450

microwave antennas
see also waveguide antennas
aperture efficiency of 6m mm-wave antenna *(Japanese)* 78−89061
atmospheric water vapour and liquid monitoring using radiometry at 21 and 32 GHz 80−26628
biomedical system, invasive, for locally-induced hyperthermia for cancer therapy 80−67193
cancer treatment appl. of microwave arrays for localised tumour heating 80−94308
cancer treatment by local microwave hyperthermia system 79−83893
coherent microwave imaging of limited fields of view, angular and aperture noise, optimum procedure 77−67045
Damping antennas for spurious RF-modes in electron-positron storage rings 78−70659
dielectric spherical radiator, horn-fed, near field characteristics 77−56543
dish antenna, modified for acoustic remote sensing, charact. 79−72770
EM field probe, miniaturised antenna 79−26136
exact time signal transmission using artificial satellites 77−79069
GEOS, IUE and METEORSAT Earth Station antennas, design, charact. *(German)* 77−56764
hemispherical antenna as microwave plasma probe 78−67438
horn aerial directional diagram, 3.2 cm, circular scanning indicator *(Russian)* 77−26328
IR and submillimetric-wave antenna design and simulation 79−30552
microstrip antenna for biomedical applications 80−89826
microstrip antennas for biomedical applications of microwaves 80−3762
microstrip slot radiator for medical appls. 80−108994
open-structure submillimetric-wave mixer props. 79−30551
plasma, focusing hog-horn antenna for microwave diagnostics in plasma machines 80−96395
radiation of cranial structure model, heat potential distrib. 79−2105
radiation pattern peculiarities in plasma *(Russian)* 78−38504
radiotelescope, quasi-optical diplexer for mm wavelength 79−21187
satellite, solar power conversion for Earth-based utility appl., 5 GW, using GaAlAs cells 79−52892
Schottky-barrier diode monolithic detector dielectric plate antenna 79−30548
semispherical monopole, immersed in plasma electrons, input admittance thermal noise *(Russian)* 77−76196
side-looking airborne radar, Earth surface remote sensing appl. 78−20561
slotted cylinder antenna, for HF tumor therapy 79−34629
solar power satellite design, use of nomograph 79−70433
spin wave excitation in ferromag. films by antenna field 80−44816
transponder dipole antennas in and near three-layered body 80−98181
water immersed, biological targets internal microwave interrogation 79−34623

microwave circulators *see circulators (microwave)*

microwave detectors
active microwave sensing of atmosphere *(Japanese)* 78−16213
active microwave sensing of Earth surface *(Japanese)* 78−16214
active microwave sensing of ocean surface phenomena *(Japanese)* 78−16215
active microwave systems for remote sensing 77−56776
airborne millimeter-wave radiometer, multi-channel, dual frequency, high altitude obs. of atmospheric water vapour 79−80061
airborne remote sensing, using 4.5 to 7.2 GHz stepped-frequency radiometer 79−80062
automatic nulling radiometer for the 3-4-mm band 80−18016
breast cancer 30 GHz and 68 GHz telethermography *(French)* 80−3765
cholesteric liquid crystal visualisation of microwave fields 78−58031
circular scanning indicator for 3.2 cm wave expts. *(Russian)* 77−26328
cm-wave radiometer, with enhanced long-term stability, for solar radio emission obs. 80−109361
conference, Zurich, Switzerland (Mar. 1979) 80−4783
discontinuous metal film millimetric-wave and IR detectors *(Japanese)* 77−49771
Earth resources, remote sensing by Skylab microwave radiometer 78−16273
EM field probe, miniaturised antenna 79−26136
far IR technology and applications, conf., Reston, USA, (Apr. 1977) 78−45711
Faraday effect in lightguide, weak microwave field meas. 80−73463

microwave detectors continued
ferromagnetic resonance probe, for eddy current detection of surface flames in metals 79−34254
glow discharge detection, gas breakdown theory 78−58035
glow discharge plasma lamp detector design, for real-time microwave holography 78−37859
glow discharge tube, EM MM-wave detection properties in mag. field 80−70059
heterodyne receiver, meas. of electron cyclotron emission from hot plasmas 79−90463
InSb subMM detector, fast response, for use in measuring electron cyclotron emission 80−27347
IR and mm wave techniques, for Cosmic Background Explorer Satellite 78−49344
Josephson contact microwave detector sensitivity and cutoff frequency rel. to capacitance 78−49902
Josephson contacts, quasi-autonomous, props. 78−88084
Josephson junction, discriminating props., use in microwave spectral anal. 77−49748
Josephson junction, externally pumped, singly and doubly degenerate microwave parametric amplifiers 79−26122
Josephson junction detector of microwave and far IR radiation, response 77−61119
Josephson junctions, applications in plasma physics 80−103194
Josephson junctions, mixing in the FIR 79−26121
Josephson junctions mounted in a waveguide, wide-band detect. characts. 80−4767
Josephson mixer receiver, at millimetre and long submillimetre wavelengths 77−34027
Josephson mixers, mm wave, using Nb point contacts 79−26123
Josephson mixers for heterodyne reception at submillimetre wavelengths present expt. status, future developments 79−26120
Josephson self-oscillator mixer 77−34026
Josephson video-detector, optimisation for mm wavelengths 80−4768
Josephson-effect differential heterodyne receiver, freq. conversion at 0.4 mm wavelength 79−26125
Josephson-effect mm wave superconducting devices, present status 79−26119
liquid crystals, thermooptical effects used to visualise EM fields 80−62723
lossy waveguide attenuation and phase meas. 77−26343
low-level microwave power detector 79−54189
microbridge SUPARAMPs, phase instability noise in Josephson junctions 79−26124
millimetre wave detector using the pyroelectric effect of PVF_2 *(Japanese)* 78−8444
millimetric and IR discontinuous-metal-film detector 78−289
MIM discontinuous metal film, fast detector for MM-wave through optical freq. range 77−18092
MIM tunnelling diode, detector performance, IR and microwave freqs. 79−12844
MM wave detector using ohmic diode *(Japanese)* 80−73464
mm waves video detection by capsule type point-contact Josephson junctions 80−13141
moisture meas. of granular and powdered materials *(Polish)* 78−12706
Nimbus 5 microwave spectrometer for atm. H_2O vapour and liquid remote sensing 77−49129
nonlinear tunnelling devices, photon detection, theory 79−6177
open-structure submillimetric-wave mixer props. 79−30551
PAM microwave field dosimetric device 80−3818
passive microwave radiometers for remote sensing 77−56775
photon detector for subMM wavelengths using Rydberg atoms 80−77867
plasma detector system for gas chromatography/emission spectroscopy in environmental pollution studies 80−26070
plasma detector-gas chromatograph, appl. to atmospheric alkyl Pb and Se compounds detect. 78−68975
point contact, in wide-band radiometer for short millimetre range 79−62750
point contact microwave detector/receiver 77−79153
point-contact diode, submillimetre wave detection, sensitivity detn. 77−37984
probe fibre optic telemetric linked, 0.2 to 12 GHz range, microwave effects obs. appl. 78−15859
PVF_2 pyroelectric device for homodyne MM wave detect. at 100 GHz, high-sensitivity *(Japanese)* 79−97432
pyroelectric detectors for submillimetre waves 79−30545
radiometer, microprocessor-based signal processing unit 80−77874
radiometer, recognition of coherence 77−74505
radiometer design with orthomode type mixer, radioastron. appls. and 1.35 cm range 79−2817
radiometer for rain attenuation measurements at X, K bands, communication appl. 80−68254
radiometers for remote sensing of Earth *(Japanese)* 78−16212
receiver design principles 78−45714
remote sensing, sensors and detectors in NASA's future mission 79−5656
remote sensing from space, synthetic-aperture radar systems and Spacelab expts. 80−36409
Rydberg atom microwave and far IR spectroscopy 80−63564
satellite scatterometer, SEASAT-A, determ. of sea-surface wind stress using algorithm 79−39883
satellite-borne, active and passive, remote sensing of Earth physical parameters 79−80060
Schottky barrier diode, submillimetre laser Thomson scatt. system for plasma diode 77−84526
Schottky diode, monolithic, submillimetre wave, printed resonant antenna 77−34025
Schottky diode concepts, heterodyne radiometry 78−45713
Schottky-barrier diode, for submmillimetre heterodyne detection 77−37983
Schottky-barrier diode, sub-micron size, for submillimetre wave detection 77−34024
Schottky-barrier diode, submillimetre heterodyne detection 77−34028
Schottky-barrier diode monolithic detector dielectric plate antenna 79−30548
self-oscillating Josephson mixer as submillimetric and far IR detector 77−38004
semiconductor, with superlattice, heating photocond. 79−19622
semiconductor superlattice microwave/infrared detectors 80−13138

microwave detectors continued
solar emission, harmonic generation and mm waves mixing for receiver *(Italian)* 77−49292
spectroscopy, analytical, instrumentation, automation, review 77−56260
strip line coupled Josephson junctions, microwave response *(Japanese)* 77−69454
subcutaneous temperature meas., for thermoregulation obs., using passive microwave sensors 79−34721
submillimeter wave heterodyne detection, with a laser LO 78−70183
submillimetre wave heterodyne radiometry, for upper atm. comp. meas. 78−49183
submillimetric Josephson mixer receivers, potentials and limitations 77−38003
submillimetric radiation, heterodyne vs. direct detection receivers 77−38006
submillimetric wire grid array Fabry-Perot interferometers 77−37974
subnormal glow discharge detection of microwaves, internal signal gain 78−16843
superconducting, space appl. 80−85836
superconducting tunnelling devices as mm wave photon detectors 79−30554
superconductivity, space applications 80−41694
superconductor-insulator-superconductor quasiparticle tunnel junctions, as microwave detectors 80−65744
superconductor-metal point junction as microwave radiation detectors 78−16847
thermoelectric, using hot carrier semicond., reactive props. and equiv. cct. 77−10109
thermography, principle and biomedical appls. *(French)* 80−30957
thermophotoindicators based on cholesteric liquid crystals, analysis of diffuse light spectra 80−73457
TIROS-N microwave sounder unit for global temp. distribution meas. 80−90265
tunnel junction mixers, quantum limited detection 80−18015
wide-band mechanically stable quasi-optical detector for 100-300 GHz 79−67382
X-band, natural emission detection, biological, medical appl. 77−32949
n-GaAs/N-GaAlAs heterojunctions, microwave detection 79−54186
Ge and Ge-diamond bolometers operated at 4.2, 2.0, 1.2, 0.3, 0.1K, design and construction 80−77868
Ge photon-drag detector submillimetric-wave performance 79−30547
n-$Hg_{0.8}Cd_{0.2}Te$, microwave bolometer heterodyne receiver based on magnetic field induced phase transition 80−13135
$Hg_{1-x}Cd_xTe$ hot-electron photoconductive detection of near mm wave radiation 80−57377
In-In_2O_3-Pb, Josephson tunnel junction fabrication for MM-wave detector 80−100427
In-In_2O_3-Pb, tunnel junction fabrication for MM-wave detector 80−100427
InP Schottky-barrier diodes appl., operation in submm. wave region 80−105707
n-InSb electronic bolometer, appl. in system for millimetre and submillimetre wave detection 78−24860
Nb_3Sn, nonstationary Josephson effect, 13-18.3K, 9-10 GHz, 20 MW *(Russian)* 78−2631
Pt-Pd discontinuous film MIM point-contact diode detector 77−5917
Si-W point diode, sub MM band, optimisation of operating conditions 79−89006
TiO_2:Fe^{3+}, microwave second harmonic generation and freq. conversion 80−50166
VO_2, film, visualisation of microwave and IR radiation 80−5839

microwave devices
see also acoustic microwave devices; circulators (microwave); Gunn devices; masers; microwave parametric devices; solid-state microwave devices; waveguides
4-port, transmission charact. utilizing total reflection, wave transmission matrix *(Czech)* 80−37937
accelerator, linear, transient behaviour of high-current relativistic electron beam 80−32541
applicator, rapid thermal fixation of murine brain 78−92689
cavities, Q-factor meas. by analytic method using reflection coeff. vs. freq. 80−98937
cavity resonator, automatic monitor of resonant freq. and bandwidth 77−22567
coaxial microwave cavity for improved EPR sensitivity with loss solvents 80−62705
conference, IR and MM waves and appls., Miami Beach, USA (Dec. 1979) 80−57009
conference on magnetism and mag. materials Cleveland, USA (Nov. 1978) 79−73651
diathermy 2.45 GHz direct-contact applicator 79−2122
diathermy applicator for irrad. of rat brain 80−94425
diathermy dielectric-loaded applicator, 915 MHz, for therapeutic heating of tissues 79−2120
diathermy direct-contact applicator, 915 MHz, for human deep-tissue heating 79−2121
dielectric irradiated by microwaves, near-field theory 79−41288
diffraction grating, two-layer asymmetrical for SHF, characts. *(Russian)* 77−54649
electro-optic microwave modulator, broadband electronically tunable, for CO_2 lasers 79−64256
electron beam switch, microwave energy compression 80−96396
ENDOR cavity for electron spin echo experiments 78−82013
EPR cavity sensitivity improvement 78−54419
ESR dual sample cavities for Q-band and spectrometers with small magnets 79−58761
exposure system for marine animals, dosimetry and reflectometric obs. 80−56319
Fabry-Perot type microwave wideband open resonator 77−57351
ferrite devices, fundamentals of operation 78−88548
flowmeter, Doppler-effect type, particle moisture content effects 78−9732
gas discharge source for production of supersonic atom and free radical beams 79−80720
Gaussian beam launcher, focal region field aberrations, biomedical appl. 78−44580
Gaussian-beam launcher for producing focused exposure field, biomedical appl. 77−40728
generator for induced hyperthermia in small animals 79−2118
heating device, for automatic analysis system 78−88666

microwave devices continued
interferometer, freq. stabilized, laser prod. plasma density decay meas. 77−84524
interferometer, improved Michelson-type operating at 140 GHz 80−31854
interferometer for electron meas. on T-II plasma device 78−55754
interferometers, for biomedical appl. physiological movement meas. 79−25137
ion source, for high-current beams prod. 78−327
ion-storage microwave and optical frequency standards 79−54101
Josephson junctions in self-pumping mode of operation 80−54839
K-band interferometer for measuring the magneto-microwave Kerr effect in semiconductors and ferrites 80−52263
laser cooled ion storage frequency standard possibilities 79−54102
microwave rapid fixation device for inactivation of enzymes in rat brain 77−81761
MM wave sensors, conf., London (Apr. 1980) 80−67441
moisture content-attenuation-voltage convertor with time-domain attenuation comparisons *(Polish)* 78−70131
p-i-n diode modulator, transient plasma instability meas. *(German)* 80−87942
particle flowmeter, Doppler effect, approx. signal theory 79−94747
plasma diagnostic interferometer with fourfold signal passage 78−87487
plasma radial carrier density profiles, determ. using microwave resonators *(German)* 78−47160
plasma source, power absorpt. charcts. 77−84464
polarimeter, for 8 mm (35 GHz) band, MnF_2 Cotton-Mouton-Voigt effect *(French)* 78−74040
power source for electrodeless discharge lamps 79−36969
power symposium, Monaco (1979) 80−3758
remote sensing expt., operation in Spacelab 80−109332
resonant cavities, thermal expansion correction methods *(French)* 77−61087
respiration monitor, microwave Michelson interferometer 79−8557
SAW components fabrication process 79−32162
scanner for soft tissue tumour detect. 80−17054
scatterometer, backscatter optimisation using complex charact. polarisation concept 79−100966
scatterometer on Seasat-A satellite for ocean wind field mapping 78−73529
self-accelerating microwave ion and plasma sources 78−66000
slab line cavity for excitation of electrodeless discharge tubes 77−7166
SLAC, microwave developments, beam-test results 77−83405
Stark modulator, zero-based half-sine wave, for analytical microwave spectrometer 77−13802
tumour and normal cell anal. systems, microwave transmission and standing waves 79−2107
waveguide system for chronic exposure of small animals to microwaves 80−56318
weak field absolute induction meas. HFS magnetometer 78−77949
Wonderstone ENDOR cavity 78−70174
X-band ESR spectrometer, microwave kit for conversion to K-band operation 78−21192
X-band supercond. cavity accelerometer for gravitational wave antenna 77−30076
$Li_{0.5}Fe_{2.5}O_4$, microwave material, mag. props., review 79−33504
Nb_3Sn superconducting microwave resonator for measuring dielectric loss in polymeric solids 79−67316

microwave filters
1.2 GHz temperature stable SAW oscillator 78−59226
bandpass interference filters for 1-3 mm window 80−109368
composite bulk acoustic resonator properties and applications 77−27434
interference filter for submillimetre astronomy 80−48393
low-pass interference filters for Tokamak plasma diagnostics 80−64783
satellite communications wideband polarisation separation network with adaptive control 77−78394
waveguide TE_{on}-mode filters for VLA radiotelescope circular waveguide system 79−66922
withdrawal weighted SAW filter design from electric field interactions in finite arrays 77−23827
YIG film filter, theory of charcts. 79−42808

microwave generation
see also microwave oscillators; relativistic electron beam tubes
acetonitrile sub mm laser, generation lines identification *(Russian)* 78−82952
acoustic waves/microwave radiation fields interaction, deflection and mixing effects 79−90056
circular waveguide, microwave generation by relativistic electron beam 80−48128
coherent microwave Cherenkov radiation generation, relativistic electron beam-dielectric loaded waveguide 77−58246
coherent millimetric radiation from relativistic beam-plasma instabilities 77−39435
coherent scattering from relativistic electron beams, submillimetre wave generation 77−34798
coherent submillimetric Cherenkov radiation generated by relativistic electron beam 77−38793
coherent tunable Josephson radiation generation, 2-18 GHz, with narrowed linewidth 78−88078
cyclotron maser instability, linear and self-consistent nonlinear theory 77−38847
cyclotron maser instability, quasi-linear theory, calc. of microwave generation efficiency 80−1783
electron beam, coherent radiation when modulated in residual gas 77−594
electron beam, hollow rotating, microwave generation and suppression 77−83797
electron beam, intense, relativistic, stimulated Raman radiation spectral props. 79−64163
electron beam, relativistic, intense, subjected to rippled elec. field, stimulated Raman scatt., submm. radiation prod. 79−98439
electron beam excitation of skew comb, mm wave generation *(Russian)* 78−22078
electron beam interaction, nonrelativistic, modulated, fast EM wave conversion, in waveguide 77−84455
enzyme inactivation system, electronic control to reduce dose variability 78−40285
free electron laser, characterisation and optimisation of gain and efficiency 79−68400

microwave generation continued
free electron laser simulations using relativistic EM plasma simulation codes 79−68376
gamma ray generation of microwaves in Zn *(Russian)* 78−2939
gyrotrons for high power millimeter wave generation, fusion reactor appl. 78−62611
high power MM wave source−gyrotron *(Japanese)* 80−23654
high-power microwave generation by relativistic electron beams 78−5444
intense microwave radiation, generation by relativistic electron beam introde 80−14887
intense relativistic electron beam generation by foilless diodes, simulation 80−63438
Josephson junction, broadband tunable microwave generation 77−72944
Josephson junction, coherent microbridges coupled by external shunts, props. 79−28460
laser-microwave two-photon spectroscopic tunable source 79−30579
methyl bromide sub mm laser, generation lines identification *(Russian)* 78−82952
millimetric generation, stimulated scatt., relativistic electron beam, zero freq. pump field 77−88687
millimetric-wave high-power optically-pumped laser performance and applic. 78−5469
millimetric-wave optically-pumped laser CW performance 78−5468
mm waves using CW FIR laser, optically pumped, analysis of efficiency 79−76667
nonisochronic reflecting electron system, high power microwave emission 78−1140
relativistic electron beam, excitation of slow cyclotron and space-charge waves 79−86118
relativistic electron beam, planar, annular, high power Ka band 77−83804
relativistic electron beam device, intense, high-power millimetre radiation generated 77−83795
relativistic electron beam generated coherent submillimetre Cherenkov radiation 77−38788
relativistic electron beam in circular waveguide, radiation efficiency in periodically inhomogeneous mag. field 77−23608
relativistic electron beam in mag. field, microwave radn. 77−79735
relativistic electron beam Raman laser 78−74877
relativistic sheet electron beam interaction with slow-wave structure 77−38795
sheet relativistic electron beam application 77−34800
spectroscopy, analytical, instrumentation, automation, review 77−56260
stimulated EM shock radiation, intense submillimetre wave generation 77−38787
stimulated EM shock radiation from relativistic electron beam 77−38997
stimulated scatt. with intense relativistic electron beam and zero frequency pump 77−38995
strip line coupled Josephson junctions, microwave response *(Japanese)* 77−69454
sub-mm CW gas laser, optically pumped, scaling 78−55341
submillimetre-wave optical design approach 79−32048
superconducting microbridges in resonant cavity, enhanced Josephson radiation and linewidth-narrowing 79−56433
thermal noise source, temp. of liq. N_2 cryostat dewars 79−58700
undulator radiation, coherence, directional pattern, wavelength spread, polaris. 79−55043
undulator radiation theory, coherence, extension to short wavelengths 79−55042
upshifted reflection, from moving ionisation front, submillimetre wave generation 77−34796
X band gigawatt microwave pulse, produced by relativistic electron beam injection into waveguide *(French)* 78−25781
X-band ENDOR cavity constructed from rectangular waveguide 79−80653
Ar microwave noise sources, new similarity rules 77−55177
CdS, subMM radiation excitation by N_2 laser pulse 80−60678
GaAs devices and their use for generation and freq. conversion of microwave oscillations 80−15534
p-InSb, high resist. compensated, generation of microwave radiation 80−34476

microwave heaters *see radiofrequency heating*

microwave heating *see radiofrequency heating*

microwave holography
3D image-construction technique and appl. to microwave diagnostics 80−83565
applications and theory review, background and current status 78−74866
by rotational scanning of object 78−42302
computer simulation and image reconstruct. *(German)* 78−46540
data processing using Fermat number transform 80−43298
development in past decade, 10 to 140 GHz 79−76649
developments, review 80−23645
Fourier transform holography 77−54676
fundamentals and appl. 78−37830
image enhancement by electronic differentiation 77−19204
image field resolution, improvement using metallic screens to increase effective area 79−94198
image reconstruction using computer tomography algorithm, numerical simulation and expt. 80−58484
imaging, influence of wave polarization and surface discontinuities 80−14305
imaging, real-time camera prospects 80−53241
imaging of subsurface cylindrical scatters from crosspolar backscatter 77−88666
imaging of water waves 78−37861
imaging through aberrating media using phase-modulated reference beam 78−37860
imaging through aberrating media with phase-modulated ref. beam 78−42303
imaging through random aberrating media 77−3551
lens for holographic imaging 80−48183
long distance, space sampling signal as reference 78−87028
long-wave imaging with super-resolution by wavelength diversity 80−102675
long-wavelength hologram image reconstruction microcomputer system 78−1196
microfiche of picture like information 77−38833
MM wave systems operating at 35, 70 and 140 GHz 80−63963
multifrequency, improved image reconstruction 80−1159
multifrequency holography, close range wide band imaging 77−42505

microwave holography continued
quadratically spaced linear antenna array 80−32938
quasi-real-time inertialess recording system 77−31076
raster choice 78−74867
real-time, glow discharge plasma lamp detector design 78−37859
reconstruction of long wave holograms using photocond. controlled liq. cryst. light valve 77−79787
subtraction for imaging of buried objects 78−46543
super resolution technique in long wavelength holography *(Japanese)* 78−66787
swept-freq. techniques, expts. on two-dimensional image reconstruction system *(Japanese)* 79−98313
techniques and appls. 77−10871
two-frequency microwave holographic imaging with axial resolution 78−1184
UHF, polarisation effects on quality of images *(Russian)* 78−29907
UHF recording method *(Russian)* 78−46541

microwave induced delayed phosphorescence *see MIDP*

microwave-infrared double resonance *see optical double resonance*

microwave integrated circuits
see also hybrid integrated circuits
analysis formulas, applic. to integrated optics modulators 77−39108
microwave compatible MIC temperature electrode for use in biological dielectrics 79−88216
substrate permittivity meas. in cylindrical cavity 78−77942
thin and thick film technology, conference, Augsburg, Germany (1977) *(German)* 78−39685
$Ca_{1-y}Sr_{y/2}Ba_{y/2}Zr_{1-x}Ti_xO_3$, ceramic system, dielectric props., microwave resonator application 80−80674
GaAlAs injection DH laser and GaAs Schottky-gate FET, monolithic integration 80−58593

microwave isolators
ferrite, magnetised, nonreciprocal refl. of EM waves, rel. to phase shifter and isolater appls. 78−71006

microwave limiters
modulation radiometer, limiting pulse noise *(Russian)* 77−67497

microwave links
11 GHz forward scattering due to rain, 9 km line of sight link 77−86995
11 GHz rain attenuation data, appl. to path engineering 78−24327
11 GHz rain attenuation distribution, from 5-min rain rate statistics 78−24326
19 GHz over 35 km attenuation meas., effects of rain and multipath propag. 79−88453
20 GHz multi relay links, simultaneous probability of rain attenuation 78−3898
60 GHz rainfall attenuation, 680 m vertically polarized link invest. 78−36238
140 GHz atmospheric attenuation by rain, obs. 78−3914
atmospheric water vapour meas. over 10 years rel. to radiowave propag. 78−3857
attenuation in rain, UK rainfall studies and data 78−11965
attenuation of signals under adverse dust-storm conditions 80−46247
BWO appl., 110 to 170 GHz, using Sm-Co ring magnets *(German)* 80−105684
CETI from Earth satellite orbit 78−61758
comparison with optical communication 79−81546
computer model for atmospheric propag. conditions, 1 to 300 GHz band 79−53505
cross-polarisation on terrestrial path, wind, raindrop size and canting angle effects 79−66736
depolarisation due to snow at 11.6 GHz 78−57239
differential attenuation and phase shift meas. for 36.5 GHz polarised waves rel. to raindrops 78−3856
differential rain attenuation prediction, adjacent microwave and mm-wave links 77−87048
Earth-satellite paths, 11.5 GHz, annual and annual-worst-month statistics of fading 78−57238
exact time signal transmission using artificial satellites 77−79069
fading due to rain, snow and multipath propag. at 11 GHz 77−91206
long-term rain rate distribution estimation, extremal statistical method 77−13096
medical communications using pre-existing statewide microwave network 77−48899
METEOSAT 1 weather satellite pictures, amateur facsimile reception *(German)* 80−81982
millimetre-wave amplitude scintillation in town environment, observations 77−78302
over-the-sea propag. hops in Republic of Indonesia 80−46245
power transmission from solar power satellite, environmental aspects 79−52896
rain attenuation, estimation of duration time distribution *(Japanese)* 80−21788
rain attenuation, terrestrial radio link freq. range 10 to 40 GHz, calcs. meas. 77−70771
rain attenuation, year and worst-month rain rate distrib. estimation method 79−5648
rain attenuation distributions on Earth-satellite paths, empirical calc. 79−5592
rain attenuation estimation in UK at freqs. 10 to 100 GHz 78−73426
rain attenuation meas., microwave radio link projected design appls. *(Slovenian)* 80−46217
rain attenuation on parallel, series, and convergent terrestrial paths 79−66735
rain attenuation on terrestrial path 79−66734
rain attenuation study on terrestrial link, weather radar appl. 77−41130
rain cell attenuation of Earth-space link 80−94586
rainfall, short and long term rates, link design implications *(German)* 78−49082
rainfall characteristics across Europe 79−66733
rainfall intensity data for radio-relay system design above 10 GHz *(French)* 78−53690
RESMAC, Mexican seismic array 77−5355
satellite, crosspolarisation phase due to ice crysts. 78−7684
satellite links rain attenuation and site diversity effect, statistical studies 78−88892
satellite to Earth path, effect of rain on crosspolarization 80−21789
satellite transmission of converted solar energy, technique developments 79−24891

microwave links continued
scintillation fading meas. at 110 and 36 GHz, wavelength depend. 77−41110
SIRIO radiowave propag. data for earth-space rain-cell modelling 80−36352
slant path rain attenuation, satellite relay broadcasts 77−86988
slant path rain attenuation characteristics in 20 and 30 GHz bands 79−8678
solar power, microwave power beaming, for long range energy transfer 79−34427
solar satellite power system, microwave power transmission design 79−52893
space communications, Voyager project 80−77263
tandem and route diversity systems, rain outage performance at 11 GHz 77−41131
trans-horizon propagation path over sea, transmission loss due to ducting at 1.8 GHz 80−105041
troposhere, Danish experimental line-of-sight propag. path, 13.5-15.0 GHz 79−48555
troposphere, 10-40 GHz, attenuation/rain-rate relationships 78−40607
tropospheric and precipitation scatter, rel. importance in interference and coordination calcs. 78−73423
tropospheric propagation, satellite-borne monitoring of atmospheric and surface characteristics 78−24353
turbulence and wavelength effect on scintillation fading at mm. wavelengths 78−85623
Voyager Project, spacecraft communication system 80−26718

microwave measurement
see also microwave reflectometry
3 GHz surface and lateral EM wave meas. 80−103742
3K blackbody cosmic background radiation meas. 77−41422
9 GHz radiometry of tumours *(French)* 80−3767
20 and 30 GHz radiometer calibration using ATS-6 satellite beacons 77−74500
22.75 GHz microwave attenuation characts. at high elevation *(Japanese)* 80−27346
100 GHz bolometer mount efficiency meas. calorimeter *(Japanese)* 78−54460
absorption by water in heterogeneous organic materials 80−15998
acoustic-microwave Doppler radar system, wind and wind shear meas. at Dulles Airport 78−32233
advances reviewed 78−57984
aerosol layer depth remote meas. by microwave-modulated laser *(Russian)* 78−57338
air pollution, pollutant gases monitoring from space using passive microwave techniques 80−76690
airborne 33 GHz radiometer system for 3K background anisotropy mapping 78−61735
AM active method for plasma density meas. 80−87948
amplitude meas. of signals up to microwave freqs. using Ge diodes 77−37905
amplitude-phase ratio meter, description *(Russian)* 78−62209
anisotropy meas. at microwave freq., experimental results 80−52279
application survey, non-conventional *(Italian)* 80−13093
aqueous soln. reaction kinetics meas. microwave apparatus 80−3470
Arctic Ocean ice characteristics meas. by microwave scatterometry 79−84298
arterial wall movement monitoring by microwave Doppler radar 79−96647
artificial satellites, effective isotropic radiated power, error anal. using calibrated radio star 78−93070
atmosphere, liquid water content from Nimbus 6 scanning microwave spectrometer data parameterisation 79−58047
atmosphere boundary layer temp. profile determ. from ground-based 60 GHz radiometry *(German)* 80−82097
atmosphere parameters, retrieval from scanning multichannel microwave radiometer obs. 80−90261
atmospheric boundary layer, vertical temp. profile determ. by ground-based microwave radiometry 79−79915
atmospheric H_2O vapour and cloud liquid determ. by dual freq. ground-based microwave radiometry 78−93007
atmospheric regional precipitation meas. by ground-based radiometer *(Chinese)* 79−84547
atmospheric surface pressure measured using microwave signals transmitted from orbiting satellite 80−94581
atmospheric temperature-pressure profile meas. by microwave remote sensing *(Chinese)* 80−4116
atmospheric vertical temp. profiles, microwave remote sensing meas. *(Chinese)* 79−84452
ATS-6 to ground link, near horizon meas. over water at 30 GHz 78−24345
attenuation at 36.8 GHz in sea ice, freshwater ice and snow *(Russian)* 77−5209
attenuation by atmospheric water vapour at 0.869 mm *(Russian)* 77−5277
attenuation in human torso, 1.8-2.7 GHz 77−70517
automatic calorimeter system for bolometer mount effective efficiency meas. in 35 GHz band 78−86272
biological effects determ., contactless meas. of temp. and absorbed energy, using fluorescent screens 80−36186
biological liquids, reflection meas. of complex dielectric const. 80−101309
biological specimen complex permittivity meas. bench for 2-10 GHz at 77-300K *(Russian)* 77−32966
biological systems, microwave radiometry applications 77−81770
biological target internal microwave imaging using water immersed microwave antennas 79−34623
biomeasurements using microwaves *(Japanese)* 80−94314
biomedical appl., bio-clutter interference effects 79−11992
biomedical respiration monitor 79−96646
bolometer mount, millimetre wave, for waveguide power meas. at 100 GHz 77−71372
broadband mm-wave calorimeter, design and calibration 79−26084
cancer detection by microwave thermography 78−24172
cancerous mouse hyperthermia meas., microwave, IR and thermocouple methods *(French)* 80−3768
cavity perturbation measurements, elimination of influence of non-ideal microwave circuit 79−88979
cavity resonator, containing dielec. sample, num. soln. of charact. eqn. *(French)* 78−13649

microwave measurement continued
ceramic low-loss foils, permitt. and dielec. loss meas. method *(Polish)* 78−37028
ceramics crack and inclusion detection, NDT microwave evaluation 78−95866
chloral, in benzene, permittivity, dielectric loss, 36 GHz 77−32323
Cicoil personal RF radiation hazard detector, evaluation 80−5337
circular discs and rectangular plates, shadow-side field meas. 77−79731
clinical microwave focusing thermography 80−3771
cloudy atmospheric parameter determination using radiometric method 80−67435
coaxial resonator technique for microwave cond. meas. 77−4384
coaxial waveguide wave impedance, USSR special standards 77−30182
complex dielec. and mag. props., modified von Hippel least square fit determ. 78−21179
complex dielectric constants, meas. at 10 GHz using cavity perturbation method 78−24815
complex dielectric data measurement using coaxial line resonator 78−8419
complex permittivity of low-to-medium loss standard liqs., meas. at 285 GHz 78−15083
complex permittivity on liquid and solid dielectrics at mm and sub mm wavelengths 77−18011
conductivity measurement by eddy current loss method, effect of permittivity 78−24817
conductivity measurement in reson. cavity, appl. to CdTe 79−51620
conference, IR and MM waves and appls., Miami Beach, USA (Dec. 1979) 80−57009
conference, Zurich, Switzerland (Mar. 1979) 80−4783
conference on microwave power appls., London, England (Nov. 1979) 80−21520
counters, modern techniques 78−32831
CROs with GHz bandpass for general purpose use 79−88936
cyclohexane loss meas. at 35, 72 and 144 GHz 77−82560
cylindrical TE_{01n} cavity, measurement of complex permittivity using approx. anal. method 79−49254
Dextrane in aqueous solution permittivity meas., dielec. relaxation study 77−77143
diathermy equipment and power indicator 77−40901
dielectric complex permittivity, two coupler method 78−21167
dielectric complex permittivity, using open transmission line resonator 77−26333
dielectric const. measurement using cavity perturbation technique 80−31802
dielectric constant of liquids, complex, with high dielectric losses, 300 MHz to 6 GHz *(German)* 80−13106
dielectric constant of low-loss solids, at 1 GHz, coaxial resonator method *(German)* 78−32834
dielectric cylinders, microwave meas. of permittivity using retarded waves *(Czech)* 80−95111
dielectric discs in rectangular waveguides, permittivity meas. *(Russian)* 77−18050
dielectric loss, low temp., expts. on polymers, 0.1-10 GHz, 2.2-4.2K 77−24786
dielectric loss, resonator bridge method 78−54391
dielectric loss angle/permittivity meas. as function of temp. at 9-10 GHz 77−82559
dielectric loss high sensitivity meas. using supercond. microwave resonators in oscillator loop 77−10043
dielectric loss meas. at 100 GHz range, precision, Fabry-Perot resonator 78−70163
dielectric loss measurements at microwave frequencies *(Russian)* 79−2788
dielectric loss tangent, cavity resonator bridge method 77−37914
dielectric material, X-band characterisation 77−2664
dielectric meas., automated, using resonance substitution techniques 77−82573
dielectric meas., precise, 10-150 GHz freq. range 79−30491
dielectric parameters, E_{010} cylindrical resonator, perturbation theory, error estimators *(Russian)* 77−18051
dielectric parameters meas. by cavity perturbation technique 80−9002
dielectric properties, von Hippel's method, appl. to Eccosorb HF-2050 77−32314
dielectric properties at millimetre wave frequencies, using inverted strip dielec. waveguides 79−26081
dielectric properties of living tissue, 10 MHz to 6 GHz meas. 77−78071
dielectric props. of organic liquids in freq. range 400 MHz to 285 GHz, internat. comparison of meas. methods *(German)* 80−68168
dielectric relaxation of compressed water at 17.613 GHz using microwave refl. meas. method *(German)* 80−71306
dielectric relaxation spectroscopy of polar fluids in microwave region, double beam interferometry method *(German)* 80−71309
dielectric spectrometer, meas. of attenuation coeffs. and permittivity of liquids 77−41646
dielectric time domain spectroscopy, transmission methods 77−67462
dielectrics, HF cavity resonator method of measuring electromagnetic parameters 79−80642
digital freq. counters and counter-timers, new range using MSI 80−27318
dispersive Fourier transform spectrometry, dielec. meas. on low-loss materials at millimetre and submillimetre wavelengths 77−37916
dispersive Fourier transform spectroscopy, submillimetre wave, with variable thickness variable temp. liquid cells 77−37915
distance meas. using mm waves, expt. *(Japanese)* 77−71298
dosimeter, evaluation of implantable elec. field probe within finite simulated tissues 78−40345
dosimetry and densitometry techniques in bioeffects research 77−78072
double electron-nuclear resonance obs. using 3 cm rectangular resonator, low-temp. 80−98956
dry calorimeter for power meas. at mm wavelengths 79−26085
dynamic microwave cavity perturbations, active freq. technique, precision 79−21769
dynamic plasma discharge microwave oscillation expt. 77−84433
electric field intensity meas. using Ne gas-discharge tube 80−9006
electric field intensity unit, 30 MHz to 1 GHz, USSR special standard 77−30181
electromagnetic meas., precision, conf., Braunschweig, Germany (Jun. 1980) 80−98903
electron-hole drop motion recorded by microwave probe meas., appl. to Ge 77−76755
EM non-ionising radiation standardisation 77−38013
environmental field intensity, automated meas. system 77−37947
ethyl trichloroacetate, in benzene, permittivity, dielectric loss, 36 GHz 77−32323
extinction cross section for single particles at 100 GHz 80−82116
Fabry-Perot interferometer, inhomogeneous, dielectric loading and general phase-frame shaping, analysis 80−13197
Fabry-Perot type microwave wideband open resonator appl. 77−57351
far IR laser line frequency meas. by klystron harmonic comparison 77−7113
feedthrough waveguide resonator Q-factor meas. 77−10053
ferrites, mag. permeability meas. at 9.5 GHz, precision test unit 77−74465
ferrites, microwave flaw detection 78−53122
ferroelectrics, dielectric props. meas. in vicinity of phase transition 78−74022
field distribution, phase modulated scattering method appl. *(Japanese)* 79−85151
film and slab-like materials, open transmission line UHF CW phase technique for meas. of thickness, permittivity and moisture content 79−35778
flowmeter, Doppler-effect type, particle moisture content effects 78−9732
forest fire sources, microwave radiation spectra 80−52314
frequency, meas. with 10 MHz resolution in upper microwave bands 77−5868
frequency counter, LSI design 80−213
frequency counters, phase-locked transfer oscillator automatic computing system 77−5862
frequency meter, UHF pulse carrier freq. meas. appl. 77−37917
full wafer magnetic bubble films, devices for characterisation 79−78461
gas refractive index meas., 150 GHz to 6 THz 77−5892
Gulf of Alaska SeaSat Experiment 14.6 GHz scatterometer surface wind obs. 80−46200
gyromagnetic ferrite materials, saturation magnetisation meas. *(German)* 79−67357
hazard survey instrumentation and meas. 78−44618
high permittivity measurement using waveguide measuring line 80−47080
high surface vels. using K-band microwave interferometry 80−77761
holography, techniques and appls. 77−10871
hot/cryogenic noise standards, preliminary design 77−82563
human thorax, mapping of transmitted microwave power 80−3756
hydration kinetics, microwave obs. 79−34255
hydrometeors, radiative props. at microwave freqs. 79−20940
imagery of isolated canine kidney, use of orthogonal polarisations 80−81783
in vivo probe measurement technique for determining dielectric properties at VHF through microwave frequencies 80−85542
instrumentation review 79−212
interferometry for biological movements *(French)* 78−53469
Josephson junction, discriminating props., use in microwave spectral anal. 77−49748
kidney, canine, isolated, microwave scattering parameter imagery 80−3755
lanoline emulsion permittivity meas. 77−77144
liquid complex permittivity meas., 100 GHz to 18 THz 77−8490
liquid dielec. complex permittivity meas. method 77−82558
liquid drops, size and dielectric const. determ., active microwave system 78−54339
lossy dielectric complex permittivity, at millimetre wave freq. 79−30492
lossy waveguide attenuation and phase meas. 77−26343
low loss liquids, loss angle temp. var. meas. at microwave freqs. 78−48114
low-loss dielectric meas. at millimetric and submillimetric wavelengths 77−37943
low-loss dielectric measurement in the E_{010} resonator, numerical error analysis *(Polish)* 78−70153
magnetic anisotropy, measurement using square resonant cavity 79−93173
magnetic-field distribution meas. using new resonant scatterer 79−49211
mapping of near-field pattern in simulated biological tissues 79−39445
marine boundary layer microwave sensing, estimation techniques 79−74993
material losses, by resonance input impedance method *(Czech)* 77−26326
material testing, nonuniformity of dielec. props., at mm wavelengths, method of determining 78−40001
microprobes, non-perturbing, based on cholesteric crystal and dielectric microthermometer 78−16791
microtransducer for temperature and power density meas. appl. *(French)* 77−61084
microwave detection of third-order nonlinearities 80−55594
MM and subMM wave appl. in 100-1000 GHz range 80−17962
MM wave radiometry for atmospheric sounding 79−84551
moisture content determ. of cloudless atmosphere, microwave radiation meas. 80−94624
moisture meas. of bulk materials using SHF moisture gauges 77−87771
moisture meas. of granular and powdered materials *(Polish)* 78−12706
multi-frequency microwave radiometer system for oceanography, performance evaluation 78−81417
murine malignant tumours, in vivo probe dielectric meas. 78−11761
narrow-band semiconductors, current-carrier conc. distrib. nonuniformity, contactless meas. 77−76853
noise standards in Japan, 10 GHz system *(Japanese)* 78−57985
nonmagnetic materials complex permittivity rapid determ. *(German)* 78−21161
nonperturbing dielectric microthermometer probes 78−11743
ocean, microwave scattering signature, aircraft measurements 77−17112
ocean passive radiometry, radio meteorology colloquium, Victoria, British Columbia, Canada (1978 June 14 to 21) 80−46724
ocean surface parameters, retrieval from scanning multichannel microwave radiometer obs. 80−90261
ocean surface wind speed, SeaSat-A scatterometer 77−29626
ocean temp. and salinity meas. by microwave radiometry 78−81416
ocean wave detection by microwave radar, gravity-capillary wave modulation 78−77333
ocean wave height meas. with satellite radar altimeter 79−44253
ocean wave spectra, remote meas., two-freq. microwave technique 78−77336

microwave measurement continued
ocean waves over North Sea, using side looking airborne radar 78−77245
oceanographic microwave remote sensing 80−56612
oceanography, microwave radiometry appls. review 78−81415
one-dimensional conductor, microwave permittivity measurement techniques 78−10825
open resonator, MM and sub MM wavelengths, imaging using thermoluminophorous sensor 79−93168
open resonator methods for microwave permittivity meas. 80−15942
particulate velocity and density meas., using microwave Doppler effect 77−27628
passive microwave radiometry from satellites 77−70882
passive microwave remote sensing of snowpacks, theory and expt. 80−26632
permittivity, submillimetre region, in polar liquids, Poley absorption interpretation 77−36167
permittivity meas. at microwave freqs., two coupler method modification 80−100632
permittivity meas. of lossy liquids at 70 GHz using precision waveguide cells 78−37032
permittivity measurement, time domain spectroscopy, transmission method 77−43926
permittivity measurement for human sera and erythrocytes 80−26424
permittivity of dielectric films and plates, nondestructive method 78−57987
permittivity of dielectric sheet materials, at 35 GHz, free-space transmission technqiue 78−62208
permittivity of liquids using modified microwave cavity perturbation technique 80−42239
phase and voltage measured at frequencies above 2 GHz using high speed sampling 78−8418
phase measurement, error anal. due to reflections error anal. due to reflections *(Bulgarian)* 79−88975
phase measurement of microwave interference signals from 0 to n.360° for plasma density meas. *(German)* 80−6278
photoconductivity recording method, simple and reliable 77−41642
physiological movements, interferometer appl. 79−25137
plane-wave microwave power density of hazard probe, precise calibration techniques 77−71341
polarised beams, meas. using mechanical polarisation modulator 77−37987
polarising submillimetric Fourier interferometer with achromatic internal modulation 78−65959
ponderomotive power meter, frequency range 8.5 to 12 GHz, power range 0.5 to 100 W, VSWR up to 1.1 *(Russian)* 77−37939
power, microwave, bolometric method *(Hungarian)* 77−18091
power, self-balancing DC-substitution RF power meter 77−18012
power leakage from microwave-excited light sources 78−36988
power meas., calorimetric method, using Ge vane loads 77−82562
power meas. at higher microwave freq., conf., London, England, (Jan 1979) 79−26082
power meter, UHF, using contact between metal probe and Ge 77−37986
power symposium, Monaco (1979) 80−3758
power using absorption spectrum of $^{14}NH_3$ gas 77−18013
precision EM measurements conference, Boulder, Colorado (June 1976) 77−18010
probe for subsurface soil moisture profiling 78−65939
PTFE, spacer material for supercond. cable, dielec. loss meas. using supercond. reson. cavity 77−8501
pulmonary diagnosis/monitoring, reflection/transmission meas. method 78−28031
pulmonary oedema diagnosis by a surgically noninvasive microwave technique 80−61659
Q-factor, EPR spectrometer appl. *(Polish)* 78−93728
Q-factor, meas. system 78−54396
radiation balance microwave thermograph for industrial and medical appls. 78−45621
radiation hazard assessment methodology for USA Army Radiation Protection Program 78−85389
radiation losses, through connecting-coupling hole in microwave cavities 77−79105
radiation monitor 77−26401
radiation monitoring instruments, evaluation and comparison 79−96667
radiation power density measurement, used in formulation of dosimetry standards 80−26377
radio interferometer system for microwave band coherent transition radiation study 79−85181
radiometer, multichannel scanning, for Nimbus-G and SeaSat-A 77−29625
radiometer calibration standard with Brewster angle impedance 77−5918
radiometer measurements, microwave brightness temperature *(Danish)* 80−26625
radiometers for ice movement measurement *(Danish)* 80−26624
radiometric determ. of ocean surface wind speed during BESEX 77−29479
radiometric measurements, passive, influence of atmosphere in 10 to 1000 GHz range 79−88465
radiometry in detect. of breast cancer 78−40384
rain attenuation for Earth-space links, comparison between radar- and radiometer-derived data 78−24343
rain slant path attenuation statistics prediction at various locations 78−24344
rainfall distrib. determ. from radiation meas. by Nimbus 6 satellite 78−3981
rainfall meas. by microwave attenuation in 1-3 cm band 78−65414
reflectance of ice and seawater at 100, 140 and 180 GHz 79−84552
reflection coefficient, waveguide standard 77−41644
refractive index of isotropic and anisotropic media, meas. at 35 GHz 80−256
refractometer, expendable, lightweight, construction and performance 79−8708
remote sensing and profiling of lower atmosphere using radiowaves, ground-based 80−56628
remote sensing atmospheric sounding of cloudy atmospheres *(Chinese)* 80−51549
remote sensing from satellites, appl. to meteorological meas. over W Australia 80−98485
remote sensing of ocean surface currents, recent progress 77−87114
microwave measurement continued
remote sensing of two-layer media, microwave radiative transfer models 77−21908
remote sensing technology for marine oil pollution surveillance *(Japanese)* 80−76685
resonator, automatic monitor of resonant freq. and bandwidth 77−22567
respiration measurement application, technique 77−5058
rotary-vane attenuator, automatic calibration on modulated subcarrier system 77−18022
sand, moisture content, microwave optics determ. 77−37684
sandy and clay soils, microwave absorption *(Russian)* 78−81162
satellite location by tone-code trilateration 77−9653
scanning passive radiometry for ocean surveillance 78−73550
scanning radiometer, improvement of performance by digital reference averaging 79−35824
scanning radiometry, appls. 78−73551
sea ice, initial forms, microwave refr. index and absorpt. 78−49036
sea ice, low-salinity, radiometer studies 78−81175
sea ice, microwave remote sensing in AIDJEX main expt. 78−81173
sea ice in Arctic Basin, time depend. of ice conc. and multiyear ice fraction 78−81174
sea surface temperature, radiometric observations at 2.65 GHz, atmospheric and surface corrections, Chesapeake Bay 77−17114
sea surface waves, remote sensing using one and two freq. microwave techniques 80−94622
sea surface wind speed and significant wave height using pulsed radar 77−29477
sea-surface wind, radar backscatter meas. at 13.9 GHz from Skylab 77−91304
SeaSat scanning multichannel microwave radiometer 80−46248
SEASAT-A satellite microwave scatterometer for wind sensing 77−5417
SEASAT-A satellite ocean surface truth expts. 77−5419
SEASAT-A satellite project 77−5414
SEASAT-A satellite scanning multichannel microwave radiometer 77−5416
seawater and wet soil complex permittivity meas. method 77−45184
seawater permittivity, modelling 77−25690
semiconductor materials, noncontacting techniques 77−2668
semiconductor microwave conductivity meas. by eddy current loss method 78−8417
semiconductor thin film conductivity monitoring by microwave resonator absorption *(Russian)* 78−23182
shelled, dielectric loss and moisture meas. 77−77142
shock flow, time analysis using dual microwave and dual schlieren systems 77−15143
single pulses of ns duration, amplitude and shape meas. instrument 77−45863
skin stratum corneum, human, linear meas. of water content using microwave probe 80−21518
small liquid biological sample microwave complex permittivity meas. 80−17222
snow, parameters investigation by radiometry in 3 to 60 mm wavelength region 80−72561
snow, water equiv. of dry snowpack, active and passive microwave response 80−72563
snow penetration and backscatter of millimetric waves 77−21877
snow wetness, active and passive microwave response 80−67382
soil, moist, dielec. relaxation model, complex permitt. meas. 77−43930
soil moisture content, microwave radiometer meas. over bare and vegetated surfaces, comparison 78−88851
soil moisture meas. by remote microwave radiometry 79−48526
soil moisture measurement, active microwave remote sensing, surface roughness and texture effects 79−12295
soil stored productive moisture, remote determ. technique 79−29795
solid dielec. loss, high sensitivity, using supercond. high-Q resonator 78−93733
solid dielectric props. meas. with superconducting resonators 78−21180
spectrum analyser model 7L18 79−30487
spectrum analysis, using microcomputer 78−41329
standards for power meas. in mm. wave region 79−26083
subcutaneous temperature meas., for thermoregulation obs., using passive microwave sensors 79−34721
submillimetric wave propagation meas. techniques 77−38007
superheterodyne tracking cct. for mm-wave measurements 80−59288
surface soil moisture remote meas. 79−70896
survey instrument evaluation and calibration 77−37946
thermoluminescence fading in $BaTiO_3$ ceramic, applic. to dosimetry 79−1792
thermometer with automatic balancing, for liquid streams temperature meas. 80−47055
tissue equivalent bolus, 1 to 10 GHz electrical prop. characterisation 80−3763
Tokamak microwave discharges, refraction losses, from measured plasma density profiles 78−22549
triangulation, microwave distance meas. in German net *(German)* 78−88792
trilateration distance measurement in German Bight *(German)* 80−8248
troposphere, temp. profiles from ground-based angular microwave meas. 80−51551
tubular dielectric, complex permittivity and loss angle meas. in X-band using H_{011} cavity resonator method *(German)* 80−62690
unit power standard for 53.57 to 78.33 GHz 80−90808
using microwave O line splitting 80−77124
voltmeter, broad-band, based on hot carrier thermoelec. effects, features 78−21166
water pollution, dielectric props. and determ. of microwave emissivity 80−101142
waveguide impedance meter verification scheme 78−37035
waveguide interferometer, for precise determ. of very low dielectric losses at 9 and 29 GHz dielectric loss, very low, waveguide interferometers for 9 and 12 GHz 77−8503
wavelength instability meter 77−10054
wavemeter calibration, Q-band, using spectrometer *(Polish)* 78−29866
wind measurements in clear air by microwave radar 77−13136
X-band frequency standard, high Q cavity resonator *(Polish)* 77−26342
zenith brightness radiometry, absorption altitude profile determ. at 2.53 mm 77−81979
GaAs hot electrons drift rate/field strength characteristic in microwave fields *(German)* 78−43430
H_2O vapour, atmospheric, microwave meas. of absolute values of absorpt. 79−66773

microwave measurement continued
NH_3 monitoring using Stark microwave cavity resonator 80−61500
SO_2 detection using thermal radiation at 53.53 GHz rot. reson. 77−78411
Se layer crystallinity meas., combination microwave resonator method *(Russian)* 78−22652
Si wafer, nondestructive method for meas. of spatial distrib. of minority carrier lifetime 80−13098

microwave-optical double resonance
see also PMDR
acridine in fluorene matrix, RF induced mag. reson. transitions, triplet state, optical nucl. polarisation 79−31561
alkali halides:Ga^+, Jahn-Teller effect, EPR study 78−43690
alkali halides:Ga^+, optically detected EPR in relaxed excited states of Ga^+ 78−72437
alkali halides, EPR in relaxed excited state of F-centres, detection via saturated optical pumping 78−6606
alkali halides, self trapped exciton, optical detection of spin relax. processes 78−60358
alkali metal, double freq. microwave reson. in hyperfine struct. of ground state *(Russian)* 77−51993
alkaline earth fluoride, EPR of triplet state of self-trapped excitons 78−43684
allylamine, laser-microwave double and triple reson. 80−83397
aniline, in p-xylene host cryst., phosphoresc. triplet state, ESR and MIDP obs. 80−66077
anthracene-dimethylpyromellite-imide, CT complex, reaction yield detect. double reson., delayed fluoresc. quenching *(Russian)* 78−88230
anthracene-dimethylpyromellitimide, cryst., triplet exciton pairs, EPR spectra 77−43906
anthracene-TCNB charge transfer cryst., phosphoresc. and delayed fluoresc. detected mag. reson. 79−33565
anthracene-tetracenebenzene, triplet excitons annihilation, mag. reson. sign reversal 79−65769
anthracene-tetracyanbenzene, charge transfer, magnetic resonant modulation of photoconductivity 78−64062
anthracene-tetracyanobenzene charge-transfer complex, RYDMR of triplet excitons annihilation 78−39448
anthracene-tetracyanobenzene cryst., triplet exciton annihilation, time correlated delay fluoresc., ODMR 80−39895
aromatic molecular crystals, optical nuclear polarization, appl. to EPR and ODMR 79−19804
$^3\pi\pi^*$benzaldehyde, zero field splitting and sublevel decay rates, deuteration and host effect 80−37750
benzene/benzene-d_6, cryst., X-trap phosphoresc., ODMR, 1.3K, triplet state struct. 77−20902
benzenoid aromatics, triplet zero field splitting parameters, ODMR obs., struct. effects 80−78636
benzil, high temp. ODMR obs. of cryst. phases 79−38407
benzil crystals, triplet state spin-lattice relaxation, zero field magnetic resonance spectrometer analysis 79−97409
benzil X-trap, ODMR, near planarity in triplet state 77−32295
1,2-benzocoronene, phosphoresc. and ODMR meas. 79−18220
benzophenone, and d_{10}, ODMR and phosphorescence spectra in organic matrix 79−36671
benzophenone, high resolution ODMR and optically detected ENDOR 79−19811
benzophenone, lowest triplet state, ODMR spectra, D- and g-tensors 77−75191
benzophenone, triplet, optically detected EPR, ENDOR and ODMR, HFS, isotope and spin-orbit effects 78−86898
benzophenone, triplet state zero-field ODMR, ^{17}O HFS 79−18216
2-benzoylpyridine, mol. cryst. triplet state selective photoexcitation, phosphoresc. spectra and microwave-optical double reson. 79−15507
2-benzoylpyridine, triplet states, phosphoresc. and ODMR 79−38603
benzo[α]pyrene-DNA complex, triplet state props., optically detected zero-field mag. reson. obs. 77−79636
benzo[α]pyrene-DNA complex, triplet state props., optically detected zero-field mag. reson. obs. 79−18222
biacetyl, triplet kinetics, EPR fine struct., ODMR 77−71824
(biphenol)$^+$/(biphenol)$^-$ ion-radical pair, ODMR, hyperfine struct. *(Russian)* 80−15829
camphor, optical isomers, separated, IR Lamb dip obs. 78−90197
carbazole, triplet state of X-traps, ODMR 79−24231
carbazolyl substituted diacetylene monomer cryst., ODMR and triplet state kinetics 78−76355
charge transfer phanes, glassy and cryst., ODMR meas. 79−19812
chloromethylethyl ether, GT isomer, microwave spectra and geom. config. 79−59444
chlorophyll, enhancement of fluorescent mag. resonance detection, under intense laser excitation *(Russian)* 78−91995
chlorophyll solutions, triplet state props., ODMR meas. 79−20517
chlorophyll-a (b), dimerisation, fluoresc. and ODMR study 80−18876
coherent radiation sources for mol. spectroscopy, review 77−3343
coherently coupled ensemble, energy exchange, density matrix calcs. 78−64298
conference on optical techniques in mag. reson. spectroscopy, Dublin, Ireland (Aug. 1977). 78−43683
cyanogen fluoride, fund., hot bands, laser microwave two photon and double reson. spectroscopy 80−32752
cyclopentanone, excited triplet state, intramolecular tunnelling, optically detected electron spin coherence 77−61774
diacetylene, luminesc. and ODMR spectra 79−38604
p-diazines, polycyclic, $T_1(\pi\pi^*)\rightarrow S_0$ intersystem crossing, isotope effects, ODMR and phosphoresc. obs. 80−91586
1,2,5,6-dibenzocoronene, phosphoresc. and ODMR meas. 79−18220
dibenzofuran, cryst., phosphoresc. spectra and ODMR meas. 80−11470
dibenzofuran, triplet state of X-traps, ODMR 79−24231
dibenzofuran-fluorene, mixed cryst., phosphoresc. spectra and ODMR meas. 80−11470
dibenzothiophene, triplet state of X-traps, ODMR 79−24231
4,4'-dibromobenzophenone, ODMR and phosphorescence spectra in organic matrix 79−36671
1,4-dibromonaphthalene, substitutionally disordered, energy localisation, optical and ODMR spectra of triplet Frenkel excitons 80−54996
p-dichlorobenzene, triplet state symmetry, geometry, ODMR, ENDOR obs. 79−18214
4,4'-dihalobenzophenone, lowest triplet state, ODMR spectra, D- and g-tensors 77−75191

microwave-optical double resonance continued
dihydroporphin free base, in n-octane cryst., zero-field optically detected mag. reson., triplet state kinetics 78−42103
dimethylbenzaldehydes in durene single crysts., ZFS D-parameters 77−55731
dinaphtho-(2′.3′:1.2);(2″3″:6.7)-pyrene, triplet state, phosphoresc. and ODMR obs. 79−27013
double radiooptical resonance, signal propag. and shape 80−87360
EEDOR triplet state zerofield transition energy, spectral diffusion 80−88893
electron spin coherence in nonphosphoresc. triplet states, optical detect. meas., TADMR and FMDR 78−25578
EPR, optical detection in excited state *(Japanese)* 77−81029
ethylene oxide, rot. relax., double reson. and Stark switching obs. 80−106340
F centre, EPR in relaxed excited state, via mag. circular polarisation of emission 79−24232
F-centres, relaxed excited state, spin polarisation, saturated optical pumping 79−15522
fluorene, cryst., phosphoresc. spectra and ODMR meas. 80−11470
fluorene, triplet state of X-traps, ODMR 79−24231
fluoroacetylene, fund. and hot bands, laser microwave two-photon and double reson. spectroscopy 80−32752
fluoroacetylene, laser Stark and IR-microwave double resonance, E1 moment, vibr. states 77−6813
fluoroacetylene-d, Stark and microwave double reson. laser spectra 80−63690
fluoromethane, excited state rot. spectroscopy and kinetics, appl. of tunable sub-MM sources 80−14162
formaldehyde, microwave-microwave double resonance 80−53029
formaldehyde and -d_1, MODR and collision-induced transitions in laser cavity 78−74686
formaldehyde-d_1, rotational transitions, IR-RF double reson. meas. 77−61775
formic acid, CW submm. laser assignment, microwave IR double reson. expt. 79−27244
formic acid, vap., laser lines identification 78−1222
free radicals, high resolution spectroscopy *(Japanese)* 79−79355
glyoxal-d_0, -d_2, triplet kinetics, microwave-saturation recovery and MIDP obs. 77−71823
ground- and excited-state, lineshapes, relative signal intensities 77−27100
haloanilines, T_1-states, EPR and zero-field ODMR obs. 78−58725
haloanisoles, T_1-states, EPR and zero-field ODMR obs. 78−58725
halobenzonitriles, T_1-states, EPR and zero-field ODMR obs. 78−58725
high temperature molecules, rotational spectroscopy 80−52236
high-temperature chemical processes, review, book contrib. 77−40545
homogeneous linewidths in ODMR and optical transitions, connection 79−91316
II-VI compounds, donor-acceptor recombination emission in cryst. subjected to mag. reson. 79−95684
II-VI semiconducting phosphors, ODMR, defect excited states 78−80254
II-VI semiconductor, recombination radiation, ODMR study, detrimental effects of high excitation intensities 80−44958
II-VI semiconductors deep centres, ODMR *(French)* 80−60461
III-V semiconductors, k.p perturbation theory 77−43484
III-V semiconductors, optical detect. of CESR, giant Overhauser shifts 78−80251
2-indanone, single cryst., ODMR and phosphoresc. of $^3n\pi^*$ state 79−78570
iodomethane-d_3, ν_2 band, laser Stark and laser-microwave double resonance spectra 77−27067
laser microwave double resonance IR spectroscopy 78−86900
laser microwave double resonance spectroscopy, wide-band intracavity microwave cells 77−82580
longitudinally detected ESR, lineshapes, density matrix formalism calcs. 79−82894
magnesium porphin, lowest triplet state, zero-field ODMR 79−31562
magnesium tetraphenylchlorin, lowest triplet state, zero-field ODMR 79−31562
magneto-optical effect, influence of ESR saturation, allowance for dipole-dipole reservoir of electron spins 79−15442
methyl acetate, microwave spectra and internal rot. 80−87100
methyl bromide, NQR and A_1-A_2 splitting, RF spectrosc. inside laser cavity 80−91579
methyldichlorosilane, Stark effect and microwave-microwave double reson., struct. *(German)* 80−47975
methylene fluoride, ν_9 fundamental band, 9.4-μm CO_2 laser Stark spectroscopy 78−9191
5-methylpyrimidine, singlet-triplet intersystem crossing, ODMR and MIDP in matrix at 1.6K 79−50055
microwave modulated saturation spectroscopy 79−68245
modern aspects, theoretical and further developments, book contrib. 80−53029
modulation technique, discrimination between homogeneous and inhomogeneous lines 79−44923
molecular cryst., phonon scatt. times below 10K, optically-detected APR 78−88228
molecular crystals, shallow traps, spin triplet population temp. depend. 77−1371
molecular cystals, triplet exciton pairs, mag. reson., fluoresc. modulation detect. 77−43906
molecular double resonance expts., off-reson. dispersion 77−58052
molecular planar structure, double reson. signals depend., appl. to microwave spectra 80−32751
molecular triplet states under optical spin orientation conditions, microwave energy transfer 80−74187
1,2-naphthacoronene, phosphoresc. and ODMR meas. 79−18220
naphthalene, in durene, photoexcited triplet state spin-lattice relax., local phonons effects 78−6605
naphthalene pair ($C_{10}H_8$) in $C_{10}D_8$ host, mini-exciton obs., electron spin echo and ODMR 77−4559
naphthalene-d_0, in naphthalene-d_8 cryst., mol. pair mini-exciton form., electron spin echo and ODMR 77−72822
off-resonant optical radiation, theory of double reson. 78−25579
one-dimensional solids, energy transfer processes, optically detected electron spin coherence meas. 79−19808
optical isomers, separated, IR Lamb dip obs. 78−90197
organic molecules in Shpolskii matrices, phosphoresc. site selection spectrosc., ODMR 79−36687

microwave-optical double resonance continued
α-oxalic acid dihydrate, low-lying excited states, ODMR and optical obs. 79−41188
palladium porphin, triplet state, optically detected EPR and Zeeman meas. 79−19809
palladiumporphin in n-octane cryst., lowest triplet state, ESR-optical detect. 77−58050
perdeuterobenzophenone, in 4,4'-dibromodiphenylether, cross-relax., microwave pulse obs. 80−53031
[2.2]phanes in glass matrices, transanular π-electron interaction, emission spectra 79−36682
phenazine, substitutionally disordered, energy localisation, optical and ODMR spectra of triplet Frenkel excitons 80−54996
phenazine, triplet state, ^{14}N quadrupole tensor, optical detection of NQR 79−18218
pheophytin-a (b), dimerisation, fluoresc. and ODMR study 80−18876
photoexcited triplet state molecules, in cryst., cross-relax., variable freq. ODMR obs. 80−53031
photon counter, microprocessor-controlled, for pulsed ODMR 79−88992
photosynthetic systems, reaction centre struct., triplet state ODMR 77−29093
polyatomic molecules in solid matrices, ODMR in triplet states, appl. of spin echoes 79−18217
polypeptide hormones, conformations, ODMR investig. 78−76356
polypeptide hormones, folding, ODMR and phosphoresc. 79−20518
porphin free base, triplet state electron spin echoes, fluoresc. detection 78−70856
propynal, ν_2 vibr. state, IR-microwave triple resonance 79−13746
propynal-d, in ground vibrational state, IR microwave double resonance spectra, rot. and centrifugal distortion const. determ. 80−83358
propynal-d, IR microwave double reson. spectroscopy 80−69172
pyrene solutions, radical ion pairs, pulse radiolysis, time resolved EPR spectra meas. by ODMR of fluoresc. 80−83395
pyridinium(-d_5) ion, triplet state obs. by ODMR, rel. to CNDO/2 STO calcs. 77−18951
pyrimidine, singlet-triplet intersystem crossing, ODMR and MIDP in matrix at 1.6K 79−50055
quinoxaline, in p-dibromobenzene, triplet state NQR, nucl. spin polarisation effects 79−18208
quinoxaline, triplet state symmetry, geometry, ODMR, ENDOR obs. 79−18214
R. spheroides, triplet state electron spin echoes, fluoresc. detection 78−70856
rare earth ions, optically excited states, EPR, ENDOR 78−43637
rare-earth magnets, low-frequency modes 78−88087
RF induced magnetic resonance transitions, in mol. triplet states, optical nucl. polarisation method 79−31561
rubrene film, excited complex with charge transfer, fluoresc. obs. of mag. reson. *(Russian)* 77−8454
ruby, ESR of Cr^{3+} excited state as function of delay time, Zeeman levels explained 78−43695
Rydberg states, fine struct. splitting, quantum beat and double reson. spectroscopy 78−86979
scandium octaethylporphyrin, μ-oxo bridged dimer, triplet states and geometrys, ODMR obs. 80−9625
scandium octaethylporphyrin, triplet states and geometrys, ODMR obs. 80−9625
semiconductor, ODMR appl. to recombination processes 79−42871
semiconductors, spin orientation by optical pumping, review 79−38410
slotted tube resonator, pulsed ESR and ODMR expts. 80−86360
solid, molecular fluoresc., phosphoresc., and ODMR line narrowing 80−43084
spectroscopy, modern aspects, book 80−51973
Stark cavity, open, for detection of microwave transitions 79−63288
tetracene, cryst., singlet exciton fission rate const. RYDMR spectra meas. 78−91619
tetracene, cryst., triplet exciton pairs, EPR spectra 77−43906
1,2,4,5-tetrachlorobenzene, excited triplet state dimer, intermol. exchange integral, isotope effect 80−15826
1,2,4,5-tetrachlorobenzene, impurity induced states, spin dephasing, spin coherence expts. 78−84498
1,2,4,5-tetrachlorobenzene, linear chain triplet excitons, electron spin-echo and ODMR 78−76357
1,2,4,5 tetrachlorobenzene, triplet excitons, high. mag. field, spin-lattice relax. study 80−20517
1,2,4,5-tetrachlorobenzene, triplet excitons, zero field ODMR 80−88891
trifluoroethane, MODR, rot. consts. 78−9177
trifluoroiodomethane, laser microwave double reson. spectroscopy with CO_2 laser lines 80−87156
triple resonance, semiclassical anal. 79−93963
triplet state, intersystem crossing rates from ODMR 78−78735
triplet state broadening, inhomogeneous and homogeneous, of optical and ODMR transitions in solids 80−32750
triplet state ODMR, spin-lattice relax. and triplet-triplet. absorpt. effects 79−19807
xanthione, optically detected mag. reson. study of lowest excited triplet state of aromatic thioketones 78−86901
Ag halide, EPR of triplet state of self-trapped excitons 78−43684
AgBr, optically-detected EPR of excitons 77−55732
AgCl, AgCl:AgBr, X-ray, ultraviolet effects, ODMR 78−79933
AgCl, and Br doped, optically-detected EPR of excitons 77−55732
AgCl crystals, optically detected 79−24233
AgCl, excited states, optically detected EPR 79−8073
AgCl, optically detected EPR of excited states rel. to luminesc. 77−12256
AgCl:Ni, optically detected double resonance, radiative recombination electron traps 80−20518
As_2S_3, amorphous, luminesc. and optically detected ESR, photoinduced struct. change 80−50399
As_2S_3, amorphous, optical detection of ESR 79−38408
As_2Se_3, amorphous and single cryst., ODMR expts. 80−50230
BO_2, gas, optically detected mag. reson. spectrum, $X^2\Pi$ rovibronic sublevels 78−82756
BaO, $A\ ^1\Sigma^+$ state, dipole moment, MODR Stark effect 77−46584
BaO, microwave-laser double reson. spectra 78−82757
CSI:Na cryst., V_K-Na^0 centre pairs, tunnelling recomb. 78−91952
$Ca^{35}Cl$, radical, rot. spectrum, $X^2\Sigma^+$ state, laser MODR 78−5257
CaF, $^2\Sigma_{1/2}^+$ ground state, spin-rot. and hyperfine splittings rot. depend., mol. beam laser-RF double reson. 80−43079
CaF, $A^2\Pi_r$-$X^2\Sigma$ band system 78−74685
CaF_2:Dy^{3+}, EPR of colour centres, spin-spin interaction of pair of Dy^{3+} ions *(Russian)* 79−69751
CaF_2:U^{3+}, anomalous magnetooptic props., optical detection of ESR and cross-relax. resonances 80−93287
CaO, $^3T_{1u}$ state of F-centre, ODMR spectra 78−43685
CaO, $^3T_{1u}$ state of F-centre, paramag. relax. optical detect. 78−43687
CaO, F-centre, selective excitation, detection of EPR 78−43688
CaO, F-centres, laser selective excitation and double reson. in Jahn-Teller systems 78−19379
CaO, line broadening of EPR and zero phonon lines of F centres 78−43686
CaO, obs. of dipolar induced spin dephasing, coherent optical-microwave spectroscopy 80−103900
CaO, phosphoresc. F-centre, phonon assisted conversion of Jahn-Teller states, ODMR under uniaxial stress 78−48084
CaO, random intrinsic strain effect on ODMR, PMDR, of F-centre in Jahn Teller states 78−84499
CaO, relax. in $^3T_{1u}$ state of F centres 80−24443
CaO, triplet state of F_A centres, ODMR obs. 79−28639
CaO:Mo, spin coherence and Stark modulation effect of F_A-Mo centre excited state 77−69733
CdS, ODMR, bound excitons 78−80253
CdS pulsed optically detected resonance, time depend. recomb. processor study 79−38411
p-CdTe, ESR optical detect., Overhauser shift, g-factor 78−80252
CdTe, optical detection of ESR 79−65770
CdTe:Mn^{2+}, luminesc. and magnetooptic reson., mag. field effect 80−93390
CdTe:Mn^{2+}, magneto-optical and microwave-optical double reson. meas. of exciton band *(Russian)* 77−81087
$^{37}ClO_2$, ν_3=1 state, laser-microwave double reson. obs. 80−95657
CsBr, F-centres, EPR in relaxed excited state, detection via saturated optical pumping 78−6606
CsBr, F-centres, relaxed excited state, ESR, detected via optical pumping 78−43693
CsBr, second relaxed excited state of F-centre, optically detected EPR 79−87335
CsBr, self-trapped excitons, magneto-optical props., 1.3-50K 80−49606
CsCl, F-centres, EPR in relaxed excited state, detection via saturated optical pumping 78−6606
CsCl, F-centres, relaxed excited state, ESR, detected via optical pumping 78−43693
CsF, EPR of self trapped exciton and MCd meas. 77−48091
CsI, self-trapped excitons, magneto-optical props., 1.3-50K 80−49606
CsI:Na, tunnelling recomb. of electron-hole pair, optical detection of ESR and circ. dichroism 79−47360
FCN, collisional transition obeying nondipolar selection rules between M-levels, laser-microwave double reson. 77−83627
$Ga_{1-x}Al_xAs$, optical detection of CESR 77−36155
GaAs, optical detection of CESR 77−36155
GaAs:Cr, far IR EPR spectroscopy, mag. field-modulation technique 80−15830
GaAs-$Al_xGa_{1-x}As$ multilayer, photoluminesc., electron spin orientation 80−25453
$Ga_{1-x}In_xAs$, optical detection of CESR 77−36155
GaP:N, spin dependent exciton recombination at N_2 isoelectronic traps 77−69734
GaP:O^-, two-electron O^- state evidence, ODMR, IR emission, phonon replicas 80−15828
p-GaP:Zn,S, spin polarisation of donors and acceptors in mag. field, optical and microwave study 80−93393
GaS, optical detection of triplet excitons 80−29650
p-GaSb, interband optical pumping, optical detection of EPR 77−28483
GaSe, optical detection of triplet exciton reson. 79−33567
GaSe, triplet excitons ODMR 80−25252
GaSe, type II crysts., triplet exciton resonances 79−47359
Ge, ODMR using luminescence of electron-hole drops *(Russian)* 77−90072
HCN, microwave-microwave double resonance 80−53029
H_2O, laser Stark and IR-RF double reson. at 6 μm 79−45760
He fine structure interval 2^3P_0-2^3P_2, optical microwave atomic beam mag. resonance meas. 80−102585
^{4}He, Rydberg states, fine struct., D, F and G states meas. 77−50418
ICl, $B^3\Pi_{0(+)}$ state, rot. transitions, quadrupole hyperfine coupling const. 79−85979
InSb, electron spin levels resonant excitation, photolum. 80−25454
KBr:Ga^+, Jahn-Teller effect in orbital triplet, optically detected EPR meas. 77−66441
KBr:Li(Na), F_A centres, optical detection of ESR 79−99793
KBr:P, colour centre fine struct., ODMR 78−6604
KCl, F centre, EPR in relaxed excited state, via mag. circular polarisation of emission 79−24232
KCl:Na, F_B centres, optical detection of ESR 79−99793
KCl:P, colour centre fine struct., ODMR 78−6604
KCl:PO_2^-, ODMR spectra at 2K, HFS tensor of P 79−87333
KCl:PO_2^-, triplet state pseudonuclear Zeeman effect, optical detections *(Russian)* 79−78571
KCl:PO_2^-, triplet state, level anticrossing and pseudonuclear Zeeman effect, microwave ODIMR 80−39896
KCl(Br), second relaxed excited state of F-centre, optically detected EPR 79−87335
K_2CuF_4, microwave excitation, optical detection of ferromagnetic reson. 80−50197
KF, self-trapped exciton, ODMR spectra 79−28286
$KMnF_3$, optically detected antiferromag. reson. 78−15029
Kr, g-factors meas. by optical pumping and mag. reson. 80−14246
LiF, self-trapped exciton, ODMR spectra 79−28286
MgO, F centre luminesc., effects of uniaxial stress and ODMR 80−20690
MgO:Cr^{3+}, ODMR, octahedral and orthorhombic site symm. 80−71243
MgO:Cr^{3+}, ODMR study, Cr^{3+} ions in tetragonal symm. sites 80−88892
MgO:Li, [Li]^0 defects, magneto-optical props., optical detection of EPR spectrum 77−12365
NH_2, hyperfine struct. of u-state, microwave optical double reson. 79−68246
NH_2, lab. obs. of 16 GHz rotational transition 77−3389
NH_2, microwave modulated saturation spectroscopy, hyperfine energy levels 79−68245

microwave-optical double resonance continued
NH_2, microwave-optical double reson., collision-induced transitions, vibronic state obs. 77−34667
NH_2, X^2B_1 rot. transition, MODR 78−66571
NH_3, IR-microwave double resonance 79−81221
NH_3, IR-microwave two-photon spectra using CO_2 lasers 78−37664
NH_3, microwave-microwave double resonance 80−53029
NH_3, molecular rotational transition, collision induced shift 77−484
NH_3+He(H_2), rot. relax. double and triple reson. obs. 78−66570
NH_3+He(H_2), rot. relax., double and triple reson. obs. 78−90196
NH_3+NH_3, vibr. and rot. energy transfer, IR-microwave double reson. study 78−46432
NHD, rotational transitions, microwave optical double resonance obs. 80−58293
$NH_2(X^2B_1)$, MODR, hyperfine coupling consts., spin rot. consts. 78−1010
NO, laser mag. reson. and IR-RF double-reson. near 5.3 μm 78−5258
NO_2, excited state, ODMR obs. 79−36670
NaCl, second relaxed excited state of F-centre, optically detected EPR 79−87335
NaF, self-trapped exciton, ODMR spectra 79−28286
$NaNO_2$, cryst., triplet excitons, localised states, zero-field ODMR, dopant effects 78−15062
$NaNO_2$:Ag^+, optical and MODR spectra, anion states spin-orbit perturbation 79−19908
Ne+^{3}He(^{4}He), $2p_4$ state alignment destroying cross sections 79−89757
OCS, dipole moment, laser microwave double reson.-Stark effect meas. 78−55191
OCS, MODOR in ν_2=1 state, nondipolar collision-induced transitions 77−6812
OCS, microwave-microwave double resonance 80−53029
RbBr(Cl) F centre, EPR in relaxed excited state, via mag. circular polarisation of emission 79−24232
$RbMnF_3$, antiferromagnetic resonance, optical detection, luminescence 80−7174
^{87}Rb double resonance, signal intensity charact. due to pumping light 77−34603
S_2 $^{35}Cl_2$, microwave spectra and double reson., assignments, distortion consts. and struct. 79−89664
Si, amorphous, glow-discharge deposited, ODMR spectrum, deposition temp. and annealing effects 80−50229
Si, amorphous, optically detected ESR obs. 78−84500
Si, amorphous, time-resolved ODMR and luminesc. 80−25254
Si amorphous film, glow-discharge, optically detected mag. reson., annealing and substrate temp. effects 80−20519
Si:P, optical excess charging $D^0 \rightarrow D^-$, photoelectron spin relaxation *(Russian)* 79−78572
SiC:Al,N (6H), ODMR for effective-mass-like acceptor 80−93213
SrF, $A^2\Pi$-$X^2\Sigma$ system, rot. anal. using CW tunable dye laser 79−31563
SrF radical, rot. spectrum of $X^2\Sigma^+$ state, MODR 78−9176
SrF_2:Tm^{2+}, modulation magnetooptic spectroscopy of cross-relaxation resonances 79−15381
SrO:Co^{2+}, EPR, optical, MCD absorpt. spectra 78−43692
Tl, in gas discharge, optical self pumping, hyperfine struct., microwave-optical spectroscopy 80−32680
Xe, $5d_{7/2} \rightarrow 6p_{5/2}$ transition struct., laser spectrosc. and double reson. obs. 78−1210
Xe, g-factors meas. by optical pumping and mag. reson. 80−14246
ZnO:Li, luminesc. donor-acceptor pairs, exchange broadened optically detected EPR spectra 78−23373
ZnO:Li, optically detected ESR, donor-acceptor pairs, line broadening 78−80256
ZnS, ODMR of Zn vacancy obs. 80−108121
ZnS, pulsed optically detected resonance, time depend. recomb. processor study 79−38411
ZnS, self activated emission, spin depend. donor acceptor pair recombination, ODMR exam. 79−42870
ZnS, time resolved ODMR, electron-hole recombination 79−42872
ZnS:Al, signal enhancement by field modulation, ODMR expts. 78−56406
ZnS:Ga, self-activated emission, A-centre ODMR 79−95685
ZnSe, ODMR expts., A and V^--centres, origin of emission bands 78−80255
ZnSe, optically detected mag. reson., donor g-factor 77−69732
ZnSe, optically detected mag. reson. of V^- centre and donors 78−10805
ZnSe:F, signal enhancement by field modulation, ODMR expts. 78−56406
ZnSe:Ga, P, optically detected mag. reson. of P_{Se}-centre 79−33566
ZnSe:Mn^{2+} Schottky barrier diodes, spin depend. cond. and photovoltage, donor reson. deep centre studies 79−91141
ZnSe:P(Ga), 1.91 eV red emission, optically detected mag. reson. study 79−69750

microwave oscillators
see also Gunn oscillators; microwave parametric oscillators; parametric oscillators; tunnel diode oscillators
0.5 GHz stripline oscillator employing $^{15}NH_3$ freq. standard 79−71418
1.2 GHz temperature stable SAW oscillator 78−59226
2.148 GHz SAW oscillator 80−74680
band I, 10 GHz, with noise compressed by acoustic delay line *(French)* 78−16818
BWO for 110 to 170 GHz, using Sm-Co using magnets, design and appl. *(German)* 80−105684
CRM-monotron, low-frequency fluctuations calc. *(Russian)* 77−88684
cyclotron resonance maser tube with transverse current, theory of oscillation 79−89877
gyrotron efficiency, CW and pulsed power achievements 79−31849
gyrotrons for high power millimeter wave generation, fusion reactor appl. 78−62611
IMPATT source, frequency-stabilised, 115 GHz 80−67573
Josephson bridge microwave oscill. regenerative effects *(Russian)* 78−2630
Josephson contacts, quasi-autonomous, props. 78−88084
Josephson junction, frequency-agile, biasing for precise freq., analogue computer study 79−28455
klystron self excited oscillator with short time delay microwave pulse 77−6578
maser, circulating resonance monotron, synchronisation *(Russian)* 77−38842
relativistic electron beam of microsecond duration for microwave oscills. 77−38057

microwave oscillators continued
stabilizing resonator of high-power klystron self-oscillator for microwave supply system of linear accelerator 80−42878
surface-skimming bulk wave controlled quartz crystal oscillator 78−59250
$Ca_{1-y}Sr_{y/2}Ba_{y/2}Zr_{1-x}Ti_xO_3$, ceramic system, dielectric props., microwave resonator application 80−80674
GaAs LSA diodes, current controlled LPE for optimum doping profiles 78−35318
InSb film cyclotron-frequency submillimetric oscillation generation model 77−80801
^{87}Rb maser and related oscillators, time- and frequency-domain stability 78−58968
n-Si, microwave and far IR hot carrier mobility, Monte Carlo calc. appl. to mm. transit time oscill. efficiency 78−72184

microwave parametric amplifiers
Josephson effect parametric amplifiers, mm wave superconducting devices, present status 79−26119
Josephson junction, externally pumped, singly and doubly degenerate microwave parametric amplifiers 79−26122
Josephson parametric amplifiers, gain-dependent noise temp. 80−84552
Josephson tunnel junction, parametric amplification at 35 GHz 79−95547
Josephson tunnel junction array parameter amplifier 79−65611
microbridge SUPARAMPs, phase instability noise in Josephson junctions 79−26124
nonperiodic bandlimited signals in three dimensional electron flow, general relations 79−68360
radioastronomy, 18 and 1.35 cm wavelengths amplifiers, charact. *(Russian)* 77−9658
superconducting, space appl. 80−85836
superconducting thin film parametric amplification region calc. 77−80860
GaAs n-n^+ epitaxial structure for CW electroacoustic amplifier 78−59235
GaAs thin-film semiconductor travelling-wave, differential mobility anisotropy effect 78−88050
n-GaAs-YIG layered structure, magnetostatic surface wave amplification 78−88107
Sn-O-Sn Josephson tunnel junction, parametric amplification on RF-induced steps 79−78266

microwave parametric devices
see also microwave parametric amplifiers; microwave parametric oscillators
n-GaAs, parametric interaction of HF waves, anal. 80−15554

microwave parametric oscillators
lasers, mm-wave Fabry-Perot tuning and freq. modulation by electrically variable external reactance 79−68409

microwave reflectometry
see also swept-frequency reflectometry; time-domain reflectometry
backscatter from ploughed soil, surface roughness meas. *(French)* 80−82072
biomaterial microwave complex permittivity meas., noninvasive selective exposure 79−20729
direct measures of small microwave signal reflections occuring on four-terminal networks and on dummy loads *(Polish)* 80−57334
dual six-port automatic network analyser, performance 80−47074
Goos Haenchen negative shifts 78−78865
human serum and erythrocyte microwave complex permittivity meas. 80−3889
K-band interferometer for measuring the magneto-microwave Kerr effect in semiconductors and ferrites 80−52263
reflection coeff. meas., calibration error evaluation 79−21768
reflection coefficients measurement *(French)* 79−67350
solid dielectric complex and power reflectivity determ., 100 GHz to 3 THz 80−15999
strip lines meas., dielectric, small standing wave ratio and losses meas. 80−77811
surface pollutants, microwave detect. of adsorpt. and spreading films 79−5690
thru reflect line, improved technique for calibrating dual six-port automatic network analyser 80−47073

microwave region *see microwaves*

microwave spectra
see also molecular rotation; molecular vibration; radiofrequency and microwave spectra of diatomic inorganic molecules; radiofrequency and microwave spectra of organic molecules and substances; radiofrequency and microwave spectra of polyatomic inorganic molecules
amorphous materials for IR and microwave absoprtion, temp. and freq. depends. 78−39539
atmospheric transparency, 3-13 cm^{-1}, rel. to water vapour conc. 80−12476
averaging method in RF-atom system interaction calcs. *(Russian)* 79−26973
2-bromo-2,3-dimethylbutane, low resolution, NMR values 79−54846
bromomethane+$OCS(SO_2)$, (cyanomethane), microwave spectral line width, dipole-dipole interaction calc. 78−74648
compounds with hindered internal rot., microwave spectra, free rotor states obs. 79−18179
Doppler-free saturated absorption microwave spectrometer 78−55256
electron storage ring coherent microwave emission fine struct. 78−78875
energy interval measurement by obs. Zeeman transition in microwave spectra 80−69274
ferromagnet, parallel pumping, in microwave field, magnon-photon interaction 79−51861
forest fire sources, microwave radiation spectra 80−52314
glass fibre reinforced plastics, dielectric const./mechanical strain relation, microwave study 77−32650
2-iodo-2,3-dimethylbutane, low resolution, NMR values 79−54846
K-band interferometer for measuring the magneto-microwave Kerr effect in semiconductors and ferrites 80−52263
laser heterodyne detector appl. in sub mm spectrosc. with harmonic generator 79−72444
magnetic system, amorphous, microwave absorption spectra 80−50469
magneto-microwave effects, rel. to EPR 77−55853
molecular forbidden rot. transitions, expt. and theory, review 77−34612
molecular geometry, minimum necessary no. of isotopic substitutions 77−3484
molecular press. broadened lines, deviations from Lorentzian line shape 77−61806

microwave spectra continued
molecular press. broadened width and shift, temp. depend. 77−61807
molecular vap., conformational changes, microwave spectroscopic intensities 77−75227
molecule, SPECAN, rot. spectra automatic assignments program, speed improvements 79−31499
molecules, short-lived, review 79−50010
molecules with internal rot., normal vibrs. classification 77−18909
Mori formalism for far IR and microwave absorption 77−24833
polyethylene, microwave photon echo 80−66330
polystyrene foam, X-band microwave dielectric spectra 79−87376
rigid linear rotor+atom, rot. relax., microwave transient T_1 and T_2 rates 79−13797
ruby, two-photon spectroscopy of reson. three-level spin system, reson. shift 79−82864
semiconductor, submillimetric magneto-optical props., strip line technique 80−60554
soil, theory for passive microwave remote sensing of near-surface moisture 77−87105
superradiance in alkali Rydberg atom medium 79−86153
symmetric top molecules, microwave transient phenomena, Bloch eqns. 79−26969
symmetric-top molecules, dilute gas, non-reson. microwave absorpt., kinetic theory 79−68901
tetramethylpyrazine-d_{12}, in durene matrix, intersystem crossing of 859.5 MHz transition 79−27015
triatomic molecules, microwave spectra, mol. parameters 79−31513
α-AgI, superionic conductor, microwave absorption spectrum 80−11515
β-Al_2O_3, Na, K and Ag substitued, lattice vibrs., ion transport spectra 77−20121
β-Al_2O_3-Ag_2O, superionic conductor, microwave absorption spectrum 80−11515
β-Al_2O_3-Na_2O, superionic conductor, microwave absorption spectrum 80−11515
$BaFe_{12}O_{19}$ powder, hysteresis of microwave absorpt. and magnetisation reversal 80−75814
Bi-Sb, semimetallic alloys 78−87908
BrF(Cl), rot. spectra in millimeter wave region, rot. transitions obs., equilib. const. determ. 80−78607
ClF, rot. spectra in millimeter wave region, rot. transitions obs., equilib. const. determ. 80−78607
Cs n=15-17 f-g interval meas. 80−91477
Cs^+ excited levels, hyperfine struct. and lifetimes 80−63590
CuTeBr, superionic conductor, microwave absorption spectrum 80−11515
p-Ge, compensated, sub mm and mm radiation absorpt., acceptor conc. depend. 77−28664
Ge, compensated, sub mm radiation absorpt., temp. depend. 80−66331
Ge, impurity spectral linewidth meas., free electron effects 80−71463
Ge:Be, P, absorption of radiation, 0.6-2.8 mm, 4.2 to 20K 80−66332
n-Ge:Ga(P), uniaxial compression, 0.6-2.9 mm radn. absorpt. 79−82629
n-Ge:P,Ga, compensated, uniaxially compressed, anisotropy of mm. and submm. wave absorpt. 78−19074
H, excited atom interacting with reson. oscill. EM field 79−76371
H-bonded complexes, microwave spectra, assignments, mol. consts. 78−62794
o-H_2, isolated in solid p-H_2 energy levels 78−2948
H_2, solid, orientational level structure of o-H_2 pairs, phonon renormalisation 79−47554
He, liquid, velocity autocorrel. time in surface electron liq. from spectral line broadening 77−20146
$Hg_{1-x}Cd_xTe$, n-surface inversion layers study 80−25017
ICl(Br), rot. spectra in millimeter wave region, rot. transitions obs., equilib. const. determ. 80−78607
n-InSb, strongly compensated, ionized donor mol. optical absorpt. spectra characts., 1.5-2.5 mm 79−11422
KD_2PO_4, microwave spectra, temp. depend. mode rel. to proton subsystem 80−24548
α-N_2, solid, $w^1\Delta_u$-$X^1\Sigma_g^+$ intensity and band shape 79−47427
Na, Rydberg levels mm resonances detected by field ionis., quantum defects, Stark shifts 77−42262
Na_2O-CaO-SiO_2 glass, mm wavelength absorpt. 79−82978
Ne-Kr mixture, collision-induced microwave absorpt. 77−88411
OCS+bromomethane, microwave spectral line width, dipole-dipole interaction calc. 78−74648
SiO_2, glass, ^{29}Si hyperfine struct. of E′ centre, microwave saturation props. 80−7165
Sr, Rydberg states, $^1D_2 \rightarrow {}^1F_3$ microwave transition meas. using selective reson. ionisation 79−72258
VO_2 film, optical and elec. props., 0.8 to 4.2 mm, near metal-semicond. transition 77−32473
VO_2, thermochromic film, visualisation of microwave radiation using metal-semiconductor phase transition 79−65845
W, single cryst., coated with ferromagnetic layer, longit. cond. electron spin waves 79−11307
YIG, intrinsic microwave emission, coupling to waveguide system, magnon system cooling 77−24912

microwave spectrometers
see also magnetic resonance spectrometers
absorption, swept-freq. system for dielectric characterisation 80−104824
absorption spectrometer with automatic tuning 80−270
acousto-optical radio astronomy spectrometer for processing of MM-wave signals 80−4253
analytical, instrumentation, automation, review 77−56260
baseline suppression using FM and harmonic detection 78−82866
bridge type, 94 GHz, used for SO_2 linewidth obs. 78−42044
bridge type superheterodyne microwave spectrometer, for transient effects investig. 80−91551
control pulse shaper for two-pulse relaxation time meas. 79−67363
dielectric spectrometer, meas. of attenuation coeffs. and permittivity of liquids 77−41646
Doppler-free saturated absorption microwave spectrometer 78−55256
double resonance modulation type with two confocal open resonators 77−53929
ELDOR spectrometer with computer-controlled scanning 77−1619
electronic sweep of magnet field 78−12717
EPR, microwave cavity variable coupling with solid construction 77−13790
EPR spectrometer, 2 mm band, with re-entrant resonator 78−86311
EPR superheterodyne spectrometer for Si defects detect. 77−43885

microwave spectrometers continued
ferromagnetic resonance, for wide band lines *(Slovak)* 79−12829
ferromagnetic resonance absorpt. lineshape 24 GHz microwave transmission apparatus 77−49755
Fourier transform spectrometer, double-pass rapid-scanning, for plasma diagnostics 80−103190
gas microwave absorption Fourier spectrometer for 300 GHz to 1.2 THz 77−5935
gas spectrometer using dielectric image waveguide 79−93229
grating spectrometer for mm waves 78−12768
interferometric microwave spectroscopy, modern aspects, book contrib. 80−52330
intrinsic sensitivity limitations, optimum attainable parameters, methods of realisation 80−37087
Ku-band microwave Fourier transform spectrometer, construction, appls. 80−68265
lamellar grating Fourier spectrometer for sub-mm and mm spectroscopy *(Japanese)* 77−67504
liquid dielec. permittivity meas., sub-mm wave, using laser- and Fourier transform-spectrometry 78−95568
low transparency samples, submm. wavelength spectroscopy 77−176
methoxy detection by submillimetric laser spectrometer 77−40623
microwave spectrometer baseline suppression using FM and harmonic detection 78−82866
moderate-pressure low-temperature spectrometer for paramag. reson. appl. 78−266
modern aspects, book 80−51973
modern aspects, book contrib. 80−52328
modulation technique, high temp. mols. 80−52236
noise considerations in millimeter-wave spectrometers, air pollution detection appl. 80−57367
NPL submillimetre-wave for precision measurements of gases 77−18111
one-dimensional wire grid and BWT spectrometers 77−38040
pressure-scanning millimetric-wave dispersion spectrometer expt. 80−61904
radar remote sensing, capability in 5-4 GHz region 79−25368
reflection-cavity paramagnetic spectrometer at 60 GHz 77−71356
regulator, wide-range magnet-current, for RE1301 microwave spectrometer 79−21779
scanning microwave spectrometer (SCAMS) on Nimbus 6 synoptic scale studies 78−16114
scanning spectrometry, submillimetre, modern aspects, book contrib. 80−52329
spin resonance spectrometer, influence of nonlinearity of microwave network characteristics 80−62707
Stark effect spectrometer, with electric molecular modulation *(Russian)* 80−9003
Stark modulator, zero-based half-sine wave, for analytical microwave spectrometer 77−13802
TWT prior to crystal detection for sensitivity increase 80−82822
$OHX^2\Pi$ radical, ground and vibr.-excited ($v \leq 6$) levels, microwave spectrum 79−63985

microwave spectroscopy
see also magnetic resonance spectroscopy; microwave spectrometers; paramagnetic resonance
3K blackbody cosmic background radiation meas. 77−41422
absorption cell, 'stripline' type, for use in microwave Stark spectrosc. 79−81305
air pollution, gaseous pollutant monitoring by mm-wave microwave rot. spectroscopy 79−48197
1-butanol, permitt., dielec. time domain spectroscopy, total transmission method study 80−27323
computer acquisition, simultaneous, of IR, microwave and Raman spectral data *(Japanese)* 80−4776
dielectric props. of biological substances, physical meas. 80−94417
dielectric relaxation spectroscopy, liquids, frequency and time domain expt. methods 80−40044
dielectric spectroscopy, combined total reflection-transmission method 78−86295
dielectric target microwave interrogation, scatt. parameters 79−20608
dielectric target microwave interrogation, time delay spectroscopy 79−20609
dielectric time domain spectroscopy, transmission method 77−74441
dispersion-absorption plots, for spectral line shape anal. 78−89511
dispersive Fourier transform, with variable thickness variable temp. liquid cells 77−37915
dispersive Fourier transform spectrometry, dielec. meas. on low-loss materials at millimetre and submillimetre wavelengths 77−37916
Earth imaging from Nimbus 6 satellite 78−12026
EPR, data handling and processing method *(German)* 77−53968
ESR spectrometry, anal., cavity loading effects 78−7253
Fabry-Perot resonator for CESR studies at 34 GHz 80−37065
fluid and solid molecular motion, submillimetric-wave spectroscopy obs. 79−31517
gas analysis by computer-controlled microwave rotational spectrometry 78−85227
glass reinforced plastic, microwave determ. of mech. strains, anisotropic props. in millimeter range 77−9023
high resolution spectroscopy in alkali metals 80−53248
high temp. molecules, modulation technique 80−52236
industrial appl. 77−67484
interferometric microwave spectroscopy, modern aspects, book contrib. 80−52330
interstellar molecules, microwave astronomy, modern aspects, book contrib. 80−56921
interstellar molecules, microwave spectrosc. obs. 79−41160
laser-microwave two-photon spectroscopic tunable source 79−30579
light-beating spectroscopy, collisionless sources, Forrester effect 77−34034
millimetric/submillimetric coherent transient spectroscopy 80−58651
modern aspects, book 80−51973
modern aspects, book contrib. 80−52328
modulation technique for CESR cavities 77−37956
molecular spectroscopy book 80−27051
molecular spectroscopy book 80−27052
molecule energy barrier to interal rotation 80−28117
multilayer dielectric microwave reflectance and transmittance, characteristic matrix formalism 80−239
network characteristics, influence of nonlinearity on shape of mag. resonance spectra 80−62707

microwave spectroscopy continued
nonlinear modulation microwave spectroscopy, press. and power correl. depend. 79−44936
one-dimensional wire grid and BWT spectrometers 77−38040
2-propanol, dielec. time domain spectroscopy, total transmission method study 80−27323
recent advances *(Chinese)* 79−71504
rotational spectroscopy, optical rot., semiclassical theory 77−75132
Rydberg atom microwave and far IR spectroscopy 80−63564
saturated spectral lines in mm and sub-mm mol. rotation spectroscopy *(Russian)* 77−75335
scanning spectrometry, submillimetre, modern aspects, book contrib. 80−52329
solar S-component spectrum in 4 to 7 GHz range, radiospectrograph for fine structure *(Russian)* 78−49320
Stark cell, broadband and low insertion loss, performance 79−17460
Stark modulated, min. detectable air pollutant conc. determ. 78−57337
stochastic NMR spectroscopy, Ito and Stratonovich calculus calcs. 77−13787
strip line mode structure influence on submillimetric-wave spectroscopy 79−30586
submillimetre spectroscopy, applic. to magnetic excitations 77−37955
submillimetre-wave precision measurement of gases at NPL 77−18111
submillimetric extension of molecular beam electric resonance spectroscopy 77−38751
submillimetric heterodyne receiver with laser local oscillator 77−38042
submillimetric wave atmospheric spectroscopy, review 77−41240
successive oscillatory fields, molecular beam resonance method 80−91706
time delay spectroscopic imagery of isolated canine kidney 80−46109
time-domain in aqueous solution, problems and solutions 77−74440
Tl, in gas discharge, optical self pumping, hyperfine struct., microwave-optical spectroscopy 80−32680

microwave tubes
see also electron bombarded semiconductor devices; electron-wave tubes; relativistic electron beam tubes
backscatter from intense relativistic electron beam 77−38794
coherent millimetric radiation from relativistic beam-plasma instabilities 77−39435
coherent scatt. from relativistic electron beams 77−42477
coherent submillimetric Cherenkov radiation generated by relativistic electron beam 77−38793
cyclotron-harmonic wave propag. in spiraling electron beam 77−19685
electron injector, high perveance, high power microwave device appl. *(Russian)* 77−38535
fusion machine application, review 80−23151
gas mixture, reacting, atom conc. reson. absorb. meas., microwave discharge lamp calibration 79−92032
gyrotron, new milliwave power tube 80−53198
gyrotron for electron-cyclotron heating in large Tokamaks 80−28751
gyrotron oscillator, TNS, electron cyclotron heating startup system, design 80−99330
gyrotron oscillator for electron cyclotron heating expt. on ISX-B Tokamak 80−99329
gyrotron power source development in MM wavelength range 80−28852
gyrotrons and gyrokylstrons, small signal theory, fusion reactor appl. 78−70633
gyrotrons for electron cyclotron reson. heating of Tokamak power reactor 80−99331
gyrotrons for high power millimeter wave generation, fusion reactor appl. 78−62611
helical electron beam in resonator of gyro device with uniform EM field, nonlinear eqns. soln. 79−81348
lasers and accelerators 79−72015
nonisochronic reflecting electron system, high power microwave emission 78−1140
O-type relativistic electron devices, linear theory 80−43242
O-type relativistic electron devices, nonlinear theory 80−43243
power capabilities for plasma heating *(French)* 78−9801
relativistic Doppler frequency conversion, on relativistic electron beam front, exptl. obs. 77−34799
relativistic sheet electron beam interaction with slow-wave structure 77−38795
space charge wave propag. along rotating electron-plasma column 77−55137
stimulated collective EM scatt. from magnetised relativistic electron beam 77−38791
stimulated EM shock radiation from relativistic electron beam 77−38997
stimulated EM shock radiation with frequency up-conversion 77−38996
stimulated scatt. with intense relativistic electron beam and zero frequency pump 77−38995
strophotronic source, radiation induction 77−46710
submillimetric magnetoresonant scatt. from relativistic electron beams 77−38792

microwaves
918 MHz rat irradiation, thermographic near field effects and behavioural studies, near field effects 78−7386
absorbed dose rate distrib. in phantom heads irrad. by aperture source 77−73581
AM, LF plasma wave excitation 77−62366
applications, in industry, science and medicine, w.r.t. economics and safety 80−3754
atmosphere, modification by space borne microwave beam at water vapour absorption line, 22.2 GHz 78−49171
atmospheric slant path propag., 15 to 40 GHz, survey of expts. 79−84465
attenuation due to rainfall, rain fine structure meas. *(French)* 78−53680
auditory perception of microwaves, contrib. of middle-ear structs. 80−67097
backscatter by sea waves, meas. at 8 mm and 30 mm *(Russian)* 77−5210
biological effects and medical applications *(Spanish)* 80−26260
biological solids, resonant interactions, physical plasma 80−101222
brain tissue, dog, dielectric props. between 0.01 and 10 GHz 80−16915
combustion bomb microwave cavity, electrically loaded with propagating flame front electron plasma, theory and expt. 79−20369
computed tomography with microwaves 80−104719
cross-polarization due to precipitation in atmosphere *(French)* 78−53674

microwaves continued
dielectric relaxation in muscle 80−51146
diffraction by various shaped conducting objects 78−29885
emission and exposure standards 78−44619
Hall mobility, microwave meas. method 79−54154
hearing mechanism hypotheses, holographic assessment 80−72178
holography, computer simulation and image reconstruct. *(German)* 78−46540
holography, fundamentals and appl. 78−37830
IEEE International Microwave Symposium, Orlando (1979) 79−68356
interaction of electron beams with microwave-frequency field, of planar gap 80−106431
interference and diffraction principles and expts. *(German)* 77−61900
International Microwave Symposium, San Diego, Calif., USA (June 1977) 78−5478
magnetic field diffr. meas. on axes of disks and apertures, Babinet principle, complex spirals 80−102599
mammalian nervous system, possible microwave mechs. 80−89738
mm wave propagation and atmospheric influences 79−84466
mm waves, attenuation due to rain at 74 GHz 79−80002
mm waves, rain attenuation measurements at 94 GHz 79−80000
mm-wave thermography, application to breast cancer 79−100693
modulation, by random fluctuations of pulse discharge plasma parameters 77−42988
near-field diffr. on the axes of disks 78−33652
nonlinear effects in polarised gases, complex dielectric constant evaluation 78−1787
plant leaves, microwave photoconductivity obs. 80−104637
in plasma, enhanced scatt. at upper hybrid freq. 77−7548
polarised, polar diagram for 3.2 cm waves, circular scanning indicator *(Russian)* 77−26328
ponderomotive effect on transverse electron beam, expt. 79−13886
power absorption differences between normal and malignant tissue 80−104640
propagation in standard atmosphere, ducting, subrefraction effects, radio links appl. *(Norwegian)* 79−29835
propagation through rain, numerical calcs. *(French)* 78−53675
radiation pattern meas. in presence of biological specimens 78−48828
radiation safety meas. and instrumentation 78−44618
radioactive waste vitrification appl. 79−18008
rain attenuation and depolarization of Earth-satellite transmissions at freq. greater than 10 GHz *(French)* 78−53689
rain effects, drop-size and temp. effects on forward and backward scattering 80−17317
recording using instant photographic technique 78−58079
remote probing for wind and struct. const., line-of-sight method 80−36426
remote sensing of Earth, radiative transfer eqns. 80−21855
sandstorms effect on microwave propagation 79−70834
soil, surface roughness effect on microwave emission 80−17264
solar power satellite, microwave power transmission technology 80−40868
solar power satellite, microwave system perform. during startup/shutdown 80−40869
submillimetre waves and applications, conf., San Juan, Puerto Rico (Dec. 1976) 78−4712
submillimetre waves and applications, conference, Guildford, England (1978) 79−31916
submillimetre waves and applications, conference, San Juan (1976) 77−38785
surface wave plasma production and appl. 79−19059
survey, propag., transmission, reflection, refraction, diffraction *(Norwegian)* 79−29834
thermal microwave emission from random inhomogeneous layer over homogeneous medium 77−42726
thermographic observability of tumours with microwave heating 78−73193
thermographic turnover detection, sweep-freq. illum. investigation 78−73194
thunderstorms, microwave radiometric detect. of corona from chaff 78−16106
tropospheric propagation, attenuation by salt water droplets 78−7725
tumour detection by microwave enhanced thermography and computer-aided image analysis 79−70604
two-frequency microwave holographic imaging with axial resolution 78−1184

mictomagnetism
see also spin glasses
alloys, review 79−24183
computer simulation 77−66365
dilute and concentrated alloys, magnetism *(Rumanian)* 78−91843
review 77−69578
Ag-Mn, spin glass alloy, elec. resist. 77−8067
Au-Cr(Mn), spin glass alloy, elec. resist. 77−8067
Au-Fe, mictomagnet, freq. depend. of susceptibility max. 78−95445
AuMn, mictomagnetic, Hall and magnetoresist. effects 78−43361
B_2O_3-PbO-GeO_2-Fe_2O_3 glasses, mag. props. and Mossbauer spectra, speromag. order at low temps. 80−80530
BaO-Fe_2O_3-B_2O_3 glass, splat cooled, low temp. micromagnetism 80−34660
BaO-Fe_2O_3-B_2O_3(Na_2O) glasses, high Fe_2O_3 content, mictomagnetic props. 80−65916
$Be_2Mn_{1-x}Fe_x$, mag. props., giant moment clusters 79−28508
$Ce_{80}Au_{20}$, metallic glass, mag. ordering and cryst. field effects, speromagnetism 80−80531
Co-Mn, FCC, magnetisation and mag. susceptibility meas. 80−60310
Cu-Mn, mag. irreversibility and metastability 78−19279
Cu-Mn, massive short-range antiferromagnetism 77−12139
Cu-Mn, spin glass alloy, elec. resist. 77−8067
Cu-Mn (15 at.%), short-range ordering, neutron scatt. polarisation anal. 80−50110
Cu-Mn (8 to 75 at.%), spin correl., neutron polarisation anal. study 80−65905
Cu-Mn mictomagnet, effect of ageing on mag. moment 77−43841
Cu-Ni alloy, critical conc. for ferromagnetism 78−14969
$EuB_{6-x}C_x$, magnetisation, effects of C 80−25163
$EuB_{6-x}C_x$, Mossbauer spectra, cond. electrons effect 80−20545
Fe-Al, ferromag.-mictomag. transition, intermediate superparamag. 77−12140
$FeAl_x$, ferromag. to mictomag. transition, Mossbauer meas. 77−24692

mictomagnetism continued
$Fe_{0.7}Al_{0.3}$, local environment effects and magnetic clustering 78−10658
FeF_3, amorphous, mag. props. and Mossbauer spectra, speromagnetism and mictomagnetism 80−75778
$(Fe_{0.04}Ni_{0.96})_{80}P_{10}B_{10}$, amorphous, mictomagnetic to ferromag. transition 78−34981
$Fe_cNi_{80-c}P_{14}B_6$, amorphous, annealing effects on mag. props. 79−78383
$Fe_xNi_{1-x}P_{14}B_6$, amorphous, spin-glass regime, magnetoresist. meas. 80−34418
$Fe_xNi_{80-x}P_{14}B_6$, amorphous, sp. ht. and susceptibility meas., spin glass and mictomag. props. 78−68274
Fe_2O_3-BaO-B_2O_3, magnetic props. of Fe-rich amorphous oxide *(French)* 80−80511
Fe_2O_3-Na_2O-BaO glass, mag. props. 4.2-295K, mictomagnetism *(French)* 80−39782
Fe_2O_3-PbO-B_2O_3 glass, X-ray and electron microscope studies, mag. and Mossbauer effect meas. 80−28919
$Ho_xY_{1-x}(Fe_{0.1}Co_{0.9})_2$, ^{57}Fe hyperfine interaction, mag. props., Mossbauer study 80−39951
$KFeF_4$, amorphous, mag. props. and Mossbauer spectra, speromagnetism and mictomagnetism 80−75778
(La,Gd)Al_2, spin glass, cluster glass and magnetisation characts. for different comps. 77−69585
La-Gd-Au, amorphous spin glasses, mag.-cluster description 79−42776
$LaNi_{1-x}Fe_xO_3$, magnetisation meas. and ^{57}Fe Mossbauer studies 80−93217
Mn-Bi mictomagnetic alloy, mag., elec. and elastic props. *(Russian)* 80−108028
Mn-Cu, mictomagnetic props., neutron diffr. obs. 80−65906
MnBi, mictomag. alloys, elastic props. *(Russian)* 80−7141
$Mn_{17.5}Cu_{82.5}$, ageing process, alternating mag. susceptibility meas. at 80K and 373K, 78−3157
Mo-Fe, spin glass and mictomag. regimes, sp. ht., resist. and susceptibility meas. 77−69581
MoFe, occurrence of spin glass and mictomagnetic regimes, props. meas. 77−16085
$NaFeF_4$, amorphous, mag. props. and Mossbauer spectra, speromagnetism and mictomagnetism 80−75778
Ni-Cu, low field magnetisation meas., mag. props. comp. depend. 78−91879
β'-NiAl B2 phase, mag. aftereffect 80−34700
$(Ti_{1-x}V_x)_2O_3$ spin glass, mag. props., metallic antiferromagnetism 79−82791
$(Ti_{1-x}V_x)_2O_3$, spin glass to antiferromag. regime 78−52276
V-Fe, ferromagnetism to mictomagnetism at low Fe conc. 78−91878
$Y(Fe_xAl_{1-x})_2$, Mossbauer spectra and mag. props. 80−39950
$Y(Fe_xCo_{1-x})_2$, $x \leq 0.2$, mag. props. and Mossbauer meas. 80−75798
$Zr(Fe_{1-x}Al_x)_x$, transition region, spin glass or long range mag. order 80−44841
$Zr(Fe_{1-x}Co_x)_2$, mag. props. and Mossbauer effects 79−91322
$Zr(Fe_{1-x}Co_x)_2$, magnetovolume effects, thermal expansion and forced vol. magnetostriction meas. 80−29595
$Zr(Fe_{1-x}Co_x)_2$, mictomagnetism 80−15863
$Zr(Fe_{1-x}Co_x)_2$, thermal expansion and forced volume magnetostriction 80−75830
$Zr(Fe_{1-x}Co_x)_y$, transition region, spin glass or long range mag. order 80−44841

MIDP
aniline, in p-xylene host cryst., phosphoresc. triplet state, ESR and MIDP obs. 80−66077
$^3\pi\pi^*$benzaldehyde, zero field splitting and sublevel decay rates, deuteration and host effect 80−37750
p-bromochlorobenzene, T_1 states, zero-field ODMR, MIDP and phosphorescence excitation spectra 80−74191
carbazolyl substituted diacetylene monomer cryst., ODMR and triplet state kinetics 78−76355
coronene, triplet mol. in n-heptane Shpol'skii sites, distortion and orientation meas. by MIDP 78−37668
coronene in n-heptane cryst., MIDP, distortion and orientation of mols. 79−31581
p-dibromobenzene, T_1 states, zero-field ODMR, MIDP and phosphorescence excitation spectra 80−74191
dichloronaphthalenes, heavy atom effects on subrates of lowest triplet states, MIDP obs. 80−91594
glyoxal-d_0, -d_2, triplet kinetics, microwave-saturation recovery and MIDP obs. 77−71823
halonaphthalenes, heavy atom effect on radiative and nonradiative decays 79−31584
5-methylpyrimidine, singlet-triplet intersystem crossing, ODMR and MIDP in matrix at 1.6K 79−50055
pyrazine, in pyrazine-d_4, p-dioxane, X-trap, p-xylene, benzene(-d_6), cryst., MIDP, PMDR, low temp., assignments 77−36154
pyrazine, vibronic bands, MIDP and polarised phosphoresc. in benzene matrix 77−6833
pyrazine triplet state, mol. distortion, MIDP using polarised light 79−10137
pyrazine-d_4, in p-dioxane, p-xylene, benzene, cryst., MIDP, PMDR, low temp., assignments 77−36154
pyrimidine, singlet-triplet intersystem crossing, ODMR and MIDP in matrix at 1.6K 79−50055
TCNB, electron donor-acceptor complex, triplet state phophoresc. kinetics, MIDP obs. 78−62839
triphenylene, triplet state, MIDP and T-S excitation spectrosc. 79−81233
p-xylene, isotopically mixed cryst., phosphoresc. triplet state, ESR and MIDP obs. 77−58071

Mie theory *see electromagnetic wave scattering*

military administrative data processing *see military computing*

military ADP *see military computing*

military computing
see also command and control systems
battlefield smoke/dust cloud temporal analysis algorithm 80−98484

military equipment
see also aircraft; military systems; ships
acousto-optic parallel channel wideband receiver 80−48447
Archimedes' mirrors, siege of Syracuse, feasibility *(French)* 79−62988
armour, lightweight ceramic, ballistic tests, computer simulation, book contrib. 78−48556
avionics interconnection fibre-optic data bus 78−46806
biomedical electronic, maintenance in forward army hospitals 79−96683

military equipment continued
C-CD image sensors, dynamic sampling of object pattern 79−50414
democratic control 79−75316
fibre optic communication system components, USA military developments, review 79−46060
fibre optics appl., West German developments 1978 survey *(Swedish)* 79−55209
fibre-optic processor serial interconnect system 78−1426
hard copy imagery from remote sensing systems, laser beam recorder appl. 79−80715
integrated electro-optical A/D convertor, using branching waveguide modulator channels 78−42474
integrated signal processor, using geodesic thin film lenses 78−42475
IR sensors and assoc. signal processing, performance evaluation 77−49313
IR source classification system, non image forming, exp., simulation results 79−49296
logic latches, mag. approach to upset prediction 77−18710
microcontroller, radiation tolerant, design, elec. and radiation tests, performance 77−18709
multielement IR detector array technology 77−45893
Navy navigation satellite system TRANSIT, on-board computer 79−29978
night vision goggles, military low-cost, design and development 80−78990
optical coating requirements in United States military specifications 80−48365
optical diamond turning and precision engineering 80−1364
optical fibre communication systems *(Italian)* 77−42601
optical fibre connectors, hot forming versus epoxy bonding of bundles, single fibre techniques 78−42482
optical fibre interconnection components 78−46812
optical fibres, connectors, standardisation 78−30083
optical glass fibre development, large-core, for military appls. 80−48451
optical precision machining commercialisation for military economy 80−1371
optical rotation rate sensors, Air Force appls. 80−9932
optical waveguides, manufacture, CAD, doped deposited SiO_2, optical fibres *(Italian)* 77−19385
portable US warning tape, perimeter warning device for combat troops 80−19200
protective headgear design, bioengineering considerations 78−11793
radar systems, space based, development, appl. 78−81525
replicated reflector for TOW anti-tank weapon's IR beacon 78−66889
ring laser gyro, military appl. 78−42370
SAW devices, US military investment and usage 77−39189
scanning sensor optimisation, SNR, sensor sizing parameters 79−58792
sonobuoys for anti-submarine warfare, design 79−3829
staring IR sensors, space and reconnaissance appln. 80−86406
submarine detection system, response to ocean waves 77−72220
T-coupler for multimode optical fibres 78−42457
tactical rugged lightweight fibre-optic cable performance 79−37025
thermoelectric power sources, technology improvements and 100 W and 500 W sources characts. 79−48151
undersea acoustics equipment, review (to 1950) 77−45667
United States Air Force infrared reconnaissance set 78−81458
US imaging sonar, design and construction 79−3831
visual simulation in training devices 79−50413
GaAs technology, MBE growth, microwave, optoelectronic devices appl. 79−52129
Li cells appl., 1979 state of art *(Spanish)* 79−96432

military systems
see also military equipment
aerospace systems and electronics, IEEE conference, Washington D.C., USA, 26-29 Sept (1976) 77−5420
airborne, reconnaissance, data collection, conf., Washington, DC, USA, March 1978 79−32078
aircraft voice communication networks, operational noise environment, expt. study 79−81662
automatic speech recognition, speaker authentication and data entry 79−94419
automatic target identification by hybrid pattern recognition 79−31829
automatic target screener for tactical thermal imaging system 79−32083
bandwidth compression effect on military target observers' detection and recognition performance 80−106484
communication, local distribution systems, use of optical fibre cables 78−9457
communications, multimode optical fibre waveguides appl. 78−55452
communications, SAW filters for signal sorting, identification in receivers 79−18615
context-dependent automatic image screening system 80−95820
defence science, effects on advance of astronomy 78−36471
electro-optics, systems aspects, seminar, Huntsville, AL, USA (May 1979) 80−94921
fibre optic connector system characteristics, aerospace user's viewpoint 78−46804
fibre optic long distance tactical communication link, injection laser transmitter appl. 78−42355
fibre optic sonar link, multichannel 78−42446
fibre optics, single mode, and integrated optics, for optical communication 78−42469
fibre optics for defence appls. in UK 78−42440
fibre optics for military appls., review and assessment 78−42438
fibre optics tasks of NASA, review 78−42441
fibre-optic communication systems progress 78−1425
Global Positioning System NAVSTAR connection to World geodetic system of DOD 79−25378
holographic one-tube goggle system engineering 80−78988
hydroacoustic sources of locally generated sound in towed arrays, hose material 80−23822
image anal., subjective and objective criteria 79−31828
image evaluation methods, project SENTINEL SIGMA for Air Force, resolution meas. 79−31826
IR system performance in airborne environment 78−82039
IR technology, conf. II (San Diego, California, 1976, August 26-7) 77−45891
IR technology utilisation, symposium, San Diego, CA, USA (Aug. 79) 80−86037
laser possibility of hitting high speed targets, shield piercing 77−68235
laser radar requirements for strategic and tactical appls. 77−38978

military systems continued
local distribution fibre-optic cable system 77−68277
Loran-C navigation system, progress report update 77−70875
man-machine interfaces, weather forecaster console for satellite data handling system 80−90205
marksmanship training, moving target screen system with laser beam firing 78−54488
moonlit object real-time optical matched filtering 77−19192
MTF anal. for post-flight image eval. 79−31827
multispectral aerial imagery capabilities for military geographic information acquisition 77−82054
NAVSTAR, satellite Global Positioning System 79−101042
NAVSTAR Global Positioning System, sea trials results 80−12645
NAVSTAR Global Positioning System satellites Doppler meas., geodetic solns. accuracy 79−100803
near-millimetric wavelength military systems 80−86428
neutron bombs, effects *(German)* 78−814
optical data bus T-system, single multimode fibre, based on access coupler 78−46810
optical data link, single fibre, multimode electro-optic guiding 78−38065
optical fibre, cost models for A-7 aircraft ALOFT project 78−59131
optical fibre applications to military and industrial systems 78−38021
optical fibre cables for use in ocean, design rel. to stresses 78−42439
optical fibre communication, A-7 ALOFT economic analysis, EM interf. and pulse tests 78−42448
optical fibre communication system, cost model 78−42447
optical fibre communication systems development 78−59158
optical fibre communications 78−42433
optical fibre digital transmission system, 2 km, for field use at 20 Mb/s 78−38064
optical fibre link for Command and Control System 280 78−42445
optical fibre multiterminal data system for aircraft, based on time division multiplexing 78−46811
optical fibre technology for military aeronautic appl. *(French)* 78−46813
optical fibre transmission, civil and military communications prototype systems 77−27375
optical fibre transmission systems appl. 77−75670
optical fibre waveguide link, colour multiplexing 78−42444
optical fibres and integrated optics, conference, London, England (May 1977) 78−38063
optical image and signal processing, United States Air Force programmes 78−74854
optical long focal length aerial reconnaissance system response to thermal shock 80−78939
optical system temperature effects and counter-measures 80−78938
passive mm wave radar detection of metallic objects in snow 79−84467
photodiode array integration with optical power spectral analysis 80−99645
physics and arms race, physicists participation explored for general education students 80−57023
radar system, forward looking IR, effect of ZnS CVD windows 78−46816
signal processing activities of United States Army 80−48172
signal processing research programme of United States Air Force 80−48171
sonar for smaller ships, clutter spatial correlation signal processor 79−3833
sonar horizontal array shape measurement using active/passive acoustic techniques 80−23824
submarine periscope optical design for laser rangefinding compatibility 80−78987
systems integration and optical design, conference, Reston, VA, USA (Apr. 1977) 78−50783
tactical reconnaissance system, real-time, KA-102A EO LOROP camera 79−30599
target IR emission meas. using versatile sensitive radiometer 77−70887
towed arrays, hydrodynamics 80−23823
underwater detection, effectiveness of distributed sensor concept 78−33944
USA Naval Observatory clock time scales, algorithm 79−21716
utilisation of IR technology, conf., San Diego (1977) 78−77984
weather chart transmission by facsimile 80−90206

Milky Way *see the Galaxy*

milliammeters *see ammeters*

mills, rolling *see rolling mills*

m.i.m. devices *see metal-insulator-metal devices*

m.i.m. structures *see metal-insulator-metal structures*

MINDO calculations
acetaldehyde, force consts., vibr. freqs., CNDO/2 and MINDO/2 calcs. 77−14607
acetylene, vibr. freqs., MINDO/3 calcs. 78−13429
acrolein, mol., conformational anal., inapplicability of MINDO/3 79−94105
aldehydes, conjugated, ethylenic, UV photoelectron spectra *(French)* 78−90215
alicyclic compounds, nucl. spin-spin coupling via nonbonded interactions, γ-substituent effects 80−69078
aliphatic compounds, nucl. spin-spin coupling via nonbonded interactions, γ-substituent effects 80−69078
alkanes, nucl. spin-spin coupling via nonbonded interactions, conformational and substituent effects 80−69077
n-alkenes, photoelectron spectra, MINDO/1, MINDO/3 and Fenske-Hall calcs. 78−5285
alkyl chlorides, proton affinity correl., ab initio SCF calc., MINDO/3, STO and G basis sets 78−33421
annulenes, MINDO calcs., electron correlations 79−45636
benzaldehyde, proton affinity, MINDO/3 results compared to ICR obs. 78−1103
benzene, vibr. freqs., MINDO/3 calcs. 78−13429
benzyl carbonium ion, internal rot. barrier, MINDO/2(3) forces method 78−9078
benzyl radical, MINDO/3-FORCES, geom. of heat of formation 78−66472
butadiene, mol., conformational anal., inapplicability of MINDO/3 79−94105
2,3-butanedione, mol., conformational anal., inapplicability of MINDO/3 79−94105
C-N spin-spin coupling consts., NMR, MINDO/3 calcs. 78−17694
carbenes, unrestricted HF calcs. of electronic structure 77−6683

MINDO calculations continued
carbon tetrachloride, low-energy X-ray emission spectra, MO anal., ionis. pot., rel. to CH_4 and $CHCl_3$ 79−85975
carbonyl compounds, ^{13}C chem. shifts, approximate SCF perturbation theory 77−6804
chloroethane diradical, MINDO/3 for optimised geometry and heat of form. 78−78830
chloromethylene radical, MINDO/3 for optimised geometry and heat of form. 78−78830
p-cyano-N,N-dimethylaniline in polar solvents, double fluorescence, theoretical model 80−58296
cyclobutadiene(-d_1), singlet and triplet ground states, vibr. freqs., MINDO/3 and ab initio SCF calcs. 78−13429
cyclopenta[h]cycl[4.2.2]azine, electronic struct., photoelectron data 78−5286
cyclopropyl carbinyl cation, internal rot. barrier, MINDO/2(3) forces method 78−9078
cyclopropyl ketones, photoelectron spectra, MO calcs. 77−27115
diamond (111) surfaces, relax. and reconstruction using C_4H_9 clusters, MINDO/3 calc. 79−42356
dichloromethylene radical, MINDO/3 for optimised geometry and heat of form. 78−78830
dimethyl sulphide dimerisation, S lone pair nonbonded contacts, EH, MINDO/3, CNDO/2 calcs. 79−773
dipole moment derivatives, MINDO/3 79−59599
dipole moment derivatives, MINDO/3 semiempirical calcs. 77−75055
electron affinity, MNDO semi-empirical SCF-MO calcs. for atoms, mols., negative ions 78−74578
ethane, localised molecular orbitals, orthogonal transformations calcs. 80−47892
ethane, photolytic decomp. to ethylene via triplet ethylidene, MINDO/2 calcs. 78−64869
ethane, vibr. freqs., MINDO/3 calcs. 78−13429
ethylene, and ^2H, ^{13}C, ^{15}N, ^{18}O isotopic derivatives, vibr. freqs. using MINDO/3 force consts. 77−71793
ethylene, dipole moment derivatives, MINDO/3 79−59599
ethylene, vibr. freqs., MINDO/3 calcs. 78−13429
fluoromethane, dipole moment derivatives, MINDO/3 79−59599
force constants, semiempirical quantum mechanical method 78−62947
formaldazine, mol., conformational anal., inapplicability of MINDO/3 79−94105
formaldehyde, force consts., vibr. freqs., CNDO/2 and MINDO calcs. 77−14607
formamide, mol. geom., self-consistent MINDO calcs., torsion and relax. effects 77−42243
formic acid, fragmentation, fragment structs. and energies calcs. 80−74124
glyoxal, mol., conformational anal., inapplicability of MINDO/3 79−94105
heat of formation calc. for C/H containing species *(German)* 78−82646
hydrocarbons, α-substituent effects in ^{13}C NMR, quantum chem. calcs. 78−74680
hydrocarbons, mol. geometry, CNDO/BW and MINDO/2 calcs. 79−41109
interstellar candidate mols. formed by NO ion-molecule reactions, MINDO/3 calcs. 78−28739
ionised molecules, geometrical and vibrational struct. changes, semiempirical MINDO/3 calcs. 79−31401
ketones, conjugated, ethylenic, UV photoelectron spectra *(French)* 78−90215
lactam-lactim tautomeric equilibria, quantum chem. calcs. 80−50833
methane, force consts., vibr. freqs., CNDO/2 and MINDO calcs. 77−14607
methane, low-energy X-ray emission spectra, MO anal., ionis. pot., rel. to CCl_4 and $CHCl_3$ 79−85975
methane, mol. cations, struct., Jahn-Teller effect, MINDO/3 calcs. 80−74135
methyl radical+ethylene(acetylene)(propene)(allene), reaction pot. surfaces, MINDO/3 calcs. 79−22601
methylamine, and ^2H, ^{13}C, ^{15}N, ^{18}O isotopic derivatives, vibr. freqs. using MINDO/3 force consts. 77−71793
methylene, photoelectron spectra, singlet and triplet state calcs. 78−42127
4-methylene-cyclohexadiene-2,6-one-1, proton affinity, MINDO/3 results compared to ICR obs. 78−1103
3-methyleneoxetane, electron structure, orbital-O interaction, MO calcs., UV photoelectron spectra 80−28058
MINDO/3, anomalous energy minima in pot. surface 77−34559
MINDO/3, limitations for unusually bonded mols. 78−25439
MNDO method, approx. and parameters 78−910
MNDO results for ground-state B-containing molecules 77−88391
MNDO results for H-, C-, N-, and O-containing mols. 78−911
molecular force fields, MINDO/3 semiempirical SDF MO calc. 79−76408
molecular geometries, reaction paths, MINDO/2(3) forces method 78−9078
molecular vibr. freqs., MINDO/3 calcs. 77−61730
molecule, electronic struct. and physicochem. props., modified partial neglect of differential overlap 78−82645
molecules, without internal rot., ground state heat capacity and entropy MINDO/3 calc. 78−33450
nicotinamide, and related compounds, dipole moments, electronic transitions, chemical and biological activity 78−90086
nicotinic acid, and related compounds, dipole moments, electronic transitions, chemical and biological activity 78−90086
nuclear spin-spin couplings between ^1H, ^{13}C, or ^{19}F, LCAO-MO-SCF-MINDO/3 approx. calcs. 79−94019
organic molecules, small, harmonic force consts., vibr. freqs., integrated intensities, MINDO/3 method 80−58411
organic mols., NMR coupling consts., MINDO/3 and perturbation theory 77−79630
3- oxetanone, electron structure, orbital-O interaction, MO calcs., UV photoelectron spectra 80−28058
phenylcarbene, singlet and triplet ground states, rearrangement to cycloheptatrienacarbene, MINDO/3 calc. 78−13430
trans-polyacetylene, electronic energy band struct., extended Huckel and MNDO studies 80−20065
β-propiolactone, electron structure, orbital-O interaction, MO calcs., UV photoelectron spectra 80−28058
quadratic potential functions, calc. MO constraint of interaction coordinates 78−74631

MINDO calculations continued
radical, small, isotropic hyperfine coupling consts., MINDO/3 calcs. 80−52894
retinal, proton donor-acceptor isomerisation coupling, bacteriorhodopsin as light driven proton pump 79−79473
semi-empirical SCF-LCAO calc. including energy minimisation, GEOMO program 77−23428
spirohydrocarbons, strained, bond angles, interatomic distances, semiempirical and ab initio calcs. 80−95533
TCNQ, infinite stacks, all valence electron band struct. 78−39001
TCNQ, semiempirical CNDO calcs. of electronic struct. and absorpt. spectra 78−995
3,3,4,4-tetramethyldiazetine, photoelectron spectra, ring size effects on azo group ionis. pots. 77−61793
triatomic inorganic mols., harmonic force consts., vibr. freqs., integrated intensities, MINDO/3 method 80−58411
trichloromethane, low-energy X-ray emission spectra, MO anal., ionis. pot., rel. to CCl_4 and CH_4 79−85975
trimethylene, singlet state, rot. barrier origin, MINDO/2 calc. 79−81170
trimethylene biradical, rot. barrier of mol., INDO calc. 79−68192
tropone, proton affinity, MINDO/3 results compared to ICR obs. 78−1103
TTF, infinite stacks, all valence electron band struct. 78−39001
vinyl isocyanate, conformers, geometrical and electronic structures, microwave spectra 78−9142
vinyl radical, MINDO/3-FORCES, geom. of heat of formation 78−66472
vinylidene+H_2, addition reaction, MINDO/3 study 80−108705
B and F chemical shifts, MINDO/3 in Pople's free electron model 79−93926
B-containing mols., MNDO calcs. for ground-state 77−88391
C-containing mols., MNDO calcs. for ground state 78−911
C_n aggregates in equilib. C vapour, MINDO/2 calc., isomerism 78−29873
CF_2 dimerisation reaction, UHF and MINDO/2′ calcs. 77−12793
CH_2, dimerisation reaction, UHF and MINDO/2′ calcs. 77−12793
$CH_2+H_2 \rightarrow CH_4$, MINDO/3-FORCES calc., acativation energy and enthalpy of reaction 78−66472
$C_2H_7^+$, ab initio SCF, CI, CEPA-PNO struct. and energy calcs. 78−94197
CHF dimerisation reaction, UHF and MINDO/2′ calcs. 77−12793
$C_2H_5O^+$ and $C_2H_5S^+$, stability, proton affinity, ab initio SCF, CEPA PNO, MINDO/3 and MNDO calcs. 79−59357
$CN^-.H_2O$, redox processes, MINDO/3 calcs. 79−47895
CO group, NMR chem. shift, solvent's dielectric const. effect, mag. anisotropy 79−42847
Cl, MINDO parameters 78−86786
F^-+methane, MINDO/3-FORCES study, reactant energy, products and paths 78−95926
H bonding, MINDO/3 approximation unsuitability 79−31400
H-bonded systems, MINDO/3 geom. optimis. calcs., heats of form. of monomer and dimer 79−31399
H-containing mols., MNDO calcs. for ground state 78−911
H_2, binding energy, MINDO/3 calcs. *(German)* 79−3366
H_2 ground state, bond breaking reaction, MINDO/3 CI *(German)* 78−21852
H_2^+, binding energy, MINDO/3 calcs. *(German)* 79−3366
$(HBr)_2$, intermol. distances, dipole moments, MINDO/3 and IR intensities and shifts calcs. 78−46335
$(HCl)_2$, intermol. distances, dipole moments, MINDO/3 and IR intensities and shifts calcs. 78−46335
$(HCl)_2$, vibr. freqs. in inert gas matrix, force const., MINDO/3 calcs. 78−41952
H_2O, and ^2H, ^{18}O isotopic derivations, vibr. freqs. using MINDO/3 force consts. 77−71793
H_2O, force consts., vibr. freqs., CNDO/2 and MINDO calcs. 77−14607
N-containing mols., MNDO calcs. for ground state 78−911
NH_3, force consts., vibr. freqs., CNDO/2 and MINDO calcs. 77−14607
O-containing mols., MNDO calcs. for ground state 78−911
P, MINDO parameters 78−86786
S, MINDO parameters 78−86786
Si (111) surfaces, relax. and reconstruction using Si_4H_9 clusters, MINDO/3 calc. 79−42356
Si, MINDO parameters 78−86786

mineral oil industry *see petroleum industry*

mineral processing industry
coal, liquefaction by hydrogenation, developments 79−92051
Colombian alluvial platina, processing historical account 80−86060
ore dressing X-ray spectrometric analysis centre 80−86541
U ore processing by filtration-free sorption method 79−26664

mineralogy *see minerals*

minerals
see also lunar rocks and minerals; mineral processing industry
β-eucrypite, glass-ceramics, internal stresses 79−15770
β-spodumene, glass-ceramics, internal stresses 79−15770
acoustic non-linearity parameter, calc. for twelve isotropic minerals 78−20392
actinolite, optical spectra obs. 77−40284
Adelaide meteorite, carbonaceous chondrite description and chemical anal. 79−2532
Adelaide meteorite, member of new carbonaceous chondrites subgroup, comp. and mineralogy 78−65573
adsorption of Tc and I radioisotopes by minerals 80−83203
afghanite, stacking variation, TEM study 79−99219
African plate, ore deposites rel. to mantle convection pattern and stress system 77−81859
aikenite, $CuPbBiS_3$, electrophysical props. 77−47822
albite, Al-Si order-disorder, electroneutrality effects in model 79−90593
albite, Li diffusion in silicate glass, ion-microprobe determ. 78−53649
albite, melt, viscosity and struct. changes at high press. 79−29754
albite, phase behaviour between 100 and 280 kbar at 1000°C 78−53644
albite, radial distribution functions, quasi-crystalline model 80−1879
albite porphyroblasts, growth rel. to deform. in Sambagawa schist, Central Shikoku, Japan 80−26509
albrittonite, new mineral from Llano County, Texas 78−65286
alinite, cryst. struct. determ. 79−19215
alkali feldspar, deformation, plastic defects, TEM investig. 78−32066
alkali feldspars, TEM study of exsolutions, review *(French)* 78−28224
alkali-Fe-Mg diagrams, magmatic trends 78−85551

minerals continued
alkaline, kinetic study of reaction with H_2S, pulsed differential reactors appl. 79−20465
allanite, metamict, phase changes on heating, age determ., x-ray fluoresc. anal. 77−51493
allanite occurrence in charnockites from Visakhapatnam, India 78−65285
Allende meteorite, mineralogy and petrology of isotopically unusual Ca-Al rich inclusion HAL 80−109399
Allende meteorite FUN inclusion Cl, search for ^{26}Al effects 79−16896
Allende meteorite minerals, Ti^{3+}/Ti^{4+} ratio as new cosmothermometer 79−12437
allophane, synthetic, amorphous mineral struct. obs. using ^{57}Fe Mossbauer effect 80−34836
almandine, synthetic, hydrostatic compression, isothermal bulk modulus 78−40545
almandine garnet, Fe-Mn interdiffusion expt. meas. rel. to compositional zoning 79−77812
almandine-pyrope garnet, elastic consts. from rectangular parallelepiped resonance method 77−56625
almandine-pyrope-grossular garnet, exsolution obs. 78−32074
aluminosilicate minerals, X-ray spectral study, emission bands, quantum yield, tetrahedra valence band 77−28660
aluminosilicates, isomorphous replacement theory 77−60113
alunite-jarosite, spcae group refinement by means of vibr. spectroscopy 79−94981
amacite, X-ray cryst. struct. determ. 80−28961
amber, natural, optical strength and laser induced rupturing 78−7039
amethyst, 3400 cm^{-1} IR spectra fine struct., H impurities 78−43910
amethyst, natural form. conditions and optimum artificial growth conditions *(French)* 79−33911
amethysts of E.Siberia, form. conditions and history *(Russian)* 80−12393
amosite fibres aerosol, collection efficiency of nuclepore filters 78−81341
amphibole, electrical resist., up to 60 kbar *(German)* 80−31032
amphibole fibre conc. in water, interlaboratory meas. by TEM 78−88590
amphiboles, high-resolution electron microscopy 80−75241
amphiboles in andesite and basalt, stability 79−66678
anadalusite, thermal expansion and cell parameters 79−90801
analcite, polyhedral tilt transitions obs. at high press. 80−6515
andalusite, shock-loaded, deform. 80−19873
andalusite+sericite+sillimanite, cyclic reactions in Willyama Complex, New South Wales 80−26508
anglesite, $PbSO_4$, crystal struct. and sulphate force consts. 78−83784
anhydrite, phonon spectroscopy, lattice dynamical calc. 80−19889
anhydrite, radioactive waste storage, anion effect on sorption of trivalent actinides 80−13717
anorthite, $CaAl_2SiO_3$, quenched from 1530°C, cryst. struct. 78−63700
anorthite, crystal growth rates from melt 77−16489
anorthite, thermal eqn. of state up to 120 GPa, appl. to Earth mantle 80−109136
anorthoclase megacrysts rel. to glass inclusions from Erebus volcano *(French)* 77−9388
anthophyllite, kinetics of Fe-Mg exchange reaction, rock cooling rates calc. 77−81875
apatite, α-induced X-ray anal. of Y, La, Ce, Nd content 79−16084
apatite, chem. anal. by secondary ion mass spectra 78−68965
apatite, fission damage detection, absorpt. spectra 78−84617
apatite, fission track retention as functions of heating time during isothermal expts. 80−36420
apatite, Indian, fission track dating and annealing, U content determ. 79−57891
apatite, influence of crystallographic struct. on annealing of fission fragment tracks 77−38577
apatite, mean etchable fission track length, high fission track densities determ. 77−82041
apatite crystal growth in skeletal tissues 80−94181
apatite in ijolitic and carbonatitic igneous rocks, comp. vars. 79−57929
apatite radioactive waste storage, anion effect on sorption of trivalent actinides 80−13717
apatite solubility in magma, laboratory expts. 80−72504
apatites, condensation of tetrahedra, IR absorpt. band exam. 77−85760
apatites, dipolar reorientations, TSD study 80−107068
aphiboles, nomenclature 79−66677
aragonite, formation through precipitation of $CaCO_3.H_2O$ 78−27427
aragonite, polymorphic transition kinetics, differential thermal anal. meas. 79−14722
aragonite, Sr/Ca ratio for ocean temp. 80−12568
aragonite, transform. to calcite in marine gasteropod 79−62485
arfvedsonite, sodic amphibole occurrence in basalt dykes, Newfoundland 78−65287
armalcolite, synthetic, stability as function of press. and O_2 fugacity 77−64275
Armorican Massif, occurrences of antimony minerals from ile de Sein and cap Sizun *(French)* 78−11888
armstrongite, X-ray cryst. atomic struct. and refinement 79−60345
arrojadite, X-ray cryst. struct. determ. 80−39058
arsenolite, As_2O_3, vapour mol. mass determ. using repulsion Knudsen cell 78−46464
asbestiform chain silicates, new minerals and struct. groups 78−28227
astrophyllite, electron diffr. characts. of polytypic forms 77−39573
astrophyllite, polytypic forms 77−39572
N.Atlantic recent sediments, volcanism effects on mineral comp. 78−44802
aubertite, X-ray cryst. struct. determ. *(French)* 80−33932
augite, influence on plagioclase fractionation in igneous rocks 80−12390
auripigment, radiography of geological specimens for determ. of α- and fission-activity 78−20540
Australia, genesis of Proterozoic U deposits 79−84270
authigenic silicate minerals in marine sediments and oceanic Mg budget 77−86858
autunite, random layer structure by grinding, X-ray powder patterns 77−78174
axial-plane slaty cleavage and schistosity development, expt. 78−7625
babefphite, cryst. struct. determ. using $P\bar{1}$ automatic diffractometer 80−107179
baddeyelite, high-press. phase transform., Earth mantle appl. 80−8296
Baltic underwater coastal slope sand grain size and mineral composition *(Russian)* 80−76963

minerals continued
banded Fe formations rel. to inverse segregation in Precambrian sea 79−20863
barite, $BaSO_4$, crystal struct. and sulphate force consts. 78−83784
barite, $BaSO_4$, thermoluminesc. glow curves after γ-ray irrad., low doses 77−63471
barite, crystal orientation determ. by Laue method, computer calc. *(Chinese)* 79−32853
barite, deposits at deep-sea hydrothermal site on strike-slip fault 80−21710
barite, in Devonian carbonate rocks, NE British Columbia, origin hypothesis 79−25240
barite rare earth composition rel. to formation conditions 80−41439
barium mordenite, dehydrated, position of cations and molecules, electron probe anal. 78−51509
Barwell meteorite, fusion crust mineralogy obs., preatmospheric size determ. 78−53893
baryta, crystal gas-liquid inclusion meas. with microscope heating stage 80−76967
basalt, compressed, appl. to shielding against soft X-ray radiation 78−41865
basaltic glass, expt. study of cationic diffusion of alkali and alkali-earth ions 78−95180
basalts from Nazca Plate, mag. props. and opaque mineralogy 78−20396
bauxite, Fe-containing, Mossbauer analysis 78−44806
bauxite, increasing contrast of secondary scatt. aureoles *(Russian)* 77−29299
bauxite, seismic exploration, analysis method for statistical distribs. *(Russian)* 77−9561
bayldonite, struct. chem., complex layer struct. 79−46609
beach and dune sands on Goa coast, mineralogy 77−41028
Bench Crater meteorite, member of new carbonaceous chondrites subgroup, comp. and mineralogy 78−65573
bentonite, selective sorption props., thermodynamics of ion-exchange reactions 79−39203
bentonite, selectivity of ion-exchange reactions 79−34360
bentonite, sorption props., appl. to radioactive fallout water deactivation 79−43995
berndtite, SnS_2, cryst. struct. and compressibility at high press. 78−67685
berthierite, $FeSb_2S_4$, anomalies in elec. and dielec. props. 77−47821
beryl, channel constituents, electronic absorption spectra of Fe^{2+} 79−69863
beryl, natural and synthetic, ion channelling transmission ratios 80−75277
beryl, single crysts., dislocations obs., X-ray topography *(French)* 79−37709
beryl, single crysts., growth defects study using X-ray topography *(French)* 79−37710
beryl, thermal expansion study 79−37857
beryllonite, Zn(Fe) analog, refined cryst. struct. allowing anisotropy of atomic thermal vibs., comparison with hurbutite 79−55722
beryls, optical absorpt. spectra in the near IR (900-2500 nm) 80−89004
biotite, deform. and recrystallisation in Woodroffe Thrust mylonite zone 80−21739
biotite, disordered mica struct. high resolution electron microscopy exam. 78−91344
biotite, excess ^{40}Ar, mobility in metamorphic terrain 80−17260
biotite, Mossbauer and optical spectra, Fe^{2+}-Fe^{3+} interactions 80−60470
biotite, thermal decomposition, stability of ferromag. products 78−57195
biotite+apatite geothermometer, re-examination 78−85704
biotite at Fleurieu Peninsula, South Australia, deform. rel. to slaty cleavage development 80−21735
biotite deformation, comparison with muscovite from optical microstruct. 80−26507
biotite stress corrosion cracking, seen in granodiorite 80−36299
biotites, Alpine, excess Ar evolution from ^{40}Ar-^{39}Ar anal. 80−94521
birnessite group mineral, new, with 14 Å spacing, in deep-sea micronodules 79−74892
bismuthinite, superheavy element search using neutron multiplicity counter 80−4011
Black Sea and Bay of Biscay, grain size and mineral comp. of shelf sediments 79−20812
boehmite, γ-AlOOD, hydrogen bond, neutron profile refinement of struct. 78−71701
boehmite, γ-AlOOH, lattice vibrs., evidence for C_{2v}^{12} space group 79−28756
boehmite, γ-ALOOH, structural variability 78−38681
bog Fe ore, Mossbauer effect exam. of annealing effect on struct. 78−19396
bornite, cathodolum. and AES, ionic diffusion obs. 80−71497
bornite-digenite series, superstructuring, vacancy clustering, high-resolution electron microscopy 78−42981
boxed sets of rock and minerals from Geological Survey of Canada 77−37203
bredigite-larnite rock from Scawt Hill, electron microprobe anal. 78−68952
bronzite, influence of crystallographic struct. on annealing of fission fragment tracks 77−38577
Bulgarian mid-Rhodopes massive, depth struct. metallogeny and main formation tendencies *(Bulgarian)* 79−34812
bulk chemical anal. calc. from mineral phases obs. in thin section, BULK computer program 79−2378
bulk modulus-volume relationship, for cation-anion polyhedra 80−41434
Burgers vector characterisation method using electron microscope contrast simulations 80−109141
bytownite, quenched from 1723K, X-ray single cryst. struct. anal. and refinement 79−19193
bytownite megacrysts., study of trapped basaltic melts, petrogenetic process study 78−95688
C1 carbonaceous chondrites, vein form. 79−2533
calaverite, Te atom splitting and modulated struct. 79−99145
calc-silicate isograds, Riondel area, SE British Columbia 77−5197
calcic plagioclase, ordering and antiphase boundaries 79−95032
calcite, A_{1g} Raman mode obs., new technique appl. 79−61354
calcite, anisotropic elastic const. meas. by uniaxial compression test *(Japanese)* 79−79822
calcite, atm. dust, imaginary refr. index rel. to particle size 78−7763
calcite, cryst. preferred orientation in marble, mag. susceptibility anisotropy development 78−56286
minerals continued
calcite, crystal intergrowth condensation-crystallisation contact bridge, between dissimilar crystals 79−65332
calcite, deform. twinning mechanisms 80−79814
calcite, elec. cond., 300 to 1200°C at CO_2 pressure of 40 bars 80−20195
calcite, formation temp. of fluid inclusions 77−56618
calcite, I-II phase transition interrelation with flow or fracture in carbonate rock deform. 80−51389
calcite, II-III transition rel. to high press. US propag. in Solenhofen limestone 79−29756
calcite, luminescence spectral anal. of polycyclic aromatic hydrocarbon impurities 80−71483
calcite, mechanical behaviour studies by stress relaxation testing method 78−96309
calcite, phase transitions rel. to calcite rock compression waves 78−81151
calcite, polished sphere as teaching aid for birefringence demonstration 77−71172
calcite, preferred orientation, review and outlook 79−83220
calcite, Quaternary, thermoluminescence dating 79−84231
calcite, skeletal, dissolution in deep sea, rate control 79−20817
calcite, source of excess Ca in rain and snow samples, Japan 79−39766
calcite, subglacially precipitated, $^{18}O/^{16}O$ palaeoclimatic implications 79−20897
calcite, thermal decomp. in vacuo, ultrastruct. and crystallography 78−71864
calcite, thermolum. dating, age relation for slices 77−34073
calcite, thermoluminesc. spatial distrib. using image intensifier technique 80−47115
calcite and aragonite precipitation, seed crystal effects 77−33054
calcite crystal as radiation-stable thermometer 78−203
calcite dating, appl. of luminesc. under N_2 laser excitation 80−60685
calcite dissolution by fossil fuel CO_2, effect of sediment mixing 78−81212
calcite microstructure, geological aspects 79−57933
calcite speleothems, stable isotope geochemistry rel. to climatic change, 230000 to 100000 BP 79−2234
calcite speleothems from Britain, palaeoclimatic and geomorphic implications of $^{230}Th/^{234}U$ dates 78−36128
calcite-depositing spring, chemical vars. and calcite precipitation 79−44202
calcium hexahydroborite, crystal struct. determ. 77−15391
Canadian mineral occurrence index 77−53205
Canadian soil characterisation of FeO compounds by Mossbauer and other methods 77−44986
cannizzarite, X-ray cryst. struct. determ. 79−23567
CaO-SiO_2-CO_2, subsolidus and liquidus phase relationships to 30 kbar 80−85643
carbonaceous chondrite mineralogies, remote spectroscopic identification in Ceres and Pallas 79−96946
carbonaceous chondrites of Ornans type, mineralogy rel. to metamorphic sequence 77−87341
carbonate, (Si, Cl)-bearing, from limestone-granite contact zone near Ikizdere, Turkey *(French)* 78−69339
carbonate mineral identification by CO_2 evolution on heating 80−90248
carbyne forms, of C, in natural graphitic formations in Ceylon and California 79−77450
carlfriesite, cryst. struct., chemical formula revision, and synthesis 79−55709
cassiterite, appl. of cathodolum. microscopy and spectrometry 77−69919
cassiterite, reduction by H_2 *(Korean)* 79−39201
celestite, colouring mechanisms 79−82998
celestite, $SrSO_4$, crystal struct. and sulphate force consts. 78−83784
α-celsian-leucospherite-tuhualite-milarite series of cpds., struct. types 79−19223
ceramic mineral, exam. by X-ray diff. at high temp. *(French)* 79−96234
Cerro Impacto, Venezuela, thermoluminescence radiation dosimetry appl. to Th prospecting 78−32244
chabazite, Cu^{2+}-exchanged, cation and water mol. positions 78−15709
chabazitic tuff, a zeolitic rock for thermal storage of solar energy 80−94117
chalcopyrite, cathodolum. and AES, ionic diffusion obs. 80−71497
chalcopyrite, NH_3-oxidation leaching, reaction kinetics 77−52639
chalcopyrite, NH_3-oxidation leaching, surface deposit effects 77−48643
chalcopyrite, nonlinear impedance of mineral-electrolyte interface 79−53338
chalcopyrite, superficial degradation in air and water, XPS obs. *(French)* 80−89110
chalcopyrite oxidation, in acidic chloride medium electrochem. study 78−95817
chalk, grain size determ., sample preparation methods 79−24694
Changbaiite−a new lead metaniobate mineral discovered in China *(Chinese)* 78−85543
chemical analysis, biotite gneiss and amphibolite mode estimation, using FISK (FORTRAN) program 77−86397
chemical analysis, energy dispersive X-ray spectrometry with Si (Li) diodes *(French)* 80−85251
chemical analysis by ion beam analysis *(French)* 77−52711
chert, Ce as indication of form. in marine environment 77−37200
chert artifacts, thermolum. determ. of prehistoric heat treatment 78−24914
chevkinite from Oslo region, Norway, cryst. struct. and chemical comp. 78−85533
E.China Sea sediments, mineral comp. and distrib. *(Chinese)* 80−8293
chlorite, ^{57}Fe Mossbauer analysis 80−40006
chlorite, cryst. struct. and compressibility at high press. 78−63717
chlorite, fission track annealing and age determ. 78−36307
chloritoid, topotactical dehydration, X-ray diffr. and TEM study 79−51057
chloritoid intergrown polytype identification by electron multiple scatt. 80−70184
chondrules, experimental reproduction of textures 80−94763
chrome ores, rapid anal. by X-ray fluoresc. 79−16065
chrome-magnesia, rapid anal. by X-ray fluoresc. 79−16065
chromian spinel lamellae in olivine from the Iwanai-dake peridotite mass, Hokkaido, Japan 78−96205
chromite, in Allende meteorite, search for fission tracks from superheavy elements 78−32415

minerals continued
chromite grains in Fe formation from Early Precambrian Isua supracrustal belt, W. Greenland, probable cosmic origin 80−72508
chromite natural samples of Brazilian, Philippine origin, chem. comp., Mossbauer spectroscopy 80−103901
chromites, electron microscopy, high-resolution observations 80−75241
chromites, from India, struct. and comp. 78−44807
chrysocolla, electronic absorpt. spectra 78−92087
citrine, 3400 cm^{-1} IR spectra fine struct., H impurities 78−43910
claudetite, As_2O_3, vapour mol. mass determ. using repulsion Knudsen cell 78−46464
clay, compressed, appl. to shielding against soft X-ray radiation 78−41865
clay, symposium (New Delhi, 1972, October 10-12) 78−7617
clay minerals, distrib. in sediments of Bay of Bengal 78−81146
clay minerals, interstratified, X-ray scattering 79−66685
clay minerals in DSDP Leg 34 basalt, form. 79−29767
Clearwater Lake impact structures, Quebec, meterotic component and impact melt comp. 78−65314
clinohedrite, cryst. struct., comparison with herstmannite 79−19228
clinohedrite, cryst. struct. study 78−79593
clinoptilolite, natural zeolite, ion-exchange, struct. rel. to heating 79−39145
clinoptilolite, sorption props., appl. to radioactive fallout water deactivation 79−43995
clinopyroxene geothermometry of spinel-lherzolites 77−2126
clinopyroxene in ophiolitic metabasalts of Mediterranean area, comp. 79 57925
clinopyroxene-orthopyroxene pairs, element partitioning in spinel peridotite xenoliths from Assab 79−62488
clinopyroxenes, in Mesozoic pillow lavas from French Alps, comp. trends, cooling rate effects 77−5154
clinopyroxenes from deep sea basalts, statistical anal. 78−88828
clinopyroxenes from deep-sea basalts, statistical anal. of chemistry 80−41437
closing temp. for fission track retention 77−64268
coal and mineral content characterisation by Fourier transform IR spectroscopy 80−104474
coesite, discovery in Vredefort Dome, S.Africa 78−53653
coesite, elasticity meas. on 100 μm cryst. 77−44978
coesite-stishovite transition determ. by in-situ X-ray meas. 77−17092
colour of gems and minerals 77−37182
colour origin, physical theories 78−69323
colour values from diffuse reflectance spectra *(French)* 78−11881
COMOD, program for standardizing mineral resource commodity data 78−20524
compressional wave velocity and damping, minerals and rocks at high-press. *(German)* 80−31031
computerised model analysis, from raw point-count data using MODES (FORTRAN IV) program 77−86880
contour map aeromagnetic data computer processing 78−7819
coral skeleton US velocity and Young's modulus anisotropy obs. 79−57837
cordierite, Brazilian, giant halos, superheavy element search 80−21752
cordierite, evidence of giant halo radioactive inclusions 80−94524
cordierite, isolation of excess ^{40}Ar effects in $^{40}Ar/^{39}Ar$ dating 77−29456
cordierite-garnet bearing assemblages in granulite facies terrains 78−44810
Cornwallis Pb-Zn District, Canada, Mississippi Valley-type deposits controlled by stratigraphy and tectonics 77−91130
Cornwallis Pb-Zn district, deposits controlled by stratigraphy and tectonics, discussion 78−73366
corundum, derived from dehydration of diaspore (α-AlOOH), periodic regular texture 79−99328
cosmic ray particle identification from tracketch rates in minerals 79−16788
Cretaceous clay minerals from S.Atlantic DSDP cores *(French)* 79−84220
cristobalites and topologically related structures, cryst. struct. 77−7688
critical mineral resources 79−5482
cryolite, hydrothermal synthesis of large synthetic single crystal, props. 78−19654
crystal growth characts. 78−32072
crystal settling in upper mantle magmas, high-press. viscosity expts. 77−29291
crystalline minerals, elastic consts. rel. to surface waves propagation over liquid and crystalline layers 80−76924
crystalline minerals, surface waves propagation over liquid and crystalline layers 80−76925
crystallisation, barometric investigation autoclave 77−86241
crystallographic defects, high-resolution TEM obs. 80−72517
cubanite, new sulphide phase in CI meteorites 78−12173
cumulate nodules from Lesser Antilles island arc, crystallisation conditions 78−65267
dating, EPR method 80−36415
deep-sea cherts and porcelanites, mineralogy of silica phases 77−86856
deformation mechanisms, international colloquium (Perros-Guirec, France, 1-5 October 1978) 79−96757
deposit evaluation with Metalog gamma-ray anal. technique 77−64446
deposition temperature, determ. via decrepitometric recorder with electronic filter *(French)* 79−48571
desert varnish, cyclic Mn deposition 79−16469
desert varnish, importance of clay minerals 77−86893
determination of C and O_2, ZAF correction procedure *(French)* 80−11983
Devonian lacustrine sediments, from Caithness, Scotland, palaeomag. and mineralogy 78−28170
Devonian old red sandstone, comparison with Euphrates and Tigris river sediments 78−81160
diamond, defect struct., recent obs. by new methods 78−30628
diamond, impurity complexes, shape and dimens., diffuse X-ray scatt. obs. 78−47398
diamond, natural, polycryst., distinctive features of struct. 79−92530
diamond with garnet inclusion, expt. crystallisation conditions study 80−46172
diamonds, artificially coloured, spectroscopic diagnostic technique 78−65281
diaspore, AlOOH, cryst. struct. refinement and electron density distrib. 80−79758
dickite, unusual crystal habit, structural disorder 80−59445
minerals continued
dickite occurrence in Jamaica, ordered and disordered varieties 78−83786
diogenesis, plate tectonic controls 80−12387
diopside, crystal growth rates from melt 77−16489
diopside, elasticity 80−6454
discovery probability, quantitative fall-backs of naturalist classifications 77−53204
dislocations and shock compression, thermodynamics 80−100235
disperse, with small specific surface, heat of wetting determ. 77−29050
dispersion staining method for refr. index meas. of a thin crystal section 80−8433
dissolution under Earth surface conditions, rate control 79−20817
djurleite, cryst. struct., X-ray study 79−42033
dolomite, $CaMg(CO_3)_2$, kinetics and thermodynamics of decomposition to metastable solid product 78−80740
dolomite, deform. twinning mechanisms 80−79814
dolomite, preferred orientation, review and outlook 79−83220
dolomite, radioactive waste storage, anion effect on sorption of trivalent actinides 80−13717
dolomite, radiography of geological specimens for determ. of α- and fission-activity 78−20540
dolomite, stacking faults obs. 78−3761
dolomite (Magneta), migration of ^{137}Cs, effect on radioactive waste storage 80−13718
dunite-peridotite mixed-oxide compositional models rel. to mantle temp. 77−2124
dusts, electron microscope anal., environmental monitoring 77−81877
dusts and asbestos fibres, health hazards 77−86732
dusts in environment, health hazards 77−87068
dyke walls minerals, ang. relations as dyke injection direction criterion 79−79843
Earth interior, mineral comp. prediction for rocks at great depths *(Russian)* 80−104956
eclogites, Rb-Sr dating in Munchberg Gneiss Massif 79−34774
economic geology management system 77−53201
elastic behaviour, near phase transitions with negative dP/dT 78−83885
elastic props., chemical comp. and crystal struct. 77−86862
elbaites, ferriferous, γ-irradiated, Mossbauer study 80−44990
electron microprobe, and ion microanalyser, appls. in mineralogy *(French)* 79−5628
electron microprobe data analysis, using FORTRAN IV programs 77−86878
electron microprobes and scanning electron microscopy, conf., Orsay, France, Dec. (1978) 80−11979
electrostatic precipitator, free-fall, motion of charged particles, determ. 78−71020
elpidite, Mongolian, cryst. struct. 78−95038
emerald, artificial single crystal, distrib. of Cr^{3+} impurity 80−59505
enorthite-albite system, crystal growth rates and processes 80−4010
enstatite, Al_2O_3 content as geobarometer for plagioclase and spinel lherzolite 77−2142
enstatite, elastic modulus and internal friction in single crystals 78−85550
enstatite, low solubility of Al_2O_3, palaeogeotherm uncertainties 78−65283
enstatite, $MgSiO_3$, high-press. phase relations, absence of oxide mixture 77−37185
enstatite, wet polycrystalline, high temp. flow 78−32082
enstatite ($MgSiO_3$), effects on IR spectra of irradiation with MeV potons 77−45534
enstatite activity and O_2 partial pressure effects on point-defect chemistry of olivine 78−40549
enstatite-diopside solvus, En pressure depend. rel. to geothermometry 77−2141
enstatite-pyrope system, high press./temp. phase behaviour rel. to Earth mantle 78−11882
enstatite-wollastonite system, phase transforms at high press. and temps. with emphasis on diopside 79−79825
enstite, elec. cond. var. with O_2 partial press., obs. and theory 79−1609
epidote, correction for single cryst. intensities for average values of multiple reflection 79−23488
epsomite, relation between soln. and growth rates of cryst. faces 79−14716
erevanit based glass, granulation and briqueting 80−60823
erionite, cryst. struct. exam., stacking faults 78−2083
ettringite, expansion by H_2O adsorption, exam. 78−64806
exploration, remote-sensing appls., book 77−37450
exploration and plate tectonics 78−7607
explosive microstructues in Pb-Zn ore deposit, Lozen, E.Rhodope mountains 77−37195
fayalite, elec. cond. obs. under shock compression 80−81873
fayalite, Fe_2SiO_4, Czochralski growth under controlled O_2 fugacity conditions 80−84843
fayalite (Fe_2SiO_4), shear strength and press. distrib. in diamond anvil press 78−12710
feldpsar in porcelain, melting behaviour *(German)* 79−90758
feldspar, dislocation image contrast in electron microscopy and X-ray topography 78−26573
feldspar, $KAlSi_3O_8$ microwedge, melting by CO_2 laser, deform. of IR absorpt. spectra 77−19984
feldspar, sintering props. 79−29006
feldspar, thermolum., anomalous fading, thermolum. dating 78−10999
feldspar crystals, anisotropy of particle-track visualisation 78−25397
feldspar dissolution under Earth surface conditions, rate control 79−20817
feldspar stress corrosion cracking, seen in granodiorite 80−36299
feldspar/water O isotope exchange, effect of fluid press. 78−57204
feldspars, ^{90}Sr diffusion studies 78−7621
feldspars, in epizonal granitic intrusions, geothermometric and geobarometric appl. 77−5140
feldspars, superplastic flow and cryst. chemistry changes 79−79831
feldspars, synthetic, cryst. struct. 78−34469
feldspars from Mt. Rokko granites, electron probe X-ray microanalysis 80−31038
feldspars in Amitsoq gneiss, initial Pb isotopic comp. and implications for Earth age 78−20371
felsic and mafic mineral separates from an Abitibi dike, $^{40}Ar/^{39}Ar$ dating 80−17237
feroxyhyte (δ-FeOOH), possible occurrence on surface of Mars 80−85879

minerals continued
ferromagnetic components comp. and struct. from coercive spectra of rock samples 79−62490
ferromagnetic mineral grain orientation model in natural slates 77−5192
ferromagnetic minerals in basalts, stability region 78−16000
ferromanganese concretion deposits in Shebandowan Lakes, Ontario 79−84257
ferromanganese deposit on basaltic glass from E.Pacific Hess Deep 77−29283
ferromanganese freshwater nodules, antiferro- to speromag. order 77−70649
ferrosilite, $FeSiO_3$, high pressure and temp. phases rel. to Earth's mantle 77−9403
fibre characterisation using energy dispersive X-ray spectrometry in TEM *(French)* 80−82857
fibre production with low dust and zero lubricant contents *(German)* 78−19678
fission fragment range and closing temp. for track retention 80−41566
fission fragment track annealing characteristics for geochronology 79−100827
fission track dating technique 77−45203
fission track dating technique 80−36417
fission track retention as function of heating time during isothermal expts. 80−36420
fission Xe isotope dating technique 79−21043
fissionable element impurities, nature and distrib., fission track method 78−44436
Fleur de Lys terrain, Newfoundland, minerals $^{40}Ar/^{39}Ar$ age spectra, rel. to metamorphism 77−70657
flint, burnt, thermolum. dating, age relation for slices 77−34073
flint artefacts, ancient heat treatment identification by ESR spectroscopy 79−12831
flotation extraction, thermoelectric power, extraction yield depend. 78−19686
flotation of hydrophobic minerals, US activation of non-polar collectors 78−63250
fluid inclusions obs., Raman laser microprobe analysis appl. 80−57390
fluorapatite, far IR reflectivity to polarised light 79−56778
fluorapatite, proton and photon induced X-ray emission anal., depth sensitivity 78−23988
fluoride-oxide analogue pairs, high-temp. behaviour of elastic moduli 77−11621
fluorite, CaF_2, radiation and thermal redox processes of Mn ions 80−55678
fluorite, crystal gas-liquid inclusion meas. with microscope heating stage 80−76967
fluorite, crystal intergrowth condensation-crystallisation contact bridge, between dissimilar crystals 79−65332
fluorite, Gruneisen parameter at high press. 80−8299
fluorite, solubility equilibria in geothermal waters 77−60368
fluorite, use of proton irrad. to reveal growth and deform. features 80−84216
fluorite mineralisation of carbonate bearing rocks, dynamic model 80−81876
fluorite-like structures of CaF_2 and BaF_2, elec. cond. of shock-compressed monocrystals 77−9404
fluorites, colouring, effect of impurities on absorpt. spectra, rel. to geochronology 79−56822
fluorites, natural colour centres and associated rare earth ions 79−61408
fluorphlogopite, synthetic, with excess Al, radiation-induced paramag. O centres 80−60417
fly ash, depth composition determ. by XPES 78−68943
forsterite, ^{18}O self-diffusion expts., high-temp. creep implications 80−81870
forsterite, decorated dislocations 80−54245
forsterite, elastic constants of single crystal, temp. var. 78−92818
forsterite, elastic modulus and internal friction in synthetic polycrystal 78−85550
forsterite, elec. props. 78−34833
forsterite, glissile splitting of dislocations, cross-slip-controlled creep and mantle rheology 78−61406
forsterite, Mg_2SiO_4, high-press. phase relations, absence of oxide mixture 77−37185
forsterite, O^2 self-diffusion coeffs. 80−70457
forsterite, pure 79−79827
forsterite, single-cryst., shock wave compression 79−84242
forsterite, temp. in high-press. shock state 80−72490
forsterite, with SiO_2 impurity, elec. and dielec. props. at high temp. 80−104953
forsterite-anorthite assemblage limits, results from peridotite hornfelses 77−5184
fosterite, grown by Czochralski method, trivalent ion distrib. between melt and single crystals 78−9972
fracture-filling calcite in granitic basement, $^{87}Sr/^{86}Sr$ ratio 77−29267
franzinite, stacking variation, TEM study 79−99219
French Western Alps, internal mineralogical and petrological investigations of Alpine metamorphism 78−36157
galena, nonlinear impedance of mineral-electrolyte interface 79−53338
galena, polycryst. synthetic, stress relax. 500 to 800°C 78−87737
galena, polycrystalline synthetic, mechanical behaviour studies by stress relaxation testing method 78−96309
galena, superficial degradation in air and water, XPS obs. *(French)* 80−89110
ganophyllite, complex manganese aluminosilicate, cryst. struct. 78−75633
garnet, from Gassetts schist, Vermont, prograde reaction histories from compositional zonation and inclusions 78−36159
garnet content of eclogite *(Chinese)* 78−20413
garnet inclusion in diamond 80−46172
garnet peridotites, fertile and sterile, density meas. 77−5193
garnet pyroxene equilibria in $CaSiO_3$-$MgSiO_3$-Al_2O_3 system 77−2143
garnet solid soln. series, elastic props. inferred from expts. on pyrope 80−76968
garnet solid-soln. series, elastic props. 78−40550
garnet-cordierite gneisses, geothermometry of granulite facies rocks from Rogaland, Norway 78−96193
garnets, comp. and zoning rel. to metamorphism temp. and press. 77−2148
garnets, cryst. symmetry, X-ray diffr. data 79−42024
garnets, fluid inclusion data rel. to thermal history around Grassy granodiorite, Tasmania 80−4012
minerals continued
garnets, in Gondwana Late Palaeozoic sediments, chattermarks rel. to nature of glaciation 79−100874
garnets, triangle diagrams for physical determ. 77−70839
garnets from granitic and migmatic rocks of Argentera Massif 78−85554
garnets from Sharns, IR absorption spectra *(Chinese)* 79−20831
garnierite, high-temp. reactions, spectrochem. anal. 77−70294
gas-mineral equilibria and Earth interior chemical model 77−9411
gehlenite, new high-press. phase, rel. to Earth interior 79−29753
gemstones, synthetic, cryst. growth, review *(German)* 79−33926
geochemical exploration using marine mineral suspensates 78−88936
geochemical haloes analysis using X-ray radiometric methods 77−53231
geological anal., nuclear track technique, B, Li, U, Th mapping 78−20553
gibbsite, synthetic, crystallinity and topotactic reactions, X-ray diffr. obs. 78−63851
glass shards from set-W tephra, Mount St. Helens, Washington, electron microprobe 78−24274
glauconite group, Norwegian-Greenland basin, age determ. by EPR and Mossbauer spectra 80−26467
glauconites, Mossbauer anal., Fe^{3+}/Fe^{2+} ratio 80−17252
glauconites, radiogenic Ar as function of mineral recrystallization 78−32090
global problems soln., scientific and social approaches 77−74185
goethite, FeO(OH), Mossbauer effect exam. of annealing effect on struct. 78−19396
goethite, transformation to maghaemite in CsI discs 79−69259
goniometry, from photographs or angle-true sketches 79−55619
grains in rocks, mechanical heterogeneities rel. to flow cleavage form. 79−57934
granite, compressed, appl. to shielding against soft X-ray radiation 78−41865
granite in W. Great Kabylia (Algeria), minerals evolution during ductile shear deform. *(French)* 79−39716
graphite, nonlinear impedance of mineral-electrolyte interface 79−53338
gratonite, single crystal, photoelectric props. 80−49822
green tuff, cylindrical beads, Japanese, trace elements, neutron activation anal., rel. to archaeological provenience 78−8492
greenalite, metamag. clay mineral, mag. props. *(French)* 78−88817
greenalite, two-dimens. mag. order 79−61188
grossular, cryst. struct. and compressibility to 60 kbar 78−63718
growth during metamorphism, rate laws 79−16467
gypsum, atm. dust, imaginary refr. index rel. to particle size 78−7763
gypsum, crystal intergrowth condensation-crystallisation contact bridge, between dissimilar crystals 79−65332
gypsum, phonon spectroscopy, lattice dynamical calc. 80−19889
gypsum, powder Jeener-Broekaert three-pulse sequence, inhomogeneous lineshapes, second rank spin interactions 80−39891
gypsum, struct., vibr. spectroscopic obs. *(Russian)* 78−15175
gypsum, thermal conductivity thermal decomposition 78−2310
gypsum from DSDP site 395 on Mid-Atlantic Ridge 79−34796
gypsum hydration water, isotopic comp. 79−20829
haematite, elec. resist. and phase transition under shock compression 80−72496
haematite, fine-grained, hard viscous remanent magnetisation 77−56623
haematite, grain size and coercive force from high temp. AF demag. 77−37189
haematite, interpretation of microcrysts. observed on faces (01.2) *(French)* 79−51038
haematite, mutual orientations and morphology obs. *(French)* 79−37647
haematite, natural and synthetic samples, thermomag. anal. 77−56622
haematite, reduction to magnetite under natural and laboratory conditions 78−65277
haematite, secondary, in Pliensbachian limestone sequence at Bakonycsernye, effects on remanent magnetisation 80−90074
haematite, single domain, defect moment origin and props. 79−16438
haematite, textures and topotactical relationships, neutron diffr. study 79−83229
haematite concentrates, peaked thermomag. curves 79−79824
haematite in Jurassic silicic rocks from Nevada, USA, thermochemical remanent magnetisation 80−98310
haematite-magnetite-fayalite nodule, stressed state parameters, stress zones, phase compositions *(Russian)* 80−40336
haemoilmenites, magnetic characts. of low-Curie point specimens 77−41022
halite, buried explosions model studies 77−52999
halite, dynamic recrystn. during compression creep, geophys. appl. 80−25772
halite from DSDP site 395 on Mid-Atlantic Ridge 79−34796
halokinesis and thermal convection 78−65308
Hawaiian olivine, petrologic data from crystallised silicate melt and other inclusions 77−2146
heavy mineral analysis rel. to evolution of modern Nile 77−17151
hectorite, Ba ion position, water effect *(French)* 77−72593
hematite, derived from dehydration of geothite (α-FeOOH), periodic regular texture 79−99328
hematite/magnetite transformation matrices, higher-order orientation relationships 80−100846
hemimorphite, phase angle determ., by four-circle diffractometer *(Japanese)* 80−1897
hemimorphite, $Zn_4Si_2O_7(OH_2)H_2O$, polarised IR refl., vibr. modes *(French)* 77−85698
hemoilmenites, mag. anisotropy, torque balance obs. 80−98309
herstmannite, cryst. struct., comparison with clinohedrite 79−19228
Hildebrand equation of state, appl. to Earth interior geophysics 80−56464
hilgardite, $Ca_2[B_5O_9]Cl.H_2O$, PMR of water mol. 80−84655
hilgardite and parahilgardite, piezoelectric zeolite type structures and composition 78−16003
hollandite type structures, rel. between β-gallia, rutile psilomelane, ramsdellite and $Ga_4Ti_{x-4}O_{2x-2}$ type structs. 79−37664
hornblende, Cumberland Peninsula, Baffin Island, grain etching, age and palaeoclimate indicator 80−8307
hornblende, grunerite and garnet comp. in Archean Fe formation, Canada 78−7630
hornblende and biotite, $^{40}Ar/^{39}Ar$ ages across Georgia Inner Piedmont, rel. to tectonothermal history 78−48990
hornblendes, highly aluminous specimens from SW.Massachusetts 79−66679

minerals continued
hornblendes, refinement of struct. characts. by reference to PMR data 78 - 22704
hulsite, cation distrib., X-ray determ. 79−19225
humite, real structs., mixed layer characts. 78−79567
hutnahorite, deform. twinning mechanisms 80−79814
hydrated minerals on Callisto, evidence from IR spectrum obs. 78−4141
hydrogen embrittling effects from acoustic emission meas. 80−11742
hydrogoethite, α-FeOOH-nH$_2$O, Mossbauer spectra, Neel point, Fe^{3+} config. 77 - 32310
hydrogoethites, weak ferromag. props. 77−53042
hydrothermal alteration minerals, near IR spectra for remote sensing use 80 - 81871
hydrothermal alteration minerals, spectral signal rel. to spectroradiometric data anal. 79−34973
hydrothermal deposit on Guaymas Basin spreading axis 80−101355
hydrothermal ore bodies, nature of porosity rel. to transport phenomena 78−36205
hydrous amphibole, presence in melt inclusions of Chassigny cumulate dunite meteorite 79−21235
hydroxyellestadite, X-ray cryst. struct. determ. 80−96485
Ibitira eucrite, mineralogy, comparison with other eucrites and lunar rocks 77−5512
Iceland high-temperature geothermal systems, mineralogy rel. to aquifer chemistry 78−96245
Iceland spar, crystal, interaction of crack and elastic twin 77−12698
identification, IR spectra appl. 79−62589
igneous minerals dating, excess ^{40}Ar identification by ^{40}Ar/^{39}Ar age spectrum technique 77−5152
ilmenite, cryst. struct. at various compositions 79−86769
ilmenite, lunar and terrestrial, cell dimensions and antiferromagnetism 77−21764
ilmenite, single cryst. growth by floating-zone method 79−19991
ilmenite upgrading, equil. phase data of $Fe_{0.394}$-$Ti_{0.606}$-O-S subsystem under reducing conditions 80−76240
ilvaite, Fe temp. depend. oxidation states, electron hopping, Mossbauer spectra, X-ray diffr. obs. 78−2779
ilvaite, temp. dependent electron delocalization, Mossbauer spectra 79−11361
ilvaites, Mossbauer spectra and mag. features 80−7248
impact abrasion by windblown dust or snow 77−70647
in situ capture gamma analysis of large mineral samples 80−61215
W.Indian Ocean, clay mineralogy and sedimentation 77−29279
E.Indian Ocean, clay minerals distrib. in sediments 79−44172
Indian Ocean, clay minerals in Cenozoic bottom sediments 79−53335
W.Indian Ocean, mantle uplifted block 79−25228
induced polarisation for geophysical exploration, book 77−41216
industrial minerals, finest grinding methods *(German)* 79−8256
inesite, cryst. struct., X-ray determ. 79−19227
Inman, McPherson County, Kansas, meteorite, mineralogy, petrology and comp. 79−2527
inorganic gas chromatography for determ. of H_2O and CO_2 in rocks and minerals 80−85767
inorganic minerals, aqueous heavy metals adsorption 78−49006
intergrowths, regular, investigation with Laves-Ernst compensator 79−96843
iodyrite, ^{129}I concs. determ. by radiogenic ^{129}Xe meas. 77−63983
IR spectra exam. 78−84567
Irish orebodies, ^{40}Ar-^{39}Ar stepheating analyses of clay concentrates 79−66684
irradiated minerals, differential thermal anal. 79−62484
isotope spatial distributions, recovery from stepwise degassing data 79−34967
Istra wall paintings in Yugoslavia, X-ray identification of pigments 77−16876
Isukasia, Greenland, C isotope comp. of graphite and carbonate minerals from metamorphosed sediments 78−11896
itabirite, exploration with integrated aeroelectromagnetic and magnetic methods 79−16690
Itapicuru Mirim chondrite, Brazilian meteorite, mineralogy, petrology, chemistry 78−81594
jade, fracture parameters and crack propag. resist., rel. to fibrous microstruct. 77−8908
jadeite, electrical resist., up to 60 kbar *(German)* 80−31032
jadeite, phase behaviour between 100 and 280 kbar at 1000°C 78−53644
jarosite, $NH_4Fe_3(SO_4)$ $(OH)_5$, decomposition 80−11624
jerfisherite, X-ray cryst. struct. determ. 80−92512
jimthompsonite and anthophyllite from Swiss Alps, disordered intermediate minerals imaging 80−72518
josephinite and assoc. rocks, anomalous noble gases 79−79761
Jurassic seafloor, Point Sal, California, rare earth and trace element geochem. 78−32094
K X-ray fluoresc. anal. 77−81449
kaersutite, sound vels. and anisotropy, rel. to upper mantle seismic struct. 80−26501
kaolinite, aq. suspension, mag. and optical props., Fe_2O_3 impure particles 78−76933
kaolinite, cation-substituted, heat of wetting 77−29050
kaolinite, hydration, lattice deform., vol. expansion due to adsorbed H_2O 80−45555
kaolinite, optical spectroscopy study of structural changes at 700-1000°C 79−65193
kaolinite rare-earth complexes, relax., molar free energy of activation for dipole relax. 80−88919
Kazakovite, cryst. struct. determ. 80−19782
Keolu Hills, Oahu, Hawaii, hydrothermal mineralogy 77−73730
komatiitic lavas, Ni partitioning between magma and cryst. phases 77−49061
kyanite, deformed, defect struct. 77−31668
kyanite-sillimanite concentrate, sintering and mullitisation of basic minerals 77−59726
kyanite-sillimanite concentration, mullitisation and sintering, props. of refractory products 80−20867
laboratory analogues to cosmic dust 79−58397
labradorite, thermal annealing of ion tracks 78−20604
labradorite feldspars, lattice parameter determ. of exosolution structs. 77−84704
Lake Lisan-Dead Sea aragonite, element and isotropic comp. rel. to pleistocene geochemical evolution 78−49047
minerals continued
laterite, Ti determ. using ^{57}Fe, energy dispsersive X-ray fluoresc. 78−76955
laterites, Venezuelan, total Fe determ. by at. absorpt. method 78−31728
lattice thermal conductivity at mantle press. and temp. 78−69338
laumontite potential of S.Island, New Zealand warm springs 79−62528
Leoville meteorite, minerals identification from ^{57}Fe Mossbauer spectroscopy 78−49404
leucite, phase diagram and thermodynamic props. 79−91985
leucosphenite, polymorphism of infinite Si_3O_7 radicals in layered stacks 79−60301
Libyan Desert Glass, redox form. conditions, EPR obs. of as-received and irrad. samples 78−28228
likasite, $Cu_3P_2H_3(NO_3)(OH)_2.H_2O$, comp. and struct. *(French)* 77−47405
limonite, optical props. compared with Mars disc IR spectra 78−85879
lodestone, microstructure and mag. props., source of mag. hardening 79−82828
lodestones, magnetic and microstructural props. 78−16004
longitudinal wave vel. and absorpt. in rocks and minerals at high press. and temp. 79−39704
lorandite, radiography of geological specimens for determ. of α- and fission-activity 78−20540
low chalcocite, cryst. struct., X-ray study 79−42033
low tridymite, SiO_2, cryst. struct. 78−36150
lower mantle, thermodynamically based eqn. of state 80−26473
lower mantle minerals, evaluation of finite strain eqns. of state using lattice models 80−96620
Macau chondrite, Brazil, mineralogy, petrology, chemistry 78−93171
Madagascar monazite, search for fission decay of superheavy elements 77 - 17105
magma genesis, mineral phases and parental rocks, ^{87}Sr/^{86}Sr ratios 77 - 25671
magnesia-chrome, rapid anal. by X-ray fluoresc. 79−16065
magnesian-spinel materials form. using heat treatment 79−38773
magnesioferrite spinels, noncubic, spinodal decomp. of Fe-rich chromites 78−72763
magnesium kurchatovite, crystal struct. determ. 77−15388
magnetic, Curie temp., HF meas. method *(Russian)* 79−39992
magnetic minerals, constraints on Curie isotherms in deep crustal mag. anomalies 78−44805
magnetic minerals, in basaltic dyke with concentric cooling zones, props. var. 77−49062
magnetic minerals, multidomain grains demagnetisation field 78−65273
magnetic minerals, psarks existence rel. to pseudo-single-domain behaviour 78−65274
magnetic minerals in DSDP Leg 37 samples, alteration rel. to field palaeointensity meas. 77−90996
magnetic minerals in Icelandic columnar basalt, long-axis alignment rel. to susceptibility anisotropy 77−86859
magnetic minerals in submarine basalts, changes in oceanic crust mag. signal 77−90995
magnetic separation of minerals using supercond. mags. *(Czech)* 78−88923
magnetite, coercive force spectrum at high temps. rel. to thermal activation below blocking temp. 77−91111
magnetite, grain size limits for pseudosingle domain behaviour, rel. to palaeomagnetism 80−11215
magnetite, in Lake Tahoe, California-Nevada, sediments, palaeomag. and sedimentological studies 80−41371
magnetite, low stress effects on susceptibility and coercive force 78−16001
magnetite, magnetisation of immobilised particles, shape factors 80−72499
magnetite, magnetisation using Neel's mol. field theory 79−87223
magnetite, multidomain particles magnetisation 79−66686
magnetite, origin and stability of drilling induced remanence 77−33059
magnetite, oxidation mechanism during roasting of nodules *(Russian)* 80−40567
magnetite, partial thermal remanent magnetisation additivity 80−26498
magnetite, particle size effect on palaeointensity determ. 77−37186
magnetite, single domain, weak field thermoremanent magnetisation intensity, cooling rate effect 80−109139
magnetite, spin polarisation, effect of temp. and photon energy 80−45221
magnetite, textures and topotactical relationships, neutron diffr. study 79−83229
magnetite, TRM props. of single-domain, pseudo-single-domain and multidomain particles 78−40544
magnetite (Fe_3O_4), mag. susceptibility under hydrostatic press. and implications for tectonomagnetism 80−26504
magnetite (Fe_3O_4), piezomag. response depth depend. rel. to tectonomagnetism as earthquake precursor 80−26465
magnetite electrochemical polarisation in surfactant solns. *(Russian)* 79−83465
magnetite in Bushveld Complex upper zone, Cr content vars. rel. to magma chambers heterogeneity 80−56421
magnetite monocrystals and rocks under high uniaxial press., mag. props. 78−73361
magnetite nodules with fayalite additives, stressed state parameters *(Russian)* 80−45352
magnetite stressed to failure, mag. behaviour rel. to earthquake prediction 78−32068
magnetite-titanomagnetite interdiffusion expts. 78−55991
magnetites, superleak behaviour in superfluid ^{4}He 77−43399
magnetites and titanomagnetites, synthetic, TRM and var. with grain size 78−65270
majorite, dislocation obs., Earth mantle implications 80−85909
malachite from patinas of ancient bronze objects, stable ^{13}C/^{12}C and ^{18}O/^{16}O ratios 79−26194
in Malvern howardite meteorite, petrology and chemistry 77−49346
manganese (II) arsenatotrisilicate, cryst. struct. determ. and refinement 80−1970
manganese minerals, photoluminesc., cryst. field theory *(Russian)* 78−84654
manganoan magnesian ilmenite from Jacupirango carbonatite, Sao Paulo, Brazil, paragenesis and comp. 78−85552
mangetite-ilmenite intergrowth, thermal magnetization of granules 79−44182
mantle, mineralogy and chemistry above 1000 km 77−33015

minerals continued
mantle minerals, interionic repulsive force and ion compressibility theory 77−11500
mantle minerals, significance of ferroelectric phase transitions 77−53045
marble, LF dielectric props. 80−34843
marble, radioactive waste storage, anion effect on sorption of trivalent actinides 80−13717
margarite, stability and compatibility relations as press.-temp. indicators 77−5183
marine heavy mineral deposits, extraction, X-ray spectrometric anal. *(German)* 78−20551
marine minerals exploration, Mobile Initial Condition Indicator approach 79−5687
marine Mn concretion growth rates, nonradiometric considerations 78−61393
Mars, clay minerals prod. by alteration of glass 78−89097
marshite, ^{129}I concs. determ. by radiogenic ^{129}Xe meas. 77−63983
massive sulphide ores genesis, geothermal model from altered volcanic rocks geochemistry at Matagami, Quebec 78−77231
melting (petrurgy) *(Czech)* 80−44298
metabasalt block from Mid Atlantic Ridge, metamorphic mineral data 77−64279
metabasites, geothermometry of granulite facies rocks from Rogaland, Norway 78−96193
metal oxide-SiO_2 systems, phase diagrams calc. from high press. phases stability study 79−90779
metal-rich deposits in oceanic lithosphere, origin 78−53634
metallic mineral deposits of Australia mag. induced polarisation survey results 80−98223
metallic mineral deposits prospecting using induced-polarization freq.-domain method *(Italian)* 79−16686
metallic ore processing, effects of ultrasonics and their appls. 78−92214
metalliferous sediments and Fe-Mn concretions, magnetomineralogical study, East Pacific Rise 79−62481
metamorphic bathograds and bathozones, diagnostic mineral assemblages rel. to regional uplift meas. 78−81113
metamorphic plagioclases from Japan, modulated microstructure 79−96760
metamorphic sodic amphibole from Newfoundland Appalachians, tectonic implications 77−29298
metasomatic anhydrite in Mississippian reservoir carbonates, age determ. 78−73328
metasomatic garnets, low-temperature, in marine sediments, paragenesis 77−86857
metastable phases, eqns. of state 77−70639
meteorite, Hoba ataxite, low temp. impact props. 79−80283
meteorite, Santa Barbara, mineralogy and petrology 79−25551
meteorite Zaisho, Japanese pallasite, mineralogical and petrographical study 80−46509
meteorites, ^{16}O enrichments in carbonaceous chondrites rel. to pre-solar component distrib. 77−37582
meteorites, minerals assemblages rel. to condensed matter re-evaporation during solar system form. 78−85864
meteorites, noble gases abundance in separated minerals 77−33429
meteorites, noble gases isotopic anomalies in separated minerals from Allende chondrite 77−33430
meteorites, Poluyamki, Rakity and Markovka chondrites, composition *(Russian)* 77−9721
meteorites, stony, electron microscopy of mineral grain substructs. 77−87349
meteorites, Yamato, constituent minerals determ. 78−77524
mica, deformed, syntectonic nucleation of new grains 79−65102
mica, metamorphic white, surface microtopography 80−54493
mica, North American, electrical cond. rel. to chem. composition 77−29285
mica, preferred orientation, review and outlook 79−83220
mica, Swedish, giant and dwarf haloes rel. to unknown radioactivity 78−81157
mica muscovite, iron latent tracks obs. by TEM 79−73235
micaceous-crystalline material, cast, prep. and props. 77−12591
micas in micaceous kimberlites, chemistry 79−16465
Michigan Basin deep hole metagabbro, mineralogy and geochemistry compared to seawater hydrothermal alteration 79−39710
microcline, continuous laser emission effects on surface, spectroscopic obs. 79−94271
microcline, laser torch effects, spectroscopic investig. *(Russian)* 78−76560
microcline, maximum, room temp. phase transition, heat capacity meas. 80−54373
microcline, maximum room temp. phase transition, unit cell parameters, thermal expansion 80−54208
microscopic intracrystalline cavities in lithospheric materials *(French)* 77−9400
microstructure, example of high resolution TEM application *(Hungarian)* 77−76267
mineral exploration, computer uses, limitations and requirements 77−53207
mineralized zones, probability and uncertain number theory appls. *(Rumanian)* 77−29509
mixed oxide and perovskite structure model of mantle 78−85507
modal analysis of rocks, error assoc. with point-counting 78−32232
modulated structures, conference, Kailua Kona, Hawaii, USA (March 1979) 79−94928
molybdenite in Ca-Al-rich inclusions in Allende meteorite 78−12170
monazite, α-spectra evidence for natural activity at 6.52 to 9.07 MeV 80−67363
monazite, from South Indian beach sand, superheavy element search, K X-ray fluoresc. anal. 80−61801
monazite, giant halo inclusions, evidence against superheavy elements 78−40554
monazite, giant haloes prod. by ^{244}Pu fission alpha particles 77−29300
monazite, high-energy alpha emitters, $E \geq 10.6$ MeV 79−48467
monazite, PIXE aval. in search for superheavy elements 79−79845
monazite, search for superheavy elements, neutron fission of mass separated samples 77−13078
monazite, superheavy elements search in bulk samples by ^{32}S ion backscattering 77−21773
monazite from Malaysia, search for $Z=126$ via X-ray spectra 77−86895
monazite from South India beach sands, superheavy elements search using X-ray fluorescence 78−16017
monazite inclusions, PIXE search for superheavy elements 77−49066

minerals continued
monazite inclusions possessing pleochroic halos, PIXE anal. 78−69350
monazite sand, determ. of Th, U, and K from spectrometry of natural γ-activity 78−20408
monazites, nuclear waste, synthesis, ideal actinide hosts for geologic disposal 79−22406
monazites, search for superheavy elements 80−36297
monozite, superheavy element search via ^{7}Li elastic scatt., upper limits 77−86896
monticellite ($CaMgSiO_4$), high-press. phase transforms. and implications for upper mantle mineralogy 80−17255
montmorillonite, clay mineral, expanding type, surface props. rel. to heat treatment 79−29406
montmorillonite, Co^{2+} form, optical spectroscopy study of structural changes at 700-1000°C 79−65193
montmorillonite, dehydration kinetics 78−76857
montmorillonite, mech. props. at high press., rel. to fault behaviour 79−84234
montmorillonite, optical props. compared with Mars disc IR spectra 78−85879
montmorillonite clay sols, structure determ. by neutron diffr. and small angle scatt. 80−40748
montmorillonite group, Norwegian-Greenland basin, age determ. by EPR and Mossbauer spectra 80−26467
Moore County, eucrite meteorite, mineralogy rel. to quench temp. 78−96444
mooreite, X-ray cryst. struct. determ. and refinement 80−92488
mordenite, dehydrated Na-exchanged, cation and molecular distrib. 79−90617
mullite, X-ray diffr. structural model 80−49191
mullite-based dispersed refractory system, rheological props. at high temp. 77−16629
mullite-corundum refractories, reactions with FeO in different media 77−24994
multielement analysis by photon or neutron activation 78−12018
muscovite, exam. of dislocations and props. using elasticity theory *(German)* 79−10854
muscovite, natural cryst., submicroblock struct., electron microscopy 79−14816
muscovite, thermal annealing of ion tracks 78−20604
muscovite deformation, comparison with biotite from optical microstruct. 80−26507
muscovite of regional metamorphic rocks in Xizhang, b_0 value and geological significance *(Chinese)* 79−74890
muskovite, disordered mica struct. high resolution electron microscopy exam. 78−91344
'mysterite' as late condensate in solar nebula, H6 chondrite evidence 78−7946
'mysterite'-bearing clast in H6 chondrite Supuhee, chemical charact. 78−7947
natrolite, cleavage etching in acid and neutral media 80−6407
nepheline, continuous laser emission effects on surface, spectroscopic obs. 79−94271
nepheline, laser torch effects, spectroscopic investig. *(Russian)* 78−76560
nepheline, phase behaviour between 100 and 280 kbar at 1000°C 78−53644
nephrite, amphibole, planar defects termination, high resoln. electron microscopy 80−79772
nephrite, mech. props. 77−44295
nephrite jade, struct. irregularities, electron microscope obs. 77−19969
neutron capture γ-ray borehole mineral anal., optimum neutron source size 80−61213
nifontovite, cryst. struct., H bonds 79−19232
nomenclature recommendations of International Mineralogical Assoc. and International Union of Crystallography 77−65927
nonsilicate, EPR, review 78−39384
nontronite in hydrothermal mounds near Galapagos Rift, chemistry and mineralogy 79−29739
Norton County enstatite achrondrite meteorite, ^{87}Rb-^{87}Sr anal. of enstatite and feldspar 77−5508
NQR analysis, appls. to mineralogy 80−67426
obsidian, characterisation by proton induced γ-ray emission 79−74442
obsidian, Japanese, trace elements, neutron activation anal., rel. to archaeological provenience 78−8492
obsidian, Li diffusion in silicate glass, ion-microprobe determ. 78−53649
obsidian glass, Lipari and Teotihuacan origin, Mossbauer, magnetisation, X-ray diffr. and fluoresc. study 80−46173
obsidian sources, chem. characterisation and hydration rates, W.Mexico 78−348
ocean floor spilites, seawater/basalt ratio effects on chem. and mineralogy 78−92819
Okhotsk Sea, clay minerals distrib. in recent sediments 79−20804
Oklo fossil nuclear reactors, radiation damage of minerals 80−21751
Oklo natural fission reactors, temp. of mineral phase assemblages and rock textures 80−21722
olivenite, $Cu_2AsO_4(OH)$, symmetry and cryst. struct. determ. 77−80457
olivine, anisotropic, seismic body waves refl. and refr. at plane interface 77−49019
olivine, anisotropic track etching of crystals using WN solution 79−26836
olivine, creep mechanisms 78−69332
olivine, diffusion and diffusion creep, rel. to upper mantle deform. 77−9409
olivine, dislocation recovery rate affected by high-press. 80−94515
olivine, fayalite rich, single cryst., UV absorpt. spectra at high press. 78−85545
olivine, Fe-rich superparamagnetic clusters, Mossbauer study, appl. to thermal histories of rocks 79−82831
olivine, fracture surface energy 79−16462
olivine, hardness var. with temp., rel. to polycryst. yield stress 80−26500
olivine, heavy ion irradiated, and amorphous, IR extinction rel. to interstellar dust 79−53873
olivine, high temp. creep, edge dislocation control 79−79815
olivine, isolated grains origin in type 2 carbonaceous chondrites 79−30020
olivine, naturally deformed, recovery process, rel. to Earth upper mantle mech. state 78−96202
olivine, nature and origin of isolated grains in carbonaceous chondrites 77−64711

minerals continued
olivine, optical absorpt. spectra and radiative heat transport at high temp. 79−79818
olivine, origin of isolated crystals in C2 carbonaceous chondrites 78−53890
olivine, plastic flow of oriented single crystals, dislocation struct. interpretation 78−36156
olivine, plastic flow of oriented single crystals, mech. data 78−36155
olivine, point defect formation 78−85547
olivine, point-defect chemistry, effect of enstatite activity and O_2 partial pressure 78−40549
olivine, preferred orientation, review and outlook 79−83220
olivine, rheology rel. to thermal stability or instability of asthenospheric shear flow 78−20370
olivine, shock deform. expts., Hugoniot data implications 80−94497
olivine, shock induced high-pressure transformation 78−11883
olivine, terrestrial and meteoritic, IR spectra rel. to 10 μ interstellar absorpt. band 77−78846
olivine, thermal annealing of ion tracks 78−20604
olivine ($Mg_{1.8}Fe_{0.2}SiO_4$), elastic consts. from free vibr. of rectangular parallelepiped cryst. 77−84849
olivine (Mg_2SiO_4), effects on IR spectra of irradiation with MeV protons 77−45534
olivine and enstatite of meteoritic and terrestrial origin, porosity determ. *(Russian)* 77−9725
olivine and garnet Fe^{2+} and Mg^{2+} partitioning 78−32091
olivine and lunar basaltic liquids, Fe and Mg distrib. 79−35158
olivine and metallic phases equilib. conditions in pallasites *(Russian)* 77−9720
olivine and molten sulphide fractionation, from komatiite magma, numerical model 78−96177
olivine and silicate melt, Ni partitioning, comments 79−88319
olivine and silicate melts; Ni^{2+}, Co^{2+}, Fe^{2+}, Mn^{2+} and Mg^{2+} partitioning 79−66683
olivine crystals in mantle, orientation rel. to seismic anisotorpy of subcrustal lithosphere 77−49039
olivine dynamic recrystallisation, applicability limits of grain size geopiezometer 78−85715
olivine flow laws rel. to lithospheric stress 77−91121
olivine fractionation equations for basaltic and ultrabasic liquids 79−20818
olivine in Archaean peridotitic komatiites, crystal forms rel. to emplacement 78−77234
olivine in Iwanai-dake peridotite mass, chromian spinel lamellae 78−96205
olivine in Japanese peridotites, appl. to uppermost mantle differential stress lateral var. determ. 80−98275
olivine in pallasite meteorites, ion microprobe anal. for Ni 79−58304
olivine inclusions in diamond, epitaxy 77−78173
olivine mixtures in Earth mantle, rel. to P-wave vel. anisotropy inversion 77−49017
olivine rheology, local nonsimilarity boundary layers rel. to shear flow beneath oceanic plates 78−40521
olivine subgrain boundaries, origin in mantle peridotites 78−85544
olivine to spinel transition kinetics, rel. to deep-focus earthquake genesis 77−5190
olivine with fixed cationic ratio, O_2 pressure effect on defect cores 78−85548
olivine-metal texture formation in pallasite meteorites 78−7944
olivine-orthopyroxene Fe/Mg partitioning in diamonds *(Portuguese)* 78−65284
olivines, cosmic ray nuclei groups Z≥ abundances, fossil tracks in meteorites 80−105139
olivines, elec. cond. meas. under defined thermodynamic activities, up to 20 kbar, 340-1100°C 80−6832
opal, ordered arrangements of SiO_2 spheres of two different sizes 78−87658
opal, Spor Mountain, Utah, U-Pb age systematics 80−46149
opals, crystal struct. and IR spectra 80−40117
opaque, alteration states correl. with temp. in active geothermal system 78−40551
ophiolitic sulphide deposits in Cyprue, ^{87}Sr enrichment confirms ore form. by circulating seawater 77−81887
ophiolitic sulphide ore deposits in Cyprus, seawater fluid inclusions 77−44997
optical constants, derivation from measured reflectances, errors in two-media method 79−58100
optical crystallography techniques, advances in spindle stage methods 78−85702
ore, Zn and Pb content determ. by universal backscattered gamma method 79−1984
ore analysis by selective gamma-gamma method, elimination of geometrical effects 78−44425
ore bodies, channel-type streaky conductivity model, polarisation 77−33063
ore body distrib. in Baisoara mine, gravity anomaly data *(Rumanian)* 78−20347
ore deposits, mineral discrimination and inductive coupling removal via multifreq. induced polarisation 79−5448
ore deposits, strata-bound, rel. to chemical speciation of Cd, Cu, Pb and Zn in freshwater-brine solns. 78−20409
ore mineralisation in Erma River Area, Bulgaria, age, genesis, Pb isotope and K-Ar investigs. 78−81115
ore minerals, recent developments in microscopic meas. of spectral reflectance *(French)* 79−5627
ore prospecting, and mining research, examples of mineralogy contrib. *(French)* 79−5475
ore-bearing structures in Krivoj Rog basin (Krivbas), gravity anomalies interpretation *(Russian)* 78−85466
ore-deposition through geological time, review 78−77235
ore-flux mixtures, automatic X-ray fluorescence monitoring of major components 77−87887
ore/pore electrolyte phase boundary layer, excess voltage time depend. *(German)* 79−84233
orebodies location in mineworkings, muon hodoscope appl. 79−84491
ores, chemical analysis methods 77−41027
ores, sediments and metamorphism 77−86889
ores, Ta chem.-spectral determ. 79−16075
orthoclase, Li diffusion in silicate glass, ion-microprobe determ. 78−53649
orthoenstatite, elastic constants 78−85546
minerals continued
orthopyroxene, occurrence and origin in some lavas from the French Massif central 78−96203
orthopyroxenes, electron irrad. effects, Mossbauer study 80−40016
orthopyroxenes, synthetic, cryst. struct. 78−42970
orthosilicate chloritoid, layered, disordered, electron microscopic and X-ray anal. 78−75511
oxide particles, single domain, as source of rocks TRM 78−65271
oxides, ABO_4 type, high press. phase transforms. and struct. types, cryst. chem. aspects 80−79940
oxides, elastic constant systematics 79−69177
oxides, thermal expansion, characterisation technique 79−70795
oxides in DSDP Leg 37 basalts, microstructs. mag. props. 77−91108
oxides in Turnagain ultramafic complex, NW. British Columbia 79−84247
palaeogeotherms from xenolith suites in basalts and kimberlites 77−2127
palaeomagnetic record carriers synthetic analogues, preparation, characterisation and mag. props. 78−65276
palaeopiezometry using recrystallized grain size 77−91317
pallasite meteorites 78−7945
palygorskite, uncoupled H_2O, isotopic dilution IR obs. 77−8568
paradamite, $Zn_2(AsO_4)(OH)$, crystal struct., anisotropic temp. factors 80−84145
paragonite, $2M_1$, cryst. struct. refinement by HV electron diffr. 78−67696
paragonite, 3T, cryst. struct., oblique texture electron diffr. 78−67697
particles, large coarse, max. midsection area determ. by photoelec. method 79−70240
particulate pollutants, identification by selected area electron diffraction 77−90970
paulmooreite, $Pb_2[As_2O_5]$, crystal struct., dimeric arsenite groups 80−84143
pectolite (hydrous silicate), lowest δD value 79−62513
pegmatite ores in Tanco mine area, SE.Manitoba, in Canada, exploration methods 79−48577
pegmatites, U^{235} estimation by homogenised fission track anal. using solid state track detector 80−97719
penninite, one-layer triclinic chlorite, neutron diffraction study 80−84144
pentlandite, prep., H_2 reduction with lime, to yield Fe-Ni alloy 78−85018
periclase, containing Fe^{2+}, visible absorpt. spectra and mantle radiative transfer 80−90039
periclase, recording of pulsed EM radiation in RF band during heating *(Russian)* 77−55837
peridot, shock-produced olivine glass, TEM obs. 78−10178
peridotite xenoliths in S.African kimberlites, structurology, upper mantle constitution implications *(French)* 78−11889
peridotite-CO_2-H_2O and carbonatitic liquids in upper asthenosphere 77−29294
perovskite, $MgSiO_3$, synthesis and cryst. chem. charact., rel. to mantle mineralogy 78−65266
perrierite from Oslo region, Norway, cryst. struct. and chemical comp. 78−85533
petroleum generation in SW block of Los Angeles Basin, rel. to thermal subsidence 80−3967
petzite, X-ray cryst. struct. refinement 79−46634
phase transformations of minerals and Earth's deep interior materials, review *(Japanese)* 78−28225
3T-phengite, existence in Xingyang metamorphic belt, tectonic significance *(Chinese)* 79−84264
phenocrystic minerals, Ca-Mg-Fe ratios, pyroclastic deposits correl. in S.Kyushu, Japan *(Japanese)* 77−64278
phenocrysts and megacrysts in basalts of Pinacate volcanic field, textures and genesis 77−81881
phenocrysts in Quaternary magmas of NE Japan, comp. rel. to H_2O contents lateral vars. 79−57899
phlogopite, cryst. struct. and compressibility at high press. 78−63717
phlogopite in S.African kimberlites, $^{40}Ar/^{39}Ar$ anals. 79−34769
phlogopite mica, press. depend. of Ar diffusion 77−86861
phlogopites, mica, Fe^{2+}, F^-, and OH^- distrib. in octahedral sheet, NMR study 79−82183
phosgenite, $Pb_2Cl_2CO_3$, natural single cryst., vibr. props. 79−24319
phosphates, U content, α-ray autoradiography, fluorimetry, estimation 78−20414
phosphophyllite, $Zn_2Fe(PO_4)_2.4H_2O$, chem., optical and X-ray data 77−15366
phosphorite nodules on sea floor off Peru and Chile, U isotopes 78−7612
photoelectron spectra rel. to bond lengths *(French)* 77−36364
phuralumite, X-ray cryst. struct. determ. 79−90606
phurcalite, cryst. struct. determ. 78−55849
phyllosilicates, dioctahedral and trioctahedral, calc. of electrostatic energy relations 80−19743
phyllosilicates, from Orgueil meteorite, Ni and S abundances correl. 78−12169
phyllosilicates, laboratory spectra comparison with interstellar 10 micron absorpt. band 79−80344
phyllosilicates, new types, in carbonaceous chondrite matrix 79−80285
phyllosilicates, struct. inheritance in transforms. under hydrothermal conditions *(French)* 79−34802
phyllosilicates in Nogoya meteorite, IR spectrum comparison with 10 and 20 μm interstellar absorpt. bands 79−48741
physical properties, investigation using high-press. apparatus *(Russian)* 77−70850
physics and chemistry, conf., Newcastle, England (April 1974) 77−37194
pigeonite, antiphase domains exptl. coarsening 80−81886
pigeonite, inverted, from SW Norway, precipitation temp. estimation 80−72500
pigeonite, occurrence and origin in some lavas from the French Massif central 78−96203
plagioclase, flotation and remelting in Kalka Intrusion, central Australia, rel. to anorthosite genesis 77−60371
plagioclase, labradorite, Al/Si distrib. in An_{66}, superstructure in An_{54} 79−94970
plagioclase, zoned, of different magmatic environments, preliminary ion-microprobe anal. 79−34815
plagioclase feldspar, deformed, elastic twinning, TEM obs. 77−62551
plagioclase feldspar, deformed in compression, dislocation substruct. and slip, TEM obs. 77−43221
plagioclase feldspars, banding, calcs., nonlinear partial differential eqns. appls. 80−4510

minerals continued
plagioclase feldspars, modulated structs., X-ray diffr. and electron microscopy obs. 79−95031
plagioclase fractionation in igneous rocks, influence of augite 80−12390
plagioclase grain size of basaltic andesite dykes, Iritono, central Abukuma plateau 78−7618
plagioclase-garnet-Al_2SiO_5-quartz assemblage, pot. geobarometer-geothermometer 77−2147
plagioclases, singularities of IR spectra, struct. and composition depend. 77−78166
plagioclases, volcanic, thermoluminescence dating 80−98475
plasma furnaces, mineralogy and extractive metallurgy appls. *(French)* 80−28849
plate phosphides in hexahedrite meteorites, growth rel. to cooling rates 78−57511
Poisson number determ., discrepancies *(German)* 78−69324
polymorphic phase boundaries effects on mantle vertical and horizontal motions 77−9395
post-shock temperatures, meas. by IR radiation detector 79−92527
powdered, adsorbed films influence on cohesion and angle of internal friction 77−25084
Precambrian zircons, metamictization and U-Pb systematics by IR absorpt. spectrometry 77−17099
preferred orientation, review and outlook 79−83220
prospecting by airborne EM method *(Japanese)* 78−24392
prospecting by tunable laser spectroscopy 77−60500
Proterozoic iron-formation, Labrador Trough, Canada, regional metamorphism rel. to mineralogy and chemistry 79−57916
protohaematite, transformation to maghaemite in CsI discs 79−69259
proton activiation analysis of B and Li local levels in minerals, rocks and ores 79−74477
proustites, optical props. and chem. comp. rel. to pyrargyrites 78−95566
pseudoboehmite, exam. of structure, using radial electron distrib. method, and X-ray diffraction 80−1977
psilomelane type structures, rel. between rutile, β-gallia, hollandite and $Ga_4Ti_{x-4}O_{2x-2}$ type structs. 79−37664
pyrargyrites, optical props. and chem. comp. rel. to pyrargyrites 78−95566
N Pyrenean metamorphism, age and tectonic implications 79−34819
pyrite, FeS_2, eqn. of state, rel. to constraints on Earth S content 79−70789
pyrite, nonlinear impedance of mineral-electrolyte interface 79−53337
pyrite, stacking faults, TEM obs. *(French)* 79−28004
pyrite, superficial degradation in air and water, XPS obs. *(French)* 80−89110
pyrite, Witwatersrand sediments, petrography and diagenesis rel. to origin Au-U deposits 79−84265
pyrite (FeS_2), glide elements study by electron microscopy and electron diffr. 78−83817
pyrite layers in coal, rel. to anisotropic elec. props. 80−98312
pyrochlore, high temperature chlorination 78−11180
pyrolusite (MnO_2), UV irradiated, simulation of Viking gas exchange reaction on Mars 80−72831
pyrope, cryst. struct. and compressibility to 60 kbar 78−63718
pyrope, elasticity of single cryst., implications for garnets 80−76968
pyrope, synthetic, hydrostatic compression, isothermal bulk modulus 78−40545
pyrope garnet, elastic consts., pressure and temp. depend. 77−70643
pyrope garnet-ilmenite transition 77−49063
pyrope-almandine garnets, elastic consts. temp. depend. 80−17251
pyrophillite, phase transform. promoted by water under ultra-high press., high temp., technical appls. *(Chinese)* 79−1499
pyrophyllite, cation-substituted, heat of wetting 77−29050
pyrophyllite, dickite and kaolinite in quartz veins of Stavelot massif 79−34813
pyrophyllite, failure precursors during anelastic deformation 78−61405
pyrophyllite, phase transitions, importance in diamond synthesis *(Chinese)* 77−70049
pyrophyllite, strength and flow props., vibrations effect 79−37237
pyroxene, containing trivalent cations, lab. meas. of elec. cond., rel. to lunar temp. profile 80−31033
pyroxene, electrical resist., up to 60 kbar *(German)* 80−31032
pyroxene, ferroelectric-like phase transformation in mantle 78−61362
pyroxene chemistry of DSDP Leg 34 basalt, cooling rate effects 79−44148
pyroxene geobarometry and geothermometry 77−2254
pyroxene geothermometry model with approx. soln. 77−2255
pyroxene geotherms, thermodynamics 78−65282
pyroxene solvus geothermometer in CaO-MgO-SiO_2 system 77−2144
pyroxene-garnet solid-soln. equilibria in $Mg_4Si_4O_{12}$-$Mg_3Al_2Si_3O_{12}$ and $Fe_4Si_4O_{12}$-$Fe_3Al_2Si_3O_{12}$ systems 77−81895
pyroxenes, antiphase domains, contrasting props. and behaviour 80−79813
pyroxenes, elec. cond. meas. under defined thermodynamic activities, up to 20 kbar, 340-1100°C 80−6832
pyroxenes, high Ca, of the diopside-hedenbergite series, cryst. struct. refinement 79−14783
pyroxenes, order-disorder interpretation 80−38987
pyroxenes in CaO-MgO-Al_2O_3-SiO_2 system, subsolidus phase relations rel. to geothermometry and geobarometry 79−16440
pyroxenes in ultramafic xenoliths from Elwin Bay kimberlite, comp. rel. to Canadian palaeogeotherm 77−91078
pyroxenites, layered, in ultramafic complexes from Ariege, France, petrology, comp., equilib. conditions *(French)* 77−86874
pyroxenites, layered, in ultramafic complexes from Ariege, France, petrogenesis 77−86875
pyrrhotite, complex refractive indices rel. to comp. of Saturn's rings 77−29716
pyrrhotite, $Fe_{0.9}S$, eqn. of state, rel. to constraints on Earth S content 79−70789
pyrrhotite, Ni recovery by thermal upgrading 77−60034
pyrrhotite, pseudosingle-domain effects and single-domain multidomain transition 77−64274
pyrrhotite ($Fe_{1-x}S$) in sulphide ores from Kambalda, W.Australia, sulphide fabrics 78−77229
pyrrhotites and Kholodninskoye ore deposit, magnetic props. 77−60367
quantitative anal. by XPS 78−35742
quantitative image analysis, applic. to mineralogy *(French)* 79−5631
quartz, ⟨a⟩ axes preferred orientations in tectonites, flow kinematics 78−96200
quartz, c-axis fabrics anal. via photometric method 80−101456
minerals continued
quartz, Dauphine twinning, stress-induced, acoustic emissions 80−6414
quartz, defects growth, study by X-ray diffr. topography *(French)* 80−39095
quartz, dislocations fine structure under electron irrad. 80−70213
quartz, dosimetric props., possibility of thermolum. dating of geological objects 79−12288
quartz, etch features for determ. of quartz grain source 77−70650
quartz, formation in closed seams, inferences from expts. on hydrothermal crystn. 80−10516
quartz, from alpine fissures, fluid inclusions, reln. to metamorphism *(German)* 77−25677
quartz, Gruneisen parameter at high press. 80−8299
quartz, high-low transition, effect on compressional and shear wave vel. in rocks under high press. 80−12380
quartz, hydrolytic weakening of natural and synthetic crystals, mech. and IR study 78−61410
quartz, low, CC Si-O bond characteristics 80−84132
quartz, low, ionicity of Si-O bond 80−84133
quartz, natural, gamma-irradiated, stress effect on thermolum. sensitivity 80−11482
quartz, natural, virgin (γ-irradiated), polarisation effect on thermolum. sensitivity 80−11483
quartz, preferred orientation, review and outlook 79−83220
quartz, rose, charge transfer mechanism for origin of colour, EPR and optical expts. 78−52537
quartz, shock-loaded, IR spectroscopic studies, solid-state glass prod. 79−19157
α-quartz 80−72490
quartz c-axis orientation in Saxony Granulites, petrofabric anal. by optical and X-ray diffr. studies 80−21740
quartz distribution in Atlantic sediments, relation to climate, last glaciation 80−8308
quartz fibres, polar orientation, stereospecific twisting 78−42930
quartz grains, from coastal plain of Rio Grande do Sul, Brazil, coaxial crescentic marks *(Spanish)* 78−92816
quartz grains, from sub-glacial and assoc. environments, characterisation using SEM 79−25238
quartz grains in Einbeck, W.Germany, loess profile, weathering rel. to stratigraphy *(German)* 79−20823
quartz grains in Moine thrust zone, deformation-induced microstructs. rel. to differential stress 80−85652
quartz in granites, cathodoluminescence rel. to granites microcracking and healing 80−51391
quartz in shear zone from Castell Odair, Scotland, orientation re-investigation 78−77216
quartz orientations in quartzite breccia, Onaping Formation, Sudbury Basin 77−9402
quartz overgrowths, on quartz, cathodoluminescence and microstruct., SEM exam. 79−25239
quartz preferred orientation and quartz content interdependence in deformed rocks 78−88818
quartz radioactive waste storage, anion effect on sorption of trivalent actinides 80−13717
quartz sand from Lasko Polje, determ. of Th, U, and K from spectrometry of natural γ-activity 78−20408
quartz-feldspar mylonite, microstruct. and fabric development 78−96201
Quaternary lavas, Snake River Plain, Idaho, mineralogy and petrology 78−20402
radioactive, prospecting, thermoluminescence radiation dosimetry appl. 78−32244
radioactive ores, effective γ-ray attenuation coeffs. 77−25680
radioactive ores, hazard indices rel. to nucl. high-level waste 78−15913
radioactive ores, specific sensitivity of NaI(Tl) scintillator in γ-ray meas. 78−81449
rare earth elements, determ. in geological materials, using thermal and epithermal neutron activation 78−7797
rare earth elements determination by neutron activation analysis 79−88492
rare earth geochemistry and mineralogy, book contrib. 80−46157
rare metal ores, quantitative relns. between Ta, U, Th and Zr 77−56629
realgar, radiography of geological specimens for determ. of α- and fission-activity 78−20540
rectorite, stacking and ordered interstratification, high-resolution TEM obs. 80−109140
red ochre, chem. anal. by Mossbauer spectroscopy, and superparamagnetism 78−20397
Red Sea geothermal system, ore transport and deposition 78−32096
redox logging for minerals, model studies 77−64466
refractory megacrysts and Mg-rich melt inclusions in spinel in oceanic tholeiites 78−32060
regional resource appraisal, statistical methods 78−28326
release-adiabat measurements, effect of viscosity 80−51388
reserve estimation, in three-dimensional deposits using FORTRAN IV Function Segment 77−87085
resource data bases 77−53203
rhodochrosite, deform. twinning mechanisms 80−79814
rhodonite, lattice imaging of struct. defects 80−49240
rhodusite, electrical resist., up to 60 kbar *(German)* 80−31032
rhonite-bearing Ca-Al rich inclusion in Allende meteorite, mineralogy 79−2530
riebeckite, low temp. Mossbauer obs. of oriented single cryst. behaviour and mag. props. 80−84674
ringwoodite, dislocation obs., Earth mantle implications 80−85909
rinneite, Rb-Sr dating of potash salt deposits 80−67429
rock salt, finite strain isotherm and vels. for single crystal and polycrystalline samples 78−53646
rock salt, progressively mined soln. cavities, struct. behaviour 78−61409
rock salt, radar detection of boreholes in advance of mining 78−96305
rock salt, radar propag. 78−96215
rock salt cavities, stress distrib. 79−48462
rock-forming minerals in metamorphic rocks, thermal overprinting of NMR and K/Ar ages 78−65278
Rother catchment, W.Sussex, fine sediment mineralogy of source rocks and suspended sediment 79−20827
rustumite, crystal struct. 77−84727
rustumite, crystal structure, X-ray anal. 80−79766
rustumite, crystal structure determ. by X-ray diffr. method 80−70182
rutile, isothermal compression under hydrostatic press. to 106 kbar 80−31035
rutile (MgF_2), high-pressure phase transformations 79−44181

minerals continued
rutile type structures, rel. between β-gallia, ramsdellite psilomelane, hollandite and $Ga_4Ti_{4-x}O_{2x}$ type structs. 79−37664
salt, deposits, of Sao Paulo Plateau, seismic survey 77−21750
salt, diapirs on E.Brazil continental margin, distrib. rel. to crustal models 77−21698
salt deposit formation *(Russian)* 79−2237
salt deposits, in W.Gulf of Mexico, multichannel seismic refl. results 77−21749
salt deposits, seismic prospecting by well logging *(Rumanian)* 78−20566
salt dome dynamics, finite element analysis 79−20789
salt-bearing sections, vertical electric sounding *(Russian)* 78−11807
sanidine, (K,Na)$AlSi_3O_8$, monoclinic-to-triclinic reversible transformation at high press. 77−17090
sanidine, phase diagram and thermodynamic props. 79−91985
sapphire, natural, origin of colour 79−70794
sapphirine, in rocks with sedimentary and volcanogenic protoliths 79−44185
sarabauite, X-ray cryst. struct. determ. and refinement 79−14754
scanning electron microscopy for mineralogy 80−82077
schorl tourmaline, elastic const. 78−68718
schreibersite, platelike, in hexahedrites, habit planes 78−65572
scolecite, from Poona, India, X-ray cryst. struct. determ. 79−90605
secondary minerals in basaltic rocks from DSDP Leg 37, geochemistry 77−91127
SEM, and assoc. microanal. by X-ray dispersive spectrometry applic. to mineralogy *(French)* 79−5630
SEM, automation, quant. anal. of elementary images *(French)* 78−78045
serpentine, D/H ratios, rel. D/H fractionation factors between serpentine and water at 100-500°C 79−34803
serpentine, solubility of inert gases, meteoritic abundance 80−12712
serpentine minerals, IR specta, comparison with Orgueil, type C-1 chondrite 80−17556
serpentine minerals, milling rel. to cryst. struct., X-ray diffr. 77−55278
serpentine rock, quarried, rel. to environmental asbestos pollution 77−91261
shale investigation as radioactive waste repository, vermiculite role 80−32354
shallow-water mineral exploration by controlled-source audiomagnetotellurics and resistivity profiling 77−5356
shock deformation of brittle solid, review of theory 80−72493
shortite, cryst. struct. and space group, pyroelec. effect 79−23573
shungite, Ar degassing to form ancient atmos., isotope fractionation 80−85749
Sikhote-Alin meteorite, chem. comp. *(Russian)* 77−9715
silica, biogenic, dissolution in deep sea, rate control 79−20817
silica, determ. respirable dust from steelmaking, silicosis 80−45832
silica shock adiabat, rel. to specimen size 77−81873
silicate, chemical analysis by ion beam analysis *(French)* 77−52711
silicate, determ. of ^{16}O and ^{18}O diffusion profiles by ion analyser *(French)* 77−55400
silicate, identification and asbestiform varieties, electron optical and X-ray techniques 80−8446
silicate, interstellar, porous grains, free-space equilib. temps. calc., rel. to optical props. 80−62223
silicate, linear variation of secondary ion yield *(French)* 80−108763
silicate, microanalysis with ion analyser *(French)* 77−52710
silicate, microscopic samples molecular analysis, with Raman microprobe 80−57391
silicate, quantitative analysis using SIMS 77−56285
silicate anal. on small samples using X-ray quantometer 78−61112
silicate dust condensation processes investigation, expt. techniques 80−26940
silicate glasses from igneous rocks, high temp. thermal props. 77−33055
silicate HV high-resolution electron microscopy 80−70096
silicate inclusions in group IAB Fe meteorites, rel. to anomalous stony meteorites 78−32416
silicate melt, ^{45}Ca tracer diffusion 79−90809
silicate minerals, Mossbauer anal. of Fe chem. state 80−20547
silicate minerals, relationship between phonon cond. and seismic parameter Φ 79−39707
silicate minerals, X-ray photoelectron diffr., quantitative anal. 80−66912
silicate minerals, X-ray spectral study, emission bands, quantum yield, tetrahedra valence bands 77−28660
silicate rocks and minerals, instrumental neutron activation anal. 78−20548
silicate slag melt, physicochemical optimisation 78−85112
silicate smokes, vapour-condensed, 800 to 130 nm extinction and interstellar extinction curve 80−82180
silicate-K-(Fe-S liquid) equilibria and K solubility, in Fe-S liq., planetary implications 78−11843
silicates, destruction by adsorption of tropospheric halocarbon and N_2O 79−12168
silicates, elastic constant systematics 79−69177
silicates, elec. field gradient at Fe^{2+} sites, Mossbauer spectra 80−15484
silicates, emission and extinction in 4-14 μ range 79−44581
silicates, entropy estimates at 298K from molar vols. 77−1243
silicates, ESR, review 78−88166
silicates, heat capacities rel. to simple lattice vibrational models 80−4005
silicates, interdepend. between tetrahedral d(T-O) bond lengths, nonbonded d(T...T) separations and TOT angles (T=Al,Si,P), using regression anal. 79−19182
silicates, IR spectra compared with astrophysical IR features 80−26728
silicates, lattice imaging 78−30522
silicates, layered, optical filtering of faulted areas in electron micrographs 80−84035
silicates, liq. immiscibility rel. to spheroidal pyroxenite aggregates in Bushveld Complex 79−88351
silicates, liquid, thermodynamic props., calc. model 79−34804
silicates, optical props. in far UV 78−53875
silicates, phonon cond. and mean sound vel., linear relationships 77−21761
silicates, thermal expansion, characterisation technique 79−70795
silicates, thermodynamics and lattice vibr. props. 79−100830
silicates, thermodynamics and lattice vibrs. 79−100831
silicates and oxides, phonon conductivity 77−73715
silicates in Fe meteorites group IAB, I-Xe dating 80−17554
silicates with branched anions, crystallochemistry distinct class 79−57917
minerals continued
sillimanite-andalusite-kyanite (Al_2SiO_5 polymorphs) thermal expansion and high-temp. cryst. chemistry 80−39319
single domain grains, mag. blocking temps. during slow cooling 80−90082
sinter mineral samples, analysis by electronic microsonde *(Croatian)* 79−29910
skarns, B distrib. as mineralisation test, (n,α) radiography 77−17091
slaty cleavage development across Nackara Arc, Adelaide Geosyncline 79−66694
sodalite, ESR and optical spectra obs. 77−32407
sodalite, $Na_8Al_6Si_6O_{24}F_2(I)(Br)(I)$, luminescence and coloration *(Russian)* 78−72578
sodalite single crystals, exam. of growth mech. in hydrothermal method, using SEM 79−52105
sodium rare earth silicates, single cryst. data and ionic cond. 80−84158
Sokoman Iron Formation near Ardua Lake, Quebec, mineralogy and petrology 78−77228
Solar Lake, Gulf of Elat, recent hot brine dolomitization 77−70634
solution rates, effects of stress 77−86865
south-east Baltic Sea silt granulometric and mineral composition *(Russian)* 79−96755
space group refinement by vibr. spectroscopy methods, possibility 78−79507
spark spectroscopy and new type of electrodes and paste specimens *(French)* 78−92563
spectral analysis by Kler method, increased accuracy 79−70393
spectral reflectance data, lab. and remote obs. comparison 77−17251
spectral signatures of particulate minerals in visible and near IR 78−7620
specularite, in sandstone, exptl. evidence for primary depositional magnetisation 80−90075
sphalerite, appl. of cathodolum. microscopy and spectrometry 77−69919
sphalerite, superficial degradation in air and water, XPS obs. *(French)* 80−89110
sphalerite geobarometer, experimental extension to 10 kbar 78−85703
sphalerite geobarometry, regionally metamorphosed terrain appls. 77−2257
sphalerite geobarometry in Balmat-Edwards district, New York 78−65261
sphene, fission track annealing, fission track age-temp. relationship 80−98316
sphene in high-pressure partial melting of hydrous mafic compositions 79−44174
sphenes, anisotropic and variable track etching characts. due to annealing 78−65435
spherical ore-bodies, total field mag. anomalies interpretation via zero-line method 79−39973
spilite and keratophyre from Oregon-Idaho Permo-Triassic volcanic arc, mineralogy and petrogenesis 79−20826
spinel, dislocation obs., Earth mantle implications 80−85909
spinel, $MgAl_2O_4$, anomalous thermal expansion, second order transition 80−84307
spinel, natural, solid soln., thermodynamic model *(French)* 78−32065
spinel, space group, electron diffr. pattern anal. 79−7594
spinel, zoned from La Perouse layered gabbro, Fairweather Range, Alaska 77−5204
spinel disproportionation reactions, elasticity and phase equilibria 77−78158
spinel lherzolites, petrology, comp., equilib. conditions *(French)* 77−86874
spinel lherzolites in upper mantle, petrogenesis, magmatic model 77−86875
sputtering rates, implications for abundances of solar elements in lunar samples 80−61797
stalactite, from Akiyoshi cave, thermoluminescence and ESR dating comparison 78−88807
stalactites, chem. decomp., ESR obs. 80−15788
stalactites and stalagmites, dating with ESR and thermolum. *(Japanese)* 77−44955
stenhuggarite, $CaFeSbAs_2O_7$, cryst. struct. 77−58983
stilpnomelane, long-period polytypes struct. by electron diffr. and microscopy 77−64266
stishovite, compression to 100 kbar, eqn. of state from bulk modulus 77−17085
stishovite, discovery in Vredefort Dome, S.Africa 78−53653
stishovite, polycrystalline, elasticity 77−5189
stishovite, synthetic polycrystalline, thermal diffusivity meas. 79−39706
stishovite (SiO_2), single cryst. anal. of struct. 78−53648
strontium weilite, $SrHAsO_4$, cryst. struct. 78−38671
strunzite, ^{57}Fe Mossbauer study of crystal chemistry 80−39975
struvite crystals, growth morphology and cryst. habit 79−41994
subducting oceanic crust, thermodynamic consequences of minerals dehydration, high press. and temp. 78−69301
sulphate deposits, stable isotopic comp. and early Archaean origins 79−20832
sulphate evaporites, Middle Proterozoic, at Mount Isa mine, Australia 78−73371
sulphide deposits from E.Pacific Rise near 21°N, mineralogy and geochemistry 80−101361
sulphide group minerals, elec. cond., four-point probe technique meas. 78−64045
sulphide mineralisation in Rajasthan, and Gujarat, India, induced polarisation surveys results 79−39714
sulphide mineralisation zones of NW Ukrainian Shield, rocks mag. props. *(Russian)* 79−96758
sulphide minerals, K-bearing, age meas. by $^{40}Ar/^{39}Ar$ technique 79−29720
sulphide minerals, superstructure and modulated struct. 79−99146
sulphide ore bodies, model for interpretation of towed-bird airborne EM system cond. meas. 79−5447
sulphide ore deposits, deep-sea discovery on E. Pacific Rise 79−34799
sulphide ore deposits, ophiolitic, in Cyprus, prod. by hydrothermal convection 79−29761
sulphide ore deposits in NW.Kola Peninsula, electric near zone field development method testing *(Russian)* 80−85761
sulphide ores, disseminated, electrochemical model of induced-polarisation phenomena 79−92526
sulphide ores, geoelectrical identification and location *(Rumanian)* 77−32997

minerals continued
sulphide-solvent boundaries, two-layer capacitance meas. *(Russian)* 78−10551
sulphides, in DSDP Leg 37 drill core from Mid-Atlantic Ridge 77−91122
sulphides *(German)* 79−29709
sulphides and sulphates from DSDP Leg 37, S isotope comps 77−91101
sulphoborite, cryst. struct. determ. 77−15389
sulphosalt minerals, exam. of crystal chemistry and morphology 79−10838
surface interactions with organic solutes, groundwater vel. determ. 80−98492
surface weathering reactions, stability, thermochem. calcs. 77−44969
surfaces, role in origin of life 77−91273
suspensions, dielectric separation of solid particles 80−16213
swelling examination method 77−53232
sylvite powder, compression in smooth faced rolling presses, preferred orientation *(German)* 79−33959
syngenite, $K_2Ca(SO_4)_2.H_2O$, thermal dehydration, isothermal kinetics 79−15982
syngenite, space group refinement by vibr. spectroscopy methods 78−79507
tabular grain shapes prod. in metamorphic rocks, shear displacement 78−96199
taconite, exploration with integrated aeroelectromagnetic and magnetic methods 79−16690
taenite, cloudy, origin in meteorites, TEM study of Santa Catharina anomalous Fe meteorite 79−66968
clear taenite in meteorites, identification as ordered FeNi 80−8604
taenite lamellae in Fe meteorite, Mossbauer study 78−65575
talc, ^{57}Fe Mossbauer analysis 80−40006
talc, cation-substituted, heat of wetting 77−29050
talc, lattice parameters meas. by back-reflection pseudo-Kossel technique 79−82124
talc, vibr. mode assignments, Raman microprobe spectra 80−88977
TEM, application to mineralogy, sample prep. methods *(French)* 79−5629
terrigenous and volcanogenic deep sea bottom sediments chem. comp., Sea of Japan 77−21758
tetraferriphlogopite, cryst. struct. refinement using least squares approx. 78−79594
thermal conductivity and thermal expansion, conference, Chicago, USA (Nov. 79) 80−31425
thermal expansion, characterisation technique 79−70795
thermal properties of dry, water-saturated and petroleum-saturated specimens *(Russian)* 78−92817
thermobarogeochemistry of inclusions *(Russian)* 80−104954
thermodynamic functions from eqns. of state for end members 80−90084
thermodynamic properties of mantle related substances at high press. and temp. 80−81874
thermoluminescence dating, error sources 78−11006
thermoluminescence dating, phototransfer technique 78−11005
thermoluminescence dating 78−11004
threadgoldite, X-ray cryst. struct. determ. 80−28969
titanian clinohumite from Jacupiranga carbonatite, Sao Paulo, Brazil, paragenesis and comp. 78−85552
titanite, lanthanides, relative concs. rel. to host rock type 79−62492
titanomaghemite, identification in rock by mag. rot. hysteresis loss 80−67428
titanomaghemite, synthetic, cation distrib. 78−55856
titanomagnetite, Al-substituted, monodomain, mag. props. 78−56346
titanomagnetite, identification in rock by mag. rot. hysteresis loss 80−67428
titanomagnetite, monodomain behaviour in multiphase oxidised material 77−60366
titanomagnetite, prepared at different oxidation conditions, hysteresis props. 78−56352
titanomagnetite, single-crystal, mag. props. of multidomain TRM 78−56345
titanomagnetite, single-domain particles identification by TEM 79−88342
titanomagnetite, TRM acquired by multi-domain single cryst. 80−36293
titanomagnetite from African rift zones, spinodal decomposition and partial self-reversal of magnetisation 77−81869
titanomagnetite in basalts, mag. coupling in partial self-reversal assoc. with increased mag. viscosity 77−73717
titanomagnetite in Waipipi ironsands, New Zealand, mag. assessment technique 80−17254
titanomagnetites, domain struct. var. with temp. 78−65272
titanomagnetites, exsolution microstructures, magnetic significance 80−98313
titanomagnetites, hysteresis props., grain size and comp. depend. 77−37187
titanomagnetites, temp. depend. cation distrib., mag. prop. obs. 80−85647
titanomagnetites from oceanic crustal layer 2, oxidation rel. to magnetisation 77−91071
titanomagnetites of oceanic basalts, low-temp. oxidation rel. to mag. anomalies statistical anal. 80−36233
todorokites, natural, new forms crysts. structs. 79−48469
topaz, thermolum. props., dosimeter appl. 78−35957
topsoil mineralogy, Ngunguru Basin, New Zealand 78−85557
torbermorite study by X-ray line profile anal. *(Japanese)* 80−33984
tourmaline, elastic consts. by US phase-comparison method 80−2108
tourmaline, fission track etching and annealing, thermal retention 77−82042
tourmaline, Mossbauer spectra, struct. 80−20566
tourmaline, proton jumps, NGR obs. 80−15921
tourmaline, pyroelectricity, struct. mechanisms 78−10850
tourmaline, Raman spectra 79−4801
tourmalines of dravite-schorl series, Mossbauer anal. 80−15920
trace element determ., neutron activation anal., coaxial, planar detectors comparison appl. 77−81443
traskite, Ba mineral of variable comp., X-ray diffr. struct. anal. 77−44981
travertine from archaeological sites, Nahal Zin, Israel, U series dating 79−34781
tremolite, optical spectra obs. 77−40284
tremolite asbestos, fibrous. elec. anisotropy 78−80273
tridymite, low, synthetic, struct. refinement, Si-O bond lengths and Si-O-Si bridging angles 77−80456
tridymite, non-integral phase from 150°-190° 79−99144
tridymite, thermal expansion meas. 80−59682
troilite, complex refractive indices rel. to comp. of Saturn's rings 77−29716
troilite in Fe meteorites group IAB, I-Xe dating 80−17554
tschermakitic clinopyroxenes, mixing props. 77−2149
tundrite, $Na_2Ce_2TiO_2[SiO_4](CO_3)_2$ new cryst. struct. and formula 77−31648
turquoise, crystalline, Nogales Mexico, SEM and TEM study 79−29760
tveitite, X-ray powder and single cryst. electron diffr. study *(German)* 79−99160
twin composition plane as extended defect, structure-building entity 80−44218
type B carbonate apatites, dehydration obs. *(French)* 79−66264
Tysnes Island meteorite, unusual clast composed of solidified immiscible Fe+FeS and silicate melts 79−2526
ultramafic inclusions, petrogenesis, geochem. and petrologic data 78−65301
ultrasonic damping due to internal friction, freq. depend. *(German)* 80−90078
ulvospinel, containing magnetized inclusions, mag. behaviour, cooling through Curie point 78−56314
ulvospinel, mag. props. weak ferromag. in 4-200K temp. range 78−56351
underground water mineralisation, reliability anal. of geophys. estimation *(Polish)* 77−73862
upper mantle mineral assemblages, implications of CO_2 high temp. and press. fugacity 79−16439
uralborite, $Ca_2(B_4O_4(OH)_8)$, accurate cryst. struct. 78−34492
uraniferous structures of Cluff Lake district, resistivity mapping *(French)* 78−69285
uraninite, Oklo phenomenon, isotopic abundances, long-term radioactive waste storage information 80−52769
uraninite from Oklo natural fission reactors, comp., evidence for mode of deposition and metamorphism 80−21747
uraninite grains, U solubility in the Oklo reactor 80−21756
uraninite in Oklo natural fission reactors, geochemistry of insoluble organic material *(French)* 80−21748
USA developments, by means of technological innovations, federal regulations influence 80−16763
USSR, tectonics and mineral resources *(Russian)* 78−40536
vapour growth and epitaxy, comparison of growth methods 79−23856
vaterite, polymorphic transition kinetics, differential thermal anal. meas. 79−14722
velikite, cryst. struct. determ. 78−2097
vermiculite, electric field gradient, Mossbauer absorption 79−73865
vermiculite, firing temp. depend. of Mossbauer parameters 80−15837
vermiculite, fission track annealing and dating 80−81885
vermiculite, interlayer space struct. anal., by replacing exchange cations with NH_4^+ 77−7700
vermiculite, sorption props., appl. to radioactive fallout water deactivation 79−43995
vermiculites, chem. treated, for liq. radioactive waste treatment by ion exchange 79−45370
violarite, $FeNi_2S_4$, mag. and elec. props., struct. determ. 77−43633
vitrinite, in bituminous coal, microporosity and micromineralogy, small-angle X-ray scatt. study 79−12117
voglite, cryst. and powder diffr. data 80−24421
volcanic glass and sanidine/plagioclase feldspars, Pb partitioning 79 74867
volcanosedimentary levels, S.Pacific, neoformation and weathering *(French)* 78−73353
wadeite, cryst. struct. refinement, X-ray diffr. meas. 78−2091
weathered Athenian schist, basic geotechnical and mineralogical props. 78−61408
weathering profile evolution simulation by aq. soln. *(French)* 77−60438
whitlockite from Bjurbole chondrite, origin of fission fragment tracks 78−81595
willemite, cryst. struct. 78−83804
wollastonite, exptly. deformed, polytype transforms. 79−65021
wollastonite, individual silicate chains obs. by high resolution electron microscopy 79−100829
X-ray anal. of microcrystallite nucleation and detection threshold 80−890
X-ray fluorescence spectrometry of geological samples, element analysis *(Rumanian)* 77−33217
X-ray $K\alpha_{1,2}$ emission spectra, chem. shift, effective charges of Al,Si,Fe and O atoms 77−28659
X-ray spectral analysis, appl. of semiconductor spectrometer 79−87902
X-ray spectral analysis, calibration method 79−87904
xonotlite, $Ca_6Si_6O_{17}(OH)_2$, polytype identification from electron diffr. patterns 80−72519
Yamato meteorites (j), (k), (l) and (m) from Antarctica, petrology 79−2528
yellow ochre, chem. anal. by Mossbauer spectroscopy 78−20397
zektzerite, silicate mineral with six-tetrahedral-repeat double chains 78−63719
zeolite:Fe^{3+}, Mossbauer effect and magnetometric exam. 78−6613
zeolite, $Na_6Al_6Si_6O_{24}$, luminescence and coloration *(Russian)* 78−72578
zeolite, surface reactions with H and O atoms, EPR anal. via ultrahigh vacuum/flow system 78−7232
zeolite (Itaya), removal of H^+, NH_4^+, Cu^{2+}, Cd^{2+} *(Japanese)* 78−95951
zeolite A, synthetic, with salt inclusions, elec. and thermal props. 79−55925
zeolite addition to cement-waste composites for ^{137}Cs immobilisation 78−82466
zeolite facies alteration of sandstones of Southland syncline, New Zealand 78−32084
zeolite inclusion complexes, LiA.$LiNO_3$ and LiX.$LiNO_3$, ^{7}Li NMR motional line narrowing 79−56618
zeolite L-D, prep. and props., from crystn. of obsidian 79−100067
zeolite minerals, filament and cluster crystals, liqs. in ultrathin channels, rel. to supercond. materials development 79−19162
zeolite-water desorption, complex reaction interphase boundary kinetics 79−57203
zeolites, and Ga analogues, IR spectroscopy to investigate structure 79−95744
zeolites, dehydrated Na-exchanged mordenite, cation and molecular distrib. 79−90617

minerals continued
zeolites, synthetic, thermal dehydration effect on physicochem. characts. 60120
zeolites in basalts, effects on compressional and shear wave vels. at high temp. and press. 79−84244
zinckenite, chem. and structural study *(French)* 77−43181
zinkenite, electrophysical properties 78−34834
zircon, (sand), thermolum., UV and γ-ray effects 78−2930
zircon, element distrib. from proton multiprobe and fission track techniques 80−17261
zircon, high-press. phase transform., Earth mantle appl. 80−8296
zircon, improved etching techniques for fission track dating 77−29457
zircon, Indian, fission track dating and annealing, U content determ. 79−57891
zircon, natural and synthetic crysts. Hf and Tb activated, capture centres and luminescence mechanism *(Russian)* 77−28626
zircon, nucl. radiation effect on elastic moduli 77−11616
zircon, radiation defect centre, EPR obs. 80−75853
zircon, thermoluminesc. glow curve and spectrum 79−33847
zircon in Uivak II gneiss from Saglek area, Labrador, age meas. 80−3958
zircon minerals, Hf determ. by neutron activation anal. *(Russian)* 77−40615
zircons, detrital, in N.Africa, no evidence of 500 Myr ages or Pan-African mountains 79−84213
zircons, from early Precambrian rocks of W.Greenland, U-Pb dates 77−29256
zircons, from gold-bearing region of Salsigne, France, thermolum. meas. *(French)* 77−28637
zircons, U-Pb dating in Munchberg Gneiss Massif 79−34774
zircons from Early Precambrian rocks of W.Greenland and Minnesota River Valley, U-Pb ages 78−11845
zircons from gneisses, radioactive dating, igneous and metamorphic events, Fiskenaesset region, Greenland 79−84250
ziron, from Kanyakumari, India, U content estimation using plastic track detector *(French)* 77−64445
zorite, X-ray cryst. struct. determ. 80−92513
zussmanite, polymorphism of infinite Si_3O_7 radicals in layered stacks 79−60301
α radioactivity, E>11 MeV emulsion and counting techniques 78−8785
Ag_3AsS_3, proustite, reflectivity and optical constants at 80K and 300K from 18 to 700 μm *(French)* 77−36235
Al electrolytes, X-ray determ. of cryolite ratio 78−3417
Al saponite, differential thermal anal., IR absorpt. spectra, chlorite-like mineral 78−88816
Al saponite, evidence for inclusion in chlorite-like mineral group, X-ray and chem. anal. 79−12108
Al_2O_3, solubility in orthopyroxenes in spinel and plagioclase peridotites and spinel pyroxenite 77−5186
$Al_2O_3.SiO_2.H_2O$, new materials from pianlinite minerals *(Chinese)* 79−95982
Al_2SiO_5, kyanite, sillimanite, mullitisation, effect of gaseous atm. 79−11604
apatites, replacement by La, Nd, Sm, Gd by Ti, Ge, Mn^{IV}, V^V *(French)* 79−69093
$^{40}Ar/^{39}Ar$ dating, appl. of isochron diagrams 79−29873
^{40}Ar-^{39}Ar systematics, temp. and pressure effects 79−44178
As determ. in ores of reduced heteropoly acids, photometric method 78−61103
Au ores, neutron activation and mathematical programming *(Rumanian)* 78−20565
Au, spectral determ. 79−70391
Au-U ores, Witwatersrand Basin, fluid inclusion study 77−86891
BaF_2, fluorite-struct. compound, high-temp. elasticity, US pulse meas. 77−81878
$Ba_2Ga_2GeO_7$, gehlenite struct., synthesis and physicochem. props. 79−43181
C_3S mineral, chem. and polymorphism 79−69051
$(Ca,Fe)SiO_3$, intracryst. Fe^{2+}-Ca^{2+} exchange, Mossbauer spectra 80−20548
Ca-Al rich inclusions in meteorites, origin rel. to cosmoradiogenic ghosts 78−12162
Ca-rich clinopyroxenes, intracrystalline Fe^{2+}-Mg equilibria 77−2145
$Ca_2Al_2GeO_7$, gehlenite struct., synthesis and physicochem. props. 79−43181
$Ca_3Al_2Si_3O_{12}$, garnet, thermophysical props., 5 to 600K 79−60517
CaF_2, fluorite-struct. compound, high-temp. elasticity, US pulse meas. 77−81878
Ca_2GeO_4, with K_2NiF_4-type struct., high press. decomp. 79−1507
$CaHPO_4$, monetite, low-temp. ordering of H atoms, X-ray and neutron diffr. study at 145K 80−39022
$Ca_2HPO_4SO_4.4H_2O$, synthetic, cryst. struct. and relation to brushite and gypsum 78−83785
$CaMg(CO_3)_2$, dolomite, reaction with ZrO_2, mineralisation during roasting 79−43180
Ca_2MnO_4, with K_2NiF_4-type struct., high press. decomp. 79−1507
CaO, solid, phase transition at high-press., lower mantle implications 80−79876
CaO, tentative evidence for high press. metallisation 80−84427
CaO-Al_2O_3-SiO_2 diffusion triangular diagram, diffusion between lime and sintered kaolinite *(French)* 79−69296
CaO-MgO, doloma, composition effect on creep, impurity effects 79−43318
$Ca_5(PO_4)_3OH$:Mn, synthesized by hydrothermal method in CaO-P_2O_5-H_2O, thermoluminescence study rel. to starting mixture 78−95612
chrysoberyl, $BeAl_2O_4$, kinetics and mechanism of formation, in presence of V_2O_5 79−11535
$Co_3(AsO_4)_2.8H_2O$, optical absorpt. spectra, spin orbit splitting and cryst. field parameters 79−38560
Cr spinellide, acid extracted, phase transform. on heating in air *(French)* 79−96003
Cr-rich pyroxenes of peridotite xenoliths, Nevada, comp. rel. to formation press. and temps. 77−5139
Cs-mordenite , dehydrated, positions of cations and molecules 79−1418
Cu content of Rumanian ores, X-ray fluorescence analysis *(Rumanian)* 77−29508
Cu deposits, exploration using LANDSAT-1 imagery 79−2398
Cu minerals suspended in ocean waters 79−74904
Cu ore processing materials, nondispersive X-ray fluoresc. anal. 78−92575

minerals continued
Cu-Ni enriched ferromanganese nodules and crusts from Bauer Basin, mineralogy and chemistry 77−86851
$CuFeS_2$, natural chalcopyrite, defect struct., TEM 77−62535
emerald:Cr^{3+}, spin-lattice coupling consts. 79−99761
Fe, concretions origin of Hepworth carboniferous sediment, geochemistry 80−17262
Fe containing minerals, basalt rocks, Mossbauer spectroscopy identification 80−8302
Fe containing minerals in oil-impregnated sedimentary rocks 77−53053
Fe meteorites, mineralogy, review 77−87348
Fe, meteoritic, first order shock induced mag. transitions characts. and discrimination from TRM 78−64205
Fe ore, adsorption methods for determ. of specific surface 78−21096
Fe ore, Calicut area, associated biotite pegmatite dating by fission track 77−13066
Fe ore, cold bound pellets, reduction using H_2 gas, 700 to 900°C *(Japanese)* 80−71907
Fe ore, strength and flow props., vibrations effect 79−37237
Fe ore band associated with meta- acidic intrusive, Himalayas, Mossbauer meas. 79−79821
Fe ore concentrates, two-layer charge, sintering conditions *(Russian)* 80−45248
Fe ore deposit integral characts. determ. from magnetic anomalies *(Russian)* 79−62621
Fe ore deposits from gravity and magnetic anomalies, determ. accuracies *(Russian)* 79−84536
Fe ore formation, Addatigala, India, mag. profiles 79−34808
Fe ore pellet, meas. of gas permeability of individual pellets 78−80711
Fe ores, determinaton of Fe content, using ionisation effect of back β-scattering 79−52824
Fe ores, grade, bulk density, porosity determ. by nuclear geophysical methods 79−48570
Fe ores and coal, nuclear activation logging for Al 79−80042
Fe-bearing olivine and pure forsterite, creep props. comparison 77−78168
Fe-Mn nodules from Pacific Ocean, sorption processes 79−16435
Fe-Ni sulphide ores, partitioning in metamorphosed olivine-sulphide assemblages 77−5185
Fe-Ni sulphides in Murchison meteorites, props. and rel. to phase Q1 79−58303
Fe-Ni-Cr-S-O compounds, occurrence in Allende chondrite *(French)* 78−32411
Fe-Ti oxide minerals from Asama volcano, Japan, in 1973 eruption 77−17065
Fe-Ti oxides, in epizonal granitic intrusions, geothermometric and geobarometric appl. 77−5140
α-Fe_2O_3 (haematite), X-ray diffr. compression studies under hydrostatic isothermal conditions 78−85539
Fe_3O_4 (magnetite), effects of mag. field on reduction rate 77−44461
Fe_3O_4, magnetite, comparison of anhysteretic remanence and thermoremanence 77−5191
Fe_3O_4-$FeAl_2O_4$-$FeTiO_3$ titaniferous magnetite, chlorination, 1273 to 2273K 80−55752
β-FeOOH, akaganeite, struct. changes due to radiation damage 79−28014
FeOOH minerals, magneto-mineralogical props. 77−81872
FeS_2 (pyrite) formation in sulphide-rich sediments, Fe diagenesis studies by Mossbauer spectroscopy 79−74917
Fe_7S_8, 3C pyrrhotite, cryst. struct. refinement 79−42017
Fe_2SiO_4, spinel, isothermal compression up to 75 kbar hydrostatic press. 77−43280
H isotope exchange between clay minerals and seawater 78−69329
haematite nodules with fayalite and Ca ferrite additives, stressed state parameters *(Russian)* 80−45352
Hg ores, determ. of Hg content using ^{57}Co isotope and scintillation counter 78−20539
$In_2Si_2O_4$, high press. pyrochlore struct. 77−47426
K concentration, electron probe analysis with low temperature sample holder *(French)* 80−85248
K feldspars from Precambrian igneous rocks, Pb isotope inhomogeneity 78−32095
K-Ar dating of intrusion gas and scheelite mineralisation, Cantung, Canada 79−5460
K-feldspar importance in polyorogenic areas, ^{39}Ar-^{40}Ar dating 79−44152
Li concentrations in McDermitt Caldera, in Nevada and Oregon, geological survey 79−48478
Li deposits and potential, Quebec and Atlantic Provinces, in Canada, report 79−48481
Li, needs and resources, conf., Corning, USA (Oct. 1977) 79−48473
Li, occurrence in flint clay and related rock types in United States, preliminary survey 79−48475
Li ores in Horse Spring Formation Miocene rocks, Clark County, Nevada, report 79−48474
Li, ores in United Kingdom, brief assessment 79−48476
Li ores resource evaluation, United States Geological Survey role 79−48477
Li pegmatite ores in Western Superior Province, in Canadian Shield, distribution and petrogenesis 79−48480
Li resources, Yellowknife area, in NW.Canada, report 79−48482
Li resources and potentials, NW.Ontario, Manitoba, Saskatchewan, in Canada, estimation 79−48483
Li rich brines in SW.Bolivia, chemical composition and distribution 79−48479
β-$(Mg,Fe)_2SiO_4$, high-press. spinel phase identification in Tenham chondritic meteorite 79−80284
Mg SiO_3 melt, instantaneous struct. simulated by mol. dynamics 80−84049
Mg silicates, high-press. phase relations, absence of oxide mixture 77−37185
Mg vermiculite, adsorbed water mol. orientation, elec. pot. calc. 78−26763
Mg-cordierites, synthetic end member, variation of refractive index with water content 80−80739
Mg_2GeO_4, determ. of olivine-spinel transition up to 20 kbar and 1300°C 77−53044
Mg_2GeO_4, geometric flow props. 78−57198
MgO (periclase), elastic consts. and internal frictions meas. by rectangular parallelepiped reson. 77−78165
MgO, longitudinal elastic vels. to 360 kbar 77−70642
MgO, thermal cond. up to 40 kbar 79−1533

minerals continued
$MgO-SiO_2$ system, high-press. phase transistions calcs. rel. to mantle discontinuities 79−90780
$MgSiO_3$ perovskite polymorph, high-press elastic consts. determ. 77−51428
Mg_2SiO_4 in Earth mantle, possible transform. to Ca ferrite struct. 77−64270
$Mg_3Si_4O_{10}(OH)_2$, talc, for hydrothermal crystn. of fibrous amphiboles 80−20810
$2Mg_2SiO_4.3Mg(OH)_2$, new high-press. struct. type, cryst. struct. 80−39028
Mn minerals, photoluminesc. 79−95829
Mn minerals in hydrothermal mounds near Galapagos Rift, chemistry and mineralogy 79−29739
Mn nodule, sediment-water interface and submergence dynamics 78−28217
Mn nodule growth rate from ^{10}Be meas. using tandem Van de Graaff accelerator 79−74967
Mn nodule growth rate meas. using radioactive ^{10}Be and ^{26}Al 78−40537
Mn nodule undersea mining data file, management and statistical anal. 77−53206
Mn nodules, deep-sea, diagenetic features, X-ray spectral and SEM anal. 79−16099
Mn nodules, deep-sea, Ni and Cu accumulation as essential elements in 10-Å manganite 79−66674
Mn nodules, from Pacific Ocean growth rates from U series and hydration-rind dating 77−29280
Mn nodules, from sea-bed, isotopic and elemental composition, U, Pa, Th, radiochem. anal. 78−77215
Mn nodules, mineralogy and comp. changes from long-term seafloor mineral exposure expts. 79−5471
Mn nodules and Deep Ocean Mining Environment Study phase I and II, prospects 78−16164
MnF_2, rutile type, polymorphism at high press., distorted fluorite phase 79−69050
$Mn_2NaSi_3O_8(OH)$, serandite, synthesis, struct., physicochem. props. 79−43187
Mo oxides, low-grade, soda roasting study *(Korean)* 80−93508
$NH_4Al(OH)_2CO_3$, NH_4-dawsonite, cryst. struct., X-ray powder diffr. *(Japanese)* 79−69096
$(NH_4)_2SO_4$, atm. dust, imaginary refr. index rel. to particle size 78−7763
Na concentration, electron probe analysis with low temperature sample holder *(French)* 80−85248
Na determ. by (p,γ) reacts., target excitation yields determ., appls. 77−44545
Na determ. in rock, mineral samples, X-ray fluoresc. quantometer modification 78−61589
Na montmorillonite, water vapour adsorption at −5°C 78−65540
Na zeolites, electronic struct., quantum chemical study 80−69058
Na-rich plagioclase microstructure and exsolution 80−72501
$Na_3Al_2Li_3F_{12}$ garnet, cryolithionite, hydrothermal growth 79−43123
$NaAlSiO_4$ (nepheline), high-press. to transform. to first silicate Ca ferrite isotype 77−64270
$NaAlSi_2O_6$, jadeite, melt, changes in viscosity and struct. at high press. 77−29290
$NaAlSi_2O_6$ melts quenched at high press., struct. from IR and Al K-radiation data 79−32907
$Na_6Al_6Si_6O_{24}$, zeolite, luminescence and coloration *(Russian)* 78−72578
NaCl, thermal cond. up to 40 kbar 79−1533
$NaF-MgF_2-MgO-SiO_2$, phase formation 78−27460
$Na_2Si_3O_7$ melt, changes in viscosity at high press. 77−29290
Nb-Ta family minerals, cryst. struct., X-ray powder diffr. study 80−107169
Ni partitioning between forsterite and aluminous silicate melts, pressure depend. 79−44176
Ni sulphide ores from Kambalda, W.Australia, sulphide fabrics 78−77229
Ni-Fe particles in chondrites, microscopic obs. *(Russian)* 77−9724
NiO ore, reduction of Ni in segregation roasting process *(Japanese)* 80−71908
O isotope partitioning among minerals in igenous and metamorphic rocks 77−86870
O isotopes rel. to diagenetic silica minerals in Monterey Shale 77−64267
O_2 self-diffusion in feldspars, ion microprobe determ. 78−69325
^{18}O distrib. among mineral triplets in igneous and metamorphic rocks 78−32071
^{187}Os isotopic anomalies from different ore deposits, LAMMA determ. 80−61800
P determ. in ores of reduced heteropoly acids, photometric method 78−61103
Pb and Zn layers in South Niger, geological features *(Croatian)* 79−29772
Pb minerals suspended in ocean waters 79−74904
Pb sulphides, isotopic composition, mineralisation time determ. 78−73372
Pb-Zn belts and their origin 79−48427
Pb-Zn minerals, carbonate-hosted, in NE British Columbia, Robb Lake deposit 79−62494
Po-haloes in Precambrian biotite and other old minerals 78−85556
^{244}Pu minerals, haloes prod. by fission alpha particles 77−29300
ramsdellite type structures, rel. between β-gallia, rutile, psilomelane, hollandite and $Ga_4Ti_{x-4}O_{2x-2}$ type structs. 79−37664
S isotope exchange between sulphate and sulphide in acid solns., expt. determ. at 300°C and 1000 bars 78−62937
$Sc_2Si_2O_7$, high press. pyrochlore struct. 77−47426
Si-O bonds, cryst. chem. at high press., rel. to Earth mantle mineralogy 79−48470
SiO_2 budget of Antarctic waters, effects of glacial weathering 78−20436
SiO_2, coesite, thermal cond. up to 40 kbar 79−1533
SiO_2 stishovite, thermal cond. up to 40 kbar 79−1533
SiO_2, vitreous, radiation behaviour of optical props. 78−21655
$SiO_2-Al_2O_3$, minerals, phase equilibrium *(German)* 77−73261
$SiO_2-Al_2O_3$, mullite, sintering behaviour and microstruct. 80−20876
$SiO_2-Al_2O_3$ based minerals, phase equilib., struct., comp. *(French)* 78−60659
SiO_6 octahedra, var. of mean Si-O bond lengths 78−18577
$Sr_2Al_2GeO_7$, gehlenite struct., synthesis and physicochem. props. 79−43181
SrF_2, fluorite-struct. compound, high-temp. elasticity, US pulse meas. 77−81878
minerals continued
Te ores, geochem. test of nucleon stability 78−8667
ThO_2, $^{233}U/Th$ ratio determ. *(Spanish)* 77−70637
Ti garnets, Mossbauer spectroscopic anal. of chem. state of Fe 80−20547
Tl minerals, ^{205}Pb assay by mass spectrometry for solar neutrino flux determ., proposed expt. 77−5447
U are at Oklo, appl. of Ep-pH diagrams to problems of retention and migration of fissiogenic elements 80−21757
U boreholes, in situ assay using prompt fission neutron technique 77−37441
U deposit, Saima alkaline massif, NE China 79−16470
U deposit at Oklo natural reactor site, anomalous Xe and Kr isotope composition 77−56630
U deposits, Canadian Uranium Reconnaissance Program 77−37439
U deposits, in situ assay logging system using delayed fission neutrons 77−37440
U deposits rel. to granitic rocks, formation and destruction during continental crust evolution 79−84201
U distribution and evolution in oceanic lithosphere 79−84226
U, exploration in Australia 79−48471
U exploration in Egypt, exploration under arid conditions 79−26538
U exploration probes, meas. spatial depend. of delayed neutron signals 79−34989
U extraction from friable ore-bearing rocks, underground leaching 77−70664
U, in Witwatersrand Triad, geochronology 77−86892
U, mineral analysis using alpha particle absorption by cellulose nitrate *(Spanish)* 77−70358
U mineral deposits, criticality study using ore model *(Spanish)* 77−70655
U mineralisation rel. granite magmatism, British Isles 79−84273
U mineralization of Witwatersrand and Dominion Reef systems 77−86890
U minerals, Pu content, ore model calcs. comparison with expt. *(Spanish)* 77−70654
U minerals, quantitative microprobe anal. 78−61126
U natural reactor in Oklo, isotopic composition 77−56628
U, nature and exploration in US sandstone deposits, educational module 80−36799
U ore, in situ mining, Wyoming State regulations and environmental monitoring 79−88510
U ore, radioisotopic X-ray anal. by K-shell fluorescence 79−79353
U ore, Ru isotopic anal. 80−21764
U ore, solution mining, effect of Environmental Protection Agency requirement for underground injection 79−92101
U ore, solution mining, environmental impact, groundwater restoration 79−88012
U ore, solution mining, in situ leach method 79−87983
U ore, solution mining facilities, operational and environmental aspects 79−87984
U ore, U content determ., radioisotopic X-ray technique using Compton scatt. 77−70357
U ore bodies, ^{235}U var. and natural abundance 77−41014
U ore body rel. to excess ^4He in Teggau Lake, NW.Ontario 78−65353
U ore deposits, fossil nuclear reactors, review 77−60377
U ore deposits, sulphide-free, unusual mineral assocs. in oxidation zone 77−25682
U ore deposits in collapse calderas, structural-geological features 77−25681
U ore detection, using trace detection sensitive to ^{222}Rn α-particles *(Hungarian)* 78−77339
U ore systems, morphogenetic grouping 78−81158
U ore zone logging, corrections for prompt fission neutron data 79−88353
U ores, $^{13}C/^{12}C$ isotope fractionation of assoc. organic matter induced by alpha irradiation 79−57932
U ores, dusts and mill tailings, simultaneous determ. of ^{238}U, ^{234}U, ^{230}Th, ^{226}Ra, and ^{210}Pb 78−15736
U ores, estimation of ratio of induced to spontaneous fission 78−53234
U ores, fissile nuclide concentration ratios *(Spanish)* 77−33067
U ores, U content rapid determ. using X-ray fluorescence anal. methods 79−88479
U prospecting, pattern recognition appl. 77−66999
U, radiogenic Pb migration in hydrothermal metamorphism 77−56627
U reserves, technological status 77−34398
U secondary minerals from Shinkolobwe, Zaire *(French)* 77−86873
U, world resources, effect on development of nuclear power 80−55826
U-bearing, isotopic composition due to terrestrial neutron flux *(Spanish)* 77−5195
U-containing, luminescence spectra, chemical bond effect 78−72597
U-containing identification in Black Sea sediments *(German)* 78−65257
UO_2, ^{236}U activity meas. *(Spanish)* 78−44822
UO_2, equilib. conc. of fission products, ^{235}U induced fission and ^{238}U spontaneous fission *(Spanish)* 78−44823
UO_2, equilib. conc. of fission products, calc. comparison with expt. values *(Spanish)* 78−44824
UO_2, pitchblende and sooty uraninite, U extraction by underground leaching with H_2SO_4 77−61626
^{238}U concentration in ore, absolute determ. by gamma-ray spectroscopy 77−13133
^{238}U, determ. of time since arrival in matrix existing at time of discovery in Pakistan 79−34822
Zn minerals suspended in ocean waters 79−74904
ZnS, sphalerite, struct. of twin seam obs. by optical microscopy 77−39596
ZnS, sphalerites, in-determ. by nondestructive neutron activation anal. 79−87929

mines (coal) *see mining*

mines (mineral) *see mining*

minicomputers
for minicomputer aaapplications see under relevantapplications; administrative data processing; computerised control; natural sciences computing see also electronic calculators
aerospace test meas. symposium, San Diego (1976) 77−41284
automatic control of photographic analysis precision using minicomputer and meas. engine 77−41710
Bermuda Eleuthera Acoustic Range environmental meas. buoy 77−41229

minicomputers continued
constant value curve tracing technique, nuclear medicine, EEG appl. 70510
control of X-ray spectrometer for steel anals. 77−56318
criteria for selecting and interconnecting micro-, mini-, midi- and maxi-computers 77−17961
data acquisition system for Princeton cyclotron facility 78−90048
emission spectroscopy signal-to noise ratio improvement and data processing *(Japanese)* 77−21448
fast signal averager based on sampling oscilloscope interfaced to minicomputer 77−57308
gamma-ray spectra evaluation, appl. of programmable calculators and minicomputers 79−9956
high-level languages and real-time operating systems for scientific instrumentation 79−12778
high-speed, economical minicomputer 79−36496
karyotyping automatic image processor *(French)* 77−40953
microcomputer interface 77−54483
Mossbauer data acquisition system using minicomputer 78−90050
multichannel data logging minicomputer switching program synthesis *(Russian)* 77−9993
multichannel precision temperature measuring device for Pt 100 resistance thermometers *(German)* 78−77914
multiuser minicomputer system for gamma-ray spectroscopy and laboratory programming 79−9952
neurophysiological experiments, fast data acquisition and processing system, minicomputer appl. *(Japanese)* 80−85536
neutron irradiation short-lived products, rapid anal. using minicomputer based pulse height analyser 79−11866
NOVA, artifical vision machine for blind people appl. *(Korean)* 79−66583
optical design education program, desktop computer appl. 79−84922
optical spectroscopy laboratory and programming, minicomputer control 77−74526
PDP-11 with RSTS/E operating system, design for nuclear fuel management 79 - 22395
phase noise meas. with high-resolution counter and online calculator 77−37945
program-controlled electronic keyboard computers, appl. to oceanographic information anal. automation 80−101439
radiochemical analysis by coincidence spectrometry, minicomputer system 79−11864
radionuclide cardiology appl. 79−96661
real-time portable minicomputer system, for dynamic ocean data acquisition and display 80−12552
Royco aerosol particle counter 225, data processing system and modified system props. 80−37005
spectroscopic data online presentation, optical multichannel vidicon spectrometric detector appl. 78−74077

minimax techniques
aperture in elastic body, optimal form *(Russian)* 78−22270
areal air pollution source shaping and location for downwind community protection 77−37380
artificial satellite nonconvex solar battery panel mounting, optimal ang. determ. 79−39291
elasticity, beam bending on Pasternak foundation, reciprocal variational inequalities 80−92091
gravimetric prospecting problem appl. of nonsmooth function minimisation methods 77−41180
MHD channel flow, minimax principle 77−15133
neutron flux, collision probability integrals, annular geometry, evaluation using analytic expansions 80−32317
NMR bandshape, complex exchange-broadened, iterative computer anal. 79−35805
plate, increase of first natural freq. and buckling load by optimal fields of initial stresses 78−13945

minimisation
see also minimum principle
algorithms, effectiveness improvement for band parameters determ. of complex spectra 79−93225
beam nonlinear elastic optimal design for minimum compliance 79−1108
beam-columns, optimal design 80−10142
bending plastic collapse, mm. cost in elastoplastic structs. 78−30197
BWR refuelling schedule, minimisation of power peaking 77−61513
cantilever beam axial vibration, min. mass structures determ. 78−63278
Choquard nonlinear eqn. minimising soln. existence and uniqueness 78−67315
composite materials, cylindrical shells, probability anal. of stability, mass minimisation 78−42553
concrete slab, reinforcement optimisation by linear programming, minimum value design 77−89022
cost of photovoltaic power supplies, self-contained 79−48098
cross-spring hinge problem, 2-D, use of minimization methods in solving 78−18163
cylinders, stiffened, subjected to pure torsion, min. weight design 78−1582
data logger mean square error minimisation by analogue computer *(Russian)* 77−9994
dynamic force measurement results, errors in deformation experiments, data reduction and anal. *(Hungarian)* 77−117
education, astronomy, orbital elements, nonlinear least squares minimisation 77−33761
eigenvalue independent partitioning and direct minimisation of SCF theory 77−26970
elastic stress conc. minimisation and const. stress surfaces 77−869
electron integrals transformation method, program in FORTRAN IV H 78−82603
energy functional, direct minimisation in LCAO-MO density matrix formalism 78−5118
fault conditions, minimisation of diagnosis time, appl. to nuclear power plants 77−6549
flexible bar, min. vol. design by dynamic programming *(Polish)* 78−13965
formaldehyde, MC SCF method in full and pseudopot. versions 77−83487
free energy minimisation method in aqueous multicomponent multiphase equil. comput. 80−40724
general-purpose molecular mechanics program construction principles 78−13411
minimisation continued
gravity complex fields interpretation via minimisation method, automated system appl. *(Russian)* 79−35006
heat transfer model, sequential estimation of thermal parameters 77−80047
image reconstruction from kinoforms and distorted holograms *(Russian)* 78−13664
ionospheric data processing, improvement of convergence of least squares method *(Russian)* 78−85700
lattice energy, comparative computations using explicit minimisation procedures 79−32944
least squares objective functions, constrained minimization technique CONGAU 79−30212
meteorological elements, ordered risk minimisation in daily var. forecasting *(Russian)* 77−60451
modal dispersion in fibres with any numerical aperture and profile dispersion 77−23746
molecular geometry optimisations, invariance criteria, symmetry conservation rules 80−58406
molecular inelastic collisions, improved quasiclassical histogram method, minimisation procedure 78−66617
molecule, mag. susceptibility, calcs. using completely minimising gauge functions 77−6702
nuclear optical model parameter searches, minimisation procedures, use of derivatives 77−10379
optimal plastic design, superposition principles and bounds on min. cost 78−42538
optimal plastic design of circular plates, linear programming appl. 78−42539
pipeline nonlinear anal. by potential minimisation 77−68552
plates, uniaxially loaded, minimising stress concentrations around circular holes 79−18806
polychromatic wave, refl. from absorbing layer, coeff. minimisation 77−82396
power reactor Xe oscillations optimal control problem *(German)* 78−46153
pure harmonic tide in canal, eqns. of motion quadratic resistance term linearisation 78−69369
radioactive waste, alpha-bearing, operational techniques for minimisation, segregation and accounting 77−61567
radiotherapy cervical intracavitary applicators, computer program for optimisation of source loading 77−13005
reactor fuel, selected enrichments for minimisation of blending losses, optimal set 78−17402
real-time urban power dispatch with ambient air quality constraints 79−57542
regional water quality management, goal programming approach 79−57514
satellite flexibility experiment design, control/flexible structure interaction 77−70970
seismic prospecting, minimisation of distortion caused by geophone-ground coupling 79−44256
soap films and analogue computers 77−17797
solenoid inductance, minimisation, mag. induction optimum profile 79−31769
spacecraft atmospheric entry, body shape for minimal radiative heat inflow *(Russian)* 78−77457
spectrometer, IR, instrumental distortion computation without measuring apparatus function 80−95159
strings, stretched, vibr. control by an external distributed force 78−83308
thermal conductivity measurement of soil by probe method, minimisation of errors 77−17259
wind tunnel transonic test section wall interference minimisation *(French)* 77−27550

minimum metallic conductivity
actinide non-stoichiometric intermetallic cpds., elec. resist. temp. depend. 79−1597
Anderson transition, electron localisation in disordered systems, review 80−29361
disordered material, elc. cond. and density of states, scaling relations 79−28329
disordered materials, thin films and wires, resist. and localisation 80−44537
disordered solids, electronic props., numerical methods 80−44538
disordered system, cond. and mobility edge, square and diamond lattice calc. 78−43347
disordered systems, Anderson localisation theory in two dimens., real space scaling method 80−44540
disordered systems, localisation using random series, Anderson transition for extended states 80−44542
disordered systems, props. of mobility edge 77−4330
glass systems, electronic props. 79−42495
group velocity and minimum metallic cond. 78−23141
localised electronic system, sp. ht., singularity at Anderson-Mott transition 80−34381
semiconductor melts, metallic cond. at high temp. 80−49832
spatially disordered system, two-dimens., localisation and cond. 78−18998
thin wires, max. metallic resist., approx. expressions 78−14663
transition metal cpds., minimum cond. and electron localisation near metal-insulator transition 78−30960
transport processes, isothermal method for static cond. of electrons 80−29373
two-dimensional disordered electron systems, transport props. in strong mag. fields 78−95318
two-dimensional electron system, Anderson localisation under strong mag. fields 77−15929
As_2Se_3-As_2Te_3, molten semicond., thermoelec. power and elec. cond. near metallic cond. transition 78−10486
$Bi_2(Te,S)_3$, thin crystal, min. metallic conductivity 79−1610
Cs-Au, disordered, min. metallic cond. 79−95372
Cs-Sn, disordered, min. metallic cond. 79−95372
Fe film, vacuum deposited, resist. minimum 80−44741
$Fe_{40}Ni_{40}B_{20}$, amorphous and crystalline, resist. minimum 79−47079
$FeSi_2$ films, structural and Anderson transitions, cond. and IR reflectance meas. 79−15200
n-GaAs, metal-insulator transition in impurity band induced by mag. field and loss of dimension 78−52042

minimum metallic conductivity continued
n-InSb, galvanomagnetic props. at low temps., mag. field induced metal-nonmetal transition 77−76845
$La_{1-x}Sr_xVO_3$, Anderson transition, elec. resist. and thermopower meas. 80−100488
Na-Sn, disordered, min. metallic cond. 79−95372
Pd, film with defects, field-induced resist. min. 80−11050
$Pd_{1-x}Pr_x$ (x=0.02 and 0.03), dil. alloy, min. resist. around 20K 79−19583
n-Si inversion layer, thermal activation of two-dimens. Shubnikov-de Haas cond. extreme 78−60218
Si inversion layers, Anderson transition, random field origin, substrate bias effect 77−28255
Si inversion layers, mag. localisation 78−43481
Si:H amorphous films, conductivity and temp. dependence of optical gap 80−100462
Si-SiO_x interface, localisation in inversion layer due to states in gap of oxide 77−12012
SiO_2-Ni granular metal films 78−56241
SmB_6, mixed valent, large low-temp. Hall effect and resist. 80−39611
VO_x, minimum cond. and electron localisation near metal-insulator transition 78−30960
W-Re, amorphous wire, elec. resist., 2-20K, dimens. and mag. field depend., quantum localisation 80−39547

minimum principle
capillary surface problems with prescribed contact angle, max. and min. principles 79−37907
extremum principles for linear initial and mixed boundary value problems of math. phys. 78−49637
linear dynamic theory of elasticity, minimum principles 78−57781
nerve membrane, steady-state finite cable model, complementary variational principles 79−34545
viscoelasticity, linear theory *(Japanese)* 80−48599

mining
see also mineral processing industry
air pollution detection and control, health hazards in India 77−41145
Akabira coal mine, stress relief boring, monitoring programme 77−9423
asbestos mining area river pollution meas. by proton-induced X-ray emission 79−100556
asbestos particulate concs. in Thetford Mines area of Quebec 77−37394
asteroids, prospects for space colony 78−61786
Baisoara mine, gravity anomaly rel. to ore body distrib. *(Rumanian)* 78−20347
Barre granite, static and dynamic fracture strength 77−44976
blasting, recording system for noise meas. 77−88984
Boksburg, S.Africa, dyke strain relief meas. near mine working 80−17263
British coalfields, geological aspects, resources and reserves 79−57931
Broken Hill, NSW, stress meas. and underground mine openings design 77−9425
brown coal, 60 years supply at Hambach open cast mine *(German)* 79−57352
caved faces of Appin Colliery, rock pressure distrib. 77−9420
coal, deep-level seams, bed rocks instability obs., by monitoring acoustic emission activity *(Japanese)* 80−10071
coal, stress meas. using borehole instrument 77−9415
coal, underground rock destruction, seismic meas. method 77−9419
coal and U, mining, processing and transportation, in Western US, impact 80−45621
coal pillars, elastoplastic anal. of stresses, finite element method 79−66691
coal seam acoustic imaging 79−53585
coal seam fault location 80−94613
coal seams fault indication using acoustic array processor 80−85778
concentrator X-ray on stream anal. design, installation and commissioning 78−35778
Deep Ocean Mining Environment Study phase I and II, prospect 78−16164
deep sea mining freedom 77−91274
diesel-powered underground mining equipment, noise control 80−53557
discovery probability, quantitative fall-backs of naturalist classifications 77−53204
disused vertical brick-lined mineshafts, geoelectrical methods of detection 77−64451
economic geology management system 77−53201
EM prospecting, harmonic and transient fields behaviour on surface of two-layer medium 79−92478
energy changes due to mining 77−64236
flame sensor-trigger device for explosion barrier in underground mines 80−52313
fractured zone dip-angle and width, seismic determ. *(Japanese)* 77−17228
geophysical prospecting by pseudobaseband pulse radar 78−24398
heat transfer in polymeric and disperse Bingham fluids during forced convection in ultradeep boreholes 79−68762
HF EM induction profiling, of boreholes in underground mines *(Polish)* 80−51547
HSLA steel crack properties 78−52943
industrial health service automated ECG analysis results 79−39563
large particle size photometric sorting machine, DATAC system, design principles 78−32853
long-hole drilling machine, noise reduction 80−53559
Lubin Cu mine, source study of mining tremor 80−41377
LWR and coal power stations, effects on ambient media from mining to waste disposal *(Spanish)* 77−75005
maps of workings on microfilm, correlation with topographic maps 78−32259
marine mining, environmental effect meas. 79−12305
methane gas interferometer for coal mine safety 78−44423
mineral processing isotope on-stream anal. 78−35777
mining tectonical forecast maps, geoelectric bed sounding method *(Hungarian)* 80−105075
mobile equipment noise control in surface mining 80−53558
Mount Isa Mine, rock pillar monitoring during ore extraction 77−9418
New York State, earthquakes related to hydraulic mining and natural seismic activity 78−48986
noise, characterization of environment, control methods 80−53556
nuclear explosives use in continuous underground operations 77−23302
ocean mining, position location system 78−45046

mining continued
oil fields, in N.Aegean region, implications of crustal shortening 77−53028
Oklo natural reactors, mining, geology and tectonics *(French)* 80−21743
opencast coal, principal environmental noise sources 80−81505
ore Au content determ., methods 78−35076
ore prospecting, and mining research, examples of mineralogy contrib. *(French)* 79−5475
permafrost, thermal amelioration tests near Schefferville, Quebec 77−33058
phosphate and related industries, need for radiation controls 77−56483
pneumatic motor noise reduction methods 77−19488
potash mine salt thickness meas. by EM depth sounding 78−28324
production in New Mexico, constraints 80−42843
quarrying, use of electronic transient recorders for meas. explosion noise and vibration 80−67023
radioactive waste disposal, Dutch policy *(Dutch)* 80−671
river basin, Monongahela, acid mine drainage problems treatment via QUAL II simulation 79−29806
rock failure, scale invariant properties 78−3758
rock salt, progressively mined soln. cavities, struct. behaviour 78−61409
rock strength in situ meas., triaxial testing 77−44975
rockburst fault gouge microscopic features, SEM obs. 79−74891
roof and walls condition study, radar appl. *(Russian)* 79−62602
salt, radar detection of boreholes in advance of mining 78−96305
satellite remote sensing appls. 77−25788
seismicity in deep-level mine, influence of mine geometry and closure volume 78−3723
seismicity increase prior to moderate rock burst 78−3722
siesmic moment and source size determ. for mining tremors 78−3717
spherical cavity, variational anal. of stability *(Russian)* 77−50885
stoper drills for coal mines, total noise-control systems 80−53560
stress meas. in bored raise at Mount Isa Mine 77−9414
subsidence and ground movement, holographic interferometry 78−57343
surface coal mine spoils areas restoration, rainfall simulation 77−33120
surface mine spoils area restoration, Wyoming, evaluation using ranfall simulation 77−49094
Szombierki coal mine, Upper Silesia, Poland, mining tremors, freq.-mag. relation 80−41378
tremors, seismic recording stations, optimal config. 78−20359
tremors in anisotropic media, optimal recording 78−3718
tunnel location by cross-borehole EM probing 77−78545
two-fold resistivity mapping of lateral inhomogeneities 78−61573
underground openings, stress release, improved method 77−9424
underground quarries, EM detection *(French)* 78−96306
ventilation fan acoustic noise spectral anal. *(Russian)* 80−53584
Mn nodule mining, environmental effects 77−33096
Mn nodule mining and processing with nuclear meas. 77−4975
Mn nodule undersea mining data file, management and statistical anal. 77−53206
Mn nodules deposits, deep sea telemetry *(German)* 80−26623
U and coal, mining, processing and transportation, in Western US, impact 80−45621
U, CEA and Cogema activities *(French)* 80−626
U, effects on groundwater in Grants Mineral Belt, New Mexico 77−56657
U extraction from UO_2 minerals, underground leaching by H_2SO_4 of explosion crushed rock 77−61626
U, in situ leach mining, environmental considerations rel. to water quality 80−3543
U, in situ mining, Wyoming State regulations and environmental monitoring 79−88510
U mine, Rn aerosol particle size distrib. *(French)* 78−32195
U mine radon control research 78−82525
U mines, radiological evaluation 80−42806
U mining, U refining and decay processes, radioactive mining waste disposal *(Dutch)* 80−21418
U, mining and milling radioactive waste management N.Australia 79−31076
U ore, solution mining, appl. of solution flow prediction computer models 79−88013
U ore, solution mining, effect of Environmental Protection Agency requirement for underground injection 79−92101
U ore, solution mining, environmental impact, groundwater restoration 79−88012
U, solution mining, in situ leach method 79−87983
U, solution mining facilities, operational and environmental aspects 79−87984
U surface mining, radiation exposures, meas. 77−64140

minmax technique *see minimax techniques*

minor planets *see asteroids*

minority carrier conduction *see minority carriers*

minority carriers
Auger recombination of carriers bound to centres involving phonons 80−107805
deep level investig. by new optical method 78−6331
degenerate materials with position depend. band struct. carrier densities and emitter efficiency calc. 78−43378
DH devices, interface recomb. effects on transient response 77−88722
DH devices, interface recomb. effects on transient response anal. 78−22127
diffusion length, spectrometric determ. *(Russian)* 78−84230
diffusion length determ., using angle-lapped p-n junctions 79−42631
diffusion length determ. near p-n junction, SEM appl. *(French)* 78−43466
diffusion lengths meas. using SEM 79−60848
DLTS, photo-excited, minority carrier trap meas. 80−96816
electron beam depth profiling in semiconductors, using carrier collection models 80−70723
generation rate meas. using transient response of MOS capacitor with guard ring 78−2576
graded composition semiconductor, minority carrier transport, rel. to transistor 78−80022
graphite, low field Hall coefficient, effect of warped energy surfaces 78−68043
graphite, minority carriers and H-point magnetorefl. spectra 77−63398
graphite, thermoelectric power, low temperature, anomaly rel. to phonon drag 80−65610

minority carriers continued
heterojunction isotypic, under transient depletion conditions, information-carrying charge 78−26944
HgCdTe/CdTe, limited diffusion volume photodiode, characterisation 80−75627
high-low junction, heavy doping effects on minority carrier reflecting props. 79−42623
III-V epitaxial layers, minority carrier lifetime, correl. with defect props. 77−89835
III-V semiconductor epitaxial structures as wide-gap substrates, minority carrier diffusion length determ. by photoluminesc. 80−103992
inhomogeneous semiconductor, negative photocond. and IR quenching of residual cond. 77−24587
injection in trap free semicond. 80−96904
LED, diffusion lengths and near-junction luminescence-efficiency profiles from SEM scans 77−77301
life-time measurement in solar-cells, open-cct. to short-cct. switching method 79−79392
lifetime determ. by relative amplitude method 77−72869
lifetime mapping by SEM 80−96903
lifetime profile measurements in heavily doped emitter structures using electron beams 80−15538
minority carrier diffusion length, Schottky barriers, electron bombard. investigation 78−68037
minority carrier recombination 80−65591
minority-carrier injection into semicond. containing traps 78−60137
MIS capacitors, theory of nonequilibrium props. including charge exchange of interface states 79−42659
MIS negative barrier contact for induced back surface field solar cell 80−101101
MIS SAW convolver, minority carrier response 77−80847
MIS Schottky barrier and conducting diodes with interface traps, capacitance and conductance 78−10564
MIS solar cells with diffused back surface field (BSF), and diffused junction solar cells with MIS BSF 80−94074
MIS structure, hysteresis pulsed C-V method for minority-carrier lifetime and surface generation velocity determ. 80−70839
MIS structure, minority carrier, lifetime and generation determ., graphical technique 78−95378
MIS structure, thermal generation of carriers through surface centres 79−69603
MIS structure minority carrier generation time constant meas. 77−89873
MIS structures, surface generation rate determ. using dynamic nonequilibrium I/V charcts. 78−64139
MIS tunnel diode, minority-carrier, pot. barrier height 80−96998
MIS-Schottky barriers, photovoltaic props. anal. 78−26966
MOS C-V data in strong inversion, surface minority carrier redistrib. 78−72266
MOS capacitor, comparison of lifetime meas. techniques 78−56232
MOS capacitor, flatband voltage shift time depend., injection of minority carrier from Si into SiO_2 79−42656
MOS capacitor, minority carrier generation time and surface generation rel. determ. from Q-t meas. 78−72265
MOS capacitor, minority carrier lifetime, effects of swirls and stacking faults 77−32088
MOS capacitor switched from inversion to accumulation, minority carrier lifetime meas. 77−39957
MOS capacitors, establishment of inversion layer in Si substrate under high oxide field conditions 77−66202
MOS diodes, minority carrier lifetime determ. from photocurrent spectra 80−49920
MOS inverted-channel carrier scatt., effect of oxidation in Cl media 78−76156
MOS pulsed capacitor, minority carrier lifetime meas. influence of Si-wafer surface state density 80−60098
MOS solar cell, IV characteristics obtained under dark and illuminated conditions 79−48126
MOS struct., nonuniform generation obs. by SEM 78−72273
MOS tunnel diodes characterisation, solar cell appls. 77−32089
n-p junctions, determ. of transport parameters of minority carriers using electron microscope 80−65665
ohmic contact, hot minority carrier effects on thermoEMF and photovoltage 77−15956
p^+-n, n^+-p solar cell structures on polycrystalline material, performance 80−89640
p-n diode minority carrier storage effect reduction by F ion implantation damage 78−72243
p-n junction, diffusion length meas. of minority carriers, accel. voltage of primary electrons effect *(Czech)* 78−34844
p-n junction, magnetic injection of minority carriers 80−107900
p-n junction minority carrier diffusion length meas. by short-circuit current ratio 80−31849
p-n junctions, partially opened, three-frequency parameter systems, equivalent conductivities *(Russian)* 80−24998
photocurrent in diffused junction, back surface field effect 78−91762
photon detector, nonuniformly doped intrinsic photoconductor, photovoltaic operation 79−224
recombination at surfaces, dislocations and microdefects, luminesc. evaluation 78−6769
recombination lifetime measurement using pulsed MOS capacitor 80−25012
Schottky barrier height approaching semicond. band gap, minority carrier injection effect 77−20434
Schottky barrier solar cell, doping density effect on efficiency 80−101100
Schottky diode, effect of thin oxide layer between metal and semicond. 77−20432
SEM measurement of minority carrier diffusion lengths in semiconds. interpretation 78−80002
semi-infinite direct-gap semiconductor optically generated minority carriers 78−95312
semiconductor, carrier diffusion length meas. using electron microprobe 77 39867
semiconductor, cathodoluminescence meas. of minority carrier lifetime, appl. to GaP 78−19572
semiconductor, inertia of Benedicks effect in carrier heating by microwave field 79−15173
semiconductor, ionization and subthreshold effects in defect creation and annihilation 77−84811
minority carriers continued
semiconductor, lifetime meas. by photoconductivity null apparatus 78−56184
semiconductor, localised defects, theory of SEM charge-collection imaging 79−1374
semiconductor, minority carrier conc. determ., integral eqn. approach to abrupt depletion approx. 77−32022
semiconductor, minority carrier exclusion 79−42561
semiconductor, minority carrier injection 78−60136
semiconductor, n-type, inhomogeneous, nonequilib. carrier diffusion and lifetime 80−60005
semiconductor, nonequilibrium carriers, diffusion in alternating elec. field 79−11133
semiconductor, nonuniform diffusion length and elec. field determ. 78−72166
semiconductor, optical absorpt. coeff. and minority-carrier diffusion length, differential photocurrent method of meas. 80−96896
semiconductor, polycryst., electronic processes at grain boundaries under optical illum. 77−55561
semiconductor, resolution of transport equation, by linearisation *(French)* 78−79989
semiconductor, SEM electron beam induced current images of dislocations and stacking faults, computer simulation 80−70198
semiconductor, spatial resolution of SEM electron beam induced conductivity images 80−6327
semiconductor, spin injection, carrier polarisation, luminesc. polarisation 77−15957
semiconductor crystals, with high quantum efficiency, minority carrier lifetime meas. *(Japanese)* 80−54711
semiconductor device, surface recombination, effect on steady-state relationships 78−39191
semiconductor diodes, minority and majority mobilities, transit time effect determ. 78−14753
semiconductor diodes in radiophysical devices, minority carrier charge-accumulation effect *(Russian)* 79−73569
semiconductor electrode, electrolum. due to hole injection from electrolyte 77−20926
semiconductor heterostructure laser, carrier diffusion length using differential electron beam induced current 79−55137
semiconductor under illumination, simple model of generation and recombination processes 79−69523
semiconductor-electrolyte solar cell, minority carrier transfer, energy levels role 78−39209
semiconductor-metal contact, minority carrier injection in strong elec. field 77−55609
semiconductors, exhibiting negative photocond., photovoltaic effects 80−96943
semiconductors, polycryst., opto-electronic processes at grain boundaries 77−43667
semiconductors, variable gap thin structs., radiative recomb. photoluminesc. spectra 79−43036
semiinsulator, minority carrier injection effect on TSC 78−10466
shallow junction devices, minority carrier diffusion lengths 78−72168
solar cell, interaction of electron beam, minority carrier diffusion length 80−7943
solar cells, metal-semiconductors contacts, collection vel. of excess minority carriers 77−15954
solar cells, minority carrier lifetime meas. from photo-induced open-cct. voltage decay 79−87990
surface wave interaction CCD prototype 77−23818
transmutation doped, stabilisation 78−10449
traps, detection using transient spectroscopy 79−65402
Al-SiO_2-Si capacitor C-V characteristic determ. of surface minority carrier lifetime *(Polish)* 77−89855
Al-SiO_x-Si, experimental verification of theoretical predictions 80−29485
Al-SiO_x-(p-)Si barrier structs., minority carrier injection ratio meas., MIS solar cell model 80−93007
AlGaAs-GaAs heterostructure effective lifetime, photon recycling effect *(Japanese)* 79−42556
p-$Al_xGa_{1-x}As$, DH under optical orientation conditions, diffusion of spin labelled electrons 77−8189
$Al_xGa_{1-x}As$ variable gap thin structs., radiative recomb. photoluminesc. spectra 79−43036
$Al_xGa_{1-x}As$-GaAs heterostructure, effect of photon recycling on diffusion length and internal quantum efficiency 77−39929
$Al_xGa_{1-x}As$-GaAs heterostructure, nonradiative large dark spots rel. to minority carrier transport 78−9378
$Al_xGa_{1-x}As$-GaAs heterostructures, nonradiative large dark spots exam. 78−23149
$Al_xGa_{1-x}As$-GaAs long life laser, initial degradation, minority carrier lifetime reduction 77−71984
BN glass transfer process 80−107459
Bi:Sb, semimetallic alloy, microwave spectroscopy 78−87908
n-$Cd_{0.3}Hg_{0.7}Te$, photoelec. props. at 78K, relax. time, minority carrier extraction 80−107864
CdS Schottky contact, photovoltage 78−95337
CdS-Cu_2S heterojunctions, photovoltaic mechanism, model 77−43715
CdS-Cu_2S solar cell, minority carrier generation and transport in emitter 77−43649
CdTe, minority carrier diffusion length from photocurrent meas. in semicond.-electrolyte boundary 80−65584
CdTe-CdS thin film p-n solar cells, spectral response temp. depend. 80−93871
Cr-SiO_x-Si MIS solar cells, photovoltaic performance and interface states, nucl. radiation effects 80−94004
$CuInS_2$, minority carriers lifetime, photoelectromag. effect meas. 79−47125
p-$CuInSe_2$, minority carrier lifetime and surface recomb. velocity, photoelectromag. meas. 78−19085
Cu_2O-Cu diode junction, Schottky barrier, electronic structure and minority carrier diffusion length *(French)* 80−65682
Cu_2S/CdS heterojunction solar cells, diffusion length determ. using minority carrier SEM 80−61359
Cu_xS-CdS solar cell, minority carrier diffusion length, SEM determ. 77−72911
GaAlAs-GaAs heteroface solar cells, 1 MeV electron irrad., analytical and expt. study 79−70450
$Ga_{1-x}Al_xAs$ n-p_3-p_2-p_1-p_0 struct., degradation electrolum. 80−50428
$Ga_{1-x}Al_xAs$-$Ga_{1-y}Al_yAs$ p-n heterojunction, minority carrier lifetime, elec. characts. and electrolum. meas. 78−2554

minority carriers continued
$Ga_{1-x}Al_xAs$-GaAs-GaAs, p-p-n junctions, variable gap solar photocell with coordinate depend. band gap gradient 79−11213
GaAs, deep centres, electron and hole capture cross sections 79−99510
GaAs, electron beam induced defect annealing 77−80790
GaAs, electron beam induced current, minority carrier generation distrib. 80−96900
p-GaAs, electron minority carrier diffusion lengths 80−29807
n-GaAs epitaxial films, residual cond. meas., struct. perfection rel. to photomemory 80−7010
GaAs film, vapour-grown, effect of gas-phase stoichiometry on deep levels 78−10393
GaAs LED, minority carrier lifetime determ. 79−42560
GaAs LED absorption effect on freq. characteristic 79−8189
GaAs MOS capacitor fabrication and transient response for minority carrier lifetime meas. 79−47103
GaAs MOS structures, props. of capacitance transient 80−25013
GaAs, minority carrier diffusion length, reabsorbed radiation effect 77−28191
GaAs, minority carrier diffusion lengths, contact metal effects 78−72260
GaAs, minority carrier diffusion length, photon absorption reemission 79−87109
GaAs, minority carrier lifetime at high temp., solar cell performance appl. 80−24947
p-GaAs, minority carrier mobility calcs., including screening, scattering mechanisms 79−99545
GaAs p^+-n^0 junction, photocurrent, hole diffusion length in lightly doped n-type region 77−28246
GaAs, polycrystalline films, meas. of effective diffusion length by SEM 80−80424
n-GaAs Schottky barrier junction, SEM meas. of hole diffusion length, surface effects 79−87110
GaAs, Schottky barrier solar cells, diffusion length meas. 79−61973
n-GaAs, Schottky barriers, minority carrier trap meas. 78−26951
GaAs solar cell polycrystalline conducting substrate, minority carrier diffusion length spatially-resolved meas. 80−94084
GaAs, surface recomb. velocity, determ. from SEM expts. on p-n junctions 77−55601
GaAs, VPE, hole diffusion lengths, surface prep. and heat treatment effects, etchant evaluation 80−15627
GaAs, VPE, hole diffusion lengths, effect of transition metal diffusional doping 80−15628
GaAs, wide-gap semiconds., HV diodes, current-voltage characts. 79−24068
p-GaAs:Cr, semi-insulating, illumination effect on mobilities 77−32043
GaAs:Cr, surface and bulk recombination parameter determ. from photoluminesc. spectra 77−55820
GaAs:Fe p^+-n junction minority carrier trap meas. by photo-excited DLTS 80−96816
GaAs:Ge, vap. grown, diatomic complex donor and acceptor model 78−80003
GaAs:Se cathodoluminescence decay obs. with SEM and streak camera, 90 to 300K 80−97348
GaAs:Si p-n light-emitting structs., soln. of general minority carrier transport eqn. 80−15597
GaAs:Te Schottky barrier solar cells, diffusion length determ. using minority carrier SEM 80−61359
GaAs-$Ga_{1-x}Al_xAs$, n^+-i-n heterojunction, radiative recombination under double injection *(Russian)* 77−77298
GaAs-$Ga_{1-x}Al_xAs$ DH lasers, electron beam induced current microscopy 80−95899
GaAs-GaAlAs double heterostruct., self-absorpt. effects on radiative lifetime 77−39928
$GaAs_{0.6}P_{0.4}$, VPE, hole diffusion lengths, surface prep. and heat treatment effects, etchant evaluation 80−15627
$GaAs_{0.6}P_{0.4}$, VPE, hole diffusion lengths, effect of transition metal diffusional doping 80−15628
GaP, epitaxial layer, thickness and diffusion length, photocurrent meas. 77−32096
GaP, frozen-in pt. defects annihilation 79−99949
n-GaP, interface-recomb.-controlled minority carrier lifetime obs. 77−12027
n-GaP, LPE, bulk lifetime and diffusion coeff. meas. 77−11932
n-GaP, LPE, non-radiative recombination 78−19565
GaP, minority carrier lifetimes at dislocations, SEM meas. using photon counting 78−23109
GaP, minority carrier quasi-Fermi level meas. in illuminated photoelectrolysis cell 77−85308
p-GaSb:Zn film, epitaxial, lifetime of nonequilib. carriers, determ. from circular polarisation of luminesc. 77−24898
p-GaSe, back wall Schottky barrier cells, diffusion length, RT spectral response meas. 80−107806
GaSe:Sn, single crystal, transient photoconductivity *(Russian)* 79−11171
Gap-Ge, compensated, photosensitivity 79−19624
p-Ge, detector-grade single crysts., impurity background effect on minority-carrier lifetime 79−11088
n-Ge, minority-carrier injection and extraction 80−49767
p-Ge:Ga(Sb), proton irradiated, kinetics of accumulation of radiation defects, minority carrier lifetime 79−10885
Ge-metal Schottky barrier photodetectors, near IR interband transitions and optical parameters 80−73449
GeS film, photocond. kinetics 77−39897
$Hg_{0.68}Cd_{0.32}Te$ photodiode, minority carrier lifetime determ. 79−38084
p-InGaAsP, on InP surface, diffusion coeff. and surface recombination velocity 80−39598
$In_xGa_{1-x}As_{1-y}P_y$ epitaxial layers, characterisation and relation to lattice matching 80−100540
InP, photoemission and LEED meas., minority carrier diffusion length 77−69959
InP/InGaAs/InP field assisted photocathode, minority carrier electron transport across p-p heterojunction 78−95651
n-InP/SiO_2 capacitors, minority carrier generation 79−95496
n-InSb, hole mobility temp. depend. after electron bombardment 79−33290
p-InSb, magnetoconcentration effect in extrinsic cond. range 80−65593
InSb p-n junction, minority carrier injection in mag. field, recomb. radiation obs. 80−11078
MIS solar cells, comparison of majority- and minority carrier 80−85280
(Pb,Sn)Te, (Pb,Sn)Se IR detector diodes, junction resist. comparison, minority carrier lifetimes 78−24858

minority carriers continued
$Pb_{0.86}Sn_{0.14}Te$/PbTe, interface recomb. velocity in DH laser diodes 79−64222
$Pb_{1-x}Sn_xTe$ DH laser, minority carrier lifetimes and lasing thresholds 80−19031
$Pb_{1-x}Sn_xTe$, epitaxial layers, carrier lifetime meas. 79−42559
$Pb_{1-x}Sn_xTe$, photomagnetic effect at low temps. 77−62960
PbTe, epitaxial layers, carrier lifetime meas. 79−42559
PbTe IR diode, epitaxially grown and ion implanted, minority carrier lifetimes, efficiency 77−20411
PbTe p-n junction, minority carrier lifetime, step pulse recovery 77−11995
Si, amorphous, solar cells, efficiency, transport props. 80−50961
Si based MOS device irradiation with γ-rays, minority carrier generation, CV characts. 80−88637
Si, carrier lifetime, comparison of meas. by photocond. decay and surface photovoltage 78−68038
Si, carrier lifetime depth distrib. due to Ar ion implantation 80−70232
Si, diode, minority-charge-carrier lifetime rel. to abrasion of surface *(Russian)* 80−11805
Si, electrical properties of single crystal, dislocation effects *(Rumanian)* 79−73504
Si, electron irrad. devices, dominant recomb. centres 77−72912
n-Si, electron radiation defect annealing, negative stage, Hall coefficient, defect levels 79−90701
Si, epitaxial, minority carrier lifetime and impurity conc. meas. *(Japanese)* 80−25025
Si epitaxial layer, minority carrier lifetime obs. *(Russian)* 80−49765
Si epitaxial layer substrate junctions, carrier lifetime and abnormal conduction phenomena *(Korean)* 78−47888
Si, epitaxial layers, minority carrier lifetime and diffusion length meas., photocurrent technique 78−95302
Si, film, polycryst., for photovoltaic appl., grain size effects 78−72034
Si, float zone, meas. of deep levels by photovoltage spectroscopy 80−103723
Si, gettering by ion damage, minority carrier lifetime and backscatt. study 80−100286
Si, heat treated, minority carrier lifetime, effect of swirl defects 77−39868
n-Si, heavily doped, meas. of minority carrier transport parameters 80−15537
Si, heavily doped, minority carrier injection, model 77−39874
Si, heavily doped, minority-carrier transport parameters meas. 80−80291
Si, heavily doped layer, electronic characts., electron beam induced current obs. 78−10473
Si, highly doped and highly exerted, Auger coeffs., radiative band to band recomb. lifetime meas. 77−85764
Si, ion beam damaged, minority carrier lifetime distribs., electron beam meas. 79−87108
Si junction diodes, fabrication by LPE on Si:B substrates, and characts. 80−80363
Si large grain films on metallurgical Si substrates, diffusion length profile 80−61357
Si, laser measurement, of semiconductor materials and devices *(Rumanian)* 78−52035
Si, lifetime and surface recomb. vel. determ. 77−89771
Si, MOS diode, dependence of minority carrier bulk generation on HCl concentration 80−88639
Si materials, advanced, preliminary evaluation for space solar cells 80−94006
Si, minority carrier lifetime and surface recomb. vel. meas. 77−28194
Si, minority carrier lifetime profiles meas. 77−39873
Si minority carrier lifetime degradation effect of $POCl_3$ emitter diffusion 77−76917
Si, minority carrier lifetime and diffusion length meas. contactless nondestructive technique 77−80789
Si, minority carrier lifetime degradation by $POCl_3$ emitter diffusion 78−2496
Si, minority carrier lifetime and surface recombination velocity meas. by photocurrent 78−10515
Si, minority carrier lifetime meas. by contactless technique 78−23102
Si minority carrier lifetime meas. methods and results *(Hungarian)* 79−56241
Si, minority carrier lifetime, effect of SiO_2 coating deposited by sputtering 80−11003
Si, minority carrier lifetime in neutron doped samples 80−20218
p-Si, minority carrier lifetime, effect of low dose ion implantation *(Japanese)* 80−54715
Si, minority carrier lifetime improvement through laser damage gettering 80−65589
Si minority carrier MIS solar cells, design and expt. results 80−81445
Si minority carrier MIS solar cells, AM1 efficiencies 80−93975
Si, minority-carrier diffusion length and drift mobility determ. using a modulated SEM beam 79−19607
Si multilayer structure dopant distrib. and minority carrier diffusion length, SEM obs. *(Russian)* 78−10543
Si, neutron irradiated, resistivity and minority carrier lifetime, radial inhomogeneity *(Russian)* 78−26881
Si, neutron transmutation doping, annealing, deep defect levels 80−20123
Si p^+n diodes, minority carrier lifetimes, gettering of Cu and Au during Ga diffusion 78−91350
Si p-n junction, charge carrier recomb. at dislocations, combined SEM and TEM study 80−15105
Si, p-n junction, dopant conc. diffusion length and lifetime variations, SEM obs. 79−82604
Si p-n junction diodes and solar cells, minority carrier diffusion length 80−107894
Si, photodiode, shallow junction n^+-p, spectral response limitation mechanisms 78−37058
Si planar structures, Haynes-Shockley expt. for students 78−28888
Si, polycryst. films, transport props. and grain boundary charact. by TEM 80−50980
Si, polycrystalline, grain boundary effects on minority-carrier diffusion length and solar-cell efficiency 79−48124
Si, polycrystalline, large grain size, gross defects effect on effective carrier lifetime 77−80793
Si, polycrystalline films, meas. of effective diffusion length, by surface photovoltage meas. 80−80424
Si, polycrystalline-metal contacts, minority carrier injection 80−103750

minority carriers continued
Si, proton irradiation, energy depend. of rate of degradation of cond. 77−62944
p-Si radiation defects due to 30 MeV proton irrad., rel. to solar energy convertors 78−71776
Si, rapidly grown RTR sheet, props. and solar cell processing 79−100048
Si ribbon crystal evaluation for solar cells 77−76813
Si ribbon solar cell, EFG, diffusion length enhancement under illum. 78−14756
Si ribbon solar cells, var. of minority-carrier diffusion length with light intensity, heavy metal doping effects 80−93937
Si, ribbons produced through capillary action shaping, elec. and struct. characts. 78−47804
Si slice, minority carrier diffusion lengths, surface photovoltage meas. 78−72168
Si, solar cell, minority carrier lifetime *(Korean)* 78−23103
Si, solar cell, minority carrier excess charge and time const. 78−30938
Si solar cell parameters, grain size dependence 80−94049
Si solar cells, inhomogeneities and their influence on cell performance 80−93967
Si solar cells, minority carrier lifetimes determ. from spectral and transient meas. 79−100533
Si solar cells, radiation damaged, origin of reverse annealing 80−76630
Si solar cells using minority carrier MISS 80−101103
Si, temporary trap characteristic after heat treatment *(German)* 80−34459
Si, trichloroethylene and HCl grown oxides compared 77−76988
Si wafer, nondestructive method for meas. of spatial distrib. of minority carrier lifetime 80−13098
Si wafers, Czochralski grown, minority carrier transport props., laser beam scan for homogeneity anal., photovoltaic cell appls. 80−92905
Si:Ar, ion implant gettering of MOS capacitors using linear voltage ramp and N^+ backscattering 79−95502
Si:B, diffusion length, SEM-EBIC/Schottky diode 79−82605
Si:B photodiode front region collection efficiency models 80−96899
Si:B radiation damage and minority carrier lifetime, SEM-EBIC obs. 80−96573
p-Si:B(Al), radiation defect form. and annealing study using Hall effect, cond. and carrier diffusion length 80−84214
Si:B(P), minority carrier diffusion coeffs. 79−99559
Si:Co, diode minority carrier lifetime, Lax method meas., effect of Co diffusion 79−69525
Si:Co, minority carrier lifetime investigation 80−80292
Si:H, amorphous, surface activated, photoemission spectra, minority carrier diffusion length 80−40235
p-Si:Li, dislocation free, minority carrier lifetime, effects of heat treatment *(Japanese)* 79−65492
Si:O, annealed, minority carrier lifetime 79−23985
Si:P(B) solar cells, minority carrier lifetime mobility rel. to impurity conc. 80−55848
Si:Zn, minority carrier lifetime investigation 80−80292
Si-SiO_2 boundary, relaxation of nonequilibrium capacitance in electrolyte in intense elec. fields 80−70845
Si-SiO_2 MIS systems, dynamic props. of switching, appl. to charge transfer devices 80−92997
Si-SiO_2 MOS interface, surface-state density and minority carrier generation rate, meas. by DLTS, hot hole effect 80−100527
α-SiC:Al diodes, ion implanted, transient characts. of electrolum. 79−24369
TiO_2 electrode, sensitised, for photoelectrolysis of water in sunlight, minority carrier diffusion length 78−19143
$Zn_xCd_{1-x}S/Cu_2S$ heterojunction solar cells, fabrication and performance 79−79397
$Zn_xCd_{1-x}S/GaAs$ heterojunction solar cells, meas. of minority carrier diffusion length 80−26158
Zn_3P_2 thin polycrystalline films for solar photovoltaic cells 80−97797
ZnSe, minority carriers diffusion length by surface photovoltage method 80−60003
ZnTe-In Schottky diodes, photocapacitance determ. of electron-hole recomb. *(French)* 79−47119
ZrO_2:Y_2O_3, solid electrolytes, charge carrier conc. and diffusion 77−11930

mirages *see atmospheric optics; light refraction*

mirrors
3 m parabolic dish heliostat system design, fabrication and testing 79−62111
5 MW Solar Thermal Test Facility 79−62113
45° scan mirror, static and dynamic equilib. *(Chinese)* 79−68423
90° phase shift beam splitter for displacement interferometer 78−87145
α-crystal quartz as IR dichroic laser mirror 79−36908
aberration, meridional, summation for spherical surfaces, arbitrary decentring angles 77−71931
ACCOS V, commercially available optical design and anal. program 79−86230
achromatic metal-dielectric mirror coating, computer synthesis 78−46750
active mirror characterisation by heterodyne interferometry 79−59799
active mirror testing by stroboscopic interferometry 79−58782
adapter mounted on CRT face for multilayer 3D display 79−18498
adaptive deformable mirror system using polyvinylidene fluoride piezoelec. film 80−74455
adaptive laser resonator techniques for CO_2 laser, phase error correction 79−59729
adaptive optical components, seminar, Washington (1978) 79−59792
adaptive optics, atmospheric compensation, book contrib. 79−31972
adaptive optics, book 79−31921
adaptive optics in astronomy, rubber mirrors to compensate for atm. aberrations, book contrib. 79−35150
adaptive optics in high energy laser systems, book contrib. 79−31971
adaptive optics technology, historical review and prospects 79−59793
adaptive optics technology overview, book contrib. 79−32030
adaptive optics technology status and prospects 80−33132
adherent dielectric coatings of diamond-turned mirrors 78−33810
adiabatic laser calorimeter design for window and mirror evaluation 79−13971
alignment testing in converging beams 78−30044
analysis of mirror-prism system, using biquaternions *(Russian)* 78−50882
animal eye technology use in better lens and mirror design 80−28295
annular, Gaussian-beam theory 78−71185

mirrors continued
annular aperture, light distrib. from diffr., aberration correction using mirror lenses *(German)* 80−69325
annular HSURIA resonators, testing with CO_2 laser, polarisation effects 80−58599
annular lapping of precision flatware 77−27396
aplanatic mirror pairs for X-ray imaging systems 77−5967
aplanatic optical system containing two aspheric surfaces, design 79−81500
aplanatic two mirror telescope from near-normal to grazing incidence, comparative performance anal. 80−58654
aplanatic waxicon insensitive to tilt errors, for high power laser beam transport 80−74460
arc motion in narrow chamber, photography with optical waveguides and rotating mirror *(German)* 77−74542
aspheric mirror optical systems for the infra-red 79−36983
aspheric mirror testing, interferometric method with computer-generated holograms 78−46845
aspheric optics low scatter finishing, polishing of f/2 paraboloids 79−59855
aspheric reflecting systems, geometrical design 80−38083
aspheric surfaces, two axis, design 79−86245
aspherical optical surface low-scatter finishing 79−14125
aspherical planoidal surface, autocollimation apparatus for testing manufacturing quality 80−10053
aspherical surface prod., review 77−7224
aspherical surface testing, interferometer optical system modification 79−7236
astronomical lightweight mirrors of glass, economical construction *(French)* 77−17370
astronomical mirror reflection coefficient checking against control samples 79−75106
astronomical mirror suspended on belt, deforms. during horizontal control 80−17494
astronomical mirror testing, portable visible-IR reflectometer 77−62033
astronomical mirrors, low-cost temp.-compensated cell 77−17369
astronomical multiple mirror telescope, design *(Norwegian)* 79−40072
astronomical optical surface control, Hartmann method, use of splines 79−35149
astronomical optical surface shaping process automation 80−105169
astronomical telescope concave mirrors, design of lens compensators for testing 80−28305
astronomical telescopes, radial support methods for large mirrors 77−49293
astronomical three mirror anastigmatic telescope design 77−87265
asymmetric, with thin absorbing film, design 80−69493
asymmetrical ideal cylindrical solar concentrator principles 79−62119
automatic target alignment of Helios CO_2 laser system 80−74416
axially mobile mirror components design *(Russian)* 77−54769
axicon combined with mirrors and lenses, laser linear, annular and radial focusing 78−66856
axisymmetric mirror class with uniform flux conc. props. along axes 80−95978
azimuth scan MTF techniques, for optical component and system evaluation 78−50900
basing in convergent beam of rays 77−72054
beam divider and mirror expt., amplitude correlation mehtod for optical polarisation meas. 80−53206
beam pointing control system, visible to IR wavelengths 79−98426
beam sampling mirror gratings, optimal design 77−14791
beamsplitters, beam inherent parameters analysis 79−36999
bent glass optics 78−45767
bicylinder mirror aberrations, effects on multipassage mag. mass spectrometer props. *(French)* 79−75651
bicylinder mirrors for appl. in multichannel mag. mass spectrometer *(French)* 78−54494
bimorph piezoelectric flexible mirror constructed from glass plates and $Pb(Zr,Ti)O_3$ ceramic 79−59787
black surface glass mirror as solar energy reflector, reflection coeff. determ. 77−34930
blank fabrication for large azimuthal telescope primary mirror, work program 78−16302
Bragg mirror, corner-reflector type, laser beam divergence reduction 80−91822
Bragg mirror emission and absorpt. losses in waveguide mode *(Russian)* 78−1272
Bragg mirror reflectance, dielectric waveguide inhomogeneity effect 80−28356
Bragg reflector statistical analysis 78−66882
Brillouin, pump wave wavefront reversal, influence of certain radiation parameters 80−9961
broadband dielectric mirror interference coatings, scatter losses 79−50365
Calver mirror remounted at Wollongong Univ. 77−91428
Cassegrain mirror system with high light grasp for Raman spectroscopy 78−78000
cassegrain solar concentrators for photovoltaics 80−61304
Cassegrainian 40 cm reflector, qualitative and quantitative examination *(Japanese)* 79−44366
cat's-eye reflectors, wavefront distortion 79−64303
catoptric objective design, testing *(German)* 80−53400
catoptric Schmidt telescope correcting mirrors, aspherisation by elastic relax. *(French)* 80−62015
Cherenkov counter, ellipsoidal mirrors, fabrication and use 80−47818
circular cylinders with longitudinal slots, rigorous solution of excitation problem *(Russian)* 79−18340
cleaning method for low scatter mirrors after silicone oil exposure 78−59167
coated metal mirrors, p-polarised light total absorpt. by surface plasma waves 78−88373
coating materials for high power laser elements, selection 77−50735
coatings, selective reflectors, and antireflection coatings for nonlinear optics, chemical method 80−28300
coelostat pointing method 80−90338
cold light mirror multilayer coating deposition 80−87464
cold light production by high vacuum deposition of multilayer interference coatings *(German)* 80−53486
coma-free two-mirror systems, astronomical appls. *(Russian)* 77−64641
compact four-mirror optical system design and testing 79−23049
compensator of image surface curvature for system centering 77−72053

mirrors continued
complex aspheric mirror testing by phase meas. interferometry 80−74467
compound circular arc concentrators, optical properties 79−29453
compound elliptical concentrator, geometrical vector flux field 80−33119
compound parabolic, cylindrical parabolic, and compound wedge solar concentrator performance 79−62117
compound parabolic concentrator, derivation of 79−72651
compound parabolic concentrator solar collector design 80−3532
compound spherical mirror for space radio telescope 80−41720
compound wedge cylindrical stationary concentrator, charact. 78−33815
computer-controlled polisher for small-tool fabrication of mirrors 80−14496
concave, vertical astigmatism correction in monochromator *(Japanese)* 79−76841
concave aspheric surfaces, quantitative test using Babinet compensator 79−98512
concave grating mirror stable resonator, approx. anal. *(Chinese)* 79−50324
concave mirror, real image demonstration device 77−41447
concave mirrors, image light reflection, optical illusion teaching demonstration 78−49604
concave paraboloidal mirror, prod. method, interferogram tests 80−58823
concave spherical mirror fabrication using flexure 77−42583
condenser synthesis, astigmatism-free, using spherical mirrors 78−50887
cone collectors for finite sources 78−46742
confocal strip resonator, diffr. performance, mirror defects effect 77−19349
confocal unstable resonator beam props., astigmation in two-mirror config. 78−46670
conic mirrors, caustic coordinates in Platzeck-Gaviola test 78−33799
conic reflectors, basic props. of meridional and sagittal caustics 78−25948
conical, for optical concentration in solar power plants *(French)* 79−24904
conical optics for radiation conversion from laser with unstable resonator 80−91831
contact problems in optical surface shaping 80−74540
continuous deformable mirror multidither coherent optical adaptive system operation 77−19296
continuous deformable mirror multidither coherent optical adaptive system characteristics 77−19297
cooled laser mirror construction, possible use of open pore structures 79−31952
corner edge mirror, vector transform., object space to image space 80−95983
coronagraph objective component surface scatt. angular distrib. obs. 80−74463
corrector element finite size rel. to wavefront compensation error 77−46693
corrosion resistance *(Polish)* 80−11811
coupling reflector, involute-related, for flash lamp pumped laser systems 78−90425
curved glass mirror manufacture for linear solar concentrators 79−62124
cylindric-paraboloid mirror, geometric parameter, focal band width 79−64302
cylindrical, adjustment of coupling coeff. in tunable open optical resonator 79−90024
cylindrical concentrating solar energy collectors, economics 77−88890
cylindrical electrostatic mirror analyser, image line aberrational expansion, nonplanar trajectories 79−41327
cylindrical mirror analyser, design and use with synchrotron radiation, autoionisation obs. 80−18049
cylindrical mirror and lens optical figure characterisation with conventional interferometer 80−78944
cylindrical parabolic focusing collector for distributed-collector solar power system 79−62108
cylindrical parabolic mirror utilisation as solar receiver *(Rumanian)* 80−7914
cylindrical-mirror confocal resonator design with high transmissivity region *(Russian)* 80−14361
damage thresholds for laser fusion pulse shapes 78−74467
damaged laser mirror reuse using simple mirror holder 79−36910
decentered concave mirror in three-mirror concentric objective, for astigmatism correction 78−46749
deflecting system, 3-slit, for isotopic spectral anal. 79−37005
deflection effect of light reflected from moving mirror in ether theory 80−91749
deformable metal mirror characterisation techniques 79−59798
deformable mirror, integrated imaging irradiance sensor for real-time wavefront messuration 80−33138
deformable mirror adaptive optical system 77−46796
deformable mirror design and resonance damping 79−59794
deformable mirror design for wavefront correction in CO_2 laser fusion system 80−74427
deformable mirror figure sensor control 77−19384
deformable mirror for wavefront error correction in Gemini CO_2 laser fusion system 80−74426
deformable mirror high-reflectance dielectric coatings 79−14085
deformable mirrors for wavefront error correction, piezoelectric material requirements 80−78928
deformable mirrors with bimorph actuators 80−33135
deformable-mirror system, computer-aided, using differential angle control 79−27356
delay line for investigation of fast processes 77−764
design, reflector computation *(German)* 78−55429
design of instrument optics from basic elements 77−58418
design of reflective and catadioptric systems 79−86242
design via principal surface, focusing optics for laser fusion 77−3641
diamond turned metal optics, book contrib. 79−32104
diamond turned optics facility 77−50782
diamond turned surface production, interferometric test repeatability 80−74538
diamond turning, technology developments, appls. 77−27400
diamond turning at large optical manufacturer, aspheric surface generation 79−23101
diamond turning of optics, past, present and future 79−23100
dichroic for high energy DF laser 77−88885
dichroic multilayer mirror for 16 μm region, design and fabrication 80−5808
mirrors continued
dielectric, for KrF excimer laser *(Japanese)* 79−72588
dielectric, Rayleigh scatt. at 441.6 nm 80−97367
dielectric coated mirrors, large-spot DF laser damage obs. 79−14022
dielectric coating adhesion improvement of diamond turned mirrors, ion polishing surface prep. 79−23102
dielectric compound parabolic concentrator 78−5533
dielectric laser mirror production with variable transmissivity *(Russian)* 80−14362
dielectric mirror, temp. field during laser radiation absorpt. 80−19063
dielectric mirrors, reflection and wavefront shaping, limits of coexistence 78−46747
dielectric multilayer mirrors, reflectance under slight absorpt. conditions 80−83655
dielectric multilayer systems for optical appls., computer program synthesis *(German)* 78−46788
dielectric semitransparent wide-band mirror, synthesis method 78−13785
differential ball screw actuator driven deformable mirror design and performance 80−33137
differential spectroscopy of charged particle beams, cylindrical mirror 77−50600
diffraction-limited CW optically-pumped far IR lasers, beam characts. 77−38953
diffuse light collection onto extended absorber, mirror designs 78−22186
dihedral corner reflector, effective scattering area calculation, radiation balance method 80−48380
discrete actuator deformable mirror 80−33133
discrete component Sagnac optical rate sensor, error sources 80−1342
double focon, concentration factor 78−1316
double-exposure collector system for solar water heating 79−62070
dual-grating direct-reading spectrograph mirror system design and performance 80−81397
dye laser, short constructional length with folded mirror beam expansion system 80−53328
dynamic-focusing mirror system, umbrella-type 79−36971
education hyperbolic mirrors, holography and Fermat's principle, geometrical anal. 77−45647
electrodynamic scanning mirror drive system for fast-scanning Fourier spectrometer 79−75630
electromagnetic fields, near wide angular lens and mirror systems 77−72051
electromechanical mirror scanning devices 77−58477
electron microscopy, contrast form. 80−68299
electron-beam and photolithographic fabrication of guided-wave optical components 78−13818
electrostatic, Bosi's method for solving Laplace's equation 79−68347
electrostatic, resolution improvement method 80−78753
electrostatic, transaxial, for large-incidence ang. ion beams 78−37798
electrostatic, two-electrode, transaxial, for large incidence ang. electron beam 78−37797
electrostatic energy filter, telescopic, with cylindrical mirror analysers 80−87296
electrostatic mirror, approx. cylindrical field, focal line correction 77−50599
electrostatic mirror, axisymmetric, two-electrode paraxial props., aberrations 78−71025
electrostatic mirror, second order focusing space charge effects 77−50598
electrostatic mirror, two-electrode, transaxial, aberrations, gap depend. 77−27242
electrostatic mirror, two-electrode, transaxial, cardinal elements, aberrations 77−27241
ellipsoidal, detector system for cathodoluminescence SEM 80−101898
ellipsoidal mirror furnace for Czochralski growth 80−60766
EM field, in focal region of wide-angular annular lens and mirror systems 78−90485
EM field quantification near plane mirror *(French)* 77−34854
empty off-axis unstable resonators with rectangular mirrors, modes 79−76787
energy coupling arrangement for parallel concentric lasers *(German)* 78−33757
extreme asymmetrical nonfocusing concentrators for solar energy utilisation, assessment 79−43746
fabrication by diamond turning 79−76899
fabrication using computer controlled polisher 78−75006
Fabry-Perot interferometer, wavefront form. by multilayered dielec. mirror 78−54449
facet surfaces of large mirror reflectors, approx. methods *(Russian)* 80−69564
faceted solar concentrator effects of reflector aperture and facet number 79−62115
fail-safe fibre optics data bus using active electrooptic mirror terminals 79−23053
far IR modular Fourier interferometer construction, very high resolution 80−57401
fast aspheric mirror figure control by profile monitor, wire tester and null lens 80−14419
fast off-axis parabolic mirrors, design and fabrication 78−46741
ferrite polished surface of gyroscope rotor, reflectivity, statistical charcts. 77−10996
fibre optical CW Raman oscillator, using two-mirror resonator config. 79−7152
fiducial system compatible with computer-controlled polishing facility 80−74539
field-widened Michelson spectrometer with no moving parts 79−93223
figuring of mirror for 6 inch reflecting telescope 77−64639
fixed mirror solar concentrator for application to a 100 MW(e) electric generating plant 80−30393
flashlamp reflectors for I photodissoc. laser 77−79848
flat circular, in marginally stable resonators, solns. of Fresnel-Kirchhoff integral equation 79−94262
flat mirror materials, specular reflectance properties and appl. 77−34917
flat mirror multivalent solar concentrator 80−61420
flat mirrors, flatness meas. theory, Foucault method 78−33802
flat mirrors, in multiple transmission attachment for Raman scatt. spectrometer 77−38036
flat plate, parabolic, and conical solar concentrator performance compared 79−62118
flat plate collector energy yield increase by planar reflector, modelling appl. 78−33813
flatness meas. by plane lattice point light source *(Japanese)* 78−9463

mirrors continued
flatness of mirror surfaces by group of line light sources *(Japanese)* 80−1294
focons and foclines as radiation concentrators for extended objects 77−88893
focusing system for synchrotron radiation from electron storage ring 77−10991
foil, with automatic phase correction, astronomical appl. *(German)* 77−88883
four-channel laser system with four-ellipsoidal-mirror set-up for focusing laser beams 79−94276
Fourier spectrometer reflector displacement precision meas., photoelectric method 77−18107
framing spotlight, optimizing the compound reflector 79−3766
Fresnel formula for dielectric multilayer mirrors 80−33118
Fresnel mirror interference method for diffr. grating generation 80−48460
galvanometer beam-scanning rotating lens system, for laser fibre drawing 79−41463
gas laser cavity light intensity optimisation for three-mirror system utilising Fabry-Perot resonators 80−48305
gas laser resonator, simple method of adjusting mirrors 80−19054
gas laser with internal mirrors, polarisation states 77−50701
gas lasers, glass-sealed tubes, Toshiba manufacture 77−14760
geosynchronous satellite plane-mirror solar concentrators 79−96474
glass-Na vap. interface, dye laser frequency locking by selective refl. 78−29992
glasses, high vol. low cost, as solar reflectors, compositions and weathering effects 80−106589
grating mirror, loss of periodic mode in IR laser resonator 80−28254
grating mirrors, periodic mode losses and optimal geom. characts. *(Russian)* 79−27434
grazing incidence spectrograph-monochromator with focusing toroidal mirror 79−75617
grazing incidence X-ray microscopy, of laser fusion targets 78−47178
grinding, as student lab. project 77−5614
grinding and polishing for 6″ reflecting astronomical telescope 77−56826
hazards to air traffic, photometric photography of dazzling heliostat mirrors *(French)* 80−61295
heat mirror on plastic sheet for radiation insulation of visible windows 80−95985
heat mirrors, spectral selectivity of conducting micromeshes 80−26160
helenoid actuators applied to deformable mirrors 80−74454
heliostat design teaching aids and demonstrations 79−62126
heliostat facets, optical characterisation 80−53485
heliostat mirrors array, in Solar Thermal Test Facility, Albuquerque 78−66887
heliostat reflected beam structure 78−90482
heliostat solar collectors, meas. of performance characts. 80−85303
heliostats for central receiver solar power stations, optical analysis 79−74543
hemianopia, new mirror design for detect. 80−108992
hemispherical, 65 ft. dia., solar gridiron electric power generation system appl. 79−87980
high-energy laser mirror thermal distortion test facility 80−14348
high-performance telescope aspheric mirror test error budget 80−48386
high-power annular lasers, uniform beam transformation, mirror system 78−94403
high-speed mirror photochronograph 78−37098
high-temperature solar compound parabolic concentrator requiring monthly tilt adjustments 79−62104
holographic Pancake Window reflective system 80−1165
holographic simulation for fabrication 80−87351
holographic simulation of ellipsoid and hyperboloid mirrors 77−71945
holographic system path length difference controller *(Russian)* 79−22916
holographic three-dimensional image prod., reversal method using reflective and lenticular screens 78−90403
Huygens-Fresnel integral in circular coords., asymptotic soln. 78−87013
hyperbolic cone-channel condenser system 78−33811
hyperbolic mirror testing, interference pattern analysis program and error elimination method 79−76894
ideal cylindrical radiation transformers and concentrators, symm. and asymm. forms 79−55200
image formation, graphical representation for teaching 77−49539
image processing on-axis coherent optical feedback system 77−50631
image quality evaluation from aspheric replica master data, using ACCOS V SPLINE program 78−66964
image-forming reflection system testing by grazing-incidence Linnik interferometry 79−76891
imaging analysis, normal to grazing incidence 77−614
imaging performance of mirrors with circular coolant channels 77−68254
imaging polarizer with spherical mirrors for VUV radiation 80−48375
imaging system with obscured pupils, OTF and point spread function 78−25809
inhomogeneous interface laser mirror coatings, durability improvement 80−1252
injection laser diode mode structure enhancement by backface plating 80−64056
integrated photovoltaic/thermal system with faceted-mirror sunlight concentrator 79−62010
interference coatings for devices transmitting colour images 78−59108
interference coatings on projector reflectors, vac. deposition 77−75725
interference coatings perpared by electron beam evaporation, UV optical strength 79−59779
interference mirror coating thickness meas. equipment 79−35676
interference mirror kinematic adjustment mechanism 78−59109
interferometer, Fabry-Perot, random defects in medium and mirrors 79−54180
interferometer, two-beam, comparison of refl. and refr. optics in condensing element 78−77968
interferometric examination of lenses, mirrors and optical systems, 3D display 80−69497
interferometry, multimode fibre optic, applications 80−86387
intermetallic coatings, possible use in power optics elements 79−14084
intracavity tip/tilt adaptive control system 79−59728
ion polishing for diamond-turned mirror dielectric coating adhesion 80−1370
IR, image scanning systems, tilting plane mirrors 77−83944

mirrors continued
IR bidirectional refl. distrib. function meas. for baffle and mirror materials, recording instrument 78−58012
IR coating for high energy laser reflector and window 79−45951
IR diffuse reflectance spectrometry, spectrochemical anal. appl. 79−34387
IR heat trap field optics, compact lens-mirror system 78−55422
IR imaging and missile-borne tracker optics, selection guidelines 79−23050
IR multidither deformable-mirror COAT system expts. 80−1289
IR multilayer partial mirrors effective from 1.3 to 16 μm, GeSe/KRS-6 and GeSe/NaF 80−9978
IR optical components, diamond turning fabrication 78−5590
IR optical components and aspherics, 10.6 μm interferometric testing 80−74523
IR optical train handling high pulse powers, thermal distortion thresholds 77−46745
isotropic dielectric mirror theory 80−102797
kinematic mirror mount 79−36979
laminated, high refl. region width calcs. for oblique light incidence *(Russian)* 77−19382
large aperture flat mirror testing, Ronchi interferometry appl. 79−85171
Large Azimuth Telescope primary mirror blank testing 79−50367
large azimuthal telescope, glass for 6 m primary mirror 77−62025
large azimuthal telescope, primary mirror testing in observatory 78−20642
large azimuthal telescope mirror, shop tests using modified Hartmann method 78−87173
Large Azimuthal Telescope mirror blank fabrication facilities 79−14123
large azimuthal telescope primary mirror, blank grinding and polishing 78−90541
Large Azimuthal Telescope primary mirror, glass blank quality 79−29991
large azimuthal telescope primary mirror, Hartmann test 77−91430
large precision mirrors, possibilities of mass reduction 78−79100
large size lightweight scanning mirror for airborne laser sensor system 79−23045
Large Space Telescope mirror figure control, adaptive optical techniques 77−22076
large-aperture holographic visual simulator 80−102679
laser, CW heterojunction, mirror surfaces degradation on 10000 hr. lifetime tests 80−106542
laser, for Fabry-Perot interferometer, coeff. of reflection meas. *(Russian)* 78−1237
laser, Q-switching, resonant vibrating mirror system 78−87082
laser, sputtered films production and props. *(Hungarian)* 80−53483
laser beam deflected by prismatic polygon mirror, focus path 77−19267
laser beam expander design corrected for Petzval curvature 80−74461
laser beam expander for short cavity dye laser 80−87532
laser beam profile measurement using spatial sampling, Fourier optics and holography 79−86201
laser beam scanning distortion correction, using parabolic mirror 79−7171
laser beam scanning using rotating mirrors, specifications and tolerances 80−9979
laser beam steerer-expander, two-mirror system design 79−18460
laser beam steerer-expander device, two-mirror afocal telescope design 78−46700
laser cavity, output mirror, low reflectance, reduced radiation loading 78−83000
laser cavity high-reflectivity mirrors, for (GaAl)As diode laser 78−82994
laser damage threshold at 10.6 μm, up to 10^{10} W/cm^2 77−50707
laser damage thresholds, 10.6 μm 77−50708
laser grating mount, compact stepping motor design 80−87402
laser gyros, low-scatter low-loss mirror prod. 80−1272
laser light source for spectroscopy, far-IR, optical coupling arrangements 80−73481
laser mirror, depth concentration profile determ. by ion microprobe mass anal. 77−31126
laser mirror, diffusive component meas. using heterodyne method 77−68217
laser mirror, SEM obs. of laser induced damage *(German)* 78−37929
laser mirror, simple high-resolution mount 77−3618
laser mirror and window absorption, reflection and transmission obs. at 10.6 μm 79−14014
laser mirror birefringence, ellipsometric meas. using stabilised two-frequency laser 80−101820
laser mirror manufacture, ion beam/plasma chemical etching mixed batch process *(French, English)* 77−83880
laser mirror reflectivity meas. technique, precision 78−17947
laser mirrors, high precision reflectivity meas. technique 77−23698
laser mirrors, optical fabrication techniques 77−65600
laser mirrors cooled by open pore structures, radiation damage 79−72603
laser multielement resonant reflector design, temp. and wavelength depend. props. 78−17945
laser optics, Shiva, system, thin film coatings technology 79−7135
laser polarisation rotator, broad band, using successive refls. from 4 mirrors 79−981
laser radar simulator for low scatter characts., three-mirror design 78−59118
laser reflector with non-quarter-wave design, enhanced damage resist. 77−88819
laser resonator formed by 90° cone and mirror, misalignment characts. 80−99757
laser resonator mirrors, optimal refl. coeffs. for intraresonator Q-switching 80−48302
laser resonator optimal output mirror 78−13735
laser system, high energy, thermally induced optical distortion 80−38051
laser unstable resonator, thermoelastic mirror deform., influence on laser characts. 78−71124
laser unstable resonator cavity, tilted mirror system 77−88790
laser unstable resonator with circular mirrors, asymptotic analysis 79−3718
laser-induced damage in optical materials, conference, Boulder, USA (Oct. 1977) 79−14048
laser-target self-adjusting system, wavefront reversal by stimulated Brillouin scatt. mirror 79−14024
lens-mirror combinations with max. conc. 78−9422
light divider phase distortion compensation improvement 78−58073
light reflection by rough surface 80−18996

mirrors continued
light weight honeycomb struct., stiffness 77−75651
light-valve projectors, mirror system use *(Russian)* 80−78930
linear echelon refractor/reflector solar concentrators 80−7929
linear focusing solar reflector, production by elastic deformation of flat sheet 80−30391
Lloyd's mirror, Goos-Hanchen shift at grazing incidence 77−71917
long fibre, mirror and hollow dielec. lightguides, photometric characts. 80−33201
low inertia scanner performance and selection 79−41429
low scatter mirror degradation by particle contamination 77−65618
Low-inertia mirrors for galvanometers 78−71191
luminaire with mirror-type cylindrical reflectors, design *(Russian)* 78−63166
luminaire with paraboloid reflectors, design, cylindrical luminous body dimensions calc. *(Russian)* 78−63165
lunar laser ranging receiving telescope mirror, polishing and Foucault test *(Japanese)* 78−89065
machining, by controlled diamond turning 79−37061
machining of nonconventional shapes, for laser systems 78−5589
magnetooptic bounce-cavity modulator, direct AM 80−5769
masked mirror imaging compared with conventional longit. tomography 78−92695
measuring projector, examination of recording heads 80−83657
mechanical devices for light beam refl. *(Japanese)* 78−5540
mechanical multimode one-to-many fibre-optic switch 79−76814
membrane mirror, vibr. electronic damping using piezoelec. transducers 79−50372
membrane mirror performance as adaptive optical element 77−46782
membrane mirrors for image compensation system, performance and manufacture 77−42587
meniscus collimator viewfinder, optimisation of mirror light transmission coeffs. 80−74469
meniscus-concave mirror systems, misaligning effects *(Russian)* 77−53426
meridional caustics from conic reflectors 77−72044
metal, for high-power appls., multithreshold damage analysis 77−88884
metal and alloy surfaces, highly reflecting, pulsed laser stress phenomena 79−14015
metal film mirror prep. by ultraclean DC sputtering, optical props. 77−50748
metal film reflection filter for CO_2 laser line selection 78−55368
metal mesh dielectric mirrors for far IR lasers 77−54727
metal mirror, diamond turned, optical figure inspection by interferometry 78−5545
metal mirror design and mounting specifications 80−48388
metal mirrors, Al, Ni and Au surfaces, EUV reflection efficiencies 79−14073
metal mirrors, diamond turned, evaporated and sputtered, surface and optical studies 78−79098
metal mirrors, diamond turned, surface, optical and laser damage characts. 77−50705
metal mirrors, dielec. enhanced, absorptance at 5.3 μm 77−50709
metal mirrors for CO_2 laser fusion systems, material constraints and fabrication 78−5476
metal mirrors for high power appls., multithreshold damage analysis 79−980
metal optics, reflective system specifications 80−48387
metal oxide/fluoride mirror coatings, light scatt. and optical strength in UV range 80−106595
metal polishing and lapping 78−5587
metal reflective optics, single-point diamond-turned, polishing 79−23104
metal surface, diamond turned, finish meas. by differential light scatt. 78−5544
metal surfaces for laser mirrors, ion polishing and vac. annealing 78−5588
metal-dielectric interference mirror coatings, high mech. strength 78−30043
metallic, laser damage, temp. depend. of absorptance, melting 79−81470
metallic, laser damage, temp. depend. of absorptance, vaporisation and vap. heating 79−81471
metallic film, IR reflectivity, mirror appl. 78−5536
metallic mirror as complex rough surface, light scatt. 80−1293
metallic mirror coatings, protected and unprotected specular reflectance 79−76792
metallic mirror surface topography determ. by Nomarski reflection microscopy, theory 79−54185
metallic mirrors for laser fusion reactors, neutron and gamma irrad. response calc. 80−23121
metallic wired grids as semitransparent flat mirrors in far IR 78−71188
metals for mirror substrates, manufacturing processes, review 78−5542
Michelson interferometer, external resonator for GaAs-$Ga_xAl_{1-x}As$ injection laser 79−81455
Michelson interferometer misalignment nonlinear phase errors 79−30535
micro-optic devices for coupling/branching in fibre optic communications 79−55211
microroughness ellipsometric determ., effect on laser cavities 79−59791
microscope, scanning mirror, with optical sectioning characts., ophthalmology appls. 80−85461
mirror, with MgF_2 overcoating, reflective scatt. and reflectance meas. in vac. UV, moisture and oil vapour influence *(German)* 79−86227
modulation-interference spectrum analyser 77−79161
monochromator, telescopic, in CTEM, with cylindrical mirror analysers 80−87296
monochromator using concave holographic grating and plane mirror, imaging props. 80−99856
monochromators with off-axis mirrors, distortion and split-image curvature 78−59141
monolithic deformable mirror/heat exchanger unit evaluation 80−33139
mount for optical instrumentation 79−80690
moving atmosphere simulation by rotating phase plate 80−79021
multi-segmented mirror for laser thermal blooming reduction vice phase correction, experimental demonstration 79−98449
multiactuator deformable mirror evaluations 80−14416
multiactuator mirrors, wavefront error compensation capabilities 79−59797
multibeam modular interferometer design 80−18004
multidimensional scan generation by single rotating component 77−58482
multidither adaptive optical system, 69-channel hybrid controller 80−33136
mirrors continued
multidither adaptive optical systems with zonal control of deformable mirrors 77−46795
multidither adaptive optics system operation 80−33141
multidither hillclimbing adaptive optical system, secondary intensity maxima correction 80−106593
multidithered segmented COAT mirror, surface wave control 78−46752
multilayer, dielectric reflectors, simplified description 79−89984
multilayer 532/1064 nm laser reflector damage resistance improvement by non-λ/4 design 79−14019
multilayer broadband dielec. coatings for Fabry-Perot spectroscopy 77−18101
multilayer coating design with reduced elec. field intensity 77−72046
multilayer dielectric enhanced mirrors for 2 to 6 μm 79−14086
multilayer dielectric mirror, light scattering due to surface roughness 80−58460
multilayer dielectric mirrors, exam. of reflectance, optical thickness and refractive index 78−59106
multilayer dielectric mirrors, phase anisotropy, temp. depend., intracavity method, meas. 80−78931
multilayer dielectric reflectors, nearly perfect, theory 79−72644
multilayer dielectric reflectors, optical props. calc. 78−30041
multilayer light scattering and laser gyro 78−33764
multilayer mirror optics of animal eyes 79−57643
multilayer mirrors, for X-ray and far UV radiation 78−1313
multilayer mirrors, high refl. at fundamental, second and third harmonic laser wavelengths 78−90490
multilayer mirrors for X-ray and far UV, optimum refl. 77−23725
multilayer systems, neutron optical props. 79−55044
multimirror system stray light mask calc. method *(Russian)* 78−1312
Multiple Mirror Telescope guide alignment system 79−75107
multiprofile buried gratings, dielec. coated metallic, use as beam sampling mirrors, theory 78−79120
multistage cylindrical analyzer for simultaneous detection of several beams with different energies 79−22891
neutron reflectivities, Ni-Mn and Ni-Ti multilayers for monochromators and supermirrors 80−22880
Newton's formula validily in Fourier transform. config. 78−42281
nonaxisymmetric, fabrication by stressed mirror polishing 80−99885
nonconcentric bispherical mirror objective, collimating props., ray path calcs. 78−90492
nonevacuated compound-parabolic-concentrator solar heating prototypes 79−62105
nonimaging concentrator design as second stages with image-forming first-stage concentrators 80−50933
nonlinear holographic gratings for high energy laser beam sampling 80−14476
nonlinear interference mirror, reflection of light 80−102761
nonlinear media, phase distortion compensation by phase conjugation 80−43392
nonorthogonal resonators, fund. mode props. w.r.t. rotating Gaussian beams 80−53336
nontracking solar collectors, wide-angle lenses and image collapsing subreflectors 80−76603
object mutual orientation using active polarisers with tetrahedral reflectors 79−26109
objective, 3-mirror design, optical scheme 78−55431
objective using a planoidal mirror 80−28297
off-axis mirrors made using conventional milling machine 79−59848
off-axis parabolic, for laser fusion expt., fabrication process 79−23103
off-axis parabolic mirror fabrication for laser function expt. 80−1374
opaque surface, roughness determ., photometric method 80−95072
open resonator with aperture in reflector, theoretical anal. 79−31955
optical beam-guide lines, elec. length instability 78−46748
optical CAD, conf., San Diego, CA, USA (Aug. 1978) 79−86228
optical component blank pressure shaping, semiautomatic apparatus 79−72731
optical component replication 79−55253
optical contamination assessment by bidirectional refl. distrib. function meas. 79−59790
optical delay line, OLZ-7 seven-frame, using multiple reflections in plane mirrors 79−23080
optical design of two-mirror systems, coupling props. 80−53396
optical fibre fracture stress and mirror size obs. 79−37020
optical fibre-laser transverse coupling and front-mirror monitoring for feedback control of laser transmitters 80−33151
optical materials, laser induced damage, symposium, Boulder, USA (Sep. 1978) 80−31417
optical resonant reflectors, two elements, expression derived for finesse 78−33809
optical resonator nonsymm. eigenvalue problems, numerical solns., Prony method 78−82992
optical rotation multiplier, lens-mirror reflector system *(Russian)* 78−46745
optical scatter meas. specification proposal 80−48390
optical switch array, mirror-type, integrated on $LiNbO_3$ substrate 79−27436
optical system for light scatt. expts. 79−76786
optical systems, entropy and neguentropy *(French)* 80−102608
optical wavefront distortion compensation in real time 77−17219
optics test chamber for cryogenic meas. at high vacuum, upgrading design 79−23098
orbiting mirrors, solar illumination after dark appl. 78−33816
oscillating beam spectrometer for organic thin film transmission 80−18022
para-ellipsoid mirrors for fan shaped beams, calc. method 80−33117
parabolic, 20 cm diam. f/3, null testing in modified scatterplate interferometer 80−79015
parabolic, for optical concentration in solar power plants *(French)* 79−24904
parabolic, TV large-screen virtual display, fabrication by rotational method 80−87465
parabolic mirror made by rotation method, fabrication and defects 79−76889
parabolic mirror segment, general Fourier transforming configuration 77−46687
parabolic mirror testing by vibration-insensitive laser unequal path interferometer 80−74537
parabolic mirror testing during fabrication by long-wavelength interferometer 80−74536
parabolic off-axis mirrors, imaging props. 79−94316

mirrors continued
parabolic reflectors, medium size, surface shape quantitative evaluation 79−72654
parabolic solar reflector for accurate and economic producibility 80−7930
parabolocylindrical focline, localised flux density calc. 79−72659
paraboloid, off-axis section, fabrication by stressed mirror polishing 80−99886
paraboloid, small-field single-lens field corrector 77−33344
paraboloid epimirror for microscope illuminator, design 80−28304
paraboloid mirror with coaxial linear source, intensity distribution 80−74456
paraboloidal, image formation determ., solar concentrator appl. 77−46780
paraboloidal, radiant heating 79−97392
paraboloidal collector arrays, shading and spacing, energy loss evaluation 79−43747
paraboloidal facets, long focus, radiant flux distribution calc. 77−50745
paraboloidal off-axis mirrors in plane grating monochromators, fourth-order aberrations 77−62056
pendulum mirror, in geodetic compensator level, systematic level errors reduction *(German)* 77−2289
penta mirror assembly, fabrication and performance description 79−81505
periscope, rearview, using two concave cylindrical mirrors, design 78−71178
Perspex for astronomical telescope mirror manufacture 78−36458
phase compensation of thermally bloomed laser beam, mirror deform. 80−8423
phase conjugate mirror, dynamic interferometry, differential holography of irregular phase objects 80−37969
phase conjugate mirror component for optical cavity, Gaussian transverse modes 80−58595
phase conjugate mirror for optical resonator, longit. and transverse modes 80−14392
phase conjugate mirror forming optical cavity, Hermite-Gaussian higher-order reson. modes 80−58594
phase-conjugate mirrors for optical resonators, degenerate four-wave mixing 80−43393
phase-conjugate reflection using TEM_{00} pump beam 80−48327
photovoltaic solar energy concentrators, image calcs. for an array of directable mirros 80−76609
piezoelectric beam deflector, basic characts., multielement 77−54808
piezoelectric beam deflector, bimorph, theory and expt. 77−54807
piezoelectric bimorph plate, adaptive optical element analysis 79−50389
piezoelectric mirror translator, stabilisation of narrow-bandwidth CW dye laser 80−33036
planar Fresnel ring mirror, focal region, solar flux redistribution visualisation 79−68426
plane, planarity deviations detection method 77−27329
plane, spatially separated, adjustment to coplanarity, interferometric technique 80−95974
plane, use in electro-optical distance meas., influence of nonperiodic errors *(German)* 77−9324
plane mirror system synthesis using biquaternions 80−9982
plane surface scanning, 4th order matrix operator formulation *(Russian)* 78−18037
plane-mirror two-beam interferometer analysis 79−2812
plasma mirror in electron beam controlled CO_2 laser 78−17976
plasma mirror refl. charact., in electron beam controlled CO_2 laser 78−59064
plastic mirror, large size lightweight, for airborne laser sensor system, fabrication 78−66891
plastic optical components and systems 78−25967
plastic optics, design patterns 79−32009
plastic parabolic concentrator, for terrestrial solar cell arrays 79−14089
point spread function energy distrib. rel. to surface deform. 77−58422
pointing and stabilisation by fine control of secondary mirror 77−82124
polarisation flipper for IR laser beams mirror and prism systems 77−75586
polisher, computer controlled, efficiency 80−91938
polygonal, precision, optomechanical scans for information storage and retrieval *(Russian)* 77−83947
porous structures for cooling laser reflectors, theoretical study 80−91809
position, in Michelson interferometer, form. of bands of equal thickness 80−52298
position control in Michelson interferometer by means of capacitor probes 78−21119
premonochromator for stray light rejection in Raman spectroscopy 77−58438
primary mirror for large azimuthal telescope, glass blank annealing 77−72101
primary mirror of large azimuthal telescope, interference testing method 77−73952
primary mirror of large azimuthal telescope, isophotometric recording 77−73953
prism-mirror system transformations by biquaternions *(Russian)* 78−55426
production technology advances, seminar, London, England (April 1979) 80−67938
Prony method for symmetric matrix in scalar resonator calc. 80−5807
proof glass superposition method for testing convex spherical surfaces, errors 77−75649
pyroceramic blanks, surface finishing 77−62079
pyroceramic lightweight mirror blank fabrication using standard metal-working equip. 80−102871
quarter-wave dielectric reflector, spectral absorptance approximation 80−33131
quarter-wave mirrors, oblique incidence reflection coefficient, small absorption of layers effect 80−64140
quasi-fixed adjustable-focus reflector array solar collectors 79−62106
radiation polarisation state calc. method *(Russian)* 79−98458
radiative transfer between mirror surface and its focal point 79−32020
ray tracing algorithm for programmable pocket calculator 79−81508
ray-optical analysis of unstable resonators with spherical mirrors 80−14415
Raytheon laser gyroscope using MnBi magnetic mirror 78−79064
rectilinear laser scanning of wide formats application of additional mirrors 78−33803
reference mirror for alignment of optical instruments 80−10054
mirrors continued
reflectance meas. using multiple wave interferometer *(French)* 77−42585
reflectance measurement, using multipath optical cavity *(French)* 77−13797
reflecting all-sky cameras, design 79−40074
reflecting interferometer design with predetermined characteristics *(Russian)* 79−93206
reflecting layers, appl. to instrument parts 79−37065
reflecting telescopes with zero expansion material mirrors, temp. defocusing *(Russian)* 79−96912
reflection anisotropy of 6320 Å laser mirrors 79−98413
reflection coefficient meas. instrument 78−18036
reflection polarisers and analysers in vac. UV, design criteria 78−55424
reflection polarisers for vacuum UV, design and performance 78−33801
reflection-transmission holograms obtained using mirror photolayers 77−58300
reflectivity, quantitative meas., undergrad. lab. expt. 78−49624
reflectivity measurement of highly reflective mirrors 78−54444
reflectometer, for laser mirrors, high accuracy 78−87118
reflectometer, versatile high-precision multiple-pass 78−93754
reflector geometrical optics design using complex coordinates 77−19380
reflectors, deep paraboloid, light intensity curves with transverse cylindrical light source, calc. *(Russian)* 80−38090
replicated and plastic optics, conf., San Diego, USA (Aug. 1977) 78−66961
replicated light weight wave flats for scanning radiometer 78−66889
replicated reflector for TOW anti-tank weapon's IR beacon 78−66889
replication of large lightweight mirrors 78−66963
replication of light-weight components, mirrors for space use 78−66965
replication process for laser scanner mirror surfaces 77−58496
resonator, annular, adaptive mirror effects on performance 80−58596
resonator, spherical optical, mirror misalignment sensitivity 80−53334
resonator with wavefront reversing mirror, oscillator modes 80−53345
resonators, cylindrical unstable, ray-optical anal. 79−72652
resonators, unstable, Fourier transform spline soln. to deal with sharply cut off fields at mirror edges 79−94263
retroreflecting mirror for dynamic compensation of optical inhomogeneities 79−31970
retroreflective array as resonator mirror 80−95973
retroreflective arrays as approximate phase conjugators 79−72508
retroreflector, temp. stability testing under space conditions 77−62078
reversible mirror design, for real time holographic interferometry 78−33705
reversing, laser beam spatial struct. reproduction inaccuracy in amplifying medium 80−14379
ring laser, perturbed cavity calcs. 80−102739
ring laser characteristics, influence of radiation interaction with reflector material 79−13993
ring laser gyroscope for missile guidance using magneto-optic bias mirror 78−79061
ring optical cavity, nearly confocal, with spatially inhomogeneous medium, threshold gain 80−43373
ring resonator with diaphragmed spherical mirror, stability of oppositely travelling waves 79−98415
Ronchi test, fringe sharpening 80−53480
rotating, for synchrospeed synchroballistic camera 78−41366
rotating, laser beam TV scanner, development programme *(Japanese)* 80−74369
rotating, scanning of light beams with parallel displacement *(Russian)* 77−34929
rotating mirror deflector design cost/performance tradeoffs 77−58485
rotating mirror deflector motor and control system selection 77−58484
rotating mirror scanners, technology and market rel. to price 79−27362
rotating prism display of multiple LED lines 79−93111
rotationally symmetrical reflector, physical modelling *(Slovak)* 80−38088
Salyut-4 orbiting solar telescope, design, obs. results 78−53783
scanners, compensated moving-coil mirror galvanometer 77−58479
scanning gauge for surface form meas., spherical and aspherical 79−32100
scanning IR microscope, photodetector field of view correction using additional mirror 80−52304
scanning mirror, in precision two-coordinate device 77−26275
scanning mirror electron microscopy, quantitative evaluation of elec. microfields 78−74110
scanning rate restrictions in monochromators 80−48430
scanning system with multifaceted mirror, tracking sweep 80−33123
scanning system with reflecting elements, angular distortions 78−37965
schlieren photography, single and two mirror systems, resolution 77−34040
second-surface mirrors, solar radiation resistance increase using filters 77−39015
secondary mirror centering of Tirgo telescope 80−101533
sectional mirror, optoelectronic control system 78−20645
SEM cathodoluminescence microscopy, mirror detector system 78−24000
semiconductor laser output stabilisation by mirror close to laser facet 79−45954
semireflecting lossless, transmitted and reflected optical fields phase shift 80−46769
shadow methods for studying turbulence using reflection from a mirror in the medium 80−95801
SHG, optimum, in thin-film external resonator 79−18485
short-wave synchrotron radiation prevention by rotatable mirrors 78−62274
sight stabilisation using microprocessor 79−27369
simulated multiple mirror telescopes, speckle interferometry, meas. of astronomical objects 80−56716
single point diamond-turned mirror polishing 79−14126
single-point diamond-turned mirror performance before and after polishing 80−74466
small grinding and polishing tool control by computer 79−98516
small nonsymmetrical aspheric surface fabrication, using grinding or polishing minipad 79−64365
soft X-ray interference mirror 78−41385
solar cells test facility using plane mirror heliostat 80−45668
solar central tower receivers, flux density distribution anal. 77−46786
solar collector, compound parabolic type, optical and thermal design 77−23735
solar collector, fixed spherical, geometrical optics *(French)* 77−83945

mirrors continued
solar collector, fixed spherical, optical simulation 80−7912
solar collector, focused, slightly curved, reflected light pattern anal. 77−23728
solar collector long-term average performance prediction method 79−62116
solar collector with cusplike compound parabolic concentrator with tubular absorber 77−23734
solar collector with flat specular mirror, optimal tilt angles with seasonal variations 80−72081
solar collector with stationary spherical reflector and tracking absorber, characts. 77−54773
solar collectors, mirror configurations for flat plate double-exposure panels 80−50999
solar collectors, parabolic cylindrical, design 77−23729
solar collectors concentrating, compound versus simple parabolic 79−64304
solar compound parabolic concentrator collectors, prediction of thermal performance 80−55905
solar compound parabolic concentrator flux distrib. nonuniformity 79−62011
solar concentrating collector optical efficiency, heat loss coeff. and heat removal factors 79−100483
solar concentration heliostat mirror field analysis and design 79−83570
solar concentrator, fixed, concentrated flux characts., expt. 77−23733
solar concentrator, fixed-mirror, with secondary concentration, design, construction and testing 79−52903
solar concentrator, fixed-mirror-distributed focus, optical-thermal performance anal. 80−30392
solar concentrator distrib. array, mirror specular reflectance 77−88886
solar concentrator image characteristics, non-uniform intensity distrib. 80−55816
solar concentrator using catenary curve reflecting surfaces 78−46744
solar concentrator with line focus segmented mirror, features 77−54772
solar concentrators, cylindrical parabolic, with flat absorbers, intensity distribution calc. 77−23730
solar concentrators, design variables, optical efficiency, heat loss coefficient and heat removal factor 80−7927
solar concentrators, paraboloid type with reduced wind drag, design 77−23731
solar concentrators, reflector shapes for truncation of nonimaging cusp concentrators 80−21385
solar concentrators with fixed focal axis and gravity-determined curvature 79−74495
solar cylindrical parabolic collector geometry 79−62109
solar energy, photo-optical instrumentation, [Conf. San Diego, CA, USA Aug. 1978] 80−7926
solar energy collecting system, cylindrical absorbers, sun following reflectors, semi-parabolic reflector *(Korean)* 80−21380
solar energy collector, reflector and absorber design, spherical stationary mirror, and automatic tracking absorber 80−50997
solar energy concentrator, for tower type solar power plant efficiency 77−19379
solar energy concentrator, spherical, irradiance distribution anal. 77−46779
solar energy concentrator designs for underdeveloped countries 79−62125
solar energy concentrator reflecting surface formation, deformation method evaluation 78−90481
solar energy concentrators, design methods analysis and classification 78−83063
solar energy concentrators, heliostatic fields, geometry *(Spanish)* 79−23037
solar energy concentrators, performance evaluation 80−87457
solar energy concentrators, segmented parabolic mirrors, optical performance anal. by THEK computer code *(French)* 80−61294
solar energy concentrators, thermal deformations 79−39277
solar energy conentrators design, American and Australian practices *(Italian)* 80−50935
solar energy enhancement, using Earth-orbiting mirrors 79−52901
solar energy parabolic trough mirrors, concentration characts. *(Japanese)* 79−79376
solar energy photothermal conversion, optical performance of absorber-reflector combinations 78−63168
solar focusing collectors, cylindro-parabolic mirrors *(Rumanian)* 80−50934
solar mirror materials, reflected beam profile characterisation 78−33814
solar planar reflector-collector array optimisation 79−62071
solar plant composite heliostat, computer anal. and optimisation 79−39283
solar point focusing concentrators, effects of tracking errors on performance, statistical anal. of intercept factor 80−61302
solar power, one and two faced symmetric sidewall booster mirrors, optimal geometries 79−43743
solar power stations appl., surface specularity obs. 78−13786
solar radiation concentrator accuracy assessment, using laser radiator and sectioned photoreceiver 79−23038
solar radiation concentrators, composite, with conical radiation sources 77−19378
solar radiation simulator, non-axial type, reflector profile calc. *(Russian)* 78−63169
solar reflecting concentrators, optical evaluation techniques 78−50893
solar reflector concentrator, Fresnel geometrical design 80−45636
solar reflector-collector system all-day performance, time-integrated calc. 79−3765
solar reflectors, solar radiation resistance increase using filters 77−39015
solar shallow pond performance with mirror on side away from Equator 79−62077
solar thermal collector, internal cusp reflector, optical anal. 80−101127
solar vacuum thermal collector with optimal conc. 78−50892
spatial variables meas., Mekometer additional equipment design, manufacture and calibration for more complete utilisation *(Italian)* 80−64129
specular reflectance standards for visible and infrared region using thin Al film vacuum deposited on optical flats *(Japanese)* 80−102789
specular reflectometer-spectrophotometer, NBS reference, mirror refl. meas. 80−68236
spherical, image forming mirror systems *(Hungarian)* 77−3644
spherical, radii, seventh-order design of a reflecting optical system 80−48378
spherical, scatt. theory *(Chinese)* 79−10243
spherical for IR imaging, astigmatism 78−33804
mirrors continued
spherical mirror folded cavities, astigmatism elimination and regulation *(Chinese)* 78−90431
spherical mirror resonator, misaligned, open, spatial struct., phase and amplitude distrib. 78−46676
spherical mirror with piezoelectrically controlled curvature 78−33796
spherical surface error absolute definition technique, use in interferogram analysis 79−86268
spherical wide angle mirror under oblique illumination, diffraction in focal region 80−1108
spontaneous emission near plane mirror, quantum formalism *(French)* 77−27267
sputter deposited, mechanically polishable damage-resistant mirror materials 79−47181
standing wave and pellicle, proposed design for very large space telescopes 79−92672
static photovoltaic concentration improvement, two-sided Transcell 79−61999
stationary spherical solar collector design 79−62107
stereoscope for viewing aerial photographs, interpretoskop optics, modifications 80−105081
stigmats using two curved Fresnel surfaces 80−38084
stimulated Brillouin scatt. complex conjugate mirror for ruby laser 80−87438
stimulated Brillouin scatt. mirror, selective props. improvement using wide band pumping 77−88863
stimulated Brillouin scatt. mirror, short high-power pulses obtained by wavefront reversal 80−99801
stimulated Brillouin scattering mirror, wave-front inversion of laser output 79−14038
stimulated Raman scatt. and optical freq. mixing, simultaneous occurrence using three-mirror config. 80−48342
stratosphere trace molecule Fourier transform spectrometer optical design 80−82099
stray light calculations, surface refl. models 78−58905
stray radiation analysis using first-order deterministic APART program 78−59116
stray radiation rejection capabilities of optical systems, GUERAP II program analysis 78−59115
student experiment in mirror prep., electroless plating of Cu on treated glass 80−36817
submillimetre laser, vibr. mirror for phase modulated pumping, amplitude stability improved 79−22967
sunlight reflected from polygonal heliostat, analytic evaluation 79−29452
surface configuration control by conc. loads applic. 79−94317
surface configuration control of nonuniformly heated shells, actuators effectiveness 79−94318
surface curvature and local distortion meas. by holographic interferometry 79−76796
surface errors rel. to optical performance, effect of mid- and high-spatial freqs. 79−59789
surface evaluation techniques for optical components 79−46094
surface high power optical damage threshold elevation by hypervapotron cooling 79−23002
surface irregularity statistics for laser component materials 79−14057
surface light scattering rel. to microtopographic features 79−59639
surface profile testing with set of spherometers, math. analysis 78−13823
surface reflectances, expt. investigation 78−83066
surface roughness evaluation, statistical approach 78−90367
surface scattering rel. to microroughness, surface transfer function 78−58917
surface testing by caustic method using phase stripe as spatial filter 79−72722
surface testing of 6m LAT mirror, Hartmann method under shop conditions 78−90540
synchrotron radiation collection mirrors, soft X-ray throughput 78−62275
synchrotron radiation vac. UV and soft X-ray mirrors 78−83071
synthetic aperture objectives, use of toroidal elements 77−75650
systematisation of mirror lenses according to extent of central obstruction *(German)* 80−102795
telescope, altazimuth mounted, primary mirror deflection and stress anal. 80−58659
telescope primary mirror manufacture, monitored null corrector 80−78946
telescope primary mirror testing by Hartmann method during manufacture 78−20641
telescope secondary mirror, flexure, elasticity theory *(French)* 77−14789
telescopic system, unstable resonator calculation, laser operating on organic compound solution 80−58600
temperature-dependent absorptance, laser-induced thermal runaway 80−91882
testing using autocollimation method with multiple pendulum mirros 80−102792
thermal blooming cell design for use in evaluating adaptive optics 80−102780
thermal imaging scanners, mirror rotation axis optimisation 80−86426
thin film Kapton mirror for concentrator enhanced solar arrays for spacecraft appls. 80−30501
three plane mirrors, transform. of vectors 77−75654
three-actuator deformable water-cooled mirror 80−33134
three-mirror image rotator use in laser produced plasma expt. 80−33814
three-mirror system as IR broadband polarisation rotator 77−58413
three-mirror telescope, design and optimisation 78−90476
three-step compound-wedge stationary solar energy concentrator optimal geometry 79−62103
tip/tilt mirror positioner, high performance 79−59795
toroidal, fabrication for projecting target surface in solar furnace *(Japanese)* 78−90534
toroidal mirror as focusing element for stigmatic grazing incidence spectrometer 79−71539
toroidal mirror fabrication for soft X-ray imaging 78−41384
toroidal mirror optical polisher 80−5848
total absorbing optical coatings using black metallic mirrors 79−3767
tower-top focus solar receiver designs 79−62114
transmissive optics for high power CO_2 lasers 78−79057
transverse structure of radiation from a laser with an additional mirror 80−58604
trihedral reflectors, for holography with local reference beam 78−37853

mirrors continued
two-component pancratic systems containing mirrors, paraxial calc. 79−72661
two-mirror anastigmatic telescopes, designs 77−60611
two-mirror corrector, well baffled, for parabolic telescope mirror 77−62030
two-mirror grazing incidence telescopes with one conical surface 79−84673
two-mirror pancratic system, extraneous image plane highlights elimination 80−87467
two-mirror system with zero spherical aberration *(Russian)* 77−64645
two-mirror telescopes, image quality estimation and utilisation in cosmic astronomy *(Russian)* 79−96911
two-sided photovoltaic solar cell static concentrators 80−35684
uncentred surface system, field aberrations of object meridional points 78−82923
underground beam-guide lines with periodic light beam corrections 80−33196
uniform radiation field on flat receiver surface, creation, design principles 78−90480
unstable optical resonators with tilted spherical mirrors, design eqns. 78−74930
unstable resonator mirrors, diffuse scatt. effect on intensity distrib. 77−58354
unstable resonators with scraper mirrors, equivalent Fresnel no. calc. 79−81460
unstable strip resonators with misaligned circular mirrors, waveguide approach 78−82991
UV optics, high intensity solar irrad. testing 77−5431
UV polariser, coating materials *(Russian)* 77−34928
UV reflecting mirrors for space appls. *(French)* 77−67022
vacuum UV and soft X-ray mirrors, for synchrotron radiation 79−3762
vacuum UV efficiency, conference on synchrotron radiation instrumentation, Orsay, France (Sept. 1977) 78−62999
vacuum UV optics, reflecting coatings and transmitting filters, review 79−46029
vector transformation by system of four plane mirrors 80−9981
vibration analysis by wavefront modulated holography using seesaw mirror 79−3652
virtual image in hyperbolic mirror, holography problem, for teachers 79−35476
visual, acuity experiments, image viewed through a rotating mirror 79−76790
wavefront meas. control, and conjugation, adaptive optical system aspects 79−59796
wavefront reversing mirrors for plane-parallel resonator, mode structure 79−86196
waxicon, nonlinear, for laser beam transform., design and fabrication 78−5543
wide field of view high resolution reflecting optics, design techniques 79−86241
wide-angle concentric dome and shell production, double-pass null test 80−79022
wide-angle spherical mirror under oblique illum., EM diffr. in focal region 78−58888
wide-angle spherical mirror under oblique illum., EM diffr. integral formal expansion 79−72464
wideband optical pathway for electron ring diagnostics using synchrotron radiation 78−78518
Wolter lens component replication 80−95972
X-ray catoptrical crossed-mirror imaging at grazing incidence 80−77923
X-ray focusing mirror for synchrotron radiation 80−90961
X-ray imaging system, surface roughness and scatt. effects 80−77921
X-ray mirror, for HEAO-B X-ray telescope, design, fabrication and expected performance 78−49330
X-ray mirror objectives, tests with soft X-rays from plasma mirror of electroionisation CO_2 laser soft X-rays from plasma mirror of electroionisation CO_2 laser 78−85850
X-ray mirror profile meas. machine 80−69496
X-ray resonator based on successive refls. of surface wave 80−99021
XUV mirror reflectivities from 50-150 eV 80−90966
Young-Fresnel double-mirror interference experiment with electrons *(German)* 78−90351
zonal Foucault test, diffr. effects 77−72099
Ag chemically deposited layer, reflectivity rel. to heat treatment 79−27366
Ag, formation on salts of carboxylic acids by photolysis 77−75720
Ag mirror, Y_2O_3 coated, for the 0.5 to 14 μm region 80−87456
Ag mirror IR reflectance at 45° incidence, obs. 79−14074
Ag-Sb alloy, reflectivity, effect of electrodeposition conditions 78−13784
(Al,Ga)As DH laser degradation, facet oxide formation 79−86185
Al and Ag, polarisation effects by overcoatings 77−72055
Al coated Pyrex double ellipse cavity 78−5503
Al coating reflectivity in vacuum UV, heating effect 80−95981
Al, diamond-turned, surface reflectivity meas. 1 to 12 μm 80−1298
Al film, enhanced mirror, high-rate sputtering, reflectance and dispersion 77−42636
Al mirror IR reflectance at 45° incidence, obs. 79−14074
Al mirror reflectance 8 to 12 μm, normal to high incident angles, Y_2O_3, HfO_2 protective layers 78−79090
Al mirrors, on metal substrates, resistance to heat and radiation 79−94319
Al reflective coating, reflectance in UV and visible 80−28307
Al spherical mirror generation with single point diamond cutting tool 80−33249
Al, with MgF_2 overcoating, reflective scatt. and reflectance meas. in vac. UV, moisture and oil vapour influence *(German)* 79−86227
Al-Ag alloy mirror for use as solar reflector, co-sputtering 80−20789
Al-Cu(Bi), multilayer mirrors, for X-ray and far UV radiation 78−1313
AlGaAs DH laser mirror degradation mechanism and lasing charact. changes 80−9919
Al_2O_3 coated Al mirrors, highly efficient refl. type polarisers for 10.6 μm laser radiation 78−71177
Al_2O_3-Si, alternating layers, dielec. facet reflector for semiconductor lasers 78−66841
Al_2O_3-Si-Te-Al_2O_3 layered apertured facet reflector, for lateral mode stabilisation of diode lasers 80−23708
Au coated surface, reflectivity in soft X-ray range 78−45221
Au plated mirror, with Si:Li detector in X-ray astronomy rocket expt. 77−5439
Be mirrors, props. and fabrication procedures 80−38138
Be substrate for lightweight mirror, surface quality and thermal props. 80−23762
Be substrate with metallic coating and dielec. overcoating 77−62034
C-Au, multilayer mirrors for X-ray and far UV radiation 78−1313
C-fibre reinforced resin laminate for IR mirror, design and fabrication *(French)* 77−54770
CO_2 laser, 10 ns pulse generation, rotating mirror technique 80−33042
CO_2 laser Antares fusion system, mirror quality specifications 80−74423
CO_2 laser bimetallic mirror coating vacuum sputtering technology 80−35086
Co-Fe laminated mirror, with Ti-Gd sublayer, in polarising neutron guide 78−9012
^{133}Cs vapour external selective mirror for semiconductor laser 79−45961
Cu film self-generation on Cu doped glass ceramics, for low-expansion IR laser mirrors 79−14127
Cu, microstructure effect on Ag overlayer deposition, 10.6 μm reflectivity 77−42543
Cu mirror, single-point diamond-turned, evaluation for 8-beam CO_2 laser, Helios 79−23044
Cu mirror acted on by laser radiation, reflectivity meas. 79−10342
Cu plated substrates for Antares CO_2 laser mirrors 80−14349
Cu, polished, optical props. ageing 77−79912
Cu, surface defect layer form. on mech. polishing 80−33122
Cu vapour deposited mirror on SiC substrate, pulsed laser damage charact. 80−48314
Cu-Sn(Al)(Ga) reflecting surface absorpt. coeffs. at 10.6 μm 80−95984
GaAs, laser, transverse modes, mirror reflectivity dependence 79−68404
GaAs laser convex micromirror mode control 79−36920
GaAs laser reliability, protective facet coatings 79−81452
HFO_2, vacuum deposited film, use in multilayer reflector for near UV 77−34924
HfO_2, vac. deposited, near UV multilayer reflector 77−39014
In_2O_3, transparent heat mirror formation by ion plating on ambient temp. substrates and props. 80−25578
LaF_3-MgF_2 multilayer mirrors, optical strength in Xe laser 77−27294
$LiNbO_3$ waveguide, Ti diffused, partial reflector, optical branch and switch fabrication 78−33834
MgF_2 coated Al mirrors, AES, UV irrad. effect 77−72047
MgO-MgF_2 multilayer stack selective mirror with high reflectivity *(French)* 80−64131
Mo, CVD films of high IR reflectance 79−52119
Mo laser mirror, optical and metallurgical characterisation 80−33129
Mo sputtering for laser mirror refurbishment 80−14498
Na vapour lamp reflector design *(Spanish)* 79−23042
$NdAl_3(BO_3)_4$ miniaturised crystals with directly applied mirrors, laser emission 79−22958
Ni plated aspheric metal mirror fabrication for IR optical systems 80−14497
PbF_2-Na_3AlF_6, semitransparent wide band dielectric mirror synthesis using dispersive and absorbing materials 79−89986
PbF_2-ZnSe multilayer 16 μm dichroic mirror, 16 μm region, mech. stress compensation 80−74465
Re-W/C multilayer films for X-ray mirrors 79−44992
Sb_2O_3-MgF_2, semitransparent wide band dielectric mirror synthesis using dispersive and absorbing materials 79−89986
SiC, CVD, polished, total integrated vac. UV scatt. 77−62029
SiO_2 lightweight 370 mm mirror fabrication and testing 78−57447
SiO_2 wideband dielectric mirror production, spectral transmission 79−76897
SiO_x protected Al mirror, far UV refl., UV irrad. effect 79−7191
TiO_2 optical coatings, deposition, performance 77−88896
TiO_2, wideband dielectric mirror production, spectral transmission 79−76897
TiO_2-SiO_2, multilayer dielec. mirrors, laser-induced damage resist. 79−10335
VO_2 variable-reflectance mirror for CO_2-N_2-He 10.6 μm scan laser 80−38026
ZnS-Ag, broad band visible heat reflecting mirror 77−39017
ZnS-Na_3AlF_6 layer achromatic interference polarizers, design, fabrication 79−55222

m.i.s. devices *see metal-insulator-semiconductor devices*

m.i.s. integrated circuits *see field effect integrated circuits*

m.i.s. structures *see metal-insulator-semiconductor structures*

miscibility *see solubility*

missiles
aerodynamic flow, vortex-induced side force on slender bodies 79−14408
ballistic trajectory algorithm, analytic, including Earth oblateness 78−4476
IR imaging and missile-borne tracker optics, selection guidelines 79−23050
laminar compressible MHD boundary layer flow, effect on heat transfer 79−14489
mirror for tactical missile, aspheric replica master evaluation using ACCOS V SPLINE program 78−66964
navigation, proportional, teaching exercises 80−82611
rain impact damage to supersonic missile radomes simulation 77−40500
replicated reflector for TOW anti-tank weapon's IR beacon 78−66889
ring laser gyro, military appl. 78−42370
simulated underwater partial launch system, photogrammetric data reduction system 77−79075
tornado generated, impact loads, nucl. plant appl. 78−51103
White Sands Missile Range, Optical Evaluation Facility 79−36981

mixed conductivity
α-$AgSbS_2$ crystals, influence of external elec. field on elec. cond. 80−60056
aluminophosphate melts with V, Fe and Co oxides 77−39903
ceramics, electron and ion conductivity, instrument for meas. up to 2000°C 79−96247
coal dispersions, solvent refined, elec. props., surface charact. 80−80333
electrochemical methods for determ. of kinetic props. of solids, book contrib. 79−65251
electrode, kinetic parameters determ., method and appl. to Li_3Sb 78−14772
electrode-electrolyte interfacial phenomena, solid electrolyte 77−77782
energy storage and conversion systems, characterisation 77−76596
fast ionic transport in solid electrolytes and mixed conductors, material stability and chem. diffusion 80−65292
hydroxyapatites, elec. cond., charge carrier identification 78−67855

mixed conductivity continued
intercalation compound electrodes, thermodynamic and transport props. 80−66963
metallic glasses, electrical resistance min. at low temp., mixed conduction model 80−44560
naphthoxazole derivatives, elec. cond., thermoelec. power, energy gap, absorpt. spectra 77−32053
polyester polymer-C black composition, elec. cond. under press. 77−28224
polymer, charge carrier species determ. using interfacial phenomena 80−24978
proton semiconductors, with H-bonds, quantum theory of proton cond. 80−65641
solid electrolyte, electronic conductivity 77−76882
superionic conducting oxides, review 80−49414
superionic-electronic solid solution electrodes, partial cond. meas. technique 80−44360
valve metal oxide-semicond. oxide, electron injection, interface reactions 77−76936
AgCNS, mixed conductor, elec. cond. props. 80−65639
$AgCrS_2$, mixed conductor props. 80−44675
$AgCrS_2(Se_2)$, superionic and electronic cond. meas. 77−89577
AgCuSe, mixed conduction 79−78140
$AgI-Ag_2O-MoO_3$ glass glass superionic cond., struct. and transport props. 80−88602
AgN_3, high-resist. explosive cpd., elec. and galvanomag. props., temp. depend. 80−103728
$AgPO_3-PbI_2$ system, elec. conductivity as function of composition and temp. *(French)* 77−69112
Ag_2S and Ag_2Se melts, electrotransfer, ionic component of elec. cond., Ag ion diffusion 79−51640
β-Ag_2S, electrogalvanic and elec. props., and range of existence *(French)* 78−43175
$Ag_2S(Se)$, changes in elec. cond. and thermoelec. power at melting point 79−15147
$Ag_2S(Se)$, ionic-electronic mixed conductor, solid state controlled growth using cryst. rotation 78−31338
Ag_3SbS_3, pyrargyrite, electronic to ionic conductivity ratio *(Russian)* 77−80818
$Ag_2Tl_6I_{10}$, one-dimensional ionic conduction, ionic and electronic conductivities 79−7707
$Ag_xV_2O_5$, thermodynamic, elec. and electrochem. props. 78−84265
Al_2O_3 polycrystalline, effects of space charge, grain-boundary segregation and mobility differences on conductivity 80−79979
$Al_2O_3-SiO_2-TiO_2-RO$ (where R=Ca, Sr, Ba) system glass-crystal material, elec. cond. 79−60876
As_2S_3 glasses, DC elec. cond. and thermo-elec. power 80−96865
As_2Se_3:Ag, amorphous, doping effect of gap states and elec. cond., dielec. relax. and DC cond. meas. 79−47098
AuI, elec. cond. 79−42302
BaF_2 solid electrolyte, n-type electronic cond., 700-900°C 80−29448
$Ba_3Sc_4O_9$, $Ba_3Sc_2WO_9$ and Ba_2ScTaO_6, elec. cond. nature, depend. on comp. and medium thermodynamic parameters 80−70773
Bi_2O_3, elec. props. of α, β, γ and δ phases 79−23771
Bi_2O_3-Mo(W)O_3 melts, electrophys. props. 77−89817
CaF_2 crystals, elec. cond., O^{2-} effect 80−2431
$CaMoO_4$, electrical cond. and ionic transport number meas., defect struct. model 80−2388
$CaO-B_2O_3-Al_2O_3-V_2O_5$ glass, cond. mechanism, current carriers, V_2O_5 conc. effects 77−62668
CeO_2, conductivity at high O press. 77−20367
Cu-CuI-graphite secondary cell, transient ionic current obs. 80−108790
Cu-CuI-graphite secondary cell, steady state hole current obs. 80−108791
CuI, elec. props. 78−56193
$Cu_xMo_6S_{8-y}$, mixed conductor, partial Cu ion cond. and chem. diffusion 80−84323
$Cu_xMo_6S_{8-y}$, mixed conductor, equilib. partial thermodynamic props. 80−85270
$Cu_2S(Se)$, ionic-electronic mixed conductor, solid state controlled growth using cryst. rotation 78−31338
$Cu_{2-x}Te$, x<0.22, phase diagram, electronic and ionic cond. meas. 80−6917
Cu_3VS_4, conducting ions as mobile donors 80−11055
p-Cu_3VS_4, mixed conduction due to cationic interstitials 80−70772
Cu_3VS_4, mixed conductor, fast ion transport at room temp. 78−72214
Cu_3VS_4, out of equil. mixed cond., electronic cond. decrease in ionic soln. 80−107874
Cu_3VS_4, out of equil. mixed cond., off-centre positions and order-disorder transition, ultrafast nucl. relax. obs. 80−108103
Cu_3VS_4, out of equil. mixed cond., chem. origin of mobile ions, spin-lattice relax. and NQR obs. 80−108104
D-T, liq., dielectric constant and elec. cond. 80−84680
$FeSO_4.7H_2O$, single cryst., elec. and dielec. props., temp. depend. 79−19826
GaAs:Cr, photoconductivity and photo Hall spectra 78−19091
InS(Se)(Te), fused, charge transfer nature 77−89757
IrO_x anodic films, electrochromism and ionic cond., model 80−59706
$K_2O_{5-x}Ga_2O_3.xFe_2O_3$, K ion cond. 78−83998
$K_2O.6Fe_2O_3$: divalent metal oxide, electronic and ionic cond. 79−87135
La_2O_3, elec. cond. and dielec. const., 400-1180K, phase transition 79−56224
$LiAlSiO_4$, β-eucryptite, one-dimens. Li ionic cond. 77−84982
$LiFe_5O_8$, elec. props. 77−80641
$LiFe_5O_8$, spinel, mixed cond. using four-point DC techniques 79−60877
$Li_xFePS_3(Se_3)$, Li_xMnPSe_3 and $Li_xNiPS_3(Se_3)$, NMR and neutron diffr. obs., mag. props. 80−60433
Li_xNiPS_3, antiferromag., mag. props. and ionic mobility, NMR meas. 79−24223
$Li_2O-Al_2O_3$, rapidly quenched glasses, Li ion cond., elec. cond. 80−100346
$Li_2O-Bi_2O_3$, rapidly quenched glasses, Li ion cond., elec. cond. 80−100346
$Li_2O-Ga_2O_3$, rapidly quenched glasses, Li ion cond., elec. cond. 80−100346
Li_3Sb, mixed conducting electrodes, kinetic parameters determ. 78−14772
$Li_3Sb(Bi)$, evaluation as electrode material, electrochem. expts., 360-600°C 78−11526
$Li_{2.33}Si$, cryst. struct. and electrochem. anal. *(German)* 80−88132

mixed conductivity continued
Lu_2O_3, elec. cond. and dielec. const., 400-1180K, phase transition 79−56224
$Mg_2Si_2O_6$, enstite, elec. cond. var. with O_2 partial press., obs. and theory 79−1609
$MnO-SiO_2-TiO_2$ melt, electrical cond. meas. and electrolytic anal. *(Japanese)* 78−38861
$Na_2O-TiO_2-SiO_2$ glass, elec. props. and energy gap 78−26921
$Nd_xZr_{1-x}O_{2-x/2}$, elec. cond. of ceramic solid solutions 80−107554
Pb-S melt, absolute thermo-emf obs. 77−85251
β-PbF_2, electrolytic props., AC cond. meas. 78−71878
PbI_2, DC elec. cond. as function of I pot. 79−24023
$PbMoO_4$, ionic and electronic cond. 79−91107
$PbWO_4$, ionic and electronic cond. 79−91107
Sb_2S_3, defect drift in elec. fields and bistable switching 80−92947
Sb_2S_3-SnS, Sb_8S_3-As_2S_3, fused mixtures, resistivity 77−80815
Sc_2O_3, at 1300°C 77−80813
Sc_2O_3, elec. cond. rel. to defect struct. 77−80814
Se, nanosecond switching investigation 80−20263
Si-Al-O-N system, ionic cond. from 850 to 1400°C 80−2203
SiO_2 thin dielectric films in MOS structures, elec. props. with DC voltage *(Slovak)* 80−88634
Sn-S melt, absolute thermo-emf obs. 77−85251
ThO_2, cationic transport number determ. *(French)* 78−84267
ThO_2 ceramics, CaO and Y_2O_3 stabilised density, elec. cond., permittivity 78−47838
ThO_2, O_2 self-diffusion and intrinsic p-type electronic conduction 79−90821
ThO_2:Ce^{3+}(Ce^{4+}), mixed ionic and electronic transport 80−107875
ThO_2:Y_2O_3, electrochem. cell, complex impedance, temp. and freq. depends. 77−1458
ThO_2-CaO electrolyte, mixed and ionic cond. regions 77−8156
TiO_2, stoichiometric single crysts., anisotropy of ion transport 80−2206
V_2O_5 containing melts, activation energy of electron mobility and electronegativity 77−35971
$YO_{1.5}-PrO_x$, phase relns. and electrophys. props. of solid solutions 78−23686
Y_2O_3, elec. cond. components 77−85272
Y_2O_3:HfO_2, elec. cond. and O ion mobility 80−34490
ZrO_2-CeO_2, semiconducting ceramics, electronic conductivity and oxido-reduction *(French)* 78−26919

mixed state
see also flux creep; flux flow; flux-line lattice; flux pinning
A15 compounds, martensitic and supercond. transition models, anisotropy of vortices and US anomaly, review *(Japanese)* 78−23216
amorphous superconductor, high-κ, upper and lower crit. fields 79−4629
current density distrib. in cylindrical sample 79−38270
cylindrical type II superconductor rotating in mag. field, dissipation determ. 77−28309
dirty superconductor, thermal cond. anisotropy 80−7036
dirty superconductor, US attenuation 77−8231
dirty superconductor in mixed state, transverse thermal conductivity 77−32117
dissipation in mixed state of pure supercond freq. depend. *(Russian)* 78−52164
film, nonequilibrium, inhomogeneous state onset 78−14875
film, resistive transition 80−7049
film, resistivity, vortex-antivortex depairing 79−69639
film, vortex-antivortex pair dissoc. in 2-dimens. superconds. 79−56457
finite superconductor, mixed state 79−99662
flux cutting in type-II superconductors, direct evidence 80−70915
fluxoid quantum number at H_{c3} 79−78275
Ginzburg-Landau parameter crit. value 78−10597
hard superconductor, critical state stability and oscillations 80−107959
hard superconductors, mag. instabilities 77−89908
ideal type II superconducting wire, macroscopic current in longitudinal field 78−84366
ideal type II superconductor, thermodynamics of inhomogeneous mixed phase 78−84365
Josephson contact, mixed state, parametric reson. 77−8245
layers, mixed state struct. rel. to Josephson effects 79−4628
local state form. along dislocation, crit. field and current for destruction *(Russian)* 78−14905
magnetic field response, intensity, and direction-varying, nonrot. vortices 80−2535
magnetic impurities in supercond. *(Hungarian)* 77−28277
pion condensate props. in mag. field, superconductivity, mixed state *(Russian)* 80−49974
resistive layer microstructure on superconducting Al surface *(Russian)* 80−34567
ring with low capacitance Josephson point contact junction, flux transition mechanisms 80−44770
stress tensor for system without volume pinning 77−36032
superconducting composite, endurance in mixed state, fatigue failure *(Russian)* 80−44778
superconducting film, memory device storage of Abrikosov vortices 79−28487
superconductor, two-dimens., topological excitations 79−56458
superconductors, tilted vortices, mixed state features in surface layers *(Russian)* 80−29512
thermally activated flux creep, effect on AC response of hard superconductor 79−33416
thin films, vortices, phase transitons, review 80−88698
transport current distrib. of mixed phase of ideal material 79−61008
two-dimensional superconductor, resistivity evidence in Monte Carlo studies 80−80434
type I, two-dimensional mixed state, influence of mag. field, Ginzburg-Landau theory 77−1523
type I superconductor, paramagnetic effects of two-dimensional mixed state *(Russian)* 79−51729
type I superconductor, two dimens. mixed state *(Russian)* 78−19193
type II superconductor, giant-vortex state, temp. depend. 80−7051
uniaxial anisotropic superconductor, stress tensor for mixed phase 79−47210
vortex deformation and reduction of Lorentz force 78−84368
vortex width broadening in long Josephson tunnel junction 79−82718
vortices, transport entropy theory 78−43534
Al, nonlinear conductivity of thin films in mixed state *(Russian)* 80−80464

mixed state continued
Al, superconducting thin film, evidence for Kosterlitz-Thouless transition 80−39721
Al, surface layer structure in magnetic field *(Russian)* 78−56268
Bi, superconducting amorphous film, Kosterlitz-Thouless transition 80−88699
Cr, antiferromagnetic, mixed state, mag. torque and magnetostriction meas. 77−89909
$ErRh_3B_4$, mag. supercond., NMR study of ^{11}B 80−107957
In, film, embedded with He particles, superconductor ion implantation study of inhomogeneities 78−52181
In film, He ion implantation effects on parallel crit. field, vortex state *(Russian)* 77−69459
In, mixed state, two-dimensional effect study, destruction current *(Russian)* 80−93054
In-Bi, mixed state, pinning centre distrib. statistics, I-V charcts. *(Russian)* 80−100571
In-Bi, single spheres, supercond. props. 79−73617
In-Bi (2.5 at.%), supercond. foils, transport current effect on magnetisation 79−56379
$(Mo_{0.5}Ru_{0.5})_{80}P_{20}$, amorphous normal and mixed supercond. state, ^{31}P NMR 79−87193
Nb, Abrikosov vortices orientation depend. of elastic props. *(Russian)* 77−40007
Nb, electron drag on mobile dislocations, flow stress meas. 79−91197
Nb, flow stress, depend. on magnetic fields 77−73311
Nb, hysteresis of US attenuation 80−84549
Nb, low temp. sp. ht. meas. 77−24638
Nb, lower critical field anisotropy 78−76201
Nb, muon spin rotation in mixed state 79−56446
Nb, nonequilib. mixed state, with pinning centres, mag. flux interactions *(Russian)* 78−39275
Nb, plastic deformation effects on superconducting specific heat transition 80−20352
Nb, sp. ht., 0.03-0.3K, electronic and nucl. contribs. 78−10621
Nb superconducting cylinder, hollow, flux-flow voltages during guided flux collapse 77−16012
Nb, US attenuation, hysteresis near and below H_{c1} 80−75676
Nb-epoxy, interface, Kapitza resist. in supercond. and normal states 77−66085
Nb-Hf(26 at.%), magnetoacoustic attenuation 77−4473
Nb-V_3Ga mixed state, Meissner effect investigation by muon method *(Russian)* 80−107954
Nb_3Ge, amorphous nongranular thin superconducting film, thermodynamic and resistive transitions 80−34571
Nb_3Ge, bridge contact, Josephson effect 80−70906
$NbSe_2$, 2H phase, layered type II supercond., NMR meas. 77−36024
Nb_3Sn, low field microwave props., H_{c1} 77−28317
NbZr, thermally activated flux creep, effect on AC response 79−33416
Pb superconducting film, interaction between crystal lattice and vortices 77−28307
Pb-In (21 at.%), dirty supercond., anisotropic thermal cond. 79−56385
Pb-In (5%), supercond. mobile dislocation density, instantaneous flux change meas. 80−15670
Pb-Sn(Bi), dirty strong-coupling supercond., Ginzburg-Landau parameters, type II behaviour deviations 77−8249
Sn, nonlinear conductivity of thin films in mixed state *(Russian)* 80−80464
Sn, superconductivity destruction by current in hollow cylindrical sample *(Russian)* 79−78278
Sn, thin layers, EM field penetration, depend. on temp. in mixed and intermediate states 79−65598
Sn-In, nonlinear conductivity of thin films in mixed state *(Russian)* 80−80464
TaS_2 (2H) single crystal, specific heat meas. in mag. field, 0.3 to 3K, AC calorimetry technique 78−43516
V, lower critical field anisotropy 78−76201
V, thermal conductivity in ultrapure normal, mixed and supercond. states *(Russian)* 79−4617
V, US attenuation purity depend., crit. temp. and energy gap 77−47935
V-Ti (42 at.%), US attenuation meas. at 4.14K 80−15657
V-Ti (42 at.%), ultrasonic vel. in mixed state 80−75689
V_3Si, A15 struct. Gibbs free energy and lower crit. field temp. depend. 77−55643
V_3Si bridge contacts, nonstationary props. 80−103793
V_3Si, hysteresis in elastic characteristics *(Russian)* 80−103799
V_3Si, normal, mixed and supercond. state, specific heat meas., thermodynamic and superconducting props. 80−49987
V_3Si, sp. ht. meas., internal heating effect obs. 77−12067
V_3Si, supercond. mixed state, low temp. tetragonal-domain-reorientation phenomena, US expts. and thermal props. 80−60141
V_3Si, thermodynamic study, intrinsic type II superconductivity 79−47193
V_3Si, ultrasonic anomaly 77−55644

mixed valence compounds
actinide, compounds, f-electron systems with fluctuating valence, phase transitions 80−6789
actinide alloys, valence fluctuation model, physical prop. response 80−6791
actinide materials, valence transitions and intermediate valence states 79−42496
Anderson model coupled to boson field, HF approx. and RPA 77−40033
asymmetric Anderson Hamiltonian, ground state 80−65503
asymmetric Anderson model, ground state, perturbation approach 80−65504
atomic limit approach to intermediate valence 80−39531
charge ordered crystals, low lying collective electronic excitations, NQR study problems 79−78561
conduction processes in magnetic and intermediate valency compounds 80−96787
Creutz-Taube complex, mixed valence, reson. Raman calcs. using vibronic coupling model 80−97249
diatomic molecule model 80−107751
dielectric-metal phase transition *(Russian)* 80−6788
disordered extended Anderson model, CPA-alloy analogue treatment 80−65506
dynamic susceptibilities 80−70653
dynamic susceptibility, RPA study of Anderson lattice 80−97075
electrical conductivity, periodic Anderson model, memory function approach 80−84458

mixed valence compounds continued
electron-hole symmetry, phase diagrams, and lattice props., periodic Anderson model 80−15481
electron-phonon coupling, theory 80−70343
electronic levels, impurity model 79−99513
electronic structure, of mixed valence state 79−11092
electronic structure, spin-orbit interaction effects, mag. susceptibility 80−54657
elementary excitation damping, electron specific heat 79−95180
entropy and phase diagram of valence transition 80−59877
exchange coupled ions, electron transfer, optical intervalence transition 80−44556
excitation mechanism in tight-binding approx., metal-insulator transition 80−10925
Falicov-Kimball model, mag. short- and long-range order 80−15480
Falicov-Kimball model at atomic limit 80−65505
Hubbard regime, at. and nearly free state hybridisation 80−44546
impurity model, Fermi liq. theory, Ward identities 80−34401
impurity states, statistical mech. treatment, phase transitions and mixed valence 78−64004
inorganic compounds with inequivalent atoms, XPS 80−2918
IR absorption, anomalous, in fluctuating valence compounds 80−66210
K_2PtI_5, synthesis and cryst. struct. *(German)* 78−79588
linear, longitudinal lattice modes 78−95119
linear mixed valence compounds, lattice modes obs. 79−46763
local mixed valence model, exact limit 77−51705
local polaron model, appl. to intermediate valence systems 80−107717
localised description of valence fluctuations 80−80225
magnetic behaviour, model calc. 77−80901
magnetic susceptibility and mag. instabilities 80−39532
magnetic susceptibility and sp. ht., periodic Anderson model, CPA alloy analogue method 80−15474
magnetic susceptibility and sp.ht., mean field theory of periodic 78−47937
magnetic susceptibility calcs. Falicov-Kimball model 79−42745
magnetic-nonmagnetic transitions, heuristic model 79−73718
magnetism conference, Freudenstadt and Bad Nauheim, Germany (March and April 1978) 79−24121
metallic substances, retention and exchange of 4f electrons *(Dutch)* 79−1587
metallomacrocytes, mixed valent, cofacial assembly, cond. polymeric material 80−70143
metals, renormalisation of collective excitations, acoustic wave vel. near electronic transition 79−82539
metatungstate anions, XPS spectra, oxidation states 78−6824
mixed valence compounds, phase diagrams, lattice props., electron hole symmetry 79−91002
Mossbauer effect in metallic and semiconducting hosts, microscopic model 79−78595
niobates, mixed metal, Eu oxidation state, mag. props., Mossbauer study 80−66080
one-dimensional conductor, Curie const. discontinuity, paramag. domain tip alignment 77−16035
paramagnetic intermediate valence compounds, sum rules and inelastic neutron scatt. 79−61037
periodic Anderson Hamiltonian, alloy analogy treatment for mixed valence states 80−75527
periodic Anderson model self-consistent treatment, specific heat, susceptibility 79−99514
phase diagram and Kondo behaviour 80−29366
phase transition with valency change, sound vel. renormalisation *(Russian)* 78−79963
phonon effect on press.-temp. phase diagram 80−24849
phonon induced instabilities, periodic Anderson model 78−79964
phonons, effect of valence changes due to f⇄d electronic transitions 79−95104
phthalocyanines, partially oxidised, highly conductive mol. solids 77−47800
polarized neutron diffractoin in high magnetic fields 79−73684
polaronic effects in mixed- and intermediate-velence cpds. 79−60732
power spectrum of valence fluctuations 78−47742
pressure-temperature phase diagram 79−28283
properties and appearance conditions, review 80−103649
rare earth alloys, mixed-valence effect, limiting model of dil. alloy 77−47768
rare earth alloys, surface effects on valence 78−91746
rare earth alloys and cpds., intermediate valence, models for anomalous systems 80−96827
rare earth compound, intermediate valence induced by alloying, CPA calcs. 78−67986
rare earth compound, valence fluctuation type, replicate core level XPS probe 80−25521
rare earth compounds, charge dominated fluctuation props. comparison, mag. moments and ordering 80−54659
rare earth compounds, electron-phonon interaction influence on electronic phase transitions *(Russian)* 78−47743
rare earth compounds, intermediate valency, review 79−91001
rare earth compounds, mag. moment and valence fluctiations 78−23244
rare earth compounds, mag. susceptibility in intermediate valence state 78−14928
rare earth compounds, mixed valence state, conduction band struct. 80−103624
rare earth compounds, mixed valent, renormalisation of transversal phonons 79−90749
rare earth compounds, spatial correlations of rare-earth ions 79−19560
rare earth compounds, spin dynamics, mag. neutron scatt., Mossbauer effect, XPS studies 80−39786
rare earth compounds, valence changes, book contrib. 80−39533
rare earth compounds, valence fluctuations, electron-phonon coupling effect 80−20134
rare earth compounds, valence instabilities rel. to electronic structure of $GaMn_3(C_{1-x}N_x)$ *(French)* 80−34596
rare earth compounds, valence mixed state, Kondo lattice, Anderson localisation models *(Japanese)* 78−51945
rare earth compounds, XPS, intermediate valence states 79−33887
rare earth cpds., RM_4Sb_{12} (R=La, Ce, Pr, Nd, Sm, Eu; M=Fe, Ru, Os), prep. and cryst. struct. 80−100211
rare earth cpds., spinless periodic Anderson model with phonons 78−84153
rare earth Cu_2Si_2, interconfiguration fluctuation system, NMR meas. 80−15817

mixed valence compounds continued
rare earth materials, valence transitions and intermediate valence states 79−42496
rare earth mixed valent compounds, lattice dynamics 79−73268
rare earth systems, neutron scatt., review 80−49674
rare earth systems with valence transitions, phonons 80−96611
rare earth-nonmagnetic metal intermetallic cpds., struct. and props., review 79−95377
renormalisation group approach 77−89734
review of theoretical situation 79−4536
semiconductor, Falicov-Kimbell model, intermediate valence states, metal-insulator transition 78−51897
semiconductor-metal phase transition, cryst. existence in intermediate mixed state *(Russian)* 79−90962
short-range-order model 79−78049
spatial correlations in simple model 79−60770
spinless model, coherent-hybridisation states and virtual-bound states 80−107749
spinless model, isolated f-level problem 80−107750
stabilisation by polaronic effects 79−4520
structural phase transitions, effect of electron-phonon coupling 79−33265
substitutional alloys of intermediate valence systems, static mag. susceptibility con. and temp. depend. 80−84586
tantalates, mixed metal, Eu oxidation state, mag. props., Mossbauer study 80−66080
theory, electronic sp. ht. calc. 80−79956
thermal expansion anomaly 79−77783
three-site, six-electron, even-parity model 80−20125
three-site, six-electron model, variational calc. 80−20126
transition metal chalcogenide, possible anionic clusters and mixed valence effects 78−43333
transition metal complexes, linear chain type, synthesis and cryst. struct. 78−6047
transition metal complexes, quasi-one-dimens. elec. props. at ultrahigh press. 78−2470
transition metal compounds, minimum cond. and electron localisation near metal-insulator transitirn 78−30960
transition metal cpds., chage-orbital ordering 78−39069
(TTF^+) radical cation, optical props. in mixed-valence and monovalent halide salts and solns. 79−61399
TTF-TCNQ, mixed valency in organic crystals *(Japanese)* 79−78051
TTT salts, IR spectra, mixed-valence salts 80−40121
Wolffram's red salt, mixed valence, reson. Raman calcs. using vibronic coupling model 80−97249
$Ag_xNa_{2-x}Te_2^{IV}Te_3^{VI}O_{14}$, (x=0,4), mixed tellurate, cryst. chem. and elec. cond. *(French)* 80−107150
$Ba_x(Ba_{1-x}Al_x)Fe_2S_6[S_{1-y}(S_2)y]$, cryst. struct., Mossbauer and mag. behaviour 77−55273
$Ba_4Ru_3MO_{12}$, (M=Ta, Nb), Ru oxidation state, Mossbauer study 80−44965
Be intermetallics, MBe_{13}, (M=Y, La, Ce, Lu, Th), lattice spacings and susceptibilities 80−65778
$CaFe_2^{2+}Fe^{3+}Si_2O_8(OH)$, Mossbauer spectra, temp. depend. electron delocalisation 80−20567
$CaFe^{3+}Fe_2^{2+}(Si_2O_7)O(OH)$, ilvaite, electronic struct., press. and temp. depend. of ^{57}Fe Mossbauer spectrum 80−108129
$CdCr_2S_4(Se_4)$, pure and Ag doped, electronic struct., mixed valence 80−70612
(Ce, La)In_3, heat capacity and elec. resist. 80−71049
Ce, chemically collapsed, valence transition 79−28325
Ce cubic intermetallics, interconfig. fluctuations 80−20130
Ce niobate, pyrochlore structure, synthesis and props., 79−11533
Ce pnictides, unusual anisotropy mechanism due to virtual valence fluctuation 80−96828
Ce, renormalisation of collective excitations, acoustic wave vel. near electronic transition 79−82539
α-Ce, susceptibility, sp. ht. and magnetisation 79−28512
Ce-based alloys, valence transition, scaling studies 80−20135
$CeAl_2$, Anderson lattice system, volume collapsed strongly mixed valent state 79−38033
$CeAl_2$, mixed valence, anisotropic magnetostriction near antiferromag. transition 78−88157
$CeAl_2$, press.-induced electronic transition 80−20147
$CeAl_2$, resistivity and volumetric meas., phase diagrams, comparison with CeS 80−107789
CeAs, evidence for valence fluctuations, ^{75}As Knight shift data 78−91966
$CeBe_{13}$, intermediate valence state, XPS, resist. and susceptibility study 80−71565
$CeCu_2Si_2$, valence fluctuations, ^{29}Si NMR and mag. susceptibility 79−61246
Ce(In, Sn)$_3$, heat capacity and elec. resist. 80−71049
Ce(In, Sn)$_3$, mag. susceptibility, temp. depend., intermediate valence 80−65779
$CeIn_{3-x}Sn_x$, conduction electrons role in valency fluctuations 78−47741
$CeIn_{3-x}Sn_x$ mixed valence system, low-temp. susceptibility, paramagnon study 80−97077
$CeIn_{3-x}Sn_x$, scaling behaviour near valence instability, mag. susceptibility and mag. transitions 80−25111
$CeIn_{3-x}Sn_x$, electrical resist. and thermal expansion meas., 1.5-300K 80−34400
$(Ce_xLa_{1-x})Be_{13}$, mag. intermediate valence behaviour 79−24131
$Ce_{1-x}La_xSn_3$ (x=0 to 1), mag. susceptibility and magnetisation, lattice parameters, X-ray and neutron diffr. meas. 80−49675
$Ce_{0.9-x}La_xTh_{0.1}$, mixed valence state, static and dynamic mag. response 80−103816
CeN, electronic struct., XPS exam. 78−6269
CeN, interconfiguration fluctuation, temp. and press. depend. 79−38031
$CePd_3$ fluctuating-valence compound, anomalous far IR absorption 80−66210
$CePd_3$, magnetic neutron scatt. 77−20552
$CePd_3$, mixed valence cpd., theory of inelastic mag. neutron scatt. 79−15284
$CePd_3$, mixed-valence, 3d and 4d core levels, XPS study 80−89111
$CePd_3$, spontanerys relax. of 4f magnetisation, neutron scatt. obs. 77−77025
$CePd_3$, susceptibility, sp. ht. and magnetisation 79−28512
$CePd_3$-MPd_3 mixed valent systems, nonlinear conc. depend. of resist. 80−65528
$CePd_{3-x}Rh_x$, resistance behaviour and intermediate valence effects 79−78068

mixed valence compounds continued
CeS, resistivity and volumetric meas., phase diagrams, comparison with $CeAl_2$ 80−107789
$Ce_{1-x}Sc_xAl_2$, fluctuating valence system, quadrupole interaction temp. depend. 80−54972
$Ce_{1-x}Sc_xPd_3$, intermediate valence of Ce, susceptibility, lattice const., ESR meas. 80−103648
$CeSn_3$, electronic struct. and mag. props. 80−70649
$CeSn_3$, induced magnetic form factor, polarised neutron studies 80−25078
$CeSn_3$, intermediate valence cpd., search for phonon anomalies, inelastic neutron scatt. 80−100317
$CeSn_3$, polarised neutron study of induced magnetisation 80−34594
$Ce_{0.74}Th_{0.26}$, induced magnetic form factor, polarised neutron studies 80−25078
$Ce_{0.74}Th_{0.26}$, spin dynamics 78−10708
CoM_2O_{4+x} (M=Rh,Mn), anomalous $^{57}Fe^m$ charge states, Mossbauer study 80−40017
Co_3O_4, Mossbauer spectra and cryst. struct. determ. 79−56637
$Cs_2Au^IAu^{III}Cl_6$, influence of high hydrostatic pressure on cryst. struct. in pressure range up to 52×10^8 Pa 79−51249
$Cs_2Au_2Cl_6$, Mossbauer high-press. study 78−52387
$CsInCl_3$, mixed-valence cpd., structural phase transition *(German)* 80−70406
Cs_2SbCl_6, mixed valence compound, ^{121}Sb Mossbauer spectroscopy 79−51890
$Cs_2Sb_{0.5}M_{0.5}C_6$, M=Se, Te, or SnI, ^{121}Sb Mossbauer effect 78−84506
Cs_2ZrBr_6, $PtBr_4^{2-}$-$PtBr_6^{2-}$ doped, mixed valence, absorpt. spectra, vibronic struct. 80−97308
Cu complex, mixed-valence, X-ray K-absorption spectra 79−33863
$CuCr_2S_4(Se_4)$, electronic struct., mixed valence 80−70612
$DyCoO_3$, anomalous $^{57}Fe^m$ charge states, Mossbauer study 80−40017
$Er_cCe_{1-c}Pd_3$, cryst. field spectra, neutron scatt. study 80−50047
Eu intermetallic compounds, valence fluctuations, role of charge screening 78−51944
Eu intermetallic compounds, valence fluctuations, thermal occupation effects 78−72118
Eu-alloys, role of phonons and Coulomb interactions 79−38032
Eu-transition metal intermetallics, valence fluctuations 78−91649
$EuCoO_3$, anomalous $^{57}Fe^m$ charge states, Mossbauer study 80−40017
$EuCu_2Si_2$, fluctuating valence system, quadrupole interaction temp. depend. 80−54972
$EuCu_2Si_2$, interconfiguration fluctuation, NMR expts. 80−66069
$EuCu_2Si_2$, mixed valence system, X-ray absorption spectroscopic study 80−80906
$EuCu_2Si_2$, XPS studies, valence band, 4-f region 78−6831
$EuFe_4Al_8$, mag. ordered, mixed valency of Eu, X-ray, susceptibility and Mossbauer spectra studies 79−19728
$Eu(Ni_{1-x}Cu_x)_5$, mixed valency, isomer shift temp. depend. 78−84511
$EuNi_xCu_{5-x}$, mixed valency of Eu, Mossbauer expts. 78−52407
$EuNi_xZn_{5-x}$, mixed valency of Eu, Mossbauer expts. 78−52407
EuO, physical and physicochem. props., review 80−96875
$Eu_3O_4(S_4)$, inelastic light scatt. 77−55788
$Eu_3O_4(S_4)$, inelastic light scatt., photoluminesc. 77−90145
$EuRh_{2x}Pb_x$, XPS of intermediate valence state 77−28687
Eu_3S_4, inelastic light scatt. and photoluminesc. 77−48229
$FeF_3.3H_2O$, α and β phase, ^{57}Fe Mossbauer study of local struct. 80−39973
$Fe_2F_5.7H_2O$ and oxidation products, ^{57}Fe Mossbauer study of local struct. 80−39973
Fe(III)M(II)$F_5.7H_2O$,M=Fe,Co,Ni,Zn, antiferromagnetism 77−59395
$Fe(Nb_{1-x}W_x)O_4$, mag. and elec. props. and Mossbauer effect 79−78590
Fe_3O_4, magnetite, valence instabilities, Mossbauer effect 80−20543
$K_2Pt(CN)_4Br_{0.3}.3H_2O$, one-dimensional cond., phys. props. 78−30916
$K_2Pt(CN)_4Br_{0.3}.3H_2O$, one dimens. cond. transition, spin susceptibility and Dc. cond. temp. depend. 78−84198
$K_2Pt(CN)_4Br_{0.3}.3H_2O$, spin-lattice model for elastic anomalies 80−15179
$K_2Te^{IV}Te_3^{VI}O_{12}$, mixed tellurate, cryst. chem. and elec. cond. *(French)* 80−107150
La atom on transition metal, surface, intermediate valence state 79−69367
La, ground state, two band Hubbard model, for almost mixed valence system 78−84171
$La_{1-x}Ce_xPd_3$, resistance behaviour and intermediate valence effects 79−78068
$La_{1-x}Ce_xSn_3$, electrical resist. and thermal expansion meas., 1.5-300K 80−34400
$LaCoO_3$, structured phase-transition involving changes in spin and valence 78−79765
$LaCoO_3$:Ca(Sr), anomalous $^{57}Fe^m$ charge states, Mossbauer study 80−40017
$(La_2O_3)_{1-x}$-$(CeO_2)_x$:Mn, valence state of Mn, effect of annealing in H_2 atm., ESR obs. *(French)* 80−71164
$La_8Ru_4O_{21}$, cryst. struct. 78−51403
$La_{0.9}Tm_{0.1}Se$, sp. ht. meas., 1.6 to 20K, mag. contrib. 80−65934
$(MgAl_2O_4)_x(AMn_2O_4)_{1-x}$, A=Mg,Mn,Zn,Cd, $0<x<1$, mixed oxide spinels, chemical shifts of Mn K-absorpt. edge 80−29828
MgEu, dil. alloy, cold worked, valence transform. of Eu due to defect association, mag. suscept. and Mossbauer meas. 77−51404
$(NH_4)_2PtI_6$, synthesis and cryst. struct. *(German)* 78−79588
$(NH_4)_2Sb_{0.5}M_{0.5}Cl_6$, M=Se, Te, or Sn, ^{121}Sb Mossbauer effect 78−84506
$(NH_4)_2Sn_{1-x}Sb_xCl_6$ (x=0.13, 0.21, 0.28, 0.33), mixed valence compound, ^{121}Sb Mossbauer spectroscopy 79−51890
Na_xWO_3 bronze, XPS of W 4f levels 78−95648
$Nb_3Se_5Cl_7$, preparation, struct. and props. 79−65040
Ni complex, bis-(1,2-benzoquinonedioximeto)$_2$Ni.05I, X-ray scatt. study 77−1101
$NiS_{2-x}Se_x$ phase diagram, intermediate valence effects 80−103834
Pd and Pt mixed valance complex, [Pd(ethylenediamine)$_2$Pt(ethylenediamine)$_2$Cl$_2$](ClO$_4$)$_4$, Raman spectra 80−84734
Pd complex, linear ionic mixed valence cpd., IR and resonance Raman spectra rel. to lattice modes 80−25393
Pt complex, linear ionic mixed valence cpd., IR and resonance Raman spectra rel. to lattice modes 80−25393
Pt-transition metal, dil., impurity resist. 80−92875
RM_4Al_8 (M=Cr, Mn, Fe, Cu), magnetism and hyperfine interactions 80−25256
α-Rb_xFeF_3, Mossbauer effect appl. to charact. 79−51883
Rb_2PtI_6, synthesis and cryst. struct. *(German)* 78−79588
$Rb_2Sb_{0.5}M_{0.5}C_6$, M=Se, Te, or SnI, ^{121}Sb Mossbauer effect 78−84506

mixed valence compounds continued
Ru complexes, intervalence charge transfer transitions, solvent effect 77−75127
$SbCu_3Si_3$, mixed valence system, X-ray absorption spectroscopic study 80−80906
$ScAl_3$:Eu, intermediate valence on Eu ions, Mossbauer isomer shift 80−84587
Sm chalcogenide, valence fluctuations 78−67985
Sm chalcogenides, metal-dielectric phase transitions involving valence changes *(Russian)* 79−51489
Sm compounds, mixed valence, metals or small gap insulators, two-band Hubbard Hamiltonian 80−34399
Sm metal, XPS evidence for weak surface divalent component 77−39808
Sm monochalcogenides, local effects and valence transitions 79−51533
Sm, surface mixed valence, XPS study 80−60753
SmB_6, crystal preparation, elec. resistance, phase transitions 80−97427
SmB_6, EPR and heat capacity obs., metal-semicond. behaviour 80−20456
SmB_6, intermediate valence, ^{11}B NMR study 80−93193
SmB_6, mixed valency cpd., f-d hybridisation, optic phonon anomalies 78−92080
SmB_6, mixed valent, large low-temp. Hall effect and resist. 80−39611
SmB_6, mixed valent semicond., transport props. and electonic struct., review 80−96877
SmB_6, resistivity press. variation, lattice consts. 80−100456
SmB_6, surface mixed valence, XPS study 80−60753
SmB_6, valence fluctuating state, sp. ht. 80−20127
SmB_6, valence fluctuation system, ground state and elementary excitations, Anderson lattice model Hamiltonian, dense Kondo problem 80−54656
SmB_6, valence mixing, XPS 77−21000
SmB_6:Gd^{3+} (Eu^{2+}), ESR g-shifts and linewidths 78−48035
$Sm_{1-x}B_xS$, valence transition induced by alloying 80−96829
Sm_4Bi_3, mixed valence system, X-ray absorption spectroscopic study 80−80906
Sm_4Bi_3, press. induced valence instability, elec. resist. transition 78−95317
Sm_4Bi_3, press.-induced valence instability 80−20261
$Sm_{0.8}Gd_{0.2}S$, valence transition, positron annihilation study 80−15454
$Sm_{1-x}Gd_xS$, press. induced electronic transitions 78−68058
$(Sm_{1-x}Gd_x)_3S_4$, mixed valence compound, elec. cond. transition 80−70777
$Sm_{1-x}La_xB_6$, valence transition, lattice parameter and mag. susceptibility meas. 80−59929
$Sm_{1-x}La_xS$, magnetoresist. in semicond. and metallic phases 80−96914
$Sm_{1-x}La_xS$, valence transitions, theoretical model 79−69474
$Sm_{1-x}M_xS$, M=transition metal, valence charges, band struct. 80−20131
SmN, magnetic props., neutron diffr. and mag. susceptibility meas. 80−50036
SmO, intermediate valence state *(French)* 80−20132
SmO, mag. props., lattice consts., and X-ray absorpt. spectra 80−44798
SmS (001) surface, mixed valency and phase transitions 80−39658
SmS, and $Sm_{0.8}Tb_{0.2}S$, resistivity and thermopower 80−20260
SmS, electronic config., Mossbauer spectra meas. 77−16228
SmS, electronic phase transition, mechanism, trivalent metal impurity effects 80−49604
SmS, f-d hybridisation, valence fluctuation and phonon spectrum, Raman scatt. expts. 78−60464
SmS, high-pressure mixed-valence phase, diagram and electronic entropy, neutron diffr. obs. 79−33267
SmS, induced mag. form factor 78−68163
SmS, induced magnetic form factor, polarised neutron studies 80−25078
SmS, intermediate valency, three-site model 79−78047
SmS intermediate valence, low lying states 80−96826
SmS, LO phonon freq. softening in semicond. and metallic phases 80−96619
SmS, metallic phase, compressibility anomalous behaviour 80−29114
SmS, mixed valence states at surface 77−20398
SmS, mixed-valency cpd., f-d hybridisation, optic phonon anomalies 78−92080
SmS, nonorthogonal orbitate in intermediate valence 78−43323
SmS, phase diagram in p-T plane, theory 79−28278
SmS, physical and physicochem. props., review 80−96875
SmS, press. effect on lattice parameter, mag. susceptibility, and reflectivity 79−56272
SmS, pressure-temperature phase diagram 79−28283
SmS, trivalent rare earth substituted, stability of Sm^{2+} 80−65508
SmS type cpd., fd mixing effect on impurity levels, local valence transition 80−24831
SmS type semiconductors, electronic struct., influence of point defects 80−70650
SmS, valence fluctuation phenomena 80−24800
SmS, valence fluctuation system, ground state and elementary excitations, Anderson lattice model Hamiltonian, dense Kondo problem 80−54656
SmS, valence transition, positron annihilation study 80−15454
SmS, valence transition, two band model 80−65507
SmS:Eu, excited-state exchange interactions, EPR meas. 78−68374
SmS:P, neutron irrad., semiconductor-metal transition 80−24975
Sm_2S_3, mixed valence compound, mag. and thermal props. 79−78400
Sm_3S_4, cryst. struct. and valence state of Sm *(German)* 78−75636
Sm_3S_4, inelastic light scatt., photoluminesc. 77−90145
Sm_3S_4, mag. susceptibility meas., valence state of Sm 80−15684
Sm_3S_4, mixed valence compound, mag. and thermal props. 79−78400
Sm_3S_4:Eu, excited-state exchange interactions, EPR meas. 78−68374
$SmS_{1-x}As_x$, magnetoresist. in semicond. and metallic phases 80−96914
$SmS_{1-x}As_x$ solid solns., intermediate valence phase, lattice const. and mag. susceptibility meas. 79−87245
$SmS_{1-x}P_x$, intermediate valence cpd., lattice parameter and mag. susceptibility 80−7091
$SmS_{1-x}P_x$, valence changes, XPS and UPS study 80−97402
$SmSb_xS_{1-x}$, mag. ordering and configuration mixing 78−68179
$SmSb_xS_{1-x}$, susceptibility and lattice parameter meas. 78−51943
SmSe:Eu, excited-state exchange interactions, EPR meas. 78−68374
Sm_3Se_4, mixed valence compound, mag. and thermal props. 79−78400
Sm_3Se_4, valence fluctuation, mag. susceptibility meas. 80−97056
$Sm_{0.25}Y_{0.75}S$, phonon anomalies and electron-lattice coupling 80−39490
$Sm_{0.75}Y_{0.25}S$, intermediate-valence-state system, phonon dispersion meas. 79−19342
$Sm_{0.75}Y_{0.25}S$, intermediate valence system, mag. excitations 79−60771
$Sm_{0.75}Y_{0.25}S$, intermediate valence compound, phonon investigation by neutron scatt. 80−6476

mixed valence compounds continued
$Sm_{0.75}Y_{0.25}S$, mixed valence, phonon dispersion theory 80−34153
$Sm_{0.75}Y_{0.25}S$, mixed-valence, electron-lattice correlations, EXAFS studies 80−76103
$Sm_{0.76}Y_{0.24}S$, induced mag. form factor 78−68163
$Sm_{0.76}Y_{0.24}S$, induced magnetic form factor, polarised neutron studies 80−25078
$Sm_{1-x}Y_xS$, anomalies in phonon dispersion 79−73268
$Sm_{1-x}Y_xS$, electron-phonon coupling, theory 80−70343
$Sm_{1-x}Y_xS$, electronic config., Mossbauer spectra meas. 77−16228
$Sm_{1-x}Y_xS$, magnetoresist. in semicond. and metallic phases 80−96914
$Sm_{1-x}Y_xS$, mixed valence, phonon softening and linewidths, calc. 80−75319
$Sm_{1-x}Y_xS$, valence fluctuations effect on lattice dynamics 78−47493
$Sm_{1-x}Y_xS$, valence transitions, theoretical model 79−69474
$Sm_{1-y}Yb_yB_6$, valence transition, lattice parameter and mag. susceptibility meas. 80−59929
$Sm_{1-x}Yb_xS$, simultaneous Sm^{2+}-Sm^{3+} and Yb^{2+}-Yb^{3+} electron transitions *(Russian)* 79−60711
Sn_2S_3, mixed valence semicond., long wavelength phonons, full space group theoretical anal. 79−65873
Sn_2S_3 mixed valence semiconductor, far IR refl. spectra 80−108191
Sn_2S_3, resistivity, Mossbauer spectra, press. effects 79−73862
TeSe, valence fluctuation system, ground state and elementary excitations, Anderson lattice model Hamiltonian, dense Kondo problem 80−54656
Tm compounds, mag. props. 79−78048
$Tm_{1-x}Eu_xSe$, semicond. with valence instabilities, cryst. chem. considerations 80−100213
$Tm_{1-x}Eu_xSe$, valence changes, semicond.-metal transition 80−20086
TmS(Se)(Te), far IR refl. and DC resist., 1-300K, interconfig. fluctuation effects 78−35136
TmSe and its mixed crysts., valence instabilities, phase diagram 80−70651
TmSe, Anderson lattice resist. for antiferromag. ordering 80−65556
TmSe, EELS and UV photoemission 78−31305
TmSe, first obs. of negative elastic const. 80−103409
TmSe, intermediate valence cpd., mag. neutron scatt. 78−68164
TmSe, intermediate valence state, resistivity of magnetically ordered ground state 79−1683
TmSe, intermediate valent, Raman scatt. 80−16038
TmSe, intermediate valence cpd., susceptibility, single-ion approach 80−70935
TmSe, mag. neutron scatt. 80−25096
TmSe, mag. ordering under press., neutron diffr. obs. 80−70947
TmSe, mixed valence, X-ray absorption study 80−76102
TmSe, mixed valence behavior 79−78050
TmSe, mixed valence state, ferromag. alignment 80−20133
TmSe, nonstoichiometry, high temp. chem. and valence instability *(German)* 79−23743
TmSe, paramag. intermediate valence cpd., single ion approach to susceptibility 79−61042
TmSe, spin dynamics, neutron scatt. study 79−24178
TmSe, spin dynamics and mag. ordering 78−68162
TmSe, susceptibility, Tm^{2+} and Tm^{3+} charact. 80−25110
TmSe, thermal, mag., and transport props. 79−61074
TmSe, valence mixing, mag. props. obs. 80−70648
Tm_xSe, magnetic, thermal, and transport props. 78−68239
Tm_xSe, magnetoresist. and Hall effect, stoichiometry effects 80−65597
Tm_xSe, residual resistivity at very low temp., composition depend. 79−82588
Tm_xSe, valence instabilities, antiferromag. order 80−20128
$TmSe_{0.83}Te_{0.17}$, spontaneous magnetisation, mag. susceptibility, magnetostriction, elec. cond. 79−24146
$TmSe_{1-x}Te_3$, semicond. with valence instabilities, cryst. chem. considerations 80−100213
$TmSe_{1-x}Te_x$, mixed-valent cpd., spontaneous magnetisation 80−20392
$TmSe_{1-x}Te_x$, phase relationships and press. induced transitions 80−19771
$TmSe_{1-x}Te_x$, valence changes, semicond.-metal transition 80−20086
$Tm_xY_{1-x}Se$, Kondo effect, Van Vleck behaviour 80−25085
UCu_5, core and valence band spectra, XPS obs. 80−50530
$UNi_{0.5}Cu_{4.5}$, core and valence band spectra, XPS obs. 80−50530
UO_{24x}, possible anionic clusters and mixed valence effects 78−43333
$U_xTh_{1-x}Sb$, valence change of U accompanied by singlet-ground-state ferromag. 80−70965
VO_x, minimum cond. and electron localisation near metal-insulator transition 78−30960
V_nO_{2n-1} ($3 \leq 3 \leq 9$), Magneli phases, mag. susceptibilities at low temp. 80−20389
$YCoO_3$, anomalous $^{57}Fe^m$ charge states, Mossbauer study 80−40017
YM_4Al_8 (M=Cr, Mn, Fe, CU), magnetism and hyperfine interactions 80−25256
$Y_{0.8}Tm_{0.2}Se$, sp. ht. meas., 1.6 to 20K, mag. contrib. 80−65934
Yb compounds, mag. props. 79−78048
Yb intermetallic compounds, mag. susceptibility, 1.4 to 1060K 77−20543
Yb-Al mixed valent film form., XPS study 80−80943
$YbAl_3$, susceptibility, sp. ht. and magnetisation 79−28512
$YbAl_3$, XPS studies, valence band, 4-f region 78−6831
$YbAu_2$, valence transition at surface of Yb 80−70652
YbCuAl, intermediate-valent, nucl. reson. and relax. 79−78550
YbCuAl, mixed valence behaviour, mag. propr. 78−68159
YbCuAl, mixed valence cpd., dynamic susceptibility, neutron inelastic scatt. 80−65807
YbCuAl, mixed-valence behaviour, mag. susceptibility and sp.ht. 77−80939
YbCuAl, mixed-valent cpd., thermal expansion and magneto-volume effects 80−66005
YbCuAl, susceptibility, sp. ht. and magnetisation 79−28512
$YbCu_2Si_2$, interconfiguration fluctuation, NMR expts. 80−66069
$YbCu_2Si_2$, mag. 4f Zeeman-level power spectrum using diffuse mag. neutron scatt. 79−60775
$Yb_{0.99}Gd_{0.01}CuAl$, intermediate Yb valence states, mag. props. 79−51743
$YbInAu_2$, magnetic susceptibility, 4.2 to 280 K 78−39288
$YbNi_2Ge_2$, magnetic susceptibility, 4.2 to 280 K 78−39288
$Yb_xSc_{1-x}Al_3$, valence fluctuation system, suscept. meas. 78−68149
$YbSi_{1.8}$, valence fluctuation cpd., X-ray anal., mag. susceptibility and linear expansion coeffs. 79−77569
Yb_3Si_5, valence fluctuation cpd., X-ray anal., mag. susceptibility and linear expansion coeffs. 79−77569

mixed valence compounds continued
$Yb_{1-x}Y_xCuAl$, disordered extended Anderson model, CPA-alloy analogue treatment 80−65506
$Yb_{1-x}Y_xCuAl$, intermediate Yb valence states, mag. props. 79−51743
^{170}Yb in some metal and metal-like compounds, Mossbauer study, isomer shift and intermediate valence state 79−33569
$Zn_{1-x}Ge_xFe_{2-x}^{3+}Fe_{2x}^{2+}O_4$, double exchange magnetism, Mossbauer study 80−66087

mixers (circuits)
see also frequency convertors; radio receivers
cryogenically cooled mixer for 80 to 120 GHz, improvements 79−40073
equipment and services, 1979 video yearbook 79−14197
far IR Josephson junction voltage-tunable differential heterodyne spectroscopy 79−30578
far-IR heterodyne radiometric measurements with quasioptical Schottky diode mixers 78−77958
Josephson effect and quasiparticle mixers, mm wave superconducting devices, present status 79−26119
Josephson junctions, mixing in the FIR 79−26121
Josephson low noise mixers at 115 GHz using recyclable point contacts 78−62224
Josephson mixer receiver, at millimetre and long submillimetre wavelengths 77−34027
Josephson mixers, mm wave, using Nb point contacts 79−26123
Josephson mixers for heterodyne reception at submillimetre wavelengths present expt. status, future developments 79−26120
Josephson self-oscillator mixer, submillimetre and far IR detector 77−34026
MIM point-contact diode harmonic generators and mixers 80−60105
MM wave radiometry conducted at Appleton Laboratory 80−67442
MM-wave and sub MM-wave receiver elements, Schottky-barrier resistive mixer devices 80−11558
open-structure submillimetric-wave mixer props. 79−30551
oxide-barrier-tunnel junctions, low-noise 115 GHz mixing 79−51722
point contact and Schottky diodes, submm. mixing for heterodyne detect. 77−5910
point-contact diode, submillimetre wave detection, sensitivity detn. 77−37984
receiver design principles 78−45714
room-temperature Schottky diode mixer for low-noise 115 GHz receiver on Columbia GISS 4 ft radiotelescope 79−53718
Schottky-barrier diode, for submillimetre heterodyne detection 77−37983
Schottky-barrier diode, sub-micron size, for submillimetre wave detection 77−34024
Schottky-barrier diode, submillimetre heterodyne detection 77−34028
Schottky-barrier diode IR capacitive mixing and detect. at high, intermediate or modulation freqs. 80−77864
self-oscillating Josephson mixer as submillimetric and far IR detector 77−38004
submillimeter wave heterodyne detection, with a laser LO 78−70183
submillimetre wave mixers, review 78−45712
submillimetric Josephson mixer receivers, potentials and limitations 77−38003
superconducting, space appl. 80−85836
superconducting point contacts, sub mm band mixer 77−49774
superconducting tunnel junctions as low noise 10 GHz mixers 79−82714
superconductor-insulator-superconductor quasiparticle mixers, conversion gain prediction 80−70901
HgCdTe diode photomixer, optical frequency conversion 77−3682
Si-W point diode, sub MM band, optimisation of operating conditions 79−89006
W-Ni(Co) point-contact diodes as harmonic generators and mixers, DC bias dependence 80−75653

mixes *see mixtures*

mixing
see also blending; dissolving; heat of mixing; mixtures; solubility; solutions
A-type stars, rot., mixing and variability 77−87397
aerated systems, oblong, flow and mixing, transverse circulating flow of liquid, longitudinal dispersion 80−69900
agitated dispersion, droplet breakage and coalescence rates during mixing 78−85205
air pollutants dispersion from area sources in convective turbulence, model 78−28303
air pollution effects on urban-rural complex, two-dimens. numerical simulation 78−81369
air/water mixing, scrubber for air pollution abatement 77−33180
alkali feldspars, TEM study of exsolutions, review *(French)* 78−28224
alloy surface composition modification by high-power CW lasers 80−93699
amalgams, liq., mixing, excess entropy, vibr. contrib. *(Russian)* 79−51263
Arctic fjord waters, mixing 79−48504
artificial kidney construction for solution mixing, heating and degassing *(German)* 79−2161
N.Atlantic central water, vertical mixing due to salt fingers 78−85571
atmosphere, buoyancy driven mixed layers modelling 77−33150
atmosphere, comment on one-dimensional models and appl. to CO 77−45086
atmosphere, convectively mixed layer, flux ratio relation to energy ratio 78−49107
atmosphere, critical evaluation of mixed-layer model with penetrative convection 80−51483
atmosphere, urban, local mixing and turbulence effects on CO_2 concs. 80−16870
atmosphere turbulent mixing, rel. to use of passive antenna system as cond. meas. device 80−85762
atmospheric boundary layer, hourly mixing depths estimation from historical meteorological data 80−51482
atmospheric transmittance model for variable-mixing-ratio absorbent gases 79−80011
Baltic Sea, mixing in thermocline and halocline layers 78−40571
Baltic Sea horizontal mixing, Lagrangian and Eulerian meas. 80−17290
benzene-cyclohexane mixture, excess vol., indirect meas. 77−29032
binary alloy melt, influence of associate formation on thermodynamic quantities 79−66329
biological fluid mixing and bottling unit improvement 78−61291
body fluid distribution, flowing-mixing compartmental hybrid model 77−44582

mixing continued
bubble columns, large diameter, liq. phase duration *(German)* 79−32632
burner with diffusive control, intermixing of gas streams with transverse swirled air flow 78−87418
tert-butyl alcohol in nonpolar solvents, liq. struct. from dielectric studies 80−38894
carbon tetrachloride-pyridine(anisole)(acrylontrile)(acetyl-acetone) mixtures, excess volume of mixing, mol. interactions 79−57281
cell for indirect meas. of excess volume 77−29032
chemical stirred-tank reactor, homogeneous p-order reactions, mixing effects, two parameters model 80−14843
chemically active additive diffusion in turbulent mixing zone, stat. characts. 77−35258
chemically coupled equilibria, thermodynamic theory of solvent-jump relax. method 79−39186
chemically reacting nonequilibrium turbulent shear flow, prediction model *(German)* 79−18973
chemically reacting turbulent shear layer between two streams obs. 80−6163
chemically reactive flow, active solute dispersion 79−60072
chloroform-ethanol solns., light scatt. spectra, conc. fluctuations, assoc. complex form. 77−40254
cloud droplet spectra evolution, effects of mixing, lab. expt. 77−70778
coalescence redispersion model for drop-size distribs. in agitated vessel 77−1950
compressible gases interface, turbulent mixing 78−1683
condensation heat transfer in horizontal tube, effect of in-line static mixer 77−41626
contaminant lateral dispersion in open-channel flow, buoyancy effects 79−50775
continuous flow stirred tank reactor, mixing model 78−63508
coolant in LMFBR fuel assembly, mixing, subchannel vels., electrolytic tracer, isokinetic sampling techniques 77−18653
cross stream-jet mixing, near field influence on mass, momentum and vorticity fluxes 77−39320
crystalline solutions, binary isostructural, thermodynamic mixing parameters computation, FORTRAN IV subroutines 77−86344
cyclohexane-benzene liquid mixing, volume changes 79−90782
cylinder wake, external turbulence effects 78−94665
deep ocean bottom boundary layer, mixing rel. to short-term variability 79−2269
deep sea carbonates, thickness and ^{14}C age of mixed layer 79−29742
deep-sea cores, bioturbation and disruption from radiocarbon and ^{210}Pb distribs. 77−37179
degree of dissociation of congruently melting compound, calc. from liquidus curve 77−84892
across density interfaces, relation to spatially decaying turbulence 77−7373
dibutylphthalate, supersaturated vapour, aerosol form. by mixing of flows 79−39212
dilution dilatometer for excess vol. meas. 77−48678
dilution refrigerator, multiple mixing chamber 80−37042
dimethylformamide binary systems, critical mixing temp. *(German)* 79−77762
directional dispersion coefficients in anisotropic porous media 77−89195
disperse systems, coagulation, slow, turbulent 78−53259
dodecane-sodium octylbenzene sulphonate phase diagram *(French)* 79−82339
eddy diffusion, explicit scale-depend. coeffs., atm. and ocean appl. 78−67191
estuarine mixing, flocculation of dissolved Fe, Mn, Al, Cu, Ni, Co and Cd 79−29774
FFTF upper-plenum mixing and stratification, comparative studies 80−583
filtering gases, mixing zone in different porous media *(Russian)* 77−51112
flame, round jet type, mass exchange between recirculation zone and outer flows, stabilisation 80−14842
flames, turbulent, calc. in one-dimensional approach 80−30236
flow, separating boundary layer, subsonic, integral prediction method 80−1623
flow, Taylor-Gortler instability and mixing layer transitions 78−90836
flow measurement, plane mixing layer vortex digital image processing 80−103095
flow measurement by dilution method with incomplete mixing 79−50821
flow mixing in finite channel 79−90336
fluid-gas spray apparatus for conical mixing chamber *(Russian)* 79−50820
fluidised bed, gas-solid, solid circulation 78−79359
fluidised bed, large scale, gas backmixing, solids movement, bubble activities 78−30349
fluidised bed, particle mixing, diffusion model for longitudinal particle transport 77−47087
fluidised bed, solids mixing, radioactive tracer design, preparation 77−35269
fluidised bed, two-dimens. gas fluidised, mixing characts. of large particles 79−86503
fluidised beds, liq., particle mixing and classification 79−90330
fluidised system, heterogeneous, aerodynamic aspects of transfer processes, crit. state 80−79394
free turbulent mixing in streamwise press. gradients, linearised k-ε anal., wakes 80−59039
freshwater, jet in salt water laboratory exptl. results on mixing *(Russian)* 77−68654
furfural-water interface, anomalous mass transfer, coupling of heat and mass transfer 77−80626
galaxy mergers, stellar populations mixing processes 80−67860
gas flow, recirculating, in packed columns, mass transfer and mixing, cell model 80−69913
gas-liquid systems, vibs. stabilisation of dynamic equilib. and mixing *(Ukrainian)* 80−10291
glass, complex raw material, hydrothermal prep. 80−104106
glass, two-phase, struct. and texture, electron microscope 79−64999
gravity current head dynamics, mixing and Kelvin-Helmholtz billows 79−37368
groundwater flow, fresh-salt water interface, mixing zone *(Japanese)* 78−11927
high-level radioactive waste, ultimate disposal on seabed, rel. to oceanographic circulation 78−13273

mixing continued
homogeneous fluid, laboratory investigations of mixed layer evolution, appl. to ocean *(Russian)* 80−94529
hypermixing nozzle in thrust augmentor, three dimens. turbulent mixing 78−51214
indices for multicomp. solid mixtures 80−39300
isobutyric acid-water system, liq.-liq. critical pts., Ising exponents, extended scaling 77−20072
isopropyl alcohol-carbon tetrachloride, mixture, dielec. const., two-sided estimate 79−42262
jet, axisymmetric, vel. distrib. and swirl effects, low speed results 79−46351
jet, coaxial round, turbulent mixing, eddy Reynolds number var. 78−75179
jet, liq., interaction with confined wet entraining vap.-liq. flow 79−32635
jet, mixing layer, axisymmetric, influence of initial and boundary conditions 79−94689
jet, transverse, turbulent mixing with high Mach number stream 79−32603
jet, turbulent mixing layer, conditional meas. 79−32598
jet exhaust noise, role of shear-layer instability waves 77−47054
jet pseudoturbulent mixing efficiency in fluidised bed 77−39342
jets, axisymmetric, turbulence mixing of gases with different densities 77−58749
jets, mixing in transverse flow 78−5779
jets, turbulent mixing, conc. fluctuations 77−39318
jets, turbulent two-dimens., parallel, mixing 78−51209
jets of different density entering air, turbulent flow 79−72922
Lake Tahoe, California-Nevada, effects of coastal front on chlorophyll distrib. 79−2301
lake upper layer mixing during heating cycle 77−29335
Lennard-Jones mixture, binary, equimolar, static (dynamic) props., mol. dynamics calc. 80−64857
liquid binary and ternary mixtures, Hildebrand fluidity eqn., viscosity calc. 78−38867
liquid metal mixing and refining in EM chute 79−77284
liquid metals, mixing volumes, pseudopotential method 79−37846
liquid mixer, consisting of rotating cylindrical tube 79−71434
liquid mixing, volume changes, review 79−90782
liquid mixing across diaphragm in normal electric field 79−10615
liquid-gas mixer, perforated disc stirring cascade type, power dissipation, mechanism and correlation 79−1238
liquid-liquid countercurrent flow in multistage vibr. disc column, axial mixing 77−3902
liquid-liquid mixing analysis, lamellar model 80−15246
liquids of different density, turbulent mixing at an accelerating interface 80−6030
LMFBR commercial plant design 78−8877
LMFBR outlet plenum mixing, 3-D numerical simulation 78−8880
LMFBR piping tee, multiple jet thermal mixing 78−8879
longitudinal diffusion in a flow through a tube 78−90974
magmas, contrasted, commingling in plutonic environment, examples from Nain anorthositic complex 80−104959
magmas convective mixing, implications of density var. among mid-ocean ridge basalts 80−56460
magneto-hydrodynamic phenomena, of mixing in the glass industry *(Polish)* 80−64647
main-sequence stars, effects of mixing on CNO isotopes in red giants 77−33475
marine sediments, mixing effect on calcite dissolution by fossil fuel CO_2 78−81212
Mars atmosphere, dynamical mixing rel. to photochemistry 77−91458
mass transfer cell with vibr. mixing for liq.-liq. systems 79−37425
mechanistic kinetic model data appl. from conventional batch solid mixers 77−77442
melting, of substrate into different miscible liq. layer, hydrodynamic instability, heat transfer 78−90695
methane, jet, free turbulent flow, diffusion coeff. variation, mixing processs velocity 77−7480
methane tracers, single-jet mixing in turbulent tube flow, similarity and scaling law 80−14765
methanol-ethanol (n-propanol)(n-butanol) binary systems, excess vol. of mixing, dilatomitric meas. 80−59656
Mississippi River and Gulf of Mexico waters, Ba non-conservative behaviour 78−32120
mixer-settler, problems of construction and operation 78−29096
molecular thermodynamics appl. to phase separation and critical phenomena *(German)* 78−14447
molten alloys, compound-forming, vol. of mixing, conc. depend. 80−103484
non-Newtonian fluid mixing, convective heat transfer theory 79−77094
non-Newtonian fluids, axial force on agitators 79−37356
non-proportionality between flux and reservoir content 80−46261
nonlinear viscoplastic media, dispersion in circular tubes for laminar motion case 77−58626
nozzle reattachment of two-dimensional turbulent jet 79−23347
nozzles, plug, turbulent shear layers, mixing 77−89182
ocean, banded salt finger struct. form. 78−85570
ocean, implications of intense mesoscale eddy containing Mediterannean water off Bahamas 79−74902
ocean, surface mixed layer, catastrophic mixing events obs. 79−16503
ocean, tidal mixing and 18.6 year cycle of shallow seas surface temp. 78−73387
ocean, wind forcing vars. rel. to mixing and sea surface temp. response 79−48505
ocean cyclonic rings, warm saline water/cooler fresher water mixing 78−44861
ocean heat and salt mixing, double-diffusive intrusions into density gradient 78−85569
ocean microstructure, transport processes and mixing 77−60420
upperocean mixed layer, temp. and salinity struct. during POLE expt. 80−72536
ocean near-surface mixing layer, microstruct. in stable heating conditions 78−85568
ocean surface layer, dye plumes diffusion, expt. 78−44871
ocean waters mixing, effects of eddies and islands 78−85572
oil-water emulsification, by US, large primary oil drop breakup 79−32644
oil-water interface, fatty alcohol adsorbed layer phase transition, high-press. effect 79−99395
mixing continued
oil-water interface, US emulsification drop form. by capillary wave instability 79−32643
open binary mixtures, fluctuation theory, entropy prod. and energy dissipation *(German)* 78−64879
optical waveguides, SAW electrostrictive mixing analysis 77−27390
particulate materials, cohesionless, mixing and segregation, microscopic mechanisms 79−37848
particulate materials, cohesionless, mixing and segregation, failure zone form. 79−42261
particulate systems, coarse and fine, ordered powder mixing 79−61530
petrogenetic mixing models and Nd-Sr isotopic patterns 80−3965
phase separation, competitive statistical and chem. mixing effects *(German)* 77−52665
photographic emulsion production, effect of mixing on diffusion rate *(Russian)* 80−3388
plane isothermal jet propagation in bounded secondary stream 77−24008
plane laminar relaxing gas jets, mixing with radiation accounted for, boundary layer eqns. 79−90349
plasma jet mixing, with surrounding gas, effect of sound radiation 79−82053
plate, flat, with suction, boundary layer eddy viscosity, mixing length, Von Karman's constant 80−1680
plume, buoyant, turbulent, issuing vertically into stratified or uniform ambients 77−58756
pollutant dispersion in oscillatory fluid flow 78−44881
polyethylene, mixing of high and low density, mixing ratio determ. by thermo-optical anal. *(German)* 78−53070
polymer additive mech. mixing in turbulent drag reduction 77−68637
polymer agglomerates, forces in dispersive mixing 77−29052
polymer melt, particulate mixing, fluid dynamics, rheological and energetic considerations 80−43686
polymer solutions, free energy of mixing, modelling, critical exponents 80−44106
powder, lattice defect effect on mixing 79−73313
powder, mixing/segregation behaviour, 2 powders of different density, quantit. anal. 78−84733
powder, ordered mixtures production, humidity effect 80−76208
powder particle motion and segregation by density difference in V-type mixer 80−45250
powders, binary, inhomogeneity-packing density relations 78−92211
powders, laboratory device 79−61828
power-law fluid, two-stream mixing along flat-plate, variational solns. 80−53817
premixed burning in diffusion flames, Libby Economos flame zone model 79−60093
propylene carbonate and dimethoxyethane mixed electrolyte solns., for high energy density batteries 80−76627
pseudoplastic fluid flow in pipes, press. loss 79−98765
pulmonary airways, longitudinal mixing, impulse response of He, SF_6 79−20568
pulmonary airways, longitudinal mixing, inspiration rel. to expiration 79−100657
pulverised coal reactors, cold flow mixing rates with recirculation 79−50762
PVC-chlorinated PVC mixtures, compatibility, mixing techniques, elastic modulus determ. 79−4943
quantum ideal gases, paradoxes 77−13728
quiescent two-phase systems, interfacial resistance to interphase mass transfer 78−67828
rain, mixing with near-surface water 79−53371
Rayleigh-Taylor instability, turbulent stage anal. 79−41669
Redlich-Kwong, eqn. of state, modified parameters, appl. to vapour-liquid equilib. 77−39659
refractory metal dichalcogenides and Ga alloys, mixing powders using US treatment 79−24454
river flows, transverse mixing coeffs., evaluation from slug tests 77−21806
rivers estuarine mixing, dissolved humic acids and Fe removal 79−34830
salt fingers, rot. effects 79−50767
shear flow, non-parallel, stability and mixing 79−10547
shear flow, stratified, free-turbulent, buoyancy effects on large scale struct. 78−90849
shear layer, turbulent mixing of passive and reactive species 77−75989
sheared particulate beds, mass transport kinetics in, Markov chains appl. 79−60057
shelf seas, vertical mixing rel. to marine fronts adjustments 79−92545
silicate, polymerised binary melts, activities and free energy of mixing 77−47596
solar interior, convective mixing rel. to interstellar dust accretion and neutrinos prod. 79−12441
solid mixture charact. discrete fourier transform, spectroscopy, computer simulation 78−63859
solids, appl. of multivariate statistical anal. 79−61529
soluble fluids in laminar, turbulent flows, stretch model appls. to mixing, diffusion, react. 79−94736
spray mixing, effect of sharp-edged orifice type and cavitation 77−51107
stars, convective, force mixing theory 80−56818
stars, main-sequence, mag. mixing rel. to CNO isotope abundances and α Bootis (Arcturus) problem 80−105229
stars, massive, convective and semiconvective mixing 80−90405
stationary system, diffusion mixing model, approx. soln. 80−79410
statistical thermodynamics, nonlinear, mixing distance, steady state stability, appls. 77−9976
stellar cores, heating and mixing by core He flash with two-dimensional convection 80−105230
stellar interiors, meridional currents penetration of mol.-weight barrier 77−33474
stellar interiors, mixing due to meridional circulation caused by stellar rot. 79−62818
stellar winds, turbulent mixing with interstellar gas 80−67701
Stepanov method, liq. mixing in shaper hole, simulation device 78−3022
stopped flow kinetic studies, problems concerning mixers and detectors 79−8585
stratified flow, turbulence, mixing 78−22400
stratified fluid, reinterpretation of entrainment process in laboratory expts. 80−51405
stratified fluid, spread of mixing and analogue in rot. fluids 79−57949
stratosphere, H_2O vapour mixing ratio, Australia, 1973-76 period 78−49116

mixing continued
stratosphere, lower, trajectory slopes, countergradient heat fluxes and mixing by waves 79−2340
suction-induced asymptotic boundary layers, exptl. and predicted props. 80−1553
supersonic transverse gas stream, penetration and mixing of secondary liq. injection 77−24018
suspension, fibre, conc., rheology of tube flow 77−58627
suspensions, fluid dynamical aspects of operating conditions of suspension stirrers *(German)* 80−26058
thermal mixing layer, intermittency 77−31283
thermal pollution by discharges into waterways, mixing problems 79−8645
thermosphere, lower, turbulent mixing rel. to O and O_2 distrib. simulation 80−4159
thin polycrystalline films, rate of mixing depend. on grain boundary struct. 80−107578
thixotropic liquid mixing, power requirement 77−15070
three-dimensional compressible mixing and reacting ducted flows, modelling 77−27621
troposphere and stratosphere, H_2 mixing ratio vertical profiles 78−32181
tube wall, gas film-cooled, turbulent heat exchange, coolant turbulence intensity influence *(German)* 79−18895
tubular reactor, effect of axial mixing on start-up time, with first order isothermal irreversible reaction 78−9723
turbulence and mixing in stably stratified waters, book contrib. 78−59444
turbulence field mixing and decay analysis, use of significant dynamic length scales 79−86404
turbulence formation in parallel blast mixing *(Ukrainian)* 80−6033
turbulent boundary layer, compressible, extended mixing length appls. 78−94655
turbulent boundary layer, mixing length in wall region 77−62242
turbulent boundary layer, supersonic, wall temp. effect 78−94765
turbulent boundary layer on flat plate mainstream turbulence, vorticity effects 78−83408
turbulent convection of scalar fields, probability density functions relax. 79−27622
turbulent flow between rot. cylinders, model eqns. calc. 78−90852
turbulent flows with coherent structs., theory of mixing mechanism 79−7369
turbulent jet mixing, effect of nozzle wall boundary-layer state 77−27568
turbulent jet mixing rates with self-excited acoustic oscills. 78−47008
turbulent mixing, zero gradient points 78−94648
turbulent mixing at fluid interface in gravity field 77−89112
turbulent mixing coefficient correlations for compressible coaxial submerged and coflowing jets 77−42883
turbulent mixing flow, simultaneous laser measurements of instantaneous vel. and conc. 77−35287
turbulent mixing in shear flow, model 78−1650
turbulent mixing layer, two-dimens., initial conditions effect 78−90848
turbulent mixing layer at high R_e, large struct. dynamics and entrainment 77−15001
turbulent mixing layers, free-stream turbulence effect 78−46949
turbulent mixing with react. of miscible reactant streams, simulation 80−64651
turbulent plane mixing layer analysis in homogeneous incompressible fluid 77−46999
turbulent premixed flame, theoretical predictions *(French)* 78−94853
turbulent reactive gas flows, two-dimens., nonequil. processes analysis 77−51129
turbulent recirculating jet flow, initial mixing region meas. 77−27570
turbulent shear flow mixing, forced convection with chemical reactions, numerical modelling 79−1272
turbulent shear flow with streamline curvature, algebraic stress-heat flux model 79−27625
turbulent stably stratified fluid, mixed layer growth 79−55358
two-phase flow, mixing and condensation in high-speed flow, review 78−47014
two-phase mixture flow in rotary mixer, optimal dimensions 78−63485
two-stream mixing, variational soln. 78−38266
two-stream mixing layer, turbulence obs., hot-wire meas. system 79−32488
unsteady turbulent boundary layer developing in oscillatory external flow *(French)* 77−72288
Venus clouds, aerosol size distrib., coagulation sedimentation and turbulent mixing effects 77−71041
vibrational mixing and periodic struct. formation in artificial weightlessness *(Russian)* 77−59118
vibratory liquid-gas mixture, nonlinear resonance expt. *(Ukrainian)* 78−90811
viscoplastic material, mixing process, Bingham model, two-dimens. flow *(German)* 80−92076
viscous fluids in static mixer, heat transfer coeffs. 79−18885
vortices, in mixing layer, numerical simulation 78−90853
water, thermally-stratified, cooled from above, free convection 79−46315
water/Na temp. fluctuation correlation mixing tee expts. 78−8878
Al-In (40, 70 wt.%), liq. phase immiscible system, solidification in microgravity 78−84770
Al_cMg_{1-c} liquid alloys, vols. and entropies of mixing, calc. 80−75363
Al_2O_3, floating zone melting, forced convection, computer simulation 78−88422
Au-M, liq. alloys, M=Ga,In,Sn,Sb,Te, ΔG^E of mixing, exptl. determ. 77−4920
CO_2 absorption in H_2O, aq. solns. with interfacial turbulence due to microstirrers 80−64527
Cd-In-Sb, liq. alloy, Cd thermodynamic activities, Gibbs free mixing enthalpy *(German)* 80−45279
CoO-MgO, cryst. oxide demixing in O pot. gradient 79−37849
Cu bearing substitutional solutions, thermodynamics, Kapoor model applicability 79−77761
Cu substrate, ion induced intermixing of Au or Ag surface film 80−15420
D_2-HCl electric discharge gasdynamic laser, turbulent mixing charact. 78−9366
Fe/zinc stearate, compacts, admixing, effect on mech. props. 80−45402
Fe/Zn stearate powder compacts, admixing effect on apparent density, mixing, compaction 80−45403
Fe-FeS-MnS-Mn reciprocal system, interaction between three liq. miscibility gaps 77−7865
Ga-Ge-Zn ternary alloys, thermodynamic props., EMF meas. 80−81033
GaTe-SnTe, phase equilib. 77−86006
HF chemical laser, CW, influence of mixing effects on energy charact. 80−9875
H_2O vapour mixing ratio in troposphere and influence on tropopause over India 77−53123
In-Te-SnTe, phase equilib. 77−86006
In-Zn, liq., Zn activity meas. by Knudsen torsion-effusion method, thermodynamic props. of mixing 79−10950
KNO_3-TlBr, fused mixture, coexistence curve and elec. cond. 77−20071
LiBr-LiF-KBr-KF, fused, miscibility gaps 79−82348
$LiCl+NaNO_3$, apparent and partial molar volumes in aq. soln. 78−44396
N_2 jet, mixing zone in continuous to free mol. transition 79−32605
N_2-Ar corona dishcharge, convection and mixing, atm. press., mass spectra obs. 80−1853
NaCl-KCl, interdiffusion and demixing, electron microprobe anal. *(French)* 80−54444
Na_2SiO_3-K_2SiO_3, molten, thermodynamics of mixing at 1100°C, CaO addition effects 77−47581
Ni-Cu semiconducting cast ingots, effect of EM stirring on struct. *(Russian)* 78−6915
O_3-O_2 mixture, significant struct. theory appl. to phase separation 77−51503
Pb-Tl-Te, liquidus of ternary system 79−8285
Pd-Al alloys, Fermi level position rel. to mixing behaviour, Al activity, thermodynamic props. *(German)* 78−75835
Pd-Th, thermodynamic stability 79−55903
Pt-Sn alloys, thermodynamic props. *(German)* 78−52769
Pu binary alloys, periodical depend. of equilibrium distrib. coeffs. of Pu admixtures on atomic number of admixture 80−18419
Si, floating zone melting, forced convection, computer simulation 78−88422
Si substrate, ion induced intermixing of Pd or Pt film 80−15420
SiO_2, three-component glass, liq. phase separation, with two oxide modifiers 80−103250
UO_2, condensed vapour following core disruptive accident, particle-size distribs. using first-generation model 78−13295
ZnO/Al_2O_3, microstratified mixing of suspensions, viscosity dependence 79−70023

mixing, heat of *see heat of mixing*

mixing circuits *see mixers (circuits)*

mixtures
see also critical mixtures; mixing; solutions
acetic acid-carbon tetrachloride, US absorption, coupled dimerisation cyclisation reaction *(French)* 79−42148
acetone-chloroform (-iodomethane) (-CS_2), liq. mixture, excess Gruneisen parameter, intermol. interaction 78−67635
acetone-methanol, acetone-CCl_4, methanol-CCl_4 and acetone-methanol-CCl_4 mixtures, acoustic and physicochem. obs. 79−96347
acetone-toluene-tetrachloromethane, mol. interaction and thermodynamic props. 80−71935
acetonitrile binary liq. mixtures, excess thermodynamic functions, complex formation 79−52736
acetonitrile-carbon tetrachloride-n-butanol, mixtures, compressibility, free length, molar and available vol., US meas. 78−2200
acetonitrile-toluene-benzene, mol. interaction and thermodynamic props. 80−71935
acetonitrile-toluene-n-butanol, mixtures, compressibility, free length, molar and available vol., US meas. 78−2200
adsorption, competitive, from binary liquid mixtures, adhesive hard sphere model 80−2265
aerodynamic isotope separation technique based on vel. slip in freejet expansions 80−19441
aerosol, spherical particle phoresis in multicomponent gas mixtures 78−22446
air-H_2 (methane), ignition energy by capacitive discharge *(French)* 80−10446
air-solids mixture in horiz. unsymmetric branches, pressure drop and solids distrib. 79−4069
air-stream mixture, direct contact dondensation on single droplet 77 68370
air-vapour flow in channel, laminar, with wall vapour-ice transition 79−94617
air-water slug flow in horizontal pipe, liquid holdup determination 79−46362
air/water mixture mass flow meas. by drag devices and γ densitometer 80−79385
air/water vertically downward slug flow distrib., bubble vel. meas. 77−51108
alcohol-inert compounds mixtures, thermodynamic props. *(German)* 79−52748
alcohol-nonassociating active component mixtures, thermodynamic props. 78−64878
alkali fluoride-LnF_3(Ln=Y, La, Yb) binary liquid mixtures, thermochemistry 80−45538
alkali halides, molten salt mixtures, enthalpy of mixing, theory, Monte Carlo calcs. 77−72691
alkali metal halides, molten binary mixtures, excess enthalpies calc. 80−3397
alkali metal-inert gas, inhomogeneous mixture, nonequilib. processes under conditions of T-layer form. 78−91079
alkali metal/alkali halide liquids, high temp. furnace for small-angle neutron scatt. expts. 77−84591
n-alkane binary mixtures, infinite dilution activity coeffs. 78−15695
n-alkane binary mixtures, melting and solid-state transition 77−72685
n-alkane-cyclohexane, liq. mixture, excess vol. by density meas. *(German)* 79−73324
alkane-silicone oil mixtures, thermal cond. 79−42323
n-alkanes, liq. mixtures, thermodynamics 80−55700
alkanes, mixtures, order, enthalpy of mixing, calorimetric obs. *(German)* 78−18773
alkanoate, Li, Na, K and Rb salt mixtures, DSC anal. 78−10192
S-alkyl-isothiouronium iodides in methanol-water mixtures, conductance at 25°C, solute-solvent interaction 79−95194
N-alkylpyridium halides-$AlCl_3$, molten, density, elec. cond. and viscosity meas. 80−24630
analysis, quantitative, IR spectrosc. method 79−96377
analysis by mass analysed ion kinetic energy spectrometry 77−36807

mixtures continued
analysis of multicomponent by method of additions 80−61187
anisole, in cyclohexane-ethanol mixtures, UV spectra, solvent effect 79−22770
anthracene-He-Xe, gaseous mixture with one low conc. component, thermal diffusion calcs. 77−19661
aqueous heterogeneous systems, NMR, substrate struct. and H_2O mol. relax. 78−7247
aqueous organic binary mixture, pseudophase transition, heat capacity evidence 78−83937
aqueous polynucleotide-protein mixture, inverted turbidity versus conc. depend. 77−9165
aqueous-organic mixed solvent structure, solvation, cation exchange *(Dutch)* 79−83500
aromatic compound-carbon tetrachloride, liq. mixture, sound vel. theories 78−2199
bases, mixtures, potentiometric titrations, computer-calc. curves, learning machine appl. 80−3426
benzene+cyclohexane (hexafluorobenzene), isotropic light scattering, excess Gibbs function 79−8150
benzene(substituted)-n-alkane mixtures, mol. orientation correls., depolarised Rayleigh scatt. 79−22714
benzene binary liquid mixtures, US study of mol. interaction 77−15494
benzene-2,5-dibromothiophene, self-association, proton mag. relax. 77−28471
benzene-acetone-chloroform ternary liq. mixture, US vels. rel. to interactions 77−69044
benzene-chloroform mixture, reorientational motion and intermolecular interaction by Raman spectroscopy 77−24839
benzene-cyclohexane(carbon tetrachloride), binary liq. mixtures, molar heat capacity isothermal compressibility 79−66328
benzene-ethylene dichloride (-CCl_4), liq. mixture, excess Gruneisen parameter, intermol. interaction 78−67635
benzene-H_2N_2 gas ternary diffusion coefficient obs. *(Japanese)* 79−10626
benzene-hexa-n-alkanoates and benzene mixture, disc-like mesogens, thermotropic mesophases 79−86699
benzene-hexafluorobenzene, mixtures, dielectric relax. and US absorpt. 77−12307
benzene-n-alkane mixtures, mol. orientation correls., depolarised Rayleigh scatt. 79−22714
benzene-n-decane-n-tetradecane, molar enthalpies of mixing *(German)* 79−42253
benzene-n-heptane-n-tetradecane, molar enthalpies of mixing *(German)* 79−42253
benzene-p-dioxan, mixtures, mol. reorientation and assoc., depolarised Raman scatt. obs. 80−7341
benzene-p-xylene, excess vol., enthalpies, Gibbs free energies 80−44335
benzene-tetrahydrofuran, soln., excess thermodynamic props. and interactions, US vel. and density meas. 80−39288
benzene-toluene and benzene-o-xylene mixtures, US vels., compressibility, expsn. coeff. 79−33038
benzene-toluene-n-tetradecane, molar enthalpies of mixing *(German)* 79−42253
benzol-paraffin, solid-liq. mixtures, phase equilib., Wilson eqn. *(German)* 79−42245
BeO Al_2O_3 V_2O_5, kinetics and mechanism of formation of chrysoberyl 79−11535
binary, anal. by computer decomposition of mol. fluoresc. spectra 78−15735
binary, close to vaporisation, hydrostatic and external field effect, anal. 80−19929
binary, excess isentropic compressibilities and isochoric heat capacities 80−21313
binary, NMR longit. relax., mole fraction depend. 77−61767
binary, of hard spheres with nonadditive diameters, Percus-Yevick eqn. approx. soln. 79−77471
binary, qualitative anal. by fluoresc. polarisation spectroscopy 79−34396
binary and ternary, activity coeffs. rel. to excess Gibbs free energies 80−96665
binary and ternary mixtures boiling, heat transfer and heat flux density *(German)* 79−68559
binary dense gaseous mixtures, struct. and thermodynamic props., molecular dynamics study 80−64866
binary dielectric mixture relative permittivity formulae compared 80−15939
binary fluid, coexistence curve from refractive index obs. 77−32823
binary fluid mixture, spinodal decomposition, theory of late stages 79−99320
binary fluid mixture, thermal diffusion ratio determ. by forced Rayleigh scatt. 78−75858
binary gas mixture, determ. gas composition, oscillating vane gauge 79−97401
binary gas mixture, intermol. force parameters 79−22784
binary gas mixtures, force consts., intermol. pots. calcs. 78−66624
binary gas mixtures, mass transfer analysis using model of convective diffusion for turbulent flow in tube 77−7454
binary gas mixtures, nonspherical mols., second virial coeffs. calc. 78−75247
binary gas mixtures, precise diffusion coeffs., appl. to two-bulb cells calibration 77−76019
binary gas mixtures, separation and isotope separation in curved shock wave 79−94753
binary gas mixtures, thermal creep between parallel planes 79−14507
binary gas mixtures epochal relax. 79−41783
binary gas systems, thermal diffusion factors meas. 80−10344
binary hard-sphere mixture, mutual isothermal diffusion Onsager reciprocity relations effect 78−30773
binary homogeneous mixtures, motion in infinite rot. cylinder, generalised diffusion theory 80−79328
binary inert gas systems, determ. of (m,6,8) pot. parameters 79−46414
binary interaction constants, thermodynamic props. 79−41917
binary ionic highly dissymmetric mixtures, phase separation 79−46425
binary liq. mixture, chain assoc., excess Gibbs free energy 77−16860
binary liquid, containing one rotational isomeric relaxing liquid, US absorption 80−70315
binary liquid, stimulated Raman scatt., intensity changes, selective excitation 78−13753
binary liquid, US evaluation of energy of vaporisation 80−65209
binary liquid mixture, glass transition temp., composition depend., theory 77−76531
binary liquid mixture, horizontal layer, surface tension driven instability in presence of Soret effect 80−10227
binary liquid mixture, surface tension, free energy density expansion 78−91509
binary liquid mixture heated from above, convective instability, optical meas. 77−42823
binary liquid mixtures, cell mol. theory for calc. of thermodynamic props. *(Spanish)* 79−68991
binary liquid mixtures, diffusion coeffs., conc. depend., theory 77−89557
binary liquid mixtures, dispersion interactions, struct. effects 79−46535
binary liquid mixtures, excess Gruneisen parameter and intermolecular interactions 77−20082
binary liquid mixtures, excess internal press. and intermolecular interaction 78−35640
binary liquid mixtures, non-aqueous solns. of non-electrolytes 79−95081
binary liquid mixtures, nonassociated, thermodynamics 78−18797
binary liquid mixtures, sp. ht., light scatt., two-scale-factor universality 79−42267
binary liquid mixtures, viscosities, comparison of eqns. 77−59135
binary liquid mixtures, viscosity, Panchenkov model calcs. *(German)* 77−31797
binary liquid mixtures, viscosity isotherm classification *(German)* 77−28033
binary liquid mixtures, viscous flow props., mol. thermodynamic theory 78−2280
binary liquid mixtures adsorption onto solid surface, effect of surface heterogeneity 80−44411
binary liquid mixtures containing cyclohexanol, US absorpt. meas. 77−27948
binary liquid mixtures nonidealities, optimal representation 79−42248
binary liquid solutions, struct. and thermodynamic props., molecular dynamics study 80−64866
binary liquid systems, apolar-apolar and polar-apolar, significant structure theory, appl. 80−1909
binary liquid systems, thermodynamic and transport props. 80−92686
binary liquids, mol., intermol. props. from excess enthalpies 77−44503
binary liquids, viscosity rel. to thermodynamic excess functions *(German)* 77−35740
binary melts, short-range order, X-ray and neutron scatt. *(German)* 78−14272
binary mixture, boiling, liq.-vapour equilib. data, circulation apparatus determ. *(German)* 77−24375
binary mixture, inert solvent and self-associating component, Wilson consts. 79−82351
binary mixture, nucleate boiling, bubble growth, saturation press.-temp. relation 77−46892
binary mixture, pretransitional effects near convective instability 77−41536
binary mixture, Van der Waals model, global phase diagram 78−59928
binary mixture of hard spheres and square-well molecules, quantum corrections to eqn. of state 80−6338
binary mixture supersaturated vapour condensation, homogeneous nucleation 78−2247
binary mixture vapour condensation, forced-free convection, finite difference treatment 78−5741
binary mixtures, condensation on finned surfaces, heat transfer 77−39198
binary mixtures, hole theory in quasichemical approx., excess function formulae *(Spanish)* 79−68992
binary mixtures, liquid-vapour equilib. data, internal consistency, automatic checking method 80−54364
binary mixtures, models, distance parameter geometric averaging, excess free enthalpies *(German)* 77−32825
binary mixtures, qualitative anal. using fluoresc. polarisation 79−24849
binary mixtures flowing through activated C, adsorpt. interference 80−107635
binary molten salt mixture, ionic and mol. mobilities, inter-diffusion and self-diffusion *(German)* 77−11720
binary nonelectrolyte liquid mixture, hard sphere eqns. of state 78−47495
binary polymeric mixtures, soln. viscosities meas. 80−54423
binary system forming simple association complexes, liq. diffusivities prediction 80−34216
binary vapour mixture condensation into immiscible liquids *(German)* 78−18760
binary vapour mixtures, simulation of unsteady state behaviour of dephlegmation 79−7285
bitumen-salt mixtures, radioactive, thermal stress. behaviour *(German, English)* 77−65290
boson mixtures, binary, ground state configs. 80−105570
bromides, and mixtures, molten, elec. cond., density, viscosity, surface tension, review 77−80638
bromobenzene+m-xylene, US vel. and adiabatic compressibility 78−51614
buffer gas mixture choice for drift tube study of ion-neutral reactions 79−57232
burning in Soundhaus' tube, radial self excited vibr. regimes *(Ukrainian)* 78−68892
butanol-methylethyl ketone, soln., excess thermodynamic props. and interactions, US vel. and density meas. 80−39288
2-butoxyethanol, aq. binary mixture, pseudophase transition, heat capacity evidence 78−83937
t-butyl alcohol, mixtures, assoc., thermodynamic study using 2-constant model 80−66789
butyl rubber ethylene propylene ternary copolymer mixture, permeability, diffusion of gases and solvents 79−95217
carbon tetrachloride-benzene, liq. mixture, excess Gruneisen parameter, intermol. interaction 78−67635
carbon tetrachloride-benzene(cyclohexane), binary liq. mixtures, molar heat capacity isothermal compressibility 79−66328
cell design for diffusion coeff. meas. in gas phase 78−55709
characterisation of ordered mixes using X-ray microanal. 80−16215
chemical analysis, direct interferogram comparison of chromatography/Fourier transform IR spectra data 79−100458
chemical kinetics, nonequilibrium, linear mixture formula, eigenvalue approx. 77−63895
chemically reacting, microfluids theory 80−14777
chemically reacting fluid mixtures, phenomenological theory 79−1268
chemically reacting ideal gases mixture, explosion and implosion analysis 77−60066

mixtures continued
chemically reacting multicomponent systems, Langevin forces and noise correls. 77−16823
chemically reactive mixtures, continuum description *(French)* 79−41765
chlorobenzene-cis-decalin, mixtures, dielec. const. and loss tangent in liq. and solid phases 80−100628
chloroform-acetone, liq. mixture, excess Gruneisen parameter, intermol. interaction 78−67635
chloroform-carbon tetrachloride mixture, Lennard-Jones pots., mol. dynamics calcs. 78−34418
chloroform-p-dioxan and chloroform-benzene mixtures, mol. reorientation and assoc., depolarised Raman scatt. obs. 80−7341
o-chlorophenol-acetone (ethyl methyl ketone), thermodynamic and transport props. 80−92686
o-chlorotoluene(-benzene), liq. and dilute soln., microwave absorption and relax. processes 79−82920
cholesteric, binary, IR rotatory dispersions 77−36194
cholesteric liquid crysts., molecular theory, intermol. pot. 77−76302
cholesteric mixtures, quasithermal crystn. 80−92652
cholesteric positive dielectric anisotropy mixture, helix pitch increase below 20 kHz 80−15997
cholesteric-nematic mixtures, helix inversion 80−24358
cholesteryl capsylate and laurate, and their mixtures, elec. cond. *(Rumanian)* 79−64988
cholesteryl chloride, binary mixtures with cholesteryl benzoate and β-halogeno cholesteryl alkanoates, reciprocal helical pitch 79−90528
cholesteryl laurate-cholesteryl caprilate mixture, elec. cond. mechanism 79−10796
cholesteryl laurate-cholesteryl caprylate (75 wt.%), polymorphic behaviour, optical, elec. and dielec. meas. 80−65208
cholesteryl nonanoate, cyclohexanone admixture effect on mesophase order parameter, refr. index meas. 80−100165
chromatography, universal gas chromatographic system, based on frontal anal. 78−61114
clay soil/sand mixtures, reflectance 80−56475
clay-water systems, NMR, substrate struct. and H_2O mol. relax. 78−7247
component anal. by retrospective computer subtraction at gas phase IR spectra 77−77824
component analysis, i.r. spectroscopic method 79−43657
compressed powder mixture electrical conductivity calc. *(German)* 80−10940
concentrated electrolyte, solutions, viscosity, mixture law 78−18818
consolidation in compressible mixtures 79−46271
convective-diffusive transfer in cylindrical channel, soln. 77−7391
COOB-cholesteric liq. cryst. mixtures, helix pitch, temp. depend. 80−64895
critical binary liq. mixture, wall phenomena *(French)* 79−16041
critical binary liquid systems, composition depend. of US absorpt. 79−4372
critical ionisation velocity in gas mixtures, lab. expt. 78−67307
critical points, analogy with pure fluids 78−67819
cryogenic binary mixture, ultrasonic velocity, compressibility, heat capacity, at 298.15K 79−10898
curved shock waves in ideal fluid mixtures with multiple temps., theory of singular surfaces 80−28533
p-cyano-p′-pentylbiphenyl/p-pentylbenzoic acid, induced smectic phase, dielec. props. 80−6498
4-cyanobiphenyl/4-cyano-p-terphenyl liq. cryst. mixture, order parameters of dissolved dyes 80−100167
α-cyclodextrin and α,β-D-xylose, absorption mode spin-echo spectra appl. 80−78634
cyclohexane+benzene, excess volume 78−47527
cyclohexane+n-hexane, effect of pressure on excess enthalpies at 298.15K 78−48689
cyclohexane-acetic anhydride mixture, impurity effects on crit. behaviour of elec. resist. 79−65527
cyclohexane-acetone-butanol ternary liq. mixture, US vels. rel. to interactions 77−69044
cyclohexane-acetone-ethanol ternary liq. mixture, US vels. rel. to interactions 77−69044
cyclohexane-benzene-carbon tetrachloride ternary liq. mixture, US vels. rel. to interactions 77−69044
cyclohexane-methanol, crit. opalescence, AC elec. field effect 78−35159
cyclohexane-tetrachloromethane, heteromolecular vibr. relax. time, Rayleigh-Brillouin spectra 78−59731
cyclopentane+isomeric octanes, excess volume 78−47527
dense gas mixtures, thermal cond., composition dependence 78−51276
dense gas mixtures, viscosity, composition depend. 77−35295
detonation cell model, geometry, kinematics, mixture kinetics 79−66296
dextran T-10 and α-cyclodextrin, absorption mode spin-echo spectra appl. 80−78634
o-dichlorobenzene, liq. mixtures, excess vols. and eqns. of state 77−29036
o-dichlorobenzene(-benzene), liq. and dilute soln., microwave absorption and relax. processes 79−82920
1,2-dichloroethane+benzene(toluene)(p-xylene), liq., molar heat capacities 78−18787
dichloromethane-cyclohexane, liq. mixture, intermol. vibrational energy transfer, US study 80−70313
dioxan-cyclohexane-chloroform, mixtures, compressibility, free length, molar and available vol., US meas. 78−2200
dioxan-methanol system, US vel., compressibility, complex form. 79−82283
dioxane-alcohol mixtures, US vel. behaviour with dioxane conc. 79−73254
p-dioxane-water mixtures, adiabatic compressibilities and sound vels., temp. depend. 79−28044
dipolar fluid mixtures, dielec. const. calcs. 79−64969
dipolar mixtures, pair distribution function 79−86668
direct analysis, MIKES method 78−44413
discontinuity surface, nonequilib. thermodynamics, appl. to n-component viscoelastic mixture 78−93638
disparate mass gas mixtures, near-normal behaviour 79−94762
disparate-mass gases description, generalised Navier-Stokes eqns. 77−51086
dodecan-1-ol+n-hexane, vap. press. and thermodynamic props., 298.230 to 342.824K 78−47528
drop dynamics in mixture with uniform temp., thermal diffusion effects 80−103097
Dufour's effect and hydrodynamic stability *(French)* 78−30284
elastic, 2-phase interpenetrating mixtures, closed system of eqns. *(Russian)* 78−16652
elastic mixtures, stability criteria 78−18514
electric conductivity of dispersed mixtures containing high-conductivity components 80−92954
electrolyte mixtures, in aq. soln., viscosity, individual electrolyte effects *(German)* 78−22881
electrolyte mixtures in aq. soln., viscosity contrib. coeffs. *(German)* 80−15287
ellipsoidal aerosol particles in binar binary gas mixture, diffusophoresis under hydrodynamic conditions 80−66888
eosin-erythrosin, soln., qualitative anal. using fluoresc. polarisation 79−24849
ethane-n-butane-n-hexane, vap.-liq. equilib. behaviour, visual cell, for 48.3-143.5°C, up to 7619 kPa 79−46790
ethanol-water mixture, Soret coeff. determ. 79−19386
ethanol-water mixtures, specific volume, compressibility, viscosity, up to 3200 bar, 15, 25°C 78−10113
ethanol-water system, metastable states, hydrates existence and props., low temp. 78−71835
ether-water mixtures, miscibilities, enthalpy of mixing, solvation *(German)* 78−18779
ethyl acetate-isopropyl bromide, IR laser induced decomposition 79−16011
ethylene dichloride-benzene, liq. mixture, excess Gruneisen parameter, intermol. interaction 78−67635
ethylene-CO_2 gaseous mixture, thermoosmotic conc. difference across membranes 79−83508
eutectic mixture, glassy nematic phase, complex permittivity tensor 79−91336
fibre-reinforced composite, quasi-one-dimens. thermal diffusion, mixture theory 78−71271
Fick's diffusion coefficients, of pseudobinary gas-steam mixtures rel. to mag. tapes prod. *(German)* 79−27735
flow of homogeneous mixtures, theory *(Russian)* 78−87326
flow rate meas. ultrasound propagation and scatt. approach 80−43806
flowing, motion in EM field *(Russian)* 79−32686
fluid, molecular basis of activity coeff., isobaric-isothermal ensemble approach 80−55690
fluid, multiphase system, vapour bubble collapse, charact. functions 78−18156
fluid, of hard convex bodies, accurate eqn. of state 80−6484
fluid, Ornstein-Zernike relation transformation 79−98855
fluid, perturbed hard chain theory, thermodynamic props., appls. in chem. technology 79−34343
fluid, simple, dense, bulk viscosity, hard spheres appl. 80−14982
fluid, viscosity and thermal conductivity coeff. prediction 77−43361
fluid 2-component mixtures, stability conditions and wave speeds 78−30344
fluid binary mixtures, phase equilibria and critical phenomena at high press. 78−51648
fluid mixtures, analytic and perturbation theories 78−18516
fluid mixtures, asymmetric, Henry's constants and second virial coeffi-cients from perturbed-hard-chain theory 80−96621
fluid mixtures, thermophysical properties prediction 80−48563
fluid mixtures, unified mol. theory, statistical thermodynamics 77−31570
fluid mixtures with dynamic interaction, basic eqns. 79−50692
fluid multicomponent mixture, number-conc. struct. factors 78−18526
fluidised beds, three-phase, heat transfer 79−60056
fluids with polar, quadrupolar, octupolar mols., thermodynamics, vapour-liq. equilibria 78−95127
fluorescein-rose bengale, soln., qualitative anal. using fluoresc. polarisation 79−24849
fluorobenzene(-benzene), liq. and dilute soln., microwave absorption and relax. processes 79−82920
fluorocarbon-hydrocarbon mixtures press. second virial coeff., graph theory prediction 80−43823
force between components 79−55439
formaldehyde-water, heuristic intermol. pot. function, ab initio MO calcs. 78−33566
furan-cyclohexane, liq. mixture, intermol. vibrational energy transfer, US study 80−70313
gas, adsorpt. by solids, review 79−28211
gas, binary, free expansion through channel, composition change 79−64709
gas, binary, moderate density diffusive creep along flat surface 80−43822
gas, binary mixture, spherical expansion into flooded space, components separation 79−81948
gas, binary mixture, thermal slip along spherical aerosol particle surface 78−34168
gas, binary mixtures, diffusion coeffs. lists 78−34254
gas, Boltzmann collision operator matrix elements 79−86545
gas, disparate mass, double sound propag., theory 80−33724
gas, large-volume prep. technique based on compressibility ratio 80−59165
gas, multicomponent gaseous diffusion coeffs., mean free path theory 78−18365
gas, multicomponent mixtures, thermodynamic equilib. 78−68909
gas, multivel. multitemp., gasdynamic eqns. 79−77052
gas, nonpolar binary mixture, calc. eqn. for thermal cond. 77−47135
gas, viscosities estimation, new simplified methods 77−80261
gas binary mixtures, flowing, probe for conc. meas. 79−4098
gas diffusion in porous bodies with press. changes 77−62662
gas mixture, binary, condensation in boundary layer flow, numerical method 79−1236
gas mixture, modified rough sphere model, rel. to sound absorpt. 78−93597
gas mixture, multicomponent, transport equations near catalytic surfaces 80−43821
gas mixture, physical and chemical process modelling 80−71892
gas mixture, separation in travelling mag. field in discharge 79−64927
gas mixture production method, composition control 78−1765
gas mixture separation by membranes *(Japanese)* 78−48691
gas mixtures, background gas penetration into underexpanded jets, densitometric obs. 79−94655
gas mixtures, coherent anti-Stokes Raman spectroscopy, anal. capabilities 77−40589
gas mixtures, detonating, symmetric piston motion 80−59073

mixtures continued
gas mixtures, eigenfunctions positivity in time depend. kinetics theory 77−19660
gas mixtures, high temp., transport prop. calc. *(Russian)* 79−37432
gas mixtures, IR absorpt. theory using hard sphere model *(Russian)* 80−14879
gas mixtures, kinetic studies rel. to gas lasers and pollutant detect. 79−48013
gas mixtures, marginal comp., thermal diffusion column performance evaluation *(German)* 80−59157
gas mixtures, pumping in high vacuum region 80−95107
gas mixtures, removal of condensing component by suction through porous walls 79−98787
gas mixtures, separation using variable-temp. cryogenic trap 79−16026
gas mixtures, standard, SMES-2 system for metrological support 79−20487
gas mixtures, thermodynamic props. prediction 78−83512
gas mixtures, third virial coeffs., nonadditive dispersion interactions effects 78−67299
gas mixtures, velocity slip in free jet expansions 79−94656
gas-dust mixture, wave eqns. of one-dimensional motion 79−86496
gas-gas immiscibility in binary fluid mixtures 78−34627
gas-liquid mixture, arbitrary amplitude acoustic wave propag. 78−38122
gas-liquid mixture, outflow from large container with a slit 80−74951
gas-liquid mixtures, flowing, gas conc. meas., acoustic method 78−59448
gas-oil mixtures trapped under ice, stable config. obs., energy meas. 80−108818
gas-solid, hydrodynamics, use of relative velocity of gas to solids *(Croatian)* 80−14799
gas-solid flowing mixtures, heat transfer 77−58773
gaseous, at high pressure, phase equilib. calc. 77−35291
gaseous, conc. fluctuations meas. using catalytic wire 77−26291
gaseous, ignition energy by capacitive discharge and through discharge of person charged with static elec. *(French)* 80−10446
gaseous binary mixtures, use of diffusion and second virial coeffs. to predict viscosities 79−14506
gaseous mixtures, equilib. at high temp., Raman scatt. obs. 80−45619
gases, dense multicomponent, diffusion eqn., approx. mass transfer description 77−47609
gases, equations of state, for gas analysis calc. 77−11294
gases, mag. ion pump operation 77−138
gases, multicomponent system, with internal energy states, kinetic eqns. 77−15145
gases, stresses produced by concentration inhomogeneities 77−31419
gases of different mass, kinetics and thermodynamics *(Russian)* 77−76015
gassy two-liq. pool., hollow sphere formation, LMFBR simulation 77−61518
gels, dynamic light scattering in poor solvent 78−88318
giant planet interiors, dense fluid mixture of nuclei, phase separation calcs. 77−56849
granular material mixtures, balance laws 77−19581
graphite-air mixture steady and oscill., mean heat transfer 80−89536
hard disc mixture, eqn. of state, compressibility and phase behaviour, mol. dynamics simulation 77−51291
hard ion mixtures, Ornstein-Zernike eqn. and Yukawa closure 80−107031
hard nonspherical molecule fluids, mixtures, conformal theory 79−94860
hard sphere fluid mixture, density fluctuations 77−19657
hard sphere mixture, Ornstein-Zernike eqn. with Yukawa closure 78−18513
hard sphere mixtures, finite angle light scatt., Percus-Yevick approx. calcs. 80−7363
hard spheres, dipolar, dielec. props. 80−24335
hard spherocylinders and spheres mixtures, Monte Carlo study 80−49073
hard-disc mixture, mol. dynamics simulation, self-diffusion coeffs. 77−89356
hard-sphere mixtures, excess thermal cond. and viscosity 77−11292
hard-sphere-like, soln. of Ornstein-Zernike eqn. 77−4028
HCl-inert gas mixtures, van der Waals molecules, far IR spectra 80−95610
n-heptane/3-pentanone mixture, vap. press. meas., thermodynamic functions calcs. 80−75345
p-n-heptyloxybenzylidene-aminofluorenone/COOB mixtures, dynamic twist viscosity near polycrit. points 79−95133
heterogeneous flows of multi-component mixtures in porous media−review 78−59471
heterogeneous solid surface, adsorption from multicomponent gas and liq. mixtures *(German)* 80−44430
hexan-1-ol+n-hexane, vap. press. and thermodynamic props. 298.230 to 342.824K 78−43129
hexane-cyclohexane mixtures, quantitative IR spectrosc. anal. 79−96377
n-hexane-n-dodecane 'ideal' mixture, viscosity, theory *(German)* 78−22882
n-hexane-n-pentadecane mixtures, solns., mech. of US absorption and viscosity *(Russian)* 79−90732
n-hexane-perfluoro-n-hexane mixtures, US vel. and absorpt. mixtures 80−88281
n-hexane/3-pentanone(acetone) mixtures, vap. press. meas., thermodynamic functions calcs. 80−75345
n-hexane/acetone mixtures, electroviscous effect, AC and DC meas. 79−14949
high-pressure asymmetric mixture vapour-liquid equilibrium calc. 79−4408
high-temperature gases, equilibrium composition calculation *(Russian)* 79−20499
homogeneous mixtures, diffusion general theory 79−90360
homogeneous mixtures, motion in EM field 79−94725
hydrocarbon+N oxide mixtures in air, photochemistry 79−53427
hydrocarbon-fluorocarbon, press. second virial coeffs., walks on graphs method 80−7841
hydrocarbon-simple fluid gas streams, second virial coeffs. calcs. 78−1777
hydrocarbons, liq. mixtures, thermodynamics *(German)* 78−20047
hydrocarbons, thermodynamic props., multiparameter conformal solution theory 78−18796
ideal mixture, viscosity, theory *(German)* 78−22882
immiscible, variational theory 79−27885
immiscible liquids, flow in helix, high press. boiler analogue 77−58763
inert binary mixtures, weak wave evolution, Burger's eqn. 78−90924
mixtures continued
inert gas, binary, μ-capture, near 5 atm., X-ray yield 80−58419
inert gas binary mixture, unlike mol. force consts. from viscosity data, thermal cond. 78−33565
inert gas liquid mixtures, collision induced absorpt. 77−4638
inert gas mixture, dipole autocorrelation function, Lennard-Jones and exponential dipole pots., classical calc. 80−64665
inert gas mixtures, interatomic pots. and interaction dipole moments, IR spectra calcs. 77−75082
inert gas mixtures for particle detection, high-pressure discharges in nonuniform elec. fields. 78−74545
inert gases, internal forced convection, numerical calcs. 77−47005
inert gases, liquid phase mixtures, dipole autocorrelation function, IR absorpt. spectra obs. 80−28903
inert gases, mixtures, dipole moments, IR absorpt. spectra obs. 80−28903
inertial coupling in dynamic eqns. of components 78−63483
interacting continua, thermodynamics and nature of 2nd law 79−26016
interparticle percolation, lateral and axial diffusion coeffs., shear cell appl. 79−61666
interparticle percolation, statistical mech. anal. 79−96281
interpenetrating EM structured continua, thermodynamic and mech. props. calcs. *(Russian)* 77−47580
iodides and mixtures, molten, elec. cond., density, viscosity, surface tension 77−80638
iodomethane, liq. (liq. mixtures), vibr. relax. and reorientation, symmetric C-H bending mode 1st overtone 78−62884
ionic mixtures, phase separation 80−77279
ionised mixture, dense, binary, dynamical props., statistical mechs. 80−43895
IR spectra, ratio method anal., computer simulation 77−71387
Ising lattice, thermal relaxation, nonideal behaviour, stochastic theory 80−22312
isobutyric acid-water binary fluid system, crit. props. 77−76563
isobutyric acid-water mixtures, phase separation, light scatt. 78−84592
isobutyric acid-water near-critical liquid mixture, nucleation 80−92664
isopropanol-n-propanol aq. mixtures, US relax., US absorpt. and vel. meas. *(French)* 80−103426
isopropyl alcohol-carbon tetrachloride, mixture, dielec. const., two-sided estimate 79−42262
kinetic behaviour, first order reactions 77−52609
Kneser liquids, vibrational energy exchange probabilities 78−38780
laminated composite, dynamic response under large deformation, nonlinear mixture theory 78−56717
large asymmetric mol. interaction with small mol., target factor, mixture thermodynamic props. 78−26225
Lennard-Jones, liq., binary, equimolar, static (dynamic) props., mol. dynamics calc. 80−64857
Lennard-Jones liq. mixtures, mol. dynamics calc. 78−55794
Lennard-Jones liquid mixture, mol. dynamics, attractive term effects 77−11454
Lennard-Jones liquid mixtures, local comp., mol. dynamics calcs. 79−82133
liquid, binary, ultrasonic approach to interaction 80−79881
liquid, binary mixture, viscosity, semi-empirical procedure, data correlation 78−34643
liquid, decomposition into components by thermal action of continuous laser irradiation 79−19362
liquid, excess Gibbs free energy, quasilattice local composition model, phase equilib. 78−31681
liquid, mol. assembly, iterational soln. to integrodifferential eqn. 79−77473
liquid, nonideality, prediction and meas. of thermodynamic excess functions 78−27818
liquid, static surface tensions, monolayer model 77−4245
liquid, US propag. parameters, effective Debye temp. 80−79882
liquid, vibr. relax., line widths, intermol. forces dephasing 77−47315
liquid, viscosities, empirical formula, continuum theory and generalised Navier-Stokes system 78−14498
liquid (isotope) mixture, isotropic Raman spectra, intermol. vibr. mode coupling 79−31535
liquid and gas mixtures, thermodynamic props., conf., Braunschweig, Germany (May 1976) 78−20046
liquid binary, viscosities, effectiveness of mixture eqns. 77−69109
liquid binary acid+base mixtures, excess vol. and viscosity 77−21408
liquid binary mixtures, evaluation of excess internal pressure, Van der Waals' constant and ultrasonic velocity from flory's theory 80−70310
liquid binary mixtures, proton mag. relax. and mol. motion 77−28471
liquid binary mixtures of optically anisotropic molecules, depolarized Rayleigh scatt. 80−40122
liquid binary mixtures theory in quasichem. approx., hole theory and thermodynamic functions *(Spanish)* 77−72534
liquid crystal, binary mixtures, phase transition, entropy, relation to smectic plane tilt angle 80−65203
liquid crystal binary mixture phase separation, statistical theory 77−4188
liquid crystal mixture phase equilibria and transition temperatures 78−63845
liquid crystals, amines and nitriles, binary mixtures, induced phases 79−90765
liquid mixture, adsorption on solid, equilib., thermodynamics correlations 78−84045
liquid mixture, binary, oscillatory convective instability, thermodynamic anal. 78−94753
liquid mixture, modified Heil-Prausnitz eqn. for excess Gibbs energy 77−62652
liquid mixture, shallow, laser separation, thermal mechanism 80−5925
liquid mixture, surface tension theory 80−88404
liquid mixture US tissue model, component selection aid 77−78066
liquid mixtures, activity coeffs. calcs. using struct. group contribs. *(German)* 78−18777
liquid mixtures, binary film boiling, theory 77−84912
liquid mixtures, excess enthalpy 79−23733
liquid mixtures, phase separation, umbrella sampling, Monte Carlo calcs. 77−35698
liquid mixtures, separation by facilitated transport through liquid membrane 78−76920
liquid mixtures, showing phase splitting, modified Wilson eqn., phase equilib. prediction 80−96636
liquid mixtures, thermodynamic props., mol. theory 78−18515

mixtures continued
liquid mixtures, thermodynamic props. for mixed fluid densities 78−18775
liquid mixtures, thin layer separation by laser heating 79−29404
liquid mixtures adsorpt. on heterogeneous surfaces 79−56073
liquid-gas mixtures, sound speed in water-air and water-steam 77−84029
liquid-liquid, crit. soln. point, sedimentation and density gradients in high gravit. field 77−59121
liquid-liquid mixing analysis, lamellar model 80−15246
liquid-liquid phase equilibria, theory, chem. models 78−18781
liquid-solid fluidised beds, particle segregation, transition regions 79−46379
liquid-solid semi-fluidisation characts. for heterogeneous mixtures 77−36792
liquid-vapour equilibrium, thermodynamic props. using modified Redlich-Kwong eqn. of state 77−36775
liquids, multicomponent, diffusion eqn., approx. mass transfer description 77−47609
local composition equations derivation and extension of UNIQUAC eqn. 79−14933
low-boiling compound separation by low-temp. gas chromatography 79−70397
2,6-lutidine-water, spinodal decomposition, light scatt. obs. 78−34625
LV dynamic scatt. display liquid crystal mixtures 77−77178
macrocontinuum model of a mixture and a discrete multi-constituent system 79−94482
magnetic mixture of triangle-bond elements, Ising model 77−69467
mass spectroscopic analysis, integrated MS/MS technique 79−34389
mass-analysed ion kinetic energy spectrometry using negative chem. ionis., direct mixture analysis 79−34397
MBBA-BBCA mixture, field-induced distortion of mol. orientation 79−99060
MBBA-EBBA mixtures, thin and mol. films, between Hg electrodes, I-V characts. 79−11253
MBBA/CC mixtures, cholesteric phase, torsional shear flow in elec. and mag. fields 79−86697
MBBA/n-hexane, isotropic-nematic transition, transient optical Kerr effect study 79−82323
MBBA/non-mesogenic cpd., binary nematic mixtures, dielec. relax. and intermolecular interaction 79−91350
metal nitrates, molten mixtures, US vel., thermodynamic interpretation *(French)* 78−79670
methane+N_2(Ar), compressed-liquid dielectric const., derived excess vol. 79−11377
methane(-ethane)(-N_2), heat transfer in nucleate boiling of liquified gases and binary mixtures *(German)* 79−18687
methane(-H_2), long path photoelec. absorpt. spectra 4200-10600 Å, appl. to Uranus 77−83592
methane-Ar, cryogenic fluid mixture, transport phenomena, shear viscosity *(Russian)* 80−29198
methane-ethane liq. mixture, phase equilib., heat of mixing, vol. change, data evaluation 80−15233
methane-ethane-propane-butane, binary and multicomponent mixtures, viscosity, diffusion coeffs. 78−94883
methane-hydrogen mixture, flow through glass bead bed, axial dispersion coefficients 79−46378
methane-Kr, mixture self-diffusion of Kr, density depend. 77−76587
methane-Kr mixtures, rot. self-diffusion and spin-lattice relax. *(Russian)* 79−69745
methane-O_2, solid mixture, electron diffraction study *(Russian)* 78−83953
methanol+water mixtures, solubility of AgCl 77−47579
methanol-ethanol mixture, dielectric const. composition depend. rel. to struct. effects 79−11378
methanol-pyridine base systems, excess enthalpies of mixing 79−42255
methylethyl ketone-butanol, soln., excess thermodynamic props. and interactions, US vel. and density meas. 80−39288
microemulsion, struct. description of liq. particle dispersion, ultracentrifugation and small ang. neutron scatt. obs. 79−5184
miscible fluid mixtures, mechanics and thermodynamics, variational approach 79−93084
molecular fluids, binary mixtures, hydrodynamics eqns., VH light scatt. 78−35158
molecular volume effects in the excess functions of binary mixtures *(Spanish)* 80−15261
molten metal binary mixtures with wide immiscibility range, gravitational layering of components *(Russian)* 80−104092
molten salt mixtures, transport props. *(German)* 78−80750
molten saltes, binary, excess thermodynamic props. and US vel. *(French)* 77−27943
molten salts, enthalpy of mixing, theory, Monte Carlo calcs. 77−72691
monolithic materials for creating high pressures, anvil device with lune toroid 80−73377
motion, general approach 79−17233
moulding, consolidated, residual stress meas. 79−87791
moulding materials and mixtures, exam. of gases released 79−52817
multicomponent, mass transfer, penetration depths 79−42286
multicomponent, quantitative analysis from absorpt. spectra, review 79−52811
multicomponent fluorescent mixtures, quantitative anal. of data 78−27833
multicomponent liquid mixture, viscosity, Panchenkov model calcs. *(German)* 77−31797
multicomponent liquid mixtures, empirical excess volume model, for estimating densities 79−1503
multicomponent mixtures, approx. methods comparison 78−65887
multicomponent mixtures, data interpretation using nonlinear sets of eqns. *(Russian)* 77−66028
multicomponent mixtures, vapour-liquid equilibria predictions, statistical thermodynamic approach 77−55335
multicomponent polymer system, liq.-liq. phase separation, thermodynamic aspects of polymer compatability 78−14469
multicomponent vapours-condensed phases, equilib., computer modelling 80−44288
multitemperature gas mixtures, Maxwell-Grad moment method calcs. 77−47134
natural gas mixtures, simulated, enthalpy and phase equil., correl. with modified Starling eqn. 80−61127
natural gas-related saturated liquid mixtures, molar vols. 79−1505
nematic liquid crystal mixture of aliphatic materials 79−90543

mixtures continued
nematic liquid crystals, binary mixture, dil., thermodynamic props., statistical model 79−94882
nematic liquid crystals, dielec. permittivity dispersion 80−88921
nematic liquid crystals and mixtures, temp. dependence of density, obs. *(Russian)* 79−14681
nematic solution, hard rigid/flexible mols. mixture, unathermal, lattice model *(Russian)* 80−54129
nematic-chiral mixtures, viscosity and electrooptical characts. 79−86682
nematic-isotropic phase equilibria in binary mixtures containing rigid rod solutes 79−86873
Newtonian fluids, mean velocity and vol. flow rate for steady 1-D flow 80−6132
nitrobenzene-aniline, US vel., sp. ht. and compressibility 79−33037
nitrobenzene-hexane mixtures, nonlinear dielec. effect beyond critical pt. 79−99816
nitroethane-isooctane mixture, depolarised Rayleigh scatt. near crit. point 80−45089
4-nitrophenyl-4-octyloxybenzoate/cholesteric liq. cryst. mixtures, helix pitch, temp. depend. 80−64895
nitroxide free radicals, neutral, EPR spectra, localised solvent-radical adducts 79−96290
non-equilibrium thermodynamics of simple mixtures 80−76543
nonadditive hard spheres, mixtures, scaled particle theory 79−44848
nonideal fluid mixtures, generalised film model for mass transfer across interfaces 77−67387
nonideal gas, dissociating, composition and thermodynamic props., initial at. method 78−40034
nonideal gaseous mixtures, prediction of acoustic vels. 78−67306
nonisothermal ideal gas mixture, stationary state, inert and dissoc.-assoc. components 77−60042
nonisothermal mixture motion through porous media, sorption dynamics and heat exchange kinetics 77−7447
nonpolar binary mixture, partial molar vol. prediction from Lee-Kesler eqn. of state 80−10632
nonpolar binary systems, generalized correl. for Henry's constants 78−67827
nonpolar solvents, binary, gas solubility, entropy of soln. 79−52745
nonracemic mixtures, theory of chirality functions, concept of qualitative completeness 80−69255
nonyloxybenzoic acid/cholesteric liq. cryst. mixtures, helix pitch, temp. depend. 80−64895
nozzle, gas mixture in quasi-one-dimens. flow, vel. slip and temp. difference 79−64735
nylon 6-inorganic salts, glass transition temp. 80−19921
octafluorocyclobutane+n-butane mixtures, 233K, surface tension meas. 79−19371
octamethylcyclotetrasiloxane-cyclohexane liq. mixtures, u.p. and excess Gibbs free energy determ. 77−30225
oil-water vibrational mixing in artificial weightlessness *(Russian)* 77−59118
oligomeric liquid mixtures, transition to, polymer systems, thermodynamics 78−20048
olivine mixtures in Earth mantle, rel. to P-wave vel. anisotropy inversion 77−49017
one-fluid approx. transport coeffs., critical region behaviour 79−14951
organic, second virial coeff. meas. using new apparatus 80−44289
organic binary liq. mixture, relax. times and dipole moments, RF and microwave obs. 77−12308
organic binary liquid mixtures, excess free vol. calcs. 80−34202
organic binary liquid mixtures, US vel. rel. to non-ideal behaviour 78−95109
organic binary mixtures, with weak charge transfer interactions, thermodynamic props. 80−54360
organic components, liquid-liquid equilibrium data, retrieval 79−46797
organic liquid mixture separation by hyperfiltration and pervaporation through polymer membrane 80−16720
organic liquid mixtures, excess free vol. US vel. meas. 77−51294
organic liquids, positronium form., spur process 78−1113
organic mixture analysis by high-resolution mass spectrometry/mass spectrometry 80−104476
overstability in horizontal layer of binary liq. mixture with Soret effect 80−106782
pair distrib. functions, modification of regular solution theory 78−67829
partial molar quantities, calc. from molar quantities *(German)* 78−85191
perfluorinated mixtures, hydrostatic liquids for obs. of NMR 79−2801
perfluorocarbon-SF_6 mixtures, sparking C inhibition, decomp. product investig. 80−89478
perfluoromethylcyclohexane-methylcyclohexane, near-critical liquid mixture, nucleation 80−92664
petroleum-acetylene-O_2 combustion products, seeded, elec. cond., for MHD power plant 78−34256
phase equilib. prediction, simplified molecular models of soln., study of binary, ternary mixtures 79−19351
phase equilibrium, augmented Van der Waals theory 78−79737
phase equlibria, molecular thermodynamics calculations, practical appls. *(German)* 78−18733
phenetole, in cyclohexane-ethanol mixtures, UV spectra, solvent effect 79−22770
phenol, in cyclohexane ethanol mixtures, UV absorption, solvent effects 79−22767
phenol-chloromethane, US absorpt., phenol cyclic assoc. 77−15501
phenol-cyclohexane (-ether), UV spectra, solvent effects, matrix rank anal., species determ. 79−22768
phenol-cyclohexane US absorpt., phenol cyclic assoc. 77−15501
phenol-organic solvent mixtures, UV spectra, solvent effects 79−22769
phenols, substituted, in cyclohexane-ethanol mixtures, UV spectra, solvent effect 79−22770
phenylenediamine-dihydroxybenzene mixtures, solid-liquid equilibria, phase diagrams 77−27986
physical-chemical separation and thermodynamics, review *(German)* 78−18774
pigment associations, conc. effects, luminesc., absorpt. spectra and dichroism obs. 80−1007
plasma, low ionised binary mixture, electron kinetics, collision processes influence *(German)* 79−14519
plasma chromatograph/mass spectrometer simultaneous electron impact/chem. ionisation carrier gas mixture 79−30600
PMMA-PVC mixtures, dielec. relax. and struct. rel. to formation *(Russian)* 77−20073

mixtures continued
polar fluid mixtures, two-absorber model of solvated electrons, spectra 78 - 85284
polar liquids, binary mixtures, Sarma and Rao's rel. for dielectric relax time 80−88914
polar solvent mixtures, solvated electron diffusion, 2-absorber model 80−85206
polar-nonpolar mixtures, pot. of mean force 79−90510
polar-polar liquid mixture, significant structure model applic. to dielec. const. correl. 77−8487
polar/nonpolar mixtures, pot. of mean force, approx. theories, clustering of solute mols. 78−26401
polyarylate-polyethylene oxide block-copolymers and mixtures, phase separation, DSC obs. *(Russian)* 79−55895
polyatomic compounds, fluoresc. in discharge 79−54891
polyatomic fluid, thermodynamics, phase equilib. calcs. 79−1485
cis-polybutadiene and butadiene-styrene copolymer mixture, effect of temp. on phase composition 79−96005
polydisperse, vapour-liquid mixtures, acoustic velocity, damping decrement 80−66881
polyethylene, high-density, mixed with gypsum, flow props. *(Japanese)* 77−7357
polyethylene, high-density, mixed with gypsum, flow props. *(Japanese)* 77−7358
polyethylene oxide 2000-200 mixtures, Raman scatt., small-angle X-ray scatt. 77−52089
polyethylene-paraffin mixtures, crystallisation kinetics 79−41985
polyethylene-polystyrene blends, crystn. characts. 80−103261
polyheteroarylene-epoxy resin, thermodynamic stability and compatibility *(Russian)* 79−65204
polymer, breakup of anisometric drops 77−40578
polymer blends, two-component, glass transition, calorimetric investig. *(Russian)* 80−39268
polymer homologue mixtures, viscosity, conc. depend. *(Russian)* 79−23761
polymer melt, cross-links effect on struct. 79−41928
polymer melt mixtures, thermodynamically incompatible, flow, specific fibre formation mechanism 77−23926
polymer mixture, particle size in dispersed phase, effect of component viscoelasticity 77−44514
polymer mixtures, molten, interface props. near consolute point 78−87792
polymer mixtures, thermodynamics, review 79−1506
polymers, heterophase mixtures, excess energy 78−53264
polymers, IR difference spectra, dispersion effects 79−96379
polymers, linear, viscoelastic props. under flow conditions, transition to highly elastic state *(Russian)* 79−50690
polymethylmethacrylate-polycarbonate blends, kneading characts. *(Japanese)* 80−104112
polynary mixtures, natural convection boiling, heat transfer 78−90658
polyoxymethylene-copolyamide blend melt, viscoelastic peculiarities *(Russian)* 78−38263
polyoxymethylene-copolyamide mixture melt, plasticiser effect on props. and fibre form. during flow 77−27500
polystyrene-polyethylene-(polymethylmethacrylate) blends, kneading characts. *(Japanese)* 80−104112
polystyrene-polypropylene(polyethylene) mixtures, elastic moduli, phase struct. effect *(Polish)* 79−70107
porous media models using thermodynamics of mixtures 80−96184
porous moist body, air-vapour mixture form., in contact heating 77−75784
powder, fine particle, morphological anal. 80−104087
precipitation of aerosol particles on a fixed evaporating droplet 80−7869
precipitation of aerosol particles on an evaporating droplet in a turbulent gas flow 80−7870
n-propanol mixtures, US vel. depend. on association compounds 79−60436
purification of materials with overlapping absorpt. spectra 80−78452
quantitative analysis by ^{13}C NMR 78−31716
quenched binary, early stage evolution, kinetic Ising model 77−69468
radionuclide corrosion and fission products, ion exchange separation 80−18460
radionuclide corrosion and fission products, liquid-liquid extractions with metal diethyldithiocarbamates 80−18459
Raman spectroscopy and liq. chromatography anal. *(French)* 80−45595
rarefied gas mixture Poiseuille flow 79−14438
rational description, theory 78−20053
real gases, thermodynamic props. and intermol. pots. *(German)* 78−17743
rhodamine 6G, delayed fluoresc. of simple associates in polar and nonpolar solvent mixtures *(Russian)* 78−48185
rhodamine 6G-ketocyanine mixed solns., wideband lasing 79−957
rhodamine dye mixtures, qualitative anal. by fluoresc. polarisation spectroscopy 79−34396
rotating binary mixture over infinite rotating disk, species distrib., existence and uniqueness of solns. 77−15044
rubber mixtures, synthetic, natural ageing effects on dielec. props. 77−24778
rubber-channel black mixtures, natural ageing effects on dielec. props. 77−24777
rubber-resin mixtures, viscoelasticity 79−43303
salts, molten, liquidus surface and eutectic pts. 78−30736
saturated densities of liqs. and mixtures, new correlation method 80−15174
scaled particle theory results for dense mixtures of convex shaped mols. 78−1969
second harmonic generation in powder mixtures 77−62009
sedimentation of binary particle mixtures 80−40757
sheared particulate beds, mass transport kinetics in, Markov chains appl. 79−60057
smectic mesophases of binary mixtures, isobaric phase diagrams, non-ideal behaviour *(French)* 79−95141
sodium-caesium acetate, molten mixture, elec. cond. and density 77−15613
sodium-rubidium acetate, molten mixture, elec. cond. and density 77−15613
soft spheres binary mixtures, equilib. and non-equilib. radial distrib. functions 80−49074
soft-sphere mixture viscosity, nonequilib. mol. dynamics 80−19680
solid, with diffusion, axiomatic theory of mech. behaviour 77−858
solid-fluid, incompressible, equilibrium theory 77−857
mixtures continued
solid-fluid, thermostatics 77−856
solid-liquid phase equilib., binary and ternary systems, excess Gibbs free energy 78−30736
solids, multicomponent mixing index and contact number estimation by spot sampling 80−16214
solvent-rod mixture, two phase, interfacial free energies, quartic van der Waals theory 80−59377
solvophobic effect in simple fluid mixtures 77−31569
soot-gas mixture, in luminous flames and smoke, IR mean absorption coeffs. calc. procedure 78−91061
specific heat of binary liquid mixtures 78−63862
steel, low C, dual-phase, law of mixtures, applicability 80−89346
stress-strain determination by high press. X-ray diffr. 77−7792
styrene-ethylbenzene system, separation by liq. membrane permeation, operating parameters influence on selectivity 79−87871
superheated binary liquid mixtures, homogeneous nucleation of bubbles 78−67818
supersonic blunt body flow of viscous perfect gas and nonequilib. gas mixture 80−28578
surface segregation, nonequilib. 80−88325
TBBA/4-n-pentylphenyl-4-(4-cyanobenzoyloxy)benzoate, mixture, possibility of smectic A-smectic A transition 79−95132
TBBA/n-hexyl-4′-n-dodecyloxy-biphenyl-4-carboxylate, mixtures, orthogonal smectic B to tilted smectic B (smectic H) transition 79−94881
ternary liquid mixtures, molecular interaction and thermodynamic props. 78−59861
ternary liquid mixtures, nonlinear effects with high amplitude US prop. 78−51613
ternary liquid mixtures, physical props., determ. by density and US vol. meas. 79−37751
ternary liquid mixtures, shear viscosity at plait points 77−35685
ternary mixtures, eutectic point localisation, thermodynamic calcs. *(French)* 78−79742
ternary system isothermal Gibbs-Duhem eqn., direct numerical soln. 79 - 1511
tetrachloromethane-cyclohexane system, interdiffusion, ternary diffusion eqn., radioactive tracer obs. 78−79792
tetrafluoromethane-inert gas, compressed fluids, ang. momentum relax., NMR 78−19355
tetrafluoromethane-trifluoromethane-chlorotrifluoromethane, vapour-liq. equilib. compositions, calc. 80−19925
tetrahydrofuran-benzene, soln., excess thermodynamic props. and interactions, US vel. and density meas. 80−39288
theory of constrained mixtures with multiple temperatures 80−62600
thermal conductivity prediction of heterogeneous mixture, digital simulation technique 78−87247
translational relaxation at shock wave front in gas mixture 80−74917
tricritical phenomena, ternary, quaternary fluid mixtures, classical models 78−91416
triethylamine/alcohol mixtures, theoretical evaluation of sound vels. and AB interactions 78−18706
triethylamine/phenol mixtures, theoretical evaluation of sound vels. and AB interactions 78−18706
trifluoroacetic acid-acetic acid, equimolar mixture, US absorpt. 77−15505
2,4,6-trimethyl pyridine-aliphatic alcohols, molar excess enthalpies and vols. 79−42254
two-component, two photon isotope separation, dynamics 80−102584
two-phase, shock wave propagation *(Russian)* 78−51196
two-phase flow through variable cross section channels, critical flow rate 79−55410
vacancy solution theory of adsorption from gas mixtures 80−65357
vapour, with or without inert gas component, condensation, heat transfer coeff. calc. *(German)* 77−39724
vapour phase organic solute conc. estimation, from rel. humidity meas. 78−34614
vapour-liquid crit. props. for pure liqs. and mixtures 80−65213
vapour-liquid equilib., high press., phenomenological description, review 78−30737
vapour-liquid equilibria, fugacity coeff. calc., pseudocritical method 77−27972
vapour-liquid equilibria, mixing rules in equations of state 80−19902
vapour-liquid equilibrium, generalised one-parameter Redlich-Kwong eqn., mixtures 78−34589
vapour-liquid mixture, outflow from large container with a slit 80−74951
vapour-noncondensible gas mixture, body force convection condensation *(Japanese)* 79−50574
vinyl polymer mixed monolayer behaviour 77−85020
viscous fluid mixture with thermomolecular diffusion, new variational-Lagrangian thermodynamics 79−49185
vortex tube efficiency, hot end inner rifling influence 79−94462
water and saturated monatomic alcohol mixtures, effects of chlorides on struct. 79−86840
water vapour, dissociating, composition and thermodynamic props., initial at. method 78−40034
water vapour-N_2, nonstationary rarefaction wave, nonequilib. condensation obs. 77−75937
water-2-propanol, density, US vel. meas. 78−18529
water-alcohol, US attenuation meas., method of streaming 80−88272
water-dioxan mixtures, positron annihilation, o-positronium pick-off quenching 79−24386
water-ethanol(methanol), nonlinear acoustic coeff. meas., 0-50°C *(French)* 80−34142
water-ethanol mixtures, hydrophobic interaction, scaled particle theory 78−22625
water-formic acid (acetic acid)(propionic acid)(n-butyric acid), PMR relax. obs., mol. assoc. 79−33553
water-methanol(ethanol)(acetic acid), liq., Verdet const., pulsed mag. field meas. 80−16012
water-methanol (n-propanol), binary mixtures, nucleation 80−44305
water-methanol mixtures, viscosity at 25°C, isotope substitution effects 80−92700
water-nigrosin black dye-Teflon spheres dispersion, laser backscatt., turbidity 80−1129
waves, miscible (immiscible) fluids, in closed horizontal (vertical) ducts 77−62263
zeolite-bearing rocks, multicomponent, quantitative thermogravimetry 79−16082

mixtures continued
$AgCl_xBr_{1-x}$, binary melt, Ag solubility, temp. and conc. depend. 80−10677
$AlCl_3$-LiCl, molten, specific cond. meas., comp. and temp. depend. 80−15279
Al_2O_3-epoxy mechanical mixtures, stress-wave propag. model, dynamic response expts. 79−1477
Ar, Ar-N_2(Xe), detection gas suitability for proportional scintillation counter *(German)* 78−41901
Ar/Co_2 counting gas mixture, electron transport coeff. calc. 79−32727
Ar/methane, counting gas mixture, electron transport coeff. calc. 79−32727
Ar-ether(acetone)(benzene)(ethanol), conc. profile and interdiffusion coeffs. meas. 79−94763
Ar-ethylene mixtures for drift chamber appl. 78−25391
Ar-He rarefied mixture in supersonic nozzle and jet, longit. translational nonequilib. 79−27678
Ar-Hg, gas mixture, diffusion coeffs. and electron temps. 77−62327
Ar-Kr, liq. mixture, excess thermodynamic props. 78−75836
Ar-Kr mixtures, liq.-vap. isotope fractionation factors 78−33626
Ar-monochlorodifluoromethane mixture, US vels. and absorption coeffs., determ. of relaxation times 78−63530
Ar-N_2 mixture, lasing at four lines 80−99713
Ar-NH_3, viscosity under press., density depend. and mol. assoc. 80−1727
Ar-Ne mixture, thermal conductivity, 400-1500K 79−18987
Ar-O_2, diffusion, search for Senftleben-Beenakker effect 77−15155
Ar-SF_6, thermophysical props., second virial and diffusion coeffs., thermal diffusion factors 78−42699
Ar-Xe, liq., Zwanzig perturbation expansion convergence, free energy 77−76274
As_2Se_3-As_2Te_3, liquid, mixture enthalpies *(German)* 79−77770
BCl_3-N_2, thermodiffusion props., effect of resonant excitation of mol. vibr. by laser, isotope separation 80−100047
$BaBr_2$-$BaCl_2$, vap. mixture, ion-mol. equilib., heat of form. of ions 80−26039
$BaCl_2$-$BaBr_2$, vap. mixture, ion-mol. equilib., heat of form. of ions 80−26039
Bi-BiI_3($BiBr_3$) liquid binary mixtures, phase separation under press. 80−34183
Bi_2O_3-CoO system, X-ray diffr., thermal anal. and metallography obs. 80−24598
Bi_2Se_3-Bi_2Te_3, liquid, mixture enthalpies *(German)* 79−77770
Br_2-Ar liquid mixture, vibr. relax., 1-D mol. dynamics study 79−73079
C mixes, extruded, preoxidation treatment effect on transverse breaking strength 77−63767
C powder, binary mixtures, bulk density, charact. curves interpret. 77−63574
C, rheological props. at very low shear rates using capillary rheometer 77−65691
C, rheological props. using capillary rheometer, binder content depend. 77−65692
C_5 hydrocarbons, in binary mixtures, phase equilibria *(German)* 79−37822
CO-N_2-^{3}He, nucl. reactor active zone, plasma and sustained discharge props. 80−5729
CO-O_2 liq. mixture, enhancement of nonlinear optical processes with double-pass tight-focusing geometry 79−18472
CO_2-air, heat transfer from cylindrical anemometer probe 77−84256
CO_2-air mixtures, mol. rot. temp. determ., absorpt. spectra calcs. 77−30851
CO_2-Ar(He), stepwise pulsed photoionisation 77−50479
CO_2-N_2, hot gas mixture, spectral and integral emission capacities calcs. *(Russian)* 77−68054
CO_2-N_2 mixture, strongly excited, vibr. relax. 80−102555
CO_2-N_2 mixture, temperature measurement by spectrum line reversal 80−73358
CO_2-N_2 mixture gasdynamic laser, energy characts. 80−69362
CO_2-N_2-He, vol. discharge, negative ions effect 80−14956
CO_2-N_2-He volume discharge, self-sustained, with UV preionis. 79−60211
CO_2-N_2-He-CO gas laser mixture, electron motion anal. 79−64199
CO_2-water vapour mixtures, 2.7 micron band absorption, 1000 to 2200K, 0.25 to 3 atm. 77−58006
CO_2+Kr(Xe), ^{13}C-mag. shielding density depend. 78−9173
CS_2-ethanol mixture, thermal diffusion ratio determ. by forced Rayleigh scatt. 78−75858
$CdBr_2$-$BiBr_3$, molten, elec. cond., 500-870K, composition depend. 78−55965
$CdCl_2$-NaCl, KCl molten salt mixtures, US velocity and adiabatic compressibility obs. 78−75730
CdI_2-Cd(I) mixture, molten, nuclear spin relax. 80−88887
$Cd(NO_3)_2$.4.1H_2O-$CoCl_2$, melt viscosity, equivalent conductivity, glass transition temp. 78−75855
$Cd(NO_3)_2$.4.1H_2O-$NiCl_2$, melt viscosity, equivalent conductivity, glass transition temp. 78−75855
^{252}Cf neutron source for water-steam mixture void fraction meas. 79−26762
Cs atomic frequency standard, optically pumped, buffer gas mixture optimisation 77−37859
CsCl-$BaCl_2$($LaCl_3$) molten binary mixtures, thermal cond. 79−86931
Cu-Al_2O_3 powder, electrolytic deposition 78−84743
$CuCl_xBr_{1-x}$, binary melt, Cu solubility, temp. and conc. depend. 80−10677
D_2-DT-T_2, three-phase region, temp.-press.-composition correlations 77−84889
D_2-DT-T_2 fusion fuel, estimated physical and chem. props. 80−8746
D_2+H_2(N_2O)(O_2), Wassiljewa coeffs., thermal conds., 50 and 100°C 79−37437
D_2O-H_2O mixing, diffusion meas. using neutron radiography 77−15605
F_2-Ar mixtures, electron attachment rate to F_2, elec. cond. meas. 79−7019
Fe-Ni-C, Redlich-Kister eqns., activity coeffs., phase equilib. 78−23664
α-Fe_2O_3-Li_2O, structural and thermal phase behaviour from mag., spectral and thermal studies 80−2673
γ-Fe_2O_3 and glass mixtures, calibration standard for magnetic susceptibility meas. 79−88989
H, thermochemical production, irreversibility anal. of separation schemes from binary gas mixtures 80−35767
H/He mixtures in interiors of Jupiter and Saturn, condensed matter physics 80−77307

mixtures continued
H-He fluid, phase diagram and transport props., planetary appl. 78−28554
H^+-He^{2+} mixture, fully ionised, two-component plasma, mean spherical model 80−87854
H_2-Ar, H_2 separation in thermogravitational column 80−45561
H_2-Ar, liq.-vapor equilib. 83 to 141K, to 52 MPa 79−42226
H_2-CO_2, turbulent flow heat transfer, expt. and numerical anal. 78−94690
H_2-D_2 gas, thermal cond. meas., 2-36 MPa 80−64668
H_2-D_2 vacuum deposited solid films, struct. study transmission electron diffr. obs. *(Russian)* 79−11035
H_2-H_2S, solubility of S in Pd, 600-1000°C, gas mixture composition depend. *(French)* 78−87791
H_2-He, nucl. shielding, ab initio coupled HF calc. 79−89690
H_2-He, thermal cond. meas., up to 14 MPa 80−64669
H_2-He(Ne), NMR longit. relax., mole fraction depend. 77−61767
H_2-methane mixture properties for hydrogen supplementation of natural gas 80−45781
H_2-N_2, liquid-vap. equilib., 63-110K and up to 57 MPa 79−55881
H_2-NH_3 mixture, viscosity meas., 25-100°C, up to 120×10^5 Pa 79−32731
H_2-thianaphthene mixtures, gas-liq. equilib. 79−65177
H_2+D_2(O_2)(N_2O), Wassiljewa coeffs., thermal conds., 50 and 100°C 79−37437
HI-H_2-I_2, H_2 separation in thermogravitational column 80−45561
HNO_3-HNO_2, aq. soln., N isotope exchange in presence of NO 80−16662
HNO_3-water, homogeneous nucleation, relative humidity depend. 78−71846
H_2O-acetic acid, liq. mixture, thermodynamic excess functions, calorimetric meas. 77−52666
H_2O-H_2SO_4, mixtures, transient nucleation, stochastic theory 77−1221
H_2SO_4-H_2O, aerosol form., nucleation calcs. 78−31709
H_2SO_4-H_2O, vapour mixture, temp. depend. of nucleation, aerosol form. 77−86350
H_2SO_4-water, homogeneous nucleation, relative humidity depend. 78−71846
$H_2(^3\Sigma_u^+)$-He(2^3S), discharge ionisation growth, diffusion coeffs. 78−83636
He-air, thermal cond. meas., conc. depend., 315K, 330K *(Russian)* 78−71421
He-Ar, corresp. states law and thermal diffusion, two-bulb meas. 77−3910
He-Ar, diffusion coeff., two-bulb meas. 77−11299
He-Ar, gas mixtures, thermal cond. meas. in the range 0.5-15 MPa 80−14874
He-Ar, positron annihilation decay consts., temp., elec., and mag. field depend., computer anal. 78−78809
He-Ar mixture, mass separation with rot. plasma 79−13842
He-Ar(N_2)(O_2)(CO_2), binary diffusion coeffs., press. depend., 300 and 323K, Thorne's eqn. 80−1724
He-Ar(Xe) mixtures, US vel. meas., phase separation 79−27738
He-Cs mixture, Cs ion conc. determ. by radn. absorpt. 79−34395
He-N_2, mutual diffusion coeff. meas. depend. on cell geometry 77−3911
He-Ne, disparate mass, double sound propag., theory 80−33724
He-O_2, diffusion, search for Senftleben-Beenakker effect 77−15155
He-O_2 diffusion coeff., two-bulb meas. 77−11299
He-Xe, eqn. of state, Monte Carlo calcs. 80−59158
^{4}He-D_2 mixture, binary diffusion coeff. near phase separation line *(Russian)* 80−6191
Hg vapour-gas mixture, Hg diffusion, data correlation 78−79403
Hg-Xe solid films, optical absorpt., localised states 79−61452
$HgBr_2$-$BiBr_3$, molten, elec. cond., 500-870K, composition depend. 78−55965
I_2-He-Xe, gaseous mixture with one low conc. component, thermal diffusion calcs. 77−19661
$In_{1-x}I_x$, molten mixture, NMR, reson. shifts, relax. rates, quadrupole relax. 80−2654
KBr-LiBr, liq. mixture, struct. and diffusion 80−24344
KCl-$AlCl_3$, molten mixture, vap. pres. meas. 78−87779
KNO_3-$RbNO_3$, liq., electromigration cation and mobility and isotope effect 80−10691
Kr, Kr-Xe, detection gas suitability for proportional scintillation counter *(German)* 78−41901
Kr mixtures, binary and ternary, viscosity meas. 78−18367
Kr-He(Ne)(Ar)(Xe), gas, diffusion coeffs. meas., 350-1200K 80−14869
Kr-NO, thermodynamics, monomer-dimer assoc. of NO, vap. press. meas. 79−90798
Kr+ethene, liquid mixture thermodynamic excess functions 78−48690
LiCl-$AlCl_3$, molten mixture, vap. pres. meas. 78−87779
LiCl-KCl, molten mixture, struct., diffusion, cond., mol. dynamics calc. 80−64871
LiCl-RbCl, molten, Chemla effect, mol. dynamics simulation, self exchange vel. 80−79967
$LiNO_3$-$NaNO_3$-$AgNO_3$, molten salt mixture, excess thermodynamic props. and US vel. *(French)* 77−31720
LiX-alcohol mixtures, (X=Cl, Br, ClO_4), OH(OD) vibr. bands in sat. solns. and crysts. 77−8564
MgO-NaCl, stress-strain determ. by high press. X-ray diffr. 77−7792
Mg_2SiO_4-Fe_2SiO_4-$CaAl_2Si_2O_8$-SiO_2 system phase relations rel. to lunar basalts origin 78−65512
N_2-CO-OCS, liq. mixture, vibr. energy relax. and exchange, laser induced fluoresc. obs. 78−70905
N_2-chloromethane mixture, binary diffusivities, 25-110°c 79−23391
N_2-ethylene, liq., Zwanzig perturbation expansion convergence, free energy 77−76274
N_2-H_2O mixtures, two-phase pressure drops in the low flowrate region 80−19480
N_2-He-CO_2, discharge ionisation growth, diffusion coeffs. 78−83636
N_2-Kr-Xe, liquefaction, retention of ^{85}Kr from fission exhaust gases, separation technique *(German)* 80−27753
N_2-methane mixture, binary diffusivities, 25-110°c 79−23391
N_2-methane mixture, US propag. vel. up to 40 kbar, additivity deviation 77−42959
N_2-NO(He), discharge ionisation growth, diffusion coeffs. 78−83636
N_2-O_2 gas mixture, weakly ionised, electron transport coeffs. anal. *(Japanese)* 80−59184
N_2+methane, liquid mixture, press. effect on excess thermodynamic functions 78−47494

mixtures continued
NH_4NO_3-$LiNO_3$-NH_4Cl-water system, cond. and viscosity *(French)* 79−51286
N_2O, pure and in mixtures, electron attachment near 1 atm., microeave cond. meas. 80−1063
N_2O-CO_2 mixtures, predicted values of viscosity and thermal cond. coeffs. 77−84383
N_2O_4, dissociating, turbulent pipe flow, heat transfer, resistance 78−91026
N_2O(-ethane)(-neopentane), gas phase N_2O electron attachment, temp. depend. 79−36757
Na-Xe, multiphoton ionisation in third harmonic generation by mode locked Nd:YAG laser 78−94413
NaCl-$AlCl_3$, molten mixture, vap. pres. meas. 78−87779
NaCl-KCl electrolyte mixtures, in aq. soln., viscosity, individual electrolyte effects *(German)* 78−22881
$NaNO_3$-$AgNO_3$, molten salt mixture, ionic and mol. mobilities, inter-diffusion and self-diffusion *(German)* 77−11720
Na_2O+GeO_2, molten mixture, EMF measurements 78−43144
NaOH-KOH eutectic molten mixture, elec. cond. and sp. mass 79−82365
Ne/methane, counting gas mixture, electron transport coeff. calc. 79−32727
Ne-Ar, gas mixtures, thermal cond. meas. in the range 0.5-15 MPa 80−14874
Ne-Ar-Kr, gas mixtures, thermal cond. meas. in the range 0.5-15 MPa 80−14874
Ne-H_2 mixture, liquid vapour phase equilib., sound vel., compressibility, thermodynamic perturbation theory obs. *(Russian)* 80−39306
Ne-Kr, partially miscible mixture, high press. mol. dynamics using Lennard-Jones pot. 79−41929
Ne-Kr, time-dependent props. near crit. mixing point, 2000 bar, mol. dynamics calcs. 80−24580
Ne-Kr Penning mixtures, Townsend ionisation coeffs. and breakdown pot. meas. 80−19641
Ne-Xe-F_2(NF_3), excited states quenching 79−18406
O_2-^{85}Kr-Xe, liquefaction, retention of ^{85}Kr from fission exhaust gases, separation technique *(German)* 80−27753
O_2-CO_2 (ethylene)(neopentane), thermal electron attachment meas., microwave cond., pulse radiolysis 80−28592
O_2-ethylene mixture, thermo-osmosis, heat of transport 79−43628
O_2-N_2 mixture, attachment cooling, press. depend. 80−91663
O_2+H_2(D_2)(N_2O), Wassiljewa coeffs., thermal conds., 50 and 100°C 79−37437
PCl_5-$SnCl_4$, mixtures, liq. and solid, Raman spectra study *(German)* 79−91451
Pb^{2+}-Cd^{2+}, solns., differential pulse and anodic stripping voltammetry, in thin-layer cell 77−36812
Rn-CO_2 mixture, ^{222}Rn conc. monitoring by proportional counter, study of thermal diffusion in Rn-CO_2 mixture 79−50839
S-benzene systems, liq.-liq. phase separation 80−96658
SF_6 partial press. meas. in mixtures with N, using separation by freezing 79−71478
SF_6-He(N_2)(CO_2), AC particle initiated breakdown, compressed gas mixture 78−87556
SF_6-N_2, elec. breakdown and corona stabilisation obs. 78−87582
SF_6-N_2, horizontal cylindrical power cable, convective heat transfer, simulation *(Russian)* 77−58676
SF_6-N_2 mixture, discharge inception voltages, calc. 79−68966
SF_6-N_2(He), dielec. props., ionisation and attachment coeffs. 80−33726
SO_2-$^{18}O_2$ mixtures, IR laser pumped, intermol. vibr. energy transfer dynamics obs. 80−87207
SO_2-alkane-H_2O gaseous mixture, photoinduced nucleation and quantum yields 79−96348
SO_2-gas mixtures, flash photolysis, H_2SO_4 aerosol form. 79−66307
SO_2+H_2O+O_2(N_2)(Ar), condensation nuclei form., ion polarity and age depend. 79−39220
$SbCl_3$/$AlCl_3$ molten mixtures, Raman spectra 80−93305
Sb_2Se_3-Sb_2Te_3, liquid, mixture enthalpies *(German)* 79−77770
$SeCl_4$-$SbCl_5$ systems, Raman spectra *(German)* 80−93324
Sr-Xe, resonant third harmonic generation anal. 78−90460
$TiCl_4$-$SiCl_4$($SnCl_4$), liq., beat effects, neutron diffr. studies 80−38897
UCl_4 molten mixtures with alkali metal chlorides, physicochemical props. 78−38915
UF_4-LiF(KF) molten binary mixtures, viscosity meas. 80−65270
UF_6-H_2, near UV and visible excitation, quantum yield from photodissociation 80−35549
Xe-He(Ne), gas mixture, element and isotope separation in impulse plasma centrifuge *(Russian)* 80−38725
Xe-inert gas mixtures, far UV spectra, press. (temp.) depends., interaction consts. 77−61698
Xe-Kr mixtures for gas proportional scintillation counters 77−83464
Xe+Ar(He)(Ne)(Kr), thermal cond., 800 to 2000K from Wassiljewa's expression 79−27736
Xe+He(Ne)(Ar)(Kr), binary mixture viscosity and diffusion coeffs. 78−38443
$ZnCl_2$ in methanol-water mixtures, thermodynamic props. from EMF meas. 79−52735
ZnO-ZnS powder mixtures, elec. cond. and Hall effect meas., percolation effects 79−7828

mm waves *see microwaves*

MO calculations *see molecular orbitals calculations*

mobile antennas
biotelemetry antenna and propagation requirements for appl. for fresh water fish 77−78074
communications satellite system measurements 78−61712
satellite, microwave, power transmission system design for solar power system 79−52893
transmitting antennas, body-mounted, design, radiation pattern, biotelemetry appl. 77−90927

mobile communication systems
see also aircraft communication; mobile radio systems
aircraft voice communication networks, operational noise environment, expt. study 79−81662
astronomical balloon-borne equipment, data communications 79−16793

mobile radio systems
EM energy deposition in biological tissue at 900 and 450 MHz 78−69222
INMARSAT marine system, satellite radio teletype communication 80−26614
marine radiofacsimile weather chart receiver and recorder 80−46297
microwave communications from outer planets, Voyager project 80−77263
operator exposure eval. at 30 MHz 79−62297
RF radiation hazards to personnel, mobile and portable transmitters, US Citizen Band Service 77−40795
selective paging systems, noise disturbance considerations 80−40944
VHF and UHF energy deposition into biological tissue, effect on radio reception 77−73541

mobility, carrier *see carrier mobility*

model reference adaptive control systems
lung, nonlinear mathematical model, parameter tracking adaptive algorithm 77−60227

modelling
see also brain models; catastrophe theory; identification; physiological models; semiconductor device models; simulation
absorption refrigeration machine driven by solar heat for air conditioning, math. modelling 80−76651
acoustic chamber reverberation time, holographic meas. 79−68519
acoustic emission signals, transient, stochastic model 79−72749
acoustic field formation by superposition with phase shift *(Russian)* 78−18087
acoustic generator, axial dynamic, model of theoretical acoustic system 79−14181
acoustic noise propagation, railway lines 80−48500
acoustic signal, pulsed, representation by ordered sequence of uniform information elements magnitudes *(Russian)* 80−38180
acoustic wave propag. through deep water, study of shadow and convergence zones *(French)* 79−41504
acoustic wave propagation stability of a doubly spread underwater channel 77−31156
acoustics model, geometric, scaling laws for hot and cold jet mixing noise 79−37306
active polarisation spectroscopy by combinational light scatt. *(Russian)* 78−78006
adenovirus hexon, three dimensional structure from electron microscopy, computer modelling 80−35833
adhesive bonds, physical modelling, US attenuation effects 78−7141
adsorbed layers, general principles of construction of structural models 80−84351
adsorption-desorption breakthrough curves, modelling 79−37916
advanced lasers for fusion, modelling and anal. 78−50819
aerial radiometric data modelling program 78−46237
aerodynamic noise, theoretical modelling 79−37077
aerodynamics, unsteady, modelling, for arbitrary motions 78−14033
aerospace propag. environment, user requirements 79−58169
aerospace propagation environment operational modelling conf., Ottawa, Canada, 1978, April 79−53651
agricultural land urbanisation hydrologic impact, distributed watershed model 77−37277
air pollutants, long-range transport modelling, OECD study 79−20970
air pollution, plume dispersion modelling for inversion breakup at power plant 78−3933
air pollution and atmospheric processes 77−37370
air pollution level prediction models based on Kalman filtering 77−29428
air pollution model, parameter estimation from simulated LIDAR data 78−28302
air quality models development for limited wind fetch, method 80−104533
air-water bubbly mixtures, press. wave propag. *(French)* 78−22402
alloy melt, impurity conc. field model, growth by Czochralski method *(Russian)* 80−75191
amorphous metals and alloys, struct. modelling 77−31596
annular climbing film flow dispersion models 78−83473
annular two-phase, two-component flow, quasi-stationary model in three-group approx. *(Bulgarian)* 80−69911
antiseismic calc., stochastic model appl. 78−96139
arcs, SF_6, optically thick, convection-loss dominated model 78−87519
Ariane launch vehicle, model firing tests, acoustic field, heat flux, press. distrib. 78−4062
articulatoty model, for vowel feature extraction 79−20561
artificially created hole in F-layer, convergent lens for radiotelescope 77−78571
astronomical doublet system resolution, random speckle structure model and expt. *(Russian)* 79−7082
AT quartz plate resonators and filters, discrete element model 79−55297
atmosphere, enstrophy transfer in two-dimens. turbulence, subgrid scales modelling 79−16586
atmosphere, mesoscale dispersion expts., trajectory-diffusion modelling 80−61837
atmosphere vertical diffusion from ground-level source, Lagrangian similarity modelling 80−51480
atmospheric attenuation and turbulence simulation in pulsed laser Doppler velocimeter system 78−73513
atmospheric boundary layer turbulence, three vel. component modelling 78−28252
atmospheric circulation and pollution analysis using hydrodynamic models *(Italian)* 79−100892
atmospheric CO_2 effect on global radiative heat balance 78−3863
atmospheric diffusion model for short distances and complex topography 77−37386
atmospheric diffusion transport models, variational imbedding soln. 77−37381
atmospheric flow prediction using nested grids 79−44240
atmospheric general circulation, global spectral model 79−53447
atmospheric models, contrast attenuation factors calc., for remote sensing 80−4135
atmospheric motion, wind tunnel characts. review *(Italian)* 80−4156
atmospheric optical transmission modelling and prediction schemes 79−53519
atmospheric pollution, photochemical numerical model 80−40943
atmospheric pollution dispersion using cubic splines and chapeau functions 79−83662
atmospheric processes in tropical zone, numerical model 78−61532
atmospheric radiative transfer in solar, IR and microwave spectral range 79−53520
atmospheric science, radiative transfer modelling techniques extension using Bayes' rule 77−78443

modelling continued
atmospheric surface layer, airflow over nonhomogeneous surfaces with discontinuities in roughness and temp., two dimens. model *(Italian)* 79−84454
atmospheric turbulence, aircraft response, math. modelling 78−81274
atomic clock long-term frequency variations, heuristic model 77−37854
atomic independent particle pots. comparison 80−52846
auditory function, mathematical model *(Dutch)* 77−9213
automobile air pollution ejections control model 77−21900
avalanche critical condition prediction by statistical analysis *(French)* 77−33104
axisymmetric plastic deformation, slip line model *(Russian)* 78−83261
baroclinic oceans, semi-implicit numerical model 77−29316
beam, double cantilever, dynamic crack propagation modelling, 1D anal. validation 79−72857
bidimensional surface waves, periodic correlational random field model *(Russian)* 78−20430
bifurcated cooling tower plume, math. model of drift deposition 79−58002
binary alloy, solidification chemical inhomogeneity *(Russian)* 80−75335
binary alloys, two phase region calcs. in solidifying melt *(Russian)* 80−65195
binary image statistical modelling, enhancement and recognition *(Russian)* 80−63929
biological cell image, Fourier transforms 78−36007
biological effects of radiation, math. models for fractionation 77−5049
biological specimens, X-ray micro anal., iso-atomic droplets as models 78−53598
biological system, optimal control theory appl. 77−40628
biomacromolecules, rigid, modelling approaches of hydrodynamic props. 80−61613
biomedical research 78−31755
biomedical signal modelling and recognition, system identification approach 80−51286
blade pump, cavitational oscill. study 77−35187
blood pressure automated control in dogs using microprocessor 80−81797
bluff-body flame-stabiliser flow modelling 77−72367
boiling, by bubbly liquid press. variation 79−1060
boiling of coolant in LMFBR subassemblies, using Claymore code 78−82473
boundary-value problems, numerical anal. 77−67257
Box-Jenkins modelling advances, appls. 77−87633
breakage distribution, in batch grinding, mathematical model determination 78−92416
bulk forces modelling, increasing effectiveness of centrifuging *(Russian)* 78−87314
buoyancy dominated wall diffusion flames, numerical model 77−68710
BWR, air clearing in H_2O-type press. suppression systems, scaling laws 79−54563
BWR coolant oscillatory flow perturbations, altered transverse momentum transport 79−608
BWR LOCA analysis, jet pump modelling using RELAP4 80−68850
BWR long-term cooling, closed form analytical model 80−78355
BWR noise anal., identifiability of dynamics using autoregressive modelling 79−45340
BWR shutdown margin prediction, multidimensional linear regression model 79−9778
BWR stochastic neutron flux fluctuation obs. and modelling, thermohydraulic parameters 78−94065
BWR subchannel code with drift flux and vapor diffusion transport 79−59149
BWR void effects, stochastic point model and zero-power reactor simulation 78−94061
CAI in physics, student response to comput. phys. teaching lab. project at Surrey Univ. 77−53724
catalysts, heterogeneous, gas phase diffusion and reaction calcs., viscous flow importance 79−47970
cavitating fluid model *(Russian)* 78−55668
ceramic mould accelerated shell heat treatment models 79−76896
ceramics, high temp. failure mechanisms, statistical model 80−39210
chemical and biological systems, network thermodynamics appl. 78−20955
chemical laser numerical modelling, book contrib. 77−10908
chemical laser resonator modelling, LAMP and BLAZER code calcs. comparison with CL XV meas. 79−36890
chemical reactions, diffusion-controlled, continuous-time random walk modelling 80−3297
chemically reacting nonequilibrium turbulent shear flow, prediction model *(German)* 79−18973
chromatographic density detector operation *(Russian)* 78−92580
chromophores, model for simulation of EPR spectra, in partially oriented membrane multilayers 78−86894
clarinet, functional model of simplified version 80−96147
classical and special relativistic physics arithmetic models formulation 78−86130
climate, numerical modelling of long-term change 78−77315
climate models, forced noise level 78−44978
climatic change, computer modelling 79−92587
climatic var., modelling and prediction 77−21882
closed basins, three-dimens. rigid-lid model 78−32131
cloud, warm cumulus, three-dimens. numerical model with microphysical processes *(Russian)* 78−88884
cloud formation and development, numerical convection model *(Russian)* 80−81987
coal conversion reactor environments, simulation 80−100831
coal liquefaction preheaters and reactors, modelling of heat transfer charcts. 80−30337
cochlear excitation, electric circuit model and overpressure meas. in guinea pigs *(French)* 78−85316
coherence function concept extension to quadratic models 79−72987
cohesive sediments, modelling of transport, erosion and deposition 78−15994
coil winding stress mathematical model 77−73430
cold rolling force model, and its adaptive control *(Chinese)* 80−55418
combined photovoltaic/thermal flat plate collectors, extended Hottel-Whillier model 80−3520
combustion, turbulent premixed and diffusion, engineering flow modelling computation 78−1756
combustion process hazard modelling and logic theory 79−91953

modelling continued
complex unsteady flow, convective modelling procedure based on quadratic upstream interpolation 79−68694
composite material viscoelastic properties modelling 78−75082
composite materials, failure predictions 80−10200
composite materials, fibre-reinforced, impact responses perpendicular to fibres *(Japanese)* 79−43377
composite mechanical systems dynamical flexibility, ficticious source method in polar coordinates *(Polish)* 79−32225
composites, thermal stresses investigation, using polymer models 80−40639
compressed air energy storage, champagne effect, improved cavern design 79−83638
concatenated fibre-optic cable, cumulative baseband frequency response models 80−78983
conducting plate surface element models 79−41290
conductive piston retardation in mag. field, electromech. energy conversion *(Russian)* 79−64145
continuous noisy signal analysis by autoregression time-series model 79−3209
convection, turbulent, numerical models based on unsteady Navier-Stokes eqns. 80−38415
convective rainfall, storm life cycle, model 79−16589
cooling pond, waste heat dissipation at nuclear power stations 79−48191
cooling tower plume models, importance of meas. *(German)* 77−66985
cooling tower plumes and drift 80−45836
corona onset and breakdown in non-uniform air gaps, physical models 77−15268
corrosion-fatigue crack propagation 78−90779
crack dislocation model 80−69741
crack growth, anal., crack tip deform. modelling 79−41626
crack growth charcts., anal. modelling 79−41622
crack tip finite element anals. 79−41624
cracked bar under torsion and shear, elastoplastic stress and strain calc. from screw dislocations 79−68654
creep damage and the remaining life concept 80−59574
creep deformation model incorporating recovery and thermally activated glide 79−64534
creep modelling incorporating initial strain and ageing 80−58939
cross-flow-heat exchanger, model of thermal mixing process 79−1078
crystal growth, topological modelling techniques 80−59418
crystal growth disorder, 3D model, rel. between Ising models 79−51025
crystal growth models, attachment energy at habit controlling factor 80−59420
crystal step motion, in the presence of a mobile impurity computer model 79−14713
crystal symmetry, stereographic projection model, construction, teaching appl. 78−86086
crystal-size distribution, population models, review 80−49153
crystallisation, technical, modern trends, computer modelling 80−66406
crystallisation process, controlled from binary melt *(Polish)* 79−14708
current transformers, oil insulated, parameters influencing heating assessment using sensibility matrix *(Hungarian)* 80−87708
cyclic queue models of semiconductor noise and vehicle fleet operations 80−80336
cylinder array, convective mass transfer with surface reaction 78−79369
Czochralski growth model, transient phenomena 80−84125
D-optimal design for quadratic regression on a hypercube 79−92921
daylight spectral quality and solar energy availability determ. model 79−58067
deep body thermometer testing and modelling 77−40816
deformation condition, modelling *(Russian)* 79−27515
dewatered pipeline coal dust pollution model 77−37401
dielectric relaxation processes, simulation using network model 80−40046
dielectrics break-up by pulsed discharges, non-ore materials milling appl. *(Russian)* 78−27653
differential eqn. teaching with interdisciplinary models and computer 78−77640
digital computer applications to process control, conference, The Hague (1977) 78−49808
digital terrain modelling, symposium (St. Louis, Missouri, 1978, May 9-11) 79−84083
dilute solutions, Monte Carlo algorithm for preferential sampling near solutes 77−51287
dimensional anal., mathematical model of process 78−54171
dimensional base selection in expt. design and planning 78−49636
discharge probability for long surges, long distance *(French)* 77−39493
dislocation motion, lattice resist., effect of impurity interstitials 80−84170
disordered crysts., optical transforms 80−78783
disordered structures, two-dimensional, computer program for modelling *(French)* 80−59337
disordered systems, mathematical models, book 80−1878
dissipative mufflers with locally reactive lining, finite element method 78−13849
dissolved O_2 in rivers, reliability parameter in probabilistic programming models 80−26179
distributed parameters, inverse problem 79−75322
domestic water and space heating by new technologies, energy and direct economic effects, evaluation 79−92049
dose-rate model testing with Chlamydomonas reinhardi 80−21543
double cantilever beam model, for K_{Ic} determ. *(Chinese)* 80−54306
double connecting channel model *(Russian)* 80−90804
drag-free satellite, anal. modelling of orbital motion *(French)* 77−73936
drainage headwater development, modelling 79−20875
dual elastic continuum model of media with quasicracks, tensional medium with mobility effects 77−72153
dynamic phase memory in self-excited wave media 79−79505
dynamic shear crack propag. mechanics, earthquake source model 79−84147
Earth, linear inference and underparameterised models 78−49000
Earth atmosphere, lower, temp. skewness budget, turbulence modelling implications 80−21816
Earth inductive logging near single and multiple conductive bodies, scale model results 79−16696
earthquake, stick slip, rupture propag. and energy focusing in foam rubber model 80−3947
earthquakes, centrifuge modelling 78−81429
earthquakes, in homogeneous half-space 79−12078

modelling continued
easy glide, computers modelling, range of permissible parameters *(Russian)* 78 47375
ECG, arrhythmia detection and classification, statistical approach 77-21644
echoes scattered by random fluctuating surface, statistical model *(French)* 77-11066
ecological system model sampling/identification, input signal anal. 78-69267
elastic radiation from spherical wave sources, seismic model 79-8612
elastic-plastic transition, model for metallic materials *(German)* 80-75295
elasticity, rel. to rubber microscopic structure, small angle neutron scattering appl. 80-3113
elastoplastic fracture modelling 80-35303
electric arc, dynamic characts. 77-35409
electric field disturbances, in conducting fluid *(Russian)* 78-231
electrical components, mathematical simulation of life *(Spanish)* 79-21532
electroacoustic analogue model of middle ear and acoustic reflex 79-83798
electrolytic, of thermal contacts behaviour *(Italian)* 77-24504
electromagnetic interference, statistical-physical modelling 77-83789
electromagnetic scale modelling, derivation of absolute units 77-14639
electron, using phase-locked cavity 79-63089
electrostatic discharges, energy determ. 80-70065
EM exploration, target near dipping contact, response modelling 79-8595
EM induction in elongated structs., analogue model expts. *(German)* 79 25199
EM power deposition in prolate spheroid models of man and animals at resonance 78-31905
end-loading ring in rigid cavity, elementary catastrophe theory modelling 79-68585
energy demand and conservation in USA, in residential and commercial buildings, National Energy Plan impact 80-26121
energy planning in Arab world, with aid of computer 80-26122
environmental system, conf., Ghent, Belgium (Aug.-Sept. 1977) 79-25250
epoxy resin insulation, adapted models selection problems for electric ageing *(German)* 80-89365
estimation aided by instrumental variables, regression model *(German)* 78-29080
estuarine P model parameter estimation for Jamaica Bay, NY 77-21777
estuary, Jamaica Bay, New York, dissolved O modelling 77-17146
estuary thermal impact of multiple power plant operations 78-96232
estuary unsteady-state two-dimensional salinity intrusion model 78-77271
evaporative cooling, on vapour cooled transmitter tubes, physical fundamentals *(German)* 77-11114
experimental design, unbiased regression, practical appls. 79-97184
exterior regions containing moving conductors, finite element models 79-41291
F_2-peak altitude determination using global model based on M3000 values 79-101020
failure, for cyclically hardenable metals and alloys, statistical model *(Bulgarian)* 80-70296
fatigue behaviour of fibre reinforced plastics, under random loadings *(Japanese)* 80-85032
fatigue crack growth, surface reaction and transport controlled, model 80-75299
fatigue crack propagation, rel. to cyclic plastic instability zone 80-71733
fatigue lives, in metals, eval. using crack initiation model *(Japanese)* 80-104258
fatigue-crack-growth-retardation model, based on critical damage approach 80-99960
FBR core seismic anal. by assumed-mode math. modelling 79-89357
ferromagnetics, magnetisation in unidirectional field *(Russian)* 77-24660
ferromagnetics in unidirectional field, magnetisation, math. model *(Russian)* 78-88140
FFTF dynamic modelling and sensitivity analysis 79-605
fibre bundle time-dependent failure, probabilistic model 77-3798
fibre reinforced composite, single ply, thickness effect on percolation and conductivity 80-92953
fibre reinforced composites, fracture processes modelling, digital computer appl. 80-65147
fibre-optic scattering loss dependence on launching condition, lossy-layer model 78-5577
field emission gun SEM column electron-optical performance obs. and model 80-68328
film, electron beam evaporation sources, emission characts., model 79-95279
film boiling, heat-exchange intensification, nitrogen in pipes 79-81876
film-grain noise degraded images, nonlinear detection and estimation 77-50627
filtration, dynamic, use of electrically conducting paper with discretely distributed capacitance *(Russian)* 78-88850
finite element, acoustic absorption models 80-53497
fission gas release and swelling in irradiated UO_2, model 77-6488
fission reactor poisoning, KS-150 with ^{135}Xe and ^{149}Sm, three-dimensional calc. *(Slovak)* 78-54850
fission-fusion electric energy supply system modelling 78-740
fission-fusion hybrid power plant economics 78-789
fixed collector, optimised design, radiation collection study 80-40839
flame, turbulent premixed with sequential chemistry, closure model 78-35683
flames, unsteady, propagation, numerical modelling 79-64794
flat plate boundary layer flow model and spherical particle drag expt. 79-18871
flat plate collector energy yield increase by planar reflector, modelling appl. 78-33813
flat plate solar collector thermal behaviour model and performance parameters 79-62045
float glass, heat transfer and temp. control in annealing, computer appl. 78-27543
flood and tidal flows, network hydraulic model 79-12162
flood flows modelling, use of Wakeby distrib. 79-84330
flow, axisymmetric body, pot. flow/boundary layer interaction models 80-1546
modelling continued
flow, free shear layer, Reynolds stress closures systematic modelling rules 80-1552
flow, gas-liquid mixtures, measurement standard system design 77-76005
flow, general discrete time compartmental model 78-1625
flow, recirculating, behind backward-facing step, mean vel. and Reynolds stresses 80-19355
flow, Reynolds stress transport eqns. 80-19320
flow, separating boundary layer, subsonic, integral prediction method 80-1623
flow, subgrid modelling with classical closures and Burgers' eqn. 80-19332
flow, subgrid scale modelling 80-17808
flow, turbulent, developing, in square duct 80-19351
flow, turbulent wall jet, algebraic Reynolds stress model calc. 80-1668
flow, unsteady, viscous, separated, laminar, numerical modelling 78-46933
flow in open channel, turbulent intensity modelling 79-1172
flow in ring nozzle, shielding technique development for arc welding 79-7497
flow of viscous electroconducting fluid in strong mag. field, free shift stationary type 80-28576
flow through isotropic granular porous media, constricted unit cell model 78-30350
fluid, of hard hetero/homonucl. diats., Monte-Carlo simulations 78-42873
fluid dielectrics impurity particle field-enhanced motion 77-43932
fluid flowmeter metrological characts. determ. *(Russian)* 77-62318
fluidised bed reactors, mathematical modelling *(German)* 79-41767
forced convective film boiling, math. model 79-18686
forced vibration model, rail/wheel noise generation 80-48496
foundational studies, A. Mostowski, book 80-57014
foundational studies, A. Mostowski, book 80-57015
fracture mechanics, elastic-plastic, finite element method appl. 80-1489
freeze-drying systems for foodstuffs and biological materials, information systems models 79-58727
fuel element bundles at coolant boiling, fuel exchange enhancement 78-94086
furnace heat transfer, 3-dimens, computer model predictions test 78-59504
fusion reactor, Shiva Faraday rot. coils, circuit and mag. anal. 78-54951
fusion reactor, Tokamak, commercial, plasma driving system requirements 78-54954
fusion reactor breeders, models for T_2 and ^4He transport 78-17424
fusion reactor TESPE coil, finite element method calc., winding package modelling 78-50376
gas, self-structure factor, kinetic modelling 79-41791
gas blast circuit breaker arcs, radiative transfer investigation 79-27864
gas blast circuit breakers, three nozzle arc models 79-27862
gas jet injection into liq. in tank, math. model 78-63473
gas lasers, computer modelling, book 79-41364
gas-liquid flows with chemical reactions in hydraulic approx., mathematical modelling 79-18972
gas-solid turbulent flow, heat transfer, model 79-1232
gasdynamic lasers, improved perform. by selective thermal pumping 79-31858
gasdynamic modeling and computational accuracy 79-72872
gaseous reactor wastes, dispersal forecasting *(French)* 78-8995
Gaussian noise, simple models 78-32763
Geminid meteor shower radar obs., statistical modelling 78-61816
geodetic networks, physical model of notion-system of information 77-64176
geology, finite element models of folding 79-20788
geomagnetic variations induced by ocean waves, analogue model 77-49003
geophysical fluid system, climate simulation 78-81353
geophysical modelling techniques, statistical tests for goodness of fit 78-57333
geophysical time series, Hurst range of independent normal summands, distribution 78-16081
geopotential with point mass anomalies, systematic approach 78-40465
geothermal reservoirs, mathematical modelling of heat and mass transfer 80-55802
glaciers-ocean-atmosphere global system, numerical modelling 79-84469
glass fibre reinforced plastic, time depend. probabilistic failure model 80-40477
glass making process, math. and phys. models, review 78-3083
Global Positioning System, computationally efficient modelling for long-term prediction of orbits 79-80198
global processes, sedimentary cycling models 78-16162
glottal sound source, self-oscillating model *(Japanese)* 78-92654
gradient index material models and exptl. verification 80-16002
grain growth, steady-state and dynamic, computer simulation 79-38836
granular media modelling by steel spheres, packing density coeff. 78-84916
graph theoretic field model, modelling and formulations 79-67165
grinding wheel life modelling, group method of data handling 80-58987
ground motion simulation and spectral representation using non-stationary amplitude modulated mathematical model *(Spanish)* 80-56397
ground water level fluctuations, influence of outer water level variations, sand aquifer model appl. 78-53663
groundwater, two-dimens. contaminant transport simulation 77-78287
groundwater flow in unsaturated noncohesive soil *(Polish)* 77-70709
groundwater flow systems, three-dimens. modelling 79-84318
groundwater natural recharge, math. modelling 78-11934
groundwater steady state flow models, theory and numerical props. 77-78483
Gulf of Gdansk, lithodynamical processes, theoretical anal. and scale model tests *(Polish)* 78-40540
Hartmann-Sprenger tube, gas temperature calc., using Lagrange equations *(Japanese)* 79-4041
heat and mass transfer experimental data acquisition system operational analysis models *(Russian)* 79-80588
heat and mass transfer systems, modelling of eigenvalues and eigenfunctions 77-14872
heat conduction, modelling of mechanical system with external unsteady thermal action 79-37124
heat conduction, nonstationary, soln. of general nonlinear problem using electrical model *(Russian)* 77-54860

modelling continued
heat exchanger, recuperative, source/sink even model *(Hungarian)* 79−14226
heat exchanger, thermal modelling for computer simulation 77−46904
heat pipes, heat and mass transfer, one-dimens. model 79−1064
heat transfer, one-dimensional, inverse soln. *(German)* 77−11115
heated stack effluents in disturbed flows, wind tunnel modelling 79−92564
helical arc column, dynamic equilibrium model 78−71593
heterogeneous chem. reactions under action of turbulent jet, modelling 78−64885
HGTR core, multiregional coupled conduction-convection model 78−94083
high current density arcs in narrow channels, calc. and appl. 78−55762
holographic aberration compensation of optical system, computer modelling 77−50640
holographic brain model for associative memory 79−74640
holographic grid production, photographic material charact. curves appl. *(Russian)* 77−631
horizontal surface solar irradiance prediction models compared 80−36384
hot strip rolling simulation, by hot torsion technique 80−29990
HTGR low power startup model development and use 77−88220
hydrologic models of long-term persistence, skew preservation 77−78273
hydrologic time series, assessment of long-term persistence models 77−64350
hydrology, deterministic models, parameter uncertainty effects, analysis 77−25724
hydrology, river quality modelling by sequential extended Kalman filters 78−81248
ideal monatomic gases, rarefied flow statistical modelling, computer simulation 79−98753
image correlation of geometric distortion, optimal window functions 79−45907
image formation, super-resolution derivation by analytical continuation methods 78−29915
image registration, practical limits assessment *(Russian)* 78−37811
image sampling/scanning, two-dimensional Fourier transform props. 78−58929
imbibition in 2-phase flow through porous medium with capillary pressure 79−20884
impurity concentration effect in MOS tetrodes, analytical model *(Spanish)* 79−99624
in-stream settling basin sediment routeing, convective dispersion model 77−37272
incident solar flux on arbitrarily oriented surface, computation models 79−57401
inductive dipole sounding anomaly, low-impedance overburden screening *(Russian)* 78−81106
inert gas mixture, collision-induced absorption, exact line shapes, appl. to He-Ar 78−66512
inertial systems constructed on double-gyroscope frame base, generalised models *(Russian)* 78−28937
information process mathematical and thermodynamic aspects *(French)* 77−5789
ingot solidification and reheating, thermal model 77−73340
ingots, cooling regime in conditions of minimal thermal stress, modelling *(Russian)* 80−65194
inner ear impulse response and basilar membrane modelling 79−34570
integrated nuclear power system, mathematical model *(Rumanian)* 79−41013
interdigital transducer design and component specification tradeoffs 77−27455
interdigital transducer design with spectral weighting frequency response 77−27454
interfacial polarisation effec. on dielectric props., sandwich capacitor model 80−15614
interferometer, two-channel, based on prismatic dividers, with aid of coupled multi-terminal networks *(Russian)* 80−52302
International Atomic Time fluctuations, autoregressive integrated moving average model 77−57297
International Reference Ionosphere, descriptive empirical model, intentions and build-up 79−58173
ionosphere, for use in administration of HF radio transmission networks *(French)* 79−58175
ionosphere, operational physical models 79−58172
ionospheric flight conditions simulation 79−16796
ionospheric radiowave scintillation, signal-statistical and morphological model 79−58185
ionospheric travelling disturbances, medium-scale, diurnal and seasonal var. modelling 79−58181
IR radiation spectral absorptance and transmittance, accurate modelling technique 78−91062
irreversible energy conversion processes, information model *(Ukrainian)* 78−89419
jet, axisymmetric, modelling of large eddies, harmonic forcing effect 78−90957
jet, noise modelling by geometrical acoustics, outside silence cone 78−34177
jet flow, three-dimensional, hydrodynamical model 80−79369
jet in wake flow, integral relns. *(Russian)* 79−77202
jets, vertical, round, effect of buoyancy on turbulence struct. 79−55403
jets discharging into quiescent ambient, finite difference anal., turbulence modelling 78−30332
Johnson-Mehl and cellular microstructure, comparative analysis, computer simulation 80−54392
kinematics and dynamics for manipulator and man's hand purposeful motion 77−78969
kinetic theory of gases, computer modelling of mol. vel. distribs. 79−30169
Kuwait hourly stochastic insolation model 79−58068
lake, wind-induced circulation and water level changes, two-dimensional finite difference model 78−77287
lake biochemical and physical model interfacing 77−21822
lake eutrophication control theory applic. 77−21820
lakes, circulation, seiches, tides and storm surges, finite element methods, book contrib. 79−34876
lakes, winter season energy balance *(Polish)* 78−24315
lakewide wind-driven circulation, numerical models 77−37243
landslides on Ryuohzan Mountain, Japan, geology, model *(Japanese)* 78−96217

modelling continued
large scale seismic network in Italy, multiple covering problem appl. 78−69540
large-area nanosecond discharge breakdown 78−71614
laser beam interaction with inclusion defects in isotropic solids 79−76741
laser compression and heating of shell target *(Russian)* 78−1860
laser fusion microspheres, computer modelling, image analysis of X-ray radiographs 78−50311
laser ionisation, modelling 78−90133
laser-fusion reactor, surface heating of 1st wall by pulsed photon and ion irrad. 78−89979
lasers, high-power, model for stable high-density discharges 79−13943
lattice linear and surface defects, math. modelling 77−89450
lattice packing of spheres, in 3D space 80−49166
lifting system cascade struct., signal flow graphs in modelling *(Polish)* 79−32224
lightning leader stroke model, electric field strength computation *(Czech)* 79−5554
lightning overvoltages in power overhead lines, pseudo-random number generator appl. *(Polish)* 77−24234
lightning return stroke, channel current modelling 77−78351
limnological, of Lake Kinneret 77−21821
linear electrical T network for 1-D Schrodinger equation, unreal components *(German)* 77−53792
LMFBR, computer modelling of piping components for transient hydrodynamic structural response 78−74449
LMFBR, fast integral modelling of HCDA 79−26555
LMFBR, HCDA exptl. modelling 80−32366
LMFBR, hypothetical loss of flow accident, computer simulation 79−3222
LMFBR, modelling in prompt burst HCDA calcs. 78−74454
LMFBR, role of scale model tests in structural dynamics 77−3141
LMFBR, squeeze flow between two adjacent subassemblies, discrete model 78−86634
LMFBR, surface temp. distrib. of peripheral fuel elements, approx. thermal modelling 80−63237
LMFBR overpower excursions, mechanistic model of fuel freezing, channel plugging and continued coolability 78−58371
LMFBR safety, local blockage formation and growth in grid spaced fuel elements, model 77−88243
LMFBR safety, scale modelling 80−32367
LMFBR simulation, parameter estimation 80−47597
LMFBR subassembly simulation, finite element computer model, safety anal. 78−70612
LMFBR vented assembly cores, appl. to nonlinear network anal. to hydraulic modelling 78−13207
load cell transducers, shear force, mathematical modelling and design 79−35722
lossless layered media state space models 77−91065
low and high pressure discharges, aspects *(French)* 78−14240
LPE film property control, regression eqns. 79−33200
LWR fuel assemblies, coolant channel closure modelling using pattern recognition techniques 80−42835
LWR fuel cycle effluent model for ENFORM system 78−94111
LWR fuel rod mechanical performance predictor, SPEAR code 79−93730
LWR LOCA, modelling of press. and temp. changes in two-phase, two-component flow *(Bulgarian)* 80−68904
machined surface time series modelling 80−36998
macroparticle impact with meteoritic vels., physical modelling principles, quasi-full laser modelling 79−52049
magnetic alloy, interface behaviour 80−84913
magnetic bubble generator modelling and optimisation 78−6547
magnetic bubble propagation modelling, domain struct. effects 79−78488
magnetic fields induced by ocean waves, laboratory analogue model study 79−66807
magnetic hysteresis, probabilistic mathematical models *(Polish)* 77−80960
magnetic hysteresis 77−85500
magnetosphere, particle (electric current) approach 80−17442
magnetospheric energetic electron environment model revision 78−61681
magnetotelluric soundings, analogue modelling 77−33197
mammography, effective modelling of diagnostic examinations 78−85366
mammography, utility of modelling 78−69188
marine circulation three-dimensional modelling 78−77267
marine modelling (vol.6 of 'The Sea') 78−16047
Mars atmosphere, thermal radiative transfer, numerical modelling 80−8574
math. and phys. models, fundamental differences and future possibilities 79−25844
mathematical, appl. in metal processing 77−73429
mathematical, influx of meteoric matter modelling with radar observations *(Russian)* 80−67664
mathematical, vibrational resonances of built-up structures, use of meas. data 80−69718
mathematical ideas and appls., book 77−5617
mathematical model, for hydraulic calc. of steam boilers 79−68816
mathematical modelling of highly parametrised integral or differential equations 79−35492
mathematical models of instruments, fundamental principles 78−93641
measurement data processing system error analysis 78−41288
mechanics expts., model for computer based data acquisition and control 77−63844
megnetic deflection yokes, mag., integral eqn. method for anal. 79−50183
membranes, composite, relaxation time, network thermodynamics formalism 78−68926
memory alloy, pseudoelastic, model for first-order phase transition 80−92642
Mercury, Monte Carlo modelling of exosphere 78−96416
metal, amorphous struct., simple computer modelling 79−19154
metal electrodeposition protrusion growth and inhibitor action model and meas. 79−96314
metallic thin films, discontinuous, field effect of electrical conductance *(Japanese)* 80−11107
metallurgical industry, mathematical models appl. 77−70276
meteorological forecasting of orographically enhanced rainfall accumulations using 10-level model 78−69420
Meteorological Office 10-level prediction model (Dec. 1975 status) 77−91250

modelling continued
meteorology, numerical modelling of the atmosphere, review 79−44234
meteorology 79−16621
metrological research on prospective measuring techniques, conf. Wroclaw, Poland, Sept. 1978 *(Hungarian)* 80−86247
MHD channel design, w.r.t. velocity, Mach number and pressure profiles 79−83604
MHD generator, simplest physical model 78−71548
MHD generator channel, liquid metal piston dynamics, math. model *(Russian)* 80−74996
MHD generator electrodes in arc regime of operation, math. model 79−86620
MHD generator excited by central exploding wire, math. model *(Russian)* 77−51245
MHD plant components, coal-fired, thermal model development 79−52946
microphone, probe-tube type, math. modelling 77−39179
microwave propag. in 1 to 300 GHz band, computer model for atmospheric propag. conditions 79−53505
microwave radiometer, multi-freq. system mathematical model and performance evaluation 78−81417
Mississippi Pascagoula Estuary water quality planning using Gauss-Seidel iterative technique 78−73402
model and full-scale cooling tower resonance tests 78−83291
molecular models, semiautomatic coordinate meas. device using laser beams 79−37573
molecular structure models, discrete optimal control 77−61694
monochromatic coherent plane wave scatt. by living cell *(Russian)* 78−48765
multilayered media, layer-indexed acoustic reflection model 80−43517
multiphoton absorption modelling, using SF_6 energy-dependent absorption cross sections 80−32789
municipal wastewater treatment plants, electrical energy consumption and heating requirements 80−26194
natural philosophy, scientific models, catastrophe theory 80−8772
natural sciences, mathematical models role *(Afrikaans)* 80−8771
natural terrain scenes, segmentation-based boundary-modelling processor 80−99661
Navier-Stokes flow with suspended particles, mathematical modelling, numerical simulation 77−72348
nearshore circulations finite element modelling 78−77270
neutron star magnetospheres, laboratory modelling 79−75240
noise transmission between dwellings, partitions and flanking structures 80−43545
non-Newtonian fluid, steady flow, numerical modelling 78−51205
nonlinear mathematical model of the propagation of tides in interlacing channels 79−39720
North Sea, mathematical and numerical hydrodynamic models 77−37216
North Sea water circulation finite element simulation 77−2162
nuclear fuel cycle environmental impact assessment, oceanic and geological disposal, use of box model method *(Japanese)* 80−9346
nuclear fuel failure prediction using POSHO model 77−46226
nuclear generating station circulator auxiliaries modelling 77−88221
nuclear material safeguards, human performance characts. 79−85741
nuclear materials safeguards, computerised chemical modelling of deviations, from mass transfer equilib. 80−83171
nuclear plant airborne effluent variable-trajectory puff advection model modifications 78−94149
nuclear plant cooling, effluent dispersion, thermal and radioactive, math. model *(Spanish)* 77−74908
nuclear power engineering development 80−7901
nuclear power plant, technical and economic calc. 77−23315
nuclear power plant siting evaluation, environmental impact probabilistic assessment model 79−79412
nuclear power reactor systems, dynamical behaviour modelling 80−91216
nuclear power station, seismic anal., slab modelling 78−50414
nuclear power station accidents, due to loss of coolant, multiple-element model and computer solution 78−66358
nuclear power station with VVER, for semi-peak load generation, mathematical model 80−68936
nuclear reactor, GCFBR, seismic model of core support structure 77−3184
nuclear reactor, LMFBR, refuelling scheme optimisation using heuristic enumeration method 77−46301
nuclear reactor, LMFBR, scram and nonlinear system seismic anal. 77−3185
nuclear reactor, press. and temp. loads on LWR containment after LOCA, scale model expts. 77−3134
nuclear reactor, pressure and temp. sensors, reactor time const. determ. by dynamic data system method 79−93750
nuclear reactor, structural shock tests, prototype FBR MONJU scale models, computer code verification 77−3131
nuclear reactor accidents, molten fuel-coolant interaction *(Czech)* 78−66352
nuclear reactor fuel elements, struct. anal. 78−41814
nuclear reactor LOCA, reflood hydrodynamics, two-velocity two-phase flow model 79−633
nuclear reactor mixed-oxide fuel, two-component gas transport within interconnected porosity 79−617
nuclear reactor noise, specialists' meeting, Gatlinburg, USA, Sept. 1977 78−94057
nuclear reactor noise analysis, time series modelling methods, comparative eval. *(Japanese)* 80−13552
nuclear reactor structural reliability, time-depend. nature modelling 79−18013
nuclear reactor structural systems modelling for transient response anal. 77−6507
nuclear reactor system anal., empirical modelling appl. 78−25284
nuclear reactor systems, scaling laws for modelling 79−93690
nuclear reactor with delayed neutrons operator eqn. 77−50213
nuclear reactor with distributed parameters, suboptimal control, singular perturbation theory, computer model 77−6530
nuclear steam generating system, seismic design, math. model 78−58339
numerical prediction of recirculation flows with free convection encountered in gas-agitated reactors 79−10602
ocean, underwater light field fluctuations under rough sea surface, numerical modelling *(Russian)* 77−33090
ocean acoustic model inputs/sensitivity 79−5492
ocean circulation, modelling expts. 79−57952
modelling continued
ocean currents, Gauss-Markov models for error analysis of inertial navigation system 80−36411
ocean currents, synoptic-scale, numerical model 80−12424
ocean currents generated by heat and momentum fluxes through surface, numerical simulation 80−26535
ocean dynamics, coastal jet conceptual model for shallow seas 78−16051
ocean general circulation models 78−16048
ocean oil spill trajectory, modelling advancements 79−5509
ocean seasonal thermocline, one-dimens. models 78−16050
ocean surface drift currents, new model, nonlinear eqns. appl. 79−53353
ocean thermal anomalies numerical study with dynamic model 80−17271
ocean tides, numerical models 78−16049
ocean tides, shelf effects parameterisation, S. Atlantic appl. *(Russian)* 79−100843
ocean wave imaging and wavelength meas. by aerial photography 80−46323
ocean waves, currents and sediments transport, near breakwater 80−51401
ocean waves, numerical model of tide and surge propag. as aid to navigation 79−12121
oceanic sediments, elastic wave propag. 77−44966
oceanic upper layer 79−84292
oceanography, continental shelf sediment transport 78−15995
offshore wind power model estimates 80−61244
once through steam generator, Na-heated, stability anal. nuclear reactor systems model 80−91218
once-through steam generator, dynamics and control studies 77−88271
open cavity heat and mass transfer 78−55640
open channel, two-dimensional tidal propagation model, difficulties 78−77272
optical component polishing process modelling *(German)* 80−87565
optical element contamination modelling, photometric characts. estimation 80−48429
optical fibre communication systems, computer design aids 80−28350
optical gauging instrument for measuring hole misalignment in flat plates, control aspects 78−57895
optical transfer function description, of photochromic hologram recording medium 80−78796
optically pumped submillimetric laser models and rate eqns. 77−38871
order-disorder structures, layer stacking 80−38981
oscillating circuit, broken, physical model 79−50187
pacemaker interference, body potentials and currents from ELF elec. fields and household appliances 78−88770
N.Pacific mesoscale phenomena, oceanographic model and acoustic survey comparison 80−46195
pack ice deformation by ridging 79−70807
paper fibre suspension US propagation 77−27447
parallel-plate sputtering system deposition rate model 79−87579
parameterization schemes in solid state physics 79−17183
particle growth, mathematical modelling, continuity eqns. for particle distribs. 78−65863
passive solar building thermal performance modelling by passive solar test boxes, expt. 80−3494
passive solar building thermal performance modelling by passive solar test boxes, theory 80−7921
PBR axisymmetric core, thermal-hydraulic anal. techniques 79−71884
perforated tube muffler components, appls. 79−98544
perforated tube muffler components, theory 79−98543
phase and frequency instabilities in precision frequency sources, characterisation and mathematical models 79−2750
phase interfaces, balance eqns. and struct. models 78−59453
phase transformations in intermediate spherical model 79−30403
phasotron, electron ring, const. guide field induction, acceleration, magnet system 77−83181
photoacoustic cell for liqs. and solids, one-dimens. model generalisation 80−82827
photogrammetric model deformation, interactive demonstration program 77−74183
photographic development, electrochem. models 79−52697
photographic development process, mathematical modelling of growth of spherical metallic particles *(Russian)* 80−50871
photometers drift errors, due to ageing and preheating *(German)* 77−10087
photoresist, positive, simultaneous exposure and development model 78−4715
photosynthesis, fluoresc. induction modelling by elec. diagram 79−57589
physics models, nature and purpose 80−42023
physics teaching curriculum development, systems approach *(French)* 77−9834
pipes, two-phase stream, stratified flow, condensation calc. 79−23349
planet thermal radiation intensity field modelling; principles 80−62056
plasma, ablative laser driven implosion heating model, struct. and scaling laws 77−43008
plasma, axially symmetric, Doppler broadened optical line emission interpretation model 78−75276
plasma, Vlasov, mathematical model 79−55503
plastic yielding, modelling at a crack tip by inclined slip planes 80−33472
plate columns with dual flow, mass transfer modelling 78−51219
polarimeter error quadratic mean value determ., statistical method *(Russian)* 77−41668
polyethylene, polymerisation kinetics math. model, mol. wt. evaluation *(Russian)* 79−52661
polymer molecule, in soln., end-to-end distance relax., Monte Carlo simulation, model depend. 78−22061
polymer radiation chemistry, computer modelling 79−74382
polymer solution, bubble behaviour, Denn model 78−79343
polymer solution, bubble behaviour, second-order fluid model 78−79344
polymer solution, bubble elongation dynamics, modelling with viscoelastic constitutive relations 79−37388
polymers, glassy, craze surface displacements, model 80−93651
polymorphic transformations kinetics model, computer modelling *(Russian)* 80−97478
polytypic structures, mathematical model, SEG-1 *(Russian)* 78−75613
pool-type reactor noise analysis and expt. 79−3195
porous media, miscible or immiscible displacements, identification and modelling 78−69392
Port of Leba, Poland, reconstructed entrance, storm tides prediction, math. modelling *(Polish)* 78−40568

modelling continued
pressure drop measurement variations, two phase flow appl. *(German)* 78−59445
primary production model including circulation influences in Lake Superior 78−49041
probabilistic vector model for identification of intervocalic stop consonants 78−69114
propane pyrolysis, model, kinetics *(French)* 79−52649
PROPHET, real-time propagation assessment system, operational environmental models 79−58170
proteins, model building procedure 80−51036
pseudospectral dispersion model, inter grid sources representation 79−12259
psychoacoustic models for automatic speech recognition 79−41529
PWR, internal vibration calc. rel to operational safety condition *(Czech)* 78−8915
PWR, loss of coolant accident, mathematical model *(Czech)* 77−3072
PWR blowdown processes, homogeneous nonequilibrium model 79−632
PWR control system design model 77−88262
PWR core mathematical model specification 79−71931
PWR crud descriptive model 79−9691
PWR dynamical behaviour modelling in FORTRAN 80−91217
PWR neutron noise meas. and modelling 79−13443
PWR plant control loop development model *(French)* 77−23218
PWR power plant dynamics, math. model *(Polish)* 79−63800
PWR pressure vessel vibration excitation, noise correlation and modelling 79−13442
PWR pressuriser behaviour during operational transient, math. model 80−63230
PWR reactor dismantling, model scheme to meet West German regulations 80−825
PWR system nonlinear model comparison with test results 78−29571
PWR temp. sensor response time characts., estimation by noise anal. method 79−59216
pyrolysis, of single solid particle accompanied by consecutive reactions, vol. reaction model 79−47896
QUAL II river model soln. algorithm characts. 78−65348
quantum-chemical π-electron system, molecules-in-molecule model *(German)* 80−5490
quasi stationary short arc, anode spot mathematical model temp. field calcs. *(Polish)* 80−19664
quasisteady primitive equations with associated upper boundary conditions, appl. to large scale atmospheric flow 79−62563
radiation damage in crystals, computer modelling methods 77−7760
radiation damage to construction materials, math. modelling of point defects 79−90703
radiation detector fluctuations, computer simulation 77−3218
radiation heat exchanger, temp. distribution, boiler appl. 77−39210
radiational swelling of fast reactor materials modelling by inert gas ion irradiation 79−40999
radiative transfer, visible light model 77−39205
radio pulse reflection from ionospheric model, distortion, compression, approximate theoretical solution 77−21969
radioactive liquid waste elimination in hospitals, math. model for decay pond design *(Italian)* 79−48345
radioactive waste, geologic disposal, modelling of radionuclide transport and decay products 80−78415
radioactive waste disposal options, modelling studies 78−41830
radioactive waste management, mathematical modelling 80−701
radioastronomical antenna systems with complex aperture form, optical modelling *(Russian)* 77−22095
radioimmunoassay, fitting of general form of fundamental physical model 80−94150
radioisotope thermoelectric generator, selenide, power degradation predictions 79−48148
radiometric system design, mathematical modelling of relevant physical processes *(Rumanian)* 79−59313
radionuclide distribution, selective determ., mathematical modelling *(Rumanian)* 79−81098
radionuclide distribution in extended medium, qualitative and quantitative anal., mathematical modelling 80−71985
radiotelescope optical modelling using coherent optics and holographic methods, expt. *(Russian)* 77−22096
radiowave propagation in troposphere, investigation using modelling technique 79−29838
rainfall, Delhi, recursive prediction model 79−79998
reacting-diffusing system, turbulent spatio-temporal dynamics 78−56880
reaction, topochem., input mechanism, statistical approach applicability, using model process 78−92446
reactor fuel, rod modelling, utility requirements 78−21747
reactor fuel cladding loading by gas pressure during TOP accident 77−42030
reactor fuel extraction processing of nuclear fuel fluxes, effect of flux oscill. on Pu accumulation, math. simulation 80−63355
reactor malfunction detection by Dynamic Data System methodology 79−622
reactor plant mathematical modelling, dynamic model verification by comparison with recorded plant transients 79−89468
rectangular catchment basin downflow and infiltration, kinematic wave models 78−81235
reflector, rotationally symmetrical physical modelling *(Slovak)* 80−38088
reflector phased array aberration effects, optical modelling *(Russian)* 78−16290
regenerative heat exchanger high temp. behaviour, numerical model 77−62140
regional health care distribution systems, systems approach 77−48896
relativistic electron ring azimuthal oscillations in resonator with stabilising medium *(Russian)* 78−29889
remote sensing of two-layer media, microwave radiative transfer models 77−21908
reservoir sedimentation process and detention structure model 78−44892
reservoirs with Markovian inflows, first passage times 78−16080
resistance furnace heat conduction with random temp. intervals, aperiodic transfer functions determ. *(German)* 77−3709
resistive films spatially distributed, current density and potential distribution algorithm *(German)* 77−55618
resistivity, arbitrary two-dimensional structures 79−92617
resonators, concentric tube, with unpartitioned cavities, anal. 78−90587
respiratory ventilator model and design optimisation 79−20713
response surface, for stat. analysis 78−4470
modelling continued
reverberation time, absorption and impedance, theoretical model used for calcs. of a room 78−90601
riffle formation model 78−63482
ring laser gyroscope, empirical model for drift estimation 79−72605
ripple noise, models of pitch and pitch strength 79−90075
ripple noise pitch detection by human, adaptive model 78−73166
river outflow to sea, 3D model, Herault river example *(French)* 78−36209
river quality study, Streeter-Phelps models sensitivity anal. 77−70715
river water quality, modelling and control problems, review 79−57519
riverbeds, channel deformations, hydraulic modelling 80−77024
rivers, O_2 and pH fluctuations, math. model 78−92866
rivers, synthetic streamflow, Bayesian generation of multivariate model 77−78274
robots and manipulators, symposium, Warsaw (Sept., 1976) 78−53574
rock friction modelling, expt. results and constitutive eqns. 79−84240
rock friction modelling, preseismic slip simulation 79−84241
rocks drape folds, partially scaled models using folding under confining press. 79−58127
rotating noise sources, correl. meas. method model *(Croatian)* 77−39150
rotational isomeric state model, diffusion dynamics, 1-dimens. periodic pot. system 78−90315
rotor, Savonious, two-dimensional vortex sheet model 79−83552
rough surface modelling and online monitoring 79−80576
rubber, dynamic mechanical properties models *(Polish)* 79−43349
satellite-to-satellite tracking, ionospheric range-rate effects 79−58174
SAW filters, mathematical design model *(French)* 77−68331
SAW interaction with discontinuities, computer model 79−68461
SAW multistrip coupler mode analysis 77−27419
SAW resonator optical waveguide model 77−39146
scale models, incoherent jet noise line source *(Japanese)* 80−33337
scale models of buildings, acoustical performance of self-protecting buildings 80−23839
scintillation levels of synchronous satellite beacons at equatorial and high latitudes 79−58182
sea ice large-scale numerical model 79−48490
sea surface scattering channel and undersea communications 79−1022
sea temp. vertical distrib., modelling and prediction on expedition *(Russian)* 78−16190
sediment transport near ocean bed, theoretical flow models 78−15996
sedimentation, three-parameter Markov model 78−34183
seeding, hygroscopic, in cumulus clouds, a model 79−88442
seismic migration velocity estimation, problems *(Russian)* 79−66622
seismic waves, P-pulse propag. in elastic media, finite difference modelling 77−73868
seismic waves *(French)* 79−74843
self-recording heat flux meter, mathematical model 78−93678
SEM/STEM cold stage thick specimen heating model 78−61289
semiconductor, low-symmetry, modelling of elec. props. 78−19036
semiconductor film, polycrystalline, modified carrier model *(German)* 80−7012
semiconductor laser nonlinear theory self-consistent calc. 77−71968
semiconductor X-ray detectors, energy depend. efficiency response modelling 79−45560
semiconductors, high-resistivity, carrier transport *(Japanese)* 80−6850
sensitivity analysis, nonlinear, of multiparameter model systems 78−28931
shallow water circulation studies in Brazil, numerical model 78−77286
ship planing hulls, model tests using recirculating water channel, resistance characts. 79−18978
shoreline changes due to dredged holes, math. and lab. models *(Japanese)* 78−11878
shoreline evolution, beach sand transport modelling 78−15993
short single-mode optical fibre polarisation effects 78−1393
signal-dependent film-grain noise, optimal image estimation 80−102659
sine wave generator giving two signals in quadrature, mathematical model *(French)* 78−86114
skin cancer incidence modelling 78−77091
sleep EEG data classification by autoregressive model 79−57628
sliding flashover at switching-wave on rod-plate arrangement *(Czech)* 77−47278
slit and crack type leaks, calc. model and results of its use 80−35490
snow avalanche motion, hydraulic model for rectangular bed *(Russian)* 79−29804
snow melting conditions, computer modelling *(French)* 77−33102
solar active corona, modelling of mag. field three-dimensional struct. 77−67085
solar air heater transient model 79−62042
solar cell array, dispersion of characts. effect calc. 79−87994
solar cell life prediction using physical chemical failure progression modelling 80−61370
solar collector system, cylindrical, parabolic, transient energy removal calc. 79−52906
solar collectors, flat-plate, dynamic modelling and verification 80−66992
solar collectors with absorbent selective surfaces, theoretical performance 79−29482
solar drying of agricultural crops, using no-glass flat plate collectors 79−70465
solar energy collector, flat-plate, transient response, efficiency evaluation 79−18676
solar energy systems for buildings, passive, use of thermal modelling and 'predicted percentage dissatisfied' 79−62145
solar flat plate collector transient heat transfer models compared 79−83632
solar global insolation, calc. model 79−16613
solar power station, tower-type, concentrating and receiving systems design modelling 80−91873
solar power system, mathematical model, operating regimes optimisation 79−83562
solar pumping system, based on Rankine cycle, performance prediction 79−70460
solar radiation, correlations between diffuse and hemispherical and between daily and hourly insolation 79−87975
solar radiation at Earth's surface, spectral distribution model 78−69456
solar radiation average diffuse component estimation method 79−57399
solar radiation data, stochastic modelling and forecasting appl. 78−36243
solar radiation from cloudy skies, Cole's model extension 79−74947
solar radiation regime energy structure 79−39285

modelling continued
solar space heating and cooling, for moderately insolated regions, European research 79−57457
solar thermal energy production, large scale, possible climatic effects 78−81357
solar wind corotating stream interaction regions obs. by Pioneer 10 and 11, dynamic MHD modelling 79−2461
solid laser, CW, actively mode locked, picosecond pulse form., computer model 79−36939
solute transport in soils, two-site adsorption-desorption model evaluation 77−41101
sonar towed array modelling, steady-state and transverse dynamic motion study 78−30112
sound propagation in shallow water, investigation using reduced scale model *(French)* 79−3825
sound sensation varying with time 80−41053
Soyuz spacecraft, modelling of boundary layer flow by reactive streams of controlling motors of Apollo spacecraft *(Russian)* 77−82098
spacecraft payload optimisation using parametric modelling 77−5410
spacecraft surface material performance modelling 78−4061
spaceship, fission-engined series-staged, overall payload-optimal control 77−2320
spaceship, fission-engined series-staged, propulsion system model 77−2321
spark, long, at switching surge, voltage and flashover distance conversion factors *(Czech)* 77−15254
spark, long, at switching surge *(Czech)* 77−1028
spatial image filter with noncoherent incandescent source, model and expt. *(Russian)* 79−7083
spectra, IR and Raman, of disordered solids, analytical models 80−7336
speech analysis by linear predictive coding, accuracy improvement 79−46133
spin combustion, mathematical model 79−29364
sputter induced surface morphology, analytical modelling 77−16445
squid statocyst cavity using plastic sheet and modelling clay 79−84037
steady state response of systems with hardening hysteresis 78−60680
steam generator, radiant heat flux distrib., light model simulation 78−94567
steam generator combustion chamber, combustion product recirculation results *(Czech)* 78−27759
steel, continuous casting machine design, based on heat flow analysis, review 77−21048
steel, electrical, mag. hysteresis representation in numerical modelling of mag. fields 80−88813
steel, stainless, crevice corrosion, mathematical model 78−95834
steel, stainless, type 316, modelling effects of fast neutron irradiation in mech. behaviour 80−84234
STEM/SEM cold storage specimens, electron beam heating temp. profiles 79−5422
stochastic, of solar systems for space and water heating 79−57459
stochastic climate model, theory 77−37347
stochastic models for density meter characteristics *(Russian)* 77−9987
Storm Water Management Model for runoff prediction 77−37275
stratified and mixed coastal water models 78−77268
stratospheric O_3 in meridional plane, distribution by two dimensional model *(French)* 77−49100
stratospheric photochemistry and kinetics, modelling 79−53495
stream pollution dissolved O concentration optimisation using instream aeration 77−17153
stream temp. modelling, 'dishonest' method 78−81454
stream-well-aquifer system groundwater flow anal., linear system models 78−77289
streamflow, shot noise models for synthetic data generation 77−64348
structural analysis constraint techniques for coupling of discrete axisymmetric and general structs. 77−3714
structural system, simulation anal. of reliability and maintenance *(Japanese)* 80−62453
structures under impact loading, finite element modelling as tool for noise analysis and control 80−43535
student experiment, evolution of theoretical models *(Polish)* 80−36819
studios, acoustic design using scale models 79−10429
subgrid modelling procedures, turbulence theory applications 79−50710
subgrid-scale model, turbulence, experimental decay simulation 79−50709
subwatershed storm response timing, runoff model 77−37274
sucrose, mathematical model of crystn. rate in pure solns. 80−49151
sunlight, atmospheric absorption and scattering, appl. 77−81965
supersonic jet, stream model 77−89180
surface temperature of sea near Azores, thermal dispersion, math. model *(French)* 77−64290
surface waveguide electrooptical deflector, high-resolution, prism model 80−48454
surface-mounted beaded thermocouple transient response models 78−8405
suspended load sedimentation in reservoirs, analysis from one dimensional model 78−53664
synthetic seismograms using finite difference techniques 78−73326
teaching, heuristic model evaluation appl. to geometrical problem 79−80385
teaching, introductory course for undergraduates 78−57717
tectonic deformation, struct.-forming props. of bedded forms. from modelling data *(Russian)* 79−8627
tectonics, Zagros collision orogeny, finite element modelling of lithosphere deformation 79−20803
temperature field of precision calorimeters with isothermal jackets, math. model 78−93687
terrain, reflexive prediction and digital modelling 79−2175
test chimney stack construction, two-phase flow model *(French)* 77−37392
thermal fluid selection for long-distance heat transmission, theoretical model 80−35761
thermal neutron research reactor-2000, mathematical model of dynamics *(Russian)* 77−38330
thermal plume modelling, review 79−4056
thermoelectric cooler, single stage, finite element thermal stress anal. 80−108807
thermoelectric heat pumps, cross flow, anal. of operation and performance using mathematical model 80−107836
theta-pinch machines, computer modelling 79−10703
theta-pinch machines, linear, computer model of plasma 77−89296
modelling continued
thin cylindrical shell, effect of cavity resonances on sound transmission 79−3850
thin film condensates coalescence, influence on morphological changes, modelling 80−107676
three dimensional flow in controlled atmosphere, mathematical model *(German)* 79−64636
three phase induction motor heat flow model, locked rotor and running-up temp. rise calcs. *(German)* 79−90115
three-stage birefringent filter, tuning over visible region 80−58667
tidal flow in channel, modelling using turbulence energy closure scheme 79−79859
tidal wave in Venice Lagoon, kinematic mathematical model *(Italian)* 79−16471
tidal waves, finite element method appl. *(French)* 80−21782
tilted solar cell under various atmospheric conditions, performance evaluation 79−29476
time scale realisation models and predictions 78−57907
Tokamak reactor modelling, time-depend. computer codes 77−34468
tokamak reactor superconducting toroidal field magnet computational model, technical and economic 78−50375
track etch imaging, model of directional effects 77−18739
traffic noise in housing estate *(Hungarian)* 79−86291
train induced ground vibration, propagation pathways 80−48491
transducer array directional response anal., model 78−66973
transfer function with several inputs, model, math. methods of investigation identification 80−62451
transient two phase thermal hydraulics in channel, model 78−94091
transistor current gain characteristic as model for living structure 79−74590
transmission line modelling of diffusion 79−26011
transmission system design, influence of optical component baseband frequency response 78−1415
transport in heterogeneous media, random dispersed phase model 78−65885
transuranic transport from environment to man modelling 79−96669
trilateral surface cell modelling of conducting scatterers 79−36826
tropical oceanic circulation 78−16055
tropospheric reflection of differently polarized transient signals 79−29839
tube, vertical, steam generating annular flow, dry-out position prediction, computer model 78−59447
tube bundles, heat transfer to three dimens. flow 79−1073
tuition process, cybernetic principles appl., comparison with other educational methods *(Croatian)* 80−12866
Tunguska catastrophe, computational modelling 80−41779
tunnel location by cross-borehole EM probing 77−78545
turbulence, free-stream, near semiinfinite flat plate, vortex array representations interaction 78−90842
turbulence, inhomogeneous, simulation, clipping approx. 80−19331
turbulence, models, two-dimens., vortex and Fourier mode 78−46945
turbulence, numerical modelling 77−80144
turbulence, subgrid-scale modelling, eddy diffusivity, eddy noise 77−72292
turbulence structure and mechanisms, conference, Berlin, Germany (Aug. 1977) 78−94647
turbulent boundary layer, periodic intermittent model for wall region 78−87336
turbulent boundary layers, two-eqn. closure models comparison 77−84236
turbulent convection in vertical layer, numerical modelling *(Russian)* 78−9636
turbulent convection mode numerical modelling 79−64653
turbulent duct flow, length-scale model 77−84233
turbulent flow, computational modelling by finite elements 79−1163
turbulent flow separation, review 80−1543
turbulent interchanges coeffs. and parameters calc. *(Dutch)* 79−55365
turbulent jet flow, mixing length calc., using finite element method 78−38295
turbulent near wake, modelling using interaction hypothesis 78−63431
turbulent reacting flow, modelling, probability approach 79−72959
turbulent shear flow mixing, forced convection with chemical reactions, numerical modelling 79−1272
turbulent shear stress generation models, three-dimens. boundary layers 80−19360
twilight sky colours, modelling 79−100944
two phase mixtures permittivity prediction 78−48107
two-bar frame, eccentrically loaded, nonlinear stability anal. 78−63343
two-dimensional flow in condensed system axisymmetric channel 77−76010
two-dimensional gas flow model, comparison of two methods of computation *(Russian)* 78−59413
two-dimensional random field model for image structural analysis *(Russian)* 80−63932
two-dimensional space isothermal and nonisothermal turbulent flow *(German)* 80−28505
two-layer target, moderate energy electron interactions, direct statistical modelling *(Russian)* 77−66561
two-phase flow of particles during crystallisation in gaseous stream, modelling by aerothermochemistry of suspension eqns. *(French)* 80−53844
type II superconductors, flux pinning investigation using one-dimens. analogue model 78−88086
underground aquifer storage of hot water from solar energy collectors 79−57477
underwater noise, determ. of spatial coherence *(French)* 79−41487
ungauged urban watershed flood frequency model parameter estimation 77−37269
unit core cable structure design, fabrication and characterisation 79−37030
urban catchment flow and water quality model predictive accuracies 77−37279
urban flooding rel. to land use change, stormwater management model 77−37280
urban noise, math. model for noise level prediction 78−90599
urban stormwater and sediment discharge, deterministic model 77−37273
US modelling of seismic wave pattern caused by lenticular low-vel. inclusion 77−41006
US transducers for medical imaging *(French)* 80−26302
V_d ratio specification atmospheric noise models 77−81992

modelling continued
Vancouver Island region, analogue model study of EM induction 80−56356
vapour/gas joint flow in pumps, cavitational oscill. 77−35186
variable area flowmeter calibration, gas flow modelling 79−90353
vegetation canopy modelling for signature correction/anal. 77−78515
velocity meas. sonar system, transfer function model 77−7275
Venus atmosphere, thermal radiative transfer, numerical modelling 80−8574
vertebral model, computer-aided technique for 3-D finite element model generation 78−92591
viscoelastic rod analysis, using Boltzmann-Volterre memory theory, second-order approximate solution *(Russian)* 78−87278
viscosity, eddy, atmospheric flow over two-dimensional obstruction description *(Italian)* 79−20956
viscous flow, over mobile base, Navier-Stokes eqns. 78−46921
visual and auditory systems *(Japanese)* 79−66474
VLF radiowave ducts in magnetosphere 79−58202
void growth modelling, in ICFR first walls 80−63377
void modelling, in FBR pins, porosity and crack effects on transient overpower anal. 80−71760
vortex boundary layer flow, atmospheric, turbulent, predictor-corrector multiple iteration 77−91237
wastewater treatment, activated sludge, process control model 77−17154
water budget modelling and effects of spatial var. of soil hydraulic props. 77−73779
water pollution, modelling, filtering and control 79−57520
water pollution, subsurface environments 77−56658
water pollution control mathematical modelling, book 78−73418
water resources, model construction for Box-Jenkins modelling 77−87632
water resources management, systems anal. and modelling techniques appl. 79−5518
water surface, long-wave propag., modelling criteria, appl. to tsunamis 78−26132
water turbines, characteristic parameters, using laboratory models 79−63186
water waves, nonlinear, dynamic properties stochastic modelling 79−23332
water-water reactor parameters optimisation 77−74912
weather data reduction for building and solar energy system optimisation 79−57397
weather forecasting as a problem in fluid dynamics 79−84359
weather modification due to waste heat release from large dry cooling towers 79−84471
welding arcs, gas velocity fields modelling 80−75039
wide aperture optical systems, irradiance field formation, comparative analysis 78−90479
wind energy conversion systems, value to electric utility, economic model 80−61257
wind magnitude and persistence, probability models 79−5583
wind turbine, horizontal axis, interaction with wind field calc. 79−83551
wind turbine, vertical axis, torque ripple analysis and obs. 79−48072
windmill, vertical axis, aerodynamic design and testing 79−43717
wing aerodynamic characts., modelling ground plane effect 79−32553
XPS, prediction model for ang. distrib. intensity and lineshape 77−41734
Al particulate combustion process model *(Russian)* 78−85164
Ar inductively-coupled RF plasma torch, computer model 78−71559
Ar isotope separation by axial flow turbomachine model 78−78500
Au, atomic struct. of large angle [001] twist boundary, determ. by computer modelling and X-ray diffr. study 80−70162
Au black optical props. rel. to structural composition, appl. to solar absorption 79−83630
CaF_2, mol. dynamics studies of superionic conductors 80−107547
^{60}Co irradiation sterilisation processing, unequal mass interchange model 79−26758
^{60}Co irradiation sterilisation processing unequal mass interchange model verification 79−26759
Cr black, coating on Cu substrate, selective solar energy absorpt., model calcs. 79−57440
Cu, single crystal sintering model evaluation, Kossel interference and digital graphic simulation appl. *(German)* 80−2980
DF-HF CW lasers, performance, computer modelling 78−71094
F+Xe, enhanced quenching in intense KrF laser light, computer modelling 78−55232
Fe, segregation of impurities, physico-chemical aspects *(Czech)* 80−60866
GaAs structures, charge accumulation and transmission *(Bulgarian)* 80−6947
$GaAs_yP_{1-y}$ alloy, composition effects in growth by MBE 80−59816
Gd-Co amorphous films, model calculations for anisotropy formation induced by resputtering processes 78−64242
H_2 oxidation reaction kinetics, thermodynamic model appl. *(German)* 79−5130
HF, pulsed laser numerical modelling, rot. relax. 80−87388
He I, cryofluid free convection, at supercritical pressures 78−26745
$InAs_yP_{1-y}$ alloy, composition effects in growth by MBE 80−59816
n-InP film, polycryst., deposited on Mo sheets, elec. props. obs., w.r.t. varying deposition conditions 79−4608
$LiNbO_3$, ion implanted, acoustic model of SAW delay lines *(French)* 78−55540
N_2^+, first negative spectra, modelling 77−61758
Na-S cells, S electrode potential distrib. model 79−96435
P pollution removal process modelling and control by multivariate time series method 79−74561
Pb, reactor radiation-induced hardening, computer modelling *(Russian)* 79−37738
SF_6 electric strength, electrode surface roughness effects *(German)* 78−63609
SO_2 regional transport, three-dimensional grid model 77−37375
Si epitaxial growth, in $SiCl_4$-HCl-H_2 system, model based on flow graph 79−42405
Si-SiO_2-$Si_xO_yN_z$ waveguide model *(Russian)* 79−10374
SiO_2, low-pressure deposition from tetraethylorthosilicate, modelling 79−87582
Sn plate rolling cold roll-force model 77−4788
UO_2 fuel modelling *(Japanese)* 77−71648
Zn-Cl_2 batteries for electric vehicles, battery design modelling 80−30452

modelling, computer *see computer-aided analysis*

models *see modelling*

modems
DC microvoltmeter based on modem 80−31798
DC nanovoltammeter based on modem 80−31797
digital modulator and synchronous demodulator system: an alternative to the analog phase detector 78−70107
electrometer, high-sensitivity, with modem amplifier 77−74447
optical communications systems *(Japanese)* 79−27407
PSK high data rate, satellite communication appl. 77−49268
X-ray picture digital transmission over voice-grade telephone channels, laser scanning system 78−80953

moderation (neutron) *see neutron moderation*

moderators
see also beryllium; graphite; heavy water
AGR, moderator corrosion problems, soln. 77−18688
beH_2 as a moderator in minimum critical mass systems 80−83151
BWR core, moderator temp. coeff. and neutron leakage, DIFFUSION-ACE calc. 78−54844
CANDU-PHW reactors, primary and secondary water chemistry, review 79−22382
components review *(Spanish)* 77−79429
cooled polyethylene moderator on pulsed neutron source 78−70666
FFHR, tailoring the breeding-fission ratio by neutron moderation with iron 78−21677
graphite, CO formation at initial stages of H corrosion 78−11355
graphite, coke source inference from neutron small angle scattering meas. 77−74923
graphite, creep irradiation expt., design, operation, initial results 77−42067
graphite, creep rig, high temp. 77−44423
graphite, diffusion of Cs 77−7901
graphite, diffusion of T *(German)* 77−24442
graphite, energetic deuteron irradiated surface struct. quantitative meas. 78−95210
graphite, energetic ion sputtering, appl. of AES-SIMS (IMA)-FDS combined systems to physical and chemical processes 78−95636
graphite, fast neutron flux effect on irradiation damage 78−22768
graphite, fast neutron irrad. damage, chem. rate theory applic. effect of annealing and thermal equilib. defect concs. 77−67804
graphite, fast neutron irrad. damage theory and modifications 77−67805
graphite, fatigue behaviour 77−56078
graphite, irradiation creep 77−42066
graphite, irradiation induced creep, UKAEA reactor group studies 77−42065
graphite, neutron effects on shrinkage 80−37456
graphite, nucl. grade, neutron small angle scatt., thermal and radiolytic oxidation effect, porosity size distrib. 79−17977
graphite, nuclear, change in ratio of thermal expansion coeffs. at elevated temps. 79−42283
graphite, polycryst., reactor-grade, neutron irradiated, isothermal annealing obs., by ESR *(Japanese)* 77−43254
graphite, prestressing effects on nuclear graphites 78−14482
graphite, pyrolytic crystals, surface topography, bombarded with Ar^+ N^+, He^+ ions 78−6820
graphite, radiation creep 77−42064
graphite, radiation damage effect on erosion by H 78−21640
graphite, reactor material, laser microemission spectroscopy for local determ. of impurities *(German)* 78−7161
graphite, reloadable creep facility for tensile or compressive expts. 77−42070
graphite, structural, impact toughness, reln. to compressive strength 78−88605
graphite, synthetic materials, radiation defects, review 77−47494
graphite, trapped neutron pseudo-decay-consts. meas. at 77, 194K 77−42007
graphite cylindrical thin shell, thermal shock, fundamental heat cond. soln. 78−29575
graphite moderator structure design and manufacturing specification 80−23110
graphite oxidation and coolant chemistry of CEGB gas-cooled reactors 80−42774
graphite pebble bed system, meas. of neutron wave propagation *(German)* 77−6481
graphite powder, characterisation, use in HTR fuel compact matrices 78−29631
graphite reflectors in PBR with OTTO fueling, neutron effects, stress anal., cooling measures *(German)* 77−34368
graphites, reactor, strength and deformation under conditions of cyclic variation in load and temp. 79−43355
heavy atom moderator, resonance capture of neutrons 80−14310
heavy water production, using laser isotope separation 77−83106
HTGR fuel elements, neutron irradiation behaviour of graphitic matrix materials 79−19283
HTR, pyrocarbon coated fuel, C density determ. by X-ray absorpt. 80−5301
HTR reactor graphite, irradiation creep 77−46279
hydrogenous, neutron slowing down length, calc. by Fick's law 79−22352
hydrogenous, neutron thermalisation 77−65253
light atom moderators, resonance capture of neutrons 80−14310
linear extrapolation distance for a black cylindrical control rod with the pulsed neutron method 80−68839
Magnox reactors, moderator graphite corrosion protection coolant comp. effect on radiolytic graphite/CO_2 reaction 77−6489
methane, 20K, cold neutron pulse emission, time dependence 77−67928
neutron maximum density and capture rate, pulsed sources 80−13522
PBR graphite structures, neutron radiation damage, mech. props., stress fields *(German)* 77−34387
pressure tube-type reactors, moderator temp. coeffs. of reactivity meas. 80−57893
pulsed spallation neutron sources for slow neutron scatt. 77−83426
PWR, appl. of moderator temp. for enhancement of operating flexibility 80−695
PWR assemblies, spectral and density components of moderator temp. coeff. 80−9356
pyrocarbon coatings, mass spectrom. determ. of fission gas permeabilities 78−12785
reactor H_2O-graphite system, neutron rethermalisation 79−97806

moderators continued
seawater distillation, heavy water concentration, numerical model calc. 79−26514
thermalization of neutrons, review of Soviet research 79−36300
void coefficient for tight water lattices, dependence of moderator type 79−26470
Au, moderator surface preparaton for increased slow positron yield 80−61011
B_4C, effect of fast neutron irradiation on struct. 78−26597
Be, anisotropy in thermal neutron scatt., anal. 80−552
Be, finite assemblies, thermal neutron wave propagation 78−58320
Be in thermonic reactor with ^{233}U fuel, neutron physics analysis 77−50281
Be, neutron diffusion in finite blocks, flux synthesis method for 3D multigroup eqn. 77−34366
BeO, finite assemblies, thermal neutron wave propagation 78−58320
D_2O leak detection, on-line infrared analyzers, CANDU report 78−82038
D_2O, neutron scatt. cross section determ. by DEUKER computer code 79−54468
D_2O, of reactor KS-150, purification from organic impurities by catalysis *(Slovak)* 77−67811
D_2O thermal column irradiation facility, in Penn State Breazeale Reactor, D_2O thermal column irradiation facility 80−9339
D_2O-H_2O mixing, diffusion meas. using neutron radiography 77−15605
Eu-B-C ternary and binary boundary systems, preparation techniques, X-ray analysis 80−60840
Eu_2O_3, mech. and physical props. rel. to reactor control rod appl. 78−21641
H_2, liq. slow neutron scatt. rel. to intermol. excitations, analyt. model 77−58941
MgO coated moderators, slow positron form. 80−62796
Si, moderator for slow positron beams 79−71888
SiC protective coatings, on graphite for HTR, corrosion *(German)* 78−3248
T buildup in D_2O of CANDU reactors, due to $^3He(n,p)^3H$ reaction 79−22389
U, reson. absorpt., effect of annular fuel elements 78−666
UO_2 rods, 4.75 wt.% ^{235}U enriched, in lattices in water, critical expts. 79−63790
ZrH rethermaliser for IVV-2 reactor hot neutron flux increase 80−37676

modes, laser *see laser modes*

modes, lattice vibrations *see lattice dynamics*

modes, vibration *see vibrations*

modular circuits *see modules*

modulation
see also amplitude modulation; angle modulation; demodulation; demodulators; modulation spectroscopy; modulators; optical modulation; pulse modulation; Schwarz-Hora effect
acoustic monochromatic waves in water *(French)* 79−41503
acoustic wave in nonlinear medium, modulation rel. to low-freq. noise waves excitation 78−9472
acoustical communication theory, computation of modulation and carrier functions of an arbitrary audio signal 80−79064
acoustical-gravity waves in plane waveguide, self-modulation *(Russian)* 78−36221
application of communication theory to acoustics, separation of sound carrier and modulating signal 80−79063
astronomical IR photometer, beam modulation via vibr. dichroic filter 77−26017
ATS-6 satellite radio beacon, modulation phase meas. at Ootacamund, India 79−48611
aurora, latitude effect in pulsating patches periodicity 80−31155
auroral pulsations, effects of precipitating electrons flux modulation 78−73562
beam brightness modulation, in Auger scanning microscopy 79−16097
boxcar integrator instruments, baseline correction via grid modulation, plasma chromatography appl. 77−52717
CESR cavities, HF modulation technique 77−37956
complementary cross modulation, new technique for ionospheric modification studies 77−2275
cross-modulation of radio cosmic noise in ionospheric propag. 77−70936
Cygnus X-3, 4.8 hour modulation period change disproved 80−8713
displacement transducer using second harmonic type magnetic modulator 78−21115
electrotactile code evaluation 77−40932
energy flux, wave props. 77−65559
FM signal modulation by smoothed random telegraph signal, appl. to underwater acoustic meas. 78−18130
heteronuclear double-resonance spectra, modulations 78−86897
ionosphere LF signals, modulated reception method for refl. coeff. determ. 78−45114
Jupiter decametre radio emission, dynamic spectrum modulation lines origin 80−67643
magnetosphere energetic particle fluxes, modulation due to long-period geomag. oscills. 79−25407
magnetosphere VLF noise intensity, modulation by hydromagnetic oscills. 78−45139
meters, history of development, selection, special features, calibration *(French)* 77−53948
meters, operation and accuracy 77−37912
microwave, by random fluctuations of pulse discharge plasma parameters 77−42988
modulational instability expt. using nonlinear transmission line 77−82397
molecular beam scattering, S/N ratio enhancement in time-of-flight anal. 78−86969
P-wave signal, complex, from underground nuclear explosions, coda power and modulation characteristics 79−79757
phase-screen, deeply modulated, theory, appl. to multiple scatter problems 79−21561
plasma Hall accelerator, with extended accel. zone, ion stream modulation at exit 78−79480
polarising submillimetric Fourier interferometer with achromatic internal modulation 78−65959
propane, vibr. combustion, modulation in injection-vibr. apparatus *(Russian)* 77−9083
pulsar signal microstructure, temporal modulation rel. to periodicities and polarisation 79−75232

modulation continued
pulsating aurora, 3 Hz modulation rel. to pitch angle diffusion instabilities 79−25391
pulse-phase, torquemeter comprising magnetically coupled pulse transducer with electronic phasemeter 80−74819
scanning Auger electron microscopy, synchronous modulation technique 79−17570
solar 22 year cycle, long period modulations by multiple-period dynamo wave oscills. 79−16813
solar moving type IV bursts, gyro-synchrotron modulation obs. 80−26833
solar type IV meter bursts microstruct., modulation of continuous emission by whistlers wavepackets 77−78761
sunspot, Wolf number amplitude and phase modulation from freq. anal. 80−56797
superconducting chopper amplifier, improved sensitivity 77−26306
US Doppler flowmeter, new modulation method 80−45989
US Doppler flowmeter employing continuous wave modulation *(Japanese)* 79−37429
VLF wave packet, cyclotron interaction with reson. electrons beam 79−53652
X-ray astronomy, automodulation collimator telescope *(Russian)* 80−62018
GaAlAs laser, modulation behaviour in Gbit/sec range 79−31900
H beam, 3 to 15 keV, system using voltage pulse generator 79−18315
KCl:Li, microwave modulation by paraelec. reson. *(Russian)* 77−20809
Ne-Xe gas discharge, LF oscillations, modulation by gravitation and inertia forces 77−11429
Ni, intermodulation generation in RF mag. field, field interaction with domain walls 79−56600

modulation factor *see modulation*

modulation index *see modulation*

modulation spectroscopy
see also appearance potential spectroscopy; electroabsorption; electroreflectance; magnetoabsorption; magnetoreflectance; piezoreflectance; thermoreflectance
acousto-optic interaction in solids, appl. to high speed anal. of spectra *(French)* 80−95156
adsorption of isolated atoms, quantum theory 78−22957
AES, electronics design 79−30615
anthracene, single cryst., piezomodulated reflection spectra 79−61392
atomic absorption, Zeeman modulated technique, appls., detect. limits 79−24876
atomic absorption, Zeeman modulation technique, line interferences 79−24877
atomic fluorescence spectrometry, wavelength modulation, using CW dye laser 78−61083
atomic lifetimes meas, two-level atom, influence of relaxation parameters and laser fluctuations 79−72273
atomic spectra, Doppler-free spectrosc. with vel. selective optical pumping 79−81304
atomic spectrochem. anal., computer modelling of wavelength modulation spectrometry 77−63974
Auger spectroscopy, tailored waveform modulation calc. for integral spectra 77−32860
automatic compensator for background and dark current in output of photomultiplier 77−87851
tris(2,2′-bipyridine) ruthenium(II) cation, IR-optical double reson. and thermal modulation spectra 78−25576
Brillouin scattering, resonant, analogy to modulation spectroscopy *(Japanese)* 78−68526
circular differential photoacoustic spectroscopy 80−47114
contactless measurements of electrical conductivity and magnetic susceptibility of solids using torsional resonance apparatus 79−75675
continuum source, for at. absorpt., selective spectral line modulation method 77−44520
critical point symmetry, use of electromodulation as probe, sensitivity 77−66477
differential optical spectra recorder using wavelength modulation method 79−2832
differential-type Brillouin scattering system, construction *(Japanese)* 78−89562
difluoromethane, microwave spectral line widths 78−70816
Doppler-free intermodulated optogalvanic spectroscopy, of gas discharges species 79−50169
double wavelength rapid scanning spectrophotometry of intact mitochondria 78−4699
echo spectroscopy in double reson. mode 80−1284
electron spin echo modulation phenomena, paramagnetic species immediate environment struct., review 78−88164
EPR, elec. field modulated, appl. to study of ferroelectrics 80−75841
EPR and saturation transfer EPR, fast computation, perturbation approx. extension for overmodulation 78−82754
fluorescence decay, meas. via modulated gain spectroscopy, appl. to rhodamine-B 79−64025
fluorescence decay meas. via modulated gain spectroscopy, appl. to rhodamine B 80−63699
Fourier spectrometers, sinusoidal interference modulation and path difference control *(Russian)* 78−29176
frequency crossing techniques appl. to high resolution phonon spectroscopy 80−107392
frequency-modulation spectroscopy: a new method for measuring weak absorptions and dispersions 80−42262
Fresnel reflection coeff. of 3-phase system determ. by modulated reflectance spectroscopy and interferometry 77−82621
gas and solid-state lasers, use in modulation spectroscopy 79−30572
gas phase, narrow nonlinear reson. production by modulated optical radiation *(Russian)* 77−67507
hollow cathode, HF modulated for atomic absorption 79−57341
HV pulse generator 78−77995
image transmission by modulation spectroscopy *(French)* 77−14663
infrared heterodyne spectroscopy in astronomy 78−85859
IR laser Stark spectroscopy, absorption of laser radiation in Stark tunable mol. gases *(Rumanian)* 79−86157
IR laser Stark spectroscopy, RF elec. field modulation effects 80−52989
Kramers-Kronig relations, anal. in modulation spectroscopy 78−23423
laser absorption spectroscopy for point monitoring of gases ambient concs. using tunable lasers 78−61607
laser wavelength-modulation spectroscopy, high sensitivity 78−24868
layered compounds, book contrib. 77−40267

modulation spectroscopy continued
magnetic resonance, coherent averaging, modulation method 77−8424
magnetically induced circular polarisation of emission meas. 78−58058
magneto-optical spectroscopy, mag. field modulation apparatus 77−34032
maleic anhydride, struct., DRM microwave spectra, isotope shifts 78−21918
MCD and Faraday effect in chemistry and physics, optical instrumentation 78−54466
metals, electromodulation spectroscopy, developments, mechs. 77−66475
microspecimens, electro-optical techniques *(Russian)* 77−36203
microwave 'stripline' absorption cell, for use in microwave Stark spectrosc. 79−81305
modulation-interference spectrum analyser 77−79161
molecular beam spatio-temporal modulation near mol. reson. *(French)* 79−49299
monochromatic EM wave, passing through reson. medium, characteristic modulation 79−27220
nematic liquid crystals, mol. orientation, spontaneous polarisation, appl. in modulation spectroscopy *(Russian)* 78−55809
nonlinear modulation microwave spectroscopy, press. and power correl. depend. 79−44936
normalising amplifier, meas. and other automated systems appl. 80−73470
ODMR technique, discrimination between homogeneous and inhomogeneous lines 79−44923
opt. freq. shifting of light and laser beams for Rayleigh scatt. spectroscopy 78−79392
optical calculi, for phase modulation spectroscopy 77−88639
optical heterodyning, for light scatt. spectra 79−6186
optical multichannel detection system, using Si target vidicon 77−41693
optically active crystal, circ. dichroism, modulated polaris. spectra 78−23429
phase-polarisation nonlinear high-resolution spectroscopy in longit. mag. field 79−41423
phase-shift-difference method, modulated, appl. to excitation absorption energy meas. in $CuGaS_2$ 78−39565
photocapacitance spectra, wavelength modulated, deep level determ. 80−76055
photon echo spectroscopy of crysts., review 80−83648
polarisation, relaxation characts. of degenerate states obs. *(Russian)* 80−27348
polarisation spectroscopy, using phase modulation spectrophotometer, optical calculi 78−45715
polarised light in chemistry, electro-optic and photoelastic modulators 77−45896
repetitively pulsed dual beam thermo-optical absorption spectrometer 78−77999
resonant Brillouin scatt. as form of modulation spectroscopy 79−91456
rhodamine 6G, aggregation, modulation Stark spectrosc. obs. 79−27030
saturated absorption spectroscopy, effects of modulation on signals 78−74066
saturation spectroscopy with multiple-frequency excitation 80−102774
saturation transfer EPR spectroscopy, source modulation, mol. reorientation effects 78−41339
Schottky-barrier diode wavelength-modulated photoresponse spectra *(Russian)* 78−84300
selective modulation interference spectrometer, far IR 80−57397
selective modulation interferometric spectrometer, theory, design 78−58054
selective spectral line modulation AAS 78−89546
semiconducting alloys, comp. profile, second derivative wavelength modulation 80−103967
semiconductor, photoluminescence, temp. modulated 79−38623
semiconductor, submillimetric magneto-optical props., strip line technique 80−60554
semiconductor surface evaluation by electroreflectance *(Japanese)* 79−82949
semiconductors, dielec. function, modulation spectroscopy and elec. field effects book contrib. 80−80201
semiconductors, examination of optical props. using wavelength-modulating spectrometer implemented with photovoltaic photodiodes 79−80699
semiconductors, modulation spectroscopy in far UV, electroreflectance and thermoreflectance 77−66516
SEMIDS, (selectively modulated interferometric dispersive spectrometer) anal. capabilities 77−44521
signal broadening in potential modulation differentiation 79−54237
SISAM, diffracted light from grating affecting modulation 79−6187
SISAMs, sinusoidal interference modulation and path difference control *(Russian)* 78−29176
solid state spectroscopy using synchrotron radiation, book contrib. 80−7375
solid-state circular dichroism spectra, phase modulation spectrosc. obs. 80−93271
spectrochemical analysis, derivative and wavelength modulation, review 79−79317
Stark modulator, zero-based half-sine wave, for analytical microwave spectrometer 77−13802
Stark spectroscopy using CW dye laser, appl. to NO_2 77−38026
strain-modulated ESR, appl. to $MgO:Cr^{3+}$ 78−88175
stress spectroscopy of resonant bandmode with far IR laser 78−2847
1,2,4-thiadiazole, struct., double reson. modulation microwave spectra 77−14424
transition metal dichalcogenides, modulation spectroscopy obs. 78−80377
transparent solids, absorpt. coeffs. by laser calorimetry, wavelength modulation spectroscopy 78−66876
two-ray methods, appl. to semicond. band struct. determ. *(Russian)* 78−54469
UV laser window material absorption obs. 79−14012
UV-visible, throughput, signal and noise spectral bandpasses calcs. 77−45897
vacuum UV, with synchroton radiation, review 78−4710
wavelength modulated derivative UV absorpt. spectrometry, improving analysis 78−45731
wavelength modulated spectrometer for reflectivity meas. in 150-900 nm range 77−13807
wavelength modulation spectrometers, modulation depth 78−89551
wavelength-modulating spectrometer implemented with photovoltaic photodiodes, comments 80−98981
wavelength-modulation Raman spectroscopy 79−12863
X-ray modulation collimators, design and construction 77−5434

modulation spectroscopy continued
Zeeman, line shape analysis 80−74197
$AgGaSe_2$ wavelength-modulated reflectance, optical electronic transitions, 1.5-5.5 eV 78−35170
$BaF_2:Pr^{3+}$, wavelength and temp.-modulated UV absorpt. 80−2799
CaCl, free radical, $A^2\Pi$-$X^2\Sigma^+$ system obs. by saturation spectroscopy 78−46353
$CaF_2:Ce^{3+}$, absorpt. peaks in the lowest 4f→5d band, effect of conc. 80−2798
$CaF_2:Pr^{3+}$, wavelength and temp.-modulated UV absorpt. 80−2799
CdS, photorefl. in exciton region, surface layer influence 78−76489
CdS(Se), magnetoreflectance spectra of anisotropic II-VI semiconds. by mag. field modulation 77−66519
Cr complex, $(-)_D$-tris(ethylenediamine) chromium (III), solid-state circular dichroism spectra, phase modulation spectrosc. obs. 80−93271
Cu-Al, optical composition modulation spectra, dielec. const. var., Fermi surface and electronic level shifts 80−6707
Cu-Zn, optical composition modulation spectra, dielec. const. var., Fermi surface and electronic level shifts 80−6707
Eu chalcogenide mag. semiconductors *(Japanese)* 77−24862
Fe-Cr alloys, passivation films, modulation spectroscopy study 80−3244
$Ga_{1-x}Al_xAs$, epitaxial layers, reflectivity meas. by wavelength modulation spectroscopy *(French)* 77−59632
GaAs, deep level photoionisation, absorpt. by derivative surface photovoltage spectroscopy 79−99575
GaP, piezo-modulated spectroscopic investigation of N and N-N pairs, bound exciton 77−66474
GaP:N, photoluminescence, temp. modulated 79−38623
Ge, spectrum of photocapacitance current near fundamental absorpt. edge 77−28217
He-Ne lasers levels, modulation spectroscopy 78−46572
$Hg(6^3P_0)+Cl_2$ reaction, reactive quenching metastable states 79−57208
$In_{1-x}Ga_xP$, quantitative characterisation of chemical disorder from wavelength-modulated no-phonon absorpt. 79−15482
NH_2, microwave modulated saturation spectroscopy, hyperfine energy levels 79−68245
NO radicals, slow rot., modulated EPR spectra 79−38382
NO, Zeeman modulation IR spectroscopy using spin-flip Raman laser 79−18181
Si (2p) optical transitions, final state effects, soft X-ray electroreflectance study 77−66553
$SrF_2:Pr^{3+}$, wavelength and temp.-modulated UV absorpt. 80−2799
$SrF_2:Tm^{2+}$, modulation magnetooptic spectroscopy of cross-relaxation resonances 79−15381
ZnS(Se), wavelength-modulated refl. spectra, 2.5 to 8 eV 77−20877
ZnTe, excitonic effects at E_0 and E_1 gaps, wavelength modulated reflectivity spectroscopic study 79−61400
ZnTe, reflectivity meas., double beam wavelength modulated technique *(Korean)* 80−50365
ZnTe, wavelength-modulated reflectance spectrum, electron-phonon and exciton-phonon interactions 79−11434
ZrS_3, thermomodulated reflectivity and transmission 80−50357

modulation transfer function *see optical transfer function*

modulator-demodulators *see modems*

modulators
see also demodulators; modems; modulation
5 MeV electron accelerator modulator charging system 79−13563
accelerator modulator charging system upgrade for 5 MeV electron accelerator 80−23182
acousto-optic, applications and device technology 77−58468
acousto-optic, laser beam transverse mode and polarisation effects on perform. 77−58469
acousto-optic modulator for optical fibres 79−98499
acousto-optical modulators for laser beams 77−19355
bidirectional square wave modulator, for NQR spectrometer 78−256
bisymmetric Zeeman modulator for NQR 80−98960
broadband optical modulator for laser range finder *(Russian)* 80−53424
coherent OCR system using spatial light modulator *(Japanese)* 80−14291
electrochromic ATR prism modulator 80−43440
electrometer ferroelectric modulator temperature stabilisation 77−82550
electrometer ferroelectric second-harmonic modulator design 77−82549
equipment and services, 1979 video yearbook 79−14197
floating deck modulators for high voltage protection of ion beam accelerators 78−66392
fusion reactor, TFTR, neutral beam source, arc current modulator design 80−102379
high-power long-pulse thyratron modulator with small off-duty factor 78−86380
holographic binary data recording with multichannel acousto-optical modulator *(Russian)* 79−94178
holographic data recording phase-random mask production by multichannel acousto-optical modulator *(Russian)* 79−94179
integrated optical elastomeric modulators 77−75715
ionisation gauges, ion collector current, analytical description 77−53924
Josephson optical modulator with weak-link diffraction grating 79−98486
laser diode modulator using current switching bipolar transistors 78−1288
low-noise magnetic, operating near Curie point temp., equivalent input noise study 77−74462
magnetic field, EPR radiospectrometer having discrete set of modulation frequencies 80−52285
magneto-optical, IR, using CaVG polycryst. 78−10900
Magnox reactors, moderator graphite corrosion protection, Hz injection into Wylfa reactor I coolant gas 77−6490
microcantilever electrostatic deflection system for transmission optical modulator array 80−87512
micropowered IC modulator for implantable biomedical telemetry 77−78000
microtrons, thyristor modulator circuit and construction 80−63422
multibeam acousto-optic modulator efficiency stabilisation 80−43439
multichannel acousto-optical modulator control system *(Russian)* 79−72525
noise reduction of second-harmonic-type magnetic modulators 78−70168
optical modulator crystal coatings 77−19431
phonocardiograph modulator design trends 78−24171
photomultiplier modulating cct. with spurious signal compensation 78−58033
Pockels cell, for laser sub ns pulse generation 77−19357

modulators continued
SAW acousto-optical total internal reflection modulator 77−19435
Stark modulator, zero-based half-sine wave, for analytical microwave spectrometer 77−13802
tape recorder three-channel modulation scheme for biological signals 78−61272
thyristor current modulator for cyclotron arc ion source 77−46438
thyristor modulator with periodically interrupted supply, microtron appl. 78−55061
two-phase PSK modulator employing SAW delay line, fundamental performance 80−33398
CdTe electro-optical modulator for CO_2 lasers 77−19443
GaAs 400 MHz TW laser modulator 80−87541
GaAs crystals appl., with nipi superstructures *(German)* 78−95064
GaAs-on-sapphire spatially distributed thermal light modulator 79−59839
KD_2PO_4, ultrafast electro-optical modulator design and application 77−19432
$LiNbO_3$ electro-optical total internal reflection diffraction industrial modulators and deflectors 77−19436
$LiNbO_3$ planar HF acousto-optic modulator construction and expts. 79−76863
$LiTaO_3$ electro-optical total internal reflection diffraction industrial modulators and deflectors 77−19436
PZT paraelectric ceramic one-dimensional spatial light modulator 79−55240
$PbMoO_4$ acousto-optical modulator for wideband laser recording system 79−89942

modules
see also CAMAC
A/D data acquisition module for microprocessor systems, high-speed, multiple channel 77−57304
block modular instrumentation aggregate, for investigating cryst. materials via low-energy proton beams 77−76266
CAMAC module for linking external equipment to computer 77−3245
coincidence circuits and shapers, parameters 79−3320
CRO design using modular system 78−93671
dead time correction system, standard 78−17532
ELMO Bumpy Torus Reactor toroidal magnet system design 79−31196
emitter-coupled integrated circuits, application to nanosecond nuclear electronics 78−5101
hybrid optoelectronic modules for OEM fibre-optic data systems 79−86259
image convertor camera, with microchannel intensifier, modular design 78−42427
instrumentation system for nuclear industry 77−67780
instruments based on standard units, mathematical aspects of design *(Russian)* 80−37021
IR detector balanced common module coolers 80−95142
IR scanning system modular design, assembly and alignment 80−78989
low-cost encapsulation materials for terrestrial solar cell modules 80−3522
multichannel time-digit conversion modules of 'Summa' system for spark chambers 77−3236
multifuel fluidised bed combustion packaged boiler to supply 10000 lb/h saturated steam at 100 psig 80−108779
NIM system for spaceflight use on Shuttle/Spacelab missions 77−70973
nuclear reactor containment, primary, electrical penetration assembly 78−716
optical transmitter laser diode module description and performance 80−64069
photogrammetric automaton 'Zenit', program-control module for interference coordinate measuring system *(Russian)* 78−21103
photovoltaic solar devices, modular system *(German)* 80−89629
plastic encapsulated and hermetic, corrosion model 80−100937
plastic modular solar energy collector with reticulated foam 80−16833
programmed, for transducer response linearisation 78−45604
pulse counter, high-speed DC coupled, sensitivity and performance 79−89524
pulse counting measurement systems, optimum parameters determ. 79−89523
solar cell, transparent, with improved glass, adhesives and heat dissipation 80−76636
solar cell arrays, shingle-type, for residential and commercial buildings 79−52907
solar energy conversion, use of flat-type Si chips *(German)* 80−55840
Summa system for information output to oscilloscope, digital display and printer 77−3244
surface meas. instrument, with indicator and strip recorder *(German)* 80−57283
telemetry system, implantable, multichannel, inductively powered, for animal cardiovascular data recording 77−86662
thermoelectric, biomedical implantable sources appl., high reliability contacts using local heat pulses 79−52952
thermoelectric convertor technology, selenide, 156-couple ground demonstration system 79−48146
thermoelectric coolers for micromodules 79−6120
transducers of electrical variables, third-generation, individual and group arrangements *(Czech)* 80−62645
US diagnostic equipment, operation principles and constructional features, advantages *(German)* 79−100684
PbS IR staring mosaic detector array module development 80−86413

modulus, Young's *see Young's modulus*

moire fringes
afocal projection measuring system, moire fringe techniques, large lathes, milling machine appl. 77−71295
Airy profile interferometric grilles, moire fringe analysis *(Spanish)* 80−27354
aortic valve study, by holographic interferometry and shadow Moire methods 80−104613
automatic pattern processor for simple and complex interference patterns 80−13129
biostereometry using parallel light beam 79−100701
bolted joints in wood, photomech. stress determ. 79−32406
brittle solid, atomically sharp cracks, TEM study 80−71729
coincidence grain boundary, lattice displacement, electron images 77−80516
computer generated moire for profile testing 80−105689
contour lining, reference plane orientation by optoelectronic methods 77−2636
moire fringes continued
contour plotting, moire technique 80−42002
contouring by Moire holography 78−1183
contouring method by parallel light Moire holography 78−33702
contouring of large objects by scanning technique 78−32791
contouring system, lateral grating movement *(Japanese)* 77−87817
contouring using virtual moving gratings simulated on computer 78−73968
contourography, computer-aided replication of human anatomy 80−67189
convex cylindrical surfaces, deformation anal. using moire fringes 80−14636
corneal topography using moire contour fringes 80−26316
crystallographic struct. factor phases from electron-microscope dark-field moire patterns 78−51396
curved surface, deform. meas. by dynamic moire method 80−14634
cutting tools, stress anal., Moire technique 78−64799
data handling system, industrial lab. appl. 79−30523
deflection measurement from moire fringes and holograms 80−32936
deformation meas., interferometric method, appl. to sheet metal and transparent plastic sheets 78−75108
deformation meas. in structural components *(German)* 78−88587
depth contouring, high resolution depth profiles, propagation mechanism of snail *(German)* 79−74816
diameter of linear configurations, meas., laser beam diffraction appl., *(Czech)* 79−40530
difference detection by digitised moire pattern processing 80−52156
diffraction grating imaging anal., displacement transducer design appl. 79−86258
diffuse surfaces, automated contouring, phase-locked moire fringe analysis 79−26023
diffusing object microstructure, moire methods extension *(French)* 79−27177
dimensional metrology of large objects by projection moire techniques 79−85122
displacement components and derivatives, holographic-moire technique 78−51140
displacement fields, strain state determ., using moire bands and deformed raster 78−63404
displacement meas. by combined holographic and double-aperture speckle interferometry *(Japanese)* 79−80670
displacement measurement using contour fringes of displacement, deflection, slope and curvature 79−80674
electronic grating moire equipment, microcomputer, contour line slope determination *(Japanese)* 79−75577
electronic processing, comparison of moire topography and photogrammetry 79−40601
Fabry Perot spectrom., transformation of interference orders 80−263
Fabry-Perot interferometer as refractometer 80−264
finite element method use in modelling Moire method effects 78−38259
flexible coupling flange geometry stress distribution optimisation appl. *(Italian)* 77−42508
fluid flow studies using stretched membrane and moire fringes 80−64658
fly's eye lens plates, superposed, image functions *(Japanese)* 77−34925
Fourier transformation, noncoherent methods 79−76624
fracture mech. techniques, review 79−41635
geometrical approach for pattern calc. 77−19164
glass, stress in working zone under biaxial compression, Moire-band method 77−81369
glass fibre reinforced plastics, stress/strain conc. round hole, Moire fringe study 77−28964
gloss appearance by means of moire patterns *(German)* 80−52300
gratings optical imaging, embedded, Fourier optics methods appl. *(German)* 80−23805
gratings without contact, Moire fringe self images, partially coherent illum. *(French)* 77−83806
historical review of moire topography 80−9024
holograms of acoustic field, moire processing 78−55539
holographic, differentiation by wavefront reconstruction with white light sources 79−86145
holographic contouring by displacing object and illum. beam 78−74864
holographic interferometry, multiple beams 79−18371
holographic interferometry, rigid body motion compensation 77−26387
holographic moire pattern differentiation 79−59951
holographic photoelasticity, using dual-hologram method 77−19198
holographic recording of microwave field, Moire technique 77−34841
holographic-moire technique, extension to 3D, to separate patterns corresponding to components of displacement 79−35661
holography, devel. and present status of moire topography 80−63960
human topography, theoretical aspects and practical appls. 79−39463
human visual system, MTF *(Japanese)* 77−73526
idiopathic scoliosis, adolescent, monitoring with Moire fringe photography 80−17047
image alignment, focus and scaling, moire technique 77−27362
image moire method for determination of partial slopes in fixed plates 80−14645
image processing of additive-obtained moire patterns *(German)* 80−47017
in-plane motion measurements with Fourier lensless holography 80−77746
in-plane vibrational analysis, time-averaged moire method 79−68665
interferometery techniques 79−63298
isopachi fringe patterns using immersion method polarisation holography 77−19196
lamellar eutectic study 77−60020
Laplacian formation by holographic zone plate moire patterns 79−13917
lattice distortion, X-ray moire pattern fine struct. study 80−79775
linear displacement meas. accuracy meas. accuracy improvement under vibration 80−90815
liquid, detection of impurities using moire patterns 78−8440
location of optical interf. fringes by digital scanning methods 80−13128
measurement sensitivity enhancement by line density increase, using two superimposed gratings *(German)* 78−21211
metal pipe, thermal strain recording at elevated temp., photographic technique 77−66731
mismatch moire grating reproduction, critical aperture openings 78−78014
moire band displacement strain determination, use of FTM type phototransformer 79−52519

moire fringes continued
Moire Rosette method for determ. of principal strain and direction 78−27695
moire topography for 3-D shape meas., opto-electronic processing technique 79−86146
multicomponent assemblies, moire inspection 80−35434
multiplied-moire-fringe system, optical arrangment and use in strain-field anal. 79−36832
natural convection heat transfer rate meas. appl. *(Japanese)* 77−26295
NDT, holomoire interferometry appl. 79−20294
optical differentiation of geometrical patterns 78−49875
optical stress analysis using moire fringe and laser speckles 80−10217
optics applied to metrology, conf., Strasbourg, France (1977) 79−6159
orthopaedics, grating−TV method, image evaluation using moire figures 80−67199
patient topography imaging system, evaluation of 79−39464
pattern detection by solid-state dynamic self-scanned photocell array 79−32084
photoelasticity anal. 78−51138
photography, appls. of slotted aperture 77−65053
photography appl., steel welds obs. at high temperature 79−74336
photokeratography using moire techniques 77−21590
photomicrometry with moire 78−4690
pipe under internal press., lens holographic moire technique for displacement component determ. 79−44900
plastic deformation measurement, moire method *(Polish)* 80−69749
plate deflection examination by moire optical contouring *(Polish)* 79−64607
plate stability under uniaxial compression *(Russian)* 79−27609
plate vibration analysis by time-averaged projection-moire method 80−79241
Poisson's ratio determ. by Moire method 78−51137
polymer, principal stress distrib. meas. at running crack tip *(Japanese)* 77−42784
posture and spinal disease documentation by moire topography *(German)* 79−16264
potential functions, contour fringes of optical surface 77−14659
profile measurement using projection of running fringes 78−93647
profile prediction method, fringe sharpening 78−87009
projection topography accuracy and sensitivity 78−45677
projection-type Moire topography theory 78−16776
pyroceramic, stress in working zone under biaxial compression, Moire-band method 77−81369
quasiregular rasters in moire techniques 80−31857
real time moire topography equipment controlled by microcomputer 78−89441
refractive index measurement using image-moire technique 80−22420
residual stress meas. appl. 79−86390
rosette method for principal strain analysis, mismatch changeable equipment 79−32396
scanning moire topography, automatic 3-D shape meas. 77−79139
scintillation camera/high energy collimator system, misleading results with a bar phantom image 80−12237
self-imaging process, partially coherent light effects *(French)* 77−23621
sensitivity in deformation meas. *(Rumanian)* 80−48654
servosystem, opto-electronic, correction of nonrectilinearity of ruling engine 78−87174
shadow microscopy, electron interference 77−18141
shadow-moire fringes, interpretation, grating rot., translation effects, surface topography appls. 79−20304
shadow-Moire method with continuously variable sensitivity 77−74361
shadow-Moire time-averaged method for vibr. amplitude determ. 77−71364
solar energy concentrators, rotation angles and curvature meas. appl. 78−90477
speckle shearing moire method, qualitative appl. for structural flow detect. *(German)* 78−82015
spiral gratings, regular interval, fringe properties and appls. *(Japanese)* 80−53434
steel, thread rolled, Moire fringe method for examining local deform. zones 80−21220
strain analysis 80−28476
strain analysis by multipurpose optical moire processor 80−9028
strain analysis in cryogenic environments 79−77029
strain distribution measurement, tip of propag. fatigue crack, Moire fringe multiplication method 77−80124
strain meas., long time high temperature applications 80−38361
strain measurement, in-plane component, combined moire fringes and photoelastic coating technique *(Japanese)* 79−32400
strain measurement, Moire band maps, processing automation peculiarities 79−50681
strain measurement, technique using fringe patterns, book contrib. 79−20333
strain measurement in elastic thin membranes moire interferometry method, appl. to human skin 80−30828
strain measurement method, sensitivity and accuracy 77−17971
strain measurement method using diffraction beams, compensation of errors 80−13068
strain studies on flat metal plates, holographic interferometry, high-freq. moire technique, and speckle correlation 79−32421
stress analysis interferometer with microprocessor 80−31858
stress/strain meas. appl., in viscoelastic plastic compounds *(German)* 78−22309
strip attainment at specified pt. on contour of stress concentrator 77−52573
strip method application, stress-strain state of Al alloys *(Russian)* 80−40648
surface contouring by addition method 79−30420
surface depth profile generation 79−75488
surface dynamic representation by TV moire topography *(German)* 78−89430
surface flatness meas., moire angular readout device 79−93209
surface rapid motion under dynamic loading, high speed photography of Moire fringes 78−32789
surface roughness, high sensitivity interferometric measurement appl. *(Japanese)* 78−37048
surface topography, null-test using synthetic deformed gratings 77−34021
surface topography meas., geometric effects *(German)* 79−2746
surface topography meas. of high speed deform. 78−36970
temperature measurement of laser irradiated transparent materials, Moire-Schlieren technique 80−53392
tensile specimen, normal mech. anisotropy meas. by Moire technique 78−16788
thin-walled cylinder, radial deform. meas. by Ligtenberg moire method 79−59949
three dimensional deformation measurement, Moire and light slicing methods 78−8382
three dimensional uneven object protrusion height and depression depth meas. *(Japanese)* 77−87730
time-average reflection-moire method for vibration analysis of plates 79−72863
tooth surface moire topography *(German)* 78−80992
topograms, real-time, video electronic generation 80−67198
topographical mapping of the human face by Moire photography 80−85462
topography, eqn. derivation 79−81359
topography, meas. accuracy evaluation 79−40528
topography, theory and applicable limit for divergent light rays 78−86237
topography appl., real-time and time-resolved, in microseconds region 80−52154
topography using grating hologram, appl. to human body 77−5893
transversal micro-vibration meas. on diffusing objects, real time, random moire principle 79−85123
tunable moire grating for optical mapping 80−5832
two-crystal system with non-diffracting zone, X-ray interferogram fine struct. 80−1887
varifocal moire zone plates for straightness meas. 77−88902
vibration analysis by multiplied moire fringes holography, expansion of meas. limitation 80−64505
vibration analysis using moire fringes holography, facilitation of fringes counting 80−64504
viscoplastic flow study, appl. of Moire fringe method *(Russian)* 77−35102
white light moire interferometry using auxiliary compensator grating 80−31847
winding terms counting 80−73428
X-ray interferometer, LLL type, interfering beam phase rels. 80−90973
X-ray interferometric moire pattern, analyser B diffusion effect *(Russian)* 79−44994
X-ray mirror profile meas. machine 80−69496
Young's experiment with n holes, appls. *(French)* 78−42274
Al, isoaxial bicrystal, Moire investigation of mechanical behaviour 77−16647
C fibre reinforced plastics, fatigue behaviour visualised by moire fringe method 80−21110
Cu film, on Ni, recrystallisation and interdiffusion, electron microscope obs., 450-600°C 80−39363
$Gd_2(MoO_4)_3$, ferroelec. and ferroelastic, electron microscopic study 77−85675
Pb, SO type, commercial purity, local deform. meas., using Moire method 80−21219
Pb-Sn superplastic alloy, cutting, stress distrib. *(German)* 79−24682

moistening *see wetting*

moisture
see also humidity
acrylic fibres, oxidative stabilisation, moisture sensitivity 80−16524
air-condenser microphone, effects of residual moisture on long-term stability 77−84091
alkaline cell, creepage rate of electrolytes, effect of external relative humidity and moisture 79−61967
atmosphere, effect on acoustic backscatter in GATE 80−85709
atmosphere, heat and moisture balance in Baltic Sea region from aerological climatology 77−87057
atmosphere, moisture profile meas. from brightness temps. in H_2O 1.35 cm reson. region *(Russian)* 78−81403
atmosphere, water vapour transport rel. to S.America water balance 79−29820
atmosphere baroclinic planetary boundary layer above sea, heat and moisture fluxes parameterisation *(Russian)* 79−16576
atmosphere moisture and heat flux in stratified boundary layer 77−21867
atmosphere moisture budget and cumulus friction in tropical wave-CISK 79−16580
atmosphere of high-mountain regions, astronomical-climatic conditions evaluation for IR astron. obs. 79−62566
by TIROS-N operational vertical sounder 80−77132
capillary porous body, drying, X-ray absorption obs., radiometry, temp. control 78−67023
carbon tetrabromide, inherent moisture as purity probe *(German)* 77−85933
cellulose fibre, moist, dielec. props. 78−76380
cellulose film, moisture effect on phys. and mech. props. 80−40450
climate, moisture cycle rel. to thermal regime during fluctuations 78−92937
climate, moisture cycle temporal fluctuations averaged for Europe and N.America 78−92958
in coal, moisture content rel. to anisotropic elec. props. 80−98312
conduction problem, domain extension method 79−90113
diffusion in activated alumina, study 78−10219
diffusion is sorbent solids, diffusion cell and pore diffusion 78−10210
diffusive sorption in dry soil 77−41077
disperse and porous materials, moistened, permittivity 79−95304
disperse solids, thermal conductivity rel. to moisture content *(Russian)* 77−54864
domestic coal, radiometric method for determ. of heating value, rel. to moisture content 78−20111
drying kinetics of moist materials, calc. method, heat (moisture) transfer 78−55555
E-glass fabric, post heat-treatment temp. on moisture adsorption and elec. cond. 79−70178
fibre reinforced plastic laminates, US evaluation of hygrothermal effects 80−7730
flow, saturated (subcooled) water, crit. discharge through differently shaped channels 78−55681
flow in porous medium being dried, generalised model *(Hungarian)* 80−83839

moisture continued
graphite fibre epoxy composites, eutectic coating moisture barriers 80−81228
graphite fibre reinforced composites, damage by moisture, diffusion anal. 80−81227
graphite reinforced epoxy composites, moisture detection by nuclear reaction anal. 80−30306
graphite-epoxy composites, Thornel 300/Fiberite 1034, effects of thermal spiking on moisture absorpt. charact., tensile strength and buckling modulus 79−43330
ground surface temperature and moisture content, prediction with inclusion of vegetation layer 78−73373
gypsum, strength changes on setting *(Japanese)* 77−36619
horizontal absorption in unsaturated soils, infiltration analysis 77−29345
Hygroscopicity of double-condensed sodium potassium phosphates 77−84939
infiltration in homogeneous isotropic porous medium, moisture profiles and wetting 78−18336
Kirlian photography, image modulation 77−5952
laminate, fibre reinforced composites, moisture diffusion, 3-D Fick's law 78−10218
loose material moisture content determ. by UHF Brewster method 77−40488
Masulipatam (Andhra Pradesh), moisture regime and water balance in drought years 77−56663
microwave absorption by water in heterogeneous organic materials 80−15998
microwave Doppler-effect flowmeter, particle moisture content effects 78−9732
microwave moisture content-attenuation-voltage convertor with time-domain attenuation comparisons *(Polish)* 78−70131
mineral, swelling examination method 77−53232
nonswelling porous body, moisture-retaining capacity and struct. 77−12773
nylon 66, fatigue crack propagation, effect of moisture 80−3166
nylon 6, effect of moisture content on glass transition temp. and Young's modulus 79−4401
nylon 6, influence of monomer and water diluents on mech. relax. 79−4993
optical fibre moisture effect on fracture strength 79−37019
optical fibres, GeO_2-$B_2O_3SiO_2$, ageing effects of moisture on fatigue and tensile strength 80−66539
optical fibres, tensile strength and static fatigue, analysis using Weibull distribution for optimum design 80−85011
optical filter, moisture penetration patterns 77−767
organic solvents, trace H_2O determ., IR spectrophotometric method 78−31731
Parana river basin, atmospheric moisture inflow and outflow rel. to water balance *(Russian)* 77−53090
perennial grasses potential yield and yield shortfall due to water deficit, agroclimatic estimate 78−61450
plastics and reinforced plastics, tabulated data as design guide 77−21087
PMMA moist surface mech. strength reduced by electric charge *(Russian)* 80−60486
polyamide 6 (polycaproamide), temp. depend. of complex permittivity rel. to moisture content 80−50251
polyester-E glass composites, types SMC-25, SMC-65 and SMC-30EA, moisture absorpt. 80−93799
polyimide, influence of monomer and water diluents on mech. relax. 79−4993
porous material, external heat transfer, calc. methods, drying kinetics 78−59467
radiative forcing of atmosphere, sensitivity to variable cloud and moisture 80−56553
refractory, ultra-lightweight, thermophys. charact., moisture effects *(Russian)* 77−55921
reliability physics, conference, Las Vegas (1977) 77−79086
resin slab, stress response, fluctuating external moisture (temp.) effects 78−55620
sands, poorly graded, moisture distrib. in capillary crack *(German)* 80−31066
sandstone, mech. props. rel. to water content *(Japanese)* 77−44980
sea surface moisture-flux parametrisation 77−73788
SEM, wet, live and frozen objects, review 79−26183
SEM, wet objects, use of gas microchamber 79−21855
silica gel regeneration by adiabatic desorption mathematical model 79−1967
snow, moisture content investigation by radiometry in 3 to 60 mm wavelength region 80−72561
sodium potassium phosphates, double-condensed, hygroscopicity 77−84939
soil, available water storage capacity with restricted subsoil permeability 77−41089
soil, diffusion eqn. soln. with exponential diffusivity comparison of iterative and perturbation techniques 77−41097
soil, freezing, effect of moisture exchange and heaving 77−25702
soil, freezing, migrational flow of moisture 77−25704
soil, hysteretical models for prediction of hydraulic conductivity of unsaturated porous media 77−41088
soil, infiltration eqn. soln., comparison of perturbation and iterative techniques 77−41096
soil, max. mol. moisture capacity correl. with plasticity 77−78267
soil, moisture change-of-state front advancement in freezing and thawing 77−91163
soil, nonlinear diffusion eqn., perturbation soln. 77−41087
soil, nonsaturated, water content rel. to surface evaporation parameterisation 79−53372
soil, pore size distrib. estimation from moisture charact. 80−12454
soil, suction press.-moisture retention relation rel. to hydraulic cond. numerical calc. *(German)* 79−2297
soil, unsaturated, coupled heat and water movement prediction, math. model 78−61446
soil, water infiltration equations for simple systems 77−78282
soil hydraulic conductivity var. of Wisconsin soil series 78−81250
soil hydraulic properties, scaling of field meas. using similar media concept 77−78278
soil moistening, one-dimensional, surface water effects *(Russian)* 80−46209
soil moisture, effect on circulation and rainfall in a tropical model 77−45133
moisture continued
soil moisture, estimation of effective capillary press. in Green and Ampt infiltration eqn. 78−3844
soil moisture, heat and salt transport, math. model 80−26563
soil moisture, hydrometeorological aspects of 1975-6 drought in UK 77−70769
soil moisture, meas. of evapotranspiration of Douglas fir using weighing lysimeter 77−64353
soil moisture calc. methods *(Russian)* 77−29493
soil moisture content, determ. by meas. of reflectance in ultrashort radio wave band 78−16075
soil moisture deficit estimation from meteorological factors 79−20890
soil moisture distillation, contrib. to dew 78−73446
soil moisture meter, development *(Japanese)* 78−88935
soil moisture movement and groundwater recharge by T tagging technique 78−61438
soil moisture profile development during water redistrib. after infiltration 77−29344
soil moisture sensitivity of cross-polarized radar backscatt. 79−25282
soil moisture vars. under bare conditions rel. to rainfall at Pune and Delhi, India 79−96777
soil stored productive moisture, remote determ. technique 79−29795
soil surface moisture determination, photographic method for polarised visible light recording 79−53557
soil survey, lowland England, moisture content and soil discrimination from air photos 79−88504
soil water, hysteretic steady state profiles 77−91172
soil water potential, detailed field monitoring of variable source areas 79−88380
soil-atmosphere boundary, heat and moisture transport 80−77023
soil-water system, thermodynamic state functions *(German)* 80−4056
soils, rel. to thermal props. meas. *(German)* 78−61619
soils, theoretical model and expts. of rainfall infiltration 78−49058
swelling soils, moisture profiles during steady vertical flows 79−5524
swelling soils, overburden potential theory 77−41095
tetraglycidyl 4,4′ diaminodiphenyl methane, diaminodiphenyl sulphone cured, failure and tensile mech. props., moisture effect 80−50735
thermal insulator corrosion behaviour, in steel-sheathed pipe system *(German)* 78−31580
tobacco shreds, fragility, filling capacity, equilibrium moisture content, glycerol addition effects *(Japanese)* 77−77727
transfer in annular vertical channels 77−15119
transient heat conduction and moisture migration problems, finite element approach 78−12653
troposphere moisture, temp., IR soundings anal. by statistical struct. and correl functions 80−8398
unsaturated soil simultaneous heat and moisture transport analysis by finite element method 78−92868
vapor-liquid energy transport in a porous medium 79−64762
wood, yield stress, strain-rate theory, moisture effects 77−16646
Al alloys, H impurities, improving productivity and detection threshold, by removing moisture with light pulse 80−26076
Al mirror, with MgF_2 overcoating, reflective scatt. and reflectance meas. in vac. UV, moisture and oil vapour influence *(German)* 79−86227
MnO_2 battery-grade, resistivity rel. to water content *(German)* 79−96431
NaCl:Ca crystals, surface recrystn., moisture effect 80−84950
PbS(Se) film, moisture drift origin 77−20187
Si, polycryst., layer structure dependence on carrier gas moisture and O_2 content *(Bulgarian)* 80−59811
soil, surface moisture content parametrization, use in atm. prediction models 78−49052

moisture content *see moisture*

moisture control
see also humidity control
ink recorder pen moisture maintenance device 77−17964

moisture measurement
see also humidity measurement
AF3 unit replacement for Karl Fischer units using peristaltic pump 80−22376
agricultural and food products, electrical methods *(Polish)* 79−2776
asbestos-cement pipes, nondestructive neutron-radiation testing of moisture content 79−75539
atmosphere, moisture flux and turbulence meas. in unstable surface layer over land 77−66962
atmosphere, radiometric meas. precision from GATE-74 data *(Russian)* 77−29368
capacitance transducer systematic error reduction 77−79082
capacitive grain moisture meter Standard Specimens 77−82481
ceramic moulding material containing SiC, testing in UHF range 79−34404
cloudless atmosphere, microwave radiation meas. from on board aircraft 80−94624
clouds, over Sierra Nevada, liquid water content meas. 77−2213
concrete, meas. by 4 electrodes *(German)* 78−60929
corn, shelled, dielec. props. at 1 MHz-2.45 GHz 77−77142
crude-oil hydrometers calibration 78−73969
dew meter, β-absorpt. type, appl. to meas. on soil and plant surfaces 78−24803
electric soil moisture gauges, testing procedure 77−78481
electronic component package, H_2O content determ., plasma chromatograph-mass spectrometer applic. 78−86379
fibre reinforced composite, moisture content under transient conditions 77−48598
film and slab-like materials, open transmission line UHF CW phase technique for meas. of thickness, permittivity and moisture content 79−35778
gases, moisture content determ. using photocolorimeter 78−56936
grain moisture content using capacitive hygrometers, analysis of errors 79−75538
granular and powdered materials, microwave method *(Polish)* 78−12706
granular material, simultaneous moisture content/thermal cond. meas. apparatus 78−53064
heat-pulse moisture meter for capillary-porous materials 77−82499
hygrometry testing scheme for the Soviet countries 80−57312
hygroscopic materials, method for drying and cooling chamber 77−61054
hygroscopicity of dusts, contaminants and corrosion products using instrumental gravimetric method 78−74118

moisture measurement continued
in gases, mass spectroscopic method, prep. techniques 77−40587
laminates, C/epoxy, moisture distribution determination, low cost method 79−65252
microwave and infrared heat measurement of soil moisture *(French)* 79−96772
microwave probe for subsurface soil moisture profiling 78−65939
moisture meas. methods using neutrons *(Chinese)* 79−57342
neutron moisture meter calibration, soil samples, neutron absorpt. cross section meas. 77−9545
neutron soil moisture meter, design and operation 79−44280
nonuniformly moist matter, reliability of meas. methods 77−29066
passive neutron activation for environmental transuranic and moisture assay 80−21431
permafrost, neutron moisture gauge for water detection *(Chinese)* 79−34997
in porous ceramic components, equipment *(German)* 78−54378
radar meas. of surface roughness, soil moisture and texture with vegetation cover 79−62534
reference materials for NMR methods 79−34403
remote sensing simulator for soil moisture meas. 78−49143
sand, moisture content, microwave optics determ. 77−37684
semiconductor packages, hermetically sealed, calibration and anal. of moisture by gas mass spectrometry 80−90928
SHF moisture gauges for bulk materials 77−87771
soil, active microwave remote sensing, surface roughness and texture effects 79−12295
soil, freq. shift dielectric moisture sensor appl. 78−53739
soil, measurement, microwave and radar techniques 79−70896
soil, thermal neutron constants, calibration of moisture gauges 77−25804
soil, using airborne imaging passive microwave radiometer 78−36310
soil and winter wheat yield on Great Plains, Landsat data 78−65351
soil beneath crop canopy, IR remote thermography 80−109147
soil moisture, basic hydrophys. charact., determ. method 80−85696
soil moisture, microwave remote sensing, sampling techniques for ground truth data 78−65439
soil moisture, near-surface, theory for passive microwave remote sensing 77−87105
soil moisture, remote sensing by Heat Capacity Mapping Mission 79−5640
soil moisture, remote sensing with air temp. compensation 77−17247
soil moisture and component estimation from spectral polarisation 79−16678
soil moisture and geology mapping, thermal intertia method 80−8344
soil moisture content, microwave radiometer meas. over bare and vegetated surfaces, comparison 78−88851
soil moisture content by microwave radiometry 80−17425
soil moisture determination, soil drying procedure 80−82109
soil moisture meas. by remote microwave radiometry 79−48526
soil moisture meter, development *(Japanese)* 78−88935
soil surface, remote sensing by visible and false colour IR photography 80−56653
soil water content, estimation via total solar reflectance and spectral band ratioing 77−60479
soil water potential in temp. gradient, thermocouple psychrometers improvement 79−74974
stratosphere, in situ meas. with new moisture sensor 79−74930
subsoil neutron moisture probe, lab. calibration, minimum soil sample size calcs. 77−57333
teledetection applications *(French)* 79−96769
teledetection methods for determination of soil water balance *(French)* 79−96773
thermovacuum aquameter appl. 77−82537
total errors of moisture meters, representation as two series transducers 80−77792
troposphere, in situ meas. with new moisture sensor 79−74930
water content determ., rapid thermal method 77−86258
water-petroleum emulsions, mean particle diameter and conc. determ. by light scatt. 80−89538
wood, electronic moisture gauge 79−70279
yaRV-2 compact automatic nuclear resonance hygrometer 80−105657
Al_2O_3 moisture sensor for sealed hybrid packages 77−87754

molar volume *see density*

molecular alignment *see molecular orientation*

molecular beam electric resonance
benzene dimer, mol. beam elec. deflection obs. 79−72336
benzene-hexafluorobenzene, mol. beam elec. deflection obs. 79−72336
dimer, partially deuterated, microwave spectra and struct. 80−74212
formaldehyde, hyperfine interactions, mol. beam elec. reson. spectra 77−88445
halogen dimers, mol. beam. elec. deflection obs. 80−53080
hexafluorobenzene dimer, mol. beam elec. deflection obs. 79−72336
inert gas complexes spectroscopic data, geometry, pot. energy curve, dissoc. energy, equilib. internuclear distance, determ. 80−53018
interhalogen dimers, mol. beam. elec. deflection obs. 80−53080
interhalogen trimers, mol. beam. elec. deflection obs. 80−53080
ketene, hyperfine interactions, mol. beam elec. reson. spectra 77−88445
Ramsey reson. obs. by linear laser spectroscopy 80−99514
RF spectroscopy, interference effects *(French)* 78−58669
saturation effects, when irradiated with stationary wave *(French)* 79−81247
submillimetric extension of molecular beam electric resonance spectroscopy 77−38751
symmetric rotor, internal rot. splitting 78−94232
thioformaldehyde, hyperfine interactions, mol. beam elec. reson. spectra 77−88445
transition probability amplitude, coherence effect *(French)* 79−45737
trifluoromethane, rot. isomerism, internal rot. splitting 78−94232
Ar-methyl chloride, mol. beam elec. reson. spectrosc. 80−23477
$ArBF_3$, microwave spectrum and struct. 79−76420
$ArCO_2$, struct. determ. by mol. beam elec. reson. spectrosc. 79−64019
$ArSO_3$, weakly bound complex, struct., MBER obs. 80−95701
Ar.HBr(DBr), van der Waals complexes, rot. spectra and struct. 80−48055
BF_3CO, microwave spectrum and struct. 79−76420
CO, $d^3\Delta$, state elec. dipole moment, vibr. depend. obs. 79−31548
ClCN, ground and first excited bending, vibr. state, props., mol. beam elec. reson. 80−37823
CsF, Stark effect, deviations from rigid rotator model 79−18234
$(H_2O)_2$, struct. from mol. beam elec. reson. spectra 77−54555

molecular beam electric resonance continued
KrHCl, van der Waals complexes, struct., RF and microwave spectra, isotope effects 80−37806
LiF, RF spectra, spin interactions and moments, mol. beam elec. reson. meas. 77−18912
$^6Li^{35}Cl$, electronic ground state, first vibration state lifetime, MBER meas. 79−86023
N_2BF_3, microwave spectrum and struct. 79−76420
ND_3, hyperfine structure of inversion transitions, molecular beam electric resonance 79−98071
$(NH_3)_n$, (n=1-6), mol. beam elec. deflection obs. 79−72371
NO, Zeeman spectrum, mol. beam elec. reson. spectrosc. 80−91621
$^{14}N_2{}^{16}O$, elec. and mag. props., hyperfine struct., mol. beam elec. reson. obs. 78−62792
N_2SO_3, weakly bound complex, dipole moments, MBER obs. 80−95701
O_3, mol. beam electric resonance, electric and mag. props. determ. 77−27055
OCS, pure and seeded beams, rot. cooling, electric reson. meas. 79−13795
OH, mol. beam electric reson., hyperfine Λ-doubling transitions 79−36628
OH, vibrationally excited, high-resolution hyperfine Λ-doubling spectrum 78−90153
OPF_3, mol. beam elec. reson. spectrum, mol. props. 79−94011
SO_2, mol. beam electric reson. in RF field, dipole moments of vibr. states 79−64116
TlF, P- and T-violating interactions in hyperfine struct., mol. beam reson. expt. 80−53019
XeHCl, microwave and RF spectra, mol. beam elec. reson. meas. 79−72302

molecular beam epitaxial growth
$Al_xGa_{1-x}As/Al_yGa_{1-y}As$ heterostructure lasers, prep. charact., and CW reliability 80−58586
angular distrib. of beam from modified Knudsen cell 78−60586
apparatus, controlled by quadrupole mass spectrometer *(French)* 78−15315
crystal growth by MBE, devices and materials, review 78−39707
design considerations for equipment 79−95940
device applications 80−25570
device fabrication by MBE 79−43154
Electrochemical Society Meeting, Boston, USA, (May, 1979) 79−91959
electron devices, appl. of MBE *(Japanese)* 79−38749
epitaxial films, condensed from vapour or molecular ion beams, impurity distrib. 80−65032
evaluation as practical cryst. growth technology *(Japanese)* 78−92201
film, epitaxial crystal growth, electron microscope obs. *(Japanese)* 78−91568
film, interfacial boundaries and transition regions *(Russian)* 80−103596
GaAs MBE growth, deep levels effect on electron and hole trap densities 80−49652
II-VI compounds *(Japanese)* 78−15317
III-V compounds and alloys, MBE process and problem areas, review 80−10815
III-V semiconductor ternary alloys, VPE growth lattice mismatch effects 79−28220
III-V semiconductors, MBE, surface reaction steps 79−77941
III-V semiconductors, MBE developments in device fabrication 79−78902
III-V semiconductors, p-n heterostructures, epitaxial growth techniques, appl. to optoelectronics, review 80−54770
integrated optical devices fabricated by MBE 79−95943
integrated optics device fabrication, MBE of injection lasers 79−90042
ionised-cluster beam epitaxy, film form. mechanism 79−28949
IV-VI optoelectronic devices, MBE techniques 79−95942
LEED-AES obs. *(Japanese)* 78−91564
metal film, ionised-cluster beam epitaxy, film charact. 79−28230
microscopic mechanism of film growth from non-condensed phases, kinetic anal. 80−54565
nonstoichiometry and carrier concentration control in MBE of compound semiconductors 79−95941
nucleation kinetics, at high supersaturations on (111) faces of crysts. with diamond struct. 80−84128
review of recent progress *(Japanese)* 77−63566
selective lift-off for preferential growth with MBE 77−90281
semiconducting thin film manufacture 80−103593
semiconductor, MBE, doping impurity transport, free carriers effect 78−26793
semiconductor, state-of-the-art 79−24450
semiconductor device growth and precision doping 80−89156
semiconductor film, growth and doping by MBE 77−73239
semiconductor film growth, multilayer systems, spectroscopic ellipsometry, review 80−103603
semiconductor films, superlattices control 80−2283
semiconductor surface and crystal physics 79−95289
semiconductor thin films, MBE, device appls. *(German)* 78−68630
semiconductors *(Japanese)* 80−55305
in space 78−35317
superlattices and barrier structures production by MBE *(Chinese)* 79−46986
technique, analytical methods 78−72027
technique, for electronic and optoelectronic devices 77−66591
thin films, deposition techniques, review 80−80964
vacuum interlock system 78−48330
Ag film, MBE deposited on InP(001), struct. using TEM and RHEED 79−82492
Ag, metal beam epitaxy, high temp. high purity sources 79−43156
Al, epitaxial growth on GaAs (001) 80−24757
Al film, MBE and field emission deposition on III-V semiconductors, comparative study 79−87016
Al, metal beam epitaxy, high temp. high purity sources 79−43156
Al-GaAs Schottky barrier diode, prep. by MBE on GaAs, and charact. 78−72257
Al-Ge (100) interfaces, MBE prep. and geometrical struct., total refl. X-ray diffr. study 80−49531
AlAs epilayers, MBE growth on GaAs, self-terminating thermal oxidation 78−92374
AlGaAs DH laser, self-pulsations due to proton bombarded region self-annealing during ageing 80−99728
p- (AlGa)As:Zn, MBE grown, elec. props., shallow junction solar cell use 79−91175

molecular beam epitaxial growth continued
$Al_xGa_{1-x}As$ CW multiwavelength TJS laser, MBE, single-longitudinal modes 80−64049
$Al_xGa_{1-x}As$, MBE grown film, in situ surface characterisation by RHEED, SIMS and AES 77−43410
$Al_xGa_{1-x}As$ MBE layers, ionized beam doping, elec. and optical charcts. 79−37721
$Al_xGa_{1-x}As$ oxidised AlAs as multidielectric for GaAs MIS devices 79−65333
$Al_xGa_{1-x}As$:O-n-GaAs heterojunction for MIS device, capacitance voltage meas. 79−87157
$Al_xGa_{1-x}As$-$Al_yGa_{1-y}As$ DH IR-visible (0.89-0.72 μm) MBE grown lasers 80−64058
$Al_xGa_{1-x}As$-GaAs, heterojunction, interface width, AES obs. 80−20290
$Al_xGa_{1-x}As$-$Al_yGa_{1-y}As$ laser struct., for integrated optics, MBE 78−13817
AlN, epitaxial film growth by MBE, physical and optical props. 80−2293
Al_2O_3 film, MBE-growth on GaAs, MOS GaAs capacitor appl. 79−77943
Al_2O_3, VPE growth by photochemical reaction by Al and O_2 under UV excitation, MOS struct. charcts. 79−60927
Au film, MBE and field emission deposition on III-V semiconductors, comparative study 79−87016
Au, metal beam epitaxy, high temp. high purity sources 79−43156
Bi film, on Si(111) substrate, MBE deposition kinetics 80−10817
CdS, epitaxial film, structural and electron transport props. 79−82481
CdS-Al_2O_3-Al diodes fabricated by MBE, junction charcts. 79−65550
CdSe films, growth kinetics and cryst. struct. during vacuum condensation 80−2305
$CuInSe_2$ film, MBE growth, AES and optical absorpt. obs. 79−78903
$CuInSe_2$, on CdS, in situ reflection electron diffr. study 79−56936
GaA-$Al_{0.27}Ga_{0.73}As$ DH lasers grown by MBE, growth conditions influence on threshold current density 80−32984
GaAlAs based heterojunctions, integrated optics appl., technology advancements *(Slovak)* 80−33226
$Ga_{1-x}Al_xAs$, alternate monolayer crysts., MBE and props. exam. 78−10289
$Ga_{1-x}Al_xAs$, self-aligned three dimensional struct. MBE growth 77−59697
GaAs, (100) surfaces, struct. and stoichiometry during molecular beam epitaxy, RHEED anal. 79−4921
GaAs (110), surface struct., LEED and AES study, comparison of MBE and ion bombard. surface prep. 80−54496
GaAs ($\bar{1}\bar{1}\bar{1}$), MBE prep., angular resolved UPS of surface states 79−47598
GaAs, and its alloys, as integrated optics materials, book contrib. 79−64362
GaAs device structures for military microwave, optoelectronic appl. 79−52129
GaAs, epitaxial layers, MBE grown, Hall mobilities, substrate temps. 80−20335
GaAs film, MBE, growth and doping kinetics 77−76682
GaAs film on GaAs substrate, uncontrolled doping obs. *(Russian)* 80−2276
GaAs film optical components, prep. by MBE using Si shadow masking technique 80−28358
GaAs, growth temp. depend. and charcts. 79−28946
GaAs layers, process anal. and appl. *(French)* 79−56937
n-GaAs, MBE, correl. between electron traps and growth processes 80−65387
GaAs, MBE, SnTe source of donor impurities 79−95035
GaAs, MBE, surface reaction steps 79−77941
GaAs, MBE, undoped, growth and characterisation 80−10836
p-GaAs, MBE grown, As_2 and As_4 effects on photolum. 80−103974
GaAs, MBE grown film, in situ surface characterisation by RHEED, SIMS and AES 77−43410
GaAs, MBE layers, H_2 effect on residual impurities, photolum. obs. and elec. charcts. 79−47636
GaAs, MBE of autoepitaxial films, temp. range for growth, RHEED monitoring 78−44025
GaAs, MBE of doped cryst., thermodynamics and kinetics interplay 80−70144
GaAs MBE physical characteristics and applications *(German)* 79−7618
GaAs, MBE prep., device props. 77−77417
GaAs, monocrystalline, lateral definition, prep. by MBE 80−108357
GaAs, ohmic contact form. to n- and p-type samples by MBE, charcts. 79−47159
GaAs patterned epilayer structures, MBE writing 78−56590
GaAs, periodic doping structure, nipi superlattices, HBE growth and charcts. 79−95484
GaAs, selective growth, MBE and self-masking method 77−52256
GaAs, shallow-homojunction solar cell by MBE, conversion efficiency 80−30476
GaAs, surface studies during MBE growth 79−90899
GaAs, technology and epitaxial layers props. 79−33945
GaAs, thin layers, growth conditions and phys. props. *(German)* 80−55307
GaAs unintentionally doped layer growth using MBE 78−72741
GaAs, unintentionally doped layer grown by MBE, elec. props. 79−91167
GaAs:Be, annealing effect during MBE 78−79898
GaAs:Cr, epitaxial layers, MBE grown, Hall mobilities, substrate temps. 80−20335
n-GaAs:Ge, film, substrate temp. depend. of Ge incorporation during MBE 80−76196
GaAs:Ge, MBE layers, complex free-carrier profile synthesis 80−54266
GaAs:Ge, mol. beam epitaxy of n- and p-types 80−10839
GaAs:Ge film, MBE grown, heavily doped, elec. props. rel. to growth parameters 80−100537
GaAs:Ge MBE power FETs with Sn surface impurities 80−80374
GaAs:Ge p-n junctions by mol. beam epitaxy 79−56289
GaAs:S(Se), MBE grown, surface exchange doping using PbS(Se) captive sources 79−10864
GaAs:Si, accelerated growth rate effect on MBE, Hall mobility and photolum. meas. 80−104067
GaAs:Si layers, MBE growth, elec. and optical props., doping charcts. 80−10819
n-GaAs:Sn, heavily doped, nonalloyed ohmic contact form. by MBE and metallisation 79−7895
molecular beam epitaxial growth continued
n-GaAs:Sn, nonalloyed and in situ Ohmic contacts for FETs 79−56307
GaAs:Sn, surface segregation of Sn during MBE, SIMS and AES 78−72031
GaAs:Sn films 80−50563
GaAs:Sn layers for MESFET, MBE growth 77−15952
GaAs:Sn(Be) MBE films, elec. characterization 79−91168
p-GaAs:Zn, luminescent, ion doped MBE growth 80−44436
GaAs:Zn, MBE with ionized beam doping 77−77418
GaAs:Zn MBE layers, ionized beam doping, elec. and optical charcts. 79−37721
GaAs/metal contacts, recent developments in investigations of preparation and props. *(French)* 80−107909
GaAs-$Al_{0.27}Ga_{0.73}As$ Dh lasers grown by MBE, influence of growth conditions on threshold current density 80−58587
GaAs-$Al_xGa_{1-x}As$ transverse junction lasers with low threshold current prep. by MBE on semi-insulating substrates 80−58588
GaAs-$Al_xGa_{1-x}As$, current transverse junction lasers, low threshold, MBE prep. 80−83614
GaAs-$Al_xGa_{1-x}As$ buried-heterostructure lasers, current injection confinement, MBE/LPE hybrid technique 80−74374
GaAs-$Al_xGa_{1-x}As$ current injection multi-quantum-well heterostructure lasers, MBE grown 80−19042
GaAs-$Al_xGa_{1-x}As$ DH lasers, MBE grown, low current threshold, high lasing uniformity 79−64223
GaAs-$Al_xGa_{1-x}As$ DH lasers, very low current threshold, MBE grown 80−43353
GaAs-$Al_xGa_{1-x}As$ DH lasers, MBE grown, substrate temp. effect on current threshold 80−48243
GaAs-$Al_xGa_{1-x}As$ DH laser, MBE grown, CW electro-optical props. 80−102725
GaAs-$Al_xGa_{1-x}As$ films for optical devices, masked MBE 78−38100
GaAs-$Al_xGa_{1-x}As$ multilayer struct., MBE, selective area growth using Si shadow masks 77−85946
GaAs-AlAs layered films, MBE prep., struct., rel. to optical props. 79−77950
GaAs-AlAs layered superlattices, deposited by MBE, exam. of crystal growth kinetics 78−72739
GaAs-$Ga_{1-x}Al_xAs$, semiconductor superlattices by MBE 79−95939
GaAs-$Ga_{1-x}Al_xAs$ multilayer struct., growth over preferentially etched channels, MBE 77−40388
GaAs-$Ga_xIn_{1-x}P$ multilayer epitaxial films, MBE technology and epitaxial layers props. 79−33945
GaAs-GaAlAs-GaAs rectifying semicond. struct., prep. by MBE and charcts. 80−65657
GaAs-Ge, heterostructure, zincblende-on-diamond type systems, MBE growth, (110) orientation as preferred orientation 80−80099
GaAs-n-$Al_xGa_{1-x}As$ heterojunctions, selectively doped, FET 80−80364
n-GaAs-n^+-$Al_xGa_{1-x}As$ heterostructure production, by MBE *(German)* 80−44711
$(GaAs)_n(AlAs)_m$ multilayers, MBE, interdiffusion, X-ray diffr. study 80−70474
$GaAs_{1-x}P_x$, MBE growth on GaP, and crystallographic evaluation 77−8762
$GaAs_{1-x}P_x$, mol. beam epitaxial growth, cryst. quality, composition investig. *(Japanese)* 77−55895
$GaAs_{1-x}P_x$, molecular beam epitaxial, effect of substrate temp. on composition ratio 77−1811
$GaAs_{1-x}P_x$, N doping using ionised beam in MBE 78−47400
$GaAs_yP_{1-y}$ alloy, composition effects in growth by MBE 80−59816
$GaAs_{1-x}Sb$, microprocessor controlled MBE growth 78−3058
$Ga_{0.47}In_{0.53}As$, MBE, InP/$Ga_{0.47}In_{0.53}As$/InP DH laser fabrication and room temp. operation 78−74906
$Ga_xIn_{1-x}As$, alloy film surface processes controlling growth by MBE RHEED and AES exam. 78−84084
$Ga_xIn_{1-x}As$-InP, MBE film growth, composition control obs. 80−84399
$Ga_xIn_{1-x}P$ alloy films, surface processes controlling growth by MBE, RHEED and AES exam. 78−84084
GaP, heteroepitaxial growth on Si substrate by MBE 78−64481
GaP, ionised-cluster beam epitaxial growth on GaP and Si, charcts. for LED 79−28951
GaP, MBE growth on GaP, and crystallographic evaluation 77−8762
GaP, mol. beam epitaxial growth, cryst. quality composition investig. *(Japanese)* 77−55895
GaP-Si, heterostructure, zincblende-on-diamond type systems, MBE growth, (110) orientation as preferred orientation 80−80099
GaSb and $GaSb_xAs_{1-x}$ films, MBE growth and elec. props. 79−23863
$GaSb_{1-x}As_x$, MBE RHEED meas. 78−18916
$GaSb_{1-y}As_y$, MBE-grown, substrate effect on lattice consts. 79−77942
P-Ge, heteroepitaxial film, galvanomagnetic effects, influence of mechanical stresses 79−91171
Ge-$Ga_{1-x}Al_xAs$, MBE of ultra thin film superlattices on GaAs substrates, TEM study 79−37932
Ge-Si structures, molecular beam method, ion sputtering method 78−3060
In film, MBE deposited, struct. by RHEED obs. 79−82491
InAs, epilayer, MBE growth parameters, relationship with elec. props. 80−2296
InAs, MBE growth, SEM, RHEED, optical microscopy and elec. meas. 78−18925
$InAs_yP_{1-y}$ alloy, composition effects in growth by MBE 80−59816
$In_{1-x}Ga_xAs$, MBE-grown, substrate effect on lattice consts. 79−77942
$In_{1-x}Ga_xAs$-$GaSb_{1-y}As_y$, semiconductor superlattices by MBE 79−95939
$In_{1-x}Ga_xAs$-$GaSb_{1-y}As_y$ superfine heterostruct., MBE 78−95348
$In_xGa_{1-x}As$ layers, on GaAs substrate, MBE fabrication and laser operation 80−10820
$In_xGa_{1-x}As$, MBE layers on InP substrates, elec. props., photoluminesc., X-ray and Auger obs. 79−51450
$In_xGa_{1-x}As$ MBE layers on InP substrate, lattice deformation, misorientation 79−90896
$In_xGa_{1-x}Sb$, molecular beam epitaxy 79−47638
$In_{1-x}GaxAs$, MBE, RHEED meas. 78−18916
InP (100) substrates, for MBE, ion-cleared, contamination, SIMS meas. 78−11353
InP, MBE, substrate temp. related degradation mechanisms 80−65385
InP, MBE from In and P_2 beams, substrate temp. limits 80−15385
InP, MBE growth, expt. *(Japanese)* 77−4743
InP, MBE growth on InP substrate, orient.-depend. faceting 77−24966
InP, MBE growth surface, singular instabilities 77−24969
InP(100) undoped homoepitaxial films grown by MBE, photoluminesc. props. 80−2809

molecular beam epitaxial growth continued
InSb film, grown by MBE, RHEED study 80−100415
InSb film, heteroepitaxial, MBE growth and elec. props. 80−2301
InSb film, MBE apparatus and AES 78−47875
$NaCl_4$ on Pt and Ir surfaces, adsorption kinetics 80−84393
$Pb_xSn_{1-x}Se(Te)$ film, Bi and Tl impurity dopant incorporation and diffusion during MBE growth 79−66012
$Pb_{1-x}Sn_xTe$ film on BaF_2, electron beam delineation effect on MBE growth, LEED and AES obs. 79−99434
$Pb_{1-x}Sn_xTe$-PbTe heterostructures, MBE produced on mica and $LiNbO_3$, elec. props. study 80−88629
PbTe film, Bi and Tl impurity dopant incorporation and diffusion during MBE growth 79−66012
PbTe, uncontaminated films prepared by mol. beam deposition, elec. props. meas. 78−15316
Sb film, MBE deposited, struct. by RHEED obs. 79−82491
Si, CVD growth surface, singular instabilities 77−24969
Si epitaxial layers, vacuum deposited, conditions for impurity migration from B, P, Sb doped sources *(Russian)* 80−107570
Si epitaxial thin film growth on sapphire and spinel by MBE 80−76186
Si film, epitaxial growth by partially ionised vapour deposition, RHEED-AES-QMS study 79−83136
Si film, MBE, cryst. defect props., substrate treatment effects 80−70551
Si from ion-molecular beams, growth mechanism 80−2299
Si, MBE, cryopumped ultra high vac. system 77−67448
Si, MBE, on n^+ Si, with wide range doping control 78−27402
Si, MBE growth and surface struct. 80−10816
Si MBE layer resistivity and carrier mobility obs. *(Russian)* 80−49962
Si MOSFET fabricated on MBE Si layer 79−78179
Si, mol. beam and solid-phase epitaxies under ultrahigh vacuum 79−28945
Si, semiconductor devices 79−83141
Si:As, MBE with simultaneous ion implant doping 80−66432
Si:As(Sb), n-type doping techniques 80−15126
Si:Ga(Al), MBE, growth, struct. and elec. props. 77−89458
n-Si:Sb, arbitrary doping profiles produced by MBE 79−7617
Si:Sb, epitaxial film, growth by mol. beam technique 80−2292
Si:Sb, MBE film, doping technique 80−79821
Si-$CoSi_2$Si, double heteroepitaxy, solid phase and MBE 80−104063
Te film, microstructure 80−103598
ZnS, epitaxial growth, appl. to electronic devices, review *(Japanese)* 80−55281
ZnSe film, MBE and resistivity 79−100059
ZnSe, MBE growth, elec. and optical props. 80−75462
ZnSe, single cryst. film, MBE, quality obs. using photoluminesc. 77−77419
ZnSe:In films, MBE growth, doping effect on photoluminesc. 80−10818
ZnSe(Te), MBE growth, growth rate and sticking coeff. 77−32532
$ZnSe_xTe_{1-x}$, comp. ratio control 79−28947
ZnTE, MBE growth, elec. and optical props. 80−75462
ZnTe MBE thin film growth, elec. and optical props. 78−47887
ZnTe(:In), single cryst. film, MBE, quality obs. using photoluminesc. 77−77419

molecular beam magnetic resonance
acetylene, sign of rot. g-factor, mol. beam expt. 79−59600
fluoromethane, rot. mag. moment spectra, mol. beam mag. reson. obs. 77−14509
isotope separation, supersonic molecular beam technique using RF spectroscopy, mag. reson. 80−47725
methane, rot. mag. moment spectra, mol. beam mag. reson. obs. 77−14509
methane, rotational state, avoided-crossing molecular beam spectroscopy 80−63730
successive oscillatory fields, molecular beam resonance method 80−91706
tetrafluoromethane, sign of rot. g-factor, mol. beam expt. 79−59600
GeF_4, sign of rot. g-factor, mol. beam expt. 79−59600
GeH_4, avoided-crossing molecular-beam spectroscopy, hyperfine and spin rot. const. and rot. g factors determ. 80−78671
$GeH_4(F_4)$, rot. mag. moment spectra, mol. beam mag. reson. obs. 77−14509
H_2, metastable state, mol. beam reson., vibr. anal., spin-rot. interaction 79−22731
H_2, ortho, high rot. states, inter- and intra-mol. effects, mol. beam mag. reson. obs. 78−70852
H_2-H_2 dimers, hyperfine struct. in zero mag. field 80−95700
He_2, $a^3\Sigma_u^+$ metastable state, fine struct., mol. beam mag. reson. obs. 78−78720
I_2, laser fluoresc. state selected and detected mol. beam mag. reson., hyperfine transitions 80−63731
I_2, polarisability anisotropy, laser assisted mol. beam spectroscopy 80−78646
SF_6, sign of rot. g-factor, mol. beam expt. 79−59600
SiF_4, sign of rot. g-factor, mol. beam expt. 79−59600
SiH_4, avoided-crossing molecular-beam spectroscopy, hyperfine and spin rot. const. and rot. g factors determ. 80−78671
$SiH_4(F_4)$, rot. mag. moment spectra, mol. beam mag. reson. obs. 77−14509

molecular beams
see also molecular beam electric resonance; molecular beam magnetic resonance; molecule-surface impact; particle velocity analysis
acetic acid vapours, clustering, effect of supersonic mol. beam sampling, mass spectrometric study 80−104481
acetylene-d_0(-d_1)(-d_2) metastable state, mol. beam elec. deflection obs. 80−74137
acrolein, s-trans and s-cis, trapping from thermal mol. beams and UV-induced isomerisation in Ar matrices, enthalpy determ. 80−97688
alignment due to optical pumping by laser beam 77−31025
alkali halides, photoelectron spectra of ionic mols. using mol. beam technique 78−50576
analogue detection device for mol. beam scatt. expts. and vel. anal. 78−33635
analyser in mass spectrometer for thermodynamic props. determ. 77−184
anisotropic intermolecular potentials, mol. beam investig., review 79−72376
aryl halides, mol. beam photodissoc., fragment translational energy distrib. 77−50481
benzene, ^{13}C substituted, mass selective two-photon ionis., mass spectroscopy obs. 80−9651

molecular beams continued
benzene, S_0-S_1 transitions, two-photon absorpt. spectra by nozzle beam-multiphoton ionisation method 80−63728
broad-frequency chopper with adjustable duty cycle, appl. in modulating mol. beams 78−22054
chemi-ionisation reactions of Ca, Sr, Ba, and Yb with halogens and interhalogens 77−32791
chemical reaction, dynamics, mol. beam obs. 79−41233
chlorobenzene, S_0-S_1 transitions, two-photon absorpt. spectra by nozzle beam-multiphoton ionisation method 80−63728
chopper, using active permanent magnet suspensions 78−24829
cluster beam, multiple stage ioniser, spatial potential distribution and electron trajectory calcs. *(Japanese)* 80−99596
cluster beam, nozzle flow formation and detection, high energy beam 80−5638
cluster beam for injector for heating and fuelling of toroidal plasma expt. 77−24179
coherent optical spectroscopy of molecules and molecular beams 78−82054
component separation, in inhomogeneous mag. field, electron impact detect. 77−6963
conference on solid-vacuum interface, Amsterdam, Netherlands (June 78) 79−42342
continuum source particle beam properties, comput. modelling 80−26062
crossed beam studies, gas kinetics 79−74388
crossed-beam meas. of reactive scatt. using short lived radioactivity 77−4969
cryopumped aerodynamic molecular beam apparatus 77−71335
detection using fast supercond. bolometer 78−86383
detection using low background cold cathode ion source 78−54506
detector with Ti sorption pump 78−21150
directivity pattern, detect. using beam modulation method 77−556
discharge characteristics from multichannel nozzle *(French)* 79−30603
education, effusive flow, vector flux density distrib. calc. for any aperture 80−22165
elastic scatt. differential cross section deconvolution by iterative van Cittert process 78−17746
electrostatic 77−50601
electrostatic space focusing 80−28118
energy parameter determination, in nozzle-formed mol. beam, time of flight method 79−64122
epitaxy apparatus, mol. beam controlled by quadrupole mass spectrometer *(French)* 78−15315
ethanol, H-bonding investigated with supersonic mol. beam using photoionisation quadrupole mass spectrometer 80−102543
ethylene dimer, CO_2 laser induced photodissoc., pulsed mol. beam obs., van der Waals bond 80−9660
excited state processes, collision rates obs. using single at. or mol. beam 78−13567
films obtained by oblique mol. beams, texture formation *(Russian)* 77−66592
fluorescence of isolated molecules, supersonic beam method 79−45750
fluorobenzene, S_0-S_1 transitions, two-photon absorpt. spectra by nozzle beam-multiphoton ionisation method 80−63728
fluoromethane, rot. mag. moment spectra, mol. beam mag. reson. obs. 77−14509
formaldehyde, mol. beam, vel. meas. by Doppler effect on RF spectrum splitting *(French)* 78−13627
formaldehyde, molecular beam rotation temp. meas. *(French)* 80−78724
formic acid, decomposition, using Ni (110) catalyst, reaction kinetics and mechanism, mol. beam relax. spectroscopy 77−70340
formic acid + $Ar(^3P_{2,0})$ crossed mol. beams, ionisation and dissociative fluorescence, energy depend. 79−52669
gas phase chemical reactions, laser obs. *(German)* 79−29365
gas-surface interactions, mol. beam apparatus 78−72675
generator for investigating rarefied gas flow 79−32717
glyoxal in supersonic jet, fluoresc. excitation, collision-induced intersystem crossing, van der Waals complex 79−81223
halogens, supersonic atomic and mol. nozzle beam source 77−31028
heterogeneous chemical kinetics by modulated mol. beam mass spectrometry 77−25305
inert gas, metastable composition of inert gas beam from ion-neutral reaction 77−29008
intermolecular interactions, mol. beam. scatt. expts. and techniques *(German)* 78−86971
ion beams mass spectrometry absorpt. spectra, review 79−89808
ion microanalyser, neutral particle beam separation, characts., anal. appl. *(Japanese)* 78−85248
ionic molecule photoelectron spectra using mol. beam technique 78−50576
IR laser spectroscopy 77−46655
IR spectroscopy 78−89570
isotope separation, at. and mol. beams in nonuniform mag. and laser fields *(Russian)* 77−6960
laser spectroscopy, high-resolution, time-resolved, of collisionless beam, energy randomisation, optical phase relax. 79−3501
laser spectroscopy using atomic and molecular beams *(Japanese)* 79−35841
linear laser spectroscopy in collimated mol. beams, single mode tunable lasers appl. to small mols. 80−52339
mass dependent molecular beam focusing by cross-jet deflection 79−93257
mass spectromatic sampling system, ion concs. in coal-fired MHD plasmas 80−52358
mass spectrometric sampling, high press., high temp. mols., review 80−52355
mass spectrometry, in situ anal. in crystal growth ambients 80−52357
mass spectrometry, IR spectral meas. of gas phase species, at high temp. 80−52235
methane, optical Ramsey resonance, in three separated fields produced by corner reflector, theory 80−74166
methane, rot. mag. moment spectra, mol. beam mag. reson. obs. 77−14509
methanol (-d), H-bonding investigated with supersonic mol. beam using photoionisation quadrupole mass spectrometer 80−102543
methylchloride, high resoln. rot spectrum, spin-rotation and nucl. mag. shielding tensors 77−27054
modulated, detect. by electron bombard. detect. 79−2885
modulated, recording using ionization detector 79−18316
modulated mol. beam mass spectrometry, reaction prod. vector, surface reaction 77−63952

molecular beams continued
monokinetic spectroscopy *(French)* 78−25751
multichannel counter for molecular beam time-of-flight experiments 80−37119
multiple charged and polyatomic ions, use in implantation accelerator 77−54017
naphthalene, fluoresc. of isolated mol. in supersonic beam 79−45750
neutral molecule motion control by electron beams 80−99582
nozzle, mass spectroscopy sampling nozzle, gas dynamics 79−49330
optical probing of excited mols. that have undergone radiationless transitions 77−27106
optical Ramsey resonance, in three separated fields produced by corner reflector, theory 80−74166
orbiting molecular beam laboratory on Space Shuttle 78−35242
orientation, detector integrated angular distrib., photoexcitation depend. on target orientation, anal. 78−56564
pentacene, intramol. dynamics and energetics in isolated ultracold state 79−98144
plasma sampling by mol. beam, fast neutral atom prod. 77−68865
polyatomic seeded supersonic beam+monatomic host gas, internal energy relax. 79−59532
polymer breakdown plasma analysis, mass-spectrometric installation 78−88670
production apparatus, for scatt. expts. on polycryst. Pt 77−16449
pulsed beam experiments employing electromechanical valve 80−63870
pulsed gas valve as 10 μs mol. beam source 78−66690
pulsed plasma injector, for intense mol. beam prod. 77−65548
quantum state selected atomic and molecular beams production, developments in techniques 80−63871
Raman spectroscopy, very high resolution CARS 79−30568
reaction cross sections, information content of mol. beam state. vs. resolved product state distrib. expts. 77−28980
reactive gas mass spectrometric analysis with free-jet expansion sampling 80−89566
recycling reactor for study of reactive molecule-surface collisions 78−1109
RF spectroscopy, interference effects *(French)* 78−42038
ring-type state selector and space focuser for mols. with positive induced dipole moment, appl. to mol. beam maser 78−54503
rotational temp. meas. by CARS 80−23423
scattering, anal. using cross-correlation time-of-flight technique 79−55000
scattering, S/N ratio enhancement in time-of-flight anal. 78−86969
scattering apparatus for total cross section meas. 77−30954
selection, by quadratic Stark effects *(Russian)* 78−78823
sources, gasdynamic, use of lasers, time-of-flight and detection techniques 80−69264
spatial-temporal modulation in molecular beam spectroscopy, phenomena near molecular resonance *(French)* 78−90149
spatio-temporal modulation near mol. reson. *(French)* 79−49299
spectroscopy, two-freq. separated oscillating fields technique 79−21715
spectroscopy technique, adiabatic passage by Zener's theory *(French)* 79−870
state reduction in passage of mol. beam through Stern-Gerlach apparatus, calculational example 79−36696
state selection and focusing, appl. to NH_3 hyperfine spectrum 80−28119
state-resolved, detector for beam anal. using optical fibres 79−54999
Stern-Gerlach apparatus, state reduction hypothesis in quantum mech. 78−77765
structure and dynamics of mols. by pulsed mol. beams 80−102563
submillimetric extension of molecular beam electric resonance spectroscopy 77−38751
supersonic, appl. to photoelectron spectroscopy of O_2 and ethylene 79−68264
supersonic, rotor accelerated 78−66686
supersonic, velocity separation of isotopic mixtures 77−54626
supersonic beam skimmers, transition regime behaviour 77−3491
supersonic jet beam, seeded with CsF, (LiF), vibr. relax. 78−37716
supersonic mol. beam, CARS rot. temp. meas. 80−23423
supersonic molecular beam apparatus for ion anal. reaction studies *(Japanese)* 79−50165
supersonic nozzle beam, high temp. and press. device 80−37907
supersonic seeded molecular beam, vibr. relax. 78−17761
supersonic source, seeded, appl. to LiF+Ar cross-sections and intermol. pots. study 79−72398
supersonic source, simple calibration method 80−82845
surface reactions, possible expts. on Space Shuttle 78−35243
surface structure, coherence length and transfer width in LEED and mol. beam diffr. 79−42347
target for ion-atom collision studies 78−70971
tetracene, intramol. dynamics and energetics in isolated ultracold state 79−98144
tetracene molecules in Ar clusters, excited state intramol. dynamics, laser-induced fluoresc. spectra obs. 80−78674
transition probability amplitude, coherence effect *(French)* 79−45737
trifluoroethanol, H-bonding investigated with supersonic mol. beam using photoionisation quadrupole mass spectrometer 80−102543
two frequency separated oscill. fields method for beam interrogation 78−89596
two-photon ionisation, ion source of mass spectrometer 79−27118
vacuum gauge calibration, attenuation meas. on buffer gas scatt. of mol. beam *(French)* 79−58669
vapour absorption cells and beam generating ovens for synchrotron radiation spectroscopy 78−66688
velocity, intensity and particle density, mass spectroscopic determination 79−67428
velocity distribution function, and moments, from TOF meas. 78−5371
velocity distribution function, residual gas effect 77−88603
wind tunnel generated, intensity dependence on stagnation temp. 77−68629
Ar, calibration of supersonic mol. beam source 80−82845
Ar, supersonic molecular beam source, simple calibration method 80−82845
AsI_3, mol. beam photodissoc. 78−56906
$Ba+Cl_2 \rightarrow BaCl^+ + Cl^-$, chemi-ionis. reaction, mol. beam obs. 80−104434
$Ba+HF \rightarrow BaF+H$, dual mol. beam excitation difference spectroscopy, state-to-state vibr. resolved dynamics 80−89474
CH_2 molecular beam source 80−37908
CO, $d^3\Delta$, v=4 state dipole moment, laser-induced transition in mol. beam 78−25513
CO, rot. distrib. in supersonic beam, IR bolometry using tunable diode laser 80−63869
CO_2, dimer, geom. struct., by mol. beam deflection 79−27102
CO_2 free jet, rarefied flow, homogeneous condensation scaling law 80−6121
$CS_2^* + CS_2 \rightarrow CS_3^+ + CS + e^-$, chemiionisation, mol. beam photoionisation 80−76495
$Cl+Br_2 \rightarrow BrCl+Br$, crossed mol. beam, translational energy depend. 78−25693
ClF, mol. beam Zeeman effect, dipole moment sign, coupling const. 77−75208
Cu_2, in supersonic free jet expansion, laser induced excitation spectrum obs. 80−14151
D_2, sticking and accommodation on low-temp. substrate, mol. beam expts. 80−84368
F_2+UO_2, reaction kinetics, molecular beam study 78−46157
$GeH_4(F_4)$, rot. mag. moment spectra, mol. beam mag. reson. obs. 77−14509
H_2 cluster beam formation, from nozzle flow, isotope effect 80−6127
H_2, cluster beam source, cryopumping 79−63258
H_2, sticking and accommodation on low-temp. substrate, mol. beam expts. 80−84368
H_2^+ differential cross section rel. to charge exchange cross sections of fragments 80−78704
H_2+heavy inert gas, small clusters, beam cluster intensity and collision cross section 77−38711
$H_2^+ + CO \rightarrow H + HCO^+$, 1.89 eV crossed beam study 80−21287
HCl+HCl(HF)(HI)(HBr), supersonic-thermal beam collision, rot. energy transfer, classical trajectory calc. 79−68302
HDO, T_1 and T_2 relax. cross sections meas. 77−34733
HF+ClF, and isotopic forms., HFClF complex form., config., bonding, spectroscopic consts. 77−30860
$H_2O+Ar(^3P_{2,0})$ crossed mol. beams, ionisation and dissociative fluorescence, energy depend. 79−52669
He-Ar mixture, mass separation during molecular beam sampling process 80−31937
I_2, effusive collisionless beam, optical Rabi coherent transient damping, time resolved obs. 77−75231
I_2, in seeded supersonic beams, vibr. and rot. relax., laser-induced fluoresc. obs. 80−23522
I_2, mol. beam, ang. momentum polarisation 77−46635
ICl, mol. beam focusing in rot. states 79−18317
InP:Sn film, mol. beam epitaxial growth 77−16505
K+trifluoroiodomethane→KI+trifluoromethane, molecular beam reactive scattering, angular distribution study 79−98198
K_2, beam, multiphoton ionisation mass selective laser spectroscopy, vibronic, gyrovibronic states, clusters 78−21985
K_2, supersonic mol. beam, isotope selective two-step photoionisation study 80−74203
KOH, beam, formed at 300-800°C, electron elastic scatt. obs., species identification 80−14231
Kr, calibration of supersonic mol. beam source 80−82845
Kr, supersonic molecular beam source, simple calibration method 80−82845
Li/Li_2 nozzle beam characts. by spectroscopic techniques 78−55255
$Li+CH_3I(CCl_4)(CH_3NO_2)$, mol. beam kinetics 77−28978
LiF, condensation and evaporation in monomers, dimers and trimers, mol. beam method *(German)* 77−85052
LiF, supersonic seeded molecular-beam, vibr. relax. 78−17761
N_2, calibration of supersonic mol. beam source 80−82845
N_2, generation in free jet, parameters rel. to stream perturbation before skimmer 79−86468
N_2 jet, freely expanding, quantum effects in rot. relax. 80−58355
N_2+heavy inert gas, small clusters, beam cluster intensity and collision cross section 77−38711
$NH_3+NH_3(ND_3)(HCl)(H_2O)$, inversion relax., isotope effects, beam-maser ang. resolution effects 77−30964
NO, mol. beam tunable diode laser sub-Doppler spectra, $^2\Pi_{1/2,3/2}$ Λ splittings 79−41180
NO+heavy inert gas, small clusters, beam cluster intensity and collision cross section 77−38711
NO_2, dissociative limit, mol. beam characts. determ. by fluoresc. excitation spectra 80−53074
NO_2, sub-Doppler spectra, laser-beam system, HFS excitation, radiative, non-radiative decay 78−90210
Na/Na_2 beam, diagnostics with internal selection, vel. distrib. and dimer form. 78−86968
Na_2, beam, multiphoton ionisation mass selective laser spectroscopy, vibronic, gyrovibronic states, clusters 78−21985
Na_2, beam anal. using detector based on lasers on optical fibres 79−54999
Na_2, mol. beam, ang. momentum polarisation 77−46635
Na_2, mol. spectroscopy by photodeflection in supersonic nozzle beam 79−54995
Na_2, supersonic mol. beam, characterisation by multiphoton ionisation 78−23946
NaCl, mol. beam condensation on Ir and Pt substrates, adsorbed C effects 77−66593
NaCl, Na time-of-flight spectrum using pulsed tunable laser fluoresc. detect. 77−49804
NaK dimer formed in supersonic beam, laser-induced emission 80−9636
NaK, laser-induced fluoresc. in supersonic nozzle beams 78−25593
Ne+heavy inert gas, small clusters, beam cluster intensity and collision cross section 77−38711
O_2, calibration of supersonic mol. beam source 80−82845
O_2+heavy inert gas, small clusters, beam cluster intensity and collision cross section 77−38711
O_3, mol. beam Stark, Zeeman effects, polarisability, moments, mag. susceptibility anisotropy 77−79649
RbKr, magnetic resonance meas. of spin-rotational interaction 78−33528
SF_6, laser pumping in collisional region of nozzle beam, internal excitation, time-of-flight anal. 80−95719
SF_6 multiphoton dissoc. by mol. beam method, energy distribution meas. by time-of-flight spectra, dissoc. dynamics 80−78670
SF_6, ν_3 band, IR spectra, in supersonic mol. beam 78−66541
SF_6, resonant single-photon dissoc. route using prelim. electron excitation 80−9662
$SiH_4(F_4)$, rot. mag. moment spectra, mol. beam mag. reson. obs. 77−14509

molecular beams continued
$Sm+N_2O$, mol. beam chemiluminescence, cross section energy depend. 77−32792
$Sn+O_2$, crossed mol. beam kinetics, SnO time of flight recoil vel. spectra 78−68883
Sn_2, modulated, for plasma diagnostics 77−27735
TaS_2, charge density waves, mol. beam diffr. obs. 79−73453
W, catalytic decomp. of NH_3 single pulses, mol. beam relax. spectrometry 80−21321
XeF_6 seeded mol. beam, transverse ionisation, space charge, mass spectra and vel. 80−78725

molecular biophysics
see also biomembrane transport; biomolecular effects of radiation; DNA; lipid bilayers; proteins
N_1-aryl-N_2-alkyl thioureas herbicides, structure-activity relationships 79−62176
ab initio molecular fragment calculations with pseudopotentials 79−93905
absorption spectra for the complexes formed from bitamin-A and β-lactoglobulin 80−30664
acetate-ferrileghemoglobin, X-ray struct. anal., 3D refinement at resoln. of 2.0 Å 80−104554
N-acetyl-D-alloisoleucine, soln. struct., dynamics, proton relaxation mechanisms 80−76708
N-acetyl-l-phenylalanine methyl ester, model for amino acid side chains internal motions in peptides and proteins 80−48017
acetylcholine, nonenzymatic hydrolysis, Raman obs. 79−29505
acetylcholine neurotransmitter, PCILO-INDO calcs. 80−58153
acetylcholine receptor from Torpedo Californica, struct. anal., low-angle neutron scatt. obs. 80−30651
acetylcholine receptor phosphorylation by membrane protein kinase in receptor-enriched T.californica membrane 77−56370
acetylcholine receptor phosphorylation in vitro, E. electricus membrane fragments 77−56371
acetylcholine receptor protein, binding kinetics and Ca ions, rel. to membrane cond. changes of acetylcholine 77−40649
acetylcholine receptor protein structure 80−85339
actin, microcrystals and tubes formed in the presence of Gd ions 79−16143
F-actin, muscle, quasi-elastic light scatt. 77−64010
F-actin, struct. changes in living muscle fibres, polarised UV fluoresc. microscopy 80−67037
F-actin subunit structural non-equiv., tension development in skeletal muscle 78−64959
actin-myosin binding, muscle mechanics thermodynamic model 78−80908
actin-myosin filament overlap rel. to number of Ca binding sites on glycerinated muscle fibres 78−44465
actin-myosin interaction, depend. of skeletal muscle energy transduction on time in tension 77−52754
actin-myosin interaction in skeletal muscle, quantitative model 77−52753
actinomycin-DNA bindings, first-neighbour specificities, circular dichroism 78−3442
active transport, rel. to second law of thermodynamics 77−9178
acto-myosin, cross-bridge slippage induced by AMP-PNP and stretch in fibrillar muscle fibres 78−77075
actomyosin, head rot. and dissoc., muscle exponential rate processes rel. to MgATP conc. 78−44468
actomyosin kinetic anal., review 80−21441
actomyosin-ATP system kinetics, energy transform. anal. 77−81476
adenine, hydroxy and methoxy derivatives, absorption UV spectroscopy and electronic struct. of ionic and tautomeric forms 80−74177
adenine, tautomeric forms protonation, ab initio HF Roothaan SCF calcs. 80−78534
adenine, UV photoelectron spectra, valence electronic struct. 77−16905
adenine tautomers, relative stabilities, nonempirical MO calcs. 80−21442
adenine-uracil polynucleotides, alternating, premelting, melting, postmelting transitions 79−57574
adenosine, association, spin label appl. 78−81086
adenosine 5′-monophosphate, UV resonant Raman spectra 78−48756
adenovirus hexon, three dimensional structure from electron microscopy, computer modelling 80−35833
adenylate cyclase regulation, depend. on sugar transport system, review 78−69031
adenylyl 3′-5′ adenosine, conform. equilib., Raman temp. jump obs. 78−8450
adenylyl cyclases, stimulation by hormones and regulation by nucleotides, review 78−15760
ADP, association, spin label appl. 78−81086
β-adrenergic receptor, molecular interactions with agonists and antagonists 80−8005
adrenocorticotropic hormone polypeptide chain left helical conform., aqueous soln. 77−70414
adsorption isotherm for study of interfacial and biological phenomena 77−59207
aequorin, Ca^{2+}-induced luminesc., inhibition by anaesthetics 78−76985
aequorin luminescence, light emission rel. to Ca^{2+} conc., Ca-independ. component 77−48750
agarose gel immunoelectrophoretic determination of molecular weights of tubulin antigens 80−67313
L-alanine:Cr^{3+}, X-irrad., thermoluminesc., ESR, UV photobleaching 77−9104
L-α-alanine, cryst., cationic radicals, EPR 78−11537
L-alanine, nucl. spin-lattice relax. of CH_3 and NH_3 groups 77−8440
alanine, oligomer, vibr. spectra rel. to polymeric form 79−83695
alanine, unionised, ab initio equilib. structs. calcs. 79−68181
alarm pheronomes, activity rel. to mol. similarity, electron density function meas. 80−91413
albumin, adsorbed layers on polystyrene, contact angle meas. 80−61508
albumin, adsorption on SiO_2 80−10777
albumin, bovine sercem, PMR spectra line narrowing, convolution and pulse methods 78−78729
albumin, bovine serum, charged macromol. translational diffusion coeff. 79−70510
albumin, bovine serum, diffusion, hydration and soln. environment effects 77−19116
albumin, bovine serum, diffusion, hydration effects, finite conc. 77−19115
albumin, bovine serum, diffusion, hydration effects 77−19114
albumin, bovine serum, hydrated, dielectric props. at 9.9 GHz 78−15758

molecular biophysics continued
albumin, bovine serum, in soln., five-component dielec. dispersion 78−15759
albumin, bovine serum, macroion soln. viscosity and diffusion, quasielastic light scatt., electrostatic interaction 79−70508
albumin, bovine serum, solutions, fluctuation transport theory 78−70057
albumin, bovine serum, use of high heating rates in study of thermal denaturation 77−81470
albumin, human serum, adsorption studies, feasibility of radiolabelling 78−85359
albumin, human serum, AsF_3^- NMR probe for anion binding sites 78−48748
albumin, human serum, elec. cond. and dielec. const., 1 to 15 MHz 78−53315
albumin, human serum, interaction with luminol. chemilum. and fluoresc. 77−21471
albumin, Reanal serum, mag. field effect on photoinduced reactions 79−92154
albumin denaturation, investigation by PMR 80−3582
albumin-fatty acid complexing rel. to struct. lability of biomembranes, using fluoresc. probes 77−25381
albumin-unsaturated fatty acid binding kinetics, fluoresc. anal., rel. to struct. lability of biomembranes 78−15755
alkaline phosphatase, slow reaction, vidicon-based spectrometer obs. 79−21817
amine microspectrofluorometry, automatic correction of excitation spectra 77−9308
amino acid, monolayer on solid, SIMS anal. 79−89038
amino acid linear sequence form., cryo-sublimation of frozen aqueous solns. 78−95993
amino acid methyl esters, photoelectron spectrosc. 79−24954
amino acid monolayers and ordered films on Cu, surface struct. LEED 78−38968
amino acid racemization, appl. to geochronology and geothermometry 78−20341
amino acid residues, contacting, ligand binding rate dependence on specific microdynamics 80−51031
amino acid residues in globular proteins, hydrophobic character 79−2001
amino acid side chains, internal motions in peptides and proteins, N-acetyl-l-phenylalanine methyl ester model 80−48017
amino acid side chains, NMR relax. due to multiple internal rots. 78−94340
amino acids, isotopic enrichment determ. by chem. ionis. mass spectra 79−79694
α-amino acids, naturally occurring, in aq. soln., Kerr constants 80−85353
amino acids, polycryst., proton mag. relax. and mol. motion 78−20139
amino acids, positron annihilation in D and L isomers 77−12887
amino acids and their complexes, corrected G-values 79−20516
4(6)-amino-uracil, IR absorpt. spectra, vibr. anal. 78−61143
α-aminoacids, stereoselective catalysed hydrolysis of esters *(French)* 79−66438
γ-aminobutyric acid, cryst., film, matrix IR spectra, low temp., neutral and zwitterion forms. 77−18920
AMP, association, spin label appl. 78−81086
amphipathic apolipoprotein ApoC-III bound to phosphatidylcholine bilayers, lateral mobility 80−97884
all-trans anhydrovitamin A, resonance enhanced Raman spectrum 79−43815
1,8-anilinonaphthalene sulphonate in bacterial suspension, fluoresc. spectra 79−88052
anthramycin-DNA adduct, proposed struct. 80−30658
antibodies, conformation in presence and absence of antigen, small angle X-ray studies 79−11890
antigens of I-E subregion, mouse, struct. polymorphism genetically determ. 79−66442
antimalarials, interaction with coenzyme-Q_{10}, theory 78−27885
apomyoglobin reconstituted with ^{111}In(III)mesoprotoporphyrin IX, rot. correl. time determ. 80−76698
apomyoglobin-arylaminonapththalenesulfonate system, fluorescent behaviour 79−39359
L-arginine L-ascorbate, X-ray cryst. struct. determ. 80−35826
ascorbic acid adduct model systems, SCF calc., rel. to protein internal charge transfer 80−69072
aspartate-transaminase, phys. state in cryst., heating curves 77−70409
astaxanthin, aq. soln., aggregate, reson. Raman spectra, and IR spectra, exciton interactions 78−31770
asymmetric syntheses, in living systems, theory, rel. to fluctuation effects on dissipative structures 79−83442
atebrin fluorescence photo-induced quenching and photosynthetic electron transport, pea chloroplast 77−56351
ATP, association, spin label appl. 78−81086
ATP, phys. aspects of intracellular energy transform. 77−86462
ATP disodium salt, hydrated, vibr. assignments, force consts., coincidence method appl. 78−62953
ATPase, Ca^{2+}-activated, of sarcoplasmic reticulum, rot. motion and evidence for oligomeric structs. 80−72124
ATPase, Ca^{2+}-depend., struct. rearrangements during function 80−81527
Na^+, K^+-ATPase, identification of membrane-embedded segment of large polypeptide chain 78−3447
Na^+,K^+-ATPase, membrane, as digitalis receptor binding model 78−40111
ATPase kinetics in E. coli cells, ^{31}P NMR meas. 78−77022
Na, K-ATPase membrane prep. struct. characts. studied by paramag. probes 78−64930
ATPase of A-laidlawii membrane, Arrhenius plot artifacts due to temp. depend. of substrate-binding affinity 78−64949
autocatalysis in stoichiometric model of energy metabolism 77−36860
axonal transport, components, mechanisms and specificity, book contrib. 79−96551
azo dyes, UV-visible spectrophotometric 80−61207
azobilirubin, form., fast reaction vidicon-based spectrometer obs. 79−21817
Azotobacter ferredoxin, struct. of Fe-S clusters at 4.0 Å resolution 79−57575
B-DNA helix, guanine-cytosine base pair, electrostatic pot. 80−8003
bacteria, photosynthesis, primary electron acceptor, EPR, ENDOR investigs. 78−77004
bacteria, photosynthetic, triplet-state EPR spin polaris., intramol. model 78−44469

molecular biophysics continued
bacterial catalase, ^{57}Fe enriched, active centre, Mossbauer spectra meas 80−8024
bacterial chemoreception, response regulator model in simple sensory system 77−73534
bacterial luminescence excitation by singlet O_2 79−39340
bacterio-opsin, changes in protonation state during reconstitution of bacteriorhodopsin 80−89707
bacteriochlorophyll, π-electronuc struct., ASMO-SCF-CI calc. 77−36868
bacteriochlorophyll, photooxidation, picosecond absorption spectroscopy investig. 78−82053
bacteriochlorophyll *b* and pheophytin pair redox potential obs. 79−39338
bacteriochlorophyll a, stimulated fluoresc. and fluoresc. quenching, pump photon density 78−27895
bacteriochlorophyll a, triplet state energy and lifetime 80−30682
bacteriochlorophyll absorption polarisation, in liq. cryst. cell 79−24950
bacteriochlorophyll cation in soln., N atom ENDOR and proton triple resonance 78−96018
bacteriochlorophyll monolayer quantum yield and image contrast in photoelectron microscopy 78−44453
bacteriochlorophyll of green bacteria, resolution of absorpt. and fluoresc. spectra into components 78−20152
bacteriochlorophyll radicals, role in primary charge separation of Rhodopseudomonas viridis 80−63688
bacteriophage DD6, contracted tail, three dimensional struct. 78−11608
bacteriophage FI-5$^+$, struct. in intact state 79−70513
bacteriophage S shape determ. from small-angle X-ray scatt. 79−39347
bacteriophages T4B and T7, determ. of rotational diffusion coeff. by depolarised dynamic light scattering 80−85549
bacteriopheophytin, π-electronic struct., ASMO-SCF-CI calc. 77−36868
bacteriopheophytin a, triplet state energy and lifetime 80−30682
bacteriopheophytin b radicals, role in primary charge separation of Rhodopseudomonas viridis 80−63688
bacteriorhodopsin, anomalous amide I IR absorpt. rel. to alpha helices distorted struct. 80−12058
bacteriorhodopsin, Debye rot. relax. times, modulation excitation spectrophotometric obs. 79−3532
bacteriorhodopsin, dynamics, of pH-induced spectral changes 79−57587
bacteriorhodopsin, effect of high press. on absorpt. spectrum and isomeric composition 80−67041
bacteriorhodopsin, emission lifetime meas. 78−96012
bacteriorhodopsin, photosynthetic cycle, time-resolved Raman spectra 78−85294
bacteriorhodopsin, purple membrane struct., Halobacterium halobium 78−15782
bacteriorhodopsin, reson. Raman evidence for secondary protein-Schiff base interactions, primary excitation mechanism 80−55981
bacteriorhodopsin, time-resolved resonance Raman characterisation 79−83705
bacteriorhodopsin, time-resolved resonance Raman spectroscopy 77−29103
bacteriorhodopsin Br570, bathochromic shift of absorpt. band in external elec. field 80−35838
bacteriorhodopsin emission lifetime, using picosec. meas. method 77−17009
bacteriorhodopsin in purple membrane, chromophore mobility 77−25366
bacteriorhodopsin in purple membrane of H. halobium, chromophore excitonic interaction 77−21497
bacteriorhodopsin membrane preps. associated with lipid-water interface, form. of elec. pot. diff. 80−81551
bacteriorhodopsin of purple membrane of H.halobium cells, luminesc. 77−36890
bacteriorhodopsin orientation in Halobacterium halobium, selective proteolysis investig. 78−77010
bacteriorhodopsin reorientation due to elec. field 77−66789
bacteriorhodopsin Schiff base deprotonation dynamics using kintic reson. Raman spectroscopy 77−48981
bases, biologically important, and derivatives, optical crystallographic props. 78−3449
basic pancreatic trypsin inhibitor, methyl group PMR, 360 MHz 78−27887
bathoproducts of rhodopsin, isorhodopsin I, and isorhodopsin II 80−51088
Bence-Jones Rhe protein (1.9 Å), phase extension and refinement 79−99168
bent molecular organic crystals, electron diffr. intensities 80−100132
benzodiazepine receptor, coupling to chloride anion channel 79−79486
benzo[α]pyrene-DNA complex, triplet state props., optically detected zero-field mag. reson. obs. 77−79636
benzo[α]pyrene-DNA complex, triplet state props., optically detected zero-field mag. reson. obs. 79−18222
bilirubin in neonatal jaundice, chemistry, biosynthesis, transport, excretion, photodecomposition and elimination 80−3578
bimolecular rate constant ionic strength dependence, effect of a molecular dipole 80−55977
biochemical model, phase transition induced by external noise 79−17377
biochemical reactions, fast, in solns. membranes and cells, conf., Airlie, USA (Apr. 1978) 79−8485
biochemical systems anal., mol. biology, book 77−21468
bioelectrets, occurrence of electret state and appl. in mol. biophysics and bioengineering 80−8007
bioenergetics, H bonded chain theory 80−76699
bioenergetics, solitons, muscle contraction mechanism 79−96508
biological macromolecules, picosec. and subpicosec. relax. and dephasing, reson. light scatt. obs. 79−45876
biological molecule models, using wavefunction electron densities 79−24937
biological molecules, ab initio calcs., small Gaussian basis sets 79−59341
biological structure studies, neutron scattering from soln. of macromols. 77−16906
biological structures, X-ray and neutron small-angle scattering 79−11889
biological systems, nonequilib. mol. vibr. excitation, electron mechanism 80−55979
biologically active molecules, photoelectron spectrosc. 79−24954
bioluminescence spectra of fireflies 80−35821
biomembrane, apparatus for direct meas. of fluoresc. decay *(French)* 77−5116
biomembrane, apparatus for meas. of fluoresc. polarisation *(French)* 77−9307
biomembrane microviscosity measurement, light scatt. effects 79−39365

molecular biophysics continued
biomembrane transport catalysis, ADP,ATP carriers of mitochondria *(German)* 79−29512
biomolecule osmosis, educational model 77−26110
biomolecules, ZDO method for very large mols., low computer time 77−14356
biomolecules+chloranil, charge transfer interaction, equilib. const., enthalpy and entropy determ., mol. polarisability 80−89708
Biophysical Society, 23rd annual meeting, conf., Atlanta, USA (Feb. 1979) 79−34468
biopolymer, electronic transport mechanisms, asymmetry role 78−6370
biopolymer, electronic-conformation interactions 80−3588
biopolymer, local mode resonance enhancement in Raman spectra 77−77204
biopolymer Brownian diffusion, fluoresc. correl. spectroscopy 79−62193
biopolymer localised modes, due to impurities, FG-matrix technique 79−34474
biopolymer motions, nonsteady hydrodynamics, damping effects 77−36861
biopolymer negative resistance, rel. to living cell props. 78−64923
biopolymer soln. heat capacity, conformational props. temp. depend. 80−8009
biopolymer synthesis on solid supports 79−29397
biopolymer thermodynamic props. in helical and coiled state, 4 to 400K, calorimetry 78−20140
biopolymers, assoc.-dissoc. phenomena, review 79−11884
biopolymers, chromophone aggregates in Frenkel exciton model, dynamic perturbation effects on circular dichroism intensity 80−93273
biopolymers, circular dichroism, optical rotatory dispersion, conformational anal., review 77−3497
biopolymers, conditions of liquid crystal formation 80−30642
biopolymers, dynamics of helix-coil transition 79−29499
biopolymers, electronic struct. and possible chem. carcinogenesis mechanisms 79−22874
biopolymers, primary structure determ. algorithms 79−48209
biopolymers, reversible unfolding, mol. field theory 79−34479
biopolymers, X-ray struct. study using synchrotron radiation and multichannel detector 78−47210
biotin, NMR of ^{13}C, spectrum assignment 80−26204
bipyridines, torsional isomerisation of biologically active bicyclic molecules 80−27996
blood, high-resolution optical props. 77−36869
blood, magnetic relax. time of H_2O protons 79−11898
blood proteinpolymer interfacial behaviour, influence of hydrophilic-hydrophobic type of microphase separated struct. *(Japanese)* 80−12051
blue proteins, activation of electron transfer reactions 78−44446
bone, hydrazine deproteinated, rat, UV induced thermolum. glow peak obs. 80−29814
bone powder and ash, PMR and IR spectra, chem. anal., bond lengths 78−3414
Bose condensation, microscopic approach to Frohlich's theory 78−24022
bose condensation, polar modes with elastic restoring forces, metastable ferroelec. state 77−81464
bose condensation of phonons in biological systems 80−30641
bovine plasma albumin, high conc. soln., quasielastic light scatt. line breadth meas., diffusion coeffs. 77−1976
bovine serum albumin, conformational changes and mol. dynamics exam. by perturbed angular correl. 80−81538
bovine serum albumin mol. wt., X-ray small angle scattering using synchrotron radiation 78−66700
brain, microtubule solns., calf, dynamic laser light scattering 79−16150
5-bromo-uracil, IR absorpt. spectra, vibr. anal. 78−61143
bromohaemin, ferric porphyrins with fifth ligands, ^{57}Fe and ^{14}N hyperfine consts. 78−50475
burn-induced leakage of macromolecules in living tissue 79−29514
n-butyl retinal Schiff bases, absorpt. spectral props., rel. to bathochromic shift in visual pigments 78−40117
butyryl cholinesterase of horse serum, quaternary struct. obs. 79−57570
C1q of human complement, neutron scatt. obs., conformational calcs. 80−81537
C-reactive protein, interaction with artificial phosphatidylcholine bilayers 80−3579
calcium adenosine triphosphate, X-ray Ca K-edge meas. 79−6950
calcium oxalate hydrates, crystn. kinetics, comparison for mono-, di-, and trihydrates 80−81528
cancer receptor sites, proof by MO method for interstrand guanine binding of DNA 80−30656
capsular polysaccharide antigen, structure investig. by ^{13}C NMR 80−35828
carbocyanine dye orientation in erythrocyte membrane, microscopic fluorescence polarisation obs. 79−83694
carbocyanine dyes, fluoresc. probes, effect on Ca-depend. K efflux 77−12896
carbonic anhydrase, active site substrate binding, environmental effects, CNDO and SCF LCAO calcs. 80−8002
carbonic anhydrase, enzyme, mechanism 78−76846
carbonmonoxyhemoglobin, spectroscopic meas. after pulsed optical excitation 79−92150
carbonmonoxymyoglobin, forzen soln., recoilless fraction, Mossbauer spectra meas. 80−8025
carbonyl-containing biological molecules, UV photoelectron spectra 77−88498
carboxyhaemoglobin, aq. soln., photolysis using nanosec. pulse, transient effects 79−79453
carboxyhaemoglobin, redox investig. using reson. Raman, visible absorption and electrochem. methods 78−76832
β-carotene, coherent anti-Stokes reson. Raman spectrum excitation profiles 77−56342
β-carotene, electronic struct., classical and double beam photoemission obs. 78−9285
β-carotene, in CS_2, reson. Raman spectra, room temp. 78−35803
β-carotene, optical absorpt., theory 79−62189
β-carotene, resonance Raman spectra intensity distribs. in soln. 79−22763
β-carotene, solubilised in lecithin liposomes, linear dichroism, absorption statistics 78−1014
β- carotene, valence bands, XPS obs. 78−24030
β-carotene, very dilute benzene soln., picosecond reson. Raman spectroscopy 79−98102

molecular biophysics continued
carotenoid molecules in living cells of chlorella, vibrational state population 80−97861
carotenoid pigments, radical ions, radiolysis generation, absorpt. spectra, MO calcs. 77−65488
β-carotin, resonance Raman effect *(Hungarian)* 78−74666
carrier-molecule complexes, probability description of electron transport processes 78−53314
cartenoprotein, lobster shell, organisation studied by photoacoustic spectroscopy 79−62192
cartilage proteoglycan, association with hyaluronic acid, elec. birefringence obs. 80−85332
β-casein, adsorpt. isotherm, at air-water and air-oil interfaces 79−79461
β-casein, adsorption kinetics, surface denaturation 79−79460
β-casein, molecular structure of adsorbed film 79−79462
casein-methylglyoxal complex, electronic props. 77−52736
κ-caseins of cow and sheep, secondary structures 78−96001
catalase, electron microscope exam. of new cryst. form, Fourier transform. method 77−11447
catalase, from the fungus penicillium vitale pidopl. et bilai, preliminary crystallographic investigation and props. 79−66444
catalase, phys. state in cryst., heating curves 77−70409
catalase crystal lattice stability 77−25380
catalysis of reversible flow reaction by oligomeric enzyme 77−36859
cation-ligand complexes and free cations in solns., calc. method 79−62169
cell adhesion models, reaction kinetics and forces 78−80844
cell membrane interaction theory of molecular level mechanics 79−92174
cell membranes, at mol. resoln., introduction 80−104841
cell membranes, effects of hydrostatic pressure, review 78−15790
cell molecular computer, coding during intracellular processes of information processing 77−70400
cell movement, molecular basis rel. to proteins 79−100586
cell surface anisotropic molecular motion 80−97883
cell surface component rotational diffusion, time-resolved phosphoresc. anisotropy 80−97885
cell surface receptors, molecular movements 80−45866
cell water polarized multilayer theory expt. confirmation 79−62213
cellulose, conform. states and IR dichroism calcs. 80−55986
cellulose, in Valonia, pole figures and orientation functions 77−86439
cellulose, mobility of adsorbed water, NMR pulse obs. 80−108835
cellulose, struct. and conform. props. of cotton fibre grown from γ-irrad. seed 77−81539
cerebron, thermotropic and lyotropic mesomorphism 80−76703
ceruloplasmin, human, calc. of rotation function for tetragonal. cryst. at 10 Å resoln. 80−108843
ceruloplasmin, human, mol. wt. determ. by hydrodynamic methods and low-angle X-ray scatt. 78−15761
charged effectors, indirect allosteric action mechanism 79−20503
chemical oscillators responding frequency switch 80−108837
chemical reactions of biological molecules, Raman difference spectroscopy 78−44368
chemical reactions with inner sphere complex charge redistrib., polar solvent reorganisation energy 80−40730
chemical rectifiers, one-way catalysis 80−71901
chemical relaxation spectrometry, new electric field methods 79−8586
chiral biomolecules, temp.-jump relaxation studies, transient CD meas. 78−5372
chiral purity, importance in self-reproduction of organisms 77−36864
chirality rel. to biological mols. origin and evolution *(Russian)* 77−52739
chitin, in lobster shell and apodeme, piezoelec. rel. to remodelling 78−64929
chlorella, delayed fluoresc., ns laser pulse excited, fast phase kinetic anal. 79−24951
chlorin, ab initio CI calcs. on ground, singlet and excited states, visible spectrum 79−16139
chlorohaemin, ferric porphyrins with fifth ligands, ^{57}Fe and ^{14}N hyperfine consts. 78−50475
chloroperoxidase, ferric form, X-ray absorpt. fine struct., Fe-N and Fe-S lengths 79−48213
chlorophyll, -a and -b, fluoresc. fading curve of lowest triplet state 79−36691
chlorophyll, -a and -b in cyclohexane soln., far IR and reson. Raman spectra 77−48753
chlorophyll, a and b, lowest singlet-singlet transition, solvent effects 79−24952
chlorophyll, aq. solns. of detergents, polarographic obs. 79−57565
chlorophyll, electron transfer across octane-water interface 77−81474
chlorophyll, energy migration between native forms at −196°C using sensitised fluoresc. 77−70429
chlorophyll, energy trapping dynamics in photosynthetic unit model 78−88697
chlorophyll, enhancement of fluorescent mag. resonance detection, under intense laser excitation *(Russian)* 78−91995
chlorophyll, fluoresc. decay time depend. on luminesc. and excitation wavelengths 79−66447
chlorophyll, fluoresc. in bilayer lipid vesicles and liposomes, conc. quenching 77−4985
chlorophyll, in maple leaf, −196-18°C, red shift explanation 78−61144
chlorophyll, native forms., var. fluoresc. at −196°C 77−70417
chlorophyll, photooxidation, triplet state mechanism 78−27791
chlorophyll, photosynthetic unit of H_2 evolution 77−77875
chlorophyll, photosystem 2, activation energy and lifetime of fluoresc. 80−35842
chlorophyll, singlet-triplet optical resonance in solid soln. 77−52741
chlorophyll, transfer of electronic excitation energy from monomer to dimer *(Russian)* 78−27289
chlorophyll a, bimol. quenching of excitons and fluoresc. in photosynthetic unit 77−16908
chlorophyll a, cation radical formation by pulse radiolysis, oxidation and demetalation rate consts. 80−61505
chlorophyll a, fluoresc. and absorpt. spectra, resolution into components 79−57584
chlorophyll a, fluoresc. decay rate obs., inhomogeneous struct. and relax. time effects 79−86007
chlorophyll a, photo-oxidation by p-benzoquinone, nature of electron-excited state 78−76991
chlorophyll a, stimulated fluoresc. and fluoresc. quenching, pump photon density 78−27895

molecular biophysics continued
chlorophyll a and analogues, triplet state, phosphoresc. polaris. 79−39358
chlorophyll a and protochlorophyll a, optical transitions anisotropy 79−43825
chlorophyll a film, charge injection and storage 78−53317
chlorophyll a in photosynthetic material, luminesc. 79−34498
chlorophyll A low-intensity two-step absorpt. in vivo 78−35801
chlorophyll a phosphorescence in cellulose triacetate polymer matrix 77−36867
chlorophyll a-n-chloranil lamellar system, heat stimulated conductivity 79−53043
chlorophyll a-water interaction, NMR obs. in CCl_4 and trichloromethane 79−34501
chlorophyll and Mg-free derivatives, lasing and stimulated emission 77−52742
chlorophyll black lipid membranes in dil. electrolyte solns., bifacial tension meas. 79−16162
chlorophyll c absorpt., fluoresc. and fluoresc. excitation spectra in alga cell at −196°C 78−53329
chlorophyll derivatives molecular transitions, effect of molecular struct. 79−92138
chlorophyll fluorescence quenching by β-carotene 77−52735
chlorophyll in leaves and algae cells, phosphorescence obs. 79−92142
chlorophyll in vesicles, energy transfer and fluorescence quenching 79−39349
chlorophyll mixed associates, intermol. interaction, energy transfer, luminesc. and absorpt. spectra 78−64924
chlorophyll orientation in chloroplast, optical and electrochromic props. of photosynthetic membrane 77−48763
chlorophyll photochemical activity, rel. to microviscosity of detergent micelles 77−21478
chlorophyll pigments, aggregated forms in soln., spectral-luminesc. charcts. *(Russian)* 78−23529
chlorophyll pigments of photosynthetising organisms redox pots. rel. to evolutionary development 77−56337
chlorophyll radical cations, NMR, hyperfine coupling 79−8482
chlorophyll solutions, photolum. of singlet O_2 78−80831
chlorophyll solutions, triplet state props., ODMR meas. 79−20517
chlorophyll special pair models, reaction centres 80−3574
chlorophyll-a, conc. quenching rel. to functional charge transfer 80−30666
chlorophyll-a, crystalline film, energy levels and carrier generation by photocond. and fluoresc. 77−16909
chlorophyll-a, fluoresc. at low concs., noise reduction by low pass filter for DC signal 80−87249
chlorophyll-a, interaction with β-carotene in phosphatidyl choline bilayers, fluoresc. quenching 79−20506
chlorophyll-a, mol. interaction in monolayers and multilayers, IR obs. 77−71799
chlorophyll-a, mols. and complexes in PMMA and MTHF matrices, optical spectra 79−3433
chlorophyll-a, monochromatic excitation, luminesc. spectra, quasilinear struct. *(Russian)* 78−74809
chlorophyll-a, nonlinear absorpt. spectra 78−25522
chlorophyll-a, soln., luminesc. spectrum, impurity bands *(Russian)* 77−88493
chlorophyll-a, solns., vis. absorpt. spectra of monomer, dimer and oligomers 77−29101
chlorophyll-a, spectral props. of liquid crystal solutions 78−27291
chlorophyll-a adsorbed on aerosil, absorpt. spectra 78−53327
chlorophyll-a arrays, exciton transition calculations 78−35802
chlorophyll-a radical cations, in disordered systems, electron spin echo envelope modulation, isotope effects 78−61141
chlorophyll-b, mols. and complexes in PMMA and MTHF matrices, optical spectra 79−3433
chlorophylls, luminesc., conference, Szeged, Hungary (Aug. 1976) 78−27279
chlorophylls, luminesc. analysis of triplet states *(Russian)* 78−27288
chlorophylls, triplet state ESR, fine struct. and rate consts. determ. 78−25574
chlorophylls, triplet state ESR, fine structs. and rate consts. determ. 78−25575
chlorophylls, zero field triplet spin sublevel ordering, magnetophotoselection obs. 77−42342
chlorophylls a and b and pheophytins, fluoresc. and phosphoresc. 80−12057
chlorophylls and pheophytins, phosphorescence and fluorescence polarisation spectra 79−70522
chloroplast fragments, fine struct. of fluoresc. spectra, derivative spectroscopy method *(Russian)* 79−34502
chloroplast photosystems, exciton annihilation at 100K 77−25371
chloroplast-ribosomal RNA, in situ hybridisation with isolated nuclei in Euglena gracilis 79−66457
chloroplasts and subchloroplast fractions, linear dichroism 77−90744
chloroquine-biopolymer binding interactions, PMR effects 80−55982
cholesteric mixtures, quasithermal crystn. 80−92652
cholesterol+water, interaction in organic media, dielec. and NMR spectroscopy 78−76979
cholesterol crystal, polymorphic transition 77−1229
cholesterol transmembrane movement in human erythrocytes, radioactive tracer expt. 78−3459
cholesteryl oleate (linoleate), solid-solid transition, glass transition, cryst. nucleation temps., DSC obs. 78−34604
choline bromide, solid, mol. dynamics, NMR obs. 78−56390
choline chloride, solid, mol. dynamics, NMR obs. 78−56390
chondroitin-4-sulphate biopolymer, adsorption on adsorbed collagen 79−79459
choroplast 16S rRNA gene, sequencing of 3′-terminal 79−70518
chromatin, DNA-protein complexes, electron microscope visualisation, book contrib. 79−5434
chromatin, low-angle X-ray and neutron diffr., interparticle effects 80−72134
chromatin, neutron scatt. rel. to higher order struct. 79−11894
chromatin, nucleosomal arrangement DNA, histones and non-histones, review 79−79464
chromatin, reversible conformational transition obs. 79−62179
chromatin nucleosome core particle, ^{31}P mag. reson. of DNA 78−40112
chromatin solubility, role of non-histone proteins 79−53021
chromatin structure and thermal denaturation profiles 77−12881

molecular biophysics continued
chromatin subunits, in glycerol/sucrose solns. containing various D_2O/H_2O mixtures, neutron scatt. study 79−11893
chromophore aggregates, optical absorpt. and circular dichroism spectra, degenerate ground state model 79−70523
chromophore orientation in micellar, liposome solns., liq. cryst. phases, dichroism, NMR 79−53059
chromophores, biochemical, in cosmic dust, contrib. to interstellar UV extinction 80−26945
chromophores, circular polarisation of luminescence, book contrib. 79−5250
chromophores in membrane suspensions, determ. of orientational order, intensity depend. of flash-induced anisotropy 80−94177
chromosome conjugation, vibratory mechanism 78−95991
chromosomes, human, satellite associations 79−34518
chymotrypsin, charge relay system, H-bond models, IR spectra 78−64935
α-chymotrypsin, e.m. mol. electronic reson.-Raman data 77−9166
chymotrypsin hydrolysis of N-succinyl-L-phenylalanine-p-nitroanilide, enzymatic reactions 78−95992
Cl Mn II complex with protein, EPR spectra and zero field splitting interaction 78−35793
classical coupled dipole oscillators, optical props., normal mode treatment 79−36611
closed duplex DNA, struct., reactions, book contrib. 79−5248
codon-anticodon interaction, at ribosomal peptidyl-site 79−83697
cofacial diporphyrins, electron transfer reactions following picosecond excitation, CT state lifetimes, optical difference spectra 80−25995
coherent phonons and excitons in biological systems, Bose condensation 80−67042
colchicine, cryst. struct., multiple soln. direct methods 78−34384
collagen, 3-dimens. struct., rel. to props. of connective tissue 80−67038
collagen, axial arrangement of α-chains, intramolecular polar and apolar interactions 78−27891
collagen, denaturing temp. as linear function of amino acid composition 79−57571
collagen, enzyme- and alkaline-soluble, optical rot. dispersion and circular dichroism 77−70411
collagen, helical and coiled, thermodynamic values, 4 to 300K 77−25379
collagen, hydrated, PMR spin-lattice relax. of water, cross-relax. effects 79−34496
collagen, hydration and intramolecular fusion, NMR and calorimetry obs., dynamic model 79−79451
collagen, interpretation of small-angle X-ray diffr. using α1 chain primary struct. 77−66792
collagen, native, phasic transition, PMR 77−25363
collagen, optical activity rel. to ordered aggregation 79−11899
collagen, polarisation, contribution of permanent and induced dipole moments, elec. birefringence 80−85351
collagen and muscle elastic moduli rel. to phonons, Brillouin sectra 77−52824
collagen biopolymer, adsorption on solid surfaces 79−79459
collagen fibres, mech. props., role of struct. organisation 80−72207
collagen fibril, ^2H NMR of mol. motion 80−67034
collagen fibril, mol. cryst. model as basis for struct. 77−48751
collagen fibril, probabilistic aspects of struct. 78−27886
collagen fibril cross-striation, thermodeform., electron microscopy and X-ray diffr. 77−86438
collagen fibrils, in connective tissue, preferred orientation and orientation distrib. function determ., high-angle X-ray diffr. patterns 79−62177
collagen fibrils as examples of smectic A biological fibres 77−90721
collagen in skin, selection of radiation for X-ray diffr. 78−81087
collagen investigations, expt. confirmation technique for calc. phases and electron density profile 79−62408
collagen molecular organisation and connective tissues props. 80−97858
collagen piezoelectricity, rel. to stress generated pots. in bone 77−32932
collagen structure in cartilage of intervertebral disc 78−56951
collagen structures, piezoelec. effect, in rel. to mol. struct. 80−41100
collagen triple helical struct. study using Fourier transform 78−7318
collagen type supramolecular structs., 2 possible mechs. of formation 80−76702
collagen-mineral axial relationship in calcified turkey leg tendon, X-ray and neutron diffr. 77−32872
collagen-water system, phasic transition invesitgation by calorimetry and NMR 79−62167
collagne fibrils, rat tail tendon, quasi-hexagonal mol. packing model 80−30660
computer graphics, protein and nucleic acid conform. 77−36865
computer simulated modelling of molecular systems 79−88049
concanavalin A receptor, of human erythrocytes, receptor function in lipid bilayers 78−48764
conference, Crystal XII, Canberra, Australia (Jan.-Feb. 1980) 80−62388
conformational analysis, solvent effects 80−3583
conformational dynamics of macromols., subnanosecond T jump and Raman spectroscopy appl. 79−66445
cooperative behaviour, Bose condensation, Frohlich model 78−35797
corneal stroma, small angle X-ray and neutron diffr. study 79−11923
coupled spin systems, selective nucl. Overhauser effects calc., use in struct. chem. 80−23588
cowpea chlorotic mottle virus packing in crystalline monolayers, electron microscopy 80−89922
CpApUpG, self complementary oligoriboncleotide, double helix form., PMR obs. 79−22873
cross-peptide bond ^{13}C-^{15}N coupling constant, NMR obs. 80−55980
γ-crystallin, calf-lens protein, single cryst., X-ray diffr. low resolution struct. anal. 79−16130
βs-crystallin, lens protein, prep. 80−16921
α-crystallin, of calf eye lens, small angle X-ray scattering study 79−11891
α-crystallin, organisation of lens proteins in fibre cell 77−90766
α-crystallin in study of mol. processes using vertebrate eye lens 77−90770
crystallography, packing anal. appl. to cyclic hexapeptide 77−2070
cyanine dyes, excited electronic states, CNDO/S CI calc., visual pigment spectra appl. 80−85333
cyanine fluorescent dye membrane probe effects on cell props., rel. to bacterial chemotaxis 78−35815
cyanohaemin, ferric porphyrins with fifth ligands, ^{57}Fe and ^{14}N hyperfine consts. 78−50475
cyclic tetrapeptides, potential energy minima 79−59527
molecular biophysics continued
cyclo-(glycine-tyrosine-glycine)$_2$, crystal struct. from packing anal. 77−2070
β-cyclodextrinylbisimidazole, ribonuclease model, catalysis of cyclic phosphate substrate 78−85287
cyclohexadepsipeptide, refinements of mol. and cryst. struct. 77−39576
cyclophosphazene-DNa complex, spectrofluorometric and spectrophotometrics investig. 80−95643
cytidine, cryst. powder, absorption spectrum, unusual narrow line FIR modes, cryogenic temps. 79−69824
cytidine monophosphate, aq. soln., spectra, 300-450 nm, polarisation study 78−96015
cytidylyl-3′,5′-cytidine, aq. soln., spectra, 300-450 nm, polarisation study 78−96015
cytochrome *a* interaction with mitochondrial matrix H^+ ions 79−43806
cytochrome b_5 rotational diffusion in lipid bilayers, influence of lipid physical state 79−83693
cytochrome c_3, anhydrous film, elec. cond., temp. and ambient press. depend. 80−85327
cytochrome c_3, haeme-haeme mag. interaction, Mossbauer obs. 80−108836
cytochrome c_3−hydrogenase, reduction kinetics, Mossbauer spectra 80−67031
cytochrome c, dilute soln., reson. Raman spectra, pulsed laser excitation; optical multichannel detection 78−76999
cytochrome c, electron tunnelling to cytochrome c peroxidase 79−20507
cytochrome c, fast Raman spectroscopy using dye laser intracavity reson. Raman amplification 77−66794
cytochrome c, ferric- and ferro-, reson. Raman excitation profile, Soret excited 79−92147
cytochrome c, low freq. modes and excitation profiles, reson. Raman spectra 80−94428
cytochrome c, metal substitution effect on mol. struct. and functional props. 79−53037
cytochrome c, protein influence on haeme, Raman difference spectroscopy 80−72125
cytochrome c, redox investig. using reson. Raman, visible absorption and electrochem. methods 78−76832
cytochrome c, trifluoroacetylated, electron transfer reactions 79−20505
cytochrome c, very dilute benzene soln., picosecond reson. Raman spectroscopy 79−98102
cytochrome c, X-ray absorpt. edge fine struct. of active site haem 79−24945
cytochrome c adsorbed on different carriers, conformation study 79−53029
cytochrome c interaction with bilayer phospholipid membranes 78−69001
cytochrome c interaction with phospholipid membranes 77−25384
cytochrome c oxidase, coupled to proton pump in mitochondria 77−25406
cytochrome c oxidase, Cu ENDOR 80−94170
cytochrome c oxidase, macromolecular struct., electron microscopy and image anal. 80−89716
cytochrome c oxidase, oxidised and reduced, X-ray absorpt., edges, using synchrotron radiation 78−48758
cytochrome c oxidase, struct. of cytochrome a_3-Cu_{a3} couple, NO binding studies 80−67039
cytochrome c-$Fe(CN)_6$ electron transfer, verification of vibronically coupled electron tunnelling 78−48750
cytochrome c-phospholipid interaction, studied by pulse radiolysis 78−48746
cytochrome oxidase as electron-proton generator of membrane potential, role of protons 79−43807
cytochrome oxidase reaction, semiconduction as mechanism 80−55983
cytochrome P-450$_{cam}$, Fe^{3+} zero-field splitting, Orbach relax. rates 77−21483
cytochrome P-450, anomalous T^7 temp. depend. of Raman spin-lattice relax. 77−21482
cytochrome P-450, ferric form, X-ray absorpt. fine struct., Fe-N and Fe-S lengths 79−48213
cytochrome P-450, non-equilib. states formed by low-temp-reduction, absorpt. spectra 80−35837
cytochrome P-450-CO complex, absorpt. spectrum, electronic transitions, PPP calcs. 77−71811
cytochrome-c, CARS near one-photon reson. 77−65466
cytochrome-c, complete resonance Raman polarisation spectroscopy, linear and circular, modulation techniques 77−61130
cytochrome-c, hydrated, dielectric props. at 9.9 GHz 78−15758
cytosine, adenine, tautomeric equilibria, in aq. solns, electrostatic model of solvation, SCF MO calc. 79−96305
cytosine, hydroxy and methoxy, derivatives, absorption UV spectroscopy and electronic struct. of ionic and tautomeric forms 80−74177
cytosine monohydrate single crystal growth, effect of pH 79−34473
cytoskeletal proteins of human erythrocyte, in vitro complex formation 79−96514
cytosol aspartate-transaminase, of chicken heart, prep. of orthorhombic crysts., X-ray determ. of unit cell 79−57577
cytosol-ribosomal RNA, in situ hybridisation with isolated nuclei in Euglena gracilis 79−66457
dense phase chem. reaction theory 80−3575
deoxyhaeme model, semiempirical calcs., EM props. rel. to electronic config. and Fe-plane distance 78−53324
deoxyhaemoglobin, Fe(II)-N_ϵ(His-F8) stretching freq. rel. to quaternary struct. 80−94160
deoxyhaemoglobin, ferrous heme of high-spin type, MCD spectra in Soret, visible and near IR regions 80−94156
deoxyhaemoglobin, high mag. field Mossbauer spectra, electronic states 80−35845
deoxyhaemoglobin, vibronic coupling, mag. susceptibility and Mossbauer data interpretation 78−70984
deoxymyoglobin, forzen soln., recoilless fraction, Mossbauer spectra meas. 80−8025
deoxymyoglobin, high mag. field Mossbauer spectra, electronic states 80−35845
deoxymyoglobin, low temp. PMR, low-lying Fe^{2+} states model 78−68997
deoxymyoglobin, single cryst., paramag. anisotropy meas. 77−21469
deoxymyoglobin, vibronic coupling, mag. susceptibility and Mossbauer data interpretation 78−70984
deoxymyoglobin single crysts., Mossbauer study with polarised γ-rays 80−40962

molecular biophysics continued
diamine oxidase solutions, proton mag. relax. dispersion obs. 80−51136
2,4-diamino-6-hydroxy-pyrimidine, IR absorption spectrum, vibr. anal., tautomerism 80−58253
dichelated protohaeme, model haemoglobin cpd., Mossbauer spectra 80−16904
digalactosyl diglyceride multipole internal rot., ^{13}C-{^{1}H} nuclear Overhauser enhancement, ^{13}C spin lattice relax. 77−479
dimethyl phosphate, potentials of internal rot. 77−16901
4- dimethylaminochalcone fluorescence, distrib. of hydrophobic mols. in artificial lipid membrane 77−16912
1,3-dimethyluracil, non-hydrogen bonding crystal, radical formation 80−35552
dimyristoyl lecithin lipid vesicles, sonicated, ^{13}C relax. times model for gauche-trans isomerisation 78−33520
1,2-dimyristoyl-sn-glycero-3-phosphoserine multilayers, phase transitions, temp. depend., ellipsometric study 80−108846
dinucleoside monophosphates, conformational anal. by nuclear Overhauser effects 79−20509
dinucleoside monophosphates, struct. and conform. in aq. soln., Raman spectra 78−78847
dinucleoside phosphates, polaris. spectra, excimer phosphoresc. and fluoresc. 79−34497
DIP-trypsin, difference Fourier refinement using minicomputer, to 1.5 Å 77−58924
dipalmitoyl phosphatidylcholine, conformational nonequivalence of chains 1 and 2 79−16133
dipalmitoyl phosphatidylcholine monodomain samples with varying concs. of water and other ingredients, prep. 78−15780
dipalmitoyl phosphatidylcholine vesicles, appl. of depolarised light scatt. theory from hollow spherical particles 80−45946
1,2-dipalmitoyl-sn-glycero-3-phosphocholine multilayers, phase transitions, temp. depend., ellipsometric study 80−108846
dipalmitoylphosphatidylcholine/glucagon (cardiolipin/insulin) systems, Raman spectra study 80−16903
dipeptide, struct. and bonding, ab initio calcs. 79−53039
dipeptides, bend form., conformational space, statistical mech. anal. 77−68146
dipeptides, reactions with hydrated electrons, EPR and spin-trapping studies 79−16124
dipotassium uridine 5′-diphosphate trihydrate, X-ray cryst. struct. determ. 79−57569
distamycin A, analog cryst. and molecular struct. 79−88051
DNA, ^{111}In bound, rot. correl. times, from γ-ray perturbed angular correl. 80−94152
DNA, AA 79−92140
CsDNA, absorpt. factor, X-ray diffr. study using 1.2 Å synchrotron radiation 78−76988
DNA, backbone vibrational mode displacements of A-DNA and B-DNA 80−8000
DNA, calf thymus, flexible polyelectrolyte, elec. birefr. meas. 79−16126
DNA, calf-thymus, diffusion coeff. meas. using quasielastic light scatt. apparatus *(German)* 80−12314
DNA, calf-thymus Na-DNA aq. solns., dielec. behaviour in 5 kHz to 100 MHz range 80−85330
DNA, cetavlon salt, cryst. struct., X-ray diffr. meas. 78−2105
DNA, circular superhelical, X-ray diffr. at 300-10000 Å resolution 77−9168
DNA, circular superhelical, X-ray scatt. calcs. 80−56109
DNA, conformation changes, soft modes 77−29097
DNA, conformation of native molecule, influence of solvent struct. 80−30655
DNA, damaged by UV or N-acetoxy-2-acetylaminofluorene, rate-limiting steps in excision repair 77−90865
DNA, double helical fragment intercalator complex, molecular struct. 79−16140
DNA, double-helical model, sedimentation coeff., X-ray scatt. 77−14629
DNA, dye labelled elec. dichroism and birefringence, comparison with mol. props. from polarised fluoresc. 80−84785
DNA, electronic interaction with N-methyl-N-nitrosourea, ESR obs. and INDO calcs. 80−94154
DNA, entropy nature of B-A transition 79−92130
DNA, helical to coiled relax., statistical mech. approach, formaldehyde denaturation 78−3443
DNA, helix-coil transition model 77−52734
DNA, Hg (II) and Ag (I) complexes in soln., theoret. interpret. of elec. dichroism obs. 80−85347
DNA, hydrodynamic shearing simulation 80−16895
DNA, intact, modified bases characterisation by mass-analysed ion kinetic energy spectrometry 80−3591
DNA, linear dichroism in pulsed elec. field, meas. apparatus 80−90875
DNA, luminescence, excitation wavelength depend. in UV/VUV region 78−31768
DNA, molecular electrostatic pots. of complementary base pairs 78−92597
DNA, mouse liver, dynamics using single clipped photon correl. 77−48748
DNA, mutations, quantum theory, proton transfer by dynamic interactions 77−77868
DNA, Na salt, freeze-dried layers, unpolarised IR spectrum, temp. dependent spectral shift 77−48755
DNA, native Hela, shear breakage, expt. determ. 79−16121
DNA, natural, hypochromic effect 77−81467
DNA, oriented films, hydration, slow neutron scatt. obs. 79−57572
DNA, phase transition, ψ transition of single coils 80−26200
DNA, phase transitions in water-ethanol solns. *(Japanese)* 80−89709
DNA, polyelectrolyte soln., appl. of Poisson-Boltzmann eqn. 79−77483
DNA, polymorphism, X-ray diffr. and computerised model building study 78−27894
DNA, possible conformations calcs. 80−76705
DNA, proton mag. relax., methyl group reorientation 77−64009
DNA, proton radiationless transitions for hydrogen bonds *(Russian)* 80−97857
DNA, repeated, homology between humans and simians 79−8474
DNA, RF II ΦX174, melting profiles 78−24027
DNA, soln., phase transitions, light absorption oscills. obs. 80−26197
DNA, sorption and desorption of water, thermal-stimulated press. and thermogravimetric anal. 80−8008
DNA, supercoiled torsional stress and local denaturation 80−72131
DNA, supercoiling, elastic model 78−15767
DNA, superconductivity, dynamical model 79−62172

molecular biophysics continued
DNA, torsionally stressed, equilibrium statistical mechanics of helix coil transition 80−67032
DNA, torsionally stressed, transitions between B- and Z-conformations, theoretical anal. 80−94166
DNA, X-ray diffr. from side-by-side model 80−35835
DNA and polydeoxyribonucleotides, thermal properties in wide range of concs. of ions of neutral salts and of polymer 78−80833
DNA and RNA fragments, selective laser multistep excitation, uses 80−61122
DNA B-form, closer definition of struct. from X-ray diffr. and energetic criteria 80−81533
DNA base pairs., Coulomb interaction energy calcs, electron correlation role 79−96509
DNA bases, polarised fluoresc. and estimated lifetimes, room temp. and in −125°C soln. 79−39352
DNA bases, selective electronic excitation using dye lasers 80−8012
DNA bases, theoretical study of electronic spectra 80−30665
DNA binding to ethidium bromide derivatives, competitive and non-competitive bonds *(German)* 79−79446
DNA calf thymus binding to cis- and trans-dichlorodiammineplatinum(II) extended X-ray absorpt. spectra 78−85291
DNA cetavlon salt, struct., small-angle X-ray diffr. meas. 78−11609
DNA compact form, tertiary struct., small angle X-ray scatt. 80−72129
DNA conformation, influence of intermol. interactions 80−16900
DNA conformational fluctuations, internal motion correl. times, ^{31}P NMR obs. 80−72135
DNA derivate melting curves, automatic recorder using real time processing *(French)* 80−104833
DNA double helix, supercoils and torsional stiffness 79−83702
DNA double helix supercoils, linking numbers, twist, writhing number 77−12882
DNA double helix unwinding during RNA polymerase binding 79−70512
DNA entrapment mechanism at air-water interface 77−60181
DNA film, dehydration and conform. state, differential scanning microcalorimetry 80−35830
cDNA for human chorionic gonadotropin α-subunit, isolation, cloning and sequence anal. 80−3587
DNA fragment length produced from deoxyribonuclease I digestion of chromatin 79−79467
DNA helix destabilising protein cryst., electron microscopy 80−85338
DNA helix-ball transition, peculiarities due to Cu^{2+} and Mn^{2+} 79−70514
DNA hybrid molecule construction and cloning 77−56559
DNA hydrate, stability studied by thermogravimetry 80−30650
DNA hydrate, struct. conversions of sugar phosphate chain and nitrogenous bases, IR spectra 80−81530
DNA hypochromic effect, oscillator strength, perturbation theory calc. 79−96515
DNA in chromatin, stereochem. model for superfolding 80−35829
DNA in conc. solns. of neutral salts, conformational transitions 80−81531
DNA in soln., mol. wt. determ. by fluctuation spectroscopy 77−10800
DNA in water-ethanol solns., enthalpy of B-A transition 77−70412
DNA interactions with cations, UV difference spectrosc. and Marcus theory 80−94153
DNA internal motions, ^{31}P NMR and PMR 80−97855
DNA length measurement using random flight theory 77−64008
DNA of fetal globin genes, man, charact. of deletions 79−70519
DNA packing in fibrils of DNP of polytene chromosomes 80−30649
DNA pyrimidines, cryst., lattice dynamics 78−75766
DNA salt with cetavlon, twin struct. obs. 78−71746
DNA secondary structure, dependence on base sequence, theoretical conformational anal. 79−53032
DNA soln., calf-thymus, time depend. correlation functions meas., three relax. components 77−40631
DNA solution, elec. birefringence, stabilised induced dipole behaviour 80−85349
DNA strand breaking and rejoining in UV irrad. normal human and xeroderma pigmentation cells 77−4986
DNA structure, evidence from electron microscopy 79−24948
DNA structure of left-handed double helical DNA fragment 80−30659
DNA synthesis in vitro, UV induced mutagenesis 79−92149
DNA thermal transition midpoint, CAA 79−74593
DNA water salt solns., microcalorimetric investigation of phase transition and eutectic fusion 79−79448
DNA with heavy atom, X-ray struct. study using synchrotron radiation and multichannel detector 78−47210
DNA-acridine complexes, laser-induced fluorescence decay obs. 79−66449
DNA-dependent RNA polymerase, determ. of intersubunit distances and subunit shape parameters by neutron small-angle scattering 79−53038
DNA-dye-complexes, UV excitation, energy transfer and mol. struct. 79−57578
DNA-lipid interaction, IR spectroscopic obs., DNA compactisation on disperse particles 80−104550
DNA-methyl green binding, linear dichroism anal. 77−88479
DNA-protein interaction, effect of cooperativeness on recognition of specific sites 77−81463
DNA-type macromolecule, melting, low mol. wt. impurity effect 80−12050
DNA-water interaction, single and double helix DNA 80−30646
DNAs, natural, hypochromism, dependence on content and sequence of nucleotides 80−76711
DNA[Cu^{2+}], ^{111}In bound, rot. correl. times, from γ-ray perturbed angular correl. 80−94152
dopamine, thermal blooming spectroscopy 80−86441
double-stranded polynucleotides, exact relations for binding calculations 79−92123
DR antigens, human, struct. polymorphism obs. 79−66441
drug-nucleic acid interactions, conformational flexibility at intercalation site 78−96005
durene-para-dibromobenzene, binary mol. system, X-ray struct. anal. 79−55734
dye solutions, mixed, fluoresc. conc. quenching, sensibilisation 79−24347
dye-detergent model systems, degree of fluoresc. polarisation 78−27287
dynein, role in enkaryotic cell motility, book contrib. 79−16178
E. coli, light scatt., ribosomal subunit diffusion coeffs. 80−21438
E. coli, membrane struct. rearrangements in presence Ca^{2+} induced by heating 79−79482

molecular biophysics continued
E. coli cells, iron-storage protein, Mossbauer spectra obs. 80−8022
elastase, globule, atomic density distrib. 79−79458
elastin, hydrated, dielectric relax. 79−5247
electric and magnetic props. of biomolecules 77−44584
electric birefringence transient, of macromol. solns. in reversing fields of arbitrary strength and duration 80−84719
electron and excitation transfer, energy gap and temp. depend. 79−62187
electron micrograph images, determ. of structs. relative orientation 79−70714
electron micrographs, computer-aided anal. 80−4813
electron microscopical analysis of macromolecular 3D struct. 80−35836
electron microscopy, 3-dimens., computer simulation 77−13046
electron microscopy, detection and resolution of atom images *(French)* 79−66595
electron microscopy, high resolution, mol. struct. determ. 80−21595
electron transfer in bacterial photosynthesis, low-temp. 78−44470
electron transfer kinetics models 79−39339
electron transfer processes, system of differential eqns., certain evaluations of solns. 80−76694
electron transfer reaction energetic coupling to endergonic reactions, mol. mechanism 78−96026
electron transport over large distance in biol. systems, medium as mediator 80−35820
electron tunnelling, thermal and photoassisted, theory, fast charge separation in photosynthesis 80−89730
electronic structural props. of mols. relevant to photosynthesis 80−16902
electrons, advantage to low mobility in biological systems 79−39346
electrostatic isopotential maps for large biomolecules, STO transferable bond calc. 80−3571
elementary biological function, localised electron subsystem interaction process theory 80−55978
ellipsometric monitoring of mol. and cellular biological processes in vitro 77−48852
energy migration in one-dimensional structures with resonance interaction 80−1092
enzymatic activity, quantum cooperative mechanism 77−40632
enzymatic activity in biomolecular nonequilibrium reactional scheme, limit cycle and dissipative structs. 77−1977
enzymatic catalysis, dynamic theory, conform. rearrangements 77−36858
enzymatic catalysis, orbital perturbation anal. 78−31623
enzymatic charge transfer across oil-water interface, effect of dielec. const. 77−70419
enzymatic open reaction, mathematical model 79−53024
enzyme, complexation, Mossbauer spectroscopy 77−12876
enzyme, diffusion-controlled reaction rate to buried active site 78−35796
enzyme, e.m. mol. electronic reson.-Raman data 77−9166
enzyme, nucl. quadrupole interaction parameter related to structure-function 77−8472
enzyme catalysis, electron pairing in thermodynamically consistent pathways 79−5179
enzyme dynamics, statistical phys. 80−21439
enzyme Ising system, two-state, crit. behaviour, Bragg-Williams approx. calcs. 78−86223
enzyme Ising system, two-state, crit. behaviour, Monte Carlo calcs. 78−86222
enzyme reaction kinetics modelling 77−4979
enzyme-catalysed reactions, network thermodynamic modelling 80−89463
enzyme-substrate interaction forces influence on reaction rates 78−31765
enzyme-substrate reaction with ferroelec. behaviour, rel. to Frohlich brain wave model 78−44490
enzyme-substrate reactions in differential scanning calorimeter, digital simulation 79−74794
enzymes, chem. active sites 79−52757
enzymes, molecular struct. reconstruction from electron microscopy images 80−89715
enzymic kinetics, rate constants estimation 79−70505
epitaxial sandwiching of biopolymers, electron microscopy specimen prep. 78−36080
epithelial mucus, rheology and mol. organisation 80−97959
epithelioid fibre system decoration by sera, immunofluorescence microscopy visualisation 78−15801
EPR, rat liver and hepatoma mitochondrial lipids, stochastic anal. 78−76984
EPR and saturation transfer EPR, fast computation, perturbation approx. extension for overmodulation 78−82754
EPR and saturation transfer EPR spectra at high microwave field intensities 79−34488
erythrocyte ghost membrane struct. effects of fusogenic agent, fusion mechanism 78−31782
erythrocyte integral membrane protein lateral mobility, human cells 77−66805
erythrocyte membrane, pulse NMR meas. of water exchange 79−43826
erythrocyte membrane protein alterations in Huntington's disease, EPR 77−56347
erythrocyte membrane struct. changes due to cAMP, spin-probe study 78−31779
erythrocytes, bound water in frozen solns., proton mag. relax. 77−28472
estriol antigen, immunoassay using differential pulse polarography method 79−79709
ethidium bromide E-DNA, intercalated birefringent fibres, microspectrophotometric investig. *(German)* 80−57392
ethylcellosol, aq. soln., light scatt. rel. to conc. fluctuations *(Russian)* 78−3450
eukaryotic ribosomes, 2 step binding to brome mosaic virus RNA3 80−3580
exciton percolation, in molecular aggregate, rel. to photosynthesis, book contrib. 77−36297
excitons and Bose-Einstein condensation in living systems 80−30640
eye lens low molecular weight protein obs. and prep. 80−16921
eye lenses, crystalline, of humans, fish and birds, state of water, NMR meas. 79−48212
factor VIII, native and modified, surface adsorption and mol. interactions, ellipsometric obs. 80−104555
fatty acid monolayers, light scatt. meas. 80−89011
fatty acid synthetase, from yeast, three-dimens. electron microscopy, struct. and image reconstruction 77−12883
fatty acid-serum albumin molecule binding kinetics, fluoresc. probe method 77−25365

molecular biophysics continued
ferredoxin, Fe atoms at active centre, exchange integral of antiferromag. interaction 80−76697
ferredoxin, from Clostridium pasteurianum, Mossbauer effect, ESR, and mag. susceptibility meas. 80−40961
ferredoxin, from Halobacterium, Mossbauer and EPR spectrum 78−76998
ferredoxin, pulse-radiolysis study of conformationally nonequilibrium states 79−70506
ferredoxin, S. platensis [2Fe-2S], struct. and evolution of chloroplast-type ferredoxins 80−94165
ferredoxin, soluble, investigation of 2 forms from pea leaves, EPR obs. 80−45851
ferredoxin synthetic analogues, $[Fe_4S_4(SR)_4]^{3-}$ clusters, Mossbauer effect, EPR, and mag. props. 80−41057
ferredoxin-like centres, membrane bound, in photosystem I of blue-green algae, Mossbauer and EPR study 80−40974
ferric cytochrome c, reson. Raman spectra, Fe^{3+} low-lying electronic levels 78−53335
ferric haeme complex of low spin, Mossbauer spectra, crystal field parameters 80−26203
ferric haeme protein, anal. of low-spin ESR spectra 77−60185
ferric haemoglobin chains, crystalline state disorder and hyperfine component line widths 79−34482
ferric haemoglobin single crystals, contribs. to EPR line width 79−34484
ferric leghaemoglobin a, proton-depend. anion binding, soybean, proton NMR study 79−74592
ferric myoglobin compounds, single crysts., Mossbauer spectrum in small mag. field 79−100571
ferric myoglobin cpds., single cryst., Mossbauer studies 80−8016
ferrichrome A, selective excitation double Mossbauer meas. 80−8015
ferricytochrome c, rate of interaction with negatively charged lecithin liposomes 77−16914
ferricytochrome c and c_3, ionis. pot. from VUV photoelectron spectra 79−43821
ferricytochrome c structure, effect of different phospholipids 78−68981
ferrihaemoglobin hydroxide, nucl. hyperfine interaction, HF LCAO calc. 79−2002
ferrihaemoglobins, $(Fe^{3+})d^5$ config. 78−39071
ferritin, mol. wt., X-ray small angle scattering using synchrotron radiation 78−66700
ferrocytochrome c_3, anhydrous, ionisation pot., UV photoelectron spectrosc. obs. 80−85328
ferrocytochrome c, horse, transient proton-proton Overhauser effects 79−43822
ferrocytochrome c, ionis. pot. from VUV photoelectron spectra 79−43821
ferrocytochrome c, picosec. and subpicosec. relax. and dephasing, reson. light scatt. obs. 79−45876
ferrohaemoglobin, R-T conformational change due to pseudo Jahn-Teller effect 79−70521
ferrous nitrosylhaemoglobin, NO binding, spin distrib., orbital model and mag. props. 80−81534
ferrous porphyrin, intermediate spin, reson. Raman spectra 79−69820
ferrous porphyrins, 4-coordinated, PMR 77−58044
fibres, natural, Brillouin scatt. shifts, comparison with synthetic polypeptide obs. 80−55991
fibrin molecule formation, thermodynamic model 79−70527
fibrinogen, adsorbed layers on polystyrene, contact angle meas. 80−61508
fibrinogen, native and modified, surface adsorption and mol. interactions, ellipsometric obs. 80−104555
fibrous materials, struct., interatomic forces calcs. 79−22875
field-desorption mass spectrometry, principle and technique, appl. to corrins and vitamin B_{12} 78−80821
fireflies, bioluminesc. spectra 80−35821
firefly chemiluminescence emissions, time-resolved spectra 80−35822
flash photolysis, appl. to biological systems, review 78−11530
flavins, meas. of sub ns fluoresc. decay by time-correl. photon counting and Ar laser 80−94429
flavins, phosphoresc. props., solvent effects 77−12885
flavins, reson. Raman spectra avoiding fluoresc. interference 79−10114
fluid density measurement techniques, macromolecules in soln. appl. 78−92751
fluorescein, excitation and emission polarisation spectra, cell cycle changes 78−96013
fluoresceindiacetate conversion to fluorescein, in living cells and in vitro, kinetics 77−56332
fluorescence, delayed emission from green algae Chlorella pyrenoidosa 77−29118
fluorescence, laser-induced, obs. of erythrocyte membrane transport props. 77−90733
fluorescence, nonexponential decay, method of moments for data anal. 80−55975
fluorescence and fluorescent probes, appls. 78−15932
fluorescence and phosphorescence spectroscopy *(Norwegian)* 78−92596
fluorescence depolarisation, E-type delayed, rotational motion probe techniques 80−36207
fluorescence picosec. kinetics in chromatophores and reaction centres from R.sphaeroides, 295 to 80K 80−35857
fluorescence polarisation decay in membranes, theory 78−20138
fluorescence polarisation meas. by flow cytometry, appl. to fluorescein in mammalian cells 77−52942
fluorescence spectroscopic investigations of the dynamic properties of proteins, membranes and nucleic acids 80−101148
fluorescence spectroscopy in study of biochem. processes review 78−11784
Fluorescent EXAFS data using solid state detector, for metals in dilute biological systems 78−66595
fluorescent probe binding to proteins error in interpretation of double-reciprocal plot and Scatchard plot 78−24021
fluorescent probe detection of cell Ca redistrib. during stimulus-secretion coupling 77−77872
fluorescent probe interaction with surface structs. of E. coli 78−69007
fluorescent probe orientation and rot. freedom in lecithin bilayer 77−44583
fluorescently labelled molecules as probes of living cells struct. and function, review 80−67321
fluorohaemin, ferric porphyrins with fifth ligands, ^{57}Fe and ^{14}N hyperfine consts. 78−50475

molecular biophysics continued
form dichroism, theoretical treatment, determ. of macromol. shape 78−60417
formyl-triglycyl amide-H_2O, analytical pot., ab initio calc. 79−48206
Forster energy transfer problem in 2D, analytic soln. 80−26195
free radical EPR saturation corrections 77−48963
free radicals, use of Dy^{3+} as relax. agent in biological tissues 78−81090
free-base porphin, S_2-S_0 transition vibronic bands, photochem. hole-burning 79−36631
FSGO calculations, tetrahedral Gaussian lobe functions and Cartesian Gaussian basis sets 79−22587
generalised Glauber-Ising chain, dynamics in a mag. field, biopolymer appl. 79−155
genes, mouse, heavy chain immunoglobulin, nuclear transcripts 80−26208
globular protein rotatory mobility meas. by spin probe method, soln. viscosity 77−16902
globular proteins, bend form., conformational space, statistical mech. anal. 77−68146
globular proteins, in solutions, new method using X-ray diffuse scattering for investigation of conformation changes 79−12054
globular proteins, micro- and macro-stabilities 79−92135
globular proteins, surface and inside volume meas. 79−34477
glutamate dehydrogenase:α-ketoglutarate, cross relax. effect on NMR spin-lattice relax. time 78−78723
L-glutamic acid, solid, amino group reorientation, PMR second moment obs. 78−35046
glutamine synthetase macromolecular struct., electron microscopy and image anal. 80−89716
glutamine synthetase reconstruction from electron micrographs using computer averaging 79−92452
glyceraldehyde 3-phosphate dehydrogenase, EPR, saturation transfer EPR 79−98124
glycine, cryst., cationic radicals, EPR 78−11537
γ-glycine, cryst. struct. by neutron diffr. at 83K and 298K 80−35825
glycine, neutral and zwitterion interaction with water, Monte Carlo simulation 79−53026
glycine, nucl. spin-lattice relax. of CH_3 and NH_3 groups 77−8440
glycine, oligomer, vibr. spectra rel. to polymeric form 79−83695
glycogen phosphorylase b activity, struct. of cryst. and complexes 78−80830
glycolysis in human erythrocyte, steady rate rel. to ATP conc., quantitative model 78−53354
glycophorin, of human erythrocytes, receptor function in lipid bilayers 78−48764
GpApGpC:GpCpUpC duplex set, helix form., PMR obs. 79−22872
gramicidin A channel struct., elec. meas. with lipid bilayer membranes 78−15783
gramicidin A in biomembrane channel, IR spectroscopic obs. 80−16901
gramicidin A monomer-dimer states, light scatt. studies 79−92143
gramicidin D-Na^+, NMR study 79−43805
gramicidin-S, dissolved in deuterated ethylene glycol, interproton nuclear Overhauser effects 79−16123
growth, self-reproduction and autoregulation model, anal. of reactions with stretchable semi-perm. walls 77−81460
guanine, ^{15}N and D substituted, in acid and base solutions, vibr. anal. 79−26994
guanine, tautomeric forms protonation, ab initio HF Roothaan SCF calcs. 80−78534
guanine tautomers, relative stabilities, nonempirical MO calcs. 80−21442
guanyl ribonucleases of fungi, crystn. and X-ray diffr. 78−71718
haematoporphyrine, complexed with chloranil and tryptophane, energy spectra, transition moments and intermolecular distances 80−72127
haeme a, low-spin ferrous, MCD, LCAO MO SCR π-electron calcs., PPP approx. 78−9178
haeme protein, reson. Raman line intensity formulae applicability 77−83609
haeme proteins, inversely polarized modes in reson. Raman scatt., depolarisation dispersion curves, vibronic interactions 78−78676
haeme proteins, resonance Raman effect *(Hungarian)* 78−74666
haeme proteins and metalloporphytins, redox chem. and oxygen binding 80−3573
haeme-liganded sickle cell haemoglobin, spin label detection of intermolecular interactions 79−16122
haemin, hyperfine interactions and related props. 78−44451
haemin, mag. interaction down to 0.03K, Mossbauer effect 78−44450
haemin-histidin, ^{57}Fe Mossbauer spectra, temp. depend. of quadrupole splittings, atom positrons *(Spanish)* 77−73098
haemocyanin of Limulus polyphemus, quaternary struct. 80−85337
haemoglobin, absorpt. spectra, light scatt. method meas. *(Russian)* 78−21939
haemoglobin, allosteric effect, mathematical description 79−64125
haemoglobin, conformational change, relation with CO binding 79−8473
haemoglobin, deoxygenated sickle cell, gels, liq. cryst. props. 78−3445
haemoglobin, dielectric props. under UV excitation 80−6912
haemoglobin, effect of adsorpt. on struct. and props. 79−92121
haemoglobin, ferrous high-spin derivatives, MCD at room and liq. N_2 temps. 78−76997
haemoglobin, human, EPR spectrum, g-value during oxygenation-deoxygenation reaction 78−53333
haemoglobin, human, liganded, kinetics of alkaline tetramer-dimer dissoc., laser scatt. obs. 78−48749
haemoglobin, human, maleimide spin labeled, proton ENDOR spectra obs. 80−89719
haemoglobin, human and Lumbricus terrestris, conc. depend. of self-diffusion 78−68984
haemoglobin, hyperfine-shifted PMR, mag. field and temp. induced line broadening 77−60184
haemoglobin, in salt soln., diffusion rel. to intermol. interactions, light scatt. investig. 77−44585
haemoglobin, Jahn-Teller pseudo effect rel. to Fe release and conformational changes 80−76701
haemoglobin, low freq. modes and excitation profiles, reson. Raman spectra 80−94428
haemoglobin, metal substitution effect on mol. struct. and functional props. 79−53037
haemoglobin, modulated excitation meas. of quaternary conformation struct. change rate 77−44589
haemoglobin, mol. interactions, Fourier transform IR absorpt. spectra 78−96007

molecular biophysics continued
haemoglobin, mol. system, with N associating particles, free energy virial expansion 77−55336
haemoglobin, mutual and tracer diffusion coeffs., photon correl. obs. 80−72123
haemoglobin, nanosec. probe of dynamics using time resolved reson. Raman scatt. 80−94162
haemoglobin, O_2 linked Cl^- binding sites, pH dependence 79−62174
haemoglobin, quaternary struct., hydration and self-association, ^1H NMR obs. 80−67040
haemoglobin, sickle cells, 3-dimens. reconstruction of fibres 78−44452
haemoglobin, structure and respiratory transport 79−57576
haemoglobin, subunit cooperative interaction, stereochemical trigger, Mossbauer study 78−53321
haemoglobin, US attenuation and dispersion, Kramers-Kronig relative 78−83135
haemoglobin as a transducer for O_2 transport in fish 79−96505
haemoglobin cooperativity, simple tension-displacement model 79−34472
haemoglobin derivatives, hyperfine interactions and related props. 78−44451
haemoglobin equilibria in soln., surface free energy model 80−81535
haemoglobin Fe-N distance determ. by EXAFS 78−68989
haemoglobin g-value change obs., EPR *(Japanese)* 77−90724
haemoglobin haem structure after photo-deligation, Raman spectra 80−61510
haemoglobin hydroxide, Fe Mossbauer quadrupole splitting 78−55192
haemoglobin in red cell suspensions, NMR relax., T_1 and T_2 meas. 78−80832
haemoglobin macroporous particle study, photoacoustic spectrometry 80−85543
haemoglobin molecule from cybernetic and thermodynamic viewpoint *(German)* 79−1998
haemoglobin oxygenation, cooperative phenomena 77−44577
haemoglobin reactions as interfacial phenomena, hydrophilic colloid model 77−9167
haemoglobin S, fibres, discs having six-fold symmetry, electron microscopy 78−76989
haemoglobin S solution, acoustical props. 78−3453
haemoglobin S solution, effect of deoxygenation on US absorpt., rel. to sickle cell blood 78−44477
haemoglobin solution, facilitated diffusion of O_2 77−48747
haemoglobin solution, proton mag. relax. meas. 77−1975
haemoglobin-CO complex, absorpt. spectrum, electronic transitions, PPP calcs. 77−71811
haemoglobin-CO reaction kinetics, relax. meas. on photolytic illum. 77−70405
haemoglobin-haptoglobin deoxygenated complexes, Mossbauer spectroscopy 78−24020
haemoglobins and chlorocruorins, extracellular respiratory, physicochemical and functional props. 80−3581
haemoproteins, allosteric effect, mathematical description 79−64125
haemoproteins, Fe-ligand binding and electronic struct., Mossbauer studies 80−8021
haemoproteins, fluoresc., reson. Raman and radiationless decay 77−30916
haemoproteins, highly oxidised Fe, electronic struct., Mossbauer spectroscopic obs. 77−88478
heart cytosol, aspartate transaminase, electron density map interpretation 80−55990
heat capacity function, of macromolecular systems, statistical thermodynamic analysis 80−61514
α-helical protein molecules, solitons *(Russian)* 78−68990
helical to coiled relax., statistical mech. approach, appl. to DNA secondary struct. 78−3443
helix-coil transitions in specific sequence biopolymers 78−35794
n-hexadecyltrimethylammonium bromide micelles, ^{13}C relax. times model, for gauche-trans isomerisation 78−33520
high density lipoprotein-3 macromolecule observation using CTEM and STEM with negative staining 80−85561
high-potential Fe protein of Chromatium vinosum, low-lying excited state, EPR 78−3448
histidine decarboxylase, determ. of molecular wt. and radius of inertia 79−53025
histidine decarboxylase quarternary struct. 79−92129
histidine-decarboxylase, molecular weight and form determ. by low angle X-ray scatter 78−76987
histidinedecarboxylase molecule, distance between heavy atom markers small angle X-ray scatt. determ. 79−55613
L-histidine.HCl.H_2O, photographic neutron diffr. by modified Laue method 77−66791
histone F2a solutions, effect of ionic composition of medium on struct. and effectiveness of intermol. interactions 78−48744
histone F2b-DNA interaction studied by X-irrad. of calf lymph nodes 78−85346
histone H4 N-terminal oligopeptide struct., circular dichroism and IR spectroscopy 78−24025
histones, conform. state in water, circular dichroism 77−56335
histones, H2A and H4, effect of molecular interactions on fluorescence intensity 80−51032
histones H_2A and H_4, mixed solns., oligomer structs. 80−30648
homopolymer, theory of 1D adsorpt. on to 80−51034
homopolymer chain adsorpt. on uniform surface 78−53316
homopolymer chain adsorption on homogeneous surface, theoretical model 77−70403
hormonal steroids, ^{13}C NMR spectra 80−81543
horseradish peroxidase cpd. II, high-field Mossbauer spectra, 4.2 to 120K 80−8026
human serum Cu, EPR spectrum obs. 80−91582
hyaluronate solns., cooperative phase transitions, review 80−45850
hyaluronic acid, Raman spectrum, primary and secondary structs. 79−59467
hydrated systems, PMR spin-lattice relax. of water, cross-relax. effects 79−34496
hydrocarbon carcinogenesis, fluoresc. meas. in cells 79−39343
hydrocarbon chain ordering in model membrane, D quadrupole splitting 78−64947
hydrocarbon chain tilt differences between hydrated bilayers 80−51038
hydrocarbon chains in a lipid bilayer conformational anal. 80−81532
hydrodynamic properties of rigid macromolecules, modelling approaches 80−61613
hydrophobic effect, organisation of living matter 79−11887

molecular biophysics continued
hydrophobic interactions, lipid-protein binding, thermodynamics, book contrib. 79−16129
3-hydroxyflavone, excited state proton transfer, luminesc. 80−35818
hydroxyhaemin, ferric porphyrins with fifth ligands, ^{57}Fe and ^{14}N hyperfine consts. 78−50475
hyperthermia effect on nonhistone proteins isolated with DNA 78−80843
imidazole, photoelectron spectra and electronic struct. 79−22758
immunoglobulin (Ig) κ chain m RNAs, identical 3′ non-coding sequences favour unique C_κ gene in mouse 80−8010
immunoglobulin G, enzyme immunoassay, electrochem. determ. with antibody-bound membrane 79−53293
immunoglobulin light-chain genes, nucleotide sequences at somatic recombination sites 79−83701
immunonephelometric assays 79−84046
immunoresponsive membrane, pot. associated with immunochem. reaction between membrane-bound antigen and free antibody 77−86453
indole, pH dependent fluoresc., quenching by histidine *(Russian)* 78−90209
indole soln. containing histidine, fluoresc. rel. to soln. pH 80−2826
inelastic electron tunnelling spectroscopy appls. 78−92770
inelastic electron tunnelling spectroscopy appls. 78−92771
informational interaction, cooperative mechanism 78−15756
informational interaction in molecular physico-biological systems 77−25362
insect flight muscle, rigor cross-bridge pattern modelling 79−20508
insulin and analogue, side-chain mobility and tyrosyl circular dichroism 78−15770
interaction cross sections for protons and electrons with H, C, N and O atoms 77−50538
interactive model building program for macromolecules 77−52738
interfaces of nuclear and chemical physics, elementary particles and biochemistry 77−6284
intermediate states responsible for specific props. 79−96511
intermolecular interactions and biomol. organisation 77−64006
interstellar molecules in prebiological evolution 80−94726
intracellular control and intercellular transfer of molecules, multichannel anal. 79−53073
iodobenzoic acid, NQR of ^{127}I and Mossbauer, spectra of ^{125}I, bonding 77−12241
iodohippuric acid, NQR of ^{127}I and Mossbauer spectra of ^{125}I, bonding 77−12241
ionone, dipole moment determ. 78−27882
IR linear dichroism of oriented nucleic acid films 80−8013
iron porphyrin chlorides, X-ray, EPR and mag. susceptibility obs., intermol. exchange interaction 78−10765
isoelectric focusing method for human globin chain separation 80−17219
isomerism, L- and D-mol. reaction rates; weak neutral currents 78−415
isorhodopsin, physiological activity in rat rods 77−60204
isorhodopsin chromophore conform. and orientation in frog disc membrane 78−64980
isorhodpsin, resonance Raman spectra 79−92148
junctional membrane channels, size limit of permeating mols. 77−36900
K-vitamins, IR absorpt. spectra, vibr. anal., quinonoid struct. 78−61139
keratin, mammalian, organisation of polypeptide chains 77−4981
keratin-NaCl, Na Auger electron spectra 78−53339
Kerr effect of charged dipolar macromolecules without condensed counterions in conducting solution 80−53171
kidney, tissue water freezing study, ^{1}H NMR obs. 80−8027
kinetic IR spectroscopy IR, appl. to biochem. systems 80−98178
L-amino acids, weak neutral currents and biological stereoselection 80−26196
laccase, mag. susceptibility 79−92125
β-lactam antibiotics, ab initio SCF-MO-LCAO calcs., amidic bond breaking, methoxy substitution effect 80−78533
large flexible macromolecule internal modes relax., near UV photon correlation spectra 79−75621
laser Raman scattering, mol. probe of contractile state of intact single muscle fibres 80−89718
lechithin-cholesterol interaction, effect of lecithin struct. 78−64922
lecithin, adsorbed monolayer on aerosil, IR spectra 78−15753
lecithin, inelastic light scattering at second micellar formation 77−21492
lecithin, rheology and structure in conc. solns. and liquid crystalline state 77−64007
lecithin+cholesterol interaction, equilib., stoichiometry of complexes in bulk systems 78−68985
lecithin+cholesterol interaction, equilib., surface film phase relations and cholesterol condensing effect 78−68986
lecithin bilayer, ion-induced changes in head group conform, ^{31}P and ^{2}H NMR 78−3452
lecithin bilayers, density and mol. interactions 78−80837
lecithin bimolecular leaflets, incorporated fluoresc. probes, PMR 77−90734
lecithin cryst. growth rel. to mol. bilayer props. 78−31780
lecithin liposomes, binding sites for $Fe(CN)_6^{3-}$ ions, PMR obs. 79−79481
lecithin translational diffusion, pulsed NMR 77−9176
lecithin-cholesterol interaction, hydrocarbon chain length and unsaturation effects, Raman spectra 77−64012
lecithin-deoxycholate mixed micelles, surface curvature and mobility, PMR study 80−21452
leghaemoglobin, thermal denaturing in cryst. and soln. 80−108849
leghaemoglobin of Lupinus luteus, cryst. struct. of first component 78−27893
leucine aminopeptidase, 3D reconstruction by photosummation of projected functions 79−62183
leucine aminopeptidase crystalline aggregates, interpretation of electron microscope images 78−68988
leucine-binding protein, rat nerve, aggregation 79−62181
LF phonons, biological functions *(Chinese)* 78−24024
librational motion effects on fluoresc. depolarisation and NMR relax. in macromols. and membranes 80−85324
ligand binding to macromolecules, allosteric and sequential models of cooperativity 80−12870
ligand distribution among multiple binding sites on different proteins in plasma 77−12877
light absorption and orientation of absorpt. momenta in biological structs. 78−53326
light scattering, dynamic, by flexible macromols. in fluctuating elec. field 80−84722

molecular biophysics continued
light scattering from macromolecular soln. in alternating elec. field, low angle approx. 80−84721
light scattering under high press. *(Dutch)* 78−27901
Linus Pauling, publications, 1968-78, bibliography 79−24932
lipid asymmetry in membranes, review 77−48768
lipid bilayer, paraffin chain dynamics, ang. correl. function decay by multiple rot. pot. diffusion 80−3569
lipid bilayer chromophore energy transfer 79−62200
lipid bilayer couple, cation-phospholipid-induced shape changes 80−108855
lipid bilayer membrane interaction forces in zone of contact 78−53345
lipid bilayer phase transition, cholesterol effect 80−85361
lipid bilayers, asymmetry, dipole pot. meas. 77−4984
lipid bilayers, cholesterol model 78−56953
lipid bilayers, D relax. rates and mol. dynamics 80−26206
lipid bilayers, dielec. const. calc. from bond polarisabilities 77−29105
lipid bilayers, planar systems, asymm. charge distribs. 77−29104
lipid bilayers, quantitation of hindered rotations of diphenylhexatriene 79−16128
lipid bilayers, spin probes EPR partitioning between lipid and aq. phases 79−79455
lipid cell membranes, thermal structural rearrangements 79−92163
lipid extract from lung surfactant, IR spectra, H-bond lengths 79−24941
lipid free radical oxidation kinetics rel. to lipid composition, photoreceptor membrane 78−80872
lipid function in excitable membranes 80−12095
lipid hydrocarbon chain, biomembrane, rot. motion and fluidity 80−76714
lipid lamellar liquid crystalline systems, orientation studies of probe molecules by linear dichroism 77−90718
lipid layers and membranes, dynamic molecular organization 79−39364
lipid membrane order, mol. theory 79−66452
lipid membranes, molecular forces between and within 80−51051
lipid monolayer, simulation using mol. dynamics 80−108838
lipid monolayers and bilayers, phase transitions, model 78−44460
lipid organisation in Acholeplasma laidlawii membranes, ^{2}H NMR 77−86456
lipid planar bilayers, Ca^{2+} interaction with negative lipids, solvent effect 77−77871
lipid planar multibilayers, spin label study of nystatin and amphotericin B action 77−29108
lipid requirement of membrane-bound enzymes 79−20521
lipid systems, anti-oxidant action mechanism determ. by chemiluminesc. 77−56330
lipid thermotropic clustering in Tetrahymena endoplasmic reticulum membranes 80−85363
lipid-protein interaction in membrane bound Na^+, K^+-ATPase, spin label anal. 79−11902
lipid-rhodopsin interactions in photoreceptor membranes 80−12094
lipids, peroxide oxidation, sarcoplasmic reticulum membrane rearrangements 78−69025
lipids in erythrocyte membrane, phys. state determ. by X-ray diffr. 78−80835
lipids of myocardium mitochondria, composition and phase transitions rel. to depth of hypothermia, rats and dogs 78−53350
lipoprotein, low density, from human serum, STEM and FE-TEM obs. 79−100566
liposomes, nanosecond relax. processes 79−8477
liquid crystal, interaction of injected macromolecules *(Russian)* 78−78848
liquid crystal, lyotropic, form. in biological systems 77−86454
liquid crystals in living and dying systems, review 77−44602
liver alcohol dehydrogenase, proton relay system, SCRF PCE theory, CNDO/2 calcs. 80−85325
liver tissue and tumour proton mag. relaxation rel. to Fe content 79−39355
lucensomycin interaction with cholesterol in membranes, spectral parameters 77−9177
lutein, aq. soln., aggregate, reson. Raman spectra, and IR spectra, exciton interactions 78−31770
lyngbyatoxin A, struct. determ. from chemical and spectral data 79−66443
lyotropic liquid crystal, struct. rel. to amphiphilic structure 78−51416
lyotropic liquid crystal properties, biological aspects *(Japanese)* 77−70407
lysozyme, 0.01% soln., mag. and radiofreq. effects on activity 78−61136
lysozyme, adsorpt. isotherm, at air-water and air-oil interfaces 79−79461
lysozyme, adsorption kinetics, surface denaturation 79−79460
lysozyme, aq. solns., H_2O ordering, NMR relax. investig. 79−62171
lysozyme, binding to bacterial cell wall trisaccharide NAM-NAG-NAM, X-ray cryst. struct. anal. 80−35834
lysozyme, electric and mag. props. 77−44584
lysozyme, hydrated, dielectric props. at 9.9 GHz 78−15758
lysozyme, molecular structure of adsorbed film 79−79462
lysozyme, nuclear Overhauser effect in ^{1}H spectra 79−43823
lysozyme, of hen egg-white, ^{13}C n.m.r., carboxyl group resonances, ionisation consts. 77−1978
lysozyme, search for superconducting regions 80−101149
lysozyme, sorption and desorption of water, thermal-stimulated press. and thermogravimetric anal. 80−8008
lysozyme, spin echo and spin lock ^{13}C Fourier transform NMR 79−43824
lysozyme, stepped character of thermal denaturing, optical density at 290 nm 78−15763
lysozyme and complex with trisaccharide inhibitor, struct. in soln. and in cryst. 77−81465
lysozyme aqueous solutions, viscosity and density 79−48208
lysozyme bound water, thermally-stimulated press. and current 78−15757
lysozyme complex with substrate-inhibitors, photosensitised electron transfer, role of Cu^{2+} 80−30638
lysozyme effect of pH on dimorphic crystal growth 79−14728
lysozyme hydration, correl. of diverse types of meas. 80−61507
lysozyme interaction with water, intermol. pot. calcs. 77−75250
lysozyme macroradicals, ultraslow diffusion in an aq. matrix, EPR obs. 79−92119
lysozyme protein solution, spectra and dye laser threshold power 79−68391
lysozyme spin-labelled preps., water-protein layer microstruct. study by mag. relax. 78−76980

molecular biophysics continued
lysozyme-salt water soln., critical mixing point, turbidity and viscosity meas. 77−86437
α-lytic protease, predicted model rel. to X-ray struct. 79−62178
macromolecualr thermodynamics and its possible relevance in physiology 80−53176
macromolecular assemblies, struct. anal. with STEM 79−16147
macromolecular concentrated systems, molecular transport 79−57567
macromolecular crystallography, method for preventing cryst. slippage 77−76258
macromolecular force constants refinement in normal coord. calcs. 77−31035
macromolecular hard-sphere system, diffusion, hydration and soln. environment effects 77−19116
macromolecular hard-sphere system, diffusion, hydration effects 77−19114
macromolecular hard-sphere system, diffusion, hydration effects, finite conc. 77−19115
macromolecular interactions, effects of intervening medium and polar mode energy feeding 79−13857
macromolecular replication processes, with selection, stochastic theory 77−68145
macromolecular solution, rot. diffusion coeff. calc. method w.r.t. mol. struct., elec. birefringence relax. time data interpret. 80−85331
macromolecular solution dynamics, photon correl. spectroscopy, review 79−59603
macromolecular structural studies, with synchrotron radiation, X-ray television area detectors 79−55610
macromolecular structure, linked-atom least-squares reciprocal-space refinement system, LALS, incorporating stereochemical restraints 78−26377
macromolecular weight determ. by fluctuation spectroscopy 77−10800
macromolecule, high resolution struct. determ. by electron microscopy 80−89717
macromolecule adsorption to charged surface, rel. to cell metabolism 77−19118
macromolecule alignment in high mag. fields 77−64163
macromolecule behaviour when introduced into liq. cryst. 80−30639
macromolecule in soln., spectroscopic meas. of energy barrier to electron transfer 77−38766
macromolecule liquid, translational friction coeffs. of rigid, symm. top mols. 80−6003
macromolecules, biological, selection models, with time varying constraints 80−67029
macromolecules, computer simulation of solvent struct. 78−40113
macromolecules, conf., Dublin, Eire (July 1977) 79−55012
macromolecules, conformation studied by calorimetry, review 80−97870
macromolecules, effects of permanent mag. field 77−25364
macromolecules, high-resolution metal replication for electron microcopy 77−25621
macromolecules, impurity action of transition metal ions in variable oxidation states 80−85329
macromolecules, nonpolar groups, solvation, correl. function anal. 80−30644
macromolecules, PMR, nuclear Overhauser enhancement difference spectroscopy 78−81091
macromolecules, relax., modified Glauber theory 77−12879
macromolecules, struct. determ. by diffr. 79−94932
macromolecules buoyant density determ. by analytical density gradient equilib. centrifugation 80−17217
macromolecules in solution, diffusion coeff. determ. by Soret effect, using optical method 77−28032
magnesium chlorin, ab initio CI calcs. on ground, singlet and excited states, visible spectrum 79−16139
magnesium porphin, lowest triplet state, zero-field ODMR 79−31562
magnesium tetraphenylchlorin, lowest triplet state, zero-field ODMR 79−31562
magnetic circular dichroism of biological molecules, review, book contrib. 80−109080
maize mutation distinguishment by EPR 79−57580
mammalian DNA, viscoelastic behaviour, rat obs. 80−8078
mammary tumours, paramagnetic changes during development in rat 79−39425
mass spectrometry appls. in struct. studies of bioactive compounds 80−51305
mechanosensitive ionic channel, model of reception and macromolecular rearrangement, effect of deform. 79−79564
melanin, electron spin-lattice relax. times, saturation recovery meas. 78−96017
melanin, wet, elec. switching, aggregated electrons emulsion inversion as possible mechanism 79−38139
β-melanocyte stimulating hormone and β-lipotropic hormone fraction, spectral study 77−36863
melanostatin, correl. between X-ray struct. and conform. in soln. 77−48752
membrane, molecular motion determ. using periodic pattern photobleaching 79−34719
membrane, plastic deformation during freeze-cleavage, reviews 78−14400
membrane electron density profiles, determ. method on an absolute scale 79−16358
membrane fluidity of fatty acid auxotroph, EPR study 79−70574
membrane H^+ channels and mol. electrostatic generators 77−21501
membrane organisation using D-NMR and spin label EPR as probes 77−44600
membrane preparatory procedures, for electron microscopic anal., at mol. level resoln. 80−104843
membrane profiles, asymmetric, struct. determ., iterative Fourier method 79−43810
membrane protein-lipid complexes, spatial organisation obs. 79−70529
membrane structural rearrangements due to anaesthetics 77−36873
membrane systems, dynamical mechanical spectroscopy, mol. interactions 77−29109
membrane thin sectioning development for electron microscopy 79−74819
membranes, dynamic aspects, review 78−69005
membranes, functions and mol. props. *(Japanese)* 77−70422
membranes, radial autocorrelation function, significance in X-ray diffr. patterns 80−51048
membranes, structural order of lipids and proteins, fluoresc. anisotropy data eval. 80−97873

molecular biophysics continued
merocyanine-oxazolone dye optical probe for simultaneous recording from several neurones 77−66880
metallo-proteins and model systems, susceptibility and struct., SQUID magnetometer uses 79−53036
metalloenzyme, metal ion geometry and mechanism from PAC expts. 78−44449
metalloenzymes, ^{113}Cd as NMR active site probe 78−68999
metalloenzymes, model for biological active sites, ab initio calcs. 80−104551
metalloenzymes and carriers, hydration effect on mobility of Mossbauer atoms 80−35819
metalloporphins, deuterated, resonance Raman spectra, vibr. and vibronic levels 78−62812
metalloporphyrin, cation radical formation by pulse radiolysis, oxidation and demetalation rate consts. 80−61505
metalloporphyrins, Soret excited, reson. Raman excitation profiles, Jahn-Teller distortion and vibronic anal. 78−58698
metalloproteins, metal nuclei, biophysical appls. of NMR, review, book contrib. 80−109081
metalloproteins, recent EPR studies 78−64936
metalloproteins, site symmetry, X-ray absorpt. spectra using synchrotron radn. 78−64938
Cd-metallothionein, test object for dark field electron microscopy of protein struct. 78−11610
methaemoglobin, struct. change on addition of inositol hexaphosphate 80−72130
methanol dehydrogenase, enzyme, electron spin echo, 35 GHz 80−13113
methanol dehydrogenase, spin echo powder ENDOR, line shape aspects 79−34485
methionine sulfoxide in protein, ^{13}C NMR anal., method and expt. obs. 80−56305
methotrexate-dihydrofolate reductase complex form., conform., laser Raman obs. 80−104553
N-methyl acetamide, Na^+, Mg^{2+} binding to carbonyl O, lipid membrane permeation mechanisms 79−16134
3-methyl lumiflavin in soln., optical absorption, theory 78−74569
5-methyl-uracil, IR absorpt. spectra, vibr. anal. 78−61143
N-methylacetamide, and isotopic forms, low-freq. Raman spectra, internal torsional mode 79−26992
methylimidazoles, photoelectron spectra and electronic struct. 79−22758
6-methylmercaptopurine riboside, 4 MeV electron irrad., 77K radicals form., EPR obs. 78−39405
metmyoglobin, dynamics study using Rayleigh scatt. of Mossbauer radiation 80−40963
Michaelis Menten mechanism, modified, global asymptotic stability of soln. 79−79456
Michaelis-Menten mechanism for quasi-steady state and quasi-equilibrium, approx. soln. 79−70511
microemulsions, struct. aspects, using dielec. relax. and spin label techniques 80−26199
microtubule structure, temp. depend. 78−85288
microwave absorption by biological material, role of water 80−17004
mitochondria, interaction of cationic dyes, absorpt. spectra 77−52752
mitochondrial cytochrome b, evidence for two or more components 79−24944
mitochondrial DNA, nucleotide sequence in human, replication origin identification 79−29502
mitochondrion, elec. props. and struct. transitions 79−24943
mobility, using fluoresc. marker conc. dynamics 77−9303
modelling, design of computing systems 77−18814
molecular probes, orientational freedom 79−62168
molecular weight determination by STEM 79−92451
monomer self-associating systems, nonideal, graphical anal. by equilibrium ultracentrifugation 80−41335
mononucleotides, conformational anal. by nuclear Overhauser effects 79−20509
Mossbauer measurements on Fe-containing mols., using ^3He-^4He refrigerator 78−24909
Mossbauer spectrometry of Fe in hepatic and splenic tissues 80−81544
Mossbauer spectroscopy 77−13047
mucopolysaccharides in collagen, small angle X-ray diffr. studies, rat tail tendon 79−16132
multi-enzyme complex carrying out electron transfer, asymptotic anal. of functioning 80−81523
multistate systems, freq. of cyclic processes 80−108834
multistranded complexes, macromolecules, relax., modified Glauber theory 77−12879
muscle, contracting, dynamic structure, X-ray scatt., time resolved, rapid data collection systems 80−61740
muscle, cross-striated, mol. mechanisms of sarcomere struct. reorganisation in contraction 77−81462
muscle, F-actin subunits of thin filaments, functional role of struct. nonequivalence 80−76704
muscle, frog, spin-lattice relax. times for ^{13}C in isotope-enriched glycine 77−44605
muscle, glycerinated, F-actin conformational changes, polarised UV fluorescence obs. 79−100567
muscle, hydrated, PMR spin-lattice relax. of water, cross-relax. effects 79−34496
muscle, mouse, ^{13}C NMR and PMR 77−86463
muscle, mouse, NMR multiwindow anal. and proton local fields and magnetisation distrib. 80−21444
muscle, of barnacle, transverse nucl. mag. reson. relax., bounds on bound water 77−4989
muscle, rat, biological paracrystalline study, spacing variances 79−11897
muscle, skeletal, water protons NMR relax. times anisotropy obs. 80−85341
muscle, striated, mol. basis of force development 78−40126
muscle chemomechanical energy transduction, mol. basis 80−72143
muscle contraction, protofibril reciprocal sliding and thick filament shortening 77−56331
muscle contraction, single, high-time resolution X-ray investigation method 80−81777
muscle contraction, time resolved studies using small angle X-ray diffr., design of data collection system 79−12052
muscle contraction, time-resolved X-ray diffr., data-collection system *(Japanese)* 80−46108
muscle contraction cross-bridge model 78−44475
muscle contraction process, 10 ms time resolution X-ray diffr. 80−61741

molecular biophysics continued
muscle cross bridge rotation during contraction, fluctuations in polarised fluoresc. 80−97856
muscle fibres, fibrillar, tension transients affected by stretch-dependent binding of AMP-PNP 79−20562
muscle fibres, rabbit psoas, stiffness and tension after sudden length changes 79−25007
muscle model ultra-relaxation in medium with high Ca ion conc. on exposure to MgATP 77−25388
muscle thermodynamic cycles, temp.-entropic relations 79−53049
muscle thin filaments, method for anal. of X-ray diffr. patterns 79−39348
muscle water, mouse, ^1H NMR anal. above and below freezing 80−56073
muscle water, study of spin-lattice and spin-spin relax. times of ^1H, ^2H, and ^{17}O 80−21443
muscle water proton and deuteron relax. over wide ranges of reson freqs. 77−52740
muscle water transverse and longit. NMR relax. rates 78−35810
myelin, frog nerve, comments on the paracrystalline nature 79−16161
myelin, paracrystalline nature 77−52748
myelin lattice swelling kinetics study X-ray diffr. obs. 80−21436
myelin membrane, frog, with paracrystalline lattice distortions, X-ray determ. of electron-density profile 79−11903
met-myoglobin:Cu^{2+}, single cryst., EPR, conform. changes 77−73505
myoglobin, electronic and mag. struct., semiempirical MO cluster calcs. 78−62733
myoglobin, Fe-O_2 bonding and oxyhaeme struct. 78−96006
myoglobin, ferrous high-spin derivatives, MCD at room and liq. N_2 temps. 78−76997
myoglobin, from Aplysia limacina, X-ray cryst. struct. determ. at 5 Å resolution 79−16131
myoglobin, hyperfine-shifted PMR, mag. field and temp. induced line broadening 77−60184
myoglobin, O_2 and CO bonds, flash light photolysis *(Hungarian)* 79−29501
myoglobin, rate of entry of O_2, CO 79−8471
myoglobin, refolding kinetics by diffusion-collision-adhesion model 80−94157
myoglobin , oxyhaeme complex, single cryst., visible spectrum, electronic struct., coord. geometry 78−44456
myoglobin solution, facilitated diffusion of O_2 77−48747
myoglobin-Fe^{3+} compounds, Mossbauer and suscept. expts. 78−24019
myoglobin-H_2O_2, high-field Mossbauer spectra, 4.2 to 120K 80−8026
myoglobin-O_2(CO), elec. field gradient tensor, Mossbauer meas. 80−8017
myoglobins, Fe-, Co-substituted, O_2 binding, comparisons, thermodynamic investig. 80−67030
myosin, column-purified, struct. studies of synthetic filaments 79−92131
myosin, conformational changes induced by inorganic salts, Raman spectra obs. 78−96002
myosin, fast and slow, in developing muscle fibres 78−64961
myosin, removal of regulatory light chains rel. to Ca control of tension in scallop striated muscle 78−53360
myosin, struct. and functional changes in chronic cardiac insufficiency 77−36887
myosin, struct. changes in living muscle fibres, polarised UV fluoresc. microscopy 80−67037
myosin, synthetic, effects of C-protein on filament struct. 79−92132
myosin conformational conversions, using acetate and acetamide spin labels 77−52733
myosin head return to thick filaments after muscle contraction 78−7319
myosin heads, evidence for cooperative interaction from O_2 exchange meas. 77−32870
myosin heads movement during a heart beat 79−48207
myosin helical fragments, stepwise pattern of thermal denaturing 80−40966
myosin interaction with a spin-labelled ATP analogue 79−57563
myosin kinetic anal., review 80−21441
myosin molecule binding to two actin filaments 78−27884
myosin muscle filaments, crustacean, struct. of backbone 79−20512
myosin projection behaviour during staircase phenomenon in heart muscle 78−53362
myosin regulated muscle, changes in crossbridge attachment 78−53361
myosin rod, and subfragments, flexibility, birefringence relax. in soln. 78−53320
myosin subfragment-1 attachment to actin, effect on equatorial X-ray refls. 78−27880
myosin-auramine O system, conform. changes and excitation energy transfer 79−96512
N-hetrocyclic biomolecules, IR absorpt. spectra, vibr. assignment 77−10671
11-cis-N-methyl PRSB-benzene complexes, spectral props., CNDO/S calcs., bathochromic shift 78−31767
NADH coenzyme, two photon absorpt. cross section meas., reaction rate modification 80−51043
NADH-Ca complex, effect of oestrogens, rel. to mitochondria membrane Ca^{2+} interaction 78−53349
natural products mass spectroscopy, conf., Rehovot, Israel, (Aug.-Sept. 1977) 78−88681
nerve action pot., lipid bilayer local phase transition 80−89744
nerve excitability, interactions between intrinsic membrane protein and elec. field 78−53377
nerve membranes, protein channels for Na and K ions, mol. mechanisms 77−4994
nerve myelin, phasing the small-angle X-ray diffr. pattern 79−57588
net repulsive van der Waals forces between different particles, macromolecular, or biological cells in liqs., appls. 80−34274
neurotoxin, snake venom, appl. mol. graphics to struct. determ. 78−27892
neutron data acquisition system, low angle, for molecular biology 79−12053
neutron diffraction appl. to biological problems, book contrib. 79−62417
neutron scattering spectroscopy, recent advances, biology and chem. phys. appls. 77−35445
nicotinamide adenine dinucleotide, and reduced form, pH induced modification, Raman spectra 80−85343
nicotinamide co-enzymes, reduced, phosphorescence obs. at −196°C 79−79471
nitrogenase, cofactor centres, Mossbauer spectra obs. 80−8023
molecular biophysics continued
nitrogenase active site, Mossbauer spectra of Mo-Fe-S clusters 80−45852
nitrogenous bases of nucleic acids, ionisation pots. 77−29094
nitrosylhaemoglobin, electron spin distrib. 80−83528
NMR dynamic frequency shifts rel. to quadrupole interaction 79−81216
NMR of rat skin, ^1H and ^{13}C obs. 80−40965
NMR of solutions exhibiting chemical exchange, spin 5/2 and 7/2 nuclei 79−65750
NMR relaxation analysis, dynamic processes in macromolecules 79−8470
NMR studies of water in biological systems 80−3886
NMR study of molecular conform. in soln., use of La ion probe 77−60324
non-centrosymmetry, optical second harmonic generation 80−72133
noninteracting system, with N associating particles, free energy, virial expansion 77−55336
nonpolar molecules, adsorption into lipid bilayer membranes 80−61517
nuclear acids, effective force constant corrections, in redundant mol. coords. 78−13634
nuclear fibre framework in interphase nucleus *(Chinese)* 79−92187
nuclear Overhauser effect, truncated driven, in presence of spin diffusion 80−1095
nuclear spin-lattice relaxation meas., variable nutation WEFT, biochemical appl. 80−20482
nuclei acid base stacked dimer, origin of excimer states in extended Huckel method 80−35832
nuclei acid phosphate group, analytical atom-pair pot., SCF-LCAO calc. 79−70516
nucleic acid, multiphoton photoreactions of aq. soln., picosec. UV pulse 79−34487
nucleic acid base interaction with Na^+, ab initio study 77−64005
nucleic acid bases, ^{14}N relax. and N-proton spin coupling, NH-proton spin-lattice relax. 80−26202
nucleic acid bases, charge carrier photoexcitation quantum yield 79−99581
nucleic acid bases, charge-transfer complexes 79−70507
nucleic acid bases, excited state geometry distortion, normal modes reson. Raman intensity anal. 79−68236
nucleic acid bases, proton mag. relax., methyl group reorientation 77−64009
nucleic acid bases, protonated, anion binding, electrostatic mol. pots. 79−1999
nucleic acid bases, Zn^{2+} binding, ab initio SCF (pseudopot.) calcs. 80−12052
nucleic acid components, pyrimidine and purine, electronic struct. 80−30654
nucleic acid components, UV resonant Raman spectra 78−48756
nucleic acid constituents, reson. Raman spectra using synchronously pumped dye laser 79−12869
nucleic acid molecules, preprocessing of electron micrographs for automatic computer anal. 79−70711
nucleic acid optical measurements in presence of phenol and protein impurities 77−56546
nucleic acid purine, pyrimidine bases, base pairs, hydration scheme 79−92127
nucleic acid subunits, simulation of inter- and intra-molecular interactions 80−30643
nucleic acid-dye complexes, energy transfer obs. using laser-induced fluoresc. 80−12054
nucleic acid-TCNQ complex, charge transfer interaction 80−3576
nucleic acid-water interactions, review 78−44448
nucleic acids, atom-atom potential parameters, determ. of nonvalent interactions 78−25648
nucleic acids, bases and base pairs, water struct. in soln., Monte Carlo simultion 80−76709
nucleic acids, discontinuous mag. field effects, room temp. superconductivity 79−62195
nucleic acids, double-helical, conformations 77−12880
nucleic acids, electron microscopy using basic protein film method 80−104844
nucleic acids, electronic absorpt. and emission spectra 80−55989
nucleic acids, H_2 exchange kinetics and internal motions 80−21440
nucleic acids, nucleosides and nucleotides, metal ions interaction, review 80−3577
nucleic acids, pulse radiolysis study of interactions with amino acridines 78−85186
nucleic acids, Raman spectroscopy obs. *(German)* 79−27119
nucleic acids, study and theoretical physics *(Chinese)* 79−81316
nucleic acids and related compounds, photoemission rel. to absorpt. and luminesc., 120 to 250 nm 77−81466
nucleic acids and their aggregates, optical activity, review, book contrib. 80−108847
nucleic acids bases, excited state dipole moments and geometries 80−95738
nucleic acids nitrogeneous bases, thin films, water content determ. using quartz resonator 79−92439
nucleic acids studies, at. coords. of helices, by computer program 79−86095
nucleic bases, interactions and self-organisation, ionisation and solvent salt comp. effects 80−55985
nucleobases stacking interaction, NMR obs. 79−62170
nucleoside anion + hydrocarbon cation, electrochemiluminescent electron transfer reaction 79−88046
nucleoside conformations from NMR studies, review 78−76990
nucleoside cyclic monophosphates, phosphodiester stretching vibrs., IR and Raman spectra 77−65461
nucleosome core particles of chromatin, struct., X-ray diffr. and electron microscopy 77−86440
nucleosomes, structs. and modes of interaction 79−62182
nucleosomes and nucleosomal DNA, electro-optical props., relax. times and chain struct. 80−85350
3′-nucleotide, calcs. to assess rigidity 80−61506
nucleotide anion + hydrocarbon cation, electrochemiluminescent electron transfer reaction 79−88046
nucleotide base stacking interactions in vacuum, field mass spectrometry 80−81526
nucleotide bases, electronic absorpt. and emission spectra 80−55989
nucleotide conformations from NMR studies, review 78−76990
nucleotide sequences of the attachment sites of bacteriophage Mu DNA 79−79463

molecular biophysics continued
nucleotide sugar-phosphate region, γ-irradiated, deoxycytidine 5′-phosphate alkoxy radical EPR 79−5249
nucleotide threadlike crystal form. 78−95994
nucleotides, interactions and self-organisation, ionisation and solvent salt comp. effects 80−55985
octaethylchlorin, metal complexes, polaris. fluoresc. and phosphoresc. spectra 79−54906
octaethylisobacteriochlorin metal complexes, polaris. fluoresc. and phosphoresc. spectra 79−54906
opiate, receptor, synaptosome, EPR study of stereospecific binding of spin labelled morphine 77−9215
optical asymmetry correl. with parity violating weak interaction 78−69000
optical microscopy of single molecules, fluoresc. tagging, appl. to γ-globulin 77−21662
optical pumping, physicochem. mechanism for mag. field detect. by birds 77−52811
optical rotatory dispersion meas. method for macromol. conformation, press. effects 77−48984
optically active molecule separation asymmetry by longitudinally polarised relativistic electrons *(Russian)* 80−94172
oriented DNA, hydration, neutron scatt. obs. 80−89714
origin of life, chem. evolution (bibliography) 80−90620
origin of life, mol. biophys. basis 80−94158
origin of life 80−4111
origins, autobiographical review 80−57052
oxidative phosphorylation, role of respiratory chain 78−15795
oxirane-acrylic bead, radical conc. gradient determ. by microinterferometry and microfluorometry *(German)* 79−100799
oxy- and deoxyhaemoglobin, optical spectra, dichroism 79−20514
oxyhaemoglobin, deoxygenation, Jahn-Teller effect 77−21474
oxyhaemoglobin, dilute soln., reson. Raman spectra, pulsed laser excitation; optical multichannel detection 78−76999
oxyhaemoglobin, evaluation of elec. field gradient tensor components 77−64004
oxyhaemoglobin, mag. props. and structure 78−48751
oxyhaemoglobin, mag. susceptibility of frozen aq. soln., 25 to 250K 78−6507
oxyhaemoglobin, normal and sickle cell, Raman spectra, polarisability difference 79−62191
oxyhaemoglobin, spin labelled, rot. correl. times, saturation transfer EPR 77−8387
oxyhaemoglobin-hydrazine (dimethylhydrazine) interaction, γ-reson. spectroscopy 80−81525
oxyhemocyanin, mag. susceptibility 79−92125
oxyhemoglobin, spectroscopic meas. after pulsed optical excitation 79−92150
oxymyoglobin, evidence for conformational and diffusional mean square displacements 80−89713
oxymyoglobin, forzen soln., recoilless fraction, Mossbauer spectra meas. 80−8025
oxymyoglobin structure determ. by X-ray diffr. 78−56950
oxytocin, H bond linking ring and tail β-turns, biofunctional evaluation 80−61511
paddy leaves, spectrochem. anal., mineral constituents rel. to brown spot disease resistance 80−12055
pancreatic trypsin inhibitor, bovine, 3D protein folding model 77−90723
pancreatic trypsin inhibitor, bovine, macromol. dynamics, high resolution NMR investig. 80−91708
pancreatic trypsin inhibitor, bovine, struct. fluctuations in 100 ps 79−34478
pancreatic trypsin inhibitor bovine, dynamics of folded globular protein 77−64003
pancreatic trypsin inhibitor tyrosine residues in soln., laser photo-CIDNP as surface probe 78−73138
papain models, active site α-helix and ion pair stability 80−74265
paracrystal disorder, in biological systems 80−51035
paramagnetic metal ions as structural probes for NMR investigation of inorganic and bioinorganic compounds 78−62828
parvalbumins, Ca-binding, lanthamide-substituted, of muscle, ^{13}C NMR obs. 79−96516
pentofuranosyl nucleosides, isomeric, ^{1}H NMR coupling consts., SCF FPT INDO approx. calc. 80−14156
pepsin crystal fusion, microcalorimetry 77−70413
peptide, NMR spectroscopy study 78−88694
peptide and glycopeptide research methods 80−51307
peptide architectural units, ab initio SCF MO calcs. 78−96004
peptide folding, model based on incipient 3_{10} helix in Piv-Pro-Pro-Ala-NHMe 79−100568
peptide linkages, H bonding effects, review 77−10783
peptide sequencing by DADI mass spectra 79−57573
peptide-Cu II interaction, EPR and optical absorpt. 78−27881
peptide-metal complexes, EPR, models of natural systems 78−64937
peptides, α-aminoisobutyric acid containing, ^{1}H NMR conform. obs. 79−81311
peptides, bradykinin-potentiating, spatial structs. 80−95736
peptides, charge transfer, 1-electron reactions, pulse radiolysis obs. 80−45848
peptides, effect of internal librational motion on ^{13}C NMR relax. times 78−85293
peptides, in soln., nuclear Overhanzer effect methods for total conformational anal. 79−16136
peptides, soln. conformation by intramolecular nuclear Overhauser effect 79−16135
peptides and derivatives, mol. electron acceptor groups 80−30637
perdeuterio-N-1-oxyl-2,2,6,6-tetramethyl-4-piperidinyl maleimide, spin label, biological EPR 80−32746
peroxidase, ferrous high-spin derivatives, MCD at room and liq. N_2 temps. 78−76997
perturbed gamma-ray angular correlations 78−44739
Pf1 filamentous bacterial virus, macromolecular structural transitions 80−3584
phage T7 RNA polymerase, base pair for recognition and initiation 79−74597
phase-shift fluorometer using laser and transverse electrooptic modulator for sub-nsec lifetime meas. 78−20319
pheophytin solutions, photolum. of singlet O_2 78−80831
pheophytin-a, fluoresc. fading curve of lowest triplet state 79−36691
pheophytins, lowest triplet state, zero field splitting consts., decay rate consts., EPR determ. 78−27896

molecular biophysics continued
pheromone:beeswax far IR maser, possible cabbage looper moth control 77−77870
pheromone, cabbage looper moth sex scent, 17 μm emission rel. to moth control 77−73507
pheromone of cabbage looper moth, IR emission, candle flame as sexual mimic 78−35871
pheromone of cabbage looper moth, IR emission, tapping modulation 78−35872
phonons, Bose condensation, microscopic approach using Frohlich model 77−16904
phosphamides, carcinostatic, ^{14}N NQR, electron distrib. and bonding configs. 80−48018
phosphates, cellular, heteronucl. two-dimens. NMR as conform. probe 80−3590
phosphatidyl ethanolamine, charge distrib., dipole moment, CNDO calcs. 78−80840
phosphatidylcholine bilayer endothermic transitions, Raman difference spectroscopy 78−40119
phosphatidylcholine bilayers, fluidity changes and phase transitions, intramol. excimer fluoresc. obs. 80−85342
phosphatidylcholine dispersion, phase transitions obs. with interference refractometer 78−44459
phosphatidylcholine hydration, adsorpt.-desorpt. isotherm and PMR 78−15781
phosphatidylcholine-cholesterol vesicles interacting with lucensomycin, PMR obs. 80−40954
phosphofructokinase from Bacillus stearothermophilus, struct. and control 79−70517
phosphoglycerate kinase, sequence, struct. and activity, hingee-bending enzyme 79−74595
phospholipid, 1,2-dilauroyl-DL-phosphatidylethanolamine, X-ray diffr. anal., crystallogrpahy, bond lengths 77−44590
phospholipid bilayer, Gramicidin antibiotics effect on Raman spectra 77−66798
phospholipid bilayer, one- and two-component, main phase transition, Landau phenomenological theory 80−97872
phospholipid bilayer surface binding centre heterogeneity, hydrophobic mol. distrib. 77−56344
phospholipid bilayers, carbonyl groups dynamics, ^{13}C chem. shift anisotropy obs. 80−85326
phospholipid bilayers, direct obs. of hydrocarbon chain tilt angle 79−34481
phospholipid bilayers, low temp. transition from fluid state 80−97871
phospholipid bilayers, selectively deuterated, neutron diffr. study of mol. struct. 78−24036
phospholipid bilayers, struct. dynamics from deuterium spin-lattice relax. time meas. 79−79485
phospholipid inter-and intra-molecular interactions, PCILOCC and pot. function calc. 80−3570
phospholipid membrane, 4-dimethylaminochalcone fluoresc. probe of H_2O mol. surface mobility 79−79450
phospholipid membrane, polar head motion, NMR and EPR linewidth study using $TCNQ^-$ ion-radical *(French)* 80−45865
phospholipid membrane thermotropic transitions, effects of bivalent cations and proteins 77−48765
phospholipid mixtures, phase transition anal. by high sensitivity differential scanning calorimetry 77−40637
phospholipid monolayers, polymorphism 78−40120
phospholipid smectic phases, defect struct., freeze-fracture electron microscopy 77−21473
phospholipid topological asymm. in biomembranes, review 77−90736
phospholipid transmembrane asymm. studied by NMR spectroscopy with displacing reagents 78−31984
phospholipid vesicles, conform. change and fusion phenomenon, dynamic light scatt. obs. 78−11615
phospholipid-d, as nonperturbing components, for Raman studies of biomembranes 78−53330
phospholipids, ^{31}p NMR, slow-motional lineshapes for very anisotropic rot. diffusion 80−5644
phospholipids of hydrocarbon yeasts, composition and struct. 79−53028
phosphoryl transfer enzymes, biophysical appls. of NMR, review, book contrib. 80−109081
photo-induced charge transfer, mechanism and range 77−60182
photoelectrochemical conversion, using bacteria reaction centre working on SnO_2 electrode 80−94092
photoelectron spectroscopy, impact on biology 78−65156
photoelectron spectroscopy, review 77−56558
photon counting and fluctuation of molecular movement 79−29686
photoreceptor membrane, protein-lipid interactions on peroxide oxidation of lipids 77−21522
photoreceptor membranes, dynamic aspects of molecular texture 79−79519
photoreceptor transduction mechanism, conf., Julich, Germany, Oct., (1976) 77−90774
photosynthesis, analogue reaction in a porphyrin-quinone linked mol. 80−89720
photosynthesis, biophysical processes, review 78−92605
photosynthesis, carbon fixation cycle, model, teaching appl. 78−73806
photosynthesis, electron transfer reactions in carrier mol. complexes, kinetics and thermodynamics 80−108859
photosynthesis, energy transport by exciton percolation, simulation 77−28124
photosynthesis, redox conversion kinetics in the electron transport chain 80−40950
photosynthesis, use of picosecond lasers 77−81480
photosynthesis primary processes, picosecond spectroscopy *(Russian)* 79−39362
photosynthetic carboxylation reactions, ^{13}C kinetic isotope effect 79−57566
photosynthetic electron transfer by radical pair mechanism, electron spin polarisation 79−34471
photosynthetic pigment, intersystem crossing 77−58057
photosynthetic reaction centre chromophore organisation, high-resolution magnetophotoselection 80−97880
photosynthetic systems, discovery of phase transitions 80−81539
photosynthetic systems, magnetoorientated, fluorescence polarisation theory 79−16165
photosynthetic systems, reaction centre struct., triplet state ODMR 77−29093

molecular biophysics continued
phototransients, modulation excitation techniques for circular dichroism meas. 77−46656
phycobilin pigment role in photosynthesis 78−48752
β-phycoerythrin crysts., twinned by merohedry, diffr. data treatment 80−108845
Physarum actin, amino acid sequence 79−16141
physical and biological science conf., Japan (Feb. 1979) 80−12846
phytochrome, autoradiographic tryptic digest maps 79−16144
phytochrome chromophore, models, absorption wavelengths and oscillator strengths calc. 77−81469
phytochrome subunit, evidence for symmetry 78−27890
picosecond relaxation measurements book contrib. 77−64166
picosecond spectroscopy, appl. to chem. and biological reactions 79−80697
pigment associations, conc. effects, luminesc., absorpt. spectra and dichroism obs. 80−1007
pigment molecule organisation and interaction in reaction centres of Rhodopseudomonas viridis 80−35843
pigment-protein complexes oriented, of photosynthetic bacterium Chromatium minutissimum, linear dichroism 80−35841
pigments, oriented molecules in spherical arrays, fluoresc. polarisation 77−44591
pigments, visual and purple membrane, charge stabilisation mechanism 79−34500
plant fibre temperature stability investigation, rotary diffusion, spin label obs. 80−81529
plant photosynthesis, signal II, electron spin-echo method 78−96118
plant tissues, adsorbed water, detection of OH groups for adsorption centres, dielectric relaxation *(Japanese)* 80−7999
plant tissues, dielec. relax. of H_2O 78−88692
plasma low density lipoproteins, human, size and surface effects rel. to phase transitions 78−3446
plasma low-density lipoprotein, human, molecules organisation of central core 77−90722
plasma protein interaction with polyion complex studied by circular dichroism and UV spectroscopy *(Japanese)* 80−12316
plasma proteins adsorbed on polymer surface, Fourier transform IR spectrometry 80−16899
plasmid DNA and DNA-histone chromatin-like complexes, conform. and soln. props. by laser light scatt. 80−55987
PMR relaxation times vs. water content for tumour and normal tissue 77−12884
polar nonvolatile bio-organic mols., anal. by laser desorpt.-mass spectrometry 78−92534
poly (N^{α},N^{ϵ}-terephthaloyl-L-lysine) membrane for artificial red blood cells, interaction with serum proteins *(Japanese)* 80−12061
poly riboadenylic acid, time dependence of triplet-singlet excitation transfer 79−57586
poly-l-glutamic acid, soln., u.s. absorpt., linear Ising chain kinetics 77−4980
poly-β-benzyl-L-aspartate, soln., ^{13}C and ^{1}H NMR dynamic study 79−69737
poly-γ-benzyl-glutamate, α-helix second-order hyperpolarisability meas. 77−14623
poly-γ-benzyl-L-glutamate, soln., ^{13}C and ^{1}H NMR dynamic study 79−69737
poly-γ-benzyl-L-glutamate helices, optical activity 80−48113
poly-γ-benzyl-L-glutamate solutions, calorimetric study of fusion of liquid cryst. struct. 79−53022
poly-L-alanine, soln., ^{13}C NMR dynamical study 79−69737
polyacrylamide gel block electrophoresis instrument 78−7549
polyadenilic acid, semi-dil. soln., slow modes 78−53319
polyamino acids, macromolecules, relax., modified Glauber theory 77−12879
polycytosine, ab initio energy band struct. 77−70415
polyelectrolyte+physiologically active substance complexation, stability, kinetics *(Russian)* 80−8006
polyelectrolyte solution, polyion-polyion interaction effects, computer simulation 80−35817
polyelectrolytes, diffusion pots., rel. to biological electrochemical phenomena 77−4978
polyenals related to visual chromophores, absorpt. spectra rel. to chain length 79−34494
polyenals related to visual chromophores, emission spectra 79−34495
polyenones related to visual chromophores, absorpt. spectra rel. to chain length 79−34494
polyenones related to visual chromophores, emission spectra 79−34495
polyglutamic acid, helix-random coil transition observed by gamma-ray ang. correlation 78−80828
polyglutamic acid molecular dynamics in soln., γ-ray perturbed angular correl. 78−94960
polyglycine, IR spectra calc. for helix and β configs. 80−45853
polyglycine chain, electronic struct. and transport props., ab initio Hartree-Fock crystal orbital calc. 79−42448
polyglycine chain with hydrated side group, electronic struct., transport props. 79−16146
polyglycyl-prolyl-prolyl, triple-helical coiled-coil conform. determ. rel. to interchain interactions, collagen models 77−38762
polymer chain, uniform, elastic, possible conformational states 80−37913
polymer chains, intramol. reacts., enzyme catalysis appl. review 80−40953
polymer globule elasticity 77−70404
polymer solution, conc.-depend. collapse in presence of second polymer 78−56949
polymer solution, low angular scatt. of synchrotron radiation, use of proportional chambers 78−65155
polymer solutions, order, conf., Midland, USA, (Aug 1973) 79−10769
polymer system, Fourier transform IR spectroscopy appl. 78−58870
polymers, aqueous, solns., IR spectra 80−2761
polymers, circular dichroism and optical rot., review 78−44457
polymers, electro-optical changes, chem. and rotational contribs. 80−85352
polymers solns., cooperative phase transitions, review 80−45850
polymethylene chain, vibr. spectra, CH stretching region, struct. and assignments 78−70991
polynucleotide, bihelical, secondary struct. stability 79−53030
polynucleotide, double-stranded, conform. inhomogeneity of sugar-phosphate chain rel. to compact particle optical activity 80−35839
polynucleotide electron energy band studies 80−72132
molecular biophysics continued
polynucleotide solution, elec. birefringence, stabilised induced dipole behaviour 80−85349
polynucleotides, bihelical, conform. anal. 77−36862
polynucleotides, double helical, conformation, pairwise pot. function calcs. 80−53173
polynucleotides, double helix, high resolution NMR, review 77−86450
polynucleotides, double-helical, conform anal. 79−96513
polynucleotides, double-stranded conformation model 77−14631
polynucleotides, interactions and self-organisation, ionisation and solvent salt comp. effects 80−55985
polynucleotides, polaris. spectra, excimer phosphoresc. and fluoresc. 79−34497
polynucleotides, potentials of internal rot. 77−16901
polynucleotides and components, temp. depend. of UV absorpt. spectra 77−21475
polyoma virion and capsid crystal structures 80−8011
polypeptide, conformational change induced by strong elec. field 80−85336
polypeptide chains, struct. of conduction and valence band 80−76700
polypeptide hormones, folding, ODMR and phosphoresc. 79−20518
polypeptide hormones, liquid chromatographic separation 79−74450
polypeptide hormones fragmentation anal. by chromatography 79−92448
polypeptide monolayers, circ. dichroism 79−74598
polypeptides, 3_1 helix-coil transition, circular dichroism obs. 78−35795
polypeptides, α-helix asymmetry, circular dichroic spectra 79−16145
polypeptides, β-form, vibronic exciton approach to NV_1 absorption band 77−79626
polypeptides, amide proton spin-lattice relax. 79−20502
polypeptides, comparison of conformational possibilities 80−94163
polypeptides, cyclic, cryst. state conformations 79−24942
polypeptides, electronic struct., side-chain disorder effect 80−76706
polypeptides, helix-coil transition dynamics, time correl. function theory 80−99591
polypeptides, helix-random coil transition rates, mean relaxation rate, internal friction 77−38763
polypeptides, in aq. poly(L-glutamic acid) soln., helix-coil transition, US relax. times 80−45849
polypeptides, mean field Ising-type model for helix-coil transition 77−70416
polypeptides, poly-L-lysine based, comb-like, struct., physicochem. props. *(Russian)* 79−55644
polypeptides, short chain conformations, long-range interactions, Monte Carlo calcs. 77−58217
polypeptides, structured, nature of 4.5 Å max. on X-ray diffuse scatt. curves 78−31769
polypeptides, unordered, circular dichroism, Green operator method 77−14467
polyriboadenylic acid, soln., Raman spectra, struct. and conformation 77−71899
polyribonucleotides, dye tagged, aqueous solns., elec. induced fluoresc. changes 80−85346
polysaccharide gels, spectral broadening of Rayleigh scattering 78−31771
polysaccharide gels and sols, PMR relax. times rel. to temp., pH and conc. 78−56952
polysaccharides, evidence in IR astronomical spectra 77−78857
polytene chromosome, stretched, stained with acridine orange, fluoresc. polarisation rel. to DNA packing 78−76995
polyurethanes, linear, in physiological soln., in vivo, degradation by ester hydrolysis *(Russian)* 80−40690
porphin, MCD, LCAO MO SCR π-electron calcs., PPP approx. 78−9178
porphin free base, triplet state electron spin echoes, fluoresc. detection 78−70856
porphins, reson. Raman spectra, selection rules, normal coord. treatment 80−53175
porphins, UV absorption and photoelectron spectra, CNDO/S3 calcs. 77−75210
porphins orientation in n-alkane Shpolskii hosts, spectra 80−48035
porphyrin, dication and dianion, spectra, quantum chem. calcs. 79−36597
porphyrin, triplet-state EPR spin polaris., intramol. model for photosynthetic bacteria 78−44469
porphyrin a, MCD, LCAO MO SCR π-electron calcs., PPP approx. 78−9178
porphyrin singlet and triplet states, quenching of O_2 79−92141
porphyrins, dark transition of reduction products by disproportionation 79−53020
porphyrins, non-radiative deactivation of lower excited states, effect of mol. struct. 78−68987
porphyrins, reduction reactions intermediate products, PMR spectra 79−53019
porphyrins and related tetrapyrroles, mass spectrometry appls. 80−51306
prealbumin, human plasma, secondary struct. refinement from circular dichroism data 78−27888
prealbumin, protein-DNA and protein-hormone interactions rel. to model of thyroid hormone nucl. receptor 77−66793
prealbumin-DNA-hormone interactions, X-ray studies, review 78−53322
prebiological molecular evolution, as physico-chemical processes 77−60331
pressure jump method for fast kinetics using optical rotation and circular dichroism 78−77175
probes for energy transduction in membranes, review 77−21666
proline, oligomer, vibr. spectra rel. to polymeric form 79−83695
protamine, electron microscopic recognition rel. to radiation exposure 79−62175
protein: Eu^{3+}, luminesc. spectra and binding centres 78−15754
protein, amino acid composition determ. by chromatography 79−44070
protein, electron-transport type, H-bonding, ab initio MO 80−51039
protein, globular, compressibility in water at 25°C 80−40951
protein, globular, in aqueous solutions, conformational mobility investigation 79−53033
protein, long-range interactions, approx. method 78−7317
protein, metal containing, chem. characts. of conformational nonequilib. states 78−95998
protein, NMR spectroscopy study 78−88694
protein, structure and bonding, quantum theory, ab initio calcs. 80−61509
protein, X-ray struct. study using synchrotron radiation and multichannel detector 78−47210

molecular biophysics continued
protein β-pleated sheet topology rel. to relatedness 77−77866
protein adsorbed layers on field-emitter tips, removal by UV radiation 80−104836
protein adsorption and immunological reactions at liq./solid interface, ellipsometry obs. 77−52948
protein aggregation in membranes, fluctuation-induced interactions in liquid crystals 77−90732
protein analysis using PIXE 80−61691
protein architectural units, ab initio SCF MO calcs. 78−96004
protein asymmetry in membranes, review 77−48768
protein bacterial bioluminescence, isolation and props. 78−92599
protein beta sheet structures, anal. and prediction by combinatorial approach 80−76710
protein biosynthesis, role of guanine nucleotides 78−68982
protein chromophores, fluoresc. props., use in macromol. equilib. struct. mobility investigs. 79−64130
protein conformation, statistical mechanical theory, appl. to homopolymers 78−64931
protein conformation, statistical mechanical theory, folding pathway 78−64932
protein conformation in nerve membrane, and energy changes, rel. to action pot. 78−44497
protein conformational transitions, temp.-depend., using fluoresc. probes 77−70410
protein crosslinking and affinity labeling, use of photoreagents 79−96517
protein. cryst. struct. analysis by electron diffr., single scatt. approx., domains of validity 80−101150
protein crystallography, in mol. biophysics course 77−33720
protein crystallography, min.-variance Fourier coeffs. from isomorphous replacement method by least squares anal. 77−52938
protein crystallography, MWPC as area detector 78−65166
protein crystallography, synchrotron radiation appl. 77−52936
protein dynamic states, role of geometry and elastic strains 78−48745
protein evolution, molecular clock test using Panamanian sea urchins 79−92134
protein folding, incorporation of 1-dimens. Ising model into 3-dimens. model 77−90723
protein folding, unfolding, expt. studies of globular and BPTI proteins 79−2003
protein hydration dynamics, quasi-elastic neutron scattering 79−16127
protein interaction with nucleic acids and sugars, studied by luminesc. 79−34476
protein internal charge transfer, ascorbic acid adduct model systems, SCF calc. 80−69072
protein isomerisation, gel permeation chromatography of interacting multicomponent systems 78−68950
protein isomerisation kinetic consts. determ. by gel permeation chromatography of interacting multicomponent systems 78−68951
protein molecule, simulation of single mol. images combining computer and electron micrograph analysis 78−37781
protein molecules, new representation for mapping chain-folding 77−44588
protein nucleic acid recognition, role of unspecific complexing 79−79449
protein periodic models, forbidden band gap calc. indicating insulating behaviour 77−25367
protein primary structure, distrib. of identical amino acid residues 77−56334
protein rotational motions, large-scale, detection by EPR and fluorescence 79−16120
protein secondary structure determ. by circular dichroism spectra 80−30653
protein sequencing, solid-phase techniques 77−56557
protein solutions, small-angle neutron scatt. using time of flight method, spectrometer 79−1371
protein structural dynamics, temp.-depend. X-ray diffraction 79−92133
protein structure, areas, vols. and packing, review 77−86441
protein structure determination, crystal bending, electron-diffraction data 78−53325
protein structure factors from electron density, test on model crystal 78−47204
protein structure factors from electron density distrib., theoretical foundations 78−47203
protein structure prediction from amino acid sequence 78−24026
protein structures, Fourier refinement 80−51037
protein supramolecular structures, calorimetric and van't Hoff enthalpies of assembly comparison 77−90717
protein synthesis, stochastic eqns., ribosome translation along mRNA and tRNA selection processes 79−66440
protein synthesis mechanisms, genetic codes 77−56353
protein titrations by NMR, pH depend. of internal reference 77−86727
protein-ligand binding parameters estimation from continuous ultrafiltration results 77−12878
protein-ligand equilibrium binding, mathematical models 78−48688
protein-lipid interaction effect on struct. of artificial vesicular membranes 77−25385
protein-lipid interactions, review 77−90719
protein-lipid model systems, chemiluminesc. on exposure to formalin 77−56329
protein-nucleic interactions in tobacco mosaic virus, spin label and fluoresc. obs. 80−40949
protein-peroxide radicals, ^{17}O-labelled, EPR obs. 80−85345
protein-solvent systems, dynamics investigation by nucl. gamma-resonance 79−62166
protein-substrate binding, linear differential equations in chemical equilibrium calculations 80−30279
protein-water interactions in aq. solns., Raman spectroscopy 77−6792
proteins, ^{13}C NMR, review 77−86449
proteins, α-helical, possible role in membrane charge transfer processes 80−81524
proteins, α-helix dipole rel. to props. 78−61140
proteins, adsorbed at interfaces, fluoresc. spectroscopy study 80−12315
proteins, adsorpt. of non-paramag. compounds, spin probe investigation 78−65153
proteins, amide unit electron organisation, mol. orbital theory 79−2000
proteins, amino acid neighbourhood relationships, breakdown into overlapping doublets, triplets, and quadruplets 80−67035
proteins, appl. of cryst. struct. refinement technique based on fast Fourier transform algorithm 78−91197
proteins, chain reversal regions conservation 79−83699
proteins, coiling and topology of the antiparallel β-struct. 80−40956
molecular biophysics continued
proteins, coiling and topology of the parallel β-struct. 80−40957
proteins, conform. anal., algorithms and data structs. for array processing 80−83530
proteins, conform. changes in aqueous soln. and in mixed solvents, IR absorpt. spectra 78−15762
proteins, conformations, quantitative approach 80−30652
proteins, diagmagnetic anisotropy, struct. origins 79−92136
proteins, effect of internal librational motion on ^{13}C NMR relax. times 78−85293
proteins, electron transfer mechanism 79−96510
proteins, electrostatic effects on behaviour 79−53027
proteins, EPR absorption of tissue constituents, colour correlation, using mouse liver 77−90727
proteins, fluoresc., equilib. structural mobility *(Russian)* 78−76986
proteins, folded, models for H exchange 78−76981
proteins, globular, cryst. growth kinetics 80−35823
proteins, globular, crystalline, intermol. interactions, denaturation, DSC and X-ray diffr. obs. 80−16897
proteins, globular, in water, proton NMR spin echo decay comparative investigation 80−81541
proteins, globular, intramol. relaxation 77−10798
proteins, globular, no. of turns and models of turn form. 77−77869
proteins, globular, prediction of β-turns by computer 79−83698
proteins, globular, struct. anal. in soln. by large-angle diffuse X-ray scatt. 77−86723
proteins, H_2 exchange kinetics and internal motions 80−21440
proteins, inductive resonance energy transfer, struct. and conform. changes 79−27120
proteins, kinetic constants of association and dissociation, theoretical determ. 80−51033
proteins, methine aromatic C sites, natural abundance ^{13}C NMR at high mag. field strength 77−86443
proteins, minimisation of functions of many variables appl. to X-ray struct. anal. 80−3589
proteins, model building procedure 80−51036
proteins, nature of 4.5 Å max. on X-ray diffuse scatt. curves 78−31769
proteins, nuclear mag. relax. dipole-quadrupole nuclei interaction, quasi-rigid and tumbling lattice 77−66434
proteins, nuclear Overhauser effect in ^{1}H spectra 79−43823
proteins, plastic deformation during freeze-cleavage, review 78−14400
proteins, PMR spin-lattice relax. time, role of cross-relax. 78−35800
proteins, props. rel. to membrane functions, review 77−44601
proteins, representation, unique method 80−67036
proteins, resolution of components of complex spectra by Alentsev-Fok method 80−1097
proteins, role in electron transport at large distances 79−34480
proteins, solid, NMR, detection of individual C resonances, appls. 80−51042
proteins, solid, PMR spin-lattice relax., mol. dynamics 80−51041
proteins, stress-induced struct. and activity changes 79−43812
proteins, thermal denaturation, use of high heating rates to separate denaturation and aggregation 77−81470
proteins, triplet state energy transfer 78−20143
proteins, UV fluorescence detect. of conformational rearrangements in plants 79−53031
proteins, UV fluorescence spectra, resolving of components, Alentsev-Fok method 80−1096
proteins, X-ray crystallography, book contrib., review 77−40958
proteins, X-ray scattering data, Soule-Porod plots 77−51273
proteins in solution, laser photo-CIDNP as surface probe 78−73138
proteins involved in active membrane transport, struct. review, book contrib. 80−108844
proteins with memory, relax. expts. 77−70406
protocatechuate 3,4-dioxygenase, reduced, Mossbauer effect zero field splitting 79−24955
protochlorophyll, fluoresc. fading curve of lowest triplet state 79−36691
protohaeme, low-spin-ferrous, MCD, LCAO MO SCR π-electron calcs., PPP approx. 78−9178
protohaeme-CO binding dynamics, flash photolysis, activation energy, entropy 77−21472
proton relaxation; solid state, activation energies, relax. consts., 50-500K 78−68998
proton relaxation enhancement, biochem. appls., review 79−89692
proton relay model systems, reaction field theory of solvent effects 78−44346
protoporphyrin, MCD, LCAO MO SCR π-electron calcs., PPP approx. 78−9178
protoporphyrin IX, triplet states, flash photolysis, obs. 80−95555
protoporphyrin IX dimethyl ester, triplet states, flash photolysis, obs. 80−95555
purines, biological, UV photoelectron spectra, valence electronic struct. 77−16905
purple membrane, orthorhombic 2D crystal form 80−85362
purple membrane, polarized IR spectroscopic struct. study 79−43809
purple membrane asymm. struct., X-ray diffr. data anal. 77−73512
purple membrane films, absorpt. and circular dichroic spectra 79−83708
purple membrane fragment suspensions, elec. dichroism obs., trimer model interpret. 80−89728
purple membrane particles, freeze-fractured, protein content 77−90735
purple membrane protein synthetic pigment analogues 77−73504
purple membrane topography of Halobacterium halobium 79−48211
pyrene, migration between lipid vesicles in aq. soln., fluoresc. stopped-flow obs. 80−85360
pyrimidine, 77K, vibr. struct. absorption and phosphorescence spectra 78−61138
pyrimidine bases, water vapour effect on struct. and amorphous-cryst. transition 77−70408
pyrimidine derivatives, absorpt., luminesc. and polarisation spectra, electronic struct. 79−85993
pyrimidine nucleotides, UV reson. Raman excitation profiles 80−58265
pyrimidines, substituted analogues, absorption UV spectroscopy and electronic struct. of ionic and tautomeric forms 80−74177
pyronin dye, use as fluorescent indicator of energetic state of mitochondria 77−66790
pyrophosphatase, inorganic, of yeast, cryst. growth, derivatives formation, heavy atoms positions 80−108842
quantum biology and pharmacology, conf., Florida, USA (1978) 79−24934
quantum chemistry, biology, and pharmacology, conference, Kiev, USSR (Sept. 1978) 79−96499

molecular biophysics continued
quercetin, excited state proton transfer, luminesc. 80−35818
quinacrine mustard, 2-step laser-induced photodamage 80−85198
quinacrine mustard-DNA complex molecule, laser-induced fluorescence 77−60187
R spheroides, triplet state electron spin echoes, fluoresc. detection 78−70856
radioassays, automated data processing 79−16299
radiolabelling of T gas, by microwave discharge, for amino acid sequence determ. of proteins 79−12057
Raman spectroscopy, appls., strategy and tactics 77−52939
Raman spectroscopy, recent advances, reivew 78−41359
rare earth bone uptake, Mossbauer study 80−8019
reaction rate theory in bioluminesc. and other life phenomena, review 77−90716
recognition model, stereochem. enhancement of specificity 77−81461
recombinant DNA, scientific and social perspectives 79−88047
red blood cells of thalassemia, sickle-cell anaemia, and haemoglobin Hammersmith, ferritin-like Fe, Mossbauer study 80−8018
redox enzyme, Fe-, Cu-, or Mo-containing, electron transfer peculiarities 80−16896
relaxation times in solid-state theory and one-dimensional molecular systems *(Russian)* 80−100640
rennin and pepsin, relative orient. of mols. in unit cells, mol. replacement method 77−36866
replication by quantum mechanical interactions 77−40626
resonance Raman scattering line intensities in vibr. spectrum 77−83609
resonance Raman spectra interpretation, review 77−90976
resonant interactions 80−72128
retina, bovine, R2 component of early receptor pot. rel. to metarhodopsin II form. 80−97904
retinal$_1$, all-trans, valence bands, XPS obs. 78−24030
retinal, all-trans, reson. Raman excitation profile 78−73137
retinal, dipole moment determ. 78−27882
11-cis-retinal, donor energy effects on triplet-sensitized isomerization 78−3353
trans-retinal, ground and excited state dipole moments, permittivity, solvent effects, spectrophotometry 78−27883
retinal, in ethanol soln., methyl groups effect optical absorpt. 79−53047
trans-retinal, picosecond photophysics 77−9169
retinal, proton donor-acceptor isomerisation coupling, bacteriorhodopsin as light driven proton pump 79−79473
all-transretinal, two-photon spectrum, rel. to photophysics of vision 79−41159
retinal chromophore, reson. Raman spectra obs. of struct. 80−94168
retinal chromophore transition dipole moment, orientational changes obs. 80−41023
retinal electronic structure 78−15764
retinal photoreceptors, small angle X-ray data processing 80−81536
11-cis-retinal prep. by irrad. of all-trans-retinal and high press. liq. chromatography 78−40453
retinal Schiff bases, Raman spectra modelling of rhodopsin and bacteriorhodopsin chromophores 79−62190
retinal Schiff-base, photochem. step of vision, H-bonds, intermol. associations 78−31812
retinals, catalysed cis-trans isomerisation by crude tissue extracts 78−64925
retinals, emission spectra, state ordering 77−25373
retinals, polarised fluoresc. at room temp. 78−96014
retinol, fluoresc., polarised emission study 79−29504
retinol-binding proteins in retinal pigment epithelium 79−20525
retinyl acetate, fluoresc., polarised emission study 79−29504
trans-retylidene-n-butylamine, ground and excited state dipole moments, permittivity, solvent effects, spectrophotometry 78−27883
review of NMR and molecular biology research *(Chinese)* 79−39459
Rhacopholus embryo yolk platelets, freeze fracture study of crystalline struct. 80−104552
rhodopsin, α-helix orientation, spectroscopic study 80−89711
rhodopsin, bacterial compared with animal, H exchange 77−29096
rhodopsin, bathochromic shift origin 78−31767
rhodopsin, bovine, conform. in situ and solubilised with detergent 77−44587
rhodopsin, bovine, interaction with Ca^{2+} 79−100564
rhodopsin, bovine, kinetics of $NaBH_3CN$ reduction 78−64926
rhodopsin, bovine, mol. wt. determ. by monolayer method 77−81492
rhodopsin, bullfrog, thermosensitive prop. 77−25431
rhodopsin, cattle, phosphorylated, isoelec. focusing 78−15766
rhodopsin, coherent states of flexible macromol., mol. basis of vision 79−79472
rhodopsin, picosecond spectroscopy obs. of primary events 80−56312
rhodopsin, presence of two closely arranged SH groups in mol. 78−53323
rhodopsin, resonance Raman effect *(Hungarian)* 78−74666
rhodopsin, resonance Raman spectra 79−92148
rhodopsin, thermal isomerisation rel. to visual transduction mechanism in retinal obs. 79−74651
rhodopsin, vertebrate, chromophore orientation obs. 80−40959
rhodopsin and bacteriorhodopsin chromophores, modelling by retinal Schiff bases, Raman spectra 79−62190
rhodopsin and bathorhodopsin, theoretical analysis of optical activity 77−52783
rhodopsin and intermediates, absorpt. spectra and orientational change of chromophore 78−7321
rhodopsin and other proteins in artificial lipid membranes 77−90730
rhodopsin bovine, interaction with Ca^{2+} 79−100563
rhodopsin chromophore, and desmethyl analogues, theory 80−94169
rhodopsin conformation, spectral studies 78−15765
rhodopsin formation, opsin recognition of longit. length of retinal isomer 78−61137
rhodopsin in digitonin, isolation of 3 isochromic forms 77−52951
rhodopsin kinetics at room temp. meas. by picosec. spectroscopy 77−64036
rhodopsin lateral diffusion in surface membrane of rat retina rod external segment 78−15828
rhodopsin orientation in photoreceptor membrane, model 77−90775
rhodopsin photosensitivity, thermal stability and metarhodopsin prod., extractant effects 78−7355
rhodopsin thermal stability in photoreceptor membrane, role of lipids, PMR spectroscopy 80−35874
rhodopsin thermal stability in photoreceptor membrane and Triton extracts, squid rhodopsin 77−32893
molecular biophysics continued
rhodopsins of oceanic decapods, absorpt. spectra 78−61182
riboflavin, transition moments in 300 nm region 79−53042
ribonucleare, PMR spectra, line narrowing, convolution and pulse methods 78−78729
ribonuclease, positron annihilation, temp. depend. meas. 79−66448
ribonuclease A, bovine, cryst. struct. determ. by X-ray and neutron diffr. 80−108841
ribonuclease A, microviscosity, mobility profile 80−91710
ribonuclease T_1 in soln., phosphoresc. at 293K *(Japanese)* 77−44595
ribonuclease-A, solid, PMR spin-lattice relax., mol. dynamics 80−51041
ribose phosphate backbone, effective partial changes calc. 80−8013
ribosomal component, cryst. struct. at 2.6 Å resolution 80−97859
ribosomal protein S4 from Escherichia coli, circular dichroism obs. of conformation 78−96003
ribosomal RNA, conformational changes induced by ribosomal subunit proteins from E. coli 79−79466
ribosomal subunit 30 S, of E coli, meas. of location and radii of gyration of proteins by neutron scattering 79−11892
ribosomes, E. coli, complexes of individual components, small angle X-ray scatt. study 79−11895
ribosomes, E. coli, contrast variation neutron scattering studies, reassembled subunits 79−20510
ribosomes, E. coli, neutron small-angle scatt., contrast variation study 79−16138
ribulose bisphosphate carboxylase, two-layered square-shaped mol. 77−56336
ribulosebisphosphate carboxylane, electron microscopy of 79−70515
$tRNA_{ycast}^{phe}$, Fourier transform PMR in aq. soln., ^1H exchange and relax. rates meas. method 78−15049
$tRNA^{Phe}$, yeast, in soln., H-bonded protons in tertiary struct., PMR, assignments 77−90728
tRNA, conformation and intensity fluctuation spectroscopy, melting curves 78−35798
RNA, conformational fluctuations, internal motion correl. times, ^{31}P NMR obs. 80−72135
tRNA, genetic code origin, kinetic proofreading 79−92126
mRNA, H2b histone, sea urchin, sequence of 5'-end 79−74594
RNA, laser Raman spectra, cloverleaf secondary struct. 79−100569
tRNA, low-resolution phase extension using matrix direct methods 77−66875
RNA, nuclear Overhauser effect and solvent exchange rate, NMR expts. using supercond. magnet 79−74811
t-RNA, rot. relax. time, 10^{-9}s range Fabry-Perot and photoelectron time of arrival method 80−21437
t-RNA, simplified molecular model for use as teaching aid 77−78936
RNA, spliced viral messenger 79−92175
RNA in cytoplasm of eukaryotic cells, circular form from electron microscopy 79−83703
RNA nucleotide sequence, determ using computer 79−29500
RNA solns., oriented in DC mag. field light scatt. 79−2004
RNA synthesis kinetics, infolding and unambiguity of soln. of inverse problems 78−64921
rod external segment membrane, phospholipid auto-oxidation during conform. changes 77−21523
rotational correlation times, photocounting pulse fluorimetric determ., statistical accuracy 77−61777
rotational diffusion, passage saturation transfer EPR 77−8387
rubredoxin, forzen soln., recoilless fraction, Mossbauer spectra meas. 80−8025
rubredoxin, reduced analogue, EHT calc., Mossbauer parameters, zero field splittings 77−79544
salivary gland cell junction, Ca^{2+} produces graded changes in membrane channel permeab. 77−64016
sarcomere shortening, laser diffr. obs. 79−43808
sarcoplasmic reticulum, temp. dependent struct. rearrangements 79−53056
sarcoplasmic reticulum membranes, small angle X-ray data processing 80−81536
satellite tobacco necrosis virus struct., detect. and idealisation procedures of non-crystallographic symmetry with phase refinement appl. 80−108840
scaffold, in bacteriophage λ head formation, small angle X-ray scatt. study 79−11896
scanning microcalorimeters for studying macromolecules 80−61747
SCF-LCAO-ASMO and CI calcs. of low-lying multiplets and excited states 80−94155
scopolamine, permeation through human skin in vitro 77−21487
self-organisation, molecular recognition and information storage at the mol. level 78−82806
self-organizing molecular system, dynamics 80−67028
self-reproducing macromolecules, selection, controlled energy fluxes constraint 80−67027
SEM cathodoluminescence probing of biomol. species at 100 Å resolution or below 78−24197
SEM study of marine whelk haemocyanin mol., effects of coating materials 79−5421
semiconducting biopolymers and their part in biochemical phenomena 80−12053
semiquinone Q_{10}, EPR signal with unusual relax. parameters 77−56338
sequential fast kinetics, relaxation methods obs. 79−43575
L-serine, in aqueous solns., US spectra using automatic recording spectrometer 78−75735
serine, neutral and zwitterion, water solvation, Monte Carlo simulation 80−76707
serine proteases, enzymatic reaction mech. mol. orbital studies 77−60183
serine proteases, enzymatic reaction mechanism, CNDO/2 mol. orbital calcs. 78−27751
L-serine-L-ascorbic acid, X-ray cryst. struct. determ. 80−35827
serum albumen, bovine, adsorption kinetics, surface denaturation 79−79460
serum albumin, bovine, 2 types of soluble complexes with polyelectrolytes 79−92120
serum albumin, bovine, adsorpt. isotherm, at air-water and air-oil interfaces 79−79461
serum albumin, bovine, binding of spin-labelled stearic acid 79−96506
serum albumin, bovine, hydrated, dielec. and elec. props. 80−97854
serum albumin, bovine, molecular structure of adsorbed film 79−79462
serum albumin, bovine, mutual and tracer diffusion coeffs., photon correl. obs. 80−72123

molecular biophysics continued
serum low density lipoprotein, human, anomalous permittivity behaviour 80−81540
SHG study of non-centrosymmetric character 79−74599
sickle haemoglobin gelation, reaction order and crit. nucleus size 78−76983
single ligand binding constant computation, regulatory enzyme exponential model 79−79454
small fluid particles, dynamic props., applicability of neutron scatt. studies 79−41936
small molecules in protein solns., spin-lattice relax. times, inversion recovery spin-echo sequence 80−21446
small protein struct. anal. by electron microscopy, valinomycin, bacitracin, LMW-CSA N and B 79−92453
small-angle scattering, of X-rays and neutrons, (fourth international conf., Gatlinburg, USA (Oct. 77)) 79−10745
smectic lipid bilayer, in cryst. matrix, phase transition 80−21453
solitons in molecular systems, biophys. effects 80−51044
solute-water-macromolecule interactions rel. to membrane props., review 78−15789
solution, aqueous bimolecular, attractive and repulsive dispersion forces 78−44447
solution X-ray scattering, review of recent developments, book contrib. 80−109077
solvent accessibility properties of complex proteins 79−83696
southern bean mosaic virus, struct. at 2.8 Å resolution 80−85334
soya protein gels and sols, PMR relax. times rel. to temp., pH and conc. 78−56952
space environment, biological materials separation, electrokinetic phenomena and electrophoresis 79−48351
space-filling molecular models constructed by computer 77−40633
spectral sensitivyt analysis, math. techniques 77−52786
spectrochemical analysis of biological solns. using wall stabilised arc source 80−41343
spectroscopy, conference, Wroclaw, Poland (Sept. 1977) 78−62951
spectroscopy of biomolecules, DNA-dye complex fluoresc. 77−86444
spin labels, water soluble, factors restricting diffusion, rel. to biological use 77−86436
spin labels and biomembranes, review 78−69265
spin probe distribution between water and membrane in different conditions 77−21491
spin-labelled fatty acid derivatives, interaction with biomembrane lipid and protein components 77−70421
starch, H_2O mol. transverse PMR, temp. effects *(German)* 77−60186
static and dynamic structure of biomolecules, Mossbauer effect 80−40952
statistical mechanics 79−66456
stearic acid, large single cryst. growth from organic soln. 78−31314
stearic acid, single cryst. growth mechanism 78−30562
STEM use for two-dimensional molecular assemblies construction 78−24201
steroid research using mass spectrometry 80−51308
steroids, ^{13}C chemical shifts, β-, γ- and δ-substituent effects 77−23509
steroids, maximum overlap. mol. orbitals versus ab initio HF-SCF-MO calc., dipole energy 78−9070
Δ^5-steroids, methyl group rot. barriers from ^{13}C relax. data, geometry effect 78−13626
stratum corneum basic protein, epidermal keratin filaments, aggregation expts. 79−16142
streptomycin oxime selenate tetrahydrate, antibiotic, cryst. and mol. struct. 78−24028
structural change dynamics in biological particles, rapid light scatt. meas. 79−39615
structural determinations using synchrotron X-rays 80−46112
structure factor calculation, by FFT 77−51268
structure-function relationships of biologically active molecules, programs *(Russian)* 79−16137
structure-property and structure-activity correlations, graph theoretical anal. 79−26868
sublicons, special aspects of struct. 79−53034
substrate, small, binding to large biomolecule, fast kinetics studied by NMR, review 80−55662
subtilisin charge-relay system, electrostatic pot. map, STO transferable bond calc. 80−3571
subtilysin, globule, atomic density distrib. 79−79458
succinic dehydrogenase Fe-S centre of submitochondrial particles, ubisemiquinone interaction, EPR 78−69016
superweak interactions and the biological time direction 79−39344
surface labelling techniques for eukaryotic cells 77−56560
symmetry in systems 80−81519
synaptic and ephaptic transmission, quantum mech. tunnelling model 77−52772
synaptic membrane, acetylcholine-activated, interaction of fluoresc. probe 77−90762
systems with dipole-dipole interactions 79−11882
tail structure of temperate phage no.1 of Bacillus megaterium, electron micrograph 3-D reconstruction 80−35831
TEM, specimen damage and dehydration, struct. retrieval, instrumental limitations in biological struct. anal. 79−20735
testosteron, dielectric props. under UV excitation 80−6912
tetrabutylammonium iodide, in aq. proline soln., elec. conductance investigation 80−10692
tetracene, fluoresc. fading curve of lowest triplet state 79−36691
tetraglycine, aq. soln., density, viscosity and dielectric const., 0-60°C 78−47462
tetramethylammonium iodide, in aq. proline soln., elec. conductance investigation 80−10692
thaumatin antibodies as model of sweet taste receptor 78−27975
thiourea, struct., hydration, ab initio SCF calcs. 80−58142
thromboxane, evidence against prostaglandin hairpin conformation 80−3585
thymopoietin active fragment in H_2O, soln. conformation by DNMR spectroscopy 80−89710
tibosomal RNA interacting sequences, expt. determ., method and results 80−3586
time-resolved X-ray scatt. method 79−62409
tissue fluorochrome meas. with He-Cd UV laser 77−77962
tissue molecular dynamics and freezing phase transition studied by proton spin relax. 78−68983
tissue of new, proton spin-lattice relax. time study, blood, liver and tail samples 79−20515

molecular biophysics continued
tissues, normal and malignant, pulsed NMR obs. 80−94171
2,6 p-TNS fluorescence probe bound to apomyoglobin, nsec decay 77−29091
tobacco mosaic virus, data quality collected using modified mirror monochromator for rotation photography 79−9269
tobacco mosaic virus, solutions, Rayleigh scatt., elec. induced variations, spectral width and intensity meas. 78−48187
tomato bushy stunt virus crystals, appl. of oscillation method to data collection 80−14961
tooth enamel, human cryst. struct. refinement, Rietveld method 80−51040
topographic analysis in FORTRAN IV 79−88050
transferrin, ^{111}In labeled, perturbed angular correls. study 79−39342
transferrin, human, ^{57}Fe Mossbauer obs., λ and D values 77−21481
transferrin, human anal. density gradient equilib. centrifugation for determ. of mol. wt., sp. vol., preferential hydration 77−64160
transferrin bound Fe^{3+} during rat lymphosarcoma development, EPR 77−77878
tri-O-ethylamylose-solvent complexes, cryst. struct., chain conforms. 79−65067
triglycine, aq. soln., density, viscosity and dielectric const., 0-60°C 78−47462
triplet states in photosystem I of spinach chloroplasts and subchloroplast particles, EPR obs. 80−85344
tRNA in soln., selected topics review, book contrib. 80−108839
tropocollagen macromolecule form., effect of soln. pH 78−95999
tropomyosin, cryst. struct. and molecular interactions 79−48210
tropomyosin, isotopic H exchange as function of state of ionisation of side groups 78−68979
α-tropomyosin, specific splitting at cysteine-190, physicochem. study of fragments 80−30647
tropomyosin, thermal denaturing, causes of heterogeneity in fusion curves 79−53023
trypsin, bovine, activation, activity and inhibition *(German)* 79−79465
trypsin crystal fusion, microcalorimetry 77−70413
trypsin inhibitor, mol. dynamics, computer simulation 78−9932
trypsin inhibitor, soybean, folded, models for H exchange 78−76981
tryptophan, Fourier transform PMR in aq. soln., ^1H exchange and relax. rates meas. method 78−15049
tryptophan, pH dependent fluoresc., quenching by histidine *(Russian)* 78−90209
DL-tryptophan, polycryst., amino group rot., reorientation, mol. struct., 77-555K, PMR obs. 78−35047
tryptophan, Raman line characterisation 79−26996
tryptophan residue in horse liver alcohol dehydrogenase, room-temp. phosphoresc., temp. and enzymic complex form. effects 80−61512
tryptophan soln. containing histidine, fluoresc. rel. to soln. pH 80−2826
tryptophanyls, singlet and triplet states, role in protein inactivation 79−57564
tubulin proto-filaments, three-dimensional struct. 79−70520
tumour-bearing mouse tissues, proton T_1 study of water coverage parameter changes 79−24953
tyrosine fluorescence at 345 nm in proteins lacking tryptophan 79−39360
umbelliferone, excited states, in ethanol-water soln., absorption and emission spectra 79−13763
N_3-undecyllumiflavin, high resolution fluoresc. and excitation spectroscopy, vibronic transitions obs. 80−78639
UPS of biological mols., ionisation energy, assignments and electron donation 78−77005
uracil, RNA component, review of props. 79−53035
urea, electro-optical coeffs. meas., rel. to nonlinear optics calcs. 80−34889
urea molecule, bond-length corrections for external and internal vibrs. 80−106402
urease shear inactivation, metal ion effect, rel. to shear deform. effects in enzyme catalysis 78−76982
uric acid occurrence, growth morphology of $C_5H_4N_4O_3$ anhydrous monoclinic modification 80−84123
uridine monophosphate, excited state geometry distortion, normal modes reson. Raman intensity anal. 79−68236
DL-α-valine in aq. soln., dielectric dispersion 78−20141
valinomycin conformation in a phospholipid bilayer, ^1H NMR obs. 80−40958
valinomycin in its Ba complex, novel conformation 80−94167
Van der Waal's interaction of 2 parallel cylinders, simple interpolation formula 79−92122
Van der Waals interaction between loose structs. 78−95996
van der Waals interactions between surfaces of biological interest 77−44609
vascular walls, physical theory of permeability rel. to atherogenesis, mech. effects 80−16908
vasopressin, dark field electron micrographs, image array filtering in reciprocal space 77−74557
vesicular bilayer membranes, gangliosides orientation, ^1H NMR, viscometric and ultracentrifugation obs. 79−92162
vibrational analysis, comparison of algorithms for soln. of secular eqns. *(French)* 79−100565
viral DNA, nucleotide sequence 78−40114
viroid RNA, covalently closed circular mols., conform. states 80−85340
virus self-assembly by collisions 77−77867
virus-cell interactions, early molecular events, fluorescence and radioactivity obs. 79−100561
virus-cell interactions, early molecular events, kinetic study 79−100562
viruses in biological fluids, real time meas. using virometer 78−48869
vision, molecular basis 80−108876
vision, molecular mechanism for initial process 80−51089
visual chromophore, optical spectra of related polyenes 77−29102
visual chromophores, two-photon absorptivities, SCF-PPP-CI calcs. 79−31631
visual excitation, mol. mechanisms exam. by tunable laser resonance Raman spectroscopy 77−56378
visual excitation, molecular mechanism for initial process 79−100598
visual photopigments and pseudo-pigments, spectral sensitivity and neural interaction 77−25425
visual pigment and photoproduct spectral absorpt., crayfish rhabdom, pH sensitivity 78−65008
visual pigment model systems, spectroscopy and photochem. 77−32871
visual pigment spectra nomograms, wavelength depend. 77−25430

molecular biophysics continued
visual pigment unprotonated chromophore-protein bond, ^{13}C NMR spectra 78−11607
visual pigments, oil droplets and spectral sensitivity, pigeon 78−11655
visual pigments, reson. Raman studies, review 77−90729
visual pigments, resonance Raman studies of the primary photochemical event 80−41020
visual pigments of Gekko, ionochromic behaviour 77−36928
visual sensitising pigment in fly photoreceptor 77−90796
vitamin A, visual chromophores, two-photon spectra, lowest excited state 78−64934
vitamin A alcohol and acetate, compensation effect 79−51573
vitamin B_{12b}:B_{12r}, cryst. growth, orientation, ESR obs. 79−34486
vitamin B_{12}, CARS near one-photon reson. 77−65466
vitamin B_{12}, electrochemical reduction of methylcobalamin and methylcobinamide, one electron intermediates 78−85286
vitamin B_{12} derivatives, vis. and UV reson. Raman spectra, rapid flow method 77−66796
vitamin B_{12r}-^{181}Hf complex, γ-ray PAC expt., crystal and liq. 79−39341
vitamin B_6 fluorescence in cells 77−21496
vitamin D, role of free radicals in conversions and mechanisms of physiological action 77−70430
vitamin V_{12r}, monomeric O_2 adduct, struct., single cryst. ESR obs. 79−39351
water, in normal and senile cataractous eye lens 78−64987
water, lyotropic phase orientation, ^{17}O and ^2H NMR study 78−27905
water, rel. to NMR in biological systems 78−56952
water+glycine(serine) zwitterions, interaction pots., ab initio SCF LCAO calcs. 78−48747
water adsorbed on proteins, new programme for NMR study of diffusion 79−92139
water diffusion in wheat grain endosperm tissue, ^1H NMR obs. 80−8001
water in cataractous eye lens, NMR *(Hungarian)* 78−64986
water localisation in a DNA mol. by differential Fourier synthesis 80−94164
water molecules in biological systems, relax. rel. to vol., pulse NMR obs. 80−40960
water rotational mobility rel. to microwave dielec. props. of tissue 77−29092
water sorbed on DNA, temp. anomaly, IR spectroscopic obs. 80−51046
wheat germ agglutinin, struct. of binding sites, ligands with heavy atoms, phosphoresc. changes 79−24947
X-ray absorption spectra, review, book contrib. 79−5436
X-ray crystallography for symm. cryst., absorption-correction technique for arbitrary orientation 77−65932
X-ray crystallography for symm. cryst., semi-empirical absorption-correction technique 77−65931
X-ray crystallography using automatic flat-bed microdensitometer 77−35438
X-ray diffraction pattern of biological mols., improved method for solvent contrib. calc. 79−16355
X-ray diffraction patterns of seed materials subjected to mag. field 80−89721
x-ray diffraction studies of the heart, review, book contrib. 80−109079
X-ray low angle diffractometry of specimens with semiconductor spectrometer SERP-1(M) 79−53288
xanthine, and biological methyl derivatives, electronic struct. from UV photoelectron spectra 79−24949
xanthines, (theophylline, theobromine, caffeine), UV PES, constitutive subunits, methylatron effects 78−29798
zeaxanthin, aq. soln., aggregate, reson. Raman spectra, and IR spectra, exciton interactions 78−31770
zeaxanthin ([3R,3′R]-β,β-carotene-3-3′diol) as optical probe of membrane struct. 79−92124
2-zinc insulin, rhombohedral, cryst. struct. refinement, experience with fast Fourier least squares 78−92595
Be complexes, binding and orbital energies, biological systems ab initio calc. 80−102442
$(Be(OH)(NH_3)_3)^+$ model for biological active sites, ab initio calcs., comparison with Zn complex 80−104551
CH_3^+, carcinogen, attack on guanine, symposium contrib., Florida, USA (March 1979) 80−51946
CO-myoglobin, mol. tunnelling, isotope effect, time resolved IR Fourier transform obs. 80−72126
C_3O_2 polymers in primitive atmosphere rel. to living systems genetic code 79−83690
^{13}C, NMR of peptides and proteins, review 78−24023
Ca salts, biological mineralization mechanism 78−31764
$Ca_{10}(PO_4)_6(OH)_2$, dissolution in water at constant pH, exam. of kinetics 78−59949
$^{111}Cd^m$ bound on DNA, perturbed, γ-γ ang. correlations 79−79457
Co complex, oxygenated CoII amino acid-imdazole, XPS 78−21968
Co(II)-octaethylporphyrin, Mossbauer emission spectra 80−8020
CsDNA of T2 phage, in classical crystn. B form, struct., amplitudes, synchrotron radiation diffraction 80−85335
Cu(I) olfactory binding site 78−96060
Cu(II)-nucleic acid base interaction, MO calcs. 79−10013
DNA, linear dichroism, strand separation determ. 79−62188
FHF ion, H-bond excited electronic states, CI calc., dissoc. and autoionising states 80−5489
Fe-containing biomolecules, appl. of spectroscopy 79−24956
Fe-containing systems, electronic and mag. struct., semiempirical MO cluster calcs. 78−62733
Fe(III) Laeme complex, EPR g-value anal. 80−30657
$Fe_4S_4(SH)_4^{0,2-,3-}$, HFS-LCAO calcs., 4-Fe active site model in high pot. Fe protein and ferredoxin 80−42929
^{57}Fe, isomer shift calibration const. rel. to biological cpds. 80−7227
^{57}Fe transport and storage compounds 77−12875
Ga complexation by amino acids, with basic or heterocyclic groups *(French)* 78−53318
H-bonded model systems, intermolecular charge transfer, biological implications 80−3572
H^+-ATPase, soluble mitochondrial, thermal stability obs. 80−55992
H_2^+, 6 MeV, PIXE anal. of organic materials 80−26087
H_2O in biological samples, PMR, fast-exchange model interpretation via diffusional kinetics clarified 80−67033
H_2O proton relaxation in normal and cataractous cryst. lens 77−60203
^2H spin lattice relaxation, mols. with multiple internal rots., limiting behaviour 79−39356

molecular biophysics continued
^{39}K pulsed NMR obs. of whole body live and dead newborn mice 80−40964
Li complexes $((C_2H_2X_2)_2Li)^n$ where X=S, O, binding and orbital energies, biological systems ab initio calc. 80−102442
Mn II complex with amino acids and peptides in D_2O, NMR line widening 77−56328
MnII-ATP system, exchange mechanism, FT NMR and EPR obs. 79−22733
N_2 fixation, semiempirical INDO study 80−16898
NO radicals as spin labels, EPR 77−44860
NO-Fe(II)haemoproteins, orbit-orbit interaction, low temp. mag. circular dichroism obs. 80−30645
Na binding to biological materials, Auger electron spectra 78−53339
$(Na^+ + K^+)$ATPase, subunit comp. 79−83704
Nd complex, Nd^{3+}:ATP, electron spin echo decay envelope anal. 79−54871
O, singlet, photosensitised luminesc. in soln. 77−70309
O_2, quenching of luminescence by porphyrins and metalloporphyrins 79−50058
PO_4 electron structure rel. to synthesis and utilisation of ATP 80−40955
^{31}P-NMR study, crayfish perfused ventral nerve cords 79−79475
Pt-nucleoside complexes, Raman spectra, vibr. anal. 77−65473
S-S bond chirality, biomolecule struct. and activity depend., review 78−27889
$(Zn(OH)(NH_3)_2)^+$, model for biological active sites, ab initio calcs., comparison with Be complex 80−104551

molecular bonds *see bonds (chemical)*

molecular clusters
acetic acid vapours, clustering, effect of supersonic mol. beam sampling, mass spectrometric study 80−104481
admolecule association on conductor surfaces *(Russian)* 80−80078
aerosol cluster, mol., sticking probability to solid surface 77−12833
aerosol formation, growth, general dynamic eqn., H_2SO_4/H_2O aerosol simulation appl. 79−47990
alkali halide, equilib. geom., form. energy and vib. spectrum 78−55269
alkali halides, cluster ions and mol. ions in salt field desorption 80−40238
alkali halides, IR absorpt. in molecules, clusters and microcrystals 78−80363
alkali halides, sputtering and cluster formation, mass spectra and SIMS 79−19959
alkali metal hydroxide clusters in gas phase, high press. mass spectrometry, atmospherical implications 80−58436
biatomic molecular gas, quantum kinetic theory *(Rumanian)* 78−91053
n-,t-butanol in alkanes, molecular relaxation processes studied by ^{13}C NMR 80−63654
canonical partition, formulation 79−41121
carbon tetrachloride, clusters, collision induced polarisability, mol. frame distortion 80−32798
carbon tetrafluoride, clusters, collision induced polarisability, mol. frame distortion 80−32798
chromophore aggregates, circular dichroism spectra, calc. involving band shape 78−46478
Clebsch-Gordan coefficients, chain $SU(2) \supset D_\infty' \supset D_4' \supset D_2'$, mol. aggregates 78−17552
cluster beam, multiple stage ioniser, spatial potential distribution and electron trajectory calcs. *(Japanese)* 80−99596
cluster beam, nozzle flow formation and detection, high energy beam 80−5638
cluster beam for injector for heating and fuelling of toroidal plasma expt. 77−24179
concentration theory, latent image formation 79−34334
diamond (111) surfaces, relax. and reconstruction using C_4H_9 clusters, MINDO/3 calc. 79−42356
diamond clusters and corresponding saturated hydrocarbon ab-initio HF and PCILO calcs. 78−42951
diatomic clusters, break-up in thin films, particle energy distrib., central peak nature 80−50490
ejection from ion-bombarded metal surfaces, model 79−87543
electron attachment to mol. and mol. clusters, electron-mol. collision, Rydberg electron exchange 80−63843
electronic structure calcs. with double self-consistency-Bersuker's method 80−69289
electrons in fluids, picosecond chromodynamics 79−35850
ethane, clusters, excess electron localisation 79−68341
ethanol, H-bonding investigated with supersonic mol. beam using photoionisation quadrupole mass spectrometer 80−102543
ethylene($-d_4$) clusters, IR photodissoc. 80−89506
fluoride salts, static SIMS, mol. rearrangement, cluster formation 78−64440
hydroxonium complexes, produced by collisional dissoc. method, mass spectrometric study, dissoc. energies determ. 80−95707
ice, electron-irrad., cluster-ion prod., lattice and fragmentation energies 77−4911
imperfect vapour, eqn. of state 77−31413
imperfect vapour, nucleation theory 77−35289
ion cluster emission in SIMS, parity rule applics. *(French)* 80−63882
ion clusters, 3-body pots., SCF energy partitioning calcs. 80−18953
ion clusters in heteromolecular nucleation, steady state thermodynamic model 78−48687
ion solvation, growth around ions, heteromolecular nucleation 79−41260
ionic clusters, struct., thermodynamic functions, energy surfaces and SIMS 80−63881
ions, mol. clustering, gaseous-condensed state, nucleation and solvation 80−28129
isomeric structures, weights and effective characts. 79−31759
linear aggregates, small, polarisability determ., CNDO method and analytical models *(French)* 80−29298
liquid organic compound ionisation under atm. press. 80−86488
liquids, medium cluster model, vapour press. isotope effects, mol. orientation effect 77−72542
liquids, medium cluster model, vapour press. isotope effects 77−65943
localised HF orbitals for mol. clusters, layers and solids 78−9076
macromolecular aggregates, estimation of locations of subunits from neutron interference data 79−86716
metal clusters, bonding topology, graph-theoretical interpretation 78−33408
metal clusters, UPS 80−80940

molecular clusters continued
methane, clusters, collision induced polarisability, mol. frame distortion 80−32798
methane, liq., medium cluster model, vapour press. isotope effects 77−65943
methane, liq., medium cluster model, vapour press. isotope effects, mol. orientation effect 77−72542
methanol (-d), H-bonding investigated with supersonic mol. beam using photoionisation quadrupole mass spectrometer 80−102543
methanol adsorbed on Si/SiO_2 surface, light scatt. from clusters 79−33721
methyl($-d_3$) ions, association reactions, isotopic exchanges, SIFT study, review 80−58435
microemulsions, aerosol OT, inhomogeneous interior, fluoresc. and polarisation decay probes 80−50891
molecule cluster fluid, phase changes, theory 77−15534
$(MX)_n$, $(MX_2)_n$ ionic clusters, struct. and vibr. freqs. calcs. 78−94348
naphthalene-h_8-naphthalene-d_8 mixed crystal, monomer cluster states 79−15089
nozzle flowfield, cluster form., reservoir temp. scaling 80−5639
nucleation, homogeneous kinetic steady state solns. 80−50873
nucleation in finite systems, theory and computer simulation 80−26038
optical absorption, by aggregates of large rigid molecules 77−79720
optical spectra, near strong coupling limit, Green's function model 77−83774
polar molecule clusters, 3-body pots., SCF energy partitioning calcs. 80−18953
polymethine-cyanine molecular aggregate, band struct. 80−53174
polynuclear clusters, programs for calc. electronic struct. by Mulliken-Wolfsberg-Helmholtz method 80−69288
polystyrene solution, binary and ternary cluster integrals, small angle neutron scattering 79−50975
positive cluster ions, photodissoc. by CW and pulsed laser radn. 77−88513
positive ion clustering in mesopause region during winter anomaly, temp. and NO density vars. effect 79−21087
purple membrane of halobacterium halobium, aggregate optical spectra, moment anal. 79−2007
scattering states of clusters, multiple scattering X_α treatment 77−30747
serine, neutral and zwitterion, water solvation, Monte Carlo simulation 80−76707
small clusters, formations, struct. and props. 80−58437
spin and charge density theoretical determ., review 77−75045
structure sensitive factors in molecular cluster formation by ion bombardment of single crystal surfaces 79−19964
styrene-sodium methacrylate copolymers, Raman spectra, ion clustering 80−71416
supersaturated gas condensation kinetic model, cluster nucleation assoc. and dissoc. 78−85151
suspension concentrates, physical stability criteria, review 80−45562
tetracene molecules in Ar clusters, excited state intramol. dynamics, laser-induced fluoresc. spectra obs. 80−78674
thiazolidine, IR spectroscopy of mol. association *(French)* 79−50178
transition metal-carbonyl cluster molecules, electronic struct., localised orbital pseudopot. method 80−39653
trifluoroethanol, H-bonding investigated with supersonic mol. beam using photoionisation quadrupole mass spectrometer 80−102543
trimer ground states, quantum exchange effects 78−1117
triplet molecular aggregates, ESR line shape in solid matrix, fine and HFS 78−58878
water cluster ions, collision-induced dissoc. at high press. 77−83679
water cluster ions form. in ionospheric D-region rel. to mesospheric temp. 77−21842
$Al^{3+}(H_2O)n$ (n=1,2,4,6), FSGO-pair-pot. calcs. *(German)* 80−74278
Ar:H crystalline matrix, Xα scattered wave cluster model 79−73468
$BaTiO_3$ crystals, octahedral TiO_6^{8-} cluster atomic population, ionisation energy, SCF MS Xα calcs. 79−72244
$Be^{2+}(H_2O)_n$, (n=1,2,3,4,6), FSGO-pair-pot. calcs. *(German)* 80−74277
Bi_n molecular clusters, laser fluoresc. spectrosc. 80−95755
CO, adsorbed on Ni (100), freq. and amplitude of localised vibrs., cluster calc. 80−6616
CO, chemisorbed on Ni(100), mol. levels, angle depend. calcs. 78−90069
CO_2 free jet, rarefied flow, homogeneous condensation scaling law 80−6121
CO_2, proton affinity, cluster ion stability, mass spectrometer obs., appl. Martian ionosphere 77−77760
CO_2, supersonic jet, $(CO_2)_n^-$ cluster formation and electron attachment 78−5385
CO_2^-, hydrated anion stable gas phase heteronuclear clusters, mass spectra, autodetachment rates 80−14266
$CO_2^+ + 2CO_2 \rightleftharpoons (CO_2.CO_2)^+ + CO_2$, reaction rates 77−36745
$(CO_2.CO_2)^+ + CO \rightarrow (CO_2.CO)^+ + CO_2$, reaction rates 77−36745
CS_2, proton affinity, cluster ion stability, mass spectrometer obs., appl. Martian ionosphere 77−77760
$CaCl_2$, cluster ions and mol. ions in salt field desorption 80−40238
CoO, ab initio SCF and CI calcs. on d-d transitions, CoO_6^{10-} cluster d-electron localisation 77−35897
$D_3O^+(H_2O)_{0,1,2}+H_2O$ reactions, SIFT studies, review 80−58435
EuO, electronic struct. and props., mol. cluster approx. 77−11852
EuS, electronic struct. and props., mol. cluster approx. 77−11852
$F^-(H_2O)_2$, 3-body pots., SCF energy partitioning calcs. 80−18953
$F^-(H_2O)n$(n=1,2), FSGO-pair-pot. calcs. *(German)* 80−74278
GaAs, eliminating α exchange parameter in multiple scatt. method 80−103652
H, chemisorbed on Be(0001) surface, mol. orbital cluster theory 79−15002
H^-, prod. from accel. cluster ions for neutral beam plasma injection heating 77−65376
H_2, cluster beam formed from nozzle flow, isotope effect 80−6127
H_2, cluster beam source, cryopumping 79−63258
H_2, solid, electron-irrad., cluster-ion prod., lattice and fragmentation energies 77−4911
H_2+heavy inert gas, small clusters, beam cluster intensity and collision cross section 77−38711
HBr-nN_2 aggregates, near IR spectra in monatomic matrix 78−21921
HCl-N_2 mixture, electron swarm, Cl^-.HCl cluster formation, dissoc. attachment, drift tube mass spectra 78−68884
HCl-nN_2 aggregates, near IR spectra in monatomic matrix 78−21921
$(HF)_3$, 3-body pots.. SCF energy partitioning calcs. 80−18953
H_3F_2 and H_3F_3 clusters, molecular structures, ab initio calcs. 80−83532

molecular clusters continued
$H^+(H_2O)_c$ ion-induced water clusters, mass spectra, IR continuum absorpt. 80−87257
$H(H_2O)_n^+$, macromol. clusters, detect. by SIMS 79−39239
$H^+(H_2O)_n$, secondary electron emission from charged clusters on 2.4 keV Ar bombarded surfaces 79−15580
$H^+(NH_3)_n$, secondary electron emission from charged clusters on 2.4 keV Ar bombarded surfaces 79−15580
H_2O, charged clathrates, model for formation and stabilisation 80−91714
H_2O, warm fog and steam clouds, emission spectra variations, evidence for clusters in vapour phase 79−39849
H_2O-H_2SO_4-ion aerosol particles, ultrafine, stratospheric form., ion-induced nucleation 80−72608
H_2O-HNO_x-NO_x^- clusters, gas phase, thermodynamic quantities, mass spectra obs. 80−50875
$(H_2O)_n$, n=2 to 8, correlation energies, ab initio and SCF calcs. semiempirically corrected 80−43223
$H_6O_4^{2-}$, cluster anion tetrahedral struct. and stability, polarisation model 80−53181
$H_3O^+(H_2O)_{0,1,2}+D_2O$ reactions, SIFT studies, review 80−58435
$H_3O^+.H_2O$, cluster ion form. mech., rate coeffs. 78−25764
K^+-$(H_2O)_n$, complex struct., coord. numbers 79−7049
K_x, $(KNa)_x$, prep. and photoionisation pots. 78−55268
Li, adsorption of methyl groups, complex form., STO calcs. 77−9124
LiCl aqueous soln., ion-water clusters, electronic struct., Compton profile 78−47227
$Li_nCl^{(n-1)+}$, energy cluster expansion convergence 80−91715
LiF, aggregation, microcryst. form., IR spectra obs. 78−46331
$Li^+(H_2O)_n$, (n=1,2,3,4,6), FSGO-pair-pot. calcs. *(German)* 80−74277
$Li^+(OH_2)_2$, 3-body pots., SCF energy partitioning calcs. 80−18953
$Mg^{2+}(H_2O)n$ (n=1,2,4,6), FSGO-pair-pot. calcs. *(German)* 80−74278
$Mo_2Cl_8^{3-}$ ($Mo_2Cl_9^{3-}$), electronic struct. and metal-metal bonding, HMO calcs. *(Russian)* 78−1118
MoO_6^{6-}, electronic struct., discrete variation and scatt. wave X_α methods 80−917
$Mo_6X_8^{4+}$ cluster cpds. (X=F, Cl, Br, I), SCF-SW-Xα calcs. 80−74276
N_2, gas with clusters, free expansion, upper rot. levels population *(Russian)* 78−33581
N_2+heavy inert gas, small clusters, beam cluster intensity and collision cross section 77−38711
N_2(-Ne), gas, 77K, positron annihilation lifetime spectra 79−10630
NH_3, cluster-ion prod. in electron-irrad. solid, lattice, and fragmentation energies 77−4911
NH_4^+, mutual neutralisation, with simple and clustered positive (negative) ions 78−44372
$(NH_3)_nBi^+(Rb^+)(K^+)$, gas phase clusters, relative bond strengths, thermodynamic props. 78−35649
NO+heavy inert gas, small clusters, beam cluster intensity and collision cross section 77−38711
$NO^+ + 2N_2 \rightleftharpoons NO^+.N_2 + N_2$, rate const., enthalpy and bond strength 77−16809
NO_2^- hydrate clusters, ground-state HF pot., Monte Carlo simulation, energy surfaces and rot. barriers 80−106412
NO_2^-, $NO_2^-.H_2O$, and peroxy isomers, photodissoc. and photodetachment 3500-8250 Å, rel. to ionosphere 80−35554
NO_3^-, $NO_3^-.H_2O$, and peroxy isomers, photodissoc. and photodetachment 3500-8250 Å, rel. to ionosphere 80−35554
$NO_3^-.(HNO_3)_n$ clusters, form. studied by mass spectrometer, thermodynamic functions, sol. struct., 80−95754
Na_2^+-$(H_2O)_n$ clusters, gas phase, high press. mass spectrometry, atmospherical implications 80−58436
Na_x, $(NaK)_x$, prep. and photoionisation pots. 78−55268
NaCl crystals, electronic and hole centres and surface, quantum-chemical calcs. 80−65489
$(NaCl)_n$ (n=1-7) equilib. configs., total energy calcs., far IR spectra 78−29872
$Na^+(H_2O)n$ (n=1,2,4,6), FSGO-pair-pot. calcs. *(German)* 80−74278
$Nb_2Cl_9^{3-}$, electronic struct. and metal-metal bonding, HMO calcs. *(Russian)* 78−1118
NbO_2, rutile phase, energy levels, momentum density, and Compton profile, embedded cluster model 80−50453
Ne+heavy inert gas, small clusters, beam cluster intensity and collision cross section 77−38711
Ni (100), chemisorption of first row atoms, molecular cluster theory 77−1309
Ni (100), chemisorption of CO, Hartree-Fock-Slater mol. cluster calcs. 79−51650
Ni, CO chemisorption, (100) surface, mol. cluster theory 77−69174
NiO, ab initio SCF and CI calcs. on d-d transitions, NiO_6^{10-} d-electron delocalisation 77−35896
NiO, bulk props., initial state MO Ni_4O_4 and $Ni_{13}O_{14}$, cluster model, lattice and force consts., photoemission and CT absorpt. spectra 80−84828
O_2, gas, vibr. Raman spectrum, anomalous behaviour near crit. point 78−55179
$O_{2,}$ singlet state, form., quenching and reactions 77−29002
O_2^+ cluster ions, photodissoc. cross sections meas., 3500-8600 Å 79−24763
O_2+heavy inert gas, small clusters, beam cluster intensity and collision cross section 77−38711
$O_4^+(O_5^+)(O_6^+)(O_2^+H_2O)$ 80−95707
$Os_6(CO)_{18}$, electronic struct., metal cluster carbonyls mol. orbital description obs. 80−63879
$Re_3Cl_9^-$, electronic struct. and metal-metal bonding, HMO calcs. *(Russian)* 78−1118
$Rh_4(CO)_{12}$, bond energy terms from thermochem. data 78−62967
$Rh_6(CO)_{16}$, bond energy terms from thermochem. data 78−62967
SF_6, clusters, collision induced polarisability, mol. frame distortion 80−32798
$(SN)_x$, mol. cluster and band struct. calc. 77−8004
Si (111), chemisorption of H, localised model, ab initio HF-LCAO calc. 80−6930
Si (111) surfaces, relax. and reconstruction using Si_4H_9 clusters, MINDO/3 calc. 79−42356
Si, ambient effect of O precipitation, self interstitial mechanisms, IR spectra, TEM study 80−66510
Si_nH_{2n+2}, silane, SCF Xα MO calc., appl. to amorphous hydrogenated Si 80−49580
Si_xO_y structures, $Si(OA)_4$ clusters, A=H,Li,K, HMO calcs., energy stability, charge distrib. *(German)* 79−89822

molecular clusters continued
Ti:C, molecular cluster approach to electronic struct. and bonding mech. for impurity C 77−20270
UO_6^{6-}, electronic struct., discrete variation and scatt. wave X_α methods 80−917
VO_2, first principles calc. of intra-atomic correlation energy 79−23920
WO_6^{6-}, electronic struct., discrete variation and scatt. wave X_α methods 80−917
Zn^{2+}-H_2O clusters, solvation, Monte Carlo simulation 80−44102
Zn^{2+}.CO_2-H_2O clusters, solvation, Monte Carlo simulation 80−44102

molecular collision processes *see elastic scattering of atoms and molecules; molecular inelastic collisions*

molecular configuration interactions *see molecular electron correlations*

molecular configurations
see also bond angles; bond lengths; inorganic molecule configurations; isomerism; macromolecular configurations; molecular orbitals calculations; organic molecule configurations; X-ray diffraction examination of molecular structure
adsorbed molecular chains, config. props. effect on surface coverage 79−42371
aggregate, Stark spectroscopy, geometry, Heitler-London approx. dipole moments 78−55200
AH_2 systems, $1b_1$ orbital effect on geometry, CNDO/2 calcs. 79−13640
algorithm perceiving topological symmetry of molecule 79−41251
algorithms, mol. fragment recognition in E maps and electron density maps 78−55772
anions, struct. and energetic predictions, modified HF procedure evaluation 78−62720
arbitrary molecular point groups, fractional parentage concept 79−10225
Aufbau principle, rel. to mol. topology 78−74556
augmented connectivity molecular formula 79−83542
automatic geometry optimisation, Slater orbital derivatives, for d-orbital mols. 79−6831
axial symmetry molecules, graph theory *(Chinese)* 79−49964
axially symmetric molecules, graph theory, no atom on symmetry axis *(Chinese)* 79−36792
bond length changes on ionisation 77−34573
bound-state properties calcs., theoretical error estimates 80−102425
branching of mol. skeletal forms, algebraic characterisation 77−38625
bridge angle, vibr. behaviour, simplified and accurate calcs. 80−95735
character formulae for isoscalar factors of point groups 79−22858
charge distribution, quantum topology, bonding theory and molecular structure 80−5463
charge transfer complexes, geometries, CNDO/2 and EHT calcs. 79−36530
chemical bonding, antisymmetrised geminal power and simple correlated wave function 80−102423
chemical bonding studied using scattering theory concepts 80−103289
chemical mechanism struct. and coincidence of stoichiometric and kinetic subspaces 78−56877
chemical reactivity, reliability of quantum mechanical predictions, config. of reaction prod., H-bonded species 80−108691
chiral molecule, optical activity as mixed parity phenomenon 79−86011
chiral molecules, mol. symmetry rel. to cryst. space group *(French)* 77−31621
chiral molecules, prochiral centres, electronic and structural chirality 80−30220
chiral representations in one-centre mol. and field models, symmetry rules 80−14095
chirality functions, qualitative completeness concept *(German)* 79−27104
chirality functions, quantitative results *(German)* 79−27103
clusters, small, formation, struct. and props. 80−58437
CNDO method including d-functions *(German)* 79−22603
comparability of structs., ordering 78−57754
complex molecules, Cartesian coords. of atoms 79−41089
computer programs, math. model of chem. 79−52620
conformational props. rel. to spatial electron density determs., computer simulations 78−70763
conformers, dynamic interaction between ground states, effect on IR spectra 78−58767
conjugated circuits, correl. with Kekule valence structures 79−89582
conjugated system, N-electron CNDO Hamiltonian, approach to exact soln. 77−26979
constrained variation of geometry, FORMAC 79−10012
contracted Gaussian basis set for correl. wave functions, appl. struct. and energies 80−52881
critical volume, rel. to mol. struct. 79−41122
crystal structures, mol., principles *(German)* 79−42000
crystallographic data, molecular geometry, computer retrieval and anal., general principles and methods 78−83643
crystallographic data, molecular geometry, computer retrieval and anal., variance and interpretation 78−83644
$D_{\infty h}$, and subgps. down to C_3, MCD/MCPL saturation theory 78−74687
data base for force fields and mol. unit definitions 77−23575
diatomic systems, reln. between internuclear distances and force constants 80−43205
dimers, intersystem crossing, struct. 78−33537
direct CI calcs. with multiconfigurational reference state 80−63506
discrete optimal control for geometry optimisation 77−61694
distance geometry calc. of mol. conformation 77−50553
dynamical groups in atomic and molecular physics 80−42362
electron density mapping in mols., cyrsts., conf., Rehovot, Israel, (Apr. 1977) 78−71622
electron diffraction struct. investig., guide for publication of expt. data 77−1048
electron distribution anal. ab initio calcs. 80−47866
electron fast scattering for mol. characts. determ. 77−50536
14-electron isoelectronic series, ab initio calcs., equilib. geometry and electronic struct. 77−83489
electron-density maps of bent bonds, in non-cyclic mols., flexible-spring model 80−1084
electron-wave holography, molecular image reconstruction 77−79705
electrostatic potential predictions, basis set depend. 78−74786
energy component hypersurfaces, local behaviour regularities 77−42256
ethylene+cis-N_2H_2, chem. reaction, intermediate geom. calcs. 78−35655
excited states, variable metric optimisation of mol. geometry 80−58178
ferrocene, new interpretation of disordered cryst. struct., X-ray anal. 79−65063

molecular configurations continued
finite chemical graphs, characterisation by isomorphism invariant 79−13623
flexible molecules, chain end diffusion 80−23569
fluids, atomic and molecular, collision induced light scatt. *(German)* 79−27057
force field iterative consistency calcs. using geometric interpretation 77−6746
forces acting upon nuclei, Fourier transform calcs. 78−86774
four-body systems, rigid and nonrigid, correl. diagrams 79−45697
fragmentary composition, determ. by IR, EPR and US mag. reson. spectra *(Russian)* 78−13624
gas electron diffr., torsional vibr. effect on determ., pot. barrier height estimation 78−25743
gas linear molecules, symmetrised Liouville basis vectors, appl. to spectral linewidths 80−83457
gas phase electron diffr., partial wave electron scatt. factors 78−86963
geometry optimisation, Newton-Raphson method algorithm 77−10612
geometry optimisation, self consistent, semiempirical force field method 77−83760
geometry optimisation in ab initio SCF calcs., appl. of Hellmann-Feynman force 79−49927
geometry optimisation in mols. with second row atoms 77−42232
geometry optimisation with explicit inclusion of electron correl. 80−37748
geometry optimisations, invariance criteria, symmetry conservation rules 80−58406
geometry predictions using simple MO theory, teaching approach 78−93497
graphical struct., matrix descriptions 77−38737
graphs, search for self-avoiding paths 79−59336
ground state props., coupled cluster and MBPT methods appl. 80−47881
HAB_2, AB_2 mols., geometry prediction from HOMO 77−3256
heteroatomic cpds., paramag. reagents for ligand mol. struct. determ. from NMR 79−13741
high temperature gas and vapour characterisation, conf., Gaithersburg, USA (Sept. 1978) 80−53910
high temperature species, molecular shape determination 80−52233
hindered internal rotational molecules, nonbonded ligand interactions, symmetry determined investigation 78−70960
historical review *(Danish)* 79−9071
homeomorphism, structural, between nuclear pot. and electronic charge density 80−42968
icosahedral cage, symmetry coords. and vibration freq. 80−47966
image formation, electron holographic method, optical spatial domain filter appl. 80−10016
influence of solvent struct. on conformations 80−91700
interactive graphics display system 77−22536
internal rotational molecules, symmetric aspects of scalar props., appl. to ethane skeleton 78−70959
internuclear parameters measurement method using total scatt. of fast electrons 80−32857
intramolecular interactions effect on transferability props. of localised description of chemical groups 80−102424
inverted file structure for searching large data bases 78−35738
ion+molecule, intramolecular selectivity, stereochemistry, gas phase ionic chemistry techniques 80−35529
ionised compounds, geometrical and vibrational struct. changes, semiempirical MINDO/3 calcs. 79−31401
IR and Raman spectroscopy, molecular structural anal. appls. 79−35859
IR spin flip laser, matrix isolated photochemistry, isotopic, stereochemical and lattice site selectivity 78−92492
iterative EHT calcs. 78−46271
linear triatomic, config. stability in reson. light wave 79−64114
liquid surface, spreading vel., rel. to mol. struct. *(German)* 78−95209
mass spectrometric investigation, using mol. rearrangement 78−86972
mass spectrometry, mechanistic studies 80−47142
matrix isolated molecules, energy accumulation by migration to geometric trap configurations 80−78691
MCD forbidden transitions, generated by struct.-vibr. perturbations 77−50459
methane+tritium reaction, reaction ergodography 77−21371
minimum necessary no. of isotopic substitutions for geometry determ. from microwave spectra 77−3484
model molecule, skeleton-ligand interactions, algebraic invariant investig. 80−52853
modelling, design of computing systems 77−18814
molecular complexes, Cartesian coords. of atoms 79−41089
molecular crystals, optimum packing in atom-atom approx., algorithm and computer program 80−1960
molecular film, electron irrad., struct. changes, tunnelling spectra 77−10781
molecular force field iterative consistency calcs. using geometric interpretation 77−6746
molecular model building, computer program MMB 80 *(Japanese)* 79−36793
molecular models, semiautomatic coordinate meas. device using laser beams 79−37573
molecular packing arrangement drawings, plot of packing program POP1 79−94839
molecular topology, branching, distance matrix, information theoretic calcs. 78−25405
molecules under static mag. field, gauge invariance 80−102587
multidimensional dimer problem, upper bound improvement 78−78607
neutron scattering conference, Gatlinburg, TN, USA (June 1976) 79−41910
NMR in undergrad. instruction, general purpose microcomputers use for hypothetical spectra synthesis 80−42009
non-rigid molecules in condensed phases, liquid struct. effects on chem. reactions and conform. changes 80−40725
nonlinear molecules, tetrahedra, symmetry constraints on configurational props. 80−63854
nonlinear symmetric XY_2 type molecules, isotopic invariants, Coriolis coupling constants, centrifugal distortion constants 80−923
nonrigid molecule, sum of states, isometric group, symmetry no., thermodynamic functions 80−58186
nonrigid molecules, dipolar relax. and nuclear Overhauser effects, fluctuating internuclear distances effect 80−91578
nonrigid molecules, isometric group rel. to permutation-inversion group 79−22581

molecular configurations continued
nonrigid polyatomic fluid, chem. equilib., struct., statistical mech. calcs. 77−9111
one-electron props. variation with changes in mol. geometry, electronic and nuclear components partitioning 77−83491
optically active mols., coherent Raman scatt., quantum theory 80−69150
optically active mols., Raman and Rayleigh scatt. angle anal. 80−69151
optimisation, of 1st row mols., using bond function augmented basis sets 78−905
optimisation of geometry, normal coordinate ab initio force relax. 79−13833
ordering, graph theoretical basis 79−59326
oriented molecules, NMR spectra, vibr. correction study 80−18840
paramagnetic metal ions as structural probes for NMR investigation of inorganic and bioinorganic compounds 78−62828
PCILO-INDO method, theory and appls. 80−58153
phosphate-H_2O-Na^+ system, interactions 77−30773
photoelectron spectroscopy, review 78−1026
planar structure, double reson. signals depend., appl. to microwave spectra 80−32751
polyatomic molecule, atomic force correlation functions for determ. vibr. relax. rates, role of mol. symmetry 80−83337
polyatomic molecules, force consts. and geometry, pot. energy surface calcs. 77−14379
polyatomic molecules, Franck-Condon factors calcs. 78−17723
polyatomic molecules, structure recognition, from IR, UV, NMR and mass spectra, computer method 78−25737
polyatomic molecules, triplet states, var. and perturbational calcs. 77−61680
polyatomic mols., vibr. total energy distribs. in terms of symm. coords., forces and momenta 80−69123
polycyclic structure fragment searches 79−50156
polyhedra characteristic eqns. of graphs, symmetry factoring 77−83517
positive core potential energy method for conformational analysis 77−57850
quantum mechanical aspects of the molecular structure hypothesis 80−102421
quantum mechanical view of molecular structure and shapes 80−102422
quantum mechanics, mol. struct. defn. 80−52843
quantum theory, concept of mol. struct., interpretation problems 80−106248
quantum topology, theory of mol. struct. and its morphogenesis 80 106247
quartic centrifugal distortion consts., upper and lower bounds 79−45699
r_m structural determ. from rot. consts., test on OCS synthetic data 78−42236
radical, MINDO/3 unrestricted open-shell calcs. 77−23429
Raman optical activity parameters, circular intensity differentials comput. by atom-dipole interaction model 79−76407
Raman spectra of gases, high-resolution, mol. struct. and orops. 80−53000
Raman spectroscopy, vap., medium resolution, appls., review 78−42065
reaction paths, heat of formation, MINDO/2(3) forces method 78−9078
resonance Raman spectra, Dushinsky effect 79−45726
Richard's box, low-cost, superimposing mol. models on 3D electron density maps 79−35495
rigid molecular frames, generic scheme of important point groups 77−18815
rigid XYX and nonrigid three-body systems, correlation diagram 80−69249
ring characterisation method 80−63853
semi-rigid molecules, isometric group rel. to permutation-inversion group 79−22581
shape, second-order Jahn-Teller effect, highest occupied mol. orbital postulate 78−86780
similarities of configurations, computer-assisted-examination of substructs. 79−81294
similarity, electron density function meas. 80−91413
simple fluid, mol. dynamics simulation, including three-body interactions 80−54100
simple mol. charge distrib., empirical method, electrostatic pots. and struct. 78−82652
simulation, computer application 79−50158
skeletal branching, topological characterisation, appls. 79−31436
small molecules, localised charge densities calcs., bond length effects 80−83256
space filling molecular models 79−18309
sparse s and p type Gaussian basis set LCAO MO SCF calc., mol. props. 80−23306
spatial models, Stuart-Briegleb type, computer construction 78−86970
spatial structure, spectra interpretation, computer method 79−49962
spectroscopy computing, PUMSM 78−62782
stable molecules, matrix isolation spectroscopy obs., appls. 78−46320
stereochemistry, extremal arrangement of points, unit charges on sphere 77−79552
stereoisomer generation, algorithm and implementation 80−1080
stereoscopic diagrams prepared by desk calculator and plotter 77−37692
strongly interacting solvents, IR band shapes, solvent-induced chirality, field theoretic Green's function method 79−27037
structural formulae for chem. cpds., program for detecting presence or absence of struct. fragments 78−62941
structural similarity in molecules, graph theory recognition 79−50157
structure and dynamics of mols. by pulsed mol. beams 80−102563
structure determ. by isotopic substitution with geometrically equiv. atoms 77−3483
structure determination by diffraction methods, philosophical aspects 78−50665
structure elucidation algorithm (ASSEMBLE), computer construction 79−18104
structure-property and structure-activity correlations, graph theoretical anal. 79−26868
substitution structure, r_s struct. 78−42237
supersonic jet spectroscopy, appls., teaching approach 80−41996
symmetric top molecules, C_{3v} and D_{3h}, rot.-vibr. wavefunctions and mol. point groups 79−93971
symmetrical molecules, reorientation spectroscopic meas. models 80−58405
symmetry coordinates, description of mol. distortions 80−10517
symmetry coordinates construction, arbitrariness limitation 78−55252
symmetry in cryst., mol. struct., shapes 78−71697
symmetry properties of non-rigid molecules, unified approach 80−1083

molecular configurations continued
template formation, using electron microscope beam for pattern writing 77−30217
ten-atom model, interaction forces 79−59528
topological indices for branching of tree-like graphs 80−57076
topological spaces, structs. 80−91701
transformations of physical systems, decay, molecular rearrangements, causality 77−2551
transition metal complexes, O containing, coordinate bonding, charge transfer electronic bands, complex struct. determ. 80−52977
transition state characterisation by struct.-reactivity coeffs. 78−40026
triangular triatomic molecules, sextic centrifugal distortion constants, planarity relations 78−58649
triatomic molecules, angle deformation, force constant of angle deformation derivation 79−98239
twisted conjugated molecule, zwitterionic excited states investig. 80−58179
two and three-centre molecules, periodicity and internal torsional conformers around single bond, symmetry analysis 80−69250
van der Waals molecules, review, book contrib. 77−38709
vibrational spectroscopy, high pressure, and conformational analysis 80−9758
vibrational spectroscopy, structure identification 79−10092
volume characts., and electron correlations, one- and two-electron systems 77−3286
VSEPR model and Pauli exclusion principle, mol. geom. determ. and validity 79−31380
WINIMAX weighting factor, for isotope chem. and mol. struct. calcs. 80−27940
X_3YO molecules, ab initio MO calcs., geometry, electronic struct. 78−41940
XY_4, tetrahedral, SU $(2s+1)\times\zeta_r$ and spin statistical weights 78−50463
XY_4 tetrahedral mol., hyper-Raman scatt. intensities calc., tensor method *(French)* 79−22712
XY_6, octahedral, SU $(2s+1)\times\zeta_r$ and spin statistical weights 78−50463
$XY_6(O_h)$ octahedral system, F-(G-) matrix elements setting-up, transformation rules *(German)* 80−58242
H-bonded complexes, geometries, CNDO/2 and EHT calcs. 79−36530
XY_5, trigonal bipyramidal, SU $(2s+1)\times\zeta_r$ and spin statistical weights 78−50463
X_3YOH molecules, ab initio MO calcs., geometry, electronic struct. 78−41940

molecular conformations *see molecular configurations*

molecular dissociation
see also heat of dissociation; molecular dissociation energies; molecular electron impact dissociation; molecular photodissociation; molecular predissociation
$A+BC(^1\Sigma)$, structured collision, quantum mech. theory 77−88527
acetaldehyde radical cation, fragmentation, MO calc. 79−18109
acetalehyde decomposition reaction, intracavity laser spectroscopy obs. 79−61858
acetic acid, chemisorbed on MgO, decomposition mechanism 78−92502
acetic acid, ionised, pot. energy profiles for unimol. reactions 80−43210
acetic acid, vapour, chem. reaction effect on speed of sound 80−103100
acetic acid, viscosity of dissociating vapour 78−5840
acetone ions, fragmentation, kinetic energy release, mass spectra 77−79192
acetonitrile, adsorbed on ZnO, IR spectrum species identification *(French)* 79−82967
acetylene, adsorption, surface dissoc. and desorption on Pt (110) 77−62749
acetylene, chemisorbed on α-Fe, struct., bonding, dissoc., UPS obs., MO calcs. 78−84050
acetylene, dissoc. chemisorption on Pt (111) surface, EHT calcs. 79−39190
acetylene, reaction with Ni (100) and (110), room temp., UPS expts. 80−61151
acid dissociation consts., computer programs 80−26005
Acree relation, re-evaluation of its conceptual foundations *(French)* 78−7172
actinide oxides, preparation of metals and refractory cpds. 80−16229
actomyosin-ATP system kinetics, energy transform. anal. 77−81476
adsorbed molecules, ratios between rates of thermal dissociation, desorption and diffusion 79−95265
aliphatic perfluorocarbons, electron attachment, fragmentation 0-12 eV 80−5618
alkali atom+halogen mol., ion pair form., trajectory model 77−16800
alkali halide (100) surface, adsorbed monomers and dimers, pot. surfaces, diffusion dissoc. 77−66769
alkali metal hexachloroniobates and hexachlorotantalates, thermodynamic props. from VP meas. 79−34345
alkanes, collisional dissoc., time of flight mass spectrometric obs. 77−74545
alkanes, low press. triboelectric discharge, decomposition products *(French)* 77−48622
alkanes, tritiated, fragmentation by β-decay, dissoc. of daughter species 78−31669
alkenes, halogen substituted, chemisorption on Pt (100), Pt (111) substrates, photoelec. spectroscopy, dissociation model 77−43429
alkyl cyclobutane hydrocarbons, multiple initial vibr. state selection by chem. activation, relax. rate 77−40538
alkyl halide and σ^* anion radicals, stability 80−89468
alkyl halide photolysis by pulsed CO_2 TEA laser, mechanism 77−12807
alkyl substituted diacetylene radical cations, optical emission and photoelectron spectra, fragmentation decay 80−53004
allylmethylether, thermal and IR laser induced unimol. decompositions 78−20012
amino acids, ^{15}N-labelled, nanomole isotopic assay by collision induced dissoc. MS 78−20095
1-aminopyrene, protonated, excited state proton dissoc., time-resolved spectrosc. obs. 79−50164
anthracenes, exciplex form. with amines, form. kinetics and luminesc. props. 80−66792
aspartate transcarbamylase, solid, sedimentation and subunit interactions, after gamma irrad. 78−53342
atom+atom collision, mol. form in presence of third particle, Morse oscill. calcs., dissoc. cross sections *(Russian)* 77−32786
atom+diatom, collision induced dissoc., multiple scatt. theory 78−21999
atom+diatom, collision-induced dissoc., quantum mech. probabilities, close coupling calcs. 77−75259

molecular dissociation continued
atom+diatom, collision-induced dissoc., quantum mech. probability calcs. 78−25657
atom+diatomic molecule, restricted 2-D Morse oscillator model, semiclassical calcs. for mol. dissoc. 80−74222
atom+molecule, dissoc. and exchange, classical and near classical rates 79−11778
benzene, doubly charged ion fragmentation, ion kinetic energy spectrum peaks, collision gas sensitive 80−40679
benzene+molecular ion, fragmentation and electron transfer collisions 79−79229
benzene cation, internal energy selected, dissoc. dynamics 79−66274
benzoyl peroxide thermolysis, CIDNP obs. in low mag. fields 77−30885
n-butane, decomposition in RF discharges, 10-40 torr 78−3318
trans-2-butene, charge transfer mass spectra and photoelectron spectra 80−40778
cis-butene, ozonolysis, radical form., matrix ESR spectrosc. 80−16653
2-butene ion, fragmentation, angular momentum in ion-mol. reacts., RRKM calc. 80−66773
N-tert-butylacrylamide-styrene copolymers, struct., composition, IR, DTA investigs. *(Polish)* 79−31751
butyric acid, viscosity of dissociating vapour 78−5840
carbazole, excited state, dissociation rate, normal isotope effect 77−32767
catalyst surface mag. field effect on mol. dissoc. rate 80−16721
chemisorbed molecules, desorpt. kinetics 79−86977
chloroacetylene decomposition, unimolecular lifetime and relative translational energy distribs. 80−25994
chlorobenzene ion fragmentation, kinetic shift and phenyl ion heat at formation, photoelectron-photoion coincidence meas. 80−25998
clusters, small, formation, struct. and props. 80−58437
CO, dissoc. sorption on Pt, XPS obs. 77−16863
collision processes, angular correlations, summary of review papers 80−63757
collision spectroscopy, book 79−27065
collision-induced, high efficiency, in RF-only quadrupole 79−67419
collision-induced, Morse oscill. model 78−37710
collision-induced, tandem mass spectrometer obs. 80−62790
collisionally induced dissociation, struct. determ. 80−66357
complexes, differentiation between poly-, mononuclear, stability consts., graphical method 79−87927
cortisol, gas phase fragmentation, high voltage scanning field desorption obs. 78−3320
cyclobutane, dissoc., frontier orbitals and activation energy, HAM/3 method 78−92452
cyclobutane, thermal decomp., unimol. reaction theory 78−80712
cyclobutane decomposition, vibr. excitation transients using variable encounter method 80−61072
cyclobutene, strong collision and thermal decomp. on surface, variable encounter method calcs. 80−50885
cyclopropane, thermal decomp., unimol. reaction theory 78−80712
cyclopropane+inert gas, reactant decomp., rot.-vibr. energy transfer, relax. analytic soln. 80−55650
decomposition of isolated mols., transition state theory 77−16786
diatom dissociation and recombination mechanisms, bound complex and triple collision mechanisms 80−23478
diatomic, dissociation and recombination involving two states, soln. method 77−23535
diatomic, dissociation and recombination involving two states, model 77−27145
diatomic dissociation equilibrium, isotopic mass depend. theory 79−74372
diatomic gas, direct molecular simulation, using Monte Carlo method 78−23934
diatomic gas, dissoc. of nonequilib. gas, two-quanta V-V exchange 79−3547
diatomic gas, dissociation past strong shock waves 78−42683
diatomic mol., vibr. relaxation, nonequilibrial dissoc. rate consts. 77−52632
diatomic molecule, dissoc. due to gamma-quantum recoil momentum 77−1941
diatomic molecule, dissoc. electron attachment, adiabatic approx. *(Russian)* 79−94052
diatomic molecule, gaseous, dissociation rate const. eqn. 77−32769
diatomic molecule dissociation in thin films *(Russian)* 78−34558
diatomic molecules, collision induced gas phase dissoc. rate consts., discrete and continuum models 77−526
diatomic molecules, dissoc., thermal unimol. reactions, energy transfer, Monte Carlo calcs. 79−81166
diatomic molecules, dissoc., vibr.-rot. excitation effects 80−102502
diatomic molecules, dissociation, weak bias and anharmonicity effects 78−82661
diatomic molecules, vibr. relax. distrib. rate, rel. to nonequilib. vibr. levels and dissoc. 77−54596
diatomic molecules at low press., dissociative instability, role of vibr. energy 80−74227
diatomics, master eqn. theory, dissoc. rate consts. 77−77742
diazomethane, electronic struct., least energy dissoc. path to CH_2 and N_2 products 78−5131
p-diazoquinone, photodecomp. 80−7827
dibromoalkanes, energy partitioning in mass spectrometric displacement reactions 80−89471
dichlorodifluromethane, dissoc. into metastable fragments following electron impact excitation 78−37757
dicyclopentadiene dissoc., kinetics, multicolumn chromatographic reactor appl. 78−92590
diffusion-controlled reaction, theory 78−64820
dioxirane, decomposition products, mass spectrometric obs. 78−11504
1,3-diphenylisobenzofuran, oxidation, dissoc. oxciplex relax., solute reencounter probabilities 79−34285
dissociation-recombination, collision induced, exactly soluble model 78−7191
dissociative adsorption, quantum chem. theory, diatom-solid potentials 78−73087
dissociative charge transfer collisions, vibr. enhancement 78−33597
DNA-Au (III) interaction, rate consts., activation energies, pH, spectrophotometric obs. 80−30228
double-charged mols., investigation of single-charged ion products 78−37753
EDA complex, photoinduced ionic dissociation, radical-anion formation 77−40556

molecular dissociation continued
education, molecular dissociation model, dynamics and time averaged behaviour 78−61968
electron gas, dissociative recombination 80−36940
electron spectroscopy, coincidence experiments, two-parameter 78−20135
electronic excitation, mol. thermal strength depend. 77−46595
electronic polarization in solids probed by dissociation of fast molecular ions 80−71530
ethane, decomposition in RF discharges, 10-40 torr 78−3318
ethane, mass spectrometric ionis., dissociation 77−3488
ethane, shift of electronic spectrum during dissoc., CNDO calc. 80−37759
ethane, two-channel dissoc., dynamical effects, classical trajectory study 78−40042
ethane, unimol. decomp., energy transfer processes, Monte Carlo simulation 80−99555
ethane, unimol. decomp., mode localised excitation, trajectory studies 78−64815
ethanol, chemisorbed on MgO, decomposition mechanism 78−92502
ethanol, dissoc. adsorption on porous glass, IR obs. 79−23830
ethanol, ion internal energy selection by angle-resolved mass spectrometry 80−53164
ethanol, vap., decomposition by HF pulses IR laser irrad., press. depend. 78−85176
ethyl acetate, gas, radiatively heated by CO_2 laser, cooling mechanism investig. 80−75021
ethyl chloride, reson. multiphoton dissoc., excitation mechanism 79−100414
ethyl chloride, thermal decomp., unimol. reaction theory 78−80712
ethyl isocyanide, thermal decomp., unimol. reaction theory 78−80712
ethyl radical decomposition, mol. dynamics, trajectory studies 80−7780
ethylacetate, thermal and IR laser induced unimol. decompositions 78−20012
ethylene, adsorption and decomposition on Ni films, coverage depend. meas. 80−96743
ethylene, adsorption on Ni, Pd and Pt films, reactivity with adsorbed H, surface pot. meas. 79−86995
ethylene, adsorption on W (100) and decomposition to acetylene, AES obs. 79−66353
ethylene, chemisorbed on α-Fe, struct., bonding, dissoc., UPS obs., MO calcs. 78−84050
ethylene, chemistry in RF discharge, mass spectrometric obs. 77−9084
ethylene, decomposition in RF discharges, 10-40 torr 78−3318
ethylene, intense IR field multiphoton dissoc., primary products, fluoresc. obs. 79−36715
ethylene, ozonolysis, intermediate struct., multiconfig. SCF CI calcs. 80−18803
ethylene, ozonolysis, radical form., matrix ESR spectrosc. 80−16653
ethylene, planar dissociation, electronic rearrangement, states, bonds, ab initio multiconfigurational SCF calcs. 80−27937
ethylene adsorbed on Re *(French)* 78−85194
ethylene chemisorption on Pt (100), Pt (111) substrates, photoelec. spectroscopy, dissociation model 77−43429
ethylene mol. Green's function Σ perturbation method for mol. calcs. 78−55123
exponential transition probilities for collision induced dissoc. and vibr.-rot. relax. 78−27749
fast molecular ion+solid (gas), excited electronic states effects 80−9687
fast molecular ions, break-up on collision with solids 80−66353
fast molecular ions, collision induced fragmentation 80−66354
ferrites, plasma sputtering, struct. props. and phys.-chem. transform. *(Russian)* 79−38739
fluoroethyl radical, unimol. dissoc., pot. energy characts. and energy partitioning calcs. 80−45488
fluoroiodomethane, vibr. excited, dissociation, trajectory calcs. using pot. energy surface parameters 80−76508
fluoromethanols (mono and tri), decomposition activation of HF, nonstatistical energy partitioning, laser emission 79−945
formaldehyde$^+$, excited state dissoc., nonadiabatic interactions, conical and Jahn-Teller intersections, classical trajectory method 80−25997
formaldehyde, adsorbed on Ru(110), UPS study, 80K 78−73080
formaldehyde, adsorbed on W(100) single cryst., XPS obs. of decomp. 77−4927
formaldehyde, anharmonic pot. function, vibr. freqs., vibr.-rot. interaction, centrifugal distortion 77−38651
formaldehyde, chemisorbed on Rh, catalytic decomposition, transmission IR spectra 79−39199
formaldehyde, decomp. and absorpt. on hot W filament 77−90641
formaldehyde→H_2+CO, reaction path and activation energy, potential energy surface for ground state of formaldehyde 80−42967
formaldehyde decomposing to H_2+CO, reaction path Hamiltonian 80−45486
formic acid, catalytic decomposition on Pt, appl. of modulated mol. beam mass spectrometry anal. 78−56944
formic acid, chemisorption and decomp. on Cu (100), EELS study 80−16729
formic acid, decomp. on W (100), flash desorption obs. 79−29402
formic acid, decomposition, using Ni (110) catalyst, reaction kinetics and mechanism, mol. beam relax. spectroscopy 77−70340
formic acid, fragmentation, fragment structs. and energies calcs. 80−74124
formic acid, on Ni surface, decomp., dipole interactions effects 80−61143
formic acid, viscosity of dissociating vapour 78−5840
formic acid ions, fragmentation, energy selected, photoelectron-photoion spectra 80−95676
formic acid-d, decomposition on partially oxidised Ni (110) surface 77−85066
formic acid-d, kinetic study of D_2 formation using flash desorption technique 77−47683
gas, dissociating, relax. press. theory 79−81994
gas, dissociating, thermal cond. meas., temp. jump at gas-solid boundary 78−42701
gas-solid barrier permeability, absorption dissoc. anomalous temp. depend. 77−7977
gases, radiatively heated by CO_2 laser, cooling mechanism investig. 80−75021
glassy polymer multi-phase Stefan problem describing swelling and dissolution 78−2263
haemoglobin equilibria in soln., surface free energy model 80−81535
half-projected Hartree-Fock model, basis effects *(Spanish)* 77−67983

molecular dissociation continued
halocarbons, decomposition by siliceous land surface, meteorological constraints 79−12168
heavy particle shock-radiational recombination, chemiluminesc., kinetics, reversed predissoc. 77−1924
1,5-hexadiyne, time-depend. mass spectra, ionisation efficiency and breakdown curves 80−95747
hexafluoro ethyl cation fragmentation, mass spectrometry 80−53070
hexanes, isomeric, unimol. decomp. processes following field ionisation, temp. depend. 80−95733
hydrazine, decomp. on Ir(111) surface, N_2 emission, ang. depend. 80−97731
hydrazine adsorbed on Al, decomp., XPS obs. 80−92783
hydrides, aq. dissoc., solvation, MINDO/S calcs. solvation theory 80−97708
hydrocarbons decomposition reaction, with Ta and α-Hf, surface segregation influence of O_2 or N_2 80−55654
indirect dissociative recomb., T-matrix element, Feshbach's projection operator technique 80−58114
induction and transient times, in shock tubes 77−12794
interstellar molecules, collision-induced dissociation 80−17632
iodomethane(-d_3)$^+ \rightarrow CH_3^+(CD_3^+)$+I, kinetic energy release distrib. meas. 77−1922
ion beam injection technique, mol. photodissoc. 77−83134
ion kinetic energy release on fragmentation, photoelectron-photoion coincidence meas. 77−79192
ion lifetime distribution, following interaction with collision gas, determ. method 79−36732
ionic fragmentation, translational energy, phase space theory 77−9051
ions, multiple dissoc. probabilities 80−40678
isopropanol, on α- and β-V_2O_5 bronzes, 186-300°C, kinetics and mechanism 78−11553
isopropylbromide, thermal and IR laser induced unimol. decompositions 78−20012
JWKB quantisation condition, appl., breakdown and near-dissoc. behaviour 78−58571
ketene, photoionis., ion fragmentation kinetic energy 78−9206
large molecular ions, dissoc. recombination 79−7012
laser induced unimolecular dissociation of octafluorocyclobutane 77−32775
linoleic acid, adsorbed on Al_2O_3, under carbon tetrachloride immersion, IR obs. 79−24822
lysozyme complex with substrate-inhibitors, photosensitised electron transfer, role of Cu^{2+} 80−30638
macromolecular weak bonds, Brownian motion theory of transition rates 77−36731
mass action law in molecular system dissociating in laser radiation 77−70298
mass spectrometric fragmentation, MO-model and simulation 77−417
mass spectrometric fragmentation processes, dispersion relation 77−79704
mass spectrometry, energetics of theory, review 78−319
mass spectrometry, mechanistic studies 80−47142
metal compounds, double discharge technique for metal atom laser operation 77−54702
metastable ion decomposition, mass spectra peak shapes 77−44475
metastable ion decomposition, mass spectra peak shapes 77−44476
metastable unimolecular transition, collision-induced transition, energetic analysis by static mass spectrometers *(Rumanian)* 78−46460
methane, decomposition in RF discharges, 10-40 torr 78−3318
methane, dissoc. by adsorption-desorption process on W 78−92511
methane, dissoc. chemisorption on Rh (111) surface, vibr. activation 79−57292
methane, ion internal energy selection by angle-resolved mass spectrometry 80−53164
methane, photoionis., ion fragmentation kinetic energy 78−9206
methane+N^+, charge transfer reaction, dissoc., isotope effects, mass spectra 77−21382
methane+X^{n+}, (X=Ar,Kr,Xe,U), Auger emission line shape after dissoc. 78−86838
methane ions, fragmentation, kinetic energy release, mass spectra 77−79192
methane-d_0(-d_4), unimol. decomp., energy transfer processes, Monte Carlo simulation 80−99555
methanol, adsorption and decomposition on W 77−31887
methanol, and deuterates, dissoc. ionisation mechanisms, photoionisation mass spectra, ionic struct., interstellar formation 79−3503
methanol, ion internal energy selection by angle-resolved mass spectrometry 80−53164
methanol, ionic dissoc., photoelectron-photoion coincidence spectroscopy 80−66774
methanol, laser-induced decomp., comparative obs. using pulsed HF and CO_2 lasers 80−11888
methyl iodide ion, induced by collision with Kr atom, mass spectra *(Russian)* 77−88549
methyl isocyanide, thermal decomp., unimol. reaction theory 78−80712
methylcyclobutane, form. by ketene (diazomethane)+cyclobutane photolyses, decomp., CH_2 vibr. energy distrib. 78−61032
micelle dissociation-recombination kinetics, stochastic model 80−30291
molecular gas, laser irrad., field avoided crossings, new transition channels 78−33477
molecular-ion beam dissociation in thin foils 77−86315
molecule+fast heavy ion, dissoc. ionisation obs. 79−47899
Morse oscillator+atom, collinear collision, T-V energy transfer, excitation and dissociation processes 78−90269
Morse oscillator collinear collision induced dissoc., vibr. enhancement, quasiclassical trajectory study 80−28089
multiphoton transitions, perturbation theory, atomic ionisation and intermediate reson., dissoc., review 79−41145
naphthylamines, abnormal fluorimetric titration behaviour, kinetic anal., fluoresc. quantum yields and lifetime meas. 80−89560
naphthylamines, excited state pK_a* values, proton-induced fluorescence quenching 78−21958
negative ion unimolecular gas-phase decomposition, field ionis., technique for 10^{-11}-10^{-5} s lifetime 79−92046
neopentylcyclobutane, $^1CH_2$-activated, decomposition rate const., press. depend., internal vibr. relax. 78−64819
nitrobenzene, collision-induced dissoc., ionisation characts. in corona discharge 77−60156
nonadiabatic interactions, conical and Jahn-Teller intersections, classical trajectory method 80−25997

molecular dissociation continued
nonequilibrium dissoc., Morse oscill. rigid rotator system, master eqn. soln. 80−40682
nonequilibrium kinetics, linear mixture formula, eigenvalue approx. 77−63895
nonequilibrium plasma chemical reaction kinetics 78−76863
nonideal gas, dissociating, composition and thermodynamic props., initial at. method 78−40034
nonisothermal ideal gas mixture, stationary state, inert and dissoc.-assoc. components 77−60042
nonradiative transitions, vibr. spectra *(Russian)* 78−21864
nylon-6 fibre, chain rupture and tensile deform. viscosity-av. mol. wt. obs. 78−76714
octafluorocyclobutane, laser induced unimolecular decomposition 77−32775
organic ion, excited electronic state correlation with mass-spectral fragmentation pattern 80−45482
organic ions, pot. energy profiles for unimol. reactions 80−43210
organic molecules containing O, chemisorption and decomp. on Pd 77−63953
oxalyl fluoride, radiative and nonradiative transitions, self-quenching, unimol. dissoc. 78−17708
pentenes, in combustion of pentane, further reactions, isotopic tracer obs. 79−8438
perfluorobenzene, electron attachment, radiative and dissoc., negative ion lifetimes, ion cyclotron reson. spectra 80−74251
perfluorocarbon-SF_6 mixtures, sparking C inhibition, decomp. product investig. 80−89478
perfluorocyclobutane, electron attachment, radiative and dissoc., negative ion lifetimes, ion cyclotron reson. spectra 80−74251
perfluoromethylcyclohexane, electron attachment, radiative and dissoc., negative ion lifetimes, ion cyclotron reson. spectra 80−74251
perfluorotoluene, electron attachment, radiative and dissoc., negative ion lifetimes, ion cyclotron reson. spectra 80−74251
peroxides in ozonised PVC, chemilum. meas. 78−68893
phenoxy radical dimer, reversible diffusion controlled dissoc., detailed equilib. principle 80−7770
phosphonium cations, quaternary, produced by field desorption, collisional activation spectra 78−56946
photochemical smog, rate parameters and computer simulation 78−48677
poly(oxycarbonylimino-1,4-phenylene), apparent sublimation: thermal decomposition+condensation repolymerisation 78−3332
polyamides, molecular breaking under load, hydrolysis 78−11519
polyatomic, high temp. effect 78−35675
polyatomic ions, energy deposition on high-energy collision, angle-resolved mass spectrometry obs. 80−32825
polyatomic molecule, dissoc., natural collision coords. 78−44373
polyatomic molecule, selected fragment vibr. energy distrib. in dissoc. processes 78−1036
polyatomic molecule dissociation, thermochemical study of thermal negative ion production *(Japanese)* 80−50495
polyatomic molecule under nonequilibrium conditions, dissoc. kinetics, unimol. decomp. rates 80−11886
polyatomic molecules, energised, mean lifetime *(German)* 78−85131
polyatomic mols., dissoc. reaction path Hamiltonian 80−45486
polyatomics, restricted intramolecular vibr. relax. and laser selective effects 80−27992
polybutadiene, cross linked, deform. below T_g, radical form. and crazing 79−52307
polycarbonate, decomposition by H_2SO_4 and grinding by ball mill, exam. of molecular chain scission *(Japanese)* 78−64827
polyethylene, low density, melt flow, mech. degradation *(Russian)* 79−50691
polyethylene film, chain rupture and tensile deform., viscosity-av. mol. wt. obs. 78−76714
polyethylene terephthalate, chain rupture and tensile deform., viscosity-av. mol. wt. obs. 78−76714
polymer matrix composites, component interaction mass spectrometry investigation *(Russian)* 80−35511
polymers, decomposition by hydrolytic mechanisms 79−55016
polymers, oligomer mass spectral charact. 80−37916
polypropylene, film and fibre, chain rupture and tensile deform., viscosity-av. mol. wt. obs. 78−76714
polystyrene solutions, US degradation obs. 78−95989
positive column, of electroneg. gas, transverse stability, effect of dissoc. attachment 79−23475
propan-1-ol, ion internal energy selection by angle-resolved mass spectrometry 80−53164
propane, ion internal energy selection by angle-resolved mass spectrometry 80−53164
propane, radiative thermal cracking on porous glass *(Russian)* 79−39205
propane mol. ion, competing slow metastable processes, tunnelling mechanism, tandem-ICR obs. 77−28976
propanol, chemisorbed on MgO, decomposition mechanism 78−92502
propionic acid, viscosity of dissociating vapour 78−5840
proteins, thermal denaturation, use of high heating rates to separate denaturation and aggregation 77−81470
R-matrix appls., quantum defect, frame transportation 78−58761
real gas, blast wave, effects of compressibility, vibr. excitation, dissoc. and ionisation 77−68622
RRKM formula correction by non Boltzmann character factors, Markov eqns. 80−71891
RX^-, radical anion stability conditions, pot. energy diagrams 80−85161
Saha equation, elementary derivation, rel. to mol. dissoc. 80−82599
shortwave emission, influence of vibrational kinetics, appl. in plasma UV lasers 77−42395
small molecule, IR laser induced collisional pumping 78−25630
small molecule IR laser induced collisional pumping 78−25629
sulphonium cations, tertiary, produced by field desorption, collisional activation spectra 78−56946
surface interaction with adsorbed molecules, dissociation 77−31875
TCNB-MTHF EDA complex, sensitized biphotonic radical anion formation 77−40556
TCNE electron donor/acceptor complexes, photoionic dissoc., photocurrents 77−14502
tetra-n-butylammonium picrate, soln. in benzene, field dissoc. effect on ion pairs 79−91061
tetrafluoroethylene, high temp. oxidation behind refl. shock waves 77−36743

molecular dissociation continued
tetrafluoromethane gas, total dissociation, in reactive ion etching system, reactant supply 79−83349
tetrahedral and octahedral complexes, mol. vibrs. and reaction pathways, min. energy coords. and compliance consts. 77−57966
tetramethyldioxetane, collisional dissoc. by supersonic Xe beam, chemiluminesc. 78−40029
tetramethyldioxetane, gas phase unimol. decomp. and chemiluminesc. initiated by TEA CO_2 laser 77−60068
tetramethyldioxetane, photolysis, unimolecular decay probed by picosec. spectroscopy 77−60083
thermal desorption and dissociation catalyzed by a solid surface 80−108734
three-particle recombination, shift of chem. equilib. in laser reson. IR radiation field 77−56224
toluene, 91^{2+} ion fragmentation, ion kinetic energy spectrum peaks, collision gas sensitive 80−40679
triatomic negative ion fragmentation, energy partitioning isotope effects, Monte-Carlo calcs. 77−27126
triatomic negative ions, dissoc. product kinetic energy, classical trajectory method 78−64809
trichlorofluoromethane, dissoc. electron attachment, pot. curves calcs. 79−98231
trichlorofluoromethane, dissoc. into metastable fragments following electron impact excitation 78−37757
trichlorofluoromethane anion, dissoc. electron attachment, pot. curves calcs. 79−98231
trifluoroiodomethane ion, induced by collision with Kr atom, mass spectra *(Russian)* 77−88549
trifluoromethane, D ultrahigh single-step enrichment by CO_2 laser photolysis 80−45527
trifluoromethanesulphonic acid, and salts, electrochem. characts. in nonaqueous solvents 80−89499
α-tropomyosin, specific splitting at cysteine-190, physicochem. study of fragments 80−30647
two-photon technique for dissoc. limit determ. 77−3425
unimolecular, master eqns., analytic theory of extrema 80−50841
unimolecular decay dynamics, pole approx. calcs. 80−35501
unimolecular decomp. kinetics, rot. effects 80−81319
unimolecular dissoc. kinetic energy distrib., photoelectron-photoion coincidence spectrometer for the study of translational energy release distributions 80−11974
unimolecular dissociation dynamics, collinear triat. system, R-matrix method 79−70315
unimolecular reaction theory mean first passage time and reaction rates 78−60986
unimolecular reactions, dynamics, short-range interfragment coupling and incomplete randomisation 78−80735
water, decomposition by fusion energy, H_2 prod., synthetic fuel 78−50335
water, vapour, dissociated, thermodynamic props. *(Japanese)* 77−80263
water cluster ions, collision-induced dissoc. at high press. 77−83679
water molecule, photoassisted decomposition at $SrTiO_3$ surface 80−85202
water splitting thermochemical cycle for synthetic fuel prod. at fusion reactors 78−58458
water vapour, dissociating, composition and thermodynamic props., initial at. method 78−40034
$2NO_2 \rightleftharpoons N_2O_4$, multiple stationary states, hysteresis 77−9074
$AgAsS_2$, dissociation pressures and their temp. depend. 79−52640
Ag_3AsS_2, dissociation pressures and their temp. depend. 79−52640
AgH, gaseous, dissociation 79−91925
AlH_3, effect of 1 MeV Co^{60} γ-irrad. on isothermal decomp. 78−92472
AlN, $(^2P)Al$-$(^4S)N$, $(^2P)Al$-$(^2D)N$, nonempirical pseudopotential, configuration interaction calcs. 79−93930
Ar^{2+} dissociative recombination in $Ar+N_2$ early afterglow 79−34305
$Ar+Ar_2$, exchange and dissoc. interactions, three-body effects calcs. 77−9069
$Ar+H_2$, 4500K dissoc. collision vibr. selectivity, Monte Carlo trajectory method 79−70307
$Ar+H_2$, dissoc., recombination and inelastic scatt. pot. energy surface and cross section Monte Carlo calc. 77−27162
$Ar+H_2$, vibr. and rot. transfer enhancement of dissoc. cross section 77−34732
$Ar+HCN(H_2O)$, electron excitation of Ar* and Ar_2*, fluoresc. and dissoc. energy transfer collisions 77−14580
Ar^++molecule (atom), dissociative reaction rate coeffs., in high-press. afterglow 79−87837
Ar_2^+, dissoc. recomb., total rate coeff. depend. on electron temp. 78−58817
ArH^+, dissociative recombination rates 77−86295
Ar*+formaldehyde thermal collisions, $CH(A^2\Delta=X^2\Pi)$ emission 77−86304
AuH, gaseous, dissociation 79−91925
BF_3, dissoc. pathways and mol. vibr., compliance consts. and min. energy coords. 78−35661
BiLi, gas phase thermodynamics, Knudsen effusion mass spectrosc. 80−100057
Br_2, dissoc. and recomb. rate consts. meas., 1200-3000K techniques comparison 77−63892
Br_2, dissociating flow in supersonic nozzles, atomic recomb. and vibr. relax. effects 78−42677
Br_2, in Ar, deactivation and dissoc., microscopic process simulation 78−11511
Br_2, vibrational relaxation and dissoc. behind a shock front, absorpt. spectroscopy *(Russian)* 77−88536
Br_2+Ar collisions, dissociation reaction, trajectory study by ensemble method 80−66765
$Br_2+Ar \rightarrow 2Br+Ar$, 3500K trajectory anal., rate const. 77−52617
$Br_2+I(5^2P_{1/2})$, deactivation kinetics, $Br(4^2P_{1/2})$ prod., time-resolved spectrosc. obs. 78−95917
Br_2+K, inelastic scatt., total cross-sections, trajectory surface hopping calcs. 78−46420
C-H, $A^2\Delta$-$X^2\Pi$, dissociative excitation, form. environment and parent mol. effects 80−78682
$CCl_2FO_2NO_2$, thermal dissoc., rel. to photodissoc. and stratospheric Cl budget 79−74931
CH^+ $X\,^1\Sigma^+$, dissoc. recomb. rate coeff., rel. to interstellar mol. form. 78−56884
CH_3^+, CD_3^+, collisional activation to form $C(H,D)_{0\text{-}3}^+$ products, energy transfer 77−44474
CH_3^++e, dissociative recomb. reaction in interstellar clouds, products, statistical theory 78−57604
CH_3^++small molecules, binary and ternary reactions at thermal energies, rate coeffs., product distribs. 78−44358
CH_4^+, CD_4^+, collisional activation to form $C(H,D)_{0\text{-}3}^+$ products, energy transfer 77−44474
$CH_4^+ \rightarrow CH_3^+ + H$, MINDO/3-FORCES calc., activation energy and reaction enthalpy 78−66472
CH_4^+, Jahn-Teller distortion, energy and angular distrib. of collisional dissociation fragment 80−66356
$CH_4+H^+(He^+)(O^+)$, 1 MeV dissociation, kinetic energy spectra 78−94302
$(CH_3)_3SnH$, radical initiated dissoc., Sn isotope separation *(Russian)* 79−59604
$(CH_3)_2X$ molecules, perturbational MO anal., methyl rot. barriers, fragmentation mode 77−88386
CO, $^1\Sigma^+$ state, ionisation pots., dissoc. energy, atoms-in-mol. calcs. 77−88410
CO, adsorbed on stepped Ni, thermal decomposition, LEED, AES, thermal flash desorption study 78−71984
CO, adsorption and dissoc. on Mo (100), comparison with carburised surface 77−15689
CO, chemisorbed on Mo (100), surface kinetics, photoemission study method 80−80941
CO, chemisorbed on Rh (111), dissociation probability, isotopic exchange and AES meas. 80−40743
CO, chemisorption on Ti (10$\bar{1}$1), XPS, UPS, flash desorption mass spectra, and active ion bombard. obs. 79−11822
CO, dissoc. chemisorption on Ni(Fe) cryst. surface *(German)* 78−53257
CO, dissociative chemisorption on Co (10$\bar{1}$2) 79−4474
CO, dissociative chemisorption of Ru, isotope exchange 79−34354
CO, nonequilib. dissoc. induced by electron-vibr. and IR laser pumping 79−86016
CO, on W (100), surface vibrs., EELS 77−62745
CO^+, exploding fast mol. ions, Auger spectra 80−32781
CO^+ in cometary coma, dissoc. recomb. rel. to C prod. 79−16885
CO+Ar, shock heated steady state dissoc. rate consts. calc. 78−40039
$CO+H_2^+(He^+)$, dissoc, charge transfer, energy transfer processes 78−74759
$CO+X^{n+}$, X=Ar,Kr,Xe,U, Auger emission line shape after dissoc. 78−86838
$CO^+ + CO$, metastable and $X^2\Sigma^+$ states dissoc. 78−33587
CO_2, C $1s^{-1}$, π^*-state decay, fragment ion relative abundance by electron-ion coincidence technique 80−9743
$CO_2 \rightarrow CO+O$, dissoc. pathways, pot. energy surface and vibr. anal. of IR and Raman spectra 78−64826
CO_2 CW laser, vibr. temp., dissoc. and gain limitation determ., new technique 80−87369
CO_2, dissoc., high temp. effect 78−35675
CO_2, dissoc. in high-press. nonequilib. plasma 79−15991
CO_2, dissoc. in nonequilib. plasma of stationary plasma-beam discharge *(Russian)* 79−99006
CO_2, dissoc. in shock tube, interferometric meas. 77−9071
CO_2 dissociation in a nonequilibrium plasma 80−87851
CO_2, dissociation into CO and O_2, H_2 production from CO+steam, fusion reactor heat 80−67014
CO_2, initial rate of decomposition in volume discharges 79−50905
CO_2, plasma radiolysis by high current relativistic electron beam 79−91947
CO_2, plasma-chemical dissoc. in nonequilib. UHF and high freq. discharges 79−15990
CO_2 sealed high-pressure pulsed laser, gas equilibrium chemical comp. 80−63972
CO_2, valence shell ionic photofragmentation, oscill. strengths, EELS and electron-ion coincidence meas. 80−37879
CO_2^-, dissoc., $^2\Sigma_g^+$ state, Wall Porter pot. surface, autodetachment and vibr. level population inversion 80−21275
CO_2^+, thin foil impact, dissoc. struct. effects in ionic fragment energy spectra 78−50631
CO_2-N_2-He, vol. discharge, negative ions effect 80−14956
CO_2+Ar^*, CO* prod., use in laser systems 80−63824
$CO_2+He^+(H_2^+)$, charge transfer, energy transfer, product ion excitation and fluoresc. 77−75288
CO_2+inert gas, reactant decomp., rot.-vibr. energy transfer, relax. analytic soln. 80−55650
CO_2+X^{n+}, (X=Ar,Kr,Xe,U), Auger emission line shape after dissoc. 78−86838
CO_3^-, formation and dissociation in CO_2 77−60058
CO_2(-He) discharge, UV-initiated, electron ion recomb. and CO_2 dissoc. 80−44068
$CO_2^+(CO_2^{2+})$+atom(mol.), dissoc. and charge transfer 77−65532
CS_2, shock heated, visible emission 80−58274
CS_2, thermochem. generation of CS for CO chem. lasers 77−23666
CS_2^+, dissociation mechanism 79−59601
CS_2+Ar^*, Penning ionisation and dissoc. fluoresc, collisional energy depend. 78−33584
$CS_2^+ + Kr$, collision-induced dissociation *(Russian)* 77−88549
CaCl, $X^2\Sigma$ pot. energy curves, polarisability and dissoc. 80−91629
$Ce(HPO_4)_2 \times 1.33H_2O$, crystalline, thermoanal. meas. 79−91938
Cl_2, electron dissoc. attachment peaks, 0−11.5 eV, Cl_2^- pot. energy curves 77−75312
Cl_2 partially dissociated, recomb. reaction freezing in supersonic nozzle, chemiluminescence *(Russian)* 77−52644
$Cl_2+Ar(He)(Cl_2)$, dissoc. in shock wave, density gradient meas. 77−83682
$ClCO_3NO_2$, synthesis by UV irrad. of Cl_2, NO_2, CO in air, decomp. kinetics 78−76880
$ClNO_2$, catalysed by ClNO, thermal decomposition spectral photometric investig. *(German)* 78−95925
$ClNO_2$, kinetics of thermal decomposition *(German)* 78−95924
ClO_2, solns., reson. Raman effect and absorption spectra 77−71807
Cr_2O_3 dissociation in presence of C in Ar, CO and vac. atm., Cr_3C_2 form. *(Russian)* 80−35570
Cs_2, thermal dissoc., optical pumping method obs. 77−16797
$Cs_2+He(Ne)(Ar)(Kr)(N_2)(CH_4)$, collision-induced dissoc., atom-mol.-exchange optical pumping 78−22008
$CsCl+SF_6$, collision induced dissoc., threshold behaviour 78−88627
$Cs_2Cl_2+SF_6$, collision induced dissoc., threshold behaviour 78−88627
CsXe excimer laser, form. and dissociation rates, fluoresc. meas. 78−1216

molecular dissociation continued
CuCl laser, dissoc. pulse cct. inductance effect 78−29936
CuH, gaseous, dissociation 79−91925
$Cu(NO_3)_2$, decomp., prod. of free Cu atoms 79−79244
$CuSO_4$, effect of press. on ion pair dissoc., cond. of aq. solns. 78−53218
D+HX (X=Cl,I), HX dissociative ionisation, H^+ signal origin, mol. beam obs. 80−66778
D_2^-, collision induced dissoc., positive and negative ions form. 78−50612
D_2^+, dissociation on impact with mylar foil 80−67164
D_2^{2+}, dissociative recombination cross sections 79−59568
D_2^+ molecular ions, dissociation in migmacells II and III, advanced fusion fuel expts. 77−83088
D_2-Ar, thermal dissoc. of dilute mols., vibr. bias mechanism 79−61854
D_2+He^+, dissociative ionisation, D^+ energy spectra 77−58154
D_3^-, collision induced dissoc., positive and negative ions form. 78−50612
D_3^+ +inert gas, ion decay, 1-40 eV *(Russian)* 78−90286
F_2-inert gas mixtures, transport and attachment processes 78−59542
FHF ion, H-bond excited electronic states, CI calc., dissoc. and autoionising states 80−5489
$Fe(CO)_5$+inert gas, dissoc. energy transfer, chemiluminesc. 80−55647
Fe_xO_y phase comp. on equilib. heating to 3300K *(Russian)* 80−16285
β-FeOOH, dehydration 80−79767
GaAs oxide, anodised native, influence of temp. on struct. and props. 77−81332
GaI, $A0^+$-$X0^+$ and $B1$-$X0^+$ transitions, isotope shifts, UV and visible spectra obs. 80−53005
H^- form. by surface and vol. processes, neg. ion source appl., review 80−58375
$H+D_2$, collinear motion, energy transfer and dissociation, collision dynamics 80−99563
$H+H_2$, collinear, collision-induced dissoc., quantum mech. probabilities calcs. 79−20359
H_2 adsorption on Ni (001) surface, mol. dissoc., calc. 80−101036
H_2, binding energy, MINDO/3 calcs. *(German)* 79−3366
H_2, D_2, photoionisation, body-frame Hund's case b description 78−94295
H_2, dissoc. chemisorption on Ni(Fe) cryst. surface *(German)* 78−53257
H_2, dissoc. sorption on stepped and unstepped surfaces 77−89636
H_2 dissociation, in discharge, as atomic H source for maser 79−86637
H_2 dissociation fronts in circumstellar dense cloud 79−5881
H_2 dissociation in microwave discharge 78−23935
H_2, dissociation rates in elec. discharge, calc. 77−46616
H_2, dissociative chemisorption on Li clusters 79−77918
H_2 dissociator envelope degradation, AES characterisation rel. to appl. in atomic clock 77−61876
H_2, electron energy distribution function, superelastic vibr. collisions and dissoc. effects 79−59589
H_2, electron impact dissoc. ionis., 75 eV emitted H^+ energy spectrum ang. depend. 78−17812
H_2 ground state, bond breaking reaction, MINDO/3 CI *(German)* 78−21852
H_2, in maser dissociator, performance characts. 78−87034
H_2 interstellar cooling, dissociation and IR emission in shocked clouds 78−41009
H_2 mol., Green's function Σ perturbation method for mol. calcs. 78−55123
H_2, on Cu, effect of surface roughness, classical trajectory calcs. 78−76925
H_2, on Cu (100) surface, classical trajectory calcs. 77−1947
H_2, on Cu(100) and (110) surfaces, classical trajectory calcs. 77−60114
H_2, thermal dissociation at heated filament at low press. 78−85156
H_2, vibro-electronic mechanisms in nonequilib. plasma 79−6992
H_2^-, collision induced dissoc., positive and negative ions form. 78−50612
H_2^+, 400 keV beam dissoc. collisions in air, ang. distribs., vibr. state effects 79−10197
H_2^+ and H_3^+ interactions with thin foils, electronic polarisation wake effects, dissoc. of mol. ions 80−16135
H_2^+, binding energy, MINDO/3 calcs. *(German)* 79−3366
H_2^+, collisional dissoc., excited electronic states effects 80−9687
H_2^+ differential cross section rel. to charge exchange cross sections of fragments 80−78704
H_2^+, dissoc. following beam-foil interaction 78−70920
H_2^+, dissoc. recombination, doubly excited Rydberg states 80−83506
H_2^+, dissociative recombination in low energy electron collisions 79−3563
H_2^+, dissociative recombination cross sections 79−59568
H_2^+, energy spectra of emergent dissoc. and recomb. products from C film 79−45819
H_2^+, hyperfine struct., refined var. calcs. 77−75067
H_2^+, internuclear separations distrib. in 3.0 MeV collisions with C foils 80−71529
H_2^+, ion beam surface interaction, H^- formation by reson. electron capture 80−40691
H_2-Ar, thermal dissoc. of dilute mols., vibr. bias mechanism 79−61854
H_2-Ar, thermal dissociation, relaxation rates, decomposition, master equation theory 79−74368
H_2-F_2-He chemical CW laser, flows *(Russian)* 78−74895
H_2-H-Ne mixture, positive column characts. and comparison with approx. diffusion theory 80−44025
H_2-like molecules, change of binding type and dissoc. in strong mag. field 78−62744
H_2+Ar, 4500K shock wave expt. simulation, vibr. state changes and dissoc. 79−61850
H_2+Ar, Arrhenius dissoc. activation energy, vibr. depend., trajectory calc., 4500K 78−35662
H_2+Ar, H_2 dissoc. rates, nonequilib. vibr. populations, elec. discharge conditions 77−88535
H_2+Cl^-, 4-11 eV, inelastic scatt. 79−98202
$H_2+H^+(H_2^+)(He^+)(O^+)$, H^+ prod., from H_2^+ dissoc. states or H_2^{2+} 78−20015
$H_2+H \rightarrow H+H+H$, two path dissoc. 78−62875
H_2+He^+, DIM approx. pot. energy surfaces and nonadiabatic coupling 80−23330
H_2+He^+, dissociative ionisation, H^+ energy spectra 77−58154
H_2+He(Ne), gas discharge plasma, H_2 dissoc. excitation, cross section anal. 80−33735
H_2+Ne, collision-induced dissociation, Monte Carlo quasiclassical trajectory calcs. 79−74357
H_2+Ne, vibr. excitation effect on dissoc. excitation efficiency 79−76495
H_2^++Ar, low energy proton transfer reactions, crossed beam studies 80−108697
H_2^++Ar(He)(H_2), 10 keV dissoc. charge exchange collisions 78−94319
H_2^++CO excited products dissoc., proton transfer dynamics, correl. diagram anal., corssed beam obs. 80−48079
H_2^++H_2, 10 keV H_2^+ dissociation, H-H^+, H^+-H and H-H fragments 77−83688
H_2^++He, 10 keV, dissoc. excitation, ionis., energy distrib. 77−61849
H_2^++He, collisional dissoc., expt. and quasiclassical trajectory calcs., eV region 78−42201
H_2^++He(Kr)(Xe), collisional dissociation, ion-pair prod., negative ion prod., cross sections 77−14529
H_2^++Kr, collisional dissoc., 6 to 60 keV *(German)* 77−10733
H_2^++methanol, dissoc. charge transfer reaction studied at rel. translational energies from 600 eV to 5000 eV 80−104432
H_3, mol. fragmentation energetics of vibr. excited mol., spatial beam profile expts. 79−96292
H_3^-, collision induced dissoc., positive and negative ions form. 78−50612
H_3, dissociating states, lowest singlet and triplet PE surfaces, HF calcs. 79−81160
H_3^+, dissoc. following beam-foil interaction 78−70920
H_3^+, dissociative recombination in low energy electron collisions 79−3563
H_3^+ expt. determ. struct., foil-induced dissoc. fast mol.-ion beam 78−74752
H_3^+ ions, collision induced, vibr.-rot. excitation 77−42383
H_3^++H_2 charge transfer collisions, 10 keV, H_2-H fragmentation 79−853
H_3^++Kr, collisional dissoc., 6 to 60 keV *(German)* 77−10733
H_n^+ multispecies beam, particle species evolution in neutral-beam injection lines 79−85846
H_n^++e, electron-ion dissoc. recomb., rate const., electron beam sustained discharge 78−50652
H_n^++N_2, (n=2 to 27), 250-900 eV collisions, fragmentation 77−88525
HBr, fine struct. in dissociative attachment cross sections 80−87248
HCC→H+C=C dissoc., trajectory calcs., random vibr. excitation 80−45491
H_2CN^+, dissociative recomb., rel. to interstellar HCN and HNC form. 78−81672
$HCNH^+$+e, dissociative recomb. reaction in interstellar clouds, products, statistical theory 78−57604
$H_2CN^+H_2 \rightarrow HCN^+H+H_2$, ab initio GO SCF pot. energy surface, saddle point, reaction path 77−50379
HCS^+-CSH^+ system, pot. surface for H abstraction, internuclear bending for ground and excited states 78−29744
HCl, dissoc. electron attachment kinetics in flame, mass spectra obs. 78−68872
HCl, dissoc. excitation in flowing afterglow, Cl form., light emission 78−90115
HCl dissociation for XeCl(B) formation in electron beam assisted Xe/HCl laser discharge 80−63988
HCl, dissociative electron attachment, differential cross section, Feshbach resons. 80−83508
HCl, in nonequilib. plasma, electron energy distrib. function and dissoc. kinetics 80−11882
HCl-N_2 mixture, electron swarm, Cl .HCl cluster formation, dissoc. attachment, drift tube mass spectra 78−68884
HCl+Ar, shock heated steady state dissoc. rate consts. calc. 78−40039
HCl+Ar, shock-heated, collision induced dissoc. 79−34290
HCl+inert gas, dissoc. induced by collision, rot. energy depend. 79−100341
HD , collision induced dissoc., positive and negative ions form. 78−50612
HD^+, dissociative recombination cross sections 79−59568
HD_2^-, collision induced dissoc., positive and negative ions form. 78−50612
HF, fine struct. in dissociative attachment cross sections 80−87248
HF, fragmentation, enhanced vibr. excitation effect, mass spectra 78−20004
HF, IR laser induced collisional pumping 78−25629
HF, IR laser induced collisional pumping 78−25630
HF, nonequilibrium dissociation in electric discharge, vibrational excitation 78−94306
HF+Ar, shock heated steady state dissoc. rate consts. calc. 78−40039
HF+inert gas, dissoc. induced by collision, rot. energy depend. 79−100341
HN_3, decomposition and ionisation in shock tube *(Russian)* 78−7182
H_2O adsorbed on pure Co surfaces, decomp. phenomena *(German)* 80−26054
H_2O dissociation by polynaphthoquinone-SO_2-I_2 system for H_2 prod. 80−16825
H_2O, dissociative adsorption on Re surface *(French)* 79−69344
H_2O, dissociative chemisorption on Ni 79−69353
H_2O, electron impact, dissoc. excitation, core pot. correction 78−25724
H_2O ice on Europa, dissoc. rel. to O and H clouds and UV emissions 79−5775
H_2O near mesopause, dissoc. during auroras rel. to ionosphere winter absorpt. anomaly 79−58152
H_2O, on Pt(111), identification of adsorbed OH species 80−49509
H_2O radiolysis, ionisation, mol. ion dissoc. *(Rumanian)* 77−48666
H_2O, Sb-I-Ca process for thermochem. prod. of H_2 80−16824
H_2O, thermochem. prep. of H_2 using S-I cycle 80−16823
H_2O^+, ab initio potential energy surface study by CI techniques, equilibrium conform. determ., mol. dissoc. pathways 80−78550
$H_2O+H^+ \rightarrow OH^*$, cross sections for 3064 Å band emission on 50-250 keV proton irrad. 77−16847
$H_2O+Kr(^3P_1)$, decomposition, $OH(A^2\Sigma^+)$ internal energy distrib. 79−10183
H_2O_2 80−34826
H_2O_2 decomposition, IO_3^- catalysed, oscillatory Bray-Liebhafsky reaction 79−91931
H_3O^+ (D_3O^+), plasma dissociative ion electron recomb., rate coeffs. 80−63747
H_3O^++e, dissociative recomb. reaction in interstellar clouds, products, statistical theory 78−57604
HOCl, ab initio MRD CI calc., electronic spectrum, dissoc., heat of reaction, formation 78−21857

molecular dissociation continued
HO_2NO, unimol. dissoc., rate consts., temp. depend., atmospheric implications 78−7175
HO_2NO_2, unimol. decomp., press. and temp. depend. 78−68887
$H_3O^+.H_2O$, mobility in He, flow drift tube obs. 78−34257
$H_3(PMo_{12}O_{40})$, decomp., in aq. soln., Raman spectra obs. 79−13719
H_2S, adsorption and dissoc. on Ru (001) 79−79292
$H_2S^+ + Kr$, collision-induced dissociation, mass spectra *(Russian)* 77−88549
H_2SO_4, dissociation and absorpt. consts., ultrahigh resolution obs. of 8.2, 11.3 μm bands 78−70825
$H_4(SiMo_{12}O_{40})$, decomp., in aq. soln., Raman spectra obs. 79−13719
HT, dissociation by T beta-decay 77−63941
He-CO_2 atomic C nuclear pumped laser collision processes, output delay 80−38002
$He+H_2$, collisional dissoc., quasiclassical trajectory calcs. 78−42172
$He+H_2$, mol. energy transfer by quasiclassical trajectory methods, vibr. relax. and dissoc., rot. effect 80−99557
$He+H_2^+$, reactive and dissociative scatt., crossed-beam and trajectory obs. 78−64833
$He^+ + CO_2$, dissociative charge exchange kinematics 80−3318
$He^+ + H_2$, dissoc. charge transfer, vibr. enhancement 78−33597
$He^+ + H_2(D_2)$, dissociative charge transfer, 78-330K 80−61079
$He^+ + H(H_2)$, H(2p) and H(2s) excitation cross sections, 5-26 keV 77−58150
He^+ + methanol, dissoc. charge transfer reaction studied at rel. translational energies from 600 eV to 5000 eV 80−104432
$He^+ + SO_2$, dissoc. charge transfer reaction, SO^+ ($A^2\Pi$-$X^2\Pi_r$) emission 80−95659
He_2 high press. afterglows, reviews 80−64823
He_2, high-order replacements inclusion in CI calc. 80−63504
He_2^{2+}, bound excited states, potential energy curves and rovibronic energy, dissociation 80−23327
$(HeH)^+$, breakup in single dissociative collision, fragment charge states 80−74226
HeH^+, collisional dissoc., excited electronic states effects 80−9687
HeH^+ dissoc. on impact at C foil, emitted light polarisation meas. 80−58361
HeH^+, fast ion dissoc. in thin foil, theory 77−19998
HeH^+, foil induced dissociation, H^0 prod. 80−66355
HeH^+, internuclear separations distrib. in 3.0 MeV collisions with C foils 80−71529
$^4HeH^+$, ro-vibr. quasi-bound levels of $X^1\Sigma^+$ state, eigenenergies, dissoc. 77−26997
HeI_2, vibr. excited mol., dissoc., predissoc., quasiclassical trajectory obs. 79−87839
$He(2^3S)+H_2O(H_2S)$, energy transfer processes, reaction products, UV and visible obs. in flowing afterglow 78−85138
Hg halide electrically excited dissociation laser, kinetic processes 80−38013
Hg_2, dissociative recomb. and optical transmissions meas. in high press. discharge 80−37816
Hg_2, optically pumped Hg laser 77−68206
$HgBr_2$ dissociation laser, elec. excited, kinetic processes 80−48231
$HgBr_2$, dissociative excitation for HgBr laser, extraction efficiency increased by N_2 addition 80−38012
$HgBr_2$ dissociative excitation by inert gas and N_2 metastables, HgBr emission intensity 80−40687
$HgBr_2$/HgBr dissociation laser, oscillator and oscillator-amplifier expts. 80−48232
$HgBr_2$ + inert gas metastable atom ($N_2(A^3\Sigma_u^+)$), dissoc. excitation 80−63774
$HgBr_2+N_2$*, dissociative excitation, mol. fluoresc. obs. 80−91634
I_2, ($B^3\pi_{0+u}$), dissoc. reaction, computer simulation 78−48639
I_2, adsorption on ZnO, γ-irrad. induced centres 80−54513
I_2, anomalous visible band effects near B state dissoc. limit 77−6816
I_2, dissociative mol. pot. functions from continuum reson. Raman spectra 77−38673
I_2, energy levels near B-state dissoc. limit, two-photon spectra 78−9210
I_2, hydrolysis, reaction rate const. 80−11883
I_2, molecular dissociation limit, two-photon technique 77−3425
I_2, vibrational relaxation and dissoc. behind a shock front, absorpt. spectroscopy *(Russian)* 77−88536
I_2^+, impact dissoc. cross-section, excitation energy, mass spectral obs. 77−3489
$^{129}I_2$, energy levels near B-state dissoc. limit, two-photon spectrosc. obs. 80−106367
I_2+Na(K)(Cs), ion-pair form., energy transfer and differential scatt. 77−75272
$I_2^+ + N_2 \rightarrow I^+ + I + N_2$, 0.65-3.2 keV, dissoc. cross-section, internal excitation effects 78−64813
ICl, energy levels, near first dissoc. limit, 2-photon sequential absorption obs. 78−90246
I2 fluoresc., Ar^+ laser excited, high resolution and sub-Doppler Fourier transform spectroscopy 80−43089
InCl disproportionation under influence of high pressure 80−16660
InI_x, x=1,2,3, thermodynamic props. 77−40572
$InX(X_2)(X_3)$, $InAlX_4$, X=Cl,Br, Raman spectra, up to 1200K 80−48003
K+Br, harpooning mechanism interactions, semiclassical optical model 79−89755
$K+Cl_2 \rightarrow K^+(Cl+Cl^-)$, 5.5−14.0 eV, energy loss, spectrum maxima, mechanism 77−75286
$K+D_2O \rightarrow OD^- + K^+ + D$, 100-200 eV, $D_2O^-(^2A_1)$, state 78−17770
$K^+ + H_2$, dissociative collision, H_α, H_β emission prod. 77−75093
$KCl+M \rightleftarrows K^+ + Cl^- + M$, rate consts. in at. press. flames 77−60036
K_2SO_4, effusion studies of vaporisation/decomposition 79−95153
Kr microwave afterglow, Kr_2^+ dissoc. recombination coeff., electron temp. depend. 78−30501
Kr-Cl_2 mixture, glow discharge positive column, electron energy distrib. and rates of inelastic processes, negative Cl ions form. 80−19632
Kr_2^+ dissoc. recomb., rate coeff. and excited state prod., electron temp. depend. 78−22040
$Li+Li_2 \rightleftarrows Li_3$, rovibronic symmetry correlation 78−92461
$Li^+ + H_2$, dissoc., multiple scatt. theory 78−21999
$Li^+ + H_2$, dissociative collision, H_α, H_β emission prod. 77−75093
$Li_2^{++} \rightarrow 2(1s^2)Li^+ + e$, Auger electrons energy width 77−23443
$Li_2(A^1\Sigma_u^+)$, dye laser excited, collision induced dissociation 79−91920
$LiBF_4$, thermal decomposition, equilib. decomposition press. and enthalpy of form. 79−91983
$Li_2(B^1\Pi_u)$ + inert gas, laser-excited collision-induced dissoc. 79−79232

molecular dissociation continued
LiBr, in anhydrous acetone, ion-pair dissoc., at high press., Shedlovsky method 78−53219
LiCl molecular dissoc., obs. by interference method 80−40684
LiH, $X^1\Sigma^+$ and $A^1\Sigma^+$ states, hybrid pot. energy curves, dissoc. limits 77−79669
Li_2H, natural orbital contour diagrams and occupation nos. for form. and dissoc. 79−18107
M_2^+ ions, dissociative collisions, mol. effects in charge state distribs. 78−17755
$MnSO_4$, effect of press. on ion pair dissoc., cond. of aq. solns. 78−53218
$MoCl_5$, pulsed discharge dissoc., for Mo I oscill. strengths meas. 78−25479
N_2 adsorbed on W, effect of SIMS sputtering induced recomb. anal. 80−55243
N_2 adsorbed on W(110) vicinals, step sites as dissoc. centres 80−6642
N_2, dissoc. chemisorption on Ni (Fe) cryst. surface *(German)* 78−53257
N_2 dissociation role in plasma positive column Mg nitridation 78−63628
N_2, dissociative electron attachment, $N^-(^3P)$ form. 78−90308
N_2, electron impact dissoc., EELS, N^- autoionisation 80−106397
N_2, oscillatory-dissoc. relax. in hypersonic shock layer at moderate Reynolds number *(Russian)* 77−39311
N_2, plasmochemical action of relativistic electron beam, calc. by degradation spectrum method *(Russian)* 79−37536
N_2, radiation chem., primary neutral dissoc. excitation, isotopic exchange mechanism 78−48670
N_2^+, dissociative recombination rates 77−86295
N_2^+, dissociative recombination in ionosphere, rate cont. 80−17435
N_2^+, exploding fast mol. ions, Auger spectra 80−32781
N_2^{n+}, Coulomb explosion following heavy ion impact, ab initio SCF calc. 79−18277
N_2-Ar plasma, diffusion separation, N_2 dissociation 77−76036
N_2+H_2, N_2 dissoc. rates, nonequilib. vibr. populations, elec. discharge conditions 77−88535
$N_2+H^+(He^+)$, 1 MeV, dissoc. ionis., time-energy spectra 77−34744
$N_2+N_2O_4 \rightarrow N_2+2NO_2$, turbulent mixing in shear layer 77−75989
N_2+X^{n+}, (X=Ar,Kr,Xe,U), Auger emission line shape after dissoc. 78−86838
$N_2^+ + H_2$, collisional dissoc. cross-section, 2.4-24.3 keV 80−58373
$N_2^+ + N_2 \rightarrow N^+ + N + N_2$, with reactant $X^2\Sigma_g^+$, $A^2\pi_u$ and excited metastable states 77−29001
$N_2^+ + O_2$, collisional dissoc. cross-section, 2.4-24.3 keV 80−58373
$NCNO \rightleftharpoons NC+NO$, ground state pot. energy surface, ab initio calcs. 77−90593
ND_3, chemisorbed on W, decomposition mechanism, isotope effect 79−29409
ND_3, photodissoc. in discharge, spectra of metastable ND radicals, rot., vibr. consts. determ. *(German)* 77−34642
NF_3, dissoc. electron attachment, rate consts. meas. 78−3326
NF_3, shock induced decomposition in Ar, IR emission, reply 77−63907
NF_3 shock-induced decomposition in Ar, IR emission, comment 77−63906
NF_3, thermal decomp. in shock waves, rate consts. meas. 77−16810
NF_3, thermal dissoc. behind shock waves, rate meas. 78−61002
NH radical formed in NH_3 dissoc., fluoresc. spectrum, rotational relaxation 80−58310
$NH_2^+ \rightarrow NH^+ + H$, pot. energy surface of NH_2^+ quintet state 78−25419
NH_3, adsorption of Al surface, NH_3 decomp., XPS obs. 80−92783
NH_3 adsorption on Mo, and catalytic decomposition, field emission study 78−14596
NH_3, catalytic decomposition of single pulses on W, mol. beam relax. spectrometry 80−21321
NH_3, chemisorbed on W, decomposition mechanism, isotope effect 79−29409
NH_3, chemisorption on Ni (111) and reaction, LEED, desorption and photoemission expts. 80−59799
NH_3, flow in steel tubes, wall heat transfer with catalytic dissoc. 78−14099
NH_3, in nitriding process, monitoring 79−52556
NH_3, on Fe (110), adsorption and decomposition 79−69345
NH_3, photodissoc. in discharge, spectra of metastable NH radicals, rot., vibr. consts. determ. *(German)* 77−34642
NH_3^+, fast mol., dissoc. in thin C foils, Doppler broadening obs. 78−22019
$NH_3+H_2^+(He^+)$, dissociative charge transfer reactions, energy transfer depend. 77−25258
NH_3+X^{n+}, (X=Ar,Kr,Xe,U), Auger emission line shape after dissoc. 78−86838
$NH_4^+ + e$, dissociative recomb. reaction in interstellar clouds, products, statistical theory 78−57604
NH_5^+, stability, ab initio calcs. 77−23419
N_2H_4, dissociative adsorption on Fe(111) 79−46956
NH_4ClO_4, incomplete thermal decomp. 79−91939
$NH_4NO_3 \rightleftharpoons NH_3 + HNO_3$ equilib. in atmosphere 79−88389
NO, adsorbed on Cu, species identification, struct., dissoc. chemisorption, desorption, UV photoelectron spectroscopy 78−52635
NO, adsorbed on MgO, dimer form., heat of dissoc., EPR obs. 78−82755
NO, adsorpt. on W (100), 300K and 100K, XPS, UPS and XAES, rel. to catalytic decomp. 79−28204
NO, catalytic decomp. over brownmillerite like compounds 79−43631
NO, chemisorption on Ni (110), LEED, AES and thermal desorption meas. 77−15695
NO, decomp. on Ru 78−18903
NO, dissociative adsorption on W, FEM obs. 77−4258
NO, dissociative adsorpt. on Ru (10$\bar{1}$0), LEED and AES expts. 77−90642
NO, dissociative adsorption on Re surface *(French)* 79−69344
NO, dissociative electron attachment, $N^-(^3P)$ form. 78−90308
NO, surface interaction with CO on Rh/Al_2O_3 catalyst, IR study 79−70369
NO^+, dissoc. recombination, $N(^2D)$ atom quantum yield 77−63905
$NO+H^+(He^+)(O^+)$, dissociative ionis. 79−10188
NO_2, gas phase, chem. relax. times for dissoc. reactions *(Russian)* 77−70288
NO_2, shock heated, visible emission 80−58274
NO_x, dissociative adsorption on W (110), 300K and 100K, XPS, UPS and XAES 79−28203
N_2O, chemisorbed on Cu (111), decomposition probability 79−65317
N_2O, dissoc. electron attachment, O^- ang. distrib. 77−75315

molecular dissociation continued
N_2O, N $1s^{-1}$, π^*-state decay, fragment ion relative abundance by electron-ion coincidence technique 80−9743
N_2O, thermal decomp., unimol. reaction theory 79−15954
N_2O, valence shell ionic photofragmentation, oscill. strengths, EELS and electron-ion coincidence meas. 80−37879
N_2O^+, fluoresc. and dissociation lifetimes of vibr. excited states 78−42108
N_2O^+, thin foil impact, dissoc. struct. effects in ionic fragment energy spectra 78−50631
N_2O+inert gas, reactant decomp., rot.-vibr. energy transfer, relax. analytic soln. 80−55650
N_2O_4, dissoc. flow in tube, heat transfer and drag 78−71402
N_2O_4, dissociated, enthalpy, 310-782K 78−73073
N_2O_4, dissociating, nonsteady flow in steam-generating channel 79−37422
N_2O_4 dissociating gas flow in channel, turbulent boundary layer *(Russian)* 79−60067
N_2O_4 gas phase, chem. relax. times for dissoc. reactions *(Russian)* 77−70288
N_2O_4, sound dispersion and velocity mol. dissoc. effects *(Russian)* 80−1730
N_2O_5, thermal dissoc. in N_2 79−96294
$NO_2(N_2O_4)$ surface decomposition, resonance and spontaneous Raman spectra 80−61144
$N_2O_4 \rightleftarrows 2NO_2$, heat transfer meas. *(Russian)* 77−84128
$N_2O_4 \rightleftarrows 2NO_2 \rightleftarrows 2NO+O_2$, precipitation of corrosion products in a fractionating column *(Russian)* 80−25707
$N_2O_4 \rightleftharpoons 2NO_2$, gas mixture turbulent concurrent double pipe heat exchanger equilib. and nonequilib. reaction 78−94856
$N_2O_4 \rightleftharpoons 2NO_2 \rightleftharpoons 2NO+O_2$, working fluid for power-producing thermodynamic cycles 80−13536
Na_2+He(Ne)(Ar), collision induced dissoc. rate, vibr. distrib. depend. 79−22791
NaCl beam thermal decomposition, Na time-of-flight spectrum using laser fluoresc. 77−49804
NaCl+Ar, dissoc.-ionis. process rates in shock tube 78−35674
NaK, $C^1\Pi$ state, spectroscopic consts., vibr.-rot. struct., K fluoresc. obs. 77−18901
$(NbF_5)_4$ mass spectra, vel. distrib. effects, mol. beam inlet method, mol. dissoc. 77−54627
$Ne+He_2^+ \rightarrow He+$products, surface-hopping trajectory calc. 79−52637
$Ne^+ + H_2(N_2)(CO)(CO_2)(N_2O)(O_2)(NO)(NH_3)(SO_2)(COS)(H_2O)$, thermal energy, reaction rate coeffs. and product distrib. 79−29333
Ne^++methane(chloromethane)(ethylene), thermal energy, reaction rate coeffs. and product distrib. 79−29333
Ne_2^++e, in recombination afterglow, line intensity decay complex struct. 79−7503
$Ni(Co)_4$+inert gas, dissoc. energy transfer, chemiluminesc. 80−55647
NiH, gaseous, dissociation 79−91925
NiO-H_2, interaction with surface, quantum chemical study 80−45549
O source with improved long term stability for chemiluminescence reaction, mol. dissoc. and recombination 80−93758
O_2, adsorbed on graphite, pot. energy curves of dissoc., CNDO/2 calcs. 79−28206
O_2, adsorption on reduced Mo_2O_3-Al_3O_3 catalyst, O^- form. 78−85197
O_2, chemisorbed on Cu (111), decomposition probability 79−65317
O_2, discharge, nonequilib. vibr. population, dissoc. rate, role of ats. and dissoc. 79−64933
O_2, dissoc. induction times, high-temp., exact simple model numerical calcs. 78−9230
O_2, dissociation in discharge plasma 79−100356
O_2, dissociation rates, nonequilib., vibr. populations in elec. discharges 78−46427
O_2, dissociation relax. behind oblique shocks 77−548
O_2 dissociation relaxation behind regular reflected and stationary oblique shocks 78−85159
O_2 glow discharge, DC, particle concs. calc. 80−1859
O_2 glow discharges, current modulated, O atom production and removal rates 79−90477
O_2, in shock tubes, induction and transient times 77−12794
O_2, RF discharge, moderate press., O production kinetics 79−64934
O_2, thermal decomposition, vibr.-rot. state depletion, Monte Carlo calc. 80−35506
O_2, two-dimensional adsorbed layer on graphite, props. calc. 80−103568
O_2, vibrational relaxation and dissoc. behind a shock front, absorpt. spectroscopy *(Russian)* 77−88536
O_2^+ dissociative recomb., $O(^1D)$ prod. in upper atm. 77−41251
O_2^+, dissociative recombination rates 77−86295
O_2^+ dissociative recombination in auroral region 80−41581
O_2-Ar, thermal dissoc. of dilute mols., vibr. bias mechanism 79−61854
O_2+Ar, shock-heated, collision induced dissoc. 79−34290
$O_2+H^+(He^+)(O^+)$, dissoc. ionisation, kinetic energy spectra 78−25684
O_2+He^+, thermal energy charge transfer, O^+ product ion obs. 79−64100
O_2+inert gas, dissoc. induced by collision, rot. energy depend. 79−100341
O_2+inert gas, reactant decomp., rot.-vibr. energy transfer, relax. analytic soln. 80−55650
O_2+X^{n+}, (X=Ar,Kr,Xe,U), Auger emission line shape after dissoc. 78−86838
O_3, decomposition flame, flat, laminar, vel., struct. 78−51256
$O_3 \rightarrow O_2+O$, MNDO semi-empirical SCF MO calc. 77−44465
O_3, stratospheric, reduction by natural NO_x and man-made pollution, model 77−60461
$O_3^-+X \rightarrow O^-+O_2+X$, X=He, Ar, CO_2, long-lived excited (or isomeric) state of O_3^- 78−5318
$O_2^+AsF_6^-$, thermal decomposition, Raman spectra study, free radical mechanism 80−55652
OH, $A^2\Sigma^+$ state, predissociation, tunnelling 78−29824
OH^+, Coulomb explosion in 11.2 MeV collisions with C foils 80−66358
OH^+ ion beam, Coulomb explosion in thin C foil, charge state depend. 79−31649
$OH^-+C(N_2)$, electron stripping and breakup, proton spectra 77−83685
OH^-+inert gas, collision-induced dissociation 78−29834
OH_2^+, and OH_3^+, fast mols., dissoc. in thin C foils, Doppler broadening obs. 78−22019
PCl_5-$TiCl_4$, gas, melt, and solid, dimer-monomer conversion, Raman spectra obs. *(German)* 79−70320
$(PMo_{11}O_{39})^{7-}$ decomp., in aq. soln., Raman spectra obs. 79−13719
P_4S_{10}, gas, vaporisation and thermal dissoc. obs. *(French)* 78−47511
P_4S_3, gas, vaporisation and thermal dissoc. obs. *(French)* 78−47511
P_4S_7, gas, vaporisation and thermal dissoc. obs. *(French)* 78−47511
PbLi, gas phase thermodynamics, Knudsen effusion mass spectrosc. 80−100057
PbS vapour, mass spectroscopic study *(Russian)* 77−65545
PsH autodissociating Rydberg states 79−76539
$Re_2(CO)_{10}$ vapour decomposition, for plasma deposited Re films 80−20799
S_2, dissociative chemisorpt. on Ag(111), surface layer struct. changes 79−42383
SF_6, arc discharge, decomposition products for SF_6 with H_2O and organic gas contaminants 79−10743
SF_6, laser-induced isotope separation, threshold intensity 77−4898
SF_6, multiphoton absorpt., energy transfer, dissoc. probability, laser field interaction, classical trajectory approx. 80−37730
SF_6, multiple-photon excited, double reson. spectroscopy 80−53030
SF_6, photon-enhanced dissociative electron attachment, isotope selectivity 80−18939
SF_6, unimolecular reaction model 78−7189
$SF_6+X^- \rightarrow SF_5^-+F+X$ (X=O, S, F, Br, I), electron affinity of SF_5 radical 80−45495
SF_6^-+He, decomposition, SF_5^- form. 78−29833
SO_2, interaction with NiO (100) surface, electron diffr. and Auger spectrosc. obs. *(French)* 80−97728
SO_2, shock heated, visible emission 80−58274
SO_2 surface reaction and decomposition on zeolites, resonance Raman study 80−61145
SO_2^+, state selected vibr. levels, fragmentation, photoelectron-photon coincidence spectroscopy 79−89707
SO_2+Ar, dissoc. rate meas. behind shock wave, laser Schlieren method 80−81296
SO_3, dissoc. pathways and mol. vibr., compliance consts. and min. energy coords. 78−35661
$SO_3+Ar \rightarrow SO_2+O+Ar$, rate const. of spin forbidden dissoc. in shock wave 79−57214
$SeCl_4$-$SbCl_5$ systems, Raman spectra *(German)* 80−93324
Si (111), 7×7 surface, chemisorption of H_2O 80−10792
SiC, dissociation in silicate bonded refractories, X-ray obs. *(German)* 79−47893
$SiCl_4$, electron bombardment and thermal dissoc., thermochem. stability 77−58185
SiH_4, $1B_1(1T_2)$ pot. energy surface calcs. 80−53085
SiH_4^+, struct, stability, ab initio calcs. 79−13632
SiO_2 decomposition and reduction, in low temp. plasma jet *(German)* 80−45499
Sr_2 dimer, photoassoc., photoluminesc., collisional dissoc. 80−58303
TiO, chemiluminesc., dissoc., heat of form., in metastable Ti collisions with O_2, N_2O, NO_2 77−40534
TlF+Kr(Xe), collision-induced ion-pair formation 78−17749
Tl_2F_2+Kr(Xe), collision-induced ion-pair formation 78−17749
UF_4 optical interference layers, electron-beam decomposition 78−34541
UF_6, emission and absorpt. spectra at 80 to 600 nm, decomp. products 77−23212
UH_3, UD_3, dissoc., isotope effect 80−26174
UO^++Ar, collision-induced dissoc. cross section and threshold 80−95706
UO_2^++Ar, collision-induced dissoc. cross section and threshold 80−95706
URu_3, sublimation thermodynamics 80−97722
$W(CO)_6$ decomposition, W needles growth 79−95302
WCl_6, dissoc. in discharge, WI lines oscill. strengths 79−63962
Xe+Cl_2, classical trajectory calcs., energy threshold for collision induced dissoc. determ., 80−95709
XeF ground-state dynamics in laser discharge, dissoc. rate 79−18404
ZnO, electron beam induced decomposition and desorption, AES and contact pot. difference meas. 78−79893
$ZnSO_4$, effect of press. on ion pair dissoc., cond. of aq. solns. 78−53218

molecular dissociation energies
ab initio effective core pot. method appl. to F_2, Cl_2 and LiCl 80−32625
acetylene, effective core potential calcs. 79−31437
alkali halide, hyperpolarizability and dissociation energy 79−72439
alkali halide, photofragmentation spectroscopic method 79−76527
alkali halides, binding energy, relativistic effects 77−14370
alkali halides, bond order correl. with dissoc. energy 80−32596
alkali halides, improved interaction pot., spectroscopic consts. calc. 79−86024
alkali hydroxides, dissoc. energies and bond lengths, ion props. depend. 78−86801
alkali metaborates, dissoc. energies and bond lengths, ion props. depend. 78−86801
alkali metal diatomics, pot. curves, selected valence electron SCF MO calc. 79−10053
alkali metal hydrides, VB calcs., equilib. internuclear separation, dissoc. energies 77−71756
alkali metal monoxides, bond distance, dissoc. energy and vibr. freq., electron gas model 77−30846
alkali metal nitrates, Raman spectra, interionic interactions effect on bond lengths, dissoc. energies and vibr. 79−36653
alkali metal quasimolecule 77−83677
alkaline earth monoxides, dissociation energy 77−550
alkaline earth oxides, dissoc. energies rel. to occurrence in cool stars and sunspots 78−85933
alkenes, π bond dissoc. energies, derivation from isomerisation kinetics, for teaching 79−58498
atomic particles, equilib. const. and parameters of interaction pot. 78−1045
butyl cation, H-elimination, energy partitioning, transition state geometry calc. using MINDO/3 80−104430
t-butyl cyanide-HF, hydrogen bonded heterodimer, spectroscopic consts. from IR and microwave spectra 80−43039
chloropentafluoroethane, multiphoton dissoc., crossed laser and mol. beam obs. 80−11908
cluster ion band-dissociation energy, review 77−81401
cyanomethane-HF, hydrogen bonded heterodimer, spectroscopic consts. from microwave spectrum 80−43038
cyclopropane, double SCF method for electron correl., ring-opening energy 78−17575
dialkalis, VB calcs., equilib. internuclear separation, dissoc. energies 77−71756

molecular dissociation energies continued
diatom, weakly bound, dissoc. energy for Morse and Lennard-Jones pots. 79−54988
diatom product, from diatom+atom, dissoc. energy from reaction cross section 80−16655
diatomic, molecules, spectrosc. determ., near-dissoc. expansions 80−83513
diatomic mol., Hellman pseudopot. calcs., dissoc. energy, ionis. pot., bond length 77−10577
diatomic molecule, pot. and spectroscopic consts. 79−94053
diatomic molecule, vibr. potential representations 79−68219
diatomic molecules, containing elements from Li to F and Na to Cl, empirical correl. 78−62943
diatomic molecules, dissoc. energy calcs., Morse and Lippincott pot. functions 77−30952
diatomic molecules, dissoc. energy determ., Simmons-Parr-Finlan pot. calcs. 80−58128
diatomic molecules, Simon-Parr-Finlan potential appls. 80−18785
diatomic molecules, universal dissoc. energy relationships 80−5493
ethane, effective core potential calcs. 79−31437
ethylene, effective core potential calcs. 79−31437
ethylene dimer, intermol. pot., dissoc. energy, CNDO/2 calcs. 79−31641
extra correlation energy, calc. by CHF method 79−76350
formaldehyde, atomisation and bond energies, LMO calc., conjugation contrib. 80−9496
formyl radical, -d_0, (-d_1), first ionis. pot., photoelectron spectrosc. determ. 80−48039
formyl radical, electronic struct., dissoc. energy and pot. energy surface many body perturbation theory and couple cluster doubles calc. 80−23296
ground state props., coupled cluster and MBPT methods appl. 80−47881
Group IA element halides, bond order correl. with dissoc. energy 80−32596
Group IIIA element halides, bond order correl. with dissoc. energy 80−32596
group IV A monosulphides 78−29733
halogen molecule, orbitals calc., correlation effects, force const., dissoc. energy, bond length 77−26964
halogen molecule negative ion, Cl_2^-, Br_2^-, I_2^-, $ClBr^-$, ClI^-, pot. curve calc. 77−10596
hexafluoropropane, isolated CH stretching freqs. and bond props. 79−94104
hydride ions, XH^+, X=first and second row elements, PNO-CI and CEPA studies of electron correlation effects 77−34561
hydroxonium complexes, produced by collisional dissoc. method, mass spectrometric study, dissoc. energies determ. 80−95707
ice, electron-irrad., cluster-ion prod., lattice and fragmentation energies 77−4911
inert gas complexes spectroscopic data, geometry, pot. energy curve, dissoc. energy, equilib. internuclear distance, determ. 80−53018
infrared multiphoton dissociation of molecules, review *(Japanese)* 80−11885
intermetallic diatomic compounds, with multiple bonds, bond energy, VB calcs. 79−31440
metal carbonyls, gaseous, metal-carbon bond, dissoc. energy and enthalpy of form. 78−44393
metal halide (oxide) dissociation energies, calc. from chemiluminesc. reactions, temp. depend. rate const. correction 77−40524
metals, atomic binding energy and surface energy rel. to prediction of physical props. 80−59434
methane, bond dissociation, MCSCF LMO calcs. 77−57886
methane, effective core potential calcs. 79−31437
nonafluoro-iso-butane, isolated CH stretching freqs. and bond props. 79−94104
open-shell systems, ionisation pots. and dissoc. energies, correl. energy calcs. 79−31413
organic compounds, heat of formation, dissociation energy from dynamic electronegativity *(Chinese)* 79−96351
polyatomic mol. force consts. and heat of atomisation, approx. separable pot. function 80−78675
propion-aldehyde ion, fragment/mol. ion current ratio, field ionis. mass spectrum, CNDO/BW calc. 77−65544
rare earth oxides, dissoc. energies rel. to occurrence in cool stars and sunspots 78−85933
rare earth oxides, polyatomic gaseous, atomisation energies and stand. ht. of formation determ. 77−54622
three-electron bonds, stability and dissoc. energies 77−78935
transition metal hydrides, homoleptic, electronic structure, ab initio calcs. 79−89601
trifluoroethane, isolated CH stretching freqs. and bond props. 79−94104
trifluoroformamide, thermal dissoc., shock wave study 79−34284
trihalide anions, VB pseudopot. calcs. on electronic states 77−26984
virial-statistical method for atomisation energies calc. 78−62697
Ag_2, AgAu, AgCu, AgH, AgLi, VB calcs. 77−57883
AgCl, bond dissoc. energy, electronegativity pot. function, pot energy curves 77−10784
AgH, bond dissoc. energy, electronegativity pot. function pot. energy curves 77−10784
AlAs, gas phase dissoc. energy, mass spectrometric determ. 79−81301
AlBr, UV emission spectrum, vibr. consts., isotope displacement and dissoc. energies 77−3381
Al_2Cl_6, matrix isolated, vibr. spectra, isotopic fine struct. and valence force field calcs. 80−58258
AlH, $A'\pi$, spectral lifetime and predissociation 79−59515
AlO, ground state, pot. energy curve, dissoc. energy 78−46286
AlO, ground state dissoc. energy, normalised temp. method *(German)* 77−476
AlO radical, ground state dissoc. energy 80−53159
Ar_2^+, from photoionisation studies of Ar_2 77−54578
Ar_2+, weakly bound excited states, dissoc. energies 78−78748
ArF^+, selected valence-electron split-shell MO calc., ground state props. 79−22585
AsF, pot. energy curves and dissoc. energy, Hulbert-Hirschfelder calc. 80−30210
AsO, dissoc. energy calcs. 77−3486
Au_2, AgAu, AuCu, AgH, AgLi, VB calcs. 77−57883
AuV, gas, bond dissoc. energy, from high-temp. mass spectra of V-Nb-Mo-Au 79−45860
BO, spectroscopic properties, PNO-CI and CEPA calcs. 78−41961
$Ba+Br_2(I_2)\rightarrow BaBr(BaI)+Br(I)$, time-of-flight chemiluminesc., mol. bond energies determ. 78−40051
molecular dissociation energies continued
$Ba^+ + D_2 \rightarrow D + BaD^+$, sequential impulse model, prod. bond dissoc. energy and cross section 80−81295
BaBr, BaCl gas equilib. mass spectra, dissoc. energy 77−65543
BaI, mol. dissoc. energy, high temp. mass spectra 78−58863
BaOH, (BaCl), mol. dissoc. energies calc. by high temp. mass spectrometer 80−83514
BaPd, BaRh, gaseous, dissoc. energies, obs. and calc. values 78−58864
Be_4, Be_2, dissoc. energy, electron correlation effect, self-consistent electron pair calc. 77−30790
$BeAr^+(X^2\Sigma^+)$, spectrosc. determ., near-dissoc. expansions 80−83513
BeO, $X^1\Sigma^+$ state pot. energy curve, ground state dissoc. energy 78−41977
BiO, dissoc. energy calcs. 77−3486
BrF, laser excitation spectrum, 4850 to 5200 Å, rot. anal. 77−6840
$C_2(C_2^-)$ pot. energy curves calc. using SCF, MCSCF and CI methods, dissoc. energies, bond lengths, electron affinity 80−95523
CF, electronic Rydberg states, dissoc. energy, multiconfig. HF calcs. 79−59360
CF, low-lying electronic valence states, dissoc. energy, multiconfig. HF calcs. 79−59359
CO^+, dissoc. energy determ. from pot. energy curve 79−13837
CO_2^+, photoionisation reson. spectra and threshold electron-ion coincidence meas. of fragmentation 77−38700
CO_3^-, O^- bond dissociation energy 78−7193
CO_3^-, photodissoc. cross-section, excited state vibr. mode determ. 77−6870
$CO_2.CO_2^+$+ethylene, rate coeffs. and product distribution determ., dissoc. energy and heat of form. 80−97693
CS, dissoc. energy by photodissociative ionisation study of CS_2 79−94044
CS_2, photoionisation and dissociative ionisation due to 60-129 nm light, mass spectra study 79−94044
CSe, atomisation energies, enthalpy of form. 78−33631
CSe, from CSe_2 photoionis. mass spectrum 77−46604
CSe_2, atomisation energies, enthalpy of form. 78−33631
Ca_2, $A^1\Sigma_u^+$-$X\Sigma_g^+$ system, laser induced fluoresc., pot. energy curve and mol. consts. 80−58307
Ca_2, ground state, multiple scatt. Xα calcs. 80−58149
Ca_2, new ground state, photolum. obs. vibr. consts., dissoc. energy 80−5576
CaBr, gas equilib. mass spectra, dissoc. energy meas. 77−65543
CaCl, form., spectral bands, dissoc. energy calcs. 77−16816
CaI, mol. dissoc. energy, high temp. mass spectra 78−58863
CaO dissoc. energy from $Ca+O_2$ chemiluminesc. 80−97697
CaO, dissociation energies, spectrometric determ. 78−74789
CaOH, dissociation energies, spectrometric determ. 78−74789
$Ca(OH)_2$, dissociation energies, spectrometric determ. 78−74789
CeO, dissoc. energy, rel. band strengths of a_2-X_2 and b_2-X_2 systems 80−99495
ClO, dissoc. energy and bond length, CI calcs., bond function effects 80−102450
ClO, MCSCF-CI electronic wavefunctions, dissoc. energy, dipole and transition moment 77−75052
$Cs_{2,}$ ground state consts., pot. curve, laser spectroscopy 79−98247
Cs_2^+, energy threshold for Cs+Cs nP, dD excited states, assoc. ionisation, state and thermal energy depend. *(Russian)* 79−5153
Cs_2^+, form. by Cs+Cs assoc. ionisation, dissoc. energy 78−58804
CsH, dissoc. energy calc. 78−90314
Cu_2, AgCu, AuCu, CuH, CuLi, VB calcs. 77−57883
CuI dissoc. energy A-X system vibr. bands 77−50434
CuO, ab initio HF-MC-SCF with GTO basis set, dissoc. energy and bond length 80−47890
Eu_2O, Eu_2O_2, Eu_2OS, dissoc. energies and ht. of formation 77−47569
EuO(g), thermochem. props. 77−14604
EuS, Eu_2S, EuS_2, Eu_2S_2, Eu_2OS, dissoc. energies and ht. of formation 77−47569
FeO, gas, thermochem. props., mass spectrosc. meas. 80−101034
FeOH, gas, thermochem. props., mass spectrosc. meas. 80−101034
H_2, $^3\Sigma_g^+$ state, improved adiabatic energy, dissoc. energy 79−10011
H_2, channel coupling theory of covalent bonding, dissoc. energy 78−13419
H_2, Compton profile, electronic energy calc. 80−37822
H_2, ground state dissociation energy, Born-Oppenheimer pot. calcs. 78−37542
H_2, solid, electron-irrad., cluster-ion prod., lattice and fragmentation energies 77−4911
H_2^+, high (10^9 G) mag. fields, dissoc. energy, electron binding energy and equilib. separation 80−52910
H_2^+, SCF multiple scatt. calc. 80−916
HCN-HF, dimer, rot. transition intensity, dissoc. energy determ. 78−46323
HCN...HF, hydrogen bonded heterodimer, spectroscopic consts. from microwave spectrum 80−43037
HF^+, ab initio valence band calcs. 79−6869
HF_2—HF+F, radical stability, ab initio SCF and CI calcs. 77−71887
$H_2(HD)(D_2)$, ab initio pot. energy curves and vibr. levels, B″, B̃, B′ states 77−6754
HN_3, ground $^1A'$ state, SCF and CI calcs., conform., geom., vibr. freqs. and dissoc. 80−18806
HNB,(HNBH), spectroscopic properties, PNO-CI and CEPA calcs. 78−41961
HNO^+, ab initio pot. surface, and isomerisation barrier of lowest states 79−22622
HNO^+, ab initio SCF and CI comparison of struct. and spectra, rel. to NOH^+ 77−26972
HNO^+, vertical spectra, heat of form., ab initio MRD-CI calcs. 79−49934
H_2O, bond dissociation, MCSCF LMO calcs. 77−57886
H_2O, Compton profile, electronic energy calc. 80−37822
HOB,(HBO), spectroscopic properties, PNO-CI and CEPA calcs. 78−41961
He_2^+, dissoc. energy calc. 79−55447
$HeCN^+$, SCF calcs., dissoc. energies, rot. and hyperfine const. determ. 80−95531
$HeCl^+$, interaction potential, HF dissociation energies, LCAO SCF calcs. 77−6880
HeH^+, $X^1\Sigma^+$ electronic ground state, pot. curve, rovibronic and dissoc. energies 79−72254
$^4HeH^+$+He, 1 keV, collision-induced dissoc., ro-vibr. assignments, proton spectra obs. 79−3556

molecular dissociation energies continued
Hg_2^+, electronic struct. and photoabsorpt. calcs. 80−27932
HgX, (X=I, Br, Cl), ground state dissoc. 77−6755
I_2Ar^*, product state distrib. and binding energy 80−63857
IF, $B^3\Pi(0^+)$-$X^1\Sigma^+$ fluoresc., predissoc. 77−34682
I_2He^*, product state distrib. and binding energy 80−63857
I_2Ne^*, product state distrib. and binding energy 80−63857
K+halogenated methane, negative ion form., electron affinities, bond dissoc. energies 78−82827
KLi, appearance pot., dissoc. energy, ionis. pot., mass spectra obs. 78−25750
Kr_2^+, from photoionisation studies of Kr_2 77−54578
Kr_2^+, weakly bound excited states, dissoc. energies 78−78748
KrF, electronic states, ab initio CI calcs., spin-orbit coupling, pot. curves, dissoc. energy, dipole moments 77−38619
KrF^+, selected valence-electron split-shell MO calc., ground state props. 79−22585
KrF^* radiative lifetime, pulsed photolysis obs. 78−29819
LaIr(g), thermodynamic stability, high-temp. mass spectra obs. 80−7781
LaO, chemiluminescence due to bimolecular oxidation of La metal 77−29011
LaS, chemiluminesc. vibr. analysis of $C^2\Pi \rightarrow X^2\Sigma^+$, D_0^0 determ. 77−48645
Li_2, $A^1\Sigma_u^+$ state, vibr. energy levels calcs. 77−83566
Li_2, $X^1\Sigma_g^+$ and $A^1\Sigma_u^+$ states, electronic struct. and spectra 79−89615
Li_2^-, electronic struct., ab initio calcs. 77−34553
Li_2^+, dissoc. energy, laser photodissoc. determ. 78−70950
Li_3, geom. struct. and binding energy, diatomic-in-molecules 78−74785
Li_4, geom. struct. and binding energy, diatomic-in-molecules 78−74785
$LiAlH_4$, $LiBH_4$, ab initio calc. of geom. struct., charge distrib., bonding and pot. energy surfaces 80−18796
LiF-NH_2 adduct, mol. consts., ab initio SCF LCAO MO calcs. *(French)* 78−13423
LiH, electron correl., double SCF method 78−17575
LiH, LiH^-, pot. energy curves, electron affinity, spectroscopic consts. 78−5129
$^7Li_2$ 77−14602
$^7Li_2$ 77−14603
$^7Li_2$ $A^1\Sigma_u^+$-$X^1\Sigma_g^+$ band system anal. 77−83565
$Li_2(g)$, thermochem. props. 77−21410
Mg_2, ground state, multiple scatt. Xα calcs. 80−58149
Mg_2, mol. consts. calcs., inverted perturbation approach 77−57969
MgD, emission spectra, 600 to 850 nm, rot. anal., dissoc. energies 78−62815
MgH, $A^2\pi - X^2\Sigma^+$ system, dissoc. energy 77−10686
MgH, emission spectra, 600 to 850 nm, rot. anal., dissoc. energies 78−62815
MgH, Morse and Lippincott pots., r-centroids, dissociation energy 78−13446
MgO, dissociation energy in range 2020 to 2160K 77−549
MgO, dissociation energy from RKRV potential energy curve 78−37768
MgOH (MgCl), mol. dissoc. energies calc. by high temp. mass spectrometer 80−83514
MnSe, vaporization, thermodynamic study by Knudsen-cell mass spectrometry, atomisation enthalpies 79−10937
MoNb, mol. dissoc. energy, mass spectrometric obs. 79−10229
N_2, MRD CI calc., lowest dissoc. limits 78−21859
N_2, nonequilibrium dissociation rates in electrical discharges, temp. depend. 78−33447
N_2, spectroscopic data review 77−38680
ND, $d^1\Sigma^+$-$c^1\Pi$, spectra, equilib. consts., dissociation energy 78−33517
ND, dissoc. energy, calc. from $c^1\Pi$ state predissoc. *(German)* 78−90237
NF, pot. energy curves and dissoc. energy, Hulbert-Hirschfelder calc. 80−30210
NH, $d^1\Sigma^+ - c^1\Pi$, $d^1\Sigma^+$-$b^1\Sigma^+$, spectra, equilib. consts., dissociation energy 78−33517
NH, dissoc. energy, calc. from $c^1\Pi$ state predissoc. *(German)* 78−90237
NH_2^+, low lying states, ab initio MRD-CI pot. surface calcs. 79−89611
NH_3 bond dissociation, MCSCF LMO calcs. 77−57886
NH_3, cluster-ion prod. in electron-irrad. solid, lattice, and fragmentation energies 77−4911
NH_3, decomposition kinetics on single cryst. planes of Pt 77−1948
NO, adsorbed on Ru (001), inelastic electron scatt. dissoc. energies adsorbed state depend. 78−95956
NO^+ ground state mol. consts., from NO $X^2\Pi(v''=0)$ UPS obs. 80−14177
NO^+, pot. energy curves, dissoc. energy 79−22623
$(NO_2)^+$, in photoionis. efficiency obs. of $(NO)_2$ 77−61811
N_2O^-, ground state potential energy surfaces 77−27175
NOH, groundstate electronic struct., MRD CI calc., dissoc. energy, isomerisation energy 80−14088
NOH^+, ab initio pot. surface, and isomerisation barrier of lowest states 79−22622
NOH^+, ab initio SCF and CI comparison of struct. and spectra with HNO^+ 77−26972
NOH^+, vertical spectra, heat of form., ab initio MRD-CI calcs. 79−49934
NS radical chemiluminescence produced by active N+S(S_2Cl_2), kinetics study 79−39151
Na_2, dimer, $B'\Pi_u$-$X'\Sigma_g^+$ band system obs. 78−62837
Na_2, laser-induced atomic fluoresc., semiclassical intensity calc., transition moments 77−18838
Na_2^+, photodissoc. and photoionisation in Na_2 multiphoton absorpt. 79−31628
$NaAlH_4$, $NaBH_4$, ab initio calc. of geom. struct., charge distrib., bonding and pot. energy surfaces 80−18796
NaAr, intramol. pot. functions of ground and excited state 79−54785
NaAu(Ag), mol. dissoc. energy, third law enthalpy and heat of formation, mass spectra 78−40033
NaK, appearance pot., dissoc. energy, ionis. pot., mass spectra obs. 78−25750
NaLi, appearance pot., dissoc. energy, ionis. pot., mass spectra obs. 78−25750
NaNe, intramol. pot. functions of first excited state 79−54785
$Nb_2(g)$, dissoc. energy, heat of form., Knudsen effusion mass spectrometric determ. 79−81297
NdO, D_0^0-state struct., dissoc. energy, mass spectrometric obs., 79−10228
Ne_2^+ formation and destruction in Townsend discharges 80−38747

molecular dissociation energies continued
$NeCN^+$, SCF calcs., dissoc. energies, rot. and hyperfine const. determ. 80−95531
Ni_2 and Ni_2^+, lowest electronic states, GVB and POL-CI calcs. 79−31409
NiAl, vapour phase mass spectra, correl. between bond strengths in liq. and gas phases 77−35466
NiCu molecule, electronic states determ. by ab initio HF and CI methods 80−69087
O_2, determ. by laser photofragment spectroscopy 78−70957
O_2^+, vibr. energy levels, dissoc. energy, photoelectron spectra 77−83651
O_3, analytical potentials from spectroscopic data, vibr., bond length, dissoc. 77−10613
O_3^-, O bond dissociation energy 78−7193
OH, Simon-Parr-Finlan potential appls. 80−18785
OH^+, Simon-Parr-Finlan potential appls. 80−18785
$O_4^+(O_s^+)(O_6^+)(O_2^+H_2O)$ 80−95707
P_2^+, electronic states pot. energy curves, dissoc. energy, ionisation pot., curve fitting 80−32796
$P_4 \rightarrow P_2 + P_2$, from photoionisation mass spectra 77−30935
PF, (PF^+), pot. energy curves and dissoc. energy, Hulbert-Hirschfelder calc. 80−30210
PO, rot. struct. of absorpt. bands 1850-1600 Å, valence $^2\Pi$ state 79−13739
PsO, stability and dissoc. energy, restricted HF and correlation correction calcs. 77−54634
PsS, stability and dissoc. energy, restricted HF and correlation correction calcs. 77−54634
Pt complex, ethylenediamine tetrahalide, reson. Raman spectra, dissoc. energy 79−26990
Pt-actinide diatomic mol., calc. dissoc. energy 78−78832
PtC, ground and first excited states, dissoc. energy and dissoc. curves, pot. energy curves 77−50555
PtO, ground and first excited states, dissoc. energy and dissoc. curves., pot. energy curves 77−50555
Rb^{2+}, dissoc. energy from ionisation rate coeffs. of Rb+Rb 80−58363
RhTh, mol. vapour above Th-U-Rh-graphite, dissoc. energy, mass spectra 78−78832
RhU, mol. vapour above Th-U-Rh-graphite, dissoc. energy, mass spectra 78−78832
SO, pot. energy curves, dissoc. energies 78−50485
S_2O, photoionis. mass spectrum, heat of form., dissoc. energy 77−46605
SSe, dissoc. energies determ. 78−33632
SbF, pot. energy curves and dissoc. energy, Hulbert-Hirschfelder calc. 80−30210
SbO, dissoc. energy calcs. 77−3486
ScO, pot. energy curves and dissoc. energy of $X^2\Sigma$ state 80−69203
ScRh, gaseous, dissociation energies, high temp. mass spectrometric determ. 80−93790
Se_2, dissoc. energies determ. 78−33632
SeO, pot. energy curves, dissoc. energies 78−50485
SeTe, dissoc. energies determ. 78−33632
SiH, A state new predissociations, improved dissoc. energy value from rot. level lifetimes 79−3496
SiH^+, oscillator strengths and dissoc. energy determ. from time resolved precision spectroscopy 80−58272
$SiH_3PH_2BD_3$, liquid and solid, vibr. analysis, spectra and structure of P-B compounds 78−84586
$SiH_3PH_2BH_3$, liquid and solid, vibr. analysis, spectra and structure of P-B compounds 78−84586
SiO molecule, true potential energy curves, dissoc. energy, ionisation potential 77−6704
SiO(g), enthalpy of formation and dissociation energy, time-of-flight mass spectra 77−16859
SiS molecule, true potential energy curves for various states, dissoc. energies 77−6704
SmO, dissoc. energy, mass spectrometric determ., rel. to EuO 77−58199
$SnSe_2$, rel. to p-T projection of phase diag. of SnSe-Se 78−27485
SrBr, gas equilib. mass spectra, dissoc. energy meas. 77−65543
SrI, mol. dissoc. energy, high temp. mass spectra 78−58863
TeO, pot. energy curves, dissoc. energies 78−50485
ThC_3, atomisation energy, stability, mass spectrometric determ. 79−7037
TiO, potential energy curves and dissociation energy 78−50531
$TiO_{(g)}$, $TiO_{2(g)}$, thermochemistry, mass spectrometry 77−16857
TlI, mol. beam photodissoc., bond order and state symm. 77−34706
UF_5, thermochem., heat of formation, dissoc. energy, ionis. pot. 77−70326
UF_6, gas phase thermal decomp., dissoc. energy of U-F bond *(German)* 79−29353
UF_6+e⁻(K)(Na)(Cs), positive and negative ion formation, electron affinity, bond dissoc. energy 77−75314
UH_4, thermochem., heat of formation, dissoc. energy, ionis. pot. 77−70326
WF_6+Na(K) electron transfer, WF_6^- form., dissoc. energies, electron affinity 77−19071
X-H bond dissociation energies from ab initio calcs. of force consts. 77−3267
X_2H^+, X=Li, Na, K, equilib. geom. and dissoc. energy, pseudopot. calc. 78−94329
X_2Y^+, X,Y=Li, Na, K, equilib. geom. and dissoc. energy, pseudopot. calc. 78−94329
$XeAr^+$, form. from Xe^++Ar, reaction equilib. and rate consts. 80−61071
XeCl, B-X and D-X band systems, vibr. anal. 79−59482
XeF^+, selected valence-electron split-shell MO calc., ground state props. 79−22585
XeO, $d^1\Sigma^+ \rightarrow a^1\Sigma^+(b^2\Pi)$, green band emission spectroscopic anal., RKR pot. curves, bond lengths and dissoc. energies 79−41181
YC_n+(n=2, 3, 4, 5, 6), atomisation energies, Knudsen cell mass spectrometric obs. 80−58409
YRh, gaseous, dissociation energies, high temp. mass spectrometric determ. 80−93790
YbO, dissoc. energy, 4.29±0.05 eV 77−44468

molecular electron correlations
σ⁻pi consistency method, appl. to furan, pyrole and pyridene 77−67957
AB_n-type molecular systems, geminal nuclear spin-spin coupling 78−74682
ab initio CI pot. curves, mol. wavefunctions and vibr. freqs. comparison of methods 80−27956

molecular electron correlations continued
acetone, ab initio CI valence and Rydberg states, spectral assignments 77−14346
acetophenone, PPP limited CT calcs. 79−31406
acetophenones, di- and trisubstituted, π^*-π systems, UV electronic absorpt. spectra 80−74132
acetophenones, mono substituted, semi empirical Π-electron calcs. 80−74131
acetophenones, spectrosc. characts. using PPP SCF CI calcs. 80−102448
acetylcholine neurotransmitter, PCILO-INDO calcs. 80−58153
acetylene, and $C_2H_2^+$, ionis. pots., photoelectron spectra, ab initio VB calcs. 77−88396
acetylene, core ionised, core-excited and shake-up states, ab initio MRD-CI methods 80−42950
acetylene, electron density distrib., electron correl. effects, approx. HF-CI calcs. *(German)* 78−33439
acetylene, electron impact ionisation, valence orbitals, momentum distrib. and correl. effects 78−5361
acetylene, force consts. of symmetric stretch motions, accurate ab initio calcs. 77−83567
acetylene, ground and triplet states, electronic and geom. struct. 78−94184
acetylene, vertical ionisation pots., CI calcs. 79−13645
acridine C-radical, polarised absorpt. and ESR spectra, dichroism and HF-CI calc. 78−50563
acrolein, triplet state vertical and adiabatic excitation energies, CI calcs. 78−9083
adenine, tautomers, polarisation, barriers and tunneling times calcs. 79−41114
adiabatic CI pot. surface LCAO calc., gradient determ., mol. dynamics 80−48056
alkanes, van der Waals dimers, PCILO calcs. 79−36542
alkylbenzenes, electronic struct., photoelectron spectra rel. to semiempirical CNDO/S CI calcs. 79−54770
allene, ionis. pots., Green's function method 77−14608
allyl radical, restricted SCF and MC SCF calc. of C_{2v} and C_s structs. 80−83289
aniline, singlet-singlet electron transitions, modified CNDO-CI method exam. 78−25552
[4N+2]annulenes, MCD spectra, B terms, semiempirical models 77−6814
annulenes, MINDO calcs., electron correlations 79−45636
anthracene, spectra, PPP approx., CI clacs. *(German)* 79−36602
antisymmetrization wave function by method of group functions 77−3278
aromatic heterocycles, MC-SCF and CI calcs. in PPP framework 79−26892
atom+ion collisions, diabatic molecular orbitals for inner-shell excitation 78−62897
atomic collisions, mol. approach, radial couplings between approx. wavefunctions 77−38713
autonitryl, electronic struct. and geometry, open-shell SCF calcs. 79−18106
azomethane, trans-cis isomerisation, INDO-SCF and CI calc. 78−25440
benzaldehyde, PPP limited CI calcs. 79−31406
benzene, ab initio non-paired spatial orbital wavefunction, π-electron correl. energy 77−54509
benzene, correl. problem, open-shell coupled-cluster approach, PPP calc. 79−81157
benzene, excitation spectra, cluster configuration method appl. 80−78546
benzene, mono-substituted, MCD, CNDO/S calcs. using capable ang. momentum operator 77−46587
benzene, noncrossing and degeneracy in Hubbard models 80−14096
benzene, UV photoelectron spectra, valence electron shake up approx. methods 80−18788
benzene, VB calc. with CI, basis sets orthogonality problem 77−23435
benzene, X-ray photoelectron spectra, C 1s shake-up struct., PPP CI calc. 78−42126
benzophenone, metastable triplet state, SCF CI calcs. 79−54776
3,4-benzphenanthrene cation radical, in boric acid glass, spectrum 200-1400 nm, MO calcs., assignments 77−75174
Bethe-Goldstone time-depend. first-order theory, short range correl., transition moments 78−25449
biacetyl, lower excited electronic states, ab initio SCF and CI calcs., absorption band assignment 78−74589
1,1′binaphthyl, electronic struct., fluoresc. CNDO/S CI calcs. 78−90084
1,1′-binaphthyl, $T_n \leftarrow T_1$ absorption spectrum in rigid and fluid media, CNDO/A study 79−76355
biological systems, containing Fe, electronic and mag. struct., semiempirical MO cluster calcs. 78−62733
biphenyl, lowest excited singlet states, polyexcited CI calc. 79−772
bond order, maximum principle, LCAO formalism 78−29728
Born-Oppenheimer adiabatic pot. energy hypersurface gradient, exact formula 79−9992
Brillouin theorem, proof 80−91415
Brueckner condition for MO selection in correlated orbitals 77−23436
1,3-butadiene, π-electron struct., generator coord. method 79−26880
trans-butadiene, all-valence-electron CI calcs. of electronic spectrum 77−10654
trans-butadiene, correl. problem, open-shell coupled-cluster approach, PPP calc. 79−81157
butadiene, excitation spectra, cluster configuration method appl. 80−78546
s-cis-butadiene, natural orbitals, photochem. cyclisation 79−85900
trans-1,3-butadiene, valence electronic excited states, SCF ab initio GVB and CI calcs. 79−31423
n-butane, vertical electronic spectra, limited CI calcs. 79−13693
butatriene, ionis. pots., Green's function method 77−14608
caffeine, semi-empirical excited state Morokuma's EHP calc., geometry and order of states 78−46256
carbazole, CNDO/S and CI calcs., photoelectron spectrum assignment 77−67982
carbenes, triplet state g-tensors and hyperfine coupling tensors 80−52895
carbonyl compounds, localisation of $n\pi^*$ excitation, config. interaction method 78−50482
carbonyl fluoride, vertical electronic states, ab initio SCF CI calc. 79−49942
carbonyl oxide, config. interaction calc., using DODS natural orbit approach 78−66476
carbonyls, electric polarisability, in excited singlet and triplet states *(Bulgarian)* 80−52897

molecular electron correlations continued
β-carotene, optical absorpt., theory 79−62189
chain molecule excitation correlator at local relaxation *(Russian)* 80−14090
chemical bond, MO-LCAO scheme for binding energy, correlation correction, physical fragmentation 77−46490
chemical bonds, RPA calcs., ground state correlation energies 80−47847
chemisorbed atoms, theory, CI calcs. *(German)* 78−31707
chlorin, ab initio CI calcs. on ground, singlet and excited states, visible spectrum 79−16139
CI calculations, Waller-Hartree method appls. 77−14363
CI limited to double substitutions with respect to no. of electrons, dependence of energy given 79−10040
CI matrix elements eval. for canonically ordered basis 79−31420
CI methods for improving unrestricted Hartree-Fock spin densities 80−32617
CI wavefunction, terms selection for pot. energy surface 77−88401
cinnamaldehydes, electronic spectra, CNDO CI calcs. 78−29774
closed shell system, limited CI calcs., spin algebra graphical method 78−46273
closed shell systems, ionis. pot., Koopman's theorem 78−906
closed shells, fast CI method calcs. 78−90090
closed-shell linear molecules, relativistic Dirac-Fock multiconfig. SCF calcs. 80−99455
closed-shell polyatomic molecules, relativistic Dirac-Fock multiconfig. SCF calcs. 80−99456
closed-shell system, polarisability and mag. susceptibility calc. by SCF and CI method 80−99443
closed-shell systems, interactions, correl. energy, RPA calcs. 78−25646
cluster expansion, electron correlations, SAC and SAC CI calcs. 80−18802
cluster expansion electron correlations, SAC and SAC CI theories 80−18801
CNDO-CI method, parameterisation role 77−46497
CNDO/S-CI method, convergence problems 77−46496
complete active space method, comparison of super CI and Newton Raphson scheme 80−47904
complex electron configurations, quasispin method, mixing configurations 80−42953
complex heteroorganic molecule, semi empirical SCF-CI MO method 79−63917
complex molecular orbitals, pairing representation 80−91454
Compton profiles, two-electron theory 79−86012
computational atomic and molecular physics, conf., Nottingham, England, (Sept. 1978) 79−59567
computer program for calculating configuration interaction in CNDO approx. 77−50372
configuration interaction, iterative variational method calcs. 78−55127
configuration interaction, perturbation theory, partial transformation 78−37562
configuration interaction calc., atoms and atomic complexes confined in spherical boxes, Hartree-Fock-Slater potential 80−47898
configuration interaction method formulation for triplet states 78−37536
configuration interactions, appl. of unitary group methods 80−27958
configuration mixing calculations, transverse interaction, vector spherical harmonics expansion calcs. 78−9086
conjugated molecules, excited state, self-consistent HMO theory *(Japanese)* 77−42253
core holes, localised-delocalised relation, ionis pot., Green's function method 77−75064
coronene, excited state Faraday values mag. circular dichroism spectra and MO CI calcs. 80−18877
correlated Π-electron systems, mol. interactions, linear response theory 80−53090
correlation energies estimation from semi-transferable orbital correlation energies 78−82650
correlation energy, many-body Rayleigh-Schrodinger perturbation theory calcs., exclusion principle violation 80−52890
correlation energy calc. by many-body diagrammatic perturbation theory 78−9087
Coulomb exchange integrals, correlation factor r_{12}^k, kinetic energy 78−62699
Coulomb exchange integrals, correlation factor r_{12}^k 78−62698
coupled cluster approach, open (closed) shell systems 80−47842
coupled electron cluster theory for closed shell systems 79−89613
coupled-pair many electron theory, quadrupole excitation in correl. energy theories 79−36538
coupling constants in direct CI method 80−9516
CT complex, equilib. distances and stabilisation energy, PCILO calc. 78−41963
cyanine dyes, all-reactive-electrons closed-shell SCF-CI MO calcs. 79−36541
cyanine dyes, excited electronic states, CNDO/S CI calc., visual pigment spectra appl. 80−85333
cyclobutadiene, noncrossing and degeneracy in Hubbard models 80−14096
cyclobutadiene(-d_1), singlet and triplet ground states, vibr. freqs., MINDO/3 and ab initio SCF calcs. 78−13429
cyclopentadienone, photoelectron spectra, ionisation pot., PERTCI method and obs. *(German)* 78−42130
cyclopentadienyl radical, pot. surface and vibronic states, ab initio CI calcs. 80−47897
cyclopenta[h]cycl[4.2.2]azine, electronic struct., photoelectron data 78−5286
cyclophanes, double and triple-layered, triplet state zero field splitting parameters, HMO calc. 77−50366
cyclopropane, electron correlation, double SCF method 78−17575
cyclopropenyl radical and anion, planar, E state pot. surfaces, CI and SCF calcs. 78−5155
cytosine, vertical interaction evaluation methods 79−54772
d^3-configuration in trigonal field, Trees correction *(Russian)* 77−46556
delocalised treatment of correl. problems, N-depend. 79−63921
density functional calculations for atoms, molecules and clusters 80−47850
deoxyhaemoglobin, ferrous heme of high-spin type, MCD spectra in Soret, visible and near IR regions 80−94156
deoxyhaemoglobin, porphin-Fe-imidazole system, SCF-LCAO-ASMO and CI calcs. of low-lying multiplets and excited states 80−94155
s-cis, s-trans-diallyl, twisted, low-lying singlet states, sudden polarisation effect 78−86792

molecular electron correlations continued
diamagnetic susceptibilties and NMR chemical shifts in terms of localised MO's 80−106256
diatomic hydrides of first and second row elements, PNO-CI and CEPA calc. 79−768
diatomic isovalent systems, pot. curves, ab initio MRD-CI method 80−83293
diatomic molecule, electron correlations, cryst. field interactions, Hubbard calc. 80−75530
diatomic molecules, compactness proof for infinite systems of linear equations 79−72247
diatomic systems, Penning and assoc. ionisation, correl. diagrams calcs. 77−50521
diatomics, TFDW eqn., correlation diagrams 79−59355
dichlorocarbene, electronic spectrum, ab initio CI calcs. 79−85948
diformamide, excited singlet and triplet states, CNDO-CI calcs. 77−26990
dihydrophenazine derivatives, in 3-methylpentane (ethanol) (PMMA), radiationless processes, temp. depend. 80−43087
dihydroxycarbene, singlet and triplet state rot. pot. surfaces 80−32627
α,ω-diphenyl-trans-polyenes, 1st excited singlet valence states, CI and extended CNDO/S calcs. 78−74807
direct CI method, generalised to Hartree-Fock interacting space for doublets, quartets etc. 79−85908
direct CI method, Hartree-Fock interacting space for doublets, quartets and open-shell singlets 80−52889
direct CI method generalisation, graphical unitary group approach 80−47900
direct CI method with contracted config. expsn. 78−5145
direct orbital optimisation for MC SCF theory by unitary transformations 80−87049
disconnected clusters of double excitations, effect on correl. energy 79−54773
dispersion energies, charge overlap effects, with freq.-depend. polarisability 79−86025
DNA base pairs., Coulomb interaction energy calcs, electron correlation role 79−96509
dodecahexenes, sudden polarisation effect, ab initio and CI calcs. 80−58160
double excitation wavefunctions, multiconfigurational SCF method 77−10604
double SCF method 78−17575
doublet and quartet states, abstraction reactions, pot. energy surfaces calcs. 78−31627
doubly excited configurations in density-matrix method 77−3280
elecronic excitation properties, RPA-CI calcs. using hypervirial relations as constraints 79−76413
electric dipole allowed transitions, amplified sector rule based on electron correlation 80−5523
electron correlation energy, approx. 4th-order perturbation theory 79−6876
electron density and density matrix approximations using potential energy error bounds 78−94180
electron in strong randomly rotating mag. field 78−37163
electron pair distrib. functions, SCF CI wavefunctions 78−41966
electron scatt., R-matrix theory 77−75298
π-electron systems, excitation spectra, cluster configuration method appl. 80−78546
electronic charge distribs., theory, review 77−75040
energy functional, direct minimisation in LCAO-MO density matrix formalism 78−5118
energy partitioning of open-shell system, INDO theory 79−68192
equations of motion, Green's function methods and config. interaction methods, comparison, appl. and anal. 80−47841
equations of motion Green's function methods, higher order terms, ionisation pots. 80−52891
equations of motion Green's function methods, higher order terms, ionisation pots., CI comparison 80−52892
ethane$^+$, stability and struct., CI-SCF ab initio calc., Franck Condon anal. 77−54575
ethane, (e,2e) spectroscopic obs., valence electron momentum distribs. and separation energies 77−3480
ethane, ab initio MRD-CI calc., 14-25 eV PES region, Rydberg states 78−41962
ethane, nuclear spin-spin coupling consts., vicinal proton-proton coupling calcs. 80−32737
ethane, vertical electronic spectra, limited CI calcs. 79−13693
ethane cation, relative stability of $^2A_{1g}$, ^2E_g states 80−58140
ethenoxy, config. interaction calc., using DODS natural orbit approach 78−66476
ethylene, $\pi\pi^*$ singlet state, using general CI method 79−36539
ethylene, (e,2e), correlation effects, electron momentum distributions in valence orbitals 79−862
ethylene, core ionised, core-excited and shake-up states, ab initio MRD-CI methods 80−42950
ethylene, ionis. pot., Green's function method and CI calcs. 79−13839
ethylene, ionis. pots., Green's function method 77−14608
ethylene, ionisation pots. and excitation energies, correl. calcs. 77−26986
ethylene, planar, V-N vertical transition, SCF and correlation energies 77−68032
ethylene, planar $^1(\pi,\pi^*)$ state, CI calcs. 77−57887
ethylene, planar dissociation, electronic rearrangement, states, bonds, ab initio multiconfigurational SCF calcs. 80−27937
ethylene, pot. energy and dipole moment surfaces, polarisation effect, ab initio CI calcs. 80−106272
ethylene, quasidegeneracy and effective Hamiltonians, canonical transformation cluster expansion formalism 80−52888
ethylene, reaction heat, HF limit energies, correlation energy 79−8447
ethylene, rot. around double bond, four orbital-four-electron model 80−95592
ethylene, singlet Rydberg states, CI calcs. 78−33437
ethylene, UV photoelectron spectra, valence electron shake up approx. methods 80−18788
ethylene, V-state config. selection methods 79−10041
ethylene, valence XPS spectrum satellite struct., C(2s) region, correlation states 78−5278
ethylene, van der Waals dimer, PCILO calcs. 79−36542
ethylene, vertical, $N(^1A_g)$, $T(^3B_{1u})$, $V(^1B_{1u})$ states, large scale CI calc. 78−70752
ethylene, vertical $^1(\pi\text{-}\pi^*)$ V-N transition, MRD-CI calc. 79−27004
ethylene ozonide, ab initio gradient and MC SCF calc., conformational anal. 80−83290
ethylene radical cation, electronic states assignments, ab initio SCF CI calcs. 77−10584
ethylene V state, ab initio study of spatial extension 80−27952
ethylene-O_2 complex, CI calcs., singlet-triplet transitions 79−63923
ethylenes, substituted, unstable twisted forms, excited states, DODS-NO CI calcs. 79−13643
ethylidene, rearrangement to ethylene, barriers, ab initio MO calcs. 80−104424
ethynol, ab initio calc., energy levels and geom. struct. of C_2H_2O isomers 78−62716
ethynyl radical, emission spectra and pot. energy surface, ab initio MRD CI calc. 79−41099
ethynyl radical, vertical electronic spectrum, CI calcs. 77−34656
exchange and correlation, density function formalism 77−14367
excitation energies calc., using renormalised Green's function method *(Japanese)* 80−83295
excitation energy, validity of excited minus ground state calcs. using HF/pair correlation 77−38620
excited state multiconfig. wavefunctions, selection of optimal configs. 77−34566
excited states, local approach calc. 79−49956
excited states, variable metric optimisation of mol. geometry 80−58178
extra correlation energy, calc. by CHF method 79−76350
extrapolation in CI calculations, using perturbation theory natural orbitals 79−85907
first-row hydrides, correl. energy difference models 77−10600
first-row hydrides (CH_n, NH_n, OH_n, FH_n), equilib. geometries calcs. 78−33435
fluorobenzene, singlet-singlet electron transitions, modified CNDO-CI method exam. 78−25552
fluorobenzenes, UV spectra calc., oscill. strengths 79−18203
formaldehyde, $^1A_2$-state, radiative and nonradiative decay calcs., rel. to photochem. decomp. 78−37669
formaldehyde, $^1A_2$-state, SVL fluoresc.-spectra, absolute radiative lifetime, ab initio CI calcs. 79−63919
formaldehyde, $^3A''$ state, zero-field splitting param., ab initio CI calcs. 80−99454
formaldehyde, adiabatic CI pot. surface LCAO calc., gradient determ., mol. dynamics 80−48056
formaldehyde, electronic struct., dipole moments, mol. polarisability, force fields, ab initio calcs. 80−78531
formaldehyde, force consts., ab initio CI calcs. *(French)* 78−90093
formaldehyde, photodissoc., pot. energy surface features 79−79271
formaldehyde, Rydberg states, excitation energies, oscillator strengths ab initio GVB-CI calcs. 77−54518
formaldehyde, semi-empirical excited state Morokuma's EHP calc., geometry and order of states 78−46256
formaldehyde, triplet state g-tensors and hyperfine coupling tensors 80−52895
formaldehyde, vertical photoexcitation and photoionisation spectra, CI calc. 78−918
formaldehyde anion radical, hyperfine coupling consts., vibr. depend., ab initio calcs. 80−87150
formaldehyde-d_0, -d_2, $^1(n\pi^*)$ radiationless transition, ab initio CI calc. 79−767
formaldehyde-d_0, -d_2, $^1(n\pi^*)$ transition, vibr. struct., ab initio CI calc. 79−766
formamide, and related cpds., INDO-CI calc., transition moments 79−45637
formamide, CI calc. of vertical ionisation and excitation energy 78−78836
formic acid, valence and Rydberg state empirically adjusted ab initio calcs. 77−10609
fourth order perturbation theory, triple substitutions to electron correl. energy 80−74133
free radical reactions, selection rules 78−7181
free radicals, RHF CI INDO spin density calc. 80−919
fulvene, correl. problem, open-shell coupled-cluster approach, PPP calc. 79−81157
fulvene, ground and excited states, electronic correl. and struct. 79−26898
Gaussian geminals basis set calc. of correlation energy 78−41960
geometry, basis set effect and approx. natural orbitals in SCF CI GTO calcs. 78−76904
geometry of electron pair correlation, Lie algebra 78−29754
geometry optimisation with explicit inclusion of electron correl. 80−37748
glyoxal, $^3n\pi^*$ states, ab initio STO-3G CI calcs., ΔE_{SCI} transition energies 78−94194
glyoxal, lowest triplet state, excitation energies, electron correl. effects 78−5147
glyoxal, triplet state excitation energy calc., modified CI method 78−37536
graphical unitary group approach, appl. to ketene 79−76324
ground state, $n\pi^*$-excited states *(Bulgarian)* 80−32614
ground state correlation energies, Green's function calcs. 77−75061
ground state props., coupled cluster and MBPT methods appl. 80−47881
Group IV-VI diatomic molecules, He(I) photoelectron spectra, calcs. 80−1023
H_20, CI calcs. using modified virtual orbitals 80−58163
halogen molecule, orbitals calc., correlation effects, force const., dissoc. energy, bond length 77−26964
halogens, van der Waals dimers, PCILO calcs. 79−36542
heat of reaction, basis set of effect and approx. natural orbitals in SCF CI GTO calcs. 78−76904
heavy ion+atom collisions, mol. M-X-rays, self-consistent relativistic HF-Slater many electron correl. diagrams 77−14567
heavy-ion collision, quasimolecular L X-rays, relativistic self-consistent correlation diagram 78−5247
Hellmann-Feynman theorem for limited CI wave function, 1st-order props. 79−59329
Hellmann-Feynman theorem for open-shell and multiconfiguration SCF wave functions 79−89591
heterocyclic conjugated compounds, electronic struct., spectra, ionisation pot., INDO-CI LACO-MO-SCF calcs. 79−54834
heteroorganic molecules, all-reactive-electrons closed-shell SCF-CI MO calcs. 79−36541
1,3,5-hexatriene, π-electron struct., generator coord. method 79−26880

molecular electron correlations continued
trans-hexatriene, correl. problem, open-shell coupled-cluster approach, PPP calc. 79−81157
hexatriene, excitation spectra, cluster configuration method appl. 80−78546
all-trans-1,3,5-hexatriene, excited electronic states calcs., spectra assignments 79−22606
trans-1,3,5-hexatriene, low-lying $\pi\pi^*$ excited states, ab initio STO method 77−3284
trans,trans-1,3,5-hexatriene, valence electronic excited states, SCF ab initio GVB and CI calcs. 79−31423
hydride ions, XH^+, X=first and second row elements, PNO-CI and CEPA studies of electron correlation effects 77−34561
hydrides, first row, $AH_2(H_3)(H_4)$, and positive ions, chemical equilibria, correl., ab initio calc. 78−35714
hydrocarbons, 6-π electron conjugated, orbital pair correlation energy calc. method 77−88374
hydrocarbons, conjugated, effect of semi-empirical parameters on simple RPA calcs. 79−10037
hydrocarbons, cyclic, non alternant, nonsingle instabilities of HF solns. 80−58164
hydrocarbons, electric polarisability, in excited singlet and triplet states *(Bulgarian)* 80−52897
hydrocarbons, saturated and unsaturated, ionisation spectral intensities, correlation effects 78−90234
hydrogen maleate ion, electronic spectra, CNDO/S CI calcs. 77−75128
hydronaphthyl radicals embedded in naphthalene cryst., optical transition energies and ionisation energies 80−78595
β-hydroxy acrolein, lower excited states, electronic struct. and H-bonding, ab initio SCF and CI calcs., photochemical mechanism 80−83278
β-hydroxyacrolein, intramol. H bonds, orbital and transition energies, ab initio SCF and SCF CI calcs. 77−14345
Hylleraas-type wavefunction transform. to momentum space, integral and expansion techniques 79−54757
hyperpolarisabilities, HF calc. with correlation method, appl. to HF mol. 80−23342
indirect evaluation by energy variance 79−36546
inert gas dimer ions, electronic struct., chem. binding 79−31376
inert gas fluorides, covalent and ionic states, ab initio CI calcs. 78−78634
inert gas monohalides, hyperfine interactions, struct., valence bond calcs. 78−66473
inert gas oxides, low-lying electronic states, ab initio CI calcs. 77−57888
inner shell hole states calc. by generalised Brillouin theorem-multiconfig. method 77−23443
integral equation numerical soln. in pair approx. 78−90065
interaction energy, direct calc. with CI wavefunctions 78−66477
intermolecular correlation, approximation scheme 79−26905
intermolecular energy, CI ab initio calc., correction for basis superposition error 79−85904
intermolecular forces, ab initio calcs. applicability and accuracy 80−18898
ion+atom collisions, diabatic correl. diagrams for quasi-mol. description 79−3525
ionisation potential, vertical, inner and valence shells, ab initio SCF MO CI perturbation calc. method 78−74800
ionisation potentials, electron affinities, perturbation theory-CI calcs. 78−9084
ions, ionisation potentials, electron affinities, perturbation theory-CI calcs. 78−9084
isotope exchange reactions, equilib. consts., adiabatic correction, electron correl. effects 78−88626
iterative natural orbitals for CI using peturbation theory 77−79549
iterative scheme for simultaneous calc. of m 1st eigenstates of real symmetry matrix 79−85888
ketene, ab initio calc., energy levels and geom. struct. of C_2H_2O isomers 78−62716
lanthanide, trivalent, hypersensitive transitions, intensity parameters, charge transfer mixing 77−55498
limited CI with optimal generalised combination of SCF MO symmetry subsets 77−42246
limited MC SCF theory 79−36537
linear Hubbard model, RPA and CI test calcs. 78−25411
linear triatomic hydrides, ab initio SCF CI electric dipole moments 79−31410
liquid, angular velocity correlation, from angular position correlation functions 79−86660
liquid, symmetric top molecule, angular velocity correlation function, from angular position correlation functions 79−86661
LNDO/S, semiempirical SCF-CI method for calc. ionis. pot. and electronic transition energies 79−18117
local approach, molecular correlation energies, intraatomic correlations 78−41967
local force densities and stress tensors, density functional theory 80−18781
local-density theory of multiplet structure 80−18776
localisation and local phenomena in excited and ionisation stationary states 77−34563
localisation of $n\pi^*$ excitation, config. interaction method 78−50482
localised orbital construction for calcs. using multiconfigurational SCF methods *(Russian)* 78−922
magnesium chlorin, ab initio CI calcs. on ground, singlet and excited states, visible spectrum 79−16139
magnesium porphine, ab initio CI calcs., electronic absorpt. spectra 78−78639
many body perturbation calculations and coupled electron pair models 79−59363
many body perturbation expansion, fourth order linked diagrams for quadruply-excited states 79−59364
many body perturbation theory fourth order calc. of correl. energy 80−14087
many electron correl. problem, unitary group approach via spin algebra graphical methods 80−47902
many-body perturbation theory, modified pots., 3- and 4-body contribs. 77−88376
many-body perturbation theory, quadrupole excitation in correl. energy theories 79−36538
many-electron theory, unitary group formulations and quantum organic chemistry 80−106270
MC SCF theory, generalised Brillouin theorem and generalised forces 77−14366

molecular electron correlations continued
MC-SCF theory, modified one-electron Hamiltonian, iteration convergence 79−6871
MC-SCF theory, orthonormality-constrained orbital optimisations 78−86766
MCSCF and CI wave functions, two-particle density matrix and graphical unitary group approach 80−63558
MCSCF functions optimisation, generalised Brillouin theorem appl., CI calcs. 77−67960
MCSCF method improvement 80−52857
metal porphin, triplet state, spin density and zero-field splitting, PPP-SCF-CI calc. 79−68200
metalloporphyrins, reson. Raman specta, intra- and inter-manifold couplings interference 80−28020
methane, bond dissociation, MCSCF LMO calcs. 77−57886
methane, elastic and inelastic electron scatt. differential cross section, obs. and calc., struct., binding energy 80−28110
methane, force consts., ab initio CI calcs. *(French)* 78−90093
methane, force consts., equilib. geom., Hartree-Fock and CEPA calcs. 78−70753
methane, localised orbital construction for calcs. using multiconfigurational SCF methods *(Russian)* 78−922
methane, multipole moments and polarisabilities 79−85910
methane, pot. energy surface of excited singlet state, appl. to photodissoc. 79−83440
methane, vertical electronic spectra, limited CI calcs. 79−13693
methane+$O(^3P)$, barrier height and transition state geometry, POL-CI calc., H abstraction reaction 80−66782
methane cation, photodissoc., ab initio RHF and MRD CI calcs. 80−95695
methanol, dissoc. ionisation mechanism, correlation diagram approach, mass spectra obs., metastable processes 80−95728
methyl anion, geometric struct., electron correlation effects, self-consistent electron pairs 78−22050
N-methyl diformamide, excited singlet and triplet states, CNDO-CI calcs. 77−26990
methyl formate($-d_1,d_3,d_4$), mol. vibr. spectrum, struct., beginning with PCILO calc. *(French)* 80−23401
methyl glyoxal, $^3n\pi^*$ states, ab initio STO-3G CI calcs., ΔE_{SCF} transition energies 78−94194
methyl group, conform. problems, correlation effects 79−97999
methyl iodide, liq., Raman meas. of transversal angular velocity correlation function 79−87422
methyl radical, hyperfine coupling consts., vibr. depend., ab initio calcs. 80−87150
methyl radical and anion, electron affinity determ., ab initio SCF and CI calcs. 78−5149
N-methylacetamide, vertical excitation energies, ab initio SCF CI calcs. 79−45647
methylene, 2^1A_1 state, CI and multiconfiguration SCF calc. 79−10052
methylene, electron affinity, $^1A_1$-$^3B_1$ T_0-value, ab initio MRD-CI method calcs. 78−50478
methylene, geometry, SCF and CI calcs., basis set effects 78−62715
methylene, optimised geometry, CI calcs. using partitioning theory 77−38616
methylene, photoelectron spectra, singlet and triplet state calcs. 78−42127
methylene, quadruple energy, self-consistent electron pairs with higher order effects 78−46276
methylene, singlet-triplet separation, ab initio calcs. 78−74582
methylene, vibronic anal., ab initio CI pot. curves calcs. 78−50479
methylene+H_2→methane, ab initio CI calc. on SCF level, insertion reaction min. energy path 80−7774
methylene*+H_2→CH_3+H, barrier height, CI with double zeta polarisation basis 78−64812
methylene anion, electron affinity, $^1A_1$-$^3B_1$ T_0-value, ab initio MRD-CI method calcs. 78−50478
methylene anion, vibronic anal., ab initio CI pot. curves calcs. 78−50479
methylene ion, pot. energy surfaces of excited states, ab initio GTO SCF CI calcs. 78−58602
methylene peroxide, multiconfig. SCF CI calcs. 80−18803
methylene peroxide, struct., energy levels, ab. initio UHF and MRUHF NO CI calcs. 80−83287
methylenimine, lowest excited state, singly excited config. interaction calcs. 79−59361
methylenimine, n→π^* transition, ab initio SCF MO CI calc. 78−58584
methylnitrene, symmetry restricted multiconfiguration annihilation of single excitations calcs. 78−62695
methylsilylene, closed shell states, isomerisation, config. calcs. 78−35652
minicomputer open ended configuration interaction program, BERKELEY 78−37563
MNDO semiempirical calcs. accuracy rel. to current MO methods 80−47893
modified virtual orbitals, for config. interaction calc. 80−58163
modified virtual orbitals, systematic CI procedure 80−83294
molecular polarisability, ground and excited state, perturbation treatment 78−5144
molecules, natural orbitals, Brillouin-Levy-Berthier theorem, multiconfigurational SCF optimisation 80−27936
moment calcs., many-electron approach 77−57884
moment summation method for natural dichroism and MCD 77−27102
MRD-CI method for electronic wavefunctions 78−46278
multi-config. SCF super-CI calc., density matrix formulation 80−78547
multiconfiguration reference states, perturbation theory calcs. 79−13644
multiconfiguration SCF theory, hierarchy eqns. for reduced transition operators 77−54516
multiconfigurational complex MO method simplification 79−85878
multiconfigurational Hartree-Fock procedure, second-order, 2-electron integral transformations 80−87045
multiconfigurational SCF method, yielding Fock-like operator 79−36540
multiple substitution effects in linked cluster theorem for CI calcs. 78−50481
multiplet ratios for photoionisation and electron attachment, shell model, LS coupling and correl. 78−17636
N^2 problem in CI calcs. 77−23437
naphthalene, inclined dimers, transition energies and moments, excitation energy, four-electron MO-CI treatment 77−42237
naphthalene, LCAO SCF MO CI calcs., integral approx. scheme using semiorthogonalised orbitals 79−6873
naphthalene, spectra, PPP approx., CI clacs. *(German)* 79−36602

molecular electron correlations continued
naphthalene, triplet excimer conformation, σ-π interaction transitions 77−6701
1,4-naphthoquinone, and derivatives, singlet electronic transitions, SCF MO CI calcs. 79−49948
negative molecular ions, theoretical calcs., review 78−37552
p-nitroaniline, core ionisation negative shake up energy, ab initio SCF CI calc. 79−64041
p-nitroanilines, intramol. charge transfer satellites, XPS 80−78650
nitroanilines electronic states, CNDO/s-CI correlative calcs. 78−58604
nitrone, config. interaction calc., using DODS natural orbit approach 78−66476
nitrosomethane, ground state and nonvertical n-π^* excitation energy calcs. 80−18804
nuclear spin-spin coupling consts., finite perturbation-CI calcs. 80−5563
nucleic acids bases, excited state dipole moments and geometries 80−95738
1,3,5,7-octatetraene, π-electron struct., generator coord. method 79−26880
one-centre two electron repulsion parameters in TL and all-valence semi-empirical theories 78−78604
one-electron functionals for correlation energies 78−25447
one-particle Green's function with multiconfiguration reference states 79−31363
open shell orbital theory with electron correl., wavefunction cluster expansion 79−13647
open shell system, limited CI calcs., spin algebra graphical method 78−46274
open shell systems, coupled cluster approach 78−58595
open shell systems, energy partitioning theory at INDO level 79−68192
open-shell electronic states, general CI program 79−36539
open-shell system, polarisability and mag. susceptibility calc. by SCF and CI method 80−99443
open-shell systems, ionisation pots. and dissoc. energies, correl. energy calcs. 79−31413
optical rotatory strength, CI role in CNDO/S calc. 77−83561
orbit-orbit interaction, new tensor expansion, matrix and graphical forms 80−14064
orbital correspondence anal. in max. symm., appl. to spin-forbidden processes 78−78631
organic carbonyls, all-reactive-electrons closed-shell SCF-CI MO calcs. 79−36541
organic compounds, excitation energies, CNDO/S-CI method calc. appls. *(German)* 80−106275
organic radicals, HFS coupling const. calcs., RHF+CI method in INDO approx. 79−770
organic system, nonlinear second-order optical susceptibility 80−9947
oscillator strength, X $^1\Sigma_g^+$-C $^1\Pi_u$ transition, upper and lower bounds 77−83654
oxirane cation, struct. rearrangement following vertical ionisation, ab initio CI calc. 80−58191
oxirene, ab initio calc., energy levels and geom. struct. of C_2H_2O isomers 78−62716
oxoniomethylene cation, rearrangement to hydroxymethyl cation, barriers, ab initio MO calcs. 80−104424
ozone, $^1A_1$ ground state, dipole moment function, ab initio SCF and CI calcs. 80−32628
pair theory and reduced Green's functions 79−54774
pairwise correlated generalised valence bond model, electron correl. model 78−41959
pairwise correlated GVB model, multiconfig. overlap approx. calcs. 79−31408
partitioning theory, energy surface 77−38616
PCILO method, modified, second-order energy using CNDO/2 and INDO Hamiltonian approxs. 79−36533
PCILO-INDO method, theory and appls. 80−58153
s-trans-1,3-pentadiene, photoisomerisation, excited state pot. energy curves, CIPSI calc. CNDO/2 parametrisation 78−11505
perturbation calc. using Gaussian-type geminals 78−17578
perturbation theory, diagrammatic, triply excited state contrib., water appl. 80−18774
phenol, H bonds to proton acceptors, PCILO calcs. 79−26895
phenol, singlet-singlet electron transitions, modified CNDO-CI method exam. 78−25552
phospholipid inter-and intra-molecular interactions, PCILOCC and pot. function calc. 80−3570
photochemistry, sudden polarisation effect 79−34328
photoelectron spectra, satellite struct., electron correl. using initial-state-CI 77−18980
photoemission, many-electron theory, in electron spectroscopy book 78−17714
photosynthetically relevant mols., electronic structural props. 80−16902
phthalazine, excited states, protonation influence, semiempirical CNDO/S CI calc. 79−76353
phthalazine, fluoresc. and phosphoresc., expt. and CNDO/S CI calcs. 79−31585
phthalic acid derivatives, excitation energies, CNDO/S-CI method calc. appls. *(German)* 80−106275
phytochrome chromophore, models, absorption wavelengths and oscillator strengths calc. 77−81469
polar mol. anion ab initio ground state pot. energy surfaces calc. 80−47923
polar molecule, excited state MCSCF wave functions, BeO appl. 80−47916
polarisability, finite-field method, correlation corrections, pseudo-two-electron systems 77−71889
polarisability, scaling and Pade approximants, many-body perturbation theory 80−42952
polarization Green's function with multiconfiguration self-consistent-field reference states 80−37724
polyacenes, electronic transition bands, Franck-Condon factors, PPP SCF MO/CI calc. 78−33430
polyacenes, spectra, correlation effects 79−81199
polyatomic systems, MC SCF computation scheme 79−10039
polyene, deformed excited state, bond length rel. to bond order 77−75071
trans-polyenes, 1st excited singlet valence states, CI and extended CNDO/S calcs. 78−74807
polyenes, $2\,^1A_g$-$1\,^1B_u$ energy gap, extended CI study 79−81159
polyenes, π-electron correlations, canonical and localised orbitals calcs. 79−36547
polyenes, energy spectrum, electron correlation effects 78−46279
polyenes, highly branched, large networks, abnormal bond orders 79−59610
polyenes, linear, π-electron system, appl. of extended RPA excitation operators 79−97993
polyenes, linear, two-photon absorptivities, SCF-PPP-CI calcs. 79−31631
polyenes, localised representation, correlation contrib. to energy 79−59370
polyenes, model results for π electrons 78−55128
polyenic aldehydes, energy spectrum, electron correlation effects 78−46279
polymeric chains and Mott insulators, similarities w.r.t. electronic correl., AMO method *(French)* 80−24775
polymers, renormalized CI for electron correlation in excited states 78−55130
porphine, ab initio CI calcs., electronic absorpt. spectra 78−78639
programmable spin-free method for CI calcs. 78−9088
programme for CI calcs. 78−9089
propane, vertical electronic spectra, limited CI calcs. 79−13693
n-propanol, preferred conformers, PCILO study 80−95542
propyleneimine, circular dichroism, optically active Rydberg transitions 77−18952
pyridines, monosubst., H_2O complexes, n-π^* transitions, H bonding, MO theory 80−95550
2-pyridyl phenyl sulphide, dipole moments, absorpt. spectra, meas. and calcs. 77−46574
2-pyridyl phenyl sulphone, dipole moments, absorpt. spectra, meas. and calcs. 77−46574
pyrrole, excited state electronic struct., ab initio SCF and CI calcs. 78−78644
pyrrole, ground state, (π-π^*) state, ab initio SCF CI calcs. 78−33438
quadrupole excitations in correlation theories 79−36538
quasiparticle theory of large-scale configuration on mixing calcs. 78−13437
quaternionic molecular orbital approach to electron correlation 79−59327
quinoxaline, excited states, protonation influence, semiempirical CNDO/S CI calc. 79−76353
Rayleigh-Ritz method, convergence of Slater, Gauss and two-electron functions 77−65419
Rayleigh-Ritz method, criteria for convergence 77−67959
reaction potential surfaces, electron correl. theories 79−39125
reactive and charge transfer collisions, between ions and molecules 78−62914
relativistic Dirac-Fock multiconfig. SCF calcs. 80−99455
retinal, proton donor-acceptor isomerisation coupling, bacteriorhodopsin as light driven proton pump 79−79473
Ritz approximation, convergence theorem for eigenvalue calcs., appls. 77−75042
satellite peaks, relationship between X-ray emission and X-ray photoelectron spectra 78−66492
scaling and Pade approximants, rel. to perturbation series higher-order terms 80−5487
SCF basis sets of moderate size, efficient methods 78−58593
second-order calculations, scaling 79−31359
second-order perturbation energy, modified HF operator, virtual MOs perturbation anal. 77−18797
second-row hydrides, correl. energy difference models 77−10600
self consistent electron pair theory, perfect pairing valence bond generalisation 80−63532
self-consistent electron pair theory, methods and appls. 77−10579
self-consistent electron pairs method, higher order effects 78−46276
self-correlation role in correl. energy estimates using one-electron functionals 79−89612
1,3-sigmatropic rearrangements, ab initio calcs., basis set and electron correl. effects 80−104428
silaethylene, singlet-triplet energy separation 78−58594
silyl radical, conform., hyperfine struct., nonempirical calcs., vibr., effects 79−97998
singlet biradical species, correl. effects, spin density wave calcs. 77−18796
singlet states, CI method 77−46502
small molecules, HMO-CI, HMO-AO-CI methods, quantum chemistry model studies *(German)* 78−29753
spectroscopic calculations for configuration interaction, general parametrisation method 78−94228
spin adapted configurations, incorporation in many-body perturb. theory formalism 77−88374
spin density functional formalism 79−18122
spin-adapted coupled cluster many-electron theory 77−75065
spin-coupled particle-hole excitation, general matrix element formulas 80−69086
spin-free CI procedure using 1-parameter alternant MOs, appl. to butadiene 79−85887
spin-free configuration interaction, representation matrix elements 80−91459
spin-orbital eqns. for anal. derivatives of config. interaction energy including double substitutions 80−78549
stilbene, diphenylpolyenes, photoisomerisation, 'phantom' photochem. singlet state, PPP SCF CI calcs. 78−73058
superoperator resolvent, alternative inner projections 79−31412
symmetry restricted multiconfiguration annihilation of single excitations calcs., applic. to methylnitrene 78−62695
syndnone, semi-empirical excited state Morokuma's EHP calc., geometry and order of states 78−46256
systems containing noninteracting mols., variational CI calcs. 77−67988
TCNQ dimers, extended Huckel hamiltonian supermol. CNDOS calcs. 80−27953
ten-electron systems, correl. energy, fourth order diagrammatic, many body Rayleigh Schrodinger perturbation theory 80−63556
p-terphenyl, lowest excited singlet states, polyexcited CI calc. 79−772
tetrafluoromethane, elastic and inelastic electron scatt. differential cross section, obs. and calc., struct., binding energy 80−28110
tetramethyl-p-benzoquinone, mol. struct., gas phase electron diffr. obs. 80−58386
1,3,6,8-tetraphenyl-pyrene, UV absorpt. spectra, SCF CI method 79−59479
theory, inverse matrix diagonal and off diagonal elements, self energy perturbation theory 78−82607

molecular electron correlations continued
thieno(3,2-b)thiophene, electronic and vibr. spectra, vapour phase and cryst. 77−34654
thioformaldehyde, electronic struct., dipole moments, mol. polarisability, force fields, ab initio calcs. 80−78531
thiophene, single cryst., UV spectrum, ab initio CI calcs. 79−19898
three-electron bonds, strengths, ab initio LCAO MO CI calcs. 80−87046
thymine, tautomers, polarisation, barriers and tunneling times calcs. 79−41114
toluene, singlet-singlet electron transitions, modified CNDO-CI method exam. 78−25552
trans-hexatriene, 6.2 eV Rydberg state symmetry, multiphoton ionis. spectrum polaris. assignment 78−70759
transition from collective motion model of π-electrons to semiempirical Pariser-Parr-Pople theory *(Russian)* 78−5146
transition metal compounds, electronic excitation energy calc., correl. energy correction 78−17576
transition metal dihydrides, gas phase geometrical struct. calcs. 80−42951
transition metal hydrides, homoleptic, electronic structure, ab initio calcs. 79−89601
transition metal nitrosyls, appl. of HF and CI calcs. 80−9513
triatomic dihydride molecules, Walsh's rules and small bond angle states 80−106255
trichlorofluoromethane, dissoc. electron attachment, pot. curves calcs. 79−98231
trichlorofluoromethane anion, dissoc. electron attachment, pot. curves calcs. 79−98231
trimethylene, singlet state, rot. barrier origin, MINDO/2 calc. 79−81170
trimethylene diradical, generalised Hartree-Fock natural orbital config. interaction approach 77−75062
trimethylene diradicals, geometry optimisation ab initio SCF CI calcs., energy gradient 79−85903
trimethylenemethane, bisected singlet state, using general CI method 79−36539
triphenylene, excited state Faraday values mag. circular dichroism spectra and MO CI calcs. 80−18877
truncated CI calcs. 80−27954
twisted conjugated molecule, zwitterionic excited states investig. 80−58179
two photon absorptivities, CNDO/S-CI calc. with second order time depend. perturbation eqns. 80−74122
two photon absorptivity, ion cyclotron reson. photodissoc. spectra, CNDO/S-CI-perturbation theory 80−74123
two-electron ions, ground state, quadratic Stark effect 80−37775
two-photon spectra, dipole-forbidden transitions, CNDO-CI cross sections 79−81244
two-photon spectroscopy, dipole-forbidden transitions, double excited configurations, CNDO-CI methods 80−58332
UHFS model, CI, CC, and MBPT approaches, appl. to weak δ-δ bonds and δ-δ^* excitation 80−32585
umbelliferone, excited states, in ethanol-water soln., absorption and emission spectra 79−13763
unitary group approach, Gelfand formalism rel. to Harter Patterson matrix representatives 77−18799
unitary group approach, matrix element evaluation 79−31411
unitary group generators and permutations, CI matrix elements, algebraic method 80−37725
unitary group generators and permutations, CI matrix elements, graphical method 80−37726
unitary group irreducible representation subduction coeffs. 80−37723
unlinked cluster corrections for configuration interaction calculations 79−3368
valence bond perturbation theory 79−18120
valence correlation energies, contributions of triply- and quadruply excited states determ. using perturbation theory 80−78545
valence states and binding energies 77−30757
Van der Waals complex, PCILO calc. of dispersion energy and geom. conf. 79−63930
van der Waals complexes, PCILO calcs. 79−36542
variational approach to correlation energy calcs. 77−30791
variational description, loop driven graphical unitary group approach 80−47903
virtual orbitals for rapid convergence, perturbational method 79−85906
visual chromophores, two-photon absorptivities, SCF-PPP-CI calcs. 79−31631
water, liq., structure and props., minimal basis set description 80−6347
wave function calculation using abelian point group symmetry in graphical unitary group approach 79−68193
wavefunction, any-spin, 1st-order, single replacements from complete CI root function 79−81144
wavefunctions, transcorrelated method 77−61678
$Al_2(Al_2^-)(Al_2^+)$ configurations, ab initio study, LCAO, STO, MO-SCF and CI calcs., binding energy *(French)* 80−91447
AlH, $X^1\Sigma^+$ states, many body effects, diagrammatic perturbation theory 77−79547
AlH^+ radical cation, EPR matrix isolation obs., hyperfine components calcs. 80−14158
AlN, $(^2P)Al$-$(^4S)N$, $(^2P)Al$-$(^2D)N$, nonempirical pseudopotential, configuration interaction calcs. 79−93930
Ar, valence shell photoelectron spectrum, CI calcs. 79−31419
Ar XV, wavefunctions and oscill. strengths, CI calcs. 80−23317
$Ar^+ + He$, $X^2\Sigma$ and $A^2\Pi$ states, CI pots. 78−74727
Ar_2, excited state pot. curves, ab initio CI calc. 78−78643
Ar_2 van der Waals dimer, intermol. pot., SCF CI ab initio calcs. 80−106274
Ar_2^+, electronic states, pot. curves, with/without spin-orbit interaction 78−33443
Ar_2^+, near UV absorption spectra, config. interaction methods 78−17680
ArC^+, pot. energy curves calcs. 79−45651
ArF, laser emission, ab initio config. interaction calcs. on electronic states 78−63083
Ar_2F, electronic states, ab initio POL CI calcs. 78−66474
ArO, lasing, low-lying electronic states, ab initio config. interaction calcs. 78−63084
Au+I, noncharacteristic X-ray emission, self-consistent relativistic many-electron correl. diagram 77−19023
B_2, ground state, multiconfig. SCF CI calcs. 78−58590

molecular electron correlations continued
BF, diagrammatic perturbation theory, using universal even-tempered basis set 80−58131
BF_3, dissoc. pathways and mol. vibr., compliance consts. and min. energy coords. 78−35661
BH, $^1\Sigma^+$ ground state, mag. susceptibility, paramag. contrib., large config. interaction wave function calcs. 80−47899
BH, CI wavefunction, terms selection for pot. energy surface 77−88401
BH, correlation energy, many-body Rayleigh-Schrodinger perturbation theory calc. 78−894
BH, correlation energy, perturbation calc. using Gaussian-type geminals 79−10042
BH, correlation energy, quadruply excited configs. effects 79−54773
BH, electron density, basis set, electron correl. effects 78−74581
BH, electronic distribution functions and correl. holes, theory 78−17562
BH, mol. electronic momentum distrib. functions and correl. holes in p-space 79−97978
BH, PE curve, spectroscopic consts., perturbation theory appl. 80−23341
BH, SCF and CI wavefunctions for electronic struct. and one-electron props. 77−67978
BH, variation-perturbation minimal Gaussian geminal basis sets correl. energy calc. 78−78629
BH, $X^1\Sigma^+$ states, many body effects, diagrammatic perturbation theory 77−79547
BH_2, Walsh's rules and small bond angle states 80−106255
BH_3, electronic wave function determ., genealogical technique using Clebsch-Gordan coeff. 80−95529
BH_3, quadrupole excitation in correl. energy theories 79−36538
BH_3NH_3, complexation energies and interatomic distances, SCF and CEPA calcs. 78−25446
BO, spectroscopic properties, PNO-CI and CEPA calcs. 78−41961
Ba, UV photoelectron spectra, config. interaction effects 77−50413
Be+FH→BeF+H, collinear, pot. energy surface study 79−11782
$Be^{2+} + H_2O$, mol. complex struct. and interaction energy, CI calc. 79−18133
Be_2, pot. curve of ground-state, many-body perturbation theory and SCF-CI method 79−36563
Be_4, Be_2, dissoc. energy, electron correlation effect, self-consistent electron pair calc. 77−30790
BeH radical, hyperfine splitting const., electronic energy, UHF-type, CCI calcs. 80−52909
BeO_1 MCSCF and CI calcs. 80−95526
$Be_2(^1\Sigma_g^+)$, binding energy, ab initio pot. curves, interacting correlated fragments method 80−63557
$Br^{25+} + Br^{25+}$, correlation diagrams, inner-shell vacancy prod., characteristic X-rays 77−83503
C_2, $^3\Pi_g$ states, large CI wavefunctions, non-adiabatic coupling matrix elements 80−37744
C_2, band system transition moment ab initio SCF and CI calcs. 79−13770
C_2, transition moments of Swan band system, SCF-CI calc. 78−58746
C_2, valence states, CI calcs. 79−45642
C_2, $X^1\Sigma^+_g$, $6^3\Sigma^-_g$ states, perturbations, ab initio CI calcs. 77−83490
C_2^-, bound electronic states and electron affinity, IC calc. 79−76349
C_3, electron spectrum, ab initio MRD CI calcs. 78−90089
C_3, ground and excited states, vibr., pot. curves, CI calcs. 77−83509
$C_2(C_2^-)$ pot. energy curves calc. using SCF, MCSCF and CI methods, dissoc. energies, bond lengths, electron affinity 80−95523
CCO radical, heat of form. calc., geometries excitation energies and vibr. freq. calc. using POL-CI wave functions 80−89512
CH, photoionis. and photodissoc. near ionis. threshold, SCF MO CI and Steltjes imaging 78−58749
CH radical, SCF theory, multiconfig., direct orbital optimisation 80−87049
CH^+, $a^3\Pi$-$b^3\Sigma^-$ transition moment, ab initio calcs. 80−87047
CH^+, electron correl. energies, Pade approximants and many-body perturbation theory 79−59366
CH^+, excited states, pot. curves and transition moments determ. by ab initio CI methods 80−106286
CH_2, CI calcs. using modified virtual orbitals 80−58163
CH_2^+, $^4A_2$ states, large CI wavefunctions, non-adiabatic coupling matrix elements 80−37744
CH_2^+, Walsh's rules and small bond angle states 80−106255
CH_3, CH_2 and CH deformation vibration group frequencies and MO electron densities, interaction force const. 80−87101
$C_2H_7^+$, ab initio SCF, CI, CEPA-PNO struct. and energy calcs. 78−94197
$CH_3(CH_3^+)(CH_3^-)$, HF, GVB and CI calcs. 77−75063
CN, radical, adiabatic electron affinity, CI calcs. 79−68197
CN^-, ground state pot. curve, CI and coupled pair method calcs. 79−68197
CN^-, ionisation pot., CI and perturbation methods 79−31734
CN^-, spectrosc. consts. for ground and excited states, ab initio, CI calcs. 80−78551
CN^+, ab initio full CI calcs. 78−50480
CN^+ ion, $^1\Sigma^+$ and $^3\Pi$ states, multi-reference CI study 80−83288
CN^+, lower states, pot. energy curves, equilib. distances SCF CI calcs. 80−27957
CN^+, lowest $^1\Sigma^+$ and $^3\Pi$ states, ab initio CI pot. curves calcs. 79−85905
C_2N_2, satellite struct. of electron spectra, CI and vibronic coupling, dynamical calc. 80−53044
CO ($^1\Sigma^+$), X-ray and electron diffr. scatt. intensities, electron correlation effects 78−17577
CO, $a^3\Pi$ and $A^1\Pi$ states, dipole moment, CI calcs. 77−79548
CO, C_{1s} ionis., CI calcs. of satellite peaks 78−916
CO, CO^+, MO correlation diagrams 77−61689
CO, dipole moment functions for $d^3\Delta$ and $a'^3\Sigma^+$ states, MCSCF calc. 78−78636
CO, one-election props., SCF and CI calcs. 80−27951
CO, polarisability derivatives, bond length depend., SCF and CI calcs. 80−58162
CO, quadrupole excitation in correl. energy theories 79−36538
CO, valence X-ray photoelectron spectrum, satellite struct. 77−61800
CO^+, ab initio pot. energy curves, full valence CI with minimal STO 79−72361
CO^+, electronic struct., CO(e, 2e) reaction meas., CI calcs. 77−34769
$CO+Li^+$, rot. excitation, ab initio CI pot. energy surface, classical mech. and coupled states calcs. 78−25665
$CO+N_2$, electronically inelastic collision, distorted wave calc. and pot. energy curve 80−9709

molecular electron correlations continued
CO_2, $^1\Delta_u$ valence state, vertical energy level MC-CI wavefunction 79−45644
CO_2, diagrammatic perturbation theory, using universal even-tempered basis set 80−58131
CO_2, elastic and inelastic electron scatt. differential cross section, obs. and calc., struct., binding energy 80−28110
CO_2, quadrupole excitation in correl. energy theories 79−36538
CO_2, stretch-stretch interaction force const., electron correlation influence, ab initio CI study 80−58161
CO_2, valence states study by (e,2e) momentum spectroscopy 78−22039
CO_2^+, $^1\Pi_g$, mixed charact. state, vertical energy level MC-CI wavefunction 79−45644
CO_2H^+, SCF CI equilib. struct. calc., CO_2 proton affinity 77−10599
CO*, $X^1\Sigma^+$ state, dipole moment functions calc. 77−65429
CS, perturbation parameters between valence states 77−26975
Ca XVII, wavefunctions and oscill. strengths, CI calcs. 80−23317
Ca_2^+, pot. energies in Ca^+ and Rydberg Ca** collisions with Ca 79−27055
Cd_2, pot. energy curve of low-lying states, MO theory 79−89624
Cl_2, ground and ionised states, Koopman's theorem and Mo relax. in ab initio calcs. 78−1035
Cl_2, one electron props. and polarisability, SCF and CI calcs. 80−58159
$ClF(ClF_2^-)(ClF_3)$, ground and ionised states, Koopman's theorem and Mo relax. in ab initio calcs. 78−1035
ClO, dissoc. energy and bond length, CI calcs., bond function effects 80−102450
Co, Auger spectrum, ab initio MO LCAO SCF CI calc. many electron contribs. 80−87169
Co complex, metal-metal bond, correl. effects, SCF calc. 77−65425
CoO, ab initio SCF and CI calcs. on d-d transitions, CoO_6^{10-} cluster d-electron localisation 77−35897
CoO, valence photoelectron spectrum, relative intensities, limited CI calcs. 79−63918
CoO_6^{10-} cluster, valence photoelectron spectrum, relative intensities, limited CI calcs. 79−63918
Cr^{3+} in octahedral fluoride lattice, optical spectrum open shell SCF MO cluster CI calc. 78−19501
$CrOCl_3$, electronic structure and valence ionisation energies, obs. by ab initio and SW-Xα methods 80−69073
$CrOCl_3$, ionisation energy, CI and ΔSCF methods 79−68194
$CsNpF_6$, optical spectrum anal. 79−26963
CuCl, bonding, ab initio pseudopot. calcs. 79−6857
CuNi molecule, electronic states determ. by ab initio HF and CI methods 80−69087
D_3^+, ab initio vibr. intervals and vibr. freq. refinement 80−47968
DCN, electronic spectra, vibr. struct., ab initio calc. 78−9166
Eu, UV photoelectron spectra, config. interaction effects 77−50413
F_2, correlated wavefunctions, ionisation pot. 77−67986
F_2, ground and ionised states, Koopman's theorem and Mo relax. in ab initio calcs. 78−1035
F_2 ground state, multiconfig. function, perturbation theory calcs. 79−13644
F_2, PE curve, spectroscopic consts., perturbation theory appl. 80−23341
F_2, statistical correlation energies 78−78637
F_2, valence electronic states, $^1\Pi_u \leftarrow X^1\Sigma_g^+$ absorption spectrum 79−63920
FH_2^+, reactive processes, ab initio MCSCF-CI and diatomics in mols. calc. 78−56881
FHF ion, H-bond excited electronic states, CI calc., dissoc. and autoionising states 80−5489
FHF radical, struct. and stability, ab initio SCF and CI calcs. 77−71887
FNO, electronic transitions, limited GSMO and ESMO CI calcs., oscillator strengths, spectra 78−70750
F_2O, geometry, electron spectrum, vert. ionis. pot. ab initio calc. 80−58187
F_2O_2, geometry, SCF CI calcs. 78−55126
Fe complexes, electronic and mag. struct., semiempiricial MO cluster calcs. 78−62733
Fe XXIII, wavefunctions and oscill. strengths, CI calcs. 80−23317
FeF, electronic states, ab initio calcs., UV spectrum elucidation 78−74570
GaKr, low-lying electronic states, PE curves, transition moments, emission coeffs. 79−6894
H+HCl, barriers for abstraction and exchange reactions 77−48629
H+methane, abstraction and exchange reactions, energy barriers, UHF-CI calcs. 78−11512
H+methane, abstraction and exchange reaction, barrier height calc. using POL-CI wave functions 80−81304
$H^+ + H_2$, vibr. excitation, ab initio CI pot. energy surface calcs. 80−74228
$H^+ + H_2$, vibr.-rot excitation, ab initio CI pot. energy surface calcs. 80−74229
H_2, atoms-in-molecules theory, non-Hermitian formulation 80−9517
H_2, CI calculations, Waller-Hartree method appls. 77−14363
H_2, Compton defect, high energy electron impact spectroscopy 77−71876
H_2, Compton profile, correl. Gaussian wave function calc. 79−81241
H_2, correl. energy and dipole polarisability, perturbation theory 79−54775
H_2, correlation energy, perturbation calc. using Gaussian type germinals 78−17578
H_2, D_2, photoionisation, body-frame Hund's case b description 78−94295
H_2, electron correl. as rot. polarisation, Heitler-London-Rosen calc., for teacher 80−4492
H_2, electron correlation, dynamic description using boson Hamiltonian 79−26897
H_2, electron total scatt. intensity, first Born approx. , SCF CI calc. 77−10755
H_2, electronic distribution functions and correl. holes, theory 78−17562
H_2, electronic energies of $D'^1\Pi_u$ and $B''^1\Sigma_u^+$ states, wave functions 77−23438
H_2, electronic states, adiabatic energy corrections, CI ab initio calc. 77−83502
H_2, electronic struct., valence bond orbital method appl. 80−106268
H_2 ground state, bond breaking reaction, MINDO/3 CI *(German)* 78−21852
H_2 H_2, intermol. energy, CI ab initio calc. 79−85904
H_2, limited MC SCF calculations 79−36537

molecular electron correlations continued
H_2, low-lying excited states, Rydberg and valence-shell characters 78−5152
H_2, mol. electronic momentum distrib. functions and correl. holes in p-space 79−97978
H_2, pair equations, perturbation contribs. to correl. energy 79−6874
H_2, pairwise correlated GVB model, multiconfig. overlap approx. calcs. 79−31408
H_2, polarisability, CI and Gaussian geminal calcs., using explicitly correlated elec.-field-variant functions 79−36561
H_2, relativistic Dirac-Fock multiconfig. SCF calcs. 80−99455
H_2, second order props., dipole polarisability nucl. coupling, fast CI method 80−27950
H_2, semiempirical model for polarisation of s-type AOs, pot. curve and surfaces determ. 77−88400
H_2, transcorrelated method, nonlinear parameters optimisation 77−14365
H_2, $X^1\sigma_g^+$, momentum distrib., electron correl. and mol. vibr. effects, theory 77−88557
H_2^+, Compton profile and momentum distribution, impulse approx. 78−25626
H_2^+, semiempirical model for polarisation of s-type AOs, pot. curve and surfaces determ. 77−88400
H_2-H_2, intermol. pot. surface, ang. depend., nonorthogonal CI calc. 77−46613
H_2-H_2 intermol. pair pot., ab initio SCF-CI surface 80−91457
H_2-like molecule, from probability theory 77−3286
H_2+H_2, van der Waals pot., electron tunnelling, charge transfer 77−54588
H_2+He potential surfaces, SCF and MRD-CI calcs. 79−10172
$(H_2)_2$, ab initio calcs., perturbation dispersion energy versus CI treatment 77−26976
H_3, CI calc. of three dimens. pot. energy surface 78−56882
H_3, correl., ionis. and attachment operators, diagrammatic method calcs. *(French)* 79−22607
H_3, semiempirical model for polarisation of s-type AOs, pot. curve and surfaces determ. 77−88400
H_3^+, ab initio vibr. intervals and vibr. freq. refinement 80−47968
H_3^+, correl., ionis. and attachment operators, diagrammatic method calcs. *(French)* 79−22607
H_4 excimer, electronic and geom. struct., ab initio CI calc. 79−76348
H_{4u} ground and excited states, SCF MO CI calcs. 77−6693
H_4^+, ground and excited state pot. energy surfaces and geom. struct., SCF and CI calcs. 78−78769
HC_2 radical, electron affinity, ab initio SCF and CI calcs. 78−50468
HCCN, a cyanocarbene, geom. struct., electron correl. effects 80−1077
HCCN, free radical, matrix isolation spectra and ab initio calcs. 78−46329
HCN, dipole moment derivatives and force consts., CI calcs. 78−90091
HCN, dipole moment derivatives of CH and CN, CI method 79−45863
HCN, electronic spectra, vibr. struct., ab initio calc. 78−9166
HCN, electronically excited states, SCF CI calc. using Slater type orbitals 78−78645
HCN, Fermi and Coulomb correl. holes, SCF and CI wave functions 80−69085
HCN, finite field method calc., moments, polarisability, field-induced shifts in mol. props. 78−74561
HCN, H-CN dissoc. curves, SCF CI calc. 79−100405
HCN, modified virtual orbitals, systematic CI procedure 80−83294
HCN, orbital calculation, SCF+CI method 79−93928
HCN, quadrupole excitation in correl. energy theories 79−36538
HCN, valence shell correl. energies, pair correls., unlinked cluster effects, CPA calc. 79−13648
HCN, vertical ionisation pots., CI calcs. 79−13645
HCN^+, $^2\Sigma^+$ and $^2\Pi$ states, SCF and CI calcs. for determ. optimum linear geometries, bond angles calc. 80−74114
HCN^+, A and B $^2\Sigma^+$ states, pot. surfaces, ab initio SCF calcs. 80−27959
HCN^+, photoelectron spectra of third electronic state, ab initio calc. of pot. energy surface 78−70871
HCS^+-CSH^+ system, pot. surface for H abstraction, internuclear bending for ground and excited states 78−29744
HCl, electrostatically interacting mols., CI multipole function calcs. convergency 80−91458
HCl, one electron props. and polarizibility, SCF and CI calcs. 80−58159
HCl, $X^1\Sigma^+$ states, many body effects, diagrammatic perturbation theory 77−79547
HCl^-, reson. states by electron impact, GO and SCF+CI methods, dissociation channels 77−71883
HCl^-, resonance states, CI calcs., pot. energy curves 78−29755
HD, nonadiabatic effects in the B, C and E, F states, rot. line strengths 78−5148
$H_2(D_2)$, Compton profile, impulse approx., electron correl., vibr. and rot. effects 78−17585
HF, Auger spectra, correl. effects, energies and wavefunctions, ab initio CI calc. 80−14125
HF, Auger transition energy calcs. 77−34704
HF, CI+B_k extrapolation method for ground state 79−97983
HF, correlation energy, many-body Rayleigh-Schrodinger perturbation theory calc. 78−894
HF, electrostatically interacting mols., CI multipole function calcs. convergency 80−91458
HF, force consts., ab initio CI calcs. *(French)* 78−90093
HF, low lying states, GVB and CI calcs. 77−14362
HF, mol. props. internucl. separation depend., MCSCF calc. 78−70965
HF, SCF theory, multiconfig., direct orbital optimisation 80−87049
HF, variation-perturbation minimal Gaussian geminal basis sets correl. energy calc. 78−78629
HF, $X^1\Sigma^+$ states, many body effects, diagrammatic perturbation theory 77−79547
HF, $X^2\Sigma^+$ state, 3- and 4-body perturbation theory modified pots. 77−88376
HF+H′→H+H′F, transition state geometry, SCF CI calcs. 78−20009
HF+Li→LiF+H, pot. energy surface, SCF and CI calcs. 80−71904
HFF radical, struct. and stability, ab initio SCF and CI calcs. 77−71887
HN_3, ground $^1A'$ state, SCF and CI calcs., conform., geom., vibr. freqs. and dissoc. 80−18806
HNB,(HNBH), spectroscopic properties, PNO-CI and CEPA calcs. 78−41961
HNC, valence shell correl. energies, pair correls., unlinked cluster effects, CPA calc. 79−13648

molecular electron correlations continued
HNC^+, $^2\Sigma^+$ and $^2\Pi$ states, SCF and CI calcs. for determ. optimum linear geometries, bond angles calc. 80−74114
HNCO, barrier to linearity, ab initio SCF and CI calcs. 79−3363
HNO, CI-SCF-MO basis function calc. 77−42246
HNO, isomerism, low lying electronic states, ab initio MRD-CI calcs. 80−83291
HNO, low-lying states, pot. energy curves 80−9533
HNO, low-lying states, pot. energy surfaces calcs. 80−102460
HNO^+, ab initio SCF and CI comparison of struct. and spectra, rel. to NOH^+ 77−26972
HNO^+, vertical spectra, heat of form., ab initio MRD-CI calcs. 79−49934
H_2NO, hyperfine coupling const. calc., double perturb. theory and CI methods 79−59362
HNSi, and HSiN, electronically excited states, MRD CI calc. 79−49947
HNSi, struct. and microwave freqs. calcs., rel. to interstellar emission lines 78−36648
HO_2, pot. energy surface for $H+O_2 \rightarrow HO_2^* \rightarrow OH+O$ reaction, MC SCF CI method 79−74353
HO_2, vertical electronic spectrum, MRD-CI calcs. 78−37646
H_2O, 1s shake-up spectrum, ab initio equiv. cores, improved virtual orbital and CI calcs. 77−46597
H_2O, ab initio SCF CI calcs., ground state energy, config. and force consts. 77−18782
H_2O, bond dissociation, MCSCF LMO calcs. 77−57886
H_2O CI, high-order many-body perturbation theory 77−88397
H_2O, CI calc. extrapolation, using perturbation theory natural orbitals 79−85907
H_2O, correlated wavefucntions 78−70755
H_2O, correlation energy, many-body Rayleigh-Schrodinger perturbation theory calc. 78−894
H_2O, correlation energy, quadruply excited configs. effects 79−54773
H_2O, double hole states POCI calc., Auger spectrum 78−78630
H_2O, double SCF method for electron correl., stretching force const. 78−17575
H_2O, electron density, basis set, electron correl. effects 78−74581
H_2O, electronic ground state, SCF HF and CI calcs, pot. energy hypersurface, spectroscopic consts. 78−50473
H_2O force consts., ab initio CI calcs. *(French)* 78−90093
H_2O, geometry, SCF and CI calcs., basis set effects 78−62715
H_2O, ground state, CI calcs. on triply and quadruply excited configs., basis set effects 80−95549
H_2O, ground state, cond. energies, higher-order excitation contribs. 80−58166
H_2O, ground state ionis. pots., generalized Mo theory 80−52907
H_2O, iterative natural orbitals for CI using perturbation theory 77−79549
H_2O, iterative natural orbital procedures, convergence props. 78−46257
H_2O, KLL Auger electron spectrum, semi-internal correl. 80−48038
H_2O, many body perturbation theory fourth order calc. of correl. energy 80−14087
H_2O, mol., ionisation pot., CI and perturbation methods 79−31734
H_2O, multi-root config. interaction calcs. 80−102451
H_2O, polarisabilities, finite-field calc., perturbation correlation 79−72249
H_2O, polarisability and mag. susceptibility calc. by SCF and CI method 80−99443
H_2O, singlet states, CI calc. 77−46502
H_2O, vertical ionisation pots., CI calcs. 79−13645
H_2O^+, ab initio potential energy surface study by CI techniques, equilibrium conform. determ., mol. dissoc. pathways 80−78550
H_2O^+, pot. energy surface, linear approach 78−41978
H_2O^+, X^2B_1 and B^2B_2 states, pot. surfaces, SCF and CI calcs. 77−3338
H_2O_2, geometry, internal rot. barriers, electron correl. calcs. 78−70751
H_2O_2, struct. and barrier to internal rot., HF and Rayleigh-Schrodinger perturbation calcs. 79−13636
H_2O_3, struct., barrier to int. rot., HF and RS-MP perturb. calcs. 79−13637
H_3O radical, stability, ab initio UHF-CI calcs. 78−5137
H_3O^+, ab initio CI calcs. of excited states 77−30796
H_3O^+, inversion barrier, high-order replacements inclusion in CI calcs. 80−63504
HOB,(HBO), spectroscopic properties, PNO-CI and CEPA calcs. 78−41961
HOCl, ab initio MRD CI calc., electronic spectrum, dissoc., heat of reaction, formation 78−21857
HOCl, photodissoc., ab intio SCF CI calcs. 78−50604
HPN-HNP, isomerisation energies, ab initio MRD-CI calcs. 80−106271
HS_2 radical, ab initio calcs. of geometry and spectra 77−34552
H_2S, double hole states POCI calc., Auger spectrum 78−78630
H_2S, electron density, basis set, electron correl. effects 78−74581
H_2S, electronic struct., ab initio CI SCF calc., spectra assignments 77−10586
H_2S, gas-phase, states in valence photoelectron spectrum 78−94284
H_2S, ground and excited states, SCF and CI calcs. 77−414
H_2S, KLL Auger spectrum, obs. and ab initio SCF CI calc. 78−50654
H_2S, L(S_2)-MM Auger energies, MC SCF calcs. 78−21977
H_2S, mol. polarisability and derivatives, ab initio SCF CI calc. 79−59597
H_2S^+, $^2B_1$, $^2A_1$ and $^2B_2$ electronic states, pot. energy curves, CI calcs. 80−87048
HSO radical, ground and excited first states, ab initio SCF and CI calcs. 77−30776
HSO-HOS, isomerisation energies, ab initio MRD-CI calcs. 80−106271
HSiC-HCSi, isomerisation energies, ab initio MRD-CI calcs. 80−106271
HSiN, struct. and microwave freqs. calcs., rel. to interstellar emission lines 78−36648
HSiN-HNSi isomers, MRD-CI calcs. of struct. and stability 78−82635
H_2SiO, electronic struct., dipole moments, mol. polarisability, force fields, ab initio calcs. 80−78531
$H'+XH \rightarrow H'X+X$, X=H, F, Cl,CH_3, collinear pot. energy barriers, PNO-CEPA calcs. 77−32777
H_2*, energy and occupation curves, wave functions, natural spin orbital anal. 77−83493
He, isoelectronic series, charge densities and 2-electron intracule functions calcs. 77−88382
He-He, Born-Oppenheimer pot. using Hylleraas-type electronic wave functions 79−31438
$He+H_2$, CI pot. energy surface, small distances 77−38708
$He+H_2$, pot. energy surface, ab initio calcs., van der Waals const. determ. 80−106372
molecular electron correlations continued
$He^+ + He$, He_2^+ mol. collision complex, pot. energy curve spectrum 77−19008
$He^{2+} + He$, 5 to 100 keV, elastic and double charge exchange, mol. treatment 78−82813
He_2, He_2^+, MO correlation diagrams 77−61689
He_2, pair polarisability correl. effects, SCF-CI-GTO-SO calc. 78−82651
He_2, pot. surface well depth calc. 77−79667
He_2 potentials, configuration interaction calculations, superposition corrections 79−72382
He_2^{2+}, autoionising states, adiabatic pot. energy curves calcs. 78−42140
He_2^{2+} quasimolecular states, radial and rot. coupling terms 79−26896
HeH^+, bond energy calcs., using density matrix partitioning 78−46417
HeH^+, excited states, variable screening models, natural spin orbital analysis of wave functions 80−37747
HeH^+, triplet Σ, Π and Δ states, config. interactions 78−78633
HeH_2^+, CI calc. extrapolation, using perturbation theory natural orbitals 79−85907
HeH_2^+, electronic struct. 79−31414
$He_2(He_2^+)$, variational electronic struct. calcs. using Hylleraas type wavefunctions 77−88375
$HeNe^+$, collisional form., excitation, pot. energy curves calcs. 77−6697
$He_2^+ X^2\Sigma_u^+$ state, ab initio CI calc., pot. energy curve, vibr. and rot. levels 77−3263
HgBr, ab initio CI calcs., spectroscopic parameters 79−72245
$HgBr_2$, electronic struct. and photodissoc., effective core pots. and POL(1) CI wave function 80−63560
HgCl, ab initio CI calcs., spectroscopic parameters 79−72245
$HgCl_2$, electronic struct. and photodissoc., effective core pots. and POL(1) CI wave function 80−63560
$I^{25+} + Te^{24+}$, $I^{43+} + Au^{69+}$, $I^{25+} + Au^{51+}$, correlation diagrams, inner-shell vacancy prod., characteristic X-rays 77−83503
I_2, band system, MC SCF pseudopot. calcs. 78−78632
I_2, vertical valence excited states, CI nonempirical pseudopotential calc. 77−71757
IrF_6, ligand field theory analysis of spectra 79−72248
KOH, MHD plasma mol., pot. energy curves and dipole moment, bond lengths 78−71462
Kr_2^+, electronic states, pot. curves, with/without spin-orbit interaction 78−33443
Kr_2^+, near UV absorption spectra, config. interaction methods 78−17680
KrF, electronic states, ab initio CI calcs., spin-orbit coupling, pot. curves, dissoc. energy, dipole moments 77−38619
KrF, electronic states, ab initio POL CI calcs. 78−66474
KrF, laser emission, ab initio config. interaction calcs. on electronic states 78−63083
KrF*, excimer electronic struct., config. interaction, electrostatic model 78−927
KrO, lasing, low-lying electronic states, ab initio config. interaction calcs. 78−63084
$Li^+ + Ar$, interaction pot. of $X^1\Sigma$ state, CI calc. 79−50100
$Li^+ + CO$, differential cross-sections, ab initio CI vibrotor pot. energy surface calcs. 78−46421
$Li^+ + CO$, pot. energy surface, equilib. distance, SCF calcs., correl. effects 77−3430
$Li^+ + CO(N_2)$, differential cross-sections, classical trajectory calcs. 78−29841
$Li^+ + He$ collisions, K-shell vacancy sharing, ab initio LCAO-SCF, CI calcs. 77−19054
Li_2, $A^1\Sigma_u^+$ state, vibr. energy levels calcs. 77−83566
Li_2 and Li_2^+, Li 1s hole states calc., dissoc. Auger electron energies 77−23443
Li_2, $B^1\Pi_u$, pot. energy curve, MC SCF approx. calcs. 77−38618
Li_2, charge distrib. anal. rel. to Berlin's binding and antibonding regions 79−6875
Li_2, core-excited states, theoretical and experimental investigation 78−37655
Li_2, lowest $^1\Pi_g$, $^1\Pi_u$, $^3\Pi_g$, $^3\Pi_u$ states 77−54517
Li_2, MCSF accurate pot. energy curves for $^3\Sigma_u^+$ and $b^3\Sigma_g^+$ states, level crossing 77−50369
Li_2, mol. polarisability, finite-field method, correlation corrections 77−71889
Li_2, second virial coeffs., Konowalow MCSCF potential calcs. 80−23312
Li_2, $X^1\Sigma_g^+$ and $A^1\Sigma_u^+$ states, electronic struct. and spectra 79−89615
Li_2^-, electronic struct., ab initio calcs. 77−34553
Li_3, electronic struct., SCF and SCF-CI calcs. 80−87044
Li_3, multibody and stability considerations, small clusters 78−90333
Li_3, potential energy surface and config., RHF CI calc. 77−34562
Li_3, spin density, Gaussian basis set 78−33427
Li_3^-, electronic struct., SCF and SCF-CI calcs. 80−87044
Li_3^+, electronic struct., SCF and SCF-CI calcs. 80−87044
Li_4, MCSCF and CI calcs. 80−95526
LiF, Li 1s ionisation pot. calc., Li 1s XUV absorpt. spectrum 77−23443
LiF^-, ground and excited states, ab initio calcs. single config. and multiconfig. SCF calcs. 80−52873
LiH, correlation energy calc. by many-body diagrammatic perturbation theory 78−9087
LiH, dipole moments and transition moments, semi-rigorous bounds, error limits 78−78635
LiH, elec. struct. by spin-adapted vector method 79−54777
LiH, electron correl., double SCF method, mol. dissoc. energy 78−17575
LiH, electronic distribution functions and correl. holes, theory 78−17562
LiH, electronic struct., valence bond orbital method appl. 80−106268
LiH, finite-field method calcs., dipole moment gradients, polarisability gradients and elec. field effects 77−88589
LiH, iterative natural orbitals for CI using perturbation theory 77−79549
LiH, LiH^-, pot. energy curves, electron affinity, spectroscopic consts. 78−5129
LiH, limited MC SCF calcs. 79−36537
LiH, many body perturbation theory fourth order calc. of correl. energy 80−14087
LiH, mol. electronic momentum distrib. functions and correl. holes in p-space 79−97978
LiH, mol. polarisability, finite-field method, correlation corrections 77−71889
LiH, one electron props., Xα multiple scattering wave functions 80−42945
LiH, pairwise correlated GVB model, multiconfig. overlap approx. calcs. 79−31408

molecular electron correlations continued
LiH, relativistic Dirac-Fock multiconfig. SCF calcs. 80−99455
LiH, variation-perturbation minimal Gaussian geminal basis sets correl. energy calc. 78−78629
LiH, variational Hylleraas-type wavefunction, correl. 78−9082
LiH, $X^1\Sigma^+$ states, many body effects, diagrammatic perturbation theory 77−79547
LiH^+, spin densities, SCF and CI calcs. 79−3362
$LiH+H \rightarrow Li+H_2$, linear LiH_2 pot. energy surface, MCSCF functions optimisation 77−67960
$LiNO_3$, mol. struct. ab initio calcs. 79−26884
LiNa, ground and excited states, model pseudopot. calcs. 77−75069
Mg IX, wavefunctions and oscill. strengths, CI calcs. 80−23317
Mg_2, Mg_2^+, electronic struct., pot. energy curves, multiconfig. SCF calcs. 78−5124
Mg_2, perturbation theory calcs. 79−13644
Mg_2, pot. energy curve for $X^1\Sigma_g^+$ state, many-body perturbation calcs. 78−55216
MgH, and MgD, $B'^2\Sigma^+$-$X^2\Sigma^+$ band system, ab initio CI calcs. 79−93970
MgH, X and $B'\ ^2\Sigma^+$ and $A\ ^2\Pi$ ab initio CI calc. 79−31415
MgH^+, CI pot. curves and cross sections for lowest singlet states 80−23343
MnO, SCF CI calcs., ground and first excited states, bonding mechanism 77−14347
Mo complex, metal-metal bond, correl. effects, SCF calc. 77−65425
N containing molecules, N NMR, nuclear mag. shielding, X-ray photoelectron spectra 78−17695
N_2, 400 eV core-excited valence states, limited CI calc., transition energies and oscillator strengths 79−68196
N_2, (e,2e) spectra, valence momentum distribs. and config. interaction 77−19101
N_2, core-ionised, core-valence excited and shake-up states, all electron MRD CI calc. 78−21858
N_2, correlated electron density using AHF GTO wavefunctions 80−23313
N_2, correlation energy, quadruply excited configs. effects 79−54773
N_2, diagrammatic perturbation theory, using universal even-tempered basis set 80−58131
N_2, elastic and inelastic electron scatt. differential cross section, obs. and calc., struct., binding energy 80−28109
N_2, electron density distrib., electron correl. effects, approx. HF-CI calcs. *(German)* 78−33439
N_2, electronic ground state correl. energy, many-body diagrammatic perturbation theory calc. 78−917
N_2, finite field method calc., moments, polarisability, field-induced shifts in mol. props. 78−74561
N_2, ground state ionis. pots., generalized Mo theory 80−52907
N_2, ionisation pots. and excitation energies, correl. calcs. 77−26986
N_2, MRD CI calc., lowest dissoc. limits 78−21859
N_2, multi-config. SCF super-CI calc., density matrix formulation 80−78547
N_2, N_2^+, MO correlation diagrams 77−61689
N_2, one-electron props., polarisabilities and polarisability derivatives, SCF and CI calcs. 80−37746
N_2, PE curve, spectroscopic consts., perturbation theory appl. 80−23341
N_2, photoelectron spectra, valence region strong shake-up bands, Koopman's theorem breakdown 79−72354
N_2, polarisabilities, quadrupole and dipole moments, nucl. geom. effects 79−63899
N_2, polarisability derivatives, SCF and CI calcs. 79−59348
N_2, quadrupole excitation in correl. energy theories 79−36538
N_2, self-consistent electron pairs with higher order effects, quadruple iteration convergence 78−46276
N_2, statistical correlation energies 78−78637
N_2, vertical electronic spectrum, MRD-CI method calcs. 78−42033
N_2, vertical ionisation pots., CI calcs. 79−13645
N_2^+, 1s hole satellite spectrum, large-scale CI calc. 77−65428
N_2^+, $C^2\Sigma_u^+$-$B^2\Sigma_u^+$ homogeneous predissoc., perturbations calcs. 79−86020
N_3^-, low-lying excited states 79−31425
$NCNO \rightleftharpoons NC+NO$, ground state pot. energy surface, ab initio calcs. 77−90593
NCO^+, CI-SCF-MO basis function calc. 77−42246
NCO^+, partial pot. energy surfaces, ab initio SCF CI calcs. 78−37554
NH, $b^1\Sigma^+$ and $d^1\Sigma^+$ states, multiconfig. wavefunctions, optimal config. selection 77−34566
NH^+, pot. curves, ab initio CI calcs., equilib. distances 78−17579
NH_2, geometry, SCF and CI calcs., basis set effects 78−62715
NH_2, pot. energy curves of X^2B_1, A^2A_1, $^2B_2$ valence-shell and $\pi_u{}^2$3s-type Rydberg states calc. by CI 80−74138
NH_2, X^2B_1, A^2A_1 and B^2B_2 states, ab initio SCF CI calcs. 78−29746
NH_2^+, low lying states, ab initio MRD-CI pot. surface calcs. 79−89611
NH_2^+, triplet state ab inito CI pot. energy surfaces 78−74729
NH_3 bond dissociation, MCSCF-LMO calcs. 77−57886
NH_3, first triplet state, photodissoc. and Rydbergisation investig. 80−53067
NH_3, ionisation pots. and excitation energies, correl. calcs. 77−26986
NH_3 low lying states, generalised VB and CI calcs., vertical excitation energies 77−30789
NH_3, lowest triplet state geometry, SCF and CEPA-PNO calc. 80−914
NH_3, photodissoc., ab initio SCF and CI calcs. 78−21984
NH_3, quadrupole excitation in correl. energy theories 79−36538
NH_3+2H_2, triplet n3S Rydberg state, ab initio UHF CI SCF calc. 80−53095
N_2H_2, CEPA-PNO calcs., band functions, correl. and polarisation roles 77−71758
N_2H_2, model rearrangement system, electron correlation and basis set effects 80−3317
N_2H_2, $N_2H_2^+$, ab initio calcs., electronic struct., geometries relative energies 77−46487
NH_4Cl, gas $^1A_1$ ground state, pot. surface 80−32626
$N_2H_2(N_2D_2)$, ground and first excited state small vibr. coupling, ab initio CI calc. 78−62791
$NH_2(X^2B_1)$ radical, and ND_2, ionisation pot., vibr. anal., ab initio calcs. and vacuum UPS obs. 80−53047
NO, $3s\sigma(A^2\Sigma^+)$, in Ar Kr Xe matrices, Rydberg state 'bubbles', reson. fluoresc. obs. 77−83636
NO dimerisation, equilib. const. anal., trans-/cis-$(NO)_2$ zero pt. correlation energy difference 78−11509
NO, N 1s photoelectron spectrum, correl. effects 77−10702

molecular electron correlations continued
NO, predissoc. rates and pertrubations in certain electronic states, time resolved spectra 77−27131
NO^+, N 1s photoelectron spectrum, correl. effects 77−10702
NO_2, core-electron excitation, absorpt. spectrum and CI calcs. 77−75181
NO_2, direct CI calcs. 80−52889
NO_2, direct CI method generalised to HF interacting space 79−85908
NO_2, electronic states, pot. energy surface calcs. 77−6673
NO_2, NO_2^+, NO_2^-, SCF and MC SCF CI calcs. 78−46280
NO_2, vertical electronic spectrum, SCF and CI calcs. 77−30878
NO_2, vertical electronic spectra, ab initio calcs. 78−66538
NO_2^-, direct CI calcs. 80−52889
NO_2^-, direct CI method generalised to HF interacting space 79−85908
NO_2^-, microwave transition probability in zero field, spin-orbit interaction 78−25518
NO_2^- triplet state lifetimes and fine structs., CNDO-CI calcs. 77−57897
NO_2^-, vertical electronic spectra, ab initio calcs. 78−66538
NO_2^+, gas phase equilib. geometry, force consts., vibr. freq., dipole moment function MCSCF/CI calcs. 80−78520
NO_2^+, vertical electronic spectra, ab initio calcs. 78−66538
NO_3^-, triplet state lifetimes and fine structs., CNDO-CI calcs. 77−57897
N_2O , ground state potential energy surfaces 77−27175
N_2O_4, second ionis. pot. by CI wavefunction 79−31732
NOF and ONF, ab initio calcs. of geometry and electronic struct. 79−76342
NOH, groundstate electronic struct., MRD CI calc., dissoc. energy, isomerisation energy 80−14088
NOH isomerism, low lying electronic states, ab initio MRD-CI calcs. 80−83291
NOH^+, ab initio SCF and CI comparison of struct. and spectra with HNO^+ 77−26972
NOH^+, vertical spectra, heat of form., ab initio MRD-CI calcs. 79−49934
$N(^4S)+O_2(^3\Sigma_g^-) \rightarrow NO(^3\pi_u)+O(^3P)$ doublet surface minimum energy path calcs. 78−7194
$^{14}NH^+(^{15}NH^+)(^{14}ND^+)$, ab initio CI calc. Λ type doubling in $X^2\Pi$ states 78−82714
Na_3, electronic struct., pot. energy surface, ab initio CI study 78−70996
NaAr, $X^2\Sigma$, $A^2\Pi$ and $B^2\Sigma$ state, ab initio CI calcs. 78−9085
NaH, $X^1\Sigma^+$ states, many body effects, diagrammatic perturbation theory 77−79547
Ne_2^+, near UV absorption spectra, config. interaction methods 78−17680
Ne_2F, energy surfaces, application of molecular electronic struct. theory 78−25452
Ne_2* excimer, transient absorption spectra assignment 79−41115
Ni complex, nickel-bis-dithiolene, pseudopot. MCSCF and limited CI calcs. 80−83292
Ni_2 and Ni_2^+, lowest electronic states, GVB and POL-CI calcs. 79−31409
$Ni(Ni)_2$-ethylene cluster complex 78−82641
NiO, ab initio SCF and CI calcs. on d-d transitions, NiO_6^{10-} d-electron delocalisation 77−35896
NiO, electronic states, VB and CI calcs. 78−62728
O_2, $^3\Pi_g$ diabatic Rydberg states, ab initio CI calcs. 80−95554
O_2, $^3\Pi_u$ states, large CI wavefunctions, non-adiabatic coupling matrix elements 80−37744
O_2, $^3\Sigma_g^-$ ground state, pot. energy curve, direct CI method appl. 80−58165
O_2, $a^1\Delta_g$ and $b^1\Delta_g^+$ state, MCSCF wavefunctions 78−37561
O_2, CI calc. of ground and $^3\Sigma_u^-$ excited states 79−81158
O_2, excited state geometries and energies, ab initio pot. energy surfaces 78−5151
O_2, ground state, ab initio pot. curve calcs. 77−83510
O_2, ionisation pots. and excitation energies, correl. calcs. 77−26986
O_2, multiconfig. HF procedure, 2nd- and approx. 2nd-order, convergency 79−93907
O_2, RH-GTO-MCSCF calc., 1s photoelectron spectra, multiplet intensity ratio 78−5134
O_2, Rydberg states, $^3\Sigma_g^-$, $^3\Sigma_u^+$, $^3\Pi_g$, $^1\Pi_g$, $^1\Sigma_g^+$ symm., ab initio CI study 80−99460
O_2, Schumann-Runge continuum, oscill. strength and electron impact excitation 80−69121
O_2, valence states, ab initio config. interaction calcs. 78−25448
O_2^-, ab initio pot. curves of $X^2\Pi_g$, $A^2\Pi_u$, $a^4\Sigma_u^-$, $^2\Sigma_u^-$ states 78−66483
O_2^+, ab initio CI STO calc. 78−74585
O_2^+, $c^4\Sigma_u^-$ state predissoc. calcs. 79−50095
O_2^+, CI calc. of ground and $^3\Sigma_u^-$ excited states 79−81158
O_2^+, electron impact dissoc. recomb., pot. energy curves calcs. 80−53150
O_3, ab initio UHF and UHF-natural orbital CI studies 80−102452
O_3, CI calc., ground and excited states, energy locations, transition probabilities 78−74584
O_3, cyclic, stability, ab initio GVB-POL-CI calcs. 78−915
O_3 depletion, ClO influence 77−75052
O_3, open and closed forms, bond angle and length, MC SCF and MC CI calcs. 78−78831
OF_2, photoelectron spectra, ionisation energies, ab initio many-body Green's function calc. 79−89709
$OH+H_2$, pot. energy surface, barrier heights and transition state geometry, POL-CI calc. 80−55649
ONF, vertical electronic spectrum, CI and SCF calcs. 77−75123
$O(^3P,^1D)+H_2(^1\Sigma_g^+) \rightarrow H_2O$, potential energy surfaces, extended basis first-order CI study 80−7776
$O(^3P)+H_2 \rightarrow OH+H$, potential energy surface, theory 80−45492
PH_3, bonding by electron impact coincidence expt. 77−65536
PH_3, core-excited states, valence-Rydberg mixing and term values, XUV spectra and CI calc. 79−76444
PH_5, rearrangements, CI calcs. in large at. orbital basis 79−94106
P_2H_4, conformation, ab initio, HF, PNO-CI and CEPA calcs. 77−46495
S_2, low lying bound molecular electronic states 79−45643
S_3, open and ring isomers, electronic struct., ab initio SCF calcs. 77−57862
SF_2, photoelectron spectra, ionisation energies, ab initio many-body Green's function calc. 79−89709
SF_6 and SF_6^+, excited states investig. 77−57882
SF_6, KLL Auger spectrum, obs. and ab initio SCF CI calc. 78−50654
SH, ionis. pot. of $(X^2\Pi_i)$ radical, ab initio ΔSCF calc. with electron correl. 79−98153

molecular electron correlations continued
SH_3^+ geometry and inversion barrier, basis set depend. 80−921
SN, electronic states, ab initio, SCF, and CI calcs. 77−75053
SN, struct., vibr. spectra, ab initio calcs. 78−66475
SN^+, struct., vibr. spectra, ab initio calcs. 78−66475
S_2N_2, electronic states, ab initio, SCF, and CI calcs. 77−75053
S_2N_2, struct., vibr. spectra, ab initio calcs. 78−66475
SO, low lying bound mol. electronic states, SCFCI calc. 80−23314
SO_2, $2^1A'$ state, electron correl. variational description, loop driven graphical unitary group approach 80−47903
SO_2, double hole states POCI calc., Auger spectrum 78−78630
SO_2, KLL Auger spectrum, obs. and ab initio SCF CI calc. 78−50654
SO_2 PMDR, CNDO CI calcs. 79−72342
SO_3, dissoc. pathways and mol. vibr., compliance consts. and min. energy coords. 78−35661
SO_3, photoelectron spectrum assignment, ionisation pot. and electron affinity, Green's function method 77−54576
SOH radical, ab initio SCF and CI calcs., electronic states and transitions 77−46488
Si XI, wavefunctions and oscill. strengths, CI calcs. 80−23317
SiH_3 radical, hyperfine coupling consts., vibr. depend., ab initio calcs. 80−87150
SiH_4, core-excited states, valence-Rydberg mixing and term values, XUV spectra and CI calc. 79−76444
SiH_4, vertical excited states, CI calcs. 79−18127
$SiO\ ^3\Pi$ valence states, struct. and perturbations 79−59369
SiO, valence ionis. energy, calc. including correl. effects 79−68185
SiO, $X^1\Sigma^+$, $A^1\Pi$, $C^1\Sigma^-$ and $E^1\Sigma^+$ states, SCF CI calcs. 79−45641
Sm, UV photoelectron spectra, config. interaction effects 77−50413
Th cpds., configuration interaction satellites in core level ESCA spectra 77−30923
UF_6^+, electronic struct., ab initio calcs. using relativistic core pots. 79−97987
$Xe^+ + Ag$, quasimolecular L and Ag L X-ray excitation thresholds, electron correl., calc. and expt. 78−78793
Xe_2^+, electronic states, pot. curves, with/without spin-orbit interaction 78−33443
Xe_2^+, near UV absorption spectra, config. interaction methods 78−17680
XeF, laser emission, ab initio config. interaction calcs. on electronic states 78−63083
XeF(Cl)(Br)(I), covalent and ionic states, spectroscopic props., ab initio CI calc. 78−90092
XeO, lasing, low-lying electronic states, ab initio config. interaction calcs. 78−63084
Yb, UV photoelectron spectra, config. interaction effects 77−50413
Zn I isoelectronic series, $4s4d\ ^1D$-$4p^2\ ^1D$ interaction, multiconfig. Hartree-Fock calcs. 79−76351
Zn_2, electronic states, CI calcs., rel. to Hg_2 77−10601
Zn_2, pot. energy curve of low-lying states, MO theory 79−89624

molecular electron impact dissociation
acetylene, electron impact, dissoc. excitation cross-sections, fragment obs. 78−62936
acetylene, electron ionisation efficiency curves, fragment ion appearance pot. 78−86959
acetylene, ionis. efficiency curves by electron impact, $CH_2^+(C_2H^+)$ form., ~10 eV 78−62935
air, O_3 generation, macroscopic props. of field-accelerated electrons 80−61118
aliphatic chlorocarbons, electron impact dissoc., ≲10 eV, negative ion prod. 78−5359
aliphatic perfluorocarbons, electron attachment, fragmentation 0-12 eV 80−5618
alkali halides, electron stimulated dissoc. 80−34301
alkali metal fluoroaluminates, dissoc. enthalpies, mass spectrometric determ., heat of form. 80−97720
alkanes, electron impact dissoc. excitation, H sublevels populations meas. 77−75073
benzene, electron impact dissoc. excitation, H_α and H_β Balmer line intensities 77−10778
bromobenzene -d_0(-d_5) radical cation, electron impact dissoc., secondary isotope effect 80−63836
chlorofluoromethanes, electron impact excitation, resons. and dissoc. attachment 79−7020
chlorofluoromethanes, negative ion form. by 0.10 eV near-monoenergetic electron impact 79−41245
chlorotrifluoromethane, electron impact dissoc., light emission from fragments 79−13826
collisional cross-sections determ. for low and intermediate energy processes 80−99579
continuum wave functions, discrete basis set method 79−22829
cyclopropane, triplet states, electron impact and photosensitised dissoc., chem. effects 77−14592
diatomic, molecule, dissoc. following optically allowed or forbidden excitation 79−59587
diatomic molecule, electron impact dissociation by vibrational excitation *(Russian)* 78−1096
diatomic molecules, electron impact, vibs. excitation and dissoc. attachment, R-matrix calcs. 79−72228
dichlorodifluoromethane, electron impact dissoc., light emission from fragments 79−13826
dichlorodifluoromethane, total ionis. and electron attachment cross sections by electron impact 79−59586
5,5′-diethylbarbituric acid, EPR and INDO-MO study of radical formation after irrad. 80−93774
discharge, dissoc. on bombardment by low energy electrons 80−43845
dissociative attachment 78−58850
dissociative recombination, energy depend. below 0.8 eV, merged beam obs. 79−31716
dissociative recombination, repulsive term, states of products 77−65537
electron dissociative capture, vibr. struct. of resonances 77−34770
electron scatt., dissoc. attachment 78−58849
electron-ion collisions, crossed beam expts. 78−58843
electronic and at. collisions, conf., Kyoto, Japan (Aug.-Sept. 1979) 80−57011
electronic and at. collisions, conference, Kyoto, Japan (Aug.-Sept. 1979) 80−62394
ethane, electron impact dissoc., absolute total cross section, 10-600 eV 79−36781
ethane, electron impact dissoc., high Rydberg fragments 77−83749

molecular electron impact dissociation continued
ethane, electron ionisation efficiency curves, fragment ion appearance pot. 78−86959
ethane, H^+, H_2^+, and H_3^+ kinetic energy distribs., electron impact dissoc. ionisation, time of flight mass spectra 80−32843
ethanol, H^+, H_2^+, and H_3^+ kinetic energy distribs., electron impact dissoc. ionisation, time of flight mass spectra 80−32843
ethylene, electron impact dissoc., high Rydberg fragments 77−83749
ethylene, electron impact dissoc., optical emission from fragments 77−83750
ethylene, electron ionisation efficiency curves, fragment ion appearance pot. 78−86959
ethylene polymerisation and dissociation in high-freq. discharge 77−70299
ethynyl cation, dissociative recomb. cross section determ., merged beam obs. 80−78715
formyl fluoride, 70 eV electron-produced gas phase species and reactions obs. 77−63900
fragment ion kinetic energies, modified ion source and mass spectrometer 77−6958
halogen mols., electron dissociative attachment 80−91694
halomethanes, electron impact dissoc., tropospheric lifetimes *(German)* 79−50141
high-Rydberg atomic fragment form. 79−68324
hydrocarbons, electron impact cross section for H_α and $CH(A^2\Delta \rightarrow X^2\Pi)$ emission 77−27189
hydrogenic ions, electron impact, cross section functions meas., hollow beam trapping, dissociation 79−72424
inert gas-halide lasers, halide mol. negative ion prod. rates 80−18938
ion cyclotron resonance spectrometer, positive ion trapping in electron beam 78−21254
ionic fragmentation, translational energy, phase space theory 77−9051
metal oxides, electron stimulated dissoc. 80−34301
metastable negative ion, electron impact decomp., kinetic energy release 77−6944
methane, 25 to 40 eV electron dissoc. ionisation, proton formation 80−91690
methane, electron impact, Balmer-α emission Doppler profile energy depend. 77−42423
methane, electron impact dissoc., excitation of H Lyman β and Balmer α radiation 78−46450
methane, electron impact dissoc., H atom sublevel excitation 77−14593
methane, electron impact dissoc., high Rydberg fragments 77−83749
methane, electron impact dissoc. excitation cross sections 77−61861
methane, electron irrad., $CH_2(b^1B_1)$ prod. and rad. lifetime from $b^1B_1 \rightarrow a^1A_1$ emission 77−3476
methane, H^+, H_2^+, and H_3^+ kinetic energy distribs., electron impact dissoc. ionisation, time of flight mass spectra 80−32843
methane and methane-d_4, low energy electron impact dissoc. autoionisation 80−9744
methane compounds, halogen-substituted, formation of excited fragments on dissociation by electron impact *(Russian)* 77−79698
methane electron impact dissoc., optical emission from fragments 77−83750
methanol, dissoc. ionisation mechanism, correlation diagram approach, mass spectra obs., metastable processes 80−95728
methanol, electron impact dissoc., optical emission from fragments 77−83750
methanol and deuterates, H^+, H_2^+, and H_3^+ kinetic energy distribs., electron impact dissoc. ionisation, time of flight mass spectra 80−32843
momentum filter for separation of electrons and negative ions 78−78034
negative ions, form. by dissoc. attachment, ang. distrib. 79−81288
phenylalanine, hydrated electron impact dissoc., laser flash photolytic investig. 80−58396
photon emission from electron + molecule collisions *(Dutch)* 78−5362
propene, triplet states, electron impact and photosensitised dissoc., chem. effects 77−14592
propylene, dissoc. on bombardment by low energy electrons 80−43845
propylene, electron impact ionisation and dissoc. 80−37894
protein, electron radiation damage on primary and secondary struct. level 80−89808
quantum system, two-fold sudden hamiltonian change, decay, excitation *(Russian)* 77−10717
resonant states form. in dissoc. attachment 78−58851
tetrafluoromethane, electron impact dissoc., light emission from fragments 79−13826
triatomic molecule, dissoc. following optically allowed or forbidden excitation 79−59587
trichlorofluoromethane, electron impact dissoc., light emission from fragments 79−13826
trifluoromethane, electron impact dissoc., light emission from fragments 79−13826
vinyl cation, dissociative recomb. cross section determ., merged beam obs. 80−78715
Ar jet, supersonic, electron beam-excited, continuous VUV emission spectrum origins 79−6964
Ar:OCS, liq., dissoc. studies 80−78716
As_2O_3, multiple reactions by single electron impact 78−22037
Br_2, dissoc. attachment by 0-8 eV electrons 78−74776
Br_2, dissociative attachment of electrons 78−62931
Br_2, thermal electron dissoc. attachment rate consts., meas., in flowing afterglow 77−10773
C_2^+, dissociative recomb. cross section determ., merged beam obs. 80−78715
$C_2H_2^+$, dissociative recomb. cross section determ., merged beam obs. 80−78715
CO, adsorbed layer on Ru (001) surface, electron induced desorption 77−59215
CO, chemisorbed on Ir(111) surface, electron beam induced desorption and dissociation 78−56043
CO discharge plasma, electron energy distrib. and kinetic coeffs., vibr. excited mols. 80−43868
CO, dissoc. attachment, differential cross-section meas. 77−50549
CO, dissociative electron attachment 77−42431
CO, dissociative excitation by electron impact, metastable fragment energy 78−66672
CO, dissociative ionisation 77−54616
CO, electron impact K-shell ionis., ionic fragmentation, Auger decay post-collision interaction 77−75316
CO, nonequilib. dissoc. induced by electron-vibr. and IR laser pumping 79−86016

molecular electron impact dissociation continued
CO on Rh (110), electron-impact props. 78−6225
CO^-, to positive ion states, negative-ion reson. effects 79−54977
CO_2 dissociation obs. in flow system with cylindrical hollow cathode 78−66674
CO_2 dissociation obs. in hollow-cathode glow discharge 78−70946
CO_2, electron energy deposition, rel. to Venus and Mars atms. 79−45857
CO_2, electron impact dissoc. excitation, O** fragment translational spectra 79−54979
CO_2, electron impact ionisation, dissoc. ionisation 78−13610
CO_2, electron swarm parameters for high E/N, Monte Carlo simulation 80−19548
CO_2-N_2-He laser mixtures, electron swarm parameters, Boltzmann eqn. anal. 79−18396
CS_2, electron impact dissoc., CS heat of form. determ. 78−73074
Cl_2, dissoc. attachment by 0-8 eV electrons 78−74776
Cl_2, electron impact dissoc. excitation, metastable fragment form. translational spectra 78−1094
Cl_2, thermal electron dissoc. attachment rate consts., meas., in flowing afterglow 77−10773
Cu/CuCl double pulse laser, dissoc. pulse, afterglow, and laser pulse model 80−91775
D_2, dissociative attachment of electrons *(Russian)* 78−13621
D_2, dissociative electron attachment, Faddeev calcs. of cross sections *(Russian)* 78−70945
D_2, electron dissociative attachment rates, rot. (vibr.) excitation depend., in plasma 80−43848
D_2, electron impact, Balmer-α emission Doppler profile energy depend. 77−42423
D_2, electron impact, H(2S) and D(2S) form., predissoc., time of flight obs. 79−86079
D_2, electron impact, threshold excitation and predissoc., electron-photon coincidence meas. 80−18941
D_2, electron impact dissoc., anticrossing signals, Doppler-profile technique 78−33619
D_2, electron impact dissoc. ionisation 80−83510
D_2, electron impact dissociative excitation 78−13618
D_2, electron impact dissociative ionisation near $^2\Sigma_g^+$ state dissoc. threshold 80−43197
D_2, excited atom kinetic energy distrib. *(Russian)* 78−22045
D_2, forming D^+, from autoionising state 79−54980
D_2^+, dissociative recombination, projection operator formalism 77−3479
D_2^+, electron impact, dissoc. recomb., highly excited atom form. *(Russian)* 78−33621
DCl dissociative-attachment cross sections, fine struct. 77−71884
D_2O, electroionisation 79−22849
D_2O, electron impact reson. observed in $A^2\Sigma^+ \rightarrow X^2\Pi$ radiation of OD 78−46455
F_2, dissoc. attachment by 0-8 eV electrons 78−74776
F_2, dissociation by electron beam or electron-beam-sustained discharge 77−68126
F_2, dissociative attachment of electrons, current density meas., in controlled discharge 77−23566
F_2, electron dissociative attachment rate consts. at 300 and 500K, in discharge plasma 80−43849
F_2, electron impact excitation, dissoc. of lowest electronic state 80−63839
F_2, influence on KrF* laser props. 78−50756
F_2, low energy dissociative attachment and vibr. excitation, reson. scatt. theory 78−46453
F_2, thermal electron dissoc. attachment rate consts., meas., in flowing afterglow 77−10773
$Fe(CO)_5$, electron impact appearance pots. for ion fragments, mass spectra obs. 79−34281
GeX_4, (X=Br,Cl), electron impact dissoc., low-energy reson. capture 78−9263
H_2, $c^3\Pi_u$ metastable state, dissociative electron attachment 79−89794
H_2, dissoc. rates in glow discharge *(French)* 79−849
H_2, dissoc. to H^+, from autoionising state 79−54980
H_2, dissociative attachment, vibr. and rot. state depend. 79−18298
H_2, dissociative attachment, vibr. and rot. state depend. 79−13829
H_2, dissociative attachment cross sections, interference struct. around 14 eV 79−45856
H_2, dissociative electron attachment, H ang. distribs. 77−19099
H_2, dissociative electron attachment 77−42431
H_2, dissociative electron attachment, Faddeev calcs. of cross sections *(Russian)* 78−70945
H_2, electron dissociative attachment rates, rot. (vibr.) excitation depend., in plasma 80−43848
H_2, electron dissociative attachment 80−91694
H_2, electron impact, Balmer-α emission Doppler profile energy depend. 77−42423
H_2, electron impact H_α and H_β lines emission, intensity decay curves meas. 80−83505
H_2, electron impact, H(2S) and D(2S) form., predissoc., time of flight obs. 79−86079
H_2, electron impact threshold excitation and predissoc., electron-photon coincidence meas. 80−18941
H_2, electron impact dissoc. excitation, H_α and H_β Balmer line intensities 77−10778
H_2, electron impact dissoc. excitation cross sections 77−61861
H_2, electron impact dissoc. ionisation, energetic protons for autoionising states 78−25728
H_2, electron impact dissoc., anticrossing signals, Doppler-profile technique 78−33619
H_2, electron impact dissoc., close-coupling method appl. 78−74778
H_2, electron impact dissoc. excitation, cross sections, mechanisms 80−37895
H_2, electron impact dissoc. ionisation 80−83510
H_2, electron impact dissociative excitation, H 3s prod. cross section 77−58183
H_2, electron impact dissociative excitation obs. 78−1090
H_2, electron impact dissociative excitation 78−13618
H_2, electron impact dissociative ionisation near $^2\Sigma_g^+$ state dissoc. threshold of H_2 80−43197
H_2, electron impact H^+ prod., kinetic energy, ang. distribs. 80−63838
H_2, electron impact partial absolute ionis. cross section, 20-350 eV, rel. to H_2O and NH_3 *(French)* 79−861
H_2, electron scatt., elastic and inelastic, Glauber approx. 80−91695

molecular electron impact dissociation continued
H_2, electron scatt., energy deposition and energy degradation, 2, 10 and 30 keV 79−31709
H_2, excited atom kinetic energy distrib. *(Russian)* 78−22045
H_2 glow discharge with variable degrees of dissoc., diffusion theory of positive column 80−44018
H_2, HD, dissociative attachment of electrons *(Russian)* 78−13621
H_2, translational energy distrib. of H* 79−98234
H_2, vel. distrib. of H(2s), $^{11}\pi_u$ autoionising state 77−79696
H_{2s}, velocity distrib. of produced excited H atoms *(Russian)* 77−10779
H_2^+, dissociative recombination, projection operator formalism 77−3479
H_3^+, dissociative recombination 79−89796
H_2^+, electron cooling through resonant collisions 80−32845
H_2^+, electron impact, dissoc. recomb., highly excited atom form. *(Russian)* 78−33621
H_2^+, electron impact dissoc. recomb. cross sections, Rydberg states form., merged-beams expt. 78−25725
H_2^+, electron impact dissociation variationally adjusted LCAO mol. orbitals calcs. 77−3473
H_3^+ dissoc. recomb., role of H_3 excited electronic states 79−89795
H_3^+, dissociative electron capture, symmetry considerations 77−46646
H_3^+, electron impact dissoc. recomb. cross sections, Rydberg states form., merged-beams expt. 78−25725
H_3^+, H^- production cross section 80−5628
H_2(-He), H production at 10 torr in pulsed discharge 80−9748
HBO_2, electron attachment, rate coeff. 77−75310
HBO_2, electron attachment, rate coeff., equilib. effects 77−75311
HBr, dissociative attachment of electrons 78−62931
HCN, and DCN, electron impact dissoc., product H(n=4) kinetic energy distrib., emission obs. 80−28106
HCN, electron impact, dissoc. excitation cross-sections, fragment obs. 78−62936
HCN, electron impact dissoc., near-threshold $CN(B^2\Sigma)$ emission 79−54975
HCl, controlled electron impact, excited H product translational energy distrib. 80−14238
HCl, dissociative-attachment cross sections, fine struct. 77−71884
HCl, electron impact dissoc., H atom sublevel excitation 77−14593
HCl, electron impact dissoc. excitation cross sections 77−61861
HCl, HCl^- reson. states, GO and SCF+CI methods, dissociation channels 77−71883
HCl.H, form. by dissoc. attachment, differential cross section 79−86077
HD, dissociative electron attachment, Faddeev calcs. of cross sections *(Russian)* 78−70945
HD, electron impact, H(2S) and D(2S) form., predissoc., time of flight obs. 79−86079
HD, electron impact dissociative excitation 78−13618
HD, electron impact dissoc. ionisation 80−83510
$H_2(D_2)$, dissociative electron attachment and vibr. excitation, low-energy 80−23565
$H_2(D_2)$, electron impact dissoc., cross sections, isotope ratios and polarisation, B H_α and H_β emission 78−25729
HF, electron impact excitation, dissoc., emission spectrum 78−90305
H_2O, and D_2O, Feshbach-reson. and dissoc. electron attachment 79−41246
H_2O, Born approx., emission cross sections determ. *(Japanese)* 77−42425
H_2O, D_2O, electron impact dissoc. excitation, Balmer-α emission obs., Doppler profile meas. 79−31706
H_2O, dissoc. excitation by electron impact, multiple scatt. effect 79−89793
H_2O, dissociative electron attachment 77−42431
H_2O, electroionisation 79−22849
H_2O, electron impact dissoc., H atom sublevel excitation 77−14593
H_2O, electron impact dissoc. excitation cross sections 77−61861
H_2O, electron impact dissoc., $OH(A^2\Sigma^+ \rightarrow X^2\Pi_i)$ emission spectra, crossed-beam investigations 80−83504
H_2O, electron impact partial absolute ionis. cross section, 20-350 eV, rel. to H_2 and NH_3 *(French)* 79−861
H_2O, electron impact reson. observed in $A^2\Sigma^+ \rightarrow X^2\Pi$ radiation of OH 78−46455
H_2O, Glauber approx. *(Japanese)* 77−42426
H_2O, slow electron scatt., rigid mol. model with exchange and polarisation, vibr. excitation, dissoc. attachment 80−43194
H_2O vapour, ionis. coeffs. and dissociative electron attachment 80−43833
H_2S, dissociative electron attachment, H^- energy and ang. distrib. 79−31710
H_2S, slow electron scatt., rigid mol. model with exchange and polarisation, vibr. excitation, dissoc. attachment 80−43194
HX (X=Cl,Br,I) dissoc. attachment, negative ion form. and removal kinetics in flame 77−52642
Hg II halides, electron impact dissoc., excited fragment emission 79−18296
I_2, dissoc. attachment by 0-8 eV electrons 78−74776
I_2, dissociative attachment, thermal energy electrons 78−82850
InBr, electron impact dissoc. ionis., In electron affinity meas. *(French)* 80−63849
InI, electron impact dissoc. ionis., In electron affinity meas. *(French)* 80−63849
KrF* excimer laser, discharge pumped, influence of electron-F_2 collisions 78−42326
LiF, electron impact fragmentation, in mass spectrometer, porous barrier obs. 77−75313
LiF vapour system, fragmentation in mass spectrometer ion source 78−70944
$MoCl_5$, dissoc, in pulsed discharge, interference method obs. 77−58186
N_2 dissociation by electron impact and EUV photoabsorpt., rel. to aurora and airglow 78−58847
N_2, electron excitation of Birge-Hopfield bands ($b^1\pi_u$-$X^1\Sigma_g^+$) 80−95731
N_2, electron impact dissoc., EELS, N^- autoionisation 80−106397
N_2, electron impact reson. dissoc., intermediate negative ion form. 79−36783
N_2, electron ionisation, N_2^{2+} form., decay to N^+, coincidence detect. 77−79695
N_2, electron scatt., elastic and inelastic, Glauber approx. 80−91695
N_2, electron scatt., reson. excitation and dissoc. attachment, vibr. state depend. 80−78717
N_2, low energy electron impact dissociative ionis., N^{2+} form. and energy distrib. 80−5626
N_2, rel. to O_3 generation in air-fed ozonisers 80−3323

molecular electron impact dissociation continued
N_2^+, dissociative recombination, ion-beam expt. 79−54981
N_2^+, electron impact dissociative recomb. coeffs. inferred from Atmosphere Explorer meas., objections 78−86957
N_2-O_2, electron impact dissoc. ionisation, N^- form., mass spectra 77−75320
N_2D^+, dissociative recomb., interstellar mols. appl. 79−31704
NF_3, electron dissociative attachment rate consts. at 300 and 500K, in discharge plasma 80−43849
NH, ND, $d^1\Sigma^+$ state lifetimes, rot. struct., electron excited emission spectra 77−79654
NH_3, dipole oscill. strengths for excitation, ionisation and fragmentation by 5-60 eV electrons 77−68129
NH_3, direct and dissociative electron impact cross-sections 77−61864
NH_3, electron impact, dissoc. excitation cross-sections, fragment obs. 78−62936
NH_3, electron impact dissoc., H atom sublevel excitation 77−14593
NH_3 electron impact dissoc. excitation cross sections 77−61861
NH_3, electron impact partial absolute ionis. cross section, 20-350 eV, rel. to H_2 and H_2O *(French)* 79−861
NH_3, ionis. coeffs. and dissociative electron attachment 80−43833
NH_4^+, dissoc. electron recombination cross-sections, 0.065-2 eV 78−66671
N_2H^+, dissociative recomb., interstellar mols. appl. 79−31704
N_2H_2, electron impact, N_2H^+ appearance pot., N_2 proton affinity 78−58869
N_2H_4, heat of form. determ. by electron impact dissoc. 78−61040
NH($A^3\Pi$, $c^1\Pi$) radicals, electron impact of NH_3, H_2NNH_2 and organic mols., emission spectra 77−83752
NO decomp. in industrial exhaust gases by electron beam irradiation 79−29490
NO, dissociative electron attachment 77−42431
NO, electron impact dissoc. ionisation, N^- form., mass spectra 77−75320
NO^+, dissociative recombination, ion-beam expt. 79−54981
NO^+, multichannel dissociative electron recombination theory 77−83753
NO_2 decomposition by electron beam irradiation treatment of exhaust gases 79−79423
N_2O, dissoc. in alternating elec. field, kinetic and energetic data *(French)* 78−13620
N_2O, electron impact, dissoc. patterns 79−7021
N_2O, electron impact ionisation and dissociation, radiation emission 78−90304
Ne_2^+, dissoc. recomb. in afterglow, prod. of Ne 2p atoms 80−43855
O_2, atom production and removal in DC glow discharge 79−77432
O_2, discharge, conditions, self-consistent electron energy distrib. functions calc. 80−38746
O_2, dissociative attachment coeff. calc. 77−19100
O_2, dissociative electron attachment 77−42431
O_2, low energy electron impact dissociative ionis., O^{2+} form. and energy distrib. 80−5626
O_2, macroscopic props. of field-accel. electrons in pure gas *(French)* 80−59161
O_2, O I $3s'\ ^3D^0$ and $3d\ ^3D^0$ levels excitation and radiative decay 79−80064
O_2, O_3 generation, macroscopic props. of field-accelerated electrons 80−61118
O_2, rel. to O_3 generation in air-fed ozonisers 80−3323
O_2^+, electron impact dissoc. recomb., pot. energy curves calcs. 80−53150
O_2+, dissociative recombination, ion-beam expt. 79−54981
O_3 generation in air-fed ozonisers 80−3323
OCS, electron impact dissoc., CS heat of form. determ. 78−73074
PH_3, electron impact dissoc. ionisation, mass spectrometric obs. 78−9264
SF_6, ionic fragmentation after S 2p shell electron impact ionis. 78−90310
SF_6, photon-enhanced dissociative electron attachment 80−9749
SF_6, photon-enhanced dissociative electron attachment, isotope selectivity 80−18939
SF_6, vibr. excitation, dissociative attachment 77−3481
SF_6^-, electron impact, nearly zero energy, probability ratio meas. 79−72433
SO_2, electron attachment processes investig. and mobility of negative ions 80−38518
$SiCl_4$, electron bombardment and thermal dissoc., thermochem. stability 77−58185
SiX_4, (X=Br,Cl), electron impact dissoc., low-energy reson. capture 78−9263
SnX_4 (X=Br, Cl, I) electron impact dissoc.-electron capture, ionis. efficiency curves 77−61865
TlBr, electron impact dissoc. ionis., Tl electron affinity meas. *(French)* 80−63849
TlI, electron impact dissoc. ionis., Tl electron affinity meas. *(French)* 80−63849
WF_5, dissoc. electron capture, electron impact mass spectra, electron affinities 77−88579
WF_6, dissoc. electron capture, electron impact mass spectra, electron affinities 77−88579
WOF_4, dissoc. electron capture, electron impact mass spectra, electron affinities 77−88579
Xe-I_2 mixtures, electron beam excitation, XeI* emission spectrum 77−6843
Xe_2^+, dissoc. recomb. in afterglow, rate coeff., excited state prod. 77−46647
XeF laser performance, ground state population effect 80−63987
XeF_2, dissociative electron attachment, rate const., flowing afterglow obs. 77−6946
XeF_2, dissociative electron attachment, 0-20 eV 79−72430

molecular electron impact excitation
see also electron spectra
$^1\Sigma^+$-eystems, rot. and vibr. excitation, frame-transformation approx. 77−42421
ab initio methods for atomic and molecular processes 80−63550
ab initio theory including polarisation 78−50640
acetonitrile, mol.excitation by electron impact, 500 and 25-70 eV, expt. and HAM/3 79−72434
acetylene, C K-shell excitation by electron impact, electron energy loss spectra 77−31014
acetylene, electron energy loss spectra, C K-shell excitation, vibr. struct. 79−22851
molecular electron impact excitation continued
acetylene, electron impact, dissoc. excitation cross-sections, fragment obs. 78−62936
acetylene, triplet states, electron impact energy-loss spectra 77−68128
acetylene-d_0(-d_1)(-d_2) metastable state, mol. beam elec. deflection obs. 80−74137
adsorbed molecule vibration excitation on metal surface 78−18910
adsorption enhancement by electron beam excitation of gas mols. 78−43238
alkanes, electron impact, threshold excitation by monoenergetic electrons 78−58854
alkanes, electron impact dissoc. excitation, H sublevels populations meas. 77−75073
alkenes, electron impact, threshold excitation by monoenergetic electrons 78−58854
alkyl substituted diacetylene radical cations, optical emission and photoelectron spectra, fragmentation decay 80−53004
alkynes, electron impact, threshold excitation by monoenergetic electrons 78−58854
anthracene, fluoresc. by electron beam excitation 79−94031
atmospheric gases, electron impact cross-sections 78−28398
atmospheric gases, yield spectra calcs. 78−28401
benzene, 50000 cm^{-1} band, electron impact study 79−86075
benzene, C K-shell excitation by electron impact, electron energy loss spectra 77−31014
benzene, elec. dipole forbidden states, high resolution electron impact obs. 80−43195
benzene, electron impact, electronic energy levels, (below 7 eV) obs. 78−17807
benzene, electron impact dissoc. excitation, H_α and H_β Balmer line intensities 77−10778
benzene, electron impact-induced generalised oscill. strength, 400 eV, 500 eV, momentum change depend. 78−1088
benzene, excited electronic states, variable angle electron impact spectroscopy 78−13612
benzene molecule, slow electron scattering, resonances to 1.1 and 1.7 eV 77−58181
benzene-acetone donor-acceptor pair, energy transfer cross sections rel. to generalised oscill. strengths 78−46452
Bethe theory, inelastic collisions of fast charged particles 78−58783
biacetyl, triplet $n\rightarrow\pi^*$ and $\pi\rightarrow\pi^*$ transitions studied by low-energy electron diffr. 80−83502
2-(4-biphenylyl)-5-phenyloxazol, vapour, electron beam excited luminesc. *(Russian)* 78−82780
2-[4-biphenyl]-5-phenyloxazole, fluoresc. by electron beam excitation 79−94031
Born partial wave amplitude for any electrostatic multipole field 80−53128
Born-Oppenheimer approx., reson. vibr. excitation, hybrid theory 77−23568
bremsstrahlung, series expsn. for intensity components 78−50648
bremsstrahlung in resonance scatt. *(Russian)* 78−37752
trans-1,3-butadiene, electron impact energy loss spectra, energy levels 79−68323
1,3-butadiene, excited singlet states, vibronic struct., electron impact energy loss spectra, 35-90 eV 78−62932
butenes, electron energy loss spectra, 0-90°, 20-150 eV impact 79−68322
1-butyne, and propyne, electron impact spectra, comparison with acetylene 79−3585
carbon tetrachloride, mol. characts. from fast low-angle scatt. 77−50537
charge density, Bethe surfaces, Compton profile via (e,e') reactions at 20-40 keV 77−88560
chiral molecules, positron interactions, selectivity between optical isomers 77−83751
chloromethanes, inner-shell excitation and EXAFS-type phenomena 79−13828
chlorotrifluoroethylenes, electronic transitions, electron impact spectra 77−10775
collisional cross-sections determ. for low and intermediate energy processes 80−99579
Compton defect in electron impact spectroscopy 77−88578
Compton defect in X-ray and electron scatt. in 1st Born approx., Compton shift 77−88428
conference, electronic and atomic collisions, Paris (July 1977) 78−58758
continuum wave functions, discrete basis set method 79−22829
1,3-cycloheptadiene, electron impact, electronic spectra 79−45855
1,3,5-cycloheptatriene, singlet→singlet (triplet) excitation, electron impact energy loss spectra 78−46451
1,3-cyclohexadiene, electron impact, electronic spectra 79−45855
1,3-cyclopentadiene, electron impact, electronic spectra 79−45855
1,4-di(2-(5-phenyloxazolyl))benzol, vapour, electron beam excited luminesc. *(Russian)* 78−82780
diatom+atom (electron) scatt., vibr.-rot. excitation, generalised field theory method 77−23537
diatomic homonuclear molecule, effect of vibr. transitions on fast electron scatt. data 77−88583
diatomic molecule, electron scatt., vibr. and rot. transitions, close coupling theory 78−22041
diatomic molecule electron scatt., iterative static exchange method 80−53155
diatomic molecule electron scatt. vibr. and rot. transitions, hybrid and close-coupling theory 78−22042
diatomic molecules, electron impact, vibs. excitation and dissoc. attachment, R-matrix calcs. 79−72228
diatomic molecules, electron reson. scatt., ang. distrib., vibr. and rot. excitation, theory 78−22043
diatomic molecules, N_2 and CO nuclear pumped lasers, electron impact cross section meas. 80−63985
diatomic polar molecules, electron scatt., calcs., Born approx. limitations 78−17794
dichlorodifluromethane, dissoc. into metastable fragments following electron impact excitation 78−37757
dielectric gas, breakdown strength, electron impact ionis. and scatt. cross section 79−82031
p-difluorobenzene, electron impact singlet-singlet transition generalised oscill. strength 78−66668
1,4-di[2-(5-phenyloxazoyl)] benzene, fluoresc. by electron beam excitation 79−94031
electron attachment to mol. and mol. clusters, electron-mol. collision, Rydberg electron exchange 80−63843

molecular electron impact excitation continued
electron degradation and yields of initial mol. species, variational calc. 79−7023
electron impact dissoc. ionisation 80−83510
electron impact spectroscopy, low-energy aspects, book contrib. 80−14243
electron-collision cross-section data for atom or molecule, rel. to radiation physics 80−63829
electron-photon angular correlation in atomic physics 79−64109
electronic and at. collisions, conf., Kyoto, Japan (Aug.-Sept. 1979) 80−57011
electronic and at. collisions, conference, Kyoto, Japan (Aug.-Sept. 1979) 80−62394
electronic-rotational molecular states, electron-impact excitation, cross sections and rate consts. 80−14241
energy deposition in a gaseous mixture 79−25380
ethane, 30-250 eV, 0-90° 79−54949
ethane, C K-shell excitation by electron impact, electron energy loss spectra 77−31014
ethylene, $\pi \rightarrow \pi^*$, electron energy loss spectroscopy 79−72432
ethylene, C K-shell excitation by electron impact, electron energy loss spectra 77−31014
ethylene, electron energy loss spectra, 0-90°, 20-150 eV impact 79−68322
ethylene, electron energy loss spectra, C K-shell excitation, vibr. struct. 79−22851
ethylene, electron energy loss spectrum, intensity distrib. 79−64110
ethylene($-d_4$), Rydberg states assignments, electron energy loss specta 80−53153
ethylene-d_0, -d_4, electron impact, vibr. excitation cross-sections, 1 MeV 79−22850
ethyne, electron energy loss spectra, excited states investig., electron impact spectrometer 78−25756
excited states, prod. by electron pulse radiolysis 79−50142
fast electron inelastic scattering and electron density of scattering molecules 77−58189
fast electron inelastic scattering factor, vibr. transitions 77−88584
fast scattering for mol. characts. determ. 77−50536
fluorobenzenes, excited electronic states, variable angle electron impact spectroscopy 78−13612
fluoroethylenes, electronic transitions, electron impact spectra 77−10775
fluorophenol cations, emission and photoelectron spectra in gaseous phase 80−58316
formaldehyde, IR intensities by electron impact spectroscopy 77−6851
formaldehyde, Rydberg states, excitation energies, oscillator strengths ab initio GVB-CI calcs. 77−54518
formyl ion, electron impact rot. excitation, Glauber approx. with Coulomb effect 80−63840
gas laser, reson. vibr. excitation by electron impact, low energy, book contrib. 77−50662
gas optical breakdown, quantum kinetic eqn. for electrons *(Russian)* 79−60092
gases, low energy positron interactions, review 78−50651
gases, molecular, total scatt. cross sections for intermediate-energy positrons 80−91692
glow discharge in diatomic molecular gas, electronic excitation rate, vibr. temp. influence 80−19633
glyoxal, triplet $n \rightarrow \pi^*$ and $\pi \rightarrow \pi^*$ transitions studied by low-energy electron diffr. 80−83502
haloacetylene cations, electron impact excitation A→X band system assignment 80−32766
halomethanes, 2.5 keV electron impact energy loss spectra, inner shell excitation 78−42232
halomethanes, C K-shell electron energy loss spectra, assignments 79−89797
1,3,5-hexatriene, electron scatt. at low-energy, vibronic struct. of triplet state 79−3574
1,3,5-hexatriene, low energy, variable angle electron-impact excitation 77−27187
1, 3, 5-hexatriene, radical cations, emission spectra of cis and trans isomers 77−6793
high-energy electron impact spectroscopy, book contrib. 80−14244
hydrocarbons, electron impact cross section for H_α and $CH(A^2\Delta \rightarrow X^2\Pi)$ emission 77−27189
5-hydroxy-2,3-dihydro-1,4-phthalazindione, electron beam excited chemiluminesc., chem. and light yields 78−53209
indirect dissociative recomb., T-matrix element, Feshbach's projection operator technique 80−58114
inelastic exchange kernels, semiclassical exchange approximation theory 78−50642
inerg gas excited molecules formation, rate const. determ. 80−9859
inert gas fluorides, excimer emission bands *(Russian)* 77−71885
inert gases, electron beam excited, absorpt. characts. 78−82948
inner-shell electron impact excitation, developments in electron energy loss spectroscopy 80−63842
interstellar clouds, collisional excitation by charged particles 77−57075
ion+electron scatt., static exchange approx. Schwinger variational principle, photoionisation cross section 80−43192
ionised gas, slow electron momentum transfer cross section in mag. field, RF cond. meas. 79−82030
ionosphere, electron cooling rates, discrepancy with heating rates 77−29564
K-shell electrons excitation with high energy resolution, review 80−37899
L^2-basis set theory with vibr. and rot. coupling 79−41247
laser field, photon correl. effects 80−83481
lifetime meas. in atoms, mols., ions 77−30832
long optical lifetimes meas., distortion effects 78−9276
long range force effects on excitation of simple at. and mol. systems 79−10170
luminol, electron beam excited chemiluminesc., chem. and light yields 78−53209
methane, 30-250 eV, 0-90° 79−54949
methane, and -d_4, electron impact K-shell excitation spectra, isotope effects 77−71879
methane, Balmer radiation production by electron impact 0-2000 eV 79−76521
methane, Compton profiles, high energy electrons impact spectroscopy 77−27188
methane, elastic and inelastic electron scatt. differential cross section, obs. and calc., struct., binding energy 80−28110
molecular electron impact excitation continued
methane, electron energy loss spectra, C K-shell excitation, vibr. struct. 79−22851
methane, electron impact, H,D(2s,2p) prod. 78−42230
methane, electron impact dissoc., excitation of H Lyman β and Balmer α radiation 78−46450
methane, electron impact spectra, C atom inner shell excitation 77−10776
methane, electron irrad., $CH_2(b^1B_1)$ prod. and rad. lifetime from $b^1B_1 \rightarrow a^1A_1$ emission 77−3476
methane, ground state, dipole oscill. strength distrib., rel. to molar refractivity and dispersion energy 77−71835
methane, large angle elastic and inelastic electron scatt. differential cross section, exchange corrections 80−28111
methane, low-energy electron scatt., total 0.16 eV cross sections, vibr. excitation 79−86076
methane, slow electron scatt., rigid mol. model with exchange and polarisation 80−43194
1,6-methano-[10]-annulene, electron spectra, triplet excitation 79−54976
methyl halides, low energy mol. Rydberg states from Feshbach reson. spectra 77−34768
methyl iodide, van der Waals mol., electron self-scavenging 80−95727
methylisonitrile, mol.excitation by electron impact, 500 and 25-70 eV, expt. and HAM/3 79−72434
molecular gases, positron scattering, 50-800 eV, total cross-section meas. 79−31680
molecular vibration excitation on resonant electron scatt., time-perturbation method *(Russian)* 80−14242
molecules, close coupling method, elastic and rot. excitation 79−10202
molecules, rot. and vibr. excitation, methods for calcs. 80−17721
momentum wave function determ. in atomic, molecular and nuclear systems 77−88556
monohalobenzenes, inner shell excitation and ionis., electron energy loss spectra, XPS, assignments 78−62934
multiple scatt. method, scatt. cross section calc. 80−63816
naphthalene vapour, resonant scatt. of slow electrons 77−58182
neopentane, 30-250 eV, 0-90° 79−54949
nitromethane, low lying electronic states, electron energy loss spectra, singlet→triplet excitation 79−27093
nitromethane, variable angle electron-impact excitation, transitions in 7-12 eV energy-loss range 80−69244
nitrosomethane-d_3, electronic excitation, conformational changes obs. 79−98233
open-shell target, electron scatt., orthogonality constraints 77−71869
optical oscillator strengths calculation, slope of generalised oscill. strength vs. momentum transfer curve 79−98155
organic molecules, triplet state electronic energy delocalisation 77−3478
1,6-oxido-[10]-annulene, electron spectra, triplet excitation 79−54976
partial resonance widths, Siegert eigenvalues, basis-set calc. 80−37880
photoelectric effect and electron diffusion in gases 78−81745
photon emission from electron+molecule collisions *(Dutch)* 78−5362
photon-electron angular correlations, Hund's case (b) coupling case 78−42231
polar diatomic molecular ions, rot. excitation by low-energy electrons *(Russian)* 79−94093
polar molecular ions, rot. excitation by slow electrons, calc. 78−5360
polar molecule, electron scatt., momentum transfer cross-sections, semi-classical perturbation theory 78−58848
polar molecule, electron scatt. cross sections, threshold behaviour *(Russian)* 78−5347
polar molecule, slow electron capture and rot. excitation 79−81287
polar molecule electron scatt., excitation and scatt. cross sections 78−58826
polar molecule electron scatt. at intermediate J, closed-form treatment 80−32846
polar molecule electron scattering, exam. of models 80−37898
polar molecules, differential scatt., vibr. excitation 78−58853
polar molecules, elastic and inelastic electron scatt. 78−94322
polar molecules, electron impact, elastic scatt. and vibr. excitation, effective range theory 80−83485
polar molecules, electron impact vibr. excitation, threshold behaviour 77−58145
polar molecules, influence of long-range interaction on vibr. excitation 79−3586
polyatomic compounds, fluoresc. in discharge 79−54891
POPOP, vap., electron energy loss spectra rel. to lasing 78−29947
POPOP vapour, electron beam excited superradiance 78−66820
positive column of glow discharge of electronegative gas, molecular excitation and ionisation by electron collisions 80−49031
propylene, electron energy loss spectra, 0-90°, 20-150 eV impact 79−68322
propyne, and 1-butyne, electron impact spectra, comparison with acetylene 79−3585
propyne, mol.excitation by electron impact, 500 and 25-70 eV, expt. and HAM/3 79−72434
pyrene, fluorescence produced by low energy electrons *(German)* 77−18967
R-matrix method, appls. to electron mol. collisions 78−58834
R-matrix method, basic concepts, rel. to other theories electron scatt. 78−58832
resonant electron scattering, vibr. excitation of mols. *(Russian)* 77−79697
resonant energy transfer cross section, form factor formalism, 1st Born approx. appraisal 77−65519
resonant phenomena, complex stabilisation method 80−78515
resonant vibr. excitation cross section in electron scatt. 77−19098
review, of expt. and theory 78−25699
rotated coordinate method use, rel. to stabilisation method 80−37845
rotational and vibrational low energy excitation, review 77−6943
rotational excitation, Glauber amplitudes, quadrupole anisotropic pots. calcs. 78−82851
rotational excitation, Glauber amplitudes for anisotropic pots. 78−74775
rotational transitions *(Russian)* 79−76524
scattering cross-sections, ab initio calcs., incl. polarisation 78−5341
spontaneous superradiance in plasma flow 77−3470
strong excitation of nucl. motions 78−58849
strongly polar molecule, low energy electron scatt., dipole moment depend. *(Japanese)* 77−42405
symmetrical molecule, interference effects in electron impact induced X-ray emission spectra 77−83640
p-terphenyl, vap., electron energy loss spectra rel. to lasing 78−29947

molecular electron impact excitation continued
tetrafluoromethane, elastic and inelastic electron scatt. differential cross section, obs. and calc., struct., binding energy 80−28110
tetrafluoromethane, electron energy loss spectra, C K-shell excitation, vibr struct. 79−22851
tetrafluoromethane, electron impact excitation, resons. and dissoc. attachment 79−7020
tetramethylethylene, electron energy loss spectra, 0-90°, 20-150 eV impact 79−68322
theory and calc. techniques 80−63841
threshold structures, non-adiabatic theory 79−72431
total inelastic scatt. cross section, detector solid angle depend., approx. bounds 78−17798
trichlorofluoromethane, dissoc. into metastable fragments following electron impact excitation 78−37757
trifluorodimethylmercury, gas phase mol. struct., electron diffr. and microwave spectra obs. 80−78609
trifluoroiodomethane nuclear pumped lasers, electron impact cross section meas. 80−63985
trimethylethylene, electron energy loss spectra, 0-90°, 20-150 eV impact 79−68322
vibrational and rotational excitation, review 80−32847
vibrational close coupling, discrete basis sets 79−13825
vibrational excitation, shape-reson.-enhanced, 10-40 eV, appl. to CO_2 80−5629
vibrational excitation by electron impact at 30-75 eV, quantum mech. and crossed beam studies 77−34767
vibrational levels, cross section for excitation by electron impact *(Russian)* 77−79699
vibrational struct. of resonance in electron-molecule scatt. 78−17813
vibrationally excited gas, in elec. discharge, sound propag. 78−18370
vibro-rotational excitation, field theoretical formulation 79−81263
water vapour electron stopping power and energy degradation 80−23276
xanthene dye N-92+inert gas buffer, electron beam excited, fluoresc., energy transfer 78−25877
zero point vibr. effect in low energy scatt. 79−22832
zero-radius potential appl. to molecule comprising spin-1/2 atoms *(Russian)* 77−34771
Ar jet, supersonic, electron beam-excited, continuous VUV emission spectrum origins 79−6964
Ar-F_2 mixtures, low-press. excimer form. and quenching by e-beam excitation 79−50071
Ar+HCN(H_2O), electron excitation of Ar* and Ar_2*, fluoresc. and dissoc. energy transfer collisions 77−14580
Ar_2, electron impact ionisation, relative cross-sections, mass spectrometric meas. 79−86078
Ar_2F, low-lying electronic states 77−65491
ArKr, electron impact ionisation, relative cross-sections, mass spectrometric meas. 79−86078
CH, radiative lifetimes, electron-photon delayed coincidence meas. 78−50594
CH^+, electron impact excitation, rot. transitions 79−41244
CH^+ polar molecular ion, electron vibr.-rot. excitation *(Russian)* 80−1053
CH^+, rot. excitation by electron impact 79−27094
CH^+, rot. excitation by low-energy electrons *(Russian)* 79−94093
CH^+, rot. excitation by slow electrons, calc. 78−5360
C_2N_2, triplet state electronic energy delocalisation 77−3478
CO, $b^3\Sigma^+$ state excitation, low-energy electron impact, $\nu'=3$ level lifetime 80−1072
CO, $b^3\Sigma^+ \rightarrow {}^3\Pi$, excitation function 79−31705
CO, $d^3\Delta$ state, low energy electron impact excitation and radiative decay 80−91691
CO discharge plasma, electron energy distrib. and kinetic coeffs., ground-state mols. 80−43867
CO discharge plasma, electron energy distrib. and kinetic coeffs., vibr. excited mols. 80−43868
CO, dissociative excitation by electron impact, metastable fragment energy 78−66672
CO, ejected electron spectroscopy of autoionising states using electron-electron coincidence technique 79−3587
CO, electron energy loss spectra, C K-shell excitation, vibr. struct. 79−22851
CO, electron impact, absolute emission cross-sections meas., calibration appls. 79−85996
CO, electron impact, energy loss spectra, electronic transitions obs. 78−17805
CO, electron impact, reson. vibr. excitation calcs. 77−14595
CO, electron impact, vibr. levels stepwise excitation 78−1095
CO, electron impact spectra, C atom inner shell excitation 77−10776
CO, electron impact vibrational excitation, 1-4 eV 80−9747
CO, electron reson. scatt., ang. distrib., vibr. and rot. excitation, theory 78−22044
CO, electron scatt. at low energy, mechanisms *(Russian)* 78−90306
CO, electron scatt. cross sections for momentum transfer and inelastic excitation 79−36782
CO, K-shell, excitation and ionisation, vibr. struct., electron energy loss spectra obs. 80−18943
CO laser pumping with high-energy particles 79−64211
CO, low energy electron scatt., ab initio study, frame-transform. theory 77−83732
CO, negative-ion resons. associated with inner-shell-excited states, electron impact 77−88580
CO, oriented molecules, vibrationally inelastic electron scatt. 78−67907
CO, radiative lifetimes and electron impact absolute emission cross-sections 77−88503
CO, resonances in metastable and UV emitting levels 78−25727
CO, triplet state electronic energy delocalisation 77−3478
CO, $\nu=0\rightarrow1$ vibr. excitation, electron impact cross sections 80−83507
CO, vibr. excitation via high-energy shape resonances 80−91693
CO_2, X-ray and electron scatt. first Born approx. calcs. 77−61867
CO^+, electron impact rot. excitation, Glauber approx. with Coulomb effect 80−63840
CO^+, electronic transition moments for ($B^2\Sigma^+$-$X^2\Sigma^+$) and ($b^3\Sigma^+$-$a^3\Pi$) systems and matrix elements for ($X^1\Sigma^+$) and ($B^2\Sigma^+$) 77−38696
CO^+, fluoresc. spectra of ion beam, laser and electron excitation 79−45743
CO-N_2 discharge, energy balance influence of N_2 rot. level reson. excitation 78−17903
CO-N_2 discharge, plasma characts. and vibr. kinetics anal. 80−59331

molecular electron impact excitation continued
CO+e, momentum transfer cross sections, effect of nonspherical short range interactions 80−9745
CO+e, static pot. calcs. by INDO/1s and INDOX/1s 77−27192
$CO^+ + 2CO_2 \rightarrow 2CO_3^+$, reactions of electronically excited CO^+ 77−1915
CO_2, 3.8 eV resonance, vibr. struct. in electron-molecule scatt. 78−17813
CO_2, [100] symmetric stretch mode excitation 79−76523
CO_2, elastic and inelastic electron scatt. differential cross section, obs. and calc., struct., binding energy 80−28110
CO_2, elastic electron scattering and rot. excitation calcs. 79−22834
CO_2, electron elastic scatt. and vibr. excitation by 4, 10, 20 and 50 eV electrons 80−83484
CO_2, electron energy deposition, rel. to Venus and Mars atms. 79−45857
CO_2, electron energy loss spectra, C K-shell excitation, vibr. struct. 79−22851
CO_2, electron impact, 3.8 eV resonance 77−42430
CO_2, electron impact, cross sections for rot. excitation 78−17809
CO_2, electron impact, energy loss spectra, electronic transitions obs. 78−17805
CO_2, electron impact, reson. vibr. excitation calcs. 77−14596
CO_2, electron impact, transitions, generalised oscill. strengths 78−94327
CO_2, electron impact excitation, electron cooling in Mars and Venus atms. 78−57481
CO_2, electron impact single and double ionisation cross-sections 79−3584
CO_2, electron impact spectra, 35 keV electrons, Bethe surface and Compton profile 79−27091
CO_2, large angle elastic and inelastic electron scatt. differential cross section, exchange corrections 80−28111
CO_2, low energy electron (positron) collisions, ab initio adiabatic polarisation pots. 80−14240
CO_2, low energy electron scatt. cross sections, vibr. excitation, Boltzmann eqn. 80−18942
CO_2, reson. electron impact vibr. excitation, 3-5 eV 78−25726
CO_2, resonant vibr. excitation cross section in electron scatt. 77−19098
CO_2 shape resonances in [100] symmetric stretch excitation *(French)* 79−86074
CO_2, vibr. excitation and de-excitation by electronic collisions, calc. of cross section 78−66669
CO_2, vibr. excitation threshold struct., low-energy electron scatt. 80−5625
CO_2-N_2-He discharge, energy balance, influence of N_2 rot. level reson. excitation 78−17903
CO_2-N_2-He laser mixtures, electron swarm parameters, Boltzmann eqn. anal. 79−18396
CO_2+e, momentum transfer cross sections, effect of nonspherical short range interactions 80−9745
COS, electron energy loss spectra, C K-shell excitation, vibr. struct. 79−22851
CS_2, electron impact excitation and ionisation 80−63837
$^{12}C^{16}O+{}^{13}C^{16}O$, vibr. distrib., electron impact excitation, isotopic composition, interaction depend. 79−29332
Cl_2, electron impact dissoc. excitation, metastable fragment form. translational spectra 78−1094
CsCl, rot. excitation by electron impact, calc. cross sections 78−66670
CsF, rot. excitation by electron impact, calc. cross sections 78−66670
D_2, electron impact, Balmer-α, β, γ radn. emission cross sections 78−1091
D_2, electron impact, H,D(2s,2p) prod. 78−42230
D_2, electron impact, threshold excitation and predissoc., electron-photon coincidence meas. 80−18941
D_2, electron impact dissociative excitation 78−13618
D_2, electron impact excitation, transfer of moment impulses, vibration-rotation states *(Russian)* 79−7024
D_2, electron scatt., isotope effects 77−58188
$DBr^+(A^2\Sigma^+)$, vibrational states, lifetimes, emission cross sections, prod. by electron impact 77−3419
DCN, in interstellar clouds, rot. excitation by electrons and H_2 77−22292
D_2O, electron impact reson. observed in $A^2\Sigma^+ \rightarrow X^2\Pi$ radiation of OD 78−46455
F_2, electron energy loss spectra, 0-17 eV, 5-140°, repulsive valence states excitation 80−32844
F_2, electron impact excitation, dissoc. of lowest electronic state 80−63839
F_2, eqns. of motion method, transition energies, oscill. strengths, electron impact Born cross section 77−18983
F_2, low energy dissociative attachment and vibr. excitation, reson. scatt. theory 78−46453
H_2, $^3\Sigma_g^+ \rightarrow b\ ^3\Sigma_u^+$ light emission meas. by electron impact excitation 78−33618
H_2 (D_2) mol. bands, electron impact excitation, rot. transitions, cross sections in plasma 80−37896
H_2, adiabatic polarisation, ab initio calc., static electric dipole polarisability 79−72229
H_2, analytic energy degradation spectrum 77−31008
H_2, Balmer radiation production by electron impact 0-2000 eV 79−76521
H_2, close-coupling method appl. 78−74778
H_2, Compton defect, high energy electron impact spectroscopy 77−71876
H_2, elastic and rot. excitation, effective pot. theory 80−5627
H_2, elec. discharge, non-equilib. ionisation rate calcs. 80−59319
H_2, electron energy distribution function, superelastic vibr. collisions and dissoc. effects 79−59589
H_2, electron energy loss spectra, $B^2H_u^+$ state cross sections, Franck-Condon factors 78−13616
H_2, electron energy-loss spectra in afterglow, ground state vibr. conc. 77−31012
H_2, electron impact, Balmer-α, β, γ radn. emission cross sections 78−1091
H_2, electron impact, cross sectional factorization expressions, close coupling input tested in sudden approximation 79−43571
H_2, electron impact, elastic scatt. and rot. excitation, close-coupling calcs. 77−6949
H_2, electron impact, H,D(2s,2p) prod. 78−42230
H_2, electron impact, H_α and H_β lines emission, intensity decay curves meas. 80−83505

molecular electron impact excitation continued
H_2, electron impact, rot. excitation, comparison of local exchange pots. 78−5346
H_2, electron impact, threshold excitation and predissoc., electron-photon coincidence meas. 80−18941
H_2, electron impact, vibr.-rot. excitation by slow electrons, multiple scatt. calcs. 78−13617
H_2, electron impact dissoc. excitation, H_α and H_β Balmer line intensities 77−10778
H_2, electron impact dissoc. excitation, cross sections, mechanisms 80−37895
H_2, electron impact dissoc. ionisation 80−83510
H_2, electron impact dissociative excitation, H 3s prod. cross section 77−58183
H_2, electron impact dissociative excitation obs. 78−1090
H_2, electron impact dissociative excitation 78−13618
H_2, electron impact excitation total cross section, oscill. strengths, independent particle model calcs. 77−61856
H_2, electron impact excitation, of E, F $^1\Sigma^+_g$ states, optical excitation functions 77−61866
H_2, electron impact excitation, high vibr. levels of ground state, decay of reson. states 77−88581
H_2, electron impact excitation, $v \leq 4$ vibr. levels, theory 80−18940
H_2, electron impact excitation, to high Rydberg states, by threshold energy collision 80−83509
H_2, electron impact excitation, low energy, distorted wave approx. cross-sections 80−83511
H_2, electron impact low energy rot. and vibr.-rot. excitation cross sections, static exchange approx. 79−89799
H_2, electron impact rot. excitation, eikonal approx. 77−10777
H_2, electron impact rot. excitation, low energy, close-coupling calcs. 78−1092
H_2, electron impact spectroscopy for Compton profile meas. 78−90299
H_2, electron irrad., emission cross-sections for $3p^3\Pi_u \rightarrow 2s^3\Sigma_g^+$ 77−3477
H_2, electron scatt., ab initio theory, elastic scatt. and rot. excitation 78−50640
H_2, electron scatt., elastic and pure rot. excitation 79−22854
H_2, electron scatt., isotope effects 77−58188
H_2, electron scatt., iterative approach to Schwinger variational principle 80−99580
H_2, electron scatt., vibr. and vibr.-rot. excitation, ab initio calcs. 79−22853
H_2, electron scatt. in intense IR field, multiphoton free-free transitions 79−81289
H_2, electron total scatt. intensity, first Born approx., SCF CI calc. 77−10755
H_2, electronic stopping power calcs. 80−2104
H_2, energy deposition and energy degradation, 2, 10 and 30 keV 79−31709
H_2, excitation of $G^1\Sigma_g^+$ state, emission cross-section meas. 78−37755
H_2, metastable level electron impact excitation, resonances *(Russian)* 80−43198
H_2, optical polarisation following electron impact 80−63831
H_2, oriented molecules, vibrationally inelastic electron scatt. 78−67907
H_2, positron scatt., rot. excitation 78−50653
H_2, positron scattering, 50-800 eV, total cross-section meas. 79−31680
H_2, radiation polarisation, electron-impact excited, Lyman and Werner emissions and Lyman-α 79−36681
H_2, relativistic yield spectra from electron impact cross sections 78−13614
H_2, total cross sections meas. for electron scatt. at very low energies 80−58398
H_2, two-step excitation, Hanle effect obs. 78−25730
H_2^-, electron cooling through resonant collisions 80−32845
H_2^+, electron scatt., Schwinger variational principle appl. 80−48086
$H_2 + e^- \rightarrow H_2^* + e^-$, Gaussian basis Glauber approx., elastic and vibrorotational excitation cross sections 80−58399
HBr, Balmer radiation production by electron impact 0-2000 eV 79−76521
HBr, electron scatt., elastic rot. scatt. and vibr. excitation 78−58822
HBr, vibr. excitation by electron impact, threshold resons. 77−68127
$HBr^-(A^2\Sigma^+)$, vibrational states, lifetimes, emission cross sections, prod. by electron impact 77−3419
HCN, electron impact, dissoc. excitation cross-sections, fragment obs. 78−62936
HCN, electron impact excitation of low lying electronic states, assignments 78−25671
HCN, in interstellar clouds, rot. excitation by electrons 77−22292
HCN, K-shell excitation by electron energy loss spectroscopy 79−31712
HCl, Balmer radiation production by electron impact 0-2000 eV 79−76521
HCl, electron impact, H,D(2s,2p) prod. 78−42230
HCl^-, HCl^- reson. states, GO and SCF+CI methods, dissociation channels 77−71883
HCl, rot. excitation, energy dependence of elastic and inelastic cross sections 78−37756
HCl, slow electron impact vibr. excitation wave function, virtual s-state 77−42429
HCl, vibr. excitation by electron scatt., virtual state interpretation 78−17808
HCl^+, emission cross sections for $A^2\Sigma^+,v' \rightarrow X^2\Pi_i,v''$ on electron impact and lifetime of $A^2\Sigma^+,v'$ state 77−38697
HD, electron impact, H,D(2s,2p) prod. 78−42230
HD, electron impact dissociative excitation 78−13618
HD, electron impact dissoc. ionisation 80−83510
HD^+, rot. excitation by slow electrons, calc. 78−5360
HF, electron impact excitation, dissoc., emission spectrum 78−90305
HF, electron impact rot. excitation 77−42427
HF, electron scatt. cross section, vibr. and rot. excitation, close coupling calc. 80−53154
HF, electron spectroscopy of resonances 79−3583
HF, rot. excitation, energy dependence of elastic and inelastic cross sections 78−37756
HF, vibr. excited, ang. distrib. of reson. scatt. electrons 77−71881
HN_3 IR multiphonon dissociation with electronic excitation 80−11934
H_2O, Balmer radiation production by electron impact 0-2000 eV 79−76521
H_2O, dissoc. excitation by electron impact, multiple scatt. effect 79−89793
H_2O, dissociative excitation by electron impact, Born approx., emission cross sections *(Japanese)* 77−42425
molecular electron impact excitation continued
H_2O, dissociative excitation by electron impact, Glauber approx. *(Japanese)* 77−42426
H_2O electron collision cross sections behind shock wave in plasma 77−11309
H_2O, electron impact, dissoc. excitation, core pot. correction 78−25724
H_2O, electron impact, H,D(2s,2p) prod. 78−42230
H_2O, electron impact, inelastic scatt., 4-6 eV energy loss region 78−90277
H_2O, electron impact, vibr. excitation, effective range theory 80−83485
H_2O, electron impact reson. observed in $A^2\Sigma^+ \rightarrow X^2\Pi$ radiation of OH 78−46455
H_2O, inelastic electron scatt., geometrical parameters determ. 77−88585
H_2O, slow electron scatt., rigid mol. model with exchange and polarisation 80−43194
H_2O, Van der Waals polymer mols., negative ions formed in nozzle expansion 78−90296
H_2O, vibrational excitation by electron impact, threshold structs. 78−22038
H_3O^+, rot. excitation by slow electrons, calc. 78−5360
H_2S, Balmer radiation production by electron impact 0-2000 eV 79−76521
H_2S, electron impact, vibr. elastic scatt. and vibr. excitation 79−13822
H_2S, slow electron scatt., rigid mol. model with exchange and polarisation 80−43194
$H_2(^1\Sigma_g^+ - {}^1\Pi_u)$ excitation, electron-polarised-photon coincidence 79−22852
$^2HN_3$ IR multiphonon dissociation with electronic excitation 80−11934
HeH^+, electron impact excitation, rot. transitions 79−41244
Hg_2, excimer fluorescence, electron beam and optically produced systems 77−27107
K_2, electron impact, vibr.-rot. excitation by slow electrons, multiple scatt. calcs. 78−13617
KI, rot. excitation by electron impact, calc. cross sections 78−66670
Kr_2, electron impact ionisation, relative cross-sections, mass spectrometric meas. 79−86078
KrF, electron beam pumped laser medium, time depend. fluoresc. spectrum in high current density range 80−78842
KrF, electron impact deexcitation cross sections and rate consts. calcs. 80−32848
KrF, excimer, electron impact deexcitation, low energy cross-sections and rate consts. 80−1071
KrF, formation and quenching of electronic excited states 77−673
KrF linac-excited gas mixture, UV fluoresc. meas. 80−28216
KrF, UV bound-free emission after electron excitation 77−27279
KrXe, electron impact ionisation, relative cross-sections, mass spectrometric meas. 79−86078
Li-like ion, in plasma, ion electron collisional radiative recomb. coeffs., bottleneck calc. 80−53942
Li_2, electron impact, vibr.-rot. excitation by slow electrons, multiple scatt. calcs. 78−13617
LiCl, rot. excitation by electron impact, calc. cross sections 78−66670
LiF, elastic and rot. excitation cross sections for electron scatt. 78−46446
LiF, electron scatt., quasiclassical close-coupling approximation 79−81280
LiF, low-energy electron impact rot. excitation, close-coupling calc. 77−58187
LiH_+ rot. excitation by electron impact, calc. cross sections 78−66670
$N_2, E^3\Sigma_g^+$ state electron excitation, collisional deactivation and energy transfer 77−10774
N_2, 2.4 eV shape resonance, vibr. struct. in electron-molecule scatt. 78−17813
N_2, (e,2e) spectra, valence momentum distribs. and config. interaction 77−19101
N_2, $B^3\pi_g$ state excitation and deactivation in positive column 77−3482
N_2, $C^3\Pi_u$ state, electron impact excitation function approx. 79−7022
N_2, $C^3\Pi_u$-state, electron impact excitation, low energy 80−9746
N_2, DC low press. positive column, electron distrib. function superelastic electron collision depend. 79−46498
N_2, diffuse plasma, population densities of triplet states, correl. with electron impact processes 80−43966
N_2, discharge, excitation efficiency of rot. and vibr. levels, heating due to elastic collisions and relax. 80−38751
N_2, elastic and inelastic electron scatt. differential cross section, obs. and calc., struct., binding energy 80−28109
N_2, elastic and inelastic electron scatt., state to state cross section 80−78708
N_2, electron energy-loss spectra, dipole-forbidden states 79−59588
N_2, electron excitation of Birge-Hopfield bands ($b^1\pi_u$-$X^1\Sigma_g^+$) 80−95731
N_2, electron impact, absolute emission cross-sections meas., calibration appls. 79−85996
N_2, electron impact, differential cross-section, converged close-coupling calcs. 78−90290
N_2, electron impact, reson. vibr. excitation, ab initio R matrix calc. 80−32842
N_2, electron impact, rot. excitation 77−58184
N_2 electron impact, spatial yield spectra, microplume model 79−98235
N_2, electron impact, spatial yield spectra, energy degradation 79−100992
N_2, electron impact enhanced vibr. excitation, continuum multiple scatt. model with Hara exchange approx. 80−43196
N_2, electron impact excitation cross section of rot. states in glow discharge plasma 77−43092
N_2, electron impact excitation total cross sections, oscill. strengths, independent particle model calcs. 77−61856
N_2, electron impact excitation, $x^1\Sigma_g^-$ and $y^1\Pi_g$ states lifetimes meas. 78−17806
N_2 electron impact excitation, rate coeffs., momentum transfer cross-section 78−78819
N_2, electron impact excitation cross-sections meas. *(Spanish)* 79−98230
N_2, electron impact excitation cross-sections for $B^3\Pi_g$, $C^3\Pi_u$ and $E^3\Omega_g^+$ states 80−1073
N_2, electron impact excitation, to high Rydberg states, by threshold energy collision 80−83509
N_2, electron impact excited, broadband photon yield meas. *(French)* 78−25723
N_2, electron impact reson. excitation of new valence state 79−36785
N_2, electron impact rot. and vibr. excitation, elastic scatt., close coupling and Born approx. 80−28108
N_2, electron impact vibr. excitation, adiabatic approximation, energy-modified 79−59523

molecular electron impact excitation continued
N_2, electron resonant scatt., total cross section function 77−50548
N_2, electron scatt., 50-500 eV, two-pot. approach 79−41242
N_2, electron scatt., reson. excitation and dissoc. attachment, vibr. state depend. 80−78717
N_2, electron scatt., vibr. excitation, rot.-vibr. close-coupling calcs. 77−6947
N_2 electron scatt. cross sections, 0.04-3.7 eV 79−54978
N_2, electron scatt. ground state vibr. levels population 78−1093
N_2, electron scattering, local-exchange approx. for intermediate-energy-differential cross sections 80−48094
N_2, electron scattering excited, hybrid theory results for 5 and 10 eV 77−27191
N_2, electronic states, 12.5-14.2 eV energy-loss region 78−17811
N_2, electronic states, differential cross sections, 10-50 eV 78−13619
N_2, electronic states, integral cross-sections, 10-50 eV 78−17810
N_2, energy transfer, source of $O(^1S)$ in aurora 79−48598
N_2, excitation efficiency for rot. states 80−102557
N_2, fluoresc. efficiencies of electrons, 4900-10500 Å wavelength range 77−61870
N_2, IR laser transition, excitation process 80−87383
N_2, in CO_2-N_2-He laser, electron impact excitation, V-V resonant transfer 78−5452
N_2 in upper atmosphere, effects of soft electron precip. on vibr. energy distrib. 77−33261
N_2, inner shell $(1s)^{-1}(\pi 2p)^1\Pi$ state, energy, vibr. struct., electron impact investig. 78−13611
N_2, K-shell, excitation and ionisation, vibr. struct., electron energy loss spectra obs. 80−18943
N_2, large angle elastic and inelastic electron scatt. differential cross section, exchange corrections 80−28111
N_2 laser UV-IR pulse time lag theory *(Japanese)* 80−14325
N_2, low energy electron (positron) collisions, ab initio adiabatic polarisation pots. 80−14240
N_2, low energy electron scatt. phaseshifts 77−31011
N_2, low energy electron scatt., N_2^- resonance at 2 eV as energy standard 77−71872
N_2, low-energy electron scatt., calcs. 77−31013
N_2, metastable level electron impact excitation, resonances *(Russian)* 80−43198
N_2, multiple scatt. method, scatt. cross section calc. 80−63816
N_2, N K-shell excitation, high-resolution electron energy loss spectra 80−53152
N_2, N_2^+ auroral bands, excitation studies from airborne spectroscopy 77−29533
N_2, N_2^+ first negative spectra excitation, modelling 77−61758
N_2, negative-ion resons. associated with inner-shell-excited states, electron impact 77−88580
N_2, oriented molecules, vibrationally inelastic electron scatt. 78−67907
N_2 plasma, electron beam energy distrib., excitation and ionisation model, Monte Carlo method *(Russian)* 79−27790
N_2 plasma, electronic excitation levels in gas-discharge 80−24280
N_2, resonances in metastable and UV emitting levels 78−25727
N_2, rot. excitation by electron impact 1-4 eV 78−55248
N_2, rot. excitation of non-polar mol. by slow electron impact, variational approach 79−31708
N_2, rot. temp. meas., rocketborne electron beam fluoresc. meas., reflected mol. effects 77−29519
N_2, triplet state electronic energy delocalisation 77−3478
N_2, vibr. populations of excited states under auroral conditions 78−42035
N_2, X-ray and electron scatt. first Born approx. calc. 77−61867
N_2^-, first $^2\Pi_u$ state form. and decay 80−58177
N_2^+, A- and B-states interactions, time-resolved obs. 80−18862
N_2^+, electron impact excitation, ionisation, rel. to auroral spectral intensities 79−84563
N_2^+, electron impact excitation cross-sections meas. *(Spanish)* 79−98230
N_2^+, excitation in RF discharges *(French)* 77−61868
N_2+Ar+POPOP, electron beam excited, energy transfer mechanisms 80−23497
$N_2+H^+(e)$, vibrational N_2^+ excitation *(Russian)* 80−53156
$N_2^+ + 2N_2 \rightarrow 2N_3^+$, reactions of electronically excited N_2^+ 77−1915
NH, radiative lifetimes, electron-photon delayed coincidence meas. 78−50594
NH_3, Balmer radiation production by electron impact 0-2000 eV 79−76521
NH_3, Compton defect for 35 keV electrons 79−27092
NH_3, Compton profile asymmetry, 35 keV electron impact spectroscopy 79−7025
NH_3, dipole oscill. strengths for excitation, ionisation and fragmentation by 5-60 eV electrons 77−68129
NH_3, electron impact, 35 keV, Bethe surface and Compton profile 80−87235
NH_3, electron impact, dissoc. excitation cross-sections, fragment obs. 78−62936
NH_3, electron impact, H,D(2s,2p) prod. 78−42230
NH_3, lowest triplet excitation, electron energy loss spectra 77−71880
N_2H^+, electron impact rot. excitation, Glauber approx. with Coulomb effect 80−63840
NO, $a^4\Pi$ and $b^4\Sigma^-$ states, electron impact spectra 78−58733
NO, adsorbed on Ru (001), inelastic electron scatt. dissoc. energies adsorbed state depend. 78−95956
NO, doublet-quartet transitions, 5-7.4 eV, electron-impact spectroscopy, 5-80° 78−37754
NO, doublet-quartet transitions, low energy variable-ang. electron scatt. obs. 78−62933
NO, electron impact, absolute emission cross-sections meas., calibration appls. 79−85996
NO, electron impact, energy loss spectra, electronic transitions obs. 78−17805
NO, electron impact excitation, high vibr. levels of ground state, decay of reson. states 77−88581
NO, Feshbach resonances, energy dependence of electronic coupling to ground state 79−89616
NO, measured lifetimes of $A\ ^2\Sigma^+$, $D\ ^2\Sigma^+$ and $C\ ^2\Pi$ states 78−90219
NO, N K-shell excitation, high-resolution electron energy loss spectra 80−53152
NO^-, $^3\Sigma^-$ and $^1\Delta$ resonances, excitation in electron scatt. 77−31010
N_2O, electron impact, energy loss spectra, electronic transitions obs. 78−17805
N_2O, electron impact excitation, ionisation, emission spectrum 77−50469
N_2O, IR intensities by electron impact spectroscopy 77−6851
N_2O, N K-shell excitation, high-resolution electron energy loss spectra 80−53152
$NO(a^4\Pi)$ dipole moment, meas. by mol. beam electron impact vibr. excitation 79−72440
$NO(b^4\Sigma^-)$, electron impact excitation energy, radiative lifetime, quenching in NO 77−79642
$^{14}N^{14}N+^{14}N^{15}N$, vibr. distrib., electron impact excitation, isotopic composition, interaction depend. 79−29332
Na_2, electron impact, vibr.-rot. excitation by slow electrons, multiple scatt. calcs. 78−13617
NaCl, rot. excitation by electron impact, calc. cross sections 78−66670
Ne, electron impact, collision freq. in ionospheric F-region 79−53641
O_2, 7 to 10 eV energy loss spectra, Rydberg states excitations 77−27193
O_2, $b^1\Sigma_g^+$ state excitation by 0.75-6 eV electrons 78−86958
O_2 electron coincidence spectrosc., valence electron momentum distrib. and binding energies 80−102583
O_2, electron excitation total cross sections, oscill. strengths, independent particle model calcs. 77−61856
O_2, electron impact, energy loss spectra, electronic transitions obs. 78−17805
O_2, electron impact excitation, high vibr. levels of ground state, decay of reson. states 77−88581
O_2, electron impact vibr. excitation, direct and stepwise, rate coeffs. 80−5630
O_2, electronic electron impact excitation, rot.-electronic coupling 78−9265
O_2, energy transfer, source of $O(^1S)$ in aurora 79−48598
O_2, fluoresc. efficiencies of electrons, 4900-10500 Å wavelength range 77−61870
O_2, indirect mechanism for $O(^1S)$ prod. in aurora 79−48597
O_2, interactions with slow electrons 79−45848
O_2, K-shell, excitation and ionisation, vibr. struct., electron energy loss spectra obs. 80−18943
O_2, metastable level electron impact excitation, resonances *(Russian)* 80−43198
O_2, optically allowed transitions from ground state 79−10216
O_2, optically forbidden transitions from ground state 79−10217
O_2, Schumann-Runge continuum, oscill. strength and electron impact excitation 80−69121
O_2, X-ray and electron scatt., first Born approx. calcs. 77−61867
O_2^+, electron impact excitation, ionisation, rel. to auroral spectral intensities 79−84563
O_2^+, second negative bands excitation cross-sections, rel. to auroral emissions 78−37745
O_3, low energy elastic and inelastic electron scatt., rot. transitions, close coupling calc. 80−78706
OCS, electron impact excitation and ionisation 80−63837
PH_3, electron impact dissoc. ionisation, mass spectrometric obs. 78−9264
PH_3-PD_3, electron impact dissoc. ionisation, mass spectrometric obs. 78−9264
SF_6, electron impact excitation, 12 eV resonance 77−88582
SF_6, electron impact excitation of inner shell, using 2.5 keV electrons 78−90303
SF_6, electron impact vibr. excitation 77−42428
SF_6 electron scatt., total absolute cross sections, 0.5-100 eV, incl. reson. struct. 79−45843
SF_6, electronic props., (e,2e) spectrosc. obs. 80−5527
SF_6, resonant single-photon dissoc. route using prelim. electron excitation 80−9662
SF_6, vibr. excitation, dissociative attachment 77−3481
SO_2, electron impact excitation of low-lying electronic states 79−10215
SO_2, resonant vibrational excitation, electron impact spectrometer obs. 78−90309
SO_2, triplet state electronic energy delocalisation 77−3478
Sb_4, vap., $M_{4,5}N_{4,5}N_{4,5}$ Auger electron spectra 79−50089
SiH_4, $L_{2,3}MM$ Auger spectrum, line width and intensities 80−58325
Te_2, vap., $M_{4,5}N_{4,5}N_{4,5}$ Auger electron spectra 79−50089
UF_6, excitation spectra after electron impact, 30-75 eV impact energy 79−45854
UF_6 nuclear pumped lasers, electron impact cross section meas. 80−63985
WF_6, excitation spectra after electron impact, 30-75 eV impact energy 79−45854
Xe-Br_2(Cl_2)(HCl) mixtures, low-press. excimer form. and quenching by e-beam excitation 79−50071
Xe_2, e-beam excited, 193 nm absorpt. studies 80−43323
Xe_2, electron beam excited, 193 nm absorpt. meas. rel. to 172 nm laser pulse termination 80−28200
Xe_2, electron impact ionisation, relative cross-sections, mass spectrometric meas. 79−86078
Xe_2, laser performance for atm. press. and microsecond electron beam excitation 80−28199
Xe_2, performance as photolytic driver at low electron beam excitation rates 80−32963
XeBr, UV bound-free emission after electron excitation 77−27279
XeCl laser, electron beam excitation *(Russian)* 78−22115
XeCl molecule excited by electron beam, stimulated emission obs. 80−32966
XeF, direct pumping by electron beam pulses, gain and laser oscill. obs. in blue-green 80−102699
XeF, electron impact deexcitation cross sections and rate consts. calcs. 80−32848
XeF, excimer, electron impact deexcitation, low energy cross-sections and rate consts. 80−1071
XeF, formation and quenching of electronic excited states 77−673
XeF linac-excited gas mixture, UV fluoresc. meas. 80−28216
XeF_6 molecules with Jahn-Teller pseudo-effect, ang. depend. of inelastic scatt. of electrons 80−69246
XeF* temp. dependent quenching rate constants 80−63701
XeI, UV bound-free emission after electron excitation 77−27279

molecular electron impact ionisation
see also electron spectra
acetylene, electron impact ionis., valence electron momentum distribs. 78−33617
acetylene, electron impact ionisation, valence orbitals, momentum distrib. and correl. effects 78−5361

molecular electron impact ionisation continued
acetylene, electron ionisation efficiency curves, fragment ion appearance pot. 78−86959
acetylene, electron momentum distribs. in π orbitals from (e,2e) expts. 80−14239
acetylene, inner shell electron energy loss obs. 79−45853
acetylene, ionis. efficiency curves by electron impact, $CH_2^+(C_2H^+)$ form., ~10 eV 78−62935
adiabatic approximation, energy-modified 79−59523
air, electron backscattering coeffs., 100 eV to 5 keV 80−9750
atmospheric gases, electron impact cross-sections 78−28398
atmospheric gases, yield spectra calcs. 78−28401
autoionising states 78−58852
benzene, ionisation by electron bombard., empirical and semi-empirical calcs. 79−36784
benzenes, substituted, gaseous, negative ion states, electron transmission spectra 77−31007
butadiene, electron momentum distribs. in π orbitals from (e,2e) expts. 80−14239
butane, ionisation by electron bombard., empirical and semi-empirical calcs. 79−36784
chlorofluoromethane negative ion products, in 0-10 eV near-monoenergetic electron impact 79−41245
chlorofluoromethanes, electron attachment, electron swarm method 80−69245
collisional cross-sections determ. for low and intermediate energy processes 80−99579
continuum wave functions, discrete basis set method 79−22829
cyclopropane, electron momentum distribs. in π orbitals from (e,2e) expts. 80−14239
dichlorodifluoromethane, total ionis. and electron attachment cross sections by electron impact 79−59586
dielectric gas, breakdown strength, electron impact ionis. and scatt. cross section 79−82031
double-charged mols., investigation of single-charged ion products 78−37753
doubly charged negative ions, electron impact 77−31006
dynamic structure, determ. using electron impact ionisation 77−3460
(e,2e) knockout reactions, electron single particle states 77−88117
(e,2e) molecular knockout reactions via electronic struct. calcs., Green's function methods 77−88577
(e,2e) offshell impulse approx., electronic momentum distribs. 77−88565
electrically excited preionisation unit with electron beam energy recuperation 78−59013
electron attachment, high temperature processes, chemical modelling 80−18937
electron attachment to mol. and mol. clusters, electron-mol. collision, Rydberg electron exchange 80−63843
electron coincidence spectroscopy, binding energy charge density meas. 80−63817
electron coincidence spectroscopy, orbital shape, charge density, mol. struct. determ. appls. 79−27113
electron degradation and yields of initial mol. species, variational calc. 79−7023
electron scatt. and photoionisation, shape-resonance enhanced nuclear motion effects 80−63603
electron wave function pair Fourier transforms, at., mol. and solids, by (γ,2e) and (e,3e) *(Russian)* 77−71878
electron wavefunctions for (γ,2e) and (e,3e) processes at high energy, double Fourier transform 78−17628
electronic and at. collisions, conf., Kyoto, Japan (Aug.-Sept. 1979) 80−57011
electrostatic electron energy analysers, cylindrical mirror appls., review 78−21265
ethane, (e,2e) spectroscopic obs., valence electron momentum distribs. and separation energies 77−3480
ethane, electron impact dissoc., absolute total cross section, 10-600 eV 79−36781
ethane, electron ionisation efficiency curves, fragment ion appearance pot. 78−86959
ethane, ionis. efficiency curves by electron impact, fragment appearance pots. 77−61863
ethane, ionisation by electron bombard., empirical and semi-empirical calcs. 79−36784
ethylene, (e,2e), correlation effects, electron momentum distributions in valence orbitals 79−862
ethylene, electron impact ionis., valence electron momentum distrib. 79−18297
ethylene, electron ionisation efficiency curves, fragment ion appearance pot. 78−86959
ethylene, electron momentum distribs. in π orbitals from (e,2e) expts. 80−14239
fast electron ionisation or attachment transition probabilities, extended statistical law 77−54613
formyl fluoride, 70 eV electron-produced gas phase species and reactions obs. 77−63900
fragment ion kinetic energies, modified ion source and mass spectrometer 77−6958
fragmentation processes in mass spectroscopy, rate constant *(Rumanian)* 77−26429
gaseous dielectrics, electron-molecule interactions and negative ion resonances 78−75480
generalised overlap amplitudes, (e,2e) spectroscopic determ. 77−61862
n-hexane, ionisation by electron bombard., empirical and semi-empirical calcs. 79−36784
hydrocarbon, (e,2e), angular correlations *(Russian)* 77−46648
inert gas Van der Waals dimers, electron impact ionis. 80−58400
inert gases, (e,2e) reactions 200 to 2600 eV as probe of atomic and molecular struct. 77−88566
inner electron resonances in molecules, roles in ionisation *(French)* 78−82660
inner shell (e, 2e) symmetric reacts. 77−19092
ionic fragmentation, translational energy, phase space theory 77−9051
methane, and -d_4, electron ionis., excited states between 18 and 22 eV 79−3588
methane, angular correl. for (e, 2e) reaction 77−6950
methane, electron transmission function and mean energy per ion pair, obs. 80−23566
methane, ionisation by electron bombard., empirical and semi-empirical calcs. 79−36784
methane, semiempirical electron impact ionis. cross-sections 78−1089
molecular electron impact ionisation continued
molecules, electron coincidence ionisation spectra, Green's function anal. 79−31714
momentum wave function determ. in atomic, molecular and nuclear systems 77−88556
monohalobenzenes, inner shell excitation and ionis., electron energy loss spectra, XPS, assignments 78−62934
organic molecular systems, polarisabilities, susceptibilities, electron impact ionis. cross-sections calcs. 80−63835
pentafluoroethyl iodide, electron impact, time of flight mass spectrometry 77−42424
n-pentane, ionisation by electron bombard., empirical and semi-empirical calcs. 79−36784
phenyl cation, struct., ion-molecule reactions studied by trapped ion mass spectroscopy 80−102586
photon emission from electron+molecule collisions *(Dutch)* 78−5362
plasma chromatograph/mass spectrometer simultaneous electron impact/chem. ionisation carrier gas mixture 79−30600
positive column of glow discharge of electronegative gas, molecular excitation and ionisation by electron collisions 80−49031
n-propane, ionisation by electron bombard., empirical and semi-empirical calcs. 79−36784
propylene, electron impact ionisation and dissoc. 80−37894
rate coefficients and ionisation cross sections 77−50547
review, of expt. and theory 78−25699
tissue equivalent gas electron transmission function and mean energy per ion pair, obs. 80−23566
total inelastic scatt. cross section, detector solid angle depend., approx. bounds 78−17798
transient species, vacuum UPS, book contrib. 80−14178
two-electron Fourier amplitudes of atomic and mol. wavefunctions using the (γ,2e) and (e,3e) processes 79−3419
two-particle-hole Tamm-Dancoff approximation (2ph-TDA) equations for closed-shell atoms and molecules 78−70937
water vapour electron stopping power and energy degradation 80−23276
yield spectra, continuous-slowing-down approx. 77−88569
Ar, electron transmission function and mean energy per ion pair, obs. 80−23566
Ar-HI, low electron beam excitation rates 79−86163
Ar-I_2, low electron beam excitation rates 79−86163
Ar_2*, electron impact ionisation cross sections in binary encounter approx. 79−68320
$AsBr_3$, electron impact positive ion form., appearance energy obs. 80−53151
$AsCl_3$, electron impact positive ion form., appearance energy obs. 80−53151
$AsF_3(AsF_5)$, electron impact positive ion form., appearance energy obs. 80−53151
$CH(CH_2)(CH_3)$, semiempirical electron impact ionis. cross-sections 78−1089
CO, adsorbed layer, electron impact, electron impulsive ionisation spectroscopy obs. 80−60720
CO discharge plasma, electron energy distrib. and kinetic coeffs., vibr. excited mols. 80−43868
CO, electron impact ionisation, metastable state mol. ion form. 77−14594
CO, electron impact K-shell ionis., ionic fragmentation, Auger decay post-collision interaction 77−75316
CO, electron scatt., absolute total cross-section meas. 78−74774
CO, ionisation by electron bombard., empirical and semi-empirical calcs. 79−36784
CO, K-shell, excitation and ionisation, vibr. struct., electron energy loss spectra obs. 80−18943
CO, optical excitation function by electron impact near threshold 77−6942
CO, single and double ionisation by electron impact, energy depend. and ionisation pot. 79−13827
CO^+, electronic struct., CO(e, 2e) reaction meas., CI calcs. 77−34769
CO_2, electron energy deposition, rel. to Venus and Mars atms. 79−45857
CO_2, electron impact, 50-400 eV, secondary electrons double differential cross section 80−37897
CO_2, electron impact ionisation, dissoc. ionisation 78−13610
CO_2, electron scatt., absolute total cross-section meas. 78−74774
CO_2, electron swarm parameters for high E/N, Monte Carlo simulation 80−19548
CO_2, electron transmission function and mean energy per ion pair, obs. 80−23566
CO_2 gas, electron impact ionisation, electronic fluoresc. spectra 80−95664
CO_2, negative Van der Waals polymer mols., formed by nozzle expansion 78−90307
CO_2, valence shell ionis. spectra, theory and dipole (e-2e) spectra expts. 79−76522
CO_2, valence states study by (e,2e) momentum spectroscopy 78−22039
CO_2^+, electron impact ionisation, cross section obs. 80−58397
CO_2-N_2-He laser mixtures, electron swarm parameters, Boltzmann eqn. anal. 79−18396
CO_2-N_2-He-O_2 discharge mixture, three body electron attachment to O_2 80−64779
CO*, metastable, electron impact ionisation cross-section calcs. 77−46644
CS_2, electron impact excitation and ionisation 80−63837
CS_2, ionisation and fragmentation by monoenergetic electron impact, mass spectrometric study 80−102581
CeI_3 vapour, negative ion formation by charge transfer and electron attachment 77−27190
CeI_3 vapour, positive ion formation (CeI^+, CeI_2^+, CeI_3^+) 77−23567
Cl_2, electron impact total ionis. and electron attachment cross sections 79−3589
Cl_2^-, formation in vibrationally excited state 77−60048
Co, orientated mol., (e,2e) spectra, electron momentum density 79−98236
D_2, electron Compton profiles from energy loss spectra 79−7013
D_2, electron impact dissoc. ionisation 80−83510
D_2, electron impact dissociative ionisation near $^2\Sigma_g^+$ state dissoc. threshold 80−43197
D_2O, electroionisation 79−22849
$Fe(CO)_5$, gas phase collisions, negative ion form., struct. 77−6945
H_2, analytic energy degradation spectrum 77−31008
H_2, degradation, energy apportionment methods calcs. 77−6951

molecular electron impact ionisation continued
H_2, electron impact dissoc. ionis., 75 eV emitted H^+ energy spectrum ang. depend. 78−17812
H_2, electron impact dissoc. ionisation, energetic protons for autoionising states 78−25728
H_2, electron impact dissoc. ionisation 80−83510
H_2, electron impact dissociative ionisation near $^2\Sigma_g^+$ state dissoc. threshold of H_2 80−43197
H_2, electron impact H^+ prod., kinetic energy, ang. distribs. 80−63838
H_2, electron impact ionis., differential cross sections 78−58839
H_2, electron impact ionisation cross section 80−78718
H_2, electron impact partial absolute ionis. cross section, 20-350 eV, rel. to H_2O and NH_3 *(French)* 79−861
H_2, energy deposition and energy degradation, 2, 10 and 30 keV 79−31709
H_2, fast electron retardation, ionisation cascade, degradation spectra, anal. *(Russian)* 79−27741
H_2, ionisation by electron bombard., empirical and semi-empirical calcs. 79−36784
H_2, positron annihilation, positron form. 79−94092
H_2, positron annihilation involving low energy positrons, lifetime spectra 79−94091
H_2, statistical fluctuations in ionisation yield, rel. to electron degradation spectrum 80−99581
H_2, $X^1\sigma_g^+$, momentum distrib., electron correl. and mol. vibr. effects, theory 77−88557
H_2^+, electron cooling through resonant collisions 80−32845
H_2-Ne, positron annihilation involving low energy positrons, lifetime spectra 79−94091
H_2-Ne, positron annihilation, positron form. 79−94092
HBr, electron impact ionisation, vibr. excitation spectra threshold peaks, negative ion effects 80−106322
HCN, inner shell electron energy loss obs. 79−45853
HCN, K-shell excitation by electron energy loss spectroscopy 79−31712
HD, electron impact dissoc. ionisation 80−83510
HF, valence orbitals momentum distribs., (e, 2e) binding energy spectra 80−14237
H_2O, (e,2e) separation energy spectra, valence orbital electron momentum distribs. 77−38736
H_2O, and D_2O, Feshbach-reson. and dissoc. electron attachment 79−41246
H_2O, binding energy, MO momentum distrib., electron impact coincidence spectrometer obs. 77−61869
H_2O, electroionisation 79−22849
H_2O, electron impact partial absolute ionis. cross section, 20-350 eV, rel. to H_2 and NH_3 *(French)* 79−861
H_2O, generalised overlap amplitudes, (e,2e) spectroscopic determ. 77−61862
H_2O, vapour, fast electron impact, secondary electron energy distrib. 77−58148
H_2O vapour, ionis. coeffs. and dissociative electron attachment 80−43833
H_2S, valence electron ionisation and momentum distribs. 80−28107
H_2S, valence momentum distribs., binding energies, binary (e,2e) spectrosc. meas. 79−31713
H_2S, valence shell binding energy spectrum, 8-34 eV, electron scatt. simulation of photoionis. 79−10213
He flow discharge, intermediate press., positive column conc. of ions and metastables 80−44017
I_2, dissociative attachment, thermal energy electrons 78−82850
InBr, electron impact dissoc. ionis., In electron affinity meas. *(French)* 80−63849
InI, electron impact dissoc. ionis., In electron affinity meas. *(French)* 80−63849
Li_2, core-excited states, UV photoabsorpt. and ejected electron spectra 78−37655
LiF vapour system, fragmentation in mass spectrometer ion source 78−70944
LiI, electron-mol. beam collisions, autoionising states, electronic spectra *(Russian)* 78−22023
N_2, continuum, energy loss cross sections for 300, 400 and 500 eV electrons 79−94090
N_2, electron backscattering coeffs., 100 eV to 5 keV 80−9750
N_2, electron impact, electron distrib. function in laser radiation field, vibr. excitation influence 80−28112
N_2 electron impact, spatial yield spectra, microplume model 79−98235
N_2, electron impact ionis., differential cross sections 78−58839
N_2, electron impact ionisation, metastable state mol. ion form. 77−14594
N_2, electron impact reson. dissoc., intermediate negative ion form. 79−36783
N_2, electron impact resonant scattering, absolute cross sections from boomerang model 79−89798
N_2, electron ionisation, N_2^{2+} form., decay to N^+, coincidence detect. 77−79695
N_2 electron scatt. cross sections, 0.04-3.7 eV 79−54978
N_2, electron swarm parameters for high E/N, Monte Carlo simulation 80−19548
N_2 gas, electron impact ionisation, electronic fluoresc. spectra 80−95664
N_2, glow discharge, ionis. mechanism 78−13613
N_2, in CO_2 laser, electron beam-ionis. optical pumping characts. 77−75477
N_2, ionisation by electron bombard., empirical and semi-empirical calcs. 79−36784
N_2, K-shell, excitation and ionisation, vibr. struct., electron energy loss spectra obs. 80−18943
N_2, low energy electron impact dissociative ionis., N^{2+} form. and energy distrib. 80−5626
N_2 mean energy expended per ion pair, Fowler eqn. 77−71882
N_2, N_2^+ first negative spectra excitation, modelling 77−61758
N_2, orientated mol., (e,2e) spectra, electron momentum density 79−98236
N_2 plasma, electron beam energy distrib., excitation and ionisation model, Monte Carlo method *(Russian)* 79−27790
N_2, rot. energy distrib. of $N_2+(X^2\Sigma_g^+)$ 79−76520
N_2^+, electron impact excitation, ionisation, rel. to auroral spectral intensities 79−84563
N_2-O_2, electron impact dissoc. ionisation, N^- form., mass spectra 77−75320
NH_3, dipole oscill. strengths for excitation, ionisation and fragmentation by 5-60 eV electrons 77−68129
NH_3, direct and dissociative electron impact cross-sections 77−61864
NH_3, electron excited Auger emission 77−88518
NH_3, electron impact ionisation, threshold to 180 eV, mass spectrometric obs. 78−13615
NH_3, electron impact ionisation, total and partial cross sections meas. 80−95729
NH_3, electron impact partial absolute ionis. cross section, 20-350 eV, rel. to H_2 and H_2O *(French)* 79−861
NH_3, ionis. coeffs. and dissociative electron attachment 80−43833
NH_3-ND_3, electron impact ionisation, threshold to 180 eV, mass spectrometric obs. 78−13615
NO, adsorbed layer, electron impact, electron impulsive ionisation spectroscopy obs. 80−60720
NO, electron impact dissoc. ionisation, N^- form., mass spectra 77−75320
NO, electron impact ionisation, metastable state mol. ion form. 77−14594
NO, Feshbach resonances, dynamic coupling to Rydberg states 79−89617
NO, ionisation by electron bombard., empirical and semi-empirical calcs. 79−36784
NO^-, $^3\Sigma^-$ and $^1\Delta$ resonances, excitation in electron scatt. 77−31010
NO_2, single and double ionisation by electron impact, ionisation pot. determ. 80−95730
NO_2, valence shell ionis. spectra, theory and dipole (e-2e) spectra expts. 79−76522
N_2O, electron impact excitation, ionisation, emission spectrum 77−50469
N_2O, electron impact ionisation and dissociation, radiation emission 78−90304
N_2O gas, electron impact ionisation, electronic fluoresc. spectra 80−95664
N_2O, ionis. by low-energy electrons and near thermal inert gas ions, emission obs. 79−31707
N_2O, negative Van der Waals polymer mols., formed by nozzle expansion 78−90307
N_2^* ($A^3\Sigma_u^+$), electron impact ionisation cross section 80−78718
N_2^*, metastable, electron impact ionisation cross-section calcs. 77−46644
Ne-Ar-I_2, low electron beam excitation rates 79−86163
Ne_2^*, electron impact ionisation cross sections in binary encounter approx. 79−68320
$Ni(CO)_4$, gas phase collisions, negative ion form., struct. 77−6945
Nz, electron transmission function and mean energy per ion pair, obs. 80−23566
O_2 discharge plasma, metastable states role, two-step ionisation, electron densities and transition pts. 80−44019
O_2, dissociative attachment coeff. calc. 77−19100
O_2, electron backscattering coeffs., 100 eV to 5 keV 80−9750
O_2, electron impact ionisation, metastable state mol. ion form. 77−14594
O_2, electron impact ionisation, in RF ion source, effective cross-sections 78−22034
O_2, ionisation by electron bombard., empirical and semi-empirical calcs. 79−36784
O_2, K-shell, excitation and ionisation, vibr. struct., electron energy loss spectra obs. 80−18943
O_2, low energy electron impact dissociative ionis., O^{2+} form. and energy distrib. 80−5626
O_2, mean energy expended per ion pair, Fowler eqn. compared with CSDA approx. 78−74777
O_2^+, electron impact excitation, ionisation, rel. to auroral spectral intensities 79−84563
OCS, electron impact excitation and ionisation 80−63837
OCS, electron scatt., absolute total cross-section meas. 78−74774
PH_3, bonding by electron impact coincidence expt. 77−65536
Rb_2^+, form. by electron impact in elec. discharge, low-press. vap. 79−10738
SF_6 electron scatt., total absolute cross sections, 0.5-100 eV, incl. reson. struct. 79−45843
SF_6, ionic fragmentation after S 2p shell electron impact ionis. 78−90310
SF_6, pure and mixtures, dielec. props., ionisation and attachment coeffs. 80−33726
SF_6^-, electron impact, nearly zero energy, probability ratio meas. 79−72433
SF_6-N_2 mixture, electron swarm development, Boltzman eqn. anal. 80−87841
SO_2XY, (X,Y=Cl,F), positive and negative ion chemistry 78−85140
SnX_4 (X=Br, Cl, I) electron impact dissoc.-electron capture, ionis. efficiency curves 77−61865
$TiO_{(g)}$, $TiO_{2(g)}$, ionisation pot. determ. 77−16857
TlBr, electron impact dissoc. ionis., Tl electron affinity meas. *(French)* 80−63849
TlI, electron impact dissoc. ionis., Tl electron affinity meas. *(French)* 80−63849
$UF_6+e^-(K)(Na)(Cs)$, positive and negative ion formation, electron affinity, bond dissoc. energy 77−75314
WF_6, electron impact, negative ion form., mass spectra *(German)* 77−88586
XeF_6, monomeric charact., electron ionisation mass spectra 77−75322
$Xe^{2+}(Xe^{3+})(Xe^{4+})(Xe^{5+})$, molecular electron impact ionisation 80−102582
Yb_2O_3, M-series soft X-ray appearance pot. spectroscopy 79−54866

molecular electron scattering *see elastic scattering of electrons by atoms and molecules; molecular electron impact dissociation; molecular electron impact excitation; molecular electron impact ionisation*

molecular electronic states
see also charge transfer states; molecular metastable states; triplet state
$^2\Pi$ state, of linear diat. mol., vibronic-spin-orbit interaction, Renner effect 78−70758
$\pi\pi^*$ and $n\pi^*$ states, rel. positions, single-triplet conversion probability, low temp. 79−816
$\pi\pi^*$ and $n\pi^*$ states relative position, optical props., singlet-triplet conversion processes 79−3484
π electron Hamiltonian, ab initio derivation by nonperturbative open shell formalism 78−21846
π-electron total energy, approx. topological formulae 77−38603
A_2B_{2N} mols. and ions, strengths of A-A single bonds symmetries 78−74790
ab initio CI pot. curves, mol. wavefunctions and vibr. freqs. comparison of methods 80−27956

molecular electronic states continued
acetaldehyde+CO_2, vibr. relax., search for unquenchable species, room temp., 5-2200 torr 78−9229
acetone, ab initio CI valence and Rydberg states, spectral assignments 77−14346
acetophenone enolate anion radicals, substituted, electron photodetachment cross sections, reson. states 80−1030
N-acetyle DL-methionine, γ-irradiated, radical cation EPR, ^{33}S hyperfine coupling 77−40559
acetylene, and $C_2H_2^+$, ionis. pots., photoelectron spectra, ab initio VB calcs. 77−88396
acetylene, chemisorbed on metal surfaces, geometric and electronic struct., UPS obs. and HF LCAO calc. 79−86988
acetylene, effective core potential calcs. 79−31437
acetylene, electron density distrib., electron correl. effects, approx. HF-CI calcs. *(German)* 78−33439
acetylene, excited state, photochem. and spectrosc. investig. 80−95553
acetylene, higher excited states, electron energy loss spectra 80−91664
acetylene, ionis. efficiency curves by electron impact, $CH_2^+(C_2H^+)$ form., ~10 eV 78−62935
acetylene, vibr. fine struct. accompanying core ionis., STO calcs. 78−62844
acetylene ($-d_1,d_2$), and isotopic forms high resolution absorption spectra, Renner-Teller interactions 79−72332
N-acetylglycine, X-irrad., stable radical electronic and mol. struct., ENDOR and ESR 80−80637
activated complexes, exp. obs., bonding MO LCAO states 80−76506
adenine, hydroxy and methoxy derivatives, absorption UV spectroscopy and electronic struct. of ionic and tautomeric forms 80−74177
adenine, tautomers, polarisation, barriers and tunneling times calcs. 79−41114
adenine, UV photoelectron spectra, valence electronic struct. 77−16905
adenine tautomers, relative stabilities, nonempirical MO calcs. 80−21442
adiabatic correction for nonlinear triatomic molecules: techniques and calculations 78−62735
aggregates, optical spectra, near strong coupling limit, Green's function model 77−83774
alkali + inert gas molecule, far wing line broadening, quasistatic theory 79−22762
alkali bromides, photofragment spectra, 266 nm, bond energies and excited state symmetries 80−53072
alkali hydrides, ionic-covalent config. mixing, pot. curves 77−34576
alkali iodides, photofragment spectra, bond energies and excited state symmetries 80−5589
alkali metal chlorides, photofragment spectra, bond energies and excited state symmetries 80−87190
alkali metal diatomic system, three states nonadiabatic coupling calcs. 77−57896
alkali metal dimers, $^1\Sigma_g^+$ ground state, density functional theory 78−37573
alkali metal halides, Born-Mayer repulsive parameters, overlap parameters, free ion electronic charge densities 79−98179
alkaline earth dimens., heteronuclear, matrix-isolated, laser photoluminesc., van der Waals ground state 79−41192
alkanes, linear, K-shell ion relax. energy chain length depend. 79−72252
n-alkanes, mol. Rydberg S←S and S←T transitions, semi-empirical SCF MO calc. 80−91453
alkanes, polycyclic, three-photon ionisation spectra, 3s Rydberg orbital 79−68282
alkyl benzenes, jet-cooled, vibr. relax., nanosecond time evolution 80−95584
alkyl cadmium, valence and core electron energies, photoelectron spectra, ab initio calc. 78−25613
alkyl iodide+K, collisional electronic excitation, time-of-flight obs. 79−86049
alkyl silanes, far UV and He I photoelectron spectra 79−18204
alkynoyl cations, struct., charge distrib., ab initio population anal. calcs. 80−58407
1H-alloxazine, and derivatives electronic struct., photoelectron spectrosc. and ab initio study 80−106261
allyl-radical, pi-electron system, appl. of UHF Green's function method 77−61684
alternant hydrocarbons, approx. calc. by spin-extended HF method 79−26889
amide C-N bond character, metal ion bonding effects 77−6801
amino acid methyl esters, photoelectron spectrosc. 79−24954
1-aminopyrene, protonated, excited state proton dissoc., time-resolved spectrosc. obs. 79−50164
aniline, vacuum UV electrochromism studies rel. to dipole moment changes 77−50562
annulenes, MINDO calcs., electron correlations 79−45636
anthracene, excited states calc., unrestricted HF theory in PPP approx. 77−50377
anthracene, Raman intensities rel. to vibronic coupling and excited electron state geometries 77−27075
antisymmetric light scattering of molecules with non-degenerate electronic state 79−18192
approximate and exact state wavefunctions, ionisation potentials, energy difference calcs. 79−97967
aromatic compounds, electrophilic substitution sites, perturbation theory calcs. 77−30800
aromatic compounds, intersystem crossing theory, El-Sayed rule extension, anomalous rate consts. 77−30911
aromatic compounds, mol. rearrangement in excited electronic state, fluoresc. with anomalously large Stokes shift 79−85983
aromatic hydrocarbon derivatives, low-temp. singlet-triplet conversion probability rel. to optical parameters 79−54898
aromatic hydrocarbon in soln., excited electronic state vibr. relax., time resolved fluoresc. 80−48024
aromatic hydrocarbons, kata-annellated, para band energy-topology empirical correlations *(German)* 79−13657
aromatic hydrocarbons, sequential coupling 80−58297
aromatic hydrocarbons, singlet-triplet conversion at low temp. 80−43094
aromatic hydrocarbons with condensed nuclei, ring current calcs. *(Chinese)* 79−93916
aromatic impurity molecule, internal conversion processes 78−82776
aromatic nitroso compounds, fluoresc. from upper singlet 79−6958
aromatic radical ion recomb., mag. field modulation, Liouville eqn. soln. 77−28995
aromatic ring ompounds adsorbed on Al-AlO_x-Pb and Mg-MgO-Pb, inelastic electron tunnelling 79−59521

molecular electronic states continued
1-arylbutadienes, lowest excited singlet states, photochemical implications 77−30795
asymmetric top molecules, doublet-quartet transitions, rot. selection rules 78−94186
atomic potentials, transferable, new general methodology 79−45624
azaaromatics, neutral and protonated, excited singlet and triplet states, charge densities, INDO calcs. 80−58152
azacyclobutadienes, conjugated mols. electronic struct. and geometry, Hartree-Fock instability 80−69055
aziridines, substituted, ^{14}N NQR, electron distribs. 77−3385
1-azo-bicyclo-2,2,2-octane, multiphoton ionis. spectra polaris. characts., two-photon symmetry assignment 78−74718
azobenzene, derivatives, photoelectron spectra, ionisation pot., electronic struct. determ. 80−1024
azobenzene, emission from $^1(n,\pi^*)$ state, spectrum and ultrashort decay time 77−30895
azulene, soln., laser-excited $S_2 \rightarrow S_1$, $S_1 \rightarrow S_0$ emission and $S_2 \rightarrow S_n$ absorption 79−10131
azulene in cyclohexane, relax. time of first excited electronic singlet state 77−6825
azulenes, substituted, internal conversion, energy gap correl. 79−54901
azuleno[5,6,7-cd]phenalene, slow internal conversion between close lying singlet state 77−30907
bacteriochlorophyll, π-electronic struct., ASMO-SCF-CI calc. 77−36868
bacteriopheophytin, π-electronic struct., ASMO-SCF-CI calc. 77−36868
bases, K^+ affinities ab initio SCF calc. 78−58585
benzaldehydes, in mixed cryst., T_1/T_2 interstate interactions, modulation polaris. phosphoresc. spectra, 4.2K 78−9185
1,2-benzanthracene, secondary reson. radiation and hot energy transfer, soln. luminesc. 80−87167
benzene, 50000 cm^{-1} band, electron impact study 79−86075
benzene, $^1B_{1u}$ state, vibronic mag. rot. strengths and oscill. strengths, CNDO/S calcs. 77−34670
benzene, π electron system, excitation energy, appl. of MBPT 80−52876
benzene, π-electron approxs. *(Russian)* 77−42244
benzene, and $-d_6$, $^1B_{2u}$ excited state, force field, normal coords. 78−5193
benzene, and methyl derivatives, $^1E_{1u}$ N-V state mag. moments, MCD obs. 80−23575
benzene, dynamic polarisabilities, calcs., superposition method of excited config., nonstationary perturbation theory eqns. 80−69257
benzene, elec. dipole forbidden states, high resolution electron impact obs. 80−43195
benzene, electronic struct., mag. susceptibilities, ab initio calcs. 78−74571
benzene, excitation spectra, cluster configuration method appl. 80−78546
benzene, excited electronic states, variable angle electron impact spectroscopy 78−13612
benzene, excited state props., by electrochromism in polymer matrix 79−22737
benzene, Jahn-Teller active states, vibronic struct., vibr. perturbation, spectral obs. 78−13440
benzene, location of $^1B_{2u}$, $^1B_{1u}$, $^1E_{2g}$ states, from two-photon spectra 77−30940
benzene, multiphoton ionis. spectra polaris. characts., two-photon symmetry assignment 78−74718
benzene, photoelectron spectra ang. distrib., π- and σ-orbital assignments 79−818
benzene, protonated, electronic struct., SCF MO LCAO calcs. 78−82638
benzene, solid, electronic struct., XPS 77−73213
benzene, variable angle electron impact energy loss spectra 79−68321
benzene ($^1B_{2u}(S_1)$)+Ar(benzene), rot. relax. to Boltzmann distrib. 78−86936
benzene (S_1)+OCS, V-V reson. energy transfer, microscopic reversibility, level degeneracies role 79−86045
benzene derivatives, atomic localisation of electronic excitation 77−18806
benzene-d_0, $-d_6$, electronic relax., absorpt. spectra 77−75129
benzene-d_6, splitting of vibrationless level in Jahn-Teller active state of D_{2h} symmetry 77−58080
benzene-Dewar benzene, lower excited states pot. energy surfaces for isomerisation 80−104429
benzenes, substituted, electronic struct., ab initio calcs., photoelectron spectra 80−58314
benzenetricarbonylchromium, neutron inelastic scatt. spectrum and valence force field 80−48096
benzonitrile, excited single state B_1, electron-vibr. spectra and electronic struct. 79−26904
benzophenone, $^3(n\pi^*)$, carbonyl ^{13}C hyperfine coupling tensor, ENDOR obs. 79−13744
p-benzoquinone, electronic struct., CNDO/S calcs. 78−70754
p-benzoquinone($-d_4$), n-π* excited states, distant intramol. interaction between identical chromophores 78−90203
benzothiazole, and homologues electronic struct., photoelectron spectra and MO calcs. *(French)* 79−31598
biacetyl, lower excited electronic states, ab initio SCF and CI calcs., absorption band assignment 78−74589
bimolecular reaction, partly diffusion-controlled, physical and chem. kinetics competition 79−43567
bimolecular reaction, partly diffusion-controlled, physical and chem. kinetics competition 79−43566
1,1′binaphthyl, electronic struct., fluoresc. CNDO/S CI calcs. 78−90084
1,1′-binaphthyl mononegative ion conformation 77−30774
biologically active molecules, photoelectron spectrosc. 79−24954
biphenyl, lowest excited singlet states, polyexcited CI calc. 79−772
biphenyl crystals, electronic and vib. states, cryst. field mixing, two-photon spectra 77−59603
biphenyl glutarate polymer, resonant Raman spectra and fluoresc. 77−24830
biphenyl gluterate diacetylene, monomer, single cryst., stable and metastable UV photoexcited states, EPR obs. 79−78522
biphenylene, fluoresc. from higher singlet levels 79−83473
tris(2,2′-bipyridine) ruthenium(II) cation, IR-optical double reson. and thermal modulation spectra 78−25576
Bohr's 1913 atomic theory, chem. aspects 77−67170
bond contributions to electronic energies, ab initio STO 3G calcs. 77−6669
book, electron theory of small mols. 77−57848
Born-Oppenheimer and true eigenstate prep. by coherent light, large mol. nonradiative relax. 77−88490

molecular electronic states continued
Born-Oppenheimer approx., perturbation theory 77−26988
Born-Oppenheimer approximation, validity 77−23440
bound and quasi-bound states in continuum 77−14329
broadening, inhomogeneous and homogeneous, of optical and ODMR transitions in solids 80−32750
bromobenzene, photoelectron spectra ang. distrib., π- and σ-orbital assignments 79−818
p-bromochlorobenzene, T_1 states, zero-field ODMR, MIDP and phosphorescence excitation spectra 80−74191
p-bromofluorobenzene, UV electronic absorption spectrum, band shape and molecular geometry 80−87147
trans-butadiene, $^1B_{1u}$-state dynamics in cooled supersonic expansion, electronic absorpt. spectra obs. 80−78629
trans-butadiene, all-valence-electron CI calcs. of electronic spectrum 77−10654
butadiene, cis- and trans-, appl. of spin-free CI procedure using alternant MOs 79−85887
butadiene, excitation spectra, cluster configuration method appl. 80−78546
1,3-butadiene, excited singlet states, vibronic struct., electron impact energy loss spectra, 35-90 eV 78−62932
trans-1,3-butadiene, multiphoton ionis. spectra polaris. characts., two-photon symmetry assignment 78−74718
s-cis-butadiene, natural orbitals, photochem. cyclisation 79−85900
butadiene, twisted zwitterionic excited states, SCF calcs. 80−58179
trans-1,3-butadiene, valence electronic excited states, SCF ab initio GVB and CI calcs. 79−31423
butadiene chromophores, cis- and trans- (α- and β-phellandrene) absorpt. and CD spectra 78−62834
butadiene-acrylonitrile copolymer, electronic struct., reactivity, SCF CNDO calc. 77−50580
1-butene oxide, gas, microwave spectrum 79−13703
1-butyne, and propyne, electron impact spectra, comparison with acetylene 79−3585
camphorquinone, cryst., PMDR and fluoresc., S_2 state, intersystem crossing 77−32296
camphorquinone, vapour, nonradiative electronic relax. rate, excess energy depend. 77−38687
carbenes, heterosubstituted, singlet-triplet splitting depend. on heteroatom electronegativity and conform. 80−63553
carbonyl compounds, localisation of nπ* excitation, config. interaction method 78−50482
carbonyl fluoride, vertical electronic states, ab initio SCF CI calc. 79−49942
carbonyl halogen substituted cpds., geometric and electronic struct., LCAO-SCF calc. 79−89603
β-carotene, excitation profile of ν_2 line in resonance Raman spectrum, solvent effects 80−74173
carotenoids related to visual chromophore, electronic struct., band shape model 78−20142
charge density, Bethe surfaces, Compton profile via (e,e′) reactions at 20-40 keV 77−88560
chemically induced magnetic polarization by $S\text{-}T_{\pm1}$ mixing in strong mag. field 80−83515
Chichibabin's hydrocarbon, ESR spectra, electron exchange integral 78−50562
chiral molecules, prochiral centres, electronic and structural chirality 80−30220
chlorobenzene, photoelectron spectra ang. distrib., π- and σ-orbital assignments 79−818
chloroethane molecular ion, laser induced photodissoc. in gas phase 79−94048
chlorofluoromethanes, valence photoelectron spectra, electronic and vibr. bands 78−50582
chlorophyll photo-oxidation, role of singlet-excited and triplet states 80−51156
chlorophyll-a, laser action and excited singlet state absorpt. 77−27288
chlorophyll-a, monochromatic excitation, luminesc. spectra, quasilinear struct. *(Russian)* 78−74809
chlorophyll-a, triplet and excited singlet optical absorpt. spectra 79−59477
chlorophylls a and b, photo-oxidation primary processes 79−79468
cholesteryl chloride, binary mixtures with cholesteryl benzoate and β-halogeno cholesteryl alkanoates, reciprocal helical pitch 79−90528
chrysene, excited electronic state, CARS obs. 79−31514
chrysene, excited singlet and triplet state, CARS obs. 80−83374
classical many-body collision model incorporating Heisenberg and Pauli principles 80−63511
closed shell system excitation function, response function approach in multiple cluster expansion formalism 79−72293
closed-shell systems, quadruply excited states, fourth order terms, perturbation theory calcs. 79−22582
closely coupled electronic states, vibronic level calcs. using derived anharmonic pots. 77−23423
cluster systems, program for calc. electronic struct. with double self-consistency-Bersuker's method 80−69289
$Co_4Sb_4(CO)_{12}$, electronic struct. calc. *(Russian)* 80−58136
CO, in glow flow discharge, electronic states, excitation mechanism 80−53040
Combination of Atomic Boxes MO model, development and testing 80−32592
completeness theorem for operator spaces 77−34536
complex anion electronic struct., outer sphere cation effects, X-ray fluoresc. spectra 78−86884
complex molecules, π-electron pair correl. of supercond. type, appl. to optical and mag. props. 79−54778
complex molecules appl. to electronics, liquid crystals and plastics 80−6355
conformational props. rel. to spatial electron density determs., computer simulations 78−70763
conformers, dynamic interaction between ground states, effect on IR spectra 78−58767
conjugate systems, atomic localisation of electronic excitation 77−18806
conjugated circuits, correl. with Kekule valence structures 79−89582
conjugated cpds., aromaticity determ. by topological reson. energy method 80−42915
conjugated heterocycles with single heteroatom, stability, graph theoret. approach 77−38604
conjugated molecule, charge distrib. calcs., refinement by exptl. quadrupole moments 77−3258

molecular electronic states continued
conjugated molecule diamagnetic anisotropy, graphical anal. 79−76360
conjugated molecules, alternant, with one heteroatom, stability, graph theory calcs. 77−3253
conjugated molecules, excited state, self-consistent HMO theory *(Japanese)* 77−42253
conjugated molecules, linear and mag. cir. dichroism interpretation 78−62835
conjugated systems, symmetry-depend. rules 79−89592
core-hole processes, electronic Hamiltonian, many-body theory 80−91443
correlated electron motion and (ħω,2e) reactions, Green's function methods 77−88431
coumarin 102, excited state interaction dynamics, picosec. time-resolved spectral shift obs. 80−78624
coumarin 6, ultrashort vib. population lifetime of ground state in vapour phase 77−30929
cyanine dyes, excited electronic states, CNDO/S CI calc., visual pigment spectra appl. 80−85333
p-cyano-N,N-dimethylaniline in polar solvents, double fluorescence, theoretical model 80−58296
6-cyanobenzquinuclidine, intramol. electron-transfer excited state 80−58295
cyanogen fluoride, fund., hot bands, laser microwave two photon and double reson. spectroscopy 80−32752
cyanomethyl radical, electronic struct. and props. 79−49938
cyclic 3- and 4-membered ring cpds., saturated, ab initio struct. anal. 80−58192
cyclic ketones, electrochromism and electric dichroism for studying transitions to second excited singlet 80−63692
cyclic molecules, localised electronic vacancies lifetimes 80−106264
cyclobutadiene($-d_1$), singlet and triplet ground states, vibr. freqs., MINDO/3 and ab initio SCF calcs. 78−13429
cyclobutenedione derivatives, photoelectron spectra, 2p lone pair delocalisation 78−46392
1,3,5-cycloheptatriene, singlet→singlet (triplet) excitation, electron impact energy loss spectra 78−46451
1,4-cyclohexadiene, excited electronic states, electron impact spectrosc. 79−45842
cyclohexane, excited electronic states, electron impact spectrosc. 79−45842
cyclohexane, liq., ps time-resolved energy transfer, ultra-fast process, ps single pulse radiolysis 79−79267
cyclopropane, IR spectra studied by tunable laser, $\nu_{10}+\nu_{11}$ band anal. 80−95615
cytosine, hydroxy and methoxy, derivatives, absorption UV spectroscopy and electronic struct. of ionic and tautomeric forms 80−74177
d-orbital basis functions role in electronic struct. description of systems containing Si, P, S and Cl 80−9484
decacyclene anion, photoexcited quartet state, transient EPR 80−78635
degenerate electron states, electron interaction with doubly degenerate vibr., optical transitions, semiclassical approx. 80−27927
delocalisation, organic chemistry courses 78−4426
delocalisation, static and dynamical aspects 77−30761
delocalisation, statistical and stochastic aspects 77−30759
delocalisation, statistical and stochastic aspects 77−30760
density functional calculations for atoms, molecules and clusters 80−47850
deoxyhaeme model, semiempirical calcs., EM props. rel. to electronic config. and Fe-plane distance 78−53324
deoxyhaemoglobin, ferrous heme of high-spin type, MCD spectra in Soret, visible and near IR regions 80−94156
deoxyhaemoglobin, porphin-Fe-imidazole system, SCF-LCAO-ASMO and CI calcs. of low-lying multiplets and excited states 80−94155
diabatic molecular states, definition basis set calcs. 79−97969
diabatic representation of one-dimens. diatomic mols. 80−23285
s-cis, s-trans-diallyl, twisted, low-lying singlet states, sudden polarisation effect 78−86792
diatomic $^1\Delta$ states, corrections to effective orbital g-factor 79−7036
diatomic fragments, from triatomic mol. photodissoc., fluoresc. polarisation excitation spectroscopy 80−28054
diatomic hydrides, quantum mechanically calculated observables, reliability determ. 80−63505
diatomic isovalent systems, pot. curves, ab initio MRD-CI method 80−83293
diatomic mol., vibr. rot. Hamiltonian expansion, Born Oppenheimer κ, explicit introduction 80−69118
diatomic mol., X-ray scatt. intensities, vibr. averaging 78−74722
diatomic molecule, electron static interaction potl., computation 77−3255
diatomic molecule, electronic states calc. using five-parameter pot. function *(Russian)* 77−3270
diatomic molecule, ground state, opt. prod. and orientation, review *(Russian)* 79−27046
diatomic molecule, homonuclear, modified simple bond charge model 79−89595
diatomic molecule, overtone intensities in reson. Raman scatt. 80−48001
diatomic molecule, quartet and quintet transitions branches, intensity distrib., rel. to Hund's rule 78−90216
diatomic molecule, rot.-vibr. hamiltonian, Born-Oppenheimer approx. breakdown 77−27051
diatomic molecule, sextet transition branches, intensity distrib., rel. to Hund's rule 78−86913
diatomic molecules, and ions, internal partition function calc. 78−55159
diatomic molecules, compactness proof for infinite systems of linear equations 79−72247
diatomic molecules, electronic states excitation, atom promotion, ab initio calcs. 78−86772
diatomic molecules, excitation energies, oscillator strengths, many body approach, eqns. of motion method 80−47969
diatomic molecules, excited states, electronic transition probabilities and lifetimes, review 80−78658
diatomic molecules, Fues pot., electronic energy partitioning 77−61674
diatomic molecules, ground, excited and ionic states, energy rels. 78−78606
diatomic molecules, laser-induced predissoc., surface mag. field effect 80−106365
diatomic molecules, modified pot. energy functions from normalised kinetic field functions 79−838
diatomic molecules, optically pumped lasers, review 80−58519
diatomic molecules, polarisabilities and dipole moment derivatives, virial theorem calcs. 77−57865

molecular electronic states continued
diatomic molecules, rotational Raman intensities and polarisability anisotropy change meas. with internuclear distance 80−63641
diatomic molecules, shortening of energy relax. time of excited mol. vibr. in dense medium by form. of H-bonds 80−91553
diatomic mols., doublet states, spin-orbit and spin-rot. coupling cals., isotope depend. 77−57902
diatomic mols., electronegativity, bond charge and chemical pot. approach 80−91703
diatomic systems, interactions, long-range dipoles, quadrupoles and hyperpolarisabilities 80−53161
diatomics, spin coupled theory of mol. wavefunctions, struct. and props. 77−50337
diatonic molecules, Stark effect variational and perturbational calcs. 80−1022
p-dibromobenzene, T_1 states, zero-field ODMR, MIDP and phosphorescence excitation spectra 80−74191
trans-dibromoethylene, VUV and photoelectron spectra, Rydberg series, vibr. fine struct. 77−6799
dibromoethylenes, vac. UV spectra 77−23507
diene-iron tricarbonyl complexes, π-orbital perturbation energies, ionisation energies; UV photoelectron spectra 80−32775
diethyl cadmium, core d-level high resolution photoelectron spectra, spin-orbit splitting 78−50579
p-difluorobenzene, electronic struct., many-body calc., photoelectron spectrum assignment 77−23421
S_1p-difluorobenzene, time resolved fluoresc. spectra, direct view of intramolecular vibr. redistribution 80−83341
difluorodiacetylene radical cation, $\tilde{A}$-$\tilde{X}$ band emission spectra, $\tilde{A}$ state lifetime 79−72327
difluoroethene, cis- and trans-, photoelectron-photoion coincidence study, fluoresc. obs. 80−95678
diformamide, excited singlet and triplet states, CNDO-CI calcs. 77−26990
dihalodiacetylene radical cations, $A^2\Pi_u$-$X^2\Pi_y$ system, emission spectra and state lifetime 79−10121
dihydroquinoxalinediones, conjugated mols. electronic struct. and geometry, Hartree-Fock instability 80−69055
dihydroxycarbene, singlet and triplet state rot. pot. surfaces 80−32627
dimers, bandshape prediction, incoherent exciton scatt. model 78−42132
dimers of Group IIA, low-lying states binding energy, local spin density functional formalism calcs. 79−97994
dimethyl cadmium, core d-level high resolution photoelectron spectra, spin-orbit splitting 78−50579
dimethyl ether, review of microwave spectrum, tabulated data 80−51965
dimethyl mercury, high resolution photoelectron spectra, 5d orbital energy ordering reassignment 78−74700
dimethyl sulphide dimerisation, S lone pair nonbonded contacts, EH, MINDO/3, CNDO/2 calcs. 79−773
dimethyl zinc, core level photoelectron spectra, electric field gradient splittings 77−88494
dimethyl zinc, valence band and Zn 3d levels, electric field gradients 77−88495
6,6′-dimethyloxyindigo, picosec. kinetics, and photostability, spectrosc. obs. 79−45748
9,10-diphenyl anthracene, cyclohexane soln., solute excited state form. kinetics in pulse radiolysis 79−79263
3,6-diphenyl-pyridazine, valence electronic structure 79−72360
3,6-diphenyl-s-tetrazine, valence electronic structure 79−72360
diphenylhexatriene, low-energy ^1A_g state obs., by two-photon matrix spectroscopy 78−74715
1,6-diphenylhexatriene, lower excited states fluoresc. quenching 80−1016
diphenylhexatriene, two-photon excitation of low-energy excited states 77−14507
diphenyloctatetraene, two photon excitation of low-energy excited states 77−14507
diphenyloctatetraene, two-photon spectra, ^1A_g state confirmation 78−17736
diphenylpolyene molecules, excited electronic states, vibronic mixing, wave functions, method of fragments anal. 80−63615
DODCI in ethanol, DQOCI added, electronic energy transfer, real-time ps meas. 80−58311
DODCI in ethanol, malachite green added, electronic energy transfer, real-time ps meas. 80−58311
donor-acceptor pairs, electron transfer, theory 80−27918
doublet state, ionis. pots., electron affinities, using electron propagator, appl. to Li, Na, and BeH 79−63933
doubly resonant three-photon spectroscopy, appls. 79−71534
DSO, radical, electronic spectrum and struct. 77−75147
(e,2e) molecular knockout reactions via electronic struct. calcs., Green's function methods 77−88577
eigenvalue sum rel. to total SCF energy for ats. and mols. 79−9993
electric dipole allowed transitions, long-range dispersion-induced circular dichroism 79−81196
electrocyclic isomerisation of ground state induced by IR laser multiphoton absorpt. 77−32811
electron coincidence spectroscopy, orbital shape, charge density, mol. struct. determ. appls. 79−27113
electron density calcs., computer program, appl. 78−70742
electron density determination from inelastic scattering of fast electrons 77−58189
electron density mapping in mols., cyrsts., conf., Rehovot, Israel, (Apr. 1977) 78−71622
p-electron density matrix, spin-tensorial components, geometric consequences 79−84986
electron density studies, quantum chem., basic concepts 78−70731
electron distribution anal. ab initio calcs. 80−47866
14-electron isoelectronic series, ab initio calcs., equilib. geometry and electronic struct. 77−83489
electron momentum densities, expt. determ., review 77−76776
electron momentum densities, theory, review 77−75039
π-electron systems, excitation spectra, cluster configuration method appl. 80−78546
electron theory, empirical, for solids and molecules *(Chinese)* 79−15061
electronic and at. collisions, conference, Kyoto, Japan (Aug.-Sept. 1979) 80−62394
electronic degrees of freedom, classical models 80−63507
electronic excitation functions by low electron impact spectroscopy, trapped electron restrictions 80−69184
electronic excitation of mols., charge transfer and localisation 79−41119
electronic excitations, degree of collectivity 78−37570

molecular electronic states continued
electronic spin orbit interaction, molecular Aharonov-Bohm effect 80−83303
electronic structure calculations by fast accurate kinetic-energy method 80−83257
electronic structure theory, 1972-75 review, book contrib. 77−38595
EM field effects, strong, review 79−49955
energy component hypersurfaces, local behaviour regularities 77−42256
energy gradient, ab initio HF program 79−89606
Epstein-Nesbet partitioning of full Hamiltonian, second-quantisation representation 77−3254
equations of motion, Green's function methods and config. interaction methods, comparison, appl. and anal. 80−47841
ethane$^+$, stability and struct., CI-SCF ab initio calc., Franck Condon anal. 77−54575
ethane, (e,2e) spectroscopic obs., valence electron momentum distribs. and separation energies 77−3480
ethane, effective core potential calcs. 79−31437
ethane, electron impact dissoc., absolute total cross section, 10-600 eV 79−36781
ethane, photoionisation spectra, cond. hole model 80−58326
ethane cation, relative stability of $^2A_{1g}$, ^2E_g states 80−58140
ethanol, conformational anal., barriers of internal rotation, electronic structure 79−63916
ethanol, conformational analysis and electronic structure 78−33429
ethanol, ion internal energy selection by angle-resolved mass spectrometry 80−53164
ethylene, $\pi\pi^*$ singlet state, using general CI method 79−36539
ethylene, and radical ion, SCF-MO calc., bonding and electronic struct. 77−38610
ethylene, C atom pyramidalisation rel. to bonding, ab initio SCF calcs. 79−93936
ethylene, chemisorbed on metal surfaces, geometric and electronic struct., UPS obs. and HF LCAO calc. 79−86988
ethylene, effective core potential calcs. 79−31437
ethylene, electron energy loss spectrum, intensity distrib. 79−64110
ethylene, electronic states, optical rot. dispersion, oscill. strength calcs. 78−9095
ethylene, electronic struct., CNDO/S2 calc., photoelectron and UV absorpt. spectra 77−30783
ethylene, excited states, spectral assignments 79−85915
ethylene, excited states, V←N spectrum 77−50446
ethylene, planar $^1(\pi,\pi^*)$ state, CI calcs. 77−57887
ethylene, planar dissociation, electronic rearrangement, states, bonds, ab initio multiconfigurational SCF calcs. 80−27937
ethylene, pot. energy and dipole moment surfaces, polarisation effect, ab initio CI calcs. 80−106272
ethylene, quasidegeneracy and effective Hamiltonians, canonical transformation cluster expansion formalism 80−52888
ethylene, singlet Rydberg states, CI calcs. 78−33437
ethylene, twisted, intervalence charge transfer and reson., sudden polarisation effect 80−69230
ethylene, V-state config. selection methods 79−10041
ethylene, valence states, effective Hamiltonian from canonical transformation 80−74130
ethylene, vertical, $N(^1A_g)$, $T(^3B_{1u})$, $V(^1B_{1u})$ states, large scale CI calc. 78−70752
ethylene($-d_4$), Rydberg states assignments, electron energy loss specta 80−53153
ethylene as singlet methylene dimer, nonempirical double zeta calculations, zwitterionic singlet excited states 80−83258
ethylene cation, state geometries, electronic vibr. coupling consts., HF calcs., comparison with Xalpha calcs. 80−27946
ethylene oxide derivatives, substituents effect on electronic state of epoxide ring, CNDO/2 calcs. 79−26891
ethylene radical cation, electronic states assignments, ab initio SCF CI calcs. 77−10584
ethylene V state, ab initio study of spatial extension 80−27952
ethyleneoxide, elec. dipole moment, g-values, mag. susceptibility, moments and charge distrib. 77−58077
ethylenes, substituted, unstable twisted forms, excited states, DODS-NO CI calcs. 79−13643
ethyne, electron energy loss spectra, excited states investig., electron impact spectrometer 78−25756
ethynyl radical, vertical electronic spectrum, CI calcs. 77−34656
excimer laser, electronic structure, pot. energy curves, radiative transition probabilities, quantum mech. calcs. 79−10284
excimer systems, electronic structure and radiative transitions, book contrib. 79−81416
excitation energies calc., using renormalised Green's function method *(Japanese)* 80−83295
excitation energy, eqn. of motion method calcs., approxs. and error anal. 79−36501
excitation energy, validity of excited minus ground state calcs. using HF/pair correlation 77−38620
excited electronic states, ultrashort T_1 and T_2 relax., reson. Raman spectrosc. obs. 79−36554
excited single state kinetics on a subnanosecond time-scale 79−36677
excited state dissociation, nonadiabatic interactions, conical and Jahn-Teller intersections, classical trajectory method 80−25997
excited state multiconfig. wavefunctions, selection of optimal configs. 77−34566
excited state natural lifetime determ. by fluoresc. light quenching 78−82775
excited state props., by electrochromism in polymer matrix 79−22737
excited state vibrational energy transfer, for optoacoustic spectroscopy 78−37724
excited states, absorption spectrum, diffusion rot. effects *(Russian)* 78−74641
excited states, generalised Brillouin theorem multiconfig. method 77−67993
excited states, interpretation charge-transfer numbers 80−78530
excited states, local approach calc. 79−49956
excited states, prod. by electron pulse radiolysis 79−50142
excited states, restricted SCF method calcs. 77−88405
excited states, SCF calcs. using Binkley-Pople-Dobosh formalism 77−6694
excited states, SCF wavefunctions 78−90099
excited states, variable metric optimisation of mol. geometry 80−58178
excited states of closed-shell systems, SCF scheme 79−6885

molecular electronic states continued
excited states time evolution in presence of nonadiabatic interactions 79−3379
exponential transformation, quadratically convergent SCF procedure, appl. to closed shell ground states 80−47875
f^N-electron system, paramag. principal susceptibilities, calcs. using ang. overlap model 77−32158
fast molecular ion+solid (gas), excited electronic states effects 80−9687
ferrocene, electronic struct., excited states, semiempirical PEEL MO calcs. 78−33431
ferrous nitrosylhaemoglobin, NO binding, spin distrib., orbital model and mag. props. 80−81534
ferrous porphyrin, intermediate (S=1) spin state, PMR characterisation 80−48014
few body methods in atomic and molecular structure calcs. 79−76330
filled shells symmetry 77−23400
first row atom-H molecules, ellipsoidal Gaussian basis in MO theory 79−93919
first-row diatomic molecules, bonding, spin density functional theory 78−17558
fixed-nuclei systems, electron transfer, propagator descriptions 79−97964
fluoranthene, in rigid glass, S_1 and S_2 fluoresc. 77−3403
fluoroacetylene, fund. and hot bands, laser microwave two-photon and double reson. spectroscopy 80−32752
fluorobenzene, multiphoton reson, ionis. spectrum, 51000 cm^{-1} assignment 79−86021
fluorobenzene, photoelectron spectra ang. distrib., π- and σ-orbital assignments 79−818
fluorobenzene, variable angle electron impact energy loss spectra 79−68321
fluorobenzene cations, fluoresc. quantum yields and lifetimes, electronic state relax. processes 80−48027
fluorobenzene radical cations in solid Ne, laser-induced fluoresc. spectra, vibr. struct. of excited and ground states 80−95671
fluorobenzenes, electronic struct., CNDO/S2 calc., photoelectron and UV absorpt. spectra 77−30783
fluorobenzenes, excited electronic states, variable angle electron impact spectroscopy 78−13612
fluorobenzenes, radical cations, $B(\pi^{-1})$ excited states, radiative relax. 78−13546
fluorophenol cations, emission and photoelectron spectra in gaseous phase 80−58316
fluorosilanes, far UV and He I photoelectron spectra 79−18204
fluorostyrene, UV Raman spectra, reson. effect in photoreactive states 80−106326
formadelhyde($-d_2$), S_1 rot. levels, collisionless nonradiative decay rates 79−72346
formaldehyde$^+$, excited state dissoc., nonadiabatic interactions, conical and Jahn-Teller intersections, classical trajectory method 80−25997
formaldehyde, $^3A_1$ and $^1A_1$ states, electrostatic mol. pot., basis set and wave function calcs. 79−10020
formaldehyde, electronic excited states, GO calcs., $\pi \rightarrow \pi^*$ transition 79−22616
formaldehyde, electronic states, oscill. strengths calcs. 78−9095
formaldehyde, electronic struct., dipole moments, mol. polarisability, force fields, ab initio calcs. 80−78531
formaldehyde, excited state photodecomp., rotationally resolved spectra 77−60088
formaldehyde, excited state vibr. freq. calcs. by method based on scaled ab initio force fields 80−87092
formaldehyde, ground and low lying excited states, CNDO/V^{N-1} method *(Russian)* 78−74576
formaldehyde, mag. rot. spectrum, A^1A_2 state, singlet-triplet perturbations 79−98126
formaldehyde, mol. Rydberg S_n←S and S_n←T transitions, semi-empirical SCF MO calc. 80−91453
formaldehyde, Rydberg states, excitation energies, oscillator strengths ab initio GVB-CI calcs. 77−54518
formaldehyde, sequential coupling 80−58297
formaldehyde, vibronic and spin-orbit coupling, radiative and non-radiative transitions 77−3414
formaldehyde, X^1A_1, a^3A'' and A^1A'' states, SCF and CI ab initio calcs. 79−36545
formaldehyde ($-d_1$,d_2), isotopic forms. vac. UV Rydberg spectra, vibr. assignments origin isotope effect 77−61763
formaldehyde in air, photodecomposition, CO and H_2 quantum yields 79−66311
formaldehyde-d_1, ν_5 and ν_6 vibr. excited states, microwave spectrum obs. 79−72304
formaldehydes, (deuterated), A^1A_2 state, photoluminesc. in low temp. matrices, vibr. relaxation 79−50070
formamide, $^1\pi\pi^*$ state, perturbation theory calcs. 78−62705
formic acid, H bonding, electronic struct., geometries, moments, dimerisation energies, charge distrib., pseudopotential calcs. 80−27942
formic acid, valence and Rydberg state empirically adjusted ab initio calcs. 77−10609
formyl chloride, rot. Zeeman effect of low-J transitions 78−25519
formyl radical, electronic struct., dissoc. energy and pot. energy surface many body perturbation theory and couple cluster doubles calc. 80−23296
formyl radical, lower electronic states, ab initio calc. of pot. energy surface, hydrocarbon flame band 79−68287
Franck-Condon factors, Wigner distrib. function 80−99520
free radical reactivity rel. to paramag. centre unpaired electron density 77−52633
fulminic acid-d_0, -d_1, rot. Zeeman effect and nucl. quadrupole coupling 78−78683
fulvene, ground and excited states, electronic correl. and struct. 79−26898
gas phase reaction consts. for electronically excited species, relax. processes, data tables 80−16644
glyoxal, $^1n\pi^*$ states, ab initio STO-3G CI calcs., ΔE_{SCF} transition energies 78−94194
glyoxal, singlet-triplet coupling, double reson. and level-anticrossing spectroscopy 80−48053
glyoxal, vapour, predissoc. in S_1 zero-point level states 80−102544
glyoxal-photoreduction-product-radicals, kinetics and intramol. dynamics 77−32808
ground state alkali molecules, mag. shielding and spin-rot. interaction 80−87186
ground state props., coupled cluster and MBPT methods appl. 80−47881

molecular electronic states continued
Group IIA hydrides and halides, ionic bonds 80−18789
guanine tautomers, relative stabilities, nonempirical MO calcs. 80−21442
haeme proteins, inversely polarized modes in reson. Raman scatt., depolarisation dispersion curves, vibronic interactions 78−78676
haemoglobin, deoxygenated, electronic term scheme using mag. susceptibility and Mossbauer data 77−44586
haemoglobin, dynamic characts. of conformational nonequilib. states, radiolysis investig. 78−58877
haemoproteins, highly oxidised Fe, electronic struct., Mossbauer spectroscopic obs. 77−88478
haloacetylene cations, electron impact excitation A→X band system assignment 80−32766
halobenzenes, singlet excited states decay, substituent effects 77−75175
halomethanes, C K-shell electron energy loss spectra, assignments 79−89797
halotoluenes, singlet excited states decay, substituent effects 77−75175
HAM/3, semiempirical MO calc. method 79−89587
Hartree problem, iterative diagonalisation soln. 79−6829
heavy ion+atom collisions, small impact parameters, K-vacancy prod., molecular theory 80−69229
heavy ion collisions, electronic states in rot. two-centre Coulomb systems 77−14561
heteroconjugated molecules, π-electron props., graph theory anal. 79−89586
heterocyclic conjugated compounds, electronic struct., spectra, ionisation pot., INDO-CI LACO-MO-SCF calcs. 79−54834
1,5-hexadiene, D-labelled, IR laser induced isomerization via electronic ground state 77−25289
hexafluoro ethyl cation fragmentation, mass spectrometry 80−53070
hexafluorobenzene anion, EPR obs. of struct. 77−58048
hexafluorocyclobutene, ground state, electrocyclic isomerisation of ground state induced by IR laser multiphoton absorpt. 77−32811
hexamethylbenzene, exciton band struct. for first singlet state 77−55483
hexatriene, excitation spectra, cluster configuration method appl. 80−78546
all-trans-1,3,5-hexatriene, excited electronic states calcs., spectra assignments 79−22606
1,3,5-hexatriene, two-photon spectra, failure to find low-lying excited ^1A state 77−79665
trans,trans-1,3,5-hexatriene, valence electronic excited states, SCF ab initio GVB and CI calcs. 79−31423
1,3,5-hexatriene radical cation, in Ne matrix, laser induced fluoresc. and emission spectra 80−87163
n-hexylamine-nickel di-acetylacetonate, ^{13}C nucl. spin relax., electron spin delocalisation 78−5248
high angular momentum Rydberg states, autoionisation rates calcs. 79−81163
high pressure effects on mol. electronic spectra 78−78754
high-resolution spectroscopy, quantum mech. description 77−6862
hole burning, photophysical and photochemical theories 80−58322
homonuclear coupled NMR spectra, pulses applied to multiplets, mutual coupling determ. 80−18873
Huckel rule, proof 77−30748
hydrocarbon ions, mass spectra, H atom scrambling, delocalisation 80−58135
hydrocarbon radicals, planar and nonplanar, g-factors, π-σ delocalisation 78−58580
hydrocarbons, associated, Electric dipole polarizability of molecules in excited electronic states 78−70966
hydrocarbons, Compton profiles, deviations from bond additivity, rel. to strain energy 79−81240
hydrocarbons, conjugated, heat of formation and reson. energies 80−7839
hydrocarbons, cyclic, non alternant, nonsingle instabilities of HF solns. 80−58164
hydrocarbons, IR intensities, polar tensors, atomic population densities 77−23497
hydrocarbons, mol. thermodynamics, information-theoretic aspects 78−13409
hydrocarbons, unsaturated, Penning electron and photoelectron spectra, relative intensities comparison 79−81237
β-hydroxy acrolein, lower excited states, electronic struct. and H-bonding, ab initio SCF and CI calcs., photochemical mechanism 80−83278
para-hydroxyaniline, mol. complex., electronic struct., basis set and correlation effects 80−91436
ortho-hydroxybenzophenone, soln., intramol. proton transfer and energy relax. photostability, transient absorption obs. 80−28032
imidazole, photoelectron spectra and electronic struct. 79−22758
incoherent resonance decay and coherent optical ringing from coherently prepared electronic states 77−10698
indigo, picosec. kinetics, and photostability, spectrosc. obs. 79−45748
indole, UV absorpt, spectra, low-lying Rydberg band 77−58037
inert gas dimer ions, electronic struct., chem. binding 79−31376
inert gas fluorides, covalent and ionic states, ab initio CI calcs. 78−78634
inert gas nuclear pumped lasers, prod. efficiency of excited states 80−63998
inert gases, (e,2e) reactions 200 to 2600 eV as probe of atomic and molecular struct. 77−88566
inner electron resonances in molecules, roles in ionisation *(French)* 78−82660
inner shell hole states calc. by generalised Brillouin theorem-multiconfig. method 77−23443
inorganic species, vibr. and electronic props., reson. Raman spectra appl. 80−52996
integrated spatial electron populations using projection function method 80−23299
inter-electron repulsion integrals for three open shell configurations in cubic symmetry 78−90061
intermediate states, far off-reson., temporal coherence in multiphoton absorpt. 78−50458
intramolecular dynamics, random coupling model, math. approach 80−58308
intramolecular dynamics, random coupling model, multiphoton excitation, kinetic eqns. 80−63700
iodobenzene, photoelectron spectra ang. distrib., π- and σ-orbital assignments 79−818
ion+molecule, electronic states, kinetic energy, molecular beams obs. 80−30230

molecular electronic states continued
ionisation and excitation energies, ΔE SCF, transition functional method 77−88404
ionised, localisation approach 77−30806
10H-isoalloxazine, and derivatives electronic struct., photoelectron spectrosc. and ab initio study 80−106261
isocyanic acid, molecular structure and centrifugal distortion constants 80−47974
isocyanomethyl radical, electronic struct. and props. 79−49938
isothiocyanic acid, $H^{15}NCS$, $HN^{13}CS$ and $HNC^{34}S$, ground state spect. constants and molecular struct. 80−47973
Kekule structure classification, partity concept evaluation 77−88366
lambda coupling in Π states of triplet or higher multiplicity 79−59429
lanthanide-porphyrin complexes, upper ππ* electronic states, fluoresc. 80−83410
large molecule, electronic struct., photoemission and optical absorpt. spectrum, CNDO/S3 model 80−53172
large molecules, excited state radiationless processes, time-resolved optoacoustic spectroscopy 78−89550
laser excitation of stationary molecular states, coupling of real eigenstates to phonons and photons 77−68084
laser techniques, vis. and UV, small mols., electronically excited states, book contrib. 78−9277
lifetime meas. in atoms, mols., ions 77−30832
ligand fields calcs., strong and intermediate fields, tensor algebra 80−42922
linear mols., π orbital electron energy contrib. to reaction heat 80−76539
linear triatomic molecule, photodissoc. dynamics, moment anal. 78−13557
lithium ethylene, SCF-MO calc., bonding and electronic struct. 77−38610
local density functional theory of atomic and mol. ground electronic states 80−23286
local-density theory of multiplet structure 80−18776
localisation in ionized and excited states, conf. 77−30750
localisation of nπ* excitation, config. interaction method 78−50482
loge theory and chemical reactivity 77−30758
lone pair localised MOs, energy contribs. and second moments in 10-electron hydrides 77−14341
long range mol., electronic and vibr. levels 78−94301
low-lying singlet states, sudden polarisation effect 78−86792
magnesium porphine, ab initio CI calcs., electronic absorpt. spectra 78−78639
malachite green leucocyanide, photoionization in polar solvents, mechanism 77−25295
malonic acid, and α-alkyl derivatives, photoelectron spectra, lone-pair interactions 80−58315
Manoxal OT-cyclohexanewater reversed micellar system, singlet-singlet energy transfer 80−9531
many-body perturbation theory, eqns. of motion formulation 77−88373
many-electron systems, ionis, pot., excitation energy, cluster expansion direct calcs. 79−26912
many-electron systems, time depend., complex scaling and resons. calcs. 79−22612
mass spectra fragments, MO-model calcs. 77−417
metal vapour excimers, book contrib. 79−81419
metalloporphyrins, two quantum fluoresc. excitation from higher excited electronic states 80−106350
methane, $1B_1(1T_2)$ state, photodissoc., extended basis calcs. 78−9093
methane, and fluoro derivatives, correl. energy rel. to valence electron no., modified PCILO method 79−36533
methane, effective core potential calcs. 79−31437
methane, electronic density, multiple scatt. method, muffin-tin approx. 80−27924
methane, ion internal energy selection by angle-resolved mass spectrometry 80−53164
methane derivatives, stabilisation of planar tetracoordinate C, substituent effects, RHF/STO-3G calcs. 77−6671
methanol, conformational anal., barriers of internal rotation, electronic structure 79−63916
methanol, dissoc. ionisation mechanism, correlation diagram approach, mass spectra obs., metastable processes 80−95728
methanol, H bonding, electronic struct., geometries, moments, dimerisation energies, charge distrib., pseudopotential calcs. 80−27942
methanol, ion internal energy selection by angle-resolved mass spectrometry 80−53164
methanol (d_3), OH stretch fund., torsion-rot. levels, IR spectra obs. 80−32711
methoxy radical, LMR spectra anal. 80−63677
methoxy species on Ni (111), photoelectron spectra, electronic struct. and orientation 80−83420
methyl allenyl sulphide, UV absorpt. spectra, role of 3d valence-shell and 4s Rydberg-type atomic orbitals 80−83384
N-methyl diformamide, excited singlet and triplet states, CNDO-CI calcs. 77−26990
methyl glyoxal, $^3n\pi^*$ states, ab initio STO-3G CI calcs., ΔE_{SCF} transition energies 78−94194
methyl halide ions, unimol. dissoc. and internal conversions, coincidence meas. 77−6869
methyl halides, low energy mol. Rydberg states from Feshbach reson. spectra 77−34768
1-methyl indole, UV absorpt. spectra, low-lying Rydberg band 77−58037
methyl iodide, UV absorpt. spectra, ionjs. limit region, assignment 78−21940
methyl lithium, equilib. geometries and electronic states, FSGO calcs. 79−10019
methyl orange, aq. soln., reson. Raman spectra of D and ^{14}N isotopes 80−91566
N-methylacetamide, vertical excitation energies, ab initio SCF CI calcs. 79−45647
methylbenzenes, 3p Rydberg transitions, multiphoton ionis. spectrosc. obs. 80−95644
methylbixin, low-lying forbidden π-electronic state, spectral evidence 77−58029
methylene, 2^1A_1 state, CI and multiconfiguration SCF calc. 79−10052
methylene, $^1B_1$-$^1A_1$ separation, ab initio 80−106251
methylene, singlet a^1A_1 state, laser-induced fluoresc. spectrum 79−18225
methylene manganese, electronic struct., equilib. geometry, ab initio SCF calcs. 77−71747

molecular electronic states continued
3-methyleneoxetane, electron structure, orbital-O interaction, MO calcs., UV photoelectron spectra 80−28058
methylenes, substituted, INDO calcs. 77−30782
methylimidazoles, photoelectron spectra and electronic struct. 79−22758
methylnitrene, symmetry restricted multiconfiguration annihilation of single excitations calcs. 78−62695
mirror image molecules, parity non-conserving energy difference 79−76366
molecular photoselected excited states, dynamics, advances using synchrotron radiation 80−37836
molecular polarisabilities calcs., superposition method of excited config., nonstationary perturbation theory eqn. 80−69257
molecule+molecule, potential well depth estimation method 79−86034
molecule core 1s and 1b, photoelectron bands, vibr. excitations, ab initio calc. 80−63543
molecules containing heavy atoms, program for calc. electronic struct. by quasirelativistic method 80−69088
molecules in degenerate electronic state, IR laser radiation effects 80−81351
momentum distributions via (e,2e), offshell impulse approx. 77−88565
momentum single particle states via (e,2e) knockout reactions 77−88117
momentum wave function determ. in atomic, molecular and nuclear systems 77−88556
MS potential from a set of overlapping densities 80−52850
multicharged ions, transitions between energy levels in strong external field, relativistic calcs. *(Russian)* 80−63547
multiconfiguration reference states, perturbation theory calcs. 79−13644
multiconfigurational wave functions, optimization scheme 77−57889
multiplet energy, calc. by Hartree-Fock-Slater method 77−61685
myoglobin , oxyhaeme complex, single cryst., visible spectrum, electronic struct., coord. geometry 78−44456
N,N′-dioxy-2, 6-diazoadamantane, exchange interaction, spin density delocalisation 78−9056
nπ*- and ππ*-states, n-electron delocalisation effect 79−63902
N-electron system, Schrodinger eqn. soln. using antisymmetrisation 80−106246
naphthacene, excited states calc., unrestricted HF theory in PPP approx. 77−50377
naphthalene, $^1B_{3u}$-state lifetime, temp. depend. under Boltzmann conditions 79−86008
naphthalene, atomic localisation of electronic excitation 77−18806
naphthalene, excited states calc., unrestricted HF theory in PPP approx. 77−50377
naphthalene, Raman intensities rel. to vibronic coupling and excited electron state geometries 77−27075
naphthalene in Ar matrix, geometry changes and multiplet struct., mol. fluoresc. and phosphoresc. obs. 80−95663
naphthalenes, methyl substituted radical cations, UHF spin densities, additivity model calcs. 80−58139
naphthol complexes, H-bonded, form. of ion pairs in presence of crown ethers, proton-transfer photoreactions 80−85199
1,4-naphthoquinone, and derivatives, singlet electronic transitions, SCF MO CI calcs. 79−49948
naphthyl group, excited singlet state, intramol. fluoresc. quenching by halogeno substituents 80−102537
1-β-naphthyl-2-N-piperidinoethane, intramol. exciplex form., ground state conform. control 80−102547
nematic-isotropic transition temp. depend. on anisotropy of C-X bond polarisability for terminal substituents 77−20058
nitroanilines electronic states, CNDO/s-CI correlative calcs. 78−58604
nitromethane, torsional barriers, electronic spectrum 79−59424
nitrosobenzene, fluoresc. quantum yields, determ. from Raman scatt. 80−58294
nitrosomethane, ground state and nonvertical n-π* excitation energy calcs. 80−18804
non-Born-Oppenheimer states, nonadiabatic coupling function, matrix elements determ. 78−74562
nonlinear oscillators, 1-D, intramolecular vibr. energy transfer, quantal, classical and statistical behaviour 80−91641
nonlinear triatomic molecule, wave functions, Born-Oppenheimer approx. adiabatic correction 77−83485
nonradiative transitions, due to electronic rearrangement, rate const. calcs. 77−3411
nonrigid inorganic molecules, pot. surfaces, CNDO and ZDO calcs. 79−41112
nonstationary state time evolution, vibr. redistrib., nonradiative mechanism 77−83575
norbornadiene, excited electronic states, electron impact spectrosc. 79−45842
norbornene, excited electronic states, electron impact spectrosc. 79−45842
nuclear charged changes, influence on energy of highly symmetrical molecules 77−26987
nucleic acid bases, excited state geometry distortion, normal modes reson. Raman intensity anal. 79−68236
1,3,5,7-octatetraene, lowest excited singlet state, dipole forbidden character 79−27024
1,3,5,7-octatetraene, UV, visible, and fluoresc. spectra and assignments, evidence for ^1A_g state 78−33518
omega like technique, Hartree Fock formalism 80−18792
one-electron density functions, many-centred finite multipole expansions 78−71624
one-electron Hamiltonian method applied in SCF theory to states with open shell 80−23302
open shell excited states, perturbation effects, restricted Hartree-Fock calcs. 78−86770
open shell RPA unitary group formulation, Hartree Fock stability eqns. 80−52860
open shell states, operators for cases not fitting Roothaan-like model 78−21848
open shells, RHF treatment without Lagrange multipliers 80−32589
operator manifolds, expansion and completeness theorems 79−59331
orbitals, max. and min. overlap, localised, and hybrid, orthonormality-constrained variation method 79−6830
organic alternant molecules with conjugated bonds, ground state multiplicity, ferromag. 79−774
organic compounds, complex, nuclear relaxation influence on stimulated emission 80−48019
organic compounds, electron delocalisation, ground and excited states, fluoresc. *(German)* 77−34567

molecular electronic states continued
organic compounds, low freq. anharmonic vibr., pot. function determ., Raman and IR spectra obs. 80−52997
organic excited singlet state fluoresc. quenching by metal ions, rate meas., mechanism 77−38685
organic ion, excited electronic state correlation with mass-spectral fragmentation pattern 80−45482
organic molecules, conjugated, nonlinear props. of new class of cpds. 79−41413
organic molecules, information content, thermodynamic props., electropy (bondtropy) theory 77−54500
organic molecules, quadrupole moments, dipole quadrupole A and C polarisabilities, perturbation theory anal. 80−27934
organic molecules in solutions, electronic energy level shift estimation 79−54919
organometallic compounds containing hydrocarbon π ligands, X-ray spectral study of electronic struct. 77−27088
orthorhombic rotating molecules, doublet-quartet transitions, Zeeman effect calcs. 78−94280
ovalene, isolated ultra cold mol., intermediate level structure of S_2 state 80−28048
α-oxalic acid dihydrate, low-lying excited states, ODMR and optical obs. 79−41188
3-oxetanone, electron structure, orbital-O interaction, MO calcs., UV photoelectron spectra 80−28058
ozone, $^1A_1$ ground state, dipole moment function, ab initio SCF and CI calcs. 80−32628
pair density analysis, applics. 77−30751
pair energy, perturbative corrections, incomplete basis set problem 80−78507
pairwise correlated generalised valence bond model, electron correl. model 78−41959
pairwise correlated GVB model, multiconfig. overlap approx. calcs. 79−31408
pentacene, excited states calc., unrestricted HF theory in PPP approx. 77−50377
pentacene, first excited singlet state, butterfly motion studied by fluoresc. spectra 80−78615
pentacene in p-terphenyl, laser excitation of stationary molecular states 77−68084
perfluorohexadiyne radical cation, $\tilde{A}$-$\tilde{X}$ band emission spectra, $\tilde{A}$ state lifetime 79−72327
perfluoropentadiyne radical cation, $\tilde{A}$-$\tilde{X}$ band emission spectra, $\tilde{A}$ state lifetime 79−72327
perturbation expansion, diagrammatic, of electronic energy, 4th-order terms 79−85882
phenol ($-d_1$, d_5, d_6), excited A state, normal vibr. freqs, force consts., compliance coeffs. 78−50534
phenoxy radicals, electronically excited states, photochem., flash photolysis obs. 77−77797
phenylacetylene, excited single state B_1, electron-vibr. spectra and electronic struct. 79−26904
phenylcarbene, singlet and triplet ground states, rearrangement to cycloheptatrienacarbene, MINDO/3 calc. 78−13430
phenylnaphthalenes isomers, fluoresc. lifetime difference and mol. geometry 80−69176
pheophytin a, photo-oxidation primary processes 79−79468
phosphamides, carcinostatic, ^{14}N NQR, electron distrib. and bonding configs. 80−48018
photochemical reactions, isomerisation, complexing, proton transfer, initiation of internal conversion processes 80−40713
photochemistry, sudden polarisation effect 79−34328
photodissociation, nonrandom sequential coupling influence on radiationless relaxation processes 78−90205
photoelectron angular distribs., oriented or rot. resolved unoriented mols., dynamic and struct. data 78−37682
photoelectron spectroscopy, charact. of vapours oven heated inorganic solids 80−52239
photosynthetically relevant mols., electronic structural props. 80−16902
phthalazine, excited states, protonation influence, semiempirical CNDO/S CI calc. 79−76353
phthalocyanine compounds, XPS and change transfer 80−95681
picosecond excited state meas. using tunable laser induced grating 77−10786
pinacyanol, picosecond photobleaching and absorpt. recovery, solvent effects 77−44493
pinacyanol dye, adsorbed on CdS substrate, aggregation effect on mol. electronic states 80−37757
pinacyanol in ethanol, electronic relax., analysing light ps spectroscopy 80−99517
planar cyclic radicals, C-H proton isotropic hyperfine consts., C hybridisation 80−95646
planar molecule, oriented in transparent polymer films, dichroism of absorpt. bands *(Russian)* 79−31506
PMDA, ab initio SCF MO wavefunctions for ground and excited states 79−10028
point groups, continuous, characters and representations 80−36809
point groups, continuous, reduction of representations 80−36808
point groups, continuous, reduction of representations 80−36810
point groups, infinite, complete reduction of representations, mol. vibrs., electronic states appls. 78−94206
polar mol. anion ab initio ground state pot. energy surfaces calc. 80−47923
polar molecule, excited state MCSCF wave functions, BeO appl. 80−47916
polar molecule-electron systems, variational method for bound state calc. 78−46261
polar solvents, equilib. electronic states, basic eqn., broken symmetry 78−37535
polyacenes, alternant, internal conversion, energy gap correl. 79−54901
polyacenes, atomic localisation of electronic excitation 77−18806
polyacenes, linear, open-shell ground state wave functions 79−762
polyacenes, spectra, correlation effects 79−81199
polyacrylonitrile, electronic struct., reactivity, SCF CNDO calcs. 77−50580
polyatomic mol. quasi line spectrum in paraffin matrix, electronic-vibr. interaction 79−85971
polyatomic molecule, Jahn-Teller theorem, adiabatic approx. calcs. 77−10575
polyatomic molecule, vibr. struct. of electronic spectra, FORTRAN programs 80−32699

molecular electronic states continued
polyatomic molecules, electron density, generalised Berlin diagram appl. to H_2O internal modes 79−98001
polyatomic molecules, electronic states, four-level scheme 79−54840
polyatomic molecules, excitation energies, oscillator strengths, many body approach, eqns. of motion method 80−47969
polyatomic molecules, highly vibrationally excited, spectra calcs. 78−90140
polyatomic molecules, nonadiabatic transitions between electronic terms of identical symmetry 80−83265
polyatomic molecules, two-parameter intramol. distribs. and props. 80−47967
polyatomic radical cations, excited states, decay processes 80−28055
polybutadiene, electronic struct., reactivity, SCF CNDO calcs. 77−50580
polycyclic aromatic hydrocarbons, electrophilic superdelocalisability rel. to carcinogenesis, Pullman theory 79−63897
polyene, infinite, electronic states under local perturbation 77−57878
polyenes, 2^1A_g-1^1B_u energy gap, extended CI study 79−81159
polyenes, highly branched, large networks, abnormal bond orders 79−59610
polyenes, linear, π-electron system, appl. of extended RPA excitation operators 79−97993
polyenes, model results for π electrons 78−55128
polyenes, substituted, spectra, four-level state scheme 79−54840
polyethylene molecule, fractured, local electron level calc. 80−14263
polyglycine chain with hydrated side group, electronic struct., transport props. 79−16146
polyisoprene, electronic struct., reactivity, SCF CNDO calcs. 77−50580
polynuclear clusters, programs for calc. electronic struct. by Mulliken-Wolfsberg-Helmholtz method 80−69288
polypeptides, electronic struct., side-chain disorder effect 80−76706
porphine, ab initio CI calcs., electronic absorpt. spectra 78−78639
positronium halides, $[X^-; e^+]$, electronic struct., annihilation characts., HF calc. 77−50567
positronium halides, $[X^-; e^+]$, electronic struct., annihilation characts., HF calc. 77−50568
prop-1, 2-dienyl radical, ab initio SCF HF MO calc., electronic struct. and one electron props. 77−42231
propan-1-ol, ion internal energy selection by angle-resolved mass spectrometry 80−53164
propane, ion internal energy selection by angle-resolved mass spectrometry 80−53164
β-propiolactone, electron structure, orbital-O interaction, MO calcs., UV photoelectron spectra 80−28058
propiolyl chloride(-d), 357-333 nm absorpt. system 80−69161
propiolyl fluoride(-d), 290 nm absorpt. system 80−87142
propyne, and 1-butyne, electron impact spectra, comparison with acetylene 79−3585
proton transfer photoreaction kinetics, in singlet excited state 78−48671
pseudopotential theory 77−42230
pseudopotentials, reliability criteria 80−49563
purines, biological, UV photoelectron spectra, valence electronic struct. 77−16905
pyrazine, physisorbed on Ni (111), UV spectroscopic ellipsometry obs. 79−86997
pyrazine, triplet-triplet absorpt. related to state splitting 80−47917
pyrazine, vap., single vibronic level fluoresc., dye laser excitation 79−18224
pyridazine, π bond order calc. using U(3) basis algebra 80−18810
pyridine, i.r. spectra and electronic struct. 77−3363
pyridine and salts, deuterium NQR, double reson. method, ring charge distrib. 80−53015
pyridine-d_0, -d_5, vap. fluoresc. spectra 78−82771
pyridine-N-oxide, electronic struct. assignment, He I/He II intensities *(German)* 80−83423
pyrimidine derivatives, absorpt., luminesc. and polarisation spectra, electronic struct. 79−85993
pyrimidines, substituted analogues, absorption UV spectroscopy and electronic struct. of ionic and tautomeric forms 80−74177
pyronine, reson. Raman scatt., normal and excited mol. struct. determ. 77−58024
pyrrole (π-π^*) and ground state, ab initio SCF CI calcs. 78−33438
pyrylium, substituted, electronic struct., CNDO/S calcs. 78−29749
quantum chemistry, spin-free, alternacy, quantum no. assignment 79−9988
quantum chemistry, spin-free, particle-hole and pairing symmetries 79−6812
quantum mechanical aspects of the molecular structure hypothesis 80−102421
quantum mechanics, mol. struct. defn. 80−52843
quantum theory of mol. struct. 78−58568
quantum-chemical π-electron system, molecules-in-molecule model *(German)* 80−5490
quasi-linear molecules, low frequency anharmonic vibrations, pot. function determ., Raman and IR spectra obs. 80−52997
quasimolecules, electronic struct. calc., CNDO approx., computer program 78−86789
quasimolecules, superheavy, inner shell electronic states calc. 79−89817
quasiparticle theory of large-scale configuration on mixing calcs. 78−13437
quinoxaline$^+$, (singly protonated), struct. and kinetics of fluoresc. and phosphoresc. states 77−30906
quinoxaline, excited states, protonation influence, semiempirical CNDO/S CI calc. 79−76353
quinoxaline, solns., excited state absorpt. kinetics 79−45734
quinoxaline in Shpolskii-type hydrocarbon matrices, vib. struct. of electronic spectra 77−85773
radiationless transitions, synchrotron radiation obs. 80−63706
radiative transitions, proximity effects, role of vibronic coupling and static crystal field interactions model 80−69126
radical, MINDO/3 unrestricted open-shell calcs. 77−23429
Raman spectra, correlation with vibronic coupling and adiabatic potential 77−71804
Raman spectroscopy, in high temp. chem., review 80−52234
rare earth ions, trivalent, in O-dominated host, high energy states, reflectance spectra 77−69849
rare-earth tetraborides, electronic structure and bonding determ. from X-ray spectra 77−59646
relativistic corrections, estimation method 80−14091
relativistic corrections, review 80−47914

molecular electronic states continued
relativistic scattered wave theory, normalisation and symmetrisation 78−62694
resonant Raman spectra, overtone intensity distrib., effect of excited electronic state 80−87128
resonant Rayleigh-type mixing spectroscopy using ps light pulses, ultrafast relax. study 80−91834
all-transretinal, two-photon spectrum, rel. to photophysics of vision 79−41159
retinal electronic structure 78−15764
retinals, emission spectra, state ordering 77−25373
RHF molecular potential eqns., interactions of open-shell systems 77−30949
rhodamine, CARS spectroscopy, vibr. spectra of electronic states 80−27964
rhodamine 6G, blue and UV luminesc., obs. and mechanism 79−3486
rhodamine 6G, lasing, reson. CARS spectra in methanol, ethanol, acetonitrile, H_2O 78−74948
rhodamine 6G dye laser, induced radiation spectral charact., effect of vibr. relax. 80−64008
rhodamine 6G soln., stimulated reson. Raman scatt., first excited and ground electronic states contrib. 79−89968
rhodamine B dissolved in D_2O, electronic state two-stage excitation by light pulse 79−64056
rhodamines, reson. Raman scatt., normal and excited mol. struct. determ. 77−58024
rhodanines, tautomeric, electronic struct. and spectra, MO calcs. 79−13629
rigid symmetric top molecules, dynamic Stark effect spectrum 80−63621
ring current theories in NMR 80−53020
ruthenium tris-bipyridyl, excited state electron transfer quenching, H_2O photoreduction mediators effects 80−102536
ruthenium trisbipyridyl ions in surfactant solns., excited state decay kinetics 80−83407
Rydberg INDO method, mol. Rydberg S_n←S and T_n←S transitions and oscill. strengths 78−17572
Rydberg states, quantum defect theory applic. 80−32700
Rydberg states and valence-shell states, interactions 77−30794
Rydberg states in condensed matter, appl. to doped solid rare gases and H_2 79−69425
Rydberg transitions, correl. algorithms for Rydberg term values 80−83277
Rydberg transitions, field effects in vacuum UV region 78−66561
Rydberg-valence mixing, oscillator strengths 79−31492
salicylamide, excited state proton transfer, kinetics, picosec. fluoresc. 79−59502
satellite struct. of electron spectra, CI and vibronic coupling, dynamical calc. 80−53044
saturated organic molecule, photolysis, primary step prediction using Rydberg and valence-shell transitions 77−21404
scattering amplitude calculations, role of radiative crossings between potentials of dressed mol. 80−63642
scattering states of clusters, multiple scattering X_α treatment 77−30747
second-order perturbation energies, modified virtual orbitals calcs. 77−88381
self-consistency accel. procedure 80−78529
self-consistent convergence, effect of electron distrib. nonuniformity 77−18778
semiempirical CNDO method, calc. progam 78−86782
silaethylene, singlet-triplet energy separation 78−58594
silaethylene, singlet-triplet energy separations 77−57866
similarity, electron density function meas. 80−91413
simple mol. charge distrib., empirical method, electrostatic pots. and struct. 78−82652
single spin-config. singlet states, wavefunctions, energies 77−83505
small molecules, detect. by magnetically tuned freq.-modulated at. line sources 79−59508
sodium nitroprusside, isomeric molecular states generated by polarised light, Mossbauer resonance obs. 77−20781
solution, nonlinear luminesc. quenching kinetics, high excitation power 79−56834
solvent effects, rel. to polarisation structure 80−43062
spectroscopy, conference, Wroclaw, Poland (Sept. 1977) 78−62951
spherical-top molecules, rot.-vibr. transition moments in excited states 78−25639
spiropyron solutions, nitro-substituted, electronic state participation in photochromy 80−81347
stability of molecular states, symmetry breaking for a non-linear Schrodinger equation 79−26867
stilbene, diphenylpolyenes, photoisomerisation, 'phantom' photochem. singlet state, PPP SCF CI calcs. 78−73058
stilbene, direct photoisomerisation theory, from fluoresc. and absorption spectra 79−79262
trans-stilbene, excited state orientational relax., sub-picosec. pulse obs. 79−50006
stilbene, ps photoisomerisation, time-resolved spectra obs. 79−57252
trans-stilbene, two-photon excitation, phantom photochemical singlet, assignment 77−75247
stilbene anion radicals, photoinduced isomerisation, 77K 80−66818
stilbenes, substituted, dipole moment calcs., in excited singlet state *(German)* 77−50367
stilbenes, substituted, donor-acceptor interaction effects on excited singlet state polarity *(German)* 80−91470
styrene, UV Raman spectra, reson. effect in photoreactive states 80−106326
sum rules in optical activity 77−26993
superheavy quasimolecules, electronic states, spectroscopy 78−37706
symmetry restricted multiconfiguration annihilation of single excitations calcs., applic. to methylnitrene 78−62695
symposium, Florida, USA (March 1979) 80−51946
TCNQ, anions, screened INDO model, appl. to photoelectron, optical, Raman spectra 79−765
TCNQ, electronic struct., HAM/3 semiempirical calcs. 79−6866
TCNQ salt, NMP-TCNQ, electronic struct., SCF calc., total energy polarisation effects 80−15469
technetium hexahalides, X_α-SW-calc. of chemically induced decay const. variation of ^{99m}Tc in TcO_4^- and hexahalides 79−54769
p-terphenyl, cyclohexane soln., solute excited state form. kinetics in pulse radiolysis 79−79263
p-terphenyl, lowest excited singlet states, polyexcited CI calc. 79−772
p-terphenyl, valence electronic structure 79−72360

molecular electronic states continued
tertiary phosphine oxide+aliphatic alcohol, $p\pi$-$d\pi$ conjugation, electronegativity and H-bond energy 78−82863
1,1,4,4-tetrachloro-1,3-butadiene, reson. Raman intensities, mol. struct., excited states, vibr. anal. 77−65470
1,2,3,4-tetrachloro-7,8-diphenylcalicene, excited states, moments anal. of electro-optical spectra 79−22698
tetrachlorobenzene, in durene, 1.6K, $S_1 \sim\!\!\rightarrow T_1$ relax. mechanism, Zeeman phosphoresc. and PMDR obs. 77−30912
tetrachloromethane, He(II) photoelectron spectra, spectral intensity patterns 79−98152
tetracyanoethylene-benzene(-toluene), and isotopic forms, excited charge-transfer state nonrad. decay, vibrs. role 78−82765
tetraethyl lead, core d-level high resolution photoelectron spectra, spin-orbit splitting 78−50579
tetraethyl lead, core level photoelectron spectra, electric field gradient splittings 77−88494
tetrafluoroethylene, electronic struct., CNDO/S2 calcs., photoelectron and UV absorpt. spectra 77−30783
tetrafluoromethane, Auger transition energies, transition state approx. SCF $X\alpha$ calc. 77−65426
tetrafluoromethane, valence electron binding energies, molecular symmetry restrictions effect 80−63528
tetramethyl-1,3-cyclobutanedithione-h_{12} and -d_{12}, visible spectra, $n\pi^*$ transitions obs., mol. vibr. 80−97297
2,2,4,4-tetramethylcyclobutane-1,3-dione, Rydberg transitions, spectra, LCRO calcs. 77−34659
tetraphenylporphyrin, free base in PVC matrix, excited state props., electrochromism obs. 80−37815
tetraselenafulvalene, monomer and dimer electronic struct. scattered wave calc. comparison with photoelectron spectra 78−50465
s-tetrazine, dimethyl-s-tetrazine, photodissoc., in hexane soln., Ar matrix, and mol. cryst. 78−73059
s-tetrazine(-d_1), and $^{15}N_2$-substituted, rot. consts., ground and $^1B_{1u}$ excited states geometries 78−82862
thieno(3,2-b)thiophene, electronic and vibr. spectra, vapour phase and cryst. 77−34654
thioacetamides, CNDO calcs., internal rot., ionisation pots., photoelectron spectra 78−5143
thiocarbonyl halogen substituted cpds., geometric and electronic struct., LCAO-SCF calc. 79−89603
thioformaldehyde, and -d_2, $\tilde{A}^1A_2$-$\tilde{X}^1A_1$ visible electronic absorpt. spectra, vibr. anal. 79−45733
thioformaldehyde, electronic struct., dipole moments, mol. polarisability, force fields, ab initio calcs. 80−78531
thiophosphoryl compounds, bond ionisation energies, mol. struct. from UV photoelectron spectra 78−82782
thiourea, ground and first excited triplet state configs., ab initio SCF calcs. 79−89597
thioxanthone, fluoresc. and internal conversion, rel. to proximity effects 80−91592
Thomas-Fermi model, neutral systems, positivity of pressure and compressibility 79−13639
Thorson-Moffitt Jahn-Teller degeneracies 77−88402
three-body system, ground state determ. 78−62710
thymine, tautomers, polarisation, barriers and tunneling times calcs. 79−41114
time of flight spectroscopy, particles in excited state produced via IR laser excitation 80−74257
Tokamak impurity problems, atomic and mol. struct. and collision data, review 80−43959
topology concept of molecular structure 78−46253
trans-butadiene, ionis. pot., π-π^* energies, open shell many-body formalism calc. 77−46508
trans-hexatriene, 6.2 eV Rydberg state symmetry, multiphoton ionis. spectrum polaris. assignment 78−70759
transition matrix, for arbitrary pots., matrix element calcs. 77−3249
transition metal chlorides, 4d-series, electronic struct. and spectra, multiple scatt. calcs. 77−83486
transition metal complexes, excited states geometrical parameters, Franck-Condon anal. 77−27047
transition metal complexes, ligand field spectroscopy, selection rules, intensity enhancement of forbidden transitions 80−45049
transition metal complexes, mol. dissymmetry, book 80−27057
transition metal complexes, tetragonal, d^5 ions, ligand fields and electronic struct., theory 77−6666
transition metal compounds, electronic excitation energy calc., correl. energy correction 78−17576
transition metal dihydrides, gas phase geometrical struct. calcs. 80−42951
transition metal hexahalide complex, polarised reson. vibr. Raman spectra, electronic degeneracy effects 78−78708
transition metal hydrate complexes, physico-chem. props. CNDO calcs. 79−41110
transition metal hydrides, homoleptic, electronic structure, ab initio calcs. 79−89601
3d-transition metal ions, s-doublet struct., appl. of exchange correlation mass operator approx. 80−106266
transition metal phosphides, valence-level struct., X-ray spectra and X-ray photoelectron spectra calcs. 79−64044
transition metal trifluorides, mol. and electronic structs., ab initio restricted Hartree-Fock calcs. 79−63900
transition metal-carbonyl cluster molecules, electronic struct., localised orbital pseudopot. method 80−39653
transition metal-oxygen compounds, salts, X-ray Lα emission spectra, excited states calcs. 79−59488
transition probability, nonadiabatic unimolecular decay, simplified semiclassical formalism 77−61804
transition-metal coordination compounds, electronic energy transfer processes 78−56907
transiton metal hydrate complexes, struct., bond energies, CNDO cals. 79−41111
triatomic dihydride molecules, Walsh's rules and small bond angle states 80−106255
triatomic isoelectronic molecules, electronic struct., one-electron props. 80−42935
triatomic linear molecule, photodissoc., products rot. distrib. 79−66309
triatomic molecule, rot. vibr. electronic Hamiltonian, Born-Oppenheimer approx., breakdown 80−87097
triatomic mols., Renner-Teller effect, orbital angular momentum 80−78513

molecular electronic states continued
sym-tribenzotridehydro [12] annulene, electronic spectra in Shpolskii type hydrocarbon matrices, electronic struct. and fluoresc. 78−66589
triethylenediamine, multiphoton ionis. and two-photon fluoresc. excitation spectra 79−98164
triethylenediamine cation radical, ESR 77−24745
trifluoroiodomethane, highly excited, intermol. vibr. energy transfer, transient UV absorpt. spectra 80−106381
trihalide anions, VB pseudopot. calcs. on electronic states 77−26984
trimeric molecular complex, excitation localisation and transfer, monomeric internal vibr. effect 78−17581
trimethyl gallium, core level photoelectron spectra, electric field gradient splittings 77−88494
trimethyl indium, core d-level high resolution photoelectron spectra, spin-orbit splitting 78−50579
trimethylene, singlet state, rot. barrier origin, MINDO/2 calc. 79−81170
trimethylenemethane, bisected singlet state, using general CI method 79−36539
trioxane, $\nu_{19}(E)=\nu_{20}(E)=1$ state, rot. spectrum assignment, microwave obs. 80−58248
triply degenerate singlet electronic states, reson. Raman scatt. 78−78714
triply excited state contrib. to correlation energy, diagrammatic perturbation theory, water appl. 80−18774
twisted conjugated molecule, zwitterionic excited states investig. 80−58179
two particle density, determ. using energy optimization *(French)* 77−88369
two-centre integrals calculation in semi-empirical INDO method 80−32611
two-centre molecules, at. charge, comparison with electron count functions 79−36568
two-particle interactions, new variation-perturbation principle 79−10006
two-particle states, Talmi transformation theory, kinematic consts., appl. to mol. electronic states 80−32588
two-photon spectroscopy, dipole-forbidden transitions, double excited configurations, CNDO-CI methods 80−58332
U(3) symmetric matrices algebra applic. to π bond order calc. 80−18810
UHFS model, CI, CC, and MBPT approaches, appl. to weak δ-δ bonds and δ-δ^* excitation 80−32585
umbelliferone, excited state tautomeric forms, solvent polarity effects 79−59377
umbelliferone, excited states, in ethanol-water soln., absorption and emission spectra 79−13763
unimolecular decay, nonadiabatic interactions, transition probability as function of Massey parameter 80−35503
unimolecular reactions, laser-induced, by multiphoton IR excitation, theory 80−9664
unitary group approach to molecular electronic structure, review 80−5467
unstable molecular states, with memory effects, prep., decay, EM pulse excitation 78−46384
uranyl complexes, fluoresc. state, rel. to electronic struct. *(Russian)* 78−5274
urea, single crystal Compton profiles, H-bonding and dimer config. effects, calc. and meas. 78−80431
uridine monophosphate, excited state geometry distortion, normal modes reson. Raman intensity anal. 79−68236
valence correlation energies, contributions of triply- and quadruply excited states determ. using perturbation theory 80−78545
vanadyl phthalocyamine dye solns., laser destruction, highly excited states participation 78−53231
variational cellular method, general formulation 78−94192
variational cellular model for mol. and cryst. elec. struct. 78−29726
vibronically coupled electronic states, radiationless decay, non-Condon effects 80−52966
vinyl cyanide, electronically excited species production via collisionless, IR laser photolysis 79−57255
vinyl isocyanate, conformers, geometrical and electronic structures, microwave spectra 78−9142
virial partitioning of mol. charge distrib., defn. of bond paths and directions 78−886
vitamin A, visual chromophores, two-photon spectra, lowest excited state 78−64934
xanthene dyes, phosphorescence and orbital nature of triplet state *(Russian)* 77−85797
xanthine, and biological methyl derivatives, electronic struct. from UV photoelectron spectra 79−24949
xanthione in benzene, second excited singlet state, ps spectra 77−3399
xylenes, singlet excited states decay, substituent effects 77−75175
y_t-base, ground and excited states, dipole moment, CNDO/S and INDO/S calcs. 79−36534
Yang's biradical, EPR, g- and D-tensors, electronic struct., deuteration and conformation effects 77−42343
π electronic states and transitions, interpretation 80−52862
σ- and pi-electron contribs. to contact proton spin-spin coupling, INDO perturbation calc. 77−50361
AcH, $^1\Sigma$ state, Dirac-Fock one-centre calcs. 80−23301
AgO, $A^2\Pi$-$X^2\Pi$ blue system, rot. anal. 77−38678
AgO, electronic spectra in rare gas matrix 78−996
Al-H_2O, mol. complex, electronic struct. calcs. 78−66465
Al_2^- $(Al_2^-)(Al_2^+)$ configurations, ab initio study, LCAO, STO, MO-SCF and CI calcs., binding energy *(French)* 80−91447
AlH, vibr. consts. of electronic states, calc. method 79−93967
AlH_3, AlH_3^-, ground electronic states and geometries, ab initio calcs. 77−57863
Al_2H_6, electron density distrib., reaction channels and bonding characts., electrostatic mol. pot, CNDO/2 calc. 80−23309
AlN, (^{2}P)Al-(^{4}S)N, (^{2}P)Al-(^{2}D)N, nonempirical pseudopotential, configuration interaction calcs. 79−93930
AlO, in Al+O_3(N_2O) chemilum., perturbations and vibr. population anomalies obs., mechanism 77−63917
AlO radical, ground state dissoc. energy 80−53159
Ar, liq., recomb. and self-trapped exciton luminesc., free electron dynamics, excited states 80−25463
Ar^-, electron capture expts. to search for long lived states 79−72410
Ar:H crystalline matrix, Xα scattered wave cluster model 79−73468
Ar+Na_2, differential cross sections meas. for rot. energy transfer process, obs. of halos 80−91643
Ar^++He, $X^2\Sigma$ and $A^2\Pi$ states, CI pots. 78−74727

molecular electronic states continued
Ar_2, excited state pot. curves, ab initio CI calc. 78−78643
Ar_2, VUV emission spectrum, rot. anal. 79−98119
Ar_2^+, bound-free absorpt. cross section for Π and Σ states 78−5140
Ar_2^+, electronic states, pot. curves, with/without spin-orbit interaction 78−33443
Ar_2+, weakly bound excited states, dissoc. energies 78−78748
ArBr, emission spectrum and chemiluminesc. 80−45508
ArBr, pot. curves, population distribs. and chemiluminesc. for B(1/2) and C(3/2) electronic states 80−45509
ArC^+, pot. energy curves calcs. 79−45651
ArF, Ar_2F, electronic struct., pot. energy curves, radiative transition probability calcs. 77−57879
ArF, laser emission, ab initio config. interaction calcs. on electronic states 78−63083
Ar_2F, electronic states, ab initio POL CI calcs. 78−66474
Ar_2F_2 low-lying electronic states 77−65491
ArH^+, transition moments, perturbation calcs. 80−102542
ArO, lasing, low-lying electronic states, ab initio config. interaction calcs. 78−63084
ArO^+, $X^4\Sigma^-$ state, pot. energy curves and correl. effects, elastic scatt. cross sections 80−23502
As_2S_3 glass, localised paramag. states, As_4S_6, As_4S_4 units, mol. analogue models 78−60087
Au, ground and excited states, pot. energy curves, relativistic effects calcs. 79−31416
Au_2, ground state, ab initio effective core pots., relativistic effects calcs. 79−31377
AuH, AuCl, relativistic effective core potentials, ab initio calcs. 78−86767
AuO, electronic spectra in rare gas matrix 78−996
B_2, ground state, multiconfig. SCF CI calcs. 78−58590
BF, isoelectronic sequence, Rydberg transitions, term value-ionisation pot. correl. 80−58276
BF, $X^1\Sigma^+$ state, many-body effects, HF STO calcs., diagrammatic perturbation theory 77−50355
BF_3, dissoc. pathways and mol. vibr., compliance consts. and min. energy coords. 78−35661
BH, $^1\Sigma^+$ ground state, mag. susceptibility, paramag. contrib., large config. interaction wave function calcs. 80−47899
BH, electron density, basis set, electron correl. effects 78−74581
BH_2, Walsh's rules and small bond angle states 80−106255
$(BH_2)_n$, energy band structure 80−5478
BH_3, electronic wave function determ., genealogical technique using Clebsch-Gordan coeff. 80−95529
B_2H_6 and $B_2H_5NH_2$, electronic struct. and bonding, comparative calcs. 79−31397
$B_3N_3H_6$, electronic struct., mag. susceptibilities, ab initio calcs. 78−74571
BO_2, $A^2\Pi_u$-state, Hanle effect, press. and Zeeman broadening 79−18239
BO_2, intermodulated fluoresc. spectra using stabilised dye laser 79−27020
BO_2, Π vibronic states, laser induced fluoresc. obs. 80−58301
BaH($N^2\Sigma$), perturbations, 3800 Å absorption band obs. 80−14154
BaO, $A\ ^1\Sigma^+$ state, dipole moment, level crossing spectroscopy obs. 79−94040
BaO, $C^1\Sigma^+$-level, perturbation, extra lines, assignment 79−18213
BaO, excited electronic states, lifetimes and transition moments 80−87177
BaX_2, X=Cl, Br, I, valence shell electronic struct., ab initio SCF calc., photoelectron spectra 79−31383
Be_2, ground state, multiple scatt. Xα calcs. 80−58149
$BeBH_5$, H bridged system, floating spherical Gaussian model 80−78518
$BeCl_2$, valence shell electronic struct., ab initio SCF calc., photoelectron spectra 79−31383
BeF, $A\ ^2\Pi$ state config., ab initio MO calcs. 80−95532
BeF_2^-, ground state, conform., electron affinity, extended basis SCF calcs. 79−72253
BeH, $^2\Sigma^+$ states, spin-coupled valence bond theory of molecular electronic struct. 80−83285
BeH radical, hyperfine splitting const., electronic energy, UHF-type, CCI calcs. 80−52909
$(BeH_2)_n$, energy band structure 80−5478
BeO, MCSCF and CI calcs. 80−95526
BeO, $X^1\Sigma^+$ state pot. energy curve, ground state dissoc. energy 78−41977
BeOH, struct. and electronic props., ab initio calcs. 80−74113
Bi_2, in Ar matrix, electronic states, vis. and near IR absorption spectra 78−5213
BiBr, $A^3(0^+)$ and $X^3Sigma^-(0^+)$ states, pot. energy functions comparison 80−43133
BiBr, empirical pot. energy curves for $A^3\pi(0^+)$ and $X^3\Sigma^-(0^+)$ states 79−22617
BiF, spectrum, 5800-6600 Å, vibr. anal., electronic transition assignment 80−992
Br_2, $B^3\Pi(O^+)$ and $^1\Pi(1)$ states, reson. Raman spectra 79−59470
Br_2, continuum reson. Raman scatt., interference effects 79−6946
Br_2, long-lived $A^3\Pi(1_u)$ state, quantum-resolved dynamics of excited states 80−69178
Br_2, pot. curves, asymptotic calcs. 77−6881
Br_2, Q branches of $\Delta n=1$ profiles, calcs., rotation effect on scatt. amplitudes 80−63643
Br_2, reson. Raman scatt. obs., excited-state interference 77−79618
Br_2, UV laser transitions, electronic designation 79−944
BrCN, vacuum UV photodissociation spectroscopy, quantum yield, fluoresc. polarisation 80−32736
BrCl, $^3\pi_0^+$ state, time-resolved fluoresc. 77−34679
BrCl, elec. dipole moment, Stark effect meas. 78−90211
BrCl, excited $B^3\Pi(0^+)$ state, excitation spectra and predissoc. 78−66593
BrCl, excited $B^3\Pi(0^+)$ state, laser-induced fluoresc., steady-state kinetics 78−66594
BrCl, time-resolved fluoresc. of $a^3\Pi_0^+$ state 78−63093
BrF, $B^3\Pi(0^+)$ states, collision-free lifetimes laser fluoresc. obs. 78−94278
BrF, He(I) photoelectron spectra, interpretation 79−13766
BrF, laser excitation spectrum, 4850 to 5200 Å, rot. anal. 77−6840
BrF, predissociation in $B^3\Pi(0^+)$ state 78−66591
BrF, stable levels of $B^3\Pi(0^+)$ state 78−66592
BrF_3, electronic struct. and ionisation pot., SCF DV Xalpha method 80−69057

molecular electronic states continued
BrF_5, electronic struct. and ionisation pot., SCF DV Xalpha method 80−69057
BrF_5, excited vibr. states, microwave spectrum, rot. const. determ. 78−94237
$Br(H_2O)_n^-$, geometric and electronic struct., CNDO/2 calcs. 77−79542
BrHe, $X^2\Sigma$ and $A^2\Pi$ states, SCF calcs. 80−23503
$BrHe^-$, $X^1\Sigma$ state, SCF calc. 80−23503
C-H bond, acidity in organic mols. and anions, SCF MO calcs. 77−83497
C_2, $^3\Pi_g$ states, large CI wavefunctions, non-adiabatic coupling matrix elements 80−37744
C_2 $a^3\Pi_u$ state quenching, laser-induced fluoresc. obs. 79−31574
C_2, conc. meas. in oxyacetylene flame rel. to saturation spectroscopy 77−60148
C_2, Swan transitions, relax. dynamics and two-photon excitation, in inert gas matrix 77−505
C_2, valence states, CI calcs. 79−45642
C_2^-, bound electronic states and electron affinity, IC calc. 79−76349
C_3, $\tilde{A}^1\Pi_u$ state, orbital angular momentum 80−78514
$C_2(A^3\Pi_g)$ vibr. relax. in He 80−53106
CF, electronic Rydberg states, dissoc. energy, multiconfig. HF calcs. 79−59360
CF, low-lying electronic valence states, dissoc. energy, multiconfig. HF calcs. 79−59359
CF_2, excitation by Hg 253.7 nm line, reson. fluoresc-spectra 80−63694
CH, $B^2\Sigma^-$ state predissoc., calcs. and time resolved spectrosc. 80−23576
CH, interstellar, ground state inversion, collisional excitation 78−28503
CH radical, sputtered, rotational and vibrational excitation 80−69224
CH^+, $a^3\Pi$ state, form. from $C^+ + H_2$, energy spectra 77−1918
CH^+, excited states, pot. curves and transition moments determ. by ab initio CI methods 80−106286
CH^+, ground state photodissoc. cross sections into $A^1\Pi$ state 78−82793
CH_2^+, $^4A_2$ states, large CI wavefunctions, non-adiabatic coupling matrix elements 80−37744
CH_2^+, ground state potential surface, analytic fit 77−50380
CH_2^+, Walsh's rules and small bond angle states 80−106255
$C_6H_6^-$, gas, laser-induced-fluoresc., rel. to photodissoc. and Jahn-Teller X and A states distortion 79−72345
$CH_2(^1A_1)$ form. by ketene (diazomethane) photolysis, react. with cyclobutane, vibr. energy distrib. 78−61032
CH_2CCH radical, electronic struct., geometry, INDO calcs. 77−14358
CH_3CO', low lying states, struct., energetics, ab initio STO calcs. 77−61682
CH_3NN', low-lying states, struct., energetics, ab initio STO calcs. 77−61682
$CH_2(a^1A_1\text{-}X^3B_1)$ energy separation 79−8443
CN, $(B^2\Sigma^+)$, polarised fluoresc. following synchrotron radiation photodissoc. of ICN 79−98130
CN, A- and B-state lifetimes, collisional transfers and perturbations 78−78756
CN, $A^2\Pi_i$ state vibr. distrib., chemiluminesc. 79−39152
CN, $B^2\Sigma^+ \rightarrow A^2\Pi$ 0-0 and 1-0 bands, laser excitation spectra 80−91588
CN free radical, $A^2\Pi\text{-}X^2\Sigma^+$ Red system, perturbation analysis 80−87247
CN, internal energy distrib. following vinyl cyanide photodissoc., temp. depend. 80−78638
CN, radical, electronic, vibr. and rot. energy partitioning obs. following ICN photolysis 77−16853
CN^-, electron density distrib., theoretical and expt. determ. 77−61683
CN^-, ground state pot. curve, CI and coupled pair method calcs. 79−68197
CN^-, spectrosc. consts. for ground and excited states, ab initio, CI calcs. 80−78551
CN^+, ab initio full CI calcs. 78−50480
CN^+, ground state, identity, ab initio CI calcs. 80−5468
CN^+, ground state, SCF pot. energy curves calcs. 79−13782
CN^+ ion, $^1\Sigma^+$ and $^3\Pi$ states, multi-reference CI study 80−83288
CN^+, lower states, pot. energy curves, equilib. distances SCF CI calcs. 80−27957
CN^+, lowest $^1\Sigma^+$ and $^3\Pi$ states, ab initio CI pot. curves calcs. 79−85905
C_2N_2, and $C_2N_2^+$, electronic struct. UV and PE spectra 80−23304
C_2N_2, $C^1\Pi_u$-state predissoc., vibronic effects 80−28078
C_2N_2, satellite struct. of electron spectra, CI and vibronic coupling, dynamical calc. 80−53044
$CN(B^2\Sigma)$ shock wave excitation, emission, excited state populations, in $CO\text{-}N_2$-Ar mixtures *(Russian)* 78−74638
$CN(^4\Sigma^+)$, identification and characterisation by anticrossing 77−6864
$CN(X^2\Sigma^+)$, translational-electronic-vibr.-rot. energy partitioning in photolysis of C_2N_2 77−48667
$CN^-.e^+$, positron energy levels, rel. to Rydberg levels of Na, NO 79−86089
CO, (4+) system, electronic transition probability 80−106332
CO, $a^3\Pi$ and $A^1\Pi$ states, dipole moment, CI calcs. 77−79548
CO, $d^3\Delta$ state, low energy electron impact excitation and radiative decay 80−91691
CO, $d^3\Delta_i$ state elec. dipole moment, vibr. depend. obs. 79−31548
CO discharge plasma, electron energy distrib. and kinetic coeffs., ground-state mols. 80−43867
CO, Dunham vibration-rotation coefficients, isotope dependence 80−83518
CO, electronic states, oscill. strengths calcs. 78−9095
CO, electronic struct., binding energy and interatomic distance, SCF variational cellular calc. 80−9498
CO, electronic structure calcs., self-consistent, accelerating convergence of iterative process 80−87037
CO, isoelectronic sequence, Rydberg transitions, term value-ionisation pot. correl. 80−58276
CO, photoelectron spectra ang. distrib., vibr. transitions, autoionis. state 79−31609
CO, vibr. struct., core and valence ESCA spectra, Frank-Condon and HF anal. 80−32602
CO, $X^1\Sigma^+$ state, diagrammatic many-body perturbation theory, pot. curves 79−10014
CO, $X^2\Sigma^+$, vibr. levels, UPS electron attachment obs. 80−95683
CO^+, $A^2\Pi\text{-}X^2\Sigma^+$ system, (2,0) band, rot. anal., $^2\Pi$ state Λ-doubling *(French)* 77−10681
CO^+, $B^2\Sigma^+$ state, radiative lifetimes of 0, 1, 2, 3 vibr. levels, intensity decay meas. 79−98157
CO^+, electronic struct., CO(e, 2e) reaction meas., CI calcs. 77−34769

molecular electronic states continued
CO^+, electronic transition moments for $(B^2\Sigma^+\text{-}X^2\Sigma^+)$ and $(b^3\Sigma^+\text{-}a^3\Pi)$ systems and matrix elements for $(X^1\Sigma^+)$ and $(B^2\Sigma^+)$ 77−38696
CO^+, rel. to dissoc. ionisation of CO 77−54616
CO^+, vibr. $(A^2\Pi_i)$ states, radiative lifetimes 77−3397
CO^+, vibr. intensity distribs. for electronic states prod. by photoionis. 78−25614
$^{12}C^{18}O$, Herzberg system of $C^1\Sigma^+$ state 78−90185
$CO\text{-}N_2$ discharge, plasma characts. and vibr. kinetics anal. 80−59331
$^{13}CO^+ + CO$, charge-exchange detection of $^{13}CO^+$ electronic absorption spectrum, hyperfine consts. calc. 78−70822
CO_2, $^1\Delta_u$ valence state, vertical energy level MC-CI wavefunction 79−45644
CO_2, $1\pi_g^3\ 2\pi_\mu^1$ config., ab initio eqn. of motion excitation energies 77−50376
CO_2, high resolution UV photoelectron spectra 80−91603
CO_2, SCF vertical spectrum for valence, mixed character and Rydberg states 77−50375
CO_2, threshold photoelectron and photoionisation spectra 77−14491
CO_2^+, dissoc., $^2\Sigma_g^+$ state, Wall Porter pot. surface, autodetachment and vibr. level population inversion 80−21275
CO_2^+, $^1\Pi_g$, mixed charact. state, vertical energy level MC-CI wavefunction 79−45644
CO_2^+, photoelectron and ion emission quantum yields, interelectronic state effects 79−6967
$CO_2\text{-}N_2$-He discharge, electron distrib. relax., numerical study 80−54070
CO_3^{2-}, electronic struct., X-ray spectra obs. 78−55185
C_3O_2, semirigid bender, rot.-vibr. energy level separations obs., struct. and pot. functions determ. 80−83446
$CO^+(A^2\Pi_i)$ vibr. relax. in He 80−53106
COS, high resolution UV photoelectron spectra 80−91603
$CO(1)+CO(\nu)\rightarrow CO(0)+CO(\nu+1)$, vibr. energy accumulation, reaction rate anal. 80−78692
CS, A $^1\pi$ state, collisional transfer and radiative decay, time resolved obs. 79−89809
CS, perturbation parameters between valence states 77−26975
CS, prompt emission and internal energy distrib. of $X^1\Sigma^+$ state 80−106364
CS, vibr. states in RF discharge plasma, microwave spectrosc. obs. 80−14133
CS, $X^1\Sigma^+$ ground state, diagrammatic perturbation theory calcs. 78−29737
CS_2, $^3A_2$ state, triplet bands, MCD spectrum, near UV absorpt. spectrum 80−48010
CS_2, $^3A_2$-state, MCD and UV spectrum, theoretical anal. 80−48011
CS_2, absorpt. spectra, Rydberg series converging to $A^2\Pi_u$ states of CS_2^+ 78−90182
CS_2, electronic transitions, solid phase UV spectra 77−3380
CS_2, high resolution UV photoelectron spectra 80−91603
CS_2, high resolution X-ray emission, valence electron struct. and chemical bonding 79−31545
CS_2, photodissoc., fragment energy distrib. 80−69200
CS_2, photoelectron spectrum, spin-orbit splitting, excited state form. 80−43102
CS_2, shock heated, visible emission 80−58274
CS_2^+, electronic transitions, solid phase UV spectra 77−3380
$CS(A^1\Pi)$ vibr. relax. in He 80−53106
CSFCl, sextic centrifugal distortion consts., microwave spectra *(German)* 77−75140
$CS(a^3\Pi)$ production, CS_2 photodissoc. below 1600 Å, quantum yield, rate const. 77−48658
CSe_2, photoionis. mass spectrum, Rydberg state props. 77−46604
Ca_2, ground state, multiple scatt. Xα calcs. 80−58149
Ca_2, new ground state, photolum. obs. vibr. consts., dissoc. energy 80−5576
CaCl, $D^2\Sigma$ and $X^2\Sigma$, two-photon vis. absorption, vibr. and rot. consts. 78−78764
CaCl, $E^2\Sigma\text{-}B^2\Sigma$ system, rot. anal., optical-optical double reson. obs., using two dye lasers 78−70855
CaF, $^2\Sigma$ ground state, laser-RF double reson. spectrosc. 80−69171
CaH absorpt. spectra 2480 to 2550 Å, new electronic states and rot. anal. 79−36662
CaH, low lying electronic states, ab initio SCF-CI calcs. 80−52893
CaH, spin doubling, SCF calcs. 80−95649
CaO, electronic struct., SCF calcs. 78−66462
CaO, form. from $Ca+O_2(CO_2)$, electronic states obs. 78−92450
Cd_2, pot. energy curve of low-lying states, MO theory 79−89624
$C_2(d^3\Pi_g)$ shock wave excitation, emission, excited state populations, in $CO\text{-}N_2$-Ar mixtures *(Russian)* 78−74638
CeO, $C_1\text{-}X_1$ and $D_3\text{-}X_3$ systems, fluoresc., vibr. spectra, laser spectroscopy obs. 80−32761
Cl_2, inner shell excited states, X-ray absorpt. spectra, HF calcs. 80−78536
Cl_2, pot. curves, asymptotic calcs. 77−6881
Cl_2, pseudopot. theory calcs. 77−42230
Cl_2, semi-empirical INDO calc. of electronic struct. 80−32611
Cl_2^-, pot. energy curves, from Cl_2 dissoc. electron attachment, 0−11.5 eV 77−75312
Cl_4, He(II) photoelectron spectra, spectral intensity patterns 79−98152
ClCN, ground and first excited bending, vibr. state, props., mol. beam elec. reson. 80−37823
ClCN, vacuum UV photodissociation spectroscopy, quantum yield, fluoresc. polarisation 80−32736
Cl_2CS, excitation, singlet and triplet states, two photon absorpt., singlet-singlet energy pooling, fluoresc. obs. 80−48032
ClFCS, second excited singlet state fluoresc., spectra 79−6957
$ClF(ClF_2^-)(ClF_3)$, localised MO ab initio calc., Gaussian orbital ab initio calc. 80−14083
$ClF^*(B^3\pi_0^+)$, electronically excited, chem. generation, B→X emission spectrum 79−57216
ClNSO, ground state geometry, ab initio calcs. 80−106259
$^{37}ClO_2$, $\nu_3=1$ state, laser-microwave double reson. obs. 80−95657
$ClO(X^2\Pi_i)$, radical, He(I) photoelectron spectrum, ΔSCF calcs. 79−72359
$Cl_nSi(CH_3)_{4-n}$, ^{35}Cl NQR, geminal and vicinal interactions on substituents electronic effect 80−63663
$Cl_nSi(OCH_3)_{4-n}$, ^{35}Cl NQR, geminal and vicinal interactions on substituents electronic effect 80−63663
Co, orientated mol., (e,2e) spectra, electron momentum density 79−98236
Co-porphine, ab initio LCAO SCF MO calcs. 79−6860

molecular electronic states continued
$Co(CN)_6^{4-}$, electronic struct., ab initio LCAO SCF MO calcs 79−18112
$Co(CN)_6^{3-}$, electronic struct., photochem. props., MS Xα calcs. 79−22600
$CoCl_n$, electronic struct., INDO theory 80−42948
CoO, vibr. IR absorption spectrum, mol. consts. 79−89666
$Cr_pC_n^+$, p=1 to 4, CrC_n^-, clusters, electronic props., mass spectra obs. *(French)* 79−45877
$CrCl_4$, ligand field states, multiple scatt. Xalpha calcs. 80−47891
$Cr(NO)_4$, bonding, shake-up intensities and shake-up energies, SCF Xα multiple scatt. calc. 80−74121
CrO, $A^5\Pi$-$X^5\Pi$ transition, rot. anal. laser induced fluoresc. and discharge emission spectra 80−69173
CrO_2Cl_2, collisionless IR multiphoton production of electronically excited parent mols. 79−41211
Cs_2, 4800 Å absorpt. band, classical method anal. 80−106330
Cs_2, ground state consts., pot. curve, laser spectroscopy 79−98247
Cs_2, He-Ne 632.8 nm radiation-induced disintegration 79−76474
Cs_2, laser-excited cross IR fluoresc. emission 79−76459
Cs_2^+, $^2\Sigma$ and $^2\Pi$ state pot. energy curves, two-centre model 79−26906
Cs_2^{2+}, interaction potential determ., comparison between all-electron frozen core and psuedo-potential results 80−69054
Cs_2^{2+}, low-lying states, MC SCF+CI 80−69053
$CsAsF_6$, γ-irrad., EPR spectra, hyperfine interactions and g-value determ. 77−81416
CsH, $X^1\Sigma^+$ and $A^1\Sigma^+$ states, pot. energy curves, Rydberg-Klein-Rees methods 78−50486
Cs_2^*, optically excited, cascade predissoc. *(Russian)* 79−10159
Cu complex, bis(N,N-diethyl-N′-benzoylthioureato)Cu(II), ESR 77−8393
Cu complex, Cu(II) dimers. temp. depend. PMR relax., singlet-triplet separation determ. 80−43073
$Cu(CN)_3^{2-}$, UV absorpt. spectra, electronic struct., MO calcs. *(French)* 77−34655
$CuCl_n$, electronic struct., INDO theory 80−42948
$CuCl_3(Cl_4^{2-})(Cl_6^{4-})$, electronic struct. studies by SCF, MSXα and INDO methods 80−74119
$CuF_2(F_6^{4-})$, electronic struct. studies by SCF, MSXα and INDO methods 80−74119
CuH, UV absorpt. spectra 80−87143
CuO, electronic spectra in rare gas matrix 78−996
CuO, fluoresc., matrix isolation spectra 78−46381
$^{63}Cu_2$, $B^1\Sigma_u^+$-$X^1\Sigma_g^+$ transition, Franck-Condon factors, r-centroids and pot. curves 80−43114
D_2, $^1\Sigma_g^+$ states, adiabatic calc. of vibronic states 78−5198
D_2, c, I and i states, pot. energy curves and vibr. levels, Born-Oppenheimer approx. 78−931
D_2, electron impact dissociative ionisation near $^2\Sigma_g^+$ state dissoc. threshold 80−43197
D_2, $G(3d)^1\Sigma_g^+$ and $g(3d)^3\Sigma_g^+$ singlet-triplet anticrossing 78−42138
D_3, emission spectra, rot. struct. obs. mol. const. determ., predissociation 80−106331
D_3^- repulsive state, form. in D_3^++Cs electron capture 79−59563
D_3^0 repulsive state, form. in D_3^++Cs electron capture 79−59563
D_3^+, ab initio vibr. intervals and vibr. freq. refinement 80−47968
D_2O, polarised photofluoresc. excitation spectra, VUV photodissoc. excited state lifetimes 78−5261
$D_2O^-(^2A_1)$, obs. in K(Cs) ionis. collisions with D_2O, 100-200 eV 78−17770
DSiCl, $^1A''$ states, geometry, bending pot. and vibr. freqs. 79−59593
DyO, UV emission spectrum, high resolution, band systems and isotopic shifts 80−87146
F_2, electron energy loss spectra, 0-17 eV, 5-140°, repulsive valence states excitation 80−32844
F_2, electron impact excitation, dissoc. of lowest electronic state 80−63839
F_2, eqns. of motion method, transition energies, oscill. strengths, electron impact Born cross section 77−18983
F_2 ground state, multiconfig. function, perturbation theory calcs. 79−13644
F_2, valence electronic states, $^1\Pi_u$←$X^1\Sigma_g^+$ absorption spectrum 79−63920
FBO, electronic struct. calcs. 77−30772
F_2CS, pot. surfaces, X^1A_1, a^3A_2 and $a^3A_2(b_1)$ states, ab initio SCF calcs. 78−86795
FNO, electronic transitions, limited GSMO and ESMO CI calcs., oscillator strengths, spectra 78−70750
F_2O, geometry, electron spectrum, vert. ionis. pot. ab initio calc. 80−58187
Fe complex, $[Fe(CN)_6]^{3-}$, electronic struct., optical transitions, XPS, Mossbauer isomer shift, valence ionisation pot., SCF-MSX calc. 79−6864
Fe complex, $FeCl_3$-tetraphenylporphyrin in PVC matrix, excited state props., electrochromism obs. 80−37815
Fe complex, tris (1,10-phenanthroline) iron(II), transient bleaching, excitation wavelength absorpt. 78−73060
Fe complexes, electronic and mag. struct., semiempiricial MO cluster calcs. 78−62733
$Fe_pC_n^+$, p=1 to 4, clusters, electronic props., mass spectra obs. *(French)* 79−45877
$FeCl_4^-$, effective charge, from IR and Raman scatt. intensity obs. 78−62809
$FeCl_n$, electronic struct., INDO theory 80−42948
FeCo molecules, matrix-isolation Mossbauer spectra 80−23448
FeF, electronic states, ab initio calcs., UV spectrum elucidation 78−74570
FeF, electronic states, anal. of rot. struct. 78−74674
FeH, FeD, matrix isolated IR spectra, mol. vibr. 79−93992
FeMn, matrix isolated Mossbauer spectra, ground state determ. 79−45740
FeO, electron affinity, ground state vibr., new assignment 77−75212
FeS_6^{10-}, electronic struct., SCF-Xα scatt. wave calcs., rel. to spectra of FeS, FeS_2 78−5138
$Fe_4S_4(SH)_4^{0,2-,3-}$, HFS-LCAO calcs., 4-Fe active site model in high pot. Fe protein and ferredoxin 80−42929
FeX_4^-, (X=F, Cl and Br), electronic struct. and isomer shift 80−63545
GaI, $A0^+$-$X0^+$ and $B1$-$X0^+$ transitions, isotope shifts, UV and visible spectra obs. 80−53005
GeF, $A^2\Sigma^+$ state, time-resolved fluoresc. 78−58732
GeH_3^-, electronic struct., electron affinity, inversion barrier, ab initio SCF Gaussian basis calc. 80−63552

molecular electronic states continued
GeO, mol., VUV photoelectron spectra, $X^2\Sigma^+$ state 79−72358
GeTe, matrix isolated absorpt. and emission visible spectra, electronic states 80−28026
H bonded species, IR line broadening, kinematic and electronic coupling mechanisms 77−68043
H-bond complex formation, enthalpy change due to electronic excitation, spectroscopic determ. 78−92496
H-bonded model systems, intermolecular charge transfer, biological implications 80−3572
H_2, $^1\pi_u$ and $^3\pi_u$ states, singlet-triplet energy difference, Hund's rule, inequality formulation 78−66482
H_2, $3p\pi D^1\Pi_u^+$ state, predissoc., Fano profile anal. 79−68274
H_2 (D_2) mol. bands, electron impact excitation, rot. transitions, cross sections in plasma 80−37896
H_2, appl. of Schrodinger eqn. *(Hungarian)* 79−3339
H_2, Bender-Wu formula, SO(4,2) dynamical group and Zeeman effect, perturbation coeffs. determ. 80−95674
H_2, $c^3\Pi_u$ metastable state, dissociative electron attachment 79−89794
H_2, diabatic and reson. states, dissociative photoionisation calcs. 80−47883
H_2, dissociative photoionisation, 19.8-40.8 eV, proton kinetic energy spectra 79−68273
H_2, $E,F^1\Sigma_g^+$ state, collisional and radiative props. 80−58357
H_2, electron impact dissociative ionisation near $^2\Sigma_g^+$ state dissoc. threshold of H_2 80−43197
H_2, electron impact excitation, to high Rydberg states, by threshold energy collision 80−83509
H_2, electron irrad., emission cross-sections for $3p^3\Pi_u$→$2s^3\Sigma_g^+$ 77−3477
H_2, electron wave function calc. with Weinbaum function supplemented by floating function 79−26882
H_2, electronic chemical pot., natural orbitals occupation numbers and electronegativity 80−63509
H_2, electronic energies of $D'\Pi_u$ and $B''\Sigma_u^+$ states, wave functions 77−23438
H_2, electronic states, adiabatic energy corrections, CI ab initio calc. 77−83502
H_2, electronic struct., valence bond model, pairwise correlation 80−78543
H_2, Fulcher system ($3p^3\Pi_u$→$2s^3\Sigma_g^+$), electronic-rot.-vibr. emission spectra, relative intensities calc. 79−6932
H_2, ground state, vibr. eigenenergies, functional form 80−27998
H_2, HD, $^1\Sigma_g^+$ states, adiabatic calc. of vibronic states 78−5198
H_2, HD, c, I and i states, pot. energy curves and vibr. levels, Born-Oppenheimer approx. 78−931
H_2, ionic-covalent config. mixing, pot. curves 77−34576
H_2, lifetimes of $3d^1\Sigma(3D)$ and $3d^1\Pi(3E)$ excited levels *(Spanish)* 77−71833
H_2, low-lying excited states, Rydberg and valence-shell characters, CI calcs. 78−5152
H_2, lowest singlet and triplet states, interactions, electronic force calcs. 80−63742
H_2, Λ doubling, $C^1\Pi_u$ states, calc. methods 78−90227
H_2, metastable level electron impact excitation, resonances *(Russian)* 80−43198
H_2 ortho-para transition as means of observing weak interaction parity nonconservation *(Russian)* 80−900
H_2, pairwise correlated GVB model, multiconfig. overlap approx. calcs. 79−31408
H_2, predissociation of $^1\Pi_u^\pm$ state vibr. and rot. levels, dissoc. yields meas. 80−32784
H_2 predissociation probabilities of $4p\pi^1\Pi_u^+ v' \geq 1$ levels, dissoc. channels interference 80−28074
H_2, quantum mechanics *(Hungarian)* 79−757
H_2 singlet superexcited levels, radiative emission 80−83415
H_2, singlet-triplet anticrossings between ungerade states 77−14498
H_2, singlet-triplet anticrossings, doubly excited 3^1K-$g(3d)^3\Sigma_g^+$ states 78−50598
H_2, states velocity auto-correl. function, relax time, neutron scatt. obs. 80−58401
H_2, two-photon positron annihilation, ang. correl. 79−81276
H_2, $X^2\Sigma_g^+$ state, vibr. energy levels, radiative corrections calcs. 78−90094
H_2^+ bound states in strong mag. field 80−99438
H_2^+, calc. of lowest vibr. states where L=0, P=+ 79−31502
H_2^+, dynamic polarisability, electronic states two centre Coulombic Green's function, continuous spectrum exclusion 78−82626
H_2^+ energy spectrum, variational cellular method calcs. 78−94192
H_2^+, extended LCAO method, 1sσg orbital *(Russian)* 79−93922
H_2^+, ground and first excited states in homogeneous magnetic field 78−925
H_2^+, ground state, asymptotic primitive function, symmetry adapted perturbation calcs. 79−6855
H_2^+, ground state energy inverse power expansion of two proton distances 79−97976
H_2^+, HD^+ electron reduced mass use in electronic Schrodinger eqn. 77−10576
H_2^+, high (10^9 G) mag. fields, dissoc. energy, electron binding energy and equilib. separation 80−52910
H_2^+, mol. electron density distrib., binding/antibinding anal. 80−95534
H_2^+, polarisability, internuclear distance depend., excluding continuous spectrum 77−10581
H_2^+, quantum mechanics *(Hungarian)* 79−757
H_2^+, repulsive states in dissociative ionis. of H_2 at 304 Å 78−82792
H_2^+, spontaneous emission lifetimes in ground electronic states 80−32810
H_2^+, variational cellular model 78−29726
H_2-Ar, states velocity auto-correl. function, relax time, neutron scatt. obs. 80−58401
H_2+He^+, DIM approx. pot. energy surfaces and nonadiabatic coupling 80−23330
H_2+He*, Penning ionisation, singlet interaction pot. anomalous struct. 77−75274
H_2^++H_2→H_3^++H, state-selected ion-molecule reactions threshold electron-secondary ion coincidence technique obs. 80−85166
H_3, electronically excited state obs., vibr. level struct. determ., predissoc. 79−41204
H_3, emission spectra, rot. struct. obs. mol. const. determ., predissociation 80−106331
H_3 excited electronic states rel. to H_3^+ dissoc. recomb. 79−89795

molecular electronic states continued
H_3, interat. pot. energy matrix elements, generalised DIM calc., ZDO approx. 80−52864
H_3, quartet states, diatomics-in-molecules theory, diatomic states mixing and overlap 79−59344
H_3, Rydberg spectrum , theory 80−5528
H_3, Rydberg states, Jahn-Teller calcs. 80−9494
H_3, Rydberg states energies and equilib. geometry calcs. 80−9493
H_3^-, dissociating states, lowest singlet and triplet PE surfaces, HF calcs. 79−81160
H_3^+, $^3\Sigma_u^+$ excited level, GO SCF calcs. 77−46507
H_3^+, ab initio vibr. intervals and vibr. freq. refinement 80−47968
H_4, excited potential energy hypersurfaces, 'triply right' (C_{2v}) tetrahedral geometries 77−83501
H_4, ground and excited states, SCF MO CI calcs. 77−6693
H_4 square, $^1B_{1g}$ and $^1B_{2g}$ states, Schrodinger eqn. solved by random walk method 79−63925
H_4, square config., $^1B_{1g}$, $^1B_{2g}$ states, quantum chem. calcs., random walk method 79−36518
HBr, fine struct. in dissociative attachment cross sections 80−87248
HCN, electron impact excitation of low lying electronic states, assignments 78−25671
HCN, electronic states, oscill. strengths calcs. 78−9095
HCN, electronically excited states, SCF CI calc. using Slater type orbitals 78−78645
HCN, H-CN dissoc. curves, SCF CI calc. 79−100405
HCN, HNC, differences 77−3260
HCN, photodissoc., photoabsorpt., photoemission and CN form. obs. 80−87141
HCN, SCF ab initio ground state pot. energy surface, geometry, rel. to HCN^- 78−78646
HCN, valence shell correl. energies, pair correls., unlinked cluster effects, CPA calc. 79−13648
HCN, vibr. fine struct. accompanying core ionis., STO calcs. 78−62844
HCN^-, SCF ab initio ground state pot. energy surface, geometry, rel. to HCN 78−78646
HCN^+, $^2\Sigma^+$ and $^2\Pi$ states, SCF and CI calcs. for determ. optimum linear geometries, bond angles calc. 80−74114
HCN^+, A and B $^2\Sigma^+$ states, pot. surfaces, ab initio SCF calcs. 80−27959
HCO′, low lying states, struct., energetics, ab initio STO calcs. 77−61682
HCl, emission K spectra, vibronic and core hole effects, nonempirical orbital defreezing calc. 78−5200
HCl, semi-empirical INDO calc. of electronic struct. 80−32611
HCl, vibr. excitation in electric discharge 80−87978
HCl^+, effective Hamiltonian, ab initio calc. 79−45632
HCl^+, emission cross sections for $A^2\Sigma^+,\nu' \rightarrow X^2\Pi_i,\nu''$ on electron impact and lifetime of $A^2\Sigma^+,\nu'$ state 77−38697
HD, electric field gradient at deuteron, numerical method 77−10578
HD, ground state props., nonadiabatic var. calcs. 78−58576
HD, nonadiabatic effects in the B, C and E, F states, rot. line strengths 78−5148
HD^+, Hellmann-Feynman theorem anomaly 80−63510
HD^+, spontaneous emission lifetimes in ground electronic states 80−32810
$H_2(D_2)$, Rydberg states, nonadiabatic effects, elec. field ionis. 80−9528
$HD(^1\Sigma_u^+)$+He, fluoresc. quenching and energy transfer processes 79−86032
$H_2(E,F^1\Sigma_g^+)$, two-photon excitation, cross section, radiative lifetime, quenching rate, IR fluoresc. obs. 78−37698
HF, emission K spectra, vibronic and core hole effects, nonempirical orbital defreezing calc. 78−5200
HF, fine struct. in dissociative attachment cross sections 80−87248
HF, highly excited, ionis. pot., mass spectrometric meas. 78−58603
HF, valence orbitals momentum distribs., (e, 2e) binding energy spectra 80−14237
HF, $X^1\Sigma^+$ state, many-body effects, HF STO calcs., diagrammatic perturbation theory 77−50355
HF, $X^1\Sigma^+$ state, 3- and 4-body perturbation theory modified pots. 77−88376
HF+Li→LiF+H, pot. energy surface, SCF and CI calcs. 80−71904
HF_2 ion, H-bond excited electronic states, CI calc., dissoc. and autoionising states 80−5489
H_2F^+, ground state, ab initio valence band calcs. 79−6869
HGeCl*, chemiluminescence obs., vibr. levels 77−81406
HI, dipole moment function, multiconfiguration SCF calc. 77−75330
HI, UV absorpt. spectra, ionis. limit region, assignment 78−21940
HNC^+, $^2\Sigma^+$ and $^2\Pi$ states, SCF and CI calcs. for determ. optimum linear geometries, bond angles calc. 80−74114
HNN′, low-lying states, struct., energetics, ab initio STO calcs. 77−61682
HNO $\tilde{A}^1A''$ excited state dipole moment, optical-optical double reson. Stark spectrosc. obs. 80−106337
HNO, isomerism, low lying electronic states, ab initio MRD-CI calcs. 80−83291
HNO, low-lying states, pot. energy curves 80−9533
HNO, low-lying states, pot. energy surfaces calcs. 80−102460
HNO^+, ab initio pot. surface, and isomerisation barrier of lowest states 79−22622
$HNO(A^1A'')$, state-selected fluoresc. lifetimes, collisional quenching rates 79−36674
HNSi, and HSiN, electronically excited states, MRD CI calc. 79−49947
HO_2^+, ab initio calc. of three lowest states 78−62711
H_2O, $(H_2O)_2$, mag. shielding rel. to hydrogen bonding 77−14348
H_2O, (e,2e) separation energy spectra, valence orbital electron momentum distribs. 77−38736
H_2O, ESCA and soft X-ray emission, vibr. excitation 80−23433
H_2O, electron density, basis set, electron correl. effects 78−74581
H_2O, electronic ground state, SCF HF and CI calcs, pot. energy hypersurface, spectroscopic consts. 78−50473
H_2O, electronic states, oscill. strengths calcs. 78−9095
H_2O, excited states, pot. energy curves w.r.t. bond ang., one-centre expansion approx. 79−6886
H_2O, ground state, CI calcs. on triply and quadruply excited configs., basis set effects 80−95549
H_2O, ground state, cond. energies, higher-order excitation contribs. 80−58166
H_2O, ground state, energy, bond parameters, diagrammatic perturbation theory calcs. 78−25414
H_2O, ground state ionis. pots., generalized Mo theory 80−52907

molecular electronic states continued
H_2O, H bonding, electronic struct., geometries, moments, dimerisation energies, charge distrib., pseudopotential calcs. 80−27942
H_2O, mol. Rydberg S←S and S←T transitions, semi-empirical SCF MO calc. 80−91453
H_2O, multiplet states, SCF theory 80−69062
H_2O, polarised photofluoresc. excitation spectra, excited state lifetimes, VUV photodissoc. 78−5261
H_2O, Rydberg states, visible spectra 78−9162
H_2O, VB minimal Slater basis set calcs., comparison with H_2S, MO calcs. 79−36536
H_2O^+, electronic spectrum, upper and lower electronic states 77−473
H_2O^+, spin and rot. fine struct., orbital angular momentum 80−83247
H_2O^+, states geometries, electronic vibr. coupling consts. HF calcs., comparison with Xalpha calcs. 80−27946
H_2O^+, vibr. and rot. struct., intensity factors and orbital angular momentum 80−83246
$H_2{}^{16}O$, interacting vibr. states, energy level fitting 78−78618
H_2O_2, electronic states, optical rot. dispersion, oscill. strength calcs. 78−9095
H_3O^+, ab initio CI calcs. of excited states 77−30796
HOO radical, lowest doublet electronic states, rel. to photodissoc. 79−93914
HPN-HNP, isomerisation energies, ab initio MRD-CI calcs. 80−106271
HPO, emission system, rot. anal. of vibr. bands 80−47957
HS_2 radical, ab initio calcs. of geometry and spectra 77−34552
HS_n^-, n=1-4, electronic struct., ab initio Hartree-Fock-Slater calcs. 80−74107
HS_n^{2-}, n=1-4, electronic struct., ab initio Hartree-Fock-Slater calcs. 80−74107
H_2S, electron density, basis set, electron correl. effects 78−74581
H_2S, electronic struct., ab initio CI SCF calc., spectra assignments 77−10586
H_2S, excitation energy, one-centre approx. calcs 78−70737
H_2S, semi-empirical INDO calc. of electronic struct. 80−32611
H_2S, VB minimal Slater basis set calcs., comparison with H_2O, MO calcs. 79−36536
H_2S, VUV absorption spectrum, Rydberg series assignments 79−64016
H_2S, valence and Rydberg excited states, SCF-Xα-SW mol. oribtal study 79−36550
H_2S^+, $^2B_1$, $^2A_1$ and $^2B_2$ electronic states, pot. energy curves, CI calcs. 80−87048
H_2S_2, rot. barriers, internal rot. and electronic struct., valence electron study 80−83344
H_2S_n, n=1-4, electronic struct., ab initio Hartree-Fock-Slater calcs. 80−74107
HSO radical, Doppler-limited dye laser excitation spectroscopy, rot., distortion and spin-rot. interaction const. determ. 80−83383
HSO, radical, electronic spectrum and struct. 77−75147
HSO radical, ground and excited first states, ab initio SCF and CI calcs. 77−30776
HSO-HOS, isomerisation energies, ab initio MRD-CI calcs. 80−106271
H_2Se_2, rot. barriers, internal rot. and electronic struct., valence electron study 80−83344
HSiBr, $^1A''$ states, geometry, bending pot. and vibr. freqs. 79−59593
HSiC-HCSi, isomerisation energies, ab initio MRD-CI calcs. 80−106271
HSiCl, $^1A''$ states, geometry, bending pot. and vibr. freqs. 79−59593
H_2SiO, electronic struct., dipole moments, mol. polarisability, force fields, ab initio calcs. 80−78531
H_2Te_2, rot. barriers, internal rot. and electronic struct., valence electron study 80−83344
$H_2(X^1\Sigma_g^+)$, semiempirical Morse pot. extension, fitting procedure appl. 79−36560
He, Pade type variational functions, appln. to ground state 80−87025
He^++He, He_2^+ mol. collision complex, pot. energy curve spectrum 77−19008
He_2, 600 Å emission continuum struct., in 700-900 Å region in glow discharge 80−95641
He_2, laser-driven transitions to high Rydberg states 80−106360
He_2, molecular spectrum and structure, singlet Π states $4p\pi$-$9p\pi$ 78−42080
He_2 optical absorpt. spectra and kinetic behaviour 80−95635
He_2, possibility of existence, Lennard-Jones pair potential 80−52869
He_2^{2+}, bound excited states, potential energy curves and rovibronic energy, dissociation 80−23327
He_2^{2+}, electronic energies, James-Coolidge method calcs. 78−17564
$HeCl^+$, interaction potential, HF dissociation energies, LCAO SCF calcs. 77−6880
HeH, HeH^+, variable screening model calcs. 78−74587
HeH^+, (HeD^+), rot. predissoc., nucl. motion effects on rovibr. energies and widths 78−70885
HeH^+, electronic momentum distribution, Coulomb shift and correl. coeffs. 80−83266
HeH^+, $X^1\Sigma^+$ electronic ground state, pot. curve, rovibronic and dissoc. energies 79−72254
HeH^{2+}, lowest 20 states, eigenvalues, electronic wavefunctions, w.r.t. internuclear separation 77−18811
$^4HeH^+$, ro-vibr. quasi-bound levels of $X^1\Sigma^+$ state, eigenenergies, dissoc. 77−26997
$^4HeH^+$+He, 1 keV, collision-induced dissoc., ro-vibr. assignments, proton spectra obs. 79−3556
HeH_2^+, electronic struct. 79−31414
$HeHe_2^+$, doublet, ab initio pot. energy surface calcs. for ground and lower excited state 79−63898
$HeNe^+$, collisional form., excitation, pot. energy curves calcs. 77−6697
$He_2(\Sigma_g^+)$, general-model-space diagrammatic perturbation theory appl. 80−47844
$^4He_3$, Efimov states and binding energies, Faddeev coord. momentum approach 78−46259
Hg_2, pseudopot. theory calcs. 77−42230
Hg_2^+, electronic struct. and photoabsorpt. calcs. 80−27932
$HgBr+O_2(N_2)(H_2)(He)(Ne)(Ar)(Kr)(Xe)$, vibr. relax., rate coeffs., fluoresc. obs. 80−63697
$HgBr_2$, electronic struct. and photodissoc., effective core pots. and POL(1) CI wave function 80−63560
$HgCl_2$, electronic struct. and photodissoc., effective core pots. and POL(1) CI wave function 80−63560
HgD, $A^2\Pi$ state radiative lifetime, pulsed dye laser excitation meas. 78−94288
HgH, $A^2\Pi$ state radiative lifetime, pulsed dye laser excitation meas. 78−94288

molecular electronic states continued
HgH, $HgCl_2$, relativistic effective core potentials, ab initio calcs. 78−86767
HgH, pseudopot. theory calcs. 77−42230
I^- in aq. soln., anthracene sulphonate sensitised photooxidation via singlet $^1O_2$ 77−32812
I_2, A-X system 79−63995
I_2, band system, MC SCF pseudopot. calcs. 78−78632
I_2, electronically excited states, vis. and UV laser techniques, book contrib. 78−9277
I_2, hyperfine struct. in B-X transition, laser spectroscopy of pure I_2 jet 79−81234
I_2, in Ar, emission spectrum interpretation 80−95634
I_2, laser dissociation, in gas and soln. *(German)* 78−90240
I_2, multiphoton reson. ionis. bands, 360-600 nm 78−90233
I_2, sequential multiphoton ionis. spectroscopy 79−50163
I_2, two-photon sequential absorpt. spectroscopy 77−54581
I_2, UV laser transitions, electronic designation 79−944
I_2, use as test mol. in modern spectroscopy, review 78−90317
I_2, vertical valence excited states, CI nonempirical pseudopotential calc. 77−71757
$^{129}I_2$, energy levels near B-state dissoc. limit, two-photon spectrosc. obs. 80−106367
I_4^{2-}, electronic struct., binding energy, charge distrib. from free electron model *(German)* 78−29741
$I_2(B^3\pi_{o^+u})$, ps excitation, in CCl_4 soln., ultrafast decay and spectrum 78−9184
IBr, $B^3\Pi(0^+)$ excited state, laser-induced fluoresc. 80−58309
IBr, $B^3\Pi(0^+)$ states, Franck-Condon factors, RKR turning pts. 77−34681
ICN, A-state photolysis, $I(^5P_{1/2,3/2})$ branching ratio wavelength depend. 80−81335
ICN, photodissoc., product rot. distribs. 79−66310
ICN, photodissoc. dynamics, moment anal. 78−13557
ICN, vacuum UV photodissociation spectroscopy quantum yield, fluoresc. polarisation vacuum UV photodissociation spectroscopy, quantum yield, fluoresc. polarisation 80−32736
ICl, $B^3\Pi(0^+)$ states, Franck-Condon factors, RKR turning pts. 77−34681
ICl, $B^3\Pi(0^+)$-$X^1\Sigma^+$ fluoresc., predissoc. 77−34682
IF, $B^3\Pi(0^+)$ states, Franck-Condon factors, RKR turning pts. 77−34681
IF, $B^3\Pi(0^+)$-$X^1\Sigma^+$ fluoresc., predissoc. 77−34682
IF, He(I) photoelectron spectra, interpretation 79−13766
$I(H_2O)_n^-$, geometric and electronic struct., CNDO/2 calcs. 77−79542
I_2He, Van der Waals mol., photodissoc. lifetime, I_2 vibr. depend. 79−6977
$I_2X^1\Sigma_g^+$, collisional relax. of highly excited vibr. levels, using I_2 optically pumped laser 80−43155
InCl, discharge excited spectrum 4100-3900 Å, vibr. anal. 80−32732
InKr, low-lying electronic states, PE curves, transition moments, emission coeffs. 79−6894
IrF 6, $\Gamma_{8g}(^2T_{1g})$ state, electronic Raman scatt. and absorption spectra at 1.6 μ, resolution of Jahn-Teller problem 79−36648
IrF_6, in mixed crysts., Jahn-Teller effect, $\Gamma_{8g}(t_{2g})^3$ state, 6800 Å 78−76032
IrO, ground state, matrix isolation spectra 78−46352
K+H, covalent and ionic states interaction, config. mixing 78−50613
K_2, absorpt. and relax. const. determ. by optical laser pumping method 80−102550
K_2, optically aligned ground state, Hanle effect obs. 79−36707
K_2, photodissoc. products of $C^1\Pi_u$ and $C^1\Sigma_u^+$ states 79−98171
K_2^+, $^2\Sigma$ and $^2\Pi$ state pot. energy curves, two-centre model 79−26906
K_2+Cl(Br)→KCl(KBr)+K* product electronic state distrib., chemiluminesc. 77−40529
$K_2(A^1\Sigma_u^+)$, form. by K(4P) ats. in K discharge 80−44013
Kr, liq., recomb. and self-trapped exciton luminesc., free electron dynamics, excited states 80−25463
Kr^-, electron capture expts. to search for long lived states 79−72410
Kr_2, kinetics of optically excited electronic states 78−63059
Kr_2^+, electronic states, pot. curves, with/without spin-orbit interaction 78−33443
Kr_2^+, weakly bound excited states, dissoc. energies 78−78748
KrAr, photoionisation spectra of ground and excited states 78−5297
KrCl, B and C states, energy ordering from temp. depend. of emission spectra 80−78837
KrF discharge pumped laser, energy extraction, collisional coupling between B, C and D-states 80−28213
KrF, electronic states, ab initio CI calcs., spin-orbit coupling, pot. curves, dissoc. energy, dipole moments 77−38619
KrF, electronic states, ab initio POL CI calcs. 78−66474
KrF, fluoresc. spectrum, theoretical modelling using electronic potential curves 78−63086
KrF, formation and quenching of electronic excited states 77−673
KrF, laser emission, ab initio config. interaction calcs. on electronic states 78−63083
KrF, laser spectrum, discharge-pumped, absorption bands and lines, assignment 78−79004
Kr_2F, semi-empirical VB calcs. of hyperfine interactions and struct. 79−85902
KrF*, excimer electronic struct., config. interaction, electrostatic model 78−927
KrO, lasing, low-lying electronic states, ab initio config. interaction calcs. 78−63084
KrO^+, $X^4\Sigma^-$ state, pot energy curves and correl. effects, elastic scatt. cross sections 80−23502
LaF^+, electronic spectra, rot. anal. and orbital configurations 80−83240
LaH, $^1\Sigma$ state, Dirac-Fock one-centre calcs. 80−23301
LaO, ground and excited states following bimolecular oxidation of La metal 77−29011
Li-H_2O(ethylene) 78−66465
Li^++He collisions, K-shell vacancy sharing, ab initio LCAO-SCF, CI calcs. 77−19054
Li_1^+, potential energy curves, exchange and ion-multipole interactions, vibrational energy levels 79−98175
Li_2, and anion, electronic struct., spin-unrestricted, spin-restricted SCF HF calc. 78−90331
Li_2, and isotopic variants, low-lying X-B transition freq. calc. 78−90180
Li_2 and Li_2^+, Li 1s hole states calc., dissoc. Auger electron energies 77−23443
Li_2, gerade excited electronic states, pulsed optical-optical double reson. spectroscopy, laser medium 79−81220
molecular electronic states continued
Li_2, lowest $^1\Pi_g$, $^1\Pi_u$, $^3\Pi_g$, $^3\Pi_u$ states 77−54517
Li_2, MCSCF and CI calcs. 80−95526
Li_2, radiative lifetimes of $B^1\Pi_u$ states, model pot. calcs. 78−46397
Li_2, $X^1\Sigma_g^+$ and $A^1\Sigma_u^+$ states, electronic struct. and spectra 79−89615
Li_2^-, electronic struct., ab initio calcs. 77−34553
Li_2^+, $^2\Sigma$ and $^2\Pi$ state pot. energy curves, two-centre model 79−26906
Li_2^+, $X^2\Sigma_g^+$, $^2\Sigma_u^+$, $A^2\Pi_u$ and $^2\Pi_g$ states, electronic struct. vibr. spectra, ab initio calcs. 79−36507
Li_3, electronic struct., SCF and SCF-CI calcs. 80−87044
Li_3^-, electronic struct., SCF and SCF-CI calcs. 80−87044
Li_3^+, electronic struct., SCF and SCF-CI calcs. 80−87044
Li_4, MCSCF and CI calcs. 80−95526
$Li_2(A^1\Sigma_u^+)$, dye laser excited, collision induced dissociation 79−91920
$Li_2(A^1\Sigma_u^+)$, state multipoles transfer following rot. inelastic He collisions, polarised emission obs. 80−5608
$LiAlH_4$, $LiBH_4$, ab initio calc. of geom. struct., charge distrib., bonding and pot. energy surfaces 80−18796
$LiBH_4$, comparison of potential surfaces, calculated ab initio and semiempirical CNDO/2 scheme 79−41112
$LiBH_4$, H bridged system, floating spherical Gaussian model 80−78518
$LiBH_4$, struct., pot. surface, ab initio calcs. 79−41092
$LiBeH_3$, H bridged system, floating spherical Gaussian model 80−78518
LiBe(Mg)(Ca), $^2\Sigma^+$ and $^2\Pi$ states, mol. binding energy curves 80−58189
LiBr, Compton profile anisotropies 79−27044
$LiCH_5$, H bridged system, floating spherical Gaussian model 80−78518
LiCl aqueous soln., ion-water clusters, electronic struct., Compton profile 78−47227
LiF, Li 1s ionisation pot. calc., Li 1s XUV absorpt. spectrum 77−23443
LiF, $X^1\Sigma^+$ state, many-body effects, HF STO calcs., diagrammatic perturbation theory 77−50355
LiF^-, ground and excited states, ab initio calcs. single config. and multiconfig. SCF calcs. 80−52873
LiH, elec. struct. by spin-adapted vector method 79−54777
LiH, pairwise correlated GVB model, multiconfig. overlap approx. calcs. 79−31408
LiH, polarisabilities and dipole moment derivatives, virial theorem calcs. 77−57865
LiH, $X^1\Sigma^+$ ground state, spectroscopic and pot. functions, method for combining spectroscopic data 79−45782
^7LiH, $A^1\Sigma^+$ state, vibr. levels, radiative and nonradiative lifetimes 78−66604
$(LiH)^+$+meson system, ground and 1st excited state pot. surfaces, quantum mech. calc. 78−5377
LiH_2O^+, geom., electronic struct. FSGO model calcs. 78−82614
LiN_2, geom., electronic struct. FSGO model calcs. 78−82614
LiNC type molecules, Born-Oppenheimer approx. applicability 80−32603
$LiNH_3^+$, geom., electronic struct. FSGO model calcs. 78−82614
LiNa, and anion, electronic struct., spin-unrestricted, spin-restricted SCF HF calc. 78−90331
LiNa, ground and excited states, model pseudopot. calcs. 77−75069
Li_2O^-, electronic struct. and config., ab initio SCF study 79−85898
LiOH, $^1A'$ pot. energy surface, diatomics-in-mols. method calcs. 79−36566
LiOH , electronic struct. and config., ab initio SCF study 79−85898
$^6Li^{35}Cl$, electronic ground state, first vibration state lifetime, MBER meas. 79−86023
LrH, $^1\Sigma$ state, Dirac-Fock one-centre calcs. 80−23301
LuF, $^1\Pi$ hyperfine struct. parameters, bonding 77−58036
LuF, vibr. anal., 3000-6500 Å *(French)* 77−23502
LuH, $^1\Sigma$ state, Dirac-Fock one-centre calcs. 80−23301
Mg_2, Ar matrix isolated laser photoluminescence spectra, electronic absorpt., emission, vibronic and vibr. relax. 78−82744
Mg_2, ground state, multiple scatt. Xα calcs. 80−58149
Mg_2, Mg_2^+, electronic struct., pot. energy curves, multiconfig. SCF calcs. 78−5124
Mg_2, perturbation theory calcs. 79−13644
Mg_2, $X^1\Sigma_g^+$ state, pot. curve, coupled pair many electron theory calc. 79−89621
MgD, $A^2\Pi$ state radiative lifetime, pulsed dye laser excitation meas. 78−94288
MgF_2, ground state, nonempirical LCAO SCF calcs. 78−66469
MgF_2^-, ground state, conform., electron affinity, extended basis SCF calcs. 79−72253
MgH, $A^2\Pi$ state radiative lifetime, pulsed dye laser excitation meas. 78−94288
MgH, and MgD, $B'^2\Sigma^+$-$X^2\Sigma^+$ band system, ab initio CI calcs. 79−93970
MgH, Morse and Lippincott pots., r-centroids, dissociation energy 78−13446
MgH, X and $B'\,^2\Sigma^+$ and $A\,^2\Pi$ ab initio CI calc. 79−31415
MgH, X→A and X→B' band systems, oscill. strengths and photodissoc. cross-sections 79−94045
MgH^+, CI pot. curves and cross sections for lowest singlet states 80−23343
MgO, dissociation energy in range 2020 to 2160K 77−549
MgO, electronic transition strengths, shock tube meas. 80−87183
MgO, KLL' Auger spectra, electronic relax., Friedel model 77−65444
MgOH, struct. and electronic props., ab initio calcs. 80−74113
MgX_2, X=Cl, Br, valence shell electronic struct., ab initio SCF calc., photoelectron spectra 79−31383
MnH(MnD), $^7\Sigma$-state, mol. parameters, ESR and optical spectrosc. 78−94264
$MnH_2(MnD_2)$, $^6A_1$ state, mol. parameters, ESR and optical spectrosc. 78−94264
MnO, $A^6\Sigma^+$-$X^6\Sigma^+$ electronic transition, rot. and hyperfine struct. 80−74134
MnO, SCF CI calcs., ground and first excited states, bonding mechanism 77−14347
MnO_4^{m-} chromophore, tetrahedral, electronic spectra 77−58032
Mo complex, hexadimethylamino molybdenum, electronic description of triple bonds and verification by photoelectron spectroscopy 78−41949
Mo complexes, electronic struct., XPS and X-ray emission spectra 77−42336
Mo complexes, μ-oxo, di-μ-oxo, di-μ-oxo-μ-carboxylato bridged oxodimolybdates (v), structures 77−76370
Mo complexs. bis(η-cyclopentadienyl) Mo halides, electronic struct., photoelectron spectra 77−75214
Mo cpds, chemistry and uses, conf., Oxford, Eng., Sep (1976) 77−77749

molecular electronic states continued
Mo_2, matrix isolated visible absorpt. spectra, electronic, vibronic and vibr. states 80−28027
$Mo_2Cl_8^{4-}$, low lying states, weak electronic coupling, Xα valence band theory 79−72237
$Mo_6Cl_{14}^{2-}$, cluster ground state electronic struct. SCF Xα SW calc. 79−3607
MoN, matrix isolated visible absorpt. spectra, electronic, vibronic and vibr. states 80−28027
$Mo_2(NH_2)_6$, electronic description of triple bonds and verification by photoelectron spectroscopy 78−41949
MoO, matrix isolated visible absorpt. spectra, electronic, vibronic and vibr. states 80−28027
$Mo_2(OH)_6$, electronic description of triple bonds and verification by photoelectron spectroscopy 78−41949
N, $3p^4S^0$-state quenching in low-press. glow discharge 80−23355
N_2 ($^1\Sigma_g^+$), charge density, X-ray scatt. factors, gas phase electron diffr. 78−930
N_2, ($C^3\Pi$) nonequilibrium rotational level distrib. in gas discharge *(Russian)* 78−86796
N_2, (e,2e) spectra, valence momentum distribs. and config. interaction 77−19101
N_2, $B^3\pi_g$ state excitation and deactivation in positive column 77−3482
N_2, $C^3\Pi_u$ excited state, lifetime determ. by phase-shift and delayed-coincidences methods 77−18988
N_2, $C^3\Pi_u$-state, electron impact excitation, low energy 80−9746
N_2, elec. field gradient electronic contrib., using generalised X-ray scatt. factors 77−75321
N_2, electron density distrib., electron correl. effects, approx. HF-CI calcs. *(German)* 78−33439
N_2, electron impact excitation, 10-50 eV, differential cross-sections 78−13619
N_2, electron impact excitation, $x^1\Sigma_g^-$ and $y^1\Pi_g$ states lifetimes meas. 78−17806
N_2, electron impact excitation, 10-50 eV, integral cross-sections 78−17810
N_2, electron impact excitation, 12.5-14.2 eV energy-loss region 78−17811
N_2, electron impact excitation, to high Rydberg states, by threshold energy collision 80−83509
N_2, electron impact reson. excitation of new valence state 79−36785
N_2, electron scatt., reson. excitation and dissoc. attachment, vibr. state depend. 80−78717
N_2, electronic density, multiple scatt. method, muffin-tin approx. 80−27924
N_2, electronic states excitation and population in glow discharge 77−487
N_2, electronic struct., binding energy and interatomic distance, SCF variational cellular calc. 80−9498
N_2, electronic structure calcs., self-consistent, accelerating convergence of iterative process 80−87037
N_2, excitation energies, eqn. of motion-Green's function calcs., 3rd order contribs. 77−65417
N_2, inner shell $(1s)^{-1}(\pi 2p)^1\Pi$ state, energy, vibr. struct., electron impact investig. 78−13611
N_2, isoelectronic sequence, Rydberg transitions, term value-ionisation pot. correl. 80−58276
N_2, isotopic forms, visible spectra, rovibronic and rot. anal., C′ $^3\Pi_u$ and C $^3\Pi_u$ interaction 77−18933
N_2, metastable level electron impact excitation, resonances *(Russian)* 80−43198
N_2 molecule, formation of $C^3\Pi_u$ and $B^3\Pi_g$ in early afterglow 79−34305
N_2, N K-shell excitation, high-resolution electron energy loss spectra 80−53152
N_2, orientated mol., (e,2e) spectra, electron momentum density 79−98236
N_2, transition moments between excited electronic states 78−5204
N_2 triplet-triplet transitions, Einstein-A coeffs., oscill. strengths, lifetimes, theory and experiment comparison 80−47876
N_2, vibr. struct., core and valence ESCA spectra, Franck-Condon and HF anal. 80−32602
N_2^-, first $^2\Pi_u$ state form. and decay 80−58177
N_2^+, A- and B-states interactions, time-resolved obs. 80−18862
N_2^+, $B^2\Sigma_u^+$ excited state, lifetime determ. by phase-shift and delayed-coincidences methods 77−18988
N_2^+ Meinel system, high resolution spectrum to 11 250 Å 80−99497
N_2^+, partial photoionisation cross section and photoelectron angular distribution for $X^2\Sigma_g^+$ state determ. 80−83429
N_2^+, produced by threshold ionis., X($^2\Sigma_g^+$), A($^2\Pi_u$) and B($^2\Sigma_u^+$) vibr. struct. and mol. parameters 78−94294
N_2^+, vibr. intensity distribs. for electronic states prod. by photoionis. 78−25614
N_2^+ $X^2\Sigma_g^+$-state, vibr. states asymmetry parameter and photoelectron spectrum 80−95591
N_2^{2+}, low-lying electronic states, pot. energy curves calcs. by SCF technique, vibr. and ionisation consts. 80−69091
N_2^{2+}, recomb. energy determ. from pot. curves 80−58335
N_2-CO_2(-He) volume discharge, N_2 vibr. levels, stepwise excitation, effect on electron energy balance 80−54071
N_2-He ion nuclear pumped lasers feasibility study and quenching 80−64001
N_2+H^-, charge transfer, ejected electron spectra 79−45828
N_2+H^+(e), vibrational N_2^+ excitation *(Russian)* 80−53156
N_3^- electronic struct., SCF Xα scatt.-wave calcs. 77−50364
N_3^-, low-lying excited states 79−31425
N_3^-, theoret. electron density distrib. cf. expt. density distribs. of NaN_3 and KN_3 77−46489
N_2^+($B^2\Sigma_u^+$), perturbation of $v=1$ vibr. level, rot. lines freqs. and intensities *(French)* 77−79640
NBr, in solid Ar, $b^1\Sigma^+ \rightleftarrows X^3\Sigma^-$ transitions 80−32702
$NCNCO_2$, geometrical struct., INDO calcs. 79−22602
NCO, $A^2\Sigma$ state, Fermi resonance and vibr. relax. in solid Ar 78−5212
NCl, in solid Ar, $b^1\Sigma^+ \rightleftarrows X^3\Sigma^-$ transitions 80−32702
ND, $b^1\Sigma^+$ state, radiative lifetime, Einstein coeff. 78−90217
NF*($a^1\Delta$ and $b^1\Sigma^+$) production in F+HN_3 reaction 79−11770
NH, 3Π states, MC wavefunctions, rot.-vibr. anal. 79−13652
NH, $b^1\Sigma^+$ and $d^1\Sigma^+$ states, multiconfig. wavefunctions, optimal config. selection 77−34566
NH, $b^1\Sigma^+$ state, radiative lifetime, Einstein coeff. 78−90217
NH, fine struct. in $X^3\Sigma^-$ and $A^3\pi$ states, STO and GTO calcs. 77−6679

molecular electronic states continued
NH, ND, $X^3\sigma^-$ state vibr. relax. Ar matrix, energy gap law breakdown 77−30963
NH_2 (A^2A_1), excited state dynamics and bimol. quenching processes 80−9681
NH_2, pot. energy curves of X^2B_1, A^2A_1, $^2B_2$ valence-shell and $\pi_u{}^23s$-type Rydberg states calc. by CI 80−74138
NH_2, spin and rot. fine struct., orbital angular momentum 80−83247
NH_2, vibr. and rot. struct., intensity factors and orbital angular momentum 80−83246
NH_2, X^1B_1 ground state, 010 level, mol. consts., emission spectra obs., 0.4-0.89 μ 78−74688
NH_2, X^2B_1, A^2A_1 and B^2B_2 states, ab initio SCF CI calcs. 78−29746
NH_2^+, low lying states, ab initio MRD-CI pot. surface calcs. 79−89611
NH_2^+, quintet states, pot. energy surfaces, ab initio SCF MO calc. 78−25419
NH_3, and ND_3, new electronic state, multiphoton ionis. obs. 78−74717
NH_3, C′-state, 3-photon gas phase spectroscopy obs. 79−89715
NH_3, ESCA and soft X-ray emission, vibr. excitation 80−23433
NH_3, expansion cooled, mol. photoionisation, rot. struct., rot. predissoc. of excited states 80−91611
NH_3 inverse level doubling mol., space and combined parity nonconservation *(Russian)* 80−52879
NH_3 low lying states, generalised VB and CI calcs., vertical excitation energies 77−30789
NH_3, mol. beam state selection and focusing, hyperfine spectrum 80−28119
NH_3, mol. Rydberg S←S and S←T transitions, semi-empirical SCF MO calc. 80−91453
N_2H_2, $N_2H_2^+$, ab initio calcs., electronic struct., geometries relative energies 77−46487
N_3H_3 radical, lowest two electronic states 80−925
$NH_2(A^2A_1)$, IR emission detection in UV laser photodissoc. of NH_3 80−11901
NH($A^3\Pi$, $b^1\Sigma$), two-photon generation in NH_3 UV laser photodissoc. 80−11901
NH_2CO', low-lying states, struct., energetics, ab initio STO calcs. 77−61682
NH_4Cl, gas $^1A_1$ ground state, pot. surface 80−32626
NHD radical, A-A′ state transitions, Stark effect contribs. 80−23455
$NH_2(F_2)(Cl_2)$, SCF-MO-HF calc., struct. and one-electron props., population anal. indices 79−76338
NH(ND) $X^1\Sigma^-$, in inert gas solid, vibr. relax., matrix and isotope effects 80−95713
$NH_3(ND_3)$ in solid Ar, UV absorption spectra, temp. depend. of matrix spectra 80−63652
$NH_2(X^2B_1)$, laser-induced fluoresc. obs. in UV laser photodissoc. of NH_3 80−11901
$NH_2(X^2B_1)$, MODR, hyperfine coupling consts., spin rot. consts. 78−1010
$NH_2(X^2B_1)$ radical, and ND_2, ionisation pot., vibr. anal., ab initio calcs. and vacuum UPS obs. 80−53047
NI, in solid Ar, $b^1\Sigma^+ \rightleftarrows X^3\Sigma^-$ transitions 80−32702
NO, $^2\Pi_{1/2}$ and $^2\Pi_{3/2}$ band centre freqs., opto-acoustic detection 77−58108
NO, $3s\sigma(A^2\Sigma^+)$, in Ar Kr Xe matrices, Rydberg state 'bubbles', reson. fluoresc. obs. 77−83636
NO, 4-photon ionis. spectrum 2- and 3-photon resons., low temp. assignments 78−70887
NO, $a^4\Pi$ and $b^4\Sigma^-$ states, electron impact spectra 78−58733
NO, and isotopic forms, $v=0$ electronic states, spin-rot. doubling 80−5540
NO, γ and β system, electronic transition probability 80−106332
NO, γ band lines, collisional broadening coeff. and optical collision diameter 80−63714
NO, $\gamma(0,0)$ band, collisional broadening parameters 80−63713
NO, $I^2\Sigma^+$ state, valence bands, absorpt. spectra 78−46361
NO, IR emission Fourier transform spectroscopy, mol. rot.-vibr., RKR potential curve calc. 80−95618
NO, in Ar and N_2 matrices, 6K, vac. UV photolysis, β and M band emissions 78−73069
NO, mol. beam tunable diode laser sub-Doppler spectra, $^2\Pi_{1/2,3/2}$ Λ splittings 79−41180
NO, N K-shell excitation, high-resolution electron energy loss spectra 80−53152
NO, positron energy levels, rel. to Rydberg levels of Na, NO 79−86089
NO, predissoc. rates and pertrubations in certain electronic states, time resolved spectra 77−27131
NO, state selective step-wise photoionis. with mass spectroscopic ion detect. 80−43119
NO, two-photon excitation to levels near and above the dissoc. limit 79−10161
NO, UV fluorescence, IR laser induced 80−53032
NO, $v=0,1$ states, spectroscopic data calc. 78−86851
NO, $X^2\Pi$ state, vibr. relax., IR-UV double reson. obs. 80−106338
NO, Zeeman spectrum, mol. beam elec. reson. spectrosc. 80−91621
NO^+ ground state mol. consts., from NO $X^2\Pi(v''=0)$ UPS obs. 80−14177
NO^+, pot. energy curves calcs. 80−5602
NO+N_2(Ar), $^2\Pi_{3/2}$, $^2\Pi_{1/2}$ states, line broadening, mag. moment effect 79−72391
NO+Ne(Ar)(N_2)(H_2)(CO), $E^2\Sigma^+$ and $B'^2\Delta$ states fluoresc. collisional deactivation 79−6965
NO+O_3, fs-states and rot. states, effect on reactivity 80−89473
NO_2, electronic states, pot. energy surface calcs. 77−6673
NO_2, electronic struct., A^2B_2←X^2A_2 and B^2B_1←X^2A_1 absorpt. bands 77−3257
NO_2, excited electronic states, time-resolved spectrosc. 79−45747
NO_2, ground state pot. surface, ab initio LCAO MO SCF calcs. 80−102461
NO_2 Hanle effect, nonstationary states in molecular spectroscopy, level splitting 80−23465
NO_2, lowest quartet state theoretical excitation energy 79−68221
NO_2, perturbed $^2B_2$ state fluoresc. lifetime, excitation energy depend. 78−90202
NO_2, shock heated, visible emission 80−58274
NO_2, VUV absorption spectra, Rydberg states assignments 77−58040
NO_2, vertical electronic spectrum, SCF and CI calcs. 77−30878
NO_2, visible spectrum simplification, rot.-vibr. levels, excitation, polarisation labelling spectroscopy 80−32730
NO_2^-, electronic struct., X-ray spectra obs. 78−55185

molecular electronic states continued
NO_2^-, solvated, in H_2O, ethanol, cyanomethane, and DMF lowest n-π^* transition 79−85960
NO_3, electronic struct., X-ray spectra obs. 78−55185
N_2O, electron energy loss spectrum, optically forbidden transitions 77−31015
N_2O, electron impact, dissoc. patterns 79−7021
N_2O, N K-shell excitation, high-resolution electron energy loss spectra 80−53152
N_2O, photoelectron spectrum, vibronic interaction and autoionis. effects 80−95680
N_2O^+, electronic ground state, INDO SCF MO calcs. 78−82644
N_2O^+, pot. energy hypersurface characts. calc. in $O^+ + N_2 \rightarrow N + NO^+$ react. 78−60996
$NO(A^2\Sigma^+)$, prod. by near reson. electronic energy transfer, initial rot. state population 79−68304
NOH, groundstate electronic struct., MRD CI calc., dissoc. energy, isomerisation energy 80−14088
NOH isomerism, low lying electronic states, ab initio MRD-CI calcs. 80−83291
NOH^+, ab initio pot. surface, and isomerisation barrier of lowest states 79−22622
$NO(X^2\Pi) + Cd(^1P_1) \rightarrow NO(A^2\Sigma^+, v=0)$ electronic energy transfer react., collisional fluoresc. quenching 77−14548
$NO(X^2\Pi) + Zn(^1P_1) \rightarrow Zn(^1S_0) + NO(A^2\Pi^+, v=0,1)$, near-resonant electronic energy transfer, fluoresc. quenching 77−14549
NO_2*, multiple IR photon fluoresc. excitation and dissoc., electronically excited 80−48050
$NO(b^4\Sigma^-)$, electron impact excitation energy, radiative lifetime, quenching in NO 77−79642
$N_3P_3Cl_6$, ionisation energy and electronic struct., UV photoelectron spectra and Xα calcs. 78−94281
NS, ground ionic state, photoelectron spectra determ. 77−46596
$N(^4S) + N^+(^3P) = N^+(^3P) + N(^4S)$, gerade-ungerade splitting of N_2^+ pots., cross sections 77−30987
$NS(B^2\Pi)$, form. kinetic in active $N + S_2Cl_2$, chemilum. obs. 79−39151
$^{14}NH^+(^{15}NH^+)(^{14}ND^+)$, ab initio CI calc. Λ type doubling in $X^2\Pi$ states 78−82714
Na $A^1\Sigma_u^+ \rightarrow X^1\Sigma_g^+$ system, transition moments and radiative lifetimes calcs. 77−34697
Na zeolites, electronic struct., quantum chemical study 80−69058
Na + H_2 covalent and ionic states interaction, config. mixing 78−50613
Na_2, $A^1\Sigma_u^+$ state, spectroscopic consts. and RKR pot. calcs. 77−75130
Na_2, absorpt. and relax. const. determ. by optical laser pumping method 80−102550
Na_2, and anion, electronic struct., spin-unrestricted, spin-restricted SCF HF calc. 78−90331
Na_2, $B^2\Pi_u$ state, pot. energy curve, shape determ. 79−31432
Na_2, dimer, $B'\Pi_u$-$X'\Sigma_g^+$ band system obs. 78−62837
Na_2, excited state identification by two-step polarisation labelling 79−76472
Na_2, ground state, vibr.-rot. relax., optical pumping transients obs. 80−28067
Na_2 in free jet expansion, internal-state distribution 80−83403
Na_2, long range mol., electronic and vibr. levels 78−94301
Na_2 molecule, Doppler-free two-photon transitions, $^1\Sigma_g^+$ state 77−3427
Na_2, optically aligned ground state, Hanle effect obs. 79−36707
Na_2, photodissoc. products of $C^1\Pi_u$ and $C^1\Sigma_u^+$ states 79−98171
Na_2, Rydberg state, two-step polarisation labelling 80−87053
Na_2, wave function and potential energy curves for lowest $^3\Sigma_u^+$, $^1\Sigma_u^+$, $^3\Sigma_{g+}^+$, $^1\Pi_u$, $^1\Pi_g$, $^3\Pi_u$ and $^3\Pi_g$ states 80−63738
Na_2^+, $^2\Sigma$ and $^2\Pi$ state pot. energy curves, two-centre model 79−26906
$NaAlH_4$, $NaBH_4$, ab initio calc. of geom. struct., charge distrib., bonding and pot. energy surfaces 80−18796
NaAr, ground and excited state pot. curves, dispersed fluoresc. spectrum 79−98140
$NaBH_4$, struct., pot. surface, ab initio calcs. 79−41092
NaBr, Compton profile anisotropies 79−27044
$NaCl^-$, $NaBr^-$, NaI^-, photodetachment cross section resons., 2-2.3 eV 79−54922
NaH, $A^1\Sigma^+$ states radiative lifetime in HF discharge 77−6841
NaK, $C^1\Pi$ state, spectroscopic consts., vibr.-rot. struct., K fluoresc. obs. 77−18901
NaNe, $X^2\Sigma$, $A^2\Pi$ and $B^2\Sigma$ states, model pot. calcs. 78−78776
Na_2*+Xe, rot. energy transfer, level-to-level dynamics, laser fluoresc. obs. 79−64029
Nd complex, Nd(2,2,6,6-tetramethyl-3,5-heptanedione), vapours, excited-state kinetics and fusion laser media prospects 79−64243
Ne^-, electron capture expts. to search for long lived states 79−72410
Ne-Xe-F_2(NF_3), excited states quenching 79−18406
Ne + D_2, energy-loss scaling in 0.5-3.5 keV 80−63768
$Ne^+ + D_2(H_2)$, energy-loss scaling in 0.5-3.5 keV 80−63768
NeF, low energy state pots. energy curves, fluores. and dipole moment 78−21991
$NeHe_2^+$, extended valence bond diatomic calcs., applications to method of diatomics-in-molecules 79−45635
Ni_2, A→X system, Ar matrix isolation fluoresc. spectrosc. obs. 80−9628
Ni_2 and Ni_2^+, lowest electronic states, GVB and POL-CI calcs. 79−31409
$Ni(CO)_4$, back donation, multiple scatt. Xalpha calcs. 79−36527
NiCu molecule, electronic states determ. by ab initio HF and CI methods 80−69087
NiF_2+CO, Ar matrix isolated, ab initio MO calcs. 78−92458
$Ni(Ni)_2$-ethylene cluster complex 78−82641
NiO, VB and CI calcs. 78−62728
$Ni_{13}(O_h)$ cluster, electronic states and X-ray spectra in Xα approx. of multiple scatt. theory 77−28645
O^+ + Ne, pot. energy curves, nonadiabatic coupling matrix elements 80−53110
O_2, $^3\Pi_g$ diabatic Rydberg states, ab initio CI calcs. 80−95554
O_2, $^3\Pi_u$ states, large CI wavefunctions, non-adiabatic coupling matrix elements 80−37744
O_2, $^3\Sigma_g^-$ ground state, pot. energy curve, direct CI method appl. 80−58165
O_2 ($^1\Sigma_g^-$), charge density, X-ray scatt. factors, gas phase electron diffr. 78−930
O_2, $a^1\Delta_g$ and $b^1\Delta_g^+$ state, MCSCF wavefunctions 78−37561
O_2, $A^3\Sigma_u^+$, $C^1\Delta_u$ and $C^1\Sigma_u^-$ states in van der Waals solids, electronic spectra, dynamics 78−1000
O_2, $A'^3\Delta_u$ state, inversion, presence in nightglow and discharges 80−63616
molecular electronic states continued
O_2, $b^1\Sigma_{g+}^+$ state excitation by 0.75-6 eV electrons 78−86958
O_2 $b^1\Sigma_g^+$ state prod. and deactivation following $O(^1D_2)$ quenching 80−76493
O_2, $b'\Sigma_g^+$-$X^3\Sigma_g^-$ electronic transition, absorpt. coeffs. and transition moments 80−43061
O_2, CI calc. of ground and $^3\Sigma_u^-$ excited states 79−81158
O_2 electron coincidence spectrosc., valence electron momentum distrib. and binding energies 80−102583
O_2, electronic electron impact excitation, rot.-electronic coupling 78−9265
O_2, electronic struct., self-consistent pseudopot. calc. 80−9508
O_2, excited state geometries and energies, ab initio pot. energy surfaces 78−5151
O_2, metastable level electron impact excitation, resonances *(Russian)* 80−43198
O_2 molecule, UHF description of ground and lowest singlet states 78−90056
O_2, multiconfig. HF procedure, 2nd- and approx. 2nd-order, convergency 79−93907
O_2, multiconfig. Hartree-Fock calcs. convergency 80−47901
O_2, Rydberg states, $^3\Sigma_g^-$, $^3\Sigma_u^+$, $^3\Pi_g$, $^1\Pi_g$, $^1\Sigma_g^+$ symm., ab initio CI study 80−99460
O_2, singlet state, form., quenching and reactions 77−29002
O_2, singlet states, quenching by $O_2(N_2)$, shock tube study 80−23511
O_2 singlet-state luminesc. in energy transfer from dissolved pigments 79−54886
O_2, valence states, ab initio config. interaction calcs. 78−25448
O_2^-, $A^2\Pi_u$ state pot. energy curve, MCSCF calcs. 80−63565
O_2^+, ab initio pot. curves of $X^2\Pi_g$, $A^2\Pi_u$, $a^4\Sigma_u^-$, $^2\Sigma_u^-$ states 78−66483
O_2^+, $A^2\Pi_u \rightarrow X^2\pi_g$ and $b^4\Sigma_g^- \rightarrow a^4\Pi_u$ emissions by photoionis. of O_2 79−94041
O_2^+, ab initio CI STO calc. 78−74585
O_2^+, $b^4\Sigma_{g-}$ state, laser-induced predissoc. in ion beam 78−70886
O_2^+, $c^4\Sigma_u^-$ state predissoc. calcs. 79−50095
O_2^+, CI calc. of ground and $^3\Sigma_u^-$ excited states 79−81158
O_2^+, $f^4\Pi_g$ state, quasi-bound levels, predissociation, band rot. anal., photofragment kinetic energy anal. 80−63650
O_2^+, vibr. intensity distribs. for electronic states prod. by photoionis. 78−25614
O_3, approximate spin extended HF calcs., singlet and triplet states 78−78621
O_3, CI calc., ground and excited states, energy locations, transition probabilities 78−74584
O_3, cyclic, stability, ab initio GVB-POL-CI calcs. 78−915
O_3, line and band strengths in IR spectra, variational calcs. 80−87112
O_3, open-shell SCF secular eqn., iterative algorithm soln. 80−52868
O_3, photolysis, primary products electronic and vibr. state distrib. 80−50865
$O_3 + NO \rightarrow NO_2^* + O_2$, kinetic energy and internal state depend. 79−66287
OCS, rot.-vibr. levels and semiclassical energy levels 80−37804
OCl_2^+, radical cation, struct. and electronic props., ab initio RHF SCF MO calc. 80−52883
$O_2(^1\Delta_g)$, 650-1650K reaction in combined discharge flow/shock tube study 79−89618
OH $(A^2\Sigma^+) + H_2(N_2)$(Ar), collisionally induced population change rates, laser-induced fluoresc. obs. 78−5326
OH, $A^2\Sigma^+$ $_{1/2}$ state, g-factor meas. by quantum beat obs. 79−18176
OH, $A^2\Sigma^+$-$X^2\Pi_i$ system, vibrational and rotational levels, transition probability determ. 80−43034
OH in flames, laser excitation dynamics 80−74201
OH, prod. by photolysis, Λ-doublets, population, rot. states, hyperfine struct., microwave spectra 80−32694
OH radical, gas phase EPR, rot. states electronic struct. and Zeeman parameters 78−86896
OH spectroscopy using freq.-doubled dye laser radiation *(Dutch)* 79−50039
OH, $X^2\Pi$ state, microwave spectrum calcs. 77−30858
OH^+, fine struct. in $X^3\Sigma^-$ and $A^3\pi$ states, GTO and STO calcs. 77−6679
OH + CO(trichloroethane), reaction rate consts. and quenching kinetics, reson. fluoresc. obs. 79−72349
OH + halomethane(haloethane), reaction rate consts., reson. fluoresc. meas. in discharge-flow system 79−72350
$OH(A^2\Sigma^+) + N_2(O_2)(H_2O)$(air), quenching rates and fluoresc. efficiency, rel. to atmosphere 80−14199
OH(OD), $A^2\Sigma^+$ state, vibrational energy transfer in collisions, rot. resolved fluoresc. 78−74742
OH(OD) radical, photoelectron spectra 77−27113
$OHX^2\Pi$ radical, ground and vibr.-excited ($v \leq 6$) levels, microwave spectrum 79−63985
ONF, J transitions, rot. Zeeman effect 80−63707
ONF, vertical electronic spectrum, CI and SCF calcs. 77−75123
$O_2(^1\Sigma_g)$, 650-1650K reaction in combined discharge flow/shock tube study 79−89618
$^{13}O^{16}O$ and $^{12}C^{18}O$, emission bands of $E^1\Pi$-$A^1\Pi$ transition 78−90177
O_2*+O_3, UV photolysis, $O(^3P)$ prod., rate const. determ. 80−55636
$O_2(b^1\Sigma^+g) + O_2(X^3\Sigma)$, quenching rate coeff. meas., density depend. 77−38721
$O_2(c^1\Sigma_u^-, C^3\Delta_u, A^3\Sigma_u^+)$ generation from at. recomb. in O_2-He afterglow, fluoresc. obs. 79−31576
P_2, perturbations in $b^3\Pi_g$ state, existence of $^5\Sigma_g^+$ state, visible and IR systems *(French)* 77−68035
P_2 radical, $b^3\Pi_g$-$a^3\Sigma_u^+$ transition, perturbed by $I^5\Sigma_g^+$ state *(French)* 80−18855
P_2^+, electronic states pot. energy curves, dissoc. energy, ionisation pot., curve fitting 80−32796
P_4, allowed multiplets, coordinate wavefunctions 78−33444
PH, $b^1\Sigma^+$ band emission visible and UV regions 78−46357
PH, fine struct. in $X^3\Sigma^-$ and $A^3\pi$ states, GTO and STO calcs. 77−6679
PH_2 radial, pot. energy curves. config., ab initio SCF-MO calcs. 77−50419
PH_2 radical, laser-induced fluoresc. 78−94277
PH_3, excitation energy, one-centre approx. calcs 78−70737
PH_3, X-ray K-fluoresc. obs. of electronic struct. 80−37818
$PH_3(F_2)(Cl_2)$, SCF-MO-HF calc., struct. and one-electron props., population anal. indices 79−76338
$PH_2(PH_2^+)(PH_2^-)$, electronic structure, ab initio LCAO MO SCF calcs. 79−10027

molecular electronic states continued
PN, absorpt. and emission spectra, electronic transition and vibr. obs. 80−91573
PN($X^1\Sigma^+$), VUV photoelectron spectrum 78−1024
PO, rot. struct. of absorpt. bands 1850-1600 Å, valence $^2\Pi$ state 79−13739
PO, Rydberg states, UV absorption spectrum 78−90184
$P^{18}O$, UV absorpt. spectra, valence and Rydberg states, rot., vibr., anal., predissoc. 79−41184
PO_4^{3-}, synchrotron radiation excited fluoresc., O K-emission spectrum, electronic struct. 77−42335
Pb-Pb quasimolecular states, inner shell ionis. spectra during form. 78−33592
$Pb^+ + Z$ ($42 \leq Z \leq 92$), 1sσ MO excitation probability and binding energy, X-ray coincidence 78−94316
Pb_2, low-lying states, energy curves, bonding 79−76367
PbO+C→CO+Pb, chemiluminesc. from gas phase reaction 79−8426
Pd_2, ab initio relativistic core pot. studies of metal-metal bonding 80−106257
PdH, ab initio relativistic core pot. studies of metal-H bonding 80−106257
PsH autodissociating Rydberg states 79−76539
PsH, positronium hydride, resonant and ground states 78−62964
Pt_2, ab initio relativistic core pot. studies of metal-metal bonding 80−106257
$PtCl_4^-$, effective charge, from IR and Raman scatt. intensity obs. 78−62809
PtH, ab initio relativistic core pot. studies of metal-H bonding 80−106257
PtO, ground state, matrix isolation spectra 78−46352
PtO, ground state identification from 3800-7000 Å emission spectrum 78−21937
pyridine, elec. dipole moment, g-values, mag. susceptibility, moments and charge distrib. 77−58077
Rb_2, $X^1\Sigma_g^+$ state, Raman spectra, fluoresc., vibr. energy 78−46345
Rb_2^+, $^2\Sigma$ and $^2\Pi$ state pot. energy curves, two-centre model 79−26906
Rb_2+Br→RbBr+Rb*, product electronic state distrib., chemiluminesc. 77−40529
$Re_3Cl_{12}^{3-}$, cluster ground state electronic struct. SCF Xα SW calc. 79−3607
Re_3Cl_9, cluster ground state electronic struct. SCF Xα SW calc. 79−3607
Re_3Cl_9 metal cluster complexes, He(I) photoelectron spectrum, SCC DV Xα calcs., $Re_2Cl_8^{2-}$ comparison 80−28063
Ru complex, (2,2'-bipyridyl)$_3$ruthenium^{2+}, excited-state redox processes, electron transfer theory 79−39126
Ru complex, Ru(II)-polypyridine, excited charge transfer states, multiple emissions 79−3468
Ru complex, $Ru(bpy)_3^{2+}$, excited, in aq. soln., optical absorption spectrum 79−50032
Ru dimers, mixed-valence, electron transfer rate consts. calc. from intervalence transfer absorpt. bands 79−81164
Ru(II) complex, carbonyl(pyridine)-phthalocyaninatoruthenium(II), optical hole burning, matrix effects 80−102522
RuO_4, SCF Xα SW calcs. of ground state 78−90081
S_2, $^1\Delta_g$ and $^1\Sigma_g^+$ states, near IR emissions 80−18852
S_2, low lying bound molecular electronic states 79−45643
S_8^{2+}, electronic struct. and localised MOs, bonding nature and geom. struct. 80−18798
$S_2(B\ ^3\Sigma_u^-)$+inert gas $(H_2)(N_2)(S_2)$, collision-induced energy transfer 79−3544
SCN^-, electron density distrib., theoretical and expt. determ. 77−61683
SF_2, generalised VB calcs. of electronic struct. 77−57881
SF_4, generalised VB calcs. of electronic struct. 77−57881
$SF_4+O^+(Cl^+)$, S highly stripped core ion outer shell arrangement, Kα X-ray spectra 77−3451
SF_6 and SF_6^+, excited states investig. 77−57882
SF_6, excited to dissoc. threshold, IR absorption 79−81245
SF_6, generalised VB calcs. of electronic struct. 77−57881
SF_6, IR multiphoton dissociation studies, inverse bottle-neck effect 80−87193
SF_6 molecule absorption of IR laser radiation *(Russian)* 80−986
SF_6, multiphoton pathways, rot.-vibr. transition moments in excited states 78−25639
SF_6, ν_3 bands, rot. fine struct., HFS spectroscopic consts. determ., saturation spectroscopy obs. 80−53008
SF_6, photoelectron ang. distrib., orbital assignments 79−819
SF_6, vibr. spectra, rot. consts., IR spectra, Raman spectra obs. 80−32719
SH^+, fine struct. in $X^3\Sigma^-$ and $A^3\pi$ states, GTO and STO calcs. 77−6679
SN, electronic states, ab initio, SCF, and CI calcs. 77−75053
S_2N_2, electronic states, ab initio, SCF, and CI calcs. 77−75053
S_2N_2, photoelectron spectrum, interpretation, Green's function calcs. 80−87175
SO, $a^1\Delta$ state, laser mag. reson. spectrosc. 78−94265
SO, low lying bound mol. electronic states, SCFCI calc. 80−23314
SO_2, $2^1A'$ state, electron correl. variational description, loop driven graphical unitary group approach 80−47903
SO_2, direct meas. of $^3B_1$ state lifetime in air at atm. press. 77−79653
SO_2, IR multiphoton excitation and inverse electronic relax., mol. vibr. and fluoresc. 80−106349
SO_2, shock heated, visible emission 80−58274
SO_2, X→A electronic absorpt. band system, non Condon effects study 80−18837
SO_3, dissoc. pathways and mol. vibr., compliance consts. and min. energy coords. 78−35661
$S^{16}O_2(S^{18}O_2)$, $^1B_2('A')$ state, force field for large amplitude motions 80−43023
SPF_3, electronic struct. of valence shell, UV photoelectron spectroscopy 78−82781
ScH, $^1\Sigma$ state, Dirac-Fock one-centre calcs. 80−23301
$^{80}Se_2$, Lande factors measurement in $B\ ^3\Sigma_u^-$ state 77−34648
Se_8^{2+}, electronic struct. and localised MOs, bonding nature and geom. struct. 80−18798
SeD, ground state, spin-orbit coupling const. vac. UV determ. 78−70847
SeH, ground state, spin-orbit coupling const. vac. UV determ. 78−70847
SeH, isotope effects, Rydberg levels-ground state transitions, rot. const., VUV spectra obs. 80−58279
SeH($X^2\Pi$), IR LMR spectrum, spin-orbit coupling const. direct determ. 79−76429

molecular electronic states continued
SeO, $X^3\Sigma^-$ state mol. parameters, Zeeman and EPR spectra 79−6966
SeO_2, HeI and II photoelectron spectrum, valence electronic struct. 77−61798
Sf_6, high resolution X-ray emission, valence electron struct. and chemical bonding, LCAO comparison 79−31545
Si_2, electronic struct. and bonding, atomic effective pot. appl. 80−95745
$SiCl_4$, He(II) photoelectron spectra, spectral intensity patterns 79−98152
SiF_3, low-lying electronic states, ab initio HF calcs. 77−54512
$SiF_4+O^+(Cl^+)$, Si highly stripped core ion outer shell rearrangement, Kα X-ray spectra 77−3451
SiH, ground state, Λ-type doubling 80−23431
SiH_2, $1B_1$-state, geometry calcs., avoided crossings 80−53085
SiH_4, $1B_1(1T_2)$ pot. energy surface calcs. 80−53085
SiH_4, excitation energy, one-centre approx. calcs 78−70737
$SiH_4+O^+(Cl^+)$, Si highly stripped core ion outer shell rearrangement, Kα X-ray spectra 77−3451
SiO $^3\Pi$ valence states, struct. and perturbations 79−59369
SiO, interaction between $G^1\Pi$ and $I^1\Pi$ states 79−50040
SiO, low-lying electronic states, vib. assigned perturbations 77−27082
SiO, test of perturbation method for vibr. assignments, low lying electronic states 77−34645
SiO, $X^1\Sigma^+$, $A^1\Pi$, $C^1\Sigma^-$ and $E^1\Sigma^+$ states, SCF CI calcs. 79−45641
Sn_2, in Ar matrix, absorpt., fluoresc. and reson. Raman spectra 80−95640
Sn_2, low-lying states, energy curves, bonding 79−76367
$SnCl_4$, He(II) photoelectron spectra, spectral intensity patterns 79−98152
SnF, $A^2\Sigma^+$ state, radiative lifetime, quenching rates 79−98156
SrH, absorption UV spectra, (0,0)-band at 2680 Å 78−50554
SrI, low-lying electronic states, vibr. anal. 80−106315
$Sr^{16}O$, ($Sr^{18}O$), $A'^1\pi$ state, vibr. anal., isotope shifts, vibr. consts. 77−18903
SrX_2, X=Cl, Br, I, valence shell electronic struct., ab initio SCF calc., photoelectron spectra 79−31383
TaN, matrix isolated, electronic and vibr. absorpt. spectra 79−64014
TaO_6^{7-}, octahedral cluster, ionisation energies and atomic populations, XPS and SCFMS Xα calc. 79−93923
Tb complex, Tb(2,2,6,6-tetramethyl-3,5-heptanedione), vapours, excited-state kinetics and fusion laser media prospects 79−64243
$TbCl_3$-$AlCl_3$, vap., high-energy laser medium props., for fusion ignition 78−63075
TcO_4^-, X_α-SW-calc. of chemically induced decay const. variation of ^{99m}Tc in TcO_4^- and hexahalides 79−54769
Te_2, $B0_u^+ - b^1\Sigma_g^+$ system, transition assignment, IR and visible spectra obs. 80−58298
$ThF_4(Cl_4)$, electronic struct., MS-SCF-Xα calcs. and VUV photoelectron spectra 80−63710
Ti_2, electronic structure of five and ten atom chains SCF-Xα-SW calcs. 80−5483
TiH, electronic structure of five and ten atom chains SCF-Xα-SW calcs. 80−5483
TiN, electronic absorpt. spectrum, rot. anal. 80−78601
$TlBO_2$, $TlNO_2$, Tl_2SO_4, $TlReO_4$, gaseous species, mol. orbital assignment of photoelectron peaks 77−18974
TmH, $^1\Sigma$ state, Dirac-Fock one-centre calcs. 80−23301
U+U, superheavy quasimolecule, direct Coulomb formation of 1sσ vacancies 77−3450
UC, electronic struct., comparison with photoemission spectra 80−91450
UCl_6, electronic struct., photoelectron spectra and SW Xα calcs. 79−72355
UF_6, gas, laser-induced fluoresc., A-X band 78−94275
UF_6, photophysical props., laser study 80−28040
UF_6, UF_6^+, and UF_6^-, electronic struct., ab initio calcs. using relativistic core pots. 79−97987
UF_6, UV spectra, electronic and vibronic states in gas and solid phases 77−14445
$UF_4(Cl_4)$, electronic struct., MS-SCF-Xα calcs. and VUV photoelectron spectra 80−63710
UN, electronic struct., comparison with photoemission spectra 80−91450
UO_2^{2+}, relativistic X_{α} scatt. wave calcs. 78−46268
$UO_2^{2+}{}_{(aq)}+UO_2NO_3^+{}_{(aq)}$, ground and excited state interaction, struct., thermodynamic functions, photochemistry obs. 80−32779
V_2, formation, spectra, electronic struct. 77−54642
$VCl_4(Br_4)$, vibronic systems, degenerate ground states, statistical sums, thermodynamic func. calcs. 80−27997
VH, electronic struct. and X-ray emission spectra 77−52201
WF_6, electronic structure, SCF-Xα-SW calcs. 77−26974
Xe, liq., recomb. and self-trapped exciton luminesc., free electron dynamics, excited states 80−25463
Xe^-, electron capture expts. to search for long lived states 79−72410
Xe_2, dispersion damping functions and interaction energy calcs. 80−78673
Xe_2^+, electronic states, pot. curves, with/without spin-orbit interaction 78−33443
XeAr(XeKr) photoionisation spectra of ground and excited states 78−5297
XeBr, B and C states, energy ordering from temp. depend. of emission spectra 80−78837
XeCl avalanche discharge laser, D and B state coupling, population depletion 80−28214
XeCl, B and C states, energy ordering from temp. depend. of emission spectra 80−78837
$XeCl_2$, electronic structure, MSW-SCF-Xα method 80−78539
XeF, (B,C) state prod. and kinetics, XeF_2 photolysis with VUV radiation 80−32975
XeF, B and C-state kinetics with self-sustained discharge pumping 80−28212
XeF, C-state radiative lifetime meas. 77−46598
XeF, formation and quenching of electronic excited states 77−673
XeF, laser emission, ab initio config. interaction calcs. on electronic states 78−63083
XeF laser performance, ground state population effect 80−63987
XeF, X, B, and D-states, spectra, vibr. and rot. consts. 78−70844
XeF_2, photodissoc. yield in solid Xe and Kr, time-resolved photolum. excitation obs. 80−3372
XeF_x, x=2, 4, 6, electronic structure, MSW-SCF-Xα method 80−78539
$XeF_2(C)$ state lifetime, quenching rate consts., photolysis in inert gas atmospheres 80−66816
XeF(Cl)(Br)(I), covalent and ionic states, spectroscopic props., ab initio CI calc. 78−90092

molecular electronic states continued
XeO, lasing, low-lying electronic states, ab initio config. interaction calcs. 78−63084
XeO^+, $X^2\Sigma$ state, pot. energy curves and correl. effects, elastic scatt. cross sections 80−23502
Xe_2^*, $Xe_2^{*\prime}$, Xe_2, pot. energy curves, relativistic ab initio effective core pots. 78−86800
Xe(nf)+SF_6, l-changing collisions obs. 80−91633
YF emission, 3400 to 3700 Å, rot.-vibr. anal., electronic struct. 77−6839
YH, $^1\Sigma$ state, Dirac-Fock one-centre calcs. 80−23301
YO, Fourier transform spectroscopy of $A^2\Pi-X^2\Sigma^+$ and $B^2\Sigma^+-X^2\Sigma^+$ electronic systems 79−22718
YSi_n, electronic struct., calc. and X-ray obs. *(Russian)* 79−13634
Zn_2, electronic states, CI calcs., rel. to Hg_2 77−10601
Zn_2, pot. energy curve of low-lying states, MO theory 79−89624
$ZnCl_2$, pseudopot. calcs. of mol. electronic props. 77−30779
ZrO, singlet-triplet separation meas. 80−78623

molecular electronic structure *see molecular electronic states*

molecular energy level calculations
see also molecular electron correlations; molecular orbitals calculations; molecular rotation calculations; molecular rotation-vibration calculations; molecular vibration calculations; VB calculations
6d metal superheavy hexafluorides, relativistic mol. calcs. 80−5484
π-electron systems, screened potential, excitation energies determ. in RPA 79−22597
acetylene, valence excitation energy and UV spectra, HAM/3 calc. 78−25453
alkynoyl cations, struct., charge distrib., ab initio population anal. calcs. 80−58407
anions, struct. and energetic predictions, modified HF procedure evaluation 78−62720
approximate and exact state wavefunctions, ionisation potentials, energy difference calcs. 79−97967
approximate energy formula 79−45629
aromatic systems, alternant, sign-alternation rule for triplet state 80 102420
atom+diatom, collinear collision with exponential repulsive interaction, generalised distorted wave calcs. 78−9060
Born-Oppenheimer approx., physics of new derivation 79−9997
bound state problems, many-body scatt. theory, arrangement channel 77−75044
Buridan's ass, weakly bound quantum-mechanical, single particle spherical limit in three nuclei field 79−9998
trans-butadiene, excitation energies, effective Hamiltonian convergence props. 79−3346
charge densities, bonded-atom fragments 77−67961
chemical reactions, quantum chemical methods appls. 80−93752
chloroethane diradical, MINDO/3 for optimised geometry and heat of form. 78−78830
chloromethylene radical, MINDO/3 for optimised geometry and heat of form. 78−78830
Clebsch-Gordan coefficients, chain $SU(2)\supset D_\infty'\supset D_4'\supset D_2'$, mol. aggregates 78 17552
closed-shell systems, effective Hamiltonian for excitation energies, convergence props. 79−3346
computer program MOLMEC, design and performance 78−13410
conditional probability amplitudes, variational principle 77−79530
conference, Boulder, Colorado, USA, June 1978 79−36511
coordinate rotation calcs., complex basis function appls. 80−95515
Coulomb potential with cut-off, exact eigenvalues 78−62692
covalent bonding from superposition of one-centre charge densities 80−37722
d-orbital basis functions role in electronic struct. description of systems containing Si, P, S and Cl 80−9484
density of states, steepest descent method, non-iterative procedure 77−54496
diabatic states from molecular properties near avoided crossing 78−82664
diagrammatic representation by method of progressive interactions by atomic orbitals 77−46482
diatomic hydrides, quantum mechanically calculated observables, reliability determ. 80−63505
diatomic molecule, wave functions and intensity factors, using effective Hamiltonian *(French)* 78−5114
diatomic molecule Hamiltonian, homogeneous derivation for spectrum anal. *(French)* 78−5113
diatomic molecules, $^2\Pi$ states, $^2\Delta$ states, $^3\Pi$ ground state, g-factor, Zeeman effect 79−98149
diatomic molecules, Born-Oppenheimer approx. 77−46478
diatomic molecules, electronic states, variable-screening method 78−25410
diatomic molecules, one-electron, automatic method 78−90064
diatomic polar molecule in electric field, energy levels 79−18136
diatomic system, Thomas-Fermi-Dirac eqn., accurate numerical soln. 77−50358
diatomic systems, correl. diagrams, Thomas-Fermi calcs. 80−23294
diatomic systems, Thomas-Fermi and Thomas-Fermi-Dirac-Weizsacker eqns., solns. 80−23293
dichloromethylene radical, MINDO/3 for optimised geometry and heat of form. 78−78830
dicyanomethane, multiple scatt. Xα calc. of electronic struct. 78−78626
dimethyl nickel, equilib. geometry, orbital energies, ab initio rel. to pseudopot. calcs. 78−82613
double antisymmetrisation 78−21836
EBIR method, two electron integral retention criterion 78−82606
effective atomic charge distribution in mols., multiple scatt. calcs. 80−83244
electric field gradient, overlap and ligand contribs. 78−58575
electron density and density matrix approximations using potential energy error bounds 78−94180
electron density distrib. maps, graphical construction from MO LCAO calculated wave functions 77−83480
electronic energies, homogeneity prop. 80−63539
electronic energy of atoms and mols., (N+1/N) Pade approximants in Rayleigh-Schrodinger perturbation theory 77−71738
electronic structures comparison, arbitrary electronic state, distance and similarity measures appl. 80−9487
ethylene, π-electron system, self-consistent many-body theory 78−25432

molecular energy level calculations continued
ethynol, ab initio calc., energy levels and geom. struct. of C_2H_2O isomers 78−62716
exact counting of internal energy levels, backtracking algorithm 78−25407
exchange perturbation theory, Eisenschitz-London type 78−41915
exchange perturbation theory, Hirschfelder-Silbey model 78−41916
exchange perturbation theory, multicentre electron systems 78−41914
excimer laser, electronic structure, pot. energy curves, radiative transition probabilities, quantum mech. calcs. 79−10284
excited molecule, energy level statistics on destruction of integrals of motion *(Russian)* 78−21864
Fermi contact interaction, by finite nucleus model 79−63887
fluoromethane, core energy levels, pseudopot. calcs. *(French)* 79−49935
formaldehyde, atomisation and bond energies, LMO calc., conjugation contrib. 80−9496
formaldehyde, bond polarity effect on other bonds and lone pairs, LMO calc. 80−9495
formyl chloride, photoelectron spectrum, vibr. struct., ionis. pots., assignments 78−9195
general SCF coupling operators, arbitrariness 80−99439
general-purpose molecular mechanics program construction principles 78−13411
generator coordinate method, soln. of Hill-Wheeler eqn. 79−26880
geometry optimisations, invariance criteria, symmetry conservation rules 80−58406
graph theory, eigenvalues of graphs with threefold symmetry 80−58123
ground state, energy functional of first-order reduced density matrix 79−10003
harmonic oscillator matrix elements, generating functions 77−23407
Heisenberg equation of motion, operator level and function level 79−6826
heterobenzenes, electronic struct., π electron mag. susceptibility anisotropy 79−59353
Hund's rule violation by spin polaris. 78−90058
hydrides, localised mol. orbital density, spatial distrib., principal lobe description evaluation 78−888
hydrides, single-centre perturbation theory calcs. 80−5470
increased valence when octet rule is obeyed 79−76323
inner-shell vacancy system, saddle point calcs. 80−23292
interconversion pot. energy surfaces, geometries, electronic structs. 78−35660
intramolecular energy transfer, crit. energy calcs. 77−9046
ionisation and excitation energies, ΔE SCF, transition functional method 77−88404
isoelectronic series, var. energy functionals involving 1-electron operators 77−83484
isotopic relations for rotational and Coriolis consts. 79−3377
JWKB quantisation condition, appl., breakdown and near-dissoc. behaviour 78−58571
ketene, ab initio calc., energy levels and geom. struct. of C_2H_2O isomers 78−62716
Kirkwood-Pople-Schofield method, appls. to polarisabilities calcs. 80−83272
l-splitting of energy levels for almost Coulombic central pots. 77−6659
local-density theory of multiplet structure 80−18776
localised molecular orbital density, spatial distrib., principal lobe description evaluation 78−888
many electron theory, state vectors and propagators, unified approach 79−6822
many-electron systems, electron density, Schrodinger inequalities and asymptotic behavior 78−21845
many-electron systems, excitation energies, linear response function theory, coupled-cluster framework 80−42936
metal hexafluorides, MF_6(M=W,Re,Os,Ir,Pt), ionisation energies and optical spectra in Dirac-Slater model 77−83488
methane, ionisation pot., quasidegenerate many-body perturbation theory calcs. 77−50346
methoxy, Jahn-Teller induced rovibronic effect, nuclear spin-electron spin hyperfine Hamiltonian 80−83298
methylene nickel, equilib. geometry, orbital energies, ab initio rel. to pseudopot. calcs. 78−82613
methylnitrene, symmetry restricted multiconfiguration annihilation of single excitations calcs. 78−62695
microscopic description 80−102433
model calculations, matching with experiment through linear regression 80−58243
molecular duplexes, graph construction yields 80−106245
molecular quantum mechanically calculated observables, reliability determ. 80−63505
molecules in molecule (MIM) model, appl. to π-electron systems *(German)* 79−36506
molecules of rows 1-3, equilib. geometries, orbital energies, ab initio rel. to pseudopot. calcs. 78−82613
molecules-in-molecules method, as extension of generalised diatomics-in-mols. 79−97970
multicentre potential, X_α scattered waves method and Schrodinger eqn. soln. 80−37740
multidimensional interpolation by polynomial roots 80−18778
multiple scattered wave method, incl. interatomic forces 79−59325
multiple scattering theory, nonspherical outer regions 79−59352
muonic mol. ions correl. wave functions calc. for pμd, pμt and dμt 77−23439
N-body excited states, Hartree-Fock eqns. derivation 79−93934
N-completeness problem, soln. for many electron systems 77−23405
N-electron system, Schrodinger eqn. soln. using antisymmetrisation 80−106246
neutral molecules, total energy and eigenvalue sums 78−21835
nitrobenzene, energy based integral repulsion method calcs. 78−82606
non-Hermitian operators, self-adjoint matrix equations 80−42916
nonadiabatic transitions, linear curve crossing problem, generalised Stueckelberg method 80−28085
nonbonded interactions, density response theory, appl. to rot. barriers 78−41913
odd electrons distrib. in ground-state mols. 78−90073
open shell polarisation propagator, for doublet-doublet transitions calcs. 80−27939
orbtial and total SCF energies, Ruedenberg's formula evaluation 78−37537
organic alternant molecules with conjugated bonds, ground state multiplicity, ferromag. 79−774

molecular energy level calculations continued
organic molecules in solution, electronic energy level shift estimation 79−54919
orthogonal trajectories of molecular electron density, critical pt. behaviour 79−9995
oxirene, ab initio calc., energy levels and geom. struct. of C_2H_2O isomers 78−62716
paraspectral molecular pairs 79−45620
phase integral approximations, advantages over JWKB approx. 80−87027
phenol-phenyl complex, electrostatic mol. pot. contour maps, MODPOT and VRDDO calcs. 80−102463
pi systems representation, efficient computer manipulation 79−81148
Poisson's equation integration for complex system with arbitrary geometry 77−47705
polyatomic, energy states, permutation group irreducible representations 77−23416
polyatomic systems, self-consistent nonorthogaonl group function approx., for closed-shell system 78−9059
polyhedral clusters, electron-rich and electron-poor 78−90057
polymers linear conjugated, π-electron energies calc. 78−17830
potentials at nuclei of atoms in molecule, relation with total energy of molecule 80−42917
pseudopotential method, SCF approx., first-row mols. 77−65420
quantum defect theory, general form 79−68177
quantum dynamics in effective system states basis, not in radiation field, perturbation theory 78−33499
quantum mechanics, molecular, book 77−79538
quantum theory, postulate of mol. structure 78−62684
quasi-energy states and stability in light wave field, adiabatic approach *(Russian)* 79−94039
relativistic scattered wave theory, normalisation and symmetrisation 78−62694
rigid molecules, allowed states by combining fragments in identical states 79−49933
rigid rotor in electric field, energy eigenvalues, Brillouin-Lowdin perturbation expansion 78−62690
Schrodinger energy functional, unification with Hohenberg and Kohn functionals 77−413
Schrodinger eqn. with double-minimum potential, numerical integration 78−58573
self-consistent electron pair theory for open shell wavefunctions 78−25408
semiclassical calc. for nonseparable systems 77−42227
semiclassical eigenvalues from classical trajectories for non-separable bound systems 77−50342
spin-degenerate system, Martin-Schwinger functional differentiation method 77−30765
stilbene aza-analogues, lowest excited states, INDO/S calcs. 80−95545
subspace quantum dynamics and the quantum action principle 78−65798
subspace quantum mechanics and the variational principle 78−70002
symmetric deorthogonalisation, constrained variation method 78−37540
symmetry restricted multiconfiguration annihilation of single excitations calcs., applic. to methylnitrene 78−62695
tetracyanomethane, multiple scatt. Xα calc. of electronic struct. 78−78626
total π-electron energy, topological formula calcs. 77−88377
total energies, virial-statistical method 78−62696
total energies and atomisation energies, virial-statistical method 78−62697
transition probability evaluation in double asymmetric pot. well 80−69120
trioxane $^{13}C(^{18}O)$ substituted, mol. consts. and rot. spectra 80−87096
two-dimensional multichannel scattering, wavefunction corrections averaging method 78−9060
two-electron integrals in molecular calcs., simplifications in generation and transformation 79−9996
two-particle density determ., energy and density matrix *(French)* 77−88368
universal variational functionals of electron densities, first-order density matrices, and natural spin-orbitals and solution of the v-representability problem 80−95516
variational method, metric-constrained 79−22579
π-electron systems, self-consistent many-body theory 78−25432
BF, matrix HF calcs. using universal basis sets 79−59354
BH, mol. electronic momentum distrib. functions and correl. holes in **p**-space 79−97978
C_2N_2, valence excitation energy and UV spectra, HAM/3 calc. 78−25454
CO, analytic RKR pot. including higher-order WKB approx. effects 77−57901
CO, electrostatic interaction energies for point charge and NaCl (100) surface 78−74592
CO, equilib. geometry, orbital energies, ab initio rel. to pseudopot. calcs. 78−82613
CO, ground state, third-order many-body perturbation theory 79−10015
CO, matrix HF calcs. using universal basis sets 79−59354
CO, valence excitation energy and UV spectra, HAM/3 calc. 78−25453
CO_2, valence excitation energy and UV spectra, HAM/3 calc. 78−25454
Co_3O_4-H_2, interaction with surface, quantum chemical study 80−45549
$CrCl_4$, ligand field states, multiple scatt. Xalpha calcs. 80−47891
Cr_2O_3-H_2, interaction with surface, quantum chemical study 80−45549
Cu complex, $Cu(NH_3)_2(NCX)_2$, X=O, S, electronic struct., stereochem. 80−58156
DBr, mol. consts., rel. to TBr mol. consts. *(French)* 77−57855
F+H_2, quenching, rot. energy transfer, quantum mech. calcs. 77−50499
FeH^+, valence electronic struct., pseudopot. method 79−68184
Fe_2O_3-H_2, interaction with surface, quantum chemical study 80−45549
H_2, electron repulsion matrix elements, asymptotic form, adiabatic representation 80−87038
H_2, electronic and vibrational structure, theoretical developments 78−62707
H_2, generator coord. method 79−26880
H_2, ground state calcs. 79−22595
H_2, mol. electronic momentum distrib. functions and correl. holes in **p**-space 79−97978
H_2^+, bound state problems, many-body scatt. theory, arrangement channel 77−75044
H_2^+, electronic energy levels calc. 77−57856
H_2^+, semiclassical quantisation for low lying electronic states 79−68183
H_3, generalised diatomics-in-mols. theory 79−97970
H_3, relative magnitudes of direct and indirect exchange, Heitler-London calcs. 80−69069
H_4 square, $^1B_{1g}$ and $^1B_{2g}$ states, Schrodinger eqn. solved by random walk method 79−63925
HBr, mol. consts., rel. to TBr mol. consts. *(French)* 77−57855
HCN, valence excitation energy and UV spectra, HAM/3 calc. 78−25453
HCl, electric field gradient at Cl, two- and one-centre wavefunction expsn. 78−17561
HCl, one-centre-expsn. SCF calc., electric field grad., Sternheimer effect 78−37550
HD, spin-spin coupling const., convergence of calc. 80−9506
HF, analytic RKR pot. including higher-order WKB approx. effects 77−57901
HF, linear response function, diagonal ARPA calcs. 78−74594
H_2O, ionisation pot., quasidegenerate many-body perturbation theory calcs. 77−50346
H_2O, linear response function, diagonal ARPA calcs. 78−74594
H_2O, many-body Green's function, electronic mol. props. 78−25417
$(H_2O)_2$, difference electrostatic mol. pot. contour maps, basis set superposition effect 80−102462
He, isoelectronic series, var. energy functionals involving 1-electron operators 77−83484
He^+, Xα statistical exchange method, orbital energies, HF method comparison 78−9071
HeH^+, electronic states, variable-screening method 78−25410
I_3^-, geom. and electronic struct., effective pot. calc. 78−74788
I_5^-, geom. and electronic struct., effective pot. calc. 78−74788
Li_2, mol. struct. 2-electron integral evaluation by Multipole Expansion of Diatomic Overlap 78−908
LiH, linear response function, diagonal ARPA calcs. 78−74594
LiH, many-body Green's function, electronic mol. props. 78−25417
LiH, mol. electronic momentum distrib. functions and correl. holes in **p**-space 79−97978
LiH, mol. struct. 2-electron integral evaluation by Multipole Expansion of Diatomic Overlap 78−908
LiNC type molecules, Born-Oppenheimer approx. applicability 80−32603
LiO_2, molecule, vibronic interaction in low-lying states, model calc. 80−32603
Mg_2, mol. consts. calcs., inverted perturbation approach 77−57969
MnO-H_2, interaction with surface, quantum chemical study 80−45549
Mo complex, μ-oxo bridged oxomolybdenum(V) dimers, conform. anal. by ang. overlap method, triplet ground states 78−5119
N-N, correl. diagrams, Thomas-Fermi calcs. 80−23294
N_2, electrostatic interaction energies for point charge and NaCl (100) surface 78−74592
N_2, matrix HF calcs. using universal basis sets 79−59354
N_2, mol. struct. 2-electron integral evaluation by Multipole Expansion of Diatomic Overlap 78−908
N_2, photoionisation of π-shell, π-π^* transition, modified static-exchange calcs. 79−98163
N_2, valence excitation energy and UV spectra, HAM/3 calc. 78−25453
NH, 3Π states, MC wavefunctions, rot.-vibr. anal. 79−13652
NH_3, linear response function, diagonal ARPA calcs. 78−74594
NO, v=0,1 states, spectroscopic data calc. 78−86851
NO_2, coupling of vibronic states induced by messenger state 79−72226
N_2O, valence excitation energy and UV spectra, HAM/3 calc. 78−25454
Ne-Ne, correl. diagrams, Thomas-Fermi calcs. 80−23294
Ni, orbital energies, ab initio rel. to pseudopot. calcs. 78−82613
Ni_3, linear system, energy based integral repulsion method calcs. 78−82606
NiO, equilib. geometry, orbital energies, ab initio rel. to pseudopot. calcs. 78−82613
NiO-H_2, interaction with surface, quantum chemical study 80−45549
NpF_6, energy levels and bonding, relativistic SCF Dirac-Slater calcs. 77−6691
O_2, equilib. geometry, orbital energies, ab initio rel. to pseudopot. calcs. 78−82613
OCS_2, rot.-vibr. levels and semiclassical energy levels 80−37804
OH, $^2\Pi$ states, $^2\Delta$ states, $^2\Pi$ ground state, g-factor, Zeeman effect 79−98149
$PtCl_2(NH_3)_2$, cis- and trans-isomers, electronic struct., SCF-Xα study 80−18795
PuF_6, energy levels and bonding, relativistic SCF Dirac-Slater calcs. 77−6691
$SeOCl_2$:Pr^{3+}(Nd^{3+})(Er^{3+}), $SbCl_5$ acidified, Racah and Judd-Ofelt parameters in laser liqs. 80−106516
Si_2H_4 ground state struct., ab initio SCF calcs., singlet silylsilylene 80−27945
TBr, mol. consts., calcs., rel. to HBr, DBr *(French)* 77−57855
ThH_4, Dirac-Fock one-centre expsn. calc. 80−5485
UF_5, electronic struct. and geometry, ab initio calcs. using relativistic ECP 80−32606
UF_6, electronic struct., relativistic MS Xα calc. 79−85911
UF_6, energy levels and bonding, relativistic SCF Dirac-Slater calcs. 77−6691
UH_6, Dirac-Fock one-centre expsn. calc. 80−5485
V_2O_3-H_2, interaction with surface, quantum chemical study 80−45549
XeF_6, energy levels, nonrigid mol. effects 78−41931

molecular energy levels
see also macromolecular energy levels; molecular electronic states; molecular energy level calculations; molecular fine structure; molecular hyperfine structure; molecular libration; molecular polarisability; molecular reorientation; molecular resonant states; molecular rotation; molecular rotation-vibration; molecular vibration; molecular vibronic states; nuclear screening
ab initio effective core potentials, all-electron calcs. 78−62704
acetylene, electron impact ionis., valence electron momentum distribs. 78−33617
alkali metal molecular, laser radiation absorpt., at. excitation processes 80−32785
alkanes, linear, elec. struct., evolution of electronic level towards band struct. *(French)* 78−5282
alkanes, linear, electronic struct., electronic relax. during photoemission *(French)* 78−5283

molecular energy levels continued
anharmonic corrections in unimolecular theory, Monte Carlo calcs. 80−83441
anthracene dimer anion, charge reson. transition anal. 80−42931
approximate energy differences from average electron densities 79−36505
approximate energy relationships 79−3345
aromaticity, reson. energy in graph theory 80−91412
atomic, molecular and solid-state theory, conf., Flagler Beach, Florida, USA (Mar. 1978) 79−31356
Aufbau principle, rel. to mol. topology 78−74556
Auger lineshape anal. of molecules and solids 80−76113
$^1\pi\pi^*$benzaldehyde, zero field splitting and sublevel decay rates, deuteration and host effect 80−37750
benzene, electron impact, electronic energy levels, (below 7 eV) obs. 78−17807
biological molecule models, using wavefunction electron densities 79−24937
biological systems, containing Fe, electronic and mag. struct., semiempirical MO cluster calcs. 78−62733
Born-Oppenheimer energy, energy states of one electron, two nuclei interaction 78−90052
bromohaemin, ferric porphyrins with fifth ligands, ^{57}Fe and ^{14}N hyperfine consts. 78−50475
trans-1,3-butadiene, electron impact energy loss spectra, energy levels 79−68323
charge density, X-ray scatt. factors, gas phase electron diffr. 78−930
charge distribution in ions and mols., inductive effect 80−47837
charge distributions and chemical effects, mol. energy formula 79−89585
chemical bonding, antisymmetrised geminal power and simple correlated wave function 80−102423
chlorohaemin, ferric porphyrins with fifth ligands, ^{57}Fe and ^{14}N hyperfine consts. 78−50475
clustering, qualitative theory of irreducible tensor operators spectra 80−28001
colour, chemical origins 79−21479
Compton profile, empirical correlation with energy 78−78758
conjugated molecules eigenvalue polynomials 80−14078
convex structure of electrons 78−62685
core regions, in linear polyatomic molecules, radial density functions calcs. 78−900
cupric mixed ligand complexes, mechanism of spin transfer to next neighbours ^{13}C and ^{31}P 78−86892
cyanohaemin, ferric porphyrins with fifth ligands, ^{57}Fe and ^{14}N hyperfine consts. 78−50475
cyclopropane-d_0, -d_6, multiphoton ionisation spectra, electronic struct. 78−82803
diagrammatic many-body perturbation expansion, computer program 78−50454
diagrammatic many-body perturbation expansion, ladder energies, computer program 78−50455
diagrammatic many-body perturbation expansion, ring energies, computer program 78−50456
diatomic molecule, quantum mech. model 78−86050
diatomic molecules, linear, substituted fragment series, electronic struct. transferability, mutual at. influence 78−9066
diatomic molecules, periodic table, spectrophysical props. 79−45621
diatomic molecules, variable screening model 78−74587
diatomic molecules with Coulomb forces, time dependent Born-Oppenheimer approximation 80−105518
dicyanoethylenes, substituted, vibr. spectra, intramol. effects 79−31528
electron density contour diagram, polarisability anisotropy 78−66681
electron pairwise interactions, energy depend. on occupation numbers 80−102427
electronic distribution and electronegativity, theory 80−23283
electronic energies, determ. from exptl. electron densities 79−31365
electronic structure, investig., electron coincidence spectrometer appls. 79−30617
electrostatic potentials, approximation using overlap multipole expansion 79−36519
energy density functional approach, kinetic energy model 79−31357
ethane, internal rot. splittings, vibr.-rot.-torsion energy levels perturbations 80−91531
ethylchloride, d_0-d_5, microwave spectra, elec. field gradient tensor at Cl nucleus *(German)* 78−46325
ethylene, electron impact ionis., valence electron momentum distrib. 79−18297
ethylenimine, multiphoton ionisation spectra, electronic struct. 78−82803
excited mol. states, preparation and decay, dephasing relax. and pulse fall time effects 78−94200
Faraday effect measurement in pulsed mag. field 80−80758
fermion expectation values, using program SCHOONSCHIP 78−74555
ferric cytochrome c, reson. Raman spectra, Fe^{3+} low-lying electronic levels 78−53335
fluorobenzenes, negative ion states, comments and reply 80−32599
fluorohaemin, ferric porphyrins with fifth ligands, ^{57}Fe and ^{14}N hyperfine consts. 78−50475
forces acting upon nuclei, Fourier transform calcs. 78−86774
fractional parentage coefficient identities, atomic, molecular spectroscopy applications 80−69050
highly correlated particle densities and idempotent one-densities 79−6815
hindered internal rotational molecules, nonbonded ligand interactions, symmetry determined investigation 78−70960
homologous linearity rule for energies of mol. orbitals and related props. 78−58569
hydroxyhaemin, ferric porphyrins with fifth ligands, ^{57}Fe and ^{14}N hyperfine consts. 78−50475
internal rotational molecules, symmetric aspects of scalar props., appl. to ethane skeleton 78−70959
intramolecular electron transfer processes 79−36565
ion-molecule equilibria in solvolysis, secondary β ^{2}H isotope effects, hyperconjugation 80−50874
isocyanates, nonbonding and π-orbital interactions, photoelectron spectra 80−32774
isolated molecules, internal energy transfer, ergodic and nonergodic behaviour 79−36499
isothiothiocyanates, nonbonding and π-orbital interactions, photoelectron spectra 80−32774
molecular energy levels continued
Koopman's theorem, corrections using energy shifted perturbation theory 79−6845
many-body scattering theory, mol. struct. calcs., channel coupling array method 79−31362
mass scaling for molecular systems, quantum mech. theory 77−83475
methane, electron pair interactions calcs. 80−23298
methylene peroxide, struct., energy levels, ab. initio UHF and MRUHF NO CI calcs. 80−83287
6-methylmercaptopurine riboside, 4 MeV electron irrad., 77K radicals form., EPR obs. 78−39405
mixed-valence system, diatomic molecule model 80−107751
model potentials, constructive theory 79−26869
Morse oscillator, matrix elements calcs. with Sturm-Liouville eqn. eigenfunctions 79−2660
N-particle system in arbitrary EM field, eqn. of change in config. space 79−36705
nonadiabatic transitions, 1-dimens. model, mol. props. appls. 80−52861
nonalternant hydrocarbons, charge distrib. rule 78−90060
noncyclic molecules, bent bonds, electron density maps 79−49960
nuclear spin-spin coupling constants in series of related mols., orbital model, perturbational approach 79−81217
O K-emission spectra, electron struct. 80−87099
occupation number dependence 78−13417
one-electron polynuclear systems, Dirac eqn., variational soln. 80−83242
open shell systems, wave operator hierarchy eqns. 79−41087
open-shell systems, many-body perturbation theory, coupled cluster approach 79−31360
orbital pairs, transformation into localised pairs, use of FORTRAN for angle selection 80−27922
orbitally degenerated electronic level instability *(French)* 79−31421
organic chemistry courses, unified approach to teaching of struct. and bonding 80−17732
organic compounds, photoelectron spectroscopy, ionis. pots., MO models 78−17716
paradichlorobenzene, electronic struct., X-ray emission obs. 78−5246
periodic table of diatomic molecules, internuclear separation 79−45859
point charge model of molecules, Mulliken population anal. 80−102429
polar molecule-electron systems, variational method for bound state calc. 78−46261
polyatomic molecule, transform. of complete electron-nuclear Hamiltonian to intramolec. coords. 78−9054
polyatomic molecules, energy levels, classification 78−9052
polyatomic organic molecules, electronic excitation transport in inhomogeneity broadened 79−54884
polyatomic systems, Cartesian coords., charge densities, field gradients 78−29771
polyatomic van der Waals molecules, struct. and dynamics calcs. 79−41097
polymer, quantum mechanical effects, due to orbital overlap 78−50670
polymethine dye lasers, optical absorpt. 80−64009
polymethinecyanines, symm., solvent effects on electronic struct., ^{1}H, ^{13}C NMR 78−13516
projection of wave functions on states with definite ang. momentum 78−12590
quantum chemistry, conf., Kyoto, Japan, 29 Oct.-3 Nov. 1979 80−101659
quantum mechanical aspects of the molecular structure hypothesis 80−102421
quantum topology, theory of mol. struct. and its morphogenesis 80−106247
quantum topology of mol. charge distribs., mol. struct. and its change 79−68175
quasiparticle picture, at. and mol. systems, breakdown for inner valence electrons 78−5112
reduced Bessel functions calcs. for multipole and overlap integrals 80−83250
rhodamine 6G, blue and UV luminesc., obs. and mechanism 79−3486
rigid rotor, asymmetric, semiclassical energy levels determ., tunnelling 78−37624
rotations and translations in isospin space 80−102431
Rydberg transitions, term value-ionisation energy correls. 78−70738
sandwich complexes, mag. props., effective Hamiltonian method 80−37731
Singer polymals, evaluation of matrix elements 79−6813
six-site Hubbard model, approximations 79−76327
spin permutation group for transpositions, elements of representation matrices 79−31358
spin-density functional formalism, correl. energies calcs., appls. and corrections 80−91433
spin-dependent operators in the spin-free quantum chemistry 79−6817
spontaneous symmetry breaking, induced representations 80−5464
symmetry, electronic energy gradient rel. to nucl. coords., HONDO calcs. 78−66463
symmetry of MO with its energy, theorems and calc. methods 78−66457
symmetry-lobe orbitals, symmetry defects and contamination 79−9990
Tamm-Dancoff approximation, 2p-h, rel. to other self energy approximants 80−83243
tetracene, intramol. dynamics and energetics in isolated ultracold state 79−98144
tetrachloromethane, electronic characts. from electron scatt. meas. 79−59576
tetrahedral molecules, clusters for $\nu_2+\nu_3$ type combination bands 79−98009
thiocyanates, nonbonding and π-orbital interactions, photoelectron spectra 80−32774
topological resonance energy is real 79−81145
total molecular energies, calcs., SCF orbital energies rel. to total SCF energies 79−59337
transitions, excitation by monochromatic laser radiation, Doppler-broadened transitions 80−78582
triatomic molecules, linear, substituted fragment series, electronic struct. transferability, mutual at. influence 78−9066
triatomic mols., bound state. mol. Aharonov-Bohm effect 80−83302
triethylamine-perfluoro-T-butanol, photoelectron and Rydberg bands, UV spectra study 80−18865
two-level molecule interacting with light, Dicke model asymptotic behaviour 79−3508
unified theory of atoms and atomic aggregates, self consistent theory 80−102418

molecular energy levels continued
unrestricted Hartree Fock equation, in mol. systems, group theoretical classification of solns. 79−36522
uranocene, reson. Raman spectra, anomalously polarised electronic band, energy level assignment 79−59451
uranyl complexes, MCD spectra, electronic struct. of lowest excited states *(Japanese)* 79−27014
valence shell electron pair repulsion model, geometry variations, ab initio calc. 80−5472
van der Waals molecules, pot. functions, level spacings and thermodynamic props. 80−14185
vanadyl mixed ligand complexes, mechanism of spin transfer to next neighbours ^{13}C and ^{31}P 78−86892
variational computations, containing nonlinear parameters, nonexistence of maxima 79−6816
weak nonorthogonal geminals, antisymmetrised product 79−6814
WINIMAX weighting factor, for isotope chem. and mol. struct. calcs. 80−27940
$(AgCl)_3$, photoelectron spectrum and valence shell struct. 78−62843
BF_3, X-ray fluorescence, electronic struct. determ. 78−86887
BH, electronic distribution functions and correl. holes, theory 78−17562
BO_3^{3-}, X-ray fluorescence, electronic struct. determ. 78−86887
$BaTiO_3$, XPS satellite spectra, mol. orbital study 80−43100
CH^+, predissociated levels obs. 80−37838
CO, chemisorbed on Ni(100), mol. levels, angle depend. calcs. 78−90069
CO, energy levels for perturbed Morse oscillators 80−78676
CO, K-shell, excitation and ionisation, vibr. struct., electron energy loss spectra obs. 80−18943
CO, one-electron props., corrections, Moller-Plesset perturbation theory calc. 80−95519
CO_3^{2-}, X-ray fluorescence, electronic struct. determ. 78−86887
$CeFe_2Si_2$, charge state of 3d shell, state of Fe atoms, atomic bonds *(Russian)* 80−47884
ClO_2, Cl $L_{II,III}$ fluoresc. X-ray spectra, mol. orbital struct. 78−70848
ClO_3, Cl $L_{II,III}$ fluoresc. X-ray spectra, mol. orbital struct. 78−70848
ClO_4, Cl $L_{II,III}$ fluoresc. X-ray spectra, mol. orbital struct. 78−70848
Co complexes, Co(III) mixed complexes, orbital angular momentum reduction, ^{59}Co NMR chemical shift 80−58137
CrO_4^{2-}, electronic struct. determ. from X-ray spectra 78−86885
Cs_2, laser-excited fluoresc. in Cs-Xe mixture, pumping, level scheme 78−86909
CsXe excimer, laser-excited fluoresc. in Cs-Xe mixture, pumping, level scheme 78−86909
Cu complexes, Cu(I)-P tetrahedral, ^{63}Cu FT-NMR 80−53021
$(CuBr)_3$, photoelectron spectrum and valence shell struct. 78−62843
$(CuCl)_3$ photoelectron spectrum and valence shell struct. 78−62843
$(CuI)_3$, photoelectron spectrum and valence shell struct. 78−62843
D_2O, energy levels and mol. vibr., internal coord. model 79−799
D_2S, energy levels and mol. vibr., internal coord. model 79−799
F isoelectronic sequence, spectra and energy levels 79−93948
Ge_2, multiplet struct. and charge distrib. 79−26881
H like molecule ion, chemical pot. asymptotic scaling, homonuclear diatomic total energy 80−47885
H_2, electronic distribution functions and correl. holes, theory 78−17562
H_2, electronic struct., valence bond orbital method appl. 80−106268
H_2, struct., channel coupling array calcs. 79−31362
H_2^+, ground state, asymptotic primitive function, symmetry adapted perturbation calcs. 79−6855
H_2^+ molecule energy level splitting, lecture demonstration based on coupled elect. reson. ccts. 79−49949
HCl, one-electron props., corrections, Moller-Plesset perturbation theory calc. 80−95519
H_2O, electron pair interactions calcs. 80−23298
H_2O, energy levels and mol. vibr., internal coord. model 79−799
H_2O, Politzer's k and V/T variations, mol. geom. effects 79−54766
H_2O, relative ionisation energies, Tamm-Dancoff approx. calcs. 80−83243
H_2S, electron pair interactions calcs. 80−23298
H_2S, energy levels and mol. vibr., internal coord. model 79−799
H_2S, valence momentum distribs., binding energies, binary (e,2e) spectrosc. meas. 79−31713
$HSiO^+$, $HOSi^+$, quantum mechanical study 78−37541
HeH^+, struct., channel coupling array calcs. 79−31362
I_2, energy levels near B-state dissoc. limit, two-photon spectra 78−9210
ICl, energy levels, near first dissoc. limit, 2-photon sequential absorption obs. 78−90246
InCl, InBr, InI, UV photoelectron spectra of valence d shells, gas-phase 78−62845
IrF_6, ligand field theory analysis of spectra 79−72248
LiH, electronic distribution functions and correl. holes, theory 78−17562
LiH, electronic struct., valence bond orbital method appl. 80−106268
LiO, struct., spectra, SCF MO calcs. 78−17559
Li_2O (LiOLi, LiLiO), struct., spectra, SCF MO calcs. 78−17559
LiOO, struct., spectra, SCF MO calcs. 78−17559
MnF, MnF_2, EPR, in inert gas matrices, high spin mag. parameters, level diagrams 78−66565
MnO_4^-, electronic struct. determ. from X-ray spectra 78−86885
N_2 ($^1\Sigma_g^+$), charge density, X-ray scatt. factors, gas phase electron diffr. 78−930
N_2, K-shell, excitation and ionisation, vibr. struct., electron energy loss spectra obs. 80−18943
N_2 relative ionisation energies, Tamm-Dancoff approx. calcs. 80−83243
NH_3, electron pair interactions calcs. 80−23298
NO_3^-, X-ray fluorescence, electronic struct. determ. 78−86887
Na_2 vapour, IR absorpt. bands 80−102507
Ni+Ni, 12-90 MeV, molecular orbital K X-rays ang. distrib. 79−10125
O_2 ($^3\Sigma_g^-$), charge density, X-ray scatt. factors, gas phase electron diffr. 78−930
O_2, K-shell, excitation and ionisation, vibr. struct., electron energy loss spectra obs. 80−18943
O_2, symmetry adapted wave function generation using group theoretical projection operators 80−102428
O_3, microwave and IR spectra, ν_2 state, $(\nu_3+\nu_2)-\nu_2$ band, 10 micron lines 78−82718
$PbCl_2$, $PbBr_2$, PbI_2, UV photoelectron spectra of valence d shells, gas-phase 78−62845
SO_3^{2-}, SO_4^{2-}, O K-emission spectra, electron struct. 80−87099
Sb (III) compounds, orbital population anal. using ^{121}Sb Mossbauer data 78−21953
SeO_3^{2-}, SeO_4^{2-}, O K-emission spectra, electron struct. 80−87099
molecular energy levels continued
Si phthalocyanine, monomer and dimer, UV photoelectron spectra, valence level splitting 77−38695
Si_2, multiplet struct. and charge distrib. 79−26881
Si_2, pseudopotential charge densities calcs. 79−31367
$SiH_4(SiF_4)$, electron rearrangement after inner shell ionisation by heavy charge particle impact 80−87043
$SnCl_2$, $SnBr_2$, UV photoelectron spectra of valence d shells, gas-phase 78−62845
T_2, solid, radiation-catalyses ortho-para transition 79−73832
Ti (III) halides, bonding, struct., ligand field splitting, electron gas calcs. 78−17557
TiO_2, XPS satellite spectra, mol. orbital study 80−43100
TlCl, TlBr, TlI, UV photoelectron spectra of valence d shells, gas-phase 78−62845
UF_5, electronic struct., Hartree-Fock-Slater and Dirac-Slater calcs. 79−31370
$UF_{6,5}$ relativistic scattered wave calculations 80−63538
VO_4^{3-}, electronic struct. determ. from X-ray spectra 78−86885

molecular excitation *see beam-foil spectra; chemical reactions; Davydov splitting; discharges (electric); molecular fluorescence; optical pumping; photoionisation; radiation quenching*

molecular fine structure
acetylene, vibr. fine struct. accompanying core ionis., STO calcs. 78−62844
9,10anthraquinone, lower triplet states, interactions and position, matrix isolation spectra 80−63634
aromatics in stretched PVA films, ESR of phosphorescent triplet state 77−30908
benzene, IR spectra, fine struct. of rot.-vibr. bands 80−102504
benzophenone, metastable triplet state, SCF CI calcs. 79−54776
benzophenones, triplet state fine struct. parameters and phosphoresc. spectra 79−50065
2-benzoylpyridine crystals, lowest triplet state, optically detected EPR 80−15827
1,2-benzpyrene, butyl bromide solid soln., phosphoresc. line struct. obs., vibr. assignments 77−58075
biaryls, model, mol. vibronic circular dichroism 78−37665
binary complex, quinone-phenol radical pair EPR, geometry calc. 78−90101
biphenyl gluterate diacetylene, monomer, single cryst., stable and metastable UV photoexcited states, EPR obs. 79−78522
bromotrifluoromethane, photoelectron spectra, spin-orbit splitting, vibr. fine struct. 78−21974
chloroperoxidase, ferric form, X-ray absorpt. fine struct., Fe-N and Fe-S lengths 79−48213
chlorophyll, and related mols., in solid solns., fine-structured vibronic spectra under tunable dye laser excitation *(Russian)* 80−74164
chlorophylls, triplet state ESR, fine struct. and rate consts. determ. 78−25574
chlorophylls, triplet state ESR, fine structs. and rate consts. determ. 78−25575
chloroplast fragments, fine struct. of fluoresc. spectra, derivative spectroscopy method *(Russian)* 79−34502
chlorotriflouromethane, UV photoelectron spectra, vibr. fine struct. 78−9196
chrysene, butyl bromide solid soln., phosphoresc. line struct. obs., vibr. assignments 77−58075
coronene, butyl bromide solid soln., phosphoresc. line struct. obs., vibr. assignments 77−58075
coronene, n-alkane matrix, up to 1.8 kbar emission multiplet struct. shift 77−34677
cyanoacetylene, photoelectron spectra, electronic states of radical cations 79−22756
cyclophanes, double and triple-layered, triplet state zero field splitting parameters, HMO calc. 77−50366
cytochrome P-450, ferric form, X-ray absorpt. fine struct., Fe-N and Fe-S lengths 79−48213
diacetylene, near UV band system, rot. and vibr. anal., rot. fine struct. 77−61761
diacetylhydrazine, ^{14}N NQR lines fine structure 80−63667
diatomic molecule, rel. to theory of high-precision Zeeman effect 77−14486
diatomic molecules, centrifugally distorted fine struct. 78−62783
diatomic molecules with $^1\Sigma^-$ ground states, use of $\langle L^2 \rangle$ to assess 2nd-order sums convergence 79−76364
trans-dibromoethylene, VUV and photoelectron spectra, Rydberg series, vibr. fine struct. 77−6799
dichlorodifluoromethane, UV photoelectron spectra, vibr. fine struct. 78−9196
difluorodichloromethane, spectral data evaluation for atm. sensing 79−62582
diformylhydrazine, ^{14}N NQR lines fine structure 80−63667
dimethylether, and d_6, microwave spectra of torsionally excited states 79−26974
disilylmethane, microwave spectrum, struct., dipole moment and internal rot. 79−13699
dyes, secondary fluoresc. under very powerful pumping, fine struct. spectra 77−58383
electron impact excitation, photon-electron ang. correlation, fine/hyperfine struct. effects 78−42231
equivalent nuclei, ENDOR fine struct., exact solns. 77−6811
ethyl radical, $^{13}C_\alpha$ and H^+ hyperfine interactions, EPR spectra, vibr. anal. 80−23443
fluorene: acridene, radical pair form. from excited states, optical nucl. polarisation obs. 80−14155
fluorene:pyrene-d_{10} cryst., magnetic resonance absorpt. of host-guest triplet paired centres 80−34750
fluoromethanes, soft X-ray absorpt. spectra, fine struct. above K-edge of C 78−42096
fluorotrichloromethane, spectral data evaluation for atm. sensing 79−62582
formaldehyde, 4_0^1 band anal., isotope effects 78−86878
formic acid ions, fragmentation, energy selected, photoelectron-photoion spectra 80−95676
gas layer, absorpt. model, fine struct. parameters *(Russian)* 77−65455
germanyl acetylenes, fine structure due to internal rotation in IR-active perpendicular bands 79−98096
haloacetylenes, photoelectron spectra, electronic states of radical cations 79−22756

molecular fine structure continued
hexa-deutero dimethyl selenide, microwave spectrum, first excited torsional states, top-top interaction 77−10668
trans-hexatriene, multiphoton ionization spectrum in 6.2 eV region 77−27133
hole-burning spectra, absorption spectra fine struct. method 77−88594
inner-shell photoabsorpt., shape resonances, extended X-ray absorpt. fine struct. 77−18979
inorganic molecules, UV photoelectron spectroscopy, spectral assignment criteria, bonding 78−17717
iodotrifluoromethane, photoelectron spectra, spin-orbit splitting, vibr. fine struct. 78−21974
ionised compounds, geometrical and vibrational struct. changes, semiempirical MINDO/3 calcs. 79−31401
methane, ν_1 fundamental, CW stimulated Raman gain spectroscopy 79−6943
methane, and -d_4, soft X-ray absorpt. spectra, fine struct. above K-edge of C 78−42096
methoxy detection by submillimetric laser spectrometer 77−40623
molecular aggregates, triplet, ESR line shape in solid matrix, fine and HFS 78−58878
multiphoton resonances, vibr.-rot. fine struct. effect *(Russian)* 79−86022
naphthalene, doped crysts., fine struct. strengths in vibronic spectra 77−44004
nonlinear resonances of accelerated atoms and molecules *(Russian)* 78−50488
organic molecule, nonuniformly broadened absorpt. spectra, hidden fine struct. 79−93999
α-oxalic acid dihydrate, low-lying excited states, ODMR and optical obs. 79−41188
perylene, solid soln. in ethanol, fine struct. in absorpt. spectra, laser technique 77−90178
phenol, in cyclohexane ethanol mixtures, UV absorption, solvent effects 79−22767
phenol-organic solvent mixtures, UV spectra, solvent effects 79−22769
4-pyridine carbaldehyde, microwave spectrum, rot. assignments, quadrupole coupling consts. 80−91548
rotation-vibration spectrum, fine struct. splitting 77−57975
silyl acetylenes, fine structure due to internal rotation in IR-active perpendicular bands 79−98096
spherical top mols., T(ν_3) rovibrational bands, level cluster patterns, centrifugal and Coriolis effects 79−18175
symmetric molecules, high resolution spectra, rot. and permutation dynamics 79−41157
$TCNQF_4$, charge transfer complexes and salts, C(1s) and N(1s) XPS anal. of shake-up satellites 77−14492
trichlorofluoromethane, UV photoelectron spectra, vibr. fine struct. 78−9196
BCl_3, ν_3 vibr. level, fine struct., nonlinear reson. 77−6783
BaCl+Ar(He)(N_2), intermultiplet energy transfer 79−27063
$BaCl(C^2\Pi_{3/2}, \nu=0)$+Ar, intermultiplet energy transfer, laser induced fluoresc. obs. 78−9227
Br_2, extended X-ray absorption fine struct. amplitude 79−59489
Br_2, extended X-ray absorption fine struct. amplitude attenuation, rel. to XPS satellites 80−37821
CN, free radical, anticrossing spectra for fine struct. consts. 79−68270
CO, X-ray K-absorpt. spectra, vibr. fine struct., ab initio restricted HF calc. 78−86883
CO, X-ray K-absorpt. spectra, reson. obs., near fine struct. 80−37817
CO_2^+, electronically excited states emission, $A^2\pi_u$ state bending vibrs. 77−3454
Ca-Ca symmetric collisions, molecular-K-X-ray anisotropy spectra, discrete struct. 77−14560
CaF, $A^2\Pi$-$X^2\Sigma^+$ transition, HFS and fine struct., intermodulated fluoresc. spectra obs. 80−63695
Cl_2, Ar ion laser excited, normal and reson. Raman spectra 79−26993
CsX, (X=F, Cl, Br), absorpt. fine struct. at Cs^+ 4d threshold 77−18940
Cu complexes, spin coupled ion pair, singlet-triplet splitting 77−85552
FO free radical, detection by CO_2 laser mag. reson. 80−45594
Fe+Fe symmetric collisions, molecular-K-X-ray anisotropy spectra, discrete struct. 77−14560
H_2 3s, 3d: $^1\Sigma$, $^1\Pi$, $^1\Delta$ complex, fine struct., Doppler-free laser spectroscopy 80−1087
H_2, $c^1\Pi_u$ metastable state, fine struct. lifetimes 79−64050
H_2, metastable state, mol. beam reson., vibr. anal., spin-rot. interaction 79−22731
H_2-inert gas, bound complex form., anisotropic intermol. pot., IR spectra anal. 78−37634
HBr, fine struct. in dissociative attachment cross sections 80−87248
HCN, vibr. fine struct. accompanying core ionis., STO calcs. 78−62844
HF, fine struct. in dissociative attachment cross sections 80−87248
H_2O vapour, visible absorpt. spectrum, fine struct. acoustooptical determ. 80−86450
H_2O^+, spin and rot. fine struct., orbital angular momentum 80−83247
$H_3SiOSiH_3$, pot. function governing low freq. bending mode 77−58016
He_2, $a^3\Sigma_u^+$ metastable state, fine struct., mol. beam mag. reson. obs. 78−78720
InCl, InBr, InI, UV photoelectron spectra of valence d shells, gas-phase 78−62845
^{24}MgH, IR rot.-vibr. bands, stellar atm. appls. 77−18918
N_2, X-ray K-absorpt. spectra, vibr. fine struct., ab initio restricted HF calc. 78−86883
N_2, X-ray K-absorpt. spectra, reson. obs., near fine struct. 80−37817
NH, fine struct. in $X^3\Sigma^-$ and $A^3\pi$ states, STO and GTO calcs. 77−6679
NH_2, spin and rot. fine struct., orbital angular momentum 80−83247
NH_3, IR spectra, fine struct. of rot.-vibr. bands 80−102504
NH_3^+, ionisation pot. of ^2E state, Jahn-Teller effect 78−62948
$NH_2(X^2B_1)$, MODR, hyperfine coupling consts., spin rot. consts. 78−1010
NO, autoionisation struct. at first ionisation limit, photoionis. data 78−58748
NO_2, fluoresc. excited by laser, spin-orbit effects 79−64030
N_2O, X-ray fluoresc. obs., ionis. pot., fine struct., LCAO SCF calc. 77−68055
Ni+Ni symmetric collisions, molecular-K-X-ray anisotropy spectra, discrete struct. 77−14560
Ni_3, in solid Ar, reson. Raman spectra 80−63638

molecular fine structure continued
O_2 rot. Raman spectra fine struct., press. broadening *(French)* 79−94003
O_2^+, $^4\Pi$ states, spin-spin coupling consts., ab initio calc. 79−97981
O_2^+, absorpt. linewidth of predissociated levels, lifetimes 79−36711
O_2^+, IR spectra, rot. anal. of b Σ_g^--$a^4\pi_u$ first negative band 78−5219
O_2^+, photofragment spectroscopy using fast ion beams 80−9755
$(O_2)_2$, struct., energy transfer, high resolution electronic spectra 78−25550
O_3, combination bands ($\nu_1+\nu_2$) and ($\nu_2+\nu_3$), anal. 78−9150
OH, laser induced fluorescence, preferential population of π^+ component of Λ doublet in $H+NO_2 \rightarrow OH+NO$ 78−31620
OH, Λ-doublet splitting calc. rel. to predicted radioastronomical freqs. accuracy 79−48666
OH, radical, far IR laser mag. reson. spectra, fine struct. transition 79−76454
OH, $X^2\Pi$ state, microwave spectrum calcs. 77−30858
OH^+, fine struct. in $X^3\Sigma^-$ and $A^3\pi$ states, GTO and STO calcs. 77−6679
OsO_4, HFS and fine struct., saturation spectroscopy obs. visible spectra 80−53008
PH, far IR laser mag. reson. of $X^3\Sigma^1$ and at $^1\Delta$ states 79−54869
PH, fine struct. in $X^3\Sigma^-$ and $A^3\pi$ states, GTO and STO calcs. 77−6679
PH_2, X^2B_1-state, rot. laser mag. reson. spectrosc. 80−28038
$PbCl_2$, $PbBr_2$, PbI_2, UV photoelectron spectra of valence d shells, gas-phase 78−62845
PbF, visible spectra, A-X_1 and B-X_1 fine struct. anal. 79−36657
S_2, microwave spectra 79-150 GHz, rot. and fine struct. parameters 79−63987
$S_2(B^3\Sigma_u^-\nu=4)$+He(Ar)(Xe), collision-induced transfer rates 79−94062
SF_6, IR double reson. with tunable diode laser 80−14160
SF_6, IR spectra, fine struct. of rot.-vibr. bands 80−102504
SF_6, $L_{II,III}$-absorption spectrum, prethreshold range fine struct. 78−86847
SF_6 molecule, resonant energy absorpt. struct. in IR laser field *(Russian)* 80−5592
SF_6, ν_3 bands, rot. fine struct., HFS spectroscopic consts. determ., saturation spectroscopy obs. 80−53008
SH^+, fine struct. in $X^3\Sigma^-$ and $A^3\pi$ states, GTO and STO calcs. 77−6679
$S^{16}O_2$,$S^{18}O_2$, (0,0) band rot. anal., a^3B_1 state electron spin fine struct. consts. 77−10687
SO_2, absorption spectrum, meas. using frequency doubled pulsed dye laser 80−87144
SO_2, absorption spectrum, meas. using frequency doubled CW dye laser 80−87145
SO_2, $L_{II,III}$ absorpt. edge, fine struct. 78−62823
SbO, B-X system fine struct. 79−50030
$SeH(X^2\pi_{3/2})$, far IR LMR spectrum 78−66564
$SnCl_2$, $SnBr_2$, UV photoelectron spectra of valence d shells, gas-phase 78−62845
TlCl, TlBr, TlI, UV photoelectron spectra of valence d shells, gas-phase 78−62845
^{238}U complex, α-induced defects, vibronic luminesc. band fine struct. 79−87489
VO, $^4\Pi$ states, spin-spin coupling consts., ab initio calc. 79−97981
Zn complex, Zn-tetraphenylporphine, absorption spectra fine struct., hole-burning method 77−88594
Zn complexes, pheophytins a and b, dual phosphorescence molecular splitting 79−89706
ZrO^+, $^2\Pi$-$^2\Sigma$ system 0.0 band spin-split components 80−23413

molecular fluorescence
$[1\text{-pyrenyl-}(CH_2)_n\text{-}N(CH_3)_3]^+Cl^-$, intramicellar fluorescence quenching 80−9627
3-amino- and 4-amino-N-methylphthalimide, effect of orientational-relax. processes in fluoresc. kinetics 80−18886
$\pi\pi^*$ and $n\pi^*$ states relative position, optical props., singlet-triplet conversion processes 79−3484
acenaphthene, vibronic spectra, electronic-vibr. interactions 78−1021
acenaphthene in n-alkane matrices, Shpolskii spectra fluorescence 78−9190
acetaldehyde, single vibronic level fluoresc., radiative lifetimes 78−82769
acetaldehyde+CO_2, vibr. relax., search for unquenchable species, room temp., 5-2200 torr 78−9229
acetaldehyde ($A,^1A_2$), laser induced fluoresc. 79−50075
acetic anhydride, multiphoton dissoc., CH_2 and C_2 prod., fluence depend. meas. 80−5586
acetones, fluorinated, absorpt., fluoresc. spectra, quantum yields, decay times meas., mechanism 77−3410
acetonitrile, low press. IR multiple photon photolysis 79−16022
acetonitrile molecule dissociation in IR field, laser-induced fluoresc. obs. 80−53075
acetophenone, highly purified, luminesc. props. 80−32764
2-acetylanthracene, soln., excitation spectra rel. to recording wave length *(Russian)* 77−12438
2-acetylanthracene solutions, excitation spectra rel. to absorption spectra, 77-300K 79−85970
acetylene, multiphoton vacuum UV photodissoc. obs. and interpret. 80−11939
acetylene, vibr. relax. study using laser-induced fluoresc. 80−74219
acetylene, VUV multiphoton dissoc., electronically excited fragment emission 78−90238
acetylene+inert gas, vibr. relax. study using laser-induced fluoresc. 80−74219
acetylene (-d_2), fluoresc., in matrix-isolated acetylene and ethylene photolysis 79−59505
acetylenic hydrocarbons, cyclohexane soln., structureless fluoresc. 80−5575
achiral molecules dissolved in cholesteric liq. crysts., fluoresc. circular polarisation *(German)* 77−42350
acridene yellow, glycerol soln., luminesc. intensity and polaris., temp. and viscosity effects 79−56833
acridine, dye solns., luminesc. spectra, conc. depend. effects 79−54885
acridine, excited state proton transfer reactions, ns fluorometry obs. 79−5132
acridine, methanol soln., edge excitation red shift, excited state proton association 79−18228
acridine, singlet state absorption profile, time resolved spectra 79−45769
acridine, solvent depend. of radiationless relax., singlet lifetime, picosecond spectroscopy 78−66582

molecular fluorescence continued
acridine, temp. depend. of fluoresc. decay meas. using picosecond techniques 80−99518
acridine orange, fluoresc. decay meas. by high repetition rate gated photon counting 80−86402
acridine orange, solvent effect on fluoresc. polaris. 79−41191
acridizinium ion, fluoresc. quenching by external heavy atom, via charge-transfer complex 78−42112
acriflavine, fluoresc. polaris., solvent effect 77−50468
acriflavine solution, fluoresc. polarisation, effect of aggregation of molecules 79−91485
acrolein, vap., visible luminesc. excited by pulsed CO_2 laser 79−54894
acrylonitrile, IR multiphoton dissoc., prod. of $CN(X^2\Sigma^+)$ and $C_2(a^3\Pi_u)$ radicals 80−63723
acrylonitrile, multiple photon dissoc., photofragment spectroscopy by laser-induced fluoresc. 80−11937
F-actin, struct. changes in living muscle fibres, polarised UV fluoresc. microscopy 80−67037
adsorbed molecules, on Ta (111), electron bombardment induced luminesc. and bremsstrahlung *(Russian)* 78−31290
adsorbed molecules, Raman and fluoresc. enhancement by surface roughness 80−102511
adsorbed molecules on metal surface, ang. intensity distrib. of emitted light 78−18907
aequorin-injected frog cardica muscle, Ca transients 78−61149
albumin, human serum, interaction with luminol. chemilum. and fluoresc. 77−21471
albumin-fatty acid complexing rel. to struct. lability of biomembranes, using fluoresc. probes 77−25381
albumin-probe complex, fatty acid binding kinetics 77−25365
aliphatic amines, tertiary, fluoresc. decay 80−91590
alkali halide: S_2^-, laser-excited spectra and reorientation of S_2^- 77−28563
alkali metal molecular, laser radiation absorpt., at. excitation processes 80−32785
alkali metal-inert gas mol., gaseous transient, D-line emission obs. 77−38688
alkaline earth dimens., heteronuclear, matrix-isolated, laser photoluminesc., van der Waals ground state 79−41192
alkanes, vap., fluoresc. lifetimes meas. 79−50064
alkyl benzenes, jet-cooled, intramol. vibr. relax., reson. fluoresc. and excitation obs. 80−14152
alkyl benzenes, jet-cooled, vibr. relax., nanosecond time evolution 80−95584
alkyl styrenes, fluoresc., ns time resolved emission spectra 77−6822
para-alkylanilines having optically active modes, vibr. relax. studied by absorpt. and fluoresc. spectra 80−83340
alkylbenzenes, jet-cooled, vibr. relax., absorpt. spectra 80−74236
alkylbenzenes, jet-cooled, vibr. relax., fluoresc. spectra 80−78694
amines, aromatic, photochem. reactions with carbon tetrachloride, initiation mechanism 79−61888
2-amino, 7-nitrofluorene, in 2-propanol, Stokes fluorescence shift time resolution 77−58060
4-amino-4′-nitrostilbene, fluoresc. emission anisotropy, solvent effects 79−3489
4-amino-4′-nitrostilbene, thermal motion of prolate luminescent molecules in solvents with different viscosities 79−83029
7-amino-4-methylcoumarin, fluoresc., solvent depend., shift of max. wavenumber 79−85997
2-amino-7-nitrofluorene, in binary solvent soln., time-resolved fluoresc. spectroscopy 79−36680
3-amino-N-methylphthalimide, in polar-nonpolar solvent mixture fluorescence band struct. 78−15213
4-amino-N-methylphthalimide, reversible induced absorpt. spectra in binary solvents 79−98117
4-amino-N-methylphthalimide in n-propanol, nanosecond laser fluorometry 80−102721
m-aminoacetophenone+t-amyl alcohol, in soln., fluoresc. and absorpt. spectra, excimer form. 78−78737
aminobenzoic acid, aqueous and dioxane solns. with nonfluoresc. impurity, fluoresc. and pH *(Russian)* 77−83635
4-aminophthalimide, soln. in n-propanol, fluoresc., orient. relax. of solvent 79−24357
4-aminophthalimide soln., fluoresc. nanosec. kinetics, dielec. relax. 79−78737
2-aminopurine, in viscous soln., fluoresc. quenching, emission, intensity and reson. transfer *(German)* 80−91599
aminoquinoline derivatives, solvent effect on absorpt. and fluoresc. spectra 79−59494
aniline, $^1B_2$ state, single vibronic level fluoresc. 79−54903
aniline+AR, $^1B_2$-state collision induced intramol. vibr. energy transfer, SVL fluoresc. obs. 79−54904
8-anilinenaphthalene-1-sulphonic acid, edge excitation red shift, temp. depend. 77−6849
anilinium ion, $C_6H_5NH_3^+$, fluoresc. and phosphoresc., pKa values 79−13755
8-anilino-1-naphthalenesulfonic acid, fluoresc. probe mol. in mixed solvent 79−45746
1-anilino-8-naphthalene sulphonate, bound to chloroplast membrane, fluoresc. study of proton and cation effects 78−24034
1,8-anilinonaphthalene sulphonate, aq. and ethanolic solns., excited singlet state decay pathway 78−17703
1,8-anilinonaphthalene sulphonate in bacterial suspension, fluoresc. spectra 79−88052
1-anilinonaphthalene-8-sulphonate fluorescent probe interaction with surface structs. of E. coli 78−69007
anisotropically polarisable molecules embedded in small particles, fluoresc. scatt. 79−76587
1-(N-p-anisyl-N-methyl)-amino-3-anthryl-(9)-propane, intramol. exciplex formation 77−58059
1,8-ANS, fluorescent probe orientation and rot. freedom in lecithin bilayers 77−44583
anthracene:2-hydroxyanthracene cryst., site selective photochem. change, fluoresc. obs. 77−40273
anthracene, chemisorbed on Al_2O_3, radiative and nonradiative processes 79−36686
anthracene, diacetyl-sensitised delayed fluoresc. 79−54888
anthracene, evaporated films, fluoresc. 77−85777
anthracene, excimer fluoresc. lifetime and quantum yield in soln. 77−6834
anthracene, excimer form. in soln. and cryst., fluoresc. study 79−45759

molecular fluorescence continued
anthracene, fluoresc., site selection spectroscopy, 2-300K 77−1731
anthracene, fluoresc. by electron beam excitation 79−94031
anthracene, fluoresc. quenching by triethylamine 79−50057
anthracene, fluorescence spectra in aq. and surfactant solns. 77−83639
anthracene, hot luminesc. in solid matrix at 4.2K, intramol. thermal bath 79−85999
anthracene, in acethylcellulose, fluorescence, time dependent emission anisotropy *(German)* 78−94279
anthracene, in n-paraffin matrices, luminesc. spectra, depend. of inhomogeneous broadening *(Russian)* 79−10145
anthracene, in stretched polyethylene film, UV-visible and fluoresc. spectral shifts 78−62852
anthracene, matrix isolated, vibr. relax., hot luminesc. obs. 79−85986
anthracene, optical determ. of vapour conc., vap. press. and heat of sublimation 78−22840
anthracene, rarefied vap., fluoresc. spectrum shape distortion in presence of intense radiation 79−3487
anthracene, Shpolskii spectra, vibronic struct., fluoresc. *(German)* 79−22754
anthracene, spectral evidence for green incipient dimers after photooxidation and photodimerisation 78−15687
anthracene, vap., laser-excited long-lifetime luminesc. 79−54887
anthracene, vap., line fluoresc. response to IR laser 79−54893
anthracene, vapour, fluoresc. spectra, mol. vibr. freq. reson. laser IR irradiation, quenching 80−18883
anthracene derivatives in soln., fluoresc. and laser parameters 79−27251
anthracene in polychlorinated alkanes photochemical study by rapid scanning fluoresc. spectroscopy 80−86440
anthracene intramolecular excimer in 1,3-dianthrylpropane, direct obs. 80−48029
anthracene vapour, conc. depend. of diffuse component of fluoresc. spectrum *(Russian)* 77−46601
9-anthracene-$(CH_2)_n$-N,N-dimethylaniline, electrogenerated chemiluminesc., intramol. exciplex form. 78−11503
anthracene-Au interface, energy transfer 77−85775
anthracene-dimethylpyromellitimide, CCT crystals, mag. field effect on fluorescence 78−19543
anthracene-N,N-diethylaniline exciplex, intersystem crossing 77−30905
anthracene-tetracyanbenzene, charge transfer, magnetic resonant modulation of photoconductivity 78−64062
anthracene-trinitrobenzene complex, neat and mixed cryst. and glass opt. spectra 77−40274
anthracene/trans, trans-2,4-hexadiene-exciplex, fluoresc. rel. to photodimerization 77−3401
anthracenes, anthronyl substituted, solvent-assisted form. of luminesc. intramol. exciplexes 78−25589
anthracenes, exciplex form. with amines, form. kinetics and luminesc. props. 80−66792
anthracenes, in soln., triplet-triplet fluoresc. 79−59501
anthracenes, meso-substituted, thermally assisted and heavy atom assisted intersystem crossing 79−31573
anthracenes, nonradiative relax. of higher excited triplet states, double excitation obs. 78−29805
anthracenophanes, fluoresc. and photoisomerisation 79−33781
9,10-anthraquinone, phosphorescence, external heavy atom in mol., 4.2 to 77K, quasiline spectra 78−82773
anthraquinone-xanthone liq. soln., upper excited singlet state, delayed fluoresc. 80−106345
9-anthroic acid, excimer-type transition polaris. 79−50062
4-(9-anthryl)-N,N-dimethylaniline, fluoresc., dipole moments and polarisabilities 80−1019
p-(9-anthryl)-N,N-dimethylaniline derivatives, excited emitting states in polar solvents, fluoresc. 78−5263
p-9-anthryl-dialkulanilines, twisted intramol. charge transfer states, dual fluoresc. 79−36683
antibunching phenomena on single-scatterer fluorescence in weak-field limit 80−63580
antimalarial drugs, lifetime meas. via reiterative convolution using fluorescence decay curves 80−57380
aromatic aldehyde, phosphorescence spectra of mol., intensity and vibronic coupling 79−76461
aromatic amides, intersystem crossing, mol. geom. effects 77−6828
aromatic compounds, absolute fluorescence quantum yield, calorimetric determ. 80−43092
aromatic compounds, heavy atom substituents at different bonding sites *(German)* 79−81236
aromatic compounds, isothermal recomb. fluoresc., decay kinetics 78−29809
aromatic compounds, mol. rearrangement in excited electronic state, fluoresc. with anomalously large Stokes shift 79−85983
aromatic compounds, oriented in stretched polyethylene film, phosphoresc. polarisation 79−6961
aromatic compounds, subpicosecond states, fluoresc. spectroscopy in liquids 79−45758
aromatic compounds luminesc. polarisation, quasilines and bands in Shpolskii spectra *(Russian)* 79−31592
aromatic esters, in ethanol, luminescence spectra, phosphoresence and fluorescence 79−54899
aromatic esters, phosphoresc. and fluoresc. spectra in organic matrices 80−32756
aromatic hydrocarbon, centrosymmetric, two photon excited upper state fluoresc. spectra, reson. fluoresc. and vibr. mode selectivity 80−18878
aromatic hydrocarbon, quenched with Ag^+ in ethanol, triplet state form. 79−11801
aromatic hydrocarbon in soln., excited electronic state vibr. relax., time resolved fluoresc. 80−48024
aromatic hydrocarbon soln., delayed fluoresc., mag. field effect, excimer form. 77−14479
aromatic hydrocarbon-dicyanobenzene, aq. micellar soln., fluoresc. quenching mechanism 79−50063
aromatic hydrocarbon-N,N-dimethylaniline, aq. micellar soln., fluoresc. quenching mechanism 79−50063
aromatic hydrocarbons, ethanol-KI solns., fluoresc. affected by I 79−13749
aromatic hydrocarbons, excimer decay dynamics, rate const. rel. to solvent 78−58729
aromatic hydrocarbons, fluorescence quenching rate constant, undergraduate expt. using Spectronic 20 77−57119
aromatic hydrocarbons, liq. solns., delayed fluoresc., mag. field induced polarisation inversion 77−88485

molecular fluorescence continued
aromatic hydrocarbons, rot. anisotropy and solvent-fluorophase bonds, differential polarised phase fluorimetric investig. 77−61779
aromatic hydrocarbons, sequential coupling 80−58297
aromatic hydrocarbons, Shpolskii systems, key and hole rule test, fluoresc. 77−42347
aromatic hydrocarbons in soln., low quantum-yield mol. fluoresc. 77−58063
aromatic hydrocarbons in soln., mag. field effects on delayed fluoresc., perturbation theory applic. 77−30913
aromatic isolated mol. nonradiative conversion, internal and S-T conversion, vibr. excitation and fluoresc. quantum yield 80−43095
aromatic molecule, electronic excitation energy degradation, electronic-vibr. spectrum 77−488
aromatic molecules, energy transfer from upper triplet states 79−10142
aromatic molecules, singlet lifetime by time resolved spectrosc. 79−45769
aromatic nitroso compounds, fluoresc. from upper singlet 79−6958
aromatic-molecules, conformeric fluoresc. and phosphoresc., rotation of chromophoric fragments around single chemical bonds 77−68068
aromatics, fluoresc. polarisation red edge effect, rot. anomaly 79−3472
atebrin fluorescence photo-induced quenching and photosynthetic electron transport, pea chloroplast 77−56351
atom+diatom, energy transfer, vibronic excitation, emission spectra 78−66578
atom+molecule, rot. inelastic collision, rot. alignment calcs., quantum formulation 77−61834
atom+molecule reaction rate meas. 80−16676
Ca^{2+},Mg^{2+}-ATPase, of sarcoplasmic reticulum, transient kinetics obs. by fluoresc. 78−61156
Na^+,K^+-ATPase preparations, tryptophan fluoresc. 77−21477
auramine O, fluoresc. efficiency, solvent viscosity effects at high press. 78−9188
2-azaanthracene in heptane, benzene and ethanol, max. intensity of fluoresc. on axis of cylindrical cell *(Russian)* 77−55814
7-azaindole dimers, photoautomerisation by double proton transfer, fluoresc. kinetics 80−11880
azastilbenes, fluoresc., excitation energy anomaly, pot. energy model. 77−50466
azoalkanes, fluoresc., solvent isotope effect 78−25591
azobenzene, emission from $^1(n,\pi^*)$ state, spectrum and ultrashort decay time 77−30895
trans-azobenzene, $S_2 \rightarrow S_0$ fluoresc. 80−28044
azulene, Shpol'skii matrix, $S_2 \rightarrow S_1$ fluoresc., spectral anal. 77−18956
azulene, soln., laser-excited $S_2 \rightarrow S_1$, $S_1 \rightarrow S_0$ emission and $S_2 \rightarrow S_n$ absorption 79−10131
azulene(-d_8), ultrafast $S_2 \rightarrow S_0$ internal conversion 79−3474
azulene in cyclohexane, relax. time of first excited electronic singlet state 77−6825
azulene in naphthalene, reson. Raman and reson. fluoresc. spectra, 30K 78−80323
azulene in naphthalene mixed cryst., $S_2 \rightarrow S_1$ fluoresc., vibr. anal. 78−66586
azulene-fluoranthene, soln., triplet energy transfer, delayed fluoresc. study of $S_2 \rightarrow S_0$ 80−23331
(2,2) (2,6) azulenophanes, mag. circular dichroism and anomalous fluoresc. spectra 80−83398
azuleno[5,6,7-cd]phenalene, slow internal conversion between close lying singlet state 77−30907
background fluorescence spectra, in continuum source at. fluoresc. spectrometry 77−81430
bacterial photosynthesis, light collection and harvesting processes investig. on psec. time scale 77−90743
bacteriochlorophyll a, stimulated fluoresc. and fluoresc. quenching, pump photon density 78−27895
bacteriochlorophyll of green bacteria, resolution of absorpt. and fluoresc. spectra into components 78−20152
bacteriorhodopsin, emission lifetime meas. 78−96012
BBOT, time-depend. fluoresc. depolarisation, mol.-rot., slip boundary conditions in soln. 78−9179
BBOT dye, vapour phase, optical props. *(Japanese)* 80−9879
Bengal pink-anthracene, mixed annihilation delayed fluoresc. 80−74193
benzaldehyde, electronic spectra, Cl and F substitution effects 80−23456
1,2-benzanthracene, monomer and excimer fluoresc. in soln., triplet-triplet annihilation and mag. field depend. 78−78738
1,2-benzanthracene, secondary reson. radiation and hot energy transfer, soln. luminesc. 80−87167
1,2-benzanthracene in polystyrene films, delayed luminesc. decay kinetics 80−43088
benzene, $^1B_{2u}(\pi\pi^*)$-$^1A_{1g}(6_0^1)$ band, in supersonic jet, rot. anal. 79−31578
benzene, $-d_0-d_6$ vapour at low press., intersytem crossing and internal conversion, press. depend. of triplet form. 77−30918
benzene, electron impact-induced generalised oscill. strength, 400 eV, 500 eV, momentum change depend. 78−1088
benzene, fluoresc., triplet state and isomerisation yields, photochem. 77−1942
benzene, fluoresc. quantum yield in soln., dipole-dipole interaction 78−25598
benzene, fluoresc. quenching by pulsed proton irrad. of cyclohexane soln. 78−5270
benzene, fluoresc. triplet state and isomerisation yields, low vibr. levels 79−64035
benzene, luminesc. yield spectra in VUV 79−36685
benzene, matrix fluoresc. spectra, rel. intensities of multiplet components 79−54882
benzene, ns time-resolved emission spectra, collisional processes 77−3490
benzene, photoluminesc. at 5K, N_2 and inert gas matrices 77−6838
benzene, S_1 state, mode to mode vibr. energy flow, low pressure fluorescence spectra exam. 78−25664
benzene, single vibronic level fluoresc. after two-photon excitation 77−6818
benzene, solid and isolated in rare-gas matrices, spectroscopic study 79−3455
benzene, SVL fluoresc. band intensities, Franck-Condon factors, Fermi reson. 77−10700
benzene, UV fluoresc. quantum yield, photoacoustic technique 77−88595
benzene, vapour-phase, absolute fluoresc. quantum yields, nonradiative processes 77−6829
benzene+benzene-d_6, electronic energy transfer between vibronic levels, fluoresc. obs. 77−38712

molecular fluorescence continued
benzene+Hg, electronically excited, mol. fluoresc., vibr. relax. cross sections and equilibration rates determ. 80−87205
benzene(-d_6) vapour, SVL fluoresc. lifetimes and quantum yields 77−10701
benzene ($^1B_{2u}(S_1)$)+Ar(benzene), rot. relax. to Boltzmann distrib. 78−86936
benzene in Xe-doped solid Ne, luminesc. 77−32416
benzene radical cation in solid Ar, fluorescence spectra obs. 80−83382
benzene-aniline gas mixture, fluoresc. spectra, lifetimes, yields, electronic energy transfer 77−14477
benzene-d_6+N_2+CO_2, electronically excited, mol. fluoresc., vibr. relax. cross sections and equilibration rates determ. 80−87205
benzil, in PMMA glass, luminesc. temp. depend. matrix controlled photorotamerism 79−22743
benzimidazole, excited states, solvent interactions, fluoresc. obs., rel. to chromophore 78−37670
benzoic acid, in acidic solns., room temp. fluoresc. 78−50568
1,12-benzoperylene, in heptane, Stokes and anti-Stokes fluoresc., transition moment 77−61781
3,4-benzophenanthrene, dual fluoresc. (S_1, S_2), collision-free conditions 79−45741
benzophenone, and d_{10}, ODMR and phosphorescence spectra in organic matrix 79−36671
benzophenone, intensity of decay rel. to laser irrad. intensity 78−82772
benzophenone betyl radical, photochem. yield mag. field effect on spin rephasing, double-pulse technique 77−90615
benzophenone vapour, fluoresc. and phosphoresc., nonradiative transitions between triplet and singlet state obs. 80−99516
benzophenones, triplet state fine struct. parameters and phosphoresc. spectra 79−50065
benzoxazole, aromatic derivatives, spectral luminesc. and lasing props. rel. to electronic struct. 80−99519
1,12-benzperylene, in benzene, 77K, quasi-line luminesc. spectra obs., Shpolskii's method 77−69894
1,12-benzperylene exciplexes, radiative and radiationless decay 77−6817
1,2-benzpyrene, in cyclohexane, 77K, quasi-line luminesc. obs., Shpolskii's method 77−69894
3,4-benzpyrene, monomer and excimer fluoresc. in soln., triplet-triplet annihilation and mag. field depend. 78−78738
3,4-benzpyrene, relative S_1* emission yield vibronic states density 77−486
benzyl radical, IR absorpt. spectra, matrix isolated at 77K 79−22706
benzyl radical-halide ions, form. by dissoc. electron attachment in matrix, charge transfer band 77−16854
benzyl radicals, monomtheyl- and dimethyl-substituted, electronic spectra and electron affinity 80−63618
betamethylnaphthalene in $C_{10}D_8$, exciton percolation and coherence 77−59258
biacetyl, aq. solns., fluoresc., phosphoresc. 77−3395
biacetyl, IR/UV double resonance, fluoresc. and phosphoresc. obs. 77−6810
biacetyl, multiphoton excitation of triplet state, fluoresc. decay 79−31632
biacetyl, single rovibronic state fluoresc., quantum beats 79−31570
biacetyl in supersonic jet, emission spectra, energy-resolved decay times 79−81224
biaryls, nonplanar, spin-orbit coupling effects, luminesc. quantum yields *(German)* 77−42349
bilayer membranes, permeation of water mols. meas. using fluoresc. quantum yield solvent-isotope effect 79−34710
bimolecular reaction, partly diffusion-controlled, physical and chem. kinetics competition 79−43567
1,1'binaphthyl, electronic struct., fluoresc. CNDO/S CI calcs. 78−90084
1,1'-binaphthyl mononegative ion conformation 77−30774
binary mixtures, anal. by computer decomposition of mol. fluoresc. spectra 78−15735
binary mixtures, qualitative anal. by fluoresc. polarisation spectroscopy 79−34396
biogenic amine microspectrofluorometry, automatic correction of excitation spectra 77−9308
biological applications of fluoresc. and fluoresc. probes 78−15932
biological probes, size limit of mols. permeating junctional membrane channels 77−36900
biomembrane, apparatus for direct meas. of fluoresc. decay *(French)* 77−5116
biomembrane, apparatus for meas. of fluoresc. polarisation *(French)* 77−9307
biomembrane microviscosity measurement, light scatt. effects 79−39365
biomolecule and membrane dynamics, fluoresc. spectroscopy 80−101148
biophysical substances, chemical and structural anal. *(Norwegian)* 78−92596
biopolymer Brownian diffusion, fluoresc. correl. spectroscopy 79−62193
biopolymer molecular dynamics and structure, fluorescence spectroscopy 77−60329
biphenyl:fluoranthene(pyrene)(chrysene), triplet and singlet transport rate ratio 79−56832
biphenyl, carbonyl derivatives, absorpt. and luminesc. spectra, solvent effects and triplet lifetimes 77−24889
biphenyl, in propylene glycol, mol. fluoresc., effect of mol. conformation 78−78736
biphenyl, luminesc. yield spectra in VUV 79−36685
biphenyl, luminescence spectrum intensity distribution 79−3476
biphenyl crystals, electronic and vib. states, cryst. field mixing, two-photon spectra 77−59603
biphenyl glutarate polymer, resonant Raman spectra and fluoresc. 77−24830
biphenyl in Ne or Ar matrix, biphenyl ring torsion by vibronically resolved spectra 79−81228
biphenyl polyenes, vibronic states, quasi-linear spectra *(Russian)* 80−95598
biphenylene, fluoresc. from higher singlet levels 79−83473
2-(4-biphenylyl)-5-phenyloxazol, vapour, electron beam excited luminesc. *(Russian)* 78−82780
2-[4-biphenyl]-5-phenyloxazole, fluoresc. by electron beam excitation 79−94031
tris(2,2'-bipyridine) ruthenium(II) cation, IR-optical double reson. and thermal modulation spectra 78−25576
1,4-bis[2-(5-phenyloxazolyl)]benzene, saturated vap. press., absorpt. and fluoresc. spectra 79−76442

molecular fluorescence continued
Born-Oppenheimer and true eigenstate prep. by coherent light, large mol. nonradiative relax. 77−88490
9-bromoanthracene, fluoresc. and phosphoresc. spectra 77−14480
bromofluoromethylene radical, laser-induced fluoresc., $^1A''$-$^1A'$ transition 80−91589
bromomethane, IR multiphotonic excitation, depend. on cell geometry, mol. fluoresc. and decomp. obs. 80−83430
Brownian rotational motion, effects on nonlinear fluoresc. characts. *(Russian)* 78−5275
camphorquinone, cryst., PMDR and fluoresc., S_2 state, intersystem crossing 77−32296
carbazole, excited state, dissociation rate, normal isotope effect 77−32767
carbazole, in presence of KI, decay functions of triplet state of fluoresc. and phosphoresc. 78−66590
carbazole, multiexponential fluorescence decay, systems theory approach to anal. 79−59495
carbazole-labelled phospholipid, fluoresc. quenching meas. of pesticide uptake into membranes 78−7323
carbocyanine dye orientation in erythrocyte membrane, microscopic fluorescence polarisation obs. 79−83694
carbohydrate soln., γ-irradiated, fluoresc. spectra obs. *(Russian)* 77−83644
carbonyl fluoride, IR laser driven reverse internal conversion 79−81230
cells, living, fluorescently labelled mols. as probes of struct. and function, review 80−67321
cetyltrimethylammonium bromide-1-butanol system, micellar conc. meas. using fluoresc. probe study 80−85217
charge-transfer, excited, ps. kinetics, geometrical and solvent polarity effects 77−30986
chemiluminescence, beam-gas, kinetics of metastable excited state products 77−56231
chlorodifluoromethane, IR multiphoton dissociation, laser intensity effects, fluoresc. obs. 79−98168
chlorodifluoromethane, laser-induced decomp. rate, laser fluoresc. investig. 79−68257
chlorofluorocarbene, ($^1A''$) state, radiative lifetime, quenching rate, press. depend., laser-induced fluoresc. obs. 78−5259
chlorofluoromethylene, radical, laser-induced fluoresc. excitation spectra 79−98131
chlorofluoromethylene radical, gas phase laser-induced floresc. spectroscopy 80−14173
chloromethanes, VUV fluoresc., UV multiphoton dissoc. 80−28076
chlorophyll, -a and -b, fluoresc. fading curve of lowest triplet state 79−36691
chlorophyll, and related mols., in solid solns., fine-structured vibronic spectra under tunable dye laser excitation *(Russian)* 80−74164
chlorophyll, energy migration between native forms at −196°C using sensitised fluoresc. 77−70429
chlorophyll, fluoresc. decay time depend. on luminesc. and excitation wavelengths 79−66447
chlorophyll, fluoresc. detection of triplet state kinetics 77−30903
chlorophyll, fluoresc. in bilayer lipid vesicles and liposomes, conc. quenching 77−4985
chlorophyll, fluorescence quenching, exciton annihilation excited state absorption and stimulated emission 79−98137
chlorophyll, for passive remote sensing of phytoplankton 77−86938
chlorophyll, native forms., var. fluoresc. at −196°C 77−70417
chlorophyll, transfer of electronic excitation energy from monomer to dimer *(Russian)* 78−27289
chlorophyll a: Cu^{2+}, in pyridine fluoresc. quenching mechanism 79−56837
chlorophyll a, absorpt. and fluoresc. spectra, observance of Stepanov relation 80−81554
chlorophyll a, bimol. quenching of excitons and fluoresc. in photosynthetic unit 77−16908
chlorophyll a, fluoresc. and absorpt. spectra, resolution into components 79−57584
chlorophyll a, fluoresc. at 685 nm, rel. to diffuse reflectance of ocean 79−66700
chlorophyll a, fluoresc. decay rate obs., inhomogeneous struct. and relax. time effects 79−86007
chlorophyll a, photoinduced changes in oxidation-reduction pot. of chloroplast suspension 77−25399
chlorophyll a, stimulated fluoresc. and fluoresc. quenching, pump photon density 78−27895
chlorophyll a and protochlorophyll a, optical transitions anisotropy 79−43825
chlorophyll a delayed fluoresc. in absence of electron transport on acceptor side of photosystem 2 77−70428
chlorophyll a fluorescence duration in chloroplasts rel. to ferricyanide and vitamin K_3 conc. 77−25393
chlorophyll a of photosystem II, fluoresc. when electron transport on acceptor side is blocked 78−7324
chlorophyll c absorpt., fluoresc. and fluoresc. excitation spectra in alga cell at −196°C 78−53329
chlorophyll fluorescence changes in isolated broken chloroplasts and involvement of elec. double layer 78−44464
chlorophyll fluorescence lifetime data rel. to stimulated emission 77−52742
chlorophyll fluorescence quenching by β-carotene 77−52735
chlorophyll in vesicles, energy transfer and fluorescence quenching 79−39349
chlorophyll-a, fluoresc. at low concs., noise reduction by low pass filter for DC signal 80−87249
chlorophyll-a, interaction with β-carotene in phosphatidyl choline bilayers, fluoresc. quenching 79−20506
chlorophyll-a, mols. and complexes in PMMA and MTHF matrices, optical spectra 79−3433
chlorophyll-a, monochromatic excitation, luminesc. spectra, quasilinear struct. *(Russian)* 78−74809
chlorophyll-a, soln., luminesc. spectrum, impurity bands *(Russian)* 77−88493
chlorophyll-a, spectral props. of liquid crystal solutions 78−27291
chlorophyll-a (b), dimerisation, fluoresc. and ODMR study 80−18876
chlorophyll-b, mols. and complexes in PMMA and MTHF matrices, optical spectra 79−3433
chlorophyll-like molecules, fluoresc. and phosphoresc. polarisation spectra 79−85980

molecular fluorescence continued
chlorophyllide fluorescence quantum yield during photochlorophyllide reduction in etiolated leaves 80−81542
chlorophylls, mag. reson., site selected fluoresc. detection 80−69164
chlorophylls a and b and pheophytins, fluoresc. and phosphoresc. 80−12057
chlorophylls and pheophytins, phosphorescence and fluorescence polarisation spectra 79−70522
chloroplast fragments, fine struct. of fluoresc. spectra, derivative spectroscopy method *(Russian)* 79−34502
chloroplast photosystems, exciton annihilation at 100K 77−25371
chlorotetracycline, fluoresc. probe detect. of cell Ca redistrib. during stimulus-secretion coupling 77−77872
chlorotetracycline fluorescence, use in demonstrating Ca^{2+} release from cardiac cells 80−3612
cholesta-4,6,8(14)-triene, fluoresc. and absorpt. spectra in UV, lifetimes 79−27017
cholesta-5,7,9(11)-triene-3β-01, fluoresc. and absorpt. spectra in UV, lifetimes 79−27017
cholesteric liquid cryst., guest mol. fluoresc. in scatt. state 80−63698
chromone, solns., pH dependent fluorescence spectra, pK_a and tautomerism 79−59506
chromophore, excited state, solvent interactions, fluoresc. obs. 78−37670
chromophores, circular polarisation of luminescence, book contrib. 79−5250
chrysene, dual fluoresc. (S_1, S_2), collision-free conditions 79−45741
cluster containing tetracene molecules, excited state intramol. dynamics, laser-induced fluoresc. spectra obs. 80−78674
CO, in glow flow discharge, electronic states, excitation mechanism 80−53040
colliding particle system, two-photon transition, stimulated Raman scatt. 80−9663
collision-induced emission with laser irrad., cooperative chemical and optical pumping 78−22012
collisions in intense light beams, quantum aspects *(Russian)* 79−6903
combustion diagnostics, laser appls. 80−16688
complex anion electronic struct., outer sphere cation effects, X-ray fluoresc. spectra 78−86884
compounds with hindered internal rotation, vibronic luminesc. and absorption spectra 79−54883
concanav A, light irrad. causing membrane damage 80−56123
concentration depolarisation, of luminescing mols. 77−65505
conference, Minsk, USSR (May 1977) 79−54878
conformational mobility, fluorescence obs. 80−63877
conjugated molecules, excited state, self-consistent HMO theory *(Japanese)* 77−42253
conjugated molecules, triplet-triplet excitation, atomic localisation calcs. 79−54830
cooling of gases, laser pumping followed by reradiation at higher freq. transitions 79−827
coordination compounds, chemistry, electronic excitation, luminesc. methods 79−54880
copperporphin, metastable quartet state radiative decay 80−23453
coronene, fluorescence spectra, zero field line splitting *(Russian)* 78−17604
coronene, in cyclohexane, 77K, quasi-line luminesc. spectra obs., Shpolskii's method 77−69894
coronene, luminesc., spin-orbit coupling perturbation by metal chlorides *(German)* 80−1021
coronene, n-alkane matrix, up to 1.8 kbar emission multiplet struct. shift 77−34677
coronene-rhodamine 6G, energy transfer in PMMA matrix, fluoresc., temp. depend. 78−13539
coumarin, aqueous solution, fast neutron irrad., dosimetry appl. 78−44613
coumarin 6, ultrashort vib. population lifetime of ground state in vapour phase 77−30929
coumarin 6 dye mols. in liq. cryst., fluoresc. intensity, orientation control 78−82759
coumarin laser dyes, fluoresc. quantum yields and lifetimes, polar solvent effects 80−87054
coumarin laser dyes, in methanol, ethanol, and water, fluoresc. lifetimes meas. 79−27252
coumarin laser dyes, solvent effects on photophysical parameters 80−91598
counter-ion quenching of organic compound fluoresc. in micellar aq. solns. of surface-active substs. *(Russian)* 77−54573
cresyl violet, rot. diffusion, picosec. saturation spectrosc. obs. 80−5634
cryptocyanine, soln., $S_2 \rightarrow S_0$ fluoresc. 78−13541
cryptocyanine, solns., fluoresc. lifetime, viscosity depend. 79−59497
cryptopleurine derivatives, absorpt. and fluoresc. obs. of photodecomp. processes, dye laser relevance 80−55686
crystal violet, fluoresc. efficiency, solvent viscosity effects at high press. 78−9188
crystal violet, soln., picosec. relax., wavelength depend. 79−99921
cyanine dye sensitisers, J-aggregate formation, spectral changes of UV bands 77−70318
cyanine dye sensitisers, J-aggregates, meso substituents effect on mol. assoc. 77−70320
cyanine fluorescent dye membrane probe effects on cell props., rel. to bacterial chemotaxis 78−35815
9-cyano anthracene-dimethyl aniline, exciplex, fluoresc. of vap., 185-231°C 78−74693
9-cyano anthracene-tributyl amine, exciplex, fluoresc. of vap., 185-231°C 78−74693
9-cyano anthracene-triethyl amine, exciplex, fluoresc. of vap., 185-231°C 78−74693
p-cyano-dialkylanilines, twisted intramol. charge transfer states, dual fluoresc. 79−36683
p-cyano-N,N-dimethylaniline in polar solvents, double fluorescence, theoretical model 80−58296
9-cyanoanthracene excimer emission, in glassy and cryst. matrices 79−11445
9-cyanoanthracenes-N,N-dimethylaniline, fluoresc. exciplex emission in gas phase 79−68250
6-cyanobenzquinuclidine, intramol. electron-transfer excited state 80−58295
4-cyanobiphenyl and 4′-alkyl- or 4′-alkoxy-substituted liq. cryst. derivatives, soln., absorpt. and fluoresc. spectra 80−87164
cyanoethylene, photofragment recoil, state selective time of flight- fluoresc. method 79−11809

molecular fluorescence continued
cyclohexane, two-photon spectra; fluoresc. spectra, decay times, intensities obs. 77−75245
cyclohexane + toluene, energy transfer, pulse radiolysis obs. 80−16714
cyclophosphazene-DNa complex, spectrofluorometric and spectrophotometrics investig. 80−95643
cyclopropane, partial vibr. energy transfer map 80−32760
cyclopropane, vibr. energy transfer processes, laser induced fluorescence exam. 78−25663
deca-2,4,6,8-tetraene, fluoresc. and absorpt. spectra, forbidden transition 78−82764
decalin, two-photon spectra; fluoresc. spectra, decay times, intensities obs. 77−75245
decay, nonexponential, method of moments for data anal. 80−55975
decay measurement using time correlation method with CW He-Cd laser 79−50072
decay measurement via modulated gain spectroscopy 80−63699
decay time of organic dyes, technique allowing for self-absorpt. 79−68255
decay times and bimolecular quenching, ultrafast kinetics expt. for students 77−26116
deconvolution nomogram for single exponential fluoresc. decays 80−67290
delayed fluorescence, quantum mech. model 78−29804
dephasing, emitting mols. coherent oscills., optical T_1 and T_2 meas. 77−79644
depolarisation, orientation factors, excitation energy transfer between isolated donor-acceptor fluorophore pairs 79−22740
1,2-di(1-naphthyl)-ethylene, cis-trans photoisomerization in condensed phase, polycryst. phase transition 79−10139
di(1-pyrenylmethyleneoxycarbonyl) alkanes, intramol. excimer emission 78−70862
1,4-di(2-(5-phenyloxazolyl))benzol, vapour, electron beam excited luminesc. *(Russian)* 78−82780
2,5-di(4-biphenylyl)oxazole, fluoresc. emission anisotropy, solvent effects 79−3489
trans-1,2-di-(1-napthyl)-ethylene, conformeric fluoresc., chromophoric fragments rot. 77−485
1,4-di-(2-naphthyl)-benzene, conformic fluoresc., chromophoric fragments rot. 77−485
diacetyl, triplet-singlet conversion, by laser spectrosc. technique 79−86002
diacetyl vapour, fluoresc. and phosphoresc., nonradiative transitions between triplet and singlet state obs. 80−99516
diacetylene radical cation, and deuterated forms, electronic spectrum in solid inert gases 79−94026
dialkylaniline derivatives, twisted intramol. charge transfer states, dual fluoresc. obs. and form., dipole moments 80−18881
dialkylanilines, p-substituted, twisted internal charge transfer excited state form. 79−22683
3,6-diaminophthalimide vapour, mol. electronic excitation energy degradation path depend. on pentane 80−74195
diarylalkane, in isooctane soln. triplet excimer form., phosphoresc., delayed fluoresc., triplet-triplet absorption 78−25597
diarylethylene, luminesc. spectra and rot. isomerism 79−85991
diatomic fragments, from triatomic mol. photodissoc., fluoresc. polarisation excitation spectroscopy 80−28054
diatomic mol., effect of anharmonicity on kinetics during spontaneous emission *(Russian)* 78−70904
diatomic molecules, catalogue of lines originating in or around stellar objects 77−23514
diatomic molecules, near saturated fluorescence, two-level model 79−50000
diatomic mols. in Ar matrix, vibr. level energy cascades 77−79598
1,3-diazaazulene, vibronic coupling, Duschinsky effect, mixed cryst. spectra 77−79622
4,10-diazachrysene, absorpt. spectra and luminesc. in cryst. and glassy matrices, 77K 78−37650
3,4,9,10-dibenzpyrene, hexane soln., UV fluoresc. line-narrowing two-photon site selective excitation 77−88484
1,3-dibiphenylpropane, intramol. excimer form., kinetic and thermodynamic obs. 79−13750
9,10-dibromoanthracene, fluoresc. and phosphoresc. spectra 77−14480
4,4′-dibromobenzophenone, ODMR and phosphorescence spectra in organic matrix 79−36671
dibromodifluoromethane, UV laser fluoresc. and photochem., CF_2, CF and Br_2 fluoresc. obs. 80−16703
dicarbocyanine solns., photoisomerisation, fluoresc. and absorpt. spectra of photoisomer 78−85181
1,3- and 1,4-dichlorobenzene radical cation, emission and photoelectron spectra, lifetimes meas. 78−86905
dichlorocarbene, $^1B_1$ state, radiative lifetime, quenching rate, press. depend., laser-induced fluoresc. obs. 78−5259
dichlorodifluoromethane, UV photolysis, free radical emission 80−30263
dichloromethane-d_2, vibr.-vibr. energy transfer, laser-induced fluoresc. obs. 80−78689
dichloromethylene, radical, emission and excitation spectra, in Ar matrix 77−34657
dichloromethylene, radical, laser-induced fluoresc. excitation spectra 79−98131
9,10-dicyanoanthracene, exciplexes, electronic struct. by electro-optical expts. 78−25581
dicyanoanthryl-naphthyl, intramol. exciplex, fluoresc. quenching by pyridine (γ-picoline), triple exciplex form. 79−50061
dielectric cylinder embedded mols., Raman and fluoresc. scatt. 80−37949
3,3-diethyl thiadicarbocyanine iodide dye, stimulated fluoresc. and stimulated reson. Raman scatt. relationship 80−91853
1,1-diethyl-2,2′-dicarbocyanine iodide, solns., fluoresc. lifetime, viscosity depend. 79−59497
N,N-diethyl-4-phenyl-butylamine, fluoresc. spectra intramol. exciplex formation, fluoresc. spectra 79−59499
3,3′-diethyloxadicarbocyanine iodide, lasing and photoisomerisation, conc. and temp. effects 77−7081
3,3′diethylthiacarbocyanine iodide-rhodamine 6G, mixed dye laser system, laser and fluorescence behaviour 78−25876
3,3'-diethylthiacarbocyanine iodide-rhodamine-6G-sodium lauryl sulphate, soln., premicellar region, energy transfer 80−20685
3,3′-diethylthiacarbocyanine iodine-rhodamine 6G, energy transfer with increased local conc., Forster mechanism 80−69220

molecular fluorescence continued
diethynylbenzene, radiative and nonradiative processes, triple bond effects 79−3481
p-difluorobenzene, $^1B_{2u}$, fluoresc. quantum yield, radiative and nonradiative lifetimes, vibronic level depend. 77−75204
p-difluorobenzene, $^1B_{2u}$, quenching by cyclobutanone, fluoresc. lifetime meas. 77−75205
S_1p-difluorobenzene, time resolved fluoresc. spectra, direct view of intramolecular vibr. redistribution 80−83341
1,3- difluorobenzene radical cation, and deuterated forms, laser-induced fluoresc. matrix, study 79−98138
difluorocarbene, $\tilde{A}^1B_1$-$\tilde{X}^1A_1$ system spectrosc. and photophysics 80−5577
1,1-difluoroethane IR photolysis product, time-resolved fluoresc. obs. 79−57254
difluoroethene, cis- and trans-, photoelectron-photoion coincidence study, fluoresc. obs. 80−95678
dihydrophenazine derivatives, in 3-methylpentane (ethanol) (PMMA), radiationless processes, temp. depend. 80−43087
dihydroporphin, single crystal Shpolskii matrix, fluoresc. anisotropy 79−85994
dimethoxyphenyl-1,1-dicyanomethylene, donor-acceptor systems, fluoresc., through-band interaction 79−13751
3,8-dimethyl-2-azaanthracene in heptane, benzene and ethanol, max. intensity of fluoresc. on axis of cylindrical cell *(Russian)* 77−55814
4-dimethyl-amino-4′-nitrostilbene, in EBBA, nematic ordering influence on fluoresc., temp. depend. *(German)* 79−81235
dimethyl-diacetylene, radical cation, fluoresc. spectra, matrix isolated 79−45752
dimethyl-POPOP, soln., and vap., fluorescence rise time, intramolecular vibrational relaxation 79−98134
dimethyl-s-tetrazine, vapour, mol. fluoresc., photodissoc. product 80−81352
4-dimethylamino-4′-nitrostilbene, thermal motion of prolate luminescent molecules in solvents with different viscosities 79−83029
4-dimethylamino-4′-nitrostilbene in solvent fluorescence lifetime meas. by picosecond optical amplification 79−81227
7-N-dimethylamino-4-methylcoumarin, fluoresc., solvent depend., shift of max. wavenumber 79−85997
1-dimethylamino-4-phenylbicyclo-[2,2,2]octane, intramolecular energy transfer, fluoresc. spectra 79−59499
p-dimethylaminoacetophenone, ps reversible isomerisation kinetics, O_2 quenching obs. 79−5133
p-N,N-dimethylaminobenzonitrile, multiple fluoresc., mechanism 79−45742
p-dimethylaminobenzonitrile, picosecond relax., fluoresc. spectroscopy, solvent effects 78−58737
4- dimethylaminochalcone fluorescence, distrib. of hydrophobic mols. in artificial lipid membrane 77−16912
dimethylaminophenyl-(methylene)$_n$-(1-pyrenyl), intramolecular charge transfer, heteroexcimer formation processes 78−27783
9,10-dimethylanthracene, conc. solns., fluoresc. quenching by anthracene and derivatives 78−17711
9,10-dimethylanthracene, Shpolskii spectra, vibronic struct., fluoresc. *(German)* 79−22754
9,10-dimethylanthracene derivative, intramol. fluoresc. quenching, attached CBr_3 groups 78−42113
1,5-dimethylnaphthalene, fluoresc. quenching by cyclic azoalkanes, micelle system probe 80−35578
2:3dimethylnaphthalene, in polystyrene matrix, singlet O_2 induced excimer fluoresc. 77−6832
2,6,dimethylpyrazine, PMMA soln., fluoresc. and phosphoresc. quantum yield and lifetime, 20-120 kbar 79−54902
dinaphthylalkanes, triplet-triplet annihilation of excimers in soln. 78−86904
dinaphthylamine, fluoresc. in soln., intramol. excimer and exciplex form. 78−62836
dinucleoside phosphates, polaris. spectra, excimer phosphoresc. and fluoresc. 79−34497
1,8(6′,7′-dioxododecamethylene) phenanthrene, intramol. electronic energy transfer, emission obs. 79−31571
1,6-diphenly-1,3,5-hextriene, mol. derivatives, absorpt. and fluoresc. spectral props. 79−72344
diphenyl, double mols. with weak reson. bonds, quasilinear spectra 79−94030
3,5-diphenyl-1,2,4-oxadiazole, saturated vap. press., absorpt. and fluoresc. spectra 79−76442
2,5-diphenyl-1,3,4-oxadiazole, fluoresc. quantum efficiency, one-photon dissociation, temp. depends. 80−69180
2,5-diphenyl-1,3,4-oxadiazole, vapour, spectral, fluoresc., photochem. and laser props. 80−106344
1,8diphenyl-1,3,5,7-octatetraene, high press. fluoresc. studies of radiative and nonradiative processes 80−1011
1,6-diphenyl-1,3,5-h-hexatriene and derivatives in n-paraffins, electronic spectra and fluoresc. 78−13509
1,6-diphenyl-1,3,5-hexatriene, high press. fluoresc. studies of radiative and nonradiative processes 80−1011
2,5-diphenyl-1,3-oxazole vapour, spectral, fluoresc., photochem. and laser props. 80−106344
diphenylanthracene, fluoresc., site selection spectroscopy 2-300K 77−1731
9,10-diphenylanthracene, refr. index meas. of frozen gas matrices, fluoresc. method 80−90884
diphenylene, n-paraffin soln., quasiline sensitised phosphoresc. spectra at 4.2K 77−68071
2,5-diphenylfuran vapour, spectral, fluoresc., photochem. and laser props. 80−106344
1,6-diphenylhexatriene, lower excited states fluoresc. quenching 80−1016
1,6-diphenylhexatriene, radiationless transitions and natural lifetimes, solvent effects 80−63622
1,6-diphenylhexatriene soln., light quenching effect on fluoresc. band shape 79−98148
1,6-diphenylhexatrienes, electronic and fluoresc. spectra, solvent effects, 77K 78−21959
diphenylketyl radical, fluoresc. lifetime and quantum yield, organic matrix, 77-130K 78−42110
2,5-diphenyloxazole, multiexponential fluorescence decay, systems theory approach to anal. 79−59495
4-diphenylphosphenylstilbenes, fluoresc., photodimerisation 80−1015
diphenylpolyene molecules, excited electronic states, vibronic mixing, wave functions, method of fragments anal. 80−63615

molecular fluorescence continued
diphenyltriafulvenes, absorpt. and fluoresc. spectra, dipole moments, solvent effects 77−75169
dipole transition, transient behaviour in intense laser field *(German)* 78−66520
dipoles, magnetic and electric, close to plane interface, radiation patterns 78−37675
dipoles, magnetic and electric, close to plane interface, total radiated power 78−37674
2,5-distyrylpyrazine, absorpt., Raman and fluoresc. spectrosc. 80−28049
1,4-di[2-(5-phenyloxazoyl)] benzene, fluoresc. by electron beam excitation 79−94031
DNA, axially symmetrical ensemble stained with acridine orange, polarisation of fluorescence 79−92140
DNA, fluorescence depolarisation, twisting and bending, rot. Brownian motion 79−70509
DNA, triplet state excited by X-rays 77−9174
DNA dye complex, spectral changes observed using microfluorometer and cryostat 80−17949
DNA in soln., mol. wt. determ. by fluctuation spectroscopy 77−10800
DNA packing in fibrils of DNP of polytene chromosomes 80−30649
DNA-acridine complexes, laser-induced fluorescence decay obs. 79−66449
DNA-acridine dye complex, fluorescence studies 80−37921
DNA-dye complexes, fluoresc. intensities, dye laser spectroscopy 77−86444
DODCI, lifetime of optically stimulated dyes, generation of time correlated picosecond laser pulses *(German)* 79−27045
DODCI, rot. diffusion time, time depend. fluoresc. depolarisation meas., photoisomer effects 77−71825
DODCI in ethanol, DQOCI added, electronic energy transfer, real-time ps meas. 80−58311
DODCI in ethanol, malachite green added, electronic energy transfer, real-time ps meas. 80−58311
Doppler-free fluorescence induced by strong quasi-resonant laser field 79−41193
Doppler-free Raman spectroscopy and suppression of laser-induced mol. Doppler broadened transitions 80−9638
durene:fluoranthene(pyrene)(chrysene), triplet and singlet transport rate ratio 79−56832
duryal radical in durene matrix, optical coherent transient spectra 79−76764
dye, fluoresc. lifetime meas. using synchronised ultrashort laser pulses and streak photography 79−44951
dye, O quenching for surface flow visualisation 80−79422
dye, two-photon fluoresc. quenching, phase fluctuations and phase modulation effect 78−50570
dye laser, nanosecond laser fluorometry 80−102721
dye mixture planar solar concentrator for solar cell, photon trapping and energy transfer 77−88946
dye molecule, excited, thermal rotations and relaxation of vibr. energy 79−81231
dye molecule direct energy transfer to surface plasmons of adjacent metal 79−91119
dye molecule relax. rates from intracavity spectroscopy *(Russian)* 78−25582
dye molecules, excited state lifetimes and lasing conditions, time resolved spectroscopy 77−71983
dye molecules excited by surface plasmon waves in Ag film, fluoresc. angular emission profiles 79−89703
dye monomolecular layers, energy transfer between sensitizers and acceptors 80−80861
dye soln., fluoresc. amplitude anisotropy, polarised light excited 79−85990
dye solns., two-component, b_fore-relax. energy transfer and absorpt. spectra overlap 78−27285
dye solution, fluoresc. yield, photoacoustic determ. method 78−42117
dye solution, mol. fluctuation distrib. function 79−36692
dye solution, nonlinear fluoresc. meas., two-photon pumping by low power laser 80−48037
dye solutions, dil., fluoresc. decay time determ. 78−68540
dye solutions, excited fluorescence film thickness meas., report 78−81945
dye solutions, mixed, energy transfer and conc. depolarisation of fluoresc. 78−25583
dye solutions, picosecond flash photolysis and very fast processes 80−30249
dye vapour, fluoresc. meas., buffer gases effect · 77−75503
dye vapour pumped by N_2 laser, fluorescence and amplified spontaneous emission characts. 79−3694
dye-detergent model systems, degree of fluoresc. polarisation 78−27287
dye-inert gas vapour mixture, electron beam pumping 77−42535
dyes, fast mode-locking, IR fluoresc. and laser action obs. 80−102717
dyes, fluoresc. conc. depolarisation, during intense excitation *(Russian)* 77−65507
dyes, secondary fluoresc. under very powerful pumping, fine struct. spectra 77−58383
dyes, substituted methane, press. effs. on viscosity-depend. fluoresc. 77−34672
dyes in micellar aq. solns., counter-ion quenching *(Russian)* 77−54573
electro-optical emission, for excited state dipole moment determ. 78−62230
electron impact excitation, photon-electron ang. correlation, fine/hyperfine struct. effects 78−42231
electronic processes and energy transfer, conf., Tallahassee, Fla., USA (Jan. 1976) 77−27042
electronically excited molecule, rot. diffusion, fluoresc. depolaris. meas. 79−24846
emission quantum yield spectrometer and program system *(Japanese)* 79−89008
energy transfer dye lasers and laser induced intermol. and intramol. energy transfer processes 80−9647
eosin, fluoresc. polarisation, solvent effects 79−36678
eosin, in glycerine-water mixture, excitation and emission peaks, concentration shifts 78−33540
erythrocyte membrane, intrinsic fluorescence obs., radiation effects on struct. 79−74724
erythrocyte suspension, laser-induced fluoresc. of intact human membrane cell 77−90733
erythrosin in water-acetone, subnanosecond fluoresc. lifetime meas., environmental effects 78−5268

molecular fluorescence continued
erythrosine dye, vibrational decay and fluoresc. in S_1 excited state 78−25605
10,10′-ethanediylidenedianthrone, fluoresc. efficiency, mol. geom. effects in two cryst. structs. 77−18953
ethenoadenosine, influence of pH and metal complexion on fluorescence parameter 79−34483
ethylene, electron impact dissoc., optical emission from fragments 77−83750
ethylene, excited with parametric oscillator, vibr. relax. obs. and interpret. 80−9702
ethylene, intense IR field multiphoton dissoc., primary products, fluoresc. obs. 79−36715
ethylene, laser-induced IR photolysis mechanism 78−56909
ethylene, multiphoton dissoc., CH_2 and C_2 prod., fluence depend. meas. 80−5586
ethylene, vibr. energy transfer, fluoresc. detect. 79−64026
ethylene+inert gas, vibr. energy transfer, fluoresc. detect. 79−64026
ethylene-d_0, -d_4, hindered internal rotation, vibronic luminesc. and absorption spectra 79−54883
N-ethylphthalimide+olefins, photochemical reaction, absorpt., fluoresc., phosphoresc. and triplet-triplet absorpt. spectra 80−85197
ethyltoluenes, fluoresc. and triplet state quantum yields, biacetyl method 78−37671
ethynylbenzene, radiative and nonradiative processes, triple bond effects 79−3481
excimer, fluorescence, relative yield following triplet-triplet annihilation, re-encounter effects 78−33538
exciplex emission, effect of polymeric matrix and temp. 77−61785
exciplex fluoresc. decay, elec. field depend., quantum theoretical model 79−98133
exciplexes, electronic struct. by electro-optical expts. 78−25581
excitation by standing wave radn. field, mol. relax. processes 78−29803
excitation spectroscopy, time-resolved photoluminescence emission and lifetime meas., synchrotron radiation use 78−66687
excited molecular ensemble, photon echoes, optical coherence in electronic transitions 77−58392
excited molecular systems, relax. processes, nanosecond time-resolved spectra 77−26992
excited single state kinetics on a subnanosecond time-scale 79−36677
excited state natural lifetime determ. by fluoresc. light quenching 78−82775
fast fluorescence spectroscopy, nanosec. range, using synchrotron radiation 80−62736
fibrinogen solution, effect of scavengers on radiation-susceptible sites 78−11701
flavin aqueous solns., fluorescence quenching by iodide ions, temp. and viscosity effects 77−34673
flavins, meas. of sub ns fluoresc. decay by time-correl. photon counting and Ar laser 80−94429
flexible chain molecules, mutual interpenetration, fluorescence obs. 80−63877
fluctuations effect on emission spectra 77−58055
fluoradene, absorpt. and fluoresc. in solvents, excimer form., aggregation 77−79625
fluoranthene, in rigid glass, S_1 and S_2 fluoresc. 77−3403
fluoranthene, vapour, laser excited fluorescence 78−29807
fluorene, in polystyrene matrix, singlet O_2 induced excimer fluoresc. 77−6832
fluorene, n-paraffin soln., quasiline sensitised phosphoresc. spectra at 4.2K 77−68071
fluorenone fluoresc. in plastic, high press. effects., quantum yield 78−25601
fluorescein, excitation and emission polarisation spectra, cell cycle changes 78−96013
fluorescein, fluoresc. quenching by rose bengal 79−78726
fluorescein dye, halogen substituted, in dimethyl sulphoxide, spectral evidence for anion-counterion association 80−71909
fluorescein dye(-Yb^{3+}), triplet state energy transfer, fluoresc. quenching obs. 79−54897
fluorescein isothiocyanate labelled integral membrane proteins, lateral mobility in human erythrocyte 77−66805
fluoresceindiacetate conversion to fluorescein, in living cells and in vitro, kinetics 77−56332
fluoresceindiacetate hydrolysis and transport in mammalian cells after UV and gamma-irrad. 77−56333
Fluorescent EXAFS data using solid state detector, for metals in dilute biological systems 78−66595
fluoroanthene in micelles soln., fluoresc., halide ion induced quenching and enhancement 80−95672
fluorobenzene cations, fluoresc. quantum yields and lifetimes, electronic state relax. processes 80−48027
fluorobenzene ions, fluoresc. quantum yields and lifetimes, meas. method ion form. 77−6815
fluorobenzene radical cations, in gas phase, laser-induced fluoresc. 79−27022
fluorobenzene radical cations, matrix laser fluoresc. spectra 80−1009
fluorobenzene radical cations in solid Ne, laser-induced fluoresc. spectra, vibr. struct. of excited and ground states 80−95671
fluorobenzenes, radical cations, B(π^{-1}) excited states, radiative relax. 78−13546
fluorobenzenes, vibr. relax. in first electronically excited singlet state 79−3535
fluoroethanes, IR multiphoton dissoc., HF vib. energy distribs. 80−53073
fluoroethylenes, IR multiphoton dissoc., HF vib. energy distribs. 80−53073
fluoromethane, ν_3 mode, laser induced fluoresc. of V→T/R transfer 77−6899
fluoromethane, laser pumped, overtone fluoresc., intermode energy flow 78−37673
fluoromethane, laser pumped, vibr. states collision dynamics fluoresc. obs. 80−53104
fluoromethane+fluoromethane, collision induced mode selective energy transfer, fluoresc. obs. 80−69177
fluoromethane-d_3, vibr. energy transfer at low temps., inert gas and N_2 matrix obs. 80−9706
fluorometric system, nanosec. time-resolved spectrometry with tunable dye laser and pulse-gated photon counter 80−11968
fluorophores, limited rot. motion, differential phase fluorometric obs. 79−22741

molecular fluorescence continued
formaldehyde(-d_2), S_1 rot. levels, collisionless nonradiative decay rates 79—[illegible]346
formaldehyde, $^1A_2$-state, radiative and nonradiative decay calcs., rel. to photochem. decomp. 78—37669
formaldehyde, $^1A_2$-state, SVL fluoresc.-spectra, absolute radiative lifetime, ab initio CI calcs. 79—63919
formaldehyde, and -d_2, lifetime of ($^1A_2$) rovibronic levels 79—3495
formaldehyde, excited state photodecomp., rotationally resolved spectra 77—60088
formaldehyde, laser-excited reson. fluoresc., rot. struct., rot. and vibr. consts. 79—54993
formaldehyde, laser-induced fluorescence, rad. transition rates from two vibronic levels 77—3400
formaldehyde, photochemistry, past and present 79—52711
formaldehyde, sequential coupling 80—58297
formaldehyde, two-step photoionisation, $^1A_2$ state lifetime 77—10711
formaldehyde, vibronic and spin-orbit coupling, radiative and non-radiative transitions 77—3414
formaldehyde+O, absolute rate consts., discharge flow and flash photolysis reson. fluoresc. meas. 80—55648
formaldehyde S_1 levels, collisionless single rot. level lifetimes, elec. field depend. 80—63566
formaldehyde-d_0, -d_1, -d_2, single vibronic level photochem., radiative and nonradiative processes 78—66583
formaldehyde-d_0, -d_2, fluoresc. quantum yields, rot. depend., single rovibronic level values 79—22748
formaldehyde-d_0(—d_2), S_1 single rot. level lifetimes, isotope, elec. field and vibr. state depend. 80—78655
formaldehyde-d_1 (-d_2), single vibronic levels, fluoresc. emission, radiative lefetimes and vibr. relax 80—23521
formaldehyde-d_2, fluoresc. quenching *(Russian)* 79—50074
formaldehyde-d_2, inert gas and N_2 matrix fluoresc. spectra, radiationless transitions and lifetimes 79—3469
formaldehyde-d_2 vapour, IR-UV double resonance 80—43078
formaldehydes, (deuterated), A^1A_2 state, photoluminesc. in low temp. matrices, vibr. relaxation 79—50070
formic acid+Ar($^3P_{2,0}$) dissociative fluorescence in crossed mol. beams, energy depend. 79—52669
gasoline-air flame, laser induced fluorescence spectra obs. 80—91587
geminate recombination of radical ions in polar solvent, mag. field modulation, fluoresc. quenching 77—4912
glyoxal, ^1A_u state energy transfer, D effects 77—58066
glyoxal, gas phase emission spectra, mag. quenching 77—18968
glyoxal, intersystem crossing in weak mag. field 78—78743
glyoxal, mag. quenching of fluoresc. 79—31582
glyoxal, radiationless transitions in weak mag. field, fluoresc. quenching 77—58062
glyoxal, relax. processes, single vibronic level fluoresc. spectroscopy 78—58789
glyoxal, S_1-S_0 fluorescence after narrow band excitation, deconvolution 78—58734
glyoxal, singlet-triplet coupling, double reson. and level-anticrossing spectroscopy 80—48053
glyoxal, vapour, predissoc. in S_1 zero-point level states 80—102544
glyoxal, vibr. energy redistrib. following internal conversion 80—23452
glyoxal (^1A_u), fluoresc. quantum yields, radiative and nonradiative lifetimes 80—32759
glyoxal in supersonic jet, fluoresc. excitation, collision-induced intersystem crossing, van der Waals complex 79—81223
haemoproteins, fluoresc., reson. Raman and radiationless decay 77—30916
haloacetylene cations, electron impact excitation A→X band system assignment 80—32766
halobenzene cations, in solid Ne matrix, slow vibr. relax., fluoresc. obs. 80—74194
halobenzenes, singlet excited states decay, substituent effects 77—75175
halofluorescein dyes, fluoresc. internal conversion, intersystem crossing 77—3405
halomethanes, UV multiphoton dissoc., photofragment fluoresc. 80—14165
halotoluenes, singlet excited states decay, substituent effects 77—75175
helicenes, fluoresc., intersystem crossing, rate parameters 77—3392
α,β-heptacyclene, double mols. with weak reson. bonds, quasilinear spectra 79—94030
α-heptacyclene, in solid matrix, photodissoc. quantum yields, fluoresc. temp. depend., phosphoresc. IR spectra 77—25292
α-(β-)heptacyclene, vibronic spectra, electronic-vibr. interactions 78—1021
heteroaromatic molecules, planar, orientation and phosphoresc. polarisation in stretched film 80—14169
heterocyclic aromatic molecules, nonradiative transitions activated by external fields 77—65501
heteroexcimers, intramolecular, picosecond time-resolved fluorescence studies 80—83401
hexafluorobenzene cation, laser fluoresc. in solid Ar 79—18229
hexahydrohexahelicene, in Shpolskii matrix, absorpt., fluoresc., phosphoresc. spectra 79—76463
hexamethylbenzene, exciton band struct. for first singlet state 77—55483
hexamethylbenzene charge-transfer complexes, heavy atom effect on radiative and radiationless transitions 78—25607
1,3,5-hexatriene radical cation, in Ne matrix, laser induced fluoresc. and emission spectra 80—87163
highly fluorescent compounds coherent antiStokes reson. Raman spectra 79—36655
histone F2a solutions, effect of ionic composition of medium on struct. and effectiveness of intermol. interactions 78—48744
histones, H2A and H4, effect of molecular interactions on fluorescence intensity 80—51032
hydrocarbons, electron impact cross section for H_α and CH($A^2\Delta$→$X^2\Pi$) emission 77—27189
7-hydroxy-2-methylchromone, solns., pH dependent fluorescence spectra, pK_a and tautomerism 79—59506
7-hydroxycoumarin, absorpt. and emission spectra, ionic forms 78—21955
7-hydroxycoumarine, one- and two-photon absorption, fluoresc. obs. 78—46407
7-hydroxycoumarine, two-photon visible absorpt. spectra, fluoresc. obs. 78—42147
hydroxyethyl cellulose, polymer segments, fluoresc. depolarisation on conjugated spin lables 80—91711
3-hydroxyflavone, excited state proton transfer, luminesc. 80—35818
molecular fluorescence continued
7-hydroxylepidone, solns., multiple fluoresc. emission 78—33547
I_2He, I_2He_2, and I_2He_3, photodissoc. products energy distrib. 79—100410
incoherent resonance decay and coherent optical ringing from coherently prepared electronic states 77—10698
indene, fluoresc., ns time resolved emission spectra 77—6822
indigo dyé, excited state lifetime, influence of inter- and intramol. H bonding 77—79659
indigo dye, S_1-lifetime determ. by two-photon fluoresc. 77—18966
indole, fluoresc. polaris., solvent effects 78—33542
indole, fluorescence quenching by chloromethanes due to electron transfer 79—94027
indole, pH dependent fluoresc., quenching by histidine *(Russian)* 78—90209
indole decapeptide luteinising hormone, high-press. liq. chromatography, fluorometric detect. 78—20096
indoles, excited states, solvent interactions, fluoresc. obs., rel. to chromophore 78—37670
indoles, fluoresc. anomalies, mixed valence-Rydberg states 78—17707
indoles, in glassy hydrocarbons, complexation vs. aggregation, absorption and fluoresc. obs. 79—98132
indoles, temp. effects on electronic transition moments in n-heptane and water 78—58744
indrr gas halogen exciplex, spontaneous and superfluoresc. emission, pumping of I laser 77—34883
inelastic collisions, calc. of fluoresc. in multilevel system in gas phase 79—98129
inelastic collisions, rot. ang. momentum distrib., reson. fluoresc. meas. 78—33580
inert gas, electronic excitation, mol. thermal strength depend. 77—46595
inert gas+hydrogen halide, energy transfer as function of collision energy, luminesc. obs. 79—86043
inert gas afterglow, excimer form., VUV emission obs. at low press. 80—38755
inert gas fluorides, excimer emission bands *(Russian)* 77—71885
inert gas halides, UV emission spectra, pressure and temp. depend. 80—28209
inert gas-H_2 mixtures, electronic excitation, mol. thermal strength depend. 77—46595
intramolecular donor-acceptor systems, fluoresc., through-band interaction 79—13751
intrastate scrambling in large mol. bound level struct., appl. to tetracene 80—63696
9-iodoanthracene, picosecond fluoresc. lifetimes, thermally activated S_1→T_n intersystem crossing 80—28045
iodomethyl radical, vibr. excited, photofragmentation IR emission obs. 80—87162
ion beam, from saddle-field ion source, gas depend. characts., at. spectroscopy appls. 78—78039
ions, radiative lifetimes, threshold electron-phonon coincidence meas. 78—13550
IR laser induced fluoresc. as spectroscopic probe, appl. to CO_2 79—89704
IR laser photolysis of polyat. mols. photochem. appls. 80—66835
IR multiple-photon dissociation, laser induced fluoresc. photofragment detect. 80—37840
isoquinoline, fluoresc., phosphoresc. and H bonding 77—79647
isoquinoline, radiationless transition branching ratio, temp. effects 79—54900
isoquinoline luminesc. in polymeric media at high press. 79—13756
isotropic rigid solutions, polarisation of fluorescence 78—31228
isotropic solutions, fluorescence emission anisotropy, time depend. 80—7391
kerosene-air flame laser induced fluorescence spectra obs. 80—91587
ketene, multiphoton dissoc., CH_2 and C_2 prod., fluence depend. meas. 80—5586
ketene+H, reaction rate consts., lab. meas., rel. to interstellar cloud processes 79—74359
ketocyanine solution lasing dyes, absorpt. and luminesc. spectra 77—75502
ketocyanines alcohol solns., spectral-luminesc. props. 80—2835
ketyl radical+benzophenone, triplet-doublet energy transfer, viscosity and mag. field effects 77—71850
kinetic spectroscopy of molecules 79—94110
kiton red S, mol. fluoresc. decay time, self-absorption 79—68255
lanthanide-porphyrin complexes, upper $\pi\pi^*$ electronic states, fluoresc. 80—83410
large molecule, novel ultrafast two-pulse excitation spectroscopy 78—94331
large molecules, nonradiative transitions activated by external fields 77—65501
large molecules, picosecond relax., fluoresc. spectroscopy, solvent effects 78—58737
laser dyes, fluorescence efficiency 77—42531
laser dyes, photochemical quantum yield determ. using fluorescence data 80—55685
laser excitation of stationary molecular states, coupling of real eigenstates to phonons and photons 77—68084
laser near-reson. scatt. from collisionally perturbed mol. 78—1033
laser optical microprobe, MOLE 77—60141
laser studies of relaxation and reaction of species in defined quantum states 80—11918
laser techniques, vis. and UV, small mols., electronically excited states, book contrib. 78—9277
laser-induced, review 78—37678
laser-irradiated gas, IR fluoresc. meas. of equilib. and vibr. temps. 78—82766
lecithin bimolecular leaflets, incorporated fluoresc. probes, PMR 77—90734
lepidopterene exciplex, luminesc. intramolecular anthracene-ethylene exciplex, mol. geometry-fluoresc. relationship 78—58728
librational motion effects on fluoresc. depolarisation and NMR relax. in macromols. and membranes 80—85324
lifetime meas., time resolved optical precision spectroscopy 77—42444
lifetime meas. in atoms, mols., ions 77—30832
lifetime measurement, using CW laser beat noise as multifreq. modulated source 77—57406
lifetime measurement with subpicosec. resolution, use of synchrotron radiation 79—72447
lifetime near diffuse surface, coupling to surface polaritons 77—69395

molecular fluorescence continued
light quenching of mol. fluoresc. spectrum, spectral distrib. of polarisation 79−85989
lipid analogues, meas. of lateral diffusion in planar lipid bilayers 77−36884
lipid bilayer chromophore energy transfer 79−62200
lipid peroxide oxidation fluorescing products, effect of UV on formation 79−57585
lipid probe and labelled protein, lateral transport on cell membrane 77−40646
liposome-cell interaction, transfer and intracellular release of trapped fluoresc. marker 77−36901
liposomes, nanosecond relax. processes 79−8477
liquid, electron-hole interactions and double proton transfer, picosec. laser obs. 79−45773
liquid crystal, uniaxial, polarised fluoresc. emission, orientational distrib. function, rot. Brownian motion 78−80390
liquid intermolecular relaxation spectroscopy 79−95844
liquid scintillators, theory of fluorescence, appl. *(Rumanian)* 79−81135
liquids, two-pulse spectroscopy with ps laser pulses 80−53041
long-range energy transfer combined with isotropic or anisotropic diffusion 79−11461
luminescence conference, Szeged, Hungary (Aug. 1976) 78−27279
luminescence decay, exchange mechanism, parameters 80−28051
luminescence of solutions under powerful excitation, intermol. relax. effect 79−85985
luminescence spectrometry, pulsed and continuous wave excitation sources, signal-noise ratios 77−71381
luminescence spectroscopy, image devices and photomultiplier detectors, signal-noise calcs. 77−81433
luminescence-vibrational relaxation interaction, master eqn. calcs., theory 78−42123
2,6-lutidine, fluoresc. of vap. phase, nonradiative electronic relax. 79−86000
lysozyme protein solution, spectra and dye laser threshold power 79−68391
macromolecular, electrically induced fluorescence depolarisation 77−27210
macromolecules and colloids, apparatus for meas. electrically induced fluorescence changes 77−46662
macromolecules in dilute soln., electrically induced fluorescence polarised component change meas. 80−32863
magnesium porphin.ethanol, in n-octane cryst., triplet state splitting, fluoresc. intensity microwave-induced changes 77−6820
magnetic and electric dipoles near dielec. interface, fluoresc. lifetime 77−34683
magnetic quenching, enhancement of radiationless decay, direct and indirect mechanisms 77−42345
malachite green in glycerol, subnanosecond fluoresc. lifetime meas., environmental effects 78−5268
malachite green leucocyanide, photoionization in polar solvents, mechanism 77−25295
Manoxol OT-cyclohexane-water reversed micellar system, singlet-singlet energy transfer 80−9531
2,6-MANS, fluorescent probe orientation and rot. freedom in lecithin bilayers 77−44583
medium-induced relaxation, laser pulse meas. 79−38667
membranes, fluoresc. polarisation decay theory 78−20138
mercurochrom, fluoresc. polarisation, solvent effects 77−14470
metal halide vapours, quantum efficiency of fluoresc. excited by photodissociation 79−81421
metalloporphyrins, two quantum fluoresc. excitation from higher excited electronic states 80−106350
methacrylate polymer, carbazolyl substituted, excimer and charge transfer complex trapping of excitons 80−34367
methane, energy transfer obs. using excitation of fund., overtone and combination bands 80−9704
methane, V-V energy transfer 80−83469
methane+inert gas (H_2)(HD)(methane), vibr. energy transfer, fluoresc. 77−519
methane electron impact dissoc., optical emission from fragments 77−83750
methane-d_2, vibr. energy transfer, laser-induced fluoresc. 79−13753
methane-d_3, vibr. energy flow, fluoresc. 78−82770
methane-d_3 + inert gas, vibr. deactivation, laser-induced fluoresc. obs. 77−42377
methane-d_3-polyatomic gas mixture, vibr. energy flow, fluoresc. 78−82770
methanol, electron impact dissoc., optical emission from fragments 77−83750
methanol, UV multiphoton dissoc., photofragment fluoresc. 80−14165
methanol (dimethyl ether)+Cl, absolute rate consts., 200-500K, stratospheric chem. appl. 79−66271
methine dyes, spectral props., solvent effects 80−69181
methoxy prod. from methyl nitrite photolysis 80−85200
methoxy radical and deuterate, vibronic level fluoresc. spectrum 80−58305
methoxy radical fluoresc. spectra induced by laser, UV region 79−59498
methoxy radical prod. from 266 nm photolysis of methyl nitrite 80−76534
methyl radical, vibr. excited, photofragmentation IR emission obs. 80−87162
methyl salicylate, vapour phase, absorption and fluorescence spectra 79−81232
methyl thiyl radical, emission spectrum, collisional quenching 78−13543
N-methyl-2-N-phenylamino-6-naphthalene sulphonates, triplet excitation, multiple fluoresc. 77−71826
m-methyl-p-cyanodimethylaniline, ps reversible isomerisation kinetics, O_2 quenching obs. 79−5133
methylamine, $CH(X^2\Pi)$ and $OH(A^2\Sigma^+)$, production by multiphoton dissociation, rate constant, laser induced fluorescence and chemiluminescence study 79−98135
methylamine, multiple-photon dissociation, laser induced fluoresc. photofragment detect. 80−37840
methylamine, photochemical conversion to HCN with ArF laser, mol. fluoresc. obs. 80−97710
9-methylanthracene, in acetylcellulose foil, time-depend. fluoresc. anisotropy, crit. transfer distance *(German)* 78−21964
9-methylanthracene, Shpolskii spectra, vibronic struct., fluoresc. *(German)* 79−22754
molecular fluorescence continued
9-methylanthracene, solubilisation in water by hypercoiled polymethacrylic acid 80−91591
2-methylchromone, solns., pH dependent fluorescence spectra, pK_a and tautomerism 79−59506
methylcyclohexane:styrene-d_0, -d_3, -d_5, d_8, fluorescence meas., 77K 78−25606
methylene, singlet a^1A_1 state, laser-induced fluoresc. spectrum 79−18225
methylene, singlet-triplet splitting 79−100407
methylglyoxal, fluoresc. mag. field effect 80−102535
1-methylindole-n-butanol (ethyl acetate), soln., ground state complex form., fluoresc. spectra, Stoke's shift origin 80−58299
N-methylphthalimide in ethanol soln., gain and induced absorpt., struct. props. 77−24890
2-methylPOPOP, soln., anisotropic fluoresc. of prolate mol. *(German)* 80−1018
1-methylpyrene, fluoresc. quenching by Cu^{2+} in micellar system, general kinetic model 80−32753
methylpyrimidines, fluoresc. quantum yield, methyl substitution effects 79−13757
1,4-Bis(2-methylstyryl)benzene, laser dye, picosec. laser obs. 79−36891
4-methylumbelliferone, excited state reaction rate, fluoresc. and decay time 77−63919
β-methylumbelliferone in ethanol solns., spontaneous luminesc. kinetics 80−74192
micelles, inverted containing water, hydrodynamic vol. determ. by fluoresc. polarisation 80−50892
microemulsions, aerosol OT, inhomogeneous interior, fluoresc. and polarisation decay probes 80−50891
microwave modulated saturation spectroscopy 79−68245
mixed molecular crystals, exciton percolation 77−28124
modulated gain spectroscopy, for fluoresc. decay meas., appl. to rhodamine-B 79−64025
molecular $\pi\pi^*$ and $n\pi^*$ states, rel. positions, single-triplet conversion probability, low temp. 79−816
molecular crystals, electronic energy transfer, review, book contrib. 77−39789
molecular crystals, spectroscopy, bibliography for 1976 78−72585
molecular crystals, trapping rates for sensitized fluoresc. 79−11455
molecular excited state relaxation processes, oscillatory versus dissipative limits, education appl. 80−31468
molecular X-rays from heavy-ion collisions, superheavy quasi-molecule spectroscopy 80−23509
molecule synthesis by ion implantation, laboratory simulation of interstellar process 77−70297
molecules embedded in particles 77−23618
moment index displacement theory 77−57395
monochromators for light scatt. and fluoresc. standard in colloid 80−57247
monodispersed particles, angular distrib. of fluoresc. 78−76927
monolayer assemblies, molecular cooperation in photo-induced electron transfer 79−73985
3-monomethylamino-N-methylphthalimide solns., fluoresc. and excitation spectra 79−61425
multicomponent solutions, solvatofluorochromism kinetics, orientation-concentrational relax. 77−65506
multilevel system, laser excitation, Wilcox-Lamb rate eqn. approx. 79−27028
multiphoton,, crossed mol. and laser beam obs. 79−41208
multiphoton dissociation products translational energy determ., laser-excited fluoresc. method 78−92491
multiphoton ionisation dynamics, rate eqn. modelling 80−48046
myosin, struct. changes in living muscle fibres, polarised UV fluoresc. microscopy 80−67037
myosin-auramine O system, conform. changes and excitation energy transfer 79−96512
N_2, Lewis-Rayleigh afterglow spectrum 79−64938
Na_2, laser-excited, emission bands obs. in visible and IR 80−48036
NAD.H-Ca complex, effect of oestrogens, rel. to mitochondria membrane Ca^{2+} interaction 78−53349
nanosecond time-resolved emission spectroscopy, appl. to gas phase collision processes 77−3490
naphthalene, absolute quantum yields, high resolution laser excitation, low press. gas 77−3404
naphthalene, adsorbed on silica gel surface, biphasic photochemistry, time-resolved spectra 80−30252
naphthalene, fluoresc. and phosphoresc., singlet/triplet excimers conform. difference 77−14469
naphthalene, fluoresc. lifetimes of single vibronic levels 79−27016
naphthalene, fluoresc. of isolated mol. in supersonic beam 79−45750
naphthalene, fluoresc. probe of micellar systems 78−95599
naphthalene, fluorescence and absorpt. spectra, deviations from Condon approx. 80−28004
naphthalene, fluorescence quenching by biacetyl, effect of viscosity 78−29810
naphthalene, inclined dimers, transition energies and moments, excitation energy, four-electron MO-CI treatment 77−42237
naphthalene, matrix fluoresc. spectra, rel. intensities of multiplet components 79−54882
naphthalene, triplet excimer conformation, σ-π interaction transitions 77−6701
naphthalene, triplet exciton annihilation and triplet spin relax. 80−29792
naphthalene, two-photon and mutiphoton excitation, UV fluoresc. spectra 77−88517
naphthalene, vapour-phase, absolute fluoresc. quantum yields, nonradiative processes 77−6829
naphthalene, vibronic fluorescence spectrum, intensity distribution 79−3477
naphthalene (-d_8), gamma irradiated soln., fluoresc. mag. field depend., spin correls. 77−44492
naphthalene crystal, vibronic spectra at 1.6K, two-photon fluoresc. excitation 77−59604
naphthalene in Ar matrix, geometry changes and multiplet struct., mol. fluoresc. and phosphoresc. obs. 80−95663
naphthalene in $C_{10}D_8$, exciton percolation and coherence 77−59258
naphthalene-d_0(−d_8), fluoresc. spectra, vibronic intensities 77−50464
2-naphthalensulphonate, fluoresc. and phosphoresc., external heavy atom effect 78−29812
naphthalimide derivatives, solutions, lasing characts. in green spectral region, photostability 80−32978

molecular fluorescence continued
naphthyl group, excited singlet state, intramol. fluoresc. quenching by halogeno substituents 80−102537
1-naphthyl methacrylate-9-vinylanthracene copolymer, time-resolved fluoresc. spectra 78−80401
naphthylalanine polypeptides, fluoresc. quenching and energy transfer 79−34332
1-naphthylamine, anisotropic rot., red edge transition moment, fluoresc. 77−10699
β-naphthylamine, fluoresc. quenching and spectra, excited state reaction, red edge effect obs. 80−83400
β-naphthylamine, soln., fluoresc., photochem. quenching, excitation wavelength depend. 77−50470
naphthylamines, abnormal fluorimetric titration behaviour, kinetic anal., fluoresc. quantum yields and lifetime meas. 80−89560
naphthylamines, excited state pK_a^* values, proton-induced fluorescence quenching 78−21958
β-naphthylmethyl amine, solvent-induced intramol. exciplex fluoresc. 78−25592
napthalene-$d_{0,8}$, fluoresc. and absorpt. Shpolskii spectra *(Russian)* 78−90208
near resonance fluorescence and Raman scatt. theory 79−3446
neutron flux energy spectrum meas. from freq. change of luminesc. line 80−23272
nitromethane molecule dissociation in IR field, laser-induced fluoresc. obs. 80−53075
nitrosobenzene, fluoresc. quantum yields, determ. from Raman scatt. 80−58294
nonradiative transitions, due to electronic rearrangement, rate const. calcs. 77−3411
α-NPO, fluoresc. spectrum light quenching factor wavelength depend. 80−18882
nucleic acid-dye complexes, energy transfer obs. using laser-induced fluoresc. 80−12054
octaethylchlorin, metal complexes, polaris. fluoresc. and phosphoresc. spectra 79−54906
octaethylisobacteriochlorin metal complexes, polaris. fluoresc. and phosphoresc. spectra 79−54906
octaethylporphin, radiationless transitions, fluoresc. and phosphoresc., isotope effects 77−65502
1,3,5,7-octatetraene, lowest excited singlet state, dipole forbidden character 79−27024
1,3,5,7-octatetraene, UV, visible, and fluoresc. spectra and assignments, evidence for ^1A_g state 78−33518
optical free induction decay, of mols. undergoing radiative and radiationless relax. 78−83040
optical microscopy of single molecules, fluoresc. tagging, appl. to γ-globulin 77−21662
optoelectronic image detectors, for mol. fluoresc. spectrometry 79−21815
organic chromophores, $^1O_2$, annihilation luminesc., in polymer matrices 77−88488
organic compound, vap., laser-excited long-lifetime luminesc. 79−54887
organic compound soln., relax. of rot. rel. to laser emission polarisation *(French)* 78−58738
organic compounds, electron delocalisation, ground and excited states, fluoresc. *(German)* 77−34567
organic compounds, fluoresc. decay in nonhomogeneous level broadening conditions *(Russian)* 79−50073
organic compounds, fluorescence quantum yield, light quenching meas. 79−98147
organic compounds, IR fluorescence under CO_2 laser radiation 80−37830
organic donor-acceptor solns., triplet-triplet energy transfer under Shpolskii effect conditions 79−64031
organic dyes, absolute fluorescence quantum yield, calorimetric determ. 80−43092
organic dyes, absorption ege struct. in stimulated fluorescence spectra, Raman scatt. 78−55350
organic dyes, fluoresc. spectra calcs., β-variation method *(German)* 80−69182
organic dyes, rot. diffusion time, fluoresc. depolaris. meas. 79−24846
organic dyes, stimulated fluoresc., four-photon parametric interaction 79−13748
organic dyes, stimulated fluorescence, energy level scheme, photoisomerisation effect 77−70310
organic dyes, two-band stimulated fluorescence, laser action and bleaching effect 79−41190
organic gases, IR fluoresc. by CO_2 laser 80−78619
organic gases, kinetics of intermolecular triplet-triplet electron energy transfer 79−10141
organic glasses, hole burning, fluoresc., struct. 79−31588
organic laser dyes, fluorescence decay, aggregation effects 78−25879
organic molecule, triplet-triplet annihilation, delayed fluoresc. in soln. *(Russian)* 79−6962
organic molecules, in MBBA matrix, polarised fluoresc. 78−90207
organic molecules, relax. phenomena, following core ionis., LCAO MO SCF calc. 79−10030
organic molecules, struct., computer-assisted interpretation, using fluoresc. spectra 77−36805
organic molecules in soln., scintillator systems 78−21966
organic molecules in solution, electronic energy level shift estimation 79−54919
organic scintillators, vap. phase dye laser media, photophysical parameters 80−95884
ovalene, isolated ultra cold mol., intermediate level structure of S_2 state 80−28048
ovalene, vibrational quasicontinuum threshold, spectrosc. criterion 80−52972
1,3,4-oxadiazole derivatives, in soln., IR absorpt. and fluoresc. spectra, vibr. anal. 78−66597
oxalyl fluoride, $^1A_u(n\pi)$-^1A_g fluoresc. excitation spectrum in pulsed supersonic jet 79−31577
oxalyl fluoride, radiative and nonradiative transitions, self-quenching, unimol. dissoc. 78−17708
oxirane-acrylic bead, radical conc. gradient determ. by microinterferometry and microfluorometry *(German)* 79−100799
2-oxyphenylbenzoxazol, proton intramolecular transfer, light absorpt. and emission, dichroism, polarised fluoresc. 80−87166
oxypyrenetrisulphonate anion, aq. soln., ps time depend. fluoresc. depolaris. obs. rot. diffusion determ. 77−81139

molecular fluorescence continued
palladium-octaethylporphyrin, gas phase delayed fluoresc. and phosphoresc., triplet excimer formation 80−18884
papain inactivated by OH radicals and H_2O_2, optical density, amino acid composition and fluoresc. 78−53344
2,2 paracyclophane, dimer vibration influence on emission spectrum 80−69133
paraterphenyl, fluoresc. quantum efficiency, one-photon dissociation, temp. depends. 80−69180
pentacene, first excited singlet state, butterfly motion studied by fluoresc. spectra 80−78615
pentacene, intersystem crossing and internal conversion rates, fluoresc. transient and optical FID spectrosc. 79−81229
pentacene, laser fluoresc. of mol., excitation bandwidth and optical dephasing 79−36679
pentacene, narrow band laser excitation, fluoresc. decay, optical free induction, dipole moment 78−21956
pentacene, vibrational quasicontinuum threshold, spectrosc. criterion 80−52972
pentacene-d_0, -d_{14}, in p-terphenyl-d_0, mixed cryst., photon-echo relax. 77−72034
n-pentadecane, two-photon spectra; fluoresc. spectra; decay times, intensities obs. 77−75245
perfluoroalkyl iodides, laser photolysis, quantum yields 79−29382
perylene, hot luminesc. in solid matrix at 4.2K, intramol. thermal bath 79−85999
perylene crystal, molecular exciton system, resonance Raman and fluorescence studies, dynamical effects 80−66169
perylene fluorescence polarisation in erythrocyte membranes, rel. to fluidity 77−36885
perylene in EBBA, nematic ordering influence on fluoresc., temp. depend. *(German)* 79−81235
perylene in n-heptane cryst., polarised fluoresc. 80−1017
perylene in n-paraffin crystal matrices, effect of heat pulses on fluoresc. 78−88360
perylene in paraffin, anisotropic rot. and libration 77−32417
perylene-tetracene in liquid crystals, temp. depend. of absorption and fluoresc. *(German)* 80−18887
PET, uniaxially drawn, comparison of polarised fluorescence, polarised Raman and IR dichroism measurements 79−99084
[2.2]phanes in glass matrices, transanular π-electron interaction, emission spectra 79−36682
phase fluorometry as a probe of diffusion-controlled molecular encounters in dense fluids 80−32799
phase-shift fluorometer using laser and transverse electrooptic modulator for sub-nsec lifetime meas. 78−20319
phenanthrene, and dideuteroisomers, vapour phase fluoresc. lifetimes, position dependent D effects 77−30901
phenol (oestrogen) compounds, high-press. liq. chromatography, fluorometric detect. 78−20096
9-phenylanthracene, fluoresc. lifetime and quantum yield in solns. 77−6834
phenylene compounds in n-paraffins, electronic spectra and fluoresc. 78−13509
2-phenylindole, in viscous soln., fluoresc. quenching, emission, intensity and reson. transfer *(German)* 80−91599
phenylnaphthalenes isomers, fluoresc. lifetime difference and mol. geometry 80−69176
pheophytin-a, fluoresc. fading curve of lowest triplet state 79−36691
pheophytin-a (b), dimerisation, fluoresc. and ODMR study 80−18876
phosphatidylcholine bilayers, fluidity changes and phase transitions, intramol. excimer fluoresc. obs. 80−85342
phospholipid bilayer surface binding centre heterogeneity, hydrophobic mol. distrib. 77−56344
photobleaching recovery for meas. of mol. motion, cell surface heating 77−48956
photon counting and fluctuation of molecular movement 79−29686
photon echoes and coherence 79−31586
photon time-correlated counting, for fluoresc. decay signal analysis 78−49910
photosynthesis, fluoresc. and energy transfer, time resolved obs. 79−48216
photosynthesis of green plants, tripartite model for photochem. apparatus 78−44474
photosynthesis primary processes, picosecond spectroscopy *(Russian)* 79−39362
photosynthetic membranes, anal. of laser-induced fluorescence with Pauli master eqn. 79−39350
photosynthetic systems, magnetoorientated, fluorescence polarisation theory 79−16165
photosynthetic systems, temperature dependence of excitation transfer 78−92598
phthalamide derivative with aromatic amine, exciplex formation and fluoresc. quenching 79−87848
phthalamide derivatives, solutions, excitation spectra rel. to absorption spectra, 77-300K 79−85970
phthalazine, fluoresc. and phosphoresc., expt. and CNDO/S CI calcs. 79−31585
phthalimide, soln., excitation spectra rel. to recording wave length *(Russian)* 77−12438
phthalimide, soln., triplet state accumulation and deactivation depend. on solvent polarity 79−85982
phthalimide derivative-tetramethyldiaminodiphenylmethane exciplexes, luminesc. props. 77−68070
phthalimide derivatives, hidden vibr. band determ. method, fluorescence and excitation spectra meas. 80−40158
phthalimide derivatives, in hexane and isopentane, vap., inversion freq. determ., from fluoresc. quantum yield obs. 79−54892
phthalimide derivatives, solns., ultrafast mol. relax. 79−85984
phthalimide derivatives, solutions, lasing characts. in green spectral region, photostability 80−32978
phthalimide solutions, fluoresc. optical quenching by ruby laser rad. *(Russian)* 77−12437
phthalimides, solns., solvent effects on absorpt. spectra and fluoresc. 77−34650
phthalocyanine, fluoresc. spectra in supersonic expansion 79−3475
phthalocyanine, free base, fluoresc. excitation spectrum, cooling in supersonic free jet 80−95670
phthalocyanine, in n-alcanes and polyethylene, absorpt. and fluoresc. spectra, 4.2 and 77K 78−976

molecular fluorescence continued
phthalocyanine, metal-free, singlet-triplet fusion rel. to carrier photogeneration 77−36276
phthalocyanine, supersonic free jet-cooled, fluoresc. obs. 79−45753
phycobilin pigment role in photosynthesis 78−48752
α-picoline, fluoresc. of vap. phase, nonradiative electronic relax. 79−86000
picosecond fluorescence spectroscopy using CW laser and radio 77−27200
picosecond phase shift measurements at 358 MHz using synchrotron radiation 79−44949
picosecond relaxation processes in chemistry, book contrib. 77−61788
picosecond spectroscopy, appl. to chem. and biological reactions 79−80697
picosecond time-resolved fluorescence techniques using mode-locked laser system 80−27359
pigments, oriented molecules in spherical arrays, fluoresc. polarisation 77−44591
pinacyanol, picosecond photobleaching and absorpt. recovery, solvent effects 77−44493
pinacyanol, solns., fluoresc. lifetime, viscosity depend. 79−59497
planar aromatic hydrocarbons in polymer films, polarisation data interpretation, photoselection spectroscopy appl. 80−58302
polar molecules, fluoresc. emission anisotropy, solvent effects 79−3489
polarimeter for flow cytometry 78−73191
polarisation anisotropy, meas. via photon counting, appl. to mol. rot. diffusion coeff. 77−18072
polarisation meas., T-format photon-counting polarisation photometer 78−54423
polarisation of fluorescence spectrum for enhanced resolution 77−6827
polarised fluorescence, polymeric noncrystalline chain orientation evaluation *(Japanese)* 80−6368
polarized nanosecond time-resolved fluorometry 79−31738
poly (ar-methylstyrene)s, steric effects on excimer formation, fluorescence spectra exam. 80−25430
poly-1-naphthyl methacrylate, time-resolved fluoresc. spectra 78−80401
poly-1-vinyl napthalene, excimer dissoc., time resolved fluoresc. spectra 78−33643
poly-9-vinyl carbazole, fluoresc. props. 78−84647
poly-N-vinylcarbazole, in polymer film, excimer fluoresc., high press. effects 80−34966
poly-N-vinylcarbazole, soln., picosecond time-resolved fluoresc. by pulse radiolysis 80−28122
polyacenes, S_1-T_1 interconversion, excitaiton indices calcs. 79−54830
polyaromatic hydrocarbons, n-alkane solvent effect on low temp. fluorescence spectra 77−36274
polyaromatic hydrocarbons, quasi-linear fluoresc. spectra, temp. effect 79−22745
polyatomic, fluoresc. spectrum excitation depend., proportionality coeff., vibr. redistrib. 77−23518
polyatomic compounds, fluoresc. in discharge 79−54891
polyatomic compounds, vibr. relax., IR band line shape obs. 79−54879
polyatomic gas, laser-induced rate processes, intermol. and intramol. relax. formalism 79−27070
polyatomic molecular vapour, rot. fluoresc. depolaris. 79−54889
polyatomic molecule, diffuse absorpt. and fluoresc., vibronic band broadening 79−98161
polyatomic molecule, luminesc. parameters, intramol. vibr.-energy redistrib. effect 79−54890
polyatomic molecule, ultrafast vibr. using laser light pulses 80−9699
polyatomic molecule, vibr. relax. probability determ. from quasi-line fluoresc. 77−50505
polyatomic molecules, inverse electronic relaxation 79−18223
polyatomic molecules, picosecond fluoresc. gating, intra- and intermol. transfer processes 78−78745
polyatomic molecules, primary photochem. processes *(French)* 77−90620
polyatomic molecules, vibr. combination states, ultrashort two-pulse spectroscopy 79−828
polyatomic molecules, vibr. energy transfer and relax., picosec. time-resolved spectra 79−50028
polyatomic molecules, vibronic spectra and luminescence kinetics 79−54881
polyatomic molecules with pronounced vibr. struct., spectral shape 79−76469
polyatomic mols., quantum beats 80−37826
polyatomic organic molecules, electronic excitation transport in inhomogeneity broadened 79−54884
polyatomic radical cations, excited states, decay processes 80−28055
polyatomics, absorpt. and luminesc. spectra, higher electronic states effect 80−9586
polyatomics, light amplification in discharge excitation *(Russian)* 79−54908
polycyclic aromatic hydrocarbons, alternant and nonalternant, fluoresc. quenching by nitro cpds. *(German)* 78−21967
polycyclic aromatic hydrocarbons, detect. using laser-induced mol. fluoresc. 77−81431
polycyclic aromatic hydrocarbons, matrix isolated, quasilinear Shpol'skii fluoresc. spectra 78−9189
polycyclic hydrocarbons, alternant and nonalternant, fluoresc. quenching by electron transfer 79−6959
polycyclic monoazines, temperature dependence, triplet formation 79−54900
polydiacetylenes, visual conformational transitions, absorpt. and fluoresc. spectra, pH and electrolyte effect 80−102590
polyenals related to visual chromophores, emission spectra 79−34495
polyenes, substituted, spectra, four-level state scheme 79−54840
polyenones related to visual chromophores, emission spectra 79−34495
polyethylene oxide, polymer segments, fluoresc. depolarisation on conjugated spin lables 80−91711
polymer film, proton intramolecular transfer, light absorpt. and emission, dichroism, polarised fluoresc. 80−87166
polymers, intra- and intermolecular nonradiative energy transfer 77−34792
polymers containing carbazole units, optically active, fluoresc. props. 78−84647
polymethacrylic acid, dye-tagged, electrically oriented solns., fluoresc. polaris. changes 78−76523
polymethine cyanine dyes, viscosity depend. fluoresc. lifetime using synchronously operated ps streak camera 80−28041
molecular fluorescence continued
polymethine dye nonequilib. protolytic forms, lasing, fluoresc. and nonradiative transitions 80−102722
polymethine dyes, excited mols., photoisomeric transformations 79−87854
polymethine dyes, highly excited states, absorption and fluoresc. *(Russian)* 77−19248
polymethine dyes, mol. struct., lasing props. 79−3693
polymethine dyes, relax. mechanisms in picosecond range *(German)* 78−33737
polymethine saturable absorbing dyes, dual component fluoresc. lifetime meas. 80−106359
polynucleotides, polaris. spectra, excimer phosphoresc. and fluoresc. 79−34497
polyphenyls, S_1-T_1 interconversion, excitaiton indices calcs. 79−54830
polystyrene, steric effects on excimer formation, fluorescence spectra exam. 80−25430
polystyrene microspheres, dye impregnated, fluoresc. spectra struct. resonances 80−50914
polytene chromosome, stretched, stained with acridine orange, fluoresc. polarisation rel. to DNA packing 78−76995
polyvinylcarbazole, fluoresc., photooxide quenching, exciton migration effects 79−56830
POPOP, fluoresc. quantum efficiency, one-photon dissociation, temp. depends. 80−69180
POPOP, fluoresc. spectrum light quenching factor wavelength depend. 80−18882
POPOP, polarisation of spontaneous and stimulated radiation 79−31583
POPOP, soln., anisotropic fluoresc. of prolate mol. *(German)* 80−1018
POPOP+Cd(5^3P_1), vap., electronic energy transfer, laser appl. 77−30980
POPOP laser, bleaching of vapour 80−19027
POPOP vapour, spectral, fluoresc., photochem. and laser props. 80−106344
porphin, free base, in n-octane crystal, S_1 from S_0 transition, freq. shift and dephasing temp. depend. 78−25584
porphin, free-base, in n-octane cryst., photochem. hole-burning, vibronic relax. 79−31587
porphin, single crystal Shpolskii matrix, fluoresc. anisotropy 79−85994
porphin ($-d_2,d_4,d_6,d_8,d_{10},d_{12},d_{14}$), nonradiative transition probabilities, deuteration effects 79−3485
porphin free base, vibr. and normal mode anal. 80−69122
porphin in host n-alkane crystals, phototautomerism, IR spectral obs. 80−34963
porphin-d_n, (n=2-14) electronic-vibr. interaction, quasi-line absorption (fluoresc.), mirror symmetry 78−55197
porphins orientation in n-alkane Shpolskii hosts, spectra 80−48035
porphyrin solns., quenching of excited states by nitro-cpds., donor-acceptor interactions 78−2899
porphyrins, solid solns., phosphoresc. rel. to solvent heavy ats. *(Russian)* 77−40286
probes, study of protein temp.-depend. conform. transitions 77−70410
prolate molecules, anisotropic fluoresc. in soln. *(German)* 80−1018
prolate molecules in solvents, anisotropic fluoresc. *(German)* 80−69183
propanolol, (adrenergic blocking agent), high-press. liq. chromatography, fluorometric detect. 78−20096
propynal, energy dispersion and relax., laser IR-visible double reson. 80−48023
propynal, rovibronic populations, collisionless IR multiphoton spectra, energy deposition, photoacoustic determ. 80−83354
protein bacterial bioluminescence, isolation and props. 78−92599
protein chromophores, fluoresc. props., use in macromol. equilib. struct. mobility investigs. 79−64130
protein rotational motions, large-scale, detection by EPR and fluorescence 79−16120
protein-probe binding, error in interpretation of double-reciprocal plot and Scatchard plot 78−24021
proteins, adsorbed at interfaces, fluoresc. spectroscopy study 80−12315
proteins, fluoresc., equilib. structural mobility *(Russian)* 78−76986
proteins, resolution of components of complex spectra by Alentsev-Fok method 80−1097
proteins, UV fluorescence detect. of conformational rearrangements in plants 79−53031
proteins, UV fluorescence spectra, resolving of components, Alentsev-Fok method 80−1096
protochlorophyl, mag. reson., site selected fluoresc. detection 80−69164
protochlorophyll, fluoresc. fading curve of lowest triplet state 79−36691
proton transfer photoreaction kinetics, in singlet excited state 78−48671
protoporphyrin: Cu^{2+}, in pyridine fluoresc. quenching mechanism 79−56837
pryazine, fluoresc. $^1B_{3u}$→$^1A_{1g}$ band, vibr. struct. and intensities 79−64033
pseudoazulenes, anomalous fluoresc., radiationless transitions 80−91593
pseudocyanine, I aggregates, fluoresc. decay time 77−27105
pulsed laser induced molecular fluorescence, exptl. configs. 78−58045
purple membrane protein chromophore, fluoresc. 78−44454
pyrazine, excited and N_{1s} ionised states, ab initio calcs. broken orbital symm. 80−27931
pyrazine, PMMA soln., fluoresc. and phosphoresc. quantum yield and lifetime, 20-120 kbar 79−54902
pyrazine, pyrazine-Kr, ground and n-π^* excited state struct. 79−68241
pyrazine, single vibronic level fluoresc., non-exponential decay 77−27108
pyrazine, vap., single vibronic level fluoresc., dye laser excitation 79−18224
pyrazine, vapour, fluoresc. quantum yields, rot. effects 80−95661
pyrazine.$(H_2O)_n$, n=1,2, ground and n-π^* excited state struct. 79−68241
pyrazine (-d_4), single vibronic level fluoresc. spectra, rel. to vibronic coupling 80−28043
pyrazine (-d_4) vapour, single vibraonic level fluoresc. from n, π^* 80−37827
pyrene, adsorbed on silica gel surface, biphasic photochemistry, time-resolved spectra 80−30252
pyrene, distinction of delayed fluorescences S_1→S_0 and S_2→S_0 by selective quenching of S_1→S_0 80−69175
pyrene, excimer fluoresc., struct. depend. in cryst. 77−75200
pyrene, fluoresc. quenching by 1,4-diazabicyclo[2-2-2]octane in cyclohexane soln. 79−31575
pyrene, fluorescence produced by low energy electrons *(German)* 77−18967
pyrene, fluorescence spectra in aq. and surfactant solns. 77−83639

molecular fluorescence continued
pyrene, in aq. micelle system, fluoresc. quenching by inorganic ion 77−10697
pyrene, in micellar environments, fluoresc. quenching by nitroxyl radical 79−13754
pyrene, in polystyrene, excimer fluorescence 79−68249
pyrene, in polystyrene matrix, singlet O_2 induced excimer fluoresc. 77−6832
pyrene, micellar solns., fluoresc. quenching 78−25588
pyrene, micellar system, fluoresc., solubilisate distrib. statistics, kinetic model 79−34366
pyrene, migration between lipid vesicles in aq. soln., fluoresc. stopped-flow obs. 80−85360
pyrene, monomer and excimer fluoresc. in soln., triplet-triplet annihilation and mag. field depend. 78−78738
pyrene, multiexponential fluorescence decay, systems theory approach to anal. 79−59495
pyrene, photoionisation in alkane liqs., laser induced fluoresc. 78−61038
pyrene, S_1, fluoresc. decay in micellar and homogeneous liq. dispersions 77−75199
pyrene+N,N-dimethylaniline (deuterate)(3,5 dimethoxy-N,N-dimethylaniline), geminate recomb., solvent, isotope, mag. field effects 78−56888
pyrene excimer fluorescence, erythrocyte membrane fluidity changes after X-irrad. obs. 80−72262
pyrene excimer formation in micellar surfactant solns., distributional effects 78−64855
pyrene excimer formation in micelle, time-resolved spectra 79−79298
pyrene solutions, emission spectra 77−30910
pyrene vapour, laser excited fluorescence 78−29807
pyrene-DMA-methanol solution, photoinduced radical ion pair geminate recombination, triplet yield 78−76879
pyrene-h_{10}, -d_{10}, dual fluoresc. quenching by O_2 and NO 78−5266
pyrene-N,N-dimethylaniline heteroexcimer systems, micellar solns., fluoresc., photoinduced electron transfer 78−25590
pyrene-sodium 5-[1-pyrenyl]pentanoate intramicellar excimer formation in CTAC and SDS micelles, fluoresc. probe 80−16733
1-pyrene-sodium sulphonate, excimer form. in inverse micelles, fluoresc. probe 77−88491
[2.2](2,7)pyrenophane, emission spectra, transannular interaction 77−489
pyrenophanes, excimer fluoresc., struct. depend. in cryst. 77−75200
pyridine, fluoresc. of vap. phase, nonradiative electronic relax. 79−86000
pyridine, vapour, $S_1(n,\pi^*)$ state fluoresc. 78−5267
pyridine and methyl derivatives, fluoresc. and nonradiative processes 79−36684
pyridine-d_0, -d_5, vap. fluoresc. spectra 78−82771
pyrimidine, $^1B_1$ state zero level fluoresc. decay, press. effects 78−13540
pyrimidine, fluoresc. quantum yield 79−13757
pyrimidine, vapour, fluoresc. quantum yields, rot. effects 80−95661
pyrimidine derivatives, absorpt., luminesc. and polarisation spectra, electronic struct. 79−85993
quantum statistical mechanics of relaxation phenomena, non-exp. decay 79−44850
quantum yield meas. using photoacoustic spectroscopy 77−88595
quantum yield meas. using reference soln. standards 77−42442
quantum yield measurements, real, observed and mol. parameters, ref. soln. standards 78−32898
quasi-linear spectra and vibronic states of molecules with end phenyl rings *(Russian)* 80−95597
quasilinear spectra of double molecules with weak reson. bonds 79−94030
p-quaterphenyl, polarisation of spontaneous and stimulated radiation 79−31583
quercetin, excited state proton transfer, luminesc. 80−35818
trans-quinacridones, absorpt. and emission spectra, struct. and solvent effects 77−478
quinacrine, fluoresc. probe interaction with acetylcholine-activated synaptic membrane 77−90762
Quinacrine Mustard, time-resolved fluoresc. spectrum 80−87165
quinacrine mustard-DNA complex molecule, laser-induced fluorescence 77−60187
quinine sulphate, acid soln., edge excitation red shift and proton migration 78−1028
quinine sulphate, fluorescence polarisation meas. at high press. 78−66576
quinoline, fluoresc., phosphoresc. and H bonding 77−79647
quinoline, radiationless transition branching ratio, temp. effects 79−54900
quinoline in alcoholic glasses, induced fluoresc. 79−33775
quinoxaline$^+$, (singly protonated), struct. and kinetics of fluoresc. and phosphoresc. states 77−30906
quinoxaline, solns., excited state absorpt. kinetics 79−45734
quinoxalinones, new class of high-efficiency laser dyes 78−46597
radiative electron transitions in photodissoc. *(Russian)* 79−98212
radiative interaction operators, translational expansion 77−75197
radiative lifetimes, polarisation propagator approach 77−18844
radiative rate consts., solvent depend. 78−66587
radicals, laser fluoresc. detection with high time resolution 80−9632
Raman and fluorescent scattering by molecules embedded in dielectric spheroids 80−99507
Raman spectroscopy, sub-nanosecond, time-resolved, background rejection, fluoresc. enhancement 77−18109
rare earth complexes, formation and props., book contrib. 80−43204
rare earth halide vapours, discharge spectra, fluoresc. lifetimes meas. 79−27025
resonance fluoresc., probe of intramolecular relax., density matrix formalism, lifetimes and quantum beats 80−32757
resonance fluorescence, saturation effects, coherent pulse calcs. 77−6785
resonance interactions of atomic and molecular systems driven by strong laser field, theory 80−14097
resonance light scattering, two level density matrix description 78−25840
resonance Raman lineshapes and fluorescence in strong radiation fields 80−87074
trans-retinal, picosecond photophysics 77−9169
retinals, emission spectra, state ordering 77−25373
retinals, polarised fluoresc. at room temp. 78−96014
retinol, fluoresc., polarised emission study 79−29504
retinyl acetate, fluoresc., polarised emission study 79−29504
retinyl acetate, high press. fluoresc. studies of radiative and nonradiative processes 80−1011

molecular fluorescence continued
rhodamine, 6G and B, low quantum yield mol. fluoresc., polarisation, excitation energy depend. 77−50462
rhodamine, soln., triplet state accumulation and deactivation depend. on solvent polarity 79−85982
rhodamine 3B solutions in polyvinyl alcohol matrix, spectrum-luminesc. characts. 79−13761
rhodamine 4C, in ethanol soln., rot. relax. time using ps. spectroscopy technique 80−1013
rhodamine $6G_2$ molecules in solution, photoluminescence study, fluorescence decay time 80−80832
rhodamine 6G, associated, in polyvinyl alcohol film and soln., emission, room temp. 79−54896
rhodamine 6G, delayed fluoresc. of simple associates in polar and nonpolar solvent mixtures *(Russian)* 78−48185
rhodamine 6G, electronic energy transfer from S_2 state to BBOT in soln. 78−88346
rhodamine 6G, fluoresc. polaris. spectra in glycerol soln. 79−76458
rhodamine 6G, fluoresc. polarisation, solvent effects 80−32755
rhodamine 6G, in ethanol, time-depend. fluoresc. spectrum, using synchrotron radiation 80−62736
rhodamine 6G, in glycerine-water solns., anti-Stokes fluoresc., conc. quenching 79−24349
rhodamine 6G, in methanol, fluoresc. lifetime meas. 78−29811
rhodamine 6G, micellar soln., aq., fluoresc. decay for rot. diffusion const. 79−11826
rhodamine 6G, mol. fluoresc. decay time, self-absorption 79−68255
rhodamine 6G, on surface of stilbene cryst., sensitised luminesc., energy migration 79−56831
rhodamine 6G, orientated relax. times, streak camera meas. 80−14168
rhodamine 6G, rot. diffusion, fluoresc. spectra, solvent effects 77−75198
rhodamine 6G+BBOT donor-acceptor system, intermol. electronic energy transfer 78−17702
rhodamine 6G+malachite green, in low viscosity solvent, ps time resolved energy transfer 78−70910
rhodamine 6G and rhodamine B adsorbed on AlH_3, luminesc. spectra during AlH_3 photolysis 80−55171
rhodamine 6G aqueous solution, surfactant effect on fluoresc. intensity *(Japanese)* 77−42536
rhodamine 6G doped polyurethane film, fluoresc., photoinduced effects 77−1727
rhodamine 6G ethanol soln., absorpt. and luminesc. spectra using picosecond excitation 80−106351
rhodamine 6G polar solution, conc., temp effect on spectral props. 79−87505
rhodamine 6G soln., delayed annihilation fluoresc., external heavy at. effect 79−99931
rhodamine 6G soln., hot luminesc. and vibr. relax. 79−22752
rhodamine 6G solns., picosec. kinetics of emission 79−76685
rhodamine 6G solution, absolute fluoresc. quantum yield determ. by calorimetric method 80−78851
rhodamine B, 6G, spectra of lowest excited singlet states 79−81424
rhodamine B, acid-base equilib., photophys., fluoresc. lifetime meas. 78−82762
rhodamine B, in glycerine-water mixtures mol. agglomeration effect on fluoresc. polaris. spectrum 78−25595
rhodamine B, mol. fluoresc. decay time, self-absorption 79−68255
rhodamine B and 6G, fluoresc. decay time meas. in different solns. 80−9637
rhodamine B in ethylene glycol, fluoresc. decay meas. via modulated gain spectroscopy 80−63699
rhodamine B lactone, dual fluoresc., solvent polarity depend. 77−3394
rhodamine C and 6G, strong base solns., electronic spectra, temp. depend. 79−85987
rhodamine dye mixtures, qualitative anal. by fluoresc. polarisation spectroscopy 79−34396
rhodamine dye solns., amplified spontaneous emission 79−45941
rhodamine dye solutions, additional heavy atom effects on triplet state transitions *(Russian)* 77−85800
rhodamine dye solutions, vibr. relax. in S_1-state 77−6826
rhodamine dyes, amplified spontaneous emission, picosecond pulse generation 79−3691
rhodamine dyes in soln., bleaching, electronic and vibr. absorpt. spectra, fluoresc. 80−42960
rhodamine G, in glycerine-H_2O mixture, fluoresc. polarisation spectra, 350 and 540 nm excitation 79−98139
rhodamine solns., anti-Stokes fluorescence 78−27284
rhodamine solutions, quenching of two-photon fluoresc. and stimulated anti-Stokes emission 79−72619
rhodamine-6G-3,3'-diethylthiacarbocyanine iodide-sodium lauryl sulphate soln., premicellar region, energy transfer 80−20685
rhodamine-B, fluorescence decay meas. via modulated gain spectroscopy 79−64025
rhodamine-B fluoresc. polarisation, solvent effects 77−54569
rhodamine-methanol soln. energy transfer to Ag film surface plasmons 79−91119
rhodamines, 5G, 6G, B, 3B in ethanol soln., luminesc. quenching by photoirradiation 80−87168
rhodamines in ethanol soln., gain and induced absorpt., struct. props. 77−24890
rhodopseudomonas sphaeroides, reaction centre triplet state fluoresc. mag. field depend. 78−53358
rhodopsin and thermal intermediates, fast struct. fluctuations in protein component 80−72137
rigid linear rotor+atom, rot. relax., microwave transient T_1 and T_2 rates 79−13797
rose bengal, excited state orientational relax., in protic and aprotic solvents 78−46383
rose bengale, fluoresc. polaris., solvent dipole moment effect 78−25596
rotational correlation times, photocounting pulse fluorimetric determ., statistical accuracy 77−61777
rotational motion probe technique using E-type delayed fluorescence depolarisation 80−36207
rubrene, sensitised photooxidation of 1,3-diphenylisobenzofuran solns., S_1 excited state O_2 quenching 80−45529
rubrene film, excited complex with charge transfer, fluoresc. obs. of mag. reson. *(Russian)* 77−8454
rubrene fluorescence, quenching by Ni complexes 79−94028
ruthenium trisbipyridyl ions in surfactant solns., excited state decay kinetics 80−83407

molecular fluorescence continued
salicylamide, excited state proton transfer, kinetics, picosec. fluoresc. 79−59502
saturated fluorescence excitation, transition probabilities and particle density determ. 78−58871
saturated laser-induced fluoresc., rot. redistrib. effect 79−81259
SEM cathodoluminescence probing of biomol. species at 100 Å resolution or below 78−24197
Shpolskii multisite luminesc. spectrum deconvolution, vibr. struct. anal. 80−58304
Shpolskii spectra, identification and struct. anal. of unknown compounds in organic mixture 79−87891
signal sampling, using ultrafast optical Kerr shutter, book contrib. 77−31140
small particles, angular distrib. of fluoresc. from embedded mols. 78−76926
sodium dodecyl sulphate micelles-ω-(α-naphthyl) dodecanoic acid soln. fluoresc. decay obs. 80−61158
sodium polystyrene sulphonate, dye-tagged, electrically oriented solns., fluoresc. polaris. changes 78−76523
solid, molecular fluoresc., phosphoresc., and ODMR line narrowing 80−43084
solutions, meas. using multichannel SIT image vidicon or photomultiplier scanning systems 77−79638
solutions, photoluminesc. decay time, donor conc. effect 80−66299
solutions, time dependent emission anisotropy *(German)* 78−94279
solvatochromism kinetics 77−30898
spectra, synchronously excited, peak wavelength and intensity prediction 78−20082
spectroscopy, in study of biochem. processes review 78−11784
spherical molecule, anisotropic mol. rot. detect., differential phase fluorometry theory 77−61778
spherical particle, surface enhanced Raman scatt. by molecules 80−95629
spin-orbit interaction, in mag. field 79−3483
state-resolved product distribution, pump and probe laser determ. 79−6956
steady-state molecular luminescence radiance assuming narrowband excitation 79−13747
stilbene, cis→trans photoisomerisation rate const., direct meas. 80−30250
stilbene, cis and trans, transient spectra, radiative lifetimes and quantum yields 80−78640
stilbene, direct photoisomerisation theory, from fluoresc. and absorption spectra 79−79262
trans-stilbene, fluoresc. decay, picosecond anal. 79−31569
stilbene, single cryst., triplet excitons, delayed fluorescence 78−63988
trans-stilbene, soln., lifetime and anisotropic fluoresc., viscosity effects *(German)* 80−106352
trans-stilbene, time resolved fluoresc. in ps. regime 80−14164
stilbene aza-analogues, lowest excited states, INDO/S calcs. 80−95545
stilbene derivatives, fluoresc. props. 79−85992
trans-stilbene photoisomerisation, ps dynamics under collision-free conditions 79−91975
stilbenes, prolate molecules in solvents, anisotropic fluoresc. *(German)* 80−69183
trans-stilbenes, triplet energy, substituents effect, singlet-triplet absorpt. and electrochemilum. obs. 79−81225
Stokes fluorescence shift time resolution, obs. of 2-amino, 7-nitrofluorene in 2-propanol 77−58060
stratospheric species monitor, review 77−9472
strong driving field, stochastic Liouville eqn. anal. 79−59503
styrene, fluoresc., ns time resolved emission spectra 77−6822
styrene (-d_3, d_5, d_8), fluoresc. quantum yields and lifetimes, 298 and 77K 79−59500
styrene-method methacrylate copolymer glassy soln., excimer form., energy migration, fluoresc. depolarisation meas. 78−70986
symmetric top molecule, two-photon excited fluoresc. spectroscopy, density matrix formalism 79−36716
symmetric top molecules, microwave transient phenomena, Bloch eqns. 79−26969
synchrotron radiation with single photon counting or phase shift techniques, for fluoresc. lifetime meas. 79−13841
TCNE aromatic donor/acceptor complexes, reson. Raman excitation and absorpt. profiles, model theory 77−18982
temperature controlled X-cell for gas phase fluorescence spectra obs. 78−66692
p-terphenyl, saturated vap. press., absorpt. and fluoresc. spectra 79−76442
p-terphenyl, triplet exciton annihilation and triplet spin relax. 80−29792
p-terphenyl vapour, spectral, fluoresc., photochem. and laser props. 80−106344
tetra-4-tert-butylphthalocyanine-H_2 mol. in solid tetradecane, electronic lines 77−18965
tetracene, fluoresc. fading curve of lowest triplet state 79−36691
tetracene, intramol. dynamics and energetics in isolated ultracold state 79−98144
tetracene, vibrational quasicontinuum threshold, spectrosc. criterion 80−52972
tetracene in liquid crystals, temp. depend. of absorption and fluoresc. *(German)* 80−18887
tetrachloromethane, UV laser photolysis 80−66826
tetrachloromethane+Xe, excitation functions and rotational polarisation, chemiluminesc., crossed beam study 80−76491
tetrachlorotetraiodofluorescein, rot. diffusion, fluoresc. spectra, solvent effects 77−75198
tetracyanobenzene+methylated benzene, fluorescent exciplex form., electronic relax. 80−5573
tetracyanoethylene(d), charge-transfer complex, fluoresc. quantum field and decay time 78−42107
1,4,5,8-tetrahydroxyanthraquinone, selective excitation, luminescence of long-wavelength component of multiplet 79−3478
tetramethyl pyrazine in durene, phosphorescent mols., quantum beats in triplet states 80−58312
3,6-tetramethyldiamino-N-methylphthalimide soln., hot luminesc. and vibr. relax. 79−22752
tetramethylpyrazine, PMMA soln., fluoresc. and phosphoresc. quantum yield and lifetime, 20-120 kbar 79−54902
tetramethylpyrazine-d_{12}, in durene matrix, intersystem crossing of 859.5 MHz transition 79−27015

molecular fluorescence continued
s-tetrazine, cooled supersonic jet, Van der Waals complex, isotope effects, fluoresc. obs. 78−55194
s-tetrazine, fluoresc. excitation spectra, 1K rot. struct. 78−1020
s-tetrazine in n-hexane, picosecond time-resolved fluoresc., vibr. relax. 80−48025
s-tetrazine-benzene, mixed cryst., 2K, lifetime limited photochem. hole burning 78−9183
thiocarbonyl chlorofluoride, second excited singlet state emission spectroscopy, resonance fluorescence obs. 80−69158
thioindigo, in nonpolar solvent, photoisomerisation mechanism, fluoresc. obs. 77−63933
thioindigo, vibronic fluoresc. spectrum, vibr. struct. 77−54571
thiophosgene, B^1A_1-state, photophys., fluoresc. lifetime meas. 80−53033
thiophosgene, photolysis, $^1A_2$-state lifetime, fluoresc. 77−52653
thiophosgene vapour, fluoresc. from S_2 single vibronic states, quantum yields and quenching 77−34675
thioxanthone, fluoresc. and internal conversion, rel. to proximity effects 80−91592
three-level molecular system, cooperative evolution, transient effects of dephasing and relax. 80−28184
three-level system, rel. tuned two- and three-photon processes 77−68198
three-level system, reson. fluoresc., superposition of adiabatic state theory 78−78734
time resolved spectrofluorometry, appl. of synchrotron radiation 78−65978
time resolved spectroscopy using new laser techniques 77−79162
time-correlated picosecond laser pulses generation, rapid sampling of optical relax. phenomena 80−9969
time-dependent effective rates for molecular processes 79−63928
time-resolved laser fluorescence spectroscopy for atomic and mol. excited states obs., review, book contrib. 80−9760
tissue fluorochrome meas. with He-Cd UV laser 77−77962
TMPD, 2,2,4-trimethylpentane, fluoresc. quenching by elec. field, above photoionis. threshold 78−33539
TMPD, fluoresc. in nonpolar organic liqs. for excitation energies above and below photoionis. threshold 78−1018
TMPD, nonpolar photoionised soln., geminate pair quantum field, recombination fluoresc. elec. field quenching 79−20389
2,6 p-TNS fluorescence probe bound to apomyoglobin, nsec decay 77−29091
toluene, fluoresc. quantum yield in soln., dipole-dipole interaction 78−25598
toluene-d_8, soln., fluoresc. quantum yields, temp. and deuteration effects 77−3396
TOPOT, 1,4-bi[2-(5-p-tolyloxazolyl)]benzene laser, bleaching of vapour 80−19027
TOPOT, fluoresc. spectrum light quenching factor wavelength depend. 80−18882
TOPOT, polarisation of spontaneous and stimulated radiation 79−31583
TP-C-DMP, new bifluorophoric laser dye with intramolecular energy transfer, lasing characts. 78−74899
TP-CSC-DMP, bifluorophoric mol. ultrafast intramolecular energy transfer 78−74900
trans-stilbene, fluoresc. lifetimes, 77-295K 78−1029
transfer of electronic excitation energy between like mols. in soln. *(German)* 78−21965
transition metal complexes, electron energy transfer processes 79−10143
tri-n-propylamine, fluoresc. decay 80−91590
triatomic ions, fluoresc. quantum yields and lifetimes, meas. method, ion form. 77−6815
sym-tribenzotridehydro [12] annulene, electronic spectra in Shpolskii type hydrocarbon matrices, electronic struct. and fluoresc. 78−66589
tricarbocyanine solns., photoisomerisation, fluoresc. and absorpt. spectra of photoisomer 78−85181
1,3,5-trichloro,2,4,6-trifluorobenzene radical cation, $B^2A_2' \rightarrow X^2E''$ laser-induced fluoresc. spectra 80−14172
1,3,5-trichlorobenzene radical cation, emission and photoelectron spectra, lifetimes meas. 78−86905
trichlorobenzene radical cation, gas and matrix isolated vibr. resolved electronic spectrum 79−68252
trichlorobenzene radical cation, symm. substituted, fluoresc. and emission spectra in Ne matrix 79−89702
trichlorofluoreomethane, UV laser photolysis 80−66826
tricycloquinazoline, excited states, fluoresc., phosphoresc. 77−61789
triethylamine, fluoresc. decay 80−91590
triethylenediamine, multiphoton ionis. and two-photon fluoresc. excitation spectra 79−98164
1,3,5-trifluorobenzene radical cation, laser induced fluoresc. spectra, vibronic anal., Jahn-Teller distortion 79−3470
trifluorobenzene radical cation, symm. substituted, fluoresc. and emission spectra in Ne matrix 79−89702
trifluoroformamide, radiationless pathways, time-resolved fluoresc. obs. 78−66577
trimethylamine, collision induced fluoresc. enhancement and quenching, relax. processes 80−83412
trimethylamine, electronically excited isolated mol., relax. and intramol. processes 80−83411
trimethylamine, fluoresc. decay 80−91590
triphenylene, in n-heptane cryst., 2-photon excitation spectrum 78−82760
triphenylene, in n-heptane cryst., polarised fluoresc. spectrum, mol. deformation 79−10135
triphenylene in Shpolskii matrix, orientation, ESR and fluoresc. spectra 79−36688
triphenylmethane dye, S_1-lifetime determ. by two-photon fluoresc. 77−18966
triphenylmethyl in triphenylamine, photon echo stimulated from optically induced nucl. spin polarisation 79−76460
tris(bipyridine)ruthenium(II)dichloride, fluoresc. decay meas. by high repetition rate gated photon counting 80−86402
tropolone, π-π^* singlet state, H^+ tunnelling dynamics and equilib. geometry 80−102539
tropolone, in water and cyclohexane, electronic relax., absorption, excitation and fluoresc. spectra 78−66588
trypaflavine solutions in polyvinyl alcohol matrix, spectrum-luminesc. characts. 79−13761
trypsin, photoluminescence after UV irradiation *(German)* 79−92137
tryptophan, fluoresc. intensity increase due to deuteration 78−78739
tryptophan, pH dependent fluoresc., quenching by histidine *(Russian)* 78−90209

molecular fluorescence continued
D-tryptophan, soln., excitation spectra rel. to recording wave length *(Russian)* 77−12438
tryptophan, stereoselective energy transfer induced by circularly polarised light 80−1010
two-atom resonance fluorescence, in strong EM field, excitation spectrum 78−82778
two-level molecular systems, optically pumped, increased inversion efficiency 80−23657
two-photon excited molecular fluorescence, in optically dense media 78−33534
two-photon excited molecular fluorescence technique in chem. analysis 80−40799
two-photon fluorescence, constrast ratio decrease depend. on laser pulse intensity 80−1255
ultrafast molecular processes, use of picosecond lasers 77−79709
umbelliferone, excited states, in ethanol-water soln., absorption and emission spectra 79−13763
umbelliferones, 3-substituted, fluoresc. spectra, pH depend. 77−88492
N_3-undecyllumiflavin, high resolution fluoresc. and excitation spectroscopy, vibronic transitions obs. 80−78639
unimolecular processes, electronic, vibr., rot. and translational energy partitioning 79−36712
upper atmosphere, in situ reson. fluoresc. meas. 79−53600
uranyl complexes, fluoresc. state, rel. to electronic struct. *(Russian)* 78−5274
UV fluorescence lifetime determ., correction of instrumental time response var. with wavelength 78−5374
van der Waals molecules, mol. fluoresc., vibr. predissoc. model 78−42120
velocity redistribution by optical processes 78−38448
vibration relaxation time measurement, by coherent Raman-induced IR fluoresc. 79−7038
vibrational relaxation of molecules in condensed media, survey, book contrib. 77−36295
vibrational relaxation rate meas. by delta *(Russian)* 77−68074
vinyl copolymers, containing fluorescent groups, optically active 80−102594
vinyl cyanide IR photolysis products, time-resolved fluoresc. obs. 79−57255
2-vinylanthracene, conform. conversion kinetics, fluoresc. 80−9631
1-vinylnaphthalene-methyl methacrylate copolymer glassy soln., excimer form., energy migration, fluoresc. depolarisation meas. 78−70986
visual pigment model systems, spectroscopy and photochem. 77−32871
vitamin B_6 fluorescence in cells 77−21496
Weber effect, and inhomogeneous spectral broadening 79−3482
X-ray, ultrasoft region, 5M grating spectrograph eval. for high resolution spectra prod. 79−27117
X-ray fluorescence polarisation 78−1003
X-ray spectra observation using 5 m grating spectrograph 80−86538
xanthene, dye solns., luminesc. spectra, conc. depend. effects 79−54885
xanthene dye, solute-solvent hydrogen bonding and temp. effects on internal conversion 77−3402
xanthene dye N-92+inert gas buffer, electron beam excited, fluoresc., energy transfer 78−25877
xanthene dyes, hidden vibr. band determ. method, fluorescence and excitation spectra meas. 80−40158
xanthene dyes, internal heavy atom effect on radiative and non-radiative rate consts. 80−32765
xanthene dyes, phosphoresc. spectra of T_1 state in ethyl alcohol soln. 79−85981
xanthene dyes in n-alcohols (ethylene glycol) (glycerol), rot. relax., time-resolved fluoresc. depolaris. obs. 80−58300
xanthione in benzene, second excited singlet state, ps spectra 77−3399
p-xylene-d_{10}, soln., fluoresc. quantum yields, temp. and deuteration effects 77−3396
xylenes, fluoresc. and triplet state quantum yields, biacetyl method 78−37671
xylenes, singlet excited states decay, substituent effects 77−75175
γ_1-base, ground and excited states, dipole moment, CNDO/S and INDO/S calcs. 79−36534
Zeeman effect, anomalous, Doppler-free standing wave saturated resonance, book contrib. 78−9279
zinc chlorophyll b, triplet state population at 4.2K, magnetic field effects 77−30915
zinc octaethylporphin, radiationless transitions, fluoresc. and phosphoresc., isotope effects 77−65502
zinc porphin, in anthracene, triphenylene, n-octane, fluoresc. and optical absorpt. spectra 79−68240
AgBi, laser induced fluoresc., vibr. anal., rot. consts. *(French)* 77−18959
Ag(II) protoporphyrin IX dimethyl ester, fluoresc. relax. after picosec. excitation 79−45751
AlO, produced by Al+O_2→AlO+O, product rot., vibr., translational energy 78−23928
Ar, condensed electron beam excited, exciton radiative lifetimes 80−6727
Ar jet, supersonic, electron beam-excited, continuous VUV emission spectrum origins 79−6964
Ar, Paschen (1s) reson. state, decay mechanism and kinetics 79−27021
Ar:$N_2O(CO)(CO_2)$, fluoresc. and thermoluminesc. after photolysis 79−89700
Ar-F_2 mixtures, low-press. excimer form. and quenching by e-beam excitation 79−50071
Ar-HI, low electron beam excitation rates 79−86163
Ar-I_2, low electron beam excitation rates 79−86163
Ar-Kr-F_2 mixture, nucl. induced excimer fluoresc. for I laser excitation 80−78846
Ar-Xe-NF_3 mixture, fluorescence from e-beam excitation at low temp. and high press. *(French)* 78−58727
Ar+HCN(H_2O), electron excitation of Ar* and Ar_2*, fluoresc. and dissoc. energy transfer collisions 77−14580
Ar^++N_2, energy transfer, vibronic excitation, emission spectra 78−66578
Ar_2, emission continua in VUV, new oscill. struct. 79−54905
ArCl*, excimer formation rate consts., B state radiative lifetimes, quenching, VUV excitation 80−55631
ArCl* fluoresc., HgCl laser, HgCl(B) state radiative lifetime meas. 78−94390
ArF, Ar_2F, electronic struct., pot. energy curves, radiative transition probability calcs. 77−57879
molecular fluorescence continued
ArF, Ar_2F, time depend. emission meas., Ar-Kr-F_2 laser mixture kinetics 80−32768
ArF, electron quenching rate consts. meas. by fluoresc. anal., laser implications 80−32969
ArF, excimers, power superluminescence, in elec. discharge *(Russian)* 77−7621
ArF*, Ar_2F*, kinetics of proton-excited Ar-F_2 mixtures, time-resolved and time-integrated spectra 79−36883
ArF*, formation and quenching kinetics 77−88482
ArF* laser, electron beam pumped, dominant formation and quenching processes 79−938
ArI_2, van der Waals mol., fluoresc. spectrum, predissoc. 78−66584
ArO, in doped inert gas matrix, photoluminesc. 79−31579
ArXeF*, gain meas. at 4416 Å 78−50758
Ar*+$Fe(CO)_5$, chemiionisation and chemiluminescence reactions, Penning ionisation and fluoresc. obs. 80−97689
Ar*+$N_2(H_2)(D_2)$, de-excitation processes, by pulse radiolysis optical emission obs. 77−65529
Ar_2* excimer, electron-beam excited, time-resolved fluoresc. spectra 79−813
BCl_3, intense IR radiation absorption singularities 79−76432
BCl_3, visible fluorescence dynamics due to IR laser irrad. *(Chinese)* 80−102534
BH, $A^1\Pi$ state, fluoresc. decay radiative lifetime meas. 79−13771
BO, radiative lifetime, first excited state 78−62848
BO_2, Doppler free spectra, backscatter fluoresc. line narrowing, theory and obs. 80−53034
BO_2, fluoresc. excitation spectra, vibronic level fluoresc., Fermi reson., force field 77−79643
BO_2, intermodulated fluoresc. spectra using stabilised dye laser 79−27020
BO_2, laser excited fluoresc. spectra assignments, vibronic and electronic states 77−46590
BO_2, photoexcitation and fluoresc. spectra, rot. transitions, assignment and deconvolution 79−27003
BO_2, Π vibronic states, laser induced fluoresc. obs. 80−58301
BO_2, radiative lifetime, first excited state 78−62848
BO_2, reson. fluoresc. assignment of vibr. and vibronic transitions 78−17663
BS, and isotopic forms, two new emission bands, mol. consts. 77−18960
Ba compounds in air-acetylene flames, dye laser-excited fluoresc. 79−68260
Ba+HBr, laser induced fluoresc. study at different collision energies 80−91632
Ba+HCl, laser induced fluoresc. study at different collision energies 80−91632
Ba+SO_2→BaO+SO reaction, laser-induced fluoresc. obs., vibronic distrib. of BaO, collisional energy depend. 80−11917
BaBr, visible spectrum, $C^2\Pi_{1/2,3/2}$−$X^2\Sigma^+$ transition, laser induced fluorescence 79−98072
BaCl($C^2\Pi_{3/2}$, v=0)+Ar, intermultiplet energy transfer, laser induced fluoresc. obs. 78−9227
BaO, excited electronic states, lifetimes and transition moments 80−87177
BaO, lowest triplet state, photoluminesc. optical-optical double reson. obs. 79−68254
BaO, optical-optical double reson. of excited states, Parkinson band system 78−70857
BaO($X^1\Sigma^+$), vibr. relax., laser-induced fluoresc. meas. 77−83631
Ba(^1S,^3D)+ halogenated methane, laser induced fluoresc. 79−66270
Bi_2, radiative lifetime and self-quenching cross sections meas. from laser induced fluorescence expt. 80−69189
Bi_n molecular clusters, laser fluoresc. spectrosc. 80−95755
Br+NOBr, primary and secondary photochemistry, vibrationally excited NO, IR fluoresc. obs. 80−48030
Br_2 (B-X) band spectrum in laser induced fluorescence 79−47931
Br_2, and isotopic forms, new rot.-vibr. lines, laser reson. fluoresc. obs. 78−991
Br_2, $B^3\pi o_u^+$ state deactivation efficiency, temp. depend. 78−70869
Br_2, fluoresc. obs. in UV laser photochem. of dibromodifluoromethane 80−16703
Br_2 in Ar matrix, reson. Raman scattering amplitude damping in discrete reson. limit 80−58262
Br_2, Kr ion laser-excited fluorescence, predissoc. 80−83414
Br_2, long-lived $A^3\Pi(1_u)$ state, quantum-resolved dynamics of excited states 80−69178
Br_2, resonant fluoresc. at 5145 Å, isotope mols., rot.-vibr. states 77−61782
Br_2, single rot. states, lifetimes and collisional quenching cross sections determ by obs. fluoresc. decay 80−91595
Br_2+Xe, excitation functions and rotational polarisation, chemiluminesc., crossed beam study 80−76491
BrCN, photodissoc. energy disposal, electronic branching, vibr. and rot. transfer, CN(B→X) fluoresc. 77−42364
BrCN, vacuum UV photodissociation spectroscopy, quantum yield, fluoresc. polarisation 80−32736
BrCl, $^3\pi_0^+$ state, time-resolved fluoresc. 77−34679
BrCl, excited $B^3\Pi(0^+)$ state, excitation spectra and predissoc. 78−66593
BrCl, excited $B^3\Pi(0^+)$ state, laser-induced fluoresc., steady-state kinetics 78−66594
BrCl laser induced fluoresc., quantum resolved level dynamics in $B^3\Pi(O^+)$ state 80−74188
BrCl, time-resolved fluoresc. of $a^3\Pi_0^+$ state 78−63093
BrF, $B^3\Pi(0^+)$ states, collision-free lifetimes laser fluoresc. obs. 78−94278
BrF, fluoresc. decay lifetimes and quenching cross-sections for excited $B^3\Pi(0^+)$ states 78−1030
BrF, laser excitation spectrum, 4850 to 5200 Å, rot. anal. 77−6840
BrF, laser excited fluoresc. 79−50077
BrF, predissociation in $B^3\Pi(0^+)$ state 78−66591
BrF, stable levels of $B^3\Pi(0^+)$ state 78−66592
$^{81}Br_2$, visible, vibr.-rot. absorption, fluoresc. decay, predissoc. quantum yield 77−18962
Br*+N_2O, electronic-vibr. energy transfer, time-resolved fluoresc. obs. 79−89753
Br($4^2P_{1/2}$)+$^{12}CO_2$($^{13}CO_2$), electronic-vibr. energy transfer, temp. depend. meas. 79−10136
Br($4^2P_{1/2}$)+CO_2(COS)(CS_2), electronic to vibrational energy transfer rates 78−29839

molecular fluorescence continued
$Br(4^2P_{1/2})+H_2(HD)(D_2)$, electronic-vibr. energy transfer, fluoresc. meas. 79−72347
$Br(4^2P_{1/2})+N_2O$, electronic-vibr. energy transfer obs. 78−55220
C in molecule, K-shell fluoresc. yield, statistical scaling 80−78644
C particle formation, C_2+C_3 as possible first step 78−68876
C_2 $a^3\Pi_u$ state quenching, laser-induced fluoresc. obs. 79−31574
C_2, conc. meas. in oxyacetylene flame rel. to saturation spectroscopy 77−60148
C_2, in comets, synthetic spectra calcs. 78−28579
C_2, in flames real time fluoresc. spectra, CW tunable dye laser excited 79−3488
C_2, laser fluoresc. detection with high time resolution 80−9632
C_2, low lying $a^3\Pi_u$ state produced in intense IR field, fluoresc. and quenching obs. 80−11931
C_2, reson. fluoresc. statistical equilib. calc., appl. to comets 78−1016
C_2 resonance fluoresc. technique for transient flame investigs. 77−30894
C_2^-, matrix isolated, vibr. relax., absorpt. spectra 77−75172
C_2^-, matrix isolated, vibr. energy transfer, fluoresc. 78−46382
C_3, ($^1\Pi_u$) radical excited state radiative lifetimes and the collisional deactivation 79−27018
C_3 production, vibr. relax., chem. kinetics, following IR multiphoton allene photolysis 80−66820
CBr_2 emission in solid Ar, laser excitation spectra and lifetimes 80−48034
CBrCl emission in solid Ar, laser excitation spectra and lifetimes 80−48034
CCN radical in solid Ar, emission and excitation spectra 78−70868
CD^+, in RF ion trap, laser induced fluoresc. spectrum, 0,0 vibr. band and rot. consts. 80−74189
CF, fluoresc. obs. in UV laser photochem. of dibromodifluoromethane 80−16703
CF_2, excitation by Hg 253.7 nm line, reson. fluoresc-spectra 80−63694
CF_2, fluoresc. and radiative lifetime obs. in dibromodifluoromethane UV laser photolysis 80−16703
CF_2, low pressure, vibrational excitation 79−47955
CF_2, matrix-isolated, vibr. unrelaxed fluoresc., lattice mode coupling 77−14485
CF_2, photoproduct, vibr. distrib., fluoresc. meas. 77−88511
CF_2 radical, UV emission in microwave discharge, assignments 77−50461
$CF_3NO \rightarrow CF_3NO$, photodissociation dynamics, two-photon laser-induced fluorescence study 80−43122
CH, collisionless form., rovibronic relax., reson. fluoresc. 78−68902
CH, in low pressure flame, laser-excited fluoresc. 78−90199
CH radical, sputtered from acetone chemisorption layer on SI, rot. and vibr. population distrib. 78−64436
CH_2, photoprod. from ketene, singlet-triplet energy separation and rovibronic level obs. 80−11936
CH_2 radical, fluoresc. induced by laser 588.9-595.6 nm, ($a^1A_1-X^3B_1$) energy separation 78−42121
$C_6H_6^+$, gas, laser-induced-fluoresc., rel. to photodissoc. and Jahn-Teller X and A states distortion 79−72345
CH($A^2\Delta$) radicals, electronically excited, lifetimes and quenching rate constants meas. 80−69188
CHF radical, $\tilde{A}^1A''$-$\tilde{X}^1A'$ transition, laser induced fluoresc. 80−95660
CH($X^2\Pi$) radical, prod., detect. and reactions 79−61842
$CH_2(b^1B_1)$, radiative lifetime from $b^1B_1 \rightarrow a^1A_1$ emission in electron irrad. methane 77−3476
CN, ($B^2\Sigma^+$), polarised fluoresc. following synchrotron radiation photodissoc. of ICN 79−98130
CN, $B^2\Sigma^+ \rightarrow A^2\Pi$ 0-0 and 1-0 bands, laser excitation spectra 80−91588
CN, fluoresc. spectra, time resolved, radiative decay and radiationless deactivation in Ar 79−98142
CN, free radical, anticrossing spectra for fine struct. consts. 79−68270
CN, from ICN photodissoc., internal state distrib., laser-induced fluoresc. 77−36773
CN, from IR photolysis of cyanomethane, photoluminesc. spectroscopy 77−73452
CN, internal energy distrib. following vinyl cyanide photodissoc., temp. depend. 80−78638
CN, prod. by RCN photodissoc., fluoresc. obs. 79−52725
CN, radical, ($A^2\pi$-$X^2\Sigma$) fluoresc. predissoc. in HCN photodissoc. 77−38691
CN, radical, $A^2\pi$ state, collisional deactivation, fluoresc. quenching obs. 77−83642
CN, radical, electronic, vibr. and rot. energy partitioning obs. following ICN photolysis 77−16853
CN radical, photofragment spectroscopy of A-X transition 79−52726
CN, radical fluoresc. excitation spectrum and laser emission from ICN photolysis 78−76892
CN radicals, time behaviour in laser-initiated thermal isomerisation of CH_3NC 80−11887
CN($B^2\Sigma$), from electron impact dissoc., of HCN, near-threshold emission 79−54975
CNN, matrix-isolated, $^3\Pi$-$^3\Sigma^-$ system, laser-induced temporal and wavelength resolved spectra 77−83637
CNN radical, matrix isolation spectra, 23.5-25.6×10^3 cm^{-1}, vibr. relax. and Renner splitting 77−83612
CN(X), free radicals, state distribs. rel. to prod. by photolysis of dicyanoacetylene 77−9107
CN*, $B^2\Sigma^+$ state, fluoresc. decay dynamics, collisional quenching and radiative lifetimes 80−58306
CO, A-X and B-X bands intensities in comets 79−35191
CO, $A^1\Pi(v'=1)$, vibr. relax. by reversible intersystem crossing, fluoresc. obs. 80−14170
CO, $A^1\Pi \rightarrow X^1\Sigma^+$, (2-0) band, three photon excitation, fluoresc. obs. 78−13481
CO, $a^3\pi$ state, IR radiative decay of vib. levels 77−30870
CO, electron impact, absolute emission cross-sections meas., calibration appls. 79−85996
CO, fluorescence, lifetime meas. for rot. levels of (0,0) band, $A^1\pi$ to $X^1\Sigma^+$ transition 78−29808
CO, from CO_2 photodissoc., CO($A^1\Pi \rightarrow X^1\Sigma^+$) transitions, vibr. population 77−58100
CO, istopically enriched, Ar matrix isolation, laser-included vibr. fluoresc. 80−9707
CO, matrix isolated, vibrational energy migration, vibr. fluoresc. obs. 79−91486
CO, multiphoton UV photolysis, isotope effects obs. 80−55679

molecular fluorescence continued
CO, optical excitation function by electron impact near threshold 77−6942
CO, radiative lifetimes and electron impact absolute emission cross-sections 77−88503
CO, solid and liq., vibr. relax. and vibr. diffusion rates, 66-79K 78−17757
CO, two-photon excited vac. UV fluoresc. 78−5264
CO, two-photon spectroscopy with tunable ArF laser 80−37843
CO, vibr. relax. in unsteady expansion wave, vibr. temp. distrib. 77−68096
CO^+, A-X and B-X bands intensities in comets 79−35191
CO^+, fluoresc. and production cross-sections by photoionis. of CO 78−9204
CO^+, fluoresc. spectra of ion beam, laser and electron excitation 79−45743
CO^+, vibr. ($A^2\Pi_i$) states, radiative lifetimes 77−3397
CO^+, vibr. relax., laser-induced fluoresc. 77−83632
CO^+, vibr.-excited $A^2\Pi$ state, radiative and radiationless vibronic deactivation rates with He 79−10134
$^{12}C^{16}O$, in Ar matrix, vibr. population time evolution temp. depend., master eqn. 78−9180
$^{12}C^{16}O$, near UV emission bands of fourth positive system, vibr. and rot. anal. 77−58054
$^{12}C^{18}O$ 78−82768
$^{12}C^{18}O$, $A^1\pi$-$X^1\sigma^+$(13,0) band, monochromatic excitation 78−82767
$^{13}C^{16}O$, fluoresc. and electronic quenching cross sections 78−82768
CO-NO mixtures, Ar matrix isolation, laser-included vibr. fluoresc. 80−9707
CO+ perfluoroalkyl halide, collisional relax 79−13799
$CO+{}^{14}N_2$ ($^{14}N^{15}N$),($^{15}N_2$), vibr. energy transfer, laser fluoresc. obs. 80−28050
$CO+{}^3He(^4He)$, vibr. relax., deactivation rates, pulsed fluoresc. meas. 79−89698
CO+CO, $d^3\Delta$ state vibr. relax. in glow discharges 79−18271
$CO+CO_2$, vibr. level depend. quenching of CO(v=1-16) 80−32808
CO+inert gas, collision-induced intersystem crossing mechanism 78−74689
$CO+Kr(^3P_1)(^1P_1)$ $A^1\Pi$-$X^1\Sigma^+$ and $b^3\Sigma^+$-$a^3\Pi$ sensitised fluorescence, isotope effects 78−82761
$^{12}C^{16}O+{}^{13}C^{16}C$, vibr. energy transfer, laser-induced fluoresc. obs. 80−78690
CO_2 (00°1) vibr. relax. in H_2 and D_2 below room temp., fluoresc. decay obs. 77−42381
CO_2, (001)→(000) fluorescence following dye laser photolysis of s-tetrazine 78−88652
CO_2, anomalous Zeeman effect, nonlinear optical techniques, book contrib. 78−9279
CO_2, antisymmetric vibr., energy relax. rate, rel. to IR luminesc. kinetics *(Russian)* 78−82826
CO_2 antisymmetric vibr. mode relax. rate, luminesc. meas 79−94067
CO_2, collisional laser-induced vib. excitation 77−27155
CO_2 gas, electron impact ionisation, electronic fluoresc. spectra 80−95664
CO_2, IR laser induced fluoresc. as spectroscopic probe 79−89704
CO_2 IR Zeeman spectra utilizing copropag. wave reson., diamag. shift obs. 80−53055
CO_2 laser, IR luminesc. of active layer *(Russian)* 79−31862
CO_2, laser excited, dealignment relaxation meas. by fluorescence 78−25587
CO_2, laser-induced fluoresc. obs. of N_2*+$H_2O(H_2S)$(methane) deactivation 80−63776
CO_2, spontaneous emission probabilities and collisional broadening of 00^01-10^00 lines 77−23649
CO_2 vibr. luminesc., excited by DC discharge, rot. and vibr. mol. consts. 78−58867
CO_2, vibr.-rot. transitions power broadening by laser irrad. 77−3420
CO_2^+, electronically excited states emission, $A^2\pi_u$ state bending vibrs. 77−3454
CO_2^+, fluoresc. quantum yields, isotope effects, photon-photoion coincidence meas. 78−90200
CO_2^+, laser excitation spectra, $A^2\Pi_u \rightarrow X^2\Pi_g$ fluoresc., rot. struct. 78−1019
CO_2^+, radiative lifetimes, threshold electron-phonon coincidence meas. 78−13550
CO_2+ perfluoroalkyl halide, collisional relax 79−13799
CO_2+CO(Ar), bending vibr. mode deactivation rate meas., 150 to 1500K 77−10738
CO_2+deuteromethane, time resolved fluoresc. for vibr. relax 79−31659
CO_2+H_2, vibr. de-excitation of $CO_2^*(v_3)$, 200K 79−45802
CO_2+HCl, vibr. relax., 300-900K, by laser fluoresc. 79−31658
$CO_2+He^+(H_2^+)$, charge transfer, energy transfer, product ion excitation and fluoresc. 77−75288
CO_2+hydrocarbon in mixtures, vibr. energy transfer, laser induced fluoresc. obs. 78−58731
CO_2+N_2, vibr. energy transfer, time-resolved laser induced fluorescence 78−29842
CO_2+polyatomic molecule, (00^01) mode deactivation, laser induced fluoresc. obs. 80−83453
$C_2O+NO(O_2)$(isobutene), absolute reaction rate consts. meas. by laser induced fluoresc. 80−93738
COF_2, laser excited IR fluoresc. C=O and C-F stretching modes 78−21960
CO* prod. from Ar*+CO_2, use in laser systems 80−63824
CO_2*+SO_2, near-reson. energy transfer, fluoresc. obs. 80−106348
CO($d^3\Delta_i$-$X^1\Sigma^+$) fluoresc. from CO_2 photodissoc. 77−6836
CS, $A^1\Pi(v=0)$, radiative lifetimes and quenching rates, laser-induced fluoresc. obs. 79−59496
CS, prompt emission and internal energy distrib. of $X^1\Sigma^+$ state 80−106364
CS^+, red emission spectrum, rot. anal. and perturbation effects 78−55193
CS+He, Penning ionisation, $CS^+(B^2\Sigma^+ \rightarrow A^2\Pi_i)$ fluoresc., flowing afterglow 80−14197
CS_2, fluoresc. from third excited singlet state 79−22749
CS_2, fluorescence due to laser excitation, Hanle effect 78−25628
CS_2, laser excited fluoresc., time and freq. resolution, assignments 77−14476
CS_2, laser fluoresc., discrete and continuum, time and freq. resolved obs. 79−41195
CS_2, mag. quenching of fluoresc. 79−31582

molecular fluorescence continued
CS_2^+, matrix isolated, laser induced fluorescence spectrum 79−50068
CS_2 + Ar*, Penning ionisation and dissoc. fluoresc, collisional energy depend. 78−33584
$^1C^{16}O$, $A^1\pi$-$X^1\sigma^+$ (13,0) band, monochromatic excitation 78−82767
$C^{17}O$ in Ar matrix, vibr. level energy cascades 77−79598
Ca + CCl_4→CaCl + CCl_3 reaction, laser-induced fluoresc. obs. 80−11916
Ca + NaCl, crossed beam reaction, collision complex lifetime internal state depend. fluoresc. 77−56217
Ca_2, $A^1\Sigma_u^+$-$X\Sigma_g^+$ system, laser induced fluoresc., pot. energy curve and mol. consts. 80−58307
Ca_2, in Kr matrix, 1- and 2-photon fluoresc. excitation 78−50567
Ca_2, laser-excited fluorescence in inert gas matrices 78−94273
Ca_2, new ground state, photolum. obs. vibr. consts., dissoc. energy 80−5576
Ca_2, van der Waals mol., in Kr matrix, absorpt. and emission spectra 77−83611
CaCl, $B^2\Sigma^+$-$X^2\Sigma^+$ system, laser excitation spectroscopy, rot. anal. 77−65500
CaCl, free radical, $A^2\Pi$-$X^2\Sigma^+$ system obs. by saturation spectroscopy 78−46353
CaCl, laser excitation and fluorescence spectra, rotational anal. of $A^2\Pi$−$X^2\Sigma$ transition 80−43098
CaF, $A^2\Pi_r$-$X^2\Sigma$ band system, MODR 78−74685
CaF, $A^2\Pi$-$X^2\Sigma^+$ transition, HFS and fine struct., intermodulated fluoresc. spectra obs. 80−63695
CaF, $B^2\Sigma^+$-$X^2\Sigma^+$ system, rot. and vibr. anal. 80−74156
CaOH, in flames real time fluoresc. spectra, CW tunable dye laser excited 79−3488
CaOH, laser excited, in an air-acetylene flame 78−86908
$C_2(a^3\Pi_u)$ + methane(acetylene)(ethylene)(ethane)(O_2), reaction rate consts. and quenching, multiphoton UV photolysis, fluoresc. obs. 79−74355
$C_2(a^3\Pi_u)$ + NO(vinyl cyanide)(ethylene), laser-generated radical kinetics 79−100352
Cd_2,(Cd_3), fluoresc. kinetics, optical excitation, energy spacings and equilib. consts. 80−43090
CdH, lifetime, Λ-doubling, hyperfine struct., in $A^2\Pi$ excited states 77−58083
CdHg, excimer kinetics and transmission meas. 80−37832
CdHg excimer system, absorpt. meas. 80−48007
CdHg, fluoresc. kinetics, optical excitation, energy spacings and equilib. consts. 80−43090
CdI_2, vapour, excited by photodissociation, fluoresc. yields 78−55138
Cd_2* excimer, fluoresc. band shape, decay rates 78−70866
CeO, C_1-X_1 and D_3-X_3 systems, fluoresc., vibr. spectra, laser spectroscopy obs. 80−32761
Cl + methane→HCl + CH_3, absolute reaction rate, flash photolysis-reson. fluoresc. obs. 77−56222
Cl + NOCl, primary and secondary photochemistry, vibrationally excited NO, IR fluoresc. obs. 80−48030
Cl_2, and isotopic forms, $B^3\Pi(0_u^+)$ state, laser-induced fluoresc., collisional energy transfer rates 80−53038
Cl_2, B-X transition, predissoc., laser-induced fluoresc. obs. 80−43093
Cl_2, B-X transition, rotationally resolved excitation spectra and predissociation in excited state 79−45754
Cl_2, fluoresc. quenching by collision-induced predissoc. 77−14472
Cl_2, laser-induced fluoresc., excited $B^3\Pi(O_u^+)$ states, collision-free lifetimes of ro-vibr. levels 79−94029
Cl_2, resonance fluoresc. by Ar ion laser excitation 78−42122
ClCF, radical in Ar matrix, vibr. relax., multiphonon processes, fluoresc. 77−65430
ClCN, vacuum UV photodissociation spectroscopy, quantum yield, fluoresc. polarisation 80−32736
Cl_2CS, excitation, singlet and triplet states, two photon absorpt., singlet-singlet energy pooling, fluoresc. obs. 80−48032
Cl_2CS, fluoresc. decay from second excited singlet state 78−25600
ClF, interhalogen UV laser on 285 nm band, fluoresc. and laser oscill. obs. 79−76674
ClF UV laser system 80−83597
ClFCS, second excited singlet state fluoresc., spectra 79−6957
ClFCS, second excited singlet state photophysics, laser excitation obs. 80−32758
ClO, laser excited fluoresc. 79−50077
Cl(^{2}P) + CH_4→CH_3 + HCl, reaction rate const., laser flash photolysis-resonance fluoresc. kinetic study 80−45485
Cl($3p^5(^2P_{1/2})$) + carbon tetrachloride (Cl_2)(He), VUV metastable state quenching, absolute rate const. 77−79641
Cn free radical, $B^2\Sigma^+$ state lifetime, photon-photon cascade meas. 78−5273
Co, fluoresc. of interstate intramol. perturbations 79−41194
CrO, $A^3\Pi$-$X^5\Pi$ transition, rot. anal. laser induced fluoresc. and discharge emission spectra 80−69173
CrO, in flames real time fluoresc. spectra, CW tunable dye laser excited 79−3488
CrO_2Cl_2, collisionless IR multiphoton production of electronically excited parent mols. 79−41211
CrO_2Cl_2, fluoresc. excitation spectrum, free jet expansion cooling effects 79−3473
CrO_2Cl_2, inert gas matrices, IR spectra, emission spectra, photoselection 77−14443
CrO_2Cl_2, multiphoton induced inverse electronic relax. 80−66836
CrO_2Cl_2, single vibronic level fluoresc. 77−3408
Cs-H_2 vapour, resonant character of laser induced formation of particles 80−89481
Cs-Xe molecular bands, time-resolved fluoresc., lifetimes 77−58068
Cs + Cs→Cs_2, inelastic light scatt. processes and mol. fluoresc. *(Russian)* 77−61787
Cs_2, fluoresc. at 6270 Å, rot. consts. 79−45744
Cs_2, fluoresc. spectra, kinetics, laser candidate 79−64027
Cs_2, fluoresc. spectra induced by laser, energy transfer and dissoc. 79−98141
Cs_2, ground state consts., pot. curve, laser spectroscopy 79−98247
Cs_2, He-Ne 632.8 nm radiation-induced disintegration 79−76474
Cs_2, laser-excited cross IR fluoresc. emission 79−76459
Cs_2, laser-excited fluoresc. in Cs-Xe mixture, pumping, level scheme 78−86909
Cs_2, laser-induced fluoresc. spectrum, diffuse band anal. 80−106346
CsXe excimer, laser-excited fluoresc. in Cs-Xe mixture, pumping, level scheme 78−86909
CsXe excimer laser, form. and dissociation rates, fluoresc. meas. 78−1216

molecular fluorescence continued
CsXe + Xe, time resolved fluoresc. decay and collisional transition rates 77−27111
Cu^{2+}-1,5-dimethyl-2,4-hexadiene, fluoresc. quenching method for determ. binding const. 80−89530
Cu_2, fluoresc., A-X system, rot. consts. *(French)* 78−33544
CuCl, Bose-Einstein condensation of biexcitons 79−56138
Cu(II) protoporphyrin IX dimethyl ester, fluoresc. relax. after picosec. excitation 79−45751
CuO, fluoresc., matrix isolation spectra 78−46381
D_2, Lyman bands, Morse Franck-Condon factors and R-centroids 77−58088
D_2, Rydberg state predissoc., Lyman and Balmer emission obs. 77−38702
DCl, matrix isolated, vibr. relax., IR fluoresc. obs. 79−45749
DCl + Cl(Br), vibr. relax. times, laser induced fluoresc. 77−27159
DF + $D_2(H_2)(N_2)$(HF)(CO_2), vibr. relax., laser-induced fluoresc. obs. 79−64028
D_2O, polarised photofluoresc. excitation spectra, VUV photodissoc. excited state lifetimes 78−5261
D_2O, vibr. relax. rates 80−95717
4-dimethyl-amino-4′-nitrostilbene, fluoresc. emission anisotropy, solvent effects 79−3489
$ErCl_3(AlCl_3)_x$, vap. complexes, absorpt. spectra, 6000-44000 cm^{-1}, relax. props. 78−62799
Eu chelate, fluoresc. lifetime, depend. on optical environment 80−9630
Eu compounds tetrahedral, ligand struct., rel. to luminesc. spectra satellite intensity *(Russian)* 78−72603
F + $CH_3I(CF_3I)(ICl)$ reactions, product state analysis using laser-induced fluoresc. 80−11915
F + $H_2(D_2)$, absolute reaction rate coeffs., time resolved IR emission meas. 79−68258
F + HCl(HBr)(DBr)(HI), H abstraction reactions, temp. depend., laser photolysis IR fluoresc. obs. 80−93744
F_2 UV laser system 80−83597
p-fluorobenzaldehyde, vap., high-resolution electronic emission spectrum assignments 78−78742
GeF, $A^2\Sigma^+$ state, time-resolved fluoresc. 78−58732
GeF, use in chemical lasers 80−64004
H-bond complex formation, enthalpy change due to electronic excitation, spectroscopic determ. 78−92496
H^+ + NO, ∼10 eV, anomalous excitation of NO Rydberg states 77−14546
H^+ + O_2, energy transfer, vibronic excitation, emission spectra 78−66578
H_2, $^3\Sigma_g^+$→b $^3\Sigma_u^+$ light emission meas. by electron impact excitation 78−33618
H_2, $B^1\Sigma_u^+$ state, selectively excited continuous vac. UV emission obs. 79−13667
H_2, density meas. by resonance fluoresc. ($X^1\Sigma_g^+$→$B^1\Sigma_u^+$ transition) 80−5570
H_2, $E,F^1\Sigma_g^+$ state, collisional and radiative props. 80−58357
H_2, electron impact, excitation of $G^1\Sigma_g^+$ state, emission cross-section meas. 78−37755
H_2, electron irrad., emission cross-sections for $3p^3\Pi_u$→$2s^3\Sigma_g^+$ 77−3477
H_2, electronic excitation, mol. thermal strength depend. 77−46595
H_2, lifetimes of $3d^1\Sigma$(3D) and $3d^1\Pi$(3E) excited levels *(Spanish)* 77−71833
H_2, liq., vibr. energy transfer, isotopic impurities, relax. 79−6993
H_2, Lyman bands, Morse Frank-Condon factors and R-centroids 77−58088
H_2, radiation polarisation, electron-impact excited, Lyman and Werner emissions and Lyman-α 79−36681
H_2, reson. fluoresc. with Lyman α, astronomical appls. 79−8821
H_2, Rydberg state predissoc., Lyman and Balmer emission obs. 77−38702
H_2 singlet superexcited levels, radiative emission 80−83415
H_2, superluminescence in surface discharge *(Russian)* 78−37676
H_2, two-photon spectroscopy with tunable ArF laser 80−37843
H_2, vibr. population relax. in gas and fluid 80−29775
H_2^+, ion-surface collision with Mo, optical radiation emission 78−95644
H_2 + Ar, near-reson. energy transfer, fluoresc. excitation 78−9187
H_2 + $D_2(N_2)$(HCl)(CO_2), V-V transfer, pulsed fluoresc. obs. 77−14540
H_2 + D(O)(Cl)(Br), relax. and chem. reaction, time resolved IR fluoresc. and mass spectrometry obs. 80−69177
H_2 + Hd, vibr. energy transfer rates, IR fluoresc. meas. 79−98145
H_3^+, ion-surface collision with Mo, optical radiation emission 78−95644
HBr, electronic to vibr. energy transfer from excited halogen atoms, IR fluoresc. 78−63113
HBr + Br, vibr. relax. times, laser induced fluoresc. 77−27159
HCN (A^1A''→$X^1\Sigma^+$), fluoresc. spectrum, using ArF laser excitation 79−36675
HCN, (001)→(000) fluorescence following dye laser photolysis of s-tetrazine 78−88652
HCN + Br_2(Ar)(HCN), electronic-vibr. energy transfer, Br($4^2P_{1/2}$) quenching and HCN (001) deactivation, fluoresc. obs. 77−518
HCN + HF(DF)(H_2), vib. energy transfer, laser-induced fluoresc. 77−58139
HCl, electronic to vibr. energy transfer from excited halogen atoms, IR fluoresc. 78−63113
HCl, matrix isolated, vibr. relax., IR fluoresc. obs. 79−45749
HCl-Br_2-Ar, flash photolytically produced Br* to HCl electronic to vibr. and rot. energy transfer 80−48069
HCl + Br, IR fluoresc. studies of state-selected energy transfer, photochemistry 77−77768
HCl + CO_2, vibr. relax., 300-900K, by laser fluoresc. 79−31658
HCl + D(O)(Cl)(Br), relax. and chem. reaction, time resolved IR fluoresc. and mass spectrometry obs. 80−69177
HCl + HCl-SF_6, nonequilib. rot. distrib. relax., fluoresc. obs. 79−36673
HCl + N_2O, vibr. relax., 300-900K, by laser fluoresc. 79−31658
HCl(ν=1,2) + O(^3P_g), reaction and deactivation, laser-induced fluoresc. obs. 78−35669
HD, Lyman bands, Morse Franck-Condon factors and R-centroids 77−58088
H(D)CN(C^1A')→H(D) + CN($B^2\Sigma^+$), polarisation, predissociation, photofragment excitation spectra measurement 79−45777
HD($^1\Sigma_u^+$) + He, fluoresc. quenching and energy transfer processes 79−86032
H_2($E,F^1\Sigma_g^+$), two-photon excitation, cross section, radiative lifetime, quenching rate, IR fluoresc. obs. 78−37698
HF (v=2, 3), vib. deactivation by H atom 77−58142
HF, collisional rot. relax. probability model 77−83697

molecular fluorescence continued
HF, electron impact excitation, dissoc., emission spectrum 78−90305
HF, time resolved fluoresc., IR energy deposition in laser irradiated SF_6-H_2 mixture 80−23454
HF, vibr. fluoresc. from SF_6H_2 collisionless multiple photon absorpt. photodissoc. 77−58099
HF-Ar mixture; HF rotational relax., laser IR fluoresc. 77−83634
HF+Ar, rot. relax. of high rot. levels at 1 torr press. 79−10181
HF+H_2(HCl)(N_2)(O_2)(CO_2) vibrs. relax., laser fluoresc. obs. 77−14484
HF+H_2(N_2)(CO_2)(O_2)(HCl), vibr. relax. laser induced fluoresc. obs. 79−64037
HF+HF (methane)(methane-d_4), collision relaxation rate constants and rot. equilibration time meas. 80−69213
HF+HF(H_2)(D_2)(CO_2)(isobutene), vibr. relax. dye laser pumping effects 80−9703
HF+I*($5^2P_{1/2}$), electronic-vibr. energy transfer fluoresc. decay meas. 77−71846
HF+O_2($a^1\Delta_g$), E-V energy transfer 77−30960
HF($v_1=1$)+HF($v_2=0$), vibrational relaxation temperature dependence, laser-induced fluorescence simulation 79−50069
HI containing radioactive ^{124}I, ^{126}I, nucl. reson. fluoresc. in ^{124}Te, ^{126}Te obs. 77−2953
HN_3, UV photolysis 80−101027
HNO, vibronic state perturbative and predissoc. mechanisms, fluoresc. excitation spectra obs. 80−9658
HNO(A^1A''), state-selected fluoresc. lifetimes, collisional quenching rates 79−36674
HO, detection by laser excited fluoresc., press. depend. of fluoresc. and photolytic interferences 80−95666
HO radical form. from H_2+N_2O reaction on Pt surface, laser-induced fluoresc. obs. 80−108738
H_2O, dissociative excitation by electron impact, Born approx., emission cross sections *(Japanese)* 77−42425
H_2O, dissociative excitation by electron impact, Glauber approx. *(Japanese)* 77−42426
H_2O, photodissociation, atomic hydrogen Lyman-α, Balmer series 79−45775
H_2O, polarised photofluoresc. excitation spectra, excited state lifetimes, VUV photodissoc. 78−5261
H_2O, Pt catalytic oxidation of H_2 and D_2, matrix isolation and laser fluoresc. obs. of prods. 80−66865
H_2O vertical distrib. in stratosphere, UV fluorescence meas. 79−34891
$H_2{}^{18}O$, vibr. relax. rate consts., fluoresc. method determ. 78−17762
H_2O+Ar($^3P_{2,0}$), dissociative fluorescence in crossed mol. beams, energy depend. 79−52669
H_2O+H_2O(He)(Ar)(N_2)(O_2)(CO_2), vibr. energy transfer temp. depend. 80−63763
H_2*+H_2, van der Waals mols., mol. fluoresc., vibr. predissoc. model 78−42120
H_2($a^3\Sigma_g^+ \rightarrow b^3\Sigma_u^+$) continuum emission excited by low-energy Ar^+ collisions, UV laser appl. 79−41200
HbBr($B^3\Sigma^+_{1/2}$), rate coeffs. for collisional quenching, time resolved emission obs. 79−89705
He-benzene, van der Waals, complexes, $^1B_{2u}(\pi\pi^*)$-$^1A_{1g}(6_0^1)$ band, in supersonic jet, rot. anal. 79−31578
He-N_2, de excitation rate consts., energy transfer, pulse radiolysis obs. 80−30303
He-N_2 plasma, N_2 $B^3\Pi_g$ state excitation, role of long lived states, luminesc. 80−37829
He+LiH, rot. inelastic collisions, state-to-state cross sections determ. 80−87210
He^++N_2, collisional excitation processes, visible emission, cross-sections 80−99571
He^++N_2, low energy collisions, vibronic excitation model 77−83689
He_2, 600 Å emission continuum 80−1012
He_2, collisional electronic and rot. relax. in afterglow of pulsed discharge 77−61784
He_2, electronic and rot. energy relax., reactive collisions by isotope selective excitation 78−33541
He_2, metastable states, laser excitation spectra 80−5578
HeI_2, rot. fluoresc. spectra, nonlinear equilib. struct. 78−37672
$HeNO_2$ van der Waals complex, fluoresc. spectrum 77−46591
Hg II halides, electron impact dissoc., excited fragment emission 79−18296
Hg-Xe(Kr)(Ar), fluoresc. emission, high press., electron beam excitation, laser appl. 77−34676
Hg_2, absorpt., fluoresc. and two-photon spectroscopy 78−998
Hg_2, dissociative recomb. and optical transmissions meas. in high press. discharge 80−37816
Hg_2, emission and form. kinetics, sequential two-photon absorpt. expt. 80−32767
Hg_2, excimer fluorescence, electron beam and optically produced systems 77 27107
Hg_2 excimers, photoassoc., spectroscopy and kinetic processes of high-lying vibronic states, laser applics. 80−9649
Hg_2, fluoresc. and absorpt. spectra-anal., pot. energy curves 78−999
Hg_2, fluoresc. decay, 335 and 485 nm 78−46387
Hg_2, fluoresc. decay of 1_u state 78−70864
Hg_2, optical pumping, continuous emission obs. 78−5296
Hg_2, photoassoc., $0_u^+ \rightarrow 0_g^+$ fluoresc., Condon internal diffraction 78−78747
HgBr emission intensity, $HgBr_2$ dissociative excitation by inert gas and N_2 metastables 80−40687
HgBr, green luminesc. and stimulated emission, prolonged optical pumping of $HgBr_2$ 79−18414
HgBr, laser photolysis prep., laser induced fluoresc., collisional quenching processes 80−38014
HgBr laser using dissociative excitation of $HgBr_2$, extraction efficiency increased by N_2 addition 80−38012
HgBr, polarised photofluoresc. spectroscopy, $HgBr_2$ photodissociation by ArF laser 80−37841
HgBr+O_2(N_2)(H_2)(He)(Ne)(Ar)(Kr)(Xe), vibr. relax., rate coeffs., fluoresc. obs. 80−63697
$HgBr_2$, photofragment fluoresc. polarisation, press. depend. 80−63720
$HgBr_2$+ inert gas metastable atom ($N_2(A^3\Sigma_u^+)$), dissoc. excitation 80−63774
$HgBr_2$+N_2*, dissociative excitation, mol. fluoresc. obs. 80−91634
HgBr(B→X) radiative lifetime, laser induced fluorescence 77−30900
HgBr*, collisional quenching by inert gas (molecule) 80−42986
HgBr*, collisional quenching by inert gas (molecules) 80−43091
HgCl*, collisional quenching by inert gas (N_2) 80−42986

molecular fluorescence continued
HgCl*(B1/2), fluoresc., collisional quenching kinetics 78−94269
Hg_2(Hg_3), violet emission, formation and decay kinetics, luminesc. time resolved spectra 79−76464
HgI_2(Br_2), vapour, excited by photodissociation, fluoresc. yields 78−55138
HgI*, collisional quenching by inert gas (N_2) 80−43091
$HgNH_3$ complex, fluoresc., lifetime meas. 78−53193
$HgNH_3$*, excited complex photosensitised luminesc. and fluoresc. phase shifts 78−33535
HgTl excimer laser, kinetics, optical excitation obs. 80−58527
HgTl optically excited excimers, upper state kinetics 80−37831
HgXe, excited molecule formation 77−23519
HgXe, fluoresc. spectra, pot. curves and binding energy 78−66581
Hg(6^3P_0)+t-butylamine, attachment mechanism, kinetics, dimer emission, luminesc. spectra 77−73442
I_2, angular momentum transfer, elastic, inelastic collisions, orientation and polarised fluoresc. 78−90271
I_2, anomalous visible band effects near B state dissoc. limit 77−6816
I_2, B state, fluorescence yield, individual hyperfine components 77−68067
I_2, B-X fluoresc. band system, intensity and relative band strengths meas. 80−102540
I_2, B-X system superfluoresc. emission obs., 1.1 to 1.3 μm 79−81412
I_2, $B^3\pi_{0_u^+}$ state deactivation efficiency, temp. depend. 78−70869
I_2, blue-green fluoresc., ArF laser excitation 80−14166
I_2, CW intracavity dye laser spectroscopy 80−13155
I_2, coherent optical transients and optical dephasing in mol. collisions 80−9966
I_2 containing radioactive ^{124}I, ^{126}I, nucl. reson. fluoresc. in ^{124}Te, ^{126}Te obs. 77−2953
I_2, electronically excited states, vis. and UV laser techniques, book contrib. 78−9277
I_2, excited by circ. polaris. light, mol. collisions, emission depolaris. 78 33577
I_2, fluoresc. and quenching of 3400 Å 77−3398
I_2, fluoresc. in 340 nm band, buffer gas press. depend. 79−13762
I_2, fluorescence, CW dye laser emission wavelength locking by intracavity gain 80−99721
I_2, hyperfine struct. in B-X transition, laser spectroscopy of pure I_2 jet 79−81234
I_2, in CCl_4 (cyclohexane) soln., ps dye laser excitation, fluoresc. and resonance Raman emission 80−28021
I_2, in seeded supersonic beams, vibr. and rot. relax., laser-induced fluoresc. obs. 80−23522
I_2, laser fluoresc., relax. of oriented ground and excited mols. 78−46390
I_2, laser fluoresc., spectral assignments at 5145 Å 78−46389
I_2, laser fluoresc. state selected and detected mol. beam mag. reson., hyperfine transitions 80−63731
I_2 lines, Franck-Condon factors, Ar^+, Kr^+ and He-Ne laser excitation 80−58320
I_2 molecule, fluorescence decay study, dye laser appl. *(Japanese)* 77−58341
I_2, picosecond relax., fluoresc. spectroscopy, solvent effects 78−58737
I_2, polarisability anisotropy, laser assisted mol. beam spectroscopy 80−78646
I_2, predissociation, electric-field induced 80−37839
I_2, reson. fluoresc. obs. of rotationally inelastic collisions selection rules 77−58133
I_2, reson. Raman scatt., time delay 77−34641
I_2, time-resolved reson. Raman and reson. fluoresc., hyperfine splitting effects 77−30874
I_2, use as test mol. in modern spectroscopy, review 78−90317
I_2 vapour low conc. detect. by laser fluoresc. excitation 78−27871
I_2+Ar(Ne)(tetrafluoromethane), D-state lifetime and UV laser action 77−14471
I_2+I_2, collisional energy transfer, selection rules for elastic collisions 77−50467
$I_2+O_2 \rightarrow IO$, flash photolysis reaction mechanism 77−32813
I_2($B^3\pi_{0_u^+}$), ps excitation, in CCl_4 soln., ultrafast decay and spectrum 78−9184
IBr, $B^3\Pi(0^+)$ excited state, laser-induced fluoresc. 80−58309
IBr, $B^3\Pi(0^+)$ states, Franck-Condon factors, RKR turning pts. 77−34681
IBr, laser fluoresc. study of $B'O^+$-$X^1\Sigma^+$ system 78−70867
IBr($B^3\pi_{0^+}$), lifetimes determ. from time resolved fluoresc. 78−46385
ICN, vacuum UV photodissociation spectroscopy quantum yield, fluoresc. polarisation vacuum UV photodissociation spectroscopy, quantum yield, fluoresc. polarisation 80−32736
ICl, $B^3\Pi(0^+)$ states, Franck-Condon factors, RKR turning pts. 77−34681
ICl, $B^3\Pi(0^+)$-$X^1\Sigma^+$ fluoresc., predissoc. 77−34682
ICl, IF, fluoresc. decay lifetimes and quenching cross-sections for excited $B^3\Pi(0^+)$ states 78−1030
ICl, laser excited fluoresc. 79−50077
ICl, lifetimes of $A^3\Pi_1$ state vibr. levels, 6070-7300 Å 78−66605
ICl($A^3\Pi_{(1)}$), zero-press. lifetimes, fluoresc. quenching 79−68266
IF, $B^3\Pi(0^+)$, radiative and predissoc. lifetimes, laser-induced fluoresc. 79−31589
IF, $B^3\Pi(0^+)$ states, Franck-Condon factors, RKR turning pts. 77−34681
IF, $B^3\Pi(0^+)$-$X^1\Sigma^+$ fluoresc., predissoc. 77−34682
IF emission spectrum and form. kinetics in electron-beam-produced plasma 80−102533
IF internal vibr.-rot. product distrib., formed in F+$CH_3I(CF_3I)$, fluoresc. obs. 80−48078
IF, laser excited fluoresc. 79−50077
I_2He, Van der Waals mol., photodissoc. lifetime, I_2 vibr. depend. 79−6977
$I_2Ne_aHe_b$ van der Waals complexes photodissoc. 80−50864
$^{127}I_2$, $^{129}I_2$, $B^3\Pi 0_u^+$-$X^1\Sigma_g^+$ systems, fluoresc., mol. consts., Franck-Condon factors 77−34680
$^{127}I_2$, B-X electronic transition, systematic hyperfine struct. meas. 78−9267
$^{127}I_2$, Doppler-free optoacoustic spectroscopy 80−57396
$^{127}I_2$, hyperfine structure obs. in saturated fluoresc. 78−50569
$^{127}I_2$, rovibronic absorpt. lines, hyperfine struct. 80−78596
$^{127}I_2$, weak rot. R(98), 58−1 line, HFS struct., saturated intermodulation fluoresc. 79−94024
$^{129}I_2$, hyperfine struct., saturated fluoresc. obs. 79−31591
$^{129}I_2$ rovibronic absorpt. lines, hyperfine struct. 80−78596

molecular fluorescence continued
I* + $H_2O(D_2O)(HDO)$, $5^2P_{1/2}$ electronic to vibr. energy transfer, quenching and time resolved IR fluoresc. 79−3537
I* + I(Br)(Cl)(IBr)(ICl)(BrCl), collisional deactivation and reaction rate consts., obs. 78−80738
I_2* + He, low energy collisions, energy redistrib. 80−63765
I2 fluoresc., Ar^+ laser excited, high resolution and sub-Doppler Fourier transform spectroscopy 80−43089
I($5^2P_{1/2}$) + HCl(HBr)(NO), electronic-vibrational energy transfer, fluoresc. obs. 78−66579
InI, vapour, excited by photodissociation, fluoresc. yields 78−55138
InKr, low-lying electronic states, PE curves, transition moments, emission coeffs. 79−6894
$IrCl_6^{2-}$, electronic Raman spectra, available excitation lines 79−47437
K_2, absorpt. and relax. const. determ. by optical laser pumping method 80−102550
K_2, $B^1\Pi_u$ state lifetimes, Hanle effect 78−90218
K_2, $B^1\pi_u$ state radiative lifetime, quenching cross section, fluoresc., single photon counting 77−75202
K_2, formed by K atoms photorecombination, luminesc. spectrum *(Russian)* 79−3531
K_2, ground state thermalisation speed, collision cross-sections meas. *(Russian)* 80−78723
K_2, in discharge plasma, anomalous 5725 Å band, photorecomb. mechanism 79−50088
KMg, laser induced fluoresc. spectra 78−74692
KN_3, fluoresc. spectrum, 30K, vibronic and vibr. assignments 79−27023
KXe, dye laser induced emission, excimer bands and uses 80−9650
KXe, fluoresc. excitation and emission spectrum 79−6947
KXe_n exciplexes (n=1-4), visible emission bands 78−78746
K(5S)Xe, K(5S)Kr, excimer, visible emission band, exptl. results relative to theory 78−82779
Kr_2, prod. and decay of 0_u^+ and 1_u states, synchrotron excited 80−43109
KrCl, B and C states, energy ordering from temp. depend. of emission spectra 80−78837
KrCl*, excimer formation rate consts., B state radiative lifetimes, quenching, VUV excitation 80−55631
KrCl* + Xe, substitution efficiency during excitation in transverse AC electric discharge 80−50850
KrF discharge pumped laser, energy extraction, collisional coupling between B, C and D-states 80−28213
KrF, electron beam pumped laser medium, time depend. fluoresc. spectrum in high current density range 80−78842
KrF, electron quenching rate consts. meas. by fluoresc. anal., laser implications 80−32969
KrF, electronic states, ab initio CI calcs., spin-orbit coupling, pot. curves, dissoc. energy, dipole moments 77−38619
KrF, excimers, power superluminesc. in elec. discharge *(Russian)* 77−7621
KrF, fluoresc. spectrum, theoretical modelling using electronic potential curves 78−63086
KrF, Kr_2F, time depend. emission meas., Ar-Kr-F_2 laser mixture kinetics 80−32768
KrF laser, collisional coupling between B, C, D states from fluoresc. meas., influence on energy extraction 80−1189
KrF, laser, e-beam pumped Kr-F_2 mixtures, form. and quenching processes 78−42322
KrF linac-excited gas mixture, UV fluoresc. meas. 80−28216
Kr_2F, absorpt. in near UV wing of 410 nm band, fluoresc. efficiency 80−14323
KrF(B), excimer, collisional quenching rates, photolysis meas. 78−63066
KrF*, bound-free emission spectra, simulation 78−29806
KrF*, Kr_2F*, kinetics of proton-excited KrF_2 mixtures, time-resolved and time-integrated spectra 79−36883
KrF* laser, electron beam pumped, dominant formation and quenching processes 79−938
KrF*, three-body quenching by Ar and broad-band emission at 415 nm 77−75486
Kr_2F*, gain meas. at 4416 Å 78−50758
Kr_2F*, radiative lifetime and quenching rate consts. 78−63056
KrO, in doped inert gas matrix, photoluminesc. 79−31579
Kr_2*, form. and UV fluoresc. under monochromatic excitation and collision processes 78−9237
Kr_2*, radiative lifetime and quenching rate consts. 78−63056
LaO, fluoresc. spectra, atom+ROH O atom abstraction reactions, fluoresc. study 78−48643
Li_2, A-X band intensity distrib. Franck-Condon calcs. validity 77−65511
Li_2, $A^1\Sigma_u^+$ state, radiative lifetime 77−27104
Li_2, circular polarisation of emission, influence of nucl. hyperfine interactions and elastic collisions 80−9635
Li_2, collisional depolarisation and rot. energy transfer, laser-induced fluoresc. obs. 80−9698
Li_2, emission circ. polaris., hyperfine coherence and elastic collisions effect 79−3471
Li_2, spectroscopy and structure, triplet excimer continuum emission 80−32769
$^7Li_2$, $B^1\Pi_u$-$X^1\Sigma_g^+$ band system, absorpt. and laser fluoresc. spectra 79−68256
Li_2+inert gas, collision induced transition rate consts., two-laser spectrosc. 80−9629
Li_2+inert gas, energy and ag. momentum transfer, polarised laser fluoresc. obs. 79−31590
Li_2+Li, collisional depolaris. and rot. energy transfer, laser-induced fluoresc. 79−13794
LiH, state selected rot. transition integral cross section, laser fluoresc. obs. 80−63770
LiH+HCl(DCl), state-to-state rot. inelastic cross sections, new laser fluoresc. technique 79−98200
^{7}LiH+HCN, rot. inelastic collision, energy transfer 80−87211
Lu porphyrin complexes, luminesc. 77−18958
LuCl, visible emission spectra, detection and characteris. 79−6963
Mg_2, $A^1\Sigma_u^+$-$X^1\Sigma_g^+$ system Franck-Condon factors, J-depend., fluoresc. pot. and predissoc. 77−58067
Mg_2 $A^1\Sigma_u^+$-$X^1\Sigma_g^+$ system, discrete and continuous Franck Condon factors, J-depend. 78−66811
Mg_2 excimer system, laser induced fluoresc. 78−33548
MgO, $B^1\Sigma^+$-$X^1\Sigma^+$ and $B^1\Sigma^+$-$A^1\Pi$ fluoresc. 78−21963
MgO, in acetylene flame, mol. conc. meas. by laser saturation spectroscopy 79−29425
MgO, laser induced photoluminesc. spectra 78−82757
molecular fluorescence continued
MnO, in flames real time fluoresc. spectra, CW tunable dye laser excited 79−3488
$N^+ + H_2$ (hydrocarbons) rotational vibrational product excitations 79−47901
N_2,$E^3\Sigma_g^+$ state electron excitation, collisional deactivation and energy transfer 77−10774
N_2 ($C^3\Pi_u$) vibr. levels radiative lifetime, transition moment internucl. distance depend. 78−1027
N_2, $B^3\pi_g$ state excitation and deactivation in positive column 77−3482
N_2, $C^3\Pi_u$ excited state, lifetime determ. by phase-shift and delayed-coincidences methods 77−18988
N_2, desorbed after N atom recomb. on Fe, vibr. energy, electron beam induced fluoresc. 80−61149
N_2, electrical discharge excitation, vibr. level population distrib., electron beam fluoresc. obs. 80−48031
N_2, electron impact, absolute emission cross-sections meas., calibration appls. 79−85996
N_2, electronic states excitation and population in glow discharge 77−487
N_2, fission fragment excitation of optical radiation, quenching by UF_6 77−23665
N_2, fission fragment excitation, delayed coincidence spectroscopy 77−24189
N_2, fluoresc. efficiencies of electrons, 4900-10500 Å wavelength range 77−61870
N_2 gas, electron impact ionisation, electronic fluoresc. spectra 80−95664
N_2, molecular centre, in Ar matrix, vacuum UV luminesc., 8K 78−10958
N_2, N_2^+ auroral bands, airborne spectroscopic studies 77−29533
N_2 photostabilised UV laser, gain, fluoresc., and energy extraction characts. 79−7118
N_2 plasma, non-equilib., excited species, vibr.-rot. anal. fluoresc. obs. 80−54034
N_2, pulsed H^+ excitation, fluoresc. decay and press. depend. 77−14483
N_2, rarefied fluid dynamics, flow meas. by electron beam-body interactions 80−6186
N_2, rot. temp. meas., rocketborne electron beam fluoresc. meas., reflected mol. effects 77−29519
N_2^-, vibr. autodetaching states, from $H^- + H_2$, excitation and decay, Franck-Condon factors 78−33620
N_2^+, 3914 Å band emission, in $H^+(He^+)$ collisions, 0.5-34 keV 77−54598
N_2^+, 3914 Å band spectra, fluoresc. efficiency 79−81226
N_2^+, $B^2\Sigma_u^+$ excited state, lifetime determ. by phase-shift and delayed-coincidences methods 77−18988
N_2^+ emission, in N_2O-He afterglow 79−68251
N_2^+, emission in $Ne^+ + N_2O$ charge transfer excitation, down to 1 eV 79−45835
N_2^+, excitation in RF discharges *(French)* 77−61868
N_2^+, fission fragment excitation of optical radiation quenching by UF_6 77−23665
N_2^+, fluoresc. and production cross-sections by photoionis. of N_2 78−9204
N_2^+, fluoresc. quantum yields and lifetimes, meas. method, ion form. 77−6815
N_2^+, radiative lifetime of $B^2\Sigma_u^+$ state 78−90220
N_2^+, UV spectral line width in rarefied free jet, for rot. temp. 80−6184
N_2-CO, electrical discharge excitation, vibr. level population distrib., electron beam fluoresc. obs. 80−48031
N_2-CO-OCS, liq. mixture, vibr. energy relax. and exchange, laser induced fluoresc. obs. 78−70905
N_2+Ar, 0.06-0.41 eV, metastable at. electronic excitation transfer 79−64071
N_2+Ar, metastable atom excitation of $C^3\Pi_u$ state, symmetry, propensity rules and alternation intensity, rot. spectrum 80−87135
N_2+Ar, proton excited, time-resolved, VUV, UV and vis. photon emission 77−14547
N_2+Ar+POPOP, electron beam excited, energy transfer mechanisms 80−23497
N_2+Ar*(He*), sensitised fluoresc., vel. depend. 77−10744
N_2+C^+ collisions, luminesc. 80−1055
N_2+C^+(N^+)(O^+), luminescent charge transfer, metastable and ground state ions 78−42202
N_2+SF_6, pulsed H^+ excitation, fluoresc. decay and press. depend. 77−14483
N_2^++H^+, fluoresc. efficiency, 3914 Å band of N_2^+ (1N), 100 eV-10 MeV 78−74697
N_2^++He, low energy collisions, vibronic excitation model 77−83689
N_2^++He, N_2^+ selectively excited, collisional deactivation 80−83338
N_2^+($B^2\Sigma_u^+$), perturbation of v=1 vibr. level, rot. lines freqs. and intensities *(French)* 77−79640
ND radical, metastable $b^1\Sigma^+$ state, tunable laser fluoresc. obs. 79−22744
ND_3, Einstein A coeff. for A→X transition 77−27127
ND_3, Hg-photosensitised luminesc. at low press. 78−13542
NF+H(NF), electronically-excited free radical reactions 80−97707
NF_2+H(O)(N), electronically-excited free radical reactions 80−97707
N_2F_4, mol. photodissoc. using CO_2-laserradiation, rate const. meas., mol. fluoresc. and time-resolved UV spectra obs. *(German)* 80−83434
N_2F_4, multiphoton excitation and vibr. energy flow, fluoresc. obs. 80−95673
NH, $c^1\Pi$ state anomalous populations following NH_3 photodissoc. 79−10133
NH, laser-excited A-X system fluoresc. 79−50060
NH, ND, $d^1\Sigma^+$ state lifetimes, rot. struct., electron excited emission spectra 77−79654
NH radical formed in NH_3 dissoc., fluoresc. spectrum, rotational relaxation 80−58310
NH+O_2 energy transfer rate const., time-resolved fluoresc. rise 79−83489
NH_2 ($\tilde{A}^2A_1$), excited state dynamics and bimol. quenching processes 80−9681
NH_2, ($\tilde{A}^2A_1$), fluoresc., form. by photolysis of $NH_3(\tilde{A}^1A_2'')$ 78−13547
NH_2 fragments, multiple photon dissoc. of CH_3NH_2 and NH_3, laser-excited fluoresc. obs. 80−11938
NH_2, microwave modulated saturation spectroscopy, hyperfine energy levels 79−68245
NH_2, vibronic levels, excited by blue CW dye laser 78−86907
NH_2, $\tilde{X}^1B_1$ ground state, 010 level, mol. consts., emission spectra obs., 0.4-0.89 μ 78−74688
NH_2+NO_2, reaction rate const. meas. 80−7772

molecular fluorescence continued
NH_3, decay of saturation reson., IR ν_2 as Q(8,7) transition 78−25609
NH_3, Hg-photosensitised luminesc. at low press., isotope effects 78−13542
NH_3, IR multiphoton dissoc., laser fluoresc. and chemiluminesc. obs. 79−68276
NH_3, mol. alignment relax. rate, laser saturation reson. technique 78−25755
NH_3, photosensitisation by Hg, fluoresc. spectrum 78−90198
NH_3 remote atmospheric sensing by multiphoton sequential photodissociative excitation 79−48199
NH_3 solution, aqueous, by Nd laser radiation *(Russian)* 77−54753
NH_3+NH_3(He)(Ar)(N_2)(O_2), ν_2 state vibr. relax., laser induced vibr. fluoresc. obs. 79−18269
NH_3+NH_3(He)(Ar)(N_2)(O_2), vibr. energy transfer temp. depend. 80−63763
$NH(A^3\Pi, c^1\Pi)$ radicals, electron impact of NH_3, H_2NNH_2 and organic mols., emission spectra 77−83752
$NH_2(X^2B_1)$, laser-induced fluoresc. obs. in UV laser photodissoc. of NH_3 80−11901
$NH(X^3\Delta^-)$ radical, form., detect. and reactions 79−64036
NO, $3s\sigma(A^2\Sigma^+)$, in Ar Kr Xe matrices, Rydberg state 'bubbles', reson. fluoresc. obs. 77−83636
NO (v=1), vibr. fluoresc. detection of trifluoroformamide photodissoc. 78−74712
NO, $A^2\Sigma^+$ two-photon excitation, radiation lifetime, quenching 77−3426
NO, $a^4\Pi$ and $b^2\Sigma^-$ states, electron impact spectra 78−58733
NO, electron impact, absolute emission cross-sections meas., calibration appls. 79−85996
NO, electronic to vibr. energy transfer from excited halogen atoms, IR fluoresc. 78−63113
NO electronically excited photofragment of VUV photodissoc. methylnitrite, identification and quantum yield 80−99527
NO, fluoresc. spectra, $3s\sigma(A^2\Sigma^+)$ Rydberg state, vibr. relax. 79−13759
NO, gamma band emission rate factor, rel. to upper atm. comp. determ. 77−54572
NO, in Ar and N_2 matrices, 6K, vac. UV photolysis, β and M band emissions 78−73069
NO in rare gas matrix, radiationless processes in luminesc. spectra 79−36689
NO measurements in CH_4-O_2-N_2 flame by laser fluorescence 80−61178
NO, optical detection in air, gamma band fluoresc. *(German)* 77−60494
NO, photodissoc. at 184.9 nm, quantum yield, and quenching by N_2 78−80773
NO, simultaneous one- and two-photon spectroscopy, Λ-doubling, spin-rot. splitting 78−66560
NO, two-photon excitation to levels near and above the dissoc. limit 79−10161
NO, UV fluorescence, IR laser induced 80−53032
NO+Ne(Ar)(N_2)(H_2)(CO), $E^2\Sigma^+$ and $B'^2\Delta$ states fluoresc. collisional deactivation 79−6965
NO+O, vibr. relaxation of NO, laser induced IR fluoresc. study 80−9626
NO+O_3*, laser excitation effects, fluoresc. meas. 77−21372
NO^++NO_2^- neutralisation reaction, spectroscopic study 79−13819
NO_2, $^2B_1$ state fluoresc., bending vibr. progression 77−83638
NO_2, $^2B_2$ state, fluoresc. anomalous mag. depolaris. 78−21962
NO_2, $^2B_2$-state excitation, fluoresc. lifetime 77−61780
NO_2, A-X band system, visible absorption, fluoresc., vibronic coupling 77−58030
NO_2, coupling of vibronic states induced by messenger state 79−72226
NO_2, dissociative limit, mol. beam characts. determ. by fluoresc. excitation spectra 80−53074
NO_2 excited, fluoresc. spectrum, IR multiphoton vibr. pumping, photon absorpt. probability distrib. study 80−18854
NO_2, excited electronic states, time-resolved spectrosc. 79−45747
NO_2, fluoresc. excited by laser, spin-orbit effects 79−64030
NO_2, fluoresc. lifetime and quenching mechanism 79−89701
NO_2, fluoresc. quenching mechanism 78−25599
NO_2, fluoresc. quenching mechanism in mag. field 78−74696
NO_2, fluoresc. spectra and collisional quenching 80−102538
NO_2, fluoresc. spectra from selectively excited HFS levels 78−21961
NO_2, fluoresc. spectra near 5000 Å, rotationally-forbidden bands 77−79639
NO_2 fluorescence monitor with flashlamp pumping atm. tests 77−64443
NO_2, IR-optical double reson., fluoresc. obs., high-energy vibr. levels 78−55188
NO_2, inter and intramolecular radiationless transitions, relax., time resolved excitation and fluoresc. spectra 80−27966
NO_2, laser and flash lamp fluoresc. monitors, comparison 80−17367
NO_2, laser excited fluoresc. lifetime 79−50076
NO_2, laser fluoresc., $^2B_1$ vibronic states 77−27109
NO_2, laser-induced fluoresc. spectrum near 6125 Å 77−58069
NO_2, laser-induced fluoresc. quenching rate const. and lifetimes 80−11930
NO_2, mag. quenching of fluoresc. 79−31582
NO_2, perturbed $^2B_2$ state fluoresc. lifetime, excitation energy depend. 78−90202
NO_2, reson. fluoresc. excited by visible laser, force consts. of ^{15}N mol. 79−72343
NO_2, reson. Raman spectra, vibr.-rot. scatt. Q branch enhancement 78−989
NO_2, rot. cooled, vibronic band lifetimes, time resolved fluoresc. excitation spectra obs. 79−94025
NO_2, sub-Doppler spectra, laser-beam system, HFS excitation, radiative, non-radiative decay 78−90210
NO_2 transitions assigned using laser-induced fluorescence 79−98146
NO_2, vibr. excited, from nitroalkane photodissoc., fluoresc. obs. 78−37693
N_2O, anomalous Zeeman effect, nonlinear optical techniques, book contrib. 78−9279
N_2O, electron impact ionisation and dissociation, radiation emission 78−90304
N_2O gas, electron impact ionisation, electronic fluoresc. spectra 80−95664
N_2O, IR combination band spectral emissivity, 1200, 1700, 1900K, shock tube obs. 78−5287
N_2O, ionis. by low-energy electrons and near thermal inert gas ions, emission obs. 79−31707

molecular fluorescence continued
N_2O quadrupole hyperfine struct., vibr. depend. obs. using twin-laser spectrometer 80−43097
N_2O^+ emission, in N_2O-He afterglow 79−68251
N_2O^+, emission in Ne^++N_2O charge transfer excitation; down to 1 eV 79−45835
N_2O^+, fluoresc. and dissociation lifetimes of vibr. excited states 78−42108
N_2O^+, fluoresc. and production cross-sections by photoionis. of N_2O 78−9204
N_2O+deuteromethane, time resolved fluoresc. for vibr. relax 79−31659
N_2O+HCl, vibr. relax., 300-900K, by laser fluoresc. 79−31658
N_2O+SF_6, vibr.-vibr. energy transfer, fluoresc. 80−78688
N_2O+X^+, charge transfer excitation channels, emission cross-sections meas. 77−61851
NOCl, vibr. energy transfer, (001) level activation/deactivation rate consts. meas. 77−79677
NO($X^2\Pi$)+Cd($^1P_1$)→NO($A^2\Sigma^+$, v=0) electronic energy transfer react., collisional fluoresc. quenching 77−14548
NO($X^2\Pi$)+Zn($^1P_1$)→Zn($^1S_0$)+NO($A^2\Pi^+$, v=0,1), near-resonant electronic energy transfer, fluoresc. quenching 77−14549
NO*+NO, van der Waals mols. in mol. fluoresc., vibr. predissoc. model 78−42120
NO_2*, multiple IR photon fluoresc. excitation and dissoc., electronically excited 80−48050
α-NPO, two-photon fluoresc. 77−30896
$N_2(X^1\Sigma_g^+)$+Ar($^3P_{2,0}$)→Ar(^1S)+$N_2(C^3\Pi_u)$, sensitised fluoresc., vel. depend. 78−90204
$^{14}NH_3$, high power vibr.-rot. emission, optically pumped off reson. 77−7068
Na_2, A-X band intensity distrib., fluoresc. spectrum Franck-Condon calcs. validity 77−65511
Na_2, absorpt. and relax. const. determ. by optical laser pumping method 80−102550
Na_2, dimer, $B'\Pi_u$-$X'\Sigma_g^+$ band system obs. 78−62837
Na_2, form., collision-produced diffuse violet emission band obs. 79−27026
Na_2, form. by excited-unexcited atom collision, emission band 4160 to 4570 Å 77−88422
Na_2, ground state, vibr.-rot. relax., optical pumping transients obs. 80−28067
Na_2 in free jet expansion, internal-state distribution 80−83403
Na_2, laser excited, atomic and molecular fluorescence with long radiative decay times 80−27976
Na_2, laser induced, conversion rate determ. comparison with molecular nuclear spin relaxation 79−43568
Na_2 molecule, Doppler-free two-photon transitions, $^1\Sigma_g^+$ state 77−3427
Na_2, spectroscopy and structure, triplet excimer continuum emission 80−32769
Na_2 supersonic beam rovibronic level population, anal. by laser spectroscopy 80−43118
Na_2, TOF spectra, molecular beam diagnostics with internal state selection 78−86968
Na_2+Ar(Ne)(He), collision induced dissoc. rate, vibr. distrib. depend. 79−22791
Na_2+He, rot. transitions differential cross sections, laser fluoresc. meas. 80−63771
Na_2+He(Ne), rot. transitions, state-resolved differential cross-sections 78−62887
NaAr, ground and excited state pot. curves, dispersed fluoresc. spectrum 79−98140
NaH, $A^1\Sigma^+$ states radiative lifetime in HF discharge 77−6841
NaK, $^1\Pi$ state perturbations, circular polarisation fluoresc. meas. 79−76462
NaK, $a^3\Sigma^+$ state, laser induced fluorescence, $D^1\Pi$ to $a^3\Sigma^+$ transition, molecular constants, dissociation energies 79−98143
NaK, $a^3\Sigma^+$ state, $X^1\Sigma^+$ state, fluorescence, visible spectrum 79−98114
NaK dimer formed in supersonic beam, laser-induced emission 80−9636
NaK, laser induced D $^1\Pi$-$a^3\Sigma$ fluorescence, mol. vibr. 80−87160
NaK, laser-induced fluoresc. in supersonic nozzle beams 78−25593
NaK, mol. transition dipole moment, from laser-induced fluoresc. spectra 79−94034
NaNe, laser spectroscopy, interat. pot. curves 78−86871
$N_2(a'^1\Sigma_u^-)$ state radiative lifetime, VUV emission 79−18226
Na_2*, fluoresc. red continuum emission, atom-mol. energy transfer 80−43086
Na_2*+Xe, rot. energy transfer, level-to-level dynamics, laser fluoresc. obs. 79−64029
Na(4S)Xe, Na(4S)Kr, excimer, visible emission band, exptl. results relative to theory 78−82779
Nd complex, Nd(2,2,6,6-tetramethyl-3,5-heptanedione), vapours, excited-state kinetics and fusion laser media prospects 79−64243
$NdCl_3$-$AlCl_3$ vap. complexes, Nd^{3+}, $^4F_{3/2}$ level deactivation 77−61786
NdO, electronic spectrum, rotational struct. anal. 80−78643
Ne, metastable state ratio in fast beam, laser-induced fluoresc. obs. 79−54801
Ne-Ar-I_2, low electron beam excitation rates 79−86163
Ne-N_2, charge transfer kinetics, weak H^+ beam effects 78−9243
Ne+He(Ar)(Xe)(N_2)(CO_2), fluoresc. spectra, mol. bands, 0.1 to 6 atm., 3000-8200 Å 79−3394
Ne_2, emission continua in VUV, new oscill. struct. 79−54905
Ne_2^++e, in recombination afterglow, line intensity decay complex struct. 79−7503
NeF, low energy state pots. energy curves, fluores. and dipole moment 78−21991
Ne*+$Fe(CO)_5$, chemiionisation and chemiluminescence reactions, Penning ionisation and fluoresc. obs. 80−97689
Ni_2, A→X system, Ar matrix isolation fluoresc. spectrosc. obs. 80−9628
O in molecule, K-shell fluoresc. yield, statistical scaling 80−78644
O+CS_2→CS+SO, vibrational distribution of CS, laser-induced fluorescence meas. 80−71895
O+H_2S, ^3P-state, absolute reaction rate, flash photolysis reson. fluoresc. obs. 79−66283
O+saturated hydrocarbon, chem. reaction dynamics. OH prod. investig. 80−101016
O+saturated hydrocarbon→OH+alkyl radical, reaction dynamics, mol. beam-laser induced fluoresc. obs. 80−97695
O_2, $b^1\Sigma_g^+$ state excitation by 0.75-6 eV electrons 78−86958
O_2, fluoresc. efficiencies of electrons, 4900-10500 Å wavelength range 77−61870

molecular fluorescence continued
O_3 in chloroform and carbon tetrachloride solns., sensitized luminesc 80 - 32762
O_2, laser excited, quenching by CO_2, H_2O and I_2 80−99515
O_2, quenching of luminescence by porphyrins and metalloporphyrins 79−50058
O_2, singlet state radiative lifetime, perturbation-variation calc. 77−14496
O_2^+, $A^2\Pi_u \rightarrow X^2\pi_g$ and $b^4\Sigma_g^- \rightarrow a^4\Pi_u$ emissions by photoionis. of O_2 79−94041
O_2+fluoromethane, vibr. energy equilibration, IR laser fluoresc. 79−846
$O_2+O(^1S)$, collisional interaction products, reson. fluoresc. obs. 78−46423
$(O_3)_2$, struct., energy transfer, high resolution electronic spectra 78−25550
O_3, UV absorpt. spectra, IR laser induced changes 80−83385
O_3+NO, laser enhanced reaction, fluoresc. obs. 79−66285
OCS, vibr. energy transfer map 80−99560
OCSe, laser photolysis using ArF laser, Se*+OCSe and Se_2*+OCSe quenching rates 79−86050
OD, A-X system, relative transition probabilities 77−6860
OD, $A^2\Sigma^+ \rightarrow X^2\Pi_i$ radiation after dissociative excitation of D_2O 78−46455
OH, $(A^2\Sigma^+ \rightarrow X^2\pi)$ fluoresc. prod. by H_2O photodissoc., cross sections 78−25604
OH $(A^2\Sigma^+)+H_2(N_2)(Ar)$, collisionally induced population change rates, laser-induced fluoresc. obs. 78−5326
OH, A-X system, rot. transition probabilities 80−43027
OH $A^2\Sigma^+$ state, laser excited, vibr. energy transfer, flame thermometry appls. 80−58349
OH, $A^2\Sigma^+ \rightarrow X^2\Pi_i$ radiation after dissociative excitation of H_2O 78−46455
OH, collisionless form., rovibronic relax., reson. fluoresc. 78−68902
OH concentration in flame, local and instantaneous meas. by laser induced fluoresc. obs. *(French)* 79−15999
OH concentration profile in methane-air flames 80−35534
OH, fluoresc. lidar instrument for stratospheric temp. and press. determ. 79−80033
OH, high resolution emission spectrum in oxyacetylene flame, mol. vibr.-rot. consts. 77−3409
OH, in inert gas matrix, H-bonding and charge transfer, fluoresc. 78−25602
OH, internal state distrib., crossed mol. beam $H+NO_2$ reaction, laser-induced fluoresc. 77−4905
OH, laser induced fluorescence, preferential population of π^+ component of Λ doublet in $H+NO_2 \rightarrow OH+NO$ 78−31620
OH, laser induced fluoresc. spectrosc. for flame temperature meas. 80−90839
OH, produced in CH_3+O_2, 368K, rate const. upper limit 80−7771
OH, product state distrib. in $O+H_2$ reaction, laser photolysis-laser induced fluoresc. meas. 79−83446
OH, Pt catalytic oxidation of H_2 and D_2, matrix isolation and laser fluoresc. obs. of prods. 80−66865
OH, radiative lifetimes of $A^2\Sigma$ state and A-X Einstein coeffs. 79−36703
OH radical, matrix-isolated, from H_2 oxidation on Pt, laser diagnostics 80−5572
OH radical in premixed laminar methane-air flame, fluoresc. meas. of rot. temp. 79−80622
OH+CO(trichloroethane), reaction rate consts. and quenching kinetics, reson. fluoresc. obs. 79−72349
OH+dimethyl sulphide, flash photolysis reson. fluoresc. rate consts. determ., pollution aspects 78−95913
$OH+H_2O_2$, reaction rate const., 298K, flash photolysis-reson. fluoresc. obs. 79−57215
$OH+H_2O_2 \rightarrow HO_2+H_2O$, reaction rate consts., laser induced fluoresc. 80−101017
$OH+HO_2 \rightarrow H_2O+O_2$ reaction rate const. determ. by resonance fluoresc. 79−24730
OH+haloalkanes (haloalkenes), reaction kinetics in microwave discharge, reson. fluoresc. obs. 77−77744
OH+halomethane(haloethane), reaction rate consts., reson. fluoresc. meas. in discharge-flow system 79−72350
$OH+NO(NO_2)(O_2)$, $OH(v=1)$ relax., time resolved spectra 80−74240
$OH+OCS(CS_2)$, flash photolysis reson. fluoresc. rate consts. determ., global S cycle 78−95914
$OH(A^2\Sigma^+)$, form. from $H_2O+Kr(^3P_1)$, internal energy distrib. 79−10183
$OH(A^2\Sigma^+)+N_2(O_2)(H_2O)$(air), quenching rates and fluoresc. efficiency, rel. to atmosphere 80−14199
$OH(C^2\Sigma^+)$, prod. by water radiolysis, time-resolved emission, quenching rate consts. 79−10138
OH(OD), $A^2\Sigma^+$ state, vibrational energy transfer in collisions, rot. resolved fluoresc. 78−74742
$OH^+(OD^+)$, $A^3\Pi_i \rightarrow X^3\Sigma^-$ emission branching ratios, r-centroid depend. 77−6830
OH(v,N) bimodal rot. distrib. from $O(^1D_2)+NH_3$ 80−76501
O(Se)(S)+inert gas, ^1S-^1D collision-induced transitions 78−33588
$O_2(c^1\Sigma_u^-, C^3\Delta_u, A^3\Sigma_u^+)$ generation from at. recomb. in O_2-He afterglow, fluoresc. obs. 79−31576
$OsBr_6^{2-}$, electronic Raman spectra, available excitation lines 79−47437
OsO_4, isotope selective dissociation by IR radiation pulses, luminesc. intensity 77−83665
PH_2 radical, laser-induced fluoresc. 78−94277
PH_3, laser photolysis, PH and PH_2 radical excited states 79−16023
PO_4^{3-}, synchrotron radiation excited fluoresc., O K-emission spectrum, electronic struct. 77−42335
Pb_2, laser induced fluoresc. *(French)* 79−13760
PbF, laser-induced fluoresc. of $A^2\Sigma$ state, chem. laser eval. 79−81222
PbS, molecule, Ne matrix environment effects on vibronic emission systems 77−58070
PrO, 0-0 band in XVII system, hyperfine splitting, visible excitation spectra 80−28028
PtAl, form. in hollow cathode discharge, emission spectrum obs. 78−27819
PtD, form. in hollow cathode discharge, emission spectrum obs. 78−27819
PtH, form. in hollow cathode discharge, emission spectrum obs. 78−27819
PtO, form. in hollow cathode discharge, emission spectrum obs. 78−27819
$Rb+Rb \rightarrow Rb_2$, inelastic light scatt. processes and mol. fluoresc. *(Russian)* 77−61787

molecular fluorescence continued
Rb+Xe system, reson. fluoresc., quasimol. states *(Russian)* 79−85935
Rb_2, B-X system vibr. consts. from mag. rot. spectra 79−76530
Rb_2, mol. spectra, population inversion, high-power laser appls. 77−3406
Rb_2, $X^1\Sigma_g^+$ state, Raman spectra, fluoresc., vibr. energy 78−46345
$ReBr_6^{2-}$, IR luminesc. spectra 79−45745
Ru complex, Ru(II)-polypyridine, excited charge transfer states, multiple emissions 79−3468
Ru complex in PMMA matrix, mag. induced circular polarisation of emission meas. 78−58058
S+inert gas $(N_2)(H_2)$, rare gas sulphide S(^{1}S) emissions 78−82828
S_2, $B^3\Sigma_u^-$ state lifetime, fluoresc. decay rate meas. 77−42346
S_2, fluoresc. quenching by He, Ar, Xe, N_2, S_2, CF_4, C_2F_6, fluoresc. lifetimes 78−46386
S_2, in Ar matrix, fluoresc. and excitation spectra 78−94271
S_2, matrix-isolated, $B^3\Sigma_u^-$ predissoc., relax. processes 80−58329
S_x vapour, x=3 to 8, UV absorption and fluorescence spectros., vibrational constants of S_2 80−78631
$S_2(B^3\Sigma_u^-, v=4)+He(Ar)(Xe)$, collision-induced transfer rates 79−94062
SF_6, collisionless fluoresc., 16 μm, following laser pumping, vibr. quasicontinuum 78−42111
SF_6, collisionless intramol. vibr. relax., time-resolved spectra 78−82777
SF_6 gas, CO_2 TEA laser-excited, slow intermol. redistrib. of vibr. energy 80−53039
SF_6, IR multiphotonic excitation, depend. on cell geometry, mol. fluoresc. and decomp. obs. 80−83430
SF_6, multiphoton excited, IR fluoresc. spectrum meas. 80−37828
SF_6 rarefied gas, coherent emission in time-separated fields 79−36954
SF_6-SO_2-fluoromethane mixture, laser irrad., IR fluoresc. meas. of equilib. and vibr. temps. 78−82766
SO, laser excited fluoresc. 79−50077
SO^+ $(A^2\Pi$-$X^2\Pi_r)$ emission following $He^+ + SO_2$ afterglow reaction 80−95659
SO_2, atmospheric, fluoresc. monitoring using NO γ-bands 78−73121
SO_2, collisional quenching of $^3B_1$ state, 8-1300 torr 78−86906
SO_2, fluoresc. and photosensitised phosphoresc. of biacetyl, quenching and triplet theory transfer 78−25608
SO_2, IR multiphoton excitation and inverse electronic relax., mol. vibr. and fluoresc. 80−106349
SO_2, laser-induced phosphoresc.-excitation spectra of vibr. bands of $(^3B_1)$-$(X,^1A_1)$ transition 80−18879
SO_2, SVL fluoresc. spectra, multiple vibronic origins 77−14474
SO_2, SVL fluoresc. spectra, 293 to 307 nm region 77−14475
SO_2, single vibronic level fluoresc. spectra 80−91597
SO_2, UV absorpt. spectrum, triplet states, phosphoresc. lifetime 79−50042
SO_2, UV excitation spectra, mol. fluoresc. meas., mol. predissoc. obs. 80−83389
SO_2^+, $(B^2A_1 \rightarrow X^2A_1)$ fluoresc., Penning excitation, vibr. and bending freqs. 77−50507
SO_2^+ fluoresc. spectra, Penning ionis. collision with $He(2^3S)$ 79−13758
SO_2-$^{18}O_2$ mixtures, IR laser pumped, intermol. vibr. energy transfer dynamics obs. 80−87207
$SO_2+N_2(CO_2)(H_2O)$, collisional quenching of $^3B_1$ state, 8-1300 torr 78−86906
S_2O, UV excitation spectra, mol. fluoresc. meas. 80−83389
SO_3F, dye laser excitation of vibr. levels of upper electronic state, mol. fluoresc. meas. 80−83402
SO_3F, laser fluoresc. spectrum 80−28047
$Sc+O_2(NO)(SO_2)$, nascent product state distribs., laser fluoresc. detect. 78−7187
ScO, fluoresc. spectra, atom+ROH O atom abstraction reactions, fluoresc. study 78−48643
ScO, optical emission spectrum, wave functions and intensity factors, using effective Hamiltonian *(French)* 78−5114
Se_2, laser induced fluoresc. in inert gas matrix 80−87161
Se_2, photolytic dissoc. obs. using inert gas halide lasers 80−11935
$SeO_2+Ar(N_2)(CO_2)$, radiative lifetime and quenching rates 80−95685
$^{80}Se_2$, $B\ ^3\Sigma_u^-$ state, Lande factor meas., mol. perturbations 79−45756
SiF, $A^2\Sigma(v'=0)$ state, radiative lifetime meas. 77−27110
SiF, use in chemical lasers 80−64004
SiF_4, CO_2 laser irrad., collision induced dissociation, visible fluoresc. 78−66613
SiF_4, CO_2 laser-irrad., dissoc. product fluoresc., wavelength depend. 80−11900
SiF_4, interaction with strong IR field, instantaneous luminescence 79−18232
SiH, A state new predissociations, improved dissoc. energy value from rot. level lifetimes 79−3496
SiO, $d^1\Pi_i$-$b^3\Pi_r$ transition, 0-1 band rot. anal. 77−18961
Sn_2, in Ar matrix, absorpt., fluoresc. and reson. Raman spectra 80−95640
SnF, use in chemical lasers 80−64004
Sr_2 dimer, photoassoc., photoluminesc., collisional dissoc 80−58303
Sr_2, Van der Waals dimer, inert gas matrix-isolated, laser excited emission spectra 78−78744
SrOH, in flames real time fluoresc. spectra, CW tunable dye laser excited 79−3488
SrOH, laser excited, in an air-acetylene flame 78−86908
Sr(^{1}S,^{3}P)+ halogenated methane, laser induced fluoresc. 79−66270
T 79−45757
TF, spontaneous emission, Einstein coeffs. determ. using chem. laser 77−58073
Tb complex, Tb(2,2,6,6-tetramethyl-3,5-heptanedione), vapours, excited-state kinetics and fusion laser media prospects 79−64243
$TbCl_3$-$AlCl_3$, vap., high-energy laser medium props., for fusion ignition 78−63075
$TbCl_3$-$AlCl_3$ complex, fluoresc. spectrum and gas-phase lasing 77−83861
Te_2, $B0_u^+ - b^1\Sigma_g^+$ system, transition assignment, IR and visible spectra obs. 80−58298
Te_2, laser excited fluoresc. Fourier transform spectrosc. obs., isotope effects 79−59504
Te_2, laser induced fluoresc. in inert gas matrix 80−87161
Th porphyrin complexes, luminescence 77−18958
TiO, β-system, radiative lifetime determ. 77−58086
TiO, $C^3\Delta_3$-X^3D_3 α system, radiative lifetime meas. 78−55202
TiO, emission spectra in chemiluminesc. flames 77−38689
TiO, photoluminesc. of $\alpha(C^3\Delta$-$X^3\Delta)$ system in chemiluminesc. flames 77−38690
TlHg excimer, fluoresc. at 4590 and 6560 Å, possible laser action 77−6837

molecular fluorescence continued
TlI, vapour, excited by photodissociation, fluoresc. yields 78−55138
UF_6, electronically excited, laser-induced time-resolved emission, self-quenching 78−42114
UF_6, electronically excited, emission quenching by organic mols. 78−42115
UF_6, electronically excited, emission quenching by inorganic mols. 78−42116
UF_6, fission fragment excitation of optical radiation 77−23665
UF_6, fluoresc. lifetime, temp. depend. 77−58065
UF_6, gas, laser-induced fluoresc., A-X band 78−94275
UF_6 in Ar matrices, fluoresc. and Raman spectra, vibr. anal. 78−66585
UF_6, matrix isolated, laser fluoresc. spectrosc. at 12K 79−68253
UF_6, matrix isolated, vibronic fine struct. in fluoresc. spectrum 80−83406
UF_6, matrix isolation spectra and photolysis 79−50043
UF_6 molecule dissociation in two-frequency IR laser field 80−66855
UF_6, near UV fluoresc., quantum efficiency, decay time 77−61776
UF_6, photophysical props., laser study 80−28040
UF_6, strong UV-visible emission and weak ionisation induced by focused KrF laser 79−64034
UF_6, UV photophysics, energy balance through quantum efficiency meas. 80−9634
UF_6, visible fluoresc. obs., 374 and 270 nm excitation 79−3490
UF_6-H_2, near UV and visible excitation, quantum yield from photodissociation 80−35549
V (III) complex, alcoholic VCl_3 soln., fluoresc. and photoreduction 78−85177
Xe, condensed electron beam excited, exciton radiative lifetimes 80−6727
Xe-$Br_2(Cl_2)$(HCl) mixtures, low-press. excimer form. and quenching by e-beam excitation 79−50071
Xe_2 excimer laser, electron beam excitation, VUV fluoresc., lasing 80−87379
Xe_2, fluoresc. decay of O_u^+ and 1_u states, rad. decay consts. 79−86009
Xe_2, laser performance for atm. press. and microsecond electron beam excitation 80−28199
Xe_2, performance as photolytic driver at low electron beam excitation rates 80−32963
Xe_2, time and energy resolved fluorescence, radiative lifetime, collisional mixing, pulsed synchrotron radiation obs. 79−98136
Xe_2, time-resolved excitation using synchrotron radiation *(French)* 77−88483
Xe_2, VUV radn. emission, radiative lifetimes 79−27089
Xe_2^+ excimer form. in pulsed discharge, visible emission obs. 80−38754
XeBr, B and C states, energy ordering from temp. depend. of emission spectra 80−78837
XeBr, emission and form. kinetics, sequential two-photon absorpt. expt. 80−32767
XeCl avalanche discharge laser, D and B state coupling, population depletion 80−28214
XeCl, B and C states, energy ordering from temp. depend. of emission spectra 80−78837
XeCl, energy curves and transition moments 80−28210
XeCl laser, B→X, form. and quenching kinetics 80−74341
XeCl, relax. and quenching rate consts., emission spectra modelling 80−28211
XeCl*+Kr, substitution efficiency during excitation in transverse AC electric discharge 80−50850
XeF, (B,C) state prod. and kinetics, XeF_2 photolysis with VUV radiation 80−32975
XeF, B and C-state kinetics with self-sustained discharge pumping 80−28212
XeF, B- and C-state fluoresc. rel. to laser efficiency 79−41368
XeF, broadband emission origin 80−38007
XeF, C-state radiative lifetime meas. 77−46598
XeF, electron beam pumped laser, gain, fluoresc. and laser output at 351, 488 nm 80−28215
XeF, electron quenching rate consts. meas. by fluoresc. anal., laser implications 80−32969
XeF electron-beam-pumped laser, characts., 300-600K 80−78839
XeF, energy curves and transition moments 80−28210
XeF, energy ordering of excited states, rel. to fluoresc. and laser action 78−74887
XeF, excimers, power superluminesc. in elec. discharge *(Russian)* 77 7621
XeF, ground state dissoc. vibr. equilibrium 80−9652
XeF ground-state dynamics in laser discharge, fluoresc. from vibr. levels 79−18404
XeF, in Ar and Ne matrices, reson. fluoresc., ground $X^2\Sigma^+$ state pot. well 77−14482
XeF laser, photoionization-stabilised self-sustained, energy extraction efficiencies 79−41369
XeF laser performance, ground state population effect 80−63987
XeF laser using XeF_2 photodissociation, fluoresc. and laser performance 80−32976
XeF linac-excited gas mixture, UV fluoresc. meas. 80−28216
XeF, relax. and quenching rate consts., emission spectra modelling 80−28211
XeF, supersonic expansion jet, B←X system rot. and vibr. anal., isotope intervals, fluoresc. spectra 80−14174
XeF+He(Ne)(Xe)(F_2)(NF_3), radiative lifetime and collisional quenching kinetics 78−94289
XeF(B), fluoresc. and quenching rel. to XeF_2 vac. UV photolysis 77−58061
XeF* ($C_{1/2}$), radiative lifetime meas. 78−63087
XeF*, $B^2\Sigma^+$ and $C^2\Pi_{3/2}$ states, fluoresc. decay dynamics, collisional quenching and radiative lifetimes 80−58306
XeF*, formation by XeF_2+Ar(Kr)(Xe) metastable states reaction, mechanisms 77−30897
XeF*, lifetime and collisional quenching meas., XeF_2 photolysis 78−33545
XeF*, two- and three-body quenching by Ar, Xe 77−58053
XeF*(C1/2), excited state radiative lifetime meas. 77−34671
XeI, covalent and ionic states, spectroscopic props., ab initio CI calc., strong fluoresc. 78−90092
XeI*, emission spectrum, from Xe-I_2 77−6843
XeI*, production via laser absorpt. processes at 193 nm, quenching kinetics 80−91466
XeO, emission kinetics 77−34684

molecular fluorescence continued
XeO, excited state spectra, subpicosec. predissoc., solvation, in solid rare gas hosts 77−68050
XeO, luminesc. meas. of O(^{1}S) absolute quantum yield in photolysis of CO_2, N_2O 80−35561
Xe_2(−Kr,He), time-resolved excitation spectra, 1500 Å region, fluoresc. lifetime 77−75195
Xe_2*, form. and UV fluoresc. under monochromatic excitation and collision processes 78−9237
Y porphyrin complexes, luminesc. 77−18958
Y+O_2(NO)(SO_2), nascent product state distribs., laser fluoresc. detect. 78−7187
YF^+ emission, 3400 to 3700 Å, rot.-vibr. anal., electronic struct. 77−6839
YO, $A^2\Pi$-$X^2\Sigma^+$ photoluminesc. 78−55195
YO, fluoresc. spectra, atom+ROH O atom abstraction reactions, fluoresc. study 78−48643
YbCl, chemiluminesc., vibr. anal. 77−30917
YbF, chemiluminesc., vibr. anal. 77−30917
Zn complexes, pheophytins a and b, dual phosphorescence molecular splitting 79−89706
Zn porphin, in triphenylene, single site fluoresc. and visible spectra, vibr. assignments 77−58031
Zn-porphin(-d_4,d_8,d_{12}), nonradiative transition probabilities, deuteration effects 79−3485
ZnH, lifetime, Λ-doubling and hyperfine struct. of $A^2\Pi$ excited states 77−58083
ZnHg excimer, optical pumping of Zn reson. line, optical and kinetic props. 78−58991
ZnI_2, vapour, excited by photodissociation, fluoresc. yields 78−55138
ZrO, $B^1\Pi$-$X^1\Sigma$ intercombination transitions rel. to singlet-triplet separation 80−78623
ZrO, $B^3\Pi$ state radiative lifetimes, transition rates and oscillator strengths, reson. fluoresc. decay 80−28053
ZrO, in Ne matrix, laser photoluminesc. 77−14481

molecular force constants
see also Coriolis force
(3×3) order systems, force const. calcs. using isotopic freqs., parametric method 78−21907
3,3,3-trifluoropropene, struct. and vibr. spectra, IR, Raman polarisation study 80−18845
ab initio calc., appl. of force relaxation method for geometry optimisation 78−66685
ab initio calcs., evaluation of X-H bond dissociation energies 77−3267
acetaldehyde, Coriolis resonance bands in IR spectrum 80−47995
acetaldehyde, force consts., vibr. freqs., CNDO/2 and MINDO/2 calcs. 77−14607
acetaldehyde, optimum geometry, force fields, CNDO/force method 77−46498
acetonitrile, quadratic force fields, MOCIC pot. functions calcs. 80−5475
acetylene, force consts. of symmetric stretch motions, accurate ab initio calcs. 77−83567
acetylene, harmonic and anharmonic stretching force consts., ab initio calcs. 78−58587
acetylene, Q-branches, diode laser IR spectra, rot. consts. and struct. 79−45723
acetylene, vibr. fine struct. accompanying core ionis., STO calcs. 78−62844
acetylene, vibr.-rot. IR spectra, mol. force field determ. ^{14}C effects 77−61748
acetylene(-d), Raman and vibr. spectra and force const. calcs. 80−108747
acetylene-d_2, IR spectra of ν_5 bending fundamental, and $^{12}C^{13}CD_2$ isotope 79−50020
alene, -d_2, -d_4, harmonic force field, ground state average struct. 77−61732
alkali halides, geometries, force consts., charge distribs., FSGO model pot. calcs. 77−88379
alkali metal diatomics, pot. curves, selected valence electron SCF MO calc. 79−10053
alkali metal halide dimers, mol. force consts. and vibr. amplitudes calc. using electron gas model data 80−87245
alkali metal tetrafluoroborates, intramol. force fields and mean vibr. amplitudes 80−2743
alkali metal uranyl nitrates, IR spectra, force constants, bond orders 77−30873
alkali trimers, LEPS pot. energy surfaces, equilib. geometries, vibr. force consts. 79−22624
alkali trimers, London pot. energy surfaces 79−6893
alkali trimers, semiempirical pot. energy surfaces calcs. 78−25649
alkali-anthracene ion-pairs and triple-ions in solution, far IR spectra 79 78663
n-alkanes, vibr. data and force field consts., review 79−31750
alkenes, IR absorpt. curves calc. using standard fragments computer library 80−982
alkynes, normal coord. calc. and valence force field 79−72294
anthracene, harmonic force fields, bond orders, normal coord. anal. 78−25418
aromatic compounds, out-of-plane mol. vibrs., force field approx. calcs. 80−91538
aromatics, condensed, new force field, appl. to pyrene inplane vibrs. 79−81201
ATP disodium salt, hydrated, vibr. assignments, force consts., coincidence method appl. 78−62953
automatic geometry optimisation, Slater orbital derivatives, for d-orbital mols. 79−6831
AX_n molecules, vibrationally-hot, bond lengths, simple treatment 79−68202
benzene, and -d_6, $^1B_{2u}$ excited state, force field, normal coords. 78−5193
benzene, and aza-substituted derivatives, out-of-plane vibrs. force field 77−83572
benzene, corrected valence force field, force constants calc. 80−63868
benzene, d_3, -d_6, vibr. freqs., force consts., CNDO/2 calcs. 77−65449
benzene, force const. calc., resonance integral distance depend. 77−88443
benzene, force constants, local mode approx. 77−71791
benzene, normal vibr. anal. 78−13487
benzene, out-of-plane mol. vibrs., force field approx. calcs. 80−91538

molecular force constants continued
benzenes, trisubstituted, valence force fields, normal modes of planar vibrations *(French)* 78−37626
binary gas mixtures, force consts., intermol. pots. calcs. 78−66624
binding force constants, CNDO-2 calcs. *(French)* 77−14381
biphenylene, harmonic force fields, bond orders, normal coord. anal. 78−25418
blue proteins, activation of electron transfer reactions 78−44446
borazines, substituted, Urey Bradley force field, pot. energy consts. 80−78588
boron trihalides, mol. force field using parametric represent. method 80−27991
bridge angle, vibr. behaviour, simplified and accurate calcs. 80−95735
bromoacetylene, microwave spectrum, r_5-struct., dipole moment, quadrupole coupling consts., vibr. excited states 77−79606
bromobenzene-d_0, -d_1, -d_4, vibr. spectra and force fields 77−65463
bromochlorofluoromethane, gas, IR band contours and intensities anal. 78−82788
bromochlorofluoromethane-d_0, -d_1, Urey-Bradley force field calcs. 77−57968
bromomethane-$d_{0,1,2,3}$, IR spectra intensities, dipole moment, bond charge, force consts. 77−83588
3-bromopropene, microwave spectra, torsionally excited mol., HFS and rot. consts. 79−63988
bromotrifluoromethane ^{79}Br (^{81}Br), vibrational spectra and force constants of symmetric tops, rotational analysis 79−98090
bromotrifluoromethane, E-species force consts., using L-F approx. method, HLFS applicability 80−962
bromotrifluoromethane-^{12}C, -^{13}C, matrix IR spectra and harmonic force fields *(German)* 79−76431
butadiynyl radical, interstellar detect., rot. and spin-doubling consts. 78−93374
cis-butene-1, microwave rot. spectrum, centrifugal distortion effects, rot. consts. 78−9137
C_{3v} symmetry excited vibr. state mol. consts., graphical method 80−52969
carbon tetrafluoride, vib. anharmonicity 78−55160
carbonyl fluoride, vibr. transition moments and force fields, gaussian basis set calcs. 79−81152
cellulose triacetate, vibr. spectra, theory 79−54836
2-chloro-3-fluoro-1-propene, struct. and conformers, force field and vibr. amplitudes 78−25747
chloroacetylene, harmonic and anharmonic stretching force consts., ab initio calcs. 78−58587
chloroalkanes, modified Urey-Bradley force field calcs. 78−25500
p-chlorobenzaldehyde and deuterated derivs., vibrational spectra 79−3441
chlorofluoromethane, mol. centrifugal distortion and Urey-Bradley force field 79−89807
chloroform −d_0, −d_1, absolute Raman intensities and force fields 77−71808
2-chloropropane, and deuterated derivatives, modified Urey-Bradley force field 77−27048
2-chloropropane, conformation, vibr. spectrum, from simple harmonic force field 78−33494
chlorotrifluoromethane, E-species force consts., using L-F approx. method, HLFS applicability 80−962
chlorotrifluoromethane, matrix IR spectra and harmonic force fields *(German)* 79−76431
cis-1-cholobutadiene-1,3, microwave spectrum, struct., nuclear quadrupole coupling, distortion const., thermodynamic functions calc. 80−99500
computer program 78−58655
computer program MOLMEC, design and performance 78−13410
conformational props. rel. to spatial electron density determs., computer simulations 78−70763
conjugated hydrocarbons, conformational analysis and heats of form. by force field method 77−60105
coupled oscillators, approx. and exact quantum energies and eigenfunctions 79−26961
cyclododecane, force field, PMR of deuterated isotopomers 79−45695
cyclopentanone, centrifugal perturbation consts., determ. from forbidden rot. transitions 79−6931
cyclopentene, mol., pot. functions of bending modes 80−9753
cyclopropane-d_0, -d_6, force fields, Raman spectra 77−71806
cyclopropane-d_0, d_6, absolute IR intensities, dipole moment derivatives and polar tensors 78−90165
data base for force fields and mol. unit definitions 77−23575
decanoic acid, mol. config. change in cryst., IR spectra, normal coord. anal. 78−33506
definition and symbolism 79−49192
deformation force constants, rel. to valence force consts. *(Russian)* 78−29742
dense media, Q-branch Raman line width, rotational relaxation, reorientation, collision strength 79−98106
determination using isotopic freq. 77−38650
di thioformic acid, cis and trans isomers, rot. microwave spectra and config. 79−63989
diamond clusters and corresponding saturated hydrocarbon ab-initio HF and PCILO calcs. 78−42951
diatom, quadratic vibr. force const., from X-ray scatt. factors 79−45864
diatomic fluorides, exact force field calcs. using at. force consts. 78−62739
diatomic mol., vibr. rot. Hamiltonian expansion, Born Oppenheimer κ, explicit introduction 80−69118
diatomic mol. pot. energy function, rot. consts. and Sutherland parameter 79−54931
diatomic molecule, force const., Morse function in pot. curve *(Russian)* 79−49968
diatomic molecule, vibr. potential representations 79−68219
diatomic molecules, force consts. evaluated in first order of perturbation theory 77−34781
diatomic molecules, harmonic force consts., calc. from zero, second-order energy, modified PCILO method 79−36533
diatomic molecules, matrix isolated, vibr. spectrosc., IR line shape calcs. 79−72307
diatomic molecules, molecular orbital theory 79−10057
diatomic molecules, spectrosc. consts., rel. to electronegativity 80−28007
diatomic molecules vibr. consts. determ., IR spectroscopic, quantum chem. teaching project 79−84914
diatomic systems, nonadiabatic coupling matrix elements by Hellmann-Feynman theory and HF 80−83263
molecular force constants continued
diatomic systems, reln. between internuclear distances and force constants 80−43205
diatomics, quadratic-quartic force consts. calc. 79−63979
diatomics, spin coupled theory of mol. wavefunctions, struct. and props. 77 50337
1-10-dicarba-closo-decarborane (10), mol. struct., vibr. and shrinkage corrections calc. from force field 80−95739
dichlorodifluoromethane, IR spectrum and mol. force field 79−72309
dichloromethane, d_{0-3}, Raman intensity, force consts. and electro-optical parameters 79−36651
1,1-dichroethane and d, IR and Raman spectra, βCH stretching interaction force consts. 77−79616
difluoroacetaldehyde, optimum geometry, force fields, CNDO/force methods 77−46498
1,2-difluorobenzene-d_0, -d_4, IR spectra, vibr. anal., force field 77−27063
cis- and trans-difluoroethylene, force consts., mean vibr. amplitudes 77−6748
2,2-dihalohexafluoropropane, IR and Raman spectra, gas, liq. and solid, normal coord. anal. 79−72314
2,5-dihydrofuran, mol., pot. functions of bending modes 80−9753
N,N-dimethyl acrylamide (−d_3,d_6,d_9), force field, IR and Raman spectra obs. 80−47979
dimethyl di(trifluoromethyl) germanium, and perdeuterated analogues, vibr. spectra, normal coord. anals. *(German)* 80−5547
dimethylether, ab initio SCF calcs., force field, IR and Raman intensities 77−79601
dimethylether, equilib. struct., ab initio SCF calcs. 77−3265
dimethylmercury, mol. force field, generalised inverse method for calc. 78−25505
dimethylphosphines, IR spectra, coupling between methyl rocking, PH bending, and PC stretching, force field interpretation 80−69141
N,N-dimethylselenourea, deuterated forms and methyl derivatives, fundamental IR vibr. assignments 80−961
dimethylsulphate, cryst., liq., and oriented film, vibr. spectra, internal rot. 79−91444
dimethylsulphite(-d_6), cryst., liq., and oriented film, vibr. spectra, force fields 79−91443
N,N-dimethylthiourea, deuterated forms and methyl derivatives, fundamental IR vibr. assignments 80−961
1,4-dioxadiene, mol., pot. functions of bending modes 80−9753
dioxane-$HgCl_2$ complexes, IR and Raman vibr. spectra, inter- and intramol. forces 77−66489
effective hamiltonians, pseudopotentials and applics. 77−30754
electric dipole moments derivatives calc. *(French)* 77−88389
electronegativity equalisation in atom-atom reactions 79−66272
ethane, $^{13}CH_3{}^{12}CD_3$, $^{12}CH_3{}^{13}CD_3$, microwave spectra, Stark effect, C-C bond length and mol. consts. 77−50428
ethane, force consts., model potential function vs. mol. orbitals calcs. 78−29829
ethane, force consts., vibr. stress and isotope effects 78−21897
ethane, inclusion of nonbonded interactions in vibr. freq. calcs. 80−95590
ethene, general valence force field, ab initio calcs., IR and Raman intensities 77−71746
ethylene, and ^{2}H, ^{13}C, ^{15}N, ^{18}O isotopic derivatives, vibr. freqs. using MINDO/3 force consts. 77−71793
ethylene, Raman spectra of ν_3 band, rot. consts. 79−26988
ethylene+cis-N_2H_2, chem. reaction, intermediate geom. calcs. 78−35655
ethylene oxide-d_0, -d_4, centrifugal distortion const., thermodynamic functions 79−41149
ethylene sulphide, centrifugal distortion const., thermodynamic functions 79−41149
fluoroacetylene, harmonic and anharmonic stretching force consts., ab initio calcs. 78−58587
fluoroaromatics, CH stretching, vibr. force fields, substitution pattern effects 77−54550
fluoroform, quadratic force fields, MOCIC pot. functions calcs. 80−5475
fluoromethane, mol. rot.-vibr. consts. of ν_3 band of $^{12}CH_3F$ 79−64118
fluoromethanes, GVFF from SCF ab initio energies 78−74635
fluoromethanes, optimum geometries, force fields, CNDO/force method 77−46498
fluoromethanes, vibr. spectra, force consts. and geom., SCF ab initio calcs. 78−62785
fluoromethyl methyl mercury-d_0, -d_3, vibr. spectra, normal coord. anal. 79−50017
force field calcs., damped least-squares method 80−91533
force field determination, Green's function method, ambiguities 80−960
force field representations, vibr. stress, isotope effects and struct. of ethane 78−21897
force fields, virial theorem appls., zero virial reaction coords. and diatomic pots. 79−31433
formaldehyde, electronic struct., dipole moments, mol. polarisability, force fields, ab initio calcs. 80−78531
formaldehyde, excited state vibr. freq. calcs. by method based on scaled ab initio force fields 80−87092
formaldehyde, force consts., ab initio CI calcs. *(French)* 78−90093
formaldehyde, force consts., vibr. freqs., CNDO/2 and MINDO calcs. 77−14607
formaldehyde, force field calcs., damped least-squares method 80−91533
formaldehyde, ground state rot. consts. 79−45701
formaldehyde, photodissoc., pot. energy surface features 79−79271
formaldehyde, rot. struct. of 3500 Å transition, large amplitude vibr. effect 79−93976
formaldehyde, unique force field, parametric representation method 77−18897
formamide, force consts. and dipole moment derivatives, ab initio MO calcs. 80−95521
formamide, mol. geom., self-consistent MINDO calcs., torsion and relax. effects 77−42243
formamide, near-IR spectra, anharmonic pot. 77−14430
formic acid, H bonding, electronic struct., geometries, moments, dimerisation energies, charge distrib., pseudopotential calcs. 80−27942
formic acid, harmonic force consts., ab initio calcs. and uniqueness problem 79−6834
formic acid, normal vibr. pot. energy distrib. 77−451
formic acid (-d), microwave spectra and rot. consts., astrophysical appl. 80−91550
formic acid anhydrides, valence force consts., IR spectra, isotope effects 79−93997

molecular force constants continued
formic acid dimer, vibr. spectra, CNDO/2 interpretation *(French)* 80−58155
cis-formic acid geometry, force fields and fundamental vibr. freq., ab initio study 80−87040
formic acid-d_0(-d_1)(-d_1)(-d_2), vibr. spectra, CNDO/2 interpretation *(French)* 80−58155
generalised inverse method for calc. 78−25505
geometry optimisation, self consistent, semiempirical force field method 77−83760
ground state props., coupled cluster and MBPT methods appl. 80−47881
group II halide-periodate complexes, force consts., compliance and Coriolis consts. calc. 78−42242
group IV halides, pot. consts. calcs. 79−36605
Group IV tetrabromides, intramol. force fields and mean vibr. amplitudes 80−106316
group IV tetrahalides, isotope shifts, Coriolis coupling and force consts., isotope substitution and matrix isolation 77−42322
group IVA tetrahalides, force consts., bond strengths, Urey-Bradley calcs. 77−50558
Group V trideuterides, Coriolis coupling consts., progressive rigidity method calcs. 78−929
Group V trihalides, Coriolis coupling consts., progressive rigidity method calcs. 78−929
halogen molecule, orbitals calc., correlation effects, force const., dissoc. energy, bond length 77−26964
Hartree-Fock-Roothaan calcs. with differentiated integral estimation 77−23573
heavy metal diatomic halides, Wasastjerna pot. function, force consts. internulcear separations and binding energies 80−14187
heptafulvene, microwave spectrum and dipole moment 77−14421
hexa(trifluoromethyl) germanium, gas and liq., IR and Raman spectra, normal coord. anal. *(German)* 79−72315
hexabromobenzene, cryst., IR and Raman spectra, vibr. normal coordinate anal. 77−79602
hexachlorodisiloxane, normal vibr. and force field calc. 79−54994
hexafluoride ions of group IIIA elements, molecular consts., normal coord. anal. 77−1187
hexafluoropropene, struct. and vibr. spectra, IR, Raman polarisation study 80−18845
hexahalo ions, octahedral, mol. consts. calcs. 80−106317
hexahaloanions of group IV A and V, mol. const. determ. 80−87093
hexaidobenzene, cryst., IR and Raman spectra, vibr. normal coordinate anal. 77−79602
hexaoxy ions, octahedral, mol. consts. calcs. 80−106317
hydrides, first row, bending pot. calc. using MINDO approx., force const., equilib. geometry 80−95544
hydrocarbons, conformational anal., modified Urey-Bradley force field, gauche-H_2 interactions 77−6749
hydrocarbons, force constants, CNDO-2 calcs. *(French)* 77−14381
ice, D_2O-H_2O, intramolecular stretching spectrum, role of Fermi resonance 79−93973
indene, microwave spectrum, assignments, rot. consts. and config. 79−31510
inert gas binary mixture, unlike mol. force consts. from viscosity data, thermal cond. 78−33565
inert gas complexes spectroscopic data, geometry, pot. energy curve, dissoc. energy, equilib. internuclear distance, determ. 80−53018
inert gases, mean force constants and rectilinear law of mean force calcs. 78−33414
inverse spectral problem, use of parameters of intermol. spectrum of condensed media to decrease nonuniqueness 77−80586
3-iodopropene, microwave spectra, torsionally excited, rot. consts. 79−63986
iodotrifluoromethane, E-species force consts., using L-F approx. method, HLFS applicability 80−962
ion-molecule equilibria in solvolysis, secondary β ^2H isotope effects, hyperconjugation 80−50874
IR and Raman band intensities, use in force const. calcs. 77−27120
iron poprhin, A_{2u} out of plane vibration, pseudo-Jahn-Teller effect 78−82712
isostructural molecules and ions, force const. set calcs. 80−23390
isotopic freqs. for evaluation, parameter representation, algebraic approach 78−33493
iterative consistency calcs. using geometric interpretation 77−6746
iterative parameter method *(German)* 79−76418
JWKB phase integrals, to high-order 80−5632
ketene-d_0, -d_2, Coriolis coupling, centrifugal distortion and force consts., mean vibr. amplitudes calcs. 79−36607
L-F approx. method, second order secular eqn. soln. 78−66458
L-F approx. method for symmetrized force consts., XY_n mols. 80−14128
light atom molecules, general quadratic force fields, semiempirical MOCIC calcs. 80−5474
maleimide, monomer, valence force field in Ar matrix at 20K, self-assoc. *(French)* 79−81165
metal ions, in complexes and biological systems, preliminary vibr. assignment method 78−62953
methane, and isotopic forms, anharmonic force field, equilib. struct. 79−76365
methane, force consts., ab initio CI calcs. *(French)* 78−90093
methane, force consts., equilib. geom., Hartree-Fock and CEPA calcs. 78−70753
methane, force consts., vibr. freqs., CNDO/2 and MINDO calcs. 77−14607
methane, mol. rot.-vibr. consts., calc. using ν_1 band data 79−76529
methane, orbital valency force field 77−34779
methane, parametric representation method 78−25503
methane(-d_4), force field representation, equilib. struct. 78−42238
methane-d_4, isotope effect on rot. and vibr. consts. 79−22688
methanethiol, ab initio force consts., anharmonic vibr. 78−21898
methanol, ab initio force consts., anharmonic vibr. 78−21898
methanol, equilib. struct., general valence force field, ab initio calcs. 77−3265
methanol, H bonding, electronic struct., geometries, moments, dimerisation energies, charge distrib., pseudopotential calcs. 80−27942
methyl bromide, and isotopic modifications, rotational spectrum in vibr. ground state 79−54853
methyl cation, force consts., ab initio calcs. with differentiated estimation of integrals 77−67974
methyl chloride, ab initio force consts., anharmonic vibr. 78−21899
methyl chloride, charge distrib., substituents effect 80−905
molecular force constants continued
methyl chloride, microwave spectrum of excited vibr. states, Coriolis coupling, rot. consts. 77−14420
methyl fluoride, ab initio force consts., anharmonic vibr. 78−21899
methyl fluoride, charge distrib., substituents effect 80−905
methyl fluoride, harmonic force field calcs. and exptl. configs. 80−63865
methyl fluoride, vibr. transition moments and force fields, gaussian basis set calcs. 79−81152
methyl formate(-d_1,d_3,d_4), mol. vibr. spectrum, struct., beginning with PCILO calc. *(French)* 80−23401
methyl halides, force consts. evaluation using gp. vibrs. and centrifugal distortion consts. 80−9580
methyl halides, harmonic force fields, high-low freq. separation calcs. 78−90067
methyl halides, mol. force field at SCF ab initio levels, quantum-mechanical calc., LCAO-MO method 80−106319
methyl halides, mol. force fields, IR intensities, and vibr. props. 80−47879
methyl iodide, rot. microwave spectra, nucl. quadrupole, spin-rot. and nucl. shielding tensors 78−42040
methyl ion, electrostatic force theory appl. to mol. geometry ab initio verification 79−98002
N-methyl thiopropionamide-N-d_3, normal coord. calcs. 79−36598
N-methyl thiopropionamides, normal coord. calcs. 79−36598
methyl tri(trifluoromethyl) germanium, and perdeuterated analogues, vibr. spectra, normal coord. anals. *(German)* 80−5547
methyl vinyl ether, microwave spectrum, quartic centrifugal distortion and rot. consts. 79−10099
methyl vinyl sulphide, syn-gauche equilib., force field and ab initio calcs., microwave and Raman spectra 80−23573
methylacetylene, quadratic force fields, MOCIC pot. functions calcs. 80−5475
methylamine, ab initio force consts., anharmonic vibr. 78−21898
methylamine, and ^2H, ^{13}C, ^{15}N, ^{18}O isotopic derivatives, vibr. freqs. using MINDO/3 force consts. 77−71793
methylborodichloride-d_0(-d_3), vibr. spectra and force constants *(German)* 79−26982
N-methylcarbamoyl chloride(-d_1), vibr. spectra, normal coord. anal. 78−33497
methylene, force consts., ab initio calcs. with differentiated estimation of integrals 77−67974
methylene chloride, microwave spectra, rot. consts. and geometric struct. 79−63990
methylene glycol(-d_A)=formaldeyhyde(-d_2)+H_2O(D_2O) Raman spectra and normal vibr. 80−58271
MgF_2, force consts., vibr. amplitude and shrinkage effects 79−22863
MINDO/3 semiempirical SDF MO calc., for small mols. 79−76408
model 78−963
molecular model building, computer program MMB 80 *(Japanese)* 79−36793
molecule, intensities dipolaris. ratios, polarisability, matrix rotation, isotopic rules 78−5288
monofluoromethane, ν_6 band, Q-branches, diode laser IR spectra, mol. consts. 79−45722
monofluoromethane, force consts. and IR intensities, ab initio SCF finite difference method 78−86783
monothioformic acid, cis-, trans-rotamers, rot. spectrum, force consts. and isotopically substituted struct. 78−9145
Morse oscillator, rotational const. B_v, asymptotic expansion 79−68289
MX_4^n-type ions, modified Urey-Bradley force field 78−21905
sym-N_2O_3, mol. vibr. in N_2 matrix, normal coord. anal. 79−59432
N=3 eigenvalue problem, appl. to XYZ bent mols. *(German)* 80−14131
naphthalene, and aza-substituted derivatives, out-of-plane vibrs. force field 77−83572
naphthalene, harmonic force fields, bond orders, normal coord. anal. 78−25418
naphthalene, out-of-plane mol. vibrs., force field approx. calcs. 80−91538
naphthalene radical anion, ethereal soln., far IR spectra 78−62796
nitrobenzene-d_0(p-d)(d_5), vibr. spectra 79−26966
p-nitrotoluene, vibr. spectra, normal mode calcs. 77−65482
nonafluorobutane(-d_1), and halo-substituted forms, gas and liq., IR and Raman spectra, normal coord. anal. *(German)* 79−72318
normal co-ordinates through coriolis coupling constants 80−28005
normal mode calcs. of crystals and molecules, coordinates and force matrices generation, computer program 78−91393
octahedral ions and molecules of 2nd and 3rd row metals, intramol. force fields and cryst. field stabilisation energy effects 77−54548
octahedral mols., anharmonic force field, decoupled rigid bender model 79−41153
octahedral systems, intramolecular force fields and vibr. amplitudes, Wilson's FG matrix method 77−31021
one-electron density functions, many-centred finite multipole expansions 78−71624
organic molecules, core ionisation and electronic redrganisations, LCAO MO SCF calcs. 79−18115
organic molecules, small, harmonic force consts., vibr. freqs., integrated intensities, MINDO/3 method 80−58411
organometallic amines, Raman and IR spectra, band intensity and assignment, force const. determ., vibr. props. *(German)* 80−87133
orthoborates, dolomite type, vibr. spectra, vibr. coupling effects *(French)* 77−65464
oxalate ion, vibr. assignments, force consts., coincidence method appl. 78−62953
oxalic acid, monomeric, IR matrix-isolation spectra, vibr. anal. 78−66550
oxalyl bromide, normal vibr. freqs., force fields 79−41155
oxalyl chloride, normal vibr. freqs., force fields 79−41155
oxalyl chloride (fluoride), centrifugal distortion consts. and thermodynamic functions, pot. energy calc. 79−22619
oxide ions XO_4^{n-}, n=1 to 4, normal vibr. freqs., prediction, force consts. calc. *(Russian)* 77−6759
perfluoroneopentane, geom. struct. of mol., gas phase electron diffr. 78−78810
perovskites, ordered cubic, cationic effect on intramolecular forces, stretching force const. 80−88979
peroxyacetic acid, and isotopic forms, matrix IR spectra, force spectrum, force const., thermodynamic props. calc. 77−14427
perylene, harmonic force fields, bond orders, normal coord. anal., mean amplitudes calcs. 78−25418

molecular force constants continued
phenanthrene, planar normal vibrs. calcs. 80−5525
phenol, H bonds to proton acceptors, PCILO calcs. 79−26895
phenol ($-d_1$, d_5, d_6), excited A state, normal vibr. freqs, force consts., compliance coeffs. 78−50534
polyatomic force fields, Ohwada's pairwise interaction model 80−106321
polyatomic mol. force consts. and heat of atomisation, approx. separable pot. function 80−78675
polyatomic molecule, anharmonic force consts., vibr.-rot. interaction consts. 80−966
polyatomic molecule, crit. consts. evaluation from intermol. force consts. 80−37844
polyatomic molecule, intramolecular coord. relax., generalised classical theory 80−78589
polyatomic molecules, force and interaction consts. of ang. coords. 79−27054
polyatomic molecules, force consts., Hellman-Feynman type calc. method 77−65451
polyatomic molecules, force consts. and geometry, pot. energy surface calcs. 77−14379
polyatomic molecules, normal coordinate problem, QM treatment, book contrib. 78−78677
polyatomic molecules, vibr. spectrum, intermolecular interaction effects *(Russian)* 78−37621
polyatomic mols., nuclear charge model and valence force consts. prediction 80−43022
polyatomic systems, Cartesian coords., charge densities, field gradients 78−29771
polyatomic XY_5 type molecules, vibr. assignment using Redington's method 80−23410
polyethylene (orthorhombic), intermol. pot. functions, force consts., vibr. assignments, thermodynamic props. 77−39639
polymer chain, elasticity for different vibr. modes, algorithm 78−66696
porphin, ground-state energies, force consts. and vibr. freqs., CNDO/2 calc. 79−18118
porphins, reson. Raman spectra, selection rules, normal coord. treatment 80−53175
potassium oxalate monohydrate, force fields and normal coords. of H_2O mols. 79−31500
propane, force const. selection, backward elimination regression-refinement procedure 79−31497
propene, force constants, SCF ab initio calcs. 77−34780
pseudo exact, high and low frequency separation method 78−50539
pyramidal molecules and ions, bond polarisability and force constants 80−69260
pyrazine, in pyrazine-d_4, p-dioxane, X-trap, p-xylene, benzene($-d_6$), cryst., MIDP, PMDR, low temp., assignments 77−36154
pyrazine-d_4, in p-dioxane, p-xylene, benzene, cryst., MIDP, PMDR, low temp., assignments 77−36154
pyridine(-d), force consts. and vibr. spectra by CNDO/2 force method 80−95540
quartic centrifugal distortion consts., upper and lower bounds 79−45699
Raman excitation profiles and mol. spectra synthesis, vibronic and exciton-in-mol. theory 78−42076
Raman spectroscopy, vap., medium resolution, appls., review 78−42065
relaxed force constants, generalised approach 79−41156
relaxed force constants, generalised approach 80−23409
rigid molecules, invariance and stability conditions, in lattice dynamical model calcs. 79−28051
rubidium tetramethylborate, vibr. spectra and force constants *(German)* 79−26981
SCF MO calculations with fixed orbital basis, H_2 mol. appl. *(French)* 79−94107
selenoacetamide ($-d_n$), IR spectra, vibr. assignments, normal coord. anal. 79−22708
semicarbazide hydrochloride, vibr. spectra, normal coord. anal. 80−58255
semicarbazide-d_0, $-d_5$, vibr. spectra, normal coord. anal. 80−58255
semiempirical quantum mechanical method 78−62947
simple symmetric complexes and mols., calc. method *(Russian)* 79−59435
spectroscopic determ., extremal props., book contrib. 78−78678
symmetry adaption, force const. matrix of symmetric mols. 79−26878
TCNQ, electron-mol. vib. coupling 77−15782
TCNQ salts, vibr. and electronic spectra 79−45704
ten-atom model, interaction forces 79−59528
terpenes, methyl groups internal rotation, ^{13}C spin lattice relaxation times and force field calcs. 80−74255
tetra(trifluoromethyl) germanium, gas and liq., IR and Raman spectra, normal coord. anal. *(German)* 79−72315
1, 2, 4, 5-tetracyanobenzene and $-d_2$, IR and Raman spectra, vibr. anal. 79−36629
tetracyanomethane, molecular vibration analysis 79−803
tetrafluoromethane, ^{19}F chem. shielding, depend. on internal coords. 78−5249
tetrafluoromethane, mol. consts. and mean vibr. amplitudes calcs. 80−106318
tetrafluoromethane, pot. consts., IR spectra 78−82808
tetrahalides of Gp.IV elements, M-X bond flexibility, by compliance scheme 80−37805
tetrahedral and octahedral complexes, mol. vibrs. and reaction pathways, min. energy coords. and compliance consts. 77−57966
tetrahedral molecules, thermodynamic isotope effect 78−20000
tetrahedral molecules and ions, parameter study for force fields 77−34778
tetrahedral XY_4 ions, normal coord. treatment and mol. consts. 79−93968
tetrahedral XY_4 type molecule, change in mean square amplitude 77−57963
tetrahydrofuran, effective force constant corrections, in redundant mol. coords. 78−13634
tetrakis(trifluoromethyl)germane, gas phase electron diffr. struct., torsional force consts., CNDO/2 calc. 79−31687
tetramethyl germanium($-d_{12}$), vibr. spectra, normal coord. calcs. 79−22717
tetramethyl lead($-d_{12}$), vibr. spectra, normal coord. calcs. 79−22717
tetramethyl silicon($-d_{12}$), vibr. spectra, normal coord. calcs. 79−22717
tetramethyl tin($-d_{12}$), vibr. spectra, normal coord. calcs. 79−22717
tetramethylcarbonyl-silane,-germanium,-tin,-lead, force fields and vibr. mean amplitudes 77−30856
molecular force constants continued
tetramethyls, of IVA metals, pseudo-exact force consts., force fields 77−31022
tetramethylurea-d_0,-d_{12}, IR spectra, normal coord. anal. 78−978
s-tetrazine, mol., pot. functions of bending modes 80−9753
tetrohydrofuran-$HgBr_2$ complexes, IR and Raman vibr. spectra, inter- and intramol. forces 77−66489
thiazolidine, valence force field transferability *(French)* 79−10091
-4 Δ-thiazoline-2 thione and N deutero homologue, force field determ. *(French)* 77−14407
thiirene and deuteroderivatives, Fourier transform IR spectra using Ar matrix isolation, vibr. band assignments 80−14142
thiocarbonyl bromide, IR spectra, gas, liq. and matrix isolated, mol. force consts. *(German)* 79−36640
thioformaldehyde, electronic struct., dipole moments, mol. polarisability, force fields, ab initio calcs. 80−78531
2-thiohydantoin-d_0, ($-d_2$), mol. vibr. and force field calcs. 78−62779
thiophosgene, IR spectra, gas, liq. and matrix isolated, mol. force consts. *(German)* 79−36640
thioureas, substituted, normal coord. anal. 79−98246
p-toluidine, vibr. spectra, normal mode calcs. 77−65482
torsional internal coordinates in normal coordinate calcs. 77−83574
transition metal ammine complex, mol. force consts. and vibr. amplitude 79−31727
transition metal oxyanions, intramol. force fields 79−45693
tri(trifluoromethyl) germanium halides, gas, liq. and solid, IR and Raman spectra, normal coord. anal. 79−72316
triatomic inorganic mols., harmonic force consts., vibr. freqs., integrated intensities, MINDO/3 method 80−58411
triatomic mol. bond-bond interaction force consts., simple MO theory 78−50452
triatomic molecule, rot. vibr. electronic Hamiltonian, Born-Oppenheimer approx., breakdown 80−87097
triatomic molecules, angle deformation, force constant of angle deformation derivation 79−98239
triatomic systems, compliance const., L matrix approx. method 78−74797
triatomic unsymmetrical mols. and ions, electrostatic models 79−22697
trichloromethoxysilane, normal vibr. and force field calc. 79−54994
trifluorochloromethane, Raman and IR spectra, $^{35/37}Cl$ isotope splitting and mol. constants *(German)* 77−83595
trifluoroethene-d_0,d_1, mol. struct., microwave and electron diffr. obs. 80−58384
trifluoromethane, quadratic CNDO force fields calcs., coord. effects 79−6877
trifluoromethyl trimethyl germanium (tin)(lead), and perdeuterated analogues, vibr. spectra, normal coord. anals. *(German)* 80−5547
trigonal and triatomic molecules, orbital valency force field const. calcs. 80−78516
trigonal planar molecules, thermodynamic isotope effect 78−20000
trimeric molecular complex, excitation localisation and transfer, monomeric internal vibr. effect 78−17581
trimethylantimony(V) dihalides, normal coord. anal., comparison of force fields 78−968
trimethylborane, vibr. spectra and force constants *(German)* 79−26981
tris(trimethylstannyl)amine, gas phase electron diffraction 80−106401
two valence-electron diatomics and triatomic ions, FSGO method calcs. using at. Fues pot. 78−62717
unlike molecules, force constants, transport and virial coefficients, law of corresponding states calcs. 79−98848
uranyl complexes, IR spectra, complexation effects on force consts. and bond lengths 78−980
uranyl complexes, IR spectra and bond distances 80−74167
uranyl pentafluoride complexes, normal coordinate anal. 79−22596
urea, force field for planar vibrs., CNDO/Force MO calcs. 79−76416
valence force constants, rel. to deform. force consts. *(Russian)* 78−29742
valence force constants, semiempirical point charge model *(German)* 78−90150
valence force constants in planar and pyramidal XY_3 molecules, effective nuclear charge model appln. 80−63864
valence force consts., computer program, least squares procedure 78−58656
valence force field evaluation by empirical constraints 77−42310
valence states and binding energies 77−30757
vibr. anal., force fields and consts. *(German)* 79−45702
vibrational intensity calcs., CNDO/2 method with extended basis set 80−91445
vinyl cyanide, microwave spectra data tables 79−59445
vinylfluoride, gas phase electron diffr. and microwave spectra, rot. consts., struct., isotope shifts 79−31686
virial theorem, appls. 78−41904
weakly coordinated molecular systems, mutual vibronic effects in chem. reactions and catalysis 78−64821
XY_2 bent symmetrical molecules, Coriolis coupling consts., centrifugal distortion consts. 80−58236
XY_2 linear symmetric mols., chem. perturbations, Green's function calcs. 80−63866
XY_2 molecule, chem. perturbation of force field, Green's function appl. 79−76417
XY_2 nonlinear symmetrical molecules, isotopic invariants 79−36599
XY_2 nonlinear system, mol. dynamics calcs. 78−41975
XY_2 type molecule, force fields using Redington method 77−18899
XY_2-type bent symmetric mols., vibr. anal., kinetic consts. method 80−18838
XY_2Z planar molecule, transformation and compliance matrices determ. 77−18898
XY_3, pyramidal, force consts. and mean amplitudes, group theoretical anal. 79−36609
XY_3, pyramidal halides, mean amplitude, Coriolis coupling const. and centrifugal distortion const. 78−29735
XY_3 planar mols., mean vibr. amplitudes, force and kinetic consts. 77−79603
XY_3 planar symmetrical molecules, isotopic invariants 79−36599
XY_3 pyramidal mols., intramol. forces, fundamental vibr. freqs., centrifugal distortion consts., PF_3 appl. 78−5202
XY_3 pyramidal-type mols., mol. consts., kinetic consts. and L-approx. methods 80−18839
XY_4, force and compliance consts. calc. 77−23572
XY_4, XY_3, mols., force field anal., parametric representation method 78−25503

molecular force constants continued
XY_4 molecules, force consts. by modified Redington and Aljibury method 80−69261
XY_4 molecules, isotope effect on rot. and vibr. consts. 79−22688
XY_4 oxygenated ions, tetrahedral, mol. consts. 79−36555
XY_4 square-planar type ions, force consts., bond polarizability 78−5201
XY_4 tetrahedral molecules, kinetic const. method appls. 79−36608
XY_4 tetrahedral mols., force and kinetic consts. calcs. 77−27053
XY_4Z (C_{4v}) molecules, force constants and mean-square amplitudes of vibration 78−66535
XY_6 force and compliance consts. calc. 77−23572
XY_6-type molecules, Coriolis coupling consts., at. mass effect, XCl_6 appls. 78−66684
XY_8 molecules of D_{2d} symmetry, G, F and Σ matrices *(French)* 80−970
XY_9 molecules, D_{3h} symm., U-, G-, F- and Σ-matrix determ. *(French)* 80−78599
XY_n, symmetrised force consts., new approx. method 77−14409
XYZ type system, bent, force field determ. Redington's method applicability 79−81168
AlBr, UV emission spectrum, vibr. consts., isotope displacement and dissoc. energies 77−3381
$AlCl_3$, force and compliance consts., OVFF, UBFF and GVFF models 78−50663
$AlCl_3$, matrix isolated, vibr. spectrum, struct., vibr. freqs. 78−46339
Al_2Cl_6, matrix isolated, vibr. spectra, isotopic fine struct. and valence force field calcs. 80−58258
AlH_4^-, AlD_4^-, intramol. force fields, F_2 vibrs., isotope shifts 77−3336
AlO, spectra, vibr. consts., pot. curves, Franck-Condon factors and r-centroids 78−42243
AlX_3 (X=Cl, Br, I), pseudo-exact force consts. 77−31022
Ar_2, mean force constants and rectilinear law of mean force calcs. 78−33414
ArHBr, ArHCl, and isotopic forms, rot. spectra, mol. struct., mol. consts. 80−58246
As-O, single bond stretching force consts. and bond orders 77−26994
$AsBr_3$, gas-phase electron diffr., mol. struct., force consts., vib. unharmonicities 77−546
$AsBr_3$, microwave spectra, rot. consts., mol. struct. 77−3485
$AsCl_3$, 100 to 200 GHz spectra, mol. struct., harmonic force field 78−42042
AsF_3, millimetre rot. spectra, vibr. excited states, anharmonic force field 78−33502
AsF_5, E′ vibr. assignments, bending modes, parameter method 77−10658
AsF_5, normal coord. anal., generalised valence force field calcs. 77−58195
$AsH_3(AsD_3)(AsT_3)$, harmonic force fields, equal coord. method calcs. 77−30845
As_4O_6, IR and Raman spectra vibr. spectra, valence force field calc., pot. function *(French)* 78−50549
$AuBr_4^-$, harmonic force field, mean vibr. amplitudes, cation effect 77−3335
$AuCl_4^-$, harmonic force field, mean vibr. amplitudes, cation effect 77−3335
$AuCl_4^-(Br_4^-)$, mean vibr. amplitudes and force field, Muller approx. 77−10659
AuLi, vibr. freq. determ., IR spectra, matrix depend. 77−75146
BF, quadratic vibr. force const., from X-ray scatt. factors 79−45864
BF_3, ^{19}F chem. shielding, depend. on internal coords. 78−5249
BF_3, dissoc. pathways and mol. vibr., compliance consts. and min. energy coords. 78−35661
B_2F_4, mol. force consts. and vibr. amplitude, force field study 79−31729
BH, mol. spectroscopic consts., FSGO calcs. 77−6758
BH, pot. curve, one-config. Hartree-Fock-Roothaam calc. for force consts. 78−82627
BH_2^+, BH_3, force consts., ab initio calcs. with differentiated estimation of integrals 77−67974
BH_4^-, BD_4^-, intramol. force fields, F_2 vibrs., isotope shifts 77−3336
B_2H_6, quadratic valence force field, rel. to ethene 79−3382
$BHBr_2$, and isotopic forms, mol. pot. consts., amplitudes, Coriolis coupling, centrifugal distortion 78−50662
$BHCl_2$, and isotopic forms, mol. pot. consts., amplitudes, Coriolis coupling, centrifugal distortion 78−50662
BHF_2, and isotopic forms, mol. pot. consts., amplitudes, Coriolis coupling, centrifugal distortion 78−50662
BI_3, mol. force field using parametric represent. method 80−27991
BO, spectroscopic properties, PNO-CI and CEPA calcs. 78−41961
BO_2, fluoresc. excitation spectra, vibronic level fluoresc., Fermi reson., force field 77−79643
B_2O_3, bipyramidal struct., stability, ab initio SCF-MO calcs. 80−99446
B_2O_3, vibrational force consts. and B-O bonding, Green's function method 77−14406
BX_3, (X=Br, Cl, F), ellipticity of symm. force field, force consts. 78−17646
BX_3, X=F, Cl, Br, I, parametric representation method 78−25503
$BaClO_3.H_2O$, force fields and normal coords. of H_2O mols. 79−31500
BaF_2, force consts., mean amplitudes of vibr. 78−17647
BeF_4^{2-}, pseudo-exact force consts., force fields 77−31022
BeH_2, force consts., ab initio calcs. with differentiated estimation of integrals 77−67974
BiCl, form., microwave spectrum, hyperfine struct., mol. rot. vibr. consts., bonding 77−14418
$BiCl_6^{3-}$, model force fields and vibr. amplitudes calcs. 78−62780
BrCN, general quartic force field, Machina-Overend parameters 78−50532
BrCN, ICN, and isotopic forms, force field calc., freqs., rot. consts. 79−22693
$BrCl(H_2O)_n$, mean vibr. amplitudes, Raman spectra, isotope effects 77−58014
BrF_5, gas phase electron diffraction and microwave rot. consts. data anal., mol. struct. 79−76363
$Br_2(H_2O)_n$, mean vibr. amplitudes, Raman spectra, isotope shifts 77−58014
BrSN, force consts. and mean amplitudes of vibr. calc. 77−30855
Br_2SO, A′-force consts., 4th-order secular eqn., L-matrix approx. vs. HLFS methods 79−36556
1-bromo-1-chloro-1-fluoroethane(-2-d_1), IR and Raman spectra, vibr. assignments, normal coord. anal. 78−42053
C-H bond containing molecules, correls. among bond lengths, stretching freqs. and bond order matrix elements 77−58192
C_2, IR flame emission spectra, Ballik-Ramsay system 79−63999

molecular force constants continued
C_3, ground state pot. surfaces, analytical functions 80−83304
CF_2S, mol. consts., kinetic consts. method calcs. 80−58235
CF_2Se, mol. consts., kinetics consts. method calcs. 80−58235
CH, force constants, local mode approx. 77−71791
CH_3, CH_2 and CH deformation vibration group frequencies and MO electron densities, interaction force const. 80−87101
C_6H_4 radical, force constants, local mode approx. 77−71791
C_6H_5 radical, force constants, local mode approx. 77−71791
CNC radical vibr. and electronic spectra, in VUV photolysis of matrix-isolated cyanomethane 78−85180
CO, carbonyl group stretching freq. force const., CNDO/2 and localised orbitals calc. 77−30784
CO, inner-shell ionisation, vibr. struct., sudden approx. calcs. 79−50002
CO, isotopic mols., Dunham pot. energy coeffs. 78−41979
CO, quadratic vibr. force const., from X-ray scatt. factors 79−45864
CO, vibr. struct., core and valence ESCA spectra, Frank-Condon and HF anal. 80−32602
CO_2, ab initio SCF calcs., force consts., vibrs., pot. energy surface 78−5209
CO_2, dipole moment functions 80−87094
CO_2, ionised states, core and valence, ab initio HF calcs. 77−79597
CO_2, stretch-stretch interaction force const., electron correlation influence, ab initio CI study 80−58161
CO_3, and isotopic forms, struct., normal coord. anal. 78−965
C_3O_2, mol., pot. functions of bending modes 80−9753
COF_2, force field analysis using parametric represent. method 80−27990
COS, mole. potential surface, evaluation from spectroscopic observations 80−43207
C_3OS, vibrational assignment, calc. of normal modes and valence force consts., IR spectra 79−50014
CSFCl, vibr. excited states, microwave spectra *(German)* 78−55167
^{13}C-^{13}C spin-spin coupling const. and stretching force consts., single and double bonds 80−63867
C*O, core hole species soft X-ray emission spectra examination 79−41186
Ca_2, $A^1\Sigma_u^+$-$X\Sigma_g^+$ system, laser induced fluoresc., pot. energy curve and mol. consts. 80−58307
CaF_2, force consts., mean amplitudes of vibr. 78−17647
$CaSO_4.2H_2O$, H_2O intramol. force fields calcs. 79−51229
$CdF_2(FCl)(FBr)$, matrix isolated IR and Raman spectra, assignments, force consts., isotope effects and thermodynamic props. 80−63631
$Cd(^{15}NH_3)_4^{2+}$, IR spectrum, force consts. *(German)* 77−6781
CdX_2, (X=Br, Cl), spectroscopic parameters of mols. from vibr. isotopic effects 78−74798
CdX_2, CdXY, (X,Y=Cl,Br,I), matrix isolated vibr. spectra, isotopic effects, force consts. 77−3358
CdX_2, CdXY, (X,Y=Cl,Br,I), matrix isolated, far IR spectra, thermodynamic props. 78−86869
CdXY, (X, Y=Cl, Br, I), spectroscopic parameters of mols. from vibr. isotopic effects 78−74798
CeF_3, force consts., Coriolis coupling consts., vibr. amplitudes 78−17650
CeF_3, mol. force, compliance and Coriolis consts. 79−31726
ClCN, and isotopic species, force field calc., freqs., rot. consts. 79−22692
ClCN, general quartic force field, Machina-Overend parameters 78−50532
$ClF^*(B^3\pi_0^+)$, electronically excited, chem. generation, B→X emission spectrum 79−57216
$Cl_2(H_2O)_n$, mean vibr. amplitudes, Raman spectra, isotope effects 77−58014
ClO, UV spectra of $C^2\Sigma^-$←$X^2\Pi$ system, rot. anal. 80−996
ClO_2F, pyramidal type mol., force field comput. using Green's function procedure 80−23407
ClSN, force consts. and mean amplitudes of vibr. calc. 77−30855
Cl_2SO, A′-force consts., 4th-order secular eqn., L-matrix approx. vs. HLFS methods 79−36556
$Cl_3SiOSiCl_3$, normal vibs. and force field, calcs. using electron diffr. struct. determ. *(Russian)* 78−46317
$Co_4(CO)_{12}$, heptane soln. Co-Co force consts., prereson. Raman spectra, rel. to solid IR spectra *(French)* 78−31193
$CrBr_4$, mol. consts. and mean vibr. amplitudes calcs. 80−106318
$Cr(CO)_6$, relative intensities of ν(CO) and ν(MC) Raman bands 78−55176
$CrCl_4$, mol. consts. and mean vibr. amplitudes calcs. 80−106318
CrO_2Cl_2, matrix isolation IR spectrum and force constants 79−3445
Cs_2, fluoresc. at 6270 Å, rot. consts. 79−45744
$Cs_2UO_2Br_4$, force consts., IR spectra 78−5216
Cu complex, $Cu(NH_3)_2(NCX)_2$, X=O, S, electronic struct., stereochem. 80−58156
$CuCl_2.2H_2O$, H_2O intramol. force fields calcs. 79−51229
$Cu_2(OH)_2CO_3$, malachite, vibr. assignments, force consts., coincidence method appl. 78−62953
DBr, IR absorpt. in 5-0 band, high-resolution spectra 77−14431
$D^{79}Br$, $D^{81}Br$, IR absorpt. spectra of 1-0, 2-0, 3-0, 4-0 bands 77−3360
DCN, self-assoc. in matrices, IR vibr. spectra of multimers 78−86858
DN_3, microwave spectra, 8-340 GHz, spectrosc. consts. for ^{13}N isotope 79−85958
EuF_3, mol. force, compliance and Coriolis consts. 79−31726
$FBrO_3$, gas-phase electron diffr., mol. struct., force field, vib. amplitudes 77−547
FCN, and isotopic forms, force field calc., freqs., rot. consts. 79−22691
FCN, general quartic force field, Machina-Overend parameters 78−50532
FCO, form. in Ar matrix, vibr. and electronic spectra, valence force potential determ., mol. photodissoc. obs. 80−85170
FH, quadratic vibr. force const., from X-ray scatt. factors 79−45864
FH-OH_2(dimethyl ether), H-bonded complexes, cubic force consts. calcs. 80−47868
F_2SO, A′-force consts., 4th-order secular eqn., L-matrix approx. vs. HLFS methods 79−36556
F_3SiAsH_2, liq. Raman, gas phase IR spectra, normal coord. anal., assignments *(German)* 77−6778
$FeCl_3$, Fe_2Cl_6, matrix isolation Raman spectra, assignments 77−65480
$FeCl_3$, intramolecular force fields, compliance consts. and vibr. amplitudes 80−58234
Ga trihalides, vibr. anal., pot. const. determ., mol., compliance and Coriolis coupling const. calc. 80−95579
$GaBr_3$, D_{3h} point group, mol. consts., struct. effects 79−54992
$GaCl_3$, D_{3h} point group, mol. consts., struct. effects 79−54992

molecular force constants continued
$GaCl_3$, force and compliance consts., OVFF, UBFF and GVFF models 78−50663
$GaCl_3(Br_3)(I_3)$, intramolecular force fields, compliance consts. and vibr amplitudes 80−58234
GaH_3 , GaD_4 , intramol. force fields, F_2 vibrs., isotope shifts 77−3336
GaI, rot. spectrum, EHF spectra obs. 80−58245
GdF_3, mol. force, compliance and Coriolis consts. 79−31726
Ge-O cpds., bond lengths rel. to force consts. 77−46653
GeCl, mol., UV spectra, band assignments and rot. consts. 80−997
GeF_2, force consts., mean amplitudes of vibr. 78−17647
GeF_4, $\nu_3(F_2)$ IR band contour, isotopically pure cpds., mol. consts. 77−61746
GeH_3-group containing mols., normal coord. anal. 80−9579
GeH_4, microwave spectra of Q-branch, rot. consts. 79−54845
GeH_4, orbital valency force field 77−34779
GeH_4, tetrahedral mol., force field calcs. 78−29734
$(GeH_3)_3P$, vibr. force fields and amplitudes zero point, structs. 77−54551
GeH_3X, (X=F,Cl,Br,I), force fields and consts., Redington's method calcs. 80−58130
GeH_3X, mol. consts. calcs. 79−36606
GeH_3NCS, mol., IR, Raman and microwave spectra, $^{70,72,74}Ge$ and $^{1,2}H$ isotopes 79−89663
GeO, UV spectra of mol., rot. anal. 79−81210
GeO_4^{4-} compounds, vibr. pot. function, force consts., isotopic shifts, mean vibr. amplitudes 80−23395
GeO_4^{4-}, normal vib. freq. and force const. calcs. *(Russian)* 78−46318
GeO_4^{4-}, normal vibr. freqs. calc. 79−54837
GeX_4, X=H, F, Cl, parametric representation method 78−25503
H_2, quadratic vibr. force const., from X-ray scatt. factors 79−45864
H_2, SCF method with fixed orbital basis *(French)* 79−94107
H_2Se, potential function and vibrational spectra 77−68030
H_2^+, SCF multiple scatt. calc. 80−916
H_2^+, $^3\Sigma_u^+$ excited level, GO SCF calcs. 77−46507
$HAlCl_2$, IR matrix spectrum, vibrs. and force consts. *(German)* 79−11786
HBF_2 and DBF_2 harmonic force field and ground-state average struct. determ. 80−83342
HBS, and isotopic forms, force consts., coriolis consts., vibr. amplitudes, shrinkage effects 80−43021
HBS, force consts., Coriolis const., vibr. amplitude, shrinkage and isotope effect 79−22863
HBr, and DBr, in monatomic matrices, near IR spectra and aggregate structs. 79−89667
HBr, Dunham pot. energy coeffs. 78−41979
HCCN, matrix isolation IR and UV spectra, vibr. anal., struct. 77−65457
HCN, and stable isotopic species, mol. struct., ground vibr. rot. transitions and consts. 77−10666
HCN, dipole moment derivatives and force consts., CI calcs. 78−90091
HCN, ground state pot. surfaces, analytical functions 80−83304
HCN, HNC, molecular electronic struct., unlinked cluster effects 78−94185
HCN, self-assoc. in matrices, IR vibr. spectra of multimers 78−86858
HCN, vibr. fine struct. accompanying core ionis., STO calcs. 78−62844
HCNO, isomers, geometry, spectra, rot. and force consts., ab initio calcs. 77−34574
HCO and HNO, pot. energy functions for ground state surfaces 79−89620
HCP, force fields and force consts. of electronically excited states 80−69116
HCl, and DCl, in monatomic matrices, near IR spectra and aggregate structs. 79−89667
$(HCl)_2$, vibr. freqs. in inert gas matrix, force const., MINDO/3 calcs. 78−41952
HD^+, Hellmann-Feynman theorem anomaly 80−63510
HF, force consts., ab initio CI calcs. *(French)* 78−90093
HF, pot. curve, one-config. Hartree-Fock-Roothaam calc. for force consts. 78−82627
HF, spectroscopic consts., FSGO calcs. 77−6758
HF-HCN, microwave spectroscopic investigations of hydrogen-bonded complexes 78−62794
$(HF)_n$, n=1-∞, ab initio hydrogen bond and electronic parameters, phonons 77−14342
HI, Dunham pot. energy coeffs. 78−41979
HNB,(HNBH), spectroscopic properties, PNO-CI and CEPA calcs. 78−41961
HNC (DNC), anharmonic force field, equilib. struct., rot. consts. and bond lengths 78−90147
HNC, and stable isotopic species, mol. struct., ground vibr. rot. transitions and consts. 77−10666
HNC, millimetre spectrum, rot. consts., force consts., U90.7 interstellar line, struct. parameters 77−57989
HNF_2, force consts., geometry, ab initio Hartree-Fock calcs. 77−57864
H_2NF, force consts., geometry, ab initio Hartree-Fock calcs. 77−57864
H_2O, ab initio SCF CI calcs., ground state energy, config. and force consts. 77−18782
H_2O, and ^2H, ^{18}O isotopic derivations, vibr. freqs. using MINDO/3 force consts. 77−71793
H_2O, dimers, IR spectra in N_2 matrix, assignments and force consts., isotope effects 77−61744
H_2O, double SCF method for electron correl., stretching force const. 78−17575
H_2O, ESCA and soft X-ray emission, vibr. excitation 80−23433
H_2O electro-optical harmonicity of OH bond 77−34634
H_2O, electronic ground state, SCF HF and CI calcs, pot. energy hypersurface, spectroscopic consts. 78−50473
H_2O, equilib. struct., ab initio SCF calcs., general valence force field 77−3265
H_2O, excited states, pot. energy curves w.r.t. bond ang., one-centre expansion approx. 79−6886
H_2O, force consts., ab initio calcs. with differentiated estimation of integrals 77−67974
H_2O force consts., ab initio CI calcs. *(French)* 78−90093
H_2O, force consts., vibr. freqs., CNDO/2 and MINDO calcs. 77−14607
H_2O, H bonding, electronic struct., geometries, moments, dimerisation energies, charge distrib., pseudopotential calcs. 80−27942
H_2O, in $CuCl_2.2H_2O$ or $CaSO_4.2H_2O$, intramol. force field calcs. 79−51229
molecular force constants continued
H_2O, isotope derivatives, mech. anharmonic problems, spectroscopic consts. 79−63983
H_2O, rot.-vibr. Schrodinger eqn. soln., bond lengths and angles, force consts. 79−41151
H_2O^+, X^2B_1 and B^2B_2 states, pot. surfaces, SCF and CI calcs. 77−3338
$H_2{}^{16}O$, $H_2{}^{18}O$, isotope fractionation, H-bonds, force consts., liq. water struct. 77−76288
$HOB_3(HBO)_3$, spectroscopic properties, PNO-CI and CEPA calcs. 78−41961
$H_3O^+(H_2O)_n$, H^+ motion energetics, ab initio calcs. 78−25413
$H_2O...HF$ complex, force field, vibr. freqs., equilib. geometry bond energy, ab initio calc. 77−65450
HPO, emission system, rot. anal. of vibr. bands 80−47957
HPO, mol. struct. and props., ab initio, calc., Gaussian lobe orbital 78−62713
HSiN-HNSi isomers, MRD-CI calcs. of struct. and stability 78−82635
H_2SiO, electronic struct., dipole moments, mol. polarisability, force fields, ab initio calcs. 80−78531
HeH^+, spectroscopic characts. in ground and first excited triplet states, Dunham pot. approach 77−42234
Hg complex, methylethynylmercury(II)(-d_1,-d_3,-d_4), vibr. spectra and normal coord. calcs. 80−58259
$HgF_2(FCl)(FBr)$, matrix isolated IR and Raman spectra, assignments, force consts., isotope effects and thermodynamic props. 80−63631
HgX_2, (X=Cl, Br), spectroscopic parameters of mols. from vibr. isotopic effects 78−74798
$HgX_2(HgXY)$, (X,Y=Cl, Br, I), IR and Raman matrix isolation spectra, bending force consts. 77−465
HgXY, (X, Y=Cl, Br, I), spectroscopic parameters of mols. from vibr. isotopic effects 78−74798
HoF_3, mol. force, compliance and Coriolis consts. 79−31726
IBr, predissoc. and photodissoc., intermed. coupling strength 77−16850
ICN, general quartic force field, Machina-Overend parameters 78−50532
ICN_3, microwave spectrum, vibr.-rot. const., equilib. struct. 78−58677
ICl, ^{35}Cl and ^{37}Cl, $B^3\Pi_{0+}$ state IR spectra, mol. consts. 80−28016
IF_7, generalised quadratic valence pot. calcs., Wilson's F-G matrix 79−93966
In trihalides, vibr. anal., pot. const. determ., mol., compliance and Coriolis coupling const. calc. 80−95579
$InCl_3$, D_{3h} point group, mol. consts., struct. effects 79−54992
$InCl_3$, force and compliance consts., OVFF, UBFF and GVFF models 78−50663
$InCl_3$ in Kr lattice, Raman and IR spectra, vibr. assignments, force consts., isotope shift and config. 79−89671
$InCl_3$, intramolecular force fields, compliance consts. and vibr. amplitudes 80−58234
InI_3, D_{3h} point group, mol. consts., struct. effects 79−54992
$KBrO_2F_2$, struct. data, vibr. spectra 77−39563
$K_2(Cd(CN)_4)$, vibr. spectra, isotope substitutions, force consts. determ. *(German)* 77−61750
K_2MoO_3S, aq. soln., Raman spectrum, MoO_3S^{2-} force consts. 78−74668
$K_2UO_2Br_4$, force consts., IR spectra 78−5216
$K_2(Zn(CN)_4)$, vibr. spectra, isotope substitutions, force consts. determ. *(German)* 77−61750
Kr_2, mean force constants and rectilinear law of mean force calcs. 78−33414
KrHBr, KrCHl, and isotopic forms, rot. spectra, mol. struct., mol. consts. 80−58246
KrHCl, van der Waals complexes, struct., RF and microwave spectra, isotope effects 80−37806
KrHCl, weak complex, rot. spectra 80−52980
LaF_3, force consts., Coriolis coupling consts., vibr. amplitudes 78−17650
LaF_3, mol. force, compliance and Coriolis consts. 79−31726
Li_2, optical-optical double reson., $^1\Sigma_g^+$ state mil. consts. 80−53027
LiCNS, ether solns., dimer struct. and force consts., IR and Raman spectra 79−72442
LiF, pot. curve, one-config. Hartree-Fock-Roothaam calc. for force consts. 78−82627
$LiF-NH_2$ adduct, mol. consts., ab initio SCF LCAO MO calcs. *(French)* 78−13423
Li_2F_2, struct., force fields and normal mode freqs., ab initio calcs. 80−83260
LiH, $LiHe^+$ and $LiHe_2^+$ systems, ab initio SCF LCAO calcs. of stability and spectroscopic consts. 77−71748
LiH, mol. spectroscopic consts., FSGO calcs. 77−6758
LiH, pot. curve, one-config. Hartree-Fock-Roothaam calc. for force consts. 78−82627
LiH, $X^1\Sigma^+$ ground state, spectroscopic and pot. functions, method for combining spectroscopic data 79−45782
$LiH_2(LiD_2)(LiT_2)$, pot. surfaces, fundamental freqs. and thermodynamic functions 80−69205
$Li_2H(Li_2D)(Li_2T)$, pot. surfaces, fundamental freqs. and thermodynamic functions 80−69205
α-$LiIO_3$, hexagonal cryst., vibrs. and force consts. 79−69220
Li_2O_2, ab initio geometry, vibr. freqs., ionis. pots., and force consts. 77−65421
$LuCl_3$, pyramidal struct. and force field coeffs., electron diffr. obs. 78−9250
LuF_3, mol. force, compliance and Coriolis consts. 79−31726
$MgBr_2$, force consts., vibr. amplitude and shrinkage effects 79−22863
$MgCl_2$, force consts., vibr. amplitude and shrinkage effects 79−22863
MgF_2, force consts., mean amplitudes of vibr. 78−17647
MgI_2, force consts., vibr. amplitude and shrinkage effects 79−22863
MgX_2 (X=F, Cl, Br, I), 2Z 80−43021
MgX_4^{2-} (X=Cl, Br, I), pseudo-exact force consts. 77−31022
MnH(MnD), $^7\Sigma$-state, mol. parameters, ESR and optical spectrosc. 78−94264
$MnH_2(MnD_2)$, $^6A_1$ state, mol. parameters, ESR and optical spectrosc. 78−94264
MnO_4^- ion, ^{18}O enriched, matrix isolated IR spectra, force consts. 80−52985
$Mo(CO)_6$, relative intensities of ν(CO) and ν(MC) Raman bands 78−55176
$Mo(CO)_6Kr$, dispersion energy, stabilisation energy, Mo-Kr separation 79−98241
MoO_3, $^{16}O^{18}O$ substitution, isotope shift, vibr. amplitudes and consts., normal coord. anal. 79−36610
Mo_7O_{24}, C_2, symmetry model, force field anal. 79−81200

molecular force constants continued
N-H bond containing molecules, correls. among bond lengths, stretching freqs. and bond order matrix elements 77−58192
N_2, quadratic vibr. force const., from X-ray scatt. factors 79−45864
N_2, solid, α- and γ-forms, Raman spectra, vibron and lattice freq. shifts, libration 80−16020
N_2, solid, Raman spectra vibron and lattice freq. shifts, librational force consts., α- and γ-phases 78−19460
N_2, vibr. struct., core and valence ESCA spectra, Franck-Condon and HF anal. 80−32602
N_3^-, high press. IR vibr. spectroscopy *(German)* 80−74170
NCS, force field in alkali halide lattices 79−51224
$NCl_3.NH_3$, force const. calcs. 79−36603
N_2F_4, centrifugal distortion effect in microwave rot. spectrum 77−30859
NH, mol. spectroscopic consts., FSGO calcs. 77−6758
NH_2, ground state mol. consts., absorption spectra 80−28030
NH_2 radical, mag. hyperfine interactions, zero-point vibrs. effects 80−58167
NH_2^-, photodetachment energy calcs. 77−27123
NH_3, ab initio SCF calcs., force consts., vibrs., pot. energy surface 78−5209
NH_3, ESCA and soft X-ray emission, vibr. excitation 80−23433
NH_3, force consts., vibr. freqs., CNDO/2 and MINDO calcs. 77−14607
NH_3, NH_3^+ ion, electrostatic force theory appl. to mol. geometry ab initio verification 79−98002
NH_3, predissociation of A''_2 state, force constants calc. 80−1034
NH_3, vibr. excitation in soft X-ray emission and core ESCA spectra 80−69163
NH_3^+ radical, mag. hyperfine interactions, zero-point vibrs. effects 80−58167
NH_3-CO_2 complex, matrix isolation IR spectrum, struct., ab initio SCF calcs. 78−5209
NH_3-lithium halide complex, ab initio calcs., Li bond rel. to H bond 77−14343
NH_4^+, mol. consts. and mean vibr. amplitudes calcs. 80−106318
N_2H_2, vibr. assignment and pot. function, cis- and trans. mols., d_0-d_2 species 79−85952
$N_2H_4^+$ radical, mag. hyperfine interactions, zero-point vibrs. effects 80−58167
$NH_3(ND_3)(NT_3)$, harmonic force fields, equal coord. method calcs. 77−30845
$(NH_4)_2S_5$, Raman spectra, vibrs. and rot. isomers of Sn^{2-} (n=4-8) *(German)* 78−13504
$NH_4UO_2(NO_3)_3$, IR spectra, force consts., bond orders 77−30873
$NH_2(X^2B_1)$, laser mag. reson. spectra, Zeeman and hyperfine effects, rot. consts. 77−30892
NO, $b^4\Sigma^- \rightarrow a^4\Pi$ band system, rot. consts. 79−72312
NO dimer, asymmetric, characterisation, Raman, IR spectroscopy 79−41176
NO_2 and isotopic forms, total quartic potential function 78−13486
$(NO)_2$, normal coordinate anal. 78−90144
NO_2, reson. fluoresc. excited by visible laser, force consts. of ^{15}N mol. 79−72343
NO_2^-, high press. IR vibr. spectroscopy *(German)* 80−74170
NO_2, solvated, in H_2O, ethanol, cyanomethane, and DMF lowest n-π* transition 79−85960
NO_2^-, molecular vibrational constants in KBr crystal, impurity effects 77−20035
NO_2^+, gas phase equilib. geometry, force consts., vibr. freq., dipole moment function MCSCF/CI calcs. 80−78520
$(NO_2)_2$, struct. and force fields of isomers, ab initio calcs. 77−18783
N_2O, dipole moment functions 80−87094
N_2O^+, force fields and force const. of electronically excited states 80−69116
N_2O_4, mol. force consts. and vibr. amplitude, force field study 79−31730
NO_2Br, formation and IR spectrum 79−98097
NO_2Cl, force fields calc. 78−42241
NO_2Cl, rot. distortion parameters for force consts. determ. in parametric method 79−76401
NO_2F, force fields calc. 78−42241
NO_2F, rot. distortion parameters for force consts. determ. in parametric method 79−76401
NO_2I, formation and IR spectrum 79−98097
NSCl, force consts. and mean amplitudes of vibr. *(German)* 79−50005
NSF_3, IR spectra, matrix isolated, force const. calc. 78−62802
NSF_3, microwave spectra in vibr. excited states, mol. consts. 79−50009
NSF_3, RF-mm wave double reson. of vibr. excited state 79−50054
N_2^*, core hole species soft X-ray emission spectra examination 79−41186
$NaIO_4$, normal coord. anal., internal and external modes 79−23684
$Na_3UO_2F_5$, IR and Raman spectra, struct. *(French)* 79−11409
$NbCl_5.POCl_3$, Raman spectra, normal coordinate treatment 77−46568
NdF_3, mol. force, compliance and Coriolis consts. 79−31726
$Ni(CO)_4$, mol. struct. by gaseous electron diffr., quadratic force field refinement 79−64115
$NiN_4S_4H_2$, vibr. anal. 78−90148
NiO, bulk props., initial state MO Ni_4O_4 and $Ni_{13}O_{14}$, cluster model, lattice and force consts., photoemission and CT absorpt. spectra 80−84828
O_2, anharmonicity const., Raman meas. 77−34637
O_2, excited state geometries and energies, ab initio pot. energy surfaces 78−5151
O_3, analytical potentials from spectroscopic data, vibr., bond length, dissoc. 77−10613
O_3, anharmonic force field and isotopic relation 77−58198
O_3, IR spectra of vibr. rot. bands 79−64001
O_3 vibr. and rot. variational calc., isotope shifts 77−57967
OAlCl and OAlF, IR matrix spectra, vibr. freqs. *(German)* 79−11785
$OCBr_2$, IR spectra in Ar matrix, force consts. *(German)* 79−36641
OCS, 5.3 μm vibr.-rot. bands, rot. consts., spin-flip Raman laser obs. 77−34631
OCS in Ar soln., IR spectra, solvent shifts, vibr. band assignment and anharmonic force consts. 80−9607
OCS, mol. consts. of ν_2 levels 77−14429
OGaF, matrix IR spectrum, vibrs. and force consts. 79−11787
OH, Dunham pot. energy coeffs. 78−41979
OH, optimum mol. consts. and term values, $X^2\Pi$ and $A^2\Sigma^+$ states, vibr.-rot. and microwave freqs. 80−95577
$OH^+(OD^+)$, $A^3\Pi_i \rightarrow X^3\Sigma^-$ emission branching ratios, r-centroid depend. 77−6830
$ON^{81}Br$, anharmonic force field from IR and microwave data 78−82809
ONCN, IR spectra isotope shifts and ab initio calc. for harmonic force field 79−13715
$ON^{35}Cl$, anharmonic force field from IR and microwave data 78−82809
ONF_3, vibr. anal. using Green function 77−57962
ONI, IR matrix isolated spectra, force consts. 79−10111
$Os^{16,18}O_4$, pseudo-exact force consts. 77−31022
OsO_4, and isotopic forms, stretching fundamental, 961 cm^{-1}, high resolution spectroscopy 78−90162
OsO_3F_2, normal coordinate anal. in Urey-Bradley force field 79−49966
P-O cpds., bond lengths rel. to force consts. 77−46653
PF_3, anharmonic force field from mm wave spectra of vibr. excited states 79−13701
PF_3 pyramidal mols., intramol. forces, fundamental vibr. freqs., centrifugal distortion consts. 78−5202
PF_5, normal coord. anal., generalised valence force field calcs. 77−58195
PH_2, laser mag. reson. spectra. 9-9.6 μm, ν_2 band 79−89694
PH_3, equilibrium structure and harmonic force field, ab initio calc. 80−9502
PH_5, equilibrium structure and harmonic force field, ab initio calc. 80−9502
$PH_3(D_3)$, ^{31}P NMR, chemical shielding, centrifugal distortion, anharmonic vibr., cubic force consts. 78−82752
$PH_3(PD_3)(PT_3)$, harmonic force fields, equal coord. method calcs. 77−30845
$PMo_{12}O_{40}^{3-}$, vibr. force const. for spectroscopically active freqs. 77−57976
P_4O_6, IR and Raman spectra vibr. spectra, valence force field calc., pot. function *(French)* 78−50549
$PbCl_6^{4-}$, model force fields and vibr. amplitudes calcs. 78−62780
$PdCl_4^{2-}(Br_4^-)$, mean vibr. amplitudes and force field, Muller approx. 77−10659
PrF_3, orbital valency force consts. and mean square amplitudes 78−74627
Pt complexes, INDO calcs. for predicting ground-state props., charge distributions and force const. determ. 80−83283
Pt complexes, XY_4Z_2 type ions, vibr. anal., force consts. 78−70812
$PtCl_4^{2-}$, vibr. force consts. calc. 78−58655
$PtCl_4^{2-}(Br_4^{2-})$, mean vibr. amplitudes and force field, Muller approx. 77−10659
PuO, in Ar and Kr matrices, IR absorption spectra, normal coord. anal., assignments, force consts. 78−78681
PuO_2, in Ar and Kr matrices, IR absorption spectra, normal coord. anal., assignments, force consts. 78−78681
ReF_6^+, force consts. and vibr. props., GVFF calcs. 77−14417
ReF_7, generalised quadratic valence pot. calcs., Wilson's F-G matrix 79−93966
RuO_4, $\nu_3(F_2)$ IR band contour, isotopically pure cpds., mol. consts. 77−61746
$(Ru_2OCl_{10})^{4-}$; reson. Raman, IR and electronic spectral studies 79−10118
$S_2{}^{35}Cl_2$, microwave spectra and double reson., assignments, distortion consts. and struct. 79−89664
S_2, at. force consts. and internuclear distance 77−42439
S_2, microwave spectra 79-150 GHz, rot. and fine struct. parameters 79−63987
S_7, Raman and IR spectra, vibr. anal., force consts., thermodynamic functions 78−50545
SCF_2, IR, Raman and matrix isolation spectra, isotopic shifts, anharmonicity consts. *(German)* 77−83600
$(SCN)_2^-$, and $(SCN)_2$, vibr. anal., bond strengths 80−9582
S_4Cl_2, Raman spectra, vibrs. and rot. isomers of S_n^{2-} (n=4-8) *(German)* 78−13504
SCl(Br), unstable radicals, matrix-isolated, IR spectra force const. *(German)* 80−43053
$^{32}SF_2$, $^{34}Sf_2$, matrix IR spectra, vibr. and force fields, bond angle *(German)* 78−74662
SF_6, hot, vibr. anharmonicity, electron diffr. study, 298-10^3K 79−68316
SF_6, vibr. anharmonicity consts., ν_4 region laser absorption obs. 78−94242
SF_6, vibr. strength, IR intensities calcs. 77−34608
$^{32}SF_6$, anharmonic splittings, vibr. energy levels, $n\nu_3$ manifold 77−30853
SN, electronic states, ab initio, SCF, and CI calcs. 77−75053
$S_4N_4H_4$ ($S_4N_4D_4$), vibr. spectra, force consts. *(German)* 78−13499
S_7NH, solid and solns. vibr. spectra, force consts. isotope effects 77−66490
SO_2, $^1B_2$ state, force field and asymm. struct. 79−22685
SO_2, force field determ. from first and second order Raman spectra *(Russian)* 77−14441
SO_2 surface reaction and decomposition on zeolites, resonance Raman study 80−61145
SO_3, dissoc. pathways and mol. vibr., compliance consts. and min. energy coords. 78−35661
SO_4, and isotopic forms, struct., normal coord. anal. 78−965
S_2O, isotopes, force consts., mean amplitudes of vibr. 78−970
SPF_3, IR spectra, matrix isolated, force const. calc. 78−62802
$SbCl_3$, dynamic coeff., molecular interaction effects of media *(Russian)* 77−83601
$SbCl_5.POCl_3$, Raman spectra, normal coordinate treatment 77−46568
SbF_3, IR spectra of solid and gas, rel. to struct. *(French)* 78−78692
$SbF_5.OSO$, force constants, normal coordinate calculations 77−61735
SbO_4^{3-}, normal vib. freq. and force const. calcs. *(Russian)* 78−46318
SbO_4^{3-}, normal vibr. freqs. calc. 79−54837
Sb_4O_6, IR and Raman spectra vibr. spectra, valence force field calc., pot. function *(French)* 78−50549
ScF_3, pyramidal struct. and force field coeffs., electron diffr. obs. 78−9250
$SeCF_2$, IR, Raman and matrix isolation spectra, isotopic shifts, anharmonicity consts. *(German)* 77−83600
SeF_6, IR vibr. band contours, isotope substitution, force consts. 78−17670
SeH, isotope effects, Rydberg levels-ground state transitions, rot. const., VUV spectra obs. 80−58279
SeO, mol., mm wave spectra, $X^3\Sigma^-$ state 79−85959
Si-H bond containing molecules, correls. among bond lengths, stretching freqs. and bond order matrix elements 77−58192
Si-O cpds., bond lengths rel. to force consts. 77−46653
Si_2, SCF Xα calcs. using pseudopots. and PW basis set 77−34558
Si_6Br_{12}, and Si_6Cl_{12}, vibrational spectra and force constants, rel. to Si_5Cl_{10} and Si_5Br_{10} *(German)* 79−22716

molecular force constants continued
Si_5Cl_{10}, and Si_5Br_{10}, vibrational spectra and force constants, rel. to Si_6Cl_{12} and Si_6Br_{12} *(German)* 79−22716
SiF_4,($SiCl_4$), parametric representation method 78−25503
SiF_4, ^{19}F chem. shielding, depend. on internal coords. 78−5249
SiF_4, $\nu_3(F_2)$ IR band contour, isotopically pure cpds., mol. consts. 77−61746
Si_2F_6, normal coord. analysis, vibr. freqs. and amplitudes, shrinkage and distortion consts., force consts. 80−27989
SiH_3-group containing mols., normal coord. anal. 80−9579
SiH_4, orbital valency force field 77−34779
SiH_4, tetrahedral mol., force field calcs. 78−29734
Si_6H_{12}, and Si_6D_{12}, Raman and IR spectra, vibr. force consts., config. *(German)* 79−22715
SiH_2DF, $SiHD_2F$, microwave spectra, harmonic force field, mol. struct. 77−18913
$SiHX_3$, (X=F,Cl,Br,I), force fields and consts., Redington's method calcs. 80−58130
$(SiH_3)_3Y$, (Y=As, P, Sb), vibr. force fields and amplitudes, zero point struct. 77−54551
SiO_4^{4-} compounds, vibr. pot. function, force consts., isotopic shifts, mean vibr. amplitudes 80−23395
SiS, and isotopes, microwave spectra and consts., review 77−23493
$SnBr_4$, matrix-isolation and $^{79/81}Br$ and $^{116/124}Sn$ isotope shifts in IR spectra 77−46561
$SnCl_3^-$, harmonic approx., force consts., electro-optical parameters and normal vibrs 78−62790
$SnCl_4N_2$ ions, force field calc., vibr. amplitude and rot. distortion consts. 79−98245
SnH_4,($SnCl_4$), parametric representation method 78−25503
SnH_4, tetrahedral mol., force field calcs. 78−29734
SnI_3^-, harmonic approx., force consts., electro-optical parameters and normal vibrs 78−62790
SnI_3 , vibr. intensities, forms and freqs. anal. SCF MO LCAO CNDO calcs. 78−9274
SnO_4^{4-}, normal vib. freq. and force const. calcs. *(Russian)* 78−46318
SnO_4^{4-}, normal vibr. freqs. calc. 79−54837
Sr+Ar, press. effect on Sr 4607 Å reson. line shape, width and shift 79−22653
SrF_2, force consts., mean amplitudes of vibr. 78−17647
$TaBr_5$, gaseous, electron diffr. obs. of vibr. assignment, mol. struct. and barrier to pseudorot. 79−81293
Te_4^{2+}, pseudopot. SCF-MO calcs., spectrum assignments 80−83269
TeO_4^{2-}, normal vib. freq. and force const. calcs. *(Russian)* 78−46318
TeO_4^{2-}, normal vibr. freqs. calc. 79−54837
TeO_4^{4-}, vibr. props. calcs. *(German)* 79−3431
$Te^{VI}O_6$ ion in $A_2B^{II}B^{VI}O_6$ perovskites vibr. anal. using isotope shifts and perturbation theory 77−59073
Ti complexes, cryst., amorphous, coordinated H_2O, mol. force field ellipses, mol. force consts. 77−34609
$TiBr_4$, (TiI_4), struct., force field and Coriolis const. calcs. 78−86843
$TiCl_5^-$, vibr. anal., force fields and consts. *(German)* 79−45702
$Ti_2Cl_{10}^{2-}$, vibr. anal., force fields and consts. *(German)* 79−45702
$(TiCl_4.POCl_3)_2$, normal coord. anal. and force consts. 79−22682
TiF_2, force consts., mean amplitudes of vibr. 78−17647
TiF_4, equilib. config., force field, Coriolis consts., vibr. freqs. and amplitudes 80−32835
TiI_4, pseudo exact force consts. 77−31022
Tl halide dimers, kinetic consts. method for vibr. analysis 79−26968
Tl_2X_2(X=F,Cl), mol. force field and const. constraints from electron diffr. data 77−27197
UBr_4O_2 ions, force field calc., vibr. amplitude and rot. distortion consts. 79−98245
UCl_4O_2 ions, force field calc., vibr. amplitude and rot. distortion consts. 79−98245
UF_5, monomer struct. and pot. consts., IR and Raman spectra in inert gas matrices 78−5215
UF_6, vibr. strength, IR intensities calcs. 77−34608
$UO_2(NO_3)_2$ complexes, IR spectra, normal coordinate anal., vibr. assignments, force consts. and ligation effects 80−9608
VF_5, normal coord. anal., generalised valence force field calcs. 77−58195
$W(CO)_6$, relative intensities of ν(CO) and ν(MC) Raman bands 78−55176
WCl_6, force fields, IR spectra, isotope shifts 77−14432
WO_3, force field, normal coord. anal., kinetic consts. method, thermodynamic props. 78−25504
WO_3, vibr. anal., mol. consts., kinetic consts. method 80−23393
XBr_4, Coriolis coupling const., at. mass effect 79−31728
XI_4, Coriolis coupling const., at. mass effect 79−31728
XY_3, XY_4 mols., harmonic force field calcs., average pot. energy criterion 77−57903
XY_4Z molecules, assignment of fundamentals of vibr. spectra for 24 mol. with C_{4v} symmetry *(French)* 79−31504
XeF_2, pseudopotential SCF-MO studies, equilib. struct., stretch-stretch interaction force const. 80−95525
XeF_4, pseudopotential SCF-MO studies, equilib. struct., stretch-stretch interaction force const. 80−95525
XeF_4, vibr. force consts. calc. 78−58655
XeF_5^+, pseudopot. SCF MO studies, steric aspects of struct. and force fields, Jahn-Teller effect 80−99444
XeF_6, pseudopot. SCF MO studies, steric aspects of struct. and force fields, Jahn-Teller effect 80−99444
XeO_3F_2, mol. consts., general valence force field calcs. 78−21906
$YC(H,D)_3$ (Y=F, Cl, Br, I) mols., applicability of bidimensional approach to force field 77−68026
YF_3, force consts., Coriolis coupling consts., vibr. amplitudes 78−17650
YbF_3, mol. force, compliance and Coriolis consts. 79−31726
ZnF_2(FCl)(FBr), matrix isolated IR and Raman spectra, assignments, force consts., isotope effects and thermodynamic props. 80−63631
ZnX_2, (X=Cl, Br, I), spectroscopic parameters of mols. from vibr. isotopic effects 78−74798
ZnX_2, ZnXY, X and Y=halogen, matrix isolation IR and Raman spectra 78−55171
ZnXY, (X, Y=Cl, Br, I), spectroscopic parameters of mols. from vibr. isotopic effects 78−74798
ZnXY, (X,Y=Cl,Br or I), matrix isolation, vibr. spectra, isotope effects, force consts. and geometry 78−46337
$Zr(BH_4)_4$, and d_{16}, mol. vibr. amplitude, normal coord. anal., T model 79−59433
$ZrBr_4$(ZrI_4), struct., force field and Coriolis const. calcs. 78−86843

molecular force fields *see molecular force constants*

molecular hyperfine structure
acetyl cyanide-d_1, microwave spectra, r_s, r_0-struct. 78−13491
N-acetyle DL-methionine, γ-irradiated, radical cation EPR, ^{33}S hyperfine coupling 77−40559
acyloxy radical ion, in irrad. Rochelle salt, decarboxylation, pulse radiolysis and EPR obs. 78−70854
alkoxy free radicals, produced by X-irrad. of hydroxy containing cpds., characterisation by ESR and ENDOR 78−95938
alkoxy radical, trapped in nucleosides or nucleotides, EPR, INDO calcs. 77−90623
anthronyl radicals, ESR, temp. depend. phenyl twist angles 79−18210
asymmetric-rotor HFS energies, Hamiltonian by irreducible tensor techniques 77−71761
azaphenanthrenes, lowest triplet state zero field splitting parameters calcs. 80−83391
bacteriochlorophyll cation in soln., N atom ENDOR and proton triple resonance 78−96018
benzenes, lowest triplet states, instability rel. to environmental effects 77−57893
benzenoid aromatics, triplet zero field splitting parameters, ODMR obs., struct. effects 80−78636
benzophenone, $^3(n\pi^*)$, carbonyl ^{13}C hyperfine coupling tensor, ENDOR obs. 79−13744
benzophenone, triplet, optically detected EPR, ENDOR and ODMR, HFS, isotope and spin-orbit effects 78−86898
benzophenone, triplet state zero-field ODMR, ^{17}O HFS 79−18216
2,1,3-benzothiadiazole, EPR of phosphorescent state 77−8405
bromoacetonitrile, ground state microwave spectrum assignments, mol. struct., rot. consts., quadrupole coupling 77−6763
bromohaemin, ferric porphyrins with fifth ligands, ^{57}Fe and ^{14}N hyperfine consts. 78−50475
bromomethane, microwave spectrum obs., B rot. and centrifugal distortion consts. 77−75135
bromomethyl methyl ether, microwave spectra, quadrupole computing effect 80−18848
bromomethyl methyl ether, microwave spectra, quadrupole coupling effect 80−14135
bromomethylsilane, microwave spectra, quadrupole computing effect 80−18848
bromomethylsilane, microwave spectra, quadrupole coupling effect 80−14135
3-bromopropene, $^{79,81}Br$, microwave spectrum, mol. struct., nucl. quadrupole coupling consts., rot. consts. 77−6767
3-bromopropene, microwave spectra, torsionally excited mol., HFS and rot. consts. 79−63988
t-butyl radicals, ab initio geometry calc., ^{13}C hyperfine coupling 77−10580
carbenes, triplet state g-tensors and hyperfine coupling tensors 80−52895
chlorohaemin, ferric porphyrins with fifth ligands, ^{57}Fe and ^{14}N hyperfine consts. 78−50475
ClF_6, EPR of matrix, isolated radical 79−85977
computational atomic and molecular physics, conf., Nottingham, England, (Sept. 1978) 79−59567
copper (II) complex, bis(dithiocarbamate), HF-Slater-LCAO calcs., mag. coupling parameters and optical spectrum 80−99447
copper porphine, Xα multiple scatt. calcs., EPR and electronic spectra 78−13426
cupric mixed ligand complexes, mechanism of spin transfer to next neighbours ^{13}C and ^{31}P 78−86892
cyanodiacetylene, interstellar, J=2-1 transition detect. and hyperfine splitting const. 79−25692
2-cyanofurane, rot. consts., dipole moments, nuclear quadrupole coupling, spectral obs. 77−34620
cyanohaemin, ferric porphyrins with fifth ligands, ^{57}Fe and ^{14}N hyperfine consts. 78−50475
2-cyanothiophene, rot. consts., dipole moments, nuclear quadrupole coupling, microwave spectra 77−34620
3-cyanothiophene, rot. spectrum and consts., elec. dipole moment, quadrupole coupling, r_0-struct. 77−79607
1,1-cyclobutanedicarboxylic acid, X- and γ-irrad. cryst., EI-EPR overlapping spectra resolution 77−16179
cyclopropyl cyanide, high-resolution microwave spectra, quadrupole hyperfine struct. of rot. transitions anal. 80−95601
cytochrome c_3, haeme-haeme mag. interaction, Mossbauer obs. 80−108836
deoxyhaemoglobin, high mag. field Mossbauer spectra, electronic states 80−35845
deoxymyoglobin, high mag. field Mossbauer spectra, electronic states 80−35845
deuterated nitroxide radical probe, synthesis and appls. *(French)* 78−76314
di-tert-butyl nitroxide, N hyperfine coupling const., solvent effect, model 79−54870
diatomic intensity factors, hyperfine struct. 77−57978
diatomic mil., hyperfine struct. transitions, quantum theory for undergraduate demonstration 80−17762
diatomic molecule, homonuclear, effective hyperfine Hamiltonian, theory and appl. to B state of I_2 78−58598
diatomic molecule, rel. to theory of high-precision Zeeman effect 77−14486
1,4-diazaphenanthrene, zero-field splitting, basic triplet states, H bond effects 78−5366
1,4-diazatriphenylene, zero field splitting, basic triplet states, H bond effects 78−5366
m-dichlorobenzene, nucl. quadrupole coupling consts., hyperfine struct., bonding 77−14422
dichlorodifluoromethane, microwave rot. absorpt. spectra, nuclear quadrupole coupling, hyperfine splitting 77−30861
electron impact excitation, photon-electron ang. correlation, fine/hyperfine struct. effects 78−42231
ethylidenimine, pyrolysis product, microwave spectra, rot. distortion and electric quadrupole const. and rot. barriers determ. 80−78608
ferrihaemoglobin hydroxide, nucl. hyperfine interaction, HF LCAO calc. 79−2002
ferrous porphyrin, intermediate (S=1) spin state, PMR characterisation 80−48014
fluorene: acridene, radical pair form. from excited states, optical nucl. polarisation obs. 80−14155

molecular hyperfine structure continued
fluorene:acridine (phenazine)(anthracene), optical nuclear polarisation, non-crossing rule, guest-host complex 77−42339
fluoroform, Zeeman effect, mag. moments and susceptibility, nuclear shielding 79−13764
fluorohaemin, ferric porphyrins with fifth ligands, ^{57}Fe and ^{14}N hyperfine consts. 78−50475
formaldehyde, $^{3}A''$ state, zero-field splitting param., ab initio CI calcs. 80−99454
formaldehyde, hyperfine interactions, mol. beam elec. reson. spectra 77−88445
formaldehyde, triplet state g-tensors and hyperfine coupling tensors 80−52895
formaldehyde anion radical, hyperfine coupling consts., vibr. depend., ab initio calcs. 80−87150
free radicals, hyperfine struct., EPR cepstra method determ. 80−102531
haemin, hyperfine interactions and related props. 78−44451
haemoglobin derivatives, hyperfine interactions and related props. 78−44451
hexafluoride radicals, prep. and EPR spectra comparison, hyperfine splitting 78−68381
hexafluorobenzene anion-radicals in squalane, ESR spectrum optical detection 80−95655
hexafluorobenzene radical anion, ^{13}C hyperfine interaction, EPR obs. 80−83392
hydrocarbon radicals, ab initio calc. of spin densities 79−93938
hydroxyhaemin, ferric porphyrins with fifth ligands, ^{57}Fe and ^{14}N hyperfine consts. 78−50475
hydroxymethyl radical, isotropic hyperfine coupling consts., temp. depend., nuclear vibrs. 78−35039
hyperfine coupling, constants, nucl. spin spin coupling const., NDDO MO calcs. 80−23310
imidazoles, reaction with photochemically generated α-hydroxyalkyl radicals, EPR study 80−35558
inert gas monohalides, hyperfine interactions, struct., valence bond calcs. 78−66473
interaction tensor components in mol. systems, evaluation using ang. momentum interactions 77−42249
β-iodophenylacetylene radical, PhC_2I^-, from γ-irrad. morpholine β-iodophenylacetylene complex, EPR obs. 77−52652
3-iodopropene, microwave spectra, rot. consts. and HFS 78−975
3-iodopropene, rot. spectra, quadrupole hyperfine struct. 80−91545
ketene, hyperfine interactions, mol. beam elec. reson. spectra 77−88445
lowest triplet state zero field splitting parameters calcs. 80−83391
methane, $^{13}CH_4$ line hyperfine splitting at 3.39 μm, laser saturated absorpt. obs. 79−76470
methane, hyperfine struct., Racah finite group algebra appls. 78−78617
methane, hyperfine struct. of $F_2^{(2)}$ line, appl. of laser spectrometer 77−58201
methane, line profile of coherent radiation in separated fields due to $F_2^{(2)}$ transition 80−37835
methane, mag. hyperfine struct., laser spectroscopy 77−88757
methane, mag. struct. of vibr.-rotational transition, review of laser appl. to precision meas. 78−42246
methane, nonlinear optical reson. shift in mag. field, vibr.-rot. transition 78−13549
methane, recoil effect, optical resolution by saturated absorpt. spectroscopy 77−18937
methane, rotational state, avoided-crossing molecular beam spectroscopy 80−63730
methane absorption cell for He-Ne laser, hyperfine struct. influence on freq. reproducibility 78−50864
methanol dehydrogenase, enzyme powder, ESR and ENDOR, 9 and 35 GHz 79−70524
methoxy, Jahn-Teller induced rovibronic effect, nuclear spin-electron spin hyperfine Hamiltonian 80−83298
methoxy detection by submillimetric laser spectrometer 77−40623
methyl bromide, NQR and A_1-A_2 splitting, RF spectrosc. inside laser cavity 80−91579
methyl chloride, Zeeman effect, mag. moments and susceptibility, nuclear shielding 79−13764
methyl cyanide, linewidth parameters in rot. spectrum, multiple differentiation calcs. 79−98070
methyl iodide, mag. hyperfine struct. of quadrupole spectra *(Russian)* 77−34622
methyl iodide, rot. microwave spectra, nucl. quadrupole, spin-rot. and nucl. shielding tensors 78−42040
methyl radical, hyperfine coupling, in ground and excited states, Green's function calcs. 77−6692
methyl radical, hyperfine coupling consts., vibr. depend., ab initio calcs. 80−87150
methyl radical, isotropic hyperfine coupling consts., temp. depend., nuclear vibrs. 78−35039
methyl radical in sodium acetate, EPR spectra, anisotropic hyperfine interaction, rot. tunnelling 80−34775
6-methylmercaptopurine riboside, S-substituted nucleoside, ESR and ENDOR obs. 77−36766
molecular aggregates, triplet, ESR line shape in solid matrix, fine and HFS 78−58878
molecular vibration, IR spectra 79−98084
monoalkylbenzenides, anion radicals, EPR, temp. depend., vibronic interaction, proton HFS 77−34666
muonium-substituted transient radicals observed by muon spin rotation 78−74678
N-methylhydroxylamine, microwave spectra, struct., moments, internal rot., HFS and rot. consts. 79−45708
nitrosylhaemoglobin, electron spin distrib. 80−83528
2-norbornyl radical, photolysis prod. and EPR, hyperfine splitting 77−56237
nuclear energy levels, observation by laser technique book contrib. 78−9212
optical nuclear polarisation, field and orientation depend., non-crossing rule, perturbation anal. 77−42337
optical nuclear polarisation, the non-crossing rule, electronic relax. perturbation anal. 77−42338
organic radicals, HFS coupling const. calcs., RHF+CI method in INDO approx. 79−770
pentacene in naphthalene, triplet state, EPR study by electron spin-echo and laser flash excitation 80−58172
pentacoordinated ferrous porphyrins, ^{1}H and ^{19}F NMR, hyperfine shift, π electron binding 78−78719

molecular hyperfine structure continued
phenanthrene, lowest triplet state zero field splitting parameters calcs. 80−83391
9-phenylanthronyl radical, ESR, temp. depend. phenyl twist angle 79−18210
planar cyclic radicals, C-H proton isotropic hyperfine consts., C hybridisation 80−95646
porphyrexide solutions, EPR meas., isotropic hyperfine coupling constants and g-factor determ. 77−81009
pyridinyl radicals, hyperfine splitting consts., vibronic effects 77−57890
pyrimidine bases, electron adducts, spin density distribs., INDO calcs. 77−71754
pyrimidine H-addition radicals in single crystals, long range proton hyperfine coupling, EPR and INDO 77−54568
quinoxaline, zero-field splitting, basic triplet states, H bond effects 78−5366
radical pair recombination reactions, spin multiplicity 77−81393
radical pairs recombination probability in liqs., HF mag. field, reson. effect 80−93737
rubredoxin, reduced analogue, EHT calc., Mossbauer parameters, zero field splittings 77−79544
saturation spectroscopy, hyperfine component intensities 80−31886
scandium octaethylporphyrin, μ-oxo bridged dimer, triplet states and geometrys, ODMR obs. 80−9625
scandium octaethylporphyrin, triplet states and geometrys, ODMR obs. 80−9625
silyl radical, conform., hyperfine struct., nonempirical calcs., vibr., effects 79−97998
spectral lines, hyperfine struct., brightness distrib., form. model verification 77−57928
Stark shift of transition freqs. in reson. optical field, hyperfine splitting 77−14487
tetrahedral molecules, hyperfine and superfine levels, elementary spin-1/2 cases, vibronic ground states 79−85954
tetramethyl pyrazine in durene, phosphorescent mols., quantum beats in triplet states 80−58312
thioformaldehyde, hyperfine interactions, mol. beam elec. reson. spectra 77−88445
three-spin systems in nematic liq. cryst., EPR 77−14463
thymine+muonium, radical form. in aq. soln., spin reson. obs. 78−74679
transition identification, coherence resonances for hyperfine struct. interpretation 79−54920
transition metal complex, ligand field problems, group theory 80−42920
triatomic molecules, microwave spectra, mol. parameters 79−31513
β,β,β-trifluoroethyl radical in Ar matrix, EPR, F and H^+ hyperfine interaction and motional effects 77−14460
trifluoroiodomethane, laser microwave double reson. spectroscopy with CO_2 laser lines 80−87156
triglycine sulphate: Cu^{2+}, cryst., struct., hyperfine coupling consts., ^{1}H ENDOR, isotope effects 77−71822
trigonal molecules, hyperfine and superfine levels, elementary spin-1/2 cases, vibronic ground states 79−85954
two-level molecules in low press. gas, nonlinear power reson., field broadening and shifts 79−45768
vanadyl mixed ligand complexes, mechanism of spin transfer to next neighbours ^{13}C and ^{31}P 78−86892
vanadyl octaethylporphyrin, radical cation EPR linewidth inversion, relax. theory 77−10693
vinyl cyanide, microwave spectra data tables 79−59445
xanthione, large zero-field splitting of lowest triplet state 80−58171
$_2$, photoluminesc. spectrum, ^{31}P Fermi interaction, hyperfine struct. 78−33536
AlF, hyperfine structure simulated by computer programme 78−50538
AlH^+ radical cation, EPR matrix isolation obs., hyperfine components calcs. 80−14158
Ar-acetylene van der Waals molecule, radiofreq. spectroscopy and Stark effect meas., equilib. struct. and props. 80−91543
BH^+, spin-extended Hartree-Fock ab initio calculations for small radicals 78−70746
BO_2, intermodulated fluoresc. spectra using stabilised dye laser 79−27020
BeH radical, hyperfine splitting const., electronic energy, UHF-type, CCI calcs. 80−52909
BeH, spin-extended Hartree-Fock ab initio calculations for small radicals 78−70746
Bi_2, vap. phase Faraday effect, P-invariance in M1 transitions, calc. 78−82805
BiCl, form., microwave spectrum, hyperfine struct., mol. rot. vibr. consts., bonding 77−14418
BiF, mm spectrum, HFS struct., HFS, vibr. and rot. consts. and equilib. distance 77−79604
BrCl, elec. dipole moment, Stark effect meas. 78−90211
^{79}BrF, (^{81}BrF), hyperfine struct., elec. dipole moment, rot. transitions, microwave spectral obs. 80−32695
BrF_6, EPR of matrix, isolated radical 79−85977
BrF_6, EPR spectra, 'NMR' transitions, mol. symmetry 77−46580
C-$^{+}NH_3$ radical, exchangeable H^+ hyperfine coupling, ENDOR obs. 79−36669
CH, far IR laser mag. reson. spectrum 79−3466
CH, interstellar, rot. levels struct., excitation mechanisms 78−21908
CN, radical, $X^2\Sigma^+$ ground state, microwave absorpt. spectrum 78−17657
$^{13}CO^+ + CO$, charge-exchange detection of $^{13}CO^+$ electronic absorption spectrum, hyperfine consts. calc. 78−70822
$COCl_2$, phosgene, Cl_2 nuclear quadrupole coupling tensor, microwave spectra 80−52982
^{13}C-labelled organic radicals, ^{13}C- and proton-ENDOR in soln. 78−55190
^{13}CH, predicted Λ-doubling spectrum 77−30857
CaF, $^{2}\Sigma$ ground state, laser-RF double reson. spectrosc. 80−69171
CaF, $^{2}\Sigma_{1/2}{}^{+}$ ground state, spin-rot. and hyperfine splittings rot. depend., mol. beam laser-RF double reson. 80−43079
CaF, $A^2\Pi$-$X^2\Sigma^+$ transition, HFS and fine struct., intermodulated fluoresc. spectra obs. 80−63695
CdH, lifetime, Λ-doubling, hyperfine struct., in $A^2\Pi$ excited states 77−58083
ClCN, Cl and N quadrupole coupling, spectroscopic meas. 79−72337
ClCN, ground and first excited bending, vibr. state, props., mol. beam elec. reson. 80−37823
ClF_6, EPR spectra, mol. symmetry, INDO calcs. 77−46580

molecular hyperfine structure continued
CrH (CrD), molecular vibration, IR spectra electron spin resonance, 4K 79−98084
CsCl, hyperfine spectrum, mol. beam elec. reson. meas. 77−71797
CsOH, quadrupole hyperfine struct., Δ-level splitting, microwave spectra 77−88446
Cu complex, bis-(salicyladoximato) Cu(II), ENDOR multiplet HFS, energy level non-crossing 79−72341
Cu complex, catena-μ-isothiocyanato-(N′-pyridylmethylene-N″-salicyloylhydrazinato-NN′O) copper (II), EPR and visible spectra 80−5566
Cu complex, N,N′-ethylenebis (salicylaldiminato) copper (II)-thiourea, in solns., bond strength and hyperfine linewidth, EPR 80−74186
Cu complex, N,N′-o-phenylenebis (salicylaldiminato) copper (II)-thiourea, in solns., bond strength and hyperfine linewidth, EPR 80−74186
CuBr, rot. spectrum hyperfine struct., coupling consts., microwave spectroscopy study 80−18844
CuCl, hyperfine struct., microwave rot. spectrum obs. 78−21917
CuI, hyperfine struct., quadrupole coupling const., rot. spectrum 77−88447
D_2O, sub mm beam maser spectrum, D hyperfine splitting 77−61874
FO free radical, detection by CO_2 laser mag. reson. 80−45594
$^{57}FeBr_2$, matrix isolation Mossbauer spectra, isomer shift, quadrupole splitting 78−42104
$^{57}FeCl_2$, matrix isolation Mossbauer spectra, isomer shift, quadrupole splitting 78−42104
$^{57}Fe_2Cl_6$, matrix isolation Mossbauer spectra, isomer shift, quadrupole splitting 78−42104
GaBr, rot. spectrum hyperfine struct. 79−13838
GeH_4, avoided-crossing molecular-beam spectroscopy, hyperfine and spin rot. const. and rot. g factors determ. 80−78671
H_2, ortho, high rot. states, inter- and intra-mol. effects, mol. beam mag. reson. obs. 78−70852
H_2^+, hyperfine struct., allowed transition freqs. 79−13630
H_2^+, hyperfine struct., refined var. calcs. 77−75067
H_2-H_2 dimers, hyperfine struct. in zero mag. field 80−95700
$(H_2)_2$, $(D_2)_2$, $(HD)_2$ and H_2-D_2, Van der Waals complexes, mol. symmetry 80−42963
HBr^+, laser mag. reson. pure rot. transition in far IR 79−89695
HBr(DBr), isotopic forms, Stark hyperfine struct., polarisability anisotropy 77−83645
HCC^+, equilib. struct., rot. const. 79−98003
HCO, microwave spectra, hyperfine struct. 77−75139
HD^+, IR hyperfine struct. of rot.-vibr. transitions calc. 77−42323
HDO, beam maser double reson., hyperfine struct. D quadrupole coupling 77−65493
HI nuclear quadrupole HFS in IR spectrum, obs. using tunable diode laser 80−58412
HNC, quadrupole coupling constant determ. 78−1101
$HN^{13}C$ and HNC, hyperfine structure in dark interstellar clouds 79−101182
H_2NO, hyperfine coupling const. calc., double perturb. theory and CI methods 79−59362
H_2O mesospheric vapour line at 22.2351 GHz, hyperfine structure 79−8666
H_2O^-, trapped in γ-irrad., Y-type zeolites, ESR obs. 77−9099
$HeCN^+$, SCF calcs., dissoc. energies, rot. and hyperfine const. determ. 80−95531
Hg_2-Pt, ^{199}Hg Mossbauer meas., isomer shift and quadrupole splitting calcs. 80−28039
Hg_2F_2, ^{199}Hg Mossbauer meas., isomer shift and quadrupole splitting calcs. 80−28039
Hz, 3d complex, radiative lifetimes, hyperfine constants 78−70873
I_2, 2-step reson. scattering, subnatural linewidths in vapour 79−76419
I_2, B state, effective hyperfine Hamiltonian 78−58598
I_2, B state, fluorescence yield, individual hyperfine components 77−68067
I_2, B-X transitions, rot.-vibr. hyperfine coupling consts., extension to other levels 80−63625
I_2 folded Doppler broadened system, interaction with two reson. laser fields 80−53007
I_2, HFS and mag. parameters of B state, ab initio calc. 79−45865
I_2, hyperfine component classification, suitability for laser wavelength stabilisation 78−86965
I_2, hyperfine predissoc., Doppler-free spectrosc. obs. 78−89558
I_2, hyperfine predissociation, saturated absorpt. expt. 77−58103
I_2, hyperfine struct. in B-X transition, laser spectroscopy of pure I_2 jet 79−81234
I_2, hyperfine structure, 612 nm and 640 nm, saturated absorpt. expt. 78−66871
I_2, hyperfine transition saturation intensities, saturated absorpt. technique 80−43208
I_2, laser fluoresc. state selected and detected mol. beam mag. reson., hyperfine transitions 80−63731
I_2, lifetime of R(127) line of 11-5 band of $B^3\Pi_{ou}^+$-$X^1\Sigma_{og}^+$ transition 77−6861
I_2, line near 520 THz, HFS, direct freq. meas. 80−53266
I_2, saturated absorpt. at 612 nm, stabilisation of He-Ne laser 79−59730
I_2, stabilised He-Ne lasers, hyperfine struct. spacings, international intercomparison meas. 78−87088
I_2, using Doppler-free stimulated-emission technique 78−93765
IBr, elec. dipole moment, rot. transition Stark shift obs. 77−75207
ICN, microwave spectrum, mag. hyperfine struct., I nucl. shielding tensor 78−17661
ICl, microwave-optical double reson. obs. in $B^3\Pi_{0(+)}$ state 79−85979
IF, elec. dipole moment, Stark effect 79−18233
$^{127}I_2$, absolute frequencies of ten hyperfine components freq. meas. in visible 79−93104
$^{127}I_2$, B-X band system, nucl. HFS, coupling consts. 77−6794
$^{127}I_2$, B-X band system, nucl. HFS, octupole coupling const. effects 77−6795
$^{127}I_2$, hyperfine struct. in electronic spectrum, saturated absorption spectroscopy 78−37645
$^{127}I_2$, hyperfine structure obs. in saturated fluoresc. 78−50569
$^{127}I_2$, visible spectra, HFS at 586.82 nm 78−9395
$^{127}I_2$, weak rot. R(98), 58−1 line, HFS struct., saturated intermodulation fluoresc. 79−94024
$^{127}I_2$ hyperfine structure components, stabilization of doubly resonant intracavity SHG of 1153 nm radiation 80−33077
$^{127}I_2$ rovibronic absorpt. lines, hyperfine struct. 80−78596
$^{129}I_2$, complete hyperfine spectrum obs. at 612 nm 80−95638
molecular hyperfine structure continued
$^{129}I_2$, hyperfine struct., saturated fluoresc. obs. 79−31591
$^{129}I_2$ rovibronic absorpt. lines, hyperfine struct. 80−78596
$^{115}In^{79}Br$, $^{115}In^{81}Br$, rot. J=1→2 hyperfine struct., quadrupole coupling consts. *(German)* 77−30866
KOH, quadrupole hyperfine struct., Δ-level splitting, microwave spectra 77−88446
Kr_2F, semi-empirical VB calcs. of hyperfine interactions and struct. 79−85902
Li_2, circular polarisation of emission, influence of nucl. hyperfine interactions and elastic collisions 80−9635
Li_2, emission circ. polaris., hyperfine coherence and elastic collisions effect 79−3471
LiF, RF spectra, spin interactions and moments, mol. beam elec. reson. meas. 77−18912
LiH^+, spin-extended Hartree-Fock ab initio calculations for small radicals 78−70746
LuF, $^1\Pi$ hyperfine struct. parameters, bonding 77−58036
MnH(MnD), $^7\Sigma$-state, mol. parameters, ESR and optical spectrosc. 78−94264
$MnH_2(MnD_2)$, $^6A_1$ state, mol. parameters, ESR and optical spectrosc. 78−94264
MnO, $A^6\Sigma^+$-$X^6\Sigma^+$ electronic transition, rot. and hyperfine struct. 80−74134
Mo complexes, mononuclear, EPR ligand superhyperfine interactions, implications for enzymes 77−86372
ND_3, hyperfine structure of inversion transitions, molecular beam electric resonance 79−98071
ND_3, sub mm beam maser spectrum, D hyperfine splitting 77−61874
N_2D^+, lab. rest frequencies 78−1102
NH_2, hyperfine level crossing spectroscopy of (0, 9, 0) and (0, 10, 0) vibr. states 78−17728
NH_2, hyperfine struct. of u-state, microwave optical double reson. 79−68246
NH_2, lab. obs. of 16 GHz rotational transition 77−3389
NH_2, microwave modulated saturation spectroscopy, hyperfine energy levels 79−68245
NH_2 radical, mag. hyperfine interactions, zero-point vibrs. effects 80−58167
NH_3, hyperfine quadrupole coupling, ro-inversional levels, inversional depend. 80−27961
NH_3 in interstellar dark clouds, hyperfine struct. 77−78852
NH_3 in Taurus dark cloud, mag. hyperfine struct. rel. to gas temp. and motion 77−78851
NH_3, mol. beam state selection and focusing, hyperfine spectrum 80−28119
NH_3^+ radical, mag. hyperfine interactions, zero-point vibrs. effects 80−58167
$^{14}NH_3$, IR saturated absorpt. spectra, vibr. depend. of hyperfine quadrupole const. 77−27072
NH_4^+, ND_4^+, in lyotropic mesophase, ^{14}N NMR, and quadrupole splitting 78−17690
$N_2H_4^+$ radical, mag. hyperfine interactions, zero-point vibrs. effects 80−58167
NH(D) radical, and isotopic species, laser mag. reson., hyperfine parameters 77−10694
NHD, rotational transitions, microwave optical double resonance obs. 80−58293
$NH_2(X^2B_1)$, MODR, hyperfine coupling consts., spin rot. consts. 78−1010
NO, hyperfine splitting const., H-bond contrib. 78−74799
NO, laser mag. reson. and IR-RF double-reson. near 5.3 μm 78−5258
NO, sub-Doppler resolution IR spectra 78−86860
NO_2, excited state, ODMR, hyperfine spectrum 79−36670
NO_2, fluoresc. spectra from selectively excited HFS levels 78−21961
NO_2, radical, ENDOR and ESR obs. ^{14}N hyperfine coupling tensor 77−50455
NO_2, sub-Doppler spectra, laser-beam system, HFS excitation, radiative, non-radiative decay 78−90210
NO_3, mag. hyperfine interactions, MO LCAO UHF calcs. 77−14369
NO_3^{2-}, coupling consts., geometry, LCAO UHF and ENDOR data calcs. 77−14369
NO_3^{2-}, ENDOR and ESR obs., ^{14}N hyperfine coupling and g-tensors 77−50455
N_2O quadrupole hyperfine struct., vibr. depend. obs. using twin-laser spectrometer 80−43097
$^{14}N_2{}^{16}O$, elec. and mag. props., hyperfine struct., mol. beam elec. reson. obs. 78−62792
$^{14}N^{16}O$, v=2←0 overtone band IR spectra, Λ doubling, hyperfine struct. 79−41165
Na_3, electronic struct., pot. energy surface, ab initio CI study 78−70996
$NeCN^+$, SCF calcs., dissoc. energies, rot. and hyperfine const. determ. 80−95531
OD, $^2\Pi_{3/2}$ state EPR spectra 78−21949
OH, $A^2\Sigma^+_{1/2}$ state, g-factor meas. by quantum beat obs. 79−18176
OH, exact hyperfine struct. and Einstein A-coefficients, astrophys. appl. 77−83762
OH, Λ-doublet transitions induced by ion collisions 78−9222
OH, mol. beam electric reson., hyperfine Λ-doubling transitions 79−36628
OH, prod. by photolysis, Λ-doublets, population, rot. states, hyperfine struct., microwave spectra 80−32694
OH spectroscopy using freq.-doubled dye laser radiation *(Dutch)* 79−50039
OH, spin-extended Hartree-Fock ab initio calculations for small radicals 78−70746
OH, vibr. ground-state, MFS, rot. spectra and electronic band anal. 78−5206
OH, vibrationally excited, high-resolution hyperfine Λ-doubling spectrum 78−90153
$OH(A^2\Sigma_{1/2}{}^+P)$, and OD, hyperfine struct. determ. by freq.-doubled dye laser radiation 79−72333
$OHX^2\Pi$ radical, ground and vibr.-excited ($v \leq 6$) levels, microwave spectrum 79−63985
OPF_3, mol. beam elec. reson. spectrum, mol. props. 79−94011
OsO_4, HFS and fine struct., saturation spectroscopy obs. visible spectra 80−53008
PF_5, total nuclear spin in rovibronic state, three calc. methods for hyperfine mag. struct 78−58658
PH, far IR laser mag. reson. of $X^3\Sigma^1$ and at $^1\Delta$ states 79−54869
PH_2, X^2B_1-state, rot. laser mag. reson. spectrosc. 80−28038

molecular hyperfine structure continued
PrO, 0-0 band in XVII system, hyperfine splitting, visible excitation spectra 80−28028
PrO, hyperfine structure, rotation, electronic spectrum obs. 79−98061
RbBr, hyperfine struct., qudrupole coupling consts., vibr. depend. *(German)* 77−34565
RbI, ground vibr. state rot. transition, quadrupole HFS and coupling consts. *(German)* 77−57990
RbOH, quadrupole hyperfine struct., Δ-level splitting, microwave spectra 77−88446
S_2 $^{35}Cl_2$, microwave spectra and double reson., assignments, distortion consts. and struct. 79−89664
SF_6, IR saturation spectrum, mag. hyperfine struct. 79−13714
SF_6, ν_3 bands, rot. fine struct., HFS spectroscopic consts. determ., saturation spectroscopy obs. 80−53008
SF_6, total nuclear spin in rovibronic state, three calc. methods for hyperfine mag. struct 78−58658
$^{32}SF_6$, point group symmetry breakdown, vibr.-rot. state, saturation spectroscopy 80−87116
ScF_2, ESR spectra of radical in Ar matrix, 12K, hyperfine splitting 79−98122
ScS, $B^2\Sigma$-$X^2\Sigma$ system, rot. struct. and hyperfine effects near IR spectrum 80−5544
SiH_3 radical, hyperfine coupling consts., vibr. depend., ab initio calcs. 80−87150
SiH_3 radical, in Ar(Kr)(N_2) matrix, anisotropic ESR spectroscopic parameters 80−63687
SiH_4, avoided-crossing molecular-beam spectroscopy, hyperfine and spin rot. const. and rot. g factors determ. 80−78671
$SiH_3{}^{81}Br$, high resolution rot. microwave spectrum, 8-40 GHz, mol. consts. 78−21916
SiH_3NCS, microwave spectrum, struct., dipole moment, ^{14}N quadrupole coupling const. 77−46560
SiH_3X^-, X=Cl, Br, I, and isotopic forms, EPR spectra, mol. struct. 79−94023
TlF, electric dipole hyperfine struct. calc. 80−53162
TlF, P- and T-violating interactions in hyperfine struct., mol. beam reson. expt. 80−53019
V complex, vanadyl ion-pyridyliminonitroxide radical mag. interactions, ESR 77−83623
$YbF(^2\Sigma^+)$, matrix isolated ESR spectra 78−86890
YbH(YbD), and isotopic forms, optical and EPR matrix isolated spectra, HFS, bonding 77−83613
ZnH, lifetime, Λ-doubling and hyperfine struct. of $A^2\Pi$ excited states 77−58083

molecular inelastic collisions
see also atom-molecule collisions; atom-molecule reactions; ion-molecule collisions; ionisation of molecules; molecular rotational-vibrational energy transfer; molecule-molecule reactions
absorption bands, collision-induced, rel. to dielec. and refr. virial coeffs. 79−86547
acetaldehyde+$H_2(N_2)(CO_2)$, rot. line broadening, mol. quadrupole moments calc. 80−28065
acetylene, triplet state quenching by foreign gases 80−91596
acetylene, vibr. relax. study using laser-induced fluoresc. 80−74219
acetylene-d_2, $\nu_4+\nu_5$ band, diode laser meas. 78−78664
adiabatic approximation, energy-modified 79−59523
alkali metal dicarboxylates, H bonding and motion, incoherent inelastic neutron scatt. spectroscopy 80−48095
alkanes, collisional dissoc., time of flight mass spectrometric obs. 77−74545
alkanes, liq., energy transfer rate parameters, emission intensity, lifetime meas. 79−86031
amplitude density function analysis, modified method 79−6987
angular correlations, summary of review papers 80−63757
angular momentum distributions in collision processes and the location of the transition state in ion-molecule reactions 78−64808
angular velocity autocorrelation function of fluid of rough spheres, long time behaviour 77−6879
anthracenes, meso-substituted, thermally assisted and heavy atom assisted intersystem crossing 79−31573
aromatic hydrocarbons, fluorescence quenching rate constant, undergraduate expt. using Spectronic 20 77−57119
asymmetric scattering, spin-1 particle by non-central field 78−55214
atom+diatom, scatt., opacity functions, J_z-conserving approx. calcs. 77−6878
atom+diatom, T-matrix element approx., j_z-CCS calcs. 77−19003
atom+harmonic oscillator, classically forbidden transitions, classical and classical path methods 77−520
atom+molecular inelastic collisions, statistical decoupling 77−517
atom-diatom collision, vibrationally inelastic scattering by quantum mechanical calculations 77−46624
atom-polyatom collisions, quantal many-body approach 77−30943
atomic, molecular and solid-state theory, conf., Flagler Beach, Florida, USA (Mar. 1978) 79−31356
atomic and molecular collisions, book 80−27058
Auger electrons in mol. ion+solid (gas) targets 79−45814
beam self-scattering cross section 77−46618
beam-foil spectroscopy, mol. effects 79−50127
benzene, ns time-resolved emission spectra, collisional processes 77−3490
benzene, total neutron cross sections for subthermal energies 78−74779
benzene+acetone, energy transfer cross-sections, generalised oscill. strength calcs. 79−10173
benzene+benzene-d_6, electronic energy transfer between vibronic levels, fluoresc. obs. 77−38712
benzene+bromomethane, microwave line width and quadrupole moments, perturbation theory 80−69190
benzene+OCS, microwave line width and quadrupole moments, perturbation theory 80−69190
benzene-d_6, intermol. dynamics, neutron scatt. obs. 79−863
benzenetricarbonylchromium, neutron inelastic scatt. spectrum and valence force field 80−48096
Bethe theory, inelastic collisions of fast charged particles 78−58783
biatomic molecular gas, quantum kinetic theory *(Rumanian)* 78−91053
bimolecular, time delay, multichannel spectral theorem 80−43144
bimolecular quasiresonant processes, impact approx. 78−33571
binary collisions, time correlation functions, influence of bounded trajectories 80−43143
body-fixed theory, two-system collision, arbitrary ang. momenta 78−25642

molecular inelastic collisions continued
Born inelastic cross sections, Pade approximants 78−17742
bound states, semiclassical study 80−9693
trans-butadiene, two-photon spectra, press. effects, transient lensing spectrosc. 78−58756
chemical ionisation, classical description, complex interaction pot., exponential representation 80−99570
chiral systems, differential scatt. of spin $\pm^1/_2$ neutrons, theory 78−33622
chiral systems, differential scatt. of spin $\pm^1/_2$ neutrons, Condon oscillator model 78−33623
chloromethane, low density gas, proton spin-lattice relax., mol. reorientation 79−3462
chlorophyll, electronic excitation, transition monopole theory 78−22016
2-chloropropane, separation of collision-induced from intrinsic mol. depolaris. Rayleigh scatt., C-Cl bond optical anisotropy 78−27244
classical scattering of charged particles, single and multiple scatt. at small angles 78−17740
closed shell chiral molecule, polarised neutron beam interaction, optical activity 79−64111
coherence transfer between collision partner mols. 77−71844
collinear, quantum mech. sudden vibr. approx. calcs. 79−98193
collinear collision of molecule with diatomic molecule, in presence of intense laser beam 78−94304
collinear scattering, information content, dynamical approach 80−23500
collision broadening, short-range interaction effects 77−42355
collision induced line shapes, hard sphere model calcs. 79−81182
collision reorientation in resonant light field *(Russian)* 80−14192
collision spectroscopy, book 79−27065
collision-induced emission with laser irrad., cooperative chemical and optical pumping 78−22012
collisional dephasing in strong radiation fields, unified theory, Karplus-Schwinger formula 80−91635
collisional ionisation in intense laser field, quasimol. state reson., quantum mechanical anal. 78−33589
collisional optical coherence transfer, laser spectroscopy 77−42360
collisional processes, nonreson. laser field effects 77−60093
complex molecular systems, collision phenomena by stochastic model, observables distribs. and information entropy 78−25640
complex scaling transformations in stationary and scattering problems 79−18124
complex solutions, stimulated radiation anisotropy, spectral depend. *(Russian)* 77−68085
compound state resonances, semiclassical calcs. 80−87031
computational atomic and molecular physics, conf., Nottingham, England, (Sept. 1978) 79−59567
correlated collisions, kinetic theory ansatz 78−70901
cosmic masers, collision-collisional pumping model *(Russian)* 80−90560
coupled equations solution method in adiabatic approx. 79−3524
critical molecules, neutron scatt., 'optical activity' 80−23567
cross-sections, computational technique, exponential distorted wave and effective Hamiltonian 78−37709
crossing electronic term problem, influence of motion 79−76499
cyclohexane+toluene, energy transfer, pulse radiolysis obs. 80−16714
cylcohexane, liq., energy transfer rate parameters, emission intensity, lifetime meas. 79−86031
damping of excited molecules located above surface of metal 78−92160
decalin, liq., energy transfer rate parameters, emission intensity, lifetime meas. 79−86031
decoupled l-dominant approximation, limit of validity 77−14528
diatom, phase shift difference, trigonometric pots. in radial Schrodinger eqn. 79−22787
diatom+diatom, effect on depolarised light scatt. linewidths 80−58321
diatom+diatom, vibr. energy transfer, collinear and 3-dimens. rate consts. 80−48065
diatomic mol. scatt., Tietz phase shift differences, semi-empirical relations, Varshni and Hulbert-Hirschfelder pots. 80−9673
diatomic molecular fluids, slow neutron scatt., models 80−83463
diatomic molecular fluids, slow neutron scattering, moment expansions 80−87201
diatomic molecular gases, slow neutron scatt., recoil corrections, time of flight, rel. to mol. liq. struct. 79−7028
diatomic molecular gases, slow neutron scatt., recoil corrections, rel. to mol. liq. struct. determ. 79−7027
diatomic molecule, dissoc. and recombination involving two states interacting via at. species, soln. 77−23535
diatomic molecule, dissoc. and recombination involving two states interacting via at. species, model 77−27145
diatomic molecule, neutron scatt. induced electronic transitions, tunnelling 80−63844
diatomic molecules, collision induced gas phase dissoc. rate consts., discrete and continuum models 77−526
diatomic one-electron mols., wavefunction calc., collision matrix elements, computer program 78−50457
diatomic rigid molecules, multipole pot. interaction cross-sections 77−6890
diatomic transition operator, separable approx., variational approach 78−42150
diatomic transition operators, L^2 basis expansions 80−63519
differential cross-sections, from classical trajectory studies, Legendre polynomial series 78−17738
differential scatt. cross sections from classical trajectories, Legendre moment method 78−3314
p-difluorobenzene+acetone, generalised oscill. strength, for reson. electronic energy transfer 78−66668
1,1-difluoroethane, unimol. decomposition, direct meas. via IR laser photolysis, collision effects 79−57254
dilute gas simulation, pattern recognition algorithm for mol. formation 77−75249
p-dimethylaminoacetophenone, ps reversible isomerisation kinetics, O_2 quenching obs. 79−5133
diphenyl, solid and liquid, total neutron cross sections for subthermal energies 78−74779
direct chemical reactions in fast molecule collisions, eikonal approx. calcs. *(Russian)* 80−3332
dissociation, collision-induced, high-efficiency, in RF-only quadrupole 79−67419
dissociation-recombination, collision induced, exactly soluble model 78−7191
distorted wave matrix elements for inverse power pots., approx. analytic evaluation 80−83442

molecular inelastic collisions continued
DODCI + malachite green (DQOCI), electronic energy transfer obs. 80−5633
dynamics of collision induced intersystem crossing 78−90276
electronic degrees of freedom, classical models 80−63507
electronic energy transfer, in excited atom collisions, review, book contrib. 77−40543
electronic excitation energy transfer by reabsorption 78−37735
electronic transitions, combined effects of tunnelling and inaccessible states 77−58147
energy level transitions, Doppler broadening, phase-destroying collisions 80−9561
energy moments of final state distrib., direct moment method 78−33562
energy transfer processes involving distorted excited states 79−45794
ergodic collision theory of intermolecular energy transfer 78−9224
ethylene, compressed gas, far IR dipolar absorpt., meas. and theory 77−14425
ethylene, liq., far IR absorption spectrum, quadrupole induced dipole interaction 78−86857
ethylene, quadrupole moment tensor determ. by collision-induced absorpt. spectrum 80−91555
excimer, fluorescence, relative yield following triplet-triplet annihilation, re-encounter effects 78−33538
excited state processes, collision rates obs. using single at. or mol. beam 78−13567
fast molecular ion+solid (gas), excited electronic states effects 80−9687
field theoretical method for mol. scatt., distorted wave formalism 79−3513
flame collisional processes, coherent optical transient spectroscopy 79−39147
fluorobenzene, mol. reorientation and weak mol. interaction influence, ^2D spin-lattice relax. obs. 80−106333
fluoroethanes, IR photodissoc. by multiphoton absorpt., collisional effects 79−36713
fluoroethylenes, IR photodissoc. by multiphoton absorpt., collisional effects 79−36713
fluoromethane, vibrational-translational transfer rate, optoacoustic meas. using short pulse CO_2 laser 80−74258
fluoromethane+fluoromethane, collision induced mode selective energy transfer, fluoresc. obs. 80−69177
fluoromethane+fluoromethane, collisionally induced relax. processes and vibr. energy transfer 80−53107
fluoromethane+SF_6(CS_2), fluoromethane laser, buffer gases collisional narrowing 80−99710
fluoromethane+SO_2, collisionally induced relax. processes and vibr. energy transfer 80−53107
formaldehyde, spectral linewidth press. broadening, Anderson-Tsao-Curnutte calcs. 77−75220
formaldehyde, vibr. and electronic energy transfers, from single vibronic level 78−82820
formaldehyde+CO_2(NH_3), cross sections meas. *(French)* 79−76487
formaldehyde and -d_1, MODR and collision-induced transitions in laser cavity 78−74686
formaldehyde-d_1, multiphoton dissociation, pulse duration and collision effects 79−835
gas, dissociating, relax. press. theory 79−81994
gas linear molecules, symmetrised Liouville basis vectors, appl. to spectral linewidths 80−83457
gas mixture, laser irradiated, anisotropy of inelastic scatt. and selective diffusion 80−53907
gas of nonspherical mols., transport processes, kinetic cross sections, temp. depend. 77−80259
gas phase chemical reactions in IR laser field, collision-induced absorpt. spectra 80−76499
gas phase collisions, dynamics, generalised Langevin eqn. theory 78−70900
gasdynamic equations, multiatomic gases with different elastic and inelastic rates 79−81993
gaseous relax. phenomena, few-level approx. validity 80−53097
gases, collision induced absorpt. spectra, integral data 79−81202
heavy atom+H_2(HD)(D_2), intramultiplet transitions 77−54597
hexafluorobenzene+bisdiphenylenephenylallyl radical, solvent effects on collisions, dynamic nucl. polaris., spin-lattice relax. 77−63303
hexafluoropropyl cation, laser multiphoton dissoc. probabilities, collisional enhancement 79−68277
induced IR spectra, overlap dipole moment determ. 77−18924
induced moments in at. and mols., polarisability density concept limitations 78−70964
inert gas, dense, rotational relax. of solute molecules reln. with local anisotropy fluc. 80−58183
inert gas excimer lasers, at. and mol. collision processes 80−53263
inert gas halide lasers, at. and mol. collision processes 80−53263
inert gas-halogen mixture, ion form., ion-mole. reactions, mass spectra 77−61841
in intense light beams, quantum aspects *(Russian)* 79−6903
interaction anisotropy, small angle scatt., spectral evidence 80−78600
intermolecular electronic energy transfer induced by optical radn. field 77−88524
intermolecular potential well depth role in collision-induced state changes 79−81257
intermolecular spectroscopy and dynamical properties of dense systems, conf., Varenna, Italy (1978) 80−82581
intermolecular spin relaxation by reorientation of off-center spins 79−42821
internal degrees of freedom collisional excitation, statistical model 79−45803
interstellar clouds, collisional excitation by charged particles, model exact soln. 77−74114
intersystem crossing, collision-induced, reduced eqn. of motion 79−18227
1-iodopropane, pyrolysis, intermol. energy transfer in two-channel unimol. reaction 79−11769
ion+ion, Coulomb-Born and unitarised Coulomb-Born cross-sections 78−82815
ion lifetime distribution, following interaction with collision gas, determ. method 79−36732
ion motion, in RF quadrupole field, collision effects 77−75261
IR-absorbing molecules, collisional cross-sections, temp. depend. 79−96787
isotropic molecular gases, binary collision-induced light scatt., rot. Raman scatt. 80−78660
isotropic molecular gases, binary collisions induced light scatt. 80−83428
isotropic tetrahedrally and octahedrally symmetric molecules, clusters, collision induced polarisability, mol. frame distortion 80−32798
j_i CCS approx., partial wave parameter identification and differential cross section simplification 77−58112
J_i-conserving coupled states approximation, mag. transitions and ang. distribs. 77−75262
ketyl radical+benzophenone, triplet-doublet energy transfer, viscosity and mag. field effects 77−71850
Lamb-dip spectroscopy, collision broadening theory 77−83659
large asymmetric mol. interaction with small mol., target factor, mixture thermodynamic props. 78−26225
laser applications to chemistry, overview 79−58800
in laser field, basis set selection and rotating-wave approx. 80−58341
laser field, multimode, intensity time variation on mol. collision processes 79−31620
in laser field, multiphoton vibrational excitation enhancement, semiclassical theory 80−58350
laser field interacting with collision dynamics, quantum mechanical model 78−62876
laser near-reson. scatt. from collisionally perturbed mol. 78−1033
laser radiation field effects, quantum mechanical close coupled expansion 77−50485
laser spectroscopy, atom and mol. interactions, conf., Zarogoza, Spain (June 1979) 80−27041
laser-assisted excitive Penning ionisation 79−41232
lasers, atomic and molecular, appl. to collision physics 80−63596
Lennard-Jones fluids, orientational and collision induced light scatt. 80−63644
light scatt., near-reson., from collisionally perturbed atoms and molecules, theory 80−1045
light scattering, collision-induced and multiple, by simple fluids 80−53919
linear molecule+methane, collisional energy transfer by octupole coupling 78−62881
linear rigid rotors, scattering calcs., ab initio intermol. pots. fitting 77−83680
lineshape analysis for collision induced spectra 78−70787
linewidths and shifts determ. by convolution method 80−102541
Liouville equation, reduced form 78−33569
liquid solutions, reaction rates, mol. mobility effects, review, book contrib. 77−40526
low-energy scattering, resonances 79−72384
magnetic scattering of neutrons on excited atoms or mols., cross sections, neutron polarisation *(Russian)* 78−55249
many channel scattering model, exactly soluble 80−43127
maser, three-level, collisional relax. times 78−13675
methane, absorpt. line profile, press. and temp. effects 77−495
methane, collision-induced light scatt., spectral features 78−13493
methane, collision-induced Rayleigh scatt. intensity calcs. 77−46569
methane, gas, liq., collision-induced microwave absorpt. 77−42312
methane, ground state, dipole oscill. strength distrib., rel. to molar refractivity and dispersion energy 77−71835
methane, V-V energy transfer 80−83469
methane+methane, ^1H and ^{13}C mag. shielding, intermol. effects 78−37571
methane+methane and methane+monatomic collisions, photoacoustic study of vibr. relaxation *(French)* 77−30969
methane+SF_6, vibr.-vibr. relax 80−99537
methane molecular pair, polarisability tensor anisotropy 79−31725
methane-d_4, vibr.-translational relax. 80−99537
methane-d_4+methane, vibr. relaxation 80−99537
methyl chloride, pressure-induced shift of the J=0→1 transition, 193 to 366K 77−14497
methyl cyanide, anomalous Senftleben effect *(Russian)* 78−71415
methyl iodide, vibrational dephasing by translational collision 80−87202
methyl thiyl radical, emission spectrum, collisional quenching 78−13543
m-methyl-p-cyanodimethylaniline, ps reversible isomerisation kinetics, O_2 quenching obs. 79−5133
microphysics to macrochemistry, discrete simulations, review 80−54102
microwave spectral lines, press. broadened, deviations from Lorentzian line shape 77−61806
microwave spectral lines, press. broadened width and shift, temp. depend. 77−61807
moderately dense gases, molecular interactions, neutron scatt. 79−50144
molecular beam scattering, S/N ratio enhancement in time-of-flight anal. 78−86969
molecular gas, laser irrad., field avoided crossings, new transition channels 78−33477
molecule+ion charge transfer, vibr. excited mol. form. 77−3455
molecule-molecule collision, effect on linear and non-linear spectroscopic line shapes 79−36735
momentum transfer rate consts. meas. by ion cyclotron resonance 77−86287
multidimensional surface intersection problem and classical surface hopping 77−14512
multilevel system, nontransient phase coherent light absorpt. effects 77−498
multiple electron transfer to highly charged ions, scaling of cross sections 77−83711
multiple time scale stochastic formulation for collision problems with more than one degree of freedom 79−36718
multipole moment relaxation, impact approx. with long range interac. 77−61828
nanosecond time-resolved emission spectroscopy 77−3490
nitrobenzene, collision-induced dissoc., ionisation characts. in corona discharge 77−60156
non-ideal gas, internal degrees of freedom, kinetic equation *(Russian)* 79−23390
nonadiabatic collision processes, electronic degrees of freedom, classical model, pseudopot. anal. of $F(^2P_{1/2})+H^+(Xe)$ 79−64062
nonadiabatic collision processes, electronic degrees of freedom, classical analogue, appl. to mol. system 79−64063
nonadiabatic transitions, linear curve crossing problem, generalised Stueckelberg method 80−28085
noncrossing interactions, Rosen-Zener model, differential cross-section calcs. 77−46621
noncrossing interactions, Rosen-Zener model, total cross-section calcs. 77−50497
nonlinear spectroscopy, collision induced resonant four photon parametric generations 77−3627

molecular inelastic collisions continued
nonreactive scatt., classical differential cross sections in Legendre polynomials 79−836
nonspherical molecule, rot. and vibr. inelastic scatt., rot. IOS approx. calcs. 78−46433
optical activity induced by right-left nonsymm. mol. collisions 78−75254
optically isotropic molecules, collision-induced Rayleigh scatt. intensity calcs. 77−46569
optically isotropic molecules, collision-induced scatt., many-body correls. 80−87127
orbital angular momentum quantum numbers in definite parity j_z CCS approx. 77−14511
organic gases, kinetics of intermolecular triplet-triplet electron energy transfer 79−10141
partial wave parameters in CS and IOS approx., mag. transitions 79−10164
perylene, vapour phase excitation energy transfer from pyrene 77−12802
phase fluorometry as a probe of diffusion-controlled molecular encounters in dense fluids 80−32799
photon angular momentum effects in laser field 79−10178
PMMA solution in isopropylbenzene, mol. mass effect on mobility and interaction parameters *(Russian)* 79−31754
polyatomic molecular vapour, rot. fluoresc. depolaris. 79−54889
polyatomic molecule+atom, many body approach 79−31645
polyatomic molecules, multiphoton excitation, collisional deactivation, information theory anal. 78−90264
polyatomic molecules, multiphoton IR absorpt., collisional effects 79−41174
polyatomic molecules, picosecond fluoresc. gating, intra- and intermol. transfer processes 78−78745
polyatomic seeded supersonic beam+monatomic host gas, internal energy relax. 79−59532
POPOP+Cd(5^3P_1), vap., electronic energy transfer, laser appl. 77−30980
positronium+N_2 (inert gas), fine struct. interval, collisional density shifts 77−34788
potential well depth estimation method 79−86034
potentials, anisotropic, from rotationally inelastic and elastic cross sections, direct inversion method 80−69090
predissociation, multichannel, and inelastic scatt., uniform WKB theory 79−72404
pressure broadened spectral line shape, effect of turning points 79−22655
prior statistical distributions implied by dynamical threshold laws for molecular collisions 78−86928
projection operator formalism, stochastic reductions 77−65521
protein dynamic states, role of geometry and elastic strains 78−48745
quantal cross-sections, j_zCCS and statistical j_z approx. surprisal anal. 77−14513
quantum three particle system, action-angle variables 80−95708
quasi-classical and quantum moments of distrib. of states, semiclassical comparison 80−23480
quasiclassical histogram method improvement, minimisation procedure 78−66617
R-matrix propag., amplitude density function and invariant bedding methods 80−91622
radiative transitions in collision processes in presence of picosecond laser pulses 80−23479
reactive, joint products' state distribs. 78−64807
reactivity band boundaries, trapped trajectories, theory 78−29836
reduced phase space approach calcs. 80−83438
relaxation, averaged j_z-conserving coupled states approx. 77−54585
relaxation processes, symposium, London, England (Dec. 1976) 80−56993
relaxation processes and spectra in liqs. and dense gases 77−58935
relaxed sudden approx., moderate collision energies 78−70902
resonance broadening due to collision-induced vel. change *(Russian)* 77−46540
resonance scatt., enhanced isotope separation 77−61825
resonance transfer rate of electron excitation, model of convergent terms, effect of diffusional motion of particles 80−8936
resonant transfer of electronic excitation, eqns. of classical system interacting with quantum system 79−76498
rhodamine 6G+malachite green, in low viscosity solvent, ps time resolved energy transfer 78−70910
rigid spherical mols., relax. of translational energy in perpendicular directions 77−72398
rotational cross-sections, energy depend., modified exponential model 79−50115
rotational infinite-order sudden-approximation, low energy appls. 78−1052
rotationally inelastic scattering, sudden approximation, theory 77−71843
rough sphere fluid dynamics, specific kinetic models 77−58936
S-matrix factorisation, in mol. collision problems 79−72380
semiclassical calculations using arithmetic mean of velocities associated with initial and final states 80−83460
semiclassical S-matrix, by generalised phase shift approach 79−89725
semiclassical scatt. matrix, Massey parameter expansion 78−58759
semiclassical theory of electronically nonadiabatic collisions, reson. effects 78−66618
semiclassical theory of mol. collisions in laser field 77−34718
shock waves, starvation kinetics 78−64841
slow neutron scattering, microscopic cross section, gas imperfection effects 79−40984
slow neutron scattering, recoil and detector corrections for mol. gases and liquids 79−41223
solution, nonlinear luminesc. quenching kinetics, high excitation power 79−56834
spectral line collisional broadening 77−88426
spectral line pressure broadening dipole moment correlation function 77−79656
spectral line shapes, linear and nonlinear, atom or mol. cross sections 78−70899
state selected molecules, sudden approx. 80−106377
statistical mechanics of nuclear and molecular collisions 79−30821
stochastic theory in perturbation limit 78−1042
strongly interacting systems, energy decomp. scheme 79−31431
structure and dynamics of mols. by pulsed mol. beams 80−102563
structureless polyatomic molecules, phenomenological energy exchange, kinetic models 78−42168
molecular inelastic collisions continued
superposition of reactive and nonreactive scattering amplitudes in the presence of a conical intersection 80−63733
symmetric-top molecular gas, non-reson. half widths, approx. calcs. 77−75221
terphenyl, ortho-, para-, meta-, total neutron cross sections for subthermal energies 78−74779
tert-butyl chloride, separation of collision-induced from intrinsic mol. depolaris. Rayleigh scatt., C-Cl bond optical anisotropy 78−27244
tetrachloromethane, separation of collision-induced from intrinsic mol. depolaris. Rayleigh scatt., C-Cl bond optical anisotropy 78−27244
tetracyanobenzene+methylated benzene, fluorescent exciplex form., electronic relax. 80−5573
tetrafluoromethane, collision-induced light scatt., spectral features 78−13493
tetrafluoromethane, collision-induced Rayleigh scatt. intensity calcs. 77−46569
tetrafluoromethane, collision-induced scatt., many-body correls. 80−87127
tetrafluoromethane, collision-induced scattering at a vibrational Raman frequency 78−62814
tetrafluoromethane, gas, liq., collision-induced microwave absorpt. 77−42312
s-tetrazine, UV and vis. photodissoc., three-body half-collision dynamics 80−78664
thermal unimolecular reactions, rate calcs., weak collisional centrifugal barrier effects, adiabatic channel calcs. 79−74348
three body problems with Coulomb interaction, adiabatic representation, two-level approx. 80−47861
three-body problem, coupled channel method calcs., Faddeev approach 78−86929
three-level system, coherently driven, collisional contrib. to dynamic Stark effect 79−13765
Tokamak impurity problems, atomic and mol. struct. and collision data, review 80−43959
transition probabilities and line width parameter of rot. transition 79−22776
transition probability amplitudes quasiclassical approx. *(Russian)* 77−79676
transition probability between two electronic states, curve crossing 77−3445
transition rates, collisionally induced, estimation from lab. data, rel. to interstellar mols. 79−45787
translation factor, parameter-free, semiclassical approach 80−23482
translational energy distrib. of products, surprisal analysis 77−38706
translational energy distribution, Brownian motion model 77−50483
trichloroethane, separation of collision-induced from intrinsic mol. depolaris. Rayleigh scatt., C-Cl bond optical anisotropy 78−27244
trichloromethane, separation of collision-induced from intrinsic mol. depolaris. Rayleigh scatt., C-Cl bond optical anisotropy 78−27244
trimethylamine, collision induced fluoresc. enhancement and quenching, relax. processes 80−83412
turning point region, approx. method 79−72373
two-level molecular gas, nonlinear absorption near gas-medium reson. 79−41409
two-photon transition in colliding particle system, stimulated Raman scatt. 80−9663
unimolecular reactions, energy transfer effects, nonsteady state solns., weak collisions 79−74351
unimolecular reactions, temperature dependence A-factor 79−74347
unlike molecules, in soln., electronic excitation energy transitions *(German)* 77−34749
vibration-rotation lineshapes, effect of elastic and reorientation collisions 79−89712
vibrational dephasing by translational collision 80−87202
vibrational-translational transfer rate, optoacoustic meas. using short pulse CO_2 laser 80−74258
water, collision-induced far IR absorpt., depolarised Rayleigh scatt. 77−81100
water cluster ions, collision-induced dissoc. at high press. 77−83679
weak interactions, competitive preferential solvation theory 79−27051
xanthene dye N-92+inert gas buffer, electron beam excited, fluoresc., energy transfer 78−25877
Ar gas, primary ionisation coeffs. in cross mag. field 80−83879
Ar+HCN(H_2O), electron excitation of Ar* and Ar_2*, fluoresc. and dissoc. energy transfer collisions 77−14580
Ar+N_2, rot. and vibr. inelastic mol. collision cross section calc. 79−59542
Ar+NO($X^2\pi$), intermol. pot. surfaces, electron gas model calcs. 77−34721
Ar^{12+}+N_2(NH_3)(CO_2)(methane)(acetylene), C and N Auger effect 77−6908
Ar_2, collision-induced Raman spectrum, absolute cross sections 78−46349
Ar_2, collision-induced Raman scatt., polarisability anisotropy 78−46350
ArF*, in Ar-F_2 proton-excited mixtures, production and quenching 78−94307
Ar_2F*, in Ar-F_2 proton-excited mixtures, production and quenching 78−94307
Ar*+N_2, metastable mol. form., emission spectra 77−19019
BO_2, $A^2\Pi_u$-state, Hanle effect, press. and Zeeman broadening 79−18239
BaCl+Ar(He)(N_2), intermultiplet energy transfer 79−27063
BaCl($C^2\Pi$)+He(Ar)(N_2), collisional quenching, laser induced fluoresc. decay meas. 79−27075
BaO+CO_2, in Ar flame, rot. and translational relax. by sub-Doppler optical-optical double reson. 80−95583
C_2+acetylene, C_2 Swan band transition probabilities, collisional energy transfer effects 80−87214
C_2+O_2, C_2($X^1\Sigma_g^+$) and C_2($a^3\Pi_u$) intersystem crossing and free radical kinetics 80−95668
CH, interstellar, rot. levels struct., excitation mechanisms 78−21908
CN, A- and B-state lifetimes, collisional transfers and perturbations 78−78756
CO, high resolution lifetime meas., perturbation and collisional transfer correl. 78−78699
$^{12}C^{18}O$ 78−82768
$^{13}C^{16}O$, fluoresc. and electronic quenching cross sections 78−82768
CO+H_2, pot. energy surface anisotropy in nonreactive region, ab initio calcs. 78−29832
CO+H_2, rot. excitation, rel. between tensorial cross sections 80−83454

molecular inelastic collisions continued
CO+H_2, thermal energy collision, ab initio pot. energy surface 79−45788
CO+N_2(CO_2), line broadening, short range force effects, semiclassical calcs. 79−98085
CO^++CO, metastable and $X^2\Sigma^+$ states dissoc. 78−33587
CO_2 R-branch line intensities and press.-broadened line widths at 15 μm 80−102508
CO_2, rot. Raman and IR lines, self-broadened linewidths 77−42357
CO_2-N_2-H_2O gasdynamic laser, water vapour condensation and mol. relax. processes 79−13946
CO_2-N_2-He discharge, electron distrib. relax., numerical study 80−54070
CO_2+Ar(N_2), 30_{III}-000 band, intensities, press.- and self-broadening coeffs. meas. 78−78695
CO_2+He^+(Ar^+)(Ne^+)(Kr^+), electronically excited CO_2^+, $A^2\pi_u$ state bending vibrs. 77−3454
CO_2+N_2, near IR absorpt., collisional broadening 77−30872
CO_2+polyatomic molecule, ($00^0$1) mode deactivation, laser induced fluoresc. obs. 80−83453
COF_2+COF_2, collisionally induced relax. processes and vibr. energy transfer 80−53107
CS, A $^1\pi$ state, collisional transfer and radiative decay, time resolved obs. 79−89809
CS+H_2, collisional excitation of interstellar molecule 78−81664
CS_2+inert gas, translational excitation, energy transfer, cross spectra 77−50559
C_2($a^3\Pi_u$)+methane(acetylene)(ethylene)(ethane)(O_2), reaction rate consts. and quenching, multiphoton UV photolysis, fluoresc. obs. 79−74355
Cl_2, fluoresc. quenching by collision-induced predissoc. 77−14472
Cs_2, fluoresc. spectra, kinetics, laser candidate 79−64027
Cs_2+halogens($SnCl_4$)(MoF_4)(UF_6), ionisation reactions, absolute cross sections 80−99565
Cs_2+methane, collision-induced dissoc., atom-mol.-exchange optical pumping 78−22008
$CsHCl_2$, H bond bending vibrs., inelastic neutron scatt. obs. 79−89800
CsHClBr, H bond bending vibrs., inelastic neutron scatt. obs. 79−89800
D_2^-, collision induced dissoc., positive and negative ions form. 78−50612
D_2+D_2, collision effect on depolarised light scatt. linewidths 80−53059
D_2+He^+, dissociative ionisation, D^+ energy spectra 77−58154
D_3^-, collision induced dissoc., positive and negative ions form. 78−50612
DCl+CO, V-V energy transfer 80−78695
DF, vibr. relax., isotope effect, quantum model 80−91460
D_2O, vibr. relax. rates 80−95717
F+H_2, electronic-to-rotational energy transfer 77−3431
H^++NO, ~10 eV, anomalous excitation of NO Rydberg states 77−14546
H_2, (oriented), scatt., total collision cross-sections, anisotropic pot. parameters calcs. 78−13568
H_2, D_2 and HD, intermol. collision process obs. using light scatt. expts. 80−53001
H_2, dissociation rates in elec. discharge, calc. 77−46616
H_2 in Seyfert, galaxy NGC 1068 nucleus, collisional excitation 80−12816
H_2, rot. Raman linewidths, self-broadening calcs. 77−42356
H_2^-, collision induced dissoc., positive and negative ions form. 78−50612
H_2^+, 400 keV beam dissoc. collisions in air, ang. distribs., vibr. state effects 79−10197
H_2^+, collisional dissoc., excited electronic states effects 80−9687
H_2-H_2, overlap parameters from IR spectrum in binary collision-induced H_2 band 77−54561
H_2+Ar, induced IR spectrum, overlap dipole moment determ. 77−18924
H_2+D_2, reactive and inelastic scatt. using repulsive model pot. energy surface 78−66620
H_2+D_2, reactive and inelastic scatt., semiempirical pot. energy surfaces calcs. 80−74140
H_2+Fe^{+q} collisions, 3.4 MeV/nucleon single electron capture and loss cross sections 77−83726
H_2+H, rot. excitation in diffuse interstellar clouds rel. to CH^+ prod. by shock waves 80−56898
H_2+H_2, collision effect on depolarised light scatt. linewidths 80−53059
H_2+H_2, coupled states approximation for scattering of two diatoms 78−62872
H_2+H_2, quadrupolar $S_1(J)+S_0(J)$ double transitions, IR fundamental band, 77K 80−52986
H_2+H_2(He), anisotropy of long-range interaction 79−36734
H_2+H_2(N_2), cross sections for electron stripping of fast H_2 meas. 77−83705
H_2+He, inelastic collisions, statistical decoupling 77−517
H_2+He^+, dissociative ionisation, H^+ energy spectra 77−58154
H_2+He(2^3S), Penning ionisation, quantum mech. scatt. calcs. rigid rotor approx. 77−34741
H_2+He(2^3S), pot. energy surfaces and autoionisation lifetimes calcs. 77−34740
H_2^++H_2, 10 keV H_2^+ dissociation, H-H^+, H^+-H^+ and H-H fragments 77−83688
H_2^++He, 10 keV, dissoc. excitation, ionis., energy distrib. 77−61849
H_2^++He(Kr)(Xe), collisional dissociation, ion-pair prod., negative ion prod., cross sections 77−14529
H_3, form. and dissoc., kinetics, historical review, book contrib. 77−40527
H_3^-, collision induced dissoc., positive and negative ions form. 78−50612
H_3^+ fast molecules, transmission through thin C foils 79−76484
H_3^++H_2, 100 to 500 eV, dissociation of H_3^+ 77−42383
H_4^+, ground and excited state pot. energy surfaces and geom. struct., SCF and CI calcs. 78−78769
H_n^++N_2, (n=2 to 27), 250-900 eV collisions, fragmentation 77−88525
HB rot. relaxation, diffusion theory 80−106313
HBr-Ar, IR fundamental region, line intensity, line breadth, tunable laser meas. 78−46328
HCN+H_2(CH_3F), HCN excited vibr. state, T_2 meas. 80−102498
HCl, del. gas, proton longit. relax. time 77−34720
HCl, linewidths and shifts in fundamental band broadened by D_2 and H_2 *(French)* 78−972
HCl, rot. relaxation, diffusion theory 80−106313
HCl, vibr.-rot. line broadening by CF_4 and SiF_4 77−27117
HCl, vibr.-rot. lines broadening and shifting by SiF_4 perturber 77−23521

molecular inelastic collisions continued
HCl+Ar, IR line width press. broadening 77−61802
HCl+CO_2, semi-empirical non-Lorentzian line shape determ. 77−34699
HCl+N_2(CO)(O_2)(HCl), HCl linewidth, impact parameter calcs. 79−89714
$H^{35}Cl$+N_2, collision broadened vibr.-rot. linewidths, and shifts in fund. band, low temp. obs. *(French)* 77−68076
HD, dipole spectrum, influence of intracollisional interference 78−33492
HD, gas, fundamental band, R and P line shapes 80−23461
HD, IR absorpt. spectra, collision induced fundamental band 77−79613
HD^-, collision induced dissoc., positive and negative ions form. 78−50612
HD+Kr(Xe), collision-induced fundamental band in room temp. IR absorpt. spectra 77−34627
HD_2^-, collision induced dissoc., positive and negative ions form. 78−50612
HF, near IR absorpt. spectra, collisional broadening, line shapes and half-widths 79−89673
HF+Ar, IR line width press. broadening 77−61802
HF+HF (methane)(methane-d_4), collision relaxation rate constants and rot. equilibration time meas. 80−69213
HF+O_2($a^1\Delta_g$), E-V energy transfer 77−30960
HNO_3, spectral linewidth, broadened in air, O_2 and N_2 at 200 and 300K 78−46399
H_2O, microwave absorption, spectral line press. broadening theory 77−30864
H_3O^+.H_2O, mobility in He, flow drift tube obs. 78−34257
H_3O^+.$2H_2O$, in 2,5-dichlorobenzenesulphonic acid trihydrate, neutron diffr. obs. 78−58855
H_2S+O^+(Cl^+), S highly stripped core ion outer shell rearrangement, Kα X-ray spectra 77−3451
H_2*+H_2, depolarisation cross-section of (1s 3p) $^3\Pi_u$ (N=1) level 77−61829
H^*_2+H_2O(SF_6), ionis. collisions 79−64088
HbBr($B^2\Sigma^+_{1/2}$), rate coeffs. for collisional quenching, time resolved emission obs 79−89705
He-Ne, laser pumping transition, mol. beam obs. 77−7064
He+H_2, final quantum state assignment, improved quasiclassical histogram method 78−66617
He+H_2, rot. and vibr. inelastic mol. collision cross section calc. 79−59542
He+H_2, scatt., opacity functions, j_z-conserving approx. calcs. 77−6878
He+H_2, T-matrix element approx., j_y-CCS calcs. 77−19003
He^++H(H_2), H(2p) and H(2s) excitation cross sections, 5-26 keV 77−58150
He_2, collisional electronic and rot. relax. in afterglow of pulsed discharge 77−61784
He_2+N_2(O_2), He_2($2^3\Sigma$) quenching reactions 78−22014
HeH^+, collisional dissoc., excited electronic states effects 80−9687
Hg+H_2(HD)(D_2), intramultiplet transitions 77−54597
Hg_2 excimers, photoassoc., spectroscopy and kinetic processes of high-lying vibronic states, laser applics. 80−9649
$HgBr_2$+N_2*, dissociative excitation, mol. fluoresc. obs. 80−91634
HgCl*(B1/2), fluoresc., collisional quenching kinetics 78−94269
Hg($^3P_0$)+N_2 fluorescence decay following pulsed laser excitation 77−30817
I+H_2(HD)(D_2), intramultiplet transitions 77−54597
I_2 collision-induced predissoc., Landau-Zener model, method of analytic continuation 77−83687
I_2, fluoresc. in 340 nm band, buffer gas press. depend. 79−13762
I_2, laser fluoresc., relax. of oriented ground and excited mols. 78−46390
I_2^+, impact dissoc. cross-section, excitation energy, mass spectral obs. 77−3489
I_2+Ar(Ne)(tetrafluoromethane), D-state lifetime and UV laser action 77−14471
I_2+I_2, optical coherent transients detected by frequency-switched tunable laser 77−54762
Ir complex, tetraethylene iridium chloride, ligand-ligand interactions; low freq. vibr. obs. 78−94255
K_2, absorpt. and relax. const. determ. by optical laser pumping method 80−102550
K_2, ground state thermalisation speed, collision cross-sections meas. *(Russian)* 80−78723
K_2+halogens($SnCl_4$)(MoF_4)(UF_6), ionisation reactions, absolute cross sections 80−99565
Kr_2, collision-induced Raman spectra, absolute cross sections 78−46351
KrF(B)+Ar(Kr)(F_2), excimer, collisional quenching rates, photolysis meas. 78−63066
Li^++N_2, (0.5 to 1.0 keV) energy loss spectra, ionisation, electronic and vibro-rot. transitions 77−14541
Li_2($B^1\Pi_u$)+inert gas, laser-excited collision-induced dissoc. 79−79232
LiF+Ar, polarised rot. selected mol., high resolution differential cross section 77−27147
LiF+Ar(Kr), anisotropic system intermol. pot. determ. 77−58121
molecular pair polarisabilities, continuum electrostatic theory 78−86769
N_2,$E^3\Sigma_g^+$ state electron excitation, collisional deactivation and energy transfer 77−10774
N_2, 1^- system bands, line broadening and shift 80−87138
N_2, ($C^3\Pi$) nonequilibrium rotational level distrib. in gas discharge *(Russian)* 78−86796
N_2, fission fragment excitation, delayed coincidence spectroscopy 77−24189
N_2, gas, liq., collision-induced microwave absorpt. 77−42312
N_2, rot. Raman linewidths, self-broadening calcs. 77−42356
N_2, rotational collision number from thermal cond., 700-2500K 80−23526
N_2 structural second virial coeff., intermol. pot. and mag. scatt. 80−78678
N_2+Ar, 0.06-0.41 eV, metastable at. electronic excitation transfer 79−64071
N_2+CO, electronically inelastic collision, distorted wave calc. and pot. energy curve 80−9709
N_2+CO(N_2)(O_2)(NO)(CO_2)(methane), ionis. at low energy 78−58791
N_2+H^+, electron ejection, energy distrib. binary encounter approx. calcs. 77−30971
N_2+H^+, energy transfer, dissoc., cross section calcs. 77−50522
N_2+H^+(He^+), 1 MeV, dissoc. ionis., time-energy spectra 77−34744
N_2+N_2(Ar)(H_2), ($A^3\Sigma_u^+$, ν=0,1) metastable state quenching rate coeffs. 78−90206
N_2+O_2 collinear collision, quantum-mech. model 77−30955
N_2+O_2 vibr. transitions, semiclassical theory 78−66633

molecular inelastic collisions continued
$N_2(A^3\Sigma_u^+)$, auroral, quenching by O and O_2 from rocket meas. of emission 78−57380
NH_2, microwave-optical double reson., collision-induced transitions, vibronic state obs. 77−34667
NH_3, collisional broadening, vel. depend., IR optical saturable absorpt. technique, book contrib. 78−9201
NH_3, collisionally induced transition rates, estimation from lab. data, rel. to interstellar mols. 79−45787
NH_3, inversion spectrum, reson. half-widths calcs. 77−75221
NH_3+2H_2, triplet n3S Rydberg state, ab initio UHF CI SCF calc. 80−53095
$NH_3+CO_2(N_2)$, collisional broadening of NH_3 inversion spectrum lines 80−99521
NH_3+H_2, NH_3 inversion transition, linewidths and T_1/T_2 ratio 80−99499
NH_3+H_2, semi-empirical non-Lorentzian line shape determ. 77−34699
NH(ND), $b^1\Sigma^+$ state, collisional quenching, isotope effects, rate coeffs. 77−19018
NO, $A^2\Sigma^+$ two-photon excitation, radiation lifetime, quenching 77−3426
NO, γ-band collisional broadening parameters from resonance line absorpt. 77−10704
NO, press. broadening coeffs., spin-flip Raman laser spectrosc. 80−43147
$NO+CO_2$ collisions in CO_2 gasdynamic laser, causing depopulationg of lower active level 80−74336
$NO+N_2(Ar)$, $^2\Pi_{3/2}$, $^4\Pi_{1/2}$ states, line broadening, mag. moment effect 79−72391
NO+NO, semi-empirical non-Lorentzian line shape determ. 77−34699
$NO+Ne(Ar)(N_2)(H_2)(CO)$, $E^2\Sigma^+$ and $B'^2\Delta$ states fluoresc. collisional deactivation 79−6965
NO_2, inter and intramolecular radiationless transitions, relax., time resolved excitation and fluoresc. spectra 80−27966
$NO_2+Ar(CO_2)(NH_3)$, continuum quenching in upper atmosphere 79−88520
$N_2O(X^1\Sigma^+)\rightarrow N_2(^1\Sigma_g^+)+O(^1S)$, photodissoc., exact collinear calcs. 77−30937
$NO(b^4\Sigma^-)$, electron impact excitation energy, radiative lifetime, quenching in NO 77−79642
N_2*+$H_2O(H_2S)$(methane), deactivation, from laser-induced CO_2 fluoresc. obs. 80−63776
Na_2, absorpt. and relax. const. determ. by optical laser pumping method 80−102550
$Na_2+Na(K)$, electron energy transfer from optically excited mols. 77−34742
Na^*+N_2, differential quenching cross-section, polarisation effects 77−27019
$Na_2^*(A\Sigma)+He(H_2)(N_2)$(methane), rot. energy transfer, power law scaling 79−98204
$Ne+N_2$, K-X-ray spectrum, collisional configuration-rearrangement 78−82816
O_2, laser excited, quenching by CO_2, H_2O and I_2 80−99515
O_2, microwave absorption, spectral line press. broadening theory 77−30864
O_2, microwave spectrum, press. broadening 80−23412
O_2, singlet state, form., quenching and reactions, review 77−29002
O_2, structural second virial coeff., intermol. pot. and mag. scatt. 80−78678
$O_2+Ar(O_2)$, collision induced UV absorpt. in Herzberg continuum, dimer form. 77−30883
O_2+H^-, energy transfer, dissoc., cross section calcs. 77−50522
O_2+N_2, collision induced UV absorpt., Herzberg continuum, dimer form. 78−9167
O_2+N_2, O_2 absorption in Herzberg region, N_2-induced, temp. effect 78−87429
$O_2+O_2(N_2)(H_2O)(Ar)(He)$, 118750 GHz transition, press. broadening 77−75136
O_2+O_3, collisional deactivation of laser excited $O_2(^1\Delta_g)$, addition effects and pathways 78−25673
OCS, microwave rot. transitions, phase shift effect, collisional effects 79−98073
OCS, vibr. energy transfer map 80−99560
$OCS+H_2$, collisional excitation of interstellar molecule 78−81664
OH collisional broadening parameter in H_2-NO flame, curve of growth calcs. 80−53052
OH, excitation in interstellar clouds 78−65669
OH, Λ-doublet transitions induced by ion collisions 78−9222
$OH+H_2O$, OH linewidth rot. depend. on UV transitions 80−91606
$OH+H_2O(NO_2)(CH_3Cl)(N_2)(H_2)$(He), mean collision cross sections from microwave spectroscopy 80−1046
$OH+NO(NO_2)(O_2)$, $OH(v=1)$ relax., time resolved spectra 80−74240
$O_2(^1\Sigma_g^+)+H_2$, collisional relax. temp. depend. 77−32783
$O_2(b^1\Sigma_g^+)+O_2(X^3\Sigma)$, quenching rate coeff. meas., density depend. 77−38721
$PH+N_2(CO)(NO)(H_2)$, collisional deactivation of $PH(b^1\Sigma^-)$, time resolved quenching 79−54948
PH^*+PH_3, collisional deactivation of PH $(b^1\Sigma^+)$ state, time resolved spectra 78−78750
$Pb+H_2(HD)(D_2)$, intramultiplet transitions 77−54597
S_2, fluoresc. quenching by He, Ar, Xe, N_2, S_2, CF_4, C_2F_6, fluoresc. lifetimes 78−46386
$SF_4+O^+(Cl^+)$, S highly stripped core ion outer shell arrangement, Kα X-ray spectra 77−3451
SF_6, collision-induced forbidden Raman transitions 77−6791
SF_6, collision-induced Rayleigh scatt. intensity calcs. 77−46569
SF_6, collisions, laser spectroscopy investig. 80−9697
SF_6, multiphoton dissoc., collision effects 80−23467
SF_6, multiphoton isotope selective dissoc., pulse shape, energy, press. and geometry effects 78−25733
SF_6, multiple IR photon absorpt., collisional effects 78−86926
SF_6, multiple photon absorpt., laser pulse intensity and collisions influence 80−95699
SF_6+H_2 chemical laser, electron beam pumping 80−91784
SO_2+alkane, $^3B_1$-state lifetime saturation, chem. and phys. quenching channels 79−814
$SO_2+N_2(CO_2)(H_2O)$, collisional quenching of $^3B_1$ state, 8-1300 torr 78−86906
$SeO_2+N_2(CO_2)$, radiative lifetime and quenching rates 80−95685
$SiF_4+O^+(Cl^+)$, Si highly stripped core ion outer shell rearrangement, Kα X-ray spectra 77−3451
molecular inelastic collisions continued
$SiH_4+O^+(Cl^+)$, Si highly stripped core ion outer shell rearr Kα X-ray spectra 77−3451
Sr_2 dimer, photoassoc., photoluminesc., collisional dissoc. 80−56
$Te+H_2(HD)(D_2)$, intramultiplet transitions 77−54597
$\{Th[(CH_3)_5C_5]_2H(\mu\text{-}H)\}_2\text{-}C_6H_4CH_3$, molecular structure by neutron α. fraction 79−89801
$Tl+H_2(HD)(D_2)$, intramultiplet transitions 77−54597
UF_6, electronically excited, emission quenching by organic mols. 78−42115
UF_6, electronically excited, emission quenching by inorganic mols. 78−42116
Xe_2, collision-induced Raman spectra, absolute cross sections 78−46351
XeCl+HCl, ground state destruction, quenching rate consts. meas. 80−63758
$XeF+F_2(NF_3)$, radiative lifetime and collisional quenching kinetics 78−94289
XeF*+$He(Xe)(NF_3)(F_2)$, quenching rates for XeF in (B) state 78−58730

molecular internal conversion *see nonradiative transitions*

molecular internal mechanics *see molecular vibration*

molecular internal rotation *see rotational isomerism*

molecular intersystem crossing *see nonradiative transitions*

molecular libration
see also macromolecular dynamics
acenaphthene, vibr. spectra, mol. crystal dynamics, librational modes 78−64356
acetic acid-d_0, -d_1, -d_4, H bonding in solid, IR spectra, vibr. and librational modes 78−43843
adamantane, deuterated single plastic cryst., coherent inelastic neutron scatt., libration damping *(French)* 79−14905
adamantane, lattice dynamics in disordered phase 78−55923
adamantane, plastic phase, librations, phonon branches, neutron scatt. study *(French)* 79−51222
adamantane-d_{16}, collective librational modes and orientational correlations 79−73266
alkali halide:NH_4^+, hindered rot. energy levels calc. 80−10514
alkali halide, lattice vibrs., effect of NO_2^- impurity molecule, theory 77−35654
alkali halides:NH_4^+, inelastic neutron scatt. 78−14407
alkali metaphosphate glasses, low frequency Raman scattering and glass transitions 79−95745
aniline, in p-xylene host cryst., phosphoresc. triplet state, ESR and MIDP obs. 80−66077
anisotropic system, paramag. to ferromag. transition, libron interactions *(German)* 78−76237
anthracene:tetracyanobenzene charge transfer complex, cryst. struct., temp. effects 80−96508
anthracene, dynamic electron densities, anharmonic contribs. from large molecular librations 79−97971
anthracene-d_{10}-s-tetracyanobenzene, rotational mode coupling in phase transition 78−71827
anthracene-pyromellitic dianhydride, mol. charge transfer cryst., Raman scatt. meas. 80−29743
anthracene-TCNB, charge transfer cryst., frequencies of librations involved in phase transition 79−19885
benzene, liq., spectral broadening of mol. transitions, librational broadening 79−51939
biphenyl, diamagnetism and thermal motion 80−25076
bipyridines, torsional isomerisation of biologically active bicyclic molecules 80−27996
1-butene oxide, gas, microwave spectrum 79−13703
chloranil, phase transition, Zeeman effect of ^{35}Cl NQR 78−59944
condensed phase mol. reorientation, correlation times, librational model 78−1968
constrained thermal motion refinement for rigid molecule with librating side groups 77−11643
crystal, librational dynamics 77−7831
crystal impurity librational relax., phonon assisted transitions, direct, Orbach and Raman processes 78−83887
cyclobutane-d_0(d_8), cryst. modifications, low. freq. Raman and IR spectra 80−7342
cyclohexane fluorinated derivatives, $C_6F_9H_3$, C_6H_{12}, mol. rot. in plastic phases 77−35495
cytidine, cryst. powder, absorption spectrum, unusual narrow line FIR modes, cryogenic temps. 79−69824
diamantane, low temp. soft librational mode, Raman spectra exam. 78−30730
diamantane, Raman study of three solid-state phase transition 79−51946
diatomic molecular crystal, librational force constants, appl. to α-N_2 and γ-N_2 80−16020
2,2-dibenzyl-1,3-dibromopropane, crystal structure and thermal motion 79−99173
dichloromethane-decalin glass, mol. dynamics, from dielec. loss meas., 107-148K, 293K 78−76379
dielectric singularity, causing Kohn anomaly and soft modes 79−60470
p-diiodobenzene, far IR single cryst. transmission spectrum, temp. and polaris. depends., assignments 78−72498
dimethylacetylene, librational motion, inelastic neutron scatt. obs. 78−75742
dimethylacetylene, tunnel splitting, rot. pot., μeV neutron scatt. study 79−41993
dynamic electron densities, anharmonic contribs. from large molecular librations 79−97971
electrolyte aq. solns., IR librational bands, struct. making and breaking 78−56476
ethers, and solid alkane solns., far IR spectra *(French)* 79−4793
ethylene crystal, partially deuterated, Raman phonon spectra 78−56470
ethylene oxide clathrate, reorientation, residence times, Debye-Waller factors, activation energy, neutron scatt. study 79−41989
ethylene oxide clathrate deuterate, rotational motion, quasi-elastic neutron scatt. study 79−51022
ethylmethylether(-d_3), low freq. vibr. spectra, methyl torsional pot. functions, internal rot. 79−26978
FTF-TCNQ, libron freqs., temp. and press. effect 79−86860
2-haloethanols, torsional interaction, IR spectra, ab initio calcs., 2-dimens. model 80−74160
hexamethyl benzene, high press., variable temp. Raman spectra 78−56488

mc **molecular libration** continued
hydracids, monatomic matrix-trapped, assoc. forms, struct. and spectral response, intermol. pot. calcs. 79−93996
hydrates, solid, librational motion from electric field gradient tensors at deuterons 77−71792
hydroxylapatites, IR spectra, stretching and librational bands of OH groups, and hindered rotation 78−2841
ice, isotopic, I_{Ih}, single crystal Raman intensities, OH bond polarisability, librational modes 78−27208
imidazole, vibr. spectra, mol. crystal dynamics, librational modes 78−64356
impurities in crysts., dynamics 79−60442
impurity molecule, in solid, vibr. relax., rot. and translational local modes 77−75118
impurity molecule in cryst. lattice, strong EM field effect on librational-rot. motion 80−80824
impurity molecules in crystals, exclusion rules for librational-tunnelling states 78−84174
intermolecular interactions, correlation with absolute Raman intensities of lattice modes in mol. crystals. 77−66502
librational reorientation, sum rules 78−71659
malononitrile, displacive phase transition, 294.7K, Raman and Brillouin-Rayleigh scatt. obs. 80−16047
methane, solid, phase II, Raman spectrum, vol. and temp. depend. 80−97260
methane, solid, phase III, Raman spectra 79−65849
beta-methane, solid, Raman spectrum in intramol. and lattice region 79−33697
methane-d_4, solid phases I, II, librational excitations 78−2212
methyl selenocyanate, and isotopic forms, microwave spectrum 79−13705
N-methylacetamide, and isotopic forms, low-freq. Raman spectra, internal torsional mode 79−26992
methylammonium chloride, torsional motion, harmonic oscillator and free rotor bases calcs. 79−72232
molecular crystal, dynamics, neutron spectroscopy appl., review 79−42166
molecular crystal, p-$Cl_3P{=}NSO_2C_6H_4Cl$, rel. to quadrupole nature of spin-lattice relax. 77−59480
molecular crystal, triplet spin-lattice relax. rate anisotrpy at low temp. and high mag. fields 79−42822
molecular crystals, effect of temp. on libron frequencies 79−86860
molecular crystals, orientational dynamics, unified theory 79−41992
molecular crystals, rot. excitations and tunnelling, review 79−46579
molecular liquids, depolarised Rayleigh-wing scatt. and far IR absorpt. spectra 78−39532
molecular motion analysis, using least square anal. of X-ray and neutron diffr. struct. factors 79−7656
naphthalene: quinoxaline, isolated triplet mol. direct spin-lattice relax., librational model 79−11444
naphthalene, external mode one-density states, low freq. Raman scatt. spectra *(French)* 80−76012
naphthalene, molecular cryst., phonon scatt. and exciton linewidths 78−15185
naphthalene, Raman active phonon freqs., linewidths and line shapes, temp. depend. 79−47432
naphthalene-TCNB, charge-transfer cryst., donor mol. orient. and dynamics 79−32926
neopentane, mol. motion in cryst., liq. and plastic phases, neutron scatt. obs. 78−6021
p-nitropyridine N-oxide, dynamic electron densities, anharmonic contribs. from large molecular librations 79−97971
NMR signal for quadrupole, chem. shift., dipole-dipole interactions, mol. solids, rigid-body vibr. effect 78−15056
octafluoronaphthalene, struct. phase transition exam. 77−47572
one-dimensional conductor, phenomenological eqns. of motion for electrons, phonons and librons 80−10955
pentacene in naphthalene (p-terphenyl), mol. mixed crysts., optical dephasing and vibronic relax. 80−95957
pentachloronitrobenzene, single cryst., far IR absorption 79−73940
peptides, effect on ^{13}C NMR relaxation times 78−85293
perylene in paraffin, anisotropic rot. and libration 77−32417
phenanthrene, molecular cryst., phonon scatt. and exciton linewidths 78−15185
phenanthrene, vibr. spectra, mol. crystal dynamics, librational modes 78−64356
polyatomic molecule, torsional motion, harmonic oscillator and free rotor bases calcs. 79−72232
polystyrene, substituted, Raman, IR and neutron spectra of LF vibs. 78−2848
potassium hydrogen oxalate, oriented single cryst., Raman spectra with very strong H-bonding 80−25359
propenoyl chloride, IR bands, torsional struct. 80−28018
isopropyl chloride, torsional pot. function, far IR and Raman obs. 80−28022
propylene, liquid, effect of libration transitions on sound absorpt. 78−2203
1,3-propylenediammonium manganese tetrachloride, vibr. study of phase transitions, IR and Raman spectra 80−40103
proteins, effect on ^{13}C NMR relaxation times 78−85293
protonated samples, rot. states, coherent neutron scatt. 77−84678
pyridine, adsorbed on Ag surface, Raman active librational modes 80−65359
quasi-one-dimensional conductor, chiral charge density waves form. 78−6302
Raman librational spectra polariation, mol. single cryst., temp. depend. 79−1760
random anharmonic system, self-consistent approx. 77−62798
rigid molecules, dil. soln. in decalin, mean librational freqs. 80−6479
rigid molecules, with large librations, dynamic density and struct. factors 79−7515
rigid-body molecules, diamagnetism and thermal motion 80−25076
sodium hydrogen oxalate monohydrate, oriented single cryst., Raman spectra with very strong H-bonding 80−25359
solid, phase transition, Raman study 78−80345
solid, rotational tunnelling, neutron scatt. theory 78−18561
structured fluid, itinerant libration in two-dimens., numerical soln. 79−14662
symmetric top molecules, microwave transient phenomena, Bloch eqns. 79−26969
TCNQ, lattice vibrs., temp. depend., NQR obs. 79−38402

molecular libration continued
tellurophene($-d_4$), cryst., struct., phonon spectrum, exciton splittings, assignments 77−81088
temperature factor for large libration, general cryst. metric and any site symmetry 78−91410
1,2,4,5-tetrabromobenzene, structural phase transition, Raman and IR spectra meas. *(French)* 77−66503
tetrabromomethane, plastic phase, neutron diffr. obs. and theory 79−77533
1,2,4,5-tetrachlorobenzene, structural phase transition, Raman and IR spectra *(French)* 77−66503
tetrahydrofuran clathrate, reorientation, residence times, Debye-Waller factors, activation energy, neutron scatt. study 79−41989
tetrahydrofuran clathrate deuterate, rotational motion, quasi-elastic neutron scatt. study 79−51022
tetramethylammonium halides, libration amplitudes, NMR second moment determ. 77−1603
tetramethyllead, tunnel splitting, rot. pot., μeV neutron scatt. study 79−41993
thiourea, commensurate-incommensurate phase transition, X-ray diffuse scatt. meas. *(French)* 79−19856
thiourea, Raman scattering spectra, soft mode frequency 79−24305
TMTTF fluoroborate, BF_4 pyramid orientation fluctuation from libration spectrum 79−19891
triethylenediamine, Raman spectra study *(French)* 80−80768
TTF-TCNQ, anharmonic effects on resistivity 78−84202
TTF-TCNQ, anharmonic props., temp. (press.) depend., rel. to naphthalene and anthracene 80−15200
TTF-TCNQ, elec. cond., role of librations 79−19580
TTF-TCNQ, Landau free energy function, CDW-libron interaction, sp. ht. near phase transitions 80−19963
TTF-TCNQ, Landau theory of phase transitions 80−92666
TTF-TCNQ, lattice distortion, displacive transform., Landau theory 77−31743
TTF-TCNQ, lattice distortion, displacive transform., Landau theory 77−84879
TTF-TCNQ, metallic conductivity temp. depend. 78−6357
TTF-TCNQ, thermal cond. above and below Peierls transition, electronic and lattice contribs. 79−95394
urea molecule, bond-length corrections for external and internal vibrs. 80−106402
vinyl aromatic polymer series, dielec. relaxs. at 220°C, −50°C and ~120°C interpret. 77−43929
Zeeman effect, effective rotorsional Hamiltonian 79−26970
Ar-HCl, Van der Waals mol., far IR spectrum, anisotropic intermol. force effects 78−62869
B_2H_6, cryst., mol. charge distrib. anal., using struct. factors from mol. densities 80−15068
Ba hexafluorometallates, $BaMF_6$, (M=Si,Ge,Sn,Ti), Raman spectra, at press. up to 25 kbar 78−6670
$BaBr_2.2H_2O$, pure and deuterated, low temp. IR and Raman spectra *(German)* 79−19874
$BaCl_2.2H_2O$, polycryst. hydrates, librational motion of H_2O mols., neutron diffr. exam. 80−10604
$BaCl_2.2H_2O(D_2O)$, lattice vibr., IR and Raman spectra 79−15443
$BeSO_4.4H_2O$ and deuterated analogue, IR spectra, 110K, 1200 to 250 cm^{-1} 77−8582
$BiCl_3$, Raman scatt. spectrum, librational and translational vibr. *(Russian)* 77−54562
CCl_3PCl_4, cryst., libration freqs., temp. depend., combination light scatt. and NQR obs. *(Russian)* 77−66436
CN^-, on Ag surface, Raman active librational modes 80−65359
CO, in Ar matrix, vibr. line shape, vibr.-phonon interaction 79−3493
CO, matrix-isolated, librational relax., IR line broadening 80−978
CO_2, solid, high press. mol. libration calc. with Kihara core pots., Gruneisen parameter and lattice 80−65173
CO_2-N_2O, mixed cryst., librational motion, Raman obs. 78−6661
$Ca_{10-x}Sr_x(PO_4)_6(OH)_2$, continuous cation migration, IR spectra study 80−93297
$CoCl_2.2H_2O$, wagging and rocking band intensities of water 78−27200
$Co(NH_3)_6X_3$, (X=Cl, Br, I), internal and lattice vibr. normal coordinate anal. 79−69203
CsB_3H_8, librational modes, IR, Raman and inelastic neutron scatt. spectra 79−42966
$CsNO_3$, Raman spectra temp. depend., NO_3^- ion external librational modes, I→II transition, Raman spectra temp. depend., NO_3^- ion external librational modes 79−78662
4-cyano-4′n-heptyl biphenyl, nematic phase, torsional absorptions 77−48161
p-D_2, anharmonic spectral density of librons 79−14899
p-D_2, roton dragging librons 78−67886
p-D_2, solid, bound libron state form., Raman scatt. data 77−80600
D_2, solid, compressed, anomalons double peaked one-phonon for IR absorption 79−56788
D_2, solid, far IR absorption by phonons and librons in ordered state 78−80331
D_2, solid, libron spectra and conversion as function of ortho-para conc., Raman scatt. spectra 78−84570
p-D_2, solid, libron spectrum calc. 78−79677
p-D_2, solid, orientationally ordered state, anomalous far IR absorption spectrum 78−10876
D_2, solid, phonon absorption line shape as function of density 80−50329
DCl, orthorhombic, nucl. quadrupole double reson. obs. and interpret. 77−90070
DI, crystalline, Raman and IR spectra, mol. vibr., libration and translation 80−2757
o-H_2, anharmonic spectral density of librons 79−14899
H_2, phonon absorption line shape as function of density 80−50329
o-H_2, roton dragging librons 78−67886
o-H_2, solid, bound libron state form., Raman scatt. data 77−80600
H_2, solid, far IR absorption by phonons and librons in ordered state 78−80331
H_2, solid, inelastic neutron scatt., theoretical analysis 78−34569
H_2, solid, libron spectra and conversion as function of ortho-para conc., Raman scatt. spectra 78−84570
0-H_2, solid, libron spectrum calc. 78−79677
H_2 solid, localised excitations due to p-H_2 impurity 79−65288
o-H_2, solid, NMR relax. and libron energy 78−88204
p-H_2, solid, rotation-libration transition under press., Monte Carlo study 80−49460
o-H_2:p-H_2, solid, isolated pH_2 effect on orientational order 77−47535

molecular libration continued
o-H_2:p-H_2, solid, librons, CPA theory 77−47536
HBr, far IR Ar matrix isolated spectra, 4.2K, press. and conc. effects 78−62801
HCl, far IR Ar matrix isolated spectra, 4.2K, press. and conc. effects 78−62801
HF(Cl)(Br)(I), ferroelec. and paraelec. phases, elec. multipole interactions 77−59522
HI, crystalline, Raman and IR spectra, mol. vibr., libration and translation 80−2757
H_2O, hydrates librational modes in IR spectra 78−48161
H_2O, IR continuum absorpt. due to librational mode of dimer 78−66542
H_2O, Raman spectra, liq. state, depolarisation ratios, libration and translational spectra 79−4797
Hf complex, tetrakis (tropolonato) hafnium (IV), mol. interactions in solid, perturbed γ-γ ang. correl. obs. *(French)* 79−8076
KBr:CN^- 80−49316
KCN, lattice dynamics in disordered cubic phase 78−38794
KCN, librational and phonon sidebands of IR CN^- stretching mode 79−15457
KCN, phonon freq. distrib., cubic and monoclinic phases 78−22800
KCN, plastic phase, Raman scatt. spectra *(French)* 80−11379
KCN-KCl mixed crystals, rel. to F-centre optical absorpt. half width 77−81134
KCN-KCl mixed system, order-disorder transition, Raman spectra obs. 78−15113
KCNS, librational modes in phase transition, Raman spectra obs. 79−55885
KCl:CN^-, coherent admixtures of phonons with impurity libronic excitations, neutron scatt. study 80−49316
KCl:Li^+, restricted interstitial motion of $H_A(Li^+)$ centre, ESR and uniaxial stress expts. 77−48053
$K_2Cu(H_2O)_6(SO_4)_2$, IR and Raman vibr. spectra 79−28743
$K_2Cu(H_2O)_6(SeO_4)_2$, IR and Raman vibr. spectra 79−28743
KI:NO_2^-, first-order Raman scatt. meas. 77−52085
K_2SnCl_6, phase instabilities and mode softening X-ray and neutron diffr. 77−7830
K(TCNQ), Raman spectra from 30 to 2300 cm^{-1} 80−11392
$K_2Zn(H_2O)_6(SO_4)_2$, IR and Raman vibr. spectra 79−28743
$K_2Zn(H_2O)_6(SeO_4)_2$, IR and Raman vibr. spectra 79−28743
$La_2(SO_4)_3.9H_2O$, and isotopic forms, water librations, Raman obs. *(French)* 79−28754
α-$LiIO_3$, hexagonal cryst., vibrs. and force consts. 79−69220
α-$LiIO_3$, pot. energy distrib. and force const. variations with temp. 80−79894
$Li_2SO_4.H_2O$, $^6Li/^7Li$ and H/D substituted, IR and Raman spectra, vibr. and librational modes 77−85716
$Li_2SO_4.H_2O$, far IR spectra, H_2O flipping motion, lattice modes 80−84258
$Li_2SO_4.H_2O$, linear pyroelectric, temp. depend. of polarisation 79−99821
methane, solid, librational tunnelling and proton relax. temp. 80−38969
methane-I plastic crystal, surface modes 78−71926
$MnCl_2.2H_2O$, Raman spectra and lattice dynamics 79−28742
$MnCl_2.2H_2O$, wagging and rocking band intensities of water 78−27200
N_2, solid, α- and γ-forms, Raman spectra, vibron and lattice freq. shifts, libration 80−16020
N_2, solid, β-phase, for IR absorption spectra 80−11385
α-N_2, solid, coherent loss of vibr. and librational excitations 79−86852
α-N_2, solid, librational motion, theory 77−43303
α-N_2, solid, librational motion, neutron scatt. 77−43304
α-N_2, solid, librational motion, spin-lattice relax. 78−15047
N_2, solid, mol. libration and α-γ phase transition, Kihara pot. calcs. 80−44312
N_2, solid, mol. libration in α and γ phases, core pot. calcs. 79−86849
α-N_2, solid, NQR meas. 77−12252
N_2, solid, Raman spectra vibron and lattice freq. shifts, librational force consts., α- and γ-phases 78−19460
α-N_2, solid, $w^1\Delta_u$-$X^1\Sigma_g^+$ intensity and band shape 79−47427
N_2-CO mixed cryst., librational motion, Raman obs. 78−6661
N_2-N_2 anisotropic interaction pot. model, comparison with solid state data 77−34712
ND_4ClO_4, librational tunnelling and proton relax. temp. 80−38969
ND_4I, librational motion of ND_4^+ ion, far IR spectra obs. *(Japanese)* 79−8142
ND_4NO_3, cubic, mol. orientation determ. by multipole anal. 79−73136
NH_3, ND_3, crystals, rotation mol. motion *(Russian)* 78−87762
NH_4 compounds, tunnelling frequency of NH_4 ion in crystals, cubic and noncubic 78−38633
NH_4^+, in NH_4Cl, ion dynamics in disordered states, neutron scatt. exam. 78−26459
NH_4^+, libration and tunnelling freq. rot. heat capacity, hindered rot. energy level calcs. 79−98058
$(NH_4)_2BeF_4$, powder, IR spectra, assignments, mol. libration, in paraelec. and ferroelec. phases 78−88299
NH_4Br and NH_4I, Raman scatt., 1 bar-7 kbar, 86-295 K 80−34909
NH_4Br, partially disordered, librational modes below 235K, Raman scatt. obs. 78−72500
NH_4Br-NH_4I mixed crysts., far IR spectra, phase transition and NH_4^+ libration 77−85719
NH_4Cl, ordered phase, press. depend. of Raman scatt. meas. 77−12388
NH_4ClO_4, NH_4 ion rot. tunnelling splitting, inelastic neutron scatt. 77−15325
NH_4F, cryst. struct., mol. wavefunction calcs. of struct. factors 77−62507
$(NH_4)_2M(SO_4)_2.6H_2O$, M=Ni, Co, Mg, IR spectra 80−97280
$(NH_4)_2PbCl_6$, librational tunnelling and proton relax. temp. 80−38969
NH_4ReO_4, ND_4ReO_4, Raman spectrum, temp. depend. 78−80335
$(NH_4)_2SO_4$, irrad., −50°C transition, librational mode softening, paramag. NH_3^+ probe obs. 77−20037
$(NH_4)_2SnCl_6$, NH_4^+ ion rot. states, inelastic neutron scatt. obs. 78−30552
$NH_4Zn(Co)F_3$, sp. hts., librational and reorientational 77−84946
NaBr.$2H_2O$, polycryst. hydrates, librational motion of H_2O mols., neutron diffr. exam. 80−10604
NaCN, FCC, orientational anisotropy of CN^- ions, Raman spectra meas. 77−36247
NaCN, lattice dynamics in disordered cubic phase 78−38794
NaCN, librational and phonon sidebands of IR CN^- stretching mode 79−15457
NaCN, plastic phase, Raman scatt. spectra *(French)* 80−11379
NaCN, Raman spectrum, hydrostatic press. effects 78−6663
molecular libration continued
Na_2CO_3, struct. changes at incommensurate phase transition 79−95158
$NaClO_3$, X-ray diffr. determ. of ClO_3^- ion dimensions and libration correction 77−80462
$Na_8(Ge_6Al_6O_{24}).CO_3.nH_2O$, linear pyroelectric, temp. depend. of polarisation 79−99821
β-NaN_3, dynamic electron densities, anharmonic contribs. from large molecular librations 79−97971
NaN_3, phase transitions and N_3^- librational motion 77−4178
NaO_2, physical mechanisms of phase transitions 80−6381
$NaPF_6.H_2O$, IR and Raman spectra 77−61749
$Ni(NH_3)_6I_2$, phase transition and rot. excitation 80−96642
$Ni(NH_3)_6X_2$, X=Cl,Br,I, rotational tunnelling by inelastic neutron scatt. 78−30553
β-O_2 crystal, thermodynamics of mol. libration motion *(Russian)* 80−70328
α-O_2, solid, quasi 2D antiferromag., magnon and libron excitation spectra *(Russian)* 77−36067
O_2, solid, struct. elementary excitation spectrum and thermodynamic props. *(Russian)* 79−55696
OH^- (D^-) in alkali halide, impurity rot. barrier height and librational modes 77−11491
RbCN, molecular motion and ordering from dielec. and Raman techniques 79−73932
RbCl:NO_2^-, first-order Raman scatt. meas. 77−52085
$RbNO_2$, Raman spectra temp. depend., NO_3^- ion external librational modes, IV→III transition, Raman spectra temp. depend., NO_3^- ion external librational modes 79−78662
SF_6, plastic phase, neutron diffr. obs. and theory 79−77533
SiH_4, plastic phase, rotational motion, quasi-elastic neutron scatt. study 79−51022
SiH_4, solid, NMR direct detection of tunnel splittings 78−56396
$SrCl_2.2(H,D)_2O$, IR and Raman spectra, force fields 80−2753
TTF-TCNQ, irradiated, libron and phonon equilibration, resistivity meas. 79−42530
$TlSbF_6$, Raman spectra, at press. up to 25 kbar 78−6670
$V(CO)_6$, cryst. and mol. struct., Jahn-Teller distortion, mol. vib. and librational correction 79−32949

molecular librational states *see molecular libration*

molecular magnetic susceptibility
acetylene, magnetic susceptibility, frost model wavefunctions with p-type Gaussians 80−5477
alkali halides, diamagnetic susceptibility, interatomic charge transfer effect 78−50660
alkanes, diamag. susceptibility, graph theoretical anal. 78−33449
alkanes, mag. susceptibility simple additive approx. calcs. 78−86775
alkenes, diamag. susceptibility, graph theoretical anal. 78−33449
aromatic hydrocarbons, localised π-bond model 79−22862
aromatic hydrocarbons, proton chemical shifts, localised π-bond model calcs. 80−43070
benzene, electronic struct., mag. susceptibilities, ab initio calcs. 78−74571
benzene, ring currents hypersusceptibilities calcs. 80−102588
calculations using completely minimising gauge functions 77−6702
carboxyhaemoglobin, carp, variability of mag. moment 80−94159
carboxylic acids, diamag. susceptibility of carbonyl group 77−75329
chromocene, solid, Raman transition assignments, mag. susceptibility, mag. moment 78−43861
closed-shell system, polarisability and mag. susceptibility calc. by SCF and CI method 80−99443
conjugated compounds, ring currents static octopole hyperpolarisabilities calcs. 80−102588
conjugated molecules and ions, diamag. susceptibility, quinonoid character 78−62945
trans-crotonaldehyde, rot. Zeeman effect, microwave spectra, mol. parameters 79−3491
cyclic polyphenylacetylene, thermally excited paramag. props. 77−88614
deoxyhaemoglobin, vibronic coupling, mag. susceptibility and Mossbauer data interpretation 78−70984
deoxymyoglobin, vibronic coupling, mag. susceptibility and Mossbauer data interpretation 78−70984
diamagnetic molecule, mag. susceptibility, nucl. mag. shielding, calc. methods *(German)* 78−33448
diamagnetic molecule, NMR shielding tensor and mag. susceptibility tensor, current density calc., appl. to H_2 *(German)* 79−76445
diamagnetic susceptibility, interatomic charge transfer in diatoms, mol. second moments, additivity formulas 78−70961
diamagnetic susceptibilties and NMR chemical shifts in terms of localised MO's 80−106256
diamagnetism, non-coupled Hartree-Fock-Roothaan method satisfying gauge invariance *(French)* 77−67984
diatomic molecules, diamag. susceptibility and second moments, intramol. charge transfer effects 80−78702
1,3difluorobenzene, rot. Zeeman effect, g-tensor, mag. susceptibility 77−497
DPPH, mag. susceptibility of solvent-free and DPPH-benzene complex 78−70963
electric current density, induced by external mag. field, gauge invariant method calcs. 78−82665
esters, diamag. susceptibility of carbonyl group 77−75329
ethylene, magnetic susceptibility, frost model wavefunctions with p-type Gaussians 80−5477
exchange coupled ions with ground $^3T_1$ term molecular field approximation 79−41093
ferrous porphyrin, intermediate (S=1) spin state, PMR characterisation 80−48014
fluoroform, Zeeman effect, mag. moments and susceptibility, nuclear shielding 79−13764
fulvene, ring currents hypersusceptibilities calcs. 80−102588
haemoglobin, deoxygenated, electronic term scheme using mag. susceptibility and Mossbauer data 77−44586
halomethanes, ^{13}C chemical shifts, diamag. susceptibility, effect of non-bonded interactions 78−78726
Hartree-Fock perturbation technique, CNDO/2 *(French)* 78−37559
heterobenzenes, electronic struct., π electron mag. susceptibility anisotropy 79−59353
HF theory, 1st-order, perturbed, use of symmetry in mol. props. calcs. 79−85916
hydrides, second row, ab initio calcs. using FSGO basis, mol. parameters correlation 78−901

molecular magnetic susceptibility continued
hydrocarbons, average elec. polarisabilities and mag. susceptibilities, ab initio valence electron calcs. 80−87033
Kirkwood equation applicability charged anisotropic harmonic oscill., mol. diamag. 78−5365
metallo-proteins and model systems, susceptibility and struct., SQUID magnetometer uses 79−53036
methane, mag. susceptibility, HF perturbation method 77−79702
methane, rotational state, avoided-crossing molecular beam spectroscopy 80−63730
methyl chloride, Zeeman effect, mag. moments and susceptibility, nuclear shielding 79−13764
methyl vinyl ether, rot. Zeeman effect, g-values, mag. susceptibility, quadrupole moments 77−490
methylamine, C-N and N-H bond nucl. mag. isoscreening line diagrams 80−78555
3-methylfurane, rot. Zeeman effect, g-tensor, mag. susceptibility 77−497
molecular multipole magnetisability, mag. shielding, multiple SCF perturbation theory 77−34549
molecular second-order mag. props. by London field-dependent orbitals calcs. 77−42225
molecules or clusters, interpretation of data from Mossbauer, ESR, susceptibility, optical and XPS meas. 80−37825
myoglobin-Fe^{3+} compounds, Mossbauer and suscept. expts. 78−24019
naphthalene, ring currents hypersusceptibilities calcs. 80−102588
NMR spectra, high resolution, mag. field induced mol. alignment effects 79−18207
open-shell system, polarisability and mag. susceptibility calc. by SCF and CI method 80−99443
optimal gauge parameters, var. calcs., appl. to mol. mag. props. 77−71760
organic molecular systems, polarisabilities, susceptibilities, electron impact ionis. cross-sections calcs. 80−63835
organic molecules, NMR spectra, mag. field induced mol. alignment effects 79−18207
organo-silicon compounds, diamagnetic susceptibility, semiempirical calcs. 78−17820
ozulene, ring currents hypersusceptibilities calcs. 80−102588
paraffins, solid and liquid, diamagnetic susceptibility 78−14923
paramagnetic intermediate valence compounds, sum rules and inelastic neutron scatt. 79−61037
paramagnetic ions, spontaneous coherent state transition, susceptibility singularities 77−40119
PMMA, effects of permanent mag. field on macromolecules 77−25364
point charge models, magnetic susceptibilities, Frost-model Lewis basis sets calcs. 79−54761
poly-γ-benzyl-L-glutamate, soln., liq. film, diamagnetic susceptibility 78−74794
polycyclic aromatic hydrocarbons, diamagnetic susceptibility NCHF (SCF-PPP) calcs. 77−6686
ring current theory 80−87240
sandwich complexes, mag. props., effective Hamiltonian method 80−37731
small molecules, diamag. susceptibility and second moments, intramol. charge transfer effects 80−78702
tetra-glycine, cyclic, mol. polaris. and diamag. suscept. calcs. 80−63858
tetra-l-alanine, cyclic, mol. polaris. and diamag. suscept. calcs. 80−63858
thioformic acid, g-values, mag. susceptibility, quadrupole moments, rot. Zeeman effect, isomer effects 78−25520
triatomic isoelectronic molecules, electronic struct., one-electron props. 80−42935
triplet state, screening and susceptibility 79−41117
vector potential variation method for calc. mag. props., effective selection of gradient transform. functions 80−69258
vinyl formate, rot. Zeeman study, g-factors, mag. susceptibility, quadrupole moments 78−50572
BH, $^1\Sigma^+$ ground state, mag. susceptibility, paramag. contrib., large config. interaction wave function calcs. 80−47899
BH coupled Hartree-Fock perturbation approach 79−868
BH, mag. field depend. susceptibility, gauge invariant GO calc. 78−1100
$B_3N_3H_6$, electronic struct., mag. susceptibilities, ab initio calcs. 78−74571
CO_2, mol. quadrupole moments, mag. shielding and spin-rot. tensors 79−22609
CS_2, mol. quadrupole moments, mag. shielding and spin-rot. tensors 79−22609
Cu-Co heterobinuclear complex, cryst., mag. susceptibility of Cu-Co(fsa)$_2$ en, $3H_2O$ 80−2556
$D_2^+(HD^+)$, g-factors and related mag. props., calc. theory 79−41124
FH, one-electron props., review of expt. and theoretical data, Hartree-Fock calcs. 77−67980
FOH, nucl. mag. shielding and susceptibility, SCF calcs. 77−14351
Fe complexes, tetraphenylporphyrins, mag. susceptibility, hyperfine mag. field value Mossbauer spectra 80−37824
H_2, harmonic oscillator model, elec. polarisability, mag. susceptibility and chem. shift tensor calcs. 79−81299
H_2, mag. field depend. orbitals for mag. screening and susceptibility of mol. 78−78611
H_2, mag. field depend. susceptibility, gauge invariant GO calc. 78−1100
H_2, mag. susceptibility calc. by distinguishable electron method 78−897
H_2, mag. susceptibility calc., vector pot. variation method, effective selection of gradient transform. function 80−69258
H_2, nucl. mag. shielding and susceptibility, elec. field depend., SCF-Hartree Fock method 80−18791
H_2, octapole magnetisability, multiple SCF perturbation calc. with STO basis set 77−34550
HCl, second order mag. props., coupled Hartree-Fock perturbation theory 80−87042
HF, mag. field depend. orbitals for mag. screening and susceptibility of mol. 78−78611
HF, mag. field depend. susceptibility, gauge invariant GO calc. 78−1100
HF, mag. shielding and susceptibility, ab initio finite perturbation calcs. using GIAOs 77−6670
HF, mol. props. internucl. separation depend., MCSCF calc. 78−70965
HF, NMR shielding consts. and mag. susceptibilities, coupled HF with extended GTO basis 80−5480
HF, nucl. mag. shielding and susceptibility, elec. field depend., SCF-Hartree Fock method 80−18791
$H_2^+(HD^+)$, g-factors and related mag. props., calc. theory 79−41124
H_2O, elec. and mag. props., equations of motion method calcs. 77−83513
molecular magnetic susceptibility continued
H_2O, elec. and mag. props. in static fields, perturbed Hartree-Fock calcs. 78−50462
H_2O, liquid, diamagnetism, temp. dependence, NMR chemical shift calcs., molecular interactions data 80−75707
H_2O, liquid, equations for mag. susceptibility, electric polarisability 80−75708
H_2O, mag. susceptibility, HF perturbation method 77−79702
H_2O, nucl. mag. shielding and susceptibility, SCF calcs. 77−14351
H_2O, one-electron props., review of expt. and theoretical data, Hartree-Fock calcs. 77−67980
H_2O, polarisability and mag. susceptibility calc. by SCF and CI method 80−99443
H_2S, second order mag. props., coupled Hartree-Fock perturbation theory 80−87042
LiH, NMR shielding consts. and mag. susceptibilities, coupled HF with extended GTO basis 80−5480
MgF_2, ground state, nonempirical LCAO SCF calcs. 78−66469
N_2, elec. and mag. props., equations of motion method calcs. 77−83513
NH_3, mag. susceptibility, HF perturbation method 77−79702
NO, Zeeman spectrum, mol. beam elec. reson. spectrosc. 80−91621
O_3, mol. beam electric resonance, electric and mag. props. determ. 77−27055
O_3, mol. beam Stark, Zeeman effects, polarisability, moments, mag. susceptibility anisotropy 77−79649
OCS, mol. quadrupole moments, mag. shielding and spin-rot. tensors 79−22609
PH_3, NMR shielding consts. and mag. susceptibilities, coupled HF with extended GTO basis 80−5480
PH_3, second order mag. props., coupled Hartree-Fock perturbation theory 80−87042
SF_2, ab initio LCAO MO SCF calcs., elec. struct., mol. props. 77−14344
SiH_4, second order mag. props., coupled Hartree-Fock perturbation theory 80−87042
SiH_3NCS, microwave spectrum, rot. Zeeman effects 79−54847
V III, fluoro complexes anomalous magnetic properties, theoretical basis using magnetic field approximation 79−41093

molecular mass *see molecular weight*

molecular metastable states
cis-acetylene, triplet state, near IR electronic absorption spectrum, and form. 79−63997
acetylene-d_0($-d_1$)($-d_2$) metastable state, mol. beam elec. deflection obs. 80−74137
atom-diatom complexes, metastable level widths, energies with lifetimes 79−89727
Auger electrons in mol. ion+solid (gas) targets 79−45814
benzophenone, metastable triplet state, SCF CI calcs. 79−54776
biphenyl gluterate diacetylene, monomer, single cryst., stable and metastable UV photoexcited states, EPR obs. 79−78522
butyl cation, H-elimination, energy partitioning, transition state geometry calc. using MINDO/3 80−104430
carbonyl compounds, metastable triplet states, var. and perturbational calcs. 77−61680
chemiluminescence, beam-gas, kinetics of metastable excited state products 77−56231
copperporphin, metastable quartet state radiative decay 80−23453
decomposition, mass spectra, peak shapes 77−44476
decomposition, mass spectra peak shapes in field-free space 77−44475
p-dichlorobenzene, in p-dibromobenzene, optical detection of Cl NQR in mag. field 80−50228
dye lasers, metastable state relaxation time determ. 80−102719
electron spectroscopy, coincidence experiments, two-parameter 78−20135
electronic field effects 80−91465
fluoromethane, laser pumping effects, translational and vibr. energy distribs. 79−844
gas laser, at. and mol. vibr. and electronic metastable states, book contrib. 77−50653
hydroperoxy-hydroxy-methane, metastable mol., IR spectra of formaldehyde photooxidation products 79−93994
interstellar molecules, metastable isomers 79−48872
low-energy scattering, resonances 79−72384
macromolecular interactions, effects of intervening medium and polar mode energy feeding 79−13857
mass spectra, modulated-field linked-scan studies of metastable ions 80−77904
multiphoton transition detection 80−58231
N_2*+NO(H_2O), vibr. excited quenching temp. depend., flowing afterglow 77−54595
negative ion, electron impact decomp., kinetic energy release 77−6944
negative ion lifetimes, review, book contrib. 80−9529
organic molecules, triplet state electronic energy delocalisation 77−3478
polyatomic molecules, laser pumping effects, translational and vibr. energy distribs. 79−844
polymeric macromolecule containing mesogroups, phase diagrams *(Russian)* 80−58433
properties, energy transfer mechanisms and exptl. techniques 80−27921
refractive index transients, laser-induced, low-temp. solns., excited triplet state polarisabilities role 79−87411
van der Waals molecules, intermediates, form. in at. and mol. collisions 79−72384
vibrational predissociation in hydrogen bonded complexes 80−61078
Ar+HCN(H_2O), electron excitation of Ar* and Ar_2*, fluoresc. and dissoc. energy transfer collisions 77−14580
$Ar_2(^3\Sigma_u^+)+N_2$, quenching, fast absorption spectrophotometry 79−54940
Ba_2^{2+}, very long lived vibr. states, lifetimes, WKB calc. 80−78560
BeF_2^-, electron binding, extended basis SCF calc. 79−49944
CH_4^+, CD_4^+, rot. predissoc., metastable peaks 79−13774
CO, electron impact ionisation, metastable state mol. ion form. 77−14594
CO^++CO, metastable and $X^2\Sigma^+$ states dissoc. 78−33587
CS, nonexponential decay of $a^3\Pi$-$X^1\Sigma^+$ luminesc., Π sublevel radiative lifetimes, matrix isolated spin-orbit 79−89699
Cd^*_2, 470 nm absorber, multiconfiguration SCF calcs. 80−27963
Cl+formaldehyde, photolysis, Fourier transform IR studies, metastable species detection 80−81293
ClONO, form., reaction kinetics, IR spectra 78−35641
cis-ClONO, microwave spectrum, rot. consts., inertial defects and config. 79−59439
Cs_2, laser-induced photodisintegration *(Russian)* 79−89719

molecular metastable states continued
$DBr^+(A^2\Sigma^+)$, vibrational states, lifetimes, emission cross sections, prod. by electron impact 77−3419
GeF, use in chemical lasers 80−64004
H_2, $c^3\Pi_u$ metastable state, fine struct. lifetimes 79−64050
H_2, Doppler-free linear single-photon spectroscopy 78−50487
H_2, electron impact excitation, two-step, Hanle effect obs. 78−25730
H_2, metastable $c^3\Pi_u$ state, population densities and quenching times meas. 78−94296
H_2, metastable state, mol. beam reson., vibr. anal., spin-rot. interaction 79−22731
H_2 metastable state, spin-rot. coupling, ab initio calcs. 77−18804
$H_2+e^-\rightarrow H_2^*+e^-$, Gaussian basis Glauber approx., elastic and vibrorotational excitation cross sections 80−58399
$HBr^+(A^2\Sigma^+)$, vibrational states, lifetimes, emission cross sections, prod. by electron impact 77−3419
HCN, H-CN dissoc. curves, SCF CI calc. 79−100405
HCOH, prediction, potential energy surface for ground state of formaldehyde 80−42967
HH, hydrogenium, -ion, metastable states, ground state energy, bound states, lifetimes 79−45868
H_2O dimers, IR spectra in N_2 matrix, temp. and IR irrad. effects 77−61745
$H_2(c^3\pi_u)$, theoretical radiative lifetime, from mag. dipole, elec. quadrupole interaction 78−33553
He, afterglow, intermediate press., plasma discharge parameter time depend. calc. 79−19102
He flow discharge, intermediate press., positive column conc. of ions and metastables 80−44017
He_2, $a^3\Sigma_u^+$ metastable state, fine struct., mol. beam mag. reson. obs. 78−78720
He_2, collisional electronic and rot. relax. in afterglow of pulsed discharge 77−61784
He_2, metastable states, laser excitation spectra 80−5578
$He_2+N_2(O_2)$, $He_2(2^3\Sigma)$ quenching reactions 78−22014
$He_2(^3\Sigma)+Ar$, press. depend. reactions, rate coeffs. 78−64823
$He_2(^3\Sigma_u)+Ne(Ar)(N_2)(CO)(C_2)(CH_4)$, excitation transfer reaction rates 78−5332
$He_2(2^3\Sigma_u^+)+He_2(Ne)$, reaction rate consts. meas. in afterglow 78−7173
Hg_2 and Hg_3 metastable states in flash photolysis of Hg vapour, electronic absorpt. spectra 79−76438
Hg_2 as energy storage medium, energy extraction from metastable excimers 79−59677
HgBr* form. from laser irrad. $K+HgBr_2$, chemiluminescence 80−55658
$Hg(6^3P_0)+Cl_2$ reaction, reactive quenching metastable states 79−57208
K_2, laser-induced photodisintegration *(Russian)* 79−89719
Kr_2*, VUV time resolved spectra, formation and decay kinetics 79−31544
N_2, B-state collisional transfer, press. effects, oscillator strengths, time resolved spectra 79−36744
N_2, electron impact ionisation, metastable state mol. ion form. 77−14594
N_2, glow discharge, ionis. mechanism 78−13613
N_2, ionisation current increase, metastable mol. induced cathode secondary electron emission 80−38830
$N_2+Ar(Xe)$, $A^3\Sigma_u^+$ state energy pooling in flowing afterglow, Herman IR system 80−83503
$N_2+N_2(Ar)(H_2)$, ($A^3\Sigma_u^+$, ν=0,1) metastable state quenching rate coeffs. 78−90206
ND radical, metastable $b^1\Sigma^+$ state, tunable laser fluoresc. obs. 79−22744
ND radicals, metastable, production in discharge, spectra, rot., vibr. consts. determ. *(German)* 77−34642
$ND(b^1\Sigma^+)$, quenching rate consts. *(German)* 79−41189
NH radicals, metastable, production in discharge, spectra, rot., vibr. consts. determ. *(German)* 77−34642
NH_3, obs. in Orion Molecular Cloud 80−36687
$NH(b^1\Sigma^+)$, quenching rate consts. *(German)* 79−41189
NO, electron impact ionisation, metastable state mol. ion form. 77−14594
NO^+ +molecule, reaction rate consts. meas. 80−7782
NO^+, ($a^3\Sigma^+$), prod. from N^++O_2 reaction 80−7784
NO^++Ar, reaction product ratios, 300K 80−7783
NO^++atmospheric gases, thermal energy reaction rates 78−92443
$NO(a^4\Pi)$ dipole moment, meas. by mol. beam electron impact vibr. excitation 79−72440
N_2* ($A^3\Sigma_u^+$), electron impact ionisation cross section 80−78718
N_2*, metastable, collisional form., C-B emission spectrum 77−19019
$N_2^*+H_2O\rightarrow N_2+H_2O^*$ 80−87212
$N_2^*+HgBr_2$, dissociative excitation, mol. fluoresc. obs. 80−91634
Na_2, laser-induced photodisintegration *(Russian)* 79−89719
O_2 $^1\Delta_g$, produced in HF low-press. plasma, use in organic cmpd. synthesis 80−61099
O_2 discharge plasma, metastable states role, two step ionisation, electron densities and transition pts. 80−44019
O_2, electron impact ionisation, metastable state mol. ion form. 77−14594
O_2, from γ-irradiated $NaClO_3$, reson. Raman scatt., excitation profile, polarisation meas. and decay kinetics 77−14437
O_2, HF discharge, prod. of cold plasma rich in metastable species *(French)* 78−14238
O_2, laser-induced photolysis of ozone reactions 80−11928
O_2, metastable emission bands 79−64015
O_2, obs. in electron-beam controlled discharge *(French)* 77−30880
O_2^+, first negative system, high-resolution photofragment spectroscopy 80−47971
O_2^++atmospheric gases, thermal energy reaction rates 78−92443
O_3, Hartley band during formation, metastable states, vibr. excitation and relax. 80−55632
O_3, metastable cyclic ozone predictions 77−46511
O_3+thiirane+olefin+SO_2, excited neutral metastable SO_2 form. mass spectrometric study 80−83300
O_x metastable and O_3 production in electron-beam-controlled high-pressure discharge 78−71607
$O_2(^1\Delta_g)$, sensitisation of $SO(^1\Delta_g, ^1\Sigma_g^+)$ chemiluminescence 80−26016
$O_2(^1\Delta_g)+O_3$, UV photolysis, $O(^3P)$ prod., rate consts. determ. 80−55636
$O_2^+(a^4\Pi_u)$+methane, 0.04-1.2 eV, reaction rate consts. 79−47911
$O_2(b^1\Sigma_g^+)$, temp. dependent quenching, photochemical study by H_2-VUV laser 80−63702
$O_2(c^1\Sigma_u^-, C^3\Delta_u, A^3\Sigma_u^+)$ generation from at. recomb. in O_2-He afterglow, fluoresc. obs. 79−31576
Rb_2, laser-induced photodisintegration *(Russian)* 79−89719
molecular metastable states continued
SO_2+active N_2, excited neutral metastable SO_2 form. mass spectrometric study 80−83300
SiF, use in chemical lasers 80−64004
SnF, use in chemical lasers 80−64004

molecular moments
1,3-butadiene-1-one, spectroscopic consts., IR and microwave spectra, prep. 80−18859
AB system, molecular calcs., electric dipole moments and electronic valence population, CNDO study 80−37742
acetaldehyde, dipole moment 78−66540
acetaldehyde, soln., C-O stretching band intensity calcs., intermol. interaction effects 77−68081
acetic acid dimer, gas phase, H-bonded complex struct. from elec. dipole moment obs. 78−74791
acetone, ab initio CI valence and Rydberg states, spectral assignments 77−14346
acetophenones, mono substituted, semi empirical Π-electron calcs. 80−74131
acetylene, and -d_2, integrated IR intensity, meas. and interpretation 78−66551
acetylene, multipole moments and polarisabilties, SCF calcs. 80−5471
acetylene(-d_1,d_2), integrated IR intensities 80−23457
adsorbed molecules, Raman and fluoresc. enhancement by surface roughness 80−102511
aggregate, Stark spectroscopy, geometry, Heitler-London approx. dipole moments 78−55200
AH system, molecular calcs., electric dipole moments and electronic valence population, CNDO study 80−37742
alkali halide mols., electronic polarisability, ionic radii and repulsive pot. parameters, mol. consts. 80−87242
alkali sulphates, SO_4^{2-} optical and spectroscopic props., cryst. environment effect 77−40224
alkanes, mol. electro-optical props. 79−50162
alkyl chlorides, mol. electro-optical props. 79−50162
alkyl halides, conform. energy calcs., polar bonds and polarisability, polaris. model appl. 80−58188
allylamine, N-cis lone electron pair trans isomer, total dipole moment, rel. orientation 80−69259
allylamine, N-cis lone-pair gauche rotamer ground state microwave spectrum anal. 78−82720
amide group molecules empirical pot. model EPEN/2, development, parameter testing 79−54935
aminobenzotrifluoride, benzene soln., permittivity and dielec. loss 78−64320
3-aminopropanol, and deuterated forms microwave spectrum, dipole moment, struct. 79−59441
2-aminopurine, triplet state, electric dipole moments 79−22742
5-aminopyrimidine triplet state, electric dipole moments 79−22742
aniline, vacuum UV electrochromism studies rel. to dipole moment changes 77−50562
anilines, substituted, in nonpolar solvent, dielec. relax. obs. 80−55022
anisometric mol. liqs., Raman spectral components, vibr. reson. coupling and noncoincidence effect 80−69149
anthracene:2-aminoanthracene, polarised guest absorpt. spectra, transition dipole moment direction, cryst. packing 77−8610
anthracene derivatives in solution, polarisability and dipole moments, emission and absorpt. spectra obs. 80−69256
4-(9-anthryl)-N,N-dimethylaniline, fluoresc., dipole moments and polarisabilities 80−1019
aromatic aldehyde, triplet state dipole moments, vibronic coupling effects 79−31493
aromatic butadienes, dipole moment and dielectric relax. meas. 80−83516
aromatic ethylenes, dipole moment and dielectric relax. meas. 80−83516
aromatic polyesters, with S atoms, configurational props. 80−74269
asymmetrical molecules, absolute rotational contributions, calc. methods, dipole moment derivatives, transferability 79−72297
azabenzenes, multipole moments, polarisabilities and long-range interaction coeffs. calcs. 79−89599
1-aziridineethanol, mol. spectrum and hydrogen bonding 78−70820
barium stearate, oriented mols. in MIM struct., determ. from intrinsic voltage 78−72277
benzaldehyde, and isomeric phthalaldehydes, dipole moments meas., config., ab initio MO calc. 80−58410
benzaldehyde, proton affinity, MINDO/3 results compared to ICR obs. 78−1103
benzene, and methyl derivatives, $^1E_{1u}$ N-V state mag. moments, MCD obs. 80−23575
benzene, excited state props., by electrochromism in polymer matrix 79−22737
benzene, FSGO calcs. of orbital energies locations, dipole moments, charge distribs. 77−67976
benzene, mol. cryst., quadrupole contribs. to lattice vibr. freqs. 79−82290
benzene, monosubstituted, dipole moments, isomerisation and H bonding, INDO calcs. 77−54515
benzene, quadrupole moments, elec. field-gradient birefringence method 80−95746
benzene+bromomethane, microwave line width and quadrupole moments, perturbation theory 80−69190
benzene+OCS, microwave line width and quadrupole moments, perturbation theory 80−69190
benzene+OCS (methyl bromide), spectral line broadening, quadrupole moment meas. 77−6848
benzene-d_0 (-d_6), polar tensors and at. effective charge, calculated from IR intensity 78−74703
benzoylacetone, dil. soln. in benzene, dielectric behaviour 79−42886
benzoylacetones, p-substituted, dil. soln. in benzene, dielectric behaviour 79−42886
bicyclo[3.1.0]hex-2-ene, microwave spectra, rot. consts., ring struct. and config. 78−42041
Δ^6-bicyclo[3.2.0]heptene, microwave spectrum and dipole moment 80−9591
biomolecules+chloranil, charge transfer interaction, equilib. const., enthalpy and entropy determ., mol. polarisability 80−89708
biopolymers, electro-optical changes, chem. and rotational contribs. 80−85352
bond magnetic rotations, Faraday effect determ. of additive props. 77−30746

molecular moments continued
bond polarity parameters, IR intensities, molecular orbital study 79−63914
bromal, in benzene soln., dielec. relax., loss, and dipole moment 80−2692
4-bromo-m-thiocresol, liq., dielectric relax. mechanisms 79−42891
bromoacetylene, microwave spectrum, dipole moment 78−17660
bromoacetylene, microwave spectrum, r_s-struct., dipole moment, quadrupole coupling consts., vibr. excited states 77−79606
bromomethane, ab initio SCF MO calcs., ionis. pots., dipole moment, config., electronic props. 78−1104
bromomethane, mol. dipole moment derivative, sign of 79−86082
bromomethane-$d_{0,1,2,3}$, IR spectra intensities, dipole moment, bond charge, force consts. 77−83588
1,3-butadiene, FSGO calcs. of orbital energies, locations, dipole moments, charge distribs. 77−67976
butadienes, optical activation energy and dipole moment, electron repelling and attracting groups 78−46341
1-butene oxide, gas, microwave spectrum 79−13703
t-butyl acetate, rot. isomerism, dielect. and Raman spectra 80−106328
tert-butyl alcohol in nonpolar solvents, liq. struct. from dielectric studies 80−38894
t-butyl cyanide-HF, hydrogen bonded heterodimer, spectroscopic consts. from IR and microwave spectra 80−43039
t-butyl formate, rot. isomerism, dielect. and Raman spectra 80−106328
t-butylphosphine, microwave spectrum, meas., determ. 78−58675
carbon tetrafluoride, intensities of binary overtones and combinations in IR spectrum 78−55172
carbonyl halogen substituted cpds., geometric and electronic struct., LCAO-SCF calc. 79−89603
carboranes, ab initio 6-3G and 3G/MODPOT LCAO-MO-SCF calcs. 79−10026
carboxyhaemoglobin, carp, variability of mag. moment 80−94159
chemical substitution effect, LCAO calc. 79−41103
4-chloro, 3-nitrotoluene, partially aligned in elec. field, ^{13}C NMR, dipole moment determ. 80−78633
4-chloro-3-nitrobenzotrifluoride-benzene (carbon tetrachloride) dilute soln., dielec. relax. time, dipole moment, microwave obs. 78−35084
4-chloro-3-nitrotoluene-benzene (carbon tetrachloride) dilute soln., dielec. relax. time, dipole moment, microwave obs. 78−35084
4-chloro-α-toluothiol, liq., dielectric relax. mechanisms 79−42891
2-chloro-p-nitroaniline, in benzene soln., dipole moment from solute relax. time-solvent viscosity relation 80−37905
2-chloroanisole and sulphur analogue, benzene dipole moment anal. 78−25748
p-chlorobenzaldehyde, p-dibromobenzene and p-dimethoxybenzene hosts, dipole moments, lowest electronic states 77−18954
chlorobenzotrifluoride, benzene soln., permittivity and dielec. loss 78−64320
chloroform-d_0(-d_1), Raman and IR intensity anal. 80−18857
chloromethane, mol. dipole moment derivative, sign of 79−86082
chloromethanes, elec. bond moments calcs. *(French)* 79−36562
chloromethyl formate, conformation potential energy surfaces, ab initio calcs. 80−69065
o-chloronitrobenzene-benzene (carbon tetrachloride) dilute soln., dielec. relax. time, dipole moment, microwave obs. 78−35084
2-chlorophenol and sulphur analogue, benzene dipole moment anal. 78−25748
chromocene, solid, Raman transition assignments, mag. susceptibility, mag. moment 78−43861
chromophoric groups, freqs., dipole strengths, rot. strengths, nonchromophoric group dipole coupling effects 79−98060
CNDO method including d-functions *(German)* 79−22603
collagen, polarisation, contribution of permanent and induced dipole moments, elec. birefringence 80−85351
conjugated hydrocarbon chains, nonlinear elec. susceptibilities calcs. 78−66484
conjugated molecule, charge distrib. calcs., refinement by exptl. quadrupole moments 77−3258
CPHB, nematogenic liq. cryst., above T_c, Kerr effect response time, temp. depend. 78−34434
crystallography, electron distributions, aspherical-at. least squares refinements combined with Fourier methods 78−71633
1-cyano-1,3-cyclopentadiene, microwave spectrum, rot. consts., dipole moment 78−42043
cyanoacetylene, microwave spectrum, mol. consts. 78−74647
cyanobutadiyne-d_0,d_1, microwave spectrum, substitution struct., dipole moment 77−3348
2-cyanofurane, rot. consts., dipole moments, nuclear quadrupole coupling, spectral obs. 77−34620
cyanomethane-HF, hydrogen bonded heterodimer, spectroscopic consts. from microwave spectrum 80−43038
2-cyanothiophene, rot. consts., dipole moments, nuclear quadrupole coupling, microwave spectra 77−34620
3-cyanothiophene, rot. spectrum and consts., elec. dipole moment, quadrupole coupling, r_0-struct. 77−79607
cyclic ketones, electrochromism and electric dichroism for studying transitions to second excited singlet 80−63692
cyclic molecules, calc. of orbital mag. moment of π-electronic terms, collective motion model *(Russian)* 77−14335
cyclobutane derivatives, heterocyclic, elec. dipole moment in benzene soln. 79−36796
1,3-cycloheptadiene, microwave spectrum, conform. 79−98074
2-cycloheptene-1-one, microwave spectrum, dipole moment and mol. conform. 79−72303
cyclopentene-3,5-dione(-d_1) microwave spectrum assignments, rot. consts., dipole moment, config. 78−55168
cyclopropane-d_0, d_6, absolute IR intensities, dipole moment derivatives and polar tensors 78−90165
cyclopropene, dipole moment, reversed sign, theory 79−59440
cyclopropyl silane, rotational spectrum (9.0-35 GHz), transitions of ground vibrational state 79−98077
Debye generalised fluid model, dielectric relax., depolarised dynamic light scatt. 80−108156
di thioformic acid, cis and trans isomers, rot. microwave spectra and config. 79−63989
dialkylaniline derivatives, twisted intramol. charge transfer states, dual fluoresc. obs. and form., dipole moments 80−18881
diamagnetic susceptibility, interatomic charge transfer in diatoms, mol. second moments, additivity formulas 78−70961

molecular moments continued
diatomic molecular spectra, conventions for defining electric transition moment and rot. line intensity factors 80−83346
diatomic molecule, photodissoc. cross section, dipole moment, Poschl-Teller oscill. model 78−55210
diatomic molecule, pot. and spectroscopic consts. 79−94053
diatomic molecules, diamag. susceptibility and second moments, intramol. charge transfer effects 80−78702
diatomic molecules, dipole moments, electronegativity and photoemission chem. shifts 79−13655
diatomic molecules, homonuclear, molecular dynamics, translation-rotation coupling 80−44094
diatomic molecules, polarisabilities and dipole moment derivatives, virial theorem calcs. 77−57865
diatomic molecules vibr. consts. determ., IR spectroscopic, quantum chem. teaching project 79−84914
diatomic mols., 2nd row, STO and HF calcs., bond length, dipole moment 77−23431
diatomic radiative transitions, electronic-vibr. dipole moment, band strength 78−46400
diatomic rigid molecules, multipole pot. interaction cross-sections 77−6890
diatomic systems, interactions, long-range dipoles, quadrupoles and hyperpolarisabilities 80−53161
diatomics, spin coupled theory of mol. wavefunctions, struct. and props. 77−50337
1,3-diazaazulene-azulene, Stark spectra, vibronic perturbations in mixed cryst. 77−79623
1,2-dibromoethane in various solvents, dipole moments, concs. of anti and gauche forms 79−27106
2,4-dichloroanisole and sulphur analogue, benzene dipole moment anal. 78−25748
2,4-dichlorophenol and sulphur analogue, benzene dipole moment anal. 78−25748
9,10-dicyanoanthracene, exciplexes, electronic struct. by electro-optical expts. 78−25581
N,N-diethyl formamide, dipole moment, dielectric relax., internal rot., microwave absorpt. 79−56716
1,2-difluoroethylenes, ab initio HF comparison of cis and trans energies 77−18786
difluoromethylborane, microwave spectra and struct. obs. 80−43036
1,3-dihalopropane, dielectric permittivity and loss, dipole moment 78−60383
dimethylamine-HCl systems, H-bonded complexes studied by ab initio MO method, dipole moments determ. 80−83253
2-dimethylaminoethanol(-d_1), microwave spectrum, hydrogen bonding, rot. consts., struct., dipole moment 77−6764
3,3-dimethylcyclopropene, microwave spectrum, dipole and quadrupole moments calcs. 79−59440
diphenyltriafulvenes, absorpt. and fluoresc. spectra, dipole moments, solvent effects 77−75169
dipole moment, additivity criteria, from fundamental tone intensity theory 77−83516
dipole moment, mean conformational dynamics and the rotational isomeric state model 78−90315
dipole moment, meas. using simple apparatus for undergraduates 77−57118
dipole moment, program for canonical MO transformation to localized MO by Boys' method 77−88394
dipole moment derivatives, MINDO/3 semiempirical calcs. 77−75055
dipole moment derivatives, unique sign set selection 78−66682
dipole properties and dispersion energies additivity, using atoms and small mol. models 80−53091
disilylmethane, microwave spectrum, struct., dipole moment and internal rot. 79−13699
doubly resonant three-photon spectroscopy, appls. 79−71534
dyes in polymer matrices, intramol. charge transfer, electrochromism 79−73901
electric dichroism spectroscopy 78−1013
electric dipole susceptibility, third order, rel. to mol. spectra 79−36624
electric multipole moment integrals, STO orbitals 77−50557
electro-optical emission, for excited state dipole moment determ. 78−62230
electron donor-acceptor complexes, excited state dipole moments, electro-optical expts. 77−46586
electronic transition dipole moments, excited state alignment in linear mols. 77−38698
ethane, multipole moments and polarisabilties, SCF calcs. 80−5471
ethaneselenol, IR, Raman and microwave spectra, barriers to internal rot. 77−38666
ethanol, conformational analysis and electronic structure 78−33429
ethyl alcohol-d_0(-d_1)(-d_1)(-d_2), internal rot. and microwave rot. spectra 80−69128
ethyl cyanoformate, conformers, dipole moments, rel. energies, microwave spectra 78−55164
ethyl hyoochloride, microwave spectrum, dipole moment, quadrupole coupling consts. 78−58673
ethyl nitrite, microwave spectra, rot. isomerism and dipole moments 79−93990
ethyl-3-chloropropionate, liq., microwave absorption and relax. 78−60386
ethyldifluoroborane, microwave, Raman, IR spectra, conform., dipole moments, vibr. assignment 78−90155
ethylene, dipole moment derivatives, IR vibr. intensities, STO-3G, 4-31G, calcs. 77−6750
ethylene, dipole moment derivatives, MINDO/3 79−59599
ethylene, imperfect gas contrib. to refractive index and quadrupole moment 78−55253
ethylene, liq., far IR absorption spectrum, quadrupole induced dipole interaction 78−86857
ethylene, multipole moments and polarisabilties, SCF calcs. 80−5471
ethylene, quadrupole moment and shape parameters, in virial coeffs. calc. 78−9743
ethylene, quadrupole moment tensor determ. by collision-induced absorpt. spectrum 80−91555
ethylene molecules, long range forces in multipole expsn., ab initio calcs. 78−9219
ethyleneoxide, elec. dipole moment, g-values, mag. susceptibility, moments and charge distrib. 77−58077
ethylenes, optical activation energy and dipole moment, electron repelling and attracting groups 78−46341

molecular moments continued
ethylgermane, microwave, IR and Raman spectra, struct., internal rot., dipole moments 77−79605
ethylidenimine, pyrolysis product, microwave spectra, rot. distortion and electric quadrupole const. and rot. barriers determ. 80−78608
exciplexes, electronic struct. by electro-optical expts. 78−25581
excitation of simple atomic and mol. systems, long-range force effects 79−10170
Fermi and molecular min. dipole moment for binding electron 78−12
field-induced molecular multipoles, local polarisation theory 80−74141
first row elements, split-valence basis set, mol. vibr. and mol. moment calcs. 80−69063
1-fluoro, 2,4-dinitrobenzene, partially aligned in elec. field, ^{13}C NMR, dipole moment determ. 80−78633
fluoroacetylene, laser Stark and IR-microwave double resonance, E1 moment, vibr. states 77−6813
fluoroacetylene-d, Stark and microwave double reson. laser spectra 80−63690
fluoroform, Zeeman effect, mag. moments and susceptibility, nuclear shielding 79−13764
fluoromethane, ν_3 band Lamb dips, effects of RF elec. field modulation on Stark spectra 80−52989
fluoromethane, dipole moment derivatives, MINDO/3 79−59599
fluoromethane, mol. dipole moment derivative, sign of 79−86082
fluoromethane, rot. mag. moment spectra, mol. beam mag. reson. obs. 77−14509
fluoromethane-d_3, laser Stark spectra, ν_6 band, vibr.-rot. consts., dipole moment 78−5277
fluoromethanes, dipole moment derivatives and infrared intensities, transferable polar tensors 78−17668
fluoromethyl formate, conformation potential energy surfaces, ab initio calcs. 80−69065
formaldehyde, $^3A''$ state, zero-field splitting param., ab initio CI calcs. 80−99454
formaldehyde, CO laser Stark and IR absorpt. spectra, dipole moment and rot. consts. 77−75150
formaldehyde, electrochromism of 1749 Å band, electric dipole moment and polarisability 78−66572
formaldehyde, electronic struct., dipole moments, mol. polarisability, force fields, ab initio calcs. 80−78531
formaldehyde, hyperfine interactions, mol. beam elec. reson. spectra 77−88445
formaldehyde, IR spectra, Coriolis-coupled ν_4, ν_6 and ν_3 fundamental bands 78−5227
formaldehyde-d_2, laser Stark spectra, Coriolis coupled ν_4 and ν_6 fundamentals 77−27065
formamide, force consts. and dipole moment derivatives, ab initio MO calcs. 80−95521
formamide, hydration by H_2O mol., point charge model 77−34569
formic acid, H bonding, electronic struct., geometries, moments, dimerisation energies, charge distrib., pseudopotential calcs. 80−27942
formic acid (-d), microwave spectra and rot. consts., astrophysical appl. 80−91550
formic acid dimer, gas phase, H-bonded complex struct. from elec. dipole moment obs. 78−74791
formic acid-acetic acid, gas phase, H-bonded complex struct. from elec. dipole moment obs. 78−74791
formic acid-water polymers, gas phase, H-bonded complex struct. from elec. dipole moment obs. 78−74791
formyl chloride, equilib. geometries and one-electron props., ab initio calcs. 80−47878
formyl fluoride, equilib. geometries and one-electron props., ab initio calcs. 80−47878
formyl fluoride (-d_1), IR absorption intensity anal. 78−70813
furan, FSGO calcs. of orbital energies, locations, dipole moments, charge distribs. 77−67976
gas, elec. dipole reson. *(Russian)* 79−22755
glycine, elec. dip. mom. lower limit for μ_a component, mm wave spectrum 79−3435
ground state alkali molecules, mag. shielding and spin-rot. interaction 80−87186
haemoglobin, deoxygenated, vibronic coupling effect on paramagnetisms 77−57899
haloalkanes, max. overlap approx., heat of form. and dipole moment 78−94198
halomethanes, -d_0 and -d_3, IR intensity anal. 77−58082
halomethanes, dipole moment derivatives, unique sign set selection 78−66682
helical wormlike chain, dipole moment, elec. birefringence, elec. dichroism, statistical mech. calcs. 80−14262
heptafulvene, microwave spectrum and dipole moment 77−14421
4′-n-heptyl-4-cyanobiphenyl, nematogenic liq. cryst., above T_c, Kerr effect response time, temp. depend. 78−34434
heterocyclic conjugated compounds, electronic struct., spectra, ionisation pot., INDO-CI LACO-MO-SCF calcs. 79−54834
hexafluorobenzene, polar tensors and at. effective charge, calculated from IR intensity 78−74703
hexafluorobenzene, quadrupole moments, elec. field-gradient birefringence method 80−95746
hexamethylbenzene, quadrupole moments, elec. field-gradient birefringence method 80−95746
N-(p-hexyloxybenzylidene)-p-toluidine, dil. soln. in benzene, dielectric behaviour 79−42893
histamine monocation, FSGO calcs. of orbital energies locations, dipole moments, charge distribs. 77−67976
hydrazine-1,2-d_2, microwave spectra, mol. structural parameters 77−27056
hydrides, diatomic, dipole moments, atomic anisotropies effective charges 78−46458
hydrides, second row, ab initio calcs. using FSGO basis, mol. parameters correlation 78−901
hydrides, ten electron, localised orbitals, moment analysis 78−41945
hydrocarbons, CH, bond moments, sense and magnitude 79−45861
hydrocarbons, dipole moments, NDDO calcs. 80−47894
hydrocarbons, IR intensities, C-H bond moments and bending modes 77−10703
hydrocarbons, IR intensities, polar tensors, atomic population densities 77−23497
hydrocarbons, unsaturated, empirical potential model EPEN/2 parameterisation, testing 79−50103
molecular moments continued
hydroxylic solvents, dielec. consts., effect of non H-bonding solutes 77−48673
ice, IR absorpt., O-H stretching vibrs., orientation polaris. 78−31177
ice III, dipolar correlation factor and dipole moment of water molecule 79−77548
ice orientational correlation parameter, water mol. dipole moment 80−59407
identical molecules, dispersion intermolecular pot. anomaly prod. by intense radiation field 80−58336
induced absorption, point charges and multipole fields 78−74637
inert gas halides, electronic transition dipole moments, excited state alignment 77−38698
intermolecular spectroscopy and dynamical properties of dense systems, conf., Varenna, Italy (1978) 80−82581
iodomethane, mol. dipole moment derivative, sign of 79−86082
iodomethane-d_3, ν_2 band, laser Stark saturation spectra 78−42125
iodomethane-d_3, Stark tuned level crossings and saturated absorpt., RF elec. field modulation effects 80−52989
ion+polar molecules, long range dipole interaction effect 80−102558
ionone, dipole moment determ. 78−27882
IR absorption band integrated intensities, ab initio and LMO studies 80−23458
IR absorption intensities, electro-optical parameters transferability to isotopic species 77−6850
IR absorption spectra intensity, polyat. mol. dipole moment additivity, parameter transferability 78−58747
IR and Raman band intensities, use in force const. calcs. 77−27120
IR band intensities and polar tensors, effective charge and dipole moment derivs. sign 77−34695
IR band moments, effect of dipole induction 77−75143
IR intensity, Mayants-Averbuch theory d-parameters, rel. to valence optical theory 77−34700
IR intensity theory *(French)* 77−88389
isopropylamine-d_0,-d_1,-d_2, microwave spectra, struct., dipole moments and quadrupole coupling consts. 77−34613
isopropylphosphine, gauche form, Stark spectra, microwave spectrum, identification 78−58674
ketene, hyperfine interactions, mol. beam elec. reson. spectra 77−88445
lanthanide ion complexes, octahedral, f-f transition intensities, vibronic coupling model 78−58659
(Li^+,-) model calcs., correl. between electron affinity and dipole moments 77−57857
linear triatomic hydrides, ab initio SCF CI electric dipole moments 79−31410
liquids, solute-solvent interactions, moment anal. of IR absorpt. bands 78−58766
lone pair localised MOs, energy contribs. and second moments in 10-electron hydrides 77−14341
macromolecular, electrically induced fluorescence depolarisation 77−27210
macromolecule monodisperse solutions, macromol. length rel. to anisotropic light scatt. in elec. field 77−32391
magnetic multipole interaction between two nonoverlapping charge distributions 79−89731
magnetic multipole moment integrals, mols., Slater-type orbitals 77−88384
magnetic multipole moment integrals for Slater-type orbitals, analytic evaluation 80−58110
magnetic properties, calcs. using completely minimising gauge functions 77−6702
many-electron calc. 77−57884
maximum overlap mol. orbitals versus ab initio HF-SCF-MO calc. dipole energy 78−9070
methane, $\nu_3=1$ state, dipole moment and IR-radiofrequency double reson. spectra 80−14161
methane, and $d_{1\ 4}$, intensity sum rules, dipole moment derative 79−13695
methane, and d_4, finite field method, mol. polarisability and moment 79−59462
methane, IR intensities, C and H atomic polar tensors 78−50592
methane, isotopic variants, IR intensity anal. 77−58081
methane, multipole moments, far IR spectrum determ., pot. function effects 77−50435
methane, multipole moments and polarisabilities 79−85910
methane, rot. mag. moment spectra, mol. beam mag. reson. obs. 77−14509
methane, rotational state, avoided-crossing molecular beam spectroscopy 80−63730
methane-d_1, dipole moment, rot. depend., IR-IR double reson. obs. 79−81298
methanes, halogenated, interacting segment model for elec. tensor props. 78−5111
methanol, H bonding, electronic struct., geometries, moments, dimerisation energies, charge distrib., pseudopotential calcs. 80−27942
2-methoxyethylomine, microwave spectra, H-bond, torsional motion and mol. vibr. obs., rot. isomerism, mol. moments determ. 80−95603
methyl acetylene, IR absorpt. intensities 79−10103
methyl chloride, charge distrib., substituents effect 80−905
methyl chloride, Zeeman effect, mag. moments and susceptibility, nuclear shielding 79−13764
methyl fluoride, charge distrib., substituents effect 80−905
methyl fluoroformate, isomer conformation, CNDO and ab initio STO calcs. 80−58151
methyl formate, microwave spectra, rot. consts., moments and struct., radio astronomy appl., review 80−17637
methyl groups, electric dipole moment, perpendicular component, orbital calcs. 77−68138
methyl groups, tunnelling, proton second moment, signal-to-noise ratio effects 78−70766
methyl hypochlorite-d_0, -d_3, microwave Zeeman spectra, dipole moment, nuclear quadrupole tensor 77−459
methyl iodide, vibrational dephasing by translational collision 80−87202
5-methyl isoxazole, microwave spectrum internal rot. barrier 78−58665
methyl selenocyanate, and isotopic forms, microwave spectrum 79−13705
methyl vinyl ether, rot. Zeeman effect, g-values, mag. susceptibility, quadrupole moments 77−490
methyl-3-bromopropionate, liq., microwave absorption and relax. 78−60386

molecular moments continued
2-methyl-pyrimidine, microwave spectrum, V_6 barrier, dipole moment, rot consts. 77−3345
methylacetylene, ν_5 band, microwave and IR laser Stark spectrosc. 80−91558
methylamine-HCl systems, H-bonded complexes studied by ab initio MO method, dipole moments determ. 80−83253
p-methylbenzaldehyde, p-dimethoxybenzene host, dipole moments, lowest electronic states 77−18954
methyldiborane, microwave spectra, bond lengths, dipole moments, rot. consts. 77−83579
methylene fluoride, ν_9 fundamental band, 9.4-μm CO_2 laser Stark spectroscopy 78−9191
methylene ketene, microwave spectrum, rot. and centrifugal distortion consts., dipole moment 78−17659
4-methylene-cyclohexadiene-2,6-one-1, proton affinity, MINDO/3 results compared to ICR obs. 78−1103
methylpropylether, trans-trans isomer, microwave spectra, struct., dipole moment and rot. barriers calcs. 80−83348
N-methylpyrazole, microwave spectrum, internal rot. barrier 78−58666
MINDO/3 dipole moment derivatives, reliability for IR intensity calcs. 79−59599
MNDO semiempirical calcs. accuracy rel. to current MO methods 80−47893
molecular crystals, Stark splitting ang. depend. dipole moment and polarisability effects 77−51711
molecular negative ion, photoelectron ejection ang. distrib. theory 77−491
N-methylhydroxylamine, microwave spectra, struct., moments, internal rot., HFS and rot. consts. 79−45708
naphthalene, mol. cryst., quadrupole contribs. to lattice vibr. freqs. 79−82290
nematic liquid crysts. of mols. containing nitrile groups, dipole moments determ. 77−19872
net atomic charges and molecular dipole moments from spherical-atom X-ray refinements, rel. between atomic charges and shapes 79−27866
3-nitro-o-anisidine, in benzene soln., dipole moment from solute relax. time-solvent viscosity relation 80−37905
nitroanilines, hyperpolarisability, second harmonic generation and four wave mixing, excited dipole moment 77−54624
nitrobenzotrifluoride, benzene soln., permittivity and dielec. loss 78−64320
nitrosomethane, microwave spectrum, structure, dipole moment and centrifugal distortion 78−66540
nonuniform arbitrary elec. field-induced moments polarisability density concept limitations 78−70964
norbornane, microwave spectrum and dipole moments 80−78606
nucleic acids bases, excited state dipole moments and geometries 80−95738
1-octanol-H-bonding solute system, chain assoc., dipole correl. theory, dielec. const. anal 77−48675
1-octanol-nonhydroxylic solvent complexes, H bonding, assoc. consts., elec. dipole moments, dielec. consts. 77−48672
one-electron density functions, many-centred finite multipole expansions 78−71624
optically active molecule, photoelectron ejection ang. distrib. theory 77−491
organic carbonyl compounds, empirical pot. model EPEN/2, development, parameter testing 79−54934
organic compounds, correl. between solubility and mol. polarities *(Chinese)* 79−37847
organic molecules, saturated, empirical potential model EPEN/2, parameterisation testing 79−54933
organic mols., IR intensities anal., hybrid orbital rehybridisation model, mol. charge distrib. 78−74630
organic mols., relative Raman intensities, CNDO/2 INDO param. effect 80−95633
organic solids, charged excitonic complexes, coupled states, exciton interaction with charge carriers study 80−20090
overlap dipole moment, determ. from induced IR spectra 77−18924
7-oxabicyclo (4.1.0) hept-3-ene, conformation, dipole moment, microwave spectrum 78−66539
oxazole($-d_1$), dipole moment, quadrupole coupling tensor, from microwave spectrum 78−55166
oxiranecarboxaldehyde, microwave spectrum, torsional excitation energy, partial struct., dipole moment 77−38655
ozone, $^1A_1$ ground state, dipole moment function, ab initio SCF and CI calcs. 80−32628
paramagnetic electronic props. of atoms and mols., orbital mag. moments, paramagnetic currents 77−46476
paramagnetic liquid, depolarized light scatt. in mag. field 80−80759
partial at. charges calc. from ab initio mol. electrostatic pots., appls. 78−70739
phase memory probe by electro-opt. single laser mode switching 77−10698
p-phenitidine, in benzene soln., dipole moment from solute relax. time-solvent viscosity relation 80−37905
phenols, ^{13}C and D substituted, microwave spectra, substitution struct. and absolute dipole moment 79−31511
phenyl isocyanate, microwave spectrum, rot. consts., dipole moment 77−61739
phosphatidyl ethanolamine, charge distrib., dipole moment, CNDO calcs. 78−80840
PMMA solution in isopropylbenzene, mol. mass effect on mobility and interaction parameters *(Russian)* 79−31754
point charge model of molecules, Mulliken population anal. 80−102429
polar liquid, electric double layer at surface 78−53212
polar liquid solns., H bonding, dielec. theory, apparent dipole moment, chem. model 77−48671
polar liquids, elec. polarisation theory 77−4596
polar liquids soln., mol. electric dipole moments, extrapolation formula 79−38437
polar molecular negative ions, thermally stable 79−7033
polar molecule, dipole moment determ. from soln. data 77−6956
polar molecule, slow electron capture and rot. excitation 79−81287
polar molecule, Stark effect in electron spin transition in zero-field 77−27099
polar molecule+high Rydberg atom, l-changing collision 79−10185
polar molecules, electron affinities, ab initio calcs., dipole moments 79−89623
molecular moments continued
polar tensors, compact formulation on bond moment hypothesis 80−58108
poly-ε-caprolactone in dioxane soln., low freq. dielec. response 77−40177
polycyclic aromatic ring systems, localised MOs and wave functions 79−31398
polydiethylene terephthalate chains, dipole moment, config. props. 78−9288
polydiethylsiloxane chains, dipole moments 78−78844
polymer chain moments, charact. function, distrib. function, numerical calc. 78−78843
polymer solution, Perrin light scatt. matrix including mag. dipole and elec. quadrupole interactions 77−77228
polymethylene, intramol. scatt. function calc. 77−38761
polypropylene sulphide, atactic chains, dipole moments, dielec. const. meas. 80−23584
polytrimethylene oxide, soln., chain dipole moment, dielec. const. meas. 77−81043
pot. curves, selected valence electron SCF MO calc. 79−10053
propanes, substituted, liq., microwave absorpt., dielectric relax., loss, permittivity, moments and reorientation 77−63362
propiolamide($-d_2$, d_3), microwave spectrum, struct., dipole moment 78−78685
purple membrane of halobacterium halobium, aggregate optical spectra, moment anal. 79−2007
pyridine, elec. dipole moment, g-values, mag. susceptibility, moments and charge distrib. 77−58077
pyridine, FSGO calcs. of orbital energies, locations, dipole moments, charge distribs. 77−67976
pyridine, in benzene single cryst., electronic spectrum Stark modulation, dipole moment 78−29814
s-trans-3-pyridinecarbaldehyde, microwave spectrum, assignments 78−21912
2-pyridyl phenyl sulphide, dipole moments, absorpt. spectra, meas. and calcs. 77−46574
2-pyridyl phenyl sulphone, dipole moments, absorpt. spectra, meas. and calcs. 77−46574
pyrrole, FSGO calcs. of orbital energies, locations, dipole moments, charge distribs. 77−67976
pyrrole-acetonitrile, H-bonded complex, ab initio MO calcs. 80−102440
quadrupole moment from K^+(Ar)(Kr)(Xe) scatt. total cross sections 77−50495
quadrupoles, axially symmetric, lattice sums, error bounds 77−30803
retinal, dipole moment determ. 78−27882
trans-retinal, ground and excited state dipole moments, permittivity, solvent effects, spectrophotometry 78−27883
trans-retylidene-n-butylamine, ground and excited state dipole moments, permittivity, solvent effects, spectrophotometry 78−27883
RNA, molecular motions investigated by ^{31}P and ^{13}C NMR relaxation 80−63657
rotamers, total dipole moment orientation calcs. 80−91705
rotational relaxation mechanism, under absorption saturation conditions, in resonance with high intensity monochromatic radiation 79−64083
second-row molecular orbital calcs., INDO calc. for Na to Cl 78−82643
semirigid molecules, Stark effect, isometric groups, elec. dipole moments theory 78−29815
silyl acetylene, microwave spectra in ground and ν_{10} vibr. state 80−78610
small mol. electro-optical parameters, dipole moment derivatives, vibr. calc. valence-optical theory 80−23406
small molecules, diamag. susceptibility and second moments, intramol. charge transfer effects 80−78702
smectic liquid crystals, role of dipole moment in smectic C phase 78−94968
solvent, polar, spherical ion radius and limiting elec. cond. Brownian motion 78−95168
sparse s and p type Gaussian basis set LCAO MO SCF calc., mol. props. 80−23306
spectroscopy quantum chem. teaching, fluctuating elec. dipoles, light absorpt. 78−73802
spherical-top molecules, single-photon transition moments in excited states 78−94291
stearic acid, insulator in MIM struct., electric dipole moment internal voltage meas. 79−76532
stilbenes, substituted, dipole moment calcs., in excited singlet state *(German)* 77−50367
stilbenes, substituted, donor-acceptor interaction effects on excited singlet state polarity *(German)* 80−91470
strongly polar molecule, low energy electron scatt., dipole moment depend. *(Japanese)* 77−42405
N-sulphinylaniline, microwave rot. spectra, torsional freq., dipole moment and internal rot. barrier 78−973
surface adsorbed molecules, internal optic modes, mol. dipole model 80−100395
symmetric top mols., gas phase IR rot. velocity correl. functions, appls. to CH_3F, CHF_3 *(French)* 78−62778
symmetrical molecules, absolute rot. contribs. calcs., dipole moment derivatives, transferability 79−72296
1,2,3,4-tetrachloro-7,8-diphenylcalicene, excited states, moments anal. of electro-optical spectra 79−22698
tetracyanoethylene in acetone-d_6, anion solvation, electron spin echo modulation 80−63676
tetracyanoethylene in dimethylsulphoxide-d_6, anion solvation, electron spin echo modulation 80−63676
tetracyanoethylene in methanol-d_3(d_1), anion solvation, electron spin echo modulation 80−63676
tetracyclo[3.2.0.$0^{2,7}$.$0^{4,6}$]heptan-3-one, microwave spectrum and effect of cyclopropyl-carbonyl group interactions on dipole moment 78−9138
tetrafluorobenzene, microwave spectra, dipole moment, centrifugal distortion consts. 77−75133
1,1,2,2-tetrafluorocyclobutane, microwave spectrum, dipole moment, rot. and vibr. modes assignments 77−18914
tetrafluoromethane, collision-induced rot. spectrum 79−98101
tetrafluoromethane, multipole moments, far IR spectrum determ., pot. function effects 77−50435
1,2,5-thiadiazole, NQR coupling const., dipole moment of mol. 79−27010
thioacetaldehyde ($-d_1$), microwave spectrum, substitution struct. internal rot. barrier, dipole moment 77−6762
thioacetic acid, $-d_1$, principle axis method anal. of microwave spectra 78−9139

molecular moments continued
thiocarbonyl halogen substituted cpds., geometric and electronic struct., LCAO-SCF calc. 79−89603
thioformaldehyde, elec. dipole moment determ. using elec. field spectroscopy 78−70870
thioformaldehyde, electronic struct., dipole moments, mol. polarisability, force fields, ab initio calcs. 80−78531
thioformaldehyde, hyperfine interactions, mol. beam elec. reson. spectra 77−88445
thioformic acid, g-values, mag. susceptibility, quadrupole moments, rot. Zeeman effect, isomer effects 78−25520
thioketen, microwave spectrum, substitution structure and dipole moment 80−975
thiopen-2,5- dicarboxaldehyde, in lyotropic mesophase, mol. struct. and orientation 78−1004
thiophen-2-carboxaldehyde, in lyotropic mesophase, mol. struct. and orientation 78−1004
o(m)-toluidine+o-chlorophenol, H-bonded mol. complex, microwave absorpt., dipole moment and relax. times 80−14134
trans-propargyl amine, microwave spectra, dipole moments and struct., isotopic species 78−974
triatomic isoelectronic molecules, electronic struct., one-electron props. 80−42935
triatomic molecules, microwave spectra, mol. parameters 79−31513
1,1,1-trichloroethane, in nonpolar solvents, permanent dipole moment determ. 77−43125
1,2,4-trifluorobenzene, microwave spectrum, dipole moment and centrifugal distortion constants 78−37630
1,3,5-trifluorobenzene, quadrupole moments, elec. field-gradient birefringence method 80−95746
trifluoromethyl bromide, microwave spectra, mol. rot., isotopic variation in bond lengths, Stark meas., dipole moments determ. 80−74165
trifluoromethyl iodide, microwave spectra, mol. rot., isotopic variation in bond lengths, Stark meas., dipole moments determ. 80−74165
2,4,5-trimethylbenzaldehyde, durene host, dipole moments in lowest electronic states 77−18954
1,3,5-trimethylbenzene, quadrupole moments, elec. field-gradient birefringence method 80−95746
tropone, proton affinity, MINDO/3 results compared to ICR obs. 78−1103
van der Waals interactions, time-depend. Hartree theory, elec. quadrupole effects 77−6882
vibrational dephasing by translational collision 80−87202
vinyl azide, microwave spectrum 77−57985
vinyl cyanide, microwave spectra data tables 79−59445
vinyl formate, rot. Zeeman study, g-factors, mag. susceptibility, quadrupole moments 78−50572
vinyl isocyanate, microwave and photoelectron study of cis- and transforms 78−70819
vinyl mercaptan -d_0, -d_1, anti rotamer, conform., microwave spectrum 80−9592
vinyl mercaptan -d_0, -d_1, synrotamer, conform., microwave spectrum 80−5535
vinyl polymers with flexible side chains, configurational statistics, dipole moments 77−38760
water, and ionic dissoc. products, polarisation model 78−91216
XY_2 molecules, nonlinear, inertia defects and dipole moments by kinetic consts. method 80−928
XY_3 molecules, electric dipole moment function 79−59598
XY_4 tetrahedral mol., IR absorption intensities, tensorial calc. *(French)* 77−18984
y_1-base, ground and excited states, dipole moment, CNDO/S and INDO/S calcs. 79−36534
AgI surface, adsorption of water, effective pair pot. model 80−100394
Ar-O_3 Van der Waals complex, struct. and props., RF and microwave obs. 80−32704
$ArBF_3$, microwave spectrum and struct. 79−76420
ArF^+, selected valence-electron split-shell MO calc., ground state props. 79−22585
ArH^+, $^1\Sigma^+$ ground state, molecular consts. calc. from pot. curves 80−9680
Ar.HBr(DBr), van der Waals complexes, rot. spectra and struct. 80−48055
B-containing mols., MNDO calcs. for ground-state 77−88391
BF_3, IR intensity anal. 77−58081
BF_3CO, microwave spectrum and struct. 79−76420
$BF(OH)_2$, identification, rot. and centrifugal consts., mol. struct., microwave spectra obs. 80−32705
BH, elec. polarisabilities and dipole moments, var. perturbation obs. 80−63527
BH, SCF and CI wavefunctions for electronic struct. and one-electron props. 77−67978
B_2H_6 and $B_2H_5NH_2$, electronic struct. and bonding, comparative calcs. 79−31397
BH_3CO, struct., quadrupole coupling consts., dipole moment, microwave spectra 77−54557
BH_2NH_2, microwave spectra, rot. consts., dipole moment, mol. struct. 79−85957
BaO, $A\ ^1\Sigma^+$ state, dipole moment, MODR Stark effect 77−46584
BaO, $A\ ^1\Sigma^+$ state, dipole moment, level crossing spectroscopy obs. 79−94040
BeO(BeO^-), electron affinity and dipole moment, ab initio calc. 78−41938
Br_2CO and Br_2CS, signs of dipole moment derivatives, semiempirical CNDO calcs. 79−26890
BrCl, elec. dipole moment, Stark effect meas. 78−90211
^{79}BrF, (^{81}BrF), hyperfine struct., elec. dipole moment, rot. transitions, microwave spectral obs. 80−32695
BrF_2^--, $BrFCl^-$-, $BrCl_2^-$, inert gas cpds., localised MOs and bonding nature 78−9061
C-containing mols., MNDO calcs. for ground state 78−911
CF_3 radical, dipole moment from beam mass spectrometric anal. 79−59596
CH bond dipole calcs. 80−69067
CN^-, finite field method calc., moments, polarisability, field-induced shifts in mol. props. 78−74561
CN^-, spectrosc. consts. for ground and excited states, ab initio, CI calcs. 80−78551
CO, $a^3\Pi$ and $A^1\Pi$ states, dipole moment, CI calcs. 77−79548
CO, adsorbed on Pt, internal optic modes, mol. dipole model 80−100395
CO, $d^3\Delta_i$ state elec. dipole moment, vibr. depend. obs. 79−31548
molecular moments continued
CO, $d^3\Delta_i$ v=4 state dipole moment, laser-induced transition in mol. beam 78−25513
CO, dipole moment expsn. determ. from vibr. intensities *(French)* 78−42240
CO, dipole moment functions for $d^3\Delta$ and $a'^3\Sigma^+$ states, MCSCF calc. 78−78636
CO, elec. and mag. props., mol. beam elec. reson. spectroscopy 77−61791
CO, finite field method calc., moments, polarisability, field-induced shifts in mol. props. 78−74561
CO, ground state, radial matrix elements and dipole moment function 77−57973
CO, ground-state, dipole moment function and absorpt. oscillator strengths for vibr.-rot. transitions 78−62846
CO, high order vib. matrix elements, for dipole moment function and transition moments 77−6757
CO, one-election props., SCF and CI calcs. 80−27951
CO, total Xα energy, LCAO calc., rel. to local density models 80−32607
CO, vibr.-rot. interaction, high excitation transitions in solar IR spectrum 77−68040
CO, $X^1\Sigma^+$ state elec. dipole moment function, transitions, vibr.-rot. band calcs. 77−14410
CO_2, collision-induced Raman spectrum, theoretical studies 80−63646
CO_2, dimer, geom. struct., by mol. beam deflection 79−27102
CO_2, dipole moment functions 80−87094
CO_2, electrooptic constants, IR absorption spectrum in $2\nu_3$ vibration band 79−3442
CO_2, IR band intensity 80−83425
CO_2, induced absorpt. spectral moment, mol. calcs. 80−63737
CO_2, laser transitions, rel. to dipole strengths calcs. 77−61937
CO_2, mol. quadrupole moments, mag. shielding and spin-rot. tensors 79−22609
CO_2, polarisabilities, quadrupole and dipole moments, nucl. geom. effects 79−63899
CO_2, Π_u symmetry transition probabilities, dipole moment and electro-optical consts. calc. 80−43115
CO_2, quadrupole moment and shape parameters, in virial coeffs. calc. 78−9743
CO_2, SCF vertical spectrum for valence, mixed character and Rydberg states 77−50375
CO_2, transition moment and probabilities of IR spectra 79−3498
$^{12}C^{16}O_2$, ν_3 band, IR single line strength 80−83370
CO_2-type cryst., transl.-vibr. absorpt., hexadecapole moment effects 77−90134
$CO_2+C_2H_4O$, mol. quad. moments from rot. line broadening 80−28065
COF_2, dipole moment from compact formulation of polar tensors on bond moment hypothesis 80−58108
CO*, $X^1\Sigma^+$ state, dipole moment functions calc. 77−65429
CS, perturbation parameters between valence states 77−26975
CS_2, excited state props., by electrochromism in polymer matrix 79−22737
CS_2, laser transition, rel. dipole strengths calcs. 77−61937
CS_2, mol. quadrupole moments, mag. shielding and spin-rot. tensors 79−22609
CS_2, ν_3 band, dipole moment correl. function, isotope splitting and band contour 78−74650
CS_2, symmetric stretch mode, moments and polarisability derivatives, SCF calcs. 80−901
CS_2+OCS (methyl bromide), spectral line broadening, quadrupole moment meas. 77−6848
Cl_2, quadrupole moment determ. by refr. index anisotropy meas. method 80−78722
ClCN, ground and first excited bending, vibr. state, props., mol. beam elec. reson. 80−37823
ClF, mol. beam Zeeman effect, dipole moment sign, coupling const. 77−75208
ClF_5, microwave spectrum, rot. transitions, dipole moment, struct., nuclear quadrupole coupling consts. 77−14423
ClF_n-, ClF_n^+-, ClF_n^-, inert gas cpds., n=1-6, localised MOs and bonding nature 78−9061
$ClNO_3$, microwave spectrum 77−57984
ClO, MCSCF-CI electronic wavefunctions, dissoc. energy, dipole and transition moment 77−75052
$ClONO_2$, laboratory microwave spectrum, atm. chem. appl. 77−6760
Co_2, electrooptical consts., $2\nu_3$ band induced component 80−78626
Cu complex, Cu(II) dimers. temp. depend. PMR relax., singlet-triplet separation determ. 80−43073
DCN, dipole moment, relative sign w.r.t. normal coords. 78−46457
DCN, integrated IR intensities of fundamental modes 79−98083
$D^{35}Cl$, $D^{37}Cl$, IR absorpt. 3←0 band, dipole moment series expsn. 77−61747
DI, dipole moment for ν=0 vibr. level, calc. 77−75330
DN_3, microwave spectra, 8-340 GHz, spectrosc. consts. for ^{13}N isotope 79−85958
DNCS, ground state spectroscopic constants and elec. dipole moment, from microwave and millimetre wave spectra 79−804
D_2O, finite field method, mol. polarisability and moment 79−59462
D_2O, isotopic species, far IR spectra, assignments, moments 77−6761
Eu(III) complexes, f-f transition probabilities, ligand polarisation model, anisotropic contribs. 80−53049
F compounds, ground states, mol. parameters, MINDO calcs. 78−41955
F_2^-, mag. dipole terms evaluation, internucl. distance depend. 78−82864
FCN, IR laser Stark spectra, C-F stretching mode, dipole moments, rot. consts. 78−1022
FCP, microwave spectrum, struct., dipole moment and vibr.-rot. props. obs. 80−91549
FH, one-electron props., review of expt. and theoretical data, Hartree-Fock calcs. 77−67980
FNO, Stark spectroscopy of ν_1 band, rot. consts., dipole moment 79−13710
GeH_2, centrifugal-distortion dipole moment, CO_2 laser spectroscopy 77−75331
$GeH_4(F_4)$, rot. mag. moment spectra, mol. beam mag. reson. obs. 77−14509
H-bonded complexes, microwave spectra, assignments, mol. consts. 78−62794
H-bonded systems, cyclic and bifurcated, ab initio MO calcs. 79−41100
H-containing mols., MNDO calcs. for ground state 78−911
H_2, $H\bar{H}\ ^1\Sigma_g^+$ state $\bar{H}\ ^1\Sigma_g^+$-$B\ ^1\Sigma_u^+$ transition, 1<R<20 a.u. 79−98094

molecular moments continued
H_2, quadrupole moment, adiabatic approx. calcs. 78−62742
H_2, quadrupole moments calcs. from line broadening collision with acetaldehyde 80−28065
H_2, second order props., dipole polarisability nucl. coupling, fast CI method 80−27950
H_2+Ar, induced IR spectrum, overlap dipole moment determ. 77−18924
$(H_2)_2$, $(D_2)_2$, $(HD)_2$ and H_2-D_2, Van der Waals complexes, mol. symmetry 80−42963
HBr, spectral intensity, vibr.-rot. bands, dipole-moment expansion 77−75228
$(HBr)_2$, intermol. distances, dipole moments, MINDO/3 and IR intensities and shifts calcs. 78−46335
HCN, dipole moment, relative sign w.r.t. normal coords. 78−46457
HCN, dipole moment derivative, sign anomaly, CGTO ab initio calc. 78−74795
HCN, dipole moment derivatives and force consts., CI calcs. 78−90091
HCN, dipole moment derivatives of CH and CN, CI method 79−45863
HCN, finite field method calc., moments, polarisability, field-induced shifts in mol. props. 78−74561
HCN, IR and Raman vibr. intensity changes due to Li^+ interaction 79−45712
HCN, integrated IR intensities of fundamental modes 79−98083
HCN, relative signs of CH/CN dipole moment derivatives 78−74796
HCN-HF, elect. dipole moment, Stark effect of linear mols. 78−70818
HCN...HF, hydrogen bonded heterodimer, spectroscopic consts. from microwave spectrum 80−43037
HCO, IR spectra of ν_2 fundamental, laser elec. reson. 78−5226
HCl, dipole moment function using wavefunction approx., error calc. 79−98063
HCl, electrostatically interacting mols., CI multipole function calcs. convergency 80−91458
$(HCl)_2$, intermol. distances, dipole moments, MINDO/3 and IR intensities and shifts calcs. 78−46335
$(HCl)_2$, vibr. freqs. in inert gas matrix, force const., MINDO/3 calcs. 78−41952
HD, dipole moment and rot. spectrum, perturbation theory calcs. 77−65454
HD, elec. dipole vibr.-rot. spectrum, line strengths, ab initio calcs. 78−25514
HD, gas, fundamental band, R and P line shapes 80−23461
HF, ab initio valence band calcs. 79−6869
HF, cluster and chain dipole moments, ab initio calc. 77−26967
HF, dipole moment function, Schrodinger eqn. soln. using Morse pot. 77−79703
HF, electrostatically interacting mols., CI multipole function calcs. convergency 80−91458
HF, hyperpolarisabilities, dipole moment, HF calc. with correlation 80−23342
HF, IR dispersion, refractive index meas., vibr.-rot. fundamental intensities, dipole moment 79−37441
HF, mag. shielding and susceptibility, ab initio finite perturbation calcs. using GIAOs 77−6670
HF, mol. props. internucl. separation depend., MCSCF calc. 78−70965
HF, vib.-rot. props. of $X^1\Sigma^+$ and $B^1\Sigma^+$ states, variational calcs. 77−50422
HF-HCN, microwave spectroscopic investigations of hydrogen-bonded complexes 78−62794
HF_2^-, dipole derivatives, rel. to refl. spectra of Na and K salts 78−80324
HI, dipole moment function, multiconfiguration SCF calc. 77−75330
HI, line strength meas., 0→4 and 0→5 absorpt. bands, dipole moment *(French)* 78−62847
HNC, finite field method calc., moments, polarisability, field-induced shifts in mol. props. 78−74561
HNO $\tilde{A}^1A''$ excited state dipole moment, optical-optical double reson. Stark spectrosc. obs. 80−106337
HNO, isomerism, low lying electronic states, ab initio MRD-CI calcs. 80−83291
$(HNO_3)_2$, gas phase, H-bonded complex struct. from elec. dipole moment obs. 78−74791
HO_2 and HOCl, struct., vibr. freqs., IR intensities, ab initio calcs. 79−98007
HO_2 free radical, dipole moments and Stark effects from microwave spectra 80−63623
H_2O aggregates, dimer and octomers, dipole moments, polaris. model calcs. 79−77482
H_2O electro-optical harmonicity of OH bond 77−34634
H_2O, electro-optical parameters determ. *(Russian)* 77−14466
(H_2O), electron affinity, ab initio SCF calcs. 79−76343
H_2O, finite field method, mol. polarisability and moment 79−59462
H_2O, H bonding, electronic struct., geometries, moments, dimerisation energies, charge distrib., pseudopotential calcs. 80−27942
H_2O, isotopic species, far IR spectra, assignments, moments 77−6761
H_2O, localised MO, basis set depend. 79−36525
H_2O, many-body Green's function, electronic mol. props. 78−25417
H_2O, one-electron props., review of expt. and theoretical data, Hartree-Fock calcs. 77−67980
$H_2{}^{16}O$, 6.3 μm region hot bands, intensities 77−75156
H_2O-(HF)(F_2) complexes, CNDO/2 calcs. for electronic struct. and props. 78−25442
H_2O-HF heterodimer, H bonding, microwave rot. spectrum, mol. geometry and moment 80−99501
$(H_2O)_2$, elec. dipole moments from Stark effect meas. 77−54555
H_2O_2, Zeeman effect and mol. quadrupole moment, beam maser spectrosc. 78−90152
$(H_2O)_3$, electric-dipole selection rules 77−54549
HOCl, ab initio MRD CI calc., electronic spectrum, dissoc., heat of reaction, formation 78−21857
HOCl, ν_1 band IR spectrum, rot. anal. 79−98095
HOO radical, lowest doublet electronic states, rel. to photodissoc. 79−93914
HPO, mol. struct. and props., ab initio, calc., Gaussian lobe orbital 78−62713
HS_2 radical, ab initio calcs. of geometry and spectra 77−34552
H_2S dipole moments, submillimetric Stark cell meas. 77−38694
HSO radical, ground and excited first states, ab initio SCF and CI calcs. 77−30776
H_2SiO, electronic struct., dipole moments, mol. polarisability, force fields, ab initio calcs. 80−78531

molecular moments continued
He+Ar(Kr), translation band spectral moments, induced dipole moments 78−55218
He+H_2, collision-induced dipole, ab initio VB calc. 78−94202
He_3, dipole moment, large separation, perturbation theory 78−62946
HeH_2 collision induced dipole IR spectra, ab initio SCF LCAO calc. 79−89737
I-containing molecules, geom. struct. and dipole moments, CNDO/2 calc. 79−94103
I_2, HFS and mag. parameters of B state, ab initio calc. 79−45865
IBr, elec. dipole moment, rot. transition Stark shift obs. 77−75207
IF, elec. dipole moment, Stark effect 79−18233
$I_2(I_2^+)(I_2^-)$, HF and SCF calcs., pot. curves, electron affinity and quadrupole moment determ. 80−95527
$^{127}I_2$ rovibronic absorpt. lines, hyperfine struct. 80−78596
$^{129}I_2$ rovibronic absorpt. lines, hyperfine struct. 80−78596
KF, ab initio SCF MO energy, dipole moment and polarisability 80−1085
KOH, MHD plasma mol., pot. energy curves and dipole moment, bond lengths 78−71462
KrF, electronic states, ab initio CI calcs., spin-orbit coupling, pot. curves, dissoc. energy, dipole moments 77−38619
KrF^+, selected valence-electron split-shell MO calc., ground state props. 79−22585
KrF*, excimer electronic struct., config. interaction, electrostatic model, dipole and transition moments 78−927
Li_2^+, $X^2\Sigma_g^+$, $^2\Sigma_u^+$, $A^2\Pi_u$ and $^2\Pi_g$ states, electronic struct. vibr. spectra, ab initio calcs. 79−36507
LiBr, pair pot., dipole moment, polarisability tensor, bond length depend., finite field SCF calcs. 80−58127
LiF, ab initio SCF MO energy, dipole moment and polarisability 80−1085
LiF, RF spectra, spin interactions and moments, mol. beam elec. reson. meas. 77−18912
LiF(LiF^-), electron affinity and dipole moment, ab initio calc. 78−41938
LiH, dipole moments and transition moments, semi-rigorous bounds, error limits 78−78635
LiH, finite-field method calcs., dipole moment gradients, polarisability gradients and elec. field effects 77−88589
LiH, $LiHe^+$ and $LiHe_2^+$ systems, ab initio SCF LCAO calcs. of stability and spectroscopic consts. 77−71748
LiH, many-body Green's function, electronic mol. props. 78−25417
LiH, mol. elec. polarisabilities and dipole moments calcs. 78−41976
LiH, numerical calc. of one-electron props. from SCF-Xα-SW calcs. 77−6688
LiH, polarisabilities and dipole moment derivatives, virial theorem calcs. 77−57865
LiH^+, spin densities, SCF and CI calcs. 79−3362
LiH_2PO_3, P-H bond dipole direction, nonlinear optical coeffs. meas. 80−69253
LiNa, ground and excited states, model pseudopot. calcs. 77−75069
LiO, struct., spectra, SCF MO calcs. 78−17559
Li_2O (LiOLi, LiLiO), struct., spectra, SCF MO calcs. 78−17559
LiOO, struct., spectra, SCF MO calcs. 78−17559
$Li_2SO_4.H_2O$, X-ray diffr., IR and Raman spectra, internal optic modes, mol. dipole model 77−76493
MgF_2, ground state, nonempirical LCAO SCF calcs. 78−66469
MgH, X and $B'\,^2\Sigma^+$ and $A\,^2\Pi$ ab initio CI calc. 79−31415
MgO(MgO^-), electron affinity and dipole moment, ab initio calc. 78−41938
N-containing mols., MNDO calcs. for ground state 78−911
N_2, collision-induced far IR absorpt., quadrupole moment 77−27163
N_2, electron excitation of Birge-Hopfield bands ($b^1\pi_u$-$X^1\Sigma_g^+$) 80−95731
N_2, finite field method calc., moments, polarisability, field-induced shifts in mol. props. 78−74561
N_2, liq., simulation of atomic and quadrupole interactions, predictions 77−11457
N_2, liq. and gas, induced absorpt. spectral moment, mol. calcs. 80−63737
N_2, multiple moments, polarisabilities and anisotropic long range interaction coeffs. 80−43206
N_2, multipole moments, far IR spectrum determ., pot. function effects 77−50435
N_2, photoabsorption, moment anal. 78−46321
N_2, polarisabilities, quadrupole and dipole moments, nucl. geom. effects 79−63899
N_2, quadrupole moment and shape parameters, in virial coeffs. calc. 78−9743
N_2 quadrupole moment calc. from N_2+OH collision cross section 80−1046
N_2, quadrupole moments calcs. from line broadening collision with acetaldehyde 80−28065
N_2, transition moments between excited electronic states 78−5204
N_2 triplet-triplet transitions, Einstein-A coeffs., oscill. strengths, lifetimes, theory and experiment comparison 80−47876
N_2BF_3, microwave spectrum and struct. 79−76420
ND_3, hyperfine structure of inversion transitions, molecular beam electric resonance 79−98071
NF_3, IR intensity anal. 77−58081
NH_3, dipole moment derivatives, polar tensors, effective charges, CNDO calcs. 77−38613
NH_3, excited vibr. states, transition dipole moments, laser Stark spectrosc. 79−68261
NH_3, IR intensity anal. 77−58081
NH_3 IR intensity formulations 77−58004
NH_3, lone pair contributions to the IR intensities, ab initio calcs. 80−63630
$^{14}NH_3$, $^{15}NH_3$, electric dipole moment, vibr. depend. 79−59598
$^{14}NH_3$, $^{15}NH_3$ and $^{14}NH_2D$, IR laser Stark spectroscopy 80−47978
$^{15}NH_3$, IR-IR double resonance, ν_2 vibr. state, electric dipole moment 77−83626
$^{15}NH_3$, modulated coherent Raman beats 80−23464
NH_3-(HF)(F_2) complexes, CNDO/2 calcs. for electronic struct. and props. 78−25442
NHD radical, dipole moment determ., optical Stark spectroscopy 80−23455
NO, self-N_2- and O_2-broadened linewidths 5.4 micron band, quadrupole moment 77−30930
NO, Zeeman spectrum, mol. beam elec. reson. spectrosc. 80−91621

molecular moments continued
NO_2^-, microwave transition probability in zero field, spin-orbit interaction 78−25518
N_2O, dipole moment functions 80−87094
N_2O, ν_3 and $2\nu_3$ IR bandshape and dipole correl. functions 80−91560
N_2O^-, ground state potential energy surfaces 77−27175
$^{14}N_2{}^{16}O$, elec. and mag. props., hyperfine struct., mol. beam elec. reson. obs. 78−62792
NOCN, struct., dipole moment, quadrupole coupling, microwave spectra 78−94238
NOF and ONF, ab initio calcs. of geometry and electronic struct. 79−76342
NOH isomerism, low lying electronic states, ab initio MRD-CI calcs. 80−83291
$NO(a^4\Pi)$ dipole moment, meas. by mol. beam electron impact vibr. excitation 79−72440
N_2SO_3, weakly bound complex, dipole moments, MBER obs. 80−95701
$^{14}NH_3$, ground state, microwave inversion lines 80−87098
NaF(NaF^-), electron affinity and dipole moment, ab initio calc. 78−41938
NaH, ground state dipole moment, elec. quadrupole state selector meas. 79−98243
Ne+Ar(Kr), translation band spectral moments, induced dipole moments 78−55218
NeF, low energy state pots. energy curves, fluores. and dipole moment 78−21991
O-containing compounds, dipole moments, NDDO calcs. 80−47894
O-containing mols., MNDO calcs. for ground state 78−911
O_2, atmospheric, electric quadrupole transitions detection in A band 80−85746
O_2, liq. and gas, induced absorpt. spectral moment, mol. calcs. 80−63737
O_2, multipole moments, far IR spectrum determ., pot. function effects 77−50435
O_3, combination bands ($\nu_1+\nu_2$) and ($\nu_2+\nu_3$), anal. 78−9150
O_3, line and band strengths in IR spectra, variational calcs. 80−87112
O_3, mol. beam electric resonance, electric and mag. props. determ. 77−27055
O_3, mol. beam Stark, Zeeman effects, polarisability, moments, mag. susceptibility anisotropy 77−79649
OCS, dipole moment, laser microwave double reson.-Stark effect meas. 78−55191
OCS, IR spectral moments and mean squared torques, rare gas effects 78−62944
OCS, laser Stark spectra, 9.5 micron, band origins, dipole moments 77−18969
OCS, microwave rot. lines, self-broadening 78−58668
OCS, mol. quadrupole moments, mag. shielding and spin-rot. tensors 79−22609
ONF, geom. and electronic struct., ab initio calcs. 79−76342
ONF, J transitions, rot. Zeeman effect 80−63707
OPF_3, forbidden transitions, mol. beam elec. reson. obs. using avoided crossings 78−29775
OPF_3, mol. beam elec. reson. spectrum, mol. props. 79−94011
$^{16}OPF_3$, microwave centrifugal distortion moment spectrum 78−78684
PH_3, dipole moment derivatives, polar tensors, effective charges, CNDO calcs. 77−38613
PH_3, dipole moment in ground and excited states, submm. spectrum obs. 80−28056
PH_3, IR intensity anal. 77−58081
PH_3, IR intensity formulations 77−58004
4′-n-pentyl-4-cyanobiphenyl, nematogenic liq. cryst., above T_c, Kerr effect response time, temp. depend. 78−34434
SF_2, ab initio LCAO MO SCF calcs., elec. struct., mol. props. 77−14344
SF_6, gas, thermodynamical and spectral props., effect of angle-dependent part of dispersion forces 80−43138
SF_6, mol. beam mag. resonance, rot. mag. moment spectrum 77−34661
SO_2, mol. beam electric reson. in RF field, dipole moments of vibr. states 79−64116
SO_2 PMDR, CNDO CI calcs. 79−72342
SiD_3F, microwave spectrum, rot.-vibr. interaction consts., Coriolis reson., E1 moment 77−6766
$SiH_3{}^{81}Br$, high resolution rot. microwave spectrum, 8-40 GHz, mol. consts. 78−21916
SiH_3F, microwave spectrum, rot.-vibr. interaction consts., Coriolis reson., E1 moment 77−6766
$SiH_4(F_4)$, rot. mag. moment spectra, mol. beam mag. reson. obs. 77−14509
SiH_3NCS, microwave spectrum, struct., dipole moment, ^{14}N quadrupole coupling const. 77−46560
SiH_3NCS, microwave spectrum, rot. Zeeman effects 79−54847
Si_2H_6O, geom. and electronic struct., ab initio MO calc. 79−97972
$(SiH_3)_2S$, microwave spectrum, r_0-struct., elec. dipole moment, internal rot. barrier 79−3439
SiS, and isotopes, microwave spectra and consts., review 77−23493
TlF, electric dipole hyperfine struct. calc. 80−53162
cis-vinylisocyanate, dipole moment from microwave spectra 79−98078
XeF^+, selected valence-electron split-shell MO calc., ground state props. 79−22585
XeX, (X=F,Cl,Br,I), Ar matrix isolated, MCD, low temp. depend., spectroscopic parameters calc. 77−38682

molecular nuclear coupling
^1H and ^{19}F dynamic polarisation, Cl scalar coupling enhancement 78−66568
AB_n-type molecular systems, geminal nuclear spin-spin coupling 78−74682
acetonitride-d_1, ^2H NMR spectra, vibr. and asymmetry corrections to quadrupole coupling consts. 80−74184
acetonitrile, ^{13}C mag. shielding from beam maser meas. of spin-rot. interaction 79−45707
acrylonitrile, dielectric constant effect on nuclear spin-spin coupling constants, INDO approx. 79−72240
adamantane, nucl. spin echoes ^{13}C magnetisation and intermol. dipolar coupling 78−35062
alicyclic compounds, nucl. spin-spin coupling via nonbonded interactions, γ-substituent effects 80−69078
aliphatic alcohols-2,2,6,6-tetramethylpiperidine nitroxide radical complexes, EPR, PMR, hyperfine coupling consts. 79−65736
aliphatic compounds, nucl. spin-spin coupling via nonbonded interactions, γ-substituent effects 80−69078
alkali halides, quadrupole coupling, vibr. and rot. effects, Morse oscill. calcs. 77−6805
alkanes, nucl. spin-spin coupling via nonbonded interactions, conformational and substituent effects 80−69077
allylamine, N-cis lone-pair gauche rotamer ground state microwave spectrum anal. 78−82720
aminoacetonitrile, microwave rot. spectrum, quadrupole hyperfine struct. 78−17658
benzene, unlabelled and ^{13}C labelled PMR, oriented in liq. crysts., r_a struct., solvent effects 79−94017
benzene-d_1, ^2H NMR spectra, vibr. and asymmetry corrections to quadrupole coupling consts. 80−74184
benzene-d_1, $(-d_2)(-d_3)$, oriented, order, D nucl. quadrupole coupling, mag. reson. spectra 78−74683
benzenes, monosubstituted, high resoln. ^1H coupled ^{13}C NMR, INDO calcs. 77−50457
benzenesenol, CCl_4 soln., PMR, barrier to internal rot. 78−1006
benzophenone, $^3(n\pi^*)$, carbonyl ^{13}C hyperfine coupling tensor, ENDOR obs. 79−13744
benzyl radical trapped in X-irrad. potassium hydrogen bisphenylacetate, ENDOR 77−10695
benzyl-phosphonium radical, EPR spectra temp. depend., H-P coupling consts., conformation and rot. *(German)* 77−18950
biradical magnetic field dependent ^{13}C and ^1H CIDNP, hyperfine coupling 79−3460
bromoacetic acid, microwave spectrum, rot. consts., nucl. quadrupole coupling, conform. 79−13702
bromoacetonitrile, ground state microwave spectrum assignments, mol. struct., rot. consts., quadrupole coupling 77−6763
bromoacetylene, microwave spectrum, r_s-struct., dipole moment, quadrupole coupling consts., vibr. excited states 77−79606
bromoallene, microwave spectra in vibr. ground state, rotational consts., nuclear quad. coupling consts. *(French)* 77−10664
bromomethane, microwave spectra, isotope substitution, Br quadrupole coupling, J=0←1 transitions 79−45709
bromomethane, microwave spectrum obs., B rot. and centrifugal distortion consts. 77−75135
bromomethanes, ^{13}C-Br spin-spin coupling consts., isotope effects 78−13522
bromomethyl methyl ether, microwave spectra, quadrupole computing effect 80−18848
bromomethyl methyl ether, microwave spectra, quadrupole coupling effect 80−14135
bromomethylsilane, microwave spectra, quadrupole computing effect 80−18848
bromomethylsilane, microwave spectra, quadrupole coupling effect 80−14135
3-bromopropene, $^{79,81}Br$, microwave spectrum, mol. struct., nucl. quadrupole coupling consts., rot. consts. 77−6767
butadiene, J_{C-H} spin-spin coupling const., bond length depend. 78−37660
cis- and trans-2-butene, proton-proton coupling consts., valence angle depend. 77−23508
t-butyl bromide, bond lengths, nucl. quadrupole coupling, microwave spectrum 79−31512
camphene, plastic cryst., ^{13}C NMR obs. 79−95667
carboranes, small cage, antipodal H-H coupling 80−1003
chemical exchange for non-bonded spin-spin coupling of groups of nuclei 79−39143
chlorinated compounds, ^{13}C T_1 meas. and scalar coupling consts. 80−18945
α-chloro radical in X-irrad. 5-chlorodeoxyuridine, ESR, ENDOR 77−4916
chlorobenzene-d_5, and isotopic forms, microwave spectrum, rot. consts. 78−58667
chloroform, CNDO approx. 79−72240
chloromethane, low density gas, proton spin-lattice relax., mol. reorientation 79−3462
chlorophyll radical cations, NMR, hyperfine coupling 79−8482
cholesterol, proton-coupled ^{13}C NMR spectrum, double Fourier transform 78−78725
cis-1-cholobutadiene-1,3, microwave spectrum, struct., nuclear quadrupole coupling, distortion const., thermodynamic functions calc. 80−99500
CIDNP, polarisation transfer, scalar paramagnetic exchange mechanism 78−25557
CNDO-MO calcs. 78−912
2-cyanoaziridine, microwave rot. spectrum, assignments 80−91546
2-cyanofurane, rot. consts., dipole moments, nuclear quadrupole coupling, spectral obs. 77−34620
cyanomethane, multiple quantum coherence in dipolar relaxation measurements 79−73845
cyanomethane-d_1, ^{13}C-D quadrupole coupling const., ^2H-NMR spectra 77−481
2-cyanothiophene, rot. consts., dipole moments, nuclear quadrupole coupling, microwave spectra 77−34620
3-cyanothiophene, rot. spectrum and consts., elec. dipole moment, quadrupole coupling, r_0-struct. 77−79607
cyclopentyl chloride, microwave spectrum, conformation, quadrupole coupling consts. 79−3434
cyclopropane, J_{C-H} spin-spin coupling const., bond length depend. 78−37660
cyclopropyl cyanide, high-resolution microwave spectra, quadrupole hyperfine struct. of rot. transitions anal. 80−95601
deuteron quadrupole coupling constants, determ. from natural abundance ^{13}C satellites in ^2H NMR 79−31556
deuteron quadrupole coupling freqs. from ab initio wavefunctions 78−29801
diatomic homonuclear mol., nuclear spin relax., intramol. quadrupole relax. 77−14450
diatomics, spin coupled theory of mol. wavefunctions, struct. and props. 77−50337
dicarboxylic acids, D quadrupole coupling constants, ENDOR study 78−90195
m-dichlorobenzene, nucl. quadrupole coupling consts., hyperfine struct., bonding 77−14422
3,5-dichlorobenzyl mercaptan, PMR, barrier to rot. about C-C bond 78−17696
dichlorodifluoromethane, microwave rot. absorpt. spectra, nuclear quadrupole coupling, hyperfine splitting 77−30861

molecular nuclear coupling continued
dichlorofluoromethane, ^{1}H and ^{19}F dynamic polarisation, Cl scalar coupling enhancement 78−66568
dichloromethane, dielectric constant effect on nuclear spin-spin coupling constants, CNDO approx. 79−72240
N,N-diethylaniline-pyrene, photochem. polarisation transfer, scalar paramagnetic exchange mechanism 78−25557
difluoromethane, dielectric constant effect on nuclear spin-spin coupling constants, INDO approx. 79−72240
difluoromethylborane, microwave spectra and struct. obs. 80−43036
1,2-difluorotetrachloroethane, mol. motions and Zeeman-quadrupole cross relax., NMR obs. 79−65751
dimethyl mercury, coupling consts., solvent depend., ^{1}H, ^{13}C and ^{199}NMR 78−76334
dimethyl mercury, indirect coupling constants, vibr. corrections 79−50050
dimethyl tellurium diiodide, ^{129}I Mossbauer spectra, coupling consts. 78−62833
dimethyldichlorosilane, microwave spectrum, rot., centrifugal distortion and quadrupole coupling consts. 80−91547
dimethylsulphide-d_3, two interacting C_3, rotor system, mol. coupling parameters, Raman spectra 78−42074
diphenylantimony radical, EPR spectral parameters, nuclear quadrupole coupling 77−81010
diphenylmethylene, triplet state, ENDOR in $P2_1$ benzophenone, conformation and spin distrib. 77−483
elastomer, segmented block, morphology, pulsed proton NMR study 80−33907
EPR of $S=^{1}/_{2}$, $I=^{3}/_{2}$ system, quadrupole effects 79−42827
ethane, nuclear spin-spin coupling consts., vicinal proton-proton coupling calcs. 80−32737
ethyl hyoochloride, microwave spectrum, dipole moment, quadrupole coupling consts. 78−58673
ethyl-trimethyl phosphines, $(C_2H_5)_{3-n}P\{E^{IVB}(CH_3)_3\}_n$, ($E^{IVB}$=C;Si;Sn; n=0,1,2,3), ($^{1}H$, ^{13}C, ^{29}Si, ^{31}P, ^{119}Sn) NMR 80−32744
ethylene, proton-proton coupling consts., valence angle depend. 77−23508
Fermi contact coupling const., second order perturbation energies 79−50046
Fermi contact interaction, by finite nucleus model 79−63887
pfluorobenzaldehyde(-d_1), in smectic mesophase, mol. struct. and reorientation, NMR 77−27093
fluoroform, Zeeman effect, mag. moments and susceptibility, nuclear shielding 79−13764
fluoromethane-$d_{1,2}$, deuteron quadrupole coupling const. 78−33522
fluoromethanes, ^{19}F shielding anisotropies, NMR of smectic mesophase solns. 77−34662
formaldehyde, O and C 1s ionis. pots., shakeup XPS spectra electron spin coupling depend. 77−30925
formaldehyde anion radical, hyperfine coupling consts., vibr. depend., ab initio calcs. 80−87150
formic acid(−d_1), dilute deuterated mixture, high-sensitivity NQR, double quadrupole reson. 78−68412
fulminic acid-d_0, -d_1, rot. Zeeman effect and nucl. quadrupole coupling 78−78683
furil + pentachlorophenol, photochem. reduction, cross-relax. and CIDNP, PMR relax. obs. 79−52694
α-glycine, irradiated, oxidation prod. N-centred π radical ERR 77−14459
ground state alkali molecules, mag. shielding and spin-rot. interaction 80−87186
haemoglobin hydroxide, Fe Mossbauer quadrupole splitting 78−55192
hexamethylenetetramine in oriented mesophases, mol. distortion, PMR 77−6802
homonuclear coupled NMR spectra, pulses applied to multiplets, mutual coupling determ. 80−18873
hydrocarbon, ^{13}C NMR shielding constants and tensors, finite perturbation calcs. 77−27092
hydroxyproline HCl, X-irrad., free radical products, ENDOR meas. 78−76883
hyperfine coupling, constants, nucl. spin spin coupling const., NDDO MO calcs. 80−23310
ice, high-pressure forms, ^{2}D and ^{17}O NQR from double reson. obs., quad. coupling consts. 77−90069
imidazole, quadrupole coupling consts. interpretation, ab initio field gradient calcs. 80−58282
3-iodopropene, microwave spectra, rot. consts. and HFS 78−975
2-iodopropene, microwave spectrum, quadrupole coupling consts., internal rot. barrier 79−45710
isoproplyiodide, microwave spectrum, quadrupole coupling 78−86848
isopropylamine-d_0,-d_1,-d_2, microwave spectra, struct., dipole moments and quadrupole coupling consts. 77−34613
isoxazole-4D, microwave spectrum, ^{14}N nucl. quadrupole coupling tensor 78−90154
J coupling from Carr-Purcell spin echo techniques 77−10690
Jahn-Teller molecules, quasiclassical dynamics 79−6880
large molecule, ^{1}H spin-spin coupling consts., accurate meas. method 79−31555
liquid crystal, chain ordering model 80−24357
liquid crystal, thermotropic mesophase, DMR chain segments assignment 80−24356
nido-metalloborane, high-resolution ^{11}B NMR obs. of $[(B_{10}H_{12})_2Ni]^{2-}$ 79−31553
methane, mol. nuclear spin-spin coupling, ab initio SCF perturbation theory 78−33525
methane, nuclear spin-spin coupling consts., finite perturbation-CI calcs. 80−5563
methane-d_0,-d_1,-d_2,-d_3,-d_4, ^{13}C NMR chem. shifts, coupling consts. 78−37657
methanol, mol., nucl. spin-spin coupling const., Hartree-Fock calc. 80−9618
methanol-d_1, ^{13}C-D quadrupole coupling const., ^{2}H-NMR spectra 77−481
methyl bromide, NQR and A_1-A_2 splitting, RF spectrosc. inside laser cavity 80−91579
methyl chloride, Zeeman effect, mag. moments and susceptibility, nuclear shielding 79−13764
methyl cyanide, microwave rot. spectra, mol. consts. 77−34615
methyl derivatives, simple, organometallic, spin-spin coupling between metal nucleus and protons 78−37656

molecular nuclear coupling continued
methyl group, ^{2}H quadrupole coupling const. by high-resolution NMR spectroscopy 78−25563
methyl group, proton spin relax. due to intermol. proton coupling, reorientation 78−25564
methyl hypochlorite-d_0, -d_3, microwave Zeeman spectra, dipole moment, nuclear quadrupole tensor 77−459
methyl iodide, and -d_1, dissolved in nematic phase, C-H bond orientation, ^{13}C NMR 78−46371
methyl iodide, mag. hyperfine struct. of quadrupole spectra *(Russian)* 77−34622
methyl radical, hyperfine coupling consts., vibr. depend., ab initio calcs. 80−87150
methylchloride, high resoln. rot spectrum, spin-rotation and nucl. mag. shielding tensors 77−27054
6-methylmercaptopurine riboside, S-substituted nucleoside, ESR and ENDOR obs. 77−36766
methylmercury nitrate, in nematic and lyotropic liq. crysts., r_{ij}-struct. and anisotropy of Hg-C coupling const. 80−43071
multiple quantum transition in relax. in coupled spin systems 78−88211
multiple-quantum coherence, selective excitation, appl. to benzene NMR 80−23439
nitrobenzene, anisotropic mol. reorient., ^{13}C, ^{14}N and ^{2}H mag. relax. 77−48070
nitrobenzene, liq., ^{14}N and D NMR, ^{14}N quadrupole coupling const., environmental effects 78−48052
nitromethyluracil reduction product of X-ray irrad., ENDOR and ESR 77−32816
nitroso and nitrosyl cpds., ^{14}N chem. shifts correl. with nuclear quadrupole coupling consts. 77−30888
NMR bandshape, complex exchange-broadened, iterative computer anal. 79−35805
NMR coupling constant, SCF INDO calc., zero overlap approx. *(French)* 79−50047
NMR dynamic frequency shifts rel. to quadrupole interaction 79−81216
NMR parameters, chem. shielding, ^{13}C chem. shifts 80−23435
NMR spin-spin coupling consts., Fermi contact contrib., mol. orbital calcs. 77−68060
nonaqueous electrolyte solutions, ionic nuclei, quadrupolar interaction, mag. relax., infinite dilution limit 78−35692
nuclear energy levels in visible spectra, observation by laser technique, book contrib. 78−9212
octahedral systems, quadratic Jahn-Teller vibronic coupling calcs. 79−6881
organic mols., NMR coupling consts., MINDO/3 and perturbation theory 77−79630
organic ring mol., INDO finite perturbation theory, contact proton spin-spin coupling 77−50361
organoindium cpds., ^{115}In nucl. quad. coupling consts., additive calcs. 77−50453
α-oxalic acid dihydrate, H_2O proton shielding tensor, multiple pulse proton NMR obs. 80−63655
oxazole(-d_1), dipole moment, quadrupole coupling tensor, from microwave spectrum 78−55166
paramagnetic metal ions as structural probes for NMR investigation of inorganic and bioinorganic compounds 78−62828
pentofuranosyl nucleosides, isomeric, ^{1}H NMR coupling consts., SCF FPT INDO approx. calc. 80−14156
phenol, PMR in absence of intermol. proton exchange, long-range coupling and conformations 77−34660
phosphates, cellular, heteronucl. two-dimens. NMR as conform. probe 80−3590
phthalozine, oriented in lyotropic mesophase, proton NMR spectra 79−82886
planar cyclic radicals, C-H proton isotropic hyperfine consts., C hybridisation 80−95646
polyisoprenes, partly deuterated, ^{1}H-NMR spectra, struct. 80−50202
polymethinecyanines, symm., solvent effects on electronic struct., ^{1}H, ^{13}C NMR 78−13516
porphin, spin-spin coupling const., MO LCAO CNDO/2 calc. 79−41108
potassium oxalate, D_2O, D quadrupole coupling, temp. depend. 79−31551
propiolamide(-d_2, d_3), microwave spectrum, struct., dipole moment 78−78685
propylene, proton-proton coupling consts., valence angle depend. 77−23508
pyridine, and -d_1, microwave spectra, mol. struct., rot. consts. 78−25517
pyridine, proton-coupled ^{13}C J spectra, strong coupling 77−68063
4-pyridine carbaldehyde, microwave spectrum, rot. assignments, quadrupole coupling consts. 80−91548
pyridinium salts, hydrogen-bonded systems, deuteron quadrupole coupling 79−78563
pyrimidine H-addition radicals in single crystals, long range proton hyperfine coupling, EPR and INDO 77−54568
qauche NMR effect in ^{13}C, ^{19}F and ^{31}P chem. shifts and directly bonded coupling consts., bond angle effects 77−68056
quadrupole-Zeeman cross-relax. between two nucl. spin species, appl. to difluorotetrachloroethane 79−65766
quinoxaline, oriented in lyotropic mesophase, proton NMR spectra 79−82886
radical, MINDO/3 unrestricted open-shell calcs. 77−23429
radical cation EPR spectra, ion-pair effects 79−13742
relativistic theory 77−61769
second-row elements, nucl. spin-spin coupling consts. to H, INDO calcs. 77−83621
second-row hydrides, nucl. spin-spin coupling consts., ab initio calcs. 80−95647
solid state NMR, selection of nonprotonated ^{13}C resons. 80−50201
spin-spin coupling constant calculations in mol. by CNDO/SP methods 80−74126
spin-spin coupling constants, directly bonded C-C and C-H, CDOE/INDO LMO calcs. 80−95546
spin-spin coupling constants in series of related mols., orbital model, perturbational approach 79−81217
spin-spin coupling consts., mol. vibr. contrib., calc. methods comparison 80−23402
spin-spin coupling consts. calcs., review 77−30889
spin-spin couplings between ^{1}H, ^{13}C or ^{19}F, LCAO-MO-SCF-MINDO/3 approx. calcs. 79−94019
spin-spin nuclear attraction integrals over Slater type orbitals, anal. calcs. 78−78722

molecular nuclear coupling continued
stibabenzene, struct., microwave spectrum and nucl. quadrupole coupling consts. 78−70817
cis-stilbene radical anion, ESR, proton coupling const. 78−21948
succinic acid, partially deuterated, ^{1}H and ^{2}H distant ENDOR obs. of mol. struct. parameters 80−23445
p-terphenyl solns., deuteration effect on scintillation in mag. field, solute ion hyperfine interac. 77−16835
transition metal complexes, proton NMR chem. shift, covalency parameters calcs. 78−42098
1,2,3-triazole, nucl. quad. coupling in microwave spectrum 77−57987
tribromofluoromethane, liq., ^{13}C and ^{19}F nucl. relax., ^{19}F-^{79}Br and ^{13}C-^{79}Br scalar coupling consts. 78−76330
1,2,3-trichlorobenzene, oriented mols., ^{13}C satellites use in proton spectra, r_{α}-structure 80−18872
2,3,4-trichlorophenol, AX spin system, two-dimens. J-resolved NMR, spin decoupling 80−31823
trifluoromethane, dielectric constant effect on nuclear spin-spin coupling constants, INDO approx. 79−72240
2,4,6-trifluoronitrobenzene, ^{19}F shielding anisotropies, nematic phase NMR 77−27090
trimethylene oxide, ^{12}C NMR, coupling consts. 78−25570
trimethylene sulphide, ^{12}C NMR, coupling consts. 78−25570
trimethylphosphonium oxide (sulphide) (selenide), chem. shift anisotropy, struct., liq. cryst. NMR 77−61768
triphenylmethyl-^{13}C phosphonium chloride, Ph_3P^{+}-$^{13}CH_2$ EPR, reorientation and hyperfine coupling tensor 78−6574
two interacting C_{3v} rotor system, mol. coupling parameters, Raman spectra 78−42074
vibronically coupled electronic states, radiationless decay, non-Condon effects 80−52966
vinyl isocyanate, conformers, geometrical and electronic structures, microwave spectra 78−9142
water molecule, nucl. spin-spin coupling consts. geometric approx. 79−59380
AF_n^{x-} compounds, A-F nucl. spin-spin coupling, ligand influence 77−14454
AgM (M=Mg, Ca, Sr, Ba, Zn, Hg) intermetallic mols., Ar matrix isolated, ESR investig. 79−811
ArHBr, ArHCl, and isotopic forms, rot. spectra, mol. struct., mol. consts. 80−58246
AsH_3, forbidden millimetre-wave transitions 78−55165
As_2I_4, ^{127}I, ^{75}As NQR freqs. meas. 80−58285
B compounds, ^{13}C NMR spectroscopy 79−89691
$BClF_2$, microwave spectrum, struct., quadrupole coupling consts. 77−57986
B_4H_{10}, ^{11}B NMR line broadening, B-B coupling 78−62826
B_5H_9, ^{11}B NMR line broadening, B-B coupling 78−62826
BH_3CO, struct., quadrupole coupling consts., dipole moment, microwave spectra 77−54557
$Ba(ClO_3)_2.D_2O$, D quadrupole coupling, temp. depend. 79−31551
BrF_6, EPR spectra, 'NMR' transitions, mol. symmetry 77−46580
CH^{-} indirect nucl. spin-spin coupling const., Hartree-Fock and polarisation propag. calcs. 78−9170
$C_5H_6NNHCSNH_2$ radical, prod. in X-irrad. 1-phenyl-3-thiosemicarbazide, ESR, ENDOR 77−36770
CO, indirect nucl. spin-spin coupling const., Hartree-Fock and polarisation propag. calcs. 78−9170
$COCl_2$, phosgene, Cl_2 nuclear quadrupole coupling tensor, microwave spectra 80−52982
^{13}C NMR spectra, ^{13}C-X coupling consts., relative signs determ. using ^{13}C satellites 79−94018
^{13}C-^{13}C spin-spin coupling consts., data compilation, meas. and appls. review 80−17725
^{13}C-^{13}C spin-spin coupling const. and stretching force consts., single and double bonds 80−63867
^{13}C-^{15}N spin-spin coupling consts. calcs., lone pair contribs. 77−480
^{13}C-^{1}H long-range coupling assignment through selective ^{1}H decoupling 77−46582
^{13}C-labelled organic radicals, ^{13}C- and proton-ENDOR in soln. 78−55190
CaH, spin doubling, SCF calcs. 80−95649
ClCN, Cl and N quadrupole coupling, spectroscopic meas. 79−72337
ClCN, ground and first excited bending, vibr. state, props., mol. beam elec. reson. 80−37823
ClF_6, EPR spectra, mol. symmetry, INDO calcs. 77−46580
$ClHCl^{-}$, deuteron quadrupole coupling const., nuclear mag. shielding, geometry depend. 78−58586
ClO, rot. spectrum, mol. parameters in $v=0$, $v=1$ states 78−70821
$^{37}ClO_2$, $\nu_3=1$ state, laser-microwave double reson. obs. 80−95657
ClO_xF_y, ^{17}O NMR, chem. shifts, indirect coupling consts. 77−14453
Co complex, Co(III) diamine, ^{13}C NMR, spin-spin coupling const. *(Japanese)* 79−6952
CsOH, quadrupole hyperfine struct., Δ-level splitting, microwave spectra 77−88446
Cs_2TeI_6, ^{129}I Mossbauer spectra, coupling consts. 78−62833
Cu complex, Cu(II) bis(dithiocarbamate), ^{1}H ENDOR 80−87154
Cu complex, Cu(II) impurity in α-glycine crysts., ligand ENDOR spectra 79−65765
Cu complexes, Cu(I)-P tetrahedral, ^{63}Cu FT-NMR 80−53021
Cu complexes, FT NMR, ^{63}Cu and ^{65}Cu chemical shifts and coupling constants 78−94260
Cu^{2+}-imidazole complex, electron spin echo, nuclear modulation effect 79−18211
CuCl, hyperfine struct., microwave rot. spectrum obs. 78−21917
CuI, hyperfine struct., quadrupole coupling const., rot. spectrum 77−88447
$CuM_2X_4.2D_2O$, MX=alkali or ammonium halide, quadrupolar interaction, 4-300K, reorientation 79−73848
D quadrupole coupling const., semiempirical MO theory 79−10128
D_2, elec. field gradient, calc. of D quadrupole moment 79−93511
DNCS, ground state spectroscopic constants and elec. dipole moment, from microwave and millimetre wave spectra 79−804
D_2O, matrix isolation spectra, vibr.-rot. lines, nucl. spin interconversion 78−46336
F, spin-spin coupling constants, review 77−23511
FH, indirect nucl. spin-spin coupling const., Hartree-Fock and polarisation propag. calcs. 78−9170
$FHCl^{-}$, deuteron quadrupole coupling const., nuclear mag. shielding, geometry depend. 78−58586
molecular nuclear coupling continued
FHF^{-}, deuteron quadrupole coupling const., nuclear mag. shielding, geometry depend. 78−58586
GeH_4, avoided-crossing molecular-beam spectroscopy, hyperfine and spin rot. const. and rot. g factors determ. 80−78671
GeI_2, ^{127}I NQR freqs. meas. 80−58285
H_2, $c^3\Pi_u$ metastable state, fine struct. lifetimes 79−64050
H_2, nucl. mag. shielding and susceptibility, elec. field depend., SCF-Hartree Fock method 80−18791
H_2, nuclear spin-spin coupling consts., finite perturbation-CI calcs. 80−5563
o-H_2 pairs, in solid H_2, microwave absorpt. 77−68034
H_2, second order props., dipole polarisability nucl. coupling, fast CI method 80−27950
H_2^{+}, floating orbital calc. of elec. field gradient, quadrupole coupling const. 77−12248
H_2-He, nucl. shielding, ab initio coupled HF calc. 79−89690
HCN, quadrupole coupling and mol. deformations 78−90191
HCN Sternheimer shielding, perturbing elec. field and field gradient effects 77−88403
HCl, quadrupole coupling and mol. deformations 78−90191
HCl, Sternheimer shielding, perturbing elec. field and field gradient effects 77−88403
HD, Hartree-Fock calc., paramagnetic orbital contrib. to spin-spin coupling const. 79−89689
HD, indirect nucl. spin-spin coupling const., Hartree-Fock and polarisation propag. calcs. 78−9170
HD, nucl. spin coupling const., MBPT theory calcs. 80−28035
HD, nuclear spin coupling const. calc., using ab initio LCAO MO SCF method 78−25558
HD, nuclear spin-spin coupling const., perturbed at. orbitals calc. *(French)* 77−27095
HD, spin-dipolar term, spin-spin coupling const. corrections, Fermi contact terms calcs. 80−99448
HD, spin-spin coupling constant convergence, comparative study 80−63536
HDO, beam maser double reson., hyperfine struct. D quadrupole coupling 77−65493
HDO molecules in solid hydrates, D quadrupole coupling consts., O-H and O-D stretching freqs., H bond distances 78−29773
HF, nucl. mag. shielding and susceptibility, elec. field depend., SCF-Hartree Fock method 80−18791
HF, nucl. spin-spin coupling consts., finite perturbation and sum-over-states calcs. 79−85893
HF, nuclear spin-spin coupling, ab initio SCF perturbation theory 78−33525
HF, nuclear spin-spin coupling const., finite perturbation calcs. 78−78616
HF, nuclear spin-spin coupling consts., finite perturbation-CI calcs. 80−5563
HNCS, ground state spectroscopic const., microwave, millimeter and IR spectra 80−28010
H_2O, matrix isolation spectra, vibr.-rot. lines, nucl. spin interconversion 78−46336
H_2O, nucl. spin-spin coupling consts., finite perturbation and sum-over-states calcs. 79−85893
H_2O, nuclear spin-spin coupling, ab initio SCF perturbation theory 78−33525
H_2O, nuclear spin-spin coupling consts., finite perturbation-CI calcs. 80−5563
$(H_2O)_2$, nucl. spin statistics effects on group theoret. classification of tunnelling-rot. energy levels 77−54549
HT, triton-proton mag. moment ratio determ. by NMR method with 10^{-6}% accuracy *(Russian)* 77−61773
^{1}H spin systems, NMR, two-dimensional Fourier transform. of spin echoes 79−3463
^{2}H NMR, deuteron quadrupole coupling constants, determ. from natural abundance ^{13}C satellites 79−31556
$Hg_2^{129}I_2$, Mossbauer effect, bonding, quadrupole coupling const., comparison with $Hg^{129}I_2$ 78−2774
I complexes, ICl.L (L=organic radical), charge transfer and quadrupole-interaction consts. calc. 77−10590
I_2, time-resolved reson. Raman and reson. fluoresc., hyperfine splitting effects 77−30874
ICl, microwave-optical double reson. obs. in $B^3\Pi_{0(+)}$ state 79−85979
$^{127}I_2$, B-X band system, nucl. HFS, coupling consts. 77−6794
$^{127}I_2$, B-X band system, nucl. HFS, octupole coupling const. effects 77−6795
$^{115}In^{79}Br$, $^{115}In^{81}Br$, rot. J=1→2 hyperfine struct., quadrupole coupling consts. *(German)* 77−30866
KDF_2, deuteron mag. reson., quadrupole coupling consts., F-D distance 77−63313
KOH, quadrupole hyperfine struct., Δ-level splitting, microwave spectra 77−88446
KrF_2, Mossbauer spectra, quadrupole coupling strengths, isomer shift and bonding 77−50458
$KrF_2.AsF_5(SbF_5)$, Mossbauer spectra, quadrupole coupling strengths, isomer shift and bonding 77−50458
KrHBr, KrCHl, and isotopic forms, rot. spectra, mol. struct., mol. consts. 80−58246
KrHCl, van der Waals complexes, struct., RF and microwave spectra, isotope effects 80−37806
KrHCl, weak complex, rot. spectra 80−52980
$KrHF_2$, ^{83}Kr nucl. quadrupole coupling, charge transfer 80−53012
^{83}Kr, $^{3}P_1$ and $^{1}P_1$ levels, quadrupole coupling consts. 80−23434
Li_2, emission circ. polaris., hyperfine coherence and elastic collisions effect 79−3471
^{25}Mg, $^{3}P_1$ and $^{1}P_1$ levels, quadrupole coupling consts. 80−23434
$Mo_2Cl_9^{3-}$ complexes, cluster exchange coupling consts. SCF-Xα-SW calcs. 80−74120
α-N_2, solid, NQR echo envelope modulation due to intramol. dipole coupling 77−48083
N_2D_4, ^{14}N quadrupole coupling consts., inversion barrier, microwave spectrum 77−54556
NH, fine struct. in $X^3\Sigma^{-}$ and $A^3\pi$ states, STO and GTO calcs. 77−6679
NH_3, mol. nuclear spin-spin coupling, ab initio SCF perturbation theory 78−33525
NH_3, nuclear spin-spin coupling consts., finite perturbation-CI calcs. 80−5563

molecular nuclear coupling continued
$^{15}NH_3$, nucl. spin-spin coupling consts. calc., vibr. averaging effects 78−33521
NH_4^+, proton-proton dipolar coupling in nematic soln. using high resolution NMR 77−3387
NH_4^+, quadrupole coupling and mol. deformations 78−90191
NH_4^+, Sternheimer shielding, perturbing elec. field and field gradient effects 77−88403
$NH_2(X^2B_1)$, laser mag. reson. spectra, Zeeman and hyperfine effects, rot. consts. 77−30892
$NH_2(X^2B_1)$, MODR, hyperfine coupling consts., spin rot. consts. 78−1010
NO_3, mag. hyperfine interactions, MO LCAO UHF calcs. 77−14369
NO_3^{2-}, coupling consts., geometry, LCAO UHF and ENDOR data calcs. 77−14369
N_2O dissolved in liq. cryst., NMR, relax. times 80−25233
NOCN, struct., dipole moment, quadrupole coupling, microwave spectra 78−94238
^{14}N NMR, single cryst., separation of dipolar and quadrupolar splittings, new technique 80−25217
^{14}N quadrupole coupling consts., ab initio calcs. 80−58283
^{15}N-^{13}C spin-spin coupling constants calc. using SCF and INDO method 80−32609
^{15}N-$^{1}H^+$ NMR, coupling consts., double reson., difference proton Fourier transform spectroscopy 79−3467
Ni complex, [Ni(niox)$_2$], ^{61}N Mossbauer spectrum, quadrupole splitting 79−76456
O_2^+ $^4\Pi$ states, spin-spin coupling consts., ab initio calc. 79−97981
OH^+, fine struct. in $X^3\Sigma^-$ and $A^3\pi$ states, GTO and STO calcs. 77−6679
P-C, one-bond couplings, orbital and spin dipolar contribs., INDO approx. 79−31552
PH, fine struct. in $X^3\Sigma^-$ and $A^3\pi$ states, GTO and STO calcs. 77−6679
PSF_3, in orienting smectic solvent, ^{19}F and ^{31}P mag. shielding anisotropies, F-P-F bond angle 77−18942
RbBr, hyperfine struct., qudrupole coupling consts., vibr. depend. *(German)* 77−34565
RbHe(Ne), spin relax., Rb hyperfine interaction in Van der Waals mol. 78−94201
RbI, ground vibr. state rot. transition, quadrupole HFS and coupling consts. *(German)* 77−57990
RbOH, quadrupole hyperfine struct., Δ-level splitting, microwave spectra 77−88446
S_3^-, stabilized on MgO surface, CNDO calcs. of g-tensors and hyperfine coupling consts. 77−83625
SF_5, anisotropic ESR spectrum in γ-irrad. SF_6 77−21400
SH^+, fine struct. in $X^3\Sigma^-$ and $A^3\pi$ states, GTO and STO calcs. 77−6679
Sb (III) compounds, orbital population anal. using ^{121}Sb Mossbauer data 78−21953
Sb complexes, $SbCl_5$.L (L=organic radical), charge transfer and quadrupole-interaction consts. calc. 77−10590
Sb halides, quadrupole-interaction consts., CNDO/2 calc. 77−10589
Si-C, one-bond couplings, orbital and spin dipolar contribs., INDO approx. 79−31552
SiH_3 radical, hyperfine coupling consts., vibr. depend., ab initio calcs. 80−87150
SiH_4, avoided-crossing molecular-beam spectroscopy, hyperfine and spin rot. const. and rot. g factors determ. 80−78671
$SiH_3^{81}Br$, high resolution rot. microwave spectrum, 8-40 GHz, mol. consts. 78−21916
SiH_3NCS, microwave spectrum, struct., dipole moment, ^{14}N quadrupole coupling const. 77−46560
SiO, low-lying electronic states, vib. assigned perturbations 77−27082
SiS, and isotopes, microwave spectra and consts., review 77−23493
Sn complexes, $SnCl_4$.L (L=organic radical), charge transfer and quadrupole-interaction consts. calc. 77−10590
Sn halides, quadrupole-interaction consts., CNDO/2 calc. 77−10589
SnI_2, ^{127}I NQR freqs. meas. 80−58285
Sn(IV)-, Sn(II) halide mols., rare gas matrix-isolated ^{119} Sn spectra 77−48097
Te compounds, dihalides, organometallics, ^{125}Te, ^{13}C, ^{1}H NMR spectra, nucl. coupling, exchange processes 79−95658
α-TeI, ^{129}I Mossbauer spectra, coupling consts. 78−62833
TeI_4, ^{129}I Mossbauer spectra, coupling consts. 78−62833
TiO, $C^3\Delta$ term anomalous triplet splitting 78−13514
VO, $^4\Pi$ states, spin-spin coupling consts., ab initio calc. 79−97981
$ZnCl_2$, ^{35}Cl NQR freqs. meas. 80−58285
ZnI_2, ^{127}I NQR freqs. meas. 80−58285
^{67}Zn, ^3D, ^1D, $^3P_1$ and $^1P_1$ levels, quadrupole coupling consts. 80−23434

molecular orbitals *see molecular energy levels*

molecular orbitals calculations
includes calculations of electronic and geometric molecular structure see also APW calculations; EHT calculations; GO calculations; GTO calculations; HMO calculations; KKR calculations; LCAO calculations; NDO calculations; OPW calculations; PNO calculations; PPP calculations; STO calculations
4f orbitals, overlap integrals evaluation 79−72225
10-electron systems, minimal basis set localised orbitals, conjugate gradients method calcs. 79−6849
π-electron, effective Hamiltonians, formal theory 79−59333
Σ perturbation method using Green's functions for mol. calcs. 78−55123
A_2B_{2N} mols. and ions, strengths of A-A single bonds symmetries 78−74790
ab initio CI pot. curves, mol. wavefunctions and vibr. freqs. comparison of methods 80−27956
ab initio effective core pots., reduction of all electron to valence electron calcs. 77−14361
acetaldehyde, first triplet state geometry, fragmentation into free radicals 80−47915
acetaldehyde, internal rotation barriers, exchange energy and orbital orthogonality effects 77−75049
acetaldehyde, proton affinity, geom. and basis set depend., MO calcs. 78−50461
acetaldehyde radical cation, fragmentation, MO calc. 79−18109
acetic acid, cryst. binding, ab initio MO SCF calc. 79−37657
acetic acid, dimer, config and energy, ab initio MO SCF calc. 79−37657
acetic acid, monomer and dimer, photoelectron spectrosc. 80−87172
acetic acid-formic acid, 'dimer', tritium β^--decay causing H^+ transfer, ab initio MO calc. 80−3391
molecular orbitals calculations continued
acetone vapour, mol. assoc., monomer-dimer equilib., thermal cond. meas., MO calcs. 79−52647
acetonitrile, mol.excitation by electron impact, 500 and 25-70 eV, expt. and HAM/3 79−72434
acetonitrile, quadratic force fields, MOCIC pot. functions calcs. 80−5475
acetophenones, di- and trisubstituted, π^*-π systems, UV electronic absorpt. spectra 80−74132
acetophenones, mono substituted, semi empirical Π-electron calcs. 80−74131
acetylene, average mol. polarisability, Frost model wavefunctions calcs using p-type Gaussians 78−41924
acetylene, chemisorbed on α-Fe, struct., bonding, dissoc., UPS obs., MO calcs. 78−84050
acetylene, electron momentum distribs. in π orbitals from (e,2e) expts. 80−14239
acetylene, ionis. by mol. orbital method, many-body calc. 79−36512
acetylene, LMO population calc. method appl., from given SCF eigenvector matrix 80−14063
acetylene, mol. and cluster Auger spectrum calc., SCF core-valence-valence spectra 80−48045
acetylene, mol. geometry basis set depend., geometry optimisation ab initio method 79−31382
acetylene, variationally deorthogonalised localised molecular orbitals, electronic struct. 79−97968
Adams-Gilbert equation, modified, expansion methods 77−34542
addition theorems of spatial functions, multicentre integrals of arbitrary atomic functions, symmetry and analytical struct. *(German)* 80−37729
adiabatic perturbation theory, mol. fixed moving coord. system, review 78−62687
adsorbed molecules, ang.-resolved photoemission, independent atomic centre approx. 78−84701
aliphatic anhydrides, photoelectron spectra, orbital energies 79−10151
alkali halide molecules, zero point Compton profile anisotropy rel. to nucl. charge 79−64054
alkali halides, electron momentum distrib. and Compton profiles 79−13631
alkali metaborates, vapour over heated solid, XPS, obs. 80−87171
alkali metal diatomics, pot. curves, selected valence electron SCF MO calc. 79−10053
alkali metal monoxides, bond distance, dissoc. energy and vibr. freq., electron gas model 77−30846
alkali metal-H, liq. and solid, solvation energies 77−4201
alkane dimer, PCILO calc. of geom. struct. and energy 79−63930
n-alkanes, mol. Rydberg S_n←S and S_n←T transitions, semi-empirical SCF MO calc. 80−91453
alkenes, 1,1-, 1,2-disubstituted, fragmentation modes in perturbational MO anal. 80−58138
n-alkenes, photoelectron spectra, MINDO/1, MINDO/3 and Fenske-Hall calcs. 78−5285
alkyl cadmium, valence and core electron energies, photoelectron spectra, ab initio calc. 78−25613
allyl radical, restricted SCF and MC SCF calc. of C_{2v} and C_s structs. 80−83289
alternant hydrocarbons, HOMO-LUMO separation, approx. topological formula 79−49928
aminoborylpolyynes, intermolecular interaction through triple bonds, internal rot. 80−106370
aminopolyynes, intermolecular interaction through triple bonds, internal rot. 80−106370
anthracene, cryst., radiation induced radicals, optical absorpt. bands, SCF-CI MO calc. 79−91463
approximate methods with accuracies comparable to exact calcs. 77−23433
aromatic heterocycles, MC-SCF and CI calcs. in PPP framework 79−26892
aromatic hydrocarbons, π-ionisation energies correl. with free electron MO energies 80−14073
aromatic hydrocarbons, excited state vibr. freqs. 79−85947
aromatic hydrocarbons, vibronic calcs. 80−58238
aromaticity, reson. energy in graph theory 80−91412
atom+ion collisions, diabatic molecular orbitals for inner-shell excitation 78−62897
atom+ion slow collisions, K-shell excitation of relativistic atoms 80−48073
atom+molecule collisions, mol. basis sets as energy approaches excitation threshold 78−78783
atom+multiply charged ion, slow collisions, MO calcs. 80−23504
atom-atom slow collisions, electron translational effect, diagonalisation calcs. 77−3441
atomic cluster total energy, diatomics-in-mol., LMTO calc. pot. curve, Lanczos eigenvalue method 78−9291
atomic collisions, momentum transfer phase factors, mol. integral evaluation with travelling GTO basis set 79−22778
atomic collisions, outershell excitation, diabatic mol. orbitals 78−62901
atomic sphere overlap, Xα-SW MO projection of LCAOC MO's 78−25422
atomic-integral calculations using spatial symmetry, efficient permutational approach 79−63888
Aufbau principle, rel. to mol. topology 78−74556
back-of-the-envelope calcs., teaching 78−16593
bases, K^+ affinities ab initio SCF calc. 78−58585
benzaldehyde, and isomeric phthalaldehydes, dipole moments meas., config., ab initio MO calc. 80−58410
benzene, ab initio model calc., variational 77−46492
benzene, dynamic polarisabilities, calcs., superposition method of excited config., nonstationary perturbation theory eqns. 80−69257
benzene, electronic struct. calc. using free-electron orbitals basis set 77−79537
benzene, LMO population calc. method appl., from given SCF eigenvector matrix 80−14063
benzene, Lowdin orthogonalisation procedure, rel. to orbital localisation procedures 79−6848
benzene, mol. semiempirical RPA calc. using PPP Hamiltonian, triplet instability 79−26893
benzene derivatives, mol. electrostatic pot., approx. evaluation 80−58337
benzenes, substituted, electronic struct., ab initio calcs., photoelectron spectra 80−58314
benzenoid aromatic hydrocarbons, ionisation pot. and electron affinities, semiempirical MO theory 79−6843

molecular orbitals calculations continued
benzoyl chloride, HeI/He photoelectron spectra, band intensity anal. 79−31601
3,4-benzphenanthrene cation radical, in boric acid glass, spectrum 200-1400 nm, MO calcs., assignments 77−75174
benzyne, struct. and IR spectrum, MNDO calc. 79−31403
Bethe-Goldstone time-depend. first-order theory, short range correl., transition moments 78−25449
binding and transition energies, expt. and theoret. comparison, review 78−50497
biomolecule conformational anal., solvent effects 80−3583
biomolecules, ZDO method for very large mols., low computer time 77−14356
biopolymer, electronic-conformation interactions 80−3588
biphenyl, lowest excited singlet states, polyexcited CI calc. 79−772
bond bending, bond orbitals rel. to nucl. motion 80−95513
bond charge parameters from integrated IR absorption intensities 77−6853
bond function augmented basis sets, appl. to 1st row mol. geometry optimisation 78−905
bond magnetic rotations, Faraday effect determ. of additive props. 77−30746
bond orbitals and intramolecular interactions, barriers to rotation and non-bonded interactions 80−32855
bond order orbitals and eigenvalues 79−41088
bonds, AH and AB (A, B=Li-F), linear momentum operator expectation values calcs. in molecules 79−7566
borazine, triplet instability, RPA calculations 80−27938
Born-Oppenheimer coupling elements, crude and adiabatic approx. 77−65415
Born-Oppenheimer electronic wave function, density matrices, electronic and nucl. motions separation 79−59332
Born-Oppenheimer Hamiltonian, resolvent matrix elements complex coord. calc. 80−52878
branching diagram and Serber type spin functions, construction algorithms 79−6828
Breit-type three-electron eqn., Pauli approx. 79−10044
bromomethane, ab initio SCF MO calcs., ionis. pots., dipole moment, config., electronic props. 78−1104
Brueckner condition for MO selection in correlated orbitals 77−23436
trans-butadiene, all-valence-electron CI calcs. of electronic spectrum 77−10654
butadiene, cis- and trans-, appl. of spin-free CI procedure using alternant MOs 79−85887
butadiene, electron momentum distribs. in π orbitals from (e,2e) expts. 80−14239
butadiene, LMO population calc. method appl., from given SCF eigenvector matrix 80−14063
trans-butadiene, mol. semiempirical RPA calc. using PPP Hamiltonian, triplet instability 79−26893
trans-butadiene, weak low-energy band, S and T levels by fragment method 78−82625
1-butanethiol, simulated ab initio MO method calcs. 80−47867
cis- and trans-2-butene, Compton profiles, theory and expt. 78−50597
butene-2-cis Li^+ complex, intermolecular interaction energy PCILO calc. 77−34572
caffeine, semi-empirical excited state Morokuma's EHP calc., geometry and order of states 78−46256
cage molecules, calc. using free-electron orbitals basis set 77−79537
cancer receptor sites, proof by MO method for interstrand guanine binding of DNA 80−30656
canonical and localized molecular orbitals *(Hungarian)* 79−13633
canonical MO transformation to localized MO by Boys' method 77−88394
carbonyl compounds, localisation of $n\pi^*$ excitation, config. interaction method 78−50482
carbonyl oxide, config. interaction calc., using DODS natural orbit approach 78−66476
carboxylic acid-fluoride system, H---F bond, ab initio MO study 79−76528
carbyne, π-electronic struct., alternant MO method 78−62708
catalysed reaction theory applic. 77−1923
catalysis, orbital perturbation approaches 78−80783
Cauchy inequalities applic. in simple MO theory 77−54498
character orders for nonorthogonal AO bases 77−34535
charge and current densities, approx. wavefunctions, valence bond, molecular orbital methods 77−3261
chelatropic reaction, intrinsic single and dual mol. orbital symmetry conservation 80−102419
chemical bond transferability, group or loge functions 78−41939
chemical bonding studied using scattering theory concepts 80−103289
chemical bonds, atomic d orbitals, symmetry considerations 77−79536
chemical substitution effect on the props., LCAO calc. 79−41103
chemisorption on transition metals, semiempirical model calcs., extended basis set 77−72793
p-(N-chlorobenzylidene)-p-chloraniline, cryst., polymorphism, cryst. struct. rel. to mol. conform. 78−75611
chromium formate, mol., Hartree-Fock instability of SCF wavefunctions 80−9492
chromophores, semiempirical rules in circular dichroism, Cotton effect sign correl. with stereochem. 80−1006
CI calculations, virtual orbitals for rapid convergence, perturbational method 79−85906
classically forbidden region, molecular-orbital X-rays, spectral distrib. 79−72334
closed shell Hartree theory with orthonormal orbitals 80−69051
closed-shell molecule, local canonical MO theory 77−88372
cluster expsn. of wavefunction, closed-shell orbital theory 79−10004
collision systems $\alpha(Z_1+Z_2)\gtrsim 1$, quasimolecular 1 $s\sigma$ orbital, excitation and spectroscopy 80−87199
Combination of Atomic Boxes MO model, development and testing 80−32592
complex heteroorganic molecule, semi empirical SCF-CI MO method 79−63917
complex molecular orbitals, pairing representation 80−91454
complex molecules, multiple scattering Xα method 77−57874
complexes, H-bonded, PCILO method calcs. 79−10035
compound state resonances, semiclassical calcs. 80−87031
Compton profile, Fourier anal. 79−89588
conference, group theory and application to spectroscopy, Nova Scotia, Canada (Aug. 1978) 80−41947

molecular orbitals calculations continued
configuration interactions, appl. of unitary group methods 80−27958
conjugated heterocycles with single heteroatom, stability, graph theoret. approach 77−38604
conjugated molecule, with proper axis of rot., MO calcs., graph theory appls. 79−76329
conjugated molecules, electronic transitions, Σ-Π separability 80−58124
conjugated molecules eigenvalue polynomials 80−14078
conjugated systems, symmetry-depend. rules 79−89592
conservation of molecular orbital symmetry, construction of energy correl. diagrams *(Chinese)* 80−910
contracted Gaussian basis set for correl. wave functions, appl. struct. and energies 80−52881
contracted Gaussian-type orbital basis sets, test with and without outer orbital splitting 80−47872
convergence in SCF calcs., reverse level shifting technique for accel. rate 78−70735
core-valence approx. scheme 80−42927
coreless pseudopots. for atoms K through Zn 78−55121
coronene, excited state Faraday values mag. circular dichroism spectra and MO CI calcs. 80−18877
correlated wave functions anal. gradients from two particle density matrix and unitary group 80−78548
correlation energy, modified bielectronic potential method calcs. 79−59365
Coulomb integral and quantum mechanical exchange redefinition from atomic and molecular orbitals 79−44787
Coulomb interaction integrals bounds 80−52856
counterintuitive orbital mixing, SCF perturbation methodology 78−74564
coupled cluster many electron theory, unitary group formulation 80−52859
coupling constants in direct CI method 80−9516
cross section by complex basis function calcs. of resolvent matrix elements 80−78662
crystal field theory connections 80−29514
CT complex, equilib. distances and stabilisation energy, PCILO calc. 78−41963
cyclic molecules, calc. of orbital mag. moment of π-electronic terms, collective motion model *(Russian)* 77−14335
cyclobutane, dissoc., frontier orbitals and activation energy, HAM/3 method 78−92452
cyclopentadiene, HAM/3 calc. of ionis. and excitation energy and electron affinity 79−26894
cyclopentanone, $n\rightarrow\pi^*$ transition, vibr. band intensities 80−74116
cyclopropane, 3e′-orbital, electron momentum distribs., mol. distortions effects 80−18773
cyclopropane, electron momentum distribs. in π orbitals from (e,2e) expts. 80−14239
cyclopropane, localisation of MOs using density matrix formalism *(Russian)* 79−93911
cyclopropanone, electronic struct., UV photoelectron spectrum 78−33428
d-orbitals importance in calc. of effective interactions and excitation spectra 79−6823
delocalised treatment of correl. problems, N-depend. 79−63921
density function method 79−41091
deoxyhaemoglobin, porphin-Fe-imidazole system, SCF-LCAO-ASMO and CI calcs. of low-lying multiplets and excited states 80−94155
diabatic mol. states, shielded diatomic orbital method 78−5121
diagrammatic many-body perturbation theory for general model spaces 80−18780
diagrammatic representation by method of progressive interactions by atomic orbitals 77−46482
diamagnetic susceptibility, interatomic charge transfer in diatoms, mol. second moments, additivity formulas 78−70961
diamagnetic susceptibilties and NMR chemical shifts in terms of localised MO's 80−106256
diamond, structure and motion of self-interstitials 79−37700
diamond clusters and corresponding saturated hydrocarbon ab-initio HF and PCILO calcs. 78−42951
diatomic, effective quasiparticle pot., Green's function method 79−49940
diatomic, shielded, parametric shielding pots. calcs. 77−54506
diatomic bound molecules with zero bond order, excited biexcitons 78−9049
diatomic molecular Hamiltonian, function of internucl. separation 79−22583
diatomic molecule, binding and excitation energy, Wigner-Seitz pot. 79−50160
diatomic molecule, with 2nd row atom, core pseudopot. valence electron method 79−72233
diatomic molecule electron scatt., iterative static exchange method 80−53155
diatomic molecules, compactness proof for infinite systems of linear equations 79−72247
diatomic molecules, electronic and vibr. functions of non-adiabatic wavefunction 79−22621
diatomic molecules, force consts. 79−10057
diatomic molecules, homonuclear, individual orbital contribs. to SCF virial 79−3349
diatomic molecules, one-electron, heteronuclear, partial wave treatment 79−10017
diatomic mols., 2nd row, STO and HF calcs., bond length, dipole moment 77−23431
diatomic mols., multipole expansion of diatomic overlap, MEDO calcs. 78−46264
diatomic orbitals, bonding criteria 78−46254
diatomic radicals, wavefunctions, populations and orbital energies, Roothaan calcs. 78−86773
diatomic system, pair polarisability curve shape, rel. to chem. bonding 80−42930
diatomic systems, Penning and assoc. ionisation, correl. diagrams calcs. 77−50521
diatomic transition operators, L^2 basis expansions 80−63519
diatomics, spin coupled theory of mol. wavefunctions, struct. and props. 77−50337
diatomics-in-molecules theory, diatomic states mixing and overlap 79−59344
diatomics-in-molecules theory, Hermitian formulation 78−90063
diatoms, homonuclear, σ_p and π level permutation, for teachers 79−40336

molecular orbitals calculations continued
dibutyl-phenyl-benzoyloxy-benzoate, nematic liq. cryst., rot. barrier, PCILO and CNDO/2 calcs. 80−33874
9,10-dicyanoanthracene, exciplexes, electronic struct. by electro-optical expts. 78−25581
dimethyl ether, O donor capacity *(Russian)* 77−71741
dimethyl ether, spin-orbital interaction *(Russian)* 78−66461
dimethyl sulphide, S donor capacity *(Russian)* 77−71741
dimethyl sulphide, spin-orbital interaction *(Russian)* 78−66461
dimethyl sulphide, sulphoxide and sulphone, electronic struct. and spectra *(Russian)* 78−66460
dimethylamine-HCl systems, H-bonded complexes studied by ab initio MO method, dipole moments determ. 80−83253
Dirac bra-ket notation for second quantisation 78−41910
direct orbital optimisation for MC SCF theory by unitary transformations 80−87049
displacement of molecular orbitals due to interaction with charged species 79−63926
distorted frozen-orbital method for diabatic mol. orbitals 78−41936
double groups, relativistic symmetry orbitals for LCAO calculations 79−10018
double zeta basis sets constrained for rapid integral evaluation 77−88370
doubly charged molecular ions, energy calc. by HAM/3 method 80−9512
dynamical damping in ab initio MO SCF calcs., energy minimisation method 80−18777
effective hamiltonian matrix parameter optimisation, least squares method 79−26874
effective hamiltonians, pseudopotentials and applics. 77−30754
eigenvalue independent partitioning and direct minimisation of SCF theory 77−26970
electric large distribs., theory, review 77−75040
electric-field-variant orbitals, Slater- and Gaussian-type 78−37543
electron correl., second-order perturbation energy, modified HF operator, virtual MOs perturbation anal. 77−18797
electron density calc., approx. differential eqn. 80−47864
electron density mapping in mols., cyrsts., conf., Rehovot, Israel, (Apr. 1977) 78−71622
electron integrals transformation method, program in FORTRAN IV H 78−82603
electron momentum distribs., mol. distortions effects 80−18773
electron repulsion integrals, computation involving Gaussian basis functions 78−58572
electron repulsion integrals, three and four centre for Slater type orbitals, spherical harmonic expansion 79−18108
electron transfer, intramol., electron propagator method 77−34560
electronic excitations, degree of collectivity 78−37570
electronic structure calculations by fast accurate kinetic-energy method 80−83257
electronic structures, omega like technique, Hartree Fock formalism 80−18792
electrostatic isopotential maps for large biomolecules, STO transferable bond calc. 80−3571
electrostatic potential, using overlap-multipole-expansion 79−63931
equations of motion Green's function methods, higher order terms, ionisation pots. 80−52891
equations of motion Green's function methods, higher order terms, ionisation pots., CI comparison 80−52892
equations of motion-Green's function methods, wave function approach 77−65416
ESCA photoionisation cross section, relative intensities calcs., comparisons 78−50464
ethane$^+$, stability and struct., CI-SCF ab initio calc., Franck Condon anal. 77−54575
ethane, (e,2e) spectroscopic obs., valence electron momentum distribs. and separation energies 77−3480
ethane, force consts., model potential function vs. mol. orbitals calcs. 78−29829
ethane, internal rotation barriers, exchange energy and orbital orthogonality effects 77−75049
ethane, localised molecular orbitals, orthogonal transformations calcs. 80−47892
ethane, one-electron props. in terms of localised mol. orbital components 79−6840
ethane, valence electronic struct., model pot. in floating spherical GO formalism 78−74563
ethane, variationally deorthogonalised localised molecular orbitals, electronic struct. 79−97968
ethenoxy, config. interaction calc., using DODS natural orbit approach 78−66476
ethylene, π-electron system photoionisation cross-section, 2nd Born approx. calcs. 77−3424
ethylene, ab initio GO calc. 78−94187
ethylene, and radical ion, SCF-MO calc., bonding and electronic struct. 77−38610
ethylene, average mol. polarisability, Frost model wavefunctions calcs. using p-type Gaussians 78−41924
ethylene, chemisorbed on α-Fe, struct., bonding, dissoc., UPS obs., MO calcs. 78−84050
ethylene, electron momentum distribs. in π orbitals from (e,2e) expts. 80−14239
ethylene, Hartree-Fock energy and Moller-Plesset perturbation energy, harmonic vibr. freq. 80−52852
ethylene, mol. and cluster Auger spectrum calc., SCF core-valence-valence spectra 80−48045
ethylene, mol. semiempirical RPA calc. using PPP Hamiltonian, triplet instability 79−26893
ethylene, quasidegeneracy and effective Hamiltonians, canonical transformation cluster expansion formalism 80−52888
ethylene, RPA hypervirial relation, ab initio minimal basis calcs. 77−18779
ethylene, transition moment closure tests of basis sets 79−6968
ethylene, V-state config. selection methods 79−10041
ethylene, valence states, effective Hamiltonian from canonical transformation 80−74130
ethylene, variationally deorthogonalised localised molecular orbitals, electronic struct. 79−97968
ethylene as singlet methylene dimer, nonempirical double zeta calculations, zwitterionic singlet excited states 80−83258
ethylene dimer, PCILO calc. of geom. struct. and energy 79−63930
molecular orbitals calculations continued
ethylene ozonide, ab initio gradient and MC SCF calc., conformational anal. 80−83290
ethylidene, rearrangement to ethylene, barriers, ab initio MO calcs. 80−104424
ethynyl radical, emission spectra and pot. energy surface, ab initio MRD CI calc. 79−41099
exchange integral, three-centre nuclear attraction integrals, STAO anal. 77−18787
exchange integral, two centre, analytical evaluation 77−18788
exchange localisation, distant orbital tails 77−412
excited states, restricted SCF method calcs. 77−88405
exponential transformation, quadratically convergent SCF procedure, appl. to closed shell ground states 80−47875
$F_m(y)$ function, improved computation 79−63892
ferrocene, electronic struct., excited states, semiempirical PEEL MO calcs. 78−33431
ferrocene, metal to ring distance, ab initio MO SCF calcs. 80−47870
first row elements, split-valence basis set, mol. vibr. and mol. moment calcs. 80−69063
first-row atoms, SCF calcs. using cusped-Gaussian basis sets, polarisation effects 80−74118
first-row hydrides (CH_n, NH_n, OH_n, FH_n), equilib. geometries calcs. 78−33435
floating basis set model, vibronic interaction, polyatomic molecule 77−10587
fluorene and 9-allyl derivations, electronic struct. and reactivity 79−36523
fluoroethyl radical, unimol. dissoc., pot. energy characts. and energy partitioning calcs. 80−45488
2-fluoroethyl to ethylene fluoronium ion interconversion, pot. energy surface, MNDO calc. 79−34296
fluoroform, quadratic force fields, MOCIC pot. functions calcs. 80−5475
fluoromethane, total energy, MOs nonempirical minimum STO-4LGF calcs. 78−9074
fluoromethanes, vibr. spectra, force consts. and geom., SCF ab initio calcs. 78−62785
FMO, applic. to exciplex quenching 77−48655
force constants, SCF method with fixed orbital basis, H_2 mol. appl. *(French)* 79−94107
formaldehyde, $^3A_1$ and $^1A_1$ states, electrostatic mol. pot., basis set and wave function calcs. 79−10020
formaldehyde, mol. orbital calcs., new set of generalised hybrid atomic orbitals 77−67962
formaldehyde, mol. Rydberg S←S and S←T transitions, semi-empirical SCF MO calc. 80−91453
formaldehyde, photoabsorpt. and ionis., intensities, assignments, ST, IVO calc. 79−31614
formaldehyde, proton affinity, geom. and basis set depend., MO calcs. 78−50461
formaldehyde, semi-empirical excited state Morokuma's EHP calc., geometry and order of states 78−46256
formaldehyde, triplet instability, RPA calculations triplet instability, RPA calculations 80−27938
formaldehyde, vertical photoexcitation and photoionisation spectra, CI calc. 78−918
formamide, force consts. and dipole moment derivatives, ab initio MO calcs. 80−95521
formamide, valence ionisation energy and electron affinity, HAM/3 calc. and photoelectron, UV spectra 79−50081
formamide dimer, tritium β^--decay causing H^+ transfer, ab initio MO calc. 80−3391
formamide-glyoxal, charge transfer theory, Mulliken population, ab initio calc., multiconfiguration scheme 80−106392
formic acid, and dimer, ab initio MO calcs., ground and excited states 77−83492
formic acid, cryst. binding, ab initio MO SCF calc. 79−37657
formic acid, dimer, config. and energy, ab initio MO SCF calc. 79−37657
formic acid, dimer, UPS, expt. and MO theory 79−86005
formic acid, dimerisation energy, non-empirical MO SCF calc. 79−37656
formic acid, lattice energy, non-empirical MO SCF calc. 79−37656
formic acid, proton affinity, geom. and basis set depend., MO calcs. 78−50461
formic acid dimer, tritium β^--decay causing H^+ transfer, ab initio MO calc. 80−3391
formic acid dimer-t_1, H bonding, β^--decay effects, ab initio calcs. 79−54763
formyl radical, lower electronic states, ab initio calc. of pot. energy surface, hydrocarbon flame band 79−68287
frontier molecular orbital theory, appl. to Hammett correls. 78−93499
fully coupled SCF perturbation theory in matrix form, simultaneous perturbations 77−34548
fulvalene, electronic structs., semi-empirical MIEHM calcs. 77−75057
furan, HAM/3 calc. of ionis. and excitation energy and electron affinity 79−26894
geminal product approx., optimisation of molecular wavefunction 80−37733
generalised hybrid atomic orbitals, new set 77−67962
geometry predictions using simple MO theory, teaching approach 78−93497
glyoxal, $^3n\pi^*$ states, ab initio STO-3G CI calcs., ΔE_{SCF} transition energies 78−94194
glyoxal-alkali (alkaline earth metal) complex, ab initio MOSCF calc., chelate effect 79−31386
graph theory, equality conditions *(Chinese)* 79−93910
graph theory, of MO, symmetrical analysis and calc., eigenpolynomials 78−29729
Green's function electronic struct. calc., improving Σ perturbation approach 79−13642
group function model for mol. electronic struct. 78−62700
group theory applications to physical and chemical systems in relation to struct. and substructs. 80−42921
H-bonded complexes-first row hydrides, ab initio calcs. *(French)* 80−5479
HAB_2, AB_2 mols., geometry prediction from HOMO 77−3256
halogen molecule, orbitals calc., correlation effects, force const., dissoc. energy, bond length 77−26964
halogenonaphthalenes, bond and mol. polarisability, semi-empirical delta-function 79−31441

molecular orbitals calculations continued
halomethanes, ^{13}C chemical shifts, diamag. susceptibility, effect of non-bonded interactions 78−78726
HAM/3 semiempirical MO theory, correl. energy, self-repulsion 78−13416
HAM/3 semiempirical MO theory, photoelectron spectra calcs. 78−13414
HAM/3 semiempirical MO theory, SCF method 78−13413
HAM/3 semiempirical MO theory, unoccupied orbitals, excitation energies and electron affinities calcs. 78−13415
Hamiltonians, effective, appl. to atomic pot. transferability in hydrocarbons 80−42933
harmonic oscill., excited states, hypervirial relations, off-diagonal 80−37728
harmonic oscillator model in predissoc., level widths, shifts and curve crossing 78−90239
Hartree-Fock approximation with pseudowavefunctions 79−3357
heavy ion collision, K-shell vacancy sharing, variation-perturbation mol. model 79−31665
heavy ion collisions, electron EM field interaction, quantised field formalism 80−83478
Hellmann-Feynman theorem for open-shell and multiconfiguration SCF wave functions 79−89591
Hermitian form of secular eqn. in complex MO method 79−10000
heteroconjugated molecule, LCAO MO graph-theoretical formulation 78−890
heterocycles, five membered ring, MCD spectra dnd π-electron approx. calcs. 79−812
heteronuclear molecules, alternant mol. orbitals energies, generalised formula 79−6867
hexafluorobenzene, slow electron attachment obs., π-orbital calcs. 77−6948
hexatriene, mol. semiempirical RPA calc. using PPP Hamiltonian, triplet instability 79−26893
trans-hexatriene, weak low-energy band, S and T levels by fragment method 78−82625
hydride ions, XH^+, X=first and second row elements, PNO-CI and CEPA studies of electron correlation effects 77−34561
hydride of Z=104, tetravalent, Dirac-Fock one-centre calcs. 77−88380
hydrides, MH^+, MH_2, M=alkaline earths: Zn, Cd, Hg, Yb, No, relativistic (non-relativistic) HF one-centre expansion calcs. 80−52908
hydrocarbons, alternant, perturbational MO calcs., appls. 78−74565
hydrocarbons, bond functions, for ab initio calcs. 80−5469
hydrocarbons, conjugated, heat of formation and reson. energies 80−7839
hydrocarbons, cyclic, ionis. pot., electron affinity, semiempirical MO theory 77−50365
hydrocarbons, effective Hamiltonians for atomic pot. transferability 80−42933
hydrocarbons, nobenzoid, ionisation pot. and heat of form., IOC-ω method 79−31733
hydrocarbons, normal, mass-spectrometric fragmentation processes, quantum field theory 80−40782
hydrocarbons, occupied mol. orbital energy levels, rel. to chemisorption activity 79−19449
hydrocarbons, saturated, topological orbitals, graph theory and ionis. pots. 78−82615
hydronaphthyl radicals embedded in naphthalene cryst., optical transition energies and ionisation energies 80−78595
hydroxymethyl cation, geom. and electronic struct., ab initio SCF calc. 79−76331
hydroxymethylene radical cation stability, $CH_2O^{+\cdot}$ isomers, ab initio MO study 80−42965
hyperfine coupling, constants, nucl. spin spin coupling const., NDDO MO calcs. 80−23310
hyperpolarizability, freq. depend., time depend. HF eqn., second order LCAO SCF pertubation theory 79−31388
IBMOL-5 service program 78−86765
ice, cubic, LCMO calc. of energy bands 77−51656
incomplete basis set problem, virtual orbitals and CIBS expansion of HF energies 80−52844
independent-particle Hamiltonian, group struct. 79−22580
inert gas diatomic molecule, excited state pots., fast calc. 80−9490
inert gas halides, emission spectra, open-shell closed-shell interaction, electron gas model 77−30879
integral explicit expressions, generalised Chong method 78−892
integrals involving continuum orbitals, numerically oriented evaluation method 77−61673
integrated spatial electron populations, evaluations for simple mols. 80−78524
integrated spatial electron populations using projection function method 80−23299
intermolecular energies calculation from delocalised pictures, artifacts and elimination 80−18899
intermolecular interaction energies, calcs. in terms of local contrib. 77−30755
intramolecular electron transfer amplitude, basis function overlap effect 78−9080
intramolecular interactions effect on transferability props. of localised description of chemical groups 80−102424
intramolecular potentials, quantum chemical calc. 78−13436
intrinsic single and dual mol. orbital symmetry conservation 80−102419
inverse Gaussian transforms, general props., Slater type orbitals appl., coord. and momentum representation 78−37549
inverse matrix diagonal and off diagonal elements, self energy perturbation theory 78−82607
ion+atom, low vel., X-ray emission ang. distrib., MO calc. 79−54803
ion+atom collision, diatom. quasimolecule form., shielded-orbital model 79−10165
ion-molecule equilibria in solvolysis, secondary β ^2H isotope effects, hyperconjugation 80−50874
ionis. pot. calc. from VB and MO wavefunctions 78−82616
ionisation potentials, natural transition orbital theory, perturbation theory anal. 77−34541
ionisation processes 79−36512
ionised, localisation approach 77−30806
isocyanates, nonbonding and π-orbital interactions, photoelectron spectra 80−32774
isothiazole, ^{14}N NQR of mol., expt. and MO calc. 79−36667
isothiothiocyanates, nonbonding and π-orbital interactions, photoelectron spectra 80−32774

molecular orbitals calculations continued
isoxazole, ^{14}N NQR of mol., expt. and MO calc. 79−36667
iterative natural orbitals for CI using peturbation theory 77−79549
ketene, UHF-INDO perturbation calc., localised spin orbitals, spin anomaly and second order substituent effect 79−68191
β-lactam antibiotics, ab initio SCF-MO-LCAO calcs., amidic bond breaking, methoxy substitution effect 80−78533
lanthanide, trivalent, hypersensitive transitions, intensity parameters, charge transfer mixing 77−55498
large molecular systems, local pot. surface and charges, parametrisation scheme for quantum mechanical computation *(German)* 80−18793
large molecules, mol. fragment basis, generalisation, for ab initio calcs. 80−91438
LCAO method, chem. bond order, ZDO approx. 79−41102
LCAO method, improvement by directed variation of exponential parameters 79−41101
LCAS MS SCF method within Gaussian basis set 80−102438
LCMO formalism 78−62693
level shift technique, unconditional convergence in SCF formalism 77−50339
(Li^+,-) model calcs., correl. between electron affinity and dipole moments 77−57857
ligand field spin-orbit coupling calcs. for d^7, d^8, d^9 five coordinated complexes 77−18781
ligand fields calcs., strong and intermediate fields, tensor algebra 80−42922
light atom molecules, general quadratic force fields, semiempirical MOCIC calcs. 80−5474
limited CI with optimal generalised combination of SCF MO symmetry subsets 77−42246
limited MC SCF theory 79−36537
linear combinations of fragment orbitals, appl. to π-systems photoelectron spectra 79−18119
linear Hubbard model, RPA and CI test calcs. 78−25411
linear triatomic hydrides, ab initio SCF CI electric dipole moments 79−31410
lithium ethylene, SCF-MO calc., bonding and electronic struct. 77−38610
local force densities and stress tensors, density functional theory 80−18781
localisation, bonds, physical models of molecular reality 77−30756
localisation and local phenomena in excited and ionisation stationary states 77−34563
localisation approach, applic. to additive props. 77−30752
localisation in ionized and excited states, conf. 77−30750
localisation in loges, cf electron pair concept 77−23401
localisation of MOs using density matrix formalism *(Russian)* 79−93911
localised and pseudo orbitals, steepest descent method 79−18102
localised fixed orbitals, construction, pseudopot. method using multi-config. SCF theory 77−14334
localised mol. orbital struct., octet rule violations, fractionality 78−25445
localised molecular orbitals, orthogonal transformations calcs. 80−47892
localised orbital density, charge distrib. charact., hydrides 77−54501
localised orbital theories, cancellation effects 80−84445
localised orbitals, moment characterisation 77−46486
localised orbitals method for describing chem. bonds *(French)* 79−89593
localised orbitals transform. to restricted alternant orbitals 79−76334
localised site cluster expansion, interacting paramagnetic sites, spin symmetry projection 79−7951
loge theory and chemical reactivity 77−30758
loge theory and wave function calcs. 77−30753
lone pair orbital explicit representation, augmented contracted Gaussian basis set 78−25423
lower bound Hamiltonians for atoms and mols., projection operator method 78−82602
magnetic circular dichroism, group theoretical techniques 80−45048
magnetic properties, London field-dependent orbitals calcs. 77−42225
magnetic susceptibility calc., vector pot., variation method, effective selection of gradient transform. function 80−69258
many-body perturbation theory, modified pots., 3- and 4-body contribs. 77−88376
many-electron spin degeneracy, recursive formula for Young's orthogonal representation 77−38596
mass spectrometric fragmentation, MO-model and simulation 77−417
mass spectrometry results comparison with MO calcs. 78−320
materials science appl. 78−29732
MC-SCF theory, modified one-electron Hamiltonian, iteration convergence 79−6871
MCSCF and CI wave functions, two-particle density matrix and graphical unitary group approach 80−63558
metal cluster, Wolfsberg-Helmholz relation analysis, reson. integral approx. 80−49566
metal clusters, electronic states and mag. props., MO calc. 77−20219
metal complex, radiationless transitions, internal ligand modes 79−22750
metal porphin, triplet state, spin density and zero-field splitting, PPP-SCF-CI calc. 79−68200
metal-insulator transition, AMO method 78−63982
metal-ligand 3-orbital-4-electron, 4-orbital-4-electron bonding, perturbation theory 79−98000
methane, $1B_1(1T_2)$ state, photodissoc., extended basis calcs. 78−9093
methane, and $-t_1$, β-decay, ab initio SCF MO calcs. 77−71842
methane, bond dissociation, MCSCF LMO calcs. 77−57886
methane, bonding, electron pairs, size and shape parameters, Gaussian basis set MO calcs. 80−27935
methane, elastic and inelastic electron scatt. differential cross section, obs. and calc., struct., binding energy 80−28110
methane, energy quantities from localised charge densities, dependence on geometry and basis set 80−63525
methane, freq. depend. polarizability, LCAO SCF perturbation theory 79−31387
methane, ionis. by mol. orbital method, many-body calc. 79−36512
methane, large angle elastic and inelastic electron scatt. differential cross section, exchange corrections 80−28111
methane, mol. and cluster Auger spectrum calc., SCF core-valence-valence spectra 80−48045
methane, orbital relax. energy for single and double ionis. from valence shells 80−106253
methane, orbitals calcs. using modified Adams-Gilbert eqn. 77−34542

molecular orbitals calculations continued
methane, pot. energy surface of excited singlet state, appl. to photodissoc. 79−83440
methane, SCF calcs. including polaris. functions 80−87034
methane+O(^{1}P), barrier height and transition state geometry, POL-CI calc., H abstraction reaction 80−66782
methane +H_2O, pairwise interaction pot. function, ab initio SCF MO calc. 79−22786
methanesulphonyl chloride, geom. struct., CNDO/2 calc., comparison with CF_3SO_2Cl 79−81295
methanol, internal rotation barriers, exchange energy and orbital orthogonality effects 77−75049
methanol, total energy, MOs nonempirical minimum STO-4LGF calcs. 78−9074
method of moments, criteria for good weight functions, appl. to correlated wave functions 77−23415
method of optimal relax., eqns. of motion method, k lowest or highest solns. 80−37727
methoxide surface complexes on Li, He(I) photoelectron spectra, MO calcs. 80−83417
methyl cyanides and isocyanides, isomerisation, ab initio (STO-3G) geometry optimised calc. 78−46265
methyl glyoxal, $^3n\pi^*$ states, ab initio STO-3G CI calcs., ΔE_{SCF} transition energies 78−94194
4-methyl-2,6-di-tertiary butylphenol, gamma-irradiated, effect of radiation damage on hindered methyl group rotation 77−35494
methylacetylene, quadratic force fields, MOCIC pot. functions calcs. 80−5475
methylamine, total energy, MOs nonempirical minimum STO-4LGF calcs. 78−9074
methylamine-HCl systems, H-bonded complexes studied by ab initio MO method, dipole moments determ. 80−83253
methylene, singlet-triplet separation, configuration interaction study 78−13438
methylene+H_2→methane, ab initio CI calc. on SCF level, insertion reaction min. energy path 80−7774
3-methyleneoxetane, electron structure, orbital-O interaction, MO calcs., UV photoelectron spectra 80−28058
methylenimine, n→π^* transition, ab initio SCF MO CI calc. 78−58584
methylisonitrile, mol.excitation by electron impact, 500 and 25-70 eV, expt. and HAM/3 79−72434
minerals, physical theories for origin of colour 78−69323
MNDO calculations, total energy, anal. first derivatives 78−86763
model potential method, STO calcs. 77−408
modified virtual orbitals, for config. interaction calc. 80−58163
mol. and cluster Auger spectrum calc., SCF core-valence-valence spectra 80−48045
molecular, relativistic orbitals for double group D_{3h} 78−41968
molecular complex, bond lengths and heat of form., INDO calc. 79−54783
molecular complex, pot. energy curves, INDO calc. 79−54784
molecular crystals, PCILO calculations 77−34571
molecular electron affinities, qualitative molecular orbital theory 78−5122
molecular ground, excited states, doubly excited configurations in density-matrix method 77−3280
molecular polarisabilities calcs., superposition method of excited config., nonstationary perturbation theory eqn. 80−69257
molecular solid, electron tunnelling, long-range electron transfer processes, orbital overlap model 80−7813
molecular solid, localisation of mol. ion or exciton states 79−47048
molecular spectra, full quantum mechanical theory, mol. eigenstates generator coordinate method 78−21895
molecular vibr. freq. calc. using MNDO method 78−25508
molecules or clusters, interpretation of data from Mossbauer, ESR, susceptibility, optical and XPS meas. 80−37825
molecules-in-molecules method, as extension of generalised diatomics-in-mols. 79−97970
molybdenum formate, mol., Hartree-Fock instability of SCF wavefunctions 80−9492
monochromatic wave perturbation, time depend. HF calcs. *(French)* 80−63516
monofluoromethane, force consts. and IR intensities, ab initio SCF finite difference method 78−86783
monothioformate anion, protonation site, ab initio SCF calc. 79−47894
muffin-tin approximation in mol. calcs. and solid state 77−409
muffin-tin potential, relativistic scattered-wave theory, elimination method calcs. 77−10607
Mulliken's magic formula, mathematical basis of approx. MO theory 79−22577
multi-config. SCF super-CI calc., density matrix formulation 80−78547
multicentre molecular integrals evaluation over hydrogen like atomic orbitals *(Russian)* 80−63548
multiconfiguration SCF theory, hierarchy eqns. for reduced transition operators 77−54516
multiconfiguration wave functions, optimisation 78−33411
multiconfigurational paired excitation SCF theory 77−42224
multiconfigurational reference states, orbitals optimisation 79−10002
multiconfigurational SCF method, yielding Fock-like operator 79−36540
multiple scattering MO method, atomic charges concept 79−18101
multiple substitution effects in linked cluster theorem for CI calcs. 78−50481
multiplet ratios for photoionisation and electron attachment, shell model, LS coupling and correl. 78−17636
multiply charged collision systems, slightly asymm., curve crossings, constraints, MO theory 78−74734
multipole magnetisability, mag. shielding, multiple SCF perturbation theory 77−34549
$n\pi^*$- and $\pi\pi^*$-states, n-electron delocalisation effect 79−63902
n-electron molecular wavefunction, Schrodinger inequalities, many-electron densities 78−94191
N-representability problem, operator endomorphisms 77−33892
N-representability problem, operator endomorphisms 77−33893
naphthalene, cryst., radiation induced radicals, optical absorpt. bands, SCF-CI MO calc. 79−91463
natural orbitals, Billouin-Levy-Berthier theorem, multiconfigurational SCF optimisation 80−27936
NDO schemes, calc. of largest mol. integrals over orthogonal hybrid orbitals 78−41956
negative molecular ions, theoretical calcs., review 78−37552
negative quantum chemical calcs. 78−62703

molecular orbitals calculations continued
Nesbet equation for molecular calculations, appl. to Hubbard model 80−87029
p-nitroaniline, core ionisation negative shake up energy, ab initio SCF CI calc. 79−64041
nitrofuranes, substituted, electron affinity, HAM/3 calc. 79−27109
nitroimidazoles, substituted, electron affinity, HAM/3 calc. 79−27109
nitrone, config. interaction calc., using DODS natural orbit approach 78−66476
NMR chemical shift, nucl. other than protons, semi-empirical calcs., review 77−75188
nonane dimer, intermolecular interaction energy, PCILO calc. 77−34572
nonlinear differential equations, similar to Schrodinger eqn., variational principle application 79−63065
nonperturbative open shell theory, mol. ionisation pot. and excitation energies, HF multiple cluster expansion 79−22599
nuclear spin-spin coupling constants, directly bonded C-C and C-H, CDOE/INDO LMO calcs. 80−95546
nuclear spin-spin coupling constants in series of related mols., orbital model, perturbational approach 79−81217
nucleic acid purine, pyrimidine bases, base pairs, hydration scheme 79−92127
numeric MCSCF method, unicentre expansion 79−45623
octachlorofulvalene, electronic structs., semi-empirical MIEHM calcs. and photoelectron spectra 77−75057
octane, first-order props. of simulated ab initio molecular orbital wave functions comparison with SCF wavefunctions 79−41094
trans-octatetraene, weak low-energy band, S and T levels by fragment method 78−82625
one-dimensional conductor, model system, polymer-bridged metal complex, MO theory 79−90940
one-dimensional molecular crystals, electronic struct., mol. orbital theory 80−54588
one-electron Hamiltonian method applied in SCF theory to states with open shell 80−23302
one-electron props. variation with changes in mol. geometry, electronic and nuclear components partitioning 77−83491
open shell orbital theory with electron correl., wavefunction cluster expansion 79−13647
open shell RPA unitary group formulation, Hartree Fock stability eqns. 80−52860
open shell systems, orbital energies, semiempirical calcs. 77−3272
open shell theory for complex mol. orbitals 77−23410
open shells, RHF treatment without Lagrange multipliers 80−32589
optimum minimal basis of exponential atomic orbitals 78−41921
orbital amplitudes of nuclei, extrapolation procedure, gaussian basis set and nucl. cusp eqn. 78−74560
orbital interaction and chemical bonds. Exchange repulsion and rehybridization in chemical reactions 78−85142
orbital SCF and total SCF energies, approx. relation 78−5123
orbital symmetry conservation, chem. appl. of field theory *(Chinese)* 79−63884
organic chemistry courses, unified approach to teaching of struct. and bonding 80−17732
organic compounds, ^{13}C NMR, chem. shift, effective excitation energy calcs. 77−14457
organic molecules, improved IOC-ω technique 77−14336
organic mols., IR intensities anal., hybrid orbital rehybridisation model, mol. charge distrib. 78−74630
organic reaction mechanisms, generalised mol. orbital theories, review 78−44366
organic semiconductors, refined AMO calcs. 79−36514
overlap integrals for AO NSTO basis set 79−31379
oxadiazoles, ^{14}N NQR of mol., expt. and MO calc. 79−36667
oxalic acid, cryst. binding, ab initio MO SCF calc. 79−37657
3- oxetanone, electron structure, orbital-O interaction, MO calcs., UV photoelectron spectra 80−28058
oxoniomethylene cation, rearrangement to hydroxymethyl cation, barriers, ab initio MO calcs. 80−104424
PAA, nematic liq. cryst., rot. barrier, PCILO and CNDO/2 calcs. 80−33874
pair density analysis, applics. 77−30751
pairwise correlated generalised valence bond model, electron correl. model 78−41959
papain models, active site α-helix and ion pair stability 80−74265
paramagnetic electronic props. of atoms and mols., orbital mag. moments, paramagnetic currents 77−46476
paraspectral molecular pairs 79−45620
PCILO method and localisation 77−30785
PCILO method at INDO level, σ-π exchange phenomena 78−62725
s-trans-1,3-pentadiene, photoisomerisation, excited state pot. energy curves, CIPSI calc. CNDO/2 parametrisation 78−11505
perovskite and tungsten bronze cryst. struct. types, ionic grouping theory, electrooptical, nonlinear optical effects *(Chinese)* 78−52472
perturbation energy, second order, environmental effects, SCRF theory 78−58609
perturbational molecular orbital analysis, hybrid lone pairs problem 79−89608
phase and population relax., semigroup formalism 80−78519
phenanthrenoid compounds, abnormal bond lengths, MO calculations 77−31020
phenol, H bonds to proton acceptors, PCILO calcs. 79−26895
phospholipid inter-and intra-molecular interactions, PCILOCC and pot. function calc. 80−3570
photochemical reaction, avoided crossings in excited states potential energy surfaces 78−76881
photoelectron spectra, localised and delocalised calcs. 80−63709
photoelectron spectra, self-consistent charge calcs. of core-electron binding energy shifts 80−69084
photoionisation cross sections, at. extrapolation, ground state inversion method appl. 80−18787
photoionisation cross-section, orthogonalised-plane-wave approx. 79−41202
pi systems representation, efficient computer manipulation 79−81148
point charge model approach to intermol. interaction coeffs. 80−18897
point charge model approach to mol. elec. polarisability 80−18797
point group coupling, coeffs., props. and application 80−43033
polarisabilities, average, empirical calc. method 80−63859
polarisability, calc. by semiempirical methods 79−36535
polarisability of molecules, differential scaling of σ and π orbitals, and geom. approx. 79−10231

molecular orbitals calculations continued
polarisability of molecules, freq. depend., Hartree-Fock theory 79−45652
polarisability of negative molecular ions 77−57860
polarization Green's function with multiconfiguration self-consistent-field reference states 80−37724
polyacetylene, band struct. valence Hamiltonian minimal STO-3G basis calc., nonempirical model pot. 80−54596
polyatomic ions, charge distributions, rel. with cohesive energies of ionic crystals 80−70161
polyatomic molecule, Eckart frame orientation by symmetric orthonormalisation 79−6818
polyatomic molecules, bond functions, for ab initio calcs. 80−5469
polyatomic molecules, IR absorpt. bands, integrated intensities, ab initio and LMO calcs. 79−72234
polyatomic mols., multipole expansion of diatomic overlap, MEDO calcs. 78−46264
polyatomic polarisability, semi-empirical delta-function method 79−31442
polyatomic systems, MC SCF computation scheme 79−10039
polycyclic aromatic hydrocarbons, benzenoid system PO-MO character and PMO localisation energy 79−54767
polycyclic aromatic ring systems, localised MOs and wave functions 79−31398
polyenes, π-electron correlations, canonical and localised orbitals calcs. 79−36547
polyenes, DODS methods with HF variations 77−23425
polyenes, highly branched, large networks, abnormal bond orders 79−59610
polyenes, linear, two-photon absorptivities, SCF-PPP-CI calcs. 79−31631
polyenes, localised representation, correlation contrib. to energy 79−59370
polyethylene, band struct. valence Hamiltonian minimal STO-3G basis calc., nonempirical model pot. 80−54596
polyethylene, band structure, linear combination of localised orbitals calc. 77−62808
polyethylene terephthalate, conformation rel. to orientation, pot. energy surfaces study 79−68338
polyglycine, total energy, conformational calc. using quantum mech. partitioning method 78−94189
polymeric chains and Mott insulators, similarities w.r.t. electronic correl., AMO method *(French)* 80−24775
polymethine-cyanine molecular aggregate, band struct. 80−53174
polypeptides, total energy, conformational calc. using quantum mech. partitioning method 78−94189
polypyridines, photoelectron spectra, SCF LCAO calcs. 78−33551
polyynes, intermolecular interaction through triple bonds, internal rot. 80−106370
porphin, electron spectra, PPDP/S approx. calc. *(Russian)* 78−13435
positive core potential energy method for conformational analysis 77−57850
potential energy first derivative, open-shell restricted HF and MC SCF calcs. 79−98004
potential energy surfaces, of mols., VB diatomics-in-mols. method 79−85919
prop-1, 2-dienyl radical, ab initio SCF HF MO calc., electronic struct. and one electron props. 77−42231
n-propanol, preferred conformers, PCILO study 80−95542
β-propiolactone, electron structure, orbital-O interaction, MO calcs., UV photoelectron spectra 80−28058
propionitriles (-O, NH, S), conformational investig., NMR, IR and semiempirical MO methods 80−95650
propyne, mol.excitation by electron impact, 500 and 25-70 eV, expt. and HAM/3 79−72434
protein, electron-transport type, H-bonding, ab initio MO 80−51039
proteins, amide unit electron organisation, mol. orbital theory 79−2000
pseudopotentiai method, nonparametrised, for Hartree-Fock-Slater calcs. 77−57859
pseudopotential method, testing of arbitrariness and limits 80−91446
pseudopotentials, improved three parameter, Li to Kr and hydrides, PSIB-MOL algorithm 77−26963
pseudopotentials, use in mol. calcs. 79−31384
pyrazine, excited and N_{1s} ionised states, ab initio calcs. broken orbital symm. 80−27931
pyrrole, HAM/3 calc. of ionis. and excitation energy and electron affinity 79−26894
pyrrole-acetonitrile, H-bonded complex, ab initio MO calcs. 80−102440
quantum defect theory, general form 79−68177
quantum mechanics, molecular, book 77−79538
quasi-energetic spectra of quantum systems in classical monochromatic fields 78−78981
random phase approximation, consistent ground state characteristics 79−59346
random walk calcs., method of successive corrections 79−68180
rare earth orthovanadates, covalency, chemical bonding and opt. spectra 77−80442
reaction barrier from overlap repulsion scheme 77−36734
reaction potential surfaces, electron correl. theories 79−39125
relativistic MO theory in Dirac Slater model *(Japanese)* 78−66480
relativistic self-consistent field theory for open-shell molecules 80−95518
RHF energy values calcs., influence of mol. integral errors 77−50354
rhodanines, tautomeric, electronic struct. and spectra, MO calcs. 79−13629
RPA hypervirial relation, sum rules for ordinary and rotatory intensities in finite bases 77−18779
RS perturbation theory, E_3 variational principles 78−58570
Ruedenberg energy relation, deviations, theory 79−93909
Rydberg transitions, correl. algorithms for Rydberg term values 80−83277
satellite struct. of electron spectra, CI and vibronic coupling, dynamical calc. 80−53044
SCF calculations, simplified extrapolation procedure 78−82604
SCF theory, sum rules for circular dichroism in spectroscopy 78−58059
Schrodinger eqn., random walk soln., electron spin effects 77−18780
Schrodinger-Infeld-Hull factorisation, quantisation condition, matrix elements and selection rules 78−41909
second-order perturbation energies, modified virtual orbitals calcs. 77−88381
second-quantisation representation, with nonorthogonal basis set of one particle functions 78−889
second-row homonuclear diatomics, photoemission energy, rel. to atoms 78−86832
second-row hydrides, equilib. geometry, FSGO model pot. calcs. 77−50347
self-consistent convergence, effect of electron distrib. nonuniformity 77−18778
semi-empirical methods based on NDO, reson. integrals 78−41907
semiconductor, defect electronic structure and lattice config., MO approaches 80−65495
semiempirical all-valency MO methods, derivation using restricted HFR theory *(German)* 78−21853
semiempirical MO theory, modified NDO model 80−52887
semiempirical molecular quantum-chemical calculations, PARAMOL programs 77−88393
semiempirical theory for ground and excited states, Fock operator expansion, STO-3G and CNDO/S calcs. 80−58154
shape, second-order Jahn-Teller effect, highest occupied mol. orbital postulate 78−86780
shielded diatomic orbitals, two-centre integrals eval. *(French)* 79−49931
shifted Hartree-Fock eigenvalues and Slater's transition-state concept 80−83261
SiH_5, SCF calcs. including polaris. functions 80−87034
silaethylene, singlet-triplet energy separations 77−57866
Simons-type model potentials, mol. calcs. appls. 78−5120
simple mol. charge distrib., empirical method, electrostatic pots. and struct. 78−82652
simulated ab initio MO method, appl. to second row elements in mols. 80−47867
simulated ab initio molecular orbital method, resolvent technique 79−41094
Singer polymal tempering methods 80−52845
singlet-triplet energy difference, Hund's rule, inequality formulation 78−66482
singlet-triplet energy difference and singlet generalised oscillator strength, Lassettre-Dillon relation 80−63508
site symmetry approach to hybridized orbitals 77−13552
Slater 1s orbital four centre mol. integrals, Fourier transforms 80−74104
Slater type orbitals, multicentre integrals 79−22590
Slater-type orbitals, expansion, electron-repulsion integrals evaluation 80−99451
small, medium and large systems, ab initio and approx. rigorous calcs. 78−62714
small molecules, localised charge densities calcs., bond length effects 80−83256
solid, correlation holes, number-sum rules and infinite system 79−23916
solvated electrons, fractional charge MO model 78−31752
solvent effects, proton pots., SCRF theory 78−58608
sp-hybrid crystals, energy bands calc. by many-neighbour approximation 77−35846
sparse s and p type Gaussian basis set LCAO MO SCF calc., mol. props. 80−23306
spectral sensitizing dye design, use of molecular orbitals calcs. 79−20425
spherical harmonics problems, identities 80−63515
spin and charge density theoretical determ., review 77−75045
spin factoring for spectroscopic term determ. 77−61695
spin-orbit formalism of Hartree-Fock energy and Moller-Plesset perturbation energy 80−52852
spin-orbital eqns. for anal. derivatives of config. interaction energy including double substitutions 80−78549
spirohydrocarbons, strained, bond angles, interatomic distances, semiempirical and ab initio calcs. 80−95533
Sternheimer effect in ligand field splitting, nucl. and electronic levels 78−70757
struct. and props., SCF calcs. 80−106260
subtilisin charge-relay system, electrostatic pot. map, STO transferable bond calc. 80−3571
superexchange, ang. depend. for frozen ion orbitals, mol. orbital model 77−32185
supermolecule calcs. with additive procedure, intermolecular interactions and binding energy 80−52880
supra-antarafacial cycloaddition intrinsic single and dual mol. orbital symmetry conservation 80−102419
symmetric group theory and Waller-Hartree spin-free method 78−41908
symmetry adapted multiconfiguration SCF wave functions, single excitation annihilation calcs. 77−46481
symmetry adaption, diagonalisation of overlap matrix 79−26877
symmetry adaption, force const. matrix of symmetric mols. 79−26878
symmetry adaption, representations on symmetric polyhedra 79−31368
symmetry coordinates and group orbitals from basis functions 79−759
symmetry of MO with its energy, theorems and calc. methods 78−66457
symmetry-lobe orbitals, symmetry defects and contamination 79−9990
syndnone, semi-empirical excited state Morokuma's EHP calc., geometry and order of states 78−46256
system, 1 s σ orbital, variational calc. 78−37707
Talmi transformation, multicentre integrals, harmonic oscillator functions 79−93908
Tamm-Dancoff approx., relativistic correction 78−9090
TCNE-benzene, charge transfer theory, Mulliken population, ab initio calc., multiconfiguration scheme 80−106392
TCNQ salt, NMP-TCNQ, electronic struct., SCF calc., total energy polarisation effects 80−15469
teaching instruction using ab initio computer program 77−78937
tempered orbital energies and pot. curve, appl. to H_2 79−89584
p-terphenyl, lowest excited singlet states, polyexcited CI calc. 79−772
tetrabiomethane, electronic struct., Xα SW calcs. 80−102447
tetrafluoromethane, elastic and inelastic electron scatt. differential cross section, obs. and calc., struct., binding energy 80−28110
tetrafluoromethane, electronic struct., Xα SW calcs. 80−102447
tetrahedral model systems, Dirac-Fock one-centre calcs. 79−6837
tetrahedral molecules, spectral line press. broadening, symm. basis set calcs. 77−3421
tetrahedrally coordinated solids, charge distrib., localised mol. orbitals 79−23560
tetraselenafulvalene, monomer and dimer electronic struct. scattered wave calc. comparison with photoelectron spectra 78−50465
thiazole, ^{14}N NQR of mol., expt. and MO calc. 79−36667
thiocyanates, nonbonding and π-orbital interactions, photoelectron spectra 80−32774
three open shell configs., inter electron repulsion integrals 77−55499
three-centre two-electron exchange integral *(Russian)* 78−37551

molecular orbitals calculations continued
three-electron model system, unrestricted and projected Hartree-Fock calcs. 79−6850
time-depend. HF model, transition energies, oscill. strengths *(Spanish)* 77−6684
time-dependent multiconfigurational Hartree-Fock theory 80−58117
topological model and orbital mapping for chemical systems 80−78512
total electronic energy, atoms and mols., SCF binding energy, Z^{-1} perturbation theory 80−83268
total energy and orbital energy, semiempirical calcs. 78−78614
total energy of molecule, local spin density functional approx., LCAO SCF calc. 79−93920
trans-butadiene, ionis. pot., π-π^* energies, open shell many-body formalism calc. 77−46508
transformation properties of molecular orbitals *(Russian)* 78−82605
transition metal, bimetallic cluster, photoselective bimetallic aggregation, review 80−53182
transition metal clusters, bonding capabilities, MO calcs. 79−22589
transition metal complex, ligand field problems, group theory 80−42920
transition metal complex ions, MY_4^{n-4}, MY_6^{n-6}, alkali metals and alkaline earth outer-sphere cations, spectroscopic splitting parameters 78−39075
transition metal complexes, octahedral, optical rot. dispersion theory 77−77164
transition metal compounds, electronic excitation energy calc., correl. energy correction 78−17576
transition metal cyanides, octahedral, electronic struct., multiple scatt. mol. orbitals calcs., ESCA satellites 77−14488
transition metal surface atom interaction with ethylene and acetylene, MO calc. 80−6623
transition metal tetrahalogeno anions, ligand field spectra, MO model 78−17654
transition state determination and characterisation ab initio calcs. 77−28975
trial wave functions, by off-diagonal hypervirial theorem 79−22578
triatomic isoelectronic molecules, electronic struct., one-electron props. 80−42935
triatomic mol. bond-bond interaction force consts., simple MO theory 78−50452
s-triazine, triplet instability, RPA calculations 80−27938
trifluoroacetic acid, monomer and dimer, photoelectron spectrosc. 80−87172
trifluoromethyl cyanides and isocyanides, isomerisation, ab initio (STO-3G) geometry optimised calc. 78−46265
trifluoromethylsulphonyl chloride, geom. struct., CNDO/2 calc., comparison with CH_3SO_2Cl 79−81295
trimethylamine, SCF calcs. including polaris. functions 80−87034
trimolecular interaction, multiple site reactivity, perturbation theory 79−52639
trioxolanes, pseudorotation surface, mol. struct. and conform. 79−45653
triphenylene, excited state Faraday values mag. circular dichroism spectra and MO CI calcs. 80−18877
triphenylene, excited state polarisabilities, electrochromism and pot. energy curves 79−7034
triphenylene derivatives, hexasubstituted, disc-like cpd., mol. conform. and arrangement, semiempirical calcs. 80−107048
TTF-TCNQ, molecular coordination along stacking directions 79−47031
two centre and three centre integrals for attraction of Slater type orbitals to nucleus, coord. systems 80−14068
two centre on electron molecular integrals, Fourier convolution theorem 78−66468
two centre one-electron system, continuum wave functions 79−93915
two identical molecules, level shifts due to overlap of MO's 77−46494
two state two mode vibronic coupling model, Born-Oppenheimer and crude adiabatic perturbation methods 80−87036
two valence-electron diatomics and triatomic ions, FSGO method calcs. using at. Fues pot. 78−62717
two-centre charge distrib., Fourier transform, STO general expression derivation 80−58119
two-centre Coulomb and hybrid integral coeffs., analytical evaluation formulae 77−67958
two-centre repulsion integrals, semiempirical model using NDDO approx. 78−78609
two-electron system, natural orbitals, pseudo-eigenvalue eqn. and long-range behaviour 79−85886
two-electron wave functions with monopole interaction, asymptotic forms 80−78528
two-parameter omega technique 78−41933
UHF orbitals, ionisation energy calcs. appls. 80−58141
undergraduate course, localised and delocalised MOs to polyatomic mols., bonding 78−32630
unitary group generators and permutations, CI matrix elements, algebraic method 80−37725
unitary group generators and permutations, CI matrix elements, graphical method 80−37726
unitary group irreducible representation subduction coeffs. 80−37723
unitary variational method 77−71743
universal basis set concept, Slater-basis set 79−36502
universal basis sets 79−10021
unlinked cluster corrections for configuration interaction calculations 79−3368
uranyl pentafluoride complexes, normal coordinate anal. 79−22596
urea, single crystal Compton profiles, H-bonding and dimer config. effects, calc. and meas. 78−80431
valence electron studies using atomic Fues potential, homonuclear diatomics 80−78544
valence only calculation, non-empirical pseudopot. method 79−49932
valence states and binding energies 77−30757
valence-shell MO calc. with pseudopot. 78−907
Van der Waals complex, PCILO calc. of dispersion energy and geom. conf. 79−63930
variable gauge at. orbitals 77−34540
variational cellular method, electronic struct. calcs. 80−54591
variational localised site cluster expansion, wave function higher ansatze, linear Heisenberg model 79−7959
variational localised site cluster expansion, wave function ansatze, many body theory 79−6827
variational method, metric-constrained 79−22579
variationally deorthogonalised localised molecular orbitals 79−97968
variations preserving orthonormality, parameter representation for first and second-order variation 79−76326

molecular orbitals calculations continued
vibrational circular dichroism theory, localised mol. orbital model 77 75192
vibronic coupling matrix element evaluation 77−14408
visual chromophores, two-photon absorptivities, SCF-PPP-CI calcs. 79−31631
water molecule, nucl. spin-spin coupling consts. geometric approx. 79−59380
water oligomers, H-bonding, PCILO calcs. 77−83500
X_3YO molecules, ab initio MO calcs., geometry, electronic struct. 78−41940
Xα method with pseudopotentials 80−83282
X-ray absorption spectra, method of coupled differential eqns. 77−88466
X-ray emission spectra, techniques and spectral interpretation, rel. to XPS, book contrib. 80−11514
Z=114, Dirac-Fock one-centre calcs., tetravlent hydride prediction 77−34551
Z-centre 1-electron integrals and Coulomb integrals over STOs 78−82608
zero differential overlap approximation, theory, parametrisation methods, review 78−82622
Ag, chemisorpt. of CO, N_2, NO, semiempirical calcs. 78−14611
Ag halides, localised MO treatment of fractional bonding 77−58970
Ag_2, Harris-Pohl selected valence electron split-shell MO calcs. 80−91439
$Al_2(Al_2^-)(Al_2^+)$ configurations, ab initio study, LCAO, STO, MO-SCF and CI calcs., binding energy *(French)* 80−91447
$Al^{3+}(H_2O)n$ (n=1,2,4,6), FSGO-pair-pot. calcs. *(German)* 80−74278
α-Al_2O_3, charge distribution determ., SCF calc., Slater-type orbitals, Madelung type const. 80−107100
Al(111), chemisorption of O_2, SCF X_α scatt. wave MO calc. 79−42374
Ar_2, excited state pots., fast calc. 80−9490
Ar_2, short range interactions between two rare gas atoms 79−26888
ArF^+, selected valence-electron split-shell MO calc., ground state props. 79−22585
ArF_2, ab initio diatomics in mols. pot. surface, spin-orbit coupling 79−3519
ArHF, van der Waals complex, ab initio RHF calc., struct. 79−76339
ArHO, van der Waals complex, ab initio RHF calc., struct. 79−76339
Au_2, Harris-Pohl selected valence electron split-shell MO calcs. 80−91439
BH, variation-perturbation minimal Gaussian geminal basis sets correl. energy calc. 78−78629
BH_2, potential energy surface, DIM method 79−18110
BH_3, variationally deorthogonalised localised molecular orbitals, electronic struct. 79−97968
BH_3-ethylene complex, semiorthogonalised orbitals, integral approx. scheme 80−83262
$B_2H_5^+$, FSGO ab initio calc. of geometry, CNDO/2 calc. 78−41943
B_2H_6, LMO population calc. method appl., from given SCF eigenvector matrix 80−14063
B_2H_6, localisation of MOs using density matrix formalism *(Russian)* 79−93911
B_2H_6, variationally deorthogonalised localised molecular orbitals, electronic struct. 79−97968
$B_nH_n^{2-}$, n=5-12, localised orbitals, bonding, PRDDO calcs. 78−13431
B_2O_3, bipyramidal struct., stability, ab initio SCF-MO calcs. 80−99446
$BaTiO_3$, photoelectron and optical spectra derived from self-consistent charge MO and band calcs. 80−96785
Be complexes, binding and orbital energies, biological systems ab initio calc. 80−102442
$Be^{2+}+H_2O$, mol. complex struct. and interaction energy, CI calc. 79−18133
BeF, A $^2\Pi$ state config., ab initio MO calcs. 80−95532
BeF_2^-, electron binding, extended basis SCF calc. 79−49944
BeH_2, potential energy surface, DIM method 79−18110
$Be^{2+}(H_2O)_n$, (n=1,2,3,4,6), FSGO-pair-pot. calcs. *(German)* 80−74277
Be(2^3P)+methane, reaction, ab initio MO calcs. 79−8431
$Br^{25+}+Br^{25+}$, correlation diagrams, inner-shell vacancy prod., characteristic X-rays 77−83503
BrF_2^-, $BrFCl^-$, $BrCl_2^-$, inert gas cpds., localised MOs and bonding nature 78−9061
$Br^-(H_2O)_n$, hydration energies, orientation, ab initio-LCAO SCF MO calcs. 80−27944
C-C bond length electron difference density depend., approx. HF calc. *(German)* 78−5127
C-C σ bonds, mag. suscept., refined variational calc. 77−68136
C-H bonds, mag. suscept., vector pot. variational calc. 77−68137
$C^{6+}+H(1s)$, low vel. cross-section, adiabatic mol. orbital basis 77−88553
C_2, pot. curves, binding and ionisation energies and config. variational cellular method 80−32597
C_2^{6+}, total SCF energy estimation from orbital energies 79−63908
$C_2B_{n-2}H_n$, n=5-12, localised orbitals, bonding, PRDDO calcs. 78−13431
CH bond dipole calcs. 80−69067
CH, one-centre integrals of semiempirical theories of valence, ab initio calcs. 80−102441
CH, photoionis. and photodissoc. near ionis. threshold, SCF MO CI and Steltjes imaging 78−58749
CH_3, CH_2 and CH deformation vibration group frequencies and MO electron densities, interaction force const. 80−87101
CH_3CO^+, ground-state, two-config. SCF wavefunction 77−46481
CH_2SiH_2, ab initio GO calc. 78−94187
$(CH_3)_2X$ molecules, perturbational MO anal., methyl rot. barriers, fragmentation mode 77−88386
C_3Li_4, structure calculations 78−5364
CN, radical, nonradiative transition rates, matrix isolated molecule 78−78740
CN^-, electron density distrib., SCF mol. orbitals calcs. 78−9058
C_2N_2, satellite struct. of electron spectra, CI and vibronic coupling, dynamical calc., equilib. geometry 80−53044
CO, $^1\Sigma^+$ state, ionisation pots., dissoc. energy, atoms-in-mol. calcs. 77−88410
CO adsorbed on Ni(001), orbital energy spectrum 78−2369
CO, electronic struct., binding energy and interatomic distance, SCF variational cellular calc. 80−9498
CO, Hartree-Fock-Slater calcs., using pseudopot. method 77−57859
CO, interaction with Cu (100), molecular orbital calc. 77−31898
CO, LCAO-Xα method calcs., comparison with Hartree Fock and MS Xα methods 80−95539

molecular orbitals calculations continued
CO, nonempirical PRDDO scheme and calcs. 80−37739
CO, numerical coupled Hartree-Fock parallel polarisability, partial wave SCF calc. 78−9079
CO, photoabsorption, photoionisation cross section, separated channel static exchange Stieltjes-Tchebycheff calc. 79−3502
CO photodesorption from metal, forming CO_2 79−52777
CO, pot. curve, variational cellular method, electronic struct. calcs. 80−54591
CO, pot. curves, binding and ionisation energies and config. variational cellular method 80−32597
CO, X-ray K-absorpt. spectra, vibr. fine struct., ab initio restricted HF calc. 78−86883
CO^+, ab initio pot. energy curves, full valence CI with minimal STO 79−72361
$CO+H^+$, ground state pot. energy surface, ab initio SCF calc., protonated equilib. geometry 80−83301
$CO+H^+$, vibr. excitation calc., close coupling and sudden approx. 80−78561
CO_2, $^1\Delta_u$ valence state, vertical energy level MC-CI wavefunction 79−45644
CO_2, elastic and inelastic electron scatt. differential cross section, obs. and calc., struct., binding energy 80−28110
CO_2 H^+, geom. struct., ab initio mol. orbital study 78−62939
CO_2, interaction with Cu (100), molecular orbital calc. 77−31898
CO_2, large angle elastic and inelastic electron scatt. differential cross section, exchange corrections 80−28111
CO_2, localised mol. orbitals, ab initio PRDDO SCF calc., isoelectronic struct. 78−25441
CO_2, nonempirical PRDDO scheme and calcs. 80−37739
CO_2^+, $^1\Pi_g$, mixed charact. state, vertical energy level MC-CI wavefunction 79−45644
$(CO_2)_2^-$, struct., stability, electron affinity of neutral dimer, Hartree Fock calc. 79−63912
CO_3^{2-}, localised mol. orbitals, ab initio PRDDO SCF calc., isoelectronic struct. 78−25441
CO_3^{2-}, molecular orbital anal., anisotropic X-ray emission obs. of components 80−18786
CaF_2:Np^{3+}(U^{3+}), cryst. field splittings, ab initio MO calcs. 77−20520
CdS:In, impurity resist., Matsubara-Toyozawa theory extension 80−80264
Cl-containing molecules, hybridisation, bonding orbitals effects 79−36510
Cl_2, Hartree-Fock-Slater calcs., using pseudopot. method 77−57859
ClCO radical, struct. and props. calcs. 80−74112
Cl_2CS, potential energy surfaces and equilibrium geometries for ground and excited states 79−45634
ClF_3, ESCA chemical shift, energy levels, SCC-MO calcs. 79−64045
ClF_4 radical, geom., ab initio MO calcs. 79−89610
ClF_n-, ClF_n^+-, ClF_n^--, inert gas cpds., n=1-6, localised MOs and bonding nature 78−9061
ClFCS, potential energy surfaces and equilibrium geometries for ground and excited states 79−45634
$ClF(ClF_2^-)(ClF_3)$, localised MO ab initio calc., Gaussian orbital ab initio calc. 80−14083
ClO_n^+, ClO_n and ClO_n^- (n=1 to 3), ab initio calcs., localised MO and nature of Cl-O bond 80−69070
ClOO radical, struct. and props. calcs. 80−74112
Co complex, O_2CoCl_4 and $O_2CoCl_4NH_3^{2-}$, struct. and bonding model, CNDO-UHF calcs. 80−95541
Co complexes, Co(III) mixed complexes, orbital angular momentum reduction, ^{59}Co NMR chemical shift 80−58137
$Co(CO)_3$, bond angles, hybrid bond orbital calcs. 78−94188
$CoCl_4^{2-}$, mol. orbital energy levels, semi-empirical calc. 77−3271
Cr^{3+} in octahedral fluoride lattice, optical spectrum open shell SCF MO cluster CI calc. 78−19501
$Cr(CO)_3$, bond angles, hybrid bond orbital calcs. 78−94188
$CrCl_4$, ligand field states, multiple scatt. Xalpha calcs. 80−47891
CrF_6^{3-}, CrF_6^{2-}, multiple scatt. calcs. methods, comparative study 79−6865
$Cr_2O_7^{2-}$ centre in lattice, optical props., mol. orbital calcs. 79−15491
$CrOCl_3$, electronic structure and valence ionisation energies, obs. by ab initio and SW-Xα methods 80−69073
Cs_2^+, $^2\Sigma$ and $^2\Pi$ state pot. energy curves, two-centre model 79−26906
CsI, self-trapped exciton electronic struct., semi-empirical mol. orbital method 80−49605
CsI:Na, electronic struct. and luminesc. 80−16080
$CsNpF_6$, cryst. field splittings for Np^{5+}, ab initio MO calcs. 77−20520
Cu, chemisorpt. of CO, N_2, NO, semiempirical calcs. 78−14611
Cu, cluster and bulk, struct. and electronic props. 78−95592
Cu-Co heterobinuclear complex, cryst., mag. susceptibility of Cu-Co(fsa)$_2$ en, $3H_2O$ 80−2556
Cu_2 contracted Gaussian-type orbital basis sets, test with and without outer orbital splitting 80−47872
Cu_2, Harris-Pohl selected valence electron split-shell MO calcs. 80−91439
$Cu(CN)_3^{2-}$, UV absorpt. spectra, electronic struct., MO calcs. *(French)* 77−34655
CuCO, linear, ab initio RHF-MO calcs., rel. to adsorption 79−26883
CuCl, electronic struct., ab initio HF SCF MO calcs. of $CuCl_4^{3-}$ cluster 78−95262
Cu(II)-nucleic acid base interaction, MO calcs. 79−10013
CuNi molecule, electronic states determ. by ab initio HF and CI methods 80−69087
CuO, ab initio HF-MC-SCF with GTO basis set, dissoc. energy and bond length 80−47890
$^{63}Cu_2$, $B^1\Sigma_u^+$-$X^1\Sigma_g^+$ transition, Franck-Condon factors, r-centroids and pot. curves 80−43114
D_2, semiempirical nonadiabatic pot. energy curves calcs. 78−17744
D_2^+, semiempirical nonadiabatic pot. energy curves calcs. 78−17744
F compounds, ground states, mol. parameters, MINDO calcs. 78−41955
F^- hydration, ab initio MO calcs., fractional charge model 77−34547
F_2, Compton scatt. profile, SCF MO theory calcs. 78−58577
F_2, MSXα calc., partial wave expansion, binding energy and orbital energy 80−37738
F_2, mag. shielding and susceptibility, finite perturbation mol. orbitals calcs. 77−46513
F_2, photoexcitation and ionisation cross sections, Stieltjes -Chebyshev static exchange calc. 80−53060
F_2, pot. curves, binding and ionisation energies and config. variational cellular method 80−32597
molecular orbitals calculations continued
FCN, CNF, isomer pairs, mol. orbitals calcs., using PLA and LEDO integral approx. methods 78−13418
FCO, radical, struct. and props. calcs. 80−74112
$FClO^+$, radical cation, struct. and electronic props., ab initio RHF SCF MO calc. 80−52883
FH-OH_2(dimethyl ether), H-bonded complexes, cubic force consts. calcs 80−47868
FH_2, pot. energy surface, valence states, VB diatomics-in-mols. method 79−85920
FH_2^+, reactive processes, ab initio MCSCF-CI and diatomics in mols. calc. 78−56881
F $(H_2O)n(n=1,2)$, FSGO-pair-pot. calcs. *(German)* 80−74278
FNO, electronic transitions, limited GSMO and ESMO CI calcs., oscillator strengths, spectra 78−70750
F_2O_2, geometry, SCF CI calcs. 78−55126
FOO radical, struct. and props. calcs. 80−74112
FSO (FOS), struct. and props., SCF calcs. 80−106260
FSS, struct. and props., SCF calcs. 80−106260
Fe complex, Fe (alkyldithiocarbamate)$_2$X, X=Cl, I, mol. orbital calc., hyperfine fields, elec. field gradient 80−39981
Fe halides, electronic charge and spin distrib. from interpretation of hyperfine interactions 79−60776
Fe^{2+} and Fe^{3+} hydrate clusters, aq. electron exchange reaction, ab initio RHF MO calc. of inner shell reorganisations, vibr. freq. 80−102564
Fe-O compounds, MO cluster calc. of charge densities and elec. field gradients 77−76783
$Fe(CO)_3$, bond angles, hybrid bond orbital calcs. 78−94188
GaAs (110) face, adsorption of one Cs atom, mol. orbital study *(French)* 78−38958
$GeBr_4$, electronic struct., Xα SW calcs. 80−102447
GeF_4, electronic struct., Xα SW calcs. 80−102447
GeH_3 , electronic struct., electron affinity, inversion barrier, ab initio SCF Gaussian basis calc. 80−63552
Ge_2H_6, valence electronic struct., model pot. in floating spherical GO formalism 78−74563
GeO, mol., VUV photoelectron spectra, $X^2\Sigma^+$ state 79−72358
(H,H) system, 1 s σ orbital, variational calc. 78−37707
H, chemisorbed on Be(0001), mol. cluster theory 79−15002
H-bonded complex, PCILO method 79−10036
H-bonded dimers involving H_2O, HF and NH_3, PCILO study 79−72238
H-like ion, elec. multipole polarisability, relativistic corrections, shielding factors, Dirac eqn. 78−13441
$H+H^+$, low energy, optimised translation factors 80−18813
H^++H_2, elastic scatt. and rot. excitation, multistate semiclassical orbital method 79−27058
H_2, $^1\pi_u$ and $^3\pi_u$ states, singlet-triplet energy difference, Hund's rule, inequality formulation 78−66482
H_2, $^3\Sigma_u^+$, Schrodinger eqn., random walk soln., electron spin effects 77−18780
H_2, AMO method at small internucl. distances 79−6838
H_2, atoms-in-molecules theory, non-Hermitian formulation 80−9517
H_2, chemisorption on defect MgO surface, quantum mechanical approach 77−62761
H_2, Compton profile, correl. Gaussian wave function calc. 79−81241
H_2, diatomic transition operators, L^2 basis expansions $^1\Sigma$ and $^3\Sigma$ state pots. 80−63519
H_2, electron correl. as rot. polarisation, Heitler-London-Rosen calc. for teachers 80−4492
H_2, electron elastic low energy scatt., ab initio pseudostates calc. 78−9247
H_2, expressions for calc. Coulomb repulsion between electrons using adiabatic basis 80−91427
H_2, Λ doubling, $C^1\Pi_u$ states, calc. methods 78−90227
H_2, mag. field depend. orbitals for mag. screening and susceptibility of mol. 78−78611
H_2, mag. susceptibility vector pot. variational method, gradient transform. function selection 80−69258
H_2 mol., Green's function Σ perturbation method for mol. calcs. 78−55123
H_2, mol. ion, Burrau approx., series solns. 77−30763
H_2, nonempirical calc. for molecules in electric field 78−25459
H_2, octapole magnetisability, multiple SCF perturbation calc. with STO basis set 77−34550
H_2, one-electron properties, basis set contraction effects 77−88383
H_2, photoionisation Born-Oppenheimer Hamiltonian, resolvent matrix elements complex coord. calc. 80−52878
H_2, pot. curves, binding and ionisation energies and config. variational cellular method 80−32597
H_2, STP basis sets, energies calc. 77−3262
H_2, semiempirical nonadiabatic pot. energy curves calcs. 78−17744
H_2, shielded diatomic orbital method, two-interacting state system 78−5121
H_2^-, free free absorpt. coeffs. dipole length formulation and two centre close coupling calc. 80−83345
H_2^+ bonding, simplest MO approx. 77−30948
H_2^+, coupled-channel Schrodinger eqn. bound states, renormalised Numerov method 79−13627
H_2^+, dynamic polarisability, electronic states two centre Coulombic Green's function, continuous spectrum exclusion 78−82626
H_2^+, exponentially small part of wave function *(Russian)* 80−9497
H_2^+, floating orbital calc. of elec. field gradient, quadrupole coupling const. 77−12248
H_2^+, high (10^9 G) mag. fields, dissoc. energy, electron binding energy and equilib. separation 80−52910
H_2^+, individual orbital contribs. to SCF virial 79−3349
H_2^+, mol. energy in strong magnetic field, MO SCF calcs. 79−6858
H_2^+, multiple scattering technique, space partitioning effects 79−85883
H_2^+, natural orbital anal. of nonadiabatic wave functions 79−81151
H_2^+, one-electron wavefunction calcs., expectation values 77−83483
H_2^+, reson. states, complex basis functions methods 79−6887
H_2^+, semiclassical quantisation for low lying electronic states 79−68183
H_2^+, semiempirical nonadiabatic pot. energy curves calcs. 78−17744
H_2^+, Temple lower bound mol. orbitals, GTO calcs. 78−41935
H_3, generalised diatomics-in-mols. theory 79−97970
H_3, quartet states, diatomics-in-molecules theory, diatomic states mixing and overlap 79−59344
H_3, relative magnitudes of direct and indirect exchange, Heitler-London calcs. 80−69069
H_3, spin-optimised SCF general spin orbitals calcs. 78−5125

molecular orbitals calculations continued
H_3^+, D_{3h} $^1A_1'$, Schrodinger eqn., random walk soln., electron spin effects 77−18780
H_3^{2+}, Temple lower bound mol. orbitals, GTO calcs. 78−41935
H_4, $^1\Sigma_g^+$, Schrodinger eqn., random walk soln., electron spin effects 77−18780
H_4 excimer, electronic and geom. struct., ab initio CI calc. 79−76348
H_4 square, $^1B_{1g}$ and $^1B_{2g}$ states, Schrodinger eqn. solved by random walk method 79−63925
H_n^+ (n=3,5,7,9,11), stability, struct., ab initio MO calcs. 78−74810
HCN, CNH, isomer pairs, mol. orbitals calcs., using PLA and LEDO integral approx. methods 78−13418
HCN, HNC, molecular electronic struct., unlinked cluster effects 78−94185
HCN, ionis. by mol. orbital method, many-body calc. 79−36512
HCN, orbital calculation, SCF+CI method 79−93928
HCN, semi-empirical excited state Morokuma's EHP calc., geometry and order of states 78−46256
HCN, valence shell correl. energies, pair correls., unlinked cluster effects, CPA calc. 79−13648
HCN-CO complex, charge transfer theory, Mulliken population, ab initio calc., multiconfiguration scheme 80−106392
HCO_2^+, geom. struct., ab initio mol. orbital study 78−62939
H_2COLi^+, geom. and electronic struct., ab initio SCF calc. 79−76331
H_2CS, potential energy surfaces and equilibrium geometries for ground and excited states 79−45634
HCl, mol. cryst., angles of H-bonded mols., ab initio calcs. 78−6037
HCl, nonempirical calc. of X-ray K-absorpt. spectra 77−88465
HCl, second order mag. props., coupled Hartree-Fock perturbation theory 80−87042
HCl^+, effective Hamiltonian, ab initio calc. 79−45632
HD, nuclear spin-spin coupling const., perturbed at. orbitals calc. *(French)* 77−27095
$H_2(D_2)$, Compton profile, impulse approx., electron correl., vibr. and rot. effects 78−17585
HF, ab initio HF-STO perturbation Auger transition rate calc. 79−72368
HF, Auger spectra, correl. effects, energies and wavefunctions, ab initio CI calc. 80−14125
HF, cluster and chain dipole moments, ab initio calc. 77−26967
HF, energy quantities from localised charge densities, dependence on geometry and basis set 80−63525
HF H-bonded dimers, PCILO calc., energies, geometries 78−37557
HF, liquid, struct. and props., intermol. pot. function calcs., basis set depend. 79−82134
HF, mag. field depend. orbitals for mag. screening and susceptibility of mol. 78−78611
HF, mag. shielding and susceptibility, ab initio finite perturbation calcs. using GIAOs 77−6670
HF, NMR shielding consts. and mag. susceptibilities, coupled HF with extended GTO basis 80−5480
HF, nonempirical calc. of X-ray K-absorpt. spectra 77−88465
HF, numerical coupled Hartree-Fock parallel polarisability, partial wave SCF calc. 78−9079
HF, one-dimens. cryst., ground state energy PCILOCC method 79−10056
HF, orbital relax. energy for single and double ionis. from valence shells 80−106253
HF, orbitals calcs. using modified Adams-Gilbert eqn. 77−34542
HF, STP basis sets, energies calc. 77−3262
HF, variation-perturbation minimal Gaussian geminal basis sets correl. energy calc. 78−78629
HF, $X^2\Sigma^+$ state, 3- and 4-body perturbation theory modified pots. 77−88376
HF-cyclic ethers H-bonded complexes, calorimetry, IR spectra and MO calcs. 79−52738
HF_2^-, mag. shielding and susceptibility, finite perturbation mol. orbitals calcs. 77−46513
$(HF)_n$, n=1-∞, ab initio hydrogen bond and electronic parameters, phonons 77−14342
HFCS, potential energy surfaces and equilibrium geometries for ground and excited states 79−45634
$H_2(H_2^+)$ and isotopes, expectation values, Born-Oppenheimer, adiabatic and non-adiabatic results 78−82624
$H_2(H_2^+)$, path integral formalism of perturbation theory, simple mols. and atoms 79−6841
$H_2(HD)(D_2)$, ab initio pot. energy curves and vibr. levels, B″, B̄, B′ states 77−6754
H_3N-BH_3, cryst., electronic struct., ab initio, MO calcs., fractional charge model 77−34547
HNC⇌HCN, transition state determination and characterisation ab initio calcs. 77−28975
HNC, valence shell correl. energies, pair correls., unlinked cluster effects, CPA calc. 79−13648
HNO, CI-SCF-MO basis function calc. 77−42246
HNO^+, ab initio pot. surface, and isomerisation barrier of lowest states 79−22622
HO_2, pot. energy surface for $H+O_2 \rightarrow HO_2^* \rightarrow OH+O$ reaction, MC SCF CI method 79−74353
HO_2, struct. and props., SCF calcs. 80−106260
HO_2^+, ab initio calc. of three lowest states 78−62711
H_2O, 1s shake-up spectrum, ab initio equiv. cores, improved virtual orbital and CI calcs. 77−46597
H_2O, bond dissociation, MCSCF LMO calcs. 77−57886
H_2O, bonding electron pairs, size and shape parameters, Gaussian basis set MO calcs. 80−27935
H_2O, double hole states POCI calc., Auger spectrum 78−78630
H_2O, electron affinity, mol. geom. effects calcs. 78−82618
H_2O, energy quantities from localised charge densities, dependence on geometry and basis set 80−63525
H_2O, excited states, pot. energy curves w.r.t. bond ang., one-centre expansion approx. 79−6886
H_2O, geom. and electronic struct., ab initio SCF calc. 79−76331
H_2O H-bonded dimers, PCILO calc., energies, geometries 78−37557
H_2O, iterative natural orbitals for CI using perturbation theory 77−79549
H_2O, iterative natural orbital procedures, convergence props. 78−46257
H_2O, many body perturbation theory fourth order calc. of correl. energy 80−14087
H_2O, mol., Compton profile, directional, polarisation functions 79−36706
molecular orbitals calculations continued
H_2O, mol. Rydberg S←S and S←T transitions, semi-empirical SCF MO calc. 80−91453
H_2O, orbital relax. energy for single and double ionis. from valence shells 80−106253
H_2O, orbitals calcs. using modified Adams-Gilbert eqn. 77−34542
H_2O, photoionis. cross section by atomic extrapolation method 79−81242
H_2O, pseudopotential calculations, parameter fitting scheme appls. 78−41928
H_2O, SCF calcs. using cusped Gaussian basis sets, polarisation effects 80−74118
H_2O, separated electron pair theory, numerical calcs. 80−87049
H_2O, shape, electrostatic force study with floating wavefunction 78−37545
H_2O, sum rule props., SCF optimizations of MO and VB calcs. 78−5156
H_2O, variationally deorthogonalised localised molecular orbitals, electronic struct. 79−97968
H_2O^-, electron affinity, mol. geom. effects calcs. 78−82618
H_2O^+, ab initio potential energy surface study by CI techniques, equilibrium conform. determ., mol. dissoc. pathways 80−78550
H_2O^+, X^2B_1 and B^2B_2 states, pot. surfaces, SCF and CI calcs. 77−3338
H_2O_2, internal rotation barriers, exchange energy and orbital orthogonality effects 77−75049
H_4O_2, intermolecular interaction energy, PCILO calc. 77−34572
HOCl, ab initio MRD CI calc., electronic spectrum, dissoc., heat of reaction, formation 78−21857
$H_3O^+(H_2O)_n$, H^+ motion energetics, ab initio calcs. 78−25413
$HOO(H_2O)$, electronic struct., and config., semiempirical UHF INDOC calc. 79−59356
$H_2O.H_2O$ and H_2O.Ne, excited, first order interaction energy, ab initio calc. 80−32598
H_2PNH_2, inversion-rot. mechanism, basis set and geometry optimisation effects 80−83273
HS_2, rotamers, electronic and geometrical structs., ab initio floating GO basis calcs. 78−74572
H_2S, double hole states POCI calc., Auger spectrum 78−78630
H_2S, excitation energy, one-centre approx. calcs 78−70737
H_2S, mol. polarisability and derivatives, ab initio SCF CI calc. 79−59597
H_2S, pseudopotential calculations, parameter fitting scheme appls. 78−41928
H_2S, second order mag. props., coupled Hartree-Fock perturbation theory 80−87042
H_2S, valence electron ionisation and momentum distribs. 80−28107
HSS, struct. and props., SCF calcs. 80−106260
H′+XH→H′X+X, X=H, F, Cl,CH_3, collinear pot. energy barriers, PNO-CEPA calcs. 77−32777
He pair, dispersion interaction, independent particle model, polarisabilities 80−37732
He+CO, nuclear mag. shielding consts., interaction geometry depend., chemical shift, gauge invariant method 78−62866
He+Ne collisions, MO calcs. for excitation processes 78−25676
He^{2+}+H, electron transfer, 0.1-20 keV, mol. orbital calc., convergence 78−42210
He_2, pair polarisability correl. effects, SCF-CI-GTO-SO calc. 78−82651
He_2, pot. curve using CEPA-PNO correl. wavefunction 79−63932
He_2, short range interactions between two rare gas atoms 79−26888
HeH^+, excited states, variable screening models, natural spin orbital analysis of wave functions 80−37747
HeH^+, Temple lower bound mol. orbitals, GTO calcs. 78−41935
$He_2^+ X^2\Sigma_u^+$ state, ab initio CI calc., pot. energy curve, vibr. and rot. levels 77−3263
$(^{3,4}He)_3$ molecular bound state, variational and exact studies 77−27214
HfH_4, Dirac-Fock one-centre calcs. 77−88380
Hg_2-Pt, ^{199}Hg Mossbauer meas., isomer shift and quadrupole splitting calcs. 80−28039
$HgBr_2$, electronic struct. and photodissoc., effective core pots. and POL(1) CI wave function 80−63560
$HgCl_2$, electronic struct. and photodissoc., effective core pots. and POL(1) CI wave function 80−63560
Hg_2F_2, ^{199}Hg Mossbauer meas., isomer shift and quadrupole splitting calcs. 80−28039
I-containing molecules, geom. struct. and dipole moments, CNDO/2 calc. 79−94103
$I^{25+}+Te^{24+}$, $I^{43+}+Au^{69+}$, $I^{25+}+Au^{51+}$, correlation diagrams, inner-shell vacancy prod., characteristic X-rays 77−83503
I_2, Phillips-Kleinmann pot. derivation, pseudopot. for ground state orbitals bond length, vibr. freq. 77−65418
K_2^+, $^2\Sigma$ and $^2\Pi$ state pot. energy curves, two-centre model 79−26906
K_2^{+}, Simons-type pseudopots. calcs. 78−5120
KCl:Tl, energy level scheme, mol. orbital model 80−10912
KF, ab initio SCF MO energy, dipole moment and polarisability 80−1085
K_2NaGaF_6:Cr^{3+}, magneto-optical study of $^2T_{1g}$, $^4T_{2g}$, ^2E_g-$^4A_{2g}$ transitions 80−71384
$KNiF_3$, electronic struct. and spectrum of NiF_6^{4-} complexes, scattered wave method calc. 77−15807
KOH, MHD plasma mol., pot. energy curves and dipole moment, bond lengths 78−71462
$KrAr^+$, quasimolecule Auger spectra 79−68269
$Kr_2Cl(F)$, ab initio diatomics in mols. pot. surface, spin-orbit coupling 79−3519
KrF^+, selected valence-electron split-shell MO calc., ground state props. 79−22585
Li clusters, dissociative chemisorption of H_2, ab initio SCF-MO calcs. 79−77918
Li complexes $((C_2H_2X_2)_2Li)^n$ where X=S, O, binding and orbital energies, biological systems ab initio calc. 80−102442
Li^+ hydration, ab initio MO calcs., fractional charge model 77−34547
Li^+-H_2O complex, charge transfer theory, Mulliken population, ab initio calc., multiconfiguration scheme 80−106392
Li^++H_2, elastic scatt. and rot. excitation, multistate semiclassical orbital method 79−27058
Li_2, and anion, electronic struct., spin-unrestricted, spin-restricted SCF HF calc. 78−90331
Li_2, and isotopic variants, low-lying X-B transition freq. calc. 78−90180
Li_2, MCSF accurate pot. energy curves for $^3\Sigma_u^+$ and $b^3\Sigma_g^+$ states, level crossing 77−50369
Li_2, total SCF energy estimation from orbital energies 79−63908

molecular orbitals calculations continued
Li_2^+, $^2\Sigma$ and $^2\Pi$ state pot. energy curves, two-centre model 79−26906
Li_2^+, Simons-type pseudopots. calcs. 78−5120
Li_{2n}, (n=1, 2, 3), stable cluster configs., ionisation pots., binding energies, vibr. freqs., al initio SCF and CEPA calcs. 80−14265
Li_3, potential energy surface and config., RHF CI calc. 77−34562
Li_n, at. cluster with H_2O mol. attached, MO study 79−76541
$LiAlF_4$, struct. pot. energy surface, Li^+ migration, ab initio LCAO SCF calcs. 80−23305
$LiBeF_3$, pot. energy surface, struct., stability and internuclear distances, ab initio calc. 80−58147
LiCN, electron density distrib., SCF mol. orbitals calcs. 78−9058
LiCl:Cu^+, luminescent centre, cluster MO calculation of energy levels 78−64411
Li_2Cl^+, mass spectra, struct., stability, expt. and theory 77−554
Li_2Cl^+, triplet polarisability, ab initio MO calc. 79−98244
LiF (001), adsorption of H_2, molecular orbital calc. 78−87878
LiF, ab initio SCF MO energy, dipole moment and polarisability 80−1085
LiF-NH_2 adduct, mol. consts., ab initio SCF LCAO MO calcs. *(French)* 78−13423
Li_2F^+, mass spectra, struct., stability, expt. and theory 77−554
LiH, adsorption of H_2, on (100 surface), FSGO calcs. *(German)* 79−33196
LiH, dipole moments and transition moments, semi-rigorous bounds, error limits 78−78635
LiH, direct optimisation of orbitals for multiconfiguration self-consistent field theory by unitary transformations 80−63544
LiH, iterative natural orbitals for CI using perturbation theory 77−79549
LiH, many body perturbation theory fourth order calc. of correl. energy 80−14087
LiH, NMR shielding consts. and mag. susceptibilities, coupled HF with extended GTO basis 80−5480
LiH, numerical calc. of one-electron props. from SCF-Xα-SW calcs. 77−6688
LiH, SCF calcs., undergraduate exercise 80−82597
LiH, STP basis sets, energies calc. 77−3262
LiH, variation-perturbation minimal Gaussian geminal basis sets correl. energy calc. 78−78629
LiH, variational Hylleraas-type wavefunction, correl. 78−9082
Li_2H, natural orbital contour diagrams and occupation nos. for form. and dissoc. 79−18107
$Li^+(H_2O)_n$, (n=1,2,3,4,6), FSGO-pair-pot. calcs. *(German)* 80−74277
LiNa, and anion, electronic struct., spin-unrestricted, spin-restricted SCF HF calc. 78−90331
LiOH, geom. and electronic struct., ab initio SCF calc. 79−76331
LiOH, potential energy surface, diatomics-in-molecule method 79−63929
$Mg^{2+}(H_2O)n$ (n=1,2,4,6), FSGO-pair-pot. calcs. *(German)* 80−74278
$Mn(CO)_3$, bond angles, hybrid bond orbital calcs. 78−94188
MnO_4^-, valence mol. orbital energy, nonempirical pseudopot. 79−22592
MnO_4^{m-}, chromophore, tetrahedral, electronic spectra 77−58032
$Mo_6Cl_{14}^{2-}$, cluster ground state electronic struct. SCF Xα SW calc. 79−3607
MoS_2, struct., XES and XPS obs. 80−43105
N_2, 400 eV core-excited valence states, limited CI calc., transition energies and oscillator strengths 79−68196
N_2, ab initio MO-LCAO-SCF and Gordon-Kim intermolecular pot. for seven different orientations 80−95522
N_2, core-ionised, core-valence excited and shake-up states, all electron MRD CI calc. 78−21858
N_2, elastic and inelastic electron scatt. differential cross section, obs. and calc., struct., binding energy 80−28109
N_2, electron elastic low energy scatt., ab initio pseudostates calc. 78−9247
N_2, electron scattering, 13.6 eV, coupled channel treatment calcs. 79−64106
N_2, electronic struct., binding energy and interatomic distance, SCF variational cellular calc. 80−9498
N_2, energy band calc. by linear combination of muffin tin orbitals method 77−4283
N_2, large angle elastic and inelastic electron scatt. differential cross section, exchange corrections 80−28111
N_2, MRD CI calc., lowest dissoc. limits 78−21859
N_2, MSXα calc., partial wave expansion, binding energy and orbital energy 80−37738
N_2, nonempirical calc. for molecules in electric field 78−25459
N_2, one-electron properties, basis set contraction effects 77−88383
N_2, pot. curves, binding and ionisation energies and config. variational cellular method 80−32597
N_2 SCF calcs. using cusped Gaussian basis sets, polarisation effects 80−74118
N_2, vertical electronic spectrum, MRD-CI method calcs. 78−42033
N_2, X-ray K-absorpt. spectra, vibr. fine struct., ab initio restricted HF calc. 78−86883
N_2^+, localised treatment of hole states 79−54765
N_3^-, theoret. electron density distrib. cf. expt. density distribs. of NaN_3 and KN_3 77−46489
NCO^+, CI-SCF-MO basis function calc. 77−42246
NF_3, mol. orbital calcs. core-valence approx. scheme 80−42927
NH_2, pot. energy curves of X^2B_1, A^2A_1, $^2B_2$ valence-shell and $\pi_u{}^2$3s-type Rydberg states calc. by CI 80−74138
NH_2^-, mol. geom., diffuse functions in SCF calcs. 79−10226
NH_3, 35 keV electron elastic differential cross section, bond formation, independent atom model 79−31683
NH_3 bond dissociation, MCSCF LMO calcs. 77−57886
NH_3, bonding electron pairs, size and shape parameters, Gaussian basis set MO calcs. 80−27935
NH_3, energy quantities from localised charge densities, dependence on geometry and basis set 80−63525
NH_3 H-bonded dimers, PCILO calc., energies, geometries 78−37557
NH_3, LMO population calc. method appl., from given SCF eigenvector matrix 80−14063
NH_3, lowest triplet state geometry, SCF and CEPA-PNO calc. 80−914
NH_3, mol. Rydberg S←S and S←T transitions, semi-empirical SCF MO calc. 80−91453
NH_3, orbital relax. energy for single and double ionis. from valence shells 80−106253
N_2H_2, variationally deorthogonalised localised molecular orbitals, electronic struct. 79−97968

molecular orbitals calculations continued
NH_4F, cryst. struct., mol. wavefunction calcs. of struct. factors 77−62507
$NH_2(F_2)(Cl_2)$, SCF-MO-HF calc., struct. and one-electron props., population anal. indices 79−76338
$N_2H_2(N_2D_2)$, ground and first excited state small vibr. coupling, ab initio CI calc. 78−62791
NH(NF)(NCl), effective spin-spin parameter and singlet-triplet transition intensities, ab initio calc. 78−9067
NH_2T, β-decay, ab initio SCF MO calcs. 77−71842
$(NO_2)_2$, struct. and force fields of isomers, ab initio calcs. 77−18783
N_2O_4, ionis. by mol. orbital method, many-body calc. 79−36512
NOH, groundstate electronic struct., MRD CI calc., dissoc. energy, isomerisation energy 80−14088
NOH^+, ab initio pot. surface, and isomerisation barrier of lowest states 79−22622
$N_3P_3Cl_6$, ionisation energy and electronic struct., UV photoelectron spectra and Xα calcs. 78−94281
Na, chemisorption of halogens, surface chemiluminesc., MO description 79−43048
Na_2, and anion, electronic struct., spin-unrestricted, spin-restricted SCF HF calc. 78−90331
Na_2^+, $^2\Sigma$ and $^2\Pi$ state pot. energy curves, two-centre model 79−26906
Na_2^+ Simons-type pseudopots. calcs. 78−5120
Na_2Cl^+, mass spectra, struct., stability, expt. and theory 77−554
Na_2F^+, mass spectra, struct., stability, expt. and theory 77−554
$Na^+(H_2O)n$ (n=1,2,4,6), FSGO-pair-pot. calcs. *(German)* 80−74278
NaNCO, val. band electronic struct., XPS meas., MOC and INDO calc. 80−95520
Nb+Nb, X-ray ang. distrib., 35-75 MeV 2 pΣ MO calc. 79−76380
NbC, chemical bonding and X-ray emission spectral analysis 77−44088
NbN, chemical bonding and X-ray emission spectral analysis 77−44088
NbO chemical bonding and X-ray emission spectral analysis 77−44088
NbO_2, rutile phase, energy levels, momentum density, and Compton profile, embedded cluster model 80−50453
Ne+HeH^+, collinear reaction, pot. energy surface SCF-LCAO-MO and DIM calc. 78−92467
Ne+Ne, distorted frozen-orbital method for diabatic mol. orbitals 78−41936
Ne+Ne^+, 2s vacancy prod., coupling state calcs. in mol. basis 79−13806
Ne_2, excited state pots., fast calc. 80−9490
Ne_2, short range interactions between two rare gas atoms 79−26888
Ne_2F, ab initio diatomics in mols. pot. surface, spin-orbit coupling 79−3519
NeH_2^+, ab initio potential surfaces, frozen orbital approximation calcs. 78−41927
Ni, chemisorpt. of CO, N_2, NO, semiempirical calcs. 78−14611
Ni_2, extended basis set LCAO Xalpha treatment 80−95537
Ni_2, Hartree-Fock-Slater calcs., using pseudopot. method 77−57859
NiCO, linear, ab initio RHF-MO calcs., rel. to adsorption 79−26883
$Ni(CO)_4$, valence orbital energies, pseudopot. calcs. 78−37546
NiF_2, ESCA, charge transfer satellite struct., hole state localisation intensity depend., MS-MO calc. 77−66139
NiH, extended basis set LCAO Xalpha treatment 80−95537
$Ni(Ni)_2$-ethylene cluster complex 78−82641
NiO, bulk props., initial state MO Ni_4O_4 and $Ni_{13}O_{14}$, cluster model, lattice and force consts., photoemission and CT absorpt. spectra 80−84828
O_2, $^3\Sigma_g^-$ ground state, pot. energy curve, direct CI method appl. 80−58165
O_2, $^3\Sigma_u^-$-$^3\Sigma_u^+$ spin-orbit mixing in Schumann-Runge predissoc. 77−6875
O_2, effective spin-spin parameter, ab initio calc. 78−9067
O_2, harmonic oscillator model in predissoc., level widths, shifts and curve crossing 78−90239
O_2, MSXα calc., partial wave expansion, binding energy and orbital energy 80−37738
O_2, multiconfig. Hartree-Fock calcs. convergency 80−47901
O_2, nonempirical calc. for molecules in electric field 78−25459
O_2, photoexcitation and photoionisation cross sections, HF Gaussian method 80−53064
O_2^+, $A^2\Pi_u$ state pot. energy curve, MCSCF calcs. 80−63565
O_2^+, $^4\Pi$ states, spin-spin coupling consts., ab initio calc. 79−97981
O_3, approximate spin extended HF calcs., singlet and triplet states 78−78621
O_3, localised natural orbitals 77−83482
O_3, wave function calc. rel. to energy separation, cyclic and open isomers 79−93929
O_5^{2-}, hypothetical, mol. self-consistent study, possible prep. method *(French)* 80−91717
OCl_2^+, radical cation, struct. and electronic props., ab initio RHF SCF MO calc. 80−52883
OF_2, photoelectron spectra, ionisation energies, ab initio many-body Green's function calc. 79−89709
OH+H_2, pot. energy surface, barrier heights and transition state geometry, POL-CI calc. 80−55649
O_3H^+, isomeric structs. ab initio MO calcs. 80−83270
OHT, β-decay, ab initio SCF MO calcs. 77−71842
ONCN, IR spectra isotope shifts and ab initio calc. for harmonic force field 79−13715
$Os_6(CO)_{18}$, electronic struct., metal cluster carbonyls mol. orbital description obs. 80−63879
PCl_3, mol. orbital calcs. core-valence approx. scheme 80−42927
PF_5, ESCA chemical shift, energy levels, SCC-MO calcs. 79−64045
PH_3, core-excited states, valence-Rydberg mixing and term values, XUV spectra and CI calc. 79−76444
PH_3, excitation energy, one-centre approx. calcs 78−70737
PH_3, NMR shielding consts. and mag. susceptibilities, coupled HF with extended GTO basis 80−5480
PH_3, second order mag. props., coupled Hartree-Fock perturbation theory 80−87042
$PH_2(F_2)(Cl_2)$, SCF-MO-HF calc., struct. and one-electron props., population anal. indices 79−76338
PH(PF), effective spin-spin parameter and singlet-triplet transition intensities, ab initio calc. 78−9067
PN($X^1\Sigma^+$), VUV photoelectron spectrum 78−1024
$P_2(X^1\Sigma_g^+)$, He I photoelectron spectrum, ab initio and semiempirical calcs. 77−34691
PbS, relativistic electronic mol. struct., calcs. 79−761
PbSe, relativistic electronic mol. struct., calcs. 79−761

molecular orbitals calculations continued
Pd, chemisorpt. of CO, N_2, NO, semiempirical calcs. 78−14611
$Pd(CO)_4$, valence orbital energies, pseudopot. calcs. 78−37546
$Pd(CO_4)_4$, valence mol. orbital energy, nonempirical pseudopot. 79−22592
Pt complexes, X-ray absorpt. spectra, mol. orbital interpretation 78−42097
$Pt(CO)_4$, valence orbital energies, pseudopot. calcs. 78−37546
Pt(O)-Pt(O) dimers, bounding in a d^{10}-d^{10} system 78−74579
Rb_2^+, $^2\Sigma$ and $^2\Pi$ state pot. energy curves, two-centre model 79−26906
$Re_3Cl_{12}^{3-}$, cluster ground state electronic struct. SCF Xα SW calc. 79−3607
Re_3Cl_9, cluster ground state electronic struct. SCF Xα SW calc. 79−3607
$Rh_2Cl_2(CO)_4$, non-empirical pseudopot., PSIBMOL algorithm 79−76335
Ru complex, HF calc., electron densities and Mossbauer isomer shift, chemical binding 78−50470
S_2, effective spin-spin parameter, ab initio calc. 78−9067
S_8, cyclic, electron deformation density distrib., SCF-Xalpha-scatt. wave method 78−33425
SF_2, photoelectron spectra, ionisation energies, ab initio many-body Green's function calc. 79−89709
SF_4, ESCA chemical shift, energy levels, SCC-MO calcs. 79−64045
SF_6, ab initio electronic struct., and photoelectron spectral assignment 79−54764
$(SN)_x$, mol. cluster and band struct. calc. 77−8004
S_2N_2, $(SN)_x$, (x=2 or 3), minimal STO-3G basis HF ab initio LCAO SCF MOC, geometry 78−903
S_4N_4, electronic struct. calc. using free-electron orbitals basis set 77−79537
SO, iow lying bound mol. electronic states, SCFCI calc. 80−23314
SO_2, double hole states POCI calc., Auger spectrum 78−78630
SO_2, effective spin-spin parameter and singlet-triplet transition intensities, ab initio calc. 78−9067
SO_2, ground state, ab initio and MOD POT calcs. 78−66466
Sb trihalides, non-empirical valence electron MO calcs., ion states spin-orbit splitting 77−34544
ScH_3, valence mol. orbital energy, nonempirical pseudopot. 79−22592
$SeCl_2$, photoelectron spectra 80−69186
Se_2Cl_2, photoelectron spectra 80−69186
Si_2, charge density and pseudo charge density, pseudopot. and SCF calcs. 78−70740
$SiBr_4$, electronic struct., Xα SW calcs. 80−102447
SiF_4, electronic struct., Xα SW calcs. 80−102447
SiH_4, core-excited states, valence-Rydberg mixing and term values, XUV spectra and CI calc. 79−76444
SiH_4, excitation energy, one-centre approx. calcs 78−70737
SiH_4, SCF calcs. including polaris. functions 80−87034
SiH_4, second order mag. props., coupled Hartree-Fock perturbation theory 80−87042
SiH_4, vertical excited states, CI calcs. 79−18127
Si_2H_4, Si-Si double bond, ab initio GO calc. 78−94187
Si_2H_6, valence electronic struct., model pot. in floating spherical GO formalism 78−74563
Si_nH_{2n+2}, silane, SCF Xα MO calc., appl. to amorphous hydrogenated Si 80−49580
SiH_3Br, mol. ionis. and excitation energy, Xalpha calc. 79−41105
SiH_3Cl, mol. ionis. and excitation energy, Xalpha calc. 79−41105
SiH_3F, mol. ionis. and excitation energy, Xalpha calc. 79−41105
SiH_3F, total energy, MOs nonempirical minimum STO-4LGF calcs. 78−9074
SiH_3I, mol. ionis. and excitation energy, Xalpha calc. 79−41105
$(SiH_3)_3N$, SCF calcs. including polaris. functions 80−87034
SiH_3NCO, geometric struct., ab initio MO calc. 79−13834
SiH_3NH_2, total energy, MOs nonempirical minimum STO-4LGF calcs. 78−9074
Si_2H_6O, geom. and electronic struct., ab initio MO calc. 79−97972
SiH_3OH, total energy, MOs nonempirical minimum STO-4LGF calcs. 78−9074
SiO, valence ionis. energy, calc. including correl. effects 79−68185
SiO^+, vac. UV photoelectron spectra, ab initio mol. orbital and Xα calcs., $(X^1\Sigma^+)$ state 78−46395
SiO_2, g-tensor of interstitial O and broken Si-O bond, MO model calc. 79−78520
Sn tetrahalides, non-empirical valence electron MO calcs., ion states spin-orbit splitting 77−34544
SnF_2, valence bands, electronic struct., UPS 78−39656
TaO_6^{7-}, octahedral cluster, ionisation energies and atomic populations, XPS and SCFMS Xα calc. 79−93923
Te_4^{2+}, pseudopot. SCF-MO calcs., spectrum assignments 80−83269
$ThF_4(Cl_4)$, electronic struct., MS-SCF-Xα calcs. and VUV photoelectron spectra 80−63710
ThO_2:Np^{4+}, cryst. field splittings, ab initio MO calcs. 77−20520
Ti:C, molecular cluster approach to electronic struct. and bonding mech. for impurity C 77−20270
TiC_x^{n-}, nonstoichiometric, ESCA spectra, MO LCAO calcs. 79−59513
$TiCl_4$, optical and Ti 2p core photoemission spectra, SCF Xα anal. 79−94032
TiH_4, Dirac-Fock one-centre calcs. 77−88380
TiH_3F, valence mol. orbital energy, nonempirical pseudopot. 79−22592
TiO_2, ESCA, charge transfer satellite struct., hole state localisation intensity depend., MS-MO calc. 77−66139
U compounds, equatorial bonds, MO calcs. 78−82621
$U^+ + U^+$, critical two-centre distance, HFS relativistic calc. 79−22801
UC, electronic struct., comparison with photoemission spectra 80−91450
UF_6, relativistic scattered wave calculations 80−63538
UF_6, UF_6^+, and UF_6^-, electronic struct., ab initio calcs. using relativistic core pots. 79−97987
UF_6, valence energy levels, SCF relativistic Xalpha calc. 79−85912
$UF_4(Cl_4)$, electronic struct., MS-SCF-Xα calcs. and VUV photoelectron spectra 80−63710
UN, electronic struct., comparison with photoemission spectra 80−91450
UO_2^+, valence energy levels, SCF relativistic Xalpha calc. 79−85912
UO_2^{2+}, electronic struct. theory, applied to solid phase $Cs_2UO_2Cl_4$ and $CsUO_2(NO_3)_3$ 79−73476
UO_2^{2+}, relativistic X_α scatt. wave calcs. 78−46268
$V(CN)_5NO^{1-}$, struct., FSGO calcs. 78−70736
$V(CN)_6NO^{4-}$, struct., FSGO calcs. 78−70736
VH, electronic struct. and X-ray emission spectra 77−52201
VO, $^4\Pi$ states, spin-spin coupling consts., ab initio calc. 79−97981

molecular orbitals calculations continued
X_3YOH molecules, ab initio MO calcs., geometry, electronic struct. 78−41940
$Xe^+ + Ag$, quasimolecular L and Ag L X-ray excitation thresholds, electron correl., calc. and expt. 78−78793
XeF^+, selected valence-electron split-shell MO calc., ground state props. 79−22585
XeF_2, pseudopotential SCF-MO studies, equilib. struct., stretch-stretch interaction force const. 80−95525
XeF_4, pseudopotential SCF-MO studies, equilib. struct., stretch-stretch interaction force const. 80−95525
XeF(Cl)(Br)(I), covalent and ionic states, spectroscopic props., ab initio CI calc. 78−90092
YIG, magnetisation density, polarized neutron expts. 78−52215
$Zn(CH_3)_2$, valence mol. orbital energy, nonempirical pseudopot. 79−22592
ZrH_4, Dirac-Fock one-centre calcs. 77−88380

molecular orientation
2,4-hexadiyne-1, 6-diol, bis(p-toluene sulphonate), dark-current meas. 80−15520
3-amino- and 4-amino-N-methylphthalimide, effect of orientational-relax. processes in fluoresc. kinetics 80−18886
acetone, soln. in EBBA, nematic liq. cryst., NMR, orientation 77−1605
acetonitrile, dissolved in nematic EBBA, oriented CH_3 group relax., multiple quantum NMR 80−66057
acetylene, chemisorbed on Ni (111), ind. vibrs., high resolution electron energy-loss meas. 79−90877
achiral molecules dissolved in cholesteric liq. crysts., fluoresc. circular polarisation *(German)* 77−42350
adamantane, Ising, diffuse scatt., hard-core correl., weak-graph method 80−49137
adamantane, orientation and deform. in nematic liq. cryst., PMR obs. 77−71815
adsorbate covered metal surface, mol. orientation, photoemission spectra selection rules 79−33896
adsorbed layer, classical octupoles on triangular lattice, orientational phases 80−2263
adsorbed monolayer of orientable molecules, lattice fluid model, real-space renormalisation group method 80−17882
aliphatic chains, mol. orientation correls. with squalane in soln., depolarised Rayleigh scatt. *(French)* 79−65885
alkali hyperoxides, low temp. phases, mag. order, EPR and antiferromag. reson., O_2 orientation 79−95630
n-alkane liquids, molecular orientational correlations 79−19131
n-alkanes, anisotropic London dispersion forces, surface effects 80−74214
n-alkoxy-α-methyl-p′-cyanophenyl cinnamate, orientational order, tricrit. behaviour 79−27907
p-n-alkoxybenzoic acids, mol. arrangement in cryst., nematic, and smectic C phases 79−32889
p-alkoxybenzylidene-p,n-butylanilines, IR absorpt. spectra, elec. field effects, orientational order parameter determ. by IR dichroism 80−80778
p-alkoxybenzylidene-p-aminocyanoanilines, IR absorpt. spectra, elec. field effect, orientational order parameter determ. by IR dichroism 80−80777
p-alkoxybenzylidene-p-n-alkylanilines, thermotropic mesophases, proton spin-lattice relax. 78−91968
4′-n-alkyl-4-cyanobiphenyls, elasticity, orientational order, and nematic-isotropic transition 77−84643
4-amino-N-methylphthalimide-decalin-n-propanol, translational relax. kinetics, luminesc. obs. 79−8180
4-aminomethylphthalimide-decalin-n-propanol, electronic spectra of 3-component solns., temp. depend. 79−4822
amorphous solids, diffusion of nonspherical particles, correl. effects 80−39337
anisotropic impurity centres, local relaxational phase transitions *(Russian)* 80−44220
anisylidene-p-aminophenyl acetate, nematic liq. cryst., refractive index, density, orientational order 78−76419
anisylidene-p-aminophenyl butyrate, nematic liq. cryst., refractive index, density, orientational order 78−76419
anthracene:2-aminoanthracene, polarised guest absorpt. spectra, transition dipole moment direction, cryst. packing 77−8610
anthracene: tetracene cryst., triplet-state EPR for isolated mol. orientation 78−26583
anthracene:naphthalene, guest mol. orientation 79−19161
anthracene, dispersed in stretched PVC, dichroic meas. of orientation 77−30867
anthracene, in stretched polyethylene film, UV-visible and fluoresc. spectral shifts 78−62852
anthracene, orientated in nematic liq. cryst., UV-visible dichroism meas. *(German)* 77−34668
anthracene, orientation in polyethylene film, linear dichroism 78−29864
anthracene crysts., mol. orientational disorder calc. vacancies, dislocations, photodimerisation 77−4915
aromatic compounds, oriented in stretched polyethylene film, phosphoresc. polarisation 79−6961
aromatic molecule, orientation and linear dichroism in stretched polyethylene 77−88480
aromatics in stretched PVA films, ESR of phosphorescent triplet state 77−30908
azoxy-4,4′-(di-undecyl α-methylcinnamate), smectic A to smectic C phase transition, optical tilt angle meas. 78−95141
p-azoxyanisole, directed crystn. in elec. and mag. fields 80−107052
p-azoxyanisole, orientated in nematic liq. crysts., UV-visible dichroism meas. *(German)* 77−34668
azoxybenzenes, nematic, mag. susceptibility, orientational order parameter 78−34426
bacteriorhodopsin orientation in Halobacterium halobium, selective proteolysis investig. 78−77010
BBOA:Sn-BBA, liquid crystal glass, unresolved Mossbauer quadrupole doublet, orientation depend. 77−84645
beam alignment due to optical pumping by laser beam 77−31025
1,2-benzanthracene in polystyrene films, delayed luminesc. decay kinetics 80−43088
benzene, excited state props., by electrochromism in polymer matrix 79−22737
benzene, monohalogenated, orientation in lyotropic surfactant soln., NMR 77−28456

molecular orientation continued
benzene, partially ordered solid, NMR line shape, orientational distrib. 78−35048
benzene, polycrystalline heteronuclear dipolar modulated chemical shift spectra, geometrical and orientational obs. 77−20750
benzene, unlabelled and ^{13}C labelled PMR, oriented in liq. crysts., r_α struct., solvent effects 79−94017
benzene(substituted)-n-alkane mixtures, mol. orientation correls., depolarised Rayleigh scatt. 79−22714
benzene adsorbed on graphite, melting and orientation, NMR study 80−100403
benzene-n-alkane mixtures, mol. orientation correls., depolarised Rayleigh scatt. 79−22714
$^3(n,\pi^*)$benzophenones in 4,4-dibromodiphenylether, oriented triplet state, LAC and cross relax., phosphoresc. 77−81143
BEPC, nematic liquid crystals, EPR of slowly tumbling VO^{2+} spin probes 79−50985
4,4′-bis(heptyloxy)azoxybenzene, nematic liq. cryst., refractive index, density, orientational order 78−76419
4,4′-bis(hexyloxy)azoxybenzene, nematic liq. cryst., refractive index, density, orientational order 78−76419
bromoethane, liq., relative mol. orientation appl. of nucl. mag. relax. data 79−41933
bromoform, liq., orientational motion, Raman spectra 77−50443
butane adsorbed on graphite, struct. and dynamics, neutron scatt. study 78−87870
4-n-butoxybenzylidine-4′-n-octylaniline, liquid cryst., smectic B phase lattice vibr. anisotropy, Mossbauer anal. 77−7666
p-n-butyl-p′-heptanoyloxyazoxybenzene oriented on NaCl MgF_2 coated NaCl, surface phenomena and IR spectra 80−79678
calcium formate, polycrystalline, heteronuclear dipolar modulated chemical shift spectra, geometrical and orientational obs. 77−20750
carbonaceous mesophase, formation at lower temps. 79−90524
carbonaceous mesophase spherules, new mol. arrangement in mag. field, orientation behaviour 79−94869
β-carotene, orientated in nematic liq. crysts., UV-visible dichroism meas. *(German)* 77−34668
CBOOA, smectic A phase, specific volume and layer spacing, X-ray diffr. and dilatometry meas. 79−55659
cellulose hydrated film, orientational heterogeneity, IR spectra and dichroism obs. *(Russian)* 78−38990
cetyl orange monolayers on water surface, reson. Raman spectra 79−91434
chemical surface reaction with orientational selectivity, diffusion controlled effective reaction rate 79−16040
chiral smectic liquid crystal, A-C phase change, electroclinic effect 79−42224
chlorobenzene, in CCl_4 soln., quadratic changes in elec. permittivity, intermol. interactions 77−73107
m-chloronitrobenzene, molecular crystals, translational and orientational vibr. determ. 80−55103
chlorophyll-a, mol. interaction in monolayers and multilayers, IR obs. 77−71799
chlorophyll-a, spectral props. of liquid crystal solutions 78−27291
cholestanyl benzoate, liq. cryst., orientational order, EPR study 78−75540
cholesteric liquid crystal, molecular polarisability, arrangement order calc. *(Polish)* 80−10495
cholesteric liquid crystal, oriented, Newtonian capillary shear flow, effective viscosity 79−18957
cholesteric liquid crystal, orienting effect of different substrates 79−46554
cholesteric liquid crystals, orientational order determ. using birefringence 79−94902
cholesteric liquid crystals, spiral twisting, orientational order effect *(Russian)* 78−42906
cholesteric mixture, solid phase, spherulite textures, optical effects and mol. ordering 79−1746
cholesteric systems, induced, intrinsic helical pitch rel. to temp. 79−64984
cholesteric systems, with nonmesogenic additives, Keating-Bottcher theory 80−84057
cholesteric-type liqiud crystals, small-angle X-ray scattering, mol. ordering determ. 79−60274
cholesteryl benzoate liq. cryst., orientational order, EPR study 78−75540
cholesteryl linoleate, dielec. props., phase transitions rel. to temp. 79−33592
cholesteryl nonanoate, cyclohexanone admixture effect on mesophase order parameter, refr. index meas. 80−100165
cholesteryl nonanoate-MBBA, liq. cryst. mixture, two colour display device 80−70116
cholesteryl pelargonate, liq. cryst. phase transitions *(Russian)* 79−37818
cholesteryl-m-fluorobenzoate, cholesteric liq. cryst., NMR, orientational order parameter 77−8429
chromophore orientation in micellar, liposome solns., liq. cryst. phases, dichroism, NMR 79−53059
COC, cholesteric liq. cryst., positron lifetimes and phase transitions 80−59383
COOB-cholesteric liq. cryst. mixtures, helix pitch, temp. depend. 80−64895
coronene, triplet mol. in n-heptane Shpol'skii sites, distortion and orientation meas. by MIDP 78−37668
coronene in n-heptane cryst., MIDP, distortion and orientation of mols. 79−31581
coumarin 6 dye mols. in liq. cryst., fluoresc. intensity, orientation control 78−82759
crystalline polymer, epitaxial crystallisation on surface of drawn polytetrafluoroethylene 78−14626
4-cyano-4′(n-amyl)-diphenyl, isotropic phase, induced molecular orientation relaxation time, Kerr effect *(Russian)* 80−19699
4-cyano-4′-octyloxybiphenyl, nematic-smetic-A transition, optical birefr. temp. coeff. 78−47505
5-cyano-biphenyl, nematic phase, effect of elec. field on flow alignment angle 79−10792
cyano-biphenyl series, nematogens and smectogens, props. characterised by even-odd effect 80−107046
9-cyanoanthracene excimer emission, in glassy and cryst. matrices 79−11445
4-cyanobiphenyl/4-cyano-p-terphenyl liq. cryst. mixture, order parameters of dissolved dyes 80−100167
cyanobiphenyls, liq. crysts. flow alignment 79−50988
molecular orientation continued
cyanobiphenyls molecular conformational mobility study by optical probing method *(Russian)* 80−92459
cyanopyridine, isomeric forms, adsorbed of Ag electrodes, Raman scatt., orientational specificity 79−69822
cyclohexylcyclohexanes, substituted, anisotropic liq. cryst. solvent for optical absorption spectroscopy 78−45724
decylammoniumchloride and bromide, lyotropic nematic struct. 78−51410
p-n-decyloxybenzoic acid p-n-hexyloxyphenyl ester, dielec. permittivity in nematic and smectic phases 79−32899
dense gas, of dipolar mols., electron localisation, density fluctuation, mol. orient. 78−38446
4,4′-di(p,n-alcoxybenzylideneamino)biphenyl series, smectic polymorphism, molecular area and tilt angle *(French)* 77−43139
diammonium oxalate monohydrate, NMR spectra, ^{13}C-^{13}C interaction, chemical shift effects 78−29800
diatomic molecules, homonuclear, molecular dynamics, time-dependent statistical props. 80−44093
diatomic molecules, homonuclear, molecular dynamics, translation-rotation coupling 80−44094
diatomic molecules, matrix isolated, vibr. energy relax., orientational motions effects 78−67776
2,3-dichloro-1,4-napthoquinone in EBBA, PMR obs., mol. struct., orientation and solute-solvent interactions 77−27806
1,5-dichloroanthracene, photodimerisation, orientational defects, lattice energy 78−80724
p-dichlorobenzene, orientation and deform. in nematic liq. cryst., PMR obs. 77−71815
3,6-dichloropyrazine, orientation and deform. in nematic liq. cryst. 77−71815
4.4-dihexylazoxybenzene, nematic liq. cryst., alignment on surfactant treated obliquely evaporated surfaces 80−49092
p,p′-dihexyloxyazoxybenzene-fluorobenzene, solute orientational order, NMR obs. 77−84627
dihydroporphin, single crystal Shpolskii matrix, fluoresc. anisotropy 79−85994
dihydroporphin free base, in n-octane cryst., zero-field optically detected mag. reson., triplet state kinetics 78−42103
4-4′-dimethoxyazoxybenzene-d_{14}, orientational order and internal rot., D NMR obs. 79−50987
dimethyl cadmium, partially oriented in nematic EBBA, mol. geom., PMR obs. 77−71819
dimethyl tin difluoride, solid, methyl group motion, neutron scatt. study 80−10607
dimethylsulphite($-d_6$), cryst., liq., and oriented film, vibr. spectra, force fields 79−91443
dipalmitoyl lecithin bilayer, mol. tilt, X-ray diffraction obs. in gel phase 80−84059
dipalmitoyl lecithin-water system, lyotropic liq. cryst., pretransitional effects, PMR second moment meas. 78−91234
diphenylpolyene, oriented in polymer film, polaris. reson. Raman spectra 79−59466
all-trans-diphenyltetradecaheptaene, oriented, photochem. reaction production and monitoring, reson. Raman spectroscopy 77−29020
disordered crystal, diffuse scatt., hard-core correl., weak-graph method 80−49137
DOBAMBC, ferroelec. liq. cryst., helical struct., elec. field depend. *(Japanese)* 80−38910
p-ndodocyloxy benzylidene p-azophenyl aniline, smectic phases, mol. order, EPR study 80−79693
dye activated CLC, distributed feedback, tunable radiation generation *(Russian)* 80−102720
dye laser amplifer, DC elec. field effects 80−64006
EBBA, IR absorpt. spectra, elec. field effects, orientational order parameter determ. by IR dichroism, bend elastic consts. 80−80778
EBBA, mematic, orientational order, effect of hexa-n-alkoxy-triphenylene disc-like solutes 80−79682
EBBA, mol. order study by means of C^{13}-H^1 double resonance 79−60275
EBBA, nematic, mol. alignment, elec. and mag. field effects, dielec. const. obs. 77−11472
EBBA, orientational order in glassy and nematic phases, IR dichroism meas. 80−64891
EBBA-MBBA mixture, differential IR spectroscopy determ. of orientation of molecules 77−7670
EBBA-non-mesogenic binary liq. cryst. system, two-phase premelting, NMR obs. *(Russian)* 78−30743
EBBA/EBCA mixed cryst., mol. alignment, field, temp. freq. depend. 78−75542
electrode surface, covalently bound molecules, redox reactions, steric effects 78−73077
epoxide compound, polymerisation in non-uniform magnetic field, exam. of structural changes 80−7791
EPR excess linewidth, of mol. cryst. triplet excitons orientational order effect 78−72389
ethanol-$d_1(d_2)(d_3)$, glassy state, solvated electron geometry, electron spin echo modulation obs. 80−66009
trans-4-ethoxy-4′-alkanoyloxyazobenzenes, nematogenic liquid crysts., birefr., order parameters, vol. changes during nematic-isotropic transitions 78−59742
ethoxyhexyltolan, Raman spectra, molecular conformational instability, internal field effects 80−54127
ethoxyoctyltolan, Raman spectra, molecular conformational instability, internal field effects 80−54127
p(p-ethoxyphenyazo)phenyl undecylenate, nematic liq. cryst., refractive index, density, orientational order 78−76419
p(p-ethoxyphenylazo)phenyl heptanoate, nematic liq. cryst., refractive index, density, orientational order 78−76419
p(p-ethoxyphenylazo)phenyl hexanoate, nematic liq. cryst., refractive index, density, orientational order 78−76419
p(p-ethoxyphenylazo)phenyl valerate, nematic liq. cryst., refractive index, density, orientational order 78−76419
ethylene, isotopically mixed, crystal, dilute guest probe orientational energy, IR, Raman spectra 78−68496
excited state props., by electrochromism in polymer matrix 79−22737
ferroelectric smectic-C liquid crystal film, freely suspended, two-dimensional mol. orientation fluctuations, light scatt. meas. 78−47236
fluid with nearly spherically symmetric molecules, thermodynamic perturbation theory 80−14985

molecular orientation continued
fluorescence, depolarisation, orientation factors, excitation energy transfer between isolated donor-acceptor fluorophore pairs 79−22740
fluorescence polarisation apparatus, for simultaneous meas. of orientation and mobility in uniaxial media 78−86320
fluorobenzenes, partially oriented in lyotropic liq. cryst. 77−68059
fluoromethanes, ^{19}F shielding anisotropies, NMR of smectic mesophase solns. 77−34662
formaldehyde-water, heuristic intermol. pot. function, ab initio MO calcs. 78−33566
furan, adsorbed on NaCl, evidence of new condensed phase, IR spectra *(French)* 80−16028
guest mol. orientation 79−19161
halobenzenes, in potassium laurate mesophase, NMR, proton distance ratios and order tensor elements calcs. 80−63672
hard rod system, improved lattice model, nematic and isotropic phases 80−33882
4-heptyl-4′-cyanobiphenyl, nematic liq. cryst., alignment on surfactant treated obliquely evaporated surfaces 80−49092
4-n-heptyl-d_{15}-oxybenzoic acid-d_1, nematic and smectic phases, mol. and relative segmental order 80−96439
p-heptyl-p′-cyanobiphenyl, refractive index, dielec. const., mag. susceptibility, orientational ordering *(Dutch)* 80−33884
heptyloxyazoxybenzene, filamentary structures 80−107051
p-n-heptyloxybenzylidene-p-aminobenzoic acid, smectic C to nematic transition 79−33076
hexamethylenetetramine, orientation and deform. in nematic liq. cryst., PMR obs. 77−71815
hexamethylenetetramine in oriented mesophases, mol. distortion, PMR 77−6802
n-hexyl 4′-n-decyloxybiphenyl-4-carboxylate, smectic C phase, tilt angle using electron reson. spectroscopy 80−33886
high speed rot., spin diffusion, NMR spin lattice relax. obs. of D 80−66056
HOAB, molecular orientatioal order in uniaxial and biaxial phases by NMR 77−84629
HOAB, smectic C liquid crystal, spin label probe obs. 77−19867
HOAB-cholesteryl benzoate mixture, twisted smectic-C and twisted nematic phases, optical and X-ray investig. 77−84634
hyper-Raman scattering by oriented molecules 79−36650
ice, IR absorpt., O-H stretching vibrs., orientation polaris. 78−31177
iodomethane, oriented in nematic liq. crystal, longit. NMR, relax. mech. 77−63302
iodomethane-d_1, ^{13}C enriched, NMR, oriented, symmetry related isotope effects 77−61772
ion-water interactions, survey of diffr. studies 80−24347
isotropic-nematic liquid crystal phase transition, theory including mol. orientation correlation 78−47508
Kevlar fibres, effect of crystallinity and orientation on mech. props. *(Japanese)* 79−38952
lamellar liquid crystal, biaxiality due to oriented defects 79−41945
lattice energy, minimisation, singularity-free, static 80−10525
lecithins, L_α phase, shear-induced biaxiality 78−95997
linear dichroism spectroscopy for mol. orientation in model membrane systems 78−29864
lipid bilayers, long-range order, phase transition, coherence lengths 78−92593
lipid lamellar liquid crystalline systems, orientation studies of probe molecules by linear dichroism 77−90718
lipid-water systems, byotropic liquid crystalline and other lamellar phases 78−92592
liquic crystals, orientational order parameter, optical birefr. meas., polarisation field problems 80−79688
liquid, cooperative mol. orientation, rel. to OH proton chem. shift 78−1974
liquid, coupling of vel. gradients to molecular orientation, light scatt. and flow birefringence anal. 80−25398
liquid crystal, deuterated compounds, molecular order and conformation changes in phase transitions 78−47237
liquid crystal, nematic, molecular theory, orientation-average pair correlations 79−60272
liquid crystal, order parameter measurement, phys. chem. lab. expt. 80−36818
liquid crystal, Rayleigh scatt. in isotropic phase, mol. orientational correl., mesophase possibilities 77−84637
liquid crystal, short rod, short range correl. and orientational energy 78−1978
liquid crystal, spiral-like, struct., PMR of dissolved mols. 78−1981
liquid crystal, theoretical foundations of chain ordering props. 80−38907
liquid crystal, uniaxial, polarised fluoresc. emission, orientational distrib. function, rot. Brownian motion 78−80390
liquid crystal alignment, use of SiO_2 critical surface tension anisotropy 79−86676
liquid crystal alignment films prod. by RF plasma beam technique 80−76198
liquid crystal cells, twisted, mol. orientation 77−27818
liquid crystal cells. pretilt influence on capacitance voltage depend. 78−83724
liquid crystal dynamic scatt. devices, initial molecular alignment effect on electro-optical props. *(Japanese)* 77−1655
liquid crystal matrix, orientational distrib. coeffs. 80−92452
liquid crystal orientation mol. ordering determ. by Raman scatt. *(Russian)* 79−19153
liquid crystal phase transition, effect of dipole-dipole interaction on translational order 77−84910
liquid crystal surface, statistical thermodynamics, local order parameter 80−88023
liquid crystal surface alignment treatment giving controlled low angle tilt 77−19871
liquid crystal symmetry and thermodynamic states, review 80−10493
liquid crystals, alignment by amphiphilic monolayers 79−37614
liquid crystals, biaxial and uniaxial, NMR 78−75552
liquid crystals, deuterated, dueteron mag. resonance mol. odering, conformational changes 80−34789
liquid crystals, hydrodynamic instabilities and neutron scattering 79−50990
liquid crystals, mol. conformation and orientational order, NMR studies, review 80−75151
liquid crystals, molecular ordering from incoherent quasi-elastic neutron scatt. 79−4241

molecular orientation continued
liquid crystals, nematic and smectic mol. dynamical investigation 78−91252
liquid crystals, stability of mol. orientational distrib. 79−94880
liquid crystals, static and dynamic props., time depend. fluoresc. depolarisation obs. 80−29786
liquid crystals, structure and dynamics, neutron diffr. studies 78−94972
liquid crystals, surface alignment using polynuclear metal complexes 80−1924
liquid crystals, thermal conductivity anistropy, forced Rayleigh light scatt. meas. 78−94991
liquid-liquid interface, adsorbed monolayer mol. orientation, electrolyte effects, reson. Raman obs. 78−60430
lyotropic liquid crystals, orientation in mag. field, glass interface effects 79−1390
lyotropic mesophase, mag.-oriented, X-ray diffr. obs. 80−1921
lyotropic systems, NMR of dissolved cations and D_2O molecules 79−22732
macromolecular chain dynamics model interpret. of dielec. relax. data 77−52014
magnetic circularly polarised emission from luminesc. mol. system, QED formalism, orientation relax. 77−46589
MBBA:trichlorobenzene, solute orientation in nematic soln., temp. and conc. depends., NMR obs. 79−46556
MBBA, anisotropic interactions with surface-treated substrates, wall effects on Freedericksz transition 79−99070
MBBA, calc. of order parameter from X-ray diffraction data 79−69009
MBBA, elec. field effect on optical indicatrix orientation 77−36202
MBBA, IR absorpt. spectra, elec. field effects, orientational order parameter determ. by IR dichroism, bend elastic consts. 80−80778
MBBA, mol. alignment in elec. and mag. fields 77−58956
MBBA, nematic, aligning props. for Si film surface tension 79−90846
MBBA, nematic, flexibility gradient of fatty acid spin labels, EPR study 80−71181
MBBA, nematic, mol. alignment on SiO film, film thickness effects 80−59384
MBBA, nematic liq. cryst., quasihomeotropic orientation induced by PTFE deposited on SiO surface 79−90525
MBBA, nematic liq. cryst., surface alignment using lecithin monolayers, contact angle meas. 79−4247
MBBA, nematic liq. cryst. alignment on domains of TGS 79−38506
MBBA, nematic liq. crysts., AC excited, dynamic light scatt., orient. fluctuations 79−1769
MBBA, orientational order in glassy and nematic phases, IR dichroism meas. 80−64891
MBBA, refractive index, dielec. const., mag. susceptibility, orientational ordering *(Dutch)* 80−33884
MBBA, tilted alignment induced by short chain surfactants 77−4037
MBBA, uniaxial, orientational order, polarised fluoresc. meas. 79−55655
MBBA nematic liq. cryst. systems, orientational order rel. to solute size, shape 77−4565
MBBA-BBCA mixture, field-induced distortion of mol. orientation 79−99060
MBBA-cholesteryl chloride mixture, liq. cryst., bubble domain texture, obs. of interference fringes 79−23520
MBBA-cholesteryl chloride mixture, mol. orientation during mag. field induced cholesteric-nematic transition 79−28086
MBBA-EBBA mixture, nematic liq. cryst., alignment on domains of TGS 79−38506
MBBA/EBBA binary liquid crystal mixture, US absorpt. and vel. dispersion, phase transition and alignment effects *(Korean)* 80−29121
MBBA/n-hexane mixtures, isotropic-nematic transition, transient optical Kerr effect study 79−82323
mesophase, degree of order rel. to cholesterol additions, chain motions 77−24260
mesophase pitch, magnetically-oriented, phys. props., mol. struct. 80−64885
mesophase thin layers, boundary effects 79−94903
methane, melting transitions, thermodynamic props., positional disordering energies 80−96452
methane, solid, orientational order of molecules in phase III 79−51042
methane, solid, thermal expansion and conversion processes *(Russian)* 78−95163
methane-d_2, orientational ordering and tunnelling states meas. 79−10963
methoxy species on Ni (111), photoelectron spectra, electronic struct. and orientation 80−83420
methoxyamyltolane, nematic phase orientation mol. ordering determ. by Raman scatt. *(Russian)* 79−19153
methyl group, calc. of optimal orientation in crystals 77−89392
methyl iodide, and -d_1, dissolved in nematic phase, C-H bond orientation, ^{13}C NMR 78−46371
molecular crystal, quadrupole analogue of Ising model 78−29063
molecular crystals, chem. shielding, spin-lattice, quadrupole interactions, ^2D NMR spin echo spectroscopy 80−34817
molecular crystals, mol. orientation defects, effect on polarised IR and Raman spectra 80−88989
molecular order and dynamics, high resolution neutron scatt. study 79−50991
monochlorobenzene, partially oriented, r_α-struct., ^{13}C satellite PMR obs. 79−50048
monolayers, polycryst., IR determ. 80−80891
monomolecular layers, Langmuir-Blodgett, mol. orientation determ. by IR absorpt. 79−11423
multiplexed twisted nematic displays, liq. cryst. material design 79−90533
naphthalene: anthracene, cryst., triplet-state EPR for isolated mol. orientation 78−26583
naphthalene:anthracene, guest mol. orientation 79−19161
naphthalene charge transfer complexes, orientational disorder, spt. ht. meas. 79−46813
naphthalene in EBBA, PMR obs., mol. struct., orientation and solute-solvent interactions 77−27806
1,4-naphthoquinone in EBBA, PMR obs., mol. struct., orientation and solute-solvent interactions 77−27806
nematic bend-splay elasticity near the nematic-smectic-A transition 80−24360
nematic cells, pretilted, Freedericksz transition in mag. field normal to director 79−99071
nematic layer, Freedericksz transition, first-order, second-order elasticity effect 79−99069

molecular orientation continued
nematic liq., cryst. cell, with asymmetrically treated electrodes, electrooptic characts. 79−55658
nematic liq. cryst. with oblique config., Freedericksz transition and anchoring effects 79−55652
nematic liq. crystals, orientational relax. calc. 78−75549
nematic liq. cysts. surface alignment, temp. depend. of pretilt angles 79−55656
nematic liquid cryst., 3D convective instability in AC field 77−62475
nematic liquid cryst., Freedericksz transition and anchoring effects for general config. 80−33875
nematic liquid cryst., orientational fluctuations effect on evanescent modes of transmitted EM wave 80−64889
nematic liquid cryst., surface alignment on TGS surface controlled by domain struct. 79−99068
nematic liquid cryst., surface alignment using lecithin monolayers, contact angle meas. 79−4247
nematic liquid cryst. display devices, with twisted and tilted arrangements, guest-host interactions 80−34891
nematic liquid cryst. mixture, ZLI-207, nonideally oriented layers, Freedericksz transition dynamics 80−100163
nematic liquid crystal, anamalous stiffness and tilt angle from nonuniform attachment angle 79−86688
nematic liquid crystal, anchoring energies determ. from surface tilt angles 79−64986
nematic liquid crystal, average orientation in three dimens. parallelepiped model 77−51315
nematic liquid crystal, diamagnetic susceptibility, refractive index, density and polarisability 77−15315
nematic liquid crystal, electroconvective flow, vel. and orientation deform. angles *(Russian)* 79−37621
nematic liquid crystal, fluorescent measurement of S_2 and S_4 order parameters 77−24262
nematic liquid crystal, homogeneous surface alignment using double SiO deposition, appl. to displays 79−4239
nematic liquid crystal, ionic conduction-induced flow alignment angle, NMR evidence 80−44125
nematic liquid crystal, orientational order of molecules, molecular dynamics method study 79−27918
nematic liquid crystal, SHG, mol. symmetry and macroscopic nonlinearity *(Russian)* 78−90457
nematic liquid crystal, spontaneous polarisation, rel. to mol. orientation, electro-reflection meas. *(Russian)* 78−55809
nematic liquid crystal, surface tension, mol. theory 77−1075
nematic liquid crystal, thermal instabilities in layer with oblique orientation at boundaries 80−44110
nematic liquid crystal, twist cell, dynamic props., voltage depend. 80−70117
nematic liquid crystal film, with two free surfaces, mol. orientation 78−47238
nematic liquid crystal layer, twisted, elastic deform. energies and reverse twist domains 79−37617
nematic liquid crystal reversely pretilted cell, conformation of molecular orientation 80−59388
nematic liquid crystal solutions, isotropic phase, orientational pair correl. obs. using depolarised Rayleigh light scatt. *(Russian)* 79−90552
nematic liquid crystal with luminesc. impurity, luminesc. and absorpt., order parameter determ. 79−4240
nematic liquid crystals, acoustic props., rotating mag. field study 80−88034
nematic liquid crystals, cause of orientation on cleavage faces of triglycine sulfate crystal 79−94899
nematic liquid crystals, coherent neutron scatt. studies, review 79−41956
nematic liquid crystals, continuum theory of disorder, intermolecular correls. 77−31591
nematic liquid crystals, Marangoni effect 78−6009
nematic liquid crystals, molecular mechanisms of dielec. polarisation and relaxation 80−34846
nematic liquid crystals, orientation fluctuations in high mag. field, quenching, birefringence effects 80−64892
nematic liquid crystals, orientation ordering, mol. dynamics obs. 78−91239
nematic liquid crystals, paramagnetic, flexomagnetoelec. effects 80−75158
nematic liquid crystals, shear flow, effect of mag. fields and boundary conditions, PAA example 77−7668
nematic liquid crystals, surface alignment, easy axis determ. and temp. depend. of field energy 79−90541
nematic liquid crystals, surface and anchoring energies, van der Waals contrib. 80−92455
nematic liquid crystals, twist effect dynamics, mol. inclination angles relaxation 79−60276
nematic liquid crystals, twofold orientations and hysteresis props. 79−82146
nematic liquid crystals, viscosity, rel. to order parameter *(Russian)* 78−91242
nematic liquid crystals on chlorosilane-coated glass 77−11466
nematic liquid crysts., behaviour in inhomogeneous elec. fields 80−44118
nematic liquid crysts., molecular alignment using alkoxysilanes, rel. to surface energy 80−100164
nematic ordering in a system of rods 79−60271
nematic-chiral-dye mixture, circular dichroism, selective light scatt. *(Russian)* 80−103944
nematic-cholesteric mixtures, spiral pitch temp. depend. *(Russian)* 80−19700
nematic-smectic A transition, orientational fluctuation effect 80−6496
nematic-smectic B mesophases, mutual orientation *(French)* 79−55660
nematics, mol. orientation, rel. between meas. and theoretical characts. 79−60273
4-nitrophenyl-4-octyloxybenzoate/cholesteric liq. cryst. mixtures, helix pitch, temp. depend. 80−64895
NMR spectra, high resolution, mag. field induced mol. alignment effects 79−18207
NMR spectra, vibr. correction study 80−18840
non-random orientation distribution functions with random pole figures 80−6320
nonpolar molecule substituting polar mol. in mol. dipole lattice, dielectric alignment 77−89359
p-n-nonyloxybenzoic acid, smectic C phase, electro-optical effect *(Russian)* 80−92458
molecular orientation continued
nonyloxybenzoic acid/cholesteric liq. cryst. mixtures, helix pitch, temp. depend. 80−64895
nuclear quadrupole spin-lattice relax. due to mol. reorientation in cryst. 80−66062
Nylon 6 and 12 films, drawn, NMR, mol. orientation, motions *(Japanese)* 77−32268
Nylon 6 gut yarn, fine struct. change in twisting, annealing and untwisting, X-ray and electron microscopy obs. 80−84904
octaphenylcyclotetrasiloxane, mesophase form., neutron diffr. obs. 78−91224
4-octyl-4′-cyanobiphenyl, liq. cryst. phases, dielec. relax. meas., short range interactions 78−94976
octyl-cyano-biphenyl, influence of laser light wave field on nematic phase *(Russian)* 80−92456
4-n-octyl-d_{17}-oxybenzoic acid-d_1, nematic and smectic phases, mol. and relative segmental order 80−96439
p-n-octyloxy benzylidene-p-toluidine, mol. order, EPR VAAC probe 80−70114
4-octyloxybenzoyloxy-4'-cyanostilbene, enantiotropic reentrant nematic behaviour at atmos. press. 79−60490
OHMBBA, nematic, dielectric behaviour at RF 79−7548
one-component system interface with directed intermol. forces, Monte Carlo calcs. *(Russian)* 77−61031
OOAB, nematic thermotropic mesophases, end-chain ordering and even-odd effects, deuterium mag. reson. 79−82890
optical nuclear polarisation, field and orientation depend., non-crossing rule, perturbation anal. 77−42337
optically active and inactive molecules, electric and mag. dispersion forces interaction 80−99533
organic molecules, NMR spectra, mag. field induced mol. alignment effects 79−18207
organic tensio-active compounds, mol. orientation correlations in hydrophobic groups *(French)* 79−73957
orientational bistability, nematic storage effects 80−70112
2-oxa-6-thiaadamantane, plastic phase, transition and fusion thermodynamics, DSC meas. 78−75603
oxalic acid dihydrate, NMR spectra, ^{13}C-^{13}C interaction, chemical shift effects 78−29800
oxazine dyes, orientation of $S_1 \rightarrow S_n$ transition moments, continuous ps photometry 79−10152
2-oxyphenylbenzoxazol, proton intramolecular transfer, light absorpt. and emission, dichroism, polarised fluoresc. 80−87166
PA-6, polymer fibre, orientation changes during stretching, IR spectra 78−75568
PAA, nematic, orientation in thick layers, continuum theory validation 77−15312
PAA, refractive index, dielec. const., mag. susceptibility, orientational ordering *(Dutch)* 80−33884
partially oriented molecules, uniaxial, two-photon processes, polarised spectrosc. 80−74209
PCP, oriented swollen soln., IR dichroism, short-range orient. order *(Russian)* 79−51941
pentacene in naphthalene, triplet state, EPR study by electron spin-echo and laser flash excitation 80−58172
p-n-pentyl-p′-cyanobiphenyl, nematic liq. cryst., Raman depolaris. ratios, order parameters 79−28733
pentylcyanobiphenyl, nematic, elastic and dielec. props. from capacitance-voltage curve 79−32894
4-n-pentyloxy-phenyl-4′-n-octyloxybenzoate, nematic, dielec. relax. and freq. depend. of threshold voltage 80−60497
perylene in n-heptane cryst., polarised fluoresc. 80−1017
PET, biaxial orientation, refr. index meas. by Raman and IR spectrosc. 80−60583
PET films, one-way drawn, constant strain effects, IR meas. 80−60584
phenylcyclohexanes, substituted, anisotropic liq. cryst. solvent for optical absorption spectroscopy 78−45724
phthalozine, oriented in lyotropic mesophase, proton NMR spectra 79−82886
planar molecules in stretched polymer films, solute orientation, transition moment direction, dichroic spectra 78−58742
plastic crystal, orientational disorder, group theory method 80−107091
plastic crystal, orientational dynamics, neutron scatt. data interpret. using functions derived from group theory 80−107092
PMMA, effect of mol. orientation on fracture toughness 78−52992
PMMA, glassy, photoelasticity 80−45034
PMMA, oriented, hypersound propag., elastic props. 78−75737
PMMA, oriented by extrusion, stress-optical study 78−47248
poly-γ-benzyl-L-glutamate, lyotropic liq. cryst., crosslinking in mag. fields, aligned orientation form. 77−43137
poly-γ-benzyl-L-glutamate, mag. oriented liq. cryst. solns., order parameter 77−15305
poly-γ-benzyl-L-glutamate, monolayers, struct. studies, IR, ATR, and TEM obs. 80−44396
poly-γ-benzyl-L-glutamate, preliq. cryst. mol. alignment, space charge effect, electro-optical obs. 77−40206
poly-γ-benzyl-L-glutamate, soln., liquid crystal transitions anal. 80−65207
poly-γ-benzyl-L-glutamate solution orientation of liq. cryst. domains, IR spectroscopy *(Russian)* 77−62477
poly-γ-benzyl-L-glutamate-dioxane liq. cryst., orientational order temp. depend., diamag. susceptibility 77−47966
poly-n-benzamide, lyotropic liq. cryst., structural orientation *(Russian)* 77−31593
polyalkyl methacrylates, oriented stretched membrane, gas diffusion, entropy correl. theory 79−69291
polyamidoimide film, thermomech. props. rel. to mol. struct. *(Russian)* 79−57029
polyarylate, F-2, film, rigid chain orientation in surface active medium *(Russian)* 78−88513
polycaproamide, oriented, molecular rearrangements during deformation, IR spectra exam. 80−7644
polycarbonate fibre, highly-oriented, drawing behaviour and mech. props. 78−76708
polyester fibres, orientation in drawn fibres, birefringence meas. 78−35344
polyethylene, amorphous-cryst., highly oriented, plastic deform. rel. to supermol. struct. *(Russian)* 79−51010
polyethylene, chain-extended, oriented, microindentation hardness 78−76728

molecular orientation continued
polyethylene, doubly oriented, low density, deformation and structure, exam. 80−11705
polyethylene, elongation, conform. set change IR obs. *(Russian)* 78−37778
polyethylene, highly oriented fibre composite, self-hardening, tensile props. 77−55939
polyethylene, lightly crosslinked, processed under mol. orient., struct., props., review 80−38957
polyethylene, linear, films, elec. cond. rel. to drawing, annealing *Japanese)* 79−15817
polyethylene, oriented, elastic stiffness constants, US meas. 78−76690
polyethylene, oriented, partially crystalline, amorphous component obs., X-ray diffr. *(Russian)* 79−23534
polyethylene, oriented, Raman active modes 78−23457
polyethylene, ultra-oriented, prep. technique, extreme moduli 77−21086
polyethylene, ultraoriented, ^{13}C-^{13}C dipolar satellites 77−28465
polyethylene, ultraoriented, prep. comments 77−85983
polyethylene films modified by polyacrylonitrile grafting before, after orientating elongation, struct. *(Russian)* 77−32554
polyethylene terephthalate, amorphous material orientation determ. *(Polish)* 79−73111
polyethylene terephthalate, elongation, conform. set change IR obs. *(Russian)* 78−37778
polyethylene terephthalate, film, two-stage orientation in monoaxial extension *(Russian)* 77−62488
polyethylene terephthalate, mech. props., influence of cryst. arrangement and noncryst. region struct. 78−76707
polyethylene terephthalate, uni- and biaxially drawn films, preferred planar orientation 78−80590
polyethylene terephthalate fibres, elastic modulus correlation with mol. orientation 79−79019
polyimide films, mol. relaxations, mol. orientation and friction characts. 77−59939
polymer, crystalline, dynamic mech. props., influence of struct. 79−4991
polymer, drawing properties, role of interfibrillar tie mols. 78−76706
polymer, noncrystalline solid, preferred orientation from scatt. ang. distribs. 78−75560
polymer, orientational ordering rel. to mech. props. *(Russian)* 78−59766
polymer, oriented, amorphous-crystalline low ang. X-ray diagrams, supermol. struct. models, schematic representation *(Russian)* 78−87630
polymer, oriented, thermostable, relax. transitions, thermomech. and isometric heating obs. *(Russian)* 79−23538
polymer, semicrystalline, model for thermal cond., orientation effects 77−85004
polymer, solid, orientation meas. and characterisation methods uing X-rays 78−75559
polymer, uniaxial, fluoresc. polarisation, orientation and mol. dynamics effects 78−76516
polymer fibre, highly oriented, struct. and mech. props. 78−75563
polymer fibres, ultra high modulus, prep. by soln. and melt spinning, review 79−11544
polymer film, noncrystalline chain orientation evaluation, with polarised fluorescence method *(Japanese)* 80−6368
polymer film, stretched, orientation and transition moment directions of small planar molecules 78−1015
polymer film, supermolecular structure and mech. stress distrib. among chem. bonds 78−75562
polymer films and sheets 78−80590
polymer matrix, decreased stabilisation energy of excimers and exciplexes 80−25431
polymer melt, flow-induced orientation freezing-in by vitrification, appl. to processing 79−23531
polymer orientation measurement, in solid, by spectroscopic techniques, mech. anisotropy 78−75558
polymer processing technology, prod. of high chain extension 78−31378
polymer solution, short-range order and solvent crystallisation; spectroscopic and microcalorimetric, methods *(Russian)* 78−26416
polymer solution, short-range solvent orientational order, IR dichroism and photoelasticity obs. *(Russian)* 78−26415
polymer solutions, order, conf., Midland, USA, (Aug 1973) 79−10769
polymers, aliphatic and aromatic, mean mol. orientation factors, from IR spectra and acoustic method 80−70142
polymers, crystn. under mol. orientation, formation of stacked lamellar structs. 80−84109
polymers, solid, orientation effects, conf., Budapest, Hungary (April 1976) 78−75557
polypeptide liquid crystal, electric field-induced phase transition 80−24571
polypropylene, extruded, chain orientation, polarised Raman scatt. 79−1756
polypropylene, homopolymer, effect of mol. orientation on fracture toughness 78−52992
polypropylene, oriented, thermooxidative degradation kinetics, durability, influence of mech. initiated processes *(Russian)* 79−24591
polypropylene film, effect of crystallinity on deformation mechanism of biaxial stretching 77−80426
polyribonucleotide complexes, mag. field orientation of nematic liq. cryst. solns., light scatt. and birefr. meas. 79−82152
polystyrene, isotactic, orientation of remaining amorphous chains during crystallisation 80−10506
polystyrene, oriented amorphous, supermol. structures rel. to mech. behaviour 78−22673
polystyrene, shrinkability, orient. 79−11660
polystyrenes, rubber modified, mech. props., mol. orientation effects 79−52331
porphin, single crystal Shpolskii matrix, fluoresc. anisotropy 79−85994
porphin in host n-alkane crystals, phototautomerism, IR spectral obs. 80−34963
porphyrin in n-octane Shpolskii matrix, defect props., Monte Carlo obs. 80−63533
N-p-propoxybenzylidene-p-pentylaniline, orientational order in glassy and nematic phases, IR dichroism meas. 80−64891
N-p-propoxybenzylidene-p-pentylaniline, Williams domains, interference study 80−44114
di-n-propyl p-terphenyl-4,4''-dicarboxylate, biaxiality of smectic E mesophase 79−41949
PTE, polymer fibre, orientation changes during stretching, IR spectra 78−75568
molecular orientation continued
PVC, amorphous, orientation study by creep thermomechanical method, computer anal. 78−75561
PVC, amorphous-cryst., highly oriented, plastic deform. rel. to supermol. struct. *(Russian)* 79−51010
PVC, filled, drawn, mol. orientation study by Raman spectroscopy 79−73919
PVC, film, uniaxially stretched, effect of mol. orientation on anisotropy of Young's modulus 77−86076
PVC, uniaxially stretched, mol. orientation, birefringence, effect of plasticizers, draw ratio 77−48500
PVC film, uniaxially stretched, mol. orientation, polarised fluoresc. investig., deform. mechanism 77−52440
pyrene, orientated in nematic liq. crysts., UV-visible dichroism meas. *(German)* 77−34668
pyridine, in benzene single cryst., electronic spectrum Stark modulation, dipole moment 78−29814
quinoxaline, oriented in lyotropic mesophase, proton NMR spectra 79−82886
Raman librational spectra polariation, mol. single cryst., temp. depend. 79−1760
Raman spectra of assembly of partially oriented scatterers 77−16295
rhodamine dyes, methanol-water solns., triplet state EPR spectra, aggregation, mol. orientation 77−48031
rubber, drawn networks, orientation averages 79−10819
Schiff base azo dyes in nematic liq. cryst. hosts, order parameters, optical density meas. 80−84055
simple cubic lattice, orientational ordering of quadrupoles 80−44157
SLC, chiral structure in electric field, dielectric permeability, spontaneous polarisation *(Russian)* 80−75159
smectic A and C phase and A-C phase transitions, diffuse-cone model 79−41952
smectic A mesophase, spin-probe longitudinal relax. 79−94871
smectic A phases, mol. tilt, layer thickness and orientational disorder 79−32897
smectic A to C phase transition, phenomenological model 79−1495
smectic C liq. cryst. film, mol. orientation fluctuations in two-dimens., light scatt. obs. 80−93355
smectic C phase, mol. director behaviour at domain EHD instability 80−15000
smectic C phase, tilt angle determ. by field-induced Freedericksz transitions and X-ray meas. 79−94884
smectic C phase, with second order transition to smectic A, molecular tilt, zigzag model 78−94986
smectic liquid crystal, chiral, electroclinic effect at A-C phase transition 77−39668
smectic liquid crystalline solvents, ESR obs. of anisotropic ordering, spin relax. and slow tumbling 79−95629
smectic liquid crystals, ferroelec., submicrosecond bistable electro-optic switching 80−84051
smectic phases ordered, structural classification, collective modes *(French)* 78−94971
smectic-C liquid crystals, biaxial mol. order, NMR meas. 80−25227
soap system, C_{18} mono-cis-unsaturated, lyotropic liq. cryst., X-ray diffr. and EPR meas., Monte Carlo simulation 78−94981
solid, partially ordered, orientational distrib. from NMR and EPR line shapes 78−35048
solute orientation in stretched polymer matrix, dichroism anal. 80−75998
spiropyrans, photochromic transform., dipolar cryst. form. 79−20386
succinonitrile, plastic, diffuse scatt., hard-core correl., weak-graph method 80−49137
succinonitrile, plastic cryst., orientational order, depolarised Rayleigh scatt. method 78−75612
sulphonic acids, adsorption and orientation on Al_2O_3, tunnelling spectroscopy obs. 78−34707
surfaces, electron spectroscopy, review 78−92169
TBACA, chiral, smectic C* and H* phases, mol. orientational ordering, ^{14}N NQR study 80−75152
TBBA, biaxial liq. cryst., orientational order, ^{14}N NQR meas. 77−32288
TBBA, biaxial smectic phases, orientational order, neutron scatt. and NQR results 78−91225
TBBA, smectic A phase, incoherent neutron quasielastic scatt. exam. of molecular ordering 77−43143
TBBA, smectic phases, orientational order, ^{14}N NQR and double NMR obs. 78−94974
TBBA mesophases, mol. orientational order 79−37619
TCOOB, smectic A and C liq. cryst., A-C phase transition, diffuse-cone model description 79−86674
p-terephthal-bis-aminocinnamate, smectic phases, orientational order, ^{14}N NQR and double NMR obs. 78−94974
tetrabutylammonium picrate, elec. cond. in nematic (smectic) 4-alkyloxy-4'-cyanobiphenyls, temp. (conc.) depends. *(German)* 78−55966
thermotropic systems of rodlike molecules with orientation-depend. interactions 80−33883
tolanes, molecular conformational mobility study by optical probing method *(Russian)* 80−92459
1,3,5-tribromobenzene mesophase, spiral-like, struct., PMR of dissolved mols. 78−1981
1,2,3-trichlorobenzene, oriented mols., ^{13}C satellites use in proton spectra, r_a-structure 80−18872
1,3,5-trichlorobenzene mesophase, spiral-like, struct., PMR of dissolved mols. 78−1981
trichlorophosphazo compound, $Cl_3P{:}NCCl(CF_3)_2$, nuclear quadrupole spin-lattice relax. 80−66062
2,4,6-trifluoronitrobenzene, ^{19}F shielding anisotropies, nematic phase NMR 77−27090
triphenylene, trapped in n-heptane single cryst., ESR and orientation *(French)* 78−91928
triphenylene in Shpolskii matrix, orientation, ESR and fluoresc. spectra 79−36688
tris-butadienyl metal D_3 complex pairwise chiral discriminations, stereochem. basis, extended transition monopole model 78−74725
twisted nematic display with cholesteric dopant, transmission characteristic temp. depend. compensation 80−103934
two-dimensional systems, order parameter from chemical shift anisotropy patterns 80−80624
urea-n-paraffin adducts, order-disorder transition, thermal anal., X-ray diffr., and NMR 79−33084

molecular orientation continued
vanadyl alkanoates, ^{51}V NMR, quadrupole splitting in nematic phases 79−28637
vapour-liquid interface, mol. orientation, theoretical and computer simulation 79−73377
vitamin B_{12b}:B_{12r}, cryst. growth, orientation, ESR obs. 79−34486
water, lyotropic phase orientation, ^{17}O and ^{2}H NMR study 78−27905
water interface, mol. orientation and surface pot. at 4°C 80−15339
BCl_2NCO, soln., force fields and normal modes, vibr. spectra, IR and Raman obs. *(French)* 80−58266
$BX_2{}^{14}NCS$ (X=Cl, Br, I), soln., force fields and normal modes, vibr. spectra, IR and Raman obs. *(French)* 80−58266
$BeSO_4.4H_2O$, p-p vector orient., PMR obs. 78−52361
CO adsorbed on Ni, adsorbed mol. bond config. and orientation, ang. resolved photoemission 77−44506
CO, Photoelectron angular distrib. of C and O K-shell ionisation 78−52628
C_2O_3, liq., mol. conform. and orientation correlation 79−32877
$Ce_2(SO_4)_3.9H_2O(D_2O)$, polarised Raman spectra, vibr. props. and role of lattice H_2O 80−66201
Co complex, triazene-1-oxide complexes, EPR spectra in frozen nematic liq. cryst. glass 80−88871
Co, orientated mol., (e,2e) spectra, electron momentum density 79−98236
$Cr(CO)_6$, linear dichroism, distortion and local field contribs. 79−87415
Cu complex, triazene-1-oxide complexes, EPR spectra in frozen nematic liq. cryst. glass 80−88871
p-D_2 adsorbed on graphite, NMR, orientational behaviour, weak crystal field 78−75935
p-D_2, orientational ordering, transition temp. and change of symm. 77−31609
DBr, orientational phase transitions, effective field approx. calcs. 77−24404
$Fe(CO)_4$, in N_2, Ar low temp. matrix, IR laser photochemistry, orientational and site selectivity 78−23954
o-H_2 adsorbed on graphite, NMR, orientational behaviour, weak crystal field 78−75935
H_2 adsorbed submonolayer, ortho-para separation coeff., mol. alignment and rot. levels 77−7971
o-H_2, orientational ordering, transition temp. and change of symm. 77−31609
H_2, solid, orientational ordering, crit. temp. and conc. density depend. 79−86725
H_2, solid, quadripolar glass, relax. time and low temp. sp.ht., computer simulations 80−49377
H_2, solid, with low ortho-fraction, ferrorotational transition *(Russian)* 79−60597
o-H_2, solid FCC, orientational ordering, SCF approx. 78−2029
o-H_2:p-H_2, solid, isolated pH_2 effect on orientational order 77−47535
HCl+He, mag. transitions, initial-l labelled CS approx. computations 79−3552
HF+HF, interaction energy, multipole anal., charge overlap, orientation and bulk props. 77−34715
H_2O, adsorbed, surface-induced NMR line splittings and augmented relax. rates 78−64288
Hbr+Cl_2(BrCl), four-centre reaction, quasiclassical trajectory study 79−57213
I_2, angular momentum transfer, elastic, inelastic collisions, orientation and polarised fluoresc. 78−90271
I_2, mol. beam, ang. momentum polarisation 77−46635
InO_3:Sn transparent conducting films, homeotropic orientation of liquid crystals *(Russian)* 80−108181
K+trifluoroiodomethane→KI+trifluoromethane, molecular beam reactive scattering, angular distribution study 79−98198
LiH+LiH, interaction energy, multipole anal., charge overlap, orientation and bulk props. 77−34715
Mg vermiculite, adsorbed water mol. orientation, elec. pot. calc. 78−26763
$MnSO_4.4H_2O$, p-p vector orient., PMR obs. 78−52361
$Mo(CO)_6$, in nematic matrix, linear dichroism, distortion and local field contribs. 79−87415
N_2, ab initio MO-LCAO-SCF and Gordon-Kim intermolecular pot. for seven different orientations 80−95522
N_2 dissolved in Ar, mol. orientation, Raman spectrosc. obs. 80−52994
N_2, liquid, mol. correl. functions, effective pair pot. evaluation 80−10476
N_2, neutron diffraction patterns at room temp., correls. and struct. factor 78−82810
N_2, orientated mol., (e,2e) spectra, electron momentum density 79−98236
β-N_2, orientational order, model 78−67667
N_2 overlayer on graphite, orientational ordering, neutron scatt. meas. 80−10783
N_2+N_2, interaction energy, multipole anal., change overlap, orientation and bulk props. 77−34715
ND_4NO_3, cubic, mol. orientation determ. by multipole anal. 79−73136
NH_3, time-delayed laser saturation IR spectroscopy 78−86976
NH_4 Br single cryst., low temp. PMR lineshapes of tunnelling NH_4^+ ions 80−25223
NH_4^+, proton-proton dipolar coupling in nematic soln. using high resolution NMR 77−3387
NH_4Br, NH_4^+ rot. motion, quasielastic neutron scatt. obs. 80−96492
Na_2, mol. beam, ang. momentum polarisation 77−46635
NaCN, diffuse scatt., hard-core correl., weak-graph method 80−49137
$NaNO_3$, N atom velocity, NO_3^- vib. and orientation, nucl. reson. photon scatt. 78−68433
Ni, CO adsorption, mol. orientation, ion scatt. 78−71949
$NiS_2O_3.6H_2O$, p-p vector orient., PMR obs. 78−52361
O_2 dissolved in Ar, mol. orientation, Raman spectrosc. obs. 80−52994
O_2, liquid, mol. correl. functions, effective pair pot. evaluation 80−10476
O_2 solid film, optical and structural props. 78−56052
O_2, two-dimensional adsorbed layer on graphite, props. calc. 80−103568
PSF_3, in orienting smectic solvent, ^{19}F and ^{31}P mag. shielding anisotropies, F-P-F bond angle 77−18942
SO_2 liquid, short range orientation effects, vibr. Raman spectra 80−2759
$Sr(NO_3)_2.4H_2O$, p-p vector orient., PMR obs. 78−52361
TaS_2(pyridine)$_{1/2}$, pyridine orientation, X-ray diffr. meas. 79−55679
W, CO adsorption, mol. orientation, ion scatt. 78−71949
$W(CO)_6$ dissolved in oriented compensated nematic mixture, distortion of cubic mol., linear dichroism obs. 79−95797
$W(CO)_6$, in nematic matrix, linear dichroism, distortion and local field contribs. 79−87415

molecular photodissociation
absorbing boundary method, Golden Rule generalisation 79−97226
acetic anhydride, multiphoton dissoc., CH_2 and C_2 prod., fluence depend. meas. 80−5586
acetone-d_6, multiphoton dissoc., recomb. to ethane 80−3371
acetonitrile, low press. IR multiple photon photolysis 79−16022
acetonitrile molecule dissociation in IR field, laser-induced fluoresc. obs. 80−53075
acetyl iodide, photodissoc., secondary product decomposition 78−25636
acetyl radical, photofragment spectroscopy, collision dynamics 78−25636
acetylene, multiphoton UV photodissoc. 78−50602
acetylene, multiphoton vacuum UV photodissoc. obs. and interpret. 80−11939
acetylene, VUV multiphoton dissoc., electronically excited fragment emission 78−90238
acrylonitrile, IR multiphoton dissoc., C_2 prod. and quenching obs. 80−11931
acrylonitrile, IR multiphoton dissoc., prod. of $CN(X^2\Sigma^+)$ and $C_2(a^3\Pi_u)$ radicals 80−63723
acrylonitrile, multiple photon dissoc., photofragment spectroscopy by laser-induced fluoresc. 80−11937
alkali bromides, photofragment spectra, 266 nm, bond energies and excited state symmetries 80−53072
alkali halide, dissoc. energy by photofragmentation spectroscopic method 79−76527
alkali iodides, photofragment spectra, bond energies and excited state symmetries 80−5589
alkali metal chlorides, photofragment spectra, bond energies and excited state symmetries 80−87190
alkali metal diatomic system, three states nonadiabatic coupling calcs. 77−57896
alkali metal dimers, photodecomp. 79−27049
alkali metal halide, UV photodissoc., metal-atom resonance-line lasers 80−58529
alkali metal molecular, laser radiation absorpt., at. excitation processes 80−32785
alkenes, IR multiphoton dissoc., IR detection of H atoms 80−83356
alkyl bromides, and perfluorinated mols., Br branching ratios, broadband flash photolysis 78−27787
alkyl iodide molecules, photodissoc. by 254 nm radiation 78−3354
alkyliodides, UV photodissoc., time-resolved obs. of $I(^2P_{1/2})$ reactions 80−11940
anharmonic molecules, excitation, by steady-state and pulsed radiation 77−50476
aryl halides, mol. beam photodissoc., fragment translational energy distrib. 77−50481
atmosphere, photon fluxes and photodissoc. rates calc. including mol. scatt. and refl. 79−53512
atmospheric negative ions, photodissoc. and photodetachment 78−66609
atmospheric negative ions, photodissoc. and photodetachment 80−69199
atmospheric positive ions, photodissoc., 5300 to 6700 Å, mass spectroscopic obs. 78−16095
atmospheric water vapour meas. in stratosphere by photodissociation with Lα 78−77369
axial-recoil photofragmentation, detector integrated angular distrib., photoexcitation depend. on target orientation, anal. 78−56564
bent triatomic mol., photodissoc. rot. distrib. 80−95694
benzaldehyde, photoionisation mass spectra formation by UV laser radiation *(Russian)* 80−93781
benzene, mol. beam, fragmentation by reson. enhanced multiphoton ionisation 79−54213
benzene, multiphoton ionisation fragmentation patterns, statistical theory 80−95693
benzene, photoionisation mass spectra formation by UV laser radiation *(Russian)* 80−93781
benzoyl peroxide, photodecomp. low temp., isotope effects 77−42365
benzyl radical, in solid Ar, absorption and photodissociation spectra 80−69156
biomotrifluoromethane, multiphoton dissoc., isotopically selective 80−28113
bond rupture reactions in multiphoton dissoc. 79−47947
bromobenzene molecular ion+neutral atom, collisional relax., 2-photon photodissoc. 79−18258
bromomethane, IR multiphotonic excitation, depend. on cell geometry, mol. fluoresc. and decomp. obs. 80−83430
bromomethane, multiphoton vacuum UV photodissoc. obs. and interpret. 80−11939
bromomethane, VUV laser multiphoton dissoc., CH excited state branching ratio, chemiluminesc. 78−70884
bromotrifluoromethane, IR multiphoton dissoc. 79−18243
bromotrifluoromethane, IR multiphoton selective dissoc., effect of acceptor radicals 80−66854
bromotrifluoromethane, multiphoton decomp., ^{13}C enrichment 79−830
bromotrifluoromethane cation, photodissoc. by quasi-continuum single IR photon absorption 80−61124
bromotrifluoromethyl cation, IR photodissoc. 80−87188
butene, cations, photodissoc., branching ratio meas., unimolecular decay theory 77−6873
t-butyllithium, dissoc. photoionis. 79−6976
by multiphoton dissociation of CF_3I 79−3592
carbon tetrachloride, isotopically selective dissociation by NH_3 laser radiation 79−41206
carbon tetrachloride, isotropically selective dissoc. by NH_3 laser radiation 78−17815
carbon tetrachloride, mol. vibr. excitation, photodissoc., in strong IR field *(Russian)* 79−89721
carbon tetrahalides, matrix photodissoc. and photoionisation by inert gas reson. radiation 77−83587
chloroacetylene dissoc. and predissoc., state selected unimolecular reaction dynamics 77−36744
chlorodifluoroethane, CW laser-induced reaction, vibr. rate enhancement obs. 80−11922
chlorodifluoromethane, IR multiphoton dissoc., mag. field effect 80−93772
chlorodifluoromethane, IR multiphoton dissociation, laser intensity effects, fluoresc. obs. 79−98168
chlorodifluoromethane, laser induced decomp., nonthermal reaction 79−20387
chlorodifluoromethane, laser-induced decomp. rate, laser fluoresc. investig. 79−68257

molecular photodissociation continued
chlorodifluoromethane, unimol. reaction by IR radiation, rate consts. and prod. yield, fluence and intensity depend. 80−97713
chloroethane, reson. multiphoton dissoc. 80−53077
chloroethane molecular ion, laser induced photodissoc. in gas phase 79−94048
chloroethane-d_1, laser multiphoton dissoc., intramolecular isotope effect 78−17733
chlorofluorocarbons, stratospheric photodissoc., residence times 78−53703
chlorofluoroethane, multiphoton dissoc. under CO_2 laser irrad., decomposing mol. energy distrib. 80−30251
chlorofluoromethanes, collision-free multiphoton dissoc., X CF_2 translational energy meas. 78−92491
chloromethane-d_3, multiphoton IR C-Cl dissoc. classical trajectory calc. 78−11532
chloromethanes, VUV fluoresc., UV multiphoton dissoc. 80−28076
chloropentafluoroethane, isotopically selective multiphoton dissoc., CO_2-laser wavelength, pressure and additives effects 80−78666
chloropentafluoroethane, multiphoton dissoc., crossed laser and mol. beam obs. 80−11908
chloropentafluoroethane-(He)(Xe)(O_2)(H_2)(NO), multiphoton dissoc., ^{13}C enrichment factor, CO_2 laser wavelength and fluence depend. 80−58331
chlorotrifluoroethane, IR photoreaction *(Japanese)* 80−11885
chlorotrifluoromethane, multiphoton dissoc., ^{13}C enrichment *(French)* 80−91615
chlorotrifluoromethyl cation, IR photodissoc. 80−87188
coherent multiphoton processes, effective two level hamiltonian 78−29921
collisionless dissociation in intense reson. wave field 77−13640
collisionless dissociation mechanism, vibr. nonlinear mechanics in high-intensity laser field 79−41207
comets neutral atmospheres, average random walk model for mol. phot. dissociation 80−77351
complex molecules, laser induced dissoc., thermal energy effects 80−53071
complex molecules, photoinstability and quenching effect on laser generation kinetics 80−3390
complex molecules, triplet state, photoinstability and quenching effects on lasing kinetics *(Russian)* 79−13778
conference, electronic and atomic collisions, Paris (July 1977) 78−58758
cyanoacetylene, photodissoc., CN radicals fluoresc. 79−52725
cyanomethane, IR laser photofragmentation $CN(X^2\Sigma^+)$ radical energy partitioning, rovibronic distrib. 77−61813
cyanomethane-d_0, -d_3, vacuum UV photodissociation spectroscopy 79−834
cyanotrifluoromethane, vacuum UV photodissociation spectroscopy 79−834
cycloalkane, mol. ion struct., photodissoc., charge transfer, ICR obs. 79−45774
cyclobutanone, absorpt. of pulsed IR radiation and decomp., joulemeter and opto-acoustic obs. 80−58328
cyclopropane, triplet states, electron impact and photosensitised dissoc., chem. effects 77−14592
decay processes, reduced model theory 77−50480
diaminoazobenzene, photodecomp., low temp., isotope effects 77−42365
dianthracene, photodissoc., electronically excited products 78−27790
diatomic hetero-nuclear molecules, dissociation in intense IR fields 77−71841
diatomic molecule, IR multiphoton dissoc. with 1 or 2 lasers 79−86015
diatomic molecule, photodissoc. cross section, dipole moment, Poschl-Teller oscill. model 78−55210
diatomic molecule, photopredissoc. fragment, ang. distrib. in mag. field 79−89716
diatomic molecule, vibr. Green's function and two-photon dissociation 80−28075
diatomic molecules, chem. relax. in dissoc. kinetics during laser excitation 79−31630
diatomic molecules, form. and dissoc. in interstellar medium 80−23471
dibromodifluoromethane, laser-induced dissoc., CF_2 vibr. distrib. 77−88511
dibromofluoromethane, photolysis, IR matrix isolation spectra of CF_2Br free radical 78−27788
dichlorodifluoromethane, dissociation by CO_2 laser radiation into trifluorochloromethane 78−40062
dichlorodifluoromethane, infrared multiphoton processes, apparent step cross-sections, pulse spatial structure, irradiation techniques 80−32792
dichlorodifluoromethane, isotopically selective photodissoc. 79−86013
dichlorodifluoromethane, laser-induced dissoc., CF_2 vibr. distrib. 77−88511
dichlorodifluoromethane, threshold multiphoton dissoc. Cl_2 elimination 80−9653
dichlorodifluoromethane, UV photodissoc. cross-section, 223 and 296K 79−52729
dichlorodifluoromethane energy threshold effects in collisionless dissociation by IR laser radiation 77−58096
1,2-dichloroethylene, photodissoc., photoisomerisation, sensitised laser-induced reactions 78−7179
dichlorofluoromethyl peroxynitrate, UV absorpt., spectra, photodissoc. lifetime meas. 80−83386
1,1-difluoroethane, IR multiphoton dissoc., inert gas collision effects 79−16021
1,1-difluoroethylene, IR multiphoton dissoc., inert gas collision effects 79−16021
dimethyl ether, multiphoton selective dissoc. induced by pulsed CO_2 laser 79−20381
dimethyl s-tetrazine, two-photon laser photochem., hole burning appls. 80−21304
dimethyl-s-tetrazine, vapour, mol. fluoresc., photodissoc. product 80−81352
2,5-diphenyl-1,3,4-oxadiazole, fluoresc. quantum efficiency, one-photon dissociation, temp. depends. 80−69180
diphenylmercury, mol. photoionisation, up to 13.5 eV, formation of $HgPh^+$ 78−25633
dye laser deterioration, effect on performance 80−83602
energy deposition by multiple IR photon absorpt. 80−66833
ethane, photolytic decomp. to ethylene via triplet ethylidene, MINDO/2 calcs. 78−64869
ethanol, collisionless production of $C_2(a^3\pi_u)$ in intense IR laser field 78−55206
ethanol, multiphoton absorpt. and dissoc. 80−99530
ethanol, multiphoton UV photodissoc. 78−50602
ethanol, vap., decomposition by HF pulses IR laser irrad., press. depend. 78−85176
ethyl cyanide, collisionless production of $C_2(a^3\pi_u)$ in intense IR laser field 78−55206
ethyl vinyl ether, IR multiphoton dissoc., branching ratio and laser pulse duration 78−80772
ethylamine, collisionless production of $C_2(a^3\pi_u)$ in intense IR laser field 78−55206
N-ethylcarbazole, soln., laser induced ionic photodissoc., transient polyelectrolyte form. 80−53068
ethylene, dimer and trimer, dissoc. following photoionis. of mol. beam 79−57212
ethylene, laser-induced IR photolysis mechanism 78−56909
ethylene, multiphoton absorption, luminesc. and dissoc. in laser pulse field 78−1040
ethylene, multiphoton dissoc., CH_2 and C_2 prod., fluence depend. meas. 80−5586
ethylene, multiphoton UV photodissoc. 78−50602
ethylene, TEA laser induced multiphoton dissoc., model and expt. 79−16016
ethylene(-d_4) clusters, IR photodissoc. 80−89506
ethylene dibromide, photoabsorption and photodissociation, 190-300 nm 79−50038
ethylene dimer, CO_2 laser induced photodissoc., pulsed mol. beam obs., van der Waals bond 80−9660
ferrocene, multiphoton dissoc. and ionisation by tuneable dye lasers 80−99524
flashtube-pumped photodissociation laser with improved characteristics 79−76712
fluoride, F atom quantum yield meas. in chem. laser 78−58753
fluorinated organic iodides, absorpt. spectra and primary photolysis processes, near and vac. UV 79−20393
fluoroethanes, IR multiphoton dissoc., HF vib. energy distribs. 80−53073
fluoroethanes, IR photodissoc. by multiphoton absorpt., collisional effects 79−36713
fluoroethylenes, IR multiphoton dissoc., HF vib. energy distribs. 80−53073
fluoroethylenes, IR photodissoc. by multiphoton absorpt., collisional effects 79−36713
fluoroform-d, laser isotope separation of D multiphoton dissoc. 79−94096
fluoroformaldehyde, pot. energy surface characts., substitution effect 80−89505
fluoromethane, deuterium separation at high press. by ns CO_2 laser multiple-photon dissoc. 80−91616
formaldehyde, $^1A_2$-state, radiative and nonradiative decay calcs., rel. to photochem. decomp. 78−37669
formaldehyde, $-d_0$, $-d_1$, $-d_2$, multiple-photon dissociation, intensity and press. depend. 77−88515
formaldehyde, excited state photodecomp., rotationally resolved spectra 77−60088
formaldehyde, ion laser induced photopredissociation, ^{17}O, ^{18}O, ^{13}C isotope separation 77−61871
formaldehyde, laser-induced photodecomposition from single vibronic levels, H atom quantum yield determ. 79−96344
formaldehyde, multiphoton dissoc. by CO_2 laser, intensity/fluence depend. 80−11913
formaldehyde, multiphoton dissoc. intensity depend. 80−28073
formaldehyde, multiphoton dissoc. using focused DF laser, H-isotope separation 79−94094
formaldehyde, near UV predissoc., appl. to heavy water production by laser isotope separation 77−83106
formaldehyde, nonradiative transition rates and predissociation process 77−54574
formaldehyde, normal and deuterated solid films, UV dissociation at 77K 77−29021
formaldehyde, photodecomposition in tropospheric clean air *(German)* 79−53405
formaldehyde, photodissoc., H_2 and CO relative quantum yields, 270-360 nm 78−44384
formaldehyde, photodissoc., pot. energy surface features 79−79271
formaldehyde, UV photopredissociation, H-laser isotope separation 79−94095
formaldehyde (A^1A_2) single vibronic level photolysis, H atom prod., HNO chemiluminescence 77−9108
formaldehyde photopredissociation, laser isotope separation of D 78−55040
formaldehyde-d_1, multiphoton dissociation, pulse duration and collision effects 79−835
formaldehyde-d_2, reson. multiphoton dissoc. 80−53077
formic acid decomposition by IR laser radn., photochem. isotope enrichment 79−52712
Franck-Condon transition amplitudes, semiclassical evaluation 78−62860
Freon, photochemical ^{13}C and ^{37}Cl isotope enrichment using CO_2 laser pulses 79−36787
Freon 123, deuterium separation at high press. by ns CO_2 laser multiple-photon dissoc. 80−91616
freons, tropospheric photodissoc. rates from solar 1950-2150 Å radiation ground level meas. 79−2345
gas laser with wide-band optical pumping, review 79−31885
gas phase ions, kinetics meas. using time of flight mass spectrometer 77−75240
glyoxal, selected state photodissoc., vibronic effects, CO quantum yield, 1-10 torr 78−37691
glyoxal, vapour, predissoc. in S_1 zero-point level states 80−102544
group IIIA metal halide, UV photodissoc., metal-atom resonance-line lasers 80−58529
haemoglobin, human, liganded, kinetics of alkaline tetramer-dimer dissoc., laser scatt. obs. 78−48749
haemoglobin, nanosec. probe of dynamics using time resolved reson. Raman scatt. 80−94162
haemoglobin-CO reaction kinetics, relax. meas. on photolytic illum. 77−70405
halides, aryl and aryl-alkyl 193 nm photodissoc., fragment translational energy distrib. 80−48048
halocarbons, multiphoton dissociation, product identification 78−37694

molecular photodissociation continued
halogenated hydrocarbon HCl elimination, three and four centre, IR multiphoton dissoc. 79−5137
halogens, dissolved complexed in liq. soln., laser-induced photodissociation for etching 80−100929
halomethanes, UV multiphoton dissoc., photofragment fluoresc. 80−14165
HeH^{2+}, photodissoc., rel. to UV flux deficiency of stellar spectra 80−9654
α-heptacyclene, in solid matrix, photodissoc. quantum yields, fluoresc. temp. depend., phosphoresc. IR spectra 77−25292
heptafluoroiodopropane, photodissoc., appl. in I ring laser 80−48236
hexafluoroacetone, IR multiphoton decomposition, press., fluence, wavelength, temp. depend. 80−7809
hexafluoroacetone, IR multiphoton dissociation, isotopic selectivity and yield, temp. effect 80−53069
hexafluoroacetone, multiphoton absorption and dissociation in strong IR CO_2 laser field 79−98172
hexafluoroacetone, multiphoton dissoc., mechanisms 79−6978
hexafluoroacetone, natural isotopic abundance, selective multiphoton decomposition at threshold 79−89723
bis(1,1,1,5,5,5-hexafluoropentane-2,4-dionato)dioxouranium (VI), isotope selective IR laser induced unimol. dissoc. 80−69197
hexafluoropropyl cation, laser multiphoton dissoc. probabilities, collisional enhancement 79−68277
highly excited molecular systems, high energy photochem. 80−66831
hole burning, photophysical and photochemical theories 80−58322
homonuclear diatomic mols., Morse pot. and vibr. level field induced, shift and broadening 80−69117
inert gas dimer ions, $A^2\Sigma_{1/2u}^+ \rightarrow D^2\Sigma_{1/2g}^+$ system, theoretical absorption spectrum 80−32734
infrared multiphoton dissociation of molecules, review *(Japanese)* 80−11885
infrared multiphoton processes, apparent step cross-sections, pulse spatial structure, irradiation techniques 80−32792
infrared multiphoton processes, reaction rate, scale factors, pulse structure 80−32791
intramolecular dynamics, random coupling model, multiphoton excitation, kinetic eqns. 80−63700
inverted triangle potential, non-symm., appl. to photodissoc. continua 79−74400
iodomethane cation, photodissoc., mass spectrometric obs., isotope effects 77−75241
iodotrifluoromethane, high vibr. state excitation in high-power laser field, spectral characts. 80−91562
iodotrifluoromethane, IR multiphoton dissoc., source of trifluoromethyl radicals 80−26036
iodotrifluoromethane, IR multiphoton selective dissoc., effect of acceptor radicals 80−66854
iodotrifluoromethane, isotope selective photodissoc. by multiphoton vibr. and electronic excitation *(Russian)* 79−59517
ion fragmentation mechanisms and photoelectron spectroscopy, book contrib. 80−14179
ion kinetics in high-pressure laser plasmas 80−64002
ion photodissociation and photofragment spectroscopy 78−66673
ionic fragmentation, translational energy, phase space theory 77−9051
ionic photofragment ang. and energy distribs. meas., ion cyclotron reson. cell 77−31026
IR laser photodissociation 79−52710
IR laser photolysis of polyat. mols. photochem. appls. 80−66835
IR multiple-photon dissociation, laser induced fluoresc. photofragment detect. 80−37840
IR multiple-photon photolysis, fluence-depend. dissociation probabilities calc. 80−32786
IR radiation induced vibr. excitation and dissoc. 77−27135
IR-laser-induced unimolecular reactions by vibr. modes excitation 78−58757
isotope enrichment, laser induced, in inert gas matrix 77−88599
isotope separation, multiphoton dissociation of mols. with high-power CO_2 laser 79−89802
isotope separation by multiphoton dissociation, CO_2 laser appl. 77−88598
isotope separation by pulse-periodic CO_2 laser, multiphoton process 80−9931
isotopically selective dissoc. polyatomic mols., intense IR laser field 77−6868
ketene, in near UV, bimolecular mechanism 78−64870
ketene, multiphoton dissoc., CH_2 and C_2 prod., fluence depend. meas. 80−5586
ketene, photodissoc. threshold energy, $CH_2(a^1A_1\text{-}X^3B_1)$ energy separation 79−8443
ketene, photolysis, methylene singlet-triplet splitting investig. 79−100407
ketene$\rightarrow CH_2+CO$, photodissoc. at 337 nm, visible fluoresc. of CH_2 78−42121
kinetic theory analysis 78−82795
kinetic treatment of molecular dissoc. rate and isotope enrichment coeff. under focused IR laser pulse *(Chinese)* 79−50093
laser, optical excitation by photodissoc. wave propag. in dense gas 80−74352
laser induced isotope separation and selective photochem. reactions 77−77800
laser induced molecular predissociation, by stimulated emission or absorpt. of IR photons 79−54925
laser induced reactions, activation energies, temps. and rate consts. 80−40710
laser ionisation mass spectroscopy, appl. to fragmentation obs. via. multiphoton ionisation 79−54213
laser isotope separation, overview 78−55257
laser isotope separation, review 77−34784
laser radiation, selective action on matter, review 80−7832
laser selective photophysics and photochemistry, book contrib. 79−79273
laser specific and thermal reactions classifications 80−11919
laser spectroscopy conf., Jackson Lake Lodge, WY, USA, 1977 July 78−82666
laser stepwise excitation, coherence versus incoherence 77−18859
laser-controlled unimolecular and bimolecular processes, field-depend. rate const. 80−11906
laser-induced, effective manifold reduction, criteria 80−43123
laser-induced, mass spectrometer design 78−82071
laser-induced fluoresc., excited $B^3\Pi(O_u^+)$ states, collision-free lifetimes of ro-vibr. levels 79−94029
molecular photodissociation continued
laser-induced selective multistep processes: impact on nuclear physics, chemistry and biology 80−61122
linear triatomic mol. photodissociation, fragment ang. distribs., theory 80−23468
linear triatomic molecule, photodissoc. dynamics, moment anal. 78−13557
linear triatomics, photodissociation, coupled eqns. calcs., final states interactions 78−25637
linear triatomics, photofragmentation, vibr. and rot. distrib., quantum anal. 77−14504
metal alkyl compounds, excited metal atom prod. by UV multiphoton dissoc. 79−6974
metal halide vapours, quantum efficiency of fluoresc. excited by photodissociation 79−81421
metal-triiodide vapour two-photon dissociation for atomic transition lasers 80−23679
methane, $1B_1(1T_2)$ state, photodissoc., extended basis calcs. 78−9093
methane, excited states, photochem., ab initio calcs. 77−14371
methane, photodissoc. ionis., 16-41 eV 77−18995
methane, pot. energy surface of excited singlet state, appl. to photodissoc. 79−83440
methane cation, photodissoc., ab initio RHF and MRD CI calcs. 80−95695
methanol, multiphoton decomposition with laser, isotope separation 79−66306
methanol, multiphoton UV photodissoc. 78−50602
methanol, UV multiphoton dissoc., photofragment fluoresc. 80−14165
methanol($-d_3$), multiphoton absorpt. and dissoc. 80−99530
methanol-d_4, dissoc. following photoionis., using coincidence spectrometer 79−54998
methyl alcohol, IR photodissoc., CH prod. 80−97690
methyl amine, photodissoc. products, Doppler spectroscopy 80−53124
methyl bromide, photoabsorption and photodissociation, 190-300 nm 79−50038
methyl chloroform, vap., multiphoton dissoc. by CO_2 laser beam 80−61123
methyl halide ions, unimol. dissoc. and internal conversions, coincidence meas. 77−6869
methyl halides, photodecomp., primary products and secondary reactions 77−90624
methyl iodide photodissoc. laser, kinetic model, cross-section calcs. 80−58530
methyl isocyanide, laser initiated thermal isomerisation, time behaviour of CN radicals 80−11887
methyl isocyanide, vacuum UV photodissociation spectroscopy 79−834
methyl isocyanide photodissoc., cyanide radical energy partitioning chemical laser determ. 78−73063
methyl nitrite, IR multiphoton dissoc., time resolved IR emission from prods. 78−29822
methyl nitrite, N-isotope separation by multiphoton dissoc. in intense IR field 77−68086
methyl peroxynitrate, UV absorpt., spectra, photodissoc. lifetime meas. 80−83386
methylamine, $CH(X^2\Pi)$ and $OH(A^2\Sigma^+)$, production by multiphoton dissociation, rate constant, laser induced fluorescence and chemiluminescence study 79−98135
methylamine, IR multiphoton dissoc., NH_2 prod. fluence depend. 79−68275
methylamine, multiphoton discoc., N isotope separation 80−35553
methylamine, multiple photon dissoc., NH_2 fragments, laser-excited fluoresc. obs. 80−11938
methylamine, multiple-photon dissociation, laser induced fluoresc. photofragment detect. 80−37840
methylbenzene cations, photodissoc. spectra, substituent effects 78−58710
methylchloride, $CH_3Cl^{\cdot+}$, photofragmentation at 366 nm 78−58752
methylchloroform, vapour phase, UV absorpt. spectrum, photodissoc., stratospheric appls. 79−81208
methylcyanide, photodissoc., CN radicals fluoresc. 79−52725
methylnitrite VUV photodissoc., NO electronically excited photofragment identification and quantum yield 80−99527
molecular laser, optical pumping in damped photodissoc. wave propag. in dense gas 80−99714
molecular photoselected excited states, dynamics, advances using synchrotron radiation 80−37836
multiphoton,, crossed mol. and laser beam obs. 79−41208
multiphoton absorption modelling, using SF_6 energy-dependent absorption cross sections 80−32789
multiphoton disso. of polyatomic mols., population distrib., phenomenological model 78−33560
multiphoton dissociation, polyatomic mols., dissoc. dynamics 78−82802
multiphoton excitation, molecular dynamics 77−29019
multiphoton high order processes, 3/2 power law, saturation effects 77−14500
multiphoton ionisation and fragmentation, UV laser induced, time of flight mass spectra 79−31625
multiphoton IR decomposition, approx. model and exact soln. of energy grained master eqn. 80−66829
multiphoton IR dissociation yields, new technique, appl. to CF_3I 79−100406
multiphoton IR photodissoc., pot. energy surface classical trajectory calcs. 78−11532
multiphoton mol. dissoc., ground state polyatomic mol. photofragmentation theory 77−27128
multiphoton photofragmentation of large mols., random coupling model 79−68281
multiphoton processes, high order, review 78−82797
naphthalene molecular ion, two and four photon absorpt., dissoc. 80−74210
neopentane, unimolecular ion dissociation branching ratios and kinetic energies 77−502
nickelocene, multiphoton dissoc. and ionisation by tuneable dye lasers 80−99524
nitromethane, multiquantum absorption in intense IR field, isotope shift 77−19000
nitromethane, photodissoc., vibr. excited NO_2 form., fluoresc. obs. 78−37693
nitromethane molecule dissociation in IR field, laser-induced fluoresc. obs. 80−53075

molecular photodissociation continued
2-nitropropane, photodissoc., vibr. excited NO_2 form., fluoresc. obs. 78−37693
nonlinear optical processes in atoms and mols. using inert gas halide lasers 79−59745
optically active chiral molecules, photodissoc. fragments, ang. distrib. theory 77−10713
organic scintillators, vap. phase dye laser media, photophysical parameters 80−95884
paraterphenyl, fluoresc. quantum efficiency, one-photon dissociation, temp. depends. 80−69180
paraterphenyl pumped by pulsed laser radiation, photodissociation 79−98353
perfluoroalkyl halides, at. I form., quantum yields 78−3355
perfluoroalkyl iodides, laser photolysis, quantum yields 79−29382
photofragment distrib. in two-photon photochem., isotope separation appl. 80−81344
photofragment spectroscopy of mol. ions using fast ion beams 80−9755
photofragments produced by tunable VUV monochromator, laser induced fluoresc. 78−90316
photoinduced recombination of atoms and radicals 79−5170
photostimulated recombination of atoms after mol. photodissoc. 79−57263
picosecond relaxation processes in chemistry, book contrib. 77−61788
poly N-vinylcarbazole, soln., laser induced ionic photodissoc., transient polyelectrolyte form. 80−53068
polyatomic, dissociation by IR laser radn. 77−6866
polyatomic ions, IR photodissoc. 80−87188
polyatomic molecule, anharmonic model for mol. photoexcitation 80−9669
polyatomic molecule, collisionless dissociation in strong IR laser field *(Russian)* 77−34709
polyatomic molecule, collisionless multiphoton dissoc., threshold behaviour, nonthermal theory 80−11905
polyatomic molecule, high vibr. level excitation and dissoc. in laser field *(Russian)* 77−27132
polyatomic molecule, laser photochem. dissoc., isotope effect rel. to dissoc. probability 80−23472
polyatomic molecule, multiphoton absorpt. resons., dynamic Stark splitting 80−9670
polyatomic molecule, multiphoton collisionless dissociation via intramolecular amplification 77−30936
polyatomic molecule, multiphoton dissoc. dynamics, classical model 80−11904
polyatomic molecule, photodissoc. probability, freq. depend. 77−14506
polyatomic molecule, radiative dissoc. in laser field *(Russian)* 78−9207
polyatomic molecule, theory of multi-photon photo-dissociation in intense IR laser field *(Chinese)* 79−50094
polyatomic molecule, vibr. excitation in strong IR field, rot. level emptying *(Russian)* 77−75235
polyatomic molecule dissociation in IR laser field *(Chinese)* 80−106363
polyatomic molecule radiactive dissociation model 80−43124
polyatomic molecules, collisionless dissoc. mechanism in laser field *(Russian)* 78−37696
polyatomic molecules, collisionless dissociation by multiphoton IR absorption 77−54580
polyatomic molecules, cyclopropane, selective bond breaking by multiple IR photon absorption 80−66834
polyatomic molecules, dissociation by intense IR laser field 77−54579
polyatomic molecules, high vibr.-rot. state excitation and dissociation by IR field 79−41205
polyatomic molecules, IR laser sensitised chem. reactions 80−11910
polyatomic molecules, IR photodecomp. mechanism 79−52716
polyatomic molecules, multiphoton dissoc. and isotope separation 78−62865
polyatomic molecules, multistage IR dissoc., collisionless energy-gathering process 80−99526
polyatomic molecules, photodissociation dynamics, review 78−37697
polyatomic molecules, photofragmentation, time depend. formulation 79−831
polyatomic molecules, photofragmentation obs. methods 80−63725
polyatomic molecules in laser radiation field, transition influence between similar energy states 79−18244
polyatomic mols., absorpt. lineshape 77−79662
polyatomic mols., excitation and dissoc., intense IR laser radiation 77−83570
polyatomic mols., laser induced isotope enrichment, selective vibr. excitation mechanisms 77−18994
polyatomic mols., multiple photon IR processes, reviews 80−43125
polyatomic photofragmentation 77−6874
polyatomic symmetric molecules, collisionless dissoc. and vibr. spectum of degenerate modes 80−18893
polyatomic symmetric molecules, selective multistep IR dissoc. 80−23473
polyatomics, polarised photofluoresc. excitation spectra 79−52727
polyatomics, small, photodissoc. dynamics, isolated mol. behaviour and collision induced effects 79−11807
polyethylene terephthalate, simultaneous mech. loading, UV rad. effects on overstrained chem. bonds 79−52706
polyurethane, dithiodiglycol-plasticised, time-crosslinked density reduction, photochem. scission obs. 78−52920
POPOP, fluoresc. quantum efficiency, one-photon dissociation, temp. depends. 80−69180
POPOP pumped by pulsed laser radiation, photodissociation 79−98353
population trapping during laser induced molecular excitation and dissociation 80−1035
positive cluster ions, photodissoc. by CW and pulsed laser radn. 77−88513
positive ions, photodissoc. 79−52715
positive ions, photodissoc. spectra with time-of-flight anal. 79−50096
PPD pumped by pulsed laser radiation, photodissociation 79−98353
propane, unimolecular ion dissociation branching ratios and kinetic energies 77−502
propane and deuteropropane, fragmentation, threshold photoelectron photoion coincidence mass spectra 77−14505
propene, triplet states, electron impact and photosensitised dissoc., chem. effects 77−14592
propynal, IR photochem. in electronically excited state 80−11923
pulsed molecular beam experiments employing electromechanical valve 80−63870

molecular photodissociation continued
purification of materials, selective dissociation by IR laser radiation 77−79708
pyrimidine N_2O aq. solns., dimer formation in γ-radiolysis, chromatographic obs. 80−7785
quantum corrections to classical models 78−55205
quantum nonlinear oscillators, theory of excitation of harmonic force *(Russian)* 77−79663
radiationless relaxation processes, nonrandom sequential coupling influence 78−90205
radiative electron transitions *(Russian)* 79−98212
recombination afterglow, quenching var., activator penetration to region inaccessible to quencher 80−64813
resonant photocatalytic effect, in laser induced uni-mol. dissoc. 80−3377
rotational heating during IR multiphoton excitation, dynamical effects on dissoc. products 80−18892
s-tetrazine, two-photon laser photochem., hole burning appls. 80−21304
selective dissociation, ionis., and chem. reaction stimulation, by ultra-short pulses, isotope separation *(Russian)* 78−29825
selective nonresonant dissociation, possible isotope separation appl. 77−75244
simple molecules, two-photon dissoc., spectrosc. obs. 80−32787
single/multiphoton dissoc., ab initio theory 78−17735
small molecules in solid matrix, cage effect 79−52728
solar heat storage using chemical reactions, review 77−86333
sub-Doppler laser spectroscopy of mol. ions in fast ion beams 80−9655
switched, for inversion of atomic and molecular species 80−74206
tetrachloromethane, UV photodissoc., mechanism and quantum yield 79−52723
1,2,4,5-tetracyanobenzene complexes, electron donor-acceptor interaction, ionic photodissoc. yield 79−6975
tetrafluorodilhietane, IR photolysis, multiphoton dissoc. models 80−30253
tetramethyldioxetane, IR laser dissociation, chemilum. spectrum 79−5171
tetramethyldioxetane, multiphoton dissoc., collisional vibr. relax., rate eqns. model 80−63729
tetramethyldioxetane, multiphoton dissoc. time depend. 79−16020
s-tetrazine, dimethyl-s-tetrazine, photodissoc., in hexane soln., Ar matrix, and mol. cryst. 78−73059
sym-tetrazine, isotope selective mol. spectroscopy and isotopically pure mols. prod. with dye laser 80−11926
s-tetrazine, laser photodissociation, product vibr. excitation 78−88652
s-tetrazine, UV and vis. photodissoc., three-body half-collision dynamics 80−78664
s-tetrazine in Ar matrix, laser induced isotope enrichment 77−88599
thiophosgene, photolysis, $^1A_2$-state lifetime, fluoresc. 77−52653
time of flight spectroscopy, particles in excited state produced via IR laser excitation 80−74257
toluene cation in solid Ar, absorption and photodissociation spectra 80−69156
triamino-trinitrobenzene, UV and shock-induced decomp. XPS obs. 79−31595
triatomic molecule, IR multiphoton dissoc., quantal and classical calcs. 80−83431
triatomic molecules photodissociation to diatomic fragments, fluoresc. polarisation excitation spectroscopy 80−28054
triatomic van der Waals complex, vibr. predissoc. and photodissoc. lifetimes 80−9661
tribromoethanol UV storage films, HBr prod. and sensitivity optimisation *(German)* 79−14068
tribromomethane, multiphoton dissoc., free radical prod. 79−61842
tricarbocyanine, laser dyes, flashlamp-pumped, photochemical stability 80−83604
1,1,2-trichloro-2,2-difluoroethane, vac. UV photodecomp. 80−66828
trichlorofluoromethane, ion pair formation by photoionisation 79−89718
trichlorofluoromethane, UV photodissoc. cross-section, 223 and 296K 79−52729
trichloromethyl peroxynitrate, UV absorpt., spectra, photodissoc. lifetime meas. 80−83386
trifluoremethane-d_1, IR photolysis, kinetics of multiphoton dissoc., ^1H isotope separation 79−79276
trifluoroacetyl iodide, UV photodissoc. into three fragments, expt. and trajectory calc. 79−70356
2,2,2-trifluoroethanol, multiphoton absorpt. and dissoc. 80−99530
trifluoroformamide, photodissoc., obs. of NO ($v=1$) 78−74712
trifluoroiodomethane, high press., selective isotope dissociation with pulsed CO_2 laser 79−72370
trifluoroiodomethane, isotopic sensitivity of IR laser photodissociation 80−7805
trifluoroiodomethane, laser, excited I atom accumulation, kinetic eqns. 77−3576
trifluoroiodomethane, laser isotope separation by multiple photon IR excitation and subsequent UV dissoc. 79−18301
trifluoroiodomethane, multiphoton dissoc., isotopically selective 80−28113
trifluoroiodomethane, multiphoton IR excitation and dissoc. *(Russian)* 80−35562
trifluoroiodomethane, multiple IR photon excitation and dissoc., primary characts. 80−11909
trifluoroiodomethane, UV absorpt. spectrum broadening by laser-induced vibr. excitation 80−53050
trifluoroiodomethane cation, photodissoc. by quasi-continuum single IR photon absorption 80−61124
trifluoroiodomethyl cation, IR photodissoc. 80−87188
trifluoromethyl chloride, IR multiphoton dissociation, isotopic selectivity and yield, temp. effect 80−53069
trifluoromethyl halides, multiphoton dissoc. products, ^{13}C enrichment 79−18302
trifluoromethyl iodide, ^{13}C isotope separation by selective multiphoton dissoc. 78−25734
bis-trifluoromethyl phosphine iodide, stimulated emission, photodissoc. laser appls. 79−10295
trihalonitromethanes, mol. dissoc. lifetime in atmosphere 79−22720
trihalonitrosomethanes, mol. dissoc. lifetime in atmosphere 79−22720
two photon absorptivity, ion cyclotron reson. photodissoc. spectra, CNDO/S-CI-perturbation theory 80−74123
unimolecular decay, laser driven polyatomic mols., rate eqn. anal. 79−87862
unimolecular decomposition, photon catalysed, first-order rate constant 80−99528

molecular photodissociation continued
unimolecular photodissociation, laser field induced, semiclassical theory 78−62863
unimolecular processes, electronic, vibr., rot. and translational energy partitioning 79−36712
unimolecular reactions, laser-induced, by multiphoton IR excitation, theory 80−9664
unimolecular reactions induced by monochromatic IR radiation, intensity and laser energy fluence influence 80−11903
uranyl hexafluoroacetylacetonate tetrahydrofuran, IR laser photodissoc., O and U isotope selective 80−50868
van der Waals molecules, photo-induced vibr. predissoc. 79−41209
van der Waals mols., vib. predissoc. 78−55215
vanadyl phthalocyamine dye solns., laser destruction, highly excited states participation 78−53231
vinyl chloride, multiple IR photon dissoc. 77−88510
vinyl cyanide, IR multiphoton dissoc., CN internal energy distrib., time depend. 80−78638
vinyl fluoride, IR multiphoton dissoc., inert gas collision effects 79−16021
water solar photodecomposition, redox reaction thermodynamics 80−35697
XY_2, collinear photodissoc., UV spectra vibr. struct. 77−18936
XY_2, symmetric triatomic molecules, photodissoc., time depend. theory 78−66610
AlH_3, photolytic decomp. using high-intensity UV light 78−92472
Ar:N_2O, $O(^1S)$ photodissociative prod., photoluminesc. excitation spectra, exciton energy transfer 80−89508
Ar:OCS, $O(^1S)$ and $S(^1S)$ photodissociative prod., photoluminesc. excitation spectra, exciton energy transfer 80−89508
Ar_2^+, photodissoc., pot. curves and photofragment spectra 77−88514
Ar_2^+, photodissoc. cross sections at 3.0 and 3.5 eV 78−62861
Ar_2^+, photodissoc. cross-section, 6200-8600 Å 78−78761
Ar_2^+, photodissoc. mass spectrometric obs. 77−6867
Ar_2^+, photodissociation cross sections, 3500-5400 Å 79−81243
Ar_2^+, vibr. excited, form. by assoc. ionisation, photodissoc. 79−68279
$AsCl_3$-CCl_4($C_2H_4Cl_2$) mixtures, purification by selective photodissociation 77−79708
AsI_3, mol. beam photodissoc. 78−56906
BCl_3, strong IR CO_2 laser field, isotopically selective dissociation 79−18245
BR_2, laser induced photodissoc. in vis. continuum 79−64059
Bi_2, three photon excitation, Bi Rydberg series 80−106280
Br+NOBr, primary and secondary photochemistry, vibrationally excited NO, IR fluoresc. obs. 80−48030
Br_2, laser-induced photodissoc. spectroscopy 77−90614
Br_2, photolytic cage effect in high-press. gases, laser wavelength depend. 80−11925
Br_2-CO_2 chem. pumped photodissociation laser, output energy increase by WF_6 addition 79−45939
BrCN, photodissoc. energy disposal, electronic branching, vibr. and rot. transfer, CN(B→X) fluoresc. 77−42364
BrCN, vacuum UV photodissociation spectroscopy, quantum yield, fluoresc. polarisation 80−32736
$BrCl_2^-$, photodissoc. and photodetachment, pot. curves. 79−64060
CD_4^+, laser photodissoc. cross sections 78−66611
CF_3NO→CF_3NO, photodissociation dynamics, two-photon laser-induced fluorescence study 80−43122
CH, photoionis. and photodissoc. near ionis. threshold, SCF MO CI and Steltjes imaging 78−58749
CH^+, excited states, pot. curves and transition moments determ. by ab initio CI methods 80−106286
CH^+, ground state photodissoc. cross sections into $A^1\Pi$ state 78−82793
CH^+, photodissoc., $A^1\Pi$ state shape resonances 79−54924
CH^+, photodissociation to C^+ and H, wavelength depend. and photofragment kinetic energies, visible obs. 80−58275
CH_4^+, laser photodissoc. cross sections 78−66611
$C_4H_6^+$, fragmentation, kinetic energy release 77−77737
$C_6H_6^+$, gas, laser-induced-fluoresc., rel. to photodissoc. and Jahn-Teller X and A states distortion 79−72345
CH_3OHF^-, IR photodissoc., fluence depend., saturation effects 80−78663
CN, form. by photodissoc. of parent mols., possible detect. in comets 78−61798
C_2N_2, multiphoton dissociation in UV light 79−54928
C_2N_2, multiphoton UV photodissoc. 78−50602
CO, nonequilib. dissoc. induced by electron-vibr. and IR laser pumping 79−86016
CO photodissoc. ionis., 16-41 eV 77−18995
CO, UV photodissoc., O I 1304 angstrom emission 80−32652
CO_2, 1060-1175 Å photodissoc. quantum yield and $O(^1S)$ decayplots 78−27798
CO_2, C I UV fluorescence spectrum obs. 79−13776
CO_2, Franck-Condon transition amplitudes for mol. dissoc., semiclassical evaluations 78−62860
CO_2 in comet comae, effect of solar photodissociative ionisation 80−90370
CO_2 in lower thermosphere, photolysis rel. to concs. 78−96336
CO_2, negative ion form., photodissoc., mass spectrometric obs. 78−13558
CO_2, photodissoc., CO fluoresc. 77−6836
CO_2, photodissoc., isotope effects 77−75238
CO_2, photodissoc. CO($A^1\Pi$→$X^1\Sigma^+$) transitions, vibr. population 77−58100
CO_2, photodissoc. ionis., 16-41 eV 77−18995
CO_2, photolysis, 1470 and 1302-1306 Å, absolute O atom yield 78−48681
CO_2, photolysis, $O(^1S)$ absolute quantum yield spectral depend. meas. using XeO luminesc. 80−35561
CO_2, selected fragment vibr. energy distrib. in dissoc. processes 78−1036
CO_2, UV photodissoc., O I 1304 angstrom emission 80−32652
CO_2^+, photoionisation reson. spectra and threshold electron-ion coincidence meas. of fragmentation 77−38700
CO_2-H_2O-O_2, gas mixture, photodetachment and photodissoc., mass spectra meas. 77−500
CO_2-O_2, negative ion form., photodissoc., mass spectrometric obs. 78−13558
CO_2-O_2-H_2O, mixture, mol. negative ions, photodissoc. and photodetachment cross section 77−27129
CO_2-O_2-H_2O, photodissoc. and photodetachment of negative ions 80−14182
$(CO_2)_2^+$, photodissoc., mass spectrometric obs. 77−6867
molecular photodissociation continued
CO_3^-, laser photodissociation, tandem quadrupole study 80−81343
CO_3^-, photodissoc. cross-section, excited state vibr. mode determ. 77−6870
$CO_2CO_2^+$, photodissoc. cross sections meas., 3500-8600 Å 79−24763
$COCl_2$, photodissociation, C isotope effects, photocatalysed isotope exchange with CO 77−36764
COS, dissoc. photoionisation, mass spectrometric obs. 79−72366
CS_2, 193 nm laser dissoc., prompt emission and internal energy distrib. of CS 80−106364
CS_2, dissoc. photoionisation, mass spectrometric obs. 79−72366
CS_2, photodissoc., fragment energy distrib. 80−69200
CS_2, photodissoc. below 1600 Å, CS($a^3\Pi$) production, quantum yield, rate const. 77−48658
CS_2, photoionisation and dissociative ionisation due to 60-125 nm light, mass spectra study 79−94044
CS_2, single-photon isotope separation using ArF laser 78−55211
CS_2, VUV photolysis in Ar matrix, thermoluminesc. 77−52659
CS_2^+, photodissociation cross section, UV and visible spectral obs. 80−28077
CdI_2, photodissoc., spectroscopy and dynamics 79−98169
CdI_2, photofragment spectroscopy 79−52718
CdI_2, vapour, excited by photodissociation, fluoresc. yields 78−55138
Cl+NOCl, primary and secondary photochemistry, vibrationally excited NO, IR fluoresc. obs. 80−48030
Cl_2^-, gas phase photodissoc. spectrum 77−58098
Cl_2^-, photodissoc. and photodetachment, pot. curves. 79−64060
Cl_3^-, photodissoc. and photodetachment, pot. curves. 79−64060
ClCN, vacuum UV photodissociation spectroscopy, quantum yield, fluoresc. polarisation 80−32736
ClO $A^2\Pi$-$X^2\Pi$ system, electronic transition moment and dissoc. cross-section meas. 77−38679
ClO^-, photodissoc. and photodetachment, pot. curves. 79−64060
$ClONO_2$, photolysis products, very-low press. meas. 79−29376
$ClONO_2$, solar photodissoc. rates, current levels in stratosphere 79−53496
ClOO, stratospheric chem., formation and loss reactions 78−16138
^{58m}Co III complexes, stability rel. to internal conversion deexcitation, inner shell ionisation 77−42361
$Cr(CO)_6$, photodissoc., Cr prod. 80−95575
CrO_2Cl_2, multiphoton induced inverse electronic relax. 80−66836
Cs orientation in CsI photodissociation by UV light *(Russian)* 80−69201
Cs_2, Cs Rydberg states, diamag. and collisional perturbations 80−58181
Cs_2, fluoresc. spectra induced by laser, energy transfer and dissoc. 79−98141
Cs_2, ion-pair form. in two-photon absorpt. 77−88507
Cs_2, laser-induced photodisintegration *(Russian)* 79−89719
Cs_2, two-photon dissoc., spectrosc. obs. 80−32787
CsI, photodissoc., UV, Cs atom orientation *(Russian)* 80−69201
CsI, saturated photodissoc. by laser pulse, laser reson. ionis. obs. 77−79661
CsX (X=Cl,Br,I), photodissoc. cross sections 77−6876
$D_{2,+}$ photodissoc., fragment Balmer series fluoresc. 77−27020
D_2^+, photodissoc. cross section, time of flight anal. of reaction products 77−83664
DCN, photodissoc., vibr. energy states population meas. 78−58751
DCN, photofragmentation, vibr. distribs. 77−18992
DCN, selected fragment vibr. energy distrib. in dissoc. processes 78−1036
DN_3, IR multiphoton dissoc., form. and reaction of electronically excited ND 78−80771
D_2O, polarised photofluoresc. excitation spectra, VUV photodissoc. excited state lifetimes 78−5261
F_2, recombination const. meas. of atomic F 77−36749
F_2, valence electronic states, $^1\Pi_u$←$X^1\Sigma_g^+$ absorption spectrum 79−63920
FCO, form. in Ar matrix, vibr. and electronic spectra, valence force potential determ., mol. photodissoc. obs. 80−85170
FNO_2, UV photoabsorption spectrum 79−10123
H^- photofragments angular distribution, parity favoured electric dipole transitions 80−58330
H_2, $B^1\Sigma_u^+$ state, selectively excited continuous vac. UV emission obs. 79−13667
H_2, diabatic and reson. states, dissociative photoionisation calcs. 80−47883
H_2 dissociation efficiency, meas. by Wrede-Harteck method 79−72369
H_2, dissociative photoionis. at 26.9 eV 77−3423
H_2, dissociative photoionisation, 19.8-40.8 eV, proton kinetic energy spectra 79−68273
H_2, H(2S)→H(2P) conversion, efficiency measurement 79−45775
H_2, H(2s)/H(2p) branching ratio, photodissoc. near threshold 78−21983
H_2 in interstellar clouds, photodestruction in H to H_2 transition region 79−25672
H_2, photodissoc., fragment Balmer series fluoresc. 77−27020
H_2 photodissociation, formation of excited H atoms *(Russian)* 79−3506
H_2, photodissociation, near threshold, excited atom prod. 79−86019
H_2, photodissociation cross section, excited atom form., 620-350 Å 79−86018
H_2, photoionisation, dissociative, at 304 Å, photoion ang. distribs. photoelectron channels 78−82792
H_2, Rydberg state predissoc., Lyman and Balmer emission obs. 77−38702
H_2^+, photodissoc., mass spectra 80−86489
H_2^+, vibr. Green's function and two-photon dissociation 80−28075
H_3^+, photofragmentation, time depend. formulation 79−831
H_3^+, photofragmentation vibr. energy levels and wavefunctions calcs. 78−42143
HBr, laser photodissociation, ^{81}Br isotope enrichment 80−1075
HBr, vibr. excited, photodissoc. cross-section meas. 79−89717
HCN, Franck-Condon transition amplitudes for mol. dissoc., semiclassical evaluations 78−62860
HCN, H-CN dissoc. curves, SCF CI calc. 79−100405
HCN in neutral cometary atmospheres, photodissoc. rel. to CN prod. 80−82303
HCN, photodissoc., CN radicals fluoresc. 79−52725
HCN, photodissoc., isotope effects 77−75238
HCN, photodissoc., photoabsorpt., photoemission and CN form. obs. 80−87141
HCN, photodissoc., vibr. energy states population meas. 78−58751
HCN, photodissociation coupled eqns. calcs., final states interactions 78−25637

molecular photodissociation continued
HCN, photofragmentation vibr. and rot. distrib., quantum anal. 77−14504
HCN, photofragmentation, vibr. distribs. 77−18992
HCN, photofragmentation, initial excitation effects calcs. 78−17734
HCN, predissoc. in photodissoc., CN radical ($A^2\pi$-$X^2\Sigma$) fluoresc. 77−38691
HCN, selected fragment vibr. energy distrib. in dissoc. processes 78−1036
HCl, photodissoc. cross section, from high vibr. levels, Poschl-Teller oscill. model 78−55210
HD^+, laser photodissoc. cross-section calcs. 77−58102
HD^+, vibr.-rot. transitions, using new two-photon IR photodissoc. technique 80−23405
HF dissociation with one and two IR lasers, classical mech. treatment 80−23470
$H_2^+(HD^+)$, IR photodissoc. cross sections, calc. and simulation expt. 80−9659
HN_3 IR multiphonon dissociation with electronic excitation 80−11934
HN_3, IR multiphoton dissoc. 78−80771
$HN_3 \rightarrow N_2^* + NH^*$, laser photolysis, primary products, energy distrib., intermediate reactions 78−61037
HN_3, photodissoc. ionis., 16-41 eV 77−18995
HNCO, 193 nm photolysis, photodissoc. products, $NH(a^1\Delta)$ internal energy distrib. reaction rate with O_2 79−83489
HNO_3 and H_2O_2, photodissociation, solar radiation effects in atmosphere 79−58045
HNO_3, VUV photodissoc., vibr. and rot. distribs. 80−87191
H_2O, atomic H Lyman-α, Balmer series fluorescence 79−45775
H_2O, D_2O, fragment ion formation on photoionisation, energetics and mechanism 77−501
H_2O, dipole oscillator strengths, 10-60 eV, for photoabsorpt., photoionis. and fragmentation 78−42133
H_2O, gaseous, photodecomposition over TiO_2 and TiO_2-RuO_2 surfaces 80−85194
H_2O, multiphoton UV photodissoc. 78−50602
H_2O, photodecomposition over Pt/TiO_2 catalysts 80−81337
H_2O, photodissoc., H Lyman-α emission 79−10158
H_2O, photodissoc. ionis., 16-41 eV 77−18995
H_2O, photodissoc. resonances, converged 3-dimens. quantum mech. calcs. 80−106366
H_2O, photodissoc. with $OH(A^2\Sigma^-)$ radical form. 79−57270
H_2O photodissociation, $OH(A^2\Sigma^+ \rightarrow X^2\Pi_i)$ yields 80−71927
H_2O, solar photochemical decomposition for H_2 prod. 80−16822
H_2O, VUV photodissoc., vibr. and rot. distribs. 80−87191
H_2O vapour, photodissoc., production cross section meas. for $OH(A^2\Sigma^+$ to $X^2\Pi)$ fluoresc. 78−25604
H_2O, vibr. excitation of OH 77−75242
H_2O_2, in atmosphere, UV absorpt. cross sections and photodissoc, coeffs. 78−42086
H_2O_2, vapour, atmospheric, UV absorpt. cross sections, photodissoc. rate 78−32222
HOCl, HOOCl, stratospheric chem., formation and loss reactions 78−16138
HOCl, photodissoc., ab intio SCF CI calcs. 78−50604
HOCl, photodissoc. cross-sections rel. to prospects as atmospheric Cl reservoir 79−12207
HOCl, photodissoc. rot. distrib. 80−95694
HOCl, UV spectrum, stratospheric lifetime rel. to photodissoc. 79−36661
$H_3O^+(H_2O)_n$, photodissoc. meas. and calc., rel. to atmospheric stability 79−86017
HO_2NO, UV absorpt., spectra, photodissoc. lifetime meas. 80−83386
HO_2NO_2, stratospheric, UV and IR absorpt. cross sections rel. to photodissoc. loss 79−13733
HOO radical, lowest doublet electronic states, rel. to photodissoc. 79−93914
$H_2S(D_2S)$ photodissoc., SH internal energy distribution 80−95697
H_2Te, in Ar matrix, Mossbauer spectra of photodissoc. products. 77−20769
$^2HN_3$ IR multiphonon dissociation with electronic excitation 80−11934
He H^+, formation and destruction in gaseous nebulae, assoc. IR emission line spectrum 79−44589
He photofragments angular distribution, parity favoured electric dipole transitions 80−58330
HeH^+, photodissoc. by electronic and vibr. transitions 78−90244
$HgBr_2$, electronic struct. and photodissoc., effective core pots. and POL(1) CI wave function 80−63560
$HgBr_2$, photodissoc., two-photon excitation of Hg atom 78−90114
$HgBr_2$ photodissociation for laser action on HgBr radical 78−13695
$HgBr_2$ photodissociation by ArF laser, characterisation of transition prod. $HgBr(B^2\Sigma^+)$ 80−37841
$HgBr_2$, photofragment fluoresc. polarisation, press. depend. 80−63720
$HgBr_2$, prolonged optical pumping, photodissociation producing stimulated emission from HgBr 79−18414
HgCl, photodissociation cross section, laser extraction efficiency 80−32972
HgCl, photodissociation calcs., laser efficiency 80−48047
$HgCl_2$, electronic struct. and photodissoc., effective core pots. and POL(1) CI wave function 80−63560
$HgCl_2$ photodissoc., HgCl laser, HgCl(B) state radiative lifetime meas. 78−94390
$HgCl_2$, photodissoc., two-photon excitation of Hg atom 78−90114
HgI_2, photodissoc., quantum yield for $I(5^2P_{1/2})$ 79−11805
HgI_2, photodissoc., two photon excitation of Hg atom 78−90114
$HgI_2(Br_2)$, vapour, excited by photodissociation, fluoresc. yields 78−55138
HgX (X=Br, I), B-state quenching rate consts. from radiative decay of photodissociated mols. 79−54877
I_2, laser dissociation, in gas and soln. *(German)* 78−90240
I_2, multiphoton ionis. and dissoc. vibronic/mass spectra method 79−3507
I_2, nonlinear photodissoc., at. reson. UV fluoresc. and photoionis. obs. 78−37692
I_2, photodissoc., atomic He (1) photoelectron spectrum 80−83325
I_2, photodissoc. cage effect, computer simulation 79−24771
I_2, photolytic cage effect in high-press. gases, laser wavelength depend. 80−11925
I_2, theory of resonant Raman scattering *(Russian)* 78−55180
I_2^+, fragmentation ang. distrib., energy disposal, branching, photoelectron-photoion coincidence spectra 79−68263

molecular photodissociation continued
I_2-aromatic complexes, photodissociation, I-aromatic complex in soln. formation ps laser studies 80−40711
I_2Ar^*, product state distrib. and binding energy 80−63857
IBr, photodissoc., curve crossing of $Br(^2P_{3/2})$ and $Br(^2P_{1/2})$ 78−62859
IBr_2 predissoc. and photodissoc., intermed. coupling strength 77−16850
IBr^+, fragmentation ang. distrib., energy disposal, branching, photoelectron-photoion coincidence spectra 79−68263
IBr:CO_2 photolysis, electron-vibr. pumping, 2.7 μm Br and 4.3, 10.6 μm CO_2 laser transitions 80−28196
ICN, A-state photolysis, $I(^5P_{1/2,3/2})$ branching ratio wavelength depend. 80−81335
ICN, A-system photodissociation mechanism 77−38701
ICN, absorpt. lineshape, intermolecular forces 77−79662
ICN, Franck-Condon transition amplitudes for mol. dissoc., semiclassical evaluations 78−62860
ICN, photodissoc., CN internal state distrib. 77−36773
ICN, photodissoc., efficient $I(5^2P_{1/2})$ prod. 79−94047
ICN, photodissoc., polarised fluoresc. from fragments 79−98130
ICN, photodissoc. and predissoc., cyanide radical fluoresc. excitation spectrum and laser emission 78−76892
ICN, photodissoc. dynamics, moment anal. 78−13557
ICN, photodissociation, coupled eqns. calcs., final states interactions 78−25637
ICN, photofragmentation, vibr. and rot. distrib., quantum anal. 77−14504
ICN, vacuum UV photodissociation spectroscopy quantum yield, fluoresc. polarisation vacuum UV photodissociation spectroscopy, quantum yield, fluoresc. polarisation 80−32736
ICl^+, fragmentation ang. distrib., energy disposal, branching, photoelectron-photoion coincidence spectra 79−68263
I_2He, Van der Waals mol., photodissoc. lifetime, I_2 vibr. depend. 79−6977
I_2He, van der Waals mol., photodissoc. 80−63765
I_2He^*, product state distrib. and binding energy 80−63857
$I_2Ne_aHe_b$ van der Waals complexes photodissoc. 80−50864
I_2Ne^*, product state distrib. and binding energy 80−63857
InI, lasing of at. In at 451 nm 77−14698
InI, vapour, excited by photodissociation, fluoresc. yields 78−55138
K_2, laser-induced photodisintegration *(Russian)* 79−89719
K_2, photodissoc. products of $C^1\Pi_u$ and $C^1\Sigma_u^+$ states 79−98171
KI, near UV photodissoc., at state determ. 79−18105
Kr:OCS, $O(^1S)$ and $S(^1S)$ photodissociative prod., photoluminesc. excitation spectra, exciton energy transfer 80−89508
Kr_2^+, photodissoc. cross sections at 3.0 and 3.5 eV 78−62861
Kr_2^+, photodissoc. cross-section, 6200-8600 Å 78−78761
Kr_2^+, photodissociation cross sections, 3500-5400 Å 79−81243
Kr_2^+, photofragment energy spectra, pot. energy curves 78−55207
Li_2^+, dissoc. energy, laser photodissoc. determ. 78−70950
Li_2^+, photodissoc., effective cross-sections calcs. 79−86014
LiH, laser irradiated, single/multiphoton dissociation, ab initio theory 78−17735
LiI UV photodissoc. cross section, reson. ionis. Li detection 80−63719
MgH, $X \rightarrow A$ and $X \rightarrow B'$ band systems, oscill. strengths and photodissoc. cross-sections 79−94045
N_2 dissociation by electron impact and EUV photoabsorpt., rel. to aurora and airglow 78−58847
N_2, multiphoton absorpt., spectroscopic evidence 80−63726
N_2 photodissoc. ionis., 16-41 eV 77−18995
N_4^+, photodissoc. cross sections meas., 3500-8600 Å 79−24763
N_2F_4, collisionless dissociation kinetics in highpower IR radiation field 80−66853
N_2F_4, mol. photodissoc. using CO_2-laserradiation, rate const. meas., mol. fluoresc. and time-resolved UV spectra obs. *(German)* 80−83434
N_2F_4, ns CO_2 laser pulse, probing by UV and IR beams 77−71840
NH_2 group, rate of dissociation at SiO_2 surface *(Russian)* 78−53233
NH_3, first triplet state, photodissoc. and Rydbergisation investig. 80−53067
NH_3, IR multiphoton dissoc., laser fluoresc. and chemiluminesc. obs. 79−68276
NH_3, multiple photon dissoc., NH_2 fragments, laser-excited fluoresc. obs. 80−11938
NH_3, NH $c^1\Pi$ state anomalous population 79−10133
NH_3 on Pt surface, heterogeneous reaction of decomp., stimulation by CO_2 laser 78−61052
NH_3, photodissoc., ab initio SCF and CI calcs. 78−21984
NH_3, photodissoc. to NH_2, ground state, off-reson. multiphoton absorption 77−14501
NH_3, photodissociation in $A \leftarrow X$ absorption region, D isotope effects 77−77790
NH_3, photodissociation in $A \leftarrow X$ absorption region, translational excitation of H atoms and predissociation mechanism 77−77791
NH_3 remote atmospheric sensing by multiphoton sequential photodissociative excitation 79−48199
NH_3, selective two-step dissoc. by laser, ^{14}N, ^{15}N separation, book contrib. 78−9208
N_2H_4, IR multiphoton dissoc., NH_2 prod. fluence depend. 79−68275
NO, photodissoc. at 184.9 nm, quantum yield, and quenching by N_2 78−80773
NO, photodissoc. in mesosphere and stratosphere, theory 80−41580
NO, photodissoc. ionis., 16-41 eV 77−18995
NO, stratospheric and mesospheric photodissoc. rate, calc. 80−51498
NO, two-photon excitation to levels near and above the dissoc. limit 79−10161
NO^+, fragmentation ang. distrib., energy disposal, branching, photoelectron-photoion coincidence spectra 79−68263
NO_2, $^2B_2$ state photodecomposition in 2nd predissoc. region 77−10712
NO_2 and NO_3, photodissociation, solar radiation effects in atmosphere 79−58045
NO_2, atmospheric, rate constant depend. on altitude 78−11949
NO_2, electronic states, pot. energy surface calcs. 77−6673
NO_2, one-photon dissoc. to NO+O, Doppler spectroscopy 80−53124
NO_2, UV photodissoc. quantum yield, absolute absorption cross section 77−90616
NO_3^-, $NO_2^-.H_2O$, and peroxy isomers, photodissoc. and photodetachment 3500-8250 Å, rel. to ionosphere 80−35554
NO_3^-, $NO_3^-.H_2O$, and peroxy isomers, photodissoc. and photodetachment 3500-8250 Å, rel. to ionosphere 80−35554
N_2O, atmospheric, instantaneous global photochemical reaction rates 80−17335
N_2O, decomposition over particulate matter 79−16014

molecular photodissociation continued
N_2O, O prod. and props. in liq. Ar and N_2 80−43063
N_2O, photoionisation and ion dissoc., isotope effects, mass spectra 78−9203
N_2O, photolysis, $O(^1S)$ absolute quantum yield spectral depend. meas. using XeO luminesc. 80−35561
N_2O, vac. UV photodissoc., kinetic energy and ang. distribs. of fragments 77−30938
N_2O^+, dissoc., threshold photoelectron-photoion coincidence obs. 80−87189
N_2O^+, photodissoc. cross section, time of flight anal. of reaction products 77−83664
N_2O^+, photodissociation 77−34705
NOBr, photoabsorption and photodissociation, 190-300 nm 79−50038
$NONO^+$, photodissoc. cross sections meas., 3500-8600 Å 79−24763
$N_2O(X^1\Sigma^+) \rightarrow N_2(^1\Sigma_g^+) + O(^1S)$, photodissoc., exact collinear calcs. 77−30937
NO_2*, multiple IR photon fluoresc. excitation and dissoc., electronically excited 80−48050
$NO^+.H_2O$, photodissoc. cross sections, mass spectrometric determ. 78−1038
$NO^+.NO$, photodissoc. cross sections, mass spectrometric determ. 78−1038
Na_2, laser-induced atomic fluoresc., semiclassical intensity calc., transition moments 77−18838
Na_2, laser-induced dissoc., polarisation of atomic fluorescence obs. 80−78569
Na_2, laser-induced photodisintegration *(Russian)* 79−89719
Na_2, photodissoc., ^2P products, at. fine struct. anal. 80−78665
Na_2, photodissoc. products of $C^1\Pi_u$ and $C^1\Sigma_u^+$ states 79−98171
Na_2, vibrationally excited, photodissociation cross section 79−13777
Na_2^+, form. from Na vapour excitation, photodissoc. 79−795
Na_2^+, photodissoc., effective cross-section calcs. 79−31627
Na_2^+, photodissoc. and photoionisation in Na_2 multiphoton absorpt. 79−31628
NaBr photodissoc., Na non-Gaussian line shape, level shifting and velocity inversion 80−58182
NaI, inversion and superfluoresc. emission of Na reson. line by selective photodissoc. 78−87040
NaI, photodissoc., perpendicular transition leading to ground state atoms 77−58097
Ne_2^+, photodissoc. mass spectrometric obs. 77−6867
Ne_2^+, photodissociation cross sections, 3500-5400 Å 79−81243
O^-, photodissoc. and photodetachment in $O_2/CH_4/H_2O$ mixtures, 3500-8600 Å 79−45776
O_2, determ. by laser photofragment spectroscopy 78−70957
O_2 in stratosphere and mesosphere, photodissoc. through solar UV radiation absorpt. 80−109248
O_2, ionisation, photodissoc. of positive and negative ions, mass spectrometric obs. 78−13559
O_2, $O(^1D \rightarrow {}^3P)$ and $O_2(b^1\Sigma_g^+ \rightarrow X^3\Sigma_g^-)$ energy transfer 79−11810
O_2, on MgO surface, O_3^- form. 79−100431
O_2, photoabsorpt., photoionis, and photodissoc., dipole oscill. strengths in UV 79−76468
O_2, photodissoc., $O(^1D)$ production quantum yields, 1160-1770 Å 78−33557
O_2, photodissoc. ionis., 16-41 eV 77−18995
O_2, vac. UV photodissoc., kinetic energy and ang. distribs. of fragments 77−30938
O_2^-, photodissoc. and photodetachment in $O_2/CH_4/H_2O$ mixtures, 3500-8600 Å 79−45776
O_2^+, absorpt. linewidth of predissociated levels, lifetimes 79−36711
O_2^+ cluster ions, photodissoc. cross sections meas., 3500-8600 Å 79−24763
O_2^+, $f^4\Pi_g$ state, quasi-bound levels, predissociation, band rot. anal., photofragment kinetic energy anal. 80−63650
O_2^+, first negative system, high-resolution photofragment spectroscopy 80−47971
O_2^+, fragmentation ang. distrib., energy disposal, branching, photoelectron-photoion coincidence spectra 79−68263
O_2^+, laser-induced photodissoc. spectrum 79−68280
O_2^+, photodissoc. by visible light, predissociation 78−66612
O_2^+, predissociated $b^4\Sigma_g^-$ state, high resolution laser spectroscopy in fast ion beam 80−9656
O_2^+, predissociation of $b^4\Sigma_g^-$, $c^4\Sigma_u^-$ states, threshold photoelectron-photoion coincidence 78−42144
O_2^+, quartet states, predissoc. photofragment spectroscopy 78−82794
O_3, atmospheric, annual var. of effects of diffuse solar radiation on photodissoc. 80−109210
O_3, effects of radiation scattered by aerosols 79−2371
O_3 in stratosphere and mesosphere, photodissoc. through solar UV radiation absorpt. 80−109248
O_3, multiphoton dissoc. dynamics, classical model 80−11904
O_3, multiphoton dissociation by IR laser 79−36710
O_3 photodissoc., $O(^1S)$ yield at 1700-2000 Å 80−97714
O_3, photodissoc. cross section, vibr. excitation effects obs. 80−95696
O_3 photolysis at 248 nm, $O(^3P_J)$ direct obs. 80−101028
O_3, UV photodissoc. rate, expt. and theory 80−40722
O_3, UV photofragment spectroscopy 79−10122
O_3^-, $(O_3^-.H_2O)$, photodetachment and photodissoc. cross-sections meas. 79−98170
O_3^-, photodissoc, cross section 79−832
O_3^-, photodissoc. and photodetachment in $O_2/CH_4/H_2O$ mixtures, 3500-8600 Å 79−45776
O_3^-, photoelectron, photodetachment and photodestruction spectra 79−64042
$O_3 + O_2(^1\Delta_g)(O_2$*), UV photolysis, $O(^3P)$ prod., rate consts. determ. 80−55636
$O_3 + O(^1D)$, UV photolysis, $O(^3P)$ prod., rate consts. determ. 80−55636
O_4^-, photodissoc. and photodetachment in $O_2/CH_4/H_2O$ mixtures, 3500-8600 Å 79−45776
O_4^+, photodissoc. cross sections meas., 3500-8600 Å 79−24763
OCS, mol. photodissoc., 142-170 nm, quantum yield of S(^{1}S) 79−83477
OCS, multiphoton dissociation by IR laser 79−36710
OCS photodissociation, S(^{1}S) prod. and props. in liq. Ar and N_2 80−43064
OCS, two photon and vibr. depend. photolytic prod. of S(^{1}S) atoms 79−13775
OCS, UV photolysis producing S($^3D_2$) 79−79274
OCS, VUV photolysis in Ar matrix, thermoluminescence 77−52659

molecular photodissociation continued
OCS^+, photodissociation cross section, UV and visible spectral obs. 80−28077
OCS-N_2-SF_6 mixture laser, OCS photodissociation, electron dipole forbidden transition, absorpt. spectra 79−68389
OCSe, quantum yields for Se, $^1S_0$, $^1D_2$, and $^3P_{0,1,2}$ atoms determ. in photolysis, lifetime and quenching rate meas. 80−97741
OH^-, and OD^-, photodissoc. and photodetachment in $O_2/CH_4/H_2O$ mixtures, 3500-8600 Å 79−45776
$^{18}O^{16}O$, in atmosphere, photodissociation as source of atmospheric O_3 80−94559
$O_{2-3}^-.H_2O$, photodissoc. and photodetachment in $O_2/CH_4/H_2O$ mixtures, 3500-8600 Å 79−45776
$O_3^-.H_2O$ and $O_3^-.2H_2O$, photodissoc, and photodetachment 79−833
OsO_4, IR laser dissociation isotope separation appl. 77−18993
OsO_4, isotope selective dissociation by IR radiation pulses, luminesc. intensity 77−83665
OsO_4, isotope separation by dissociation in two-freq. IR laser field 78−25638
OsO_4, multiphoton absorpt. under two CO_2 laser pulse excitation 78−86925
OsO_4, multiphoton dissociation by two freq. tunable CO_2 laser pulses 78−50606
OsO_4, multiple photon excitation by dissociation yield saturation 79−3505
OsO_4, two IR pulse multiphoton absorpt. selective dissoc., obs. 78−82798
P_4, photoionisation, mass spectra 77−30935
PH_3, laser photolysis, PH and PH_2 radical excited states 79−16023
Pb salts, inorganic 80−77081
Pb_2, three photon excitation, Pb Rydberg series 80−106280
$PbBr_2(I_2)$ photodissociation, stimulated emission obs. on Pb 405.8, 368.3 and 364.0 nm lines 80−87387
Rb_2, laser-induced photodisintegration *(Russian)* 79−89719
Rb_2, photodissoc., ^2P products, at. fine struct. anal. 80−78665
S isotope separation, multiphoton process using high-power CO_2 laser radiation 80−9657
SF_5^+ ion-molecules, IR multiple-photon dissoc., lifetime meas. 80−28072
SF^+_5, ion-mols. in beam, IR multiple-photon dissociation, mass spectroscopic detect. 79−89720
SF_6, absorption of intense IR radiation, statistical model 77−34626
SF_6, CO_2 laser induced dissociation, energy and press. depend. 77−23523
SF_6, collisionless dissociation and isotopic enrichment, using CO_2 laser 77−18999
SF_6, collisionless dissoc. using two reson. freq. CO_2 laser fields 78−5305
SF_6, collisionless dissociation, spectral struct. of low level excitation 78−74714
SF_6, collisionless multiphoton laser dissoc. mechanism 77−503
SF_6, collisionless multiphoton dissoc. rate, statistical thermodynamic process 77−50482
SF_6, collisionless multiphoton dissoc., statistical theory 78−62862
SF_6, collisionless multiphoton dissoc., statistical thermodynamic process 78−82799
SF_6 cooled gas, multiphoton dissociation with CO_2 laser, enrichment with ^{33}S 80−14245
SF_6 dissoc. by multiphoton IR absorption, focused beam approach 78−42369
SF_6, dissociation probability for ultra-short CO_2 laser pulses 77−18998
SF_6 dissociation processes using one or two TEA CO_2 lasers 78−74713
SF_6, dissociation rate increase by red shift of nonresonant freq. under two freq. laser action *(Russian)* 77−58104
SF_6, Doppler-limited spectroscopy, of $3\nu_3$ band 80−58244
SF_6, Doppler-limited spectroscopy of $3\nu_3$ band, rot. const. and anharmonic parameters calcs., mol. photodissoc. 80−83361
SF_6, emission spectrum of ν_3 band, 1780K, dissoc. effects 78−62795
SF_6, energy threshold effects in collisionless dissociation by IR laser radiation 77−58096
SF_6, IR double resonance and energy transfer obs. 77−58105
SF_6, IR laser radiation induced dissoc., isotope separation 77−29026
SF_6, IR multiphoton dissoc., energy randomization 78−21982
SF_6, IR multiphoton dissociation F atoms obs. by chemi-ionis. method 78−31661
SF_6, IR multiphoton dissociation studies, inverse bottle-neck effect 80−87193
SF_6, IR multiphotonic excitation, depend. on cell geometry, mol. fluoresc. and decomp. obs. 80−83430
SF_6, IR photodissoc., hydrogen halides form., IR chemiluminesc. 77−63932
SF_6, in strong IR field, appl. of CO_2 laser for isotope separation 77−83755
SF_6, infrared multiphoton processes, apparent step cross-sections, pulse spatial structure, irradiation techniques 80−32792
SF_6, isotope separation, laser induced multiphoton dissoc. 77−16839
SF_6, isotope separation, selective dissociation using compressed H_2 Raman laser 77−34708
SF_6, isotope separation, TEA CO_2 laser irradiation *(Japanese)* 80−11885
SF_6, isotopic enrichment, coherent multiphoton vibr. excitation and dissociation 77−88512
SF_6, isotopically selective photodissociation under CO_2 laser pulses, geometrical effects 77−16852
SF_6, isotopically selective collisionless laser induced dissoc. 78−1037
SF_6 laser isotope separation, rot. and vibr. relax. in mixture 78−25634
SF_6, laser photodissoc. energy depend. 77−10710
SF_6, laser-irrad., high-resolution double-reson. spectroscopy, collisionless multiphoton dissoc. 80−9623
SF_6, matrix isolated, CO_2 laser irrad., IR absorpt. spectra obs. *(Russian)* 77−6877
SF_6, matrix isolated, IR photodissoc. 78−90245
SF_6, mol. beam, selective dissoc. in intense IR laser field, wavelength and energy depends. 78−73065
SF_6, multiphoton dissoc., producing $SF_5 + F$, ang. and vel. distribs. 77−27130
SF_6, multiphoton dissoc., selective mechanism, mol. beam obs. 79−41210
SF_6, multiphoton dissoc., anharmonic force field, decoupled rigid bender model 79−41153
SF_6, multiphoton dissoc., unified dynamical model 80−5587
SF_6, multiphoton dissoc., collision effects 80−23467
SF_6, multiphoton dissoc., classical model 80−53076

molecular photodissociation continued
SF_6 multiphoton dissoc. by mol. beam method, energy distribution meas. by time-of-flight spectra, dissoc. dynamics 80−78670
SF_6, multiphoton excitation and dissociative ionisation, model 78−58754
SF_6, multiphoton isotope selective dissoc., pulse shape, energy, press. and geometry effects 78−25733
SF_6, multiphoton reaction, laser mode-locking effect 77−46606
SF_6, multiple photon dissociation threshold behaviour, chemilum. obs. 78−42145
SF_6, multiple photon excitation, collisionless 80−53079
SF_6, multiple-photon dissoc. rate determ. 77−60079
SF_6, photoabsorption and ionic fragmentation, 5-63 eV, absolute oscill. strengths 79−72367
SF_6, photodissoc. by IR laser pulse, selectively excited vibr. levels 78−9209
SF_6, photodissociation by IR laser beam *(Chinese)* 78−90236
SF_6, radiative dissoc. in laser field *(Russian)* 78−9207
SF_6, resonant single-photon dissoc. route using prelim. electron excitation 80−9662
SF_6, selective dissoc. in two freq. i.r. laser field 77−504
SF_6, selective multiphoton dissociation by CO_2 laser irradiation 77−34707
SF_6, two IR pulse multiphoton absorpt. selective dissoc., obs. 78−82798
SF_6 type molecule, multiphoton absorption in continuum 78−90247
SF_6, unimolecular reaction model 78−7189
SF_6, vibrationally excited, collisionless intramolecular energy transfer 78−37663
$^{32}SF_6$, infrared multiphoton processes, reaction rate, scale factors, pulse structure 80−32791
$^{32}SF_6$, multiphoton dissoc. by laser pulse, Ar, N_2 and CF_4 environments 78−73061
SF_6-H_2 mixtures, laser irradiated, IR energy deposition and HF fluoresc. 80−23454
SF_6-H_e mixtures, collisionless multiple photon absorpt. photodissoc., HF fluoresc. 77−58099
SF_6-hydrocarbon mixtures, IR laser induced ionis., mechanism 77−81415
SF_6-methane, mixture, CO_2 laser induced multiphoton dissociation and chemilum., laser fluence depend. 79−57233
SF_6+Si(surface), IR laser induced reaction, mol. vibr. and mol. dissoc. obs. 80−93798
SF_5Cl, multiphoton dissoc., real-time Cl atom fluoresc. detect. 78−86923
SO_2, 193 nm photodissoc., photofragment translational energy distrib. 79−74402
SO_2-containing ions, photodestruction 80−63722
$SOCl_2$, photoabsorotion and photodissociation, 190-300 nm 79−50038
SO_2Cl_2, photoabsorption and photodissociation, 190-300 nm 79−50038
$S_2O_6F_2$, heating and laser excitation fluorosulphate radical prod. and spectrum 78−35647
$^{32}SF_6$, multiphoton dissoc., temp. depend. 79−89722
Se_2, photolytic dissoc. obs. using inert gas halide lasers 80−11935
SeF_6, isotopically selective IR photodissociation 78−42142
SiF_4, CO_2 laser irrad., collision induced dissociation, visible fluoresc. 78−66613
SiF_4, dissociation rate increase by red shift of nonresonant freq. under two freq. laser action *(Russian)* 77−58104
SiF_4, energy threshold effects in collisionless dissociation by IR laser radiation 77−58096
SiF_4, interaction with strong IR field, instantaneous luminescence 79−18232
SiH_4, irrad. by CO_2 laser, Si film deposition 80−16190
TlBr, selective photodissoc. branching ratios at 2660 Å, Raman up-convertor appl. 78−90243
TlI, atomic fluorescence, D_2 pressure effect on width and shift 80−99475
TlI, mol. beam photodissoc., bond order and state symm. 77−34706
TlI, photodissoc., Tl 535.0 nm line shift by H_2 perturber 80−91506
TlI photodissociation, Tl atomic fluorescence, pressure and Doppler broadening 80−5504
TlI, photofragment spectroscopy 79−52718
TlI, pumping of Tl atomic laser 79−18411
TlI, vapour, excited by photodissociation, fluoresc. yields 78−55138
U complex, bis-hexafluorocetylacetonate uranyl tetrahydrofuran, laser-induced dissoc. 80−53071
UF_6, collisionless multiple photon absorpt. photodissociation using IR lasers 79−22772
UF_6, IR multiphoton dissociation using 16 μm CF_4 laser 79−22773
UF_6, laser chemistry 80−69198
UF_6, matrix isolation spectra and photolysis 79−50043
UF_6 molecular dissociation by DF_4 laser radiation 80−91619
UF_6 molecule dissociation in two-frequency IR laser field 80−66855
UF_6, photodissoc. through light scatt. of UF_5 particles, influence of N_2 as collisional partner 80−95698
UF_6, photodissociation dynamics at 266 nm, recoil flight time 78−73062
UF_6, UF_6-H_2 gas dissociation in pulsed IR and UV laser fields 80−91620
UF_6-H_2, near UV and visible excitation, quantum yield from photodissociation 80−35549
$W(CO)_6$, photodissoc., W prod. 80−95575
Xe_2^+, photodissoc. cross sections at 3.0 and 3.5 eV 78−62861
Xe_2^+, photodissoc. cross-section, 6200-8600 Å 78−78761
Xe_2^+, photodissociation cross sections, 3500-5400 Å 79−81243
XeF, ground state dissoc. vibr. equilibrium 80−9652
XeF, photodissociation by Xe_2*, excimers inducing blue-green excimer lasing, laser spectra 79−68382
XeF_2, for XeF laser 80−32976
XeF_2, photodissoc. to XeF, stimulated emission 78−71097
XeF_2 photodissociation forming XeF, laser action due to bound-free C(3/2)-A(3/2) transition 80−14334
ZnI_2, vapour, excited by photodissociation, fluoresc. yields 78−55138

molecular polarisability
see also molecular moments
π-bonded mol., atom monopole-dipole interaction model with charge transfer 79−22860
AB_2 and AB_4 molecules Raman overtone and combination transition intensities, bond-polaris. approach 78−42034
acetaldehyde, soln., C-O stretching band intensity calcs., intermol. interaction effects 77−68081
acetic acid amides, polarisabilities and π-π* transitions, dipole interaction calcs. 80−23411
molecular polarisability continued
acetylene, average mol. polarisability, Frost model wavefunctions calcs. using p-type Gaussians 78−41924
acetylene, mean polarisability derivatives, variational calc. procedure 79−27108
acetylene, multipole moments and polarisabilties, SCF calcs. 80−5471
acetylene, near HF dipole polarizability, using EFV GTOs 79−31395
additive-orbital scheme for calculating atomic and molecular polarizabilities 77−3273
alkali halide, hyperpolarizability and dissociation energy 79−72439
alkali halide mols., electronic polarisability, ionic radii and repulsive pot. parameters, mol. consts. 80−87242
alkali halide solutions in DMSO, modelling of interactions 79−77469
alkali metal halide, zero point Compton profile anisotropies and bond polarities, correl. 80−78659
alkali sulphates, SO_4^{2-} optical and spectroscopic props., cryst. environment effect 77−40224
n-alkane gases, depolarised light scatt., internal field effects 79−76471
alkanes, mol. electro-optical props. 79−50162
p-n-alkoxybenzoic acid, homologs, principal mol. polarisabilities calc., refr. indices of nematic mesophase meas. 78−2004
alkyl chlorides, mol. electro-optical props. 79−50162
alkyl halides, conform. energy calcs., polar bonds and polarisability, polaris. model appl. 80−58188
alternant hydrocarbons, polarisabilities rel. to bond orders using Huckel's method *(French)* 79−31405
14-aminopyridine-I_2, charge-transfer complexes, hyperpolarisability 77−34568
anisotropic, optical study *(Rumanian)* 80−74256
anisotropic atom point dipole interaction model calcs., involving electron repulsion 80−78521
anisotropically polarisable molecules embedded in small particles, fluoresc. scatt. 79−76587
anisotropy parameter, rel. to electron density contour diagram 78−66681
anthracene derivatives in solution, polarisability and dipole moments, emission and absorpt. spectra obs. 80−69256
4-(9-anthryl)-N,N-dimethylaniline, fluoresc., dipole moments and polarisabilities 80−1019
antisymmetric light scattering of molecules with non-degenerate electronic state 79−18192
aromatic hydrocarbon crysts., effective mol. polarisability 77−88590
aromatic hydrocarbons, mol. polarisability, INDO calc. 80−52886
asymmetric top molecules, complex polarisabilities, NMR line dipolar broadening 79−54058
atom abstraction reactions, empirical correlation of activation energy and mol. polarisability 78−40038
average, empirical calc. method 80−63859
azabenzenes, multipole moments, polarisabilities and long-range interaction coeffs. calcs. 79−89599
azobenzene, polarisability optical anisotropy 79−72441
benzalaniline, polarisability optical anisotropy 79−72441
benzene, dipole polarisability, finite-field SCF MO calcs. 80−83255
benzene, dynamic polarisabilities, calcs., superposition method of excited config., nonstationary perturbation theory eqns. 80−69257
benzene, excited state props., by electrochromism in polymer matrix 79−22737
benzene, mol. hyperpolarisability meas. by optical SHG 79−22861
benzene, Raman scatt. cross sections 79−6945
benzene, reson. Raman cross sections, forbidden electronic transitions, depolaris. ratios 78−42075
benzene, SCF-EHT polarisability calc. 80−47895
benzene, substituted benzenes, liq., Kerr effect in UV region, mol. optical anisotropy dispersion 78−72488
benzene and monosubstitutes, hyperpolarisabilities, perturbed INDO calc. 79−68189
benzene monosubstitutes, hyperpolarisabilities, perturbed INDO calc., substituent effects, σ-π contributions 79−68190
benzenes, para-disubstituted, liq., 2nd order hyperpolarisabilities, regularities, intramol. charge transfer 79−10353
benzenes, substituted, average mol. polarisability, δ-function calcs. 77−551
benzocondensed five-membered heterocycles continuing S and O, optical anisotropy, depolarised Rayleigh scatt. obs. *(French)* 79−31533
benzyl bromide and chloride, bond orders estimation, bond polarisability derivative 80−32594
benzyl chloride, mol. polarisability, bond polarisability derivatives 78−74793
biomolecules+chloranil, charge transfer interaction, equilib. const., enthalpy and entropy determ., mol. polarisability 80−89708
bond polarity parameters, IR intensities, molecular orbital study 79−63914
bounds on van der Waals coeffs., oscillator strength sum rules 80−27941
bromobenzene, mol. polarisability, bond polarisability derivatives 78−74793
trans-butadiene, polarisability, nonlinear elec. susceptibility, SCF calcs. 80−95547
carbon tetrachloride, clusters, collision induced polarisability, mol. frame distortion 80−32798
carbon tetrachloride, optical props. under press., molecular polarisability depend. on thermodynamical state 78−80312
carbon tetrafluoride, clusters, collision induced polarisability, mol. frame distortion 80−32798
carbonyls, electric polarisability, in excited singlet and triplet states *(Bulgarian)* 80−52897
charge distribution in ions and mols., inductive effect 80−47837
charge transfer complex, Raman scatt. intensity enhancement model 79−13720
chemically induced magnetic polarization by S-$T_{\pm 1}$ mixing in strong mag. field 80−83515
chloroform-d_0(-d_1), Raman and IR intensity anal. 80−18857
chloromethanes, vapour phase, Kerr effect temp. depend., polarisability and hyperpolarisability 79−31568
cholesteric liquid crystal, molecular polarisability, arrangement order calc. *(Polish)* 80−10495
chymotrypsin, charge relay system, H-bond models, IR spectra 78−64935
classical fluid, collision-induced and multiple light scatt. 80−53919
closed shell system, response function approach in multiple cluster expansion formalism 79−72293
closed-shell system, harmonic oscillator model for mag. props., shielding tensor 79−81299

molecular polarisability continued
closed-shell system, polarisability and mag. susceptibility calc. by SCF and CI method 80−99443
CNDO calculations including polarisation functions in the basis set 79−6891
CNDO/2 calculation 78−913
colloids, electro-optic studies, stability 80−85222
complex frequency polarisability, bounds, bivariational calcs. 78−58611
conducting spheres, polarisability spatial extension in two body collision induced light scattering 79−98174
conjugated compounds, mol. polarisability additive scheme, CNDO approximation calcs. 77−50363
conjugated hydrocarbons, dipole polarisabilities, tensor components 79−36795
conjugated hydrocarbons and aromatics, PPP calc. of static and dynamic polarisability 79−98242
conjugated molecules, large second-order polarisability, SHG 78−66683
coumarin laser dyes, solvent effects on photophysical parameters 80−91598
crystal, calcs. using submolecule concept 77−12298
crystal, molecular lattice vibr. IR intensities, mol. polarisability calc. 80−11372
p-cyanophenyl p-n-alkylobenzoates, nematic, birefringence, polarisability and order parameter 80−100642
cyclic ketones, electrochromism and electric dichroism for studying transitions to second excited singlet 80−63692
delta function equation, bond order rel. to bond polarisability 77−61693
s-cis, s-trans-diallyl, twisted, low-lying singlet states, sudden polarisation effect 78−86792
diatomic molecule, polarisability anisotropy derivative determ. from relative Raman intensities 78−55177
diatomic molecules, electric polarisabilities, EFV GTO basis set 78−50661
diatomic molecules, polarisabilities and dipole moment derivatives, virial theorem calcs. 77−57865
diatomic molecules, polarisability correl. with mol. dimens. 80−23288
diatomic molecules, rotational Raman intensities and polarisability anisotropy change meas. with internuclear distance 80−63641
diatomic system, pair polarisability curve shape, rel. to chem. bonding 80−42930
diatomic systems, interactions, long-range dipoles, quadrupoles and hyperpolarisabilities 80−53161
diazines, cavity radius and mean polarisability 79−45862
dichloromethane, $d_{0\text{-}3}$, Raman intensity, force consts. and electro-optical parameters 79−36651
dielectric friction in plasma, harmonic oscillator and rigid dipole dielectrics 80−53928
dielectric solids, molecular optics model, electrodynamic eqns. derivation 78−27151
2,5-dimethoxy-4-nitrostilbene, hyperpolarisability meas. by DC induced second harmonic generation 78−87096
dimethyl ether, nonlinear optical polarisability meas. 79−54991
trans-4-dimethylamino-4′-nitrostilbene, mol. hyperpolarisability in soln., UV dispersion of charge transfer contrib. 79−31986
dipolar media, 0-10^{12} Hz freq. polarisation, dipole-dipole interaction effects 79−59525
dipolar molecular lattice, dielec. absorpt. of disordered mol. solids, electrodynamic influences 80−40040
dipolar molecules, zero-THz liq. phase dielec. absorpt. and rot. Langevin eqn. 80−40032
disordered media, LF spectrum study from Raman scattering cross section 80−25363
dodecahexenes, sudden polarisation effect, ab initio and CI calcs. 80−58160
dye molecule, excited, thermal rotations and relaxation of vibr. energy 79−81231
dynamic polarisabilities calcs., superposition method of excited config., nonstationary perturbation theory, eqn. 80−69257
dynamic variational calc. method, below 1st excitation freq. 77−50552
electric polarisabilities, hyperpolarisabilities, nonlinear optical coeffs., MNDO calc. 79−13641
electric polarisation in strong field for mol. with two hindered rot. groups 79−76361
electric-field-variant orbitals, Slater- and Gaussian-type 78−37543
electron+molecule, scatt., polarisation pot. determ. 80−17721
electron density contours from FSGO model wave functions, nonbonded radius of atoms, mol. anisotropy of polarisability 79−85897
electronic multipole molecular polarisabilities, variational calcs. 79−7035
electronic polaron, excess electron transport, polarisation dynamical self consistency depend. 79−47030
electrostatic interactions in liquid state, effect on frontier orbitals and chem. reactivity 80−84046
electrostatic potentials influence of polarisation functions 79−839
ethane, mean polarisability derivatives, variational calc. procedure 79−27108
ethane, multipole moments and polarisabilties, SCF calcs. 80−5471
ethene, dipole polarisability, finite-field SCF MO calcs. 80−83255
ethylene, average mol. polarisability, Frost model wavefunctions calcs. using p-type Gaussians 78−41924
ethylene, mol. hyperpolarisability meas. by optical SHG 79−22861
ethylene, multipole moments and polarisabilties, SCF calcs. 80−5471
ethylene, near HF dipole polarizability, using EFV GTOs 79−31395
ethylene, polarisability, nonlinear elec. susceptibility, SCF calcs. 80−95547
ethylene, pot. energy and dipole moment surfaces, polarisation effect, ab initio CI calcs. 80−106272
ethylene, rot. around double bond, four orbital-four-electron model 80−95592
ethylene mean polarisability derivatives, variational calc. procedure 79−27108
ethylene molecules, long range forces in multipole expsn., ab initio calcs. 78−9219
excitation of simple atomic and mol. systems, long-range force effects 79−10170
ferrocene, quantum mechanical delta-function potential study 77−23571
finite-field calcs., SCF and Galerkin treatments 77−54497
finite-field method, correlation corrections, pseudo-two-electron systems 77−71889
fluid, polar, equilib. theory, graph theoretical treatment 78−6002
fluorene, mol. polarisabilities and opt. props. of cryst. 79−24285

molecular polarisability continued
formaldehyde, electrochromism of 1749 Å band, electric dipole moment and polarisability 78−66572
formaldehyde, electronic struct., dipole moments, mol. polarisability, force fields, ab initio calcs. 80−78531
formaldehyde, first hyperpolarisability, Hartree-Fock-Slater calc. *(French)* 78−78625
formic acid amides, polarisabilities and π-π^* transitions, dipole interaction calcs. 80−23411
free radical reaction, chemically induced dynamic polarisation in strong mag. field, radical rotation influence 80−76509
frequency dependent dipole optical polarisability, time dependent adiabatic approx., Born-Oppenheimer approx. 77−23491
frequency dependent polarisability, time depend. Hartree-Fock calc. 79−45652
gas molecules, meas. of depolarisation rates and polarisability anisotropies 79−45770
gases, anisotropy, Rayleigh scattering depolarisation ratio 79−45730
Gaussian basis set with external elec. field perturbation depend., for polaris. calcs. 77−38740
Gaussian basis sets 78−58865
geometric approximation, various perturbation theories 78−17819
ground and excited state, perturbation treatment 78−5144
ground state props., coupled cluster and MBPT methods appl. 80−47881
group IVA tetrahalides, force consts., bond strengths, Urey-Bradley calcs. 77−50558
group-dipole interaction model, hyperpolarisabilities 77−34777
haloalkanes, mol. second hyperpolarisability, atom-dipole interaction model 77−34543
halogenonaphthalenes, bond and mol. polarisability, semi-empirical delta-function 79−31441
heteroconjugated molecules, π-electron props., graph theory anal. 79−89586
hexachlorobenzene, mol. cryst., calcs. using submolecule concept 77−12298
n-hexane, optical props. under press., molecular polarisability depend. on thermodynamical state 78−80312
hexatriene, mol. hyperpolarisability meas. by optical SHG 79−22861
hexatriene, polarisability, nonlinear elec. susceptibility, SCF calcs. 80−95547
HF theory, 1st-order, perturbed, use of symmetry in mol. props. calcs. 79−85916
homonuclear diatomic ions, static polarisabilities, internuclear separation effects 80−5494
hydrazonium tartrate enantiomers, and deuterates, struct. and opt. props. 77−68954
hydrides, second row, ab initio calcs. using FSGO basis, mol. parameters correlation 78−901
hydrocarbon molecules, mutual polarisability of two atoms *(French)* 78−78834
hydrocarbons, associated, Electric dipole polarizability of molecules in excited electronic states 78−70966
hydrocarbons, average elec. polarisabilities and mag. susceptibilities, ab initio valence electron calcs. 80−87033
hydrocarbons, bond polarisation charcts. 77−3487
hydrocarbons, conjugated, dynamic polarisability and eigenfreqs. in one-electron approx. 79−64117
hydrocarbons, deuterated, mol. polarisability and intermol. dispersion energy, 1-D delta pot. function 78−29862
hydrocarbons, electric polarisability, in excited singlet and triplet states *(Bulgarian)* 80−52897
hydrocarbons, mol. Raman intensities calcs. 80−52993
hyperpolarisabilities, HF calc. with correlation method, appl. to HF mol. 80−23342
hyperpolarisability contrib. to optical activity 78−70890
hyperpolarizability, freq. depend., time depend. HF eqn., second order LCAO SCF pertubation theory 79−31388
hyrocarbons, on activated C, rel. between adsorption and polarizabilities 80−76558
ice, isotopic, I_H, single crystal Raman intensities, OH bond polarisability, librational modes 78−27208
1,3-indandione derivatives, higher-order harmonic generation, laser-induced nonlinear optical effects *(Russian)* 78−55412
intermolecular spectroscopy and dynamical properties of dense systems, conf., Varenna, Italy (1978) 80−82581
ion-induced dipole pot. scatt. calcs., electronic and nuclear contribs. to mol. polarisability 77−50488
IR and Raman band intensities, use in force const. calcs. 77−27120
IR band moments, effect of dipole induction 77−75143
Kirkwood equation applicability charged anisotropic harmonic oscill., mol. diamag. 78−5365
Kirkwood-Pople-Schofield method, appls. to polarisabilities calcs. 80−83272
Lennard-Jones fluids, orientational and collision induced light scatt. 80−63644
lipid bilayers, dielec. const. calc. from bond polarisabilities 77−29105
liquid crystals, polarisability anisotropy of nematic homologous series 78−38614
liquid mixtures, associating, mol. hyperpolarisability, SHG 77−552
liquid structure and dynamics from light scatt. spectra 80−55105
liquids, nonpolar, b.p. calc. as function of mol. polarisability, ionisation energy, and size 79−95148
Longuet-Higgins-Pople theory extension using isotropic polarisability 79−31617
Lorenz-Lorentz relation, series expansion 77−40199
low-lying singlet states, sudden polarisation effect 78−86792
macromolecules in soln., Rayleigh scatt., elec. reorient. rel. to spectral line rot. broadening 79−1774
merocyanine dye, solvent-depend. hyperpolarisability, polar (nonpolar) solvents 78−70962
metalloporphyrins, mol. origin of anomalous polarisation in reson. Raman spectra 77−3368
methane, and d_4, finite field method, mol. polarisability and moment 79−59462
methane, and deuterates, absolute Raman intensities, depolaris. ratios, bond polaris. theory 77−10705
methane, clusters, collision induced polarisability, mol. frame distortion 80−32798
methane, collision induced rot. Raman scatt., polarisability effects 78−86874

molecular polarisability continued
methane, elec. dipole polaris., near Hartree-Fock value, using EFV GTOs 77−88591
methane, elec. dipole polarisability, coupled and uncoupled Hartree-Fock calcs. 77−34539
methane, first hyperpolarisability, Hartree-Fock-Slater calc. *(French)* 78−78625
methane, freq. depend. polarizability, LCAO SCF perturbation theory 79−31387
methane, ground state, dipole oscill. strength distrib., rel. to molar refractivity and dispersion energy 77−71835
methane, mean polarisability derivatives, variational calc. procedure 79−27108
methane, mol. multipole polarisabilities, extended variational method calcs. 79−36558
methane, multipole moments and polarisabilities 79−85910
methane, slow electron scatt., rigid mol. model with exchange and polarisation 80−43194
methane($-d_4$), liq., Brillouin scatt. and refr. index measurements 80−76035
methane ($-d_1,d_2,d_3,d_4$) Raman electro-optical parameters, overlay least squares calcs. 78−42105
methane and halogen derivatives Raman scatt. parameters at.-dipole interaction model calcs. 77−65465
methane molecular pair, polarisability tensor anisotropy 79−31725
methanes, halogenated, interacting segment model for elec. tensor props. 78−5111
methanes, substituted, Kerr consts., depolarisation ratios and hyperpolarisabilities meas. 78−25624
methanol, nonlinear optical polarisability meas. 79−54991
methyl acetylene, Kerr consts., depolarisation ratios and hyperpolarisabilities meas. 78−25624
molecular crystals, microscopic dielec. theory 80−97186
molecule, intensities dipolaris. ratios, polarisability, matrix rotation, isotopic rules 78−5288
multipole electric polarisability, variational calc. *(French)* 77−542
multipole polarisabilities, extended variational method calcs. 79−36558
naphthalene, dipole polarisability, finite-field SCF MO calcs. 80−83255
naphthalene, hyperpolarisability meas. by DC induced second harmonic generation 78−87096
naphthalene, mol. cryst., calcs. using submolecule concept 77−12298
negative ions, dynamic polarisability, many-centre short-radius model pots. 78−25735
negative molecular ions, calculation method 77−57860
nematic homologous series, molecular polarisability anisotropy, depend. on alkyl chain length 79−23518
nematic liquid crystals, refractive index, order parameter, density 79−38513
nematic liquid crysts., polarisabilities, Lippincot δ-function pot. model 80−79686
nematic-isotropic transition temp. depend. on anisotropy of C-X bond polarisability for terminal substituents 77−20058
nitriles, nonlinear 3rd-order elec. susceptibility calcs. 79−54786
p-nitroaniline, mol., second-order hyperpolarisability CNDO/S calc. 79−76358
p-nitroaniline, mol. hyperpolarisability in soln., UV dispersion of charge transfer contrib. 79−31986
nitroanilines, hyperpolarisability, second harmonic generation and four wave mixing, excited dipole moment 77−54624
1-nitronaphthalene, hyperpolarisability meas. by DC induced second harmonic generation 78−87096
nonpolar molecules, adsorbed on metal surface, depolarisation interaction 78−51820
nonpolar polarisable fluids, effective field of a dipole, rel. to mol. polaris. 80−79659
nonuniform arbitrary elec. field-induced moments polarisability density concept limitations 78−70964
olefins, zwitterionic states, polaris. and vibronic interactions 80−32620
open-shell system, polarisability and mag. susceptibility calc. by SCF and CI method 80−99443
orbital method, differential scaling of σ and π orbitals, and geom. approx. 79−10231
organic molecular systems, polarisabilities, susceptibilities, electron impact ionis. cross-sections calcs. 80−63835
organic molecules, quadrupole moments, dipole quadrupole A and C polarisabilities, perturbation theory anal. 80−27934
organic molecules, Raman spectra intensities, electronic polarisabilities, quantum mech. calc. 79−27041
organic molecules, semi-empirical delta-function method 79−31442
organic mols., relative Raman intensities, CNDO/2 INDO param. effect 80−95633
organic solids, charged excitonic complexes, coupled states, exciton interaction with charge carriers study 80−20090
organic system, nonlinear second-order optical susceptibility 80−9947
orientational correlation parameter for liquid 79−73090
oscillating electric dipole contrib. to light scatt. and interpret. in terms of polarisability and hyperpolarizability 80−53212
oxalic acid diamide, mol., PMR and IR spectra, easy polarisable H-bonds 79−31516
pair polarisabilities, continuum electrostatic theory 78−86769
pentacene, in p-terphenyl, polarisability calcs., from Stark meas., anisotropic Lorentz approx. breakdown 78−5276
n-pentane, optical props. under press., molecular polarisability depend. on thermodynamical state 78−80312
p-n-pentyl-p′-cyanobiphenyl, nematic ordering effect on hyperpolarisabilities 79−60263
perfluorobenzene, orientational correlation parameter for liquid 79−73090
(+)-(S)-2-phenyl-3,3-dimethylbutane, optical activity, circular dichroism, polarisability model 80−43082
phenylpolyenes, donor-acceptor disubstituted, INDO calc. of hyperpolarisability 79−93924
phthalic acid diamide, mol., PMR and IR spectra, easy polarisable H-bonds 79−31516
PMMA, piezobirefringence, optical and mech. relaxations, temp. depend. 80−34885
point charge model approach to mol. elec. polarisability 80−18797
polar fluid, translationally invariant correlation function, thermodynamic and dielectric props. 77−35457
polar liquids, elec. polarisation theory 77−4596
polar mol., freq. depend. of polarisability calc. 77−6957

molecular polarisability continued
polar molecules with fluctuating polarisability, dielec. theory 80−97178
polarisation propagator calculations of frequency-dependent polarisabilities, Verdet constants, and energy weighted sum rules 78−58647
poly(p-phenylene terephthalamide) fibres, optical anisotropy determ. 79−4786
poly-γ-benzyl-glutamate, α-helix second-order hyperpolarisability meas. 77−14623
poly-N-vinyl imidazole solution, light scatt., viscosity and dynamic birefringence, mol. wt. obs. *(Russian)* 79−33665
polyatomic, spin polarisation effect on thermal cond. 78−71422
polyatomic gas, viscous flow in mag. field, vector polarisation 77−42438
polyatomic molecule, crit. consts. evaluation from intermol. force consts. 80−37844
polyatomic molecules containing transition elements, delta function strength 78−46459
polyatomics, semi-empirical delta-function method 79−31442
polydisperse dilute suspensions, of rod-like particles, anisotropy of electric polarisability 80−85224
polyethylene glycol, mol. polarisability from Faraday effect 78−58726
polypeptides, α-helical, π-π^* absorpt. and circular dichroism spectra 80−23398
pyrazine absorbed on electrode, surface enhanced Raman spectra, symmetry and polarisability changes 80−50310
pyridine iodine complexes, charge transfer complexes, vibr. spectra, laser Raman obs. 80−52990
pyridine-I_2(ICl), charge-transfer complexes, hyperpolarisability 77−34568
pyridine-I_2 charge transfer complex, hyperpolaris., SHG obs. 77−553
di-α-pyridyl hydroperchlorates, intramol. H bonds, steric conditions and polarisability obs. 80−53160
quadrupole, semi-empirical calc. method 77−83761
quadrupole polarisability, using elec. field variant GTO basis set 79−76359
quinazolines, enzyme inhibitory, structure-activity quantitative study 80−78540
Raman and fluorescent scattering by molecules embedded in dielectric spheroids 80−99507
Raman scatt. theory, vibr. state summation, polarisability tensor upper and lower bounds 80−48000
Raman spectra intensity analysis, electrooptical parameters transferability 78−29820
Raman spectra of gases, high-resolution, mol. struct. and orops. 80−53000
rhodamine dye, coherent ellipsometry determ. of third order polarisability 79−71511
RNA solns., oriented in DC mag. field light scatt. 79−2004
rotational Brownian motion of spherical polar mol., diffusion eqn. study, complex polarisability 77−67381
rotational Raman scattering, collision-induced and dipole-quadrupole polarisabilities 78−25546
scaling and Pade approximants, many-body perturbation theory 80−42952
semiempirical calculation methods 79−36535
sepiolite, electric polarisability, anisotropy, length depend. of ionic contrib. 80−85224
single bond lengths and polarisation, a relationship *(Chinese)* 79−89806
spherical tops, chiral discrimination 80−106314
static polarisability, ab initio SCF wave functions 80−74106
stilbene, polarisability optical anisotropy 79−72441
stilbene derivatives, hyperpolarisabilities, four-wave mixing and SHG meas. 77−83925
Stockmayer fluid, mol. dynamics and thermodynamic perturbation theory, mol. polarisability effects 78−71419
styrene derivatives, hyperpolarisabilities, four-wave mixing and SHG meas. 77−83925
succinic acid diamide, mol., PMR and IR spectra, easy polarisable H-bonds 79−31516
tangential isotropic polarisable atomic unit model, optical rotation calc. *(French)* 79−54989
TCNQ salt, NMP-TCNQ, electronic struct., SCF calc., total energy polarisation effects 80−15469
tetra-glycine, cyclic, mol. polaris. and diamag. suscept. calcs. 80−63858
tetra-l-alanine, cyclic, mol. polaris. and diamag. suscept. calcs. 80−63858
tetracene, in p-terphenyl, polarisability calcs., from Stark meas., anisotropic Lorentz approx. breakdown 78−5276
tetrafluoromethane, collision induced rot. Raman scatt., polarisability effects 78−86874
thioformaldehyde, electronic struct., dipole moments, mol. polarisability, force fields, ab initio calcs. 80−78531
tolan, polarisability optical anisotropy 79−72441
toluenes, substituted, average mol. polarisability, δ-function calcs. 77−551
triphenylene, excited state polarisabilities, electrochromism and pot. energy curves 79−7034
unsaturated hydrocarbons, dipole polarisabilities, STO-4G calcs. 80−83255
van der Waals coeff., two-body combination rules 80−78677
vapour-liquid equilibria, and intermol. forces, semi-empirical approach 80−54359
water, and ionic dissoc. products, polarisation model 78−91216
water, optical props. under press., molecular polarisability depend. on thermodynamical state 78−80312
water elec. dipole polaris., near Hartree-Fock value, using EFV GTOs 77−88591
XY_4 square-planar type ions, force consts., bond polarizability 78−5201
Ar_2, collision-induced Raman scatt., polarisability anisotropy 78−46350
BH, elec. polarisabilities and dipole moments, var. perturbation obs. 80−63527
Be_2, generalised London formula for dispersion coeff. 78−82662
CN^-, first hyperpolarisability, Hartree-Fock-Slater calc. *(French)* 78−78625
C_2N_2, $2\nu_4$ band overtones, Raman intensities, bond polarisability theory 80−63639
CO, ab initio calcs. of the derivative of the static polarisability 79−3597
CO, finite field method calc., moments, polarisability, field-induced shifts in mol. props. 78−74561
CO, first hyperpolarisability, Hartree-Fock-Slater calc. *(French)* 78−78625
CO, freq.-depend. polarisabilities and Verdet consts., calcs. 78−62781
CO, nonlinear optical polarisability meas. 79−54991

molecular polarisability continued
CO, numerical coupled Hartree-Fock parallel polarisability, partial wave SCF calc. 78−9079
CO, polarisability derivatives, bond length depend., SCF and CI calcs. 80−58162
CO_2, collision-induced Raman spectrum, theoretical studies 80−63646
CO_2, Kerr consts., depolarisation ratios and hyperpolarisabilities meas. 78−25624
CO_2, low energy electron (positron) collisions, ab initio adiabatic polarisation pots. 80−14240
CO_2, nonlinear optical polarisability meas. 79−54991
CO_2, polarisabilities, quadrupole and dipole moments, nucl. geom. effects 79−63899
CO_2, static polarisabilities, ab initio SCF HF calcs., internucl. separation depend. 78−9073
CS_2, excited state props., by electrochromism in polymer matrix 79−22737
CS_2, liq., Kerr effect in UV region, mol. optical anisotropy dispersion 78−72488
CS_2, orientational correlation parameter for liquid 79−73090
CS_2, symmetric stretch mode, moments and polarisability derivatives, SCF calcs. 80−901
CaCl, $X^2\Sigma$ pot. energy curves, polarisability and dissoc. 80−91629
Cl_2, one electron props. and polarisability, SCF and CI calcs. 80−58159
DCl, polaris. anisotropy 77−83645
D_2O, finite field method, mol. polarisability and moment 79−59462
$D_5O_2^+$, isotope effects, easily polarisable H and D bonds 78−94231
Eu(III) complexes, f-f transition probabilities, ligand polarisation model, anisotropic contribs. 80−53049
FH, freq.-depend. polarisabilities and Verdet consts., calcs. 78−62781
FH, numerical coupled HF hyperpolarisabilities, basis set depend. 79−76357
FH, one-electron props., review of expt. and theoretical data, Hartree-Fock calcs. 77−67980
H halides, ab initio SCF calc. of dipole polarisabilities 79−89600
H halides, polarisability, correl. with mol. dimens. 80−23288
H-like ion, elec. multipole polarisability, relativistic corrections, shielding factors, Dirac eqn. 78−13441
H_2, adiabatic polarisation, ab initio calc., static electric dipole polarisability 79−72229
H_2, CI and Gaussian geminal calcs., using explicitly correlated elec.-field-variant functions 79−36561
H_2, dipole polarisability, coupled perturbed Hartree-Fock method improvement 80−58148
H_2, dynamic dipole polarisabilities calcs. 80−74110
H_2, dynamic polarisabilities, variation-perturbation calcs. 80−87243
H_2, dynamical optical susceptibility, third-order 79−31724
H_2, electric dipole polarisabilities and hyperpolarisabilities, perturb. theory calcs. 78−17563
H_2, electric dipole polarisability, many-body perturbation theory calcs. 78−21839
H_2, generalised London formula for dispersion coeff. 78−82662
H_2, harmonic oscillator model, elec. polarisability, mag. susceptibility and chem. shift tensor calcs. 79−81299
H_2, many-body perturbation theory 79−54775
H_2, nonlinear optical polarisability meas. 79−54991
H_2, optical polarisation following electron impact 80−63831
H_2, polarisabilities, higher, static, calc., wave-function quality depend. 80−18814
H_2, polarisability, finite field MC SCF calcs. 80−14075
H_2, polarisability anisotropy derivative determ. from relative Raman intensities 78−55177
H_2, second order props., dipole polarisability nucl. coupling, fast CI method 80−27950
H_2, static polarisability determ. by optimised rot. method 79−54990
H_2, triplet state, molecular polarisability, ab initio calcs. 80−63860
H_2^+, dynamic dipole polarisability, variational perturbation theory 78−94330
H_2^+, dynamic polarisability, electronic states two centre Coulombic Green's function, continuous spectrum exclusion 78−82626
H_2^+, hyperpolarisabilities, quadrupole and field-gradient quadrupole polarisabilities 80−1086
H_2^+, moment functions calcs. and radiative corrections 78−90141
H_2^+, polarisability, internuclear distance depend., excluding continuous spectrum 77−10581
H_2^+, polarisability, numerical two-centre calc. 79−10232
H_2^+, static polarisability determ. by optimised rot. method 79−54990
H_2+H_2, interaction polarisability comparison with the He diatom, ab initio SCF calcs. 80−27943
H_2+H_2, quadrupolar $S_1(J)+S_0(J)$ double transitions, IR fundamental band, 77K 80−52986
H_3^+, dipole polarisabilities, variational perturbation theory calcs. 78−70765
HBr(DBr), isotopic forms, Stark hyperfine struct., polarisability anisotropy 77−83645
HCN, finite field method calc., moments, polarisability, field-induced shifts in mol. props. 78−74561
HCN, IR and Raman vibr. intensity changes due to Li^+ interaction 79−45712
$HCN+He(H_2)(CH_3F)$, HCN excited vibr. state, T_2 meas. 80−102498
HCl, bond dependence of dipole polarisabilities 78−74573
HCl, electron elastic scatt., exchange and polarisation 80−91668
HCl, one electron props. and polarizibility, SCF and CI calcs. 80−58159
HCl, polar liqs. models, mol. polarisability effect 80−92444
HF, bond dependence of dipole polarisabilities 78−74573
HF, elec. dipole polaris., near Hartree-Fock value, using EFV GTOs 77−88591
HF, hyperpolarisabilities, dipole moment, HF calc. with correlation 80−23342
HF, mol. hyperpolarisability, second-order SCF perturbation method, coupled Hartree-Fock calc. 78−33422
HF, mol. props. internucl. separation depend., MCSCF calc. 78−70965
HF, numerical coupled Hartree-Fock parallel polarisability, partial wave SCF calc. 78−9079
HF, polar liqs. models, mol. polarisability effect 80−92444
HNC, finite field method calc., moments, polarisability, field-induced shifts in mol. props. 78−74561
H_2O, elec. and mag. props., equations of motion method calcs. 77−83513
H_2O, elec. and mag. props. in static fields, perturbed Hartree-Fock calcs. 78−50462

molecular polarisability continued
H_2O, elec. dipole polarisability, coupled and uncoupled Hartree-Fock calcs. 77−34539
H_2O, finite field method, mol. polarisability and moment 79−59462
H_2O, liquid, equations for mag. susceptibility, electric polarisability 80−75708
H_2O, nonlinear optical polarisability meas. 79−54991
H_2O, one-electron props., review of expt. and theoretical data, Hartree-Fock calcs. 77−67980
H_2O, polarisabilities, finite-field calc., perturbation correlation 79−72249
H_2O, polarisability and mag. susceptibility calc. by SCF and CI method 80−99443
H_2O, polarisability tensor components, virial theorem calcs. 80−53087
H_2O, refractive index, temp. depend., relationship to mol. polarisability 78−56448
H_2O, SCF calcs. using cusped Gaussian basis sets, polarisation effects 80−74118
H_2O, slow electron scatt., rigid mol. model with exchange and polarisation 80−43194
H_2O, vap., depolarised Rayleigh scatt., rot. Raman spectra, mol. polarisability 78−33513
$H_5O_2^+$, aq. soln., IR continua with polarisable H-bonds 79−26979
H_2S, mol. polarisability and derivatives, ab initio SCF CI calc. 79−59597
H_2S, nonlinear optical polarisability meas. 79−54991
H_2S, slow electron scatt., rigid mol. model with exchange and polarisation 80−43194
H_2SiO, electronic struct., dipole moments, mol. polarisability, force fields, ab initio calcs. 80−78531
He pair, dispersion interaction, independent particle model, polarisabilities 80−37732
He_2, collision induced Raman spectrum, polarisability anisotropy 79−72320
He_2, generalised London formula for dispersion coeff. 78−82662
He_2, ground state, generalised dipole polarisability, bivariational calcs. 78−58611
He_2, pair polarisability correl. effects, SCF-CI-GTO-SO calc. 78−82651
He_2, polarisability and collrision induced Raman spectra 80−48005
He_2, Raman spectra, collision-induced, diatom polarisability 79−64011
He_2^{2+}, static polarisability determ. by optimised rot. method 79−54990
HeH^+, dynamic dipole polarisabilities calcs. 80−74110
HeH^+, static polarisability determ. by optimised rot. method 79−54990
I_2, mol. cryst., calcs. using submolecule concept 77−12298
I_2, polarisability anisotropy, laser assisted mol. beam spectroscopy 80−78646
KCl, charge transfer and pair polarisability anisotropy 80−43173
KCl, polarisability, near-Hartree-Fock limit SCF MO calc., bond length 78−42239
KF, ab initio SCF MO energy, dipole moment and polarisability 80−1085
Li_2, finite-field method, correlation corrections 77−71889
Li_2, generalised London formula for dispersion coeff. 78−82662
Li_2 SCF polarisability, polarisation potentials, ab initio calc. 79−89602
$LiBH_4$, non-rigid complex molecule, ab initio calcs. of pot. energy surface and geometric struct. 77−6678
LiBr, pair pot., dipole moment, polarisability tensor, bond length depend., finite field SCF calcs. 80−58127
LiCl, charge transfer and pair polarisability anisotropy 80−43173
LiCl, polarisability bond length depend. 77−23422
Li_2Cl^+, triplet polarisability, ab initio MO calc. 79−98244
LiF, ab initio SCF MO energy, dipole moment and polarisability 80−1085
LiH, electric dipole polarisabilities and hyperpolarisabilities, perturb. theory calcs. 78−17563
LiH, finite-field method, correlation corrections 77−71889
LiH, finite-field method calcs., dipole moment gradients, polarisability gradients and elec. field effects 77−88589
LiH, mol. elec. polarisabilities and dipole moments calcs. 78−41976
LiH, polarisabilities and dipole moment derivatives, virial theorem calcs. 77−57865
N-containing heterocycles, nonlinear 3rd-order elec. susceptibility calcs. 79−54786
N_2, ab initio calcs. of the derivative of the static polarisability 79−3597
N_2, elec. and mag. props., equations of motion method calcs. 77−83513
N_2, electron-mol. adiabatic polarisation pots. and ab initio SCF polarisabilities 80−9499
N_2, finite field method calc., moments, polarisability, field-induced shifts in mol. props. 78−74561
N_2, internuclear depend. of α_0 and α_2 78−58866
N_2, light polarisability parameters, Raman scatt. ang. meas. 80−37814
N_2, low energy electron (positron) collisions, ab initio adiabatic polarisation pots. 80−14240
N_2, multiple moments, polarisabilities and anisotropic long range interaction coeffs. 80−43206
N_2, nonlinear optical polarisability meas. 79−54991
N_2, one-electron props., polarisabilities and polarisability derivatives, SCF and CI calcs. 80−37746
N_2, polarisabilities, quadrupole and dipole moments, nucl. geom. effects 79−63899
N_2, polarisability anisotropy derivative determ. from relative Raman intensities 78−55177
N_2, polarisability derivatives, SCF and CI calcs. 79−59348
N_2, polarisability tensor anisotropy, Raman spectra differential scatt. cross section 80−18860
N_2, Raman intensity, ab initio calc. 80−1028
N_2 SCF calcs. using cusped Gaussian basis sets, polarisation effects 80−74118
N_2, static polarisabilities, ab initio SCF HF calcs., internucl. separation depend. 78−9073
N_3, polarisability correl. with mol. dimens. 80−23288
ND_4Cl, ordered phase, Raman spectrum, dipole and polarisability derivatives 77−52072
NH_3, elec. dipole polarisability, coupled and uncoupled Hartree-Fock calcs. 77−34539
NH_3, elec. dipole polaris., near Hartree-Fock value, using EFV GTOs 77−88591
NH_3, freq. depend. hyperpolarisability, time-depend. Hartree-Fock calcs. 79−36559
NH_3, nonlinear optical polarisability meas. 79−54991
N_2H_2, CEPA-PNO calcs., band functions, correl. and polarisation roles 77−71758

molecular polarisability continued
NH_4Cl, ordered phase Raman spectrum, dipole and polarisability derivatives 77−52072
NO, nonlinear optical polarisability meas. 79−54991
Ne_2, collision induced Raman spectra and diatom polarisability 80−63647
Ne_2, pair polarisability tensor, extended Gaussian basis set, perturbation coupled HF calc. 77−75058
Ne_2, Raman spectra and polarisability 79−98107
NiF_2+CO, Ar matrix isolated, ab initio MO calcs. 78−92458
O_2, light polarisability parameters, Raman scatt. ang. meas. 80−37814
O_2, nonlinear optical polarisability meas. 79−54991
O_2, polarisability tensor anisotropy, Raman spectra differential scatt. cross section 80−18860
O_3, mol. beam electric resonance, electric and mag. props. determ. 77−27055
O_3, mol. beam Stark, Zeeman effects, polarisability, moments, mag. susceptibility anisotropy 77−79649
OH_n, LCAO-MO-SCF with Gaussian polarisation functions, energetic effect of p-, d-, and f-functions 78−41944
Pd complex, $Pd^{I}Pt^{I}(CNCH_3)_6(PF_6)_2$, vibr. spectra, M-M bonds. *(French)* 80−47997
Pt complex, $Pt^{II}(CNCH_3)_4(PF_6)_2$, $Pt_2^{I}(CNCH_3)_6(PF_6)_2$, and $Pt^{I}Pd^{I}(CNCH_3)_6(PF_6)_2$, vibr. spectra, M-M bonds. *(French)* 80−47997
SF_6, clusters, collision induced polarisability, mol. frame distortion 80−32798
SF_6, collision induced rot. Raman scatt., polarisability effects 78−86874
SF_6, collision-induced forbidden Raman transitions 77−6791
SF_6, liq., depolarised light scatt., dipole-induced dipole effect 77−12395
SF_6, nonlinear optical polarisability meas. 79−54991
SF_6, pair polarisability anisotropy, point atom polarisability approx. calcs. 80−87244
SH_n, LCAO-MO-SCF with Gaussian polarisation functions, energetic effect of p-, d-, and f-functions 78−41944

molecular positron scattering *see elastic scattering of electrons by atoms and molecules; molecular electron impact dissociation; molecular electron impact excitation; molecular electron impact ionisation*

molecular potentials *see potential energy functions*

molecular predissociation
acetaldehyde-d_1(-d_3), fragmentation processes, H scrambling, photoionis. mass spectra 78−42139
alkali metal molecular, laser radiation absorpt., at. excitation processes 80−32785
chloroacetylene dissoc. and predissoc., state selected unimolecular reaction dynamics 77−36744
collision-induced state-changes, intermol. pot. well depth role 79−81257
diatomic molecule, photopredissoc. fragment, ang. distrib. in mag. field 79−89716
diatomic molecule, predissoc. at intermediate coupling strengths, semiclassical theory 78−50601
diatomic molecules, form. and dissoc. in interstellar medium 80−23471
diatomic molecules, laser-induced predissoc., surface mag. field effect 80−106365
diatomic molecules, predissoc., simplified model 79−6892
diatomic molecules, shifts and widths of predissoc. levels 78−5304
diazonium salts in aqueous solns. and polymer matrices, IR absorpt. spectra 80−76030
double curve crossing model, predissoc. linewidths and level shifts 77−75070
formaldehyde, appl. to heavy water production by laser isotope separation 77−83106
formaldehyde, ion laser induced photopredissociation, ^{17}O, ^{18}O, ^{13}C isotope separation 77−61871
formaldehyde, nonradiative transition rates and predissociation process 77−54574
formaldehyde, UV photopredissociation, H-laser isotope separation 79−94095
formaldehyde photopredissociation by Ne II ion laser for ^{17}O enrichment 77−19112
formaldehyde predissoc., from reson. multiphoton dissoc. of small mols. 80−53077
formaldehydes, (deuterated), A^1A_2 state, photoluminesc. in low temp. matrices, vibr. relaxation 79−50070
glyoxal, vapour, predissoc. in S_1 zero-point level states 80−102544
harmonic oscillator, v=0 level predissociation, by linear pot., line width and shift 77−75239
harmonic oscillator, relative line widths and level shifts 80−23469
harmonic oscillator model in predissoc., level widths, shifts and curve crossing 78−90239
highly excited molecular systems, high energy photochem. 80−66831
laser induced molecular predissociation, by stimulated emission or absorpt. of IR photons 79−54925
laser-induced nonreson. predissoc., quantum theory, selection rules 78−82796
laser-induced of diatomic and polyatomic mols., photocatalytic effect 80−11907
methane+Ar, rot. compound state resons. 80−28090
methylchloride, CH_3Cl^+, photofragmentation at 366 nm 78−58752
molecular gas, laser irrad., field avoided crossings, new transition channels 78−33477
molecular ion gas prestripping in tandem accelerator 78−46185
multichannel, and inelastic scatt., uniform WKB theory 79−72404
photorecombination emission reaction mechs. during atomic collisions 80−18914
polyatomic mol. gas, laser-induced rate processes, collision-free dynamics 77−30934
polyatomic molecules, photofragmentation obs. methods 80−63725
polyatomic molecules, vibr. predissoc., rel. to van der Waals triatomic mol. theory 78−55208
polyatomic molecules, vibr. predissoc. rel. to van der Waals mol. theory, anharmonicity effects 78−55209
polyatomic photofragmentation 77−6874
preassociation, laser induced, in presence of natural predissociation 78−85174
preionis. and predissoc., rel. to spectral line shape 80−63724
radiative preassociation, in presence of natural predissociation 78−85174
reflection method of calculating energy shifts and linewidths in predissociation 77−75237
resonant photocatalytic effect, in laser induced uni-mol. dissoc. 80−3377

molecular predissociation continued
rotational predissociation, Weyl's theory and Jeffrey's approx., resons. 78−926
small molecules, detect. by magnetically tuned freq.-modulated at. line sources 79−59508
spectroscopic interferences, unified description 77−23524
sub-Doppler laser spectroscopy of mol. ions in fast ion beams 80−9655
thiophosgene vapour, fluoresc. from S_2 single vibronic states, quantum yields and quenching 77−34675
triatomic van der Waals complex, vibr. predissoc. and photodissoc. lifetimes 80−9661
triatomic van der Waals molecules, vibr. predissoc., rel. to polyatomic complexes, theory 78−55208
triatomic van der Waals mols., rot. predissoc. 80−63721
two-channel model, resonances with complex rot. method 80−58327
two-state model, uniform semiclassical wave function approach, and preassoc. 78−90241
type I unimolecular predissociation, level widths and shifts, quantum-mech. method 79−31629
Van der Waals cluster, gas phase, vibr. predissoc., rel. to matrix-isolated O_2 multiphonon vibr. relax. 80−18861
Van der Waals dimers, intermol. V-V energy transfer in vibr. predissoc. 79−94060
van der Waals dimers, intramolecular vibr. dynamics, vibr. predissociation 80−28083
van der Waals mol. rot. predissociation study, complex coord. method 80−74205
van der Waals molecule, linear triatomic, vibr. predissoc. model 77−71838
van der Waals molecules, mol. fluoresc., vibr. predissoc. model 78−42120
van der Waals molecules, photo-induced vibr. predissoc. 79−41209
van der Waals molecules, vibrationally excited, lifetimes, momentum gap 80−5601
van der Waals mols., vib. predissoc. 78−55215
van der Waals T-shaped mol., perpendicular vibr. predissoc., vibr. relax., Morse pots. 78−82659
vibrational predissociation in hydrogen bonded complexes 80−61078
AlD, $A'\pi$, spectral lifetime and predissociation 79−59515
AlH, $A'\pi$, spectral lifetime and predissociation 79−59515
ArH_2, van der Waals mols., rot. predissoc. 80−63721
ArI_2, van der Waals mol., fluoresc. spectrum, predissoc. 78−66584
ArN_2, van der Waals mols., rot. predissoc. 80−63721
BeCl, $^2\Sigma^+$ predissoc. state, vibr. and rot. calcs. 77−42363
BeH, BeD, linewidth, indirect predissoc., anomalous isotope effect, ab initio calc. 77−58101
Br_2 (B-X) band spectrum in laser induced fluorescence 79−47931
Br_2, absorpt. spectrum, rel. to laser isotope separation 77−10683
Br_2, $B^3\Pi(O_u^+)$ predissoc. rates, analytical interpretation 80−91617
Br_2, Kr ion laser-excited fluorescence, predissoc. 80−83414
Br_2, single rot. states, lifetimes and collisional quenching cross sections determ. by obs. fluoresc. decay 80−91595
BrCl, excited $B^3\Pi(0^+)$ state, excitation spectra and predissoc. 78−66593
BrCl laser induced fluoresc., quantum resolved level dynamics in $B^3\Pi(O^+)$ state 80−74188
BrF, $B^3\Pi(0^+)\leftarrow X^1\Sigma^+$ absorption spectrum, high-resolution anal. 79−59478
BrF, laser excitation spectrum, 4850 to 5200 Å, rot. anal. 77−6840
BrF, predissociation in $B^3\Pi(0^+)$ state 78−66591
$^{81}Br_2$, visible, vibr.-rot. absorption, fluoresc. decay, predissoc. quantum yield 77−18962
C^+ predissociations, anal. line profile and energy shifts, linear pot. approx. 77−6871
C^+ predissociations, anal. line profile and energy shifts, linear pot. approx. 77−6871
C^+ predissociations, Fano line profiles, linear pot. calcs. 77−6872
CD_4^+, rot. predissociation, observed by metastable peak struct. in translational spectra 78−25635
CH, $B^2\Sigma^-$ state predissoc., calcs. and time resolved spectrosc. 80−23576
CH^+, photodissoc., $A^1\Pi$ state shape resonances 79−54924
CH^+, photodissociation to C^+ and H, wavelength depend. and photofragment kinetic energies, visible obs. 80−58275
CH^+, predissociated levels obs. 80−37838
CH_4^+, CD_4^+, rot. predissoc., metastable peaks 79−13774
CH_4^+, rot. predissociation, observed by metastable peak struct. in translational spectra 78−25635
C_2N_2, $C^1\Pi_u$-state predissoc., vibronic effects 80−28078
CO, dissociative ionisation 77−54616
CO_3^-, photodissoc. cross-section, excited state vibr. mode determ. 77−6870
$CO_2^+(C^2\Sigma_g^+)$, formation and predissoc., photoelectron spectra 78−5300
Cd_2, quenching and predissociation, possible excimer laser 80−32770
Cl_2, B-X transition, predissoc., laser-induced fluoresc. obs. 80−43093
Cl_2, B-X transition, rotationally resolved excitation spectra and predissociation in excited state 79−45754
Cl_2, fluoresc. quenching by collision-induced predissoc. 77−14472
Cl_2, laser-induced fluoresc., excited $B^3\Pi(O_u^+)$ states, collision-free lifetimes of ro-vibr. levels 79−94029
ClO, predissociation in stratosphere, cross sections and rate consts. 77−70763
ClO_2, predissoc. mechanism determ. from rot. level lifetimes 79−13732
Cs_2, fluoresc. spectra, kinetics, laser candidate 79−64027
Cs_2, fluoresc. spectra induced by laser, energy transfer and dissoc. 79−98141
Cs_2, He-Ne 632.8 nm radiation-induced disintegration 79−76474
Cs_2*, optically excited, cascade predissoc. *(Russian)* 79−10159
CuH, UV absorpt. spectra 80−87143
D_2, electron impact, threshold excitation and predissoc., electron-photon coincidence meas. 80−18941
D_2, predissoc. linewidths and shapes for $3p\pi D^1\Pi_u^+$ state 80−53066
D_2, Rydberg state predissoc., Lyman and Balmer emission obs. 77−38702
D_3, emission spectra, rot. struct. obs. mol. const. determ., predissociation 80−106331
DCN, photofragmentation, vibr. distribs. 77−18992
H_2, $3p\pi D^1\Pi_u^+$ state, predissoc., Fano profile anal. 79−68274
H_2, $c^1\Pi_u$ metastable state, fine struct. lifetimes 79−64050
H_2, electron impact, threshold excitation and predissoc., electron-photon coincidence meas. 80−18941
H_2, electron impact dissociative excitation obs. 78−1090

molecular predissociation continued
H_2, ion source, duoPIGatron, H^+ fraction enhancement by predissoc. 77−13816
H_2, photoabsorption, photoionisation, predissoc., high resolution obs. 77−477
H_2, predissoc., interference effects, lineshape obs. 80−83432
H_2, predissoc. linewidths and shapes for $3p\pi D^1\Pi_u^+$ state 80−53066
H_2, predissociation of $^1\Pi_u^+$ state vibr. and rot. levels, dissoc. yields meas. 80−32784
H_2, predissociation of $4p\pi^1\Pi_u^+$ state, due to UV radiation 78−37695
H_2, predissociation of $c^1\Pi_u$ state, H_2^+ impact, flight time difference obs. 77−27164
H_2 predissociation probabilities of $4p\pi^1\Pi_u^+ v' \geq 1$ levels, dissoc. channels interference 80−28074
H_2, preionis. and predissoc., rel. to spectral line shape 80−63724
H_2, Rydberg state predissoc., Lyman and Balmer emission obs. 77−38702
H_2^++He(Kr)(Xe), collisional dissociation, ion-pair prod., negative ion prod., cross sections 77−14529
H_3, electronically excited state obs., vibr. level struct. determ., predissoc. 79−41204
H_3, emission spectra, rot. struct. obs. mol. const. determ., predissociation 80−106331
HCN, H-CN dissoc. curves, SCF CI calc. 79−100405
HCN, photofragmentation, vibr. distribs. 77−18992
HCN, photofragmentation, initial excitation effects calcs. 78−17734
HCN predissoc. Frank-Condon amplitudes 80−95694
HCN, predissoc. in photodissoc., CN radical ($A^2\pi$-$X^2\Sigma$) fluoresc. 77−38691
HCN(DCN), photodissoc. dynamics, rot. (vibr.) energy disposal 78−48672
H_2CO^+ ion, unimolecular decay paths of electronically excited species 79−3359
HD, isotopic effects in predissociations 78−86924
HD, predissoc., interference effects, lineshape obs. 80−83432
HD, predissoc. linewidths and shapes for $3p\pi D^1\Pi_u^+$ state 80−53066
H(D)CN(C^1A')→H(D)+CN($B^2\Sigma^+$), photofragment excitation spectra measurement 79−45777
HF, Feshbach resons., predissoc. investig. 80−83433
H_2(HD), predissoc., Feshbach resons., spin-aligned atom form., stability 77−10723
HNO, predissoc., absorpt. spectrum line broadening 77−14503
HNO, vibronic state perturbative and predissoc. mechanisms, fluoresc. excitation spectra obs. 80−9658
H_2*, vibr. excited mols., time-of-flight spectra 78−42146
H_2*+H_2, van der Waals mols., mol. fluoresc., vibr. predissoc. model 78−42120
HeH^+, (HeD^+), rot. predissoc., nucl. motion effects on rovibr. energies and widths 78−70885
HeI_2, van der Waals mol., vibr. predissoc. lifetimes 79−68278
HeI_2, Van der Waals mol. vibr. predissoc. anharmonicity effects 80−52971
HeI_2, vibr. excited mol., dissoc., predissoc., quasiclassical trajectory obs. 79−87839
$HeNO_2$, vibr. predissoc., rel. to van der Waals triatomic mol. theory 78−55208
$HeNO_2$, vibr. predissoc. rel. to van der Waals mol. theory, anharmonicity effects 78−55209
Hg_2, photoassociated, collision-induced predissoc. with Hg 79−31626
Hg_2, quenching and predissociation, possible excimer laser 80−32770
HgH, predissoc. by rot., continuous rot.-vibr. spectrum, Weyl's theory 77−18996
HgH, predissoc. by rot., continuous rot.-vibr. spectrum, resons. and eigenvalues, Weyl's theory 77−18997
HgH, rot. predissociation, Weyl's theory and Jeffreys' approx., resons. 78−926
I_2, B state, fluorescence yield, individual hyperfine components 77−68067
I_2 collision-induced predissoc., Landau-Zener model, method of analytic continuation 77−83687
I_2, hyperfine predissoc., Doppler-free spectrosc. obs. 78−89558
I_2, hyperfine predissociation, saturated absorpt. expt. 77−58103
I_2, predissociation, electric-field induced 80−37839
I_2, use as test mol. in modern spectroscopy, review 78−90317
I_2, vibr.-translational relax., collisional predissoc., opto-acoustic effect obs. 80−43157
IBr, $B^3\Pi(0^+)$ excited state, laser-induced fluoresc. 80−58309
IBr, predissoc. and photodissoc., intermed. coupling strength 77−16850
ICN, photodissoc. and predissoc., cyanide radical fluoresc. excitation spectrum and laser emission 78−76892
ICl, $B^3\Pi(0^+)$-$X^1\Sigma^+$ fluoresc., predissoc. 77−34682
$I^{35}Cl$, predissociations in $B^3\Pi_{0+}$ state 80−1033
$I^{37}Cl$, predissociations in $B^3\Pi_{0+}$ state 80−1033
IF, $B^3\Pi(0^+)$, radiative and predissoc. lifetimes, laser-induced fluoresc. 79−31589
IF, $B^3\Pi(0^+)$-$X^1\Sigma^+$ fluoresc., predissoc. 77−34682
$^{127}I_2$, B-X electronic transition, systematic hyperfine struct. meas. 78−9267
I_2*He, vibrational predissociation, van der Waals molecules, vibration-translation scaling theory 80−43135
KrH_2 van der Waals mols., rot. predissoc. 80−63721
Mg_2, $A^1\Sigma_u^+$-$X^1\Sigma_g^+$ system Franck-Condon factors, J-depend., fluoresc. pot. and predissoc. 77−58067
N_2, preionis. and predissoc., rel. to spectral line shape 80−63724
N_2, spectroscopic data review 77−38680
N_2^+, $C^2\Sigma_u^+$-$B^2\Sigma_u^+$ homogeneous predissoc.; perturbations calcs. 79−86020
ND, $d^1\Sigma^+$-$c^1\Pi$, spectra, equilib. consts., dissociation energy 78−33517
ND, dissoc. energy, calc. from $c^1\Pi$ state predissoc. *(German)* 78−90237
ND_3, Einstein A coeff. for A→X transition 77−27127
ND_3, predissoc. mol., rot. resolved IR reson. scatt. 77−30882
NH, $d^1\Sigma^+$−$c^1\Pi$, $d^1\Sigma^+$-$b^1\Sigma^+$, spectra, equilib. consts., dissociation energy 78−33517
NH, dissoc. energy, calc. from $c^1\Pi$ state predissoc. *(German)* 78−90237
NH, lower valence states, predissociations, Franck-Condon anal. 80−5590
NH, ND, $d^1\Sigma^+$ state lifetimes, rot. struct., electron excited emission spectra 77−79654
NH_3, ($\tilde{A}^1A_2''$) predissoc., vac. UV photolysis, NH_2 form. 78−13547
molecular predissociation continued
NH_3, expansion cooled, mol. photoionisation, rot. struct., rot. predissoc. of excited states 80−91611
NH_3, photodissociation in A←X absorption region, translational excitation of H atoms and predissociation mechanism 77−77791
NH_3, predissociation of A''_2 state from UHF calcs. of potential energy surface 80−1034
NO, 4-photon ionis. spectrum 2- and 3-photon resons., low temp. assignments 78−70887
NO $C^2\Pi(v'=0)$, lifetime meas., predissoc. and non-predissoc. rot. levels 78−62849
NO molecular predissociation, quantum mechanics expt. test 79−17274
NO, photoionis. resonant processes, preionis. and predissoc. 77−65516
NO, predissoc. rates and pertrubations in certain electronic states, time resolved spectra 77−27131
NO predissociation in mesosphere and stratosphere, photochemistry 80−21802
NO_2, $^2B_2$ state photodecomposition in 2nd predissoc. region 77−10712
NO_2, dissociative limit, mol. beam characts. determ. by fluoresc. excitation spectra 80−53074
$^{15,14}NO_2$, predissoc. rot. struct. in 2490 Å band 80−87192
N_2O, preionis. and predissoc., rel. to spectral line shape 80−63724
N_2O, vac. UV photodissoc., kinetic energy and ang. distribs. of fragments 77−30938
$(N_2O)_2$, photo-induced vibr. predissoc. of van der Waals mol. 78−90242
NO*+NO, van der Waals mols. in mol. fluoresc., vibr. predissoc. model 78−42120
NeH_2, van der Waals mols., rot. predissoc. 80−63721
No, $C^2\Pi(v=0)$ state, two-photon absorpt. spectra, predissociation 77−79664
O_2, $^3\Sigma_u^-$-$^3\Sigma_u^+$ spin-orbit mixing in Schumann-Runge predissoc. 77−6875
O_2, double curve crossing model, predissoc. linewidths and level shifts 77−75070
O_2, harmonic oscillator model in predissoc., level widths, shifts and curve crossing 78−90239
O_2, predissoc. of $B'^3\Sigma_u^-$ state, Rydberg-valence crossing model 80−1032
O_2, reson. cross-sections, predissoc. and preassoc., isotope effects 78−58750
O_2, Schumann-Runge band system, oscill. strengths and linewidths 79−98120
O_2, Schumann-Runge bands, predissoc. linewidths and oscill. strengths, vibr. level depend. 79−45735
O_2, vac. UV photodissoc., kinetic energy and ang. distribs. of fragments 77−30938
O_2^+, absorpt. linewidth of predissociated levels, lifetimes 79−36711
O_2^+, $b^4\Sigma_g^-$ state, laser-induced predissoc. in ion beam 78−70886
O_2^+, $c^4\Sigma_u^-$ state predissoc. calcs. 79−50095
O_2^+, $f^4\Pi_g$ state, quasi-bound levels, predissociation, band rot. anal., photofragment kinetic energy anal. 80−63650
O_2^+, first negative system, high-resolution photofragment spectroscopy 80−47971
O_2^+, laser-induced photodissoc. spectrum 79−68280
O_2^+, laser-induced predissoc. spectrum, rot. anal. 77−71839
O_2^+, photodissoc. by visible light, predissociation 78−66612
O_2^+, photofragment spectroscopy using fast ion beams 80−9755
O_2^-, predissociated $b^4\Sigma_g^-$ state, high resolution laser spectroscopy in fast ion beam 80−9656
O_2^+, predissociation of $b^4\Sigma_g^-$, $c^4\Sigma_u^-$ states, threshold photoelectron-photoion coincidence 78−42144
O_2^+, quartet states, predissoc. photofragment spectroscopy 78−82794
O_2^+, radiative lifetimes and UV spectra, $b^4\Sigma_g$-$a^4\Pi_u$, $A^2\Pi_u$-$X^2\Pi_g$ transitions 78−17724
OD, reson. cross-sections, predissoc. and preassoc., isotope effects 78−58750
OH, $A^2\Sigma$ state, predissoc. rates, high freq. deflection meas. 78−62864
OH, $A^2\Sigma^+$ state, predissociation and tunnelling 78−29823
OH, multipredissoc. of $A^2\Sigma^+$ state, multichannel scatt. theory 79−94046
OH, reson. cross-sections, predissoc. and preassoc., isotope effects 78−58750
$O_2(b^4\Sigma_g^-, v'=4, N', F')$ predissociation fragments, ang. distribs., separation energies 80−5588
$O_2^+(b^4\Sigma_g^-)$ predissociation, branching ratio determ. 80−14181
PO, rot. struct. of absorpt. bands 1850-1600 Å, valence $^2\Pi$ state 79−13739
$P^{18}O$, UV absorpt. spectra, valence and Rydberg states, rot., vibr., anal., predissoc. 79−41184
S_2, matrix-isolated, $B^3\Sigma_u^-$ predissoc., relax. processes 80−58329
SO_2, UV excitation spectra, mol. fluoresc. meas., mol. predissoc. obs. 80−83389
S_2O, UV excitation spectra, mol. fluoresc. meas. 80−83389
SiH, A state new predissociations, improved dissoc. energy value from rot. level lifetimes 79−3496
SiO, nearly degenerate $G^1\Pi$-$I^1\Pi$ energy spectra, predissoc., extended virial theorem 79−22771
SrH (0,0)-band at 2680 Å, R-branch predissociation 78−50554
XeO, excited state spectra, subpicosec. predissoc., solvation, in solid rare gas hosts 77−68050
Zn_2, quenching and predissociation, possible excimer laser 80−32770

molecular quadrupole moments *see molecular moments*

molecular relaxation *see chemical reactions; molecular fluorescence; molecular inelastic collisions; molecular spectra; time resolved spectra*

molecular reorientation
see also macromolecular dynamics
acetic acid, $-d_1(=d_4)$ liquid, molecular motion, proton spin echo study *(Russian)* 80−32745
acetic acid, Rayleigh-Brillouin scatt., 20-115°C, viscoelastic theory anal. 79−28774
acetone, ^{17}O chemical shift and NMR linewidth meas., self-association equilib. const. determ., mol. reorientations obs. 80−87148
acetone, liq., rot. motion, nucl. mag. relax. obs. 78−88209
acetone, solid, effects of tunnelling on spin-lattice relax. of methyl protons 77−12216
acetonitrile, ^{13}C relaxation times anal. using J-diffusion model of mol. reorientation 80−87149
acetonitrile, dissolved in liq. cryst., NMR, ^{13}C, ^{14}N relax. times, temp. depend. 79−94016
acetonitrile, dissolved in nematic EBBA, oriented CH_3 group relax., multiple quantum NMR 80−66057

molecular reorientation continued
acetonitrile, IR and Raman spectra, vibr. and reorientational and energy transfer width separation, rot. const. determ. 80−87131
acetonitrile, liq., Brownian reorientation barriers *(Russian)* 79−27901
acetonitrile, liq., rotational motions, diffusion coeffs., quasi-elastic neutron scatt. study 79−50979
acetonitrile, soln., high press., mol. reorientation, correl. times, depolarised Rayleigh scatt. obs. 80−29748
2-acetylanthracene solutions, excitation spectra rel. to absorption spectra, 77-300K 79−85970
acridene yellow, glycerol soln., luminesc. intensity and polaris., temp. and viscosity effects 79−56833
adamantane, mol. reorientation activation parameters, determ. by NMR method under press. 77−89393
adamantane, plastic cryst., rotational motion, elastic incoherent struct. factor determ. 77−4056
adamantane, plastic cryst. rotational motion, quasielastic neutron scatt. study 79−41991
adamantane, plastic phase, C_4 rot. jumps, existence and uniqueness 80−88067
adamantane, plastic-phase transition, cell model 77−11665
adamantane-d_{16}, collective librational modes and orientational correlations 79−73266
adamantane-d_{16}, in soln., deuteron spin-lattice relax. time, mol. rotational correl. time 78−84491
2-adamantanone, cryst. struct. in plastic phase 80−88065
adsorbed layers, bitransitions in molecule reorientation processes *(Russian)* 79−99416
adsorption one-dimensional lattice model, thermodynamic functions calc., matrix method 79−37917
L-alanine, nucl. spin-lattice relax. of CH_3 and NH_3 groups 77−8440
L-alanine, solid, H bonding, wide line NMR obs. 78−52362
alcohol, dielec. const., hindered mol. rot. influence 78−43767
alcohols, monohydric, dielec. polarisation 79−99818
alcohols, OH-stretching vibr. band in overtone region, IR-Fourier spectral investig. *(German)* 80−976
alcohols, vapour and liq. IR spectra, bandwidth, directional mol. rot., H-bonding 79−78661
alignment relaxation rate, laser saturation reson. technique 78−25755
aliphatic, in dil. solns., dielectric relax. dipole reorientation, rot., microwave obs. 77−28516
aliphatic ethers, dil. solns., dielec. loss meas. for dielec. relax. 78−68451
alkali halide: S_2^-, laser-excited spectra and reorientation of S_2^- 77−28563
alkali halide:NH_2^-, paraelectric alignment, UV electroabsorpt. and Kerr effect 77−12413
alkali halide:NH_4^+, hindered rot. energy levels calc. 80−10514
alkali halide:VO^{2+}, impurity behaviour, elec. cond. and IR absorpt. obs. 77−8607
alkali halide, doped, AC field induced impurity-vacancy dipole relax. 79−11385
alkali halides:NH_4^+, inelastic neutron scatt. 78−14407
alkali halides, luminesc. polarisation and low-temp. photoinduced orientation change in O_2 and S_2 mol. centres 78−6735
alkali hyperoxides, ionic π-electron systems, magnetogyration 80−93155
n-alkane, order-disorder phase transition bits. calc. 77−72684
alkane chains in liquids, rot. and torsional dynamics, Riemann tensor theory 80−54084
n-alkanes, depolarised Rayleigh spectroscopy 79−4808
alkanes, liquid, chain reorientation, Brownian dynamics simulation, comparison of models 80−49067
n-alkanes, orientational phase transitions with mol. config. change 78−14444
alkoxybenzoic acids, liq. crystal, solid phase, methyl group C_3 reorientation, proton spin relax. 77−1071
p-alkoxybenzylidene-p-aminocyanoanilines, IR absorpt. spectra, elec. field effect, orientational order parameter determ. by IR dichroism 80−80777
p-alkoxybenzylidene-p-n-alkylanilines, solid state, nuclear spin relax. 78−76337
alkyl chains, ^{13}C longitudinal relax. times and nuclear Overhauser enhancement anal. 80−83390
alkylammonium cadmium tetrachloride, struct. phase transition, PMR, spin-lattice relax. time 77−35688
alkylene diammonium cadmium tetrachloride, struct. phase transition, PMR, spin-lattice relax. time 77−35688
allene, liq., orientational dynamics, Raman obs. *(French)* 79−28746
allene, rot. diffusion in CS_2 soln., IR spectral profiles 79−87426
alternating copolymer of styrene and N-substituted maleimides, NMR relax. studies of mol. motion 77−85608
amino acids, polycryst., proton mag. relax. and mol. motion 78−20139
4-amino-4′-nitrostilbene, thermal motion of prolate luminescent molecules in solvents with different viscosities 79−83029
ammonium compounds, rotational tunnelling, temp. dependence 80−38970
ammonium hydrogen oxalate hemihydrate, single cryst., DNMR obs., elec. field gradients, reorientation 77−85618
ammonium ions, tunnelling, model of spin-lattice relax. time 77−63305
ammonium salts, proton spin relax. and phonons 78−84493
anilines, substituted, in benzene soln., dielectric relax. time, dipole moment 80−50259
anilines, substituted, in nonpolar solvent, dielec. relax. obs. 80−55022
anilinium chloride, NH_3^+ intraionic C_3 reorientation, NMR and rot. frame expt. 79−28630
anilinium halides, and anilinium sulphate, proton mag. relax. obs. 80−34800
p-anisidine, polycryst., intramol. reorientations, PMR 78−64279
anisotropic liq. ang. correl. functions, memory function approach, Mori theory and extended diffusion eqn. 80−10489
anisotropic rotational diffusion studied by passage saturation transfer EPR 80−60403
anthracene:tetracyanobenzene charge transfer complex, cryst. struct., temp. effects 80−96508
anthracene dianions in dimethyl ether, rotational diffusion meas. 80−65262
anthracene-TCNB, charge transfer cryst., Raman study of phase transition 79−19885
anthracene-TCNB charge transfer crystal, EPR spectra of triplet excitons, and Raman spectra 78−26817
anthranilic acid, solid, amino group reorientation, PMR second moment obs. 78−35046

molecular reorientation continued
apatites, dipolar reorientations, TSD study 80−107068
assembly of molecules, orientational correl. functions, dipole-dipole coupling 79−36798
atom+diatom collisions, reorientation cross section calc., distorted wave and Bernstein Kramers approx. 79−843
atomic and plastic crystals, melting transitions, thermodynamic props. 80−96452
autocorrelation functions, planar itinerant oscill. model 77−80400
azobenzenes, substituted, isotropic, nucl. spin-lattice relax. 79−23519
azoxybenzenes, substituted, isotropic, nucl. spin-lattice relax. 79−23519
barriers, in crystals, determ. from data on LF spectra of lattice vibrs. 77−69824
BBOA, smectic B phase, fluidlike mol. dynamics, Raman scatt. study 80−20630
benzaldehydes in EBBA liq. cryst., NMR, mol. struct., reorientation and order matrix 78−5251
benzene, cryst., press. depend. of nuclear spin-lattice relax. time 79−28635
benzene, liq., Brownian reorientation barriers *(Russian)* 79−27901
benzene, liq., mol. motion at high press. 80−103509
benzene, mol. reorientationally disordered phases, thermodynamics 79−46782
benzene, polycrystalline heteronuclear dipolar modulated chemical shift spectra, geometrical and orientational obs. 77−20750
benzene, rot. motions and cryst. growth, Monte Carlo calcs. 79−46577
benzene in 3-methylpentane glass, phosphoresc. polarisation and intensity, 77K 77−46588
benzene submonolayer on silica gel, PMR and DMR dynamics and surface heterogeneity 79−69735
benzene-chloroform mixture, Raman spectroscopy 77−24839
benzene-d_0, -d_6, in glass matrix, phosphoresc. lifetime and polarisation, rot. relax. time meas. 77−79648
benzene-d_6, liq., reorientational motion, Raman obs. 78−70841
benzene-p-dioxan, mixtures, mol. reorientation and assoc., depolarised Raman scatt. obs. 80−7341
benzenes, nitrohalide substituted, dipole orientation 78−75522
benzenes, substituted, cryst., reorientation motion, site models with non-equivalent sites, dielec. relax. 79−11382
benzenes, substituted, dense liq., mol. reorientation and shear viscosity 77−4213
benzenes, substituted, dielectric absorpt. and NMR 78−88251
benzil, NMR of cryst., 77-367K 79−38387
n-benzoates, MP and rot. mobility of struct. groups *(Russian)* 77−69074
benzonitrile, depolarised Rayleigh scatt. 78−68522
1,1′-binaphthyl, $T_n \leftarrow T_1$ absorption spectrum in rigid and fluid media, CNDO/A study 79−76355
binary liquids, coupled mol. reorientational relax. kinetics, Kerr effect 78−67636
biomolecular components, proton relaxation; solid state, activation energies, relax. consts., 50-500K 78−68998
biomolecular EPR and saturation transfer EPR spectra at high microwave field intensities 79−34488
biradical metal chelates, rot. motion in polar solvents, rel. to ESR lineshape 80−27994
BPBAC, smectic B phase, neutron diffr. and X-ray obs. 78−94973
4-bromo-m-thiocresol, liq., dielectric relax. mechanisms 79−42891
9-bromo-meta-carborane, mol. reorientation, ^1H and ^{11}B NMR 77−16185
4-bromobiphenyl, dielectric const., mol. reorientation in solid 78−72448
bromomethanes, ^{13}C-Br spin-spin coupling consts., isotope effects 78−13522
n-butane, liq., temp.-depend. free vol. 79−99052
n-butane, solid, mol. reorientation, PMR 77−8431
tert-butanol, mol. dynamics, liq. and cryst. states, neutron inelastic scatt. obs. 78−75599
2-butanol adsorption on Al_2O_3, PMR spectra 79−19457
t-butyl bromide, vibr. relax. in pure liq. and soln., Raman spectra 80−66167
t-butyl chloride, rotational motions, cold neutron scatt.study 79−51023
t-butyl chloride, solid phases, mol. motion, cold neutron scatt obs. 78−26460
t-butyl chloride, vibr. relax. in pure liq. and soln., Raman spectra 80−66167
t-butyl derivatives, liq., reorientational correlation times, Hubbard model 79−61353
n-butyl-4-(4′-phenylbenzylideneamino)cinnamate-d_9, smectic E, B and A phases, quasielastic neutron scatt. obs. 78−75539
calcium copper acetate hexahydrate, and deuterated cpd., tunnelling reson. effects in nonreson. spin-lattice relax. 79−86726
calcium formate, polycrystalline, heteronuclear dipolar modulated chemical shift spectra, geometrical and orientational obs. 77−20750
d-camphor, high resolution ^{13}C NMR spectra, 275 to 343K 79−56621
d-camphor systems, mol. reorientation dynamics, Raman spectra 78−31178
carbon tetrabromide, plastic phase, orientational disorder 79−73115
carborane, ortho- and para-, phase transition and mol. reorientation, isomer effects, PMR obs. 80−80628
cellulose, mol. motions, role of water, temp. and morphology 77−89386
cetyliodide, cryst. phase transitions, mol. dynamics, spectroscopic and dielectric meas *(Russian)* 79−51965
charge transfer complexes, polycryst., NMR spin-lattice relax. *(French)* 77−32279
chloral, in benzene, permittivity, dielectric loss, 36 GHz 77−32323
chloral, liq., permittivity, dielec. loss, up to 60 GHz 78−60384
chloranil, mol. cryst., soft mode and central peak neutron scatt., struct. transition 79−42209
2-chloro-2-nitropropane, far IR-microwave estimation of binary collision approx. 80−55095
4-chloro-α-toluothiol, liq., dielectric relax. mechanisms 79−42891
chlorobenzene-d_0, -d_1, mol. reorientation and D nucl. relax. time, temp. depend. 78−39424
o-chlorobenzoic acid, solid, H bonding, wide line NMR obs. 78−52362
3-chlorodiphenyl, in dipolar aprotic solvent, internal rot. barrier, ^{13}C T_1, obs. 78−29860
chloroform, and d, polar soln., Raman line shape of ν_1 band 78−74705
chloroform, dense liq., mol. reorientation and shear viscosity 77−4213
chloroform, in isotropic MBBA, nucl. spin-lattice relax., reorientation 79−4735

molecular reorientation continued
chloroform, solns., vibr. dephasing and reorientational relax., solvent depend., Raman spectra 79−85968
chloroform and -d, Raman spectra study of mol. reorientation 79−24303
chloroform diluted in CS_2, proton transverse relax. time and reorientation of chloroform *(French)* 77−32280
chloroform-d_1, D NMR relax., in nematic liq. cryst., motion spectral densities determ. 77−63304
chloroform-He(Ar)(N_2) gaseous compressed mixture, mol. reorientation, Raman spectra 80−23422
chloroform-hexamethylphosphoramide complex, mol. motion and assoc., PMR obs. *(French)* 78−72429
chloroform-p-dioxan and chloroform-benzene mixtures, mol. reorientation and assoc., depolarised Raman scatt. obs. 80−7341
chloromethane, low density gas, proton spin-lattice relax., mol. reorientation 79−3462
2-chloropropane, separation of collision-induced from intrinsic mol. depolaris. Rayleigh scatt., C-Cl bond optical anisotropy 78−27244
2-chloropyrimidine, CS_2 soln., nucl. mag. relax. of ^1H, ^{13}C 78−27105
cholesteric liquid crystal, non-sterol, helical twist sense, absolute config. and mol. struct. 77−72552
choline bromide, solid, mol. dynamics, NMR obs. 78−56390
choline chloride, solid, mol. dynamics, NMR obs. 78−56390
choline salts, mol. motion, proton spin-lattice relax. 77−59474
chromophore emission spectra, exciting wavelength depend., hydroxylated solvent reorientation 78−76514
classical octopolar solid, temp. effect, Monte Carlo calc. 78−75598
classical quadrupole solids, correl. effects 80−10628
clathrate hydrates, containing ethylene, oxide, mol. rot. motion, quasielastic neutron scatt. 78−91274
clathrate hydrates, containing ethylene oxide, mol. rot., inelastic neutron scatt. 78−91275
collagen fibril, ^2H NMR of mol. motion 80−67034
condensed phase mol. reorientation, correlation times, librational model 78−1968
condensed phases, molecular rototranslation, single particle theory 80−64932
conformational dynamics and the rotational isomeric state model 78−90315
copper formate tetradeuterate, deuterated, paraelec. and antiferroelec. phases, neutron diffr. obs. of struct. 79−87404
coupled molecular rotational diffusion and conform. change 78−22613
CPHB, nematogenic liq. cryst., above T_c, Kerr effect response time, temp. depend. 78−34434
cresyl violet, rot. diffusion, picosec. saturation spectrosc. obs. 80−5634
crystal, non-rigid impurity centres, symmetry groups 79−77534
crystal orientational disordering, thermodynamic props., stat. mech. model 80−96453
crystals, anomalous thermoelastic behaviour, mol. reorientation, theory 77−84676
cubic crystal, self-diffusion and melting 77−31803
cuminaldehyde, dil. soln., dielectric relax., solid rotator phase 79−42890
4-cyano-4′-d_{17}-n-octylbiphenyl, D spin-lattice relax. time, partially averaged quadrupole tensors 77−1076
4-cyano-4′-n-octylbiphenyl, smectic A liq. cryst., electrically induced scatt. textures and elec. reversal 78−83725
cyanoacetylene, liquid, mol. pot. and translational motion, anal. using slip and stick boundary conditions and Perrin correction *(French)* 79−38394
4-cyanobiphenyl and 4′-alkyl- or 4′-alkoxy-substituted liq. cryst. derivatives, soln., absorpt. and fluoresc. spectra 80−87164
cyanobiphenyl nematic homologous series, Kerr consts., relax. times, refr. index, dielectric const. 79−19863
cyanomethane-d_0,-d_3, soln., for IR spectra, band shape and moment anal. 80−58252
4-cyanphenylene-4′-n-alkoxybenzoates, pulsed NMR Fourier spectroscopy 77−24266
cyclodiphosphazane, cryst., NQR study, intramol. interaction geom. and CCl_3 group dynamics 79−78564
cyclohexane, in benzene soln., mol. motion, correl. functions 80−96431
cyclohexane, mol. motion, press. and temp. depend., PMR relax. obs. 78−64289
cyclohexane, plastic and liquid crystal phase, rot. correl. func. by Raman spectroscopy 80−23403
cyclohexane, rotational reorientation anisotropy near phase transition *(Russian)* 79−4261
cyclohexane, thermal cond. and sp. ht. under press. 78−22906
cyclohexane-d_0(d_6), plastic crystal phase transition, mol. reorientation, Raman scatt. phonon spectra 80−20631
cyclooctane, solid, NMR lineshape and spin-lattice relax. 77−24757
cyclopropane, liq., molecular motion, incoherent neutron scatt. study 79−50978
cytidine, cryst. powder, absorption spectrum, unusual narrow line FIR modes, cryogenic temps. 79−69824
n-decylammonium cadmium chloride, perovskite-type layer cmpd. n-decylammonium chain dynamics 79−99313
decylammonium chloride micelles, ^{13}C longitudinal relax. times and nuclear Overhauser enhancement anal. 80−83390
dense fluid, hydrodynamics, high freq., small wavelength 77−19860
dense media, Q-branch Raman line width, rotational relaxation, reorientation, collision strength 79−98106
depolarised Rayleigh-Brillouin spectra, theory for molecular liqs. and solids 79−69850
deuterated nitroxide radical probe, synthesis and appls. *(French)* 78−76314
deuteriochloroform, Raman spectra, mol. orientational relax. 79−65865
deuterochloroform, solns., vibr. dephasing and reorientational relax., solvent depend., Raman spectra 79−85968
di-(2-ethylhexyl)phthalate, ^{13}C and ^1H relax., reorientational correlation times 79−51869
2,4-di-p-bromophenyl pentane, polystyrene model mol., US relax., mol. dynamics 79−73258
1,1′-diacetylferrocene, MBBA soln. nematic glass-supercooled nematic transition, Mossbauer temp. obs. 79−95687
diamantane, NMR meas. of mol. motion 79−42858
diamantane, Raman study of three solid-state phase transition 79−51946
diatomic mol., vibr. relax. in condensed media, mol. rot. effects 78−91388
dibenzenechromium, cryst. and soln., dynamic struct., NMR expts. 77−15328
molecular reorientation continued
dibenzenechromium-dibenzenevanadium, proton HFS data, ENDOR obs. 80−66073
4,4′-dibromobiphenyl, dielectric const., mol. reorientation in solid 78−72448
dibutyl-phenyl-benzoyloxy-benzoate, nematic liq. cryst., rot. barrier, PCILO and CNDO/2 calcs. 80−33874
2,6-dichloroanisole, anisotropic reorientation, nucl. relax. in coupled spin systems 77−40145
o-dichlorobenzene, dil. soln. in CS_2, nucl. relax. and anisotropic mol. reorientation 79−95669
p-dichlorobenzene(−d_4), mixed cryst. phases, mol. reorientations and intermol. interactions, Raman obs. 79−28751
1,2-dichloroethane, enclathrated, conform., reorientation, PMR line shape anal. 79−91300
1,2-dichloroethane, orientationally disordered crystal., mol. orientation 78−34448
trans-1,2-dichloroethane, solid, NQR at high press., hindered rot. 79−95672
dichloromethane, liq. and dil. CCl_4 soln., far IR spectra and Rayleigh scatt. for planar itinerant oscillator 78−47229
dichloromethane, liq. dynamics, neutron inelastic scatt. 78−71664
dichloromethane-d_0,-d_2, soln., far IR spectra, band shapes and moment anal. 80−58252
dichloromethane-d_2, spectral densities determ. from spin-lattice relax. and spin-echo decay rates 80−75877
dichloromethane-decalin glass, mol. dynamics, from dielec. loss meas., 107-148K, 293K 78−76379
2,6- dichlorophenol, soln., anisotropic reorientation, H-bonding effect, NMR obs. 79−99782
2,6-dichlorophenol-O-d_1, anisotropic reorientation, nucl. relax. in coupled spin systems 77−40145
3-dichlorophenyl, in DMSO, NMR spin-lattice relax. obs. *(German)* 78−31121
dicyanoacetylene, solns., NMR and mol. reorientation 79−73840
dicyanoalkanes, in benzene soln., microwave absorption, internal rot. 78−60385
α,α-dideuterotetrabutylammonium iodide, in soln., deuteron spin-lattice relax. time, mol. rotational correl. time 78−84491
α,α-dideuterotetraethylammonium iodide, in soln., deuteron spin-lattice relax. time, mol. rotational correl. time 78−84491
dielectric and piezoelectric relax., difference between 78−72458
dielectric friction theory 78−87599
N,N′-diethyl-p-nitroso aniline, dil. benzene soln., dielec. props., microwave region, mechanisms 78−35085
diethylcarbonate, liq., alkoxy group internal torsion, extended microwave/far IR anal. 78−19457
1,2-difluorotetrachloroethane, mol. motions and Zeeman-quadrupole cross relax., NMR obs. 79−65751
1,2-difluorotetrachloroethane, orientationally disordered, mol. reorientation, depolarised Rayleigh scatt. obs. 78−88316
diheptyloxyazoxybenzene, smectic-C phase, proton NMR 77−11474
2,4-dihydroxy benzoic acid, PMR obs., proton second moment, 77 to 383K effect of OH group rot. 78−10784
1,4-dimethoxy-2,6-dimethylbenzene, methyl reorientations, NMR relax. and inelastic neutron scatt. obs. 79−61253
dimethyl tin difluoride, crystallographic phase transition, 70K, Mossbauer obs. 79−47366
dimethyl tin difluoride, solid, methyl reorient., low temp. phase transition, neutron scatt. obs. 79−27932
N,N′-dimethyl-p-methyl aniline, dil. benzene soln., dielec. props., microwave region, mechanisms 78−35085
dimethylacetylene, tunnel splitting, rot. pot., μeV neutron scatt. study 79−41993
4-dimethylamino-4′-nitrostilbene, thermal motion of prolate luminescent molecules in solvents with different viscosities 79−83029
dimethylcarbonate, liq., alkoxy group internal torsion, extended microwave/far IR anal. 78−19457
1,1-dimethylcyclopropane-d_0,-d_6, internal rot., Raman spectra 78−985
dimethyldihalostannanes, cryst., IR spectra bandwidth, CH_3 group internal rot. 78−52490
dimethylsulphate, cryst., liq., and oriented film, vibr. spectra, internal rot. 79−91444
dimethyltin difluoride, neutron scatt. exam. methyl group motion 78−59769
N,N-dimethyltrichloroacetamide, two-site exchange system, total line shape anal. 80−35519
2,6-dioxaadamantane, plastic phase, transition and fusion thermodynamics, DSC meas. 78−75603
1,4-dioxane, liq., reorientational correl. times from light scatt. 77−32385
dipolar hindered rotators, dielec. response calcs. 77−24781
dipolar liquid time-variation of dispersion and absorption of third-order electric polarisation, mol. relax. times 80−60487
dipolar molecular lattice, dielec. absorpt. of disordered mol. solids, electrodynamic influences 80−40040
dipolar molecules, zero-THz liq. phase dielec. absorpt. and rot. Langevin eqn. 80−40032
dipolar solids, nuclear spin-lattice relax. from hindered rot. 78−52373
dipolarly coupled spin pairs, correlation function and relaxation time, group theory approach 78−48068
dipole, spherical, steadily rot., dielec. friction 78−87600
dipole-dipole coupling, inertial effect 80−40049
DMBCA, nematogen, incoherent neutron quasielastic scatt. 79−32887
DNA, mutations, quantum theory, proton transfer by dynamic interactions 77−77868
DNA, proton mag. relax., methyl group reorientation 77−64009
DOBAMBC, polarized Raman scatt. and elec. field effects in aligned smectic phases 79−94873
double oscillatory tunnelling, soln. by effective Hamiltonian method 77−20109
dyes, rot. diffusion of prolate, oblate mols. from absorpt. relax. 80−1008
dyes in rigid matrices, solvent reorientation relax. effect on luminesc. 79−43009
EABAC, smectic-A, mol. motions, incoherent quasielastic neutron scatt. obs. 78−59740
EBBA: nitroxide, mol. reorientation in nematic and isotropic phases, EPR study *(French)* 79−91297
EBBA, isotropic phase, order fluctuations, self-diffusion, and rot. motion, proton spin relax. meas. 79−87328
EBBA, liq. cryst., rapid cooling and mag. field effects on NMR relax. and thermal behaviour 79−82321

molecular reorientation continued
EBBA, macroscopic and microscopic orientations, EPR of nitroxide probe *(French)* 78−75546
EBBA, nematic, ordering parameter temp. depend. 79−23517
EBBA, NMR and Raman scatt. studies in nematic phase 80−100619
elastin, hydrated, dielectric relax. 79−5247
elastomer, relaxation processes, statistical description *(Russian)* 79−23229
electrode-electrolyte interface, orient. models for solvent 78−61017
electronic spectra of molecules, pure elec. quadrupole transition polaris. 80−63691
electrostatic space focusing of molecular beam 80−28118
erythrosine B, dye soln., transient dichroism, rot. diffusion anomalies 79−87414
ethane, solid, mol. reorientational motions, incoherent neutron scatt. studies 80−107070
ethanol, polymorphic forms, mol. motion, NMR obs. 80−88885
ethanol, US studies of mol. relax. 78−22790
ethanol mols. reorientation in ethanol-water mixtures, Raman and Rayleigh spectra 78−76449
N-p-ethoxybenzylidene-p′-cyanoaniline, nematic, mol. reorientation in DC elec. field, IR ATR spectra study 80−45064
p-p-ethoxyphenylazophenyl hexanoate, dielec. relax. in stable and metastable solid phases 80−34851
ethyl trichloroacetate, in benzene, permittivity, dielectric loss, 36 GHz 77−32323
ethyl-3-chloropropionate, liq., microwave absorption and relax. 78−60386
ethylene, adsorbed on Na zeolite, uniaxial rot., translational dynamics 78−91538
ethylene oxide clathrate, reorientation, residence times, Debye-Waller factors, activation energy, neutron scatt. study 79−41989
ethylene oxide clathrate deuterate, rotational motion, quasi-elastic neutron scatt. study 79−51022
ethyltrichloroacetate, liq., permittivity, dielec. loss, up to 60 GHz 78−60384
eutectic mixture, glassy nematic phase, complex permittivity tensor 79−91336
ferrocene, cryst. and soln., dynamic struct., NMR expts. 77−15328
flexible three-bond mols., orientational dynamics 79−7537
fluid, correlation functions in mol. acoustics 77−51451
fluid, extended rot. diffusion, unified all-symmetry models 77−51285
fluid, mol. acoustics, light scatt. 77−52111
fluid, molecular, multiphoton Raman scatt. spectra 77−63404
fluid, of rough spheres, translational and rot. motion, particle roughness depend. 78−26403
fluid, rotational and translational diffusion, stochastic Liouville eqn. formalism 79−64971
fluid molecular reorientation, extended rotational diffusion models, unified treatment, review 77−27797
fluid of partially rough spheres, translational and rot. diffusion coeffs. 78−26404
fluid-like viscoelastic liquid, coupling of orientational and translational motions, LF depolarised (VH) scatt. 77−7642
fluids, stochastic differential eqns. 79−82132
p-fluoranil, ^{19}F NMR and spin-lattice relax. meas., pot. profile calc., mole. reorientation 80−29634
fluorescein 27, rot. diffusion and level kinetics separation in transient absorpt. spectroscopy 77−30877
fluorescence solvatochromism kinetics 77−30898
fluoroapatite, IR spectra, H motion in nonstoichiometric cryst. 78−35125
pfluorobenzaldehyde(-d_1), in smectic mesophase, mol. struct. and reorientation, NMR 77−27093
fluorobenzene, mol. reorientation and weak mol. interaction influence, ^2D spin-lattice relax. obs. 80−106333
Fokker-Planck fluid, dilute, ang. and orientational correlation times 77−84380
Fokker-Planck fluid of symmetric top mols., orientational relax. 78−5996
formic acid, liq., microdynamic behaviour, struct., nucl. spin-lattice relax. 77−76270
furan, mol. reorientationally disordered phases, thermodynamics 79−46782
furfuryl alcohol resins, PMR study of mol. motion 79−8062
gas of nonspherical mols., transport processes, kinetic cross sections, temp. depend. 77−80259
glassy polar matrix, electron trap relaxation model 80−15470
L-glutamic acid, solid, amino group reorientation, PMR second moment obs. 78−35046
glycerol, reorientation in associated liqs. 79−77481
glycerol-d_3(-d_4), compressed viscous liq., reorientational motion, NMR obs. 80−7183
glycine, nucl. spin-lattice relax. of CH_3 and NH_3 groups 77−8440
graphite nitrate, $(C_{3.24})^+(NO_3)^-3HNO_3$, DTA, NMR and refl. meas., dynamical and electronic props. 77−59478
graphite-DNO_3, intercalation cpd., mol. dynamics 79−28631
H-halide, phase transition theory 77−15580
HAB, dielectric and calorimetric investig. in solid, liq. cryst. and liq. phases 77−84639
halloysite, $Al_2O_3(SiO_2)_3(H_2O)_2$, NMR study of adsorbed water, molecular motions 78−95226
Haupt effect, coupled rotational and dipolar relaxation of methyl groups 77−32292
4-n-heptyl-4′-β-cyanovinylbiphenyl, liq. cryst., isotropic mechanism of mol. rot., dielec. permitt. meas. 80−10491
n-heptyl-4-cyanobiphenyl, nematic phase, dielec. loss, diffusion equations 80−71305
4′-n-heptyl-4-cyanobiphenyl, nematogenic liq. cryst., above T_c, Kerr effect response time, temp. depend. 78−34434
n-heptyl-cyanobiphenyl, dielec. relax. in nematic and isotropic phases 79−82151
n-heptyloxy-cyanobiphenyl, dielec. relax. in nematic and isotropic phases 79−82151
heterocyclics, in polystyrene matrices, energy barriers, dielec. absorpt. meas. 78−70958
2,4-hexadiyne, solid, methyl group tunnelling and torsion, neutron scatt. 78−18560
hexafluorobenzene, cryst., press. depend. of nuclear spin-lattice relax. time 79−28635
hexafluorobenzene-benzene, liq., mol. interactions, IR and Raman lineshape obs. 80−28907
molecular reorientation continued
hexamethyldialuminium, methyl group rotation and bonding, CW proton second moment and line shape studies 79−47346
hexamethyldisilane, mol. motion, press. and temp. depend., PMR relax. obs. 78−64289
hexamethylenetetramine, mol. ultraslow rot. obs. using D probe spin alignment tech. 80−88890
hexamethylenetetramine, ultraslow tetrahedral jumps, deuteron NMR spin alignment obs. 80−66046
hexamethylethane, mol. motion, press. and temp. depend., PMR relax. obs. 78−64289
hexanetriol 1,2,6, liq., light scatt. study of struct. relax., viscosity and dielec. relax. 79−86672
4-n-hexyl-4-cyanobiphenyl, liq. cryst., isotropic mechanism of mol. rot., dielec. permitt. meas. 80−10491
4-n-hexyloxybenzylidene-4′-n-propylanilene, smectic S_H and S_m phase structs. 79−14673
hindered rotational energy levels of a linear ion in octahedral and tetrahedral crystalline fields 78−59767
hindered rotator in mag. field, mag. moment due to orientational tunnelling 77−68931
HOAB-d_{30}, biaxial liq. cryst., NMR of spinning sample 79−64987
hydrate, struct. I clathrate hydrate, H_2O mol. reorientation and diffusion, PMR and dielectric relax. 77−36142
hydrocarbon chain, gauche-trans isomerisation, ^{13}C relax. times and nucl. Overhauser enhancement model 78−33520
hydrodynamic boundary conditions and radii, appl. to rot. rough sphere friction with chloroform 78−9926
hydrogen-bond systems, near-equilib. behaviour, model 77−30961
hydrogenous molecules in crysts. and liquids, neutron spectra, book contrib. 77−89573
hydroxyapatites, dipolar reorientations, TSC study 80−60491
hydroxylapatites, IR spectra, H motion in nonstoichiometric cryst. 78−35125
hydroxylapatites, IR spectra, stretching and librational bands of OH groups, and hindered rotation 78−2841
IBPBAC, dynamics of smectic phases, quasi-elastic neutron scatt. meas. 79−86700
IBPBAC, smectic B phase, neutron diffr. and X-ray obs. 78−94973
ice orientational correlation parameter, water mol. dipole moment 80−59407
impurities in crysts., dynamics 79−60442
impurity molecule in cryst. lattice, strong EM field effect on librational-rot. motion 80−80824
impurity molecule reorientation at phonon excitation *(Russian)* 79−51019
in-cage reactions controlled by mol. reorientation 78−44362
intermolecular spectroscopy and dynamical properties of dense systems, conf., Varenna, Italy (1978) 80−82581
intermolecular spin relaxation by reorientation of off-center spins 79−42821
iodomethane, liq. (liq. mixtures), vibr. relax. and reorientation, symmetric C-H bending mode 1st overtone 78−62884
isopropanol, US studies of mol. relax. 78−22790
isotropic-nematic transition, model, mol. shape, vol. effects on orientational ordering 78−30741
ketones, in soln., IR spectral line halfwidths determ., rot. Brownian motion investig. 77−36248
librational reorientation, sum rules 78−71659
light quenching of mol. fluoresc. spectrum, spectral distrib. of polarisation, orientational relax. 79−85989
linear diatomic rigid mol. chain, mol. dynamics, rot. phase transformation, struct. factors 78−26635
linear molecules, forced rot. diffusion, nonlinear aspects 79−90503
lipid membranes, orientational phase transitions with mol. config. change 78−14444
liquid, anisometric, light scatt. obs. of orientational pair correlations 77−36252
liquid, barrier to internal rot., IR spectral linewidths meas. 78−72507
liquid, conditional pair distrib. function, irreducible expansion, symmetries 77−47317
liquid, configurational heat capacity, correlation formula, corresponding states method 78−30766
liquid, dielec., Kerr effect relaxation rel. to mol. reorientations 77−4599
liquid, dynamic and static orientational pair correls., depolarised light scatt. 77−16321
liquid, electron spin echo phase memory decay, generalised cumulant expansions appl. 79−11334
liquid, far IR absorpt., rot. dynamics studies *(French)* 78−39534
liquid, IR absorpt. lineshape, orientation density fluctuation effects 78−48171
liquid, IR and Raman studies, model 80−11390
liquid, IR spectra, calc. involving vibr. and reorientational relax. 78−48170
liquid, orientational correlation functions for dipolar and induced dipolar absorpt. in far IR 77−11451
liquid, polyatomic molecular, intermol. dipolar mag. interactions effect on nucl. relax. *(French)* 77−32277
liquid, reorientation on C_∞ group 77−1053
liquid, vibr. dephasing and gas-liq. crit. density fluctuations 79−51954
liquid, vibr. relax., line widths, intermol. forces dephasing 77−47315
liquid crystal, ferroelec., helicoidal, smectic-C, dynamics 79−1396
liquid crystal, nematic, reorientation time in magnetic fields, two methods *(German)* 78−59736
liquid crystal, relaxation eqns. for mean orientation *(Russian)* 77−11483
liquid crystal, rotary motion about short axis, dielectric and splay viscosity meas. 77−43145
liquid crystal display, with dichroic dye guest, field-induced colour switching 80−1327
liquid crystals, molecular ordering from incoherent quasi-elastic neutron scatt. 79−4241
liquid crystals, static and dynamic props., time depend. fluoresc. depolarisation obs. 80−29786
liquid crystals, uniaxial, molecular dynamics 79−19141
liquid memory functions for ang. motions 80−59358
liquid phase band contours, data processing, band shape corrections 78−27215
liquid short chain molecules, optical investig. of mol. motions 80−40123
liquid structure and dynamics from light scatt. spectra 80−55105

molecular reorientation continued
liquid-state dipoles in weak const. elec. field, orientation relaxation *(Russian)* 78−43886
liquids, collective molecular motion from depolarized light scatt. 80−60614
liquids, depolarised Rayleigh scatt., review 77−40256
liquids, rotational relaxation, molecular hydrodynamics, long time tails 80−59357
lithium acetate dihydrate, nearly free methyl rotors, rot. energy states, nucl. reson. props. 80−34784
lithium oxalate hydrate, proton spin-lattice relax., 180° flips and diffusion of water mol. 77−15327
luminescent system, orientation factor in conc. effects due to nonradiative energy transfer 80−25425
macromolecular, solutions, mol. orientation, time-depend. torque, rot. diffusion eqn. 78−68471
macromolecular rotational diffusion, ^{13}C spin-lattice relax. data anal., computer program, appls. 79−95664
macromolecular solutions, orient. in laser beam elec. field, anisotropic light scatt. 79−1768
macromolecule monodisperse solutions, macromol. length rel. to anisotropic light scatt. in elec. field 77−32391
macromolecules, scatt. methods, conf., Prague, Czechoslovakia, (July 1976) 79−1764
macromolecules in soln., Rayleigh scatt., elec. reorient. rel. to spectral line rot. broadening 79−1774
magnetic relaxation depend. on internal motion in solid, correlations 80−25239
magnetic reson. lineshape, with slow mol. motion, asymptotic method, strong collision limit 77−48063
magnetic resonance line shape, effect of anisotropic motion 80−7144
maleic acid-styrene copolymer, aq. soln., conform. transition 78−75526
MBBA, dielec. relax. in nematic phase 79−82153
MBBA, dielectric and calorimetric investig. in solid, liq. cryst. and liq. phases 77−84639
MBBA, isotropic, depolarised Rayleigh doublet, de Gennes viscosity coeffs. 78−31207
MBBA, isotropic phase, order fluctuations, self-diffusion, and rot. motion, proton spin relax. meas. 79−87328
MBBA, nematic, freq. depend. of proton T_1, rot. diffusional mechanism interpret. 77−12219
MBBA, nematic, ordering parameter temp. depend. 79−23517
MBBA, nematic liq. cryst., ^2H NMR, mol. order and reorientation 79−27906
MBBA, nematic liq. cryst., nonlinear optical amplification above Frederiks transition 80−95937
MBBA, NMR and Raman scatt. studies in nematic phase 80−100619
MBBA, order fluctuations, self-diffusion, rot. motion, proton spin T_1 relax. 77−32285
MBBA, solid, metastable, wide-line NMR 77−51966
MBBA, solid, NMR and thermal behaviour, cooling and mag. field effects 78−76336
MBBA-d_{13}, nematic phase, mol. order and director fluctuations, ^2D NMR meas. 79−90529
MBBA/EBBA, nematic, mol. interaction energy 80−33881
mesitylene-d_{12}, extended diffusion with internal rot., NMR test 79−31549
methane:O_2, crystal field, O_2 catalysis of spin-species conversion 77−51706
methane, adsorbed on graphitised C black, rot. tunnelling, neutron scatt. obs. 79−15000
methane, and methane-d_4, rotational transition in condensed Xe, 6K, optical excitation 78−60494
methane, entropy and sp. ht., 0.4 to 28K, spin-species conversion 77−28015
methane, heavy, cryst., temp. depend. of Debye-Waller factor, Monte Carlo calc. 78−47492
methane, in alkane soln., ^{13}C nucl. spin-spin relax., for mol. correl. times 79−95661
methane, liq., temp.-depend. free vol. 79−99052
methane, phase II, nuclear spin-lattice relax. and site symm. 80−97155
methane, solid, high press. NMR obs. 80−50214
methane, solid, lattice distortions and phase transitions 77−19882
methane, solid, phase II, Raman spectrum, vol. and temp. depend. 80−97260
methane, solid, phase II, theory of phase transitions 77−51494
beta-methane, solid, Raman spectrum in intramol. and lattice region 79−33697
methane, solid, rot. ordering and proton spin-lattice relax. 78−91967
methane, solid, theory of nucl. spin conversion in β phase 77−31608
methane and methane-d_4, solid, thermal cond. calc. 78−51753
^{13}C-methane-d_1:O, annealed, spin conversion and proton 2nd moment time-depends. 80−11283
methane-d_1, and -d_3, reorientation in simple fluids, IR band profiles 77−36237
methane-d_4, critical behaviour at orientational order-disorder transitions, neutron scatt. 77−43308
methane-d_4, solid, rot. tunnelling, neutron scatt. obs., isotope effect 80−92468
methane-d_4, solid, tunnel splittings, heat capacity meas. 80−96451
methane-d_4, solid, US attenuation, phase transitions 79−51204
methanol, ^{13}C spin-lattice relax., cross correlation of rot. motion 79−42855
methanol, US studies of mol. relax. 78−22790
methanol glass, H atom abstraction by methyl radicals, 15-100K, limiting rate const. rel. to tunnelling 77−60037
methanol molecule enclosed in β-quinol clathrate, dielec. meas. 78−2026
methanol-β-quinol clathrate, orientation and reorientation dynamics, dielec. and NMR obs. 79−99783
p-methoxybenzoate-p′-n-pentyl benzene, slow non-critical mol. reorientation in isotropic phase 80−84062
4-methyl 2,6 di-tertiary butyl phenol, gamma-irradiated, electron-methyl group dynamical interactions 77−43161
4-methyl 2,6-di-tertiary butyl phenol, change in barrier to methyl group rotation near cryst. surface 78−38634
methyl (CH_3D) group tunnelling in solids, quantum model rel. to two T_1 temp. depend. minima 78−2028
methyl bromide, ^{13}C relaxation times anal. using J-diffusion model of mol. reorientation 80−87149
methyl bromide, liq., NMR relax., anisotropic mol. reorientation 78−2764

molecular reorientation continued
methyl compounds, rotational tunnelling, temp. dependence 80−38970
methyl group, ^2H quadrupole coupling const. by high-resolution NMR spectroscopy 78−25563
methyl group, proton spin relax. due to intermol. proton coupling, reorientation 78−25564
methyl group nuclear spin symmetry species, torsional relax. 79−60287
methyl groups, detection of proton NMR at arbitrary temps. of tunnelling system 78−39432
methyl groups, dynamical coupling between dipolar and tunnelling at high temps. 77−65959
methyl groups, flip-flop motion and spin symmetry conversion 77−15326
methyl groups, reorientation in solids, nonexponential Zeeman relax. 78−6589
methyl groups, spin symmetry species, neutron scatt. transitions 80−92470
methyl groups in solids, proton spin-lattice relax. mechanisms at low temp. 77−51982
methyl groups in solids, reorienting and tunnelling, spin-lattice relax. 80−50217
methyl groups in solids, tunnelling freq. for internal rotation in pot. function 80−49134
methyl halides, liq., orientational dynamics, local coherence 77−27805
methyl halides, Raman spectra and lattice motions 77−77197
methyl iodide, ^{13}C relaxation times anal. using J-diffusion model of mol. reorientation 80−87149
methyl iodide, dense liq., mol. reorientation and shear viscosity 77−4213
methyl iodide, liq., expt. comparison with rough sphere rot. diffusion model 78−30532
methyl iodide, liq., mol. reorientation, dielec. and viscosity meas. 80−100157
methyl piperidines, PMR spin-lattice relax. times and lineshapes, 100-300K 77−81027
methyl protons, in solids, spin-lattice relax., torsional vibr. effects calcs. 77−16196
methyl rotator in isotropic fluid, motional asymm. determ. from ^{13}C spin dynamics 77−69718
methyl symmetric stretching vibr. bandwidths, vibr. and reorientational effects, IR and Raman spectra 78−78686
4-methyl-2,6-di-tert-butylphenol, methyl group rot. mechanisms, Raman effect 78−71691
4-methyl-2,6-di-tertiary butylphenol, gamma-irradiated, effect of radiation damage on hindered methyl group rotation 77−35494
4-methyl-2,6-ditert-butylphenol, temp. depend. of methyl tunnelling spectrum by inelastic neutron scatt. 79−51015
4-methyl-2,6-ditertiarybutyl phenol, proton spin relax., 80-340K methyl rot. 79−78553
4-methyl-2,6-ditertiarybutylphenol, methyl group reorientation, classical dynamics, NMR relax. and inelastic neutron scatt. 80−88066
4-methyl-2,6-ditertiarybutylphenol, proton spin-lattice relax. and activation energies of tunnelling CH_3 groups 77−48071
4-methyl-2,6-t-butylphenol, γ-irrad., electron-methyl group spin-spin interaction 77−85572
4-methyl-2, 6-ditertiarybutylphenol, tunnelling methyl group, inelastic neutron scatt. study 79−46580
methyl-3-bromopropionate, liq., microwave absorption and relax. 78−60386
methyl-containing mol. solids, proton NMR line shape, methyl group tunnelling 78−6588
methyl-d groups, reorienting or tunnelling spin-lattice relax. 80−97156
3,5-methyl-pyridine, rot. pot., proton spin-lattice relax., inelastic neutron scatt. study 79−47351
N-methylacetamide, and isotopic forms, low-freq. Raman spectra, internal torsional mode 79−26992
methylcyclohexane, dense liq., self-diffusion and viscosity 80−15278
methylene chloride, partially deuterated, NMR, T_1 meas. and anal., −96 to 40°C 78−80237
methylene iodide, benzene soln., spin-lattice relax., struct., dynamics 77−1610
methyltrifluorosilane-d_3, extended diffusion with internal rot., NMR test 79−31549
mixed ion-dipole systems, rot. diffusion, statistical theory *(Russian)* 77−80403
mobile liquids, coupled vibr. and reorientational dephasing 79−22686
molecular crystal, anomalous thermoelastic behaviour and orientational transition 77−76334
molecular crystal, orientationally disordered, translation-rot. dynamics, soft modes 78−83906
molecular crystal, p-$Cl_3P{=}NSO_2C_6H_4Cl$, rel. to quadrupole nature of spin-lattice relax. 77−59480
molecular crystal, quadrupole ordered phase, thermodynamic props. *(Russian)* 79−82353
molecular crystal, semiflexible long-chain mols., phase transition 77−80615
molecular crystals, orientational dynamics, unified theory 79−41992
molecular crystals, rot. and sp. ht. anomalies 80−28932
molecular crystals, rot. excitations and tunnelling, review 79−46579
molecular crystals, rotational and translational dynamics 79−51215
molecular crystals, thermal motion computer simulation 79−46577
molecular dynamics of nematics and thin films *(Russian)* 79−27903
molecular fluid, itinerant oscillator model, non-Markovian probability density function 78−47222
molecular liquid, reorientation PAC, nonadiabatic effects 77−12274
molecular rotation and reorientation, microscopic and hydrodynamic contrib. 79−1379
molecular solid, dynamic struct., NMR 79−73829
molecule, tetrahedral, in cryst. field, torsional ground state splitting, appl. to methane and $(NH_4^+)_2SnCl_6^{2-}$ 80−15019
Monte Carlo calcs. *(French)* 77−62491
Mossbauer spectroscopic studies of mol. motion in solids 80−39915
motions in liquids, review and anal., hydrodynamics 80−59356
trans,trans-mucodinitrile solid, NMR relax., mol. motions between unequal pot. wells 78−19353
trans,trans-muconodinitrile, mol. reorientation, unequal well pot. energy calcs. 78−26461
multicomponent solid solution, mean field approx. 78−22688
naphthalene, melting of rotational degrees of freedom near cryst.-liq. transition 80−54352
naphthalene in nonpolar solvent, vibr. and reorientational relax., correl. function 80−45065

molecular reorientation continued
naphthalene-TCNB, charge-transfer cryst., donor mol. orient. and dynamics 79−32926
naphthalene-TCNB (PMDA), Raman spectra orientational disorder, charge transfer cryst. 78−19459
naphthalene-tetracyanobenzene, doped cryst., EPR of triplet state for mol. reorientation 79−38368
β-naphthylamine, cryst., amino group reorientation, PMR obs., 77-373K 79−82881
nematic liq. crystal spin-relaxation, composite Markov process, rot. reorientation and director fluctuations 77−62471
nematic liquid cryst., rot. diffusion and freq. spectra 77−84631
nematic liquid crystal, circular random walk motion, comparison with neutron scatt. data 77−43146
nematic liquid crystal, domains due to mag. field 77−58951
nematic liquid crystal, ESR of symmetrical three-spin systems, slow motional spectra 77−36135
nematic liquid crystal, mol. reorientation, Fourier tranform NMR 77 35479
nematic liquid crystal, orientational order in two-dimens. elec. and mag. field effect 78−79530
nematic liquid crystal, oriented, transient behaviour of field induced reorientation 78−30536
nematic liquid crystal mixtures with low-freq. dielec. relax., phase behaviour 78−91246
nematic liquid crystal moment singularities at angular corners 77−51320
nematic liquid crystals, reorientation times, in mag. field. optical method determ. *(German)* 78−91240
nematic liquid crystals, shear flow in presence of electric AC field, elastic and viscous const. determ. 77−43144
nematic oriented film, birefringent stripe pattern generation by ultrasonic waves 77−76301
nematic to cholesteric transition, elec. field induced, transient phenomena of relax. 78−75811
nematic-cholesteric liq. cryst. mixture, NMR, reordering, nucleation and growth model 77−72546
nematics, nonlinear effects above electrohydrodynamic instability threshold *(Russian)* 78−75551
nematogen, isotropic phase, fast ps reorientation, optical Kerr signal 77−15313
nematogenic substances in solid state, NMR spectra 77− 16186
nematogens, isotropic phase, direct obs. of picosecond mol. reorientation 78−1991
nematogens, molecular motion in solid phase 79−61239
neopentane, mol. motion in cryst., liq. and plastic phases, neutron scatt. obs. 78−6021
neopentane, plastic crysts., rot. correlation functions, neutron scatt. obs. 79−46578
neopentane, rotational motions, cold neutron scatt.study 79−51023
neutron scattering, incoherent-quasielastic, coherent-quasielastic and coherent-inelastic, data anal. 78−63640
neutron scattering studies of mol. rotational motion in solid state 80−24384
nitrobenzene, anisotropic mol. reorient., ^{13}C, ^{14}N and ^{2}H mag. relax. 77−48070
nitrobenzene, liquid and CCl_4 soln. shear waves and translation-rotation coupling obs. by depolarised Rayleigh scattering 80−71432
nitrobenzene, oscill. optically induced Kerr kinetics 80−1286
nitrobenzene, rot. relax. times of anisotropic mols., optical Kerr effect and viscosity expts. 77−79906
nitrobenzene-n-hexane, crit. mixtures, reorientation spectra, linewidths and intensities 79−28777
t-nitrobutane, phase, II, quasielastic neutron scatt. 78−26458
nitromethane, 1-dimens. reorientation and tunnel splitting in solid 79−99086
nitromethane, proton spin-lattice relax. time, methyl group rot., 1 to 10K 77−48080
nitromethane, solid, tunnel states investig. 80−103274
m-nitrotoluene, pure and in soln., rot. relax. times of anisotropic mols., optical Kerr effect and viscosity expts. 77−79906
nitroxide free radical spin label EPR spectra, determ. of rot. correl. time and HFS coupling 80−74260
nitroxyl radical, slow anisotropic tumbling in ESR spectra 77−28448
nitroxyl radical rotation in liquids, ESR, dielec. relax. 77−28447
NMR line shapes, motionally narrowed, in solids 78−76325
NMR slow motional lineshape for very anisotropic diffusion, I=1 nuclei 79−78533
NMR spin echo, rotating solid sample, Fourier transform anal. 79−65759
noble metal complexes, hexafluoro, review of struct. obs., pseudorot., press. effects 78−6045
nonadecane, mol. motion in solid, ^{1}H spin relax. 78−15048
nonlinear molecules, tetrahedra, symmetry constraints on configurational props. 80−63854
nonlinear symmetric XY_2 type molecules, isotopic invariants, Coriolis coupling constants, centrifugal distortion constants 80−923
nonspherical mol., in dense fluid, depolarised light scatt. due to orientational fluctuations 77−47318
nonspherical mol., in dense fluid, depolarised light scatt. due to orientational fluctuations 77−47319
NQR, molecular reorientations between unequal potential wells 80−54989
NQR, NMR and EPR, spectral parameters, influence of mol. motion dynamics, review 80−20486
NQR spin-lattice relax. due to mol. fragments reorientation *(Russian)* 80−7189
nuclear quadrupole relaxation of I=1 nuclei in mol. crysts. 77−12247
nuclear relaxation in symm. groups, phonon-induced transition model 78−38635
nuclear spin relaxation and molecular rotation, review, book contrib. 79−31557
nuclear spin-lattice relax., effects of hindered rotation of NH_4^+ 77−8433
nucleic acid bases, proton mag. relax., methyl group reorientation 77−64009
nylon 6, influence of monomer and water diluents on mech. relax. 79−4993
n-octane, relax. about porphyrin defects and vacancies, Monte Carlo calcs. 79−46577
n-octane fluid, gauche-trans. relax. 79−69002

molecular reorientation continued
octylcyanobiphenyl, smectic liq. cryst., orientation between different interface and induced struct. *(French)* 77−51310
OHMBBA, solid phase dielectric relax. times and strength, mol. rot. 78−72456
organic compound, two-dimensional condensation with adsorbed mol. reorient. 78−61051
organic crystal, molecular rearrangements, intermol. cooperation and dipole-dipole interactions 77−1087
organic free radical solutions, mol. motions, dynamic nucl. polarisation 78−91991
organic homologous series, mol. orientational interaction, Maxwell effect 79−65833
organic liquid systems, dielectric and dynamic Kerr-effect studies 80−60496
organic liquids, Brownian reorientation barriers *(Russian)* 79−27901
organic molecular crystals, use of atom-atom pots. in interpreting behaviour, book contrib. 80−84136
organic nitriles, in soln., IR spectral line halfwidths determ., rot. Brownian motion investig. 77−36248
organic ortho compounds, solid, H bonding, wide line NMR obs. 78− 52362
organic reactions in solid state 80−21309
organic solid state chemistry, conf., Waltham, USA (June 1978) 79−46990
organic surfactant molecules reorientation on electrode surface, electrochem. kinetics 80−45522
organo tin dichlorides, tetrahedral, dilute soln., dielec. and thermodynamic behaviour, microwave region 77−36170
orientational autocorrelation functions, appl. to rot. Brownian motion 78−18520
orientational correlation times of nonrigid molecules, tensor correlations 79−4220
orientational phase transition in system of flexible mols. 79−82311
2-oxaadamantane, plastic phase, transition and fusion thermodynamics, DSC meas. 78−75603
oxalic acid dihydrate, PMR, water mols., reorientation 79−42856
oxalic acid dihydrate, proton spin-lattice relax., 180° flips and diffusion of water mol. 77−15327
oxalic and dihydrate, monocrystals, high resolution PMR 78−64283
oxypyrenetrisulphonate anion, aq. soln., ps time depend. fluoresc. depolaris. obs. rot. diffusion determ. 77−81139
PAA, deuterated, mol. reorientation, quasielastic neutron scatt. study 79−86705
PAA, isotropic, nucl. spin-lattice relax. 79−23519
PAA, methoxy deuterated, reorientational correl. times, comparison of neutron scatt. and dielec. relax. data 79−7545
PAA, methyl group rotation in solid and nematic phases, NMR obs. 78−6595
PAA, nematic, freq. depend. of proton T_1, rot. diffusional mechanism interpret. 77−12219
PAA, nematic and crystalline phases, NMR and relax. 79−4740
PAA, nematic liq. cryst., rot. barrier, PCILO and CNDO/2 calcs. 80−33874
PAA, selectively deuterated, proton spin-lattice relax. temp. freq. depend., diffusion 77−43132
PAA with deuterated methyls, nematic phase, quasieleastic neutron scatt. study of fast reorientations 78−14280
n-paraffin, cryst., first-order phase transition 77−80615
paraffin crystals, molecular motion, thermal expansion and phase transitions *(German)* 78−67837
paramagnetic liquid, depolarized light scatt. in mag. field 80−80759
pentacene dianions in dimethyl ether, rotational diffusion meas. 80−65262
pentachloro aniline, far IR spectra, mol. crystal orientational dynamics 78−60428
pentachloronitro benzene, far IR spectra, mol. crystal orientational dynamics 78−60428
pentachloronitrobenzene, single cryst., far IR absorption 79−73940
pentachloronitrobenzene crystal, anomalous microwave permittivity, IR absorption and Raman spectra *(Japanese)* 78−15169
4-n-pentyl-4′-cyanobiphenyl, nematogen, incoherent neutron quasielastic scatt. 79−32887
perdeuterobenzene, liquid, reorientation and spin-rotation interaction 78−39423
perovskite crystal, ABX_3, transition involving BX_6 octahedra rot., distorted phase symm. 77−4197
perovskite structure, phase transitions due to octahedra rot., model 79−99103
perylene in paraffin, anisotropic rot. and libration 77−32417
Phase V, nematic, transient response to redirected mag. field, EPR study 80−33879
phenanthrenequinone, NMR of cryst., 77-480K 79−38387
4-phenyl n-pentyl ester, Nematel 105, nematogen, isotropic phase, Rayleigh scatt. and mol. reorientation 78−34429
phenylene sulphides, NMR relaxation for mol. motions *(German)* 80−11288
phospholipids, ^{31}p NMR, slow-motional lineshapes for very anisotropic rot. diffusion 80−5644
phosphoranes, cryst., NQR study, intramol. interaction geom. and CCl_3 group dynamics 79−78564
photoluminescence of solutions, decay and self-depolarisation 79−24351
photoselection, orient. relax. rel. to emission mag. induced circular polarisation 78−70860
phthalamide derivatives, solutions, excitation spectra rel. to absorption spectra, 77-300K 79−85970
phthalimide acetyl derivatives in polar solvents, luminesc. kinetics and phosphoresc. quenching 80−18885
picoline compounds, proton spin-lattice relax. time, methyl group rot., 1 to 10K 77−48080
picosecond relaxation processes in chemistry, book contrib. 77−61788
piperazines, PMR spin-lattice relax. times and lineshapes, 100-300K 77−81027
pivalic acid, orientationally disordered crystal., mol. orientation 78−34448
pivalic acid($-d_1$, d_9), liq. and soln., Raman assignments, CH_3 rot. barrier, dimerisation 79−26991
pivalic anhydride, liq. and soln., Raman assignments, CH_3 rot. barrier, dimerisation 79−26991
planar molecules, anisotropic reorientation, nucl. relax. in coupled spin systems 77−40145

molecular reorientation continued
plastic crystal, critical behaviour at orientational order-disorder transitions 77−43308
plastic crystal, dipolar autocorrelation function, phonon contrib., IR absorption 78−42928
plastic crystal, k-independent Rayleigh diffuse line and orientational order 77−36253
plastic crystal, long time behaviour for chain of colliding rotators 78−75602
PMA, phosphorescence depolarisation, segmental relax. time 78−95606
PMMA, amorphous, reorientational relax., 6-165°C, polarised laser beam scatt. correlation 78−2864
PMMA, effect of fillers on molecular motions, dielectric relax. meas. 80−80691
PMMA, EPR of NO radicals, rot. mobility 79−33539
PMMA, mol. motions in benzene soln., ^{13}C NMR and EPR 79−78551
PMMA, multicomponent network, pulsed NMR study of mol. motions 77−55724
PMMA, phosphorescence depolarisation, segmental relax. time 78−95606
polar fluids, intermol. and thermodynamic potentials, angle-depend. pot. 78−22618
polar fluids, intermol. and thermodynamic potentials, preaveraged pot. 78−22617
polar fluids, rigid, dielectric relaxation theory 80−60495
polar liquid, IR absorpt. spectra and hydrodynamic model *(Russian)* 79−78689
polar liquids, solns., mol. rot., kinetics 77−51984
polar molecule, dielec. friction effect on reorientation in liq. 80−40048
polar symmetric-top molecules, reorientation, theoretical models 78−83707
poly(L-histidine), molecular motions in solid state, NMR and dielec. meas. 80−11332
poly(methacrylic acid)-D_2O soln., proton and deuteron relax. rates, temp. and freq. depends 77−88472
poly-α-methyl styrene, viscoelastic relaxation and methyl group tunnelling 79−57038
poly-p-phenylene sulphide, NMR relaxation for mol. motions *(German)* 80−11288
polyatomic fluid, local dynamics, spectroscopic studies, summer school lecture series 80−6343
polybut-1-ene and but-1-ene-polypropylene copolymers in solution, ^{13}C spin-lattice relax. and mol. motions 79−95670
polybutadiene, mol. motion in solid and soln., ^{13}C NMR relaxation meas. *(Japanese)* 80−2666
polycarbonate, amorphous morphology, from NMR obs. of swelling penetrant mol. motion 79−27929
polydiethylsiloxane, mol. motion, NMR spin relax. data re-interpret. 80−84664
polydimethylsiloxanes, liq., proton spin relax., mol. motion, network form. 79−15369
polydisperse rod suspension, elec. birefringence relax. 78−23430
polyethylene, dielec. loss below 4.2K arising from proton tunnelling 77−52015
polyethylene, EPR of NO radicals, rot. mobility 79−33539
polyethylene, linear, nuclear relaxation, mol. motion *(Russian)* 80−44949
polyethylene crystals, plastic deformation, molecular mech., TEM obs. 80−21022
polyethylene glycol, depolarised Rayleigh scatt., orientational motion, pure and soln. 77−44008
polyethylene oxide in benzene solns., ^{1}H relaxation times, intermol. interactions 77−32281
polyglycidyl methacrylate, soln., mol. dynamics, by spin mark method *(Russian)* 79−60260
polyimide, influence of monomer and water diluents on mech. relax. 79−4993
polymer, mol. motion, fluctuational network of nodes *(Russian)* 79−51011
polymer, solid, rot. degrees of freedom affecting physical props. 79−69029
polymer, uniaxial, fluoresc. polarisation, orientation and mol. dynamics effects 78−76516
polymer chains with rigid bonds, local relax. times, mol. dynamics study *(Russian)* 80−59373
polymer dynamics simulation, relax. rates and dynamic viscosity 78−91211
polymer relaxation phenomena, conference, San Francisco, CA, USA (Aug. 1976) 79−4257
polymer solns., entangled, relax. dynamics, viscoelastic response functions 77−31578
polymeric solids, mech. retardation time spectrum, thermostimulated creep 79−5014
polymers, glassy, amorphous, secondary loss peaks, mol. motions 79−11649
polymers, network, low freq. mol. mobility, quadratic electrochromism method *(Russian)* 78−71688
polymethyl acrylate, multicomponent network, pulsed NMR study of mol. motions 77−55724
polyoxymethylene, low-strain deform., transmission electron microscope exam. 79−5013
polyoxymethylene copolymers, solid, mol. motions, 4-315K, dynamic-mech. study 79−4258
polyphenylquinoxaline, soln., conform., equilib. rigidity *(Russian)* 79−55643
polypropylene, EPR of NO radicals, rot. mobility 79−33539
polypropylene, TSC meas. of relax. modes, apparent double glass transition 80−11323
polystyrene, atactic, chain length depend. of hypersonic relax., Brillouin spectra 77−55797
polystyrene, end group modified, chain dynamics studied by fluorescence depolarization 80−19724
polystyrene, EPR of NO radicals, rot. mobility 79−33539
polystyrene, glassy state, relax., free vol. fluctuations effect 80−19722
polystyrene, isotactic crystals, plastic deformation, molecular mech., TEM obs. 80−21022
polystyrene, molecular motion obs. during thermal polymerisation of styrene, PMR 80−3342
polystyrene in dil. sol., solvent depend. of molecular motion, three-band conformational jumps and rot. diffusion 79−41932
molecular reorientation continued
polystyrene soln., monosubstituted, mol. chain dynamics, NMR meas. 78−56393
polystyrene-trans-decalin system, ^{13}C spin-lattice relax., solvent rot. diffusion 79−33556
polystyrene-wood, polymer composite, dielec. props. at low temperature range *(Japanese)* 78−95541
polyvinylidene fluoride, correlated mol. motion in dielec. props. 77−55749
polyvinylidene fluoride, TSC and thermoluminescence, reln. to molecular motion *(Japanese)* 80−55200
polyvinylidene fluoride film, cryst. dipole orientation in elec. field 78−80286
potassium palmitate-d_{31}, spin-lattice relax., chain position and temp. depends. 78−68405
propane, liq., temp.-depend. free vol. 79−99052
propanes, substituted, liq., microwave absorpt., dielectric relax., loss, permittivity, moments and reorientation 77−63362
1-propanol, low temp. pulse radiolysis, solvated electrons, absorpt. spectral changes 77−12813
n-propanol, US studies of mol. relax. 78−22790
propyl-1,3-diamino manganese chloride, structural phase transitions at 336 and 305K, NQR meas., DTA 78−63855
n-propylammonium chloride, NMR, spin-lattice relax., cation dynamics 79−11353
protein-solvent systems, dynamics investigation by nucl. gamma-resonance 79−62166
proton spin-lattice relax. and activation energies of tunnelling, CH_3 groups 77−48071
protonated samples, rot. states, coherent neutron scatt. 77−84678
PTFE, NMR and X-ray diffr. investig. of press. induced III-I transition and mol. motion 77−51969
PVC, EPR of NO radicals, rot. mobility 79−33539
pyrazine, cryst., mol. reorientation, NMR meas., pot. energy calc. 78−76335
pyridazine, liq., nucl. relax. and mol. reorientation, nucl. Overhauser enhancement 78−60351
pyridine, cyclohexane soln., depolarised Rayleigh scatt. 79−47467
pyridine, liq. and in CCl_4 soln., depolarised Rayleigh scatt. 79−51973
pyridine-water soln., reorientational relax. and activation energy of pyridine, depolarised Rayleigh scattering 80−76037
pyridinium iodide, order-disorder phase transition and reorientation fluctuations studied by Raman spectra 80−80764
pyrimidine, liq., nucl. relax. and mol. reorientation, nucl. Overhauser enhancement 78−60351
pyrogallol, PMR, OH group rot., H-bonds 79−47339
pyrrole, liq. and nonaq. solns., ^{14}N NQR, ^{1}H line shape anal. 78−6598
quasiquadrupolar echoes in solid with dipolar coupled rotating methyl groups 78−23366
quinine sulphate, acid soln., edge excitation red shift and proton migration 78−1028
β-quinol clathrate, CH_3OH mol. reorientation investig. by IR and dielec. meas. 77−12369
β-quinol clathrate, single cryst., double NMR obs. of mol. motion of trapped methanol 79−87332
quinuclidine, cubic phase disorderd struct., X-ray diffr. study 79−69037
quinuclidine, plastic phase, mol. reorientations, ^{1}H and ^{14}N NMR relax. 79−69039
quinuclidine, plastic phase, rot. motion, quasielastic neutron scatt. 79−69038
Raman band shapes in liq., rot.-vibr. coupling effect for reorientation 78−72491
reduced reorientational correl. times, extended diffusion, Langevin, Ivanov, strong collision models 77−54520
relaxation processes, symposium, London, England (Dec. 1976) 80−56993
resonance Raman lineshape studies of vibrational and rotational relaxation in soln. 80−60560
resorcin, Raman line intensity as function of mol. orientation 80−11383
rhodamine 4C, in ethanol soln., rot. relax. time using ps. spectroscopy technique 80−1013
rhodamine solution, picosec. spectroscopy with antiStokes excitation, orientational rearrangement *(Russian)* 79−42984
ribonuclease-A, solid, PMR spin-lattice relax., mol. dynamics 80−51041
rigid macromolecule, in soln., depolarised Rayleigh spectroscopy 79−94119
RNA solns., oriented in DC mag. field light scatt. 79−2004
rod-shaped molecules, restricted rot. diffusion, time correl. functions 80−79655
rose bengal, excited state orientational relax., in protic and aprotic solvents 78−46383
rotational barrier, calc. for molecular crystals 78−75601
rotational barriers, calc. for molecular crystals 78−79541
rotational diffusion and level kinetics separation in transient absorpt. spectroscopy 77−30877
rotational diffusion in periodic potentials, dynamic correlation functions 77−59138
rotational phase transition in ferroelectrics and other crysts., Ising model 77−4605
rotational tunnelling, neutron scatt. theory 78−18561
rotational tunnelling and diffusion in condensed mol. systems, neutron scatt. 78−63658
rough sphere, rot. in bath of spheres, microscopic boundary layers 78−18521
ruthenocene, cryst. and soln., dynamic struct., NMR expts. 77−15328
saturation transfer EPR spectroscopy, source modulation, mol. reorientation effects 78−41339
short chain molecule, dielectric relax. 79−95706
siloxane, temp. transitions, linear dilatometry and X-ray diffr. obs. *(Russian)* 80−59404
smectic C phase, tilt angle determ. by field-induced Freedericksz transitions and X-ray meas. 79−94884
smectic phases, long mol. axis reorientation, LF dielec. dispersion 80−70124
sodium decanoate-n-decanol-water system, lamellar G-phase, orientational-order, EPR investigation 80−24355
solid, ultraslow mol. rot. obs. using D probe spin alignment tech. 80−88890
solid containing spin-1/2 triads undergoing hindered reorientation, quasiquadrupolar echoes 79−4744

molecular reorientation continued
solid torsional oscillators, rotating frame, nucl. spin polarisation losses, torsional spectroscopy 80−31821
solid with reorienting mol. groups, effective decay time for multipulse NMR 79−61238
solutions, dynamic orientational correlation functions, coupled translational-rot. diffusion model 77−84604
sp. hts., librational and reorientational 77−84946
spherical particles, hydrodynamic interaction, translational, rot. and translational-rot. diffusion 78−26405
spin-lattice relax., effect on mol. groups in solids of symm.-restricted spin diffusion 78−39431
stability constraints on potential function and rotational invariance in external mode formalism 80−24543
trans-stilbene, excited state orientational relax., sub-picosec. pulse obs. 79−50006
succinonitrile, orientationally disordered crystal., mol. orientation 78−34448
succinonitrile, plastic cryst. and liq., Kerr effect for relax. kinetics 78−59768
succinonitrile, plastic phase, mol. reorientation and rotational isomerization, anal. of elastic incoherent struct. factor 78−22674
succinonitrile, plastic phase, molecular reorientation, rotational isomerism, incoherent neutron scatt. study 79−51021
symmetric top mol. with internal rot., extended diffusion and reorientation in fluids 77−20101
symmetric top molecules in liquid state, book contrib. 78−22623
symmetric-top molecules in liquids, Coriolis coupling 77−10657
symmetrical molecules, reorientation spectroscopic meas. models 80−58405
TBBA, smectic, proton ^{14}N nuclear double reson. 77−58947
TBBA, smectic and cryst. phases, far IR absorpt., struct. and dynamical props. 77−84636
TBBA, smectic liq. cryst., polarised Raman spectra, 90-300K, 0-400 cm^{-1} 77−12383
TBBA, smectic VI and H phases, orientational order 77−84648
TCNQ salt, $(N(CH_3)_3H)(I)(TCNQ)$, proton spin-lattice and spin-spin relax. times 79−8065
o-terphenyl, dipolar solutes, reorientational motions, dielectric relax. below glass transition 80−19706
tert-butyl chloride, separation of collision-induced from intrinsic mol. depolaris. Rayleigh scatt., C-Cl bond optical anisotropy 78−27244
tert-butylchloride-d_9, extended diffusion with internal rot., NMR test 79−31549
tetraalkylammonium halides, mol. reorientation, spin lattice relax. time study 80−18875
tetrabromomethane, plastic phase, neutron diffr. obs. and theory 79−77533
tetracene dianions in dimethyl ether, rotational diffusion meas. 80−65262
tetrachloromethane, separation of collision-induced from intrinsic mol. depolaris. Rayleigh scatt., C-Cl bond optical anisotropy 78−27244
tetrafluoromethane, liq., mol. reorientation 80−106320
tetrahedral four spin $^1/_2$ systems, Zeeman and tunnel system reson., coupled and uncoupled relax. 80−50214
tetrahedral molecule, hindered rot. energy levels in trigonal field 77−7678
tetrahedron, hindered rot. energy levels in orthoorhombic crystalline field 77−76332
tetrahydrofuran clathrate, reorientation, residence times, Debye-Waller factors, activation energy, neutron scatt. study 79−41989
tetrahydrofuran clathrate deuterate, rotational motion, quasi-elastic neutron scatt. study 79−51022
tetramethyl germanium, methyl reorient., lattice vibrs., neutron scatt. obs. 79−51016
tetramethyl gruop VIa cation silicon hexafluorides, ^1H and ^{19}F nucl. spin lattice relax. 78−80234
tetramethyl silicon, methyl reorient., lattice vibrs., neutron scatt. obs. 79−51016
tetramethyl tin, methyl reorient., lattice vibrs., neutron scatt. obs. 79−51016
tetramethylammonium chlorate, order-disorder transitions, DTA and NQR meas. 77−66022
tetramethylammonium octahydrotriborate, NMR study of proton and B dynamics 80−93200
tetramethyllead, tunnel splitting, rot. pot., μeV neutron scatt. study 79−41993
tetraoxane, NMR obs. of mol. motion, rel. to polymerisation temp. effects on polytetraoxane texture 77−84663
tetrolyl fluoride, free internal rot. of CH_3 group, IR spectra 79−41171
2-thiaadamantane, plastic phase, transition and fusion thermodynamics, DSC meas. 78−75603
1,2,5-thiadiazole, liq., light scatt. from orientational and density fluctuations, hypersonic vel. 77−81110
thiourea, ferroelec., soft mode and Debye relax., IR reflection spectra 77−90111
thiourea-cyclohexane inclusion compound, phase changes, molecular motion exam. 78−31116
thiourea-d_4-ferrocene inclusion cpd. mol. motion, PMR spectrum 80−84656
three-spin systems in nematic liq. cryst., EPR 77−14463
time-dependent distribution functions, pictorial representation, correlation functions 80−55021
TMNC, restriction of free internal motions of methyl groups 79−24309
tolualdehyde, dil. soln., dielectric relax., solid rotator phase 79−42890
toluene, in benzene soln., mol. motion, correl. functions 80−96431
toluene, liq., Brownian reorientation barriers *(Russian)* 79−27901
toluene-d_0, -d_1, mol. reorientation and D nucl. relax. time, temp. depend. 78−39424
5d-transition metal antifluorite cryst., struct. props. and lattice dynamics, mag. struct. 80−44268
translation and rot. dynamics, microscopic Hamiltonian anal., inelastic neutron scatt. elastic consts. 78−38632
triamantane, phase transistions, X-ray diffr. meas. 79−14930
s-triazene, second order phase transition, mol. reorientation, ^{14}N NQR 78−48074
s-triazine, mol. cryst., low temp. mol. reorientation, phase transition, ^{14}N NQR 77−36150
sym-triazine cryst., PMR determ. 79−73114
bis-triazolopyridazines, deformation, rot. angles and intramolecular steric factors 80−69079
molecular reorientation continued
bis-triazolyls, deformation, rot. angles and intramolecular steric factors 80−69079
tribromofluoromethane, liq., ^{13}C and ^{19}F nucl. relax., ^{19}F-^{79}Br and ^{13}C-^{79}Br scalar coupling consts. 78−76330
1,2,3-trichlorobenzene, anisotropic reorientation, nucl. relax. in coupled spin systems 77−40145
1,2,4-trichlorobenzene liq., mol. reorientation, translation and vibr. relax., Rayleigh and Raman spectra 80−95632
trichloroethane, separation of collision-induced from intrinsic mol. depolaris. Rayleigh scatt., C-Cl bond optical anisotropy 78−27244
trichloromethane, separation of collision-induced from intrinsic mol. depolaris. Rayleigh scatt., C-Cl bond optical anisotropy 78−27244
trichloromethane-d_0,-d_1, soln., far IR spectra, band shape and moment anal. 80−58252
trichloromethane-d_1, in nonpolar solvents, vibrational and rotational relax. 79−10182
trichlorophosphazenes, ^{35}Cl NQR spectra and reorientational motion of PCl_3 group 78−25567
trichlorophosphazoperfluoro-1,1-dimethylethane, cryst., ^{19}F NMR and mol. mobility, fluorination influence 80−34809
triethylene, in polystyrene matrix, energy barriers, dielec. absorpt. meas. 78−70958
trifluoroacetates, methyl and ethyl, intramol. relax. at microwave freqs. 80−55020
2,2,5-trimethyl-1,3-dioxane-4,6-dione, cryst., X-irradiated, methyl group hindered rot. tunnelling, EPR, ENDOR, and ELDOR 79−68328
trimethylammonium chloride, cation and CH_3 groups rot. diffusion, quasielastic neutron scatt. 77−27840
trimethylammonium chloride, cation and CH_3 groups rot. diffusion, quasielastic neutron scattering 77−27841
trimethylphosphate, plastic and hard crysts., liq., nucl. spin-lattice relax. mol. motion 78−48065
trioxane, NMR proton relax., mol. rot., rel. to polymerisation 79−73843
triphenylmethyl-^{13}C phosphonium chloride, Ph_3P^+-$^{13}CH_2$ EPR, reorientation and hyperfine coupling tensor 78−6574
triplet oriented mols. in solid matrix, slow mol. motion, ESR spectra 77−90014
tris(3-deutero-2,4-pentadionato)aluminium, in soln., deuteron spin-lattice relax. time, mol. rotational correl. time 78−84491
trithiane, NMR proton relax., mol. rot., rel. to polymerisation 79−73843
n-tritriacontane, C-phase, mol. motion obs., incoherent quasielastic neutron scatt. 79−4260
n-tritriacontane, non periodic molecular motions, neutron scatt. study 79−51024
DL-tryptophan, polycryst., amino group rot., reorientation, mol. struct., 77-555K, PMR obs. 78−35047
tunnelling centres, nonadiabatic props. 78−79705
tunnelling molecular groups in solids, symmetry of rotor part of rotor-phonon interaction 80−84114
uniaxial rotator in N-fold cosine pot., correlation functions, neutron incoherent scatt. law 78−9970
urea, aqueous soln., mol. reorientation, Raman spectra 78−64354
urea in NaI aq. soln., Raman scatt., mol. reorientation relax. time 79−8136
vibration-rotation lineshapes, effect of elastic and reorientation collisions 79−89712
water, liq., NMR proton spin-lattice relax. and shear viscosity press. depend., −15 to 10°C 77−40144
water, quadrupolar relax. of ^{27}Al in aqueous soln., formulation of relax. rate 77−85600
water, reorientational motion, quadrupolar relax. of ^{27}Al in aqueous soln. 77−85601
water, supercooled, sound vel. dispersion, struct. relax. effect, Brillouin scatt. obs. 80−107375
xanthene dyes in n-alcohols (ethylene glycol) (glycerol), rot. relax., time-resolved fluoresc. depolaris. obs. 80−58300
xanthrene, dye soln., transient dichroism, rot. diffusion anomalies 79−87414
Ag, adsorption of aromatic hydrocarbons, heat of adsorption, coating and fine struct. *(German)* 79−23844
Ag, and Ag^+, solvation in deuterated-ice matrices, electron spin echo obs. 80−15780
$Ag(NH_3)_2Ag(NO_2)_2$, and deuterate, proton and deuteron mag. reson., reorientation 79−11351
$Ag(NH_3)_2Ag(NO_3)_2$, phase transition, mol. motion, PMR obs. 78−88203
$Ag_2SO_4.4NH_3$, mol. motion, proton mag. reson. 79−47349
Al_2Cl_6 molten, nuclear mag. relax., mol. rot. 80−71209
β-Al_2O_3-H_3O^+, pulsed ^1H NMR study, 77 to 440K 79−87329
β-Al_2O_3-NH_4^+, PMR relax. time obs. of ionic motion 80−71213
β-Al_2O_3-NH_4^+ proton dynamics neutron scatt. study 80−59408
β-Al_2O_3-OH_3^+, proton dynamics neutron scatt. study 80−59408
β-$Al_2O_3.(NH_4)_2O$, neutron scatt. study of NH_4^+ motion 78−30785
Ar, solid, NH and ND impurities, role of rotational and translational modes in vibr. relax. 78−10132
Ar:methane, impurity rotational states, inelastic neutron scatt. study 79−51020
o-$As_2B_{10}H_{10}$, ^1H and ^{11}B CW NMR, mol. reorientation in cryst., phase transition 77−85583
AsD_3, IR spectra, vibr. relax., rot. reorientation in solid phase 78−19463
AsH_3, IR spectra, vibr. relax., rot. reorientation in solid phase 78−19463
AsH_3, plastic cryst., dipolar autocorrelation function, phonon contrib., IR absorption 78−42928
BH_4^- motion in solids, nucl. spin-lattice relax. exam. 78−56388
$BaBr_2.2H_2O:VO^{2+}$, EPR meas. 77−16145
$BaCl_2.2H_2O:VO^{2+}$, EPR meas. 77−16145
$Ba[Fe(CN)_5NO]_2.2H_2O$, NMR, H_2O orient. *(French)* 78−52366
CO, collision-induced reorientation, direct meas. by IR double reson. 80−32800
CO_2, liq., 100 to 3000 atm., depolarised Rayleigh spectra, orientation dynamics, wings 78−92084
CS_2, in alkane soln., ^{33}S NMR linewidth for mol. correl. times 79−95661
CS_2, in CCl_4, orientational fluctuations, depolarised Rayleigh relax. time obs., temp. and conc. depends. 79−4809
CS_2, in carbon tetrachloride soln., Raman scatt. 79−65850
CS_2, liq., ^{33}S NQR, quadrupole coupling const. from linewidth data 78−91985
CS_2, liq., props. from allowed light scatt. spectra 80−25364

molecular reorientation continued
^{13}C-labelled organic radicals, ^{13}C- and proton-ENDOR in soln. 78−55190
$CaSO_4.2H_2O$, mol. reorientations and mol. diffusion, PMR 78−43671
Cd complex, aminoacetate, PMR, activation energy for NH_3 reorientation determ. 78−31119
$Cd(NH_3)_6Cl_2(Br_2)(I_2)$, crit. behaviour of light scatt. intensity at phase transitions 77−90141
$Cd(NH_3)_6X_2$, X=Br, Cl, I, orientational phase transitions, Raman spectra 80−11382
Cl_2, liq., mol. motion, Raman spectrum 78−5236
Cl_2, liq., mol. reorientation, Raman spectra obs. *(French)* 78−31192
ClF, gas, rot. frame NMR, reorientational and ang. correl. times 78−78721
ClO_3F, ^{19}F NMR line shape temp. depend. and spin-lattice relax. 78−91969
$Cl_3PNCCl(CF_3)_2$, cryst., ^{35}Cl NQR obs. of molecular reorientations between unequal potential wells 80−54989
$Cl_3PNPO(CCl_3)_2$, NQR spin-lattice relax. study of PCl_3 and CCl_3 group reorientation 78−2767
Co complex, $Co(NH_3)_5FCl_2$, mol. motions, NMR 77−36145
$Co(NH_3)_6Cl_3$, proton second moment meas., 96 to 404K 79−95652
CsB_3H_8, transients reorientation, calc. using simple harmonic approx. 79−42966
CsBr(I), single crysts., polarisation of luminesc. and reorientation of NO_2^- centres 79−95823
$CsHF_2$, struct. and phase transformation, NMR study 77−90047
$Cs_2MFe(CN)_6$, M=Ba, Mg, Ca, Sr, lattice instabilities 77−72668
Cs_2TiF_6, Raman spectra, internal and lattice vibrs. 77−8569
$CuM_2X_4.2D_2O$, MX=alkali or ammonium halide, quadrupolar interaction, 4-300K, reorientation 79−73848
Cu_2O, NQR freq. of ^{63}Cu, temp. depend., mol. dynamics 77−12227
t-cyanobutane, solid, uniaxial molecular reorientation, quasielastic neutron scatt. 78−42927
D_2, solid, quadrupolar glass ordering NMR adsorption line shapes 80−7178
D_2, solid, Raman scatt. meas. of rotational spectrum under press. 77−69814
DCl, liquid, on coexistence line, light scatt., orientational correlation function 80−20632
$DF(\nu=n)+DF(\nu=0)\rightarrow DF(\nu=n-1)+DF(\nu=1)+\Delta E$, applic. of hydrogen-bond interac. model 77−30961
Fe dicyclopentadienyl-dibenzenevanadium, coalescence temps., full proton HFS tensor, ENDOR obs. 80−66073
$FeSiF_6.6D_2O$, ^2H NMR spectrum, correl. effects 78−76324
GeH_4, crystalline, determ. of mol. symm. from IR spectrum 78−9969
H_2, solid, heat capacity and configurational entropy at low ortho concs. 77−35706
H_2, solid, neutron scattering expts. 78−79693
H_2, solid, Raman scatt., meas. of rotational spectrum under press. 77−69814
p-H_2, solid, rotation-libration transition under press., Monte Carlo study 80−49460
HBr, liquid, on coexistence line, light scatt., orientational correlation function 80−20632
HCl aqueous soln., H^+ mobility, 15, 25, 40°C, up to 5000 atm 78−10207
HCl, liquid, on coexistence line, light scatt., orientational correlation function 80−20632
HCl, solid, incoherent neutron scatt. of proton motions 78−75600
HN_4^+, in crystalline cpds., tunnelling, PMR, generalised line shape, theory 79−73827
$HNO_3.H_2O$, devitrification crystallisation, fast Raman and wide-line NMR obs. *(French)* 79−73915
$HNO_3.H_2O$ glassy form, stochastic rot. motions 79−7551
H_2O, adsorbed, surface-induced NMR line splittings and augmented relax. rates 78−64288
H_2O at interfaces, mol. struct. and dynamics 77−31873
H_2O, force bias Monte Carlo simulation 79−77487
H_2O molecules free from H-bonding, reorientation, IR absorpt., dielectric loss 77−36233
H_2O reorientation in HCl aq. soln., 15, 25, 40°C, up to 5000 atm 78−10207
$HSiCl_3$($DSiCl_3$), Raman and IR spectra, mol. motion 78−64353
^2H spin lattice relaxation, mols. with multiple internal rots., limiting behaviour 79−39356
Hf complex, with N-benzoyl N-phenyl hydroxylamine, mol. reorientation in soln. 77−16218
I_2 solutions, vibr. and rot. relax., reson. Raman lineshape meas. 79−31616
K+NaK collisions studied using circularly polarised laser fluorescence, molecular reorientation obs. 80−69215
KCN, inelastic neutron scatt. by coupled rot. and translational modes 80−79895
KCN, liq., mol. dynamics computer simulation 78−38609
KCN, plastic phase, Raman scatt. spectra *(French)* 80−11379
KCN, single cryst., orientationally disordered, Brillouin scatt., elastic consts. 77−85732
KCN-KCl mixed crystals, rel. to F-centre optical absorpt. half width 77−81134
KCN-KCl mixed system, order-disorder transition, Raman spectra obs. 78−15113
$(KCN)_{0.25}(KBr)_{0.75}$, rot.-translation interactions, neutron scatt., 0-300K 78−67783
KCl:NH_4Cl, PMR, NH_4^+ ion proton spin-lattice relax. time temp. depend. 78−27104
$KClO_3$, NQR freq. of ^{35}Cl, temp. depend., mol. dynamics 77−12227
$K_3Co(CN)_6$, Raman scatt. and electronically-induced phase transition at 130K 77−90142
$K_3Fe(CN)_6$, Raman scatt. and electronically-induced phase transition at 130K 77−90142
$K_4Fe(CN)_6.3H_2O$, reorientation of H_2O trimer, restriction by temp. depend. pot. barrier 79−51959
KH_2AsO_4:Cr^{3+}, ferroelec. phase transition, EPR intensity and linewidth meas. 79−4721
KH_2PO_4, elec. cond. and diffusion, Co dopant effects 77−72716
$KH_3(SeO_3)_2$:Cr^{3+}, EPR, ferroelectric phase transition 79−65716
$K_2HgCl_4.H_2O$ proton spin-lattice relax., 180° flips and diffusion of water mol. 77−15327
KI:S_2, Raman spectra, orientational dynamics 78−56482

molecular reorientation continued
$K_xRb_{1-x}HF_2$, nuclear spin-lattice relax. and internal motion mechanism 79−99787
K_2SnCl_6, structural phase transitions, Raman spectra 77−73143
Kr:methane, impurity rotational states, inelastic neutron scatt. study 79−51020
LiCl, aqueous, proton, deuteron and ^7Li relax. times, mol. motion obs. 79−28632
α-$LiIO_3$, in electrostatic field, X-ray double cryst. spectrometric investigation *(Chinese)* 78−67666
$LiNO_3$, soln. in organic liq. or D_2O, Raman lineshape, solvent-solute interaction 78−76448
methane, solid, librational tunnelling and proton relax. temp. 80−38969
$Mg(NH_3)_6(ClO_4)_2$, solid, mol. rot., Raman contour, quasielastic neutron scatt., and PMR obs. 79−87444
Mg_2NiH_x, PMR exam. of motion of H 78−56383
MoF_5, mol. and electronic struct., vitreous, liq., and tetrameric states, ^{19}F NMR obs., mol. mobility 80−34787
β-N_2, dynamical struct. factor $S(Q,\omega)$, digital simulation 77−76502
N_2, liq., computer-simulated ang. correlations and rot. motion 77−11461
N_2, liq., dephasing of mol. vibr. related to correl. functions 78−75523
N_2, liq., simulation of atomic and quadrupole interactions, predictions 77−11457
α-N_2 simulation of dynamical props. of molecular solids 78−30710
α-N_2, solid, mol. dynamics simulation 77−47519
N_2, solid, self-localisation of high frequency triplet excitations *(Russian)* 79−8176
ND_3 dissolved in poly-γ-benzyl-L-glutamate-chloroform, NMR study 80−34805
ND_3, in $TaS_2(TiS_2)$, intercalation system, wideline NMR, temp. effects 77−16184
ND_4^+ ions, rapidly reorienting deuteron NMR lineshape 79−19800
β-ND_4Br, ND_4^+ orientational fluctuations, neutron scatt. obs. 79−7557
ND_4ClO_4, librational tunnelling and proton relax. temp. 80−38969
ND_4NO_3, Raman spectra meas., 250-420K 77−20845
$(ND_4)_2PbCl_6$-ND_4Cl polycryst. mixture, D spin-lattice relax. times, ND_4^+ reorientation activation energies 78−6587
ND_4ReO_4, nucl. quadrupole coupling, ND_4 ion rot. motion 79−65756
NG_4HgCl_3, NQR freq. anomalous temp. depend., reorientation 80−54976
NH_3, mol. alignment relax. rate, laser saturation reson. technique 78−25755
NH_3, ND_3, crystals, rotation mol. motion *(Russian)* 78−87762
NH_4 compounds, tunnelling frequency of NH_4 ion in crystals, cubic and noncubic 78−38633
NH_4^+, hindered rot. energy levels in trigonal field 77−7678
NH_4^+, in crystal lattice, tunnelling effect on proton spin-lattice relax. time 79−61252
NH_4^+, in NH_4Cl, ion dynamics in disordered states, neutron scatt. exam. 78−26459
NH_4^+ ions undergoing slow tunnelling rotations, proton NMR line shapes 79−90576
NH_4^+ motion in solids, nucl. spin-lattice relax. exam. 78−56388
NH_4^+, NMR absorpt. lineshape rel. to ion reorientation 77−48074
NH_4^+, NMR line shapes at low temp., composite tunnelling, reorientation 78−48054
NH_4^+, tetrahedron, hindered rot. energy levels in orthorhombic crystalline field, rot. heat capacity 77−76332
NH_4-ion rotation, quantum effect on spin-lattice relax. time 80−75875
$N_2H_6^{2+}$ salts, NMR spin lattice relaxation study, ^{14}N-^1H dipole-dipole contrib. to relax. 80−75878
$(NH_4)_2Al(SO_4)_2$, ^1H spin-lattice relax., 100-500K 79−38398
$NH_4Al(SO_4)_2.12H_2O$, dielectric losses, proton spin lattice relaxation by NH_4^+ hopping 79−56721
NH_4BF_4, H^+ relax. and tunnelling, nucl. spin-lattice relax. obs. 79−51876
N_2H_5Br, mol. ion motion and barriers to rot., PMR and neutron scatt. meas. 79−24226
$(NH_4)_2Ce(NO_3)_6$, proton tunnelling frequencies from nuclear spin-lattice relaxation 78−6591
NH_4Cl, NH_4^+ ion rotation, near order-disorder transition, quasielastic neutron scatt. obs. *(German)* 77−84679
NH_4Cl, ordered phase, press. depend. of Raman scatt. meas. 77−12388
NH_4Cl single crystals, quasielastic neutron scattering expts. near order-disorder phase transition 79−4410
N_2H_5Cl, mol. ion motion and barriers to rot., PMR and neutron scatt. meas. 79−24226
NH_4ClO_4, γ-irrad., motions of trapped NH_3^+ radical, ESR study 79−95648
NH_4ClO_4, instantaneous jump reorientations, neutron scatt. study 79−41990
NH_4ClO_4, NH_4 ion rot. tunnelling splitting, inelastic neutron scatt. 77−15325
NH_4ClO_4, proton tunnelling frequencies from nuclear spin-lattice relaxation 78−6591
$(NH_4)_2Cr_2O_7$, proton tunnelling frequencies from nuclear spin-lattice relaxation 78−6591
NH_3D^+, IR spectrum in NH_4ClO_4 and weakly H-bonded cpds., mol. motion 77−36232
$(NH_4)_2GeF_6$, H^+ relax. and tunnelling, nucl. spin-lattice relax. obs. 79−51876
$(NH_4)_2HAsO_4$, $(NH_4)_2HPO_4$, molecular motion, PMR meas. 77−85591
$NH_4H_2AsO_4$:Cr^{3+}, antiferroelec. phase transition, EPR intensity and linewidth meas. 79−4721
NH_4HF_2, powder, proton and fluorine 2nd moments meas., 77-395K 80−34803
$(NH_4)_2HPO_4$, NH_4^+ motions, PMR relax. times obs., 77-430K, struct. transition 77−85599
$NH_4H_2PO_4$, elec. cond. and diffusion, Co dopant effects 77−72716
NH_4HSO_4, NH_4^+ movement 77-388K 77−28524
$(NH_4)_3H(SO_4)_2$, movement of NH_4^+ in all phases over 77 to 388K, NMR study 77−28524
α-NH_4HgCl_3, NQR freqs., anomalous temp. depend. NH_4^+ ion reorientation 79−56624
NH_4I, $(NH_4)_{0.16}K_{0.84}I$ and $(NH_4)_{0.16}K_{0.84}Br$, reorientation motion of NH_4^+ 78−79542
NH_4I, coexisting phases and NH_4^+ dynamics, neutron scatt. exam. 79−42158
NH_4I, reorientation dynamics of NH_4 ions, quasielastic neutron scatt. obs. 77−31610

molecular reorientation continued
NH_4I, reorientational motion of ammonium ions in octahedral environments, neutron scatt. exam. 79−42159
NH_4I_3, NQR freq. anomalous temp. depend., reorientation 80−54976
$(NH_4)_{0.16}K_{0.84}I(Br)$, reorientation motion of ammonium ions in octahedral environments, neutron scatt. exam. 79−42159
$((NH_4)_{0.16}K_{0.84})_2SO_4$, reorientational relax. times, quasielastic neutron scatt. obs. 78−55821
$((NH_4)_xK_{1-x})_2SO_4,NH_4^+$ dynamics, neutron scatt. study 79−42167
NH_4LiSO_4, ferroelec., PMR line shape and spin-lattice relax. 78−88205
$(NH_4)_2MoO_4$, ^1H spin-lattice relax., 100-500K 79−38398
$NH_4NH_2SO_3$, ^1H spin-lattice relax., 100-500K 79−38398
NH_4NO_3 crystals, NH_4^+ ion symmetry in phases II-V, Raman spectra obs. 80−66200
NH_4NO_3, Raman scatt. in region of extended IV-V phase transition 79−99887
NH_4NO_3, Raman spectra meas., 250-420K 77−20845
NH_4PF_6, H^+ relax. and tunnelling, nucl. spin-lattice relax. obs. 79−51876
$(NH_4)_2PbCl_6$, inelastic neutron scatt. and pot. shape 80−1946
$(NH_4)_2PbCl_6$, librational tunnelling and proton relax. temp. 80−38969
$(NH_4)_2PbCl_6$, temp. depend. of tunnel freq. 80−1947
$(NH_4)_2PdCl_6$, inelastic neutron scatt. and pot. shape 80−1946
$(NH_4)_2PtCl_6$, inelastic neutron scatt. and pot. shape 80−1946
NH_4ReO_4, NQR freqs., anomalous temp. depend. NH_4^+ ion reorientation 79−56624
NH_4ReO_4, NQR freq. anomalous temp. depend., reorientation 80−54976
NH_4ReO_4, PMR, NH_4^+ tunnelling, ground torsional level struct. 78−27097
NH_4ReO_4, proton absorpt. lineshape and spin-lattice relax., ^{187}Re anomalous temp. depend. 78−48067
$(NH_4)_2SO_4$, ferroelec., ion group reorientation temp. and press. depend., PMR obs. 78−72470
$(NH_4)_2SO_4$, irrad., −50°C transition, librational mode softening, paramag. NH_3^+ probe obs. 77−20037
$(NH_4)_2SO_4$, NH_4^+ dynamics, neutron scatt. study 79−42167
$(NH_4)_2SO_4$, reorientational relax. times, quasielastic neutron scatt. obs. 78−55821
$(NH_4)_2SiF_6$, cubic, trigonal, proton tunnelling frequencies from nuclear spin-lattice relaxation 78−6591
$(NH_4)_2SiF_6$, trigonal, proton and ^{19}F relax, 30 to 200K 77−76549
$(NH_4)_2SnCl_6$, ^1H spin-lattice relax., 100-500K 79−38398
$(NH_4)_2SnCl_6$, $^{35,37}Cl$ NQR, Raman spectra and spin lattice relax., hindered rot. 80−54974
$(NH_4)_2SnCl_6$, inelastic neutron scatt. and pot. shape 80−1946
$(NH_4)_2SnCl_6$, NH_4^+ ion rot. states, inelastic neutron scatt. obs. 78−30552
$(NH_4)_2SnCl_6$, proton tunnelling frequencies from nuclear spin-lattice relaxation 78−6591
$(NH_4)_2TeCl_6$, inelastic neutron scatt. and pot. shape 80−1946
$(NH_4)_2TiF_6$, ^1H-^{19}F coupled NMR, line shapes, spin-lattice relax. 79−73839
$(NH_4)_2TiF_6$, H^+ relax. and tunnelling, nucl. spin-lattice relax. obs. 79−51876
$(NH_4)_2TiF_6$, Raman spectra, internal and lattice vibrs. 77−8569
NH_4ZnF_3, hindered rot. sp. ht. of NH_4^+, 2.5-300K 77−62648
NH_4ZnF_3, rot. motion of NH_4^+ in lattice, neutron scatt. 79−37773
NO radicals, slow rot., modulated EPR spectra 79−38382
NO· radicals, saturation transfer EPR effects anal. using hole-burning concept 79−94022
NO_2^-, impurity in alkali halide, linear dichroism *(Russian)* 80−45127
NO_3^-, Raman spectrum of ν_1 mode in soln., reorientation 78−92067
N_2O, in soln., IR and Raman band shapes, mol. dynamics, ν_3 band 77−36238
N_2O, in soln., Raman and IR ν_1 and ν_2 band shapes, mol. motion dynamics 78−64352
N_2O, pure liq., mol. motion, anisotropic interaction 80−24345
$Na_8Al_6Ge_6O_{24}(CO_3).3H_2O$, water molecule dynamics and hydrogen bonds, PMR spectra 79−90577
NaCN, FCC, orientational anisotropy of CN^- ions, Raman spectra meas. 77−36247
NaCN, plastic phase, Raman scatt. spectra *(French)* 80−11379
NaCN, single cryst., orientationally disordered, Brillouin scatt., elastic consts. 77−85732
NaCl, aq. soln., isothermal compressibility, hydration parameters, up to 350°C and 10^3 kg cm^{-2} 78−10112
$NaClO_3$, γ-irradiated, ESR of trapped O_3^- 79−29381
$NaClO_4.H_2O$, ^1H NMR second moment, H_2O dynamic disorder 80−25221
NaN_3, orientational motion and elastic anomaly 79−46803
NaN_3, struct. phase transform., microscopic model 79−65022
$NaNO_2$, mechanism of ordering type ferroelec. transition, vibr. spectroscopy 78−76402
$NaNO_2$, mechanism of order-disorder transition, opt. spectra 78−76403
$NaNO_2$, ν_1 Raman linewidth and reorientation of NO_2^-, temp. depend. 78−72522
$NaNO_2$, polarisation reversal by time-resolved X-ray diffr., NO_2 radical rot. 77−63382
$NaNO_2$, rot. behaviour of NO_2 radicals in order-disorder transition, Fourier synthesis study of neutron data 79−56739
$NaNO_3$, rel. to ^{23}Na spin-lattice relax. time −75.5 to +320°C *(Japanese)* 77−43897
$NaNo_3$, aq. soln., Raman spectra, vibr., orient. relaxation *(French)* 78−62808
NaOH, cubic, reorientational motion of OH^- ion, neutron scatt. 79−51017
Ni complex, $[Ni(OCH_3)(acac)(CH_3OH)]_4$, sp. ht., 0.4-285K, methyl group internal rotation 78−47531
Ni complexes, $[Ni(NH_3)_6](ClO_4)_2$ and $[Ni(ND_3)_6](ClO_4)_2$, phase transitions, Raman spectra meas. 77−66501
Ni^{2+} aqueous complex, EPR, PMR and spin-spin relax. 79−69713
$Ni(NH_3)_6(ClO_4)_2$, stochastic NH_3-rotation, neutron incoherent scatt. 77−51331
$Ni(NH_3)_6I_2$, phase transition and rot. excitation 80−96642
$Ni(NH_3)_6X_2$, X=Cl,Br,I, rotational tunnelling by inelastic neutron scatt. 78−30553
$NiSiF_6.6H_2O$, dielec. loss and relax., 100-270K, reorient. mech. 78−35088
$NiSiF_6.6H_2O$, dynamical props. of H_2O below 300K, Raman spectroscopic obs. 79−8140

molecular reorientation continued
$(Ni[NH_3]_6)(ClO_4)_2$, reorient. correlation times of NH_3 and ClO_4 groups, Raman obs. 79−28748
O_2, adsorbed on Ag, EPR of O_2^-, rate of angular reorientation 78−72413
O_2^-, impurity in alkali halide, linear dichroism *(Russian)* 80−45127
$OH^-(D^-)$ in alkali halide, impurity rot. barrier height and librational modes 77−11491
PF_3, cryst., mol. motion, ^{19}F NMR investig. 77−73093
P_4S_3, ^{31}P NMR spectrum and spin-lattice relax. time, 77 to 500K and 7 to 25 MHz 79−8064
4′-n-pentyl-4-cyanobiphenyl, nematogenic liq. cryst., above T_c, Kerr effect response time, temp. depend. 78−34434
cis-$Pt(NH_3)_2Cl_2$, torsions, metal-metal interactions, inelastic neutron scatt. study 79−46581
$(Pt(NH_3)_4)[PtCl_4]$, torsions, metal-metal interactions, inelastic neutron scatt. study 79−46581
RbCl:NH_4Cl, PMR, NH_4^+ ion proton spin-lattice relax. time temp. depend. 78−27104
RbI:AgI, thermal reorientation kinetics of I_2^-, decay of optical anisotropy 77−52138
$RbNH_4SO_4$, ferroelec., ion group reorientation temp. and press. depend., PMR obs. 78−72470
SF_6, dissolved in O_2 and Kr, cryogenic liqs., mol. motions, IR and Raman spectra 79−69823
SF_6, plastic phase, neutron diffr. obs. and theory 79−77533
SF_6, plastic phase, orientational disorder 79−73115
SF_6, solid, NMR line shape and relax. 77−51978
SF_6, vibr. coupling in collision-induced Raman scatt. 80−83373
Se and Se-As, amorphous, dipolar activity at glass transition temp., AC method 77−66454
Si biradical, six-coordinate, mol. mobility two-spin probe investig. 80−102529
$SiCl_4$ molecule, NMR relaxation expts. 80−63673
SiH_3 radical, in Ar(Kr)(N_2) matrix, anisotropic ESR spectroscopic parameters 80−63687
SiH_4, NMR linewidths and relax. times at 6.7 to 124K 77−85602
SiH_4, plastic phase, rotational motion, quasi-elastic neutron scatt. study 79−51022
SiH_4, plastic phases I and II, neutron inelastic scatt. 79−7558
SiH_3D, in polycryst. SiH_4, mol. motions and symmetries, IR obs. 78−48163
$SnCl_2.2H_2O$, protonic order-disorder transition, inelastic light scatt. obs. 78−68497
$SrCl_2:S_2^-(S_3^-)$, thermally activated reorientation of centres between equivalent equilib. positions 79−51855
$Sr(NH_3)_6$, PMR linewidth, proton tunnelling and NH_3 rot., rapid NH_3 diffusion 78−35045
SrO:Cu^{2+}, phonon-induced tunnel hopping, ESR obs. 79−69714
TaS_2:NH_3, mol. motion, neutron quasielastic scatt. obs. 79−90827
TaS_2-NH_3 intercalation complex, press. induced diffusion effects, NMR study 79−19797
$TaS_2(NH_3)$, intercalation complex, wideline NMR obs., translational and reorientational effects 77−1602
$TiS_2(NH_3)$, intercalation complex, wideline NMR obs., translational and reorientational effects 77−1602
WF_6, effect of high hydrostatic press. in reorientation and internal motion, ^{19}F NMR spectra 79−15364
Xe hydrate, reorientation and diffusion of H_2O, PMR and dielectric relax. 77−36142
Xe:methane, impurity rotational states, inelastic neutron scatt. study 79−51020
$YFe_{1-x}Co_xO_3$, reorientation transitions, neutron diffr., mag. behaviour *(Russian)* 77−24678
Zn complex, aminoacetate, PMR, activation energy for NH_3 reorientation determ. 78−31119
ZnSe:Cr, piezodichroism due to reorientation of Jahn-Teller centres 80−11363

molecular reorientational states *see molecular reorientation*

molecular resonant states
see also Fermi resonance; molecular vibronic states
absorption line shape, coupling strength incoherence 78−17721
acetaldehyde, Coriolis resonance bands in IR spectrum 80−47995
acetophenone enolate anion radicals, substituted, electron photodetachment cross sections, reson. states 80−1030
adsorbed mols., effective reson. Raman spectra 80−97730
aliphatic perfluorocarbons, electron attachment, fragmentation 0-12 eV 80−5618
alkali homonuclear dimers, quasi-static wing profiles of self-broadening reson. lines 80−48042
alkali metal molecular, laser radiation absorpt., at. excitation processes 80−32785
allylamine, laser-microwave double and triple reson. 80−83397
aromaticity, reson. energy in graph theory 80−91412
Autler-Townes effect, coupled 1- and 2-photon resons., theory 77−83649
autoionisation, vibr.-excited ions form. in Franck-Condon gaps, threshold photoelectron spectra obs. 79−68262
autoionising resonances, vac. UV nonlinear optical props. 77−50565
benzene, ground, singlet and triplet states, ab initio VB STO, GTO calcs. 77−75060
benzene, reson. Raman effect in gas, liq., and solid phases 79−31531
benzene, resonance-enhanced multiphoton ionis. and fragmentation of mol. beam 79−100411
benzene (S_1)+OCS, V-V reson. energy transfer, microscopic reversibility, level degeneracies role 79−86045
benzene molecule, slow electron scattering, resonances to 1.1 and 1.7 eV 77−58181
benzenoid hydrocarbons, reson. energy calcs. 78−70762
bimolecular quasiresonant processes, impact approx. 78−33571
biomolecule resonant interactions 80−72128
Bixon-Jortner approx. limitation, coupling strength incoherence 77−57960
bromochlorofluoromethane, narrow saturated reson. absorpt., weak current detection 77−14433
butadiene, resonance-enhanced multiphoton ionis. and fragmentation of mol. beam 79−100411
C_{3v} molecules, l-reson. perturbations in overtone and combination vibr. systems 80−52962
$^{12}C^{16}O_2$, Herman-Wallis coeff. for band affected by reson. *(French)* 77−61805

molecular resonant states continued
CARS, reson.-enhanced, and coherent anti-Stokes hyper-Raman spectroscopy 78−86980
chloroethane, reson. multiphoton dissoc. 80−53077
chloroform molecule, liq. phase, Faraday rot. dispersion near vibr. reson. 79−91413
coherent optical spectroscopy, by 90° photon echo, during reson. scatt. and radiationless transitions 78−86978
collisionless dissociation in intense reson. wave field 77−13640
complex scaling method, theory 79−18123
compound state resonances, semiclassical calcs. 80−87031
coronene, mono- and dianions, reson. spontaneous Raman spectra, vibronic interactions 79−3451
cytochrome c, dilute soln., reson. Raman spectra, pulsed laser excitation; optical multichannel detection 78−76999
decacyclene, mono- and dianions, reson. spontaneous Raman spectra, vibronic interactions 79−3451
definition of molecular resonance curves by method of exterior complex scaling 79−63903
diatomic ion+molecule, reson. charge exchange *(Russian)* 79−98218
diatomic molecule, resonance multiphoton processes of laser radiation interaction 80−37800
p-difluorobenzene+acetone, generalised oscill. strength, for reson. electronic energy transfer 78−66668
dissociative electron attachment, H^- ang. distribs. 77−19099
dynamic electrooptical effects, reson. modulation of light *(Russian)* 78−9192
elastic scattering, nonlinear reson. freq. shift in rot.-vibr. transitions 79−36731
elastic scattering, nonlinear reson. profiles *(Russian)* 79−68295
elastic scattering, reson. width, stabilisation method, variational calc. 77−19011
electron dissociative capture, vibr. struct. of resonances 77−34770
electron elastic scatt., Feshbach resonances 78−58831
electron elastic scatt., resonances, use of high-Rydberg at. as spectroscopic probe 77−58162
electron impact shape-reson.-enhanced vibr. excitation, 10-40 eV, appl. to CO_2 80−5629
electron scatt., dissoc. resonant states 78−58851
electron scatt., strong excitation of nucl. motions 78−58849
electron scatt. reson. using dilatation transforms., dilatation stability condition 78−46445
electron scatt. using dilatation transforms., restricted perturbation methods 78−50639
electron scattering from ats.(mols.), partial resonance widths, Siegert eigenvalues, basis-set calc. 80−37880
electrostatically induced, pertubation theory 1-D model 77−75077
ethyl chloride, reson. multiphoton dissoc., excitation mechanism 79−100414
ethylene, excited states, continuum embedded, SCF-stabilisation approach 78−928
ethylene, multiphoton absorption, luminesc. and dissoc. in laser pulse field 78−1040
ethylene, narrow resonances of multiple-photon IR absorpt. 80−99529
ethylene, twisted, intervalence charge transfer and reson., sudden polarisation effect 80−69230
excited molecules, coherent anti-Stokes reson. Raman scatt. 79−59475
ferrous porphyrin, intermediate spin, reson. Raman spectra 79−69820
Feshbach resonances, many-electron systems, complex-coord. method extension 78−74591
flavins, reson. Raman spectra avoiding fluoresc. interference 79−10114
formaldehyde, laser-excited reson. fluoresc., rot. struct., rot. and vibr. consts. 79−54993
formaldehyde($-d_1$, d_2), and isotopic forms, microwave spectrum, ν_4-ν_6 vibr. states Coriolis reson. 78−82719
formaldehyde-d_2, reson. multiphoton dissoc. 80−53077
furan, resonantly enhanced multiphoton ionisation 80−106362
gas of two-level molecules, reson. interaction of standing freq. modulated wave 79−94295
haeme protein, reson. Raman line intensity formulae applicability 77−83609
Hamiltonian, complex-rotated, reson. props. 79−31427
hydrocarbons, non-alternant, reson. energies 80−106278
impurity crystal, in-band resonance states 78−27268
inner electron resonances in molecules, roles in ionisation *(French)* 78−82660
inner-shell photoabsorpt., shape resonances, extended X-ray absorpt. fine struct. 77−18979
ionisation spectroscopy, reson. chem.-physics appls. 80−68259
isotope separation, microwave reson., triplet state photochem. technique 77−32818
isotope separation by resonance scattering 77−61825
laser field interaction, Floquet theory 80−63716
laser near-reson. scatt. from collisionally perturbed mol. 78−1033
laser spectroscopy, high-resolution, time-resolved, of collisionless beam, energy randomisation, optical phase relax. 79−3501
light wave resonant interaction with atoms and molecules *(Ukrainian)* 78−66515
linear triatomic, config. stability in reson. light wave 79−64114
many-photon resonances, coherent excitation dynamics of mol. vibrs. 79−27050
metalloporphyrins, reson. Raman specta, intra- and inter-manifold couplings interference 80−28020
methane, and $-d_4$, electron ionis., excited states between 18 and 22 eV 79−3588
methane, $F_2^{(2)}$ doublet Zeeman effect obs., nonlinear reson. *(Russian)* 77−38027
methane, narrow reson., elastic scatt., spectroscopic studies 80−53094
methane, saturated absorpt. reson. shape, geometry and field intensity effects *(Russian)* 80−32778
methane+Ar, rot. compound state resons. 80−28090
methane absorber in He-Fe ring laser, narrow nonlinear resonances at low press. *(Russian)* 79−76722
methane absorption cell for He-Ne laser, reson. freq. shift with methane press. 77−50687
methyl bromide, l-reson. perturbations in overtone and combination vibr. systems 80−52962
methyl chloride, pressure-induced shift of the J=0→1 transition, 193 to 366K 77−14497
methyl halides, low energy mol. Rydberg states from Feshbach reson. spectra 77−34768
molecular resonant states continued
methyl iodide, van der Waals mol., electron self-scavenging 80−95727
methyl isocyanide, microwave spectrum, anal., N isotope effects 77−50430
N-methyl pyrrole, resonantly enhanced multiphoton ionisation 80−106362
N-methylthioacetamide($-d_1$), reson. Raman spectra obs. and mechanism 78−17672
molecular electron scatt., dissoc. attachment 78−58850
molecule-photon interaction, techniques and calcs. for reson. determ. 80−17721
multi-level excitation theory, analytic approximations 78−29922
multichannel threshold structures in scattering theory 80−58334
multiphoton ionisation, resonance peaks strengths 77−42293
multiphoton ionisation dynamics, rate eqn. modelling 80−48046
multiphoton resonances, vibr.-rot. fine struct. effect *(Russian)* 79−86022
N-level molecules, coherent dynamics, anal. solns. 78−22105
N-level molecules, coherent dynamics, numerical expts. 78−22104
naphthalene $^1B_{2u}$ resonance pairs, energy denominator depend. of excitons absorpt. 77−39783
naphthalene mixed crysts., dimer reson. self-energy 80−99459
naphthalene vapour, resonant scatt. of slow electrons 77−58182
near reson. Raman lines, relative intensities, A-term method 79−81205
near resonance fluorescence and Raman scatt. theory 79−3446
negative ions, Feshbach type reson. scatt., Glauber approx. calcs. 80−102570
nonadiabatic multiquantum excitation by reson. radiation 77−19001
nonlinear resonances of accelerated atoms and molecules *(Russian)* 78−50488
optical nutation in gases *(Russian)* 79−27225
optical nutation in standing wave, Rabi oscillations *(French)* 79−31999
optical transient signals, saturation dips 78−18020
oxyhaemoglobin, dilute soln., reson. Raman spectra, pulsed laser excitation; optical multichannel detection 78−76999
perfluoromethylcyclohexane, electron attachment, ≲3 eV, rel. to perfluoro-1-heptene 79−36755
polar molecule, electron scatt. cross sections, threshold behaviour *(Russian)* 78−5347
polar molecule, slow electron capture and rot. excitation 79−81287
poly-β-ethynylnaphthalene, insoluble, reson. Raman spectrum, struct. models 78−70981
polyatomic molecule, multiphoton absorpt. resons., dynamic Stark splitting 80−9670
polyatomic molecules, nonadiabatic transitions between electronic terms of identical symmetry 80−83265
potential surfaces, complex coord. calcs. in adiabatic approx. 80−102464
potential surfaces, complex coord. calcs. using stationarity condition 80−102465
predissociated two-channel model, resonances with complex rot. method 80−58327
predissociation, multichannel, and inelastic scatt., uniform WKB theory 79−72404
predissociation, spectroscopic interferences, unified description 77−23524
pyrazine, multiphoton ionisation spectra, of three-photon ionisation region 78−37689
pyrazine, reson. Raman and absorpt. spectra to $S_2(\pi,\pi^*)$ state, excited state geometry 79−76433
pyrazine, reson. to the $S_2(\pi,\pi^*)$ state, Raman spectra calcs. 80−69147
pyridine, multiphoton ionisation spectra, of three-photon ionisation region 78−37689
pyrimidine nucleotides, UV reson. Raman excitation profiles 80−58265
pyrrole, resonantly enhanced multiphoton ionisation 80−106362
quantum mechanical theory of resonance in chem. 77−75038
Raman gain spectroscopy, stimulated, Doppler broadening at electronic resonance 80−38065
resonance calculations for arbitrary potentials 79−22779
resonance eigenvalues, accuracy criteria 80−91423
resonance levels prediction, stabilisation technique 77−61818
resonance Raman spectra, Dushinsky effect 79−45726
resonance Raman spectra intensity distribs. in soln. 79−22763
resonant energies and width from discrete states in spherical box 80−47918
rhodamine 6G, lasing, reson. CARS spectra in methanol, ethanol, acetonitrile, H_2O 78−74948
rhodamine 6G+malachite green, in low viscosity solvent, ps time resolved energy transfer 78−70910
rhodamine 6G soln., stimulated reson. Raman scatt., first excited and ground electronic states contrib. 79−89968
rhodamine B, 6G, resonance CARS line shape, scatt. processes in ground or excited states 80−48043
rose bengal, adsorbed on ZnO electrode, reson. Raman spectra 78−76446
rotated coordinate method use, rel. to stabilisation method 80−37845
rotational coherence, reson. collisional exchange, time-resolved microwave obs. 80−23525
Rydberg spectra, resonance line shape 78−17720
Rydberg-valence mixing, oscillator strengths 79−31492
soft photon approx. accuracy for resonances in electron scatt. in laser field 78−70935
spatial-temporal modulation in molecular beam spectroscopy, phenomena near molecular resonance *(French)* 78−90149
spatio-temporal modulation near mol. reson. *(French)* 79−49299
stilbene, monoanions, reson. spontaneous Raman spectra, vibronic interactions 79−3451
sub-Doppler laser spectroscopy of mol. ions in fast ion beams 80−9655
three-level coupled Doppler-broadened system, optical time-delayed laser saturation spectroscopy 78−54472
transition identification, coherence resonances for hyperfine struct. interpretation 79−54920
triethylenediamine, multiphoton ionis. and two-photon fluoresc. excitation spectra 79−98164
triphenylene, mono- and diamons, reson. spontaneous Raman spectra, vibronic interactions 79−3451
tryptophan, Raman line characterisation 79−26996
twisted conjugated molecule, zwitterionic excited states investig. 80−58179
two- and three-photon resonances, Doppler-free power broadening 78−5308
two-atom resonance fluorescence, in strong EM field, excitation spectrum 78−82778

molecular resonant states continued
two-level molecules in low press. gas, nonlinear power reson., field broadening and shifts 79−45768
two-level system, power broadened Doppler-free saturation resons., transit time effects 77−79657
variational calc. of energies and widths of reson. 77−83506
variational calculation of reson. width and energy 78−33445
variational method for reson. width and energy calc. 77−61690
vibrational excitation cross section in electron scatt. 77−19098
vibrational struct. of resonances in electron-molecule scatt. 78−17813
vibronic state short lifetime, determ. from reson. Raman excitation profiles 79−98103
wavefunctions of complex coord. method 80−106282
widths, purely L^2 method 78−46283
ddμ mesic mol. form. in gas D_2, reson. depend. *(Russian)* 79−50171
BCl_3, ν_3 vibr. level, fine struct., nonlinear reson. 77−6783
BCl_3, vibr. excited states distrib. in reson. radiation, photodissoc. rate 78−50603
Br_2, condensed phases, spontaneous and stimulated Raman scatt., weak and strong radiation fields 79−3450
Br_2, dissoc. attachment by 0-8 eV electrons 78−74776
Br_2 in Ar matrix, reson. Raman scattering amplitude damping in discrete reson. limit 80−58262
Br_2, resonant fluoresc. at 5145 Å, isotope mols., rot.-vibr. states 77−61782
C_2, reson. fluoresc. statistical equilib. calc., appl. to comets 78−1016
CO, electron impact, reson. vibr. excitation calcs. 77−14595
CO, electron impact excitation, resonances in metastable and UV emitting levels 78−25727
CO, negative-ion resons. associated with inner-shell-excited states, electron impact 77−88580
CO, optical excitation function by electron impact near threshold 77−6942
CO, oscill. strengths for shape resonances near K edges 77−75224
CO, photoionis., vibr. intensity distrib., shape reson. effects 79−98167
CO, vibr. excitation via high-energy shape resonances 80−91693
CO, X-ray K-absorpt. spectra, reson. obs., near fine struct. 80−37817
CO+inert gas, collision-induced intersystem crossing mechanism 78−74689
CO_2, 3.8 eV resonance, vibr. struct. in electron-molecule scatt. 78−17813
CO_2, electron impact, 3.8 eV resonance 77−42430
CO_2, electron impact, reson. vibr. excitation calcs. 77−14596
CO_2 IR Zeeman spectra utilizing copropag. wave reson., diamag. shift obs. 80−53055
CO_2, narrow reson., elastic scatt., spectroscopic studies 80−53094
CO_2, photoionisation, nuclear motion effects 80−58324
CO_2, reson. electron impact vibr. excitation, 3-5 eV 78−25726
CO_2, resonant vibr. excitation cross section in electron scatt. 77−19098
CO_2 shape resonances in [100] symmetric stretch excitation *(French)* 79−86074
CO_2, VV processes, estimation of almost resonant molecular energy transfer due to multipolar pot. 80−91642
CdH, lifetime, Λ-doubling, hyperfine struct., in $A^2\Pi$ excited states 77−58083
Cl_2, Ar ion laser excited, normal and reson. Raman spectra 79−26993
Cl_2, dissoc. attachment by 0-8 eV electrons 78−74776
ClO_2, laser mag. reson. spectra tuned by Zeeman level crossing avoidance, perp. spectra 79−68229
ClO_2, laser mag. reson. spectra tuned by Zeeman level crossing avoidance, high-field spectra 79−76424
Cs_2, laser-induced photodisintegration *(Russian)* 79−89719
CsAr, 6dσ states, multiphoton laser spectrosc. obs. 79−85974
CsKr, 6dσ states, multiphoton laser spectrosc. obs. 79−85974
D_2, electron scatt., low energy, rot. resons. 78−33608
DF, threshold photoelectron spectra, photoionis. threshold, resonant autoionis. 77−499
DF-HBr CW optical resonance transfer laser 80−64003
D_2O, electron impact reson. observed in $A^2\Sigma^+ \rightarrow X^2\Pi$ radiation of OD 78−46455
F_2, dissoc. attachment by 0-8 eV electrons 78−74776
F_2, threshold photoelectron spectra, photoionis. threshold, resonant autoionis. 77−499
GeAs+Cl_2(Br_2)(I_2), high temp. Raman spectra, cryst. growth mechanism *(French)* 79−26999
H_2, autoionising states, complex scaling method calcs. 80−9527
H_2, diabatic and reson. states, dissociative photoionisation calcs. 80−47883
H_2, electron impact excitation, high vibr. levels of ground state, decay of reson. states 77−88581
H_2, electron scatt., low energy, rot. resons. 78−33608
H_2, photoionisation, resonant, dissociative 79−68272
H_2^-, autoionising states, complex scaling method calcs. 80−9527
H_2^- resonant states, Feshbach projection-operator calc. 78−5153
H_2^+, variational calcs. of resonant states 79−3571
H_2^+, reson. states, complex basis functions methods 79−6887
H_2+I→HI+H, collinear reaction, reson. effects, quantum mech. calcs. 77−52625
HBr, vibr. excitation by electron impact, threshold resons. 77−68127
HCl and HBr, low-lying reson. states in 0.25-1.15 eV electron scatt. 79−45844
HCl, dissociative electron attachment, differential cross section, Feshbach resons. 80−83508
HCl, dissociative-attachment cross sections, fine struct. 77−71884
HCl elastic electron scatt., short-lived resons., theory 77−14578
HCl^-, electron impact excitation, GO and SCF+CI methods, dissociation channels 77−71883
HCl^-, resonance states, CI calcs., pot. energy curves 78−29755
HCl^-, resonance states, interpretation of low energy HCl-electron scatt. 78−17808
HD^++HD^+, 0.1-1 eV, rot. transitions and reson. transfer, first-order perturbation theory 77−83698
H_2(D_2), dissociative electron attachment and vibr. excitation, low-energy 80−23565
H_2(D_2), electron dissociative attachment rates, rot. (vibr.) excitation depend., in plasma 80−43848
HF, elastic electron scatt., short-lived resons., theory 77−14578
HF, electron scatt. cross section, vibr. and rot. excitation, close coupling calc. 80−53154
HF, electron spectroscopy of resonances 79−3583
HF, Feshbach resons., predissoc. investig. 80−83433
HF, threshold photoelectron spectra, photoionis. threshold, resonant autoionis. 77−499
HF, vibr. excited, ang. distrib. of reson. scatt. electrons 77−71881
H_2(HD), predissoc., Feshbach resons., spin-aligned atom form., stability 77−10723
HNCO, rot. spectrum, ground and vibr. state reson., centrifugal distortion coupling 80−83364
H_2O, and D_2O, Feshbach-reson. and dissoc. electron attachment 79−41246
H_2O, atmospheric, IR attenuation, lab. study of role of molecular and aerosol contribs. *(Russian)* 79−34945
H_2O, electron impact reson. observed in $A^2\Sigma^+ \rightarrow X^2\Pi$ radiation of OH 78−46455
H_2O, photodissoc. resonances, converged 3-dimens. quantum mech. calcs. 80−106366
H_2S, electron impact, vibr. elastic scatt. and vibr. excitation 79−13822
$^4HeH^+$, ro-vibr. quasi-bound levels of $X^1\Sigma^+$ state, eigenenergies, dissoc. 77−26997
HgH, predissoc. by rot., continuous rot.-vibr. spectrum, resons. and eigenvalues, Weyl's theory 77−18997
HgH, rot. predissociation, Weyl's theory and Jeffreys' approx., resons. 78−926
I_2, dissoc. attachment by 0-8 eV electrons 78−74776
I_2, doubly resonant third harmonic generation, spectrosc. 79−93984
I_2, reson.-enhanced CARS, band contours, assignments 78−86980
I_2, reson.-enhanced three-photon absorption, CW intracavity absorption 79−10160
I_2, resonance-enhanced multiphoton ionis. and fragmentation of mol. beam 79−100411
$^{127}I_2$, saturation resons., recoil shift meas. 79−93985
IBr, elec. dipole moment, rot. transition Stark shift obs. 77−75207
K_2, laser-induced photodisintegration *(Russian)* 79−89719
N_2, 2.4 eV shape resonance, vibr. struct. in electron-molecule scatt. 78−17813
N_2, $3\sigma_g$ photionis., shape-reson.-induced non-Franck-Condon vibr. intensities 80−43120
N_2, elastic electron scatt. from 0 to 1000 eV, energy dependent exchange pots., continuum multiple scatt. method 80−43182
N_2, electron impact enhanced vibr. excitation, continuum multiple scatt. model with Hara exchange approx. 80−43196
N_2, electron impact excitation, resonances in metastable and UV emitting levels 78−25727
N_2, electron resonant scatt., total cross section function 77−50548
N_2, electron scatt., absolute total cross-sections 80−83486
N_2 electron scatt. cross sections, 0.04-3.7 eV 79−54978
N_2, molecule, electron impact resonant scattering, absolute cross sections from boomerang model 79−89798
N_2, negative-ion resons. associated with inner-shell-excited states, electron impact 77−88580
N_2, oscill. strengths for shape resonances near K edges 77−75224
N_2, rot. excitation by electron impact 1-4 eV 78−55248
N_2, X-ray K-absorpt. spectra, reson. obs., near fine struct. 80−37817
N_2^-, $^2\Pi_g$ resonance effect on N_2 electron impact rot. excitation 77−58184
N_2^-, 2 eV resonance as energy standard in low energy electron scatt. 77−71872
N_2^-, resonances in N_2 electron impact excitation *(French)* 78−25723
ND_3, predissoc. mol., rot. resolved IR reson. scatt. 77−30882
NH_3, and ND_3, new electronic state, multiphoton ionis. obs. 78−74717
NH_3, inversion spectrum, reson. half-widths calcs. 77−75221
NH_3, time-delayed laser saturation IR spectroscopy 78−86976
NH($X^3\Delta^-$) radical, form., detect. and reactions 79−64036
NO, 4-photon ionis. spectrum 2- and 3-photon resons., low temp. assignments 78−70887
NO, electron impact excitation, high vibr. levels of ground state, decay of reson. states 77−88581
NO, Feshbach resonances, energy dependence of electronic coupling to ground state 79−89616
NO, Feshbach resonances, dynamic coupling to Rydberg states 79−89617
NO, γ-band collisional broadening parameters from resonance line absorpt. 77−10704
NO, resonance-enhanced multiphoton ionis. and fragmentation of mol. beam 79−100411
NO^-, $^3\Sigma^-$ and $^1\Delta$ resonances, excitation in electron scatt. 77−31010
Na_2, Doppler-free three-photon cross reson. obs. 77−58107
Na_2, laser-induced photodisintegration *(Russian)* 79−89719
Na_2, mol. spectroscopy by photodeflection in supersonic nozzle beam 79−54995
$NaCl^-$, $NaBr^-$, NaI^-, photodetachment cross section resons., 2-2.3 eV 79−54922
O_2, electron impact excitation, high vibr. levels of ground state, decay of reson. states 77−88581
O_2, I and I′ resonance series, vibr. level populations in autoionisation, photoelectron spectra, bond length determ. 80−91612
O_2, interactions with slow electrons 79−45848
O_2, reson. cross-sections, predissoc. and preassoc., isotope effects 78−58750
O_2^+, predissociated $b^4\Sigma_g^-$ state, high resolution laser spectroscopy in fast ion beam 80−9656
OD, reson. cross-sections, predissoc. and preassoc., isotope effects 78−58750
OH, reson. cross-sections, predissoc. and preassoc., isotope effects 78−58750
OH($A^2\Sigma^+$), form. from H_2O+Kr($^3P_1$), internal energy distrib. 79−10183
PsH, positronium hydride, resonant and ground states 78−62964
Rb_2, laser-induced photodisintegration *(Russian)* 79−89719
SF_6, collisionless dissociation, spectral struct. of low level excitation 78−74714
SF_6, electron elastic scatt., shape resonances 79−18289
SF_6, electron impact excitation, 12 eV resonance 77−88582
SF_6 electron scatt., total absolute cross sections, 0.5-100 eV, incl. reson. struct. 79−45843
SF_6, narrow reson., elastic scatt., spectroscopic studies 80−53094
SF_6, resonant single-photon dissoc. route using prelim. electron excitation 80−9662
SO_2, resonant vibrational excitation, electron impact spectrometer obs. 78−90309

molecular resonant states continued
SeF_6, IR photolysis, $NH_3^- + CO_2^-$ laser isotope separation and dissoc. enhancement 79−29377
$SiAs + Cl_2(Br_2)(I_2)$, high temp. Raman spectra, cryst. growth mechanism *(French)* 79−26999
SiF_4, XUV spectra, overlapping core-valence and core-Rydberg transitions and resons. 80−32735
UF_4, absorption spectrum indicating presence of resonantly localised continuum state 80−58173
ZnH, lifetime, Λ-doubling and hyperfine struct. of $A^2\Pi$ excited states 77−58083

molecular rotation
see also macromolecular dynamics; molecular force constants; molecular reorientation; molecular rotation calculations; molecular rotational-vibrational energy transfer; molecular spectra; rotational isomerism
α,β-trifluoroacetonitrile, liq.-liq. transition rel. to mol. motion, NMR study 80−70383
AB_4 tetrahedral molecule, rot. transition intensities, nucl. spin statistics 79−93969
acetaldehyde, T_2-relax. meas. press. depend. for rot. transitions, pulse spectrometer 80−78612
acetaldehyde + $H_2(N_2)(CO_2)$, rot. line broadening, mol. quadrupole moments calc. 80−28065
acetic acid-d_1(-d_2), equilib. config. from microwave spectrum 79−59442
acetonitrile, ^{13}C mag. shielding from beam maser meas. of spin-rot. interaction 79−45707
acetonitrile, IR and Raman spectra, vibr. and reorientational and energy transfer width separation, rot. const. determ. 80−87131
acetonitrile, soln., IR perpendicular bands, profiles, rot. models 78−58695
acetyl cyanide, (^{15}N), microwave spectrum, rot. consts., internal rot. barrier 77−75141
acetyl cyanide-d_1, microwave spectra, r_s, r_0-struct. 78−13491
acetylene, absorpt. spectrum, 9240-9520 cm^{-1}, rot. anal. and consts. 79−54855
acetylene, and -d_1, 1.1 μm band, rot. struct. 77−27069
acetylene, IR spectra, rot. and vibr. struct. 78−21922
acetylene, Q-branches, diode laser IR spectra, rot. consts. and struct. 79−45723
acetylene, Raman spectra, high resolution using laser source 78−42072
cis-acetylene, triplet state, near IR electronic absorption spectrum, and form. 79−63997
acrylonitrile, NMR and relax. props., liq.-liq. transition rel. to mol. motion 80−70382
alcohols, vapour and liq. IR spectra, bandwidth, directional mol. rot., H-bonding 79−78661
aliphatic, in dil. solns., dielectric relax. dipole reorientation, rot., microwave obs 77−28516
alkali hydride molecules, pot. energy function, rot. const., vibr. const., and binding energy 80−99532
alkali hydrides, Woodcock pot. calcs. 80−43136
allylamine, laser-microwave double and triple reson. 80−83397
allylamine, N-cis lone-pair gauche rotamer ground state microwave spectrum anal. 78−82720
allylamine, NGLT, rot. and centrifugal distortion consts., microwave spectrum 78−74644
2-amino-5-chloropyridine, rot. modes, ^{35}Cl NQR 78−74677
aminoacetonitrile, microwave rot. spectrum, quadrupole hyperfine struct. 78−17658
2-aminoethanol(-d_2)(-d_3), microwave spectra, hydrogen bonding, rot. const. 77−6765
3-aminopropanol, and deuterated forms microwave spectrum, dipole moment, struct. 79−59441
aniline, amino group inversion and torsion, far IR spectra 77−10670
anilines, substituted, in benzene, dielectric relax. and mutual viscosity, obs., rot. resistance 79−38449
antisymmetric light scattering of molecules with non-degenerate electronic state 79−18192
aromatic hydrocarbons, rot. anisotropy and solvent-fluorophase bonds, differential polarised phase fluorimetric investig. 77−61779
aromatics, fluoresc. polarisation red edge effect, rot. anomaly 79−3472
BBOT, time-depend. fluoresc. depolarisation, mol.-rot., slip boundary conditions in soln. 78−9179
bent triatomic mol., photodissoc. rot. distrib. 80−95694
benzene, $^1B_{2u}(\pi\pi^*)$-$^1A_{1g}(6_0^1)$ band, in supersonic jet, rot. anal. 79−31578
benzene in solution, rotational motion, Raman study 80−44104
benzoxazole, polarisation of 274 nm absorpt. system, band contour analysis 79−27043
bicyclo[3.1.0]hex-2-ene, microwave spectra, rot. consts., ring struct. and config. 78−42041
Δ^6-bicyclo[3.2.0]heptene, microwave spectrum and dipole moment 80−9591
biradical metal chelates, rot. motion in polar solvents, rel. to ESR lineshape 80−27994
bond charge parameters from integrated IR absorption intensities 77−6853
bond magnetic rotations, Faraday effect determ. of additive props. 77−30746
bromoacetic acid, microwave spectrum, rot. consts., nucl. quadrupole coupling, conform. 79−13702
bromoacetonitrile, ground state microwave spectrum assignments, mol. struct., rot. consts., quadrupole coupling 77−6763
bromoacetylene, microwave spectrum, r_s-struct., dipole moment, quadrupole coupling consts., vibr. excited states 77−79606
bromoallene, microwave spectra in vibr. ground state, rotational consts., nuclear quad. coupling consts. *(French)* 77−10664
bromomethane, and isotopic forms, self-broadening and self-shifting of rot. spectra 78−13551
bromomethane, microwave spectra, isotope substitution, Br quadrupole coupling, J=0←1 transitions 79−45709
bromomethane, microwave spectrum obs., B rot. and centrifugal distortion consts. 77−75135
bromomethane, rotational spectrum in ground state of vibr., 18 to 350 Hz *(French)* 77−57980
Brownian rotational motion, effects on nonlinear fluoresc. characts. *(Russian)* 78−5275
Brownian rotational motion effect on anisotropic props. of absorpt. and luminesc. from excited states 79−93978

molecular rotation continued
1-1-d_2-but-1-ene skew form, microwave spectra, rot. const. and centrifugal distortion coefficients determ. 80−83351
1,3-butadiene, UV spectra, polarisation of strongest Rydberg transitions 78−46360
trans-2-butene, Raman and IR spectra, torsional mode pot. function 79−89676
1-butene oxide, gas, microwave spectrum 79−13703
t-butyl bromide, bond lengths, nucl. quadrupole coupling, microwave spectrum 79−31512
t-butylphosphine, microwave spectrum, meas., determ. 78−58675
C_2, vibr. and rot. anal. of vis., UV spectra, RF discharges in N_2, H_2, CH_4 mixtures 78−5241
centrifugal distortion in weakly bound linear triatomic molecules 78−9136
cetyltrimethylammonium bromide, micelles, solubilised nitroxide spin probes, ESR 78−21950
chain mols., conformational transition kinetics 80−83339
chlorobenzene-d_5, and isotopic forms, microwave spectrum, rot. consts. 78−58667
3-chlorodiphenyl, in dipolar aprotic solvent, internal rot. barrier, ^{13}C T_1, obs. 78−29860
chlorofluoromethane, mol. centrifugal distortion and Urey-Bradley force field 79−89807
chlorofluoromethylene radical, gas phase laser-induced floresc. spectroscopy 80−14173
chloroform molecule, liq. phase, Faraday rot. dispersion near vibr. reson. 79−91413
chloromethane-d_2, microwave spectrum, rot. consts. 78−9140
chloromethane-d_3, and isotopic forms, optically pumped mm laser transition assignments, 792 micron line 78−42328
chloromethyl formate, conformation potential energy surfaces, ab initio calcs. 80−69065
chloromethyl oxirane, microwave spectra and conformations of cis and gauche-2 forms 80−5534
chromophoric groups, freqs., dipole strengths, rot. strengths, nonchromophoric group dipole coupling effects 79−98060
compounds with hindered internal rot., microwave spectra, free rotor states obs. 79−18179
condensed phases, molecular rototranslation, single particle theory 80−64932
condensed system, rotational tunnelling and diffusion in condensed mol. systems, neutron scatt. 78−63658
correlation times, photocounting pulse fluorimetric determ., statistical accuracy 77−61777
coumarin laser dyes, fluoresc. quantum yields and lifetimes, polar solvent effects 80−87054
trans-crotonaldehyde, rot. Zeeman effect, microwave spectra, mol. parameters 79−3491
1-cyano-1,3-cyclopentadiene, microwave spectrum, rot. consts., dipole moment 78−42043
p-cyano-N,N-dimethylaniline in polar solvents, double fluorescence, theoretical model 80−58296
cyanoacetylene, ^{13}C and ^{15}N isotopic species, rot. transitions, 8-220 GHz 77−61740
cyanoacetylene, microwave spectrum, mol. consts. 78−74647
2-cyanoaziridine, microwave rot. spectrum, assignments 80−91546
cyanocyclopentane, microwave spectral study of axial and equatorial conformers 80−95604
N-cyanoformimine-d_2, struct., microwave transitions 80−973
cyanomethane, collisional rot.-line widths and shifts, microwave region 78−25619
3-cyanothiophene, rot. spectrum and consts., elec. dipole moment, quadrupole coupling, r_0-struct. 77−79607
3-cyanothiophene-^{34}S(-^{15}N), partial r_0-struct., microwave spectra 80−91552
cyclic 4-ring rotation-puckering, use of spherical coords. 80−58193
1,3-cycloheptadiene, microwave spectrum, conform. 79−98074
cycloheptane, cyclooctane, high resoln. rot. Raman spectra 77−75163
cyclohexane, liquid, density effect on transport properties 80−65264
cyclohexane, rot. correl., Raman scatt. 77−83603
cyclohexanecarbonitrile, rot. consts., conformers, struct., microwave spectrum 77−42314
1,5-cyclooctadiene, gas, high resolution Raman spectroscopy with laser sources, rot. spectra 79−27000
cyclooctanone, vibr., rot. spectra and conformations, pot. function 78−78707
1,3,5,7-cyclooctateraene, gas, high resolution Raman spectroscopy with laser sources, rot. spectra 79−27000
cyclopentadienylhafniumdichloride, gaseous, far IR and Raman spectra 80−95624
cyclopentadienyltitanium dichloride, gaseous, far IR and Raman spectra 80−95624
cyclopentadienyltitaniumtrichloride, gaseous, far IR and Raman spectra 80−95624
cyclopentadienylzirconiumdichloride, gaseous, far IR and Raman spectra 80−95624
cyclopentene-3,5-dione(-d_1) microwave spectrum assignments, rot. consts., dipole moment, config. 78−55168
cyclopentyl chloride, microwave spectrum, conformation, quadrupole coupling consts. 79−3434
cyclopopane, conformations, rot. consts., microwave spectrum 79−98075
cyclopropane, rot. Raman spectrum 78−86873
cyclopropyl cyanide, high-resolution microwave spectra, quadrupole hyperfine struct. of rot. transitions anal. 80−95601
cyclopropyl silane, rotational spectrum (9.0-35 GHz), transitions of ground vibrational state 79−98077
dense media, Q-branch Raman line width, rotational relaxation, reorientation, collision strength 79−98106
diacetylene, near UV band system, rot. and vibr. anal., rot. fine struct. 77−61761
diatom-atom gas mixture, infrared line shape, rotational lines, influence of collision duration 80−43110
diatom-surface scatt., rot. inelastic, impulsive collision limit calc. 80−104030
diatomic astrophysical molecules, review of spectroscopic information in visible and UV regions 77−88459
diatomic hetero-nuclear molecules, dissociation in intense IR fields 77−71841
diatomic mol. pot. energy function, rot. consts. and Sutherland parameter 79−54931

molecular rotation continued
diatomic molecular spectra, conventions for defining electric transition moment and rot. line intensity factors 80−83346
diatomic molecules, and ions, internal partition function calc. 78−55159
diatomic molecules, homonuclear, molecular dynamics, time-dependent statistical props. 80−44093
diatomic molecules, homonuclear, molecular dynamics, translation-rotation coupling 80−44094
diatomic molecules, near saturated fluorescence, two-level model 79−50000
diatomic molecules, rotational Raman intensities and polarisability anisotropy change meas. with internuclear distance 80−63641
diatomic molecules, spectral line collisional broadening, numerical method 78−25622
diatomic molecules, spectrosc. consts., rel. to electronegativity 80−28007
1,3-diazaazulene, vibronic coupling, Duschinsky effect, mixed cryst. spectra 77−79622
dichlorodifluoromethane, microwave rot. absorpt. spectra, nuclear quadrupole coupling, hyperfine splitting 77−30861
1,3-dichloropropyne and -d_1, vibr. spectra, normal coord. anal. and centrifugal distortion constants 78−70832
1,1'-dicyanoethene(-d_2), microwave spectrum, Coriolis interaction, rot. assignments 78−82721
1,3difluorobenzene, rot. Zeeman effect, g-tensor, mag. susceptibility 77−497
1,2-difluoroethane, internal rotation temp. frozen in supersonic jet, matrix IR spectroscopy 80−9594
1,1 difluoroethylene, -d_1, -d_2, mol. struct., rot. consts., gas phase electron diffr., microwave data 77−65542
dimethyl ether, review of microwave spectrum, tabulated data 80−51965
dimethyl selenide, r_s-struct., methyl top axis tilt 77−46554
dimethyl selenide-d_6, microwave spectrum in ground and excited torsional states *(German)* 77−57992
dimethylacetylene, laser Raman spectra, pure rot. anal. 79−59468
2-dimethylaminoethanol(-d_1), microwave spectrum, hydrogen bonding, rot. consts., struct., dipole moment 77−6764
dimethyldiacetylene, laser Raman spectra, pure rot. anal. 79−59468
dimethyldichlorosilane, microwave spectrum, rot., centrifugal distortion and quadrupole coupling consts. 80−91547
dimethylether, and d_6, microwave spectra of torsionally excited states 79−26974
dimethylphosphine, microwave spectra, internal rot. barrier 78−5205
dimethylsulphide, Raman spectra, torsional pot. consts. and kinetic coeffs. 78−5233
disilylmethane, microwave spectrum, struct., dipole moment and internal rot. 79−13699
DNA, ^{111}In bound, rot. correl. times, from γ-ray perturbed angular correl. 80−94152
DNA, molecular motions, investigated by ^{31}P and ^{13}C NMR relaxation 80−63657
DNA[Cu^{2+}], ^{111}In bound, rot. correl. times, from γ-ray perturbed angular correl. 80−94152
DODCI, rot. diffusion time, time depend. fluoresc. depolarisation meas., photoisomer effects 77−71825
dyes, rot. diffusion of prolate, oblate mols. from absorpt. relax. 80−1008
education, rigid rotator, account suitable for basic quantum mechanics course 77−33773
electron scattering, L^2-basis set theory with vibr. and rot. coupling 79−41247
electronically excited molecule, rot. diffusion, fluoresc. depolaris. meas. 79−24846
energy loss spectra, state-to-state rot. transition cross sections 80−91665
ethane, CH bond orbitals, internal rot. barriers, antisymmetrization effects 80−63529
ethane, doubly degenerate torsional states, pure rot. transitions, theory 79−72299
ethane, intensity of $^RQ_0$ branch in ν_9 fundamental 77−6856
ethane-1,1,1-d_3, gas-phase IR spectra, rot. fine struct. obs. 80−83359
ethane-d_n, IR spectra, r_0, r_z and r_e structs. 79−59453
ethanol, alcoholic electrolytic solutions, Dielectric constants 79−99813
ethyl alcohol-d_0(-d_1)(-d_1)(-d_2), internal rot. and microwave rot. spectra 80−69128
ethyl fluoroformate, microwave spectra of rot. isomers 79−10097
ethyl formate, microwave rot. spectrum, centrifugal distortion effects 80−52979
ethyl iodide, microwave spectra and internal rot. anal. 80−69130
ethylene, IR absorpt. spectra of ν_1, ν_{10} and ν_4 interacting band 80−83369
ethylene, laser-induced IR photolysis mechanism 78−56909
ethylene, Raman spectra of ν_3 band, rot. consts. 79−26988
ethylene, rot. around double bond, four orbital-four-electron model 80−95592
ethylene oxide, ^{13}C and D variants, T_2-relax., 2_{20}-2_{11} rot. transition by microwave pulse spectrometer 80−47976
ethylene ozonide-d_4, isotopic species, microwave rot. spectrum assignments, struct. 77−57982
ethylene-d_1, ν_9 B-type band analysis, ground state rot. parameters 77−42316
ethylene-d_1, IR absorpt., ν_{12} and $\nu_2+\nu_9$ bands, rot. consts., Fermi and Coriolis coupling consts. 77−27070
ethynyl compounds, vibr. dephasing of C-H stretching vibrs. 79−6927
excited states, absorption spectrum, diffusion rot. effects *(Russian)* 78−74641
flame temperature meas. by Raman scattering 77−16822
fluids, atomic and molecular, collision induced light scatt. *(German)* 79−27057
fluorescence depolarisation, E-type delayed, rotational motion probe technique 80−36207
fluorescent molecule, rot. diffusion coeff. from polaris. anisotropy meas., photon counting technique 77−18072
fluoroacetylene, IR absorpt. spectra, rot. anal. of hot bands 77−75151
fluoroacetylene, laser Stark and IR-microwave double resonance, E1 moment, vibr. states 77−6813
fluoroacetylene-d_1, ν_4 band, IR spectrum, rot. anal. of hot bands 77−75149
4-fluoroaniline, amino group inversion and torsion, far IR spectra 77−10670
o-fluoroaniline, conformation by microwave spectroscopy, rot. consts. 78−9144
fluorobenzene, mol. reorientation and weak mol. interaction influence, ^{2}D spin-lattice relax. obs. 80−106333
molecular rotation continued
fluoroform, ν_3, ν_6 and hot bands, high resolution IR spectrum 79−81204
fluoromethane, ν_3 band Lamb dips, effects of RF elec. field modulation on Stark spectra 80−52989
fluoromethane, chem. shielding, mol. rot. and anharmonic vibr. 78−94258
fluoromethane, excited state rot. spectroscopy and kinetics, appl. of tunable sub-MM sources 80−14162
fluoromethane, microwave spectrum, and 2nd order Coriolis reson., mol. consts. 77−18915
fluoromethane, rot. mag. moment spectra, mol. beam mag. reson. obs. 77−14509
fluoromethyl formate, conformation potential energy surfaces, ab initio calcs. 80−69065
forbidden rot. transitions, expt. and theory, review 77−34612
formadelhyde(-d_2), S_1 rot. levels, collisionless nonradiative decay rates 79−72346
formaldehyde, 4_0^1 band anal., isotope effects 78−86878
formaldehyde, a^3A_2-X^1A_1 system, rot. anal. 78−62818
formaldehyde, anharmonic pot. function, vibr. freqs., vibr.-rot. interaction, centrifugal distortion 77−38651
formaldehyde, CO laser Stark and IR absorpt. spectra, dipole moment and rot. consts. 77−75150
formaldehyde, excited state photodecomp., rotationally resolved spectra 77−60088
formaldehyde, IR spectra, Coriolis-coupled ν_4, ν_6 and ν_3 fundamental bands 78−5227
formaldehyde, IR spectrum, rot. anal., P-and Q-branch assignments 77−18923
formaldehyde, laser-excited reson. fluoresc., rot. struct., rot. and vibr. consts. 79−54993
formaldehyde, mag. rot. spectrum, A^1A_2 state, singlet-triplet perturbations 79−98126
formaldehyde, microwave-microwave double resonance 80−53029
formaldehyde, molecular beam rotation temp. meas. *(French)* 80−78724
formaldehyde(-d_1, d_2), and isotopic forms, microwave spectrum, ν_4-ν_6 vibr. states Coriolis reson. 78−82719
formaldehyde and -d_1, MODR and collision-induced transitions in laser cavity 78−74686
formaldehyde and its isotopic species, rot. spectra of ground vibr. state, rot. const. determ. 80−83350
formaldehyde S_1 levels, collisionless single rot. level lifetimes, elec. field depend. 80−63566
formaldehyde substituted with ^{17}O and ^{18}O, microwave spectra of ground vibr. states, rot. and distortion const. determ. 80−83349
formaldehyde-^{13}C, A^1A_2-X^1A_1 system, UV absorpt. spectra, rot. anal. 80−9614
formaldehyde-d_0, -d_2, fluoresc. quantum yields, rot. depend., single rovibronic level values 79−22748
formaldehyde-d_0(−d_2), S_1 single rot. level lifetimes, isotope, elec. field and vibr. state depend. 80−78655
formaldehyde-d_1, rotational transitions, IR-RF double reson. meas. 77−61775
formaldehyde-d_2, laser Stark spectra, Coriolis coupled ν_4 and ν_6 fundamentals 77−27065
formaldoxime, centrifugal distortion effects, microwave rotational spectrum 79−22699
formic acid, ^{16}C, ^{18}O, microwave spectra and centrifugal distortion consts. 80−83352
formic acid and isotopic species, microwave spectra, Coriolis reson. between vibr. excited states 79−13700
formyl chloride, rot. Zeeman effect of low-J transitions 78−25519
formyl ion, electron impact rot. excitation, Glauber approx. with Coulomb effect 80−63840
formyl radical-d_0,-d_1, microwave spectroscopy, high field Zeeman effect 78−37631
free radical reaction, chemically induced dynamic polarisation in strong mag. field, radical rotation influence 80−76509
fulminic acid-d_0, -d_1, rot. Zeeman effect and nucl. quadrupole coupling 78−78683
gas, rot. temp. decrease due to stimulated transitions *(Russian)* 79−86152
gases, high resolution rotational Raman spectra, review 80−23425
gases, Raman line broadening, rotational structure, vibrational relaxation 79−98105
germanyl acetylenes, fine structure due to internal rotation in IR-active perpendicular bands 79−98096
glyoxal, 4550Å bond system, rot. anal. mol. consts. and geometry 77−42330
glyoxal, internal conversion, energy redistrib. 80−53036
ground state alkali molecules, mag. shielding and spin-rot. interaction 80−87186
Hamiltonian of a molecular type system with internal rotation 80−18842
heat capacity and entropy, mol. without internal rot., MINDO/3 calc. 78−33450
heavy ion collisions, electronic states in rot. two-centre Coulomb systems 77−14561
heptafulvene, microwave spectrum and dipole moment 77−14421
hexa-deutero dimethyl selenide, microwave spectrum, first excited torsional states, top-top interaction 77−10668
hexafluoroethane, far IR multipole induced absorpt. 78−37639
hydrazine-1,2-d_2, microwave spectra, mol. structural parameters 77−27056
hydrogen, and isotopic forms, cryogenic data rel. to mag. fusion energy 80−8746
identical molecules, dispersion intermolecular pot. anomaly prod. by intense radiation field 80−58336
indane, 271 nm spectrum, rot. band contour anal., puckering vibr. 78−1001
indene, microwave spectrum, assignments, rot. consts. and config. 79−31510
inert gas, dense, rotational relax. of solute molecules reln. with local anisotropy fluc. 80−58183
interaction of molecular rotation and translation 80−69262
interstellar masers, Λ-doublet population inversion in OH, OD, CH, CD and NH^+ collisions 80−22065
iodomethane, and isotopic forms, self-broadening and self-shifting of rot. spectra 78−13551
iodomethane, collisional rot.-line widths and shifts, microwave region 78−25619

molecular rotation continued
iodomethane-d_3, Stark tuned level crossings and saturated absorpt., RF elec. field modulation effects 80−52989
3-iodopropene, microwave spectra, rot. consts. and HFS 78−975
3-iodopropene, microwave spectra, torsionally excited, rot. consts. 79−63986
3-iodopropene, rot. spectra, quadrupole hyperfine struct. 80−91545
ion+atom collision, electron spin coupling in rot. frame, X-ray emission 79−36724
ion+atom slow collision, atomic excitation by quasimolecular orbital rot. coupling, uniform Airy approx. 78−25644
ion+polar molecule collision, low-energy, rot. state approach 80−74224
ion+polar molecules, long range dipole interaction effect 80−102558
ion cyclotron motion, Coriolis coupling of ion internal degrees of freedom 80−87246
ionic equilibria in water and mol. dynamics of pure liqs. using high-press. Raman spectroscopy 79−24301
IR and Raman studies in liqs. and gases 80−11390
IR intensity data reduction, use of reference mols. 79−13772
IR molecular absorption spectra, effect of rotational coupling on torsional bands 78−13497
IR multiphoton excitation, rot. heating, dynamical effects on dissoc. products 80−18892
isocyanic acid, molecular structure and centrifugal distortion constants 80−47974
isocyanoacetylene theoretical study and rot. const. 78−33633
isocyanoethynyl radical, theoretical study and rot. const. 78−33633
isopropyl fluoroformate, microwave spectrum and conformation 79−10098
isopropylphosphine, gauche form, microwave spectrum, identification 78−58674
isothiazole, rot. Zeeman effect, localised susceptibilities 80−91600
isothiocyanic acid, $H^{15}NCS$, $HN^{13}CS$ and $HNC^{34}S$, ground state spect. constants and molecular struct. 80−47973
isotopic substitution, rot. and Coriolis consts. 79−3377
ketene-d_1(d_2), microwave and millimetre spectra, rot. transition, centrifugal distortion anal. 77−57991
laser IR excited mols., excited fraction determ. 80−78661
laser Stark spectroscopy, technique for molecular vibration-rotation spectra *(Japanese)* 77−494
linear triatomic mol. photodissociation, fragment ang. distribs., theory 80−23468
linear triatomics, photofragmentation, vibr. and rot. distrib., quantum anal. 77−14504
lipid hydrocarbon chain, biomembrane, rot. motion and fluidity 80−76714
liquid crystal, uniaxial, polarised fluoresc. emission, orientational distrib. function, rot. Brownian motion 78−80390
liquid rot. and transl. correl. time discrimination by ELDOR 77−1619
liquids, Raman line broadening, rotational structure, vibrational relaxation 79−98105
macromolecule rotational diffusion props., validity of general ellipsoid model 80−95751
magnetic circularly polarised emission from luminesc. mol. system, QED formalism, orientation relax. 77−46589
magnetic resonance spectra, averaging for quantum finite motion with large amplitude 77−58046
methane, $\nu_1(a_1)$ vibrational state rotational structure, CARS obs. 79−98109
methane, microwave Q branch distortion moment Stark spectrum, rot. transitions, C isotope shifts 77−455
methane, phase II, IR and Raman spectra of ν_3 and ν_4 modes 78−2834
methane, pure rot. Raman scatt. 78−86875
methane, rot. mag. moment spectra, mol. beam mag. reson. obs. 77−14509
methane, rotational anal. of ($\nu_3+\nu_4$) combination bands *(French)* 78−21900
methane, rotational state, avoided-crossing molecular beam spectroscopy 80−63730
methane, vibr. induced rot. spectrum in ($u_4=1$) state 79−18184
methane-d_1, 9613 Å band rot. anal. 78−86861
methane-d_1, dipole moment, rot. depend., IR-IR double reson. obs. 79−81298
methane-d_1, high resolution spectra, line intensities, ground-state rot. const. determ. 80−83517
methane-d_1, laboratory rotational spectrum and upper limits on abundance in (OMC-1) 80−56705
methane-d_2, IR spectrum, ν_2 and ν_8 bands, rot. struct. and consts. 77−27066
methane-d_4, ν_2 and ν_4 IR bands meas. and anal. 80−18851
methane-O_2-N_2 flames, OH radical conc., hook method meas. 77−77762
methanol, alcoholic electrolytic solutions, Dielectric constants 79−99813
methanol, vap., rot. spectrum, 8-50 cm^{-1}, 293K 79−72305
methanol (d_3), OH stretch fund., torsion-rot. levels, IR spectra obs. 80−32711
methanol laser, optically pumped, use of crystalline reflector in cavity 80−64080
methanol-^{13}C, torsion-rotation transitions, C-O stretch fundamental, FIR spectra obs. 79−93998
methanol-d_1, (CH_2DOH), microwave torsional-rot. spectrum, rel. to interstellar search 80−99498
methanols, labelled, proton T_1 in presence of intramol. rots., intermol. relax. rate 80−2656
3-methoxypropionitrile, microwave spectrum, rot. conformer, rot. consts., vibr. state 77−14419
methyl acetate, microwave spectra and internal rot. 80−87100
methyl azidoformate, microwave rot. spectrum, satellite transitions 80−69127
methyl bromide, pure rot. spectrum, fundamental and $\nu_3=1$ levels *(French)* 77−18919
methyl bromide, rot. absorption spectrum of ν_3 and $2\nu_3$ excited vibr. states, mol. consts. determ. 78−82732
methyl bromide, rot. spectrum, microwave region *(Russian)* 78−70823
methyl bromide, rot. Zeeman effect 79−54909
methyl chloride, microwave spectrum of excited vibr. states, Coriolis coupling, rot. consts. 77−14420
methyl chloride, pressure-induced shift of the J=0→1 transition, 193 to 366K 77−14497
methyl chloride, rot. anal. of IR absorpt. spectra, mol. vibr., rot. const. determ. 80−99505
molecular rotation continued
methyl chloride-d_3, 9.4 μm region laser Stark spectrum, ν_2 and ν_5 bands 77−27112
methyl cyanide, linewidth parameters in rot. spectrum, multiple differentiation calcs. 79−98070
methyl cyanide, submm. rot. spectra in ground vibr. state *(Russian)* 77−34636
methyl fluoride, second-order Coriolis resonance between ν_2 and ν_5 states, microwave spectra 78−74646
methyl fluoroformate, isomer conformation, CNDO and ab initio STO calcs. 80−58151
methyl formate, microwave spectra, rot. consts., moments and struct., radio astronomy appl., review 80−17637
methyl iodide, rot. microwave spectra, nucl. quadrupole, spin-rot. and nucl. shielding tensors 78−42040
methyl isocyanide, and ^{15}N derivative, microwave spectra in $4\nu_8$ state 77−83582
methyl isocyanide, microwave spectrum, anal., N isotope effects 77−50430
methyl isocyanide-d_2, IR spectrum, rovibr., ground state struct. 78−25537
N-methyl m-fluoroaniline, conformational anal., microwave spectra obs. 80−58247
methyl nitrite, internal rotation temp. frozen in supersonic jet, matrix IR spectroscopy 80−9594
methyl radical in sodium acetate, EPR spectra, anisotropic hyperfine interaction, rot. tunnelling 80−34775
methyl selenocyanate, and isotopic forms, microwave spectrum 79−13705
methyl vinyl ether, microwave spectrum, quartic centrifugal distortion and rot. consts. 79−10099
methyl vinyl ether, rot. Zeeman effect, g-values, mag. susceptibility, quadrupole moments 77−490
2-methyl-pyrimidine, microwave spectrum, V_6 barrier, dipole moment, rot. consts. 77−3345
methylacetylene, ν_5 band, microwave and IR laser Stark spectrosc. 80−91558
methylchloride, high resoln. rot spectrum, spin-rotation and nucl. mag. shielding tensors 77−27054
methyldiborane, microwave spectra, bond lengths, dipole moments, rot. consts. 77−83579
methylene chloride, microwave spectra, rot. consts. and geometric struct. 79−63990
methylene fluoride, excited vibr. state, microwave spectrum 78−58672
methylene ketene, microwave spectrum, rot. and centrifugal distortion consts., dipole moment 78−17659
methylene radicals, rotational transitions, laser mag. resonance spectra 80−5538
3-methylfurane, rot. Zeeman effect, g-tensor, mag. susceptibility 77−497
methylphosphinosilane, IR and Raman spectra, vibr. assignment and asymmetric potential function 79−85962
microwave rotational spectroscopy, of high temp. mols. 80−52236
microwave spectral lines, press. broadened, deviations from Lorentzian line shape 77−61806
microwave spectral lines, press. broadened width and shift, temp. depend. 77−61807
molecular electron impact, close coupling method, elastic and rot. excitation 79−10202
molecular fluids, coupling of rotation and translation 80−38892
molecular rotation and reorientation, microscopic and hydrodynamic contrib. 79−1379
molecules, isolated, intersystem crossing, rot. motion effect 80−95669
molecules D_{6h}, D_{3h} and D_{3d}, appln. of Aliev-Watson maxima-minima criteria for quartic centrifugal distortion const. 80−87132
monofluoromethane, ν_6 band, Q-branches, diode laser IR spectra, mol. consts. 79−45722
monothioformic acid, cis-, trans-rotamers, rot. spectrum, force consts. and isotopically substituted struct. 78−9145
morpholine, centrifugal distortion consts., microwave spectrum 80−5531
N-methylhydroxylamine, microwave spectra, struct., moments, internal rot., HFS and rot. consts. 79−45708
naphthalene, absolute quantum yields, rot. excitation 77−3404
naphthalene, nonradiative transition rates, rot. struct. 78−42119
naphthalene-h_8, gas phase two-photon spectra calcs. 78−94298
1-naphthylamine, anisotropic rot., red edge transition moment, fluoresc. 77−10699
neutron scatt. studies of near-spherical mols., translational and rotational parameters 77−61734
nitromethane, liq., NMR relax. obs. of internal mol. rot. 79−95668
nitrosomethane, microwave spectrum, structure, dipole moment and centrifugal distortion 78−66540
3-nitrothiophene, rot. transitions, torsion, microwave spectra 77−42313
nitroxide radicals, q- and A-tensor components, rot. mobility 2 mm EPR spectrosc. determ. 80−102530
nitroxide spin labels in rigid-lattice limit, EPR and ST-EPR spectra, rapid computer simulation 79−93189
nonlinear polyatomic molecules, centrifugal distortion, phenomenological consts. 77−75120
nonrigid molecules, dipolar relax. and nuclear Overhauser effects, fluctuating internuclear distances effect 80−91578
nonspherical molecules, rot. diffusion tensors determ. from rot. friction tensor calcs. 80−63861
norbornane, microwave spectrum and dipole moments 80−78606
nuclear spin relaxation and molecular rotation, review, book contrib. 79−31557
OCS, submillimetre rot. lines, press. shifts 80−23463
n-p-octyloxybenzylidene-p-toluidine, dielectric behaviour in nematic mesophase at RF 80−34842
optical activity, rotational 79−72298
organic compounds, structural energy characteristics, rotational isomerism, mol. motion *(Russian)* 79−56602
organic dyes, rot. diffusion time, fluoresc. depolaris. meas. 79−24846
oxide semiconducting glass, structural energy characteristics, rotational isomerism, mol. motion *(Russian)* 79−56602
oxiranecarboxaldehyde, microwave spectrum, torsional excitation energy, partial struct., dipole moment 77−38655
parity-violating effects of weak interactions 80−52455
phenolic Mannich bases, dielec. relax. study 80−97196
phenyl isocyanate, microwave spectrum, rot. consts., dipole moment 77−61739

molecular rotation continued
picosecond intramolecular dynamics in solution, Fokker Planck eqn. 80 - 28891
planar structure, double reson. signals depend., appl. to microwave spectra 80 - 32751
polar diatomic molecular ions, rot. excitation by low-energy electrons *(Russian)* 79 - 94093
polar molecule, slow electron capture and rot. excitation 79 - 81287
polar molecule electron scatt. at intermediate J, closed-form treatment 80 - 32846
poly-4-vinyl-pyridine in ethanol, spin label obs. of local density of monomer units and mol. dynamics 80 - 44099
polyatomic molecular vapour, rot. fluoresc. depolaris. 79 - 54889
polyatomic molecule, vibr. excitation in strong IR field, rot. level emptying *(Russian)* 77 - 75235
polyatomic molecules, high intensity IR absorpt. 80 - 14183
polyatomic molecules, intensity distribution in vibronic bands, Dushinsky effect 79 - 93983
predissociated two-channel model, resonances with complex rot. method 80 - 58327
premixed H_2-O_2-N_2 laminar flames, temp. profiles, Raman, absorpt. and line reversal obs. 80 - 42227
pressure-induced spectral linewidth and line shifts, vibr. depend., IOS scatt. approx. 79 - 68267
prolate molecules in solvents, anisotropic fluoresc. *(German)* 80 - 69183
propargyl mercaptan ($-d_1$), microwave spectra, struct., rot. anal. 77 - 18916
propenoyl chloride, IR bands, torsional struct. 80 - 28018
propiolamide(-d_2, d_3), microwave spectrum, struct., dipole moment 78 - 78685
propynal, IR-microwave double reson. and two-photon expts. 80 - 83396
propynal-d, in ground vibrational state, IR microwave double resonance spectra, rot. and centrifugal distortion const. determ. 80 - 83358
propynal-d, IR microwave double reson. spectroscopy 80 - 69172
propyne, ^{13}C isotopic species, microwave spectra, rot. consts. 78 - 86850
pulsed molecular beam experiments employing electromechanical valve 80 - 63870
pyrazine, vapour, fluoresc. quantum yields, rot. effects 80 - 95661
pyridine, and -d_1, microwave spectra, mol. struct., rot. consts. 78 - 25517
4-pyridine carbaldehyde, microwave spectrum, rot. assignments, quadrupole coupling consts. 80 - 91548
s-trans-3-pyridinecarbaldehyde, microwave spectrum, assignments 78 - 21912
pyridizine, 0-0 bands in n-π^* absorption, rot. contour anal. 78 - 55184
pyrimidine, vapour, fluoresc. quantum yields, rot. effects 80 - 95661
quantum state selected atomic and molecular beams production, developments in techniques 80 - 63871
r_m structural determ. from rot. consts., test on OCS synthetic data 78 - 42236
racemic liq. soln., mirror isomeric mol. separation by RF rot. polarisation elec. field 78 - 80317
Raman high-resolution molecular spectroscopy, review 78 - 42064
Raman spectra of gases, high-resolution, mol. struct. and orops. 80 - 53000
reaction product initial rot. state distrib., pump and probe laser obs. 80 - 85158
RF spectroscopy in laser cavity, pure nucl. quadrupole spectra 78 - 90320
rhodamine 6G, rot. diffusion, fluoresc. spectra, solvent effects 77 - 75198
rigid asymmetric molecule, rotational partition function 79 - 84899
rigid XYX and nonrigid three-body systems, correlation diagram 80 - 69249
rot. spectra, 714-1667 μm, Fourier interferometric spectrometer 77 - 83765
rotational selection rules for nonradiative processes 78 - 62838
rotations and translations in isospin space 80 - 102431
saturated spectral lines in mm and sub-mm mol. rotation spectroscopy *(Russian)* 77 - 75335
selenoacetaldehyde, microwave spectrum, struct. internal rot. barrier 78 - 74645
shock wave, rot. distrib., exponential gap law 77 - 89156
silyl acetylenes, fine structure due to internal rotation in IR-active perpendicular bands 79 - 98096
spectra, unresolved rot. struct., use in flame temp. meas. 80 - 86300
spherical molecule, anisotropic mol. rot. detect., differential phase fluorometry theory 77 - 61778
spherical top mols., with electronic degeneracy, rot. Raman spectrum 79 - 72322
spherical top type molecules, rot. spectra, CARS *(Russian)* 77 - 75168
spherical tops, chiral discrimination 80 - 106314
stibabenzene, struct., microwave spectrum and nucl. quadrupole coupling consts. 78 - 70817
stilbenes, prolate molecules in solvents, anisotropic fluoresc. *(German)* 80 - 69183
N-sulphinylaniline, microwave rot. spectra, torsional freq., dipole moment and internal rot. barrier 78 - 973
symmetric top, rigid, rot. partition function 78 - 46260
symmetric top molecule, radiationless processes, angular momentum constraints 80 - 28052
symmetric-top dipole molecule, Stark effect in strong field *(Russian)* 77 - 61792
tertiarybutylisocyanide-borane, vibr., rot. consts., moment of inertia, microwave spectra obs. 80 - 32706
tetrachlorotetraiodofluorescein, rot. diffusion, fluoresc. spectra, solvent effects 77 - 75198
tetracyclo[3.2.0.$0^{2,7}$.$0^{4,6}$]heptan-3-one, microwave spectrum and effect of cyclopropyl-carbonyl group interactions on dipole moment 78 - 9138
tetrafluorobenzene, microwave spectra, dipole moment, centrifugal distortion consts. 77 - 75133
1,1,2,2-tetrafluorocyclobutane, microwave spectrum, dipole moment, rot. and vibr. modes assignments 77 - 18914
tetrafluoromethane, $\nu_2+\nu_4$ band, high resolution diode laser spectra 80 - 69138
tetrafluoromethane, ν_4 fundamental of three isotopic species 78 - 70835
tetrafluoromethane, collision-induced rot. spectrum 79 - 98101
tetrafluoromethane, liq., mol. reorientation 80 - 106320
tetrakis(trifluoromethyl)germane, gas phase electron diffr. struct., torsional force consts., CNDO/2 calc. 79 - 31687
s-tetrazine, fluoresc. excitation spectra, 1K rot. struct. 78 - 1020
s-tetrazine(-d_1), and $^{15}N_2$-substituted, rot. consts., ground and $^1B_{3u}$ excited states geometries 78 - 82862

molecular rotation continued
1,2,4-thiadiazole, struct., double reson. modulation microwave spectra 77 - 14424
thiazole, rot. Zeeman effect, localised susceptibilities 80 - 91600
thioacetaldehyde (-d_1), microwave spectrum, substitution struct. internal rot. barrier, dipole moment 77 - 6762
thioformaldehyde, $\tilde{a}^3A_2 \leftarrow \tilde{X}^1A_1$ IR absorpt. spectra 80 - 83362
thioformaldehyde-d_0, -d_2, A^1A_2-X^1A_1 vis. absorpt. system, rot. anal. 80 - 5559
thioformic acid, g-values, mag. susceptibility, quadrupole moments, rot. Zeeman effect, isomer effects 78 - 25520
thioformyl ion, theoretical study 78 - 37553
thioketen, microwave spectrum, substitution structure and dipole moment 80 - 975
trans-propargyl amine, microwave spectra, dipole moments and struct., isotopic species 78 - 974
triatomic linear molecule, photodissoc., products rot. distrib. 79 - 66309
triatomic molecule, rot. vibr. electronic Hamiltonian, Born-Oppenheimer approx., breakdown 80 - 87097
triatomic molecules, microwave spectra, mol. parameters 79 - 31513
triatomic molecules, rotating, semiclassical eigenvalues 80 - 9588
triatomic van der Waals mols., rot. predissoc. 80 - 63721
trifluoroethane, MODR, rot. consts. 78 - 9177
trifluoroethene-d_0,d_1, mol. struct., microwave and electron diffr. obs. 80 - 58384
trifluoroiodomethane, laser microwave double reson. spectroscopy with CO_2 laser lines 80 - 87156
trifluoromethane, and -d_1, microwave spectra in $\nu_6=1$ state, accidental degeneracy, mol. struct. 79 - 3436
trifluoromethyl bromide, microwave spectra, mol. rot., isotopic variation in bond lengths, Stark meas., dipole moments determ. 80 - 74165
trifluoromethyl hydroperoxide(-d), CF_3 torsional vibrs., low freq. Raman spectra 80 - 91565
trifluoromethyl hypofluorite (hypochlorite), CF_3 torsional vibrs., low freq. Raman spectra 80 - 91565
trifluoromethyl iodide, microwave spectra, mol. rot., isotopic variation in bond lengths, Stark meas., dipole moments determ. 80 - 74165
trifluoromethyl peroxyfluoride (peroxychloride), CF_3 torsional vibrs., low freq. Raman spectra 80 - 91565
trimethylbromosilane, microwave spectra, struct., chemical bonding 80 - 95602
trimethylene sulphoxide, microwave spectrum, mol. struct., methylene group, bends, tilts, twists 77 - 50431
trinitromethane, microwave and rot. spectra, effect of twist of NO_2 groups, rot. and centrifugal distortion const. determ. 80 - 95605
trioxane, $\nu_{19}(E)=\nu_{20}(E)=1$ state, rot. spectrum assignment, microwave obs. 80 - 58248
trioxane $^{13}C(^{18}O)$ substituted, mol. consts. and rot. spectra 80 - 87096
triplet-singlet transitions in mag. field, rot. struct. 77 - 61790
two and three-centre molecules, periodicity and internal torsional conformers around single bond, symmetry analysis 80 - 69250
unimolecular decomp. kinetics, rot. effects 80 - 81319
van der Waals mol. rot. predissociation study, complex coord. method 80 - 74205
vinyl alcohol-d_0, -d_1, microwave spectrum, centrifugal distortion 77 - 71796
vinyl azide, microwave spectrum 77 - 57985
vinyl cyanide, microwave spectra data tables 79 - 59445
vinyl isocyanate, microwave and photoelectron study of cis- and trans-forms 78 - 70819
vinylfluoride, gas phase electron diffr. and microwave spectra, rot. consts., struct., isotope shifts 79 - 31686
XY_4 oxygenated ions, tetrahedral, mol. consts. 79 - 36555
XYZ type system, bent, force field determ. Redington's method applicability 79 - 81168
Ag_2, dispersion absorption spectra, 1500 to 5300 Å, rot. anal. 78 - 42089
AgBi, laser induced fluoresc., vibr. anal., rot. consts. *(French)* 77 - 18959
AgO, $A^2\Pi$-$X^2\Pi$ blue system, rot. anal. 77 - 38678
AlF, $a^3\Pi$-$X^1\Sigma^+$ transition, rot. anal. 77 - 18938
AlH^+, spectrum at 3632 Å, rot. anal. 80 - 78632
AlS, $B^2\Pi$-$X^2\Sigma^+$ transition, assignment of UV bands, vibr. and rot. anal. 80 - 58278
AlSe, $A^2\Sigma^+$-$X^2\Sigma^+$ transition, rot. anal. 79 - 72325
Ar-HCl, van der Waals mol., far IR spectra 77 - 79611
Ar-O_3 Van der Waals complex, struct. and props., RF and microwave obs. 80 - 32704
Ar+HCl, inelastic scatt. exponential perturbation theories 80 - 74217
Ar+N_2, inelastic scatt. exponential perturbation theories 80 - 74217
Ar_2, VUV emission spectrum, rot. anal. 79 - 98119
ArH_2, van der Waals mols., rot. predissoc. 80 - 63721
ArHBr, ArHCl, and isotopic forms, rot. spectra, mol. struct., mol. consts. 80 - 58246
ArN_2, van der Waals mols., rot. predissoc. 80 - 63721
$AsBr_3$, microwave spectra, rot. consts., mol. struct. 77 - 3485
AsF, molecular constants determ. from $b^1\Sigma$-$X^3\Sigma$ transition, nonlinear least squares procedure 79 - 798
AsF, UV band system, $e0^-$-X_21 and $f0^+$-X_21 rot. anal. 77 - 27083
AsF_3, millimetre rot. spectra, vibr. excited states, anharmonic force field 78 - 33502
AsH_3, forbidden millimetre-wave transitions 78 - 55165
AuCa radicals, rotational analysis for near IR bands *(French)* 77 - 61741
AuSi radicals, rotational analysis for near IR bands *(French)* 77 - 61741
$BClF_2$, microwave spectrum, struct., quadrupole coupling consts. 77 - 57986
B_2F_4, molecular structure, barrier to internal rotation, temperature effects 78 - 13625
$BF(OH)_2$, identification, rot. and centrifugal consts., mol. struct., microwave spectra obs. 80 - 32705
BH, $A^1\Pi$ state, fluoresc. decay radiative lifetime meas. 79 - 13771
$BHBr_2$, and isotopic forms, mol. pot. consts., amplitudes, Coriolis coupling, centrifugal distortion 78 - 50662
$BHCl_2$, and isotopic forms, mol. pot. consts., amplitudes, Coriolis coupling, centrifugal distortion 78 - 50662
BHF_2, and isotopic forms, mol. pot. consts., amplitudes, Coriolis coupling, centrifugal distortion 78 - 50662
BH_2NH_2, microwave spectra, rot. consts., dipole moment, mol. struct. 79 - 85957
$B_3N_3H_6$, isotopic variants, pure rot. Raman spectra 77 - 71803

molecular rotation continued
BO_2, photoexcitation and fluoresc. spectra, rot. transitions, assignment and deconvolution 79−27003
Ba+HF, product rot. and vibr. distributions and reaction cross sections depend. on reagent translational energy 80−93745
BaBr, visible spectrum, $C^2\Pi_{1/2,3/2}-X^2\Sigma^+$ transition, laser induced fluorescence 79−98072
BaH, new absorpt. band at 2991 Å, electronic transition, rot. consts. 77−83616
BaO, excited electronic states, lifetimes and transition moments 80−87177
BaO+Ar(CO_2), in Ar flame, rot. and translational relax. by sub-Doppler optical-optical double reson. 80−95583
BeCl, $^2\Sigma^+$ predissoc. state, vibr. and rot. calcs. 77−42363
BeI, reinvestigation of $A^2\Pi-X^2\Sigma^+$ band system 77−23503
BeKr$^+$, $A^2\Pi_r-X^2\Sigma^+$ system, rot. anal., Λ-doubling consts. 77−27078
BiCl, form., microwave spectrum, hyperfine struct., mol. rot. vibr. consts., bonding 77−14418
BiF, mm spectrum, HFS struct., HFS, vibr. and rot. consts. and equilib. distance 77−79604
BiF, spectrum, 5800-6600 Å, vibr. anal., electronic transition assignment 80−992
Br_2, Q branches of Δn=1 profiles, calcs., rotation effect on scatt. amplitudes 80−63643
Br_2, rotationally dependent lifetimes 79−47931
Br_2, single rot. states, lifetimes and collisional quenching cross sections determ. by obs. fluoresc. decay 80−91595
Br_2-Ar system, mol. rot. effects on V-T energy transfer 80−14195
BrF, $B^3\Pi(0^+)\leftarrow X^1\Sigma^+$ absorption spectrum, high-resolution anal. 79−59478
BrF, laser induced fluorescence 78−66591
BrF, laser induced fluorescence 78−66592
^{79}BrF, (^{81}BrF), hyperfine struct., elec. dipole moment, rot. transitions, microwave spectral obs. 80−32695
BrF_5, gas phase electron diffraction and microwave rot. consts. data anal., mol. struct. 79−76363
BrF_5, microwave spectrum, Coriolis interaction, A_1-A_2 splitting of kl levels 77−38657
BrF(Cl), rot. spectra in millimeter wave region, rot. transitions obs., equilib. const. determ. 80−78607
C-H, $A^2\Delta-X^2\Pi$, dissociative excitation, form. environment and parent mol. effects 80−78682
C_2, ($A^3\Pi_g-X'\ ^3\Pi_u$) band system, vibr. and rot. intensity distrib. 77−42332
C_2, $A^3\ pi_g-X'^3\ pi_u$ bands, rot. struct., intensity alternation 79−41158
C_2, interstellar, rot. fine-struct. lines obs. towards ζ Persei 80−67811
C_2, Phillips system, 2.3-0.9 μm, rot. consts. 78−21925
C_2 rotational temp. and solar photospheric models 80−62099
C_2, solar rotational temperatures, centre to limb behaviour 79−84758
C_2 vapour, Swan bands, oscillator strength 80−63712
C_3, $\tilde{A}^1\Pi_u$ state, orbital angular momentum 80−78514
CD_3, Λ-type doubling in excited rot. levels 77−57979
CD^+, $A^1\Pi-X^1\Sigma$ band system, spectroscopic consts. and isotope shifts 79−59485
CD^+, in RF ion trap, laser induced fluoresc. spectrum, 0,0 vibr. band and rot. consts. 80−74189
CD_4^+, rot. predissociation, observed by metastable peak struct. in translational spectra 78−25635
CF_2, $X\ ^1A_1$ radical, form. in chlorofluoromethane collision-free multiphoton dissoc., translational energy meas. 78−92491
CH, far IR laser mag. reson. spectrum 79−3466
CH, Λ-type doubling in excited rot. levels 77−57979
CH radical, sputtered from acetone chemisorption layer on SI, rot. and vibr. population distrib. 78−64436
CH^+, $a^1\Pi-b^3\Sigma^-$ transition moment, ab initio calcs. 80−87047
CH^+, electron impact excitation, rot. transitions 79−41244
CH^+, rot. excitation by electron impact 79−27094
CH^+, rot. excitation by low-energy electrons *(Russian)* 79−94093
CH_3-d_n, matrix isolation IR spectra, rot. and vibr. struct. 77−83589
CH_4^+, rot. predissociation, observed by metastable peak struct. in translational spectra 78−25635
CH_2F, far IR laser mag. reson. spectrum 78−9174
CN, internal energy distrib. following vinyl cyanide photodissoc., temp. depend. 80−78638
CN, radical, electronic, vibr. and rot. energy partitioning obs. following ICN photolysis 77−16853
CN, time resolved chemilum., in C_2+NO(vinyl cyanide)(ethylene), laser-generated radical kinetics 79−100352
CN, vibr. and rot. anal. of vis., UV spectra, RF discharges in N_2, H_2, CH_4 mixtures 78−5241
C_2N_2, gas, high resolution Raman spectra 78−17673
CN(X), free radicals, state distribs. rel. to prod. by photolysis of dicyanoacetylene 77−9107
CN($X^2\Sigma^+$), translational-electronic-vibr.-rot. energy partitioning in photolysis of C_2N_2 77−48667
CO, and isotopic forms, fundamental bands, absolute wavenumbers, mol. consts. 79−59458
CO, centrifugal distortion calcs. by perturbed Morse oscillator model including Dunham parameters 80−63862
CO, collision-induced reorientation, direct meas. by IR double reson. 80−32800
CO discharge plasma, electron energy distrib. and kinetic coeffs., ground-state mols. 80−43867
CO in solar faculae, rot. temp. of mols. 77−78740
CO molecular layer optical depth and rotational temp. on Sun 79−96988
CO, pressure-induced spectral linewidth and line shifts, vibr. depend., IOS scatt. approx. 79−68267
CO, rot. distrib. in supersonic beam, IR bolometry using tunable diode laser 80−63869
CO, rot. transitions obs. in interstellar molecular clouds 77−33612
CO^+, electron impact rot. excitation, Glauber approx. with Coulomb effect 80−63840
CO^+, electronic absorpt. spectrum, rot. lines, laser/ion beam reson. 77−54564
CO^+, violet-degraded B-A bands, rotational analysis 79−18199
$^{12}C^{16}O$, $^{13}C\ ^{16}O$, Heizberg system, rot. anal. 79−59423
$^{12}C^{16}O$, near UV emission bands of fourth positive system, vibr. and rot. anal. 77−58054
$^{12}C^{18}O$, $A^1\pi-X^1\sigma^+$(13,0) band, monochromatic excitation 78−82767
$^{13}C^{16}O^+$ (2,0) band, comet-tail system, rot. anal. 80−74157
molecular rotation continued
^{14}CO, pure rot. far IR spectra, rot. consts. 80−47996
CO-HBr, weakly bound, rot. spectra 80−91544
CO-HCl, weakly bound, rot. spectra 80−91544
CO-HF, weakly bound, rot. spectra 80−91544
CO+H_2, rot. excitation, rel. between tensorial cross sections 80−83454
CO^++H_2, ion-molecule reaction detection of laser-induced ion spectrum, rot. components 78−74671
$^{13}CO^+$+CO, charge-exchange detection of $^{13}CO^+$ electronic absorption spectrum, hyperfine consts. calc. 78−70822
CO_2, absorption, spectrum calibration, 14-15 μm, using diode laser source 77−18917
CO_2, and isotopic forms, bending fund. region, IR spectra, rot. consts. 80−47988
CO_2, IR absorption spectrum using Nd:glass intracavity spectrometer *(Russian)* 78−33512
CO_2 laser heterodyne meas. of 01^11-11^10 hot band transition frequencies 77−7063
CO_2 lasers, optically pumped, use of crystalline reflector in cavity 80−64080
CO_2 multi-rotational line TEA laser, theoretical model 80−69361
CO_2 multiatmosphere UV preionized laser, elec. and gain characts. 80−14313
CO_2, P-branch transitions, accurate wavelength meas. 77−38667
CO_2, press. broadening coeffs. at 4.2 μm, rot. quantum number 78−74704
CO_2, pure rotational stimulated Raman photoacoustic spectroscopy 80−32724
CO_2 TEA laser, injection tuning and mode locking on low gain rot. lines 80−95928
CO_2 vibr. luminesc., excited by DC discharge, rot. and vibr. mol. consts. 78−58867
CO_2^+, laser excitation spectra, $A^2\Pi_u\rightarrow X^2\Pi_g$ fluoresc., rot. struct. 78−1019
$^{12}CO_2$, absorpt. spectrum at 4.3 microns 78−58692
$^{13}C^{16}O_2$, emission spectrum near 4.5 μm, nu_3 region spectroscopic consts. 77−38664
CO_2-N_2-He discharge, electron distrib. relax., numerical study 80−54070
C_3O_2, ν_7 vibrational states, rigid-bender model 80−47964
C_3O_2, vibr. IR spectra anal. 80−47984
$COCl_2$, microwave spectra, 24-154 GHz, rot. and centrifugal distortion consts. 78−46324
$COCl_2$, phosgene, Cl_2 nuclear quadrupole coupling tensor, microwave spectra 80−52982
CS, near UV spectra, rot. anal. of $a^3\pi_r=X^1\Sigma^+$ transition 78−5242
CS^+, red emission spectrum, rot. anal. and perturbation effects 78−55193
CS_2, $^3A_2$ state, triplet bands, MCD spectrum, near UV absorpt. spectrum 80−48010
CS_2, $^3A_2$-state, MCD and UV spectrum, theoretical anal. 80−48011
CS_2, isotopic variants, $2\nu_1+\nu_3$ band IR spectra, rot. and rovibr. consts. 79−41166
CS_2, photodissoc., fragment energy distrib. 80−69200
CS_2+He(Ar)(N_2), perturbed rot. diffusion of CS_2, IR spectra 78−75245
CSFCl, sextic centrifugal distortion consts., microwave spectra *(German)* 77−75140
$^{13}C^{16}O$, $A^1\pi-X^1\sigma^+$(13,0) band, monochromatic excitation 78−82767
CaCl, $B^2\Sigma^+-X^2\Sigma^+$ system, laser excitation spectroscopy, rot. anal. 77−65500
CaCl, $B^2\Sigma-X^2\Sigma$ transitions, rot. anal. by laser spectroscopy 80−91536
CaCl, $D^2\Sigma$ and $X^2\Sigma$, two-photon vis. absorption, vibr. and rot. consts. 78−78764
CaCl, $E^2\Sigma-B^2\Sigma$ system, rot. anal., optical-optical double reson. obs., using two dye lasers 78−70855
CaCl, $E^2\Sigma-X^2\Sigma$ transition, rot. anal. 78−37652
CaCl, laser excitation and fluorescence spectra, rotational anal. of $A^2\Pi=X^2\Sigma$ transition 80−43098
$Ca^{35}Cl$, radical, rot. spectrum, $X^2\Sigma^+$ state, laser MODR 78−5257
CaF, $^2\Sigma_{1/2}{}^+$ ground state, spin-rot. and hyperfine splittings rot. depend., mol. beam laser-RF double reson. 80−43079
CaF, $A^2\Pi_r-X^2\Sigma$ band system, MODR 78−74685
CaF, $A^2\Pi-X^2\Sigma^+$ transition, HFS and fine struct., intermodulated fluoresc. spectra obs. 80−63695
CaF, $B^2\Sigma^+-X^2\Sigma^+$ system, rot. and vibr. anal. 80−74156
CaH absorpt. spectra 2480 to 2550 Å, new electronic states and rot. anal. 79−36662
CaH, $D^2\Sigma^+-X^2\Sigma^+$ band system 80−18847
CaO, form. from Ca+O_2(CO_2), electronic states obs. 78−92450
CaO, millimetre wave spectrum, spectrosc. consts. 77−61737
Cd+$H_2\rightarrow$CdH+H, product initial rot. state distrib., pump and probe laser obs. 80−85158
CdH, lifetime, Λ-doubling, hyperfine struct., in $A^2\Pi$ excited states 77−58083
chloromethane, collisional rot.-line widths and shifts, microwave region 78−25619
Cl_2, liq., mol. reorientation, Raman spectra obs. *(French)* 78−31192
ClBS, form., photoelectron and microwave spectra 78−90214
ClCN, and isotopic derivatives, rot. depend. of Fermi resonance 78−94227
ClF, rot. spectra in millimeter wave region, rot. transitions obs., equilib. const. determ. 80−78607
ClF_5, microwave spectrum, rot. transitions, dipole moment, struct., nuclear quadrupole coupling consts. 77−14423
$ClNO_3$, far IR rot. and torsional spectra 77−79609
$ClNO_3$, microwave spectrum 77−57984
ClO, rot. spectrum, mol. parameters in $\nu=0$, $\nu=1$ states 78−70821
ClO, UV spectra of $C^2\Sigma^-\leftarrow X^2\Pi$ system, rot. anal. 80−996
^{35}ClO, microwave spectrum in excited vibr. state, centrifugal distortion const. 77−83580
ClO_2, gas-phase electron g-tensor, magic doublet rot. Zeeman spectra 78−90212
ClO_2, predissoc. mechanism determ. from rot. level lifetimes 79−13732
$^{37}ClO_2$, $\nu_3=1$ state, laser-microwave double reson. obs. 80−95657
cis-ClONO, microwave spectrum, rot. consts., inertial defects and config. 79−59439
$^{35}Cl^{35}Cl$, $B^3\Pi(0^+)\rightarrow X^1\Sigma^+$, 6300 to 9900 Å, rot. anal., mol. consts., equilib. internuclear separation 78−42082
$^{35}Cl^{37}Cl$, $B^3\Pi(0^+)\rightarrow X^1\Sigma^+$, 6300 to 9900 Å, rot. anal., mol. consts., equilib. internuclear separation 78−42082
$^{37}Cl_2$, pure rot. Raman spectrum 78−94252

molecular rotation continued
CoO, vibr. IR absorption spectrum, mol. consts. 79−89666
CrO, $A^5\Pi$-$X^5\Pi$ transition, rot. anal. laser induced fluoresc. and discharge emission spectra 80−69173
CrO molecule, $B^5\pi$ and $X^5\pi$ states, potential energy curves 80−42962
Cs_2, fluoresc. at 6270 Å, rot. consts. 79−45744
Cs_2, ground state consts., pot. curve, laser spectroscopy 79−98247
Cs_2, rot. consts., Doppler-free polarisation spectrosc. 80−5555
CsF, Stark effect, deviations from rigid rotator model 79−18234
Cu_2, fluoresc., A-X system, rot. consts. *(French)* 78−33544
Cu_2, in supersonic free jet expansion, laser induced excitation spectrum obs. 80−14151
CuBr, rot. spectrum hyperfine struct., coupling consts., microwave spectroscopy study 80−18844
CuCl, hyperfine struct., microwave rot. spectrum obs. 78−21917
CuCl, mol. emission spectrum, 5900-6800 angstrom, rot. anal. of A-X system 80−58273
CuF from Cu+F_2 chemiluminesc. reactions, mol. beam study 80−97702
CuI, hyperfine struct., quadrupole coupling const., rot. spectrum 77−88447
CuO, $^4\Sigma_{1/2}$-$^2\Pi_{1/2}$ transition, rot. anal. 78−82748
CuO, 4182 Å band spectrum, rot. anal. 79−89685
CuO, $C^2\Pi_i$-$X^2\Pi_i$ and $D^2\Delta_i$-$X^2\Pi_i$ band systems, rot. anal. 78−82747
CuO, rot. anal. of red $A'\,^2\Sigma^+$−$X\,^2\Pi_i$ system 78−13508
CuS, emission spectra, rotational analysis of O-O band of green system *(French)* 77−3372
D_2, electron dissociative attachment rates, rot. (vibr.) excitation depend., in plasma 80−43848
D_2, electron scatt., low energy, rot. resons. 78−33608
D_2, Fulcher band system, rot. struct. 79−98986
D_2, in zeolitic matrix, IR active fundamentals obs. 77−71800
D_2, matrix isolated, IR spectra, mol. rot. and vibr. const. determ. 80−78617
D_2, matrix rot. and vibr.-rot. spectra, free and hindered rot. 77−83607
D_2, photoabsorpt. spectra, rovibronic interactions 78−992
D_3, emission spectra, rot. struct. obs. mol. const. determ., predissociation 80−106331
DCl, vib.-rot. spectra in hexadecane solvents of different mol. shapes 77−34623
DN_3, microwave spectra, 8-340 GHz, spectrosc. consts. for ^{13}N isotope 79−85958
DNCS, ground state spectroscopic constants and elec. dipole moment, from microwave and millimetre wave spectra 79−804
DO_2, ν_2 fundamental band, 9.8 micron, laser mag. reson. spectroscopy 79−85961
$D_2{}^{16}O$, IR spectra, ν_2 band, rot. struct. 78−982
DT, vibr. rot. Raman anal. 80−87126
DyO, UV emission spectrum, high resolution, band systems and isotopic shifts 80−87146
F+I_2→IF+I, energy partitioning, vibr. populations and rot. temp., population inversion 80−50832
F^++H_2→FH^++H, rot. effects 78−27744
FCN, IR laser Stark spectra, C-F stretching mode, dipole moments, rot. consts. 78−1022
FNO, Stark spectroscopy of ν_1 band, rot. consts., dipole moment 79−13710
FO free radical, detection by CO_2 laser mag. reson. 80−45594
FeF, electronic states, anal. of rot. struct. 78−74674
GaBr, rot. analysis of $^3\Pi_{0,1}$-$X^1\Sigma^+$ transition 80−69129
GaBr, rot. spectrum hyperfine struct. 79−13838
GaI, $A0^+$-$X0^+$ and $B1$-$X0^+$ transitions, isotope shifts, UV and visible spectra obs. 80−53005
GaI, rot. spectrum, EHF spectra obs. 80−58245
GaO, B-X band system, electronic spectrum, struct. and anal. 79−45732
GdO, high resolution visible emission spectrum 77−18932
GeCl, mol., UV spectra, band assignments and rot. consts. 80−997
GeH_2, centrifugal-distortion dipole moment, CO_2 laser spectroscopy 77−75331
GeH_4, avoided-crossing molecular-beam spectroscopy, hyperfine and spin rot. const. and rot. g factors determ. 80−78671
GeH_4, IR-microwave double reson., rot. assignments 77−75190
$^{74}GeH_4$ mol. vibr., IR and CARS spectra *(Russian)* 80−102509
$GeH_4(F_4)$, rot. mag. moment spectra, mol. beam mag. reson. obs. 77−14509
GeO, UV spectra of mol., rot. anal. 79−81210
H-bonded complexes, microwave spectra, assignments, mol. consts. 78−62794
H+Br_2→HBr+Br, HBr ang. momentum alignment, scatt. ang. depend. 78−3323
H+ClBr→HCl+Br(HBr+Cl), product energy distrib., rate const., IR chemilum. obs. 77−81391
H+ICl→HCl+I, IR chemiluminesc., product energy distrib. 78−23926
H+ICl→HCl+I, product energy distrib., rate const., IR chemilum. obs. 77−81391
H^++H_2, rot. and vibr. excitation, energy loss obs. 80−63773
H_2 3s, 3d: $^3\Sigma$, $^3\Pi$, $^3\Delta$ complex, fine struct., Doppler-free laser spectroscopy 80−1087
H_2 (D_2) mol. bands, electron impact excitation, rot. transitions, cross sections in plasma 80−37896
H_2 adsorbed submonolayer, ortho-para separation coeff., mol. alignment and rot. levels 77−7971
H_2, CARS, optical Stark effect on vibr., and rot. transitions 80−99512
H_2, electron dissociative attachment rates, rot. (vibr.) excitation depend., in plasma 80−43848
H_2, electron impact rot. excitation, low energy, close-coupling calcs. 78−1092
H_2, electron scatt., low energy, rot. resons. 78−33608
H_2, fluid, Raman meas., 0.2-630 kbar, at room temp. 80−58269
H_2, Fulcher band system, rot. struct. 79−98986
H_2, high resolution electron spectroscopy 80−62740
H_2 in interstellar clouds, photodissoc. from excited states in H to H_2 transition region 79−25672
H_2, interstellar, rot. transitions rel. to hot gases cooling 79−12505
H_2, matrix isolated, IR spectra, mol. rot. and vibr. const. determ. 80−78617
H_2, metastable state, mol. beam reson., vibr. anal., spin-rot. interaction 79−22731
H_2, ortho, high rot. states, inter- and intra-mol. effects, mol. beam mag. reson. obs. 78−70852
H_2, photoabsorpt. spectra, rovibronic interactions 78−992
H_2, photoelectron ang. distrib., rot. states anal. 78−33550

molecular rotation continued
H_2 photoelectron spectra, rot. intensity distrib. 80−91605
H_2, predissociation of $^1\Pi_u^+$ state vibr. and rot. levels, dissoc. yields meas. 80−32784
H_2 predissociation probabilities of $4p\pi\,^1\Pi_u^+\nu' \geq 1$ levels, dissoc. channels interference 80−28074
H_2, recombination on interstellar grains, translational and rot. energy 79−17045
H_2, rot. energy, specific heat, temp. depend. determ., demonstration 78−12465
H_2, $S_0(3)$ pure rot. quadrupole transition, obs. using tunable diode laser 78−82723
H_2, stimulated Raman scatt. gain of Nd laser radiation by rot. levels 80−69464
H_2^+, rot lines and rot. consts. 80−91605
H_2-H_2 dimers, hyperfine struct. in zero mag. field 80−95700
H_2+CO_2, exponential gap relation, rot. inelasticity 80−78693
H_2+H, exponential gap relation, rot. inelasticity 80−78693
H_2+H_2, exponential gap relation, rot. inelasticity 80−78693
H_2+He, exponential gap relation, rot. inelasticity 80−78693
H_2+Li, exponential gap relation, rot. inelasticity 80−78693
H_2+Li^+, exponential gap relation, rot. inelasticity 80−78693
H_2^++Ar, low energy proton transfer reactions, crossed beam studies 80−108697
H_3, emission spectra, rot. struct. obs. mol. const. determ., predissociation 80−106331
HB rot. relaxation, diffusion theory 80−106313
HBS, force consts., Coriolis const., vibr. amplitude, shrinkage and isotope effect 79−22863
HBr^+, laser mag. reson. pure rot. transition in far IR 79−89695
HCCl, IR spectra, ν_4 and ν_5 vibr. bands, rot. struct., rot. and vibr. consts. 77−38665
HCN, absorption, spectrum calibration, 14-15 μm, using diode laser source 77−18917
HCN, and isotopic derivatives, rot. depend. of Fermi resonance 78−94227
HCN, and stable isotopic species, mol. struct., ground vibr. rot. transitions and consts. 77−10666
HCN, laser plasma, microwave spectra of excited vibr. states 78−17656
HCN, photofragmentation vibr. and rot. distrib., quantum anal. 77−14504
HCN predissoc. Frank-Condon amplitudes 80−95694
$HC^{14,15}N$ dimer, and $(DCN)_2$, microwave rot. spectrum identification and struct. 77−50427
HCN-HF, dimer, rot. transition intensity, dissoc. energy determ. 78−46323
HCN-HF, elect. dipole moment, Stark effect of linear mols. 78−70818
HCN+He(H_2)(CH_3F), HCN excited vibr. state, T_2 meas. 80−102498
$(HCN)_2$, and isotopic forms, microwave spectroscopic investigations of hydrogen-bonded complexes 78−62794
HCO, IR spectra of ν_2 fundamental, laser elec. reson. 78−5226
HCP, ν_3 band, high-resolution IR absorption spectrum 80−47994
HCl, intermol. partial struct. factors, isotopic substitution and neutron diffr. obs. 80−53157
HCl, pure rot. lines, press. induced shift perturbed by Ar 77−79652
HCl, rot. relaxation, diffusion theory 80−106313
HCl-Kr, rot. for IR spectra, anisotropic density fluctuations 79−54848
HCl+Ar, rot. linewidth calcs., using different pots. 78−66602
HCl+Ar(Xe), infrared line shape, rotational lines, influence of collision duration 80−43110
HCl+HCl(Ar), pure rot. Raman lines, press. broadening cross sections 78−74702
HCl+K, mol. beam reaction, rot. state depend. 79−74365
HCl+methane, pure rot. line broadening obs., transition cross sections 77−75134
HCl+N_2(O_2)(D_2)(H_2), HCl ν_0-ν_1 band perturbations, linewidth and shifts calcs., IR spectra obs. *(French)* 80−58251
HD, dipole spectrum, influence of intracollisional interference 78−33492
HD, interstellar rotationally excited, towards ζ Ophiuchi, column density 79−25674
HD, nonadiabatic effects in the B, C and E, F states, rot. line strengths 78−5148
HDO, beam maser double reson., hyperfine struct. D quadrupole coupling 77−65493
HDSe, high resolution IR spectra, anal. of $2\nu_1$ band, rot. ground state const. determ. 80−95616
HF chain reaction laser energetics, C_5F_{12} mol. addition and rot. nonequilib. *(Russian)* 77−42530
HF, in ClF-H_2 chem. laser, rot. laser emission 79−98349
HF, rot. population transfer using IR-laser double-resonance expt. 79−55128
HF rotational line shift, far IR Fourier transform spectrometry improvement 79−30582
HF-cyanomethane, microwave spectroscopic investigations of hydrogen-bonded complexes 78−62794
HF+HF (methane)(methane-d_4), collision relaxation rate constants and rot. equilibration time meas. 80−69213
HF*+NF*, microscopic vibrotational-electronic energy transfer, IR chemiluminesc. obs. 79−31662
H_2(HD)(D_2), matrix rot. and vibr.-rot. spectra, free and hindered rot. 77−83607
HN_3, and DN_3 pure rot. Raman spectra, rot. consts., K-depend. parameters 78−29791
HNC, and stable isotopic species, mol. struct., ground vibr. rot. transitions and consts. 77−10666
HNC, millimetre spectrum, rot. consts., force consts., U90.7 interstellar line, struct. parameters 77−57989
HNCO, a-type rot. spectrum in excited bending states, rot. consts. 78−21915
HNCO, microwave and RF spectra, b-type rot. transitions 78−21914
HNCO, rot. spectrum, ground and vibr. state reson., centrifugal distortion coupling 80−83364
HNCS, a-type rot. spectrum in excited bending vibr. states 79−3437
HNCS, microwave spectrum, K_a=0 and 1 rot. levels inversion 77−38656
HNCSe, struct., microwave spectrum 79−18178
HNF, $\tilde{A}\,^2A'$-$\tilde{X}\,^2A''$ emission spectrum 79−50033
HNO $\tilde{A}\,^1A''$ excited state dipole moment, optical-optical double reson. Stark spectrosc. obs. 80−106337
HNO, low-lying states, pot. energy curves 80−9533

molecular rotation continued
HNO_2, trans and cis, ν_2 fundamental vibrational bands, intracavity CO laser Stark spectroscopy 80−47992
HNO_3, centrifugal perturbation in microwave spectrum 77−57981
HNO_3, ν_5 band rot. struct., anal., band centre and rot. consts. 79−10109
HNO_3, VUV photodissoc., vibr. and rot. distribs. 80−87191
$HNO(A^1A'')$, state-selected fluoresc. lifetimes, collisional quenching rates 79−36674
HNSO, centrifugal distortion anal. 79−59438
HO_2 radical, microwave spectrum 77−57983
H_2O 79−72308
H_2O, 22 GHz rot. transition relax. rate consts. 79−18180
H_2O, effect of mag. field on rotational IR spectra 79−54849
H_2O, electron impact dissoc., $OH(A^2\Sigma^+ \rightarrow X^2\Pi_i)$ emission spectra, crossed-beam investigations 80−83504
H_2O, electronic ground state, SCF HF and CI calcs, pot. energy hypersurface, spectroscopic consts. 78−50473
H_2O, IR spectra, linewidths 79−59454
H_2O, IR spectrum, rot. anal., isotope effects 78−78694
H_2O, IR spectrum rot. nonequilib. *(Russian)* 79−50023
H_2O spectrum, 4200 to 5000 cm^{-1} 77−58005
H_2O, VUV photodissoc., vibr. and rot. distribs. 80−87191
H_2O^+, electronic spectrum, vibr. levels, rot. consts. 77−473
H_2O^+, spin and rot. fine struct., orbital angular momentum 80−83247
H_2O^+, vibr. and rot. struct., intensity factors and orbital angular momentum 80−83246
$H_2{}^{17}O$ and $H_2{}^{18}O$, centrifugal distortion anal. of ground vibr. states 78−70834
$H_2{}^{18}O$, $H_2{}^{17}O$, rot. spectra, 650-50 cm^{-1} 77−65458
$H_2{}^{18}O$, line positions and intensities, $\nu_1+\nu_2$ and $\nu_2+\nu_3$ bands 78−74656
H_2O-HF heterodimer, H bonding, microwave rot. spectrum, mol. geometry and moment 80−99501
$H_2O^+ + H_2$, ion-molecule reaction detection of laser-induced ion spectrum, rot. components 78−74671
HOCl, ν_1 band IR spectrum, rot. anal. 79−98095
HOCl, photodissoc. rot. distrib. 80−95694
$H_2O(D_2O)$, VUV absorption spectra, Rydberg series, rot. line shapes, quantum defect 78−5244
H_2O...HF complex, force field, vibr. freqs., equilib. geometry bond energy, ab initio calc. 77−65450
H_2S_2, rot. barriers, internal rot. and electronic struct., valence electron study 80−83344
$H_2S(D_2S)$ photodissoc., SH internal energy distribution 80−95697
HSO radical, Doppler-limited dye laser excitation spectroscopy, rot., distortion and spin-rot. interaction const. determ. 80−83383
H_2Se, UV absorpt. spectra, 148.3 nm band, rot. contour anal. 77−75179
H_2Se_2, rot. barriers, internal rot. and electronic struct., valence electron study 80−83344
HSiN-HNSi isomers, MRD-CI calcs. of struct. and stability 78−82635
$HSiO^+$, $HOSi^+$, rot. consts. from theoretical study 78−37541
H_2Te, mol., submm. rot. microwave spectrum 79−59443
H_2Te_2, rot. barriers, internal rot. and electronic struct., valence electron study 80−83344
$^1H^3H$ and $^2H^3H$, pure rot. and vibr.-rot. Raman spectra 80−14145
$Hbr + Cl_2(BrCl)$, four-centre reaction, quasiclassical trajectory study 79−57213
He-benzene, van der Waals, complexes, $^1B_{2u}(\pi\pi^*)$-$^1A_{1g}(6_0^1)$ band, in supersonic jet, rot. anal. 79−31578
$He + H_2$, inelastic scatt. exponential perturbation theories 80−74217
$He + H_2$, mol. energy transfer by quasiclassical trajectory methods, vibr. relax. and dissoc., rot. effect 80−99557
He+LiH, rot. inelastic collisions, state-to-state cross sections determ. 80−87210
$He + Na_2$, optically pumped state to state differential cross sections for rot. transitions, rainbow phenomena 80−5609
$He + Na_2$, rotational inelastic scatt., uniform semiclassical sudden approx. 80−99544
$He^+ + He$, interference struct., optical emission interpretation 79−45816
$HeCN^+$, SCF calcs., dissoc. energies, rot. and hyperfine const. determ. 80−95531
HeH^+, electron impact excitation, rot. transitions 79−41244
HeI_2, rot. fluoresc. spectra, nonlinear equilib. struct. 78−37672
$HeNe^+$, visible spectrum obs. in discharge 79−13729
$He_2{}^+ X^2\Sigma_u^+$ state, ab initio CI calc., pot. energy curve, vibr. and rot. levels 77−3263
HfN, vibr. IR spectrum, mol. consts. 79−68230
Hz, 3d complex, radiative lifetimes, hyperfine constants 78−70873
I_2, 5350 Å band rot. anal., Fourier transform spectroscopy 77−27081
I_2, B-X system, mol. consts. and Dunham expansion parameters 80−87095
I_2, energy levels near B-state dissoc. limit, two-photon spectra 78−9210
I_2, two-photon sequential absorpt. spectroscopy 77−54581
I_2, $X^1\Sigma_g^+$ ground state, Le Roy's theory, continuous wave oscillation 79−94006
$^{129}I_2$, energy levels near B-state dissoc. limit, two-photon spectrosc. obs. 80−106367
IBr, elec. dipole moment, rot. transition Stark shift obs. 77−75207
IBr, magnetic rot. spectrum, rot. and vibr. anal. 78−70861
IBr, predissoc. and photodissoc., intermed. coupling strength 77−16850
ICN, photodissoc., product rot. distribs. 79−66310
ICN, photofragmentation, vibr. and rot. distrib., quantum anal. 77−14504
ICl, $A^3\pi(1)$-$X^1\Sigma^+$ emission spectrum, near-IR, rotational analysis 80−47991
ICl, microwave-optical double reson. obs. in $B^3\Pi_{0(+)}$ state 79−85979
ICl, mol. beam focusing in rot. states 79−18317
ICl(Br), rot. spectra in millimeter wave region, rot. transitions obs., equilib. const. determ. 80−78607
IF internal vibr.-rot. product distrib., formed in $F + CH_3I(CF_3I)$, fluoresc. obs. 80−48078
IF_5, gas phase electron diffr. and B_0 rot. const., struct. determ. 79−89782
IF_5, microwave spectra obs., rot. assignments, mol. parameters *(French)* 78−55163
$^{127}I_2$, weak rot. R(98), 58−1 line, HFS struct., saturated intermodulation fluoresc. 79−94024
I2 fluoresc., Ar^+ laser excited, high resolution and sub-Doppler Fourier transform spectroscopy 80−43089
$^{115}In^{79}Br$, $^{115}In^{81}Br$, rot. J=1→2 hyperfine struct., quadrupole coupling consts. *(German)* 77−30866
InCl, B→X system, rot. anal. 79−36619

molecular rotation continued
$InX(X_2)(X_3)$, $InAlX_4$, X=Cl,Br, Raman spectra, up to 1200K 80−48003
K+CO, rotational inelastic scatt., uniform semiclassical sudden approx. 80−99544
K+CsF collision complex, reactive decay branching ratio, rot. energy effect 77−66752
K_2, $B^1\Pi_u$ state lifetimes, Hanle effect 78−90218
KCNS, single cryst., IR and Raman multiphonon bands, factor group anal. 77−4644
KOD, mm wave spectrum, rot. transitions in excited vibr. states 77−3351
KOH, electron collisions, integrated and momentum transfer cross sections, cond. integrals 79−41238
KOH, mm wave spectrum, rot. transitions in excited vibr. states 77−3351
KrH_2 van der Waals mols., rot. predissoc. 80−63721
KrHBr, KrCHl, and isotopic forms, rot. spectra, mol. struct., mol. consts. 80−58246
KrHCl, van der Waals complex, prod. and rot. spectra assignments 80−5532
KrHCl, van der Waals complexes, struct., RF and microwave spectra, isotope effects 80−37806
KrHCl, weak complex, rot. spectra 80−52980
LaF^+, electronic spectra, rot. anal. and orbital configurations 80−83240
$Li^+ + H_2$, quasiclassical approx. for scatt. amplitude, rot. degrees of freedom *(Russian)* 77−79676
$Li^+ + K$, rot. coupling, Fraunhofer diffraction effects 77−65526
$^7Li_2$, $B^1\Pi_u$-$X^1\Sigma_g^+$ band system, absorpt. and laser fluoresc. spectra 79−68256
LiF+Ar, polarisation cross section, close-coupling calcs. 80−69214
LiH, $X^1\Sigma^+$ ground state, spectroscopic and pot. functions, method for combining spectroscopic data 79−45782
LiH+He, rot. inelastic collisions, rigid shell models 80−99545
MgD, emission spectra, 600 to 850 nm, rot. anal., dissoc. energies 78−62815
MgH, $A^2\pi - X^2\Sigma^+$ system, dissoc. energy 77−10686
MgH, emission spectra, 600 to 850 nm, rot. anal., dissoc. energies 78−62815
MgH rotational temp. and solar photospheric models 80−62099
MgH(D), spectra in 230-235 nm region 80−48012
MgO, new electronic band system in UV 77−14447
$^{24}MgH^+$, rot.-vibr. spectra, equilib. rot. consts. for $X^1\Sigma^+$ state 77−18939
MnO, $A^6\Sigma^+$-$X^6\Sigma^+$ electronic transition, rot. and hyperfine struct. 80−74134
N_2, $(C^3\Pi)$ nonequilibrium rotational level distrib. in gas discharge *(Russian)* 78−86796
N_2, $B^3\Pi_g$ state, Hanle effect on rot. level 77−58090
N_2, $B'^3\Sigma_u^- \rightarrow B^3\Pi_g$ (0,0) emission band 78−58690
N_2, CARS, optical Stark effect on vibr., and rot. transitions 80−99512
N_2, diffuse plasma, population densities of triplet states, correl. with electron impact processes 80−43966
N_2, elastic and inelastic electron scatt., state to state cross section 80−78708
N_2, electron scatt., 50-500 eV, two-pot. approach 79−41242
N_2, excitation efficiency for rot. states 80−102557
N_2 fluid, light scatt. orientational memory function at moderate density 80−102521
N_2 gas, stimulated Raman scatt. on rotational and vibrational transitions 79−27330
N_2, gaseous, density behaviour of rototranslational spectrum, IR spectra obs. 80−28002
N_2, high energy electron spectroscopy techniques 80−62740
N_2, in zeolite matrix, IR active fundamentals obs. 77−71800
N_2, isotopic forms, visible spectra, rovibronic and rot. anal., $C'\,^3\Pi_u$ and $C\,^3\Pi_u$ interaction 77−18933
N_2 laser 337.1 nm transition, rotational struct. variation 80−78836
N_2, N_3, spectra, review 77−38680
N_2, polarisability tensor anisotropy, Raman spectra differential scatt. cross section 80−18860
N_2, pure rot. CARS obs. 80−99511
N_2, rot. excitation by electron impact 1-4 eV 78−55248
N_2, rot. excitation of non-polar mol. by slow electron impact, variational approach 79−31708
N_2, rotational collision number from thermal cond., 700-2500K 80−23526
N_2, supersonic mol. beam, CARS rot. temp. meas. 80−23423
N_2, VUV absorpt. spectrum, homogeneous perturbation between $c_4'(0)$ $^1\Sigma_u^+$ and $b^1(1)\,^1\Sigma_u^+$ levels 77−83618
N_2, vibr. and rot. anal. of vis., UV spectra, RF discharges in N_2, H_2, CH_4 mixtures 78−5241
N_2^+, first negative spectra, modelling 77−61758
N_2^+, perturbation of $B^2\Sigma^+$ rotational levels by $^4\Sigma^+$ level, lifetimes meas. *(French)* 77−88437
N_2^+, spectroscopic consts., remeas. 77−58197
N_2+Ar, metastable atom excitation of $C^3\Pi_u$ state, symmetry, propensity rules and alternation intensity, rot. spectrum 80−87135
$N_2^+(B^2\Sigma_u^+)$, perturbation of $\nu=1$ vibr. level, rot. lines freqs. and intensities *(French)* 77−79640
ND radicals, metastable, production in discharge, spectra, rot., vibr. consts. determ. *(German)* 77−34642
NF_2, IR spectra, ν_1 and ν_2 bands, vibr. excitation and spin-rot. interaction, doublet splitting 80−28011
NF_3, Raman spectra, Coriolis coupling and transition dipole 78−39533
N_2F_4, centrifugal distortion effect in microwave rot. spectrum 77−30859
NH, ND, $d^1\Sigma^+$ state lifetimes, rot. struct., electron excited emission spectra 77−79654
NH, photofragment, energy distrib., chemiluminesc. reaction rates 77−90618
NH radical formed in NH_3 dissoc., fluoresc. spectrum, rotational relaxation 80−58310
NH radicals, metastable, production in discharge, spectra, rot., vibr. consts. determ. *(German)* 77−34642
NH_2 (A^2A_1), excited state dynamics and bimol. quenching processes 80−9681
NH_2 fragment internal energy distrib. in NH_3 UV laser photodissoc. 80−11901
NH_2, ground state mol. consts., absorption spectra 80−28030
NH_2, lab. obs. of 16 GHz rotational transition 77−3389
NH_2, spin and rot. fine struct., orbital angular momentum 80−83247

molecular rotation continued
NH_2, vibr. and rot. struct., intensity factors and orbital angular momentum 80−83246
NH_2, $X\ ^2B_1$ rot. transition, MODR 78−66571
NH_2, X^2B_1 ground state, 010 level, mol. consts., emission spectra obs., 0.4-0.89 μ 78−74688
NH_3, adsorbed on silica gel, neutron scatt. investig., mol. vibrs., rots. 77−51608
NH_3, and -d_n IR matrix isolation spectra, rotation and inversion 78−5218
NH_3, expansion cooled, mol. photoionisation, rot. struct., rot. predissoc. of excited states 80−91611
NH_3 forbidden vibr.-rot. transitions, ν_2 band, IR-microwave two-photon spectra 77−3428
NH_3, hyperfine quadrupole coupling, ro-inversional levels, inversional depend. 80−27961
NH_3, IR-microwave double reson., rot. and vibr. relax., inversion layers 78−86902
NH_3, microwave-microwave double resonance 80−53029
$^{14}NH_3$, $^{15}NH_3$ and $^{14}NH_2D$, IR laser Stark spectroscopy 80−47978
NH_3+H_2, NH_3 inversion transition, linewidths and T_1/T_2 ratio 80−99499
NH_3+He(Ne)(Ar)(Kr), pure rot. line, press. broadening calcs. 80−78656
N_2H^+, electron impact rot. excitation, Glauber approx. with Coulomb effect 80−63840
NHD, electronic absorption spectrum, 5750-6450 Å, rot. assignments 79−64013
NH(D) radical, and isotopic species, laser mag. reson., hyperfine parameters 77−10694
NHD, rotational transitions, microwave optical double resonance obs. 80−58293
NH_2D, dipole moments effects of RF elec. field modulation on IR stark spectroscopy 80−52989
$NH_3(ND_3)$ in solid Ar, UV absorption spectra, temp. depend. of matrix spectra 80−63652
$NH_2(X^2B_1)$, laser mag. reson. spectra, Zeeman and hyperfine effects, rot. consts. 77−30892
$NH_2(X^2B_1)$, MODR, hyperfine coupling consts., spin rot. consts. 78−1010
NO, and isotopic forms, $\nu=0$ electronic states, spin-rot. doubling 80−5540
NO, $b^4\Sigma^- \rightarrow a^4\Pi$ band system, rot. consts. 79−72312
NO, electronic spectrum, press. induced config. demixing 78−42090
NO, far IR spectral lines and absorptance calcs. 77−46564
NO, fundamental band spectrum, determ. of rotational, spin-orbit coupling and Λ type doubling consts. *(French)* 77−6768
NO, $\gamma(0,0)$ band, collisional broadening parameters 80−63713
NO, Rydberg absorpt. bands 800-850 Å, isotope shift 79−13734
NO, spectroscopic consts., rot. const. of fundamental band 77−68027
NO, state selective step-wise photoionis. with mass spectroscopic ion detect. 80−43119
NO, Zeeman modulation spectroscopy, line shape analysis 80−74197
$NO+N_2(CO_2)(CO)(CH_4)(Ar)$, NO $\gamma(0,0)$ band, oscillator strength and line broadening 80−106356
$NO+O_3$, fs-states and rot. states, effect on reactivity 80−89473
NO_2, $^2B_2$ state photodecomposition in 2nd predissoc. region 77−10712
NO_2, 6480 Å absorption, rot. anal. 79−45731
NO_2, 8170-8280Å absorption spectrum, rot. struct., assignments 79−6937
NO_2, 8920 Å band temp. depend., location of 000-000 band of A^2B_2-X^2A_1 transition 78−70826
NO_2, excited-state rot. const., 5933 Å vibronic band reassignment 77−58196
NO_2, fluoresc. spectra and collisional quenching 80−102538
NO_2, laser-induced fluoresc. spectrum near 6125 Å 77−58069
NO_2, Ne matrix isolated, 6K, B←X band system 78−993
NO_2, rot. cooled, vibronic band lifetimes, time resolved fluoresc. excitation spectra obs. 79−94025
NO_2, rot. Q-branch effective line strength at 37.7 cm^{-1} 77−6859
NO_2, visible fluoresc., rotational structure of vibronic bands 79−98146
$^{15,14}NO_2$, predissoc. rot. struct. in 2490 Å band 80−87192
N_2O, in soln., IR and Raman band shapes, mol. dynamics, ν_3 band 77−36238
N_2O, pure rotational stimulated Raman photoacoustic spectroscopy 80−32724
N_2O, submillimetre rot. lines, press. shifts 80−23463
N_2O, submm wave spectra, 375-565 GHz, isotopic species, mol. consts. 77−3346
NS, spectrum, perturbations in $A^2\Pi_{1/2}$-$X^2\Pi_{1/2}$ transitions, constants of $B'^2\Sigma^+$ state 78−70845
NSF_3, microwave spectra in vibr. excited states, mol. consts. 79−50009
NSF_3, RF-mm wave double reson. of vibr. excited state 79−50054
$^{14}NH_3$, ground state, microwave inversion lines 80−87098
$^{14}NH^+(^{15}NH^+)(^{14}ND^+)$, ab initio CI calc. Λ type doubling in $X^2\Pi$ states 78−82714
$^{15}NH_3$, T_2/T_1 determ. for inversion transitions, power-broadened line shape 77−38654
$Na+HX(J;v)\rightarrow NaX+H$, (X=F,Cl), reaction rate, rot. excitation depend. 78−64818
Na_2, dimer, $B'\Pi_u$-$X'\Sigma_g^+$ band system obs. 78−62837
Na_2, rot. level repopulation rate by laser-induced depopulation 77−65528
NdO, electronic spectrum, rotational struct. anal. 80−78643
$NeCN^+$, SCF calcs., dissoc. energies, rot. and hyperfine const. determ. 80−95531
NeH_2, van der Waals mols., rot. predissoc. 80−63721
Ni complex, nickel-bis-dithiolene, pseudopot. MCSCF and limited CI calcs. 80−83292
NiF $^2\Delta$-$^2\Pi$ system, rot. anal. 79−98115
$O+H_2O\rightarrow OH+OH$, energy partitioning 80−101009
O+saturated hydrocarbon→OH+alkyl radical, reaction dynamics, mol. beam-laser induced fluoresc. obs. 80−97695
O_2, electronic electron impact excitation, rot.-electronic coupling 78−9265
O_2, in zeolite matrix, IR active fundamentals obs. 77−71800
O_2 isotopes, $^{17}O_2$, $^{16}O^{17}O$, $^{17}O^{18}O$, pure rot. Raman spectra, bond lengths 78−42071
O_2, polarisability tensor anisotropy, Raman spectra differential scatt. cross section 80−18860
O_2, pure rot. CARS obs. 80−99511

molecular rotation continued
O_2, Raman spectra of fundamental vibr. band, rot. consts. 78−21932
O_2 rot. Raman spectra fine struct., press. broadening *(French)* 79−94003
O_2, rot. struct. in Zeeman effect 79−50078
O_2^+, $b^4\Sigma_g^-$ state, laser-induced predissoc. in ion beam 78−70886
O_2^+, $b^4\Sigma_g^-$-$a^4\Pi_u$ band, rot. lines, rel. intensities, theoretical and exptl. results 78−13505
O_2^+, $f^4\Pi_g$ state, quasi-bound levels, predissociation, band rot. anal., photofragment kinetic energy anal. 80−63650
O_2^+, first negative system, high-resolution photofragment spectroscopy 80−47971
O_2^+, IR spectra, rot. anal. of $b\ \Sigma_g^-a^4\pi_u$ first negative band 78−5219
O_2^+, laser-induced predissoc. spectrum, rot. anal. 77−71839
O_2^+, photofragment spectroscopy using fast ion beams 80−9755
O_2^+, rotational analysis of $A^2\Pi_u$-$X^2\Pi_g$ band system of $(^{16}O\ ^{18}O)^+$ 78−58678
O_2^+, second negative ($A^2\Pi\ _u$-$X^2\Pi_g$) band system, rot. anal. 77−18911
O_2^+, spectroscopic consts., remeas. 77−58197
O_3, line position and intensities of $2\nu_3$, $\nu_1+\nu_3$ bands 80−87181
O_3, mol. beam electric resonance, electric and mag. props. determ. 77−27055
O_3, sextic centrifugal distortion consts. calc. 79−59430
OCS, collisional rot.-line widths and shifts, microwave region 78−25619
OCS, IR spectra using spin-flip Raman laser, combination band near 1890 cm^{-1} 78−37640
OCS, M-resolved rot. Stark levels, four-level microwave-microwave double reson., collision induced 77−10696
OCS, MM wave spectrum, centrifugal distortion const. 77−34618
OCS, microwave rot. lines, self-broadening 78−58668
OCS, microwave rot. transitions, phase shift effect, collisional effects 79−98073
OCS, microwave spectra, rot. Q-band *(Polish)* 78−29866
OCS, microwave spectral lineshape of J 1→2 line 79−68225
OCS, millimeter wave rot. spectra, isotope shifts, freqs. and mol. consts. 80−78611
OCS, r_m struct. determ. from rot. consts. 78−42236
OCSe, isotopic species, microwave and IR spectra 77−38658
OH, ($A^2\Sigma^+$), abnormal rot. following H_2O photodissoc., semiclassical calcs. 78−40069
OH, (0,0) UV transitions, band oscill. strength 80−69162
OH, $A^2\Sigma^+$-$X^2\Pi_i$ system, vibrational and rotational levels, transition probability determ. 80−43034
OH, band oscill. strength, rot. excitation effects 80−23460
OH, excitation and band rot. temp. of plasma jet light source 77−44555
OH, internal state distrib., crossed mol. beam $H+NO_2$ reaction, laser-induced fluoresc. 77−4905
OH maser sources, interstellar, radiative transport effects on inversion 80−17681
OH, methane-air flame, conc., temp. and rot. temp., laser absorption spectroscopy 78−76862
OH, prod. by photolysis, Λ-doublets, population, rot. states, hyperfine struct., microwave spectra 80−32694
OH radical, gas phase EPR, rot. states electronic struct. and Zeeman parameters 78−86896
OH, rot. transitions broadened by press., laser mag. reson. study 79−94020
OH rotational temp. determ., successive approx. 80−23389
OH, vibr. ground-state, MFS, rot. spectra and electronic band anal. 78−5206
OH, $X^2\Pi$ state, microwave spectrum calcs. 77−30858
$OH+H_2O$, OH linewidth rot. depend. on UV transitions 80−91606
OH($^2\Pi$), rot and translational temps. in gas discharge 78−5243
OHX $^2\Pi$ radical, ground and vibr.-excited ($\nu\leq6$) levels, microwave spectrum 79−63985
$OH(v,N)$ bimodal rot. distrib. from $O(^1D_2)+NH_3$ 80−76501
ONCN, far IR spectra, pure rot. and vibr.-rot. bands 78−82731
OPF_3, distortion moment microwave obs., rot. consts., mol. config. 77−50426
OPF_3, forbidden transitions, mol. beam elec. reson. obs. using avoided crossings 78−29775
OSC_2N_2O, submillimetre rot. lines, press. shifts 80−23463
^{16}O, $^{18}O_2$, vac. UV absorpt. spectra, band intensities and designations 78−5245
$^{16}O_3$ and ^{18}O isotopic species, rot. spectra 18 to 382 GHz, force and Coriolis coupling consts. 77−75137
$^{18}O_2$, Herzberg transition I in absorpt. spectrum 79−72313
OsO_4, and isotopic forms, stretching fundamental, 961 cm^{-1}, high resolution spectroscopy 78−90162
P_2, intersystem transition obs. in absorpt. spectrum 80−48008
P_2 radical, $b^3\Pi_g$-$a^3\Sigma_u^+$ transition, perturbed by $1^5\Sigma_g^+$ state *(French)* 80−18855
PBr_3, Raman scatt. spectra in gas, liq. and solid states, mol. dynamics *(Russian)* 77−55779
$P^{35}Cl_3$, microwave, rotational spectra, excited vibrational states 79−98080
PD^+, IR emission spectra, rot. anal. and mol. parameters 80−69134
PD_3, forbidden rot. spectra, spectal consts., bond lengths and angles 77−83581
PF_3, anharmonic force field from mm wave spectra of vibr. excited states 79−13701
PF_3, microwave l-type reson. transitions in $v_4=1$ state 77−57988
PH^+, IR emission spectra, rot. anal. and mol. parameters 80−69134
PH_2 radical, laser-induced fluoresc. 78−94277
PH_2, X^2B_1-state, rot. laser mag. reson. spectrosc. 80−28038
PH_3, forbidden rot. spectra, spectal consts., bond lengths and angles 77−83581
PH_3, liq. and solid, Raman spectra., vibr. correl. functions, rot. motions 80−55087
PH_3, millimeter spectra, $\nu_2=1$, $\nu_4=1$ excited vibr. states, J=0→1 rot. transition 79−6936
PN, valence state interactions, ab initio and semiempirical estimates 78−74567
PO, rot. struct. of absorpt. bands 1850-1600 Å, valence $^2\Pi$ state 79−13739
$P^{18}O$, UV absorpt. spectra, valence and Rydberg states, rot., vibr., anal., predissoc. 79−41184
PS, electronic transition $B^2\Pi$-$X^2\Pi$, vibr. and rot. anal. *(French)* 78−78716
PbBr, $b^1\Sigma^+$-$X^3\Sigma^-$ band system, microwave discharge obs., mol. consts. 79−81203

molecular rotation continued
PbCl, rot. analysis of $A\text{-}X_1$ system 80−32703
PbF, rot. anal. of $B\text{-}X_2$, $B\text{-}X_1$ and $A\text{-}X_1$ systems 77−58001
PbO, laser excitation IR spectra, photoluminescence obs., rot. anal., rot. const. determ. 80−95619
PrO, hyperfine structure, rotation, electronic spectrum obs. 79−98061
PrO, visible spectra, 7500-8500 Å, VII and X systems, rot. anal. *(French)* 78−46355
Rb_2, B-X system vibr. consts. from mag. rot. spectra 79−76530
RbCNS, single cryst. factor group anal. of IR and Raman multiphonon bands 77−4644
RbF+K collision complex, rot. energy effect on branching fraction for reactive decay 78−73023
S_2 $^{35}Cl_2$, microwave spectra and double reson., assignments, distortion consts. and struct. 79−89664
S_2 B-X system, Franck-Condon factors 79−94035
SCl_2, microwave spectrum, quadratic pot. function, average struct. 77−65456
SF_6, ^{19}F NMR vibr. anharmonicity effects 80−91580
SF_6, collisionless multiple-photon excitation, mol. rot. and vibr.-rot. interaction effects 78−74720
SF_6, collisionless multiphoton excitation, anharmonic oscill. model rot. effects 78−86845
SF_6, Doppler-limited spectroscopy, of $3\nu_3$ band 80−58244
SF_6, Doppler-limited spectroscopy of $3\nu_3$ band, rot. const. and anharmonic parameters calcs., mol. photodissoc. 80−83361
SF_6, highly excited, time-resolved IR absorpt. obs. 80−9666
SF_6, IR radiation induced mol. excitation and heating effects, time resolved 77−75142
SF_6, IR rot. spectra, orbital level splitting in octahedral symmetry, high J levels 77−69815
SF_6, IR rot. spectra orbital level splitting in octahedral symmetry, high J levels 77−69816
SF_6, mol. beam mag. resonance, rot. mag. moment spectrum 77−34661
SF_6, multiphoton dissoc., classical model 80−53076
SF_6, ν_3 bands, rot. fine struct., HFS spectroscopic consts. determ., saturation spectroscopy obs. 80−53008
SF_6, vibr. spectra, rot. consts., IR spectra, Raman spectra obs. 80−32719
SF_5Cl, pure rot. spectra, 300 GHz, isotope effects 80−5533
SO_2, absorpt. coeffs. for ν_2 and ν_3 bands 77−38668
SO_2 in Orion Molecular Cloud-1 (OMC-1), rot. temp. 79−25670
SO_2, T_2 relax. time meas. by microwave transient nutation 77−30862
SO_2+$H_2O(N_2)(SO_2)$, linewidths, intensities, isotope shifts, 91.5-95.5 GHz 78−42044
SO_3, rotational Raman spectrum, rot. consts. and bond lengths 79−18195
S_2O, 3400 Å bands, rot. anal., upper state struct. 78−13506
SPF_3 band contours of E fundamentals, IR spectra 79−98089
SPF_3, isotopic forms, microwave spectra, centrifugal distortion consts., vibr. and rot. states, IR matrix spectra 77−10665
SbF, ($f0^+$, $e0^-$)-X_2^1 transition, rot. anal. 78−74657
SbN, 3300-4000 Å, rot. and vibr. perturbations and rot. anal. *(French)* 78−37651
ScOH, electron collisions, integrated and momentum transfer cross sections, cond. integrals 79−41238
ScS, $B^2\Sigma\text{-}X^2\Sigma$ system, rot. struct. and hyperfine effects near IR spectrum 80−5544
Se_2, 3d absorption spectra, mol. damping of centrifugal barrier effects 77−61736
$^{80}Se_2$, Lande factors measurement in $B\ ^3\Sigma_u^-$ state 77−34648
SeH, isotope effects, Rydberg levels-ground state transitions, rot. const., VUV spectra obs. 80−58279
SeO, $A^3\pi\text{-}XO^+$, 1 band system 77−58039
SeO, IR bands of 10296 and 10491 Å, rot. struct. 78−5224
SeO, molecular constants determ. from $b^1\Sigma\text{-}X^3\Sigma$ transition, nonlinear least squares procedure 79−798
SeO_3, rotational Raman spectrum, rot. consts. and bond lengths 79−18196
Si biradical, six-coordinate, mol. mobility two-spin probe investig. 80−102529
SiBr, $B^2\Sigma^+ \rightarrow X^2\Pi$ transition, rot. anal. *(French)* 79−50013
SiCl, ($A^2\Sigma^+\text{-}X^2\Pi$) transition, rot. anal., equilib. consts. 78−37648
SiF, D-X transition, rot. anal. 79−72331
SiH, A state new predissociations, improved dissoc. energy value from rot. level lifetimes 79−3496
SiH_4, avoided-crossing molecular-beam spectroscopy, hyperfine and spin rot. const. and rot. g factors determ. 80−78671
SiH_4, proton spin relax. rate, centrifugal distortion 77−75184
SiH_3Br, rot. Zeeman effect 79−54909
SiH_3 ^{81}Br, high resolution rot. microwave spectrum, 8-40 GHz, mol. consts. 78−21916
$^{28}SiH_3D$, IR spectrum ν_1 and ν_4 bands, rot. const. 77−83590
SiH_2DF, $SiHD_2F$, microwave spectra, harmonic force field, mol. struct. 77−18913
$SiH_4(F_4)$, rot. mag. moment spectra, mol. beam mag. reson. obs. 77−14509
SiH_3NCS, microwave spectrum, struct., dipole moment, ^{14}N quadrupole coupling const. 77−46560
SiH_3NCS, microwave spectrum, rot. Zeeman effects 79−54847
$(SiH_3)_2S$, rot. consts., internal rot. parameters, anal. of microwave spectra 78−46316
$(SiH_3)_2S$, microwave spectrum, r_0-struct., elec. dipole moment, internal rot. barrier 79−3439
SiO, $d^2\Pi_i\text{-}b^3\Pi_i$ transition, 0-1 band rot. anal. 77−18961
SiO, rot. and vibr. consts., millimetre-wave spectrum 77−34619
SiO^+, rot. spectrum, isotope shift, mol. consts. 79−59483
SiS, and isotopes, microwave spectra and consts., review 77−23493
SiS, chemiluminescent flame spectra, electronic states and rot. struct. obs., vibr. assignments, Franck-Condon factors determ. 80−85179
SnF, rotational struct. of UV (O,O) bands 77−34658
Sr+HF→SrF+H, product state distrib., reagent orientation and rot. effect 79−20361
SrD, UV absorpt. spectra, rot. consts. 77−14448
SrF, $A^2\Pi\text{-}X^2\Sigma$ system, rot. anal. using CW tunable dye laser 79−31563
SrF, $B^2\Sigma^+\text{-}X^2\Sigma^+$ system, rot. anal. using a cw tunable dye laser 78−9165
SrF radical, rot. spectrum of $X^2\Sigma^+$ state, MODR 78−9176
$^3T_2$, pure rot. and rot.-vibr. Raman spectrum 78−94253
Te_2, $B0_u^+ - b^1\Sigma_g^+$ system, transition assignment, IR and visible spectra obs. 80−58298
molecular rotation continued
ThO, $L^1\Pi\text{-}^1\Sigma^+$ and $N^1\Pi\text{-}X^1\Sigma^+$ systems, spectra, rot. anal. 80−23430
TiN, electronic absorpt. spectrum, rot. anal. 80−78601
TiN, vibr. IR spectrum, mol. consts. 79−68230
TiO, rot. anal. of (0,0) (1,0) (0,1) (1,1) bands of $\gamma'(B^3\Pi\text{-}X^3\Delta)$ 79−22719
U+Pb, K-vacancy form., rot. coupling effect in quasimol. L-shell 78−25692
^{186}WO, electronic spectra following flash photolysis, intracavity laser technique, rot. consts. 79−31538
XeF, supersonic expansion jet, $B\leftarrow X$ system rot. and vibr. anal., isotope intervals, fluoresc. spectra 80−14174
XeF, X, B, and D-states, spectra, vibr. and rot. consts. 78−70844
XeF_2, pure rot. Raman spectrum 78−94254
YD, electronic spectra *(French)* 77−14442
YF, $^3\Phi - ^3\Delta$ system, rot. anal. 78−9149
YH, electronic spectra *(French)* 77−14442
YH, YD, 3800-9000 Å negative glow spectra, triplet and singlet systems 77−79608
YO, rot. anal. of $A^2\Pi - X^2\Sigma^+$ and $B^2\Sigma^+ - X^2\Sigma^+$ systems 79−22718
ZnH, lifetime, Λ-doubling and hyperfine struct. of $A^2\Pi$ excited states 77−58083
ZrN, vibr. IR spectrum, mol. consts. 79−68230
ZrO, band identifications in $^1\pi\text{-}X^1\Sigma^+$ system 77−18931
$^{90,92,94}ZrO^+$, rot. anal. in near IR 80−74162

molecular rotation calculations
3j and 6j coeffs., recursive computation 77−5687
absolute rotational contributions, calc. methods, dipole moment derivatives, transferability 79−72297
absorption intensities, rot. averages, ensemble method 79−89658
alkali halides, quadrupole coupling, vibr. and rot. effects, Morse oscill. calcs. 77−6805
asymmetric top molecules, doublet-quartet transitions, rot. selection rules 78−94186
asymmetric top molecules, R_S-struct., bond length mass depend. 78−94230
asymmetric top molecules, type B band envelopes, QQ and RQ-QP branch separation 79−802
asymmetric top mols., semi-rigid, rotational hamiltonian *(French)* 77−30848
asymmetric tops, spin-rotation Hamiltonian in reduced form 79−63976
asymmetrical molecules, absolute rotational contributions, calc. methods, dipole moment derivatives, transferability 79−72297
asymptotic eigensolutions of fourth and sixth rank octahedral tensor operators 79−93975
atom+molecule, rotational inelastic scattering, effect of interaction pot. 79−59533
atom+molecule rot. inelastic scatt., coupled eqns. for single initial state, variation-iteration method 79−68301
benzene-d_0,-d_6, $^1B_{2u}$ excited states, high resolution two-photon spectra 77−506
bipyridines, torsional isomerisation of biologically active bicyclic molecules 80−27996
bond orbitals and intramolecular interactions, barriers to rotation and non-bonded interactions 80−32855
3-bromopropene, $^{79,81}Br$, microwave spectrum, mol. struct., nucl. quadrupole coupling consts., rot. consts. 77−6767
carbon tetrafluoride laser, emission spectrum in 16 micron range, CO_2 laser stimulation 80−9870
centrifugal distortion analysis including P^6-terms 77−14413
chloroform, internal field factor, rot. correlation calc. 77−449
1-chloronaphthalene, $A^1A'\text{-}X^1A'$ electronic transition, rot. band contour 79−6935
classical radiative damping of symmetric and asymmetric rotor mols. 77−18907
coherent anti-Stokes Raman spectroscopy, selection rules, depolarisation ratios, rot. struct. 77−34640
cyanobutadiyne-d_0,d_1, microwave spectrum, substitution struct., dipole moment 77−3348
2-cyanofurane, rot. consts., dipole moments, nuclear quadrupole coupling, spectral obs. 77−34620
2-cyanothiophene, rot. consts., dipole moments, nuclear quadrupole coupling, microwave spectra 77−34620
cyclopentanone, centrifugal perturbation consts., determ. from forbidden rot. transitions 79−6931
diatomic mol. parity breaking in rot. levels *(Russian)* 79−2954
diatomic molecular dilute solns., IR and Raman spectra temp. depend. anal. model *(French)* 77−88456
diatomic molecule, pots. superposition, rel. to lattice dynamics, mol. consts. calcs. 80−5598
diatomic molecule, rot. perturbed Morse oscillator, eigenfunctions and Franck-Condon factors 77−42309
diatomic molecule, Stark effect calcs., rigid rotator rotational levels in asymmetric potential well 80−5580
diatomic molecules, centrifugally distorted fine struct. 78−62783
diatomic molecules, rot. line strengths in multiphoton transitions 80−48051
diatomic molecules, rot. temp. determ., absorpt. spectra calcs. 77−30851
diatomic molecules, rot. transition probabilities calc. using Morse pot. 79−86046
diatomic molecules, soluble potential 78−21996
diatomic polar mol., rot. level Stark effect in strong field 78−25611
diatomics, vibr. correction and effective moment of inertia, a correl. 79−89662
dichlorodifluoromethane, study of ν_6 fundamental 79−31526
difluoramine, centrifugal distortion anal., microwave rot. spectrum 78−58650
dimethyl ether-d_0,d_3,-d_6, microwave spectra, torsional splittings 77−3347
DMSO, centrifugal distortion analysis including P^6-terms 77−14413
effective Hamiltonians for rot. absortion spectra 79−6930
electric dipole $^4\Sigma$(int)-$^4\Sigma$(int) transitions, rot. intensities 80−9642
electron impact excitation, rot. transitions *(Russian)* 79−76524
electron spin-rotation coupling, phase problem *(French)* 79−36612
electronic-rotational molecular states, electron-impact excitation, cross sections and rate consts. 80−14241
energy level clustering, qualitative theory of irreducible tensor operators spectra 80−28001
ethanol, conformational anal., barriers of internal rotation, electronic structure 79−63916

molecular rotation calculations continued
ethyl cyanide, isotopic species, rot.-torsion-vibr. interaction in rot. spectra 77−458
ethylene, compressed gas, far IR dipolar absorpt., meas. and theory 77−14425
ethylene oxide-d_0, -d_4, centrifugal distortion const., thermodynamic functions 79−41149
ethylene sulphide, centrifugal distortion const., thermodynamic functions 79−41149
9H-fluorene, soln., correl. times from ^{13}C relax. 80−23438
fluoromethanal, visible spectrum, rot., vibr. and vibronic anal., double min. pot. 79−41182
formaldehyde, ground state rot. consts. 79−45701
formaldehyde, unique force field, parametric representation method 77−18897
formaldehyde-d_1, rot. transitions, millimetre wave spectrum 77−34617
formaldehyde-d (d_2) submillimetre lasers, optically pumped, assignment of laser lines 80−58513
heavy-ion collisions, electron slip effects on quasimolecular X-ray emission 77−19040
impurities in crysts., dynamics 79−60442
IR spectra 77−18910
least-squares parameters, stepwise merging method 78−89319
linear molecules in inert solvent, collapse of rot. struct. of Raman scatt. spectra *(Russian)* 77−3371
linear polar molecule, rotational Brownian motion, spherical harmonics 79−30368
melanostatin, correl. between X-ray struct. and conform. in soln. 77−48752
methane, quantum mech. rot. partition function 80−102501
methane, rotational partition function, isotope effects 80−14130
methane+Ar, low energy collision, close coupling and coupled states, rot. transitions 78−78784
methane-d_4, isotope effect on rot. and vibr. consts. 79−22688
methanol, conformational anal., barriers of internal rotation, electronic structure 79−63916
methyl bromide, far IR laser lines, rot. anal. of ν_6 perpendicular band 77−3359
methyl cyanide, microwave rot. spectra, mol. consts. 77−34615
methyl cyanide and isocyanide, microwave spectra, rot. consts. 79−36627
methyl groups correlated quantum rotation effects on ESR spectra 77−18948
methyl oxirane, centrifugal distortion consts. and struct. parameters calcs. 77−34616
methylamine, vibr.-inversion-internal rot.-rot. Hamiltonian 78−86840
molecular fluid, computer simulation of liquid-vapour surface 80−54478
monomer self-associating systems, nonideal, graphical anal. by equilibrium ultracentrifugation 80−41335
Morse oscillator, rotational const. B_v, asymptotic expansion 79−68289
nonlinear XYX molecules, quartic centrifugal distortion consts., rot. const. depend. 78−62784
nonrigid rotation IR band absorption, appl. to CO, NO, N_2O and CO_2 78−91060
optical torsion transitions, barrier heights from vibr. optical freqs. 77−42308
orthorhombic rotating molecules, doublet-quartet transitions, Zeeman effect calcs. 78−94280
oxalyl chloride (fluoride), centrifugal distortion consts. and thermodynamic functions, pot. energy calc. 79−22619
planar mols., sextic centrifugal distortion consts. calcs., planarity relation 77−57970
polar mol. rot. relax., dielectric friction, Onsager cavity model 80−64664
polyacetylene compounds, rot. consts. 78−86841
polyatomic molecule, anharmonic force consts., vibr.-rot. interaction consts. 80−966
polyatomic molecule, radiative dissoc. in laser field *(Russian)* 78−9207
polyatomic molecule, sextic centrifugal distortion consts., Watson Hamiltonian, perturbation method 77−10785
polyatomic molecule, transform. of complete electron-nuclear Hamiltonian to intramolec. coords. 78−9054
polyatomics, vibr. correction and effective moment of inertia, a correl. 79−89662
n-propanol, centrifugal distortion constants, OH-trans-trans and OH-trans-gauche conformers *(Russian)* 79−10089
propionitrile, quartic and sextic centrifugal distortion consts., microwave spectrum 78−94236
propyne, microwave spectra and mol. consts., rot. anal. 79−76411
pyramidal XY_3 molecules, mol. geometry calcs. using centrifugal distortion const. 80−18841
quartic and sextic centrifugal effects, book contrib. 78−21910
quartic centrifugal distortion consts., upper and lower bounds 79−45699
Raman scattering, spontaneous and stimulated, by forbidden rotational and vibr.-rot. transitions in strong optical field 80−74174
Raman spectra, C_{3v} and T_d mols., foribdden rot. line intensity 77−58019
real symmetry coordinates, groups having complex representations 78−82715
rigid rotor, asymmetric, semiclassical energy levels determ., tunnelling 78−37624
rotational isomerism, torsional pot. anal., from spectrosc. data 78−62787
rotational isomers, transformation of operators of coordinates and momenta 79−63982
rotational predissociation, Weyl's theory and Jeffrey's approx., resons. 78−926
simple oscillator, correl. functions, IR band shapes 79−26960
SPECAN, rot. spectra automatic assignments program, speed improvements 79−31499
spectral line broadening, semiclassical straight line vs. curved trajectories 79−45765
spherical top molecule, triply degenerate fundamentals, line freq. expression for lage ang. momentum 79−36614
spin-rotation parameters for homonuclear diatomic mols. 77−88438
sum rules for the turning forces of pure rotational transitions 80−78597
symmetric molecules, high resolution spectra, rot. and permutation dynamics 79−41157
symmetric polyatomic mols., frame transform. relations and multipole transitions 78−58661
symmetric rotor, internal rot. splitting 78−94232
symmetric top and linear molecules in inert solvents, far IR absorpt., free rotational models 77−450
symmetric top mol., overlapping press. broadening, nonreson. microwave absorpt. line radii 78−17662
molecular rotation calculations continued
symmetric top molecules, microwave transient phenomena, Bloch eqns. 79−26969
symmetric top molecules, rovibronic 2-photon transitions, rot. line strengths 78−78762
symmetrical molecules, absolute rot. contribs. calcs., dipole moment derivatives, transferability 79−72296
tetrahydrothiophene, microwave spectrum, centrifugal perturbation effects 77−3350
s-tetrazine(-d_1), and $^{15}N_2$-substituted, rot. consts., ground and $^1B_{3u}$ excited states geometries 78−82862
triatomic molecule, nonlinear, transform. of vibr. and rot. coords. during electronic transition *(Russian)* 79−93980
trifluoromethane, rot. transitions, self-broadening and self-shifting meas. 79−59426
triptycene, soln., correl. times from ^{13}C relax. 80−23438
vanadyl octaethylporphyrin, radical cation EPR linewidth inversion, relax. theory 77−10693
X_2Y nonlinear mols., isotopic relations, anharmonicity, reson. interaction, vibr.-rot. consts., rot. energy levels 77−10663
XY_2 bent symm. nonhydride mols., centrifugal distortion constants, approx. method 77−30854
XY_3 type molecules, centrifugal distortion constants and inertia defects *(Russian)* 79−800
XY_4 molecules, centrifugal consts., isotope relations 79−59427
XY_4 molecules, isotope effect on rot. and vibr. consts. 79−22688
AsF_3, mol. geometry calcs. using centrifugal distortion const. 80−18841
BF_3, pure rot. spectra of ground vibronic state, calc. 79−63975
BH, mol. spectroscopic consts., FSGO calcs. 77−6758
BrCN, ICN, and isotopic forms, force field calc., freqs., rot. consts. 79−22693
BrF, laser excitation spectrum, 4850 to 5200 Å, rot. anal. 77−6840
C_2, Phillips system, rot. depend. of Franck-Condon factors 77−27058
CH, $A^2\Delta$ state, radiative lifetime 77−34698
CH, interstellar, rot. levels struct., excitation mechanisms 78−21908
CO, CO-air, mol. rot. temp. determ., absorpt. spectra calcs. 77−30851
CO, population inversion mechanism for rot. levels, interstellar medium appl. 79−21406
CO, rot. line strengths in multiphoton transitions 80−48051
CO rotational-level populations of interstellar molecule 79−97054
CO^+, $A^2\Pi$-$X^2\Sigma^+$ system, (2,0) band, rot. anal., $^2\Pi$ state Λ-doubling *(French)* 77−10681
$^{12}C^{18}O$, Herzberg system of $C^1\Sigma^+$ state 78−90185
CO+H^+, vibr. excitation calc., close coupling and sudden approx. 80−78561
CO_2, 9.6 μm region emission spectrum, rot. consts. 77−3353
CO_2, rot. Raman spectra, 01^10 state effects on intensity distrib. *(German)* 77−10679
CO_2+He, rot. transition classical integral cross section, surprisal predictions 77−54594
C_3O_2, large amplitude bending mode, rot.-vibr. calc., assignments 77−18905
COF_2, centrifugal distortion analysis including P^6-terms 77−14413
COS, mole. potential surface, evaluation from spectroscopic observations 80−43207
CS, population inversion mechanism for rot. levels, interstellar medium appl. 79−21406
CS, rotation analysis of $d^3\Delta_i$-$a^3\Pi_r$ transition, IR spectra 80−78591
CS, rotational-level populations of interstellar molecule 79−97054
CS, spin-orbit and spin-spin parameter calcs. 77−27044
CSiH, matrix Hartree-Fock calcs. 79−5874
Ca_2, rot. perturbed Morse oscillator eigenfunctions and Franck-Condon factors 77−42309
Cl_2, liquid-vapour surface, computer simulation 80−54478
ClCN, and isotopic species, force field calc., freqs., rot. consts. 79−22692
$ClONO_2$, laboratory microwave spectrum, atm. chem. appl. 77−6760
D_2, Lyman bands, Morse Franck-Condon factors and R-centroids 77−58088
D_2, rot. levels and consts., nonadiabatic corrections 77−18906
$D^{79}Br$, $D^{81}Br$, IR absorpt. spectra of 1-0, 2-0, 3-0, 4-0 bands 77−3360
D_2O, isotopic species, far IR spectra, assignments, moments 77−6761
FCN, and isotopic forms, force field calc., freqs., rot. consts. 79−22691
H+H_2, planar reaction, cross section calcs., vibr. and rot. convergences 77−21376
H+H_2, three dimens. reaction, Porter-Karplus pot. energy surface, rot. distribs., rate consts. 77−21378
H^++H_2, elastic scatt. and rot. excitation, multistate semiclassical orbital method 79−27058
H^++H_2, rot. excitation and vibr. transitions, coupled state approx. 77−61835
H_2, $c^3\Pi_u$ metastable state, fine struct. lifetimes 79−64050
H_2, Lyman bands, Morse Frank-Condon factors and R-centroids 77−58088
H_2, ortho-para mixtures, 10 to 23K, rot. Raman spectra, quantum calcs. 77−6700
H_2, spin-rotation parameters 77−88438
H_2, static polarisability determ. by optimised rot. method 79−54990
H_2^+, electron cooling through resonant collisions 80−32845
H_2^+, static polarisability determ. by optimised rot. method 79−54990
HCC^+, equilib. struct., rot. const. 79−98003
HCN, HNC, molecular electronic struct., unlinked cluster effects 78−94185
HCN(DCN), photodissoc. dynamics, rot. (vibr.) energy disposal 78−48672
HCNO, isomers, geometry, spectra, rot. and force consts., ab initio calcs. 77−34574
HCl, Ar-perturbed rot. linewidths, temp. depend. 79−45766
HCl, in inert solvents, far IR absorpt., free rotational models 77−450
HCl+He, mag. transitions, initial-l labelled CS approx. computations 79−3552
HCl+N_2(CO)(O_2)(HCl), HCl linewidth, impact parameter calcs. 79−89714
HCl^+(DCl^+), spin-rot. consts., Van Vleck approx., ab initio calcs. 77−34610
HD, Lyman bands, Morse Franck-Condon factors and R-centroids 77−58088
H_2(D_2), Compton profile, impulse approx., electron correl., vibr. and rot. effects 78−17585
HF, spectroscopic consts., FSGO calcs. 77−6758

molecular rotation calculations continued
HF, vib.-rot. props. of $X^1\Sigma^+$ and $B^1\Sigma^+$ states, variational calcs. 77−50422
$HF^+(DF^+)$, spin-rot. consts., Van Vleck approx., ab initio calcs. 77−34610
$H_2(HD)$, rot. levels and consts., nonadiabatic corrections 77−18906
HNNN, substitution struct., rot. consts. calcs. 80−91534
HNO_3, microwave spectra, centrifugal distortion effect 77−34621
HO_2, mol., spin-rot. Hamiltonian in reduced form 79−63976
H_2O, centrifugal distortion 77−57974
H_2O, classical radiative damping 77−18907
H_2O, isotopic species, far IR spectra, assignments, moments 77−6761
H_2O, matrix of rotational energy Hamiltonian, calc. *(Russian)* 78−37622
H_2O, pure rot. band, exponential wide band parameters 79−31498
H_2O, rot. consts. for ground states and (110) and (011) interacting states 78−21902
H_2O_2, lone pair orbital explicit representation, augmented contracted Gaussian basis set 78−25423
$(H_2O)_2$, tunnelling-rotational energy levels, group theoretical classification 77−54549
HPO, vibrational freqs., by rot. anal. of spectra 79−54831
H_2S, centrifugal distortion 77−57974
He+CO, rot. inelastic scatt., coupled eqns. for single initial state, variation-iteration method 79−68301
He_2^{2+} quasimolecular states, radial and rot. coupling terms 79−26896
He_2^{2+}, static polarisability determ. by optimised rot. method 79−54990
HeH^+, static polarisability determ. by optimised rot. method 79−54990
HgH, predissoc. by rot., continuous rot.-vibr. spectrum, Weyl's theory 77−18996
HgH, predissoc. by rot., continuous rot.-vibr. spectrum, resons. and eigenvalues, Weyl's theory 77−18997
HgH, rot. predissociation, Weyl's theory and Jeffreys' approx., resons. 78−926
I_2, ($B^3\pi_{0+u}$), dissoc. reaction, computer simulation 78−48639
I_2 B-X transitions near 5145 Å, reassignment 77−3374
$^{127}I_2$, $^{129}I_2$, $B^3\Pi0_u^+$-$X^1\Sigma_g^+$ systems, fluoresc., mol. consts., Franck-Condon factors 77−34680
LaF, Franck-Condon factors and R-centroids, rot.-vibr. effects 78−50596
LaO, Franck-Condon factors rot. depend. 80−58319
$Li^+ + H_2$, elastic scatt. and rot. excitation, multistate semiclassical orbital method 79−27058
$Li^+ + H_2$, rot. inelastic scatt., body frame partitioning approx. calcs. 80−23527
LiH, mol. spectroscopic consts., FSGO calcs. 77−6758
MgO, Franck-Condon factors rot. depend. 80−58319
N_2, electron impact rot. and vibr. excitation, elastic scatt., close coupling and Born approx. 80−28108
N_2, electron scattering, local-exchange approx. for intermediate-energy-differential cross sections 80−48094
N_2, energy levels, low lying triplet states, infrared emission analysis 78−58691
N_2, liquid-vapour surface, computer simulation 80−54478
N_2, rot. line strengths in multiphoton transitions 80−48051
N_2, rot. perturbed Morse oscillator, eigenfunctions and Franck-Condon factors 77−42309
N_2, rot. temp. meas., rocketborne electron beam fluoresc. meas., reflected mol. effects 77−29519
N_2, transverse excited $C^3\Pi_u \rightarrow B^3\Pi_g$(0-0) UV laser band, spectroscopic rot. anal. 79−7115
NF_2H, centrifugal distortion anal., microwave rot. spectrum 78−58650
NH, mol. spectroscopic consts., FSGO calcs. 77−6758
NH_3, in inert solvents, far IR absorpt., free rotational models 77−450
NH_3, rot.-inversion Raman spectra, K-splitting 80−9611
NH_4^+, libration and tunnelling freq. rot. heat capacity, hindered rot. energy level calcs. 79−98058
N_2H_4, lone pair orbital explicit representation, augmented contracted Gaussian basis set 78−25423
NH(NF)(NCl), effective spin-spin parameter and singlet-triplet transition intensities, ab initio calc. 78−9067
NO, rot. line strengths in multiphoton transitions 80−48051
NO, v=0,1 states, spectroscopic data calc. 78−86851
NO_2, mol., spin-rot. Hamiltonian in reduced form 79−63976
N_2O, rot. Raman spectra, 01^10 state effects on intensity distrib. *(German)* 77−10679
N_2O, rot. transitions, self-broadening and self-shifting meas. 79−59426
NO_2Cl, force fields calc. 78−42241
NO_2Cl, rot. distortion parameters for force consts. determ. in parametric method 79−76401
NO_2F, force fields calc. 78−42241
NO_2F, rot. distortion parameters for force consts. determ. in parametric method 79−76401
Na_2, rot. perturbed Morse oscillator eigenfunctions and Franck-Condon factors 77−42309
O_2, effective spin-spin parameter, ab initio calc. 78−9067
$^{18}O_2$, Raman spectrum and mol. parameter 77−46565
O_2+La(Y)(Sc), crossed beam chemiluminescence reaction, spectral simulation, hyperthermal energy meas. 78−80732
O_3, and isotopic substitutions, rot. spectra calcs. 77−38659
O_3, low energy elastic and inelastic electron scatt., rot. transitions, close coupling calc. 80−78706
O_3, sextic centrifugal distortion constants 77−57972
O_3 vibr. and rot. variational calc., isotope shifts 77−57967
OH, A_2-X system, rot. transition probabilities 80−43027
OH, $A^2\Sigma$ state, predissoc. rates, high freq. deflection meas. 78−62864
OH Meinel bands, in airglow, rot. temp., radiative lifetime 78−61643
OH, nightglow emissions, rot. temp. calc. 77−64507
OH, nightglow emissions, equilib. nature of rot. temp. 77−64508
OH radical, in Earth's atmosphere, pure rot. lines 79−92593
OH radicals in glow discharge, rot. levels distrib., temp. meas. 78−47169
OH(OD), spin-rot. consts., Van Vleck approx., ab initio calcs. 77−34610
$OH(^2\Pi)$+H, rel. to interstellar OH maser action 79−101186
PF_3, mol. geometry calcs. using centrifugal distortion const. 80−18841
PH(PF), effective spin-spin parameter and singlet-triplet transition intensities, ab initio calc. 78−9067
PS, UV bands, rotational anal. 79−76443
PtH(D), pot. energy curves, r-centroids, Franck Condon factors, rot. depend. 80−28082
S_2, effective spin-spin parameter, ab initio calc. 78−9067
SF_6, rot. spectra, asymptotic level clusters, quantum model 77−23490

molecular rotation calculations continued
SIO, Franck-Condon factors rot. depend. 80−58319
$S^{16}O_2S^{18}O_2$, (0,0) band rot. anal., a^3B_1 state electron spin fine struct. consts. 77−10687
SO_2, $^1B_2$ state, force field and asymm. struct. 79−22685
SO_2, effective spin-spin parameter and singlet-triplet transition intensities, ab initio calc. 78−9067
$^{32}SF_5{}^{35}Cl$, microwave rot. spectra, mol. parameters *(French)* 77−456
ScF, Franck-Condon factors and R-centroids, rot.-vibr. effects 78−50596
SiCH, matrix Hartree-Fock calcs. 79−5874
SiD_3F, microwave spectrum, rot.-vibr. interaction consts., Coriolis reson., E1 moment 77−6766
SiH, rot. transition freqs. calc., rel. to search in interstellar space 78−93100
SiH^+, rot. transition freqs. calc., rel. to search in interstellar space 78−93100
SiH_3F, microwave spectrum, rot.-vibr. interaction consts., Coriolis reson., E1 moment 77−6766
SiO, population inversion mechanism for rot. levels, interstellar medium appl. 79−21406
SiO, rotational-level populations of interstellar molecule 79−97054
TiO, Franck-Condon factors rot. depend. 80−58319
TiO, rot. temp. in sunspots, rel. to photospheric and sunspot models 78−69766
YF, Franck-Condon factors and R-centroids, rot.-vibr. effects 78−50596
YF^+ emission, 3400 to 3700 Å, rot.-vibr. anal., electronic struct. 77−6839
ZrO, Franck-Condon factors rot. depend. 80−58319

molecular rotation in solids *see molecular reorientation; nuclear magnetic resonance; plastic crystals*

molecular rotation-vibration
see also macromolecular dynamics; molecular force constants; molecular rotation-vibration calculations
(3×3) order systems, force const. calcs. using isotopic freqs., parametric method 78−21907
ab initio methods for atomic and molecular processes 80−63550
acetyl cyanide, rot. spectrum, rot.-torsion-vibr. interaction, A-E rot. splittings 77−10667
acetylene, ν_2 band, Q-branch, high resolution CW CARS 77−42329
acetylene, Raman spectra, high resolution using laser source 78−42072
acetylene, rot. vibr. anal., Raman spectra obs. 80−69146
acetylene, vibr.-rot. IR spectra, mol. force field determ. ^{14}C effects 77−61748
acetylene-d_2(d_1), rot.-vibr. Raman spectra 80−83372
alkali dimer laser, continuous, optically pumped 78−87046
alkali halides, improved interaction pot., spectroscopic consts. calc. 79−86024
allene(-d_4), IR absorption intensities 80−1026
allene-1,1-d_2, rot.-vibr. Raman spectra 77−65477
allene-d_4, Raman and IR spectra, rot.-vibr. bands, ground state constants 78−25545
allylamine, anomalous Stark effect for torsional splitting 79−64040
allylamine, N-cis lone-pair gauche rotamer ground state microwave spectrum anal. 78−82720
asymmetric rotor molecule, props., vibr.-rot. effects 79−98066
asymmetric top molecules, Raman spectra, vibr.-rot. selection rules and general band contours 77−58020
atom+polyatom systems, rotation-vibration symmetry correlation 80−61074
atomic polar tensors and the effective charge-charge flux model of infrared intensities 78−70875
benzene, doubly degenerate high-resolution rot.-vibr. Raman bands 79−6941
benzene, IR spectra, fine struct. of rot.-vibr. bands 80−102504
benzene, mol. transilicon consignment, two-photon gas-phase spectra 77−54582
benzene, totally symm. bands, high resolution rot.-vibr. Raman spectra 78−70838
benzene, totally symmetric rot.-vibr. Raman bands 79−59474
benzene-d_6, high resolution rot.-vibr. Raman spectra 79−64006
benzenetricarbonylchromium, neutron inelastic scatt. spectrum and valence force field 80−48096
biacetyl, single rovibronic state fluoresc., quantum beats 79−31570
bimolecular reactions, rot.-vibr. symmetry correlation, building-up principle from mol. fragments 78−76849
bromoacetylene, microwave spectrum, r_5-struct., dipole moment, quadrupole coupling consts., vibr. excited states 77−79606
bromochlorofluoromethane, narrow saturated reson. absorpt., weak current detection 77−14433
bromomethane, IR spectra, $2\nu_2$, $2\nu_5$ and $\nu_2+\nu_5$ 78−42059
carbon tetrafluoride $^{12}CF_4$ laser, Doppler-limited absorption spectroscopy 80−74347
carbon tetrafluoride laser, CF_4 molecule $\nu_3+\nu_4$ band optical pumping 80−74349
carbon tetrafluoride laser, weakly forbidden vibr.-rot transitions 79−55121
chloromethane, IR spectrum, evidence for $2\nu_3$ overtone 79−68226
chlorotrifluoromethane, IR rovibr. spectrum *(German)* 80−47998
chromocene, solid, Raman transition assignments, mag. susceptibility, mag. moment 78−43861
correlation spectroscopy, rotational and vibrational relaxation autocorrelation functions 80−32856
cyanoacetylene, ν_3 vibr.-rot. band, diode laser spectrum 80−91563
cyanoacetylene, and deuterate, microwave spectrum, ground and excited vibr. states 78−90157
cyanomethane, IR laser photofragmentation $CN(X^2\Sigma^+)$ radical energy partitioning, rovibronic distrib. 77−61813
cyclohexane, plastic and liquid crystal phase, rot. correl. func. by Raman spectroscopy 80−23403
cyclopropane, gaseous phase, vibration-rotation spectra, anal. of ν_9 and ν_{10} bands 79−41172
cyclopropane-d_6, high resolution IR spectra, vibr. rot. band anal. 80−95621
diatomic, photoelectron ang. distrib. and intensity, vibr.-rot. struct. 78−42128
diatomic mol., vibr. rot. Hamiltonian expansion, Born Oppenheimer κ, explicit introduction 80−69118
diatomic molecule, Autler-Townes power splitting of rovibr. lines, direct obs. using intense IR laser 79−54854
diatomic molecule, bound-states, new trigonometric pots. 79−72383

molecular rotation-vibration continued
diatomic molecule, Franck Condon factors, vibr. rot. interaction effect 80−74198
diatomic molecules, dissoc., vibr.-rot. excitation effects 80−102502
diatomic molecules, excitation by intense reson. EM wave 77−61733
diatomic molecules, parity nonconservation effects and Λ doubling *(Russian)* 79−3432
diatomic molecules, rotational Raman intensities and polarisability anisotropy change meas. with internuclear distance 80−63641
diatomic molecules, spectrosc. consts., rel. to electronegativity 80−28007
diatomic mols., internal partition functions for O_2, N_2, NO and their ions, max. summation indices 80−27995
3,5-dichlorophenol, torsional-vibr. freq., ^{35}Cl NQR 78−70851
1,1′-dicyanoethene(-d_2), microwave spectrum, Coriolis interaction, rot. assignments 78−82721
electron+molecule, rot. and vibr. excitation 80−17721
electron scattering, L^2-basis set theory with vibr. and rot. coupling 79−41247
ethane, internal rot. splittings, vibr.-rot.-torsion energy levels perturbations 80−91531
ethylene, intracavity IR absorpt. in CO_2 laser, enhanced sensitivity 78−78835
ethylene, Raman spectra, ν_1, ν_3 and ν_5 bands, polarisability 77−58021
ethylene, Raman spectra, vibr.-rot. selection rules and general band contours 77−58020
trans-1,2-ethylene-d_2, Raman spectra, vibr.-rot. selection rules and general band contours 77−58020
ethylene-d_4, Raman spectrum, fundamental bands 79−59473
Feynman quantisation in curved space, vibr.-rot. spectra *(Russian)* 77−75121
fine structure splitting of rot-vibr. spectrum 77−57975
fluoroacetylene, laser Stark and IR-microwave double resonance, E1 moment, vibr. states 77−6813
fluoroacetylene-d_1, bending vibr.-rot. band ν_4, IR spectrum 77−75149
fluorobenzene, 2644 Å band system, rovibronic anal., isotope effects 79−6949
fluoromethane, mol. rot.-vibr. consts. of ν_3 band of $^{12}CH_3F$ 79−64118
fluoromethane, very high resolution IR spectrum anal. 77−34630
fluoromethane ν_2, ν_5 rot.-vibr. Raman bands, anisotropic components, ^{13}C shifts 78−74667
fluoromethane-d_3, laser Stark spectra, ν_6 band, vibr.-rot. consts., dipole moment 78−5277
formaldehyde, anharmonic pot. function, vibr. freqs., vibr.-rot. interaction, centrifugal distortion 77−38651
formaldehyde, IR spectrum, rot. anal., P-and Q-branch assignments 77−18923
formaldehyde, T_2-relax., rot. transitions, time resolved spectra, microwave pulsed spectrometer study 80−18846
formaldehyde and -d_1, MODR and collision-induced transitions in laser cavity 78−74686
formaldehyde-d_2, laser Stark spectra, Coriolis coupled ν_4 and ν_6 fundamentals 77−27065
formaldehyde-d_2 vapour, IR-UV double resonance 80−43078
formic acid, vibr. states, rot. and Coriolis parameters IR Fourier transform spectra 80−32709
formyl radical, laser mag. reson. spectrum at 5.3 micron 80−47981
four-body systems, rigid and nonrigid, correl. diagrams 79−45697
Freon 14, roto-vibr. mol. laser, low-temp. performance 80−9871
glyoxal, S_1-S_0 fluorescence after narrow band excitation, deconvolution 78−58734
halomethylsilanes, internal torsion modes, inelastic neutron scatt. 77−19105
intramolecular nonradiative transitions of gaseous small molecules, rovibronic level, lineshapes 80−95667
IR band moments, effect of dipole induction 77−75143
ketene, IR spectra, rot.-vibr. anal. of Coriolis coupled bands 78−86859
laser scaling, CO_2-TEA laser pumped 80−5728
line broadening by monatomic gas 80−9643
methane, $\nu_1+\nu_4$ vibration-rotation spectrum, spectroscopic constants *(French)* 79−13709
methane, absorption spectra, 6000-6500 Å, intracavity laser detection 79−89684
methane, mag. struct. of vibr.-rotational transition, review of laser appl. to precision meas. 78−42246
methane, narrow reson., elastic scatt., spectroscopic studies 80−53094
methane, solid, Raman spectra and II-III phase transition 80−2745
methane in condensed inert gas matrices, optical excitation of rotational transition, far IR absorption spectra 80−37808
methane-d_1, ν_6 band at 8.6 μm, vibr.-rot. band 78−21923
methane-d_4, B_0 determ., from ν_3 Raman band and IR spectrum 77−88455
methane-d_4, IR laser sideband obs., ro-vibr. struct., isotope shifts, line widths 79−72306
methane-d_4, Stark effect, rot. transitions in vibr. ground state, isotope shift 79−27029
methane-d, 4.5 μm absorpt., $2\nu_6$ overtone band anal. 80−91557
methanes, substituted, internal torsion modes, inelastic neutron scatt. 77−19104
methanol, rot.-torsional-vibr. quantum nos. for FIR laser action 80−14320
methoxy, Jahn-Teller induced rovibronic effect, nuclear spin-electron spin hyperfine Hamiltonian 80−83298
methyl azidoformate, microwave rot. spectrum, satellite transitions 80−69127
methyl bromide, ν_6 band, CO_2 and N_2O laser Stark spectroscopy 78−78698
methyl chloride, ν_1 band absorpt. strengths 77−75226
methyl chloride-d_3, 9.4 μm region laser Stark spectrum, ν_2 and ν_5 bands 77−27112
methyl cyanide, far IR laser line assignments 80−69380
methyl cyanide, IR rot.-vibr. spectrum, ν_2 and ν_3 and ν_4 bands anal. 77−75159
methyl isocyanide, microwave spectrum, anal., N isotope effects 77−50430
methyl isocyanide-d_2, IR spectrum, rovibr., ground state struct. 78−25537
methylacetylene, ν_5 band, microwave and IR laser Stark spectrosc. 80−91558
molecules, isolated, intersystem crossing, rot. motion effect 80−95669
multiphoton ionisation spectroscopy, sequential, appl. to I_2 79−50163

molecular rotation-vibration continued
multiphoton resonances, vibr.-rot. fine struct. effect *(Russian)* 79−86022
naphthalene, vap., Doppler free two-photon absorption spectra 78−5307
phosphine, IR spectrum, ν_1 and ν_3 band analysis 80−83366
photoelectron angular distribs., oriented or rot. resolved unoriented mols., dynamic and struct. data 78−37682
polyacetylenes, symm. top, microwave spectra 78−58676
polyatomic molecules, absorpt. forbiddenness removal in strong light fields *(Russian)* 79−36616
polyatomic molecules, collisionless dissoc. mechanism in laser field *(Russian)* 78−37696
polyatomic molecules, high vibr.-rot. state excitation and dissociation by IR field 79−41205
polyatomic molecules, vibr.-rot. coupling, modified Eckart conditions 80−27993
propylene, intracavity IR absorpt. in CO_2 laser, enhanced sensitivity 78−78835
propynal, energy dispersion and relax., laser IR-visible double reson. 80−48023
propynal, IR-microwave double reson., rot.-vibr. transitions, microwave assignment, mol. consts. 78−86902
propynal, rovibronic populations, collisionless IR multiphoton spectra, energy deposition, photoacoustic determ. 80−83354
Raman high-resolution molecular spectroscopy, review 78−42064
Raman spectroscopy, in high temp. chem., review 80−52234
reactive collisions, symmetry selection rules for ro-vibronic states 77−81385
rotation vibration emission turbulent flowfield spectral absorpt. coeff., temp. depend. 80−52987
small molecules, detect. by magnetically tuned freq.-modulated at. line sources 79−59508
spectroscopic and molecular consts., extremal props., book contrib. 78−78678
spectroscopy, finite symmetry adaptation 80−43032
spherically symmetric molecules, many-photon excitation in IR laser field 80−95596
symmetric bands, profile anal., correl. functions and moments *(French)* 77−71836
symmetric top molecules, C_{3v} and D_{3h}, rot.-vibr. wavefunctions and mol. point groups 79−93971
tetrafluoromethane, ^{19}F NMR, chem. shielding, intermol. interactions and rovibr. motion effects 78−9171
tetrafluoromethane, ν_4 fundamental of three isotopic species 78−70835
tetrafluoromethane, spherical top mol. vibr.-rot. spectrum with tunable diode laser 78−82734
triatomic molecule, rot. vibr. electronic Hamiltonian, Born-Oppenheimer approx., breakdown 80−87097
triatomic molecules, vibr.-rot. energy level calc. method 79−93974
1,3,5-trifluorobenzene, IR rot.-vibr. band contours 79−76430
van der Waals molecules, vibr.-rot. spectrum 79−13698
vinyl chloride, intracavity IR absorpt. in CO_2 laser, enhanced sensitivity 78−78835
Zeeman effect, anomalous, Doppler-free standing wave saturated resonance, book contrib. 78−9279
Ar+HF, state-to-state cross sections for rot. to translational energy transfer determ. 80−91644
Ar+N_2, projectile reduced mass variation, rotor state, collision energy, potential anisotropy influence 79−43571
Ar*+H, assoc. ionis., rovibronic struct. in electron energy spectrum 80−106380
BF_3, ^{19}F NMR, chem. shielding, intermol. interactions and rovibr. motion effects 78−9171
BO_2, gas, optically detected mag. reson. spectrum, $X^2\Pi$ rovibronic sublevels 78−82756
BaO+Ar(CO_2), in Ar flame, rot. and translational relax. by sub-Doppler optical-optical double reson. 80−95583
$BeKr^+$, $A^2\Pi_r$-$X^2\Sigma^+$ system, rot. anal., Λ-doubling consts. 77−27078
BiCl, form., microwave spectrum, hyperfine struct., mol. rot. vibr. consts., bonding 77−14418
Br_2, and isotopic forms, new rot.-vibr. lines, laser reson. fluoresc. obs. 78−991
Br_2, long-lived $A^3\Pi(1_u)$ state, quantum-resolved dynamics of excited states 80−69178
Br_2, reson. Raman spectrum, vibr.-rot. struct. 78−17674
Br_2, resonant fluoresc. at 5145 Å, isotope mols., rot.-vibr. states 77−61782
BrCN+N_2*, vibr. energy transfer, α_3 vibr.-rot. const., microwave meas. 77−83578
BrF_5, microwave spectrum, Coriolis interaction, A_1-A_2 splitting of kl levels 77−38657
$^{81}Br_2$, visible, vibr.-rot. absorption, fluoresc. decay, predissoc. quantum yield 77−18962
C_3, linear, high temp., rot.-vibr., anharmonicity, thermodynamic function calcs. 80−43830
CD^+, $A^1\Pi$, rot.-vibr. population distrib. 80−23396
CH^+, $A^1\Pi$, rot.-vibr. population distrib. 80−23396
CH_2, photoprod. from ketene, singlet-triplet energy separation and rovibronic level obs. 80−11936
CN free radical, $A^2\Pi$-$X^2\Sigma^+$ Red system, perturbation analysis 80−87247
CN, from ICN photodissoc., internal state distrib., laser-induced fluoresc. 77−36773
C_2N_2, gas, high resolution Raman spectra 78−17673
CO, absolute intensity meas., 4-0 vibr.-rot band 77−6854
CO, Autler-Townes power splitting of rovibr. lines, direct obs. using intense IR laser 79−54854
CO, Dunham vibration-rotation coefficients, isotope dependence 80−83518
CO electric discharge laser using single vibr.-rot. transition, laser line selection 79−59687
CO, ground-state, absorpt. oscillator strengths for vibr. rot. transitions 78−62846
CO, hole burning in single quantum power spectrum due to Autler-Townes splitting 80−9671
CO laser, multiphoton amplification, HF removal of forbiddenness *(Russian)* 80−53262
CO, rovibr. multiphoton spectra comput., hole burning effect 80−9672
CO supersonically driven chem. laser, kinetics of physical processes 79−45937
CO, vibr.-rot. absorpt. line., shock tube spectroscopy 77−71890

molecular rotation-vibration continued
CO, vibr.-rot. interaction, high excitation transitions in solar IR spectrum 77−68040
CO-alkane, liq. soln., vibration-rot. IR spectra, rot. diffusion 77−83584
CO-Ar(-N_2), C_2 and CN form. by optical pumping, room temp. 80−16701
CO-cycloalkane solns., CO IR vibr.-rot. spectra, solvent mol. struct. 77−83585
CO-N_2 and CO lasers, energy and spectral characteristics 80−14327
CO_2, ^{13}C NMR, chem. shift., determ. of virial coeffs., rovibr. motion 78−58720
CO_2, $20^0 1_{II}$←000 band, press. broadened coeffs. and absolute intensities, temp. depend., IR obs. 80−53054
CO_2, $30^0 1_{II}$←$00^0 0$ band, meas. at different temps. of absolute intensities, line half-widths and broadening by Ar and N_2 78−86865
CO_2, $30^0 1_I$←$00^0 0$ and $30^0 1_{IV}$←$00^0 0$ bands, absolute intensity meas. at different temps. 78−86864
CO_2, 4854 cm^{-1} $20 1_{III}$←000 band, intensities and half-widths, 197, 233, 294K 79−89713
CO_2 and isotopic species, high-resolution Fourier spectra near 4.3 micron 80−47982
CO_2, IR absorpt. spectrum, line parameters, spectral transmittance function *(Russian)* 77−57998
CO_2, IR spectra, 401←000 and 411←010 absolute intensities 78−21976
CO_2, isotropic Raman scatt., Fermi reson. vibr.-rot. spectra 77−38741
CO_2 laser, multiphoton amplification, HF removal of forbiddenness *(Russian)* 80−53262
CO_2 laser, output characts. at high pump levels 80−58509
CO_2, linear, high temp., rot.-vibr., anharmonicity, thermodynamic function calcs. 80−43830
CO_2, narrow reson., elastic scatt., spectroscopic studies 80−53094
CO_2, optically pumped laser, simultaneous lasing in bands of sequence 80−5725
CO_2, turbulent flow field, mol. vibr.-rot. bands, spectral absorpt. coeff., temp. depend. 80−52987
CO_2, Venus IR absorpt. bands, 3900-10000 cm^{-1}, assignment 78−7896
CO_2 vibr.-rot. band shape calcs. 80−969
CO_2, vibr.-rot. spectrum, absolute line intensity, vibr. transition moment 77−83655
CO_2, vibr.-rot. transitions power broadening by laser irrad. 77−3420
CO_2, vibr.-rot. transition overtones, active Raman spectra obs. 78−50550
$^{12}CO_2$, absorpt. spectrum at 4.3 microns 78−58692
$^{12}C^{16}O_2$, vibr.-rot. Raman spectrum, in Fermi reson. region 78−42073
$^{13}C^{16}O_2$, emission spectrum near 4.5 μm, nu_3 region spectroscopic consts. 77−38664
C_3O_2, bending pot. function, vibr. depend. 80−48058
C_3O_2, $\nu_2+\nu_7$ bands, Q-branch spectra, 12 μm region, l-doubling const. 77−65459
C_3O_2, semirigid bender, rot.-vibr. energy level separations obs., struct. and pot. functions determ. 80−83446
C_3O_2, vibr. IR spectra anal. 80−47984
CS, isotopic variants, IR absorpt. spectra, $\nu=2$←1 hot band 79−45721
CS, isotopic variants, IR absorpt. spectra, vibr.-rot. transitions 79−45720
CS^+, red emission spectrum, rot. anal. and perturbation effects 78−55193
$^{12}C^{32}S$, ($^{12}C^{34}S$), IR spectra, 2-0 vibr.-rot. bands, spectroscopic consts. 77−75153
CS_2, isotopic variants, $2\nu_1+\nu_3$ band IR spectra, rot. and rovibr. consts. 79−41166
CS_2, ν_3 band, dipole moment correl. function, isotope splitting and band contour 78−74650
CS_2, vibr.-rot. bands at .46 μm, isotope effects 78−94245
$^{12}CS_2$, $^{13}CS_2$, vibration-rotation bands 2700-2900 cm^{-1} *(French)* 78−25521
CSFCl, vibr. excited states, microwave spectra *(German)* 78−55167
C_3O_2, vibr.-rot. band, microwave, spectrum obs. 80−5536
^{13}CH, predicted Λ-doubling spectrum 77−30857
CaF, $B^2\Sigma^+$-$X^2\Sigma^+$ system, rot. and vibr. anal. 80−74156
Cl_2, and isotopic forms, $B^3\Pi(0_u^+)$ state, laser-induced fluoresc., collisional energy transfer rates 80−53038
Cl_2, B-X transition, rotationally resolved excitation spectra and predissociation in excited state 79−45754
Cl_2, laser-induced fluoresc., excited $B^3\Pi(O_u^+)$ states, collision-free lifetimes of ro-vibr. levels 79−94029
Cl_2+H(D), uni- and bimodal product energy distribs. 79−57207
Cl_2+muonium (H)(D), pot. energy surfaces, inversion calcs. 80−93734
ClCN+N_2*, vibr. energy transfer, α_3 vibr.-rot. const., microwave meas. 77−83578
ClO, bandstrength determ. of fundamental vibr.-rot. spectrum 78−70872
ClO, fundamental vibr.-rot. spectrum, rel. to remote sensing 77−42317
ClO, laser spectroscopy relevant to stratospheric photochemistry 78−88951
ClO radical, 2-0 vibrational overtone band, laser magnetic resonance spectroscopy study 80−48021
ClO radical, IR vibr.-rot. spectra, background data for atm. meas. 78−58679
ClO, vibr.-rot. bands, intensity parameters 78−17722
ClO_2, laser mag. reson. spectra tuned by Zeeman level crossing avoidance, perp. spectra 79−68229
ClO_2, laser mag. reson. spectra tuned by Zeeman level crossing avoidance, high-field spectra 79−76424
D_2, elec. quadrupole vibr.-rot. spectrum, 2.8 to 3.9 μm 79−805
D_2, electron impact excitation, transfer of moment impulses, vibration-rotation states *(Russian)* 79−7024
D_2, matrix rot. and vibr.-rot. spectra, free and hindered rot. 77−83607
D_3^+, IR spectrum, vibr.-rot. assignment 80−95627
DCl and $(DCl)_2$, matrix isolated Raman spectra 78−42063
DCl-cycloalkane solns., CO IR vibr.-rot. spectra, solvent mol. struct. 77−83585
D_2^+(HD^+), g-factors and related mag. props., calc. theory 79−41124
DI, IR absorption bands 4←0 and 5←0 79−98091
D_2O, $(D_2O)_2$, isotopic forms, Ar matrix isolated IR spectra, assignments, config. 77−6779
D_2O, matrix isolation spectra, vibr.-rot. lines, nucl. spin interconversion 78−46336
DT, vibr. rot. Raman anal. 80−87126
FCP, microwave spectrum, struct., dipole moment and vibr.-rot. props. obs. 80−91549
FO free radical, detection by CO_2 laser mag. reson. 80−45594
GeH_4, IR laser sideband obs., ro-vibr. struct., isotope shifts, line widths 79−72306
molecular rotation-vibration continued
GeH_4, Stark effect, rot. transitions in vibr. ground state, isotope shift 79−27029
GeH_4, ν_2 fundamental, isotope effect 80−43024
$^{74}GeH_4$, transition moment for ν_3, rel. to Jovian atmosphere 79−72363
H+H_2, projectile reduced mass variation, rotor state, collision energy, potential anisotropy influence 79−43571
H_2, 3d-triplet complex, Zeeman effect, eigenvectors and g-factors, rovibronic states 79−72353
H_2, electron impact, projectile reduced mass variation, rotor state, collision energy, potential anisotropy influence 79−43571
H_2, electron impact, vibr.-rot. excitation by slow electrons, multiple scatt. calcs. 78−13617
H_2, electron impact excited singlet-g states, optical and time resolved spectra, radiative lifetimes, quenching rates for rovibronic levels 80−23564
H_2 formation by H+H^- assoc. detachment rot-vib. levels population 79−44351
H_2, Fulcher system ($3p^3\Pi_u$→$2s^3\Sigma_g^+$), electronic-rot.-vibr. emission spectra, relative intensities calc. 79−6932
H_2, photoionisation cross-sections, ang. distrib. and intensity, vibr.-rot. struct. 79−50091
H_2^+, hyperfine struct., refined var. calcs. 77−75067
H_2-inert gas, bound complex form., anisotropic intermol. pot., IR spectra anal. 78−37634
H_2+Ne, collision-induced dissociation, Monte Carlo quasiclassical trajectory calcs. 79−74357
H_{22} quadrupole vibration-rotation transition probabilities 78−25512
HBr, fundamental IR band, solvent effect *(Russian)* 78−13501
HBr, spectral intensity, vibr.-rot. bands, dipole-moment expansion 77−75228
HBr, vibr.-rot. absorpt. spectra at very high foreign gas densities 78−78687
HCN, and isotopic forms, l-type doublet transitions 79−13704
HCO, IR spectra of ν_2 fundamental, laser elec. reson. 78−5226
HCO, ν_2 fundamental band, laser mag. reson. spectra 78−5256
HCO, vibr.-rot. transitions, IR laser mag. resonance 77−27098
HCP, ν_1 and $\nu_1+\nu_2-\nu_2$ IR absorpt. bands 78−42060
HCl, 1-0 absorption bands, absolute wavenumber meas. 77−3361
HCl and $(HCl)_2$, matrix isolated Raman spectra 78−42063
HCl, in dil. solution IR absorpt. fundamental shape temp. depend., solvent-solute interaction 79−26977
HCl, overtone vibr.-rot. bands, intracavity dye laser techniques meas. 80−91532
HCl, rot.-vibr. lines collision broadening, in He, Ar, N_2, O_2, CO, temp. depend. 77−58084
HCl, vibr.-rot. absorpt. spectra at very high foreign gas densities 78−78687
HCl, vibr.-rot. line broadening by CF_4 and SiF_4 77−27117
HCl, vibr.-rot. lines broadening and shifting by SiF_4 perturber 77−23521
$H^{35}Cl$, collision broadened vibr.-rot. linewidths and shifts in fund. band, low temp. obs. *(French)* 77−68076
HCl+Ar(Xe), spectral line shift of vibr.-rot. lines. press. shift 79−18237
HCl+iert gas, weak collisions, HCl spectral line broadening of IR spectra 80−74161
HCl+$N_2(O_2)(D_2)(H_2)$, HCl ν_0-ν_1 band perturbations, linewidth and shifts calcs., IR spectra obs. *(French)* 80−58251
HD_2, vibr.-rot. transitions, possible laser appl. 79−55122
HD^+, ground state vibr.-rot. spectrum, high resolution laser-ion beam reson. expt. 78−82733
HD^+, IR hyperfine struct. of rot.-vibr. transitions calc. 77−42323
HD^+, vibr.-rot. transitions, using new two-photon IR photodissoc. technique 80−23405
$H_2(D_2)$, Rydberg states, nonadiabatic effects, elec. field ionis. 80−9528
HF, 1-0, 2-0 absorption bands, absolute wavenumber meas. 77−3361
HF, dipole moment function, Schrodinger eqn. soln. using Morse pot. 77−79703
HF, IR dispersion, refractive index meas., vibr.-rot. fundamental intensities, dipole moment 79−37441
HF in absorption, anomalous dispersion meas. 80−95881
HF, vibr.-rot. band, absorpt. line self-broadening, rot. relax. 80−87213
HF, vibr.-rot. emission, from highly rot. excited states, in ClF_x-H_2 chem. laser 78−17926
H_2^+(HD^+), g-factors and related mag. props., calc. theory 79−41124
$H_2(HD)(D_2)$, matrix rot. and vibr.-rot. spectra, free and hindered rot. 77−83607
HI, 7-0 vibr.-rot. band in near-IR absorpt. spectrum, equilib. mol. consts. 78−21936
HI, line strength meas., 0→4 and 0→5 absorpt. bands, dipole moment *(French)* 78−62847
$H^{14}N_3$, rotational-vibrational Raman spectrum of ν_2 band 80−91564
HNO_3, high resolution spectral meas. of 11.3 μm band, using tunable diode lasers 78−33504
HNO_3, high resolution spectral meas. of 5.9 μm band using tunable diode laser 80−32707
HNO_3, vibr.-rot. spectrum, 855-915 cm^{-1} *(French)* 78−50543
H_2O,$(H_2O)_2$, isotopic forms, Ar matrix isolated IR spectra, assignments config. 77−6779
H_2O, $4\nu_2$ band, hot vap., Fourier transform spectrum, rot. consts. 80−32712
H_2O, electro-optical parameters determ. *(Russian)* 77−14466
H_2O, higher ro-vibr. levels, high resolution flame spectra 77−58033
H_2O, IR line intensities and widths, ν_2 rot.-vibr. band 78−9200
H_2O, isotope derivatives, mech. anharmonic problems, spectroscopic consts. 79−63983
H_2O, laser Stark and IR-RF double reson. at 6 μm 79−45760
H_2O, matrix isolation spectra, vibr.-rot. lines, nucl. spin interconversion 78−46336
H_2O, roto-vibrational structure, correlated bender theory 78−37627
H_2O, rovibr. Raman spectrum, ν_2 and $2\nu_2$ vibrs. 77−58022
H_2O vapour, rovibrational Raman spectrum 78−90174
$H_2{}^{16}O$, $H_2{}^{18}O$, determ. of line intensities from Fourier absorpt. spectra *(French)* 79−18186
$H_2{}^{16}O$, vibr.-rot. intensities of $3\nu_2$, $\nu_1+\nu_2$, and $\nu_2+\nu_3$ bands 78−5291
H_2O-H_2 cooling in supersonic nozzle, submillimetre wave generation 80−48229
$^1H^3H$ and $^2H^3H$, pure rot. and vibr.-rot. Raman spectra 80−14145
He+HF(DF)(HCl)(DCl), projectile reduced mass variation, rotor state, collision energy, potential anisotropy influence 79−43571
He_2^{2+}, bound excited states, potential energy curves and rovibronic energy, dissociation 80−23327

molecular rotation-vibration continued
HeH^+, (HeD^+), rot. predissoc., nucl. motion effects on rovibr. energies and widths 78−70885
HeH^+, $X^1\Sigma^+$ electronic ground state, pot. curve, rovibronic and dissoc. energies 79−72254
$^4HeH^+$, IR rot.-vibr. spectrum obs. 80−23420
$^4HeH^+$+He, 1 keV, collision-induced dissoc., ro-vibr. assignments, proton spectra obs. 79−3556
I_2, B state, fluorescence yield, individual hyperfine components 77−68067
I_2, B-X transitions, rot.-vibr. hyperfine coupling consts., extension to other levels 80−63625
I_2, high-dispersion polarisation-labelled spectrum 80−990
I_2, sequential multiphoton ionis. spectroscopy 79−50163
I_2, stepwise two-photon excitation, E-state vibr. bands, B-state vibr. rot. levels 79−26962
I_2, use as test mol. in modern spectroscopy, review 78−90317
I_2+I_2, collisional energy transfer, ground and excited states, polarisation spectra 80−32805
IBr, $B^3\Pi(0^+)$ excited state, laser-induced fluoresc. 80−58309
ICN, microwave spectrum, vibr.-rot. const., equilib. struct. 78−58677
ICl, $A^3\pi(1)$-$X^1\Sigma^+$ absorption spectrum, rotational analysis 80−47990
$^{127}I_2$, two photon excitation, rot.-vibr. structure of E-state 79−41213
$^{127}I_2$ rovibronic absorpt. lines, hyperfine struct. 80−78596
$^{129}I_2$ rovibronic absorpt. lines, hyperfine struct. 80−78596
$InX(X_2)(X_3)$, $InAlX_4$, X=Cl,Br, Raman spectra, up to 1200K 80−48003
K_2, absorpt. and relax. const. determ. by optical laser pumping method 80−102550
K_2, electron impact, vibr.-rot. excitation by slow electrons, multiple scatt. calcs. 78−13617
Li_2, electron impact, vibr.-rot. excitation by slow electrons, multiple scatt. calcs. 78−13617
LiH, isotopic species, $A^1\Sigma^+ \rightarrow X^1\Sigma^+$ bands 78−42091
$^{24}MgH^+$, high resolution rot.-vibr. spectra, solar atm. appl. 77−18939
$^{98}Mo_2$, electronic spectra after flash photolysis of $Mo(CO)_6$ 79−36622
N_2, 250 MW 0.53 micron laser pulse scatt. spectra, vibr.-rot. transitions *(Russian)* 77−46570
N_2, discharge excited vibr.-rotation states meas. by CARS *(Russian)* 79−3429
N_2, elastic and inelastic electron scatt., state to state cross section 80−78708
N_2, liquid, vibrational dephasing, computer simulation, Raman spectra, pair potential effect 80−63863
N_2 plasma, non-equilib., excited species, vibr.-rot. anal. fluoresc. obs. 80−54034
N_2, Raman spectra, intermol. torques and orientational correlation times 80−48006
N_2, rot. excitation by electron impact 1-4 eV 78−55248
N_2, rot. temps. determ. in diffusion flames using CARS 79−29358
ND_3, predissoc. mol., rot. resolved IR reson. scatt. 77−30882
$^{14}ND_3$, $^{15}ND_3$, ν_2 fundamentals and isotope shift 79−59456
NH, ND, $X^3\sigma^-$ state vibr. relax. Ar matrix, energy gap law breakdown 77−30963
NH_2, hyperfine struct. of u-state, microwave optical double reson. 79−68246
NH_2, radical, laser mag. reson. spectra in 9 μm region, ν_2 band 79−45724
NH_2, vibr.-rot. transitions, IR laser mag. resonance 77−27098
NH_2, X^1B_1 ground state, 010 level, mol. consts., emission spectra obs., 0.4-0.89 μ 78−74688
NH_3, absorption spectra, 6000-6500 Å, intracavity laser detection 79−89684
NH_3, and ND_3, new electronic state, multiphoton ionis. obs. 78−74717
NH_3, Coriolis and l-type interactions, ν_2, $2\nu_2$ and ν_4 states, IR spectra 80−47993
NH_3 forbidden vibr.-rot. transitions, ν_2 band, IR-microwave two-photon spectra 77−3428
NH_3, IR spectra, fine struct. of rot.-vibr. bands 80−102504
NH_3, molecular beam, IR-IR double reson., laser spectroscopic method appl. 79−68243
NH_3, ν_2 IR band, vibr,-rot. lines, self-broadening and intensities 77−34635
NH_3-$N_2(H_2)(Ne)(Ar)(Kr)(Xe)$, as R(1,1) vibr-rot. line parameters, ν_2 band, using CO_2 laser light 79−3444
$^{14}N^{14}N$, Raman spectra, direct determ. of rotation-vibration coupling coeff. α_e 77−38675
NO, $^2\Pi_{1/2}$ and $^2\Pi_{3/2}$ band centre freqs., opto-acoustic detection 77−58108
NO, and isotopic forms, $X^2\Pi$ state, IR obs., mol. consts. 78−42045
NO, fundamental band spectrum, determ. of rotational, spin-orbit coupling and Λ type doubling consts. *(French)* 77−6768
NO, IR emission Fourier transform spectroscopy, mol. rot.-vibr., RKR potential curve calc. 80−95618
NO, laser mag. reson. and IR-RF double-reson. near 5.3 μm 78−5258
NO, photofragment of NO_2, Doppler spectroscopy 80−53124
NO, rot.-vibr. fundamental obs., mol. consts. 77−57971
NO, selectively excited rovibrational states, multiphoton ionisation spectra 80−69202
NO, simultaneous one- and two-photon spectroscopy, Λ-doubling, spin-rot. splitting 78−66560
NO, $v=2\leftarrow1$ absorption band two-and multiphoton spectra, Λ-doubling const. vibr. depend. 77−30942
NO, vibr.-rot. bands of Raman spectra 78−29173
^{15}NO, vibr.-rot. transitions, Λ-doubling, optoacoustic spectroscopy meas. 78−42062
NO_2, (101) band, line strengths, spin-splittings and forbidden transitions 80−47987
NO_2, excited state, ODMR signal, occurrence in rovibronic manifold of $^2B_2$ state 79−36670
NO_2, fluoresc. spectra and collisional quenching 80−102538
NO_2, reson. coherent antiStokes Raman and absorpt. spectra 79−54860
NO_2, reson. Raman spectra, vibr.-rot. scatt. Q branch enhancement 78−989
NO_2, visible spectrum simplification, rot.-vibr. levels, excitation, polarisation labelling spectroscopy 80−32730
$^{14}N^{16}O_2$, IR spectra, $2\nu_2+\nu_3$ and $\nu_1+\nu_2+\nu_3$ bands, vibr. and vibr.-rot. consts. 78−983
$^{14}N^{16}O_2$, $\nu_1+\nu_3$ band, IR absorpt. spectra 78−78693
N_2O, ^{15}N NMR, chem. shift., determ. of virial coeffs., rovibr. motion 78−58720
molecular rotation-vibration continued
N_2O, 40°00-00°0 band, IR high press. absorpt. spectra profiles 80−52988
N_2O, as mol. probe in MBBA, solute solvent interaction, IR spectra vibr.-rot. fundamental 80−29155
N_2O laser, new lines in 10 μm region, rot.-vibr. transitions in (00^02-10^01) band 77−27281
$^{14}N^{16}O$, $^{15}N^{16}O$ isotopic species determ. using Zeeman scanning of atomic line, vibr.-rot. line profiles 79−49983
$^{14}N^{16}O$, overtone region IR emission spectra, vibr.-rot. Dunham coeffs. 79−41164
$^{14}N^{16}O$, $v=2\leftarrow0$ overtone band IR spectra, Λ doubling, hyperfine struct. 79−41165
$^{14}NH_3$, high power vibr.-rot. emission, optically pumped off reson. 77−7068
$^{14}NH_3$, ν_2-band Doppler-free two-photon resons. in Stark field 77−23527
Na_2, absorpt. and relax. const. determ. by optical laser pumping method 80−102550
Na_2, Doppler-free three-photon cross reson., intermediate and ground rot-vibr. levels 77−58107
Na_2, electron impact, vibr.-rot. excitation by slow electrons, multiple scatt. calcs. 78−13617
Na_2 in free jet expansion, internal-state distribution 80−83403
Na_2, Rydberg state, two-step polarisation labelling 80−87053
Na_2 supersonic beam rovibronic level population, anal. by laser spectroscopy 80−43118
Na_2 vapour, near reson. two-photon absorption, polaris. depend. 77−79666
NaK, $a^3\Sigma^+$ state, $X^1\Sigma^+$ state, fluorescence, visible spectrum 79−98114
NaK, $C^1\Pi$ state, spectroscopic consts., vibr.-rot. struct., K fluoresc. obs. 77−18901
Ne_2, van der Waals mol., vibr.-rot. spectrum 79−13698
Ne^*+H, assoc. ionis., rovibronic struct. in electron energy spectrum 80−106380
O_2, thermal decomposition, vibr.-rot. state depletion, Monte Carlo calc. 80−35506
O_2, vibr.-rot. Raman spectrum, Q-branch resolution, direct recording spectrometry *(German)* 79−85967
$(O_2)_2$ formation, rot.-vibr. symmetry correlation, building-up principle from mol. fragments 78−76849
O_3, IR and microwave spectra, ν_3 vibr.-rot. band 77−38663
O_3, infrared spectra of vibr.-rot. bands 79−64001
O_3, line and band strengths in IR spectra, variational calcs. 80−87112
O_3, line position and intensities of $2\nu_3$, $\nu_1+\nu_3$ bands 80−87181
OCS, 5.3 μm vibr.-rot. bands, rot. consts., spin-flip Raman laser obs. 77−34631
OCS, IR spectra using spin-flip Raman laser, combination band near 1890 cm^{-1} 78−37640
OCS, laser Stark spectra, 9.5 micron, band origins, dipole moments 77−18969
OCS, ν_3 band absolute wavenumbers *(French)* 79−98099
OCS, roto-vibr. mol. laser, low-temp. performance 80−9871
OCS, vibr.-rot. bands of Raman spectra 78−29173
OH, free radical, vibr.-rot. level population determ., including unresolved doublet struct. *(Russian)* 77−68033
OH, optimum mol. consts. and term values, $X^2\Pi$ and $A^2\Sigma^+$ states, vibr.-rot. and microwave freqs. 80−95577
OH radical, in Earth's atmosphere, pure rot. lines 79−92593
OH radical in premixed laminar methane-air flame, fluoresc. meas. of rot. temp. 79−80622
OH, vibr. ground-state, MFS, rot. spectra and electronic band anal. 78−5206
OH, vibrationally excited, high-resolution hyperfine Λ-doubling spectrum 78−90153
$OHX^2\Pi$ radical, ground and vibr.-excited ($\nu\leq6$) levels, microwave spectrum 79−63985
$ON^{81}Br$, anharmonic force field from IR and microwave data 78−82809
ONCN, far IR spectra, pure rot. and vibr.-rot. bands 78−82731
$ON^{35}Cl$, anharmonic force field from IR and microwave data 78−82809
$^{16}O^{16}O$, Raman spectra, direct determ. of rotation-vibration coupling coeff. α_e 77−38675
$^{18}O^{18}O$, Raman spectra, direct determ. of rotation-vibration coupling coeff. α_e 77−38675
OsO_4, and isotopic forms, stretching fundamental, 961 cm^{-1}, high resolution spectroscopy 78−90162
OsO_4, IR vibr.-rot. spectrum, theoretical interpretation 77−6776
OsO_4, multiple IR photon absorpt., rovibr. transitions 79−54926
PH_3, $3\nu_2$ and $4\nu_2$ states, K=3n A_1-A_2 centrifugal splitting 79−59484
POF_3, IR rot.-vibr. spectrum, mol. consts., laser Stark spectroscopy obs. 78−33508
RbKr, magnetic resonance meas. of spin-rotational interaction 78−33528
SF_6, ^{19}F NMR, chem. shielding, intermol. interactions and rovibr. motion effects 78−9171
SF_6, collisionless multiple-photon excitation, mol. rot. and vibr.-rot. interaction effects 78−74720
SF_6, collisions, laser spectroscopy investig. 80−9697
SF_6, excited state levels, perturbation through higher-order vibration-rotation order 79−36702
SF_6, IR laser multiphoton excitation, weak transitions in rot. band struct. 78−66614
SF_6, IR saturation spectrum, mag. hyperfine struct. 79−13714
SF_6, IR spectra, fine struct. of rot.-vibr. bands 80−102504
SF_6 molecule absorption of IR laser radiation *(Russian)* 80−986
SF_6, multiphoton excitation due to vibr.-rot. transitions 80−102546
SF_6, multiple-photon excited, double reson. spectroscopy 80−53030
SF_6, narrow reson., elastic scatt., spectroscopic studies 80−53094
SF_6, nonlinear absorpt. spectrum using Doppler-free polarisation spectroscopy 79−3440
SF_6, spherical top mol. vibr.-rot. spectrum with tunable diode laser 78−82734
SO, $a^1\Delta$ state, laser mag. reson. spectrosc. 78−94265
SO, and isotopic forms, $X^3\Sigma^-$ state, CO_2 laser mag. reson. spectroscopy 80−9602
SO_2, 4 μm $\nu_1+\nu_3$ band, Doppler-limited and atmospheric spectra 77−27064
SO_2, IR spectra, $\nu_1+\nu_2$ combination band, rot.-vibr. anal. 78−5225
SO_2, T_2-relax., rot. transitions, time resolved spectra, microwave pulsed spectrometer study 80−18846
SbO, B-X system fine struct. 79−50030
Sc+NO_2, chemiluminesc., nonequilib. product distrib. 80−101014
$^{80}Se_2$, $B\ ^3\Sigma_u^-$ state, Lande factor meas., mol. perturbations 79−45756

molecular rotation-vibration continued
SiD_3F, microwave spectrum, rot.-vibr. interaction consts., Coriolis reson., E1 moment 77−6766
SiF_4, ^{19}F NMR, chem. shielding, intermol. interactions and rovibr. motion effects 78−9171
SiH, optically derived lambda splitting rel. to interstellar existence 77−17657
SiH, SiH^+, line positions and oscill. strengths of rot.-vibr. bands, interstellar medium appl. 78−58644
SiH^+, rot.-vibr. consts. and dissoc. energy determ. from time resolved precision spectroscopy 80−58272
SiH_4, Stark effect, rot. transitions in vibr. ground state, isotope shift 79−27029
SiH_3F, microwave spectrum, rot.-vibr. interaction consts., Coriolis reson., E1 moment 77−6766
$^3T_2$, pure rot. and rot.-vibr. Raman spectrum 78−94253
TiO, $X(^3\Delta)$ state, vibrational IR spectrum using microwave powered molecular source, rotational analysis 80−9596
XeF, supersonic expansion jet, B—X system rot. and vibr. anal., isotope intervals, fluoresc. spectra 80−14174
XeO, $d^1\Sigma^+ \rightarrow a^1\Sigma^+$ $(b^2\Pi)$, green band emission spectroscopic anal., RKR pot. curves, bond lengths and dissoc. energies 79−41181
YI, IR $^1\Pi \rightarrow {}^1\Sigma$ system, Fourier spectrometry, rovibrational anal. 80−83360
YS, $A^2\Pi$-$X^2\Sigma$ and $B^2\Sigma$-X^2Sigma transitions vibr. anal. and B-X(0,) band rot. anal. 79−31537
ZrO, $X(^1\Sigma)$ state, vibrational IR spectrum using microwave powered molecular source, rotational analysis 80−9596

molecular rotation-vibration calculations
acetaldehyde, Coriolis resonance bands in IR spectrum 80−47995
acetylene, relationships between higher-transition frequencies 80−69119
anharmonic oscillator, three-dimens., interpolative perturbation theory 79−45703
asymmetric rotators, sextic centrifugal distortion consts. 79−72295
atom+rigid rotor collision, sudden rot. approx. 77−30966
atom+vibrator, stochastic theory, master or Fokker-Planck eqn. numerical solns. 77−30965
bromochlorofluoromethane, gas, IR band contours and intensities anal. 78−82788
Clebsch-Gordan coefficients, chain $SU(2) \supset D_\infty' \supset D_4' \supset D_2'$ 78−17552
composite particle, vibr. amplitude and vibr.-rot. anal. 80−74158
computational atomic and molecular physics, conf., Nottingham, England, (Sept. 1978) 79−59567
contact transformation technique 79−72295
Coriolis coupling, diagonal, in degenerate vibr. states of symm. or spherical tops 79−63977
diatomic molecular dilute solns., IR and Raman spectra temp. depend. anal. model *(French)* 77−88456
diatomic molecule, electronic pot. rot.-vibr. eigenfunction, analytic expression 80−52964
diatomic molecule, line intensities by perturbation calc. 79−85945
diatomic molecule, pots. superposition, rel. to lattice dynamics, mol. consts. calcs. 80−5598
diatomic molecule, rot.-vibr. hamiltonian, Born-Oppenheimer approx. breakdown 77−27051
diatomic molecule, vib.-rot. wavefunctions and matrix elements, pot. function effects 77−453
diatomic molecule, vibr.-rot. interaction effect on Franck-Condon factors 77−23485
diatomic molecule, vibr.-rot. states, high accuracy wave functions and energies 80−74159
diatomic molecule Hamiltonian, homogeneous derivation for spectrum anal. *(French)* 78−5113
diatomic molecules, rot.-vibr. matrix elements, fourth-order contribs. 77−46553
diatomic molecules, vibr. relaxation, vibr.-rot. levels, population relationships *(Spanish)* 80−959
diatomic molecules, vibr.-rot. coupling const. calc. 79−31503
diatomic molecules vibr. consts. determ., IR spectroscopic, quantum chem. teaching project 79−84914
diatomic mols., doublet states, spin-orbit and spin-rot. coupling cals., isotope depend. 77−57902
diatomic vibr. rot. expectation values, inversion 79−45700
1,1-difluoroethylene, vibration-rotation parameters in ν_4 and ν_9 states 79−36694
dimethylsulphoxide, r_3-struct. calcs. 78−70770
dipole moment matrix element for C_{2v} symmetry molecules 80−91537
Dunham coeffs., nuclear mass depend., Born-Oppenheimer approx. breakdown 78−21904
Eckart frame relation to Eulerian angles 79−59428
elastic scattering, nonlinear reson. freq. shift in rot.-vibr. transitions 79−36731
ethyl cyanide, isotopic species, rot.-torsion-vibr. interaction in rot. spectra 77−458
excitation in field of intense reson. wave, vibr.-rot. spectra *(Russian)* 77−75126
exothermic triatomic exchange reactions, prod. energy distrib., statistical dynamic model 78−92455
finite difference perturbation anal. 77−50420
fluoromethane gas phase IR rot. velocity correl. functions *(French)* 78−62778
formaldehyde, rot. struct. of 3500 Å transition, large amplitude vibr. effect 79−93976
formaldehyde-d (d_2) submillimetre lasers, optically pumped, assignment of laser lines 80−58513
formic acid, vap., laser lines identification 78−1222
formyl fluoride, and isotopic forms, mol. struct., from electron diffr. and microwave data 80−23570
Fues potential, vibr.-rot. spectra, Schrodinger eqn. soln., pot. energy curves *(Spanish)* 78−36784
fulminic acid, semirigid bender Hamiltonian, rot.-vibr. level separations, config., bending pot. 79−41152
group II halide-periodate complexes, force consts., compliance and Coriolis consts. calc. 78−42242
halomethanes, collision induced vibr.-rot. transitions, semiclassical theory 78−78785
high symmetry molecules, vibration rotation spectra, qualitative theory of clusters *(French)* 78−58645
inhomogeneous molecular gas radiation calc. using spectral comp. modelling 80−32697

molecular rotation-vibration calculations continued
interaction anisotropy, small angle scatt., spectral evidence 80−78600
ion, spontaneous IR rot.-vibr. emission probability 78−50535
isolated molecules, vibration relax. theory, adiabatic approx. 80−58237
lambda coupling in Π states of triplet or higher multiplicity 79−59429
linear molecular gases, IR radiation in Q branch 79−54850
lineshapes, effect of elastic and reorientation collisions 79−89712
methane, ^{13}C enriched, IR spectrum, ν_3-band forbidden lines, ground state consts. 77−18922
methane, ν_2 and ν_4 bands Coriolis interaction, using a general Hamiltonian formalism *(French)* 78−5192
methane, mol. rot.-vibr. consts., calc. using ν_1 band data 79−76529
methane, nonlinear optical reson. shift in mag. field, vibr.-rot. transition 78−13549
methane, simultaneous analysis of ν_2 and ν_4 bands 77−10662
methane, vibration-rotation ν_3-ν_4 band, theoretical spectra 78−42037
methane, vibration-rotation energies, $2\nu_2$ and $\nu_2+\nu_4$ bands 80−47963
methane, vibration-rotation energies of harmonic and combination levels 80−47962
methane-d_0(-d_4) vibrational state rotational struct., CARS spectra *(Russian)* 80−99513
methane-d_2, rotation-vibration constants, C−H bond length 79−94055
methane-d_4, isotope effect on rot. and vibr. consts. 79−22688
methyl halides, force consts. evaluation using gp. vibrs. and centrifugal distortion consts. 80−9580
molecular crystals, theory of IR spectra of H-bond 77−40223
molecular gas, laser-stimulated cooling 80−5594
$^{14}N^{16}O$, 1-0 band at 1900 cm^{-1}, meas., interpret. 78−58651
non-linear molecule, off reson., Wilson-Howard Hamiltonian, appl. of projector formulation for Van Vleck transform. 79−36613
non-reactive heavy particle collision calculations, review 79−59541
nonlinear molecule rotation-vibration motion, sum rules calculations 79−98062
nonpolar molecules in degenerate vibr. states, pure rot. absorpt. spectra 80−78598
nonrigid molecules, rot.-vibr. study, rigid core with nearly-free atoms 78−62789
1-phosphapropyne, microwave spectrum, vibration-rotation analysis, dipole moment, structural parameters 79−93989
polyatomic molecule, anharmonic force consts., vibr.-rot. interaction consts. 80−966
polyatomic molecule, semirigid, Watson hamiltonian expansion 80−23404
polyatomic molecule, sextic centrifugal distortion consts., Watson Hamiltonian, perturbation method 77−10785
polyatomic molecules, forbidden rotation-vibration transitions *(Russian)* 80−5593
polyatomic mols., ground rot.-vibr. energy, internal coord. Morse oscill. 77−79596
radiation escape kinetics, radiation captured by plane optically thick layer 80−95593
Raman scattering, spontaneous and stimulated, by forbidden rotational and vibr.-rot. transitions in strong optical field 80−74174
Raman spectra, C_{3v} and T_d mols., forbidden rot. line intensity 77−58019
real symmetry coordinates, groups having complex representations 78−82715
rotational energy levels, quartic and sextic centrifugal effects, book contrib. 78−21910
rotational line width of vibr. bands, self- and foreign gas-broadening 78−33552
silylacetylene, centrifugal distortion consts., thermodynamic functions 80−47959
spectral line intensities, accidental resonance effect 77−18987
spherical top molecules, low-resolution spectra of triply degenerate vibr.-rot. fundamental bands 78−82713
spherical top mols., matrix elements for vibr.-rot. operators 78−5194
spherical top mols., $T(\nu_3)$ rovibrational bands, level cluster patterns, centrifugal and Coriolis effects 79−18175
spherical top mols., vibr.-rot. eigenvalue spectrum, energy level cluster anal. 79−18174
Stark shift of transition freqs. in reson. optical field, hyperfine splitting 77−14487
symmetric-top molecules in liquids, Coriolis coupling 77−10657
symposium contrib., Florida, USA (March 1979) 80−51946
tetrahedral molecules, vibr.-rot. spectral parameters 77−3341
thermochemical properties of atoms and molecules in specific quantum states 78−68911
triatomic linear mol., parallel bands, band model parameters 80−43026
triatomic molecule, large-amplitude Hamiltonian for vibr.-rot. 78−25511
triatomic molecules, model with two large-amplitude coords. 78−5196
triatomic molecules with diatomic rigid core, vibr-rot. hamiltonian 78−74629
vibrational-rotational line profiles, theory 80−1029
vinyl bromide, mol. struct., from gas-phase electron diffr. and microwave data 80−23571
viscous gases, simplified transport coeffs. for vibr.-rotational relaxation *(Russian)* 78−51270
water, vap., rot.-vibr. levels, nonperturbative multimode model, 2 interacting Morse oscills. 78−9135
X_2Y nonlinear mols., isotopic relations, anharmonicity, reson. interaction, vibr.-rot. consts., rot. energy levels 77−10663
XY_4 molecule, tetrahedral, effective vib.-rot. Hamiltonian for triply degenerate vib. 77−10661
XY_4 molecules, isotope effect on rot. and vibr. consts. 79−22688
XY_4 molecules, tetrahedral, vibration-rotation energies of harmonic and combination levels 80−47962
XY_4 spherical top mols., general rot.-vibr. Hamiltonian formalism *(French)* 78−5192
XY_4 tetrahedral mol., IR absorption intensities, tensorial calc. *(French)* 77−18984
AlH, vibr. consts. of electronic states, calc. method 79−93967
AlO, Franck-Condon factors, rot. quantum number effect 79−31613
Ar+H_2, 4500K dissoc. collision vibr. selectivity, Monte Carlo trajectory method 79−70307
Ar+N_2, rot. and vibr. inelastic mol. collision cross section calc. 79−59542
Ar.HBr(DBr), van der Waals complexes, rot. spectra and struct. 80−48055
BH, Franck-Condon factors, rot. quantum number effect 79−31613
BH, mol. spectroscopic consts., FSGO calcs. 77−6758
BO, Franck-Condon factors, rot. quantum number effect 79−31613

molecular rotation-vibration calculations continued
C_2, Franck-Condon factors, rot. quantum number effect 79−31613
C_2, Swan band system, vibr.-rot. interaction on pot. energy curves 80−27965
CH^+, $^1\pi^-{}^1\Sigma$ band systems, vibr.-rot. interaction on pot. energy curves 80−27965
CN (0,0) vibr. band in Comet Mrkos (1957 V) 78−20734
CN, spectral absorpt. coeffs for fundamental and first overtone vibr.-rot. bands 77−14405
CN violet system, rotational and vibrational analysis 80−52961
CO, computation of multiphoton IR rovibration spectrum 79−89660
CO, Franck-Condon factors, rot. quantum number effect 79−31613
CO, ground state, radial matrix elements and dipole moment function 77−57973
CO, IR band absorpt. derivation from vibr.-rot. band spectroscopic variables 77−14434
CO pulsed laser emission with line selection, analytical theory 80−53277
CO, rot.-vibr. matrix elements, fourth-order contribs. 77−46553
CO, $X^1\Sigma^+$ state elec. dipole moment function, transitions, vibr.-rot. band calcs. 77−14410
CO_2, absorption spectrum line parameters *(Rumanian)* 77−42326
CO_2, rot.-vibr. bands, absorpt. coeff. calc. method, Fermi reson. effect on spectral lines 80−32696
$^{14}C^{16}O_2$, band centre at 4.5 μm, tunable diode laser spectroscopy 78−33503
C_3O_2, large amplitude bending mode, rot.-vibr. calc., assignments 77−18905
$^{13}C^{16}O$, IR emission, vibr.-rot. lines 77−3355
Ca_2, mol., vibr. quantum numbers of rotating vibrator 79−85949
Ca_2, vibr.-rot. states, high accuracy wave functions and energies 80−74159
CaH, Franck-Condon factors, rot. quantum number effect 79−31613
Cl_2, B-X transition, predissoc., laser-induced fluoresc. obs. 80−43093
ClCF, radical in Ar matrix, vibr. relax., multiphonon processes, fluoresc. 77−65430
ClH-dimethyl ether, vibr.-rot. IR spectra, quantum and classical mechanics 80−91561
CuH, vibr.-rot. interaction influence on band intensity parameters 79−49999
D_2, effective vibr.-rot. hamiltonian 77−27052
D_{2+}, semiempirical nonadiabatic pot. energy curves calcs. 78−17744
D_3^+, rot.-vibr. spectrum, ab initio calcs. 80−95595
DT^+, adiabatic relativistic rot.-vibr. energy levels 77−57964
DT^+, HT^+, HD^+, accurate energy and transition moment calcs. 77−14412
GeH_4, vibrational state rotational struct., CARS spectra *(Russian)* 80−99513
H bonded species, IR line broadening, kinematic and electronic coupling mechanisms 77−68043
$H+H_2 \rightarrow H_2+H$ three dimens. chem. reaction, distorted-wave calcs. 80−81294
H_2, effective vibr.-rot. hamiltonian 77−27052
H_2, electron impact low energy rot. and vibr.-rot. excitation cross sections, static exchange approx. 79−89799
H_2, $H\bar{H}^1\Sigma_g^+$ state $\bar{H}^1\Sigma_g^+$-$B^1\Sigma_u^+$ transition, $1<R<20$ a.u. 79−98094
H_2, photoelectron angular distrib. and intensity, vibr.-rot. struct. 78−46393
H_2Se, potential function and vibrational spectra 77−68030
H_2^+, HD^+ electron reduced mass use in electronic Schrodinger eqn. 77−10576
H_2^+, semiempirical nonadiabatic pot. energy curves calcs. 78−17744
$H_2+e^- \rightarrow H_2^* + e^-$, Gaussian basis Glauber approx., elastic and vibrorotational excitation cross sections 80−58399
$(H_2)_2$, $(D_2)_2$, $(HD)_2$ and H_2-D_2, Van der Waals complexes, mol. symmetry 80−42963
H_3^+ rot.-vibr. spectrum, ab initio calcs. 80−95595
H_3^++Ne, Petty-Moran ion-impact expt. reinterpretation re vibr. intervals 79−94063
HCN, relationships between higher-transition frequencies 80−69119
HCl-inert gas rot.-vibr. line pressure broadening and shift calc. 80−69124
HCl+N_2(CO)(O_2)(HCl), HCl linewidth, impact parameter calcs. 79−89714
HD, elec. dipole vibr.-rot. spectrum, line strengths, ab initio calcs. 78−25514
HD, $v=0$ to $v=5$ rot.-vibr. band, photoacoustic spectrosc. obs. 80−9589
HD^+, HT^+, adiabatic relativistic rot.-vibr. energy levels 77−57964
HD^+, HT^+, DT^+, accurate energy and transition moment calcs. 77−14412
HD^+, spontaneous IR rot.-vibr. emission probability 78−50535
HF, pot. curves, diagrammatic perturbation theory, spectrosc. consts. 78−25458
HF, spectroscopic consts., FSGO calcs. 77−6758
HF^+, Λ-type doubling and spin-doubling 78−74633
HNC (DNC), anharmonic force field, equilib. struct., rot. consts. and bond lengths 78−90147
H_2O, dimer config., vib.-rot. band intensities, rel. to 8-13 μm atmospheric extinction 80−9610
H_2O, rot.-vibr. Hamiltonian, rigid and semirigid bender models 78−5197
H_2O, rot.-vibr. Schrodinger eqn. soln., bond lengths and angles, force consts. 79−41151
H_2O_2(D_2O_2), vibr. consts rot. struct. doubling, Raman spectra assignment 77−54563
HPO, emission system, rot. anal. of vibr. bands 80−47957
He+H_2, rot. and vibr. inelastic mol. collision cross section calc. 79−59542
He+H_2, stochastic theory, master or Fokker Planck eqn. numerical solns. 77−30965
He+H_2, sudden rot. approx., rot. and vibr. cross sections 77−30966
He+I_2^*, sudden rot. approx., rot. and vibr. cross sections 77−30966
He+I_2^*, sudden rot. total rot. inelastic cross section 77−30967
He_2, vibr.-rot. interaction factor 78−42036
HeH^+, spectroscopic characts. in ground and first excited triplet states, Dunham pot. approach 77−42234
$^4HeH^+$, ro-vibr. quasi-bound levels of $X^1\Sigma^+$ state, eigenenergies, dissoc. 77−26997
K_2, ground state thermalisation speed, collision cross-sections meas. *(Russian)* 80−78723
LaF, Franck-Condon factors and R-centroids, rot.-vibr. effects 78−50596
$Li+Li_2 \rightleftarrows Li_3$, rovibronic symmetry correlation 78−92461
Li^++CO, differential cross-sections, ab initio CI vibrotor pot. energy surface calcs. 78−46421
LiCN, vibr.-rot. spectra, model with two large-amplitude coords. 78−5196
LiH, $LiHe^+$ and $LiHe_2^+$ systems, ab initio SCF LCAO calcs. of stability and spectroscopic consts. 77−71748
LiH, mol., vibr. quantum numbers of rotating vibrator 79−85949
LiH, mol. spectroscopic consts., FSGO calcs. 77−6758
Mg_2, mol. consts. calcs., inverted perturbation approach 77−57969
^{24}MgH, transition probabilities, oscill. strengths, rot.-vibr. bands fine struct., stellar atm. appl. 77−18918
N_2, asymptotic expansion for Morse-Pekeris oscillators, band strength factors, electronic transition moment 78−78755
N_2, electron impact rot. and vibr. excitation, elastic scatt., close coupling and Born approx. 80−28108
N_2, electron scatt., vibr. excitation, rot.-vibr. close-coupling calcs. 77−6947
N_2, Franck-Condon factors, rot. quantum number effect 79−31613
N_2, Raman intensity, ab initio calc. 80−1028
N_2^+, Franck-Condon factors, rot. quantum number effect 79−31613
NH, 3Π states, MC wavefunctions, rot.-vibr. anal. 79−13652
NH, mol. spectroscopic consts., FSGO calcs. 77−6758
NH, rot.-vibr. anal. by finite difference perturbation method 77−50420
NH_3, time-resolved four-level double-reson. signal, coherent transients effects 78−78732
NO, gamma band emission rate factor, rel. to upper atm. comp. determ. 77−54572
NO, IR band absorpt. derivation from vibr.-rot. band spectroscopic variables 77−14434
NO, $v=0,1$ states, spectroscopic data calc. 78−86851
$^{14}N^{16}O$, overtone bands, determ. mol. consts. 78−58652
NO_2 and isotopic forms, total quartic potential function 78−13486
O_2, Franck-Condon factors, rot. quantum number effect 79−31613
$^{18}O_2$, Raman spectrum and mol. parameter 77−46565
OCS, rot.-vibr. levels and semiclassical energy levels 80−37804
OH, high resolution emission spectrum in oxyacetylene flame, mol. vibr.-rot. consts. 77−3409
OH^+, rot.-vibr. bands, line positions, oscill. strengths transition probabilities 80−67828
O_3O_2, $3\nu_7{}^{1f}+\nu_2 \leftarrow 2\nu_7{}^0$ $4\nu_7{}^0+\nu_2 \leftarrow 3\nu_7{}^{1f}$ Q-branches, diode laser analysis 78−74660
$^{12}O^{16}O$, $^{12}C^{18}O$, IR emission, vibr.-rot. lines 77−3355
$^{13}O^{16}O$ and $^{12}C^{18}O$, emission bands of $E^1\Pi$-$A^1\Pi$ transition 78−90177
PF_5, total nuclear spin in rovibronic state, three calc. methods for hyperfine mag. struct 78−58658
PO, $B^2\Sigma^+$ state perturbations 77−30849
SF_2, microwave spectrum inertia defects, ν_1, ν_3, ν_2, equilibrium structure, vibration rotation constants, anharmonic potential functions 79−93988
SF_6, comparison of multiple-photon excitation models 78−94297
SF_6, pumped by OC_6 laser, transition strengths 77−14416
SF_6, total nuclear spin in rovibronic state, three calc. methods for hyperfine mag. struct 78−58658
ScF, Franck-Condon factors and R-centroids, rot.-vibr. effects 78−50596
SiH_4, ν_3 band assignment in IR and Raman spectra, ν_1-ν_3 coupling 77−75124
SiO, isotopic lines in sunspots, $^{28}Si/^{29}Si/^{30}Si$ isotopic abundance ratio determ. 79−30044
TbF, absorption spectrum, vibr. and rot. anal. 78−55181
YF, Franck-Condon factors and R-centroids, rot.-vibr. effects 78−50596
ZrO, vibr.-rot. interaction influence on band intensity parameters 79−49999

molecular rotational energy transfer *see molecular rotational-vibrational energy transfer*

molecular rotational states *see molecular rotation*

molecular rotational-vibrational coupling *see molecular rotation-vibration*

molecular rotational-vibrational energy transfer
see also atom-molecule reactions; molecule-molecule reactions
$^1\Sigma^+$-eystems, rot. and vibr. excitation, frame-transformation approx. 77−42421
acetaldehyde+CO_2, vibr. relax., search for unquenchable species, room temp., 5-2200 torr 78−9229
acetone, Raman scatt., intermol. vibr. coupling effects 77−58026
acetonitrile, ν_2, ν_3 and $2\nu_3$ bands, vibr. relax., Raman spectra of liq. and dil. soln. 78−9154
acetonitrile, IR and Raman spectra, vibr. and reorientational and energy transfer width separation, rot. const. determ. 80−87131
acetonitrile, soln., vibr. relax., isotropic Raman spectrosc. obs. 79−50025
acetonitrile-carbon tetrachloride solns., rot. and vibr. relax., Rayleigh and Raman scatt. 77−66513
acetylene, triplet states, electron impact energy-loss spectra 77−68128
acetylene cation+methane, reaction, vibr. and translational energy depend., mass spectrosc. obs. 79−47908
acrolein, vap., visible luminesc. excited by pulsed CO_2 laser 79−54894
air, afterglow plasma, interaction with glass, Cu, steel walls, calorimetric method obs. 78−14177
air, vibr. energy transfer rates rel. to HF sound absorpt. meas. 78−1475
air-water fogs, rot. and vibr. relaxation rel. to audible sound propag. 78−1473
alicyclic ketones, triplet state behaviour, non-RRKM photochemical decay, vibr. relax. 78−61030
alignment relaxation rate, laser saturation reson. technique 78−25755
alkali halide+inert gas, inelastic scatt., short-lived complex form. 79−13796
alkanes, vap., fluoresc. lifetimes meas. 79−50064
alkylbenzenes, jet-cooled, vibr. relax., absorpt. spectra 80−74236
alkylbenzenes, jet-cooled, vibr. relax., fluoresc. spectra 80−78694
angular momentum distributions in collision processes and the location of the transition state in ion-molecule reactions 78−64808
anharmonic molecule, selective multiphoton absorpt. by vibr. mode theory 77−83669
anharmonic molecules, vibr. relax. under strongly pumped conditions, anal. theory 78−5328
anharmonic oscillator in inert gas, vibr.-translational relax., low temp. 77−75270
anharmonic oscillators, two-component system, diffusion description of vibr. relax. 80−23528
anharmonic oscills., vibr. relax. eqns. *(Russian)* 77−34739
aniline+AR, $^1B_2$-state collision induced intramol. vibr. energy transfer, SVL fluoresc. obs. 79−54904

molecular rotational-vibrational energy transfer continued
anthracene vapour, conc. depend. of diffuse component of fluoresc. spectrum *(Russian)* 77−46601
anthrone, 533 nm excited state absorpt. kinetic, triplet quenching solvent, internal conversion, vibr. relax. 78−21935
$Ar+SO_2$, vibr. relax., shock tube study 80−48062
aromatic hydrocarbon in soln., excited electronic state vibr. relax., time resolved fluoresc. 80−48024
asymmetric diatom+atom, phase shift affecting vibr. transfer 79−64080
asymmetric top molecules, collisional selection rules, perturbation calcs. 77−61838
atom+diatom, collinear, vibr. energy transfer, stochastic theory, nonmarkovian effects 79−81262
atom+diatom, collinear collision, vibr.-translation energy transfer, model calc. 78−66634
atom+diatom, inelastic cross-sections, rot. quantum number, energy scaling 77−83692
atom+diatom, inelastic scatt., initial rot. and vibr. excitation effects 77−14543
atom+diatom, rot. and vibr. excitation, S-matrix element calcs. 78−17763
atom+diatom, rot. excitation, fixed nuclei approximation calcs. 79−6990
atom+diatom, rot. inelastic cross sections, ang. and rot. energy moments 79−81261
atom+diatom, rot. inelastic scatt., mag. transitions, time reversal symm. 80−48066
atom+diatom, rot. state distrib. interference effects, propensity and inverse propensity 77−83694
atom+diatom, rot. transitions, body-fixed formulation for close coupling calc. 78−78786
atom+diatom, sudden approx. of Cross, computational tests, cross section factorisation, scatt. phenomena 80−58352
atom+diatom, vibr.-translational energy transfer, mol. rot. effects calcs. 77−34736
atom+diatom, vibr.-translational energy transfer, self-consistent and stochastic treatment 77−83693
atom+diatom collision, vibr. and rot. excited states, field theory 77−14533
atom+diatom collisions, reorientation cross section calc., distorted wave and Bernstein Kramers approx. 79−843
atom+diatom inelastic scattering, exponential gap law 77−10737
atom+diatom reaction, endoergic, vibr. energy consumption 77−52621
atom+diatomic molecule, coupled states, P-helicity, and effective pot. methods comparison 77−30944
atom+diatomic molecule, rot.-vibr. excitation, theory 77−75271
atom+harmonic oscillator, classically forbidden transitions, classical and classical path methods 77−520
atom+harmonic oscillator, vibrational excitation, sudden approx. theory 80−53103
atom+harmonic oscillator collinear collisions with attractive interactions, semiclassical theory 77−522
atom+linear molecule, rot. excitation, classical and quantum calcs. 78−1059
atom+molecule, 3-dimens. vibrot. reaction probabilities from collinear results, information theoretic synthesis 79−74354
atom+molecule, electronic to vibrational/rotational/translational energy transfer, crossed beam expt. 79−89750
atom+molecule, IR induced vibr. transition, Schrodinger eqn. distorted wave calc. 77−23538
atom+molecule, linear rotor excitation, infinite order sudden approx. 78−74740
atom+molecule, optical potential approach 78−62885
atom+molecule, rot. excitation, body-fixed approx. 77−19015
atom+molecule, rot. excitation, classical transition probabilities calc. 77−88533
atom+molecule, rot. excitation, M-conserving approx. in time depend. theories 79−3546
atom+molecule, rot. excitation cross sections, use of rot. and orbitally adiabatic basis functions 79−59543
atom+molecule, rot. inelastic collision, rot. alignment calcs., quantum formulation 77−61834
atom+molecule, rotational rainbow maxima: a time dependent study 80−58353
atom+molecule, vibrational transition probability, information theoretic and collision dynamics calcs. 77−34728
atom+molecule chemical reaction, vibrational-translational energy transfer, forced harmonic oscill. model 79−59540
atom+molecule collisions, mol. basis sets as energy approaches excitation threshold 78−78783
atom+molecule collisions, rot. energy transfer 79−50118
atom+molecule collisions, theory, book 79−72394
atom+molecule inelastic collisions, statistical decoupling 77−517
atom+molecule rot. effect on polar mol. collisional ionis. 77−83702
atom+molecule rot. inelastic scatt., coupled eqns. for single initial state, variation-iteration method 79−68301
atom+polyatomic molecule, pair correlation function role 79−64082
atom+polyatomic molecules, vibr.-translational energy transfer in thermal reactions 78−23924
atom+symmetric harmonic oscillator, vibr. energy transfer, 1-D and 3-D rate consts. calcs. 78−50611
atom+symmetric top, rot. excitation, IOS approx. calcs. 79−45801
atom+symmetric top, rot. inelastic collisions, physical anal. 79−6991
atom + molecule inelastic differential cross sections, rotational rainbows 79−50114
atom-diatom kinetic cross section, ES, CS and IOS approx. with translational-internal coupling, viscomag. effect 80−63764
atom-molecule collisions, rotational transitions, classical cross sections, sudden approx. calcs. 79−89751
bacteriorhodopsin, Debye rot. relax. times, modulation excitation spectrophotometric obs. 79−3532
1,2-benzanthracene in soln., luminesc. and vibr. relax. 79−52007
benzene, $^1B_{2u}$ and $^3B_{1u}$ states nonradiative decay, collisional deactivation 77−6819
benzene, liq., vibr. excitons, reson. energy transfer and local struct., IR spectra 77−75145
benzene, ns time-resolved emission spectra, collisional processes 77−3490
benzene, S_1 state, mode to mode vibr. energy flow, low pressure fluorescence spectra exam. 78−25664
benzene, vapour, transport coeffs., theoretical study 77−3904
benzene, vapour-phase, absolute fluoresc. quantum yields, nonradiative processes 77−6829

molecular rotational-vibrational energy transfer continued
benzene, vib. relax. and Raman line widths 77−32359
benzene, vibr. relax. in soln., ν_1 C-H stretching band Raman spectra 78−25540
benzene+Hg, electronically excited, mol. fluoresc., vibr. relax. cross sections and equilibration rates determ. 80−87205
benzene+$O_2(^1\Sigma_u^-)$, photo-oxidation mechanism, optoacoustic determ. 77−12808
benzene ($^1B_{2u}(S_1)$)+Ar(benzene), rot. relax. to Boltzmann distrib. 78−86936
benzene (S_1)+OCS, V-V reson. energy transfer, microscopic reversibility, level degeneracies role 79−86045
benzene and deuterates, highly vibr. excited intramolecular V-V transfer, visible and photoacoustic spectra 80−32729
benzene-d_0, -d_6, intramol. vibr. energy relax. calcs. 78−33574
benzene-d_6, liq., Raman spectra vibr. relax. and band widths 78−23440
benzene-d_6+N_2+CO_2, electronically excited, mol. fluoresc., vibr. relax. cross sections and equilibration rates determ. 80−87205
benzonitrile, depolarised Rayleigh scatt. 78−68522
benzonitrile, transverse sound wave and mol. motion, light scatt. obs. 77−79621
biacetyl in supersonic jet, emission spectra, energy-resolved decay times 79−81224
bimolecular reactions, rot.-vibr. symmetry correlation, building-up principle from mol. fragments 78−76849
binary liquid mixtures, vibr. and rot. relax., crit. point effects 79−50969
binary reactive gas, in laser field, vibr. energy distrib. 79−6972
boundary relaxation of vibrationally excited gas *(Russian)* 79−3549
bromochloromethane, ultrasonic absorption obs. 79−98537
bromomethane, vibr., rot. and translational energy exchange, semiclassical theory 80−48067
bulge effect, in rot. inelastic scatt., isotope shift 79−86047
n-butane, freejet flow, vibr. relax. time 79−98760
n-butane-CO_2, freejet flow, vibr. relax. time 79−98760
t-butyl bromide, vibr. relax. in pure liq. and soln., Raman spectra 80−66167
t-butyl chloride, vibr. relax. in pure liq. and soln., Raman spectra 80−66167
camphor, separated optical isomers, rot.-vibr. transitions, IR-RF double reson. obs. 78−21951
carbon tetrachloride, polarized light scatt., relaxation processes 80−60615
CARS, effect of rot. relax. in continuous media *(Russian)* 79−10186
catalysis, heterogeneous, vibr. excitation, classical trajectory calcs. 80−26045
chemical laser efficiency, in limits of fast and slow rot. relax. 77−14700
chemical reaction dynamics, Franck-Condon factors rel. to information theory for vib.-rot. distribs. and isotopic branching ratios 77−60041
2-chloro-2-nitropropane, far IR-microwave estimation of binary collision approx. 80−55095
chlorobenzene, polarized light scatt., relaxation processes 80−60615
chlorofluoromethanes, laser photolysis, product vibr. relax. rates and diffusion coeffs. 80−55680
chloroform, liq. vibr.-translational energy exchange, temp. depend., Brillouin scatt. obs. 79−73959
chloroform-d_1, Raman scatt., intermol. vibr. coupling effects 77−58026
chloromethane, rot. dynamics, far IR spectra 77−19864
chloromethane, vibr., rot. and translational energy exchange, semiclassical theory 80−48067
chlorotrifluoroethylene, multiphoton dissoc., fragment energy partitioning 80−55681
classical trajectories, use of perturbation theory in asymptotic region, appl. to HF+HF 79−98199
classical versus quantum calcs., forced quantum oscillator and moment methods 80−28095
coherent radiation sources for mol. spectroscopy, review 77−3343
collinear collisions, vibr. energy transfer, exact classical and quantal calcs. 77−19014
collisional energy transfer, stochastic reductions, generalised cumulant expansion calcs. 77−71847
collisional line broadening of microwave spectra, semiclassical theory 78−29776
collisional relax. of highly excited states, laser-induced fluoresc. obs. 80−58205
competitive decomposition and stabilisation models for collisional efficiency in external activation systems 80−25989
condensed systems, vibrational relaxation times calc. from low-freq. mol. spectrum 78−2205
coumarin 6, ultrashort vib. population lifetime of ground state in vapour phase 77−30929
cyanomethane, collisional rot.-line widths and shifts, microwave region 78−25619
cyclobutane decomposition, vibr. excitation transients using variable encounter method 80−61072
cyclobutane-t, chem. activated by nucl. recoil reaction, energy transfer interpret. 80−25985
cyclobutane-t, chemically activated by nuclear recoil, vibr. energy transfer 77−66763
cyclohexane, liq., vibr. relax. at high press., Raman obs. 79−50026
cyclohexane-tetrachloromethane, heteromolecular vibr. relax. time, Rayleigh-Brillouin spectra 78−59731
cyclopropane, partial vibr. energy transfer map 80−32760
cyclopropane, thermal unimol. isomerisation, vibr. energy transfer, diffusion cloud method 80−26001
cyclopropane, vibr. energy transfer processes, laser induced fluorescence exam. 78−25663
cyclopropane+inert gas, reactant decomp., rot.-vibr. energy transfer, relax. analytic soln. 80−55650
1,1-cyclopropane(-d_2), isomerisation in He bath, vibr. transfer, temp. depend. 79−24723
1,1-cyclopropane-d_2, isomerisation transient vibr. energy distrib., collisional relax., variable encounters method 80−50836
1,1-cyclopropane-d_2, rearrangement, collisional vibr. energy transfer, temp. depend. 78−15668
1,1-cyclopropane-d_2, struct. isomerisation, vibr. distrib. collisional relax. dynamics, surface collisions 79−91926
dense media, energy transfer between coupled mol. vibrs. *(German)* 78−37719
dense media, Q-branch Raman scattering impact theory, collisional rotational relaxation, line broadening 79−98104
dense media, radiationless vibr. phase relax. theory *(German)* 78−37720

molecular rotational-vibrational energy transfer continued
diacetyl, triplet-singlet conversion, by laser spectrosc. technique 79−86002
diatom, resonance Raman scatt. amplitude, coupled channel eqns., collision theory 78−94248
diatom+atom, rot. transitions, mols. in II state 78−82825
diatom+atom (electron) scatt., vibr.-rot. excitation, generalised field theory method 77−23537
diatom+diatom, ang. momentum decoupling approximations and factorisation 79−72397
diatom+diatom, optical pot. theory 79−86041
diatom+diatom, quantum vibr. transition probabilities from classical trajectories 77−34730
diatom+diatom, vibr. energy transfer, collinear and 3-dimens. rate consts. 80−48065
diatom+diatom, vibrorot. energy transfer, optical pot. theory, distinguishable mols. 78−13575
diatom+molecule, laser-induced vibr. excitation 79−98205
diatomic+atom, rot. polarisation, spectator model 77−30970
diatomic+polar diatomic, vibr.-rot. absorpt. line shift 77−27160
diatomic beam, scatt. on solid surface, rot. energy distrib., hard cube model 77−34717
diatomic gas, dissoc. of nonequilib. gas, two-quanta V-V exchange 79−3547
diatomic gas, thermal cond. in high temp. region, effect of vibr.-rot. collisions 77−42955
diatomic gas, vib. energy transfer calcs. *(French)* 77− 27153
diatomic gas, vibr. cross section, orientation depend. of interaction pot. *(French)* 77−515
diatomic gas, vibr. excited, large V-T relax. and isotope effect 79−3548
diatomic gas, weak nonlinear wave propag., effect of convection, vibr. relax. 77−27623
diatomic gas mixture, perturbation soln. of vibr. relax. eqn. 77−10741
diatomic gases, harmonic oscill. system, vibr. energy relax. 78−66632
diatomic homonuclear molecules, vibr. relax. in nozzle expansions *(French)* 78−62877
diatomic mol., effect of anharmonicity on kinetics during spontaneous emission *(Russian)* 78−70904
diatomic mol., vibr. relaxation, nonequilibrial dissoc. rate consts. 77−52632
diatomic mol.+diat. mol., rot. inelastic collisions, symmetry considerations in quantum treatment 77−46623
diatomic molecular gas, vibr. excited, on surface, accommodation coeff. *(Russian)* 78−38973
diatomic molecule, bulk rot. or vibr. relax. processes, information theoretic approach 77−58132
diatomic molecule, electron scatt., vibr. and rot. transitions, close coupling theory 78−22041
diatomic molecule, polarisability anisotropy derivative determ. from relative Raman intensities 78−55177
diatomic molecule, rot. and vibr. relax., quasiclassical rot. relax. model 79−76491
diatomic molecule+identical mol., vibr. inelastic collision, semiclassical theory 77−14537
diatomic molecule+triatomic mol. combination levels, V-V exchange 77−27165
diatomic molecule electron scatt. vibr. and rot. transitions, hybrid and close-coupling theory 78−22042
diatomic molecules, binary mixture, thermodynamic description of vibr. relax. 77−34724
diatomic molecules, electron reson. scatt., ang. distrib., vibr. and rot. excitation, theory 78−22043
diatomic molecules, in inert matrices, vibr. energy transfer, theory 78−82822
diatomic molecules, matrix isolated, vibr. relax., rot.-translational coupling 80−53102
diatomic molecules, rot. transition probabilities calc. using Morse pot. 79−86046
diatomic molecules, rotational transitions in collisions, semiclassical theory 78−29843
diatomic molecules, theory of vibrational relax. in quasi-equilib. approx. *(Russian)* 78−58790
diatomic molecules, vibr. relax. at intermediate energies 79−10180
diatomic molecules, vibr. relax. distrib. rate, rel. to nonequilib. vibr. levels and dissoc. 77−54596
diatomic molecules, vibr. relaxation, vibr.-rot. levels, population relationships *(Spanish)* 80−959
diatomic molecules, vibr.-translation relax. calcs., classical vs. quantum diffusion 80−14196
diatomic molecules, vibr.-vibr. energy transfer probabilities 78−22009
diatomic molecules at low press., dissociative instability, role of vibr. energy 80−74227
diatomic molecules in monatomic matrix, vibr. relax. 79−18263
diatomics, vibr.-translational relax., diffusion description 79−41225
diazanaphthalenes, excited state absorpt. spectra and intersystem crossing kinetics 80−74176
dibenzene-naphthalene, relax. time of vibr. levels of ground state *(Russian)* 77−44054
dibromomethane, ultrasonic absorption obs. 79−98537
dichloromethane, vibr. population lifetimes in liqs. anti-Stokes Raman scatt. 78−74665
dichloromethane-cyclohexane, liq. mixture, intermol. vibrational energy transfer, US study 80−70313
dichloromethane-d_0(d_1), ultrasonic absorption obs. 79−98537
dichloromethane-d_2, vibr.-vibr. energy transfer, laser-induced fluoresc. obs. 80−78689
3,3′-diethylthiacarbocyanine iodine-rhodamine 6G, energy transfer with increased local conc., Forster mechanism 80−69220
diffusional theory of vibr. relax., non-single-quantum transitions 79−36745
p-difluorobenzene, $^1B_{2u}$, quenching by cyclobutanone, fluoresc. lifetime meas. 77−75205
p-difluorobenzene+ketone reson. energy transfer cross section, 1st Born approx. appraisal 77−65519
1,1-difluoroethane, rot. relax., anharmonic shifts and excited state absorpt. 80−43154
1,1-difluoroethylene, rot. dynamics, far IR spectra 77−19864
dimethyl ether, optical saturation characts., using CO_2 laser radiation 78−30027
dimethyl-POPOP, soln., and vap., fluorescence rise time, intramolecular vibrational relaxation 79−98134
molecular rotational-vibrational energy transfer continued
dissociation reaction, shift of chem. equilib. in laser reson. IR radiation field 77−56224
dissociative charge transfer collisions, vibr. enhancement 78−33597
distorted wave infinite order sudden approx. method, symmetrix T matrix 77−75265
donor-acceptor transition kinetics, with allowance for vibr. struct. 80−144
DWBA calcs. of V-V transfer cross section 79−3542
dye molecule, excited, thermal rotations and relaxation of vibr. energy 79−81231
electron impact excitation, cross section *(Russian)* 77−79699
electron transfer reactions, damping mechanisms effects calcs. 77−21381
electron-molecule low energy rot. and vibr. excitation, review 77−6943
electron-vibration system, nonequilib. first-order type phase transition 80−9633
electronic to vibrational energy transfer, vibr. state anal., review 78−37725
electronic-vibrational energy transfer and quenching, modified model 77−14534
endothermic reactions, extreme mass combinations LH+H→L+HH and HH+L→H+HL 79−43570
energy redistribution in quasiperiodic and ergodic regimes 79−41227
energy transfer relative rates, opposing dynamical constraints 77−79678
entropy and macroscopic disequilibrium, isothermal vibr. relax 77−6896
entropy and macroscopic disequilibrium, Markovian relax. 77−14539
ethane, unimol. decomp., energy transfer processes, Monte Carlo simulation 80−99555
ethanol, vibr. population lifetimes in liqs. anti-Stokes Raman scatt. 78−74665
ethanol in CCl_4, vibr. energy redistrib. after ultrashort IR excitation 77−6894
ethyl isocyanide, thermal isomerisation in presence of at. gases, vibr.-translational energy transfer 78−23924
ethylene, excited with parametric oscillator, vibr. relax. obs. and interpret. 80−9702
ethylene, intense IR field multiphoton dissoc., primary products, fluoresc. obs. 79−36715
ethylene, laser-induced IR photolysis mechanism 78−56909
ethylene, line selective excitation with CO_2 laser light and vibr. relax. 80−9705
ethylene, multiphoton absorption, luminesc. and dissoc. in laser pulse field 78−1040
ethylene, vibr. energy transfer, fluoresc. detect. 79−64026
ethylene+inert gas, vibr. energy transfer, fluoresc. detect. 79−64026
ethylene glycol, vibrational dephasing time of subgroup, transient stimulated Raman scatt. 78−37718
ethylene oxide, rot. relax., double reson. and Stark switching obs. 80−106340
ethylene-N_2, gas, vibr. relax. time by US meas. 79−98852
excitation cross-sections, meas. and calcs., review, book contrib. 77−38720
excitation to coherent state, resonant energy transfer calcs. 79−98178
excited state vibrational energy transfer, for optoacoustic spectroscopy 78−37724
exothermic triatomic exchange reactions, dynamics, anal. theory 78−3322
exponential transition probilities for collision induced dissoc. and vibr.-rot. relax. 78−27749
extended diffusion and 'sticky' collisions 78−86940
fast molecular ions, break-up on collision with solids 80−66353
flows with vibrational relaxation, sudden-freezing analysis 77−58806
fluid and solid molecular motion, submillimetric-wave spectroscopy obs. 79−31517
fluorobenzene, polarized light scatt., relaxation processes 80−60615
fluorobenzenes, vibr. relax. in first electronically excited singlet state 79−3535
fluoroform, vib. relax., 183-295K, US absorpt. meas. 77−34722
fluoromethane, $^{13}CH_3F$ and $^{12}CH_3F$, vibr. energy transfer between ortho- and para-mols. *(Russian)* 78−29845
fluoromethane, ν_3 mode, laser induced fluoresc. of V→T/R transfer 77−6899
fluoromethane, in Kr matrix, vibr. relax., IR double reson. 77−79635
fluoromethane, in liq. O_2(Ar), vibr. energy relax. obs. 78−5208
fluoromethane, laser excitation, energy storage and vibr. heating 77−58137
fluoromethane, laser pumped, vibr. states collision dynamics fluoresc. obs. 80−53104
fluoromethane, laser pumping effects, translational and vibr. energy distribs. 79−844
fluoromethane, molecular pumping, thermal lens phenomena 80−9708
fluoromethane+Ar, vibr. time depend. on equilib. and vibr. temps. *(Russian)* 79−27071
fluoromethane+D(H)(O), reactions, selective vibr. excitation effects 78−35643
fluoromethane+fluoromethane, collision induced mode selective energy transfer, fluoresc. obs. 80−69177
fluoromethane+fluoromethane, collisionally induced relax. processes and vibr. energy transfer 80−53107
fluoromethane+O_2, laser induced translational-vibr. energy conversion obs. 79−72396
fluoromethane+SO_2, collisionally induced relax. processes and vibr. energy transfer 80−53107
fluoromethane-^{12}C+fluoromethane-^{13}C, vibr. energy transfer, IR double resonance monitor 77−61833
fluoromethane-d_0, -d_1, vibr. relax. in matrix, rot. effects, double reson. obs. 78−46375
fluoromethane-d_2, matrix isolated, vibr. energy transfer at low temps. 80−37860
fluoromethane-d_3, vibr. energy transfer at low temps., inert gas and N_2 matrix obs. 80−9706
fluoromethylene+NO→HF+CNO, vibr. energy distrib., lasing action in dichlorofluoromethane-O_2 78−48644
fluoromethylene+O_2→HF+CO_2, vibr. energy distrib., lasing action in dichlorofluoromethane-O_2 78−48644
fluorotrichloromethane, optical saturation characts., using CO_2 laser radiation 78−30027
form-factors, l-dominant, analytical formulae, appl. to Ar+N_2 80−1052
formaldehyde, vibr. and electronic energy transfers, from single vibronic level 78−82820
formaldehyde+He, interstellar, collisional excitation 78−89237

molecular rotational-vibrational energy transfer continued
formaldehyde+He, rot. excitation, coupled-channel calcs., microwave doublets cooling 77−3436
o-formaldehyde+He, rot. excitation at interstellar temps., coupled states cross sections 77−54593
formaldehyde+He, rot.-translational energy transfer, nonlinear vs. linear rotors, surprisal anal. 79−76492
formaldehyde+He(H_2), collisional relax. times and lineshape distortion, Stark absorpt. linewidth obs. 78−74744
formaldehyde(-d_2), S_1 state, collisionless decay, vibr. relax., quenching 79−27019
formaldehyde-d_1 (-d_2), single vibronic levels, fluoresc. emission, radiative lefetimes and vibr. relax 80−23521
formaldehydes, (deuterated), A^1A_2 state, photoluminesc. in low temp. matrices, vibr. relaxation 79−50070
formyl radical, form., vibr. relax., spectrosc. 79−36746
Franck-Condon factors in reactive collision dynamics, general theory and applic. 77−36741
Franck-Condon factors in reactive collision dynamics, vibr.-rot. distribs. in atom-diatom reactions 77−36742
freon 113, 114 and 115, thermal cond., rot. relax., investigation *(Russian)* 77−89226
freons of methane series, pulsed US investigation of vibr. relaxtion 77−39397
furan-cyclohexane, liq. mixture, intermol. vibrational energy transfer, US study 80−70313
gas, diatomic, spherical source expansion 80−58356
gas, dilute, reacting, mass and momentum transport, DIPR model extension 78−35666
gas, molecular, kinetic coeffs. calc. from ultrasonic data 78−42703
gas jet expsn. into vacuum, rot. relax. 79−32625
gas mixtures with vibr. relax., nozzle flow 79−64727
gas phase nucl. mag. relax., DWBA cross sections from S-matrix formalism 77−27151
gas phase reaction consts. for electronically excited species, relax. processes, data tables 80−16644
gaseous transport coefficients, rot. inelastic collisions effects 79−82020
gases, vibr. relax. rate meas. by luminesc. attenuation, using stroboscopic synchronous integrator *(Russian)* 77−68074
gases induced scattering and self-action, effect on optical radiation propagation 79−72628
glyoxal, ^1A_u state energy transfer, D effects 77−58066
glyoxal, gas phase emission spectra, mag. quenching 77−18968
glyoxal, relax. processes, single vibronic level fluoresc. spectroscopy 78−58789
glyoxal, vibr. energy redistrib. following internal conversion 80−23452
glyoxal, vibr. relax. of ^1A_u state in gaseous environments 79−45800
glyoxal in supersonic jet, fluoresc. excitation, collision-induced intersystem crossing, van der Waals complex 79−81223
H+FH(FD), low barrier quantum model, vibr. deactivation 80−69216
haemoproteins, fluoresc., reson. Raman and radiationless decay 77−30916
halobenzene cations, in solid Ne matrix, slow vibr. relax., fluoresc. obs. 80−74194
halobenzenes, liquid, vibr. relaxation, Brillouin spectra 80−108219
halogen hydride lasers, vibr. energy transfer, from metastable diatomic molecules 79−31882
halomethanes, collision induced vibr.-rot. transitions, semiclassical theory 78−78785
harmonic oscillator, average energy, time evolution eqns. 77−34738
HCl-NOCl gas mixture, vibr. relaxation, collisional de-excitation *(French)* 78−86934
He_2, collisional electronic and rot. relax. in afterglow of pulsed discharge 77−61784
$^4He+H_2(v=0,j=0)\rightarrow{}^4He+H_2(v'=1,j')$, fully converged sudden rotation total integral cross sections 77−58135
hexafluorobenzene, IR multiphoton excitation, vibr. energy redistrib. and hot band spectrum 80−95656
hydrogen halides, rot. relax. rate consts., information theoretic synthesis 79−86044
hydrogen halides rot. relax. with inert buffer gas, comment 80−69221
hydrogen halides rot. relax. with inert buffer gas, reply 80−69222
impurity molecule, in solid, vibr. relax., rot. and translational local modes 77−75118
inelastic collision cross section, adiabatic distorted wave infinite order sudden approx. calcs. 79−94066
inert gas+CO(O_2)(N_2), state-to-state rates from press.-broadened linewidths, data reduction method 78−46430
inert gas+diatomic (triatomic) mol., Penning ionis. process from electron spectroscopy 77−14555
inert gas+hydrogen halide, energy transfer as function of collision energy, luminesc. obs. 79−86043
inert gas atom+diatomic molecule, collision in laser field, vibr. excitation 78−86937
information theory anal., vibr. population distribs. in laser excited system 77−42380
intermolecular electronic excitation transfer, vibr. relax. effects, master eqn. theory 77−88548
intermolecular potential, rot. energy transfer, sensitivity anal. 80−63762
intermolecular potential well depth role in collision-induced state changes 79−81257
intermolecular potentials, vibr. coupling behaviour 78−25668
internal degrees of freedom collisional excitation, statistical model 79−45803
interpolation schemes comparison for rot. transfer 79−18268
interstellar masers, Λ-doublet population inversion in OH, OD, CH, CD and NH^+ collisions 80−22065
interstellar molecules, collisional excitation theory 77−67119
interstellar molecules collisional excitation by H_2, theory for linear mols. CO, OCS, SiO, HCN and HC_3N in $^1\Sigma$ state 80−109508
intramolecular longit. relax. in mol. system with Rabi oscills., transient regime theory 78−46404
iodomethane, collisional rot.-line widths and shifts, microwave region 78−25619
iodomethane, liq. (liq. mixtures), vibr. relax. and reorientation, symmetric C-H bending mode 1st overtone 78−62884
iodomethane, vibr., rot. and translational energy exchange, semiclassical theory 80−48067
iodomethane, vibr. population lifetimes in liqs. anti-Stokes Raman scatt. 78−74665
iodomethane, vibr. relax., Raman overtone band obs. 77−14436

molecular rotational-vibrational energy transfer continued
ion+molecule, electronically elastic collisions, scaling law in sudden approx. 78−37723
ion+polar molecule, perturbed rotational state approach 78−92469
ion pair form., vibr. energy depend. 79−34287
IOS opacities and integral cross sections for rotational collision, partial wave parameter identification effects 77−38719
IR band shapes, reson. relax. effects 78−13576
IR laser absorption initiated collision, vibr. inversion generation 77−10707
IR laser isotope separation appls. 79−64113
isobutylene, liq., vibr. phase relax. and freq. shifts, density and temp. effects 80−74235
isolated molecules, vibration relax. theory, adiabatic approx. 80−58237
isothermal bulk relaxation, entropy production monotonicity 77−68097
isothermal system with δ-function source of mols., vibr. relax. 78−1061
isotope separation, by selective laser-induced mol. vibr. excitation effect on reaction kinetics 78−33627
ketene-d_0,-d_2, mol. ion reactivity, vibr. energy effects, mass spectrometric obs. 77−44470
kinetic spectroscopy of molecules 79−94110
kinetically controlled chemical activation, multistep deactivation processes applic. in energy transfer interpret. 80−25985
Kneser liquids, vibrational energy exchange probabilities 78−38780
Laguerre uniform approximation for vibrational transition probabilities 77−71849
laser amplifier, vibr. relax. effect on laser pulse energy characts. 78−17921
laser studies of relaxation and reaction of species in defined quantum states 80−11918
laser systems, vibr. interaction of diatomic and triatomic mols., theory 77−23670
laser-controlled unimolecular and bimolecular processes, field-depend. rate const. 80−11906
laser-induced unimolecular decomposition of octafluorocyclobutane 77−32775
laser-irradiated gas, IR fluoresc. meas. of equilib. and vibr. temps. 78−82766
liquid, IR absorpt. lineshape, orientation density fluctuation effects 78−48171
liquid, IR spectra, calc. involving vibr. and reorientational relax. 78−48170
liquid, rate of relaxation of vibrational energy 78−17764
liquid, vibr. relax., line widths, intermol. forces dephasing 77−47315
liquid, vibrational energy relax. of excited probe mol., density fluctuation interaction 78−63653
liquid, vibrational relaxation. appl. of Bogoliubov's relaxation time hierarchy idea *(Russian)* 77−15297
liquid media, vibr. two-photon reson. linewidths 77−88516
liquid vibrational modes, direct and indirect modes, reson. energy transfer, population decay 78−48162
liquids, molecular, vibr. dephasing and reson. energy transfer 78−18519
liquids, vibr. energy relax., nonMarkovian effects 80−74230
luminescence-vibrational relaxation interaction, master eqn. calcs., theory 78−42123
macroscopic system, vibrational relaxation, information-theoretic approach 77−58156
maser, three-level, collisional relax. rates between rot. states 78−22106
master equation energy transfer transition probabilities and moments 79−3533
matrix isolated molecules, energy accumulation by migration to geometric trap configurations 80−78691
matrix isolated molecules, vibr. relax. 78−46425
metal surface, mol. vibr. energy transfer, classical EM theory 80−96806
metal vapours, excitation energy transfer, sensitised fluoresc. 80−23358
methane, (methane-Xe)(methane-NH_3), mol. relax., optoacoustic reson. meas. 80−27351
methane, collision induced rot. Raman scatt., polarisability effects 78−86874
methane, energy transfer, multi-dimens. harmonic oscillator model 78−42174
methane, energy transfer obs. using excitation of fund., overtone and combination bands 80−9704
methane, gas, Rayleigh-Brillouin scatt., hydrodynamic effects calcs. 77−470
methane, harmonic and anharmonic matrix elements comparison, appl. to vibrational energy transfer 80−63760
methane, photoacoustic Raman spectroscopy under pulsed laser excitation 80−82825
methane, vibr. relax. time, spectrophone meas. 77−38669
methane+CO, vibr. relax. rates, energy transfer 80−37862
methane+d_2, Ar vibr.-vibr. energy transfer process diagnostics 80−32807
methane+inert gas, vibr. relax. time, spectrophone meas. 77−38669
methane+inert gas (H_2)(HD)(methane), vibr. energy transfer, fluoresc. 77−519
methane+linear molecule (one-electron atom) collisional energy transfer by octupole coupling 78−62881
methane+methane, vibr. energy transfer, Morse pot. 79−31653
methane+methane and methane+monatomic collisions, photoacoustic study of vibr. relaxation *(French)* 77−30969
methane+methyl fluoride, intermol. vibr. energy transfer, double reson. investig. *(Russian)* 77−61839
methane+SF_6, vibr.-vibr. relax 80−99537
methane isotopic mixtures, enrichment of D using vibrationally sensitized reaction 80−76532
methane-d_0(-d_4), unimol. decomp., energy transfer processes, Monte Carlo simulation 80−99555
methane-d_2, vibr. energy transfer, laser-induced fluoresc. 79−13753
methane-d_3 + inert gas, vibr. deactivation, laser-induced fluoresc. obs. 77−42377
methane-d_4, selectively excited, cooling, vibr.-vibr., vibr.-translational relax. 80−33723
methane-d_4, vibr.-translational relax. 80−99537
methane-d_4+Ar, vibr.-translational relax. 80−99537
methane-d_4+methane, vibr. relaxation 80−99537
methane-d+methane-d_4 (inert gas), vibr. relax. time meas. by photoacoustic effect 77−88541
methane-N_2, gas, vibr. relax. time by US meas. 79−98852
methanol, collision-induced rot. energy transfer, M-resolved microwave double reson. 79−6955

molecular rotational-vibrational energy transfer continued
methanol, vibrational dephasing time of subgroup, transient stimulated Raman scatt. 78−37718
methanol 70 and 118 μm laser line diagnostic expts. 80−69387
methanol and deuterated methanols, vibr. energy transfer probabilities, breathing-space theory 79−86039
methyl bromide-^{81}Br+nonpolar perturber, JK0,0-1,0 line broadening 77−6848
methyl chloride, mode-matching model of collisional-induced vibr. transitions 77−10735
methyl cyanide, vibr. relax., Raman overtone band obs. 77−14436
methyl cyanide ($-d_3$), vib. dephasing, Raman obs. 77−59566
methyl fluoride, laser collision-induced energy absorpt. and vibr. excitation 80−74233
methyl halide+inert gas, vibr. relax. transition rates, anharmonicity effects 79−89747
methyl halides, semiclassical theory for collision induced vibr.-rot. transitions 80−63767
methyl halides, vibr. energy relax., opto-acoustic obs. 80−95711
methyl iodide, liq., A_1 modes, vibr. relax., temp. depend. Raman spectra obs. 80−32806
methyl iodide, liq., vib. relax., A_1 Raman bands 77−40220
methyl iodide, liquid, rough sphere rot.-diff. model, relax. times 77−15294
methyl iodide, vib. relax. and Raman line widths 77−32359
methyl iodide in CCl_4, vibr. energy redistrib. after ultrashort IR excitation 77−6894
methyl isocyanide, thermal isomerisation in presence of at. gases, vibr.-translational energy transfer 78−23924
mixture, strongly excited, vibr. relax. 80−102555
molecular, vibrational dephasing time of subgroup, transient stimulated Raman scatt. 78−37718
molecular gas, nonequilib., thermal conductivity 78−94885
molecule, O_2, ($b^1\Sigma_g^+$-$X^3\Sigma_g^-$) system in auroras, vibr. development 77−2293
molecule+ion, Λ-doublets transitions 80−14132
molecule+molecule, rotational transitions theory 79−81260
molecule-molecule reaction, ergodic energy transfer, vibr. quantisation effects 78−85137
monofluoromethane+Ar, vibr.-vibr. energy transfer process diagnostics 80−32807
Morse oscillator, collinear V-T energy transfer, initial vibr. state 79−27066
Morse oscillator+atom, collinear collision, T-V energy transfer, de-excitation process 78−90268
Morse oscillator+atom, collinear collision, T-V energy transfer, excitation and dissociation processes 78−90269
Morse oscillator collinear collision, inelastic vibr. energy transfer, mol. continuum influence 80−106383
multiphoton absorption modelling, using SF_6 energy-dependent absorption cross sections 80−32789
multiphoton excitation, molecular dynamics 77−29019
multiple photon photochemistry in low temp. matrices 80−76533
N_2*+$NO(H_2O)$, vibr. excited quenching temp. depend., flowing afterglow 77−54595
nanosecond time-resolved emission spectroscopy 77−3490
naphthalene:β-naphthyl-n-biphenyl-ethylene, relax. time of vibr. levels of ground state *(Russian)* 77−44054
naphthalene, in nonpolar solvents, IR absorpt. bands 79−6939
naphthalene, vapour-phase, absolute fluoresc. quantum yields, nonradiative processes 77−6829
naphthalene in nonpolar solvent, vibr. and reorientational relax., correl. function 80−45065
nitrobenzene, liquid and CCl_4 soln. shear waves and translation-rotation coupling obs. by depolarised Rayleigh scattering 80−71432
nitromethane, vibr. relax., Raman overtone band obs. 77−14436
non-adiabatic transitions induced by rotational coupling 80−106385
non-Markovian theory of vibr. relax. and dephasing in condensed media 79−41224
nonisothermal system, equilib. distribs. and detailed balance relations 79−36737
nonlinear oscillators, 1-D, intramolecular vibr. energy transfer, quantal, classical and statistical behaviour 80−91641
nonradiative transition of molecule in condensed medium, vibr. relax. effect 80−80848
nonspherical molecule, rot. and vibr. inelastic scatt., rot. IOS approx. calcs. 78−46433
nozzle flow, hypersonic, vibr. relax. in air 79−68781
nucleic acid-dye complexes, energy transfer obs. using laser-induced fluoresc. 80−12054
octafluorocyclobutane, laser induced unimolecular decomposition 77−32775
photodecomposition, by MW IR laser, nonstatistical behaviour 77−73455
photoelectron recoil effects in light atom mols., X-ray photoelectron vibr., rot. excitation 78−42129
phthalimide derivatives, in hexane and isopentane, vap., inversion freq. determ., from fluoresc. quantum yield obs. 79−54892
picosecond phenomena, conf., Hilton Head, USA (May 1978) 79−44940
picosecond transient spectroscopy of molecules in solution 79−36621
picosecond vibrational and electronic relaxation processes 79−45808
picosecond vibrational relaxation times, Raman scatt. meas., book contrib. 77−65057
plasma, nonequilib., diat. mols. vibr. excited state population, rel. to plasma chem. 80−19553
polar mol. rot. relax., dielectric friction, Onsager cavity model 80−64664
polar molecular ion, charged particle vibr.-rot. excitation *(Russian)* 80−1053
polar molecule+high Rydberg atom, l-changing collision 79−10185
polar molecules, electron impact, influence of long-range interaction on vibr. excitation 79−3586
polar molecules, vibr. relax., Raman overtone band obs. 77−14436
polyatomic, vibr. relax. in monochromatic radn. field behind shock wave 78−42177
polyatomic compounds, vibr. relax., IR band line shape obs. 79−54879
polyatomic fluid, nonassociated, vibr. relax. density depend., simple model 80−32809
polyatomic gas, laser-induced rate processes, intermol. and intramol. relax. formalism 79−27070
polyatomic liquids, vibr. relax. and energy transfer, ultrafast dynamics obs. 77−50506

molecular rotational-vibrational energy transfer continued
polyatomic molecule, dissoc., natural collision coords. 78−44373
polyatomic molecule, mode-matching model of collisional-induced vibr. transitions 77−10735
polyatomic molecule, multiphoton excitation by two IR lasers 80−91607
polyatomic molecule, multiphoton excitation from many rot. states by IR laser pulse 78−21986
polyatomic molecule, multiple-photon IR laser pumping, collisional effects 80−9668
polyatomic molecule, ultrafast vibr. using laser light pulses 80−9699
polyatomic molecule, vibr. relax. probability determ. from quasi-line fluoresc. 77−50505
polyatomic molecule in solution, vibr. population relax. model 78−17756
polyatomic molecules, applic. of classical perturbation theory of good action-angle variables 80−23481
polyatomic molecules, intramolecular vibr. relax., restricted quantum exchange theory 80−63610
polyatomic molecules, IR laser sensitised chem. reactions 80−11910
polyatomic molecules, laser pumping effects, translational and vibr. energy distribs. 79−844
polyatomic molecules, multistage IR dissoc., collisionless energy-gathering process 80−99526
polyatomic molecules, vibr., rot. and translational energy exchange, semiclassical theory 80−48067
polyatomic molecules, vibr. theory, kinematic anharmonicity spectrum 77−50504
polyatomic molecules, vibrational distrib. 77−88540
polyatomic molecules in condensed phases, origin of vibr. dephasing 79−27069
polymethin cyanine dyes, vibronic energy relax., picosec. spectrosc. obs. 80−5526
potential well depths, intermolecular, effect on molecular vibration energy transfer 80−43156
propane, freejet flow, vibr. relax. time 79−98760
propane-CO_2, freejet flow, vibr. relax. time 79−98760
propynal, energy dispersion and relax., laser IR/visible double reson. obs. 80−53028
propynal, internal energy distrib., collisional effects, IR-vis. double reson. obs. 80−14159
quantum collision theory, time-depend., using classical path approx. 79−13798
quantum interpretation of fully state-selected rotationally inelastic collisions 77−34726
quantum statistical mechanics of relaxation phenomena, non-exp. decay 79−44850
quasiequilibrium vibr. distrib. of polyatomic mols., max. entropy principle 78−58786
radiating molecules, in upper atm., rot. relax., IR emission and vibr.-rot. transitions calcs. 77−65462
radiationless relaxation processes, appl. to mol. vibs. in dense media *(German)* 78−1055
radiationless vibrational energy relax. processes and appl. to mol. vibrs. in dense media *(German)* 78−1057
Raman spectra, isotropic, of liq. (isotope) mixture, intermol. vibr. mode coupling 79−31535
Raman spectra in liqs., vibr. relax. *(Russian)* 79−64012
rarefied gas flow, nonequilib. flow expts. at Novosibirsk 79−98824
rarefied nonequilibrium flow, transport coeffs. and relax. phenomena 79−98825
reacting gas mixtures, kinetic coeffs. determ. by Enskog-Chapman method *(Russian)* 77−36733
reaction product rot. distribs., relax. rates and chem. laser threshold times 80−28222
reactive collisions, joint products' state distribs. 78−64807
reactive mixture of viscous gases, vibr. relax. *(Russian)* 77−36735
real gas, blast wave, effects of compressibility, vibr. excitation, dissoc. and ionisation 77−68622
relaxation of strongly excited mols. 78−1060
relaxation processes in fluoresc. excited by standing wave radn. field 78−29803
resonance fluoresc. meas., rot. ang. momentum distrib., polarisation and intensity, theory 78−33580
resonant electron scattering, vibr. excitation of mols. *(Russian)* 77−79697
resonant electronic-vibrational energy transfer and use in pumping IR mol. lasers 80−9700
resonant exchange of molecular rotational coherence 80−23525
resonant vibr. excitation cross section in electron scatt. 77−19098
rhodamine, dye soln., photoinduced dichroism and vibronic relax. 77−14465
rhodamine 6G dye laser, induced radiation spectral characts., effect of vibr. relax. 80−64008
rhodamine dye solutions, vibr. relax. in S_1-state 77−6826
rigid linear rotor+atom, rot. relax., microwave transient T_1 and T_2 rates 79−13797
rotational band, line shape, collisional broadening, impact approx. 78−42134
rotational energy diffusion in gas of nearly spherical rot. mols. 77−964
rotational energy transfer, power scaling law 79−54942
rotational excitation, planar trajectory approx. calcs. using body-fixed coords. 77−75267
rotational line width of vibr. bands, self- and foreign gas-broadening 78−33552
rotational mechanism for vibr. relax. in rigid media 77−58138
rotational relaxation, press.-broadened linewidth data deconvolution using scaling theories 78−82823
rotational relaxation in mol. gas, selection rules for nonspherical scatt. *(Russian)* 77−68099
rotational relaxation mechanism, under absorption saturation conditions, in resonance with high intensity monochromatic radiation 79−64083
rotational spectral line shift and widths, collision induced phase shifts 77−75222
rotationally inelastic collision cross section, centrifugally decoupled exponential distorted wave approx. 79−842
rotationally inelastic collisions, tensorial factorisation 80−28096
rotationally inelastic rate const. determ. by direct inversion of pressure-broadened half-widths 78−74745
rotationally inelastic scattering, mag. transitions, time reversal symm. 80−53105
roto-vibrational molecular laser, optically pumped, rate eqn. model 78−37874

molecular rotational-vibrational energy transfer continued
saturated laser-induced fluoresc., rot. redistrib. effect 79−81259
scaling of energy and quantum no. for nonreactive collisions 80−9695
self-sustained gas discharge, mol. vibr. relax. effect on thermal stability 80−10358
semiclassical methods for low energy inelastic scatt. 79−10184
semiclassical model of vibr. energy relax. in simple liqs. and compressed fluids 80−33865
semiclassical theory of electronically nonadiabatic collisions, reson. effects 78−66618
small molecule, IR laser induced collisional pumping 78−25630
small molecule IR laser induced collisional pumping 78−25629
solution, of polar mols., local order and vibr. coupling, Raman bands, dielec. const. 79−99868
sonic nozzle expansions, rot. relax. theory 80−43827
spectral line breadth, combined effect of collision and Doppler broadening 77−71832
spectral line broadening, semiclassical straight line vs. curved trajectories 79−45765
spectral pressure broadening, Liouville space methods 77−27116
spherical-top molecules, rot.-vibr. transition moments in excited states 78−25639
starvation kinetics, thermally activated processes and vibr. relax. rate consts. temp. depend. 78−95908
state change collisions, attractive intermolecular forces, temp. depend. 80−23515
stochastic reductions, projection operator formalism, classical quantum forced oscill. model 77−65521
sudden rotational approximation, reactive and inelastic, body-fixed frame, exchange reaction extension 80−61073
supersonic flow of inverted population gas flow round blunt bodies, amplification factor 78−5828
supersonic seeded molecular beam, vibr. relax. 78−17761
surface deactivation in gas-aerosol system, rel. to two-phase gasdynamic lasers 79−45807
tetracyanobenzene+methylated benzene, fluorescent exciplex form., electronic relax. 80−5573
tetrafluoromethane, collision induced rot. Raman scatt., polarisability effects 78−86874
tetrafluoromethane, US absorpt. for vibr. self-relax., 139-183K 78−63529
tetrafluoromethane+CO, vibr. relax. rates, energy transfer 80−37862
tetrahedral molecules, spectral line press. broadening, symm. basis set calcs. 77−3421
tetramethyldioxetane, multiphoton dissoc., collisional vibr. relax., rate eqns. model 80−63729
s-tetrazine in n-hexane, picosecond time-resolved fluoresc., vibr. relax. 80−48025
thermal conductivity, vibr. energy diffusion coeff., 400-1600K 77−27644
thermal lens phenomena in mol. pumping expts., time-resolved geom. optics approach 80−9708
thermally available vibrational energy levels, energy transfer, photoacoustic and IR emission obs. 79−72402
time evolution calcs. for medium size mols. 77−54592
time-dependent effective rates for molecular processes 79−63928
toluene+OH(D), vibrational and rotational energy effect 80−76497
toluene-d_8, liq., vibr.-vibr. near resonant energy transfer, Raman spectra 77−61836
triatomic exchange reactions, exothermic, semiclassical dynamics calcs. 80−25999
triatomic mol. in solvent, rot. induced vibr. energy relax., Coriolis effect 80−47921
trichloroethane, CH_3-stretching modes, Raman spectra reson. energy transfer obs. 78−48162
1,1,1-trichloroethane, Raman spectra, vibr. dephasing 79−59465
trichloroethane, vibr. population lifetimes in liqs. anti-Stokes Raman scatt. 78−74665
trichloromethane, and -d_1, liq., vibr. relax., Raman spectra 78−19471
trichloromethane, vibr. population lifetimes in liqs. anti-Stokes Raman scatt. 78−74665
trichloromethane-d_1, in nonpolar solvents, vibrational and rotational relax. 79−10182
trifluoroformamide, electronically excited, vibr. relaxation, stochastic description 78−37715
trifluoroformamide+NO (v=1), vibr. relax. rate, in trifluoroformamide photodissoc. 78−74712
trifluoroiodomethane, highly excited, intermol. vibr. energy transfer, transient UV absorpt. spectra 80−106381
trifluoromethane, pure and mixtures, vibr. relax. times at 298K 77−525
trifluoromethane, US absorpt. for vibr. self-relax., 163-299K 78−63529
triiodomethane, polarized light scatt., relaxation processes 80−60615
1,3,5-trimethylbenzene+OH(D), vibrational and rotational energy effect 80−76497
two quanta vibr.-vibr. transitions, translation distortion effects, DWA calc. 79−3541
two-level system coupled to thermal bath, quantum dynamics of relax. 77−3437
unimolecular reactions, nonequil. time-depend., model calc., single collision approx. 80−25987
unimolecular reactions induced by monochromatic IR radiation, intensity and laser energy fluence influence 80−11903
upper atmosphere, IR radiation from mol. vibr.-rot. transitions 79−5695
V-V energy transfer, perturbed wave eqn. soln. H_2+H_2 appl. 80−1051
V-V master equation, numerical inversion, information theoretic approach 79−18265
Van der Waals dimers, intermol. V-V energy transfer in vibr. predissoc. 79−94060
van der Waals mols., vib. predissoc. 78−55215
van der Waals T-shaped mol., perpendicular vibr. predissoc., vibr. relax., Morse pots. 78−82659
vibration-rotation transitions, perturbation theory framework 79−31661
vibrational dephasing, polyat. mols. in condensed phases, intermol. energy exchange mechanism 78−74737
vibrational energy transfer in solids, rot. mode participation 78−63815
vibrational excitation by electron impact at 30-75 eV, quantum mech. and crossed beam studies 77−34767
vibrational excitation calcs. by sudden approx., pot. energy surface choice 77−27158
vibrational kinetics of dissociating mols., effect on short wave emission 77−42395
vibrational nonequilib. in gases, review 79−18270
molecular rotational-vibrational energy transfer continued
vibrational relax. in dense media, memory functions approach 78−37722
vibrational relax. in liqs., Raman spectra *(Russian)* 79−59476
vibrational relax. in supersonic flow, meas. using high temp. spectropyrometric unit 78−9275
vibrational relaxation, scaling theoretical anal., rot. effects, long-range collisions 80−14194
vibrational relaxation in liqs., hydrodynamic theory 77−35734
vibrational state distribution from classical trajectory calcs. 77−32773
vibrationally inelastic collision, rot. energy sudden approx. 79−68303
vibrationally inelastic collisions, 3D impact parameter approach 77−75268
vibrationally inelastic scattering, 3-dimens., adiabatic semiclassical perturbation theory 79−94065
vibrationally inelastic scattering, collinear, adiabatic semiclassical perturbation theory 79−94064
vibro-rotational excitation, field theoretical formulation 79−81263
vinyl fluoride, vibr. excitation effects on ion-molecule reaction pathways, photoionisation mass spectra 77−16804
water, structure and motion at high pressure 78−87606
weakly bonded molecular complexes, intermol. transfer and relax. of vibr. energy *(German)* 78−1056
xanthene dyes in n-alcohols (ethylene glycol) (glycerol), rot. relax., time-resolved fluoresc. depolaris. obs. 80−58300
$AR(^3P_1)+H_2$, energy transfer rate const. expts., reverse reaction effect 77−65520
Al+TlF, rot. excitation, M-conserving approx. 79−3546
$Ar+CO_2$, rot. inelastic wide angle scatt., differential cross sections 77−14536
$Ar+CO_2$, rot. transitions, classical trajectory calcs. 77−50501
$Ar+H_2$, vibr. and rot. transfer enhancement of dissoc. cross section 77−34732
$Ar+H_2$, vibr. transition rates, thermally averaged, Monte Carlo trajectory calcs. 80−23519
$Ar+H_2(HD)(D_2)$ reson. energy transfer cross section, 1st Born approx. appraisal 77−65519
Ar+HCl, rotationaly inelastic collision, planar trajectory, classical centrifugal decoupling calcs. 78−58788
Ar+HF, state-to-state cross sections for rot. to translational energy transfer determ. 80−91644
$Ar+N_2$, collinear collision, vibr.-translation energy transfer, model calc. 78−66634
$Ar+N_2$, IOS opacities and integral cross sections, partial wave parameter identification effects 77−38719
$Ar+N_2$, rot. excitation, classical transition probabilities calc. 77−88533
$Ar+N_2$, rot. excitation, planar trajectory approx. calcs. using body-fixed coords. 77−75267
$Ar+N_2$, rot. inelastic collision, orientation depend., close coupling calcs. 78−9232
$Ar+N_2$, rot. inelastic collision cross section, centrifugally decoupled exponential distorted wave approx. 79−842
$Ar+N_2$, rot. inelastic cross section, classical trajectory calc. surprisal anal., pot. energy surface depend. 77−14542
$Ar+N_2$, rot. inelastic cross-section, IOS calcs., partial wave parameters 78−50616
$Ar+N_2$, rotational excitations, close-coupling calcs. 77−27157
$Ar+N_2$, vibr. cross-section, exponential distorted wave and effective Hamiltonian 78−37709
$Ar+N_2$, vibr. excitation of $N_2(C)$ and $N_2(B)$, reaction rate and branching ratio determ. 78−25662
$Ar+N_2$ rotational excitation, differential cross sections and orientation effects, classical trajectory method 80−23523
$Ar+Na_2$, differential cross sections meas. for rot. energy transfer process, obs. of halos 80−91643
Ar+TlF, rot. excitation, body-fixed approx. 77−19015
$Ar(^3P_{0,2})+N_2$, rate consts. and $N_2(C):N_2(B)$ branching ratio 78−5327
$Ar(^3P_2)+N_2(C^3\Pi_u)$ excitation transfer cross section, radiative lifetimes, in N_2 laser, transitions 79−27246
Ar^*+N_2, excitation transfer collision, vibronic energy partitioning 77−75264
$Ar^*+N_2 \rightarrow Ar+N_2^*$, electronic to vibr. energy transfer, time depend. theory 80−23514
$Ar^*(^3P)+Co_2(X^1\Sigma_g^+)$, T-R and T-V energy transfer, collisional energy depend. 79−18262
AsD_3, IR spectra, vibr. relax., rot. reorientation in solid phase 78−19463
AsH_3, IR spectra, vibr. relax., rot. reorientation in solid phase 78−19463
AsH_3, vibr. relax. in dense media, memory functions approach 78−37722
$BF_3+BF_3(D_2)$ (inert gas), US dispersion meas. 78−17758
Ba+trifluoromethyl iodide, BaI vibr. states bimodal distrib. 78−27743
BaCl+Ar(He)(N_2), intermultiplet energy transfer 79−27063
$BaCl(C^2\Pi_{3/2}, v=0)+Ar$, intermultiplet energy transfer, laser induced fluoresc. obs. 78−9227
BaO, ground state vibr. pop. distribs. from photoluminesc. in $Ba+O_2$ and $Ba+N_2O$ 77−34731
$BaO(X^1\Sigma^+)$, vibr. relax., laser-induced fluoresc. meas. 77−83631
BaO*, quenching of excited species formed by $Ba+NO_2$ chemiluminesc. reaction 77−58140
$Br+CO_2(HCl)$, quenching of $4^2P_{1/2}$ state, vib. excitation, temp. depend. 78−58792
Br+HCl(DCl), relax. rates, vibr. photochem. 79−66290
$Br+HCl(v')$, $Br+DCl(v')$, reaction and relax., classical trajectory calcs. 77−48625
Br_2, dissociating flow in supersonic nozzles, atomic recomb. and vibr. relax. effects 78−42677
Br_2, kinetics of excited states using laser excitation, radiative lifetimes and collisional deactivation 80−74237
Br_2, vibrational relaxation and dissoc. behind a shock front, absorpt. spectroscopy *(Russian)* 77−88536
Br_2-Ar system, mol. rot. effects on V-T energy transfer 80−14195
Br_2-CO_2 IR laser with $Br^* \rightarrow CO_2$ electronic-vibr. energy transfer as pump mechanism 80−53260
Br_2+Ar, collision de-energisation of highly vibr. excited Br_2, mol. dynamics simulation 77−42378
Br_2+Ar, ergodic deactivation, anharmonic effects on transfer rate 78−82818
Br_2+Ar, vibr. excited Br_2, de-energisation in high press. Ar 77−71845
Br_2+H, classically forbidden vibr. excitation, S-matrix 77−516
BrCN, photodissoc. energy disposal, electronic branching, vibr. and rot. transfer, $CN(B \rightarrow X)$ fluoresc. 77−42364

molecular rotational-vibrational energy transfer continued
BrCN+N_2*, vibr. energy transfer, α_1 vibr.-rot. const., microwave meas. 83578
BrCl laser induced fluoresc., quantum resolved level dynamics in $B^3\Pi(O^+)$ state 80−74188
BrF, fluoresc. decay lifetimes and quenching cross-sections for excited $B^3\Pi(0^+)$ states 78−1030
Br*+N_2O, electronic-vibr. energy transfer, time-resolved fluoresc. obs. 79−89753
Br*($4^2P_{1/2}$) yield, in Br_2(1Br) photodissoc., wavelength depend., collisional release 78−64857
Br($4^2P_{1/2}$)+$^{12}CO_2$($^{13}CO_2$), electronic-vibr. energy transfer, temp. depend. meas. 79−10136
Br($4^2P_{1/2}$)+CO_2(COS)(CS_2), electronic to vibrational energy transfer rates 78−29839
Br($4^2P_{1/2}$)+H_2(HD)(D_2), electronic-vibr. energy transfer, fluoresc. meas. 79−72347
C_2, low lying $a^3\Pi_u$ state produced in intense IR field, fluoresc. and quenching obs. 80−11931
C_2, Swan transitions, relax. dynamics and two-photon excitation, in inert gas matrix 77−505
C_2^-, matrix isolated, vibr. relax., absorpt. spectra 77−75172
C_2^-, matrix isolated, vibr. energy transfer, fluoresc. 78−46382
C_2+He, $C_2(A^3\Pi_g)$ vibr. relax. 80−53106
C_3, matrix isolated, vibr. relax. 78−66637
C_3 production, vibr. relax., chem. kinetics, following IR multiphoton allene photolysis 80−66820
CF_2+He(Ne)(N_2)(SF_6), vibr. deactivation of CF_2 first excited single state 79−94061
CH, collisionless form., rovibronic relax., reson. fluoresc. 78−68902
CH, interstellar, ground state inversion, collisional excitation 78−28503
CH radical, sputtered, rotational and vibrational excitation 80−69224
CH^+, rot. excitation by slow electrons, calc. 78−5360
CH+p-H_2(He), collisional pumping of Λ-doublet transitions, pot. energy surface 80−23516
$CH_2(^1A_1)$ form. by ketene (diazomethane) photolysis, react. with cyclobutane, vibr. energy distrib. 78−61032
$CH_3C^{15}N$, rot. relax. time meas., self- and foreign-gas collisions, Stark-switched microwave, obs. 79−86048
CN, radical, $A^2\pi$ state, collisional deactivation, fluoresc. quenching obs. 77−83642
CN in solid Ne, internal conversions and relax. dynamics 77−34678
CN+H^+, rot. excitation, decoupled l-dominant calcs. 77−6900
CNN radical, matrix isolation spectra, 23.5-25.6×10^3 cm^{-1}, vibr. relax. and Renner splitting 77−83612
CN*, $B^2\Sigma^+$ state, fluoresc. decay dynamics, collisional quenching and radiative lifetimes 80−58306
CO, $a^3\pi$ state, IR radiative decay of vib. levels 77−30870
CO, chem. form. from CS_2-O_2, laser dynamics and rot. relax. 77−10898
CO, collision-induced reorientation, direct meas. by IR double reson. 80−32800
CO electric discharge lasers, vibr. kinetics, modelling and expts. 80−69374
CO, electron impact, reson. vibr. excitation calcs. 77−14595
CO, electron impact, vibr. levels stepwise excitation 78−1095
CO, electron reson. scatt., ang. distrib., vibr. and rot. excitation, theory 78−22044
CO, highly excited vibr. states, double quantum V-V transitions *(French)* 77−61837
CO, in solid N_2, phonon-assisted v-v transfer rates 79−10901
CO, istopically enriched, Ar matrix isolation, laser-included vibr. fluoresc. 80−9707
CO laser, steady state operation, vibr. distrib., numerical calc. 79−36884
CO laser pumping with high-energy particles 79−64211
CO lasers, scaling laws 80−95878
CO, near resonant V-V transfer rates for high-lying vibr. states 79−3536
CO, solid and liq., vibr. relax. and vibr. diffusion rates, 66-79K 78−17757
CO supersonic lasers, CW double elec. discharge performance 80−69416
CO, vibr. excitation using steady state chemical reaction between CO and N_2O 80−50851
CO, vibr. population distrib. in supersonic expansion 78−71364
CO, vibr. relax. in unsteady expansion wave, vibr. temp. distrib. 77−68096
CO^+, vibr. relax., laser-induced fluoresc. 77−83632
CO-Ar(-N_2), C_2 and CN form. by optical pumping, room temp. 80−16701
CO-He low press. mixture, CO vibr. distrib. to high level 78−58985
CO-He-O_2-H_2O laser discharge, stability, influence of recombination and ion chem. 78−17915
CO-N_2-Ar mixture, supersonic expansion, CO vibr. level populations, gasdynamic laser appl. *(French)* 77−23659
CO-NO mixtures, Ar matrix isolation, laser-included vibr. fluoresc. 80−9707
CO+ perfluoroalkyl halide, collisional relax 79−13799
CO+$^{14}N_2$ ($^{14}N^{15}N$),($^{15}N_2$), vibr. energy transfer, laser fluoresc. obs. 80−28050
CO+^{3}He(^{4}He), vibr. relax., deactivation rates, pulsed fluoresc. meas. 79−89698
CO+Ar, vibr. relax. in supersonic stream, gasdynamic laser action 77−14697
CO+Ar(CO), rot. band, line shape, collisional broadening, impact approx. 78−42134
CO+aromatic molecule, vibr. energy transfer, quenching efficiency 79−3539
CO+CO, $d^3\Delta$ state vibr. relax. in glow discharges 79−18271
CO+CO, V-V master equation, numerical inversion 79−18265
CO+CO, vibr. energy transfer, collinear and 3-dimens. rate consts. 80−48065
CO+CO, vibr.-vibr. energy transfer, rot. effects and long-range collisions 80−14194
CO+H_2, rot. excitation, rel. between tensorial cross sections 80−83454
CO+H_2, vibr. deactivation, 250 to 2000K, Morse pot. calcs. 78−46428
CO+H^+, computed cross section vibr. threshold effects 80−63759
CO+H^+, vibr. excitation, 5-90 eV, forward scatt. differential cross section 78−9228
CO+H^+, vibr. excitation, differential scatt., low energy meas. 79−89749
CO+He, press. broadening, rot. energy transfer, infinite order sudden approx. 78−22011
CO+He, rot. excitation, infinite order sudden approx. 78−74740
molecular rotational-vibrational energy transfer continued
CO+He, rot.-translational energy transfer, nonlinear vs. linear rotors, surprisal anal. 79−76492
CO+He, vibr.-rot. energy transfer, stochastic theory 79−54944
CO+Hg(6^3P_1)(6^3P_0), electronic-vibr. energy transfer collision, IR obs. 79−45716
CO+inert gas, collision-induced intersystem crossing, reversibility 77−50465
CO+Li^+, 4-7 eV, final rot. state distrib., small ang. depend. 79−68300
CO+Li^+, rot. excitation, ab initio CI pot. energy surface, classical mech. and coupled states calcs. 78−25665
CO+N_2O, CO_2 vibr. temps. under gasdynamic laser conditions 80−21276
CO+NO(O_2)(D_2), (v=1) relax., temp. depend. 78−17760
CO+O, vibr. deactivation 78−94305
CO+O_2, vibr. deactivation of CO, 80-300K, laser fluoresc. study 78−25661
CO^++He collisions, $CO^+(A^2\Pi_i)$ vibr. relax. 80−53106
$^{12}C^{16}O$+$^{13}C^{16}C$, vibr. energy transfer, laser-induced fluoresc. obs. 80−78690
CO_2, 4.3 μm airglow, excitation mechanism involving OH and N_2 79−16731
CO_2 (00°1) vibr. relax. in H_2 and D_2 below room temp., fluoresc. decay obs. 77−42381
CO_2, antisymmetric vibr., energy relax. rate, rel. to IR luminesc. kinetics *(Russian)* 78−82826
CO_2 antisymmetric vibr. mode relax. rate, luminesc. meas 79−94067
CO_2, bending vibr. quanta intramol. exchange, interpretation of obs. 77−58144
CO_2, collision induced Raman scatt. at ν_2 and ν_3 inactive vibrs. 78−90175
CO_2, collision relax. 180-400K, spectrophone method 77−61832
CO_2, collisional laser-induced vib. excitation 77−27155
CO_2 dissociation in a nonequilibrium plasma 80−87851
CO_2, electron impact, cross sections for rot. excitation 78−17809
CO_2, electron impact, reson. vibr. excitation calcs. 77−14596
CO_2, free expsn. of jet, nonequilib. effect 79−27676
CO_2 gasdynamic laser, gain prediction, comparison of vibr. models 78−29928
CO_2, kinetic cooling by laser radiation 79−31621
CO_2 laser, effects of added gases on vibrational energy transfer *(Rumanian)* 77−27273
CO_2 laser, vibr. energy transfer by current modulation 78−1204
CO_2 laser amplifier multipulse energy extraction 80−78832
CO_2 lasers, high-power, book contrib. 77−50651
CO_2, nonequilib. expansion, retardation temps. ≤1200K, vibr. relax. and condensation influences 78−5777
CO_2, photoacoustic Raman spectroscopy under pulsed laser excitation 80−82825
CO_2, resonant vibr. excitation cross section in electron scatt. 77−19098
CO_2, saturable absorpt. and rot. relax., (00°0) vibr. level 77−19367
CO_2 shape resonances in [100] symmetric stretch excitation *(French)* 79−86074
CO_2, supersonic chem. laser, energy transfer from vibr. excited OD 77−676
CO_2, threshold photoelectron and photoionisation spectra 77−14491
CO_2, VV processes, estimation of almost resonant molecular energy transfer due to multipolar pot. 80−91642
CO_2, vibr. distrib., effect of laser radiation 77−34868
CO_2, vibr. excitation and de-excitation by electronic collisions, calc. of cross section 78−66669
CO_2 vibrational temps. at 40 to 140 km altitude 77−70762
CO_2-F_2-Ar mixture, vibr. relax. in shock wave, 4.3 μm radn. 78−1062
CO_2-N_2 mixture, strongly excited, vibr. relax. 80−102555
CO_2+ perfluoroalkyl halide, collisional relax 79−13799
CO_2+Ar, press. broadening, rot. energy transfer, infinite order sudden approx. 78−22011
CO_2+Ar, rot. energy transfer, power scaling law 79−54942
CO_2+CO, bending mode excitation 77−10738
CO_2+CO(Ar), bending vibr. mode deactivation rate meas., 150 to 1500K 77−10738
CO_2+CO(N_2), vibr. relax., optoacoustic obs. *(French)* 78−42178
CO_2+D_2, near reson. V-V exchange 77−27165
CO_2+deuteromethane, time resolved fluoresc. for vibr. relax 79−31659
CO_2+H_2, rot. transfer, ab initio intermol. pot. energy surface 80−58354
CO_2+H_2, vibr. de-excitation of CO_2*(ν_3), 200K 79−45802
CO_2+H_2(CO_2)(Ne)(NH_3)(CH_3F), rot. transfer collisions, momentum transfer distributions 77−523
CO_2+H_2(D_2), ab initio LCAO-MO-SCF intermolecular pot. energy surface, V→T transfer 77−50489
CO_2+H^+, vibr. excitation in differential scatt. 77−50503
CO_2+H^+(D^+), vibr. excitation, isotope and time effects 80−63773
CO_2+HCl, vibr. relax., 300-900K, by laser fluoresc. 79−31658
CO_2+He, rot. transition classical integral cross section, surprisal predictions 77−54594
CO_2+He, translational-vibrational energy transfer, quantum dynamical study 80−63746
CO_2+He(Ar), rot. relax. rates and cross sections 79−848
CO_2+hydrocarbon in mixtures, vibr. energy transfer, laser induced fluoresc. obs. 78−58731
CO_2+inert gas, intramol. energy transfer, 153-393K, photoacoustic obs. 79−54943
CO_2+inert gas, reactant decomp., rot.-vibr. energy transfer, relax. analytic soln. 80−55650
CO_2+inert gas, vibr. and rot. energy transfer, quasiclassical trajectory study 78−33578
CO_2+Kr, vibr. energy transfer rate, anharmonicity, quasi-classical calc. 78−46431
CO_2+N_2, energy transfer, semiclassical calc. 79−86042
CO_2+N_2, semiclassical energy transfer method, Coriolis coupling 78−90266
CO_2+N_2, vibr. energy transfer, time-resolved laser induced fluorescence 78−29842
CO_2+N_2(CO), CO_2 1st vibr. levels collisional deactivation, photoacoustic study 79−98187
CO_2+Ne, energy transfer rate consts., semiclassical method 80−91640
CO_2+O_2(N_2)(air), bending mode vibr. deactivation rate, 1500-350K, shock tube meas. 77−38714
CO_2+propyl alcohols, collisional deactivation, of CO_2 (00^01), 303-514K 78−17759

molecular rotational-vibrational energy transfer continued
COF_2+COF_2, collisionally induced relax. processes and vibr. energy transfer 80−53107
$CO(^1\Sigma^+)+O(^1D_2)$, collisional quenching, energy transfer processes 80−23501
$CO_2(00^00)+Br_2$, vibr. relax. rate consts. 77−6898
$CO_2(00^01)+H_2(D_2)$, intramol. vibr.-vibr. transfer cross sections calc. 100-3000K 78−1053
$CO_2(01^10)+N_2(CO)(O_2)$, collisional deactivation rate const., 160-375K, photoacoustic obs. 79−10179
CO_2*+SO_2, near-reson. energy transfer, fluoresc. obs. 80−106348
$CO(1)+CO(\nu)\rightarrow CO(0)+CO(\nu+1)$, vibr. energy accumulation, reaction rate anal. 80−78692
$CO(\nu=1)+Br_2$, vibr. relax. rate consts. 77−6898
$CO(\nu=1)$+He, vibr. relax., collinear and 3D rate consts., temp. depend. 77−38717
$CO(\nu=1)$+He, vibr. relax., collinear and 3D rate consts., temp. depend. 77−38718
CS+H_2, rot.-translational energy transfer, nonlinear vs. linear rotors, surprisal anal. 79−76492
CS+He, $CS(A^1\Pi)$ vibr. relax. 80−53106
CS_2+O_2, vibr. relax., effect of atomic O 79−66300
Ca+HF(DF), beam reaction, vibr. excitation 78−68877
Ca_2, in solid Kr, discrete reson. Raman scatt. and vibr. relax. 79−18188
Ca_2, vibr. relax. in rare gas matrices 78−58711
Cd+N_2, $A^3\Sigma_u^+$ state, vibr. excitation 80−1054
Cd+N_2, electronic-vibrational process, state-resolved products distrib. determ. 79−6956
$Cd(^1P_1)$ excited state quenching by mols., cross sections, chem., phys. exit channels 79−779
chloromethane, collisional rot.-line widths and shifts, microwave region 78−25619
Cl-HBr chemical laser, pulsed, computer simulation, effects of rot. nonequilib. 77−40547
Cl+HI→HCl+I, Monte Carlo quasiclassical trajectory anal., product distribs. 77−16783
Cl^-+HBr(HI)→HCl+$Br^-(I^-)$, vibr. product state distribs., IR chemiluminesc. obs. 80−81309
Cl_2, and isotopic forms, $B^3\Pi(0_u^+)$ state, laser-induced fluoresc., collisional energy transfer rates 80−53038
Cl_2, rot. relax. classical trajectory computation, using Lennard-Jones pot. 78−62880
Cl_2-HI-He chemical laser system, rot. nonequilibrium, kinetic modelling, three model comparison 80−53281
ClCF, radical in Ar matrix, vibr. relax., multiphonon processes, fluoresc. 77−65430
ClCN+N_2*, vibr. energy transfer, α_3 vibr.-rot. const., microwave meas. 77−83578
ClF+Ar, shock wave, vibr. relax., laser schlieren meas. 78−90267
Cs+H_2, rot. excitation, infinite order sudden approx. 78−74740
CsF, rot. inelastic collisions, mol. beam meas. 80−1049
CsF, seeded in supersonic beam, vibr. relax. 78−37716
CsF+Ar, 87.7 meV, reorientation effects by approx. quantum methods 77−79680
CsF+Ar, elastic and rot. inelastic scatt., quantum mech. calcs. 77−14525
CuH, vibr.-rot. interaction influence on band intensity parameters 79−49999
D+$D_2(\nu)$, vibr. relax. in at. exchange reactions, classical trajectory calcs. 77−44467
D+FD(FM), low barrier quantum model, vibr. deactivation on chemically reactive potential surfaces 80−69216
D_2, electric discharge, vibr. excitation spontaneous Raman scatt. obs. 78−5234
D_2, electron scatt., isotope effects 77−58188
D_2, rot. and vib. relax., semiclassical calcs. 77−34723
D_2-Ar, thermal dissoc. of dilute mols., vibr. bias mechanism 79−61854
D_2+chloroform, energy transfer laser 77−88701
D_2+D_2, ladder operators in vibr.-vibr. and vibr.-translational transitions at high collisional energies 80−106382
D_2+D_2, rot. relax., close coupling calc. 77−58141
D_2+D_2, V→T rate constants, deconvolution 77−27152
D_2+He, vibr. relax., 400-80K 77−10736
D_2+He, vibr. relax. times, 3D semiclassical theory 78−25667
D_2+Li^+, vibr. excitation cross sections, 100-1200 eV 79−27077
D_2+Ne(Ar)(HD), state-resolved $\Delta j=2$ rot. transitions 80−63772
DBr, vibr. energy transfer, laser selective isotope excitation 78−82790
DBr+DBr, vibr. energy transfer, dissimilar isotopic species 79−27067
DCN, in interstellar clouds, rot. excitation by electrons and H_2 77−22292
DCl, matrix isolated, vibr. relax., IR fluoresc. obs. 79−45749
DCl, vibr. energy transfer, laser selective isotope excitation 78−82790
DCl+Cl_2(DCl), vibr. relax., Monte Carlo quasiclassical trajectory calcs. 77−50502
DCl+Cl(Br), vibr. relax. times, laser induced fluoresc. 77−27159
DCl+DCl, vibr. energy transfer, dissimilar isotopic species 79−27067
DF, IR chemiluminesc. quenching, (V-V) and (V-T, R) energy transfer rates 78−20018
DF, IR chemiluminesc. quenching, (V-V) energy transfer rates 78−20019
DF-CO_2, chem. laser, vibr. energy transfer from DF to CO_2 mols. 77−23669
DF+CO_2, vibr. relax. rate, chemiluminescence depletion method meas. 79−72399
DF+$D_2(H_2)(N_2)(HF)(CO_2)$, vibr. relax., laser-induced fluoresc. obs. 79−64028
DF+DF, vibr. energy transfer collisions, trajectory calc. 79−64079
DF+DF(HF), DF vibr. deactivation, semiclassical calcs. 80−48061
$DF(1\leq n\leq 7)+HF(0)$, vibr. deactivation calc., 300-3000K 79−31655
$DF(\nu=1)+DF(\nu=0)$, deexcitation probability, low temp., hindered rot. and H-bond effects 77−88531
$DF(\nu=1)+F\rightarrow DF(\nu=0)+F$, isotope effect 77−30959
$DF(\nu=n)+DF(\nu=0)\rightarrow DF(\nu=n-1)+DF(\nu=1)+\Delta E$, applic. of hydrogen-bond interac. model 77−30961
D_2O, far IR absorpt. coeffs. meas., press. broadening 80−9599
D_2O, vibrational and rotations meas. by laser spectrosc. 80−43050
D_2O+D_2O, (010) vibr. relaxation 79−36741
$^nD_2$, compressed fluid, vibrational population relaxation time obs. 80−69219
$Dy(NO_3)_3$ in nonaqueous solvents, anharmonic vibrs. in electronic energy degradation 77−23541

molecular rotational-vibrational energy transfer continued
F+carbonyl compounds, HF IR chemiluminesc., vibr. and rot. energy disposal 77−86318
F+D_2, electronic-to-rot. energy transfer cross sections 78−86935
F+H_2, electronic-rot. energy transfer, for $F(^2P)$ 79−36740
F+H_2, electronic-rot. energy transfer, partial cross-section interweaving 79−59538
F+H_2, Franck-Condon factors in reactive collision dynamics 77−36741
F+H_2, Franck-Condon factors in reactive collisions dynamics, vibr.-rot. distribs. 77−36742
F+H_2, in pulsed HF chem. laser evolution, irreversible thermodynamic anal. 79−31887
F+H_2, quenching, rot. energy transfer, quantum mech. calcs. 77−50499
F+H_2, rotationally inelastic transitions enhancement 77−3431
F+H_2 chemical laser, vib. populations in V→V, V→R,T energy transfer corrections 77−32794
F+H_2 dynamics, Franck-Condon factors rel. to information theory for vib.-rot distribs. and isotopic branching ratios 77−60041
F+H_2 nonadiabatic effects, scatt. theory, coupled-channel calcs. 78−22010
F+muonium (H)(D)(T), exothermic triatomic exchange reactions, dynamics, anal. theory 78−3322
F_2, rot. relax., in free jet expansion, rot. temp. meas. 77−88538
F_2+He(Ar), vibr. relax. times, 3D semiclassical theory 78−25667
FCN+N_2, rot. spectra and geom. struct. of FCN 78−82725
$F^*(^2P_{1/2})+H_2$, appl. of classical model for electronic degrees of freedom 79−98192
H halides, $I^*(5^2P_{1/2})$ quenching, electronic-vibr. energy transfer 78−63114
H+CO, scattering cross-sections, factorisation and fitting, IOS approx. 78−33575
H+Cl_2, collinear reaction, quantal transition probabilities from classical trajectories 77−32773
H+Cl_2, Franck-Condon factors for reactive collision processes 77−36741
H+Cl_2, Franck-Condon factors in reactive collision dynamics, vib.-rot. distribs. 77−36742
H+Cl_2 dynamics, Franck-Condon factors rel. to information theory for vib.-rot. distribs. and isotopic branching ratios 77−60041
H+F_2→HF+F, vibr. adiabatic and static distorted wave Born approx. calcs. 80−7768
H+H_2, body-fixed coordinates collision theory, asymptotic scatt. matrix solns. 79−64070
H+H_2, collinear classical dynamics, chemically accurate pot. energy surface 77−48620
H+H_2, Franck-Condon factors in reactive collision dynamics, vibr.-rot. distribs. 77−36742
H+H_2, rot. cross-section, linear surprisal plots, theory 77−50498
H+H_2, rot. excitation 79−89746
H+H_2, sudden rot. reactive scatt., 3-dimens., approx. quantum mech. calcs. 80−76498
H+H_2 dynamics, Franck-Condon factors rel. to information theory for vib.-rot. distribs. and isotopic branching ratios 77−60041
H+$H_2(\nu)$, vibr. relax. in at. exchange reactions, classical trajectory calcs. 77−44467
H+HF (v=2, 3), vib. deactivation 77−58142
H+$N_2(CO)(O_2)$, vibr. state distrib., charge exchange 150-2400 eV 78−42195
H^++CN, perturbed rotational state approach 78−92469
H^++H_2, collisions at 3.7 eV, rotational transition probabilities 77−27156
H^++H_2, coupled states calcs. of inelastic collisions at 3.7 eV 77−14538
H^++H_2, elastic of rot. excitation, semiclassical treatment 79−31657
H^++H_2, inelastic collisions at 3.7 eV, close cou-ing calcs. 77−34734
H^++H_2, rot. and vibr. excitation 78−33579
H^++H_2, rot. and vibr. excitation, energy loss obs. 80−63773
H^++H_2, rot. excitation and vibr. transitions, coupled state approx. 77−61835
H^++H_2, rot. quantum transitions 79−845
H^++H_2, rotational excitations, close-coupling calcs. 77−27157
H^++H_2, rotational quantum excitation, time of flight spectra 77−27154
H^++H_2, time depend. close coupling, vibr. excitation, impact parameter calcs. 77−88534
H^++H_2, vibr. excitation, ab initio CI pot. energy surface calcs. 80−74228
H^++H_2, vibr. excitation, energy loss spectra, rot. sudden impact calcs. 77−88537
H^++H_2, vibr.-rot excitation, ab initio CI pot. energy surface calcs. 80−74229
H^++$H_2(CO_2)$, vibr. excitation, 10-30 meV 80−58358
H_2 dissolved in Ar, far IR spectra, density narrowing of rot. line 79−50086
H_2, E,$F^1\Sigma_g^+$ state, collisional and radiative props. 80−58357
H_2, electric discharge, vibr. excitation, spontaneous Raman scatt. obs. 78−5234
H_2, electron impact, elastic scatt. and rot. excitation, close-coupling calcs. 77−6949
H_2, electron impact excitation, high vibr. levels of ground state, decay of reson. states 77−88581
H_2, electron impact rot. excitation, eikonal approx. 77−10777
H_2, electron scatt., ab initio theory, elastic scatt. and rot. excitation 78−50640
H_2, electron scatt., isotope effects 77−58188
H_2, electron scatt., vibr. and vibr.-rot. excitation, ab initio calcs. 79−22853
H_2 in Ar, vibr. energy relax. 80−106384
H_2, interstellar, collisional excitation of rot. transitions 78−77586
H_2, interstellar, J=2 rot. level excitation rel. to departure from translational equilib. 78−8081
H_2, interstellar, rot. excitation rel. to CH^+ prod. by interstellar shocks 80−56898
H_2 interstellar cooling, dissociation and IR emission in shocked clouds 78−41009
H_2, p- and o-, calc. of thermal cond. 77−54587
H_2, polarisability anisotropy derivative determ. from relative Raman intensities 78−55177
H_2, positron scatt., rot. excitation 78−50653
H_2, rot. and vib. relax., semiclassical calcs. 77−34723
H_2, rotation-translation relax. rates *(French)* 79−849
p-H_2, rotational 0-2 transaction cross-sections *(Russian)* 80−32812
H_2, solid, vibr. energy transfer, isotopic impurities, relax. 79−6993

molecular rotational-vibrational energy transfer continued
H_2, vib. excited state production in charge transfer reactions 77−30968
H_2, vibr. population relax. in gas and fluid 80−29775
H_2, vibr. relax., optical dispersion *(Spanish)* 79−23394
H_2, vibr. relax. in H_2-Ar mixtures, mechanism, computer simulation 78−46434
H_2, vibrational relax. time meas. *(French)* 79−13791
H_2, vibro-electronic mechanisms in nonequilib. plasma 79−6992
H_2, $X^1\sigma_g^+$, momentum distrib., electron correl. and mol. vibr. effects, theory 77−88557
H_2^+, spontaneous emission lifetimes in ground electronic states 80−32810
H_2^+, vibr. excitation, cooling mechanism for hot protogalactic gas *(Russian)* 79−17149
H_2-Ar, thermal dissoc. of dilute mols., vibr. bias mechanism 79−61854
p-H_2+^{4}He, vibr. relax., 50-2000K, coupled channel, coupled states and effective pot. methods comparison 79−6995
p-H_2+^{4}He, vibr. relax., analytical approx. 80−63761
H_2+A, vibr.-vibr. energy transfer, stimulated Raman excitation obs. 79−64086
H_2+alkali metal, exchange reactions and rot. transfer effects on transfer coeffs. 77−66749
H_2+Ar, 4500K shock wave expt. simulation, vibr. state changes and dissoc. 79−61850
H_2+Ar, H_2 dissoc. rates, nonequilib. vibr. populations, elec. discharge conditions 77−88535
H_2+Ar, vibr. energy transfer rate, ab initio calcs. 78−82821
H_2+CO_2, exponential gap relation, rot. inelasticity 80−78693
H_2+CO_2, rot. excitation, semiclassical calc. using exponential approx. 77−42379
H_2+CO(CS)(OCS), rot. excitation, classical and quantum calcs. 78−1059
H_2+CO(CS)(OCS), scattering cross-sections, factorisation and fitting, IOS approx. 78−33575
H_2+Cl^-, 4-11 eV, inelastic scatt. 79−98202
H_2+$D_2(N_2)(HCl)(CO_2)$, V-V transfer, pulsed fluoresc. obs. 77−14540
H_2+D(O)(Cl)(Br), relax. and chem. reaction, time resolved IR fluoresc. and mass spectrometry obs. 80−69177
H_2+F, in pulsed HF chem. laser, kinetic modelling, rot. nonequilib. 79−36888
H_2+H, exponential gap relation, rot. inelasticity 80−78693
H_2+H_2, exponential gap relation, rot. inelasticity 80−78693
H_2+H_2, quadrupolar $S_1(J)+S_0(J)$ double transitions, IR fundamental band, 77K 80−52986
H_2+H_2, rot. cross sections 78−37717
H_2+H_2, rot. energy transfer, classical trajectory calc. 79−31652
H_2+H_2, rot. relax., close coupling calc. 77−58141
H_2+H_2, rot. relax. collision, scaling theory anal. 80−74232
H_2+H_2, V-V and V-T rate coeffs., semiclassical model 77−14535
H_2+H_2, V→T rate constants, deconvolution 77−27152
H_2+H_2, vibr.-trans. rate const. and vibr. excitation cross section 79−50116
H_2+H_2, vibrational energy transfer, adiabatic approx. calcs. 77−14532
H_2+H_2(HBr), collinear collisions, anharmonicity effects, vibr. excitation 79−31656
H_2+H^+, combined rot. sudden and vibr. exact quantum treatment 78−74739
(H_2+H^+, H_2^++H) collinear system, electronically nonadiabatic effects 78−1063
H_2+H^+, inelastic forward scattering, vibr. excitation, glory oscills. 79−22799
H_2+H^+, low energy rot. excitation, ab initio differential inelastic cross section calcs. 77−88542
H_2+H^+, vibrationally inelastic collisions, 3D impact parameter approach 77−75268
H_2+HCD, vibr. excitation cross-sections, rot. averaging calcs. 78−9231
H_2+HCl(DCl)(CO),(NO_2)(HBr)(DBr)(NO)(CO)(^{13}CO), vibr. relax. rate, stimulated Raman scatt. obs. 77−75269
H_2+H(He)(OCS)(CS), rot.-translational energy transfer, nonlinear vs. linear rotors, surprisal anal. 79−76492
H_2+Hd, vibr. energy transfer rates, IR fluoresc. meas. 79−98145
H_2+He, exponential gap relation, rot. inelasticity 80−78693
H_2+He, inelastic collisions, statistical decoupling 77−517
H_2+He, rot. relax. time, <300K, classical trajectory method invalidity 77−10739
H_2+He, rot.-vibr. energy transfer collisions, distorted wave infinite order sudden approx. method 77−75265
H_2+He, vibr. excitation, classical trajectory problem, Fourier transform method 79−98189
H_2+He, vibr. inelastic cross-section, para-H_2, threshold behav. 79−45804
H_2+He, vibr. relax., pot. surface depend. 77−75266
H_2+He, vibr. relax. times, 3D semiclassical theory 78−25667
H_2+inert gas, vibr. relax. mechanism, master eqn. anal., density changes 79−76493
H_2+Li, exponential gap relation, rot. inelasticity 80−78693
H_2+Li^+, exponential gap relation, rot. inelasticity 80−78693
H_2+Li^+, rot. energy transfer, power scaling law 79−54942
n-H_2+Li^+, rot. excitation, 150-750 eV 79−45805
o-, p-H_2+Li^+, rot. excitation and ang. depend. transition probabilities, time of flight spectra 80−23517
H_2+Li^+, vibr. excitation cross sections, 100-1200 eV 79−27077
H_2+Ne, vibr. excitation effect on dissoc. excitation efficiency 79−76495
H_2+O→OH+H, vibr. energy effects, classical trajectory calcs. 77−63904
p-H_2+p-H_2, vibr.-rot. relax. 77−34729
H_2+SF_6 (tetrafluoromethane), collision-induced simultaneous transitions, IR spectra 77−50438
H_2^++H_2, predissociation of $c^3\Pi_u$ state, flight time difference obs. 77−27164
H_2^++H_2→H_3^++H, state-selected ion-molecule reactions threshold electron-secondary ion coincidence technique obs. 80−85166
H_2^++H^-→H_2^*+H recombination react., calcs. *(Russian)* 80−55659
H_2^++He, 10 keV, dissoc. excitation, ionis., energy distrib. 77−61849
H_3^+ ions, dissociation, collision induced 77−42383
H_3^++HD, rot. inelastic collision, classical trajectory calc. 79−64078
H_3^++Ne, Petty-Moran ion-impact expt. reinterpretation re vibr. intervals 79−94063
HBr, electronic to vibr. energy transfer from excited halogen atoms, IR fluoresc. 78−63113
HBr, vibr. energy transfer, laser selective isotope excitation 78−82790

molecular rotational-vibrational energy transfer continued
HBr, vibr. excitation by electron impact, threshold resons. 77−68127
HBr+Br, vibr. relax. times, laser induced fluoresc. 77−27159
HBr+CO_2, V-V energy transfer, 300-900K 79−59539
HBr+$CO(CO_2)(N_2O)(NO)(N_2O)(O_2)$, rate consts. for vibr. energy transfer meas. using laser. induced fluorescence technique 80−87206
HBr+D, vibr. energy transfer, phase shift 79−64080
HBr+HBr, vibr. energy transfer, dissimilar isotopic species 79−27067
HBr+He, classically forbidden vibr. excitation, S-matrix 77−516
HBr+N_2O, V-V energy transfer, 300-900K 79−59539
HCN (001)+HCN(Ar)$(N_2)(CO_2)$(CO), relax. rate consts., using Cs vap. IR source 80−9696
HCN, in interstellar clouds, rot. excitation by electrons 77−22292
HCN+Br_2(Ar)(HCN), electronic-vibr. energy transfer, Br($4^2P_{1/2}$) quenching and HCN (001) deactivation, fluoresc. obs. 77−518
HCN+HCN, collisional line broadening of microwave spectra, semiclassical theory, calcs. 78−25516
HCN+HF(DF)(H_2), vib. energy transfer, laser-induced fluoresc. 77−58139
HCN+He, press. broadening, rot. energy transfer, infinite order sudden approx. 78−22011
HCN+He, rot. excitation, infinite order sudden approx. 78−74740
HCN+He, translational-vibrational energy transfer, quantum dynamical study 80−63746
HCO, prod. by formaldehyde photolysis, vibr. relax., chem. kinetics and spectra 79−11808
HCO^++H_2, J=0-1 transition press. broadening, microwave absorpt. 80−52981
HCl, Ar-perturbed rot. linewidths, temp. depend. 79−45766
HCl, electron bombard., rot. excitation, energy dependence of elastic and inelastic cross sections 78−37756
HCl, electronic to vibr. energy transfer from excited halogen atoms, IR fluoresc. 78−63113
HCl, in nonequilib. plasma, electron energy distrib. function and dissoc. kinetics 80−11882
HCl, isotopic transfer laser, intercavity cold gas isotope filter 78−46590
HCl, liq., vibr. relax., IR double reson. 80−95712
HCl, matrix isolated, vibr. relax., IR fluoresc. obs. 79−45749
HCl, slow electron impact vibr. excitation wave function, virtual s-state 77−42429
HCl, vibr. emission from ClF-H_2 chem. laser 80−97709
HCl, vibr. energy transfer, laser selective isotope excitation 78−82790
HCl, vibr. excitation by electron scatt., virtual state interpretation 78−17808
HCl^-, reson. states by electron impact, GO and SCF+CI methods, dissociation channels 77−71883
HCl+Ar, elastic and rot. inelastic collisions, quasiclassical and quantum mech. results 77−79679
HCl+Ar, rot. excitation, quasiclassical close coupling approx. 79−27068
HCl+Ar, shock-heated, collision induced dissoc. 79−34290
HCl+Ar(He), rot. energy transfer, quasiclassical trajectory calcs. 78−42173
HCl+Ar(He), rot. excitation, classical and quantum calcs. 78−1059
HCl+Ar(He), rot. excitation, infinite order sudden approx. 78−74740
HCl+Br, IR fluoresc. studies of state-selected energy transfer, photochemistry 77−77768
HCl+CO_2, vibr. relax., 300-900K, by laser fluoresc. 79−31658
HCl+CO_2, vibr. relax. rate, chemiluminesc. depletion method meas. 79−72400
HCl+Cl, vibr. energy transfer to oscilltory, rstricted rot. and translational motion 78−70908
HCl+Cl_2(DCl)(HCl), vibr. relax., Monte Carlo quasiclassical trajectory calcs. 77−50502
HCl+D(O)(Cl)(Br), relax. and chem. reaction, time resolved IR fluoresc. and mass spectrometry obs. 80−69177
HCl+H_2, translational and pot. relax., statistical calcs. 77−3435
HCl+H_2, vibr. energy transfer, collinear and 3-dimens. rate consts. 80−48065
HCl+H_2 (o- and p-), press. broadening and alternate ang. momentum coupling, rot. excitation 77−42375
HCl+HBr, single quantum vibr. energy transfer 80−69223
HCl+HCl, rot. energy transfer, quasiclassical trajectory calc. 80−23524
HCl+HCl, rot. transitions, semiclassical strong-coupling method 77−58143
HCl+HCl, rot. transitions, 0.025 eV, semiclassical exponential approx. 78−62883
HCl+HCl, vibr. energy transfer, dissimilar isotopic species 79−27067
HCl+HCl-SF_6, nonequilib. rot. distrib. relax., fluoresc. obs. 79−36673
HCl+HCl(Ar), pure rot. Raman lines, press. broadening cross sections 78−74702
HCl+HCl(HF)(HI)(HBr), supersonic-thermal beam collision, rot. energy transfer, classical trajectory calc. 79−68302
HCl+He(Ar), press. broadening, rot. energy transfer, infinite order sudden approx. 78−22011
HCl+He(Ar), rot.-translational energy transfer, nonlinear vs. linear rotors, surprisal anal. 79−76492
HCl+inert gas, dissoc. induced by collision, rot. energy depend. 79−100341
HCl+N_2O, vibr. relax., 300-900K, by laser fluoresc. 79−31658
$H^{35}Cl$+$H^{37}Cl$, reson. isotopic vibr. energy transfer, temp. depend. 79−72395
HCl(ν=1,2)+O(^3P_g), reaction and deactivation, laser-induced fluoresc. obs. 78−35669
HCl(ν=1)+H(D)(Cl)(Br) reactions, selective vibr. excitation effects, kinetics *(German)* 77−21364
HD^+, rot. excitation by slow electrons, calc. 78−5360
HD^+, spontaneous emission lifetimes in ground electronic states 80−32810
HD+D_2, rot. inelastic differential cross sections, diffr. oscills. in elastic and inelastic scatt. 78−74743
HD+HD, rot. inelastic collision, classical trajectory calc. 79−64078
HD+HD, state-resolved rot. excitation differential cross sections, crossed pulsed beams techniques 78−17766
HD+HD(^{4}He)(D_2), vibr. relax., 80 to 400K 80−5607
HD+He, press. broadening, rot. energy transfer, infinite order sudden approx. 78−22011
HD+He, rot. excitation, classical trajectory study 78−25666
HD+inert gas, isotropic Raman Q branch, vibr. dephasing effects and motional narrowing 78−74738
HD+Kr(Xe), collision-induced fundamental band in room temp. IR absorpt. spectra 77−34627

molecular rotational-vibrational energy transfer continued
HD+Ne, j=0 to 1 scatt. differential cross section, interaction pot. anisotropy 77−42382
$HD^+ + HD^+$, 0.1-1 eV, rot. transitions and reson. transfer, first-order perturbation theory 77−83698
HD^++He collisions, rotational transitions 78−70909
$H_2(D_2)$, dissociative electron attachment and vibr. excitation, low-energy 80−23565
$H_2(D_2)$+Ag(111), energy transfer, quantum mech. theory 77−8699
HDO, T_1 and T_2 relax. cross sections meas. 77−34733
$HD(^1\Sigma_u^+)$+He, fluoresc. quenching and energy transfer processes 79−86032
HF, atm., pulsed chem. laser, model including rot. nonequilib. effects 79−55127
HF, chemical laser, rot. population transfer effect obs. 78−79013
HF, colliding system initiated by IR laser absorpt., vibr. inversion generation 77−10707
HF, collisional rot. relax. probability model 77−83697
HF dimer, stabilisation energies, harmonic force constants, intermolecular vibrations, SCF and CEPA PNO calcs. 79−98177
HF, electron bombard., rot. excitation, energy dependence of elastic and inelastic cross sections 78−37756
HF, electron impact rot. excitation 77−42427
HF, IR chemiluminesc. quenching, (V-V) and (V-T, R) energy transfer rates 78−20018
HF, IR chemiluminesc. quenching, (V-V) energy transfer rates 78−20019
HF, IR laser induced collisional pumping 78−25629
HF, IR laser induced collisional pumping 78−25630
HF laser, H_2+F_2 chain reaction, rotational nonequilibrium mech. vibr.-rotational energy exchange effect 80−48230
HF, laser, pulsed, rot. relax. rate effect on efficiency *(Russian)* 77−10900
HF laser, rotationa nonequilibrium efficient model 79−22945
HF, nonequilibrium dissociation in electric discharge, vibrational excitation 78−94306
HF, pulsed H_2+F_2 chain reaction laser, rot. nonequilib. mechanisms effect on performance 78−82958
HF, pulsed laser numerical modelling, rot. relax. 80−87388
HF, rot. relax., IR double reson. obs. 77−10740
HF, rot.-vibr. transitions, theoretical expressions 77−71881
HF, vibr. relax., microscopic and macroscopic anal. of non-linear master eqns. 79−36743
HF, vibr. relax. rates, $v=3, 4$ 78−82817
HF, vibr.-rot. band, absorpt. line self-broadening, rot. relax. 80−87213
HF-Ar mixture; HF rotational relax., laser IR fluoresc. 77−83634
HF+Ar, rot. relax. of high rot. levels at 1 torr press. 79−10181
$HF+CO_2$, vibr. relax. rate, chemiluminescence depletion method meas. 79−72399
HF+DF, DF vibr. deactivation, semiclassical calcs. 80−48061
$HF+H_2(D_2)(CO_2)$, vibr. relax. of HF ($v=3,4$) 79−50117
$HF+H_2(D_2)(N_2)$, 200K and 295K vibr. relax. rates 80−63766
$HF+H_2(HCl)(N_2)(O_2)(CO_2)$ vibrs. relax., laser fluoresc. obs. 77−14484
$HF+H_2(N_2)(CO_2)(O_2)(HCl)$, vibr. relax. laser induced fluoresc. obs. 79−64037
$HF+HCl(CO_2)(N_2O)(CO)(N_2)(O_2)$, HF(v=3) relax. and rate consts. 80−61069
HF+HF, ab initio pot. surface, ang. depend. fit calcs. 77−19006
HF+HF, momentum exchange rate, Boltzmann eqn. predictions 78−78781
HF+HF, rot. inelastic collisions, partial opacities, integral cross sections, pot. surface 77−38716
HF+HF, rot. relax. collision, scaling theory anal. 80−74232
HF+HF, rotationally inelastic scattering, classical trajectory study 78−82819
HF+HF, vibr. relax., temp. depend. calcs. 78−70906
HF+HF, vibr.-vibr., vibr.-rot., and vibr.-translational energy transfer calcs. 78−70907
$HF+HF(H_2)(D_2)(CO_2)$(isobutene), vibr. relax. dye laser pumping effects 80−9703
HF+He, rot. excitation cross sections, use of rot. and orbitally adiabatic basis functions 79−59543
HF+inert gas, dissoc. induced by collision, rot. energy depend. 79−100341
HF+inert gas, press. broadening and shifting of vibr.-rot. absorpt. lines 77−27161
$HF+O_2(a^1\Delta_g)$, E-V energy transfer 77−30960
$HF(^1\Sigma^+)+Xe(^1S_0)$, expt. and computational study, 0.044 and 0.153 eV 79−89748
HF*, interaction with ClFx, relax. consts., stimulated emission delay 77−7077
HF*+ethylene (fluoroethylenes), vibr. deactivation rate constant 78−50615
HF*+NH*, microscopic vibrotational-electronic energy transfer, IR chemiluminesc. obs. 79−31662
$HF(1\leq n\leq 7)+DF(0)$, vibr. deactivation calc., 300-3000K 79−31655
$HF(v_1,J_1)+HF(v_2,J_2)$ collisions, energy transfer, reaction rates 78−29844
$HF(v=1)+F\rightarrow HF(v=0)+F$, vibr. relax. rate const., 100-3000K 77−3434
$HF(v_1=1)+HF(v_2=0)$, vibrational relaxation temperature dependence, laser-induced fluorescence simulation 79−50069
HN_2^++He, rot.-translational energy transfer, nonlinear vs. linear rotors, surprisal anal. 79−76492
H_2O cosmic masers collisional pumping, influence of dust 78−54030
H_2O, far IR absorpt. coeffs. meas., press. broadening 80−9599
H_2O, harmonic and anharmonic matrix elements comparison, appl. to vibrational energy transfer 80−63760
H_2O, IR laser, electronic-vibr. energy transfer from $Br(4^2P_{1/2})$ 77−31094
H_2O, relaxation by IR and microwave coherent transients 80−28092
H_2O, vibr. relax. at high temps. 77−79681
H_2O, vibrational excitation by electron impact, threshold structs. 78−22038
$H_2{}^{18}O$, vibr. relax. rate consts., fluoresc. method determ. 78−17762
H_2O+Ar, collisional energy transfer in unimol. reaction, classical trajectory calcs. 78−62882
H_2O+H_2O, vibr. relax. near room temp. 78−86939
$H_2O+H_2O(He)(Ar)(N_2)(O_2)(CO_2)$, vibr. energy transfer temp. depend. 80−63763

molecular rotational-vibrational energy transfer continued
H_2O+He, rot.-translational energy transfer, nonlinear vs. linear rotors, surprisal anal. 79−76492
$H_2O+N_2(CO_2)$, collision broadened H_2O absorpt. line, laser radiation intensity effects 77−83661
H_2O+O, rot. excitation, classical Monte Carlo calcs. 77−34727
H_3O^+, rot. excitation by slow electrons, calc. 78−5360
H_2S, electron impact, vibr. elastic scatt. and vibr. excitation 79−13822
H_2S, rot. transitions, press. broadening, microwave spectra 77−50429
$H_2S+H_2S(N_2)(O_2)$, press. broadening of spectral linewidth, calcs. 77−30932
$H_2S(D_2S)$ photodissoc., SH internal energy distribution 80−95697
HX+ inert gas atom, (X=halide), rot. excitation 77−10742
$^nH_2$, vibr. relax. at low temps., gas, liq. and solid phases 77−83691
$H_2(1)+H_2(1)\rightarrow H_2(2)+H_2(0)$, V-V energy transfer temp. and rot. depend., semi-empirical pot. calc. 80−28094
He + H_2, vibr. inelastic integral cross-sections calcs. 79−31660
He-H_2, rot. relax and spectral line shapes, coupled states calcs. 77−50500
He-LiH, rot. inelastic collisions, ab initio pot. energy surface calcs. 80−87208
He+CO, rot. inelastic scatt., coupled eqns. for single initial state, variation-iteration method 79−68301
$He+CO_2$, IOS opacities and integral cross sections, partial wave parameter identification effects 77−38719
$He+CO_2$, rot. and vibr. inelastic scatt., rot. IOS approx. calcs. 78−46433
He+CO(HCl), rot. excitation, classical and quantum calcs. 78−1059
He+CO(HCl)(HCN)(HD), press. broadening cross-section, ang. momentum approx. calcs. 77−34696
$He+CO(HCl)(HCN)(N_2H^+)$, scattering cross-sections, factorisation and fitting, IOS approx. 78−33575
He+CO(HF), vibr. relax., unitary distorted-wave approach 79−36738
$He+H_2$, collisional dissoc., quasiclassical trajectory calcs. 78−42172
$He+H_2$, collisional energy transfer, stochastic reductions, generalised cumulant expansion calcs. 77−71847
$He+H_2$, distorted wave integrals approx., analytic formulae 78−42175
$He+H_2$, inelastic scatt., vibr. effects, classical mech. calcs. 77−34735
$He+H_2$, mol. energy transfer by quasiclassical trajectory methods, vibr. relax. and dissoc., rot. effect 80−99557
$He+H_2$, rot. excitation, 0.403-1.900 eV total energy, classical trajectory method 77−30962
$He+H_2$, rot. excitation, effective pot. and classical trajectory calcs. 77−88539
$He+H_2$, rot. transitions, quantum mech. and semiclassical cross-sections calcs. 77−83690
$He+H_2$, simultaneous rot. and vibr. transitions, cross-sections calc. 77−68098
$He+H_2$, V→T rate constants, deconvolution 77−27152
$He+H_2$, vibr. inelastic integral cross-sections, transitions to $v=2$ level 80−99559
$He+H_2$, vibr.-rot. inelastic cross section adiabatic distorted wave IOS calcs. 79−94066
$He+H_2$, vibr.-rot. relax., high temp., exponential distorted wave technique 78−37721
$He+H_2$, vibrationally inelastic collision, rot. energy sudden approx. 79−68303
$He+H_2(CO_2)$, rot. inelastic, moments of final state distrib., direct method 78−33562
$He+H_2(O_2)$, rot. cross-section, exponential distorted wave and effective Hamiltonian 78−37709
$He+H_2$ rot. and vibr. distorted wave integrals, stationary pt. struct. 78−46436
$He+H_2^+$, collision in laser field, vibr. excitation 78−86937
$He+H_2^+$, endothermic reactive and vibr. inelastic collisions, pot. well effects 79−8430
$He+H_2^+$, vibr. and rot. transitions, trajectory calcs. 79−13793
$He+H_2(D_2)$, vibr. deexcitation, cross sections, rate consts., vibr. rot. model 78−62879
$He+H_2(D_2)(T_2)$, vibr.-rot. transitions, optical potential approach 78−62885
$He+H_2(\mu H)$, interaction pots. and rot. scatt. calcs. 80−43158
He+HCl(HF)(DCl)(DF), slow collisions, rot. excitation cross-sections, quantum mech. calcs. 77−12795
He+HD, thermal energy scatt., distorted-wave and close coupling calcs. 78−86938
He+HD, vibr.-rot. relax. from high vibr. states 79−54945
He+HD collisions, single quantum rot. excitation by pulsed molecular beams 78−29840
He+I*, low energy collisions, energy redistrib. 80−63765
He+LiH, rot. inelastic collisions, dynamics 80−87209
He+LiH, rot. inelastic collisions, state-to-state cross sections determ. 80−87210
$He+N_2(CO)(O_2)$, vibr. state distrib., charge exchange 150-2400 eV 78−42195
$He+NH_3$, rot. excitation rate consts., semiclassical method 79−3538
$He+NH_3$(formaldehyde), rot. excitation, IOS approx. calcs. 79−45801
$He+Na_2$, elastic scatt. and rot. excitation, model pot. energy surface 77−6895
$He+Na_2$, rot. excitation, rainbow oscills., coupled states and IOS approx. calcs. 80−23518
$He+O_2$, long lived collision complexes, exact classical and quantum mech. calcs. 78−33576
$He+O_2$, vibr. energy transfer, exact classical and quantal calcs. 77−19014
$He+p\text{-}H_2$, vibr.-rot. inelasticity, stochastic theory 77−71848
$He+SO_2$, vibr. relax., shock tube study 80−48062
$He^+ + H_2$, dissoc. charge transfer, vibr. enhancement 78−33597
$He^+ + N_2$, low energy collisions, vibronic excitation model 77−83689
He_2, electronic and rot. energy relax., reactive collisions by isotope selective excitation 78−33541
HgBr+$O_2(N_2)(H_2)$(He)(Ne)(Ar)(Kr)(Xe), vibr. relax., rate coeffs., fluoresc. obs. 80−63697
$H_2(j=0)+F(^2P_{1/2})$ quenching, quantum mech. study, ortho-para mixing role 79−76485
$I(5^2P_{1/2})$+HBr, reactive and inelastic channels rate, temp. depend., AAS obs. 78−35657
I+methane $^-d_0(^-d_3)$,$(^-d_4)$, excited atoms, quenching, isotope effects, time resolved reson. fluoresc. 80−32656
I_2, angular momentum transfer, elastic, inelastic collisions, orientation and polarised fluoresc. 78−90271

molecular rotational-vibrational energy transfer continued
I_2, coherent optical transients and optical dephasing in mol. collisions 80−9966
I_2, excited by circ. polaris. light, mol. collisions, emission depolaris. 78−33577
I_2, in seeded supersonic beams, vibr. and rot. relax., laser-induced fluoresc. obs. 80−23522
I_2, recomb. shock heating in unsteady Ar expansion, vibr. relax. effect 77−16794
I_2, reson. fluoresc. obs. of rotationally inelastic collisions selection rules 77−58133
I_2 seeded in supersonic free jet, collision-induced rotational relax. 80−102556
I_2 solutions, vibr. and rot. relax., reson. Raman lineshape meas. 79−31616
I_2, vibr.-translational relax., collisional predissoc., opto-acoustic effect obs. 80−43157
I_2, vibrational relaxation and dissoc. behind a shock front, absorpt. spectroscopy *(Russian)* 77−88536
I_2+Ar, mol. rot. axes, collisional alignment calcs. 77−42376
I_2+CO_2, collisional energy transfer, quenching effects 80−14193
I_2+H_2, vib. relax. in supersonic jet 77−58134
I_2+He, collisional relax. of vibr. excited mol., reson. enhanced 79−64081
I_2+He, energy transfer, centrifugal sudden approx., classical infinite order sudden approx. 80−27933
I_2+He, vibr. relax. cross section, in I_2He_n photodissoc. expt. 79−100410
I_2+I_2, collisional energy transfer, ground and excited states, polarisation spectra 80−32805
I_2+Na(K)(Cs), ion-pair form. cross section, 15-120 eV, mol. props. depend. 77−28996
IBr-CO_2 IR laser with Br*→CO_2 electronic-vibr. energy transfer as pump mechanism 80−53260
ICN, rotational distribs. in photodissociation 77−9097
ICl_2 IF, fluoresc. decay lifetimes and quenching cross-sections for excited $B^3\Pi(0^+)$ states 78−1030
I_2He, van der Waals mol., photodissoc. 80−63765
I_2He* Van der Waals complex, vibr. relax. processes and decomposition 80−63765
$I(^2P_{1/2})$ energy transfer and reactive collisions, laser pumping possibility 79−949
$I_2X^1\Sigma_g^+$, collisional relax. of highly excited vibr. levels, using I_2 optically pumped laser 80−43155
I*+$H_2O(D_2O)(HDO)$, $5^2P_{1/2}$ electronic to vibr. energy transfer, quenching and time resolved IR fluoresc. 79−3537
I_2*+He(Ne), energy depend. of collision induced intramolecular energy transfer 80−83470
$I(5^2P_{1/2})$+benzene-d_0(-d_6), fluoresc. quenching, spin-orbit interaction, isotope effect obs. 78−62763
$I(5^2P_{1/2})$+$H_2O(D_2O)(HX)(DX)$, collisional quenching, isotope effects 77−34583
$I(5^2P_{1/2})$+$H_2(HD)(D_2)$, electronic to vibrational energy transfer 79−68259
$I(5^2P_{1/2})$+HCl(HBr)(NO), electronic-vibrational energy transfer, fluoresc. obs. 78−66579
$I(5^2P_{1/2})$+iodomethane-d_0(−d_3), temperature dependence for quenching 79−45755
K+Br_2(BrI)(I_2), stripping reactions, vibr. distribs. 77−16815
K+CO, bulge effect, in rot. inelastic scatt., isotope shift 79−86047
K+N_2(CO), anisotropy of the repulsive intermolecular potential from rotationally inelastic scattering 79−41226
K+N_2(CO), rot. inelastic scatt., quantum effects, simple model surfaces 80−48064
K+$N_2(H_2)(O_2)$, excited atom quenching, semi-empirical model 78−1065
K+NH_3, rot. inelastic, time-of-flight spectra 78−5325
K_2, optically pumped, relax. in at. collisions 78−17765
KBr*+Ar, inelastic collision, classical trajectory anal., vibr. excitation effects 77−34737
KBr*+Ne(Ar)(CO)(N_2)(CO_2), information theoretic anal. 77−521
Kr+CO_2, collisional energy transfer, anharmonicity effects 80−28097
Kr+CO_2(001), deactivation pathways, quantal close-coupling calcs. 78−58787
KrF discharge pumped laser, energy extraction, collisional coupling between B, C and D-states 80−28213
KrF, form., relax. and quenching 80−81314
KrF laser, collisional coupling between B, C, D states from fluoresc. meas., influence on energy extraction 80−1189
KrF*, oscillatory bound-free emission spectra, semiclassical anal. method 80−7799
Kr**+HCl rot. effect on collisional ionis. 77−83702
Li+H_2, rot. and vibr. transitions, close-coupling calcs. 77−58136
Li+H_2, vibr. excitation, rotationally sudden calcs. 79−22797
Li+N_2, optical pot. method 78−62886
Li+$N_2(H_2)(O_2)$, excited atom quenching, semi-empirical model 78−1065
Li^++CO, rot.-vibr. energy transfer, 1-10 eV, calc. 79−45799
Li^++CO_2, collisional excitation, quasiclassical trajectory calcs. 80−83467
Li^++CO_2, rot. vibr. energy transfer, 1 to 10 eV, many body theory 80−28093
Li^++CO(N_2), differential cross-sections, classical trajectory calcs. 78−29841
Li^++H_2, rot. excitation dynamics, quasi-classical phase space density functions 77−88532
Li^++H_2, rot. inelastic scatt., body frame partitioning approx. calcs. 80−23527
Li^++H_2, vibr.-rot. excitation at intermediate energies 79−3534
Li^++H_2 78−9234
Li^++methane, vibrational excitation, time of flight measurements 79−45826
Li^++N_2, (0.5 to 1.0 keV) energy loss spectra, ionisation, electronic and vibro-rot. transitions 77−14541
Li^++N_2, rot-vibr. transitions, semiclassical calc. of cross sections 79−22798
Li_2, collisional depolarisation and rot. energy transfer, laser-induced fluoresc. obs. 80−9698
Li_2+inert gas, collision induced transition rate consts., two-laser spectrosc. 80−9629
Li_2+inert gas, energy and ag. momentum transfer, polarised laser fluoresc. obs. 79−31590

molecular rotational-vibrational energy transfer continued
Li_2+Li, collisional depolaris. and rot. energy transfer, laser-induced fluoresc. 79−13794
$Li_2(A^1\Sigma_u^+)$, state multipoles transfer following rot. inelastic He collisions, polarised emission obs. 80−5608
$Li_2(B^1\Pi_u)$+inert gas, rot. inelastic collision, classical trajectory calc. 78−1054
LiF, low-energy electron impact rot. excitation, close-coupling calc. 77−58187
LiF, seeded in supersonic beam, vibr. relax. 78−37716
LiF, supersonic seeded molecular-beam, vibr. relax. 78−17761
LiF+Ar, polarised rot. state-selected cross sections, anisotropic intermol. pots. 79−72398
LiH, state selected rot. transition integral cross section, laser fluoresc. obs. 80−63770
LiH+Ar, rot. energy transfer, power scaling law 79−54942
LiH+Ar, rot. transition cross-section, 0.8 eV 79−36742
LiH+Ar, rotationally inelastic cross-sections, state resolved, determ. 78−13577
LiH+HCl(DCl), rot. inelastic collisions, sudden theories 79−98201
LiH+HCl(DCl), state-to-state rot. inelastic cross sections, new laser fluoresc. technique 79−98200
^{7}LiH+HCN, rot. inelastic collision, energy transfer 80−87211
Li^+H_2, elastic of rot. excitation, semiclassical treatment 79−31657
Mg_2, Ar matrix isolated laser photoluminescence spectra, electronic absorpt., emission, vibronic and vibr. relax. 78−82744
MgF+HF, V-V energy transfer collisions, 'triple beam' expt. 79−98197
N^++H_2 (hydrocarbons), rotational-vibrational product excitation 79−47901
N_2 (-CO_2 mixture), jet, molecular rot. level population during condensation 79−86481
N_2, afterglow plasma, interaction with glass, Cu, steel walls, calorimetric method obs. 78−14177
N_2, anharmonic molecules in disturbed thermosphere, vibr. relaxation rel. to NO conc. 79−12322
N_2, B-state collisional transfer, press. effects, oscillator strengths, time resolved spectra 79−36744
N_2, collision induced far IR absorption at high press. 78−5161
N_2, collision-induced far IR absorpt., quadrupole moment 77−27163
N_2, discharge, excitation efficiency of rot. and vibr. levels, heating due to elastic collisions and relax. 80−38751
N_2, electron impact, rot. excitation 77−58184
N_2, electron scatt. ground state vibr. levels population 78−1093
N_2, electron scattering excited, hybrid theory results for 5 and 10 eV 77−27191
N_2, excitation efficiency for rot. states 80−102557
N_2 free jet expansion, rot. level population kinetics, electron-beam diagnostics 78−5776
N_2, gas with clusters, free expansion, upper rot. levels population *(Russian)* 78−33581
N_2, gas-discharge plasma, meas. of electron energy loss distrib. 77−35418
N_2, glow discharge, ionis. mechanism 78−13613
N_2 HP collision-induced translational-rotational far IR absorption obs. 77−38628
N_2, in CO_2-N_2-He laser, electron impact excitation, V-V resonant transfer 78−5452
N_2 jet, freely expanding, quantum effects in rot. relax. 80−58355
N_2, liq., ang. freq. autocorrelation function for mol. oscillator 79−90511
N_2, liq., near BP, vibr. reson. energy transfer and dephasing, Raman spectra 77−6790
N_2, nonequilibrium dissociation rates in electrical discharges, temp. depend. 78−33447
N_2, oscillatory-dissoc. relax. in hypersonic shock layer at moderate Reynolds number *(Russian)* 77−39311
N_2 plasma heating in electrodeless RF capacitative discharge, mechanism, impurity effect 80−59312
N_2, polarisability anisotropy derivative determ. from relative Raman intensities 78−55177
N_2, relax. time in presence of water vap. *(Russian)* 78−74741
N_2, rot. relax. classical trajectory computation, using Lennard-Jones pot. 78−62880
N_2, rot. relax. in viscous shock layer *(Russian)* 77−89162
N_2, V-V and V-T/R energy transfer rate coeffs. by semiclassical collision model 80−9694
N_2, vibr. excitation using steady state chemical reaction between CO and N_2O 80−50851
N_2 vibrational temps. at 40 to 140 km altitude 77−70762
N_2:$CO_2(N_2O)$(methane-d_4), liq., vibr. relax., Raman scatt. obs. 78−92061
N_2-Ar liq. mixtures, coherently excited mol. vibrs., dephasing time 78−62813
N_2-Ar mixtures in 300-1050K range, rot. energy relaxation 78−50617
N_2-Ar plasma, coupled thermal-chem. relax., thermodynamic nonequilib. 78−34265
N_2-CO_2 nonequilibrium aerosol flux mixing, inverse population of vibrational levels *(Russian)* 77−10743
N_2-CO-OCS, liq. mixture, vibr. energy relax. and exchange, laser induced fluoresc. obs. 78−70905
N_2+alkali metal atom, temp. depend. of vibr. relax. time 77−34725
N_2+Ar, 0.06-0.41 eV, metastable at. electronic excitation transfer 79−64071
N_2+Ar, rot. energy transfer, power scaling law 79−54942
N_2+Ar, rot. relax., approx. treatments 79−76494
N_2+Ar, rotational cross-sections, energy depend., modified exponential model 79−50115
N_2+Ar, total differential cross section, diffr. oscills. quenching 78−66625
N_2+Ar*($^3P_{0,2}$), rot. and vibr. energy transfer, relative reaction rates 78−9233
N_2+Cu, preferential energy transfer from N_2 to specific Cu energy levels 80−43152
N_2+H_2, N_2 dissoc. rates, nonequilib. vibr. populations, elec. discharge conditions 77−88535
N_2+H_2O, vibr.-translation relax. cross section in glow discharge plasma 77−43092
N_2+H_2O 78−66631
N_2+$H_2(D_2)$, vibr. relax. in liquid phase 79−847
N_2+H^+, vibr. excitation, differential scatt., low energy meas. 79−89749
N_2+K collision, electronic excitation and energy transfer, time of flight spectra 80−43151

molecular rotational-vibrational energy transfer continued
N_2+Li^+, inelastic scatt., initial rot. and vibr. excitation effects 77−14543
N_2+Li^+, rot. polarisation, spectator model 77−30970
N_2+Li^+, vibr. excitation cross sections, 100-1200 eV 79−27077
N_2+N_2, isotopic variants, V-T and V-V exchanges 78−90270
$N_2+N_2(CO)$, in matrix, vibr. energy transfer and relax. 78−46426
$N_2+N_2(CO)(O_2)$, collinear collisions, anharmonicity effects, vibr. excitation 79−31656
$N_2+Ne(Ar)$, rot. excitation, body-fixed approx. 77−19015
N_2+O_2 vibr. transitions, semiclassical theory 78−66633
$N_2^{+}+He$, low energy collisions, vibronic excitation model 77−83689
$N_2^{+}+He$, vibronic excitation, curve-crossing trajectories 80−23520
$N_2^{+}+Li(Na)(K)$, 50-1000 eV, crossed beams, electron transfer and excitation 80−14226
$^{14}N_2+CO$, vibr.-vibr. energy transfer, long and short range pot. effect 80−99556
$^{15}N_2+CO$, vibr.-vibr. energy transfer, long and short range pot. effect 80−99556
N_3, moist, sound tube meas. of relaxation freq. 78−1058
$N_2(A^3\Sigma_u^{+}, v_i)+N(^4S)\rightarrow N(^2P \text{ or } ^2D)+N_2(X^1\Sigma_g^{+}, v_f)$, energy partitioning 78−66636
NCO, $A^2\Sigma$ state, Fermi resonance and vibr. relax. in solid Ar 78−5212
ND_3, relax. rates determining the inversion spectra 77−454
NH, ND, $X^3\sigma^-$ state vibr. relax. Ar matrix, energy gap law breakdown 77−30963
NH+CO, vibrational energy transfer in solids, rot. mode participation 78−63815
$NH+O_2$ energy transfer rate const., time-resolved fluoresc. rise 79−83489
NH_2, ($\tilde{A}^2A_1$ state), rot. energy transfer, absolute rate coeffs. 79−50119
NH_2 ($\tilde{A}^2A_1$), excited state dynamics and bimol. quenching processes 80−9681
NH_2+H rot. energy transfer in vibronic levels, absolute transfer rates 80−9701
NH_3, Doppler free coherent two-photon transients, collision induced relax. time, meas., Stark switching 78−90249
NH_3, gas-phase Auger electron spectrum 77−31005
NH_3, mol. alignment relax. rate, laser saturation reson. technique 78−25755
NH_3, molecular beam, IR-IR double reson., laser spectroscopic method appl. 79−68243
NH_3, relaxation by IR and microwave coherent transients 80−28092
NH_3, rotational transition, collision induced shift 77−484
NH_3 sensitiser, excitation in MW region using CO_2 laser, pumping models 80−11911
NH_3, time-resolved four-level double-reson. signal, coherent transients effects 78−78732
NH_3+H_2O, collision-induced energy transfer, IR-microwave double reson. obs. 78−42171
$NH_3+He(H_2)$, rot. relax. double and triple reson. obs. 78−66570
$NH_3+He(H_2)$, rot. relax., double and triple reson. obs. 78−90196
NH_3+NH_3, vibr. and rot. energy transfer, IR-microwave double reson. study 78−46432
$NH_3+NH_3(He)(Ar)(N_2)(O_2)$, ν_2 state vibr. relax., laser induced vibr. fluoresc. obs. 79−18269
$NH_3+NH_3(He)(Ar)(N_2)(O_2)$, vibr. energy transfer temp. depend. 80−63763
$NH_3+NH_3(ND_3)(HCl)(H_2O)$, inversion relax., isotope effects, beam-maser ang. resolution effects 77−30964
NH_3+O, rot. excitation, classical Monte Carlo calcs. 77−34727
NH(ND) $X^3\Sigma^-$, in inert gas solid, vibr. relax., matrix and isotope effects 80−95713
$^{14}N^{15}N+CO$, vibr.-vibr. energy transfer, long and short range pot. effect 80−99556
NO ($a^4\Pi$), condensed phase vibr. relax., isotope effect, time resolved obs. 78−94233
NO, electron impact excitation, high vibr. levels of ground state, decay of reson. states 77−88581
NO, electronic to vibr. energy transfer from excited halogen atoms, IR fluoresc. 78−63113
NO excited state vibrational energy transfer, for optoacoustic spectroscopy 78−37724
NO, fundamental intensity and linewidth of IR absorpt. spectra, press. broadening 78−25530
NO, IR laser, electronic-vibr. energy transfer from $Br(4^2P_{1/2})$ 77−31094
NO, $X^2\Pi$ state, vibr. relax., IR-UV double reson. obs. 80−106338
$NO+H^+$, vibr. excitation, differential scatt., low energy meas. 79−89749
NO+Hg, vibr. relax. of states ν=2-10 79−89752
$NO+Hg(6^3P_1)(6^3P_0)$, electronic-vibr. energy transfer collision, IR obs. 79−45716
NO+I, vibr. relax. rate const. determ. 77−19013
$NO+Li^+$, vibr. excitation cross sections 79−54946
NO+O, vibr. relaxation of NO, laser induced IR fluoresc. study 80−9626
$NO+O_3$, (001), laser enhanced reaction, temp. depend., reactive and non-reactive channels 78−48642
$NO+O_3$(001), laser-enhanced reaction, rates, temp. depend. 78−48675
$NO+O_3\rightarrow NO_2^*$, mol. beam chemiluminesc., kinetic and internal energy depend. 78−31638
$NO^{+}+N_2$, vibrational radiation quenching in upper atmosphere 79−3543
NO_2, laser-induced fluoresc. quenching rate const. and lifetimes 80−11930
$NO_2^{-}+O_2(CO_2)(NO_2)$, photodetachment and de-excitation rates 77−75236
NO_3^{-}, in aq. nitrate solns., vibr. dephasing process, Raman obs. 79−51936
N_2O, IR laser, electronic-vibr. energy transfer from $Br(4^2P_{1/2})$ 77−31094
N_2O-CO_2(-ethane), gas phase thermal electron N_2O attachment mechanism, 5-120 torr 79−27085
N_2O+CO_2, vibr. energy transfer, relax. times 79−72401
N_2O+deuteromethane, time resolved fluoresc. for vibr. relax 79−31659
N_2O+HCl, vibr. relax., 300-900K, by laser fluoresc. 79−31658
N_2O+inert gas, reactant decomp., rot.-vibr. energy transfer, relax. analytic soln. 80−55650
N_2O+N_2, vibr. population distrib. energy depend., ν_3, ν_2 and ν_1 mode exchanges *(French)* 79−10187

molecular rotational-vibrational energy transfer continued
N_2O+N_2, vibr. transfer from N_2O ν_3 to ν_1 and ν_2 modes, rate const. 79−22796
N_2O+N_2, vibroluminesc., V-V transfer consts., quadrupolar transition moment, IR spectra 79−10112
N_2O+N_2*, vibr. population studied by IR emission spectra *(French)* 77−14544
NOCl, vibr. energy transfer, (001) level activation/deactivation rate consts. meas. 77−79677
$NO(X^2\Pi)+Ar(NO)$, lower vibr. states relax. rates meas. 77−65527
$NO(X^2\Pi)+Zn(^1P_1)\rightarrow Zn(^1S_0)+NO(A^2\Pi^{+}, \nu=0,1)$, near-resonant electronic energy transfer, fluoresc. quenching 77−14549
$NO(X^2\Pi)+Zn(^1P_1)\rightarrow Zn(^1S_0)+NO(A^2\Sigma^{+})$, near reson. electronic energy transfer, initial rot. state population 79−68304
$N_2O(X^1\Sigma^{+})\rightarrow N_2(^1\Sigma_g^{+})+O(^1S)$, photodissoc., exact collinear calcs. 77−30937
$NO(a^4\Pi)$ dipole moment, meas. by mol. beam electron impact vibr. excitation 79−72440
$NO^{+}(\nu=1,2)+N_2$, vibr. transfer, vibr. absorption coeff. 79−6994
$^{15}NH_3$, $\nu_2R(2,0)$ line freq. coincidence with R(42) CO_2 laser line collisional relax., double reson. obs. 77−46562
N_2*+CO, vibr. excitation and quenching, long contact time effect 79−86040
N_2*+H_2O, vibr. deactivation rate, hard core calc. 79−31651
N_2*+$H_2O\rightarrow N_2+H_2O$* 80−87212
N_2*+SO_2, quenching of vibr. excited N_2, photoionis. detect. technique 78−46388
$Na+H_2$, electronic to vibr. energy transfer, close coupling calcs. 79−98203
Na+molecule, likelihood of vibr. or electronic excitation, model 79−76496
$Na+N_2$, rot. excitation and fine struct.-changing collisions 78−42176
$Na+N_2(H_2)(O_2)$, excited atom quenching, semi-empirical model 78−1065
Na+NO, energy transfer collisions via collision complex 77−83695
$Na+Na_2$, reaction probability, energy transfer 77−28998
$Na^{+}+HCN$, rotational excitation, Stark shifted level transitions, energy transfer calcs. 79−98059
Na_2, ground state, vibr.-rot. relax., optical pumping transients obs. 80−28067
Na_2+Ar, rot. level repopulation rate by laser-induced depopulation 77−65528
Na_2+He, rot. transitions differential cross sections, laser fluoresc. meas. 80−63771
Na_2+He, rotationally inelastic scatt., state-to-state differential cross sections 80−74234
$Na_2+He(Ne)$, rot. transitions, state-resolved differential cross-sections 78−62887
Na_2+Xe, rot. energy transfer, scaling law 78−90272
Na_2+Xe, rot. inelastic collision, rate correls., scaling theory 79−36736
NaF+HF, V-V energy transfer collisions, 'triple beam' expt. 79−98197
$NaNO_3$, aq. soln., Raman spectra, vibr., orient. relaxation *(French)* 78−62808
Na_2*+Xe, rot. energy transfer, level-to-level dynamics, laser fluoresc. obs. 79−64029
Na_2*+Xe, rot. energy transfer, vel. depend. 80−95715
$Na_2^*(A\Sigma)+He(H_2)(N_2)$(methane), rot. energy transfer, power law scaling 79−98204
$Na^*(3^2P)+H_2(D_2)(O_2)(N_2)(CO)(CO_2)(N_2O)(C_2H_4)$, electronic to vibr.-rot. energy transfer, differential cross sections 77−38715
$Na(3^2P)$, electronic to vibrational energy transfer in collisions with simple molecules 80−63769
$Na(3^2P)+CO(X^2S^{+})$, electronic-vibr. energy transfer reaction 79−64084
$Ne+CO_2$, energy transfer, anharmonic coupling terms, semiclassical calcs. 80−37861
$Ne+D_2$, anisotropic inversion pot., rot. inelastic cross sections 80−78696
$Ne+D_2$, energy-loss scaling in 0.5-3.5 keV 80−63768
Ne+HD, j=0 to 1 rot. excitation, differential cross sections, time of flight obs. 80−48104
$Ne^{+}+D_2(H_2)$, energy-loss scaling in 0.5-3.5 keV 80−63768
$Ne_2^{+}+He$, pot. energy surface, reaction cross sections, ab initio calcs. 80−11881
$O+N_2$, quenching of $O(^1D)$ state, at 300K, semiclassical study 79−45823
$O+N_2(^1\Sigma_g^{+})$, energy transfer, classical trajectory model *(Spanish)* 79−89745
O_2, discharge, conditions, self-consistent electron energy distrib. functions calc. 80−38746
O_2, discharge, nonequilib. vibr. population, dissoc. rate, role of ats. and dissoc. 79−64933
O_2, dissoc. induction times, high-temp., exact simple model numerical calcs. 78−9230
O_2, dissociation rates, nonequilib., vibr. populations in elec. discharges 78−46427
O_2, electron impact excitation, high vibr. levels of ground state, decay of reson. states 77−88581
O_2, liq., vibr. energy relax., 53-96K 79−77477
O_2, relaxation by IR and microwave coherent transients 80−28092
O_2, rotational collision number, diffusion coeffs. 79−1281
O_2, vibrational relaxation and dissoc. behind a shock front, absorpt. spectroscopy *(Russian)* 77−88536
O_2-Ar, thermal dissoc. of dilute mols., vibr. bias mechanism 79−61854
O_2+Ar, gas, intermol. pot. for spectral props. and rot. energy transfer 79−68224
O_2+Ar, shock-heated, collision induced dissoc. 79−34290
O_2+fluoromethane, vibr. energy equilibration, IR laser fluoresc. 79−846
O_2+inert gas, dissoc. induced by collision, rot. energy depend. 79−100341
O_2+inert gas, reactant decomp., rot.-vibr. energy transfer, relax. analytic soln. 80−55650
O_2+Li^+, vibr. excitation cross sections, 100-1200 eV 79−27077
O_2+O_2, gas, intermol. pot. for rot. energy transfer and spectral props. 79−68224
$O_2+O_2(H_2)$, vibr. energy transfer, collinear and 3-dimens. rate consts. 80−48065
$(O_2)_2$, struct., energy transfer, high resolution electronic spectra 78−25550
$(O_2)_2$, struct., vibr. relax., local modes, isotope effects 78−25669
O_3, UV absorpt. spectra, IR laser induced changes 80−83385
O_3+CO, O_3+OCS, double-quantum vib. energy transfer 77−6897
O_3+HCl, nonreactive vibr. relax. rate of O_3 (001), 173-419K 79−3545

molecular rotational-vibrational energy transfer continued
O_3+He(Ar)(Xe), collisional energy transfer in unimol. reaction, classical trajectory calcs. 78−62882
O_3+He(D_2)(H_2), vibr. relax. rate consts. 80−74231
O_3+inert gas, rot. energy transfer, centrifugal sudden approx. 80−27933
O_3+p-H_2(n-H_2), vibr. relax. quenching rate consts. meas. 79−13792
OCS, collisional rot.-line widths and shifts, microwave region 78−25619
OCS in n-alkane, rot. relax., solvent hydrodynamic props., Raman and IR spectra 80−45055
OCS, M-resolved rot. Stark levels, four-level microwave-microwave double reson., collision induced 77−10696
OCS, MODOR in ν_2=1 state, nondipolar collision-induced transitions 77−6812
OCS, microwave rot. transitions, phase shift effect, collisional effects 79−98073
OCS mixtures, rot. energy collisional transfer, M-depend., microwave double reson. 78−46435
OCS, pure and seeded beams, rot. cooling, electric reson. meas. 79−13795
OCS, relaxation by IR and microwave coherent transients 80−28092
OCS, rot. relax. cross section, beam maser meas. 79−31654
OCS, seeded beam, rot. cooling 79−18266
OCS, self-broadening linewidth parameters 79−18268
OCS, T_2 relax. meas. using budge-type superhet. microwave spectrometer 80−91551
OCS+CO_2, collisional line broadening of microwave spectra, semiclassical theory 78−29776
OCS+CO_2(H_2)(N_2)(OCS), collisional line broadening of microwave spectra, semiclassical theory, calcs. 78−25516
OCS+H_2, rot. excitation, infinite order sudden approx. 78−74740
OCS+H_2(CO_2) (fluoromethane), rot. relax. parameters, microwave spectra linewidth parameters 80−28009
OCS+He, translational-vibrational energy transfer, quantum dynamical study 80−63746
OCS+He(Ar), rot. lines, collisional broadening 79−18267
OCS+methanol (H_2)(He), collisional rot. energy transfer, microwave-microwave double reson. obs. 77−19016
OCS+N_2* 80−48063
OCS+nonpolar perturber, J1-2 line broadening 77−6848
OCS+nonpolar perturbation, J=1→2 microwave line press. broadening 80−9644
OCS+OCS, rot. transition, interpolation scheme 79−22776
OCS+OCS(He)(Ar), rot. spectral line shift and widths, collision induced phase shifts 77−75222
OD laser, pure rot. lasing intensity, pumping by collision induced energy transfer 78−74897
$O_2(^1\Delta)$+H_2O, atmospheric, collisional emission rel. to new diffuse bands in twilight 80−72662
OH ($A^2\Sigma^+$)+H_2(N_2)(Ar), collisionally induced population change rates, laser-induced fluoresc. obs. 78−5326
OH $A^2\Sigma^+$ state, laser excited, vibr. energy transfer, flame thermometry appls. 80−58349
OH, collisionless form., rovibronic relax., reson. fluoresc. 78−68902
OH, interstellar, rot. excitation by H_2 rel. to maser emission 80−62232
OH laser, pure rot. lasing intensity, pumping by collision induced energy transfer 78−74897
OH Meinel bands, in airglow, rot. temp., radiative lifetime 78−61643
OH-CH rotationally inelastic collisions, maser action 79−94068
OH+Ar, colisional relax., laser mag. reson. study of press. broadening 79−94020
OH+Ar, pure rot. collisionally pumped laser, vibr.-rot. transfer 77−42523
OH+H, interstellar, role in OH 18 cm maser lines pumping 79−48892
OH+H(H_2), rot. excitation in interstellar medium 78−4306
OH+He, colisional relax., laser mag. reson. study of press. broadening 79−94020
OH+He, O_2, N_2, H_2, NO_2, H_2O, NH_3, SO_2, chloromethane, rot. inelastic collision, microwave spectra 79−45806
OH+NO_2, colisional relax., laser mag. reson. study of press. broadening 79−94020
OH+p-H_2(He), collisional pumping of Λ-doublet transitions, pot. energy surface 80−23516
OH($A^2\Sigma^+$), form. from H_2O+Kr($^3P_1$), internal energy distrib. 79−10183
OH(OD), $A^2\Sigma^+$ state, vibrational energy transfer in collisions, rot. resolved fluoresc. 78−74742
OH^+(OD^+), $A^3\Pi_i$→$X^3\Sigma^-$ emission branching ratios, r-centroid depend. 77−6830
OH($^2\Pi$)+H, rel. to interstellar OH maser action 79−101186
O(^3P)+CO($X^1\Sigma^+$), vibr. deactivation and atom exchange, rate. consts., Monte Carlo anal. 77−48627
PHD_2, vibr. dephasing in liq. and solid PD_3, calcs. 80−19884
S_2, selectively excited, coherence retention during rotationally inelastic collisions 77−46622
S_2($B^3\Sigma_u^-$)+inert gas (H_2)(N_2)(S_2), collision-induced energy transfer 79−3544
S_2($B^3\Sigma_u^-$ ν=4)+He(Ar)(Xe), collision-induced transfer rates 79−94062
SF_6 and S_2F_{10}, multiple-photon IR laser pumping, collisional effects 80−9668
SF_6, collision induced rot. Raman scatt., polarisability effects 78−86874
SF_6, collisionless intramolecular vibr. relax. obs. 79−45706
SF_6, collisionless multiphoton excitation and V-V energy transfer, coherent versus stochastic theories 78−82804
SF_6, electron impact vibr. excitation 77−42428
SF_6, excited to dissoc. threshold, IR absorption 79−81245
SF_6 gas, CO_2 TEA laser-excited, slow intermol. redistrib. of vibr. energy 80−53039
SF_6, gas, heating effect on optical props., transmittance meas., intermolecular vibr. energy transfer 79−27737
SF_6, highly excited, time-resolved IR absorpt. obs. 80−9666
SF_6, IR double resonance and energy transfer obs. 77−58105
SF_6, in cryogenic liqs., vibr. kinetics, IR spectrosc. obs. 79−18182
SF_6, laser excited, vibr. relax., optoacoustic meas. of energy absorpt. 77−83667
SF_6 laser isotope separation, rot. and vibr. relax. in mixture 78−25634
SF_6, laser pumping in collisional region of nozzle beam, internal excitation, time-of-flight anal. 80−95719
SF_6 multiphoton dissoc. by mol. beam method, energy distribution meas. by time-of-flight spectra, dissoc. dynamics 80−78670
SF_6, relax. mechanism, narrow reson. obs. by amplitude-modulated wave method 79−10155

molecular rotational-vibrational energy transfer continued
SF_6, soln. in liquid Kr, resonant IR radiation, nonlinear absorpt., vibr. relaxation estimate 79−36642
SF_6, vibr.-translational relax. at high excitation rates 79−41201
SF_6, vibrational-translational relaxation, depend. on intensity of selective laser excitation *(Russian)* 78−9235
SF_6-SO_2-fluoromethane mixture, laser irrad., IR fluoresc. meas. of equilib. and vibr. temps. 78−82766
SF_6+He(Ar), mol. vibrational-translational energy transfer, mass spectrometric meas. 79−36739
SF_6+Li^+(H^+), mode selective vibr. excitation 80−58351
SF_6+N_2O, vibr.-vibr. energy transfer, fluoresc. 80−78688
SF_6+NO+O_3, laser sensitised reaction, time-resolved NO_2* emission obs. 78−20017
SO_2, harmonic and anharmonic matrix elements comparison, appl. to vibrational energy transfer 80−63760
SO_2, liq., vibr. relax., US absorpt. and vel. meas. 80−34147
SO_2, T_2 relax. meas. using budge-type superhet. microwave spectrometer 80−91551
SO_2, T_2 relax. time meas. by microwave transient nutation 77−30862
SO_2, vibr. relax., phase spectrophone method obs. 80−87059
SO_2, vibr. relax. time, 300-2000K, SSH-Tanczos calc. 79−45798
SO_2-$^{18}O_2$ mixtures, IR laser pumped, intermol. vibr. energy transfer dynamics obs. 80−87207
SO_2+H_2O(N_2)(SO_2), linewidths, intensities, isotope shifts, 91.5-95.5 GHz 78−42044
SO_2+O(^3P), vibr. excited, collision induced intramol. deactivation 78−25670
SO_2+SO_2 vibr. relax., shock tube study 80−48062
Se_2, laser induced fluoresc. in inert gas matrix 80−87161
SF_6, third harmonic generation at 10.6μ 77−14775
SiH_4, vibr. energy transfer in pure SiH_4 and mixtures 77−524
SiO, nonmaser emission lines from expanding envelopes around evolved stars 78−28650
Sm+N_2O, mol. beam chemiluminescence, cross section energy depend. 77−32792
Sr+HF(DF), beam reaction, vibr. excitation 78−68877
Sr+N_2, $A^3\Sigma_u^+$ state, vibr. excitation 80−1054
TF-CO_2, chem. laser, rate const. of energy transfer from TF(ν=1) to CO_2(00°0) 77−675
Te_2, laser induced fluoresc. in inert gas matrix 80−87161
U+molecule, collisional relax. of highly excited states, laser-induced fluoresc. obs. 80−58205
UF_6, vibr. relax., US meas. 77−83696
UF_6 vibrational relaxation, ultrasonic meas. in UF_6-Ar-N_2 mixtures 80−1050
U(f^3ds^2)+molecule, collisional relax. of $^5K_5^0$ and $^5L_7^0$ states, laser-induced fluoresc. obs. 80−52925
Xe+Cl_2, classical trajectory calcs., energy threshold for collision induced dissoc. determ., 80−95709
Xe_2, time and energy resolved fluorescence, radiative lifetime, collisional mixing, pulsed synchrotron radiation obs. 79−98136
XeCl, form., relax. and quenching 80−81314
XeCl* emission spectrum obs., in Xe(6s,$^3P_2$)+RCl reactive quenching 79−100344
XeF, form., relax. and quenching 80−81314
XeF, ground state kinetics, multilevel model of energy transfer 80−99707
XeF_2+Ar(Kr)(Xe) metastable atoms→XeF*, mechanisms 77−30897
XeF*, $B^2\Sigma^+$ and $C^2\Pi_{3/2}$ states, fluoresc. decay dynamics, collisional quenching and radiative lifetimes 80−58306
Xe(6s,$^3P_2$)+Cl_2(PCl_3)(CCl_4)($COCl_2$), vibr. energy disposal from XCl* spectrum 79−100345
Xe(nf)+NH_3, at. Rydberg state further excitation by rot. transfer, field ionis. obs. 78−58795
Zn+N_2, $A^3\Sigma_u^+$ state, vibr. excitation 80−1054
ZrO, vibr.-rot. interaction influence on band intensity parameters 79−49999

molecular rotational-vibrational states *see molecular rotation-vibration*

molecular spectra
see also macromolecular spectra; molecular fluorescence; molecular rotation; molecular spectral line breadth; molecular vibration; multiphoton spectra; optical double resonance; radiative corrections; spectra of inorganic molecules; spectra of organic molecules and substances
$^1\Sigma$ state, anomalous Zeeman effect, Doppler-free standing wave saturated resonance, book contrib. 78−9279
absorption, emission, linebreadths, EM radiation interaction with atoms and mols. 78−13448
absorption intensities, rot. averages, ensemble method 79−89658
absorption profiles, relax. mechanisms effects 78−58664
achiral molecular system, elec. quadrupole transition moment, circ. polaris. spectroscopy 77−75219
active Raman spectroscopy, high resolution molecular methods 80−52998
adsorbed molecule, IR multiple refl. spectra recording via cuvette attached to UR-20 spectrophotometer 78−298
anharmonically coupled oscills., time depend. Hartree theory, susceptibility, absorpt. and Raman spectrum 80−58241
asymmetric top molecules, type B band envelopes, QQ and RQ-QP branch separation 79−802
atmospheric pollutants, Zeeman and Stark tuning for laser perturbation spectroscopy 78−69526
atom+atom collisions, adiabatic satellites of at. lines 77−50513
atom+diatomic molecule, collinear collision, light absorption 79−76486
autoionising resonances, vac. UV nonlinear optical props. 77−50565
beams, monokinetic spectroscopy *(French)* 78−25751
benzoic acid, spectral shift due to electron-repelling substituents 79−72362
bimolecular mixed-valence metal complex, intramol. intervalence charge transfer 79−76405
binary reactive gas, in laser field, vibr. energy distrib. 79−6972
Bixon-Jortner approx. limitation, coupling strength incoherence 77−57960
book, summaries and reviews of recent work, fields of interest 78−21894
Born-Oppenheimer and true eigenstate prep. by coherent light, large mol. nonradiative relax. 77−88490
Born-Oppenheimer approx., IR absorption, circ. dichroism using vibronic gauge function 78−967
Born-Oppenheimer approximation, breakdown, spectroscopic effects 77−27045

molecular spectra continued
bound states, semiclassical study 80−9693
bromomethane ($-d_1$, d_2, d_3), exptl. vibr. intensity data error indication by F and G sum rules 79−72364
Brownian rotational motion effect on anisotropic props. of absorpt. and luminesc. from excited states 79−93978
charge transfer transitions, solvent effect, appl. to Ru complexes 77−75127
chemical dynamics, laser probe investigs. 79−43580
chemical reaction wave, propag. of coherent probe light pulse 80−61190
chemisorbed molecules, on metal surface, spectrosc., electron gas effects 80−54504
chemistry and spectroscopy 78−89556
chiral representations in one-centre mol. and field models, symmetry rules 80−14095
circular polarisation of emission, magnetically induced, appl. to inorganic complexes 78−78005
classical coupled dipole oscillators, optical props., normal mode treatment 79−36611
classical model for vibr. transition dynamics, absorpt. of IR radiation 80−52965
coherent and nonlinear optics, conf., Leningrad, USSR (Jun. 1978) 80−98753
coherent anti-Stokes Raman spectroscopy, selection rules, depolarisation ratios, rot. struct. 77−34640
coherent optical spectroscopy of molecules and molecular beams 78−82054
collision free triplets, spectrum, temporal evolution 78−33441
collision-induced light scatt., moments of three-body portion 77−57961
collisional optical coherence transfer, laser spectroscopy 77−42360
complex, (E+A)*e systems, Jahn-Teller, pseudo Jahn-Teller coupling and circular dichroism 79−68247
complex molecules, harmonic oscillator model for band contours 78−82717
complex spectra, band parameters determ., minimisation algorithms effectiveness improvement 79−93225
compounds with hindered internal rot., microwave spectra, free rotor states obs. 79−18179
compounds with hindered internal rotation, vibronic luminesc. and absorption spectra 79−54883
compressed gases, intermol. interactions, translation absorption spectra, temp. depend. 78−46419
computational atomic and molecular physics, conf., Nottingham, England, (Sept. 1978) 79−59567
computing, PUMSM 78−62782
Condon approximation deviation in fluoresc. and absorption spectra, appl. to naphthalene 80−28004
conference, group theory and application to spectroscopy, Nova Scotia, Canada (Aug. 1978) 80−41947
configuration interaction, spectroscopic calcs., general parametrisation method 78−94228
continuous spectra, electronic transition freq. determ. method 77−50425
cooling and trapping of atoms and mols., by reson. laser field 77−3321
cooling and trapping of atoms and mols. by reson. light field *(Russian)* 77−46544
coupling coefficients, f-coeffs. 77−3344
crystal field theory, finite symmetry adaptation in spectroscopy 80−43032
data analysis, phenomenological and theoretical 80−52963
degenerate electron states, electron interaction with doubly degenerate vibr., optical transitions, semiclassical approx. 80−27927
diatomic, singlet-triplet perturbations, spin-orbit interaction 77−10653
diatomic, transition moments, systematics 77−6857
diatomic intensity factors, hyperfine struct. 77−57978
diatomic molecular spectra, conventions for defining electric transition moment and rot. line intensity factors 80−83346
diatomic molecular spectra, space and time parity nonconservation *(Russian)* 79−50098
diatomic molecule, intensity distrib. in branches of septet transitions 79−85944
diatomic molecule, quartet and quintet transitions branches, intensity distrib., rel. to Hund's rule 78−90216
diatomic molecule, resonant and near-resonant Rayleigh and Raman scatt. 78−78705
diatomic molecule, rot. temp. determ., absorpt. spectra calcs. 77−30851
diatomic molecule, sextet transition branches, intensity distrib., rel. to Hund's rule 78−86913
diatomic molecules, $^2\Pi$ states, $^2\Delta$ states, $^2\Pi$ ground state, g-factor, Zeeman effect 79−98149
diatomic molecules, excitation energies, oscillator strengths, many body approach, eqns. of motion method 80−47969
diatomic molecules, excited states, electronic transition probabilities and lifetimes, review 80−78658
diatomic molecules, generator-coordinate theory 79−22689
diatomic molecules, laser spectroscopy, mol. consts. determ., review 77−46602
diatomic molecules, potential energy functions, spectroscopic consts., correls. 79−18253
diatomic molecules, spectrosc. consts., rel. to electronegativity 80−28007
diatomic mols., photoabsorpt. cross-section, photoionis. continuum 77−68029
diatomic radiative transitions, electronic-vibr. dipole moment, band strength 78−46400
dielectric model for electronic spectra solvent effects 77−26991
dielectric sphere with embedded molecule, fluoresc. and Raman scatt. 79−76435
diffuse electron-vibrational spectra, approximation method *(Russian)* 77−65452
dimer, adiabatic theory of exciton interactions 77−30852
dimers, circ. dichroism spectra, quadratic vibronic coupling effect 79−76402
dipole transition, transient behaviour in intense laser field *(German)* 78−66520
Doppler-free two-photon spectroscopy, appl. to mol. electronic transitions 77−74525
double molecules, with weak reson. bond, quasilinear *(Russian)* 78−74640
electric dipole allowed transitions, amplified sector rule based on electron correlation 80−5523
electric dipole susceptibility, third order, rel. to mol. spectra 79−36624
molecular spectra continued
electro-optic laser technique for probing coherent and incoherent decay processes 77−75338
electronic and magnetic structure, interpretation of data obtained from Mossbauer, ESR, susceptibility, optical and XPS meas. 80−37825
electronic emission spectroscopy, appl. of composite wall hollow cathode source 77−19376
electronic excitation of mols., charge transfer and localisation 79−41119
electronic processes and energy transfer, conf., Tallahassee, Fla., USA (Jan. 1976) 77−27042
electronic relax. of large mols. in strong EM field 77−34703
electronic spectra, parity nonconservation effects *(Russian)* 78−13488
electronic spectra, vibr. struct. determ. by Franck-Condon method, book contrib. 78−21911
electronic spectra of molecules, pure elec. quadrupole transition polaris. 80−63691
electronic transition dipole moments, excited state alignment in linear mols. 77−38698
electronic-vibrational transitions in laser radiation field 80−99522
emission and absorption, RF and visible regions predictions from dressed-molecule theory 78−42124
energy level clustering, qualitative theory of irreducible tensor operators spectra 80−28001
energy level transitions, Doppler broadening, phase-destroying collisions 80−9561
excitation of mols. interacting with own radiation fields, stochastic mechanism *(Russian)* 79−85955
excitation of simple atomic and mol. systems, long-range force effects 79−10170
excited mols. that have undergone radiationless transitions, optical probing 77−27106
excited states, absorption spectrum, diffusion rot. effects *(Russian)* 78−74641
Fermi resonance theory 77−1666
fluid and solid molecular motion, submillimetric-wave spectroscopy obs. 79−31517
Fourier transform IR spectroscopy, use in atm. chem. 80−55743
fragmentary composition, determ. by IR, EPR and US mag. reson. spectra *(Russian)* 78−13624
Franck-Condon effects in resonance Raman spectra and excitation profiles, appl. to CrO_4^{2-} and β-carotene 80−14129
Franck-Condon integral for bound-free transitions between harmonic and flat pots. 78−969
free induction decay and optical nutation, short-term behaviour *(French)* 77−75117
Fues potential, vibr.-rot. spectra, Schrodinger eqn. soln., pot. energy curves *(Spanish)* 78−36784
full quantum mechanical theory, mol. eigenstates generator coordinate method 78−21895
gas lasers, computer modelling, at. and mol. processes 80−23661
gas layer, absorpt. model, fine struct. parameters *(Russian)* 77−65455
gas phase chemical reactions in IR laser field, collision-induced absorpt. spectra 80−76499
gas-pressure shifts, Stark displacements 80−23463
gases, collision induced absorpt. spectra, integral data 79−81202
gases, nonuniform vols., IR emission calcs. 80−78657
gases, Raman line broadening, rotational structure, vibrational relaxation 79−98105
generator coordinate method, nonadiabatic mol. dynamics 79−31495
generator coordinate theory, nonadiabatic effects 80−23391
generator-coordinate theory 79−22689
group frequencies study of chem. mechanism, bonds, liq. struct. 79−98057
hexagonal symmetry doubly degenerate mode systems, excitation profiles, depolarisation ratios, reson, Raman scatt. 79−98108
Hierarchically Ordered Spherical Description of Environment, substructure code, spectra estimation 79−50001
high pressure effects, Morse potential formulation 80−63617
high resolution IR mol. spectroscopy with difference frequency generation, refinements 78−90321
high-overtone spectra, reson. struct. and background absorption 79−54833
high-resolution spectroscopy, quantum mech. description 77−6862
high-temperature molecules, matrix isolation spectra, review 78−46340
hole-burning spectra, absorption spectra fine struct. method 77−88594
holographic recording 78−62954
hook spectra, evaluation limitations 80−90905
hydrogen bond absorption spectra, interaction between two harmonic oscills. 79−6929
hyper-Raman scattering by chiral molecules 79−45727
induced absorption, point charges and multipole fields 78−74637
inert gases, electron beam excited, absorpt. characts. 78−82948
inner level spectroscopy with synchrotron radiation, theoretical aspects, book contrib. 80−4778
intensities, IR, rel. to Raman 78−94290
intensity of IR and Raman spectra, efficient ab initio computation method 79−45698
interferometer calibration for atomic and molecular transition wavelength meas. 79−80696
interstellar molecular line intensities, appl. to kinetic temp. and density determ. 79−97056
interstellar molecules, discovery, chemistry and identification 77−82300
interstellar molecules, matrix isolation spectra, review 78−46340
intramolecular dynamics, random coupling model, math. approach 80−58308
intramolecular dynamics, random coupling model, multiphoton excitation, kinetic eqns. 80−63700
intramolecular dynamics, random coupling model 78−94226
intramolecular hydrogen bond, calc. of electronic absorption spectra 80−42949
intramolecular memory effects in second-order optical processes 78−94270
inverse Raman scattering spectroscopy and chem. appls. 80−37094
inverse spectral problem, use of parameters of intermol. spectrum of condensed media to decrease nonuniqueness 77−80586
ion, spontaneous IR rot.-vibr. emission probability 78−50535
ion beams mass spectrometry absorpt. spectra, review 79−89808
IR, in liq. Ar soln., 2 m multiple refl. cell 77−83766
IR, molecular rotation calcs. 77−18910
IR, operator perturbation method, effective Hamiltonian *(Russian)* 77−79599

molecular spectra continued
IR, operator perturbation method, effective Hamiltonians *(Russian)* 77−83563
IR absorpt. intensities, symmetry considerations on electrooptical parameters 77−75225
IR absorption intensities, bond charge parameters determ. 77−6853
IR absorption intensities, electro-optical parameters transferability to isotopic species 77−6850
IR absorption spectra intensity, polyat. mol. dipole moment additivity, parameter transferability 78−58747
IR absorption vibration spectra, true parameters of isolated bands calc. *(Russian)* 77−83586
IR and Raman band intensities, use in force const. calcs. 77−27120
IR and Raman vibrational intensity changes due to long-range interactions 80−53084
IR band nonrigid rot. absorption, appl. to CO, NO, N_2O and CO_2 78−91060
IR band shape, statistical, modelling methods 79−50087
IR Doppler free molecular spectroscopy, two photon coherence and pumping 80−48052
IR integrated intensities, rel. to mol. consts., isotopic sum rule 77−27118
IR intensities, atomic polar tensors, effective charge-charge flux model 78−70875
IR intensities, relationship with vibronic coupling integrals 79−36596
IR intensities, theory, rel. to mol. moments and vibr. 77−10703
IR intensities, vibronic calcs. 79−10108
IR intensities of fundamental bands, polar tensor calcs. 79−13708
IR intensity, Mayants-Averbuch theory d-parameters, rel. to valence optical theory 77−34700
IR intensity data reduction, use of reference mols. 79−13772
IR interaction with mols., classical/semiclassical theory 78−90164
IR lasers and laser techniques in mol. spectroscopy, book contrib. 78−8455
IR molecular absorption spectra, effect of rotational coupling on torsional bands 78−13497
IR radiation, interaction with molecular system, classical/semiclassical theory challenged 80−43117
IR radiation transfer in nonequilib. mol. gas *(Russian)* 78−50599
IR spectra, vibr. freq. shift, press. and solvent effects 78−74709
IR spectra calibration using spline functions 77−27050
isotope spectra, from unseparated natural mixture, spectrosc. technique 79−31736
isotopic isomers, spectroscopic obs. 80−53009
kinetic spectroscopy of molecules 79−94110
L^ discretisation of atomic and mol. electronic continua, review 79−59425
Landau-Zener effects in optical spectra *(Russian)* 78−55162
lanthanide (III) complex, octahedral, f-f transitions, mag. dipole intensities, vibronic coupling model 80−25404
large molecule, novel ultrafast two-pulse excitation spectroscopy 78−94331
large molecules, reson. Raman scatt. cross-section calcs. 79−31532
large molecules, Rydberg spectra, antireson. lineshapes 77−50424
laser applications to chemistry, overview 79−58800
laser interaction with matter, nature of light, nonlinear spectroscopy 77−50712
laser spectroscopy, multiphoton and multistep methods, review 79−35842
laser spectroscopy 79−55002
laser-induced processes in molecules, conf., Edinburgh, Scotland (Sept. 1978) 80−9577
least-squares parameters, rounding errors 78−158
linear atom chain, mixed spectrum of correlated pulse sequences 79−84944
liquids, Raman line broadening, rotational structure, vibrational relaxation 79−98105
liquids, solute-solvent interactions, moment anal. of IR absorpt. bands 78−58766
LNDO/S, semiempirical SCF-CI method for calc. ionis. pot. and electronic transition energies 79−18117
Lowtran molecular absorption empirical transmission function analysis 79−76400
macroscopic system, vibrational relaxation, information-theoretic approach 77−58156
matrix isolated molecules, vibr. relax. 78−46425
matrix isolation vibr. spectroscopy, complex form. studies 78−62952
methane, ground state, dipole oscill. strength distrib., rel. to molar refractivity and dispersion energy 77−71835
micelle formation model, relaxation spectra 80−71934
microwave, geometry determ., minimum necessary no. of isotopic substitutions 77−3484
microwave spectrometer baseline suppression using FM and harmonic detection 78−82866
microwave spectroscopic intensities, free energy of conformational changes 77−75227
microwave spectroscopy of short-lived molecules, review 79−50010
millimetric/submillimetric coherent transient spectroscopy 80−58651
model calculations, matching with experiment through linear regression 80−58243
molecular, electronic spectra, projected-unrestricted Hartree-Fock theory 78−46313
molecular crystals, nonlinear optical susceptibility, second order, calc. from mol. spectra *(Russian)* 79−27318
molecular crystals, spectroscopy, bibliography (1977) 80−7317
molecular ions, gas phase, spectroscopic props, review 78−33501
molecular spectroscopy, conf., Columbus, Ohio (June, 1978) 79−35848
molecular spectroscopy using synchrotron radiation, book contrib. 80−4780
molecule, intensities dipolaris. ratios, polarisability, matrix rotation, isotopic rules 78−5288
molecule+ion, Λ-doublets transitions 80−14132
molecule+molecule, enhancement by collision induced absorpt. of IR laser radiation 80−66798
molecules, distortions of decay curves in delayed coincidence techniques 78−17620
molecules adsorbed on electrode surfaces, Raman scatt. theory 79−13724
monochromatic laser radiation, excitation of atomic, mol. energy level transitions, inhomogeneous and mixed line broadening 78−55147
monochromatic laser radiation, excitation of atomic or mol. energy level transitions, strictly homogeneous line broadening 78−58629
Mori formalism for far IR and microwave absorption 77−24833

molecular spectra continued
multilevel system, laser excitation, Wilcox-Lamb rate eqn. approx. 79−27028
multiphoton,, crossed mol. and laser beam obs. 79−41208
multiphoton absorption, model 79−31633
multiphoton processes, high-order, rot. wave approx. 79−59518
multiphoton processes, stochastic reduction 79−81246
multiphoton resonances of anharmonic molecule 79−54927
N-level molecules, coherent dynamics, anal. solns. 78−22105
N-level molecules, coherent dynamics, numerical expts. 78−22104
neutral molecules, adsorbed on metal surfaces, excitation spectrum 79−23832
neutral molecules adsorbed on dielec. surface, excitation spectrum 78−71943
neutron scattering by molecules, polymers and absorbed species, review 79−41911
nongrey molecular gases, total IR band absorption, anal. and approx. models 80−14141
nonlinear absorbing medium, spatial freq. response, diagnostics appls. 79−27314
nonlinear laser spectroscopy, book 77−71894
nonlinear oscillator, fluctuational transitions between stable states *(Russian)* 79−93981
nonlinear resonances of accelerated atoms and molecules *(Russian)* 78−50488
nonpolar molecules in degenerate vibr. states, pure rot. absorpt. spectra 80−78598
normal vibrations classification in mols. with internal rot. according to microwave spectra data 77−18909
optical double resonance Stark spectroscopy, using modulation sidebands 77−58051
optical properties in resonant low freq. laser radiation field *(Russian)* 80−78628
optical rotation, semiclassical theory, appls. to pure rot. spectroscopy 77−75132
optical rotation, semiclassical theory, near reson. absorpt. 77−75131
optical torsion transitions, barrier heights from vibr. optical freqs. 77−42308
optical transition energies, Koopman's theorem, ionis. pot. 77−18908
optogalvanic double-resonance spectroscopy 80−57385
organic chemistry courses, unified approach to teaching of struct. and bonding 80−17732
organic molecules, IR spectral intensity calc. for electro-optical parameters 79−54835
oscillating electric dipole contrib. to light scatt. and interpret. in terms of polarisability and hyperpolarizability 80−53212
overlapping lines in Raman and IR bands, separation *(French)* 79−3499
overlapping Raman lines resolution by coherent ellipsometry 79−98110
partially ordered ensembles, spectrosc. props., theory, 1-vector problems 80−42261
pentagonal symmetry doubly degenerate mode systems, excitation profiles, depolarisation ratios, reson, Raman scatt. 79−98108
photoelectron spectroscopy, of transient species generation 79−31739
photofragment, ion photodissociation 78−66673
photofragment spectroscopy of mol. ions using fast ion beams 80−9755
photon emission from mol. and electronic transitions, quantum dynamics, semiclassical description 80−105466
photoselection, orient. relax. rel. to emission mag. induced circular polarisation 78−70860
picosecond chemistry, review 77−5933
picosecond emission spectroscopy, appls. 78−86350
picosecond phenomena, conf., Hilton Head, USA (May 1978) 79−44940
picosecond spectroscopy, appl. to chem. and biological reactions 79−80697
picosecond vibrational and electronic relaxation processes, spectrosc. obs. 79−45808
planar molecule, oriented in transparent polymer films, dichroism of absorpt. bands *(Russian)* 79−31506
plasma vibrational spectroscopy, data gathering and processing system 79−31737
point group coupling, coeffs., props. and application 80−43033
polarisation propagator calculations of frequency-dependent polarisabilities, Verdet constants, and energy weighted sum rules 78−58647
polyatomic, excitation and dissoc., intense IR laser radiation 77−83570
polyatomic, IR excitation to vibr. levels *(Russian)* 79−26915
polyatomic, radiative lifetimes from absorpt. spectral data 77−6852
polyatomic asymmetric top molecules, solns., IR spectra 78−58694
polyatomic gas, laser-induced rate processes, intermol. and intramol. relax. formalism 79−27070
polyatomic molecule, absorption of intense IR radiation, statistical model, appl. to SF_6 77−34626
polyatomic molecule, continuous and diffuse spectra, freqs. of 0,0 transitions, review 79−93965
polyatomic molecule, diffuse absorpt. and fluoresc., vibronic band broadening 79−98161
polyatomic molecule, Franck-Condon principle and sum rules for vibronic transitions 77−30927
polyatomic molecule, multiphoton excitation by two IR lasers 80−91607
polyatomic molecule, nuclear γ-transitions, Franck-Condon principle *(Russian)* 79−59522
polyatomic molecule, quasicontinuum, coherent and mode selective excitation by laser pulse 78−1032
polyatomic molecule, vibr. struct. of electronic spectra, FORTRAN programs 80−32699
polyatomic molecules, 0-0 transition freqs. in continuous and diffuse spectra *(Russian)* 78−74639
polyatomic molecules, absorpt. forbiddenness removal in strong light fields *(Russian)* 79−36616
polyatomic molecules, calc. of spectral absorpt. curves 79−10093
polyatomic molecules, excitation energies, oscillator strengths, many body approach, eqns. of motion method 80−47969
polyatomic molecules, excited state spectra, vibronic coupling, non-adiabatic model 78−25509
polyatomic molecules, highly vibrationally excited, spectra calcs. 78−90140
polyatomic molecules, intensity distribution in vibronic bands, Dushinsky effect 79−93983
polyatomic molecules, intramolecular dephasing processes 78−74695
polyatomic molecules, IR absorpt. bands, integrated intensities, ab initio and LMO calcs. 79−72234

molecular spectra continued
polyatomic molecules, mol. parameters isotopic depend. 80−9522
polyatomic molecules, multiphoton ionisation spectroscopy 79−41203
polyatomic molecules, multiphoton IR absorpt., collisional effects 79−41174
polyatomic molecules, multiple-photon absorption, quantitative comparison 80−32790
polyatomic molecules, multistep or multiphoton laser vibr. spectrosc. 78−90151
polyatomic molecules, non resonance vibronic coupling of excited states rel. to electronic spectra 77−18900
polyatomic molecules, normal coordinate problem, QM treatment, book contrib. 78−78677
polyatomic molecules, overtone spectra, local mode anal. 77−27046
polyatomic molecules, vibr. absorpt. spectra, diffusivity due to crowding of sequence of levels *(Russian)* 77−38652
polyatomic overtone spectra, local mode theory 79−36618
polyatomic system, multiple scattering method for photoelectron and absorpt. spectra 77−88501
polyatomics, absorpt. and luminesc. spectra, higher electronic states effect 80−9586
polymer film, proton intramolecular transfer, light absorpt. and emission, dichroism, polarised fluoresc. 80−87166
programs for identification of chem. compounds from mol. spectra *(Russian)* 77−52727
pseudo Jahn-Teller effect, rel. to vibronic coupling model, for mol. spectra 78−94234
quantum dynamics in effective system states basis, not in radiation field, perturbation theory 78−33499
quantum intramolecular dynamics: criteria for stochastic and nonstochastic flow 80−53082
quasi-classical quantisation of multidimens. systems, adiabatic invariants *(Russian)* 79−3343
quasi-energy states, and stability of mol. in field of light wave *(Russian)* 79−94039
quasilattice theory of solutions, use in mol. spectroscopy, thermodynamic parameters determ. 79−96350
Quasimolecule formation in heavy ion collisions *(Russian)* 78−33568
quasimolecules, X-ray continua from coalescing atoms 77−530
quasistationary states decay, electron and photon spectra *(Russian)* 79−49969
radiationless processes, model *(German)* 77−38686
radiative transitions, classical theory appl. 78−74597
Raman, vibrational relax. in liqs. *(Russian)* 79−59476
Raman and IR intensities relation 77−65514
Raman and IR intensity, relation in matrix notation 78−62853
Raman excitation profiles, vibronic theory 77−23501
Raman excitation profiles and mol. spectra synthesis, vibronic and exciton-in-mol. theory 78−42076
Raman microprobe analysis, principles and appl. 80−57390
Raman scatt., excitation profiles by vibronic theory, preresonance scatt. 77−79619
Raman scatt. time depend. theory 80−28023
Raman selection rules, spin degeneracy and vibronic states 78−987
Raman spectra, correlation with vibronic coupling and adiabatic potential 77−71804
Raman spectra of gases, high-resolution, mol. struct. and orops. 80−53000
Raman spectroscopy, high-resolution, using tunable spin flip Raman laser, review 80−55762
Raman spectrum, dispersion of depolaris. and conversion factors 79−72323
Ramsey reson. obs. by linear laser spectroscopy 80−99514
random velocity fields, radiative transfer and line form., intensity moment transfer eqn. derivation 80−52967
rapid intramolecular radiationless transitions, decay rate by time resolved reson. Raman spectra 79−76434
relaxation processes and spectra in liqs. and dense gases 77−58935
resonance interactions of atomic and molecular systems driven by strong laser field, theory 80−14097
resonance light pressure, anal. of forces and applications, reviews 79−18156
resonance Raman scatt. from mols., temp. effect, displaced harmonic oscillator model 80−23424
resonance Raman scatt. in mols. with double minimum pots. 77−58011
resonance Raman scattering, of totally symmetric vibr., depolarisation dispersion, vibronic coupling 77−65472
resonance Raman spectra, mols. with vibronically coupled excited states 77−6784
resonance Raman spectra, saturation effects, coherent pulse calcs. 77−6785
resonant coherent Raman scatt. spectra of excited molecules 80−87129
resonant Raman scatt., strong vibronic coupling limit, Green's function 77−83605
resonant Raman scatt., strong vibronic coupling limit, overtones, hot bands 77−83606
resonant Raman spectra, overtone intensity distrib., effect of excited electronic state 80−87128
RF field, modulated amplitude, transition probabilities oscills. *(French)* 78−42039
RF spectroscopy, interference effects *(French)* 78−42038
rotational coherence, reson. collisional exchange, time-resolved microwave obs. 80−23525
rotational forbidden transitions, review 77−34612
rotational intensities in $^4\Sigma$(int)-$^4\Sigma$(int) transitions 80−9642
rotational spectra, doublet splittings caused by tunnelling, perturbation treatment 80−91541
rotatory strengths, higher-order sum rules 77−27119
Rydberg spectra, resonance line shape 78−17720
Rydberg states, quantum defect theory applic. 80−32700
Rydberg-valence mixing, oscillator strengths 79−31492
saturated spectral lines in mm and sub-mm mol. rotation spectroscopy *(Russian)* 77−75335
scattering by EM field 78−954
selection rules for spectra and photochemical reactions *(Chinese)* 80−21308
selective excitation by laser pulses, dynamic theory of radiationless transitions 77−54570
shake-up and UV charge transfer transitions, comparison 80−102567
simple oscillator, correl. functions, IR band shapes 79−26960
small molecules, spectroscopic techniques, review 77−54554
molecular spectra continued
soft photon approx. accuracy for resonances in electron scatt. in laser field 78−70935
solvated electron, in D_2O, IR and vis. spectra, 292 to 445K 78−74672
solvated electron energy characteristics, absorpt. spectra analysis 79−34320
solvated electrons, optical absorption spectra, temp. depend. moments, many-particle theory 79−72301
solvated electrons, optical spectra and model potentials 80−30318
spatial structure, spectra interpretation, computer method 79−49962
spatial-temporal modulation in molecular beam spectroscopy, phenomena near molecular resonance *(French)* 78−90149
SPECAN, rot. spectra automatic assignments program, speed improvements 79−31499
spectral density, time-depend. perturbation theory calcs. 77−13525
spectroscopic channel basis for radiative and radiationless processes, absorpt. spectra 77−14411
spectroscopic constants, merging results of separate least-squares fits 78−5195
spectroscopic data analysis, phenomenological and theoretical 80−52963
spectroscopy, conf. Frankfurt, Germany (Sept. 1979) 80−51948
spectroscopy and crystal physics, generating function techniques 80−44162
spectroscopy of small molecules, recent developments 79−3426
spherical top molecules, IR spectra, diagonal $F^{(4)}$ and $F^{(6)}$ coeffs., computer listing 78−17669
spherical top mols., $T(\nu_3)$ rovibrational bands, level cluster patterns, centrifugal and Coriolis effects 79−18175
spherical top mols., vibr.-rot. eigenvalue spectrum, energy level cluster anal. 79−18174
spherical top mols., with electronic degeneracy, rot. Raman spectrum 79−72322
spin-flip Raman laser appl. 79−72571
spontaneous emission fluctuations, data extraction 77−434
strongly interacting solvents, IR band shapes, solvent-induced chirality, field theoretic Green's function method 79−27037
sub-Doppler laser spectroscopy of mol. ions in fast ion beams 80−9655
subpicosecond techniques, chem. meas. appls. 79−35849
superheavy quasimolecules, electronic states, spectroscopy 78−37706
symmetric molecules, high resolution spectra, rot. and permutation dynamics 79−41157
symmetric polyatomic mols., frame transform. relations and multipole transitions 78−58661
symmetric top and linear molecules in inert solvents, far IR absorpt., free rotational models 77−450
symmetric top molecules, microwave transient phenomena, Bloch eqns. 79−26969
symmetry analysis in vibr. and electronic spectroscopy computing *(Russian)* 77−46555
synchrotron radiation, techniques and appls., book 80−5668
tensorial calculations 80−18836
tetrahedral molecules, vibr., charge and charge flux 80−47961
thermally available vibrational energy levels, energy transfer, photoacoustic and IR emission obs. 79−72402
thin window gas absorption apparatus for molecular K-edge synchrotron radiation absorption 78−62955
third order perturbation theory, simplification 79−98064
time-resolved resonance Raman spectroscopy and vidicon Raman spectrography, vibr. spectra on nsec scale 80−37095
transition energy, direct calc., response function approach, multiple cluster expansion formalism 79−72293
transition identification, coherence resonances for hyperfine struct. interpretation 79−54920
transition metal complexes, O containing, coordinate bonding, charge transfer electronic bands, complex struct. determ. 80−52977
transition probabilities, conf., Lund, Sweden, (March 1977) 77−79555
transition probabilities, non-adiabatic, calc. 79−49926
transition probability, nonadiabatic unimolecular decay, simplified semiclassical formalism 77−61804
transition probability studies, review of recent advances 78−17655
triatomic molecule, nonlinear, transform. of vibr. and rot. coords. during electronic transition *(Russian)* 79−93980
triatomic molecules, motion, regular and irregular spectra, theory 80−9590
triatomic mols., Renner-Teller effect, orbital angular momentum 80−78513
trigonal symmetry doubly degenerate mode systems, excitation profiles, depolarisation ratios, reson, Raman scatt. 79−98108
triplet-triplet transitions role in spin-orbit interactions 79−63915
two-level system, interaction with polarised light, Floquet's theorem 77−57939
two-level system, one-photon optical absorpt. theory 77−34651
two-level system, strongly coupled, induced transition probabilities and energy 78−66598
two-level system in coherent field, quantum description 79−64053
two-level system in two periodic fields, kinetics 79−64188
two-photon Doppler-free technique, for mol. electronic transitions 77−79167
two-photon resonant processes, conserved quantity 79−45688
two-photon spectra, theory 78−94298
two-photon spectroscopy, dipole-forbidden transitions, double excited configurations, CNDO-CI methods 80−58332
two-photon spectroscopy, ultra-high-resolution, Doppler-free 78−49909
ultra-soft X-ray emission spectroscopy, correl. with electron spectroscopy 78−50558
unresolved rot. struct., use in flame temp. meas. 80−86300
UPEAK spectral decomposition routine 78−32798
valence and core photoionisation, spectral lines, many body effects 80−47853
van der Waals molecules, vibr.-rot. spectrum 79−13698
vibration rotation spectra, qualitative theory of clusters, high symmetry mols. *(French)* 78−58645
vibrational classical trajectories, spectral anal. 77−83564
vibrational selective excitation in time-varying freq. EM field 77−50423
vibrational spectra and structure, book 78−78700
vibrational spectra calculations, mol. fragments effects *(Russian)* 78−5203
vibrational spectroscopy, high pressure, and conformational analysis 80−9758
vibrational-rotational line intensities, accidental resonance effect 77−18987

molecular spectra continued
vibronic coupling model, nontotally symm. harmonic mode 77−3337
X-ray, chemical shift, influence of inner level vacancy 77−27085
X-ray absorption, use of synchrotron radiation from storage ring 77−27199
XY_2, collinear photodissoc., UV spectra vibr. struct. 77−18936
XY_4 tetrahedral mol., IR absorption intensities, tensorial calc. *(French)* 77−18984
Ag-electrolyte interface, enhanced Raman scatt. of adsorbed molecules, background continuum obs. 79−73926
Bi^{3+}-HCl solution, metal cation influence on spectra and luminescence kinetics *(Russian)* 80−78627
C_2+acetylene, C_2 Swan band transition probabilities, collisional energy transfer effects 80−87214
CO_2-N_2, hot gas mixture, spectral and integral emission capacities calcs. *(Russian)* 77−68054
ClO, $A^2\Pi_r$-$X^2\Pi_i$ absorpt. cross-sections and oscill. strengths, f-values 77−38649
F_2O, geometry, electron spectrum, vert. ionis. pot. ab initio calc. 80−58187
H bond system, charge transfer theory, relation between vibr. spectra and energy 77−3334
H bonded ν_{X-H} band, dynamic theories survey 80−52983
H bonded systems, IR spectra, theoretical interpretation 79−31519
H bonds, IR spectra, theoretical interpretation 79−31519
H-bond, symmetric $AHA^{(\pm)}$, A-H stretching vibr., liq. IR band shape, strong coupling phonon model 78−64358
H-bonds, IR spectra, ν_s band interpretation 78−58653
H_2 dissociative photoionisation, 19.8-40.8 eV, proton kinetic energy spectra 79−68273
HCl+Ar(Xe), spectral line shift of vibr.-rot. lines, press. shift 79−18237
$K_2Pt(CN)_4$, muonic X-ray radiation anisotropy *(German)* 80−69267
NO_2, heavy cation effect on singlet-triplet intercombination 79−85946
Na $A^1\Sigma_u^+ \rightarrow X^1\Sigma_g^+$ system, transition moments and radiative lifetimes calcs. 77−34697
O_2 (0-0) atmospheric band, laboratory discharge lamp source 80−4148
OHO H-bond, IR spectra, stochastic model 77−27060
S_x vapour, x=3 to 8, UV absorption and fluorescence spectros., vibrational constants of S_2 80−78631
XeF(Cl)(Br)(I), covalent and ionic states, spectroscopic props., ab initio CI calc. 78−90092

molecular spectral line breadth
absorption, emission, linebreadths, EM radiation interaction with atoms and mols. 78−13448
absorption line profiles, instrumental spectral resolution effects 77−6726
absorption line shape of two coupled oscillators decaying in two different mediums 78−62850
absorption line variation across planetary disc with inhomogeneous atm. 80−8569
absorption profiles, relax. mechanisms effects 78−58664
acetaldehyde+$H_2(N_2)(CO_2)$, rot. line broadening, mol. quadrupole moments calc. 80−28065
acetic acid, Rayleigh-Brillouin scatt., 20-115°C, viscoelastic theory anal. 79−28774
acetic acid-d_0, -d_1, -d_4, H bonding in solid, IR spectra, vibr. and librational modes 78−43843
acetone, liq., C-C stretching mode relax., Fermi reson. influence 80−25352
acetonitrile, ν_2, ν_3 and $2\nu_3$ bands, vibr. relax., Raman spectra of liq. and dil. soln. 78−9154
acetonitrile, in liq. phase, Ramon band profiles, calc. using IR intensities 80−2741
acetonitrile, IR and Raman spectra, vibr. and reorientational and energy transfer width separation, rot. const. determ. 80−87131
acetonitrile, soln., vibr. relax., isotropic Raman spectrosc. obs. 79−50025
acetylene, ν_2 band, Q-branch, high resolution CW CARS 77−42329
acetylene, Q-branch of CARS, form and width alteration due to press. *(Russian)* 78−29795
acetylene(-d_2) solns., IR absorpt. band profile *(French)* 77−83597
acetylene-air flame, Li(Na)(K)(Mg)(Ca) damping consts., Lorentz collisions, mag. field effect 80−66805
acetylene-d_2, $\nu_4+\nu_5$ band, diode laser meas. 78−78664
acetylene-d_2(d_1), rot.-vibr. Raman spectra 80−83372
alcohols, monohydric saturated, vibrational bandshapes 78−90226
alcohols, OH-stretching vibr. band in overtone region, IR-Fourier spectral investig. *(German)* 80−976
alcohols, vapour and liq. IR spectra, bandwidth, directional mol. rot., H-bonding 79−78661
alkali homonuclear dimers, quasi-static wing profiles of self-broadening reson. lines 80−48042
alkali-inert gas system, mol. band profiles of induced dipole transitions 78−42135
alkanes, $\nu(CH_2)$ and (CH_3) Raman bands, global integrated intensity, dilution effects *(French)* 77−61755
alkyl benzenes, jet-cooled, intramol. vibr. relax., reson. fluoresc. and excitation obs. 80−14152
alkynes, $\nu(CH_2)$ and (CH_3) Raman bands, global integrated intensity, dilution effects *(French)* 77−61755
anharmonic molecules, stochastic multiphoton absorpt. processes, classical model 79−45778
anthracene, fluoresc., site selection spectroscopy, 2-300K 77−1731
anthracene, fluorescence spectra in aq. and surfactant solns. 77−83639
anthracene, in n-paraffin matrices, luminesc. spectra, depend. of inhomogeneous broadening *(Russian)* 79−10145
anthracene, melt and dil. soln., UV spectra, line broadening and shift vibr. struct. 78−17684
anthracene, rarefied vap., fluoresc. spectrum shape distortion in presence of intense radiation 79−3487
anthracene vapours, shape of absorpt. bands, temp. depend. 78−82743
9,10-anthraquinone, Shpolskii quasi-line phosphoresc. spectra, electronic-vibrational interactions 78−55196
aromatic hydrocarbons, absorpt. spectra, electronic-vibr. sequence band broadening 77−65453
aromatic molecule, in aromatic (aliphatic) solvent, 77K, triplet-triplet absorption spectra, anomalous broadening 77−88502
asymmetric top molecules, Raman spectra, vibr.-rot. selection rules and general band contours 77−58020
atom-atom (molecule) collision, effect on linear and non-linear spectroscopic line shapes 79−36735

molecular spectral line breadth continued
bacteriochlorophyll a, stimulated fluoresc. and fluoresc. quenching, pump photon density 78−27895
benzene, 260 nm absorpt. spectrum, band contours, vibr. ang. mom. components 79−13736
benzene, $\pi\pi^*$ and Rydberg bands, cryogenic solvent effects 78−55182
benzene, liq., C-H stretch vibr. overtones, optoacoustic spectrosc. obs. 79−93982
benzene, liq., spectral broadening of mol. transitions, librational broadening 79−51939
benzene, liq., visible region absorpt. spectra, overtones meas. 80−78625
benzene, molecule translational mobility in depolarised Raman spectra 80−14150
benzene, overtone spectrum, intramol. lineshape narrowing 79−45705
benzene, photoluminesc. at 5K, N_2 and inert gas matrices 77−6838
benzene, reson. Raman cross sections, forbidden electronic transitions, depolaris. ratios 78−42075
benzene, vibr. overtone lineshape 79−27040
benzene, vibr. relax. in soln., ν_1 C-H stretching band Raman spectra 78−25540
benzene+bromomethane, microwave line width and quadrupole moments, perturbation theory 80−69190
benzene+OCS, microwave line width and quadrupole moments, perturbation theory 80−69190
benzene and deuterates, highly vibr. excited intramolecular V-V transfer, visible and photoacoustic spectra 80−32729
benzene in solution, rotational motion, Raman study 80−44104
benzene-carbon tetrachloride, mixture, mol. and Raman scatt., profile shape, conc. depend. 77−58025
1,12-benzoperylene, phosphoresc. in solid matrix, electronic transition multiplets 77−3413
benzophenone, in DDE at 2K, vibr. overtone characterisation and local modes by emission spectroscopy 79−89682
3,4-benzphenanthrene cation radical, in boric acid glass, spectrum 200-1400 nm, MO calcs., assignments 77−75174
bilirubin, soln. luminesc. 79−31572
biradical metal chelates, rot. motion in polar solvents, rel. to ESR lineshape 80−27994
bromochlorofluoromethane, gas, IR band contours and intensities anal. 78−82788
bromomethane, and isotopic forms, self-broadening and self-shifting of rot. spectra 78−13551
bromomethane+$OCS(SO_2)$, (cyanomethane), microwave spectral line width, dipole-dipole interaction calc. 78−74648
bromomethane-$d_{0,1,2,3}$, IR spectra intensities, dipole moment, bond charge, force consts. 77−83588
trans-butadiene, two-photon spectra, press. effects, transient lensing spectrosc. 78−58756
β-carotene, ν_1 line shape, CARS and CSRS 78−82727
carotenoids related to visual chromophore, electronic struct., band shape model 78−20142
CARS, effect of rot. relax. in continuous media *(Russian)* 79−10186
CARS, spectral profile interpretation 79−83523
CARS spectroscopy, laser linewidth effects 79−89012
chemisorbed molecules, IR line shape, dynamical theory 79−824
chloroform, and d, polar soln., Raman line shape of ν_1 band 78−74705
chloroform-d in soln., vibr. and reorientational relax., Raman study 80−63636
chloromethane, microwave spectrum, width and shift parameters 77−18985
chlorophyll a, stimulated fluoresc. and fluoresc. quenching, pump photon density 78−27895
chlorophyll-a, solns., vis. absorpt. spectra of monomer, dimer and oligomers 77−29101
chromophore aggregates, circular dichroism spectra, calc. involving band shape 78−46478
coherent anti-Stokes Raman scatt. for mol. homogeneous linewidth meas. 77−71810
collision and Doppler broadening, combined effect 77−71832
collision broadening, approx. trajectories calc. 78−46413
collision broadening, short-range interaction effects 77−42355
collision broadening in gases 77−88426
collision-broadened lineshape theory, reson. to far wings, appl. to CO_2 79−89711
collisional dephasing in strong radiation fields, unified theory, Karplus-Schwinger formula 80−91635
complex molecules, harmonic oscillator model for band contours 78−82717
complex spectra, band parameters determ., minimisation algorithms effectiveness improvement 79−93225
complex spectral bands, separation into components, Alentsev-Fock method *(Russian)* 78−90229
complex spectral bands, separation into components, Alentsev-Fock method *(Russian)* 78−90230
computation scheme, based on Fourier representation of Voigt profile 78−90223
copper tetraphenylporphyrin, reson. Raman spectra, vibronic coupling 79−26985
cyanoacetylene, ν_3 vibr.-rot. band, diode laser spectrum 80−91563
cyanodiacetylene (HC_5N) is Heiles's cloud 2, line widths and relative intensities 80−22054
cyanogen fluoride, fund., hot bands, laser microwave two photon and double reson. spectroscopy 80−32752
cyanomethane, collisional rot.-line widths and shifts, microwave region 78−25619
cyanomethane-d_0,-d_3, soln., for IR spectra, band shape and moment anal. 80−58252
cyclohexane, liq., vibr. relax. at high press., Raman obs. 79−50026
cyclohexane, rot. correl., Raman scatt. 77−83603
cyclohexane-d_{12}, Raman linewidth and molecular diameter meas. 80−69153
cyclooctatetraene, anions, in condensed media, electronic spectra 79−22723
dense media, exchange dephasing and motional narrowing of vibr. modes 79−68222
dense media, Q-branch Raman line width, rotational relaxation, reorientation, collision strength 79−98106
dense media, Q-branch Raman scattering impact theory, collisional rotational relaxation, line broadening 79−98104
dense polyatomic molecular systems, vibr. correl., HF band exchange dephasing 80−37803

molecular spectral line breadth continued
depolarised Rayleigh bands, permanent series expansion for correl. functions 77−61752
diatom+diatom, effect on depolarised light scatt. linewidths 80−58321
diatom-atom gas mixture, infrared line shape, rotational lines, influence of collision duration 80−43110
diatomic liquid, vibr. dephasing calc., diatom anharmonicity 78−94959
diatomic molecular dilute solns., IR and Raman spectra temp. depend. anal. model *(French)* 77−88456
diatomic molecule in strongly interacting solvent, IR band shape, field theoretic methods appl. 79−27038
diatomic molecules, $^2\Pi$-$^2\Pi$ band intensity distribs. calcs. 78−66601
diatomic molecules, matrix isolated, vibr. spectrosc., IR line shape calcs. 79−72307
diatomic molecules, shifts and widths of predissoc. levels 78−5304
diatomic molecules, spectral line collisional broadening, numerical method 78−25622
diatomic Morse mol., inhomogeneous broadening in liqs., temp. depend 77−61803
diatomic polar molecules, in simple liquids, interactions, far IR absorpt. spectra 78−25527
diatomics in rare gas matrices, vibr. modulation effects 77−23496
3,4,9,10-dibenzpyrene, hexane soln., UV fluoresc. line-narrowing two-photon site selective excitation 77−88484
dichlorodifluoromethane, diode laser spectra near 10.8 μm, air-broadening effects 78−61555
dichlorodifluoromethane, IR spectrum and mol. force field 79−72309
dichloromethane-d_0,-d_2, soln., far IR spectra, band shapes and moment anal. 80−58252
dichroism in chiral molecule, interference effects 78−82758
difluorodichloromethane, spectral data evaluation for atm. sensing 79−62582
1,2-difluoroethane in Ar matrix, IR hole burning and lineshape, vibr. transition 79−76425
difluoromethane, microwave spectral line widths 78−70816
difluoromethane, microwave spectral lines, line-width parameters 77−68077
2,2-dihalohexafluoropropane, IR and Raman spectra, gas, liq. and solid, normal coord. anal. 79−72314
dimer triplet state line shape, small excitons, appl. to phenazine, naphthalene, tetrachlorobenzene 80−48041
dimers, bandshape prediction, incoherent exciton scatt. model 78−42132
dimethyl ether.HCl, gas-phase Raman spectra, profile of stretching vibr. 79−45728
dimethyl sulphoxide, 1:1 and 1:2 complexes with H_2O and D_2O, H-bonding, IR and Raman vibr. spectra 77−34633
dimethylether-HCl complex, gaseous, H-bond IR spectra, temp. depend. theory 78−62804
dioxane, 1:1 and 1:2 complexes with H_2O and D_2O, H-bonding, IR and Raman vibr. spectra 77−34633
diphenylanthracene, fluoresc., site selection spectroscopy 2-300K 77−1731
dipolar molecules, IR absorpt. bands., temp. effects *(Russian)* 78−90228
dispersion-absorption plots, for spectral line shape anal. for RF and microwave spectrometry 78−89511
Doppler line convolution by Gaussian instrument function, appl. to diode laser 80−82830
Doppler-free saturated absorption microwave spectrometer 78−55256
electronic spectral shape, intramol. vibrs. effect 79−64052
electronic transitions, band shape in multimode weak coupling limit, multidimens. subspace theory 80−87178
emission spectra of molecules accelerated by stationary external field *(Russian)* 77−3319
energy level transitions, Doppler broadening, phase-destroying collisions 80−9561
energy loss spectra, state-to-state rot. transition cross sections 80−91665
ethane, in air, IR spectra, optical-acoustic investig. *(Russian)* 78−74663
ethylene, 10 μm absorption line profile, high resolution meas. 77−42359
ethylene, in air, IR spectra, optical-acoustic investig. *(Russian)* 78−74663
ethylene, narrow resonances of multiple-photon IR absorpt. 80−99529
ethylene, near IR absorption at high press. and temps. 77−14435
ethylene, press. broadened linewidths 79−6971
ethylene, Raman spectra, vibr.-rot. selection rules and general band contours 77−58020
ethylene(d_4) clusters, IR photodissoc. 80−89506
ethylene glycol, vibrational dephasing time of subgroup, transient stimulated Raman scatt. 78−37718
trans-1,2-ethylene-d_2, Raman spectra, vibr.-rot. selection rules and general band contours 77−58020
excited molecules, coherent anti-Stokes reson. Raman scatt. 79−59475
far-wing line spectra undulations, semiclassical methods 77−61808
ferric cytochrome c, reson. Raman spectra, Fe^{3+} low-lying electronic levels 78−53335
flavin adenine dinucleotide, resonance CARS line shapes, excited state parameters 79−3448
fluids, atomic and molecular, collision induced light scatt. *(German)* 79−27057
fluorescence of multilevel system in gas phase, calc. including inelastic collision 79−98129
fluorescence spectra, synchronously excited, peak wavelength and intensity prediction 78−20082
fluoroacetylene, fund. and hot bands, laser microwave two-photon and double reson. spectroscopy 80−32752
fluorobenzene, two-photon contours comparison with band contours of toluene 79−41212
fluoromethane, vel.-tuned multiphoton processes in laser cavity 77−27134
fluorotrichloromethane, spectral data evaluation for atm. sensing 79−62582
formaldehyde, 17(2,15)→17(2,14) line press. broadening relationship 79−98093
formaldehyde, in Ar, 0.17-1.4 gm cm^{-3}, VUV absorpt. spectra, Rydberg excitations 77−79627
formaldehyde, interstellar, collisional excitation and lines pressure-broadening widths 78−89237
formaldehyde, interstellar, line profiles towards bright rims in diffuse nebulae 77−87510
formaldehyde, IR Doppler-limited spectrum, wavenumbers, line strengths and assignments 79−72310
molecular spectral line breadth continued
formaldehyde, isolated Voigt line, off-peak spectral absorpt. coeff. 80−106355
formaldehyde, spectral linewidth press. broadening, Anderson-Tsao-Curnutte calcs. 77−75220
formaldehyde+Ar(N_2O), mol. isolated Voigt line, off-peak spectral absorpt. coeff. 80−106355
formaldehyde+He(H_2), collisional relax. times and lineshape distortion, Stark absorpt. linewidth obs. 78−74744
formaldehyde-d_2 733 μm line, Autler-Townes effect in laser interacting with RF field 80−53269
formic acid (-d), microwave spectra and rot. consts., astrophysical appl. 80−91550
Franck-Condon effects in resonance Raman spectra and excitation profiles, appl. to CrO_4^{2-} and β-carotene 80−14129
free-base porphin, S_2-S_0 transition vibronic bands, photochem. hole-burning 79−36631
gas linear molecules, symmetrised Liouville basis vectors, appl. to spectral linewidths 80−83457
gases, coherent Raman scatt., quantum theory of line shapes 79−64049
gases, nonuniform vols., IR emission calcs. 80−78657
gases, Raman line broadening, rotational structure, vibrational relaxation 79−98105
halide vapour, discharge, potential fusion laser systems 78−63074
harmonic oscillator, ν=0 level predissociation, by linear pot., line width and shift 77−75239
harmonic oscillator model in predissoc., level widths, shifts and curve crossing 78−90239
heavy ion+atom collisions, quasimol. X-ray line tails 77−14564
heavy-ion collision, quasimolecular L X-rays, relativistic self-consistent correlation diagram 78−5247
hexafluorobenzene-benzene, liq., mol. interactions, IR and Raman lineshape obs. 80−28907
hexafluorobutene, vibrational broadening, dense fluid region, Raman and NMR study 80−43056
hexafluoropropane(-d_2), IR and Raman spectra, gas and liq., normal coord. anal. 79−68235
high pressure effects on mol. electronic spectra 78−78754
high-overtone spectra, reson. struct. and background absorption 79−54833
hole burning into molecular velocity distribution due to monochromatic radiation and molecular elastic collision 80−43116
homogeneous linewidths in ODMR and optical transitions, connection 79−91316
homonuclear diatomic molecules, CARS spectral profiles, computer program 79−13723
hydrated electron, optical absorpt. spectrum, shape, temp. depend. 77−65489
hyperfine structure, brightness distrib., form. model verification 77−57928
impact broadening of nonlinear reson. due to collision-induced vel. change *(Russian)* 77−46540
indane, 271 nm spectrum, rot. band contour anal., puckering vibr. 78−1001
inert gas+$CO(O_2)(N_2)$, state-to-state rates from press.-broadened linewidths, data reduction method 78−46430
inert gas halide excimer laser, operating and beam characts. including spectral narrowing 79−59715
inhomogeneous molecular gas radiation calc. using spectral comp. modelling 80−32697
inorganic molecules, UV photoelectron spectroscopy, spectral assignment criteria, bonding 78−17717
interaction anisotropy, small angle scatt., spectral evidence 80−78600
intermolecular forces Raman scatt. obs., review 80−23427
intramolecular nonradiative transitions of gaseous small molecules, rovibronic level, lineshapes 80−95667
intramolecular radiationless transitions, theory, line broadening effects 78−90201
iodomethane, and isotopic forms, self-broadening and self-shifting of rot. spectra 78−13551
iodomethane, collisional rot.-line widths and shifts, microwave region 78−25619
iodomethane, liq. (liq. mixtures), vibr. relax. and reorientation, symmetric C-H bending mode 1st overtone 78−62884
iodomethane, P-line and ν_6 band spectra using CO_2 laser absorpt. 80−69142
iodomethane, Raman band shapes, mol. oscill. bands *(German)* 80−69154
iodomethane, vibr. relax., Raman overtone band obs. 77−14436
iodotrifluoromethane, continuous absorpt. band contour, temp. depend. 78−70876
IR absorption band shape characterisation, expts. 78−86919
IR absorption band shape characterisation, methods 78−86918
IR absorption vibration spectra, true parameters of isolated bands calc. *(Russian)* 77−83586
IR and Raman band contours in soln., self-assoc. and complex form., book contrib. 78−21931
IR band shape, statistical, modelling methods 79−50087
IR band shapes, reson. relax. effects 78−13576
IR molecular absorption spectra, effect of rotational coupling on torsional bands 78−13497
IR multilevel absorpt., field broadening and pump line selection effects 77−46599
isobutylene, liq., vibr. phase relax. and freq. shifts, density and temp. effects 80−74235
isotropic molecular gases, binary collision-induced light scatt., rot. Raman scatt. 80−78660
isotropic molecular gases, binary collisions induced light scatt. 80−83428
ketones, in soln., IR spectral line halfwidths determ., rot. Brownian motion investig. 77−36248
Lamb dip, transit time broadening, perturbation theory calcs. 77−647
Lamb-dip spectroscopy, collision broadening theory 77−83659
large molecules, Rydberg spectra, antireson. lineshapes 77−50424
laser saturation molecular spectroscopy in time-delayed mode, appl. to NH_3 78−86976
laser spectroscopy conf., Jackson Lake Lodge, WY, USA, 1977 July 78−82666
line formation, radiative transfer effects in interstellar molecular clouds 79−5884
line profile, spectral absorption coeff. calc., statistical modeling in semiclassical approx. 80−52865

molecular spectral line breadth continued
linear molecules in inert solvent, collapse of rot. struct. of Raman scatt. spectra *(Russian)* 77−3371
lineshape analysis for collision induced spectra 78−70787
lineshape calc. for stratospheric emission model 79−62586
liquid, hot bands, vibr. correlations, dephasing 79−85966
liquid media, vibr. two-photon reson. linewidths 77−88516
liquids, and dense gases IR and Raman spectra 80−11390
liquids, coherent Raman scatt., quantum theory of line shapes 79−64049
liquids, Maxwell effect relax. timeand light scatt. line broadening 80−76040
liquids, Raman line broadening, rotational structure, vibrational relaxation 79−98105
Lorentzian lineshapes and isotropic distrib. of molecules, analytical expressions derived for powder samples 80−60401
Lorentzian Raman lines, eqn. for correcting finite slit width effect 80−63593
lysozyme protein solution, spectra and dye laser threshold power 79−68391
macromolecules in soln., Rayleigh scatt., elec. reorient. rel. to spectral line rot. broadening 79−1774
magnetic reson. lineshape, with slow mol. motion, asymptotic method, strong collision limit 77−48063
malononitrile, displacive phase transition, 294.7K, Raman and Brillouin-Rayleigh scatt. obs. 80−16047
matrix isolated molecules, IR spectral line broadening, theory 78−46332
matrix isolation spectra, homogeneous IR line shape, Debye approx., space time phonon correl. functions 79−823
methane, 4350-10600 Å bands, intensity profile, vibr. assignments, rel. to major planets spectra 78−42084
methane, 6190 Å spectral line, press. broadening detected by photoacoustic 79−94033
methane, ν_1 line contour anomalous behaviour on pressure changes *(Russian)* 80−43052
methane, ν_4 fundamental band strength, line-intensity meas. 79−22700
methane, absorpt. line profile, press. and temp. effects 77−495
methane, and isotopic forms, ν_4 band, line parameters, Jovian atmosphere transmission, 7.7 micron 78−85894
methane, in air, IR spectra, optical-acoustic investig. *(Russian)* 78−74663
methane, in liq. SF_6, ν_3 band IR profile, temp. depend. 78−58696
methane, in major planets atms., Raman scatt. profiles 78−28571
methane, in SF_6, CCl_4 soln. and Ar, IR band profile *(French)* 79−54913
methane, IR line intensities 78−58687
methane, Jovian line profiles near 1.1 μ as probe of cloud struct. and C/H ratio 80−62067
methane, line profile of coherent radiation in separated fields due to $F_2^{(2)}$ transition 80−37835
methane, liq. and solns., Raman spectra, vibr. anal. 79−27001
methane, optical Ramsey resonance, in three separated fields produced by corner reflector, theory 80−74166
methane, saturated absorpt. profile using methane-stabilised laser spectrometer 79−98446
methane, saturated absorpt. resonances, shift and broadening due to curvature of laser wave fronts 77−18981
methane, single mode 3.39 μm laser obs. of absorpt. lineshape 77−46600
methane (methane-^{13}C) band strength, spectral line breadth in ν_3 bands 79−98069
methane-d_1, and -d_3, reorientation in simple fluids, IR band profiles 77−36237
methane-d_1, high resolution spectra, line intensities, ground-state rot. const. determ. 80−83517
methanol, vibrational dephasing time of subgroup, transient stimulated Raman scatt. 78−37718
methanol-acetonitrile, solns., H bonding, IR and Raman band profiles 77−42320
methyl bromide-^{81}Br+nonpolar perturber, JK0,0-1,0 line broadening 77−6848
methyl cyanide, linewidth parameters in rot. spectrum, multiple differentiation calcs. 79−98070
methyl cyanide, vibr. relax., Raman overtone band obs. 77−14436
methyl cyanide (-d_3), vib. dephasing, Raman obs. 77−59566
methyl iodide, in Ar, 0.25-1.38 gm cm^{-3}, VUV absorpt. spectra, Rydberg excitations 77−79627
methyl symmetric stretching vibr. bandwidths, vibr. and reorientational effects, IR and Raman spectra 78−78686
methylene, singlet-triplet splitting, ab initio calc. 78−5128
methylfluoride, rot. IR spectra, line width study 79−76426
microwave region, press. broadened, deviations from Lorentzian line shape 77−61806
microwave region, press. broadened width and shift, temp. depend. 77−61807
mobile liquids, coupled vibr. and reorientational dephasing 79−22686
MODR, ground- and excited-state, lineshapes, relative signal intensities 77−27100
molecular, vibrational dephasing time of subgroup, transient stimulated Raman scatt. 78−37718
molecular crystals, two particle exciton-phonon interactions, optical absorpt. line shapes theory 80−55120
monochromatic laser radiation, excitation of atomic, mol. energy level transitions, inhomogeneous and mixed line broadening 78−55147
monochromatic laser radiation, excitation of atomic or mol. energy level transitions, strictly homogeneous line broadening 78−58629
monofluoromethane, X-ray photoelectron spectral linewidth of F core, ab initio HF calc. 78−62841
naphthalene, in nonpolar solvents, IR absorpt. bands 79−6939
naphthalene, Rydberg spectra, antireson. lineshapes 77−50424
naphthalene, vap., Doppler free two-photon absorption spectra 78−5307
neutral molecules adsorbed on dielec. surface, excitation spectrum 78−71943
nickel-octaethylporphyrin, in benzene soln., reson. CARS and CSRS line shapes 80−74432
nitrobenzene, in acetone-isopropanol soln., Rayleigh scatt. and viscosity 80−5550
nitromethane, vibr. relax., Raman overtone band obs. 77−14436
nitromethane in carbon tetrachloride, polarised line widths (intensities) in Raman scatt., conc. depend. 78−70879
n-nitrophenol, H-bonded complexes, IR absorpt. band struct., freqs. and intensities *(Russian)* 77−18928

molecular spectral line breadth continued
NMR, line-broadening mechanisms, dispersion-absorption plots 78−89512
non-Markovian theory of vibr. relax. and dephasing in condensed media 79−41224
nongrey molecular gases, total IR band absorption, anal. and approx. models 80−14141
OH 1667 MHz, line width in unusual maser source OH 205.1−14.1 during flare 80−98734
optical Autler-Townes effect, time depend., finite bandwidth laser appl. theory 80−91499
optical Ramsey resonance, in three separated fields produced by corner reflector, theory 80−74166
optical triple resonance, semiclassical anal. 79−93963
organic compounds, complex, nuclear relaxation influence on stimulated emission 80−48019
organic compounds, fluoresc. decay in nonhomogeneous level broadening conditions *(Russian)* 79−50073
organic compounds, IR absorpt. bands halfwidths transferability in related mols. series 79−54921
organic compounds, solns., line struct. of broad absorption bands 79−54841
organic molecule, nonuniformly broadened absoprt. spectra, hidden fine struct. 79−93999
organic molecules, C-H Raman stretching bands in soln., vibr. freqs. and linewidth 80−78622
organic molecules in solid matrices, local vibr. inhomogeneous broadening 77−58087
organic nitriles, in soln., IR spectral line halfwidths determ., rot. Brownian motion investig. 77−36248
organometallic amines, Raman and IR spectra, band intensity and assignment, force const. determ., vibr. props. *(German)* 80−87133
overlapping lines in Raman and IR bands, separation *(French)* 79−3499
oxymyoglobin, evidence for conformational and diffusional mean square displacements 80−89713
pentacene-d_0, -d_{14}, in p-terphenyl-d_0, mixed cryst., photon-echo relax. 77 -72034
perturbed band spectrum, extra lines, assignment using power-broadened line widths 79−18213
perylene, solid soln. in ethanol, fine struct. in absorpt. spectra, laser technique 77−90178
phase and population relax., semigroup formalism 80−78519
phenol, H-bonded complexes, IR absorpt. band struct., freqs. and intensities *(Russian)* 77−18928
photodissociation, polyatomic mols., absorpt. lineshape 77−79662
polar molecules, vibr. relax., Raman overtone band obs. 77−14436
polarisation spectroscopy, high resolution, in strong saturation regime 79−55189
polyatomic, fluoresc. spectrum excitation depend., proportionality coeff., vibr. redistrib. 77−23518
polyatomic compounds, vibr. relax., IR band line shape obs. 79−54879
polyatomic molecule, diffuse absorpt. and fluoresc., vibronic band broadening 79−98161
polyatomic molecule, vibr. relax. probability determ. from quasi-line fluoresc. 77−50505
polyatomic molecules, 0-0 transition freqs. in continuous and diffuse spectra *(Russian)* 78−74639
polyatomic molecules, dil. solns., IR spectral band shapes of fundamentals 78−66544
polyatomic molecules, intramolecular vibr. relax., restricted quantum exchange theory 80−63610
polyatomic molecules, vibr. absorpt. spectra, diffusivity due to crowding of sequence of levels *(Russian)* 77−38652
polyatomic molecules, vibr. overtone lineshape 79−27040
polyatomic molecules, vibr. spectrum, intermolecular interaction effects *(Russian)* 78−37621
polyatomic molecules, vibronic spectra and luminescence kinetics 79−54881
polyatomic molecules in condensed phases, origin of vibr. dephasing 79−27069
polyatomic molecules with pronounced vibr. struct., spectral shape 79−76469
polyene chromophones, band broadening in electronic-vibr. absorpt. spectra 80−28003
polyenes, absorpt. spectra, electronic-vibr. sequence band broadening 77−65453
polymethine dyes, mol. struct., lasing props. 79−3693
polymethylene chain, vibr. spectra, CH stretching region, struct. and assignments 78−70991
polynuclear aromatic hydrocarbons, synchronous excitation spectrofluorometry *(Japanese)* 80−86452
polypeptides, unordered, circular dichroism, Green operator method 77−14467
porphin, free base, in n-octane crystal, S_1 from S_0 transition, freq. shift and dephasing temp. depend. 78−25584
porphin-d_n, (n=2-14) electronic-vibr. interaction, quasi-line absorption (fluoresc.), mirror symmetry 78−55197
porphyrin free base in n-octane, $S_1 \leftarrow S_0$ transition homogeneous linewidth, photochemical hole burning 78−7217
predissociated two-channel model, resonances with complex rot. method 80−58327
predissociating harmonic oscillator, relative line widths and level shifts 80−23469
predissociation, reflection method of calculating energy shifts and linewidths 77−75237
predissociation, spectroscopic interferences, unified description 77−23524
predissociation, unimolecular, type I, level widths and shifts, quantum-mech. method 79−31629
preionis. and predissoc., rel. to spectral line shape 80−63724
pressure broadened half-width, rot. inelastic rate consts. 78−74745
pressure broadened spectral line shape, effect of turning points 79−22655
pressure broadening, dipole moment correlation function 77−79656
pressure broadening, Liouville space methods 77−27116
pressure broadening, overlapping spectral lines, criteria 77−68082
pressure broadening in Doppler limit 79−50083
pressure-induced spectral linewidth and line shifts, vibr. depend., IOS scatt. approx. 79−68267
propane-Ar, reson. absorpt. of 10.6 μm light, shock wave in Ar mixture 79−64002

molecular spectral line breadth continued
pyrene, excimer fluoresc., struct. depend. in cryst. 77−75200
pyrene, fluorescence spectra in aq. and surfactant solns. 77−83639
pyrenophanes, excimer fluoresc., struct. depend. in cryst. 77−75200
pyridine, on Ag (100), (111) and polycryst. electrode surfaces intense Raman spectra 78−72492
quasiline shape distortion, anisotropic absorpt., meas. using unpolarised light *(Russian)* 78−94292
quasistatic theory, for line wing and core regions 78−90222
radiative transfer in real spectrum, calc. using integration over freq. method 80−33430
Raman band shape characterisation 78−86920
Raman band shapes in liq., rot.-vibr. coupling effect for reorientation 78−72491
Raman excitation profiles and mol. spectra synthesis, vibronic and exciton-in-mol. theory 78−42076
Raman scattering, continuum, time-depend. excitation profile 79−41175
Raman scattering, polarised line widths (intensities), conc. depend. 78−70879
Raman scattering, reson., coherent, lineshape, 3rd order nonlinear optical susceptibility 78−42378
Raman spectra in liqs., vibr. relax. *(Russian)* 79−64012
Raman spectra of liq. phase weak H-bonds, short range order and anharmonicity effects 78−64357
Ramsey fringes in spectroscopy without Doppler broadening *(French)* 77−50560
Ramsey reson. obs. by linear laser spectroscopy 80−99514
relaxation processes and spectra in liqs. and dense gases 77−58935
resonance absorpt. line shape, coupling strength incoherence 78−17721
resonance coherent Raman scattering, excitation profile, inhomogeneous broadening effects 79−35840
resonance fluoresc., probe of intramolecular relax., density matrix formalism, lifetimes and quantum beats 80−32757
resonance line shape in Rydberg spectra 78−17720
resonance Raman excitation profiles, vibronic state short lifetime determ. 79−98103
resonance Raman scattering, polarisation dispersion, inhomogeneous broadening effects 77−6787
resonance Raman spectra intensity distribs. in soln. 79−22763
resonance Raman spectra lineshapes, first order, rel. to optical absorpt. lineshapes 80−5548
resonant CARS, line shape and Doppler broadening 79−94002
RF mol. beam electric reson., interference effects *(French)* 78−42038
RF spectroscopy, interference effects *(French)* 78−58669
rhodamine, 6G and B, low quantum yield mol. fluoresc., polarisation, excitation energy depend. 77−50462
rhodamine 6G, blue and UV luminesc., obs. and mechanism 79−3486
rhodamine 6G polar solution, conc., temp effect on spectral props. 79−87505
rhodamine B, 6G, resonance CARS line shape, scatt. processes in ground or excited states 80−48043
rotational band, line shape, collisional broadening, impact approx. 78−42134
rotational line width of vibr. bands, self- and foreign gas-broadening 78−33552
rotational relaxation, press.-broadened linewidth data deconvolution using scaling theories 78−82823
rotational spectral line shift and widths, collision induced phase shifts 77−75222
satellite line shape, classical broadening theory including Doppler effect, pot. effect 79−22764
saturation spectroscopy, with delayed pulses, Lamb dip profiles 78−21221
scattered light spectrum Rayleigh lines, density fluctuations in two component reacting fluid 80−25397
self reversal contours, use in determ. of line broadening and shift consts. 80−52940
semiclassical broadening theory, straight line vs. curved trajectories 79−45765
Shpolskii system, 77K, sensitised phosphoresc. spectra 79−815
Shpolskii systems, sensitised phosphoresc., triplet-triplet energy transfer *(Russian)* 78−76527
simple oscillator, correl. functions, IR band shapes 79−26960
small molecules, detect. by magnetically tuned freq.-modulated at. line sources 79−59508
solid, molecular fluoresc., phosphoresc., and ODMR line narrowing 80−43084
solution, electronic bands statistical broadening depend. on intermol. interaction 77−71837
solution, excess electron optical absorption spectrum model, band shape 78−33500
solution, mol. vibr. spectral linewidth, conc. fluctuations effect 78−70880
solvated electrons, Raman spectrum modification, polarisation CARS obs. 80−5549
solvent effect, band shape, rot. diffusion model 79−64048
solvent effects, rel. to polarisation structure 80−43062
spectral line narrowing of triplet state, in laser excited experiments 80−63703
spectral line shapes, linear and nonlinear, atom or mol. cross sections 78−70899
spherical top molecules, fluid vibr. spectra, repulsive force depend. line broadening *(Russian)* 80−47970
strongly interacting solvents, IR band shapes, solvent-induced chirality, field theoretic Green's function method 79−27037
styrene, anions, in condensed media, electronic spectra 79−22723
subnatural linewidth spectra by optical double reson. with two-photon pumping 80−74200
sultams, characteristic band in IR region, Raman obs. 78−29784
symmetric top mol., overlapping press. broadening, nonreson. microwave absorpt. line radii 78−17662
symmetric vibration-rotation bands, profile anal., correl. functions and moments *(French)* 77−71836
symmetric-top molecular gas, non-reson. half widths, approx. calcs. 77−75221
symmetric-top molecules, dilute gas, non-reson. microwave absorpt., kinetic theory 79−68901
TBBA, smectic liq. cryst., polarised Raman spectra, 90-300K, 0-400 cm^{-1} 77−12383
tetra-4-tert-butylphthalocyanine-H_2 mol. in solid tetradecane, luminesc. 77−18965
molecular spectral line breadth continued
tetrabromomethane, in disordered phases, IR active mode Raman line shape, dipole-dipole interaction 80−9603
tetrachloromethane, fluid vibr. spectra, repulsive force depend. line broadening *(Russian)* 80−47970
tetrafluoromethane, in disordered phases, IR active mode Raman line shape, dipole-dipole interaction 80−9603
tetrafluoromethane, spectral shape of collision-induced scatt. 78−37687
tetrafluoromethane, X-ray photoelectron spectral linewidth of F core, ab initio HF calc. 78−62841
tetrahedral molecules, spectral line press. broadening, symm. basis set calcs. 77−3421
s-tetrazine-benzene, mixed cryst., 2K, lifetime limited photochem. hole burning 78−9183
thioamides, characteristic pattern in IR and Raman spectra 78−29818
three-level coupled Doppler-broadened system, optical time-delayed laser saturation spectroscopy 78−54472
three-level system, coherently driven, collisional contrib. to dynamic Stark effect 79−13765
toluene, molecule translational mobility in depolarised Raman spectra 80−14150
transient signals, saturation dips 78−18020
transition metal ions, in complexes, vibronically allowed d-d transitions, band shape calcs. 77−50472
trialkyl silanes, IR absorption vibration spectra, true parameters of isolated bands calc. *(Russian)* 77−83586
triatomic linear mol., parallel bands, band model parameters 80−43026
triatomic van der Waals mols., rot. predissoc. 80−63721
1,2,4-trichlorobenzene liq., mol. reorientation, translation and vibr. relax., Rayleigh and Raman spectra 80−95632
trichlorofluoromethane, 8-12 μm band model calcs. 80−43112
trichloromethane, and -d_1, liq., vibr. relax., Raman spectra 78−19471
trichloromethane-d_0,-d_1, soln., far IR spectra, band shape and moment anal. 80−58252
trichloromethane-d, Raman band shapes, mol. oscill. bands *(German)* 80−69154
1,3,5-trifluorobenzene, IR rot.-vibr. band contours 79−76430
trifluoroiodomethane, UV absorpt. spectrum broadening by laser-induced vibr. excitation 80−53050
trifluoromethane, rot. transitions, self-broadening and self-shifting meas. 79−59426
trimethylcarbinol complexes in soln., weakly H-bonded, IR bandshapes 80−106354
triphenylcarbinol complexes in soln., weakly H-bonded, IR bandshapes 80−106354
triplet state broadening, inhomogeneous and homogeneous, of optical and ODMR transitions in solids 80−32750
triplet-singlet transitions in mag. field, rot. struct. 77−61790
two coupled oscillators, decaying in the same bath, absorpt. line shape 79−10088
two level model theory, extended, appl. to Doppler-, laser and collision-broadened bound-bound multiphoton absorption 79−3423
two level system, homogeneously broadened, saturable absorpt., coherence effects 80−95958
two- and three-photon resonances, Doppler-free power broadening 78−5308
two-atom resonance fluorescence, in strong EM field, excitation spectrum 78−82778
two-dimensional spectra, eval. of peak volume, position and width, computer program 80−18890
two-level molecules in low press. gas, nonlinear power reson., field broadening and shifts 79−45768
two-level system, one-photon optical absorpt. theory 77−34651
two-level system, power broadened Doppler-free saturation resons., transit time effects 77−79657
two-level system coupled to thermal bath, quantum dynamics of relax. 77−3437
two-photon spectra, Doppler-free, occurrence of split spectra 78−292
van der Waals interaction, spectral line broadening, growth curves 80−102548
vibration-rotation lineshapes, effect of elastic and reorientation collisions 79−89712
vibrational dephasing, polyat. mols. in condensed phases, intermol. energy exchange mechanism 78−74737
vibrational spectra, linewidth, temp. depend. calcs. 77−83594
vibrational-rotational line broadening by monatomic gas 80−9643
vibrational-rotational line profiles, theory 80−1029
water vapour-N_2, absorption at CO_2 laser frequencies 79−50011
Weber effect, and inhomogeneous spectral broadening 79−3482
XH_2 molecules 1:2 complexes, H-bonding fluctuation hypothesis, IR and Raman vibr. spectra 77−34632
XY_2, symmetric triatomic molecules, photodissoc., time depend. theory 78−66610
Zeeman effect, orthorhombic rot. mols., doublet-doublet transitions 78−74698
AlF, hyperfine structure simulated by computer programme 78−50538
Ar:O_2 (6%) cryst., vibr. Raman spectra 80−60558
Ar+HCl, line broadening, short range force effects, semiclassical calcs. 79−98085
Ar_2, Raman spectra, press. broadened transitions, calc. 79−64009
ArH_2, van der Waals mols., rot. predissoc. 80−63721
ArN_2, van der Waals mols., rot. predissoc. 80−63721
$^{10,11}B_5H_9$ gas (liq.) phase, vibr. dephasing and Raman spectra 80−48101
BO_2, Doppler free spectra, backscatter fluoresc. line narrowing, theory and obs. 80−53034
BO_2, gas, optically detected mag. reson. spectrum, $X^2\Pi$ rovibronic sublevels 78−82756
Ba compounds in air-acetylene flames, dye laser-excited fluoresc. 79−68260
BaO, $C^1\Sigma^+$-level, perturbation, extra lines, assignment 79−18213
BeH, BeD, linewidth, indirect predissoc., anomalous isotope effect, ab initio calc. 77−58101
Br_2, Ar matrix reson. Raman excitation profile, red shift rel. absorption spectrum 77−14440
Br_2, $B^3\Pi(O_u^+)$ predissoc. rates, analytical interpretation 80−91617
Br_2, organic solvent effects on Raman parameters 79−26998
BrF, $B^3\Pi(0^+)\leftarrow X^1\Sigma^+$ absorption spectrum, high-resolution anal. 79−59478
C^- predissociations, anal. line profile and energy shifts, linear pot. approx. 77−6871

molecular spectral line breadth continued
C predissociations, anal. line profile and energy shifts, linear pot. approx. 77−6871
C predissociations, Fano line profiles, linear pot. calcs. 77−6872
C, Swann band profiles in spectra of two comets 78−85909
CD, Λ-type doubling in excited rot. levels 77−57979
CH, CH^+ lines in solar facula models, equivalent widths 79−66972
CH, interstellar, in bright rimmed mol. clouds, line widths rel. to post-shock gas emission 80−62238
CH, Λ-type doubling in excited rot. levels 77−57979
CO, absolute intensity meas., 4-0 vibr.-rot band 77−6854
CO, in Ar matrix, vibr. line shape, vibr.-phonon interaction 79−3493
CO, in galactic refl. nebulae, emission line profiles 77−53658
CO in IR C star CIT 6 (IRC+30219), line profile rel. to mass outflow 80−12761
CO in interstellar mol. clouds, J=2-1 emission line width rel. to optical depth 79−92827
CO, in interstellar shock assoc. with H II region NGC 281, line profiles 79−25688
CO, in solar spectrum, centre to limb behaviour of first overtone vibr.-rot. transitions 79−8889
CO in stars, equivalent widths of lines of (A-X) band 77−87368
CO, inner-valence ionisation, correl effects calcs. 78−9198
CO, line broadening, short range force effects, semiclassical calcs. 79−98085
CO line profiles for dark molecular clouds 79−5877
CO, matrix-isolated, librational relax., IR line broadening 80−978
CO, microwave spectral line profiles, rotation effects in CRL 437 peculiar IR source 78−45426
CO, P(6) line absorpt. coeff. and halfwidth, temp. depend. 80−78618
CO, pressure-induced spectral linewidth and line shifts, vibr. depend., IOS scatt. approx. 79−68267
CO, rovibr. multiphoton spectra comput., hole burning effect 80−9672
CO, thermal and maser emission lines profiles in evolved stars expanding envelopes 80−82334
CO+Ar(CO), rot. band, line shape, collisional broadening, impact approx. 78−42134
CO+He, press. broadening, rot. energy transfer, infinite order sudden approx. 78−22011
$CO+N_2(CO_2)$, line broadening, short range force effects, semiclassical calcs. 79−98085
CO_2, 10 μm absorption line profile, high resolution meas. 77−42359
CO_2, 10^00-$00^00_{1,11}$ absorpt. band profile temp. depend., integral and spectral binary absorpt. coeffs. 80−43049
CO_2, 10.6, 9.4 μm laser bands high-press. absorpt-spectra 78−66543
CO_2, 201_{III}←000 band, press. broadened coeffs. and absolute intensities, temp. depend., IR obs. 80−53054
CO_2, 30^01_{III}←00^00 band, meas. at different temps. of absolute intensities, line half-widths and broadening by Ar and N_2 78−86865
CO_2, 4854 cm^{-1} 201_{III}←000 band, intensities and half-widths, 197, 233, 294K 79−89713
CO_2, absorption spectrum line parameters *(Rumanian)* 77−42326
CO_2, band model parameters prediction, 4.3 micron, 200-3000K 80−43047
CO_2, IR absorpt. in regions of weak absorpt., lab. meas. rel. to atm. windows 79−64005
CO_2, IR absorpt. spectrum, line parameters, spectral transmittance function *(Russian)* 77−57998
CO_2, IR band intensity 80−83425
CO_2, IR bands transmission functions 80−106324
CO_2, IR spectra, lineshape and Q-branch head absorpt. profile 79−59452
CO_2, in N_2, 20-140 bar, dipolar correlation function meas., IR band shape anal. 77−61743
CO_2 induced absorpt., 3-4μm, temp. depend. 80−983
CO_2 laser, transitions, linewidth, temp. depend. 80−69360
CO_2, lifetimes from collision induced absorption spectra, IR line broadening 78−33554
CO_2, line width effect on atmospheric 15 μm emission 77−21903
CO_2, near IR absorpt. band props. 77−30872
CO_2, optical reson. widths, nonlinear press. depend. 77−42358
CO_2, press. broadening coeffs. at 4.2 μm, rot. quantum number 78−74704
CO_2 pulsed laser with continuously tunable radiation frequency 80−48292
CO_2 R-branch line intensities and press.-broadened line widths at 15 μm 80−102508
CO_2, rot. Raman and IR lines, self-broadened linewidths 77−42357
CO_2, rot.-vibr. bands, absorpt. coeff. calc. method, Fermi reson. effect on spectral lines 80−32696
CO_2, spectral line breadth in 15 μm band, N_2 broadened, 200-300K 79−22765
CO_2, spontaneous emission probabilities and collisional broadening of 00^01-10^00 lines 77−23649
CO_2 vibr.-rot. band shape calcs. 80−969
$^{12}C^{16}O_2$, ν_3 band, IR single line strength 80−83370
$^{13}C^{16}O_2$, IR line strength 80−83371
CO_2+Ar, press. broadening, rot. energy transfer, infinite order sudden approx. 78−22011
$CO_2+Ar(N_2)$, 301_{III}-000 band, intensities, press.- and self-broadening coeffs. meas. 78−78695
CO_2+He(Ar), dipole and Raman line press. broadening temp. depend. 79−68265
CO_2+N_2, near IR absorpt., collisional broadening 77−30872
CS_2, in carbon tetrachloride soln., Raman scatt. 79−65850
CS_2, ν_3 band, dipole moment correl. function, isotope splitting and band contour 78−74650
CS_2, $\pi\pi^*$ and Rydberg bands, cryogenic solvent effects 78−55182
CaCl, form., spectral bands, dissoc. energy calcs. 77−16816
CaF, $B^2\Sigma^+$-$X^2\Sigma^+$ system, rot. and vibr. anal. 80−74156
CdH, lifetime, Λ-doubling, hyperfine struct., in $A^2\Pi$ excited states 77−58083
$^{113}Cd_2$, two-level system, absorpt. spectrum, subradiative struct. *(Russian)* 80−28008
Cd_2^* excimer, fluoresc. band shape, decay rates 78−70866
chloromethane, collisional rot.-line widths and shifts, microwave region 78−25619
Co complex, X-ray K-absorpt. edge, ligand field splitting, spectrochemical series 77−10688
Cs_2, 6^2S-7^2P doublet, mol. satellites 79−85956
CsCl, hyperfine spectrum, mol. beam elec. reson. meas. 77−71797
CsN_3, Raman spectra, weaker features obs. 77−68045
CsXe excimer, laser-excited fluoresc. in Cs-Xe mixture, pumping, level scheme 78−86909
Cu complex, Cu(II) acetylacetonates, X-ray K-absorpt. edges, edge widths and shifts 78−50556
Cu compounds, ESCA shake-up satellites, spin density intensity ratio relation 78−50590
D_2, $G(3d)^1\Sigma_g^+$ and $g(3d)^3\Sigma_g^+$ singlet-triplet anticrossing 78−42138
D_2, high resolution CW CARS spectra of Q-branch 77−58023
D_2, predissoc. linewidths and shapes for $3p\pi D^1\Pi_u^+$ state 80−53066
D_2/CCl_4, inhomogeneous broadening of Morse oscillator, temp. depend. 77−61803
D_2+D_2, collision effect on depolarised light scatt. linewidths 80−53059
D_2O, far IR absorpt. coeffs. by H_2O laser meas., foreign gas and self broadening 80−9599
D_2O, IR spectra, $\nu_2+\nu_3$ band shape 78−62855
$Fe(CO)_4$, IR spectra and laser photochem., matrix isolated at 20K 78−74651
FeH, 9900 Å band profile rel. to identification in M dwarfs and S stars 77−45418
GeF_4, $\nu_3(F_2)$ IR band contour, isotopically pure cpds., mol. consts. 77−61746
GeH_4, IR laser sideband obs., ro-vibr. struct., isotope shifts, line widths 79−72306
H bonded species, IR absorption broadening, intramol. interactions effect 78−50595
H bonded species, IR line broadening, kinematic and electronic coupling mechanisms 77−68043
H-bond, symmetric $AHA^{(\pm)}$, A-H stretching vibr., liq. IR band shape, strong coupling phonon model 78−64358
H_2 2.1 μm emission line vel. profiles in Orion Molecular Cloud 79−71094
H_2 2.121 μ emission line vel. and width meas. towards Orion Nebula 79−17061
H_2, (4,0) S(1) quadrupole line intensity and pressure shift 78−90178
H_2, D_2 and HD, intermol. collision process obs. using light scatt. expts. 80−53001
H_2 dissolved in Ar, far IR spectra, density narrowing of rot. line 79−50086
H_2, gas, radiative light scatt., approx. line shapes 78−90221
H_2 in stars, equivalent widths of Lyman band line 77−87368
H_2, lifetimes from collision induced absorption spectra, IR line broadening 78−33554
H_2, linewidth determ. by integrated power meas. of CARS 79−3744
H_2, Λ doubling, $C^1\Pi_u$ states, calc. methods 78−90227
H_2, ortho-para mixtures, 10 to 23K, rot. Raman spectra, quantum calcs. 77−6700
o-H_2 pairs, in solid H_2, microwave absorpt. 77−68034
H_2 photoelectron spectra, rot. intensity distrib. 80−91605
H_2, predissoc., interference effects, lineshape obs. 80−83432
H_2, predissoc. linewidths and shapes for $3p\pi D^1\Pi_u^+$ state 80−53066
H_2, preionis. and predissoc., rel. to spectral line shape 80−63724
H_2, rot. Raman linewidths, self-broadening calcs. 77−42356
H_2, $S_0(3)$ pure rot. quadrupole transition, obs. using tunable diode laser 78−82723
H_2^+, satellite line shape, classical broadening theory including Doppler effect, pot. effect 79−22764
H_2/CCl_4, inhomogeneous broadening of Morse oscillator, temp. depend. 77−61803
H_2-H_2, overlap parameters from IR spectrum in binary collision-induced H_2 band 77−54561
H_2-inert gas, bound complex form., anisotropic intermol. pot., IR spectra anal. 78−37634
H_2+H_2, collision effect on depolarised light scatt. linewidths 80−53059
HBr, far IR Ar matrix isolated spectra, 4.2K, press. and conc. effects 78−62801
HBr-Ar, IR fundamental region, line intensity, line breadth, tunable laser meas. 78−46328
$(HBr)_2$, intermol. distances, dipole moments, MINDO/3 and IR intensities and shifts calcs. 78−46335
HCN, (3-2) line in Orion Molecular Cloud, low-intensity broad vel. wings obs. 79−25669
HCN+HCN, collisional line broadening of microwave spectra, semiclassical theory, calcs. 78−25516
HCN+He, press. broadening, rot. energy transfer, infinite order sudden approx. 78−22011
HCO, (3-2) line in Orion Molecular Cloud, low-intensity broad vel. wings obs. 79−25669
$HCO^+ + H_2$, J=0-1 transition press. broadening, microwave absorpt. 80−52981
HCl, Ar-perturbed rot. linewidths, temp. depend. 79−45766
HCl, far IR Ar matrix isolated spectra, 4.2K, press. and conc. effects 78−62801
HCl, in dil. solution IR absorpt. fundamental shape temp. depend., solvent-solute interaction 79−26977
HCl, pure rot. lines, press. induced shift perturbed by Ar 77−79652
HCl, Raman spectra in various solvents, depolaris. ratio and profiles 79−59464
HCl, rot.-vibr. lines collision broadening, in He, Ar, N_2, O_2, CO, temp. depend. 77−58084
HCl, spectral line parameters in IR 79−22766
HCl, vibr.-rot. line broadening by CF_4 and SiF_4 77−27117
HCl, vibr.-rot. lines broadening and shifting by SiF_4 perturber 77−23521
$H^{35}Cl$, collision broadened vibr.-rot. linewidths and shifts in fund. band, low temp. obs. *(French)* 77−68076
$HCl/SF_5(CCl_4)$, inhomogeneous broadening of Morse oscillator, temp. depend. 77−61803
HCl-Kr, rot. for IR spectra, anisotropic density fluctuations 79−54848
HCl+Ar, IR line width press. broadening 77−61802
HCl+Ar, line broadening, short range force effects, semiclassical calcs. 79−98085
HCl+Ar, rot. linewidth calcs., using different pots. 78−66602
HCl+Ar(Xe), infrared line shape, rotational lines, influence of collision duration 80−43110
$HCl+CO_2$ collisions, semi-empirical non-Lorentzian line shape determ. 77−34699
HCl+HCl(Ar), pure rot. Raman lines, press. broadening cross sections 78−74702

molecular spectral line breadth continued
HCl+He(Ar), press. broadening, rot. energy transfer, infinite order sudden approx. 78−22011
HCl+iert gas, weak collisions, HCl spectral line broadening of IR spectra 80−74161
HCl+Kr(Ar), pot. energy surface determ. from rot. line broadening data 79−13784
HCl+methane, pure rot. line broadening obs., transition cross sections 77−75134
HCl+$N_2(O_2)(D_2)(H_2)$, HCl ν_0-ν_1 band perturbations, linewidth and shifts calcs., IR spectra obs. *(French)* 80−58251
$(HCl)_2$, intermol. distances, dipole moments, MINDO/3 and IR intensities and shifts calcs. 78−46335
HD, gas, fundamental band, R and P line shapes 80−23461
HD, IR absorpt. spectra, collision induced fundamental band 77−79613
HD, predissoc., interference effects, lineshape obs. 80−83432
HD, predissoc. linewidths and shapes for $3p\pi D^1\Pi_u^+$ state 80−53066
HD, Q-branch band shapes, motional narrowing and overlapping effects 78−29785
HD-inert gas mixtures, $R_1(J)$ and $P_1(J)$ absorpt. spectra, positive intercollisional interference 79−54843
HD-Kr, $R_1(1)$ absorpt. spectra, positive intercollisional interference 79−54843
HD+He, press. broadening, rot. energy transfer, infinite order sudden approx. 78−22011
HD+inert gas, isotropic Raman Q branch, vibr. dephasing effects and motional narrowing 78−74738
$H_2(D_2)$, Q-band line shape 79−33707
HF, laser field interaction, Floquet theory, dynamic Stark shift, broadening 80−63716
HF, near IR absorpt. spectra, collisional broadening, line shapes and half-widths 79−89673
HF, pressure broadened linewidths in 2.5 μm band, influence of polymer form. 80−32777
HF rotational line shift, far IR Fourier transform spectrometry improvement 79−30582
HF, vibr.-rot. band, absorpt. line self-broadening, rot. relax. 80−87213
HF+Ar, IR line width press. broadening 77−61802
HF+inert gas, press. broadening and shifting of vibr.-rot. absorpt. lines 77−27161
HNC, (3-2) line in Orion Molecular Cloud, low-intensity broad vel. wings obs. 79−25669
HNO, predissoc., absorpt. spectrum line broadening 77−14503
HNO_3, high resolution spectral meas. of 11.3 μm band, using tunable diode lasers 78−33504
HNO_3, high resolution spectral meas. of 5.9 μm band using tunable diode laser 80−32707
HNO_3 IR spectra, 865.5-871.0 and 884.5-887.0 cm^{-1} regions, equiv. width meas., atm. spectrum appl. *(French)* 80−87114
HNO_3, spectral linewidth, broadened in air, O_2 and N_2 at 200 and 300K 78−46399
HNO_3 vapour line parameters meas. by CO laser transmittance 79−26976
H_2O 79−63992
H_2O, 22 GHz rot. transition relax. rate consts. 79−18180
H_2O, atmospheric, narrowing of collision shape of mol. absorpt. line in powerful laser field 79−29860
H_2O, far IR absorpt. coeffs. by H_2O laser meas., foreign gas and self broadening 80−9599
H_2O, IR absorpt. in regions of weak absorpt., lab. meas. rel. to atm. windows 79−64005
H_2O, IR and Raman spectra, bonding, vibr., band shapes 79−6938
H_2O, IR line intenisties and widths, ν_2 rot.-vibr. band 78−9200
H_2O, IR spectra, linewidths 79−59454
H_2O, interstellar, in Orion Nebula, 183 GHz emission line vel. profile 80−41869
H_2O, linewidths and press. shifts, in N_2 and air, Anderson theory and quantum many-body theory 78−74708
H_2O, microwave absorption, spectral line press. broadening theory 77−30864
H_2O, $\nu_1+\nu_3$ combination band, evolution with temp. 78−66548
H_2O, spectral line shape changes in vapour with buffer gas *(Russian)* 78−46402
H_2O, spectral line wave number, intensity and width near 5.3 μm *(French)* 77−50432
H_2O, ultrahigh resolution IR absorpt. spectra using tunable PbTe laser diode 79−75628
H_2O vapour, IR bands transmission functions 80−106324
H_2O vapour, line shape functions in absorpt. coeff. calc. 80−9600
H_2O vapour, spectral line broadening by N_2, CO_2, Ar, intraresonator laser spectroscopy method 79−54863
H_2O-CO_2, IR radiation transfer 79−80028
H_2O-formaldehyde complex, IR spectrum in solid Ar, N_2 matrix 80−43042
$H_2O+N_2(CO_2)$, collision broadened H_2O absorpt. line, laser radiation intensity effects 77−83661
$H_2O(D_2O)$, VUV absorption spectra, Rydberg series, rot. line shapes, quantum defect 78−5244
H_2S, rot. transitions, press. broadening, microwave spectra 77−50429
$H_2S+H_2S(N_2)(O_2)$, press. broadening of spectral linewidth, calcs. 77−30932
He-H_2, rot. relax and spectral line shapes, coupled states calcs. 77−50500
He+CO(HCl)(HCN)(HD), press. broadening cross-section, ang. momentum approx. calcs. 77−34696
Hg discharge, high-pressure, NaI and TlI additives, line broadening and radiative transport 80−74199
I_2, 2-step reson. scattering, subnatural linewidths in vapour 79−76419
I_2, RF optically heterodyned saturation spectroscopy, reson. degenerate four-wave mixing 80−74211
I_2, reson.-enhanced CARS, band contours, assignments 78−86980
I_2, saturated absorpt. lines press. and power broadening 79−76765
I_2 solutions, vibr. and rot. relax., reson. Raman lineshape meas. 79−31616
I_2 vapour, absorpt. lines meas. using FM spectrosc. 80−42262
IBr-benzene in n-decane soln., IR line broadening by chemical exchange 80−87111
ICN, photodissociation, absorpt. lineshape 77−79662
$I^{35}Cl$, predissociations in $B^3\Pi_{0+}$ state 80−1033
$I^{37}Cl$, predissociations in $B^3\Pi_{0+}$ state 80−1033

molecular spectral line breadth continued
I_2He, Van der Waals mol., photodissoc. lifetime, I_2 vibr. depend. 79−6977
I2 fluoresc., Ar^+ laser excited, high resolution and sub-Doppler Fourier transform spectroscopy 80−43089
In complexes, chlorocomplexes, digitised Raman band profiles 77−71802
KN_3, Raman spectra, weaker features obs. 77−68045
K(5S)Xe, K(5S)Kr, excimer, visible emission band, exptl. results relative to theory 78−82779
KrF, 25 J unstable resonator oscillator, injection locking 80−28218
KrH_2 van der Waals mols., rot. predissoc. 80−63721
Li_2, A-X band intensity distrib. Franck-Condon calcs. validity 77−65511
MgO, red and near UV bands calc., rel. to sunspot spectra 80−12736
^{24}MgH, IR rot.-vibr. bands, stellar atm. appls. 77−18918
N^{2+}, spectral line breadth in molecular nonequilibrium plasma *(Russian)* 80−48044
N_2, 1^- system bands, line broadening and shift 80−87138
N_2, core photoelectron line shape, localisation role 79−59512
β-N_2 cryst., vibr. Raman spectra 80−60558
N_2 inner-valence ionisation, correl effects calcs. 78−9198
N_2, line broadening, short range force effects, semiclassical calcs. 79−98085
N_2, liq. spontaneous Raman scatt., vibr. dephasing, review 77−28568
N_2, liquid, Q-band position, width in cryogenic mixtures *(Russian)* 78−46401
N_2, liquid, vibrational dephasing, computer simulation, Raman spectra, pair potential effect 80−63863
N_2, preionis. and predissoc., rel. to spectral line shape 80−63724
N_2, rot. excitation by electron impact 1-4 eV 78−55248
N_2, rot. Raman linewidths, self-broadening calcs. 77−42356
N_2^+, first negative spectra, modelling 77−61758
N_2^+, reson. absorpt., 1st negative band, in irrad. air, calcs. 77−30850
N_2^+, UV spectral line width in rarefied free jet, for rot. temp. 80−6184
N_2-Ar, liq. mixture, isotropic Raman line shape theory 78−88298
N_2-Ar(Kr)(O_2)(CO)(CH_4), liquid, high resolution CW CARS spectra 80−63635
NF_2, IR spectra, ν_1 and ν_2 bands, vibr. excitation and spin-rot. interaction, doublet splitting 80−28011
NH_3, 10 μm absorption line profile, high resolution meas. 77−42359
NH_3, collisional broadening, vel. depend., IR optical saturable absorpt. technique, book contrib. 78−9201
NH_3, decay of saturation reson., IR ν_2 as Q(8,7) transition 78−25609
NH_3 in benzene(CCl_4)(pentane) Fermi resonance, solvent and phase depend. 80−47960
NH_3 in Taurus dark cloud, line widths rel. to gas temps. and motion 77−78851
NH_3, interstellar, nonmetastable levels line profiles 79−25665
NH_3, inversion spectrum, reson. half-widths calcs. 77−75221
NH_3, inversion spectrum collisional line broadening, general theory 80−87184
NH_3, laser saturation time-delayed IR spectroscopy 78−86976
NH_3, linewidth parameter $\Delta\nu/p$ for the J=13, K=13 inversion line *(French)* 78−42131
NH_3, magnetic relaxation rates for microwave spectrum and contributions to linewidth 80−5564
NH_3, microwave spectrum, width and shift parameters 77−18985
NH_3, ν_2 band as R(1, 1) line self-broadening coeff. 79−98158
NH_3, ν_2 IR band, vibr,-rot. lines, self-broadening and intensities 77−34635
NH_3, optical band strengths and curves of growth rel. to spatial distrib. on Jupiter 80−46386
NH_3, parameters of $S^RR(8,3)$ transition of ν_4 band 79−54916
NH_3^+, two-mode Jahn-Teller effect calcs. 80−83297
$^{14}NH_3$, J=13, K=13 inversion line displacement as function of pressure *(French)* 78−70815
$^{15}NH_3$, IR-IR double resonance, ν_2 vibr. state, electric dipole moment 77−83626
NH_3-$N_2(H_2)$(Ne)(Ar)(Kr)(Xe), as R(1,1) vibr-rot. line parameters, ν_2 band, using CO_2 laser light 79−3444
$NH_3+CO_2(N_2)$, collisional broadening of NH_3 inversion spectrum lines 80−99521
NH_3+H_2, NH_3 inversion transition, linewidths and T_1/T_2 ratio 80−99499
NH_3+H_2 collisions, semi-empirical non-Lorentzian line shape determ. 77−34699
NH_3+He(Ar), ammonia inversion spectrum press. broadening 78−86915
NH_3+He(Ne)(Ar)(Kr), pure rot. line, press. broadening calcs. 80−78656
NH(NF)(NCl), effective spin-spin parameter and singlet-triplet transition intensities, ab initio calc. 78−9067
NO, core photoelectron line shape, localisation role 79−59512
NO, fundamental intensity and linewidth of IR absorpt. spectra, press. broadening 78−25530
NO, gamma system in sunspots, equivalent widths calcs. 79−12457
NO, γ band lines, collisional broadening coeff. and optical collision diameter 80−63714
NO, γ-band collisional broadening parameters from resonance line absorpt. 77−10704
NO, $\gamma(0,0)$ band, collisional broadening parameters 80−63713
NO, intracavity Zeeman modulation detect., passive Q-switching, CO IR laser obs. 80−9597
NO, mol. beam tunable diode laser sub-Doppler spectra, $^2\Pi_{1/2,3/2}$ Λ splittings 79−41180
NO, press. broadening coeffs., spin-flip Raman laser spectrosc. 80−43147
NO, press.-broadened linewidths of $R(9.5)_{3/2}$ transition 78−70824
NO $R_{1/2}(25/2)$ transition, extinction coeff. at 8-7 P(11) CO laser line 79−45711
NO, self-N_2- and O_2-broadened linewidths 5.4 micron band, quadrupole moment 77−30930
NO, υ=0,1 states, spectroscopic data calc. 78−86851
NO, Zeeman modulation spectroscopy, line shape analysis 80−74197
NO+N_2(Ar), $^2\Pi_{3/2}$, $^2\Pi_{1/2}$ states, line broadening, mag. moment effect 79−72391
NO+$N_2(CO_2)$(CO)(CH_4)(Ar), NO $\gamma(0,0)$ band, oscillator strength and line broadening 80−106356
NO+NO collisions, semi-empirical non-Lorentzian line shape determ. 77−34699
NO_2, optical RF double reson. showing nonstationary state 79−59492
NO_2, rot. Q-branch effective line strength at 37.7 cm^{-1} 77−6859

molecular spectral line breadth continued
NO_2, rot. spectra at 93 GHz, press. broadened hyperfine multiplet 78−90156
NO_3^-, solvated, in H_2O, ethanol, cyanomethane, and DMF lowest n-π^* transition 79−85960
N_2O, 40°00-00°0 band, IR high press. absorpt. spectra profiles 80−52988
N_2O, IR absorpt. spectra, N_2-broadened lines of ν_3 band 78−5228
N_2O, IR bands, parametric deconvolution method 78−78697
N_2O, IR combination band spectral emissivity, 1200, 1700, 1900K, shock tube obs. 78−5287
N_2O, IR emissivity and band-model parameters, 200-500K 77−83591
N_2O, in soln., IR and Raman band shapes, mol. dynamics, ν_3 band 77−36238
N_2O, in soln., Raman and IR ν_1 and ν_2 band shapes, mol. motion dynamics 78−64352
N_2O, ν_3 and $2\nu_3$ IR bandshape and dipole correl. functions 80−91560
N_2O, preionis. and predissoc., rel. to spectral line shape 80−63724
N_2O, pure liq., mol. motion, anisotropic interaction 80−24345
N_2O, rot. transitions, self-broadening and self-shifting meas. 79−59426
$^{14}N^{16}O$, elec. and mag. props., hyperfine struct., mol. beam elec. reson. obs. 78−62792
$^{14}N^{16}O$, v=2←0 overtone band IR spectra, Λ doubling, hyperfine struct. 79−41165
$^{15}NH_3$, T_2/T_1 determ. for inversion transitions, power-broadened line shape 77−38654
Na^++Ti(Ni)(Zn)(Fe), 0.2-3.0 MeV, united-at. limits, mol.-orbital continua 77−19030
Na_2, A-X band intensity distrib., fluoresc. spectrum Franck-Condon calcs. validity 77−65511
Na_2, triplet satellite band obs. in self-broadened D-line very far blue wing 80−95688
$NaNO_3$, in liq. NH_3, Raman spectra, curve resolution anal. 77−82610
$NaNo_3$, aq. soln., Raman spectra, vibr., orient. relaxation *(French)* 78−62808
Na(4S)Xe, Na(4S)Kr, excimer, visible emission band, exptl. results relative to theory 78−82779
Nb complexes, F-containing, X-ray K absorption edges, chem. interpretation 78−74676
NeH_2, van der Waals mols., rot. predissoc. 80−63721
Ni porphin, reson. Raman excitation profiles, simulation, vibronic coupling consts. 77−65471
O_2, core photoelectron line shape, localisation role 79−59512
γ-O_2 cryst., vibr. Raman spectra 80−60558
O_2, effective spin-spin parameter, ab initio calc. 78−9067
O_2, Fourier representation of Voigt profile 78−90223
O_2, gas, intermol. pot. for spectra, acoustic absorpt., rot. relax., etc. 79−68224
O_2, harmonic oscillator model in predissoc., level widths, shifts and curve crossing 78−90239
O_2, liq. spontaneous Raman scatt., vibr. dephasing, review 77−28568
O_2, microwave absorption, spectral line press. broadening theory 77−30864
O_2, microwave spectrum, press. broadening 80−23412
O_2, oscillator strengths and linewidths, Schumann-Runge bands 78−90186
O_2 rot. Raman spectra fine struct., press. broadening *(French)* 79−94003
O_2, Schumann-Runge band system, oscill. strengths and linewidths 79−98120
O_2, Schumann-Runge band system in sunspots UV spectrum 80−12735
O_2, Schumann-Runge bands, predissoc. linewidths and oscill. strengths, vibr. level depend. 79−45735
O_2^+, 1NG bands spectral synthesis, for auroral obs. anal. 77−2296
O_2^+, absorpt. linewidth of predissociated levels, lifetimes 79−36711
O_2^+, $b^4\Sigma_g$ state, laser-induced predissoc. in ion beam 78−70886
O_2+Ar, gas, intermol. pot. for spectral props. and rot. energy transfer 79−68224
O_2+$O_2(N_2)(H_2O)$(Ar)(He), 118750 GHz transition, press. broadening 77−75136
O_3, stratospheric, spectroscopy with CO_2 waveguide laser 77−13117
OCS, collisional rot.-line widths and shifts, microwave region 78−25619
OCS, microwave rot. lines, self-broadening 78−58668
OCS, microwave rot. transitions, phase shift effect, collisional effects 79−98073
OCS, microwave spectrum, width and shift parameters 77−18985
OCS, microwave spectral lineshape of J 1→2 line 79−68225
OCS, self-broadening linewidth parameters 79−18268
OCS+bromomethane, microwave spectral line width, dipole-dipole interaction calc. 78−74648
OCS+CO_2, collisional line broadening of microwave spectra, semiclassical theory 78−29776
OCS+$CO_2(H_2)(N_2)$(OCS), collisional line broadening of microwave spectra, semiclassical theory, calcs. 78−25516
OCS+$H_2(CO_2)$(fluoromethane) rot. relax. parameters, microwave spectra linewidth parameters 80−28009
OCS+He(Ar), rot. lines, collisional broadening 79−18267
OCS+nonpolar perturber, J1-2 line broadening 77−6848
OCS+nonpolar perturbation, J=1→2 microwave line press. broadening 80−9644
OCS+OCS(He)(Ar), rot. spectral line shift and widths, collision induced phase shifts 77−75222
OH, 13.4 GHz absorpt. line width *(French)* 77−61801
OH maser lines from long-period variable stars, struct. and saturation 78−93264
OH masers, interstellar, line profiles rel. to saturation effects 77−91657
OH, methane-air flame, conc., temp. and rot. temp., laser absorption spectroscopy 78−76862
OH, microwave spectral line breadth in NH_3, H_2O, NO_2, SO_2, O_2, H_2, He, N_2, chloromethane 79−45806
OH, rot. transitions broadened by press., laser mag. reson. study 79−94020
OH+H_2O, OH linewidth rot. depend. on UV transitions 80−91606
$OH(^2\Pi)$, rot and translational temps. in gas discharge 78−5243
PH(PF), effective spin-spin parameter and singlet-triplet transition intensities, ab initio calc. 78−9067
POF_3, level anticrossing effects, vibr., laser Stark spectra obs. 80−32771
RbN_3, Raman spectra, weaker features obs. 77−68045
RbXe*, far-wing line spectra undulations, semiclassical methods 77−61808

molecular spectral line breadth continued
RuO_4, $\nu_3(F_2)$ IR band contour, isotopically pure cpds., mol. consts. 77−61746
S_2, effective spin-spin parameter, ab initio calc. 78−9067
SF_6, $3\nu_3$ band anal., IR spectra 78−90161
SF_6, double IR reson. line shape, freq. and time decay 77−88477
SF_6, IR double reson. with tunable diode laser 80−14160
SF_6, ν_3 band, IR spectra, in supersonic mol. beam 78−66541
SF_6, relax. mechanism, narrow reson. obs. by amplitude-modulated wave method 79−10155
SF_6, vibr. Raman spectrum, Q branches shapes 78−42077
SO_2, effective spin-spin parameter and singlet-triplet transition intensities, ab initio calc. 78−9067
SO_2, IR bands, emissivity, line shape and band model parameters 78−94246
SO_2, IR bands, line-shape parameters, 300-1200K 79−36704
SO_2, matrix isolated, ν_3 vibr. spectrum, diode laser spectroscopy, temp. depend. 77−50433
SO_2+$H_2O(N_2)(SO_2)$, linewidths, intensities, isotope shifts, 91.5-95.5 GHz 78−42044
SO_4^{2-}, ν_1 Raman linewidth, in acidic aq. soln. 77−65481
S0 in Orion Molecular Cloud, line profile rel. to rotational explanation of high-vel. mol. emission 80−36688
SeF_6, IR vibr. band contours, isotope substitution, force consts. 78−17670
SiC, Si K_α X-ray emission spectra chemical shifts, linewidths and intensities 78−13461
SiF_4, $\nu_3(F_2)$ IR band contour, isotopically pure cpds., mol. consts. 77−61746
SiH_4, $L_{2,3}MM$ Auger spectrum, line width and intensities 80−58325
SiH_4, ν_4 fundamental, laser sideband direct freq. reading IR spectra, electro-optical, press. broadening 78−21920
Si_3N_4, Si K_α X-ray emission spectra chemical shifts, linewidths and intensities 78−13461
SiO in stars, equivalent widths of lines of (A-X) band 77−87368
SiO_2, Si K_α X-ray emission spectra chemical shifts, linewidths and intensities 78−13461
Sn_2, matrix isolation Raman spectrum, overtone bands breadth 78−33515
TiO in sunspots, equiv. width meas. theoretical interpretation, line form. process 80−72902
UF_5, transient species formed in UF_6 laser flash photolysis, 17 micron IR spectrum 79−45715
XeF_6, UV absorpt. band shape 78−5289
$ZnCl_2$, aq. solns., complex IR refr. indices, IR spectra, mechanisms, spectrometer system 78−43831
ZnH, lifetime, Λ-doubling and hyperfine struct. of $A^2\Pi$ excited states 77−58083
ZrO, IR spectrum band strengths rel. to possible presence in S-type stars 80−62124
ZrO, in Ne matrix, laser photoluminesc. 77−14481

molecular structure (electronic) *see molecular electronic states*

molecular structure (geometrical) *see molecular configurations*

molecular vibration
see also Fermi resonance; macromolecular dynamics; molecular force constants; molecular rotational-vibrational energy transfer; molecular spectra; molecular vibration calculations; molecular vibration in solids; potential energy curves and surfaces of molecules; potential energy functions
2-furanmethanethiol, mol. struct., electron diffr. and IR spectroscopic examination 79−10106
absorption bands, vibronic intensification obs., floating-orbital method 80−63619
acenaphthalene, mol. and cryst., vibr. anal., normal coord. calcs. 79−47428
acenaphthene in n-alkane matrices, Shpolskii spectra fluorescence 78−9190
acetaldehyde, adsorbed on Al_2O_3, inelastic electron tunnelling spectra, surface vibr. struct. determ. 80−35572
acetaldehyde, carbonyl addition, model transition states, vibr. anal. 80−71898
acetaldehyde, dichroic effects, computational expts. 80−83424
acetaldehyde, lowest Rydberg state, multiphoton ionisation spectra 80−83435
acetaldehyde, torsional fundamental and combination bands, K-struct. anal. 78−78696
acetamide, IR spectra, amino group inversion transitions and pot. functions 80−43041
acetic acid, adsorbed on Al_2O_3, inelastic electron tunnelling spectra, surface vibr. struct. determ. 80−35572
acetic acid, and derivatives, vibr. spectra in soln. 80−63633
acetic acid, chemisorbed on Cu(100), acetate species struct. obs. 79−98232
acetone, absorption bands, vibronic intensification obs., floating-orbital method 80−63619
acetone, liq., C-C stretching mode relax., Fermi reson. influence 80−25352
acetonitride-d_1, ^2H NMR spectra, vibr. and asymmetry corrections to quadrupole coupling consts. 80−74184
acetonitrile, electrolyte solns., IR and Raman spectra interpretation, CN-stretching region 79−73941
acetonitrile, in liq. phase, Ramon band profiles, calc. using IR intensities 80−2741
acetonitrile, IR and Raman spectra, vibr. and reorientational and energy transfer width separation, rot. const. determ. 80−87131
acetonitrile, Raman spectral study of aq. soln. struct., H-bond effects 77−88454
acetonitrile-phenol($-d_1$), in CCl_4 ($CDCl_4$) solns., H-bonds vibr. relax. bands anal. 78−84560
acetophenone, liquid, far IR absorpt., mol. vibrs., internal rot., dipoles *(French)* 77−24827
acetophenone, T_1-S_0 intersystem crossing, nonradiative decay rate, excitation energy depend. 80−63609
acetophenones, spectrosc. characts. using PPP SCF CI calcs. 80−102448
acetophenones, substituted, IR absorpt. spectra, vibr. anal. 77−10672
acetyl cyanide, IR and Raman spectra, vibr. spectrum and vibr. anal. 77−10676
acetylcholine, nonenzymatic hydrolysis, Raman obs. 79−29505
acetylene, adsorbed on Ni (111), vibr. spectra from electron energy loss *(French)* 78−34696

molecular vibration continued
acetylene, chemisorbed on Ni (111), ind. vibrs., high resolution electron energy-loss meas. 79−90877
acetylene, chemisorbed on W, IR vibration spectroscopy 78−14603
acetylene, chemisorption on Pt (111), ethylidyne group form., LEED and ELS obs. 78−73075
acetylene, electron energy loss spectra, C K-shell excitation, vibr. struct. 79−22851
acetylene, IR spectra, rot. and vibr. struct. 78−21922
acetylene, pure rot. Raman spectra of ground and vibr. Π states, intensity distrib. 77−65476
acetylene, Q-branches, high resolution pulsed CARS 78−17676
acetylene, vibr. fine struct. accompanying core ionis., STO calcs. 78−62844
acetylene, vibr. relax. study using laser-induced fluoresc. 80−74219
acetylene+inert gas, vibr. relax. study using laser-induced fluoresc. 80−74219
acetylene($-d_1,d_2$), integrated IR intensities 80−23457
acetylene on Pt (111), nature of adsorption state, surface vibrs. meas. 77−76657
acetylene-d_1, vibr. bands, IR spectrum in region of bending fundamental ν_4 80−23418
acetylene-d_2, $\nu_4+\nu_5$ band, diode laser meas. 78−78664
acetylene-d_2, microwave spectrum, P-branch transitions, Stark shifts 77−27057
acetylpyridines, vibr., IR and Raman spectra 78−74653
acid oxalate ion in aq. soln., vibr. studies, IR and Raman spectra 80−95589
acrolein, vap., visible luminesc. excited by pulsed CO_2 laser 79−54894
actinide (VI) ions, AnO_2^{2+}, in CO_3^{2-} media, Raman scatt. 79−13718
adsorbate concentration dependence of IETS intensity 79−68284
adsorbed diatomic molecule, coupled-harmonic-oscillator model for vibr. modes 79−82461
adsorbed molecules on metal surface, inelastic scatt. of electrons, model 78−34718
aggregates, optical spectra, near strong coupling limit, Green's function model 77−83774
alanine-d_3, vibr. circ. dichroism, mechanism 78−33505
alcohol H-complexes interactions, H-bond vibr. freq., anharmonic calcs. 80−99453
alcohols, monohydric saturated, vibrational bandshapes 78−90226
alcohols, opt. consts. in IR, stretch band obs. 79−91421
alcohols, saturated, list of OH stretching frequencies, using averages and least squares approx. methods 79−53966
alicyclic ring cpds., vibr. spectra, conformational props., book contrib. 78−78702
alkali + inert gas molecule, far wing line broadening, quasistatic theory 79−22762
alkali halides, improved interaction pot., spectroscopic consts. calc. 79−86024
alkali hydride molecules, pot. energy function, rot. const., vibr. const., and binding energy 80−99532
alkali metal halide dimers, mol. force consts. and vibr. amplitudes calc. using electron gas model data 80−87245
alkali metal nitrates, Raman spectra, interionic interactions effect on bond lengths, dissoc. energies and vibr. 79−36653
alkali metal uranyl nitrates, IR spectra, force constants, bond orders 77−30873
alkanes, liq., mol. struct., selective deuteration and IR vibr. spectra 80−96432
alkanes, overtone spectra, local mode anal., discrete excitation of nonequivalent CH oscills. 78−78688
alkanes, polycyclic, three-photon ionisation spectra, 3s Rydberg orbital 79−68282
alkanes, thermal accommodation coeffs., on cc Al(Fe), translational (internal) gas-solid energy exchange 78−92506
n-alkanes, vibr. data and force field consts., review 79−31750
alkene-halogen, matrix isolation vibr. spectroscopy, complex form. studies 78−62952
alkyl benzenes, jet-cooled, intramol. vibr. relax., reson. fluoresc. and excitation obs. 80−14152
alkyl benzenes, jet-cooled, vibr. relax., nanosecond time evolution 80−95584
alkyl cyclobutane hydrocarbons, multiple initial vibr. state selection by chem. activation, relax. rate 77−40538
alkyl halide+K potentially reactive collisions, electronic excitation 80−74239
alkyl metal carbonyls, phosphine monosubstituted, LF vibrs., IR and Raman spectra 80−95585
alkyl substituted diacetylene radical cations, optical emission and photoelectron spectra, fragmentation decay 80−53004
alkyl sulphides, C-S stretching vibrs. 78−25533
para-alkylanilines having optically active modes, vibr. relax. studied by absorpt. and fluoresc. spectra 80−83340
1-alkynes+$O(^3P)$, CO prod., vibr. population distrib., rate consts., laser reson. absorpt. technique 80−40676
allene, liq., orientational dynamics, Raman obs. *(French)* 79−28746
allylamine, laser-microwave double and triple reson. 80−83397
2-amino-5-chloropyridine, IR absorption, vibr. assignments 80−979
4(6)-amino-uracil, IR absorpt. spectra, vibr. anal. 78−61143
γ-aminobutyric acid, aq. soln., low freq. vibrs. Raman spectra obs. 80−987
γ-aminobutyric acid, cryst., film, matrix IR spectra, low temp., neutral and zwitterion forms. 77−18920
3-aminophthalimide, continuous spectra, electronic transition freq. determ. 77−50425
3-aminopropanol, and deuterated forms microwave spectrum, dipole moment, struct. 79−59441
aminopyrazine, far IR spectra, barrier to planarity, pot. function and energy levels 80−69137
2-aminopyrimidine($-d_1$), amino inversion vibr., planarity, far IR obs. 79−31515
amplitudes, mean square, extreme value determ. appl. to 1,3-butadiene 78−25507
analysis, mixing parameter calcs. 77−42311
anharmonic molecules, multiple photon absorption in CW laser beams 78−58755
anharmonicity effect on mol. geometry parameters 79−50159
aniline, prereson. Raman effects, intensity enhancement mechanism 78−42069
molecular vibration continued
aniline-chlorophenol complexes, ^{35}Cl NQR, inter- and intramol. interactions 80−63666
anisole and $-d_3$, Raman spectra, low freq. vibrs., torsional barrier 78−25543
anisometric mol. liqs., Raman spectral components, vibr. reson. coupling and noncoincidence effect 80−69149
anthracene, electronic vibr. spectra, stochastic description, numerical modeling, comparison with expt. 80−63620
anthracene, inelastic-electron tunnelling spectroscopy, exptl. test of symmetry selection rules 77−83671
anthracene, matrix isolated, vibr. relax., hot luminesc. obs. 79−85986
anthracene, melt and dil. soln., UV spectra, line broadening and shift vibr. struct. 78−17684
anthracene, Raman spectrum, in-plane vibr. force fields, five-parameter approx. calcs. 79−59436
anthracene, rarefied vap., fluoresc. spectrum shape distortion in presence of intense radiation 79−3487
anthracene, vapour, fluoresc. spectra, mol. vibr. freq. reson. laser IR irradiation, quenching 80−18883
antimony ethyl derivative, Et_3Sb, IR and Raman spectra, rot. isomerism 79−41167
aromatic hydrocarbon, centrosymmetric, two photon excited upper state fluoresc. spectra, reson. fluoresc. and vibr. mode selectivity 80−18878
aromatic hydrocarbons, Morse oscill., transition probabilities for mol. bond modes 79−18172
aromatic hydrocarbons, vibronic coupling model, nontotally symm. harmonic mode 77−3337
aromatic isolated mol. nonradiative conversion, internal and S-T conversion, vibr. excitation and fluoresc. quantum yield 80−43095
aromatic molecule, electronic excitation energy degradation, electronic-vibr. spectrum 77−488
arsenic ethyl derivative, Et_3As, IR and Raman spectra, rot. isomerism 79−41167
atom+diatomic molecule, restricted 2-D Morse oscillator model, semiclassical calcs. for mol. dissoc. 80−74222
atom-diatom van der Waals complex, Born-Oppenheimer separation of radial and ang. motion 78−29828
azo dyes, tautomerisation, structs., laser Raman spectra 77−38672
azobenzene, parasubstituted derivatives, reson. Raman spectra *(French)* 79−59472
azulene($-d_8$), ultrafast $S_2 \rightarrow S_0$ internal conversion 79−3474
azulene in naphthalene mixed cryst., $S_2 \rightarrow S_1$ fluoresc., vibr. anal. 78−66586
benzaldehyde, prereson. Raman effects, intensity enhancement mechanism 78−42069
benzaldehyde derivatives, Raman intensities obs., phenyl ring-carbonyl group conjugation 78−29792
benzaldehyde gas, nonradiative electronic transition 80−83413
benzaldehyde in methylcyclohexane, $n^3\pi^*$ spectra 80−63627
benzaldehydes, in mixed cryst., T_1/T_2 interstate interactions, modulation polaris. phosphoresc. spectra, 4.2K 78−9185
benzaldehydes, para-halogenated, IR and Ramam spectra, vibr. assignments, thermodynamic functions 80−14139
benzene, 260 nm absorpt. spectrum, band contours, vibr. ang. mom. components 79−13736
benzene, Ar and Kr matrix isolated, IR spectra, vibr. freqs. and intensities 78−50548
benzene, benzene-d_6, vibrational anharmonicity, condensation effect, vap. press. isotope effect 78−58657
benzene, C-H stretching overtones, thermal lensing spectrosc. obs. 79−35851
benzene, chemisorbed on Ni(100) and (111), LEED and high resoln. EELS 78−6224
benzene, deuterated and chemisorbed on glass, vibr. bands, Raman scatt. study 80−84737
benzene, excited state props., by electrochromism in polymer matrix 79−22737
benzene, fluoresc. triplet state and isomerisation yields, low vibr. levels 79−64035
benzene, Jahn-Teller active states, vibronic struct., vibr. perturbation, spectral obs. 78−13440
benzene, liq., C-H stretch vibr. overtones, optoacoustic spectrosc. obs. 79−93982
benzene, liq., visible region absorpt. spectra, overtones meas. 80−78625
benzene, liquid, C-H stretch, seventh harmonic, absorption profile 79−56806
benzene, local mode combination bands and local mode mixing 80−27999
benzene, low lying $^1A_{2u}(\sigma,\pi^*)$ and $^1E_{2g}(\pi,\pi^*)$ states, Raman line intensities 78−78709
benzene, normal vibr. anal. 78−13487
benzene, overtone spectrum, intramol. lineshape narrowing 79−45705
benzene, prereson. Raman scatt. of overtones in μV 79−59471
benzene, valence electron spectra, vibr. band struct. 77−23520
benzene+Hg, electronically excited, mol. fluoresc., vibr. relax. cross sections and equilibration rates determ. 80−87205
benzene($-d_6$), prereson. Raman effects, intensity enhancement mechanism 78−42069
benzene chemisorbed on Raney Ni, struct., neutron inelastic spectroscopy study 80−101038
benzene radical cation in solid Ar, fluorescence spectra obs. 80−83382
benzene-^{13}C, liq., vibr. spectra, band assignments 78−13500
benzene-$Br_2(Cl_2)$ π-σ complexes, low freq. spectra 78−78713
benzene-d_0,-d_6, $^1B_{2u}$ excited states, high resolution two-photon spectra 77−506
benzene-d_0($-d_6$), radiationless triplet decay, non-Condon effects 80−83405
benzene-d_1, ^2H NMR spectra, vibr. and asymmetry corrections to quadrupole coupling consts. 80−74184
benzene-d_5, C-H vibr. states, thermal lensing spectra, local mode model test 77−71812
benzene-d_6+N_2+CO_2, electronically excited, mol. fluoresc., vibr. relax. cross sections and equilibration rates determ. 80−87205
benzenes, trisubstituted, valence force fields, normal modes of planar vibrations *(French)* 78−37626
1,3-benzodioxole, far IR spectrum anal., pot. function 79−76427
benzoic acid, dimer, cryst., IR and Raman spectra, vibr. assignments 78−31191
benzoic acid, IR absorpt. spectra, fundamental assignments 80−5542

molecular vibration continued
benzophenone, in DDE at 2K, vibr. overtone characterisation and local modes by emission spectroscopy 79−89682
5,6- and 7,8-benzoquinoline trapped in n-paraffins at 77K, quasilinear absorption spectra 78−90179
benzotrifluoride, and mono-substituted derivatives, vibr. spectra, internal rot. 77−83598
1,2-benzpyrene, butyl bromide solid soln., phosphoresc. line struct. obs., vibr. assignments 77−58075
1,1′-bianthryl derivatives, dimer optical activity, vibronic circ. dichroism, theoretical anal. 78−62821
biaryls, dimer optical activity, vibronic circ. dichroism, theoretical anal. 78−62821
bicyclo(3.2.0)hept-6-ene, LF vib. spectra, conformations 78−58685
bicyclobutyl+methylene, products decomposition, competitive channels and vibr. relax. 80−83336
bioenergetics, solitons, muscle contraction mechanism 79−96508
biological molecule vibrational analysis, comparison of algorithms for soln. of secular eqns. *(French)* 79−100565
biological systems, nonequilib. mol. vibr. excitation, electron mechanism 80−55979
biomolecule resonant interactions 80−72128
biomolecules, struct. and vibr. Raman spectra 77−52939
biopolymers, dynamics of helix-coil transition 79−29499
biphenyl, vibr. level classification by Longuet-Higgins group 80−43030
bond charge parameters from integrated IR absorption intensities 77−6853
bond order rel. to vibr. 79−36498
book, summaries and reviews of recent work, fields of interest 78−21894
Born-Oppenheimer approx., IR absorption, circ. dichroism using vibronic gauge function 78−967
Born-Oppenheimer approx., IR absorption, vibr. intensity using vibronic gauge function 78−966
bridge angle, vibr. behaviour, simplified and accurate calcs. 80−95735
bromanil and radical anion, Raman and IR freq. shifts 78−33516
1-bromo-2,2-dimethylpropane, Raman and IR spectra, vibr. anal. 78−90173
1-bromo-2,3 dimethylbenzene, IR vibr. spectrum, internal modes, overtones, combination freqs. 78−9146
1-bromo-2,4 dimethylbenzene, IR vibr. spectrum, internal modes, overtones, combination freqs. 78−9146
1-bromo-2,5 dimethylbenzene, IR vibr. spectrum, internal modes, overtones, combination freqs. 78−9146
1-bromo-2,6 dimethylbenzene, IR vibr. spectrum, internal modes, overtones, combination freqs. 78−9146
1-bromo-2,6-dimethyl benzene, IR and Raman spectra, vibr. anal. 77−57997
2-bromo-4-nitrotoluene, IR absorpt. spectra, vibr. assignments 78−42048
2-bromo-5-nitrotoluene, IR absorpt. spectra, vibr. assignments 78−42048
5-bromo-uracil, IR absorpt. spectra, vibr. anal. 78−61143
bromoacetylene, microwave spectrum, r_s-struct., dipole moment, quadrupole coupling consts., vibr. excited states 77−79606
bromobenzene-d_0, -d_1, -d_4, vibr. spectra and force fields 77−65463
bromochlorofluoromethane, struct., vibr. amplitudes, gas phase electron diffr. obs. 79−31690
bromodifluoromethyl radical, IR matrix isolation spectrum, stretching fundamentals 78−27788
bromoform, highly excited vibr. states, thermal lensing spectrosc. and local mode model 80−87140
bromoform, Raman spectra, intermol. interactions 79−76436
4-bromoisoquinoline, UV and IR spectra, f-values and ground state vibr. freqs. 78−58714
bromomethane(-d_1,d_2,d_3), F and G sum rules as vibr. intensity data error indicators 79−3494
bromomethane (-d_1, d_2, d_3), exptl. vibr. intensity data error indication by F and G sum rules 79−72364
bromomethane-$d_{0,1,2,3}$, IR spectra intensities, dipole moment, bond charge, force consts. 77−83588
α-bromotoluene, liq., IR absorpt. spectrum 78−979
bromotrifluoromethane ^{79}Br (^{81}Br), vibrational spectra and force constants of symmetric tops, rotational analysis 79−98090
bromotrifluoromethane cation, photodissoc. by quasi-continuum single IR photon absorption 80−61124
bromoxylenes, near UV absorption spectra, assignments 79−81209
trans-1,3-butadiene, electronic spectra vibr. struct. calc. 79−63981
1,3-butadiene, molecular vibration, mean. square amplitude, extreme value determ. 78−25507
butadiene, UV and photoelectron spectra, first Rydberg states, vibr. components 77−46573
1,3-butadiene-1-one, spectroscopic consts., IR and microwave spectra, prep. 80−18859
n-butane, LF vibr. spectrum, methyl torsional pot. function, internal rot. 79−89670
n-butane, vibr. shrinkages, mol. struct., electron diffr. obs. 77−50535
1-butanol, IR and Raman spectra, vibr., conformers 78−25532
1-butene oxide, gas, microwave spectrum 79−13703
4-n-butoxybenzylidine-4′-n-octylaniline, liquid cryst., smectic B phase lattice vibr. anisotropy, Mossbauer anal. 77−7666
t-butyl acetate, rot. isomerism, dielect. and Raman spectra 80−106328
t-butyl alcohol, and deuterates, gaseous and matrix IR spectra, liq. Raman spectra, vibr. assignment 79−10113
t-butyl alcohol, struct. determ. from vibr. spectra, H-bonding and heat of mixing *(Russian)* 78−3368
n-butyl bromide conformers, IR and Raman spectra, vibr. anal. *(German)* 77−88451
t-butyl formate, deuteration effects, IR and Raman spectra 79−50016
t-butyl formate, rot. isomerism, dielect. and Raman spectra 80−106328
t-butyl radical, VUV photoelectron spectrum, geometry, vibr. struct. and ionisation pots. 78−50577
t-butylphosphine, microwave spectrum, meas., determ. 78−58675
butylsilane-d_0,(−d_n), vibr. spectra, normal vibrs. and rot. isomerism 79−31523
3-butyn-1-ol, vibr. spectra, assignments, rot. isomerism 80−58257
C_2, vibr. and rot. anal. of vis., UV spectra, RF discharges in N_2, H_2, CH_4 mixtures 78−5241
C_{3v} molecules, l-reson. perturbations in overtone and combination vibr. systems 80−52962
calcium oxalate monohydrate, IR and Raman spectra, vibrational studes 80−69139
carbon tetrafluoride, compressed gas, ν_1 vibr. Raman line 78−32884
carbonyl compounds, interpretation of Raman spectra 79−18193
molecular vibration continued
carbonyl frequency correlation of aromatic derivatives with nonaromatic analogues 79−22709
β-carotene, coherent anti-Stokes reson. Raman spectrum excitation profiles 77−56342
carotenoid molecules in living cells of chlorella, vibrational state population 80−97861
Cartesian displacement coords., Coriolis and transition moment calcs. 77−83573
cellobiose, vibr. spectrum, freq. calcs. *(Russian)* 78−21909
chalcogen and pseudochalcogen mols., stereochem. using nonrigid mol. model 78−62788
charge transfer complex, Raman scatt. intensity enhancement model 79−13720
chemical reaction wave, propag. of coherent probe light pulse 80−61190
chemical reactions in mixture of mol. gases by cooling translational-rotational degrees of freedom, stimulation 78−7202
chloranil and radical anion, Raman and IR freq. shifts 78−33516
chloro(ethyl)silanes and its C derivatives, Raman spectra, mol. vibr. and rot. isomerism 80−87134
3-chloro-1-butene, rot. isomerism, vibr. spectra assignments 78−58702
1-chloro-2,2-dimethylpropane, IR and Raman spectra, vibr. assignment 80−74169
1-chloro-2-methylpropane, IR and Raman spectra, vibr. assignment 80−74169
2-chloro-3-fluoro-1-propene, struct. and conformers, force field and vibr. amplitudes 78−25747
4-chloro-3-nitrotoluene, IR absorpt. spectra, vibr. assignments 78−42048
2-chloro-6-methyl benzonitrile, vibr. spectra 79−89665
chloroanisoles, ^{35}Cl NQR, inter- and intramol. interactions 80−63666
chlorobenzaldehyde, $a^3A'' \rightarrow X^1A'$ phosphoresc., conformations and ground state fundamentals 80−78642
p-chlorobenzaldehyde and deuterated derivs., vibrational spectra 79−3441
4-chlorobutyrylchloride, Raman and vibr. IR spectra of solid and liq., rot. isomerism 78−62810
chloroethane, reson. multiphoton dissoc. 80−53077
chloroethane-d_1, laser multiphoton dissoc., intramolecular isotope effect 78−17733
2-chloroethanol, IR and Raman spectra, normal coord. anal., isomerism 78−74661
chlorofluoromethanes, ideal gas thermodynamic props., mol. struct. 77−3912
chlorofluoromethanes, valence photoelectron spectra, electronic and vibr. bands 78−50582
chloroform, highly excited vibr. states, thermal lensing spectrosc. and local mode model 80−87140
chloroform-d in soln., vibr. and reorientational relax., Raman study 80−63636
chloroform-He(Ar)(N_2) gaseous compressed mixture, mol. reorientation, Raman spectra 80−23422
chloromethane-d_3, and isotopic forms, optically pumped mm laser transition assignments, 792 micron line 78−42328
chloromethyl formate(-d_1,d_2,d_3), gas, solid. and liq., IR spectra assignments and struct. 80−32715
β-chlorophenetole, UV and IR electronic and vibr. spectra, model assignments 77−10673
chlorophenols, ^{35}Cl NQR, inter- and intramol. interactions 80−63666
chlorophyll-a, monochromatic excitation, luminesc. spectra, quasilinear struct. *(Russian)* 78−74809
2-chloropropane, conformation, vibr. spectrum, from simple harmonic force field 78−33494
chrysene, butyl bromide solid soln., phosphoresc. line struct. obs., vibr. assignments 77−58075
cinnoline, prereson. Raman spectra, vibr. band intensities obs. 80−102515
circular dichroism, vibr. anharmonic effects 78−29769
classical trajectories, spectral anal. 77−83564
coherent, parametric excitation 79−18241
coherent interaction with strong monochromatic laser light, classical calc. 80−28079
collisions in laser field, multiphoton vibrational excitation enhancement, semiclassical theory 80−58350
collodion, film, IR spectrum, vibr. assignments, chain config. 77−34789
complex molecules, reson. Raman spectra, vibr. scatt., review 78−37644
complex molecules, vibr. spectra, stochastic description, appl. to optically active Brownian oscillator 80−52974
condensed aromatics, in-plane vibr. force fields, five-parameter approx. calcs. 79−59436
conjugated molecules, linear and mag. cir. dichroism interpretation 78−62835
copper porphins, vibr. spectra, planar vibrs., normal coord. anal. 77−65474
core electron ionis., vibronic coupling, symmetry breaking, vibr. struct. 78−5279
coronene, butyl bromide solid soln., phosphoresc. line struct. obs., vibr. assignments 77−58075
coronene, in-plane vibr. force fields, five-parameter approx. calcs. 79−59436
coumarin 6, ultrashort vib. population lifetime of ground state in vapour phase 77−30929
coumarin dye molecules, CH stretching modes, population lifetime meas. 80−58185
coupled vibration systems, eigenvalues, semi-classical SCF calcs. 80−27929
m-cresol, vibr. spectrum determ. using Al-insulator-Pb tunnel junction 77−6782
croconate ion, Jahn-Teller coupled vibrs., reson. Raman profiles 77−83602
cryogenic liquids, vibr. kinetics, nonlinear optics appls. 80−13082
crystal violet, prereson. Raman spectra 80−32721
cyanoacetylene, IR absorpt. bands, integrated intensities, ab initio and LMO calcs. 79−72234
cyanoacetylene, vibrational excitation in Orion molecular cloud 80−22067
α-cyanoacrylate adhesive in first monolayer on bulk Al surface, IR spectra, H-bond form., stretching vibr. 80−87119
cyanobutadiyne-d_0,d_1, microwave spectrum, substitution struct., dipole moment 77−3348
cyanodiacetylene cation, gas phase, UV emission spectra of $\tilde{A}(\pi^{-1}) \rightarrow \tilde{X}(\pi^{-1})$ band system 80−95636

molecular vibration continued
cyanogen fluoride, fund., hot bands, laser microwave two photon and double reson. spectroscopy 80−32752
cyanomethane, matrix-isolated, VUV photolysis, CNC radical vibr. and electronic spectra 78−85180
cyanopyridine, isomeric forms, adsorbed of Ag electrodes, Raman scatt., orientational specificity 79−69822
cyclic ethers-HF H-bonded complexes, calorimetry, IR spectra and MO calcs. 79−52738
cycloalkanones, carbonyl charact. freqs., kinematic and pot. energy effects 80−95578
cyclobutane(-d_8), centrifugal distortion const. calc., rel. to struct. and mol. wt. 80−95580
cyclobutanol-d_0,-d_1, conformation, microwave spectrum 78−86852
cyclobutanone, clathrate hydrate, struct. II, for IR spectra, 4-100K 79−13707
cyclobutene, strong collision and thermal decomp. on surface, variable encounter method calcs. 80−50885
cyclobutylmethylether, IR and Raman spectra, config. 79−31525
1,3-cycloheptadiene, microwave spectrum, conform. 79−98074
1,3-cycloheptadiene, Raman and IR spectra, normal coord. analysis, conform. 77−77203
cycloheptane, geom. struct. by electron diffr. 79−31682
cycloheptanone, vibr. spectra, pot. functions and conformers 77−83569
cycloheptatriene, and substituted forms, vibr. highly excited, steady-state photoisomerisation 80−16704
cycloheptatrienes, highly vibr.-excited thermal isomerisation in shock waves 79−79236
cyclohexane, IR absorption in Ar matrices and perdeutero-cyclohexane, vibrational anal. *(French)* 77−6769
cyclohexanol, struct. information from OH-stretching freqs., axial/equatorial hydroxyl ratio 79−72438
2-cyclohexene-1-one, planarity barrier, from LF Raman spectrum 79−54859
cyclohexene-Br_2 (Cl_2) π-σ complexes, low freq. spectra 78−78713
cyclooctanone, vibr., rot. spectra and conformations, pot. function 78−78707
cyclopentadienylhafniumdichloride, gaseous, far IR and Raman spectra 80−95624
cyclopentadienyltitanium dichloride, gaseous, far IR and Raman spectra 80−95624
cyclopentadienyltitaniumtrichloride, gaseous, far IR and Raman spectra 80−95624
cyclopentadienylzirconiumdichloride, gaseous, far IR and Raman spectra 80−95624
cyclopentene-3,5-dione(-d_1) microwave spectrum assignments, rot. consts., dipole moment, config. 78−55168
cyclopentyl chloride, microwave spectrum, conformation, quadrupole coupling consts. 79−3434
cyclopentylamine, vibr. spectra and struct. 80−102516
cyclopropane, clathrate hydrate, struct. II, for IR spectra, 4-100K 79−13707
cyclopropane, direction between H atom, group displacement vector and dipole moment vector for stretching and deform. vibr. 79−41172
cyclopropane, IR spectra studied by tunable laser, $\nu_{10}+\nu_{11}$ band anal. 80−95615
cyclopropane, partial vibr. energy transfer map 80−32760
cyclopropane, surface isomerisation to propylene, role of vibr. energy 79−74376
cyclopropane(-d_6), centrifugal distortion const. and thermodynamic functions calc. 80−95582
cyclopropane-d_0, d_6, absolute IR intensities, dipole moment derivatives and polar tensors 78−90165
cyclopropyl bromide, IR absorption, Raman scatt., assignments, thermodynamic functions 80−984
cyclopropyl silane, rotational spectrum (9.0-35 GHz), transitions of ground vibrational state 79−98077
cytochrome c, protein influence on haeme, Raman difference spectroscopy 80−72125
decanoic acid, mol. config. change in cryst., IR spectra, normal coord. anal. 78−33506
decyloxybenzoic acid, vibr. bands., IR dichroism, phase change effects *(Russian)* 78−15174
degenerate electron states, electron interaction with doubly degenerate vibr., optical transitions, semiclassical approx. 80−27927
dense polyatomic molecular systems, vibr. correl., HF band exchange dephasing 80−37803
dephasing dynamics, of Raman active ground state mol. vibr. 79−44942
diacetylene, near UV band system, rot. and vibr. anal., rot. fine struct. 77−61761
diacetylene radical cation, and deuterated forms, electronic spectrum in solid inert gases 79−94026
2,4-diamino-6-hydroxy-pyrimidine, IR absorption spectrum, vibr. anal., tautomerism 80−58253
9,9'-dianthryldisulphide, UV/visible absorption spectrum *(German)* 79−59487
diatom, quadratic vibr. force const., from X-ray scatt. factors 79−45864
diatomic asymmetric mol., vibr. self-ionisation and recomb. *(Russian)* 77−79700
diatomic gas, vibr. nonequilib. radiation, master eqn. approxs. 78−33496
diatomic gas, vibr. nonequilib. radiation 78−33495
diatomic hetero-nuclear molecules, dissociation in intense IR fields 77−71841
diatomic homonuclear molecule, effect of vibr. transitions on fast electron scatt. data 77−88583
diatomic homopolar molecules, light scatt. *(Hungarian)* 77−50442
diatomic molecular gas, electron elastic scatt. intensity calc., vibr. coord. averaging method 77−68114
diatomic molecule, electron impact dissociation by vibrational excitation *(Russian)* 78−1096
diatomic molecule+solid surface, energy transfer, internal vibr. energy effects 78−35234
diatomic molecules, and ions, internal partition function calc. 78−55159
diatomic molecules, electron impact, vibs. excitation and dissoc. attachment, R-matrix calcs. 79−72228
diatomic molecules, shortening of energy relax. time of excited mol. vibr. in dense medium by form. of H-bonds 80−91553
diatomic molecules, spectrosc. consts., rel. to electronegativity 80−28007
diatomic mols., electronic transition probabilities, isoelectronic, isovalent correls. for transition strength and vibr. consts. 80−87182

molecular vibration continued
diatomic mols., internal partition functions for O_2, N_2, NO and their ions, max. summation indices 80−27995
diatomics, harmonic oscillators, R-centroid props. 77−50421
diatomics in rare gas matrices, vibr. modulation effects 77−23496
4,10-diazachrysene, absorpt. spectra and luminesc. in cryst. and glassy matrices, 77K 78−37650
meso-2,3-dibromo-1,4-dichlorobutane, rot. isomerism, IR and Raman spectra 80−981
1,3-dibromobutane, IR and Raman spectra, normal coord. anal., C-halogen stretch bands and conformers 79−31522
cis-dibromoethylene, vac. UV spectrum, Rydberg transitions, ionisation limits 78−78718
trans-dibromoethylene, VUV and photoelectron spectra, Rydberg series, vibr. fine struct. 77−6799
dibromofluorobenzene, IR absorpt. spectra, vibr. assignments 78−17665
dibromomethane, highly excited vibr. states, thermal lensing spectrosc. and local mode model 80−87140
dibromomethane, IR spectra, local mode description for overtone spectra 78−42047
1-10-dicarba-closo-decarborane (10), mol. struct., vibr. and shrinkage corrections calc. from force field 80−95739
dichloroaniline (2,3- and 3,5-) IR absorpt. spectra 250 to 4000 cm^{-1}, vibr. anal. 79−13717
dichloroanilines, vibr. assignments, Raman spectra obs., thermodynamic functions 80−52992
2,6-dichlorobenzamide, IR spectrum, vibr. assignment 80−95608
3,4-dichlorobromobenzene, liq., laser Raman spectrum, LF band assignments 80−48002
dichlorobromobenzenes, IR absorpt. spectra, vibr. assignments 78−17665
1,3-dichlorobutane, IR and Raman spectra, normal coord. anal., C-halogen stretch bands and conformers 79−31522
2,2-dichlorobutane, liquid and solid., vibr. spectra, IR and Raman obs. 80−60567
1,1-dibromo-2,2-dichlorocyclopropane, normal modes, IR and Raman spectra 79−41170
2,2-dichloroethanol, vibr. spectra, normal coordinate anal. 79−22694
dichlorofluorobenzene, IR absorpt. spectra., vibr. assignments 78−17665
dichloromethane, high press. and temp. IR absorpt. spectra, stretching fundamentals *(German)* 80−47999
dichloromethane, highly excited vibr. states, thermal lensing spectrosc. and local mode model 80−87140
dichloromethane, IR spectra, local mode description for overtone spectra 78−42047
dichloromethylene, radical, emission and excitation spectra, in Ar matrix 77−34657
2,4-dichlorophenoxyacetic acid, NQR of ^{35}Cl, 77-300K 78−50560
2,2-dichloropropane, normal coordinate calcs. 80−60567
1,3-dichloropropyne and -d_1, vibr. spectra, normal coord. anal. and centrifugal distortion constants 78−70832
3,6-dichloropyridazine, liq. and solid soln. spectra, fundamental freqs. and assignments 80−5541
dichloropyrimidines, UV-vis. absorpt. spectra, anal. 77−50445
1,1-dichroethane and d, IR and Raman spectra, βCH stretching interaction force consts. 77−79616
dicyanoacetylene radical cation, $\tilde{A}^2\Sigma_g^+ \rightarrow \tilde{X}^2\Pi_u$ emission band system 79−22721
dicyanobenzene, deuterated isomers, vibr. spectra 79−31521
dicyanodiacetylene radical cation, photoelectron and emission spectra 80−5558
dicyanoethylenes, substituted, vibr. spectra, intramol. effects 79−31528
dicyclopentadienyl Ti^{3+}-N_2 compound complexes, reson. Raman scatt. 80−99510
diethylcyanine, vibrational Raman bands, excitation profiles *(French)* 80−83380
diethylsilane-d_0(−d_n), vibr. spectra, normal vibrs. and rot. isomerism 79−31524
diethynylbenzene, radiative and nonradiative processes, triple bond effects 79−3481
diethynylbenzenes, vibrational spectra, deuterated isomers 78−58705
S_1p-difluorobenzene, time resolved fluoresc. spectra, direct view of intramolecular vibr. redistribution 80−83341
1,3- difluorobenzene radical cation, and deuterated forms, laser-induced fluoresc. matrix. study 79−98138
1,2-difluorobenzene-d_0, -d_4, IR spectra, vibr. anal., force field 77−27063
1,2-difluoroethane, gauche-trans conformers, IR and Raman spectra, vibr. 78−17667
1,1-difluoroethane, mol. struct., gas phase electron diffr. obs. 80−58385
1,2-difluoroethane in Ar matrix, IR hole burning and lineshape, vibr. transition 79−76425
2,2-difluoroethanol, vibr. spectra, normal coordinate anal. 79−22694
1,1-difluoroethylene, CO_2 laser Stark spectra of ν_4 and ν_9 bands 79−36694
1,1-difluoroethylene, optically pumped, far IR laser line assignment 79−31865
1,1-difluoroethylene, optically pumped mm laser transition assignments 78−42328
difluoromethane, IR spectra, local mode description for overtone spectra 78−42047
dihalogenoacetylene radical cations, $C_2X_2^+$, emission spectra, $A^2\Pi \rightarrow X^2\Pi$ band systems 78−17679
2,2-dihalohexafluoropropane, IR and Raman spectra, gas, liq. and solid, normal coord. anal. 79−72314
2-5-dihydrofuran, liq. phase far IR spectra, ring puckering *(French)* 78−92068
1,2-diidobenzene, vibr. spectra, packing calcs. and crystal structure investig. 80−28938
diiodomethane, IR spectra, local mode description for overtone spectra 78−42047
dimethoxymethane, vibr. spectra and rot. isomerism 80−106325
dimethyl aniline, IR spectra, 250-4000 cm^{-1}, vibr. anal. 78−62797
dimethyl ether, review of microwave spectrum, tabulated data 80−51965
dimethyl ether.HCl, gas-phase Raman spectra, profile of stretching vibr. 79−45728
dimethyl mercury, indirect coupling constants, vibr. corrections 79−50050
dimethyl phosphine-d_4, isolated CH stretching freqs. 78−90167
dimethyl sulphide-d_4, isolated CH stretching freqs. 78−90167
dimethyl sulphoxide-d_6, intensities in inelastic electron tunnelling, IR, and Raman spectroscopy *(French)* 79−822

molecular vibration continued
dimethylallene, excited states, microwave spectrum and strong Coriolis coupling 78−9141
dimethylboric anhydride, IR and Raman spectra, vibr. and struct. 78−25531
trans-dimethyldiazene-1, 1, 1-d_3, IR and Raman spectra, vibr. assignments and pot. functions 78−33507
trans-dimethyldiazene-d_0,d_6, IR and Raman spectra, vibr. assignments and pot. functions 78−33507
3,3-dimethyloxetan, far IR spectra, ring puckering vibration 78−42058
dimethylphosphine, microwave spectra, internal rot. barrier 78−5205
dimethylsolphoxide, effects on water struct., Raman and IR spectral study 80−14143
dimethylsulphite(-d_6), cryst., liq., and oriented film, vibr. spectra, force fields 79−91443
2,12-dimethyltridecahexaene, optical spectra, vibr. anal., rel. to visual chromophore 77−29102
2,10-dimethylundecapentaene, optical spectra, vibr. anal., rel. to visual chromophore 77−29102
dioxan-phenol(-d_1), in CCl_4 solns., H-bonds vibr. relax. bands anal. 78−84160
dioxane, Raman spectral study of aq. soln. struct., H-bond effects 77−88454
1,3-dioxolane, clathrate hydrate, struct. II, for IR spectra, 4-100K 79−13707
diphenyl, double mols. with weak reson. bonds, quasilinear spectra 79−94030
diphenylpolyene, oriented in polymer film, polaris. reson. Raman spectra 79−59466
1,3-disilacyclobutane, ring-puckering combination band spectra in SiH_2 stretching region 78−70836
1,2-disubstituted imidazole compounds, IR and Raman spectra, vibr. anal. *(French)* 79−45713
DNA, proton radiationless transitions for hydrogen bonds *(Russian)* 80−97857
double well damped motion, proton tunnelling, transfer rate temp. depend. *(German)* 80−87058
dye solutions, mixed, energy transfer and conc. depolarisation of fluoresc. 78−25583
EBBA, liq. cryst., IR and far IR spectra, vibr. assignments 77−16298
EBBA, NMR and Raman scatt. studies in nematic phase 80−100619
electron dissociative capture, vibr. struct. of resonances 77−34770
electron impact excitation, threshold structures, non-adiabatic theory 79−72431
electron impact shape-reson.-enhanced vibr. excitation, 10-40 eV, appl. to CO_2 80−5629
electron scatt. resons., near threshold, vibr. induced narrowing 80−91673
electron scattering, L^2-basis set theory with vibr. and rot. coupling 79−41247
electronic spectra, vibr. struct. determ. by Franck-Condon method, book contrib. 78−21911
erythrosine dye, vibrational decay and fluoresc. in S_1 excited state 78−25605
ethane, doubly degenerate torsional states, pure rot. transitions, theory 79−72299
ethane, force consts., vibr. stress and isotope effects 78−21897
ethane, inclusion of nonbonded interactions in vibr. freq. calcs. 80−95590
ethane, liq., IR torsion band, 98-173K mechanism, Coriolis coupling 77−38662
ethane, long path photoelec. absorpt. spectra 4200-10600 Å, appl. to Uranus 77−83592
ethane, unimol. decomp., energy transfer processes, Monte Carlo simulation 80−99555
ethane gas, local mode overtone bands 80−83444
ethanedithiol, mol. vibr., conformational anal., Raman spectra 79−31534
ethaneselenol, IR, Raman and microwave spectra, barriers to internal rot. 77−38666
ethanol, adsorbed on Al_2O_3, inelastic electron tunnelling spectra, surface vibr. struct. determ. 80−35572
ethanol, adsorption on Ag islands on Al_2O_3 substrate, inelastic electron tunnelling spectra and TEM obs. 79−90884
ethers, Raman spectra, interpretation 77−65483
ethyl alcohol, solution, struct. determ. from vibr. spectra, H-bonding and heat of mixing *(Russian)* 78−3368
ethyl fluoroformate, microwave spectra of rot. isomers 79−10097
ethyl formate, microwave rot. spectrum, centrifugal distortion effects 80−52979
ethyl methyl sulphide, low freq. vibr. spectra, methyl torsional pot. functions and internal rot. 80−5543
ethyl radical, $^{13}C_\alpha$ and H^+ hyperfine interactions, EPR spectra, vibr. anal. 80−23443
ethyl-furan-2-carboxylate, skeletal vibr. of IR spectra, conformational props., solvent polarity effect 80−87118
ethylcyanodiacetylene cation, gas phase, UV emission spectra of $\tilde{A}(\pi^{-1})\rightarrow\tilde{X}(\pi^{-1})$ band system 80−95636
ethylcyclopropane, solid, liquid, vapour phase, IR and Raman vibr. spectra 80−84740
ethylene, $^2B_{3u}+e^-\leftarrow{}^1A_g$ transition, appl. of photoelectron spectroscopy using supersonic mol. beam source 79−68264
ethylene, adsorbed on Ni (111), vibr. spectra from electron energy loss *(French)* 78−34696
ethylene, autoionisation and photoemitted electron ang. distrib., cylindrical mirror analyser study 80−18049
ethylene, chemisorption on Pt (111), ethylidyne group form., LEED and ELS obs. 78−73075
ethylene, CW CO_2-laser irrad., low-press., chem. relax. 79−74404
ethylene, electron energy loss spectra, C K-shell excitation, vibr. struct. 79−22851
ethylene, IR absorpt. spectra of ν_1, ν_{10} and ν_4 interacting band 80−83369
ethylene, laser spectroscopy with CO_2 and N_2O lasers 79−59455
ethylene, laser-induced IR photolysis mechanism 78−56909
ethylene, near IR absorption at high press. and temps. 77−14435
ethylene, pure, IR absorption obs. of C-H stretching fundamentals up to 2 kbar and 200°C 79−22701
ethylene, S_0,S_1-states, twisting vibrs., pot. curve calcs., absorpt. spectra 77−83576
ethylene(−d_4), Rydberg states assignments, electron energy loss specta 80−53153
molecular vibration continued
ethylene(-d_1,d_2), high-resolution UPS, mol. ion vibr. assignments, symmetry 79−27032
ethylene cation, state geometries, electronic vibr. coupling consts., HF calcs., comparison with Xalpha calcs. 80−27946
ethylene glycol, IR spectra, ab initio calcs., vibr. anal., conformations of isotopic modifications 78−5210
ethylene-Br_2(Cl_2) π-σ complexes, low freq. spectra 78−78713
ethylene-d_0, -d_4, electron impact, vibr. excitation cross-sections, 1 MeV 79−22850
ethylene-d_1, ν_9 B-type band analysis, ground state rot. parameters 77−42316
ethylene-d_1, IR absorpt., ν_{12} and $\nu_2+\nu_9$ bands, rot. consts., Fermi and Coriolis coupling consts. 77−27070
ethylene-d_4, Raman spectrum, fundamental bands 79−59473
ethylmethylether(-d_3), low freq. vibr. spectra, methyl torsional pot. functions, internal rot. 79−26978
ethylmethylsilane-d_0(−d_n), vibr. spectra, normal vibrs. and rot. isomerism 79−31524
ethyloxirane, solid, liquid, vapour phase, IR and Raman vibr. spectra 80−84740
ethynylbenzene, radiative and nonradiative processes, triple bond effects 79−3481
excitation of vibrations, by varying laser pulse intensity 78−86844
excited mols., laser induced photochem., review 80−71925
excited state props., by electrochromism in polymer matrix 79−22737
fast electron inelastic scattering factor, vibr. transitions 77−88584
fatty acids, LF Raman spectra, accordion vibrs. *(French)* 77−27074
flame temperature meas. by Raman scattering 77−16822
flavin adenine dinucleotide, resonance CARS line shapes, excited state parameters 79−3448
flow, in nozzle, vibr. nonequilib., computational methods comparison 79−60073
fluid, molecular, multiphoton Raman scatt. spectra 77−63404
1-fluoro 2·4-dinitrobenzene, laser Raman and infrared spectra 79−22711
2-fluoro ethanol, Ar matrix, induced conformational isomerisation by IR irrad. 80−101010
3-fluoro-4-chloroaniline, Raman and IR spectra, vibr. anal. 79−81198
3-fluoro-4-methyl aniline, near UV electronic absorpt. spectra, line shift, vibr. anal. 77−10682
2-fluoro-5-bromotoluene, IR and Raman spectra 78−70830
2-fluoro-5-chloro-toluene, IR vibr. spectra 79−68232
2-fluoro-5-methyl aniline, near UV electronic absorpt. spectra, line shift, vibr. anal. 77−10682
3-fluoro-6-chloro-toluene, IR vibr. spectra 79−68232
fluoroacetylene, and -d_1, vibr. Zeeman effect, g-factors 78−46391
fluoroacetylene, fund. and hot bands, laser microwave two-photon and double reson. spectroscopy 80−32752
fluoroacetylene, IR absorpt. spectra, ν_4 C-H bending fundamental near 17 μm 77−75151
fluoroacetylene-d_0,-d_1, microwave spectrum, laser enhancement effects 79−41161
fluoroacetylene-d_1, ν_4 band, IR spectrum, vibr. consts. 77−75149
fluoroacetylene-d, Stark and microwave double reson. laser spectra 80−63690
m-fluoroaniline, vap. (liq)., Raman and IR spectra, vibr. assignments 78−58699
fluoroanilines, isomers, thermodynamic functions and fundamental vibr. freqs. 80−9581
fluorobenzene, IR vibr. spectra 79−13713
fluorobenzene radical cations, in gas phase, laser-induced fluoresc. 79−27022
fluorobenzene radical cations in solid Ne, laser-induced fluoresc. spectra, vibr. struct. of excited and ground states 80−95671
fluoroethanes, IR multiphoton dissoc., HF vib. energy distribs. 80−53073
2-fluoroethanol-d_0,-d_1, IR spectra in Ar, N_2 and Ar-N_2 matrices, normal coordinate anal. 78−25538
fluoroethylenes, IR multiphoton dissoc., HF vib. energy distribs. 80−53073
fluoroethylenes, variable angle photoelectron spectra, ionisation pot. asymmetry parameter 80−28064
fluoroform, absolute IR intensities of fundamental vibrs. 77−79655
fluoroiodomethane, vibr. excited, dissociation, trajectory calcs. using pot. energy surface parameters 80−76508
fluoromethane, chem. shielding. mol. rot. and anharmonic vibr. 78−94258
fluoromethane, excited state rot. spectroscopy and kinetics, appl. of tunable sub-MM sources 80−14162
fluoromethane, laser pumped, overtone fluoresc., intermode energy flow 78−37673
fluoromethane, liq., transient stimulated vibr. Raman scatt. 78−71144
fluoromethane+D(H)(O), reactions, selective vibr. excitation effects 78−35643
fluoromethane+fluoromethane, collision induced mode selective energy transfer, fluoresc. obs. 80−69177
fluoromethane-d_3, laser Stark spectra, ν_6 band, vibr.-rot. consts., dipole moment 78−5277
fluoromethanes, dipole moment derivatives and infrared intensities, transferable polar tensors 78−17668
fluoromethyl methyl mercury-d_0, -d_3, vibr. spectra, normal coord. anal. 79−50017
fluorophenol cations, emission and photoelectron spectra in gaseous phase 80−58316
2-fluoropyridine, IR and Raman spectra, vibr. assignments 78−25534
fluorostyrene, UV Raman spectra, reson. effect in photoreactive states 80−106326
force field representations, vibr. stress, isotope effects and struct. of ethane 78−21897
formaldehyde, 3.5 μ region spectrum, ground state consts. 79−13712
formaldehyde, 4_0^1 band anal., isotope effects 78−86878
formaldehyde, Doppler-limited spectra of C-H stretching fundamentals 78−70831
formaldehyde, emission spectrum, forbidden n-π^* transition, electronic-vibr. struct., CNDO/2 calcs. 77−58035
formaldehyde, excited state vibr. freq. calcs. by method based on scaled ab initio force fields 80−87092
formaldehyde, in Ar, 0.17-1.4 gm cm^{-3}, VUV absorpt. spectra, Rydberg excitations 77−79627
formaldehyde, IR spectra, Coriolis-coupled ν_4, ν_6 and ν_3 fundamental bands 78−5227

molecular vibration continued
formaldehyde, laser-excited reson. fluoresc., rot. struct., rot. and vibr. consts. 79−54993
formaldehyde, mag. rot. spectrum, A^1A_2 state, singlet-triplet perturbations 79−98126
formaldehyde, vibr. excited states, RF spectrum *(French)* 77−30863
formaldehyde(-d_1, d_2), and isotopic forms, microwave spectrum, ν_4-ν_6 vibr. states Coriolis reson. 78−82719
formaldehyde (−d_1,d_2), isotopic forms. vac. UV Rydberg spectra, vibr. assignments origin isotope effect 77−61763
formaldehyde and -d_1, MODR and collision-induced transitions in laser cavity 78−74686
formaldehyde and its isotopic species, rot. spectra of ground vibr. state, rot. const. determ. 80−83350
formaldehyde anion radical, hyperfine coupling consts., vibr. depend., ab initio calcs. 80−87150
formaldehyde substituted with ^{17}O and ^{18}O, microwave spectra of ground vibr. states, rot. and distortion const. determ. 80−83349
formaldehyde-d_0, -d_2, $^1(n\pi^*)$ transition, vibr. struct., ab initio CI calc. 79−766
formaldehyde-d_0(−d_2), S_1 single rot. level lifetimes, isotope, elec. field and vibr. state depend. 80−78655
formaldehyde-d_1, ν_5 and ν_6 vibr. excited states, microwave spectrum obs. 79−72304
formaldehyde-d_1, absorpt. spectra, 9-11 μm, ν_5 and ν_6 fundamental bands 78−70827
formaldehyde-d_2, laser Stark spectra, Coriolis coupled ν_4 and ν_6 fundamentals 77−27065
formaldehyde-d_2, reson. multiphoton dissoc. 80−53077
formamide, force consts. and dipole moment derivatives, ab initio MO calcs. 80−95521
formamide, IR spectra, amino group inversion transitions and pot. functions 80−43041
formamide, near-IR spectra, anharmonic pot. 77−14430
formamide(-d_2), vibr. spectra NH_2 stretching modes assignment 79−89675
formic acid, ^{16}C, ^{18}O, microwave spectra and centrifugal distortion consts. 80−83352
formic acid, monomer, cyclic dimer, charge transfer through H bonds, Hartree-Fock calcs. 77−58157
formic acid and isotopic species, microwave spectra, Coriolis reson. between vibr. excited states 79−13700
formic acid anhydrides, valence force consts., IR spectra, isotope effects 79−93997
formic acid dimer, vibr. spectra, CNDO/2 interpretation *(French)* 80−58155
trans-formic acid geometry, force fields and fundamental vibr. freq., ab initio study 80−87040
formic acid ions, fragmentation, energy selected, photoelectron-photoion spectra 80−95676
formic acid monomer, vib. spectra and normal coordinate analysis 77−58003
formic acid-d_0(-d_1)(-d_1)(-d_2), vibr. spectra, CNDO/2 interpretation *(French)* 80−58155
formyl chloride, photoelectron spectrum, vibr. struct., ionis. pots., assignments 78−9195
formyl fluoride (-d_1), IR absorption intensity anal. 78−70813
Fourier transform IR spectroscopy, use in polymer research as vibr. spectroscopy tool 80−55744
free radicals, photolysis, excimer laser UV obs. 80−16711
frequency shift in IR spectra, press. and solvent effects 78−74709
frequency shifts in polyatomic solutes 78−58654
frequency tables, up to 13 atom mols., and Raman, and IR values 77−79614
furan, resonantly enhanced multiphoton ionisation 80−106362
furane, cryst., low freq. vibr. spectrum, temp. depend., 12 to 253K 80−84743
gas in electric discharge, vibr. excited, sound propag. 78−18370
gas laser, at. and mol. vibr. and electronic metastable states, book contrib. 77−50653
gas laser, reson. vibr. excitation by electron impact, low energy, book contrib. 77−50662
gas-solid surface sticking probabilities, internal mode depend. 78−6213
gases, Raman line broadening, rotational structure, vibrational relaxation 79−98105
germylacetylene-d_0(-d_3), centrifugal distortion const. and thermodynamic functions calc. 80−95581
glow discharge in diatomic molecular gas, electronic excitation rate, vibr. temp. influence 80−19633
glycylglycines, isotope substituted, IR and Raman vibr. spectra 78−42051
glyoxal, 4550Å bond system, rot. anal. mol. consts. and geometry 77−42330
glyoxal, gas phase emission spectra, mag. quenching 77−18968
glyoxal, vibr. energy redistrib. following internal conversion 80−23452
group frequencies study of vibr. coupling 79−98057
guanine, ^{15}N and D substituted, in acid and base solutions, vibr. anal. 79−26994
haeme protein, reson. Raman line intensity formulae applicability 77−83609
haemoglobin, nanosec. probe of dynamics using time resolved reson. Raman scatt. 80−94162
haloacetylene cations, electron impact excitation A→X band system assignment 80−32766
haloanilines, far IR spectra, vibr. assignments 78−82726
halobenzenes, in potassium laurate mesophase, NMR, proton distance ratios and order tensor elements calcs. 80−63672
2-haloethyl ethers, relative conformational energies, Raman obs. 79−27002
halogen molecule negative ion, Cl_2^-, Br_2^-, I_2^-, $ClBr^-$, ClI^-, pot. curve calc. 77−10596
halogenated propanes, IR and Raman spectra, LF vibrs. 79−10105
halogenoacetylene radical cations, C_2HX^+, emission spectra, $A^2\Pi \rightarrow X^2\Pi$ band systems 78−17678
halomethanes, multiphoton dissoc., energy deposition 78−82800
halomethanes, Raman spectra, totally symmetric vibr. bands depolaris. ratios 79−89677
halomethanes, synchrotron radiation photoabsorption cross sections, Rydberg states 80−28033
halomethanes, valence photoelectron spectra, vibr. and vibronic struct. 78−50581

molecular vibration continued
halomethylstannanes, internal torsion modes, inelastic neutron scatt. 77−19105
heat capacity and entropy, mol. without internal rot., MINDO/3 calc. 78−33450
heavy atom substitution, vibr. freqs. and anharmonicity consts., general isotopic rules 77−75122
Henon-Heiles Hamiltonian system, vibr. energy levels in quasiperiodic and stochastic regimes, props. 80−91529
α,β-heptacyclene, double mols. with weak reson. bonds, quasilinear spectra 79−94030
heptafulvene, microwave spectrum and dipole moment 77−14421
heterocyclic compounds, bond lengths, fifth overtone of C-H stretching vibrs. obs. 80−91528
hexa(trifluoromethyl) germanium, gas and liq., IR and Raman spectra, normal coord. anal. *(German)* 79−72315
hexabromobenzene, cryst., IR and Raman spectra, vibr. normal coordinate anal. 77−79602
hexafluoroacetone, IR multiphoton dissociation, isotopic selectivity and yield, temp. effect 80−53069
hexafluorobutene, vibrational broadening, dense fluid region, Raman and NMR study 80−43056
hexafluorocyclopropane, centrifugal distortion const. and thermodynamic functions calc. 80−95582
hexafluorohalopropanes, gas and solid, IR and Raman spectra, normal coord. anal. *(German)* 79−72317
hexafluoropropane, isolated CH stretching freqs. and bond props. 79−94104
hexafluoropropane(-d_2), IR and Raman spectra, gas and liq., normal coord. anal. 79−68235
hexafluoropropene, struct. and vibr. spectra, IR, Raman polarisation study 80−18845
hexahydrohexahelicene, in Shpolskii matrix, absorpt., fluoresc., phosphoresc. spectra 79−76463
hexaidobenzene, cryst., IR and Raman spectra, vibr. normal coordinate anal. 77−79602
hexamethylbenzene in tetrachloromethane soln., local mode overtone bands 80−83444
P-hexamethylcyclotriborophosphanes, substituted, struct., vibr. spectra 77−65460
trans-1,3,5-hexatriene, electronic spectra vibr. struct. calc. 79−63981
1,3,5-hexatriene radical cation, in Ne matrix, laser induced fluoresc. and emission spectra 80−87163
high temperature electron diffraction, review 80−52237
high-overtone spectra, reson. struct. and background absorption 79−54833
holomethylgermanes, internal torsion modes, inelastic neutron scatt. 77−19105
homonuclear diatomic mols., Morse pot. and vibr. level field induced, shift and broadening 80−69117
homonuclear molecules, vibrs. excitation by IR radiation 80−28068
homopolar dipoles, changes during vibration, estimation 79−45861
hydrocarbons on Pt and Ni, C-H stretch vibration, broadened and softened, dehydrogenation 78−47666
hydrogen chloride/dimethyl ether complex, temp. depend. of IR spectra of H bond in gaseous state 77−34624
hydrogen halide+unsaturated hydrocarbon, vibr. stimulated addition reaction 79−91928
hydrogen-bonded ion-pair complex, anomalous isotropic freq. ratio of stretching $\nu_{N(+)H}$ vibrs. 77−3366
hyper-Raman effect, vibr. mode classification and spectral line assignment, QED method 78−58703
indane, 271 nm spectrum, rot. band contour anal., puckering vibr. 78−1001
1-indanone, T_1-S_0 intersystem crossing, nonradiative decay rate, excitation energy depend. 80−63609
inelastic electron tunnelling, vibr. spectra, review 77−54632
inelastic electron tunnelling spectroscopy, effect of cooperative behaviour 78−90258
inelastic electron tunnelling spectroscopy, model for electron-molecule interaction 78−90257
inorganic and coordinated cpds., IR and Raman spectra, book 79−807
inorganic species, vibr. and electronic props., reson. Raman spectra appl. 80−52996
intermolecular spectroscopy and dynamical properties of dense systems, conf., Varenna, Italy (1978) 80−82581
intermolecular triplet excitation transfer in diffusive limit 80−28046
internuclear element-H distance, rel. to vibr. amplitude 77−88444
interstellar H_2, vibrationally excited, search for 8150 Å emission line 78−93346
intramolecular energy transfer, stochastic, crit. point anal. of Hamiltonian system instabilities 79−98005
intramolecular vibrs. effect on electronic spectral shape 79−64052
intrastate scrambling in large mol. bound level struct., appl. to tetracene 80−63696
1-iodo-2-methylpropane, IR spectra, vibrational anal., stretching bands 78−90168
1-iodo-3-methylbutane, IR spectra, vibrational anal., stretching bands 78−90168
iodomethane-d_3, ν_2 band, laser Stark and laser-microwave double resonance spectra 77−27067
iodomethane-d_3, ν_2 band, laser Stark saturation spectra 78−42125
iodomethyl radical, vibr. excited, photofragmentation IR emission obs. 80−87162
2- and 3-iodopyridine, IR and Raman spectra, vibr. assignments 78−25534
iodotrifluoromethane, high vibr. state excitation in high-power laser field, spectral characts. 80−91562
iodotrifluoromethane, isotope selective photodissoc. by multiphoton vibr. and electronic excitation *(Russian)* 79−59517
ion, spontaneous IR rot.-vibr. emission probability, vibr. selective excitation 78−50535
ion+molecule, charge transfer, energy disposal and reaction mechanisms 80−28103
ion-molecule reactions, vibr. energy effects on kinetics, phase space model 78−11508
ion-molecule reactions vibrational product states determination, infrared chemiluminescence 78−88625
IR absorption spectra, true parameters of isolated bands calc. *(Russian)* 77−83586

molecular vibration continued
IR and Raman vibrational intensity changes due to long-range interactions 80-53084
IR integrated intensities, rel. to mol. consts., isotopic sum rule 77-27118
IR intensities of fundamental bands, polar tensor calcs. 79-13708
IR radiation induced vibr. excitation and dissoc. 77-27135
IR radiation transfer in nonequilib. mol. gas *(Russian)* 78-50599
IR-laser-induced unimolecular reactions by vibr. modes excitation 78-58757
iron poprhin, A_{2u} out of plane vibration, pseudo-Jahn-Teller effect 78-82712
isomer identification by vib. spectra analysis, for similar structs. *(Russian)* 77-83577
isopropyl fluoroformate, microwave spectrum and conformation 79-10098
isopropylcyclopropane, solid, liquid, vapour phase, IR and Raman vibr. spectra 80-84740
isoquinoline, quasilinear absorpt. spectrum, in Shpolskii system 77-46571
isoquinoline, radiationless transitions, internal conversion, energy depend. 78-94272
isoquinoline semiperchlorate, H-bonding, strong, stochastic model and IR spectra temp. effects 78-62805
isotope separation, by selective laser-induced mol. vibr. excitation effect on reaction kinetics 78-33627
isotopic molecules, new sum rule connecting vibr. freq. parameters 79-36615
isotopic sum rules for frequencies, band intensities and Coriolis coupling constants 80-83343
isotopically tagged molecules, normal vibr. freq. calc., eigenvalue behaviour, perturbation theory obs. 80-52973
K-vitamins, IR absorpt. spectra, vibr. anal., quinonoid struct. 78-61139
ketene($-d_2$), radical cations, doublet electronic states, photoelectron spectra 77-88496
ketones, saturated, MCD spectra, forbidden transitions generated by struct.-vibr. perturbations 77-50460
Landau-Zener effects in optical spectra *(Russian)* 78-55162
large molecule, novel ultrafast two-pulse excitation spectroscopy 78-94331
laser frequency tripling based on mol. gas vibr. nonlinearity *(Russian)* 79-72618
laser Stark spectroscopy, technique for molecular vibration-rotation spectra *(Japanese)* 77-494
laser-chemical reaction kinetic mechanism *(Russian)* 80-101007
laser-excited molecules, reactive behaviour 77-60097
level classification by Longuet-Higgins group 80-43030
linear triatomics, photofragmentation, vibr. and rot. distrib., quantum anal. 77-14504
liquid, dephasing of coherently excited mol. vibrs. *(Dutch)* 78-72505
liquid, hot bands, vibr. correlations, dephasing 79-85966
liquid, Raman band profile, vibr. dephasing and intermolecular interactions 80-60556
liquid, vibr. dynamics using picosecond Raman techniques 80-52325
liquid phase band contours, data processing, band shape corrections 78-27215
liquid polyatomic molecule vibrational mode obs. with picosecond laser pulses 77-58007
liquid structure and dynamics from light scatt. spectra 80-55105
liquids, Raman line broadening, rotational structure, vibrational relaxation 79-98105
liquids, two-pulse spectroscopy with ps laser pulses 80-53041
local mode mols., normal mode spectra 80-95687
$M^{I}M^{IV}IO_6$, vibr. spectra (M^{I}=Na,K,Rb,Cs,NH_4; M^{IV}=Ge,Sn,Pb) 77-42325
M-C-O deformation modes, no. and symmetry determ., group theoretical method, for teaching 78-11
macromolecular interactions, effects of intervening medium and polar mode energy feeding 79-13857
macromolecules, torsional oscills., HF, investig., polarised luminesc. method *(Russian)* 77-31039
magnetic resonance spectra, averaging for quantum finite motion with large amplitude 77-58046
many-photon resonances, coherent excitation dynamics of mol. vibrs. 79-27050
MBBA, liq. cryst., IR and far IR spectra, vibr. assignments 77-16298
MBBA, NMR and Raman scatt. studies in nematic phase 80-100619
MCD forbidden transitions, generated by struct.-vibr. perturbations 77-50459
mesogenic materials, tails or smear effects in X-ray diffr. photographs 80-96438
metal complex, radiationless transitions, internal ligand modes 79-22750
metal ions, in complexes and biological systems, preliminary vibr. assignment method 78-62953
metal phthalocyanines, IR spectra, vibr. transitions during intermol. interactions 79-54857
metal-ligand bonds, frequencies, predominantly stretching vibrations 79-41154
metallooctaethylporphyrin, ^{15}N-enriched, reson. Raman spectra, haemoprotein oxidation state marker bands 77-58008
metalloporphins, deuterated, resonance Raman spectra, vibr. and vibronic levels 78-62812
methane, $2\nu_4$ band, IR spectral assignments *(French)* 77-42319
methane, $2\nu_4$ band anal. *(French)* 79-41168
methane, 4350-10600 Å bands, intensity profile, vibr. assignments, rel. to major planets spectra 78-42084
methane, $\nu_1(a_1)$ vibrational state rotational structure, CARS obs. 79-98109
methane, ν_1 fundamental, CW stimulated Raman gain spectroscopy 79-6943
methane, ν_3=1 state, dipole moment and IR-radiofrequency double reson. spectra 80-14161
methane, ν_3 band, IR spectrosc. meas. and anal. 79-98098
methane, ν_4 band, high resolution spectrosc. 80-5529
methane, ν_4 band Q-branch spectrum 80-5530
methane, ν_4 fundamental, Q and R branch absolute line intensities 80-5539
methane, and d_1-d_4, absolute Raman intensities of fundamental, overtone and combination bands 77-65468
methane, chemisorption on Rh, vibr. excitation and surface reactivity 79-73393
methane, coherent spectroscopy of anharmonic vibrations 79-18187

molecular vibration continued
methane, CW vibr. photchem. for D enrichment, economic aspects 80-11920
methane, dissoc. chemisorption on Rh (111) surface, vibr. activation 79-57292
methane, electron energy loss spectra, C K-shell excitation, vibr. struct. 79-22851
methane, high resolution coherent anti-Stokes Raman scatt. *(Russian)* 77-75168
methane, high resolution photoelectron spectra, vibr. progression 78-74700
methane, intensity pertubations due to ν_3/ν_4 coriolis interaction 79-98087
methane, IR anal. of ν_2 and ν_4 bands *(French)* 80-87113
methane, J-multiplet intensity meas., ν_4 fundamental at 300K 77-68080
methane, liq., pure vibr. Raman spectra 80-97262
methane, liq. and solns., Raman spectra, vibr. anal. 79-27001
methane, low-energy electron scatt., total 0.16 eV cross sections, vibr. excitation 79-86076
methane, photoacoustic Raman spectroscopy using CW laser sources 79-44947
methane, Raman intensity from electro-optical parameters 79-36645
methane, Raman spectra, 2850-3100 cm^{-1}, ν_3 band anal. 77-75162
methane, rotational anal. of ($\nu_3+\nu_4$) combination bands *(French)* 78-21900
methane, solid, phase II and in Kr, Ar matrices, IR spectra, quantum rot. 77-28562
methane, V-V energy transfer 80-83469
methane, vibr. induced rot. spectrum in (u_4=1) state 79-18184
methane+SF_6, vibr.-vibr. relax 80-99537
methane($-H_2$), long path photoelec. absorpt. spectra 4200-10600 Å, appl. to Uranus 77-83592
methane-d_0($-d_4$), unimol. decomp., energy transfer processes, Monte Carlo simulation 80-99555
methane-d_3, activation, dissoc., internal energy distrib., trajectory calcs. 77-4899
methane-d_3, vibr. energy flow, fluoresc. 78-82770
methane-d_3-polyatomic gas mixture, vibr. energy flow, fluoresc. 78-82770
methane-d_4, selectively excited, cooling, vibr.-vibr., vibr.-translational relax. 80-33723
methane-d_4, vibr.-translational relax. 80-99537
methane-d_4+Ar, vibr.-translational relax. 80-99537
methane-d_4+methane, vibr. relaxation 80-99537
methane-d_4 4.5 μm absorpt., $2\nu_6$ overtone band anal. 80-91557
methanes, $^{12}CH_4$ and $^{13}CH_4$, IR spectra obs., anal of $\nu_2+\nu_3$ band 80-95614
methanol, and $-d_{1,3,4}$, thermodynamic props. struct. and spectroscopic data 77-39396
methanol, aqueous, damped coupled oscillator model used to study Fermi resonance 80-69152
methanol, free O-H overtone absorpt. in vis. region, thermal lensing spectra 77-34644
methanol, H-bonded struct., IR spectra, assignments 78-62800
methanol, IR spectra in soln., OH group fundamental and first overtone bands *(French)* 77-27071
methanol, optical-optical double reson., CO stretching band origin, assignments 79-31864
methanol, valence photoelectron spectra, vibr. and vibronic struct. 78-50581
methanol solns., IR spectroscopic detection of free lone-pair groups or terminal methanol mols., PMR 79-19869
methanol-^{13}C, torsion-rotation transitions, C-O stretch fundamental, FIR spectra obs. 79-93998
methanol-acetonitrile, solns., H bonding, IR and Raman band profiles 77-42320
methanol-d_1, H-bonded in soln., ν_s(OD) band 79-18183
methanol-d_1, laboratory freqs. of J=2-1, a-type transitions 80-63624
methanol-proton acceptor binary systems, hydrogen bonded, anharmonicity of OH stretching vibr. 77-6772
methoxide-d_0($-d_3$) anion, electron affinity, vibr. struct., photodetachment electron spectra 78-94282
p-methoxy benzonitrile, IR absorpt. spectra, vibr. assignments 80-95609
methoxy radical fluoresc. spectra induced by laser, UV region 79-59498
methoxydifluorophosphine-d_0 and -d_3, IR and Raman spectra, mol. vibr. and struct. obs. 80-87103
2-methoxyethylomine, microwave spectra, H-bond, torsional motion and mol. vibr. obs., rot. isomerism, mol. moments determ. 80-95603
3-methoxypropionitrile, microwave spectrum, rot. conformer, rot. consts., vibr. state 77-14419
methoxytrifluorosilane and -d_3, IR and Raman spectra, vibr. anal., barrier to internal rot. 79-18185
methoxytrimethylsilane-d_0,($-d_3$) 78-86853
methyl alcohol-d_3, Fermi resonance due to large amplitude vibrs. 80-83519
methyl anilines, IR spectra, 250-4000 cm^{-1}, vibr. anal. 78-62797
methyl anion, pyramidal inversion pot. and inversion barrier, electron correlation 78-22050
methyl azidoformate, microwave rot. spectrum, satellite transitions 80-69127
methyl bromide, l-reson. perturbations in overtone and combination vibr. systems 80-52962
methyl bromide, rot. absorption spectrum of ν_3 and $2\nu_3$ excited vibr. states, mol. consts. determ. 78-82732
methyl chloride, absorption strength of perturbed ν_4 band 78-70833
methyl chloride, far IR laser lines, vibr. isotopic shift value 78-42055
methyl chloride, microwave spectrum of excited vibr. states, Coriolis coupling, rot. consts. 77-14420
methyl chloride, rot. anal. of IR absorpt. spectra, mol. vibr., rot. const. determ. 80-99505
methyl chloride-d_3, activation, dissoc., internal energy distrib., trajectory calcs. 77-4899
methyl chloroform, vap., multiphoton dissoc. by CO_2 laser beam 80-61123
methyl compounds, vibr. dephasing of C-H stretching vibrs. 79-6927
methyl cpds., MeP, MeS, isolated CH stretching freq., bond strength, bond length 78-90167
methyl cyanide, isotopically substituted species, IR spectra, vibr. freq. displacements, harmonic pot. function 78-42057
1-methyl cyclohexanol, struct. information from OH-stretching freqs., axial/equatorial hydroxyl ratio 79-72438

molecular vibration continued
methyl furan-2-carboxylate, skeletal vibr. of IR spectra, conformational props., solvent polarity effect 80−87118
methyl furan-2-thiolcarboxylate, skeletal vibr. of IR spectra, conformational props., solvent polarity effect 80−87118
methyl group tunnelling and coupling to internal vibrations 78−79675
methyl halides, mol. force field at SCF ab initio levels, quantum-mechanical calc., LCAO-MO method 80−106319
methyl indoles, UV and IR absorpt. spectra, f-values and ground state vibr. freqs. 78−58716
methyl iodide, in Ar, 0.25-1.38 gm cm^{-3}, VUV absorpt. spectra, Rydberg excitations 77−79627
methyl iodide, liq., vib. relax., A_1 Raman bands 77−40220
methyl iodide, vibrational dephasing by translational collision 80−87202
methyl isocyanide, and ^{15}N derivative, microwave spectra in $4\nu_8$ state 77−83582
3-methyl l-butanethiol, Raman and vibr. IR spectra of solid and liq., rot. isomerism 78−62810
methyl mercapto acetate, Raman and vibr. IR spectra of solid and liq., rot. isomerism 78−62810
methyl phosphine-d_2, isolated CH stretching freqs. 78−90167
N-methyl pyrrole, resonantly enhanced multiphoton ionisation 80−106362
methyl radical, hyperfine coupling consts., vibr. depend., ab initio calcs. 80−87150
methyl radical, vibr. excited, photofragmentation IR emission obs. 80−87162
methyl selenocyanate, and isotopic forms, microwave spectrum 79−13705
methyl symmetric stretching vibr. bandwidths, vibr. and reorientational effects, IR and Raman spectra 78−78686
methyl thionine chloride, intramol. vibr. spectra 80−977
N-methyl thiopropionamide-N-d_3, normal coord. calcs. 79−36598
N-methyl thiopropionamides, normal coord. calcs. 79−36598
methyl vinyl ether, and -d_3, IR and Raman spectra, vibr., torsion and internal rot. 78−94250
5-methyl-uracil, IR absorpt. spectra, vibr. anal. 78−61143
N-methylacetamide, vibr. spectra and normal coord. calcs. 79−36632
N-methylacetamide-N-d_3, vibr. spectra and normal coord. calcs. 79−36632
methylacetylene, ν_5 band, microwave and IR laser Stark spectrosc. 80−91558
methylalkanes, CH stretching local mode anharmonicity, intramol. perturbation overtone spectra 79−18171
N-methylanilines, substituent effects on geometry, IR spectra obs. 79−10107
methylbicyclobutyl decomposition intramolecular vibr. relax., competitive channels 80−83336
methylcyanodiacetylene cation, gas phase, UV emission spectra of $\tilde{A}(\pi^{-1})\rightarrow\tilde{X}(\pi^{-1})$ band system 80−95636
methylcyclohexane:styrene-d_0, -d_3, -d_5, d_8, fluorescence meas., 77K 78−25606
(+)-(3R)-methylcyclohexanone, vibr. optical activity, Raman obs. 80−102499
methyldisilylamine, and -d_3, vibr. assignment and barriers to internal rot., IR and Raman spectra 78−13496
methylene fluoride, ν_9 fundamental band, 9.4-μm CO_2 laser Stark spectroscopy 78−9191
methylene fluoride, excited vibr. state, microwave spectrum 78−58672
methylenimine, ν_4 fundamental band, laser Stark spectroscopic obs. 79−64039
3-methylisoquinoline, quasilinear absorpt. spectrum, in Shpolskii system 77−46571
3-methylisoquinoline, semiperchlorate, H-bonding, strong, stochastic model and IR spectra temp. effects 78−62805
methylmercuric halides, partially oriented, ^1H and ^{13}C NMR obs. 80−23437
3-methylpentane, C-H stretching diagonal local mode anharmonicity, intermol. perturbation 78−25524
methylphosphinosilane, IR and Raman spectra, vibr. assignment and asymmetric potential function 79−85962
methylpropylsilane, vibr. spectra, normal vibrs. and rot. isomerism 79−31524
methylpyridine adsorbed on Ag, surface enhanced Raman spectra 80−83376
N-methylthioacetamide(-d_1), reson. Raman spectra obs. and mechanism 78−17672
methyoxy radical, electronic absorpt. spectra, visible, vibr. freqs., vibronic intensities and oscill. strengths 80−28025
minimum energy reaction paths, reactive domains of energy hypersurfaces and stability 80−71893
mobile liquids, coupled vibr. and reorientational dephasing 79−22686
model of AB_2 mol., for teachers 78−32633
mol. target internal motion 80−78697
molecular gas, vibr. instability on optical excitation *(Russian)* 80−100065
molecular internal stresses, stress tensor, one electron system 78−62686
molecular ions, interaction with thin solid targets 78−59844
molecular structure identification 79−10092
molecule, intensities dipolaris. ratios, polarisability, matrix rotation, isotopic rules 78−5288
monochlorobenzene, prereson. Raman effects, intensity enhancement mechanism 78−42069
monohalobenzenes, circularly polaris. Raman spectra, vibr. symmetries assignment 78−29787
Morse oscillator collinear collision induced dissoc., vibr. enhancement, quasiclassical trajectory study 80−28089
multiphoton absorption modelling, using SF_6 energy-dependent absorption cross sections 80−32789
MX_2 and MX_3 mols., vibr. freq. and geom. struct. 80−1081
N_2, Lewis-Rayleigh afterglow spectrum 79−64938
N-hetrocyclic biomolecules, IR absorpt. spectra, vibr. assignment 77−10671
Nafion cation exchange membranes, IR spectrum assignment 79−89818
naphthalene, cryst., laser reson. Raman effect, near 3200 Å, B_{3g} vibr. enhancement 77−52067
naphthalene, in-plane vibr. force fields, five-parameter approx. calcs. 79−59436
naphthalene, prereson. Raman spectra, vibr. band intensities obs. 80−102515
molecular vibration continued
naphthalene, two-photon and mutiphoton excitation, UV fluoresc. spectra 77−88517
naphthalene-d_0(-d_8), radiationless triplet decay, non-Condon effects 80−83405
naphthalene-h_8 (-d_8), two-photon excitation spectra, vibronic coupling 77−75246
1- and 2-naphthol, ideal gas thermodynamic props., vibr. fundamentals, rot. isomerism 79−24813
naphthols, IR spectra, assignments 78−58681
neopentane liq., local mode overtone bands 80−83444
neopentylcyclobutane, $^1CH_2$-activated, decomposition rate const., press. depend., internal vibr. relax. 78−64819
nicotinamide adenine dinucleotide, and reduced form, pH induced modification, Raman spectra 80−85343
nitriles, intermolecular interaction, band contour exam. *(Russian)* 79−808
p-nitroaniline, Raman spectra, mol. struct. in molten state 79−91435
nitrobenzene, intensities in inelastic electron tunnelling, IR, and Raman spectroscopy *(French)* 79−822
nitrobenzene, substituted, IR spectra, vibr. modes 77−68039
nitrobenzene-d_5, vibr. spectra 79−22695
nitrocyclopropane, vibr. spectra struct. and bonding 80−102520
nonadiabatic multiquantum transitions, reson. excitation of vibr. 77−19001
nonafluoro-iso-butane, isolated CH stretching freqs. and bond props. 79−94104
nonafluorobutane(-d_1), and halo-substituted forms, gas and liq., IR and Raman spectra, normal coord. anal. *(German)* 79−72318
noncyclic molecules, bent bonds, electron density maps 79−49960
nonlinear molecules, bending vibrs., correlated bender theory 78−37627
nonlinear vibrations, selective laser excitation 77−23522
nonstationary state time evolution, vibr. redistrib., nonradiative mechanism 77−83575
nucleic acid bases, excited state geometry distortion, normal modes reson. Raman intensity anal. 79−68236
nucleic acids, Raman spectroscopy obs. *(German)* 79−27119
nucleoside cyclic monophosphates, phosphodiester stretching vibrs., IR and Raman spectra 77−65461
octamethylcyclotetrasilazane, gas, liq., cryst., CCl_4 soln. IR and Raman spectra, assignments, struct. *(French)* 78−29790
1,3,5,7-octatetraene, UV, visible, and fluoresc. spectra and assignments, evidence for ^1A_g state 78−33518
4-octyloxy-4′-cyanobiphenyl, CN stretching in liq. cryst. phases, vibr. spectra 78−80325
optoacoustic laser spectroscopy of excited vibr. molecular states 77−19106
organic compounds, IR fluorescence under CO_2 laser radiation 80−37830
organic compounds, low freq. anharmonic vibr., pot. function determ., Raman and IR spectra obs. 80−52997
organic dye solutions, vibronic struct. in two-photon absorpt. spectra *(Russian)* 79−64004
organic dyes, reson. stimulated Raman spectra, transverse pumping, mol. vibrs. 77−88453
organic gases, IR fluoresc. by CO_2 laser 80−78619
organic molecules, C-H Raman stretching bands in soln., vibr. freqs. and linewidth 80−78622
organic molecules, inelastic electron tunneling spectroscopy meas. in MIM junction 77−14510
organic molecules in solid matrices, local vibr. inhomogeneous broadening 77−58087
organo-arsenic compounds, $(CF_3)_2AsSCH_3$ and $(CF_3)_2AsSeCH_3$, gas phase IR and liq. Raman spectra, normal coord. anal. *(German)* 80−32725
organometallic amines, Raman and IR spectra, band intensity and assignment, force const. determ., vibr. props. *(German)* 80−87133
organometallic compounds, vibr. spectra, book 77−38671
organophosphorus compounds, $(CF_3)_2PSCH_3$ and $(CF_3)_2PSeCH_3$, gas phase IR and liq. Raman spectra, normal coord. anal. *(German)* 80−32725
oriented molecules, NMR spectra, vibr. correction study 80−18840
orthoborates, dolomite type, vibr. spectra, vibr. coupling effects *(French)* 77−65464
ovalene, vibrational quasicontinuum threshold, spectrosc. criterion 80−52972
1,3,4-oxadiazole derivatives, in soln., IR absorpt. and fluoresc. spectra, vibr. anal. 78−66597
oxalate ion, vibr. assignments, force consts., coincidence method appl. 78−62953
oxalate ion in aq. soln., vibr. study and Raman bands 80−95588
oxalic acid, monomeric, IR matrix-isolation spectra, vibr. anal. 78−66550
oxalic acid in aq. soln., vibr. studies, IR and Raman spectra 80−95589
oxalyl bromide, normal vibr. freqs., force fields 79−41155
oxalyl chloride, normal vibr. freqs., force fields 79−41155
oxetane, clathrate hydrate, struct. II, for IR spectra, 4-100K 79−13707
2-oxybicyclo(3.2.0)hept-6-ene, LF vib. spectra, conformations 78−58685
2,2 paracyclophane, dimer vibration influence on emission spectrum 80−69133
parity-violating effects of weak interactions 80−52455
pentacene, vibrational quasicontinuum threshold, spectrosc. criterion 80−52972
pentafluorobenzene, C-H vibr. states, thermal lensing spectra, local mode model test 77−71812
pentafluorophenol, liq. IR absorpt. spectrum, fundamental freqs. and combinations 79−36633
p-n-pentyl-p′-cyanobiphenyl, nematic liq. cryst., Raman depolaris. ratios, order parameters 79−28733
perdeuteropolyethylene, IR and Raman intensities by electro-optical parameters, single chain 78−1115
perfluoro-1,3-butadiene, vibr. spectra, struct. and barrier to planarity 78−9147
perfluorocyclobutanone, IR and Raman spectra, vibr. anal. 77−38661
perfluorotertiarybutanol, IR spectra in soln., OH group fundamental and first overtone bands *(French)* 77−27071
perhalonitrosomethanes, gas phase IR spectra, assignments, isomerism 80−28017
peroxyacetic acid, and isotopic forms, matrix IR spectra, force spectrum, force const., thermodynamic props. calc. 77−14427

molecular vibration continued
perylene, harmonic force fields, bond orders, normal coord. anal., mean amplitudes calcs. 78−25418
phenacyl halides, IR spectra, $\delta(CH_2)$ vibrs. correlation with structs. *(French)* 80−23417
phenazine, prereson. Raman spectra, vibr. band intensities obs. 80−102515
phenol, in cyclohexane ethanol mixtures, UV absorption, solvent effects 79−22767
phenol(-d_1)-dioxan(-acetonitrile), in carbon tetrachloride ($CDCl_3$) solns., H-bonds vibr. relax. bands anal. 78−84560
phenols, chemisorbed on Al-Al_2O_3-Pb oxide layer, electron tunnelling spectra, 2K 77−62736
phenols, halogenated, internal rot. barriers, torsional vibr. freqs. 77−68041
phenyl acetylene, liq., phase relax., vibr. dephasing, Raman spectra obs. 80−91567
phenyl isocyanate, electronic absorpt. spectrum, vibr. struct., f-values, spectroscopic moment and config. 78−58715
phenyl isocyanate, microwave spectrum, rot. consts., dipole moment 77−61739
p-phenylenediamine, reson. Raman spectra 77−58009
phenylsilanetriol-d_0,(-d_3), cryst. and liq. vibr., IR and Raman spectra 78−86855
phosphine, IR spectrum, ν_1 and ν_3 band analysis 80−83366
photoacoustic detection, multiphoton mol. absorpt. in strong i.r. field 77−507
photoelectron spectra, ang. distrib. asymmetry parameter, vibr. state depend. 77−75218
photoionisation, vibrationally-excited ions form. in Franck-Condon gaps, threshold photoelectron spectra obs. 79−68262
phthalazine, prereson. Raman spectra, vibr. band intensities 80−102514
phthalic acid, IR absorpt. spectra, fundamental assignments 80−5542
phthalimide derivatives, hidden vibr. band determ. method, fluorescence and excitation spectra meas. 80−40158
phthalocyanine, free base, fluoresc. excitation spectrum, cooling in supersonic free jet 80−95670
picosecond, mol. dynamics and electron localisation in liquids 79−46548
picosecond spectroscopy, anal. using polarisation method 80−13152
pivalic acid(-d_1, d_9), liq. and soln., Raman assignments, CH_3 rot. barrier, dimerisation 79−26991
pivalic anhydride, liq. and soln., Raman assignments, CH_3 rot. barrier, dimerisation 79−26991
plasma, atomic ion-electron recomb. in presence molecules, appl. to HCl 80−28601
plasma vibrational spectroscopy, data gathering and processing system 79−31737
polar molecules, electron impact vibr. excitation, threshold behaviour 77−58145
polar organic molecules, external doping in MIM tunnel junctions, inelastic tunnelling spectroscopy obs. 79−3510
poly-ynes, struct., vibr. freqs., ionis. energies, MNDO calc. 77−88390
polyatomic chain molecules, vibr. freqs. 79−31731
polyatomic mol. photoelectron ang. asymmetry parameter vibr. state depend., vibronic coupling 79−36698
polyatomic molecule, collisionless multiphoton dissoc., threshold behaviour, nonthermal theory 80−11905
polyatomic molecule, high vibr. level excitation and dissoc. in laser field *(Russian)* 77−27132
polyatomic molecule, luminesc. parameters, intramol. vibr.-energy redistrib. effect 79−54890
polyatomic molecule, multiphoton excitation by two IR lasers 80−91607
polyatomic molecule, selected fragment vibr. energy distrib. in dissoc. processes 78−1036
polyatomic molecule, vibr. excitation in strong IR field, rot. level emptying *(Russian)* 77−75235
polyatomic molecules, atomic pot. energy distrib., Kyong calcs., parameter for mol. vibr. studies 78−58762
polyatomic molecules, bond distribution functions, anharmonicity effects of electron diffr. pattern 80−69234
polyatomic molecules, calc. of spectral absorpt. curves 79−10093
polyatomic molecules, dil. solns., IR spectral band shapes of fundamentals 78−66544
polyatomic molecules, high intensity IR absorpt. 80−14183
polyatomic molecules, highly vibrationally excited, spectra calcs. 78−90140
polyatomic molecules, intramolecular dephasing processes 78−74695
polyatomic molecules, laser-induced energy distribs. 80−5591
polyatomic molecules, multistage IR dissoc., collisionless energy-gathering process 80−99526
polyatomic molecules, multistep or multiphoton laser vibr. spectrosc. 78−90151
polyatomic molecules, nonradiative transitions, theory, anharmonicity effects 77−58072
polyatomic molecules, numerical soln. of nonharmonic pot. problem 77−34607
polyatomic molecules, refinement of model for overtone spectra 78−66534
polyatomic molecules, vibr. absorpt. spectra, diffusivity due to crowding of sequence of levels *(Russian)* 77−38652
polyatomic molecules, vibr. combination states, ultrashort two-pulse spectroscopy 79−828
polyatomic molecules, vibr. energy transfer and relax., picosec. time-resolved spectra 79−50028
polyatomic molecules, vibr. predissoc., rel. to van der Waals triatomic mol. theory 78−55208
polyatomic molecules, vibr. predissoc. rel. to van der Waals mol. theory, anharmonicity effects 78−55209
polyatomic molecules, vibr. spectra, theory *(Russian)* 78−13502
polyatomic molecules, vibr. spectrum, intermolecular interaction effects *(Russian)* 78−37621
polyatomic molecules, vibrations, anharmonic problem, soln. by direct diagonalisation of Hamiltonian 80−52975
polyatomic molecules with pronounced vibr. struct., spectral shape 79−76469
polyatomic mols., excitation and dissoc., intense IR laser radiation 77−83570
polyatomic mols., laser induced isotope enrichment, selective vibr. excitation mechanisms 77−18994
polyatomic mols., vibr. total energy distribs. in terms of symm. coords., forces and momenta 80−69123
molecular vibration continued
polyatomic mols. in liqs., vibr. energy relax. 80−63611
polyatomic overtone spectra, local mode theory 79−36618
polyatomic rarefied gases, vibrational modes, energy exchange *(Russian)* 80−32811
polyatomic symmetric molecules, collisionless dissoc. and vibr. spectrum of degenerate modes 80−18893
polyatomic van der Waals molecules, struct. and dynamics calcs. 79−41097
polycyclic monoazines, temperature dependence, triplet formation, radiationless transitions 79−54900
polydeoxyribonucleotides, poly(dA).poly(dT) and poly(dAT).poly(dAT), HF vibr. modes, Raman and IR spectra 80−32698
polydimethysilcxane, conc. soln. in benzene, polarised Raman scattering 78−9286
polyenes, electronic absorpt. spectra, charact. spectral band criteria 80−63651
polyenes, electronic absorpt. spectra, intensity distrib. anal. 77−58034
polyethylene, IR and Raman intensities by electro-optical parameters, single chain 78−1115
polymer, branched and crosslinked molecules, mol. description of dynamics 80−9767
polymethine dye layer, vibr. spectrum anal., inelastic electron tunnelling spectroscopy 79−13716
polymethylene, extended chain, C-H stretching band struct., Fermi reson., Raman spectrum 80−5552
polystyrene and model cpds., conformational struct. influence on normal modes of benzene ring, Raman study 80−14144
polyvinyl formate, far IR molecular vibrational spectroscopy by inelastic electron tunnelling 78−50546
porphin, ground-state energies, force consts. and vibr. freqs., CNDO/2 calc. 79−18118
porphin, hypersurface of adiabatic pot. calc. by CNDO/2 method, vibr. freqs., absorpt. spectra calc. 80−95543
porphin free base, vibr. and normal mode anal. 80−69122
porphyrin free base, spin-dependent D isotope effect in triplet state decay, N-H vibrs. 77−30909
potassium oxalate monohydrate, force fields and normal coords. of H_2O mols. 79−31500
premixed H_2-O_2-N_2 laminar flames, temp. profiles, Raman, absorpt. and line reversal obs. 80−42227
propanal, methyl torsional pot. functions, LF Raman and IR vibr. spectra 80−95612
propenoyl chloride, IR bands, torsional struct. 80−28018
propiolamide(-d_2, d_3), microwave spectrum, struct., dipole moment 78−78685
propiolyl chloride(-d), 357-333 nm absorpt. system 80−69161
propiolyl fluoride(-d), 290 nm absorpt. system 80−87142
n-propyl alcohol-α-picoline, donor-acceptor complex form., solvent effects, IR spectra 77−38660
propylsilane-d_0(−d_n), vibr. spectra, normal vibrs. and rot. isomerism 79−31523
propynal, ν_2 vibr. state, IR-microwave triple resonance 79−13746
propynal, IR-microwave double reson. and two-photon expts. 80−83396
propynal-d, in ground vibrational state, IR microwave double resonance spectra, rot. and centrifugal distortion const. determ. 80−83358
propynal-d, IR microwave double reson. spectroscopy 80−69172
propyne-d_0(-d_3), absolute and integrated IR intensities of fundamental modes 80−87179
protein-water interactions in aq. solns., Raman spectroscopy 77−6792
pryazine, fluoresc. $^1B_{3u}\rightarrow{}^1A_{1g}$ band, vibr. struct. and intensities 79−64033
pyrazine, multiphoton ionisation spectra, of three-photon ionisation region 78−37689
pyrazine, physisorbed on Ni (111), UV spectroscopic ellipsometry obs. 79−86997
pyrazine, prereson. Raman spectra, vibr. band intensities obs. 80−102515
pyrazine, reson. Raman and absorpt. spectra to $S_2(\pi,\pi^*)$ state, excited state geometry 79−76433
pyrazine, reson. to the $S_2(\pi,\pi^*)$ state, Raman spectra calcs. 80−69147
pyrazine, vibr. struct. and nonlinear vibronic coupling, pseudo Jahn-Teller effect 78−94234
pyrazine (-d_4) vapour, single vibraonic level fluoresc. from n, π^* 80−37827
pyrazole and deuterated species, CH stretching vibrs., anharmonicity, pseudo-symm. 78−78710
pyridazine, prereson. Raman spectra, vibr. band intensities 80−102514
pyridine, deuterium substituted, Raman and IR vibr. spectra 80−84739
pyridine, i.r. spectra and electronic struct. 77−3363
pyridine, multiphoton ionisation spectra, of three-photon ionisation region 78−37689
pyridine, vibr. reson. lasing threshold, complex form. and solvent effects *(Russian)* 77−75507
pyridine(-d), force consts. and vibr. spectra by CNDO/2 force method 80−95540
4-pyridine carboxaldehyde-doped Al-Al_2O_3-Ag tunnel junction, surface enhanced Raman spectra, surface plasmons 79−98111
pyridine iodine complexes, charge transfer complexes, vibr. spectra, laser Raman obs. 80−52990
pyridine-2,3,5,6-d_4, vibr. spectra, IR and Raman, assignment 80−102519
pyridine-3,4,5-d_3, vibr. spectra, IR and Raman, H exchange rates meas. 80−102518
pyridine-3,5-d_2, vibr. spectra, IR and Raman, H exchange rates meas. 80−102518
pyridine-bromine charge transfer complexes, Raman spectra 77−6788
pyridine-d_5, vibr. spectra, IR and Raman, assignment 80−102519
pyridine-I_2(Br_2) charge transfer complexes, vibr. spectra, vibronic contrib., intensity enhancement 80−53048
s-trans-3-pyridinecarbaldehyde, microwave spectrum, assignments 78−21912
2-pyridyl phenyl sulphide, dipole moments, absorpt. spectra, meas. and calcs. 77−46574
2-pyridyl phenyl sulphone, dipole moments, absorpt. spectra, meas. and calcs. 77−46574
pyrimidine, 77K, vibr. struct. absorption and phosphorescence spectra 78−61138
pyrimidine, bi-exponential decay, methylation and vibr. excitation, proximity effects 80−78641
pyrimidine, vapour, phosphoresc. 80−83408
pyrrole, resonantly enhanced multiphoton ionisation 80−106362

molecular vibration continued
quasi-linear molecules, low frequency anharmonic vibrations, pot. function determ., Raman and IR spectra obs. 80−52997
quasicontinuum threshold, spectrosc. criterion for large mols. 80−52972
quasilinear spectra of double molecules with weak reson. bonds 79−94030
quinazoline, in n-pentane (isooctane) Shpolskii matrices, luminesc. props., vibr. struct. 79−22739
quinazoline, prereson. Raman spectra, vibr. band intensities obs. 80−102515
quinoline, radiationless transitions, internal conversion, energy depend. 78−94272
quinoxaline, prereson. Raman spectra, vibr. band intensities 80−102514
radiationless relaxation processes, nonrandom sequential coupling influence 78−90205
radiationless transitions, proximity effect, vibrational tuning, vibronic interaction probe, QSM approach 78−94274
Raman band shapes in liq., rot.-vibr. coupling effect for reorientation 78−72491
Raman scattering, pre-reson., by t-type mode near A→T electronic transition 80−58261
Raman selection rules, spin degeneracy and vibronic states 78−987
Raman spectra, reflection symmetry violation for crysts. and mols. 78−48184
Raman spectra of gases, high-resolution, mol. struct. and orops. 80−53000
Raman spectra of liq. phase weak H-bonds, short range order and anharmonicity effects 78−64357
Raman spectroscopy, of IR multiple-photon excited mols. 80−74207
Raman spectroscopy of chiral molecules in mag. fields 80−102532
Raman spectrum, dispersion of depolaris. and conversion factors 79−72323
rare earth oxyphosphates, IR and Raman spectra, vibr. assignments, cryst. struct. charcts. 80−97258
resonance π-bond movement, conjugated linear cryst., vibr. barrier 77−14377
resonance Raman lineshape studies of vibrational and rotational relaxation in soln. 80−60560
resonance Raman scattering, of totally symmetric vibr., depolarisation dispersion, vibronic coupling 77−65472
resonances in vibrational struct. electron-molecule scatt. 78−17813
resonant Raman scatt. vibr. interference 77−42328
retinal chromophore, reson. Raman spectra obs. of struct. 80−94168
rhodamine, CARS spectroscopy, vibr. spectra of electronic states 80−27964
rhodamine dye solutions, vibr. relax. in S_1-state 77−6826
rhodamine dyes in soln., bleaching, electronic and vibr. absorpt. spectra, fluoresc. 80−42960
rigid symmetric top molecules, dynamic Stark effect spectrum 80−63621
ring compounds, three-membered, vibr. spectra and struct., book control 78−78701
salicylic acid, IR absorpt. spectra, fundamental assignments 80−5542
selective excitation, by time-varying freq. EM field 77−50423
selective excitation using stimulated Raman scatt. Cs vap. source, appl. to HCN (001) 80−9696
selenoacetamide (-d_n), IR spectra, vibr. assignments, normal coord. anal. 79−22708
semicarbazide hydrochloride, vibr. spectra, normal coord. anal. 80−58255
semicarbazide-d_0, -d_6, vibr. spectra, normal coord. anal. 80−58255
L-serines-d_0 and -d_4, IR and Raman spectra, rot. isomers *(French)* 79−45714
shock layer, hypersonic, vibr. nonequilib., near stagnation streamline, low Reynolds no. flow 78−87417
1-silabicyclo 2,2,2 octane, double-min. skeletal torsion, microwave spectroscopy 80−47972
silacyclopentane, Raman spectra, pot. energy surface, barrier to interconversion 78−25541
silane coupling agent deposited on E-glass fibre, hydrolysis and drying effect on siloxane bonds 80−85072
silyl acetylene, microwave spectra in ground and ν_{19} vibr. state 80−78610
simple fluids under influence of quasi-static elec. fields, vibr. Raman bands 79−8139
solution, mol. vibr. spectral linewidth, conc. fluctuations effect 78−70880
spectra separation into individual components 79−93979
spectral vibr. anal. using Cartesian coords. 77−88442
spherical top molecules, IR spectra, diagonal $F^{(4)}$ and $F^{(6)}$ coeffs., computer listing 78−17669
spin-spin coupling consts., mol. vibr. contrib., calc. methods comparison 80−23402
stilbene anion radicals, photoinduced isomerisation, 77K 80−66818
stimulated Raman scattering, appls. *(German)* 79−27320
styrene, and isotopic forms, IR and Raman spectra, normal vibr. assignments 77−18930
styrene, UV Raman spectra, reson. effect in photoreactive states 80−106326
styrene-β-d_2, IR and Raman spectra, vibr. assignments 79−13711
succinic acid and its alkaline salts in aqueous soln., Raman and IR spectra *(French)* 80−32723
sulphones, group electronegativities, empirically estimated from geometrical and vibr. data 79−81300
sulphonyl compounds, H-bonding by methyl groups, Raman spectra obs. 79−24320
TCND, IR and Raman spectra, vibr. anal. 79−36630
TCNE, Raman active fundamental vibrations, revised assignment 77−68049
TCNQ salts, vibr. and electronic spectra 79−45704
tertiarybutylisocyanide-borane, vibr., rot. consts., moment of inertia, microwave spectra obs. 80−32706
tetra(trifluoromethyl) germanium, gas and liq., IR and Raman spectra, normal coord. anal. *(German)* 79−72315
meso-1,2,3,4-tetrabromobutane, IR and Raman spectral studies 80−32722
1,1,2,2-tetrabromocyclopropane, fundamental vibr., IR and Raman spectra 79−41170
tetracene, vibrational quasicontinuum threshold, spectrosc. criterion 80−52972
1,1,4,4-tetrachloro-1,3-butadiene, reson. Raman intensities, mol. struct., excited states, vibr. anal. 77−65470
molecular vibration continued
meso-1,2,3,4-tetrachlorobutane, IR and Raman spectral studies 80−32722
2,2,3,3-tetrachlorobutane, vibr. spectra, liq. and solid-state, conform. struct. 79−73936
tetrachlorocyclopropene, A_1 vibrs., laser Raman obs. 79−76437
tetrachloroethylene, liquid, twisting vibration, direct obs. via hyper-Raman effect 77−28559
tetracyanobenzene+methylated benzene, fluorescent exciplex form., electronic relax. 80−5573
s-tetracyanobenzene+p-xylene, photoassoc., exciplex form., excitation energy and isotope depend., vibr. effects 80−55634
1, 2, 4, 5-tetracyanobenzene and -d_2, IR and Raman spectra, vibr. anal. 79−36629
tetracyanoethylene-benzene(-toluene), and isotopic forms, excited charge-transfer state nonrad. decay, vibrs. role 78−82765
tetracyanomethane, molecular vibration analysis 79−803
1,1,2,2-tetrafluorocyclobutane, microwave spectrum, dipole moment, rot. and vibr. modes assignments 77−18914
1,1,2,2-tetrafluoroethane, anti- and gauche-rotamers, struct., spectra, electron diffr. 77−50439
1,1,1,2-tetrafluoroethane, mol. struct. studied by gas-phase electron diffr., vibr. amplitudes, bond angles and lengths calc. 80−95740
tetrafluoromethane, ^{19}F chem. shielding, depend. on internal coords. 78−5249
tetrafluoromethane, $\nu_2+\nu_4$ band, high resolution diode laser spectra 80−69138
tetrafluoromethane, collision-induced scattering at a vibrational Raman frequency 78−62814
tetrafluoromethane, electron energy loss spectra, C K-shell excitation, vibr. struct. 79−22851
tetrafluoromethane, liq., pure vibr. Raman spectra 80−97262
tetrafluoromethane, pot. consts., IR spectra 78−82808
tetrahedral and octahedral complexes, mol. vibrs. and reaction pathways, min. energy coords. and compliance consts. 77−57966
tetrahedral molecules, energy level clusters for $\nu_2+\nu_3$ type combination bands 79−98009
tetrahydrofuran, clathrate hydrate, struct. II, for IR spectra, 4-100K 79−13707
tetramethyl germanium(-d_{12}), vibr. spectra, normal coord. calcs. 79−22717
tetramethyl lead(-d_{12}), vibr. spectra, normal coord. calcs. 79−22717
tetramethyl silicon(-d_{12}), vibr. spectra, normal coord. calcs. 79−22717
tetramethyl tin(-d_{12}), vibr. spectra, normal coord. calcs. 79−22717
tetramethyl-1,3-cyclobutanedithione-h_{12} and -d_{12}, visible spectra, $n\pi^*$ transitions obs., mol. vibr. 80−97297
2,3,5,6-tetramethyl-p-phenylenediamine, reson. Raman spectra 77−58009
tetramethylammonium chloride solns., aq. and methanolic, Raman spectra 79−28750
tetramethylbutane in hexachlorobutadiene soln., local mode overtone bands 80−83444
tetramethylsilane, IR and visible spectral intensity data and the universal intensity concept 80−28066
tetramethylsilane, local mode combination bands and local mode mixing 80−27999
tetramethylurea-d_0,-d_{12}, IR spectra, normal coord. anal. 78−978
s-tetrazine, laser photodissociation, product vibr. excitation 78−88652
s-tetrazine, pot. surface of low-freq. out-of-plane modes 78−62741
s-tetrazine, visible absorpt. band assignment, vibr. anal. 78−994
tetrazine-Ar, van der Waals bond, nonstatistical vibr. energy distrib., photochemical reaction effects 80−30255
tetrolyl fluoride, fund. vibr. freq., IR and Raman spectra 79−41171
thermal instability of vibr.-excited mol. gas, appl. to surface ignition *(Russian)* 78−56895
thiazolidine, IR spectroscopy of mol. association *(French)* 79−50178
Δ-2 thiazoline and alkyl derivatives, IR and Raman vibr. spectra, conformation *(French)* 79−10104
thieno(3,2-b)thiophene, electronic and vibr. spectra, vapour phase and cryst. 77−34654
thiirene and deuteroderivatives, Fourier transform IR spectra using Ar matrix isolation, vibr. band assignments 80−14142
2-thio alkyl (allyl, benzyl) pyrimidines, IR and Raman spectra anal., mol. vibr. and symmetry *(French)* 80−87123
thioacetamide, IR spectra, amino group inversion transitions and pot. functions 80−43041
thioformaldehyde, $\tilde{a}^3A_2 \leftarrow \tilde{X}^1A_1$ IR absorpt. spectra 80−83362
thioformaldehyde, and -d_2, $\tilde{A}^1A_2$-$\tilde{X}^1A_1$ visible electronic absorpt. spectra, vibr. anal. 79−45733
thioindigo, vibronic fluoresc. spectrum, vibr. struct. 77−54571
thioketen, microwave spectrum, substitution structure and dipole moment 80−975
thiomethoxide anion, electron affinity, vibr. struct., photodetachment electron spectra 78−94282
thiomethoxyl anion, and deuterate, electron photodetachment, affinities, vibr. freq. and spin-orbit splitting 80−53063
thiones, N-H-S weak and medium strong H bonds, IR spectra 80−69132
thiophene, flash photolysis, new transient absorption spectrum, C_4H_3 radical, assignments 78−46354
thiophosgene, laser Raman spectra, vibr. anal., Cl isotope splitting 77−65486
thiourea, ground and first excited triplet state configs., ab initio SCF calcs. 79−89597
thioureas, alkyl and phenyl groups trisubstituted, conformation, steric and stacking interaction 80−95587
third row element mols., general harmonic force field, SCF-MO-MNDO and freq. calc., MOCIC pot. 80−27948
third-row oxyanions, tetrahedral, kinetic and pot. consts. calcs. 77−30951
1,2,3-timethoxybenzene, weak electronic transition, solid, and in rigid glass, UV assignments 78−17681
toluene, electronic-vibr. spectra calcs., Franck-Condon and Herzberg-Teller approx. 80−37735
toluene, two-photon ionisation spectrum, of $^1L_b \leftarrow S_0$ transition 80−14180
transition metal ammine complex, mol. force consts. and vibr. amplitude 79−31727
transition metal cluster carbonyls. fluxionality, collective oscills. and low energy spectra 80−78738
transition metal complex anion, vibr. spectra in solid and soln., struct. and fundamental mode assignment 78−62803

molecular vibration continued
transition metal complex anions, ligand-bridged, binucl., reson. Raman spectra 78−42067
transition metal complexes, isothiocyanates with pyridine, far IR spectra, vibr. bands 78−25535
transition metal complexes, of 4-methylpyridine, IR and Raman spectra, vibr. anal. 78−25536
transition metal complexes, vibronic coupling and spin relax. NMR decay rate study 80−18870
transition metal hexahalide complex, polarised reson. vibr. Raman spectra, electronic degeneracy effects 78−78708
transition metal niobates, columbite struct., normal coord. anal. 78−964
transition metal oxyanions, tetrahedral, kinetic and pot. consts. calcs. 77−30951
transition metal trifluorides, mol. and electronic structs., ab initio restricted Hartree-Fock calcs. 79−63900
transition probabilities for mol. bond modes 79−18172
transition probability evaluation in double asymmetric pot. well 80−69120
tri(trifluoromethyl) germanium halides, gas, liq. and solid, IR and Raman spectra, normal coord. anal. 79−72316
tri-i-propygermylamine, and isotopomers, IR and Raman spectra, normal coord. anal. *(German)* 80−32716
tri-t-butylstannylamine, and isotopomers, IR and Raman spectra, normal coord. anal., Mossbauer spectrum *(German)* 80−32716
trialkyl silanes, IR absorption vibration spectra, true parameters of isolated bands calc. *(Russian)* 77−83586
trialkylthioureas, N-H stretching vibrs. and conformation 80−95586
triallylarsine, vibr. spectra 79−22696
triallylphosphine, vibr. spectra 79−22696
triatomic van der Waals complex, vibr. predissoc. and photodissoc. lifetimes 80−9661
triatomic van der Waals molecules, vibr. predissoc., rel. to polyatomic complexes, theory 78−55208
tribromotrifluoroethane, IR and Raman spectra, normal coord. anal. *(German)* 80−32726
1,3,5-trichloro,2,4,6-trifluorobenzene radical cation, $B^2A_2' \rightarrow X^2E''$ laser-induced fluoresc. spectra 80−14172
trichlorobenzene cation, selectively excited wavelength resolved emission spectra 80−87136
1,2,4-trichlorobenzene liq., mol. reorientation, translation and vibr. relax., Rayleigh and Raman spectra 80−95632
trichlorobenzene radical cation, gas and matrix isolated vibr. resolved electronic spectrum 79−68252
2,2,2-trichloroethanol(-d_2), vibr. spectra and normal coord. anal. 79−72319
trichloromethane, and -d_1, liq., vibr. relax., Raman spectra 78−19471
trichlorosilane liquid, Si-H stretching mode vibr. dephasing, Raman study 80−84736
trichlorotrifluoroethane, IR and Raman spectra, normal coord. anal. *(German)* 80−32726
tricyclo(3.3.0.$0^{2,6}$)octane, liq., Raman spectrum, vibr. assignments 77−61753
triethylenediamine, multiphoton ionis. and two-photon fluoresc. excitation spectra 79−98164
triethylsilylamine, and isotopomers, IR and Raman spectra, normal coord. anal. *(German)* 80−32716
trifluorobenzene cation, selectively excited wavelength resolved emission spectra 80−87136
trifluorobronomethane, $CF_3{}^{79}Br$, precision IR spectra from IR-microwave double reson. 77−14428
trifluorochloromethane, Raman and IR spectra, $^{35/37}Cl$ isotope splitting and mol. constants *(German)* 77−83595
trifluoroethane, isolated CH stretching freqs. and bond props. 79−94104
trifluoroethane(-d_3), IR and Raman spectra, normal coord. anal. *(German)* 80−32726
2,2,2-trifluoroethanol(-d_2), vibr. spectra and normal coord. anal. 79−72319
trifluoroethene-d_0,d_1, mol. struct., microwave and electron diffr. obs. 80−58384
trifluoroiodomethane, IR multi-photon excited mols. 80−74207
trifluoroiodomethane, laser microwave double reson. spectroscopy with CO_2 laser lines 80−87156
trifluoroiodomethane, molecular vibration energy stochastization in intense IR laser field by Raman spectroscopy *(Russian)* 80−14149
trifluoroiodomethane, multiphoton IR excitation and dissoc. *(Russian)* 80−35562
trifluoroiodomethane, UV absorpt. spectrum broadening by laser-induced vibr. excitation 80−53050
trifluoroiodomethane, UV absorption induced by excitation of ν_1 vibrational mode 78−50552
trifluoroiodomethane cation, photodissoc. by quasi-continuum single IR photon absorption 80−61124
trifluoromethane, and -d_1, microwave spectra in ν_6=1 state, accidental degeneracy, mol. struct. 79−3436
trifluoromethyl chloride, IR multiphoton dissociation, isotopic selectivity and yield, temp. effect 80−53069
trifluoromethyl hydroperoxide(-d), CF_3 torsional vibrs., low freq. Raman spectra 80−91565
trifluoromethyl hypochlorite, vibr. spectra and normal coord. anal. 80−102517
trifluoromethyl hypofluorite, vibr. spectra and normal coord. anal. 80−102517
trifluoromethyl hypofluorite (hypochlorite), CF_3 torsional vibrs., low freq. Raman spectra 80−91565
trifluoromethyl peroxyfluoride (peroxychloride), CF_3 torsional vibrs., low freq. Raman spectra 80−91565
trifluoromethylperoxy radical, in Ar:O_2 matrix, IR spectra 80−50845
3,3,3-trifluoropropene, struct. and vibr. spectra, IR, Raman polarisation study 80−18845
trifluorotriiodoethane, IR and Raman spectra, normal coord. anal. *(German)* 80−32726
triglycerides, diacid and triacid, IR spectra, diathesis (vibr. moieties) anal. 77−44525
trigonal and triatomic molecules, orbital valency force field const. calcs. 80−78516
1,3,5-trimethoxybenzene, solid, and in 77K glass, electronic absorption spectra interpretation 79−36659
1,1,1-trimethoxyethane, mol. struct., electron diffr., vibr. spectra 78−37765
trimethyl phosphine-d_6, isolated CH stretching freqs. 78−90167
molecular vibration continued
trimethyl-d_9-vinylsilane, IR and Raman spectra, struct., vibr. assignment, barriers to internal rot. calc. 80−87102
trimethylamine, and analogues, struc. struct. and vibr. force fields, electron diffr. and microwave spectra 77−54609
trimethylamine, collision induced fluoresc. enhancement and quenching, relax. processes 80−83412
trimethylaminegallane, microwave, IR and Raman spectra, struct., vibr. assignment 80−95600
trimethylene sulphoxide, ring puckering vibr., IR spectra obs. 80−32710
trimethylsilyl azide, vibr. spectra, normal mode assignment 78−86867
trimethylsilyl isocyanate, vibr. spectra, normal mode assignment 78−86867
trimethylsilyl isothiocyanate 78−86867
trimethylvinylsilane, IR and Raman spectra, struct., vibr. assignment, barriers to internal rot. calc. 80−87102
trimethyoxybenzenes, liq. and solid, IR and Raman spectra, vibr. assignments 78−58701
s-trioxane, Raman spectra of single crystal, liquid and chloroform-d solution 79−94000
triphenylmethane dyes, IR and Raman vibr., spectra, vibr. anal., vibronic theory of Raman scatt. 77−68048
triply degenerate singlet electronic states, reson. Raman scatt. 78−78714
tropolone, π-π^* singlet state, H^+ tunnelling dynamics and equilib. geometry 80−102539
tropolone vibr. spectra and proton tunneling 80−28014
tryptophan, Raman line characterisation 79−26996
TTF-d_0, -d_4, IR and Raman spectra, vibr. assignments 78−23436
two-level system, in nonstationary field, fluctuation and relax. props. 78−33715
N_5-undecyllumiflavin, high resolution fluoresc. and excitation spectroscopy, vibronic transitions obs. 80−78639
unimolecular reactions, laser-induced, by multiphoton IR excitation, theory 80−9664
uranocene, reson. Raman spectra, anomalously polarised electronic band, energy level assignment 79−59451
urea molecule, bond-length corrections for external and internal vibrs. 80−106402
ureas, alkyl and phenyl groups trisubstituted, conformation, steric and stacking interaction 80−95587
uridine monophosphate, excited state geometry distortion, normal modes reson. Raman intensity anal. 79−68236
van der Waals molecule, linear triatomic, vibr. predissoc. model 77−71838
van der Waals molecules, vibrationally excited, lifetimes, momentum gap 80−5601
vibrational dephasing by translational collision 80−87202
vibrational spectroscopy, high pressure, and conformational analysis 80−9758
vibronic coupling model, nontotally symm. harmonic mode 77−3337
vibronically coupled electronic states, radiationless decay, non-Condon effects 80−52966
vinyl acetate, monomer and polymer, Raman and IR spectra, liq. and solid 78−58700
vinyl fluoride, vibr. excitation effects on ion-molecule reaction pathways, photoionisation mass spectra 77−16804
vinyloxirane, Raman and IR vibr. spectra and conformations 80−83379
vinylsilanetriol-d_0,(-d_3), soln., vibr., IR and Raman spectra 78−86854
visible region thermo-optical spectroscopy 79−50036
water, adsorbed on Pt(100), bonding, electron energy loss spectra 80−34311
water, coherent Raman ellipsometry, vibr. stretching region and liq. struct. obs. 80−93341
water, H-bonded struct., IR spectra, assignments 78−62800
water, high-pressure Raman spectra, bending and librational bands 78−68499
water association, in superheated vap., equilib. consts., H bond vibr. 77−66750
water-carbon tetrachloride soln., fundamental H_2O IR spectrum, liq. struct. 80−23419
water-HF(HBr)(HCl) complex, in supersat. soln., Raman spectra assignments 78−70840
Wurster's cation dimers, reson. Raman spectra 77−58009
XY_2 nonlinear symmetrical molecules, isotopic invariants 79−36599
XY_2 nonlinear system, mol. dynamics calcs. 78−41975
XY_3 planar symmetrical molecules, isotopic invariants 79−36599
XY_4, XY_3, mols., force field anal., parametric representation method 78−25503
XY_4 oxygenated ions, tetrahedral, mol. consts. 79−36555
p-xylene, electronic-vibr. spectra calcs., Franck-Condon and Herzberg-Teller approx. 80−37735
zinc tetraphenylporphin anion, IR spectra and vibr. anal. 79−54852
$_2$, photoluminesc. spectrum, ^{31}P Fermi interaction, hyperfine struct. 78−33536
acetone-d_0, d_6, Raman spectral study of aq. soln. struct., H-bond effects 77−88454
AgBi, laser induced fluoresc., vibr. anal., rot. consts. *(French)* 77−18959
$Ag(CO)_2^+$, laser Raman spectra, CO stretching region 79−59469
$AgNO_3$, cryst. and molten salt, Raman and IR spectra, vibr. anal. 77−16311
$Al+O_3 \rightarrow AlO+O_2$, chemiluminesc., $A^2\pi$-$X^2\Sigma^+$ transition obs. 78−31639
$AlBr_2$, IR spectra in Ar matrix, struct. 79−31520
Al_2Br_6, Br_2Al-Br-$AlBr_3$, vibr. obs., normal coordinate anal. *(German)* 79−26967
$AlCl_3$, force and compliance consts., OVFF, UBFF and GVFF models 78−50663
$AlCl_3$, matrix isolated, vibr. spectrum, struct., vibr. freqs. 78−46339
$AlCl_4^-$, IR spectra in $AlCl_3$-MCl (M=Li, Na, K) melts 79−806
Al_2Cl_6, matrix isolated, vibr. spectra, isotopic fine struct. and valence force field calcs. 80−58258
AlClBr, IR spectra in Ar matrix, struct. 79−31520
$AlCl_2Br$, IR spectra in Ar matrix, struct. 79−31520
AlO, in $Al+O_3(N_2O)$ chemilum., perturbations and vibr. population anomalies obs., mechanism 77−63917
AlO, spectra, vibr. consts., pot. curves, Franck-Condon factors and r-centroids 78−42243
AlS, $B^2\Pi$-$X^2\Sigma^+$ transition, assignment of UV bands, vibr. and rot. anal. 80−58278
AlSe, $A^2\Sigma^+$-$X^2\Sigma^+$ transition, rot. anal. 79−72325

molecular vibration continued
Ar jet, supersonic, electron beam-excited, continuous VUV emission spectrum origins 79−6964
Ar-O_3 Van der Waals complex, struct. and props., RF and microwave obs. 80−32704
Ar_2^+, vibr. excited, form. by assoc. ionisation, photodissoc. 79−68279
$ArBF_3$, microwave spectrum and struct. 79−76420
ArHX, (X=F,Cl,Br,I) van der Waals mols. vibr. and thermodynamic props., WKB calcs. 77−71740
$AsBr_3$, gas-phase electron diffr., mol. struct., force consts., vib. unharmonicities 77−546
$AsBr_3(AsCl_3)$, Raman scatt. spectrum, intermol. interaction and dimeric assoc. *(Russian)* 77−54562
AsD_3, solid and liq., vibr. relax., Raman ν_1 band, 54, 160K 78−27198
As_4O_6, high temp. Raman band contours, vibr. anal. 79−10116
As_4O_6, IR and Raman spectra vibr. spectra, valence force field calc., pot. function *(French)* 78−50549
AuLi, vibr. freq. determ., IR spectra, matrix depend. 77−75146
BCl_3, high-resolution IR Ar matrix-isolation spectra, 10K 80−32708
BCl_3, vibr. excited states distrib. in reson. radiation, photodissoc. rate 78−50603
BCl_3-N_2 mixtures, thermodiffusion props., effect of resonant excitation of mol. vibr. by laser, isotope separation 80−100047
BCl_2NCO, soln., force fields and normal modes, vibr. spectra, IR and Raman obs. *(French)* 80−58266
BCl_2SH, BCl_2SD, Raman and IR spectra, barrier to internal rot. 78−5223
BF_3, ^{19}F chem. shielding, depend. on internal coords. 78−5249
BF_3, threshold photoelectron, photoionisation and coincidence ion-threshold photoelectron spectra 79−820
BF_3CO, microwave spectrum and struct. 79−76420
$^{10,11}B_5H_9$ gas (liq.) phase, vibr. dephasing and Raman spectra 80−48101
BO_2, reson. fluoresc. assignment of vibr. and vibronic transitions 78−17663
$BX_2{}^{14}NCS$ (X=Cl, Br, I), soln., force fields and normal modes, vibr. spectra, IR and Raman obs. *(French)* 80−58266
Ba compounds in air-acetylene flames, dye laser-excited fluoresc. 79−68260
Ba+HBr, laser induced fluoresc. study at different collision energies 80−91632
Ba+HCl, laser induced fluoresc. study at different collision energies 80−91632
Ba+HF, product rot. and vibr. distributions and reaction cross sections depend. on reagent translational energy 80−93745
Ba+HF→BaF+H, dual mol. beam excitation difference spectroscopy, state-to-state vibr. resolved dynamics 80−89474
Ba+trifluoromethyl iodide, BaI vibr. states bimodal distrib. 78−27743
Ba_2^{2+}, very long lived vibr. states, lifetimes, WKB calc. 80−78560
BaBr, visible spectrum, $C^2\Pi_{1/2,3/2}-X^2\Sigma^+$ transition, laser induced fluorescence 79−98072
$BaClO_3.H_2O$, force fields and normal coords. of H_2O mols. 79−31500
BaF_2, force consts., mean amplitudes of vibr. 78−17647
BaI molecule UV band systems 79−22728
BaI, visible emission spectrum, vibr. consts. 77−34643
BaI, visible spectra, 5200-5700 Å, vibr. consts. 78−25549
BaO, excited electronic states, lifetimes and transition moments 80−87177
BaO, mm wave spectrum, spectroscopic consts. 78−37629
BaO_3, visible absorpt. and reson. Raman spectra in Ar and N_2 matrices 77−65487
$Ba_3V_2O_7$, V-O-V bridge stretching freq. correl. with bond angle 78−74636
BeCl, $^2\Sigma^+$ predissoc. state, vibr. and rot. calcs. 77−42363
BeF_2, molten, symm. stretching freq. calc. using mol. dynamics method 77−71790
Bi_n molecular clusters, laser fluoresc. spectrosc. 80−95755
$BiCl_3$, Raman scatt. spectrum, librational and translational vibr. *(Russian)* 77−54562
BiF, mm spectrum, HFS struct., HFS, vibr. and rot. consts. and equilib. distance 77−79604
BiF, spectrum, 5800-6600 Å, vibr. anal., electronic transition assignment 80−992
Br+NOBr, primary and secondary photochemistry, vibrationally excited NO, IR fluoresc. obs. 80−48030
Br_2, $2g^3\Pi$-$2u^3\Pi$ UV laser transition, vibr. anal. 77−75170
Br_2, Ar matrix reson. Raman excitation profile, red shift rel. absorption spectrum 77−14440
Br_2 in Ar, solvent effects on equilibrium props. 80−61128
Br_2 in Ar matrix, reson. Raman scattering amplitude damping in discrete reson. limit 80−58262
Br_2 in liq. Ar, effective intramol. pot. 80−69208
Br_2, organic solvent effects on Raman parameters 79−26998
Br_2-pyridines, charge transfer complexes, $\nu_{Br\text{-}Br}$ vibr., Raman intensity obs. 79−36644
BrCl laser induced fluoresc., quantum resolved level dynamics in $B^3\Pi(O^+)$ state 80−74188
$BrCl(H_2O)_n$, mean vibr. amplitudes, Raman spectra, isotope effects 77−58014
BrF, laser induced fluorescence 78−66591
BrF, laser induced fluorescence 78−66592
BrF_5, IR intensities, fundamental, overtone and combination band calcs. 78−29780
BrF(Cl), rot. spectra in millimeter wave region, rot. transitions obs., equilib. const. determ. 80−78607
$Br_2(H_2O)_n$, mean vibr. amplitudes, Raman spectra, isotope shifts 77−58014
BrO, free radical, Ar matrix absorpt. spectra, mol. vibronic states obs., spectroscopic const. determ. 80−83387
$BrO^+(X^3\Sigma^-)$, vibr. struct. of photoelectron spectrum 78−25612
1-bromo-1-chloro-1-fluoroethane(-2-d_1), IR and Raman spectra, vibr. assignments, normal coord. anal. 78−42053
C-H, $A^2\Delta$-$X^2\Pi$, dissociative excitation, form. environment and parent mol. effects 80−78682
C-H, isolated IR stretching freqs., LeFevre bond parameter anal. 77−57965
C_2, ($A^3\Pi_g$-$X'\ ^3\Pi_u$) band system, vibr. and rot. intensity distrib. 77−42332
C_2, electron affinity, vibr. struct. in radiative electron attachment spectra 77−88592
C_2, reson. fluoresc. statistical equilib. calc., appl. to comets 78−1016

molecular vibration continued
C_3, ($^1\Pi_u$) radical excited state radiative lifetimes and the collisional deactivation 79−27018
C_3, ground and excited states, vibr., pot. curves, CI calcs. 77−83509
C_3 production, vibr. relax., chem. kinetics, following IR multiphoton allene photolysis 80−66820
CBr_2 emission in solid Ar, laser excitation spectra and lifetimes 80−48034
CBrCl emission in solid Ar, laser excitation spectra and lifetimes 80−48034
CCN radical in solid Ar, emission and excitation spectra 78−70868
CD^+, $A^1\Pi$-$X^1\Sigma$ band system, spectroscopic consts. and isotope shifts 79−59485
CD^+, in RF ion trap, laser induced fluoresc. spectrum, 0,0 vibr. band and rot. consts. 80−74189
CF_2, absolute IR intensity of fundamental vibrs. 78−58743
CF_2, photoproduct, vibr. distrib., fluoresc. meas. 77−88511
CF_2, $X\ ^1A_1$ radical, form. in chlorofluoromethane collision-free multiphoton dissoc., translational energy meas. 78−92491
CF_3, absolute IR intensity of fundamental vibrs. 78−58743
CF_2Br^+, CF_2Cl^+, IR spectra, matrix isolation study, C-F stretching fundamentals 78−37632
CF_2Cl^+, and parent cations, IR spectra in matrix radiolysis and photoionis. of Freons 78−80767
CF_3I, I laser medium, UV absorption profile modification by vibr. excitation, for fusion ignition 78−58717
CH radical, sputtered from acetone chemisorption layer on SI, rot. and vibr. population distrib. 78−64436
CH^+, $a^3\Pi$-$b^3\Sigma^-$ transition moment, ab initio calcs. 80−87047
CH^+, ground state photodissoc. cross sections into $A^1\Pi$ state 78−82793
CH_3, CH_2 and CH deformation vibration group frequencies and MO electron densities, interaction force const. 80−87101
CH_3-d_n, matrix isolation IR spectra, rot. and vibr. struct. 77−83589
$C_5H_9^+$, highly vibr.-excited, intermol. pot. well depth estimation method 79−86034
$C_6H_6^+$, gas, laser-induced-fluoresc., rel. to photodissoc. and Jahn-Teller X and A states distortion 79−72345
CN, $A^2\Pi_i$ state vibr. distrib., chemiluminesc. 79−39152
CN, radical, electronic, vibr. and rot. energy partitioning obs. following ICN photolysis 77−16853
CN, time resolved chemilum., in C_2+NO(vinyl cyanide)(ethylene), laser-generated radical kinetics 79−100352
CN, vibr. and rot. anal. of vis., UV spectra, RF discharges in N_2, H_2, CH_4 mixtures 78−5241
$CN(B^2\Sigma)$, from electron impact dissoc., of HCN, near-threshold emission 79−54975
CNN, matrix isolation spectrum, 2600-1900 Å 78−86880
CNN radical, matrix isolation spectra, 23.5-25.6×10^3 cm^{-1}, vibr. relax. and Renner splitting 77−83612
CN(X), free radicals, state distribs. rel. to prod. by photolysis of dicyanoacetylene 77−9107
$CN(X^2\Sigma^+)$, translational-electronic-vibr.-rot. energy partitioning in photolysis of C_2N_2 77−48667
CO, (4+) system, electronic transition probability 80−106332
CO, $A^1\Pi(v'=1)$, vibr. relax. by reversible intersystem crossing, fluoresc. obs. 80−14170
CO, $a^3\pi$ state, IR radiative decay of vib. levels 77−30870
CO, adsorbed on metal surface, collective vibr. modes, dipole interactions 78−50533
CO adsorbed on Ni, bonding struct., vibr. excitations 77−15687
CO, adsorbed on Ni, high press., low temp. Raman spectra 78−6219
CO, adsorbed on Ni (111) face, CO stretching vibr., high resolution electron loss spectroscopy 78−14605
CO, adsorbed on Pt, low temp. vibr. mode, site occupation, electron energy loss spectra 80−29263
CO adsorbed on stepped Ni surface, vibrs. from electron energy loss spectra 79−73406
CO, CO^+, emission spectra, 2100-5600 Å, electronic band systems and assignments 80−5560
CO chemisorbed on Cu (001) surface, vibr. spectrum 79−69347
CO chemisorbed on Fe, low energy vibr. modes studied by tunnelling spectroscopy 80−78590
CO, chemisorbed on Ni(111), vibr. spectra from electron energy loss spectra *(French)* 78−22951
CO, chemisorbed on Pt {111}, IR spectra, evidence for strong absorbate coupling interactions 78−14604
CO, chemisorbed on W, IR vibration spectroscopy 78−14603
CO, chemisorption on Pt (111) and Ni (100), (111), C-O bond lengths, electronic struct. 78−6210
CO, chemisorption on Ru (001), electron stimulated desorption ion ang. distribs. bonding geometry and bending vibrs. 79−33189
CO, $d^3\Delta$ state, low energy electron impact excitation and radiative decay 80−91691
CO, $d^3\Delta_i$ state elec. dipole moment, vibr. depend. obs. 79−31548
CO, dipole moment expsn. determ. from vibr. intensities *(French)* 78−42240
CO discharge plasma, electron energy distrib. and kinetic coeffs., ground-state mols. 80−43867
CO discharge plasma, electron energy distrib. and kinetic coeffs., vibr. excited mols. 80−43868
CO, Doppler-free two-photon vac. UV absorption spectra 78−86882
CO, electron energy loss spectra, C K-shell excitation, vibr. struct. 79−22851
CO, emission intensity, CS_2-O_2 flame, rate of population of CO vibr. levels 78−7186
CO, from CO_2 photodissoc., $CO(A^1\Pi \rightarrow X^1\Sigma^+)$ transitions, vibr. population 77−58100
CO, in Ar matrix, vibr. line shape, vibr.-phonon interaction 79−3493
CO, inner-shell ionisation, vibr. struct., sudden approx. calcs. 79−50002
CO isotopes in Ar matrix, vibr. energy accumulation 78−13485
CO, K-shell, excitation and ionisation, vibr. struct., electron energy loss spectra obs. 80−18943
CO, laser, vibr. distribs., O_2 addition effect 78−50757
CO laser output power, active species and buffer He isotope effects *(Russian)* 80−63986
CO, liq., pure vibr. Raman spectra 80−97262
CO liq. and CO-O_2 (N_2)(Ar) mixtures, polarised vibr. Raman scatt. lineshapes 78−27199
CO, matrix-isolated, librational relax., IR line broadening 80−978
CO, nonequilib. dissoc. induced by electron-vibr. and IR laser pumping 79−86016

molecular vibration continued
CO, one-election props., SCF and CI calcs. 80−27951
CO, oriented molecules, vibrationally inelastic electron scatt. 78−67907
CO, photoelectron ang. distributions, wavelength and vibr. state depend., reson. effects, asymmetry parameters 80−91602
CO, photoelectron spectra ang. distrib., vibr. transitions, autoionis. state 79−31609
CO, photoionis., vibr. intensity distrib., shape reson. effects 79−98167
CO, pressure-induced spectral linewidth and line shifts, vibr. depend., IOS scatt. approx. 79−68267
CO pulsed TE laser, vibr. bands 79−31876
CO reduction in nonequilibrium plasma, effect of non-Boltzmann population vibrationally excited states 79−20362
CO room temperature nuclear pumped laser, parameter optimisation and spectral props. obs. 80−63995
CO, $\nu=0\rightarrow1$ vibr. excitation, electron impact cross sections 80−83507
CO, vibr. excitation via high-energy shape resonances 80−91693
CO, vibr. intensity meas. in photoelectron spectra for ionic ground states 77−18972
CO, vibr. relax. in unsteady expansion wave, vibr. temp. distrib. 77−68096
CO, vibr. struct. of K_α emission spectra 78−86886
CO, $X^2\Sigma^+$, vibr. levels, UPS electron attachment obs. 80−95683
CO^+ ^{14}C and ^{18}O isotope shifts, vibr. anal. of first negative, comet-tail and Baldet Johnson systems 80−28029
CO^+, $B^2\Sigma^+$ state, radiative lifetimes of 0, 1, 2, 3 vibr. levels, intensity decay meas. 79−98157
CO^+, vibr. ($A^2\Pi_i$) states, radiative lifetimes 77−3397
CO^+, vibr. intensity distribs. for electronic states prod. by photoionis. 78−25614
CO^+, vibr.-excited $A^2\Pi$ state, radiative and radiationless vibronic deactivation rates with He 79−10134
$^{12}C^{16}O$, in Ar matrix, vibr. population time evolution temp. depend., master eqn. 78−9180
$^{12}C^{16}O$, near UV emission bands of fourth positive system, vibr. and rot. anal. 77−58054
CO-Ar(-N_2), C_2 and CN form. by optical pumping, room temp. 80−16701
CO-N_2 discharge, plasma characts. and vibr. kinetics anal. 80−59331
CO-UF_6 nuclear pumped laser, expansion cooled, vibr. excitation distrib. 80−63997
CO+$^{14}N_2$ ($^{14}N^{15}N$),($^{15}N_2$), vibr. energy transfer, laser fluoresc. obs. 80−28050
CO+Ar(He)(Ne)(Kr)(Xe), intermol. pot. energy surfaces from electron gas model, ang., distance, and vibr. depend. 79−3520
CO^+ +D_2, state selected reaction cross-sections, coincidence technique obs. 80−66797
CO_2 00^01-10^00 transition in CO-N_2O reacting gas mixture, gain 80−74337
CO_2, $201_{II}\leftarrow000$ band, press. broadened coeffs. and absolute intensities, temp. depend., IR obs. 80−53054
CO_2, 3.8 eV resonance, vibr. struct. in electron-molecule scatt. 78−17813
CO_2, [100] symmetric stretch mode excitation 79−76523
CO_2, ab initio SCF calcs., force consts., vibrs., pot. energy surface 78−5209
$CO_2\rightarrow CO+O$, dissoc. pathways, pot. energy surface and vibr. anal. of IR and Raman spectra 78−64826
CO_2 CW laser, vibr. temp., dissoc. and gain limitation determ., new technique 80−87369
CO_2, collision induced Raman scatt. at ν_2 and ν_3 inactive vibrs. 78−90175
CO_2, core electron ionis., vibronic coupling, symmetry breaking, O1s line vibr. struct. 78−5279
CO_2, electro-optical parameters determ. from IR absorpt. 79−98128
CO_2, electron elastic scatt. and vibr. excitation by 4, 10, 20 and 50 eV electrons 80−83484
CO_2, electron energy loss spectra, C K-shell excitation, vibr. struct. 79−22851
CO_2, electrooptic constants, IR absorption spectrum in $2\nu_3$ vibration band 79−3442
CO_2, Fermi reson, effect on vibr. bands relative intensities 80−965
CO_2, fundamental vibr. bands in liq. phase 79−54856
CO_2 gasdynamic laser, IR spectroscopic determ. of vibr. level populations 80−32952
CO_2 gasdynamic laser, vibr. temp. meas. method 80−9854
CO_2, high resolution UV photoelectron spectra 80−91603
CO_2, IR spectra, lineshape and Q-branch head absorpt. profile 79−59452
CO_2 IR Zeeman spectra utilizing copropag. wave reson., diamag. shift obs. 80−53055
CO_2, isolated CH stretching freqs. 78−92506
CO_2 laser heterodyne meas. of 01^11-11^10 hot band transition frequencies 77−7063
CO_2, liq. phase vibr. spectra, anharmonicity effects 79−50022
CO_2, matrix isolated Raman and IR spectra, fundamental freqs., isotope effects 77−88457
CO_2 multiatmosphere UV preionized laser, elec. and gain characts. 80−14313
CO_2, ν_2 fundamental, absolute IR intensities, Fourier transform spectrosc. obs. 79−93993
CO_2, photoionisation, nuclear motion effects 80−58324
CO_2, polarisabilities, quadrupole and dipole moments, nucl. geom. effects 79−63899
CO_2, reson. electron impact vibr. excitation, 3-5 eV 78−25726
CO_2, saturable absorpt. and rot. relax., (00°0) vibr. level 77−19367
CO_2, vibr. excitation threshold struct., low-energy electron scatt. 80−5625
CO_2 vibr. luminesc., excited by DC discharge, rot. and vibr. mol. consts. 78−58867
CO_2 vibrational temps. in reaction products of CO+N_2O under gasdynamic laser conditions 80−21276
CO_2^+, photoionisation reson. spectra and threshold electron-ion coincidence meas. of fragmentation 77−38700
$^{12}C^{16}O_2$, absorpt. spectrum at 4.3 microns 78−58692
$^{12}C^{16}O_2$, ν_3 band, IR single line strength 80−83370
$^{13}C^{16}O_2$, emission spectrum near 4.5 μm, nu_3 region spectroscopic consts. 77−38664
$^{13}C^{16}O_2$, ν_3 fundamental at 4.4 μm 78−86862
$^{13}C^{16}O_2$, Q-branch spectrum of ($01^{1d}0$-00^00) transition 78−42061
CO_2-N_2-He discharge, electron distrib. relax., numerical study 80−54070
molecular vibration continued
CO_2-N_2-He laser, vibr. population distrib. of N_2, vibr. temp. determ. 77−14688
CO_2-N_2-He laser mixtures, electron swarm parameters, Boltzmann eqn. anal. 79−18396
CO_2+H_e, collinear atom-triatom transition probabilities for anharmonic triatom pots., quantum mech. calcs. 80−83455
CO_2+$H^+(D^+)$, vibr. excitation, isotope and time effects 80−63773
CO_2+Kr, collinear atom-triatom transition probabilities for anharmonic triatom pots., quantum mech. calcs. 80−83455
C_3O_2, far IR and Raman spectra, vibr. mode and quasilinear config. 78−62940
C_3O_2, IR Fourier transform spectroscopy, interaction between vibr. levels 77−75152
C_3O_2, ν_2, $\nu_2+2\nu_7{}^0$ and $2\nu_7{}^0$ Raman band-accumulations 79−3449
C_3O_2, $\nu_2+\nu_7$ bands, Q-branch spectra, 12 μm region, l-doubling const. 77−65459
C_3O_2, $\nu_4+2\nu_7{}^0$ and $\nu_4+3\nu_7{}^1-\nu_7{}^1$ bands, high resolution IR spectrum 79−72311
C_3O_2, Raman bands, vibr. assignments 79−59463
C_3O_2, vibr. IR spectra anal. 80−47984
CO_2^+($C^2\Sigma_g^+$), formation and predissoc., photoelectron spectra 78−5300
COF_2, laser excited IR fluoresc. C=O and C-F stretching modes 78−21960
COS, electron energy loss spectra, C K-shell excitation, vibr. struct. 79−22851
COS, high resolution UV photoelectron spectra 80−91603
COS^+, photoionis. reson. study of ($^2\Pi$) and ($^2\Sigma^+$) states, vibr. freqs., ionis. pot 78−29821
C_3OS, vibrational assignment, calc. of normal modes and valence force consts., IR spectra 79−50014
CO* prod. from Ar*+CO_2, use in laser systems 80−63824
CS, vibr. states in RF discharge plasma, microwave spectrosc. obs. 80−14133
CS_2, absorpt. spectra, Rydberg series converging to $A^2\Pi_u$ states of CS_2^+ 78−90182
CS_2, condensation vibr. shift, intermol. interaction, vap. press. isotope effect 77−61742
CS_2, fundamental vibr. bands in liq. phase 79−54856
CS_2, high resolution UV photoelectron spectra 80−91603
CS_2, IR spectra, $\nu_1+2\nu_2{}^0+\nu_3$ band *(French)* 79−41162
CS_2, laser excited fluoresc., time and freq. resolution, assignments 77−14476
CS_2, liq., props. from allowed light scatt. spectra 80−25364
CS_2, liq. phase vibr. spectra, anharmonicity effects 79−50022
CS_2, matrix isolated Raman and IR spectra, fundamental freqs., isotope effects 77−88457
CS_2, ν_2 bending fundamental, high resolution IR spectrum 80−91559
CS_2, photodissoc., fragment energy distrib. 80−69200
CS_2, vibrational dephasing meas. with CW mode-locked dye lasers 79−65846
CS_2^+, and $(CS_2)_2^+$, photoionis. in supersonic mol. beam 79−98165
CS_2^+, photoionis. reson. study of ($^2\Pi$) and ($^2\Sigma^+$) states, vibr. freqs., ionis. pot. 78−29821
CS_2-O_2 chemical laser, vibr. bands 79−31876
CSFCl, vibr. excited states, microwave spectra *(German)* 78−55167
CSFCl, vibr. spectrum, anharmonicity corrections *(German)* 79−41173
$^{12}C^{16}O+^{13}C^{16}O$, vibr. distrib., electron impact excitation, isotopic composition, interaction depend. 79−29332
Ca_2, new ground state, photolum. obs. vibr. consts., dissoc. energy 80−5576
Ca_2, vibr. relax. in rare gas matrices 78−58711
CaCl, $B^2\Sigma-X^2\Sigma$ transitions, rot. anal. by laser spectroscopy 80−91536
CaCl, $D^2\Sigma$ and $X^2\Sigma$, two-photon vis. absorption, vibr. and rot. consts. 78−78764
CaCl, $X^2\Sigma$ pot. energy curves, polarisability and dissoc. 80−91629
CaF, $B^2\Sigma^+$-$X^2\Sigma^+$ system, rot. and vibr. anal. 80−74156
CaF_2, force consts., mean amplitudes of vibr. 78−17647
CaH, $D^2\Sigma^+$-$X^2\Sigma^+$ band system 80−18847
Ca^+NO^-, $Ca^+NO_2^-$ in solid Ar, IR spectra at 15K 77−57996
$CaNb_2O_6$, columbite struct., normal coord. anal. 78−964
CaO, millimetre wave spectrum, spectrosc. consts. 77−61737
CaO_3, visible and absorpt, and reson. Raman spectra in Ar and N_2 matrices 77−65487
Cd complexes, Cd(II) mixed halide complex anions, Raman spectra 80−58270
Cd etiochlorin complex, visible spectrum, intracomplex electron phototransfer, vibr. effects 79−72330
Cd_2, in Ar and Kr matrices, 10K, UV spectrum, vibr. assignments 77−58038
CdFCl, CdFBr, existence and vibr. characterisation, IR and Raman matrix isolation obs. 78−78706
$CdFe(CO)_4$, IR and Raman spectra, vibr. anal. 78−66553
$CdGa_2$, excimer visible emission spectra in RF discharge, vibr. struct. 79−18201
$CdNb_2O_6$, columbite struct., normal coord. anal. 78−964
$Cd_2V_2O_7$, V-O-V bridge stretching freq. correl. with bond angle 78−74636
CeF_3, force consts., Coriolis coupling consts., vibr. amplitudes 78−17650
CeO, C_1-X_1 and D_3-X_3 systems, fluoresc., vibr. spectra, laser spectroscopy obs. 80−32761
Cl+NOCl, primary and secondary photochemistry, vibrationally excited NO, IR fluoresc. obs. 80−48030
Cl+vinyl bromide-d_3 reaction, IR chemiluminesc. 80−102506
Cl_2, isolated CH stretching freqs. 78−92506
Cl_2, liq., transient stimulated vibr. Raman scatt. 78−71144
Cl_2, resonance Raman spectrum, Q-branches of $^{35}Cl_2$ and $^{35}Cl^{37}Cl$ 78−25542
ClCF radical in solid Ar, emission and excitation spectra, vibr. anal. 78−9164
ClCN, ground and first excited bending, vibr. state, props., mol. beam elec. reson. 80−37823
ClF, rot. spectra in millimeter wave region, rot. transitions obs., equilib. const. determ. 80−78607
ClH-dimethyl ether, H bonded complex, IR and Raman spectra, mech. and elec. anharmonicity 79−89672
$Cl_2(H_2O)_n$, mean vibr. amplitudes, Raman spectra, isotope effects 77−58014
$ClNO_3$, microwave spectrum 77−57984
ClO, free radical, Ar matrix absorpt. spectra, mol. vibronic states obs., spectroscopic const. determ. 80−83387

molecular vibration continued
^{35}ClO, microwave spectrum in excited vibr. state, centrifugal distortion const. 77−83580
ClO_2, laser-microwave double reson. of ν_1 band 80−48022
ClO_2, solns., reson. Raman effect and absorption spectra 77−71807
ClO_3^-, in $MClO_3$ and $MClO_4$ matrix, vibr. spectra, anion site asymmetry 77−27062
ClO_3F, vap. phase Raman spectrum, single isotopic species bands 78−78712
ClONO, form., reaction kinetics, IR spectra 78−35641
$ClO(X^2\Pi_i)$ radical, first ionis. pot., photoelectron spectrosc., vibr. struct., bond length 77−14495
$Cl_3SiOSiCl_3$, normal vibs. and force field, calcs. using electron diffr. struct. determ. *(Russian)* 78−46317
Co complex, C0(l-spartein)Cl_2, IR circular dichroism spectra, vibr.-electronic interaction 80−55074
CoIII salen complexes, O binding, reson. Raman obs. 80−58267
CoO, matrix isolated IR spectra, ground state vibr. freqs. 80−28015
CoO, vibr. IR absorption spectrum, mol. consts. 79−89666
$CoSO_4.H_2O$, IR spectra, H_2O external modes temp. depend. 78−58683
$Co_2V_2O_7$, V-O-V bridge stretching freq. correl. with bond angle 78−74636
$Cr(CO)_6$, ν(CO) region, IR and Raman spectra in organic solvents 79−41169
$Cr(CO)_6$, solid and matrix isolated, Raman spectra 79−28755
CrH (CrD), molecular vibration, IR spectra, electron spin resonance, 4K 79−98084
CrH_2 (CrHD)(CrD_2) (CrH D), molecular vibration, IR spectra, electron spin resonance, 4K 79−98084
CrO_2Cl_2, collisionless IR multiphoton production of electronically excited parent mols. 79−41211
CrO_2Cl_2, inert gas matrices, IR spectra, emission spectra, photoselection 77−14443
CrO_2Cl_2, matrix isolation IR spectrum and force constants 79−3445
CrO_2F_2, determ. of thermodynamic props. from vibrational freqs. and moments of inertia 77−31415
Cs_2, ground state consts., pot. curve, laser spectroscopy 79−98247
CsBrICN, Raman and IR vibr. spectra, struct. 80−102513
CsClICN, Raman and IR vibr. spectra, struct. 80−102513
$CsHCl_2$, H bond bending vibrs., inelastic neutron scatt. obs. 79−89800
CsHClBr, H bond bending vibrs., inelastic neutron scatt. obs. 79−89800
CsI_2CN, Raman and IR vibr. spectra, struct. 80−102513
Cu complex, glycylglycine, isotope substituted, IR and Raman vibr. spectra 78−42051
Cu_2, in supersonic free jet expansion, laser induced excitation spectrum obs. 80−14151
$CuAl_2Cl_8$, Raman resonance spectra of vapour 78−94251
CuBr, new bands in emission spectrum 77−68052
$Cu(CO)_4^+$, laser Raman spectra, CO stretching region 79−59469
CuF from Cu+F_2 chemiluminesc. reactions, mol. beam study 80−97702
D+H_2 reaction, transition state theory calculations, kinetic isotope effect explanation 80−66784
D+H_2 rearrangement collision, vibr. excitation effects 80−71910
D_2, electron dissociative attachment rates, rot. (vibr.) excitation depend., in plasma 80−43848
D_2, G, K double-minimum excited state, vibr. eigenvalues 78−33442
D_2, matrix isolated, IR spectra, mol. rot. and vibr. const. determ. 80−78617
D_2, predissoc. linewidths and shapes for $3p\pi D^1\Pi_u^+$ state 80−53066
D_2, Q(2) line, absolute Raman freq. meas. using CW CARS 78−29794
D_2, Raman spectra, vibr. freq. press. shifts 78−78703
D_3^+, vibr. spectra, ab initio calcs. 77−83562
DBr, IR absorpt. in 5-0 band, high-resolution spectra 77−14431
$DBr^+(A^2\Sigma^+)$, vibrational states, lifetimes, emission cross sections, prod. by electron impact 77−3419
DCN, dipole moment, relative sign w.r.t. normal coords. 78−46457
DCN, electronic spectra, vibr. struct., ab initio calc. 78−9166
DCN, integrated IR intensities of fundamental modes 79−98083
DCN, $\nu_1+\nu_3$ combination bands, transition moments, integrated intensities 77−79610
DCN, photodissoc., vibr. energy states population meas. 78−58751
DCN, photofragmentation, vibr. distribs. 77−18992
DCl and $(DCl)_2$, matrix isolated Raman spectra 78−42063
DCl+CO, V-V energy transfer 80−78695
DF, form., initial vibr. energy distrib., IR chemiluminescence. obs. 80−45497
DF, vibr. relax., isotope effect, quantum model 80−91460
DNSO, IR spectra obs., mole. vibr., anharmonicity constant determ. 80−83357
DO_2, ν_2 fundamental band, 9.8 micron, laser mag. reson. spectroscopy 79−85961
D_2O, $(D_2O)_2$, isotopic forms, Ar matrix isolated IR spectra, assignments, config. 77−6779
D_2O, collective excitations in 10^8 cm^{-1} momentum range, neutron scatt. expt. 78−43087
D_2O, energy levels and mol. vibr., internal coord. model 79−799
D_2O, IR spectra, $\nu_2+\nu_3$ band shape 78−62855
D_2O, vac. UV absorption spectra, Rydberg series vibr. anal. 78−42093
D_2O, vibr. relax. rates 80−95717
$D_2{}^{16}O$, IR spectra, ν_2 band, rot. struct. 78−982
$(D_2O)_2$, isotopic forms, Ar matrix isolated IR spectra, assignments, config. 77−6780
$D_5O_2^+$, isotope effects, easily polarisable H and D bonds 78−94231
DOD, vibr. intensities, ab initio and empirical calcs. 80−78592
DOD, vibr. intensities, ab initio and empirical calcs., band strengths 80−78593
D_2S, energy levels and mol. vibr., internal coord. model 79−799
D_2SO_4, pure, IR and Raman spectra in liq. state, assignments and cryst. spectra comparison *(French)* 79−33699
D_3SiNCO, low freq. bending mode, pot. function 78−82728
D_3SiNCS, IR and Raman spectra, vibr. anal., LF bending mode 78−70842
Dy^{3+}, in soln., non-radiative transitions as Forster's energy transfer to solvent vibrations 80−1014
Eu complex Eu dibenzoylmethane chelate with piperidine, vibronic and IR spectra 79−82981
Eu^{3+}, in soln., non-radiative transitions as Forster's energy transfer to solvent vibrations 80−1014
F+ethylene (benzene) derivatives, deuterated, IR chemiluminesc. 80−102506

molecular vibration continued
F+H_2 chemical laser, vib. populations in V→V, V→R,T energy transfer corrections 77−32794
F+HCl(DCl)→HF(DF)+Cl, dynamical props., pot. energy hypersurface computer anal. 77−77735
F+I_2→IF+I, energy partitioning, vibr. populations and rot. temp., population inversion 80−50832
F_2, continuous UV absorpt. spectrum, temp. depend. 77−23506
$FBrO_3$, gas-phase electron diffr., mol. struct., force field, vib. amplitudes 77−547
FCN, IR laser Stark spectra, C-F stretching mode, dipole moments, rot. consts. 78−1022
FCO, form. in Ar matrix, vibr. and electronic spectra, valence force potential determ., mol. photodissoc. obs. 80−85170
FHF^-, H bonds, vibr. dynamics calcs. 80−23397
FNO, Stark spectroscopy of ν_1 band, rot. consts., dipole moment 79−13710
$FO(X^2\Pi_i)$ radical from F+O_3 reaction, VUV photoelectron spectra 80−104455
Fe^{2+} and Fe^{3+} hydrate clusters, aq. electron exchange reaction, ab initio RHF MO calc. of inner shell reorganisations, vibr. freq. 80−102564
$FeBr_4^-$, circularly polarised Raman spectra, spin-orbit induced vibr. antisymmetry 78−5232
$Fe(CO)_2(NO)_2$, vib. assignment using ^{15}N isotopic substitution, solid, liq. and soln. spectra 77−48152
$FeCl_2$, internal motion, mol. vibr. calcs. 80−106323
$FeCl_3$, Fe_2Cl_6, matrix isolation Raman spectra, assignments 77−65480
$FeCl_3$, internal motion, mol. vibr. calcs. 80−106323
Fe_2Cl_4, internal motion, mol. vibr. calcs. 80−106323
Fe_2Cl_6, internal motion, mol. vibr. calcs. 80−106323
FeH, FeD, matrix isolated IR spectra, mol. vibr. 79−93992
FeO, electron affinity, ground state vibr., new assignment 77−75212
FeO, matrix isolated IR spectra, ground state vibr. freqs. 80−28015
FeO, vibr. IR spectra, $X(^3\Delta)$ and the ground state 79−63998
FeO_2, matrix isolated IR spectra, cyclic complex struct. 77−88449
FeOOH, H-bonding, strong, stochastic model and IR spectra temp. effects 78−62805
p-fluorobenzaldehyde, vap., high-resolution electronic emission spectrum assignments 78−78742
Ga trihalides, vibr. anal., pot. const. determ., mol., compliance and Coriolis coupling const. calc. 80−95579
$GaCl_3$, force and compliance consts., OVFF, UBFF and GVFF models 78−50663
GaI, $A0^+$-$X0^+$ and $B1$-$X0^+$ transitions, isotope shifts, UV and visible spectra obs. 80−53005
GdO, high resolution visible emission spectrum 77−18932
GeAs+Cl_2(Br_2)(I_2), high temp. Raman spectra, cryst. growth mechanism *(French)* 79−26999
GeF_2, force consts., mean amplitudes of vibr. 78−17647
GeF_4, $\nu_3(F_2)$ IR band contour, isotopically pure cpds., mol. consts. 77−61746
GeH_2, centrifugal-distortion dipole moment, CO_2 laser spectroscopy 77−75331
$^{74}GeH_4$ mol. vibr., IR and CARS spectra *(Russian)* 80−102509
GeH_4+Cl_2, HGeCl* chemilum. obs., vibr. levels 77−81406
$(GeH_3)_3P$, vibr. force fields and amplitudes zero point, structs. 77−54551
GeO_4^{4-} compounds, vibr. pot. function, force consts., isotopic shifts, mean vibr. amplitudes 80−23395
GeO_4^{4-}, normal vib. freq. and force const. calcs. *(Russian)* 78−46318
Ge_3O_3, isotopically substituted, IR freq. and intensity patterns 78−21926
GeS, band system vibr. anal. 80−48009
H bonded ν_{X-H} band, dynamic theories survey 80−52983
H bonded species, IR absorption broadening, intramol. interactions effect 78−50595
H bonding molecules, self assoc., intermolecular interactions, matrix isolation vibr. spectra obs. Raman and IR spectra 80−52995
H-bond, dynamical model, Green function method 77−65447
H-bond, dynamical model, inclusion of proton vibr. 77−65446
H-bond, symmetric $AHA^{(\pm)}$, A-H stretching vibr., liq. IR band shape, strong coupling phonon model 78−64358
H-bonded complexes, microwave spectra, assignments, mol. consts. 78−62794
H-bonded complexes, OH stretching vibr. band, temp. effect 78−90158
H-bonded species, in soln., vibr. relax. model 78−84559
H-bonded systems, frequency shift rel. to IR bandwidth 80−99502
H-bonds, IR spectra, ν_s band interpretation 78−58653
H+ClBr→HCl+Br(HBr+Cl), product energy distrib., rate const., IR chemilum. obs. 77−81391
H+D_2, collinear motion, energy transfer and dissociation, collision dynamics 80−99563
H+D_2 reaction, transition state theory calculations, kinetic isotope effect explanation 80−66784
H+F_2, vibr. prod. distrib., Einstein coeffs. 78−92448
H+H_2(HD)(D_2), exchange reaction rate consts. meas., vibr. effects 79−5134
H+H_2(v=1, j=0) exchange reaction, 0.9-1.1 eV, sudden rot. calcs. 79−79230
H+ICl→HCl+I, IR chemiluminesc., product energy distrib. 78−23926
H+ICl→HCl+I, product energy distrib., rate const., IR chemilum. obs. 77−81391
H^++H_2, rot. and vibr. excitation, energy loss obs. 80−63773
H_2 adsorbed on Pd black, vibr. spectrum assignments, inelastic neutron scatt. obs. 78−71942
H_2, CARS, optical Stark effect on vibr., and rot. transitions 80−99512
H_2 chemisorbed on W, vibr. states, electron energy loss spectra 77−31877
H_2, elec. discharge, non-equilib. ionisation rate calcs. 80−59319
H_2, electron dissociative attachment rates, rot. (vibr.) excitation depend., in plasma 80−43848
H_2, electron energy loss spectra, $B^2H_u^+$ state cross sections, Franck-Condon factors 78−13616
H_2, electron energy-loss spectra in afterglow, ground state vibr. conc. 77−31012
H_2, electron impact ionisation cross section 80−78718
H_2, excited G+$K^1\Sigma_g^+$ double minimum state, Born-Oppenheimer pot. energy curve 77−30847
H_2, field ionisation under nonequilibrium conditions 80−74244
H_2, fluid, Raman meas., 0.2-630 kbar, at room temp. 80−58269
H_2, four-body system, adiabatic representation 80−91530
H_2, G, K double-minimum excited state, vibr. eigenvalues 78−33442

molecular vibration continued
H_2, many electron systems, chem. binding, local stresses and force densities 80−27920
H_2, matrix isolated, IR spectra, mol. rot. and vibr. const. determ. 80−78617
H_2, metastable state, mol. beam reson., vibr. anal., spin-rot. interaction 79−22731
H_2, oriented molecules, vibrationally inelastic electron scatt. 78−67907
H_2 photoelectron spectra, rot. intensity distrib. 80−91605
H_2, photoionisation cross-section, calc. for vibr. excited mol. 78−17732
H_2, photoionisation cross-sections, involving vibr. states, data tables 79−18242
H_2, predissoc. linewidths and shapes for $3p\pi D^1\Pi_u^+$ state 80−53066
H_2, predissociation of $^1\Pi_u^+$ state vibr. and rot. levels, dissoc. yields meas. 80−32784
H_2 predissociation probabilities of $4p\pi^1\Pi_u^+ v' \geq 1$ levels, dissoc. channels interference 80−28074
H_2, Raman spectra, vibr. freq. press. shifts 78−78703
H_2, vibr. autoionisation and H_2^+ vibr. state distrib. depend. 77−48628
H_2^+, 400 keV beam dissoc. collisions in air, ang. distribs., vibr. state effects 79−10197
H_2^+ beam form., selected vibr. states, by electron impact in high press. Ne 77−65547
H_2+ He (metastable), Penning ionisation *(French)* 80−1060
H_2+Ar, Arrhenius dissoc. activation energy, vibr. depend., trajectory calc., 4500K 78−35662
H_2+He, vibr. relax. cross section 80−99494
$H_2^+ + H_2$, state selected reaction cross sections, coincidence technique obs. 80−66797
$H_2^+ + He \rightarrow H + HeH^+$, reaction dynamics, vibr. state channels, beam expt., trajectory calcs. 77−77739
H_3, electronically excited state obs., vibr. level struct. determ., predissoc. 79−41204
H_3, photoelectron spectra, ang. distrib. asymmetry parameter, vibr. state depend. 77−75218
H_3^+, IR spectrum, ν_2 band obs. 80−99506
H_3^+, photofragmentation vibr. energy levels and wavefunctions calcs. 78−42143
H_3^+, uncoupled symmetric stretching freq. calcs. 78−66532
$HAlCl_2$, IR matrix spectrum, vibrs. and force consts. *(German)* 79−11786
HBS, force consts., Coriolis const., vibr. amplitude, shrinkage and isotope effect 79−22863
HBr, CW chemical laser, vibrationally excited molecules *(French)* 77−14699
HBr, electron impact ionisation, vibr. excitation spectra threshold peaks, negative ion effects 80−106322
HBr, far IR Ar matrix isolated spectra, 4.2K, press. and conc. effects 78−62801
HBr, isotopic struct. and spectral characts. of vibr. band, using liq. N_2 Raman laser source 78−50859
HBr, liq., transient stimulated vibr. Raman scatt. 78−71144
HBr, vibr. excited, photodissoc. cross-section meas. 79−89717
$HBr^+(A^2\Sigma^+)$, vibrational states, lifetimes, emission cross sections, prod. by electron impact 77−3419
HBr*+I, reaction rate, vibr. excitation effect, isotope enrichment 77−90581
HCC→H+C=C dissoc., trajectory calcs., random vibr. excitation 80−45491
HCCN, matrix isolation IR and UV spectra, vibr. anal., struct. 77−65457
HCCl, IR spectra, ν_4 and ν_5 vibr. bands, rot. struct., rot. and vibr. consts. 77−38665
HCN ($A^1A'' \rightarrow X^1\Sigma^+$), fluoresc. spectrum, using ArF laser excitation 79−36675
HCN, dipole moment, relative sign w.r.t. normal coords. 78−46457
HCN, electronic spectra, vibr. struct., ab initio calc. 78−9166
HCN, IR and Raman vibr. intensity changes due to Li^+ interaction 79−45712
HCN, integrated IR intensities of fundamental modes 79−98083
HCN, laser plasma, microwave spectra of excited vibr. states 78−17656
HCN, $\nu_1+\nu_3$ combination bands, transition moments, integrated intensities 77−79610
HCN, photodissoc., vibr. energy states population meas. 78−58751
HCN, photofragmentation vibr. and rot. distrib., quantum anal. 77−14504
HCN, photofragmentation, vibr. distribs. 77−18992
HCN, self-assoc., matrix isolation vibr. spectroscopy, complex form. studies 78−62952
HCN, vibr. fine struct. accompanying core ionis., STO calcs. 78−62844
HCN^+, photoelectron spectra of third electronic state, ab initio calc. of pot. energy surface 78−70871
HCN+He(H_2)(CH_3F), HCN excited vibr. state, T_2 meas. 80−102498
$(HCN)_2$, IR spectra in Ar matrix, vibr. bands, H-bonds 78−29782
HCO and HNO, pot. energy functions for ground state surfaces 79−89620
HCO, IR spectra of ν_2 fundamental, laser elec. reson. 78−5226
HCP, ν_3 band, high-resolution IR absorption spectrum 80−47994
HCl, 6,0 band, highly forbidden optical transitions using intracavity laser spectroscopy 77−42331
HCl and $(HCl)_2$, matrix isolated Raman spectra 78−42063
HCl and HBr, low-lying reson. states in 0.25-1.15 eV electron scatt. 79−45844
HCl, coherent spectroscopy of anharmonic vibrations 79−18187
HCl, electron elastic scatt., exchange and polarisation 80−91668
HCl, far IR Ar matrix isolated spectra, 4.2K, press. and conc. effects 78−62801
HCl, from H+Cl^-, vibr. state distrib. 80−66794
HCl, K-emission and -absorpt. spectra, vibr. struct., ab initio calcs. 77−79629
HCl, liq., transient stimulated vibr. Raman scatt. 78−71144
HCl, vibr. emission from ClF-H_2 chem. laser 80−97709
HCl, vibr. excitation in electric discharge 80−87978
HCl^+, emission cross sections for $A^2\Sigma^+,\nu' \rightarrow X^2\Pi_i,\nu''$ on electron impact and lifetime of $A^2\Sigma^+,\nu'$ state 77−38697
HCl-D_2, vibr. relax. time meas., by coherent Raman-induced IR fluoresc. 79−7038
HCl-dimethylether complex, gaseous, H-bond IR spectra, temp. depend. theory 78−62804
HCl-He, discharge, possible laser action on vibr. transitions 80−14332

molecular vibration continued
HCl-X, matrix isolation vibr. spectroscopy, complex form. studies 78−62952
HCl+Cl(Br)(H), vibr. relaxation and reaction rates determ. 80−108698
$HClO_4$-H_2O, aq. soln., IR and Raman spectra, conc. depend. *(Russian)* 80−53002
HD, dipole spectrum, influence of intracollisional interference 78−33492
HD, G, K double-minimum excited state, vibr. eigenvalues 78−33442
HD, predissoc. linewidths and shapes for $3p\pi D^1\Pi_u^+$ state 80−53066
HD^+, Hellmann-Feynman theorem anomaly 80−63510
HD_2^+, vibr. spectra, ab initio calcs. 77−83562
HD^+, vibr. spectra, ab initio calcs. 77−83562
$H_2(D_2)$(HD) chemisorbed on Ni (100), vibr. excitation and struct., electron energy loss spectra 78−47660
HDSe, high resolution IR spectra, anal. of $2\nu_1$ band, rot. ground state const. determ. 80−95616
HF, fluoromethanols (mono and tri), decomposition activation of HF, non-statistical energy partitioning, laser emission 79−945
HF, fragmentation, enhanced vibr. excitation effect, mass spectra 78−20004
HF, H-bonded chains, vibr. modes in liq. and solids 78−59873
HF, IR absorption in Born-Oppenheimer approx., vibronic gauge function for vibr. intensity 78−966
HF, K-emission and -absorpt. spectra, vibr. struct., ab initio calcs. 77−79629
HF-cyanomethane, microwave spectroscopic investigations of hydrogen-bonded complexes 78−62794
HF-HCN, microwave spectroscopic investigations of hydrogen-bonded complexes 78−62794
HF+HF (methane)(methane-d_4), collision relaxation rate constants and rot. equilibration time meas. 80−69213
HF+Li→LiF+H, pot. energy surface, SCF and CI calcs. 80−71904
HF_2^-, matrix isolated, IR spectra and struct. 78−74655
$H_2{}^F(HD^+)$, IR photodissoc. cross sections, calc. and simulation expt. 80−9659
HNCO, rot. spectrum, ground and vibr. state reson., centrifugal distortion coupling 80−83364
HNCS, ground state spectroscopic const., microwave, millimeter and IR spectra 80−28010
HNF, $\tilde{A}^2A'$-$\tilde{X}^2A''$ emission spectrum 79−50033
HNF_2 and DNF_2, photoelectron spectra, vibr. struct. obs, ionisation pot. determ., ab initio calcs. of ionic geometry 80−83418
HNO_2, trans and cis, ν_2 fundamental vibrational bands, intracavity CO laser Stark spectroscopy 80−47992
HNO_3, aqueous soln., reflectance and complex refractive index, IR spectra, vibr. modes 80−66168
HNO_3, ν_5 band rot. struct., anal., band centre and rot. consts. 79−10109
HNO_3, VUV photodissoc., vibr. and rot. distribs. 80−87191
HNO_3-H_2O, liq. and glass, mol. assoc., ion pairs, Raman obs. 79−28749
HNO(A^1A''), state-selected fluoresc. lifetimes, collisional quenching rates 79−36674
HO_2 radical, near IR emission bands, vibr. and vibronic transitions 78−37633
HO_2 radical, ν_3 fundamental band, laser mag. reson. 78−66566
$H_2O_2(H_2O)_2$, isotopic forms, Ar matrix isolated IR spectra, assignments config. 77−6779
H_2O 79−72308
H_2O, (D_2O)(HDO), photoelectron spectrum, Franck-Condon, factor calc., geometry and vibrs. *(French)* 77−83652
H_2O, collective excitations in 10^8 cm^{-1} momentum range, neutron scatt. expt. 78−43087
H_2O, D_2O, fragment ion formation on photoionisation, energetics and mechanism 77−501
H_2O, dimers, IR spectra in N_2 matrix, assignments and force consts., isotope effects 77−61744
H_2O, ESCA and soft X-ray emission, vibr. excitation 80−23433
H_2O electro-optical harmonicity of OH bond 77−34634
(H_2O), electron affinity, ab initio SCF calcs. 79−76343
H_2O, electron impact dissoc., $OH(A^2\Sigma^+ \rightarrow X^2\Pi_i)$ emission spectra, crossed-beam investigations 80−83504
H_2O, electronic ground state, SCF HF and CI calcs, pot. energy hypersurface, spectroscopic consts. 78−50473
H_2O, energy levels and mol. vibr., internal coord. model 79−799
H_2O, excited stretching vibrs., quantum mechanics. 80−91535
H_2O, IR and Raman spectra, bonding, vibr., band shapes 79−6938
H_2O, isotope derivatives, mech. anharmonic problems, spectroscopic consts. 79−63983
H_2O, liq., broad band vibr. struct., polarisation CARS obs. 79−85963
H_2O, multiplet states, SCF theory 80−69062
H_2O spectrum, 4200 to 5000 cm^{-1} 77−58005
H_2O, VUV photodissoc., vibr. and rot. distribs. 80−87191
H_2O, vac. UV absorption spectra, Rydberg series vibr. anal. 78−42093
H_2O, vibr. anal., normal coord. calcs., nucl. corrections to mol. props. 77−88441
H_2O, vibr. energy levels, semiclassical trajectory method calcs. 78−58660
H_2O, vibr. Raman scatt. signature in flames 78−25539
H_2O^+, form. in $Ar^+ + H_2O$, kinetic and vibr. energy distrib. 80−16654
H_2O^+, states geometries, electronic vibr. coupling consts. HF calcs., comparison with Xalpha calcs. 80−27946
H_2O^+, vibr. and rot. struct., intensity factors and orbital angular momentum 80−83246
H_2O^-, X^2B_1 and B^2B_2 states, pot. surfaces, SCF and CI calcs. 77−3338
$H_2{}^{16}O$, 6.3 μm region hot bands, intensities 77−75156
$H_2{}^{17}O$ and $H_2{}^{18}O$, centrifugal distortion anal. of ground vibr. states 78−70834
$H_2{}^{17}O$, $H_2{}^{18}O$, Stark spectra with CO laser, Lamb dip spectra of ν_2 band 78−62840
H_2O-HF, microwave spectroscopic investigations of hydrogen-bonded complexes 78−62794
$H_2O+D_2O \rightleftharpoons 2HDO$, vibr. anharmonicity effect on equilib. 79−74410
$(H_2O)_2$, isotopic forms, Ar matrix isolated IR spectra, assignments config. 77−6780
H_3O^+ (D_3O^+), plasma dissociative ion electron recomb., rate coeffs. 80−63747
$H_4O_2^+$, aq. soln., IR continua with polarisable H-bonds 79−26979
HOCl, photolysis product of Cl_2-O_3-H_2 dil. mixtures, absolute integrated IR band intensities 80−26033
HOD, IR band intensities in ice and water 79−3443
HOD, IR spectra in D_2O, combination vibr. 80−9609
HOD, vibr. intensities, ab initio and empirical calcs. 80−78592

molecular vibration continued
HOD, vibr. intensities, ab initio and empirical calcs., band strengths 80−78593
$H_3O^+(H_2O)_n$, H^+ motion energetics, ab initio calcs. 78−25413
$H_3O^+(H_2O)_n$, IR spectra, OH stretching vibrs. 78−25529
HOI, $O_3(O)+HI$ matrix reaction, IR spectra, isotope shifts and band assignments 78−80737
HOT, vibr. intensities, ab initio and empirical calcs. 80−78592
HOT, vibr. intensities, ab initio and empirical calcs., band strengths 80−78593
HPO, in Ar matrix, IR and UV absorpt. spectra 80−47985
HPO, vibrational freqs., by rot. anal. of spectra 79−54831
H_2S, energy levels and mol. vibr., internal coord. model 79−799
H_2S, VUV absorption spectrum, Rydberg series assignments 79−64016
H_2SO_4, pure, IR and Raman spectra in liq. state, assignments and cryst. spectra comparison *(French)* 79−33699
H_3SiNCO, low freq. bending mode, pot. function 78−82728
H_3SiNCS, far IR and Raman spectra, vibr. mode and quasilinear config. 78−62940
H_3SiNCS, IR and Raman spectra, vibr. anal., LF bending mode 78−70842
$H_3SiOSiH_3$, pot. function governing low freq. bending mode 77−58016
H_20, vibr. transition moment and band intensity 79−27036
$Hbr+Cl_2(BrCl)$, four-centre reaction, quasiclassical trajectory study 79−57213
$He+H_2$, mol. energy transfer by quasiclassical trajectory methods, vibr. relax. and dissoc., rot. effect 80−99557
He^++CS_2, dissoc. charge-transfer, $CS^+(B^2\Sigma^+\text{-}A^2\Pi_i)$ emission prod., Morse pot. Franck-Condon factors calc., vibr. anal. 80−99539
He^++OCS, dissoc. charge-transfer, $CS^+(B^2\Sigma^+\text{-}A^2\Pi_i)$ emission prod., Morse pot. Franck-Condon factors calc., vibr. anal. 80−99539
He_2 optical absorpt. spectra and kinetic behaviour 80−95635
HeH^+, vibrational self-ionisation of mol. and recomb. processes *(Russian)* 77−79700
HeI_2, van der Waals mol., vibr. predissoc. lifetimes 79−68278
$HeNO_2$, vibr. predissoc. rel. to van der Waals mol. theory, anharmonicity effects 78−55209
$HeNe^+$, visible spectrum obs. in discharge 79−13729
$He_2^+X^2\Sigma_u^+$ state, ab initio CI calc., pot. energy curve, vibr. and rot. levels 77−3263
HfF_4, mol. struct. and vibr. freqs., gaseous electron diffr. obs. 80−32836
HfN, vibr. IR spectrum, mol. consts. 79−68230
Hg-N_2, optical pumping, vibr. excitation, laser theory 78−66517
$HgBr+O_2(N_2)(H_2)(He)(Ne)(Ar)(Kr)(Xe)$, vibr. relax., rate coeffs., fluoresc. obs. 80−63697
$Hg(CN)_3^-$ ion, CN and HgC stretching vibrations and HgCN bending vibration assignments 80−69140
HgCl, ab initio CI calcs., spectroscopic parameters 79−72245
HgFCl, HgFBr, HgFI, existence and vibr. characterisation, IR and Raman matrix isolation obs. 78−78706
$HgFe(CO)_4$, IR and Raman spectra, vibr. anal. 78−66553
HgI_2, mol. struct. and vibr. pot. function, gas-phase electron diffr. obs. 79−31689
I_2, $2g^3\Pi\text{-}2u^3\Pi$ UV laser transition, vibr. anal. 77−75170
I_2, A-X system 79−63995
I_2, B-X fluoresc. band system, intensity and relative band strengths meas. 80−102540
I_2, B-X system, mol. consts. and Dunham expansion parameters 80−87095
I_2, electron attachment coeff., 35-110°C, vibr. states interpretation 79−98219
I_2, in CCl_4 and cyclohexane solns., higher vibr. levels, dephasing lifetimes, from reson. Raman spectrum 78−42068
I_2, predissociation, electric-field induced 80−37839
I_2, reson.-enhanced three-photon absorption, CW intracavity absorption 79−10160
I_2, two-photon sequential absorpt. spectroscopy 77−54581
I_2, $X^1\Sigma_g^+$ ground state, Le Roy's theory, continuous wave oscillation 79−94006
$^{129}I_2$, energy levels near B-state dissoc. limit, two-photon spectrosc. obs. 80−106367
IBr, $B^3\Pi(0^+)$ excited state, laser-induced fluoresc. 80−58309
IBr, magnetic rot. spectrum, rot. and vibr. anal. 78−70861
$IBr:CO_2$ photolysis, electron-vibr. pumping, 2.7 μm Br and 4.3, 10.6 μm CO_2 laser transitions 80−28196
ICN, photofragmentation, vibr. and rot. distrib., quantum anal. 77−14504
ICl(Br), rot. spectra in millimeter wave region, rot. transitions obs., equilib. const. determ. 80−78607
IF internal vibr.-rot. product distrib., formed in $F+CH_3I(CF_3I)$, fluoresc. obs. 80−48078
IF_5, IR intensities, fundamental, overtone and combination band calcs. 78−29780
I_2He, Van der Waals mol., photodissoc. lifetime, I_2 vibr. depend. 79−6977
$I_2Ne_aHe_b$ van der Waals complexes photodissoc. 80−50864
IO, free radical, Ar matrix absorpt. and emission spectra, mol. vibronic states obs., spectroscopic const. determ. 80−83387
$I_2X^1\Sigma_g^+$, collisional relax. of highly excited vibr. levels, using I_2 optically pumped laser 80−43155
$I_2^*+He(Ne)$, energy depend. of collision induced intramolecular energy transfer 80−83470
I_2*He, vibrational predissociation, van der Waals molecules, vibration-translation scaling theory 80−43135
In trihalides, vibr. anal., pot. const. determ., mol., compliance and Coriolis coupling const. calc. 80−95579
InCl, discharge excited spectrum 4100-3900 Å, vibr. anal. 80−32732
$InCl_3$, force and compliance consts., OVFF, UBFF and GVFF models 78−50663
$InCl_3$ in Kr lattice, Raman and IR spectra, vibr. assignments, force consts., isotope shift and config. 79−89671
Ir complex, tetraethylene iridium chloride, ligand-ligand interactions; low freq. vibr. obs. 78−94255
$IrCl_6^{2-}$, circularly polarised Raman spectra, spin-orbit induced vibr. antisymmetry 78−5232
$(IrCl_6)^{2-}$, electronic Raman spectra, spin-orbit components of ground state, vibr. 78−5231
K salt of β-ketoaldehyde, configurations of anions in solutions studied by IR spectroscopy, H-bond form. 80−87117
$K+I_2(IBr)(Br_2)(ICl)(Cl_2)$, ion-pair form., bond stretching effect on cross sections 78−1064

molecular vibration continued
$K+O_2$, mol. target internal motion 80−78697
KBr:CN^-, neutron scatt. studies of $(CN)^-$ defects 80−92620
$K^+CF_3SeO_2^-$, IR and Raman spectra, normal coordinate anal. for $CF_3SeO_2^-$ anion 80−87122
KCl:OH, low temp. spectrophotometry, impurity absorpt. band *(Russian)* 79−40635
KF, KCl and KI, monomers and dimers, Ar matrix-isolated, IR spectra, vibr. assignments and calcs. 79−45718
K_2MoO_3S, aq. soln., Raman spectrum, MoO_3S^{2-} force consts. 78−74668
KN_3, fluoresc. spectrum, 30K, vibronic and vibr. assignments 79−27023
$K_2(RuCl_5NO)$, polarised Raman and IR spectra, vibr. anal. 77−69819
$K_2[B_{12}D_{12}]$, in aqueous soln., laser Raman spectra 78−15158
$K_2[B_{12}H_{12}]$, in aqueous soln., laser Raman spectra 78−15158
Kr_2, prod. and decay of 0_u^+ and 1_u states, synchrotron excited 80−43109
KrF*, bound-free emission spectra, simulation 78−29806
KrHCl, van der Waals complexes, struct., RF and microwave spectra, isotope effects 80−37806
KrHCl, weak complex, rot. spectra 80−52980
LaF_3, force consts., Coriolis coupling consts., vibr. amplitudes 78−17650
LaS, chemiluminesc. vibr. analysis of $C^2\Pi\rightarrow X^2\Sigma^+$, D_0^0 determ. 77−48645
Li salt of β-ketoaldehyde, configurations of anions in solutions studied by IR spectroscopy, H-bond form. 80−87117
$Li^++CO_2(N_2O)$, vibr. excitation, time of flight meas. 77−79682
Li_1^+, potential energy curves, exchange and ion-multipole interactions, vibrational energy levels 79−98175
Li_2, $A^1\Sigma_u^+$ state, vibr. energy levels calcs. 77−83566
Li_2, far UV photoabsorpt. spectra, core-excited states and CI calcs. 78−37655
Li_2, optical-optical double reson., $^1\Sigma_g^+$ state mil. consts. 80−53027
Li_2^+, $X^2\Sigma_g^+$, $^2\Sigma_u^+$, $A^2\Pi_u$ and $^2\Pi_g$ states, electronic struct. vibr. spectra, ab initio calcs. 79−36507
Li_2F_2, struct., internuclear-distances and mean amplitude of vibr. determ. by electron diffr. 80−69252
Li_3F_3, isotopically substituted, IR freq. and intensity patterns 78−21926
^7LiH, $A^1\Sigma^+$ state, vibr. levels, radiative and nonradiative lifetimes 78−66604
$LiH_2(LiD_2)(LiT_2)$, pot. surfaces, fundamental freqs. and thermodynamic functions 80−69205
$Li_2H(Li_2D)(Li_2T)$, pot. surfaces, fundamental freqs. and thermodynamic functions 80−69205
$Li^+NO_3^-$ ion pairs and hydrated ion pairs, MO calcs., matrix isolation data 78−46267
$^6Li^{35}Cl$, electronic ground state, first vibration state lifetime, MBER meas. 79−86023
$^7Li_2$ $A^1\Sigma_u^+\text{-}X^1\Sigma_g^+$ band system anal. 77−83565
LuBr, visible emission spectra, detection and characteris. 79−6963
methane $2\nu_4\text{-}\nu_4$ and $\nu_2+\nu_4\text{-}\nu_2$ hot bands, difference bands 80−63632
$MgBr_2$, force consts., vibr. amplitude and shrinkage effects 79−22863
$MgCl_2$, force consts., vibr. amplitude and shrinkage effects 79−22863
MgF_2, force consts., mean amplitudes of vibr. 78−17647
MgF_2, force consts., vibr. amplitude and shrinkage effects 79−22863
MgH, X→A and X→B′ band systems, oscill. strengths and photodissoc. cross-sections 79−94045
$MgHPO_4.3H_2O$ and $MgDPO_4.3D_2O$, IR absorpt. and Raman spectra, vibr. assignments 80−97257
MgI_2, force consts., vibr. amplitude and shrinkage effects 79−22863
$MgNb_2O_6$, columbite struct., normal coord. anal. 78−964
MgO_3, visible absorpt. and reson. Raman spectra in Ar and N_2 matrices 77−65487
$Mg_2V_2O_7$, V-O-V bridge stretching freq. correl. with bond angle 78−74636
Mn III chloro complexes, IR and Raman vibr. spectra 77−68038
Mn^{2+}, in soln., non-radiative transitions as Forster's energy transfer to solvent vibrations 80−1014
$Mn(CO)_5Br$, ν(CO) region, IR and Raman spectra in organic solvents 79−41169
$MnHPO_4.3H_2O$ and $MnDPO_4.3D_2O$, IR absorpt. and Raman spectra, vibr. assignments 80−97257
MnO, $A^6\Sigma^+\text{-}X^6\Sigma^+$ electronic transition, rot. and hyperfine struct. 80−74134
$MnSO_4.H_2O$, IR spectra, H_2O external modes temp. depend. 78−58683
Mo_2, matrix isolated visible absorpt. spectra, electronic, vibronic and vibr. states 80−28027
$MoCl_6^{n-}$, n=1,2,3, vibr. freqs., Raman and IR meas. 79−68234
MoF_6, valence electron spectra, vibr. band struct. 77−23520
MoN, matrix isolated visible absorpt. spectra, electronic, vibronic and vibr. states 80−28027
MoO, matrix isolated visible absorpt. spectra, electronic, vibronic and vibr. states 80−28027
MoS_4^{2-}, anharmonicity consts., reson. Raman spectra 77−61754
$MoSe_4^{2-}$, anharmonicity consts., reson. Raman spectra 77−61754
$Mo_2[(CH_2)_2P(CH_3)_2]$, $\delta\text{-}\delta^*(^1A_{2u}\text{-}^1A_{1g})$ transition, vibr. struct. anal. 80−53006
N^{2+}, spectral line breadth in molecular nonequilibrium plasma *(Russian)* 80−48044
N-containing organic compounds, Raman spectra, systematic interpretation 79−26995
N_2, 2.4 eV shape resonance, vibr. struct. in electron-molecule scatt. 78−17813
N_2, $3\sigma_g$ photionis., shape-reson.-induced non-Franck-Condon vibr. intensities 80−43120
N_2 ($C\ ^3\Pi_u$) vibr. levels radiative lifetime, transition moment internucl. distance depend. 78−1027
N_2 adsorbed on W(100), vibr. spectra, bonding struct., LEED study 80−84387
N_2 arc plasma, stabilised by gas injection, thermochem. nonequil., particle excitation, vibr. temps. 80−19634
N_2, B^3pi_g state vibr. levels, obs. in Lewis-Rayleigh afterglow 77−6797
N_2, $B^3\pi_g$ state excitation and deactivation in positive column 77−3482
N_2, $B'^3\Sigma_u^-\rightarrow B^3\Pi_g$ (0,0) emission band 78−58690
N_2, $C^3\Pi_u$ vibr. level, perturbation in relative intensity 79−36785
N_2, CARS, optical Stark effect on vibr., and rot. transitions 80−99512
N_2, desorbed after N atom recomb. on Fe, vibr. energy, electron beam induced fluoresc. 80−61149
N_2 discharge, non-Boltzmann vibr. level populations, CARS determ. 78−5968

molecular vibration continued
N_2, elastic and inelastic electron scatt., state to state cross section 80−78708
N_2, electrical discharge excitation, vibr. level population distrib., electron beam fluoresc. obs. 80−48031
N_2, electron impact, electron distrib. function in laser radiation field, vibr. excitation influence 80−28112
N_2, electron impact, reson. vibr. excitation, ab initio R matrix calc. 80−32842
N_2, electron impact enhanced vibr. excitation, continuum multiple scatt. model with Hara exchange approx. 80−43196
N_2, electron scatt., 50-500 eV, two-pot. approach 79−41242
N_2, electron scatt., reson. excitation and dissoc. attachment, vibr. state depend. 80−78717
N_2, excited kinetic investigation of vibr. distrib. function, Raman scatt. *(Russian)* 78−66557
N_2, first negative system, Deslandres table 79−98118
N_2 gas, stimulated Raman scatt. on rotational and vibrational transitions 79−27330
N_2, high-speed Raman spectroscopy, condensed discharge vibr. excitation, vibr. temp. 78−82740
N_2 in aurorae, vibrational distrib. 79−80068
N_2 in nonequilibrium gas-dynamic current, vibr.-level populations determ. by Raman scatt. 80−99509
N_2 in premixed laminar methane-air flame, Raman scatt. meas. of vibr. temp. 79−80622
N_2, inner shell $(1s)^{-1}(\pi 2p)^1\Pi$ state, energy, vibr. struct., electron impact investig. 78−13611
N_2, K-shell, excitation and ionisation, vibr. struct., electron energy loss spectra obs. 80−18943
N_2, light polarisability parameters, Raman scatt. ang. meas. 80−37814
N_2, liq., pure vibr. Raman spectra 80−97262
N_2, liq. spontaneous Raman scatt., vibr. dephasing, review 77−28568
N_2, liquid, in Kr, methane, and CO, Raman scatt. parameters, high-resolution coherent active spectroscopy 80−66207
N_2, liquid, Q-band position, width in cryogenic mixtures *(Russian)* 78−46401
N_2, liquid, vibrational dephasing, computer simulation, Raman spectra, pair potential effect 80−63863
N_2, matrix isolated, fundamental vibr. Raman spectra 80−272
N_2, microwave discharge at high press., vibr. excitation *(French)* 78−14239
N_2, N K-shell excitation, high-resolution electron energy loss spectra 80−53152
N_2, N_3, spectra, review 77−38680
N_2, oriented molecules, vibrationally inelastic electron scatt. 78−67907
N_2, photoelectron spectra, ang. distrib. asymmetry parameter, vibr. state depend. 77−75218
N_2 positive column, superelastic collisions and electron distrib. function 80−1858
N_2, Q-branches, high resolution pulsed CARS 78−17676
N_2, vibr. and rot. anal. of vis., UV spectra, RF discharges in N_2, H_2, CH_4 mixtures 78−5241
N_2, vibr. energy diffusion coeff., 900-2000K 78−26227
N_2, vibr. intensity meas. in photoelectron spectra for ionic ground states 77−18972
N_2, vibr. struct. of K_α emission spectra 78−86886
N_2, vibr. temp. meas. in CO_2 fast flow laser 80−32955
N_2, vibration stimulated Raman scatt., four photon parametric effects 80−33087
N_2^-, first $^2\Pi_u$ state form. and decay 80−58177
N_2^-, vibr. autodetaching states, from $H^- + H_2$, excitation and decay, Franck-Condon factors 78−33620
N_2^+ 1 NG emissions from proton aurora, anomalous vibr. distrib. 80−67448
N_2^+, partial photoionisation cross section and photoelectron angular distribution for $X^2\Sigma_g^+$ state determ. 80−83429
N_2^+, produced by threshold ionis., $X(^2\Sigma_g^+)$, $A(^2\Pi_u)$ and $B(^2\Sigma_u^+)$ vibr. struct. and mol. parameters 78−94294
N_2^+, spectroscopic consts., remeas. 77−58197
N_2^+, vibr. intensity distribs. for electronic states prod. by photoionis. 78−25614
N_2^+ $X^2\Sigma_g^+$-state, vibr. states asymmetry parameter and photoelectron spectrum 80−95591
N_2^{2+}, recomb. energy determ. from pot. curves 80−58335
N_2-Ar liq. mixtures, coherently excited mol. vibrs., dephasing time 78−62813
N_2-Ar mixture, picosecond dephasing of coherently excited vibrations 78−22172
N_2-CO, electrical discharge excitation, vibr. level population distrib., electron beam fluoresc. obs. 80−48031
N_2-CO_2(-He) volume discharge, N_2 vibr. levels, stepwise excitation, effect on electron energy balance 80−54071
$N_2+H_2+N_2H_4$, mixtures with nonthermal vibr. excitation of mol. N_2 80−76545
$N_2+H^+(e)$, vibrational N_2^+ excitation *(Russian)* 80−53156
$N_2+N_2(Ar)(H_2)$, $(A^3\Sigma_u^+, \nu=0,1)$ metastable state quenching rate coeffs. 78−90206
N_2+O_2+NO, mixtures with nonthermal vibr. excitation of mol. N_2, formula for calc. equilib. const. 80−76545
$N_2^+ + He$, N_2^+ selectively excited, collisional deactivation 80−83338
$N_2^+(A^2\Pi_u$-$X^2\Sigma_g^+)$ system in aurora, vibr. development and quenching effects 78−88967
N_2BF_3, microwave spectrum and struct. 79−76420
$N_2(B^3\Pi_g$-$A^3\Sigma_u^+)$ system in aurora, vibr. development and quenching effects 78−88967
$N_2^+(B^2\Sigma_u^+)$, perturbation of $\nu=1$ vibr. level, rot. lines freqs. and intensities *(French)* 77−79640
ND radicals, metastable, production in discharge, spectra, rot., vibr. consts. determ. *(German)* 77−34642
$^{14}ND_3$, $^{15}ND_3$, ν_2 fundamentals and isotope shift 79−59456
N_2D_2, near UV spectrum, vibr. assignment 78−78717
$ND_2(NH_2)$, ν_2 band, laser mag. reson., 9-10 micron 80−9601
NF_2, IR spectra, ν_1 and ν_2 bands, vibr. excitation and spin-rot. interaction, doublet splitting 80−28011
NF_3, gas and liquid Ar soln., IR spectra, binary overtone and combination band intensities 77−79658
NF_3, IR spectrum in liquid Ar, vibr. anal. 78−21927
N_2F_4, multiphoton excitation and vibr. energy flow, fluoresc. obs. 80−95673

molecular vibration continued
NH, photofragment, energy distrib., chemiluminesc. reaction rates 77−90618
NH radicals, metastable, production in discharge, spectra, rot., vibr. consts. determ. *(German)* 77−34642
NH_2 (A^2A_1), excited state dynamics and bimol. quenching processes 80−9681
NH_2 fragment internal energy distrib. in NH_3 UV laser photodissoc. 80−11901
NH_2 radical, mag. hyperfine interactions, zero-point vibrs. effects 80−58167
NH_2, vibr. and rot. struct., intensity factors and orbital angular momentum 80−83246
NH_2^+, low lying states, ab initio MRD-CI pot. surface calcs. 79−89611
NH_3, ab initio SCF calcs., force consts., vibrs., pot. energy surface 78−5209
NH_3, adsorbed on silica gel, neutron scatt. investig., mol. vibrs., rots. 77−51608
NH_3, and -d_n IR matrix isolation spectra, rotation and inversion 78−5218
NH_3, ESCA and soft X-ray emission, vibr. excitation 80−23433
NH_3, excited vibr. states, transition dipole moments, laser Stark spectrosc. 79−68261
NH_3, IR spectra, $\nu_3+\nu_4$ band anal. 77−75154
NH_3, IR-microwave double reson., rot. and vibr. relax., inversion layers 78−86902
NH_3, inversion spectra, ν_4 state 80−47965
NH_3, inversion-vibration interactions, pot. energy function calcs., isotope effects 78−33567
NH_3, isolated CH stretching freqs. 78−92506
NH_3, laser saturation time-delayed IR spectroscopy 78−86976
NH_3, line intensities in 2 μ band, Doppler broadened lines 77−75155
NH_3, ν_2 band as R(1, 1) line self-broadening coeff. 79−98158
NH_3, pure, Raman scatt., high press., high temp. 77−27077
NH_3, self-assoc., matrix isolation vibr. spectroscopy, complex form. studies 78−62952
NH_3, symmetric bending mode, Raman intensity, electrolyte solvent effects 77−34638
NH_3, vibr. excitation in soft X-ray emission and core ESCA spectra 80−69163
NH_3^+ radical, mag. hyperfine interactions, zero-point vibrs. effects 80−58167
NH_3^+, two-mode Jahn-Teller effect calcs. 80−83297
$^{14}NH_3$, $^{15}NH_3$, submm-wave rot.-inversion transition, ν_2 state 77−75138
$^{14}NH_3$, Doppler free spectroscopy, 16 micron generation applications 79−94049
$^{14}NH_3$, IR saturated absorpt. spectra, vibr. depend. of hyperfine quadrupole const. 77−27072
$^{15}NH_3$, IR-IR double resonance, ν_2 vibr. state, electric dipole moment 77−83626
$^{15}NH_3$, modulated coherent Raman beats 80−23464
$^{15}NH_3$, nucl. spin-spin coupling consts. calc., vibr. averaging effects 78−33521
NH_3-CO_2 complex, matrix isolation IR spectrum, struct., ab initio SCF calcs. 78−5209
$NH_3^{\cdot+} + H_2O \rightarrow NH_4^+ + OH^\cdot$, statistical phase space theoretical anal., vibr. depend. cross section 78−15660
$NH_3^{\cdot+} + NH_3 \rightarrow NH_4^+ + NH_2^\cdot$, statistical phase space theoretical anal., vibr. depend. cross section 78−15660
N_2H_2, isomers, photoelectron spectra, vibr. struct., ionisation pots., Green's function calcs. 77−75213
N_2H_2, near UV spectrum, vibr. assignment 78−78717
$N_2H_4^+$ radical, mag. hyperfine interactions, zero-point vibrs. effects 80−58167
$NH_4^+CF_3SeO_2^-$, IR and Raman spectra, normal coordinate anal. for $CF_3SeO_2^-$ anion 80−87122
$NH_4I(ND_4I)$.dioxane complexes, Raman spectra, vibrs., H-bonding 78−25544
$NH_4(NH_3)_n^+$, n=0 to 4, gas phase IR spectra 80−43044
NH_4NO_3, IR spectra and vibr. bands 80−69144
$(NH_4)_2(RuCl_5NO)$, polarised Raman and IR spectra, vibr. anal. 77−69819
$(NH_4)_2S_5$, Raman spectra, vibrs. and rot. isomers of Sn^{2-} (n=4-8) *(German)* 78−13504
$NH_4UO_2(NO_3)_3$, IR spectra, force consts., bond orders 77−30873
$NH_2(X^2B_1)$ radical, and ND_2, ionisation pot., vibr. anal., ab initio calcs. and vacuum UPS obs. 80−53047
NO (υ=1), vibr. fluoresc. detection of trifluoroformamide photodissoc. 78−74712
NO, adsorbed on Ru (001), inelastic electron scatt. dissoc. energies adsorbed state depend. 78−95956
NO, and isotopic forms, $X^2\Pi$ state, IR obs., mol. consts. 78−42045
NO, ang. distrib. valance photoelectron spectra, vibr. depend., autoionisation and Franck-Condon factors 79−72356
NO, chemiexcited, form. in $N(^2D)+O_2$, 90-180K, IR obs. 78−90163
NO, electronic spectrum, press. induced config. demixing 78−42090
NO, Fourier transform spectra, intensity and self-broadening coeff. meas. 80−102503
NO, γ and β system, electronic transition probability 80−106332
NO, IR spectra in O_2 matrix, vibr. freqs. 78−23936
NO, ionic ground state, photoelectron spectra vibr. intensity Franck-Condon factors 77−79650
NO, N K-shell excitation, high-resolution electron energy loss spectra 80−53152
NO, photoionisation and ionisation pot., mol. beam meas. 77−10709
NO, Q-branch spectra, external-resonator controlled Raman laser pumped by CW CO laser 80−9624
NO, Rydberg absorpt. bands 800-850 Å, isotope shift 79−13734
NO, UV fluorescence, IR laser induced 80−53032
NO, UV irrad. photoionisation, NO^+ high vibr. excitation, photoelectron spectra 77−71830
NO, UV photoelectron spectrum, autoionisation from Rydberg state, vibr. progressions, Franck-Condon factors 78−50583
NO, $\upsilon=2\leftarrow1$ absorption band two-and multiphoton spectra, Λ-doubling const. vibr. depend. 77−30942
NO vibr. overtone band, mag. rot. spectrosc. obs. 80−86446
NO $X^2\Pi(\nu''=0)$, ionis. energies to NO^+ $X^1\Sigma^+(\nu=0\text{-}34)$, NO^+ mol. consts., UPS obs. 80−14177
NO^+, symmetric charge transfer reaction cross section, selected kinetic energies, vibr. states 77−16813

molecular vibration continued
NO^+, $X^1\Sigma^+$ state, UV irrad., high vibr. excitation, photoelectron spectra 77−71830
$NO+Kr^+$, charge-transfer reaction rel. to vibr. state of NO^+ 77−1916
$NO+O_3(001)\rightarrow NO_2(^2B_{1,2})+O_2$, laser enhanced reaction, temp. depend. 77−81397
NO_2, $^2B_1$ state fluoresc., bending vibr. progression 77−83638
NO_2, $^2B_2$ state photodecomposition in 2nd predissoc. region 77−10712
NO_2 excited, fluoresc. spectrum, IR multiphoton vibr. pumping, photon absorpt. probability distrib. study 80−18854
NO_2, fluoresc. spectra and collisional quenching 80−102538
$(NO)_2$, IR spectra in O_2 matrix, vibr. freqs. 78−23936
NO_2, IR-optical double reson., fluoresc. obs., high-energy vibr. levels 78−55188
NO_2, laser-induced fluoresc. spectrum near 6125 Å 77−58069
NO_2, Ne matrix isolated, 6K, B←X band system 78−993
NO_2, vacuum ultraviolet absorpt. spectra, absorpt. coeffs. 78−70846
NO_2, vibr. excited, from nitroalkane photodissoc., fluoresc. obs. 78−37693
$^{14}N^{16}O_2$, IR spectra, $2\nu_2+\nu_3$ and $\nu_1+\nu_2+\nu_3$ bands, vibr. and vibr.-rot. consts. 78−983
$^{14}N^{16}O_2$, ν_1 band, high resolution IR spectra 78−55173
NO_3^-, aq. soln., vibr. width and dephasing, conc. depend. 80−43029
NO_3^-, in $MClO_3$ and $MClO_4$ matrix, vibr. spectra, anion site asymmetry 77−27062
NO_3^-, Raman spectrum of ν_1 mode in soln., reorientation 78−92067
N_2O, fundamental vibr. bands in liq. phase 79−54856
N_2O, IR absorpt. spectra, N_2-broadened lines of ν_3 band 78−5228
N_2O, IR emissivity and band-model parameters, 200-500K 77−83591
N_2O, IR spectrum in liquid Ar, vibr. anal. 78−21927
N_2O, in soln., IR and Raman band shapes, mol. dynamics, ν_3 band 77−36238
N_2O, liq. phase vibr. spectra, anharmonicity effects 79−50022
N_2O, N K-shell excitation, high-resolution electron energy loss spectra 80−53152
N_2O quadrupole hyperfine struct., vibr. depend. obs. using twin-laser spectrometer 80−43097
N_2O, $X_2\Pi$ state, Ne I photoelectron spectra 77−30924
N_2O^+, dissoc., threshold photoelectron-photoion coincidence obs. 80−87189
N_2O-N_2-He, population inversion of N_2O vibr. levels behind shock wave front 79−31886
N_2O+N_2, vibr. population distrib. energy depend., ν_3, ν_2 and ν_1 mode exchanges *(French)* 79−10187
N_2O+N_2*, vibr. population studied by IR emission spectra *(French)* 77−14544
$(N_2O)_2$, photo-induced vibr. predissoc. of van der Waals mol. 78−90242
N_2O_4, IR spectra in O_2 matrix, vibr. freqs. 78−23936
N_2O_4, vibr. assignment 79−6940
N_2O_5, IR spectra in O_2 matrix, vibr. freqs. 78−23936
NS radical chemiluminescence produced by active $N+S(S_2Cl_2)$, kinetics study 79−39151
$^{14}N^{14}N+^{14}N^{15}N$, vibr. distrib., electron impact excitation, isotopic composition, interaction depend. 79−29332
$^{14}NH_3$, two-photon excitation, collisional processes in excited vibr. levels 77−10890
N_2* ($A^3\Sigma_u^+$), electron impact ionisation cross section 80−78718
Na salt of β-ketoaldehydes, configurations of anions in solutions studied by IR spectroscopy, H-bond form. 80−87117
Na_2, $A^1\Sigma_u^+$ state, spectroscopic consts. and RKR pot. calcs. 77−75130
Na_2, dimer, $B'\Pi_u$-$X'\Sigma_g^+$ band system obs. 78−62837
Na_2, vibrationally excited, photodissociation cross section 79−13777
$Na_2+He(Ne)(Ar)$, collision induced dissoc. rate, vibr. distrib. depend. 79−22791
NaAr, ground and excited state pot. curves, dispersed fluoresc. spectrum 79−98140
$(NaCl)_n$ (n=1-7) equilib. configs., total energy calcs., far IR spectra 78−29872
$Na_2Fe(CN)_5NO.2H_2O$, new isomeric mol. state, Mossbauer data 77−23513
NaH, $A^1\Sigma^+$-$X^1\Sigma^+$ electronic transition, spectroscopic anal. and potential energy curves 80−48102
NaK, laser induced D $^1\Pi$-$a^3\Sigma$ fluorescence, mol. vibr. 80−87160
$NaPF_6.H_2O$, IR and Raman spectra 77−61749
$NbCl_5$, mol. struct., vibr. assignments, barries to pseudorotation 78−29858
$Nb_nW_{6-n}O^{(n+2)-}$, config., IR and Raman spectra 77−42324
Ne_2^++e, in recombination afterglow, line intensity decay complex struct. 79−7503
Ni catalyst, chemisorption of benzene, Raman and vibr. spectra 80−108747
Ni complex, Ni(l-spartein)Cl_2, IR circular dichroism spectra, vibr.-electronic interaction 80−55074
Ni complex, octaethylporphyrinato-Ni(II), meso-deuterated and ^{15}N substituted derivs., reson. Raman spectra 79−13725
Ni complex, octaethylporphyrinato-Ni(II), meso-deuterated and ^{15}N substituted derivs., reson. Raman spectra 79−13726
Ni complexes, Ni(glycinate)$_2$(pyrazine) and Ni(glycinate)$_2$(pyridine)$_2$, and isotopic forms, IR band assignments 79−22710
Ni_2, A→X system, Ar matrix isolation fluoresc. spectrosc. obs. 80−9628
Ni_n clusters, Ar matrix, UV-visible spectra pot. energy curves 77−65552
NiBr, band system in near UV, vibr. analysis 80−32733
NiO, matrix isolated IR spectra, ground state vibr. freqs. 80−28015
$Ni(PF_3)_4$, force fields, mean vibr. amplitude calcs. 77−54552
$NiSO_4.H_2O$, IR spectra, H_2O external modes temp. depend. 78−58683
$Ni_2V_2O_7$, V-O-V bridge stretching freq. correl. with bond angle 78−74636
$O+CS_2\rightarrow CS+SO$, vibrational distribution of CS, laser-induced fluorescence meas. 80−71895
$O+H_2O\rightarrow OH+OH$, energy partitioning 80−101009
O+HCl, vibr. excited, laser enhanced reaction rate, OH vibr. distrib. obs. 78−95912
$O+O_3$ reaction, vibr. enhancement 80−30215
O+saturated hydrocarbon→OH+alkyl radical, reaction dynamics, mol. beam-laser induced fluoresc. obs. 80−97695
$O^-+CO\rightarrow CO_2^++e^-$, vibr. chemiluminesc. 78−3340
O_2, $^3\Pi_g$ diabatic Rydberg states, ab initio CI calcs. 80−95554
O_2, 2,0 band, highly forbidden optical transitions using intracavity laser spectroscopy 77−42331
O_2, $A^3\Sigma_u^+$, $C^3\Delta_u$ and $C^1\Sigma_u^-$ states in van der Waals solids, electronic spectra, dynamics 78−1000
molecular vibration continued
O_2, anharmonicity const., Raman meas. 77−34637
O_2 $C^3\Delta_u-a^1\Delta_g$ band system, vibr. anal. 80−5556
O_2, electron attachment threshold photoelectron spectra, vibr. excitation 80−83422
O_2, electron impact vibr. excitation, direct and stepwise, rate coeffs. 80−5630
O_2, excited state geometries and energies, ab initio pot. energy surfaces 78−5151
O_2, I and I′ resonance series, vibr. level populations in autoionisation, photoelectron spectra, bond length determ. 80−91612
O_2, inert gas matrix, visible emission spectra, $c^1\Sigma_u^-\rightarrow a^1\Delta g$ and $C^3\Delta u\rightarrow X^3\Sigma_g^-$ transitions 77−14444
O_2, K-shell, excitation and ionisation, vibr. struct., electron energy loss spectra obs. 80−18943
O_2, light polarisability parameters, Raman scatt. ang. meas. 80−37814
O_2, liq., pure vibr. Raman spectra 80−97262
O_2, liq. spontaneous Raman scatt., vibr. dephasing, review 77−28568
O_2, Q-branches, high resolution pulsed CARS 78−17676
O_2, Raman spectra of fundamental vibr. band, rot. consts. 78−21932
O_2, Rydberg states, $^3\Sigma_g^-$, $^3\Sigma_u^+$, $^3\Pi_g$, $^1\Pi_g$, $^1\Sigma_g^+$ symm., ab initio CI study 80−99460
O_2, singlet, energy transfer in quenching, statistical theory of vibr. energy distrib. 77−68073
O_2 singlet energy transfer in quenching, vibr. excited mols. 77−71828
O_2^+, $A^2\Pi_u\rightarrow X^2\pi_g$ and $b^4\Sigma_g^-\rightarrow a^4\Pi_u$ emissions by photoionis. of O_2 79−94041
O_2^+, electron impact dissoc. recomb., pot. energy curves calcs. 80−53150
O_2^+, IR spectra, rot. anal. of $b\,\Sigma_g^-a^4\pi_u$ first negative band 78−5219
O_2^+, photoelectron spectra, vibronic transition ionisation energies, ground state mol. consts. 79−89710
O_2^+, spectroscopic consts., remeas. 77−58197
O_2^+, symmetric charge transfer reactions, selected states, photo-ion, electron coincidence 78−73028
O_2^+, vibr. energy levels, dissoc. energy, photoelectron spectra 77−83651
O_2^+, vibr. intensity distribs. for electronic states prod. by photoionis. 78−25614
O_2^+, $X^2\Pi_g$ photoelectron spectra, vibr. intensity, Franck-Condon factors 77−42352
$(O_2)_2$, van der Waals mol., WKB vibr. eigenvalues 78−33498
O_3, combination bands $(\nu_1+\nu_2)$ and $(\nu_2+\nu_3)$, anal. 78−9150
O_3, Huggins bands, vibr. anal. 78−42085
O_3, line position and intensities of $2\nu_3$, $\nu_1+\nu_3$ bands 80−87181
O_3, microwave and IR spectra, ν_2 state, $(\nu_3+\nu_2)-\nu_2$ band, 10 micron lines 78−82718
O_3, photodissoc. cross section, vibr. excitation effects obs. 80−95696
O_3, photoelectron spectrum, vibr. struct., ionos. pot. 77−75217
O_3, photolysis, primary products electronic and vibr. state distrib. 80−50865
O_3, spectroscopy with CO_2 waveguide laser 77−13117
O_3, UV absorpt. spectrum, Hartley continuum, IR laser induced changes 80−95639
O_3, UV absorption bands, new vib. quantum no. assignments, based on isotope effect 79−94008
O_3, vibr. energy anal., form. by recomb. 77−75119
O_3^-, photodissoc, cross section 79−832
OAlCl and OAlF, IR matrix spectra, vibr. freqs. *(German)* 79−11785
OCS, dipole moment, laser microwave double reson.-Stark effect meas. 78−55191
OCS, fundamental vibr. bands in liq. phase 79−54856
OCS, IR spectral moments and mean squared torques, rare gas effects 78−62944
OCS in Ar soln., IR spectra, solvent shifts, vibr. band assignment and anharmonic force consts. 80−9607
OCS laser, two-quantum excitation, photolysis, energy transfer, for fusion expts. 78−59003
OCS, mol. consts. of ν_2 levels 77−14429
OCS, two photon and vibr. depend. photolytic prod. of $S(^1S)$ atoms 79−13775
OCS, vibr. energy transfer map 80−99560
$^{16}O^{12}C^{34}S$ and $^{16}O^{13}C^{34}S$, IR spectra, ν_3 band anal. 80−95620
OGaF, matrix IR spectrum, vibrs. and force consts. 79−11787
OH, ($A^2\Sigma^+$), abnormal rot. following H_2O photodissoc., semiclassical calcs. 78−40069
OH, $A^2\Sigma^+$-$X^2\Pi_i$ system, vibrational and rotational levels, transition probability determ. 80−43034
OH, fundamental vibr. band, mag. rot. spectrosc. obs. 80−86446
OH, internal state distrib., crossed mol. beam $H+NO_2$ reaction, laser-induced fluoresc. 77−4905
OH Meinel bands, in airglow, rot. temp., radiative lifetime 78−61643
OH, radical, far IR laser mag. reson. spectra, fine struct. transition 79−76454
OH, radical $v=1^2\Pi_{3/2}$ state, microwave spectrum 79−26972
$OH+H_2\rightarrow H_2O+H$, reaction product vibr. distribs, quasiclassical trajectory, calcs. 80−85162
$OH(A^2\Sigma^+\rightarrow X^2\Pi_i)$ yields from H_2O photodissoc. 80−71927
$OHX^2\Pi$ radical, ground and vibr.-excited ($v\leq 6$) levels, microwave spectrum 79−63985
$OH(v=0, 1)+H_2(v=1)$, rate consts., 298K 79−11768
ONCN, IR spectra isotope shifts and ab initio calc. for harmonic force field 79−13715
ONCl, vibr. freq., anharmonic ab initio/empirical pot. energy functions 80−99457
$O(^3P)+C_3O_2\rightarrow 3CO$, reaction dynamics and monoxide vibr. distrib., laser reson. absorpt. method 78−68882
$O(^3P)+O_3^*$, bimolecular reaction rate coeff. reactant vibr. excitation depend., reson. fluoresc. obs. 78−76837
$OPBr_3$, mol. struct., electron diffr. and spectroscopic vibr. amplitude 80−58387
OPCl radical, absorpt. spectra, PO (β and B′-X) systems, vibr. numbering 77−75173
OPF_3, mol. beam elec. reson. spectrum, mol. props. 79−94011
$^{16}O_3$, $^{18}O_2$, vac. UV absorpt. spectra, band intensities and designations 78−5245
$^{18}O_2$, Herzberg transition I in absorpt. spectrum 79−72313
O_2*, vibrationally excited, study by variable temp. photoelectron spectroscopy 78−21972
O_2^{-*}, vibr. excited, lifetime obs. 77−42422
$O_2(a^1\Delta_g)$, vibr. constants from O_2-He afterglow 79−31576

molecular vibration continued
$O_3(c^1\Sigma_u)$, in Ar(Kr)(Ar-Kr) matrices, multiphonon vibr. relax. time-resolved emission obs. 80−18861
OsO_4, and isotopic forms, stretching fundamental, 961 cm^{-1}, high resolution spectroscopy 78−90162
P_2, electron affinity, vibr. struct. in radiative electron attachment spectra 77−88592
P_2 radical, $A^1\Pi_g$-$X^1\Sigma_g^+$ transition, vibr. consts. *(French)* 77−75176
P_2 radical, emission spectrum, perturbations in $c^3\Pi_u$ and $C^1\Sigma_u^+$ states *(French)* 77−23484
PBr_3, Raman scatt. spectrum, intermol. interaction and dimeric assoc. *(Russian)* 77−54562
PBr_3, Raman scatt. spectra in gas, liq. and solid states, mol. dynamics *(Russian)* 77−55779
PCl, visible and near IR emission, $A^3\Pi\rightarrow X^3\Sigma^-$ and $b^1\Sigma^+\rightarrow X^3\Sigma^-$ systems vibr. anal. 78−21938
$P^{35}Cl_3$, microwave, rotational spectra, excited vibrational states 79−98080
PD_3, liq. and plastic cryst. states, vibr. dephasing and correl. functions 79−69036
PF_3, microwave l-type reson. transitions in $v_4=1$ state 77−57988
PF_2D, normal coordinate analysis of vibrational spectra 79−68233
PF_2H, normal coordinate analysis of vibrational spectra 79−68233
$PF_2H(D)$, vibr. spectra and normal coordinate anal., Raman and IR spectra 80−14147
$(PF_2)_2O$, IR and Raman spectra, vibr. assignment 78−50544
PH_2 radical, laser-induced fluoresc. 78−94277
PH_3, millimeter spectra, $v_2=1$, $v_4=1$ excited vibr. states, $J=0\rightarrow1$ rot. transition 79−6936
PN, absorpt. and emission spectra, electronic transition and vibr. obs. 80−91573
PO, in Ar matrix, IR and UV absorpt. spectra 80−47985
$P^{18}O$, UV absorpt. spectra, valence and Rydberg states, rot., vibr., anal., predissoc. 79−41184
P_4O_6, IR and Raman spectra vibr. spectra, valence force field calc., pot. function *(French)* 78−50549
POF_3, level anticrossing effects, vibr., laser Stark spectra obs. 80−32771
PS, electronic transition $B^2\Pi$-$X^2\Pi$, vibr. and rot. anal. *(French)* 78−78716
Pb_2, in Ar matrix, excitation and emission spectra, vibr. freq. 78−13507
$Pb_2V_2O_7$, V-O-V bridge stretching freq. correl. with bond angle 78−74636
Pd complex, $Pd^IPt^I(CNCH_3)_6(PF_6)_2$, vibr. spectra, M-M bonds. *(French)* 80−47997
$PdAl_2Cl_8$, Raman resonance spectra of vapour 78−94251
$Pd(PF_3)_4$, force fields mean obs. amplitude calcs. 77−54552
Pt complex, $Pt^{II}(CNCH_3)_4(PF_6)_2$, $Pt_2^I(CNCH_3)_6(PF_6)_2$, and $Pt^IPd^I(CNCH_3)_6(PF_6)_2$, vibr. spectra, M-M bonds. *(French)* 80−47997
Pt complexes, cyano and cyanohalide hydrates, IR absorpt. spectra 77−6771
Pt complexes, XY_4Z_2 type ions, vibr. anal., force consts. 78−70812
Pt-nucleoside complexes, Raman spectra, vibr. anal. 77−65473
$Pt(PF_3)_4$, force fields, mean vibr. amplitude calcs. 77−54552
PuN, in Ar matrix, IR spectra, stretching freq. and isotope shifts 78−78690
PuN_2, in Ar matrix, IR spectra, stretching freq. and isotope shifts 78−78690
Rb_2, B-X system vibr. consts. from mag. rot. spectra 79−76530
Rb_2, $X^1\Sigma_g^+$ state, Raman spectra, fluoresc., vibr. energy 78−46345
$Rb^+CF_3SeO_2^-$, IR and Raman spectra, normal coordinate anal. for $CF_3SeO_2^-$ anion 80−87122
RbF, RbCl and RbI, monomers and dimers, Ar matrix-isolated, IR spectra, vibr. assignments and calcs. 79−45718
RbI, ground vibr. state rot. transition, quadrupole HFS and coupling consts. *(German)* 77−57990
ReO_4^- molecules in alkali halide matrices, CO_2 laser saturation of internal vibr. modes 78−86922
$(Re_2OCl_{10})^{3-}$, reson. Raman, IR and electronic spectral studies 79−10118
RuO_4, $\nu_3(F_2)$ IR band contour, isotopically pure cpds., mol. consts. 77−61746
S compounds, unstable, forbidden transitions, laser optoacoustic spectroscopic obs. 77−61756
S_2, matrix-isolated, $B^3\Sigma_u^-$ predissoc., relax. processes 80−58329
S_2 vibrational constants, UV absorption and fluorescence spectros. of S_x vapour, x=3 to 8 80−78631
S_7, Raman and IR spectra, vibr. anal., force consts., thermodynamic functions 78−50545
S_8 rings, vibr. spectra and thermodynamic functions *(German)* 78−82742
S_n, (n=2-12), vibr. spectra and thermodynamic functions *(German)* 78−82742
SCN^-, associated with metallic cations in aq. soln., press. effect, Raman spectra *(French)* 78−80333
$(SCN)_2^-$, reson. Raman spectrum, vibr. freqs. 79−18189
SCl_2, microwave spectrum, quadratic pot. function, average struct. 77−65456
S_4Cl_2, Raman spectra, vibrs. and rot. isomers of S_n^{2-} (n=4-8) *(German)* 78−13504
SF_2, microwave spectrum inertia defects, ν_1, ν_3, ν_2, equilibrium structure, vibration rotation constants, anharmonic potential functions 79−93988
$^{32}SF_2$, $^{34}SF_2$, matrix IR spectra, vibr. and force fields, bond angle *(German)* 78−74662
SF_6, $3\nu_3$ band anal., IR spectra 78−90161
SF_6, absorpt. structs. in VUV region 79−3458
SF_6 and S_2F_{10}, absorpt. of intense laser radiation, vibr. excitation 80−9667
SF_6, collisionless fluoresc., 16 μm, following laser pumping, vibr. quasicontinuum 78−42111
SF_6, collisionless intramol. vibr. relax., time-resolved spectra 78−82777
SF_6, collisionless intramolecular vibr. relax. obs. 79−45706
SF_6, collisionless multiphoton laser dissoc. mechanism 77−503
SF_6, collisionless multiphoton dissoc. rate, statistical thermodynamic process 77−50482
SF_6, collisionless multiple-photon laser excitation, anharmonic splitting effect 77−61815
SF_6, collisionless multiphoton dissoc., statistical thermodynamic process 78−82799
SF_6, dissolved in O_2 and Kr, cryogenic liqs., mol. motions, IR and Raman spectra 79−69823
SF_6, Doppler-limited spectroscopy, of $3\nu_3$ band 80−58244
molecular vibration continued
SF_6, dynamics of 10.4 μm absorption, vibr. bath model 78−17666
SF_6, electron impact, vibr. excitation, dissociative attachment 77−3481
SF_6, ground state, mol. consts., ν_2 Raman band calcs. *(French)* 78−9156
SF_6, ground state and vibr. heated mols., CO_2 laser pulse absorption 77−46607
SF_6, high-resolution IR Ar matrix-isolation spectra, 10K 80−32708
SF_6, highly excited, time-resolved IR absorpt. obs. 80−9666
SF_6, IR absorpt. spectra of vibr. excited mols. *(Russian)* 79−36643
SF_6, IR double resonance, V-V energy transfer from ν_3 mode 77−482
SF_6, IR multiple-photon excited molecules, Raman spectroscopy 80−74207
SF_6, IR radiation induced mol. excitation and heating effects, time resolved 77−75142
SF_6, IR spectra, ν_4 vibr. band strength 78−94240
SF_6, inhibition of homogeneous condensation by vibr. excitation, isotope separation appl. 78−37688
SF_6, intramode anharmonicity const., vibr. linear absorpt. spectrum 80−18893
SF_6, isotopically selective collisionless laser induced dissoc. 78−1037
SF_6, laser isotope separation model 77−31016
SF_6, laser pumped, mol. vibr. amplitude changes, gas phase electron diffr. obs. 79−76513
SF_6, laser-irrad., high-resolution double-reson. spectroscopy, collisionless multiphoton dissoc. 80−9623
SF_6, mean amplitude of vibr., from electron diffr. study 78−29859
SF_6, molecular vibration energy stochastization in intense IR laser field by Raman spectroscopy *(Russian)* 80−14149
SF_6, mulitphoton absorpt., pulsed CO_2 laser radiation absorpt., press., freq., fluence depend. 80−28080
SF_6, multiphoton dissoc., energy deposition 78−82800
SF_6, multiphoton dissoc., classical model 80−53076
SF_6 multiphoton dissoc. by mol. beam method, energy distribution meas. by time-of-flight spectra, dissoc. dynamics 80−78670
SF_6, multiphoton-excited in mol. beam, photoionsation probe of vibr. energy distrib. 79−76476
SF_6, ν_3 band, IR spectra, in supersonic mol. beam 78−66541
SF_6, ν_3 bands, rot. fine struct., HFS spectroscopic consts. determ., saturation spectroscopy obs. 80−53008
SF_6, ν_3 manifold, $3\nu_3$ transition, 3-quantum transition probabilities, IR spectrum 78−86866
SF_6, ν_3 mode 2nd vibr. overtone absorpt. spectrum 77−88463
SF_6, ν_3 Q-branch, CO_2 laser pumped 78−21924
SF_6, partial saturation of ν_3 ladder in IR absorpt., rate process model 80−58645
SF_6, photon-enhanced dissociative electron attachment 80−9749
SF_6, photon-enhanced dissociative electron attachment, isotope selectivity 80−18939
SF_6, population of excited vibr. level, nonequilib. absorpt., 140K *(Russian)* 79−36708
SF_6, spectroscopic consts. calc. from saturated absorption spectrum *(French)* 78−971
SF_6, valence electron spectra, vibr. band struct. 77−23520
SF_6, vibr. coupling in collision-induced Raman scatt. 80−83373
SF_6, vibr. Raman spectrum, Q branches shapes 78−42077
SF_6, vibr. relax., 150 to 320K, IR double reson. study *(Russian)* 78−86899
SF_6, vibr. spectra, rot. consts., IR spectra, Raman spectra obs. 80−32719
SF_6, vibrationally excited, collisionless intramolecular energy transfer 78−37663
SF_6+N_2, simultaneous vibr. transition, absorpt. band intensity 77−50474
SF_6+Si(surface), IR laser induced reaction, mol. vibr. and mol. dissoc. obs. 80−93798
SF_5Br, vibr. spectrum and normal coord. anal. 77−18926
SH, $(X^2\Pi_i)$ radical, UPS in VUV region showing vibr. struct. 79−98153
SN, struct., vibr. spectra, ab initio calcs. 78−66475
SN^+, struct., vibr. spectra, ab initio calcs. 78−66475
S_2N_2, struct., vibr. spectra, ab initio calcs. 78−66475
$S_{8-x}(NH)_x$, (x=1,2,3,4), and deuterates, IR and Raman spectra, isotope shifts, mol. vibr. assignment 79−10110
$(SN)_n$* radicals polymerisation to $(SN)_x$ in thin films, optical spectra 80−16656
SO_2, absorpt. coeffs. for ν_2 and ν_3 bands 77−38668
SO_2, IR multiphoton excitation and inverse electronic relax., mol. vibr. and fluoresc. 80−106349
SO_2, laser-induced phosphoresc.-excitation spectra of vibr. bands of $(^3B_1)$-$(X,^1A_1)$ transition 80−18879
SO_2, matrix isolated, ν_3 vibr. spectrum, diode laser spectroscopy, temp. depend. 77−50433
SO_2, photoelectron spectrum, vibr. struct., ionos. pot. 77−75217
SO_2, SVL fluoresc. spectra, multiple vibronic origins 77−14474
SO_2, SVL fluoresc. spectra, 293 to 307 nm region 77−14475
SO_{2+}, vibr. energy levels, semiclassical trajectory method calcs. 78−58660
SO_2^+, $(B^2A_1\rightarrow X^2A_1)$ fluoresc., Penning excitation, vibr. and bending freqs. 77−50507
SO_2^+, state selected vibr. levels, fragmentation, photoelectron-photon coincidence spectroscopy 79−89707
$^{34}SO_2$, $\nu_1+\nu_3$ band, high resolution IR spectrum *(French)* 77−71801
$SPBr_3$, mol. struct., electron diffr. and spectroscopic vibr. amplitude 80−58387
SPF_3 vibr. spectrum, assignment using matrix isolation and isotope substitution *(German)* 78−13498
$SSCl_2$, IR spectra, prod. in S_2Cl_2 photolysis 78−61033
SSF_2, FSSF, and ^{34}S isotropic forms, matrix IR and Raman spectra *(German)* 79−89674
$S_{12}(S_{12}.CS_2)$, vibr. spectra and thermodynamic functions *(German)* 78−82742
$S(SiD_3)_2$, Raman spectra of gaseous, liquid, solid phases, IR spectra of gaseous and solid phases 78−25547
$S(SiH_3)_2$, Raman spectra of gaseous, liquid, solid phases, IR spectra of gaseous and solid phases 78−25547
SbO_4^{3-}, normal vib. freq. and force const. calcs. *(Russian)* 78−46318
Sb_4O_6, IR and Raman spectra vibr. spectra, valence force field calc., pot. function *(French)* 78−50549
Se_2, $b^1\Sigma^+\rightarrow X^3\Sigma^-$ near IR emission obs. 80−91556
$^{80}Se_2$, Lande factors measurement in $B\ ^3\Sigma_u^-$ state 77−34648
SeF_6, IR vibr. band contours, isotope substitution, force consts. 78−17670

molecular vibration continued
- SeF_6, in Kr matrix, temp. reversible IR spectral changes, site struct. dynamics 80−102505
- SeO, $A^3\pi$-XO^+, 1 band system 77−58039
- SeO, $b^1\Sigma^+ \rightarrow X^3\Sigma^-$ near IR emission obs. 80−91556
- SeO, IR bands of 10296 and 10491 Å, rot. struct. 78−5224
- SeS, $b^1\Sigma^+ \rightarrow X^3\Sigma^-$ near IR emission obs. 80−91556
- Sf_6, integrated IR band intensities and transition moments 80−95611
- $SiAs+Cl_2(Br_2)(I_2)$, high temp. Raman spectra, cryst. growth mechanism *(French)* 79−26999
- Si_6Br_{12}, and Si_6Cl_{12}, vibrational spectra and force constants, rel. to Si_5Cl_{10} and Si_5Br_{10} *(German)* 79−22716
- Si_5Cl_{10}, and Si_5Br_{10}, vibrational spectra and force constants, rel. to Si_6Cl_{12} and Si_6Br_{12} *(German)* 79−22716
- $(SiCl_3)_2O$, IR matrix isolation spectrum, Raman spectrum 78−82730
- SiF_4, ^{19}F chem. shielding, depend. on internal coords. 78−5249
- SiF_4, $\nu_3(F_2)$ IR band contour, isotopically pure cpds., mol. consts. 77−61746
- SiF_4, valence electron spectrum, vibr. struct. 77−75209
- SiH_3 radical, hyperfine coupling consts., vibr. depend., ab initio calcs. 80−87150
- SiH_4, IR spectra, ν_2 and ν_4 band anal. 78−9153
- SiH_4, ν_3 and ν_1 IR bands, anal. 79−22704
- $^{28}SiH_4$, analysis of ν_4 band interacting with ν_2 band *(French)* 78−9152
- Si_6H_{12}, and Si_6D_{12}, Raman and IR spectra, vibr. force consts., config. *(German)* 79−22715
- $^{28}SiH_3D$, IR spectrum ν_1 and ν_4 bands, rot. const. 77−83590
- SiH_3NCS, microwave spectrum, mol. consts., isotope effects 77−46559
- SiH_3NCS, microwave spectrum, struct., dipole moment, ^{14}N quadrupole coupling const. 77−46560
- $(SiH_3)_2O$, and d_6, Raman spectra, vibr. mode and config. 78−62940
- $SiH_3PH_2BD_3$, liquid and solid, vibr. analysis, spectra and structure of P-B compounds 78−84586
- $SiH_3PH_2BH_3$, liquid and solid, vibr. analysis, spectra and structure of P-B compounds 78−84586
- $(SiH_3)_3Y$, (Y=As, P, Sb), vibr. force fields and amplitudes, zero point struct. 77−54551
- SiO in Ar matrix, vac. UV spectrum, vibr. progression 80−23432
- SiO, interaction between $G^1\Pi$ and $I^1\Pi$ states 79−50040
- SiO, rot. and vibr. consts., millimetre-wave spectrum 77−34619
- SiO, test of perturbation method for vibr. assignments, low lying electronic states 77−34645
- SiO^-, rot. spectrum, isotope shift, mol. consts. 79−59483
- SiO_4^{4-} compounds, vibr. pot. function, force consts., isotopic shifts, mean vibr. amplitudes 80−23395
- Si_3O_3, isotopically substituted, IR freq. and intensity patterns 78−21926
- $Si_2O(Cl_3)_2$, IR and Raman spectra, vibr. anal. 78−66552
- SiS, and isotopes, microwave spectra and consts., review 77−23493
- SiS, chemiluminescent flame spectra, electronic states and rot. struct. obs., vibr. assignments, Franck-Condon factors determ. 80−85179
- Sm complex, mono-, di-, tri-glycolate, IR absorpt. spectra, vibr. freq. and co-ordination number 78−58684
- Sn_2, matrix isolation Raman spectrum, overtone bands breadth 78−33515
- SnI_3^-, vibr. intensities, forms and freqs. anal. SCF MO LCAO CNDO calcs. 78−9274
- SnO, $D\ ^1\Pi$-$X^1\Sigma$ transition 79−41179
- SnO, $D^1\Pi$-$X^1\sigma$ transition, vibr. temp. under const. and varying electronic transition moments 79−41197
- SnO_4^{4-}, normal vib. freq. and force const. calcs. *(Russian)* 78−46318
- SrF_2, force consts., mean amplitudes of vibr. 78−17647
- SrI, low-lying electronic states, vibr. anal. 80−106315
- SrO, mm wave spectrum, spectroscopic consts. 78−37629
- SrO_3, visible absorpt. and reson. Raman spectra in Ar and N_2 matrices 77−65487
- β-$Sr_2V_2O_7$, V-O-V bridge stretching freq. correl. with bond angle 78−74636
- TOT, vibr. intensities, ab initio and empirical calcs. 80−78592
- TOT, vibr. intensities, ab initio and empirical calcs., band strengths 80−78593
- $TaBr_5$, gaseous, electron diffr. obs. of vibr. assignment, mol. struct. and barrier to pseudorot. 79−81293
- $TaCl_5$, mol. struct., vibr. assignments, barries to pseudorotation 78−29858
- TaN, matrix isolated, electronic and vibr. absorpt. spectra 79−64014
- Te_2, $B0_u^+ - b^1\Sigma_g^+$ system, transition assignment, IR and visible spectra obs. 80−58298
- TeO_4^{2-}, normal vib. freq. and force const. calcs. *(Russian)* 78−46318
- $TeOCl_2$ from $TeO_{11}Cl_2$ pyrolysis, normal coord. anal. 80−81306
- Ti complex, $Ti(IV)$-H_2O_2, H_2SO_4-aq. soln., reson. Raman spectrum, vibr. assignments, molar absorptivity 77−65469
- $TiBr_4$, reson. Raman spectrum, vibr. analysis, Jahn-Teller coupling 79−85965
- $TiCl_5^-$, vibr. anal., force fields and consts. *(German)* 79−45702
- $Ti_2Cl_{10}^{2-}$, vibr. anal., force fields and consts. *(German)* 79−45702
- $Ti_2Cl_9^-$, vibr. anal., force fields and consts. *(German)* 79−45702
- TiF_2, force consts., mean amplitudes of vibr. 78−17647
- TiF_4, equilib. config., force field, Coriolis consts., vibr. freqs. and amplitudes 80−32835
- TiN, vibr. IR spectrum, mol. consts. 79−68230
- TiO β system, electronic transition moment and effective vibr. temp. 77−68078
- Tl_2Cl_2, mol. consts., IR and Raman freqs. assignments 78−17648
- Tl_2F_2, mol. consts., IR and Raman freqs. assignments 78−17648
- $Tl_2F_2(Cl_2)$, assignment of vibr. Raman and IR spectra bands 80−58268
- $TlNO_3$, molten and aqueous soln., Raman spectra 79−78673
- U complexes, tetranuclear halogenocomplexes, preparation, vibr. spectra *(French)* 77−83596
- UF_5, transient species formed in UF_6 laser flash photolysis, 17 micron IR spectrum 79−45715
- UF_6 ($^{235,238}U$), vibrational overtone spectra calc. 78−66534
- UF_6 in Ar matrices, fluoresc. and Raman spectra, vibr. anal. 78−66585
- UF_6, room temp., IR absorpt. obs., isotope shift of fund. band and combination bands, freq. depend. 80−23421
- UF_6, valence electron spectra, vibr. band struct. 77−23520
- UN, identification in AR matrix, IR spectra, vibr. freqs. 77−9066
- UO_2, molecular geometry determ. from IR spectra vibr. assignments 77−50437
- VO^{2+}+alkyl dinitriles, reaction, CN stretching freqs., bonding effects 77−16820

molecular vibration continued
- W (100), H adsorbate low energy electron vibrational excitation 80−84375
- WCl_6^{n-}, n=1,2, vibr. freqs., Raman and IR meas. 79−68234
- WF_6, valence electron spectra, vibr. band struct. 77−23520
- WO_3, IR spectra, normal coord. anal. 78−58682
- WSe_4^{2-}, anharmonicity consts., reson. Raman spectra 77−61754
- $Xe+Cl_2$, classical trajectory calcs., energy threshold for collision induced dissoc. determ., 80−95709
- XeCl+HCl (inert gas atom), ground state destruction, quenching rate consts. meas. 80−63758
- XeF, 3500 Angstrom band, vibr. anal. 78−70843
- XeF, B-X transition vibr. anal., flash photolysis UV absorpt. spectroscopy 78−42088
- XeF, ground state dissoc. vibr. equilibrium 80−9652
- XeF, matrix-isolated, search for IR fundamental 77−58017
- XeF, supersonic expansion jet, B←X system rot. and vibr. anal., isotope intervals, fluoresc. spectra 80−14174
- XeF, X, B, and D-states, spectra, vibr. and rot. consts. 78−70844
- XeHCl, microwave and RF spectra, mol. beam elec. reson. meas. 79−72302
- XeO_2F_2, mean amplitudes of vibr. and molar thermodynamic functions 78−17649
- XeO_3F_2, mol. consts., general valence force field calcs. 78−21906
- Xe_2^*, synchrotron radiation excited, time resolved spectroscopy 80−69092
- YD, electronic spectra *(French)* 77−14442
- YF_3, force consts., Coriolis coupling consts., vibr. amplitudes 78−17650
- YH, electronic spectra *(French)* 77−14442
- YH, YD, 3800-9000 Å negative glow spectra, triplet and singlet systems 77−79608
- YO, spectra, 4500-6900 Å, mol. consts. 78−50551
- $Y^{16}O$ and $Y^{18}O$, vibr. anal. of blue and red system 79−809
- Yb^{3+}, in soln., non-radiative transitions as Forster's energy transfer to solvent vibrations 80−1014
- YbBr, emission spectra in arc discharge, vibr. anal. 78−74670
- YbCl, emission spectra in arc discharge, vibr. anal. 78−74670
- YbI, emission spectra in arc discharge, vibr. anal. 78−74670
- Zn complex, Zn(l-spartein)Cl_2, IR circular dichroism spectra, vibr.-electronic interaction 80−55074
- Zn porphin, in triphenylene, single site fluoresc. and visible spectra, vibr. assignments 77−58031
- Zn_2, in Ar and Kr matrices, 10K, UV spectrum, vibr. assignments 77−58038
- $ZnCl_2$, aq. solns., complex IR refr. indices, IR spectra, mechanisms, spectrometer system 78−43831
- ZnFCl, existence and vibr. characterisation, IR and Raman matrix isolation obs. 78−78706
- $ZnGa_2$, excimer visible emission spectra in RF discharge, vibr. struct. 79−18201
- $ZnNb_2O_6$, columbite struct., normal coord. anal. 78−964
- $Zn_2V_2O_7$, V-O-V bridge stretching freq. correl. with bond angle 78−74636
- ZnX_2, ZnXY, X and Y=halogen, matrix isolation IR and Raman spectra 78−55171
- ZrF_4, mol. struct. and vibr. freqs., gaseous electron diffr. obs. 80−32836
- ZrN, vibr. IR spectrum, mol. consts. 79−68230
- ZrO bands, integrated intensity meas. and effective vibr. temp. 80−43111

molecular vibration calculations
- AB_2, bent molecule, ab initio force fields, appl. of Simons-Parr-Finlan expansions 79−41218
- AB_2 and AB_4 molecules Raman overtone and combination transition intensities, bond-polaris. approach 78−42034
- ab initio calcs., evaluation of X-H bond dissociation energies 77−3267
- ab initio Cl pot. curves, mol. wavefunctions and vibr. freqs. comparison of methods 80−27956
- acetaldehyde, soln., C-O stretching band intensity calcs., intermol. interaction effects 77−68081
- acetic acid dimer, vibr. spectra at low temp., Witkowski-Marechal theory 78−46314
- acetonitrile, liq. and solns., IR absorpt. band intensity, temp. depend., CC and CN bonds 77−75157
- acetylene, core ionised, core-excited and shake-up states, ab initio MRD-CI methods 80−42950
- acetylene, quartic anharmonic pot. energy function 78−58662
- acetylene, vibr. freqs., MINDO/3 calcs. 78−13429
- acetylenes, substituted, CH wag group freqs., CNDO/2 calcs. 77−6745
- aliphatic alcohols, conform., rot. isomerism calcs. *(German)* 78−50541
- alkali halide, monomer to tetramer, far IR region, polarisable ion model 78−66545
- alkali halide molecular clusters, equilib. geom., form. energy and vib. spectrum 78−55269
- alkali halides, quadrupole coupling, vibr. and rot. effects, Morse oscill. calcs. 77−6805
- alkali metal dicarboxylates, H bonding and motion, incoherent inelastic neutron scatt. spectroscopy 80−48095
- alkali metal monoxides, bond distance, dissoc. energy and vibr. freq., electron gas model 77−30846
- alkanes, IR spectral intensity for electro-optical parameter 79−54835
- n-alkanes, longitudinal acoustic modes, Raman intensities 80−32718
- n-alkanes, vibr. calcs. and nonrigid mol. symmetry groups 77−6756
- alkenes, IR absorpt. curves calc. using standard fragments computer library 80−982
- alkynes, normal coord. calc. and valence force field 79−72294
- allene, ionis. pots., Green's function method 77−14608
- allene, non-degenerate vibr. mode induced Jahn-Teller effect, photoelectron spectra calc. 79−817
- anharmonic molecule, high-order multiphoton excitation features 79−54927
- anharmonically coupled oscills., time depend. Hartree theory, susceptibility, absorpt. and Raman spectrum 80−58241
- aniline-ND_2(-NHD), far-IR vap. phase spectra, assignments pot. function calcs. 77−75144
- anthracene, normal coord. calcs., simplified valence force field models 78−94229
- aromatic compounds, out-of-plane mol. vibrs., force field approx. calcs. 80−91538
- aromatic hydrocarbons, excited state vibr. freqs. 79−85947
- aromatic hydrocarbons, vibronic calcs. 80−58238

molecular vibration calculations continued
aromatics, condensed, new force field, appl. to pyrene inplane vibrs. 79 - 81201
asymmetric top molecules, transition moment between nondegenerate states 79 - 27036
atom + molecule, IR induced vibr. transition, Schrodinger eqn. distorted wave calc. 77 - 23538
atom + triatom collisional energy transfer, ergodicity in mol. vibr., Henon-Heiles pot. 80 - 18906
azulene, Shpol'skii matrix, $S_2 \rightarrow S_1$ fluoresc., spectral anal. 77 - 18956
benzene, $^1A_{1g} \rightarrow {}^1B_{2u}$ absorption band, Franck-Condon factors calc. 79 - 36701
benzene, and deuterated forms local mode oscill. strengths 79 - 27039
benzene, d_3, -d_6, vibr. freqs., force consts., CNDO/2 calcs. 77 - 65449
benzene, mean amplitude of mol. vibration, approx. calc. method 79 - 13697
benzene, nonplanar vibr., force field calcs. 79 - 41148
benzene, normal coord. calcs., simplified valence force field models 78 - 94229
benzene, out-of-plane mol. vibrs., force field approx. calcs. 80 - 91538
benzene, third channel decay mechanism, radiationless transitions 77 - 50463
benzene, vibr. freqs., MINDO/3 calcs. 78 - 13429
benzene, vibr. overtone lineshape 79 - 27040
benzene-d_3, gas phase Raman spectrum, E′ and E″ species, Coriolis consts. *(French)* 78 - 5235
benzenes, IR spectral intensity for electro-optical parameter 79 - 54835
benzenes, substituted, CH wag group freqs., CNDO/2 calcs. 77 - 6745
benzenoid hydrocarbons, normal coord. calcs., simplified valence force field models 78 - 94229
benzonitrile, excited single state B_1, electron-vibr. spectra and electronic struct. 79 - 26904
p-benzoquinones, chlorinated, transferable force field for in-plane vibrs. 80 - 964
biharmonic oscillator, coincident energy levels, for teachers 79 - 40324
binuclear double bridged complexes, $[Y_2XZ_2XY_2]D_{2h}$, normal coord. anal. *(French)* 79 - 81194
biphenyl, diamagnetism and thermal motion 80 - 25076
biphenyl cryst., nonbonded atom-atom interact. model, low freq. vibr. modes 77 - 1188
bond polarity parameters, IR intensities, molecular orbital study 79 - 63914
borazines, substituted, Urey Bradley force field, pot. energy consts. 80 - 78588
Born-Oppenheimer coupling elements, crude and adiabatic approx. 77 - 65415
boron trihalides, mol. force field using parametric represent. method 80 - 27991
bound continuum vibr. transitions, Franck Condon matrix elements calcs. 80 - 69191
• 1-bromo-1-chloroethylene, vibr. assignment, IR and Raman spectra 77 - 18925
bromoacetonitrile, ground state microwave spectrum assignments, mol. struct., rot. consts., quadrupole coupling 77 - 6763
o-bromobenzene, electronic absorpt. spectra, vibr. anal. 77 - 3379
bromochlorofluoromethane, Raman optical activity parameters, circular intensity differentials comput. 79 - 85950
bromoethane, mol. parameters, vibr., pot. barrier height etc., data tables 79 - 76409
n-butane, skeletal alkane fluid simulation, vibr., rot., torsional gauche/trans relax., diffusion const. 79 - 1378
butatriene, ionis. pots., Green's function method 77 - 14608
t-butyl radicals, ab initio geometry calc., ^{13}C hyperfine coupling 77 - 10580
C_{3v} symmetry excited vibr. state mol. consts., graphical method 80 - 52969
carbon tetrafluoride, vib. anharmonicity 78 - 55160
carbonyl fluoride, vibr. transition moments and force fields, gaussian basis set calcs. 79 - 81152
carboxylic acid dimer, Fermi reson. 79 - 31501
cellulose macromolecule, conform. states and IR dichroism calcs. 80 - 55986
cellulose triacetate, vibr. spectra, theory 79 - 54836
chemisorbed molecule, vibr. freq. rel. to interaction with surface 80 - 54519
1-chloro-2-methylbutane, conformer depend. C-C1 stretching vibrs., Raman optical activity spectrum simulation 80 - 14146
chloroethanes, electro-optical parameters, Raman spectra absolute intensities and depolaris. 77 - 10678
chloromethane, radial distrib. function of vibr. excited mol. 79 - 85951
chromophoric groups, freqs., dipole strengths, rot. strengths, nonchromophoric group dipole coupling effects 79 - 98060
classical model for vibr. transition dynamics, absorpt. of IR radiation 80 - 52965
collisionless dissociation mechanism, vibr. nonlinear mechanics in high-intensity laser field 79 - 41207
composite particle, vibr. amplitude and vibr.-rot. anal. 80 - 74158
conformations of rotational isomers, interactive access data program 78 - 62786
conjugated molecules, excited state, self-consistent HMO theory *(Japanese)* 77 - 42253
copper porphin, IR spectra and vibr. anal., and deutero-derivatives 79 - 22705
coupled isotope effects in exchange reactions, vibr. freq. and atomic masses 80 - 18843
coupled oscillator system, SCF-state interaction method 80 - 58239
coupled oscillators, approx. and exact quantum energies and eigenfunctions 79 - 26961
cubic anharmonicity constants, normal coord. ab initio calcs. 79 - 36595
cyclobutadiene(-d_1), singlet and triplet ground states, vibr. freqs., MINDO/3 and ab initio SCF calcs. 78 - 13429
cyclohexane, mean amplitude of mol. vibration, approx. calc. method 79 - 13697
cyclopentanone, n - π^* transition, vibr. band intensities 80 - 74116
cyclopentene, mol., pot. functions of bending modes 80 - 9753
1,1-cyclopropane-d_2, isomerisation transient vibr. energy distrib., collisional relax., variable encounters method 80 - 50836
dense media, exchange dephasing and motional narrowing of vibr. modes 79 - 68222
diatom, $^1\Sigma$ state vibr. matrix elements, Dunham pot. *(French)* 79 - 54832
molecular vibration calculations continued
diatomic, Morse oscill. eigenstates, coherent states and uncertainty products 79 - 59434
diatomic fluorides, exact force field calcs. using at. force consts. 78 - 62739
diatomic liquid, vibr. dephasing calc., diatom anharmonicity 78 - 94959
diatomic long-range molecules, highly vibr. excited state 78 - 29768
diatomic molecular dilute solns., IR and Raman spectra temp. depend. anal. model *(French)* 77 - 88456
diatomic molecular form factors, vibr. average, study of convolution approx. 79 - 50926
diatomic molecule, electronic states calc. using five-parameter pot. function *(Russian)* 77 - 3270
diatomic molecule, hetero- or homonucl., empirical rel. for vibr. freqs. 79 - 81197
diatomic molecule, pot. and spectroscopic consts. 79 - 94053
diatomic molecule, vib.-rot. wavefunctions and matrix elements, pot. function effects 77 - 453
diatomic molecule, vibr. eigenenergies representation, functional form 79 - 68220
diatomic molecule, vibr. energies and functions, cubic splines method calcs. 80 - 78594
diatomic molecule, vibr. Green's function and two-photon dissociation, appl. to H_2^+ 80 - 28075
diatomic molecule, vibr. potential representations 79 - 68219
diatomic molecule, vibrational transitions, Franck-Condon matrix elements 80 - 9645
diatomic molecule, vibrational wave function, anal. expressions of canonical functions *(French)* 78 - 21901
diatomic molecule, with ang.-depend. pot., vibr. matrix element calcs. *(French)* 78 - 13484
diatomic molecule vibr. pots., representations accuracy 78 - 66531
diatomic molecules, dipole matrix elements for vibrational transitions, numerical calc. 80 - 95594
diatomic molecules, electronic and vibr. functions of non-adiabatic wavefunction 79 - 22621
diatomic molecules, Franck-Condon factors for high J, Morse oscill. calcs. 78 - 37548
diatomic molecules, r-centroid method appl. 80 - 102500
diatomic molecules, soluble potential 78 - 21996
diatomic molecules, vibr. matrix elements, 0→0 to 0→7 78 - 90143
diatomic molecules, vibrational distrib. *(Russian)* 79 - 36617
diatomic mols. in Ar matrix, vibr. level energy cascades 77 - 79598
diatomic photoelectron spectra, vibr. struct. calcs., cost-effective program 77 - 18973
diatomics, vibr. correction and effective moment of inertia, a correl. 79 - 89662
2,5-dichloro-1,4-benzoquinone, mol. cryst., transition moment directions 78 - 64351
1,2-difluoroethane, vibr. amplitude optimised force field calc. 79 - 76514
• cis- and trans-difluoroethylene, force consts., mean vibr. amplitudes 77 - 6748
dihalomethanes, mol. vibr. spectra internal coord. model, and d_2 substitution 79 - 63974
2,5-dihydrofuran, mol., pot. functions of bending modes 80 - 9753
1,5-dihydroxyanthraquinone-d_0,-d_2, mol. vibr., IR spectra 77 - 467
N,N-dimethyl acrylamide (-d_3,d_6,d_9), force field, IR and Raman spectra obs. 80 - 47979
dimethyl di(trifluoromethyl) germanium, and perdeuterated analogues, vibr. spectra, normal coord. anals. *(German)* 80 - 5547
dimethyl sulphoxide, 1:1 and 1:2 complexes with H_2O and D_2O, H-bonding, IR and Raman vibr. spectra 77 - 34633
N,N-dimethylselenourea, deuterated forms and methyl derivatives, fundamental IR vibr. assignments 80 - 961
N,N-dimethylthiourea, deuterated forms and methyl derivatives, fundamental IR vibr. assignments 80 - 961
1,4-dioxadiene, mol., pot. functions of bending modes 80 - 9753
dioxane, 1:1 and 1:2 complexes with H_2O and D_2O, H-bonding, IR and Raman vibr. spectra 77 - 34633
dissociating molecule, vibr. spectra, nonradiative transitions *(Russian)* 78 - 21864
dithiosuccinimide-d_0,-d_1, normal coord. anal. calcs. 77 - 30844
DNA, backbone vibrational mode displacements of A-DNA and B-DNA 80 - 8000
double minimum vibr. pot., FORMAC program 77 - 23444
doubly degenerate vibr. levels of spherical top, basis functions as irreducible tensors of O(3) 77 - 14414
Eckart frame, mol. symm. and motions 78 - 74634
electron transfer reactions, free energy, anharmonic intramol. quantum mode depend. 77 - 12781
energy deposition by multiple IR photon absorpt. 80 - 66833
energy distribution in vibr. systems, coordinate choice 78 - 21903
energy level clustering, qualitative theory of irreducible tensor operators spectra 80 - 28001
energy transfer, classical versus quantum calcs., forced quantum oscillator and moment methods 80 - 28095
ESR of vibrationally excited diatomic radicals 77 - 18949
ethane, mean amplitude of mol. vibration, approx. calc. method 79 - 13697
ethane, vibr. anal. using torsional coords. 79 - 93977
ethane, vibr. freqs., MINDO/3 calcs. 78 - 13429
ethane(-d_6,d_3,d_1), electro-optical parameters from IR intensities, least-squares calc. 80 - 9584
ethane-d_0,-d_6, normal coord. and IR intensity anal. 79 - 36604
ethylene, and ^2H, ^{13}C, ^{15}N, ^{18}O isotopic derivatives, vibr. freqs. using MINDO/3 force consts. 77 - 71793
ethylene, core ionised, core-excited and shake-up states, ab initio MRD-CI methods 80 - 42950
ethylene, dipole moment derivatives, IR vibr. intensities, STO-3G, 4-31G, calcs. 77 - 6750
ethylene, Hartree-Fock energy and Moller-Plesset perturbation energy, harmonic vibr. freq. 80 - 52852
ethylene, ionis. pots., Green's function method 77 - 14608
ethylene, IR and Raman intensities calc., efficient ab initio computation method 79 - 45698
ethylene, mean amplitude of mol. vibration, approx. calc. method 79 - 13697
ethylene, vibr. freqs., MINDO/3 calcs. 78 - 13429
ethylsilane, redundancy coeffs. for vibrs. involving atoms with four bonds 77 - 27049

molecular vibration calculations continued
exothermic reactions, Marcus eqn., Born approx., strong vibr. nonadiabatic transitions 77−56214
first row elements, split-valence basis set, mol. vibr. and mol. moment calcs. 80−69063
fluid, dense, isotropic Raman polaris., correlation function, kinetic eqn. 77−28567
fluorinated ethylenes, valence bond polar parameters, IR intensities, MO calc. 80−28013
fluoroacetylene, laser Stark and IR-microwave double resonance, E1 moment, vibr. states 77−6813
fluoroform(-d_1)-trimethylamine-Ar(Kr), cryospectroscopic IR study of association 77−468
fluoromethanal, visible spectrum, rot., vibr. and vibronic anal., double min. pot. 79−41182
fluoromethane-d_2, matrix isolated, vibr. energy transfer at low temps. 80−37860
fluoromethanes, vibr. spectra, force consts. and geom., SCF ab initio calcs. 78−62785
force const. adjuster program for least squares fit to observed frequencies of molecules and crystals 78−91395
force constant evaluation using isotopic freq. 77−38650
force constants, semiempirical quantum mechanical method 78−62947
force field determination, Green's function method, ambiguities 80−960
force field iterative consistency calcs. using geometric interpretation 77−6746
force fields, MINDO/3 semiempirical SDF MO calc. 79−76408
formaldehyde, adiabatic CI pot. surface LCAO calc., gradient determ., mol. dynamics, vibr. freqs. 80−48056
formaldehyde, anharmonic pot. function, vibr. freqs., vibr.-rot. interaction, centrifugal distortion 77−38651
formaldehyde, photodissoc., pot. energy surface features 79−79271
formaldehyde, unique force field, parametric representation method 77−18897
formaldehyde, vibrational band intensities of $^1A_2$-$^1A_1$ transition, ab initio calc. 80−43028
formaldehyde-d_1, ν_3 fundamental band, IR absorpt. and laser Stark spectra 77−34629
formic acid, microwave spectrum, 10-200 GHz, vibrational excited states, ν_6, ν_8 79−93987
formic acid, normal vibr. pot. energy distrib. 77−451
formic acid crystals $\nu_{O\text{-}H\ldots O}$ and $\nu_{O\text{-}D\ldots O}$ vib. anharmonicities 77−48154
formic acid-d_0, -d_2, OH(OD) stretching, vibr. band struct. 77−6751
formyl fluoride, and isotopic forms, mol. struct., from electron diffr. and microwave data 80−23570
four centre elimination reactions, HX vibr. state distribs., surprisal anal. and synthesis 80−25993
Franck-Condon effects in resonance Raman spectra and excitation profiles, appl. to CrO_4^{2-} and β-carotene 80−14129
frequency shift during gas-soln. phase change, intermolecular interaction pot. 77−23487
frequency shift during gas-soln. phase change, Onsager-Bottcher model 77−23488
furoyl chloride, normal in plane coord. calc. *(French)* 79−68218
Group IIIA metal tetrahalide ions, vibr. anal. 80−63608
Group IV tetrabromides, intramol. force fields and mean vibr. amplitudes 80−106316
Hamiltonian diagonalisation method, eigen functions of Morse oscillator 79−3427
harmonic and Morse oscillator freq. change influence on Franck-Condon factors 80−106312
harmonic oscillator basis, arbitrary pot., matrix elements 78−5199
harmonically vibrating, vibr. mean square amplitudes of mol. internal coords., perturbation theory 79−89659
heteroaromatic mol. radiationless transition decay rate freq. shift depend., quantum statistical mechanics anal. 78−74691
hexachlorodisiloxane, normal vibr. and force field calc. 79−54994
hexahalo ions, octahedral, mol. consts. calcs. 80−106317
hexaoxy ions, octahedral, mol. consts. calcs. 80−106317
high and low frequency separation method, reformulation 78−50539
homonuclear molecular ions, adiabatic pot. curves 80−929
hydracids, monatomic matrix-trapped, assoc. forms, struct. and spectral response, intermol. pot. calcs. 79−93996
hydrates, solid, electric field gradient tensors at deuterons 77−71792
hydrocarbons, IR intensities, C-H bond moments and bending modes 77−10703
hydrocarbons, vibr. intensities, G sum rule appls. 80−32776
hydrogen bond absorption spectra, interaction between two harmonic oscills. 79−6929
icosahedral cage, symmetry coords. and vibration freq. 80−47966
independent-particle Hamiltonian, group struct. 79−22580
inert gas dimer ions, $A^2\Sigma_{1/2u}^+ \rightarrow D^2\Sigma_{1/2g}^+$ system, theoretical absorption spectrum 80−32734
inert gas halides, emission spectra, open-shell closed-shell interaction, electron gas model 77−30879
information theory anal., vibr. population distribs. in laser excited system 77−42380
inorganic molecules with polytopic bonds, motion of nuclei 79−41125
intensity calcs., CNDO/2 method with extended basis set 80−91445
intramolecular dynamics, random coupling model, math. approach 80−58308
intramolecular dynamics, random coupling model, multiphoton excitation, kinetic eqns. 80−63700
intramolecular energy transfer and stability of mol. motion 79−45779
inverse vibr. problem, Lowdin orthogonalisation, Kashiwagi-Sasaki generalisation 79−6928
inversion splitting, generalised WKB method 80−9585
iodoethane, mol. parameters, vibr., pot. barrier height etc., data tables 79−76409
ionic type function ν(XH), non-monotonic freq. variations, effect on Hammett freq. factors *(French)* 79−22690
ionised compounds, geometrical and vibrational struct. changes, semiempirical MINDO/3 calcs. 79−31401
IR band intensities and polar tensors, effective charge and dipole moment derivs. sign 77−34695
IR intensity, at. polar tensor method, F containing mols. 78−62854
IR interaction with mols., classical/semiclassical theory 78−90164
isostructural molecules and ions, force const. set calcs. 80−23390
isotopic frequency ratios, using high- and low-freq. separation method 79−26971

molecular vibration calculations continued
isotopic molecules reduced partition function ratio, generalised finite polynomial approx. 78−66529
isotopic rules for heavy atom substitution, perturbation theory 77−83660
ketene-d_0, -d_2, Coriolis coupling, centrifugal distortion and force consts., mean vibr. amplitudes calcs. 79−36607
kinematic anharmonicity in exact and approx. coords., H_2O molecule example 78−17653
kinematic anharmonicity in normal coordinates 79−54838
L-F approximation method extension HLFS applicability, appl. to CF_3Cl, CF_3Br and CF_3I 80−962
large mol. reaction with intermediate complex, vibr., translational distrib., pot. hypersurface calc. 77−52612
large mol. reaction with intermediate complex, vibr. distrib., R-matrix, hybrid quantum statistical mechanics 77−52611
least-squares parameters, stepwise merging method 78−89319
Lennard-Jones mol., WKB vibr. energy level calc. 78−9057
level populations, quasi-energy method 79−98067
linear molecule in reson. light field, bending vibr. 80−968
linear triatomic, isotopic relations, harmonic freq. calc. 77−23486
liquid two-dimensional itinerant oscillator model testing by molecular dynamics 79−32868
local mode approx. 77−71791
local-mode description, symmetry aspects 79−36600
long chain molecule, Szigeti's method using matrix partitioning 78−90139
long range mol., electronic and vibr. levels 78−94301
low symmetry molecule, vibr. Hamiltonian 79−22687
macromolecule, force constants refinement in normal coord. calcs. 77−31035
matrix isolation spectra, homogeneous IR line shape, Debye approx., space time phonon correl. functions 79−823
mean amplitude of vibration, approx. method 79−13697
metalloporphyrins, mol. origin of anomalous polarisation in reson. Raman spectra 77−3368
methane, and d_{1-4}, intensity sum rules, dipole moment derative 79−13695
methane, and deuterates, absolute Raman intensities, depolaris. ratios, bond polaris. theory 77−10705
methane(-d_1,d_2,d_3), electro-optical parameters from IR intensities, least-squares calc. 80−9584
methane (-d_1,d_2,d_3,d_4) Raman electro-optical parameters, overlay least squares calcs. 78−42105
methane and halogen derivatives Raman scatt. parameters at.-dipole interaction model calcs. 77−65465
methane-d_1, A_0 determ. from ν_4 Raman band 77−83608
methane-d_4, isotope effect on rot. and vibr. consts. 79−22688
methane-d_4 *(Russian)* 80−91540
methanol, and dimer, CNDO/2 calcs. of O-H stretching vib. freqs. and intensities 77−18927
methyl bromide, far IR laser lines, rot. anal. of ν_6 perpendicular band 77−3359
methyl ethyl ether, charact. vibrs., isomer and isotope effects, rel. to reverse spectral problem 80−63613
methyl fluoride, vibr. transition moments and force fields, gaussian basis set calcs. 79−81152
methyl formate(-d_1,d_3,d_4), mol. vibr. spectrum, struct., beginning with PCILO calc. *(French)* 80−23401
methyl halides, force consts. evaluation using gp. vibrs. and centrifugal distortion consts. 80−9580
methyl torsion modes, vibrational optical activity, inertial contrib. 80−5524
methyl tri(trifluoromethyl) germanium, and perdeuterated analogues, vibr. spectra, normal coord. anals. *(German)* 80−5547
methylamine, and ^2H, ^{13}C, ^{15}N, ^{18}O isotopic derivatives, vibr. freqs. using MINDO/3 force consts. 77−71793
methylamine, vibr.-inversion-internal rot.-rot. Hamiltonian 78−86840
N-methylcarbamoyl chloride(-d_1), vibr. spectra, normal coord. anal. 78−33497
methylene, photoelectron spectra, singlet and triplet state calcs. 78−42127
methylene glycol(-d_4)⇌formaldeyhyde(-d_2)+H_2O(D_2O) Raman spectra and normal vibr. 80−58271
methylene radical, classical stretching dynamics 80−23400
MINDO/3 calcs. of vibr. freqs. 77−61730
mixing parameter matrix, of Green's function vibr. anal., determ. 79−31494
MNDO calculations, vibr. freq. 78−25508
mol. consts. and mean vibr. amplitudes calcs. 80−106318
molecular spectroscopy book 80−27051
molecular spectroscopy book 80−27052
molecular vibration excitation on resonant electron scatt., time-perturbation method *(Russian)* 80−14242
molecule+ion charge transfer, vibr. excited mol. form. 77−3455
Morse oscillator, 1-D, semi-analytic solns. for wavefunction and energy 78−25502
multicomponent polyanions, PMo_9O_{34} model vibr. freqs. 80−23408
multilevel molecular system, light pulse interaction 77−38699
multilevel system, band type, excitation dynamics in laser field *(Russian)* 78−21980
multiphonon relaxation, statistical anal. 79−79223
$(MX)_n$, $(MX_2)_n$ ionic clusters, struct. and vibr. freqs. calcs. 78−94348
MXY type molecules, vibr. isotope effect 78−25506
sym-N_2O_3, mol. vibr. in N_2 matrix, normal coord. anal. 79−59432
N=3 eigenvalue problem, appl. to XYZ bent mols. *(German)* 80−14131
naphthalene, and d_4 and d_8, vibr. anal. using best struct. and spectroscopic data 79−76410
naphthalene, high-energy C-H vibr. overtones, intensity 79−76404
naphthalene, nonplanar vibr., force field calcs. 79−41148
naphthalene, normal coord. calcs., simplified valence force field models 78−94229
naphthalene, out-of-plane mol. vibrs., force field approx. calcs. 80−91538
naphthalenes, substituted, CH wag group freqs., CNDO/2 calcs. 77−6745
near reson. Raman lines, relative intensities, A-term method 79−81205
non-linear molecule, γ and q consts. for linear vibr. depend. of quartic and sextic distortion consts. 79−36613
non-rigid molecule vibration, FORTRAN FORMAC products of non-numerical matrices 78−50540

molecular vibration calculations continued
nonclassical compounds, complete calc. method 77−79600
nonequilibrium dissoc., Morse oscill. rigid rotator system, master eqn. soln. 80−40682
nonseparable system, energy levels, semiclassical method using Birkhoff-Gustavson normal form 79−97224
normal coordinate calcs., computer program for Z-matrix determ. 80−23388
normal mode calcs. of crystals and molecules, coordinates and force matrices generation, computer program 78−91393
normal mode calcs. of molecules, crystal phonon dispersion relns. and structure factors for neutron inelast. scatt., computer program 78−91394
normal vibrations classification in mols. with internal rot. according to microwave spectra data 77−18909
NQR freq. anomalous positive temp. coeff., vibr. depend. 80−53016
octahedral mols., anharmonic force field, decoupled rigid bender model 79−41153
octahedral systems, intramolecular force fields and vibr. amplitudes, Wilson's FG matrix method 77−31021
trans, trans-1,3,5,7-octatetraene, low freq. normal modes, CFF-π calcs. 79−68217
optical probing of excited mols. that have undergone radiationless transitions 77−27106
optical torsion transitions, barrier heights from vibr. optical freqs. 77−42308
organic molecules, IR spectral intensity calc. for electro-optical parameters 79−54835
organic molecules, small, harmonic force consts., vibr. freqs., integrated intensities, MINDO/3 method 80−58411
7-oxabicyclo-[4,1,0]-hept-3-ene, far IR spectrum, Q-branch transitions calcs. 77−6770
oxide ions XO_4^{n-}, n=1 to 4, normal vibr. freqs., prediction, force consts. calc. *(Russian)* 77−6759
palladium porphin, IR spectra and vibr. anal., and deutero-derivatives 79−22705
partition function, upper and lower bounds, for mols. with double min. pots. 78−42032
pentatetraene, non-degenerate vibr. mode induced Jahn-Teller effect, photoelectron spectra calc. 79−817
perfluorocyclobutane, matrix isolation Raman and IR spectra, pot. function 77−3352
phase and population relax., semigroup formalism 80−78519
phenanthrene, planar normal vibrs. calcs. 80−5525
phenol ($-d_1$, d_5, d_6), excited A state, normal vibr. freqs, force consts., compliance coeffs. 78−50534
phenylacetylene, excited single state B_1, electron-vibr. spectra and electronic struct. 79−26904
phthalimide derivatives, in hexane and isopentane, vap., inversion freq. determ., from fluoresc. quantum yield obs. 79−54892
point groups, continuous, characters and representations 80−36809
point groups, continuous, reduction of representations 80−36808
point groups, continuous, reduction of representations 80−36810
point groups, infinite, complete reduction of representations, mol. vibrs., electronic states appls. 78−94206
polyacenes, planar vibrs. classification using potential energy distrib. anal. 79−98065
polyatomic, fluoresc. spectrum excitation depend., proportionality coeff., vibr. redistrib. 77−23518
polyatomic, kinetic energy operator in exact vibr. coordinates 79−63984
polyatomic excited molecules, vibrational energy exchange *(Russian)* 80−91539
polyatomic force fields, Ohwada's pairwise interaction model 80−106321
polyatomic molecule, atomic force correlation functions for determ. vibr. relax. rates, role of mol. symmetry 80−83337
polyatomic molecule, exact to approx. coordinate relationship *(Russian)* 77−54553
polyatomic molecule, intramolecular coord. relax., generalised classical theory 80−78589
polyatomic molecule, quartic anharmonic pot. energy function 78−58662
polyatomic molecule, quasicontinuum, coherent and mode selective excitation by laser pulse 78−1032
polyatomic molecule, radical vibr. calc. method 79−31505
polyatomic molecule, SCF-SI theory applic. to coupled vibr. motion 80−23399
polyatomic molecule, sextic centrifugal distortion consts., Watson Hamiltonian, perturbation method 77−10785
polyatomic molecule, transform. of complete electron-nuclear Hamiltonian to intramolec. coords. 78−9054
polyatomic molecule, vibr. struct. of electronic spectra, FORTRAN programs 80−32699
polyatomic molecule anharmonic pot. theory, spatial matrix method 78−55161
polyatomic molecule dissociation in IR laser field *(Chinese)* 80−106363
polyatomic molecules, applic. of classical perturbation theory of good action-angle variables 80−23481
polyatomic molecules, force consts., Hellman-Feynman type calc. method 77−65451
polyatomic molecules, fundamental stretching freq., isotope shift 78−50530
polyatomic molecules, intensity distribution in vibronic bands, Dushinsky effect 79−93983
polyatomic molecules, isotopic reduced partition function ratio approx., by polynomial perturbation method 78−66530
polyatomic molecules, kinematic anharmonicity corrections, algorithm 79−76415
polyatomic molecules, normal coordinate problem, QM treatment, book contrib. 78−78677
polyatomic molecules, overtone spectra, local mode anal. 77−27046
polyatomic molecules, particle displacement momenta, quantum equilib. distrib. 78−32751
polyatomic molecules, two-parameter intramol. distribs. and props. 80−47967
polyatomic molecules, vibr. quantisation calcs., semiclassical EBK method 77−10660
polyatomic mols., Hamiltonian for nuclear motion 79−26965
polyatomic mols., nuclear charge model and valence force consts. prediction 80−43022
polyatomic XY_5 type molecules, vibr. assignment using Redington's method 80−23410
polyatomics, anharmonicity consts., parametric representation 79−31496
molecular vibration calculations continued
polyatomics, restricted intramolecular vibr. relax. and laser selective effects 80−27992
polyatomics, vibr. correction and effective moment of inertia, a correl. 79−89662
polyatomics, Wilson GF matrix method 80−9578
polyethylene($-d_4$), vibr. freqs., MNDO semiempirical SCF calcs. 78−1114
polymers and crysts., vibr. anharmonicity, intensities of overtones and component freqs. 77−69052
polyvinylidene chloride, normal vibr. analysis using conform. model 80−83529
porphins, reson. Raman spectra, selection rules, normal coord. treatment 80−53175
potential energy distrib. among atoms in normal vibr. 77−451
predissociating harmonic oscillator, relative line widths and level shifts 80−23469
predissociation, vibrational, in H-bonded complexes 80−61078
propane, force const. selection, backward elimination regression-refinement procedure 79−31497
proteins, role in electron transport at large distances, vibr. excitation 79−34480
pyramidal XY_3 molecules, mol. geometry calcs. using centrifugal distortion const. 80−18841
pyrazine, vibronic bands, MIDP and polarised phosphoresc. in benzene matrix 77−6833
pyridine N-oxide, 341 nm band system, out-of-plane modes assignment 77−34646
2-pyridone, dimer, vibr. Hamiltonian for IR spectra of H bonding 78−37620
quadratic potential functions, calc. MO constraint of interaction coordinates 78−74631
quartic anharmonic oscillator, semiclassical and quasiclassical particle function 80−99434
quartic potential function with finite BE, props. 79−26913
quasi-energy states and stability in light wave field, adiabatic approach *(Russian)* 79−94039
r-centroid approximation accuracy 79−89661
radial distribution functions, mols. in vibr. excited states 79−85951
radial matrix element generating function for mol. vibr. calcs. 77−18904
Raman and IR intensity, relation in matrix notation 78−62853
Raman optical activity parameters, circular intensity differentials comput. by atom-dipole interaction model 79−76407
Raman scatt. theory, vibr. state summation, polarisability tensor upper and lower bounds 80−48000
rate process theory, role of coherent mechanical vibr. 77−509
real symmetry coordinates, groups having complex representations 78−82715
redundancy coeffs. for vibrs. involving atoms with four bonds 77−27049
redundant coordinates, Lagrange eqns. 77−27043
resonant Raman spectra, overtone intensity distrib., effect of excited electronic state 80−87128
reverse spectral problem, charact. vibrs. effects calcs. 80−63613
rigid-body molecules, diamagnetism and thermal motion 80−25076
rotational isomers, transformation of operators of coordinates and momenta 79−63982
second anharmonicity coeffs. 77−23489
semiclassical eigenvalues in nonseparable systems, good action angle variables 79−13694
separated product rules for high and low vibr. freqs. in isotopic mols. 77−34611
silyl radical, conform., hyperfine struct., nonempirical calcs., vibr., effects 79−97998
simple oscillator, correl. functions, IR band shapes 79−26960
small mol. electro-optical parameters, dipole moment derivatives, vibr. calc. valence-optical theory 80−23406
spectral line broadening, semiclassical straight line vs. curved trajectories 79−45765
spectral line shape, vibr. overtone lineshape of polyatomic mols. 79−27040
spherical top molecules, fluid vibr. spectra, repulsive force depend. line broadening *(Russian)* 80−47970
statistical mechanics, flexible vs. rigid constraints 80−31658
subbarrier transitions in energy space as mechanism of build-up of nonlinear oscillator by external harmonic force 77−75125
superposition state in regular and irregular spectrum, time evolution, intramolecular dynamics 80−83335
symmetry coordinate construction method, atomic orbital symm. of point group, M_4X_6 78−46312
symmetry group of nonrigid molecules, completely reduced representation 80−9587
symmetry properties of non-rigid molecules, unified approach 80−1083
TCNQ, anions, screened INDO model, appl. to photoelectron, optical, Raman spectra 79−765
tetra-glycine, cyclic, mol. polaris. and diamag. suscept. calcs. 80−63858
tetra-l-alanine, cyclic, mol. polaris. and diamag. suscept. calcs. 80−63858
tetrachloromethane, fluid vibr. spectra, repulsive force depend. line broadening *(Russian)* 80−47970
tetrafluoromethane, IR spectrum, Fermi reson. sequences, cubic pot. energy, anharmonicity consts. 77−10674
tetrafluoromethane, mol. consts. and mean vibr. amplitudes calcs. 80−106318
tetrahalide of group IV A, molecular consts. 78−66528
tetrahalides of Gp.IV elements, M-X bond flexibility, by compliance scheme 80−37805
tetrahedral molecules, thermodynamic isotope effect 78−20000
tetrahedral molecules, vibr., charge and charge flux 80−47961
tetrahedral XY_4 ions, normal coord. treatment and mol. consts. 79−93968
tetrahedral XY_4 type molecule, change in mean square amplitude 77−57963
1,4,5,8-tetrahydroxyanthraquinone-d_0,-d_4, mol. vibr., IR spectra 77−467
tetrakis(trifluoromethyl)germane, gas phase electron diffr. struct., torsional force consts., CNDO/2 calc. 79−31687
tetramethylcarbonyl-silane,-germanium,-tin,-lead, force fields and vibr. mean amplitudes 77−30856
s-tetrazine, mol., pot. functions of bending modes 80−9753
thermochemical properties of atoms and molecules in specific quantum states 78−68911
2-thiapyridone, dimer, vibr. Hamiltonian for IR spectra of H bonding 78−37620

molecular vibration calculations continued
thiazolidine, mol., vibr. anal., IR and Raman spectra *(French)* 79−26964
thioformamide(-d_2), photoelectron and absorption spectra, vibr. struct., excited state configs. 77−6847
2-thiohydantoin-d_0, (-d_2), mol. vibr. and force field calcs. 78−62779
thiosemicarbazide, mol. cryst., transition moment directions 78−64351
thiosuccinimide-d_0,-d_1, normal coord. anal. calcs. 77−30844
thioureas, substituted, normal coord. anal. 79−98246
time dependent adiabatic approx., Born-Oppenheimer approx. 77−23491
toluene, asymmetric bending vibrs. 79−13696
torsional coordinates in vibrational analyses 79−93977
torsional internal coordinates in normal coordinate calcs. 77−83574
transition metal complexes, excited states geometrical parameters, Franck-Condon anal. 77−27047
transition moments, vibrational, of diatomic and polyatomic mols., elec. and mech. anharmonicity influences 80−23459
triangular triatomic molecules, sextic centrifugal distortion constants, planarity relations 78−58649
triatomic inorganic mols., harmonic force consts., vibr. freqs., integrated intensities, MINDO/3 method 80−58411
triatomic molecule, large amplitude vibr. model, appl. to H_2O 79−41150
triatomic molecule, nonlinear, transform. of vibr. and rot. coords. during electronic transition *(Russian)* 79−93980
triatomic molecules, vibr. energies, wavefunctions, ab initio calc. 78−17652
triatomic nonlinear mols., stretching vibrs., partial Morse oscills. 80−967
triatomic systems, compliance const., L matrix approx. method 78−74797
triatomic unsymmetrical mols. and ions, electrostatic models 79−22697
s-triazine(-d_3), gas phase IR band contours obs., computer simulation 77−6774
trichloromethane(-d_1), electrooptical parameters and Raman intensities obs., bond polaris. calcs., vibr. force field 77−50441
trichloromethoxysilane, normal vibr. and force field calc. 79−54994
1,3,5-trichlorotrifluorobenzene, IR and Raman vibr. spectra 77−3356
trifluoromethyl trimethyl germanium (tin)(lead), and perdeuterated analogues, vibr. spectra, normal coord. anals. *(German)* 80−5547
trigonal planar molecules, thermodynamic isotope effect 78−20000
trihalide anions, VB pseudopot. calcs. on electronic states 77−26984
trimethylantimony(V) dihalides, normal coord. anal., comparison of force fields 78−968
two linear harmonic oscillators, coupled by interaction pot., SCF calc. 78−37625
two quanta vibr.-vibr. transitions, translation distortion effects, DWA calc. 79−3541
two-dimensional oscillators with C_{4v} pot. functions 77−61731
urea, force field for planar vibrs., CNDO/Force MO calcs. 79−76416
van der Waals dimers, intramolecular vibr. dynamics, vibr. predissociation 80−28083
van der Waals molecules, vibr. level spacings calc. from Lennard-Jones pot. 77−42369
vanadyl porphyrins, anion radicals and dianions, reson. Raman spectra 77−471
vibrational potentials, non-Dunham series expansions, radii of convergence 77−18902
vibrational spectra calculations, mol. fragments effects *(Russian)* 78−5203
vibronic coupling, totally symmetric harmonic mode, exactly solvable model 78−21896
vibronic coupling model, nontotally symm. harmonic mode 77−3337
vinylchloride, mol. struct., gas-phase electron diffraction and microwave spectra, vibr. amplitudes 79−76421
water, nine isotopes, harmonic vibr. of unsymmetrical forms calc. 77−452
wave functions, semiclassical Gaussian basis set method 80−9583
Wilson-Decius s-vectors with out-of-plane wag, derivation 78−74628
X_2Y nonlinear molecule, isotope effect in harmonic vibrs. 77−452
XH_2 molecules 1:2 complexes, H-bonding fluctuation hypothesis, IR and Raman vibr. spectra 77−34632
XY_2, collinear photodissoc., UV spectra vibr. struct. 77−18936
XY_2 bent symmetrical molecules, Coriolis coupling consts., centrifugal distortion consts. 80−58236
XY_2 bent symmetrical systems in different environments, force consts. and mean amplitudes 79−18170
XY_2 molecule, chem. perturbation of force field, Green's function appl. 79−76417
XY_2 molecules, nonlinear, inertia defects and dipole moments by kinetic consts. method 80−928
XY_2-type bent symmetric mols., vibr. anal., kinetic consts. method 80−18838
XY_2Z planar molecule, transformation and compliance matrices determ. 77−18898
XY_3, pyramidal, force consts. and mean amplitudes, group theoretical anal. 79−36609
XY_3 planar mols., mean vibr. amplitudes, force and kinetic consts. 77−79603
XY_3 pyramidal molecules, change in mean square amplitude values, calc. 78−55158
XY_3 pyramidal mols., intramol. forces, fundamental vibr. freqs., centrifugal distortion consts., PF_3 appl. 78−5202
XY_3 pyramidal-type mols., mol. consts., kinetic consts. and L-approx. methods 80−18839
XY_4 molecules, isotope effect on rot. and vibr. consts. 79−22688
XY_4 tetrahedral molecules, kinetic const. method appls. 79−36608
XY_4 tetrahedral mols., force and kinetic consts. calcs. 77−27053
XY_4Z (C_{4v}) molecules, force constants and mean-square amplitudes of vibration 78−66535
XY_5 trigonal bipyramidal mols., kinetic consts. 79−18173
$XY_6(O_h)$ octahedral system, F-(G-) matrix elements setting-up, transformation rules *(German)* 80−58242
$XY_6(O_h)$ systems, lower limit and estimation of the inactive vibr. freq. $\nu_6(F_{2u})$ *(German)* 79−3430
XY_6 molecules, octahedral, cubic and quartic anharmonic pot. energy functions 79−98185
XYZ and XY_3Z type mols., at. pot. energy distrib. 79−72292
zinc porphyrins, anion radicals and dianions, reson. Raman spectra 77−471
ZXF_5, heavy central atom, vibr. mean amplitudes and mol. geometry, charact. vibr. method 80−5522
$AlBr_3$, Raman IR spectra, organic solvent effect *(German)* 77−3370

molecular vibration calculations continued
AlCl, A-X system, vibr. anal. 80−23394
AlH, vibr. consts. of electronic states, calc. method 79−93967
AlH_4^-, AlD_4^-, intramol. force fields, F_2 vibrs., isotope shifts 77−3336
AlO, A-X transition, Franck-Condon factors computation, iterative method compared with Langer's method 78−86762
Ar, Hulburt-Hirschfelder pot. function 80−63612
Ar+Br_2, effective vibr. pot. of Br_2 in Ar gas, Monte Carlo simulation 79−59526
ArBr, pot. curves, population distribs. and chemiluminesc. for B(1/2) and C(3/2) electronic states 80−45509
ArF^+, selected valence-electron split-shell MO calc., ground state props. 79−22585
ArH^+, $^1\Sigma^+$ ground state, molecular consts. calc. from pot. curves 80−9680
$Ar_nH(H^+)$, excited and ground state struct. energies and binding energy, vibr. modes, LCAO-SCF-MO calc. 79−3608
$Ar^*+N_2 \rightarrow Ar+N_2^*$, electronic to vibr. energy transfer, time depend. theory 80−23514
AsF_3, mol. geometry calcs. using centrifugal distortion const. 80−18841
AsF_5, E′ vibr. assignments, bending modes, parameter method 77−10658
$AuBr_4^-$, harmonic force field, mean vibr. amplitudes, cation effect 77−3335
$AuCl_4^-$, harmonic force field, mean vibr. amplitudes, cation effect 77−3335
$AuCl_4^-$ (Br_4^-), mean vibr. amplitudes and force field, Muller approx. 77−10659
BCl_3, ν_3 vibr. level, fine struct., nonlinear reson. 77−6783
BF, vibrational structure in X-ray spectra, calcs. 77−30884
BF_3, dissoc. pathways and mol. vibr., compliance consts. and min. energy coords. 78−35661
BF_3, mean amplitude of mol. vibration, approx. calc. method 79−13697
B_2F_4, mol. force consts. and vibr. amplitude, force field study 79−31729
BH, mol. spectroscopic consts., FSGO calcs. 77−6758
BH_4^-, BD_4^-, intramol. force fields, F_2 vibrs., isotope shifts 77−3336
$B_{12}H_{12}^{2-}$, icosahedral cage, symmetry coords. and vibration freq. 80−47966
BI_3, mol. force field using parametric represent. method 80−27991
B_2O_3, vibrational force consts. and B-O bonding, Green's function method 77−14406
BX_3, (X=Br, Cl, F), ellipticity of symm. force field, force consts. 78−17646
$BiCl_6^{3-}$, model force fields and vibr. amplitudes calcs. 78−62780
BrCN, ICN, and isotopic forms, force field calc., freqs., rot. consts. 79−22693
BrF_5, excited vibr. states, microwave spectrum, rot. const. determ. 78−94237
BrSN, force consts. and mean amplitudes of vibr. calc. 77−30855
Br_2SO, A′-force consts., 4th-order secular eqn., L-matrix approx. vs. HLFS methods 79−36556
C-C, C-H, vibr. amplitudes-internucl. distance relation validity, Badger's rule 77−68028
CCO radical, heat of form. calc., geometries excitation energies and vibr. freq. calc. using POL-CI wave functions 80−89512
CF_2S, mol. consts., kinetic consts. method calcs. 80−58235
CF^2Se, mol. consts., kinetics consts. method calcs. 80−58235
C_2H_3 species formed in chemisorption of ethylene on Pt, vibr. anal. 80−61150
$CH_3(CH_3^+)(CH_3^-)$, HF, GVB and CI calcs. 77−75063
CN, RKR Franck-Condon factors and r-centroids for $B^2\Sigma$-$A^2\pi$ transition 79−81195
C_2N_2, $2\nu_4$ band overtones, Raman intensities, bond polarisability theory 80−63639
CO, $^1\Sigma$ state vibr. matrix elements, Dunham pot. *(French)* 79−54832
CO, carbonyl group stretching freq. force const., CNDO/2 and localised orbitals calc. 77−30784
CO, dipole moment functions for $d^3\Delta$ and $a'^3\Sigma^+$ states, MCSCF calc. 78−78636
CO, flowing laser plasma, spontaneous emission, A coeffs. 77−7070
CO, high order vib. matrix elements, for dipole moment function and transition moments 77−6757
CO in Ar matrix, vibr. freq. shift and interaction pot., force-field calcs. 80−47958
CO, vibr. excitation calc., in gas mixture discharge 79−77442
CO, vibr. struct., core and valence ESCA spectra, Frank-Condon and HF anal. 80−32602
CO, vibrational structure in X-ray spectra, calcs. 77−30884
CO, vibrational transitions dipole matrix elements, numerical calc. 80−95594
CO, X-ray K-absorpt. spectra, vibr. fine struct., ab initio restricted HF calc. 78−86883
$CO+H^+$, vibr. excitation calc., close coupling and sudden approx. 80−78561
CO_2, combination and difference bands, IR intensities 77−466
CO_2 conc. and temp. in flames, Raman spectroscopy 80−32720
CO_2, ionised states, core and valence, ab initio HF calcs. 77−79597
CO_2, isotopic relations, harmonic freq. calc. 77−23486
CO_2 laser resonator, gasdynamic, optimal parameters determ. from vibr. energy exchange kinetics 80−14317
CO_2, low energy electron scatt. cross sections, vibr. excitation, Boltzmann eqn. 80−18942
CO_2, nonbending, vibr. motion calc. using SCF-SI theory 80−23399
CO_2, Rayleigh-Schrodinger and contact transform. techniques *(French)* 77−3340
CO_2, thermal conductivity, 400 to 1500K, vibr. internal energy calc. 79−18986
CO_2, vibr. excitation calc., in gas mixture discharge 79−77442
CO_2^+, electronically excited states emission, $A^2\pi_u$ state bending vibrs. 77−3454
CO_3, and isotopic forms, struct., normal coord. anal. 78−965
CO_3^-, photodissoc. cross-section, excited state vibr. mode determ. 77−6870
C_3O_2, CCC bending mode, two-dimens. anharmonic oscill. calcs. 77−14415
C_3O_2, large amplitude bending mode, rot.-vibr. calc., assignments 77−18905
C_3O_2, mol., pot. functions of bending modes 80−9753
C_3O_2, ν_7 vibrational states, rigid-bender model 80−47964
COF_2, force field analysis using parametric represent. method 80−27990
COS, mole. potential surface, evaluation from spectroscopic observations 80−43207

molecular vibration calculations continued
$C(^1P)+O_2(^1\Sigma_g^-)\rightarrow CO(^1\Sigma^+)+O(^1D)$, pot. energy surface, vibr. population inversion, classical dynamics 77−52630
CS, CS^+, emission band systems after $He(2^1S)+CS_2$ reaction 77−14473
CS molecule, calc. of HeI photoelectron spectrum, ionisation pot., vibr. struct. 77−3415
CS, vibr. struct. calcs. from photoelectron spectra 77−18973
CS_2, symmetric stretch mode, moments and polarisability derivatives, SCF calcs. 80−901
$^{12}C^{16}O$ in Ar matrix, vibr. level energy cascades 77−79598
Ca+NaCl, crossed beam reaction, collision complex lifetime internal state depend. fluoresc. 77−56217
CaI, electronic band spectrum 6100 to 6600 Å 78−90176
CdX_2, CdXY, (X,Y=Cl,Br,I), matrix isolated vibr. spectra, isotopic effects, force consts. 77−3358
ClCN, and isotopic species, force field calc., freqs., rot. consts. 79−22692
ClO_2F, pyramidal type mol., force field comput. using Green's function procedure 80−23407
ClSN, force consts. and mean amplitudes of vibr. calc. 77−30855
Cl_2SO, A′-force consts., 4th-order secular eqn., L-matrix approx. vs. HLFS methods 79−36556
$CrCl_4$, mol. consts. and mean vibr. amplitudes calcs. 80−106318
CrO_2Cl_2, single vibronic level fluoresc. 77−3408
$Cs_{11}O_3$, ionic clusters in alkali metal suboxide cryst., struct., vibr. freqs., Raman spectra 79−37772
Cu complex, $Cu(NH_3)_2(NCX)_2$, X=O, S, electronic struct., stereochem. 80−58156
Cu_2, emission band spectra and vibr. const. 79−36656
CuI dissoc. energy A-X system vibr. bands 77−50434
D_2, c, I and i states, pot. energy curves and vibr. levels, Born-Oppenheimer approx. 78−931
D_2, Lyman bands, Morse Franck-Condon factors and R-centroids 77−58088
D_2 matrix shift, CoM freq., in solid Ar, Kr and Xe 79−6969
D_2/CCl_4, inhomogeneous broadening of Morse oscillator, temp. depend. 77−61803
D_3^+, ab initio vibr. intervals and vibr. freq. refinement 80−47968
DNO, fundamental vibr. bands, laser Stark spectra 77−38692
D_2O, cubic anharmonicity constants, normal coord. ab initio calcs. 79−36595
D_2O, isotopic species, far IR spectra, assignments, moments 77−6761
$(D_2O)_2$, and isotopic species, Ar isolation IR spectra, band assignments, struct. 77−3364
$(D_2O)_2$, and isotopic species, Ar matrix IR spectra, Xe, HCl, $(CH_3)_2O$ doping, struct. 77−3365
D_2S, separated product rules for high and low vibr. freqs. in isotopic mols. 77−34611
DSiCl, $^1A''$ states, geometry, bending pot. and vibr. freqs. 79−59593
$F_2+H(D)(T)(Mu)$, impulsive triatomic reaction, vibr. state distrib., impulsive energy release model 78−92456
FCN, and isotopic forms, force field calc., freqs., rot. consts. 79−22691
F_2CS, pot. surfaces, X^1A_1, a^3A_2 and $a^3A_2(b_1)$ states, ab initio SCF calcs. 78−86795
F_2SO, A′-force consts., 4th-order secular eqn., L-matrix approx. vs. HLFS methods 79−36556
F_3SiAsH_2, liq. Raman, gas phase IR spectra, normal coord. anal., assignments *(German)* 77−6778
$F_3SiOSiF_3$, vibr. bands, normal coord. calcs. *(Russian)* 78−70814
$F_3SiOSiF_3$, vibr. anal., normal coordinates, siloxane bridge vibr. band struct. 79−50003
$FeBr_4^-$, complex Raman tensors, irreducible tensor method, antisymmetric scatt. 78−37623
GaH_4^-, GaD_4^-, intramol. force fields, F_2 vibrs., isotope shifts 77−3336
GeH_3-group containing mols., normal coord. anal. 80−9579
GeH_4, IR spectra of ν_3 band, molecular const. determ. *(French)* 77−462
GeH_3X, mol. consts. calcs. 79−36606
GeO, RKRV Franck-Condon factors and r-centroids, $(A^1\Pi-X^1\Sigma^+)$ transition, pot. energy curves 78−29817
GeO_4^{4-}, normal vibr. freqs. calc. 79−54837
H bond length and vibr. freq., deuteration effect 79−26911
H bond system, charge transfer theory, relation between vibr. spectra and energy 77−3334
H bond two-dimensional model dynamics, vibrs. freq. rel. to equil. interatomic distances 79−26910
H bonded systems, IR spectra, theoretical interpretation 79−31519
H bonds, IR spectra, theoretical interpretation 79−31519
H bonds, linear triatomic model, adiabatic approx., freqs. and isotope effects 77−65448
H-bonding, strong, stochastic model and IR spectra temp. effects 78−62805
$H+Cl_2$, impulsive triatomic reaction, vibr. state distrib., impulsive energy release model 78−92456
$H+H_2$, planar reaction, cross section calcs., vibr. and rot. convergences 77−21376
$H+H_2(v=1)\rightarrow H_2+H$, exchange reaction, classical trajectory method, vibr. excitation, partial rate consts. 78−60993
H^++H_2, rot. excitation and vibr. transitions, coupled state approx. 77−61835
H_2, D_2, photoionisation, body-frame Hund's case b description 78−94295
H_2, electronic and vibrational structure, theoretical developments 78−62707
H_2, electronic states, adiabatic energy corrections, CI ab initio calc. 77−83502
H_2, ground state, vibr. eigenenergies, functional form 80−27998
H_2, HD, c, I and i states, pot. energy curves and vibr. levels, Born-Oppenheimer approx. 78−931
H_2, Lyman bands, Morse Frank-Condon factors and R-centroids 77−58088
H_2 Se, potential function and vibrational spectra 77−68030
H_2, $X^2\Sigma_g^+$ state, vibr. energy levels, radiative corrections calcs. 78−90094
H_2^+, calc. of lowest vibr. states where L=0, P=+ 79−31502
H_2^+, electron cooling through resonant collisions 80−32845
H_2^+, moment functions calcs. and radiative corrections 78−90141
H_2^+, nonadiabatic vibrational energies, ab initio calcs. 78−90142
H_2^+, nonexponential wavefunctions for $1s\sigma_g$ and $2p\sigma_u$ states 77−415
molecular vibration calculations continued
H_2^+, nonexponential wavefunctions for $2p\pi_u$, $3d\pi_g$ and $3d\delta g$, $4f\delta_u$ states 77−416
H_2^+, vibr. eigenenergies representation, functional form 79−68220
H_2^+, vibr. excited, form. by stimulated radiative assoc. of $H+H^+$ 79−100346
H_2/CCl_4, inhomogeneous broadening of Morse oscillator, temp. depend. 77−61803
$H_2+I\rightarrow H+HI$, quasiclassical tragectory vs. quantum calcs., vibr. state depend., kinetics 78−80733
H_3^+, ab initio calcs. of vibr. spectrum 77−6753
H_3^+, ab initio vibr. intervals and vibr. freq. refinement 80−47968
HBS, and isotopic forms, force consts., coriolis consts., vibr. amplitudes, shrinkage effects 80−43021
HCN, isotopic relations, harmonic freq. calc. 77−23486
HCN, vibr. energies, wavefunctions, ab initio calc. 78−17652
HCN(DCN), photodissoc. dynamics, rot. (vibr.) energy disposal 78−48672
HCNO, far IR spectrum, weak vibr. transitions 77−3357
HCNO, IR spectrum, ν_1 and $3\nu_1$ bands 77−3354
HCP, force fields and force consts. of electronically excited states 80−69116
HCl, Poschl-Teller oscillator, matrix element of vibr. transitions 78−25510
HCl, vibr. state distrib., phase space sampling approach in statistical mech. 78−32753
$HCl/SF_5(CCl_4)$, inhomogeneous broadening of Morse oscillator, temp. depend. 77−61803
HD, Lyman bands, Morse Franck-Condon factors and R-centroids 77−58088
HD^+, nonadiabatic vibrational energies, ab initio calcs. 78−90142
$H_2(D_2)$, Compton profile, impulse approx., electron correl., vibr. and rot. effects 78−17585
HF, Poschl-Teller oscillator, matrix element of vibr. transitions 78−25510
HF, spectroscopic consts., FSGO calcs. 77−6758
HF, vib.-rot. props. of $X^1\Sigma^+$ and $B^1\Sigma^+$ states, variational calcs. 77−50422
HF, vibr. relax., microscopic and macroscopic anal. of non-linear master eqns. 79−36743
$H_2(HD)(D_2)$, ab initio pot. energy curves and vibr. levels, B″, B̄, B′ states 77−6754
HN_3, ground $^1A'$ state, SCF and CI calcs., conform., geom., vibr. freqs. and dissoc. 80−18806
HNO, fundamental vibr. bands, laser Stark spectra 77−38692
HNO, vibr. freqs. from anharmonic ab initio/empirical PE functions 79−76406
H_2O, and ^2H, ^{18}O isotopic derivations, vibr. freqs. using MINDO/3 force consts. 77−71793
H_2O, and D_2O, local model vibrs. 79−76414
H_2O, anharmonic vibr. spectroscopic coeffs. contribs. 78−86846
H_2O, cubic anharmonicity constants, normal coord. ab initio calcs. 79−36595
H_2O, electron density, generalised Berlin diagram internal modes 79−98001
H_2O, energy levels, triat. large amplitude vibrs. model appl. 80−23392
H_2O, fundamental freq., local mode structure 78−29770
H_2O, isotopic species, far IR spectra, assignments, moments 77−6761
H_2O, kinematic anharmonicity in exact and approx. coords. 78−17653
H_2O, radial distrib. function of vibr. excited mol. 79−85951
H_2O, slow electron scatt., rigid mol. model with exchange and polarisation, vibr. excitation, dissoc. attachment 80−43194
H_2O, theoretical IR transition matrix elements 79−85953
H_2O, vibr. freqs. from anharmonic ab initio/empirical PE functions 79−76406
H_2O, vibr. motion, local- vs. normal-mode description 80−5521
H_2O^+, electronic spectrum, vibr. levels, rot. consts. 77−473
$(H_2O)_2$, and isotopic species, Ar isolation IR spectra, band assignments, struct. 77−3364
$(H_2O)_2$, and isotopic species, Ar matrix IR spectra, Xe, HCl, $(CH_3)_2O$ doping, struct. 77−3365
HOCl, vibr. freqs. from anharmonic ab initio/empirical PE functions 79−76406
HOF, vibr. freqs. from anharmonic ab initio/empirical PE functions 79−76406
H_2O...HF complex, force field, vibr. freqs., equilib. geometry bond energy, ab initio calc. 77−65450
HS_2 radical, ab initio calcs. of geometry and spectra 77−34552
H_2S, separated product rules for high and low vibr. freqs. in isotopic mols. 77−34611
H_2S, slow electron scatt., rigid mol. model with exchange and polarisation, vibr. excitation, dissoc. attachment 80−43194
HSiBr, $^1A''$ states, geometry, bending pot. and vibr. freqs. 79−59593
HSiCl, $^1A''$ states, geometry, bending pot. and vibr. freqs. 79−59593
He, vibr. excitation calc., in gas mixture discharge 79−77442
$He+H_2^+\rightarrow HeH^++H$, diatomics-in-mols. and spline fitted ab initio surface, vibr. effects 78−20010
HeI_2, Van der Waals mol. vibr. predissoc. anharmonicity effects 80−52971
Hg complex, methylethynylmercury(II)($-d_1$,$-d_3$,$-d_4$), vibr. spectra and normal coord. calcs. 80−58259
HgH, predissoc. by rot., continuous rot.-vibr. spectrum, Weyl's theory 77−18996
HgH, predissoc. by rot., continuous rot.-vibr. spectrum, resons. and eigenvalues, Weyl's theory 77−18997
HgX, (X=I, Br, Cl), ground state dissoc. 77−6755
$HgX_2(HgXY)$, (X,Y=Cl, Br, I), IR and Raman matrix isolation spectra, bending force consts. 77−465
I_2, $(B^3\pi_{0+u})$, dissoc. reaction, computer simulation 78−48639
I_2, Phillips-Kleinmann pot. derivation, pseudopot. for ground state orbitals bond length, vibr. freq. 77−65418
I_2, reson. Raman lines, Stokes-antiStokes intensity ratio meas. 77−6786
ICN, A-system photodissociation mechanism 77−38701
IF_7, generalised quadratic valence pot. calcs., Wilson's F-G matrix 79−93966
IF_7, generalised valence potential consts. 79−18169
$^{127}I_2$, $^{129}I_2$, $B^3\Pi0_u^+-X^1\Sigma_g^+$ systems, fluoresc., mol. consts., Franck-Condon factors 77−34680
$IrBr_6^{2-}$, complex Raman tensors, irreducible tensor method, antisymmetric scatt. 78−37623

molecular vibration calculations continued
$IrBr_6^{2-}$, Raman tensor patterns, vibr. reson. Raman scatt., group theoretical calcs. 78−986
$IrCl_6^{2-}$, complex Raman tensors, irreducible tensor method, antisymmetric scatt. 78−37623
KF, KCl and KI, monomers and dimers, Ar matrix-isolated, IR spectra, vibr. assignments and calcs. 79−45718
KOD, mm wave spectrum, rot. transitions in excited vibr. states 77−3351
KOH, mm wave spectrum, rot. transitions in excited vibr. states 77−3351
KrF^+, selected valence-electron split-shell MO calc., ground state props. 79−22585
Li_2, $A^1\Sigma_u^+$-$X^1\Sigma_g^+$ band system transition dipole moments and radiative lifetimes, model pot. calcs. 78−9160
Li_2, $X^1\Sigma_g^+$ and $A^1\Sigma_u^+$ states, electronic struct. and spectra 79−89615
Li_{2n}, (n=1, 2, 3), stable cluster configs., ionisation pots., binding energies, vibr. freqs., al initio SCF and CEPA calcs. 80−14265
Li_2F_2, struct., force fields and normal mode freqs., ab initio calcs. 80−83260
LiH, mol. spectroscopic consts., FSGO calcs. 77−6758
LiH^+, spin densities, SCF and CI calcs. 79−3362
LiNC, mols. with polytopical bond, spatial distrib. and motion of Li 78−66533
LiNC, struct. vibr. states and pot. energy calcs. 78−86776
Li_2O_2, ab initio geometry, vibr. freqs., ionis. pots., and force consts. 77−65421
LiOH, fundamental vibr. freqs. 79−98068
LuF, mol. electronic states, 3000-6500 Å *(French)* 77−23502
MgX_2 (X=F, Cl, Br, I), 2Z 80−43021
MnO_4^-, reson. Raman lines, Stokes-antiStokes intensity ratio meas. 77−6786
MoO_3, $^{16}O^{18}O$ substitution, isotope shift, vibr. amplitudes and consts., normal coord. anal. 79−36610
Mo_7O_{24}, C_{2v} symmetry model, force field anal. 79−81200
N_2, $C^3\Pi_u$ state, electron impact excitation function approx. 79−7022
N_2, DC low press. positive column, electron distrib. function superelastic electron collision depend. 79−46498
N_2, electron impact rot. and vibr. excitation, elastic scatt., close coupling and Born approx. 80−28108
N_2, energy levels, low lying triplet states, infrared emission analysis 78−58691
N_2, liq., near BP, vibr. reson. energy transfer and dephasing, Raman spectra 77−6790
N_2, non-self-maintained glow discharge ionisation instability, vibr. states excitation calc. 77−19805
N_2 plasma, mol. vibr. excited, electron distrib. function, temp., drift vel., kinetic coeffs. *(Russian)* 79−7445
N_2, thermal conductivity, 400 to 1500K, vibr. internal energy calc. 79−18986
N_2, vibr. excitation calc., in gas mixture discharge 79−77442
N_2, vibr. populations of excited states under auroral conditions 78−42035
N_2, vibr. struct., core and valence ESCA spectra, Franck-Condon and HF anal. 80−32602
N_2, X-ray K-absorpt. spectra, vibr. fine struct., ab initio restricted HF calc. 78−86883
N_2^{2+}, low-lying electronic states, pot. energy curves calcs. by SCF technique, vibr. and ionisation consts. 80−69091
N_2/CCl_4, inhomogeneous broadening of Morse oscillator, temp. depend. 77−61803
NBr, mol. pot., r-centroids, $A^1\Sigma^+$-$X^3\Sigma^-$ band system 77−3373
ND_3, inversion splitting, generalised WKB method 80−9585
NF_3, mol. vibr., G-intensity sum rule 78−74632
NH, mol. spectroscopic consts., FSGO calcs. 77−6758
NH_2, A^2A_1-X^2B_1 absorpt. spectrum, 6250-9500 Å, rot. and vibronic anal. 77−472
NH_3, double min. vibr. pot., FORMAC program 77−23444
NH_3, IR absorption band integrated intensities, ab initio and LMO studies 80−23458
NH_3, inversion spectrum collisional line broadening, general theory 80−87184
NH_3, inversion splitting, generalised WKB method 80−9585
NH_3, mol. vibr., G-intensity sum rule 78−74632
NH_4^+, mol. consts. and mean vibr. amplitudes calcs. 80−106318
N_2H_2, vibr. assignment and pot. function, cis- and trans. mols., d_0-d_2 species 79−85952
NH_4Cl, gas $^1A_1$ ground state, pot. surface 80−32626
$N_2H_2(N_2D_2)$, ground and first excited state small vibr. coupling, ab initio CI calc. 78−62791
NO, high resolution absorpt. spectrum in region of first ionization limit 77−461
$^{14}N^{16}O$, overtone bands, determ. mol. consts. 78−58652
NO_2 and isotopic forms, total quartic potential function 78−13486
NO_2, electronic states, pot. energy surface calcs. 77−6673
$(NO)_2$, normal coordinate anal. 78−90144
NO_2^-, solvated, in H_2O, ethanol, cyanomethane, and DMF lowest n-π^* transition 79−85960
N_2O, and isotopic forms, pot. energy function determ. from vibr. data 77−18812
N_2O, combination and difference bands, IR intensities 77−466
N_2O, submm wave spectra, 375-565 GHz, isotopic species, mol. consts. 77−3346
N_2O^-, ground state potential energy surfaces 77−27175
N_2O^+, force fields and force const. of electronically excited states 80−69116
N_2O_4, mol. force consts. and vibr. amplitude, force field study 79−31730
NO_2Cl, force fields calc. 78−42241
NO_2F, force fields calc. 78−42241
NSCl, force consts. and mean amplitudes of vibr. *(German)* 79−50005
$^{14}NH_3$, ν_2-band Doppler-free two-photon resons. in Stark field 77−23527
Na_2, long range mol., electronic and vibr. levels 78−94301
NaAr, intramol. pot. functions of ground and excited state 79−54785
NaNe, intramol. pot. functions of first excited state 79−54785
$NbCl_5OPCl_3$, vibr. amplitude and normal coord. anal. *(German)* 78−66536
Ne_2, vibr. spectra, calc. from pot. curve 80−1040
NiCu molecule, electronic states determ. by ab initio HF and CI methods 80−69087
O_2, Schumann-Runge bands, predissoc. linewidths and oscill. strengths, vibr. level depend. 79−45735

molecular vibration calculations continued
O_2, thermal conductivity, 400 to 1500K, vibr. internal energy calc. 79−18986
O_2^+, 1NG bands spectral synthesis, for auroral obs. anal. 77−2296
O_2+La(Y)(Sc), crossed beam chemiluminescence reaction, spectral simulation, hyperthermal energy meas. 78−80732
O_3, radiative electron attachment spectra, vibr. stretching, electron affinity, theory 77−54617
O_3 vibr. and rot. variational calc., isotope shifts 77−57967
OCS, semiclassical energy levels calc., vibr. freqs. 78−46315
OH, A-X system, rot. transition probabilities 80−43027
OH, in lower atm., vibr. energy distrib. 77−25735
OH, vibr. excitation by H_2O photodissoc. 77−75242
$OH^+(OD^+)$, $A^3\Pi_i \rightarrow X^3\Sigma^-$ emission branching ratios, r-centroid depend. 77−6830
ONF_3, vibr. anal. using Green function 77−57962
$O(^3P)+CS_2 \rightarrow CS+SO$, reaction rate enhancement, triat. mol. symmetric vs. asymmetric stretch excitation 79−91927
OsO_3F_2, normal coordinate anal. in Urey-Bradley force field 79−49966
P_2, vibr. struct. calcs. from photoelectron spectra 77−18973
P_4 normal coordinates, allowable representations 79−2595
PD_3, $n\nu_2$ vibrational levels, prediction of inversion splittings 78−90146
PF_3, mol. geometry calcs. using centrifugal distortion const. 80−18841
PF_3, mol. vibr., G-intensity sum rule 78−74632
PF_3 pyramidal mols., intramol. forces, fundamental vibr. freqs., centrifugal distortion consts. 78−5202
PH_3, mol. vibr., G-intensity sum rule 78−74632
PH_3, $n\nu_2$ vibrational levels, prediction of inversion splittings 78−90146
$PMo_{12}O_{40}^{3-}$, vibr. force const. for spectroscopically active freqs. 77−57976
PMu_3, (Mu=muonium), $n\nu_2$ vibrational levels, prediction of inversion splittings 78−90146
PN, photoelectron spectra, ionisation pot., vibr. struct., Green's function method 77−61799
PN, vibr. struct. calcs. from photoelectron spectra 77−18973
$PbCl_6^{4-}$, model force fields and vibr. amplitudes calcs. 78−62780
$PdCl_4^{2-}$ (Br_4^{2-}), mean vibr. amplitudes and force field, Muller approx. 77−10659
PrF_3, orbital valency force consts. and mean square amplitudes 78−74627
$PtCl_4^{2-}$ (Br_4^{2-}), mean vibr. amplitudes and force field, Muller approx. 77−10659
RbBr, hyperfine struct., qudrupole coupling consts., vibr. depend. *(German)* 77−34565
RbF, RbCl and RbI, monomers and dimers, Ar matrix-isolated, IR spectra, vibr. assignments and calcs. 79−45718
Rb_9O_2, ionic clusters in alkali metal suboxide cryst., struct., vibr. freqs., Raman spectra 79−37772
ReF_6^+, force consts. and vibr. props., GVFF calcs. 77−14417
ReF_7, generalised quadratic valence pot. calcs., Wilson's F-G matrix 79−93966
ReF_7, generalised valance potential consts. 79−18169
$(SCN)_2^-$, and $(SCN)_2$, vibr. anal., bond strengths 80−9582
SF_6, $3\nu_2$ vibr. spectra 78−55183
SF_6, collisionless dissociation in intense IR field 79−87858
SF_6 gas, excited molecule vibr. translational relaxation, nonlinear processes *(Russian)* 80−91540
SF_6, multiphoton dissoc., anharmonic force field, decoupled rigid bender model 79−41153
SF_6, radial distrib. function of vibr. excited mol. 79−85951
SF_6, vibr. anharmonicity consts., ν_4 region laser absorption obs. 78−94242
SF_6, vibr. strength, IR intensities calcs. 77−34608
$^{32}SF_6$, anharmonic splittings, vibr. energy levels, $n\nu_3$ manifold 77−30853
S_2F_{10} 77−6775
SF_5Br, Ar matrix and solid phase Raman and IR spectra, vibr. assignments 77−6775
SF_5Cl AR matrix and solid phase Raman and IR spectra, vibr. assignments 77−6775
SO_2, $^1B_2$ state, force field and asymm. struct. 79−22685
SO_2, radiative electron attachment spectra, vibr. stretching, electron affinity, theory 77−54617
SO_3, dissoc. pathways and mol. vibr., compliance consts. and min. energy coords. 78−35661
SO_4, and isotopic forms, struct., normal coord. anal. 78−965
S_2O, isotopes, force consts., mean amplitudes of vibr. 78−970
$S^{16}O_2(S^{18}O_2)$, $^1B_2$('A') state, force field for large amplitude motions 80−43023
SPF_3, isotopic forms, microwave spectra, centrifugal distortion consts., vibr. and rot. states, IR matrix spectra 77−10665
$SbCl_5$, nitrile addition compounds, mol. vibr., IR and Raman spectra *(French)* 77−23499
$SbCl_5OPCl_3$, vibr. amplitude and normal coord. anal. *(German)* 78−66536
SbO_4^{3-}, normal vibr. freqs. calc. 79−54837
ScO, chemiluminesc. from Sc+O_2 reactions 77−1927
ScS, IR spectrum, vibr. consts. 77−10669
$(SeCl_4)_4$, vibr. anal., cubane-like T_d model 78−66537
SiD_3F, microwave spectrum, rot.-vibr. interaction consts., Coriolis reson., E1 moment 77−6766
Si_2F_6, normal coord. analysis, vibr. freqs. and amplitudes, shrinkage and distortion consts., force consts. 80−27989
SiH_3-group containing mols., normal coord. anal. 80−9579
SiH_3F, microwave spectrum, rot.-vibr. interaction consts., Coriolis reson., E1 moment 77−6766
$(SiH_3)_2O$, vibr. spectra, coupling of large amplitude vibrs. 78−37619
SiO, low-lying electronic states, vib. assigned perturbations 77−27082
SiO, vibr. struct. calcs. from photoelectron spectra 77−18973
SiO, vibr. wavefunctions, Franck-Condon factors, at low quantum numbers 78−55203
SiO_2, mol., ab initio SCF calcs., ground state stability, struct., vibr. freqs. 78−86781
SiS, Franck-Condon factors and r-centroids for ($D^1\Pi$-$X^1\Sigma^+$) transition using R-K-R-V 78−5293
$SnCl_3^-$, harmonic approx., force consts., electro-optical parameters and normal vibrs 78−62790
$SnCl_4N_2$ ions, force field calc., vibr. amplitude and rot. distortion consts. 79−98245
SnI_3^-, harmonic approx., force consts., electro-optical parameters and normal vibrs 78−62790
SnO_4^{4-}, normal vibr. freqs. calc. 79−54837

molecular vibration calculations continued
SnX_3, (X=F, Cl, Br, I), vibr. freqs. and intensities anal. *(Russian)* 77−23492
$Sr^{16}O$, ($Sr^{18}O$), $A'^1\pi$ state, vibr. anal., isotope shifts, vibr. consts. 77−18903
$I_2^- + T_2$, charge transfer reactions rel. to vibr. states 77−9070
$TaCl_5OPCl_3$, vibr. amplitude and normal coord. anal. *(German)* 78−66536
Te_4^{2+}, pseudopot. SCF-MO calcs., spectrum assignments 80−83269
$TeCl_4$, vibr. anal., cubane-like T_d model 78−66537
$(TeCl_4)_4$, vibr. anal., cubane-like T_d model 78−66537
TeO_4^{2-}, normal vibr. freqs. calc. 79−54837
TeO_4^{2-}, vibr. props. calcs. *(German)* 79−3431
$TiCl_4$, IR absorpt. bands, absolute integrated intensities, obs. and calc. 78−78689
$(TiCl_4.POCl_3)_2$, normal coord. anal. and force consts. 79−22682
TiO, potential energy curves and dissociation energy 78−50531
Tl halide dimers, kinetic consts. method for vibr. analysis 79−26968
UBr_4O_2 ions, force field calc., vibr. amplitude and rot. distortion consts. 79−98245
UCl_4O_2 ions, force field calc., vibr. amplitude and rot. distortion consts. 79−98245
UF_6, $3\nu_2$ vibr. spectra 78−55183
UF_6, ν_3 manifold 3-quantum transition probabilities, spectral assignment 78−58648
UF_6, vibr. strength, IR intensities calcs. 77−34608
$UO_2(NO_3)_2.6H_2O$, 420 nm absorpt. band, electronic-vibr. struct. calc. 79−10119
WO_3, vibr. anal., mol. consts., kinetic consts. method 80−23393
XY_4Z molecules, assignment of fundamentals of vibr. spectra for 24 mol. with C_{4v} symmetry *(French)* 79−31504
XeF^+, selected valence-electron split-shell MO calc., ground state props. 79−22585
YF^+ emission, 3400 to 3700 Å, rot.-vibr. anal., electronic struct. 77−6839
YO, chemiluminesc. from Sc+O_2 reaction 77−1927
YbCl, chemiluminesc., vibr. anal. 77−30917
YbF, chemiluminesc., vibr. anal. 77−30917
$Zr(BH_4)_4$, and d_{16}, mol. vibr. amplitude, normal coord. anal., T model 79−59433
$Zr(BH_4)_4$, mol. vibr., T_d model and force field 79−801

molecular vibration in solids
1,4-dithiane-1-oxide, cryst., IR and Raman spectra 79−69839
acenaphthalene, mol. and cryst., vibr. anal., normal coord. calcs. 79−47428
acenaphthene, vibr. spectra, mol. crystal dynamics, librational modes 78−64356
acetic acid, cryst., and isotopic species, H-bond, ν_s-ν_σ coupling and ν_s anharmonicity, IR spectra at 10K 79−15450
acetic acid-d_0, -d_1, -d_4, H bonding in solid, IR spectra, vibr. and librational modes 78−43843
acetic acid-d_0(-d_1,-d_3,-d_4), cryst., H bonds, stretching, temp., isotope effects 79−51938
adamantane, plastic-phase transition, cell model 77−11665
adipic acid crystals, H bonds, harmonic couplings, IR vibr. modes, isotope effect origin 80−34902
adipic acid crystals, IR spectra, O-H(O-D) stretching bands 79−91422
adsorbed molecules, photoelectron line shapes, vibr. excitation and hole delocalisation effects 79−95905
adsorbed molecules on solid surface, effect on electron capture by deep levels 80−29458
DL-alanine, cryst., Raman spectra and lattice dynamics 79−28741
L-alanine and DL-alanine, cryst., Raman band intensities of local group modes 80−93298
DL-alanine-α,β-d_4, Raman spectra, intermol. pot. 79−91432
alkali aluminometaphosphate glass, $MPO_3.Al(PO_3)_3$:U (M=Li,Na,K), vibronic excitation, absorption and emission spectra 78−52524
alkali bisulphites, and disulphites, and isotopic forms, solid and soln., Raman spectra assignments 79−42968
alkali borates, vitreous and cryst., vibr. spectra and struct. comparison 78−23470
alkali cyanide crystals, lattice dynamics calc. 79−77705
alkali halide:CN radical, impurity effects on ion-induced luminesc. 77−16402
alkali halide:NCS, force field calc. 79−51224
alkali halide:O_2^-(NO_2^-), effect of press. on vibronic spectra 78−52532
alkali halide:VO^{2+}, impurity behaviour, elec. cond. and IR absorpt. obs. 77−8607
alkali halides, cryst., force consts., IR absorpt. freq., logarithmic pot. function calcs. 78−2832
alkali halides, molecular centre symm. groups, roto-vibronic spectra *(Russian)* 80−88283
alkali hexahalogeno compounds: $ReCl_6^{2-}$($ReBr_6^{2-}$), low symm. splittings in vibronic spectrum due to phase transitions 80−55161
alkali metal hexachlorotellurates, $A_2(TeCl_6)$, (A=Cs, Rb, K), IR and Raman spectra, lattice and internal modes, phase transition 78−6659
alkali metal tetracyanoplatinate (FHF), one-dimens. conductors, IR spectra 77−77184
alkali metal tetrafluoroborates, intramol. force fields and mean vibr. amplitudes 80−2743
alkali sulphates, SO_4^{2-} optical and spectroscopic props., cryst. environment effect 77−40224
alkali tetrafluoroaluminates, matrix isolated IR spectra 80−985
n-alkyl carboxylic acids, vibr. spectra, C-H stretching mode assignments 79−47429
π-allyls, LF vibr. modes of hydrogeneous ligands, incoherent inelastic neutron scatt. 78−6229
aluminates with tetrahedrally coordinated Al atoms, normal vibs. 77−51456
aluminophosphate glass, multicomponent, 3.2 micron broad absorption band computer anal., residual H_2O vibr. 78−52478
ammonium oxalate monohydrate, IR refl. and Raman spectra, internal and external modes *(French)* 77−36231
ammonium oxalate monohydrate, Raman spectrum, internal and external vibrs. 79−73924
anharmonic molecules in condensed media, vibronic dephasing, intra- and intermolecular processes 80−2127
anharmonic molecules in low temp. matrices, vibronic dephasing 80−6469

molecular vibration in solids continued
anomatic hydrocarbon high density excitation effects on fluoresc. 79−1782
anthracene:tetracene, upper excited vibronic states optically pumped energy transfer matrix fluoresc. 78−76512
anthracene, in n-hexane, Shpolskii absorpt. spectra at 77K, vibronic struct. *(German)* 79−59507
anthracene, phonon-assisted mobility due to intermol. vibrs. 78−6383
anthracene, polarised reflection spectra, surface and vol. exciton coupling, vibronic states 78−72543
anthracene, polariton effects in transmission and absorpt. spectra in thin crysts. 77−20886
anthracene, Shpolskii spectra, vibronic struct., fluoresc. *(German)* 79−22754
anthracene, vibr. amplitude of mol. in condensed phase, five-parameter approx. 79−82295
anthracene crystal, stimulated emission and Raman scatt. 78−1303
anthracene in 2 methyl-THF glass, low temp. fluoresc. bandshape, excess energy effects 78−76509
apatites, condensation of tetrahedra, IR absorpt. band exam. 77−85760
aromatic molecular crystal, electron-intramol. vibr. coupling, rel. to carrier mobility 77−15854
L-ascorbic acid, cryst. isolated OH iscillators, IR absorption, temp. and H-bond effects 80−7351
ATP disodium salt, hydrated, vibr. assignments, force consts., coincidence method appl. 78−62953
benzamide, single cryst., far i.r. absorpt. spectrum *(French)* 77−4637
benzene-hexa-n-hexanoate, phase transitions and mesophase form., sp. ht. and IR spectra, 13 to 393K 80−79955
benzoic acid, dimer, cryst., IR and Raman spectra, vibr. assignments 78−31191
2-benzoyl-1,3,4-triphenyl-1-cyclopentanol, cryst., thermal vibr. of mols., rigid body anal. 78−38787
biphenyl, incoherent inelastic neutron scatt. time of flight spectra, vibr. spectra model calc. 78−63816
biphenyl, luminescence spectrum intensity distribution 79−3476
biphenyl cryst., nonbonded atom-atom interact. model, low freq. vibr. modes 77−1188
biphenyl crystals, electronic and vib. states, cryst. field mixing, two-photon spectra 77−59603
bis(trifluoromethyl)peroxide, gas and solid, Raman, IR spectra, internal rot. barrier of CF_3 78−29789
bond anharmonicities, Gruneisen parameters and pressure-induced frequency shifts 80−107397
1-bromopentane, low freq. mol. vibrs., neutron inelastic scatt. study 79−46760
calcium dipicolinate trihydrate, IR and Raman spectra, isotopic frequency shift, mol. vibr. obs., point groups determ. 80−89001
carbon tetrabromide, solid, Raman spectrum, temp. depend. 78−52488
carbon tetrachloride, solid, Raman and far IR spectra 79−33680
n-carboxylic acid, IR-spectra and dimeric molecules normal vibr. *(Russian)* 77−77218
n-carboxylic acids, IR spectra, normal vibrs. forms and freqs. *(Russian)* 79−91450
charge transfer complex high density excitation effects on fluoresc. 79−1782
chloro(ethyl)silanes and its C derivatives, solid, Raman spectra, mol. vibr. and rot. isomerism 80−87134
chloroacetanilides, NQR freqs., torsional vibr., temp. var. 78−2766
chloroacetoacetanilides, NQR freqs., torsional vibr., temp. var. 78−2766
chloroaluminium phthalocyanine, sublimed layer, IR absorption, vibr. assignments 78−55174
p-chlorobenzaldehyde in methylcyclohexane, matrix perdeuteration effects on $^3\pi\pi^* \rightarrow S_0$ phosphoresc. 77−20903
p-chlorobromobenzene, single cryst., polarised Raman and IR spectra, assignments 78−60431
trans-1,4-chlorobromocyclohexane, liquid, crystalline and amorphous state, conformation and vibr. spectra, IR obs. 80−60568
trans-1,4-chloroiodocyclohexane, liquid, crystalline and amorphous state, conformation and vibr. spectra, IR obs. 80−60568
chloromethoxyyaniline, NQR freqs., torsional vibr., temp. var. 78−2766
chloromethyl formate(-d_1,d_2,d_3), gas, solid. and liq., IR spectra assignments and struct. 80−32715
m-chloronitrobenzene, cryst., low freq. vibrs., polarised Raman and IR spectra study *(French)* 80−16029
m-chloronitrobenzene, molecular crystals, translational and orientational vibr. determ. 80−55103
chlorophyll, and related mols., in solid solns., fine-structured vibronic spectra under tunable dye laser excitation *(Russian)* 80−74164
chromocene, solid, Raman transition assignments, mag. susceptibility, mag. moment 78−43861
condensed media, vibrational relaxation studied by picosecond or Raman spectros., review 80−80797
constrained thermal motion refinement for rigid molecule with librating side groups 77−11643
coronene, mol. vibr. amplitude of condensed phase, five-parameter approx. 79−82295
coronene-TCNQ, solid complexes, spectra, stoichiometry 78−23435
correlation field effect in two-phonon excitations 77−72660
coupled molecular normal vibr. system, radiationless energy relax. *(German)* 78−35184
cryst., vibr. spectrosc. *(French)* 78−6667
crystal lattice, interaction of mode-locked pulse train, helium temps. 79−23012
crystallography, charge density, spatial partitioning 78−71638
crystallography, charge density models 78−71695
crystallography, electron densities, thermal smearing, limited resolution effects 78−71635
crystallography, X-ray neutron, charge deformation, vibr. smearing 78−71634
crystals, vibr. spectra, approx. calc. method *(Russian)* 78−35148
cubic crystal, Jahn-Teller effect, soft mode influence 80−59937
cyclobutadiene iron tricarbonyl, LF vibr. modes of hydrogeneous ligands, incoherent inelastic neutron scatt. 78−6229
cyclobutane-d_0(d_8), cryst. modifications, low. freq. Raman and IR spectra 80−7342
cyclohexanol, low temp. solid phases, far IR absorpt. spectra, 93 to 303K 79−56785
1,5-cyclooctadiene, liq. and solid phases, IR and Raman spectra 79−19877
cyclopentylamine, vibr. spectra and struct. 80−102516

molecular vibration in solids continued
Debye-Waller factors, contrib, of internal modes 79−73263
degenerate vibration, biphonons in region of overtone 77−69059
dense media, absorpt. profiles of mol. transitions 80−59589
dense media, absorption and dispersion profiles of molecular transitions 77−80585
diacetylene polymers, high freq. vibr. mode modelling 79−19346
diamond, impurity centres, vibronic spectra, Van Hove singularities, quasi-local vibrs. 77−85782
diatomic mol., vibr. relax. in condensed media, mol. rot. effects 78−91388
diatomic mol., X-ray scatt. intensities, vibr. averaging 78−74722
diatomic molecule in crystal, rate of radiationless electronic transitions 80−93373
diatomic molecule in solid lattice, nonradiative relax. of intramolecular vibr. 77−52178
diatomic molecules, matrix isolated, vibr. energy relax., orientational motions effects 78−67776
diatomic molecules, matrix isolated, vibr. spectrosc., IR line shape calcs. 79−72307
diatomic molecules, shortening of energy relax. time of excited mol. vibr. in dense medium by form. of H-bonds 80−91553
diatomic molecules, vibr. excited, in inert matrix, information theoretic anal. 78−91386
dibenzene-naphthalene, relax. time of vibr. levels of ground state *(Russian)* 77−44054
dibenzofuran, single cryst. 2-photon excitation spectrum, 4.2K 79−56807
2,2-dibenzyl-1,3-dibromopropane, crystal structure and thermal motion 79−99173
1,5-dibromopentane, low freq. mol. vibrs., neutron inelastic scatt. study 79−46760
1,12-dicarbaclosododecaborane, plastic solid, phase transitions, 10-320K, Raman and IR obs. 79−28744
2,5-dichloro-1,4-benzoquinone, mol. cryst., transition moment directions 78−64351
p-dichlorobenzene, cryst., Raman spectra , intensity of low freq. line 78−2846
p-dichlorobenzene($-d_4$), mixed cryst. phases, mol. reorientations and intermol. interactions, Raman obs. 79−28751
2,2-dichlorobutane, liquid and solid., vibr. spectra, IR and Raman obs. 80−60567
1,1′-diethyl-2,2′-cyanine iodide, neat and mixed crysts., visible absorption and emission spectra assignments 77−1692
difluoromethane cation, in solid Ar, IR spectra, vibr. modes 79−68231
difluoromethyl cation, in solid Ar, IR spectra, vibr. modes 79−68231
diglycine, cyclic, solid phase laser Raman spectrum 77−85695
2,2-dihalohexafluoropropane, IR and Raman spectra, gas, liq. and solid, normal coord. anal. 79−72314
1,4-dihalonaphthalenes, binary solid solns. lattice stability, mol. motions 78−31182
p-diiodobenzene, far IR single cryst. transmission spectrum, temp. and polaris. depends., assignments 78−72498
dimerized organic linear chain conductor, electron mol. vibr. coupling consts. 78−14686
dimethyl ether-d_0,($-d_6$), solid solns., vibr. Raman spectra and intermol. pot. function 78−68494
9,10-dimethylanthracene, in n-hexane, Shpolskii absorpt. spectra at 77K, vibronic struct. *(German)* 79−59507
9,10-dimethylanthracene, Shpolskii spectra, vibronic struct., fluoresc. *(German)* 79−22754
dinaphtho-(2′.3′:1.2);(2″3″:6.7)-pyrene, triplet state, phosphoresc. and ODMR obs. 79−27013
m-dinitrobenzene, oriented film, intermol. vibr. coupling, polarised IR spectra 80−97264
4,4′-dinitrobiphenyl complexes, intermol. interacts. and geometry of non-rigid mols., vibr. spectra 78−88294
dioxane-$HgCl_2$ complexes, IR and Raman vibr. spectra, inter- and intramol. forces 77−66489
dipicolinic acid, IR and Raman spectra, isotopic frequency shift, mol. vibr. obs., point groups determ. 80−89001
dipole-dipole interaction rel. to internal vibr. 78−47476
DNA pyrimidines, cryst., lattice dynamics 78−75766
dynamics, neutron spectroscopy appl., review 79−42166
electronically degenerate states, asymmetric scattering tensors of normal modes, selection rules 77−12381
energy transfer between coupled mol. vibrs. in dense media *(German)* 78−37719
energy transport, molecular dynamical calc. 78−95117
ethers, and alkane solid solns., dielec. props. and IR spectra *(French)* 79−4378
ethers, and solid alkane solns., far IR spectra *(French)* 79−4793
ethylammonium cadmium tetrachloride, order-disorder transition, far IR reflectivity obs. 79−65870
ethyldifluoroborane, microwave, Raman, IR spectra, conform., dipole moments, vibr. assignment 78−90155
ethylene oxide clathrate deuterate, rotational motion, quasi-elastic neutron scatt. study 79−51022
fluorene, near 6K, two-photon excitation spectrum, g-exciton states location 78−64393
fluoromethylene cation, in solid Ar, IR spectra, vibr. modes 79−68231
formic acid, cryst., H bonded, IR spectrum computer simulation 80−97253
formic acid crystals, low temp. IR spectra 77−48153
formic acid crystals $\nu_{O\text{-}H\ldots O}$ and $\nu_{O\text{-}D\ldots O}$ vib. anharmonicities 77−48154
furane, cryst., low freq. vibr. spectrum, temp. depend., 12 to 253K 80−84743
gamma-ray resonant scatt. cross section frequency of normal modes 80−18060
gas-solid surface sticking probabilities, internal mode depend. 78−6213
glass:Eu^{3+}, vibronic spectra, impurity complex model 78−19516
glass, alkali-alkaline earth nitrates, Raman spectra, vibr. perturbations effect 79−8132
glycerol($-d_3$), single cryst., glassy, and supercooled, polarised Raman spectra, anharmonic multiphonon interactions 79−91419
X-glycine, cryst., Raman band intensities of local group modes 80−93298
α-glycine, deuterated, low freq. intermol. modes, neutron diffr. obs. 80−15086
α-glycine, natural and ^{15}N-substituted, solid, Raman spectra, normal vibrs. 77−63408
α-glycine-C-d_2, Raman spectra, intermol. pot. 79−91432

molecular vibration in solids continued
graphite-Br_2, in-plane intercalate lattice modes, Raman scatt. 79−42163
graphite-$FeCl_3$ intercalation complex, IR and Raman spectra study of optical modes 79−56797
graphite-HSO_3F intercalation compound, Raman spectral study *(French)* 80−60581
hexabromobenzene, cryst., IR and Raman spectra, vibr. normal coordinate anal. 77−79602
hexafluoride ions of group IIIA elements, molecular consts., normal coord. anal. 77−1187
hexafluorohalopropanes, gas and solid, IR and Raman spectra, normal coord. anal. *(German)* 79−72317
hexaidobenzene, cryst., IR and Raman spectra, vibr. normal coordinate anal. 77−79602
hexamethylbenzene, cryst., Raman spectra, intensity of low freq. line 78−2846
hexamethylbenzene, IR polarised spectra 79−28758
hydrates, electric field gradient tensors at deuterons 77−71792
hydrates, H_2O vibration in crystal lattice, model calc. 78−75741
ice, amorphous, 2500-4000 cm^{-1} Raman and IR spectra, vibr. anal. 77−59562
ice, cryst. Ic and Ih phases, diffr. patterns and far IR spectra, isotope effects 78−6662
ice, D_2O, H_2O, intramolecular potential from overtone spectrum anal., H-bonding dependence 79−93972
ice, D_2O-H_2O, intramolecular stretching spectrum, role of Fermi resonance 79−93973
ice, hexagonal, i.r. polarisability rel. to mol. vibrs. anharmonicity 77−4639
ice, Ih, polycryst., vibr. spectrum anal., OH stretching region 79−11412
ice, Ih-phase, oriented single cryst., proton distrib., light scatt. obs. 77−16318
ice, II and IX, deuterated forms, 10K, OD stretching bands interpretation 78−2836
ice, IR absorpt., O-H stretching vibrs., orientation polaris. 78−31177
ice, isotopic, I_H, single crystal Raman intensities, OH bond polarisability, librational modes 78−27208
ice, IV, 4000-400 cm^{-1} IR spectra, H-bonding and assignments, orientational disorder 80−16022
ice, O-H and O-D bond stretching vibrs., Raman spectra at atmospheric press. 80−66166
ice, press. effects on Raman spectrum 78−95582
ice I, OH stretching region anal. of vibr. spectra 77−59563
ice I, polycryst., 2500-4000 cm^{-1} Raman and IR spectra, vibr. anal. 77−59562
ice Ih, polycryst., IR spectrum, OH stretching region 79−11411
ice Ih, polycryst., Raman spectra, OH stretching region 79−11410
ice VI, high-pressure Raman spectra, bending and librational bands 78−68499
ice VI, OH stretching peak freq. press. depend., Raman spectra using diamond anvil cell 80−16023
imidazole, vibr. spectra, mol. crystal dynamics, librational modes 78−64356
impure molecular crystals, ground electron state, vibr. levels, relax. time determ. *(Russian)* 78−15195
impurities in crysts., dynamics 79−60442
impurity molecule in solid matrix, vibr. relax., stochastic classical trajectory approach 78−79707
impurity molecules in Debye solids, vibr. relax., stochastic classical trajectory calcs. 79−1482
impurity spectrum under Fermi reson. with compound tones 78−34583
indigoid dyes, Raman, IR and Shpolskii spectra 79−65866
inorganic molecular crystals, metal complexes electronic spectra and intermolecular interactions 80−55137
intra-site vibration effects on elec. cond. in disordered Hubbard model 80−107775
lithium formate monohydrate, temp. depend. Raman spectra, H bonds 78−6673
magneto-optical effect in cryst. 80−45043
malononitrile, cryst., phase transitions, Raman and IR obs. 80−88980
malononitrile, displacive phase transition, 294.7K, Raman and Brillouin-Rayleigh scatt. obs. 80−16047
matrix isolated molecules, vibr. relax. 78−46425
MBBA, Raman spectra in cryst., frozen glassy, and liq. cryst. states 80−60601
medium-induced relaxation, laser pulse meas. 79−38667
melting curve extrema from repulsive step potential, molecular dynamics calc. 77−59102
metal ions, in complexes and biological systems, preliminary vibr. assignment method 78−62953
metal surface, mol. vibr. energy transfer, classical EM theory 80−96806
metal-NH_3 mixture, attractive electron-electron interaction from molecular tunnelling mode 79−37793
methane, phase II, IR and Raman spectra of ν_3 and ν_4 modes 78−2834
methane, solid, Raman spectra and II-III phase transition 80−2745
methane, solid phase II Raman spectrum, lattice vibr. and ν bands 78−19456
methanol, C-O-H bending mode in α- and β-forms at 85K 77−8588
methanol-CO-H_2O-NH_3 solid mixture vibr. modes, IR spectra 80−90504
methoxydifluorophosphine-d_0 and -d_3, solid, IR and Raman spectra, mol. vibr. and struct. obs. 80−87103
methyl ammonium chloride, Raman spectra, 70 to 300K, H stretching vibrs. 80−20628
methyl chloride, cryst., Raman band anomalous splitting, isotope effects 77−8562
methyl group tunnelling and coupling to internal vibrations 78−79675
N-methylacetamide, and isotopic forms, low-freq. Raman spectra, internal torsional mode 79−26992
N-methylacetamide, solid, Fermi resons. 80−97266
9-methylanthracene, in n-hexane, Shpolskii absorpt. spectra at 77K, vibronic struct. *(German)* 79−59507
9-methylanthracene, Shpolskii spectra, vibronic struct., fluoresc. *(German)* 79−22754
3-methylpentane, C-H stretching diagonal local mode anharmonicity, intermol. perturbation 78−25524
molecular crystals, IR absorpt. spectra, intermol. reson. interaction, temp. depend. 78−72506
molecular crystals, neutron scatt. obs., book contrib. 77−89505
molecular crystals, non-dipole vibr., Raman effect *(Russian)* 78−76471
molecular crystals, spectroscopy, bibliography for 1976 78−72585
molecular crystals, theory of IR spectra of H-bond 77−40223

molecular vibration in solids continued
molecular crystals, two particle exciton-phonon interactions, optical absorpt. line shapes theory 80−55120
molecular glass, density of states for IR active internal modes of tetrahedral mols. 78−75788
molecules, condensed, vibr. excitation in photoemission spectra, appl. to CO 77−28689
molybdates, hydrated, water mol. bending vibrs. at low freqs. *(French)* 79−78670
sym-N_2O_3, mol. vibr. in N_2 matrix, normal coord. anal. 79−59432
[n-]alkanes, cryst., vibr. correl. splitting and chain packing 80−7338
naphthalene:β-naphthyl-n-biphenyl-ethylene, relax. time of vibr. levels of ground state *(Russian)* 77−44054
naphthalene: quinoxaline, isolated triplet mol. direct spin-lattice relax., librational model 79−11444
naphthalene:azulene, reson. fluoresc., Raman spectra, single vibronic level relax. 79−38588
naphthalene, $C_{10}H_8$ and $C_{10}D_8$, optical absorpt. spectra of hydronaphthyl radicals, isotope effects 78−60487
naphthalene, cryst., vibronic absorpt. spectrum with totally symm. phonons 79−4817
naphthalene, solid, high-energy vibr. overtone spectra, local modes, intramol. relax. 79−28052
naphthalene, vibr. amplitude of mol. in condensed phase, five-parameter approx. 79−82295
naphthalene, vibr. dephasing and Raman active localised internal mode temp. depend. 80−45060
naphthalene charge transfer complexes, cryst., vibr., factor group splittings 79−7658
naphthalene-d_0, (-d_4), (-d_8), inequivalent local C-H modes, subpicosec. dephasing, high energy overtones 79−86850
naphthalene-d_8, Raman active vibrs. 77−32358
naphthalene-d_8 and -h_8, Davydov splitting of Raman-active vibr. levels 77−36210
neopentane, diamond force const., rel. to crystal elastic consts., Raman freq., bulk compressibility and freq. assignments 80−65183
NH_4 halides, halides, simple, complex, polycryst., hydrogen bonding, NH_3D^+ probe ion IR spectra 79−82966
nitrate salts, Raman spectra, thermally disordered energy states 78−35122
n-nitroaniline, IR and Raman spectra, internal modes 79−61366
nitromethane-d_0,-d_3, polycryst., methyl torsion, Raman spectra 79−82970
NMR signal for quadrupole, chem. shift, dipole-dipole interactions, mol. solids, rigid-body vibr. effect 78−15056
n-nonane:H_2-tetra-4-tert-butylphthalocyanine, thermal broadening of zero phonon lines, hole burning 78−71803
nonradiative electron transitions in crystal, impurity molecule vibr. 80−103645
norbornadienes, LF vibr. modes of hydrogeneous ligands, incoherent inelastic neutron scatt. 78−6229
NQR, NMR and EPR, spectral parameters, influence of mol. motion dynamics, review 80−20486
octafluoronaphthalene crystals, phase transition, Raman spectra 77−24829
octamethylcyclotetrasilazane, gas, liq., cryst., CCl_4 soln. IR and Raman spectra, assignments, struct. *(French)* 78−29790
one-dimensional crystal lattice, nonlinear interaction of ps light pulses with lattice vibrations 78−30032
palladium porphin, in n-alkane crystal, Zeeman and crystal field effects, absorpt. vibr. anal. 80−7372
palygorskite, uncoupled H_2O, isotopic dilution IR obs. 77−8568
PAN fibre, pre-oxidised, IR absorpt. 77−28561
particle displacement momenta, quantum equilib. distrib. 78−32751
pentacene, in naphthalene (p-terphenyl), picosec. coherent transients obs. 79−46013
perfluoro-1,3-butadiene, vibr. spectra, struct. and barrier to planarity 78−9147
perovskite, ordered, $A_2^{II}BMO_6$ type, MO_6 octahedra, mean vibr. amplitudes *(German)* 80−54320
(perylene)$_3$TCNQ, prep. and spectra, electron-mol. vib. coupling 77−16290
phase and population relax., semigroup formalism 80−78519
phenanthrene, cryst., Raman spectra, intensity of low freq. line 78−2846
phenanthrene, IR and Raman spectra, lattice and internal mode coupling 77−20843
phenanthrene, two-photon excitation spectra, exciton-phonon and intramol. vibronic coupling 80−84774
phenanthrene, vibr. spectra, mol. crystal dynamics, librational modes 78−64356
phenol, cryst., mol. vibrs., factor group splittings 80−16021
phenylsilanetriol-d_0,(-d_3), cryst. and liq. vibr., IR and Raman spectra 78−86855
phonon-assisted radiative electronic transitions 79−24348
phosphates, vib. calcs. 77−51457
picolines, freq. assignment, vibr. spectra interpretation *(Russian)* 79−22684
polar semiconductor crystalline thin films, surface vibr. states, IR absorpt. spectra obs. *(Russian)* 80−60606
Polaroid K, oriented analogue of polyacetylene, reson. Raman spectroscopy 80−66208
poly γ-methyl L-glutamate films, thermal motion of α-helical mols. 79−64133
polyacetylene:I, pure and doped, reson. Raman spectroscopy 80−66208
polyacetylene, doped and neutral, resonance Raman scatt. 80−55107
polyacetylene, lightly doped, donor and acceptor states, IR absorpt. obs. 79−73979
polyatomic molecules in condensed medium, vibr. relax., coherence transfer processes 79−60461
polyatomic molecules in condensed phases, origin of vibr. dephasing 79−27069
polycrystalline samples, Raman intensities and Raman tensor invariants 77−85696
polyethylene, intermolecular force field and normal vibrs. 79−73265
polyethylene, linear, far IR absorpt. spectrum, temp. depend., 14K to melting pt. 79−1758
polyethylene (orthorhombic), intermol. pot. functions, force consts., vibr. assignments, thermodynamic props. 77−39639
polyethylene single cryst., FT IR spectra, CH_2 rocking mode 78−2843
polyethylene single cryst., FT IR spectra, CH_2 wagging mode 78−2842
polymer, amorphous, translational motion and lattice vibr. obs. by Raman scatt., T_g phenomena 78−23469
molecular vibration in solids continued
polymer, LF vibration spectrum, effect of dimensional quantisation *(Russian)* 79−1480
polymers and crysts., vibr. anharmonicity, intensities of overtones and component freqs. 77−69052
polymers and molecular crysts., vibronic spectra exam. 78−67778
polymethineimine, all-trans, ab initio cryst. orbital calcs. 79−77530
polyperdeuteroethylene, IR and Raman spectra, 77K and room temp., vibr. anal. 78−72517
polyphenylacetylene, cryst., resonant Raman scatt., opt. absorpt. 77−4630
polypropylene, extruded, chain orientation, polarised Raman scatt. 79−1756
polystyrene, amorphous, low temp. sp. ht. calcs. 77−28014
polystyrene, substituted, Raman, IR and neutron spectra of LF vibs. 78−2848
polystyrene amorphous film, cyclically fatigued, molecular behaviour 80−35310
polystyrene and model cpds., conformational struct. influence on normal modes of benzene ring, Raman study 80−14144
polyurethanes under tension loads, spectral exam. *(Ukrainian)* 78−92058
polyvinylidene fluoride-PTFE, thermoelectret, IR spectra, struct. modifications and dielec. props. 77−55785
potassium chloranil, IR spectra, mag. and optical props., phase transition and solvation 77−43983
potassium hydrogen malonate single cryst., IR and Raman spectra 78−60444
potassium hydrogen oxalate, oriented single cryst., Raman spectra with very strong H-bonding 80−25359
potassium oxalate, anhydrous, phase II, vibr. spectra and cryst. struct. 80−34901
potassium oxalate, D_2O, D quadrupole coupling, temp. depend. 79−31551
potassium oxalate monohydrate, cryst., O-H bond lengths, H-O-H angles, corrections 79−32945
pseudomolecules in vibrational relaxation, quantum theory of vibr. relax. 79−65161
PTFE, vib. assignment, far IR spectrum 77−48170
PVC, Raman spectrum, C-Cl stretching region 78−84583
PVC, structural studies by Raman spectroscopy 79−7044
PVC film, metal doping effect on chain vibrs. 79−95868
pyrazine, cryst., 3300 Å reson. Raman band, vibr. assignments 77−1684
pyrazine, in pyrazine-d_4, p-dioxane, X-trap, p-xylene, benzene(-d_6), cryst., MIDP, PMDR, low temp., assignments 77−36154
pyrazine, pyrazine-Kr, ground and n-π^* excited state struct. 79−68241
pyrazine.$(H_2O)_n$, n=1,2, ground and n-π^* excited state struct. 79−68241
pyrazine-d_4, in p-dioxane, p-xylene, benzene, cryst., MIDP, PMDR, low temp., assignments 77−36154
pyromellitic dianhydride-anthracene, cryst., charge transfer exciton transitions, refl. spectra obs. 78−72540
quinoxaline in Shpolskii-type hydrocarbon matrices, vib. struct. of electronic spectra 77−85773
radiationless, electron transition, diatomic molecule in crystal at zero temperature, rate const. 79−43011
radiationless phase relaxation, transverse relaxation time *(German)* 77−40275
radiationless vibr. phase relax. theory in dense media *(German)* 78−37720
radiative electronic transitions of impurities, effects of hydrostatic press. 80−11446
radical radiation formation in solid organic compounds 80−85201
Raman and IR obs., review 78−43079
Raman scattering, effect of inter- or intramol. energy exchange on vibr. dephasing times 77−66506
Raman spectra, reflection symmetry violation for crysts. and mols. 78−48184
Raman spectra line polarisations, impurity mol. orientational tunnelling effect 77−77208
rare earth perrhenates, $(ReO_4)^-$ ion vibrs. rel. to static field, Raman investig. *(Russian)* 78−76470
rare earth phosphates:Eu, electronic-vibr. spectra rel. to struct. 79−56850
rare-gas crystals, intensity and band shape of depolarised scattered light 77−51458
relaxation mechanism in mol. solids 77−7817
resonance Raman scattering, appl. to ultrafast dephasing and relax. obs., phonon scatt. effects 80−7337
rigid lattice, vibr. relax., rot. mechanism, impurity interaction pots. 77−72664
rigid-body vibrations, simple test based on generalisation of Hirshfeld's rigid bond postulate 78−91385
rotational mechanism for vibr. relax. in rigid media 77−58138
scheelite crysts., Davydov splitting of vibr. levels, short range interaction 80−71418
semicarbazide hydrochloride, vibr. spectra, normal coord. anal. 80−58255
semicarbazide-d_0, -d_6, vibr. spectra, normal coord. anal. 80−58255
Shpolskii multisite luminesc. spectrum deconvolution, vibr. struct. anal. 80−58304
silane molecules, substituted, chemical effects on freq. of Si-H vibrations 79−51227
silicate glass: Cr^{3+}, optical props., 88-273K, energy levels in crossing region 78−6709
sodium acetate trihydrate, press. depend. of methyl tunnelling motion 80−10603
sodium formate, vibr. spectrum, lattice modes 79−28759
sodium hydrogen oxalate monohydrate, oriented single cryst., Raman spectra with very strong H-bonding 80−25359
sodium uranyl acetate, fluoresc., circ. dichroism 79−38598
solid phase chemical reactions, low temp. and fast, mol. motion effect 80−97681
squaric acid, vibr. props., 2D model 79−90735
squaric acid and deuterated derivative, vibrational study, IR and Raman spectra 78−92076
stability constraints on potential function and rotational invariance in external mode formalism 80−24543
stearyl alcohol, H bonding effects on skeletal optical and longitudinal acoustical modes 80−34914
structural phase transition in two dimens. model 77−20038

molecular vibration in solids continued
surface vibrational spectroscopy using stimulated Raman scatt. 80−38062
talc, vibr. mode assignments, Raman microprobe spectra 80−88977
$TCNQ_2$-TEA, quasi 1-D cryst., interaction between electronic and vibr. states 77−52102
TCNQ, electron-mol. vib. coupling 77−15782
TCNQ, optical IR antireson. absorption, characts. rel. to cryst. parameters 77−77183
TCNQ alkali salts, charge transfer enhanced IR absorpt. spectra 77−28558
TCNQ complexes with pyridine, polarised IR refl. spectra, evidence for electron-vibr. coupling 79−47448
TCNQ salt, K-TCNQ, energy gap, electron-phonon interaction, IR spectrum 78−15167
TCNQ salt, MTPA $(TCNQ)_2$, IR refl., dielec. function and cond. 80−34924
TCNQ salt, n-methyl-n-ethylmorpholinium, unpaired electron states, IR refl. study 80−75491
TCNQ salts, anomalous infra-red activity and the determination of electron-molecular vibration coupling constants 80−25389
TCNQ salts, charge transfer, mode shift study, Raman scatt. *(German)* 79−28731
TCNQ salts, electron-vibrational interaction consts. 79−28054
TEA$(TCNQ)_2$, elec. cond. and thermoelec. power under hydrostatic press. 80−11024
TEA $(TCNQ)_2$, mixed electronic-vibr. states in far IR spectra, dielec. const. *(Russian)* 77−36249
tellurophene(-d_4), cryst., struct., phonon spectrum, exciton splittings, assignments 77−81088
p-terphenyl, far IR absorption spectra, 300-1.3K, phase transition obs. *(French)* 77−90140
tetrabromoethylene, cryst., IR spectra in polarised light, cryst. struct. 78−27223
tetrabromomethane, in disordered phases, IR active mode Raman line shape, dipole-dipole interaction 80−9603
tetrabromomethane, monoclinic monocryst., polarised Raman spectra *(French)* 80−93302
tetracene, unrelaxed fluoresc., direct picosecond obs. 80−89046
sym-tetrachlorobenzene, LF Raman bands and space symmetries 77−66504
2,2,3,3-tetrachlorobutane, vibr. spectra, liq. and solid-state, conform. struct. 79−73936
tetrachloroethylene, cryst., IR spectra in polarised light, cryst. struct. 78−27223
tetrafluoromethane, in disordered phases, IR active mode Raman line shape, dipole-dipole interaction 80−9603
tetrahydrofuran clathrate deuterate, rotational motion, quasi-elastic neutron scatt. study 79−51022
tetramethyl-1,3-cyclobutanedithione-h_{12} and -d_{12}, visible spectra, $n\pi^*$ transitions obs., mol. vibr. 80−97297
tetramethylaminoborane, $B_3H_8^-$ large-angle anisotropic motion, ^{11}B BMR, temp. depend. 77−90045
tetramethylammonium hexachlorotellurate, IR and Raman spectra, lattice and internal modes, phase transition 78−6659
s-tetrazine-benzene, mixed cryst., 2K, lifetime limited photochem. hole burning 78−9183
tetrohydrofuran-$HgBr_2$ complexes, IR and Raman vibr. spectra, inter- and intramol. forces 77−66489
TGFB, IR spectra and optical consts. *(French)* 79−95748
TGS, cryst., vibr. bands, ferroelec. and paraelec. phase H bonds *(Russian)* 78−15172
thieno(3,2-b)thiophene, electronic and vibr. spectra, vapour phase and cryst. 77−34654
thiosemicarbazide, mol. cryst., transition moment directions 78−64351
thiourea, phonon modes near phase transitions, IR and Raman spectra 80−45084
Toda lattice, excitation spectrum, molecular dynamics study 80−105588
toluene-d_0,-d_8, polycryst., methyl torsion, Raman spectra 79−82970
toluene-sulphonate-diacetylene, thermal polymerisation, near IR absorpt. and low lying states obs. 80−71399
transition metal complex anion, vibr. spectra in solid and soln., struct. and fundamental mode assignment 78−62803
transition metal hexafluorides, density of exciton states, two-particle and mixed cryst. spectra 78−2829
tri(trifluoromethyl) germanium halides, gas, liq. and solid, IR and Raman spectra, normal coord. anal. 79−72316
1,3,5-trichlorobenzene, lattice vibr., Raman spectra line intensities calc. 77−69825
tricosane, single cryst., polarised Raman spectra 77−61888
trimethylammonium chloride and deuterated forms, cryst., inelastic neutron scatt. H bond vibr. obs. 77−7796
s-trioxane, Raman spectra of single crystal, liquid and chloroform-d solution 79−94000
triphenylphosphine compounds, $(C_6H_5)_3PM_xM'_{1-x}(CO)_5$, M,M'=Cr, Mo, W, mixed cryst., CO vibr. spectra, modal anal. 78−35128
TTF^+, cryst., vibr. assignments, IR spectra 79−99869
$(TTF^+)_2$ dimer, cryst., vibr. assignments, IR spectra 79−99869
TTF, cryst., vibr. assignments, IR spectra 79−99869
TTF and derived cpds., intramolecular vibrs. and vibronic effects, IR and Raman spectra 80−25387
TTF halides, charge transfer effect on internal modes, Raman scatt. 80−25392
TTF salts, charge transfer, mode shift study, Raman scatt. *(German)* 79−28731
TTF-Cu bis-dithiolene, dimer, mol. displacements at 4.2K 80−10539
TTF-d_0, -d_4, IR and Raman spectra, vibr. assignments 78−23436
TTF-TCNQ, ^{15}N, ^2H isotope labelled, IR, Raman spectra, mol. vibrs., electron-phonon interactions 77−69835
TTF-TCNQ, anharmonic props., temp. (press.) depend., rel. to naphthalene and anthracene 80−15200
TTF-TCNQ, charge transfer, mode shift study, Raman scatt. *(German)* 79−28731
TTF-TCNQ, charge transfer determ. from spectral line shift using Raman scatt. 80−25392
TTF-TCNQ, electron-molecular distortion coupling near Peierls transition, IR spectra obs. 80−25390
TTF-TCNQ, one-dimensional conductor, Raman scatt. 78−80355
TTT, neutral, cation and conducting complex reson. Raman spectra, vibr. lines, charge transfer 79−4794
tungstates:Eu, electronic-vibr. spectra rel. to struct. 79−56850

molecular vibration in solids continued
two-phonon resonances, bound states absorpt. coeff. 78−47486
two-phonon resonances, bound-states, general theory 78−47485
urea, internal modes contrib. to Debye-Waller factors 79−73264
vanadyl phthalocyanine, sublimed layer, IR absorption, vibr. assignments 78−55174
vibrational relaxation, local phonon and roton receiving modes 79−46759
vibrational relaxation, rot. and translational local modes 77−75118
vibrational relaxation of molecules in condensed media, survey, book contrib. 77−36295
vibrationally hot molecules, local mode relax. in cold environments 79−86851
vinyl acetate, monomer and polymer, Raman and IR spectra, liq. and solid 78−58700
water, low-density amorphous solid, OH stretching spectrum 79−11413
xanthene dyes, hidden vibr. band determ. method, fluorescence and excitation spectra meas. 80−40158
zeolites, type Y, containg catalysts, cryst. struct., IR spectra 79−42958
$AgClO_3$, mol. torsional oscills., cooperative study by NQR 80−25244
$Ag_2H_3IO_6$, paraelec. and antiferroelec. phases, IR vibrational study 77−85697
Ag_2HgI_4, polycryst., Raman spectra, press. depend. 77−73137
Ag_2HgI_4, Raman line shape and ionic cond., coupled mode model 80−66171
$AgNO_3$, cryst. and molten salt, Raman and IR spectra, vibr. anal. 77−16311
$AgNa(NO_2)_2$, ferroelectric transitions, group theoretic comparison with $NaNO_2$ 80−7311
$AgNa(NO_2)_2$, Raman spectrum, NO_2^- bending vibr. 79−28737
Ag_2SO_4:CrO_4^{2-}, polarised electron spectrum assignments, red colour explained 77−85753
$Al(NO_3)_3.9H_2O$, cryst., deuteration rel. to NO_3^- ion vibr. spectrum *(Russian)* 77−40240
β-Al_2O_3, stoichiometric, Raman and IR spectra, Frenkel defects, order-disorder transition and cation cond. 80−55086
β-Al_2O_3-Na_2O, low freq. Raman scatt. from NH_4^+ ions 78−43878
Ar jet, supersonic, electron beam-excited, continuous VUV emission spectrum origins 79−6964
Ar, solid, NH and ND impurities role of rotational and translational modes n vibr. relax. 78−10132
Ar:Eu, matrix isolated, obs. of Stokes and anti-Stokes vibrational sidebands in emission spectra 77−73164
Ar:NO_2, Raman spectra, high press., low temp. effects 78−52479
Ar:O_2 (6%) cryst., vibr. Raman spectra 80−60558
Ar:S_2, absorption spectra of matrix-isolated S_2 molecules 77−52139
AsD_3, solid and liq., vibr. relax., Raman ν_1 band, 54, 160K 78−27198
As_2O_3-SO_3, polarised Raman and IR spectra, force field calc. *(French)* 78−6674
$(As_2O_3)_n$, claudetite I, vibr. spectra, force field calc. *(French)* 78−60447
As_4S_4, vibrational spectra, effect of temp. and press. on phonons 79−37776
$As_2S_3(Se_3)$, dispersion curve calc. 79−7659
As_2Se_3, glassy, Cu, Ag and O impurities influence on electronic energy spectrum and mol. vibr. spectrum 77−90181
B_2O_3, vitreous and crystalline, Raman spectra exam. 77−66491
Ba hexafluorometallates, $BaMF_6$, (M=Si,Ge,Sn,Ti), Raman spectra, at press. up to 25 kbar 78−6670
$BaBr_2.2H_2O$, pure and deuterated, low temp. IR and Raman spectra *(German)* 79−19874
$Ba(ClO_3)_2.D_2O$, D quadrupole coupling, temp. depend. 79−31551
$Ba(ClO_3)_2.H_2O$, cryst., O-H bond lengths, H-O-H angles, corrections 79−32945
$Ba(ClO_3)_2.H_2O(HDO)(D_2O)$, hydrate group vibr., IR spectra, isotope effects 77−8557
$BaCl_2.2H_2O(D_2O)$, lattice vibr., IR and Raman spectra 79−15443
$BaNB_2O_6$, IR and Raman spectra, vibr. anal. *(French)* 79−91446
$Ba(NO_3)_2$, Raman spectra temp. depend. anomalies in symmetric stretch region 79−61361
$Ba_2NaNb_5O_{15}$, phase transition at high press., Raman scatt. obs. 79−55884
$BaSO_4$, polarised IR refl., absorpt. and laser Raman spectra 77−43997
$BaSO_4$, single cryst., SO_4^{2-} vibr. levels, cryst. field effects, laser Raman spectroscopy 78−43847
$BaTiO_3$, OH^- impurity IR spectra meas. 80−20679
$BeSO_4.4H_2O$ and deuterated analogue, IR spectra, 110K, 1200 to 250 cm^{-1} 77−8582
25 $Bi_2O_3.P_2O_5$, hydrothermal growth, vib. spectrum 77−63555
Br_2, condensed phases, spontaneous and stimulated Raman scatt., weak and strong radiation fields 79−3450
BrO_3^- in $NaClO_3$, Raman spectra, fundamental vibr. modes 78−78711
CF_2, matrix-isolated, vibr. unrelaxed fluoresc., lattice mode coupling 77−14485
$C(NH_2)_3Al(SO_4)_26H_2O$:Cr^{3+}, isotope effect, zero field splitting, vibr. coupling temp. depend. 78−6570
α-CO, IR and Raman spectra, vibron band, vibron-phonon combination bands 78−68495
CO, in Ar matrix, vibr. line shape, vibr.-phonon interaction 79−3493
CO, in solid N_2, phonon-assisted v-v transfer rates 79−10901
CO, matrix isolated, vibrational energy migration, vibr. fluoresc. obs. 79−91486
CO, solid, CO laser excited, strong vibr. population inversion 80−58547
CO, solid and liq., vibr. relax. and vibr. diffusion rates, 66-79K 78−17757
CO, vibr. excited, in Ar matrix, information theoretic anal. 78−91386
$^{12}C^{16}O$:CO isotopes, IR and Raman spectra, vibron band, vibron-phonon combination bands 78−68495
CO_2, isotopically mixed crysts., IR spectra ν_2 vibr. exciton band 77−73136
CO_2, solid, Fermi reson. press. tuning, Raman spectra 80−93293
CO_2-type cryst., transl.-vibr. absorpt., hexadecapole moment effects 77−90134
CS_2, second order Raman spectrum in condensed phase 80−93299
$Ca(ClO_3)_2$, mol. torsional oscills., cooperative study by NQR 80−25244
$Ca(NO_3)_2$, Raman spectra temp. depend. anomalies in symmetric stretch region 79−61361
$Ca(OH)_2$ and $Ca(OD)_2$, molecular and lattice dynamics by IR^2 and Raman spectra 77−73134
$CaSO_4$, in KBr(KI) crysts., SO_4^{2-} vibr. spectra, press.-scanned Fermi reson. spectroscopy appl. 79−73937
$CaSO_4.2H_2O$, H_2O intramol. force fields calcs. 79−51229

molecular vibration in solids continued
$CaSO_4(.2H_2O)$, single cryst., SO_4^{2-} vibr. levels, cryst. field effects, laser Raman spectroscopy 78−43847
$Ca_{10-x}Sr_x(PO_4)_6(OH)_2$, continuous cation migration, IR spectra study 80−93297
$Ca(UO_2PO_4)_2.6H_2O$, calc. and meas. of vibr. spectrum 77−76499
$CdS_{1-x}Se_x$ film, resonance between Se atom dipole vibr. and interference modes, IR spectra obs. *(Russian)* 80−2888
$Cd_{1-x}Zn_xTe$, solid soln., vibr. spectra restructuring anomalies 79−4803
$Ce_2(SO_4)_3.9H_2O(D_2O)$, polarised Raman spectra, vibr. props. and role of lattice H_2O 80−66201
Cl_2, Ar matrix, vibronic dephasing 80−6469
Cl_2 in Ar matrix, vibr. relax., stochastic classical trajectory approach 78−79707
ClO_3^- in $NaBrO_3$, Raman spectra, fundamental vibr. modes 78−78711
$CoSiF_6.6H_2O(.6D_2O)$, near IR spectrum, 80K, assignments 78−48164
Co_2SiO_4, IR absorpt. spectra 80−60591
$Cr(CO)_6$, solid and matrix isolated, Raman spectra 79−28755
$Cr_2O_7^{2-}$ centre in lattice, optical props., mol. orbital calcs. 79−15491
$CsAlCl_4$, solid state Raman spectra, 298-80K, vibr., struct. 79−28745
$Cs_2GeF_6:Mn^{4+}$, magnetically circularly polarised emission and MCD of vibronic lines 77−16377
CsH_2AsO_4, and deuterated isomorph., ferroelectric mode and molecular vibr. press. depend. 78−19424
$CsH(NO_3)_2$, inelastic neutron scatt. spectra, H bonds bending vibrs. 79−14893
$CsHSeO_3$, and deuterated analog, vibr. spectra 79−24311
$CsHg(CN)_3$, CN and HgC stretching vibrations and HgCN bending vibration assignments 80−69140
$Cs_2LiCo(CN)_6$, mol. vibr. in cryst., normal mode anal., Raman and IR obs. 77−76494
CsNCS, vibr. spectra, multiphonon modes 77−40230
$Cs_2NaErCl_6$, mag. susceptibility and IR and Raman spectra meas., crystal field splitting determ. 80−100652
$Cs_{11}O_3$, ionic clusters in alkali metal suboxide cryst., struct., vibr. freqs., Raman spectra 79−37772
$Cs_{1.75}(Pt(CN)_4).1.5H_2O$, 1-D cond., IR spectra 77−85703
Cs_2SO_4, cryst., coord. and Raman intensity anal. 78−2831
Cs_2SO_4, IR absorpt. spectra, polymorphism, site group approx. and SO_4 stretching mode 78−52510
Cs_2SeO_4, single cryst., orthorhombic, Raman spectra 77−73140
$Cs_2SiF_6:Mn^{4+}$, IR absorpt. band, electron-vibr. effect 80−108238
$Cs_2SnCl_6:ReCl_6^{2-}$, luminesc. and absorpt. spectra, relax. processes 77−85779
Cs_2TiF_6, Raman spectra, internal and lattice vibrs. 77−8569
$CsUF_6$, D_{3d} distortion on octahedral UF_6^- complex 77−47779
$Cs_4(UO_2)_2F_8.2H_2O$, IR absorpt. and Raman spectra, normal coordinate anal. *(French)* 78−52509
$CsUO_2(NO_3)_3$, ^{15}N isotope shifts in electronic spectrum, internal mode identification 80−55098
$Cs_2Zn(N_3)_4$, IR and Raman spectra 77−43999
Cu complex, bis(1,5-cyclooctadiene)copper(I) perchlorate, IR and Raman spectra 79−19877
Cu complex, di-μ-chlorobis[(1,5-cyclooctadiene)copper(I)], IR and Raman spectra 79−19877
$Cu(ClO_3)_2$, mol. torsional oscills., cooperative study by NQR 80−25244
$CuCl_2.2H_2O$, H_2O intramol. force fields calcs. 79−51229
Cu_2HgI_4, polycryst., Raman spectra, press. depend. 77−73137
$CuInS_2$ crystals, growth, struct., and elec. props. 79−38729
$Cu_2(OH)_2CO_3$, malachite, vibr. assignments, force consts., coincidence method appl. 78−62953
$CuSO_4.5H_2O$ and $CuSO_4.5D_2O$, Raman and IR spectra, mode assignments 77−66493
$CuSO_4.5H_2O$, IR spectra, internal modes and pot. environment, isotope effects 77−8563
$CuSeO_4.5H_2O$, Raman and IR spectra, mode assignments 77−66493
DF, cryst., Raman spectra 80−55075
DI, crystalline, Raman and IR spectra, mol. vibr., libration and translation 80−2757
D_2O, isolated in glassy H_2O, IR spectrum 78−27207
D_3SiNCS, IR and Raman spectra, vibr. anal., LF bending mode 78−70842
$Dy_2(SeO_4)_3.8H_2O$, thermal decomp. and IR spectra 80−3319
$Er_2(SeO_4)_3.8H_2O$, thermal decomp. and IR spectra 80−3319
Fe complex, Fe(II), 2,2′-bipyridyl complexes, reson. Raman spectra, vibr. anal. 79−61363
Fe hexacyanoferrates, $M_4Fe(CN)_6.nH_2O$, Mossbauer and IR spectra 80−2739
$FeCO_3$, vibronic coupling at Neel temp. 80−15491
$Fe_2(CO)_9$, solid, Raman and IR spectra, vibr. exam. 78−27214
$FeCl_3$, intramolecular force fields, compliance consts. and vibr. amplitudes 80−58234
$Fe(H_2O)_6SiF_6$, Raman spectra, vibr. modes 79−61369
$FeSiF_6.6H_2O(.6D_2O)$, near IR spectrum, 80K, assignments 78−48164
$FeSiO_4$, spinel, IR absorpt. spectra 80−60591
$GaCl_3(Br_3)(I_3)$, intramolecular force fields, compliance consts. and vibr. amplitudes 80−58234
B-Gd_2O_3, monoclinic single cryst., Raman spectrum 80−103953
Ge, hydrogenated amorphous and cryst., IR spectra 79−61359
$GeH_4:SiHD_3$, symmetries of GeH_4 cryst. phases, IR spectra meas. 79−19886
H-bonded crystal, IR absorpt. spectra band shape, X-H stretching vibr. temp. depend., isotope effect 78−76445
H_2, IR fundamental band, U-branch transitions 78−64361
H_2, solid, compressed, vibr. Raman spectrum 79−47422
H_2, solid, equation of state, intramol. zero pt. energy contrib., total sublimation energy 78−71829
p- H_2, solid, induced near IR absorption spectrum, freq. shift, intensity, up to 10 kbar 78−6658
p-H_2, solid, time-resolved CARS, disorder effects on coherent vibr. states 80−93342
H_2, solid, vibr. energy transfer, isotopic impurities, relax. 79−6993
$HAl_{11}O_{17}$, H β-alumina, IR absorpt. study 80−100655
HCl, cryst., internal vibr. electrostatic interactions and IR bandshape 79−91417
HCl-DCl mixed crystal, IR spectra, freqs., bandwidths and ν_{01} simultaneous transition 77−28564
$(HCl)_2$, vibr. freqs. in inert gas matrix, force const., MINDO/3 calcs. 78−41952
$H_3Co(CN)_6$, strong NHN hydrogen bond, vibr. lattice and mol., incoherent inelastic neutron scatt. 80−39232

molecular vibration in solids continued
HDO molecules, stretching vibrs., freq. meas. in hydrates 78−29772
HDO molecules in solid hydrates, D quadrupole coupling consts., O-H and O-D stretching freqs., H bond distances 78−29773
HF, cryst., Raman spectra 80−55075
HF, H-bonded chains, vibr. modes in liq. and solids 78−59873
HF-fluoromethylene anion, in solid Ar, IR spectra, vibr. modes 79−68231
HI, crystalline, Raman and IR spectra, mol. vibr., libration and translation 80−2757
α-HIO_3, dispersion anal. of IR reflection spectrum *(Russian)* 78−56493
$H_2O:D_2O$, ice Ic, vibr, decoupling, IR spectrum 79−13706
HOD, IR band intensities in ice and water 79−3443
H_2SeO_3, and deuterated analog, vibr. spectra 79−24311
H_3SiNCS, IR and Raman spectra, vibr. anal., LF bending mode 78−70842
$^nH_2$, vibr. relax. at low temps., gas, liq. and solid phases 77−83691
Hf complex, tetrakis (tropolonato) hafnium (IV), mol. interactions in solid, perturbed γ-γ ang. correl. obs. *(French)* 79−8076
$Ho_2(SeO_4)_3.SH_2O$, thermal decomp. and IR spectra 80−3319
I_2, lattice dynamics, internal and external modes 78−18719
IO_3^- in $NaClO_3$, Raman spectra, fundamental vibr. modes 78−78711
$InCl_3$, intramolecular force fields, compliance consts. and vibr. amplitudes 80−58234
InSe, second order Raman spectrum and phase transition 79−38545
IrF_6, in mixed crysts., Jahn-Teller effect, $\Gamma_{8g}(t_{2g})^3$ state, 6800 Å 78−76032
$KAlCl_4$, cryst., Raman spectra, orthorhombic space group, Cl splitting of $AlCl_4$ 77−85700
$KAl(SO_4)_2.12H_2O$, single cryst., Raman spectra, temp. depend., SO_4^{2-} site dynamic disorder 77−40219
K_3AsO_4-$KAsO_3$, glass and cryst., Raman and IR spectra 79−99862
$KBr:HS^-(HF_2^-)$, anharmonic interaction of impurity intramol. vibrs. with cryst. phonons 77−77217
$KBr:In^+$, mag. circular dichroism spectra line shape, lattice mode calcs. 79−82957
$KBr:MnO_4^-$, optical and IR absorpt. spectra, internal vibr. of MnO_4^-, freq. and type of symm. 79−15466
$KBr:MnO_4^-$, vibronic spectra interpretation 79−37770
$KBr:No_2^-$, effects of Mg, Ca, Sr, Ba, Pb impurities on vibrational constants of NO_2^- ion 77−20035
$KBrO_2F_2$, struct. data, vibr. spectra 77−39563
KCN, disordered ordinary and metastable phases, light scatt., press. depend. 78−95151
KCN, dynamics of CN^- ions near phase transitions at 83K 80−80717
KCN-KCl mixed system, order-disorder transition, Raman spectra obs. 78−15113
$(KCN)_x(KBr)_{1-x}$, Brillouin scatt. of elastic anomaly 79−28779
KCNS, single cryst., IR and Raman multiphonon bands, factor group anal. 77−4644
$KCl:CN^-$, Raman scatt. from tunnelling and hindered rotational sites 77−66507
$KCl:Na^+$, OH^-, IR absorpt. spectra, Na^+ ions rel. to OH^- stretching vibr. 79−47442
$KCl:PO_2^-$, phosphoresc. and PMDR spectra, electronic and vibr. states 79−65768
$KClO_4:MnO_4^-$, reson. Raman excitation profiles for totally symmetric mode, vibronic struct. 80−50309
$K_3Co(CN)_6$, ^{59}Co quadrupole coupling const., temp. depend. 80−44557
$KDy(MoO_4)_2$, polarised IR and Raman struct., $^{92}Mo/^{100}Mo$ isotope effect 80−108198
$KF(HF)_n$, (n=2,3,4), cryst., anion struct., H bonding, IR spectra 77−54560
$K_4Fe(CN)_6.3H_2O$, C-N vibrs., Raman study 80−40106
$K_4Fe(CN)_6.3H_2O$ ferroelectric cryst., vibrational spectrum of $[Fe(CN)_6]^{4-}$ anion 77−69839
KH_2AsO_4, and deuterated isomorph, ferroelectric mode and molecular vibr. press. depend. 78−19424
$KHCO_3$, inelastic neutron scatt. spectra, H bonds bending vibrs. 79−14893
KHF_2, IR refl. spectra 78−80324
KHF_2, vibr. spectra, Davydov splitting, absorpt. band shift 79−8147
KH_2PO_4, ferroelec., Raman internal-mode line broadening by proton jumps 77−43981
$KHSeO_3$, and deuterated analog, vibr. spectra 79−24311
$K_2HgCl_4.H_2O$, cryst., IR spectra, water mol. struct., H-bonding 77−81089
$KI:NO_2^-$, Raman spectra, high press., low temp. effects 78−52479
$KI:S_2$, Raman spectra, orientational dynamics 78−56482
KIO_3, temp. depend. Raman spectra and phase transitions *(Russian)* 78−15171
$KMgCl(ClO_4)_2.nH_2O$, IR spectra and struct. features 79−15452
$KMgCl_3.nH_2O$, IR spectra and struct. features 79−15452
KNCO, polycryst., IR and Raman spectra, lattice and internal modes 77−32369
KNCSe, IR and Raman spectra, internal and external modes 77−16312
$K_3N(SO_3)_3.2H_2O$ and ^{15}N derivative, Raman and IR spectra, $N(SO_3)_3^{3-}$ normal coord. anal. 79−91433
$K_{1.75}(Pt(CN)_4).1.5H_2O$, 1-D cond., IR spectra 77−85703
$K_2PtCl_6:Os^{4+}$, sharp line luminesc. band at 10K, vibr. assignment 78−95600
$K_{1-x}Rb_xCl:HF_2^-$, dynamic inhomogeneous broadening of bands of local vibr. 78−92102
$KReO_4$, vibr. spectrum, Raman and IR spectra obs. 80−55104
$K_2(RuCl_5NO)$, polarised Raman and IR spectra, vibr. anal. 77−69819
K_2SO_4, IR absorpt. spectra, polymorphism, site group approx. and SO_4 stretching mode 78−52510
KSO_3F, disordered cryst., IR and Raman spectra, internal modes assignment, space group *(French)* 79−95742
K_2SeO_4, Raman spectra, 77-300K *(Japanese)* 77−43988
K_2SeO_4, single cryst., orthorhombic, Raman spectra 77−73140
$K_2SnCl_6:ReCl_6^{2-}$, $(K_2PtCl_6:ReCl_6^{2-})$, luminesc. and absorpt. spectra, relax. processes 77−85779
$KTaO_3:OH^-(OD^-)(OT^-)$, IR spectra, spectrosc. consts. 80−100671
$K_5(UO_2)F_9$, optical spectra, vibr. freqs. calcs. *(Russian)* 78−31205
$K_3(UO_2)_2F_7.2H_2O$, single cryst., polarised Raman spectra, vibr. modes assignment *(French)* 80−29728
$Kr:S_2$, absorption spectra of matrix-isolated S_2 molecules 77−52139
$La(BrO_3)_3.9H_2O$, IR and Raman spectra, vibr. asignments 78−84569
$LaCl_3$, Raman intensity anal. 79−33710

molecular vibration in solids continued

$La_2(SO_4)_3.9H_2O$, and isotopic forms, water librations, Raman obs. *(French)* 79−28754

$^7Li_2CO_3$, and $^6Li_2CO_3$, polycryst., low freq. IR and Raman bands assignments 79−42970

$^7Li_2CO_3$, and $^6Li_2CO_3$, polycryst., Li-O Raman bands 79−42969

$LiHSeO_3$, and deuterated analog, vibr. spectra 79−24311

$LiH_3(SeO_3)_2$, IR and Raman spectra, internal modes, intra- and inter-H-bond tunnelling 78−43853

α-$LiIO_3$, hexagonal cryst., vibrs. and force consts. 79−69220

$LiKSO_4$, polarised Raman and IR reflection spectra, internal and external mode assignments 77−16293

$^{6,7}LiNO_3$, cryst. vibr., Raman and IR spectra 79−15445

$LiNbO_3$, Raman spectra and dielec. props. near Curie point 79−38530

$^{6,7}LiOH$, LiOD, polycryst., Raman active modes and isotopic effects 79−87424

Li_2SO_4, IR absorpt. spectra, polymorphism, site group approx. and SO_4 stretching mode 78−52510

$Li_2SO_4.H_2O$, $^6Li/^7Li$ and H/D substituted, IR and Raman spectra, vibr. and librational modes 77−85716

$Li_2SO_4.H_2O$, far IR spectra, H_2O flipping motion, lattice modes 80−84258

$Li_2SO_4.H_2O$, X-ray diffr., IR and Raman spectra, internal optic modes, mol. dipole model 77−76493

Li_2SiO_3, IR and Raman spectra, normal coord. anal. of unit cell vibrs. 77−81090

$LiTaO_3$, Raman spectra and dielec. props. near Curie point 79−38530

$Li_4WO_5:U^{6+}$, vib. fine struct. in luminesc. spectra 77−8620

LiX-alcohol mixtures, (X=Cl, Br, ClO_4), OH(OD) vibr. bands in sat. solns. and crysts. 77−8564

$Lu_2(SeO_4)_3.8H_2O$, thermal decomp. and IR spectra 80−3319

$Lu_2Si_2O_7$, IR and Raman spectra, internal and external modes 79−61365

$MgCl_2.nH_2O$, IR spectra and struct. features 79−15452

$Mg(H_2O)_6SiF_6$, Raman spectra, vibr. modes 79−61369

MgO:Fe crysts., oxidised and reduced, optical absorpt. spectra at low temps. 77−63436

$Mn(C0)_5$ Br-$Re(C0)_5$Br, polycryst., ν(C0) vibr. intermol. Raman intensity transfer 80−60564

$Mn_3(Co(CN)_6)_2.xH_2O$, mol. vibr. in cryst., normal mode anal., Raman and IR obs. 77−76494

$MnSiF_6.6H_2O$, optical absorption spectra, 77-300K, assignments 77−36259

$MnSiF_6.6H_2O(.6D_2O)$, near IR spectrum, 80K, assignments 78−48164

Mo complexes, oxo-bridged dimers, ^{16}O and ^{18}O-substituted synthesis, IR spectra 77−77188

Mo halides, $[Mo_6X_8]$ cluster group identification in IR spectra of solids, normal vibrs. 78−64359

MoF_6, cryst., overall vibr. band struct., excitons 77−90136

MoF_6 crysts., density of exciton states, two-particle and mixed cryst. spectra 78−2829

MoF_6, orthorhombic crysts., Raman spectra, int./external mode separation and factor group anal. 77−90135

β-N_2 cryst., vibr. Raman spectra 80−60558

N_2 matrix N-N stretching vibr., IR activation, guest mol. depend. 80−60570

α-N_2, mol. dynamics simulation 77−47519

N_2, solid, α- and γ-phases, Raman intensities of internal and external modes 79−33706

α-N_2, solid, coherent loss of vibr. and librational excitations 79−86852

N_2, solid, electron impact excited, luminesc. spectra 77−48252

N_2, solid, Raman spectra vibron and lattice freq. shifts, librational force consts., α- and γ-phases 78−19460

α-N_2, solid, Raman spectra vibron bands, a priori calcs. 78−31181

N_2, solid, Raman spectroscopy up to 374 kbar 80−7353

α-N_2 solid, time-resolved CARS, disorder effects on coherent vibr. states 80−93342

α-N_2, temp. depend. of IR spectra, Gruneisen parameters determ. 80−84730

N_2-Ar, liq. mixture, isotropic Raman line shape theory 78−88298

$N_2+N_2(CO)$, in matrix, vibr. energy transfer and relax. 78−46426

ND_4DS, polycryst., vibr. spectrum, lattice dynamics 77−90138

ND_4I, Raman spectrum, press. effects 80−97261

NH, ND, vib. relax. in amorphous solid inert gas systems 77−7817

$NH_4Ag_4I_5$, Raman spectra, internal vibrs. of NH_4^+ ions 78−72497

NH_4AlCl_4, crystal struct., X-ray, Raman, IR and NMR 78−63720

$(NH_4)_2BeF_4$, powder, IR spectra, assignments, mol. libration, in paraelec. and ferroelec. phases 78−88299

NH_4Cl, Raman scatt. at polarons near intramol. vibrs. 77−44003

$(NH_4)_2CuCl_4.2H_2O$, HDO and NH_3D^+ species, IR spectrum, low-temp., phase transitions 77−77182

$(NH_4)_2GeF_6$, cryst., highly bent H bonds, IR spectrosc. investig. 80−93292

$(NH_4)_2H_3IO_6$, paraelec. and antiferroelec. phases, IR vibrational study 77−85697

NH_4HS, polycryst., vibr. spectrum, lattice dynamics 77− 90138

NH_4I, coexisting phases and NH_4^+ dynamics, neutron scatt. exam. 79−42158

NH_4I, Raman spectrum, press. effects 80−97261

NH_4I, reorientational motion of ammonium ions in octahedral environments, neutron scatt. exam. 79−42159

$(NH_4)_{0.16}K_{0.84}I(Br)$, reorientation motion of ammonium ions in octahedral environments, neutron scatt. exam. 79−42159

$((NH_4)_xK_{1-x})_2SnCl_6$, mixed cryst., spectroscopic study 79−33712

$(NH_4)_2M(SO_4)_2.6H_2O$, Tutton's salts, IR spectra, correl. of vibr. freq. and N...O distance for NH_3D^+ 78−92066

$(NH_4)_5Mo_2Cl_9.H_2O$, resonance Raman spectra, $MO_2Cl_8^{4-}$ vibrs. 78−64350

NH(ND) $X^3\Sigma^-$, in inert gas solid, vibr. relax., matrix and isotope effects 80−95713

$NH_3(ND_3)$ in solid Ar, UV absorption spectra, temp. depend. of matrix spectra 80−63652

NH_4NO_3, Raman spectra of low temp. phases 78−92081

NH_4ReO_4, ND_4ReO_4, Raman spectrum, temp. depend. 78−80335

$(NH_4)_2(RuCl_5NO)$, polarised Raman and IR spectra, vibr. anal. 77−69819

$(NH_4)_2SiF_6$, cryst., highly bent H bonds, IR spectrosc. investig. 80−93292

$(NH_4)_2SnF_6$, cryst., highly bent H bonds, IR spectrosc. investig. 80−93292

molecular vibration in solids continued

$(NH_4)_2(TeCl_6)$, IR and Raman spectra, lattice and internal modes, phase transition 78−6659

$(NH_4)_2TiF_6$, cryst., highly bent H bonds, IR spectrosc. investig. 80−93292

$(NH_4)_2TiF_6$, Raman spectra, internal and lattice vibrs. 77−8569

NH_4ZnF_3, rot. motion of NH_4^+ in lattice, neutron scatt. 79−37773

NO ($a^4\Pi$), condensed phase vibr. relax., isotope effect, time resolved obs. 78−94233

N_2O crystal, vibrational exciton bands, impurity modes 77−28560

N_2O_2, IR spectra of solid, Raman spectra of solid and liq., vibr. anal. 77−81093

$(^{14}NO)_2$ and $(^{15}NO)_2$ solids, Raman spectra at 20K 77−73139

$NaAl(CO_3)(OH)_2$, cryst. struct., IR spectral investig. 77−8567

$NaBrO_3$, IR and Raman spectra, vibrs., dipolar coupling effect 78−43852

$NaBrO_3$, Raman spectra, intramolecular vibrs. and lattice vibrs. *(Russian)* 77−1683

$NaClO_3$, IR and Raman spectra, vibrs., dipolar coupling effect 78−43852

$NaClO_3$, mol. torsional oscills., cooperative study by NQR 80−25244

$NaClO_4$, anhydrous, Raman, IR and FIR spectra, 90 to 600K *(German)* 79−78687

$Na(D_xH_{1-x})_3(SeO_3)_2$, Raman spectra and nature of phase transitions 78−80341

NaF:U, luminesc. spectra, Vibr. struct. 80−80840

$NaHF_2$, IR refl. spectra 78−80324

$NaHSeO_3$, and deuterated analog, vibr. spectra 79−24311

$NaH_3(SeO_3)_2$, IR and Raman spectra, internal modes, intra- and inter-H-bond tunnelling 78−43853

$NaIO_4$, normal coord. anal., internal and external modes 79−23684

$NaMO_2$, Stark shift of visible absorpt. of NO_2^- 78−19499

$Na^{15}N_x{}^{14}N_{1-x}O_3$, reflection spectra, Kramers-Kronig anal. with preliminary dispersion anal. 78−49915

$NaNO_2$, ferroelectric transitions, group theoretic comparison with $AgNaNO_2$ 80−7311

$NaNO_2$, fine struct. in luminesc. spectra in UV region 77−59607

$NaNO_2$, X-irradiated IR, UV and visible absorption 79−95811

$NaNO_3$, N atom velocity, NO_3^- vib. and orientation, nucl. reson. photon scatt. 78−68433

$NaNO_3$, Raman scatt. band lineshape, orientational disorder of NO_3^- ion in pre-transition region 77−8589

Na_2O-Li_2O-β-$Al_2O_3.H_2O$, water mol. vibrs., IR and Raman spectra 80−89006

$NaPF_6.H_2O$, Raman spectra 79−19875

Na_2SO_4, IR absorpt. spectra, polymorphism, site group approx. and SO_4 stretching mode 78−52510

Na_3SbS_4, vibrational spectra, internal SbS_4 vibr. assignments 80−66199

$Na_3SbS_4.9H_2O(D_2O)$, vibrational spectra, internal SbS_4 and $H_2O(D_2O)$ vibr. assignments 80−66199

$Na_3UO_2F_5$, IR and Raman spectra, struct. *(French)* 79−11409

$Na_4[M^{II}(NH_3)_4][M^I(S_2O_3)_2]_2.L$, ($M^{II}$=Cu, Ni), ($M^I$=Cu, Ag), (L=$H_2O$, NH_3), IR spectra, vibr. anal. *(French)* 78−52477

$Na_4[UO_2(CO_3)_3]$, vibr. and low temp. optical spectra, rel. to U recovery from oceans 79−73939

$NbCl_5.POCl_3$, Raman spectra, normal coordinate treatment 77−46568

$Nd(BrO_3)_3.9H_2O$, IR and Raman spectra, vibr. asignments 78−84569

Ni, Raney, chemisorpt. of H_2, neutron inelastic spectroscopy investig. 77−48686

$Ni(H_2O)_6SiF_6$, $Ni(D_2O)_6SiF_6$, Raman spectra, vibr. modes 79−61369

$Ni(NH_3)_6X_2$, (X=Cl, Br, I, ClO_4, BF_4) and d, far IR, Raman spectra, 80-300K 78−31190

$NiN_4S_4H_2$, vibr. anal. 78−90148

$NiSiF_6.6H_2O$, dynamical props. of H_2O below 300K, Raman spectroscopic obs. 79−8140

$NiSiF_6.6H_2O(.6D_2O)$, near IR spectrum, 80K, assignments 78−48164

γ-O_2 cryst., vibr. Raman spectra 80−60558

OH^- vibr. dipole field and ion-pair processes with rare earth ions 79−38624

$O_2(c^1\Sigma_u^-)$, in Ar(Kr)(Ar-Kr) matrices, multiphonon vibr. relax., time-resolved emission obs. 80−18861

$(P,As)_2O_7^{4-}$, vibr. calc. by method of normal coordinates 78−22796

PD_3, liq. and plastic cryst. states, vibr. dephasing and correl. functions 79−69036

$PF_2H(D)$, Raman and IR spectra 80−14147

γ-$PH_{3-x}D_x$, Raman and IR spectra, phase transition, internal and external modes 77−77191

PH_3, liq. and solid, Raman spectra., vibr. correl. functions, rot. motions 80−55087

PHD_2, vibr. dephasing in liq. and solid PD_3, calcs. 80−19884

$PMo_{12}O_{40}$, vibr. anal., symmetry coords. and force field anal., IR and Raman spectra 77−15522

$Pb_5(AsO_4)_3Cl$, mimetite, vibr. spectra, normal coord. anal. 78−88305

$Pb_5Ge_3O_{11}$, Raman spectrum factor group anal., external and librational modes 77−36240

$PbMoO_4$, Raman scatt. obs. of external and internal modes 79−69842

$Pb(NO_3)_2$, Raman spectra temp. depend. anomalies in symmetric stretch region 79−61361

$Pb_5(PO_4)_3Cl$, pyromorphite, vibr. spectra, normal coord. anal. 78−88305

PbS, molecule, vibr. anal., in neon matrix *(Russian)* 79−10094

$PbTi_{1-x}Zr_xO_3$, low freq. vibrational modes and ferroelec. transitions 79−33637

$Pb_5(VO_4)_3Cl$, vanadinite, vibr. spectra, normal coord. anal. 78−88305

Pd-Au:$H_2(D_2)$, thermodynamic props. at 555 and 700K, vibr. freqs. and excess entropies 80−29186

Pt complex, $[Pt(en)_2][Pt(en)_2Cl_2](ClO_4)_4$, reson. Raman spectra 80−2760

Pt complex, $PtCl_3$ (9-methyladeninium), laser Raman spectra 77−66499

Pt complex, $Pt(NH_3)_4Cl_2.H_2O$, Raman spectrum *(French)* 79−19876

Pt complexes, $Pt(NH_3)_4Cl_2$, $Pt(ND_3)_4Cl_2$, Raman spectra in solid state and aq. soln. *(French)* 79−19876

Pt-nucleoside complexes, Raman spectra, vibr. anal. 77−65473

cis-$Pt(NH_3)_2Cl_2$, torsions, metal-metal interactions, inelastic neutron scatt. study 79−46581

$(Pt(NH_3)_4)[PtCl_4]$, torsions, metal-metal interactions, inelastic neutron scatt. study 79−46581

$RbAlCl_4$, solid state Raman spectra, 298-80K, vibr., struct. 79−28745

RbCNS, single cryst. factor group anal. of IR and Raman multiphonon bands 77−4644

$RbCaF_3$, cubic to tetragonal phase transition, neutron diffr. obs. 79−23730

molecular vibration in solids continued
$RbGa_3Br_{10}$, cryst., vibr. spectrosc. *(French)* 78−6667
RbH_2AsO_4, and deuterated isomorph, ferroelectric mode and molecular vibr. press. depend. 78−19424
RbI:HF_2^-, anharmonic interaction of impurity intramol. vibrs. with cryst. phonons 77−77217
$Rb_{71}K_{29}$, lattice dynamics, molecular dynamics study 79−37782
RbNCO, polycryst., IR and Raman spectra, lattice and internal modes 77−32369
Rb_9O_2, ionic clusters in alkali metal suboxide cryst., struct., vibr. freqs., Raman spectra 79−37772
$Rb_{1.75}(Pt(CN)_4)_2.1.5H_2O$, 1-D cond., IR spectra 77−85703
Rb_2SnCl_6:$ReCl_6^{2-}$, luminesc. and absorpt. spectra, relax. processes 77−85779
$Rb_4(UO_2)_2F_8.2H_2O$, IR absorpt. and Raman spectra, normal coordinate anal. *(French)* 78−52509
Re complex, $((C_2H_5)_4N)_2$ [ReI_6], electronic resonance Raman spectrum, 80K *(German)* 79−82982
$ReBr_6^{2-}$ doped K_2PtCl_6 type crystals, vibronic side band intensity distrib., $\Gamma_7(^2T_{2g})\rightarrow\Gamma_8(^2A_{2g})$ transition 80−10609
$ReBr_6^{2-}$, in cubic crysts., luminesc. spectra and relax. processes 78−68552
$ReCl_6^{2-}$ doped K_2PtCl_6 type crystals, vibronic side band intensity distrib., $\Gamma_7(^2T_{2g})\rightarrow\Gamma_8(^2A_{2g})$ transition 80−10609
ReF_6, cryst., Raman and absorpt. spectra, Jahn-Teller effect 78−6675
Rh, adsorption of $C^{16}O$ and $C^{18}O$, inelastic electron tunnelling spectra obs. 79−65331
Rh complex, di-μ-chlorobis[(1,5-cyclooctadiene)rhodium (I)], IR and Raman spectra 79−19877
Ru complexes, carbonyl hydrides, pre-reson. Raman spectra, Ru-Ru and Ru-C modes 78−43854
S, orthorhombic, far IR absorpt. spectrum 77−8560
α-S, zone-centre lattice vibrs., including hydrostatic press. effects 80−49314
S_8 rings, vibr. spectra and thermodynamic functions *(German)* 78−82742
SF_6, film, IR laser induced processes at low temp. and under ultrahigh vac. 79−69914
$(SN)_x$, IR transmission spectrum assignment 78−15160
S_2N_2, cryst. and partly polymerised films, Raman scatt., optical absorption 77−8673
S_4N_4, Raman scatt., press. and temp. depend., 0-10 kbar, 10-295K 78−15160
S_4N_4, Raman scatt. and opt. absorpt., press. and temp. depend. 77−36227
S_4N_4, vibrational spectra, effect of temp. and press. on phonons 79−37776
S_7NH, solid and solns. vibr. spectra, force consts. isotope effects 77−66490
$S_{8-x}(NH)_x$, (x=1,2,3,4), and deuterates, IR and Raman spectra, isotope shifts, mol. vibr. assignment 79−10110
SO_2, IR and Raman spectra, mol. and lattice vibrs. 78−19464
$SbCl_5.POCl_3$, Raman spectra, normal coordinate treatment 77−46568
$Sc_2Si_2O_7$, IR and Raman spectra, internal and external modes 79−61365
Si, amorphous, chemical effects on freq. of Si-H vibrations 79−51227
Si:B, ion implanted, laser annealed, Raman scatt., Fano interactions, lattice damage 79−78711
Si-C:H, amorphous film, vibr. spectrum 79−61450
SiH_4, plastic phase, rotational motion, quasi-elastic neutron scatt. study 79−51022
$SiH_3PH_2BD_3$, liquid and solid, vibr. analysis, spectra and structure of P-B compounds 78−84586
$SiH_3PH_2BH_3$, liquid and solid, vibr. analysis, spectra and structure of P-B compounds 78−84586
SiO_2, amorphous, chemical effects on freq. of Si-H vibrations 79−51227
SiO_2, OH group interactions, IR and Raman spectra 78−80383
SiO_2 vitreous, Raman spectrum, bound OH, Si-O stretch vibr. 78−19462
Sn tetrahedral molecular solids, ^{119}Sn Mossbauer and Raman spectra 78−15070
$SnCl_2.2H_2O$, protonic order-disorder transition, H-bond vibr. Raman spectra temp. depend. 78−23437
SnS_2, Mossbauer spectra, vibr. amplitudes anisotropy 80−15904
$SnSe_2$, Mossbauer spectra, vibr. amplitudes anisotropy 80−15904
$Sr(ClO_3)_2$, mol. torsional oscills., cooperative study by NQR 80−25244
$SrCl_2.2(H,D)_2O$, IR and Raman spectra, force fields 80−2753
$SrCl_2.2H_2O$, IR and Raman spectra, force fields 80−2753
$Sr(NO_3)_2$, Raman spectra temp. depend. anomalies in symmetric stretch region 79−61361
TCNQ salts, $Cs_2(TCNQ)_3$, quasi-one-dimens , IR spectra, electron-vibr. interaction 78−88309
$Tb_2(SeO_4)_3.8H_2O$, thermal decomp. and IR spectra 80−3319
TeO_2, paratellurite, atomic motions corresponding to zone centre phonons 78−76461
$Te^{VI}O_6$ ion in $A_2B^{II}B^{VI}O_6$ perovskites vibr. anal. using isotope shifts and perturbation theory 77−59073
1,2,4,5-tetramethylbenzene, liq. and solid, vibr. dephasing, intermol. energy exchange mechanism 78−74737
tetraselenatetracene, neutral, cation and conducting complex reson. Raman spectra, vibr. lines, charge transfer 79−4794
Ti complex, $Ti_2Cl_8(CH_3NO_2)_2$, single cryst., struct., IR and Raman spectra, X-ray diffr. 78−43000
$(TiCl_4.POCl_3)_2$, solid, IR and Raman spectra, vibr. assignments 78−43868
TiO_2, rutile, mechanisms for H diffusion 79−73341
$TlBrO_3$, polycryst., Raman and IR spectral assignments, room temp. 78−15156
$TlClO_3$, polycryst., Raman and IR spectral assignments, room temp. 78−15156
$TlIO_3$, polycryst., Raman and IR spectral assignments, room temp. 78−15156
$TlSbF_6$, Raman spectra, at press. up to 25 kbar 78−6670
$Tl_2(TeCl_6)$, IR and Raman spectra, lattice and internal modes, phase transition 78−6659
$Tm_2(SeO_4)_3.8H_2O$, thermal decomp. and IR spectra 80−3319
UF_6, cryst., overall vibr. band struct., excitons 77−90136
UF_6 crysts., density of exciton states, two-particle and mixed cryst. spectra 78−2829
UF_6, matrix isolated, laser fluoresc. spectrosc. at 12K 79−68253

molecular vibration in solids continued
UF_6, orthorhombic crysts., Raman spectra, int./external mode separation and factor group anal. 77−90135
UO_2 complexes, cubic crysts., low temp. optical spectra *(Russian)* 78−92083
UO_6^{6-} in oxides, excitation and emission transitions involved in green luminesc. obs. 77−16372
$UO_2(NH_2O)_2(H_2O)_2.H_2O$, cryst., Raman and IR spectra 77−63409
V phosphate glasses, vibr. spectra 77−52064
$V(CO)_6$, cryst. and mol. struct., Jahn-Teller distortion, mol. vib. and librational correction 79−32949
VPO_5, cryst., vibr. spectra 77−52064
WF_6, cryst., overall vibr. band struct., excitons 77−90136
WF_6 crysts., density of exciton states, two-particle and mixed cryst. spectra 78−2829
WF_6, orthorhombic crysts., Raman spectra, int./external mode separation and factor group anal. 77−90135
$Y_2(SeO_4)_3.8H_2O$, thermal decomp. and IR spectra 80−3319
$Yb_2(SeO_4)_3.8H_2O$, thermal decomp. and IR spectra 80−3319
$Yb_2Si_2O_7$, IR and Raman spectra, internal and external modes 79−61365
$ZnSiF_6.6H_2O(.6D_2O)$, near IR spectrum, 80K, assignments 78−48164
$Zn_4Si_2O_7(OH)_2H_2O$, hemimorphite, polarised IR refl., vibr. modes *(French)* 77−85698
ZnTe:Li(As), electronic Raman scatt., mag. field depend. 79−73928

molecular vibrational energy transfer *see molecular rotational-vibrational energy transfer*

molecular vibrational relaxation *see molecular rotational-vibrational energy transfer*

molecular vibrational states *see molecular vibration*

molecular vibronic states
$\pi\pi^*$ and $n\pi^*$ states relative position, optical props., singlet-triplet conversion processes 79−3484
AB_4 tetrahedral molecule, rot. transition intensities, nucl. spin statistics 79−93969
acenaphthene, vibronic spectra, electronic-vibr. interactions 78−1021
acetaldehyde, single vibronic level fluoresc., radiative lifetimes 78−82769
acetaldehyde ($A,^1A_2$), laser induced fluoresc. 79−50075
cis-acetylene, triplet state, near IR electronic absorption spectrum, and form. 79−63997
acridine, solvent depend. of radiationless relax., singlet lifetime, picosecond spectroscopy 78−66582
alkali halide:CrO_4^{2-}(MoO_4^{2-})(MnO_4^-)(ReO_4^-), frozen solns., absorption spectra, 4.2-300K 79−87467
alkali halide:O_2^-, frozen soln., impurity luminesc., zero-phonon lines interpretation 79−87488
alkali metal hexahalogenostannate: $ReBr_6^{2-}$, vibronic transition $\Gamma_7(^2T_{2g})\rightarrow\Gamma_8(^4A_{2g})$, intensity distrib. 80−45142
anharmonic molecules in condensed media, vibronic dephasing, intra- and intermolecular processes 80−2127
anharmonic molecules in low temp. matrices, vibronic dephasing 80−6469
aniline, $^1B_2$ state, single vibronic level fluoresc. 79−54903
aniline, vibronic perturbations of UV spectrum 78−37654
aniline+AR, $^1B_2$-state collision induced intramol. vibr. energy transfer, SVL fluoresc. obs. 79−54904
anthracene:tetracene, absorpt. spectra, energy transfer over highest vibronic levels 79−65904
anthracene:tetracene, upper excited vibronic states optically pumped energy transfer matrix fluoresc. 78−76512
anthracene, in n-hexane, Shpolskii absorpt. spectra at 77K, vibronic struct. *(German)* 79−59507
anthracene, polarised reflection spectra, surface and vol. exciton coupling, vibronic states 78−72543
anthracene, Raman intensities rel. to vibronic coupling and excited electron state geometries 77−27075
anthracene, Shpolskii spectra, vibronic struct., fluoresc. *(German)* 79−22754
anthracene, soln. and melt, second vibronic transition, spectroscopic characts., effective field dispersion calcs. 80−55102
anthracene, vibronic absorpt. spectra in soln. and cryst., universal mol. interactions effects 77−68031
9,10-anthraquinone, electronic-vibr. interaction between close excited electronic states 79−63980
β-F-9,10-anthraquinone, internal heavy atom effect, vibronic phosphoresc. spectrum, intermol. spin-orbit coupling 78−82774
9,10-anthraquinone, Shpolskii quasi-line phosphoresc. spectra, electronic-vibrational interactions 78−55196
aromatic aldehyde, triplet state dipole moments, vibronic coupling effects 79−31493
aromatic compounds, intersystem crossing theory, El-Sayed rule extension, anomalous rate consts. 77−30911
aromatic hydrocarbon derivatives, low-temp. singlet-triplet conversion probability rel. to optical parameters 79−54898
aromatic hydrocarbons, absorpt. spectra, electronic-vibr. sequence band broadening 77−65453
aromatic hydrocarbons, intersystem crossing mechanism, rate consts. 77−65497
aromatic hydrocarbons, sequential coupling 80−58297
aromatic hydrocarbons, vibronic calcs. 80−58238
aromatic hydrocarbons, vibronic coupling model, nontotally symm. harmonic mode 77−3337
aromatic hydrocarbons in Shpolskii matrices, $S_0\rightarrow T_1$ absorpt. spectra 79−85995
aromatic molecule, in aromatic (aliphatic) solvent, 77K, triplet-triplet absorption spectra, anomalous broadening 77−88502
aromatic molecule with nonbonding electrons, $T_1(\pi\pi^*)\rightarrow S_0$ radiationless transition, vibr. coupling 77−18957
astaxanthin, aq. soln., aggregate, reson. Raman spectra, and IR spectra, exciton interactions 78−31770
atom+diatom, energy transfer, vibronic excitation, emission spectra 78−66578
benzaldehyde, electronic spectra, Cl and F substitution effects 80−23456
benzaldehydes, in mixed cryst., T_1/T_2 interstate interactions, modulation polaris. phosphoresc. spectra, 4.2K 78−9185
benzene, 260 nm absorpt. spectrum, band contours, vibr. ang. mom. components 79−13736
benzene, 260 nm absorpt. spectrum, band maxima positions and intensities 79−13735
benzene, 260 nm absorpt. spectrum, vibronic anal. 79−13737

molecular vibronic states continued
benzene, 50000 cm^{-1} band, electron impact study 79−86075
benzene, $^1A_{1g}\rightarrow{}^1B_{2u}$ absorption band, Franck-Condon factors calc. 79−36701
benzene, $^1B_{1u}$ state, vibronic mag. rot. strengths and oscill. strengths, CNDO/S calcs. 77−34670
benzene, $^1B_{2u}$ and $^3B_{1u}$ states nonradiative decay, collisional deactivation 77−6819
benzene, $^1B_{2u}$-$^1A_{1g}$ transition, vibronic coupling, Duschinsky effect 77−88439
benzene, $\pi\pi^*$ and Rydberg bands, cryogenic solvent effects 78−55182
benzene, first-ionisation Rydberg spectrum assignment via John-Teller splitting 80−69155
benzene, photoluminesc. at 5K, N_2 and inert gas matrices 77−6838
benzene, reson. Raman cross sections, forbidden electronic transitions, depolaris. ratios 78−42075
benzene, Rydberg series, second ionis. process assignment, vibronic coupling 77−42333
benzene, single vibronic level decay rate, analytical representation 77−79645
benzene, single vibronic level fluoresc. after two-photon excitation 77−6818
benzene, SVL fluoresc. band intensities, Franck-Condon factors, Fermi reson. 77−10700
benzene, symmetry forbidden transitions in MCD and electronic spectra 77−65494
benzene, T_1-S_0 intersystem crossing vibronic interactions IR absorpt. spectrum obs. 80−28042
benzene, third channel decay mechanism, radiationless transitions 77−50463
benzene, vibronic coupling and IR intensities, CNDO/S semiempirical calc. 79−36596
benzene+benzene-d_6, electronic energy transfer between vibronic levels, fluoresc. obs. 77−38712
benzene(−d_6) vapour, SVL fluoresc. lifetimes and quantum yields 77−10701
benzene(-d_1,d_2,d_4), two-photon $^1B_{2u}\leftarrow{}^1A_{1g}$ spectrum, deuterium effect 80−32788
benzene p-dihalogen derivatives, electron-vibr. spectra *(Russian)* 79−89686
benzene soln., UV Raman scatt., forbidden states 78−9155
benzene-d_0(-d_3)(-d_6), vibronic coupling, hot band absorpt. spectra 78−58708
benzene-d_0-d_6, pre-reson. Raman effect and vibronic coupling 77−83604
benzene-d_6, splitting of vibrationless level in Jahn-Teller active state of D_{2h} symmetry 77−58080
benzene/benzene-d_6, cryst., X-trap phosphoresc., ODMR, 1.3K, triplet state struct. 77−20902
benzenes, lowest triplet states, instability rel. to environmental effects 77−57893
benzonitrile, vibronic spectrum, semiempirical method 80−43031
3,4-benzophenanthrene, dual fluoresc. (S_1, S_2), collision-free conditions 79−45741
p-benzoquinone(-d_4), n-π^* excited states, distant intramol. interaction between identical chromophores 78−90203
3,4-benzpyrene, relative S_1* emission yield vibronic states density 77−486
biacetyl, single rovibronic state fluoresc., quantum beats 79−31570
1,1′-bianthryl derivatives, dimer optical activity, vibronic circ. dichroism, theoretical anal. 78−62821
1,1′-bianthryl derivatives, theoretical analysis of UV, circular dichroism and optical rotating dispersion vibronic spectra 77−34652
bianthryls, vibronic anal. of circular dichroism and absorption spectra 77−38683
biaryls, dimer optical activity, vibronic circ. dichroism, theoretical anal. 78−62821
biaryls, model, mol. vibronic circular dichroism 78−37665
biological photo-induced charge transfer, mechanism and range 77−60182
biphenyl crystals, electronic and vib. states, cryst. field mixing, two-photon spectra 77−59603
biphenyl polyenes, vibronic states, quasi-linear spectra *(Russian)* 80−95598
blue proteins, activation of electron transfer reactions 78−44446
Born-Oppenheimer and true eigenstate prep. by coherent light, large mol. nonradiative relax. 77−88490
Born-Oppenheimer approx., IR absorption, circ. dichroism using vibronic gauge function 78−967
Born-Oppenheimer approx., IR absorption, vibr. intensity using vibronic gauge function 78−966
Born-Oppenheimer approx., reson. vibr. excitation, hybrid theory for electron scatt. 77−23568
Born-Oppenheimer approximation, breakdown, spectroscopic effects 77−27045
p-bromofluorobenzene, UV electronic absorption spectrum, band shape and molecular geometry 80−87147
1,3-butadiene, excited singlet states, vibronic struct., electron impact energy loss spectra, 35-90 eV 78−62932
C_{3v}-type mols., double degenerate electronic states, Jahn-Teller and spin-orbit coupling 78−50537
C_{3v}-type mols., doubly degenerate electronic states, Jahn-Teller interaction 78−50536
β-carotene, excitation profile of ν_2 line in resonance Raman spectrum, solvent effects 80−74173
chlorofluoromethylene radical, gas phase laser-induced floresc. spectroscopy 80−14173
chlorophyll, and related mols., in solid solns., fine-structured vibronic spectra under tunable dye laser excitation *(Russian)* 80−74164
chloroquinolines, photophys. behaviour, substituent and solvent effects 80−106342
chromium tetraphenylporphyrin, reson. Raman spectra, excitation profiles, nucl. distortion and Jahn-Teller effects 77−58018
chromocene, solid, Raman transition assignments, mag. susceptibility, mag. moment 78−43861
chrysene, dual fluoresc. (S_1, S_2), collision-free conditions 79−45741
circular dichroism, vibrational vibronic interaction theory 78−46380
closely coupled electronic states, exact calcs. using derived anharmonic pots: 77−23423
complex, (E+A)*e systems, Jahn-Teller, pseudo Jahn-Teller coupling and circular dichroism 79−68247

molecular vibronic states continued
complex molecules, vibr. spectra, stochastic description, appl. to optically active Brownian oscillator 80−52974
compounds with hindered internal rotation, vibronic luminesc. and absorption spectra 79−54883
core electron ionis., vibronic coupling, symmetry breaking, vibr. struct. 78−5279
coronene, luminesc., spin-orbit coupling perturbation by metal chlorides *(German)* 80−1021
coronene, mono- and dianions, reson. spontaneous Raman spectra, vibronic interactions 79−3451
coronene, n-alkane matrix, up to 1.8 kbar emission multiplet struct. shift 77−34677
coronene, sub psec radiationless relax. in soln. 77−18955
coupling model, adiabatic Born-Oppenheimer states, nonadiabatic terms calc. 77−88440
crystal, Frenkel exciton, coupled coherent and incoherent motion 77−35870
cyclobutanone, ring puckering in $^1B_2$(n,3s) Rydberg state, VUV spectrum 78−74675
cyclopentadienyl radical, pot. surface and vibronic states, ab initio CI calcs. 80−47897
cyclopentadienyl radical, vibronic valence isomerisation, Jahn-Teller effect, D_{5h} symmetry 79−97986
cyclopentanone, n−π^* transition, vibr. band intensities 80−74116
cytochrome C, vibronic theory of reson. Raman scatt. 79−94004
cytochrome c-Fe(CN)$_6$ electron transfer, verification of vibronically coupled electron tunnelling 78−48750
decacyclene, mono- and dianions, reson. spontaneous Raman spectra, vibronic interactions 79−3451
degenerate electronic state, vibronic coupling between nucl. vibr. and electronic motion 77−83568
degenerate Jahn-Teller active mode, depolaris. dispersion in resonance Raman scatt. 77−58012
delayed fluorescence, quantum mech. model 78−29804
deoxyhaemoglobin, vibronic coupling, mag. susceptibility and Mossbauer data interpretation 78−70984
deoxymyoglobin, vibronic coupling, mag. susceptibility and Mossbauer data interpretation 78−70984
diacetylene radical cation, and deuterated forms, electronic spectrum in solid inert gases 79−94026
dialkylanilines, p-substituted, twisted internal charge transfer excited state form. 79−22683
diatomic mol., vibr. relaxation, nonequilibrial dissoc. rate consts. 77−52632
diatomic mol., X-ray scatt. intensities, vibr. averaging 78−74722
diatomic molecule, semiempirical methods of calculating electron-transition moments 80−52970
diatomic molecules, electronic and vibr. functions of non-adiabatic wavefunction 79−22621
diatomic radiative transitions, electronic-vibr. dipole moment, band strength 78−46400
diatomics, harmonic oscillators, R-centroid props. 77−50421
1,3-diazaazulene, vibronic coupling, Duschinsky effect, mixed cryst. spectra 77−79622
1,3-diazaazulene-azulene, Stark spectra, vibronic perturbations in mixed cryst. 77−79623
p-dibromobenzene, cryst. electronic and vibr. energy transfer and relax. 78−31229
p-difluorobenzene, $^1B_{2u}$, fluoresc. quantum yield, radiative and nonradiative lifetimes, vibronic level depend. 77−75204
p-difluorobenzene, $^1B_{2u}$, quenching by cyclobutanone, fluoresc. lifetime meas. 77−75205
p-difluorobenzene, $^1B_{2u}$-^1A_g transition, two-photon spectra 78−46408
difluorocarbene, $\tilde{A}^1B_1$-$\tilde{X}^1A_1$ system spectrosc. and photophysics 80−5577
dihydroporphin, single crystal Shpolskii matrix, fluoresc. anisotropy 79−85994
dimer triplet state line shape, small excitons, appl. to phenazine, naphthalene, tetrachlorobenzene 80−48041
dimerized organic linear chain conductor, electron mol. vibr. coupling consts. 78−14686
dimers, circ. dichroism spectra, quadratic vibronic coupling effect 79−76402
9,10-dimethylanthracene, in n-hexane, Shpolskii absorpt. spectra at 77K, vibronic struct. *(German)* 79−59507
9,10-dimethylanthracene, Shpolskii spectra, vibronic struct., fluoresc. *(German)* 79−22754
dimethylbenzaldehydes in durene matrix, phosphoresc., $^3n\pi^*$ and $^3\pi\pi^*$ states vibronic coupling 79−22746
diphenylene sulphide, phosphoresc. vibronic struct., solvent heavy at. effect 78−17710
diphenylpolyene molecules, excited electronic states, vibronic mixing, wave functions, method of fragments anal. 80−63615
Duschinsky effect, vibronic coupling through two active modes 77−14330
electron elastic scattering, vibronic effects 78−9249
ethylene, photoelectron spectrum, vibronic coupling effects 79−10090
ethylene, V←N transition origin determ. 78−13510
ethylene-d_0, -d_4, hindered internal rotation, vibronic luminesc. and absorption spectra 79−54883
excited state, vibronically coupled, reson. Raman scatt. calcs. 79−54858
exciton-phonon interaction, molecular crystal, one-dimensional model 80−24542
fluorene, exciton band struct., two-photon fluoresc. excitation 78−64402
fluorene, near 6K, two-photon excitation spectrum, g-exciton states location 78−64393
fluorobenzene, 2644 Å band system, rovibronic anal., isotope effects 79−6949
fluorobenzene, cryst., absorpt. spectrum, vibronic states 77−59588
fluorobenzene, multiphoton ionisation spectrum in one-photon wavelength region 80−63727
fluorobenzene, vap., two-photon excitation spectrum assignments 79−59519
fluorobenzene cations, emission spectra, Jahn-Teller effects and vibronic coupling 79−10120
fluorobenzene crystal, localised excitons 77−31963
fluoromethanal, visible spectrum, rot., vibr. and vibronic anal., double min. pot. 79−41182
p-fluorostyrene, 288 nm electronic absorpt. spectra, vibr. assignment 79−13738
forbidden rot. transitions, expt. and theory, review 77−34612

molecular vibronic states continued
formaldehyde, 4_0^1 band anal., isotope effects 78−86878
formaldehyde, excited state photodecomp., rotationally resolved spectra 77−60088
formaldehyde, laser-induced fluorescence, rad. transition rates from two vibronic levels 77−3400
formaldehyde, laser-induced photodecomposition from single vibronic levels, H atom quantum yield determ. 79−96344
formaldehyde, sequential coupling 80−58297
formaldehyde, vibr. and electronic energy transfers, from single vibronic level 78−82820
formaldehyde, vibronic and spin-orbit coupling, radiative and non-radiative transitions 77−3414
formaldehyde(-d_2), photolysis quantum yields, radical production, NO reactions, freq. depend. 78−44387
formaldehyde (A^1A_2) single vibronic level photolysis, H atom prod., HNO chemiluminescence 77−9108
formaldehyde in air, photodecomposition, CO and H_2 quantum yields 79−66311
formaldehyde-d_0, -d_1, -d_2, single vibronic level photochem., radiative and nonradiative processes 78−66583
formaldehyde-d_0(−d_2), S_1 single rot. level lifetimes, isotope, elec. field and vibr. state depend. 80−78655
formaldehyde-d_1 (-d_2), single vibronic levels, fluoresc. emission, radiative lefetimes and vibr. relax 80−23521
formaldehyde-d_2 vapour, IR-UV double resonance 80−43078
free-base porphin, S_2-S_0 transition vibronic bands, photochem. hole-burning 79−36631
glyoxal, ^1A_u state energy transfer, D effects 77−58066
glyoxal, relax. processes, single vibronic level fluoresc. spectroscopy 78−58789
glyoxal, selected state photodissoc., vibronic effects, CO quantum yield, 1-10 torr 78−37691
glyoxal (^1A_u), fluoresc. quantum yields, radiative and nonradiative lifetimes 80−32759
haeme proteins, inversely polarized modes in reson. Raman scatt., depolarisation dispersion curves, vibronic interactions 78−78676
haemoglobin, deoxygenated, vibronic coupling effect on paramagnetisms 77−57899
haloacenaphthenes in n-heptane, quasi-line phosphoresc. spectra, vibronic spin-orbit interaction 80−43096
halomethanes, valence photoelectron spectra, vibr. and vibronic struct. 78−50581
halomethanes, vibronic struct. in electron spectra, Jahn-Teller and spin-orbit coupling 78−50537
α-(β-)heptacyclene, vibronic spectra, electronic-vibr. interactions 78−1021
Herzberg-Teller expansion over floating-orbital zero-order wavefunctions, coupling integral deriv. 77−14408
heteroaromatic mol. radiationless transition decay rate freq. shift depend., quantum statistical mechanics anal. 78−74691
heteroaromatic molecules, planar, orientation and phosphoresc. polarisation in stretched film 80−14169
N-heterocyclic aromatic compounds, with nonbonding electrons, proximity effect and radiationless transitions 78−58736
heterocyclic N compounds, radiationless transitions, isotope effects 80−48033
N-heterocyclics, radiationless transitions, vibronic coupling effect 78−33543
1,3,5-hexatriene, electron scatt. at low-energy, vibronic struct. of triplet state 79−3574
β-hydroxy acrolein, lower excited states, electronic struct. and H-bonding, ab initio SCF and CI calcs., photochemical mechanism 80−83278
I_2He, I_2He_3, and I_2He_3, photodissoc. products energy distrib. 79−100410
induced electronic transitions, radiative lifetimes, non-Condon effects 80−53051
intersystem crossing rates, triplet sublevel decay, vibronic coupling 78−5271
intramolecular longit. relax. in mol. system with Rabi oscills., transient regime theory 78−46404
inverse electronic relaxation, theory 80−23474
IR intensities, vibronic calcs. 79−10108
Jahn-Teller linear E-e effect, canonical transformation 78−67993
Jahn-Teller molecules, quasiclassical dynamics 79−6880
Jahn-Teller mols., fast electron scatt. theory 79−89784
lanthanide (III) complex, octahedral, f-f transitions, mag. dipole intensites, vibronic coupling model 80−25404
lanthanide ion complexes, octahedral, f-f transition intensities, vibronic coupling model 78−58659
large molecule, novel ultrafast two-pulse excitation spectroscopy 78−94331
laser techniques, vis. and UV, small mols., electronically excited states, book contrib. 78−9277
level mixing, under electronic coupling operator 80−52968
lifetimes (short), determ. from reson. Raman excitation profiles 79−98103
light quenching of mol. fluoresc. spectrum, spectral distrib. of polarisation, electronic-vibr. interactions 79−85989
linear approximations, nonBorn-Oppenheimer coupling 77−10656
linear triatomic molecule, $^2\Pi$ state, vibronic-spin-orbit interaction, Renner effect 78−70758
liquid intermolecular relaxation spectroscopy 79−95844
localisation in ionized and excited states, conf. 77−30750
lutein, aq. soln., aggregate, reson. Raman spectra, and IR spectra, exciton interactions 78−31770
metalloporphins, deuterated, resonance Raman spectra, vibr. and vibronic levels 78−62812
metalloporphyrin, low symmetry environment, Raman excitation spectra and absorpt. spectrum 80−74172
metalloporphyrin, vibronic coupling, Raman scatt. 78−21933
metalloporphyrins, reson. Raman specta, intra- and inter-manifold couplings interference 80−28020
metalloporphyrins, Soret excited, reson. Raman excitation profiles, Jahn-Teller distortion and vibronic anal. 78−58698
methanol, valence photoelectron spectra, vibr. and vibronic struct. 78−50581
methoxy, Jahn-Teller induced rovibronic effect, nuclear spin-electron spin hyperfine Hamiltonian 80−83298
methoxy radical and deuterate, vibronic level fluoresc. spectrum 80−58305

molecular vibronic states continued
9-methylanthracene, in n-hexane, Shpolskii absorpt. spectra at 77K, vibronic struct. *(German)* 79−59507
9-methylanthracene, Shpolskii spectra, vibronic struct., fluoresc. *(German)* 79−22754
methylene, vibronic anal., ab initio CI pot. curves calcs. 78−50479
methylene anion, vibronic anal., ab initio CI pot. curves calcs. 78−50479
methylene radical, vibronic bands obs. in pulsed supersonic jet 80−28024
methyoxy radical, electronic absorpt. spectra, visible, vibr. freqs., vibronic intensities and oscill. strengths 80−28025
mixed valence system, far IR intervalence tunnelling transition, vibronic coupling model 78−58646
molecular aggregates, nonvalidity of SCF vibronic spectra calcs. 77−10655
molecular cryst., dipolar exciton band struct., optical model 77−15770
monoalkylbenzenides, anion radicals, EPR, temp. depend., vibronic interaction, proton HFS 77−34666
monohalonaphthalenes, electronic transition spectra forbidden charact., symmetric vibr. interaction 78−58663
multimode Jahn-Teller effect for E-term with strong vibronic coupling, local and resonant states 80−24858
naphthalene, $^1B_{3u}$-state lifetime, temp. depend. under Boltzmann conditions 79−86008
naphthalene, cryst., laser reson. Raman effect, near 3200 Å, B_{3g} vibr. enhancement 77−52067
naphthalene, cryst., vibronic absorpt. spectrum with totally symm. phonons 79−4817
naphthalene, doped crysts., fine struct. strengths in vibronic spectra 77−44004
naphthalene, fluorescence and absorpt. spectra, deviations from Condon approx. 80−28004
naphthalene, Raman intensities rel. to vibronic coupling and excited electron state geometries 77−27075
naphthalene, reson. Raman scatt. from non-totally symm. mode 78−37641
naphthalene, soln. and melt, second vibronic transition, spectroscopic charcts., effective field dispersion calcs. 80−55102
naphthalene, triplet state time evolution after radiationless transition, initial vibronic distrib. effects 80−23450
naphthalene, two-photon and mutiphoton excitation, UV fluoresc. spectra 77−88517
naphthalene, vibronic fluorescence spectrum, intensity distribution 79−3477
naphthalene and −d_8, vibronic spectra 79−51956
naphthalene crystal, vibronic spectra at 1.6K, two-photon fluoresc. excitation 77−59604
naphthalene molecule in durene and xylene crystals, vibronic interactions 80−84755
naphthalene vapour, fast obs. of primary triplets with tandem laser pulse absorption 77−58056
naphthalene-d_0(−d_8), fluoresc. spectra, vibronic intensities 77−50464
naphthalene-h_8 (-d_8), two-photon excitation spectra, vibronic coupling 77−75246
near reson. Raman lines, relative intensities, A-term method 79−81205
nickel etioporphyrin, reson. Raman spectra, excitation profiles, nucl. distortion and Jahn-Teller effects 77−58018
nickel-octaethylporphyrin, in benzene soln., reson. CARS and CSRS line shapes 80−74432
nonradiative decay rates, single level, analytical representation 77−79645
octaethylchlorin, phosphoresc. polarisation spectra obs. 77−18963
octaethylporphin, phosphoresc. polarisation spectra obs. 77−18963
octahedral systems, quadratic Jahn-Teller vibronic coupling calcs. 79−6881
trans, trans-1,3,5,7-octatetraene, low freq. normal modes, CFF-π calcs. 79−68217
olefins, zwitterionic states, polaris. and vibronic interactions 80−32620
one-dimensional systems, electronic collective excitons, EPR response 77−31960
one-dimensional systems electronic collective excitations 77−31959
organic dye solutions, vibronic struct. in two-photon absorpt. spectra *(Russian)* 79−64004
organic solid, vibronic excitons, rigid lattice calcs. 77−31958
palladium porphin, in n-alkane crystal, Zeeman and crystal field effects, absorpt. vibr. anal. 80−7372
palladiumporphin, in n-alkane, S_1←S_0 absorpt. spectrum, vibronic coupling and avoided crossing, field splitting 78−84613
2,2 paracyclophane, dimer vibration influence on emission spectrum 80−69133
pentacene in naphthalene (p-terphenyl), mol. mixed crysts., optical dephasing and vibronic relax. 80−95957
pentacene in naphthalene crystal, relax. of vibronic states, photon-echo and ab absorpt. relax. expts. 79−95807
(perylene)$_3$TCNQ, prep. and spectra, electron-mol. vib coupling 77−16290
phenanthrene, two-photon excitation spectra, exciton-phonon and intramol. vibronic coupling 80−84774
phenanthrenequinone, in n-paraffin matrix, electronic-vibr. interaction in phosphoresc. 79−27027
phenanthrolines, in Shpolskii matrices, phosphoresc. spectra 78−94276
phonon-impurity interaction, molecular crystal, one-dimensional model 80−24542
phthalocyanine, supersonic free jet-cooled, fluoresc. obs. 79−45753
polar molecule, Stark effect in electron spin transition in zero-field 77−27099
polyatomic, floating basis set model 77−10587
polyatomic mol. photoelectron ang. asymmetry parameter vibr. state depend., vibronic coupling 79−36698
polyatomic mol. quasi line spectrum in paraffin matrix, electronic-vibr. interaction 79−85971
polyatomic molecule, diffuse absorpt. and fluoresc., vibronic band broadening 79−98161
polyatomic molecule, electronic relax. process, energy depend., book contrib. 77−34688
polyatomic molecule, Franck-Condon principle and sum rules for vibronic transitions 77−30927
polyatomic molecule, vibronic transitions, dynamical symm., Franck-Condon theory 77−34575
polyatomic molecules, energy levels, classification 78−9052
polyatomic molecules, excited state spectra, vibronic coupling, non-adiabatic model 78−25509

molecular vibronic states continued
polyatomic molecules, intensity distribution in vibronic bands, Dushinsky effect 79−93983
polyatomic molecules, non resonance vibronic coupling of excited states rel. to electronic spectra 77−18900
polyatomic molecules, vibronic spectra, stochastic model 79−50004
polyatomic molecules, vibronic spectra and luminescence kinetics 79−54881
polyatomic molecules with pronounced vibr. struct., spectral shape 79−76469
polyatomic mols., isolated, radiationless transitions and vibronic level width 77−79646
polyatomic organic molecules, electronic excitation transport in inhomogeneity broadened 79−54884
polyatomics, electronic-vibr. interaction between close excited electronic states 79−63980
polydiacetylene, cryst., one-dimens. conjugated semicond., vibronic coupling, Fano interference effects 80−34939
polyene chromophones, band broadening in electronic-vibr. absorpt. spectra 80−28003
polyenes, absorpt. spectra, electronic-vibr. sequence band broadening 77−65453
polymethin cyanine dyes, vibronic energy relax., picosec. spectrosc. obs. 80−5526
polymethine dye solns., phonon-free electron-vibration transitions, stimulated emission *(Russian)* 77−79660
polymethine dyes, mol. struct., lasing props. 79−3693
polypeptides, β-form, vibronic exciton approach to NV_1 absorption band 77−79626
population inversion during chemiluminesc. 80−3351
porphin, free-base, in n-octane cryst., photochem. hole-burning, vibronic relax. 79−31587
porphin, single crystal Shpolskii matrix, fluoresc. anisotropy 79−85994
porphin free base, vibr. and normal mode anal. 80−69122
porphin free base in cryst. anthracene, site selective optical spectra, vibronic freqs. 79−13730
porphin-d_n, (n=2-14) electronic-vibr. interaction, quasi-line absorption (fluoresc.), mirror symmetry 78−55197
porphine-d_4, vibronic transitions, polaris. determ. 80−63614
propynal, rovibronic populations, collisionless IR multiphoton spectra, energy deposition, photoacoustic determ. 80−83354
proteins, electron transfer mechanism 79−96510
pseudo Jahn-Teller effect, rel. to vibronic coupling model, for mol. spectra 78−94234
pyraozine, vibronic coupling via C-H bending mode 79−76403
pyrazine, in pyrazine-d_4, p-dioxane, X-trap, p-xylene, benzene(-d_6), cryst., MIDP, PMDR, low temp., assignments 77−36154
pyrazine, $n\pi^*$ transitions, vibronic coupling 78−25501
pyrazine, physisorbed on Ni (111), UV spectroscopic ellipsometry obs. 79−86997
pyrazine, PMDR due to single defect species, vibronic structs. 78−19535
pyrazine, pyrazine-Kr, ground and n-π^* excited state struct. 79−68241
pyrazine, Raman spectrum, correlation with vibronic coupling and adiabatic potential 77−71804
pyrazine, reson. Raman and absorpt. spectra to $S_2(\pi,\pi^*)$ state, excited state geometry 79−76433
pyrazine, reson. Raman spectra, vibronic theory of Raman intensity 78−37643
pyrazine, single vibronic level fluoresc., non-exponential decay 77−27108
pyrazine, vap., single vibronic level fluoresc., dye laser excitation 79−18224
pyrazine, vibr. struct. and nonlinear vibronic coupling, pseudo Jahn-Teller effect 78−94234
pyrazine, vibronic and spin-orbit coupling interaction 80−14126
pyrazine, vibronic bands, MIDP and polarised phosphoresc. in benzene matrix 77−6833
pyrazine, vibronic coupling by out-of-plane modes 77−6747
pyrazine.$(H_2O)_n$, n=1,2, ground and n-π^* excited state struct. 79−68241
pyrazine (-d_4), single vibronic level fluoresc. spectra, rel. to vibronic coupling 80−28043
pyrazine triplet state, mol. distortion, MIDP using polarised light 79−10137
pyrazine-d_4, in p-dioxane, p-xylene, benzene, cryst., MIDP, PMDR, low temp., assignments 77−36154
pyrene, fluorescence spectra in aq. and surfactant solns. 77−83639
pyridine, $\pi\rightarrow\pi^*$ transition, 1800 Å, electronic absorpt. spectrum 77−71813
pyridine, vibronic coupling by out-of-plane modes 77−6747
pyridine-d_0-d_5, nπ^* excited state vibronic coupling, vis. and Raman spectra 77−14438
pyridine-I_2(Br_2) charge transfer complexes, vibr. spectra, vibronic contrib., intensity enhancement 80−53048
pyridinyl radicals, hyperfine splitting consts., vibronic effects 77−57890
pyrimidine, and derivatives, intersystem crossing rates, triplet sublevel decay, vibronic coupling 78−5271
pyrimidine, bi-exponential decay, methylation and vibr. excitation, proximity effects 80−78641
pyromellitic dianhydride-anthracene, cryst., charge transfer exciton transitions, refl. spectra obs. 78−72540
quasi-linear spectra and vibronic states of molecules with end phenyl rings *(Russian)* 80−95597
quinazoline, in n-pentane (isooctane) Shpolskii matrices, luminesc. props., vibr. struct. 79−22739
quinoxaline, vibronic coupling by out-of-plane modes 77−6747
radiationless decay of vibronically coupled electronic states 79−22747
radiationless transition rate constants, effect of geometry change in molecular vibrational promoting modes 80−5569
radiationless transitions, proximity effect, vibrational tuning, vibronic interaction probe, QSM approach 78−94274
radiationless transitions, synchrotron radiation obs. 80−63706
radiationless transitions, vibronic interactions 78−17705
radiative transitions, proximity effects, role of vibronic coupling and static crystal field interactions model 80−69126
Raman excitation profiles, vibronic theory 77−23501
Raman excitation profiles and mol. spectra synthesis, vibronic and exciton-in-mol. theory 78−42076
Raman scatt., excitation profiles by vibronic theory, preresonance scatt. 77−79619
Raman selection rules, spin degeneracy and vibronic states 78−987

molecular vibronic states continued
Raman spectra, correlation with vibronic coupling and adiabatic potential 77−71804
rare earth ions, ligand-induced pseudoquadrupole absorpt., vibronic contribs. 80−52978
Renner-Teller effect, effective vibronic Hamiltonian 78−17651
reson. spontaneous Raman spectra, vibronic interactions 79−3451
resonance Raman scatt. in mols. with double minimum pots. 77−58011
resonance Raman scattering, of totally symmetric vibr., depolarisation dispersion, vibronic coupling 77−65472
resonance Raman scattering from small molecule, vibronic theory 79−94004
resonance Raman spectra, Dushinsky effect 79−45726
resonance Raman spectra intensity distribs. in soln. 79−22763
resonant Raman effect, appls. and theories, review, book contrib. 77−38676
resonant Raman scatt., strong vibronic coupling limit, Green's function 77−83605
resonant Raman scatt., strong vibronic coupling limit, overtones, hot bands 77−83606
resorufin, in PMMA, site selection spectra, hole burning and Stark effect 78−9159
11-cis-retinal, donor energy effects on triplet-sensitized isomerization 78−3353
rhodamine, dye soln., photoinduced dichroism and vibronic relax. 77−14465
rhodamine 6G dye laser, induced radiation spectral characts., effect of vibr. relax. 80−64008
rhodamine-B and -6G, sub psec radiationless relax. in soln. 77−18955
ruby, luminescence, red emission intensity at various temps., mag. field depend. 77−32423
satellite struct. of electron spectra, CI and vibronic coupling, dynamical calc. 80−53044
semiconductor, conjugated, one-dimens., vibronic coupling, Fano interference effects 80−34939
sodium uranyl acetate, fluoresc., circ. dichroism 79−38598
solvent effect on electronic spectrum 79−54839
spin relaxation in photo-excited triplet states via vibronic excitation: rotation of spin axes 79−78503
styrene, styrene-β-d_2, 288 nm electronic absorpt. spectra, vibr. assignment 79−13738
symmetric molecule, quasiclassical energy and momentum range *(Russian)* 77−3342
symmetric molecules, high resolution spectra, rot. and permutation dynamics 79−41157
symmetric top molecules, rovibronic 2-photon transitions, rot. line strengths 78−78762
TCNE aromatic donor/acceptor complexes, reson. Raman excitation and absorpt. profiles, model theory 77−18982
TCNE-benzene, charge-transfer complex, change of C≡N and C=C band intensities 77−88448
TCNE-paraxylene, charge-transfer complex, change of C≡N and C=C band intensities 77−88448
$TCNQ_2$-TEA, quasi 1-D cryst., interaction between electronic and vibr. states 77−52102
TCNQ, electron-mol. vib. coupling 77−15782
TCNQ, metallic reflection band, vibronic struct. 78−19502
TCNQ salts, electron-vibrational interaction consts. 79−28054
TCNQ salts, K(TCNQ), Ba$(TCNQ)_2$ and Ca$(TCNQ)_2$, electronic absorpt. spectra, vibronic struct., charge transfer bands 79−24331
TCNQ-perylene, electronic absorpt. spectra, vibronic struct., charge transfer bands 79−24331
p-terphenyl:pentacene, optical coherence and resonance decay 77−24859
tetrahedral molecules, hyperfine and superfine levels, elementary spin-1/2 cases, vibronic ground states 79−85954
1,4,5,8-tetrahydroxyanthraquinone, selective excitation, luminescence of long-wavelength component of multiplet 79−3478
s-tetrazine-benzene, mixed cryst., 2K, lifetime limited photochem. hole burning 78−9183
thiocarbonyl chlorofluoride, second excited singlet state emission spectroscopy, resonance fluorescence obs. 80−69158
thioformamide(-d_2), photoelectron and absorption spectra, vibr. struct., excited state configs. 77−6847
thioindigo, vibronic fluoresc. spectrum, vibr. struct. 77−54571
thiophosgene, second excited singlet state emission spectroscopy, Franck-Condon anal. 80−69157
thiophosgene, vibronic anal. of electronic transition, inversion doubling splittings obs. 80−83388
thiophosgene vapour, fluoresc. from S_2 single vibronic states, quantum yields and quenching 77−34675
1,2,3-timethoxybenzene, weak electronic transition, solid, and in rigid glass, UV assignments 78−17681
toluene, two-photon ionisation spectrum, of $^1L_b\leftarrow S_0$ transition 80−14180
transition metal complexes, ligand field spectroscopy, selection rules, intensity enhancement of forbidden transitions 80−45049
transition metal hexahalide complex, polarised reson. vibr. Raman spectra, electronic degeneracy effects 78−78708
transition metal ion system, induced transitions, structural form of intensities 78−90145
transition metal ions, in complexes, vibronically allowed d-d transitions, band shape calcs. 77−50472
triatomic mols., Renner-Teller effect, orbital angular momentum 80−78513
1,3,5-trichloro,2,4,6-trifluorobenzene radical cation, $B^2A_2'\rightarrow X^2E''$ laser-induced fluoresc. spectra 80−14172
sym-1,3,5-trichlorobenzene, cation, emission spectrum, Jahn-Teller effect 79−89681
trichlorobenzene cation, selectively excited wavelength resolved emission spectra 80−87136
trichlorobenzene cations, Jahn-Teller distortions, quadratic and mode mixing effects., distortion geometry determ. 80−91462
trichlorobenzene radical cation, gas and matrix isolated vibr. resolved electronic spectrum 79−68252
symtrifluorobenzene cation, Jahn-Teller effects, intermode interactions and intensity anomalies 80−78553
sym-trifluorobenzene cation, Jahn-Teller effects, quadrupole coupling 80−78554
trifluorobenzene cation, selectively excited wavelength resolved emission spectra 80−87136
trifluorobenzene cations, Jahn-Teller distortions, quadratic and mode mixing effects., distortion geometry determ. 80−91462

molecular vibronic states continued
1,3,5-trifluorobenzene-d_0(-d_3), cation, emission spectrum, Jahn-Teller effects 79−89680
trifluoroiodomethane, X→B Rydberg transition, Jahn-Teller coupling parameter, vibronic level calc. 78−50536
trigonal molecules, hyperfine and superfine levels, elementary spin-1/2 cases, vibronic ground states 79−85954
triphenyl phosphonium ytterbium chloride, $Yb^{3+}(4f^{13})$ absorpt. spectrum, cryst. electric field splitting 77−73151
triphenylene, in PMMA matrix, one-photon absorpt. spectrum, vibronic anal. 77−42366
triphenylene, mono- and diamons, reson. spontaneous Raman spectra, vibronic interactions 79−3451
triphenylene, triplet state, MIDP and T-S excitation spectrosc. 79−81233
triphenylene(-d_{12}), lowest $T_1[^3A_2'(\pi\pi^*)]$ state vibronic coupling 80−47955
triphenylmethane dyes, IR and Raman vibr., spectra, vibr. anal., vibronic theory of Raman scatt. 77−68048
two state two mode vibronic coupling model, Born-Oppenheimer and crude adiabatic perturbation methods 80−87036
two-electron level with quasidegenerate levels, local phase transitions and temp. effects in lattice dynamics 80−10666
N_3-undecyllumiflavin, high resolution fluoresc. and excitation spectroscopy, vibronic transitions obs. 80−78639
unimolecular radiationless decay, coupling strength incoherence 78−70865
vibronic coupling, totally symmetric harmonic mode, exactly solvable model 78−21896
vibronic systems with localised electrons, reson. Raman scatt., hot luminesc. 79−38616
vibronically coupled electronic states, radiationless decay, non-Condon effects 80−52966
vibronically coupled excited states, resonance Raman scatt. 77−6784
weakly coordinated molecular systems, mutual vibronic effects in chem. reactions and catalysis 78−64821
zeaxanthin, aq. soln., aggregate, reson. Raman spectra, and IR spectra, exciton interactions 78−31770
Zeeman effect, orthorhombic rot. mols., doublet-doublet transitions 78−74698
$Ag_2SO_4:CrO_4^{2-}$, polarised electron spectrum assignments, red colour explained 77−85753
$Ar^+ + N_2$, energy transfer, vibronic excitation, emission spectra 78−66578
$Ar^* + H$, assoc. ionis., rovibronic struct. in electron energy spectrum 80−106380
2-azaanthracene and methyl derivatives, electron-vibr. props., UV spectra *(Russian)* 77−75177
BO_2, fluoresc. excitation spectra, vibronic level fluoresc., Fermi reson., force field 77−79643
BO_2, gas, optically detected mag. reson. spectrum, $X^2\Pi$ rovibronic sublevels 78−82756
BO_2, intermodulated fluoresc. spectra using stabilised dye laser 79−27020
BO_2, laser excited fluoresc. spectra assignments, vibronic and electronic states 77−46590
BO_2, photoexcitation and fluoresc. spectra, rot. transitions, assignment and deconvolution 79−27003
BO_2, Π vibronic states, laser induced fluoresc. obs. 80−58301
BO_2, reson. fluoresc. assignment of vibr. and vibronic transitions 78−17663
BaO produced in $Ba+SO_2$ reaction, vibronic distrib., collisional energy depend., laser-induced fluoresc. obs. 80−11917
BaO_3, visible absorpt. and reson. Raman spectra in Ar and N_2 matrices 77−65487
BrO, free radical, Ar matrix absorpt. spectra, mol. vibronic states obs., spectroscopic const. determ. 80−83387
C_2, $X^1\Sigma^+_g$, $6^1\Sigma^-_g$ states, perturbations, ab initio CI calcs. 77−83490
C_3, ($^1\Pi_u$) radical excited state radiative lifetimes and the collisional deactivation 79−27018
C_3, $\tilde{A}^1\Pi_u$ state, orbital angular momentum 80−78514
C_3, Renner effect, vibronic levels and wavefunctions, ab initio variational method 80−14127
CCN radical in solid Ar, emission and excitation spectra 78−70868
$(CD)_x$, polymer, heavily doped, IR spectra, vibronic intensity enhancement 80−28124
CH, collisionless form., rovibronic relax., reson. fluoresc. 78−68902
CH_2, photoprod. from ketene, singlet-triplet energy separation and rovibronic level obs. 80−11936
$(CH)_x$, polymer, heavily doped, IR spectra, vibronic intensity enhancement 80−28124
CHF radical, $\tilde{A}^1A''$-$\tilde{X}^1A'$ transition, laser induced fluoresc. 80−95660
$(C_2H_5)_2Fe^+$ complexes, vibrational electronic (Franck-Condon) Raman transitions 78−42070
CN free radical, $A^2\Pi$-$X^2\Sigma^+$ Red system, perturbation analysis 80−87247
C_2N_2, $C^1\Pi_u$-state predissoc., vibronic effects 80−28078
C_2N_2, satellite struct. of electron spectra, CI and vibronic coupling, dynamical calc. 80−53044
CNN, matrix-isolated, $^3\Pi$-$^3\Sigma^-$ system, laser-induced temporal and wavelength resolved spectra 77−83637
CO, $A^1\Pi(v'=1)$, vibr. relax. by reversible intersystem crossing, fluoresc. obs. 80−14170
α-CO, IR and Raman spectra, vibron band, vibron-phonon combination bands 78−68495
CO^+, vibr.-excited $A^2\Pi$ state, radiative and radiationless vibronic deactivation rates with He 79−10134
$^{12}C^{16}O$:CO isotopes, IR and Raman spectra, vibron band, vibron-phonon combination bands 78−68495
CO+inert gas, collision-induced intersystem crossing mechanism 78−74689
CO_2, core electron ionis., vibronic coupling, symmetry breaking, O1s line vibr. struct. 78−5279
CO_2^+, fluoresc. quantum yields, isotope effects, photon-photoion coincidence meas. 78−90200
CS, near UV spectra, rot. anal. of $a^3\pi_r$=$X^1\Sigma^+$ transition 78−5242
CS, spin-orbit and spin-spin parameter calcs. 77−27044
CS, ultraviolet vibronic spectra, for ^{34}S isotopic anal. *(Russian)* 79−50041
CS_2, laser excited fluoresc., time and freq. resolution, assignments 77−14476

molecular vibronic states continued
CS_2, $\pi\pi^*$ and Rydberg bands, cryogenic solvent effects 78−55182
Ca_2, mol., vibr. quantum numbers of rotating vibrator 79−85949
Ca_2, optical spectra, inert matrices 78−58712
$CaF_2:Co^{2+}$, parity-forbidden transitions, elec. field effect on electronic-, vibr. spectrum 79−65905
CaO_3, visible and absorpt, and reson. Raman spectra in Ar and N_2 matrices 77−65487
$CdF_2:Co^{2+}$, parity-forbidden transitions, elec. field effect on electronic-vibr. spectrum 79−65905
Cl_2, Ar matrix, vibronic dephasing 80−6469
ClFCS, second excited singlet state photophysics, laser excitation obs. 80−32758
ClO, free radical, Ar matrix absorpt. spectra, mol. vibronic states obs., spectroscopic const. determ. 80−83387
CrO_2Cl_2, multiphoton induced inverse electronic relax. 80−66836
CrO_2Cl_2, single vibronic level fluoresc. 77−3408
$Cs_3Cr_2Cl_9$, optical absorpt., MCD, exchange interactions 78−10917
$Cs_2GeF_6:Mn^{4+}$, magnetically circularly polarised emission and MCD of vibronic lines 77−16377
Cs_2MX_6(M=Se, Te, X=Cl, Br), $\Gamma_4^-(^3T_{1u})$ state, Jahn-Teller effect, luminesc. obs. 80−60650
$Cs_2SnCl_6:UO_2Cl_4^{2-}$, luminesc., vibronic anal. 79−33767
$Cs_2ZrCl_6:UO_2Cl_4^{2-}$, luminesc., vibronic anal. 79−33767
D_2, $^1\Sigma_g^+$ states, adiabatic calc. of vibronic states 78−5198
D_2, Fulcher band system, rot. struct. 79−98986
D_2, photoabsorpt. spectra, rovibronic interactions 78−992
DNC, vibronic coupling and linear to bent transitions 79−45694
D_2O, Rydberg states, visible spectra 78−9162
Eu complex Eu dibenzoylmethane chelate with piperidine, vibronic and IR spectra 79−82981
$FeBr_4^-$, in various solvents, $^4A_1$ ^4E d-d band reson. Raman spectra, solvent depend., vibronic coupling 80−55085
$FeCO_3$, vibronic coupling at Neel temp. 80−15491
$H^+ + O_2$, energy transfer, vibronic excitation, emission spectra 78−66578
H_2, electron impact excited singlet-g states, optical and time resolved spectra, radiative lifetimes, quenching rates for rovibronic levels 80−23564
H_2, Fulcher band system, rot. struct. 79−98986
H_2, HD, $^1\Sigma_g^+$ states, adiabatic calc. of vibronic states 78−5198
H_2, HD and D_2, nonadiabatic coupling of EF and GK $^1\Sigma_g^+$ states 79−59431
H_2, photoabsorpt. spectra, rovibronic interactions 78−992
$H_2+e^-\rightarrow H_2^*+e^-$, Gaussian basis Glauber approx., elastic and vibrorotational excitation cross sections 80−58399
HCl, emission K spectra, vibronic and core hole effects, nonempirical orbital defreezing calc. 78−5200
$H(D)CN(C^1A')\rightarrow H(D)+CN(B^2\Sigma^+)$, photofragment excitation spectra measurement 79−45777
HF, emission K spectra, vibronic and core hole effects, nonempirical orbital defreezing calc. 78−5200
HF, IR absorption in Born-Oppenheimer approx., vibronic gauge function for vibr. intensity 78−966
$H_2(H_2^+)$ and isotopes, expectation values, Born-Oppenheimer, adiabatic and non-adiabatic results 78−82624
HNC, vibronic coupling and linear to bent transitions 79−45694
HNO $\tilde{A}^1A''$ excited state dipole moment, optical-optical double reson. Stark spectrosc. obs. 80−106337
HNO, vibronic state perturbative and predissoc. mechanisms, fluoresc. excitation spectra obs. 80−9658
HO_2 radical, near IR emission bands, vibr. and vibronic transitions 78−37633
H_2O, Rydberg states, visible spectra 78−9162
H_2O^+, ab initio potential energy surface study by CI techniques, equilibrium conform. determ., mol. dissoc. pathways 80−78550
H_2O^+, vibr. and rot. struct., intensity factors and orbital angular momentum 80−83246
H_2O^+, vibronic A^2A_1 states, lifetimes, delayed coincidence meas. 78−70874
HSO radical, Doppler-limited dye laser excitation spectroscopy, rot., distortion and spin-rot. interaction const. determ. 80−83383
$He^+ + N_2$, low energy collisions, vibronic excitation model 77−83689
HeH^+, $X^1\Sigma^+$ electronic ground state, pot. curve, rovibronic and dissoc. energies 79−72254
Hg_2 excimers, photoassoc., spectroscopy and kinetic processes of high-lying vibronic states, laser applics. 80−9649
Hg_2, photoassociated, collision-induced predissoc. with Hg 79−31626
HgCl, HgBr, HgI, $B^2\Sigma$-$X^2\Sigma$ systems, Franck-Condon factors and r-centroids 79−64051
I_2, energy levels near B-state dissoc. limit, two-photon spectra 78−9210
I_2, matrix samples, laser spectroscopy, evidence for $(I_2)_2$ species 78−58735
I_2, two-photon excitation of rovibronic levels and gerade states 77−14508
I_2, use as test mol. in modern spectroscopy, review 78−90317
IO, free radical, Ar matrix absorpt. and emission spectra, mol. vibronic states obs., spectroscopic const. determ. 80−83387
$IrBr_6^{2-}$, Raman tensor patterns, vibr. reson. Raman scatt., group theoretical calcs. 78−986
IrF_6, in mixed crysts., Jahn-Teller effect, $\Gamma_{8g}(t_{2g})^3$ state, 6800 Å 78−76032
K_2, beam, multiphoton ionisation mass selective laser spectroscopy, vibronic, gyrovibronic states, clusters 78−21985
K_2, supersonic mol. beam, isotope selective two-step photoionisation study 80−74203
$KClO_4:MnO_4^-$, reson. Raman excitation profiles for totally symmetric mode, vibronic struct. 80−50309
KN_3, fluoresc. spectrum, 30K, vibronic and vibr. assignments 79−27023
$LaF_3:Dy^{3+}$, laser excited fluoresc., lifetimes meas. 79−24353
$Li+Li_2\rightleftarrows Li_3$, rovibronic symmetry correlation 78−92461
Li_3, BO hypersurface and vibronic states, coupled electron pair approx. 78−94203
LiH, mol., vibr. quantum numbers of rotating vibrator 79−85949
LiO_2, molecule, vibronic interaction in low-lying states, model calc. 80−32603
LuF, electro-vibr. levels mol. consts., global fit *(French)* 77−3339
Mg_2, Ar matrix isolated laser photoluminescence spectra, electronic absorpt., emission, vibronic and vibr. relax. 78−82744
MgO_3, visible absorpt. and reson. Raman spectra in Ar and N_2 matrices 77−65487
$MnCl_2$ in soln., luminesc., strong vibronic coupling 79−65922

molecular vibronic states continued
MnF_6^{2-}, $A_2{}^1M^{IV}F_6$ hosts, luminesc., IR and Raman spectra, 5K, assignments 77−20904
Mo_2, matrix isolated visible absorpt. spectra, electronic, vibronic and vibr. states 80−28027
MoN, matrix isolated visible absorpt. spectra, electronic, vibronic and vibr. states 80−28027
MoO, matrix isolated visible absorpt. spectra, electronic, vibronic and vibr. states 80−28027
N_2, diffuse plasma, population densities of triplet states, correl. with electron impact processes 80−43966
N_2, isotopic forms, visible spectra, rovibronic and rot. anal., $C'\,{}^3\Pi_u$ and $C\,{}^3\Pi_u$ interaction 77−18933
N_2, solid, Raman spectra vibron and lattice freq. shifts, librational force consts., α- and γ-phases 78−19460
N_2, solid and matrix isolated mol., triplet state spectra *(Russian)* 80−5574
N_2 UV spectra, new band, ${}^3\pi_u$ state lower vibronic levels 78−17682
N_2:CO, IR and Raman spectra, vibron band, vibron-phonon combination bands 78−68495
N_2^+ + He, low energy collisions, vibronic excitation model 77−83689
N_2^+ + He collisions, vibronic excitation, curve-crossing trajectories 80−23520
ND_3, predissoc. mol., rot. resolved IR reson. scatt. 77−30882
NH_2, A^2A_1-X^2B_1 absorpt. spectrum, 6250-9500 Å, rot. and vibronic anal. 77−472
NH_2, hyperfine struct. of u-state, microwave optical double reson. 79−68246
NH_2, microwave-optical double reson., collision-induced transitions, vibronic state obs. 77−34667
NH_2, vibr. and rot. struct., intensity factors and orbital angular momentum 80−83246
NH_2, vibronic levels, excited by blue CW dye laser 78−86907
NH_2 + H rot. energy transfer in vibronic levels, absolute transfer rates 80−9701
NO, doublet-quartet transitions, 5-7.4 eV, electron-impact spectroscopy, 5-80° 78−37754
NO, doublet-quartet transitions, low energy variable-ang. electron scatt. obs. 78−62933
NO, measured lifetimes of $A\,{}^2\Sigma^+$, $D\,{}^2\Sigma^+$ and $C\,{}^2\Pi$ states 78−90219
NO_2, 7390 Å band, vibronic transition within ground state manifold 78−21919
NO_2, 8170-8280Å absorption spectrum, rot. struct., assignments 79−6937
NO_2, A-X band system, visible absorption, fluoresc., vibronic coupling 77−58030
NO_2, coupling of vibronic states induced by messenger state 79−72226
NO_2, electronic states, pot. energy surface calcs. 77−6673
NO_2, excited-state rot. const., 5933 Å vibronic band reassignment 77−58196
NO_2, fluoresc. spectra near 5000 Å, rotationally-forbidden bands 77−79639
NO_2, laser fluoresc., $^2B_1$ vibronic states 77−27109
NO_2, rot. cooled, vibronic band lifetimes, time resolved fluoresc. excitation spectra obs. 79−94025
NO_2, visible fluoresc., rotational structure of vibronic bands 79−98146
N_2O, photoelectron spectrum, vibronic interaction and autoionis. effects 80−95680
N_2O^+, fluoresc. and dissociation lifetimes of vibr. excited states 78−42108
$NO(A^2\Sigma^+, v'=0,1,2)$ lifetimes, $A^2\Sigma^+$-$X^2\Pi$ transition moment, oscill. strengths, internucl. separation depend. 78−82787
Na_2, beam, multiphoton ionisation mass selective laser spectroscopy, vibronic, gyrovibronic states, clusters 78−21985
Nd^{3+} complexes, hypersensitive transitions 79−36620
Ne^* + H, assoc. ionis., rovibronic struct. in electron energy spectrum 80−106380
Ni porphin, reson. Raman excitation profiles, simulation, vibronic coupling consts. 77−65471
α-O_2, antiferromagnetic polycrystal, splitting of exciton absorpt. lines in mag. field *(Russian)* 80−103943
O_2^+, photoelectron spectra, vibronic transition ionisation energies, ground state mol. consts. 79−89710
$(O_2)_2$, struct., energy transfer, high resolution electronic spectra 78−25550
$(O_2)_2$, struct., vibr. relax., local modes, isotope effects 78−25669
OH, collisionless form., rovibronic relax., reson. fluoresc. 78−68902
OH^+, $^3\Pi_i$ state, lifetime, delayed coincidence meas. 78−70874
OPF_3, forbidden transitions, mol. beam elec. reson. obs. using avoided crossings 78−29775
OPF_3, mol. beam elec. reson. spectrum, mol. props. 79−94011
$^{16}OPF_3$, microwave centrifugal distortion moment spectrum 78−78684
PH_2, X^2B_1-state, rot. laser mag. reson. spectrosc. 80−28038
PbS, molecule, Ne matrix environment effects on vibronic emission systems 77−58070
PuF_6, near IR spectrum, isotope shifts, vibronically induced transitions 77−6773
ReF_6, cryst., Raman and absorpt. spectra, Jahn-Teller effect 78−6675
SO, S isotope composition, vibronic spectroscopic determ. *(Russian)* 79−10124
SO_2, nonradiative transitions and intersystem crossing rates in gas phase, theory 80−23451
SO_2, SVL fluoresc. spectra, multiple vibronic origins 77−14474
SO_2, SVL fluoresc. spectra, 293 to 307 nm region 77−14475
SO_2, single vibronic level fluoresc. spectra 80−91597
SO_2, X→A electronic absorpt. band system, non Condon effects study 80−18837
SO_3F, dye laser excitation of vibr. levels of upper electronic state, mol. fluoresc. meas. 80−83402
$SO_3(SO_3^+)$, Jahn-Teller interaction, Franck-Condon factors and vibronic energy level calc. 78−50536
Sr_2, Van der Waals dimer, inert gas matrix-isolated, laser excited emission spectra 78−78744
SrO_3, visible absorpt. and reson. Raman spectra in Ar and N_2 matrices 77−65487
TeF, chemiluminesc. from oxidation in F_2+$H_2Te(D_2Te)$ emission spectrum obs. 80−43058
UF_6, matrix isolated, vibronic fine struct. in fluoresc. spectrum 80−83406
UF_6, UV spectra, electronic and vibronic states in gas and solid phases 77−14445

molecular vibronic states continued
^{238}U complex, α-induced defects, vibronic luminesc. band fine struct. 79−87489
VBr_4, mol. struct., vibronic interactions, dynamic Jahn Teller effect, gas phase electron diffr. 79−31711
$VCl_4(Br_4)$, vibronic systems, degenerate ground states, statistical sums, thermodynamic func. calcs. 80−27997
XeF ground-state dynamics in laser discharge, vibronic transitions 79−18404
XeF, in Ar and Ne matrices, reson. fluoresc., ground $X^2\Sigma^+$ state pot. well 77−14482
XeF_6 molecules with Jahn-Teller pseudo-effect, ang. depend. of inelastic scatt. of electrons 80−69246
Zn porphin, in triphenylene, single site fluoresc. and visible spectra, vibr. assignments 77−58031
ZnS:Co Mossbauer source, Fe^{2+} abnormal populations and vibronic props. 80−15912

molecular weight
see also mass spectra; molecular weight determination
acrylonitrile-styrene copolymer melts, rheological behaviour *(German)* 77−51012
adsorbed polymer chains, surface restricted self avoiding walks span, mol. weight depend. 80−65360
alkali halides, boiling, melting points rel. to mol. wt. 79−46785
aromatic polyamides, rigid and nonrigid, ultrahigh modulus fibres 79−95992
bovine serum albumin mol. wt., X-ray small angle scattering using synchrotron radiation 78−66700
butyryl cholinesterase of horse serum, quaternary struct. obs. 79−57570
caprolactam oligomers, low-mol. wt., crystallisation kinetics from melt, solid structs. *(Russian)* 79−69034
catalase, from the fungus penicillium vitale pidopl. et bilai, preliminary crystallographic investigation and props. 79−66444
cellulose fibre, gamma-irrad., and storage effects on props. *(Russian)* 80−61121
cellulose nitrate foils, personnel neutron dosimetry meas. by induced molecular wt. changes 79−59269
copolymers, triblock, lamellar domain dimensions, prediction 77−39547
trans-decahydronaphthalene-polystyrene system, press. and mol. wt. depend. of polymer solubility 79−23734
dextran fractions, production, characterisation and solution properties 80−59368
dextrane, aq. solns., H_2O diffusion, PMR investig. *(Russian)* 79−51290
diepoxide-diamine network polymers, chem. props. and average mol. wt. 80−37915
distribution function, polynomial series expansion 80−58116
DNA, mol. wt. determ. by fluctuation spectroscopy 77−10800
DNA, radiolysis of chromatin extracted from cultured mammalian cells 78−77003
ethylene-polyethylene mixtures, phase behaviour under high-press., polymer mean mol. wt. influence 79−24745
ethylene-propylene terpolymers, vulcanized, cond. of props. with mol. weight distrib. function parameters *(Polish)* 79−50175
ferritin, mol. wt., X-ray small angle scattering using synchrotron radiation 78−66700
finite polycondensing system, mean chain length distrib., probabilistic theory 79−70324
fluid, classical, elementary molecular theory 77−19859
glycerides, high mol. wt. species prod. after contact with lunar grains 78−3333
histidine decarboxylase, determ. of molecular wt. and radius of inertia 79−53025
histidine-decarboxylase, molecular weight and form determ. by low angle X-ray scatter 78−76987
isocyanate polymers, partitioning between isotropic and anisotropic phases 80−24343
keratin, mammalian, organisation of polypeptide chains 77−4981
macromolecule, branched, particle scatt. factor, light, computer simulation 79−64128
macromolecule, semirigid, dynamo-optic const. MW depend. *(Russian)* 77−20821
macromolecules, molecular structure, conformation and properties 80−63874
macromolecules, thermal rotations of mols. in soln. mol. wt. depend. 79−13847
magnesium alginate, light scatt., wt.-average mol. wt., charge density 77−61882
α methyl styrene-acrylonitrile, molecular mass determ., solubility studies *(German)* 80−23590
multi-molecular clusters, isomeric structures, weights and effective characts. 79−31759
nylon 6,6, selective degradation, mol. wt. determ., gel permeation chromatography, TEM 78−71682
nylon 6, oriented glassy, mol. wt. influence on cryst. rate 80−44156
oligobutenes, critical mol. weight for liq.-like behaviour 77−63704
paraffins, solid and liquid, diamagnetic susceptibility 78−14923
phenolic resins, average molecular weight and viscosity of acetone solns. *(Japanese)* 79−65234
PMMA, fracture morphology in notched tension, mol. wt. effects 77−52487
PMMA, laser initiated polymerisation kinetics, mol. wt. distrib. of resultant polymer 78−15673
PMMA, neutron and gamma irradiation effects 80−66839
PMMA, partial draining of low-molecular weight polymers with flexible chains 80−23592
PMMA, struct.-prop. relationship between mol. wt. and fracture surface energy 78−80633
PMMA electron resists, depend. of developed contours 79−87859
PMMA solution in isopropylbenzene, mol. mass effect on mobility and interaction parameters *(Russian)* 79−31754
poly(β-methylalanine), methacrylamide polymerisation by H transfer, catalyst sodium-napththalene *(Japanese)* 78−95726
poly(aminiumphosphate)s, mol. wts., and cond. studies 80−14264
poly(azomethines), thermotropic mesophases *(French)* 79−77507
poly(ethylene oxide), partial draining of low-molecular weight polymers with flexible chains 80−23592
poly(N-vinylcarbazole), glass transition temp., mol. wt. relation 80−19922
poly [2-(p-azidobenzoyloxy)ethyl methacrylate], MW distrib. effects on photosensitivity *(Japanese)* 78−94418

molecular weight continued
poly-1-olefin melts, steady-state and dynamic rheology 79−59956
poly-4,4-diphenylphthaleinterephthalamide, mol. mass distrib., sedimentation and fractionation method meas. *(Russian)* 80−71957
poly-N-vinyl imidazole solution, light scatt., viscosity and dynamic birefringence, mol. wt. obs. *(Russian)* 79−33665
poly-p-phenyleneterephthalamide, diffusion in conc. H_2SO_4 *(Russian)* 79−65232
polyacrylamide, aq. soln., thermodynamic props., light scatt. obs. *(Russian)* 80−71439
polyacrylamide, high mol. wt., prep. by electron beam irrad. 80−76222
polyazomethines, dil. soln. props. 80−19972
polybut-1-ene and but-1-ene-polypropylene copolymers in solution, ^{13}C spin-lattice relax. and mol. motions 79−95670
polybutadiene-polystyrene block copolymer, anionic prep., random coupling struct. 79−64134
polycarbonate, γ-irradiated, dielec. behaviour and glass transition 80−97182
polycarbonate, effect of mol. weight on craze shape and fracture toughness 80−25858
polycarbonate, impact behaviour, effects of thermal pre-treatment and mol. wt. 78−95798
polydichlorophenylsiloxane, cyclolinear, flow birefringence and orientation angles in soln. *(Russian)* 79−65835
polydimethyl siloxane solns., limiting viscosity no.-mol. wt. relations 78−18267
polydimethylsiloxane oligomers, Brillouin scatt. obs. of hypersonic sound speed and loss, mol. wt. depend. 79−91457
polydisperse polymer, anal. of mol. mass. distrib. *(Russian)* 77−31038
polydodecane amide soln., viscosity, mol. wt. *(Russian)* 79−51296
polyelectrolyte complexes, nonstoichiometric water-soluble structure *(Russian)* 80−54112
polyethylene, cryst., soln. grown, neutron scatt., mol. dimens. rel. to mol. wt. 79−41258
polyethylene, effects of mol. rot. and crosslink on specific draw ratios *(Japanese)* 79−96099
polyethylene, extended chain, prep. and study of separated single crystals 78−42924
polyethylene, high density, durability, in emulsifier soln., effect of mol. mass and polydispersity *(Russian)* 79−66191
polyethylene, high-density, solid-state coextrusion, mol. wt. distrib. effect 80−104212
polyethylene, linear, bulk-crystallised, morphology study 79−32918
polyethylene, linear, draw temp. and mol. wt. effect on draw ratio and Young's modulus 80−84998
polyethylene, linear, in theta solvents, Mark-Houwink eqn., chain dimensions 77−38764
polyethylene, low density, melt flow, mech. degradation *(Russian)* 79−50691
polyethylene, low-density, mol. characterisation 79−52843
polyethylene, meas. of high chain extensions by gel permeation chromatography 77−88611
polyethylene, mol. wt. averages determ. by temp. drop turbidimetry 79−39207
polyethylene, partial draining of low-molecular weight polymers with flexible chains 80−23592
polyethylene, photodegradation study by Fourier transform IR spectroscopy *(Japanese)* 79−24772
polyethylene, polymerisation kinetics math. model, mol. wt. evaluation *(Russian)* 79−52661
polyethylene, standard reference material, number average mol. wt. 79−13854
polyethylene, standard reference material, weight average mol. wt. 79−13855
polyethylene, ultra-high modulus, drawing behaviour, effect of drawing temp. 80−35232
polyethylene, ultradrawing, effects of temp. and drawing rate *(Japanese)* 79−91760
polyethylene, ultrahigh draw ratios, mol. wt. effects 79−74211
polyethylene oxide, aq. salt soln., meas.-based thermodynamic quantities 78−75525
polyethylene oxide, dilute aq. soln., laminar viscous tube flow, scale-depend. effect 79−7367
polyethylene oxide, mol. wt. averages and polydispersity determ. by temp. drop turbidimetry 77−63959
polyethylene solutions, conc., flow behavior in laminar steady flow field, mol. wt. numerical freq. distrib. *(German)* 79−68673
polyethylene terephthalate, radiation grafting 79−96342
polyglycidyl methacrylate, soln., mol. dynamics, by spin mark method *(Russian)* 79−60260
polyheteroarylenes, linear, conform. and struct., statistical calcs. *(Russian)* 80−69284
polyisobutylene, ^{13}C spin-relaxation parameters rel. to effect, mol. wt., temp. 77−40146
polyisobutylene, undiluted, mol. wt. influence on creep behaviour 80−45370
polyisobutylenes, dilute solns., turbulent drag reduction, influence of mol. wt. and mol. conformation 77−80189
polymer, adhesion phenomena and influence of various factors, work of adhesion *(Polish)* 80−3292
polymer, amorphous, struct. determ. by small-angle X-ray and neutron scatt. 77−84668
polymer, dil. soln., light scattering charact. of thermodynamic props., solvent and mol. wt. effect 80−16717
polymer, end-to-end distribution function, for most probable molecular weight distribution 78−13635
polymer, film and fibre, chain rupture and tensile deform., viscosity-av. mol. wt. obs. 78−76714
polymer, glass transition temperature, rel. to mol. wt. 80−34176
polymer, melt and solution, molecular weight distribution correlations 77−84207
polymer, mol. wt. depend. of glass transition 79−95144
polymer, molecular weight meas., improved graphical method 79−36806
polymer, molecular weight ratio, number-average: weight-average, polydispersity 80−74274
polymer, polydisperse, glass transition temp., mol. mass depend. 80−92656
polymer, synthetic, solns., assoc., quantitative evaluation, review 79−10773
polymer, viscosity v. molecular weight, linear plot 78−67844

molecular weight continued
polymer films, mol. wt. distrib. by gel-permeation chromatography *(German)* 78−85252
polymer in mixed solvents, viscosity data as function of mol. wt. 78−18266
polymer microstructure morphogenesis, book contrib. 78−83757
polymer property-molecular weight distribution relation, non uniqueness, blending expts. 77−36445
polymer semicrystallised chains, small-angle neutron scatt., mean dimension evaluation 80−43220
polymer solns., phase diagrams, pulse-induced critical scatt. 79−1490
polymer solution, adsorption at plane surface, computer rel. to real expts. *(Russian)* 79−56077
polymer solution, individual bead contribution to intrinsic viscosity 77−84206
polymer solution, intermolecular interpenetration and entanglement, crit. concs. 79−27900
polymer solution, intrinsic viscosity, mol. wt. and temp. dependence 80−34222
polymer solution, light scatt. for macromol. characts. in Rayleigh-Gans-Debye region 77−42452
polymer solution, molecular weight distrib. effect on drag reduction in turbulent stream 78−83437
polymer solution, sedimentation rates for low mol. wt. materials in dilute region 80−108756
polymer solutions, mod. wt. depend. of partial specific vol. 80−99594
polymer solutions, solvation, preferential, effect on polymer dimensions 79−10771
polymer solutions, viscosity data represented as function of mol. wt. 78−26716
polymer solutions light scatt. rel. to mol. wt. distrib. function type *(German)* 79−1767
polymer solutions viscosity rel. to mol. mass *(Russian)* 80−2190
polymer structure and optical behaviour 80−106583
polymeric systems, fluid, rheology, characterised by mol. int. distrib., review 80−1504
polymeric thin coating, mechanochem. degradation, substrate effects 79−79134
polymerisation, laser initiated, mol. wt. distrib. 78−15673
polymerisation chemistry, mol. wt., chain-unit struct. control, review 77−40544
polymers, adaptive control of molecular weight distribution 80−58434
polymers, flexible, solns., shear flow, dielec. anisotropy, appls. 79−15393
polymers, linear, viscoelastic props. under flow conditions, transition to highly elastic state *(Russian)* 79−50690
polymers, mol. wt. distrib., generalised exponential distrib. description 78−94346
polymers, multi-functional, mol. wt. distrib. 80−83531
polymers, polydisperse, mol. wt. distrib. correl. with props. *(Russian)* 80−69286
polymers, semi-crystn., radius of gyration variation rel. to mol. wt. 80−38936
polymers in mixed solvents, preferential adsorpt. coeff. rel. to mol. dimens. 80−103237
polymers in mixed solvents, viscosity data as function of mol. wt. 79−37866
polyolefine, liq., memory effect 80−103268
polyolefins, ultra-high modulus, production by tensile drawing and hydrostatic extrusion 80−81022
polyphenylquinoxaline, synthesised in different media, mass-mol. distrib. *(Russian)* 79−61862
polypropylene, (Moplen) influence of temp. and mol. wt. on high speed fracture mechanics 80−76341
polypropylene, ultrahigh modulus, tensile drawing, mol. wt. effect 80−104211
polypropylene solns., viscosity-mol. wt. relation 79−37867
polysaccharide gel, anomalous behaviour of PMR line width of water *(Russian)* 80−11962
polystyrene, benzene soln., self-diffusion, test for scaling and reptation 79−77789
polystyrene, in solns., intrinsic viscosity rel. to mol. wt., unperturbed dimensions 80−65268
polystyrene, isotactic, conformation in bulk crystallised state 80−43221
polystyrene, mechanical degradation, limiting degree of polymerisation 77−85985
polystyrene, melt, bulk diffusion, local diffusion *(Japanese)* 78−95170
polystyrene, mol. wt., distrib. rel. to glass transition temp., ESR spin-probe investig. 79−8041
polystyrene, oriented high-molecular, physicocomech. props. *(Russian)* 79−33028
polystyrene, partial draining of low-molecular weight polymers with flexible chains 80−23592
polystyrene, polydisperse, quasielectric light scatt. obs., mol. wt. and polydispersity 79−96376
polystyrene films, UV irrad., struct. changes, gel permeation chromatogram computer manipulation, substraction 79−96387
polystyrene in benzene or cyclohexane, zero shear-rate intrinsic viscosities 80−75376
polystyrene in cyclohexanol, polydispersities from temp.-drop turbidimetry 77−25314
polystyrene melt, molecular weight effects in die swell and in shear rheology 79−94575
polystyrene melt dynamic viscoelastic props., mol. weight distrib. 78−63407
polystyrene melts, low mol. mass, dynamic viscoelastic behaviour, alternating shear expts. 77−62226
polystyrene networks, glass networks, glass transition temp., mol. wt. depend. 77−11680
polystyrene solution in benzene, laser light scatt. meas. 79−91458
polystyrene solution in benzene, thermodyn. interaction coeff. determ. 78−3367
polystyrene solutions, light scatt., mol. parameters, computer anal. assessment 79−1766
polystyrene solutions, US degradation obs. 78−95989
polystyrene-co-divinylbenzene microgels in dimethylformamide, diffusion coeff., viscosity and mol. wt. meas. 80−30286
polystyrene-methylcyclohexane, coexistence curve, comparison obs. and free energy calc. 80−88323
polystyrene-methylcyclohexane, coexistence curves, range of simple scaling and critical exponents 80−88322

molecular weight continued
polystyrenes, blends, molten, rheology, dynamic viscoelastic props. in terminal zone 77−31268
polystyrenes, in toluene 79−1773
polystyrenes, monodisperse, static and dynamic props., mol. wt. effect 78−84938
polystyrenes, toluene soln., turbulent drag reduction, mol. wt. and struct. influence 79−7373
polysytene, neutron and gamma-irradiation effects 80−66839
polyvinyl acetate, partial draining of low-molecular weight polymers with flexible chains 80−23592
polyvinyl carbazole, and ring chlorinated derivatives, dielectric and NMR relaxation 79−73883
polyvinylbutyral, elec. and dielec. props., mol. wt. effect on charge storage 80−97192
PVC, effects of mol. wt. and plasticiser on fatigue cracking 79−5044
PVC, flow behaviour, particulate and melting flow, rheology 79−3981
PVC, in chlorinated aromatic solvents, mol. wt. characteris., ref. materials, soln. props. 79−7045
PVC in DMF, THF solns., mol. wt., aggregation, light scatt. investig. *(Polish)* 77−28587
PVC-THF-H_2O, precipitation fractionation, influence of stereoregularity 79−7046
recent advances in polymer characterization by GPC 80−16740
rhodopsin, bovine, mol. wt. determ. by monolayer method 77−81492
rigid chain polymer solns., flow birefringence rel. to mol. wt. and chain length *(Russian)* 79−33664
small protein struct. anal. by electron microscopy, valinomycin, bacitracin, LMW-CSA N and B 79−92453
sodium alginate, light scatt., wt.-average mol. wt., charge density 77−61882
styrene-acrylonitrile copolymer, of azeotropic composition, Mark-Kuhn-Houwink relations *(Russian)* 79−50176
styrene-isoprene block copolymers, mol. wt. from frictional props. 78−90329
styrene-p-chlorostyrene triblock copolymers in dil. soln., conform. behaviour, temp. depend. 79−90519
surfactant vesicles, low-ang. light scatt. and photon correlation spectroscopy 79−79484
tetrahydrofuran-propylene oxide copolymers, prep., ^{13}C NMR, end group anal. 79−66293
thermosetting resin, estimation of diff. co-eff. distrib. and mol. wt. distrib. by computer *(Japanese)* 77−66042
tripeptides, synethetic, hormone models, field desorption mass spectrometry using needleless emitters 79−34398
vinylpyrrolidone-tert-butylphenyl methacrylate copolymers, prep., soln. props. 79−18854
$CaSO_4$, thermal decomposition, torsion-effusion cell obs. 77−77741
$MgSO_4$, thermal decomposition, torsion-effusion cell obs. 77−77741
$Na_xH_2P_xO_{3x+1}$, conversion products in presence of orthophosphate effect on melt props. 77−25355
Te rich ternary chalcogenides, glass transition temp. predictions 78−38823

molecular weight determination
see also mass spectra
acrylonitrile Na methallylsulphonate copolymer electrolytes in dimethylformamide, gel permeation chromatography appl. 80−21345
agarose gel immunoelectrophoretic determination of molecular weights of tubulin antigens 80−67313
alkali metal polyphosphates, vitreous, mol. weight distrib. determ. by gel-chromatography 79−50173
arsenolite, As_2O_3, vapour mol. mass determ. using repulsion Knudsen cell 78−46464
block-copolymer, mol. wt. distrib. and comp. determ., gel permeation chromatography method *(Russian)* 79−31755
ceruloplasmin, human, mol. wt. determ. by hydrodynamic methods and low-angle X-ray scatt. 78−15761
claudetite, As_2O_3, vapour mol. mass determ. using repulsion Knudsen cell 78−46464
DNA, sedimentation constants, direct meas. by analytical ultracentrifugation *(French)* 80−8004
education, gas pressure gauge for student expt., mol. weight determ. by law of atm. 79−25795
fluctuation spectroscopy, appl. to DNA 77−10800
gel permeation chromatography, calibration, appl..to polycarbonate 80−58424
heterodisperse polymers, mol. wt. distribution and viscosity average mol. wt. 80−35530
histone lysine-rich, determ. via diffusion coeff. from laser scattering spectra 77−29095
hydrocarbon resin, mol. wt., chem. constitution investigation by gel permeation chromatography *(German)* 78−64910
laboratory system for mol. wt. determ. in microgram quantities 78−33634
macromolecular solution, light scattering measurements, computer processing *(Rumanian)* 79−82990
macromolecules, fluid density meas. technique 78−92751
macromolecules, mol. wt. meas., light transmission meas. 78−17828
mass spectrometry, current status and future trends 80−55665
mass spectroscopy, peak matching for known mass difference ion unit mass determ. 80−77906
osmometry, membrane and vapour press. methods 77−88593
plasmid molecular weight determ. from UV sensitivities 78−44458
poly(vinyl alcohol), high-speed aq. gel-permeation chromatography 79−61922
poly(vinyl pyrrolidone), high-speed aq. gel-permeation chromatography 79−61922
polyacrylamide, high-speed aq. gel-permeation chromatography 79−61922
polycarbonate, bisphenol-A, mol. wt. determ. using gel permeation chromatography 80−58424
polydimethylsiloxanes, linear, mol. wt. determ. from density and viscosity 79−81310
polyethylene, photodegradation mechanism, from yield strength, elongation and mol. wt. studies *(Japanese)* 80−76311
polyethylene, ultrahigh mol. wt., artificial joint appl., mol. wt. determ. 79−84001
polyethylene glycol, high-speed aq. gel-permeation chromatography 79−61922

molecular weight determination continued
polyethylene terephthalate, mol. wt. determ. by GPC *(Chinese)* 79−55009
polymer, absolute mol. wt. and mol. heterogeneity determ. from sedimentation vel. in ultracentrifugation *(German)* 80−14261
polymer, using recording thermistor cryoscope based on standard components 77−50572
polymer molecular weight correlation with physical and rheological props. 77−51011
polymer molecular weight distrib. low angle laser light scatt. combined with gel permeation chromatography 78−92230
polymer solution, determ. using SPEKOL spectrocolorimeter 79−79301
polymers, struct. determ. from elastoosmometric parameters 80−64923
polymers in soln. from US meas. *(German)* 77−54641
polymethyl methacrylate, mol. wt. determ. by activation anal. of Cl in end group 79−66377
polypropylene, isotropic, molten and cryst., small-angle neutron scatt., chain-folding 78−63680
polystyrene, in cyclohexane soln., mol. wt. distrib., photon correl. obs. 79−10239
polysulfonamide, optically active, synthesised by interfacial polycondensation, mol. wt. determ. 80−99595
protein molecular weight and ultrastruct. determ. in STEM 80−85562
proteins, mol. wt. determ. by monolayer surface press. meas. technique 80−89526
repulsion Knudsen cell to determ. vapour mol. masses without condensation 78−46464
size exclusion chromatography in polymer characterisation 78−11580
STEM determ. of biological macromol. mass 79−92451
transferrin, human anal. density gradient equilib. centrifugation for determ. of mol. wt., sp. vol., preferential hydration 77−64160
vapour pressure osmometry 77−46658

molecule-atom collisions *see atom-molecule collisions*

molecule-ion collisions *see ion-molecule collisions*

molecule-ion reactions *see ion-molecule reactions*

molecule-molecule reactions
see also molecular rotational-vibrational energy transfer
acetylcholine, nonenzymatic hydrolysis, Raman obs. 79−29505
alcohol/water mixtures, NMR and IR obs., low temp., shifts, interpretation 77−52065
alkali dimer+halogen mol. (IBr)(ICl) thermal chemi-ionisation reactions, products, energies 77−63903
amino acids, ^{15}N-labelled, nanomole isotopic assay by collision induced dissoc. MS 78−20095
anthracenes, exciplex form. with amines, form. kinetics and luminesc. props. 80−66792
benzene+molecular ion, fragmentation and electron transfer collisions 79−79229
benzophenone-Eu complex, triplet-triplet energy transfer, viscosity and temp. depend. 79−87847
bicyclobutyl+methylene, products decomposition, competitive channels and vibr. relax. 80−83336
bimolecular, complex and direct reaction mechanisms, unified statistical model 77−1914
bimolecular nonequilib. reaction, stability anal., Hinshelwood-Langmuir law 78−11517
bimolecular reaction, partly diffusion-controlled, physical and chem. kinetics competition 79−43567
bimolecular reactions, diffusion-controlled reaction kinetics 79−79226
bimolecular reactive system, pot. surface, incorporation of electronic nonadiabatic effects 77−40536
bimolecular thermal rate coefficients, Monte Carlo calcs. 77−16789
biomolecules+chloranil, charge transfer interaction, equilib. const., enthalpy and entropy determ., mol. polarisability 80−89708
bis(cyclopentadienyl)Ti(IV)chloride, reactions with oximes, IR spectra 78−92471
bromomethane+Rb(K), product translational energy calcs., energy depend. 79−70314
catalytic heterogeneous, bimolecular surface reactions, defect renormalised propagator stochastic theory 78−95955
cellulose fibre hydrolysability increase on gamma-irrad. *(Russian)* 80−61121
p-chloranil+tetrachlorohydroquinone, H atom abstraction by p-chloranil triplet 78−80720
chloromethyl methyl ether, on-column reaction GC determ. in ambient air 78−20093
competitive decomposition and stabilisation models for collisional efficiency in external activation systems 80−25989
cosmic dust condensation onset, role of association reactions 80−26931
coupled states approximation for scattering of two diatoms 78−62872
decarbonation reactions, CO_2 fugacity determ. at high temps. and press. 79−16439
diatom+molecule, laser-induced vibr. excitation 79−98205
1,5-dichloroanthracene, photodimerisation, orientational defects, lattice energy 78−80724
p-dichlorobenzene, collision induced photodecomposition with ethane, CO_2 and SF_6, quantum yields 79−79270
Diels-Alder reaction, benzogenic, of polycyclic aromatic hydrocarbons, PMO treatment *(German)* 79−15994
differential scatt. cross sections from classical trajectories, Legendre moment method 78−3314
2,6-diphenyl-1,4-benzoquinone+aromatic amine, triplet exciplex quenching, H-transfer mechanism 79−79228
enhancement by collision induced absorpt. of IR laser radiation 80−66798
ergodic energy transfer, vibr. quantisation effects 78−85137
esterification kinetic study by monitoring pitch changes in cholesteric liq. cryst. solvent 80−7786
ethane hydrogenolysis mechanism and kinetics on evap. Ir film 79−100436
ethylene+cis-N_2H_2, chem. reaction, intermediate geom. calcs. 78−35655
ethylene+HBr, low temp. chain hydrobromination, kinetics and mechanism 80−93735
exponential transition probilities for collision induced dissoc. and vibr.-rot. relax. 78−27749
formaldehyde+ClO radical, expt. showing no reactivity, stratospheric implications 80−90119
formaldehyde+formaldehyde, medium distance interaction, SCF LCAO MO, supermol., perturbation and MCF calc. 79−837

molecule-molecule reactions continued
formamide+formamide, medium distance interaction, SCF LCAO MO, supermol., perturbation and MCF calc. 79−837
four centre elimination reactions, HX vibr. state distribs., surprisal anal. and synthesis 80−25993
gasdynamic equations, multiatomic gases with different elastic and inelastic rates 79−81993
N-heteroarenium cations B, resonant, nonradiative energy transfer *(German)* 78−25659
hexafluoroethane+H_2(hexane), multiphoton induced chemistry 79−20382
hydrogen halide+unsaturated hydrocarbon, vibr. stimulated addition reaction 79−91928
in-cage reactions controlled by mol. reorientation 78−44362
intermolecular triplet excitation transfer in diffusive limit 80−28046
interstellar shocked mol. clouds, nonequilib. chemistry 79−21377
interstellar synthesis of cyanopolyynes and related molecules, gas-phase form. pathways 80−12793
iodomethane+Rb(K), product translational energy calcs., energy depend. 79−70314
kinetics of partly diffusion-controlled reactions, physical and chem. kinetics competition 79−43566
laser specific and thermal reactions classifications 80−11919
laser-controlled unimolecular and bimolecular processes, field-depend. rate const. 80−11906
metastable and unstable states relax., analytical theory of extrema 80−50829
methane, fluid, collision-induced light scatt. 78−68509
methane+H(HO)(O)(O_2), H abstraction, rate consts. calcs. 78−95921
methoxy+NO, reaction rate upper limit, laser induced fluoresc. 80−85200
methoxy radical+NO, reaction rate meas. 80−76534
methylene+H_2→CH_3+H, triplet methylene abstraction, partial open shell FSGO calc. 78−80719
methylene+H_2→methane, ab initio CI calc. on SCF level, insertion reaction min. energy path 80−7774
methylene*+H_2→CH_3+H, barrier height, CI with double zeta polarisation basis 78−64812
micellar diffusion-controlled reaction kinetics 80−30213
microphysics to macrochemistry, discrete simulations, review 80−54102
muonium, bimol. rate consts., Larmor precession relax., kinetic isotope effect rel. to H 77−38752
phthalamide derivative with aromatic amine, exciplex formation and fluoresc. quenching 79−87848
polyatomic excited molecules, vibrational energy exchange *(Russian)* 80−91539
polyatomic systems, statistical phase space theory, energy and ang. momentum conservation 77−48630
POPOP+Ar+N_2, electron beam excited, energy transfer mechanisms 80−23497
potential energy surfaces, qualitative, from linear comb. of fragment configs. 78−44349
R-matrix propag., amplitude density function and invariant bedding methods 80−91622
reversible bimolecular diffusion-controlled reactions, detailed equilib. principle 80−7770
rotation-vibration symmetry correlation, building-up principle from mol. fragments 78−76849
second-order reactions, in turbulent fluid, model, appl. to atm. plumes 79−20350
second-order reactions, in turbulent fluid, model, formulation and validation 79−20349
semiclassical theory for near adiabatic photon assisted mol. collisions 79−5141
small bimolecular systems, reversible reactions, numerical anal. of statistical functions 78−64831
state change collisions, attractive intermolecular forces, temp. depend. 80−23515
stimulation of chemical reactions by cooling translational-rotational degrees of freedom 78−7202
s-tetracyanobenzene+p-xylene, photoassoc., exciplex form., excitation energy and isotope depend., vibr. effects 80−55634
thionine triplet+haloanilines, electron transfer reaction, radical yield meas. 80−3330
toluene+OH, rate constant under simulated atmospheric conditions 80−50846
translationally driven reactions, transition state theory, cross section curve 80−26000
triethylamine, gas (soln.), fluoresc. quenching by 'inert' perfluoromethylcyclohexane 78−46438
trifluoroacetophenone+dimethoxy benzene. in acetonitrile photoreaction, nuclear spin polarisation, criterion for triplet-Overhauser mechanism 80−69168
trimolecular interaction, multiple site reactivity, perturbation theory 79−52639
two component bimolecular reaction system, stable limit cycles, choice of chem. pot. differences 80−66779
vinyl chloride+O_3 reaction, IR matrix and microwave spectroscopy 77−90587
$2NO_2+Br_2$→$2NO_2Br$, formation and IR spectrum 79−98097
$2NO_2+I_2$→$2NO_2I$, formation and IR spectrum 79−98097
$2NO_2$⇌$2NO+O_2$, gas mixture turbulent concurrent double pipe heat exchanger equilib. and nonequilib. reaction 78−94856
AlCl+HCl, matrix reaction, $HAlCl_2$ IR spectrum *(German)* 79−11786
Al_2O_3+tetrafluoroethylene, AlF radical, form. in arc plasma, spectra 77−28989
ArF*, in Ar-F_2 proton-excited mixtures, production and quenching 78−94307
Ar_2F*, in Ar-F_2 proton-excited mixtures, production and quenching 78−94307
ArH^++H_2→Ar+H_3^+, crossed beam reaction, energy distrib. 77−52626
BCl_3+methane reaction, laser-induced, vibr. excitation influence on reactivity, isotope selectivity 80−11921
BH_3NH_3, complexation energies and interatomic distances, SCF and CEPA calcs. 78−25446
BaF_2+BCl_3, crossed beam metathesis, total cross sections 77−21354
BaI_2+Cl_2(HCl)(1,1-dichloroethane)(chloroethene), crossed beam metathesis, total cross sections 77−21354
Br_2+acetylene, laser-induced photochemistry 80−45498
C_2+NO→CN+CO, chemiluminesc. reaction, crossed beam study 79−66299
C_2+O_2, $C_2(X^1\Sigma_g^+)$ and $C_2(a^3\Pi_u)$ intersystem crossing and free radical kinetics 80−95668
C_3+O_2→C_2*+CO+O, chemiluminesc., rate consts. 77−44466
CCl_2FO_2+NO(NO_2), reaction, photolysis obs. 79−74931
CCl_3O_2+NO+NO_3, photolysis, $CCl_3O_2NO_2$ thermal decomposition in stratosphere 79−57256
$CCl(\tilde{X}^2\Pi)$+methylhalosilanes, reaction rate const. determ. by kinetic absorpt. spectroscopy 80−97683
CN(ν)+O_2 react., prod. energy distribs. meas., CO vibr. level population *(German)* 78−76833
CO+I_2(ICl)(NO_2), E-V energy transfer reactions, electronically excited target mol. 78−64814
CO+N_2O, CO_2 vibr. temps. under gasdynamic laser conditions 80−21276
CO^++NO→CO_2^++N, crossed beam study 80−104436
C_2O+NO(O_2)(isobutene), absolute reaction rate consts. meas. by laser induced fluoresc. 80−93738
CO(1)+CO(ν)→CO(0)+CO(ν+1), vibr. energy accumulation, reaction rate anal. 80−78692
CS_2-O_2 flame, rate of population of CO vibr. levels, CO emission intensity 78−7186
CS_2*+CS_2→CS_3^++CS+e^-, chemiionisation, mol. beam photoionisation 80−76495
$C_2(a^3\Pi_u)$+NO(vinyl cyanide)(ethylene), laser-generated radical kinetics 79−100352
Cl_2+H_2(H_2S)(methanethiol), laser-initiated chain reactions, rates, mechanisms, chemiluminesc. obs. 80−55651
ClF+SF_4 (perfluoroethane)(Xe), thermal and photochem. reactions investig. 80−61117
ClNO+Cl_2O→ClONO+Cl, reaction kinetics, IR spectra 78−35641
ClO+NO_2+M, reaction rate constants 79−100350
ClO+NO_2→$ClONO_2$, fall-off curves, N inclusion effects 77−63910
ClO+NO_2→$ClONO_2$, reaction kinetics 77−86303
ClO+O(NO)→Cl+O_2(NO_2) rate consts. meas. 77−60059
Cl_2O+H_2O→2HOCl, equilib. const., UV spectrum investig. 79−79238
$ClONO_2$, form., reaction with OH, kinetics 77−86303
$ClONO_2$+NO(ClNO) react., gas phase, kinetics, mechanism, IR photometric investig. *(German)* 78−76834
CrO_2Cl_2+carbon tetrachloride+acetone, intermediate complex form., electronic spectra 80−61075
CsCl+SF_6, collision induced dissoc., threshold behaviour 78−88627
Cs_2Cl_2+SF_6, collision induced dissoc., threshold behaviour 78−88627
Cu clusters, interaction with CO, Cu_nCO form., chemisorpt. bond 78−31631
Eu-W-O, reaction system, thermodynamics, mass spectrometric obs. 77−77748
Fe(CO)$_5$+O_3, modulated chemilumiesc. by CO addition 80−40692
GeAs+Cl_2(Br_2)(I_2), high temp. Raman spectra, cryst. growth mechanism *(French)* 79−26999
GeH_4+Cl_2, HGeCl* chemilum. obs., vibr. levels 77−81406
H_2+CO_2, exponential gap relation, rot. inelasticity 80−78693
H_2+D_2, reactive and inelastic scatt. using repulsive model pot. energy surface 78−66620
H_2+D_2, reactive and inelastic scatt., semiempirical pot. energy surfaces calcs. 80−74140
H_2+D_2→2HD, transition state, study of Jahn-Teller instability of H_4 78−60995
H_2+F, collinear trajectories, statistical behaviour and detailed dynamics 80−16664
H_2+F_2, branched chain reaction, role of thermally nonequilibrium atoms and molecules 80−76507
H_2+F_2 chain reaction, rotational nonequilibrium mech. vibr.-rotational energy exchange effect 80−48230
H_2+H_2, exponential gap relation, rot. inelasticity 80−78693
H_2+N_2, nitrogen fixation, semiempirical INDO study 80−16898
H_2+N_2O, HO radical form. on Pt surface, laser-induced fluoresc. obs. 80−108738
H_2^++CO excited products dissoc., proton transfer dynamics, correl. diagram anal., corssed beam obs. 80−48079
H_x+H_2, hexadecapolar U-branch transitions in IR fundamental band 80−91631
HBr+CO(CO_2)(N_2O)(NO)(N_2O)(O_2), rate consts. for vibr. energy transfer meas. using laser. induced fluorescence technique 80−87206
HCN+acetylene, cyanodiacetylene form. in RF discharge 79−5156
HD(v=5)+HD(v=0)→H_2+D_2, mol. H_2 exchange, reaction mechanism 80−85167
HF+formyl fluoride, multiple site reactivity, ab initio GO supermol. calc. 78−11498
HF+HF, medium distance interaction, SCF LCAO MO, supermol., perturbation and MCF calc. 79−837
HI+O_3, HOI formation, matrix reaction, IR spectra, isotope shifts and band assignments 78−80737
HN_3+$NH(NH_2)$, rate consts. from HN_3 UV photolysis data 80−101027
HNO_2+O_3, rate consts. determ. with diode laser 79−70310
HNO_2+O_3 reaction kinetics under stratospheric conditions 78−11499
HNO_3+NO, rate consts. determ. with diode laser 79−70310
HO_2+ClO, reaction product distrib. 80−72586
HO_2+NO, reaction kinetics meas. 78−31624
HO_2+NO laser-induced fluoresc. of NO_2, quenching rate consts. and lifetimes 80−11930
HO_2+NO reaction rate constant effects on O_3 perturbations, model of stratosphere 78−73474
HO_2+NO_2 form. and react. in aq. soln., pulse radiolysis 79−24805
HO_2+O_3, reaction kinetics, laser mag. reson. obs. 80−102528
HO_2+O_3→OH+$2O_2$, rate coeff., effects on stratospheric O_3 78−96275
H_2O+Cl_2O=HOCl, equilib. const., Fourier transform IR determ. 80−7765
H_2O+H_2O, medium distance interaction, SCF LCAO MO, supermol., perturbation and MCF calc. 79−837
H_2O_2+catalase ($[Fe^{3+}(EDTA)]_2$), effect of mag. field on decomposition rate 79−52631
HO_2NO_2+N_2⇌HO_2+NO_2+N_2 react., kinetics, RRKM theory appl. 78−73032
H_2S+NO_2, SO chemiluminesc. in Ar matrix 79−5146
H_2SO_4+atmospheric species, collisional reaction probabilities rel. to H_2SO_4 aerosols as tropospheric sinks 80−72612
Hbr+Cl_2(BrCl), four-centre reaction, quasiclassical trajectory study 79−57213
He^*_2 diatom, optical absorpt. spectra and kinetic behaviour 80−95635

molecule-molecule reactions continued
$He_2(2^3\Sigma_u^+)+He_2(Ne)$, reaction rate consts. meas. in afterglow 78−7173
$HgBr_2+N_2$ metastables, dissociative excitation, HgBr emission intensity 80−40687
$HgBr_2+N_2(A^3\Sigma_u^+)$, dissoc. excitation 80−63774
$HgH+NO\rightarrow HNO+Hg$, reaction rate temp. depend., chemiluminescence 78−68885
I_2+acetylene, laser-induced 1,2-diiodoethylene form., isomerisation 80−85157
$K_2+Br_2(Cl_2)$, collisional ionisation reactions 77−50508
K_2+halogen mol., thermal energy mol. beam chemi-ionisation 77−9065
$KrF+He(Ne)(Xe)(NF_3)$, quenching rate consts. meas. 79−24718
$MgI_2+Cl_2(HCl)$, crossed beam metathesis, total cross sections 77−21354
N_2+HgX_2 (X=halide), $A^3\Sigma_u^+$-state quenching obs. 80−108693
N_2+methane, N_2 fixation, catalytic processes in non-equilibrium plasma chemical reactors *(French)* 80−89483
N_2+methylmercury halides, $A^3\Sigma_u^+$-state quenching obs. 80−108693
N_2+O_2, N_2 fixation, catalytic processes in non-equilibrium plasma chemical reactors *(French)* 80−89484
N_2+O_2 collinear collision, quantum-mech. model 77−30955
$N_2^+ + H_2$, collisional dissoc. cross-section, 2.4-24.3 keV 80−58373
$N_2^+ + O_2$, collisional dissoc. cross-section, 2.4-24.3 keV 80−58373
$^{14}N_2+CO$, vibr.-vibr. energy transfer, long and short range pot. effect 80−99556
$^{15}N_2+CO$, vibr.-vibr. energy transfer, long and short range pot. effect 80−99556
NH_2+O_3, reaction rate const., rel. to atmospheric processes 80−85155
NH_3, inversion spectrum collisional line broadening, general theory 80−87184
NH_3+Br_2, gas phase reaction, $NHBr_2$ identified by ESCA 79−31599
NH_3+SO_3, donor-acceptor adduct form., ab initio calcs. 78−82612
N_2H_2+ethylene reaction, H transfer, ab initio SCF GO calcs. 77−44469
NH*+HCl(methane)(ethylene)(cyclopropane) (cyclohexane), rate const., time resolved chemiluminesc. 78−60982
$NH^*+HN_3\rightarrow NH_2^*+N_3^*$, rate const., time resolved chemiluminesc. 78−60982
$^{14}N^{15}N+CO$, vibr.-vibr. energy transfer, long and short range pot. effect 80−99556
NO synthesis, reactions of fibr. excited N_2 in nonequilib. plasmachem. system 77−86310
$NO+BrO$, temp. depend. kinetic study, stratospheric Br photochemistry implication 80−50866
$NO+C_2H_4$, HNO excitation by $O_2(^1\Delta_g)$ 79−52674
$NO+CO(N_2)$, electronic energy transfer, spectroscopic obs. 78−82716
$NO+O_3$, (001), laser enhanced reaction, temp. depend., reactive and non-reactive channels 78−48642
$NO+O_3$, fs-states and rot. states, effect on reactivity 80−89473
$NO+O_3^*$, laser excitation effects, fluoresc. meas. 77−21372
$NO+O_3(001)$, laser-enhanced reaction, rates, temp. depend. 78−48675
$NO+O_3(001)\rightarrow NO_2(^2B_{1,2})+O_2$, laser enhanced reaction, temp. depend. 77−81397
$NO+O_3\rightarrow NO_2^*$, mol. beam chemiluminesc., kinetic and internal energy depend. 78−31638
$NO+O_3\rightarrow NO_2^*+O_2\rightarrow NO_2+h\nu+O_2$, chemiluminesc., translational and rot. energy effects 80−30218
NO_2+HO_2, reaction rate consts. by laser mag. reson. 78−27748
$NO_2+O^-(O_2^-)$, charge exchange excited NO_2^- formation 77−75236
$NO_2+OH+M\rightarrow HNO_3+M$, rate constant under simulated atmospheric conditions 80−50846
NO_x interaction with airborne particles 78−81342
N_2O+CO, Na catalysed, Na chemiluminesc., excitation mechanism, appl. chem. laser 77−63916
N_2O+CO, nonequilibrium reaction in shock waves *(Russian)* 78−76845
N_2O+CO, use of steady state chemical reaction for vibr. excitation of CO_2 and N_2 80−50851
$NO_2^*+CO\rightarrow NO+CO_2$, laser stimulated reaction, rate const. 78−40044
$Na_2+Br_2(Cl_2)$, collisional ionisation reactions 77−50508
$Ni(CO)_4+O_3$, modulated chemiluminesc. by CO addition 80−40692
NiF_2+CO, Ar matrix isolated, ab initio MO calcs. 78−92458
O_2, singlet state, form., quenching and reactions, review 77−29002
O_2+O_3, laser-induced photolysis of ozone reactions 80−11928
$(O_2)_2$ formation, rot.-vibr. symmetry correlation, building-up principle from mol. fragments 78−76849
O_3 interaction with airborne particles 78−81342
O_3+ethylene, dioxirane form., decomp. products, mass spectrometric obs. 78−11504
O_3+ethylene, dioxirane form., identification by microwave spectra 78−15659
$O_3+H_2S(OCS)$, SO chemiluminesc. in Ar matrix 79−5146
O_3+NO, IR laser enhanced reaction rate, vibr. excitation 77−1911
O_3+NO, laser enhanced reaction, fluoresc. obs. 79−66285
$O_3+NO(\nu=1)$, IR laser enhanced reactions 79−66286
$O_3+NO\rightarrow NO_2^*+O_2$, kinetic energy and internal state depend. 79−66287
$O_3+O_2(^1\Delta_g)(O_2^*)$, UV photolysis, $O(^3P)$ prod., rate consts. determ. 80−55636
$O_3+OH\rightarrow HO_2+O_2$, reaction rate const., 238-357K 79−47902
O_3+thiirane, autocatalytic reaction, stopped-flow study, reaction rate meas. 80−85152
$O_2(^1\Delta_g)$, 650-1650K reactions in combined discharge flow/shock tube study 79−89618
$O_2(^1\Delta_g)$+HNO, excitation in NO+C_2H_4 system 79−52674
$O_2(^1\Delta_g)+O_2$, deactivation rate const. meas. 78−5262
$OH+Br_2$, hydroxyl radicals reactive scatt. 80−85172
OH+CO(trichloroethane), reaction rate consts. and quenching kinetics, reson. fluoresc. obs. 79−72349
OH+dimethyl sulphide, flash photolysis reson. fluoresc. rate consts. determ., pollution aspects 78−95913
$OH+H_2$, pot. energy surface, barrier heights and transition state geometry, POL-CI calc. 80−55649
$OH+H_2\rightarrow H_2O+H$, rate constant, ab initio calc. 80−45478
$OH+H_2\rightarrow H_2O+H$, reaction product vibr. distribs, quasiclassical trajectory, calcs. 80−85162
OH+halomethane(haloethane), reaction rate consts., reson. fluoresc. meas. in discharge-flow system 79−72350
$OH+NO_2+M\rightarrow HNO_3+M$, reaction kinetics, temp. and press. depend. 79−66284
$OH+OCS(CS_2)$, flash photolysis reson. fluoresc. rate consts. determ., global S cycle 78−95914
$OH+OCS(CS_2)$, lower atmosphere chem. 80−61870
$OH(\nu=0,1)+H_2(\nu=1)$, rate consts., 298K 79−11768
$O_2(^1\Sigma_g)$, 650-1650K reaction in combined discharge flow/shock tube study 79−89618
$O_2(^1\Sigma_g^+)+H_2$, collisional relax. temp. depend. 77−32783
$O_2(b^1\Sigma_g^+)$ quenching by $O(^3P)$ and O_3, rate coeffs. 79−70309
$POCl_3$+N,N-dimethylformamide or N,N-dimethylbenzamide, reaction products 78−7199
RPO_4+3PBr_3, exam. of diffusion coefficients of gas mixture resulting, using chemical transport theory 79−1945
S compounds homogeneous oxidation in atmosphere 78−96258
SF_6+NO+O_3, laser sensitised reaction, time-resolved NO_2^* emission obs. 78−20017
SO_2, homogeneous oxidation mechanism in troposphere 78−96257
SO_2 oxidation in clouds and rain, O_2, O_3 and H_2O_2 role 79−84351
SO_2 oxidation rate, CO effect, smog chamber expt. 79−74925
SO_2+NH_3, atmospheric aerosols direct form. 77−29377
$SO_2+O_2(O_3)$, in aq. soln., kinetics, rel. to atm. rate processes 79−20905
$SO_2+O_2=SO+O_2$, gas phase reaction, rate coeffs. meas. 80−97704
$SO_3+H_2O\rightarrow H_2SO_4$, gas phase kinetics, CNDO/2 calc. of H_2SO_4 and $SO_3.H_2O$ struct. 78−76840
$SO(^1\Delta_g, ^1\Sigma_g^+)+O_2(^1\Delta_g)$, chemiluminescence and energy pooling 80−26016
SbF_5+benzyl chloride, chemi-ionis. reaction, temp. depend., flow tube investig. 80−108701
Se_2^*+OCSe, radiation quenching rates 79−86050
$SiAs+Cl_2(Br_2)(I_2)$, high temp. Raman spectra, cryst. growth mechanism *(French)* 79−26999
$SiBr_4+H_2$, SiH_nBr_{4-n} heat of form., mass spectrometric determ. 79−20455
SiF_4+H_2, SiF_xH_{4-x} heats of form., mass spectrometric determ. 78−7221
$SiH_4(SiD_4)+F_2$, chemilum., at. absorption, and laser-induced fluoresc. obs. 80−3315
$SiO+F_2$, matrix reaction, $OSiF_2$ prod., IR spectra and force consts. calcs. *(German)* 80−97718
$SrBr_2(SrI_2)+Cl_2$, crossed beam metathesis, total cross sections 77−21354
$UF_5\rightarrow UF_5AU_2F_{10}$, dimerisation equilib. of gas phase, 600-870K 79−87838
UF_6+SiH_4, photoinduced reaction in low temp. SiH_4 matrix 80−30256
XeF^*+XeF_2, lifetime and collisional quenching meas., XeF_2 photolysis 78−33545

molecule-surface impact
see also sputtering
alkali halide adsorbate motions and reactions at surface defects, mol. beams 77−59205
coherence length and transfer width in mol. beam scatt. 79−83090
coherence length and transfer width in mol. beam scatt. 79−83091
cooled surface, CO_2 mol. beam interaction, AC excitation effects *(Russian)* 77−62744
cyclobutene, strong collision and thermal decomp. on surface, variable encounter method calcs. 80−50885
damping of excited molecules located above surface of metal 78−92160
diatom-surface scatt., rot. inelastic, impulsive collision limit calc. 80−104030
diatomic beam, scatt. on solid surface, rot. energy distrib., hard cube model 77−34717
diatomic molecule+solid surface, energy transfer, internal vibr. energy effects 78−35234
diffraction of molecular beams, developments *(Japanese)* 80−60746
diffraction scattering of rigid rotor, quasi classical trajectory method 77−36332
dissociation of molecular-ion beam in thin foils 77−86315
formic acid, decomposition, using Ni (110) catalyst, reaction kinetics and mechanism, mol. beam relax. spectroscopy 77−70340
gas-metal interactions, scatt. dynamics 80−92787
gas-solid energy transfer, internal vibr. energy effects 78−35234
gas-solid interactions, rel. to reduction of aerodynamic friction and aerothermal heating 79−95896
gas-surface interactions, mol. beam apparatus 78−72675
graphite, reaction with H_2, mol. beam-surface expt., quasi-equilib. treatment 77−86376
graphite (0001), scattering and selective adsorption of H_2 (D_2) 80−71553
ion formation, apparatus for solid and surface anal. using high energy molecular beams 77−21443
ionisation, kinetic energy of ions 77−10751
metal surface, thermal negative ion production through polyatomic mol. dissociation, thermochemical study *(Japanese)* 80−50495
metals, atomic and mol. beam scatt., review 80−40203
modulated mol. beam mass spectrometry, reaction prod. vector, surface reaction 77−63952
oscillating surface, thermal accommodation coeffs., translational and internal energy 77−86354
rarefied gas of fast particles interacting with cryst., kinetic eqn. *(Russian)* 77−55440
reactive scattering, surface reaction kinetics and mechanisms 77−24469
recycling molecular beam reactor for study of reactive molecule-surface collisions 78−1109
reflection and sticking coeffs., short range forces, low energy limit 80−40208
scattering, appls., review 78−39653
scattering from cryst. surfaces in quantum regime, review 78−35244
scattering from surface with regular one-dimens. roughness elements 78−92166
scattering of atoms and mols. by solid surfaces, review 78−31291
simulation by classical stochastic propagator model 77−32482
solid, surface, modulated mol. beam scatt., pulse testing method 79−89032
Space Shuttle, expts. on mol. and atomic beam interactions with surfaces 78−35243
structure determination expts. 79−47971
vacuum deposition, evaporation source mol. distrib. and refl. at surface *(French)* 77−69999
vacuum system, molecular flow rate 78−76570

molecule-surface impact continued
vacuum system, rate of molecular impact on surface or orifice, possible conflict with second law of thermodynamics 80−46954
vibrational relaxation of mols. in gas-aerosol system, rel. to two-phase gasdynamic lasers 79−45807
Ag (111) plane, specular refl. of beams, Debye-Waller factor and surface Debye temp. 79−47580
Ag surface, scatt. of H_2, Debye-Waller factors, expt. 80−60736
AgI, water vapour mol. beam refl., nucleation and condensation 77−52212
Cu (100), diatomic mol. scatt., energy transfer and dissociative adsorption 79−46961
Ge (111), epitaxial growth of Cd, simultaneous RHEED-mol. beam obs. 77−7986
$H_2(D_2)$+Ag(111), energy transfer, quantum mech. theory 77−8699
H_2SO_4 bulk surfaces, reactions with atmospheric species rel. to aerosols role as tropospheric sinks 80−72612
LiF, diffr. scatt. of H_2 and D_2, quasiclassical trajectory method 77−36332
LiF, H_2 scatt. from surface, qudrupole interaction and rot. transitions 79−74041
NaCl, mol. beam, on hot W(Re), surface, Na_2Cl^+ ion form. 79−56907
Ni, surface, polycryst., mol. beam scatt. 79−95895
NiO, catalytic decomp. of methanol, mol. beam relax. spectrometry using surface temp. modulation 79−29401
Pd (111), scattering, adsorption, and absorpt. of H_2 and D_2, mol. beam study 80−29277
Pd(111) surface, chemisorption of He(CO)(O_2), mol. beam scatt. expts. 78−79878
Pt, H_2+D_2 mol. beam exchange recation on stepped Pt surface, incidence angle depend. 78−31686
Pt, scattering of Ar and N_2 mol. beams 77−16449
Si surface, N_2^+ bombardment, 500 eV chem. reactions, XPS and UPS 78−48265
SiO surface, N_2^+ bombardment, 500 eV chem. reactions, XPS and UPS 78−48265
SiO_2 surface, N_2^+ bombardment, 500 eV chem. reactions, XPS and UPS 78−48265
SiO_2-Si, low-energy neutral particle bombardment of SiO_2 film, degradation 80−54790
U, mol. beam bombardment, aggregate form. *(French)* 79−74047
W, catalytic decomp. of NH_3 single pulses, mol. beam relax. spectrometry 80−21321
W, clean and H_2-covered, Cl_2 scatt. 80−20743
W, direct inelastic and trapping-desorpt. scatt. of N_2, elementary steps in N_2 chemisorpt. 80−60737

molecules
see also excimers; hydrogen neutral molecules; macromolecules; mesic molecules; muonic molecules; quasimolecules
excitation processes by fluctuating light 80−9646
positrons and positronium atoms bound to mols., approx. MO theory 77−23583

Mollier diagrams *see thermodynamic properties*

molten metals *see liquid metals*

molten polymers *see polymer melts*

molybdenum
see also nuclei with .....
(110) surface, molecular adsorbed CO, electronic states, photoemission spectra 80−65363
δ_R criterion for brittle fracture in single crystals. *(Russian)* 78−56732
absorption of N_2 in induction and plasma-arc heating *(Russian)* 77−16732
adsorbed layer of Ba on (011) face, surface diffusion *(Russian)* 80−6658
adsorption and dissoc. of CO on (100) surface, comparison with carburised surface 77−15689
adsorption of CO_2 and trimethylamine on (100), adsorbed O effect, LEED and AES obs. 80−39443
adsorption of CO, O_2, metastable He de-excitation spectroscopy and UPS study 80−34314
adsorption of CO on (110) face, adsorption/desorpt. expt. obs. *(French)* 77−85075
adsorption of CO on (110) face, Auger yield attenuation interpret. *(French)* 77−85077
adsorption of CO on (110) face, model *(French)* 77−85076
adsorption of Cs and O_2, work function and thermal stability 80−44427
adsorption of Hg, work function change 77−7966
adsorption of K, work function depend. on surface coverage 77−11788
adsorption of Li, Na, Cs, Sr and La on (011) face, disordering of submonolayer film, LEED obs. *(Russian)* 77−89655
adsorption of N_2, surface coverage 78−60036
adsorption of NH_3, and catalytic decomposition, field emission study 78−14596
adsorption of NH_3 on (111) planes, preferential nitriding, FEM study 80−66877
adsorption of O_2, low energy SIMS and electron induced desorpt. exam. 77−76667
adsorption of O_2 and Cs, struct., emission props., thermal stability 80−66878
adsorption of O_2 on (100) surface, AES, LEED, work function, and desorption meas. 80−6654
adsorption of Sr, interaction of adatoms 79−7754
adsorption of Sr and La on (011) face, influence of substrate electronic struct. on props. 78−60032
adsorption of Sr on (112) face 80−2271
adsorption on (211) planes, direct obs. of atomic processes by field ion microscopy 77−59219
adsorption on W (100), effect on surface reson. 79−65983
adsorption sites of CO on Mo (100), electron stimulated desorption and LEED meas. 80−49516
AES and characteristic energy loss spectra, expt. and interpretation 78−27354
AES expts., chem. shift and beam effects for Mo and MoO_x 79−15566
air contamination effect on compatibility with liquid Li in stainless steel vessels at 600°C 78−25285
alpha-particle irradiation in He, micropore and dislocation loop form. 79−14859
amorphous, reflection of D and T, Monte Carlo study 80−40197
annealing in stage I, dose depend. and radiation doping defects 78−47422

molybdenum continued
anodic behaviour in methanolic solns. 77−73368
anodisation, oxide struct., electronic current, and const. current efficiency 78−15575
anodised layer, structure and stoichiometry, thickness effects 77−77634
arc, vac., stabilised, plasma props. 78−51384
atom, Ar matrix isolation spectroscopy using sputtering apparatus 77−26407
atom, highly ionised, mean wavelength and spectral width of transition arrays 79−6913
atom, integral Compton scatt. cross sections, of γ-rays from K-shell electrons 78−58643
atom, integral K-shell Compton scattering, cross-section, for 1250 keV photons 78−90128
atom, isotope shift meas. 78−42010
atom, $K\beta_3/K\beta_1$ and $K\beta_2/K\beta_1$ relative intensities 77−75088
atom, K-shell photoelectric cross section 79−22676
atom, K-shell X-ray spectra, $K\beta_2/K\beta_1$ determ. 77−23456
atom, Lα X-ray spectra, $_{40}Zr$ to $_{48}Cd$, linewidths 79−41131
atom, Rayleigh scattering at 59.34 keV through 60° to 150° 77−83547
atom, relative oscill. strengths in dissoc. $MoCl_5$ pulsed discharge 78−25479
atom, reson. Raman X-ray scatt., K-vacancy excited state widths 79−45661
atom, X-ray spectra, Kα hypersatellites 80−63576
atomic displacements and electronic struct. of (001) surface 78−30963
atomic X-ray spectra, parity violation, from electron-nucleus weak currents *(Russian)* 79−22642
atomisation, for graphite furnace AAS, using graphite platform 78−32877
atoms, $N_2N_3N_{45}$ super Coster Kronig processes 80−106303
backscattering of H_1^+, H_2^+, H_3^+, 4-30 keV, O_2 effect 78−15268
band structure, X-ray emission bands, self-consistent calc. 77−28104
band structure and X-ray emission spectra calcs. 77−28105
barrier metal for sintered Pt-GaAs contacts 77−8193
BCC, neutron-irradiated, Frenkel defect spontaneous recomb. volumes 79−60355
BCC, structural singularities rel. to solid soln. behaviour *(Russian)* 77−11696
BCC, void nucleation following electron irrad. 80−29054
BCC lattice, texture form. by drawing and pulling through nonpowered rolls *(Russian)* 77−25100
beam-foil EUV spectra 5 to 55 nm using 22 to 200 MeV beams 79−46481
binding energy, lattice parameters bulk modulus, self-consistent pseudopot. calc. 79−60748
blister erosion reductin by multi-groove surface microstruct. 78−95211
blistering and surface roughening, room temp. ageing effects, Ar^+ ion bombardment 78−34550
Bloch waves, corresponding atomic and mol. orbitals, in HEED 79−27880
block boundary dislocation struct. singularities under high temp. steady state creep conditions *(Russian)* 79−90670
bombardment by 1 to 30 keV ions, emitted radiation spectral comp. *(Russian)* 77−81159
boriding, Cu influence 80−21165
borosilicate cladding compatibility *(Russian)* 77−66741
brazing to type 1Kh18N10T stainless steel 79−43551
bremsstrahlung spectra, 10 to 30 keV, thick target expts. 77−8687
candidate current collector for Li-FeS_x battery, anodic corrosion rate in LiCl-KCl eutectic 79−100513
candidate refractory for Tokamak, thermal fatigue failure testing 80−32454
carbonyl coating, deposition and props. 77−28725
cast, distribution of C *(German, English)* 79−20059
catalyst, unsupported, for isomerisation of n-hexane 77−86361
cathode, H_2 glow discharge, FCC surface layer form., electron diffr. obs. 77−55311
cathode, H penetration of Mo cathode in glow discharge, point defect depend. 79−41903
cathode, ns voltage pulse breakdown of emitting sites, field emission microscopy obs. *(German)* 77−63547
cathode, production of D ion beam impurities 79−86592
cathode erosion components, vac. arc, fusion temp. and charge transfer depend. 77−4010
cathode surface contamination effect on erosion by nanosecond vacuum discharge 78−75463
cathodes arced in vacuum, erosion structs. 80−1872
cellular structure, initial stages of formation in rolled single crystals 79−23611
CESR, prediction of obs. 80−29369
chemical binding to dinitrogen and dinitrogen hydrides 77−86368
chemisorbed CO on (100), surface kinetics, photoemission study method 80−80941
chemisorption of C, N, and O, SXAPS obs. 79−52048
chemisorption of CO, low energy SIMS and electron impact desorption expts. 78−38941
chemisorption of H_2S and growth of MoS_2 film 77−1329
chemisorption of H on surface (100), phase changes, LEED obs. 79−77911
chemisorption of O on (100) surface, Cs submonolayers effect on electron stimulated desorption of O^- 79−86991
chromizing, formation of ordered solid soln. *(Russian)* 78−11402
coadsorption of CO_2 and O_2, AES and SIMS obs. 79−46928
coated diamond powders, X-ray diffr. study 80−100936
coated system, Nb on Mo, Ti, evaporation, carburisation and diffusion behaviour 77−44410
coating, soldered to diamond surface, contact strength, device 78−60910
coating by CVD of BP, comp. and microhardness of coating 79−28942
coating on EN8 C steel, fretting wear and fatigue strength assessment 78−88583
cohesive properties, augmented-spherical-wave calcs. 79−94952
cold worked, dislocation struct. change during postdeform. at 493K 79−43271
combustion under CW CO_2 laser radiation action 80−30241
compact, on H_2 permeated backing, precipitation *(Russian)* 78−27520
composite, sapphire fibre reinforced, strength at rupture 80−104286
condensation of Cu and Ag on (100), early stage comparison with W(100) 80−80072
condensed layers, restricted growth texture formation singularities *(Russian)* 77−7982

molybdenum continued
contact junction formation by ion evaporation 77−90285
container for leucosapphire synthesis, recrystallisation 78−2151
core level binding energies 80−71564
corrosion behaviour in high temp. impure He gas 80−76402
corrosion by O_2 containing H_2O and gaseous NaCl, volatile products 78−27674
corrosion in high purity liquid Na containing ≈1 ppm O, at 700°C for 500 h 79−8383
corrosion susceptibilities in synthetic geothermal brines 77−86223
creep, high temp., influence of thermomechanical treatment *(Russian)* 79−79034
creep deformed single crysts., subboundary struct. obs., dislocation sets 80−103348
creep of single crystal 78−15478
crystal growth, effect of C and Ir impurities on fine struct. *(German)* 77−28714
crystallographic feature of brittle fracture, AE study on single crystal 79−43415
CVD, thin film fabrication for photothermal solar convertors 80−11573
CVD coating on W-Re wire covered with SiO_2 film, for neurological microelectrode 78−11752
CVD films of high IR reflectance 79−52119
CVD for appl in high temp. photothermal conversion 79−79403
CVD thin films for solar photothermal conversion 80−7503
cyclotron effective mass and identification of carriers on Fermi surface 79−65372
cyclotron resonance, Doppler shifted, doppleron-phonon reson. *(Russian)* 77−32262
cyclotron resonance by microwave transmission and carrier identification on Fermi surface 79−60685
damage profile resulting from Ni^{2+} and He^{+} ion bombardment 78−10100
Debye-Waller exponents, modified ang. force model 77−76515
Debye-Waller factor, temp. variation, lattice dynamical calc. 78−55925
defect struct. in plane strain deformed single crystal 77−63751
deformation and fracture patterns under complex stress conditions 77−70134
deformation in fatigue loading of single crystal 80−35328
deformed, ^{57}Fe doped, positron annihilation exam. 79−15556
deformed, dislocation-free channels prod. by heat pulses, electron microscope obs. and hardness meas. *(Russian)* 79−52251
deformed single crystal, correlation of textural and microstructural changes 77−32586
deformed single crysts., struct. state and dislocation splitting *(Russian)* 80−29029
density change during plastic deformation in monocrystal *(Russian)* 79−87689
desorption kinetics of halogens, pulsed ion beam method 80−34300
desorption of He, Mo-He and He-He interaction pot. 79−19459
determ. by atomic absorption, using low temp. flames 80−30307
determination, in hydrodesulphurisation catalysts, by at. absorpt. spectroscopy 77−9145
determination, in Mg alloy, emission spectrographic DC arc-powder technique 78−48713
determination by intracavity at. emission spectroscopy 79−52830
dielectric function and energy loss function, APW band struct. calc. 77−62850
diffuse electron scatt. *(Russian)* 80−103438
diffusion, of Li, mechanism 78−84007
diffusion and solubility of C *(French)* 79−55932
diffusion and trapping of H(D) at ion implantation induced defects 77−47622
diffusion anomalies, vacancy model *(French)* 77−43366
diffusion in Fe rel. to transforms. 77−4214
diffusion in molten Fe *(Japanese)* 77−51531
diffusion of Cs, AES, SIMS depth profile study *(German)* 78−84008
diffusion of H_2, 900-1100°C *(Russian)* 78−79811
diffusion of H_2 enhanced by self-interstitial atoms, surface reaction const. determ. 80−75386
diffusion of Li, Cs, vacancy and divacancy mechanisms *(Russian)* 80−70472
diffusion of volatile fission products ^{140}Ba and ^{132}Te, 1400-2000K *(Russian)* 78−91485
diffusivity of C 77−43384
discontinuous film, room temp. oxidation rate consts., resist. meas. 77−32723
dislocation (100) density variation, deformation effects, dislocation stability *(Russian)* 80−15108
dislocation a ⟨100⟩ stability, plastic deformation at high-press. 78−43030
dislocation dynamics, HVEM in situ obs. 78−83822
dislocation interactions during parallel shear in (011) plane *(French)* 78−43029
dislocation motion, study by internal friction *(Russian)* 77−1133
dislocation structure, changes during work softening, HVEM 80−103336
dislocation structure, temp. depend., at crack tip, of fractured single cryst. 79−29210
dislocation structure evolution near electro-eroded crater *(Russian)* 80−100237
dislocation structure inhomogeneity in electromachining crater zone *(Russian)* 80−16326
dislocation structure of block boundaries in single crystals *(Russian)* 79−77603
dislocation structure of diffusional welding zone *(Russian)* 80−96531
divacancy binding energy, appl. stress effect, computer simulation 77−15408
doped rod, surface tension driven flow in electron beam floating zone expts. 80−19731
ductile fracture, microcrack formation, statistical description *(Russian)* 77−66689
ductility and high temp. strength of single crystal in routine tests 77−90427
edge dislocation interaction with interstitial atoms, influence on Peierls stress 78−34537
effective mass meas. and electron velocities 80−96773
elastic aftereffect after fast neutron irrad. at 5K 77−89431
elastic moduli meas. *(Russian)* 78−75704
electric arc sprayed coating on wire, elastic and elastic-plastic props. *(German)* 79−34089
molybdenum continued
electric field gradient tensor, electronic contrib., nucl. acoustic reson. determ. 78−48059
electrical resistance data in the region 300 to 2800K 77−43555
electrical resistivity, quadratic contrib., 2 to 40K *(Russian)* 80−92874
electrochemical behaviour in alcoholic KOH soln. 79−87762
electrocrystallisation from fused salts, growth rate and struct. 77−77438
electrode, disc, in KOH soln., anodic soln. kinetics *(Russian)* 78−11523
electrode, Mo extraction grid for high power ion source 80−102372
electrode reactions with molten glass 80−85186
electrodes, in glow discharge, H penetration and diffusion 77−7629
electrolytic dissolution at high anodic potentials, surface quality *(Russian)* 79−39025
electron backscatter fractions 78−87717
electron beam melted, C charge effect on ductility *(Japanese)* 80−35264
electron beam melted with C additions, mech. props. *(Japanese)* 77−48449
electron current density localisation and effect on damage prod. 78−22763
electron energy loss mechanism, surface and volume losses, anal. 79−91547
electron energy loss spectra, vol. and surface plasmon excitation 77−52207
electron field emission energy distrib. from surface oxide clusters 77−63548
electron irrad., anisotropic damage prod. 80−2071
electron irradiated, energy and orientation depend. of at. displacement 79−99244
electron irradiated, positron trapping in vacancies and vacancy clusters 79−52039
electron irradiated, recovery studies of pure and radiation doped crystals 79−19280
electron irradiated in HVEM, anisotropy of damage prod. 80−107322
electron radiation damage and props. of point defects 77−11590
electron spectroscopy, energy loss and photoemission 78−72682
electron states, calc. using SCF-Xα-SW method 77−15797
electron stimulated desorption of negative ions from adsorbed gases 78−91549
electron-electron scattering, doppleron damping meas. 79−37963
electron-phonon coupling and supercond. transition temp. 79−56360
electronic and struct. props., nonlocal pseudopot. calc. 80−34349
electronic density of states, optical mass and DC elec. resist., Slater-Koster interpolation 77−15731
electronic props., first-principles nonlocal pseudopot. approach 79−95319
electronics industry applications, prep. processing and props. 80−89171
electropolishing in alcoholic soln. of H_2SO_4 77−16718
electropolishing soln., comp. and evaluation 78−15576
emissivity, integral hemispherical degree of blackness, 1200-3000K 78−43154
emitter, radiant heat exchange, design of heater-substrate system for vapour deposited coatings *(Russian)* 78−95701
endotaxy during carburisation of single crystals 77−70228
energetic deuteron irradiated surface struct. quantitative meas. 78−95210
enthalpy and heat capacity, standard ref. material 78−18792
epitaxial growth of Rh, Ir, Pd and Pt on (001) surface 79−99450
epitaxial layer production by electron beam deposition in vacuum *(Russian)* 77−59228
evaporated film, refl. and struct. 78−72021
evaporation rate determ. by tip profile change meas. 77−24403
extinction length ζ_{200} meas., electron energy influence 80−90935
fatigue, substruct. variation kinetics for single crysts. *(Russian)* 78−60742
fatigue charact., effect of Ni and Re surface doping on mech. props. *(Russian)* 80−7660
fatigue of single crystals, dislocation struct. and strain localisation *(Russian)* 80−71741
Fermi surface, electron scatt. mech., RF size effect study *(Russian)* 79−37965
Fermi surface, homogeneous strain response 78−34753
Fermi surface, precision investigation using RF size effect 79−77984
Fermi surface ang. shear deform. 79−77985
Fermi surface curvature *(Russian)* 79−87038
Fermi surface parameters, RF size effect meas. *(Russian)* 79−95311
Fermi surface press. depend., surface impedance and US attenuation oscills. in mag. field 77−43476
Fermi surface stress depend., hybridised nearly-free-electron tight-binding model 77−15757
Fermi surface vol. depend. of extremal cross sectional areas from de Haas-van Alphen meas. 80−70589
fibre, brittle to tough transition, impact strength meas. 80−40527
fibre reinforced Cu, rule of mixtures of deform. parameters in stage III 80−97532
fibre reinforced Cu with weak interfaces, stability of tensile deform. 80−97533
fibres reinforced Al and Al alloys, SEM study *(Slovenian)* 78−84923
field emission anomalies in mag. field *(Russian)* 80−93462
field emitter, adsorption of Se, field emission meas. 77−31889
field emitter, adsorption of Te on single cryst. faces 78−34714
field emitter, Te adsorption 77−69177
field evaporation, search for high ionic charges 78−35269
field evaporation patterns, multilayer 77−59675
field ion emitter, calibration using energy distrib. of free space field ionisation 77−69971
filament, coated with thin Ni film, creep and recrystn. *(Russian)* 78−19822
film, BCC, optical props. 79−78781
film, cc preparation by H_2 reactive sputtering *(Japanese)* 79−95929
film, characteristics of elastic reflection of slow electrons 79−14657
film, CVD, optical props., solar absorber appl. 77−55844
film, CVD, passivating against IR reflectance losses caused by oxidation 79−3758
film, CVD, with high IR refl. and large solar absorpt., prep. and props. 80−26163
film, deform. in electron microscope, dislocation mechanism 79−82227
film, deposited by cylindrical magnetron sputtering, internal stresses, optical reflectance and elec. resist. 77−43449
film, electron beam deposition on Si, X-ray obs. of silicide form., diffusion processes *(German)* 77−1341

molybdenum continued
film, electron beam evaporator for in situ deposition studies in UHV electron microscope 80−40264
film, epitaxial growth on cooled W tips at 78K, struct. obs. 77−28723
film, evaporated, annealing behaviour, SEM obs. 80−65397
film, evaporated, grain size and resist. 80−88650
film, evaporated, optical props., rel. to struct. 80−55211
film, formation by reduction of $MoCl_5$, influence of electric field 80−93491
film, laser induced reactions with Si 79−70365
film, on pyrex, surface roughness meas. by ellipsometry and TEM 77−20205
film, on Si, X-ray line-shape anal., simplifications using Fourier series 79−82123
film, on SiO_2/Si substrate, effect of heat treatment after deposition on internal stress 78−22973
film, optical absorption meas. using synchrotron radiation, 20-250 eK 77−12457
film, polycryst., energy loss function, Kramers-Kronig anal., reflectivity, optical props., EELS 80−40194
film, RF impedance temp. and freq. depend. 77−4453
film, silicide formation during growth by electron beam evaporation *(German)* 78−84717
film, specularity coefficient of conduction electrons, angular dependence *(Russian)* 79−87167
film, sputtered, elec. resist., annealing and struct. effects 80−60109
film, sputtered on Si, annealing effect on uniform and nonuniform strains 79−82504
film, vacuum deposited, elec. cond., internal stresses, surface corrosion, MOS gate appl. *(Japanese)* 78−80073
film, vacuum deposited onto SiO_2-Si substrates, elec. resist. 78−76166
film, vacuum deposition on fluorophlogopite at 650 to 1050°C, orientation rels. *(Russian)* 77−48342
film, with Nb, Ni or Al_2O_3 impurity, prod. by simultaneous condensation from 2 sources, growth direction *(Russian)* 77−21026
film, work function, effects of O_2 sorption 78−19125
film deposited by low temp. carbonyl pyrolysis, struct. 78−72039
film field emission cathode with cones, phys. props. 77−24931
film on sapphire substrate, orientational growth, epitaxial textures, nucleation textures *(Russian)* 80−75454
film on Si, silicide form. 78−43261
film on Si substrate, laser irrad., cellular struct. and silicide form 80−10710
film on Si surface, $MoSi_2$ form. conditions *(French)* 78−43270
films, sputtered from cylindrical-post magnetron with Ne, Ar, Kr and Xe, compressive stress and presence of inert-gas obs. 80−80140
films, vac. evaporated, optical cond. 80−76100
fine particles formed by gas-evap. technique, cryst. struct. and habit 79−27935
fine tip cathode, field emission stability, rel. to passivation 80−100760
fission fragment bombardment, channelling effects *(Russian)* 78−38762
flame sprayed coatings, comp., microstruct. and mech. props. 80−16598
flameless atomic absorption spectrophotometric determination of Ni and Co traces 77−90674
flow stress temp. depend., effect of interstitial atom clustering and embrittlement *(Russian)* 78−34538
foil, electron energy loss spectra 80−7452
foil dislocation struct. of rolling texture *(Russian)* 78−59810
foil electrolytic perforation, surface film phase composition obs. *(Russian)* 80−61004
foils, device for electrolytic thinning from wire, for electron microscopy 80−85105
fractographic peculiarities in ductile brittle transition 78−39910
fracture and crack propag. tested in tension along [001] axis *(Russian)* 80−50697
fracture and crack tip plastic zones, in situ obs. 80−108686
fracture and ductile-brittle transition, hydrostatic press. effects 78−60735
fracture surface, effect of plastic deform. by rolling at 950°C *(Russian)* 77−59893
fragmented structure formed during plastic deform., TEM investig., dislocation model *(Russian)* 77−32634
friction, He environment 4.2-80K 78−48543
fusion reactor material, low energy ion erosion expts., Kaufman source appl. 80−68942
fusion reactor shield, neutron induced activity and γ-ray source investigation 78−54872
fusion reactor wall, microexplosion of pellet, energy deposition 78−54890
gamma irradiated defects, interaction with positrons *(Russian)* 80−97372
gamma-ray attenuation meas. using Ge(Li) detector 78−17539
gamma-ray irrad. positron annihilation during radiation defect annealing *(Russian)* 79−99970
gas driven blister growth on He ion bombardment, SEM obs. 77−76473
gas permeability (H, He, Ar) through monocrystalline and polycrystalline specimens *(Russian)* 79−60554
glow-discharge surface treatment, struct. defect prod. 77−63832
grain boundaries, electron microscope obs. *(Russian)* 79−4311
grain boundary, atomic structure determ. 79−33003
grain boundary segregation, competition between interstitial atoms, AES obs. *(Russian)* 77−25008
grain boundary segregation obs. by atom imaging probe 78−21276
grain boundary segregation of O, atom probe FIM study 80−37134
grain structure characteristics analysis using Quantimet-720 79−52496
Hall effect, effect of electron-phonon scatt. anisotropy *(Russian)* 80−10947
hardened substructure, high-temp. radiation resist. *(Russian)* 78−56654
HEED, Bloch functions rel. to at. or mol. orbitals 78−83662
high purity single crystal doped with C, low temp. mech. props. 77−77544
high temp. radiative props., expt. determ., spectral emissivities 80−74718
high temperature properties 78−44173
hole ellipsoid scatt. rate temp. dependence, magnetoacoustic obs. 79−51472
Hugoniot data, ultrahigh press. (TPa) shockwave from underground nuclear explosion 80−59580
hydrogen embrittlement mechanisms, exam., effect on mech. props. 78−39891
hydrometallurgical plant effluent waters, Mo and W determ. by activation analysis with low-power neutron sources 78−7279
molybdenum continued
implantation in Al and Al-Zn-Mg-Cu, effect on corrosion behaviour 80−71794
impurities, interaction mechanism and saturation limit *(Russian)* 77−55358
impurity diffusion in JIPP T-II tokamak plasma during H_2 gas puffing 80−28602
impurity flux, time resolved, in DITE Tokamak 80−63373
impurity interactions with C, N, and O, struct., mech. props. and purification 79−52277
in-situ coating, vacuum deposition on Hastelloy-X substrate expt. study 79−3237
interaction with gases, H_2, N_2, O_2, CO, water vapour and hydrocarbons *(German)* 79−74296
interatomic pair potential, phonon spectra 80−33927
interatomic pot. from phonon spectrum 78−67784
interatomic potential from phonon spectra 77−76355
interface with Ag and Cu films, S impurity segregation 78−84076
internal friction and segregation effects, cellular struct. *(Russian)* 77−66669
internal friction peaks, induced by work hardening, low temp. relax. spectra *(French)* 77−1844
ion bombard., ion and photon yields, CO adsorption effect 80−89098
ion bombardment, damage profile, void size and density, TEM 78−47451
ion bombardment, energy distrib. of positive secondary ions and sputtered atoms 77−32485
ion bombardment by Ni^{2+}, TEM study of damage depth distrib. 78−10101
ion bombardment effect on superconducting transition temp. in single crystal 78−52136
ion impact, radiative spectrum of sputtered particles *(Russian)* 79−91504
ion implanted, energy dependent channelling and backscatt. anal., $^4He^+$ ions, 1 to 2.8 MeV 79−4360
ion incorporation into TiO_2 matrix, ESR, UV, and ESCA spectral anal. 79−43670
ion irradiated, defect anal., electron microscopy, appl. of theory of non-edge loop image contrast 80−70200
ion irradiated, dislocation loops and stacking fault tetrahedra, electron microscope image contrast 80−6326
ion irradiated, ordered arrangement of micropores on dislocations 77−19943
ion irradiated, radiation-induced damage, microhardness and lattice consts. meas. 78−2170
ion plated on V-Mo alloy, effect on corrosion in liquid Na 78−53020
ion plating, on ceramic substrate, and coating struct. 78−11132
ion prod. in hollow cathode source 78−74525
ion-electron emission yield, ang. depend., atomic order effects 77−85877
ion-plated orthopaedic En58J stainless steel, corrosion fatigue 80−66694
ionic siliciding, diffusion layer prod. 78−23855
ionisation equilibrium, radn. losses, in high temp. plasma 77−72422
ions, beam-foil spectra from 20 to 238 MeV energy, 5 to 60 nm, lifetime meas. problems 80−9722
irradiated, defect configurations, PAC study 79−86817
irradiated, small edge dislocation loops, electron microscope image contrast, Burger's vector determ. 77−76410
irradiated between 425 and 1000°C, ductility in bending 80−39164
irradiated by H^+ and H_2^+ ion beams, grain ejection from surface 78−6819
irradiated with fission fragments, creep, 20-30K *(French)* 77−48493
irradiation induced defects, electron microscope images 78−83854
islet films, effect of external elec. field on electron emission 80−80952
isomer shift values of implanted $^{133}Xe/^{133}Cs$, Mossbauer spectra 80−7240
isotopically enriched target preparation using electron gun 80−23226
ISSEC selection for fusion reactor 80−57950
K-edge photoabsorption spectra, linear APW calc. 78−43960
Knight shift and mag. suscept. temp. depend. 78−15043
Knight shift and mag. susceptibility, temp. depend. *(German)* 78−10791
L shell prod. cross section of Zr, Mo, Ag, Cd and In for 75 to 150 keV p and e excitation 79−47552
laser induced dislocation struct. in single cryst. 80−70210
laser mirror, optical and metallurgical characterisation 80−33129
laser shock induced microstructural changes, rel. to explosive shock induced phenomena 78−67768
lattice defects, relax. studies, computer simulation 78−79604
lattice dynamical models, phonon dispersion curves 77−89506
lattice dynamics, improved Fielek model 80−59598
layer, grain size depend. on thickness *(Czech)* 77−47695
limiter for JFT-2 Tokamak 79−85768
linear expansion coefficient, at low temp. 78−83977
liquid, elec. resist., melting pt. to boiling pt., temp. depend. 80−96839
liquid, exptl. determ. of crit. data 78−75531
liquid, spectral emissivity and brightness-temp. meas. at MP 77−43356
liquid, thermal volume expansion, MP to BP 79−90802
liquid, thermophysical measurements, up to 4300K 78−43136
liquid and solid, thermophysical props. 78−75808
localised electronic states near dislocations 79−33257
localized electronic states near ⟨100⟩ edge dislocation compared with perfect lattice 78−30888
longwave dopplerons, nonlocal Hall effect, surface impedance, size effect *(Russian)* 80−80253
luminescence characteristics of pure surfaces acted on by flux of field emission electrons 80−100695
magnetoacoustic effect shear wave selectivity 79−47131
magnetoacoustic studies for longit. and shear waves 78−91604
magnetothermopower meas. 77−76795
mechanical eqn. of state *(Japanese)* 78−91375
mechanical properties, effect of exposure to high temp. He containing O_2, room temp. study 80−93639
mechanical properties, influence of temp. on singularities of deform. *(Russian)* 78−6970
mechanical props. and dislocation struct., mag. field effect 80−54935
mechanical props. and dislocation struct., mag. field effects *(Russian)* 79−42818
membrane, polycryst., LiH form. on surface from diffusing Li+H_2 77−66771
metallised amorphous GeSe junctions, electrical contact effects on properties *(German)* 80−93010

molybdenum continued
microcrack formation, structural singularities, TEM obs. *(Russian)* 79−1905
microhardness and charact. hardness 79−52376
microhole working by laser irrad., accuracy increase *(Russian)* 80−55434
microstructure, swelling induced by ion bombard., He injection effects 80−29083
microvoid form., gaseous impurity atom effects, positron annihilation study 80−49275
migration in GaAs, ESCA study *(French)* 78−75885
monocrystalline, exam. of microplasticity of ambient temps. *(French)* 78−52888
monolayer, oxidation, quasisimultaneous SIMS, AES, XPS 78−72919
Mossbauer absorpt. spectrum in deformed cryst. 77−16234
neutron activation analysis of Mo content in 12-molybdophosphoric acid 80−15148
neutron bombard., radiation damage, electron microscopy obs. *(Russian)* 80−44235
neutron damage, 14 MeV 77−15460
neutron dose depend. of elec. resist., vacancy-interstitial recomb. *(Russian)* 77−80546
neutron effects, inertial confinement reactor first wall response to thermonuclear radiation 79−76133
neutron irradiated, extended low temp. annealing 79−79014
neutron irradiated, high-temp., annealing study by positron lifetime 77−51413
neutron irradiated, influence on X-ray diffr. patterns *(Russian)* 78−22764
neutron irradiated, positron annihilation at temps. 350 to 1000°C 78−55894
neutron irradiated, radiation anneal hardening mechanism 80−71678
neutron irradiated, radiation softening and hardening 80−34083
neutron irradiated, relationship between void size and positron lifetime 77−15454
neutron irradiated, vacancy reactions in III recovery 79−73220
neutron irradiation effects on microcracks *(Ukrainian)* 79−77639
neutron irradiation induced length change, 40 to 450 degrees C 78−47433
neutron irradiation induced voids, irrad. temp. determ. from void lattice const. 77−46289
neutron irradiation induced voids, positron lifetime meas. 77−7766
neutron irradiation temp. determ. by electrical resistivity meas. 78−58354
neutron low energy interaction cross sections, gravitational spectrometer meas. 80−24521
neutron-bombarded, diffuse X-ray scattering *(Russian)* 80−92560
neutron-irradiated, high-temp., positron annihilation charact. meas. 77−89480
neutron-irradiated, positron lifetime study 79−23654
nitriding, kinetics 80−35415
nitrogenase enzyme, role of Mo 77−86367
nonstationary temperature fields due to moving heat sources, heat capacity, thermal cond. *(Russian)* 80−107448
nuclear indirect interaction, NMR line shape anal. 78−52360
optical constants 12 to 24 μm, anomalous skin effect region 77−20842
optical emission, broadband, due to heavy ion bombardment 77−28635
ordered void obs. 79−86786
orientation distrib. function depend. on deform. during cold rolling *(Russian)* 80−50647
orientation distribution function after longitudinal and cross cold rolling *(Russian)* 79−70076
oxidation, combination anal. using ESCA, AES and SIMS 78−72924
oxidation, IR emission spectrosc. obs. 78−68942
oxidation, reflectance IR study rel. to component of stainless steel 79−47811
oxidation, staged flow of O_2 interaction process, secondary ion emission obs. 78−11386
oxidation 77−70227
oxidation in flow conditions at 1000 to 6000K 78−11445
oxidation kinetics, Mossbauer study 80−40005
oxidation of (110) face 78−92402
oxidation of adsorbed C, electron diffr., contact pot. difference, and AES obs. *(Russian)* 79−52430
oxidation of single cryst., effect of high elec. fields, field emission and TEM obs. 77−90258
oxidation resistant coating of Nichrome, electrophoretic deposition *(Japanese)* 79−20270
oxidised surface, adsorbed amines and hydrazines identification by surface ionis. 77−21456
pair potentials calcs., elastic props. calc. 80−49176
partial recrystallisation 45° brittleness, 45° crack formation and propagation *(Russian)* 79−100238
particle formation, ultrafine, via pulsed laser breakdown of $MO(CO)_6$ 80−84881
particles sputtered with low energy Ne^+ ions, surface microstructure effect on angular distrib. 79−100004
phase transition on (100) surface, LEED exam. 77−55433
phonon density of states determ. from heat capacity *(Russian)* 80−29131
phonon dispersion, anomalous struct., tight-binding calcs. 78−10137
phonon dispersion, Debye temp. and Debye-Waller factors, lattice dynamical model 78−55920
phonon dispersion, lattice phonons three body interaction model 79−99280
phonon dispersion curves, extended de Launay model 77−4162
phonon dispersion relations, modified tensor force model 80−103428
phonon frequencies, seventh-neighbour tensor force model 78−91402
photodesorption of CO forming CO_2 79−52777
photoelectric cross sections of low energy photons 78−46309
photoemission, two-photon, induced by picosecond laser pulses 77−77347
photoemission peak near Fermi level on (100) face 77−52220
photon absorption and photoelectric cross-sections calcs. 79−31486
photon emission from inert gas-surface impact 78−11059
plasma impurity, flux on wall of DITE Tokamak 80−28688
plasma impurity, from Tokamak neutraliser plate, recycling effect in scrape-off plasma 80−10421
plasma impurity, high-temp. ionis. equilib. and radiative cooling 78−42712
plasma impurity, in TFR Tokamak current plateau, effect of O_2 injection 78−22565
molybdenum continued
plasma impurity, radiation loss effects on Tokamak expts. 78−22465
plasma Tokamak discharge, impurity emission spectra for diagnostics 77−11403
plastic deformation, flow of crystalline mat. *(Russian)* 78−76705
plastic deformation by rolling at 293K, dislocation struct. *(Russian)* 77−48481
plastic deformation during rolling at 293K, crystallographic of slip *(Russian)* 77−32588
plastic deformation mechanism during hydrostatic extrusion *(Russian)* 77−8879
plastic flow, early stages in single crystals 77−36584
plastic strain mechanism, in single crysts., in hydroextrusion *(Russian)* 80−21009
plastically deformed single cryst., mag. susceptibility *(Russian)* 80−93074
plate, microhardness and resist. to chem. attack of CVD Ni_2P coating 79−66009
point defect migration, stage III annealing 77−80548
point emitter, surface microrelief under explosive electron emission 78−2973
poisoning effect on LaB_6 work function 79−52070
polishing in H_2SO_4+methanol, polarisation curves 78−56851
polycrystalline, type MCh-1, fractography of static and fatigue fracture 79−87729
polycrystals, grain misalignment, electron microscope determ. *(Russian)* 80−103358
polygonisation and recrystallisation in rolled single cryst., strain depend. *(Russian)* 77−81270
porous, permeability, deform. effects 79−100229
porous high temp. props. 77−11894
positive ions, photoionisation and Auger effect 78−90135
positron annihilation and residual resistivity, effect of microvoid size 77−48272
positron annihilation and vacancy formation 80−16119
positron annihilation radiation angular correl., band struct. and Fermi surface study 78−6260
positron lifetime and pair momentum, investig. of radiation induced voids 77−8679
positronium-like states *(Russian)* 77−89737
powder, struct. changes under action of high-power pulses 79−70018
powder, struct. facators, time of flight neutron diffr. 78−47212
powder metallurgy prep. 80−29904
powder properties for plasma-sprayed coatings 78−48548
powder sintering, transition metal activators, 1000-1350°C, heterodiffusion model 78−44044
powders, defective structure and activated sintering, exam. 80−16240
power law creep, exam. of whether creep is diffusion controlled 78−52890
production by MoO_2 reduction reaction kinetics 80−16230
protective Si_3N_4 coating, RF reactive ion plating 78−3250
proton energy loss, 0.1-1.0 MeV 80−42909
proton irradiated, annealed and rolled, void form. 78−22774
proton-induced L-shell ionisation cross-sections 80−100707
quenched sample, UV photoelectron spectra, exoelectron-like emission 79−15587
radiation damage by 0.3-2 keV D_2^+, use of 300 eV D_2^+ as ion microprobe 77−43260
radiation induced vacancies and D_2^+ implantation 80−65076
radiation-induced voids and dislocations, annealing, theory *(Russian)* 78−47418
range of $^{27}Al^+$ ions, meas. by (p,γ) reson. broadening 79−46729
reaction with sintered Li_2O pellets 79−47913
reactions with LiO_2 in fusion blanket feasibility tests 80−26055
reactive sputtering yield 77−66566
recrystallisation texture of single crystals, effect of fine precipitates 78−88480
recrystallised sintered sheet, C addition effect on ductility 79−8319
reflection of H, D and He ions 78−95640
refractory fibre, effect on high-temp. strength of refractory coatings *(Russian)* 77−52536
reinforced Al and Cu based composites fatigue strength, surface layer effects 77−12697
resistivity, temp. depend., electron-electron scatt. 78−68025
resonant Raman X-ray scatt., evidence for K-M scatt. 79−61466
RF sputtered, diffusion barrier props. 78−71887
RF surface impedance, new type of oscills. 79−15070
sample chamber for ultrasonic vels. and elastic consts. meas., 4.2 to 300K *(German)* 78−46868
scattering rate temp. depend. from magnetoacoustic expts. 79−65522
screw dislocation, $^1/_2\langle 111\rangle$, in pure Mo and Mo with He interstitials, at. config. 79−65081
secondary electron emission, effect of ion implantation with K^+ and Ba^+ ions 79−91544
secondary electron emission, on proton and deuteron irrad., 0.5-2.5 MeV 77−63512
secondary recrystallisation grain structure, effect of conditions of annealing *(Russian)* 78−6945
segregation of impurities and alloy elements at surface *(French)* 79−47697
self-diffusion, 1360 to 2773K 79−86919
self-diffusion and electromigration, 1100-1300°C *(Russian)* 77−47613
self-ion damage, influence of material purity and irradiation temp., electron microscope exam. 77−35562
self-weldability in high temp Na *(Japanese)* 80−89392
sewage sludge land disposal, Mo hazard 77−33115
sheet, conc. of interstitial elements on lamination surface 77−86038
sheet, shock-induced intergranular cracks 79−57087
shock compression to 2.0 TPa, by nuclear explosion 77−84841
shock deformation twinning, shock loaded BCC and FCC metals comparison 80−104413
shock deformation twinning, shock press., pulse duration and grain size effects 79−5021
shock loaded, peak press. and press. pulse duration effect on crystallographic transform. 78−67769
shock wave depth of form. due to laser radiation interaction 77−81180
shock wave formation relationships, surface propagation, elastoplastic wave effects 79−55825
siliconised, thermal stress and thermal expansion 77−21324
siliconization, effect on adhesive interaction with Nb and unprotected Mo 77−48569

molybdenum continued
single crystal, effect of prior ultrasonic working on hardness, crystal orientation and creep resistance *(Russian)* 79−34056
single crystal, subjected to plastic deform., substruct. using X-ray diffr. 79−[illegible]
single crystal growth by plasma heating 78−60569
single crystals, orientation and alloying effect on mech. *(Russian)* 80−71706
sintered, fusion reactor blanket struct. material, low cycle fatigue behaviour 80−30073
sintered, gas evolution and degassing 80−100814
sintered, grain boundary segregation of S and N 79−56982
sintered, pure, work hardening 77−16607
sintered, thermal and elec. conds., 50-800°C, microstructure 78−43352
sintered, thermally induced surface composition variations 79−5078
sintered composite, Mos, containing, friction and wear props. 80−11786
sintering, effect of Ni activator grain size 77−63590
skin effect, Gantmakher-Kaner effect peculiarities *(Russian)* 80−49796
slip geometry, HVEM straining 80−39207
slip line study of pure single crystal compressively deformed at low temps. 79−43361
slip rosettes and dislocation struct. formed by microindentations 78−14349
solid solubility of N_2 determ. using high-pressure autoclaves 77−15592
solid-state bonding, tensile strength of bond *(German)* 79−47756
specific heat near melting point, rapid pulsed heating method 77−35704
specific volume meas., for ruby R_1 fluoresc. press. gauge calibration, 0.06-1 Mbar 78−70150
specimen preparation for TEM, two-stage jet-stagnant electrolytic thinning, Ti, Mo appls. 77−71405
spectrochemical analysis, atomic-absorption, tubes design with hollow cathode *(Bulgarian)* 80−85232
spray coating form. in pure Ar atm. 77−32709
sputter deposition, isotope enrichment 77−27198
sputtered, angular distrib. during He^+ and Ar^+ ion bombardment 78−95624
sputtered atom angular distrib., mass effects in Mg plasma 79−87538
sputtered film., internal stresses, effect of substrate orientation and rotation 79−77968
sputtering, negative ion form., Cs overlayer effect 78−39645
sputtering by fusion neutrons meas. 77−36321
sputtering by Hg ions, isotope enrichment 77−59656
sputtering for laser mirror refurbishment 80−14498
sputtering yield at low energy for light-ions 78−19620
sputtering yield meas. on first wall materials of thermonuclear fusion devices *(Japanese)* 77−85865
sputtering yields for light ions 79−87537
steel, alloyed with Cr, Mo, Co, Mn, martensitic point position depend. on cooling rate *(Russian)* 79−70063
steel, ferritic (17 wt.% Cr), influence of Mo on intergranular corrosion 80−30139
steel, maraging, 0Kh6N8M7S, effect of Cr, Ni and Mo on hardness 80−21093
steel, Ni-Cr low alloy, effect of Mo on tempered martensite embrittlement 80−3187
steels, high-purity and commercially based, containing 10 wt.%W or 5 wt.%Mo, tempering behaviour 80−7600
stopping power for 0.3-1.5 MeV protons 79−55801
stopping power for 28 MeV α-particles, re-evaluation 78−79651
stopping power nucl., in ferromag. Gd, transient mag. field 78−34555
stopping powers for 28.8 MeV α-particles 77−80556
strain hardened metal and microalloys, low temp. brittleness 79−96140
strain induced damping, micro- and macro-, and dislocation structures in single crystals 78−19797
strain localisation and fatigue, glide plane shearing stress 80−7683
stray X-rays from Mo components in transmission electron microscope, reduction 80−73550
strength, temp. depend. 78−3193
strength and internal friction 77−63711
stress measurement, in single cryst., using ψ-ϕ goniometer 80−64837
stress-to-rupture strength at high temps., struct. effect 77−70175
structural singularities of plastic deform. at localised flow stage, TEM obs. *(Russian)* 78−6968
structure of large single crystal produced by electron beam spot welding *(Russian)* 77−44136
substitution and redox reactions in oxidation states III to VI, role in enzymes 77−86364
substrate, film coated characterisation by atom probe FIM, atomic clusters, voids 80−33863
substrate, preferentially etched, initial growth behaviour of CVD InP films 78−51855
substrate, TiB_2 coating prep. by CVD and interaction with substrate 79−24680
substrate for W-Al_2O_3 composite films, oxide evaporation deposited, struct., props. 80−25581
substrate limiting temp. during vaporisation and condensation coating in vacuum *(Russian)* 80−100787
sulphidation, cryst. struct. of MoS_2 77−52539
sulphiding with H_2S 78−3078
sulphidization, coating growth kinetics and mechanism 77−86220
superconducting, isotopic vol. effect confirmation by energy-dispersive X-ray diffr. 77−36019
superconducting film, amorphous and crystalline, transition temp. exam. by UPS 79−28433
superconducting film, T_c and residual resist., variation with coating thickness 78−47900
superconducting transition temp., perturbative corrections, direct and indirect ladder diagrams 80−49979
superconducting transition temperature, ab initio calc. 80−25036
superconducting weak leak, ion-implanted, Josephson to depairing behaviour transition 77−1522
superconductivity and phonon softening, between electron bands and phonons 78−14859
surface, 10-30 keV H ion bombardment, energy refl. meas. 78−27359
surface, 2 keV Ne^+ ion bombard., dose and microstruct. effects on surface topography and sputtering yield 79−65124
surface, {100}, anisotropy of secondary electron emission from oblique incidence of electrons 79−99999
surface, (001), electronic origin of reconstruction 80−11065
surface, (001), electronic struct. 77−72902
molybdenum continued
surface, (001), electronic susceptibility and surface phase transition 79−33169
surface, (001), surface CDW phase transitions 78−43455
surface, (001), surface states and photoemission 79−60887
surface, (011), submonolayer Ba film, surface diffusion, manifestation of phase states *(Russian)* 78−91539
surface, (100), adsorbed H_2, photoemission rel. to surface resonances and surface reconstruction 80−44417
surface, (100), anisotropic ionisation loss of electrons, orientational effects 79−69935
surface, (100), clean and O_2 covered, electron energy loss spectra meas. 77−16440
surface, (100), O-covered, electron-stimulated desorption of O^+ and O^- ions 79−82444
surface, (100), surface reson. 78−72226
surface, (100) and (110), directional UPS obs. 77−8722
surface, (110), electron production by metastable rare gas atom impact 77−32486
surface, (110), surface densities of states for normal photoemission 78−35251
surface, (110) and (100), surface reson. states and adsorption of 4d atoms 78−71982
surface, adsorbed C^+ layer removal, by 20-30 keV Ar^+ bombardment, in plasma 77−76103
surface, adsorbed Ga and Sn, struct., FIM obs. 80−103576
surface, Ag cluster growth and nucleation, UHV-SEM, ASE/(RHEED or LEED) obs. comparison 78−63956
surface, ang. distrib. of desorbed mol. using directional detector 79−80626
surface, anisotropy of elastic refl. of electrons from single cryst. 79−28870
surface, Ar^+-bombarded, 40 keV, excited at. emission 80−11481
surface, backscatt. of excited H atoms in the presence of oxygen 79−3388
surface, clean and gas covered, He* impact, deexcitation, pot. energy transfer mechanism 80−60743
surface, dual beam ion bombardment 79−7634
surface, electron-stimulated desorption of negative ions, work function 78−72654
surface, electron-surface-plasmon scatt. using parabolic nontouching trajectory 77−28228
surface, electronic struct., self-consistent pseudopot. calcs. 78−76128
surface, excited state formed by B^+ impact, light emission coeffs. 78−64417
surface, field depend. of spectral line energy of He-H_2 adsorbate 79−78853
surface, $H^+(H_2^+)(H_3^+)$ impact, backscattered H Balmer-β line intensity 77−23470
surface, $H^-(H_2^+)$ ion impact, energy refl. coeffs. 78−54969
surface, H^- production by low energy H atom bombardment 79−100006
surface, low energy ion scattering of absorbed layers 79−1807
surface, low-temperature thermionic converter with an expanded-area collector 80−70045
surface, Lyman-α emission from proton bombard. 79−91503
surface, metastable He atom beam contamination by fast neutral atoms, effect on secondary emission 80−55253
surface, polycryst., CO chemisorption, substrate mediated C-O interaction, photoelectron spectra 79−34353
surface, polycryst., $H^+(H_2^+)(H_3^+)$ impact, optical radiation emission 78−95644
surface, pulsed laser atom-probe FIM, expts. 80−66402
surface, refl. of metastable He atoms, O_2 adsorption effects 79−11493
surface, rolled, H_2^+ ion bombard, large blister form. 80−75274
surface, secondary ion emission mechanism, under Hg^+ ion bombardment 79−100013
surface, SiC coatings, deposition by RF sputtering 80−25563
surface, struct. of secondary electron emission characts. 77−16439
surface (001), clean and H chemisorbed, atomic displacements, LEED obs. 80−70514
surface (001), H chemisorbed, self-consistent electron struct. 80−44693
surface (001), self consistent electronic struct., pseudopotential calcs. 79−42606
surface (001), struct., LEED anal. 80−34282
surface (001), struct. determ. using LEED 79−42351
surface (001), surface electron struct., matching Green function method calcs. 78−88014
surface (001), with adsorbed S layer, struct. and effect on CO adsorption 79−86981
surface (001) with saturated H adsorption, band structure self-consistent calc. 80−15585
surface (100), adsorpt. of CO, LEED, AES, study 78−87873
surface (100), chemisorpt. of O_2, low-energy SIMS, ion yields depend. on surface chem. and primary ion energy 78−73105
surface (100), clean, electron struct., positron annihilation obs. 80−24988
surface (100), emission and work function, K adsorption effects 78−11060
surface (100), surface resonances, photoemission and field emission meas. 79−4593
surface (100) with adsorbed O, obs. of O^- and O^+ during electron bombardment 79−95883
surface (110), Au film growth, AES, LEED, thermal desorption study 80−80130
surface (111), electroluminescence in 200 to 630 nm range 80−103997
surface (111), work function temp. coeff. 80−100499
surface (112), adsorption of Li, LEED and contact pot. method 80−10794
surface blistering, SEM and TEM obs., ion energy, dose and target temp. depends., review 77−43261
surface blistering by 75 to 350 keV He ions, SEM study 78−72657
surface deformation, He implanted, integrated lateral stress 77−31697
surface density of states 78−52047
surface erosion, by H_2^+ bombardment 77−15464
surface erosion due to H_2^+ and He^+ bombardment 79−85769
surface geometry and emission parameters, changes during directional mass transport 78−2344
surface impurities, depend. on prep. method, ion scatt. spectroscopy 80−40200
surface irregularity statistics for laser component materials 79−14057

molybdenum continued
surface machined, struct., electron diffr., TEM *(German)* 77−73371
surface orientation effect as high temp. creep and fracture type 80−16403
surface oxide softening in single crystals 78−95860
surface reconstruction, physical realisation of two-dimensional Ising and X-Y model 80−15351
surface relaxation and electronic structure of (100) surface 79−73561
surface resonances of (100) plane, field emission energy distrib., LCAO calc. 77−32507
surface resonances on (100) plane, angle-integrated photoemission spectra 77−85894
surface sensitive structure in angular resolved photoemission *(French)* 77−40326
surface structure changes due to ionic bombardment, LEED and AES obs. *(Russian)* 77−1775
surface thermoelectrotransport of atoms 80−2448
surface [110], metastable He impact, secondary electron spectra 78−95642
surface-electron beam interaction, 0.4-5 mA ion beam extraction 77−84456
surfaces, Van der Waals forces computation 79−15204
surfaces (110) and (111), joint adsorption of Cs and O, and emission props. 78−2364
temperature standard reference material, USA National Bureau of Standards 80−47009
TFTR protective plate, sputtering and surface damage by D^+ irrad. 80−18645
thermal conduct. of high-purity single crystals in temp. range 2-70K 80−75545
thermal conductivity and electrical resistivity, 300 to 2600K 77−35913
thermal desorption of CO, effect of temp. gradient along sample 77−62735
thermal expansion, 100-2000°C, as standard samples for dilatometry 78−26699
thermal expansion, 971-2153°C, vac.-melted MChVP, impurity effect 78−26700
thermal expansion, linear coeff., 100-2546°C, cast and metal-ceramic, impurity depend. 77−66032
thermal fatigue test, quick heating, sintered, electron-beam melted, vac. arc melted, fusion reactor appl. *(Japanese)* 80−93716
thermal shock resistance, original struct. effects 77−63803
thermionic emission, integral, meas. using modified high vacuum electron emission microscope 79−9263
thermionic emission, work function in atmospheric pressure gases 78−76575
thermocyclic strength of high temps. of single crystal 77−16685
thermophysical data at high temps., submicrosecond-pulse-heating method 80−103459
thermophysical meas. above 2500K, apparatus 77−45845
thermopower, 200-1600K 79−65446
thermoreflectance spectra, 0.3 to 6 eV, rel. to band struct. calcs. 77−66521
thin crystal, anomalous transmission of high energy electrons *(Japanese)* 77−43117
thin film, chemical cpd. form. by N_2^+ and Ar^+ ion bombardment *(Russian)* 79−73225
thin film deposition by high current ion beam sputtering, struct. and elec. props. 80−59837
Tokamak, TFR, variable-radius Mo and graphite limiters 78−63600
Tokamak fusion reactor, mag. limiter plate, electron irrad. and thermal shock 78−66416
Tokamak impurity in fusion reactor, at. (mol.) struct. and collision data, review 80−43959
Tokamak limiter, surface observation, infrared techniques 80−38693
Tokamak plasma, highly ionised Mo ions, recomb. and ionisation rate coeffs. determ. 78−71427
Tokamak reactor ISSEC 78−41860
transverse galvanomag. and thermomag. coeffs. 77−20298
trapping of ^{3}He and D and mutual replacement 80−59493
twin and stacking fault energies calc. 80−2038
twin boundary and twinning dislocation struct., computer simulation 78−30644
unipolar arc damage in hot, dense D plasma 79−3235
UPS, angle-resolved, surface resonances on (100) face 78−2987
US attenuation meas. of mean free path temp. dependence 77−39825
US vibrations, anomalous damping under hydrostatic press. 79−14890
US working effect on single cryst. during deform., strengthening effect, plasticity resource *(Russian)* 79−34107
vacancy annealing stage after heavy ion implantation, Mossbauer meas. 78−39463
vacancy diffusion along single edge dislocations, computer modelling *(Russian)* 77−47612
vacancy diffusivity from width of grain boundary void denuded zone 77−47615
vacancy model for stage III annealing, He desorption meas. 77−1123
vacancy mutation to divacancies by He trapping, percolation onset 78−51601
vacancy recovery stage, radiation doping, elec. resistivity meas. 79−51102
vaporisation, influence of inert gases on losses *(Russian)* 79−55878
vapour press. above different crystallographic planes *(Russian)* 78−18762
void containing, positron annihilation characts. 80−80898
void lattice and depend. of vacancy porosity on irradiation dose *(Russian)* 79−27972
voids, effect of impurities on positron lifetime 77−15453
voids, in neutron-irradiated Mo, small-angle X-ray and TEM study 79−14849
voids, neutron radiation-induced shrinkage 79−51158
volt ampere characteristics during electron melting process *(Russian)* 80−75336
wear resistance, effect of surface hardening 77−59985
wetting by Cu-Ag-P alloy 79−82417
whisker crystal growth incorporated with field electron emission 80−44458
wire, US inspection, immersion method 80−66757
wires, drawn and annealed, tensile fatigue and tensile strength under cyclic stress *(Japanese)* 78−15507
work hardening and softening in cyclic strain 80−20957

molybdenum continued
X-ray absorption, discontinuities and limits, chem. combination effects 80−93435
X-ray absorption edge, chem. shift, electron binding energy in compounds 78−62822
X-ray electron spectra, paramag. susceptibility, depend. on plastic deform. for single crysts. 77−28683
X-ray emission spectra, detect. from Alcator-A Tokamak 80−92389
X-ray L_1, L_2 and L_3 absorption limits 77−90218
X-ray $M\zeta$ energy, revised values 80−14102
X-ray reflection intensities, charact. temps. and Debye-Waller factors, 100-370K 78−18731
X-ray spectra, $K\alpha_{1,2}$ $K\beta_{1,3}$ lines, using diffractional focusing 78−5988
Young's modulus and shear modulus, temp. depend. 78−27553
zone refining effect on recryst. grain orient. in rolled and annealed cryst. 77−36532
Al-GeSe-Mo effect of contact material on DC and AC behaviour of sputtered amorphous GeSe film 79−95513
Al-Si-Mo, photovoltaic props. of sputtered amorphous Si films 77−24623
AlN-Mo cermets, ZrO_2 and mullite whisker reinforced, strength var. with temp. 80−104232
Al_2O_3, Mo-refined single crysts., fabrication 80−16250
Al_2O_3:Mo^{3+}, zero field splitting study by ESR 80−7159
Al_2O_3-Mo (20 wt.%) cermet, ZrO_2 crystal addition effect on thermal fatigue resistance 80−40528
Al_2O_3-Mo cermets, effect of processing factors on props. 79−100103
Al_2O_3-Mo cermets, ZrO_2 and mullite whisker reinforced, strength var. with temp. 80−104232
Au-Mo-Si multiple layer structure, bombarded with P ions, calc. of P ion profile in substrate *(Russian)* 79−55771
$Ba_2NaNb_5O_{15}$:Fe,Mo, photorefraction mechanism and photoelec. props. 80−71381
BaO-Al_2O_3-SiO_2-Ta_2O_5-Mo glass ceramic metal composites, cermet prep. 80−11618
BaO-P_2O_5:Mo^{5+} glass, EPR spectra, computer simulation 80−88872
$BaWO_4$:Mo, P, thermoluminesc. traps, EPR meas. 77−90032
$Bi_{12}SiO_{20}$:Mo, Raman scatt. spectra, impurity effect 80−80795
$Bi_2W_2O_9$:Mo, energy transfer and luminesc. props. 80−55177
C content determ., isotope-spectral method *(Russian)* 80−55766
C doped sheet, electron beam welded, low temp. ductility 79−87685
$CaMoO_4$:Mo^{5+}, g-factor, ground state, line broadening, EPR obs. 80−39863
CaO:Mo, spin coherence and Stark modulation effect of F_A-Mo centre excited state 77−69733
CaV_2O_6:W^{6+},Mo^{5+}, g-factors and hyperfine coupling parameters of V^{4+}, ESR 77−12196
$CaWO_4$:Mo, P, thermoluminesc. traps, EPR meas. 77−90032
CeO_2-Mo-CeO_2 thin-film selective coatings for solar energy collectors 78−94422
(Co,Mo)/Al_2O_3, hydrodesulphurisation catalyst, prep., props. and appls. 77−86360
(Co,Mo)/Al_2O_3 hydrodesulphurisation catalysts, physical props. and activities 77−86358
(Co,Mo)/Al_2O_3(SiO_2), and unsupported, catalyst for hydrodesulphurisation 77−86355
Co-Cr-Mo, eutectic alloys, charact. by melting, oxidation resistance and composition 78−52768
Co-Mo, multilayer films, depth resolution determ. in Auger depth profiling meas. 79−78800
CsMgCl:Cr^{3+},Mo^{3+}, Cr^{3+}-Mo^{3+} exchange coupled pair, EPR study 79−42830
D^+ impact, surface blistering, SEM study 78−71774
Fe-Co-Cr-Mo (20, 15, 5 wt.%), maraging, stainless alloy fracture toughness 77−73326
Fe-Cr-Mn-Mo, influence of Mo on defect conc. energy *(Russian)* 80−54241
$GdCu_2Si_2$/Mo, point contact spectroscopy of magnons 79−38312
Ge/Mo substrates, device quality epitaxial growth of polycrystalline GaAs 79−69988
H and D trapping, enhancement due to He ion damage 77−31698
He ion irradiated, TEM 77−19994
LuAl garnet:Mo^{3+}, single crysts., EPR *(Russian)* 77−63267
MgO:Mo catalyst, adsorpt. of propylene, oxidation reactions, surface structs., IR absorpt. spectra obs. 80−66868
MnO_2:Mo, Zn^{2+} ion specific adsorpt. kinetics, ^{65}Zn γ-ray scintillation investig. 80−70529
Mo (100), orientation effects in Auger electron spectroscopy 79−69928
Mo, arc, steady, vac., plasma ion mass and energy diagnostics 78−51385
Mo, cast, purification of C, O_2 and N_2 using thermal cycling *(Russian)* 79−70114
Mo, cast state, interaction nature between C, O_2 and N_2 *(Russian)* 79−70114
Mo crystals, joined by compression during heating, structural changes *(Russian)* 80−108513
Mo electrode, corrosion rate in molten glass *(Chinese)* 80−66687
Mo, electron-surface plasmon scattering using a parabolic non-touching trajectory 78−95328
Mo I spectrum, lifetime meas. of excited states of $4d^55p$ and $4d^45s5p$ config. 79−13683
Mo IX, 4p-5d,6d and 4p-6s,7s transitions, grazing incidence spectrograms 79−36576
Mo IX, 4p-5s transition 77−27010
Mo IX, energy levels, $4s^24p^4$ to $4s4p^5$ transitions obs. 77−3288
Mo IX, X, XI, 4p-4d transitions obs. 78−82669
Mo, macroscopic heterogeneity of plastic deform., metallographic examination *(Russian)* 79−100210
Mo oxycyano complex, reaction with reducible substrates, biological N_2 fixation 77−86369
Mo polycrystn., cyclically deformed, dislocation arrangements 80−108506
Mo powder, influence of powder reduction processes on props. 80−89175
Mo, recrystallisation kinetics, deform. degree effects *(Russian)* 78−6943
Mo, sputtering yield meas. by AES 78−95633
Mo VI, $4p^64d$-$4p^54d5s$ transitions, level assignments 79−22631
Mo VX-XIV, transition array and energy level distribs. variance 80−37767
Mo wire, struct. and high-temp. creep, dopant elements influence 80−66603
Mo XIII and XVII, spectra, perturbation theory with model pot. 78−58579

molybdenum continued
Mo XIII-XVIII, spectrum 20 to 90 Å from laser-prod. plasma and low-inductance vac. spark 80−102473
Mo XIV, ionisation energy, multiplet strengths, diagrammatic MBPT theory calcs. 80−9500
Mo XIV to Mo XXIX, extreme UV spectra 80−87068
Mo XLI, Mo XL, X-ray emission from vacuum-spark plasma 78−41991
Mo XV, E2 transitions, rel. to soft X-ray spectrum of TFR Tokamak 78−79470
Mo XV, electronic struct. of complex ion, relativistic perturbation theory 79−22610
Mo XV to Mo XXXIII identification in soft X-ray spectrum of TFR Tokamak 77−72504
Mo XXX, XXXI, XXXII, X-ray emission spectra, from laser produced plasma, line identification via HF calcs. 78−33459
Mo XXX to Mo XXXII, XUV spectra in laser prod. plasma 78−50493
Mo XXXI-XXXIV spectra from exploded Mo wire plasmas 79−1295
Mo XXXII, electron impact excitation, transition probabilities, oscill. and collision strengths 78−25718
Mo XXXIII, dielectronic recombination rate calc. 80−14232
Mo XXXIII, XXXIV, XXXV, transition identification X-ray spectra 80−32648
Mo XXXIX, energy levels and transition 79−59383
Mo X(XI), 4p-5s transitions 77−23453
Mo^{12+}, VUV reson. lines, transition probabilities calcs. 78−41989
Mo^{13+}, determination of spectrum using low-inductance spark and laser-produced plasma 80−19610
Mo^{13+}, energy levels for transition probabilities, oscillator strengths, rad. lifetimes 78−17589
Mo^{24+}, electron impact ionis., dominant Auger process 77−68120
Mo^{29+} to $^{39+}$, photoionis. cross sections, radiative recomb. rate coeffs., rel. to plasma diagnostics 80−52953
Mo^{30+}, VUV reson. lines, transition probabilities calcs. 78−41989
Mo^{32+}, dielectronic recomb. rate coeffs. in plasma 80−43853
Mo^{32+}, Na like ions, dielectronic recombination rate, scaling props. 80−32668
Mo^{33+}, X-ray spectra, $2p^5$-$2p^43d$, laser plasma 78−86806
Mo^{38+}, dielectronic recomb. rate coeffs. in plasma 80−43852
Mo^{39+}, electron impact excitation, relativistic Coulomb-Born approx. 79−68318
Mo^{39+}, partial photoionis. cross-sections and radiative recomb. rate coeffs. 80−52951
Mo^{5+}, ESR obs., on used hydrodesulphurisation catalysts 77−70342
Mo^{5+}, form. on reduced MoO_3-TiO_2 surface 77−90590
Mo^{n+} ($n \leq 42$) radiative electron capture calcs. 77−6928
Mo:Ba^+, secondary electron coefficients, temp. depend. 77−69947
Mo:C (110) surface, segregation, precip. and desorpt. of C, AES and LEED study *(French)* 80−103480
Mo:H(He), depth profiles of implanted atoms, proton backscatter meas. 79−51136
Mo:He, accumulation and distrib., monolayer conc. by sputtering quantitative anal. 80−49253
Mo:He, interaction of He with edge dislocation, influence of interatomic pot. 79−33014
Mo:N, ion implanted proton-irradiated, annealing behaviour 78−91362
Mo:N, single cryst., interaction of N with vacancies 79−82261
Mo:N film, high T_c amorphous phase stabilisation by interstitial nitrogen 78−23622
Mo:N film, implantation effect on supercond. and struct. transform. 77−4462
Mo:Xe, BCC, heavy ion implanted, vacancy recovery, Mossbauer spectroscopy 79−82896
$Mo/MgO(SiO_2)(\gamma\text{-}Al_2O_3)$ catalyst, diffuse refl. spectra 77−86363
Mo/Nb welded joints in sheet metal, detect. and exam. of cracks, initiation, development 77−73385
Mo/SiO_2, supported catalyst, EPR and UV-visible spectra of $Mo_6O_{19}^{3-}$ 79−99764
Mo-Al, thin film system, phase growth kinetics *(Russian)* 77−43390
$Mo\text{-}Al_2O_3$, catalysts, reducing and sulphiding treatments, XPS obs. 78−85196
$Mo\text{-}Al_2O_3$, vaporis. at elevated temp., mass spectrometric obs. 79−29388
Mo-C film layer structure obs. of supercond. transition temp. and crit. mag. field oscills. 77−69438
Mo-CdSe Schottky barrier, characts. study 79−51673
Mo-chalcogenide glass-Mo-Al struct., strong elec. field effects 80−97004
Mo-Cu cathode, spot motion and nature in UHV 80−79597
Mo-Cu nonmiscible system, sputter yields 79−87546
Mo-dimethyl terephthalate contacts, effect of elec. field on contact electrification 79−19660
Mo-Ge granular metal-amorphous semicond. film system, elec. transport and thermopower 77−76984
Mo-He and He-He Born-Mayer interaction potentials derived from He desorption expts. 79−99409
Mo-n-Si Schottky barrier, sputtered, freq. cond. charact. 77−20426
Mo-Ni film system, diffusion reaction, phase form. 77−84999
Mo-Ni thin film junction, phys. vap. deposition parameters effect on thermoelec. power 77−39922
Mo-Si, interface modification by ion implantation 80−70475
Mo-Si diffusion couples, $MoSi_2$ or Mo_3Si/Mo_5Si_3 form. 79−77836
Mo-Si film-substrate interface, reaction on heat treatment, silicide formation 80−79999
Mo-Si junctions, metallurgical boundary props. and elec. resistivity 78−2568
Mo-Si Schottky barrier diode, sputtering damage effects on I-V and C-V characts. 77−39940
Mo-Si sputtered contacts, contact resistance 80−92970
Mo-Si-Mo and Mo-Si structs., non-volatile memory switching 80−54814
$Mo\text{-}SiO_2$-Si, Mo-Si pelicular structures, struct. transitions during vacuum thermal treatment *(Russian)* 78−95238
$Mo\text{-}SiO_2$-Si, R/MOS struct., heat treatment effects 78−76683
$Mo\text{-}SiO_2$-Si, thermally stimulated ionic cond. 78−10565
Mo-TiC lamellar eutectic composite, deformation and strength, room temp. to 2073K *(Japanese)* 80−71702
Mo-transition metal admixtures, equilib. distrib. coeff., functional dependence *(German)* 77−76566
Mo-W system, short-range order calc. *(Russian)* 79−23566
Mo+Nb, K-shell vacancy prod., impact parameter depend. 80−14225
Mo^{n+} + H, single electron capture cross-section 79−59560
Mo^{n+} + H_2, single electron capture cross-section 79−59560
Mo_{12} cluster, one-dimens condensation of Mo_6 octahedral clusters, prep. and struct. of $Tl_2Mo_9S_{11}$ and $K_2Mo_9S_{11}$ 80−107168
molybdenum continued
Mo_2, matrix isolated visible absorpt. spectra, electronic, vibronic and vibr. states 80−28027
Mo_2 metal-metal bond energy, SCF-Xα-SW calcs. 80−78538
Mo_6 clusters, electronic struct., scattered wave-Xα calc. 79−11053
Mo_2C precipitates in Mo, TEM exam., exam. of crystallographic relationships 78−52811
$Mo(CO)_6$, pyrolysis for CVD of Mo_2C, laser fusion target appls. 78−60861
$MoGe_2$-Mo diffusion couple, nucleation of $Mo_{13}Ge_{23}$ *(French)* 77−55398
MoO_3 topotactic transform into MoO_2, electron microscopy, X-ray anal. 80−107417
MoS_2 intercalation compounds, reaction with alkali and alkali earth metals, band struct., superconductivity 78−26541
$Mo_{70}Si_{20}B_{10}$, amorphous alloys obtained by liq. quenching, superconductivity 80−75670
^{A}Mo, A=92, 94-98, 100, muonic atom X-ray transitions, nuclear charge radii 80−27545
^{A}Mo, A=95, 97, nucl. quadrupole moments from laser-RF double reson. spectroscopy 80−57682
^{95}Mo, ^{97}Mo, Fourier transform NMR, chem. shifts and Larmor freqs. *(German)* 77−59473
^{95}Mo, ^{97}Mo, quadrupole moments, hyperfine B factors, laser-Rf double reson. meas. 78−33452
$^{98}Mo_2$, electronic spectra after flash photolysis of $Mo(CO)_6$ 79−36622
^{99}Mo, airborne short-lived radionuclides of unknown origin in Sweden (1976) 78−32219
^{99}Mo, atomic-beam mag. reson. nuclear spin and hyperfine structure meas. 79−776
^{99}Mo fission product, sequential cation-exchange separation from neutron irrad., U_3O_8 77−90898
^{99}Mo, generation of ^{99m}Tc, influence of radiation dose on elution yield 79−29624
^{99}Mo impurities in ^{99m}Tc, gamma camera array 80−36100
^{99}Mo separation from neutron irradiated ^{235}U, HNO_3 soln., S collector 77−42161
^{99}Mo, separation regeneration of breeder reactor fuel *(Czech)* 78−82496
$NH_4Al(SO_4)_2.12H_2O$:Mo^{3+}, EPR, X-band, ion position and spin-Hamiltonian parameters 77−48042
Nb_2O_5:Mo^{5+}, ESR obs. on B-form single crysts. 80−54946
Ne-Ne and Ne, negative afterglows, microwave quenching and recombination processes, Mo emission 77−80307
$(Ni,Mo)/Al_2O_3$, hydrodesulphurisation catalyst, prep., props. and appls. 77−86360
Ni-Cr-Mn alloy solidification, effects of Si, Mo and Co alloying 79−83193
Ni-Fe-Cr-Nb-Ta-Mo alloy, fatigue crack growth, stress ratio and hold-time effects 80−40531
Ni-Mo, multilayer films, depth resolution determ. in Auger depth profiling meas. 79−78800
Pt-Mo bimetal sheet specimens, interdiffusion, 1500°C *(Russian)* 77−62683
Re-Mo bimetal sheet specimens, interdiffusion, 1500°C *(Russian)* 77−62683
Si:Mo contaminated solar cells, $POCl_3$ gettering 80−94010
$Si\text{-}SiO_2$-Mo-Si_3N_4-Al MNOS structures with metal grains, charge transport at SiO_2-Si_3N_4 interface 80−65693
SiC coating 80−7500
SiO_2-Mo-SiO_2 thin-film selective coatings for solar energy collectors 78−94422
SnO_2:Mo^{5+}, direct mechanism in supertransferred hyperfine interaction 79−23936
SnO_2:Mo^{5+}, hyperfine and superhyperfine interactions, EPR 77−8398
Tb/Mo, point contact spectroscopy of magnons 79−38312
TiO_2:Mo^{5+}, interstitial EPR, g-tensor and hyperfine tensor 80−84647
TiO_2:Mo anatase, single cryst., ESR of Mo^{5+} 79−28603
U, Mo and V, complex recovery from sedimentary ores 79−26701
VO_2:Ga, Mo, conductivity transitions 78−76121
W, powder, cold isostatic compaction effect on thermophysical props. 78−52717
with W surface film, vacuum-deposited strengthening *(Russian)* 77−66714
W-Mo-Co high-speed cutting steels, Co determ. 78−3416
YBe_{13}-Mo, solid state reaction, 1000 to 1400°C *(Russian)* 78−18845
ZrN-Mo, cermet, sintering reaction thermodynamics 80−2989

molybdenum alloys
see also molybdenum compounds
brazing to stainless steel 1Kh18N10T of type VM1 79−43551
cast alloy, shape, size, distrib. of carbides and oxides 79−24528
cast iron, white, high Cr-Mo, fracture toughness 80−50726
compatibility with Si_3N_4, solid-solid reactions 79−28151
Cr-Mo-V steel turbine rotor, fatigue tests 78−39912
creep rate in vacuum, grain size effect, for TsM-6 80−108514
dilute, HVEM bombarded, neutron damage simulation, defect cluster and dislocation obs. 80−107330
dispersed nitride strengthening anomalies *(Russian)* 77−21154
dispersion hardened with ZrC, thermally activated plastic deform. *(Russian)* 77−36612
dispersion-strengthened, plastic deform. and hardness, temp. depend. 80−3087
distribution of C *(German, English)* 79−20059
Fe-Cr-Co-Si-Mo, plastic deform. influence on structure and mag. props. *(Russian)* 79−70176
filamentary crystal prep. from brittle high-strength mats., mech. props. *(Russian)* 77−59712
fractography of deformed samples *(Russian)* 78−19889
fusion reactor first wall and blanket material, props. for struct. appl. 80−30071
fusion reactor first-wall and blanket material, mech. props. 80−34074
fusion reactor material, long term radioactivity minimisation 78−772
Hastealloy X, relations between weld heat affected zone cracking and microstruct., Gleeble test *(Japanese)* 78−52858
Hastelloy, C-276, H transport rel. to ageing treatment 80−75384
Hastelloy, C-276, H-induced crack growth 80−71747
Hastelloy, H_2 embrittlement in H_2S environments, impurity segregation effects 80−71724
Hastelloy B-2, corroded surface, electron bombardment effect during Auger electron anal. 80−61014

molybdenum alloys continued
Hastelloy B-2, decomposition of metal oxide films under electron bombardment 78−19928
Hastelloy C, stress corrosion cracking in high temp. caustic soln. 77−59964
Hastelloy C-276, cold worked, annealed, surface segregation, Auger spectroscopy study 79−83204
Hastelloy C-276 and C-4 cold worked high alloy material, factors affecting H_2 embrittlement in H_2S environments 78−31502
Hastelloy C-276 and G, accelerated H_2 charging in aq. H_2SO_4 at 0.2% yield stress 80−30144
Hastelloy C-276/Bi_2Te_3 contacts, elevated temp. compatibility, appl. to radioisotopically powered thermoelec. generator 79−49680
Hastelloy C-4, loaded at high temp., useful life 80−40523
Hastelloy N, air contamination effect on compatibility with liquid Li in stainless steel vessels at 600°C 78−25285
Hastelloy N, Si additions, comp. of eta carbide after ageing 78−52816
Hastelloy X, carburisation and dimens. stability in HTGR, He environment 80−45366
Hastelloy X, creep, effect of He environment and grain size *(Japanese)* 77−48488
Hastelloy X, creep props. and appl. to structural design *(Japanese)* 77−59862
Hastelloy X, H permeability using permeation method, effects of heat treatment *(Japanese)* 78−51740
Hastelloy X, heat resistant superalloys, for nuclear plants in He, creep props. *(Japanese)* 79−83263
Hastelloy X, high temp. low cycle fatigue strength *(Japanese)* 77−59910
Hastelloy X, high temp. low cycle fatigue tests, ductility, fracture 77−90523
Hastelloy X, thermal fatigue props. 80−21071
Hastelloy-X, carbonisation and carburisation in high press. He environment *(Japanese)* 79−26516
Hastelloy-X, fatigue crack propag. at elevated temps. in solid solution strengthened superalloys 78−39895
Hastelloy-X, low cycle fatigue crack propagation at 25°C and 760°C 80−104270
Hastelloy-X, Ni-Cr-Fe-Mo, cyclic oxidation resist. improvement by high temp. etching treatment 80−97627
Hasteloy B, equilibrium surface bombarded with high dose He^+ ions 78−95091
Hayes alloy no.716, Fe-Cr-Ni-Co-W-Mo-Si-C-B (26, 22, 12, 3.5, 3, 1.2, 1.1, 0.4 wt.%), hardfacing alloy 80−100802
Incaloy 623, cold worked, factors affecting embrittlement in H_2S 78−31502
Inconel, sputtering and blistering from H^+ and He^+ bombardment 78−79649
Inconel 617, creep, morphological changes of carbides, affect on creep props. 80−108509
Inconel 617, microstruct., mech. props., thermal ageing effect 77−36557
Inconel 625, electron yields under ion bombardment for clean and oxidised surfaces 80−66368
Inconel 706 and 718, relations between weld heat affected zone cracking and microstruct., Gleeble test *(Japanese)* 78−52858
Inconel 718, grain growth during sintering 80−97449
Inconel alloy 718, exam. of struct., properties and continuum synthesis of ductile fracture 78−76736
Inconel hardfacing materials, friction characts. in high temp. Na *(Japanese)* 80−89356
induced codeposition from aqn. soln. *(Japanese)* 79−4924
intercryst. fracture in ductile-brittle transition region, local internal stresses effect 80−81200
lattice dynamical models, phonon dispersion curves 77−89506
mag. props. after isothermal thermomag. treatment *(Russian)* 80−25159
metallic glass, Mo-based, development 80−89172
metallurgical stability and corrosion in impure He atmospheres, HTR appl. 79−36329
Mo-Ni powder mixtures, form. using electric discharge sintering 77−12563
Multimet, fatigue crack propag. at elevated temps. in solid solution strengthened superalloys 78−39895
Ni-Cr-Mo-Ti-Al, quenching and ageing effects on props. of type 36NkhTYuM8 79−52275
Nilomag alloy 771 coloured, X-ray photoelectron spectroscopy of surface film 78−64899
Nimonic PE16, irradiation creep data obtained in fast and thermal neutron spectra correlation with displacement cross-sections 80−84993
Nimonic PE-16, electron irrad. in HVEM, void growth, vacuum environment influence 80−107323
Permalloy-Mo, galvanomag. props. 77−39822
pipe, creep-resistant, influence of chem. comp. on formability *(German)* 78−84900
precipitated, finely dispersed, distrib. change due to homogenisation annealing 77−70056
precipitation hardened, yield stress in tension and compression, SD-effect *(Ukrainian)* 77−56021
reaction with sintered Li_2O pellets 79−47913
recrystallisation, crystallographic and structure texture of Mo alloy with dispersed HfN phase *(Ukrainian)* 80−71668
Rene 41, Ni-Cr-Co-Mo-Ti-Al-Fe (18.96, 11.09, 9.65, 3.06, 1.59, 0.89 wt.%) formation of Cr_2O_3 monocrystals on heat treatment 79−52455
Rene 41, volatilisation of oxides during oxidation at 1200°C 78−23873
solid-state bonding, tensile strength of bond *(German)* 79−47756
sphere, three-body abrasive wear with small size diamond abrasives 80−76373
steel, 30KhG and 30KhN, carbide formation, Mo alloying effects *(Russian)* 78−48402
steel, 30N9K4, effects of Mo, V, and N on grain growth, tempering, hardenability, strength and toughness 78−44202
steel, Al-Ti-(V)-Mo, Al-V-Mo and Al-Ti-Nb-Mo low-alloy, toughness improvement through Ti additions 80−66525
steel, alloy, Cr-Mo, alloy SCM3, hydrogen embrittlement, delayed fracture, exam. *(Japanese)* 78−64620
steel, alloy, Cr-Mo, pitting and crevice corrosion, exam. *(Japanese)* 78−64769
steel, alloy, Cr-Mo-V, fatigue, failure probability based on residual strength 78−68797
steel, alloy, Cr-Mo-V-P, quenched, temper brittleness in relation to V and P concs. 78−52986

molybdenum alloys continued
steel, alloy, Fe-Cr-Mo-Si-V, various steels, short rod stress intensity factor tests up to 700K, exam. 78−60815
steel, alloy, Fe-Cr-Ni-Mo-Al, (13, 8, 2, 1, wt.%), H_2 effects on fracture, exam. 78−60809
steel, alloy, Fe-Ni-Cr-Mo-V-C, H_2S stress corrosion cracking, effects of overload, exam. 78−60886
steel, alloy, Fe-Ni-Cr-Mo-V-C, HY130, effect of H_2 and impurities on brittle fracture, review 78−60765
steel, alloy, Fe-Ni-Mn-Si-Cr-Ni-Mo, effect of metallurgy on stress corrosion cracking, and hydrogen embrittlement 78−60885
steel, alloy, maraging, 250-grade, ductility and toughness of hot isostatically pressed powder 78−52925
steel, alloy, Ni-Cr-Mo, alloys SNCM8, SAE 4161, heat treated, residual stress at fatigue fracture surface *(Japanese)* 78−64622
steel, alloy, Ni-Cr-Mo, SNCM8, mech. stre-ngth under combined alternating strength 78−64690
steel, alloy, V-W-Mo-Cr, exam. of carbide transformation 80−16299
steel, alloy, W-Mo-Cr-V, blanks welded to steel 45, optimal high temp. tempering 80−16351
steel, alloy type N24M5, martensitic transform. microkinetics 78−56637
steel, austenitic, Cr-Ni-Mo, Mo effect on lattice parameters and chem. comp. of σ-phase and $M_{23}C_6$ carbides 77−70072
steel, austenitic, DIN X8 CRNIMONB 1616 mech. props., FBR safety anal. 78−60966
steel, austenitic, high-temp. crack resist., B and Mo influence *(Russian)* 80−16435
steel, austenitic stainless, Cr-Ni-Mo (21,6,9 wt.%), N_2-strengthened, surface segregation of B, Auger and XPS spectra 79−90854
steel, austenitic stainless, Cr-Ni-Mo-Mn, Mo, Mn and ageing effects 78−35413
steel, austenitic stainless, influence of varying Cr, Mo, N contents on resist. to pitting corrosion 78−80668
steel, austenitic stainless, Mo effect on mech. behaviour in inert medium and hot Cl^- medium *(French)* 79−43482
steel, austenitic stainless, Mo-bearing, ellipsometric meas. of passive films, optical constants *(Japanese)* 78−85041
steel, C-Mn-Cr-Mo (0.4, 0.8, 1.1, 0.25 wt.%) C, Ni, Mo, Cr addition effects on toughness of bainite 78−11327
steel, C-Mo-P, intergranular fracture and grain boundary segregation, P, H, Mo effects *(Japanese)* 79−15775
steel, cast, high speed, solidification, $(Fe,Mo)_6C$ form., struct. 79−24514
steel, CC Cr-Mo (2.25, 1 wt.%) effect of heat treatment on tensile props. 78−23745
steel, CC Cr-Mo-V, creep fatigue interaction 78−60841
steel, CC Cr-Mo-V, creep/fatigue interaction 78−64632
steel, CC Cr-Mo-V, low alloy, creep fatigue interaction 78−64673
steel, CC Cr-Mo-V, stress relief cracking mechanism 78−64669
steel, CC Cr-Mo-V press. vessel, crack growth under creep 78−60827
steel, Co-Cr-Mo, maraging, age hardening, Mossbauer study 80−40002
steel, Co-Cr-Ni-Mo-Mn (39.65, 20.25, 15.33, 7.08, 1.9 wt.%) carbide formation during tempering after plastic deformation 80−16330
steel, Cr, and Cr-Mo-Ni, austenite decomposition, deform. effects, ferrite reaction 79−1842
steel, Cr, ferritic, corrosion morphology, electrochem. pot. and Mo additions effect *(French)* 80−45439
steel, Cr (17 wt.%), influence of Mo on intergranular corrosion *(French)* 80−21182
steel, Cr-Mn-Mo, Mo addition effect on carbide form. in type 30 KhG *(Russian)* 79−87638
steel, Cr-Mo, annealed, creep and rupture, heat treatment effects 79−24548
steel, Cr-Mo, annealed, interaction solid soln. hardening, precipitation effects on creep 79−4974
steel, Cr-Mo, cast and forged, difference in mech. props. 77−48465
steel, Cr-Mo, creep resistant, creep, effect of carbide precipitation *(German)* 77−52398
steel, Cr-Mo, effect of Mo on high-temp. props. 80−85005
steel, Cr-Mo, ferritic, grain boundary segregation, X-ray microanal. by STEM 80−66740
steel, Cr-Mo, grain size effect on ductile brittle transition 79−24615
steel, Cr-Mo, H embrittlement in H_2S environment, Mo effect 80−76415
steel, Cr-Mo, high-temp. props. and constitutive equations 79−34146
steel, Cr-Mo, kinematic hardening models, use in multi-axial cyclic plasticity 80−25717
steel, Cr-Mo, low alloy, stress corrosion cracking and corrosion fatigue 79−47806
steel, Cr-Mo, materials specifications for AGR steam generators 80−42772
steel, Cr-Mo, toughness of heat treated steels of equal tensile strength *(German)* 80−25727
steel, Cr-Mo, vacuum deposited Al film 79−70231
steel, Cr-Mo(2.25, 1 wt.%), corrosion behaviour in simulated HTGR He environment 79−54495
steel, Cr-Mo(-V), ductility and heat resistant prop. prediction rel. to fine struct. and solid soln. state 79−15751
steel, Cr-Mo (1.25, 0.5 wt.%), creep, fracture, Ti and Ti+B effects 77−36603
steel, Cr-Mo (1.25, 0.5 wt.%), creep and rupture, temp. and stress effects 77−86096
steel, Cr-Mo (1, 0.5 wt.%), heat treated creep failure, role of stress state 79−5047
steel, Cr-Mo (2.25,1 wt.%), exposed to H_2-H_2O-H_2S environment, fatigue crack growth 80−40623
steel, Cr-Mo (2.25, 1.0 wt.%), C transfer between structural steels and Na in LMFBR 79−97805
steel, Cr-Mo (2.25, 1.0 wt.%), thermally aged and Na decarburised, stress-rupture props. 80−21102
steel, Cr-Mo (2.25, 1 wt.%), annealed, heat treatment effect on tensile props. 78−11243
steel, Cr-Mo (2.25, 1 wt.%), creep-fatigue testing from thermal transient effects in CRBRP reactor 78−21660
steel, Cr-Mo (2.25, 1 wt.%), decarburization, carbide effects in high temp. Na *(Japanese)* 78−15403
steel, Cr-Mo (2.25, 1 wt.%), in high temp. Na, heat treatment and metallurgical struct. effects 77−16619
steel, Cr-Mo (2.25, 1 wt.%), relationship between minimum creep rate and time to fracture 78−56759
steel, Cr-Mo (2.25, 1 wt.%), strain hardening shakedown load during bending 80−20958

molybdenum alloys continued
steel, Cr-Mo (2.25, 1 wt.%), weld metal, high temp. crack growth, effect of tempering, prestrain and grain refinement 78−27622
steel, Cr-Mo (2.25, 1 wt.%) annealing, high strain rate tensile props. 77−25117
steel, Cr-Mo (3 wt.%), temper embrittlement 77−36647
steel, Cr-Mo (9,1 wt.%), austenitized in $\gamma+\delta$ phase field, secondary hardening and tempering 78−11247
steel, Cr-Mo (9, 1 wt.%) appl. of electron energy loss spectrometry to precipitate morphology 78−48414
steel, Cr-Mo (9, 1 wt.%) microstructural instability during creep, heat treatment effects 78−48472
steel, Cr-Mo and Cr-Ni-Mo, V effects on recrystallisation *(Russian)* 77−66654
steel, Cr-Mo and Ni-Cr-Mo, quenched and tempered struct. effect on H diffusion coeff. and solubility *(Japanese)* 78−52857
steel, Cr-Mo and Ni-Cr-Mo-V low-alloy, additive remedy for temper brittleness 80−66659
steel, Cr-Mo low alloy ferritic, meas. of alloy and impurity elemental distrib. using STEM 80−35601
steel, Cr-Mo weld metal, reheat cracking, residual elements and microstruct. influence 80−66553
steel, Cr-Mo weld metal, trace element embrittlement suppression by creep strength effects 80−66656
steel, Cr-Mo-(V) austenitic, creep resist., high-temp. props. residuals effect 80−66600
steel, Cr-Mo-V, 1% Cr, chem. comp. and struct. effect on deform. props. *(German)* 79−1888
steel, Cr-Mo-V, austenite to bainite transformation under cooling conditions, effect on creep 80−3033
steel, Cr-Mo-V, biaxial cyclic deformation behaviour 80−16431
steel, Cr-Mo-V, brittle failure resistance obs. influence of cold plastic deform. 78−72858
steel, Cr-Mo-V, cast, strain intensity approach of high temperature fatigue crack growth and failure 79−20175
steel, Cr-Mo-V, combined Cr-Mn addition effects on hardenability 78−7046
steel, Cr-Mo-V, creep, effect of microstruct., heat treatment, transform. temp. 78−11248
steel, Cr-Mo-V, creep crack growth temp. depend., 525 to 600°C 78−64634
steel, Cr-Mo-V, creep deform. under const. and cyclic temp. 79−38914
steel, Cr-Mo-V, creep fatigue interactions obs., strain controlled and load controlled tests 78−44214
steel, Cr-Mo-V, creep fracture, microstruct. effects 78−64668
steel, Cr-Mo-V, cyclic oxidation and crack growth during high strain fatigue 78−31586
steel, Cr-Mo-V, environmental crack growth during isothermal high strain fatigue and temp. cycling 79−5082
steel, Cr-Mo-V, fatigue crack growth rate and threshold under oxidising conditions 79−20272
steel, Cr-Mo-V, high temp. main steam pipe, residual stresses in butt welds 80−21059
steel, Cr-Mo-V, high temp. steam pipe weld, defect distrib. and growth 80−25979
steel, Cr-Mo-V, high-temp. cumulative damage for stage I crack growth 78−19883
steel, Cr-Mo-V, low alloy, V effect on creep *(Czech)* 77−86088
steel, Cr-Mo-V, medium strength, correlation between crack initiation, propag. and microstruct. 78−60787
steel, Cr-Mo-V, normalised and tempered, size and geometry effect on creep cracking behaviour 78−64630
steel, Cr-Mo-V, press. vessel, fracture, effect of tempering 78−60799
steel, Cr-Mo-V, rupture ductility rel. to cavitation, density and SEM obs. 79−34142
steel, Cr-Mo-V, strength and ductility in creep, purity influence 80−66598
steel, Cr-Mo-V, stress rupture strength at high temps. *(German)* 80−40474
steel, Cr-Mo-V, thermal fatigue and rupture strength 78−72857
steel, Cr-Mo-V (0.5, 0.5, 0.25 wt.%), comparison of methods of correlating creep crack growth 78−60826
steel, Cr-Mo-V (0.5, 0.5, 0.25 wt.%), creep crack growth, temp. effect 78−64667
steel, Cr-Mo-V (0.5, 0.5, 0.25 wt.%), heat treated, microstructure effect on threshold region fatigue 78−56757
steel, Cr-Mo-V (1, 0.5, 0.25 wt.%), long-time stress relaxation props. 77−12666
steel, Cr-Mo-V (1 wt.%) oxidation assisted crack growth during high cycle fatigue at 550°C 77−16742
steel, Cr-Mo-V alloy, crack growth during strain fatigue at 825K 78−39890
steel, Cr-Mo-V creep crack growth, relation between engineering and metallurgical factors 78−11321
steel, Cr-Mo-V low-alloy, high-temp. ductility and crack growth, impurities effect 80−66652
steel, Cr-Mo-V low-alloy, mech. props. and stress relief cracking, effects of impurities and deoxidation practice 80−66599
steel, Cr-Mo-V low-alloy, prior austenite grain boundary embrittlement by B 80−66657
steel, Cr-Mo-V low-alloy, stress relief cracking, impurity and alloy content effects 80−66654
steel, Cr-Mo-V low-alloy with high residual element content, cavitation control 80−66663
steel, Cr-Mo-V-W, crack-growth and thermal-mech. fatigue 80−21072
steel, Cr-Mo-W-V, long term creep rupture props., turbine blade *(Japanese)* 77−59909
steel, Cr-Mo-W-V, long time stress relaxation props. *(Japanese)* 77−59841
steel, Cr-Ni-Mo, 'light spots', fractographic anal. 79−29204
steel, Cr-Ni-Mo, dynamic and static softening behaviour at hot forming temp. *(German)* 80−25728
steel, Cr-Ni-Mo, for boiler tubes, austenisation conditions effects obs., on structure and mechanical props. 80−3151
steel, Cr-Ni-Mo, handbook data for type 34KhN1M 79−78960
steel, Cr-Ni-Mo, Mo addition effect on carbide form., X-ray obs. *(Russian)* 79−87639
steel, Cr-Ni-Mo-Mn, wetting of TiC, expt. planning investigation 80−60822
steel, Cr-Ni-Mo-V, magnetic induction, struct. dependence *(Czech)* 80−50141
molybdenum alloys continued
steel, Cr-Ni-Mo-V, Mossbauer austenitometry and mag. props. 80−40003
steel, Cr-Ni-Mo-V-Nb (12,8,1,1.5,0.4 wt.%) Ce addition effects on strength and hardness *(Russian)* 78−15454
steel, Cr-W-Mo-Co, high-speed, from atomised powders, mech. and cutting props. 80−66556
steel, Cr-W-V-Mo (3.9 to 4.5, 1.5 to 2, 0.9 to 1.2, 3.9 to 4.4 wt.%), heat resistant, type 8Kh4M4V2F1-Sh, mech. props. 80−16464
steel, CrMo, cast, fatigue tests under varying stress amplitude and varying temp., amplitude damage *(Japanese)* 78−27605
steel, CrMoNi, cantilever beam method to determ. J_{Icc} and J_{Iscc} *(Chinese)* 78−15488
steel, CrMoV, compact tension specimen, thickness effect 78−68764
steel, CrMoV, creep and creep strength under alternate tension/compression *(Czech)* 77−63728
steel, CrMoV, failure in post yield regime using single edge notched tension specimens 78−68765
steel, CrMoV, low alloy, dispersed phase of VC, hardening mechanism *(Czech)* 78−60676
steel, CrMoV (1 wt.%), high temp. creep and fracture 77−36598
steel, Croloy Cr-Mo, stress corrosion cracking in high temp. caustic soln. 77−59964
steel, Cu-Ni-Mo (2, 2, 0.25 wt.%), sintering, kinetic charcts. 80−60805
steel, Fe-Mo-C low-alloy, photoelectron microscopy of diffusional transformations 77−44242
steel, ferritic, Cr-Mo (2.25, 1 wt.%), annealed, time depend. strain controlled fatigue, nuclear steam generator appl. 77−8915
steel, ferritic, Mo addition effect on corrosion resistance, X-ray photoelectron study 79−74285
steel, high speed, W-Mo-Cr-V, production by powder metallurgy 77−12574
steel, high strength, low C, with N_2, yield strength, Mo effects 77−90410
steel, high V-W-Mo, high speed, phase composition and struct. of atomized powders 77−90323
steel, low alloy Cr-Mo, heat fatigue, effect of technical factors 79−79058
steel, maraging, grain refinement due to cyclic heat treatment 78−52971
steel, maraging, heating of thin samples with brief ageing, N6G4M, ON18K9M5T 78−52866
steel, maraging, Ni-Co-Mo (18,10,5 wt.%) precipitation *(Japanese)* 78−15402
steel, maraging, solubility of Fe-Mo-Co (10, 0 to 20 wt.%) Laves phase, depend. on Co *(Russian)* 79−100145
steel, maraging, type 200, effect of freq. on cyclic crack growth in salt water environment 78−64680
steel, maraging 250-grade, fatigue crack growth model, notch analysis of fracture approach 78−52984
steel, maraging Ni-Co-Mo, precipitation, elec. resist. meas. *(Japanese)* 78−11228
steel, martensitic, Cr-Co-Ni-Mo, notch toughness, rel. to sensitivity to stress conc. 78−31532
steel, martensitic, Cr-Ni-Co-Mo-Ti, Kh12N8K5M3TYu, ageing of C free martensite *(Russian)* 79−1884
steel, martensitic, Ni-Cr-Mo, fatigue crack initiation and propag. in water 77−9000
steel, Mn-Mo, castings, mech. props., Cu and Sn trace elements effect 80−66596
steel, Mn-Mo (3, 0.4 wt.%), specimen fracturing device for ion microprobe analyser, appl. to grain boundary segregation 77−21341
steel, Mn-Mo-Nb, high strength, ductile, acicular ferrite struct. 77−21191
steel, Mn-Mo-Ni, embrittling effects of residual elements 80−66655
steel, Mn-Ni-Mo low alloy steels for nuclear appl., toughness and heat treatment 80−5239
steel, MnMoNi(Cr), pressure vessel, stress relief cracking 79−43404
steel, Mo and Cr-Mo, X-ray elasticity constants at high specimen temp. *(German)* 80−35239
steel, Mo and Mo-Cr, X-ray elastic consts. function of plastic strain *(German)* 78−31436
steel, Mo-bearing, intercritically annealed dual-phase strip, props. and appl. 78−84858
steel, Mo-Cr (3 wt.%), CrC formation in isochronal tempering, electron microscope study 80−7584
steel, Mo-Nb (2.5, 0.035 wt.%) Mo content effect on sulphide stress cracking resistance 80−21157
steel, Mo-V, creep rupture strength, heat treatment effects *(German)* 78−72834
steel, Mo-V, creep rupture strength, rel. to microstruct. *(German)* 78−35467
steel, Ni-Co-Cr-Mo-C (10,14,2,1,0.16 wt.%), stress corrosion cracking at 22°C in 3.5% NaCl 79−8390
steel, Ni-Co-Mo-Ti, maraging, electron diffr. obs. of second phase *(Chinese)* 80−11655
steel, Ni-Cr, P induced temper embrittlement, Mo effect 77−86148
steel, Ni-Cr-Mo, cleavage fracture toughness, temperature and notch sharpness influence *(German)* 80−35291
steel, Ni-Cr-Mo, exam. of delayed fracture using fracture mechanics *(Japanese)* 78−52961
steel, Ni-Cr-Mo, fracture toughness determ. from yield strength and cleavage fracture strength *(German)* 80−35292
steel, Ni-Cr-Mo, impact strength, effect of modified ausforming *(Japanese)* 79−11692
steel, Ni-Cr-Mo, Ni effect on fracture toughness, heat treatment effect *(Korean)* 79−91781
steel, Ni-Cr-Mo, quenched and tempered, nothced bar tensile tests *(German)* 80−35247
steel, Ni-Cr-Mo, weld, stress corrosion cracking, metallurgical effects 79−43468
steel, Ni-Cr-Mo (11, 5, 3 wt.%), maraging, corrosion cracking in chloride and alkaline solutions 80−55576
steel, Ni-Cr-Mo (2.5 wt.%), elevated temp. fatigue, effect of zero load rest period 77−8943
steel, Ni-Cr-Mo increase of crack initiation time in delayed fracture by fatigue accumulation *(Japanese)* 78−11312
steel, Ni-Cr-Mo-V, stress corrosion cracking 77−52542
steel, Ni-Cr-Mo-V, turbine rotor shaft, fracture toughness, validity criterion for K_{IC} 78−72861
steel, Ni-Mo, powder forged, as-forged props., effect of process variables 77−59715

molybdenum alloys continued
steel, Ni-Mo, powder forged, fracture processes and fracture toughness 78−72870
steel, Ni-Mo-C (2.0, 0.2, 0.4 wt.%) sintered, struct. transforms. and mech. props. after quenching 80−66557
steel, Ni-Mo-Cr, embrittling effects of residual elements 80−66655
steel, NiCrMoV, stress corrosion cracking, cold work effects 78−11383
steel, pearlitic, Cr-Mo, Cr-Mo-V, and Mo-V, heat resist., Mo content rel. to mech. props. 79−20134
steel, Si-Cr-Mo-W-V (2,4,1,3,2 wt.%), heat treatment and props. 80−16349
steel, Si-Mn-Ni-Cr-Mo, acoustic emission during stress corrosion cracking appl. to materials testing 78−53042
steel, sintered, Cr-Mo, CaF addition effects on struct. heterogeneity 78−60611
steel, sintered, Ni-Cr-Mo additions, struct., props., thermomechanical treatment effects 77−12657
steel, solubility of W and Mo in $Ti(C,N)_x$ 80−16276
steel, stainless, austenitic, Cr-Ni-Mn-Si-Mo-C alloy, 13Khi8N10G3S2M2, elastic moduli exam. after thermomechanical treatment *(Russian)* 79−24558
steel, stainless, Cr, Mo effects on passivation AES and electrochemical anal. 79−74292
steel, stainless, Cr-Ni, maraging, effect of Mo, Co additions on hardening 78−84835
steel, stainless, Cr-Ni-Mo (16, 14, 3 wt.%), corrosion resist., vacuum heat treatment effect 79−87754
steel, stainless, Cr-Ni-Mo-N, phase diagrams 80−35161
steel, stainless, ferritic, corrosion in formic acid at 70°C, effect of Mo additions 78−35551
steel, stainless, ferritic, corrosion resistance improvement by Mo and Ti additions 77−90505
steel, stainless, Ni-Cr-Mo, two-phase, compositional charge of ferrite and austenite *(Japanese)* 79−4948
steel, stainless, Ni-Cr-Mo-W (29, 13, 3, 2 wt.%), long-term strength in H at high pressure 80−55485
steel, stainless, resulphurated, Cr-Mo (18,2 wt.%), Mo effect on corrosion resistance *(French)* 77−63830
steel, stainless, type Kh17N13M2T, strengthening by plastic deformation and cold working *(Russian)* 78−52839
steel, stainless complex alloy, hot ductility, B effect 80−30038
steel, stainless ferritic, Cr-Mo, corrosion behaviour, review 79−39018
steel, temper embrittlement and embrittling intergranular segregates, Mo effects *(French)* 79−91788
steel, tool, W-Mo, heat treatment effect on props. 80−50656
steel, W-Mo, high speed, hot deform. and heat treatment effect on props. 77−90372
steel, W-Mo, sintered high-speed, naphthalenelike grain form., quenching effect on fracture toughness 80−30103
steel, W-Mo, tool, hydrostatic extrusion and tempering, wear resistance effect 80−50728
steel, W-Mo-Co, high-speed tool, struct. and props., cooling rate effect at primary crystn. temp. 80−76241
steel, W-Mo-Cr-V tool, laser surface melted, struct., heat treatment effect 80−76424
steel Cr-Mo (2.25, 1 wt.%), duplex LMFBR steam generator tubing, US equipment for NDT 78−11469
steel Cr-Mo low-alloy, material selection for nuclear steam generator 78−54834
steel W-Mo-V-TiC, powder, TiC effect on milling, pressing and sintering 78−60607
strain hardening depend. on temp. and structural state in type MT *(Russian)* 79−91664
strengthening by modified ausforming 78−76665
superalloy, high temperature properties 78−44173
Supermalloy, 24 GHz ferromagnetic antiresonance transmission 77−51957
Supermalloy, 9, 24 and 38 GHz ferromagnetic reson. absorpt., line shapes 77−51958
supermalloy, foil, microwave transmission, parallel RF and mag. fields 77−59462
thermally degenerated Schottky diodes, resonant tunnelling 80−100503
β-Ti-Mo (15wt.%) metastable alloy, strength enhancement 77−66650
TsM10VD, erosion, effect of ion bombardment dose and previous surface treatment 80−89419
TsM-10 alloy, fatigue fracture mechanism, dislocation struct. *(Russian)* 77−32674
TZM, blistering under He ion bombard. 80−92567
TZM bonding to Fe by vacuum rolling, corrosion protection appl. 79−29283
TZM-Mo alloy, mech. props., effect of exposure to high temp. He containing O_2, room temp. study 80−93639
Udimet 700, high temp. fatigue crack growth, fracture mech. approach 79−52340
Vitallium, surgical implant, SCC and corrosion fatigue in Tyrode's soln. 79−29263
Vitallium alloy, fretting corrosion of surgical implant material, electrochemical investigation 79−66197
VM-1, thermal fatigue rel. to struct. change *(Russian)* 78−11302
VN-2M, vac.-melted, thermal expansion meas., 971-2153°C, impurity effect 78−26700
VT22, hot deform., microstruct. form. and mech. props. *(Russian)* 77−28830
Ag-Mo, optical props., DC resist. and thermoelec. power 77−85824
Al-Mo, struct. and props. of alloys obtained from granules 80−50717
Al-$MoSi_2$-Si system, diffusion, compound form., and microstructure 80−34253
Al-$MoSi_2$-n-Si system, Schottky-barrier height 80−34520
C-Mo, dil., brute-force nucl. orientation meas. 77−59466
Co-B-Mo-Cr, amorphous, Mo and Cr addition effect on corrosion behaviour 80−16568
Co-Cr-Mo shoulder prosthesis, wear and fatigue tests 80−26415
Co-Cr-Mo-Ni-Fe-Si-Mn-C, protective coatings by B diffusion, microstruct. and mech. props. 78−11427
Co-Fe-Nb-Mo, semihard magnetic alloy, magnetic props. 78−95469
Co-Gd-Mo, amorphous film, mag. props., temp. depend. 78−10734
Co-Gd-Mo, film, amorphous Hall effect 77−85347
Co-Gd-Mo amorphous films, resist. and extraordinary Hall effect, thermal annealing effect 80−70852
Co-Gd-Mo films, sputtered, O effects on mag. props. during annealing 80−89374

molybdenum alloys continued
Co-Gd-Mo-Ar film, amorphous, mag. props. 78−80182
Co-Mo, dendritic segregation 80−76260
Co-Mo, sintering, limited solid solubility, peritectic diagram 77−28754
Co-Mo (26 wt.%), magnetic alloys for high temp. appl. 77−85503
Co-Mo alloy electrodeposits, codeposited impurities rel. to H_2 permeation, props. 79−19493
Co-Mo catalyst, Mossbauer spectra 80−7222
Co-Mo-B metallic glass ribbons, tensile strength, crystn. temp. 80−89173
Co-Mo-Cr-Si, plasma and detonation coatings, Laves- and carbide-strengthened, comparative props. 78−15562
Co-Mo-Cr-Si Laves phase, sputter deposited, struct. and wear props. 77−40477
Co-Mo-Si, directionally solidified eutectics 79−61575
Co-Ni-Cr-Mo, mech. props., effect of twinning and FCC to HCP transform. 77−4779
Co-Ni-Cr-Mo (35, 20, 10 wt.%), MP35N, TEM study of phase transformations 80−81054
Co-Ni-Mo-C, amorphous alloys, med. props. and thermal stability *(Japanese)* 80−85049
CoCrMo, artificial hip joints, fatigue strength 79−48375
$(Co_{0.89}Fe_{0.11})_{72}Mo_3Si_{15}B_{10}$, metallic glass, strain- and field-induced mag. anisotropy 80−108004
$Co_{73}Mo_2Si_{15}B_{10}$, metallic glass, strain- and field-induced mag. anisotropy 80−108004
CoNiCrMo, artificial hip joints, fatigue strength 79−48375
Cr-Mo, behaviour of mag. impurities 79−4672
Cr-Mo, binary continuous solid solution, elec. resist. and thermoelec. power behaviour 79−69492
Cr-Mo, elec. resist. and thermo-EMF, conc. depend., 4.2 to 1500K *(Russian)* 80−80247
Cr-Mo, electrical resistivity, spin density wave gap, Neel temp. 80−88534
Cr-Mo (2.25, 1 wt.%) steel, T permeation rate at 400 to 500°C, rel. to LMFBR conditions 78−17319
Cr-Mo low C steel forgings, material capabilities 77−42105
Cr-Mo pressure vessel steel, improvement through electroslag remelting 77−42104
Cr-Mo steel types JIS SCMV 2, SCMV 3 and SCMV 4, high-temp. high-cycle fatigue props., press. vessel appls. *(Japanese)* 80−93650
Cr-Mo-Fe (2, 14 wt.%), spin density wave and spin glass ordering coexistence at low temps. 79−61059
Cr-Mo-Ni-Ti alloy A-286, stress-rupture data correlation 77−44346
Cr-Mo-V, steamline bends, restorative heat treatment effects 78−68716
Cr-Mo-V steel, creep rupture tests on notched cylindrical specimens at 600°C 77−32670
Cr-Mo-V-Nb, supercooled austenite isothermal decomp., struct., strength and fracture characts. 80−60966
Cr-Mo-W-Mo, heat resistant weld seam metal, tensile strength, thermophysical characts. 79−91769
Cr-Nb-Mo system, comp. and temp. depend. alterations in mech. props., phase diagram interpret. *(Russian)* 80−85045
Cr-Ni-Mo-Cr_xC_y wear resistant coating prep. by laser beam melting, and props. 80−40607
Cr-Ni-Mo-Cu-Nb steel, martensitic precipitation hardenable, corrosion-resistant, heat treatment, structure and props. 79−74169
$Cr_{1-x}Mo_xCo$, $x \lesssim 0.25$, antiferromag., nucl. mag. relax. 78−6590
$(Cr_{98}Mo_2)_{90}Fe_{10}$, spin glass behaviour obs. 79−61157
$(Eu,Sn)Mo_6S_8$, ternary superconductor, mag. interactions 79−73613
$(Fe,Mo)_{80}B_{20}$, glassy alloy, Curie temp. and crystn. temp., Mo additions effect, Mossbauer spectra 78−68428
Fe, cast, with acicular struct., Mo distrib. 78−92269
Fe solid solution, substitution strengthening by Cr and Mo *(Czech)* 80−30080
Fe-B-Mo metallic glasses, mag., struct., and elec. props. 80−88751
Fe-B-Mo-Cr, amorphous, Mo and Cr addition effect on corrosion behaviour 80−16568
Fe-C amorphous alloys, corrosion resistance improvement by Cr and/or Mo addition 79−66211
Fe-C-Cr-Mo, white cast, effect of abrasion on carbide microstructure *(German)* 78−88540
Fe-C-Mo, dynamics of transform. interface, ferrite-austenite interface 78−52795
Fe-C-Mo, dynamics of transform. interface, at intermediate temps. 78−52796
Fe-C-Mo-Nb-Al-Ti-B (0.015, 5.75, .7, 1.6, 2.5, 0.1 wt.%), TZM sheet, wear resistance, effect of surface hardening 77−59985
Fe-Co-Mo, phase relations in system at 1100°C 80−108392
Fe-Co-Mo ternary system, phase diagram *(Russian)* 80−16269
Fe-Co-Mo-C, amorphous alloys, med. props. and thermal stability *(Japanese)* 80−85049
Fe-Co-Mo-Nb(Ta) semihard mag. alloy, mag. props., thermal expansion, elec. resistivity and hardness *(Japanese)* 80−88789
Fe-Cr-Co-Mo, melted in open induction furnace, microstruct. and magnetic props. 79−61626
Fe-Cr-Co-Mo, microstruct., hardness, mag. props., influence of isothermal tempering and heat treatment 79−79129
Fe-Cr-Co-Mo alloys, struct. transform. and mag. props. *(Russian)* 77−76543
Fe-Cr-Co-Mo high energy permanent magnets, mag. props. 80−97119
Fe-Cr-Mo, (30,2 wt.%) Bridgman-type, unexpected embrittlement phenomena, hydrostatic tensile test *(Japanese)* 80−55517
Fe-Cr-Mo, grey cast, pearlitic, isothermal transform. of austenitic in bainitic range *(Rumanian)* 78−23698
Fe-Cr-Mo, passivated single crystal, selective dissolution and surface enrichment 80−16543
Fe-Cr-Mo, sputtering effect on surface comp., AES obs. 80−6601
Fe-Cr-Mo, white cast, optimising fracture toughness and abrasion resist. 80−85042
Fe-Cr-Mo (26, 1 wt.%), single crysts. and polycrysts. strain rate influence on low cycle fatigue props. 80−3126
Fe-Cr-Mo alloy castings, thick-section, factors affecting 80−108374
Fe-Cr-Mo and Fe-Cr-Mo-Si, amorphous films, corrosion resist. and ion plating use 80−89423
Fe-Cr-Mo sintered, damping capacity and mech. props. 78−44161
Fe-Cr-Mo-C, X-ray investigation after friction and oxidation 78−52997
Fe-Cr-Mo-Ti (13, 1.5, 3.5 wt.%), equilibrium studies on chi-phase strengthening 79−24496
Fe-Cr-Mo-(Ni), AES using peak-to-peak value *(Japanese)* 79−20485
Fe-Cr-Ni-Mn-Mo, liquid, N_2 solubility 78−44087

molybdenum alloys continued
Fe-Cr-Ni-Mo, liquid, N solubility, AlN precipitation 79−11630
Fe-Cr-Ni-Mo-V, Mo and V effects on segregation *(German)* 77−55942
Fe-Cr-Ti-Mo, sintered, mech. props. *(French)* 79−91726
Fe-Cr-Ti-Mo ferritic alloy, annealed, cold rolled, fast reactor material, mech. props. 78−21646
Fe-Cr-Ti-Mo-TiO_2 (13, 3.5, 1.5, 2 wt.%) dispersion hardened, void swelling 80−65046
Fe-Mo, carburised, austenite-carbide colonies struct. *(Russian)* 79−52449
Fe-Mo, cryst. struct. and defects, high resolution electron microscopy obs. 79−94961
Fe-Mo, damping capacity 77−86082
Fe-Mo, damping capacity *(Japanese)* 78−11259
Fe-Mo, dil., high freq. induction melting and centrifugal casting, working curve sample prep. photoemission anal. *(Japanese)* 78−53050
Fe-Mo, dislocation mobility and internal friction, effect of alloying in α-Fe *(Russian)* 77−31671
Fe-Mo, ferritic, thermodynamics and solubility of C and ferrite 77−36456
Fe-Mo, hyperfine field distrib., spin echo NMR meas. 78−76351
Fe-Mo, magnetic transition effect on alloying element solubility *(Japanese)* 79−42256
Fe-Mo, nitrided by const. activity ageing, X-ray studies 77−32720
Fe-Mo, semihard magnetic alloys, magnetic, elec. mech. props. *(Japanese)* 79−70078
Fe-Mo, solid soln., cyclic stress-strain props., depend. of fatigue crack growth rate 77−4853
Fe-Mo, split bands evidence from sp. ht. and elec. transport data 77−24515
Fe-Mo (0 to 6 wt.%), in chloride solns., role of Mo as localised corrosion inhibitor 79−20255
Fe-Mo (0.54 to 2.50 wt.%) ferromag. ordering effect on Fe diffusion *(Czech)* 77−62665
Fe-Mo (13-20 at.%) binary alloys, spinodal decomp. on ageing, TEM and X-ray diffr. study 80−97503
Fe-Mo (15.5 and 19.5 at.%), modulated struct., heat treatment effects, TEM obs. 79−100192
α-Fe-Mo (1.5 and 1.8 at.%), deform., testing mode effect at stages prior to steady states 77−66721
Fe-Mo (1.8 at.%), high temp. creep mech., use of stress exponent 79−5025
Fe-Mo (1.8 at.%), recovery creep theory estimation using high temp. creep data 79−15747
Fe-Mo (1.8%), creep, absence of instantaneous plastic strain upon stress changes 78−75718
Fe-Mo (3 wt.%), substitutional solid soln. with cubic faced symmetry, Portevin-Le Chatelier effect *(French)* 78−23785
Fe-Mo (3at.%), internally nitrided, precipitate, morphology and chemistry 78−44128
Fe-Mo (4.1 wt.%), substructs. developed during steady state creep at 1100-1200K, TEM obs. *(Japanese)* 79−38900
Fe-Mo (5 wt.%), Auger anal. of passive films in neutral aqu. soln. 80−16605
Fe-Mo alloy, TZM, doped, Ni activated recrystallisation, ion probe mass spectrometer obs. 77−44280
Fe-Mo alloys, pitting 80−16549
Fe-Mo alloys, spinodal decomp. and modulated struct. form. on ageing *(Japanese)* 79−100184
Fe-Mo austenite, thermodynamics of C 77−36457
Fe-Mo catalyst, Mossbauer spectra 80−7222
Fe-Mo doping surfaces of Fe with Mo under laer emission *(Russian)* 77−70211
Fe-Mo quenched alloy, electron microscope exam. of planar defects 79−79000
Fe-Mo system, self-diffusion 77−4214
Fe-Mo system, thermomech. props. 80−89208
Fe-Mo systems, galvanic cell meas., 1160 to 1366K 78−61042
Fe-Mo-Au, orienting of precipitating Au particles by external elastic stress 77−73279
Fe-Mo-B metallic glass ribbons, tensile strength, crystn. temp. 80−89173
Fe-Mo-C, eutectoid transform. of δ-ferrite 77−16570
Fe-Mo-C, lattice parameters of cementite, annealing effect 80−29007
Fe-Mo-C (0 to 4, 1 wt.%), phase equilibria at 1143, 1198 and 1253K 80−60835
Fe-Mo-C alloy, splat cooling, microstruct. changes 78−84855
Fe-Mo-C amorphous alloys, Mo effect corrosion resistance in HCl *(Japanese)* 79−96214
Fe-Mo-C system, isothermal sections, 973 to 1273K, thermodynamic analysis 78−6895
Fe-Mo-CaF_2 sintered composite, struct. and mech. props., heat treatment effect 80−66526
Fe-Mo-Co, solubility anomaly due to magnetic transition, Co effects *(Japanese)* 79−42257
Fe-Mo-Cr alloys, creep tests *(German)* 79−61648
Fe-Mo-Cr(Ni)(Mn)-C, carbide-austenite equilibria, 1173 to 1373K, microscopic and X-ray obs. 78−44085
Fe-Mo-P, P-induced temper embrittlement, Mo role 80−35316
Fe-Mo-P-C, amorphous, corrosion resist. in 1N HCl 78−80678
Fe-Mo-P-C, amorphous, XPS study of passivity 79−96185
Fe-Mo-Ta, ternary Laves phase strengthening 80−108466
Fe-Mo-(C)-(Ni), sintering 78−35333
Fe-Mo(4.1 wt.%), steady state creep at high temps. 80−89316
Fe-Ni-B-Mo, crystn. temp. and elec. cond. correl., Mo effect 80−75179
Fe-Ni-Co-Mo (18.65, 8.99, 4.87 wt.%), ageing characts., 380-530°C 80−60876
Fe-Ni-Co-Mo alloys, struct. transform. produced during tempering 77−86058
Fe-Ni-Co-Mo phase diagram and structure *(Russian)* 80−20899
Fe-Ni-Co-Mo-Ge alloy 40NKM, excess mag. noise after various thermomag. treatments *(Russian)* 80−29575
Fe-Ni-Cr-Al-Ti-W-Mo (35, 15, 2.4, 2.3, 2.2 wt.%) wrought superalloy, freckles *(Chinese)* 80−104137
Fe-Ni-Cr-Mo superalloy, mech. props., η-phase form. effect *(Chinese)* 80−20925
Fe-Ni-Cr-Ti-Mn-Mo, (25.8, 14.04, 2.17, 1.27, 1.30 wt.%), superalloy A-286, precipitation hardening, exam. of fracture toughness and mech. props. 78−92355
Fe-Ni-Mo, austenite, annealing effect on atom redistrib., Mossbauer anal. *(Russian)* 80−66529

molybdenum alloys continued
Fe-Ni-Mo, ferrite plus martensite structures, exam. of mech. props. 78−56709
Fe-Ni-Mo, formation of austenite structure in relation to α to γ transformations 79−100142
Fe-Ni-Mo, high-strength ferritic, for cryogenic service, mech. characteris. 77−70143
Fe-Ni-Mo, inhomogeneous solid solns., annealed and work hardened states, X-ray K-absorption spectra *(Russian)* 78−56544
Fe-Ni-Mo, martensitic transformation, annealing, influence on struct. of austenite *(Russian)* 80−81057
Fe-Ni-Mo, ordered, low temp. $\alpha \rightarrow \gamma$ transform. *(Russian)* 78−19740
Fe-Ni-Mo, phase relations in system at 1100°C 80−108392
Fe-Ni-Mo, small angle X-ray scatt. study, pre-precipitation phenomenon obs. *(French)* 78−19757
Fe-Ni-Mo, two-stage martensitic transformation kinetics, depend. on austenite initial state *(Russian)* 79−74151
Fe-Ni-Mo (16.4, 8.1 wt.%), effect of substituting Mo by W during ageing 80−29991
Fe-Ni-Mo-C, amorphous alloys, med. props. and thermal stability *(Japanese)* 80−85049
Fe-Ni-Mo-C, Mossbauer investig. of secondary hardening, carbide form. *(Russian)* 77−44260
Fe-Ni-Mo(13,3wt%), welded alloy, fracture and strength for cryogenic service 79−38930
Fe-Ni-Si-Mn-Co-Mo, effect of prolonged aging on mag. props. 80−16513
Fe-W-Cr-Mo system, mag. and mech. props. rel. to production methods *(Japanese)* 80−71107
Fe-W-Cr-Mo-Co (18,12,3,x wt.%) magnetisation and hardness, cold working effect obs. *(Japanese)* 77−40428
Fe-W-Cr-Mo-Co with austenitic phase, magnetic and mech. props., cold working and ageing effects *(Japanese)* 78−60678
$(Fe\text{-}Ni\text{-}Mo)_{80}(P\text{-}B)_{20}$, amorphous, mag. aftereffects and struct. instabilities 80−88833
$Fe_{36}Cr_{12}Ti_7Mo_3$, high temp. precipitation kinetics, internal friction study 79−43254
Fe_2Mo, standard Gibbs energies, enthalpies, entropies of formation 78−61042
Fe_3Mo_2, standard Gibbs energies, enthalpies, entropies of formation 78−61042
$Fe_{76}Mo_4B_{20}$, quenched ferromag. ribbon, Brillouin spectra 80−2776
$Fe_{78}Mo_2B_{20}$, amorphous, transverse magnetoresist., stress effect 80−15501
$Fe_{78}Mo_2B_{20}$, amorphous, fast neutron and fission fragment irrad., effect on elec. resist. 80−19846
$Fe_{78}Mo_2B_{20}$, amorphous ferromag., $T^{3/2}$ depend. of hyperfine field 78−39474
$Fe_{78}Mo_2B_{20}$, amorphous ferromag., mag. props. 79−38309
$Fe_{78}Mo_2B_{20}$ amorphous ribbons, magnetoelastic effects in as-quenched and stress-relieved states 80−80588
$Fe_{78}Mo_2B_{20}$, Elinvar-type behaviour 79−66091
$Fe_{78}Mo_2B_{20}$, exam. of mag. props. between 300 and 900K 78−85010
$Fe_{78}Mo_2B_{20}$ glass, thermal expansion, glass transform. and crystn. temps. 80−2183
$Fe_{78}Mo_2B_{20}$ glasses, internal friction and shear modulus 79−52287
$Fe_{78}Mo_2B_{20}$, glassy, ferromag. anisotropy of resistivity 79−23939
$Fe_{78}Mo_2B_{20}$, metallic glass, elec. resist., 78 to 1000K, probe of crystn. process 77−76787
$Fe_{78}Mo_2B_{20}$, metallic glass, triplet correlation, field-ion microscopy study 80−38921
$Fe_{78}Mo_2B_{20}$, metallic glass, Doppler broadening of positron annihilation γ-radiation and elec. resist. 80−66321
$Fe_{78}Mo_2B_{20}$, Metglas 2605 A, amorphous ferromag., resistivity down to 60 mK 79−60783
$Fe_{80-x}Mo_xB_{20}$ metallic glasses, Curie temp., crystn. temp., elec. cond. as function of composition 79−60285
$(Fe_{93}Mo_7)_{80}B_{10}P_{10}$, amorphous, neutron scatt. investig. of spin waves, magnetisation 77−47984
$(Fe_xMo_{1-x})_{75}P_{16}B_6Al_3$, amorphous, effects of Mo on mag. props., Mossbauer meas. 79−73859
$Fe_{40}Ni_{38}$-Mo_4B_{18} amorphous alloys, compatibility of DC and AC mag. props. 80−34695
$Fe_{40}Ni_{40}(Mo,Si,B)_{20}$, amorphous, soft mag. props., switched-mode power supply appls. 80−88850
$Fe_{0.49}Ni_{0.415}Mo_{0.095}$, Vibralloy, high-temp. vibrating reed meas. 79−55811
$Fe_{40}Ni_{38}Mo_4B_{18}$ amorphous ribbons, magnetoelastic effects in as-quenched and stress-relieved states 80−80588
$Fe_{40}Ni_{38}Mo_4B_{18}$, amorphous, crystallization, heat treatment and irradiation effects *(French)* 79−90558
$Fe_{40}Ni_{38}Mo_4B_{18}$, amorphous, mag. anisotropy, Mossbauer study 80−65864
$Fe_{40}Ni_{38}Mo_4B_{18}$, amorphous, reversible enhancement of mag. directional ordering rate 80−103829
$Fe_{40}Ni_{38}Mo_4B_{18}$ glassy alloy, high permeability, low field mag. characts. 78−68301
$Fe_{40}Ni_{38}Mo_4B_{18}$ metallic glass, reorientation kinetics of magnetization 79−24155
$Fe_{40}Ni_{38}Mo_4B_{18}$, metallic glass, mag. and transport props. 80−39752
$Fe_{40}Ni_{38}Mo_4B_{18}$ ribbon, magnetic characterisation 80−34680
Gd-Co-Mo, amorphous, sputtered very thin film struct. 77−15707
Gd-Co-Mo, amorphous films, thermal stability of mag. props. *(Japanese)* 79−47307
Gd-Co-Mo, sputter deposited amorphous alloy, substrate bias, magnetic anisotropy, annealing 78−48006
Gd-Co-Mo amorphous film, MCD, oxide surface layer effect 77−90132
Gd-Co-Mo film, amorphous, bubble and stripe domain wall vel. meas. 77−40094
Gd-Co-Mo film, amorphous, mag. props., ion implantation damage effects 77−89991
Gd-Co-Mo film, amorphous, mag. bubble dynamics 77−89997
Gd-Co-Mo film, amorphous, Ar sputtered, struct. 78−63946
Gd-Co-Mo film, amorphous, mag. props., annealing effects 78−64235
Gd-Co-Mo film, amorphous, in-plane susceptibility near compensation point 78−64238
Gd-Co-Mo films, amorphous, inhomogeneities of mangetization and anisotropy 79−65698
Gd-Mo-Mo amorphous film, domain drag effect obs. 78−91911
a-GdCoAu films, perpendicular anisotropy temp. depend., Lorentz microscopy 77−28419

molybdenum alloys continued
GdCoMo amorphous alloy films, mag. cobalt alloys susceptibility, uniaxial anisotropy field 80−54930
GdCoMo film, amorphous, sputtered, ferrimag., in-plane susceptibility near compensation point 78−64240
GdCoMo film, sputtered amorphous, incorporation of Ne, Ar and Kr 77−44163
$Gd_{6.9}Co_{74.0}Mo_{12.8}Ar_{6.3}$, amorphous film, spin wave reson. 79−73823
Hf-Mo, high temp. phase diagrams 77−44217
Hf-Mo-C, isothermal section of phase diagram at 1400°C, X-ray phase analysis determ. 79−34006
Hf-Mo-C, phase diagram, crystallisation patterns of partial system Mo-HfC-Hf 77−12598
Hf-Mo-C, phase diagram and crystallisation of partial system Mo-HfC-C 77−12599
Hf-Mo-C system, isothermal section of phase diag. at 1700°C 78−68674
MO-B, B effects, rolled, segregation of implanted elements, Auger spectroscopy exam. *(Russian)* 78−35389
Mn-Cr-Mo-C, master alloys, development for low alloyed PM steel 80−50576
Mn-V-Mo-C master alloys, development for low alloyed PM steel 80−50576
$(Mo,W)C-(Mo,W)_2C$, hard facing alloys 79−24667
Mo alloy, long-term ageing effects on ductility and microstruct. 77−44348
Mo alloy TsMb, mech. props., effect of gaseous H_2 *(Russian)* 78−31508
Mo alloy:Re, effect of Re on mechanical props. 80−35196
Mo-(Zr+V+C) (1.1 wt.%) alloy, phase composition, carbide phase microhardness *(Russian)* 80−60834
Mo-Al, couple phase diagrams and thermochemical data 79−66037
Mo-Al-Ge, new compounds, structure and props. 80−39003
Mo-Al-Ge, phase equilibria, X-ray and microstructural anal. 80−93536
Mo-AlN, dispersion hardened, erosion resistance 77−12637
Mo-B, Mo-B-Fe(Ni), microalloying influence on mechanical props., cold rolling, plasticity *(Russian)* 80−40502
Mo-B alloys, B distrib. in welds, nuclear track autoradiography study 79−43282
Mo-B-Al-C, alloy TsM-10 rolled, recrystallised, deformed system, behaviour under cyclic loading 79−91795
Mo-B-Al-C system, fractography of static and fatigue fracture 79−87729
Mo-Be solid solutions, superconducting transition, temp. changing peculiarity due to press. *(Russian)* 80−70878
Mo-C, coupled phase diagrams and thermochemical data 79−66036
Mo-C (0.07 wt.%), two-phase alloy, fracture and deform. characts., struct. depend. *(Russian)* 77−32635
Mo-C dilute alloy defect cluster nucleation and growth under 1250 keV electron microscope *(Japanese)* 78−87663
Mo-C-Zr (0.03, 0.17 wt.%), thermal treatment effect on yield drop 77−90382
Mo-C-Zr-B (0.004, 0.12, 0.002 wt.%) effect of grain size, cellular dislocation structure, on mech. props. *(Russian)* 79−34105
Mo-C(Ti)(B)(Zr)(Ru)(Pt), electron beam melted, alloying addition effects on brittleness and ductility 79−61728
Mo-Ca, ion implanted, range distrib. of Ca^+ ions, work function and AES obs. 78−27365
Mo-Co Kondo alloy, Co impurity susceptibilities, Knight shift 80−88721
Mo-Co-Al, phase diagram *(Russian)* 78−19722
Mo-Co-Si, cryst. struct. and defects, high resolution electron microscopy obs. 79−94961
Mo-Cr, cracking in NH_3 at 600°C 79−70207
Mo-Cr, fusibility diagram *(Russian)* 80−20897
Mo-Cr, powder mixture, activating effect of Group VIII metals on alloy form. during sintering 77−59728
Mo-Cr powder mixture, electric discharge sintering, struct. changes 77−77446
Mo-Cr-V-P, load curves, structure states boundaries and strain hardening *(Russian)* 80−89241
Mo-Cu, electrical erosion resistance during electrospark machining 78−35531
Mo-Cu-Al, phase equilibrium *(Russian)* 78−15361
Mo-Fe, dil., Kondo effect of RKKY interaction 78−31052
Mo-Fe, Kondo system, magnetisation, Mossbauer expts. 77−77028
Mo-Fe, local magnetisation from Mossbauer meas. 77−20549
Mo-Fe, local moment system, low temp. susceptibility, Mossbauer effect meas. 77−43810
Mo-Fe, spin glass and mictomag. regimes, sp. ht., resist. and susceptibility meas. 77−69581
Mo-Fe alloy powders, densification and alloy formation on sintering 77−63597
Mo-Fe metalloceramic alloy, brittle fracture investigation, segregation, morphology, struct. *(Russian)* 80−55503
Mo-Fe-O-H system, thermodynamic equilib. 78−60657
Mo-Ge-B, phase diag., struct. of $Mo_{1.7}Ge_{0.3}B$ 77−52285
Mo-Ge(Bi) amorphous films, supercond. transition temp. and residual elec. resist. *(Russian)* 79−19680
Mo-Hf (0.3 wt.%), strength, plasticity and microhardness, internal nitriding effect *(Russian)* 80−40433
Mo-Hf-B-C, low C, sheet, strength 77−1859
Mo-Hf-C, superior powder metallurgy die alloys for isothermal forging mech. props. 79−74201
Mo-Hf-C-Ni, electrochemical phase composition anal., precip. of HfC phase *(Russian)* 80−20901
Mo-HfC, eutectic formation of regular struct., crystn. *(Russian)* 80−66496
Mo-HfC-C, projection of solidus surface, partial system of Hf-Mo-C 77−1834
Mo-iron group metal, binary and ternary alloys, induced codeposition from aq. soln. 79−95954
Mo-low alloys, C enrichment mechanism of intercrystallite zones *(Russian)* 80−20963
Mo-Mb, thermoelectric alloy for in pile temp. meas. *(French)* 79−67894
Mo-Mn alloy, plasticity, fracture, strength depend. on C content *(Russian)* 80−35257
Mo-Mn metalloceramic alloy, brittle fracture investigation, segregation, morphology, struct. *(Russian)* 80−55503
Mo-Mn powder mixture, X-ray diffr. exam. of reaction between Mo and Mn, during sintering 80−16242
Mo-Mn-Fe-Si/Al_2O_3 ceramic seal, interfacial phases 78−72011

molybdenum alloys continued
Mo-Mo_2C, eutectic formation of regular struct., crystn. *(Russian)* 80−66496
Mo-N, nonporous metal production accompanying arc plasma nitriding *(Russian)* 80−7712
Mo-N solid solution, exam. of enthalpy of solution, variation with temp. 79−10947
Mo-N solid solution, thermodynamic props., 1618 to 1883K 80−65230
Mo-N system, phase diagram of solid and liq., high and low press. 78−44083
Mo-Nb, binary continuous solid solution, elec. resist. and thermoelec. power behaviour 79−69492
Mo-Nb, dil., impurity diffusion and vacancy-impurity binding energy 80−15307
Mo-Nb (Re), thermoelec. power, 4.2 to 300K 80−70683
Mo-Nb alloy, secondary electron emission coefficient 77−77333
Mo-Nb solid solutions, enthalpy of soln. of H meas. 80−2166
Mo-Nb-C, mech. props., effect of alloying and Mo cryst. orientation *(Russian)* 80−71706
Mo-Nb-Ti-N alloy, with dispersed second phase, ductile-brittle transition 80−93653
Mo-Nb-TiN, dispersion hardened with strong interface, fracture mechanism 79−5058
Mo-Nb(V)(Cr), thermopower composition depend. 79−65445
Mo-Ni (40 at.%), exam. of ion transfer *(Russian)* 79−28127
Mo-Ni film system, diffusion reaction, phase form. 77−84999
Mo-Ni sputter deposited, amorphous and crystn., Ni^{++} ion irradiation effects, TEM study 79−65128
Mo-Ni two phase alloys, elec. and mass transport *(Russian)* 78−76044
Mo-Ni-Fe-Co-Zn alloys, Ni, Fe, Co and Zn distrib. using neutron-activation anal. 79−52531
Mo-Ni(Fe,Co,Cr,Ti) powder based composite, high temp. strength of W reinforcing fibres 79−70021
Mo-O system, grain boundary segregation and intergranular fracture 80−55516
Mo-O-C system, grain boundary segregation and intergranular fracture 80−55516
Mo-permalloy, magnetic permeability and order form. kinetics under annealing, conc. depend. 77−8356
Mo-Re, cold worked, strength 78−31426
Mo-Re, integral hemispherical degree of blackness, 1200-3000K 78−43154
Mo-Re, prep. from reduction in Mo-Re-O system *(Russian)* 80−16225
Mo-Re, solid soln., dislocation internal friction *(Russian)* 78−23748
Mo-Re, supercond. energy gap and transition temp., tunnelling meas. 79−56405
Mo-Re, σ phase alloy, critical mag. field, elec. resistance 80−54850
Mo-Re (5 at.%), enhanced lattice sp. ht. due to LF reson. modes 78−14882
Mo-Re alloy, type MR47VP, fractographic of static and fatigue fracture 79−87729
Mo-Re alloy MR47-VP, dislocation struct. and fatigue damage during room temp. deform. *(Russian)* 79−20111
Mo-Re alloys, Re determ., electrochem. method 79−16073
Mo-Re film, electron beam deposited, supercond. transition temp. conc. depend. 77−28279
Mo-Re wire, high-strength, fracture mechanism *(Russian)* 77−25126
Mo-Re-C (0.3, 0.2 at.%) time-of-flight atom-probe expts. 80−55741
Mo-Re(Os)(Ru), recovery after deform. and annealing, destrengthening mechanism *(Russian)* 80−97546
Mo-Rh, secondary electron emission and inelastic refl. coeffs. 78−15264
Mo-Ru-C, deformed, singularities of fragmented structs. *(Russian)* 77−44289
Mo-Ru-V alloys, phase equilib. and corrosion resist. *(Russian)* 79−52165
Mo-Ru(-Si), amorphous superconductors, prep. by electron beam evaporation and liq. quenching, crit. temp. 80−103776
Mo-Ru(Rh) film, amorphous, temp. stability 78−63948
Mo-Si coating on Nb and Nb alloys, protection against high temp. oxidation *(Russian)* 79−39029
Mo-Si-Cu, struct. and supercond., Cu influence 80−50592
Mo-Si(Ge)(Al), amorphous supercond. alloy, produced by coevaporation, struct. and supercond. 79−91179
Mo-Sn-Se system, supercond. crit. temp. and cryst. struct. *(Russian)* 80−107947
Mo-Tc system, supercond. behaviour, quick-quench production technique 78−56251
Mo-Ti, internally nitrided, lattice expansion by precipitation 78−68700
Mo-Ti, irrad. between 425 and 1000°C, ductility in bending 80−39164
Mo-Ti (1 wt.%), fast neutron irradiated, direct obs. of solute segregation to voids 79−78971
Mo-Ti (3.5 wt.%), load curves, structure states boundaries and strain hardening *(Russian)* 80−89241
Mo-Ti (3.6 wt.%), absorption of N_2 in induction and plasma-arc heating *(Russian)* 77−16732
Mo-Ti (up to 5.48 wt.%), internal nitriding, hardness, nitride type, precipitation *(Japanese)* 79−79157
Mo-Ti-La-C, influence of high pressure on mech. preps. after nitriding *(Russian)* 79−57137
Mo-Ti-N alloy, with dispersed second phase, ductile-brittle transition 80−93653
Mo-Ti-Zr, alloy TZM, polycrystalline, anal. of elastic anisotropy and microyielding 80−30050
Mo-Ti-Zr, D trapping in fusion reactor materials, temp. dependence 80−37577
Mo-Ti-Zr, diffusion and solubility of C *(French)* 79−55932
Mo-Ti-Zr, fusion reactor first wall material, compatibility with impure He 80−32469
Mo-Ti-Zr, TZM, corrosion behaviour in high temp. impure He gas 80−76402
Mo-Ti-Zr (TZM), fusion reactor materials, radioactivity minimization by elemental substitution and isotopic tailoring 79−22463
Mo-Ti-Zr (0.5, 0.1 wt.%), neutron irradiated, void swelling and shrinkage, TEM study 80−34079
Mo-Ti-Zr (0.5, 0.7 wt.%) alloy TZM, props. and appl. *(German)* 80−21040
Mo-Ti-Zr alloy, neutron radiation-induced shrinkage of voids 79−51158
Mo-Ti-Zr alloy TZM, fatigue and plastic flow, irradiation effects 77−52466
Mo-Ti-Zr alloys TZM and TZC, superior powder metallurgy die alloys for isothermal forging mech. props. 79−74201

molybdenum alloys continued
Mo-TiC, eutectic formation of regular struct., crystn. *(Russian)* 80−66496
Mo-TiC-Ni phase equilibria, subsolidus temp., metallographic and X-ray anal. 80−16278
Mo-TiC(ZrC)(TiN), phase diagram *(Russian)* 78−27476
Mo-TiN (3.5 vol.%), failure characts. exam. 78−68788
Mo-Ti(B)-Zr(Al)-C, stress cycling at room temp. *(Russian)* 77−25148
Mo-Ti(Zr)(Hf)-N, exam. of phase equilibria *(Russian)* 79−29018
Mo-Tic(ZrC)(HfC), thermionic emission, surface structural characts. after prolonged use, work function variation 80−20758
Mo-V, binary continuous solid solution, elec. resist. and thermoelec. power behaviour 79−69492
Mo-V, elec. resist. and thermo-EMF, conc. depend., 4.2 to 1500K *(Russian)* 80−80247
Mo-V-C, hot-worked, substructural hardening and high-temp. strength *(Russian)* 80−25731
Mo-W, calibration line introduction for comp. determ. by AES 79−56892
Mo-W, fatigue and threshold behaviour under high cycle fatigue 80−40487
Mo-W, integral hemispherical degree of blackness, 1200-3000K 78−43154
Mo-W, oxidation 77−70227
Mo-W (30 wt.%), wrought, fracture, characteristic features 80−104278
Mo-W (50 wt.%), emissivity, 1200-3000K, effects of annealing and surface treatment 78−43154
Mo-W alloy type MW25N, crystallisation form, globular dendrites, grain boundaries *(Russian)* 80−66494
Mo-W solid soln., joint solubility of C and Zr 77−25025
Mo-W-C, phase equilibria calc., line compounds 80−10638
Mo-W-Mo (4.74, 2.17 wt.%), creep resistance in ultrahigh vacuum 79−5027
Mo-W-N system, nitrided annealed samples, W replacement of Mo 80−76227
Mo-Zr, heavy ion irradiated, void swelling, phase instability 80−29084
Mo-Zr, interaction with $MoSi_2$ diffusion coating, at elevated temps. *(Russian)* 79−28150
Mo-Zr, nitride form. in N_2 atmos. *(Russian)* 78−19938
Mo-Zr, nucleation conditions, effect on formation of oxide phase during internal oxidation *(Russian)* 80−81064
Mo-Zr (0.15 wt.%), wrought, fracture, characteristic features 80−104278
Mo-Zr (6 wt.%), absorption of N_2 in induction and plasma-arc heating *(Russian)* 77−16732
Mo-Zr alloys, TsM-6, Zr segregation at grain boundaries, carbide precipitation, X-ray spectral anal. *(Russian)* 79−74154
Mo-Zr-B, neutron irrad. at 780-1080°C, porosity, hardening and embrittlement *(Russian)* 80−29062
Mo-Zr-B, porosity and mech. props. after neutron bombard., 780-1080°C *(Russian)* 80−24502
Mo-Zr-B-C, dil. alloy, struct. changes under prolonged high temp. annealing *(Russian)* 78−6944
Mo-Zr-C, deformed, singularities of fragmented structs. *(Russian)* 77−44289
Mo-Zr-C (0.063, 0.06 wt.%) alloys, ageing, effect of cold deform. by hydrostatic extrusion 79−57001
Mo-Zr-C (0.08, 0.02 wt.%), struct. and banding tendency, thermomechanical treatment effects 77−86063
Mo-Zr-C (0.12, 0.002 wt.%), prep. of diffusion metal coating on alloy, oxidation rates *(Russian)* 78−56816
Mo-Zr-C (0.63, 0.06 wt.%), quenched and deformed, structural changes during heating to ageing temp. *(Russian)* 79−1879
Mo-Zr-C alloys, carburising and annealing effects *(Russian)* 77−59828
Mo-Zr-C-B, dilute, electron microscope obs. of planar defect diffr. contrast patterns 77−43227
Mo-Zr-Nb-C, polythermal sections *(Russian)* 78−15365
Mo-Zr-Nb-C alloys, phase diagram and comp., Zr and Nb influence *(Russian)* 79−52167
Mo-Zr-Nb-C and Mo-Zr-C, carbide precip. hardening kinetics, ageing singularities *(Russian)* 77−25059
Mo-Zr-Ti (0.5, 0.1%), adhesive wear polishing of 25 mm spheres 80−89397
Mo-Zr-Ti-C(0.1, 0.15, 0.004 wt.%), alloy TsM2A, cavitation failure mechanism 77−70169
Mo-ZrC, eutectic formation of regular struct., crystn. *(Russian)* 80−66496
Mo-ZrC, internal oxidation, struct. formation law, microstruct. examination 78−84836
Mo-ZrO_2 dispersion hardened, rolled, grain struct. and props. 77−77492
Mo_2B_5-based alloys, mech. props., rel. to appl. as electrodes in electrospark machining 80−21174
$Mo_{70}B_{30}$, amorphous, local symmetry around glass-former sites, elec. quadrupole effects, NMR 80−80618
MoC coatings, produced by plasma flux deposition in vacuum, exam. *(Russian)* 80−11567
Mo_3CoSi, TEM study 79−51047
MoFe, occurrence of spin glass and mictomagnetic regimes, props. meas. 77−16085
$MoGe_2$-Mo diffusion couple, nucleation of $Mo_{13}Ge_{23}$ *(French)* 77−55398
$Mo_{13}Ge_{23}$, nucleation in Mo-$MoGe_2$ diffusion couples *(French)* 77−55398
Mo_3Ge, A15 cpd., normal state, low temp. resist. 80−107762
Mo_3Ge, RF sputtered, supercond. crit. temp. 78−14853
Mo_3Ge, superconductivity, T_c related to disorder and density of states 79−15249
Mo_cNb_{1-c}, is the rigid-band model valid? 78−95258
Mo_3Os, effect of high energy neutron irradiation on supercond. transition temp. 77−36012
$Mo_{80}P_{10}B_{10}$, amorphous supercond. high-κ, upper and lower crit. fields 79−4629
Mo_5PbS_8 embedded in resin, composite supercond., high transition temp. 80−88660
Mo_xRe_{1-x}, (x=0.4 and 0.6), search for strong coupling superconductivity 79−28441
$Mo_{1-x}Re_xCo$, mag. state of Co impurity, NMR exam. 78−27100
$(Mo_{0.6}Ru_{0.4})_{82}B_{18}$, supercond. metallic glass, neutron irrad. effects 80−29060
$Mo_{48}Ru_{32}B_{20}$, amorphous, local symmetry around glass-former sites, elec. quadrupole effects, NMR 80−80618

molybdenum alloys continued
$(Mo_{0.6}Ru_{0.4})_{0.8}G_{0.2}$-Fe (G=P,B), amorphous supercond., upper crit. field as function of temp. 79−73646
$(Mo_{0.5}Ru_{0.5})_{80}P_{20}$, amorphous normal and mixed supercond. state, ^{31}P NMR 79−87193
$(Mo_{1-x}Ru_x)_{80}P_{20}$, amorphous, liq. quenched, mag. susceptibility, supercond. and electronic props. 79−56376
$(Mo_xRu_{1-x})_{80}P_{20}$, amorphous supercond., high-κ, upper and lower crit. fields 79−4629
$(Mo_{0.6}Ru_{0.4})_{80}Si_{10}B_{10}$, amorphous supercond. matrix, flux pinning by MoRu precips. 80−65756
$MoSi_2$, diffusion grown layers, texture 79−74095
$MoSi_2$, effect of Al on oxidation behaviour *(German)* 78−31587
$MoSi_2$, form in Mo layer on Si surface *(French)* 78−43270
$MoSi_2$, SiO_2 coating effect on oxidation, AES study *(German)* 79−74298
$MoSi_3$, high temp. material, coatings, powder metallurgy, review *(German)* 79−74295
Mo_3Si, Mo_5Si_3 and $MoSi_2$, ultrasoft X-ray emission bands, empirical band schemes 78−15249
Mo_3Si, $MoSi_2$, form., Mo thin film on Si, He^+ backscattering, X-ray diffr. study 78−43261
Mo_5Si_3 based coating, interaction *(Russian)* 80−21167
Mo_5Si_3 layer growth, effect of DC density, temp. 79−43160
Mo_3Sn, thin films with A-15 struct., prep. 78−80478
$Mo_{0.4}Tc_{0.6}$, A15 and BCC, sp. ht., 4-20K 78−68111
$Mo_{1-x}Tc_x$, BCC, sp. ht. in normal and supercond. phases 79−87190
$Mo_{1-x}V_x$, supercond., NMR and mag. susceptibility meas. 79−56388
Nb-Mo, AC loss minimum, pinning, flux distribution 80−84574
Nb-Mo, and Nb-V-Mo, supercond. crit. temp. and crit. field, Mo alloying effect 77−85375
Nb-Mo, BCC, press. derivatives of elastic moduli, Fermi surface topological changes, band struct. 79−61639
Nb-Mo, BCC, struct. singularities rel. to solid solution behaviour *(Russian)* 77−11696
Nb-Mo, diffusion of N, effect of Mo and struct. defects 79−55938
Nb-Mo, dil., neutron irradiation at 4.6K, influence of impurities on defect prod. 79−55790
Nb-Mo, elastic moduli of single crystals 77−31712
Nb-Mo, electronic density of states, temp. depend. of elec. resist. and mag. susceptibility 77−11891
Nb-Mo, electronic struct., thermoreflectance meas. 0.5-5.0 eV 80−45050
Nb-Mo, internal impurity adsorption effect on bond type of intercrystallite zones 77−16684
Nb-Mo, kinetics and thermodynamics of reaction with N_2 *(German)* 79−74415
Nb-Mo, nitriding, diffusive saturation, lattice spacing and activation coeffs. *(Russian)* 80−21168
Nb-Mo, optical props., 0.1-25 eV, band models 78−10892
Nb-Mo, prod. by simultaneous carbothermic reduction of oxides/electron beam melting method *(Japanese)* 80−11590
Nb-Mo, resistivity due to H incorporation 80−70666
Nb-Mo, specific heat enhancement and electron-phonon interaction 80−65242
Nb-Mo, superconductivity and phonon softening, between electron bands and phonons 78−14859
Nb-Mo, vacuum heat treatment effects on gas content and elec. and mech. props. *(Russian)* 79−43281
Nb-Mo alloy, single crysts. slip geometry on straining in tension *(Russian)* 77−66678
Nb-Mo alloy, solubility of H_2 77−89542
Nb-Mo alloys, phonon dispersion, anomalous struct., tight-binding calcs. 78−10137
Nb-Mo film, amorphous, temp. stability 78−63948
Nb-Mo monocrystal, elastic moduli, 4.2 to 300K *(Russian)* 77−52381
Nb-Mo solid soln., single cryst., yield point and dislocation struct., temp. depend. *(Russian)* 77−81290
Nb-Mo steel, HSLA, low temp. fatigue props. 80−40490
Nb-Mo system, electron-phonon coupling const. and supercond. transition temp., average T-matrix approx. 80−39707
Nb-Mo-Al-(Cr) eutectic directionally crystallised alloy, heat resistance, alloy struct. *(Russian)* 80−40481
Nb-Mo-C, phase comp. and precip. after heat treatment 79−57020
Nb-Mo-Fe, dil., local environment and mag. props. 78−64187
Nb-Mo-Fe, dil., local moment formation 78−43562
Nb-Mo-Si, ductile amorphous, superconductivity 80−60131
Nb-Mo-Tc alloys, supercond., point-group symmetry 78−64163
Nb-Mo-Ti-Zr, influence of C content on creep charact. and creep-rupture strength *(Russian)* 77−48483
Nb-Mo-Ti-Zr-C, work function temp. and phase depend. *(Russian)* 80−2449
Nb-Mo-Zr-Ti, Zr and Ti effects on struct. and mech. props. 77−70061
Nb-W-Mo-Zr, long-term strength props., vac. level effect 80−55484
Nb-W-Mo-Zr (5, 2, 1 wt.%), surface-layer struct. and mech. props., effect of O_2 diffusion saturation 79−5087
Nb-W-Mo-Zr (5, 2.1, 0.92 wt.%), creep resist., high temp. ageing in vacuum 80−71716
Nb-W-Mo-Zr-C, strength and ductility, prolonged high-temp. soaking effect 80−55483
Nb-W-Mo-Zr-C(5,2,1,0.02 wt.%) alloy 5 BMTs, short-time tensile strength in liquid Bi and Li *(Russian)* 77−25186
Nb_3Ge-Mo, synthesis from thermalised sputtering and changes in Tc and depend. of H_{c2} on temp. 79−56350
$Nb_{0.5}Mo_{0.5}$, soft X-ray spectra, theoretical considerations 80−11511
$Nb_{80}Mo_{20}$, $Nb_{75}Mo_{25}$, supercond., phonon cond. below 1k 78−14881
$NbMo_2Be$, predicted A15 struct. and T_c=30K 78−76182
$(Nb_{0.99}Mo_{0.01})_{1-x}Ge_x$, supercond. transition temp. and crit. field 79−38220
$(Nb_{1-y}Mo_y)_{1-x}Ge_x$, transition metal atom stabilised superconductivity 79−7924
$(Nb_{1-y}Mo_y)_3Ge$ system, composite transition metal atom supercond. 77−39984
$Nb_{1-x}Mo_xSe_2$, supercond. transition temp. and mag. susceptibility 77−12043
Ni base alloy IN792, carbide morphology 77−36508
Ni-Al-Cr-Mo-Ti-W-(Co) alloys EhI 826 and EhI 929, reverse elastic after effect under loading 78−39829
Ni-Al-Cr-Ti-W-Mo, US vibration applied during solidification, improved strength, corrosion resistance *(Russian)* 78−15382
Ni-Al-Mo, eutectic form., struct. and mech. props. *(Russian)* 77−21129
Ni-Al-Mo, heat resist., solidification range 80−35177

molybdenum alloys continued
Ni-Al-Mo (12.7, 21.6 wt.%), directionally solidified eutectic composite, precipitation 80−108454
γ-αNi-Al-Mo eutectic, γ' precipitation 77−12629
Ni-Co-Cr-Al-Ti-Mo superalloy IN738, casking porosity removal using hydrostatic press. sintering 80−55322
Ni-Co-Cr-Mb-W-Ta, Cr, Mb, W, Ta effects on σ phase occurrence 77−36507
Ni-Co-Cr-Mo-Al, Astroloy, extruded powder metallurgy superalloy, recrystallisation study 79−4976
Ni-Co-Cr-Mo-Al-Ti (17.5, 15.1, 4.9, 4.15, 3.25 wt.%), creep and stress rupture behaviour in air and vacuum 80−60918
Ni-Co-Cr-Mo-Ti-Al Nimonic 105, loading frequency and environmental effects on high temp. fatigue crack growth 78−64675
Ni-Co-Cr-Ta-Al-W-Mo-Ti, cast, phase volume fraction determ. using manual point count practice 78−53052
Ni-Co-Mo, phase relations in system at 1100°C 80−108392
Ni-Co-Mo alloys, electrodeposition, struct. 79−28970
Ni-Co-Mo-Al-Cr, melt, effect of Al, Cr on O_2 activity, electrochemical determ. 79−11556
Ni-Cr-Al-Ti-Mo, low temp. mech. behaviour, precipitation 78−39860
Ni-Cr-Co-Al-Ti-W-Ta-Mo, IN 738 LC, loading frequency and environmental effects on high temp. fatigue crack growth 78−64675
Ni-Cr-Co-Al-W-Mo-Ti-Ta, heat resist. and struct., Ta effect 80−76312
Ni-Cr-Co-Mo, long-term corrosion stability rel. to use in joint endoprostheses 78−36059
Ni-Cr-Co-Mo alloy MP35N alloys, cold worked, factors affecting embrittlement in H_2S environments 78−31502
Ni-Cr-Co-Mo alloy MP35N, accelerated H_2 charging in aq. H_2SO_4 at 0.2% yield stress 80−30144
Ni-Cr-Co-Mo-Al-Ti (10, 15, 3, 5.5, 4.5 wt.%), superalloy, exam. of creep and fracture behaviour 78−48464
Ni-Cr-Co-Mo-Al-Ti alloys, Waspaloy, Astroloy, exam. of microstruct. effect on crack growth 78−52977
Ni-Cr-Co-Mo(-Ti), oxidation depend. on alloying element, cohesion strength *(Russian)* 80−40587
Ni-Cr-Co-Ti-Mo-W-Al (14, 9.8, 5, 4, 3.9, 3 wt.%), low cycle fatigue, prior heat treatment effect 80−60962
Ni-Cr-Fe-Mo-Co (21.41, 19.28, 8.64, 2.16 wt.%), Hastelloy alloy X, exam. of thermal stability 78−84865
Ni-Cr-Mo, creep parameters, high temp. 80−50685
Ni-Cr-Mo (74, 20, 4 wt.%), long-term strength in H at high pressure 80−55485
Ni-Cr-Mo steel, corrosion and cavitation-erosion resist. *(Russian)* 78−11395
Ni-Cr-Mo-C hardfacing alloy, hardness and abrasive wear resistance 79−79117
Ni-Cr-Mo-Fe-Mn, Kh12M23, intermetallic phases exam. *(Russian)* 78−39740
Ni-Cr-Mo-Mn alloy 02KhN40MB, corrosion-resist, heat-resist., phys. and mech. props. 80−35411
Ni-Cr-Mo-Ti (19,11,3 wt.%) for TiC reactively sputtered coatings, adherence, XPES and wear study 80−25565
Ni-Cr-Mo-V steel disc, rolling contact fatigue and residual stress on contact surface 77−32671
Ni-Cr-Mo-W-Al-Ti, heat-resist., phase comp. 80−76250
Ni-Cr-Ti-Al-Mo-Nb-Fe (13-16, 2.35-2.75, 1.3-1.7, 2.8-3.2, 1.8-2.2, 2.0 wt%), heat resistant props, mech props. struct., stepwise ageing effects *(Russian)* 78−76666
Ni-Cr-Ti-Co-W-Al-Mo alloys AF-115 and AF2 1DA, superalloy powder compacts, fatigue origins 78−48521
Ni-Cr-W-C-Mo, Vickers hardness and crystallisation temp. 80−16361
Ni-Cr-W-Co-Mo, high-temp. sulphide corrosion 80−76408
Ni-Cr-W-Mo-Al-Ti (15,6,3,2,2, wt.%), wrought, Si effect on transition brittleness *(Chinese)* 80−55491
Ni-Cr-W-Mo-Ti-Al, heat-resist., recovery and recrystn. 80−76268
Ni-Cr-W-Mo-Ti-Al alloy KhN67MVTYu, heat treatment effect on mech. props. 77−70082
Ni-Fe-Cr-Mo-Ti-Al, PE 16, thermally activated domain wall motion 80−88777
Ni-Fe-Mo, determ. of preferential locations of Mo or Cr on Fe and Ni sublattices, by X-ray intensity study 79−37662
Ni-Fe-Mo, K-effect, Mossbauer study 80−39998
Ni-Fe-Mo, magnetic alloy, TEM and X-ray obs. *(Chinese)* 80−24401
Ni-Fe-Mo film, anal. of main component by atomic absorpt. spectrophotometry 77−70381
Ni-Fe-Mo-Cu (79, 16, 4.3, 0.7 wt.%) K-state formation, physical props. exam. 78−47761
Ni-Fe-Nb-Al-Mo, wear resisting mag. head material, mag. props. and struct. 80−35350
Ni-Fe-Nb-Mo (11.42, 6.92, 1.54 wt.%), Hardperm, high magnetic permeability alloys 77−8361
Ni-Fe-Nb-Mo-Al, head material for mag. recording, DC and AC mag. props. 80−88812
Ni-Mo, and Ni-Mo-V, struct. changes on annealing *(Russian)* 77−21145
Ni-Mo, discontinuous precipitation as internal sulphidation mode 77−8835
Ni-Mo, effect of solute misfit and temp. on irradiation induced segregation 78−72779
Ni-Mo, eutectic form., struct. and mech. props. *(Russian)* 77−21129
Ni-Mo, off-stoichiometric, ordering 78−52752
Ni-Mo, oxidation effect on magnetic props. *(Russian)* 78−23868
Ni-Mo, phase boundary motion kinetic during interdiffusion *(Russian)* 79−60559
Ni-Mo, powder mixture, electric discharge sintering, struct. changes 77−77446
Ni-Mo, short range order considerations and development of long range order 77−16574
Ni-Mo, sintering limited solid solubility, peritectic diagram 77−28754
Ni-Mo, solid soln., US deform., electron microscope exam. *(Russian)* 78−35447
Ni-Mo, solid soln., US effect on mech. props. *(Russian)* 78−23819
Ni-Mo, solubility of H_2, 500-1000°C *(Japanese)* 78−38845
Ni-Mo, spin wave stiffness consts., RPA CPA band model 79−61088
Ni-Mo, sputtering rate, radiation-induced segregation and preferential sputtering effects, kinetic model 80−40199
Ni-Mo, variation in absolute thermoelec. power under heat/treatment *(Ukrainian)* 79−38051
Ni-Mo, weak ferromag., stiffness const., low-temp. meas., rel. to RPA-CPA theories 78−31063
molybdenum alloys continued
Ni-Mo, wear tracks, TEM obs., tested in simulated face seal 77−52508
Ni-Mo (10.7 wt.%) alloy, ordering energy calc. 80−10522
Ni-Mo (14.4 wt.%) single crystals, ordered phase precipitates influence on deformation character, mechanical props. *(Russian)* 79−74155
Ni-Mo (17.5 at.%), discontinuous precipitation reaction *(German)* 79−87643
Ni-Mo (20.8 wt.%), order, heat treatment effects 80−40406
Ni-Mo (5.8-24 at.%) solid soln. struct. and strength charact. *(German)* 79−4975
Ni-Mo alloy electrodeposits, codeposited impurities rel. to H_2 permeation, props. 79−19493
Ni-Mo binder of binary carbide hard alloy, physicomech. props. 77−90461
Ni-Mo melt, N_2 diffusion *(Russian)* 78−18812
Ni-Mo-Al and Ni-Mo-Al-V, high-resist., struct. transforms., TEM *(Russian)* 78−19762
Ni-Mo-Al eutectics, unidirectional solidification 77−4769
Ni-Mo-B metallic glass ribbons, tensile strength, crystn. temp. 80−89173
Ni-Mo-C(-Cr)(W), Vickers hardness and crystallisation temp. 80−16361
Ni-Mo-Cr-Si, plasma and detonation coatings, Laves- and carbide-strengthened, comparative props. 78−15562
Ni-Mo-MoS_2 composite, Mo alloying effect on physicochem. interactions 80−7692
Ni-Mo-W, diagram of state, W solubility, dispersion hardening *(Russian)* 80−66477
Ni-Mo-W, type N55M20V25, quenched at various cooling rates, phase transformations *(Russian)* 79−66052
Ni-Ni_4Mo, strengthening by ordered precipitates 77−86041
Ni_3-Mo, transport props. and magnetisation, effect of Mo alloying *(Russian)* 78−39095
Ni_3Al-Mo, powder, X-ray spectral analysis exam. 80−16239
NiCr-MoAl-ThO_2 (13,3 wt.%), powder, mech. alloying 78−84744
Ni_3(Fe,Mo), kinetic phenomena rel. to ordering and electron struct. *(Russian)* 78−76043
Ni_3(Fe,W), elec. resist., temp. depend. anomalies, Hall and Nernst-Ettinghausen effects *(Russian)* 80−10942
Ni_3(Mo,Ta), quenched alloys, DO_{22} type ordered phase form. 78−95768
Ni_3Mo, modulated struct. phenomena, survey 79−95033
Ni_4Mo alloy, high temp. oxidation, oxide layer growth, struct., mech. behaviour 78−44269
Ni_4Mo, antiphase domains growth kinetics, TEM and electron diffr. *(Russian)* 77−32557
Ni_4Mo, coherent phase form. at stress concentrators *(Russian)* 80−49356
Ni_4Mo, domain struct. on annealing, and dislocation struct. during deform. *(Russian)* 77−16640
Ni_4Mo, electron irrad. in electron microscope, radn. ordering 79−86818
Ni_4Mo, ionisation states of field evaporated ions 77−81200
Ni_4Mo, order-disorder phase transform., X-ray diffr. *(Russian)* 79−1855
Ni_4Mo, ordered, electrical resistivity and thermal EMF, temp. depend. *(Russian)* 77−55513
Ni_4Mo, ordering near Kurnakov point, form. of coherent phase in stress concentrators 79−7691
Ni_4Mo, quenched, short-range order, electron diffraction study 77−39560
Ni_4Mo, statistically homogeneous ordering, computer-simulated field ion images 78−9991
Ni_4Mo, stoichiometric and quenched, short range order and order-disorder transform. 79−78955
$Ni_{65}Mo_2Fe$, O_2 effect on secondary recrystallisation and mag. props. 80−35201
Pb-Mo amorphous films, supercond. transition temp. and residual elec. resist. *(Russian)* 79−19680
Pd-Mo, dilute, low temp. sp. ht. and mag. susceptibility 77−62650
Pt_2Mo-type superstructure, interaction of reacting dislocations *(Russian)* 78−83814
Re-Mo (up to 4.4 wt.%), X-ray diffr. study of conc. and temp. depend. of lattice parameters 79−94965
Re-Ta-Mo, phase diag. *(Russian)* 77−59747
(Re-Mo)-Pt bimetal sheet specimens, interdiffusion, 1500°C *(Russian)* 77−62683
SiC fibre reinforced Ti, effect of Al, Zr and Mo alloying additions on reaction rate of Ti with fibres 80−16249
Tl-Mo (11 wt.%), alpha precipitation kinetics 78−68697
TZM, D^+ impact, surface blistering, SEM study 78−71774
TZM, diffusion of Cs, AES, SIMS depth profile study *(German)* 78−84008
TZM, fatigue and threshold behaviour under high cycle fatigue 80−40487
TZM, irrad. between 425 and 1000°C ductility in bending 80−39164
Ti alloy VT3-1, large forgings, heat treatment, struct. and mech. props. 78−52864
$\alpha+\beta$ Ti alloy VT9, influence of phase comp. on fracture *(Russian)* 78−56665
Ti-Al (14 at.%), with precipitate free zones, tensile props., grain size effects 77−16690
Ti-Al-Cr-Mo (6, 2.0, 2.5 wt.%), microstructural changes and mech. props. 77−25080
Ti-Al-Cr-Mo alloy VT3-1, reactions with some refractory compounds 80−16585
Ti-Al-Cr-Mo system, VTZ-1 alloy, microstruct. influence on fatigue charcts. 80−3195
Ti-Al-Cr-Mo-Fe(V)(Zr), effect of structure and heat treatment on tensile strength, ductility, fatigue limit and notch sensitivity 78−56711
Ti-Al-Cr-Mo-U, alloy VT22, phase composition and fatigue strength 78−3219
Ti-Al-Cr-Mo-V, alloy VT22M, exam. of ageing and phase transitions *(Russian)* 79−11641
Ti-Al-Cr-Mo-V alloy VT-22, effect of heating rate on phase recrystallisation *(Russian)* 79−34077
Ti-Al-Cr-Mo-Zr hard alloy VK15, shot blasting in strength improvement 77−81272
Ti-Al-Mo, impact strength anisotropy, influence of texture *(Russian)* 80−20952
Ti-Al-Mo, phase relations 80−108398
Ti-Al-Mo, thermomechanical treatment effect on mech. props., strengthening mechanisms 80−55441
Ti-Al-Mo, type BT22, phase transformations under step-by-step heat treatment *(Russian)* 80−108436

molybdenum alloys continued
Ti-Al-Mo, type Ti-6242S, irrad. induced creep 80−39163
Ti-Al-Mo (31, 13 wt.%), transform. microstruct. 78−48394
Ti-Al-Mo alloy VT-14, spherical pressure vessel, correlation between fracture stresses and mech. laboratory charcts. 80−25838
Ti-Al-Mo alloy VT14, fracture anisotropy, with varying H_2 content, rel. to loading condition *(Russian)* 77−70148
Ti-Al-Mo-Cr, weldment containing orthorhombic martensite, autotempering behaviour and alpha precip. strengthening 80−84976
Ti-Al-Mo-Cr (4.5, 5, 1.5 wt.%), CORONA-5, effect of microstructure and heat treatment on fracture 78−60805
Ti-Al-Mo-Cr (4.5, 5, 1.5 wt.%), weld metal, α/β interace sliding 80−108512
Ti-Al-Mo-Cr-Fe, distrib. of Sn, Zr between phases, temp effect. 80−55357
Ti-Al-Mo-Cr-Fe (6.4, 2.7, 1.6, 0.4 wt.%), quenched VT3-1, decomposition kinetics of α'' and β in annealing *(Russian)* 77−66662
$(\alpha+\beta)$-Ti-Al-Mo-Fe alloy VT-22, behaviour during creep testing, solid soln. dissoc. *(Russian)* 80−40346
Ti-Al-Mo-Sn, environmental effects in alloy fretting, effect on fatigue props. 78−56787
Ti-Al-Mo-Sn alloy, elastically and plastically deformed, positron annihilation meas. of deformation 80−21038
Ti-Al-Mo-Sn-Si, type IMI 680 and 551, internal friction study of martensitic transformations 80−7573
Ti-Al-Mo-Sn-Si, type IMI 680 and 551, stability of martensitic phases 80−7574
Ti-Al-Mo-Sn-Si (4,4,2,0.5 wt.%), fracture toughness and crack propag. 78−39892
Ti-Al-Mo-V, crack resistance in chloride soln., electrochem. protection, polarization effect 80−55589
Ti-Al-Mo-V (8, 1, 1 wt. %), stress corrosion cracking and slow strain rate H_2 embrittlement 78−48569
Ti-Al-Mo-V (8, 1, 1 wt.%), environmental fatigue crack propag., texture influence 79−91802
Ti-Al-Mo-V (8, 1, 1 wt.%), Widmanstatten colonies, fracture toughness 80−85031
Ti-Al-Mo-V (8,1,1 wt.%), Widmanstatten, quantitative anal. of microstruct. effect on fatigue crack growth 79−79071
Ti-Al-Mo-Zr, compressor disk, surface plastic deform., optimal method 80−60924
Ti-Al-Mo-Zr, type VT-9, creep eqns. rel. to extension and compression props. 80−100875
Ti-Al-Mo-Zr (Cr-Fe), effect of heating on thermal stability of phases, lattice constants and chem. comp. 78−56672
Ti-Al-Mo-Zr alloy, VT9, decomp. kinetics of metastable β-phase, X-ray and mech. props. obs. *(Russian)* 78−48368
Ti-Al-Mo-Zr alloy VT9, Cu-Cr(Ni) coated, plastic deform. and diffusion annealing effect on props. *(Russian)* 78−35425
Ti-Al-Mo-Zr SiC fibre reinforced composites, matrix selection *(Russian)* 80−35192
Ti-Al-Mo-Zr-Si (6.6, 3.3, 1.8, 0.3 wt.%)-SiC fibrous composite, component interaction kinetics *(Russian)* 80−55364
Ti-Al-Mo-(Cr), etching as a function of struct. *(Russian)* 78−15568
Ti-Al-Nb-Ta-Mo (6, 2, 1, 0.8 wt.%), elevated temp. flow strength, creep resist., diffusion welding charcts. 80−30033
Ti-Al-Sn-Zr, Ti-680, O contamination under high temp. *(Chinese)* 80−66688
α-βTi-Al-Sn-Zr-Mo (6, 2, 4, 6 wt.%), interface struct. 77−44212
α-βTi-Al-Sn-Zr-Mo (6, 2, 4, 6 wt.%), deformation associated with surface cracks and α particles 79−79107
Ti-Al-Sn-Zr-Mo (6,2,4,6 wt.%), α-β type 6246, fusion zone fracture behaviour in weldments 80−30093
Ti-Al-Sn-Zr-Mo (6,2,4,6 wt.%) fusion weldment, substruct. charcts. 80−84183
Ti-Al-Sn-Zr-Mo (6,2,45 wt.%), surface cracking under unidirectional loading 78−56753
Ti-Al-Sn-Zr-Mo alloy, Ti-6242, $\alpha+\beta$, creep property improvement by Pt ion plating 80−16408
$\alpha+\beta$-Ti-Al-Sn-Zr-Mo-Cr, low cycle fatigue crack nucleation and early growth 79−8354
Ti-Al-Sn-Zr-Mo-Si (6, 2, 4, 2, 0.1 wt.%), effect of elevated temperature and environment on fatigue crack growth 80−40486
Ti-Al-Sn-Zr-Mo-Si-O-H, Si, O, H effects on fatigue, fracture and creep charact. 79−11697
Ti-Al-V-Cr-Mo-Zr (3,8,6,4,4 wt.%), beta-C, microstruct. effect on mech. props. 78−27577
Ti-Al-V-Cr-Zr-Mo (3, 8, 6, 4, wt.%), phase transforms. 79−100113
Ti-Al-V-Cr-Zr-Mo-Fe (3.4, 8.3, 5.8, 3.9, 4.2, 0.06 wt.%), shock loaded, residual strength 77−36589
Ti-Al-V-Mo, electrochemical behaviour under tensile stress in boiling H_2SO_4 and acidic chloride solns. 78−95851
Ti-Al-Zr-Mo alloy 685, phase at α/β interface *(French)* 80−25661
Ti-Al-Zr-Mo-Si (6,5,0.5,0.25 wt.%) fracture toughness and crack propag. 78−39892
Ti-B-Mo, annealed at 1400°C, exam. of phase diagram, using X-ray phase and metallographic analysis 79−1847
Ti-B-Mo system, phase equilibria at 1400°C 78−35354
Ti-CrB_2-Ni-Mo, interphase reactions, electron probe anal., metallography and hardness exam. 80−2990
Ti-Cu-Mo, heat treatable alloys, effect of alloying on strength, tensile props. 78−56671
Ti-M-V-Cr-Mo, RMI 38644, shock loaded, age hardening 79−29112
β-Ti-Mo, alloy, struct. changes during deformation and ageing *(Russian)* 78−39791
Ti-Mo, boronizing, reaction kinetics 79−61797
Ti-Mo, diffuse electron scatt. *(Russian)* 80−103438
Ti-Mo, dilute, superconducting transition temp. and mag. susceptibility 78−47899
Ti-Mo, fine cryst. struct. by diffuse X-ray and electron scatt. *(Russian)* 79−99329
Ti-Mo, fracture behaviour and tensile props. at elev. temp. 78−60822
Ti-Mo, lattice parameter and Debye temp., comp. depend. *(Russian)* 78−47280
Ti-Mo, martensitic alloy, decomposition by nucleation and growth and spinodal mechanisms 79−61590
Ti-Mo, martensitic transform., water quenched from β-region 79−38826
Ti-Mo, metastable β-phase, stress induced products formed by cold rolling *(Japanese)* 78−84843
Ti-Mo, metastable diffusionless equilibria, high press. conditions 80−71627

molybdenum alloys continued
Ti-Mo, phase diagram investigation *(Japanese)* 77−63632
Ti-Mo, sintered, manufacture and exam. of props. 79−95975
Ti-Mo, structure associated with BCC to omega transform. *(Russian)* 80−108432
β−Ti-Mo, thermal instability, hardness and tensile deform. *(Japanese)* 80−71703
Ti-Mo (15 wt.%) alloy, metastable β-phase, deform. charcts. 78−6975
Ti-Mo (15.2 at.%), swaged and recrystallized, grain growth 80−3092
Ti-Mo (16 at.%), effect of H impurities on lattice spacing, hardness, and plastic strain *(Russian)* 79−11664
Ti-Mo (20 at.%), incommensurate struct., stacking soliton 80−107109
Ti-Mo (3 to 35 wt.%), high pressure influence on transition temp. to supercond. 80−107952
Ti-Mo (5 at.%) based alloy, supercond. transition temp. enhancement by varying struct. state 77−20483
Ti-Mo alloy, thin anodic oxide, AES depth profile 80−71801
Ti-Mo alloys, elasticity moduli, 80-300°C *(Russian)* 78−80574
Ti-Mo alloys, structural stability under high-pressure soaking 80−104151
β-Ti-Mo alloys, thinning transformation 77−44438
Ti-Mo binary system, solid state phase transform. and miscibility gap, phase diagram 79−8298
Ti-Mo-Al, determ. of interaction parameters from EPMA data 77−63635
β-Ti-Mo-Cr-Al (8, 4.5, 2.5 wt.%), metastable, tensile ductility, α-phase morphology and distrib. effect 77−86098
Ti-Mo-Fe (3, 0.13 at.%), metastable phases, Mossbauer study 80−7243
Ti-Mo-Fe-Cr-Al, alloy VT3-1, influence of constitution on fracture toughness *(Russian)* 77−77559
Ti-Mo-V (8 wt.%, 8 wt.%), FCC phase, decay of β-solid soln., electron microdiffr. 79−15670
Ti-Mo-V-Al-Cr-Fe (4.8, 4.7, 5.2, 1.1, 1.0 wt.%), structural changes during heating up to 1000°C, DTA study *(Russian)* 80−93552
β-Ti-Mo-V-Fe-Al (8, 8, 2, 3, wt.%), exam. of stress induced H_2 migration 78−87823
Ti-Mo-V-Fe-Al (8,8,2,3, wt.%), exam. of stress controlled fatigue response 79−61734
β-Ti-Mo-V-Fe-Al (8,8,2,3 wt.%), metastable, high cycle fatigue crack initation, grain size effect 77−86145
β-Ti-Mo-V-Fe-Al (8,8,2,3 wt.%), metastable alloy, microstruct. and mech. props. ageing time and temp. effect 78−64569
Ti-Mo-V-Fe-Al (8823 wt.%), heavy section extrusion, fabrication and mech. props. 78−6985
β-Ti-Mo-V-Fe-Al(8,8,2,3 wt.%), metastable factors affecting stress corrosion cracking 77−28928
Ti-Mo-Zr-Al (15,5,3 wt.%), phase transform. kinetics study by X-ray diffr. 79−56960
Ti-Mo-Zr-Sn, alloy, βIII, struct. transform. in thermally affected zones after electron beam welding 78−23919
β-Ti-Mo-Zr-Sn (10.2, 5.8, 4.7 wt.%) heat treated, tensile yield, fracture behaviour, primary deform. mode, exam. 78−60724
Ti-Mo-Zr-Sn (11.5, 6, 45 wt.%), plastically strained regions, decoration 77−28864
Ti-Mo-Zr-Sn (11.5, 6, 4.5 wt.%), metastable beta III phase, recrystallization and grain growth 80−3091
Ti-Mo-Zr-Sn (11.5, 6.0, 4.5 wt.%), mech. property, microstruct. relationships 80−84961
Ti-Mo-Zr-Sn (11.5, 6.0, 4.5 wt.%) alloy, struct. as affected by processing history 80−84972
Ti-Mo-Zr-Sn-Fe-C-Si alloy, β-III, cold deform. and annealing, effect on struct. and mech. props. *(Russian)* 79−24533
β-Ti-Mo-Zr-Sn(11.5, 6, 4.5 wt.%), metastable phase III, microstruct. and age hardening response 80−84945
Ti-Mo-Zr(-Al) (15, 5 (3) wt.%), quenched and aged metastable β-phase, crystallography, morphology and decomposition 80−76262
Ti-Nb alloys, Fe, Mo, V, Ta alloying additions on microstruct. after combined treatment *(Russian)* 77−59826
Ti-Nb-Zr-Fe-Mo-V, cold worked, struct. and phase transform. during ageing 78−3153
Ti-Ni-Mo (1.5, 2 wt.%), Mo effect on microstructure 77−36536
Ti-TiO_2-ZrO_2-Mo, sintered struct. and mech. props. 78−60618
Ti-V-Cr-Mo, fracture resistance at low temps. 80−104284
Ti-V-Mo alloy system, phase equilibria and interstitial effects, TEM and X-ray diffr. study 79−43204
Ti-V-Mo-Cr system, β-phase stability 80−55353
Ti-Zr-Mo alloy, effect of O_2 on elec. resistivity, microhardness, mech. props. 77−56092
Ti-Zr-Mo-V, alloy VT20, exam. of plasticity in temp. range 20 to 1000°C 78−56712
α-β TiAl-Sn-Zr-Mo (6,2,4,6 wt.%), age hardening 79−61604
Ti_3Al, Cu, Fe, Mo (1 at.%) additions, oxidation resistance, 700 to 800 degrees C 77−12744
Ti_3Al-Mo (0.5 at.%), ordering, Mo effect 77−28841
TiC-(Mo-Cr-Ni-Mn) steel alloy, optimum comp. and manufacture conditions, Mn effect 80−84896
TiC-Ni-Mo, cemented carbides, grain growth, metallographic obs. 77−24982
TiC-Ni-Mo, hard alloy mixtures, pressing 77−63596
TiC-Ni-Mo hard alloy, wear resistance under end face friction cond. 78−60846
TiC-Ni-Mo hard alloys, use in hard layer prod. by electrospark alloying 77−59998
TiC-Ni-Mo sintered hard alloy TN-20, fracture surfaces 80−7684
U/(Zr-Cu-Mo alloy) welded joints, mech. charcts. determ. 20 to 750°C 79−29113
U-Mo, absolute thermoelec. power values 77−20303
α-U-Mo, dil., electronic properties depend. on $2^1/_2$-th order phase transition under high press. *(Russian)* 80−11128
U-Mo, high temp. phase diagram, thermodynamic props. of refractory metal solutes in liquid U 77−25022
U-Mo (10 wt.%), commercial alloys, influence of metallurgical factors on fracture processes *(French)* 78−60751
U-Mo (10 wt.%), gaseous O_2 and hydrogen embrittlement, exam. 78−60811
U-Mo (1.5 wt.%), superplastic behaviour 450 to 720°C *(French)* 79−74203
U-Mo (1.5 wt.%) metallurgical study of forging *(French)* 78−21737
U-Mo (2 wt.%), depleted, effect of microstruct. on mech. props. 80−108497

molybdenum alloys continued
U-Mo and U-Mo-Zr, shear martensitic transform. during quenching, plastic deform. and annealing 77−28815
U-Mo-Nb-Zr-Ti (0.75, 0.75, 0.75, 0.5 wt.%), heat treatment effect on microstruct. and mech. props. 78−23729
U-Mo-(Zr), ductile-brittle transition *(French)* 77−66693
U-Mo(Q^4)(Q^5), Q^4=quad, Q^5=quint, stress corrosion cracking in moist air, salt water, salted moist air 78−35562
U-Mo(2 wt.%), mech. props., effect of ageing 77−8914
V-Mo, and V-Nb-Mo, supercond. crit. temp. and crit. field, Mo alloying effect 77−85375
V-Mo, corrosion in high purity liquid Na containing ≈1 ppm O, at 700°C for 500 h 79−8383
V-Mo, effect of ion plated Mo on corrosion in liquid Na, mech. props. 78−53020
V-Mo, effects of heat treatment on mech. props. 77−21176
V-Mo, mechanical properties, O, N_2 and C addition effects 79−52356
V-Mo, X-ray K-emission spectra *(Russian)* 77−55851
V-Mo (25 wt.%), corrosion behaviour in high temp. impure He gas 80−76402
V-Mo effect of alloying additive on thermoelectric props. 77−35927
V-Nb-Mo (20,10wt.%), corrosion in liquid Na, O_2 effects 77−8987
V-Ni-Mo, structure in alloy crystallisation region, peritectic equilibria *(Russian)* 80−50622
V-Ni-Mo alloy, annealed at 1150°C, isothermal section *(Russian)* 79−52154
V_xMo_{1-x} solid soln., mag. susceptibility 79−91208
V_3Si-Mo solid soln., supercond. T_c and paramag. susceptibility *(Russian)* 77−59348
V_3Si-SiO_x-Mo_3Re_2, supercond. tunnel junctions 80−107961
Vitallium, orthopaedic implant material, metallurgical cond. effect on pitting resistance 79−70704
W-Mo, powder mixture, electric discharge sintering, struct. changes 77−77446
W-Mo, refractory, surface investigation by FIM and atom probe *(German)* 79−55623
W-Mo, vapour deposited, long-term strength and thermocyclic creep 80−16405
W-Mo alloys, positron interactions with component atoms *(Russian)* 77−63486
W-Mo alloys, thermal conductivity and diffusivity, sp. ht., 100-2400°C 78−75842
W-Mo powder mixture, activated sintering 77−21058
W-Mo powder mixtures, form. using electric discharge sintering 77−12563
W-Mo-Re heat resisting alloy MVR-27-VP2, high-temp. emissivity and resistivity 77−35727
W-Re(Mo)(Cr), powder mixture, activating effect of Group VIII metals on alloy form. during sintering 77−59728
Zr-Mo, high temp. phase diagrams 77−44217
Zr-Mo, Zr-Sn-Mo, creep characts., influence of Sn and Mo *(Czech)* 80−81119
Zr-Mo (3 wt.%), β-phase stability 78−39742
Zr-Mo film, amorphous, temp. stability 78−63948
β-Zr-Mo oxidised alloys, high temp. deformation, X-ray study 79−79045
Zr-Mo-Al (3, 1 wt.%), β-phase stability 78−39742
Zr-Mo-H, catalytic props. 80−30274
Zr-Mo-Nb-V-Sn (1,2,2,2 wt.%), heat treatment, transform. reactions and mech. props. 79−24545
Zr-Mo-Sn (3,2 wt.%), heat treatment, transform. reactions and mech. props. 79−24545
β-Zr-Mo-(Al)(Ti)(La), metastable, deform. induced transform. 78−52805
Zr-Nb-Mo, phonon spectra anomalies, lattice dynamics calculations, superconductivity parameters 79−7655
Zr-Nb-Mo alloys, decomp. of β solid soln., metastable and equilib. phases 79−11632
Zr-Nb-Mo-Re, alloying effect on dislocation core struct., determ. by discrete lattice modelling 78−30618
Zr-Sn-Mo (4.5,1 wt.%) and (4.5,2 wt.%), creep behaviour at room temp. *(Czech)* 79−24590
Zr-Sn-Mo (6, 1 wt.%), creep and creep rupture 78−23778
Zr-Sn-Mo-(Nb), creep and creep fract. at 623 to 823K *(Czechoslovakian)* 77−32643
Zr-Sn-Mo-(Nb), fracture in creep 77−36581
Zr-Sn-Mo(Nb), creep and creep fracture, 623 to 823K *(Czech)* 77−59916
Zr-Sn-No-(Nb), steady state creep 77−36580
ZrC-NbC-MoC_{1-x} alloys, physicomech. props., comp. depend. 79−66097

molybdenum compounds
see also molybdenum alloys
alkali halide:MoO_4^{2-}, frozen solns., absorpt. spectra, 4.2 to 300K 79−87467
alkali metal ternary sulphides, A_xMoS_2 and $A_xMo_3S_4$, cryst. struct. 78−42989
anodised layer, structure and stoichiometry, thickness effects 77−77634
boride coatings, reaction with Mo substrate 77−32716
borides, chemical vapour deposition *(French)* 77−36406
chalcogenide superconductors with T_c>10K 79−33381
chalcogenides, crit. mag. fields *(Russian)* 78−34936
chalcogenides, layered, soln. mechanism of metals 79−42249
chalcogenides, multicomponent, physical props. 80−84577
chalcogenides, supercond., prop. preparation and struct. *(French)* 79−73619
chemical reactions, stoichiometric and catalytic, with azobenzene 77−86370
chemical structures, thermodynamic props., reactions 77−77750
chemistry and uses, conf., Oxford, Eng., Sep (1976) 77−77749
chloride layered compound with graphitised PAN fibre, struct. and elec. cond. 79−91600
complex, $MoOCl_3.2Ph_2SO$, prep. and characterisation 78−30592
complexes, electronic struct., XPS and X-ray emission spectra 77−42336
dichalcogenide, valence band nature, elec. and mag. props. 78−39014
enzymes, investigation using EPR 77−86373
flame and smoke retardation formulations 77−77761
halides, [Mo_6X_8] cluster group identification in IR spectra of solids, normal vibrs. 78−64359
molybdates, alkaline earth, U activated, scheelite struct. luminesc. props. vibr. modes and quenching temp. 80−60651
molybdates, hydrated, water mol. bending vibrs. at low freqs. *(French)* 79−78670
molybdates, $Me^{II}MoO_4$ (Me^{II}=Cd, Cz, Sr, Ba, Pb), refr. index, single crystals having scheelite struct. 78−79082
molybdates, nonstoichiometric, IR spectra rel. to vacancy struct. *(French)* 78−43867
molybdates (double), of mono- and tri-valent metals, polymorphism, X-ray diffr. obs. 78−87642
molybdenates, X-ray photoelectron spectra 77−44121
molybdenum formate, mol., Hartree-Fock instability of SCF wavefunctions 80−9492
oxide, catalysis of graphitisable C graphitisation 80−89166
oxide clusters on surface, electron field emission energy distrib. 77−63548
oxide reduction by electron cyclotron reson. plasma of H, model study on discharge cleaning 80−76548
oxides, low-grade, soda roasting study *(Korean)* 80−93508
oxides, magnetic susceptibility meas., temp. effect 80−103822
oxides, oxysalts, reduction kinetics and mechanism 77−77733
precipitation, during evaporation of highly active nitrate solns. 78−37426
protein, containing Mo, Fe and labile S, isolation from Desulphovibrio gigas, sulphate reducer 77−86375
rare earth chalcogenides, $R_xMo_6Se_8$, coexistence of superconductivity and long-range magnetic order 79−11264
rare earth compounds, RMo_6X_8, (X=S, Se), supercond. and long range mag. order coexistence 80−15642
rare earth compounds, RMo_6X_8, X=S,Se, coexistence of supercond. and antiferromag. order 79−65579
rare earth cpds., $RMo_6S_8(Se_8)$, coexistence of supercond. and mag. ordering *(Russian)* 80−84542
refractory carbides, borides and nitrides, wetting by and interactions with liq. metals 80−54473
sulphides, supercond. ternary $M_xMo_6S_8$, crit. currents in strong mag. fields *(Russian)* 77−43796
superconducting ternary chalcogenides, structures and properties survey *(Czech)* 80−70870
ternary chalcogenide, MMo_6X_8 (M=metal, X=chalcogen) Chevrel phase, supercond. and normal state props. 78−56267
ternary chalcogenides, supercond., muffin-tin orbitals and atomic-sphere approx. 78−51871
ternary chalcogenides, supercond. props. 79−38230
ternary compounds, $R_xSn_xMo_6S_8$ (R=La, Ce, Pr, Eu, Gd, Ho, Lu, Y, In, U), supercond. props. 80−97023
ternary selenides, Chevrel phase supercond., compressibility and vol. depend. of Tc 78−31008
ternary sulphides, Chevrel phase, synthesis and superconductivity *(German)* 80−25038
ternary sulphides, Chevrel phase supercond., compressibility and vol. depend. of Tc 78−31008
ternary sulphides, influence of Fe on superconduction transition temp., and mag. props. *(Russian)* 79−42686
ternary sulphides, $M_xMo_6S_8$, (M=Pb, Sn, Sn-Al, Cu), prep. and supercond. props. 79−28434
transition metal compounds, $M_{2-x}Mo_xAs(P)$, crystal struct. *(French)* 77−47429
triphenylphosphine compounds, $(C_6H_5)_3PM_xM'_{1-x}(CO)_5$, M,M'=Cr, Mo, W, mixed cryst., CO vibr. spectra, modal anal. 78−35128
AgI-Ag_2O-MoO_3, comparison of ionic conductivity between glassy and crystalline solid electrolytes 78−30786
AgI-Ag_2O-MoO_3, superionic conducting glass, IR spectra and struct. 79−10804
AgI-Ag_2O-MoO_3 glass glass superionic cond., struct. and transport props. 80−88602
AgI-Ag_2O-MoO_3 glassy electrolyte galvanic cells 80−104513
AgI-Ag_2O-MoO_3 system, glass form. with high ionic conductivity 77−89379
Al-MoO_3-Al structure, current-voltage characts., 251K-301K 79−91156
Al_2O_3-Mo, dielectric cermet, thermophysical props. 77−51557
Al_2O_3-$MoSi_2$, for use as heating element, fabrication method and prop. *(Japanese)* 79−95989
BaO-MoO_3, solid phase reaction, thermal analysis 80−55639
Bi_2O_3:MoO_3 sintered, oxide ion conduction 77−80646
$CaMoO_4$, scheelite struct., intrinsic hole centres, EPR study 78−64274
CaO-Al_2O_3-SiO_2 glass-$MoSi_2$ filler, vitreous composite prod. 77−90313
$Ce_6Mo_{10}O_{39}$, 22 77−76373
$(Co,Mo)S_2$ hydrodesulphurisation catalyst, defect struct. and activity 77−86357
Co complexes with H_2S, formation and mol. struct. 77−75323
Co-Mo oxidic precursory state, supported on SiO_2 and γ-Al_2O_3 hydrotreating catalysts 79−61898
CoMo/γ-Al_2O_3 catalyst, ESCA and EPR meas. after hydrodesulphurization reaction *(French)* 79−52755
CoMoP, X-ray cryst. struct. anal. *(French)* 79−4281
CoO-MoO_3, catalyst pellets, Raman spectra 77−40216
Cr-Mo compound, susceptibility to thermal embrittlement 77−21458
Cr-Mo-N system, at high-pressure, temp., X-ray anal., phase diagram 80−50607
Cr_2O_3-MoO_3, physicochem. investig. of phase struct. 77−8807
$Cu_{1.8}Mo_6S_8$, supercond. energy gap and phonon-induced structs. in tunnelling density of states 79−51728
$Cu_{1.8}Mo_6S_8$, supercond. Chevrel phase, electron tunnelling spectroscopy expts. *(German)* 80−107966
$Cu_{1.8}Mo_6S_8$, superconducting state, triclinic struct., X-ray powder diffr. anal. 80−6388
$Cu_{2-x}Mo_3S_4$, X-ray cryst. struct. exam., effect of Cu conc. variation 78−2071
$Cu_2Mo_6S_8$, normal state and superconducting property measurements 78−91660
$Cu_2Mo_6S_8$, phonon density of states, mode softening correl. with supercond. transition temp. 79−51714
$Cu_xMo_3S_4$, superconductivity and cryst. struct. 79−78250
$Cu_xMo_6S_8$, 1.5≤x≤3.55, low temp. phase diagram, 1.2-320K 77−85371
$Cu_xMo_6S_8$, evaporated films, superconducting upper crit. fields, crit. currents 79−42714
$Cu_xMo_6S_8$, Hall effect and magnetoresistivity 78−95400
$Cu_xMo_6S_8$, inhomogeneous superconductor, scaling laws for pinning forces 79−47214
$Cu_xMo_6S_8$, prep. by topotactic electrode reactions, struct., supercond. 79−99158
$Cu_xMo_6S_8$, sintered and sputtered, supercond. upper crit. field 78−23215

molybdenum compounds continued
$Cu_xMo_6S_8$, supercond., two-phase, upper crit. field meas. 80−29509
$Cu_xMo_6S_8$, superconducting reactively evaporated film, crit. currents 79−28492
$Cu_xMo_6S_8$ system, low temp. modifications *(French)* 80−50606
$Cu_xMo_6S_8$, thin films, low temp. normal state, resist., temp. depend. 78−91783
$Cu_xMo_6S_{8-y}$ electrodes, thermodynamic and transport props. 80−66963
$Cu_xMo_6S_6I_2$, x=0 to 1.2, superconducting Chevrel-phase system, synthesis and transition temps. 79−69618
$Cu_xMo_6S_8(Se_8)$, prep., metallurgical and supercond. props. 77−32102
Cu_2O-CuO-MoO_3, subsolidus phase diagram, mag. props. 80−50615
$DyMo_6S_8$, long range mag. order in supercond. state 79−65653
$DyMo_6S_8$, supercond. and antiferromag. coexistence, neutron study 78−95401
$DyMo_6S_8$, superconductor, neutron scatt. exam. of mag. phase 79−73680
$Dy_{1.2}Mo_6S_8$, long-range mag. order and supercond., neutron diffr. obs. 79−78320
Dy_2O_3-K_2O-MoO_3, melt, viscosity meas. 79−99346
$ErMo_6S_8$, long range mag. order in supercond. state 79−65653
$ErMo_6S_8(Se_8)$, ternary superconductor, paramagnetic relax. effects 78−68112
$ErMo_6Se_8$, crystal field excitations, inelastic neutron scatt. obs. 79−78321
$ErMo_6Se_8$, mag. ordering and supercond., neutron diffr. 78−68125
$Er_xMo_6Se_8$, long-range antiferromag. order and supercond. coexistence 78−10715
$EuMo_6S_8$, Chevrel phase, RE mag. isolation and supercond. 80−44470
Eu_2O_3-MoO_3, phase diag. 77−48408
$Eu_xSn_{1-y}Mo_6S_y$, supercond., mag. props. 77−69447
$Eu_xSn_{1-x}Mo_6Sn_8$ (Se_8), ternary superconductor, paramagnetic relax. effects 78−68112
Fe-Mo-CaF (15, 9 and 6 wt.%), sintered, elevated temp. mech. props. 77−28878
Fe-MoS_2, exam. of props., using differential thermal analysis, and metallography *(Russian)* 79−15653
Fe-X-MoS_2 (X=WC, HfC, Al_2O_3, ZrO_2, HfB_2, ZrB_2), self lubricating coatings, exam. of props. 79−96217
Fe_2O_3-MoO_3, on SiO_2 and Al_2O_3, Mossbauer effect 79−47365
$GaMo_4S_6$, mag. and struct. transition temps., press. effects, 0-6 kbar *(Russian)* 77−89956
$GdMo_6S_8$, Chevrel phase, RE mag. isolation and supercond. 80−44470
$GdMo_6S_8$, long range mag. order in supercond. state 79−65653
$Gd_{0.1}Mo_6Se_8$, mag. supercond., low temp. sp. ht. meas. 79−56380
$H_{1.6}MoO_3$ bronze, form., kinetic, thermodynamic investig. *(French)* 80−45247
$H_{1.6}MoO_3$ bronzes, proton mobility 78−39426
H_xMoO_3, structural anal. by neutron diffr. 79−65043
H_xMoO_3, thermochemistry and electrochemical behaviour 79−100427
$H_3PO_4(MoO_3)_{12}.29H_2O$, electrochromic solid-state cells 80−2724
$Ho_{1.15}Lu_{0.05}Mo_6S_8$, long range mag. order in supercond. state 79−65653
$HoMo_6S_8$, long range mag. order in supercond. state 79−65653
$HoMo_6S_8$, reentrant supercond., direct. obs. of long range ferromag. order 78−76190
$HoMo_6S_8$, superconductor, neutron scatt. exam. of mag. phase 79−73680
$Ho_{1.2}Mo_6S_8$, re-entrant ferromag. supercond., heat capacity and AC mag. susceptibility 79−60948
$Ho_{1.2}Mo_6S_8$, supercond. destruction by mag. ordering 77−69449
$Ho_{1.2}Mo_6Se_8$, crystal field excitations, inelastic neutron scatt. obs. 79−78321
KCl(Br):MoO_4^{2-}, vibronic absorption spectra 78−10924
$K_2M(MoO_4)_3$, M=Zr, Hf, synthesis and struct. 77−36386
$K_{0.3}MoO_3$, thermochemistry 77−77801
$K_2Mo_2O_7.H_2O$, cryst. and mol. struct. 77−76373
$K_2Mo_9S_{11}$, prep. and struct., Mo_{12} cluster in $Mo_{12}S_{14}$ unit 80−107168
$K_2O.3MoO_3.3H_2O$, fibrillar crysts., morphology and struct. 78−63959
K_2SO_4-Cs_2SO_4-MoO_3 system, fusibility diagram 79−87619
$K_6[MnMo_9O_{32}].6H_2O$, cryst. struct. 77−76374
$LaCrO_3$-Mo eutectics, prep. and microstruct. 80−108380
$LaMo_6S_8$ thin films, crit. currents and pinning forces 80−34575
$LaMo_6X_8$ (X=S, Se), supercond., sp. ht., 1 to 14K 79−51720
LiAl-NaAlCl$_4$-$MoCl_5$ thermal battery evaluation and optimisation 79−29458
LiAl-NaAlCl$_4$-$MoCl_5$ thermal battery test results 79−29459
$Li_xMo_6S_{8-y}$ electrodes, thermodynamic and transport props. 80−66963
$Li_2O.3MoO_3.5.7H_2O$, fibrillar crysts., morphology and struct. 78−63959
$LuMO_6X_8$ (X=S, Se), supercond., sp. ht., 1 to 14K 79−51720
$MOSe_2$, optical phonon modes and localised effective charges, reflection spectra 78−76453
$MgMo_2O_7$, cryst. struct. 78−18596
$Mn_{0.394}$-$Ti_{0.606}$-O-S system, 1380 and 1485K, phase equilib. study 80−50616
$Mn_{8-x}Mo_{3+y}Sj_8$, cryst. struct. *(French)* 78−38675
Mo complex, ^{97}Mo and ^{95}Mo nuclear elec. quadrupole moment, nuclear quadrupole double reson. spectra 78−10802
Mo complex, [triply bridged binuclear Mo (V) cation][$MoOCl_4(H_2O)$]$^-$ struct. 77−76371
Mo complex, dithiocarbamate, model for molybdoenzymes, thermochem. meas. 77−86365
Mo complex, halogenoxomolybdenum (V), cryst. and electronic struct., reactivity 77−76369
Mo complex, hexadimethylamino molybdenum, electronic description of triple bonds and verification by photoelectron spectroscopy 78−41949
Mo complex, influence of anisotropy of spin-Hamiltonian parameters on EPR spectra *(Russian)* 77−28432
Mo complex, metal-metal bond, correl. effects, SCF calc. 77−65425
Mo complex, $MoOCl_3L_2$ (L=Ph_3PO or $(Me_2N)_3PO$), O transfer reactions and molybdoenzymes 77−86306
Mo complex, Mo(V) cysteine, reduction of cytochrome c 77−86371
Mo complex, μ-oxo bridged oxomolybdenum(V) dimers, conform. anal. by ang. overlap method, triplet ground states 78−5119
Mo complex, $Na[Mo_2O_5(O_3(OH)C_6H_8(OH)_2)].2H_2O$, struct. determ. and refinement 78−2073
Mo complex, nitrate reductase, reduction mechanism and kinetics in dimethylformamide 77−86366
Mo complex, nitrate reductase form. by recomb. with apoprotein fraction by Mo-deficient plant 77−86374
Mo complex, redox enzyme, electron transfer peculiarities 80−16896
Mo complex, tetrakis (formamidinato) dimetal, formation 77−77753

molybdenum compounds continued
Mo complex formation on oxidation of polyketo cpds., kinetics mechanism 77−77732
Mo complexes, aquo ions in solutions, isolation, characterisation 77−77847
Mo complexes, bis-carboxylate Mo(V), struct. and catalytic reactivity 77−77804
Mo complexes, chemistry and uses, conf., Oxford, Eng., Sep (1976) 77−77749
Mo complexes, dinitrogen type and derivs., XPS 77−75216
Mo complexes, dinuclear, chem. and spectroscopic props. 77−77239
Mo complexes, electron-rich bis(phosphine) dicarbonyl, chemistry and props. 77−77754
Mo complexes, hydrazine, hydrazido, amido, alkoxy 77−75324
Mo complexes, monomeric Mo(V) and Mo(IV) species 77−77803
Mo complexes, mononuclear, EPR ligand superhyperfine interactions, implications for enzymes 77−86372
Mo complexes, μ-oxo, di-μ-oxo, di-μ-oxo-μ-carboxylato bridged oxodimolybdates (v), structures 77−76370
Mo complexes, nitrosyl allyl, synthesis 77−77751
Mo complexes, organic derivs. of heteropolymolybdates 77−79701
Mo complexes, oxo- and sulphido-bridged, binuclear, in aprotic media, electrochem. and redox mechanisms 77−86324
Mo complexes, oxo-bridged dimers, ^{16}O and ^{18}O-substituted synthesis, IR spectra 77−77188
Mo complexes and catalytic activity, synthesis 77−77805
Mo complexes derived from electron-rich olefins, cryst. chem. 77−76372
Mo complexes organonitrogen derivs., chem. reactions, struct. 77−77752
Mo complexes with poly(iminoethylene)-dithiocarbamate polymer, synthesis and spectra 77−77189
Mo complexes with thousands and L-cystein, formation and Ir-spectra 77−81096
Mo complexs. bis(η-cyclopentadienyl) Mo halides, electronic struct., photoelectron spectra 77−75214
Mo halides and complexes, low oxidation state, XPS 77−75215
Mo nitrido complex, with multiple Mo-N bonds, prep., struct. and reactivity 77−83758
Mo-Al_2O_3 based hydrosulphurisation catalyst, used, ESR of SO_2^- and Mo^{5+} 77−70342
Mo-alkali earth oxides, multiple phase system calc. of phase equilibria using thermodynamic analysis *(Russian)* 79−56964
Mo-Mn-SiO_2 mixture, premetallizing of high alumina ceramics 79−47792
Mo-Mo bonds, review 77−76352
Mo-Mo_2C-La_2O_3-Pt cathode, Pt effect on work function *(German)* 79−74048
Mo-N, bond-strength bond-length relationships 80−91702
Mo-O crystals, electron microscopy study 80−28889
Mo-oxide, slow-electron-stimulated desorption 79−60623
Mo-Si, film deposition by reactive sputtering, characteris. *(Japanese)* 80−93485
Mo-Sn-S system, phase relationships, 500-800°C 79−24503
Mo-W-S system, phase relationships, 500-800°C 79−24503
Mo-Y(La)(Ce)-B, X-ray diffr., reciprocal lattice, crystal struct., phase equilibria 77−21122
$Mo_5(B,Si)_3$, stability of heatproof coating 77−86201
α-MoB, crystallographic relationship with CrB, UBC, ThBC 79−42025
MoB_2, hexagonal, form. by plasma heating and props. 79−28996
Mo_2B_5 and MoB_4, thermal, elec., and mag. props. 80−20187
Mo_2B_5, monocryst., grain size, abrasive and strength props. 80−11787
$Mo_2BC_{\frac{1}{4}}$ planar intergrowth defects and nonstoichiometry 78−2145
$Mo_2Br_8^{4-}$, electronic and reson. Raman spectra, Mo-Mo band 78−82745
MoC, precipitates in Ni-base superalloy, STEM microanal. 80−81067
Mo_2C, and $(Mo,Fe)_6C$, determ. in cementite by annealing in moist H_2 *(German)* 79−39231
Mo_2C, bond energy and ionization efficiencies from SIMS 79−24400
Mo_2C, charge transfer from XPS core level chem. shift anal. 77−72837
Mo_2C coatings, phase and struct. transformations on heating 79−96206
Mo_2C, corrosion and electrochem. props. in aq. H_2SO_4, HCl, HNO_3 and KOH solns. 80−11813
Mo_2C, free energy of form. and thermodynamic props. of C in solid Mo 80−15266
Mo_2C, magnetron-sputtered, solar selective absorbing surfaces 79−92079
Mo_2C powder form. by CVD 77−12590
Mo_2C powders, prop. from vapour phase reaction of $MoCl_4$-methane-H_2 system 79−100068
Mo_2C, RF sputtered, comp. by XPS 78−51839
Mo_2C RF sputtered wear-resistant coatings, XPS study of adherence 79−34191
Mo_2C, synthesis by ion bombard. of Mo film 78−48357
Mo_3C_2, pressing regime influence on high-temp. creep *(Russian)* 80−100852
Mo_3C, cathodic needle growth, at lower electric fields from $Mo(CO)_6$ vapour 80−76161
$Mo(CO)_6$, electronic spectra following flash photolysis, intracavity laser technique 79−31538
$Mo(CO)_6$, flash photolysis, Mo_2 form. and electronic spectra 79−36622
$Mo(CO)_6$, in nematic matrix, linear dichroism, distortion and local field contribs. 79−87415
$Mo(CO)_6$, MCD spectra, charge transfer transitions 80−95658
$Mo(CO)_6$, mol. vibrs. and reaction pathways, min. energy coords. and compliance consts. 77−57966
$Mo(CO)_6$, multiphoton ionisation, mol. cooling in pulsed supersonic beam 80−28070
$Mo(CO)_6$, physisorption and reaction on γ-Al_2O_3, IR spectra obs. 80−80064
$Mo(CO)_6$, polarised absorption, field effects in condensed media 78−997
$Mo(CO)_6$, relative intensities of ν(CO) and ν(MC) Raman bands 78−55176
$Mo(CO)_6$, second-order quadrupole splittings of ^{95}Mo NMR signal 77−28461
$Mo(CO)_5Kr$, dispersion energy, stabilisation energy, Mo-Kr separation 79−98241
$MoCl_5$, dissoc, in pulsed discharge, interference method obs. 77−58186
$MoCl_5$, photoelectron spectra 79−821
$MoCl_5$, pulsed discharge dissoc., for Mo I oscill. strengths meas. 78−25479
$MoCl_5$, reduction by H_2, influence of electric field on Mo film deposition 80−93491

molybdenum compounds continued
- $MoCl_5$-MoF_5 system, magnetochem. and IR study of phase struct. 77−85710
- $MoCl_6^{n-}$, n=1,2,3, vibr., IR meas., Raman spectra obs. 79−68234
- $Mo_2Cl_8^{4-}$, δ-δ bond, δ-δ* excitation, CI, CC, and MBPT approaches to UHFS model 80−32585
- $Mo_2Cl_8^{4-}$, low lying states, weak electronic coupling, Xα valence band theory 79−72237
- $Mo_2Cl_8^{4-}$, metal-metal bond energy, SCF-Xα-SW calcs. 80−78538
- $Mo_2Cl_9^{3-}$ complexes, cluster exchange coupling consts. SCF-Xα-SW calcs. 80−74120
- $Mo_6Cl_{14}^{2-}$, cluster ground state electronic struct. SCF Xα SW calc. 79−3607
- $Mo_2Cl_8^{3-}$($Mo_2Cl_9^{3-}$), electronic struct. and metal-metal bonding, HMO calcs. *(Russian)* 78−1118
- $Mo_6Cl_{10}S$, struct., dielec. and diamag. props. *(French)* 78−67691
- $Mo_6Cl_{10}Se$, struct., dielec. and diamag. props. *(French)* 78−67691
- $Mo_6Cl_{10}Te$, struct., dielec. and diamag. props. *(French)* 78−67691
- $MoCr_2O_6$, hydrothermal cryst. growth, 40 kbar, 873K, cryst. struct. *(French)* 78−35342
- $MoF_4+K_2(Cs_2)$, ionisation reactions, absolute cross sections 80−99565
- MoF_5, gas, thermodynamic stability 80−26041
- MoF_5, mol. and electronic struct., vitreous, liq., and tetrameric states, ^{19}F NMR obs., mol. mobility 80−34787
- MoF_5, prep., melting temp., vapour density, press., enthalpy of fusion, meas., assoc. 78−38813
- MoF_5, vapour, thermodynamic props. calc. 78−38826
- MoF_6, critical parameters determ. using thermodynamic and mol. similarities 77−43310
- MoF_6, cryst., overall vibr. band struct., excitons 77−90136
- MoF_6 crysts., density of exciton states, two-particle and mixed cryst. spectra 78−2829
- MoF_6, electron affinities from collisional ionisation with alkali atoms 78−55226
- MoF_6, in Ar matrix, photolysis, MoF_5 form., IR spectrum 80−87115
- MoF_6, isotope separation by laser, multiple-photon 78−58858
- MoF_6, orthorhombic crysts., Raman spectra, int./external mode separation and factor group anal. 77−90135
- MoF_6, reduction as method for synthesis of MoF_3 77−86307
- MoF_6 reduction by H, chemical kinetics eqn., adsorbed component interactions *(Russian)* 80−35569
- MoF_6, reduction by H in the presence of HF *(Russian)* 80−61076
- MoF_6, reduction by H_2 at 500-1200°C to Mo, exam. of Mo props. and MoF_6 props. *(Russian)* 80−7516
- MoF_6, second virial coeff. meas., Lennard-Jones pot. determ. *(German)* 77−19658
- MoF_6, universal eqns. of state and thermodynamic similarity 77−35290
- MoF_6, valence electron spectra, vibr. band struct. 77−23520
- MoF_6, vapour press., phase transform. enthalpy *(German)* 78−51654
- MoF_6-graphite intercalation cpd. 78−27441
- MoF_6+alkali atom(dimer), ionis. reactions, electron affinity 77−81398
- MoF_6+K(Cs), crossed beam reaction cross section 77−77740
- MoF_6(l), enthalpy of form. by soln. calorimetry 79−47962
- Mo_5GaS_6, specific heat temp. depend. 77−63199
- Mo_5GaS_6, struct. and mag. anomalies, 15 to 300K *(Russian)* 77−7864
- MoH_6, Dirac-Fock one-centre calcs. 79−6837
- MoN, interatomic interactions from XPS 80−49171
- MoN, matrix isolated visible absorpt. spectra, electronic, vibronic and vibr. states 80−28027
- MoN, superconducting diffusion wires, high field expts. on press. effects up to 15 kbar 79−61006
- MoN_x, ion condensing metal plasma stream, coating microhardness, chemical reactions 79−42426
- Mo_3N, synthesis by ion bombard. of Mo film 78−48357
- $Mo_2(NH_2)_6$, electronic description of triple bonds and verification by photoelectron spectroscopy 78−41949
- Mo_6NaS_8, specific heat and supercond. critical field *(Russian)* 77−77004
- MoNb, mol. dissoc. energy, mass spectrometric obs. 79−10229
- MoO, matrix isolated visible absorpt. spectra, electronic, vibronic and vibr. states 80−28027
- MoO_2, cryst., neutron diffr., mag. props. 77−16038
- MoO_2, crystal growth by vapour phase transport in I_2, 800 to 1000°C *(French)* 77−4725
- MoO_2, crystn. from gas phase in presence of I_2 79−52090
- MoO_2, effect of pressure on Fermi surface *(Russian)* 79−77988
- MoO_2, Fermi surface calcs. 78−67934
- MoO_2, Gibbs energies of form., form. enthalpies and standard entropies 79−52742
- MoO_2, MoO_3 and Mo_xO_{3x-1} single cryst. growth by chem. transport, elec. resist. meas. 77−59681
- MoO_2, optical conductivities and dielec. functions in 0.2-6 eV range, rel. to band struct. 79−42938
- MoO_2 powder bed, H_2 reduction kinetics 80−16230
- MoO_2:Re(V), current carrier sign, Fermi surface cross section variations *(Russian)* 80−84420
- MoO_2:V, growth by VO_2 transfer reacts. 79−43116
- MoO_2-I_2, heterogeneous equilib., vapour transport and cryst. growth 78−27405
- MoO_3, $^{16}O^{18}O$ substitution, isotope shift, vibr. amplitudes and consts., normal coord. anal. 79−36610
- MoO_3, addition to Mn-Zn ferrite, effect on grain growth and densification 79−61550
- MoO_3, adsorption of water 79−77898
- MoO_3 amorphous films, EPR of Mo^{5+} centres 80−34771
- MoO_3, catalysts, supported on aluminas, Raman obs. of struct. 79−28734
- MoO_3, dielec. and thermophys. props. 77−52009
- MoO_3, diffusion of C 77−11734
- MoO_3, EPR investig. of defect centres 77−59457
- MoO_3, ESCA of surface composition changes under ion bombardment 77−20974
- MoO_3, ESCA on H_2 reduction *(French)* 77−36365
- MoO_3, electric quadrupole interaction, TDPAC meas. 78−39455
- MoO_3, film, colour centre studies, optical absorpt. spectra 78−71724
- MoO_3 film, electrochromism, X-ray electron spectra 78−48146
- MoO_3 film, evaporated, electrochromism *(Japanese)* 79−38686
- MoO_3 film, optical absorpt. after ion irrad., appl. to ion beam profile monitoring 79−26181
- MoO_3, film and cryst., long range potential centres 78−30920
- MoO_3, fluidised bed roasting, operating variables effect 77−4933

molybdenum compounds continued
- MoO_3, highly dispersed, produced by plasmochemical method, adsorption props. *(Russian)* 77−70275
- MoO_3, Raman scatt. and struct. props. 77−55780
- MoO_3, reduced crystals, planes of crystallographic shear, TEM study 79−46683
- MoO_3, reduction at low temps., surface defects obs. in HV electron microscope 77−35564
- MoO_3, reduction at low temp., role of defects, electron microscope obs. 77−77755
- MoO_3 reduction to MoO_2 by electron beam, electron difrr., microscope investigs. *(French)* 78−95945
- MoO_3, smoke particles, coalescence growth by gas-evaporation 78−47256
- MoO_3 smoke particles prepared by gas evap., morphology and coalescence growth 80−97738
- MoO_3, thin cryst. obs. by convergent beam electron diffr. 78−38670
- MoO_3, ultrafine crystals, exam. of reduction using electron microscopy *(Russian)* 79−29394
- MoO_3, X-ray absorption, discontinuities and limits, chem. combination effects 80−93435
- MoO_3:Li, elec., catalytic props. 78−60122
- MoO_3:Re, ESR and optical absorption obs. 77−36127
- MoO_3-Al_2O_3 catalyst, state during thiophene hydrogenolysis 77−86359
- MoO_3-M_2O_3 system, M=trivalent metal, solid-state chem., review 77−24288
- MoO_3-MO system, M=alkaline earth metal, eutectic coordinates on phase diag. 77−44227
- MoO_3-P_2O_5, glass, DC cond. meas. high temp. range 78−6376
- MoO_3-P_2O_5 glass, thermoelec. power meas. 78−84242
- MoO_3-Si photodiode, fabrication as function of O_2 partial press. 80−29464
- MoO_3-TiO_2, reduction, Mo^{5+} and O_2^- form. 77−90590
- MoO_3+CaO→$CaMoO_4$, solid state reaction 79−43579
- MoO_3+Fe_2O_3 coreduction kinetics, thermodynamic equilib. in Mo-Fe-O-H system 78−60657
- MoO_3+Ni^{2+} interaction on Al_2O_3, Raman spectrum 80−108742
- MoO_{3-x}, single cryst. growth by physical vapour transport 79−28903
- MoO_4^{2-}, aq. soln., O isotope substitution, ^{95}Mo NMR 77−30890
- MoO_4^{2-}, in halide salt aqueous solution, absorpt. spectra, 4.2 to 290K *(Russian)* 78−60499
- MoO_4^{2-}, valence level electron struct. by XPS 77−4712
- MoO_6^{6-}, electronic struct., discrete variation and scatt. wave X_α methods 80−917
- MoO_x, AES expts., chem. shift and beam effects 79−15566
- Mo_2O_3-Al_2O_3, reduced catalyst, adsorption of O_2, O^- form. 78−85197
- Mo_2O_3-Cr_2O_3, catalyst, effect of Al_2O_3 additives on catalytic activity, in oxidation of methanol to formaldehyde *(Russian)* 79−66346
- Mo_4O_{11}, anodic dissolution, periodic phenomena 77−16735
- Mo_4O_{11}, Gibbs energies of form., form. enthalpies and standard entropies 79−52742
- $Mo_6O_{19}^{3-}$, in Mo/SiO_2 supported catalyst system, EPR, UV-visible spectra 79−99764
- Mo_7O_{24}, C_{2v} symmetry model, force field anal. 79−81200
- $Mo_2(OH)_6$, electronic description of triple bonds and verification by photoelectron spectroscopy 78−41949
- $MoO_{4-n}S_n^{2-}$ in aqueous soln., ^{95}Mo NMR identification 77−48069
- $MoO_{4-n}Sn^{2-}$, (n=0-4), $^{17}O(^{33}S)(^{95}Mo)(^{97}Mo)$ NMR investig. 80−53022
- Mo_2OsB_2, cryst. chem. and struct. 78−42995
- $MoRh_2O_6$, crystn. and cryst. struct., paramag. and elec. cond. props. *(French)* 77−80480
- $Mo_{6-x}Rh_xTe_8$, synthesis, struct., and elec. props. 80−92877
- $Mo_4Ru_2Se_8(Te_8)$, synthesis, struct., and elec. props. 80−92877
- MoS_2, 2H phase, far IR magnetoabsorption and refr. index meas. 77−24847
- MoS_2 (2H), elec. cond. press. depend. 78−43394
- MoS_2 (2H), low energy electron energy loss spectra 79−95885
- MoS_2 (2H), refl. of electrons from surface, total current spectroscopy 79−61479
- MoS_2 (2H), surface struct. determ. by dynamical LEED 77−43415
- MoS_2 (2H), surface struct. and interplanar separation by LEED 77−59191
- MoS_2 (2H), surface struct. refinement via reliability factors for surface crystallography 77−59193
- MoS_2 additive to lubricant, friction and frictional temp. reduction 80−21125
- MoS_2, adsorption of Cs and O_2, LEED, Auger and work function meas. 78−71994
- MoS_2, amorphous, cathode, electrochem. props. rel. to secondary Li battery 80−40851
- MoS_2, angular loss studies on natural surfaces by low-energy electron spectroscopy, surface cleavage influence *(French)* 79−56898
- MoS_2, bulk contact ice nucleation threshold under illum. 77−55343
- MoS_2, catalytic activity of basal and edge planes 77−86356
- MoS_2, clean surface, AES and LEED exam. 80−10762
- MoS_2 containing sintered Mo composite, friction and wear props. 80−11786
- MoS_2, effect of uniaxial stress on excitonic optical spectra 78−84606
- MoS_2, elec. cond. and Hall coefficient temp. depend. 77−28180
- MoS_2, electronic struct. by photoelectron spectroscopy using line and synchrotron sources 79−87560
- MoS_2, enthalpy and specific heat, temp. depend. 80−54406
- MoS_2, entropy, enthalpy and specific heat, temp. depend. 500 to 1700K 80−15260
- MoS_2, excitons, mag. circular dichroism and wavelength modulated reflectance meas. 79−23900
- MoS_2, factor-group analysis of high-symmetry layer dynamics 79−42160
- 2HMoS_2, far IR optical and magneto-optical absorpt. 77−52078
- MoS_2 filled polyvinyl furfural, contact area, filler effect 79−57040
- MoS_2 film, adhesion to oxidised metal surfaces, XPS meas. 78−22972
- MoS_2 film, growth on Mo(111) surface following chemisorption of H_2S 77−1329
- MoS_2 film, non-stoichiometry and sputtering conditions 78−87891
- MoS_2 film, sputtered, solid lubricant, morphological growth 77−35825
- MoS_2, friction coeff. temp. depend., 300 to 80K 77−35631
- MoS_2, homogeneity size estimation, stacking fault conc. effect 80−96661
- MoS_2 hydrotreating catalysts, Co, Fe and Ni effects on microstruct., TEM, SEM and EPMA obs. 79−52762
- MoS_2, KKR calc. of energy bands 80−34355

molybdenum compounds continued
- MoS_2, lattice images of defects and radiation damage applics. 80−107210
- MoS_2, layer cryst. surface, for solar energy assisted electrochem. splitting of H_2O 77−90612
- MoS_2, layer dynamics of high-symmetry crystals with atom-atom interactions 78−71799
- MoS_2, lubricating properties in CO_2 medium 77−86194
- MoS_2 MoS_3 catalysts struct. ESCA, binding energies 77−21420
- MoS_2, $MoSe_2$, texture and lubricating props. 77−44368
- MoS_2 molybdenite band structural props. rel. to supercond. and semicond. 80−96781
- MoS_2, molybdenite crystal, direct imaging of atom configuration projected onto the basal plane 80−64847
- MoS_2 on Mo, cryst. struct. and thermal stability 77−52539
- MoS_2 on Mo, sulphate coating growth kinetics and mechanism 77−86220
- MoS_2, optical phonon modes and localised effective charges, reflection spectra 78−76453
- MoS_2, Pd epitaxial growth, epitaxial orientation variation *(French)* 78−43256
- MoS_2, poorly crystalline 'rag' struct. 80−6391
- MoS_2, prep. and mag. props. *(French)* 80−93072
- MoS_2, RF sputtered, comp. by XPS 78−51839
- MoS_2, RF sputtered, solid lubricant on mild steel, morphology 78−6239
- MoS_2, RF sputtered layers with variable stoichiometry, lubrication props. 80−40557
- MoS_2, RF sputtered lubricant, wear life, sputtering parameter effects 80−40558
- MoS_2, self-propag. high-temp. synthesis, wear props. 80−2975
- MoS_2, sliding charact., friction and wear *(Japanese)* 78−56778
- MoS_2 solid lubricant, antifriction and elec. props. depend. on oxidation temp., dopant influence 80−108584
- MoS_2, spatial symm. of valence band struct. by angularly resolved XPS 77−69961
- MoS_2, specific surface energy determ. 77−28073
- MoS_2, struct., XES and XPS obs. 80−43105
- MoS_2, surface electronic struct., slow electron reflection, total current spectroscopy *(Russian)* 80−54759
- MoS_2, synthetic molybdenite single crystals, growth from vapour, elec. props. 80−34446
- 2H-MoS_2, thermal expansion between 10 and 320K, cell dimensions meas. 79−65222
- MoS_2, UPS meas. band struct. determ. 78−35250
- MoS_2, unsupported hydrosulphurization catalyst promoted by group VIII metals, catalytic, structural and textural props. 79−79289
- MoS_2-electrolyte, contact, electrolytic decomposition and photodecomposition 78−95357
- MoS_3, amorphous struct., X-ray radial distrib. anal. and XPS 80−49115
- $MoS_{3.2}$ prep., use as Li battery cathode 80−29892
- MoS_4^{2-}, anharmonicity consts., reson. Raman spectra 77−61754
- MoS_4^{2-}, S isotope effect on ^{95}Mo nucl. mag. shielding 77−63301
- MoS_x RF reactively sputtered film, struct. and comp. 78−60038
- Mo_6S_8 and halogen substituted cpds., sp. ht. capacity 80−49986
- Mo_6S_8 Chevrel phases with group IIIa metals, Nb, Hg, Pb and Cu, synthesis, stability and charcts. 80−71608
- Mo_6S_8, heat capacity and mag. props., 2-30K 79−42692
- Mo_6S_8, phonon density of states, mode softening correl. with supercond. transition temp. 79−51714
- Mo_6S_8, relationship between electronic struct. and supercond. transition temp. 77−85368
- $Mo_6S_6Br_2$, supercond., crit. temp. meas. 77−85367
- $Mo_6S_6Br_2$, X-ray cryst. struct. anal. *(French)* 80−33965
- MoSCl, thermal expansion and thermal transform. 78−26696
- $MoSCl_3$, prep. and characterisation 77−59705
- $Mo_6S_6I_2$, supercond., crit. temp. meas. 77−85367
- $MoS_2(Se_2)$ and Ga alloys, mixing powders using US treatment 79−24454
- $MoS_2(Se_2)$, layer type dichalcogenides, reflectivity, 6 to 40 eV, electronic deep level excitation 77−55801
- $Mo_3S_4(Se_4)$, channel-type, topotactic redox reactions 77−90598
- $MoS_2(Se_2)(Te_2)$ coatings, growth kinetics and friction coeffs. 77−16731
- $Mo_3S_4(Se_4)(Te_4)$, Chevrel-phase low temp. struct. stability rel. to supercond. 77−47919
- Mo_6S_8Sn, triple chalcogenide, NMR spectra in supercond. state *(Russian)* 80−93194
- MoS_2(2H), elastic consts., from dispersion curve and linear compressibility data 77−11618
- MoS_2(2H), electro-absorpt. edge spectra, cryst. thermal modulation, exciton state field ionisation 79−61395
- MoS_2(2H), Kramers-Kronig anal. of reflectivity spectra, 0-30 eV, band model 79−51976
- MoS_2(2H), lattice dynamics, Coulomb and quasi-harmonic effects 80−39245
- MoS_2(2H), Raman spectra, phonon modes, high press. effects 80−40111
- Mo_3Sb_7, Sb decomp. press. and enthalpy of form., Knudsen effusion meas. 79−87840
- $MoSe_2$ (2H), low energy electron energy loss spectra 79−95885
- $MoSe_2$ and other layer structs. containing hohlstellen, electron diffr. 77−80397
- n-$MoSe_2$ based liq. junction solar cell, nonaqueous electrolyte system employing Cl_2/Cl^- couple 80−81432
- $MoSe_2$ coating, on Mo, support annealing influence on orientation, texture and hardness *(Russian)* 80−20961
- $MoSe_2$, effect of uniaxial stress on excitonic optical spectra 78−84606
- $MoSe_2$, elec. cond. and Hall coefficient temp. depend. 77−28180
- $MoSe_2$, evaporation, mass spectroscopic investigation 77−76530
- $MoSe_2$, exciton spectra 80−97296
- $MoSe_2$, excitons, mag. circular dichroism and wavelength modulated reflectance meas. 79−23900
- $MoSe_2$, IR and Raman spectra, lattice vibrs. interlayer bonding 80−40110
- $MoSe_2$, imperfections from TEM study 80−79800
- $MoSe_2$, layer cryst., electrochem. solar cell, electron transfer mechanism 78−52077
- $MoSe_2$ layer-type electrochem. solar cells, electrode material performance, doping effect 79−74532
- $MoSe_2$ lubricant, synthesis by Mo+Se vapour reaction, process kinetics 79−33942
- $MoSe_2$, lubricating coatings, texture, prep. by $Se_{(g)}$+Mo 78−53018
- $MoSe_2$, Schottky barrier, photovoltaic props. 79−7854

molybdenum compounds continued
- $MoSe_2$, single cryst., growth, struct. obs. 79−90607
- n-$MoSe_2$, synthetic, performance in electrochemical solar cells 79−66412
- $MoSe_2$, TEM exam. 77−35548
- $MoSe_2$:Nb(Re), layered, elec. props., semicond.-metal transition 77−11922
- $MoSe_2$-I^-, photoelectrode, time resolved photocurrent, nanosecond excitation 80−45708
- $MoSe_2$-WSe_2, cryst. struct. parameters and growth conditions 79−86759
- $MoSe_{2-x}$, transport meas. and band structure 77−69361
- $MoSe_4^{2-}$, anharmonicity consts., reson. Raman spectra 77−61754
- Mo_6Se_8 and halogen substituted cpds., sp. ht. capacity 80−49986
- Mo_6Se_8, Chevrel phase, anisotropy of H_{c2} 79−56460
- Mo_6Se_8, Chevrel phase, isotope effect on supercond. T_c 78−52141
- Mo_6Se_8, Chevrel phase, isotope effect on supercond. transition temp., phonon modes 79−51713
- Mo_6Se_8, Chevrel phase, supercond. isotope effect meas. *(German)* 80−25038
- Mo_6Se_8, Chevrel phase supercond., compressibility and vol. depend. of Tc 78−31008
- Mo_6Se_8, Chevrel phase supercond., phonon spectra, neutron scatt. meas. 79−42174
- Mo_6Se_8, heat capacity and mag. props., 2-30K 79−42692
- Mo_6Se_8, isotope effect, theory 78−91806
- Mo_6Se_8, isotope effect on transition temp. 79−73615
- Mo_6Se_8, phonon density of states, mode softening correl. with supercond. transition temp. 79−51714
- Mo_6Se_8, relationship between electronic struct. and supercond. transition temp. 77−85368
- $Mo_6Se_{8-x}Br_x$, supercond. obs. crit. temp. determ. 77−85367
- $Mo_6Se_{8-x}I_x$, supercond. obs. crit. temp. determ. 77−85367
- Mo_6Se_8Sn, triple chalcogenide, NMR spectra in supercond. state *(Russian)* 80−93194
- $MoSe_2$(2H), Kramers-Kronig anal. of reflectivity spectra, 0-30 eV, band model 79−51976
- $MoSi_2$, ceramic additives effect on sintering, recrystallisation 80−40306
- $MoSi_2$ coating for Nb alloy, oxidation protection, diffusion-slip casting appl. method 80−21187
- $MoSi_2$, coating for oxidation resistance 77−32704
- $MoSi_2$ coating for SiC heating elements 80−21137
- $MoSi_2$, diffusion marker for backscatt. studies of W+Mo bilayer film 78−87828
- $MoSi_2$ film, elastic stiffness and thermal expansion coeffs. 80−107451
- $MoSi_2$, integrated intensities and lattice parameters, X-ray anal. 78−63733
- $MoSi_2$ layer, formation kinetics on Mo, effect of direct elec. current 79−99436
- $MoSi_2$ on Mo, coating by local heating 77−81335
- $MoSi_2$, oxidation behaviour, Ge additions effect *(German)* 80−71782
- $MoSi_2$, oxidation in CO_2, 1200-1700°C 77−40454
- $MoSi_2$ oxide film, dielec. props. and growth kinetics 80−81215
- $MoSi_2$, RF sputtered, comp. by XPS 78−51839
- $MoSi_2$, reactions with Ti-Al-Cr-Mo alloy VT3-1 80−16585
- $MoSi_2$, reactive diffusion of Si, kinetics and mechanism 77−35751
- $MoSi_2$ refractory formation by As^+ ion beam bombardment 80−107286
- $MoSi_2$, self-propag. high-temp. synthesis 80−2988
- $MoSi_2$, self-propag. high-temp. synthesised, sintering and props. 80−11616
- $MoSi_2$, silicides formation in Mo-W bilayer films on Si substrates 79−99376
- $MoSi_2$, sputtered films, microstruct. and wear props. 78−64733
- $MoSi_2$ sputtered films, protective layer form. on oxidation, Auger anal. and backscatt. meas. 79−15029
- $MoSi_2/TiGe_2$ mixed crystals, direct obs. of surface oxide form. *(German)* 77−12721
- $MoSi_2$-$CrSi_2$, phase equilib., struct. and props. 80−50608
- $MoSi_2$-$TiSi_2$, high-temp. oxidation 79−83341
- $MoSi_2$-Y_2O_3, ceramics, fireproof, direct energy conversion appl. *(Czech)* 79−70455
- $MoSi_3$ crystalline layers, diffusion growth kinetics at 1700°C under influence of direct elec. current 79−52112
- Mo_3Si, layer growth, effect of DC density, temp. 79−43160
- Mo_3Si, self-propag. high-temp. synthesis 80−2988
- Mo_5Si_3 based coating, interaction with Mo alloy substrate *(Russian)* 80−21167
- Mo_5Si_3, layer electrotransfer of Si 80−92708
- Mo_xSi_y films, magnetron DC reactive sputtering, struct. and props. 80−80966
- $Mo_5SnGa_{0.5}S_6$, specific heat temp. depend. 77−63199
- $Mo_5SnGa_xS_6$ heat capacity from 2 to 25K 78−43518
- Mo_5SnS_6, supercond., at 2 to 25K, lattice and electron contrib. to sp. ht. 77−77003
- α-$MoTe_2$, band struct. photoelectron spectroscopy 77−51653
- β-$MoTe_2$, domain struct., dislocation fine struct., phase transitions 79−82332
- $MoTe_2$, elec. cond. and Hall coefficient temp. depend. 77−28180
- $MoTe_2$, elec. cond. and thermoelec. power 79−91047
- α-$MoTe_2$, electronic struct. by photoelectron spectroscopy using line and synchrotron sources 79−87560
- $MoTe_2$, IR and Raman spectra, lattice vibrs. interlayer bonding 80−40110
- α-$MoTe_2$, KKR calc. of energy bands 80−34355
- β-$MoTe_2$, layer cryst., dislocations and domain struct. 80−39102
- β-$MoTe_2$, low-temperature structural phase transition, X-ray meas. 79−14928
- β-$MoTe_2$, metallic in-plane resistivity meas. indicate first-order phase transition 78−30903
- $MoTe_2$, single cryst. growth by chem. vapour transport using $TeCl_4$ as transport agent 79−28903
- $MoTe_2$, thermal cond., rapid meas. method *(French)* 78−12689
- $MoTe_2$:V, single cryst. growth by chem. vapour transport using $TeCl_4$ as transport agent 79−28903
- $MoTe_{2-x}$, thermal switching mechanism 77−15920
- $MoTe_{2-x}$, thermoelec. power and resist. meas., band struct. 77−1438
- Mo_6Te_8 and halogen substituted cpds., sp. ht. capacity 80−49986
- $Mo_6Te_{8-x}I_x$, supercond obs., crit. temp. determ. 77−85367
- Mo_5TeO_{16}, cryst. struct. *(French)* 77−72586
- $MoTe_2$(2H), Kramers-Kronig anal. of reflectivity spectra, 0-30 eV, band model 79−51976
- $(Mo_xV_{1-x})_2O_5$, mag. and spectroscopic investigation 80−25206
- $Mo_{0.5}W_{0.5}Se_2$ single cryst. vapour growth, characterisation 80−93466

molybdenum compounds continued
$Mo_6X_8^{4+}$ cluster cpds. (X=F, Cl, Br, I), SCF-SW-Xα calcs. 80−74276
$Mo(ZrO_2.La_2O_3)$ structural changes during reduction and sintering 80−25636
$Mo_2[(CH_2)_2P(CH_3)_2]$, δ-$\delta^*(^1A_{2u}$-$^1A_{1g})$ transition, vibr. struct. anal. 80−53006
$NH_4Cl:[MoOCl_5]^{2-}$, single cryst., struct. investigations 77−66524
$(NH_4)_2MoO_4$, ^1H spin-lattice relax., 100-500K 79−38398
$(NH_4)_4Mo_8O_{26}.4H_2O$, Lindqvist octamolybdate, cryst. and mol. struct. 77−76373
$(NH_4)_2MoS_4$, aq. soln., Raman intensity, scatt. frequency depend. 79−28747
$Na_5HMo_5P_2O_{23}(H_2O)_{11}$, mol. and cryst. struct., X-ray diffr. anal. 79−32951
$Na_4Mo_{12}GeO_{40}(H_2O)_8$, X-ray diffr. cryst. struct. exam. 78−2075
$NaMo_6O_{17}$, thermochemistry 77−77801
$Na_2MoO_4(S_4)(Se_4)$ crystals, charge transfer spectra of MoX_4^{2-} complexes 80−54658
$Na_6Mo_5P_2O_{23}(H_2O)_{14}$, X-ray diffr. cryst. struct. determ., refinement 78−2074
Na_2O-B_2O_3-SiO_2-MoO_3 glass containing high level radioactive waste, phase separation 80−25683
Na_2O-MoO_3, melt, EMF meas., rel. partial molar thermodynamic props. 80−6526
$Na_20.3MoO_3.3H_2O$, nucleation and growth from soln. 77−84682
Nb-V-Mo-Au, gaseous AuV obs. and dissoc. energy by high-temp. mass spectrometry 79−45860
NbSe (2H), surface struct. refinement via reliability factors for surface crystallography 77−59193
$NdMoO_4$, photoacoustic spectroscopy, dichroism meas. 78−62227
Nd_2O_3-MoO_2-MoO_3 system, phase equilibria *(French)* 79−52176
NiMoP, cryst. struct. determ. 77−80468
$PMo_{12}O_{40}$, vibr. anal., symmetry coords. and force field anal., IR and Raman spectra 77−15522
P_2O_5-MoO_3 glasses, EPR study 79−82866
P_2O_5-MoO_3-CaO glasses, EPR study 79−82866
$PbMo_{5.1}S_6$, high supercond. T_c, soft mode behaviour 78−14855
$PbMo_{5.1}S_6$, supercond. wire prep. by powder technique 78−52705
$PbMo_6S_6$, cold-worked core-wires, supercond. transition temp. and lattice instability 78−6469
$PbMo_6S_8$ and ternary sulphides, lattice parameter rel. to supercond. T_c 78−52119
$PbMo_6S_8$, Chevrel phase supercond., phonon spectra, neutron scatt. meas. 79−42174
$PbMo_6S_8$, Hall effect and magnetoresistivity 78−95400
$PbMo_6S_8$, influence of Fe on superconduction transition temp., and mag. props. *(Russian)* 79−42686
$PbMo_6S_8$, inhomogeneous superconductor, scaling laws for pinning forces 79−47214
$PbMo_6S_8$, normal state and superconducting property measurements 78−91660
$PbMo_6S_8$, projected critical current, comparison with Nb_3Ge 79−69642
$PbMo_6S_8$, relationship between electronic struct. and supercond. transition temp. 77−85368
$PbMo_6S_8$, supercond. Chevrel phase, electron tunnelling spectroscopy expts. *(German)* 80−107966
$PbMo_6S_8$, supercond. wires prod. and characteris. 77−69462
$PbMo_6S_8$, thin films, low temp. normal state, resist., temp. depend. 78−91783
$PbMo_6S_8$ wire, powder processed, crit. current density and field 80−80466
$PbMo_6S_8$:Fe, elec. cond. anomalous temp. depend., mag. moments *(Russian)* 80−92878
$PbMo_6S_8$:Gd_3 EPR meas. *(French)* 80−54947
$PbMo_6S_8$:Gd^{3+}, powder EPR spectra, cryst. field, supercond. energy gap 80−34769
$Pb_xMo_6S_{8-y}$, phase relns., stoichiometry, T_c 78−15378
$Pb_xMo_6S_8(Se_8)$, prep., metallurgical and supercond. props. 77−32102
$PbMo_6Se_8$, relationship between electronic struct. and supercond. transition temp. 77−85368
$Pb_{1.125}Mo_6Se_{7.5}$, Chevrel phase supercond., NMR study 80−49989
$Pb_{1.2}Mo_6Se_8$, Chevrel phase supercond., phonon spectra, neutron scatt. meas. 79−42174
$PbMo_6Se_8(S_8)$, anisotropy of H_{c2} 78−39274
$PbMo_6X_8$ (X=S, Se), phonon density of states, mode softening correl. with supercond. transition temp. 79−51714
PbO-MoO_3-MO system, M=Ca, Ba, Mg, Sr, perovskite type cpds. detection 80−108404
PbO-MoO_3-P_2O_5, glass phase investigation, density determ. *(Polish)* 77−70039
$Pb(WO_4)_{1-x}(MoO_4)_x$ mixed crystal, growth by Czochralski method, props. 78−60566
$R_{1-x}Mo_6S_8$, magnetically ordering, supercond. props. magnetically ordering, supercond. props. 79−56373
$Sb_{0.2(0.4)}MoO_{3.1}$, synthesis, struct. and oxidation state *(French)* 80−64971
$ScMo_6X_8$ (X=S, Se), supercond., sp. ht., 1 to 14K 79−51720
$SeMoOCl_2$, prep., cryst. struct., characterisation *(French)* 78−63722
$Sn_{1-x}Eu_xMo_6S_8$, supercond., Mossbauer effect, struct. phase transition 77−12290
$Sn_{1-x}Ga_xMo_5S_6$, heat capacity meas., singularities at low temp. 80−49985
$SnMo_5S_6$, high supercond. T_c, soft mode behaviour 78−14855
$SnMo_6S_8$, Chevrel phase supercond., phonon spectra, neutron scatt. meas. 79−42174
$SnMo_6S_8$, Chevrel phase, RE mag. isolation and supercond. 80−44470
$SnMo_6S_8$, cryst. struct., superconducting characts. changes 79−86773
$SnMo_6S_8$, isotope effect props. *(Russian)* 80−37751
$SnMo_6S_8$, lattice softening, vibr. anisotropy 78−14428
$SnMo_6S_8$, phonon density of states, mode softening correl. with supercond. transition temp. 79−51714
$SnMo_6S_8$:Gd_3 EPR meas. *(French)* 80−54947
$SnMo_6S_8$:Gd^{3+}, powder EPR spectra, cryst. field, supercond. energy gap 80−34769
$Sn_xMo_5S_6$, supercond. props., effect of W and Re alloying additions, Mossbauer and X-ray diffr. meas. *(Russian)* 79−15245
$Sn_xMo_6S_8$, struct. anal. supercond. props. 80−97023
$SnMo_6S_8(Se_8)$ Chevrel phase supercond., hyperfine interaction, microscopic study 79−56650
$Sn_xMo_6S_8(Se_8)$, prep., metallurgical and supercond. props. 77−32102
$SnMo_6Se_8$, anisotropy of H_{c2} 78−39274
molybdenum compounds continued
$SnMo_6Se_8$, Chevrel phase, RE mag. isolation and supercond. 80−44470
$TbMo_6S_8$, long range mag. order in supercond. state 79−65653
$TbMo_6S_8$, superconductor, neutron scatt. exam. of mag. phase 79−73680
$Tb_{1.2}Mo_6S_8$, long-range mag. order and supercond., neutron diffr. obs. 79−78320
$Tb_{1.2}Mo_6Se_8$, crystal field excitations, inelastic neutron scatt. obs. 79−78321
TeO_2-MoO_3-M_nO_m, glass formation range 78−71680
TeO_2-MoO_3-V_2C_5, phase comp. determ. using X-ray diffr., electron microscopy and DTA *(German)* 80−88046
Th(U)-Mo, high temp. phase diagram, thermodynamic props. of refractory metal solutes in liquid Th 77−25022
TiC-Mo_2C-Ni cermets, influence of anomalous phases on strength 78−92228
TiC-Mo_2C-TiN-Co, fracture toughness, effect of microstructural defects *(Japanese)* 77−56087
$Tl_2Mo_9S_{11}$, prep. and struct., Mo_{12} cluster in $Mo_{12}S_{14}$ unit 80−107168
$TlR(MO_4)_2$, R=Eu, Dy, Er; M=Mo, W, luminesc. *(Russian)* 78−48229
TmO_6S_8, low temp. Mossbauer study and mag. susceptibility 80−80656
UF_6MoF_6, dil. sol., liq.-vap. equilib. 77−62632
$V_{1-x-z}Fe_xMo_zO_2$, Mossbauer effect exam., Fe conc. and precise struct. characteristics 78−31141
V_2O_5-MoO_3, solid soln. thermogravimetric anal., ion formation on crystallisation 77−20076
V_2O_5-MoO_3 solid soln., number of V^{4+} ions, magnetic and thermogravimetric exam. 78−52199
V_2O_5-MoO_3 solid solns., small polaron cond., elec. resist. and thermoelec. power meas. 80−34447
V_2O_5-MoO_3 system, X-ray diffr., IR absorption spectra, NMR and thermal analysis 77−24379
V_2O_5-MoO_3-P_2O_5 glass, semicond., DC cond., dielec. props 79−91044
$(V_2O_5)_{0.93}(MoO_3)_{0.07}$ solid soln., struct. transform. in oxidizing and reducing gas atm. 79−23740
(W, Mo)C, hard-facing applications, effect of Mo on struct and hardness of WC 80−108474
$W_xMo_{1-x}O_3$, absorpt. spectra and optical gap energies 79−91464
$W_xMo_{1-x}O_3$, mixed cryst., structural phase transition, Raman and IR spectra 78−79766
$W_xMo_{1-x}O_3$, reduction and temp. effect on electronic core levels, XPES 79−91564
WO_3-MoO_3, film, evaporated, electrochromism *(Japanese)* 79−38686
WO_3-MoO_3, glass film compositions, electrochromism *(Russian)* 79−28721
WO_3-MoO_3 film, amorphous, electrochromic optical absorpt., expt. results and model 78−27341
WO_3-MoO_3 system, on glass substrate, electrochromism of glass film compositions 80−29720
Xe-MF_6, M=W, Mo, U, Re, Ir, charge transfer interactions, VUV and IR obs. 78−50664
$YCrO_3$-Mo eutectics, prep. and microstruct. 80−108380
YMo_6X_8 (X=S, Se), supercond., sp. ht., 1 to 14K 79−51720
$YbMo_6S_8$, low temp. Mossbauer study and mag. susceptibility 80−80656
$YbMo_6S_8$, supercond., low temp. thermal and mag. props. 78−14904
$YbMo_6S_8$, ternary superconductor, paramagnetic relax. effects 78−68112
ZrC-NbC-MoC_{1-x} system, thermal expansion coeff. up to 2500°C 79−69267

moments (electric) *see electric moments*

moments (magnetic) *see magnetic moments*

moments (molecules) *see molecular moments*

momentum
see also angular momentum
air track direct vel. readout, conservation of momentum demonstration 77−82346
atmosphere, planetary wave heat and momentum fluxes rel. to stratosphere and mesosphere meridional circulations 80−109219
education, light momentum density in refracting medium, electrostriction, Peierls method 77−33772
education, momentum flow as force, alternative conceptualisation for teaching mechanics 80−67993
elastic collisions, theory 77−67264
impact ball apparatus, teacher's demonstration 78−8195
incompressible laminar boundary layer, three-dimensional, hyperbolicity of integral equations of momentum 77−27505
interfaces, pure, thermodynamics and dynamics rel. to Spacelab 79−28910
Large Space Telescope optimal fine pointing control using Annular Momentum Control Device 77−73934
laser-produced plasma, momentum meas. by ballistic and torsion pendulums 78−83611
ocean momentum transport, diffusion parameterisation of mesoscale eddy effects from numerical expt. 79−48508
operator, in nonCartesian coords., for teaching 78−24620
position operators, systems exhibiting special relativistic relation between momentum and vel. 78−89335
predictive relativistic mechanics, two particle case 77−2540
quantisation and measurement of momentum observables 80−98815
quantum momentum operator in curvilinear coordinates *(Russian)* 78−36862
relativistic energy and momentum triangles, modified versions applicable to accelerated motions 79−88803
relativistic thermodynamics, density, momentum and energy laws 77−82424
special relativity, mass and momentum density transform. 77−30005
theory, generalised formulation for transient phenomena 80−62474
transfer from waves to particles 80−18977

monitor programs *see supervisory and executive programs*

monitoring
see also patient monitoring; radiation monitoring
AC voltage phase lead-lag and phase sequence detection 78−65942
accelerator ion beam position monitor 79−89040
acoustic emission activities in deep-level coal seams, bed rocks instability obs. *(Japanese)* 80−10071
acoustic noise, development of temporal sampling strategies 79−98542
action potentials from two different sources, distinction using dual channel audio monitor 78−61293
aerosol monitoring and control, using size distrib. 79−57534
air ionisation in rooms due to physiotherapy apparatus 77−78035

monitoring continued
air pollutant monitoring system design by spatial sample stratification 79−83680
air pollutants monitoring from municipal wastewater plants 79−80050
air pollution, Dutch national monitoring system, focal and reference point 78−69465
air pollution, incoherent optical heterodyne detection 79−16679
air pollution, laser monitoring techniques for trace gases 78−69521
air pollution, laser systems appl. 78−69520
air pollution, long-path monitoring, using tunable lasers 78−69522
air pollution, monitoring instrums. including chemiluminescent NO_x monitor 80−72118
air pollution, $NO/NO_2/O_3$ monitors intercalibration 78−69529
air pollution, non-methane hydrocarbons monitoring via photoionisation 78−73549
air pollution, philosophy 79−70492
air pollution, pollutant gases monitoring from space using passive microwave techniques 80−76690
air pollution, survey aircraft for sample collection and anal. *(Dutch)* 78−81366
air pollution, using IR PbSe diode laser spectrometer 77−82044
air pollution above urban site, monitoring by Lidar meas. *(French)* 77−25780
air pollution automatic monitoring network, statistical approach to online control 77−41164
air pollution background characts. 79−57531
air pollution meas. network, nontelemetric, in Hungary *(Hungarian)* 77−64422
air pollution monitoring by pulsed lasers, numerical filters *(Japanese)* 79−43801
air pollution networks 78−93009
air pollution survey vehicle *(Dutch)* 78−81365
air quality baseline, Australian initiative 79−96490
air quality surrounding thermoelec. plant, VHF telemetering station *(Italian)* 77−82064
air quality system in Melbourne 77−70819
air-bath enclosure for standard cell group monitoring by AC Josephson effect 77−82556
air/water pollution detection and law enforcement 77−91263
airborne contaminants monitoring in chem. labs., USA regulations 80−12869
aircraft engine emission surveillance 79−74562
aircraft noise, concepts of instrumentation 80−33397
aircraft noise monitoring systems, requirements 80−23849
ambient air analysis, area survey and sampling mobile laboratory 80−104528
animal movement monitoring in enclosure, photocell sensing devices, chart recording 77−81765
artificial heart, system for continuously monitoring pumping diaphragms 77−44844
atmosphere, point monitoring of gases ambient concs. using tunable lasers 78−61607
atmosphere, using discretely-tunable IR gas lasers and heterodyne detect. techniques 78−61605
atmosphere SO_2, long-term monitoring method using permeation sampling, development 80−26189
atmospheric aerosol automatic mass conc. meas. techniques 77−64459
atmospheric and Earth surface characteristics affecting tropospheric propagation of microwaves, satellite techniques 78−24353
atmospheric magnetic particle fallout recorded in recent ombrotrophic peat sections 78−61519
atmospheric pollution, centralised supervision system in Fos-Etang de Berre region 78−81410
atmospheric pollution in Paris streets, survey network 78−81463
atmospheric trace gas IR monitor, airborne, nondispersive 79−8719
automated plating stress monitor 79−24696
battery monitor, operates on only a few microamperes 77−18005
beam power monitor system, for neutral beam injection fusion reactor 78−54944
Biblis Nuclear Power Station, meas. and control system, fault statistics evaluation *(German)* 79−97819
bidirectional optical-fibre transmission used for control appls. *(Japanese)* 78−66917
bilge water oil pollution monitoring system development 77−5246
blasting, recording systems for noise overpress. and vibr. monitoring 77−88984
boiler tube corrosion using gamma-ray transmission meas. instrument 77−9011
bubble chamber, H MIRABELLE, minicomputer applic. *(French)* 77−10531
bubble chamber 25 valve expansion system 77−6617
buried convective heat source, in semiinfinite solid, steady temp. distrib., surface temp. 77−58534
capacitance sensor use for monitoring resonance vibr. amplitude in dynamic elastic moduli meas. 77−23923
chemical, complete laboratory, installation 78−61123
citrus orchards aerial photography monitoring for diseases and insect pest infestations 77−56749
coal gasification, in situ, diagnostic and remote monitoring instrumentation development 79−48055
coal seam, gasified, burn front monitoring via EM refls. 77−41212
coating process, thickness monitoring using bremsstrahlung from fast electron irrad. 77−77609
combustible gas and vapours, MOS sensors 79−16104
compact test pieces, optimization of electric potential technique for crack growth monitoring using finite element anal. 79−87799
component shape monitoring, tolerance field image production *(Russian)* 79−94154
conference on analysis instrumentation, Charleston, West Virginia, USA (May 1977) 79−16100
controllable real-time data collection system for coastal oceanography 77−5329
corrosion, techniques 79−83404
corrosion field testing, NBS program 80−76427
corrosion of structural materials in nuclear power stations with RBMK reactors 79−9756
cosmic ray variation spectrograph, redundancy and hardware monitoring rel. to data reliability 79−84610
crack growth gauge for assessing flaw growth potential in structural components 78−68859
monitoring continued
data logging system requirements for noise and vibr. monitoring 77−68351
DC voltage monitor for standard cell using AC Josephson effect 77−82552
deep body temperature measurement in rodents, inexpensive telemetry system 78−24185
desert environment mapping, worldwide 77−78489
detonation deposition of coatings, monitoring method 80−60780
dialysis expts., model, monitoring using chromatography refractive index detector 79−96724
diffusion pump, CMOS monitor cct. 77−5855
dosimeter, remote-reading operational amplifier type, elec. constancy checking 78−3613
drugs, therapeutic, using high performance liquid chromatography 79−79334
ear internal sound pressure, monitoring for noise exposure meas. 77−52799
Earth albedo monitoring technique from LANDSAT data 77−78516
Earth crust stress changes, in situ monitoring 79−29884
Earth surface albedo change, LANDSAT monitoring 78−32104
effluent tank contents anal. by HPLC 80−71982
elbow meters for flow monitoring, description 79−37426
electron emission spectroscopy based instrument applic. to rate controlled deposition of alloy films *(German)* 80−89152
electrothinning, laser-monitored, for preparing ultrathin metal foils 78−53074
EM radiation, liquid crystal calorimeter appl. 77−79514
environmental impact of nuclear fuel cycle, monitoring and control 79−57504
environmental noise monitoring installation 80−33396
fast aspheric mirror figure control by profile monitor, wire tester and null lens 80−14419
feedback monitoring, normal conditions for linear and angular measurements 79−75492
ferromagnetic DC convertor for process monitoring 77−57359
Finnish river water pollution monitoring network 80−89686
fish surgery, low-cost audible heart rate monitor 77−70575
fission reactor pressure vessel and circuit development, conf. report 80−47541
flaw detection methods, planning statistical acceptance monitoring 79−91901
fossil-fuelled power stations, air pollution detection and control, opacity monitoring 79−100557
Fourier IR air monitor, description and appls. 79−16106
fusion power plant, vacuum outer containment, safety, T control and monitoring 78−74498
fusion reactor, beam-profile fast scan monitor 78−54941
fusion reactor 150 kV negative ion test stand, electronics system 78−54934
fusion reactor laser, Shiva pulse power, isolation and control system 78−54935
gas trace monitor with ion sensitive electrodes, continuous and highly responsive *(German)* 79−24878
gaseous criteria pollutant methodology and standards for USA Clean Air Act 80−94133
gaseous emission from in situ sources, field experience 79−16660
glass melting furnace, gas consumption through ports, monitoring and control system 79−58692
glass melting process, TV monitoring, equipment protection 79−58756
glass water resistance, rapid meas. method 79−61812
halocarbons in atmosphere, global monitoring stations 79−57555
heart electrical and mechanical monitoring on extensometer 80−45944
heat treatment, automatic US crack detection system 77−90542
heat treatment, coercivity meter attachment, with automatic current setting and recording 77−87795
Hydrometeorological monitoring in weather modification programs 78−69544
industrial chemical waste at deep water dump site, acoustic monitoring 79−34466
industrial pollutant source emission meas. needs 77−41165
iontophoresis circuit isolated current monitor for cell membrane studies 77−60311
Kawasaki City air pollution monitoring and telemetry system 77−37464
BL Lacertae, optical monitoring by three-colour photographic photometry 78−16525
lake quality monitoring, multidate Landsat data extraction progrm 80−17299
lake Superior, organic C as nonspecific water quality indicator 79−25287
LANDSAT agricultural monitoring program to monitor corn in Iowa 77−78495
LANDSAT and weather satellite data monitoring at new Canadian receiving station, Newfoundland 77−78600
laser beam energy monitoring, photoacoustic detector, construction and calib. *(Czech)* 78−29156
laser beam indicator/visualiser made from new thermochromic material 80−9976
laser beam profile monitor system using photodiode or pyroelec. array 77−58364
lasers, spectrum monitoring during tuning via spectrum analyser 77−26403
level of liquid N_2, automatic, in Dewar flasks 80−57309
lidar system, two-freq. downward looking, for atm. monitoring 78−69523
light filter optical density, photometer appl. *(Russian)* 78−86317
Limb Infrared Monitor of Stratosphere (LIMS) radiometer, design and performance, expt. goals 78−61601
line isolation monitor with adjustable alarm level for hospital elec. systems 77−56496
line sensor used to monitor a distant transducer 79−6145
liquid level monitor with optical coupler isolation *(German)* 78−73963
liquid system monitoring for particulate contamination 77−28956
liquid-borne solids, optical instrument general principles 79−37424
LMFBR, Na purification system, cold traps and plugging indicator 80−99209
load cell monitor for liquid N meas. with Li drifted Ge detectors 78−29122
magnetic field, Hall effect transducer *(Polish)* 79−85130
magnetic iron concentration in flowing ore suspension, digital instrum. *(Russian)* 77−53879

monitoring continued
magnetic susceptibility instrument, supercond., automatic, biological appl. 78−57153
Magnox reactors, remote corrosion monitoring, laser based instrument 78−41822
maintenance-free water test stations, aspects *(German)* 78−65403
marine environment test range semi-automatic data recording and monitoring (SADRAM) system 79−39993
marine pollution, automatic shipboard oil pollution monitor 78−53662
material with fluctuating parameters, by radiometric method, smoothing filter synthesis 77−90553
medical, uterine activity in induced labour, analogue technique 77−13021
metal fatigue monitoring by US velocity and attenuation meas. 78−60970
meteorological observation system using telephone switching network 79−80031
microwave resonator, automatic monitor of resonant freq. and bandwidth 77−22567
Moscow River basin, automated surface water quality monitoring system 77−78266
multipeak residual gas analysis monitoring system 79−79342
MW impulse generator system, for ion cyclotron heating, fusion reactor 78−70635
national environmental monitoring system 78−77329
Netherlands water quality monitoring 79−24920
night sky, monitoring by photometer of NASA-NMSU Meteor Observatory 77−74014
nitriding process, monitoring systems 79−52556
nitroglycerine, in waste water, monitoring continuous electrochem. analyser 77−60147
noise in general aviation airport, abatement technique 77−65653
nonsinusoidal periodic current meas. using standard DC shunt with magnetic powder monitoring, frequency errors 80−104398
NQR spectrometer, super-regenerative, continuous freq. monitoring 79−63190
nuclear fuel cladding tube deformation monitoring, photodiode image scanning technique 79−30938
nuclear power station thermal plume monitoring by drogues 77−3192
nuclear reactor, mild steel structures, oxide thickness monitor 77−67806
nuclear reactor spent fuel bundle absence from position in storage basket, monitor for detection 77−61511
nuclear targets, thin, techniques used in preparation 79−85201
ocean moorings, acoustic phase tracking techniques 78−30138
ocean thermal structure and current, NORPAX project weather/climate prediction appl. 79−84517
ocean waste disposal in Mid-Atlantic Bight, control and monitoring 79−5511
ocean wave directional spectra monitoring horizontal-spar buoy, design 79−21083
ocean-dumping studies, strategies and tools 79−12138
oceanography, remote acoustic monitoring of natural suspensates and slope/shelf water intrusions 79−2241
offshore disposal of dredged material, sediment props. as tracers 77−5245
oil pollution in water, solid-state laser/fibre optic system 78−96301
one-sided thermal monitoring crack detection 79−5122
online shade monitor, strip materials 79−30526
optical fibre drawing, semi-automatic machine development 79−27449
outdoor noise monitoring microphone installation and calibration *(Japanese)* 78−42504
oxygen monitoring in process gas streams, sensor 80−52181
p-n junction struct., X-ray topography visualisation during prep. *(Russian)* 78−26386
Pacific Ocean, equatorial currents strength monitoring from XBT sections and sea level obs. 78−73383
Paris regional air pollution monitoring network optimisation *(French)* 77−37387
particulate emission monitor calibration in gas-solid suspension 77−37454
particulate velocity and density, using microwave Doppler effect 77−27628
permafrost near Schefferville, Quebec, monitoring during thermal amelioration tests 77−33058
pH, instrument research, stability, buffering and electrode designs 77−81438
photochemical smog, minicomputer based prediction system for reducing acute damage 79−57541
piezoceramic radiators, defects visualisation using holographic interferometry *(Russian)* 78−1530
plant and soil monitoring, from tethered balloon, multispectral radiometry 78−3958
plating line Co concentration monitoring, by automatic colorimeter 80−105691
point defect concentrations during low-temp. irradiations and anneals using integrated system 80−7741
pollutant gases, stack monitor performance tests and specifications 79−16659
pollution, environmental, metrological support to monitors, pesticide control 79−21060
pollution, of coastal waters, Italian methods *(Italian)* 78−3828
pollution measurement, automated systems 77−21885
power stations, stack emission monitoring systems, for air pollution detection and control 79−100558
proton beam position monitor, based on detection of wall currents 79−58675
proton beams in NAP-M storage ring, accelerating system and parameters monitoring 77−65364
pulsed magnetic analyser, IMA-5 80−104399
PWR acoustic monitoring instrumentation 78−17309
PWR acoustic monitoring instrumentation 79−89488
quartz mass/thickness detector using ICs, principle, design 79−17393
radar meteor A/D filter characts. *(Italian)* 79−80032
radioactive contamination, use of Xe probe 80−27826
radioactive discharges from nuclear plants, state of art *(German)* 77−42174
radioisotope measuring convertor, parameter calc., thickness monitoring appl. *(Russian)* 78−25403
rail quality testing, US, using EM acoustic convertors 77−90551
rainfall, using dual freq. radar *(Japanese)* 78−57358
monitoring continued
regenerative fibre-optic transmission system supervisory line codes *(German)* 78−33884
remote automatic station on radio link for wind and temp. monitoring 78−85726
river water quality monitoring, pollution sources estimation 79−52970
river water quality monitoring, sampling freq. 79−53380
rolling mill performance extensometer appl. 77−41590
rotating machine in nuclear power plants, vibration monitor 78−13299
rotating machine vibration monitors 77−68352
rough surface modelling and online monitoring 79−80576
salt concentration, monitored by one-chip conductivity meter 78−232
satellite solar cell panel monitoring by ground station telemetry 79−62003
scintillation camera performance monitoring, equally-spaced parallel-bar phantom 77−2041
seismic P-waves, millisecond travel time vars. systematic monitoring near Palmdale, California 79−57863
shipboard pollution monitoring system, automatic Beckman Model 915 organic carbon analyzer 79−16521
Shiva laser beam diagnostics 78−59037
single-electrode monitors of intense relativistic electron beams 79−6216
slip monitoring along major faults in southern California 79−48388
small liquid flow rate monitor using displacement transducer and float 79−68836
smoking pattern recorder, portable 80−94385
solar EUV image, TV monitoring by Skylab Apollo Telescope Mount 77−60600
solar heating systems, instrumentation principles for performance meas. 80−35743
solar XUV instantaneous images, obs. and recording on ATM television monitors 77−60605
solid-liquid pipe flow, cross correlation method anal. 79−32638
sound and vibration monitoring, signal processing developments 78−83181
sound field, stationary, in 2-dimens. enclosure, continuous obs. *(Japanese)* 79−32143
sound quality, cinematography appl. 78−33961
spectral filter thickness optical monitoring 78−55476
spectrometric channel control using blocks 78−866
spin scan camera system, on geostationary satellite, for global weather monitoring 78−61600
SQUID RF sensor, automatic monitoring circuitry 77−18044
stack dust monitor based on particle counting and sizing 79−83683
stack gas monitoring system for warning and control in Chiba Prefecture 79−57561
steel, HSLA and Low C, weldment, AE monitoring 79−87800
steel articles thickness and continuity monitoring by neutron radiometry 79−93100
steel penstock, large diameter, embedded in rock, strain measurements, using strain gauges 79−43544
stratosphere, O_3 and aerosol monitoring using orbiting photodetectors 77−78445
stratospheric O_3 monitoring, satellite benefit assessment 77−78613
stress/duress automated detect. system 80−76852
structural fatigue crack acoustic emission monitoring 77−32755
surface quality of glazed ceramic insulators 79−61813
surface thickness monitoring, electron beam backscatter 78−60944
surface water continuous analysis by NH_4^+-sensitive plastic membrane electrode 80−89701
tanker oily discharge at sea, deballasting monitoring system appl. 77−45020
temperature, using low-temperature radiometer, with conical light pipe, IC manufacture appl. 80−47105
thermal monitoring with maximal temperature differences over flaws 78−60945
thermometer, multiple thermistor unit for use with data loggers 78−41303
thin film deposition control, thickness monitor using freq. demodulation technique 79−67249
thin film growth measurement using galvanically separated quartz monitor probe *(German)* 80−11576
time-interval analyser monitor, of nanosecond range 78−77868
total artificial hearts, pneumatic powered, telemetric monitoring system, in calves 77−90956
total ion monitoring method, for secondary ion intensity correction 78−12796
USA coastal zone water quality monitoring, aircraft vs. spacecraft 77−78233
vacuum deposited layers, thickness monitoring techniques *(Japanese)* 80−60783
vinyl chloride suspension polymerisation monitoring by US attenuation and velocity 79−70328
voltage, standard cell group enclosure monitored by AC Josephson effect 79−26076
water monitoring systems in Taiwan 79−57511
water quality monitoring, modular system *(German)* 80−26186
water trihalomethanes content, comparison of dynamic and static head space and solvent extraction techniques 79−92114
wear debris analysis for machinery health monitoring 79−61807
welds, in-process, with acoustic emission 80−16620
wind energy prospecting in Prince Edward Island, programme overview and status report 80−61243
X-ray tube thermal monitoring system, LOADIX, features 78−3658
C fibre reinforced plastic, fatigue failure mechanism identification, AE detection using piezoelectric strain gauge 79−96239
CO using automatic functional check *(German)* 77−53883
CO_2, atmospheric, conc. meas. at Baring Head, New Zealand 79−100931
CO_2 laser control using Ge and InSb 78−1203
Cl monitoring, TAGA 3000 mobile test unit 80−72114
HCl, gas monitoring ion-selective electrode analyser 77−60146
H_2SO_4 mist monitor, semicontinuous 80−61495
Hg vapour monitor, personal piezoelec. cryst. dosimeter 77−21672
NH_3 dissociation in nitriding process 79−52556
NH_3, using Stark microwave cavity resonator 80−61500
NO_2 monitoring in stack gas, chemiluminescence appl. 79−57560
O_2 analyser, OTOX 90, operation, and multipoint monitoring 80−55736
O_3 calibration reference instrument calibration 78−73524
OH, laser absorption spectrum, scanning technique, appl. to atmospheric monitoring 78−17664

monitoring continued
^{18}O tracer diffusion coeff. determ. in Ti_nO_{2n-1}, continuous mass spectrometry 77−20124
Ra for earthquake prediction *(Japanese)* 78−28181
Rn concentration in groundwater continuous monitor using ionisation chamber 79−21068
^{222}Rn, atmospheric, two-filter continuous monitor 80−58097
SO_2, automatic meas., luminescence appls. *(Dutch)* 79−88041
SO_2 concentrations of Venice air, time series anal. 79−57540
SO_2 in atmosphere, monitors number and siting rel. to pollution zones definition 78−81383
SO_2 in atmosphere, practical experiences with small automatic monitoring network 78−81462
SO_4^{2-} aerosols, ambient, laser-Raman monitoring 78−69532

monitoring, computerised *see computerised monitoring*

monitors *see monitoring*

monitors (computer software) *see supervisory and executive programs*

monochromators
see also X-ray monochromators
θ-θ diffractometer with monochromator *(French)* 79−32058
aberrations in spectra recorded with Seya-Namioka monochromator, correction using inverse convolution 80−23629
atomic absorption two-wave and dispersionless spectrophotometric systems *(Russian)* 78−27862
automation of high-intensity monochromator using wavelength-scan and intensity-control system 80−86366
Barr Stroud double prism monochromator spectral anal. of skin IR radiation 79−88057
bicrystal monochromator of moderate wavelength resolution for use with X-rays or thermal neutrons 77−76254
combined monochromator instrument, synchrotron electron current determ. and light source calibration 78−65954
compact double, for atm. diffuse-direct UV ratios meas. 78−49144
concave grating efficiency in VUV region, diffusion pump oil contamination effect 80−14429
conical diffraction mounting for synchrotron radiation monochromators 80−91910
constant-deviation, defocusing compensation with concave diffr. grating 78−46792
construction, spectrosc. appl. *(Hungarian)* 80−43478
Czerny-Turner grating monochromator, Cary principle dynamic dispersion determ. 80−58666
diffraction grating monochromator for UV-visible spectrophotometer, stray light 78−94445
diffraction gratings, efficiency synchrotron radiation monochromisation 78−63189
digital stepping motor control system for repetitive scanning of a monochromator 78−54355
distortion and split-image curvature with off-axis mirrors, plate diagram analysis 78−59141
double monochromator, instrumental profile 79−68444
double monochromator systems for fluoresc. X-ray anal. 78−62280
double monochromator with nonclassical concave diffraction gratings 80−38110
double-beam UVI spectrophotometer specifications 79−26144
double-grating monochromator, theory 80−58708
double-pass solar monochromator, with digital device for obs. and spectrum processing automation *(Russian)* 80−72777
double-scanning, noncoherent optical signals coding method appl. *(Russian)* 80−5697
Drabkin neutron monochromator optimisation 79−22518
dual toroidal grating XUV monochromator, performance 80 to 1280 Å 80−90941
dual-prism, scanning attachment, appl. to cytospectrofluorometric installation 80−101837
Ebert parabolised monochromator, coma compensation 79−81526
Ebert-Fastie, alignment using He-Ne laser and Fresnel diffraction pattern 80−99853
echelle grating monochromator, spectral efficiency 79−98461
far UV transmission grating monochromator for use with reson. radiation lamps 77−27364
fluorescent materials, reflective radiance factor meas. by two-monochromator method *(Japanese)* 80−68237
Fourier transform spectrometer performance, instrumentation for assessment 80−95165
Fresnel zone plate support UV window as lens and monochromator 80−1326
gamma photons, monochromatisation method based on Compton scattering *(Russian)* 79−89516
glancing incidence, with corrections for astigmatism and spectral-line curvature 80−43466
grating double monochromator, GDM 1000, spectral anal. of low intensity emissions 79−80701
grating monochromator, real instrumental function 80−43452
grating monochromators, servocontrolled and automated scanning system, using microcomputers. 78−33852
grating type monochromators, spectrophotometry and colorimetry errors caused by polarisation of meas. system *(Japanese)* 80−101815
grazing incidence and normal incidence, intensity calibration in VUV for plasma diagnostics 80−48995
grazing incidence far UV monochromator for differentially pumped discharge lamps 77−3677
grazing incidence monochromator, polarisation by gratings 78−87129
grazing incidence monochromator, ultra high vac., SSRL, design considerations and operating experience 78−62269
grazing incidence monochromator FLIPPER, ultra high vac., for synchrotron radiation 78−62237
grazing incidence monochromator for synchrotron radiation 78−38005
grazing incidence spectrograph-monochromator with focusing toroidal mirror 79−75617
grazing incidence spectromonochromator for XUV region 78−5572
grille filtering method and associated spectometers, capability study, double grille monochromator 80−48427
heated vacuum monochromator for 40-280 nm spectroscopy 80−33176
high energy electron spectroscopy techniques 80−62740
high flux grazing incidence monochromator based on holographic grating for synchrotron radiation 78−62271
high resolution, for vacuum UV radiation from DORIS storage ring 77−7165

monochromators continued
high resolution double monochromator, for light scatt. and fluoresc. standard in colloid 80−57247
holographic concave grating monochromator, design *(Chinese)* 80−58676
holographic grating monochromator for 5 to 1000 eV synchrotron radiation 78−18049
holographic transmission gratings appl. to UV and X-ray synchrotron radiation monochromators 78−63186
horizontally curved analyser crystal, neutron scatt. monochromator appl. 79−50412
imaging properties, monochromator using concave holographic grating and plane mirror 80−99856
intensity calibration of grazing incidence monochromator *(Japanese)* 79−32062
interdependent parameters and performance tradeoffs 79−90006
IR, monochromatic line isolation methods for refr. index meas. 77−74489
IR and MM wavelengths, very rapidly scanning instrument 80−5829
IR spectrophotometer, digital data acquisition/analysis system 80−73482
laser monochromator-interferometer, protable high-resolution, with multichannel electronic readout 80−33153
light source radiance spectral density meas. using DMR-4 double monochromator 79−30527
luminescence measuring setup with GDM 1000 grating double monochromator for semicond. 78−21226
luminescence spectrum recording monochromator wavelength reference marker generator 78−58050
MAXIMOC grazing incidence monochromator for XUV investigations with synchrotron radiation 78−62238
microcomputer based scanning instrument controller, for grating monochromator 78−93764
mounting with ruled diffr. grating at 45° off-plane 80−87479
MRD-2 based polychromator for plasma diagnostics 78−5924
multilayer systems, neutron optical props. 79−55044
multiple, construction *(Hungarian)* 80−102812
neutron, curved crysts., comparison of data with simple model 77−39515
neutron, curved Cu comb 80−63427
neutron, moving cryst., design and operation 77−74552
neutron, multilayer, fabrication and neutron diffr. expts. 77−84589
neutron beam facility, 2, 24 keV neutron beams prod., filter comps. and configs. 77−6597
neutron crystallography, multiplane analyser, reflectivity calcs. 79−44984
neutron curved monochromators, reflectivity data 79−45515
neutron double monochromator for diffraction studies 78−1957
neutron double monochromator with periodically bent single Si crystals 77−58927
neutron monochromator, development of Institut Laue Langevin 79−45514
neutron polarising monochromator with Fe/Ge multilayers 77−19841
neutron powder high-resolution diffractometer, D1A, mylar collimators 77−4024
neutron reflectivities, Ni-Mn and Ni-Ti multilayers for monochromators and supermirrors 80−22880
normal incidence monochromator, 2m high throughput, for SURF II storage ring 80−90951
normal incidence monochromator, intensity calibration by double monochromator method 79−94341
normal incidence monochromator for synchrotron radiation, charact. modification using holographic concave gratings 78−62236
normal incidence monochromators for synchrotron radiation sources, experimental uses 78−62235
optical monochromator using single graded interference filter 78−94444
OTF measurement and image correction in spectroscopic system 78−37083
photodetector relative spectral sensitivity meas. method using two tandem monochromators *(Japanese)* 80−101840
photodetector spectral sensitivity meas. using two tandem monochromators *(Japanese)* 80−47107
photon counting, solar radiation UV limit meas. at Earth surface 78−49134
plane grating monochromators, fourth-order aberrations 77−62056
plane-grating, optical transfer functions, direct meas. 78−74849
polarisation ratio of crystal monochromators, method eliminating its relevence 78−55775
polarised neutrons, monochromatisation by spatial spin reson. technique *(Russian)* 77−79497
premonochromator for stray light rejection in Raman spectroscopy 77−58438
prism Littrow monochromator, wavelength calibration 78−25950
prismatic double monochromator 80−23796
Raman spectrometer, monochromator adjustable intermediate slit, Zeiss GDM 1000 *(German)* 79−9245
scanning rate restrictions in monochromators 80−48430
Seya-Namioka, polarisation characts. of concave gratings 79−18526
Seya-Namioka monochromators, automatic design of holographic gratings 79−10390
Seya-Namioka type, vertical astigmatism correction *(Japanese)* 79−76841
single, appl. in modern spectroscopy *(Hungarian)* 80−91905
solar irradiance, multispectral measurements, atm. total ozone determ. 79−53401
space telescopes, using monochromators of concave grating mounting, VUV region 78−73629
spectral instrument choice in plasma and flame emission spectrometry of traces 80−35613
spectral line profile recording, high resolution, using Fabry-Perot interferometer and monochromator 80−42268
spectral slit width correction for precision energy measurements 80−96020
spectrofluorometer components, state of the art *(Slovak)* 78−56940
spectrometer with random rasters, S/N ratio 79−54193
spectrophotometer, reference for analysis of diffuse transmittance and reflectance 77−38023
spectrophotometer, single-beam, holographically recorded concave diffraction grating appl. 78−54468
spectrophotometer for measuring small sharp absorption bands in solids at low temps. 80−86456
spectroscopic, 1980 state and selection criteria *(Hungarian)* 80−73469
spread function, graphical representation, stray light concept 80−33198

monochromators continued
step height measurement in μm range by two-ray interferometry with adjustable light wavelength *(German)* 77−82489
stray light by scattering 79−32056
stray light obs., optical techniques 79−30569
stray light transmission meas. and evaluation 77−38030
subtractive dispersion monochromator for Fourier transform spectroscopy *(French)* 78−83079
synchrotron radiation, with three-wave Bragg diffr. 80−87993
synchrotron radiation wavelength dispersion monochromator for fluorescence spectroscopy 78−296
synchrotron spectroscopy, normal incidence monochromator and order sorting problems 77−31129
synchrotron VUV and X-radiation, polarising effect of monochromators 78−66732
telescopic, in CTEM, with cylindrical mirror analysers 80−87296
thermal neutron monochromators, Monte-Carlo simulation of mechanical velocity selectors 78−24886
toroidal holographic gratings, design and performance *(Japanese)* 79−27412
total spread function description of props. 80−19100
triple monochromator a spectrometer in Raman scatt. *(French)* 80−96007
trochoidal electron monochromator, optimization of parameters 80−86511
tunable radiation sources in interferometry 80−23787
tunable vacuum UV photofragment monochromator 78−90316
twinned neutron monochromator 78−840
UHV beam line at SSRL for spectral range 4-4000 eV, monochromatised radiation 78−62673
UM-2, garnet-ferrite film thickness meas. with interference attachment 78−3035
UV, integration with 1000 W H discharge lamp into vacuum UV light source 77−42582
UV vacuum spectrofluorimeter design for luminescience meas. from thin films 79−71538
vacuum monochromator, grazing-incidence, absolute calibration using Tokamak discharges 78−87492
vacuum monochromator for investigating scattering objects 77−74523
vacuum monochromator low-temp. attachment construction and optics 80−31764
vacuum UV, conference on synchrotron radiation instrumentation, Orsay, France (Sept. 1977) 78−62999
vacuum UV 6 m, photoabsorpt. obs. in atm. gases 78−37969
VM-2 vacuum monochromator for 400-7000 Å range 78−25971
VUV 4 m normal incidence monochromator 80−90950
VUV monochromator for coherent signals *(Russian)* 79−46036
VUV monochromators, 10 to 300 Å for synchrotron radiation, evaluation 80−90907
VUV monochromators with toroidal holographic gratings, Strehl criterion 80−90949
wavelength dispersion system for synchrotron radiation 78−296
wavelength meter, He-Ne laser/monochromator/interferometric system 77−18086
Wisconsin Synchrotron Radiation Center, UHV Seya-Namioka and adjustable slit 'Grasshopper' monochromators 78−62234
X-ray focusing, for small-angle diffr. studies with synchrotron radiation 77−39508
XUV spectroscopy, grazing incidence spectrograph-monochromator, 5-900 Å region 79−17506
zone plate with circular sensor, spectral resolution 77−42591
Cu-Ge neutron monochromator 78−71643
Fe/Ge multilayer neutron polarizing monochromator 79−45513
NaCl curved crystal-monochromator, influence of elastic element area on reflecting surface relief *(Russian)* 80−64157
Si, harmonic-free single cryst., neutron and X-ray physics appl. 78−75493

monolayers
see also adsorbed layers
absorbed on liquid-liquid interfaces, interfacial tension *(French)* 79−73376
acetylene adsorbed on Fe containing segregated C, hydrogenation, C-1s XPS spectra obs. 80−84366
acoustic phonons, obs. method using Brillouin scatt. in adsorbed monolayers 80−59804
adsorbed, classification of continuous order-disorder transitions 79−7743
adsorbed, directional photoemission, book contrib. 78−95674
adsorbed, Lennard-Jones system, melting in external field 80−65362
adsorbed, many-body interactions 78−84068
adsorbed atoms, props. 78−84057
adsorbed film monolayer melting, dual symm. systems, periodic struct. *(Russian)* 80−107405
adsorbed gas films on grafoil, neutron scatt., lattice gas *(Japanese)* 77−47685
adsorbed layers, two dimensional incommensurate crystal theory, thermodynamics *(Russian)* 80−49524
adsorbed monolayer, classification of continuous order-disorder transitions 80−19910
adsorbed monolayer, substrate-induced strain and orientational ordering 79−82460
adsorbed monolayer of orientable molecules, lattice fluid model, real-space renormalisation group method 80−17882
adsorbed monolayer parameter determ. by full current spectroscopy method *(Russian)* 80−70539
adsorbed monolayers, intrinsic defects, deep potential relief surface *(Russian)* 79−99415
adsorbed monolayers, neutron scatt. meas. 79−65306
adsorbed monolayers, order-disorder transitions, classification and characterisation, review 80−52149
adsorption isotherms of partially localised, partially mobile, monolayer films, temp. depend., theory 80−107646
air-water interface, microwave detect. of adsorpt. and spreading films 79−5690
air/water interface, monolayer transfer to rot. square pillar 77−59184
aliphatic surface monolayer, on water, phase transition model 79−56041
alkali metal on metals and semiconductors, negative ion prod. on Cs^+ sputtering 78−46204
alkali metal submonolayer on metal substrate, geom. struct. rel. to electronic props. 77−85080
amino acid, monolayer on solid, SIMS anal. 79−89038

monolayers continued
amino acid monolayers and ordered films on Cu, surface struct. LEED 78−38968
amphiphilic molecules and liquid crystals, review 79−99062
anomalous thermal effects, statistical mechanics 80−15367
arachidate monolayers, optical props. integrated optics meas. 78−35214
Auger electron spectroscopy 77−85851
bacteriochlorophyll monolayer quantum yield and image contrast in photoelectron microscopy 78−44453
barium stearate film, low energy electron range meas. using radioisotope Auger electrons 80−70257
behenic acid monolayers, mol. orientation determ. by IR absorpt. 79−11423
benzene submonolayer on silica gel, PMR and DMR dynamics and surface heterogeneity 79−69735
bimolecular films, matrix effects of solid surfaces 78−84114
cadmium arachidate, monolayer, electron mean free path length, XPS obs. 79−74051
cadmium arachidate monolayer, Ag(Au) substrate, reson. surface plasmon reflection 78−56536
cadmium arachidate monolayer, surface plasmon spectra, refractive index dispersion 78−64424
cadmium arachidate monolayer transfer from air-water interface to solid, contact angles 77−55424
calcium behenate monomolecular layers between Al electrodes, nonlinear dielec. props. 80−80405
cell cycle and topography in nonsynchronised monolayers, autoradiography and time-lapse use for rigorous SEM obs. 78−24212
cetyl orange monolayers on water surface, reson. Raman spectra 79−91434
charged, surface pressure, electrostatic contrib. of divalent ions 79−24752
chemisorbed on W, anomalous Auger shifts 80−20738
chlorophyll *a*-lecithin mixed monolayer coated electrodes, highly efficient quantum conversion, solar energy appl. 79−39314
chlorophyll a, Langmuir-Blodgett films, deposition onto SnO_2 optically transparent electrode 80−80093
chlorophyll a in monolayers at water-air interface 79−47912
chlorophyll in aqueous solns., electrochem. behaviour, cathodic reduction 79−29373
cholesterol, adsorbed monolayer on aerosil, IR spectra 78−15753
cobalt stearate, monomolecular layer, electron escape depth, XPS *(Japanese)* 80−11532
cobalt stearate, monomolecular multilayers, XPS escape length depend. on emission angle, elastic scatt. role *(Japanese)* 80−84833
condensed on foreign substrate, structural aspects 77−20209
coverage, determ. by AES, appl. to C on Pt 79−46916
cyanine dye monolayer/p-chloranil crystal, charge carrier injection rate const. determ., energy transfer vs. charge transfer method 79−83031
α-cyanoacrylate adhesive in first monolayer on bulk Al surface, IR spectra, H-bond form., stretching vibr. 80−87119
cyclohexane, monolayers and thin crystals grown on Pt (111), LEED obs. 77−59230
damping effect on surface wave motion in liquid 78−67206
dense fluid monolayer, eqn. of state, appl. to alcohol monolayer on water 78−6195
designed monolayers assemblies 79−37915
desorption, Brownian motion of particles near free surface 80−54503
desorption kinetics at air-water interface, humidity effects 79−52770
diamond, sub-surface contamination by hot-atom recoil in neutron activation anal. 77−60144
N,N′-dioctadecyloxacarbocyanine monolayers on Ag surface, attenuated total refl. 79−11480
L-α-dipalmitoyl phosphatidyl choline, laser-ripplon scatt. at air-water interface 79−99894
dipolar hard spheres, adsorpt. onto smooth hard wall in elec. field, density profile 79−67221
dye, energy transfer between sensitizers and acceptors 80−80861
dye, on Ag film, effect on surface plasmons, ATR obs. 79−87001
dye molecule monolayer displaced from metal surface, light refl., coupling with metal surface modes 78−48246
dye monolayers, reson. interaction with surface plasmons 78−84674
dynamic surface tension excess at compressed interface, bulk-to-surface diffusion interchange 79−56042
effective two particle potential 79−11012
elastic and viscoelastic monolayers, dynamic surface potentials 80−3603
electrolyte double layer potential change meas., transistor method 77−85298
electron beam damage in chemisorbed layers, tunnelling spectra 77−76672
electron microscopy, light microscope attachment for isolating small specific areas from slide embedded monolayers 78−53596
electron transfer in monolayer assemblies 80−3383
electronic spectrum of ordered monolayers over metal surfaces 77−85293
ellipsometry of clean surfaces, submonolayer and monolayer films, review 80−103546
epitaxial, 2-D, and 1-D electron gas and 2-D Coulomb gas, family of mappings 80−34346
ethane, on graphite, struct. and melting, elastic neutron scatt. 80−29266
ethylene, adsorbed monolayer on Cu surface, UV-visible polarised modulation spectra obs. 78−72619
ethylene, adsorption on Ag (111) surface, XPS and UPS investigation 80−103573
fatty acid monolayers, capillary waves, photon correlation spectroscopy, viscoelastic props. 79−75608
fatty acid monolayers, electron tunnelling 77−69428
fatty acid monolayers, light scatt. meas. 80−89011
fatty acid-cyanine dye mixed monolayer, on metal electrodes, photocond. 78−68050
fatty acids, long chain, spread monolayers, rheological behaviour 79−95245
fatty alcohol solid monolayers in H_2O, interface struct., model 80−54505
fatty-acid monolayer, on water, eqn. of state, liq.-gas crit. region 77−76520
film pressure of insoluble monolayer at air/water interface, effects on wetting at solid surface 77−85017
film-deposition model of correlated percolation 80−107679
films, partially mobile and partially localised, adsorpt. of binary gas mixtures on solids 78−91551

monolayers continued
films partially mobile and partially localised, adsorpt. of single gases on solids 78−91550
fluid monolayer at solid surface, density distrib. calcs. 80−49492
fluid-fluid interfaces, hydrodynamic stability, dipole interactions 80−6599
fluid-fluid interfaces, hydrodynamic stability, ion interactions 80−6598
gas, formation on solid surface as friction protection 78−47663
gas adsorption theory for flat surface 77−28074
gases on solid surfaces, mobile and localized adsorption, theory 80−65379
graphite, dissolution into (110) face of Ni, 600-913K 80−49504
graphite on Ni (110) surface, oxidation mechanism 80−101037
hard-sphere fluid, monolayer adsorption profile, adsorption isotherm 79−33182
heterogeneous surfaces, adsorpt. of atoms, monomol. adsorpt. thermodynamic functions *(German)* 79−90891
hydrocarbon chains on aq. substrate, phase transition model 78−51795
hydrocarbon monolayer effects on wetting of Au, macroscopic continuum model 77−85018
incommensurate two-dimensional crystal, ground state, spectrum, phase diagram 79−19458
inert gas monolayers on graphite, nonregistered-registered phase transition 79−77894
insoluble, on water, effect on evaporation coeff. 78−75909
insoluble, on water, effect on evaporation coeffs., comment 78−75911
insoluble, on water, effect on evaporation coeffs., comments 78−75910
insoluble, on water, effect on evaporation coeffs., reply to comments 78−75912
insoluble, on water surface, meas. of temp. gradients in water during evaporation 80−88402
insoluble, surfactant adsorpt., Gibbs eqn. calcs. 80−59781
insoluble monolayers, thermodynamic eqn. of state for uncharged films 78−85195
interaction between monolayer and dielec. adsorbent, dispersion forces 77−4259
interfacial, thermodynamic treatment, excess quantities, adsorbed and spread layers 80−40732
ionised surfactant film, insoluble, thermodynamic eqn. of state 79−8450
IR spectroscopy, reflection-absorption, of adsorbed layer systems, review, book contrib. 80−84747
Ising model for monolayers of coadsorbed atoms, phase transitions 80−19909
Langmuir film deposition, dipping and raising device, new design 77−24954
Langmuir monolayer, phase separation without gravity effects *(French)* 80−54534
Langmuir-Blodgett, monolayer to multilayer 80−80031
lecithin, adsorbed monolayer on aerosil, IR spectra 78−15753
lecithin surface films, equilib. and metastable states rel. to use as biological model 77−60188
LEED, surface struct. determ. 77−24469
lipid, monolayer, backfolding, self-consistent field theory 79−8451
lipid monolayer, statistical mech. theory 78−73141
lipid monolayer phase transitions, model 78−2338
lipid monolayers and bilayers, phase transitions, model 78−44460
liquid crystal, lyotropic, form. of mesophases in presence of water, monolayer anal. 77−86454
liquid crystal alignment by amphiphilic monolayers 79−37614
liquid mixtures, static surface tensions, monolayer model 77−4245
liquid-liquid interface, adsorbed monolayer mol. orientation, electrolyte effects, reson. Raman obs. 78−60430
localized monolayer adsorpt. of gas-mixtures on heterogeneous surfaces, stat. thermodyn. 78−2371
long-chain compounds, on water surface, depend. of evaporation resist. on chain length 79−28196
macromolecular epitaxial crystallisation, review 79−42409
magnetic, possibility of formation on nonmag. transition metal surface 78−15009
magnetic surfactant monolayer, motion in mag. field *(Russian)* 79−1260
magnetised fluid surface monolayer motion 79−76545
manganese stearate, two-dimensional mag., prep. and characterisation 78−31097
melting transition in two-dimens. cryst. 78−51645
merocyanine dye monolayer on p-chloranil cryst. in sandwich cell, electrochromic detection of internal charges 78−11549
metal, BCC, chemisorption of monolayer of atoms, charge in density of states determ. 77−47682
metal, on metal cryst. surfaces, surface struct., review 80−80067
methane, adsorbed monolayer on graphite, two-dimens. diffusion by mol. dynamics method 79−90873
methane, adsorbed on graphite, substrate deform. meas. 80−54520
methane, submonolayer on graphite, two-dimens. fluid 79−37920
methane-d_4 monolayer films on graphite, neutron diffr. studies of phases 80−96739
methanol adsorption on Cu(110), XPS, UPS and thermal desorpt. study 80−84388
mixed protein phospholipid films, viscoelastic behaviour and Marangoni effect 80−3602
mobile adsorption, 2-D hard disc model, perturbational method 78−38932
mobile monolayer adsorption, critical props. of Bergmann's model *(German)* 78−84073
molecular, IR absorpt. enhancement by thin metal overlayers, ATR technique 80−88995
molecular cooperation in photo-induced electron transfer 79−73985
molecules, on metal surface, effect on reflectivity 79−65877
monolayer on graphite, sp. ht. and u.p., size and steric effects 77−85073
monomolecular and multimolecular built-up film, present status and future potential 78−71906
nonregistered monolayers, lateral compression effects calc. 80−6641
one-dimensional, Frank-van der Merwe model, incommensurate-commensurate crossover, transfer integral method 80−88426
organic dye on Ag, excited mol. decay near metal surface, energy transfer to plasmon surface polaritons 80−50440
organic molecular monolayer in MIM tunnel junction, anomalous surface 79−72324
organic molecules in monolayers, reactivity 80−81367
organic monolayer/metallic substrate, exciton-surface plasmon interaction 79−69569
organised molecular systems, monomolecular layers, micellar and bilayer membranes, conf., Elmau, W.Germany (April 1978) 79−39188
organosilane binding to TiO_2 electrode surface, effect on semicond. props. 79−96364
orientational ordering of incommensurate structures, static distortion waves 77−59235
oriented phase transitions *(Russian)* 78−75936
oriented second order phase transitions *(Russian)* 79−65315
overgrowth obs. in Auger electron spectra 77−85081
palmitic acid on water, characterisation by multiple wavelength ellipsometry 78−92136
n-paraffins, monolayers and thin crystals grown on Pt (111), LEED obs. 77−59230
n-paraffins, thin crysts. and monolayers on Ag(111) surface, LEED 79−11014
pentadecanoic acid, insoluble monolayer, phase transition, simple lattice model 80−70527
pentadecanoic acid, monolayer on water, surface pot. meas. in coexistence region 77−28236
permeation and evaporation resistance, hard disc fluid model 78−34678
phase transitions, review 80−44433
phase transitions in adsorbed monolayer *(Russian)* 79−95269
phenol, adsorbed layer, inelastic electron tunnelling spectral lineshapes below 100 mK 78−31000
pheophytin containing monolayers, phase separation and domain interaction, surface press. and fluoresc. meas. 79−100580
phosphatidylcholine monolayer vesicles, US irradiation formation, quasielastic laser light scatt., dynamics 77−48764
phospholipid monolayers, polymorphism 78−40120
physisorbed monolayer on graphite, neutron scatt. studies 80−107655
physisorbed monolayer rotation, pseudoharmonic theory of orientational instabilities 78−71975
PMMA, monolayers collapse mechanism, surface press. and ellipsometric obs. 78−43214
poly-γ-benzyl-L-glutamate, monolayers, struct. studies, IR, ATR, and TEM obs. 80−44396
poly-γ-methyl-L-glutamate, interfacial conformational modifications 78−2339
polycrystalline, mol. orientation, IR determ. 80−80891
polymer film, adsorbed monolayer, rheological behaviour 79−95245
polypeptide monolayers, circ. dichroism 79−74598
propyl stearate monolayers, elasticity and viscosity determ. by laser light scatt. 77−72749
protein monolayer desorption 77−85053
pyrazine, electronic energy transfer to metal surface, classical image dipole theory 80−97318
pyrene dodecanoic acid, lateral diffusion at air-water interface, monomer excimer dynamics 80−92693
4-pyridinecarboxaldehyde, in inelastic electron tunnelling spectroscopy junctions, Raman scatt. 80−93344
Raman scattering, giant, by mols. adsorbed on metals, review 80−93343
Raman scattering, giant, by mols. adsorbed on metals, theory 80−93345
Raman spectroscopy of mol. monolayers in inelastic electron tunnelling spectroscopy junctions 80−93344
random packing of circles in a plane 77−59208
rare earth element submonolayer films, electronic phase transitions, heat of absorption 80−24736
rare gas (111) adsorbate-substrate systems, thermal expansion and stability, soft phonons 79−69352
rare-gas, adsorbed on graphite, commensurate-incommensurate transition, effect of domain-wall crossing 79−69244
rigid rodlike molecules adsorption onto planar surface, dispersion interactions, statistical mech. anal. 80−29265
semiconductor electrode, sensitised photocurrent by energy and electron transfer in dye monolayers 79−38119
SIMS, primary ion beam profile effects on monolayer analysis 78−68589
SIMS apparatus for investigation of monolayers 79−89038
single gases, monomolecular adsorption on homogeneous solid surface, model 79−4477
solid surface monolayers, anal. by mass and energy spectrometry methods 77−56248
sphere crowded monolayer, multiple EM wave scatt., migration imaging film appl. 80−99627
sputtering models, depth resolution in profiling of sandwich structures 78−92165
static AES technique, appls. 78−84685
stearic acid, detection by harmonic generation of SAW 77−80688
stearic acid layers, charge transport processes 78−84316
stearic acid monolayers on HCl subsoln., surface diffusion by ^{14}C-tracer 78−34679
stearic acid-based, layer periodic structure, prep. and optical props. 77−69199
STEM use for two-dimensional molecular assemblies construction 78−24201
stimulated Raman gain spectroscopy, ultrahigh sensitivity 80−48337
structure determination, LEED anal., book contrib. 79−42358
Styrofoam spheres, diameter determ., mol. monolayer experiment, teaching appl. 79−44678
submonolayer films on metallic surface, struct. and props. review 78−38972
surface balance, monolayer parameters meas. in radiation field 78−82092
surface diffusion, influence on surface anal., model calc. 79−15016
surface pressure at air-water interface, meas. technique 80−89526
surface segregation in monolayer regime, model of kinetics and equilib. 79−7739
surface tension and spreading press. for mobile and registered layers 78−38960
surface tension meas. using filter paper Wilhelmy plates with insoluble monolayers 78−357
tetradecanoic acid, liq.-expanded/liq.-condensed phase changes press., effect of temp. diff. between liq. substrate and air 80−54476
thermodynamics props. of adsorbed monolayer, vibr. contrib. *(French)* 77−4261
uniaxial film on nonabsorbing substrates, characterisation by multiple wavelength ellipsometry 78−92136
valinomycin monolayers, struct., area and compressibility determ. 78−44461

monolayers continued
valinomycin-cholesterol (stearic acid) monolayers, struct., area and compressibility determ. 78−44461
vinyl polymer mixed monolayer behaviour 77−85020
water droplets, atmospheric, sources and effects of surface organic monolayers 78−69412
water-liquid system, solid-adsorbed, dispersion medium density changes 77−9137
Ag film, on Au substrate, monolayer overgrowth, quantitative AES method 80−10813
Ag monolayer on (111)Si surface, Schottky barrier, interface electronic nature and epitaxy 79−77934
Ag, on rough Au surface, adsorbed pyridine giant Raman effect 80−63637
Ag/CN, coverage meas. using surface enhanced Raman scatt. and radioisotope meas., electrochemical treatments 80−29260
AgBr emulsion, latent image speck size, characteristic curve anal. 79−34338
Al, effect on atomic modulation of interdiffusion at Au-GaAs interface 80−49432
Al, on Si (111) surface, local density of states 79−47142
Al-monolayer-Pb, supercond. junction, electron tunnelling meas. 79−28482
Al_2O_3, core excitons and inner well resonances in surface soft X-ray absorpt. spectra 80−40187
Ar, adsorbed on graphite, lattice dynamics 78−75946
Ar, adsorbed on graphite, monolayer two-dimensional phase change, calorimetric investig. 77−47669
Ar adsorbed on graphite, nonregistered-registered phase transition 80−39414
Ar, adsorbed on graphite, orientational ordering of incommensurate monolayers, LEED obs. 78−95233
Ar adsorbed on graphite, overlayer-substrate spacing, LEED determ. 80−103579
Ar adsorption on graphite, orientational epitaxy in self-consistent phonon approx. 79−95261
Ar, adsorption on graphitised C black, eqns. of state predictions vs. expt. 79−69223
Ar, condensation and compression on graphite 79−65316
Ar monolayer adsorbed on graphite basal planes, heat capacity 80−6636
Ar monolayer coated Grafoil, sp. ht. of adsorbed submonolayer ^{4}He film 79−51379
Ar, on graphite, condensation and compression, high resolution LEED obs. 79−77906
Ar, on graphite, equilib. config. and lattice consts. 80−54524
Ar, on graphite, lattice spacing and isosteric heat below 50K, LEED obs. 80−34303
Ar, on graphite, neutron diffr. study 78−34705
Ar, two-dimensional freezing, on differently graphitised carbon 79−77896
Ar-graphite system, effects of dynamic coupling 80−10771
Au, on W(001), elec. struct. 78−72236
Ba, conc. depend. of characteristic loss spectrum 77−15938
Ba, on W(100) surface, struct. transformation stages 77−47681
Ba submonolayer film on Mo (011) face, surface diffusion, manifestation of phase states *(Russian)* 78−91539
BaO, monolayer on W (110), film struct. and electron state 80−100498
Be film, on Cu substrate, monolayer overgrowth, quantitative AES method 80−10813
Bi, with Pb, on Cu (100), LEED and AES study 79−15017
C monolayer phase condensation on Ni (111), LEED and AES obs. 79−46960
C, on Pt, determ. of monolayer coverage by AES 79−46916
C, on Pt, stability and struct. of high Miller index forces in vacuum and with adsorbed C and O 77−76651
C, on Pt(111) surface, diffusion, AES 78−71954
CN on Ag, picosecond Raman gain spectroscopy 80−25351
CN, on Ag surface, vibr. spectra, picosec. Raman gain technique 80−91859
$(CN)^-$, monolayer on Ag, Raman spectra 78−72520
CO, on Pd (100), electronic states, tight-binding method appl. 80−49564
Cl, adsorbed on Ag, enhanced Raman intensity 79−95766
Co, atomic layers, Pauli paramagnetism to band ferromagnetism transition thickness depend. 78−72377
Co, monolayer, oxidation, quasisimultaneous SIMS, AES, XPS 78−72919
Cu (001) monolayer, electronic struct., self-consistent LCAO calc. 79−4606
Cu (001) monolayer, level ordering of states 78−91748
Cu (100), self consistent electronic struct. 80−6926
Cu, deposition on Au electrode in underpotential region, RHEED investig. 80−54539
Cu, form. on Pt (100), (110), and (111), optical and electrochem. studies 79−99419
Cu on Ag (001), ultrathin film electronic states calc. 78−6318
Cu, on Zn (0001), electronic struct., photoelectron spectra 78−39660
CuO, monolayer on Cu, SIMS anal. of oxidation 79−89038
Fe, adsorption on W foil, complex composition of annealed monolayer film 79−15023
Fe, atomic layers, Pauli paramagnetism to band ferromagnetism transition thickness depend. 78−72377
Fe, epitaxy on Au, growth processes, ultra high vac. in situ electron microscopy 78−30842
$FeCl_2$, adsorbed monolayers, gamma-ray reson. 77−8478
Ga, on W, field ion image qualities and work function 78−35272
H (1×1), adsorbed on Ti (0001) film, electronic struct., surface geometry 80−54750
H, adsorbed monolayer on Cu surface, UV-visible polarised modulation spectra obs. 78−72619
H, on Ni(111), geometry, LEED anal. 79−28200
H, on Sc (0001) and Ti (0001), geometric vs. electronic factor in surface electronic structure 80−70788
H, on Si (111) surface, electronic struct. 78−39182
H, on Si(100) 1×1, electronic props., self-consistent calc. 77−43690
H, on W (001), surface phonons, lattice dynamical model 80−39405
H, partial monolayers on Si(111), UV photoemission, disordering effect 77−1308
H_2 monolayer, on triangular lattice, orientational phases 78−75934
H_2, monolayers adsorbed on charcoal, graphite, H_2 dynamics 79−66341
He, adsorbed monolayer struct., neutron scatt. 77−7942
He film, from two to three dimens.,, review 78−47633
He films, on graphite, ordering 79−65287
He monolayer, phase diagram, order-disorder transition 80−107604
^{3}He, adsorbed, on MgO, nucl. mag. relax. props. 80−49457
^{3}He, adsorbed film on Grafoil, NMR, intermediate and near-monolayer coverages 79−46878
^{3}He, adsorbed monolayers, dipolar anisotropy effects in spin relax 77−7940
^{3}He, adsorbed monolayers on Grafoil, NMR, low coverage 78−91503
^{3}He and ^{4}He monolayer systems, book contrib. 79−99390
^{3}He film, submonolayer and multilayer, adsorbed on Grafoil, pulsed NMR study 80−49456
^{3}He film, theory of motional inhibition of interlayer quantum tunnelling 80−54466
^{3}He films adsorbed on Grafoil, NMR relax. times 79−28171
^{3}He, liq. confined in Al_2O_3 and Pt powders and Grafoil, NMR expts. 79−51371
^{3}He, monolayer film, adsorbed on Grafoil, pulsed NMR meas. 79−33152
^{3}He, monolayer on grafoil, NMR relaxation time study 78−75902
^{3}He, on Grafoil, phase determ. by sp. ht. meas. 77−11764
^{3}He, on solid Ar, desorption heat capacity 80−10735
^{3}He, quantum tunnelling, NMR linewidth 77−39720
^{3}He, submonolayer on Grafoil, vacancy induced ferromag. 78−14536
^{3}He, two-dimens. solid, melting mechanism 80−10643
^{4}He, monolayer adsorbed on Kr-plated graphite, possible Ising transition 80−34298
^{4}He monolayer superfluid films, third sound modes, superfluid solitons 79−10998
^{4}He, on Grafoil, phase determ. by sp. ht. meas. 77−11764
^{4}He, on graphite, quasi-2-dimens. quantum solid theory, lattice dynamics, thermal props. 78−84024
^{4}He, on graphite, quasi-2-dimens. quantum solid theory, vibr. props. 78−84025
^{4}He, on solid Ne, desorption heat capacity 80−10736
^{4}He, solidification, theory 77−20158
^{4}He submonolayer film adsorbed on Grafoil coated with monolayer Ar, sp. ht. 0.4-4.0K 79−51379
^{4}He superlattices on graphite, ground-state energy, variational calc. 80−24710
Hg, on W (100), fractional and zero order desorption kinetics 79−60634
In, on W, field ion image qualities and work function 78−35272
In submonolayer growth on Si(111)7 surface, superstruct. 79−77930
Ir (111), $(\sqrt{3}\times\sqrt{3})30°$ S overlayer struct., LEED obs. 80−15365
Kr absorption on graphite, monolayer regime phase diagram 80−49507
Kr, adsorbed on Cu surface, many-body interactions 78−84068
Kr adsorbed on graphite, commensurate-incommensurate transitions, low temp. theory 80−103582
Kr adsorbed on graphite, nonregistered-registered phase transition 80−39414
Kr adsorbed on graphite, overlayer-substrate spacing, LEED determ. 80−103579
Kr, adsorbed on graphite, substrate deform. meas. 80−54520
Kr, epitaxial monolayer on graphite, second order phase transform. obs. by LEED 77−76687
Kr, mono- and bilayers on graphite, two-dimens. struct., neutron diffr. study 79−42393
Kr monolayer on graphite, disregistry transition 78−30825
Kr, monolayer on graphite, commensurate-incommensurate transition, X-ray scatt. 79−73382
Kr, on graphite, commensurate to incommensurate transition 80−80079
Kr, on graphite, finite size effect and temp. depend., multicritical phase diagrams 79−42372
Kr, on graphite, misfit dislocations and lattice parameters, model 78−34708
Kr, on graphite, phase transition from localised to nonlocalised solid 77−11787
Kr, on graphite, X-ray diffr. from 2-D solid 78−75498
Kr, on graphite (0001), liq. state model appl. 77−69185
Kr, on graphite basal face, fluid-registered solid transition 80−49491
Kr submonolayer films on graphite, mol. dynamics simulation 80−88425
La, on W (112) face, contact pot. difference, LEED and field-emission microscopy meas. *(Russian)* 78−14618
La, on W (112) face, LEED and contact pot. difference meas. *(Russian)* 77−1316
LaB_6:C, AES, LEED and energy-loss spectra study of C layer on (100) surface 77−62715
Mo, monolayer, oxidation, quasisimultaneous SIMS, AES, XPS 78−72919
Mo:C (110) surface, segregation, precip. and desorpt. of C, AES and LEED study *(French)* 80−103480
MoO_3, catalysts, supported on aluminas, Raman obs. of struct. 79−28734
N, adsorbed monolayer on Cu surface, UV-visible polarised modulation spectra obs. 78−72619
N_2, adsorbed monolayer on Cu surface, UV-visible polarised modulation spectra obs. 78−72619
N_2, adsorbed on graphite, lattice dynamics 78−75946
N_2, adsorbed on graphite, monolayer two-dimensional phase change, calorimetric investig. 77−47669
N_2 adsorption on polycryst. W, α and β adsorption states 80−100404
N_2, dense monolayer on graphite cleavage face, phase transition 78−56034
N_2, on graphite, phonon dispersion curves for postulated four sublattice struct. 78−47667
N_2, two-dimensional freezing, on differently graphitised carbon 79−77896
NO, first monolayer on MgBr cleavage face, triple point 78−6227
Na, on Cu (111), UPS study of surface electronic struct. 80−80350
Ni (111) surface, C interaction, monolayer form. and struct. stability 80−10756
Ni, atomic layers, Pauli paramagnetism to band ferromagnetism transition thickness depend. 78−72377
Ni on TiO_2, interface electronic props., struct., comp., chemical bonding 80−84499
No, on graphite, melting and polymorphism 78−84063
O, 1/4 monolayer on Ir (110) unreconstructed surface, LEED study 79−14990
O, adsorbed monolayer on Cu surface, UV-visible polarised modulation spectra obs. 78−72619
O, adsorbed on Ni(100), RHEED study 79−77912

monolayers continued
O, half-monolayer on W (100), surface reconstruction kinetics 80−65375
O, on GaAs, influence of cleavage defects on interaction 80−66684
O, on Ni (001) surface, angle-resolved UV photoemission calc. 77−24927
O_2 adsorbed monolayers, antiferromag. struct. obs. by neutron diffr. 77−66257
O_2 covered metals, secondary ion yield, quantitative determ. *(German)* 79−48003
O_2, on graphite, mag. α-phase and α-β-phase transition 80−70530
O_2, on Ni (100) O K-edge surface EXAFS, secondary electron yield meas. 79−47544
O_2, on Pt, stability and struct. of high Miller index forces in vacuum and with adsorbed C and O 77−76651
O_2, solid, lattice dynamics 79−95095
O_∞ on graphite, partially localised, partially mobile monolayer films, adsorption isotherms 80−107646
Pb, deposition on Au, quantitative Auger electron spectroscopy, substrate and instrumental effects 80−71523
Pb monolayer, double layer with Sn, growth on Al (111), struct. 80−70567
Pb, on Au, sandwiching $AuPb_2$, formed during adsorpt., LEED, AES study 78−71988
Pb, on Au (100), initial stages of condensation 78−91569
Pb on Cu, Auger electron spectroscopy 77−85851
Pb, with Bi, on Cu (100), LEED and AES study 79−15017
Pb, with Sn, on Al (100) surface, prep. and props. of monolayers 79−15018
Pd on Ag (001), ultrathin film electronic states calc. 78−6318
S, adsorbed on Al (111), angle resolved UPS obs. of 2-dimens. band struct. 80−60059
SF_6, physical adsorption on Ru (001), XPS expts. 77−69178
Se, adsorbed on Al (111), angle resolved UPS obs. of 2-dimens. band struct. 80−60059
Se sphere monolayer, multiple EM wave scatt., migration imaging film appl. 80−99627
SiO_2, core excitons and inner well resonances in surface soft X-ray absorpt. spectra 80−40187
Sn, monolayer, double layer with Pb on Al (111), layer growth, struct. 80−70567
Sn, on Ge(111) surface, induced 7×7 superlattice struct. 78−91521
Sn, on W, field ion image qualities and work function 78−35272
Sn, with Pb, on Al (100) surface, prep. and props. of monolayers 79−15018
Te, adsorbed on Al (111), angle resolved UPS obs. of 2-dimens. band struct. 80−60059
Te, and $Pb_xSn_{1-x}Te$, Raman scatt. meas. 77−48211
TeO_2-PbO, and $Pb_xSn_{1-x}Te$, Raman scatt. meas. 77−48211
Ti, monolayer, oxidation, quasisimultaneous SIMS, AES, XPS 78−72919
W epitaxy on W(110) substrate, work function meas., LEED investigation 80−80103
Xe adsorbed monolayer, two-dimens. Lennard-Jones system, melting 79−28071
Xe adsorbed monolayers, thermodynamic props. and lattice const., quasi-harmonic theory 79−42380
Xe, adsorbed on graphite, substrate deform. meas. 80−54520
Xe adsorbed on graphite (0001) surface, monolayer liquid and solid struct. 80−65400
Xe, adsorbed on graphitised spheron, X-ray diffr. patterns 77−43433
Xe, adsorption on Ag (111), LEED obs. 77−1307
Xe, adsorption on Ag (111), statistical mech. 80−34306
Xe, adsorption on Cu(100), thermodynamics and kinetics, LEED and AES obs. 79−99423
Xe, on graphite, finite size effect and temp. depend., multicritical phase diagrams 79−42372
Xe, on graphite, misfit dislocations and lattice parameters, model 78−34708
Xe, on graphite, phase transition from localised to nonlocalised state 77−11787
Xe, on graphite (0001), liq. state model appl. 77−69185
Xe, physisorbed monolayer on graphite, dynamical and thermal props. 80−34292
Zr source for ultrahigh vacuum surface expts. 79−12810

monolithic integrated circuits
see also bipolar integrated circuits; field effect integrated circuits; large scale integration
automatic focusing of cameras using self-contained IC 78−82069
capacitive pressure sensors for deep-body biomedical appls., pulse-period output 80−67274
cascade CCD ultrasonic lens applications 78−22231
crystal defects in integrated circuits, review 78−88547
custom IC fabrication for implantable multichannel neural stimulator 80−85534
CW Doppler US vel. meter for implantable telemetry, blood flow meas. appl. 77−86565
defects, SEM, automation of comparative morphological analysis 79−23509
digitised layouts and impurity profiles, particle induced X-ray fluoresc. obs. 79−52804
failure source, localised cond. regions in SiO_2 film, obs. by liq. cryst. technique 77−1507
flowmeter, direction-sensitive, small size, wide flow speed range *(Dutch)* 77−55120
gas-sensitive sensor with ultrafine particle film deposited on monolithic IC chip *(Japanese)* 80−105630
heat conduction in layered struct., with local heat sources, analytic soln. 79−94456
linear, implantable CW Doppler US flowmeter appls., blood flow meas. 78−11749
matched filter device development using monolithic integration of SAW and semiconductor ccts. 79−32164
microminiature monolithic capacitive pressure sensor with pulse-period output electronics on same chip 80−81752
MWPC, high-flux fast readout system based on new monolithic integrated ccts. 78−37491
operational amplifier, linear-scale ohmmeter appl. *(Czech)* 77−61093
optical, based on Si, fabrication 77−19461
oxide thickness measurement in monolithic ICs, scanning electron microscope appl. 79−30619
piezoresistive pressure pickup *(German)* 77−49717
plasma-removal of polymeric layers 80−1851
quasimonolithic and hybrid integrated optical circuits on Si substrates 80−64218
radiation effects, conf., Williamsburg, USA (July, 1977) 78−26594
signal generator from IC chip 79−48998
social effects of microelectronics *(Dutch)* 80−20
solid-state device conference, Tokyo, Japan (Sept. 1976) 77−76901
stellar magnitude simulator, IC device 78−81742
temperature controller 77−67432
Vishnya type coincidence selection element appl. 77−18755
AlGaAs/GaAs monolithic series-connected solar cell arrays 80−97794
GaAlAs injection DH laser and GaAs Schottky-gate FET 80−58593
GaAs, ion implantation, trends 80−39132
GaAs, semi-insulating substrates, monolithic integration of optical and electronic devices, review 80−58543
GaAs-GaAlAs, injection laser and MESFET monolithic integration on GaAs substrate 79−64242
P in PSG protective film, X-ray fluoresc. technique for rapid determ. 77−40612
Si integrated resistors, both p-type and n-type, temp. coeff. of resist. calc. 78−91698
Si monolithic US transducer array 79−3877
ZnO/SOS monolithic SAW amplifier 78−6205

monomers *see molecules*

monomolecular films *see monolayers*

monomolecular layers *see monolayers*

Monte Carlo methods
^{252}Cf based nondestructive assay system for fissile material 78−73119
Abelian lattice gauge theories, Monte Carlo anal. 80−18079
absorbed energy distrib. in γ-irradiated layered target, Monte Carlo program 79−19279
accumulation dose factor for scattered γ-radiation in two-layer cylindrical shielding blocks 79−18058
acetone-chloroform solution, Monte Carlo calcs. for interface struct. with directed intermol. forces *(Russian)* 78−1975
acoustic propag. in random ocean, normal mode amplitudes, comparison with Monte Carlo simulation 78−87179
adjoint Boltzmann eqn., stochastic models for Monte Carlo integration 78−21618
adjoint photon transport, Monte Carlo biasing scheme, Compton scatt. and absorpt. 78−77819
adlayer-induced LEED beams near order-disorder transitions, Monte Carlo study 79−82438
adsorbate diffusion on single crystal surfaces, influence of lateral interactions 78−38953
adsorbed chain structure, Monte-Carlo simulation *(Russian)* 77−19122
adsorbed film, on BCC cryst., modelling of order-disorder transition, Monte-Carlo method 78−60033
adsorbed layer, classical octupoles on triangular lattice, orientational phases 80−2263
adsorbed molecular chains, config. props. effect on surface coverage 79−42371
adsorbing walls separated by Lennard-Jones liq., Monte Carlo calc. of force 80−15363
adsorption, computer simulation 79−65308
adsorption systems, Monte Carlo calcs., grand canonical ensemble, long-range corrections 78−30826
aerosol scattering indicatrices under clear sky conditions in 0.55 to 2.4 μ spectral region, determ. *(Russian)* 80−94600
AES, backscattering factor, Monte Carlo method calc. 80−7449
AES, quantitative 80−84813
agglomeration, Monte Carlo simulation *(Japanese)* 78−95707
air electron backscattering coeffs., 100 eV to 5 keV 80−9750
air pollution, steady-state distrib. 77−78415
β-Al_2O_3-Na_2O, Monte Carlo calc. of Na diffusion 77−89579
albedo dosimeter response to monoenergetic neutrons 77−90905
alkali halides, anomalous sp. ht. Ising model and Monte Carlo calcs. 78−47989
alkali halides, molten salt mixtures, enthalpy of mixing, theory, Monte Carlo calcs. 77−72691
alkali halides, secondary electron emission statistics, photomultiplier appl. 79−47564
alkali metal, bulk properties, computer simulation 78−30729
alkali metal, liq. struct., from 1st-principles pseudopot. calc. 79−41941
alkaline earth halides, thermodynamic and structural props., computer simulation 78−75849
n-alkane liquids, molecular orientational correlations 79−19131
alloy, binary, conc., with short and long range order, computer simulation of diffusion 78−30778
alloy, binary, crystallisation kinetics, Monte Carlo computer simulation 80−16294
alloy, binary, magnetic, interface struct., Monte Carlo simulation 80−60317
alloy, FCC, binary, on Ising system, sublattice magnetisation, tricrit. point, simulation 79−33491
alloy, FCC, Monte Carlo simulation of surface segregation 78−31413
alloy random, binary, diffusion correlation factors calc., comparison of matrix inversion, Monte Carlo and diffusion of probability techniques 78−30779
aluminates and aluminosilicates, thermodynamic props. determ. by Monte Carlo calc. 77−47597
ammonium halides, phase transitions by Monte Carlo method using cubic Ising model 80−70408
amorphous ferromagnet, effective-field distrib. and resistivity minima 79−73501
amorphous ferromagnet, metastable states in random anisotropy model 79−19710
amorphous solid, anomalous transit time dispersion, Monte Carlo simulation 77−47827
amorphous solid, supercooled liquid-glass transition region, short-range order, simulation 80−44127
amorphous targets, energetic in transport, Monte Carlo program 80−102411
amorphous thin film on crystalline substrate, computer simulation 79−15045
an algorithm of Monte Carlo methods for design of critical systems 79−40501
analysis of backscattering and sputtering in vacuum systems 80−235

Monte Carlo methods continued
anharmonic corrections in unimolecular theory, Monte Carlo calcs. 80−83441
anharmonicity, low-temp. model, Debye-Waller factors of Mossbauer effect 78−55927
anisotropic magnet mixture, Heisenberg spin system by Monte Carlo simulation 79−78408
anisotropic system, computer simulation, energy and specific heat temp. depend. 78−9947
anthracene, fluoresc. of cryst., Monte Carlo computer method, refl. and reabsorpt. *(German)* 78−68561
anthracene, single cryst., fluoresc. decay, Monte-Carlo simulation *(German)* 79−61440
antiferromagnet, FCC, Ising model, mag. phase diagram, ordering, Monte Carlo calc. 80−103833
antiferromagnet, Ising model, crit. props., calc. 80−65946
antiferromagnet, phase transition crossover from first- to second-order in symmetry-breaking field 79−82805
antiferromagnet, three-dimensional, fluctuation-induced first-order phase transitions, Monte Carlo calc. 77−85465
antiferromagnets, order parameter of dimens. 6 and 3 79−42762
aperture-type light conductor, photometric charact., computerised calc. by Monte Carlo method *(Russian)* 80−1339
aqueous solutions, Monte Carlo simulation, convergence of new algorithm 78−63649
asbestos-cement pipes, nondestructive neutron-radiation testing of moisture content 79−75539
astrophysics, appl. of Monte Carlo calcs. to high-energy nuclear reactions cross sections 78−28505
athermal model chains, pair distrib. function, Metropolitan Monte Carlo calcs. 78−17827
atmosphere photon transport problems, modified Monte Carlo procedure 78−61560
atmosphere proton and H atom precipitation in equatorial region 80−51596
atmosphere turbulent transport, Monte Carlo simulation and comparison with exptl. data 79−53479
atmospheric optics, book 80−77115
atmospheric scatt. of middle UV radiation from an internal source, Monte Carlo model 79−12263
atmospheric UV polarisation characteristics using Monte Carlo methods *(Russian)* 78−32224
atom, highly excited, linearly polarised elec. field ionisation, freq. (amplitude) depend. 80−32630
atom+atom recombinations, energy transfer mechanisms studied using trajectory calcs. and Monte Carlo method 80−66785
atomic aggregates, small, melting transition charact., random walk Monte Carlo calc. 77−75355
atomic clusters, free energy, compared to Becker-Doring and Lothe-Pound theory 78−22063
atomic elastic scattering, laboratory differential cross section data anal. via Monte Carlo averaging 78−21997
atoms diffusing in periodic lattices, quasi-elastic neutron scatt., use of Monte Carlo calcs. 79−60557
attenuated gas flow round plate, Monte Carlo soln. of Boltzmann eqn. 79−68754
austenite, computer simulation of C diffusivity 79−77803
autocatalytic reaction system, sustained oscills., deterministic and stochastic theories 78−95922
average solid angle subtended by right circular cylinder from distrib. sources 77−67950
axisymmetric plasma spectral emission and absorpt. coeffs., algorithm 79−37461
backscattering channelling surface peak calc. 79−8219
backscattering of γ-rays, atomic number depend., Monte Carlo calcs. 77−67734
bars, cylindrical and prismatic, stochastic, holonomic, elastoplastic torsion *(German)* 79−37192
BCC Ising model with competing interactions, fluction-induced first-order transition 80−20424
benzene-d_0, -d_6, intramol. vibr. energy relax. calcs. 78−33574
biased transport calcs. optimisation, prediction of statistical error 79−58654
bimolecular thermal rate coefficients, Monte Carlo calcs. 77−16789
binary BCC lattice model, order-disorder transition temp. 77−62614
binary collision model for plasma simulations, Monte Carlo method particle code 78−9824
binary microcluster, struct. and thermodynamics, Monte Carlo simulation 79−7736
binary triangular lattice solution, phase stratification statistical modeling 80−65239
biological macromolecules, computer simulation of solvent struct. 78−40113
blackbody cavities, directional emissivity calc., Monte Carlo method 80−83729
blackness of cylindrical cavity containing gas, calcs. using Monte Carlo method 80−106711
bond percolation, 2D, cluster size crit. exponent 80−68144
bond percolation, Monte Carlo anal. of scaling 78−77804
book 79−80528
Boson system, hard spheres, condensed phase, Jastrow wave function 78−84018
bounded flux-at-a-point estimators 79−587
bounded Monte Carlo estimator for reaction rates in finite volume elements 79−85571
brain O_2 transport, nonlinear simulation, hybrid computer implementation 78−40131
bremsstrahlung in bulk media, shielding study, Monte Carlo anal. of thick target spectra 78−59839
Brownian motion with viscous drag, for teachers 78−61984
Brusselator, dynamic correl. functions, Mori-Zwanzig formalism 80−25988
n-butane in tetrachloromethane, gauch-trans equilib. const., mol. dynamics and Monte Carlo anal. 79−70308
BWR physics methods compared with ^{232}Th lattice benchmarks 79−9711
BWR/6 axial reflectors, Monte Carlo modelling 80−22939
capture gamma-ray detector, neutron sensitivity 80−18767
cascade showers, three-dimens., Landau-Pomeranchuk-Migdal effect 78−49993
cascade showers in Pb and Fe, hadron-induced 77−60561

Monte Carlo methods continued
Chakravarty-Woo eqn., extension and appl. to liq. ^4He, liq. ^3He, and nucl. matter 80−68124
chalcogenide glass structure modelling by Monte Carlo method *(Russian)* 79−55672
charged hard spheres in uniform neutralising background, Monte Carlo and perturbation theories 77−55223
charged particle flux-at-a-point in complex geometries, numerical method 77−26249
charged particles in thin solid layer, ang. deflection due to multiple scatt. 78−79650
charmed quark fragmentation functions in a Monte Carlo quark recombination model 79−97570
chemical reaction kinetics, discrete simulation methods, appl. 78−48627
chemical reaction kinetics, teaching, Monte Carlo method, computer program 77−24
chemical reactions, quasiclassical trajectory calculations 79−15958
chemical system far from equilibrium, stochastic simulation 80−3339
chemisorption of O on W, atom interactions, Monte Carlo simulation 77−52667
circumstellar dust shells, Monte Carlo simulation of polarised light transfer 78−81608
circumstellar dust shells, polarisation by Mie scatt., Monte Carlo anal. 80−98650
classical fluid structure, Monte Carlo simulations, review, book contrib. 79−82140
classical harmonic oscillators, microcanonical ensemble, Monte Carlo sampling 80−102459
classical mag. moment system, antiferromag. phase transition, secular dipole interactions 80−80551
classical one-component plasma, screening pot., lattice model 78−22453
classical planar spin chain, dynamic props., Monte Carlo calc. 79−61144
classical planar spin model, two-dimens., Monte Carlo study 80−25147
classical quadrupoles on triangular net, orientational ordering calcs. 80−2262
classical stretching dynamics of methylene 80−23400
classical trajectory calcs., empirical testing of nonrandom integration method 78−50607
climatic change detect. and impact on hydrologic design 79−53396
cluster statistics for random and Ising percolation 78−32766
clusters of atoms, phase transitions, thermodynamics calcs. 77−59096
cobalt stearate, monomolecular multilayers, XPS escape length depend. on emission angle, elastic scatt. role *(Japanese)* 80−84833
colloid, electrostatically stabilised, very dilute, struct. and ordering, Monte Carlo method 77−36795
colloid, excess press., calc. and expt. 77−86386
colloids, model, elastic moduli, Monte Carlo methods 80−108754
colloids, phase transition, statistical mechanics approach 80−40749
colloids, solvation force between particles, Monte Carlo calc. 80−21328
comets, long-period, statistical study of orbits evolution 79−53775
comets, orbital evolution of short-period objects, Monte Carlo simulations 80−62073
complex particle transport problem soln., general-purpose Monte Carlo codes 79−583
Compton effect, multiple scattering, Monte Carlo calcs. 77−94
Compton scatter tissue densitometry, calc. of single and multiple scatter photon fluences 78−28048
Compton scattering simulation including γ-ray polarisation 77−34476
Comptonization of X-rays by low-temp. electrons, Monte Carlo calc. 80−12653
computational methods, book 78−81820
computer modelling of matter, conf., Anaheim, USA (March 1978) 80−51954
computer modelling of optical data transmission systems, principles 77−54675
computer simulation of vacancy annealing kinetics, for deformed Au 78−47353
concrete-paraffin shielding, fast neutron leakage, use of Monte Carlo method 77−23309
configurational free energy of chains Monte Carlo approach 78−16742
continuous slowing down theory params. in highly absorbing media 78−29559
contributon Monte Carlo methods, appls. to neutron deep-penetration transport problems 80−47530
convergence props. of new Monte Carlo simulation method, Brownian dynamics appl. 79−12719
copolymers, self-replicating, temporal evolution, Monte Carlo calcs. 77−83773
cosmic radiation, theoretical proton spectra at atm. depths 40 g $cm^{-2} \leq h \leq 350$ g cm^{-2} *(German)* 79−12367
cosmic ray EAS proton-initiated EM component at 690 g.cm^{-2}, Monte Carlo simulation 77−91390
cosmic ray energy spectra meas. with thin ionisation calorimeters 77−30713
cosmic ray fast timing ang. distrib. meas., data anal. 78−49256
cosmic ray hadron interactions, 0.5-5 TeV, XTR-detector, Monte-Carlo simulation *(Russian)* 79−49564
cosmic ray muons angular distrib. underground 78−40786
cosmic ray neutron detector, efficiency determ. by Monte Carlo method 78−21809
cosmic ray propagation in interplanetary space 80−12623
cosmic ray showers, calcs. of gamma ray and hadron families charact. 77−53377
cosmic ray showers, comparison with one-dimensional cascade theory *(Russian)* 79−96871
cosmic ray showers, sea-level expt. Monte Carlo anal. 77−67016
cosmic ray-nucleus reacts., 20 TeV, balloon-borne chamber, Monte Carlo simulation 80−9309
cosmic rays, atmospheric nuclear cascade charact. calc. for Pamir expt. 79−80157
cosmic rays, high-energy gamma-quantum and hadron families Monte Carlo studies 79−80158
cosmic rays, velocity diffusion, turbulent mag. field, Monte Carlo calc. 78−53777
cosmic-ray high-energy EM air showers 77−64577
Coulombic systems, charged hard sphere system, rel. to restricted primitive model 80−64854
Coulombic systems, restricted primitive model, Monte Carlo simulations, ergodic problems 78−36923
coupled chemical reactions, stochastic time evolution, Monte Carlo simulation procedure 77−9047

Monte Carlo methods continued
coupled Ising chains, Monte Carlo anal. 79−42721
covalent semiconductor, heating of charge carriers, energy dissipation 80−49755
crack growth in concrete, computer simulation using Monte Carlo method 78−76764
crater saturation and equilibrium, Monte Carlo simulation 77−71038
critical arrays, effects of packaging materials 79−26567
critical dynamics, Monte Carlo anal. of renormalisation group, scale transform. 77−22513
criticality calculations, random geometry model of fissile solns. containing borates Raschig rings 79−36310
crystal growth, computer simulation 78−26463
crystal growth, imperfect faces, Monte-Carlo growth rates 77−11493
crystal growth, Monte Carlo simulation, review, book contrib. 79−80532
crystal growth, Monte Carlo simulation nucleation, comparison with normal growth theories 77−68932
crystal growth, stochastic models, diffusion and relax. kinetics 79−37642
crystal growth from vapour, simulation 78−31312
crystal surface nucleation growth processes, Monte Carlo simulation 77−58965
crystal surface structures, Monte Carlo simulations, appl. of statistical tests, cryst. growth 77−4060
crystal surfaces, and cryst. growth, Monte Carlo computer simulations 79−14710
crystal-met interface of Lennard-Jones substance, Monte Carlo simulation 79−60622
CTR, model blanket expt., neutron spectra sensitivity analysis 78−29648
cyclotron isochronous, bunch phase behaviour, Monte Carlo simulation 77−54382
deep penetration shielding problems, calc. of contribution flux and current spatial distrib. 79−59283
deep-penetration radiation transport, event and point value in Monte Carlo importance sampling 78−8869
defect interactions, reaction constants 78−71754
defective solids, Haven ratio in athermal lattice gas;, Monte Carlo method 80−84313
delayed neutron theoretical pulse height spectra 78−78328
dendrite development and growth in very small crystals, Monte Carlo study 80−107683
dendrites, Monte Carlo simulation of growth from melt 80−15427
dense fluids, solvation forces between two solids 80−64855
dense Lennard-Jones fluids, solvent struct. and solvation forces between rigid particles 80−30287
dense liquids, structure at solid wall interface, NVT Monte Carlo method 79−65310
dense simple fluid near wall, density profile calc., integral eqn.−Monte Carlo comparison 80−54083
depletion stabilisation and depletion flocculation, theory 80−89534
deposition profiles of irradiated materials interfaces, Monte Carlo calcs., photo Compton current 79−24383
depth profiling under ion bombard., sputter broadening Monte Carlo simulation *(Japanese)* 79−83089
depth-dose relationships near the skin resulting from parallel beams of fast neutrons 80−30902
diamond, natural, anisotropy and saturation of hot carrier drift velocity 80−6867
diamond, natural, electron effective mass and lattice scatt., Monte Carlo anal. 80−44484
diamond, natural, lattice scattering and effective mass of holes 79−60842
diamond solid-fluid interface roughening transition 79−99088
diamond-like semiconductor film epitaxial growth, computer simulation 80−70560
diatomic gas, molecular dissociation, recombination reactions simulation 78−23934
diatomic molecules, dissoc., thermal unimol. reactions, energy transfer, Monte Carlo calcs. 79−81166
diffuse light scattering, mathematical modelling 80−106450
diffusion and evaporation on (100) surface of FCC crystal 78−30836
diffusion correlation factor calc. 79−82375
diffusion correlation in random primitive cubic alloys 77−80640
diffusion via vacancies, correl. factors calc. using Monte Carlo computer simulation 77−15615
dilute aqueous solutions, Monte Carlo studies of struct., review 80−54101
dilute frustrated lattice, spin-glass ordering, triangle and FCC lattices, Monte Carlo simulation 80−15746
dilute simple cubic lattice, short-range quadrupolar order 79−65681
dilute solutions, Monte Carlo algorithm for preferential sampling near solutes 77−51287
diluted Ising and Heisenberg magnets with competing interactions, phase diagrams and mag. props. 80−34672
dipolar lattice, 2-D, Monte-Carlo calc., lattice energy 78−14308
discharge, luminescent, in He, electrons energy distribution function evaluation *(French)* 77−19795
dislocation motion through random array of point obstacles, thermally activated, computer simulation 78−30636
disordered media, elec. transport theories, effective medium approx. improvement 79−47071
disordered system, spectral and spatial diffusion, Monte Carlo calc. 79−4848
disordered systems, Coulomb gap computer simulation 79−51465
disordered systems, dispersive hopping transport, Monte Carlo calcs., variable range percolation 80−44587
disordered systems, time dependent spectral transfer, Monte Carlo calc. 80−11464
displacement spike annealing, Mont Carlo method computer expteriments 78−30672
dose and LET distributions due to neutron and photons from stopped $pion^-$ 77−52878
dose factors for radiosensitive tissues in bone irrad. by surface-deposited radionuclides 78−53512
dosimetry, cylinders irrad. by $pion^-$ beams, effects of tissue inhomogeneities 77−9266
dosimetry, improvement of linear accelerator depth-dose curves 79−20681
dosimetry, isotropic and cloud source irrad. by monoenergetic neutrons and photons 78−24138
drift tube, parallel-plate, Monte Carlo simulation 77−58914
dual gauging using penetrating and scattered photon fluxes 77−41551
Monte Carlo methods continued
Durham air shower array, Monte Carlo anal. of response 78−36460
dynamic fatigue tests, statistical reproducibility of crack propag. parameter 80−25842
EAS, obs. of energetic delayed hadrons, comparison of data with Monte Carlo simulation 79−66897
education, solid state diffusion, atomistic model, pedagogical use of Monte Carlo method 79−25797
elastic-plastic frames, deformation anal. Monte Carlo technique 79−7295
electric field automatic computation, three methods, comparative study *(French)* 79−68346
electric field calc. appl. *(Italian)* 79−94124
electric field calculation by floating random walk method 80−95760
electrical double layer, Gouy-Chapman-Stern theory, Monte Carlo calc. 79−96315
electrochemistry application of kinetic model for renewal of the elements of a set leading to stable space segregation 79−20373
electrolyte soln. grand canonical ensemble Monte Carlo 80−54092
electrolyte solution, Monte Carlo calcs. of ion pair region boundary 77−36760
electron and photon transport, SANDYL program, statistical accuracy, optimisation 77−8675
electron avalanche in gas under uniform electric field, simulation *(Japanese)* 77−39399
electron avalanche simulation in hydrogen 80−38521
electron beam, energy coupling to expanding thick-shelled target 80−96365
electron beam lithography, energy loss calcs., Bethe and Spencer-Fano theories 78−87728
electron beam scattering, in organic specimen 80−100148
electron behaviour in solids, simulation 79−33274
electron channelling patterns, contrast mechanisms, lattice-defect images, in SEM 79−27884
electron diffraction crystallography, multiple inelastic scatt. in thick crysts., Monte Carlo simulation 77−7637
electron diffusion and drift in gases Monte Carlo simulation 77−84392
electron diffusion to absorbing electrodes, Monte Carlo and Boltzmann calc. comparison 80−6204
electron diffusion to anode, Monte Carlo and Boltzmann calcs. comparison 80−38519
electron displacement damage simulation in HVEM irrad. 80−107325
electron dosimetry below 50 MeV 78−7453
electron dosimetry in tissue equiv. phantoms 78−7454
electron drift velocities simulation in inert gas mixtures, rel. to neutron counters 80−48843
electron energy loss spectra, yield calcs. in H_2O, bioligical implications 79−7641
electron gas, ground state, stochastic method calcs. 80−95031
electron mean free path, stopping and straggling 78−91367
electron probe microanalysis and SEM, use of Monte Carlo calcs. 77−74562
electron random motion in molecular materials, Monte Carlo anal. 77−31703
electron resist failure, energy deposition functions, Monte Carlo simulation of electron scatt. 79−56897
electron scatt. in thin foils, depth selection, Monte Carlo calc. of energy distrib. 79−45598
electron scattering, 1.2 to 3 MeV, in amorphous materials *(French)* 79−99037
electron scattering calculations in solids, high energy 80−96422
electron slowing down in water, spatial correlation of energy deposition events 80−9473
electron sources, plane infinite oblique, Monte Carlo calcs. on dose distribs. 77−65339
electron swarms in gases with large inelastic cross sections, accuracy of numerical solns. of Boltzmann's eqn. 79−94756
electron trajectory simulation in solids, particle size anal. appl. 79−43693
electron transmission and backscatt. in solid layers, energy loss, 10 to 30 keV 77−59653
electron transport, continuous-slowing-down approx., adjoint Monte Carlo model 80−49269
electron transport, diffusion theory and Monte Carlo calcs., depend. on initial ang. distrib. of injected electrons 80−53136
electron transport calculations, orthogonal function expansion technique 77−26248
electron transport in air and N_2 78−90042
electron transport in solids, book contrib. 80−100458
electron transport simulation in liq. water, appl. to microdosimetry and radiobiology *(French)* 80−12202
electron-photon cascade simulation by Monte Carlo programs 79−54330
electron-photon cascades, Monte Carlo simulation of cascade development 79−44322
electron-solid interactions, appl. to electron probe microanal. 77−12853
electronic transport in substitutionally disordered systems, MCPA and Monte Carlo calc. 78−84185
elemental sensitivity data modeling for in situ neutron capture gamma-ray experiments 79−61928
elementary particle events with limited transverse momentum 79−3001
elementary particle inclusive interactions, multiple production processes regularities, Monte Carlo model 80−102082
ellipsometry, inversion problem solution using simple Monte Carlo procedure 77−41669
EM scattering, hybrid computation by Unimoment/Monte Carlo technique 77−14646
EM wave scattering, space structure of directed radiation field in scatt. media, calc. *(Russian)* 77−14643
empirical relationships for random self-avoiding walks on lattices 79−9190
ENDF/B-IV benchmark analyses with full spectrum three-dimensional Monte Carlo models 79−9701
ENDF/B-V cross section data for shielding appls., Monte Carlo MCNP integral calcs. 80−47744
energy distribution simulation, of low energy protons passing through Cu film 77−15466
energy doubler dipole, sensitivity to beam induced quenches 79−68084
energy loss of atomic particles in solids, fluctuation in spatial distrib. 79−90709
energy transfer models in solids 80−76074

Monte Carlo methods continued
ensemble of two-body random Hamiltonians, nonzero mean matrix elements, eigenvalue density, Monte Carlo calcs. 78−81920
ensemble of two-body random Hamiltonians, spectrum shape, Monte Carlo calcs. 78−81919
entropy calculation with computer simulation 77−22504
epithermal-neutron field in medium with inhomogeneous water distribution 79−17957
EPMA correction procedure, Monte Carlo derivation of surface ionisation function 78−20119
ethane, unimol. decomp., energy transfer processes, Monte Carlo simulation 80−99555
ethyl radical decomposition, mol. dynamics, trajectory studies 80−7780
eutectic crystal-melt system, interphase boundary struct., Monte Carlo method study 80−1950
evaporation neutrons in paraffin and lead layers, Monte Carlo methods 79−89346
exospheres of Moon and Mercury, Monte Carlo simulation methods 80−67588
exospheres of Moon and Mercury, Monte Carlo simulation methods 80−67589
exponential biasing method, optimal choice of parameters 79−40498
fallout gamma radiation, effectiveness of soil as shielding 78−5059
fast ions, behaviour during H-neutral-beam-injection in large Tokamak plasma 80−28713
fast liner reactor conceptual design, nucleonics 80−13790
fast neutron albedo for Fe, concrete and Fe-covered concrete radiation shields 79−76151
fast proton track energy deposition and ionisation calc. and obs. 80−12196
fatigue crack initiation, model using probabilistic technique 78−68800
FBR, Monte Carlo benchamrk program for anal. of critical assemblies 79−89405
FBR safety related slowing down problems 78−678
fcc alloy, A_3B ordering process time evolution, Monte Carlo simulation 79−86869
FCC Blume-Capel model, Monte Carlo study 80−103453
fermion one-component plasma ground state, two and three dimens. Monte Carlo study 79−33248
ferroelectric, anomalous sp. ht. Ising model and Monte Carlo calcs. 78−47989
ferromagnet, Ising model, diamond lattice, phase transition, crit. props. 80−93127
ferromagnet, with liq.-like disorder, excitations 79−61084
fibre reinforced composites, Monte Carlo study of strength 80−25844
fibre-optic system repeater error rate calc. approaches compared 77−54672
fibrous material failure kinetics, internal stresses, computer simulation *(Russian)* 80−40479
fields solution using transmission line matrix, random walks appl. 79−53991
film, thin, combinatorial-statistical topology of films with pores and islands 79−56096
film, transition from island to layer growth, a Monte Carlo simulation 77−85104
films, thin, on substrate, thickness meas., electron probe anal. technique *(French)* 78−41276
fission reactor criticality safety quality assurance, need for exptl. studies 79−63770
fission reactor fast systems with cylindrical geometry, Monte-Carlo method anal. 78−46132
fission reactor reactivity perturbation calc by difference iterations in the Monte Carlo method 80−5210
fission reactor safety, cooling system, fault tree anal. using Monte Carlo and anal. methods *(Spanish)* 80−57870
fission reactor spent-fuel shipping casks, Monte Carlo radiative heat transfer 79−59193
fission reactor theory, multiplication coeff. calc. by quotient matrix method *(Russian)* 77−42047
fission reactors, integral experiments for testing Th and ^{233}U data 80−27707
flow prediction, Monte Carlo and Bayesian probability techniques 78−30256
fluid, cavity-biased (T,V,μ) Monte Carlo method, computer simulation 80−92434
fluid, dense, of polarisable dipolar hard spheres, Monte Carlo study 79−86665
fluid, hard dumbbell mols., reference pot., perturbation theories, spherical reference systems 80−28898
fluid, hard polyat. mols., virial press., Monte Carlo method 77−89357
fluid, hard sphere, nonspherical mols., dielectric const., Monte Carlo simulation 78−23385
fluid, hard-core plus Yukawa tail pot., eqn. of state 78−26410
fluid, of hard hetero/homonucl. diats., Monte-Carlo simulations 78−42873
fluid, of hard prolate spherocylinders, pair distrib. function expansion validity 80−24336
fluid, optimisation of sampling algorithms 80−54099
fluid dynamics, Rayleigh-Benard convection, randomly forced 80−79314
fluid structure, ionic, boundary conditions distorting effects in simulation 79−50968
fluid structure and dynamical props., computer simulation, using Monte Carlo and mol. dynamic methods *(German)* 80−69757
fluid with periodic boundary conditions, error in computer simulation determ. 77−15296
fluids, dipolar hard spheres, dielectric const., pair distrib. function, Monte Carlo study 78−6001
fluoroscopy, organ dose per unit exposure, estimation method for artificial pneumothorax 78−96097
foil, electron scatt., appl. of Monte Carlo type calc. *(French)* 77−7636
foliated chemical inhomogeneous media, electron and γ interaction ranges, Monte Carlo calc. *(Russian)* 79−12370
forward Monte Carlo heat conduction, known-temp. boundary condition treatment 79−158
fracture, intense electron-beam pulse, initiated, Monte Carlo modelling 77−69038
fracture processes and fibre strength, in brittle fibre reinforced alloys, anal. by Monte Carlo computer simulation *(Japanese)* 78−80634
free molecular flows, Monte Carlo functional expansion calc. 79−72912
Frenkel pair formation in solids, due to passage of relativistic electrons, computer simulation *(Russian)* 80−6402
Monte Carlo methods continued
fused hard sphere fluids, equations of state, virial coeffs., Monte Carlo simulation 80−54095
fusion blanket models, calc. of T breeding per source neutron 79−67934
fusion blanket neutronics, acceleration of Monte Carlo simulation 77−23280
fusion neutron heating in laser compressed DT spheres 77−6553
fusion pellet-target system, optimum material and design for relativistic electron beam 78−17416
fusion reactions in deformed nuclei, γ-multiplicities, collective and statistical γ-rays 79−578
fusion reactor, FINTOR-D, T breeding blanket, Monte Carlo calcs. 80−99283
fusion reactor, microscopic behaviour and neutral beam heating of Tokamak 77−79476
fusion reactor blanket thickness, improvements to cellular design 80−18630
fusion reactor blanket thickness, minimization calcs., implication of cellular struct. 80−18629
fusion reactor cryo-pumps, nucl. heat deposition 78−66414
fusion reactor gross blanket breeding ratio, by 3-D methods 79−18033
fusion reactor in toroidal geometry, design calcs. 77−34456
fusion reactor Li blanket models, Monte-Carlo and discrete ordinates calcs. *(German)* 77−83096
fusion reactors, TFTR test cell, calc. dose rates from induced activity 80−57967
galactic cosmic rays, particle drift effects on solar modulation 77−37488
galaxies in clusters, Monte-Carlo simulation of orientations 80−90528
galaxy correlation function evolution, N-body Monte Carlo model 80−62292
galaxy groups, ellipticity index Monte Carlo determ. rel. to avarage ellipticities 80−12820
gamma Compton experiment, with annular ^{241}Am source, momentum resolution and reliability meas. 80−312
gamma radiation field induced in air by fast neutrons, intensity and absorbed energy calc. method 77−50310
gamma ray source, solid angle, self-absorption factors, evaluation by Monte Carlo method *(Rumanian)* 78−58526
gamma sources in walls of dwelling rooms, exposure rate calc. 78−73260
gamma spectrometry, low-level, in vivo, optimum detector size and position 78−28075
gamma spectrum average energy and numerical buildup factors meas. 77−54397
gamma-gamma logging problems with large probe length, splitting method 77−37437
gamma-ray absorpt. coeff. for non-homogeneous materials 77−34527
gamma-ray angular correlation, intrasource absorpt. and scatt. effects 79−97958
gamma-ray backscattering, survey of principal research 77−65340
gamma-ray backscattering coefficients, Monte Carlo calcs. 77−61171
gamma-ray detector, nonhydrogenous organic liquid scintillator sensitivity function calc. 78−78572
gamma-ray emitters, point isotropic, dose in surrounding water 79−62363
gamma-ray radiation in dwelling rooms, Monte Carlo code REBEL-2 77−40793
gamma-ray self-absorption in vol. shaped source for NaI detectors 77−26909
gamma-ray sources, narrowly collimated, radiation fields in Al and H_2O *(Russian)* 77−30549
gamma-rays albedo, number and energy calcs. 79−31221
gas, terminal speed ratio prediction for spherical-source expansions 77−84285
gas dynamics, compressible inviscid ideal gas flow, direct simulation methods 80−48733
gas flow, Monte Carlo simulation, book contrib. 78−59365
gas proportional detectors, relativistic charged particle energy loss 77−88362
gas-discharge cathode region transfer process simulation 78−71600
gas-liquid system, digital simulation 78−2341
gases, electron motion, Boltzmann eqn. soln. two-term approx., validity 77−35309
Gaussian polymer molecule config., stars and random regular nets, distrib. functions 79−13849
GCFR lattice, Monte Carlo and diffusion theory calcs. of steam worth 79−80991
giant stars, late-type, semi-theoretical density profiles along galactic radius through Sun 79−35253
glass, minimum life prediction, uncertainty 77−16665
glass transition, empirical criterion, Monte Carlo simulation 79−1496
glycine, neutral and zwitterion interaction with water, Monte Carlo simulation 79−53026
graphite, neutron penetration, Monte Carlo calculations for 30, 45 MeV *(Japanese)* 80−18677
graphite assembly exposed to 52 MeV protons, penetration of secondary neutrons and photons 79−76152
graphite ionisation chamber with CO_2 filling, Monte Carlo anal. of fast neutron irradiation 78−82583
Green's function Monte Carlo method for quantum hard spheres radial distrib. function 79−54005
ground surface profile, crest and trough height distrib., Monte Carlo simulation *(Japanese)* 79−34180
ground surface profile power spectrum, Monte Carlo simulations *(Japanese)* 79−34179
growing lattice animals and Monte-Carlo methods 80−57207
hadron transmission through absorbers, Monte Carlo simulator of hadron cascade 77−30736
hadronic charm prod. cross section and particle lifetimes, Monte Carlo anal. 78−89679
hard core diatomic system, pair correl. functions, Monte Carlo and RISM calcs. 77−72537
hard diatomic fluid mixtures, dense, orientational struct. 78−34415
hard disc fluid, infinite dilution solute chemical pot. by Monte Carlo simulation 80−88009
hard oblate spherocylinders, Monte Carlo virial coeffs. 78−26400
hard quadrupolar diatomics, free energy, perturbation theory and Monte Carlo calc. 79−90361
hard sphere fluid, dielectric const., Monte Carlo simulations, mol. dynamics calcs. 80−28897
hard sphere fluid, in contact with soft repulsive wall, struct. calcs. 78−1967

Monte Carlo methods continued
hard sphere fluid, y(r) function, Monte Carlo calc. 78−18523
hard sphere fluid contacting soft repulsive wall, Monte-Carlo method 78−67632
hard sphere-spherocylinder equimolecular mixture, Monte Carlo simulation of fluids 80−44088
hard spherocylinder fluid, Monte Carlo calcs. 78−91208
hard spherocylinder fluid, Monte Carlo simulation, ang. correl. functions 80−75140
hard spherocylinders, Monte Carlo simulation 78−91046
hard spherocylinders and spheres mixtures, Monte Carlo study 80−49073
hard-sphere fluid, reduced density, radial distrib. function calcs. 77−3903
hard-sphere fluid near hard wall, Monte Carlo calcs. 78−55795
hard-sphere solid, radial distrib. function, Monte Carlo calc. 78−6022
heat conduction, multimedia problems, Monte Carlo soln. method 80−74704
heat conduction using transport eqn. approximation 79−159
heat conduction with convective boundary conditions 78−680
heavy ions in low energy region, expt. and theoretical range comparison 80−32257
heavy isotope separation using nozzles, jets and channels, investig. 79−94097
Heisenberg ferromagnet, magnetisation calc. 78−23229
Heisenberg magnet, dil. three dimensional, static behaviour at finite temps., Monte Carlo calc. 79−73752
Heisenberg magnet, two-dimens., glasslike ordering Monte Carlo calcs. 79−82740
Heisenberg magnet, two-dimensional classical, mag. props., Monte Carlo calc. 78−23231
Heisenberg model, antiferromag., phase diagram and multicrit. behaviour 78−56337
Heisenberg model, two-dimensional classical, Monte Carlo evidence for inhomogeneous states 80−44790
Heisenberg spin glass model, Monte Carlo exam. 77−24698
heteronuclear hard dumbbells, eqn. of state derivation 77−30085
heteropolymer in random mag. field, Ising chains, statistical mechanics, free energy, numerical calcs. 78−77803
n-hexyl chain bound to macromol., ^{13}C spin-lattice relax. 77−23510
n-hexylamine.Gd(FOD)$_3$, flexible chain dynamics, NMR, steric effects calcs. 77−6800
highly attenuated gas flow around body, surface interactions, free molecular conditions 79−90285
hole burning into molecular velocity distribution due to monochromatic radiation and molecular elastic collision 80−43116
hopping conduction, random one-dimens. system, Monte Carlo computer simulation 80−80278
hopping transport for random spatial distrib. of localised sites, simulation 79−23971
hot atom reactions, nonequilib. vel. distrib. and reaction rate, Monte Carlo anal. 77−16855
hot electron phenomena, calc., review 78−26870
hot-atom collisional energy density function, stochastic calc. 79−29342
hydration, hydrophobic, of nonpolar mols. in dilute aq. soln., Monte Carlo simulation 80−3314
hydrocarbon scintillators, Monte Carlo predictions of neutron detection efficiency 79−68150
hydrologic systems, linear model stable estimator development and expt. 77−5259
hydrology, resource system, Monte Carlo simulation, variance reduction techniques 78−81244
ice, two-dimens. square, correl. function calcs., approx. methods, Bjerrum fault conc. effects 80−10513
III-V semiconductors, negative resistance and peak velocity in central (000) valley 79−73522
III-V semiconductors, quaternary and ternary, alloy scatt., high field transport 78−30929
importance sampling with parametric depend. 80−13013
impurity diffusion, correl. factor, computer simulation 79−19404
incompressible Kramers problem, direct simulation 79−94666
inert gas atom+highly stripped ion, multiple-ionis. cross sections, Monte Carlo calcs. 79−64091
inert gas crystallites of 5, 6, 7, 8 atoms, metastable states, Monte Carlo method 78−22687
inert gas crystals, internal energy, Monte Carlo calcs. 77−72577
inert gas crystals, Monte Carlo calc. of conc. of lattice vacancies, method of overlapping distribs. 80−39077
insulating films, hot electron energy distribs., Monte Carlo study 77−51832
Intense Neutron Source Facility skyshine analysis 79−9931
interface between liquid and vapour, surface of tension location 79−37909
interfaces, liq.-cryst. and liq.-rigid wall, Monte Carlo simulation 79−27896
interpretation using averaged continuum pot. 78−30683
interstellar clouds, Oort model, Monte Carlo simulation 78−12331
interstellar gas heating and ionization by X-ray photoelectrons 80−46383
ion+neutral neutron, ion speed effects in flow-drift tubes, Monte Carlo simulation 77−56221
ion acoustic wave, large amplitude coherent, heating mechanism 79−23432
ion bombardment collision cascades, computer simulation, Monte Carlo code 78−67756
ion clusters, equilib. props. and struct., Monte Carlo calcs. *(Russian)* 79−27745
ion energy deposition in simulated biological matter 77−81584
ion motion and charge exchange in quadrupole elec. field, Monte Carlo calcs. 77−9060
ion reflection from metal surfaces 80−40197
ion system, internal energy, Debye temp. function, Monte Carlo method data 77−35314
ion-Rydberg atom collision cross sections, classical trajectory Monte Carlo calcs. 80−43174
ion-surface impact, low energy light ions, anal. of interaction by Monte Carlo simulation 78−23570
ionic and plasma cluster equilibrium and kinetic props., computer simulation 78−71533
ionic crystal growth, fast growth of ordered AB crystals, Monte Carlo simulation 79−19165
Monte Carlo methods continued
ionic impurity, drift mobility in electric field, computer simulation 79−82388
ionic system with mild repulsion, Monte Carlo calc. 78−94891
ionisation chambers, wall correction factors, ^{60}Co γ-ray beam standardisation 79−3288
ionosphere positive ion detection, with rocket-borne mass spectrometer 80−8459
IR sensor noise reduction algorithms, Monte Carlo evaluation 80−95824
Ising antiferromagnet, BCC, crit. behaviour in mag. field, Monte Carlo calc. 78−31088
Ising antiferromagnet, BCC, in mag. field, Monte Carlo calcs. 78−31032
Ising antiferromagnet, FCC, nearest neighbour interactions, Monte Carlo method 80−80544
Ising antiferromagnet, phase boundary, crit. temp. field depend., Monte Carlo anal. 78−34995
Ising antiferromagnet with next-nearest-neighbour interactions, tricritical exponents and crossover behaviour 77−16089
Ising chain, spin-1, sp. ht. in presence of impurities and mag. field 80−93128
Ising chain with random bonds, remanence and non-exponential relax. 79−73751
Ising clusters, small, Monte Carlo calc. of critical temp. 77−63209
Ising ferro and antiferromagnet random bond mixture, on s.c. lattice, phase transition 77−12131
Ising ferromagnet, 4-D, correction to leading singularity of order parameter 80−25061
Ising ferromagnet, four-dimensional logarithmic correction to mean-field order parameter 79−73754
Ising ferromagnet, randomly dilute, determ. of transition temp. by Monte Carlo simulations 77−12130
Ising ferromagnet, two-dimensional, with second-neighbour interaction, computer simulation, series-expansion method 77−63052
Ising lattice, triangular, with next nearest neighbour interactions, Monte Carlo calc. of order 77−53836
Ising model, bond-dilute two-dimensional, crit. behaviour 79−8009
Ising model, classical, in transverse field, Monte Carlo simulation, statical props. 78−56326
Ising model, crit. props., appl. of real space renormalisation techniques 79−78420
Ising model, dipolar antiferromag., phase transition at negative absolute temp. *(Russian)* 78−43594
Ising model, interface roughening transition, Monte Carlo study 77−67384
Ising model, Kadanoff block transformation by Monte Carlo technique 77−69574
Ising model, kinetic with triplet interactions 80−7061
Ising model, logarithmic exchange interaction, Monte Carlo simulation 79−19712
Ising model, Monte-Carlo method appl. to evaluation of Niemeijer-van Leeuwen cumulant expansion 78−16751
Ising model, n≥2, Monte Carlo renormalisation group 79−75470
Ising model, nonequilib., intensive parameters and detailed balance, theoretical estimate 78−76209
Ising model, nonequilib. intensive parameters and detailed balance, computer simulation calcs. 78−76208
Ising model, quenched two-dimensional single spin-flip kinetic, Monte Carlo simulation 78−34943
Ising model, spatially modulated phase, Monte Carlo study 79−95598
Ising model, two dimens., metastability, dynamic Monte Carlo method, transfer matrix 78−72354
Ising model, two-dimens., ferromagnet-spin glass transition, Monte Carlo calc. 80−60287
Ising model for monolayers of coadsorbed atoms, phase transitions 80−19909
Ising model simulation, random mixture critical props. 77−69573
Ising model spin glass, Monte Carlo calc. of mag. suscept. 78−31079
Ising model spin glass, phase transitions 77−8327
Ising model with biquadratic interaction, phase transition, Monte Carlo method 80−60352
Ising models, spatially modulated phase, with competing interactions 80−60334
Ising site model, random mixtures, Monte Carlo simulation 78−73935
Ising site model, random mixtures, Monte Carlo simulation 78−73936
Ising spin glass, nature of ordering 78−80172
Ising spin glass, remanent magnetisation, Monte Carlo exam. 79−61166
Ising spin glass, three-dimensional mag. correlations 80−103849
Ising spin glass, vanishing of Edwards-Anderson parameter 78−43597
Ising spin glasses, Monte Carlo simulation 79−78428
Ising square lattice, phase transitions, next nearest neighbour interactions 80−50128
Ising system, Lifshitz points, phase diagram transition temp. determ. interface free energy vanishing 79−99716
Ising two-dimens. random bond model, evidence against spin-glass order 80−15747
Ising-Glauber model with competing interactions, tricrit. relax. 77−8326
Ising-system, two-state, crit. behaviour, Monte Carlo calcs. 78−86222
isotope separation, by probe in supersonic flow, Monte Carlo simulation 79−94098
jellium, one-dimensional, wall effects 79−46468
kinetic Ising model, quenched relaxing impurities, critical dynamics 79−40484
Knudsen flow, through periodically constricted pores *(Japanese)* 79−72911
laminate, strength anal. and distribution, failure prediction 78−88522
LAMPF radiation effects facility, total neutron flux, energy spectrum, meas. and calc. 77−23331
large cell renormalisation groups for percolation 80−46994
largest cluster at two dimensional percolation threshold, Hausdorff dimens. and fluctuations 80−46982
laser, electron beam controlled, electron beam parameter optimization and choice of foil 80−48269
laser, nonuniform amplification effects *(Russian)* 77−14722
laser driven fusion reactor, Monte Carlo study of asymmetric effects of LiO_2 blanket 78−74464
laser fusion-fission reactor, lattice calcs. and three dimens. effects 79−81088
laser induced fission, Monte Carlo anal., critical mass and radius for bare spheres 78−62583

Monte Carlo methods continued
laser rangefinder radiometric efficiency, optomechanical tolerance analysis 79−21705
laser reactor Li_2O blanket, Monte Carlo and discrete ordinate scoping models 78−62603
lattice gas, Ising-like, thermodynamic props., Monte Carlo calcs. 79−6054
lattice gas models, cluster statistics 77−13706
lattice gauge theory, 4-D Z_2 gauge, verification of first order phase transition 79−58876
lattice model polymer chain Monte Carlo study, Rouse coord. distrib. and dimens. 79−89814
lattice models, LJD model, fine-grained lattices and continuum 79−12734
lattices, finite, with traps, random walks, Monte Carlo simulations 80−52131
Lennard Jones liquid, simulation by force bias and Monte Carlo methods 79−86666
Lennard Jones system, nonphysical sampling distribs., Monte Carlo free energy estimation, umbrella sampling 77−26229
Lennard-Jones fluid, eqn. of state, Monte Carlo and perturbation theory 77−76519
Lennard-Jones fluid, thermodynamic props. calc. by modified Monte-Carlo method 77−35662
Lennard-Jones fluid in contact with Lennard-Jones wall, interfacial density profile 78−67901
Lennard-Jones pot. liquid, high-temperature vapour line using Monte Carlo methods 79−37826
lens design code, CLIMB, using Monte Carlo sampling 77−3642
lidar, multiple scatt. from turbid atm., Monte Carlo anal. 77−25779
Lifshitz points, crit. behaviour near, Monte Carlo calc. 79−24170
light, polarized, radiative transfer eqns., adjoint Monte Carlo treatment 78−37799
light propogation in turbulent medium, space struct. of strong intensity fluctuations 79−98278
lightly doped semiconductors, impurity band struct. 79−69461
lightning return strokes, EM radiation simulation, tortuosity effects 79−8672
LIMITS−a fast Monte Carlo code for system reliability 79−49783
linear chain, two-sublattice, hopping particle occupancy correlation function normal modes 80−49402
linear chain of oscillators, disordered, physical props., Monte Carlo approach 77−4177
linear radiation-flux functionals, estimation of local perturbations using Monte Carlo method 80−5457
liquid, associated, radial correlations, comparison of Monte Carlo and Ewald mol. dynamics calc. methods 80−14984
liquid ionic salt, Monte Carlo simulation using multipole series *(Russian)* 77−62339
liquid metals core polarisation and struct., model potentials and simulation methods 79−77492
liquid mixtures, phase separation, umbrella sampling, Monte Carlo calcs. 77−35698
liquid phase sintered systems, particle coalescence probability estimation 80−104086
liquid-vapour co-existence, dipolar hard sphere fluid, Monte Carlo method 79−99293
liquid-vapour interface, fluid phase coexistence, Monte Carlo computer simulation 80−49349
liquid-vapour interface, pair correl. function at triple pt., Monte Carlo method 80−10753
liquid-vapour interface, struct. at 110K 80−54477
liquid-vapour interface structure near hard wall 80−14983
liquids, diatomic, hard and soft core, free energy difference, Monte Carlo calcs. 80−92436
liquids, long-range dipolar interactions in computer simulations of polar liquids, Monte Carlo method 78−87603
LMFBR, bubble collapse reactivity increases in boiling fuel/steel pools 79−31025
LMFBR, intermediate Na activation 78−4997
LMFBR fuel subassembly temp. noise prediction 79−13392
LMFBR spent fuel shipping cask designs, subcriticality guidelines, Monte Carlo calcs. 78−82470
long chain paraffins, thermodynamic functions, Monte Carlo method appl. *(German)* 80−19962
low statistics expts. anal. 79−18095
low-temperature plasma production by electron beam ionisation of gas mixture 80−87908
luminescence band, deform. and shift, impurity centres, migration of excitations, math. modelling 78−48225
LWR fuel assembly, lattice calculation by double sampling Monte Carlo approach 80−606
LWR lattices, Monte Carlo radiation transport program for reactor bundle gamma transport and energy deposition analysis 80−22915
LWR safety, Monte Carlo calc. of gamma ray heating 77−50272
Lyapunov characteristic numbers and Kolmogorov entropy of a four-dimensional mapping 80−46978
macromolecular chains confined to strips or tubes, configs. 77−61883
macromolecular dimensions, mean square end-to-end distance, Monte Carlo calcs. 79−68337
magnetic alloys, binary, spinodal decomp., computer simulation study of interface behaviour 80−84913
magnetic disordered systems, Monte Carlo anal., review, book contrib. 79−82809
magnetic fluids, particle cluster configuration, Monte Carlo study 80−88827
magnetic model systems, computer simulations 80−65924
magnetic system, Lifshitz point, phase diagrams and crit. behaviour 80−65928
magnetic systems and mixtures, phase diagrams, Monte Carlo studies, book contrib., review 79−82313
magnetic transitions, in systems with competing interactions 78−14963
magnetoresistance, in semiconductors and plasmas, density or conc. nonuniformity calcs. 78−47099
magnetotelluric study, S.Scotland, Monte-Carlo data inversion 79−29706
Maier-Saupe model on square and triangle lattices, phase transitions 78−32771
mammography, absorbed dose evaluation, Monte Carlo simulation studies 80−98143
many-fermion system, Monte Carlo simulation 78−12644
Monte Carlo methods continued
marine reactor systems, Monte Carlo reliability anal. of power and heat removal systems *(Japanese)* 78−58396
master eqn. description of finite fluctuations 77−87693
material minimum lifetimes, failure probability after proof testing, exam using Monte Carlo method 78−79273
Mattis model, modified, mag. relax. 80−65947
measurement errors, random, simulation (Monte Carlo) method, teaching appl. 78−86062
Mehta-Dyson statistics, appl. to sequences of neutron resonances 77−30543
melting, Lennard-Jones two-dimensional systems, Monte Carlo study 80−49338
melting and freezing, computer simulation of simple systems using array processor 80−54353
melting curve maximum phenomenon, computer simulation using two species soft core model 78−6146
metal, He ion implanted, statistical model of low temp. blister formation 78−67754
metal, secondary electron emission, Monte Carlo calc. 79−69932
metal cylindrical wire, elec. resist., scatt. processes, Monte Carlo calc. 80−75560
metal surface, near point-defect, annealing, diffusion theory and Monte Carlo anal. 78−47646
metallic glass, packing models and structural specificity 79−37629
metamagnet, two-dimens., tricritical spinodal decomp., Monte Carlo study 80−93117
metastable peak shapes in mass spectra 78−70968
methane, aq. soln., Monte Carlo simulation of isothermal-isobaric ensemble 78−30531
methane, conversion in H_2 plasma flow, Monte Carlo study 78−61010
methane, dil. aqueous soln., Monte Carlo calcs. on struct. 79−32874
methane, heavy cryst., Debye-Waller factor temp. depend. 78−47492
methane, pot. energy curves, Monte Carlo and SCF LCAO MO calcs. 80−63526
methane-d_0($-d_4$), unimol. decomp., energy transfer processes, Monte Carlo simulation 80−99555
microbeam analysis developments, application of Monte Carlo calc. method *(Japanese)* 78−3431
microclusters, computer simulation of nucleation and thermodynamics, mol. dynamics and Monte Carlo 78−51656
microdosimetric distributions for small sites 78−3617
MIM system, electron emission modelling *(Czech)* 80−2479
minimizing splitting costs in Monte Carlo particle transport 80−47532
minority carrier diffusion length determ. near p-n junction, SEM appl. *(French)* 78−43466
missing values in time series, effect on autocorrelation analysis 79−17197
mixed crystal, coexistence of different spin structures, computer simulation 77−8276
mixed problems in theory of harmonic functions, Monte Carlo method appl. 79−10464
model nuclear matter, hypernetted chain integral eqns. 79−490
modification, radiative flux local characteristics calculation *(Russian)* 79−35648
modification for radiation field calc. behind thick shields 79−93760
molecular collisions, differential scatt. cross sections from classical trajectories, Legendre moment method 78−3314
molecular crystals, thermal motion computer simulation 79−46577
molecular dynamics simulation, sp. ht., thermal press. coeffs., compressibilities 77−28013
molecular flow in vacuum valve, conductance 78−71398
molecular flow through cylindrical channel, Monte Carlo calc. 77−55042
molecular fluid, hard-core triatomic, Monte Carlo simulations 80−38880
molecular orientational dynamics in dense media *(French)* 77−62491
molecular systems, electron density, spatial, rel. to conform. props., computer simulation 78−70763
molten salts, enthalpy of mixing, theory, Monte Carlo calcs. 77−72691
monatomic gas, rarefied flows in axisymmetric expansion nozzle 80−92182
monatomic gas, rarefied flows in two-dimens. expansion nozzle 80−28547
Monte Carlo estimation of free energy differences between canonical ensembles 77−2632
Monte Carlo shielding calcs., biased selection of particle flight directions as variance resolution technique 78−29653
MOSFET, electron and hole drift velocities in high elec. field, Monte Carlo calc. 78−60224
multi-parameter Monte Carlo computations, adaptive estimation procedures 80−105572
multichain polymer system, simulating dynamic and equilib. props. 80−53179
multidimensional integrals in many-body theory 77−57164
multidimensional integration, algorithm, iterative and adaptive Monte Carlo scheme 78−57762
multidimensional neutron transport computation 77−82980
multigroup Monte Carlo computer codes, bounded flux-at-a-point estimators 79−40499
multigroup photon cross section technique 78−4570
multiparticle prod. charge distribs. and fluctuations, Monte Carlo quark-parton model 79−93363
multiparticle prod. in quark-parton model, Monte Carlo method 78−41607
multiple graybody resolution from spectrally sampled optical systems 79−76615
multisite adsorption, mean field theory and Monte Carlo simulation 79−60630
multitarget association problem, image reconstruction approach 79−72522
multiwire proportional quantameters, performance predictions 79−3294
n-particle relativistic phase space integral, invariant variables, Monte Carlo calc. algorithm 79−9312
natural gamma-ray dose rate distribs., effect of male-female body-size diff. 78−24139
NE213 liquid cylindrical neutron spectrom., anisotropy of response 80−5434
NE 213 scintillator, neutron response functions, energy range to 40 MeV *(Japanese)* 80−18756
nematic liquid cryst., two-dimensional, Monte Carlo simulation 80−100168
nematic-isotropic phase transition, Monte Carlo calculation 77−43316

Monte Carlo methods continued
nematics, uniaxial and biaxial, formed by non-cylindrically symm. mols., computer simulation 80−79680
neutral beam injector, simulation of neutral particle transport 80−37600
neutral gas transport in infinite cylindrical plasma, Tokamak model, Monte Carlo algorithm 78−79459
neutrino energy equilibration models in supernova core collapse, Monte Carlo simulations 80−105265
neutrino transport, direct simulation and aspects of equilibration 78−89050
neutron activation anal., self attenuation of neutrons and gammas, Monte Carlo determ. 79−1980
neutron activation analysis for coal ash content measurement in moving wagons 80−3431
neutron capture probabilities for thick samples at resonance energies 78−46123
neutron coincidence counting, removal of multiplication effects 80−37715
neutron detection, efficiency meas. using Monte Carlo simulator program 78−17045
neutron detector efficiency calc. using Monte Carlo computer program 79−63874
neutron diffraction, multiple scatt. correction, Monte Carlo simulation 78−9913
neutron diffraction, pulsed source expts., optimized Monte Carlo simulation 78−9914
neutron dose distributions in pion$^-$ irradiated tissue, Monte Carlo calc. 79−16310
neutron elastic angular data, equal probability steps 78−668
neutron fictitious scatt. radiation transport model for deep penetration calcs. 78−29526
neutron field charact. calc., beyond Fe barrier, effect of scatt. indicatrix approx. and consts. representation 78−17272
neutron flux perturbation due to a 5 cm×5 cm NE213 scintillation spectrometer in a LiF assembly 79−85855
neutron guide tubes, effect of sharp bend on transmission 77−385
neutron leakage in presence of voids 77−38324
neutron multiplication effects on variable dead time counter response 79−22570
neutron physics code VIM, cross section preparation 77−23166
neutron polarisation expts., multiple scatt. effects 78−13052
neutron polarisation meas. with high press. He scintillation counter 80−14061
neutron reactions in pellet centre burnup of fission reactor waste 79−31181
neutron reflection, plane-parallel concrete interfaces, Monte Carlo calc. 80−27686
neutron reflection and transmission for homogeneous slabs, dosimetric quantities and spectra 77−38319
neutron resonance escape probability, Monte Carlo importance sampling technique 77−61471
neutron response functions of organic scintillators 80−14047
neutron scatt. and gamma-ray prod. on N 77−26682
neutron slowing-down problem, comparison of VIM and MC^2-2 codes 77−23167
neutron source, 14 MeV, skyshine anal., Monte-Carlo computer code 78−66429
neutron streaming through ducts in shields, Albedo-Monte-Carlo method usefulness 79−89345
neutron TOF spectrom., scatt. simulation 77−34509
neutron track length estimators, comparison 78−82413
neutron tracking technique for slab cells 79−85580
neutron transport, contribution Monte Carlo, exponential biasing model 80−5195
neutron transport, contribution Monte Carlo technique, variational derivation 80−5194
neutron transport, error prediction from track length estimator theory 78−29527
neutron transport, fluctuating cross sections in Monte Carlo calcs. 77−65265
neutron transport, multigroup, Monte Carlo game, moments method 80−52720
neutron transport, probability table method extension 79−584
neutron transport, state-space splitting in Monte Carlo calcs. 77−65264
neutron transport calculations, error prediction 79−59109
neutron transport equation soln., influence of group averaging of consts. *(Russian)* 77−65242
neutron transport in upper atmosphere, Monte Carlo calcs. 80−8468
nonuniform neutron transport problems, estimation of perturbations in solving 78−17271
neutron transport simulation for design studies and integral expt. anal. 77−26828
neutron transport theory, contributions, volumetric distrib. Monte Carlo calc. 79−36295
neutron transport theory, Monte Carlo method applicability *(Spanish)* 79−6721
neutron transport theory, reduction of computational time for point detector estimator 80−68724
neutronic analysis of the NBS intermediate-energy standard neutron field (ISNF) 80−27692
neutrons elastic and nonelastic scatt. on nuclei of rock-forming elements in borehole-layer system 78−61582
NMR spin-lattice relax., effect of correlated atomic diffusion 80−107495
noise calc., in III-V semiconductors 80−75575
nonanalogue Monte Carlo games, conditions concerning nonanalogue transition kernels and estimators 78−62594
nongrey, nondiffuse surfaces, 3-dimens. radiative exchange factors, Monte Carlo method 80−10128
nonideal plasma, electron degeneracy, Monte Carlo calcs. 77−35316
nonlinear kinetic eqns. soln. *(Russian)* 77−5735
nonlinear radiation transport, soln. by renormalisation group method 80−67555
nonuniform one dimensional classical fluids, Lennard-Jones pot. interactions, Percus Yevick approx. and density functional calcs. 80−64864
nosetip recession meas. using implanted radioactive sources, error analysis 78−16272
novel Monte Carlo binning technique 79−160
nuclear backward π^+ prod., momentum depend., scaling, Monte Carlo calcs. 79−13305

Monte Carlo methods continued
nuclear criticality safety, misleading assumption in array analysis 79−63772
nuclear criticality safety, uncertainties in K-effective calcs. 79−63771
nuclear cross-section probability tables generation in unresolved resonance energy range 79−80986
nuclear fuel reprocessing facilities continuous criticality control, dynamic approach 78−50291
nuclear interactions around 20 TeV, charact., comparison with Monte Carlo simulation 79−58991
nuclear materials safeguarding, isotopic inventory prediction employing a Monte Carlo Dancoff factor 80−73924
nuclear materials safeguards, Monte Carlo simulation of MUF distrib. 80−83170
nuclear matter theory, technical aspects, review of theoretical techniques, nuclear interaction investigation 78−62497
nuclear measurements, errors of parameters in least squares fitting procedure 78−16768
nuclear power plant components, probabilistic design, Monte Carlo simulation approach 78−94056
nuclear reaction rate Monte Carlo estimators, unified definition 78−58334
nuclear reactions, ^{40}Ca(^{40}Ca,x), relativistic, compression and pion distrib., Monte Carlo calc. 80−73853
nuclear reactor, energy contribs. of absorbed fast neutrons calc. *(Russian)* 77−42049
nuclear reactor, fuel rod arrays, radiative heat transfer, Monte Carlo method 78−78447
nuclear reactor, Monte Carlo heat conduction solution using transport theory approx. 77−65260
nuclear reactor criticality calc. appl., algorithm *(Czech)* 77−50209
nuclear reactor criticality calc. by Monte Carlo methods *(Czech)* 77−50259
nuclear reactor heat conduction problems with internal sources, Monte Carlo soln 77−65259
nucleation and crystal growth, two-dimensional, simulation using kinetic Ising model 80−54156
nucleic acids, bases and base pairs, water struct. in soln., Monte Carlo simultion 80−76709
ocean atmosphere system, sea foam effect on albedo 77−81899
ocean colour, Monte Carlo model including atm. and ocean scatt., absorpt. 78−61421
off-lattice polymer chains 78−5382
one-component system interface with directed intermol. forces, Monte Carlo calcs. *(Russian)* 77−61031
one-dimensional amorphous solid, short-range order effect on spectral density of excitations 77−76514
orbit evolution simulations for comets becoming asteroids 80−82261
ordered magnetic cpds., selective sublattice dilution, percolation problem 80−103850
organic scintillator efficiency using Monte Carlo code 80−889
oriented bond percolation, threshold probability and correlation length exponent calc. 80−68146
outgassing from surface, Monte Carlo method in one-dimens. 78−47001
pair correlation function of the liquid-vapour interface 79−55633
parallel optical fibre channels, pulse skew model 77−68279
particle absorption rates at high cell concs., Monte Carlo simulation 80−94141
particle generation, Monte Carlo model of proton high energy collisions *(Hungarian)* 80−13336
particle passage through thin layers, Monte Carlo calc. 80−100708
particle range in matter, T-expansion soln. of transport eqn. 79−54752
particle track record of lunar regolith history 77−33369
particle tracks, search statistics, Monte Carlo study of random scatt. problem 78−58561
particle transport calcs., error anal. 79−80548
particulate material, spectral reflectance, Monte Carlo model with asperity scatt. 78−37804
PBF reload core cell calc., failure of Wigner Seitz approx. 78−25264
PEP storage ring vac. system, synchrotron-radiation-induced heating effects, Monte Carlo based computer code 79−81107
percolation, cluster size distrib. 79−75465
percolation clusters, as teaching aid for Monte Carlo simulation and crit. exponents 78−12477
percolation clusters, spanning lengths, Monte Carlo calcs. 79−2730
percolation clusters and lattice animals, similarity laws for density profile, Monte Carlo data anal. 79−44881
percolation clusters density profiles, lattice animals 79−93075
percolation conductivity in anisotropic systems, infinite cluster struct. 79−93063
percolation lattice, diffusion, random walk method, Monte Carlo method 78−60098
percolation phenomena, simple cubic lattice, Monte Carlo study, cluster shapes and sizes 77−17919
percolation with nearest neighbour interaction 78−73934
perturbation computation with correlated sampling, nuclear reactor neutron transport 79−588
phase connectivity in two-phase microstruct., Monte Carlo calc. of topological and percolation props. 78−30765
phase separation kinetics, percolation effects 80−65233
phase space integral, n-particle, relativistic, Monte Carlo integration program 78−33001
phase transitions, percolation clusters and lattice animals 79−6057
photoinduced radical pair recombination in high mag. field, Monte Carlo method 79−87861
photon, electron and positron prod. from primary proton beams 80−32555
photon beam dose calcs., power law tissue-air ratio algorithm for inhomogeneity corrects., verification 80−56222
photon collimation problems 78−70724
photon penetration, photon backscatt. incidence angle depend. 80−104008
photon scattering angles selection in MORSE, rejection technique 78−4571
photon source in lungs of phantom, external detector response calcs. 80−8132
photon transport, adjoint, energy sampling method 77−22503
photoproduction of lepton pairs in thick target, Monte Carlo simulation 78−21432
photosensitised reacts. in continuous chem. processes, scatt. effects 78−73057

Monte Carlo methods continued
physics experiment design 79−89577
planar model, F-model and related systems, Monte Carlo test 79−9192
plane rotator model, Monte Carlo simulation 80−73295
plane rotator model, two dimens., mag. equilib. props. 78−47990
plane rotor model, static and dynamic crit. behaviour, Monte Carlo simulation 79−38334
planetary doublet craters expected frequency 78−61777
plasma, classical one-component, improved equation of state 80−83887
plasma, classical two dimensional one-component, Monte Carlo simulation, solid-liquid phase study 79−94814
plasma, laser-target interaction, Monte Carlo (hybrid) suprathermal electron transport 80−24200
plasma, Monte Carlo Lorentz collision operator 77−76028
plasma, neutral beam injection heating, computer simulation, Monte Carlo method 77−68859
plasma, neutral injection kinetics, Monte Carlo anal., local liberation to wall 77−42992
plasma, $O^+ + H$ charge exchange, Monte Carlo simulation 78−34260
plasma, one-component asymptotic fluid eqn. of state, Monte Carlo calcs. 77−24527
plasma confinement in mirror and cusp fields, Monte Carlo simulation 80−96379
plasma confinement time investigation using Monte Carlo simulation, for mag. mirror 80−64770
plasma containment vessels, backscatt. and sputtering from pocket and finned structs. 79−14558
plasma microfield 77−68743
plastic flash chambers, particle identification 79−59301
PMMA electron resists, molecular weight depend. of developed contours 79−87859
PMMA film, Monte Carlo simulation of electron penetration 79−23659
point defect trapping, reaction consts. sink conc. depend., random walk theory model 79−65072
point defects short term annealing, in α-Fe, computer simulation 80−54282
point neutron flux, Monte Carlo schemes evaluated 79−586
polar lattices, free energy, dielectric constant 77−4594
polar liqs. permittivity, computer simulation with hard sphere point dipole pot. 80−103911
polar liquid surface tension calcs. 77−31841
polyatomic gases, transport props., Monte Carlo method 77−89223
polycondensation copolymers, block length distribs. 79−31752
polydisperse system, turbulent coagulation in force field 79−57297
polyethylene, conformation, Monte Carlo simulation 77−10797
polyethylene, neutron penetration, Monte Carlo calculations for 30, 45 MeV *(Japanese)* 80−18677
polyethylene terephthalate, conform. statistics *(Russian)* 78−70993
polymer, amorphous, conform. from simulation of filling diamond lattice with chains *(German)* 78−75595
polymer, amorphous, segmental distrib., light-, neutron- and X-ray scatt., piezooptical and dielec. meas., review 78−51444
polymer, freely jointed chain, with excluded vol. interaction, Monte Carlo studies 80−10475
polymer and fibre systems, entanglement density, statistical theory 78−5381
polymer between planes, crossover between dimensionalities, Monte-Carlo study 80−74272
polymer chain in restricted environment, Monte Carlo simulation 77−46663
polymer chain statics and dynamics, Lennard-Jones interaction, calcs. 80−58425
polymer chains, intramolecular cross-linking reactions, Monte Carlo calcs. *(Russian)* 78−31636
polymer chains, scaling props., excluded-volume expansion 80−96435
polymer chains in cubic lattice solvent, thermodynamic props., Monte Carlo method, computer simulation *(Russian)* 77−31787
polymer fluid, static bulk props., reptation Monte Carlo method, LJ pot. 80−64868
polymer foil, electron irradiated, charge dynamics, computer simulation 79−82915
polymer lattice dynamics, relax. time Monte Carlo anal. 78−5380
polymer melts, defect fluctuations, reptation, Monte Carlo investig., NMR autocorrel. function 77−3499
polymer molecule, in soln., end-to-end distance relax., Monte Carlo simulation, model depend. 78−22061
polymer network formation, struct. and mech. props., computer simulation 80−38965
polymer off-lattice chains, Monte Carlo anal. of excluded vol. problem 80−5647
polymer solution, concentrated, computer-aided simulation of individual chain conforms. *(Russian)* 77−42454
polymer solution, simulation of macromol. dynamics, Monte-Carlo method, conc. depend. *(Polish)* 78−51404
polymer solutions, coil dimensions, Monte Carlo calc., computer simulation *(Polish)* 79−3606
polymerisation, radiation-induced, solid state, computer modelling 79−66294
polymers, adsorbed, excluded vol. effects, Monte Carlo investigation 79−95259
polymers, adsorbed molecules, configurational behaviour, computerised dynamic display 79−874
polymers, adsorption transition, excluded vol. effects, Monte Carlo and enumeration calcs. 78−67906
polymers, branched, mean end to end distance 79−86097
polymers, Monte Carlo renormalisation group 80−42148
polymers, simulation by self-avoiding nonintersecting random chains, conc. effect 78−12639
polymers attached to inert interface, conformations 79−94120
polymethylene, intramol. scatt. function calc. 77−38761
polymethylene, short chain mean reciprocal distances, Monte Carlo calc. 77−14626
polymethylene coils in solution, dimension and shape, computer simulation *(Russian)* 80−54111
polypeptides, short chain conformations, long-range interactions, Monte Carlo calcs. 77−58217
polystyrene, epimerised isotactic, methylene C mag. resonance spectra 80−63878
polystyrene, gamma photon backscattering, energy dependence *(Rumanian)* 79−76316
polytypes, Monte Carlo simulation 78−6024

Monte Carlo methods continued
porous media, water circulation, models *(Rumanian)* 80−69917
porous solids, diffusion of gases, Monte Carlo simulation 80−65299
porphyrin in n-octane Shpolskii matrix, defect props., Monte Carlo obs. 80−63533
positron annihilation in matter, Monte Carlo calcs. 77−88558
positron energy spectra and ang. distrib., 0.2-2 GeV electron conversion on W targets 78−86713
positron in condensing He, Monte Carlo lifetime spectra, temp. and elec. field effects 78−55263
positron scattering by atoms, computer simulations, review 77−79692
positronium relativistic beam intensity determ. from high energy accelerators *(Russian)* 77−388
Potts model, first order phase transitions, Monte Carlo renormalisation group method 80−34645
Potts model, first-order phase transform., three-state model, Monte Carlo renormalisation group method 79−99709
Potts model, Monte Carlo simulation in three dimens. 80−163
Potts model, three-state, first order phase transitions 80−60333
Potts model, three-state, phase transition continuity 80−22302
Potts models, q-state, two-dimens., Monte Carlo renormalisation-group studies 80−77727
powder specimens, oxidised and unoxidised layers, X-ray irradiated electron emission intensities, Monte Carlo calc. *(Russian)* 78−6825
press. by Monte Carlo computer simulation 78−4564
primary cosmic-radiation spectrum from 10^{12} eV to 10^{15} eV from atmospheric Cerenkov-radiation measurements 79−66895
primitive model electrolytes, grand canonical Monte Carlo calculations 80−92427
primitive model electrolytes, symmetrical, canonical Monte Carlo calcs. 80−92428
protein folding, incorporation of 1-dimens. Ising model into 3-dimens. model 77−90723
proton flux precipitating in equatorial ionosphere, estimation of energy release 78−32268
pseudo-random number generators, statistical test 78−86125
PWR, release of radioactive material, ability to meet appendix I to 10CFR50 77−46306
PWR cavity shield design, radiation streaming, calc., appl. of Monte Carlo and discrete-coordinates technique 79−89364
PWR core, thermal analysis, Monte Carlo method 80−47603
PWR pressure components reliability and residual life evaluation and precipitation 79−20191
PWR reliability prediction in design, empirical and Monte Carlo techniques 78−54827
quantised SU(2) gauge theory, Monte Carlo study 80−77973
quantum chemistry, optimum scaling in a Monte Carlo method 79−6832
quantum fluids and crystals, Monte Carlo methods and results, book contrib. 79−82405
quantum liquids and crystals, computer modelling 80−54472
quantum many-body problems, nuclear physics 80−22727
quantum mechanical corrections to classical equilibrium statistical-mechanical results 80−135
quantum statistical Monte Carlo method, Green's function path integrals with hard boundaries 79−67223
quark confinement and lattice calculation 79−13023
quark fragmentation functions in Monte Carlo quark parton model of e^+e^- annihilation 79−80791
quasars, Comptonised spectrum, Monte Carlo simulation 80−90566
quasiclassical stochastic models, analytic extensions of Monte Carlo calcs. 79−13277
radiation detector efficiency calc. for extended flat sources 80−9469
radiation dose from syringes, computer code for calc. 80−41246
radiation shielding calculations, deep penetration problem, event-value path length biasing 77−38421
radiation therapy, computer program for negative pion beam calcs. 80−46061
radiation transport, ang. biasing of collision process in multigroup calcs. 78−4975
radiation transport, solid-angle subtended at point by cylinder, eval. method 79−59110
radiation transport calc., Monte Carlo approach for engineers 79−585
radiation transport theory, tracklength biasing in Monte Carlo methods 80−5335
radiative heat transfer between isothermal parallel plates, flow models, numerical analysis 80−14547
radiative transfer, emission freqs. simulation from angle-dependent partial freq. redistribs. 78−32333
radiative transfer, freq. redistrib. in externally excited medium 78−20628
radiative transfer, inverse soln. by F_N and Monte Carlo methods 80−109352
radiative transfer, Monte Carlo method appl. to non-LTE problems 79−44357
radiative transfer, resonance scattering with absorpt. or differential expansion, Monte Carlo calcs. 80−21901
radiative-convective heat transfer from extended surface, Monte Carlo method 78−67005
radioactive materials, risk anal. of transport using Monte Carlo and probability methods *(Norwegian)* 79−13437
radiography, photon path visualisation by Monte Carlo simulation 77−66848
radiometer, absolute, with uniform response, fabrication, characts. and anal. 80−268
radiotherapy treatment planning, inhomogeneity correction methods compared with Monte Carlo data 80−61698
Ramsauer chamber, positron scatt., optimisation study using Monte Carlo method 78−70706
random anisotropy model in Ising model, Monte Carlo simulation 80−80546
random coil polymer chains, asphericity relax., Monte Carlo calcs. 77−75354
random flight theory, appl. to DNA length measurement 78−35799
random lattices, bond percolation and cluster form. 77−45798
random number generation using minicomputers 79−81122
random sampling of scattering angle in neutron transport 79−85574
random scanning problem with visibility distrib. 79−49915
random walks with residence time dependent transition probability rates, Monte Carlo simulation 79−2722
random walks without self-intersection, distrib. function 78−8350

Monte Carlo methods continued
range distributions of energetic protons in Si, Monte Carlo computer simulation 78−22777
rare earth amorphous alloys, random mag. anisotropy, antiferromag., Monte Carlo calcs. 79−33471
rare earth-Fe alloy, amorphous, random anisotropy model, generalised mol. field calcs. 77−28345
rare-earth alloys, amorphous study of hysteresis effects using Monte Carlo technique 79−1686
rarefied flat plate flow, direct simulation and expt. 79−94667
rarefied gas flow, intermolecular interaction, Boltzmann eqn., Monte Carlo simulation *(German)* 78−34165
rarefied gas flow with chemical reaction, Monte Carlo simulation of homogeneous dissociating diatomic gas 77−51128
rarefied hypersonic flow past flat-plate, numerical simulation 77−19626
rarefied transition flow, past bluff faced cylinder, Monte Carlo calcs. 79−94670
RCP01 Monte Carlo program, neutron capture and photon heating rates 79−71912
reaction rate constants, quasi-classical trajectory calcs. 79−74366
reactive scattering, trajectory calcs., Monte Carlo sampling method for initial values 78−41147
reactivity calcs., Monte Carlo perturbation source method 78−37398
reactor cavity radiation streaming, albedo Monte Carlo methods 79−89363
reactor containment leakage from Na fire anal., response surface method, SPOOL-FIRE code 79−18004
reactor criticality problems soln., MONK code description 77−14226
reactor radiation streaming anal. using spherical harmonics expansion of albedo data 79−89367
reactor reactivity calcs., correlated sampling Monte Carlo methods 79−22368
reactor shielding materials, Pb and steel, γ leakage spectra, Monte-Carlo calc. 78−58350
REBEL-3, code for dose calcs., phantom standing in dwelling room 80−94377
recursive, optimal strategies for appl. 80−13014
recursive method appl. to neutron geometrical imaging and surface sources 79−85578
recursive Monte Carlo technique for generating importance functions 79−59272
reflection nebulae, multiple scatt., Monte Carlo approach 78−12320
Reggeon field theory on a lattice, critical behaviour, Monte Carlo calc. 80−18126
relativistic charged particle identification by ionisation energy loss with delta ray suppression 79−85863
relativistic electron beam relaxation in dense gas, radiative energy transfer 80−69968
relaxation phenomena, Monte Carlo studies, review, book contrib. 79−80531
reliability calc., importance sampling and Monte Carlo advantages 79−606
renormalisation group analysis, Ising model and three state Potts model calcs. 79−44880
resonance integral calc. in reactor cell lattice, Monte Carlo code, RISO 77−3088
response functions of spherically moderated neutron detectors 80−37687
review of techniques and methods *(Spanish)* 78−86126
ring point detector, Monte Carlo flux-at-a-point estimates for axisymmetric problems 79−59282
roughening transition, crit. slowing down of solid on solid cryst. surface model 77−5773
Rutherford 180° backscatt. anomaly in solid, Monte Carlo simulation 80−45189
Rydberg atom+Rydberg atom, ionisation cross sections 79−81267
Rydberg atom+Rydberg atom, ionisation cross-section calcs. 79−31664
scanning Auger electron microscope, Monte Carlo calc. of spatial resolution 78−41383
scanning Auger electron microscope, spatial resolution, Monte Carlo calcs., Ag edge on W profiles 79−85204
scanning Auger electron microscopy, Monte Carlo calc. 78−19610
schlieren instrument, amplitude transfer charact., Monte Carlo method 80−28336
Schrodinger equation for molecular systems, comparison of Grimm Storer and Anderson techniques 78−46255
scintillation counter, energy resolution optimisation at high energies 80−37697
scintillation counter NE213, organic liquid, Monte Carlo calcs. of electron energy loss spectrum for incident gamma-rays 77−6613
secondary electron emission from various targets 79−28868
sedimentology, ellipsoidal grain thin sections, Monte Carlo simulation 77−5332
segmented calorimeter, high energy performance, Monte Carlo simulation 80−58029
self-absorption effects in X-ray fluoresc. anal., Monte Carlo simulation 77−60165
self-avoiding random walk, external spatial constraints, 'slithering snake' calcs. 77−89
self-avoiding random walks, eigenvalues Monte Carlo determ. 78−57849
self-avoiding random walks, exact enumeration method and Monte Carlo sampling 79−67228
self-avoiding random walks, excluded vol. effect 79−44845
self-avoiding walk, asymptotic behaviour in continuous space 77−13700
self-avoiding walks of macromolecules confined to strips and capillaries 78−94345
self-diffusion, correlated, via randomly migrating vacancies, in cubic crysts., computer simulation 78−2283
self-powered gamma-ray detector with directional discrimination 79−30895
self-replicating macromolecules, Monte Carlo computer models 78−46473
self-replicating macromolecules, temporal evolution, Monte Carlo calcs. 77−83773
SEM, electron channelling patterns 78−83697
SEM, signal treatment, backscattered electron spectral distrib. *(French)* 80−42305
semiconducting photocathodes, carrier transport simulation, Monte Carlo method 80−71575
semiconductor, cubic, bulk hot-electron props., soln. of Boltzmann eqn. 79−99553
Monte Carlo methods continued
semiconductor, electron distrib. function in alternating fields, single particle Monte Carlo method 77−89791
semiconductor, electron-donor recombination, Monte Carlo studies of transitions between excited donor states 79−38093
semiconductor, electron-runaway and quasi-stationary states in electric field 77−4359
semiconductor, hot electron energy tails, Monte-Carlo calcs. 77−62931
semiconductor, lightly doped, compensated, percolation level, Monte Carlo calc. 80−59923
semiconductor, lightly doped compensated, electric fields at impurity centres *(Russian)* 80−84198
semiconductor, nonparabolic, Monte Carlo transport calcs., acoustic scatt. inelasticity effects 77−51754
semiconductor detector active volume, determ. from gamma ray interactions, Monte Carlo method 80−63448
semiconductor laser, electron beam pumping efficiency, coating effect 80−91795
serine, neutral and zwitterion, water solvation, Monte Carlo simulation 80−76707
shadow device, charact., scattering medium effects, Monte Carlo calcs. 80−99630
shielding of structures against initial nuclear radiation: Monte Carlo methodology 80−47741
shock wave reflection, regular to Mach transition, Monte Carlo simulation 77−75936
signal detection analysis, in nuclear medicine examination of image quality 77−86626
silicate and alumino silicate melt, Monte Carlo calc. of ionic struct. 79−60256
silicate melt, Monte Carlo calc. of ionic struct. 79−60256
silicates and aluminosilicates, thermodynamic props. determ. by Monte Carlo calc. 77−47597
SIMON, FORTRAN Monte Carlo program for time-of-flight neutron diffractometer simulation 79−50955
simple cubic lattice, drift mobility correlation of interacting ions 79−37868
simple cubic lattice, orientational ordering of quadrupoles 80−44157
simple fluid, struct. and thermodynamics, Monte Carlo calcs. 80−59365
simple liqs. with repulsive forces, thermodynamically selfconsistent theory 80−75139
simulation of Ising chain showing several phase transitions 79−12732
simulation of photon transport in a heterogeneous phantom 80−26257
simulation of quantum spin systems, two dimens. X-Y model 78−27011
simulation of system with charge-charge interaction, boundary condition 78−62144
Singer polymal tempering methods 80−52845
site-bond problems in percolation and cluster distributions, Monte Carlo calcs. 80−42160
sky intensity and polarisation at right angles to solar direction, Monte Carlo simulation 78−81401
small systems, Monte Carlo simulation, book contrib. 79−80530
SNR-300, coolant outlet duct design from neutron transport experiments *(German)* 78−29566
soil infiltration, spatial var. of hydrological effects, Monte Carlo anal. 80−8363
solar irradiance three-dimens. transfer in clouds, finite geometry effect 79−58085
solar radiation transfer under cumulus cloud conditions application *(Russian)* 80−21793
solar radiation transmission through atmosphere, Monte Carlo simulation *(Russian)* 79−12265
solar thermal power plants, dispersed, performance and economic risk evaluation 79−52902
SOLASE laser fusion reactor, Monte Carlo shielding calc. for mirror-laser beam duct system 80−23174
solid, classical octopolar, temp. effect on struct., Monte Carlo calc. 78−75598
solid, Monte Carlo simulation of energy distrib. of transmitted or backscatt. keV electrons 78−43057
solid angle integrals for rad. detectors, Monte Carlo solns. 80−9468
solid layers, conversion electron scatt. processes anal. 80−45181
solid-on-solid representation, planar model Monte Carlo simulation 80−96727
solid-state diffusion in elec. field, Monte Carlo demonstration 80−27072
solids, X-ray prod. range by 2 to 15 keV electrons, thin film and bulk targets 79−19298
Soller collimators, appl. to small angle neutron scatt., Monte-Carlo simulation 78−29701
solution, aq., hydrophobic apolar spheres interaction, Monte Carlo simulation 80−6335
solution, aq., hydrophobic hydration around apolar species pair, Monte Carlo simulation 80−6336
solutions, dilute, Monte Carlo free energy calcs. in isothermal-isobaric ensemble 78−92498
source biasing optimisation technique using Monte Carlo calc. 79−26005
spectral transport, time-dependent, Monte Carlo study 79−33826
spent fuel waste products, delayed neutron nondestructive assay instrumentation, Monte Carlo calculational design 80−81271
spin glass, classical, Heisenberg, Monte Carlo calc. of internal energy and sp. ht. 77−20612
spin glass, computer simulation 77−66370
spin glass, dipolar, anomalous sp. ht. Ising model and Monte Carlo calcs. 78−47989
spin glass, five-dimensional, Edwards-Anderson ordering possibility 80−60295
spin glass, Ising, two-dimensional, Monte Carlo evidence for absence of phase transition 78−19260
spin glass, remanent magnetisation using Monte Carlo methods 79−78421
spin glass behaviour in conc. binary mag. systems 78−2694
spin glasses, mag. props. of Sherrington-Kirkpatrick model 80−88774
spin glasses, recent progress in numerical simulation 79−69689
spin glasses, susceptibility, time dependent, rel. to spin self-correlation, Monte Carlo model simulations 79−47290
spin glasses, theory, review 78−2696
spin glasses, time translation, spatial scaling and nonexponential relaxation 80−97110
spin system, cubic model, Monte Carlo simulation, phase transitions 80−34646
spin systems, model, Monte Carlo simulation appl. 80−20421

Monte Carlo methods continued
spinels, percolative phenomena in cationic B-sublattice 80−17893
SPODE radiation transport code, comparison of electron transport models 80−23030
spontaneously fissioning material, Monte Carlo neutronic and electronic model for thermal-neutron coincidence counting 80−23165
sputtering, high-energy, Monte Carlo calc. 77−40319
sputtering study, computer program 78−95627
square lattice, no. of configs. for nonoverlapping rods 79−21674
square lattice, percolation and cluster distrib. variable range interactions, exciton cluster model, layers 79−30379
square lattice site problem, percolating cluster, Monte Carlo study 80−77720
square well fluid, eqn. of state well width depend., Monte Carlo calc. 80−64853
standard variance reduction techniques in Monte Carlo transport problems, leakage estimator 78−78443
star clusters containing massive central black holes, dynamical simulations with self-consistent potentials 80−26915
star clusters containing massive central black holes, Monte Carlo simulations 79−8955
static properties of spin systems with truncated secular dipolar coupling 78−88130
statistical mechanics, Monte Carlo and mol. dynamics calcs., review, book contrib. 77−37807
steel, ferritic, FeC form. kinetics, Monte-Carlo simulation *(German)* 78−39779
stereology, quadrat choice for geometrical struct. determ. of two-phase specimen 78−12793
stilbene crystal, fast neutron counting efficiency 77−71719
stochastically macro-inhomogeneous medium, integral equation of mean radiation intensity *(Russian)* 78−5639
stratigraphic correlation by principal components, effects of missing data 79−25350
stratosphere, model, Monte Carlo anal. of imprecisions due to reaction rates 78−85635
stray light phenomena, GUERAP III Monte Carlo simulation 78−58907
stray light simulation with advanced Monte Carlo techniques 78−58906
strongly coupled charged Bose gas, ground state energy calcs. 79−6050
structural system, simulation anal. of reliability and maintenance *(Japanese)* 80−62453
SU(2) and SO(2) gauge fields in 4-, 5- space-time dimens., confinement, critical dimensionality 79−89064
SU(2) theory, asymptotic freedom scales calc. using Monte Carlo methods 80−90988
SU(3) theory, asymptotic freedom scales calc. using Monte Carlo methods 80−90988
succinonitrile, plastic phase, mol. motions correlation times, incoherent neutron scatt. 80−49138
supersaturated vapour, critical clusters, theory and Monte Carlo simulation, review 80−82734
surface field calc., floating random walk method 79−41273
surface flow of dilute gas in model pores, free mol. flow calc. in adsorbent force field 80−6100
surface migration of small crystallites, Monte Carlo calc. with continuous time 78−26783
surface physics applications, book contrib. 79−82426
surface roughness effect on transmission of microwave radiation through plaentary surface 79−75126
surface segregation, bond and strain energy effects, Monte Carlo method 79−74161
surfaces, multicritical phenomena 77−32208
suspension, random behaviour simulation, interval of quiescence method 78−31708
systems of soft diatomic mols., eqn. of state, Monte Carlo simulation 77−26262
teaching, two-dimens. Brownian motion simulation on micro-computer *(Japanese)* 80−31461
theory and technical aspects of Monte Carlo simulation, book contrib. 79−80529
thermal neutron monochromators, Monte-Carlo simulation of mechanical velocity selectors 78−24886
thermal neutron self-shielding factors, Monte Carlo calc. for TLD probes 79−45431
thermal radiation, geometric-optics coeff. determ. 77−50867
thermodynamic activity of C in austenite, computer simulation 79−37852
thermonuclear reactions, rate enhancement due to strong screening, ionic mixtures case 80−36613
thermonuclear reactions in laser fusion, emitted particle spectra, Monte Carlo calcs. *(Russian)* 80−52780
thermonuclear target, calc. of charged particle spectra by Monte Carlo method *(Russian)* 79−37445
thick inhomogeneity effects on charged particle beams 79−25041
thin elastic bar, impact buckling, Monte Carlo calcs. 79−32317
thin film electron microprobe analysis *(French)* 77−32856
thin foils, electron scatt., Monte Carlo study 79−67745
thin Pb-Ar calorimeter, hadronic and EM cascade discrimination 77−65401
three body ion-ion recombination probability, Monte Carlo simulation 80−85160
three body phase space distribs. 80−37393
three-dimensional Ising model, crit. behaviour 80−4672
TIGERP, 1-D multilayer electron/photon Monte Carlo transport code 79−54079
tissue equivalent phantom, dose distrib. calc. using Monte Carlo programme 80−78457
TLD, self-shielding factors for TLD-600 and TLD-100 in isotropic flux of thermal neutrons 77−6638
Tokamak, fusion reactor, axisymmetric, slowing-down alpha particle loss, Monte-Carlo calc. 78−59653
Tokamak, neutral beam injection, low density ignition scenarios 80−48937
Tokamak fusion reactor, effects of blanket-shield penetration on performance 78−21765
Tokamak fusion test reactor, dose rates from induced activity in test cell 80−23144
Tokamak Fusion Test Reactor diagnostic penetrations, neutron streaming calc. 79−9877
Tokamak scrape-off plasma, metal impurity recycling effect 80−10421

Monte Carlo methods continued
toroidal plasma, Monte Carlo treatment for neutral particle transport 80−33750
Townsend discharge, electron back diffusion 77−68884
Townsend discharge, macroscopic quantities, Boltzmann eqn. and Monte Carlo calcs. 80−38848
track rotation estimator, calc. of total flux at point 79−71385
transition matrices for Markov chain sampling, model systems, convergence rate comparisons 77−57165
transition probabilities, functional form 80−27234
transport calcs., second moment functionals for last event and collision estimators 80−13012
transport equations, Monte Carlo game, variance versus efficiency 80−27238
transport phenomena calc., in semiconductor junction lasers 80−98766
transport processes optimization method for exponential biasing in Monte Carlo calculations 79−54080
transport simulation of fast electrons slowing down in thin Al slab *(French)* 78−26610
transport theory, optimum biasing of integral equations in Monte Carlo calculations 79−54078
transuranic waste assay, low-level, Monte Carl calcs. of ^{3}He detector design 79−54542
triatomic negative ion fragmentation, energy partitioning isotope effects, Monte-Carlo calcs. 77−27126
tropical cyclone statistical prediction models, Monte Carlo significance testing 78−44943
tropical cyclones, gust speeds along N.Australian coast 77−86997
TSEE from insulating layers, Monte Carlo method simulation *(German)* 80−2932
turbulence, Burgers' model, energy decay 77−909
turbulent atmospheric transport, Monte Carlo simulation, radioactive pollution appl. 78−61550
twilight observations, Monte Carlo simulation *(Russian)* 77−33186
two-component ionic mixture, eqn. of state and phase separation in uniform background 78−21058
two-dimensional Ising model, Monte Carlo renormalisation-group method 80−4673
two-dimensional order-disorder phenomena, Monte Carlo simulation 78−67904
two-dimensional superconductor, resistivity evidence in Monte Carlo studies 80−80434
two-layer plate, random temp. fields and heat conduction, Monte Carlo method 80−33417
two-phase flow void fraction determ., simulation of neutron scatt. method 79−90321
two-point adsorption on binary metal alloy surface, Monte Carlo simulation 79−46940
ultra cold neutron production, by Bragg reflection from moving crystal, Monte Carlo simulation 79−701
underwater sound, Monte Carlo comparison of FFT and Prony algorithms processing 77−46855
undisturbed meas., Monte Carlo study of rejection of outliers on estimated mean value and standard deviation 79−26856
uniaxial dipole system, order-disorder transition, computer expt. and high temp. expansion 79−38494
uniaxial Lifshitz point, Monte Carlo calcs. 78−39353
unperturbed dimensions of branched cahin, star and ring polymers 78−66701
variance anal. 79−93079
variance reduction techniques using adjoint Monte Carlo method in shielding problem 79−63759
vegetation canopy modelling for signature correction/anal. 77−78515
velocity filter SHIP, efficiency for unslowed evaporation residues 80−23244
vinyl polymers with flexible side chains, configurational statistics, dipole moments 77−38760
viscous solution, conc. depolarisation of fluoresc. *(Russian)* 77−85799
water, liq., force bias Monte Carlo simulation 79−77487
water, liq., H bond distrib., Monte Carlo simulation calcs. 80−54106
water, liq., Monte Carlo simulation, convergence of new algorithm 78−63649
water, liq., Monte Carlo studies of struct., review 80−54101
water, liq., Monte Carlo-Metropolis computer simulation, convergence characts. 80−10485
water, liq., structure and props., minimal basis set description 80−6347
water, machine simulation, book contrib. 79−60249
water, Monte Carlo simulation 80−54113
water, Monte Carlo simulation of isothermal-isobaric ensemble 78−30530
water, Monte Carlo simulation of struct. and thermodynamic props. 80−88017
water, simulation, Monte-Carlo method, 1 g cm^{-3}, 300K, using Rahman Stillinger ST2 pot. 77−51290
water, structure, theory based on quasi-component distrib. functions 78−38606
water, X- and γ-irrad., electron slowing-down spectra and photon RBE 80−12197
water irradiated by photons up to 2 MeV, initial energies of Compton electrons and photoelectrons 80−108320
water quality models 80−8367
water slabs, fast neutron penetration spectra 78−29535
water/air mass stopping power ratios for megavolt. photon and electron beams 78−28082
Wiener path integrals, approx. evaluation 80−8829
X-radiation therapy, computer simulation of central axis dose distributions 79−8531
X-ray astronomy, point-like sources lunar occultations data anal. 79−88567
X-ray binary systems, models, X-ray transfer, Monte Carlo study 78−93463
X-ray close enhancement at material interfaces, Monte Carlo calc. verification 79−22484
X-ray clusters of galaxies, vel. dispersions correl. with X-ray luminosities 77−9804
X-ray emission from plasma, multiple Compton scatt. effect 78−96389
X-ray fluoresc. anal., energy dispersive, least squares, Monte Carlo methods, mathematical anal. techniques 78−85243
X-ray fluorescence, Monte Carlo simulation, inter-element effects determ. 80−26080

Monte Carlo methods continued
X-ray fluorescence anal., energy-dispersive, appl. of mathematical techniques 79−11837
X-ray fluorescence anal., matrix effects, reduction by Monte Carlo, fundamental parameters method 80−3460
X-ray photoelectron spectra relative intensities, elastic scatt. in solid effect on free path and ang. distrib. 80−11531
X-ray sources, Comptonization and radiation spectra, Monte Carlo calc. *(Russian)* 79−80372
X-ray spatial resolution, for SEM and STEM specimens 80−101066
X-ray spectral lines profile evolution due to Comptonisation, Monte Carlo computations 79−66916
X-ray structure analysis, Monte Carlo method for phase determ. 79−27869
X-rays transfer through optically thick shell 78−65488
X-Y classical model, vortex pair formation 79−63168
X-Y model, classical one-dimens., computer simulations 79−78396
X-Y model, critical properties near Lifshitz point, Monte Carlo study 79−28543
X-Y model, two dimensional, Monte Carlo simulation and phenomenological theory of phase transition 78−6534
X-Y model, two-dimens., vortex formation in Monte Carlo calcs. 77−63224
xeromammography, calc. of integral radiation dose 80−41248
XY Lifshitz point region, crit. exponents 80−65898
Yukawa Bose fluids, Jastrow wave function, Monte Carlo computation 79−73375
Yukawa fluid, fluid-solid interface 80−38883
Yukawa potential-ground state boson interaction, Monte Carlo study 78−51768
Z_2 lattice gauge Higgs theories, Monte-Carlo calcs. 80−86593
Zeeman resonance lineshapes, motional narrowing, lineshape in absence of motion 77−38636
Zeeman resonance lineshapes, motional narrowing, Monte Carlo simulation 77−38635
zero-variance multigroup Monte Carlo quadratures 80−5196
β-delayed neutron decay, statistical model, Monte Carlo techniques, fictional pandemonium nucleus calcs. 78−89830
e^+e^- annihilation and quark fragmentation functions, Monte Carlo quark-parton model 79−22119
$e^+e^-\rightarrow$hadron jets, QCD, Monte Carlo model 80−27514
$e^+e^-\rightarrow$jets, exclusive calcs. for QCD jets, Monte Carlo approach 80−105911
$e^+e^-\rightarrow\mu 3\pi$, above 6 GeV, Monte Carlo analysis 78−50042
$e^+e^-\rightarrow\tau^+\tau^-\rightarrow\mu e+4\nu$, Monte Carlo method for the analysis of low statistics experiments 79−18095
γ-ray cascades prod. at 10^{13} eV 77−61322
γ-ray detection by NE-213 liquid scintillator, Monte Carlo calc. of response function 79−97926
γ-ray families, multiparticle prod. above 10^{14} eV, Monte Carlo anal. 78−49257
$K^+p\rightarrow\pi^-\pi^-X$, 32 GeV/c, two-pion correlations, Monte Carlo model 80−83008
Λ hyperon polarisation, meas. by hybrid Monte Carlo tech. 80−99431
(n,2n) reactions, ang. distribs. and energy spectra, evaporation model, Monte Carlo calc. 79−45271
$np\rightarrow nn\pi^+$, 790 MeV, deviation from T=1 matrix element, π centre of mass ang. distrib. 78−70392
$np\rightarrow pp\pi^-$, 790 MeV, deviation from T=1 matrix element, π centre of mass ang. distrib. 78−70392
p beam impact on current-carrying target, Monte Carlo anal. 77−82775
$\bar{p}p$, 22.4 GeV/c, multiparticle prod., Monte Carlo quark-parton model 79−97639
$p\bar{p}$, $\pi^\pm$ inclusive spectra, comparison with Monte Carlo quark-parton model 79−30755
pp collisions, Monte Carlo approach to multiparticle prod. in a quark-parton model 79−13171
$pp\rightarrow D\bar{D}$ cross sections, Monte Carlo anal., particle lifetime for detection in emulsion 78−82229
pp→jets, 400 GeV, p_T plots, Monte Carlo and parton model predictions 78−89747
$pp\rightarrow\pi X$, 23 GeV, Monte Carlo anal., parton Fermi motion 78−45977
$(\pi,X\gamma)$ reaction at 70 MeV on s-d shell nuclei 78−29504
$\pi^-p\rightarrow\phi\phi n$, 22.6 GeV/c, cross section meas. 78−37242
$\Sigma^-\rightarrow\Delta e^-\nu$, branching ratio meas., Monte Carlo prediction 78−54631
$\Xi^-\rightarrow\Delta e^-\nu$ branching ratio meas., Monte Carlo prediction 78−54631
Ag (100), underpotential adsorption of Tl and Pb, mean field theory and Monte Carlo simulation 79−60630
Ag, spectral distrib. of X-ray braking radiation, due to electrons, calc. using Monte Carlo method 78−56538
AgBr, molten, Monte Carlo computer simulation 78−26426
AgBr, streaming cyclotron motion of hot electrons, at intense microwave fields 80−6703
α-AgI, superionic conductor, soft-core model, Monte Carlo study 80−54430
Al (001) and (110), secondary electron emission anisotropy, Monte Carlo calc. 79−99996
Al alloys, fatigue crack initiation, computer simulation 80−100893
Al and Al-alloy films, struct. induced electromigration failure, Monte Carlo calcs. 80−49405
Al, Auger electron microscopy, edge effect, Monte Carlo simulation 79−1801
Al, Compton profile, multiple scatt. correction 79−61456
Al foil, 150-400 keV electron transmission coeffs. Monte-Carlo calc. continuous deceleration model 77−50604
Al, gamma photon backscattering, energy dependence *(Rumanian)* 79−76316
Al, liq., calc. of neutron scatt. law 77−47330
Al, liq., pair correl. function calc., with pseudopot. satisfying compressibility sum rule 77−15300
Al, secondary electron emission, Monte Carlo calc. 79−69933
Al, stopping power of valence electrons, Monte Carlo calcs. 79−10886
Al, thin foil, Monte Carlo calcs. of electron transmission 77−80555
Al, vacancy distribution, interbonding atoms, heat peaks in scattered cascades *(Russian)* 80−39169
β-Al_2O_3-Na_2O, calculation of simultaneous ionic cond. and tracer diffusion 78−43178
β''-Al_2O_3-Na_2O, computer simulation of ionic conductivity 77−89580
$^{27}Al(n,\alpha)^{24}Na$, recoil escape efficiency, evaporation model, Monte Carlo calc. 79−45271

Monte Carlo methods continued
Ar, aqueous soln., dil., energy and struct., pair pot. energy function, Monte Carlo calc. 80−54107
Ar, electron avalanches at high E/N values, Monte Carlo simulation 77−35310
Ar, electron drift and diffusion, Monte Carlo simulation 79−7441
Ar, solid, equilib. props., uncorrel. pairs approx. 80−84303
$Ar+H_2$, 4500K dissoc. collision vibr. selectivity, Monte Carlo trajectory method 79−70307
$Ar+H_2$, dissoc., recombination and inelastic scatt. pot. energy surface and cross section Monte Carlo calc. 77−27162
$Ar+H_2$, vibr. and rot. transfer enhancement of dissoc. cross section 77−34732
$Ar+H_2$, vibr. transition rates, thermally averaged, Monte Carlo trajectory calcs. 80−23519
Au condensed films on NaCl, ion bombarded, film growth, thermally stimulated exoelectron emission 80−50537
Au, polycrystn., deformed, computer simulation of vacancy annihilation to dislocations *(Japanese)* 80−88205
Au, spectral distrib. of X-ray braking radiation, due to electrons, calc. using Monte Carlo method 78−56538
Au, transmission sputtering by $Ag^+(Ar^+)(He^+)$ ions 79−4885
Au-Si, spatial origin of electrons in internal photoemission struct. *(French)* 78−91770
Be, ion-implanted, impurity lattice location, channelling meas., Monte Carlo calc. 80−107291
Be+d, 14-40 MeV, Monte Carlo calc. of neutron yields 79−49887
BeF_2 glass transition, Monte Carlo study 80−75343
BeF_2:Eu^{3+} glass, struct. and optical props. 80−84067
BeF_2:Eu^{3+} glass, struct., Monte Carlo simulations 80−96448
Br_2 in liq. Ar, effective intramol. pot. 80−69208
Br_2, liq., entropy, computer simulation, Widom method 79−77486
Br_2+Ar, effective vibr. pot. of Br_2 in Ar gas, Monte Carlo simulation 79−59526
$CH^+ + H_2$, reaction products translational energies 77−86298
$CH_2^+ + D_2$, reaction products translational energies 77−86298
CO, electron swarm motion simulation for high E/N 77−19667
CO_2, electron swarm parameters for high E/N, Monte Carlo simulation 80−19548
CS_2, liq., struct. and equilib. optical props. 80−45026
$^A Ca(\pi^\pm,\pi^\pm N)$, A=40, 44, 48, 291 MeV, quasielastic scatt., differential cross sections, Monte-Carlo data fit 80−68703
Cd cut off energies, Monte Carlo code CDCUTOF 77−50211
^{252}Cf, heavy metal shielding for neutron sources 79−9892
^{252}Cf, spontaneous ternary fission scission config. from trajectory calcs., Monte Carlo calcs. 79−6718
$Cl+HI\rightarrow HCl+I$, Monte Carlo quasiclassical trajectory anal., product distribs. 77−16783
Cl_2, liq., entropy, computer simulation, Widom method 79−77486
^{60}Co source irradiation of 2 media, absorbed dose in vicinity of an interface 80−30894
CsCl(Br)(I), photoemission, electron-phonon interaction effects, Monte-Carlo calc. and expt. 78−11071
Cu, EXAFS Debye-Waller factors 80−45168
Cu, electron irradiated, void nucleation, Monte Carlo simulation method *(French)* 77−59046
Cu, liquid, struct. factor, neutron diffr. meas. and Monte Carlo calc. 80−38903
Cu, spectral distrib. of X-ray braking radiation, due to electrons, calc. using Monte Carlo method 78−56538
Cu-Ni, crystal growth from melt Monte-Carlo method modelling, surface roughness *(Russian)* 79−77536
Cu-Ni, surface composition cluster size distrib., Monte Carlo method calc. 78−63915
$Cu(\pi^-,\psi'(3700))$, 50 GeV, formation cross-sections *(Russian)* 80−106082
D-T plasma, Monte Carlo anal. of particle spectra 79−72992
$DCl+Cl_2(DCl)$, vibr. relax., Monte Carlo quasiclassical trajectory calcs. 77−50502
$^{18}F+H_2$, hot-atom reaction, nonequilib. vel. distrib. and reaction rate calcs. 77−63942
Fe, EXAFS Debye-Waller factors 80−45168
Fe, gamma photon backscattering, energy dependence *(Rumanian)* 79−76316
Fe slab *(Japanese)* 80−18595
Fe-Al, spin glass transition, Monte Carlo study 80−39801
$Fe^{n+}+H(H_2)$, 50-1200 keV amu^{-1}, impact ionis. and electron capture cross-sections 78−42204
^{57}Fe backscatt. electron Mossbauer spectroscopy 80−29661
GaAs, carrier diffusion in transient response regime 80−103688
GaAs, circuit effects in time-of-flight diffusivity measurements 80−88563
GaAs, diffusion and power spectral density and correl. function of vel. fluctuation for electrons 80−65576
n-GaAs, diffusion coeff., Monte Carlo calc., rel. to trapped domain behaviour 78−56152
GaAs, diffusion coeff. of hot electrons 79−15156
GaAs, electron transient vel. characts., Γ-L-X cond. band ordering 78−79997
GaAs, Γ_6^c-L_6^c-X_6^c cond. band ordering, velocity field characts., Monte Carlo calcs. 78−18957
GaAs, hot electron distrib. function, inter-carrier scatt. effect 80−2395
n-GaAs, limiting freq. of Gunn effect in polyharmonic LSA mode 80−6856
n-GaAs, non-Maxwellian electron distribution function, from electric field-depend. photolum. spectrum 79−11450
GaAs, self-scattering in Monte Carlo calcs. of transient dynamic response 80−103687
GaAs, transient and steady-state electron transport props. 77−39812
GaAs, transient dynamic response calculation by Monte Carlo techniques 80−107796
$Ga_{1-x}In_xP_{1-y}As_y$, drift vel. elec. field characts., Monte Carlo simulation 77−39839
$Ga_xIn_{1-x}Sb$, electron transport props. calc. by Monte Carlo method 77−76834
$Ga_xIn_{1-x}Sb$, electron transport in RF field, Monte Carlo simulation 80−96932
$Gd_3Ga_5O_{12}$, magnetic interactions and short range order 79−78401
Ge, charge carrier diffusion coeff. 78−84218
Ge, hole diffusion 78−6372
Ge, hot light hole distrib. function and light absorpt. 79−60844

Monte Carlo methods continued
Ge, intervalley diffusion of hot electrons 78−84227
Ge low energy X-ray detectors, entrance windows 77−71718
p-Ge, noise calc. in strong elec. field using Monte Carlo method 80−15578
Ge(Li), calc. of finite angle correction coeffs. and linear polarisation sensitivity 79−736
Ge(Li) detector pulse formation, Monte-Carlo anal. of multiple interaction processes 77−399
^{76}Ge double beta decay expt., Monte Carlo evaluation 79−49892
H atom in mag. field, Schrodinger eqn., Monte Carlo soln. 80−31545
H, atomic, gaseous, spin aligned, low-density props. 79−18255
H, electron impact excitation, Born and classical cross-sections *(German)* 78−86952
H, neutron scattering, 0.1 to 14 MeV, slowing down times and distances calcs. 77−65409
$H+B^{4+}(C^{5+})(O^{7+})$, excitation distrib. following electron capture 79−36763
$H+Br_2 \rightarrow HBr+Br$, HBr ang. momentum alignment, scatt. ang. depend. 78−3323
$H+H^+$, classical 3 body collision, cross section, energy transfer, computer calcs. 78−17783
$H+H^+(Arq^+)(Kr^{q+})(B^{q+})(C^{q+})(N^{q+})(O^{q+})$ charge transfer and impact ionis. cross sections calcs. 77−88555
H_2, electron swarm motion simulation for high E/N 77−19667
H_2, electron swarm transport coeffs. determ. by Boltzmann and Monte Carlo methods 79−90359
H_2, electron swarms, motion, Monte Carlo simulation 77−39398
H_2, gas, electron swarms, anisotropic scatt. model 78−91059
H_2, metallic, ground-state energies of liq. and solid phases, variational and Monte Carlo methods 80−70502
p-H_2, solid, rotation-libration transition under press., Monte Carlo study 80−49460
H_2+Ar, 4500K shock wave expt. simulation, vibr. state changes and dissoc. 79−61850
H_2+Ar, vibr. energy transfer rate, ab initio calcs. 78−82821
H_2+N_2, rot. excitation, fixed nuclei approximation calcs. 79−6990
H_2+Ne, collision-induced dissociation, Monte Carlo quasiclassical trajectory calcs. 79−74357
$HCl+Cl_2(DCl)(HCl)$, vibr. relax., Monte Carlo quasiclassical trajectory calcs. 77−50502
$HCl+H_2$, translational and pot. relax., statistical calcs. 77−3435
HD, mol., nucl. spin-spin coupling, diamag. contrib. 79−36665
HF, liquid, Monte Carlo simulations 79−64967
HF, liquid, struct. and props., intermol. pot. function calcs., basis set depend. 79−82134
H_2O aggregates, dimer and octomers, dipole moments, polaris. model calcs. 79−77482
H_2O, free energy of liq. water, ab initio Monte Carlo calc. 78−83975
H_2O, ST2, discrepancy between Monte Carlo and mol. dynamics calc. using truncated pot. anal., internal energy determ. 80−95702
H_2O+O, rot. excitation, classical Monte Carlo calcs. 77−34727
$(H_2O)_n$, n=8, 64, cluster thermodynamics calcs. using Monte Carlo method 77−58219
He glow discharge, electron behaviour in cathode fall, Monte Carlo simulation 78−1941
He, positron annihilation, average energy, lifetime spectrum, Monte-Carlo calcs. 77−88558
He-He, Born Oppenheimer pot. using Hylleraas-type electronic wave functions 80−91442
He-He, Born-Oppenheimer pot. using Hylleraas-type electronic wave functions 79−31438
He-Xe, eqn. of state, Monte Carlo calcs. 80−59158
$He+2I \rightarrow I_2+He$, energy transfer mechanisms studied using trajectory calcs. and Monte Carlo method 80−66785
He+multiply charged ions, electron capture and impact-ionis. cross sections, Monte Carlo calcs. 79−27083
$He^{2+}+Li$, electron capture, ionis. cross section, low-vel. $He^+(3l)$ production, X-ray production 79−22822
^{3}He gridded fast neutron ionisation chambers, Monte Carlo calc., of energy dependent efficiency 80−99417
^{3}He, ground state of polarised and unpolarised fluid, Monte Carlo calcs. 80−92748
^{3}He, solid, Monte Carlo method of energy calc. 79−56030
^{4}He, HCP, ground-state props. 80−44389
^{4}He, liq., variational Monte Carlo calcs. with three body correl. 80−96711
^{4}He, liq. film and solid, hypernetted chain generalised eqn. optimal solns. 80−75396
^{4}He, liquid, Jastrow wave function optimisation 79−7719
^{4}He, liquid and solid, Lennard-Jones model at 0K, props. using Monte Carlo method 79−82401
^{4}He, solid, thermodynamic props., Monte Carlo studies 79−65290
I_2 liq., static structure factor, neutron diffraction 80−103236
InAs, transient dynamic response calculation by Monte Carlo techniques 80−107796
InP, diffusion and power spectral density of velocity fluctuations for electrons, Monte Carlo calc. 79−51572
p-InP field-assisted photocathodes, quantum efficiency 80−84831
InP, hot carrier noise, Monte Carlo simulation 77−51792
InP, transferred electron effects under high press. 80−34453
InP, transient and steady-state electron transport props. 77−39812
InSb, current-voltage characteristics at room temperature and high hydrostatic pressure 80−88560
InSb, electron mobility, low-field, Monte Carlo calc. 80−10973
InSb, HF props. of hot electrons at 77K, calc. using Monte Carlo method 80−15553
n-InSb, high field electron diffusion, Monte-Carlo calc. 78−10455
n-InSb, hot electron noise temp., Monte Carlo calc. 80−107877
InSb, hot electrons, Monte Carlo calc. of transport characts. and distrib. functions of hot electrons 80−6853
K, liq., radial distribution function, Monte Carlo calcs. 77−55230
$K_L^0 \rightarrow (\pi\mu)\bar{\nu}$, energies and intensities of π-μ atoms *(Russian)* 78−54629
KD_2PO_4, ferroelectric, longit. and transverse props., Monte Carlo study 79−51912
Kr, gas structure by neutron diffr., three-body pot. contrib. 79−90358
LiF dosimeter energy response to high energy electrons <30 MeV 77−86637
LiF dosimeters for high energy electrons, Monte Carlo calc. of energy dependence 77−46421
Monte Carlo methods continued
LiF thermoluminescent dosimeters, response to ground-level cosmic-ray background 79−59265
Li_xTiS_2, Li ordering in intercalation battery, theory 79−77580
$Mg+H^+$, electron capture and impact ionisation cross sections, CI calc. 80−23343
$N^{q+}+H$,(q=1 to 7), electron capture and impact ionisation cross sections 77−75290
N_2, electron backscattering coeffs., 100 eV to 5 keV 80−9750
N_2, electron swarm parameters for high E/N, Monte Carlo simulation 80−19548
N_2 gas, electron energy degradation, Monte Carlo study 80−69969
N_2, O_2, O, electrons elastic scatt. cross sections, analytical representations 78−42213
N_2 plasma, electron beam energy distrib., excitation and ionisation model, Monte Carlo method *(Russian)* 79−27790
$NH_2^++H_2$, reaction products translational energies 77−86298
NH_3+O, rot. excitation, classical Monte Carlo calcs. 77−34727
NO_2^- hydrate clusters, ground-state HF pot., Monte Carlo simulation, energy surfaces and rot. barriers 80−106412
Na, ions in liquid, Born-Oppenheimer pot. derivative, Monte Carlo calcs. 80−54117
$Na+Na_2$, reaction probability, energy transfer 77−28998
NaI absolute photopeak efficiency, relationship between point- and extended source geometries 77−26944
NaI detector efficiency for 10 to 150 keV gammas, 4π geometry vs. well- and face-type cryst. 77−3214
NaI face-type detector efficiencies for 10 to 150 keV γ-rays 77−3215
NaI scintillation detectors, efficiency values Monte Carlo calc. method 78−13387
NaI:Tl, right-circular cylindrical detector, Monte Carlo calc. of efficiency 79−734
NaI(Tl) double crystal gamma ray spectrom., efficiency calibration 79−717
NaI(Tl) Polyscin module detector arrays, Monte Carlo code for design, use in γ-ray spectroscopy 77−54436
$Na_2O.5Al_2O_3$, diffusion of Na, computer simulation based on Monte Carlo method 77−24431
Ne, microwave breakdown field calc. 78−67551
Ne^++Co_2, three dimens. quadrupole ion storage, ion mobility, effect of charge exchange reactions, Monte Carlo calcs. 80−55738
$Ne(^3P_2)$ elastically scattered, metastable, ang. distrib., conventional rel. to Doppler shift methods 80−58418
^{21}Ne, strength function calcs. in many fermion systems, Monte-Carlo method 80−86820
Ni (110), chemisorption of O, Monte Carlo calcs. 79−69357
Ni (111), O adlayer phases and binding sites 80−80069
$Ni:K^+(Ba^+)$, ion implantation, effect on inelastic refl. and energy losses of fast primary electrons 78−55900
Ni_4Mo, statistically homogeneous ordering, computer-simulated field ion images 78−9991
$^{58}Ni+^{32}S$, 110, 132 MeV, fusion evaporation residues, Monte Carlo simulation 78−41799
O, adsorbed on W (110), three-adatom non-pairwise interaction, Monte Carlo simulations 79−82466
O^- and O_2^- ion swarm in O_2, reactions and transport, Monte Carlo calc. 78−59539
O^{q+}-He^{2+} collisions, electron capture and impact ionisation cross sections, loss of alpha particle in Tokamak plasmas 79−68936
$O^-+O_2 \rightarrow O_2^-+O$, cross section kinetic energy depend., rate consts. meas. and Monte Carlo calcs. 80−78701
O_2, electron backscattering coeffs., 100 eV to 5 keV 80−9750
O_2, thermal decomposition, vibr.-rot. state depletion, Monte Carlo calc. 80−35506
$O(^3P)+CO(X^1\Sigma^+)$, vibr. deactivation and atom exchange, rate. consts., Monte Carlo anal. 77−48627
$O_2(b^4\Sigma_g^-, \nu'=4, N', F')$ predissociation fragments, ang. distribs., separation energies 80−5588
Pb, gamma photon backscattering, energy dependence *(Rumanian)* 79−76316
Pb glass detectors for high-energy photons, Monte Carlo calc. of energy resolution 79−18072
Pb, muon angular distrib., Monte Carlo calc. 79−78600
Pb shield, effects of thickness and geometry var. on neutron spectra 78−33300
Pd, H(D) interstitial interactions rel. to diffusion and ordering transition 80−34249
Pd-Mn dilute alloys, mag. ordering, sp. ht. calc. by Monte Carlo method 77−77030
PdH_x, incoherent phase transition, lattice gas model 80−29171
Pt, EXAFS Debye-Waller factors 80−45168
Pu in situ array for electropolishing bath., Monte Carlo calcs. 80−37524
Rb, expanded fluid, struct., Monte Carlo study 78−83720
Rb, liquid, static struct. and electronic transport props., determ. by Monte Carlo simulation 79−7543
Rb, specific heat at high temp., Monte Carlo calc. 80−29182
Se, liquid and amorphous, struct. modelling using Monte Carlo method 80−59391
Si (100) inversion layer, hot electron drift velocity, Monte Carlo calcs. inc. 3 subbands 78−91752
Si, amorphous, implanted ion trajectory and spatial distrib., Monte Carlo simulation 77−11611
Si amorphous film, hole carrier transport 80−2500
Si, blistering due to 400 to 1800 keV $^4He^+$ ions, modal range determ. 80−100289
Si, diffusion and power spectral density and correl. function of vel. fluctuation for electrons 80−65576
Si, electrical conductivity, inertia of electron heating, expt. and theory 80−65613
Si, electron beam annealing, beam voltage effect modeling 80−75275
Si, energy loss to valence electrons of channelled protons, dielec. calc. 77−55312
Si, feeding-in and blocking of 2 MeV protons, simple diffusion model 78−22782
Si inversion layer, high field drift vel., Monte Carlo calc. 77−32087
n-Si, microwave and far IR hot carrier mobility, Monte Carlo calc. appl. to mm. transit time oscill. efficiency 78−72184
Si, polycryst. and amorphous, sputtering with keV Ar^+ ion, meas. and Monte Carlo calc. of sputtering yield 79−95886
Si:B, ion implanted, depth and lateral profiles of B atoms, Monte Carlo simulation 77−55297

Monte Carlo methods continued
Si:B sputtering by Ar^+, computer simulation of sputter broadening in impurity depth profiling 80−2908
Si:H, ion implanted Monte Carlo calcs. of profiles of H ions 78−55889
Si:O, ion-implanted between 2 and 20 MeV, range and range straggling 80−44241
Si-B-O film, electron probe microanal., Monte Carlo calcs. 79−83533
^{28}Si, strength function calcs. in many fermion systems, Monte-Carlo method 80−86820
^{119}Sn, thin foil, 19.6 keV conversion e^- energy, ang. contrib., Monte Carlo calc. 79−11360
Ti foil, 150-400 keV electron transmission coeffs., Monte-Carlo calc., continuous deceleration model 77−50604
$^{233,235}U(n,f)$, Monte Carlo anal. of Mn bath meas. of η_{2200} 77−23142
U, prospecting by active neutron logging, evaluation models 80−98480
UC_x, self-diffusion and nonstoichiometry, modified Monte Carlo method 77−69114
UF_6, U isotope separation by velocity slip process, calcs. 79−94100
UH_3 critical mass calc. by Monte Carlo methods as function of ^{238}U enrichment 79−36320
^{235}U-Al castings in water, pulsed reactivity meas., Monte Carlo anal. 79−26522
$^{235}U+^{233}U$, classical microscopic description 77−14160
W (110), chemisorption of O, Monte Carlo modelling of phase changes 78−71969
W (110), O adsorption, adatom interaction energies, Monte Carlo calc. 78−71948
W (110), order-disorder transform. in chemisorbed O, theory compared with LEED data 79−7748
W support film for high resoln. electron microscopy, phase contrast, computer modelling 78−1144
W+p, 25 GeV, antiproton prod., flux optimisation using hadron cascade calcs. 77−83411
Xe, solid, elastic consts., thermodynamic props., Monte Carlo simulation 77−62575
XeF_6, UV absorpt. band shape 78−5289
Zn, electronic band struct., pseudopotential calcs. 79−19510

Moon
see also lunar seismology; lunar structure
18.6 year nodal cycle, effect on shallow seas surface temp. due to tidal mixing vars. 78−73387
1978 March 24 total eclipse, S.African obs. 79−44384
age discrepancy between highlands and maria 77−73982
ALSEP-quasar differential very long baseline interferometry, for lunar position meas. 78−45245
ancient magnetic field, intensity and origin 77−60656
ancient magnetic field inferred from palaeomagnetism 77−60686
ancient magnetic field intensity determ. from NRM and surface field meas. 77−37530
Annual review of Earth and planetary sciences, vol.5 77−64174
Apennines and regional surroundings, isostatic state 78−77503
Apollo 17 KREEPy basalt, rock type intermediate between mare and KREEP basalts 77−87286
Apollo 17 landing site, Camelot crater and crater cluster ages 79−40101
Apollo lunar surface science stations shutdown 78−57425
Apollo programme, review 77−64679
Aristarchus crater obs. in 1975-6 period 77−33367
Aristarchus-Harbinger region, surface geology and history 78−20662
astrometry, equatorial coords. for 1972-4 period *(French)* 78−81577
atmosphere and ionosphere in geomagnetic tail 78−28553
atmosphere and meteoritic flux transformation 78−61768
auroral occurrence freq. incl influence 77−87149
Babylonian lunar theory 80−94729
basaltic magmatism and bulk comp., major and heat-producing elements 78−7891
basaltic magmatism and bulk comp., siderophile and volatile elements 78−7892
basin-forming impacts, global seismic effects 78−12122
bistatic radar surveillance with FM signal, Rocco crater 79−5758
blue Moon phenomenon, due to atm. light scatt. and mixed plate interference 77−2244
brightest crater, reason for name Aristarchus 79−49004
brightness at 2 and 6 cm wavelength, centre to limb var. 78−81572
brightness distrib. over lunar disc at 6 cm 77−37518
brightness distribution over lunar and planetary discs, determ. from light refl. meas. 80−17512
Brown-Eckert Improved Lunar Ephemeris, Fourier series fast evaluation 80−56711
bulk melting hypothesis rejection 77−64680
capture by Earth rel. to solar mass var. in 3-body problem 80−56728
cartography of limb regions *(French)* 80−12696
celestial mechanics, ELP soln. of Moon main problem *(French)* 80−62044
centre of mass displacement from geometric centre, comment 78−69937
centre-of mass offset 77−2353
charged particle albedo, Luna 22 data 80−56729
chemical composition, rel. to Earth and eucrite parent body comps. 77−60636
chemical history, rel. to Earth and parent body of achondrites 77−60639
chemistry, element correls. and bulk comp. 77−60637
Chernier Crater, lava-like material nature and origin 78−81569
chronology, basis for interpreting ages of Serenitatis, Imbrium and Orientale events 77−60642
chronology, determ. from ages of returned lunar samples 77−60644
colorimetric map, absorpt. strip intensity distrib. at 0.95 μm *(Russian)* 79−44381
colour photographs from space probe *(German)* 77−53445
cometary collision, origin of swirl patterns on surface 80−51675
composition determ. by solar nebula conditions and processes 79−2492
core dynamo, rel. to superheavy elements 78−65521
core formation in terrestrial planet, appl. to Moon 80−17514
core size from Moon-magnetosphere interaction 79−25525
crater arcs, catalogue and distribs. 77−41333
crater depth/diameter ratio, morphological charcts. 80−62049
crater dimensions catalogue from Apollo data 77−37527
crater doublets expected frequency 78−61777
crater Giordano Bruno, AD 1778 impact obs. consistent with laser ranging results 78−69717
crater Giordano Bruno, interpretation of eye witnesses account of formation 77−71174
Moon continued
crater morphology and size relation 77−41332
crater morphology from impact spacecraft imagery 80−62052
crater rim topography, radial variation 77−60633
crater saturation and equilibrium, Monte Carlo simulation 77−71038
crater shapes formed by high-speed impact 77−33364
crater size-shape profiles, terrain effects, interplanetary comparisons 79−66936
crater/stars superimposed photography using automatic device, lunar coords. meas. *(Russian)* 79−92675
cratered terrain, thermal regimes and impact melt 77−2125
cratering by meteorite impact 79−21244
craters, evolutionary tracks 77−91134
craters, floor fractured, morphologic classes 77−37516
craters, image edge determ. algorithm 80−98581
craters, rel. to standard crater curve for Mars and possible new time scale 77−33391
craters, simultaneous position and diam. determ. 77−82134
craters and plains, comparative studies of Moon, Mars and Mercury 77−53439
crescent first visibility prediction 78−24442
crustal evolution, major impact processes contrib. 77−60658
crustal evolution in silicate planets, review 78−61774
crustal magnetic anomalies, sources 80−8566
crustal tectonics, relation to internal evolution 78−12116
crustal tidal stresses rel. to lineaments 78−89087
density, vol. distrib., theoretical anal. 80−8567
density structure, max. entropy inversion 80−67602
differentiation, evidence from trace element abundances 77−60651
differentiation processes of interior, trace elements as probes, review 80−98584
distance and shape, laser ranging results 80−21933
distance meas. by laser 77−9673
distortion due to convection unlikely 78−61761
dolines, form. by expansion of Moon *(French)* 77−86826
dynamical evolution of Earth-Moon system from shell growth rings 78−96122
dynamics studies before laser ranging 77−64183
early chronology, evidence for early collisional history of solar system 77−60640
early collisional heating 80−8563
Earth tides observations, lunar gravit. field screening effects *(Russian)* 78−88787
Earth-Moon distance, extreme values for 1970-1979 period 77−37498
Earth-Moon system, Moon position change, evidence from geological time considerations 80−3916
Earth-Moon system, palaeodynamics from nautiloid growth 80−41713
Earth-Moon system history, palaeontological data 80−17224
Earth/Moon system, satellite aided capture of external body 79−75087
Eckert's lunar ephemeris, numerical evaluation 79−75124
eclipse, 1975, May 24-25, UBV photometry 77−22126
eclipsed Moon brightness, Danjon relation correl. with gegenschein brightness *(French)* 79−96968
electrical conductivity, inverse theory appl. 78−12113
EM heating, EM heating in early solar system 80−36555
EM induction, modelling, solar wind parameters limitations 78−36415
EM induction, variable surface EM field calc. 77−82135
EM induction in Earth and Moon, workshop proc. (Murnau, W.Germany, 1978 September 7-13) 79−79741
EM induction source, forcing by diamagnetic cavity 77−87288
EM induction studies, effects of magnetometer data errors 79−96932
EM sounding using surface magnetometer meas. 78−65518
ephemeris, Earth oblateness effects, corrections 77−22043
ephemeris correction for solar terms 80−12684
EUV albedo, comparison with Mercury 77−33378
evolution, major igneous events 77−87294
evolution and structure, review 80−4278
exosphere, Monte Carlo modelling 78−96416
exosphere simulation, Monte Carlo methods 80−67588
exosphere simulation, Monte Carlo methods 80−67589
expansion and gravit. constant changes, limits 78−28155
exploration and post-Apollo prospects 77−17329
exploration programs, United States 78−77461
Fahrenheit crater ejecta, emplacement at Luna-24 site 80−8564
far UV albedo, Apollo 17 meas. 77−37513
far-side magnetised regions, correl. with ringed impact basins 80−36521
far-side radii determ. from Apollo photography, topographic map 79−66934
first telescopic obs. by Galileo (December 1609) 77−29978
fission from Earth origin, geochemical evidence 77−60693
fission origin, cause and timing 78−85867
fission origin, lunar devolatilisation model 79−30000
fission origin from Earth mantle, geosynchronous phase, consequences for Moon 80−101537
formation, implications for solar system origin and transneptunian planets 79−8856
formation and early evolution theories 77−2355
fossil bulge to explain gravity field anomaly 80−56733
free librations determined from laser range meas. 77−37521
Galileo's lunar observations, dating rel. to 'Sidereus nuncius' composition 79−8853
gamma ray quantum flux var. calc. as function of surface relief and distance 79−80249
gamma-ray emission, observational and physical review 79−80373
gas venting, locations on maria rims and various craters 77−71029
gaseous emissions, 19 month search 77−71030
general props. and understanding 77−56847
geologic evolution of terrestrial planets 77−53442
geomagnetic Ci index (1906-1976), solar eclipse perturbations 79−100811
geometric albedo and full Moon magnitude 77−33374
geometrical figure, expansions, spherical and sampling functions 79−35159
geosynchronous revolution and terrestrial continent form. 80−101348
Giordano Bruno crater, possible impact obs. on June 18, 1178 77−33370
Giordano Bruno crater and 1178 event 79−48694
global tectonics, following tidal despinning 77−60698
global tectonics, of Mercury and the Moon 78−12128
gravimetric surveying process optimization 79−8846
gravitation theory testing by lunar laser ranging and planet radar ranging 77−53823

Moon continued
gravitational field, model based on Luna 10, 12, 14, 19 and 22 data 78−45249
gravitational field, stationary points coordinates 78−53805
gravitational field model, harmonic anal. 80−72799
gravitational potential harmonics, effects on Earth rot. axis precession angle 78−48953
gravity anomalies and tectonics, review 80−98593
gravity anomalies assoc. with large young craters 78−7889
gravity determinations and their implications 77−60653
gravity field, harmonic anal. 77−87290
gravity field, long-term Keplerian rate method 77−87291
gravity field, mass point model 77−87289
gravity field modeling from spacecraft tracking data 79−21132
gravity gradient mapping from Lunar Polar Orbiter, simulation 77−41329
gravity meas., gradiometer systems on polar orbiting satellite 80−94730
grazing occultation of ξ Sagittarii 77−33368
halo orbits in Earth-Moon restricted three body problem 80−36483
Harbinger Mountains region, topography of sinuous rilles 77−78683
Harriot's lunar maps drawn in 1609 and 1610 78−81783
heat flow and regolith struct. from radio interferometric obs. 77−5469
Heiligenschein and albedo differences at zero phase angle 79−21205
highlands, general cratering history model 78−53843
highlands crust 80−109381
Hill's problem in Lunar theory 78−77473
hypervelocity particle impact, heating and vaporisation, lab. expt. 78−59290
ice and trapped volatiles in lunar polar regions 80−26759
Imbrian-age highland volcanism, Gruithuisen and Mairan domes 78−77504
Imbrium sculpture and lunar basin radial texture, evidence for sedimentary origin 77−37526
impact basin rings formation theory 78−61766
impact crater size-frequency distrib., age determ. 77−60659
impact craters, use of equivalency in estimation of historical size distrib. 78−45250
impact ejecta parameters depend. on primary vel., lab. expt. 78−59291
impact flows and crater scaling 78−61769
impacts by objects in parabolic low inclination order, distrib. 79−2493
intercrater plains on Moon and Mercury, origin and relative ages 78−12117
interior, solid-state convection, obs. evidence 79−84692
interior melting, heat source, ^{26}Al from nearby supernova explosion 78−40849
interior structure, rel. to mag. field origin 78−12115
internal structure evolution, calc. 77−82137
internal temp., solid state convection models 77−60688
ionosphere/exosphere modulation by solar wind and EUV radiation 77−17390
IR map of disk 79−25526
Jacobi integral constant, annual and monthly vars. 78−49301
Kazan heliometric obs. (1895-1958), new reduction *(Russian)* 79−92688
large impact structures, numbers and isostasy rel. to average crustal viscosity 78−12120
largest crater, Schiller annular plain 77−17391
laser lunar ranging, scientific progress, 1969-77 period 78−36476
laser ranging, future developments 77−64483
laser ranging, McDonald Observatory results 77−64678
laser ranging, polishing and Foucault test of receiving telescope mirror *(Japanese)* 78−89065
laser ranging, reference frame for positional astronomy 77−64618
laser ranging, review 77−5459
laser ranging obs., universal time meas. results 78−85854
late heavy bombardment in inner solar system 77−71019
lava flow effects on crater populations 77−37514
Letronne-Montes Riphaeus region, tectonic pattern of mare ridges 79−66935
libration, Cassini's laws 79−8812
libration, literal theory for laser ranging interp. 77−64677
librational stability, effect of external disturbing torques 77−71021
light plains, different ages 78−81571
limb automatic meas. with Nice Obs. microdensitometer *(French)* 80−12692
Linne controversy, possible variations rejected 77−78680
lunar and planetary science, ninth conference, Houston, Texas, (1978 March 13 to 17) 80−17711
lunar eclipses, transitory phenomena obs. 78−61770
lunar exploration, status after 18 years 78−61767
lunar halos, geometrical optics of formation 77−45634
lunar megalithic sites in Britain, reconsideration 79−8854
lunar theory, accelerated elimination technique for soln. of perturbed Hamiltonian systems 77−60585
lunar theory, new soln. to main problem 79−75083
lunar theory of Hill and Brown 80−46370
M_2 ocean tide parameters and Moon's meas. longit. decel. from artificial satellite orbit data 80−31048
M_2 tide eqn. deduced from artificial satellite obs. 77−41337
magnetic anomalies, solar wind interaction 78−4125
magnetic anomalies detected by Apollo subsatellite 80−36525
magnetic field, charact. of first order shock induced mag. transitions in Fe, discrimination from TRM 78−64205
magnetic field, dimensional anal., simple model 79−58286
magnetic field, primitive remanence model 78−12125
magnetic field, spacecraft meas. 79−2503
magnetic field anomalies, comparison with Earth 78−4122
magnetic field calculation of cosmological bodies 79−12399
magnetic field determination from lunar fines 80−36526
magnetic field origin, conf., Nov. 1978, Texas USA 80−36234
magnetic field origin, constraints set by Apollo 15 and 16 subsatellite obs. 80−36523
magnetic field origin theories 80−36522
magnetic permeability and Explorer 35 magnetometer sensitivity 77−56846
magnetisation, non-random vector orientations 78−61764
magnetosphere, laboratory simulation 78−28550
main lunar problem, comparison between ELP and SALE *(French)* 80−85844
mantle, seismic vels. rel. to constitution 78−85866
map of J.D. Cassini 80−8769

Moon continued
mapping, conf., Lagonissi, Greece (May 1978) 80−12688
mapping, from Schmidt's 1878 map to Apollo photography 80−12689
mapping program of United States and Apollo project 80−12690
mare basins vertical movements, rel. to emplacement, tectonics and thermal history 79−80250
Mare Crisium, radar-detected subsurface interface stratigraphic correlation 79−16848
Mare Crisium, regolithic radioactivity 80−62045
Mare Crisium, view from Luna 24, conference, Houston, Texas (1977, December 1 to 3) 80−17710
Mare Crisium regolith, Luna 24 basalt age rel. to crater density data 77−22119
mare grounds relative spectral reflectivity 80−12695
Mare Serenitatis, elec. cond. anomaly detect. by Lunokhod 2 and Apollo 16 magnetometers 80−56730
Mare Serenitatis multiringed basin, struct. and selenology 80−77304
marginal zone, absolute elevations from stellar occultations 80−62047
marginal zone relief maps from stellar occultation obs. *(Russian)* 77−73984
Maria Serenitatis and Crisium, orbital radar evidence for subsurface layering 78−85868
Mariner 10 UV spectrometry results 77−45337
megalithic lunar site a Callanish, Lewis 80−77300
Mercury and the Moon, conference, Houston, Texas (15-17 November 1976) 78−12126
meteorite impact and explosion craters 78−45296
meteorite impact ejecta, depend. of mass and energy lost on planetary escape vel. 78−45295
meteorite impacts, review 79−8884
meteoritic material in near-Moon space, meas. from spacecraft 77−53486
micrometeorite impact, ion emission 80−77362
micrometeoroid distrib. and flux at 1 AU from lunar crater obs. 77−60730
microwave spectrum, effect of subsurface inhomogeneities 77−82133
moment of inertia and gravity field, study of Earth-Moon system 80−105184
moment of inertia determ. improvement, proposed strategy 78−24477
moment of inertia from time variation of ascending node of Explorer 49 77−53440
moments of inertia, origin of differences 78−45247
moments of inertia calc. 77−25961
moments of inertia rel. to global melting 77−60692
morphology of fresh crater landforms, form. and modification 78−40847
Mosting A posn. determ., plate reduction *(French)* 78−20661
motion, literal soln., formal convergence *(French)* 80−36482
motion and Earth shrinking effects 80−46182
nearside, multispectral maps and ratio images 79−40099
noise effects assessment, on satellite links *(Japanese)* 80−82239
normal albedo, digital file from photographic data 77−78684
observational ephemeris, 1977, September to October *(French)* 77−87241
occultation of Crab Nebula, obs. at decametre wavelengths 80−62248
occultation of hard X-ray source, in Crab Nebula balloon obs. *(Japanese)* 77−82319
occultation of Saturn, normal reflectances of Rhea, Titan and Iapetus 78−85897
occultation scans, object shape retrieval from new algorithm 80−105149
occultations, appl. of deconvolutation method 80−105174
occultations, comparison of profiles of Watts and Weimer *(French)* 77−41330
occultations, obs. at Sydney Observatory during (1974-1976) 78−69658
occultations, photoelec. obs., diffraction, stellar diameters and double stars 78−7866
occultations, photoelectric obs. at McDonald Observatory 77−2331
occultations during 1943-74, anal., rel. to Brown's theory, FK4 right ascension system and Watt's charts corrections 79−48696
occultations of 3C radiosources, 327 MHz obs. 77−45588
occultations of ψ Virginis (SAO 139033) and χ^1 Orionis (SAO 077705), ang. dias. meas. 78−20825
occultations of GX9+1, X-ray source position 77−45612
occultations of Kepler's supernova remnant and Crab Nebula, struct. at 327 MHz 78−12339
occultations of late-type stars, ang. dias. determ. 77−74048
occultations of planets by eclipsed Moon, 100 BC to 3000 AD period 77−49319
occultations of radio sources as ang. struct. investigation technique, resolving power 78−65712
occultations of stars, 1974 to 1977, photoelectric obs. summary 79−88642
occultations of stars, double and multiple stars obs. 78−4079
occultations of stars, new technique for photoelec. obs. of dark limb reappearances 78−4115
occultations of stars, summary of obs. 78−7982
occultations of stars (1943 to 1971), catalogue 79−88606
occultations of X-ray sources, first and last dates (1980 to 1985) 80−77513
Oceanus Procellarum, Ti rich basalt geology of Flamsteed region 80−105183
optical characteristics, interpretation rel. to surface material props. 78−12130
orbit computation, appl. of Urabe's method to Moon and artificial satellite cases 80−17477
orbit evolution, relation of contracting Earth 77−41331
orbital evolution, anal. 80−8565
orbital evolution 77−29671
orbital gamma-ray data rel. to large-scale lunar problems 78−12123
orbital history rel. to palaeogravimetry and palaeofigure 77−71023
orbital motion, Earth tidal potential multiple expansion 79−12062
orbital stability, Hill's concept generalisation 79−92656
orbital stability limits, restricted three body problem for Sun-Earth-Moon system 79−75084
orbital theory rel. to lunar laser ranging 77−64676
orbiter mission, NASA 1980 polar orbiter global survey study 78−4064
Orientale basin, comparison with Caloris basin on Mercury 78−12121
origin, fission theory and geosynchronous release 80−101536
origin, growth of large, late-stage planetesimals 79−96931
origin, lunar capture hypothesis revisited 78−81570
origin, rel. to Earth early history 79−20739

Moon continued
origin and composition, information from Apollo and Luna projects *(French)* 78−40846
origin from solar nebula, book 80−17266
palaeomagnetism, pole positions rel. to lunar core dynamo processes 78−93132
palaeotides, Earth-Moon system origin determ. 79−40098
palaeotides and Earth-Moon system origin 79−62769
partial eclipse of 1977, April 3-4, amateur obs. reports 77−73985
particulate surface, multiple light scatt. effects, lab. expt. 78−58912
periodic motion rel. to centre of mass in evolutionary circular orbit 80−21899
permanent magnetic field, cratered-shell model 78−4124
phase relation rel. to asteroidal regolith props. 80−36551
phases correl. with rainfall freq. 77−13112
photography for amateur astronomers 78−45238
photometric and polarimetric obs., 1976 April to 1977 December 80−51677
photometric anomalies from 1962 obs., possible transient phenomena 80−67587
physical librations, resonances in analytical soln. for libration in longit. 79−84648
planetary perturbations, formulation and Brown separation *(French)* 77−29664
planetary terms in lunar ephemeris 79−84645
plasma near surface, radiosource occultation obs. 80−8559
plasma screening length and surface potential near terminator 77−60635
plasma sheet interactions at Apollo 14 site, mag. shadowing effects 77−2354
plasma wake three-dimens. struct. 77−29613
position computation algorithm 79−25452
positional photographic obs. at Pulkovo with long-focus horizontal telescope *(Russian)* 78−28533
positions, low-precision formulae 80−61990
post-Apollo understanding 77−33373
pre-capture orbits 77−37525
primaeval melting, by superheavy elements 78−24478
radar backscatter from lunar surface, results from automatic stations 77−53438
radar contact in 1946 80−85866
radar map at 7.5 m wavelength 79−25523
radar mapping, Earth-based, review 80−12694
radar obs. technique *(Spanish)* 79−5759
radar scatter data rel. to surface parameters from images 79−40100
radial velocity determ. from parallax and phase, instrument design 77−67038
radiogenic heat source content and cooling 80−90007
radiowave propag. for composition anal. 79−21204
radiowave propagation along surface 79−5768
rayed craters on Moon and Mercury, interpretation 78−12119
recent activity, conf., Houston, USA, 1976, March 77−71024
reflectance meas. in thermal emission region, thermal component removal 80−17497
regolith, C chemistry 77−60670
regolith, particle size distrib. anal., Rosin's law 77−78682
regolith, physical characts. and dynamics 77−60660
regolith, solar wind and micrometeorite effects 77−60669
regolith dissipation during cratering, stochastic model 79−70974
regolith evolution, compositional aspects 77−60663
regolith light element chemistry of Apollo 12 site 78−65515
regolith mixing extent 80−8561
relief and selenoid deform., harmonic anal. 80−72800
remanent magnetic field 77−60685
resitricted three-body lunar theory, non-Newtonian corrections *(German)* 77−25960
reverse side surface relief from Zond 8 photographs 77−64672
Rima Sirsalis, linear magnetisation feature 77−29668
Rima Sirsalis magnetic anomaly 80−36524
ring structures, rock mechanics theory 77−64675
ringed basin formation mechanics 79−16850
rock magnetism, palaeointensity method and lunar sample 10017135 application 80−36527
rotation around centre of mass, historical development of understanding 80−57064
rotation theory, tidal effect 77−13259
β Scorpii occultation, multiple star astrometry appl. 78−57583
secondary crater size-range relationships 79−44383
secondary craters preservation states, comparison with Mercury 78−12118
secular accel. rel. to Earth-Moon tidal friction, Earth moment of inertia change 80−81803
secular acceleration, calc. from oceanic tide semidiurnal waves *(French)* 79−8634
secular motion of mean longit. and perigee due to perturbations in terrestrial and lunar gravit. fields 77−78679
selenodesic work in France 80−12693
selenodesy, results from anal. of VLBI and laser data 77−29672
selenodetic control network 77−37515
selenodetic coord. system based on Kazan heliometric obs. *(Russian, English)* 80−41738
selenodetic investigations in USSR, bibliography (1928 to 1975) 79−88609
selenodetic reference network construction, choice of coordinate system *(Russian)* 80−72797
selenographic control points location definition based on craters 77−73981
selenographic coords. determ. of ALSEPs using RATAN-600 equipment *(Russian)* 79−25517
semirestricted three body problem 77−25932
siderophile elements indigenous abundances in lunar highlands, rel. to lunar origin 79−5767
solar radiowaves diffraction and refl. from lunar limb during solar eclipses *(Russian)* 78−65586
solar system formation, supernova trigger, evidence from meteorites isotopic anomalies 78−77499
solar wind induction, primeval and present day 77−60689
solar wind interaction, enhanced mag. field fluctuations at low altitudes 78−89030
solar wind sputtering, comments 78−61763
solar wind sputtering, fractionation on lunar surface 78−61762
solar wind sputtering rate 80−85835
Moon continued
Soviet lunar and planetary exploration, handbook 80−62398
spacecraft exploration results, review 77−2356
spectral photometry during max. solar activity 77−37522
star occultations, 1965-71 events recorded at Poltava *(Russian)* 78−4083
Stonehenge I and lunar apogee tracking 77−22116
sunset terminator region, electric pots. and fields in localised photoelectric charging 77−45330
sunset terminator region, photoelectric supercharging with progression of sunset 77−45331
superheavy elements in early Moon, possible evidence from Fe meteorites 79−48742
superheavy elements in primaeval Moon 78−96412
supernova γ-ray ablation, debris deposited on Earth 80−56731
surface, chem. changes at impact-induced phase transitions 77−60662
surface, interaction with exospheric atmosphere 78−49351
surface, spherical glass particles form. by impact melting 77−60661
surface, structure, atmosphere, magnetic field, development *(Hungarian)* 77−73987
surface albedo, soil and rock chem. comp. effects, solar wind darkening mechanism 78−28552
surface brightness fluctuations, photometric and polarimetric obs. 77−78681
surface chemical composition from albedo and colour index 77−87296
surface chemistry, weighted-filter imaging technique appl. to X-ray fluoresc. data 78−12124
surface colour differences, Tycho and Alpine valley areas 78−20663
surface dust movements, evidence and causes 77−60667
surface elemental anal. via orbital gamma-ray spectroscopy 79−12412
surface elemental composition, analytical determ. from Apollo X-ray and γ-ray spectrometer data 79−2495
surface features designation, near unified system 77−53441
surface features mapping at Kottamia obs. 80−12691
surface impact erosion and solar wind sputter erosion 77−60664
surface in-situ experiments, solar wind data review 80−77556
surface layers, validity of radiative-conductivity, theory 77−17354
surface magnetisation determ. from orbital surveys 77−37531
surface mapping from side looking orbital radar images 77−37520
surface mass fractionation by solar wind sputtering 78−49350
surface origin and evolution 77−60691
surface radio reflection, Luna 23 meas. at 3.1 cm wavelength 80−8560
surface reflective props. 77−33366
surface structure forecast, based on thermal conditions 78−77502
surface texture from scatt. light polarisation meas. 77−60673
surface unit definition and characterization using remote sensing 78−28551
swirl patterns produced by comet collision 80−51675
synodic month length, palaeontological evidence rel. to rate of var. of gravit. const. 77−45307
synthetic-aperture mapping from Earth-orbiting telescope 79−75119
tectonic pattern of Cruger/Rima Sirsalis-Rima De Gasparis area 78−65520
temperature inferred from gravity, stress state and tectonics 80−56732
temperature profile, rel. to lab. meas. of elec. cond. of pyroxene containing trivalent cations 80−31033
terminator configuration, rel. to electrostatic soil transport 79−35157
thermal convection in heterogeneous planetary interior 79−30001
thermal emission at 350 μ 77−73980
thermal evolution, calc. 79−2501
thermal evolution, latitude effects 78−4126
thermal evolution of planet growing by planetesimal impacts 79−70968
thermal history, evolutionary model 78−65522
thermal history, present state and tectonics, fission origin model 80−98582
thermal history, tidal dissipation contrib. 79−25524
thermal history rel. to fission origin 78−24476
thermal images obs. Meteosat in-orbit calibration appl. 80−17511
tidal acceleration, lunar laser ranging data results 79−16849
tidal acceleration determ. from laser range meas. 78−69718
tidal acceleration from satellite-derived ocean tide parameters 78−73662
tidal energy dissipation by Antarctic ice shelf flexing 78−88845
tidal evolution of Earth-Moon system 80−82240
tidal force acting on Moon due to Earth and Sun *(Russian)* 77−78616
tidal stresses rel. to moonquakes 78−40848
tidal-friction theory of the Earth-Moon system 80−81802
topocentric aberration, reduction method for astrometric obs. 78−4081
topographic changes on airless bodies, meteorite impact and ejecta deposition 78−65523
topography, harmonic anal. 77−60634
total eclipse, 1974 November 29, obs. in Ussuriisk 77−67051
total eclipse, 1975 November 18, obs. in Tadzhikstan 77−67052
total eclipse, 1978 March 24, 3.4 mm obs. 80−31220
total eclipse, 1978 March 24, 3.4 mm wavelength obs. *(Japanese)* 79−101095
transient lunar events, possible mechanisms 80−82238
transient lunar phenomena, review 77−60683
transient lunar phenomena rel. to deep moonquakes and HF teleseismic events 77−60684
transient phenomena, catalogue of observations, 1178-1977 period 79−21208
transient phenomena, critical vel. in gas-plasma interactions 77−71035
transient phenomena, distrib. and possible causes 77−71026
transient phenomena, physical processes in recent activity 77−71036
transient phenomena, possible causes, gas borne dust clouds 77−71034
transient phenomena, survey 77−71025
transient phenomena, upper limits to gas emission 77−71033
transient phenomena observations, fourth list (1821 to 1978) 80−62038
translational-rotational resonance motion in sphere gravit. field, intermediate theory 79−96899
translatory-rotatory motion, peculiarities caused by force function third and higher harmonics *(Russian)* 80−90349
UV spectrum, International Ultraviolet Explorer (IUE) obs. 78−93133
volatile emissions, detect. techniques 79−44385
volcanism and thermal tectonics on one-plate planets 78−77507
volume distribution of density 79−70972
Watts datum centre determ. rel. to lunar centre of mass 77−71020
X-ray and gamma-ray remote sensing spectrometers, data analysis system for planetary mission appl. 79−12411
young crescents, obs. and photographs 77−73986
zero age lunar thermal profiles from electrical induction 77−64673

Moon continued
^{40}Ar gas release 77−71031
K distribution, implications of K solubility in Fe-S and silicate-K-(Fe-S) equilibria 78−11843
Li abundance in Luna 24 soil samples 80−67590
$^{143}Nd/^{144}Nd$ initial ratio, lunar crust and mantle differential evolution 79−35156
^{222}Rn emanation as indicator of current activity 77−71032
TiO_2 distrib. over surface from anal. of Mikhail's photometric catalogue *(Russian)* 78−73661

Moon structure *see lunar structure*

moonquakes *see lunar seismology*

Morin temperature
see also weak ferromagnetism
$DyFe_{1-x}Co_xO_3$, magnetostriction, thermal expansion and elastic moduli near Morin point 77−8383
$DyFeO_3$, spin reorientation transitions induced by magnetic fields, Mossbauer study 80−71246
$DyFeO_3:Al^{3+}$, Morin transition, mag. vacancies effect *(Russian)* 78−27039
$Dy_{0.5}Ho_{0.5}FeO_3$, mag. transitions, influence of Dy^{3+}, Ho^{3+} ground states 77−89955
$(Fe_{1-x}Cr_x)_2O_3$, Mossbauer exam. of mag. struct. 77−24694
α-Fe_2O_3 and α-Fe_2O_3:Mn, linear mag. birefringence near Morin transition 77−52052
α-Fe_2O_3, haematite, mag. susceptibility meas. near Morin temp. 77−59404
Fe_2O_3, haematite, single domain, defect moment components rel. to Morin transition 79−16438
α-Fe_2O_3, haematite, substituted, Morin transition, neutron diffr. study 80−54897
α-Fe_2O_3, haematite, temp. mag. hysteresis near Morin temp. 79−56566
α-Fe_2O_3, hematite, interdomain phase transition 79−65675
Fe_2O_3, shocked hematite, Mossbauer exam. 78−64304
α-Fe_2O_3, X-ray diffr. exam. at phase transition from weakly ferromag. to pure antiferromag. state 77−51904
α-$Fe_2O_3:Al^{3+}(Ga^{3+})(Cr^{3+})(In^{3+})$, substitution effect on Morin transition, neutron diffr. study 80−44827
$Ho_{0.5}Dy_{0.5}FeO_3$ orthoferrite, domain wall struct., stability conditions, Morin transition, anisotropy const. 80−34684

Morse potential
see also intermolecular mechanics; kinetic theory
alkali halides, quadrupole coupling, vibr. and rot. effects, Morse oscill. calcs. 77−6805
alloy, substitutional, low conc., volume change calc. using Morse pot. function 77−15342
anharmonic corrections in unimolecular theory, Monte Carlo calcs. 80−83441
anharmonic Morse oscillator, multiphoton excitation, quantum vs. classical treatment 78−5306
aromatic hydrocarbons, Morse oscill., transition probabilities for mol. bond modes 79−18172
atom+atom collision, mol. form in presence of third particle, Morse oscill. calcs., dissoc. cross sections *(Russian)* 77−32786
atom+diatom, collision-induced dissoc., quantum mech. probability calcs. 78−25657
atom+harmonic oscillator collinear collisions with attractive interactions, semiclassical theory 77−522
atom+Morse oscillator, inelastic vibr. energy transfer, mol. continuum influence 80−106383
atom + diatom, A+BC, rotated Morse curve-spline pot. function 78−80729
atom-atom pots., Hilbert Schmidt expansion, transition operators 78−66621
AX_n molecules, vibrationally-hot, bond lengths, simple treatment 79−68202
benzene, and deuterated forms local mode oscill. strengths 79−27039
collinear collisions of Morse oscillators, dissoc. vibr. enhancement, quasi-classical trajectory study 80−28089
collinear triatomic system, binding, crit. pot. strengths 77−6883
crystal, one-dimens., stability, for teaching 78−54134
cubic metal, elastic shear modulus, temp. depend. 78−10118
cubic pure metals, thermal expansion coeffs., Morse pot. calcs. 79−77775
desorption, thermal, one-phonon at. scatt., 3-dimens., continuum model 78−87860
diamond, compressibility, appl. of Murnaghan eqn. of state, Morse pot. 80−79861
diatom, weakly bound, dissoc. energy for Morse and Lennard-Jones pots. 79−54988
diatomic gas, vibr. cross section, orientation depend. of interaction pot. *(French)* 77−515
diatomic mol. gases, quantum partition functs., virial coeffs., by path integration 77−15146
diatomic molecule, analytic model potentials, extended accuracy 79−64066
diatomic molecule, force const., Morse function in pot. curve *(Russian)* 79−49968
diatomic molecule, rot. perturbed Morse oscillator, eigenfunctions and Franck-Condon factors 77−42309
diatomic molecule, vibr. eigenstates, coherent states and uncertainty products 79−59434
diatomic molecule, vibr. Green's function and two-photon dissociation, appl. to H_2^+ 80−28075
diatomic molecule, with ang.-depend. pot., vibr. matrix element calcs. *(French)* 78−13484
diatomic molecule+diatomic molecule, collinear collision, anharmonicity effects 79−31656
diatomic molecule system, scattering contrib. to internal partition functions 79−81253
diatomic molecules, dissoc. energy calcs., Morse and Lippincott pot. functions 77−30952
diatomic molecules, equilibrium parameters and Morse anharmonic consts., electron diffr. determ. 78−58818
diatomic molecules, Franck-Condon factors for high J, Morse oscill. calcs. 78−37548
diatomic molecules, Franck-Condon factors for Morse pots. 79−72365
diatomic molecules, Morse oscill. vibr. matrix element calcs. *(French)* 77−27144

Morse potential continued
diatomic molecules, rot. transition probabilities calc. using Morse pot. 79−86046
diatomic Morse mol., inhomogeneous broadening in liqs., temp. depend 77−61803
diatomic potential, modified Morse function fitting procedure, appl. to $H_2(X^1\Sigma_g^+)$ 79−36560
diatomics, master eqn. theory, dissoc. rate consts. 77−77742
electron transfer reactions, free energy, anharmonic intramol. quantum mode depend. 77−12781
ensemble of Morse oscillators, density matrix, semiclassical phase space representation 79−9135
homonuclear diatomic mols., Morse pot. and vibr. level field induced, shift and broadening 80−69117
inert gas atoms, pot. energy curves analysis 80−53083
inert gas trimers and tetramers, ground state energies, pairwise Morse pot., few-body methods 79−72378
infi-nitelinear array of atoms, props., Morse pairwise pot. calcs. 77−76331
insulating materials, thermal expansion, Morse pot. model 80−107449
intramolecular energy transfer, stochastic, crit. point anal. of Hamiltonian system instabilities 79−98005
inverted potential, barrier permeabilities 78−66623
isolated small particles, struct. stability, atomistic studies 79−77957
lattice constant fluctuations, influence on thermal props. of cryst. 79−77715
matrix elements for Morse oscillators 80−83451
metal, limiting elastic moduli, Morse pot. appl. 77−69025
metal, pair pot. calc. using cryst. state props. 77−7692
metals, Morse potential appl. in molecular-metallic framework 80−79742
methane+methane, vibr. energy transfer, Morse pot. 79−31653
molecular dissociation, collision-induced, Morse oscill. model 78−37710
molecular electronic spectra, high pressure effects, Morse potential formulation 80−63617
molecular vibration, Hamiltonian diagonalisation method 79−3427
molecular vibration frequency change influence on Franck-Condon factors 80−106312
non-bonded potential functions, Morse curve, exp-6 and 12-6 pots. comparison 79−10166
nonequilibrium dissoc., Morse oscill. rigid rotator system, master eqn. soln. 80−40682
normalisation of Morse functions, Gamma function series summation 79−76477
off-shell K-matrix, computation method 78−74164
one-dimensional oscillator, excited rot. states, semi-analytic solns. 78−25502
one-dimensional quiescent lattices, shock profiles, end condition effects 80−34138
oscillator, classical motion, calcs. 78−73796
oscillator transition probabilities for mol. bond modes 79−18172
polyatomic mols., ground rot.-vibr. energy, internal coord. Morse oscill. 77−79596
polymers, breaking down of anharmonic chain, computer calc. 80−106410
position-momentum uncertainty products for exactly solvable potentials 80−12939
radiationless, electron transition, diatomic molecule in crystal at zero temperature, rate const. 79−43011
radical radiation formation in solid organic compounds 80−85201
rainbow scatt. props., semiclassical estimation 77−88523
rotational const. B_μ, asymptotic expansion 79−68289
satellite line shape, classical broadening theory including Doppler effect, pot. effect 79−22764
surface, adsorbed atoms thermal desorption, one dimens. microscopic model, weak binding case 80−96729
transition metals, amorphous, density of electronic states, effect of struct. variation due to interatomic pot. softness 80−54597
triatomic nonlinear mols., stretching vibrs., partial Morse oscills. 80−967
two body T matrices derived from strong potentials 80−63732
unimolecular decomp. kinetics, rot. effects 80−81319
unimolecular dissociation dynamics, collinear triat. system, R-matrix method 79−70315
van der Waals T-shaped mol., perpendicular vibr. predissoc., vibr. relax., Morse pots. 78−82659
water, vap., rot.-vibr. levels, nonperturbative multimode model, 2 interacting Morse oscills. 78−9135
weakly bonded molecular complexes, intermol. transfer and relax. of vibr. energy using Morse pot. *(German)* 78−1056
XH-Y complexes, IR absorpt. spectra, intramol. coupling influence, pot. energy surfaces derivation 80−91624
zincblende structure group IVA covalent crystals, Murnaghan parameter estimates from Morse pot. 78−95014
Al, stability and strength of FCC metal using Morse pot. 80−59430
AlH, vibr. consts. of electronic states, calc. method 79−93967
AlO, Franck-Condon factors and r-centroids for $D^2\Sigma$-$X^2\Sigma$ transition 79−94037
Ar, Hulburt-Hirschfelder pot. function 80−63612
Au, thermal expansion coeffs., Morse pot. calcs. 79−77775
Au, tilt boundary, Σ=11, simulated and observed struct., vibr. of individual atoms at grain boundary 80−88167
BiBr, $A^3(0^+)$ and $X^3Sigma^-(0^+)$ states, pot. energy functions comparison 80−43133
CN, r-centroids for $B^2\Sigma^+$-$X^2\Sigma^+$ transition 78−70811
CO, $A^1\pi$-$X^1\Sigma$ system, Franck-Condon factors, r-centroids calc. program 77−27121
CO, centrifugal distortion calcs. by perturbed Morse oscillator model including Dunham parameters 80−63862
CO, ejected electron spectroscopy of autoionising states using electron-electron coincidence technique 79−3587
CO, energy levels for perturbed Morse oscillators 80−78676
CO, ground states, anal. pot. function calcs. 78−78775
CO, mol. potential energy functions, extended accuracy 79−64066
$CO+H_2$, vibr. deactivation, 250 to 2000K, Morse pot. calcs. 78−46428
ClO_2, solns., reson. Raman spectra, appl. of Morse pots. 77−65485
CrO molecule, $B^5\pi$ and $X^5\pi$ states, potential energy curves 80−42962
CrOOH(D), barrier to proton or deuteron tunnelling 80−70156
Cu, entropy factors for vacancy formation and migration 78−75866
Cu, thermal expansion coeffs., Morse pot. calcs. 79−77775
Cu, vacancies, formation entropy, diffusion const. by determinant and Green's function methods 79−77595

Morse potential continued
D_2, Lyman bands, Morse Franck-Condon factors and R-centroids 77−58088
Fe, BCC, shock wave simulation using Morse pot. 78−2196
Fe, equation of state determ., high temp. and pressure, computer expt. 78−75800
Ge, self-diffusion, activation energy and entropy factors 80−88353
GeS, band system vibr. anal. 80−48009
H bonded species, IR absorption broadening, intramol. interactions effect 78−50595
$H+D_2$, collinear motion, energy transfer and dissociation, collision dynamics 80−99563
$H^-+Cs(6s)$, elastic scatt., pot. determ. from differential cross-sections meas. 78−78778
H_2, Lyman bands, Morse Frank-Condon factors and R-centroids 77−58088
H_2, scattering contrib. to internal partition functions 79−81253
HCl, scattering contrib. to internal partition functions for Morse potential 79−81253
HCl-dimethylether complex, gaseous, H-bond IR spectra, temp. depend. theory 78−62804
HD, Lyman bands, Morse Franck-Condon factors and R-centroids 77−58088
HF, dipole moment function, Schrodinger eqn. soln. using Morse pot. 77−79703
H_2O, excited stretching vibrs., quantum mechanics. 80−91535
$He+CO_2$, translational-vibrational energy transfer, quantum dynamical study 80−63746
He+HCN, translational-vibrational energy transfer, quantum dynamical study 80−63746
He+OCS, translational-vibrational energy transfer, quantum dynamical study 80−63746
He^++CS_2, dissoc. charge-transfer, $CS^+(B^2\Sigma^+-A^2\Pi_i)$ emission prod., Morse pot. Franck-Condon factors calc., vibr. anal. 80−99539
He^++OCS, dissoc. charge-transfer, $CS^+(B^2\Sigma^+-A^2\Pi_i)$ emission prod., Morse pot. Franck-Condon factors calc., vibr. anal. 80−99539
HeI_2, van der Waals mol., vibr. predissoc. lifetimes 79−68278
^4He, liq., ground state energy and struct. 77−66051
I_2, A-X system 79−63995
I_2, equilibrium parameters and Morse anharmonic consts., electron diffr. determ. 78−58818
LaO molecule, potential energy curves, Rapid method by Morse function 77−26998
LiF surface, diffractive scatt. of H atoms, meas., Debye temp. and Morse pot. determ. 80−76124
MgH, Morse and Lippincott pots., r-centroids, dissociation energy 78−13446
N_2^-, vibr. autodetaching states, from H^-+H_2, excitation and decay, Franck-Condon factors 78−33620
NO^+, $A^1\Pi-X^1\Sigma$ system, Franck-Condon factors, r-centroids calc., program 77−27121
Ni perfect crystal, stability under various stresses 80−104208
PO, $C^2\Sigma^+-X^2\pi_r$ state, Franck-Condon factors and r-centroids 77−65512
Pd, metal cluster, calculated structural stability 78−95268
Pt, surface diffusion of single atoms of Pt, Ir and Au, FIM expts. and Morse potential calcs. 78−34717
SF_6, vibr. anharmonicity consts., ν_4 region laser absorption obs. 78−94242
Si, self-diffusion, activation energy and entropy factors 80−88353
SiO, vibr. wavefunctions, Franck-Condon factors, at low quantum numbers 78−55203
SnO, $D^1\Pi-X^1\sigma$ transition, Franck-Condon factors and r-centroids, calc. using Morse pot. 79−41197
Sr_2 dimer, photoassoc., photoluminesc., collisional dissoc. 80−58303

m.o.s. devices *see metal-insulator-semiconductor devices*

m.o.s. integrated circuits *see field effect integrated circuits*

m.o.s. structures *see metal-insulator-semiconductor structures*

mosaic structure (microstructure)
alloy steel, complex, X-ray diffr. determ. of fine struct. changes during quenching and tempering 77−56004
copper phthalocyanin, thermal behaviour *(Japanese)* 80−24753
corundum, spherical ground samples, extinction effects, inhomogeneous mosaicity 78−75494
mica, defects effect on epitaxial film struct. 78−26794
polyethylene terephthalate, differential scanning calorimetry of melting, mosaic block struct. of cryst. layers 78−26452
polymer crystal, paracrystallinity, mosaic block concept 77−84673
pyrocarbon coatings, TEM anal. 77−79463
quartz, spherical ground samples, extinction effects, inhomogeneous mosaicity 78−75494
rapid X-ray determ. in large single crystals 79−37584
sapphire, profiled growth, struct. perfection 78−68621
Al, high purity single cryst., etch pit morphology and their correl. with microstruct. *(French)* 79−69106
Al_2O_3, cryst. subgrain misorientations, X-ray diffr. microscopy technique 77−70272
B_2O_3-Nb_2O_5 system, phase equil. and phase struct. obs. by high resolution TEM 80−108419
$BaTiO_3$, mosaic struct. charge at ferroelec. phase transition *(Russian)* 77−32335
C, microscopic features of carbons obtained from aromatic hydrocarbons using carbonisation catalysts 77−66597
C, obtained from aromatic hydrocarbons using $AlCl_3$ catalyst. 77−63572
CdS, epitaxial layers on (111) Ce, growth and defect struct. 78−18920
Co, amorphous ferromag. film, resist. anisotropy rel. to struct. 77−72926
Cu (220), mosaic single cryst., neutron integrated reflectivities 79−86656
Cu, single crystals, deformed, extinction, γ-ray diffractometry and neutron struct. refinement 77−84588
α-Fe_2O_3, prod. by α-FeOOH dehydration, mosaic struct. and twin form. 79−86802
Ge (111), mosaic single cryst., neutron integrated reflectivities 79−86656
KCl, X-ray diffr. exam. 77−7740
$KZnF_3$ single crystal growth, Czochralski method 80−97421
Ni, deformed, work-hardening, dislocation and mosaic struct., X-ray and electron microscopy 77−35625
Pb (220), mosaic single cryst., neutron integrated reflectivities 79−86656
Pb film, monocryst., heteroepitaxial growth, struct. defects, and elec. props. *(Russian)* 80−84403

mosaic structure continued
Pd_2Si films on Si, lattice imaging obs. of structural details 80−103604
RbI, mosaic struct. in metastable press. region, gamma-ray diffr. meas. 77−20065
RbI, single crysts., mosaic struct. changes, press. induced 77−51507
Si, epitaxial, on sapphire, characterisation, X-ray rocking curves 80−75458
SiC (6H) epitaxial layers, growth by CVD, morphology 79−24446
$TbVO_4$, Jahn-Teller phase transition, γ-ray diffractometry 78−91205
V_3O_5, increase of X-ray refl. intensities and profile widths at phase transition temp. 79−69052
WC-Co compacts and sintered alloy, fine struct. of carbide phases, preforms re-pressing under high press. effect 79−28987
YAG:M^{3+}, ESR absorption spectra, line broadening of Fe^{3+}, Cr^{3+}, Gd^{3+} 78−91940
Zn (0002), mosaic single cryst., neutron integrated reflectivities 79−86656
Zn cryst. subgrain misorientations, X-ray diffr. microscopy technique 77−70272
ZnO heteroepitaxial films, grown on Al_2O_3 substrates, X-ray topographic study of struct. 79−15048

m.o.s.f.e.t *see insulated gate field effect transistors*

m.o.s.i.c. *see field effect integrated circuits*

Mossbauer effect
4f substances, rel. to electronic props. at config. crossover 77−47775
absolute Mossbauer fraction, determ. and transmission integral 80−37143
absorbers, deformation induced texture 79−8074
absorption spectra, thickness and polarisation effects, line intensities of a multiple line absorber *(French)* 80−77924
absorption spectra variations induced by LF acoustic excitations 80−102904
acoustic excitation of Mossbauer nuclei, for acoustic freq. less than linewidth 77−24773
actinide hydrides, Mossbauer studies, book contrib. 79−82906
actinide intermetallics, $AnFe_2$, (An=U, Np, Pu, Am), magnetisation, neutron diffr. and Mossbauer expts. 77−63137
actinide ions, electronic props., Dirac-Fock studies 78−60094
actinides, Mossbauer isomer shifts, book contrib. 79−87362
active data acquisition 80−9079
β-AgI, valence state and impurity-vacancy dipole formation, Mossbauer effect meas. 78−68435
alkali borate glass, Mossbauer expts., 85-500K 78−80260
alkali borate glasses, alkali cations role 78−39476
alkali halides, implantation of ^{57}Fe, conversion electron Mossbauer spectroscopy technique 80−40012
alkali metal nitroprussides, Mossbauer spectra, dehydration effects 79−24237
alkaline earth ferricyanide hydrates, $M_3[Fe(CN)_6]_2.12H_2O$, Mossbauer spectra 79−99805
allophane, synthetic, amorphous mineral struct. obs. using ^{57}Fe Mossbauer effect 80−34836
alloy, many-body atomic correlations, Mossbauer spectroscopy study 80−15934
alloy structure determ. using high-temp. chamber 77−17982
alloys, phase analysis by Mossbauer spectra 80−15922
Alnico 5, two-phase separation during ageing, Mossbauer study 80−7533
amorphous alloys and semiconductors, Mossbauer spectrometry *(French)* 80−80660
amorphous magnet, magnetisation, mag. moment temp. distrib. 80−15848
amorphous materials, Mossbauer spectra anal. 77−20762
amorphous materials props. and investigation methods *(French)* 80−80652
amorphous metals, geometric struct. models and diffraction exam. techniques 80−79700
amphiboles, Mg and Mn rich, Mossbauer spectra 79−38412
ancient Japanese roofing tiles, characterisation by ^{57}Fe Mossbauer spectroscopy 79−26191
ancient pottery anal. using transmission spectroscopy 77−48734
anharmonic US vibrations excited in crystal, effect on Mossbauer emission and absorption spectra 78−72443
anharmonicity, low-temp. model, Debye-Waller factors of Mossbauer effect 78−55927
anisotropic NiAs-CdI_2 type structure, Mossbauer line broadening due to diffusion 77−12281
antimonates, $M_4^{II}M^{III}Sb^VO_8$ spinels, struct. determ., IR and Mossbauer spectra 79−91431
apparatus for low-temp./high pressure Mossbauer absorber study, modified 79−17591
apparatus for resonance studies at high press. and low temps. 78−49943
applications in metallurgy, solid state and interface chemistry, structure of ion-containing proteins 77−12292
archaeological investigations, mag. oxides in first American civilisation 77−60886
atom in solid, mean square amplitude and velocity 80−62813
atomic hyperfine coupling consts., calc. 77−39810
austenitic steel, pearlitic transformation incubation effect, Mossbauer spectra *(Russian)* 79−70061
automated complex, Mossbauer spectra information retrieval and processing *(Russian)* 78−82091
bacteria, freshwater magnetotactic, identification of magnetite, Mossbauer obs. 80−3657
bacteria magnetotaxis, Mossbauer study 80−41056
bacterial catalase, ^{57}Fe enriched, active centre, Mossbauer spectra meas. 80−8024
basalt, deep-sea, Mossbauer study of core-to-rim alteration 79−66688
bauxite, Fe-containing, Mossbauer analysis 78−44806
BBOA:Sn-BBA, liquid crystal glass, unresolved Mossbauer quadrupole doublet, orientation depend. 77−84645
BBOA, smectic liq. cryst. glass-supercooled transition and Debye temp., ^{57}Fe Mossbauer effect 80−54999
BCC metal, heavy ion implanted, vacancy annealing stage, Mossbauer meas. 78−39463
benzene-I_2, π-σ charge-transfer complex, frozen soln., Mossbauer spectra obs. 80−91655
beryl, channel constituents, electronic absorption spectra of Fe^{2+} 79−69863
(2,2′-bi-2-thiazoline) iron thiocyanate, high spin to low spin transition, X-ray diffr. and Mossbauer obs. 79−38418

Mossbauer effect continued
bimetal foil, magnetic-transforms., Mossbauer spectroscopy *(Russian)* 78−6607
biochemical systems 77−13047
biological systems, very low temp., meas. using ^{3}He-^{4}He refrigerator 78−24909
biomolecular ^{57}Fe transport and storage compounds 77−12875
biomolecules, determ. of static and dynamic struct. 80−40952
biomolecules, Fe-containing, appl. of spectroscopy 79−24956
biotite, anisotropy of Mossbauer absorpt. 78−80263
biotite, elec. field gradient Mossbauer absorption 77−85629
biotite, Mossbauer and optical spectra, Fe^{2+}-Fe^{3+} interactions 80−60470
blackbody absorber in Mossbauer spectroscopy using SnO_2 with isotope ^{119}Sn 80−2669
Brownian particles, magnetic theory of Mossbauer effect *(Russian)* 78−68436
bubble garnet film, ion-implanted, mag. struct., conversion-electron Mossbauer spectroscopy 80−84628
butadiene, styrene, 4-vinylpyridine terpolymer, cross-linked by coordination with Fe (III) chloride, ion clustering 78−83748
butadiene iron tricarbonyl, adsorbed on graphite, diffusion and melting, Mossbauer meas. 79−61270
4-n-butoxybenzylidine-4′-n-octylaniline, liquid cryst., smectic B phase lattice vibr. anisotropy, Mossbauer anal. 77−7666
calibration constants in Mossbauer diffr. expts. 78−24906
CAMAC data acquisition system 79−30439
Canadian soil characterisation of FeO compounds by Mossbauer and other methods 77−44986
carbonaceous chondrites, reduction kinetics, Mossbauer obs. 80−41777
carbonmonoxymyoglobin, forzen soln., recoilless fraction, Mossbauer spectra meas. 80−8025
carburised and carbonitrided surface layer structure and phase composition 78−95830
chalcogenide glass, Fe, doped in equil. conditions, impurity cond. and Mossbauer effect 80−49726
chamber of Mossbauer spectra investig. at 50 kbar 77−41634
chemical relaxation, tunnelling, Mossbauer emission spectroscopy studies 80−40683
Cherenkov and transition radiation in gamma-ray resonance frequency range *(Russian)* 78−80432
Chevrel-phase superconductors, lattice dynamical calcs. 79−33056
chlorite, ^{57}Fe Mossbauer analysis 80−40006
chromindur, origin of coercivity, Lorentz microscopy, magnetisation and Mossbauer effect 78−64219
chromite natural samples of Brazilian, Philippine origin, chem. comp., Mossbauer spectroscopy 80−103901
chromites, from India, struct. and comp. 78−44807
Clauser-Blume model for Mossbauer line shape with non-stationary relax. effects 80−34827
coal, mag. and Mossbauer characterisation 78−64903
coal, mag. susceptibility and Mossbauer meas. 80−60464
coal liquefaction residues, Mag. separability enhancement, thermomagnetic anal. and Mossbauer study 79−83544
coherence and interference 78−27123
coherent γ-radiation generation, collective and stimulated processes *(Russian)* 78−9356
combination type maxima, hyperfine interactions on nuclei 80−25263
complementary techniques: EXAFS, determ. of struct. of disordered regions *(French)* 80−80905
complementary techniques: positron annihilation, review of appls. *(French)* 80−80899
complementary techniques muon spin rotation appl. to physics of condensed matter *(French)* 80−80667
computer program 79−56631
computerised analysis, collaboration collection report 80−73106
condensed matter scatt., review 79−78596
conference, Cracow, Poland (Aug. 1975) 77−24774
conference, Kyoto, Japan (Aug.-Sept. 78) 80−7199
conference, Portorez, Yugoslavia, (Sept. 1979) 80−36768
conversion electron depth selective Mossbauer spectra 79−35909
conversion electron Mossbauer spectra, electrons below 10 eV 80−37145
conversion electron Mossbauer spectra, X-ray prod. of secondary electrons 77−59498
conversion electron Mossbauer spectrometry, back-scatter-type gas flow detector 80−37680
conversion electron Mossbauer spectroscopy, appl. to surface props. and reactors 78−60359
conversion electron Mossbauer spectroscopy, cryogenic proportional He counter 80−69010
conversion electron Mossbauer spectroscopy, dynamic theory 77−51997
conversion electron Mossbauer spectroscopy, electron transport anal. 78−94159
conversion electron Mossbauer spectroscopy, electrostatic spectrometer 78−88238
conversion electron Mossbauer spectroscopy down to 4.2K, applications to thin film and surface studies 78−84504
conversion electron scatt. in thin foils, depth selection, Monte Carlo calc. of energy distrib. 79−45598
conversion electron spectroscopy at high temp., proportional counter 80−27886
cooling unit, continuous flow, for Mossbauer experiments, 4.2 to 300K 80−31954
cooling unit, continuous flow liq., He, for Mossbauer expts. 77−33992
core electron contribution to Mossbauer isomer shift, variation with ionic size 79−73866
correlation counting in time-domain Mossbauer spectroscopy 80−47161
corrosion and interfacial reactions, spectroscopy applics. 77−12749
corrosion processes and products Mossbauer study 80−40572
critical fluctuations obs. using Mossbauer spectroscopy 80−39955
critical scattering of Mossbauer radiation 78−15073
critical scattering of Mossbauer radiation in condensed matter 79−56635
cryostat, Mossbauer effect study at 65 and 77K 79−67364
crystal, line broadening due to correlated diffusion 77−73097
cubic alloys, anisotropic hyperfine interactions, Mossbauer spectra 80−15854
cubic crystal, second-order Doppler shift 79−56633
cubic metals, impurity-host force-constant changes from Mossbauer data, review 78−48097
cyclohexane, dynamic props. investig. by Rayleigh scatt. of Mossbauer radiation *(Russian)* 77−69760

Mossbauer effect continued
cytochrome c_3, haeme-haeme mag. interaction obs. 80−108836
cytochrome c_3−hydrogenase, reduction kinetics, Mossbauer spectra 80−67031
data acquisition and processing system 80−18061
data calibration using laser interferometer 77−88326
data centre 80−37148
Debye-Waller factor evaluation from recoilless fraction 77−59090
deformation induced texture in absorbers 80−7214
cis-dekalin, dynamic props. investig. by Rayleigh scatt. of Mossbauer radiation *(Russian)* 77−69760
deoxyhaemoglobin, high mag. field Mossbauer spectra, electronic states 80−35845
deoxyhaemoglobin, vibronic coupling, mag. susceptibility and Mossbauer data interpretation 78−70984
deoxymyoglobin, forzen soln., recoilless fraction, Mossbauer spectra meas. 80−8025
deoxymyoglobin, high mag. field Mossbauer spectra, electronic states 80−35845
deoxymyoglobin, vibronic coupling, mag. susceptibility and Mossbauer data interpretation 78−70984
deoxymyoglobin single crysts., Mossbauer study with polarised γ-rays 80−40962
depth profiled ^{57}Fe conversion electron Mossbauer spectra, method for distinguishing overlayer and substrate signals 79−28661
depth selective, influence of atomic number of inert component in surface layer 80−15931
depth selective, low energy electrons in matter 80−15930
depth selective Mossbauer effect spectroscopy empirical method of quantitative anal. using conversion electrons 78−20130
derivative spectroscopy, detectability *(Japanese)* 79−28652
1,1′-diacetylferrocene, MBBA soln. nematic glass-supercooled nematic transition, Mossbauer temp. obs. 79−95687
diamond:Xe, quadrupole interaction of implanted Xe 79−61279
diamond, amorphisation during ^{133}Xe implantation 80−40010
diamond, amorphization process, ^{133}Cs Mossbauer spectra 79−99809
diamond, implanted ^{129m}Xe, lattice location, combined Mossbauer and IPAC meas. 78−43733
dichelated protohaeme, model haemoglobin cpd., Mossbauer spectra 80−16904
dichroism of polarised Mossbauer rays 80−7201
dielectric permittivity in X- and γ-ray regions, review 80−44998
diffractometer using microcomputer 80−7210
diffusion data obtained by NMR and Mossbauer expts., interpretation, mol. dynamics study 78−47567
digital based triangular wave generator for Mossbauer spectroscopy 78−55113
dimethyl stannous chloride di(pyridine 1-oxide), ^{119}Sn Mossbauer spectra, elec. field gradient 80−15909
dimethyl tellurium diiodide, ^{129}I Mossbauer spectra, coupling consts. 78−62833
dimethyl tin difluoride, crystallographic phase transition, 70K, Mossbauer obs. 79−47366
dimethyl tin diisothiocyanate, ^{119}Sn Mossbauer spectra, elec. field gradient 80−15909
dimethylammonium iron chloride, two-dimens. antiferromag., ^{57}Fe Mossbauer obs., sublattice magnetis. 77−66443
dimethylammonium iron tetrachloride, Mossbauer study of struct. phase transition 80−39278
dispersion effects, in thick absorber, for arbitrary direction of propag. *(French)* 78−10806
dithioferrates (III), electronic struct. and hyperfine interactions, Xα calcs. 80−100448
Doppler shift, 2nd-order, 1-100K, appl. to Au, Pt, W, Ta, Sn, Pd, Ge, and Zn 79−91317
Doppler shift, second order, press. depend. 80−66088
double Mossbauer spectrometer for small resonance line shift meas. 78−82560
E. coli cells, iron-storage protein, Mossbauer spectra obs. 80−8022
elbaites, Zn-Fe, γ-irradiated, Mossbauer study 80−44990
electric field gradient sign, possibility of obtaining from combined TDPAC and Mossbauer meas. 78−24907
electric field gradient sign, possibility of obtaining from combined TDPAC and Mossbauer meas. 78−24908
electric field gradients, shielding for various elements and electronic configurations 80−39535
electron Mossbauer spectroscopy, scatt. technique 77−81035
electron re-emission Mossbauer spectroscopy, appl. to surface films 77−1622
electron spectrometer, internal conversion electrons detect. 80−7202
elemental semiconductors, group IV, Mossbauer spectroscopy of defects, radiation damage and deep levels 80−59533
EM vel. drive for Mossbauer spectroscopy 78−66022
energy spectrum of resonance gamma-rays obtained by time measurements *(Russian)* 79−19815
enzyme, complexation, Mossbauer spectroscopy 77−12876
exchange narrowing 77−85627
exchange narrowing of Mossbauer line 77−85627
Faraday effect for Mossbauer radiation at oblique incidence 80−50236
fast γ-ray detection systems for Mossbauer spectroscopy 78−25376
^{57}Fe, isomer-shift calibration by lifetime variations in electron capture decays of ^{52}Fe 80−75902
Fe particles in glass-like C matrix, identification and props. 80−11229
Fe-Cr-Co-Si-Mo, plastic deform. influence on structure and mag. props. *(Russian)* 79−70176
ferredoxin, from Clostridium pasteurianum, Mossbauer effect, ESR, and mag. susceptibility meas. 80−40961
ferredoxin synthetic analogues, $[Fe_4S_4(SR)_4]^{3-}$ clusters, Mossbauer effect, EPR, and mag. props. 80−41057
ferredoxin-like centres, membrane bound, in photosystem I of blue-green algae, Mossbauer and EPR study 80−40974
ferric haeme complex of low spin, Mossbauer spectra, crystal field parameters 80−26203
ferric myoglobin compounds, single crysts., Mossbauer spectrum in small mag. field 79−100571
ferric myoglobin cpds., single cryst., Mossbauer studies 80−8016
ferrichrome A, selective excitation double Mossbauer meas. 80−8015
ferrite, hexagonal, local lattice distortions, use of Mossbauer effect 78−43745
ferritin, iron core particle size distrib., Mossbauer determ. 78−92696
ferritometer, design 79−17453

Mossbauer effect continued
ferrocene, dynamics in liquid and glassy o-terphenyl, Mossbauer obs. 80-55000
ferrocene, proton irradiated, Mossbauer study of induced chemical changes 79-28656
ferrocene derivatives, exhibiting mesomorphic props., synthesis, appl. in Mossbauer spectroscopy 77-31589
ferrocene derivatives, mixed and averaged valence types, Mossbauer spectra 80-15906
ferrocene derivatives in smectic B phase liquid cryst. BBOA, ^{57}Fe Mossbauer study 78-27136
ferrocene related compounds, $C_5R_5Fe(I)$-$C_6R'_6$ paramag. sandwiches, Mossbauer study 80-39982
ferrocenecarbaldehyde, plastic cryst. state, Mossbauer spectroscopy and microscopic obs. 77-76333
ferroelectric, Mossbauer spectrum parameters, Fe^{3+} 4s shell polarisation by electric field 79-95698
ferroelectric transitions, Mossbauer spectroscopy study 80-39911
ferromagnet, amorphous and crystalline, evaluation of complex Mossbauer spectra 78-43755
ferromagnet, amorphous and crystalline, evaluation of complex Mossbauer spectra 78-60370
ferromagnet, Mossbauer effect at temp. close to Curie temp. *(Russian)* 79-87339
ferromagnet, shape of Mossbauer line 80-71251
ferromagnet with impurity atoms *(Russian)* 77-48098
ferromagnetic film, electric-charge-induced magnetisation, mag. balance and Mossbauer effect meas. 79-69700
ferromagnetic metallic glass, hyperfine field and spin wave excitations, $T^{3/2}$ depend. 78-10672
ferromagnets, domain struct. effects on dynamic props., review 80-34678
ferrous alloys, phase transforms. and ordering, Mossbauer spectroscopy 77-12619
ferrous oxalate dihydrate, Mossbauer spectrum, hyperfine fields 78-39483
ferrous rubredoxin, high spin, spin fluctuation rates from Mossbauer spectra 79-29506
ferrous tetraphenylporphyrin, Mossbauer effect, mag. hyperfine interaction 79-24236
fluorosilicate, Mossbauer polarimetry, double motion drive and effective thickness meas. 78-23379
free surfaces, apparatus for Mossbauer effect emission and AES, appl. to ^{57}Co on Ni (111) 79-80735
friction, lubrication and wear studies, Mossbauer spectroscopy appl. 80-40547
function generator using IC, for Mossbauer effect work 80-68334
furnace, high-precision for use up to 1100K 78-66021
gamma resonance phase anal., background allowance using total resonance absorpt. filter 78-33363
gamma-quantum coherent scatt. in field of US waves, kinematic theory 80-80649
gamma-ray laser, nuclear orientation techniques for directed emission 77-27268
gamma-ray laser appl. *(German)* 78-1201
gamma-ray lasers, direct pumping by resonance capture of neutrons 80-14310
gamma-ray scattering under double γ-reson. conditions 79-73873
gamma-ray source design, calibration and polarimeter 80-86535
gamma-rays guides by total external refl. appl. 80-7200
gamma-X ray coincidence Mossbauer measurements 80-14041
garnet: ^{57}Fe, electric field gradient, Mossbauer exam. 79-1732
garnets, ^{57}Fe and ^{119}Sn spectra 80-20568
geochronology, possible appl. of ^{57}Fe Mossbauer spectroscopy 80-41416
glass: ^{57}Fe, 2-parameter distrib. analysis using general inversion method 80-66079
glass, $Fe^{2+(3)}$ impurity ions struct.-chem. state, Mossbauer data 80-40028
glass, struct. formation during crystallisation, Mossbauer obs. 77-48106
glasses, elec., mag., and optical props., conference, Troy, NY, USA (Aug. 1979) 80-105417
glauconite group minerals, Norwegian-Greenland basin, age determ. by EPR and Mossbauer spectra 80-26467
glauconites, Mossbauer anal., Fe^{3+}/Fe^{2+} ratio 80-17252
glissile dislocations, prod. by impurity atoms, Debye-Waller factor calcs. 78-2214
glycerol, Mossbauer and neutron scatt. 80-20559
glycerol, supercooled, Mossbauer effect and model of mol. motion 78-64301
glycerol, supercooled liq., dynamical struct. factor, Mossbauer spectroscopy 78-27126
glycerol, supercooled liq., mol. motion, Mossbauer effect, Rayleigh scatt. obs. 77-73099
gold complex, AuI (triphenylphosphine)$_n$ chlorates (n=2,3,4,), Mossbauer spectra 79-54874
graphite, mol. orientation of adsorbed trimethyl tin chloride, recoilless gamma reson. 77-76663
graphite, pyrolytic, elastic and inelastic scatt. of Mossbauer γ quanta *(Russian)* 79-61287
graphite, pyrolytic, thermal diffuse scatt., Mossbauer γ-ray diffr. 80-40026
graphite, X-ray monochromator crystal, TDS, Mossbauer obs. *(German)* 77-16230
graphite-$FeCl_2$($FeCl_3$) intercalation cpds., lattice dynamics, Mossbauer spectra 80-15925
graphite-$FeCl_{3-x}$ intercalation compounds, Mossbauer spectra 80-20538
gravimeter based on Mossbauer effect for mineral exploration 77-37444
gravitational red shift meas. using ^{67}Zn and ^{181}Ta 78-24905
greenalite, two-dimens. mag. order 79-61188
group IV elements, ^{57}Fe isomer shift, quadrupole coupling and interat. distance correl. 78-52408
haemin, mag. interaction down to 0.03K 78-44450
haemin-histidin, ^{57}Fe Mossbauer spectra, temp. depend. of quadrupole splittings, atom positrons *(Spanish)* 77-73098
haemoglobin, deoxygenated, electronic term scheme using mag. susceptibility and Mossbauer data 77-44586
haemoglobin, subunit cooperative interaction, stereochemical trigger, Mossbauer study 78-53321
haemoglobin hydroxide, Fe Mossbauer quadrupole splitting 78-55192
haemoglobin-haptoglobin deoxygenated complexes 78-24020
Mossbauer effect continued
haemoproteins, Fe-ligand binding and electronic struct., Mossbauer studies 80-8021
haemoproteins, highly oxidised Fe, electronic struct., Mossbauer spectroscopic obs. 77-88478
Halobacterium, whole cells and ferredoxin 78-76998
HBPA, smectic liq. cryst. glass-supercooled transition and Debye temp., ^{57}Fe Mossbauer effect 80-54999
heart tissue, thalassaemic, Mossbauer spectra of Fe deposits 78-73202
hexadecapole spin resonance in cubic symm. cryst. by NQR, NMR, nuclear gamma reson. 80-20500
HF excitation, review 77-48113
high counting rate studies using modified ECIL preamplifier 78-74546
high field Mossbauer spectroscopy, recent developments 79-73863
high magnetic field behaviour of solids and plasmas, conference, Cambridge, MA, USA (Sept. 1978) 79-60667
horseradish peroxidase cpd. II, high-field Mossbauer spectra, 4.2 to 120K 80-8026
hot luminescence and relaxation processes 79-38619
hydrazinium iron tri(hydrazoformate) monohydrate single cryst., effective EFG tensor, Mossbauer spectra obs. 79-56628
hyperfine interactions at ultralow temps. 78-43742
hyperfine structure parameters program 79-15383
Icelandic igneous rocks, Mossbauer anal. 80-17253
ilvaite, electron delocalisation obs. in Mossbauer spectrum 79-33581
ilvaite, Fe temp. depend. oxidation states, electron hopping, Mossbauer spectra, X-ray diffr. obs. 78-2779
ilvaite, temp. dependent electron delocalization, Mossbauer spectra 79-11361
ilvaites, Mossbauer spectra and mag. features 80-7248
implanted atoms, Mossbauer studies 80-39913
in-beam implantation, method and appl. 78-25372
in-beam time-gated Mossbauer expt. 80-40021
industrial analysis applications *(Hungarian)* 79-16070
inelastic scattering intensity meas. of gamma quanta 80-71245
inhomogeneous waves in Mossbauer absorber 79-73871
inorganic compounds, chemical bonds using $K\alpha_1$ line chem. shifts, Mossbauer isomer shifts 77-27089
integrating counting technique, appl. to ^{197}Au Mossbauer spectroscopy 78-25377
interference effects in E2 transitions 77-59491
interference effects in relaxation spectra 77-63326
interference parameters in γ-ray optics 78-19395
intermediate valence, phase diagram and Kondo behaviour 80-29366
intermediate valence compounds, microscopic model 79-78595
intermediate valence materials, autocorrelation, line shapes, power spectrum due to occupancy variations 78-47742
Invar, deformed, magnetism and temp. depend. of effective field on ^{57}Fe *(Russian)* 79-24234
Invar, Fe-Ni-C, spin pinning effect in RF collapse studies, Mossbauer spectroscopy 80-44971
Invar, hyperfine field at Fe nucleus, effect of deform. by cold rolling 77-48556
Invar, magnetic structure, absorbed H_2 effect 80-20534
Invar, magnetic structure, depend. on absorbed H, Stoner's band model calcs., Mossbauer spectra 80-65787
Invar, magnetisation reversal, fast, forced by external RF mag. field, Mossbauer obs. 78-52311
Invar, Mossbauer effect at high press. 80-15858
Invar, RF collapse studies, skin depth effect, Mossbauer spectroscopy 80-39953
Invar, stainless, thermal expansion, elastic props. and Mossbauer effect 79-56502
Invar problem, conf., Nagoya, Japan (Sept. 78) 79-56481
inverse problem of Mossbauer spectroscopy in RF vibrating crystals 79-78574
iodobenzoic acid, NQR of ^{127}I and Mossbauer spectra of ^{125}I, bonding 77-12241
iodohippuric acid, NQR of ^{127}I and Mossbauer spectra of ^{125}I, bonding 77-12241
ionic compounds, amorphous, Mossbauer study, frozen mag. state and hyperfine interaction *(French)* 80-80661
iron(II)-A-zeolites, reduction, mag. and Mossbauer study 80-71115
iron (III) salicylates, Mossbauer and IR spectra, mag. susceptibility 80-50242
iron oxalate, γ-ray and neutron irrad. effects, Mossbauer spectra obs. 79-65778
iron oxalate, quadrupole splitting, Mossbauer spectroscopy 79-11365
iron-transition metal oxinates, Mossbauer spectra 77-90082
isomer shift, energy equivalents of one mm/sec, tabulation, book contrib. 79-87365
isomer shift, for calc. of charge and spin densities in solids, book contrib. 79-87350
isomer shift, introduction, book contrib. 79-87347
isomer shift, rel. to orbital occupation numbers 80-39983
isomer shift cancellation with resonant detectors 80-80664
isomer shift expressions, tabulation of consts., book contrib. 79-87367
isomer shift measurement, book contrib. 79-87349
isomer shift reference scales, book contrib. 79-87368
isomer shift reference scales, Mossbauer Effect Data Centre 80-37147
isomer shift theory book contrib. 79-87348
isomer shifts, book 79-87346
isomer shifts, total conversion coefficients, nuclear electron and gamma transitions importance 79-85411
isomer shifts and nuclear models, book contrib. 79-85385
isomeric molecular states generated by polarised light, Mossbauer resonance obs. 77-20781
isomeric nuclear state excitation by synchrotron radiation, Mossbauer effect 79-42508
isotope shifts, electron density at nuclear determ., book contrib. 79-87351
K-22 solid catalyst, H_2O_2 decomp. rel. to Mossbauer spectra 80-34826
$KFeF_4$, reflections of new type in Mossbauer diffraction pattern 79-78594
$KFeF_5$, one dimensional antiferromagnets, field depend. spin reduction temp. variation, spin flopping 79-78586
Kirin meteorite shower, Mossbauer anal. *(Chinese)* 79-62797
Lamb-Mossbauer factor for crystalline lattice 79-78592
lattice atom interactions from resonance γ-ray fluoresc., theory 80-71278

Mossbauer effect continued
lattice isolation of impurities from hyperfine interaction and channelling results 78−43731
lattice parameters, mag. and elec. props. 80−100578
Leoville meteorite, type III carbonaceous chondrite, ^{57}Fe Mossbauer spectroscopy 78−49404
liberation from electrolytic Ni during vacuum heating, Mossbauer spectra *(Russian)* 80−35594
line broadening, influence of diffusion *(German)* 78−84510
line broadening due to Mossbauer atom diffusion via vacancies 79−73868
line intensity fluctuations accompanying coherent US modulation *(Russian)* 78−10815
line narrowing by resonant filter 80−77922
line narrowing due to motion of emitting atoms in periodic field 77−43914
line profile, effect of diffusion in external force field *(Russian)* 78−19382
line shape, in presence of ionic charge relax., perturbation calc. 77−28495
line shape, Liouville relax. supermatrices 79−28649
line shape in presence of external periodic perturbation 78−84502
line-broadening of Mossbauer spectra 80−93221
lineshape, in presence of electronic relaxation *(Rumanian)* 78−60368
lineshapes, stochastic model for classical bath variables 77−85631
Lorentzian function fitting using non-iterative method 80−93220
lunar samples, assessment of results from Mossbauer spectra 77−60655
lunar soil samples Fe content via Mossbauer studies, Luna 16 and 20 samples 77−22124
magnetic critical phenomena, hyperfine expts., selective review 78−43722
magnetic Debye crystal, with magnon-phonon coupling, crit. changes in vibr. modes 79−95094
magnetic fluids, mag., optical, and hydrodynamic props.,, expt. study, review 80−60376
magnetic ion exchange interaction effects 79−95696
magnetic materials, determ. of spin arrangements, ^{57}Fe Mossbauer spectroscopy 79−33568
magnetic metals, hyperfine mag. fields at ^{119}Sn nuclei 80−60248
magnetic ordering temp. and order parameter exponent meas. method using Mossbauer effect 79−51776
magnetically ordered crysts., mag. pendulum beats in Mossbauer scatt., theory 79−69760
magnetism, conference, Munich, Germany (Sep. 1979) 80−56997
magnetites, cond. mechanisms *(Russian)* 79−42539
matrix isolation of atoms and ions, Mossbauer isomer shift calibration scheme for ^{57}Fe and ^{119}Sn, book contrib. 79−85924
matrix isolation spectroscopy, Mossbauer effect appls. 78−46376
matrix isolation system for rare gas Mossbauer spectroscopy 77−12285
measurement apparatus for use at high press. and low temps. 77−67548
measurement using multiple purpose 7T NbTi split coil supercond. mag. system 79−71486
measuring installation for pressure at low temp. 77−77129
mechanical press for Mossbauer spectroscopy at low temps. 78−21803
memointerference or vibrointerference phenomenon and application 78−55313
metal: ^{119}Sn, impurity force const. changes from Mossbauer parameters 77−85630
metal hydrides, rare earth and intermetallic, electronic and mag. props., Mossbauer study 80−34830
metal isomer shift, pseudopot.-Born-Oppenheimer theory development 78−2775
metal-H systems 79−82906
metal/solution reactions, possible Mossbauer studies 80−39988
metallic fine particles, Mossbauer fraction, anharmonic lattice vibr. 78−47489
metallic glass, short-range order, hyperfine field distrib. determ. by Mossbauer spectroscopy 80−39962
metallic glasses, ferromag., Mossbauer investigation of electronic struct. 78−92009
metallic glasses, Mossbauer spectra, hyperfine field distrib. determ. 80−39965
metallic glasses, Mossbauer studies 80−39917
metallic substances, retention and exchange of 4f electrons *(Dutch)* 79−1587
metalloenzymes and carriers, hydration effect on mobility of Mossbauer atoms 80−35819
metals, phase analysis by Mossbauer spectra 80−15922
meteorite, Cape York, Fe, Mossbauer and X-ray spectra of ordered Fe-Ni phase 77−78727
meteorite, Mossbauer anal. of Louisville chondrite 79−21238
meteorite, Santa-Catharina, Fe-Ni alloy detection *(French)* 79−16895
meteorite, Toluca octahedrite, Mossbauer spectra petrological study 80−36589
Metglas 2826A, Invar related system, high press. Mossbauer spectra 79−56642
methane, solid, probing phase transition with Mossbauer effect in ^{57}Fe impurities 79−4751
methylated benzene-I_2, π-σ charge transfer complex, frozen soln., Mossbauer spectra obs. 80−91655
metmyoglobin, dynamics study using Rayleigh scatt. of Mossbauer radiation 80−40963
$Mg_{1.34}Fe_{0.16}Al_{0.12}Ti_{0.38}OBO_3$, warwickite, cation distrib. from X-ray struct. and Mossbauer spectra anal. 79−1424
mica, Mossbauer spectra of Fe 78−23380
micas, Mg and Mn rich, Mossbauer spectra 79−38412
microfoil conversion electron detector for Mossbauer spectroscopy 78−70698
mixed valence cpds. $M_2^{I}Sb_{0.5}M_{0.5}^{IV}Cl_6$, ($M^{I}$=$NH_4$, Rb or Cs, M^{IV}=Se, Te or Sn), ^{121}Sb Mossbauer effect 78−84506
$Mn_{1.98-x}Cr_xFe_{0.02}Sb$, Mossbauer effect exam. 78−68432
molecular motion in solids, Mossbauer spectroscopic studies 80−39915
molecules or clusters, interpretation of data from Mossbauer, ESR, susceptibility, optical and XPS meas. 80−37825
montmorillonite group minerals, Norwegian-Greenland basin, age determ. by EPR and Mossbauer spectra 80−26467
Mossbauer spectra, struct., electronic and mag. props. 79−91320
Mossbauer spectral anal. *(German)* 79−19818
Mossbauer spectrometer and its applications *(Chinese)* 79−35913
Mossbauer spectroms., multi-purpose velocity transducer 77−38544

Mossbauer effect continued
multilayer metal films, EM excitation of sound, Mossbauer study *(Russian)* 79−99795
myoglobin, atomic vibr. mean square displacement, Rayleigh scatt. of Mossbauer radiation meas. *(Russian)* 80−100665
myoglobin-Fe^{3+} compounds, Mossbauer and suscept. expts. 78−24019
myoglobin-H_2O_2, high-field Mossbauer spectra, 4.2 to 120K 80−8026
myoglobin-O_2(CO), elec. field gradient tensor, Mossbauer meas. 80−8017
Nafion per fluorosulphonic acid ion exchange membranes, Mossbauer spectroscopy 80−80659
NDT appl. 78−3295
neopentane:tetramethyl tin, Mossbauer exam. of plastic phase transition 77−20778
neopentane:tetramethyltin, Mossbauer exam. of plastic phase transition 77−69759
Ni_2SiO_4, reaction with Fe to produce Ni gamma resonance spectroscopy *(Russian)* 78−15332
niobates, mixed metal, Eu oxidation state, mag. props., Mossbauer study 80−66080
nitrogenase, cofactor centres, Mossbauer spectra obs. 80−8023
nitrogenase active site, Mossbauer spectra of Mo-Fe-S clusters 80−45852
nomenclature and conventions for reporting Mossbauer spectroscopic data, IUPAC recommendations 77−68066
non-Arrhenius self-diffusional behaviour effect on quasielastic neutron scatt. and Mossbauer linewidth 78−67853
non-coherent resonant scattering in crystals *(Russian)* 78−15081
non-equilibrium phonon distrib., in cryst., spectral line shape theory 80−60530
noncubic metals, ^{178}Hf Mossbauer transition, electric quadrupole interaction 80−39928
nuclear energy level shift non-measurability due to pion diamagnetism in Mossbauer effect 80−73808
nuclear reactor corrosion products phase composition determ. 80−5237
obsidian, Japanese, ^{57}Fe Mossbauer spectra of naturally occurring glasses 80−67364
obsidian, Lipari and Teotihuacan origin, Mossbauer, magnetisation, X-ray diffr. and fluoresc. study 80−46173
omphacite, Mossbauer spectra study 79−65771
optical isomer crystal, energy difference due to parity nonconservation *(Russian)* 80−106405
optically active chiral molecules containing ^{57}Fe, optical activity analogy 78−27124
organometallics, intermolecular interaction, Mossbauer spectra 80−15899
organometallics, Mossbauer spectra of spin crossover 80−15903
organonitrogen derivatives of Sn, prep. and props. 78−60456
organotin compounds, mol. and cryst. struct., X-ray diffr., NMR and Mossbauer spectra meas. 77−47441
oscillation of absorpt. spectrum with acoustic modulation 79−87345
oxide phase identification and layer thickness meas. 77−16752
oxyhaemoglobin-hydrazine (dimethylhydrazine) interaction, γ-reson. spectroscopy 80−81525
oxymyoglobin, evidence for conformational and diffusional mean square displacements 80−89713
oxymyoglobin, forzen soln., recoilless fraction, Mossbauer spectra meas. 80−8025
paramagnetic metals, EM excitation of sound, Mossbauer study *(Russian)* 79−99794
pentaerythritol, Bragg reflection, thermal diffuse scatt. meas. *(German)* 78−75509
periodic amplitude and phase modulation of Mossbauer radiation 77−63332
Permalloy, magnetisation reversal, fast, forced by external RF mag. field, Mossbauer obs. 78−52311
Permalloy, proton radiation effects, Mossbauer obs. 80−40008
perovskite, Re containing, new seignettomagnets and ferroelectrics 78−19425
perovskite compound combination, Mossbauer spectroscopy study *(Russian)* 80−80666
perovskites, (AA′)(BB′)O_6, ion valency pairs determ. from lattice consts. 77−43195
perturbed ang. correl. of scattered radiation, hyperfine field determ. 77−81032
phase anal. appl. in heterogeneous systems 79−28648
phase coherence of freq. modulated Mossbauer γ-rays 80−7211
phase diagrams, construction, use of NMR, Mossbauer effect, and gamma ray perturbed angular correlation 79−8417
phase transitions, isomer shift, book contrib. 79−87352
plasma, magnetised, applic. to gamma-ray lasers 80−28186
plastic crystal, Rayleigh scatt. of Mossbauer radiation 78−27125
PMMA, amorphous polymer, Rayleigh scattering of Mossbauer γ-rays 80−39926
PMMA, Rayleigh scatt. of Mossbauer γ-rays 79−73864
polarimetric resonance electron spectroscopy, theory 79−99808
polarisation analysis of emission lines in presence of relax. 78−10813
polarisation density matrix of resonantly scatt. Mossbauer radiation in presence of relax. 79−82904
polarised nuclei system, nonthreshold and amplification *(Russian)* 79−98332
polyacrylic acid:Fe^{3+}, electron state of Fe^{3+}, Mossbauer and magnetisation obs. 79−73872
polycrystalline cubic BN plunger chamber for high-pressure Mossbauer meas. 80−31786
polycrystals, hyperfine interaction determ. from Mossbauer spectra in applied mag. field 77−28497
polyethylene, crystalline, Mossbauer anisotropic elastic scatt. fraction 78−6616
polymer science applics. 77−12798
polymetallomethacrylates, Mossbauer spectra, long-range ordering 79−65776
potassium iron tri(hydrazoformate), Debye-Waller factor, Mossbauer spectra obs. 79−56627
powder sample, Mossbauer absorpt. in external mag. field, polarisation effects 77−48099
powder spectra analysis, ambiguity problem *(Japanese)* 77−66449
press. depend. of effective mag. fields on ^{57}Fe nuclei 78−52383
pressure effects on isomer shifts, book contrib. 79−87353
principles 77−12293
probability determ. using resonance detectors 78−94160

Mossbauer effect continued
propane-(1,2)diol: $^{57}Fe^{2+}$, dil. solution, Mossbauer exam. of struct. relax. at glass transition 77−66016
proportional counter for efficient backscatter Mossbauer effect spectroscopy 79−76289
protocatechuate 3,4-dioxygenase, reduced, Mossbauer effect zero field splitting 79−24955
Prussian blue analogues, Mossbauer spectra 80−15898
pyridine-I_2, n-σ charge-transfer complex, frozen soln., Mossbauer spectra obs. 80−91655
pyrite structured 3d-transition metal chalcogenide mag. props. from Mossbauer effect obs. *(Japanese)* 80−15933
pyrite type dichalcogenides, ^{57}Fe isomer shift, quadrupole splitting, Mossbauer study 80−15832
pyrochlore compounds, EFG and Mossbauer quad. splitting calcs. 77−62877
quadrupole splitting calcs. using cryst. field model, applic. to ferrous complexes 77−32301
quadrupole splitting-isomer shift linear rel., elec. field gradient sign 77−1624
quantitative analysis including effective absorber thickness 79−65779
quantitative analysis of Mossbauer data 78−56410
quantum beats, recoil-free γ-radiation 80−22498
quantum beats of recoil-free γ-radiation 80−37142
rare earth, heavy calibration of isomer shifts by conversion electron spectroscopy 80−39918
rare earth alloys, amorphous, mag. props. rel. to struct., review 79−15298
rare earth alloys, $R(Fe_xRh_{1-x})_2$, mag. props., Mossbauer spectra 80−25108
rare earth alloys, RFe_4Al_8, cryst. struct. mag. props. and hyperfine interactions 78−87648
rare earth alloys, RFe_4Al_8, mag. props., Mossbauer spectra, ordering effects 77−63179
rare earth amorphous alloys, mag. props., Mossbauer spectra 80−7225
rare earth bone uptake, Mossbauer study 80−8019
rare earth complexes, formation and props., book contrib. 80−43204
rare earth dihydrides and dideuterides, electronic and mag. props. 80−25260
rare earth ferromagnet, mag. hyperfine field interaction, ^{197}Au Mossbauer effect 77−8463
rare earth hydrides, Mossbauer studies, book contrib. 79−82906
rare earth intermetallic, $R(Fe_{1-x}Mn_x)_2$, phase struct., mag. and Mossbauer meas. 77−20563
rare earth intermetallics, R_xFe_y, conc. depend. of Fe moments 78−56413
rare earth intermetallics, RFe_2 and $R(Co_{0.98}Fe_{0.02})_2$, magnetostrictive material, changes in vibr. modes near mag. phase transition 79−90736
rare earth ions, Dirac-Fock exam. of electronic props. 79−56106
rare earth iron intermetallics, R_2Fe_{17} and $R_2Fe_{17-x}Ni_x(Co_x)$, mag. anisotropy and hyperfine interactions 77−8298
rare earth metals, alloys, and cpds., book 80−36785
rare earth metals, Mossbauer isomer shifts, book contrib. 79−87361
rare earth mixed valence compounds, spin dynamics, mag. neutron scatt., Mossbauer effect, XPS studies 80−39786
rare earth orthochromites, mag. interactions and weak ferromagnetism 78−52220
rare earth systems, high pressure studies, review 79−69193
rare earth systems, NMR, EPR, and Mossbauer effect, book contribs. 80−39883
rare earth tellurides, electron density distrib. from Mossbauer spectra 78−23374
rare earth-Au, dil., Mossbauer exam. of mag. hyperfine field at ^{197}Au impurity 78−88244
rare earth-Co, RCo_2: ^{57}Fe, easy magnetisation directions, Mossbauer meas. and cryst. field calc. 77−63168
rare earth-Fe, intermetallic compounds, mag. props. *(Rumanian)* 78−92007
rare earth-Fe alloy, RFe_2 (R=Tb, Dy, Ho and Y) crit. phenomena, Mossbauer exam. 78−52403
rare earth-Fe-Al alloys, RFe_4Al_8, mag. props. 78−52250
rare earth-nonmagnetic metal intermetallic cpds., struct. and props., review 79−95377
rare earth-transition metal alloys, amorphous, struct. and mag. props., book contrib. 80−39818
rare earth-transition metal alloys, cryst. and amorphous, mag. props. 77−73008
rare earth-transition metal alloys, $RM_2Si_{2-x}Ge_x$ and $RM_{4+x}Al_{8-x}$, magnetism and hyperfine interactions, magnetisation and Mossbauer effect studies 80−75892
rare earth-transition metal intermetallics, H absorpt., Mossbauer studies 80−39987
rare earth-transition metal intermetallics, struct. and props. review 78−10668
rare-earth metals and oxides, very-short-lived radiation effects following Coulomb excitation 79−60411
rare-earth-Ni alloy, RNi_2 (R=Gd, Tb, Dy, Ho or Er), Mossbauer effect of ^{57}Fe 77−69743
ratio of $\Delta\langle r^2\rangle$ for pairs of elements with analogous electronic structure, tabulation, book contrib. 79−85410
ratios of $\Delta\langle r^2\rangle$ for two transitions in the same element or nuclide, tabulation, book contrib. 79−85409
Rayleigh and Compton contribs. to nuclear resonance scattering of gamma rays, line inversion 80−39919
recoilless fraction and second-order Doppler shift anomalies, localised mode relax. 77−12279
red blood cells of thalassemia, sickle-cell anaemia, and haemoglobin Hammersmith, ferritin-like Fe, Mossbauer study 80−8018
red ochre, chem. anal. by Mossbauer spectroscopy, and superparamagnetism 78−20397
relaxation spectra, breakdown of white noise approx. 78−27141
relaxation theory 80−39954
resonance detectors, spectral params. determ. 77−79502
resonance energy shift for Mossbauer impurity atoms trapped by vacancies 80−25265
resonance scattered radiation time distrib., meas. with resonance scintillation detector 77−48093
resonance scattering of neutrons and γ-quanta, high recoil energies *(Russian)* 78−35075
resonant propagation of gamma-radiation in matter, control, suppression with acoustic excitations *(Russian)* 79−4748
Mossbauer effect continued
review, and complementary techniques, muon spin rotation and Mossbauer effect 80−39912
review, nuclear moments, and moment ratios determ. by Mossbauer spectroscopy 77−22885
review of development in Soviet Union of Mossbauer spectroscopy 77−32311
review of literature 1976-1977 78−84501
RF vibr. crystals, inverse problem of Mossbauer spectroscopy 79−37081
rubredoxin, forzen soln., recoilless fraction, Mossbauer spectra meas. 80−8025
rubredoxin, reduced analogue, EHT calc., Mossbauer parameters, zero field splittings 77−79544
Santa Catharina, Fe-Ni (50 wt.%) superstructure obs. 79−30024
scattering spectra, numerical analysis 80−75899
sediment core, sulphide-rich, Mossbauer spectral study of Fe diagenesis 79−74917
selective excitation method, basic considerations and appl. 78−25375
self-absorpt. effects, simple formula 79−22532
self-diffusion by vacancy mechanism, Mossbauer line broadening 77−40161
semiconductor, crystal-glass transition influence on local struct., Mossbauer and X-ray spectra 77−36163
semiconductors, radiation damage studies on implanted Te, Sb and Sn by Mossbauer spectroscopy 78−2176
semiconductors and metals, spectra of implanted ^{83}Kr, line widths, isomer shifts 80−39899
shutter model, ultrafast, for resonant gamma rays 80−31955
silicate glasses of geologic interest; Mossbauer absorpt. of Fe III, effect of glass chem. comp. *(French)* 80−80658
silicate minerals, Mossbauer anal. of Fe chem. state 80−20547
silicates, elec. field gradient at Fe^{2+} sites, Mossbauer spectra 80−15484
single line Mossbauer absorption spectrum, simple formula for area 77−59497
small metal clusters, isomer shift of ^{57}Fe, nearest neighbour effect 80−44988
smectic-B liquid crystal, supercooled monotropic, Mossbauer studies of ^{57}Fe bearing solute 77−81041
sodium iron fluorophosphate glasses, EPR and Mossbauer resonance study 80−39968
sodium nitroprusside, isomeric molecular states generated by polarised light, Mossbauer resonance obs. 77−20781
soils from archaeological sites, Mossbauer and mag. susceptibility studies of Fe oxides 77−30224
solid, radiation defect exam. by Mossbauer spectroscopy 78−31139
solid solution, heterogeneous short-range order parameters, Mossbauer meas. *(Russian)* 79−4418
solid solutions, interpretation of spectra allowing for at. interaction in lattice *(Russian)* 77−69738
solid state properties of target 80−18060
solid state reaction monitoring by Mossbauer effect 77−12796
in solid-state physics, overview *(French)* 78−2782
source preparation, tabulation, book contrib. 79−87366
source velocity meas. errors, effect on spectral parameters 79−24244
special relativity test, indistinguishability from Lorentz electron theory 77−45695
spectra, effect of gate setting of recording apparatus on spectral parameters 80−90938
spectra fitting, influence of errors of vel. meas. on results 80−37144
spectra obtained at US excitations of source and absorber *(Russian)* 79−47364
spectra of 1/2→3/2 transitions, determ. of angle $\theta=(V_{ZZ},H)$ 79−15385
spectrometer, constant acceleration, with spring reaction compensation, circuit and construction 80−47158
spectrometer, design and construction 79−75668
spectrometer, electronic control block for moving system 77−38075
spectrometer, high field, with Bitter magnets, arrangements, problems 78−89608
spectrometer, piezoelec., with fast channel advance rates 78−24904
spectrometer, velocity nonuniformity meas. 78−848
spectrometer based on Motorola MEK 6800D1 microprocessor 78−37120
spectrometer design, use of resonance and selective ionisation chambers 77−48094
spectrometer drive systems, improved interferometric calibration 77−18151
spectrometer system with data processing capability 77−30699
spectrometer using Bitter magnets 79−51888
spectrometer with 2-4 T electromagnet 78−847
spectrometry *(Japanese)* 80−29660
spectroscopic investigation of catalysts and small particles using in situ cell 79−49357
spectroscopy, cryostat and proportional counter design 79−54238
spectroscopy, glass liquid He cryostat 79−58853
spectroscopy, new directions, workshop, Argonne, USA (1977) 78−24903
spectroscopy, spherical electrostatic electron spectrometer 78−25378
spectroscopy, using multi-purpose split-coil 7 T NbTi superconducting magnet system 79−58746
spectroscopy drive system, low cost, using μA747 ICs 79−89049
spectroscopy using sectional flow proportional counter for γ-ray detection 79−727
spectrum of Mossbauer radiation passed through vibr. resonant medium 80−40022
spherical nuclei, isomer and isotope shifts, theory of finite Fermi systems 80−39929
spin glasses, spin dynamics, EPR, NMR, muon precession, Mossbauer, and neutron scatt. results 79−65689
spin-spin relaxation complications in theory of Mossbauer spectra *(Russian)* 78−43757
spinels, electron exchange between Fe^{2+} and Fe^{3+} on octahedral sites 77−69752
spinels, ligand field stabilisation evaluation using Mossbauer determ. cation distrib. 78−31126
spinels containing Fe^{3+} and Sb^{5+}, $M_4^{2+}Fe^{3+}Sb^{5+}O_8$, Mossbauer spectra 80−15892
steel, alloy, Mn (Ni), Mossbauer, X-ray and electron microscope studies of martensite 78−56621
steel, austenite, γ and neutron irradiation, Mossbauer spectra anal. 78−692

Mossbauer effect continued
steel, austenitic, Al-C, microstruct., Mossbauer obs. *(Russian)* 80−29655
steel, austenitic, Ni-Ti, alloy N35T5, ageing, magnetisation and Curie temp. depend. on plastic deform., Mossbauer studies *(Russian)* 79−69669
steel, austenitic and martensitic, corrosion under boiled conditions, Mossbauer spectroscopy study 79−47800
steel, bainite and martensite, ^{57}Fe Mossbauer spectra 80−15051
steel, C, corrosion products, chem. state anal. by conversion electron Mossbauer spectroscopy 80−40595
steel, C, Mossbauer effect exam. of effect of alloying elements 78−2781
steel, C martensite, electron irrad., reversible C at. redistrib. 77−65991
steel, cementite precipitation from binary alloys, hardness and Mossbauer effects 77−70054
steel, Co-Cr-Mo, maraging, age hardening, Mossbauer study 80−40002
steel, cold-worked, alloying elements effect on cementite decomp. during plastic deform., Mossbauer study 79−82900
steel, cold-worked, Mossbauer obs. of cementite decomp. and restitution 78−64558
steel, cold-worked, state of cementite, nucl. gamma reson. meas., plastic deform. *(Russian)* 78−68706
steel, corroded, Mossbauer effect anal. of corrosion products 78−19943
steel, corrosion and organic coatings, possible Mossbauer studies 80−39988
steel, Cr bearing, carbide phase precipitation during tempering, Mossbauer, X-ray diffr. studies *(Russian)* 79−87636
steel, Cr-Ni-Mo-V, magnetic induction, struct. dependence *(Czech)* 80−50141
steel, Cr-Ni-Mo-V, Mossbauer austenitometry and mag. props. 80−40003
steel, Fe-C martensite, quenched, and heated to 293K, struct. obs. *(Russian)* 77−59784
steel, galvanized, Fe-Zn phases, Mossbauer study 80−50233
steel, Hadfield, Mossbauer spectra meas., 25-250°C *(Russian)* 77−51994
steel, high C, investigation of transformations during tempering by nuclear gamma resonance method *(Russian)* 80−76256
steel, hydrogenated austenitic stainless 77−7758
steel, low alloy, rust analysis by Mossbauer spectroscopy 79−43487
steel, low C, low alloy, Mossbauer study of retain austenite 78−48434
steel, martensite, high C, tempering, nuclear gamma reson. meas. *(Russian)* 79−1883
steel, medium C, hardened, Mossbauer spectroscopy study of austenite and carbide 79−56646
steel, N32, $\alpha \rightarrow \gamma$ transform., struct., texture conc. var. depend. on plastic deform. *(Russian)* 79−66050
steel, Ni (9 wt.%), tempered, mech. stability of retained austenite 79−24521
steel, Ni-Sn temper embrittled, interaction detect. by Mossbauer spectroscopy 77−86176
steel, scoring and scuffing on lubricated sliding surfaces, Mossbauer study 80−7690
steel, Si, commercial, ordering after heat treatment, Mossbauer meas. 80−7556
steel, Si, nonoriented elec. sheet, solute oxidation effect on mag. props., electron and X-ray re-emission Mossbauer spectroscopy 79−83335
steel, stainless, Cr-Ni, maraging, effect of Mo, Co additions on hardening 78−84835
steel, stainless, ferritic and duplex, Mossbauer effect study of 475°C embrittlement 78−52933
steel, stainless, Invar related system, high press. Mossbauer spectra 79−56642
steel, stainless, Mossbauer effect at high press. 80−15858
steel, stainless, Mossbauer radiation modulation by coherent US excitation 79−61277
steel, stainless, type 310, antiferromag. ordering, press. depend., Mossbauer meas. 79−73861
steel, stainless, US excitation for Mossbauer absorpt. line-width reduction 78−27148
steel, stainless 310, proton induced radiation damage investigation by Mossbauer effect 79−1735
steel, structural changes after deformation and annealing, Mossbauer spectroscopic exam. *(Russian)* 78−35446
steel, W-Co-Mo-Cr-V-C (8.5, 8.1, 4.5, 3.5, 2.2, 1.02 wt.%), phase composition, struct. and props. 80−104163
steel 1095, quenched, Mossbauer study of surface martensite 77−32578
steel alloyed with carbide formers, retained austenite determ. 80−20551
steel fibres, polycrystalline, Mossbauer spectroscopy 80−44959
steel surface, nitrided, chem. state anal. by conversion electron Mossbauer spectrometry 80−7718
steel surfaces, corrosive reactions obs. by polarimetric Mossbauer spectroscopy 80−40594
steel transformer, Mossbauer atomic struct. anal., decarburising annealing, cold rolling *(Russian)* 80−11294
steels, high Cr, type 304, high C, low C, backscatter Mossbauer spectroscopy 80−40001
Sternheimer valence shielding-antishielding factor including exchange, ions of interest in Mossbauer spectra 77−85182
stochastic theories for hyperfine spectra in presence of relax. 78−43743
superparamagnetic FCC particles, hyperfine interaction, relax. Mossbauer spectra 79−78573
superparamagnetic FCC particles, relaxation times in external mag. fields 78−95482
superparamagnetic particles, magnetic moment time development and discrete orientation model 80−60378
superparamagnetic particles, Mossbauer relax. spectra 77−66448
superparamagnetic particles, Mossbauer spectra, magnetisation vector precession 80−15872
superparamagnetism, magnetisation vector diffusion coeff., anisotropy energy, vol. distrib. of particles by Mossbauer effect 78−48099
superparamagnetism, Mossbauer effect study of relaxation of magnetisation vector 78−19402
surface analysis, using SIMS, Mossbauer spectra and spectrometry 79−16050
surface and interface magnetism by Mossbauer spectroscopy 80−7218
surface electronic structure, surface magnetism and surface phase transitions 80−39916
surface magnetisation, size effect 78−15008
synchronous digital triangle generator and servo loop pre-amp 77−88351
Mossbauer effect continued
synchrotron radiation filtering for Mossbauer source production 78−25374
synchrotron radiation resonance scatt. by nuclei, time delay 79−15386
tabulation of characts. of Mossbauer transitions, book contrib. 79−87364
taenite lamellae in Fe meteorite Cape York 78−65575
talc, ^{57}Fe Mossbauer analysis 80−40006
tangential channel for nucl. gamma-reson. spectroscopy by thermal neutrons capture *(Russian)* 79−67819
tantalates, mixed metal, Eu oxidation state, mag. props., Mossbauer study 80−66080
tektites and natural glasses, Mossbauer anal. 80−21952
tektites-irgizites, Fe ions state rel. to form. conditions 78−61420
tellurium-thiourea compounds, Mossbauer investig. of ^{129}I, quadrupole interactions and bonding 77−48111
ternary superconductor, mag. interactions 79−73613
tetrabutylammonium iron tetraiodide, structural and mag. props., ^{57}Fe and ^{129}I Mossbauer spectra 79−61282
tetraethylammonium iron tetraiodide, structural and mag. props., ^{57}Fe and ^{129}I Mossbauer spectra 79−61282
tetraethylammonium neptunium hexachloride, Mossbauer spectra and mag. susceptibility meas. 80−108140
tetramethylammonium neptunium hexachloride, Mossbauer spectra and mag. susceptibility meas. 80−108140
tetramethylene bridged ferrocene derivatives, mol. struct., Mossbauer expt. 78−60372
tetramethyltin, adsorbed on graphite, nature of 2 D diffusion, Mossbauer meas. 80−84372
texture problem, preferred crystallographic and spin orientation determ. 77−69735
texture problem and Goldanskii-Karagin effect, intensity matrix method 80−7215
thermal motion effect on linewidth, second order Doppler shift *(German)* 77−43924
thermal spike, effect in Mossbauer reson. obs. through Coulomb excitation 78−27132
thermometer, high temp., based on line broadening 80−52202
thickness dependence of absorption and scatt. line shapes 78−15079
thin film Mossbauer spectroscopy with commercially available spectrometer 77−10152
thin film thickness meas. by in-depth-selective Mossbauer spectroscopy 79−63188
three-level Mossbauer gamma-ray lasers, two-stage pumping 80−78857
time dependent PAC Mossbauer effect, theory of combined method 79−28645
time differential Mossbauer reson., theory of phonon relax. effects 77 - 20777
time-dependence of reson. scatt. radiation 77−14060
tin containing organic compounds, $[R^{I}R^{II}R^{III}PO]_2SnR_nCl_{4-n}$, $[R^{I}R^{II}R^{II}PO]SnR_3Cl$, Mossbauer spectra, isomer shift and quadrupolar splitting *(Russian)* 79−61285
tinplate, electron reemission Mossbauer spectra 79−19820
tourmaline, Mossbauer spectra, struct. 80−20566
tourmaline, proton jumps, NGR obs. 80−15921
tourmalines of dravite-schorl series, Mossbauer anal. 80−15920
transferrin, human, ^{57}Fe Mossbauer obs., λ and D values 77−21481
transition metal, change of charge radius for 2^+-0 transitions of ^{178}Hf, ^{182}W and ^{186}Os 78−25109
transition metal based amorphous mag. alloys, elec. field gradient 78−39475
transition metal compounds, silicides, germanides and antimonides 79−91324
transition metal dichalcogenides: ^{57}Fe, Mossbauer spectra, isomer shift 80−15885
transition metal diiodides, (V, Cr, Mn, Fe, Co, Ni, Cd), Mossbauer spectrum, electronic and mag. props. 77−32302
transition metal hydrides, Mossbauer studies, book contrib. 79−82906
transition metal impurities, volume corrected isomer shift, orbital electronegativity scale 77−73103
transition metal impurities, volume-corrected Mossbauer isomer shifts 78−68434
transition metal intermetallic cpds., H absorption and mag. props. 80−60224
transition metal nitroprussides, Mossbauer spectra, dehydration effects 79−24237
3d-transition metal-metalloid cryst. and glassy alloys, electronic struct. from magnetisation and Mossbauer meas. 80−29363
transition metals, 4d and 5d, Mossbauer isomer shifts, book contrib. 79−87355
transition metals, vol. corrected isomer shifts, effects in alloys 78−39470
transition metals ^{57}Fe study via conversion electron Mossbauer spectroscopy 77−55735
tri-t-butylstannyl hydroxide, Mossbauer spectrum, tin coordination *(German)* 80−32716
tri-t-butylstannylamine, and isotopomers, IR and Raman spectra, normal coord. anal., Mossbauer spectrum *(German)* 80−32716
triethylamine-I_2, n-σ charge-tranfer complex, frozen soln., Mossbauer spectra obs. 80−91655
trimethyl tin chloride adsorbed on grafoil, Mossbauer study 80−80643
trimethyl tin cyanide, ^{119}Sn Mossbauer spectra, elec. field gradient 80−15909
trinuclear exchange clusters, Dzyaloshinsky coupling effects in Mossbauer spectra *(Russian)* 80−108142
triphenyl tin chloride adsorbed on grafoil, Mossbauer study 80−80643
tris (N,N'-diethyldithiocarbamate) iron II, high field Mossbauer study 79−54873
ultrarelativistic particle radiation in cryst., γ-γ correlations obs. 80−71274
ultrasonic excitation, phase effect on Mossbauer resonance 80−55004
ultrasonic satellites of Mossbauer radiation calc. 78−27143
ultrasonic sideband intensity depend. on acoustic field statistics 80−75905
vermiculite, electric field gradient, Mossbauer absorption 79−73865
vermiculite, firing temp. depend. of Mossbauer parameters 80−15837
yellow ochre, chem. anal. by Mossbauer spectroscopy 78−20397
^{159} Tb, 58 keV level, nuclear reson. fluorescence 78−33121
$(2CdTe)_x$-$(In_2SnTe)_{1-x}$, x=0.25, 0.5, 0.75, tetrahedral semiconductor, chem. interaction of Sn atoms, Mossbauer study 80−39977
Ag, contact charge density, press. depend., trends for Ag-Te 78−39077
Ag, fine particles, Mossbauer fraction from Gaussian potential 78−47489

Mossbauer effect continued
Ag foils, polycryst. and bicrystals, grain boundaries, ^{119}Sn Mossbauer anal. 80−7229
Ag-Co, dil., binding and caging of impurities and trapped interstitials 78−39462
Ag-Fe, dil., ion implanted, phase comp., Mossbauer study 80−7244
Ag-Fe, implanted, Mossbauer conversion electrons spectroscopy, rel. to dose and annealing temp. 78−52397
Ag-Fe, Kondo system, magnetisation, Mossbauer expts. 77−77028
Ag-Fe alloy, local moment system, low. temp. susceptibility, Mossbauer effect meas. 77−43810
$Ag_{0.25}Cu_{0.25}In_{0.50}Sn_{0.50}S_2$, Mossbauer spectra *(French)* 80−44326
$AgFeO_2$, EFG tensor, nucl. quadrupole coupling const., O^{2-} polarisability 77−72844
$AgFeTe_2$, Mossbauer parameters in phase-transition region 80−11308
$Ag_2SnS_3(Se_3)(Te_3)$, lattice dynamics obs. 77−43923
^{109}Ag, Mossbauer resonance at 88 keV, temp. depend. 80−7213
Al, Bragg diffraction, anharmonic contributions, Mossbauer study 78−76358
Al, hyperfine interactions of implanted Fe, conversion electron Mossbauer spectroscopy 78−52391
Al, interaction between ^{57}Co atoms and quenched-in vacancies, Mossbauer meas. 80−7234
Al, quenched-in lattice defects, Mossbauer anal. of associated ^{57}Co 78−39820
Al, self-interstitial interaction with solutes, resistivity meas. 78−47331
Al:^{57}Fe study via conversion electron Mossbauer spectroscopy 77−55735
Al:Kr foil, ion implantation, low-temp. on-line Mossbauer meas. of ^{83m}Kr 78−35071
Al-^{57}Co, implanted, Mossbauer effect obs. of annealing 80−39126
Al-Co, defect structs. introduced by electron irrad., Mossbauer study 80−7239
Al-Co, dil., binding and caging of impurities and trapped interstitials 78−39462
Al-Co, dil., electron and neutron irradiation, interstitital atom clustering at ^{57}Co impurity, Mossbauer meas. 78−30607
Al-Co, electron irradiated, self-interstitials trapped at Co impurities, Mossbauer line shape anal. 78−6615
Al-Co, electron irradiated, quadrupolar relaxation effect in Mossbauer effect 78−39459
Al-Co alloy, dil., fast neutron radiation damage, interstitial trapping, Mossbauer spectra and elec. resist. meas. 77−27914
Al-Cu-Sn, ageing process, effect of Sn atoms, ^{119}Sn Mossbauer spectra obs. 80−7598
Al-Cu-Sn (3.4, 0.28 wt.%), Mossbauer anal. of Sn behaviour during ageing 78−31431
Al-Dy, dil., ion implanted, crystal hyperfine field interaction, Mossbauer spectroscopy study 80−44968
Al-Er, dil., lattice location of ^{169}Er ions after implantation, Mossbauer effect of ^{169}Tm 78−39460
Al-Fe, dil., annealing after cold working, impurity-vacancy interactions, Mossbauer meas. 80−7236
Al-Fe, dil., defects and phases, Mossbauer studies 80−40004
Al-Fe, dil., Mossbauer spectra of implanted ^{57}Fe, ageing behaviour 80−7233
Al-Fe, dil. solid soln., vacancy-trapped Mossbauer impurity Debye Waller factor 80−60468
Al-Fe (0.02 at.%), rapidly quenched, ^{57}Fe Mossbauer spectrum associated with vacancy 78−23378
Al-Fe (0.02 wt.%), Mossbauer spectrum of ^{57}Fe associated with vacancies 77−85636
Al-Fe (1 wt.%), depth resolved ^{57}Fe conversion electron Mossbauer spectra 79−38413
Al-Sn alloys, heat treatment effect on ^{119}Sn Mossbauer spectrum 80−7228
Al-steel, cementite isolation, Mossbauer anal. 80−93225
$AlFeF_5.7H_2O$, Mossbauer spectra, thermal decomp. products 78−80258
$Al_2Mn_3Si_3O_{12}$ glass, mag. ordering effects at low temps., Mossbauer and neutron diffr. meas. 77−16047
$Al(NO_3)_3.9H_2O:Fe^{3+}$, nucl. level hyperfine struct., reson. RF field effect *(Russian)* 77−77133
Al_2O_3-Fe_2O_3:Cr^{3+}, dil. paramag. system, Cr^{3+} conc., effect on cross relax. 79−15387
Al_2O_3-Fe_2O_3(:Cr^{3+}) paramag. system, cross relax. temp. and mag. field effects on Mossbauer spectra 79−33576
β-Al_2O_3-Na_2O:Fe, coordination site, oxidation state, Mossbauer, absorpt., emission spectra, mag. susceptibility meas. 78−68431
Al_2O_3:^{57}Co, Mossbauer study of the charge state and symmetry of $^{57}Fe^m$ in diverse cobalt spinels *(Spanish)* 79−69754
(Al_2O_3-Fe_2O_3):Cr^{3+}, (0.04 mol.% Fe_2O_3), paramag., cross relax., annealing temp. effect from Mossbauer meas. 80−44983
$Al_6Si_2O_{13}:Fe^{3+}$, mullite:Fe^{3+}, Mossbauer exam. of relaxation behaviour of Fe^{3+} 77−1620
α-Am, after-effects of ^{241}Am α-decay, ^{237}Np Mossbauer spectra obs. 79−61271
Am, Debye-Waller factor, temp. depend. 78−83902
Am-Pt intermetallics, after-effects of ^{241}Am α-decay, ^{237}Np Mossbauer spectra obs. 79−61271
AmB_2 (B=Al, Co, Fe, Rh, Ru), crystal structure, mag. props. of Laves phases 77−27851
AmO_2, Am_2O_3, after-effects of ^{241}Am α-decay, ^{237}Np Mossbauer spectra obs. 79−61271
^{241}Am, α-radiation self-damage effect on hyperfine interaction and Debye-Waller factor, Mossbauer meas. 80−7230
As-Se:^{197}Au, glassy, Au impurity influence, elec. cond., optical absorpt. and Mossbauer meas. 77−24558
As-Se-Sb, crystallised glasses, struct. from Mossbauer spectra 80−64917
As_2Se_3:Pt, glass, effect of impurities on elec. props. 80−103699
As_2Se_3-$GeSe_x$-$SnSe_x$ (x=1,2), exam. of Sn valency and physical props. 79−4753
$AsSe_{1.5}Sn_x$ glasses, crystallisation, Mossbauer obs. 77−47557
As_2Te_3, $As_4Te_5I_2$, $TlAsTe_2$, local struct. changes on crystal-glass transition, Mossbauer spectra 77−36157
$As_2Te_{3-x}Se_x$, amorphous and cryst. phases, ^{125}Te Mossbauer expts. 78−88232
Au (I) compounds, electronic config. and nucl. quadrupole interaction, atomic SCF Hartree-Fock calcs. 79−60777
Au alloy, charge density perturbations, ^{197}Au isomer shift obs. 77−20771
Au alloys, ^{197}Au Mossbauer isomer shifts, theory, book contrib. 79−87357

Mossbauer effect continued
Au, Co-hardened, characterisation by Mossbauer spectroscopy, Co precip. formation 80−80108
Au complex, paramag., ^{197}Au mag. and elec. hyperfine interactions 78−39471
Au compounds, ^{197}Au Mossbauer isomer shifts, book contrib. 79−87356
Au, electrodeposit, Co-hardened, state of Co in as-deposited material, Mossbauer obs. 80−15397
Au, fine particles, Mossbauer fraction from Gaussian potential 78−47489
Au, matrix for Mossbauer effect on ^{119}Sn and ^{197}Au 78−15080
Au small particles, embedded in gelatin, phonon spectrum obs. 77−43921
Au-Co, electrodeposit, characterisation by ^{57}Co-^{57}Fe Mossbauer spectroscopy 80−39989
Au-Co, electrodeposit, Mossbauer meas. of Co chem. state 80−39990
Au-Co electrodeposits, Co hardened, chemical state of Co, Mossbauer emission spectra 79−90897
Au-Cs(Mg)(Rb)(Zn), charge transfer, Mossbauer effect ^{197}Au isomer shifts, XPS valence-band spectra 80−2676
Au-Dy, dil., hyperfine interaction of Γ_8 quartet, Mossbauer expt. 78−43718
Au-Dy, dil., hyperfine interaction, Mossbauer study, Kramers quartets 80−66083
Au-Fe, dil., ion implanted, phase comp., Mossbauer study 80−7244
Au-Fe, Kondo system, magnetisation, Mossbauer expt. 77−77028
Au-Fe (17 at.%) alloy, fission fragment irrad., simulation of neutron effects 77−80549
Au-Fe alloy, dil., Mossbauer exam. in spin glass regime 79−61289
Au-Fe ion implanted alloy, Mossbauer conversion electron scatt. 80−88898
Au-Fe solid soln., props. during preparation by diffusion heating 77−12260
Au-M (M=Cd, In, Sn, Sb, Te), charge-transfer and valence-band behaviour using ^{197}Au Mossbauer and X-ray photoemission spectra 79−60695
Au-Te, elec. field gradients and charge transfer, Mossbauer spectra 80−25268
Au-transition metal alloys, ^{197}Au Mossbauer isomer shift cellular atomic model 80−84673
$AuAl_2(Ga_2)(In_2)(Sn_2)(Sb_2)(Te_2)$, core-level binding energy shifts and charge transfer 80−25268
Au_2MnAl, Heusler alloy, Mossbauer, determ. of Au hyperfine field 77−4586
AuMnSb, ferromag. Heusler alloy, mag. hyperfine fields at Au and Sb sites, Mossbauer spectra 77−32303
$(Au_xPb_{1-x})_{1-c}Fe_c$, ferromag. and spin glass ordering 78−56335
B_2O_3-Fe_2O_3 glass, Fe_2O_3 crystallite formation, Mossbauer obs. 78−68429
B_2O_3-PbO-GeO_2-Fe_2O_3 glass, Mossbauer exam. of Fe valence states 79−78597
B_2O_3-PbO-GeO_2-Fe_2O_3 glasses, mag. props. and Mossbauer spectra, speromag. order at low temps. 80−80530
$Ba_x(Ba_{1-x}Al_x)Fe_2S_6[S_{1-y}(S_2)_y]$, cryst. struct., Mossbauer and mag. behaviour 77−55273
Ba_2CoS_3, linear chain antiferromag., mag. susceptibility meas. and Mossbauer spectra 80−107992
BaF_2, Eu^{2+} isomer shift, Mossbauer spectroscopic anal. 79−56649
$Ba_3Fe_2BO_9$ (B=Re, Te, W, Mo), siegnette magnets with hexagonal barium titanate structure 78−76397
$BaFe_{12}O_{19}$, Ca^{2+} substitution effect on hexaferrite lattice and mag. props. 80−60243
$BaFe_{12}O_{19}$, hexagonal ferrite, local lattice distortions, use of Mossbauer effect 78−43745
$BaFe_{12}O_{19}$, high field Mossbauer effect on ^{57}Fe at room temp. and 4.2K 79−24238
$BaFe_{12}O_{19}$, M type hexaferrite, Fe ion dynamic characts. in bipyramidal position, nucl. γ reson. 79−95697
$Ba_2Fe_{18}O_{27}$, hexagonal ferrite, W-struct., Mossbauer spectra of Fe^{3+} and Fe^{2+} 78−88242
$Ba_2Fe_7O_{11}$, antiferromagnet, exam. of mag. props. by mag. meas., and Mossbauer spectroscopy 78−52256
Ba_2FeS_3, linear chain antiferromag., mag. susceptibility meas. and Mossbauer spectra 80−107992
Ba_2FeSbO_6, siegnette magnets with hexagonal barium titanate structure 78−76397
$Ba_3Fe_{0.2}Si_{0.8}S_5$, stabilisation of tetravalent Fe 79−60326
$Ba_3FeTa_2O_9$, Mossbauer and X-ray diffr. studies 80−103905
$BaFe_4Ti_2O_{11}$, R-type hexaferrite, spin struct. and mag. props. 78−52216
$BaLa_2Fe_2O_7$, Mossbauer exam. of mag. struct. 77−40157
BaLaMRuO$_6$, (M=Mg, Fe, Co, Ni, Zn), cubic ordered perovskites, Mossbauer and mag. susceptibility meas. 80−75889
Ba_2MnS_3, linear chain antiferromag., mag. susceptibility meas. and Mossbauer spectra 80−107992
BaO-Fe_2O_3-B_2O_3 glass system, mag. struct., Mossbauer study 78−39485
BaO-Fe_2O_3-B_2O_3 glass, Mossbauer study of struct. and mag. props. 79−47369
BaO-Fe_2O_3-B_2O_3 glass, struct. and mag. props., Mossbauer spectra 80−7226
BaO-Fe_2O_3-B_2O_3 glass, splat cooled, low temp. micromagnetism 80−34660
BaO-Fe_2O_3-Na_2O glass, mag. props. 78−88123
$Ba_3Ru_2MO_9$, (M=Mg, Ca, Sr, Co, Ni, Cu, Zn, Ca), Mossbauer spectra 80−108136
$Ba_4Ru_3MO_{12}$, (M=Ta, Nb), Ru oxidation state, Mossbauer study 80−44965
$BaSnO_3$, powder, electron scatt. from ^{119}Sn, effective range, Mossbauer obs. 77−63345
$Ba^{119m}SnO_3$ Mossbauer source, resonant self-absorpt. correction 77−28498
$BaSr_xCa_{1-x}Fe_4O_8$, substituted hexagonal ferrites, mag. split Mossbauer spectra obs. and X-ray struct. data 80−71250
$Ba_{0.54}Sr_{0.46}Nb_2O_6$, line broadening effect in Rayleigh scatt. of Mossbauer radiation 80−50238
$Ba_xSr_{1-x}Nb_2O_6$, single crystal, Mossbauer diffraction *(Russian)* 79−56644
$BaTiO_3$, diffr. of Mossbauer radiation near Curie point *(Russian)* 79−8079
$BaTiO_3$, line broadening effect in Rayleigh scatt. of Mossbauer radiation 80−50238
$BaTiO_3$, Mossbauer spectrum, internal elec. field effects, quadrupolar splitting and isomer shift 79−56648

Mossbauer effect continued
$BaTiO_3$, Mossbauer spectroscopy, sample prep. and results 80−66078
$BaTiO_3$-based ceramics, impurity atoms chem. state, Mossbauer spectra 80−15902
$BaVS_3$, elec. resist., mag. susceptibility, structural transition and Mossbauer effect meas. 77−84923
$BaVS_3$, exam. of ferromagnetic, antiferromagnetic behaviour, depending on stoichiometry 78−52233
$BaVS_3$:Fe, Mossbauer and mag. studies, electronic state of Fe 80−108130
Ba_2XRuO_6(X=La,Eu), ^{99}Ru Mossbauer spectra and other techniques 80−29659
$Ba_2Zn_{2-2(x+y)}Cu_{2x}Cd_{2y}Fe_{12}O_{22}$, mag. props. and Mossbauer spectrum 80−75765
$Ba_2Zn_{2-2x}Cu_{2x}Fe_{12}O_{22}$, hexagonal ferrites, prep. and mag. characterisation 79−1727
$BaZn_2Fe_{16-x}Al_xO_{27}$, saturation magnetisation, anisotropy field and Mossbauer meas. 77−69508
$BaZn_2Fe_{16-x}M_xO_{27}$ (M=Al, Ga, In, Sc), mag. props. and Mossbauer effect 80−75766
Be-Au, dil., quadrupole interactions and lattice location, ^{197}Hg TDPAC and Mossbauer expts. 78−43726
Be-Ir, dil., elec. field gradient, Mossbauer meas. 80−80665
$BiBi_4Ti_3FeO_{15}$, perovskite-like layer-type ferroelec. magnetic cpd., Mossbauer expts., 80-1200K 78−64329
Bi_2O_3, anharmonicity effect, Debye temp. determ. from Mossbauer spectra 77−63335
$Bi_9Ti_3Fe_5O_{27}$, combined hyperfine interaction 79−28663
$Bi_7Ti_{2.5}Sn_{0.5}Fe_3O_{21}$, layered ferroelec. antiferromag., superparamagnetism, Mossbauer spectra obs. 77−51999
C_2O_3:$^{125}Te^{6+}$, mag. hyperfine interactions, Mossbauer study *(French)* 79−24247
(Ca,Fe)SiO_3, intracryst. Fe^{2+}-Ca^{2+} exchange, Mossbauer spectra 80−20548
$CaBaFe_4O_8$, Mossbauer study 79−38414
$CaBaFe_4O_8$, overlap contribution to $^{57}Fe^{3+}$ isomer shifts, nuclear size change 80−39903
$CaCO_3$:Fe^{2+}, Mossbauer spectra 80−108138
CaF_2:Eu^{2+} isomer shift, Mossbauer spectroscopic anal. 79−56649
CaF_2:^{241}Am, alpha-decay induced ^{237}Np charge state, Mossbauer obs. 79−47367
CaF_2:^{57}Co, γ-irradiated, Mossbauer spectra 77−81036
CaF_2:Dy^{3+}, Mossbauer obs. 78−64303
CaF_2:Fe^{2+}, electronic props., Mossbauer and far IR spectroscopy 79−99803
CaF_2:Fe^{2+}, relax. meas., Mossbauer spectroscopy, 10-30K 80−44977
$Ca_3Fe_xCr_{2-x}Ge_3O_{12}$, antiferromagnetic order below 12K, Mossbauer study 80−39945
$CaFeF_{5+}$ one-dimens. magnetism *(French)* 79−73670
$CaFe_2^{2+}Fe^{3+}(OH)O(Si_2O_7)$, ilvaite, IR spectrum and Mossbauer effect obs. *(French)* 78−80321
$CaFe_2^{2+}Fe^{3+}Si_2O_8(OH)$, Mossbauer spectra, temp. depend. electron delocalisation 80−20567
$CaFe^{3+}Fe_2^{2+}(Si_2O_7)O(OH)$, ilvaite, electronic struct., press. and temp. depend. of ^{57}Fe Mossbauer spectrum 80−108129
$Ca_3Fe_2Ge_3O_{12}$ garnet, light absorpt. spectral study 80−93322
$CaFeO_3$, charge disproportionation, Mossbauer obs. 78−2778
$CaFeO_3$, preparation, cryst. struct., mag. and elec. props. 78−44066
$CaFe_2O_4$, overlap contribution to $^{57}Fe^{3+}$ isomer shifts, nuclear size change 80−39903
$Ca_xFe_{3-x}O_4$, Ca^{2+}, Mossbauer study 78−10814
$CaLaFeO_4$, X-crystallog. and Mossbauer spectrum *(French)* 77−66447
$Ca_2LaFe_3O_8$, physico-chemical characterisation, Mossbauer exam. and mag. props. *(French)* 77−28494
$CaMg_{0.95}Fe_{0.05}Si_2O_6$, pyroxene, integrated intensity ang. depend. 77−90083
CaO:Fe^{2+}, octahedral symm., vibronic effects from Zeeman field induced Mossbauer spectra 77−8477
$CaO-Al_2O_3-Fe_2O_3$, and resonance spectroscopy study *(Russian)* 77−55733
$CaO-Fe_2O_3-SiO_2$ glass, struct. behaviour at melting, Mossbauer exam. 79−10802
$CaO-SiO_2-Fe_2O_3$ glass, Mossbauer spectra 80−15850
$2CaO(Al_2O_3)_x(Fe_2O_3)_{1-x}$, Fe^{3+} distrib. in struct. 79−94980
$CaSnO_3$, powder, electron scatt. from ^{119}Sn, effective range, Mossbauer obs. 77−63345
$Ca_{1-x}Sr_xFeO_3$, Mossbauer spectra, charge disproportionation 80−15891
$Ca_{1-x}Sr_xFeO_3$, Mossbauer spectra, charge disproportionation 80−20542
$CaTiO_3-Ca_2Fe_2O_5$, Mossbauer resonance exam. of structure, phase equilibrium 78−76640
Ca_2XRuO_6 (X=Y,La,Eu), ^{99}Ru Mossbauer spectra and other techniques 80−29659
Cd, contact charge density, press. depend., trends for Ag-Te 78−39077
Cd nitroprussides, Mossbauer spectra, dehydration effects 79−24237
$CdCO_3$:Fe^{2+}, Mossbauer spectra 80−108138
CdF_2:^{241}Am, alpha-decay, ^{237}Np charge state, Mossbauer obs. 79−47367
$Cd_{1-x}Fe_xCr_2S_4$, Fe II electronic struct., Mossbauer spectra 80−15876
$Cd_xFe_{3-x}O_4$, collective electron states, ^{57}Fe Mossbauer meas. 77−69748
$Cd_xFe_{3-x}O_4$, cond. mechanism, collective electron description 77−4588
$CdGeAs_2$, amorphous and cryst., short-range order, Mossbauer expts. 78−22648
$Cd_2Nb_{2-2x}Sn_{2x}O_{7-2x}F_x$, solid soln., X-ray diffr. and Mossbauer study *(French)* 78−87659
CdNi ferrite, quadrupole interaction, cation distrib. influence 78−2776
$Cd_{0.8}Ni_{0.2}Fe_2O_4$ ferrite, Fe spin relaxation Mossbauer study, mag. hyperfine struct. *(Russian)* 80−15932
$Cd_{1-x}Ni_xFe_2O_4$, solid soln., mag. and structural characterisation 80−103906
$Cd_xNi_{1-x}Fe_2O_4$, mag. behaviour, Mossbauser meas. 78−52390
CdTe, diamond-like semicond., Mossbauer isomer shift meas. 77−16233
$(CdTe)_x$-$(CdSe)_{1-x}$, diamond-type semiconductor, Mossbauer spectra, quadrupole interaction of ^{125}Te 80−44992
$CeFe_2$, H_2 absorption effect on mag. props. and struct. 77−40045
$CeFe_2Si_2$, CeFeSi, absence of effective mag. field at Fe nuclei *(Russian)* 78−19397
$Ce_{0.73}Ho_{0.27}Ru_2$:Co, spontaneous mag. order below superconducting transition temp., Mossbauer study 80−39701
CeO_2-$LaCrO_3$, and CeO_2-La_2O_3, quadrupole interactions and moments, ^{137}La Mossbauer obs. 78−27121
$(Ce_xY_{1-x})Fe_2$, mag. susceptibility and Mossbauer meas., lattice parameters 80−97068

Mossbauer effect continued
Co, Bragg diffraction, anharmonic contributions, Mossbauer study 78−76358
Co complex, $[^{57}Co(1,10\text{-phenanthroline})_3](ClO_4)_2.2H_2O$, time differential Mossbauer spectra, aftereffects 78−27131
Co complex, bis-(β-diketonato) Co(II) dihydrate, Fe chem. states, Mossbauer emission 80−15917
Co complex, $Co(acac)_3$, ^{57}Co labelled, ^{57}Fe(III) species prod. by electron capture decay, spin relax. 77−63329
Co complex, diimine complexes with ^{57}Co II, ^{57}Fe II anomalous spin states, Mossbauer spectroscopy 77−12261
Co complex, diimine complexes with ^{57}Co (II), Mossbauer spectra, temp. depend. 77−12262
Co complex, Werner complexes, ^{57}Fe partial quadrupole splitting, emission Mossbauer spectra 80−15919
Co complexes, acetylacetonates, ^{57}Fe absorption and emission spectroscopy 80−40018
Co complexes, tris(oxinato) Co(III) and tris(β-diketonato) Co(III), after effects of EC decay 80−15915
Co implantation in Al, replacement collision probability at 4.2K 80−70237
β-Co superparamag. FCC particles, hyperfine interaction, relax. Mossbauer spectra 79−78573
Co^{2+} $[Fe(CN)_6]^{3-}$, time depend. phenomena caused by EC decay, Mossbauer study 80−44978
Co:^{129m}Xe, mag. hyperfine field determ. by Mossbauer effect 77−8460
Co-C, ferromag., prep. by splat-quenching, obs. of electronic struct. of interstitial C 77−62868
Co-Fe, dil., hyperfine mag. fields, press. effect, Mossbauer meas. 80−71277
Co-Mo catalyst, Mossbauer spectra 80−7222
Co-P alloys, geometric struct. models and diffraction exam. techniques 80−79700
Co-Sn, dil., hyperfine field, press. depend., Mossbauer spectra meas. 79−95375
$CoAl_{2-x}Fe_xO_4$ system obs. *(Rumanian)* 79−78575
$CoAl_2O_4$, cation distribution, Mossbauer and X-ray diffr. obs. 78−95532
$CoCl_2.2H_2O$, gamma-X-ray coincidence Mossbauer spectra 80−15913
$CoCr_2O_4$, Mossbauer spectra and cryst. struct. determ. 79−56637
CoFeCN.xH_2O, electron irrad., Mossbauer spectra 80−29652
$Co_x^{2+}Fe_{1-x}^{2+}Fe_2^{3+}O_4$ ferrites, effect of Fe^{2+} on Mossbauer parameters 78−76360
$Co_x^{2+}Fe_{1-x}^{2+}Fe_2^{3+}O_4$, Mossbauer parameters, effect of Fe^{2+}, Zeeman patterns 79−28647
Co_2FeGa, alloy, site preference of Co and Fe, Mossbauer and neutron study 79−78577
$(Co_xFe_{1-x})_5Ge_3$, Mossbauer investig. of hyperfine field at Fe nuclei 77−20776
$CoFe_2O_4$ formation rate consts. meas. by Mossbauer effect 78−68875
$CoFe_2O_4$ mag. fluid particles, comp., struct., and mag. props. 80−60374
$CoFe_2O_4$, mag. hyperfine fields, Mossbauer spectra 80−108139
$CoFe_2O_4$ ultrafine particles, prep. and mag. props. 80−71116
$Co_{1-x}Fe_{2+x}O_4$, prep. by wet and ceramic methods, struct., mag. and surface props. 78−52307
$Co_{2.94}Fe_{0.06}S_4$ Mossbauer ^{57}Fe spectrum, mag. transition, lattice atomic occupancy 77−48095
$Co_2Ga_{1.95}Fe_{0.05}$, mag. behaviour, Mossbauer effect and DC magnetisation meas. 80−50244
Co_2HfAl, hyperfine fields of Fe impurities, Mossbauer spectra 80−71255
Co_2HfSn-Fe, dil., Heusler alloy, Fe hyperfine fields, Mossbauer obs. 78−68424
Co(II)-octaethylporphyrin, Mossbauer emission spectra 80−8020
CoM_2O_{4+x} (M=Rh,Mn), anomalous $^{57}Fe^m$ charge states, Mossbauer study 80−40017
$Co_2Mn_xFe_{1-x}M$, (M=Ga,Ge,Si,Sn), hyperfine fields of Fe impurities, Mossbauer effect meas. 78−31130
$^{57}CoMn_2O_4$, after effects of orbital electron capture 79−73870
$Co(N_2H_5)_2(SO_4)_2$:Co, Mossbauer effect and paramag. relax., superparamag. behaviour of correl. spin domains 77−69756
$Co_{2-x}Ni_xTiSn$, mag. ordering, ^{119}Sn Mossbauer spectroscopy and magnetisation meas. 78−43753
CoO, Mossbauer lines, quadrupole splitting due to defects 80−2670
CoO, relax. valence averaging, Mossbauer spectra evidence 77−1626
$CoO-Al_2O_3-SiO_2$ glass, mag. ordering, Mossbauer exam. 77−24764
CoO_2, anodically formed, emission Mossbauer studies 79−61268
Co_3O_4, Mossbauer spectra and cryst. struct. determ. 79−56637
Co_3O_4:^{119}Sn, hyperfine field exam., Mossbauer meas. 77−69753
$Co_xPd_{80-x}Si_{20}$, amorphous, structural and mag. heterogeneities 80−80484
$CoRh_2O_4$, Mossbauer spectra and cryst. struct. determ. 79−56637
CoS_2, hyperfine parameters and quadrupole splitting determ., ^{57}Fe Mossbauer spectra 77−77131
$CoSO_4.7H_2O$, time differential Mossbauer coincidence technique, time depend. of electron capture aftereffects 80−39927
$CoSe_2$, hyperfine parameters and quadrupole splitting determ., ^{57}Fe Mossbauer spectra 77−77131
$CoSe_2$, paramag. metal, sp. ht., Mossbauer effect, absence of ordering 77−16036
$CoSeO_4$, electron capture and γ-radiolysis, radn. damage 80−16705
Co_2SiO_4, reaction with Fe to produce Co *(Russian)* 78−15332
$Co_{1-x}Te$, fluctuating localised mag. moments, d band motion, Mossbauer study 80−65768
Co_2TiAl, hyperfine fields of Fe impurities, Mossbauer spectra 80−71255
Co_2TiSn-Fe, dil., Heusler alloy, Fe hyperfine fields, Mossbauer obs. 78−68424
Co_2VAl, hyperfine fields of Fe impurities, Mossbauer spectra 80−71255
CoV_2O_4:Fe, spinel, prep. and Mossbauer spectra 79−28660
$^{57}CoY_2O_4$, after effects of orbital electron capture 79−73870
Co_2ZrSn-Fe, dil., Heusler alloy, Fe hyperfine fields, Mossbauer obs. 78−68424
^{57}Co complexes, phenanthroline and ethylenediamine ligands, Auger processes, Mossbauer obs. 77−12277
^{57}Co implantation in Si and Ge, Mossbauer spectra, dose dependence 79−82899
^{57}Co, Mossbauer absorpt. and emission spectra, hyperfine struct. and relax. effects 80−71279
^{57}Co source, quantum beats of recoil-free γ radiation 78−43748
^{57}Co:Fe Mossbauer source linear polarisation rate meas. *(French)* 79−30633
$^{57}Co_3O_4$, Mossbauer study of the charge state and symmetry of $^{57}Fe^m$ in diverse cobalt spinels *(Spanish)* 79−69754

Mossbauer effect continued
$CoCr_2O_4$, Mossbauer study of the charge state and symmetry of $^{57}Fe^m$ in diverse cobalt spinels *(Spanish)* 79−69754
CoO, compact single-line Mossbauer source preparation 77−10518
$CoRh_2O_4$, Mossbauer study of the charge state and symmetry of $^{57}Fe^m$ in diverse cobalt spinels *(Spanish)* 79−69754
$Co^{2+}[Fe(CN)_6]^{3-}$, struct. determ. 80−15901
$Co^{2+}[Fe^{III}(CN)_6]^{y-}$, time depend. linewidth of Mossbauer spectrum 80−15911
Cr chalcogenide spinels, $ACr_{1.9}Sn_{0.1}X_4$, Sn hyperfine interactions 80−15485
Cr, spinelides, effect of cation distribution on Mossbauer spectra parameters 79−8082
Cr-Co-Fe, low Co, phase separation, TEM and Mossbauer spectra obs. 80−71269
Cr-Fe, antiferromagnetic, effect of press. on hyperfine mag. fields at Fe nuclei *(Russian)* 80−15936
Cr-Fe, electronic struct., Mossbauer and positron annihilation study 79−82518
Cr-Fe (20 to 30 at.%), Mossbauer spectra temp. var. and ferromag. props. 77−81037
$Cr\text{-}Fe_x$ (x=0.5, 1.5 and 3.5 at.%), antiferromag., Kondo anomaly 80−11163
$Cr_{1-x}Fe_x$, Mossbauer spectra, mag. behaviour 80−20532
$Cr_xFe_{3-x}O_4$, spin and charge density oscillations due to impurities *(Korean)* 80−20565
$Cr_{1-x}Fe_xOOH$, $0 \leq x \leq 10$, prep., Mossbauer effect, Neel temp. 80−108134
CrI_3, ferromagnetic, origin of magnetic hyperfine field transferred at iodine 78−92000
$Cr_{1-x}Mn_xO_2$, hyperfine mag. fields at ^{119}Sn, Mossbauer study 80−71260
CrO_2 amorphous thin films, Mossbauer and magnetisation data 80−34712
Cr_2O_3:$^{119}Sn^{4+}$, Mossbauer spectra *(French)* 79−24248
Cr_2O_3-Fe_2O_3 solid soln., completely annealed, reclustering of Fe^{3+} ions 79−33578
Cr_2TeO_6, CC ^{57}Fe Mossbauer spectrum, hyperfine field, Neel temp. 79−56636
$CrTiNdO_5$, distrib. of Cr^{3+} and Ti^{4+} ions, Mossbauer spectrum 77−69747
$CrTiRO_5$, R=Pr,Nd,Sm,Eu,Gd,covalency contribs. 78−10808
Cs-graphite intercalated compounds, anisotropy of Debye-Waller factor, Mossbauer meas. 77−55738
$Cs_2Au_2Cl_6$, ^{197}Au Mossbauer high press. study of mixed valence compound 78−52387
$Cs_2Au_2Cl_6$, electronic state of Au at high press., Mossbauer spectra 80−60467
$Cs_3BiSbBr_9(Cl_9)$, ^{121}Sb Mossbauer chem. shifts, optical reflectance spectra, solid state band populations 77−40162
CsCl:Fe, defect struct., Mossbauer spectra and X-ray diffr. obs. 80−7237
$CsCrI_3$, Mossbauer spectra, struct., electronic and mag. props. 79−91320
$CsFeCl_3.2H_2O$, rectangular Ising cpd., Mossbauer meas. 80−71252
$CsFeCrF_6$, $CsFeVF_6$, crystal struct., Mossbauer hyperfine spectra 78−52381
Cs_2FeF_5, mag. struct. and one-dimens. antiferromagnetism 80−60209
Cs_2IrCl_6, hyperfine spectra of mag. ordered state at very low temp., Mossbauer meas. 77−69744
$CsLi_{0.5}(Al,Fe)_{1.5}F_6$ pyrochlore, Mossbauer contrib. to exam. of cationic order *(French)* 80−93224
$CsLi_{0.5}Fe_{1.5}F_6$ pyrochlore, Mossbauer contrib. to exam. of cationic order *(French)* 80−93224
$CsMi_3$, (M=V, Cr, Mn), Mossbauer spectra, struct., electronic and mag. props. 80−15908
$Cs_2NaYbCl_6$, freq. depend. of spin-spin relax. rate from Mossbauer spectroscopy 78−48095
$Cs_2NaYbCl_6$, Mossbauer spectral lineshape in presence of paramag. relax. effects 77−69755
$Cs_2NaYbCl_6$, Mossbauer relax. spectra, breakdown of white noise approx. 78−27141
$CsNiFeF_6$ pyrochlore, Mossbauer contrib. to exam. of cationic order *(French)* 80−93224
Cs_2NpCl_6, Mossbauer spectra and mag. susceptibility meas. 80−108140
Cs_2SbCl_6, mixed valence compound, ^{121}Sb Mossbauer spectroscopy 79−51890
Cs_2TeI_6, ^{129}I Mossbauer spectra, coupling consts. 78−62833
$CsVI_3$, Mossbauer spectra, struct., electronic and mag. props. 79−91320
^{133}Cs, Mossbauer isomer shifts, book contrib. 79−87363
Cu film, on Cu, Mossbauer emission spectra 78−19387
Cu, grain boundaries, nucl. gamma reson. *(Russian)* 79−8080
Cu, press. depend. of Mossbauer fraction for ^{57}Fe 77−16226
Cu, press. depend. of Mossbauer fraction 77−59493
Cu, self-interstitial interaction with solutes, resistivity meas. 78−47331
Cu-Au-Fe, ferromag. ordering in FCC γ-Fe precipitates, Mossbauer study 80−71267
Cu-Co, dil., binding and caging of impurities and trapped interstitials 78−39462
Cu-Fe, dil., diffusion and ageing processes, Mossbauer study 80−7245
Cu-Fe, dil., ion implanted, phase comp., Mossbauer study 80−7244
Cu-Fe, dil., local susceptibility, Mossbauer meas. 78−19400
Cu-Fe, force constant change with pressure, relative Mossbauer fraction 80−34163
Cu-Fe, implanted, Mossbauer effect meas. 78−31134
Cu-Fe, implanted, Mossbauer study, rel. to annealing temp. 78−31135
Cu-Fe, Kondo system, magnetisation, Mossbauer expts. 77−77028
Cu-Fe, mixed cryst., Debye-Waller factors, Mossbauer spectra obs. *(German)* 78−52412
Cu-Fe, Mossbauer studies of ageing and precip. 79−38415
Cu-Fe, supersaturated, spontaneous magnetisation region development, Mossbauer obs. *(German)* 78−64306
Cu-Fe (0.2 at.%), clustering, precipitation, and oxidation, 298 to 919K, Mossbauer study 80−7242
Cu-Fe (0.2 at.%), quenched, Fe dimers and defects 80−40007
Cu-Fe (0.2 at.%), surface oxidation, Mossbauer obs. 80−55564
Cu-Fe alloy, cluster form., Fe solubility determ., 450 to 1000°C, Mossbauer spectra obs. *(German)* 79−29021
Cu-Fe alloy, local moment system, low temp. susceptibility, Mossbauer effect meas. 77−43810
Cu-Fe alloys, Kondo system, static and dynamic susceptibilities, NMR and Mossbauer spectra 77−63090
Cu-Te system, cryst. chem., Mossbauer investig. 77−16220

Mossbauer effect continued
Cu-Zn(Ga)(Ge)(As), Mossbauer effect of Fe impurities 78−31131
$CuCr_{2-x}Fe_xO_4$, charge transfer, Mossbauer spectroscopy 80−15836
$CuCr_2O_4$-$CuFe_2O_4$ (2 mol.%), Mossbauer expts., existence of Fe^{2+} 78−43721
$CuFeO_2$, EFG tensor, nucl. quadrupole coupling const., O^{2-} polarisability 77−72844
$CuFe_2O_4$, Jahn-Teller type crystal distortions 80−103904
$Cu_{0.5}Fe_{2.5}O_4$-$ZnFe_2O_4$, cation distrib., mag. moment, Mossbauer spectra, chem. anal. 80−75210
$CuFeS_2$, electronic struct., Mossbauer expt. 78−27150
Cu_5FeS_4, mag. ordering and vacancy clustering, mag. susceptibility and Mossbauer spectra meas. 77−85625
$Cu_2MnAl_{1-x}Sn_x$, Mossbauer effect study 80−60473
$Cu_2MnIn_{1-x}Sn_x$ alloy, compositional SRO, hyperfine interactions 80−71065
Cu_2SnS_3-CdSe, diamond-type semiconductor, Mossbauer spectrum of ^{119}Sn 80−44991
$(Cu_2SnS_3)_x$-$(3CdS)_{1-x}$, diamond-type semiconductor, Mossbauer spectrum of ^{119}Sn 80−44991
$(Cu_2SnS_3)_x$-$(3ZnS)_{1-x}$, diamond-type semiconductor, Mossbauer spectrum of ^{119}Sn 80−44991
$Cu_2SnS_3(Se_3)(Te_3)$, lattice dynamics obs. 77−43923
$(Cu_2SnS_3)_x(3CdS)_{1-x}$, second co-ordination sphere atoms effect on ^{119}Sm Mossbauer spectra *(Russian)* 77−63348
$(Cu_2SnS_3)_x(3ZnS)_{1-x}$, second co-ordination sphere atoms effect on ^{119}Sn Mossbauer spectra *(Russian)* 77−63348
Cu_2SnSe_3-CdS, diamond-type semiconductor, Mossbauer spectrum of ^{119}Sn 80−44991
$(Cu_2SnSe_3)_x$-$(Cu_2SnS_3)_{1-x}$, diamond-type semiconductor, Mossbauer spectrum of ^{119}Sn 80−44991
Cu_xZn_{1-x}, positron annihilation and Mossbauer effect exam. 79−65775
D NaCl:Fe, defect struct., Mossbauer spectra and X-ray diffr. obs. 80−7237
Dy, and $DyMn_2(Fe_2)(Co_2)(Ni_2)$, H_2 absorpt., Mossbauer study 80−44987
Dy, magnetic anisotropy and ^{161}Dy Mossbauer effect 78−92001
Dy-Sc, magnetic relax. phenomena 79−33579
Dy-Sn alloy, hyperfine fields acting on diamag. impurities and anisotropic exchange, Mossbauer spectra 77−1625
$DyAlO_3$:Yb^{3+}, Mossbauer relax. 80−15875
$DyCo_2$, magnetocryst. anisotropy props. by ^{57}Fe Mossbauer spectroscopy 77−63328
$DyCo_3$, mag. and quad. interactions, Mossbauer spectra 77−12267
Dy_2Co_{17}, hyperfine interactions and cryst. field effects, Mossbauer spectra 80−2369
$DyCoO_3$, anomalous $^{57}Fe^m$ charge states, Mossbauer study 80−40017
DyFe amorphous film, Mossbauer and mag. meas. 80−15844
$DyFe_2$, phonon softening below Curie temp. 77−4589
$DyFe_3$, Mossbauer spectra, easy magnetisation axis temp. rot. 80−15859
Dy_2Fe_{17}, hyperfine interactions and cryst. field effects, Mossbauer spectra 80−2369
$Dy_2(Fe_{1-x}Co_x)_{17}$, hyperfine interactions 78−2780
$DyFe_2H_2$, mag. props., ^{57}Fe and ^{161}Dy Mossbauer spectra and magnetisation meas. 79−78579
$Dy(Fe_xNi_{1-x})_2$, mag. behaviour, susceptibility and Mossbauer expts., 4.2-1300K 78−52235
$Dy_2(Fe_{1-x}Ni_x)_{17}$, hyperfine interactions obs. 78−6614
$DyFeO_3$, field induced spin reorientation, Mossbauer spectroscopy 80−65878
$DyFeO_3$, spin reorientation transitions induced by magnetic fields, Mossbauer study 80−71246
Dy_2FeSbO_7, supertransferred hyperfine mag. fields and relax. of Dy^{3+} ions by Mossbauer spectroscopy of ^{57}Fe 77−59494
DyH_2, mag. and crystal field props. from ^{161}Dy Mossbauer studies 79−95692
DyH_2, mag. and electronic props., ^{161}Dy Mossbauer spectroscopy 78−80262
DyH_3, mag. and crystal field props. from ^{161}Dy Mossbauer studies 79−95692
$Dy_{1-x}Ho_xNi_2$, cryst. field quenching of Dy^{3+} 4f shell, Mossbauer effect meas. 78−39480
DyIG, non-cryst., Mossbauer and magnetisation studies 80−44979
DyIG, noncrystalline, Mossbauer and magnetisation data 80−34828
DyM_2Si_2, (M=Mn, Fe, Co, Ni, Cu), Mossbauer spectra 80−20558
DyMg, Mossbauer spectroscopy and mag. props. 77−85624
Dy_2Ni_{17}, hyperfine interactions and cryst. field effects, Mossbauer spectra 80−2369
Dy_2Ni_{17}, magnetic struct. by neutron diffr. and Mossbauer spectra *(French)* 77−32165
Dy_2O_3, ^{161}Dy hyperfine parameters for C_2 and C_{3i} site symmetries 77−20770
$Dy(OH)_3$, Mossbauer spectra, cryst. field and mag. props. 80−15873
DyO_2X, X=S,Se,Te, mag. and quadrupole hyperfine interactions 77−63336
$Dy_2Sn_2O_7$, supertransferred hyperfine mag. fields and relax. of Dy^{3+} ions by Mossbauer spectroscopy of $^{119}Sn^m$ 77−59494
$Dy_{1-x}Y_xAl_2$, cryst. field quenching of Dy^{3+} 4f shell, Mossbauer effect meas. 78−39480
^{161}Dy polarised nuclei system, nonthreshold and amplification *(Russian)* 79−98332
$ErAl_3$, 15 layer rhombohedral struct., mag. struct. 77−63104
$ErCo_2$, magnetocryst. anisotropy props. by ^{57}Fe Mossbauer spectroscopy 77−63328
$ErFe_2$, lattice dynamics, Mossbauer spectra 80−19888
$ErFe_3$, H_2 sorption, mag. and struct. props. of hydrides 80−34831
$ErFe_3$, mag. anomalies at 47 and 131K 77−63134
$ErFe_3$, Mossbauer and magnetisation investig. of 47K mag. anomaly, atomic rearrangement 77−20766
$Er(Fe_{1-x}Co_x)_3$, spin reorientation, easy axis of magnetisation 80−25144
$ErFe_2H_{3.65}$, $ErFe_2H_{4.12}$, Mossbauer spectra, electronic and structural studies 80−15860
$Er_3Fe_{5-x}In_xO_{12}$, lattice consts., T_c, mag. saturation, K-absorpt. and Mossbauer spectra, 80K *(Russian)* 77−20954
$ErFeO_3$, field induced spin reorientation, Mossbauer spectroscopy 80−65878
ErH_3, Mossbauer spectra of Er^{3+}, gyromagnetic ratios and cryst. field parameters determ. 78−19388
$ErH_2(D_2)$, mag. props., 1.5 to 10K, Mossbauer meas. 79−78578
ErMg, Mossbauer spectroscopy and mag. props. 77−85624

Mossbauer effect continued
$ErMo_6S_8(Se_8)$, ternary superconductor, paramagnetic relax. effects 78−68112
$Er(OH)_3$, Mossbauer spectra, cryst. field and mag. props. 80−15873
$ErRh_4B_4$, Mossbauer spectra 80−15926
$ErRh_4B_4$, supercond., electronic props. of Er^{3+} using Mossbauer effect in ^{166}Sr 79−56651
$ErRh_4B_4$, superconducting, magnetic dilemma 80−75680
$ErRh_4B_4$, ternary superconductor, paramagnetic relax. effects 78−68112
Eu complex, Eu(III) β-diketonates, Mossbauer studies 79−61286
Eu intermetallic compounds, Mossbauer effect isomer shift, charge density at nucleus, trends 77−48112
Eu intermetallic compounds, hyperfine interactions, high press. Mossbuaer expts. 78−43714
Eu, Mossbauer isomer shift and magnetic hyperfine field, press. effect 78−52386
Eu pyrochlores, $Eu_2Z_2O_7$, (Z=Ti, Ru, Ir, Mo, Sn, Zr, Pb, Pt and Hf), elec. field gradient, Mossbauer expt. 79−8077
Eu^{3+} compounds, chloride, sulphate, nitrate, carbonate, oxalate and acetate, Mossbauer study 79−99801
Eu-Cd compounds, Mossbauer effect, mag. props. and lattice consts. 77−36164
Eu-salt solutions, frozen, Mossbauer parameters depend. on pH and halide conc., Eu(III) complexes form. 78−3330
$Eu+t_2$, high press. Mossbauer spectra, interconfig. charge fluctuations 77−63341
$Eu(Al_{0.5}Ta_{0.5})O_3$, mag. props. 77−4587
EuB_6, pure single crystals, magnetic and electric props. 80−11260
$EuB_{6-x}C_x$, Mossbauer spectra, cond. electrons effect 80−20545
$Eu_{0.95}Ba_{0.05}Pt_2$, Mossbauer studies on ^{151}Eu at high press. 80−39923
Eu_xCa_{1-x}, mag. ordering temp. conc. depend., Eu mag. hyperfine field temp. depend. 78−14971
$EuCl_2$, matrix isolated, Mossbauer effect, isomer shift and quadrupole splittings obs. 78−46377
$EuCoO_3$, anomalous $^{57}Fe^m$ charge states, Mossbauer study 80−40017
$EuCo_2Si_2$, cryst. struct. and valence state 77−76375
$EuCu_2Ge_2$, cryst. struct. and valence state 77−76375
$EuCuSi_3$, cryst. struct. and valence state 77−76375
$EuFe_4Al_8$, mag. ordered, mixed valency of Eu, X-ray, susceptibility and Mossbauer spectra studies 79−19728
$EuFe_2Si_2$, cryst. struct. and valence state 77−76375
EuIG, non-cryst., Mossbauer and magnetisation studies 80−44979
EuIG, noncrystalline, Mossbauer and magnetisation data 80−34828
$Eu_{0.25}La_{0.75}Rh_2$, high press. Mossbauer spectra, interconfig. charge fluctuations 77−63341
$Eu(Lu_{0.5}Ta_{0.5})O_3$, mag props. 77−4587
$Eu(Lu_{0.5}Ta_{0.5})O_3$, mag. props. 77−4587
EuM_2Ge_2, M=Mn, Fe, Co, Ni, Cu, magnetism and hyperfine interactions 78−76228
$EuMg_5$, Mossbauer effect, effective moments, mag. ordering temp. and isomer shifts 80−34833
Eu_2Mg_{17}, Mossbauer effect, effective moments, mag. ordering temp. and isomer shifts 80−34833
$EuMg_2H_x$, Mossbauer effect exam. 78−48094
$Eu(Mg_{0.5}W_{0.5})O_3$, mag. props. 77−4587
$Eu(Ni_{1-x}Cu_x)_5$, mixed valency, isomer shift temp. depend. 78−84511
$EuNi_xCu_{5-x}$, mixed valency of Eu, Mossbauer expts. 78−52407
$EuNi_2Ge_2$, cryst. struct. and valence state 77−76375
$EuNi_5H_x$, Mossbauer effect exam. 78−48094
$EuNiSi_3$, cryst. struct. and valence state 77−76375
$EuNi_2Si_2$, cryst. struct. and valence state 77−76375
$EuNi_xZn_{5-x}$, mixed valency of Eu, Mossbauer expts. 78−52407
EuO:Gd, pure and doped, elec., mag., and optical props. rel. to electronic conc. 80−96880
EuO-RN solid soln., (R=Nd,Eu,Gd), ^{151} Mossbauer spectroscopy 78−6610
$EuO_{1-x}N_x$, blocking of valence fluctuations, ^{151}Eu Mossbauer spectra 80−2678
EuPd, mech. of H absorption, Mossbauer, mag. and X-ray diffr. meas. 78−38846
$EuPt_2$, ^{151}Eu Mossbauer studies at high press. 80−39923
$EuPt_x$ compounds, partial valence change, ^{151}Eu Mossbauer and magnetisation obs. 80−70167
$EuRh_2$, mech. of H absorption, Mossbauer, mag. and X-ray diffr. meas. 78−38846
EuS, transferred hyperfine interacs. 77−69741
EuS:Sn^{2+}, Mossbauer spectra, Sn^{2+} transferred hyperfine fields 80−15887
$Eu_zSn_{1-z}Mo_6S_y$, supercond., mag. props. 77−69447
$Eu_xSn_{1-x}Mo_6Sn_8$ (Se_8), ternary superconductor, paramagnetic relax. effects 78−68112
$(Eu_{1-x}Sn_x)S$, high press. Mossbauer exam. of Curie temp. and transferred hyperfine field 79−56643
$(Eu_{1-x}Sn_x)Se$, high press. Mossbauer exam. of Curie temp. and transferred hyperfine field 79−56643
$Eu_xSr_{1-x}S$, mag. ordering temp. conc. depend., Eu mag. hyperfine field temp. depend. 78−14971
$Eu_xSr_{1-x}S$, non-metallic spin glass system 79−61175
$Eu_xSr_{1-x}SO_4$, mag. ordering temp. conc. depend., Eu mag. hyperfine field temp. depend. 78−14971
EuTe, Neel temp. and hyperfine interactions, press. depend. up to 60 kbar, ^{151}Eu Mossbauer obs. 77−63181
EuTe:Sn^{2+}, Mossbauer spectra, Sn^{2+} transferred hyperfine fields 80−15887
Eu_xWO_3-Sn_yWO_3, prep. and struct. of mixed W bronzes 77−4085
EuX_5, X=Cu, Zn, Ag, Au, cond. electron spin polarisation effects 77−63136
β-FEOOH, Mossbauer spectra obs., chemical and thermal anal., X-ray diffr., saturation magnetisation 80−88896
α-F_2O_3:alkali metal hydroxides, reduction, Mossbauer spectra 80−16672
$(Fe,Mn)WO_4$, mixed cryst., magnetically disordered system, Mossbauer and neutron diffr. meas. 77−16225
$(Fe,Mo)_{80}B_{20}$, glassy alloy, Curie temp. and crystn. temp., Mo additions effect, Mossbauer spectra 78−68428
(Fe, Ti) silicate glasses, optical absorption and Mossbauer spectra 80−55136
Fe, ^{155}Tb sources produced by recoil implantation, ^{155}Gd Mossbauer transition 80−40009
Fe $(H_2O)_6^{2+}$, in crystals and aqueous soln., asymmetrical quadrupole spectra 80−44974

Mossbauer effect continued
Fe $(NO_3)_3.9H_2O$, spin-spin relax., Mossbauer effect studies, 4.2K 78−31128
Fe aerosol powders, oxidised, nucl. gamma reson. study *(Russian)* 79−1725
Fe aerosoled fine particles, Mossbauer spectra 80−7223
Fe, air pollution, conc. and sources determ. by Mossbauer technique 79−79442
Fe alloys, BCC, Mossbauer spectra, local mag. moments 80−15861
Fe, Armco, borided surface layers, Mossbauer and metallographic anal. 80−50769
Fe armcotype, Mossbauer spectrum linewidth, influence of dislocations 79−99806
Fe, cast, ferritic, Ce addition effect on impurity distrib. Mossbauer study *(Russian)* 78−18673
Fe, characterisation in environmental samples by Mossbauer technique 79−66433
α-Fe, chem. interaction with aluminophosphate and alumino-chromo-phosphate adhesives, Mossbauer obs. 80−40596
Fe clusters, supported, Mossbauer spectra 80−7220
Fe complex, ^{57}Fe Mossbauer spectra, temp. depend. 77−12262
Fe complex, ^{57}Fe(2-aminomethylpyridine)$_3Cl_2.C_2H_5OH$, temp. depend. spin state, ^{57}Fe Mossbauer emission spectroscopy 80−39980
Fe complex, $[Fe(CN)_6]^{3-}$, electronic struct., optical transitions, XPS, Mossbauer isomer shift, valence ionisation pot., SCF-MSX calc. 79−6864
Fe complex, $[Fe(S_2C_2O_2)_2X]^{2-}$, (X=Cl,Br,I), Mossbauer effect, EPR, mag. susceptibility 79−11366
Fe complex, anomalous spin states, Mossbauer spectra 77−12261
Fe complex, binuclear ferricyanides, Mossbauer effect 79−78576
Fe complex, bis(N,N-dialkyldithiocarbamato) iron III halides, short range antiferromag. coupling, Mossbauer spectra 77−90076
Fe complex, bis[2-(2-pyridylamino)−4-(2-pyridyl)thiazole]Fe(II) complexes, high spin-low spin transitions 77−8456
Fe complex, dithiocyanato bis(4-methyl-1, 10-phenanthroline) iron, Mossbauer effect and magnetism down to 0.98K 77−28490
Fe complex, FE II cyclohexanone thiosemicarbazone, Mossbauer spectrum, quadrupole splitting 79−28641
Fe complex, Fe (II) pseudo-tetragonal high-spin cpds., paramag. susceptibility amd Mossbauer quadrupole splitting 78−26834
Fe complex, Fe (alkyldithiocarbamate)$_2$X, X=Cl, I, mol. orbital calc., hyperfine fields, elec. field gradient 80−39981
Fe complex, Fe_xM_{1-x}(1,10-phenanthroline)$_2$(NCS)$_2$, M=Mn,Co,Ni, spin crossover, Mossbauer and magnetism study 80−44980
Fe complex, Fe^{2+} chelate of hydrazinecarboxylic acid, Mossbauer effect, cryst. field splitting 79−78591
Fe complex, $FeCl_3L_3$ type, L=ligand, Mossbauer study 78−2783
Fe complex, Fe(III) Schiff-base complexes, mag. relax., Mossbauer spectra 80−15897
Fe complex, Fe(III) tris diseleno chelates, sextet doublet Boltzmann equilib. Mossbauer spectra 78−60366
Fe complex, Fe(II) oxalato-bridged chain compounds, Mossbauer spectra 80−15890
Fe complex, Fe(5-methylpyrazole)$_4X_2$, X=Cl, Br, I, mag. susceptibility, mag. saturation; Mossbauer and ligand field spectra, single model interpretation 78−23064
Fe complex, Fe(pyrazole)$_4X_2$, X=Cl, Br, I, mag. susceptibility, mag. saturation; Mossbauer and ligand field spectra, single model interpretation 78−23064
Fe complex, ferrous pseudo-tetrahedral compounds, paramag. relax., Mossbauer spectra 80−15869
Fe complex, halobis(morpholyldithiocarbamato)Fe(III), solvation effects, mag. susceptibility and Mossbauer spectra 78−27129
Fe complex, halobis(morpholydithiocarbamato)Fe(III), Mossbauer HFS spectra, mag. relax. and cooperative transitions 78−27130
Fe complex, iodobis(morpholyldithiocarbamate), allotropes, intermol. exchange interactions 77−8455
Fe complex, iron 4,7-$(CH_3)_2$-(1,10-phenanthroline)$_2$(NCS)$_2$, spin state transition, X-ray and Mossbauer obs. 80−7195
Fe complex, perchlorato(meso-tetraphenylporphinato) iron (III), mag. props., Mossbauer study 79−99802
Fe complex, pyridine-n-oxide perchlorate, Mossbauer spectra, site distortions enhanced by grinding 80−15883
Fe complex, tris-(4-morpholinecarbodithioate-S,S')Fe(III), and dichloromethane solvate, Mossbauer and EPR spectra, spin 3/2 state 78−9169
Fe complex, tris(monothio-β-diketonato) Fe (III), spin equilib., Mossbauer spectra 80−15910
Fe complex (2, 9-dimethylphenanthroline) sulphate, mag. props., Mossbauer spectra 80−66081
Fe complexes, 1-(2-pyridylazo)-2-naphthol and 1-(2-pyridylazo)-2-phenanthrol, back co-ordination, Mossbauer study 80−20572
Fe complexes, 2- or 3-pyridyl imine complexes of $FeCl_2$, Mossbauer and mag. props. 80−15896
Fe complexes, Fe (III) bis(dithiocarbamato) iodides, transferred hyperfine interactions and mag. ordering 77−20759
Fe complexes, FeOCl[Co(cyclopentadienyl)$_2$]$_{0.16}$ and FeOCl[Fe(cyclopentadienyl)$_2$]$_{0.16}$, Mossbauer and mag. susceptibility meas. 80−44176
Fe complexes, high spin ionic with halogen ligands, Mossbauer isomer shift calibration 77−16210
Fe complexes, M[Fe$(C_2O_4)_3$].XH_2O, M=Li, Na, K, Rb, Cs, NH_4, Mossbauer studies of electronic relax. phenomena 80−44973
Fe complexes, mag. susceptibility, Mossbauer spectra 78−15071
Fe complexes, Mossbauer isomer shift and core electron binding energies of Fe 78−82620
Fe complexes, tetraphenylporphyrins, mag. susceptibility, hyperfine mag. field value Mossbauer spectra 80−37824
Fe complexes, tris and bis dithiocarbamates, quad. splitting, Mossbauer obs. 77−59489
Fe complexes with dimethylformamide, dimethylthioformamide, Mossbauer and mag. props. 80−39974
Fe containing minerals, basalt rocks, Mossbauer spectroscopy identification 80−8302
Fe, conversion electron meas. of core polarisations 80−20530
Fe, conversion spectrum anal., outer-shell s-electron density, ACSEMP program 80−7208
Fe, corrosion and oxidation, new technique for simultaneous acquisition of Mossbauer spectra and microbalance data 78−44252
Fe, corrosion product analysis by Mossbauer spectroscopy 77−28927
Fe, crit. fluctuations, Mossbauer obs. 78−43724
Fe crystalline systems and metallic glasses, Mossbauer spectroscopy, effect of neighbours on hyperfine field 80−39931

Mossbauer effect continued
Fe, deoxidation of liq. by Al, Mossbauer meas. 80−20553
Fe dilute alloys, with s-p elements of third or fourth periods, Mossbauer spectra meas. 77−63344
Fe discontinuous film, Mossbauer effect exam. of magnetic state 77−24769
Fe epitaxial film, Mossbauer effect, depth profiling of mag. hyperfine field 80−11295
Fe epitaxial film, Mossbauer effect, interface magnetism 80−11297
Fe film, antiferromagnetic ordering, Mossbauer spectroscopy 78−14990
Fe film, coated, interface magnetism by Mossbauer spectroscopy 80−75890
Fe, film, FCC, antiferromag. ordering, Mossbauer expts. 77−85508
Fe film, nuclear spin system dynamics Mossbauer study in FMR conditions *(Russian)* 80−80651
Fe film, on Cu and Ag substrates, mag. props., Mossbauer spectra meas. 80−11233
Fe film, ultra-thin Mossbauer spectroscopic studies of mag. props. 80−44970
Fe film, vacuum-evaporated contamination, conversion electron Mossbauer spectroscopic obs. 78−23985
Fe film coated by MgO, MgF_2 and Sb, surface mag. 80−7196
Fe film coated by MgO, Mossbauer spectra, mag. hyperfine field 80−7221
Fe, fine particles, chemisorption of CO, H_2, Mossbauer study 80−39415
Fe fine particles in matrices, lattice vibr., Mossbauer effect 80−15924
Fe, finely dispersed, superparamagnetism, Mossbauer meas. 78−68303
Fe foil, Lamb-Mossbauer factor at 4.2K 80−20561
Fe garnets, sublattice magnetisation curves, Mossbaeur study 80−75808
Fe hexacyanoferrates, $M_4Fe(CN)_6.nH_2O$, Mossbauer and IR spectra 80−2739
Fe, high purity, boriding with cryst. B powder 80−84951
Fe hydroxides, crystallogenesis, Mossbauer study 79−31564
Fe in hepatic and splenic tissues 80−81544
α-Fe, laser irrad., Mossbauer effect and positron annihilation *(Russian)* 78−19390
Fe, mag. hyperfine field at ^{129}I, press. depend., nucl. gamma reson. 80−71256
γ-Fe, mag. struct., Mossbauer studies. 80−39917
Fe, mag. surface props. 77−69757
Fe, metal and alloys, X-ray absorption spectra, Mossbauer spectra, comparison *(Russian)* 78−64299
Fe, microcrystal, Mossbauer Debye-Waller factor size and temp. depend. 78−15065
Fe, microcrystal, temp. dependent lowering of Debye-Waller factor 79−1736
Fe, Mossbauer absorpt. spectrum, domain struct. effect 79−69758
Fe, Mossbauer effect at high press. in α-, ε- and γ-phases 80−15858
Fe, Mossbauer energy shift near Curie temp. 78−52388
Fe, Mossbauer spectra, demagnetising field effect on magnetic splitting 80−39932
Fe multilayer films stability, Mossbauer spectra 80−29651
Fe, nitrided, X-ray and Mossbauer study of surface 78−48568
Fe, noncrystalline, mag. hyperfine data from Mossbauer spectra 78−39477
Fe ore band associated with meta- acidic intrusive, Himalayas, Mossbauer meas. 79−79821
Fe organometallics, interaction of naked Fe atoms with small mols., Mossbauer study of bonding in products 80−43080
Fe, oxidation, conversion electron Mossbauer spectroscopy, appl. to surface props. and reactors 78−60359
Fe, oxidation, electron re-emission Mossbauer spectroscopy 77−16752
Fe, oxide film thickness determ. by electron backscatt. Mossbauer spectroscopy 78−72933
Fe, oxide overlayer thickness determ. by ^{57}Fe conversion elec. Mossbauer spectroscopy 79−57142
Fe, oxidised aerosoled ultrafine particles, X-ray and Mossbauer examination 80−21183
Fe particles, spin collinearity, Mossbauer spectra study 80−71114
Fe, phosphites, polycryst. EPR and Mossbauer spectra 78−76369
Fe powder, Mossbauer spectra parameter calc. with aid of computer *(Russian)* 78−76361
Fe powder, passivating oxide layer comp. 78−31558
γ-Fe precipitates, antiferromag. ordering, press. depend., Mossbauer meas. 79−73861
γ-Fe precipitates in Cu, Invar related system, high press. Mossbauer spectra 79−56642
Fe, segregation of ^{119m}Sn at grain boundaries, Mossbauer effect 78−15414
Fe $SiF_6.6H_2O$, phase transform., temp. depend. of Mossbauer parameters 77−73102
Fe small, particle motion effect on Mossbauer spectra 80−84671
Fe, small particles, Mossbauer effect study of lattice vibr. 80−44963
Fe, sponge, oxidation kinetics by nuclear γ-resonance method *(Russian)* 80−40681
Fe sputtered film, amorphous, Mossbauer study and electron diffr. obs. 80−75897
Fe, surface, contamination in vac. depth selective conversion electron Mossbauer spectroscopy 80−2671
Fe, thin film, core electron polarisation measurement 79−4756
Fe, ultrathin film, mag. hyperfine field, temp. and thickness depend. 78−39478
α-Fe, uniaxial stress effect on Mossbauer spectrum 80−71244
Fe, whiskers, polycrystn., Mossbauer study 80−20571
Fe^{2+} compounds, Mossbauer spectra, spin-lattice relax. effects 80−50239
Fe^{2+}, in octahedral symm., vibronic effects from Zeeman field induced Mossbauer spectra 77−8476
Fe^{3+} compounds, Mossbauer spectra, temp. depend. of isomer shift *(Russian)* 78−39479
Fe^{3+} in crystals, quadrupole hyperfine struct., screening coeffs. 77−52000
Fe^{3+} ion compounds, effect on Mossbauer spectra of thermal vibrs. rel. to covalently populated 4S shell nucleus 78−72444
Fe^{3+} ions, in frozen aq. solns., spin-spin relax., Mossbauer obs. of effect of paramag. impurity ions 79−33573
Fe: ^{119}Sn, pressure dependence of effective magnetic fields 78−52382
Fe: ^{116}Er, hyperfine interaction of impurities, Mossbauer spectra 77−48105
Fe: ^{129m}Xe, mag. hyperfine field determ. by Mossbauer effect 77−8460

Mossbauer effect continued
Fe: ^{129}Cs, implanted atom sites and hyperfine interactions, Mossbauer obs. 77−20753
Fe: ^{129}Te, implanted atom sites, Mossbauer obs. 77−20756
Fe: ^{129}Tm, implantation below 15K, in situ Mossbauer obs. 77−20754
Fe: ^{129}Xe, implanted atom site populations, Mossbauer, NO and NMR/ON obs. 77−20755
Fe: ^{133}Xe, heavy ion implantation, recovery, Mossbauer effect meas. 78−52393
Fe: ^{57}Fe, suppression of nuclear reaction in direct γ-quantum beam 77−20780
Fe: ^{83}Rb, implanted atom sites and hyperfine interactions, Mossbauer obs. 77−24765
Fe:N, ion implanted foil, Mossbauer effect study, nitride form. 78−27149
Fe:Xe(Te) interaction of impurities with point defects, Mossbauer spectroscopy exam. 78−47414
Fe^{3+}/Fe^{2+} in frozen solns., stabilisation on ^{57}Co decay, electron scavenger effects, Mossbauer obs. 77−40562
Fe^{3+}/Fe^{2+} ratio, quantitative Mossbauer spectra 80−7209
Fe-Al, electron density distrib. vs. at. order 79−60309
Fe-Al, high temp. Mossbauer study of order-disorder transform. 79−100137
Fe-Al, Mossbauer spectra, local mag. moments 80−15861
Fe-Al, Mossbauer study of ordering *(Japanese)* 79−19822
Fe-Al (15 at.%), short range order form. kinetics *(Russian)* 78−3146
Fe-Al (25 at.%), anomalous magnetic behaviour *(Japanese)* 77−48011
Fe-Al (25 at.%), double Curie point phenomena 77−73030
Fe-Al alloys, cold-worked, Mossbauer study of recovery 80−7593
Fe-Al alloys, ordering studied by Mossbauer effect 77−63342
Fe-Al_2O_3 granular film, interface props., Mossbauer spectroscopy 80−34336
Fe-Al-Si alloy, order-disorder transform. exam. by Mossbauer spectroscopy 77−63334
Fe-Al(Si)(Ga)(Ge)(As)(Sn)(Sb) dil. alloys, mag. hyperfine fields, Curie temps. and Mossbauer meas. 77−63190
Fe-alloys, Mossbauer isometric effects *(Dutch)* 79−1731
Fe-As system, mag. props., Mossbauer study 80−88897
Fe-B, amorphous, short-range order, Mossbauer meas. 80−44986
Fe-B, amorphous paramag. alloys, hyperfine field distrib., Mossbauer study 80−39958
Fe-B, rapidly quenched, metastable phases 80−76234
Fe-B (15-25 at.%) glass, quasicryst. struct. Mossbauer expts. 79−4255
Fe-B amorphous alloy, mag. anisotropy temp. depend. 80−15846
Fe-B amorphous alloys, Mossbauer spectra, soft ferromag. props. 80−11302
Fe-B amorphous alloys, Mossbauer spectra, mag. moment conc. depend. 80−15847
Fe-B metallic glass, role of Fe_3B in crystn., mag. and Mossbauer expts. 78−94997
Fe-B metallic glass, struct. and crystallisation, Mossbauer spectra, calorimetry and magnetisation meas. 79−23528
Fe-B metallic glasses, struct., stability and crystn. 80−75173
Fe-B metastable alloys, Mossbauer spectroscopy and electron microscopy 79−28653
Fe-B-Si, amorphous ferromag. alloys, mag. struct., Mossbauer study 80−39746
Fe-B(Si) amorphous alloys, Mossbauer spectra, struct. 80−15840
Fe-based alloys, volume interactions between substitutional sp and 3d solutes 79−78069
Fe-C, ferromag., prep. by splat-quenching, obs. of electronic struct. of interstitial C 77−62868
Fe-C, martensite, struct., Mossbauer meas. 80−40000
Fe-C (1.2 wt.%), Mossbauer study of early stages of tempering 80−16342
Fe-C (1.86 wt.%), exam. of C clustering in martensite, using Mossbauer spectroscopy 78−84821
Fe-C-(Si), splat quenched, electron diffr. and Mossbauer study of retained ε-phase 77−52354
Fe-Co, dil., Mossbauer source, self-absorption effects *(French)* 79−24246
Fe-Co, equiatomic, atomic order, Mossbauer study *(French)* 78−27135
Fe-Co, Mossbauer investig. of order-disorder and α-γ transitions 77−48110
Fe-Co (25-35%), ordering, Cr addition effects, Mossbauer expts. *(Russian)* 78−19741
Fe-Co based alloys, redistrib. of elements, combined appl. of emission and absorption Mossbauer spectroscopy *(Russian)* 78−6031
Fe-Co films, ordered and disordered, Mossbauer study 79−24241
Fe-Co-Cd(Sn), mag. hyperfine fields at Fe, Cd and Sn sites, Mossbauer and TDPAC meas. 78−60363
Fe-Co-Cr, 25KKh15 alloy, nuclear γ-reson. investig. of atomic redistrib. during annealing *(Russian)* 77−12640
Fe-Co-Cr, alloy K25Kh15, phase tranforms., nucl. gamma reson. and X-ray diffr. meas. *(Russian)* 77−44241
Fe-Co-Cr, Cr effect on struct. of ordering, Mossbauer effect meas. 78−35407
Fe-Co-Cr alloys, atomic mag. moment, magnetisation, Mossbauer spectra and NMR spin echo spectra 77−63127
Fe-Co-Cr-Si, structural transform. and mag. props. following heat treatment *(Russian)* 77−81274
Fe-Co-Mn alloys, BCC, atomic mag. moment, magnetisation, Mossbauer spectra and NMR spin echo spectra 77−63127
Fe-Co-Ni, at. mag. moments, neutron scatt. and Mossbauer meas. 79−42744
Fe-Co-Si solid solutions, BCC, atomic configs., Mossbauer study 80−39006
Fe-Co-V alloys, effect of V on struct., electron diffr. and Mossbauer meas. *(Russian)* 77−77507
Fe-Co(Ni)(Cu) bimetallic molecule, matrix isolated 78−68425
Fe-Co(Ni)(Cu) bimetallic molecule, matrix isolated 78−88233
Fe-containing minerals, in coals, mag. hyperfine fields meas. 78−88234
Fe-containing minerals in coals, magnetic hyperfine fields meas. 78−68427
Fe-Cr, BCC, local moments in Mossbauer study 80−108125
Fe-Cr, decomposition Mossbauer study *(French)* 77−63678
Fe-Cr, disordered, mag. order, Mossbauer study 80−39992
Fe-Cr, hyperfine magnetic fields, Mossbauer spectra 80−97165
Fe-Cr, segregation of ^{121}Sb, Mossbauer spectroscopy 79−47698
Fe-Cr (1.20, 3.63, 7.98 wt.%), Mossbauer spectra shape depend. on deformations 79−61272

Mossbauer effect continued
Fe-Cr-Co, mag. alloys, Mossbauer spectra 78−19386
Fe-Cr-Co alloy, Mossbauer exam. of spinodal decomposition 77−69742
Fe-Cr-Co-Al (27.5, 17.5, 0.5) alloy, mag. props. and microstruct. obs. 78−72367
Fe-Cr-Ni, Fe-Co-Mn, Fe-Cr-Co and Fe-Ni-Mn alloys, BCC, atomic mag. moments determ. 77−59396
Fe-Cr-Ni, spin system, relaxation props. at low temp. 79−82758
Fe-Cu clusters, mag. interaction, Mossbauer study 79−82895
Fe-Cu metastable dil. alloy film, hyperfine interactions 78−52398
Fe-Dy, dil., implanted impurity hyperfine interaction 78−68417
Fe-Eu, dil., hyperfine interaction of ^{153}Eu, Mossbauer effect meas. 78−43703
Fe-Ga, Mossbauer effect for phase transitions, 20-720°C, 25.7-28.3 at.% Ga *(German)* 78−68437
β-Fe-Ge, mag. props. from X-ray, magnetisation and Mossbauer meas. 79−42755
Fe-Ge amorphous films, conversion electron Mossbauer spectra, mag. moments 77−16231
Fe-implanted alloys, residence sites of Fe, Mossbauer data 80−39299
Fe-La(Zr) amorphous films, mag. props., Mossbauer effect and magnetisation meas. 79−69701
Fe-M-SiO_2 (M=Ru,Pt), supported catalysts, Mossbauer spectra 80−11296
Fe-Mn, annealed, α-γ phase transformation obs. 78−75831
Fe-Mn, dilute, short-range ordering and segregation, Mossbauer spectra intensity *(Russian)* 77−24406
Fe-Mn, electron redistrib. and BCC struct. stability, Mossbauer meas. *(Russian)* 79−42873
Fe-Mn, γ to ε phase transform. induced by high press. and plastic deform. 78−68686
Fe-Mn, Mossbauer spectroscopy of temp. hysteresis of phase transformations *(Czech)* 80−29949
Fe-Mn, Mossbauer study near martensitic transform. temp. 78−3128
Fe-Mn (12% Mn), decomposition during plastic deform., Mossbauer parameters *(Russian)* 77−36166
Fe-Mn (18.6 wt.%), HCP-FCC martensitic transform., Mossbauer effect meas. 78−44121
Fe-Mn (8.25 wt.%), irreversible temper embrittlement, Mossbauer spectra, impact strength depend. on interstitials *(German)* 79−74235
Fe-Mn (9 to 20 wt.%), ^{57}Fe Mossbauer spectroscopy in phase transformations 80−29948
Fe-Mn base alloy, mag. preferred directions 78−39370
Fe-Mn-C alloy, martensitic transform. obs. *(Russian)* 78−6927
Fe-Mn-C austenite, spectra interpretation allowing for at. interaction in lattice *(Russian)* 77−69738
Fe-Mn-Cr(Ni), mag. and crystallographic transformation depend. on Cr-Ni addition *(Russian)* 79−83334
Fe-Mn-Ti-Al, magnetic texture rel. to annealing temp., Mossbauer investig. 77−28499
Fe-Mo catalyst, Mossbauer spectra 80−7222
Fe-N, hexagonal, ferromag. Mossbauer spectroscopy 77−63331
Fe-N(C), solid soln., metastable and stable, interstitial atom config. 77−36512
Fe-Nb alloys, mag. and Mossbauer meas. 77−63133
Fe-Ni, hydrogenated, Mossbauer effect meas. 78−92002
γ-Fe-Ni, local magnetisation of Fe atoms, Mossbauer effect meas. 80−75891
Fe-Ni, martensitic transform. dynamic, quasi-static atomic displacements, NGR, X-ray and electron scatt. meas. *(Russian)* 78−68688
γ-Fe-Ni, Mossbauer exam. 79−56640
Fe-Ni, ordered phase, Llo superstruct., Mossbauer spectrum, Debye-Scherrer pattern from LL-chondrite 80−50241
Fe-Ni, oxidation, Mossbauer spectroscopy, metallography, SEM and X-ray diffr. anal. 78−15577
Fe-Ni, segregation of ^{121}Sb, Mossbauer spectroscopy 79−47698
Fe-Ni, taenite, superstruct. in Fe meteorites 78−61820
Fe-Ni (25 to 50%), FCC, meteorites and thermodynamic equilib., Mossbauer and X-ray diffr. study 80−88087
Fe-Ni (28 at.%), martensitic transformations, Mossbauer scattering evidence of soft modes 80−93223
Fe-Ni (6-8 at.%) 80−75888
Fe-Ni alloy, anisotropic hyperfine interactions, Mossbauer spectra 80−15854
Fe-Ni alloy, α→γ transform., role of grain boundary diffusion, Mossbauer obs., homogenisation effect *(Russian)* 79−52197
Fe-Ni alloy, fluorination kinetics and fluoride film form., chem. nature obs. 80−101035
Fe-Ni alloy near crit. conc., Mossbauer γ-rays small angle scatt. 80−7217
Fe-Ni alloys, cold rolled, exam. of phase composition using Mossbauer spectroscopy 80−21204
Fe-Ni alloys, struct. of γ and α-phases near martensitic transform. point *(Russian)* 78−64541
Fe-Ni austenite, α→γ transform and stabilisation, Mossbauer and electron microscopy obs. *(Russian)* 78−23703
Fe-Ni based metallic glass, Metglas 2826 MB, Mossbauer study 80−75897
Fe-Ni film, α→γ transition *(Russian)* 77−40154
Fe-Ni Invar, Mossbauer exam. 79−56639
Fe-Ni Invar alloy, effect of hydrogenation, Mossbauer spectra 79−56641
Fe-Ni Invar alloy, electron irrad. effects 79−56638
Fe-Ni Invar alloys, Mossbauer spectra, heat treatment effect 80−15855
Fe-Ni ordered phase in meteorites, Mossbauer studies 80−41776
Fe-Ni superstructure in metal particles in chondrites 80−12713
Fe-Ni-Al, magnetic anisotropy form. and struct. changes by annealing, Mossbauer obs. 80−39994
Fe-Ni-Al, strong elastic stress effects on Mossbauer line 77−90084
Fe-Ni-Al (30, 4wt.%), ageing, peculiarities of struct. state *(Russian)* 79−57008
Fe-Ni-Al-Co-Ti base alloys, highly coercive, phase comp., Mossbauer meas. 80−39996
Fe-Ni-C, Invar, coated, Mossbauer spectra, effect of applied RF mag. field 80−80645
Fe-Ni-C (9, 0.1 wt.%), effect of intercritical tempering on impact energy, exam. of mech. props. 78−52861
Fe-Ni-C alloy, martensitic transform. obs. *(Russian)* 78−6927
Fe-Ni-Cr, Invar alloy, ^{57}Fe effective field distrib., Mossbauer obs. *(Russian)* 78−19381
Fe-Ni-Mn, Invar RF collapse and thermal effects, study 80−100624
Mossbauer effect continued
Fe-Ni-Mo-C, Mossbauer investig. of secondary hardening, carbide form. *(Russian)* 77−44260
Fe-Ni-Mo(Si), austenite, annealing effect on atom redistrib., Mossbauer anal. *(Russian)* 80−66529
Fe-Ni-P-B, amorphous ferromag. alloys, mag. struct., Mossbauer study 80−39746
Fe-Ni-P-B, amorphous paramag. alloys, hyperfine field distrib., Mossbauer study 80−39958
Fe-Ni-Si-B, amorphous paramag. alloys, hyperfine field distrib., Mossbauer study 80−39958
Fe-Ni-V alloy, ageing of martensite *(Russian)* 78−39808
Fe-Ni(41.3 at.%) Invar alloy, asymmetric Mossbauer spectra 77−63346
Fe-P alloys, amorphous, Mossbauer spectra 79−51886
Fe-P-B, amorphous alloy, Mossbauer effect and short-range order 80−2675
Fe-P-C, amorphous, struct. and mag. props., Mossbauer, X-ray diffr. and elec. resist. meas. 78−2009
Fe-P-C, amorphous alloy, Mossbauer effect and short-range order 80−2675
Fe-P-C alloys, amorphous, mag. anisotropy, Mossbauer obs., prior cooling effects *(Russian)* 77−32300
Fe-P-C amorphous alloys, Mossbauer spectra, struct. 80−15840
Fe-Pd (1-2 wt.%), solution of ^{119}Sn, study by Mossbauer spectroscopy 80−75888
Fe-Pd (50 at.%), ordering under load, nuclear gamma reson. obs. *(Russian)* 78−92258
Fe-Pd alloy, mag. struct. determ., neutron scatt., Mossbauer and mag. meas. *(Russian)* 78−2648
Fe-Pd alloy, uniaxial ferromag., anisotropic component of localised mag. field, Mossbauer meas. *(Russian)* 79−15382
Fe-Pt, Invar type, strong ferromagnetism, mag. props. 78−64197
Fe-Pt, Mossbauer exam. 79−56639
Fe-Pt-Ir, ^{193}Ir and ^{57}Fe, hyperfine field, isomer shift 78−15072
Fe-Rh(Os), mag. hyperfine interactions Mossbauer effect meas. 77−66442
Fe-Ru (30-60 at.%) alloy, mag. ordering obs. 77−4585
Fe-Ru(Os), CC hexagonal phase, ^{57}Fe Mossbauer study, saturated hyperfine fields and Neel temp. determ. 79−91321
Fe-Ru(Os) alloys, antiferromag. ordering, hyperfine fields 80−15867
Fe-S (34.0-41.0 wt.%), Mossbauer investigations 79−47376
Fe-Sb amorphous films, Mossbauer effect study 80−75896
Fe-Sb-Ti(V)(Cr)(Mn)(Co)(Ni), dil., interactions and precip., Mossbauer study 80−39997
Fe-Sb-Ti(V)(Cr)(Mn)(Co)(Ni), interactions and segregations, Mossbauer and X-ray diffr. study 80−70415
Fe-Se, low conc. binary system, Mossbauer spectroscopy meas. 79−24239
Fe-Si, electron density distrib. vs. at. order 79−60309
Fe-Si, hyperfine fields, Mossbauer meas. 80−40024
Fe-Si, Mossbauer study of mag. ordering 79−24245
Fe-Si, thin cryst., domain struct. behaviour during magnetisation *(Russian)* 78−2697
Fe-Si, type B_1 domain struct., Mossbauer exam. 77−51931
Fe-Si (3 wt.%), elec. field gradient by trigonal and tetragonal distortions 77−8474
Fe-Si (3 wt.%), grain-oriented, stacking effect on power loss, mag. props. 80−88795
Fe-Si (3 wt.%), Mossbauer spectra, domain magnetisation vector rotations, domain struct. 79−69761
Fe-Si (3 wt.%), texture, Mossbauer expts. 80−71262
Fe-Si (3 wt.%) domain struct., tensile load effects *(Russian)* 78−47995
Fe-Si (3 wt.%) layers, with ceramic coating, interface struct., electron microscopy and Mossbauer obs. *(Russian)* 79−28216
Fe-Si alloys, ordering studied by Mossbauer effect 77−63342
Fe-Si amorphous film, conversion electron Mossbauer effect 78−72440
Fe-Si amorphous film, crystallisation, Mossbauer studies 80−33900
Fe-Si amorphous film, struct. and crystallisation, Mossbauer study 80−11300
Fe-Si film, amorphous, conversion electron Mossbauer study 78−84507
Fe-Si-Al sendust type alloys, Co preferred substitution sites, Mossbauer spectra 79−91328
Fe-Si-B amorphous alloys, Mossbauer spectroscopy *(French)* 80−80653
Fe-SiO_2, granular compund, superpara- to ferromag. transition temp. meas. 77−69633
Fe-SiO_2 granular film, interface props., Mossbauer spectroscopy 80−34336
Fe-SiO_2 supported catalysts, Mossbauer spectra 80−11296
Fe-SiO_2-(Al_2O_3)(ZrO_2) granular films, superparamag., Mossbauer effect 80−7131
Fe-Sn, grain boundary embrittlement by Sn segregation, Mossbauer study 80−7239
Fe-Sn system, Sn binding state, using segregated ^{119m}Sn, Mossbauer anal. *(Japanese)* 80−20525
α-Fe-V, dilute alloy, Mossbauer diffusion line broadening, exponential fitting evaluation 78−52379
Fe-V (10 to 50 at.%), solid soln., tempered, exam. of long and short range order, using Mossbauer effect *(Russian)* 79−29105
Fe-V alloys, hyperfine fields at solute and solvent sites rel. to mag. moments 77−8461
Fe-V alloys, Mossbauer study, hyperfine field effect on formation of local moments 78−27134
Fe-X-Sn dilute alloy, Mossbauer meas. of Sn interaction with solute atoms 80−15856
Fe-Y(Lu) amorphous films, mag. props., Mossbauer effect and magnetisation meas. 79−69701
Fe-Y(Th)(Zr), amorphous, charge transfer and mag. props., ^{57}Fe Mossbauer spectra 79−19719
Fe-Zn, stable and metastable alloys, order-disorder, mag. interactions and corrosion behaviour 78−68422
Fe-ZrO_2 granular film, interface props., Mossbauer spectroscopy 80−34336
Fe+N_2(NH_3) interaction, chemical species formed studied by Mossbauer effect 80−43080
FeAl, isomer shift, electronic charge density 78−80264
$FeAl_x$, ferromag. to mictomag. transition, Mossbauer meas. 77−24692
Fe_3Al-M, ternary ordered solid solns. with M=Ti, Mn, Ni, Cu, Ge substituent 77−43177
$Fe_{1-x}Al_xOOH$, Mossbauer study, determ. of Al content and mag. props. 80−39938

Mossbauer effect continued
FeAs, Mossbauer spectra of paramag. and ferromag. states, helimagnetic spin ordering 80−7197
Fe_2As, antiferromagnet, Mossbauer spectra determ. 77−8480
$Fe_{1-x}B_x$, amorphous, hyperfine fields and local mag. moments, Mossbauer study 80−75895
$Fe_{1-x}B_x$ metallic glasses, struct. and cryst., Mossbauer spectra, DSC, and magnetisation meas. 79−94906
Fe_3B, distinctness of magnetic hyperfine fields associated with structurally unique Fe sites 77−63330
Fe_3B, mag. props., ^{57}Fe Mossbauer spectra meas. 79−95693
$Fe_{80}B_{20}$, amorphous, crystn. 80−75187
$Fe_{80}B_{20}$, amorphous, elec. and mag. hyperfine field distribs., Mossbauer study 80−39964
$Fe_{80}B_{20}$, amorphous ferromag., temp. depend. of hyperfine field distrib. 78−43756
$Fe_{80}B_{20}$, amorphous ferromag., hyperfine field distrib., Mossbauer effect 78−60371
$Fe_{80}B_{20}$, amorphous ferromag. metallic glass, stress-induced rot. of magnetisation, Mossbauer study 80−20445
$Fe_{80}B_{20}$, amorphous ferromagnet, Mossbauer hyperfine fields, mag. struct. 80−75894
$Fe_{80}B_{20}$, amorphous struct., Mossbauer spectroscopy investigation 80−84677
$Fe_{80}B_{20}$, amorphous to cryst. transorm. 80−34188
$Fe_{80}B_{20}$, binary amorphous ferromagnet, Mossbauer spectra 79−4749
$Fe_{80}B_{20}$ glass, magnetisation reorientation, Mossbauer effect 80−66092
$Fe_{80}B_{20}$, METGLAS 2605, mag. anisotropy and electronic struct., Mossbauer meas. 77−28384
$Fe_{80}B_{20}$, metallic glass, ferromag. props. 77−16107
$Fe_{80}B_{20}$ metallic glass, spin texture determ. 80−15842
$Fe_{80}B_{20}$ metallic glass, crystn. and struct. relax., Mossbauer effect study 80−75182
$Fe_{80}B_{20}$ Metglass, Mossbauer spectra line broadening 78−52400
Fe_xB_{100-x}, amorphous, mag. props., ^{57}Fe Mossbauer spectra and magnetisation meas. 79−95693
$Fe_{84}B_{16-x}C_x$, amorphous, hyperfine interaction and Curie temps., Mossbauer meas. 79−73858
$Fe_{84}B_{16-x}C_x$, amorphous alloys, short range order, Mossbauer and DSC study 80−39960
$FeBO_3$, crit. behaviour, Mossbauer and magnetisation meas. *(Russian)* 79−61106
$FeBO_3$, dynamical diffraction of gamma rays, enhanced nuclear reson. scatt. 80−108127
$FeBO_3$, Laue refl. of Mossbauer radiation, depend. on mag. field direction 80−40020
$FeBO_3$, Mossbauer coherent scatt. polaris., rel. to cryst. mag. struct. *(Russian)* 79−11368
$FeBO_3$, nuclear reaction suppression, Mossbauer spectra for Laue diffr. *(Russian)* 80−66093
$FeBO_3$, suppression effect under hyperfine quadrupole splitting, Mossbauer study *(Russian)* 80−75906
$^{57}FeBO_3$ single cryst., weakly ferromag., diffr. of Mossbauer emission *(Russian)* 77−81038
$FeBO_6$, critical indices splitting of sublattice magnetisation *(Russian)* 78−60299
Fe_3BO_6, canted mag. struct. near Neel point, Mossbauer meas. 78−35073
Fe_3BO_6, MOssbauer spectra in spin reorientation region 77−52002
Fe_3BO_6, Mossbauer exam. of electric field gradients 77−40163
Fe_3BO_6, spin reorientation by mag. field, Mossbauer meas. 78−35074
Fe_3BO_6, weak ferromag. state, Mossbauer determ. of mag. struct. 77−40164
$Fe_{78}B_{12}Si_{10}$, amorphous, continuous versus discrete hyperfine field distrib., Mossbauer spectra 79−33583
$Fe_{78}B_{12}Si_{10}$, amorphous, Mossbauer study of hyperfine interaction and mag. anisotropy 80−40027
$Fe_{78}B_{12}Si_{10}$, amorphous ferromagnet, long and short range exchange interactions, Mossbauer spectra and interpretation 79−56526
$FeBr_2$, hyperfine interaction, ^{57}Fe Mossbauer expts., mag. transition obs. 78−43720
$^{57}FeBr_2$, matrix isolation Mossbauer spectra, isomer shift, quadrupole splitting 78−42104
FeC_x ($x \leq 0.05$), splat-quenched, struct., elec. and mag. props. 77−21187
Fe_3C, alpha-particle irrad., Mossbauer study of nucl. reaction aftereffects 80−40015
$Fe(CN)_6$, Mossbauer isomer shift const., ab initio SCF calcs. 78−43751
$FeCO_3$, Mossbauer quadrupole splitting of ^{57}Fe, vibronic effects 79−19813
$FeCO_3$, siderite, Fe^{2+} Mossbauer spectrum, ligand field theory 77−16212
$FeCO_3$, siderite, powder, Mossbauer spectra, acoustic-excitation-induced asymmetry of quadrupole splitting 78−27145
$Fe_2Ca_3Si_3O_{12}$ glass, mag. ordering effects at low temps., Mossbauer and neutron diffr. meas. 77−16047
$FeCl_2$, adsorbed monolayers, gamma-ray reson. 77−8478
$^{57}FeCl_2$, matrix isolation Mossbauer spectra, isomer shift, quadrupole splitting 78−42104
$FeCl_2$-graphite, intercalation compound, formation by reduction of Fe(III) compounds with $Fe(CO)_5$ 78−63721
$FeCl_3$, nonaq. solns., solvent-solute interactions, Mossbauer investig. of equilib. consts. 79−1729
$FeCl_4$ on Dowex 1×2, Mossbauer study of Fe complexes and Cl^- soln. effects *(Russian)* 79−19817
Fe_2Cl_6, matrix isolated, Mossbauer effect, isomer shift and quadrupole splittings obs. 78−46377
$^{57}Fe_2Cl_6$, matrix isolation Mossbauer spectra, isomer shift, quadrupole splitting 78−42104
$Fe(ClO_4)_2$, frozen aq. soln., Mossbauer spectra, ligand field calc. for $Fe(H_2O)_6^{2+}$ complex 80−39971
$Fe(ClO_4)_2.6H_2O$, paramag., Mossbauer absorpt. in external mag. field, polarisation effects 77−48099
$FeCl_2.4H_2O$, antiferromag., Mossbauer exam. 77−16221
$FeCl_2.4H_2O$, finite thickness cryst., evaluation by intensity matrix method 77−43912
$FeCl_2.4H_2O$, frozen solns., isotope effect of Mossbauer parameters 80−34835
$FeCl_2.4H_2O$, polarisation effects in Mossbauer absorption in external mag. field 78−31137
$FeCl_2.4H_2O$, pressure effects on hyperfine interaction in single crysts. in mag. field 77−16211

Mossbauer effect continued
$FeCl_2.4H_2O$, proton radiation effects, Mossbauer spectra meas. 77−11603
$FeCl_2(pyrazole)_2$, linear-chain cpd., low-temp. mag. behaviour 80−71253
FeCo disordered alloys, Mossbauer spectra, hyperfine mag. field distrib., Curie temp. 80−7198
FeCo molecules, matrix-isolation Mossbauer spectra 80−23448
$Fe_{50}Co_{50}$, disordering by laser irradiation, Mossbauer transmission spectroscopy and electron microscopy study *(French)* 79−23639
$Fe_{3-x}Co_xAl$, site preference and local environment effects, Mossbauer and NMR meas. 80−71264
$(Fe_{0.5}Co_{0.5})_{1-x}B_x$, amorphous, hyperfine fields and local mag. moments, Mossbauer study 80−75895
$Fe_{1-x}Co_xCl_2.2H_2O$, random mixture with competing spin anisotropies, tetracrit. behaviour 80−60324
$FeCoCrO_4$, ^{57}Fe Mossbauer spectra, cation distrib. 80−15879
$FeCoCrO_4$, Mossbauer study, cation distrib. and Neel temp. determ. 79−33571
Fe_2CoGa, alloy, site preference of Co and Fe, Mossbauer and neutron study 79−78577
$FeCo_2O_4$, spinel, cation distrib., Mossbauer spectra meas. 78−31127
$Fe_{0.5}Co_{2.5}O_4$, spinel, cation distrib., Mossbauer spectra meas. 78−31127
$Fe_{3-x}Co_xO_4$, charge transfer, ion distribs. 77−20767
$Fe_{3-x}Co_xO_4$, Mossbauer spectra, effect of Fe^{2+} conc. 77−69754
$(Fe_{0.2}Co_{0.8})_{80}P_{17}Al_3$, Mossbauer spectra, isomer shift, mag. hyperfine field 80−11301
$Fe_{2-x}Co_xP_{1-y}As$, mag. props., Mossbauer effect 77−40156
$Fe_xCo_{1-x}Rh_2S_4$, spinel struct., X-ray, mag., elec. and Mossbauer spectra meas. 77−12278
$Fe_{1-x}Co_xSi$, mag. props., sp. ht., n.m.r. and Mossbauer effect meas. 77−12129
$Fe_{1-x}Co_xSn$, transferred hyperfine fields at ^{119}Sn, Mossbauer spectroscopy 79−33582
$Fe_{0.5}Co_{0.5}TiH_x$, transmission Mossbauer spectra 80−44964
$Fe_{1-x}Cr_x$, Mossbauer exam. 77−16222
$Fe_{65.4}Cr_{20.5}Al_{10.7}V_{3.4}$, effect of Al and V on form. of $L2_1$ superstructure and stratification 77−77474
$FeCr_2O_4$, Mossbauer spectra and cryst. struct. determ. 79−56637
$(Fe_{1-x}Cr_x)_2O_3$, Mossbauer exam. of mag. struct. 77−24694
$Fe_{3-x}Cr_xO_4$, electron transfer and spin density distribs., Mossbauer spectra 79−24243
$Fe_{3-x}Cr_xO_4$, Mossbauer study above Verwey transition 78−43750
$Fe_{2-x}Cr_xP_{1-y}As_y$ mag. props., Mossbauer obs. 77−40156
$FeCr_2S_4$, ionic distrib. and band struct., Mossbauer study 80−80646
$FeCr_2S_4$, Mossbauer spectra, second order phase transition 80−20539
$Fe_xCu_{1-x}Cr_2Se_4$, crystallographic and image props. 80−39049
$Fe_xCu_{1-x}Rh_2S_4$, mag. tetrahedral intrasublattice interaction, X-ray, magnetisation and Mossbauer expts. 78−52241
FeF_2, Mossbauer effect at high press. 80−15858
FeF_3, amorphous, characterisation by thermal, mag. and Mossbauer study 79−42782
FeF_3, amorphous, mag. props. and Mossbauer spectra, speromagnetism and mictomagnetism 80−75778
FeF_3, amorphous, noncryst. magnet with antiferromag. interactions 79−91228
FeF_3, amorphous, struct. and mag. props., computer model 80−96446
FeF_3, antiferromag., Mossbauer spectrum, effect of mag. hyperfine struct. at low temps. 79−28662
FeF_3, overlap contribution to $^{57}Fe^{3+}$ isomer shifts, nuclear size change 80−39903
FeF_6, Mossbauer isomer shift const., ab initio SCF calcs. 78−43751
$FeF_3.3H_2O$, α and β phase, ^{57}Fe Mossbauer study of local struct. 80−39973
$Fe_2F_5.7H_2O$ and oxidation products, ^{57}Fe Mossbauer study of local struct. 80−39973
$FeGa_2O_4$, magnetic props. by Mossbauer effect, neutron diffr. and magnetisation meas. 77−43918
FeGe, hyperfine interactions of ^{119}Sn atoms, Mossbauer spectra *(Russian)* 80−29665
$FeGe_2$, antiferromag., biquadratic exchange 80−2371
$FeGe_2$, mag. struct., Mossbauer method 78−60268
$Fe_{1.67}Ge$, Mossbauer and X-ray expts. 79−1734
Fe_3Ge, ^{119}Sn mag. hyperfine interaction, Mossbauer spectra *(Russian)* 79−38420
Fe_3Ge, mag. props. of cubic and hexagonal phases 77−8475
Fe_5Ge_3, collinear mag. struct. from Mossbauer effect meas. 77−63343
β-Fe_5Ge_3 formation in isothermal sintering, phase transition kinetics 80−89197
Fe_xGe_{1-x}, amorphous, conversion electron Mossbauer spectra down to 4.2K 80−7205
Fe_xGe_{1-x} amorphous alloys, appl. of spectrom. using Bitter magnets 79−51888
Fe_xGe_{1-x} amorphous alloys, high field mag. meas. 79−82765
Fe_xGe_{1-x} amorphous film, low temp. conversion electron Mossbauer spectroscopy 78−48101
Fe_xGe_{1-x} amorphous film, XPS and Mossbauer exam. 79−56577
$Fe_3(HCOO)_6(OH)_2HCOO.4H_2O$, thermal decomp. 78−80741
$Fe(H_2O)_6^{3+}$, in frozen aqueous soln., Mossbauer spectrum, hyperfine struct. 77−77130
$Fe(H_2O_6)^{3+}$ ion, amorphous frozen soln., Mossbauer study, hyperfine struct. 80−80644
$Fe(H_2O)_6.SiF_6$, pressure-induced orbital ground state inversion, Mossbauer study 80−39979
$Fe(H_2PO_2)_2$, γ-ray and electron radiolysis, Mossbauer study 80−7816
FeI_2, hyperfine interaction, ^{57}Fe Mossbauer expts., mag. transition obs. 78−43720
FeI_2, magnetic phase transitions, Mossbauer spectra in high mag. fields 80−39936
Fe(III) salt soln., hydrolysis products, Mossbauer spectra 80−16671
$FeLu_2S_4$, structural study, X-ray diffr., Mossbauer spectroscopy 80−107159
$FeMF_5.7H_2O$ (M=Zn, Co, Fe), Mossbauer spectra, thermal decomp. products 78−80258
$(Fe_{1-x}M_x)_2O_3$, yH_2O, M=Cr,Cu,Ni, crystal growth, characterisation by Mossbauer spectroscopy, mag. meas. and electron microscopy *(French)* 80−80655
$FeMO_2S_4$, Mossbauer investigation, Neel point, superparamag. effects 80−97170
$FeMgBO_4$ and $FeMg_2BO_5$, mag. props., spin glass behaviour 79−61145
$FeMgBO_4$, and $FeMg_2MO_5$, imperfect 1D mag. systems, Mossbauer expts. 80−60466

Mossbauer effect continued
$(Fe_{0.19}^{2+}Mg_{0.56}^{2+}Mn_{0.25})$ $[Fe_{1.87}^{3+}Al_{0.13}^{3+}]O_4^{2-}$, influence of Fe^{2+} ion substitution on electron hopping, Mossbauer study 80−71247
$(Fe_{0.55}^{2+}Mg_{0.32}^{2+}Mn_{0.03}^{2+}Cu_{0.10}^{2+})$ $[Fe_{1.74}^{3+}Al_{0.26}^{3+}]O_4^{2-}$, influence of Fe^{2+} ion substitution on electron hopping, Mossbauer study 80−71247
$Fe_{3-x}Mg_xO_4$, Verwey transition, Mossbauer study 80−39942
$Fe_xMg_{1-x}SO_4.7H_2O$, EFG tensor evaluation, ^{57}Fe single crystal Mossbauer meas. 78−88237
$Fe_{0.55}Mg_{0.47}SiO_3$, orthopyroxene, electron irrad. effects, Mossbauer study 80−40016
$Fe_{0.2}Mg_{1.9}Ti_{0.9}O_4$, Mossbauer parameters temp. depend. 78−23381
$Fe_{0.4}Mg_{1.8}Ti_{0.8}O_4$, Mossbauer parameters temp. depend. 78−23381
$Fe_{1.2}Mg_{1.4}Ti_{0.4}O_4$, mag. ordering, Mossbauer effect in external mag. fields 80−71257
$Fe_{2(1-y)}Mg_{1+y}Ti_yO_4$ spinel, incomplete mag. ordering, static magnetisation and Mossbauer meas. 77−16056
$Fe_{2(1-y)}Mg_{(1+y)}Ti_yO_4$, Mossbauer spectra anal., model 80−20560
$Fe_{1.4}Mg_{1.3-x}Zn_xTi_{0.3}O_4$ spinel system, X-ray diffraction study 80−88900
FeMn, matrix isolated Mossbauer spectra, ground state determ. 79−45740
$(Fe_{1-x}Mn_x)_3Al$, mag. moments determ. from magnetisation and neutron and electron diffr. expts. 79−56520
$Fe_{3-x}Mn_xAl$, ordering of Fe atoms, X-ray diffr. meas. and mid gamma reson. anal. *(Russian)* 80−96469
$Fe_{2-x}Mn_xP_{1-y}As_y$, mag. props., Mossbauer obs. 77−40156
$(Fe_xMn_{1-x})_{75}P_{16}B_6Al_3$, amorphous, mag. ordering temp., hyperfine field distrib., elec. resist. 80−34633
$(Fe_{1-x}Mn_x)_{75}P_{15}C_{10}$, amorphous, mag. ordering, Mossbauer study 80−39747
$(Fe_{1-x}Mn_x)_3Si$, $(Fe_{1-x}Co_x)_3Si$, order distrib., hardening effect *(Russian)* 77−89410
$Fe_{3-x}Mn_xSi$, Mossbauer and NMR exam. of site substitution and mag. struct. 77−12092
$Fe_{1-x}Mn_xSn$, spin reorientation, Mossbauer study, 77 to 400K 80−97172
$Fe_{1-x}Mn_xSn$, transferred hyperfine fields at ^{119}Sn, Mossbauer spectroscopy 79−33582
$(Fe_{1-x}Mn_x)_2Y(B)$, Mn effect on Fe mag. moments, Mossbauer and mag. meas. 80−71016
$Fe_78Mo_2B_{20}$, amorphous ferromag., $T^{3/2}$ depend. of hyperfine field 78−39474
Fe_2MoO_4, ^{57}Fe Mossbauer spectra, cation distrib. 80−15879
Fe_2MoO_4, electron exchange between $Fe^{2+}-Fe^{3+}$ ions on tetrahedral and octahedral sites, Mossbauer spectra 79−78585
$Fe_2(MoO_4)_3$, ^{57}Fe Mossbauer effect obs. 77−48108
$(Fe_xMo_{1-x})_{75}P_{16}B_6Al_3$, amorphous, effects of Mo on mag. props., Mossbauer meas. 79−73859
$FeMo_2S_4$, Mossbauer spectra, 79-300K, Neel pt. determ. 78−60360
$Fe(N_3)_5^{2-}$, paramag. relax. in trigonal bipyramidal environment, Mossbauer spectra 80−15871
$Fe(N_2H_5)_2(SO_4)_2$:Co, Mossbauer effect and paramag. relax., superparamag. behaviour of correl. spin domains 77−69756
$FeNH_4(SO_4)_2.12H_2O$, Mossbauer study mag. transition in region 0.024-0.029K 79−38417
$Fe(NH_4)_2(SO_4)_2.4H_2O$, rehydration kinetics, Mossbauer effect study 80−61081
$Fe(NH_4)_2(SO_4)_2.6H_2O$, Mohr salt, elec. field gradient determ., appl. of intensity tensor to thick single cryst. 80−44966
$FeNb_2O_6$, low temp. Mossbauer exam. 79−28659
$Fe_{0.33}NbS_2$, lattice dynamics and hyperfine interactions, Mossbauer spectra study 80−108135
$Fe(Nb_{1-x}W_x)O_4$, mag. and elec. props. and Mossbauer effect 79−78590
$Fe_{1-x}Ni_x$ (x<29at.%), γ-phase dispersion, Mossbauer spectra 78−52399
$Fe_{65}Ni_{35}$, H-infused, internal mag. field determ., Mossbauer effect 78−23382
$(Fe_{1-x}Ni_x)_{75}B_{25}$, amorphous and cryst., short range order, Mossbauer study 80−39961
$Fe_{40}Ni_{40}B_{20}$ alloys, crystalline and amorphous, resistivity minimum, X-ray, Mossbauer studies 79−73489
$Fe_{40}Ni_{40}B_{20}$, amorphous, hyperfine field distrib., Mossbauer effect meas. 79−4755
$Fe_{40}Ni_{40}B_{20}$, amorphous, hyperfine field distrib., Mossbauer study 79−28657
$Fe_{40}Ni_{40}B_{20}$, amorphous, RF annealing effects 80−108037
$(Fe_xNi_{1-x})_{80}B_{20}$, amorphous, Mossbauer spectra, mag. props. 80−15843
$FeNiBO_4$, $FeNi_2BO_5$, Mossbauer spectra, mag. relax. 80−15889
$FeNiBO_4$, mag. and Mossbauer studies 79−65661
$FeNi_2BO_5$, mag. and Mossbauer studies 79−65661
$(Fe_{1-y}Ni_y)_{0.8}B_{0.2-x}P_x$, amorphous, hyperfine fields and local mag. moments, Mossbauer study 80−75895
$Fe_{0.65}(Ni_{1-x}Co_x)_{0.35}$, Mossbauer spectra, ^{57}Fe hyperfine field distrib. 80−20533
$Fe_{32}Ni_{36}Cr_{14}P_{12}B_6$, amorphous ferromagnet, long and short range exchange interactions, Mossbauer spectra and interpretation 79−56526
$Fe_{32}Ni_{36}Cr_{14}P_{12}B_6$, amorphous mag. solids, Mossbauer exam. 79−61281
$Fe_{32}Ni_{36}Cr_{14}P_{12}B_6$, Metglass 2826A, mag. props. under high press., Mossbauer meas. 79−73860
$Fe_{0.65}(Ni_{1-x}Mn_x)_{0.35}$, Mossbauer spectra, ^{57}Fe hyperfine field distrib. 80−20533
$Fe_{65}(Ni_{1-x}Mn_x)_{35}$, magnetic struct. and inhomogeneities by neutron scatt. and Mossbauer effect *(Russian)* 77−63122
$Fe_{65}Ni_{28}Mn_7$, disordered, mag. struct. near ferro-antiferromagnetic transition 80−60211
$Fe_{66}Ni_{31}Mn_3$, H-infused, internal mag. field determ., Mossbauer effect 78−23382
$Fe_{40}Ni_{38}Mo_4B_{18}$, amorphous, mag. anisotropy, Mossbauer study 80−65864
$Fe_{3-x}Ni_xO_4$, low temp. Mossbauer spectra, electron transfer and spin density distribution 78−52404
$Fe_{3-x}Ni_xO_4$, Mossbauer spectra, effect of Fe^{2+} conc. 77−69754
$(Fe_{1-x}Ni_x)_{80}P_{20}$, amorphous, ferromagnetic alloys, mag. anomalies of Invar type *(Russian)* 80−93089
$Fe_{2-x}Ni_xP_{1-y}As_y$, mag. props. Mossbauer obs. 77−40156
$Fe_{40}Ni_{40}P_{14}B_6$, amorphous, thermal stress effect on mag. easy axis 77−80928
$Fe_{40}Ni_{40}P_{14}B_6$, amorphous, stress-induced mag. easy axis 79−33516
$Fe_{40}Ni_{40}P_{14}B_6$, amorphous, continuous versus discrete hyperfine field distrib., Mossbauer spectra 79−33583
$Fe_{40}Ni_{40}P_{14}B_6$, amorphous ferromagnet, Mossbauer hyperfine fields, mag. struct. 80−75894
$Fe_{40}Ni_{40}P_{14}B_6$, glassy ferromag. 4.2-1000K 78−10812

Mossbauer effect continued
$Fe_{40}Ni_{40}P_xB_{20-x}$, amorphous, mag. props. effect of metalloid elements 79−28658
$(Fe_xNi_{1-x})_{80}P_{14}B_6$, amorphous, hyperfine field distrib., ^{57}Fe Mossbauer spectra 79−11367
$(Fe_xNi_{1-x})_{80}P_{14}B_6$, magnetic hyperfine interaction, Curie temps. 78−6617
$(Fe_xNi_{1-x})_{75}P_{16}B_6Al_3$, amorphous, spin wave excitations and low temp. magnetisation 79−33468
$(Fe_{1-x}Ni_x)_{80}PyB_{20-y}$, local struct. disorder and crystallisation, Mossbauer exam. 79−1728
$FeNi_2S_4$, violarite, mag. and elec. props., struct. determ. 77−43633
$Fe_{0.5}Ni_{0.5}S_2$, hyperfine field at ^{57}Fe *(Japanese)* 77−43916
$Fe_{62.4}Ni_{15.6}Si_7B_{15}$ amorphous ferromagnetic alloy, anomalous magnetisation possible reasons, Mossbauer spectra *(Russian)* 79−78441
$Fe_{1-x}Ni_xSn$, transferred hyperfine fields at ^{119}Sn, Mossbauer spectroscopy 79−33582
FeO_4^{2-} ion, electronic struct., hyperfine interactions, SCF Xα calcs. 79−37951
Fe_2O_3, amorphous, temp. depend. of hyperfine field, Mossbauer spectroscopy 78−84508
Fe_2O_3 amorphous film, Mossbauer spectra, mag. props. 80−15851
Fe_2O_3 amorphous layer on graphite, Mossbauer spectra, superparamag. props. 80−60474
Fe_2O_3 amorphous RF sputtered thin films, Mossbauer and mag. study 80−34711
Fe_2O_3 amorphous thin films, Mossbauer and magnetisation data 80−34712
α-Fe_2O_3, analysis of car exhaust by Mossbauer spectroscopy 78−92963
α-Fe_2O_3, Bragg diffr. of 14.4 keV reson. γ-quanta in inclined mag. field *(Russian)* 78−2784
β-Fe_2O_3 film, CVD and characterisation 77−44172
β-Fe_2O_3 film, hyperfine interactions below and above mag. ordering temp., Mossbauer obs. 77−69745
α-Fe_2O_3 film, prep. by reactive condensation and mag. props. 78−64241
Fe_2O_3, haematite, Morin transition, Mossbauer expt. using selective excitation method 78−25375
α-Fe_2O_3, haematite, reduction by H_2, mag. field effect 77−12827
α-Fe_2O_3, hematite, Morin transition, Mossbauer mag. diffr. spectra 80−20562
γ-Fe_2O_3, hyperfine mag. field at ^{119}Sn, Mossbauer expt. 80−50232
α-Fe_2O_3, Morin transition, Mossbauer spectra meas. 78−31071
α-Fe_2O_3, Mossbauer spectra near Neel temp., critical indices, magnetisation *(Russian)* 80−66094
γ-Fe_2O_3 recording tapes, orientation, Mossbauer, X-ray and electron microscope meas. 77−16219
Fe_2O_3, shocked hematite, Mossbauer exam. 78−64304
γ-Fe_2O_3 small particles, hyperfine field below superparamag. blocking temp., Mossbauer obs. 78−19392
γ-Fe_2O_3 small particles, noncollinearity as crystallite-size effect, Mossbauer study 80−39939
γ-Fe_2O_3, small particles, vacancy sintering 77−65975
α-Fe_2O_3, solubility in BeO, Al_2O_3 and synthetic chrysoberyl, Mossbauer studies 77−7867
Fe_2O_3 ultrafine particles in PTFE matrix, EPR and Mossbauer study 80−100625
α-Fe_2O_3:Al, hematite, spin reorientation, Mossbauer spectra obs. 78−72356
α-Fe_2O_3:Sn, Mossbauer investig. of mag. hyperfine interactions 77−32306
xFe_2O_3-$(1-x)PbO$-$3B_2O_3$ glass, Mossbauer study of Fe cations 79−91325
Fe_2O_3-BaO-B_2O_3, magnetic props. of Fe-rich amorphous oxide *(French)* 80−80511
Fe_2O_3-BaO-B_2O_3 glass, Mossbauer spectra, ^{57}Fe hyperfine interactions 80−39969
Fe_2O_3-Bi_2O_3 system, mag. props., hyperfine parameters, Mossbauer spectrum 77−69746
α-Fe_2O_3-Cr_2O_3 solid solution, Mossbauer effect studies 80−71249
α-Fe_2O_3-Li_2O, structural and thermal phase behaviour from mag., spectral and thermal studies 80−2673
Fe_2O_3-MoO_3, on SiO_2 and Al_2O_3, Mossbauer effect 79−47365
γ-Fe_2O_3-organic interfaces, mag. struct., Mossbauer effect, IR absorpt., and magnetisation meas. 80−44869
Fe_2O_3-PbO-B_2O_3 glass, X-ray and electron microscope studies, mag. and Mossbauer effect meas. 80−28919
Fe_3O_4, electronic struct. and charge density oscills. near Verwey transition 78−27150
Fe_3O_4 film, prep. by reactive condensation and mag. props. 78−64241
Fe_3O_4, hyperfine field temp. depend., Mossbauer meas. near Verwey transition 77−69749
Fe_3O_4, hyperfine fields and spin densities below 20K 78−52405
Fe_3O_4, hyperfine mag. field at ^{119}Sn, Mossbauer expt. 80−50232
Fe_3O_4, low temp. phase, EFG meas. *(Japanese)* 77−43917
Fe_3O_4, low temp. phase 77−69751
Fe_3O_4 mag. fluid particles, comp., struct., and mag. props. 80−60374
Fe_3O_4, magnetite, Mossbauer spectra of Fe^{2+} 79−91319
Fe_3O_4, magnetite, Mossbauer spectra of low temp. phase 80−20541
Fe_3O_4, magnetite, valence instabilities, Mossbauer effect 80−20543
Fe_3O_4, magnetite Mossbauer spectra, mag. dipolar and elec. quadrupole effects 80−20544
Fe_3O_4, Mossbauer linewidth of octahedral Fe 77−66446
Fe_3O_4, Mossbauer spectra at 80K, Fe electronic states and hyperfine interactions *(Russian)* 78−43696
Fe_3O_4, Mossbauer spectra above Verwey transition 78−68415
Fe_3O_4, multistage phonon softening in Verwey transition region, Mossbauer spectra 77−72670
Fe_3O_4, nuclear gamma reson. investig. of high temp. electronic struct. 77−20751
Fe_3O_4 particles, nonstoichiometric, morphology and enhanced coercivity, Mossbauer meas. 80−7132
Fe_3O_4, relax effects, Mossbauer expt. using selective excitation method 78−25375
Fe_3O_4, selective excitation double Mossbauer exam. of electron hopping 77−69750
Fe_3O_4 single cryst., Mossbauer γ-ray diffr. 77−84600
Fe_3O_4:^{119}Sn, hyperfine field exam., Mossbauer meas. 77−69753
Fe_3O_4:^{119}Sn, magnetic interactions, Mossbauer spectra 79−15301
Fe_3O_4:Sn, hyperfine field temp. depend., Mossbauer meas. near Verwey transition 77−69749

Mossbauer effect continued
Fe_3O_4:Zn, and pure, influence of mag. order on charge delocalisation, Mossbauer spectra 78−68423
$Fe_3O_4/\gamma Fe_2O_3$ surface layers formed on small Fe particles, Mossbauer expts. 79−8081
FeOCl, Mossbauer spectra, lattice dynamics, hyperfine interactions 80−44985
$Fe_3O_{4-x}F_x$ ($0 \leq x \leq 0.25$), spectra 78−15075
$Fe_3O_{4-x}F_x$, low temp. Mossbauer spectra, electron transfer and spin density distribution 78−52404
$Fe(OH)_3$ thin films, Mossbauer spectra obs., chemical and thermal anal., X-ray diffr., saturation magnetisation 80−88896
α-FeO_2H, asymmetric line shapes of Mossbauer spectra *(Chinese)* 80−103902
$FeOHSO_4$, mag. props., Mossbauer spectra meas. 79−19824
β-FeOOH, colloidal suspension, ionic spin relax. theory for Mossbauer spectra 78−19384
FeOOH gels, Mossbauer spectra, mag. props. 80−11303
FeO(OH), goethite, Mossbauer effect exam. of annealing effect on struct. 78−19396
α-FeOOH, goethite small particles, mag. hyperfine field, bulk and surface contribs. 77−69758
β-FeOOH, Mossbauer investigation of the quadrupole splitting 78−76370
δ-FeOOH, structure and phase transform., Mossbauer, X-ray, DTA study *(Chinese)* 80−54368
β-FeOOH, ultrafine particles, mag. struct., Mossbauer spectroscopy 78−72372
α-FeOOH ultrafine particle NGR spectra, size distrib. and surface effects 80−11299
FeOOH:Cl(F), quadrupole interaction, Mossbauer spectra 80−15895
$Fe_2O(OH)_4$, Mossbauer spectra obs., chemical and thermal anal., X-ray diffr., saturation magnetisation 80−88896
α-$FeOOH.nH_2O$, hydrogoethite, Mossbauer spectra, Neel point, Fe^{3+} config. 77−32310
$xFe_2O_3(1-x)[PbO.3B_2O_3]$ glasses, mag. props. 77−73012
$FeO.Fe_2O_3.MgO.P_2O_5$ glass, conversion electron Mossbauer anal. of surfac struct. and chem. state 77−63333
$2Fe_2O_3.3H_2O$, bog Fe ore, Mossbauer effect exam. of annealing effect on struct. 78−19396
$20Fe_2O_3.80[3B_2O_3.(1-x)PbO.xGeO_2]$ glass, phys. props. 80−49119
α-FeP_4, diamag., semicond., Mossbauer study 80−50243
Fe_2P, Mossbauer spectra and mag. props., Curie temp. dispersion 77−36162
Fe_2P:Cu, Mossbauer spectra, mag. transition 80−50240
$Fe_{80}P_{20}$, binary amorphous ferromagnet, Mossbauer study 80−34829
$Fe_2P_{1-y}As$, mag. props., Mossbauer effect 77−40156
$Fe_{79}P_{13}B_8$ amorphous alloys, splat cooled, Mn, Cr and V substituted, mag. and transport props. 80−84593
$Fe_{75}P_{16}B_6Al_3$, aged metallic glass, Mossbauer effect 79−91318
$Fe_{80}P_{16}B_1C_3$, ferromag. metallic glass, Mossbauer spectra, crystn. 77−12276
$Fe_{75}P_{15}C_{10}$ amorphous foil, ferromag. domain orientation, Mossbauer exam. 78−52402
$Fe_{75}P_{15}C_{10}$ foils, amorphous, ferromag. domain orientation, Mossbauer study 78−15000
$Fe_2(PO_4)Cl$, Mossbauer study of mag. ordering and local co-ordination 80−39972
$Fe_3(PO_4)_2(OH)_2$ synthetic barbosalite, temp. depend. quadrupolar and mag. hyperfine interactions 80−25255
$FePS_3$, Goldanskii-Karyagin effect, Mossbauer spectra 79−99798
$Fe_{50}Pd_{50}$, order-disorder transition, Mossbauer study 80−71268
$Fe_xPd_{80-x}Si_{20}$, amorphous, structural and mag. heterogeneities 80−80484
Fe_3Pt, Invar alloy, elastically stressed, ^{57}Fe effective field, anomalous behaviour *(Russian)* 77−8485
Fe_3Pt, non-linear local environment effect, Mossbauer effect of ^{57}Fe and ^{195}Pt 80−39910
Fe_3Pt:Sn Invar alloy, Mossbauer shift temp. depend. 80−100626
$Fe_{76}Pt_{24}$ Invar alloy, ferromag., fine-powdered, Mossbauer effect 79−56634
$Fe_2Pu(Np)(U)(Zr)(Tm)$, Mossbauer diffr., combination type maxima, hyperfine interactions on nuclei 80−25263
$FeRO_3$, enhanced nuclear resonance scattering in dynamical diffraction of gamma-rays 80−44982
$Fe_{48}Rh_{52}$, hyperfine mag. field at ^{57}Fe and ^{119}Sn nuclei, press. depend. *(Russian)* 78−80266
FeS, quadrupole splitting and ground state, Mossbauer spectra 80−29657
FeS, zinc blende type, crystallographic and Mossbauer obs. 78−87650
Fe^{3+} (^6S) paramagnetisations, spin lattice relaxation Mossbauer study, dynamic spin Hamiltonian formalism 80−97173
FeS_2, (pyrite), angle-independent Mossbauer effect 80−20570
FeS_2, electric field gradient and mean-square displacement of Fe sites 79−95690
FeS_2, in mag. field, absence of mag. moment 77−12288
FeS_2, marcasite, Mossbauer elec. field gradient meas. 78−56407
FeS_2, Mossbauer elec. field gradient and mean square displacement 80−39991
FeS_2, oxidation, Mossbauer spectroscopic and magnetokinetic studies, 400-500°C 80−44880
FeS_2, pyrite, elec. field gradient, Mossbauer spectrum 80−15493
FeS_2, pyrite, semiconducting props., energy gap press. and lattice parameter depend., Mossbauer obs. 80−44494
$Fe_{0.9}S$, ferrimag. transition, mag., thermodynamic props., kinetics 79−47280
$Fe_{0.996}S$, $Fe_{0.93}S$, determination of quadrupole splitting sign, ground state appl. 78−76363
Fe_2S_3, existence and thermal stability, Mossbauer study 78−83733
Fe_9S_{10}, antiferro- to ferrimag. transition, Mossbauer and mag. exam., diffusion of Fe during transition 79−73716
FeS−Li_2S−Cu_2S system, Mossbauer spectra and lattice parameters 79−78584
$FeSO_4$, anhydrous, γ, β and γ-phases, Mossbauer spectra, polymorphism 77−12287
$Fe_2(SO_4)_3$, Mossbauer isomer shift in rhombohedral and monoclinic forms 78−6609
$Fe(SO_3F)_2$, Mossbauer and electronic spectra, cryst. field splittings, mag. hyperfine interactions 77−48096
$FeSO_4.4H_2O$, Fe sites asymmetry parameter, mean square displacement, Mossbauer spectra 78−6608

Mossbauer effect continued
$FeSO_4.7H_2O$ and $FeSO_4.7D_2O$, frozen solns., isotope effect of Mossbauer parameters 80−34835
$FeSO_4.7H_2O$, γ-ray irradiated, Fe^{3+} formation, Mossbauer study *(Russian)* 78−84509
FeSb alloy films, vapour-deposited, formation of metastable phase 80−44437
FeSb solid solution, supersaturated, mag. hyperfine field, Mossbauer study 80−44961
$Fe_{0.545}Sb$, temperature effect on lattice consts., Mossbauer spectra and density 80−88124
$Fe_{1+x}Sb$, hyperfine interactions of ^{57}Fe, room temp. Mossbauer meas. 79−47374
$Fe_{1+x}Sb$, Mossbauer meas. of lattice and interstitial Fe atom mag. ordering 79−99807
$Fe_{1+x}Sb$-CoSb solid soln., mag. props., Mossbauer spectra, solubility limits, and lattice consts. *(Russian)* 77−59394
$Fe_{1+x}Sb$-NiSb solid soln., mag. props., Mossbauer spectra, solubility limits, and lattice consts. *(Russian)* 77−59394
$FeSb_2O_4$, Mossbauer spectra, molecular field effects 78−91997
$FeSb_xO_{4-y}$, defect struct. and mag. transition, elec. transport and Mossbauer expts. 78−59803
$Fe(Sb_{1-x}Te_x)_3$ system cpds., prep., cryst. struct., elec. and mag. characteris. 80−108349
$Fe_{0.96}Se$, Mossbauer diffusional line-broadening 77−55734
Fe_3Se_4, Fe_7Se_8, phase gap, Mossbauer spectra 80−20552
Fe_3Se_4, Mossbauer diffusional line broadening 77−43370
Fe_7Se_8, test of Okazaki's 3c and 4c superstruct. model 77−66445
$FeSeO_4$, electron capture and γ-radiolysis, radn. damage 80−16705
$FeSi_2$ films, Mossbauer investig. of struct. 79−87341
α-$Fe_{1-x}Si_2$, many-body atomic correlations, Mossbauer spectroscopy study 80−15934
α-$Fe_{1-x}Si_2$, vacancy ordering, cryst. stabilisation energy aspects 80−103325
Fe_xSi_{1-x}, amorphous, struct. and mag. props., giant moment form. at mag. ordering 78−68192
$Fe_3Si_xAl_{1-x}$-Co, dil., site preference of ^{57}Co impurities, Mossbauer study 80−39999
Fe_5SiB_2, Mossbauer spectra, 140-784K, spin rotation 78−52409
$Fe_{79.5}Si_{1.5}B_{19}$ alloy at room temp., evaluation of hyperfine parameter distribs. from overlapped Mossbauer spectra 79−99804
$FeSiF_6$, isotropy of Lamb-Mossbauer factor, Debye model 80−60465
$FeSiF_6$, phase transform. and relax., EFG and quadrupole spectra 77−51995
$FeSiF_6.6H_2O$, Lamb-Mossbauer factor isotropy in the Debye model *(French)* 80−44962
Fe_2SiS_4, Mossbauer effect and magnetisation meas. of mag. struct. *(French)* 77−12282
Fe_3Sn_2, ^{57}Fe anisotropic hyperfine field variation 79−11294
Fe_3Sn_2, magnetic properties, ^{119}Sn Mossbauer study 79−91323
Fe_3Sn_2, Mossbauer effect and magnetisation meas. 78−31132
Fe_xSn_{1-x} amorphous alloy films, magnetisation meas. and Mossbauer spectra 78−95489
Fe_xSn_{1-x}, amorphous alloy, Mossbauer spectra, charge transfer and atomic vol. effects 80−39959
Fe_xSn_{1-x}, amorphous film, struct. and mag. props. 80−65972
$FeSnO_3$, Mossbauer spectral anal. *(German)* 79−19819
$FeSnO_3$ particles in EBBA liq. cryst., Mossbauer study of Brownian motion 79−95691
$Fe_2(SnO_3)_2$, Mossbauer spectral anal. *(German)* 79−19819
$Fe_{3-x}Sn_xO_4$, mag. hyperfine fields, ^{57}Fe and ^{119}Sn Mossbauer spectra 80−39944
$FeSn(OH)_6$, mag. props. 78−43574
$FeSnO(OH)_5$, mag. props. and cryst. struct. 78−43574
1T-$Fe_{0.1}Ta_{0.9}S_2$, mag. modulation of lattice electric field gradient 77−85628
$Fe_xTa_{1-x}S_2$ (1T), low-spin high-spin equilib., susceptibility and Mossbauer expts. 77−48109
FeTe film, on amorphous substrates, Mossbauer obs. of struct. 78−27142
$FeTe_2$, Mossbauer spectroscopy and nonstoichiometry 78−31125
$FeTe_x$, Mossbauer spectra, 80 to 750K, quadrupole splitting and isomer shift 77−4590
$Fe_{1-x}Te$, fluctuating localised mag. moments, d band motion, Mossbauer study 80−65768
$Fe_{1+x}Te$, ^{129}I transferred hyperfine field, Mossbauer spectroscopy study 80−44972
$FeTe_2Fe_2Te_3$, defect struct. compounds, room temp. ^{57}Fe Mossbauer spectra 79−47371
Fe_2TeO_6, CC ^{57}Fe Mossbauer spectrum, hyperfine field, Neel temp. 79−56636
$Fe_{1-x}Ti_{1+x}$, Mossbauer study, superparamag. clusters 77−85633
$FeTiNdO_5$, isomer shift, hyperfine field and distrib. of Fe^{3+} ions, Mossbauer spectrum 77−69747
$FeTiO_3$, electronic struct., Mossbauer expt. 78−27150
Fe_2TiO_4 magnetisation, Mossbauer spectra 79−87244
Fe_2TiO_5, anisotropic spin glass behaviour 79−99707
Fe_2TiO_5, anisotropic spin glass type behaviour 80−60296
Fe_2TiO_5, spin glass system, cation distrib. Mossbaeur spectra 80−71248
$Fe_{3-x}Ti_xO_4$, Mossbauer study at low temp. 78−27133
$Fe_{3-x}Ti_xO_4$, Mossbauer spectra in paramag. phase 80−39943
$FeTiRO_5$, R=Pr,Nd,Sm,Eu,Gd,covalency contribs. 78−10808
$Fe_{(1+x)}Ti_{2(1+x)}S_4$ non-stoichiometric cpds., vacancy-cation distrib., Mossbauer spectra 80−15900
Fe_xTiS_2, lattice dynamics and hyperfine interactions, Mossbauer spectra study 80−108135
$Fe_xV_{1-x}O_2$, mag. props. and Mossbauer spectra meas. 78−31136
θ-$Fe_xV_2O_5$, spin glass and paramag. props., susceptibility, EPR and Mossbauer studies 80−75782
$Fe_{3-x}V_xSi$, selective site substitution and spin polarisation 79−78583
$(Fe_xV_{1-x})V_2S_4$, and $(Fe_xV_{1-x})V_4S_8$, mag. props. 78−27034
$^{57}FeX_2$, (X=Cl,Br), matrix isolated, Mossbauer effect, isomer shift and quadrupole splittings obs. 78−46377
$FeYb_2S_4$, cryst. struct. determ. 79−77572
$FeYb_2S_4$, structural study, X-ray diffr., Mossbauer spectroscopy 80−107159
$Fe_{1+x}Yb_{2-x}S_4$, X-ray and Mossbauer obs. 77−77132
$Fe_{3-x}Zn_xO_4$ low temp. Mossbauer spectra, electron transfer and spin density distribution 78−52404
$FeZrF_6$, phase transition at 212.3K, Mossbauer, EPR study, quadrupole splitting, Jahn-Teller effect *(German)* 78−68430

Mossbauer effect continued
^{57}Fe,, Mossbauer spectra 77−73100
^{57}Fe, absorption line function for polycrystalline quadrupole split absorber in large applied mag. field 79−87340
^{57}Fe backscatt. electron Mossbauer spectroscopy 80−29661
^{57}Fe conversion electron Mossbauer spectroscopy at low temps., proportional counter 77−10542
^{57}Fe, hyperfine fields in Xe matrix, Mossbauer spectroscopy, Hartree-Fock calcs. 78−43749
^{57}Fe, hyperfine interactions in implanted metals, Mossbauer spectra 80−108141
^{57}Fe implantation in metals, electric hyperfine interactions, conversion electron Mossbauer meas. 80−7241
^{57}Fe, implanted in 3d, 4d and 5d metals, conversion electron Mossbauer spectra 77−12286
^{57}Fe interstitial cpds. and solid solns., Mossbauer spectra 80−20557
^{57}Fe, isomer shift, book contrib. 79−87354
^{57}Fe, isomer shift calibration const. rel. to biological cpds. 80−7227
^{57}Fe, Mossbauer absorpt. and emission spectra, hyperfine struct. and relax. effects 80−71279
^{57}Fe, Mossbauer effect-time dependent PAC technique, theory of combined method 79−28645
^{57}Fe Mossbauer isomer shift from electron capture rate of ^{52}Fe 80−7203
^{57}Fe Mossbauer level excitation using synchrotron radiation 80−7204
^{57}Fe Mossbauer spectroscopy, added precision 77−88327
^{57}Fe, nuclear inelastic channel suppression, nuclear reson. and electronic scatt. of γ-quanta, hyperfine transitions 78−60361
^{57}Fe paramagnetic ions sorbed on cation exchange resin, chem. information from relax. Mossbauer spectra 77−70332
^{57}Fe resonant absorber, anomalous γ-ray transmission, energy spectrum *(Russian)* 77−28501
^{57}Fe spectra, ferrous charact., cryst. field interactions 80−108133
$^{57}Fe^{m}$, Mossbauer level excitation using specific characts. of synchrotron radiation 78−66447
$^{57}Fe(III)$ species, prod. by electron capture decay in ^{57}Co labelled Co(III) cpds. 77−63329
$FrCr_2S_4$, second-order phase transition, Mossbauer spectra 80−20569
Ga-Fe dilute alloy, Mossbauer spectrum 77−90080
GaAs:$^{119}Sn^{m}$, Mossbauer spectra 80−29667
GaAs:Fe, impurity atom charge exchange 79−47050
GaAs:Sn, implantation, annealing, impurity-defect struct., Mossbauer study 80−54269
GaAs:Sn^{+}, impurity-defect complex from ^{119}In implantation, Mossbauer study 80−59486
Ga_2O_3-Fe_2O_3 system, anomalous Mossbauer lineshapes, incomplete annealing 77−51998
Ga_2O_3-Fe_2O_3 system, anomalous Mossbauer line shapes, incomplete annealing 78−92006
GaP, complex ^{119}Sn impurity-defect, Mossbauer study 80−75898
GaP:Fe, electron exchange via val. band between Fe acceptor centres, Mossbauer spectra 77−55741
GaP:Fe, impurity atom charge exchange 79−47050
GaP(As)(Sb), site selective doping by ion implantation of radioactive nuclei 80−34023
Ga_2Te_3, nuclear gamma resonance of ^{57}Fe, isomer shift scale construction *(Russian)* 78−35070
Ga_2Te_3:Sn, impurity atom electron shell compression by matrix *(Russian)* 77−28146
$(Gd_{1-x}R_xXCo_{1-y}M_y)_5$, R=rare earth, M=Cu,Ni,Pt, origin of hyperfine fields acting on Gd 80−44967
Gd alloys, hyperfine fields, Mossbauer meas. 77−85635
Gd, hyperfine interaction of ^{197}Au, Mossbauer obs. 77−20773
^{155}Gd:^{155}Tb sources produced by recoil implantation in Fe and Ni 80−40009
Gd-Fe(Co) film, amorphous, preferential resputtering effect induced anisotropic distrib. of atomic pairs 78−63950
Gd-Ir, dil., hyperfine interaction of ^{193}Ir, Mossbauer effect meas. 78−52413
Gd-Ni, amorphous, Mossbauer spectra 80−25262
Gd-Yb(Ir), dil., ferromag., mag. hyperfine fields of ^{170}Yb and ^{193}Ir, Mossbauer effect meas. 79−24242
$Gd(Al_xFe_{1-x})_2$, intermetallic compounds, pseudobinary, Mossbauer studies 80−75887
$GdAlO_3$, ^{155}Gd excited states, determ. of nuclear parameters using Mossbauer effect 79−28646
$GdAlO_3$, canted antiferromagnetic, Mossbauer meas. 80−97171
$Gd_xCe_{1-x}Ru_2$, magnetic ordering by ^{155}Gd Mossbauer spectroscopy 78−27139
GdCo amorphous sputtered film mag. props. from Mossbauer effect obs. *(Japanese)* 80−15933
$Gd(Co_xNi_{1-x})_2$, Mossbauer spectra, mag. props. 80−20563
GdFe amorphous film, Mossbauer and mag. meas. 80−15844
$GdFe_2$, easy direction of magnetisation 80−20535
$GdFe_2$ films, electron beam deposited, amorphous and cryst., mag. and struct. props. 79−4710
$GdFe_2$, Mossbauer sample, X-ray diffr. obs. 78−22737
$(Gd_{65}Fe_{35})_{90}B_{10}$, amorphous, mag. props., Mossbauer study 80−93093
$Gd(Fe_xCo_{1-x})_2$, Mossbauer effect at 78 and 300K, ^{57}Fe hyperfine fields 80−2677
$Gd_2(Fe_{1-x}Co_x)_{17}$, hyperfine interactions 78−2780
$Gd_2(Fe_{1-x}Ni_x)_{17}$, hyperfine interactions obs. 78−6614
$Gd_3Fe_5O_{12}$, nucl. gamma reson., anomalous behaviour of intensity 77−12289
$Gd(Fe_xT_{1-x})_2$, Mossbauer spectra, mag. props. 80−20563
GdIG, amorphous, Mossbauer specfra, mag. props. 80−15849
$Gd_{0.1}La_{0.9}Ni_5H_x$, $Gd_{0.1}La_{0.9}Co_5H_x$, ^{155}Gd Mossbauer spectra 77−63340
GdM_x, M=3d transition metal, hyperfine interactions 78−19401
GdM_2Ge_2, M=Mn, Fe, Co, Ni, Cu, magnetism and hyperfine interactions 78−76228
$GdRh_2H_x$, $GdRu_2H_x$, struct. and mag. props., Mossbauer and magnetisation meas. 80−71271
$Gd_{1-x}Sc_xI_2$, Mossbauer spectra, hyperfine interactions 80−15923
$GdVO_4$, ^{155}Gd excited states, determ. of nuclear parameters using Mossbauer effect 79−28646
$GdVO_4$, hyperfine field and exchange interactions, Mossbauer meas. 79−47370
$Gd_{1-x}Y_x$, Mossbauer spectra, hyperfine interactions 80−15923
$Gd_xY_{1-x}Co_2$, transferred hyperfine interactions, ^{155}Gd Mossbauer effect and ^{165}Ho NMR expts. 77−63339
$Gd_{1.8}Y_{1.2}Fe_5O_{12}$, nucl. gamma reson., anomalous behaviour of intensity 77−12289

Mossbauer effect continued
Ge, ^{57}Co ion implantation, Mossbauer spectra, dose depend. 79−82899
Ge, ^{57}Fe isomer shift, quadrupole coupling and interat. distance correl 78−52408
Ge:^{119m}Sn, impurity lattice dynamics, Mossbauer spectra, Debye temp. 80−84262
Ge:^{125}I(^{125}Te), implanted atom sites and quadrupole interaction, Mossbauer spectra 77−20758
Ge:^{57}Co, ion-implanted, Mossbauer study, annealing effects 80−7231
Ge:^{57}Fe, quadrupole interac. 78−92005
Ge:^{57}Fe study via conversion electron Mossbauer spectroscopy 77−55735
Ge:Fe, amorphous film or ion-implanted, comparison of ^{57}Fe Mossbauer data 77−40159
Ge:Fe, implanted, Mossbauer spectra, conversion electron, temp. dependence 80−40025
Ge:Fe, recoil implantation Mossbauer expt. in presence of external mag. field 80−44981
Ge:Sn, ion implantation of radioactive ^{119}Sn 80−59495
Ge:Sn, Mossbauer spectra of ^{119}Sn impurity atoms 80−15935
Ge-Fe, laser annealing of implanted ^{57}Co sources, Mossbauer obs. 80−39139
Ge-Te and Ge-Te-As system glasses, local struct., ^{119}Sn Mossbauer obs. 79−41968
Ge_2FeGa, and Fe_2CoGa, site preference and local environment effects, Mossbauer and NMR expts. 78−43710
$GeFeO_3$, field induced spin reorientation temp. depend. 77−63200
$GeSe_2$-$SnSe_2$-As_2Se_3, GeSe-SnSe-As_2Se_3, Mossbauer investigation 77−20052
^{73}Ge, 13.3 keV Mossbauer resonance, dispersive interference effects 78−25145
^{73}Ge, gamma-ray detection with Si(Li) and Ge detectors 77−10530
^{73}Ge Mossbauer transition, large E2 dispersive interference 77−40158
H_2Te, solid, and photodissociated H_2Te in solid Ar, quadrupole splitting and isomer shift 77−20769
He refrigerator for temp. varying Mossbauer meas., 20-300K 80−4726
^3He cryostat, continuously operating for Mossbauer investigation of biological samples 79−96725
Hf-Ir, dil., elec. field gradient at ^{193}Ir, Mossbauer meas. 80−66090
Hf_2Fe, moment form. on H_2 absorpt. 79−87343
$Hf(Fe_{1-x}Co_x)_2$, mag. props., Mossbauer spectra and magnetisation meas. 80−39948
$HfFe_{2-x}Si_x$, Mossbauer spectra, hyperfine interactions 80−15862
^{178}Hf, 2^{+}-0^{+} transitions, mean square nuclear charge radius change, Mossbauer expt. 78−25109
$Hg_2^{129}I_2$, Mossbauer effect, bonding, quadrupole coupling const., comparison with $Hg^{129}I_2$ 78−2774
HgTe, diamond-like semicond., Mossbauer isomer shift meas. 77−16233
$(HgTe)_x$-$(CdTe)_{1-x}$, diamond-type semiconductor, Mossbauer spectra, quadrupole interaction of ^{125}Te 80−44992
^{197}Hg source for Mossbauer studies 79−26796
Ho:^{119}Sn, mag. hysteresis of hyperfine field, compensation in mag. field *(Russian)* 77−81039
Ho-Sn, dil. alloy, hyperfine interaction of ^{119}Sn, Mossbauer meas. 78−91998
$HoAlO_3$:Yb^{3+}, Mossbauer relax. 80−15875
$HoCo_2$, cryst. field induced spin rot., Mossbauer meas. 77−16227
$HoCo_2$, easy direction of magnetisation, Mossbauer data, 4.2K 78−43584
$Ho(Fe_xNi_{1-x})_2$, mag. behaviour, susceptibility and Mossbauer expts., 4.2-1300K 78−52235
$HoFeO_3$, field induced spin reorientation, Mossbauer spectroscopy 80−65878
$HoH_2(D_2)$, mag. props., 1.5 to 10K, Mossbauer meas. 79−78578
$Ho(OH)_3$, Mossbauer spectra, cryst. field and mag. props. 80−15873
$Ho_xY_{1-x}(Fe_{0.1}Co_{0.9})_2$, ^{57}Fe hyperfine interaction, mag. props., Mossbauer study 80−39951
I, atoms, Mossbauer isotopes, isomer shift 80−78573
I complexes, charge transfer states, Mossbauer spectra 80−15907
$^{129}I_2$, frozen soln. in o- or p-xylene, Mossbauer effect obs. 80−78637
^{A}I, A=127, 129, Mossbauer isomer shifts, book contrib. 79−87360
^{127}I, isomer shift calibration, using lifetime variations in electron capture decay of ^{123}I 80−39925
^{127}I, Mossbauer isomer shift 80−39922
^{129}I impurities implanted in semiconductors, isomer shift 80−20522
^{129}I in transition metals, calibration of Mossbauer isomer shift 80−20520
^{129}I, internal conversion electron and Mossbauer spectra, calibration of isomer shift 80−39921
^{129}I, isomer shift calibration, using lifetime variations in electron capture decay of ^{123}I 80−39925
^{129}I, Mossbauer isomer shift 80−39922
In, contact charge density, press. depend., trends for Ag-Te 78−39077
In, recoilless fraction calc. of ^{57}Fe impurity atoms from mean-square displacements 78−2216
InP(Sb)(As), site selective doping by ion implantation of radioactive nuclei 80−34023
$(In_2SnTe)_x$-(2InSb)$_{1-x}$ system, semicond., Mossbauer absorption line of ^{119}Sn 78−27146
In_2Te_3, nuclear gamma resonance of ^{57}Fe, isomer shift scale construction *(Russian)* 78−35070
Ir-Fe, dil., local magnetisation, Mossbauer meas. 80−66091
$Ir_{1.07}Mn_{1.07}Sn_{0.88}$, ferromag. Heusler alloy, ^{193}Ir and ^{119}Sn hyperfine fields 79−78581
^{191}Ir, excited nuclei mean precession time depend. on γ-spectral width, g-factors *(Russian)* 80−78211
KAl[Fe(CN)$_6$], isomer shift of Mossbauer spectra 80−29662
KBr, Bragg diffraction, anharmonic contributions, Mossbauer study 78−76359
KBr(I):Co, coloured and uncoloured, Mossbauer effect, inhomogeneous hyperfine fields 77−32307
KCl, Bragg diffraction, anharmonic contributions, Mossbauer study 78−76359
KCl:$Fe(CN)_6^{4-}$, electron irrad., Mossbauer and ESR study 80−7238
$KCoF_3$, strain sensitive props., Mossbauer spectra obs. 77−20765
K_2CoO_3:^{57}Co Mossbauer source 77−6592
$(KF)_n$-FeF_3, antiferromagnetic systems, dimensionality and spin reduction effects, Mossbauer study 80−39947
$K_3Fe(CN)_6$, electronic struct., elec. field gradient tensor 80−15483
$K_3Fe(CN)_6$, mag. ordering and spin struct., Mossbauer obs. 77−40038
$KFeF_3$, strain sensitive props., Mossbauer spectra obs. 77−20765

Mossbauer effect continued
$KFeF_4$, amorphous, mag. props. and Mossbauer spectra, speromagnetism and mictomagnetism 80−75778
$KFeF_4$, amorphous, Mossbauer study 80−39970
K_2FeF_4, antiferromag., Mossbauer study of mag. ordering 79−28655
K_2FeF_4, two-dimensional antiferromag., cryst. field effects, Mossbauer spectroscopy 80−71254
K_3FeF_5, mag. struct. and one-dimens. antiferromagnetism 80−60209
K_3FeF_5, Mossbauer spectra, 1D antiferromag. 80−15886
K_3FeF_5, one dimens. antiferromag., zero point spin reduction 77−85456
K_3FeF_5, one dimensional antiferromagnet, Mossbauer effect, mag. and electric field gradient axes 79−78587
K_2FeF_5, one-dimens. antiferromag., single cryst. Mossbauer spectra 78−23376
K_2FeF_5, one-dimensional antiferromag. systems, Mossbauer studies 80−71266
$K_3Fe_2F_7$, two-dimensional antiferromag., cryst. field effects, Mossbauer spectroscopy 80−71254
$K_{1+x}Fe_xGa_{11-x}O_{17}$, electron hopping and excitation at room temp., ^{51}Fe Mossbauer spectra 80−25257
$KFeO_2$, cryst. and mag. struct., neutron and X-ray powder diffr., and Mossbauer effect meas. 77−84722
$KFeO_2$, overlap contribution to $^{57}Fe^{3+}$ isomer shifts, nuclear size change 80−39903
KFe_2O_3, β''' phase, mag. props., hyperfine interactions, Mossbauer study 80−20524
K_2FeO_4, antiferromag., critical fluctuations obs. using Mossbauer spectroscopy 80−39955
K_2FeO_4, crit. slowing down of spin fluctuations, Mossbauer spectra and relax. theory 80−65882
$KFeS_2$, quadrupolar hyperfine anisotropy, Mossbauer spectra meas. 78−19393
$KFeS_3$, quadrupolar and mag. hyperfine anisotropy, Mossbauer meas. 78−56408
K_2IrF_6, hyperfine spectra of mag. ordered state at very low temp., Mossbauer meas. 77−69744
$K_6LiFe_{24}S_{26}Cl$, Mossbauer spectra and lattice parameters 79−78584
$KM^{II}M^{III}F_6$ (M=1st row transition metal, Zn, or Mg), diavalent and trivalent ion distribs. obs. 78−2777
$KMgF_3:Fe^{2+}$, octahedral symm., vibronic effects from Zeeman field induced Mossbauer spectra 77−8477
$KMnF_3$, gamma quanta scattering near 186K transition 80−108126
$KMnF_3$, Mossbauer effect in ^{57}Fe, struct. and mag. transition investig. 77−20779
$KMnF_3$, width of central peak in crit. scatt. of γ-rays 77−1623
K_2O-B_2O_3-Fe_2O_3, γ-irrad., Mossbauer spectroscopic study 80−108132
K_2O-B_2O_3-Fe_2O_3 glasses, nonbridging O formation, Mossbauer spectroscopy 80−55001
$KTl[Fe(CN)_6]$, isomer shift of Mossbauer spectra 80−29662
^{40}K Mossbauer isomer shifts, book contrib. 79−87363
KrF_2, Mossbauer spectra, quadrupole coupling strengths, isomer shift and bonding 77−50458
$KrF_2.AsF_5(SbF_5)$, Mossbauer spectra, quadrupole coupling strengths, isomer shift and bonding 77−50458
^{83}Kr Mossbauer isomer shifts, book contrib. 79−87363
$LICr_{0.99}Fe_{0.01}O_2$, layer oxide, dimensionality of mag. interactions, Mossbauer study *(French)* 78−23377
La-Au, splat-quenched, Mossbauer effect and elec. resist., amorphous struct. 80−84676
La-Au liq.-quenched alloys, Mossbauer spectra, struct. 80−15841
La-Fe, FCC, Mossbauer spectra, Fe atom position 80−20549
La-Fe, liquid quenched, X-ray diffr. and Mossbaeur effect exam. of structure 78−76678
$La_xCa_{1-x}RuO_3$, metallic, mag., electronic and structural props., ^{99}Ru Mossbauer spectroscopy 77−48107
La_2Co_7, mag. props. changes upon H_2 absorpt. 80−71270
$LaCoO_3$:Ca(Sr), anomalous $^{57}Fe^m$ charge states, Mossbauer study 80−40017
LaEu, mag. supercond., phase diagram, bulk susceptibility meas. 77−59353
$LaFe_{1-x}D_xO_3$:Sn, D=Al, Ga or Sc, Mossbauer effect, hyperfine mag. fields at Sn 77−24772
$LaFeO_3$, doped, effect of doping on hyperfine fields, supertransfer model 79−47057
$LaFeO_3$, electronic struct., super transfer effects, Mossbauer expt. 78−27150
$LaFe_{12}O_{19}$, high field Mossbauer effect on ^{57}Fe at room temp. and 4.2K 79−24238
$La_2Li_{0.5}Co_{0.5}O_4$ phase, intermediate electronic configuration 80−80226
La_2MRuO_6, (M=Mg, Co, Ni, Zn), cubic ordered perovskites Mossbauer obs. and absence of mag. order 80−75889
$La_{1-x}Na_xFeO_{3-x}$, defect perovskite system, Mossbauer effect 77−36159
$LaNi_{5-x}Fe_x(Cr_x)$, Fe and Cr electron hydride formation, X-ray and SEM obs. *(Japanese)* 79−43202
$LaNi_{1-x}Fe_xO_3$, magnetisation meas. and ^{57}Fe Mossbauer studies 80−93217
$LaNi_{1-x}Fe_xO_3$, Mossbauer spectra, mag. hyperfine field 80−20537
$LaRu_xFe_{1-x}O_3$ perovskites, cryst. struct., elec., mag. and Mossbauer behaviour 77−55274
$La_{0.98}Sn_{0.02}Mo_6Se_8$, Chevrel phase supercond., hyperfine interaction, microscopic study 79−56650
$La_{0.98}Sn_{0.02}Mo_6Se_8$, Mossbauer spectra 80−15926
$La_xSr_{1-x}RuO_3$, metallic, mag., electronic and structural props., ^{99}Ru Mossbauer spectroscopy 77−48107
^{137}La, possibility of obs. of Mossbauer effect 78−39457
Li-Zn ferrites, (Li, Zn, Ti, Cr substituted), Mossbauer spectrometry, effect of supertransferred hyperfine fields and relaxation *(French)* 80−80654
$Li+KFeS_2$, electrochemical reaction, in situ Mossbauer spectra study 79−100397
Li_xAmO_{1+x}, after-effects of ^{241}Am α-decay, ^{237}Np Mossbauer spectra obs. 79−61271
$Li_2B_2O_4$-$LiFe_5O_8$, borate glass, mag. props. of Fe^{3+} cations 80−100599
LiCl:Fe, defect struct., Mossbauer spectra and X-ray diffr. obs. 80−7237
$Li_xCr_yV_{1-y}S_2$, Mossbauer and mag. studies 79−73869
LiF (200) Bragg peak, Mossbauer diffraction meas., calibration 79−82897
LiF, Bragg diffraction, anharmonic contributions, Mossbauer study 78−76359
LiF:Fe, dispersed ions, absorber Mossbauer spectra 78−15077
LiF:Fe, Mossbauer study of Fe precipitates 79−91327

Mossbauer effect continued
$LiFeO_2$, quadrupole splitting in Mossbauer ^{57}Fe spectrum, geometric anal. and computer simulation 79−1730
$LiFeS_2$, magnetic hyperfine interactions, Mossbauer spectra and mag. susceptibility meas. 80−29658
Li_2FeS_2, Mossbauer spectra and lattice parameters 79−78584
$Li_xFe_yV_{1-y}S_2$, Mossbauer and mag. studies 79−73869
$Li_{0.5}Ga_xFe_{2.5-x}O_4$, superexchange interaction parameters, Mossbauer spectra obs. 77−51899
LiI_3 Mossbauer charge density of $^{129}I^-$ 79−61275
$Li^{129}I$, Ar matrix isolated and cryst., Mossbauer verification of distortion overlap 77−63325
$Li_2IrCl_6.xH_2O$, hyperfine spectra of mag. ordered state at very low temp., Mossbauer meas. 77−69744
$LiNbO_3$, Mossbauer radiation modulation by coherent US excitation 79−61277
$LiNbO_3:^{57}Fe^{2+}$, Mossbauer spectroscopy 77−20782
$LiNbO_3:^{57}Fe^{2+}$ Mossbauer spectra, EFG axis 77−20760
$LiNbO_3$:Fe, calc. of photorefraction *(Russian)* 78−92032
$LiNbO_3$:Fe, electron spin relaxation study, Mossbauer effect, mag. and crystal field effects 80−39902
$LiNbO_3$:Fe, ferroelectric, treated in Li_2CO_3, formation of Fe^{2+} state, Mossbauer effect 78−92003
$LiNbO_3$:Fe, impurity valence state charge on X-ray irrad., Mossbauer meas. 80−7235
$LiNbO_3$:Fe, impurity charge states after UV irradiation 80−60462
$LiNbO_3$:Fe, Mossbauer spectra quadrupole doublet asymmetry 80−44960
$LiNbO_3$:Fe, state of impurity Fe cation, nucl. gamma reson. study 80−40014
$LiNbO_3$:Fe, X-ray and γ-ray irradiation effects on Fe charge state, Mossbauer study 80−40013
$LiNbO_3$:Fe(Cu), photorefractive centres, optical absorption, EPR and Mossbauer spectra meas. 77−32403
$LiScO_2:Fe^{3+}$, Mossbauer exam. of relaxation behaviour of Fe^{3+} 77−1620
$LiTaO_3$, electric field gradients and isomer shift ^{181}Ta 78−39453
LiTi ferrite, Mossbauer study, relax. and supertransferred hyperfine fields 80−39941
LiTi, substituted ferrite, cation distribution, Mossbauer, X-ray, neutron diffr. study 80−28975
$Li_xV_{1-y}Fe_yS_2$, intercalated battery cathode material, Mossbauer studies 80−44984
LiZn ferrite, Mossbauer study, relax. and supertransferred hyperfine fields 80−39941
LiZn, substituted ferrite, cation distribution, Mossbauer, X-ray, neutron diffr. study 80−28975
Lu-Ir, dil., elec. field gradient at ^{193}Ir, Mossbauer meas. 80−66090
$LuFe_2$, mag. props. changes upon H_2 absorpt. 80−71270
(Mg, Fe)SiO_3, orthopyroxenes, cation distrib., electronic and Mossbauer spectra 80−7370
$MgAl_ySc_xFe_{2-x-y}O_4$, X-ray spectra Mossbauer spectra, electronic struct. of Fe and Sc 77−28647
MgEu, dil. alloy, cold worked, valence transform. of Eu due to defect association, mag. suscept. and Mossbauer meas. 77−51404
$MgFe_2O_4$, Mossbauer effect determ. of cation distrib. temp. depend. 77−8481
$MgFe_2O_4$, Mossbauer study 79−47375
$Mg_xFe_{3-x}O_4$, polycryst., Verwey type transition, resist., magnetisation, Mossbauer effect and permeability obs. 80−75764
$(Mg_yFe_{1-x})_2SiO_4$, olivine, Fe-rich superparamagnetic clusters, Mossbauer study 79−82831
$MgIn_xFe_{2-x}O_4$ and $MgSc_xFe_{2-x}O_4$, Mossbauer spectra, elec. and mag. props. *(Russian)* 77−69737
$Mg(OH)_2$:Fe, crystal field properties, Mossbauer spectra, isomer shift and quadrupole splitting 79−61278
$MgSiF_6$, phase transform. and relax., EFG and quadrupole spectra 77−51995
Mg_2Sn, Mossbauer effect exam. under press. up to 75 kbar 79−69759
Mg_2Sn, phase transition under hydrostatic pressure, Mossbauer effect and electric resistance 78−51665
Mg_2Sn, phase transitions under high hydrostatic press., Mossbauer spectra 79−87628
Mn ternary carbides, Mn_3MC, M=metal, mag. props. 77−63116
Mn ternary nitrides, Mn_3MN, M=metal, mag. props. 77−63116
β-Mn-^{57}Fe-^{119}Sn alloy mag. props. from Mossbauer effect obs. *(Japanese)* 80−15933
β-Mn-Fe-Sn alloys, weak itinerant electron antiferromagnetism, Mossbauer spectra meas. 77−36158
β-Mn-Sn, Mossbauer and neutron diffr. exam. 77−66253
$Mn_3Al_2(SiO_4)_3$, Mossbauer spectra and absorpt. bands 80−55144
$Mn_{1-x}Fe_xCr_2S_4$, Fe II electronic struct., Mossbauer spectra 80−15876
$MnFe_{2-x}In_xO_4$, magnetic props., In substitution effects *(Russian)* 78−91849
$MnFeO_4:^{57}Co$, Mossbauer spectrum, 4s covalent bonding 80−20540
$MnFe_2O_4$:Sn, hyperfine mag. fields at ^{119}Sn and ^{57}Fe nuclei, influence of press. 79−99811
$Mn_xFe_{3-x}O_{4+\gamma}$, average directional order, cation valency and repartition on A- and B-sites *(French)* 78−39369
$MnFe_2(PO_4)_2(OH)_2.6H_2O$, strunzite, cryst. chem., Mossbauer study 80−39975
$Mn_{2-x}Fe_xSb$, mag. struct. and spin flop transition, ^{57}Fe Mossbauer expts. 77−66261
$Mn_{2-x}Fe_xSb$, Mossbauer effect exam. 78−68432
$(Mn_{1-x}Fe_x)_5SiC$, magnitude of quadrupole splittings, Mossbauer study 78−43747
$MnGd_2S_4$, mag., struct. and Mossbauer effect study 78−51507
MnO, alpha-particle irrad., Mossbauer study of nucl. reaction aftereffects 80−40015
Mn_3O_4:^{119}Sn, hyperfine field exam., Mossbauer meas. 77−69753
MnSb, hyperfine interactions, ^{119}Sn Mossbauer obs. 77−40160
MnSb, hyperfine interactions at ^{57}Fe and ^{119}Sn, Mossbauer spectroscopy 78−23375
Mn_2Sb, hyperfine fields of ^{121}Sb in several mag. phases 79−28650
Mn_2Sb, large anisotropy in mag. hyperfine field at ^{121}Sb, Mossbauer spectra meas. 77−73101
$Mn_{1+x}Sb_{1-x}Sn_x$, nuclear Zeeman effect, Mossbauer meas. 79−28654
$Mn_2Sb_{1-x}Sn_x$, mag. transitions, Mossbauer meas. 78−52406
$MnSiF_6$, phase transform. and relax., EFG and quadrupole spectra 77−51995

Mossbauer effect continued
Mn_3SnN, perovskite type struct., mag. props., neutron and Mossbauer meas. 77−32159
$MnTe_2$, Mossbauer spectra, hyperfine field 80−15866
$MnTiNdO_5$, distrib. of Mn^{3+} and Ti^{4+} ions, Mossbauer spectrum 77−69747
$MnTiRO_5$, R=Pr,Nd,Sm,Eu,Gd,covalency contribs. 78−10808
MnZn ferrite, natural, intrasite cation ordering and clustering 77−12259
MnZn ferrite, prep. and magnetic props. 78−19254
$Mn_{1-x}Zn_xFe_2O_4$, noncollinear mag. structure, Mossbauer spectrum 77−69501
$Mn_{1-x}Zn_xFe_2O_4$, prepared by wet method, neutron diffr. and high field Mossbauer expts. 80−75719
Mo, Mossbauer absorpt. spectrum in deformed cryst. 77−16234
Mo, oxidation kinetics, Mossbauer study 80−40005
Mo:Xe, BCC, heavy ion implanted, vacancy recovery, Mossbauer spectroscopy 79−82896
Mo-Fe, Kondo system, magnetisation, Mossbauer expts. 77−77028
Mo-Fe, local magnetisation from Mossbauer meas. 77−20549
Mo-Fe alloy, local moment system, low temp. susceptibility, Mossbauer effect meas. 77−43810
MoFe, occurrence of spin glass and mictomagnetic regimes, props. meas. 77−16085
N_2 solid matrix, ^{57}Fe Mossbauer spectra, Fe_xN mol. form., IR spectra confirmation 77−59496
$(N(CH_3)_3H)_2SnF_6$, phase transition and temp. effects, Mossbauer and NMR spectra 78−88236
NH_3:^{57}Fe, solid, Mossbauer study of iron bonding to solid ammonia and its photofragments 80−15833
$NH_4Al(SO_4)_2.12H_2O$:Fe^{3+}, spin-lattice relax. of paramag. ions 79−95688
$(NH_4)_2BeF_4$, incommensurate phase, Mossbauer spectrum 79−61276
$(NH_3)_2FeF_5$, one-dimensional antiferromag. systems, Mossbauer studies 80−71266
$(NH_3)_2FeF_5$, quasi two-dimens. antiferromagnet, Mossbauer study 80−39947
NH_4FeF_4, mag. and Mossbauer obs. *(French)* 78−19389
NH_4FeF_4, Mossbauer and optical evidence for crystallographic transition 79−14931
NH_4FeF_4, two-dimens. antiferromagnetism 77−66444
$N_2H_6FeF_5$, Mossbauer spectra, 1D antiferromag. 80−15886
$N_2H_6FeF_5$, one-dimens. magnetism, mag. suscept. and Mossbauer reson. exam. 77−51893
$N_2H_6FeF_5$, one-dimens. antiferromagnetism 77−66444
$N_2H_6FeF_5$, one-dimensional antiferromagnetism, Mossbauer study 80−65872
$NH_4H_2PO_4$, crysts., mechanism of habit change due to Fe^{3+}, Mossbauer study 79−19821
$NH_4H_2PO_4$:^{57}Fe, Mossbauer study, Fe^{3+} effect in habit 80−100627
NH_4MnCl_3, X-ray single crystal analysis, phase transitions, Mossbauer effect 79−19366
$(NH_4)_2Sn_{1-x}Sb_xCl_6$ (x=0.13, 0.21, 0.28, 0.33), mixed valence compound, ^{121}Sb Mossbauer spectroscopy 79−51890
NI_3Al, structural order and homogeneity, X-ray, mag. susceptibility and Mossbauer meas. 77−63663
Na-Fe fluorophosphate glass, EPR and Mossbauer resonance study 80−15838
NaCl, Bragg diffraction, anharmonic contributions, Mossbauer study 78−76359
NaF:Fe, dispersed ions, absorber Mossbauer spectra 78−15077
NaF:Fe, Mossbauer study of Fe precipitates 79−91327
$Na_2(Fe,Mg)_5Si_8O_{22}(OH)_2$, riebeckite, low temp. Mossbauer obs. of oriented single cryst. behaviour and mag. props. 80−84674
$Na_2Fe(CN)_5NO.2H_2O$, new isomeric mol. state, Mossbauer data 77−23513
$Na_2Fe(CN)_5NO.2H_2O$, absolute Mossbauer fraction of ^{57}Fe nuclei 80−80648
$Na_2(Fe(CN)_5.NO).2H_2O$, powder, Mossbauer absorption in mag. field 78−68418
$NaFeF_2$, Mossbauer and low-temp. dilatometry study *(French)* 80−80662
$NaFeF_4$, amorphous, mag. props. and Mossbauer spectra, speromagnetism and mictomagnetism 80−75778
$NaFeF_4$, amorphous, Mossbauer study 80−39970
$NaFeF_4$, two-dimens. antiferromagnetism 77−66444
α-$NaFeO_2$, EFG tensor, nucl. quadrupole coupling const., polarisability 77−72844
α-$Na_3Fe_2(PO_4)_3$ orthophosphate, cryst. and vitreous, Mossbauer spectroscopy and mag. susceptibility *(French)* 80−80657
$NaFeS_2$, mag. hyperfine fields and covalency, Mossbauer effect meas. 77−90077
NaI, temp. varying Mossbauer spectra, isomer shift 80−4726
$Na_3M_2Li_3F_{12}$, M=Al, Fe, fluoride garnets, high press. form 77−76554
$Na_3M_2^{3+}Li_3F_{12}$ garnets, M=Al,Cr,Fe, synthesis from aq. soln., props. 77−44184
$NaNbO_3$, energy width of central peak near phase transition 78−79724
Na_2O-$3SiO_2$:Fe^{2+}, Fe^{3+} glasses, Mossbauer and ESR spectra and internal friction 80−100865
Na_2O-CaO-SiO_2 glass:Fe, Mossbauer spectra of Fe^{2+}, Fe^{3+} impurities *(French)* 79−51893
Na_2O-Fe_2O_3-SiO_2, Mossbauer spectra, crystallisation study *(Russian)* 79−19816
Na_2O-Fe_2O_3-SiO_2 glass and crystals, leucite type, Mossbauer ESR study of Fe^{3+} distrib. 79−65774
Na_2O-Li_2O-B_2O_3:Fe_2O_3, Mossbauer spectra, isomer shift and quadrupole splitting *(Korean)* 79−51889
Na_2O-PbO-SiO_2 glass-ceramic composite, directionally crystallised 80−107058
Na_2O-SiO_2, disilicate glass reaction with Fe 78−11190
Na_2O-SiO_2, disilicate glass, Fe ion introduction 78−11191
Na_2O-SiO_2-CaO:Fe_2O_3, Mossbauer spectra, isomer shift and quadrupole splitting *(Korean)* 79−51889
$5Na_2O.Fe_2O_3.8SiO_2$, glass crystallisation study by Fe^{3+} EPR and Mossbauer spectra 80−64904
$Na_2O.2Al_2O_3.5SiO_2$:Fe^{3+}, Mossbauer effect and magnetometric exam. 78−6613
$Na_2O.2B_2O_3$-Fe_2O_3 glass, Fe_2O_3 crystallite formation, Mossbauer obs. 78−68429
Na_3RuO_4, ^{99}Ru Mossbauer spectra, antiferromag. order, mag. relax. 80−50234
$NaTaO_3$, electric field gradients and isomer shift ^{181}Ta 78−39453

Mossbauer effect continued
$Na_20.3B_2O_3.xFe_2O_3$, borate glass, Fe^{3+} spin state and distrib. meas 80−39966
$Na_2[Fe(CN)_5(NO)]$ powder, Mossbauer spectroscopic study of ultrasonic anharmonicity 78−52411
$Na_2[Fe(CN)_5NO].2H_2O$, powder, Mossbauer spectra, acoustic-excitation-induced asymmetry of quadrupole splitting 78−27145
Nb-Fe, formed on laser irradiation of Nb-Fe interface, Mossbauer spectra *(Russian)* 79−60560
Nb-Sn, supercond. foils, phase anal. by Mossbauer spectra 78−64305
Nb-Sn(Ge), A-15 compound formation by ion implantation 78−51572
NbS_2.Sn, $NbS_2.Sn_{1/3}$ intercalation cpds., lattice dynamics, hyperfine interactions 79−61273
Nb_3Sn, 2-MeV proton-irradiated, Mossbauer effect studies 79−69757
Nb_3Sn, lattice microstrain induced metastable phase, low temp. struct. and props. 77−8482
Nb_3Sn, O^{4+} bombarded, Mossbauer studies 80−2672
Nb_3Sn, produced by Sn implantation, supercond. and Mossbauer effect 79−4612
Nb_3Sn, proton and γ-irradiated, lattice dynamics from ^{119}Sn Mossbauer studies 78−39458
Nb_3Sn, proton irradiated, Mossbauer effect at 78K 78−19394
Nb_3Sn, supercond. tape, crit. current, effect of Sn-Nb phase, annealing 79−24119
NbZr, energy anal. of diffuse ω-reflections, Mossbauer, X-ray scatt. 78−60369
$NdCo_2$, cryst. field induced spin rot., Mossbauer meas. 77−16227
Nd_xCo_{1-x} film, amorphous, mag. props. meas. 78−68312
$(NdCu_3)(Ti_3Fe)O_{12}$, synthesis, cryst. struct. and Mossbauer exam. 78−84505
$NdFe_2$, Curie temp., elec. quadrupole couplings, Mossbauer study 80−39949
$NdFe_2$, high field Mossbauer study 80−75893
$NdFe_2$, preparation and mag. props. 80−25259
Nd_xFe_{1-x} film, amorphous, mag. props. meas. 78−68312
Ni (111), Mossbauer effect emission spectroscopy and AES 79−91329
Ni, alpha-particle irrad., Mossbauer study of nucl. reaction aftereffects 80−40015
Ni complex, $[Ni(niox)_2]$, ^{61}N Mossbauer spectrum, quadrupole splitting 79−76456
Ni microcrystals, H_2 chemisorption effect on superparamagnetic relax. time, Mossbauer meas. 79−61284
Ni:^{116}Er, hyperfine interaction of impurities, Mossbauer spectra 77−48105
Ni:^{119}Sn, 78−52382
Ni:^{129m}Xe, Mossbauer obs. of mag. hyperfine field 77−8460
Ni:^{129}Te, implanted atom sites, Mossbauer obs. 77−20756
Ni:^{57}Fe, meas. near Curie temp. 78−10817
Ni:^{83}Rb, implanted atom sites and hyperfine interactions, Mossbauer obs. 77−24765
Ni-Al system, Mossbauer spectroscopy investigation *(Russian)* 80−20523
Ni-C, ferromag., prep. by splat-quenching, obs. of electronic struct. of interstitial C 77−62868
Ni-Co (25 wt.%), short range order parameters from Mossbauer data 79−56645
Ni-Dy, dil., implanted impurity hyperfine interaction 78−68417
Ni-Fe, dil., hyperfine mag. fields, press. effect, Mossbauer meas. 80−71277
Ni-Fe, dil., temp. depend. of Mossbauer absorpt. near Curie point *(French)* 80−11305
Ni-Fe film, mag. and hyperfine field exam. of uniaxial anisotropy 77−66391
Ni-Fe Invar, thermal expansion and spontaneous magnetisation, Invar anomalies, low spin model 80−71001
Ni-Fe-Al type B2 lattice alloys, Fe atom distribution, Mossbauer study *(Russian)* 79−99796
Ni-Fe-Mo, K-effect, Mossbauer study 80−39998
Ni-SiO_2 supported catalysts, particle size, H_2 chemisorption, Mossbauer study 80−7219
Ni_3Al, Mossbauer experiments on homogeneity 78−48395
Ni_3Al, Mossbauer spectra, exam. of struct., superlattice population anal. 78−88240
Ni_3Al-Fe, Fe effect on Mossbauer effect study 77−32298
$Ni_{1-x}Au_x$-Co, dil., hyperfine field and isomer shift, precip. process, Mossbauer expts. 80−25267
$Ni_{1-x}Au_x$-Co, dil., Mossbauer effect, mag. hyperfine field 80−20528
$NiCr_2O_4$, ^{61}Ni Mossbauer effect studies of hyperfine interactions, mag. dipole and elec. quadrupole 78−43746
$NiCr_2O_4$, sign of net mag. hyperfine field, ^{61}Ni Mossbauer study 80−39946
$NiCr_2O_4$:Fe, Mossbauer effect 80−15874
NiFe disordered alloys, Mossbauer spectra, hyperfine mag. field distrib., Curie temp. 80−7198
Ni_3Fe, atomic order, Mossbauer effect obs. 77−69736
Ni_3Fe disordered alloys, Mossbauer spectra, hyperfine mag. field distrib., Curie temp. 80−7198
Ni_3Fe, influence of order on Mossbauer spectra of ^{119}Sn 79−42876
Ni_3Fe, long range order, X-ray anal. comparison 78−10810
Ni_3Fe, non-linear local environment effect, Mossbauer effect of ^{57}Fe 80−39909
Ni_3Fe, order-disorder transition 78−10811
Ni_3Fe, order-disorder transition phase diagram, Mossbauer meas. 80−39995
Ni_3Fe-Sn, dil., atomic order detection by ^{119}Sn spectroscopy 80−39993
$Ni_{73}Fe_{27}$, order-disorder transition, Mossbauer study 79−95163
$NiFe_{2-t}Al_tO_4$, cryst. and mag. props. 78−14940
$NiFe_{2-x}Al_xO_4$, ^{57}Fe and ^{61}Ni Mossbauer spectra 80−39940
$Ni_{0.6}Fe_{2.4}B_7O_{13}I$, boracite, orthorhombic-trigonal transition region, Mossbauer investig. 79−87342
$Ni_{0.6}Fe_{2.4}B_7O_{13}I$, boracite, mag. hyperfine interactions, Mossbauer study 80−39935
$Ni_{36}Fe_{32}Cr_{14}P_{12}B_6$ metallic glass, mech. props. and thermal stability 80−76362
$NiFeO_4$, induced ferrimagnetism, temp. depend. of sublattice magnetisation, Mossbauer study 77−66280
$NiFe_2O_4$ mag. fluid particles, comp., struct., and mag. props. 80−60374
$NiFe_2O_4$ precipitation from silicate glass, Mossbauer study 80−54998
$Ni_{0.98}{}^{57}Fe_{0.02}S_{1.0}$, quadrupole splitting and ground state, Mossbauer spectra 80−29657

Mossbauer effect continued
$(Ni_{1-x}Fe_x)S$, solid solns., electronic props., X-ray, thermal and Mossbauer study 79−78376
$Ni_2Mn_{0.9}Fe_{0.1}Sn$, Fe site hyperfine field and mag. moment, Mossbauer effect meas. 78−76365
$Ni_2Mn_xM_{1-x}Sn$ (M=Ti,V) mag. hyperfine fields, ^{119}Sn Mossbauer spectra study 80−55003
$Ni_2Mn_xTi_{1-x}Sn$, Mossbauer spectra, mag. hyperfine field 80−15857
NiO, relax. valence averaging, Mossbauer spectra evidence 77−1626
NiO:Fe, estimation of 4s covalent bonding of Fe^{2+} and Fe^{3+} ions, Mossbauer spectra 78−72441
NiS_2, hyperfine parameters and quadrupole splitting determ., ^{57}Fe Mossbauer spectra 77−77131
$Ni_{1-x}S$, metal-semimetal transition, lattice dynamics and thermodynamic props. 80−29324
$NiS_{2-x}Se_x$, mag. struct., ^{57}Fe Mossbauer study 78−56409
$Ni_{1+}Sb$, temperature effect on lattice consts., Mossbauer spectra and density 80−88124
$NiSe_2$, hyperfine parameters and quadrupole splitting determ., ^{57}Fe Mossbauer spectra 77−77131
NiSn, thermally prepared Mossbauer spectroscopy 79−61269
Ni_3Sn_2, thermally prepared Mossbauer spectroscopy 79−61269
Ni_3Sn_4, thermally prepared Mossbauer spectroscopy 79−61269
$NiSnF_6.6H_2O$, probability anisotropy of Mossbauer effect 79−42874
$Ni_{1-x}Te$, fluctuating localised mag. moments, d band motion, Mossbauer study 80−65768
NiZn ferrites, Mossbauer effect and IR spectra 78−64300
$Ni_{0.25}Zn_{0.75}Fe_2O_4$, Mossbauer study, spin fluctuations 80−60471
$Ni_{0.25}Zn_{0.75}Fe_2O_4$, Mossbauer study, noncollinear spin struct. 80−60472
$Ni_{0.38}Zn_{0.62}Fe_2O_4$, preparation, Mossbauer study 80−50231
$Ni_{1-x}Zn_xFe_2O_4$ spinel, low-temp. transitions and spin configurations, Mossbauer study 78−27144
^{61}Ni, isomer shift, book contrib. 79−87354
Np intermetallics, NpM_2Si_2, (M=Cr, Mn, Fe, Co, Ni, Cu), Mossbauer and magnetization expts. 78−31138
Np, ternary oxides, electronic and structural props., ^{237}Np Mossbauer spectroscopy 79−33570
$NpAs_2$, magnetic props., 4.2 to 77K, Mossbauer study 80−39937
$NpBa_6Zr_{12}F_{64}$ glass, Mossbauer spectrum, evidence for charge states 3+ and 4+ *(French)* 78−88231
$NpBa_6Zr_{12}F_x$ glass, Mossbauer spectrum 80−11304
$NpCo_2Si_2$ and $NpFe_2Si_2$, itinerant magnetism obs. 77−28406
$NpCo_2Si_2$, mag. props., high press. studies with $^{237}Np(60)$-resonance 80−39924
$NpFe_{2-x}Co_xSi_2$, mag. and hyperfine props. 79−51887
$NpFe_{2-x}Co_xSi_2$, mag. and hyperfine props. 80−7247
NpM_2Ge_2, Neel point and hyperfine interactions, Mossbauer and magnetisation meas. 77−1555
$NpPd_{3-x}Rh_x$, hyperfine interactions and mag. ordering 77−20783
$NpSn_3$, itinerant f-electron antiferromag. obs. 77−8315
$(Np_{1-x}U_x)Fe$, Mossbauer spectra, magnetism and hyperfine interactions 80−20529
^{237}Np charge state, alpha-decayed ^{241}Am, in $CaF_2(CdF_2)$ host, Mossbauer obs. 79−47367
^{237}Np, lineshape, dispersion amplitudes 78−25146
^{237}Np, lineshape analysis of 60 keV Mossbauer resonance, interference effects 79−28644
Os, Mossbauer meas., elec. field gradients at ^{186}Os nuclei 79−47373
Pa, Mossbauer resonance, electric field gradient 79−19823
^{231}Pa Mossbauer resonance, elec. field grad. 80−7207
^{231}Pa Mossbauer resonance, elec. field gradient 80−15927
Pb, recoilless fraction calc. of ^{57}Fe impurity atoms from mean-square displacements 78−2216
$PbFe_{12}O_{19}$, Mossbauer spectra, domain magnetisation vector rotations, domain struct. 79−69761
$PbFe_{12}O_{19}$, single crystal, Mossbauer spectra 80−84670
$Pb_2Fe_2O_5$, IR absorpt., Mossbauer spectra, Neel temp., cryst. cell *(French)* 79−42759
$Pb(FeTa)_{1/2}O_3$, Mossbauer spectra, 78-480K 79−51885
$PbFe_{2/3}W_{1/3}O_3$-$BaTiO_3$ system, ferroelec., antiferromag., nucl. gamma reson. spectra 77−40172
$PbFe_{(2/3}W_{1/3)}O_3$-$Pb(Co_{1/2}W_{1/2})O_3$ solid soln., crystallographic, dielectric, magnetic props., Mossbauer spectra 78−43807
$PbMnFeF_7$ and Pb_2MnFeF_9, vitreous, insulating, evidence of spin-glass transition 80−97112
$Pb_2MnSb_{0.99}Sn_{0.01}$, ^{119}Sn Mossbauer study, compositional and heat treatment effects 79−42875
PbO, anharmonicity effect, Debye temp. determ. from Mossbauer spectra 77−63335
PbO-$2B_2O_3$-Fe_2O_3 glass, Mossbauer study, struct., crystallite formation, broadened quadrupole doublet 78−59761
$Pb_{0.2}Sn_{0.8}S$, Mossbauer spectra, effect of optical emission *(Russian)* 78−60367
$Pb_{1-x}Sn_xTe$, Mossbauer investig. of phonon softening at semicond.-semimetal transition 77−43908
$Pb_{1-x}Sn_xTe$:^{119}Sn, symm. breaking of Sn local environment, Mossbauer splitting obs. *(Russian)* 77−40166
$Pb_xSn_{1-x}Te$, thin film, oxidation, appl. of Mossbauer method 80−45410
$xPb0.(1-x)B_2O_3$:Fe_2O_3, Mossbauer spectra 79−87338
Pd concentration determ. by gamma-ray absorption from $^{119}Sn^m$ 80−108123
Pd, matrix for Mossbauer effect on ^{119}Sn and ^{197}Au 78−15080
Pd-Co, dil., Mossbauer emission spectra, fast relaxation regime, ^{57}Co hyperfine field 78−60362
Pd-Co, dil., relax. of oriented ^{57}Co nuclei, meas. using ^3He-^4He refrigerator 78−24909
Pd-Co, Mossbauer effect under press. for ^{119}Sn impurity atoms and hyperfine mag. field model *(Russian)* 77−55742
Pd-Co, very dil., Mossbauer emission spectra of ^{57}Co, relax. effects 80−29656
Pd-Fe, del. alloy, Mossbauer obs., 0.018-300K 77−69740
Pd-Fe, highly dil., mag. behaviour, 0.06-300K, Mossbauer expt. 78−43711
Pd-Fe, Mossbauer effect under press. for ^{119}Sn impurity atoms and hyperfine mag. field model *(Russian)* 77−55742
Pd-Fe, Mossbauer spectra, scatt. and transmission geometries, differences in crit. behaviour near T_c 78−76367
Pd-Fe, Pd-Fe-H and Pd-Fe-D, Mossbauer effect, internal hyperfine field temp. depend. 77−12283
Pd-Fe, scatt. and transmission Mossbauer spectra near Curie temp. 80−15864

Mossbauer effect continued
Pd-Fe, very dil., Mossbauer emission spectra, relax. effects 80−66084
Pd-Fe (25-55 at.%) ^{57}Fe effective field and mag. struct., Mossbauer and magnetisation expts. *(Russian)* 77−90085
Pd-Fe alloys, dil., spin polarisation effect on hyperfine interactions, anal. of Mossbauer meas. *(Russian)* 79−47055
Pd-Fe-H alloy, Mossbauer line shift with H conc. *(Russian)* 77−40165
Pd-H, Mossbauer study of local environment of substitutional Co and Fe impurities 80−60475
Pd-H-Fe, Mossbauer effect, hyperfine field, effect of changing spin susceptibility 77−20494
Pd-Ni, local susceptibilities, ^{61}Ni Mossbauer spectroscopy 78−95536
Pd-Si-Fe amorphous alloy, Mossbauer spectra, struct. and bonding 80−7224
$Pd_{1-x}Ag_{1-x}$-Au, dil., electron density at Au, Mossbauer reson. 78−39473
Pd_3Fe, hyperfine interactions during atomic ordering, Mossbauer obs. *(Russian)* 78−56630
$(Pd_{0.9965}Fe_{0.0035})_{1-x}Mn_x$, mag. behaviour at Fe sites, Mossbauer effect meas. 80−66085
$Pd_{70}Fe_{10}Si_{20}$ alloy, amorphous to cryst. transition, 350 to 450°C, Mossbauer spectra 78−59758
PdH_x $(\alpha')Fe_{0.003}$ 79−61054
β-PdH_x, diffusion-induced reduction of ^{57}Fe Mossbauer fraction 80−108131
PdH_x:Co(Fe), diffusion and interstitial site occupancy, Mossbauer spectra 80−20555
PdH_x-Au, dil., electron density at Au, Mossbauer reson. 78−39473
PdH_x-Fe, dil., Kondo system, local moment hyperfine studies, Mossbauer expt. 80−39908
$PdH_xFe_{0.003}$, Kondo system, local moments, hyperfine fields, Mossbauer study 80−80478
$Pd(M_nCo)$, giant moments, Mossbauer study of ^{57}Fe 80−44969
$Pd_2MnIn_{1-x}Sb_x(Sn_x)$, Heusler alloy, Mossbauer effect exam., mag. coupling 79−69755
$Pd_2MnIn_{1-x}Sb_x(Sn_x)$, Heusler alloy, Mossbauer effect exam., hyperfine interactions in ferromag. phase 79−69756
PdMnSb, Heusler alloy, hyperfine fields of 5sp shell impurities substituting Sb, Mossbauer spectra 78−80261
PdMnSb, hyperfine field at ^{125}Te, Mossbauer expts., compared with Jena-Geldart model 78−43707
PdMnSb, Pd_2MnSb, Heusler alloys, ^{129}I mag. hyperfine struct., Mossbauer meas. 79−33580
Pd_2MnSb, ferromag. Heusler alloy, mechanical and heat treatment effects 79−78582
Pd_2MnSb, Heusler alloy, hyperfine fields of 5sp shell impurities substituting Sb, Mossbauer spectra 78−80261
Pd_2MnSb:^{119}Sn, ferromag., mag. hyperfine structure, Mossbauer obs. 77−32309
$Pd_2MnSb_{1-x}Sn_x$, Mossbauer meas. of ^{119}Sn mag. hyperfine struct. 77−12258
$Pd_2Mn_{0.95}Sn_{1.05}$, hyperfine mag. fields, Mossbauer spectra 80−15870
$Pd_2MnSn_{1-x}Sb_x$, Heusler alloy, Mossbauer effect exam., hyperfine interactions in ferromag. phase 79−69756
$Pd_2MnSn_{1-x}Sb_x$, Mossbauer spectra, mag. hyperfine field 80−15868
$Pd_2Mn_xV_{1-x}Sn$, Heusler alloy, structural disorder, Mossbauer study 80−80650
$Pd_{100-x-y}Si_xFe_y$, amorphous, ^{57}Fe Mossbauer spectra, X-ray diffr., ageing behaviour 79−28651
$Pd_{0.99}Sn_{0.01}$, lattice dynamics of ^{119}Sn impurities, Mossbauer meas. 77−76507
Pd_xSn_y (x=0.95, y=0.05; x=3, y=1), Mossbauer spectra, high press. effects, force consts. 80−84669
(1,10-phenanthroline-2-carbaldehyde phenylhydrazone) iron perchlorate, high spin to low spin transition, X-ray diffr. and Mossbauer obs. 79−38418
Pr-Eu, dil., magnetisation, Mossbauer spectra 80−15928
$PrCo_2$, magnetocryst. anisotropy props. by ^{57}Fe Mossbauer spectroscopy 77−63328
PrEu(Gd), magnetic interactions, Mossbauer spectra quadrupole splitting, crystal field parameters 80−39907
$PrFe_2$, Curie temp., elec. quadrupole couplings, Mossbauer study 80−39949
$PrFe_2$, high field Mossbauer study 80−75893
$PrFe_2$, Laves phase, mag. props., Mossbauer spectra, crystalline field mag. anisotropy 80−65851
$PrFe_2$, preparation and mag. props. 80−25259
Pt, matrix for Mossbauer effect on ^{119}Sn and ^{197}Au 78−15080
Pt-Fe, very dil., Mossbauer emission spectra, relax. effects 80−66084
Pt-Mn-Sn alloy, mag. hyperfine fields 79−1737
Pt-Sn/Al_2O_3 catalyst, Mossbauer effect, reactivity 80−11298
$Pt_{0.72}Fe_{0.28}$, isomer shift and effective mag. field at ^{57}Fe, press. depend. 77−16232
PtMnSn, ^{197}Au and ^{119}Sn hyperfine fields, Mossbauer expt. 78−72439
^{195}Pt, lineshape, dispersion amplitudes 78−25146
PuO_2, Mossbauer resonance 80−20554
$PuO_2C_2O_4$, Mossbauer resonance 80−20554
^{240}Pu, 42.9 keV γ transition, Mossbauer reson. obs. 79−36229
RM_4Al_8 (M=Cr, Mn, Fe, Cu), magnetism and hyperfine interactions 80−25256
$RbCaF_3$, crit. scatt. at phase transition, Mossbauer diffraction 79−1733
$RbCaF_3$, critical scatt. at struct. phase transition, Mossbauer diffr. 80−20546
$RbCaF_3$, cubic to tetragonal phase transform., X-ray, neutron, Mossbauer diffr. study 80−49360
Rb_2CoF_4:^{57}Fe, Ising antiferromag., Mossbauer spectra, critical dynamics 80−15884
Rb_2CoF_4:^{57}Fe, Mossbauer spectra, critical region anal. 80−15888
$Rb_2Co_{0.95}Mg_{0.05}F_4$:$^{57}Fe$, Mossbauer spectra, critical region anal. 80−15888
$(RbF)_n$-FeF_3, antiferromagnetic systems, dimensionality and spin reduction effects, Mossbauer study 80−39947
$RbFeCl_3.2H_2O$, 2D Ising system, crit. fluctuations, Mossbauer spectra study 80−44842
$RbFeCl_3.2H_2O$, rectangular Ising cpd., Mossbauer meas. 80−71252
$RbFeF_3$, antiferromag., Mossbauer study of mag. axis 79−4752
$RbFeF_3$, appl. of spectrom. using Bitter magnets 79−51888
$RbFeF_3$, Mossbauer spectra, mag. phases 80−15878
$RbFeF_4$, Mossbauer and optical evidence for crystallographic transition 79−14931
$RbFeF_4$, Mossbauer spectra, struct. and hyperfine field 77−12266

Mossbauer effect continued
$RbFeF_5$, one dimensional antiferromagnets, field depend. spin reduction temp. variation, spin flopping 79−78586
Rb_2FeF_5, 1D antiferromagnetic system, Mossbauer investigation 78−95533
Rb_2FeF_5, mag. struct. and one-dimens. antiferromagnetism 80−60209
Rb_2FeF_5, Mossbauer spectra, 1D antiferromag. 80−15886
Rb_2FeF_5, one-dimensional antiferromag. systems, Mossbauer studies 80−71266
α-Rb_xFeF_3, mixed valence compound, Mossbauer effect appl. to charact. 79−51883
$RbFeS_2^+$, ^{57}Fe Mossbauer hyperfine interaction, covalency effects, point charge model 78−39484
Rb_2IrCl_6, hyperfine spectra of mag. ordered state at very low temp., Mossbauer meas. 77−69744
$RbNiFeF_6$, pyrochlore, Mossbauer spectra in paramag. and mag. ordered states 77−52003
Re, Mossbauer meas., elec. field gradients at ^{186}Os nuclei 79−47373
Rh_2CoSn, ferromag., crit. exponent of ^{119}Sn hyperfine field, Mossbauer obs. 78−92008
Rh_2CoSn, ferromag., mag. hyperfine fields of ^{119}Sn, Mossbauer meas. 78−10816
Rh_2CoSn, hyperfine mag. fields at ^{119}Sn, under press., Mossbauer expts. 79−99812
Rh_2CoSn, metallic ferromagnet, hyperfine mag. field temp. depend. *(Russian)* 78−80265
Rh_2FeSn, ferromag., mag. hyperfine fields of ^{119}Sn, Mossbauer meas. 78−10816
Rh_2FeSn, Heusler alloy, Sn and Fe hyperfine field, Mossbauer exam. 77−43920
Rh_2FeSn, hyperfine mag. fields at ^{119}Sn and ^{57}Fe, under press., Mossbauer expts. 79−99812
Rh_2FeSn, metallic ferromagnet, hyperfine mag. field temp. depend. *(Russian)* 78−80265
Rh_2MnPb, hyperfine fields, ferromag., NMR and Mossbauer effect studies 80−71259
Rh_2MnSb, hyperfine fields, ferromag., NMR and Mossbauer effect studies 80−71259
Rh_2MnSn, Heusler alloy, Sn hyperfine field, Mossbauer exam. 77−43920
Rh_2MnSn, mag. hyperfine fields at Rh and Sn sites, and their temp. depend. 78−43708
Rh_2MnSn, Rh_2NiSn, Heusler alloys, hyperfine mag. field at Sn 78−39482
Ru complex, HF calc., electron densities and Mossbauer isomer shift, chemical binding 78−50470
Ru-Fe, dil., local magnetisation, Mossbauer meas. 80−66091
Ru_2FeSn, ferromag. Heusler alloys, hyperfine fields at nonmagnetic atoms in various sites, Mossbauer effect and NMR meas. 80−66089
Ru_2FeSn, hyperfine mag. field, Mossbauer spectra 80−15865
Sb (III) compounds, Mossbauer spectra, direct population of solid-state bands 80−15905
Sb (III) compounds, orbital population anal. using ^{121}Sb Mossbauer data 78−21953
Sb complexes, dithiocarbamates, lone pair electrons, ^{121}Sb Mossbauer spectroscopy study 80−39984
Sb compounds, Mossbauer effect, isomer shifts, quadrupole splitting, CNDO/II calcs. 77−24766
Sb, contact charge density, press. depend., trends for Ag-Te 78−39077
Sb, Mossbauer radiation, Rayleigh scatt., Debye-Waller factor determ., annealing effect 80−39963
Sb, press. depend. of Mossbauer isomer shift 78−56411
Sb-containing glasses, ^{121}Sb Mossbauer spectra 77−20764
$(Sb_2F_4^{2+})[SbF_6^-]_2$ and $[Sb_3F_{14}^-]$ ion containing cpds., ^{121}Sb Mossbauer obs. of mixed oxidation state cpds. 79−28640
SbI_3, intermolecular bonding study using ^{129}I Mossbauer effect 78−72438
Sb_2Te_3, Mossbauer radiation, Rayleigh scatt., Debye-Waller factor determ., annealing effect 80−39963
^{121}Sb, Mossbauer isomer shifts, book contrib. 79−87360
^{125}Sb in Pd_2MnSb, orientation meas. with ^{125}Te Mossbauer effect 77−55713
Sc-Fe(ru)(Au), dil., elec. field gradient, Mossbauer meas. 80−80665
Sc-Ir, dil., elec. field gradient at ^{193}Ir, Mossbauer meas. 80−66090
$ScAl_2$-Eu, intermediate valence on Eu ions, Mossbauer isomer shift 80−84587
$ScFe_2$, Mossbauer effect of ^{57}Fe 80−75903
$ScFe_2H_2$, Mossbauer effect of ^{57}Fe 80−75903
$Sc_xY_{0.95-x}Sm_{0.05}$, ^{153}Eu isomer shift, at. vol. depend. 77−43915
Si, ^{57}Co ion implantation, Mossbauer spectra, dose depend. 79−82899
Si, ^{57}Fe isomer shift, quadrupole coupling and interat. distance correl. 78−52408
Si, subthreshold irrad., migration of Sn, Mossbauer obs. 77−15462
Si:^{119m}Sn, impurity lattice dynamics, Mossbauer spectra, Debye temp. 80−84262
Si:^{119}Te(^{119}Sb), implanted atom site changes with time, Mossbauer obs. 77−20757
Si:^{57}Co, ion-implanted, Mossbauer study, annealing effects 80−7231
Si:^{57}Co/^{57}Fe, Mossbauer spectra, deep level Co impurity study 80−29666
Si:^{57}Co(^{57}Fe), implanted, Mossbauer spectra, study of dose dependence 80−75900
Si:^{57}Fe, electric quadrupole coupling at Fe nuclei 78−27137
Si:^{57}Fe, quadrupole interac. 78−92005
Si:^{57}Fe study via conversion electron Mossbauer spectroscopy 77−55735
Si:Co, diffused distrib. and state of Co atoms, Mossbauer spectra meas. 77−1146
Si:Co, high-temp. ion-implanted and diffused samples, Mossbauer spectra of ^{57}Co 79−51891
Si:Co, implanted or diffused, and annealed, localisation of Co atoms, Mossbauer obs. 80−39140
Si:Co, substitutional Co and Co precipitates, identification by Mossbauer spectroscopy 79−11631
Si:Fe, implanted, annealing and stripping, Mossbauer expts. 80−39141
Si:Fe, implanted, Mossbauer spectra, conversion electron, temp. dependence 80−40025
Si:Fe, ion implanted, laser annealing studies using Mossbauer spectroscopy 80−79827
Si:Fe, laser annealing of implanted ^{57}Co sources, Mossbauer obs. 80−39139
Si:Fe, laser implantation, Mossbauer obs. 80−39125

Mossbauer effect continued
Si:Sb, Mossbauer spectra of ^{119}Sn defect struct. 80−97174
Si:Sn, Mossbauer spectra of ^{119}Sn impurity atoms 80−15935
Si:Sn, Mossbauer study of defects due to ^{119}In implantation 80−80641
Si:Te(Sm), implanted impurity location, Mossbauer and channelling expts. 80−39128
n-Si-^{119}Sn resonant detector for Mossbauer spectroscopy 80−883
Si-Pb heterojunction, RHEED, Mossbauer spectroscopy and I-V characts. 80−70828
Si-Sn heterojunction, RHEED, Mossbauer spectroscopy and I-V characts. 80−70828
Si-Te, laser and thermal annealing, Mossbauer resonance lines 79−99810
Si-Te system glasses, local struct., ^{119}Sn Mossbauer obs. 79−41968
SiC, α- and β-phases, isomer shift in Mossbauer spectra of implanted ^{129}I 78−15067
Si_3N_4:Fe, α- and β-phases, Mossbauer and Raman obs. of state of Fe 79−33572
SiO_2-Al_2O_3-Fe_2O_3-CaO, basalt glass ceramics, crystallite form. due to heat treatment 80−38917
SiO_2-Al_2O_3-Fe_2O_3-Na_2O-K_2O-CaO-MgO glasses, Mossbauer spectra study 80−39967
$((SiO_2)_{45}(CaO)_{55})_{65}$ $(Fe_2O_3)_{35}$ glass, effect of melt atmosphere on mag. props. 78−68299
$SmFe_2(Co_2)(Ni_2)$, hyperfine interactions and exchange fields acting on Eu^{3+}, Mossbauer obs. 77−63338
SmIG, mag. phase transitions, Mossbauer spectroscopy obs. 80−80509
SmS, divalent and trivalent ion doped, electronic struct., Mossbauer spectroscopy 78−39022
SmS, electronic config., Mossbauer spectra meas. 77−16228
$Sm_{1-x}Y_xS$, electronic config., Mossbauer spectra meas. 77−16228
Sn (II) compounds, Mossbauer spectra, direct population of solid-state bands 80−15905
Sn (IV) in glassy aq. soln., Mossbauer spectra 80−15894
β-Sn, anisotropy of Mossbauer effect and quad. splitting 77−12268
Sn, anodically treated in borate buffer, passive film form., Mossbauer meas. 80−39990
Sn, α- and β-phases, isomer shift in Mossbauer spectra of implanted ^{129}I 78−15067
Sn, binding state of atoms segregated at boundary of Fe and Fe alloys, Mossbauer study 80−7232
Sn borate glasses, IR and ^{119}Sn Mossbauer spectra 78−60438
Sn complex containing P, $L_2Sn(CH_3)_nCl_{4-n}$, Mossbauer parameters, quadrupole splittings *(Russian)* 78−76362
Sn compounds, influence of nonuniform electronic absorption on Mossbauer line intensity 79−47372
Sn compounds, Mossbauer effect, isomer shifts, quadrupole splitting, CNDO/II calcs. 77−24766
Sn compounds, Sn(II) valency config., Mossbauer and X-ray electron determ. *(Russian)* 77−8483
β-Sn, configuration of ^{57}Fe, Mossbauer effect measurements 78−47333
Sn, contact charge density, press. depend., trends for Ag-Te 78−39077
β-Sn, dissociative diffusion of ^{57}Fe, Mossbauer expts., 90-462K 79−7714
Sn, electric field gradient, Debye model calc. 80−49682
Sn, filtered reson. radiation, time depend. 80−7216
α-Sn, implanted with Sn, Sb or Te, impurity-defect structs., Mossbauer expts. 80−39129
Sn in $SnSO_4$ anodised Al 78−35582
α-Sn, ion implanted, defect struct., Mossbauer spectra 80−80214
Sn isomer shifts, book contrib. 79−87359
Sn, metallic thin film, oxidation mechanism, depth selective Mossbauer spectroscopy method 78−35549
Sn, nucl. quadrupole interactions, ^{119}Sn Mossbauer spectra 78−56412
Sn organometallic cpds., chem. shifts in ESCA and Mossbauer spectra *(French)* 77−28685
Sn, press. depend. of Mossbauer isomer shift 78−56411
Sn tetrahedral molecular solids, ^{119}Sn Mossbauer and Raman spectra 78−15070
Sn, X-ray diffraction study of thermal motion of atoms in β-Sn 80−39243
α-Sn:^{119m}Sn, impurity lattice dynamics, Mossbauer spectra, Debye temp. 80−84262
Sn-Ni, electrodeposit, Mossbauer meas. 80−39990
Sn-Ni alloys, electrodeposited Mossbauer spectroscopy 79−61269
Sn-O system, amorphous, characterisation by appl. of Mossbauer effect 79−61283
Sn-Pb alloy, dil., lattice dynamics, sp. ht., resist., thermal expansion and nuclear γ reson. expts. *(Russian)* 78−87749
Sn-Pb alloys, dil., low-freq. phonon spectrum peculiarities 79−60463
$SnBaO_3$, resonantly scatt. gamma radiation from ^{119}Sn, energy spectrum with time parameters 80−108122
$^{119m}SnCl_2$ adducts with O and N containing cpds., Mossbauer emission 80−15918
$SnCo_2O_4$ spinel, mag. props. 77−1543
$Sn_{0.5}Eu_{0.5}Mo_6S_8$, supercond., spin polarisation, NMR, Mossbauer effect and bulk magnetisation meas. 77−43782
$Sn_{0.75}Eu_{0.25}Mo_6S_8$, Chevrel phase supercond., spin-depairing interaction, Mossbauer obs. 80−25258
$Sn_{1-x}Eu_xMo_6S_8$, supercond., Mossbauer effect, struct. phase transition 77−12290
SnF_2^{2-}, Mossbauer effect 77−85626
$SnFe(CN)_6$, Mossbauer spectral anal. *(German)* 79−19819
$Sn_2Fe(CN)_6$, Mossbauer spectral anal. *(German)* 79−19819
$Sn_xGe_{1-x}Se$, ^{119}Sn Mossbauer and elec. conductivity study 79−19595
$Sn_{0.9}Ge_{0.1}Te$, Mossbauer spectra, soft modes 80−20550
$Sn_{1-x}Ge_xTe$, solid soln. series, Mossbauer study 80−39985
$Sn(HPO_4)_2.H_2O$ and its alkali metal salts, struct. and vibr. spectra 80−39030
SnI_4, mol. solid, dynamics, press. and temp. depend. 78−79691
SnI_7 crysts., dynamical props. of ^{119}Sn by Mossbauer spectroscopy 77−59495
Sn(IV)-, Sn(II) halide mols., rare gas matrix-isolated ^{119} Sn spectra 77−48097
$SnMo_6S_8$, lattice softening, vibr. anisotropy 78−14428
$Sn_xMo_5S_6$, supercond. props., effect of W and Re alloying additions, Mossbauer and X-ray diffr. meas. *(Russian)* 79−15245
$SnMo_6S_8(Se_8)$ Chevrel phase supercond., hyperfine interaction, microscopic study 79−56650
$SnMo_6S_8(Se_8)$, Mossbauer spectra 80−15926
SnO chlorination, Mossbauer and X-ray phase anal. 80−21266

Mossbauer effect continued
SnO, disproportionation, thermoEMF, Mossbauer spectroscopic, X-ray diffr. anals. 79−11776
SnO, under hydrostatic press. up to 41 kbar, Mossbauer study 79−51892
SnO-GeO_2 system, glass form., compound anal. 77−35486
SnO_2 aerosols, Lamb-Mossbauer factor *(French)* 80−81375
SnO_2, anharmonicity effect, Debye temp. determ. from Mossbauer spectra 77−63335
SnO_2, defect, resonance filter for line width reduction 77−24767
SnO_2, finely dispersed, Lamb-Mossbauer factor 80−39930
SnO_2, from rocks, quantitative determination by Mossbauer effect *(Rumanian)* 78−49178
SnO_2 layers, study using Mossbauer effect 78−31124
SnO_2, powder, electron scatt. from ^{119}Sn, effective range, Mossbauer obs. 77−63345
SnO_2, quantitative determ. by Mossbauer effect, using portable analyser 78−20131
SnO_x films, non-stoichiometric, DC reactively sputtered, elec. props. 80−80415
SnO_x films, phase composition, Mossbauer spectra 80−20051
SnO_x films reactive DC sputtering prep., phase comp., X-ray diffr. and Mossbauer meas. 79−90914
$SnO_2(F_4)$, elec. field gradient at Sn^{4+} site, Mossbauer quadrupole splitting and anionic polarisability calc. *(French)* 79−15384
SnPb eutectic alloy, Mossbauer spectra, isomer shifts 79−82903
$Sn_{1-x}Pb_xSe(Te)$ films, of ^{119}Sn, spectral charact., conc. depend. 80−103903
$Sn_{1-x}Pb_xSe(Te)$ films, oxidation rel. to annealing temp. and time, Mossbauer spectra, X-ray and microstruct. obs. 80−104311
$Sn_{1-x}Pb_xSe(Te)$ thin films, resistance to oxidation, Mossbauer study 80−39986
SnS-SnTe, solid solns., synthesis, Mossbauer spectra 77−24768
SnS_2, Mossbauer spectra, vibr. amplitudes anisotropy 80−15904
Sn_2S_3, resistivity, Mossbauer spectra, press. effects 79−73862
$SnS_{2-x}Se_x$, ($0 \le x \le 2$), ^{119}Sn Mossbauer spectrum, lattice dynamics 78−71809
SnS(Se)(Te)(S_2)(Se_2), oxidation, thermal decomp., Mossbauer spectra 79−11713
SnS(Te):O, impurity assoc. with Fe microtraces, Mossbauer effect meas. 77−20763
SnSe, Mossbauer spectra, effect of optical emission *(Russian)* 78−60367
SnSe-SnTe, solid solns., synthesis, Mossbauer spectra 77−24768
$SnSe_2$, Mossbauer spectra, vibr. amplitudes anisotropy 80−15904
$SnSnO_3$, Mossbauer spectral anal. *(German)* 79−19818
SnTe, displacive phase transition at 22K, Mossbauer spectra and elec. resist. meas. 80−6514
SnTe, mechanochem. and thermal oxidation comparison 80−104310
SnTe, phase transition at high hydrostatic pressure, Mossbauer study 79−95162
SnTe, phase transition obs. by Mossbauer spectroscopy 77−55740
SnTe, temp.-depend. ^{119}Sn isomer shift, calcs. 77−8457
SnX_2, (X=Br,Cl,F,I), matrix isolated, Mossbauer effect, isomer shift and quadrupole splittings obs. 78−46377
SnX_4, (X=Br,Cl,I), matrix isolated, Mossbauer effect, isomer shift and quadrupole splittings obs. 78−46377
^{119}Sn conversion electron Mossbauer spectroscopy in β-Sn, $CaSnO_3$ and SnO_2 79−33575
^{119}Sn, magnetic moment, of $I=+^3/_2$ level *(Russian)* 78−50083
^{119}Sn, Mossbauer spectra 77−73100
^{119}Sn resonance from inert gas matrix, Mossbauer isomer shift calibration 77−46530
^{119}Sn temp. depend. isomer shift, pseudopot. approach 80−84675
^{119}Sn, thin foil, 19.6 keV conversion e^- energy, ang. contrib., Monte Carlo calc. 79−11360
^{119}Sn, total mass absorpt. coeff. of gamma quanta, chem. binding influence, determ. using Mossbauer effect 80−99467
^{199}Sn, Mossbauer effect thermometer, rel. to Cu nuclear susceptibility thermometer, 6 mk to 1K 79−35737
^{119m}Sn in FCC metals, isotope separator implanted, Mossbauer spectroscopy 79−24240
$SrCoO_3$:Fe^{4+}, ferromag., sign of Fe^{4+} hyperfine field, spin struct., Mossbauer study 80−39933
SrEuFeO$_4$, Neel temp. and spin reorientation, Mossbauer study 80−39934
$SrEu_2Fe_2O_7$, ferrite, Mossbauer effect study of hyperfine interactions, spin reorientation 78−19383
SrF_2, Eu^{2+} isomer shift, Mossbauer spectroscopic anal. 79−56649
$SrFe_{12-x}Cr_xO_{19}$, effects of substitution of Fe by Cr, Mossbauer spectra 80−2674
$SrFe_{12-x}Cr_xO_{19}$, hexagonal ferrite series, Mossbauer study 80−71258
Sr_2FeEuO_5, ^{57}Fe Mossbauer study 80−39976
$SrFe_6Ga_6O_{19}$ ferrite, mag. struct., Mossbauer study 80−93087
$SrFe_{12}O_{19}$ and $Sr_4Fe_6O_{13}$, Mossbauer spectra 80−15882
$SrFe_{12}O_{19}$, Ca^{2+} additives effect on hexaferrite lattice and mag. props. 80−60243
$SrFe_{12}O_{19}$ ceramic compact, sublattice magnetisation and textures 78−68426
$SrFe_{12}O_{19}$, M type hexaferrite, Fe ion dynamic charact. in bipyramidal position, nucl. γ reson. 79−95697
$Sr_7Fe_{10}O_{22}$, mag. props. and spin order 78−52232
$Sr_2Fe_xRu_{1-x}O_4$ solid soln., Mossbauer spectrosc. study 80−50235
$Sr_3FeTa_2O_9$, Mossbauer and X-ray diffr. studies 80−103905
$Sr(Fe_{0.766}W_{0.234})O_3$, cryst. growth, mag. and Mossbauer studies 79−42743
SrGdFeO$_4$, Neel temp. and spin reorientation, Mossbauer study 80−39934
$Sr_{1-x}La_xFeO_3$, Mossbauer spectra, charge disproportionation 80−20542
$Sr_{0.5}La_{1.5}Li_{0.5}Fe_{0.5}O_4$, high spin configuration stabilisation for Fe^{4+} *(French)* 80−88519
SrO-Fe_2O_3, EMF meas. with solid state cell, Mossbauer effect and magnetic props. *(Korean)* 77−28493
SrO-Fe_2O_3 system, non-existence of single phase $SrFe_2O_4$, Mossbauer expts. 80−29178
SrRFeO$_4$, (R=La,Pr,Nd), Mossbauer spectra, spin reorientation 80−15880
SrRFeO$_4$, R=La, Pr, Nd, Sm, Eu, Gd, Mossbauer effect, Neel temp. and internal mag. field 77−12284
$SrR_2Fe_2O_7$, (R=Pr,Nd,Sm,Eu,Gd or Tb), Mossbauer exam. of mag. struct. 77−40157

Mossbauer effect continued
$SrR_2Fe_2O_7$ series, mag. struct. and spin reorientation, neutron diffr. and Mossbauer meas. 77−69503
$SrTb_2Fe_2O_7$, ferrite, Mossbauer effect study of hyperfine interactions, spin reorientation 78−19383
$SrTb_2Fe_2O_7$, hyperfine parameters, ordering temp. 77−90079
$SrTiO_3$, energy width of central peak near phase transition 78−79724
$SrTiO_3$, Mossbauer spectroscopy, sample prep. and results 80−66078
Sr_2YRuO_6, ^{99}Ru Mossbauer spectra and other techniques 80−29659
Ta, 6.2 keV Mossbauer transition of ^{181}Ta at high temps. 77−12269
Ta, Knight shifts obs. with 6.2 keV ^{181}Ta Mossbauer resonance 79−11369
Ta, Mossbauer states at 6.2 keV, freq. modulation 80−7212
Ta, NMR-Mossbauer double reson. 80−40019
Ta, NMR-γ double resonance, Mossbauer absorpt. spectra *(Russian)* 80−34824
Ta, static and dynamic props. of O and H impurities, Mossbauer meas. 80−7246
Ta, surface layers, Mossbauer conversion electron studies 78−15068
Ta:Xe, BCC, heavy ion implanted, vacancy recovery, Mossbauer spectroscopy 79−82896
$TaD_{0.06}$, D diffusion, 6.2 keV Mossbauer reson. of ^{181}Ta 78−39472
TaS_2.Sn, intercalated, Mossbauer effect, hyperfine interaction, lattice dynamics 77−8473
$TaSe_2$ (1T), CDW obs. by Mossbauer reson. of ^{57}Fe impurity 77−73104
1T-$TaSe_2$, CDW obs. by ^{181}Ta Mossbauer effect 78−39469
^{181}Ta, 6.2 keV level, Mossbauer spectroscopy, source prep. 78−25373
^{181}Ta 6.2 keV Mossbauer resonance, prep. of narrow line sources 79−76253
^{181}Ta, freq. modulation of 6.2 keV Mossbauer states 79−13202
^{181}Ta, gamma-ray detection with Si(Li) and Ge detectors 77−10530
^{181}Ta, isomer shifts of 6.2 keV γ-rays, book contrib. 79−87358
^{182}Ta Mossbauer sources *(French)* 80−74064
Tb, phonon spectrum, obs. of one phonon transitions by nucl. reson. fluoresc. 79−38416
$TbAlO_3$:Yb^{3+}, Mossbauer relax. 80−15875
$TbCo_2$, magnetocryst. anisotropy props. by ^{57}Fe Mossbauer spectroscopy 77−63328
$Tb_{1-x}Dy_xFe_2$, pseudobinary Laves cpds., spin-orientation diagram, Mossbauer effect meas. 77−55739
$TbFe_2$, amorphous, Mossbauer spectra *(French)* 80−25261
Tb-$^{57}Fe_{1-x}Cr_xO_3$ mag. props. from Mossbauer effect obs. *(Japanese)* 80−15933
$Tb(Fe_{1-x}Rh_x)_2$, Fe sublattice spin reorientation possibility, Mossbauer spectra *(Russian)* 79−78335
TbO_x, Mossbauer spectra of localised modes 79−73874
$Tb_{0.2}Y_{2.8}Fe_5O_{12}$, Mossbauer investigation of spin-reorientation transition 78−88243
Tc:^{51}Fe, dilute, quadrupole splitting and isomer shift 78−48096
Tc-Fe, dil., local magnetisation, Mossbauer meas. 80−66091
Tc-Fe alloy, Mossbauer spectra, hyperfine field 80−20526
Tc-Fe dilute alloys, supercond. and mag. props. 80−29494
Te (IV) compounds, Mossbauer spectra, direct population of solid-state bands 80−15905
Te, amorphous, Rayleigh scatt. of Mossbauer radn., lattice dynamics 80−15845
Te complexes of thiourea, Mossbauer spectra 80−15914
Te compounds, X-ray photoemission, core level binding energy shifts rel. to Mossbauer isomer shifts 78−2984
Te, contact charge density, press. depend., trends for Ag-Te 78−39077
Te, elec. field gradient and lattice location of Sn, TDPAC and Mossbauer effect meas. 78−52395
Te, Mossbauer spectra under press. up to 8000 MPa 80−80647
Te, single cryst., influence of nucl. reson. absorption on Mossbauer diffr. spectra 77−43922
Te, trigonal, nucl. elec. field gradient ellipsoid, extended Huckel approx. calc., comparison with Mossbauer spectra 77−55736
Te, trigonal, of ^{129}I, high press. expts., phase transition and electronic changes 80−55005
α-TeI, ^{129}I Mossbauer spectra, coupling consts. 78−62833
TeI_4, ^{129}I Mossbauer spectra, coupling consts. 78−62833
α-TeO_2, anisotropy of atomic vibrations, Mossbauer absorption spectra 78−27147
TeO_2-Fe_2O_3 system, glass structure 79−90562
$Te_{1-x}S_x$, ^{125}I and ^{129}Te Mossbauer spectra obs. 77−90075
Te_xS_{1-x}, chemical bonding from ^{129}I and ^{125}Te Mossbauer spectra 79−73867
$Te_{1-x}Se_x$, ^{125}I and ^{129}Te Mossbauer spectra obs. 77−90075
Te_xSe_{1-x}, chemical bonding from ^{129}I and ^{125}Te Mossbauer spectra 79−73867
^{125}Te, Mossbauer isomer shifts, book contrib. 79−87360
Th-Dy, dil., supercond. Th, paramag. relax. of Dy moments, Mossbauer study 80−39957
Th-Dy, dil., type I superconductor, paramag. Dy moment relax., Mossbauer spectra study 80−65755
$(ThCu_3)(Mn_2Fe_2)O_{12}$, synthesis, cryst. struct. and Mossbauer exam. 78−84505
$ThFe_3$, H_2 absorption effect on mag. props. and struct. 77−40045
$ThFe_5$, mag. props., ferrimag. moment arrangement 79−33475
$Th_{1-x}Fe_x$ amorphous alloys, mag. props. and Mossbauer spectra 79−91326
Th_7Fe_3, Mossbauer spectra, mag. props. 80−15852
$Th_7Fe_3H_{14.2}$, Mossbauer spectra, mag. props. 80−15852
Ti, diffusion of Fe, plastic deform., anomalous mass transfer mech., Mossbauer spectra *(Russian)* 79−28146
Ti, press. depend. of Mossbauer fraction for ^{57}Fe 77−16226
Ti, press. depend. of Mossbauer fraction 77−59493
Ti:^{57}Fe, quadrupole interaction, Mossbauer and PAC meas. 77−48101
Ti-Al alloys, comp. depend. *(Russian)* 78−6611
β-Ti-Fe, (7.1 wt.%) exam. of ω phase formation, by X-ray diffr. and Mossbauer spectroscopy 78−52800
Ti-Fe, diffusion of stored H, Mossbauer study 80−34838
Ti-Fe, force constant change with pressure, relative Mossbauer fraction 80−34163
αTi-Fe, plastically deformed, $\alpha \rightarrow \omega$ transform. 78−3095
Ti-Fe-D system, phase anal. *(German)* 79−56963
α-Ti-Fe(0.22 wt.%), ω phase form. during ageing 77−52355
Ti-H, deposited on carriers, synthesis, structure and catalytic props. 80−29890
Ti-Ir, dil., elec. field gradient at ^{193}Ir, Mossbauer meas. 80−66090
Ti-Mo-Fe (3, 0.13 at.%), metastable phases, Mossbauer study 80−7243

Mossbauer effect continued
α-Ti-V(Al)(Sn), Mossbauer spectra, metastable θ- and ω-phases 80−20556
TiAl, Mossbauer effect on impurity nuclei of ^{57}Fe *(Russian)* 77−1621
Ti(Fe,Co)H_3, mag. and ^{57}Fe Mossbauer studies 80−71272
TiFeD, cryst. struct., Mossbauer and neutron diffr. obs. 80−34839
$TiFeH_x$, metallurgical and electronic struct., Mossbauer effect meas. 77−16223
TiO_2:Sb(Fe), Mossbauer effect exam. of impurities 78−31140
TiO_2-based ceramics, impurity atoms chem. state, Mossbauer spectra 80−15902
Tl, recoilless fraction calc. of ^{57}Fe impurity atoms from mean-square displacements 78−2216
$TlAsTe_2$, local struct. changes on crystal-glass transition, Mossbauer spectra 77−36157
Tl_2Se-As_2Se_3-SnSe system alloys, covalent component of chem. bond effect in vitrification processes 77−36156
Tl_2SnSe_3, preparation, Mossbauer spectra 77−28489
Tl_4SnSe_4, preparation, Mossbauer spectra 77−28489
Tm and Tm compounds, electronic relaxation 80−39914
Tm, and Tm cpds., Mossbauer expt. in ^{3}He-^{4}He dilution refrigerator 78−27127
Tm-3d transition metal intermetallics, ^{169}Tm Mossbauer effect 80−71261
TmAG, Mossbauer study of crystal field props. 80−66082
$TmAlO_3$:Yb^{3+}, mag. relax., Mossbauer expts. 79−8078
$Tm_2Fe_{17-x}Co_x$, and related cpds., easy magnetisation direction, Mossbauer spectra 77−63169
$Tm_3Ga_5O_{12}$, Mossbauer study of crystal field props. 80−66082
TmH_{2+x}, ^{169}Tm Mossbauer studies 80−44975
TmH_3, ^{169}Tm Mossbauer study 80−44976
TmO_6S_8, low temp. Mossbauer study and mag. susceptibility 80−80656
TmTe, hyperfine struct. of Tm^{2+} 78−76368
$TmZn_2$, Mossbauer effect meas. in antiferromag. and paramag. states 80−71265
$UFe_3B_2(B_4)$, Mossbauer effect of ^{57}Fe nuclei, mag. props. 80−103907
$V_3Ga_{1-x}Sn_x$, lattice props. supercond., ^{119}Sn Mossbauer shift meas., 5-300K 77−1627
V, press. depend. of Mossbauer fraction for ^{57}Fe 77−16226
V, press. depend. of Mossbauer fraction 77−59493
V-Fe, ^{57}Co Mossbauer spectra, diffusion mechanism of Fe 80−15292
V-Fe, force constant change with pressure, relative Mossbauer fraction 80−34163
$V_{75-x}Fe_xGa_{25}$, Mossbauer exam. 77−90078
$V_{1-x-z}Fe_xMo_zO_2$, Mossbauer effect exam., Fe conc. and precise struct. characteristics 78−31141
$V_{1-x}Fe_xO_{2-y}$, Mossbauer effect exam., Fe conc. and precise struct. characteristics 78−31141
$V_{1-x}Fe_xO_{2-x}F_x$, 0<x<0.2, phase diagrams, ^{57}Fe-Mossbauer spectra, X-ray diffr. studies *(German)* 80−29663
$V_{1-x}Fe_xO_{2-x}F_x$, mag. susceptibility *(German)* 79−78305
VI_2, mag. struct., long- and short-range order and Mossbauer spectroscopy 80−65803
V_2O_{3+x}, 0≤x≤0.08, mag. and elec. props. 80−49833
V_2O_{3+x}, nonstoichiometric compositions, mag. transition exam. by Mossbauer effect 77−28385
$^{57}CoV_2O_4$, after effects of orbital electron capture 79−73870
V_2O_5-Fe_2O_3 solid solution, Mossbauer investig. of cryst. props. *(French)* 77−4592
V_2O_5-Fe_2O_3-Li_2O ternary system, charge compensation of Fe ions, Mossbauer obs. 78−52410
V_2O_5-Fe_2O_3-LiO_2 system, physical properties 78−84503
V_2O_5, struct. and electronic aspects of cond. transition 78−15078
V_5S_8:Fe, Mossbauer and mag. studies, electronic state of Fe 80−108130
$V_{2-x}Sb_xO_4$, defect struct. exam. 78−18635
V_2Si, Mossbauer spectra of ^{57}Fe *(Russian)* 79−24235
$(V_{1-x}Ti_x)_2O_3$, solid solution, phase transition exam. 77−15590
$(V_{1-x}Ti_x)_2O_3$:Fe, metallic antiferromagnetism, Mossbauer spectra 80−15881
W, implantation effects of ^{133}Xe, annealing behaviour, Mossbauer study 80−40011
W, Mossbauer recoilless fractions, temp. depend. 78−15076
W:Xe, BCC, heavy ion implanted, vacancy recovery, Mossbauer spectroscopy 79−82896
^{182}W, 2^+-0^+ transitions, mean square nuclear charge radius change, Mossbauer expt. 78−25109
^{182}W, lineshape, dispersion amplitudes 78−25146
^{182}W, reson. γ-quanta absorption and emission probabilities *(Russian)* 78−23383
Xe compounds, Xe chemical and isomer shifts, electron valence struct. *(Russian)* 80−53056
Xe: ^{57}Co, solid, ion implantation for rare gas matrix isolation, Mossbauer spectroscopy study 80−54271
Xe(II, IV, VI and VIII) compounds, Mossbauer study 79−65772
^{A}Xe, A=129, 131, Mossbauer isomer shifts, book contrib. 79−87360
^{133}Xe/^{133}Cs, implanted in various hosts, isomer shift values, Mossbauer spectra 80−7240
$(Y,Sm,Lu,Cu)_3(Fe,Ge)_5O_{12}$, ion implanted, hard bubble suppression 80−11238
Y-Fe, rapid diffusion, Mossbauer exam. 78−27138
Y-Ir, dil., elec. field gradient at ^{193}Ir, Mossbauer meas. 80−66090
$(Y_{3-x}Ca_x)(Fe_{2-x}Sn_x)(Fe_3)O_{12}$, long and short range magnetic order 79−38419
$(Y_{3-x}Ca_x)[Fe_{2-x}Sn_x](Fe_3)O_{12}$, Mossbauer spectra of Fe^{27} and Sn^{119} nuclei 79−95578
$Y_{3-x}Ca_x[Fe_{2-x}Sn_x]Fe_3O_{12}$, Mossbauer spectra, Sn hyperfine mag. field 80−15893
$YCoO_3$, anomalous $^{57}Fe^m$ charge states, Mossbauer study 80−40017
Y_2F_{17}, hyperfine interactions, 5 to 300K 77−85634
YFe_2, amorphous, mag. order, cluster phenomena, hyperfine struct. 77−16079
YFe_2, amorphous concentrated spin glass, susceptibility, Mossbauer and neutron scatt. meas. 80−39783
YFe_2, phonon softening below Curie temp. 77−4589
$Y_{1-x}Fe_x$, amorphous, Mossbauer spectra, appearance of magnetism 78−52401
$Y(Fe_{1-x}A_x)_2$, A=Al or Ni, Laves phase, mag. props. and Mossbauer effect 77−85632
$Y(Fe_{1-c}Al_c)_2$, mag. and Mossbauer study, local environment effects 78−27033
$Y(Fe_xAl_{1-x})_2$, Mossbauer spectra and mag. props. 80−39950
Mossbauer effect continued
$Y(Fe_{0.022}Co_{0.978})_2$, ferromag. relax. model, Mossbauer spectra 80−15853
$Y(Fe_{0.022}Co_{0.978})_2$ mag. props., Mossbauer expts., 0.15-4.2K 78−43712
$Y(Fe_{1-x}Co_x)_2$, mag. hyperfine field, conc. depend. 77−63337
$Y(Fe_xCo_{1-x})_2$, 0.5≥x≥0.2, Mossbauer effect meas., 5 to 300K *(German)* 77−24771
$Y(Fe_xCo_{1-x})_2$, Mossbauer effect at 78 and 300K, ^{57}Fe hyperfine fields 80−2677
$Y(Fe_xCo_{1-x})_2$, x≤0.2, mag. props. and Mossbauer meas. 80−75798
$Y_2(Fe_{1-x}Co_x)_{17}$, hyperfine interactions 78−2780
$Y_3Fe_{5-x}Ga_xO_{12}$, garnet, magnetically inequivalent positions of cations in external mag. field 80−11307
$Y_3Fe_{5-x}In_xO_{12}$, K absorpt. and Mossbauer spectra *(Russian)* 77−32467
$Y(Fe_{1-x}Ir_x)_2$, magnetisation, mag. hyperfine field 80−20531
$Y(Fe_{1-x}Mn_x)_2$, Mossbauer spectra and mag. props. 80−39952
$Y_6(Fe_{1-x}Mn_x)_{23}$, Mn-rich compounds, Mossbauer effect study 80−71276
$Y_2(Fe_{1-x}N_x)_{17}$, magnetic properties, Mossbauer spectra *(Chinese)* 78−95433
$Y_2(Fe_{1-x}Ni_x)_{17}$, hyperfine interactions obs. 78−6614
$YFeO_3$, hydrothermal synthesis, mag. struct. 77−47972
$YFeO_3$, induced spin reorientation near Neel point 78−19267
YFe_2O_4, Mossbauer spectra of ^{51}Fe in antiferromag. and paramag. states 80−15834
$Y_3Fe_5O_{12}$, amorphous, mag. moments, susceptibility, Mossbauer studies 79−78345
$Y_3Fe_{5-x}Sc_xO_{12}$, local spin struct., Mossbauer obs. 77−32305
$Y(Fe_xT_{1-x})_2$, Mossbauer spectra, mag. props. 80−20563
YH_3:Er, Mossbauer spectra of Er^{3+}, gyromagnetic ratios and cryst. field parameters determ. 78−19388
YIG, Al substituted, transferred hyperfine fields, Mossbauer effect meas. 79−1726
YIG, cation sites distrib. and valence states 79−99167
YIG, crit. behaviour, Mossbauer and magnetisation meas. *(Russian)* 79−61106
YIG, press. depend. of effective mag. fields on ^{57}Fe nuclei 78−52383
YIG, Si substituted, spin reorientation, Mossbauer spectroscopy obs. 80−44989
YIG, vitreous electric-field-gradient distrib., Mossbauer quadrupole splitting meas. 80−75901
$Y_{2.85}La_{0.15}Fe_{3.85}Ga_{1.15}O_{12}$ garnet, mag. props., ion implantation effect, Mossbauer study 80−97166
YM_4Al_8 (M=Cr, Mn, Fe, CU), magnetism and hyperfine interactions 80−25256
$Y_{3-x}Sm_xFe_5O_{12}$:^{57}Fe film, ion implanted, Mossbauer conversion spectra study 80−80663
$YbAl_3$, Mossbauer effect obs. of induced hyperfine field 78−52396
YbB_4, mag. props. *(French)* 77−20566
$YbCl_3.6H_2O$, paramag. relax., Mossbauer spectra 80−20536
$YbFe_2$, cryst. elec. field and exchange interac., ^{170}Yb Mossbauer obs., magnetostriction contrib. 80−108124
$YbFe_2$, Curie temp., elec. quadrupole couplings, Mossbauer study 80−39949
$YbFe_2$, high field Mossbauer study 80−75893
$YbFe_2$, Laves phase compounds, synthesis, mag. props., ^{57}Fe Mossbauer effect 78−10807
$YbFe_2$, Mossbauer spectra, cryst. elec. field and exchange interaction 79−47368
$YbFe_2$, preparation and mag. props. 80−25259
$YbMo_6S_8$, low temp. Mossbauer study and mag. susceptibility 80−80656
$YbMo_6S_8$, ternary superconductor, paramagnetic relax. effects 78−68112
$Yb_2Ti_2O_7$, cryst. field props., Yb^{3+} hyperfine spectra, Mossbauer effect meas. 78−67990
$Yb_2Ti_2O_7$, crystal field props., ^{170}Yb Mossbauer spectroscopy 79−4750
^{170}Yb in some metal and metal-like compounds, Mossbauer study, isomer shift and intermediate valence state 79−33569
^{170}Yb, Mossbauer line shape, Liouville relax. supermatrices 79−28649
Zn ferrite, production by mechanochemical reactions by grinding in ball mill 79−20014
Zn, Mossbauer spectra, quadrupole interaction 80−7206
Zn nitroprussides, Mossbauer spectra, dehydration effects 79−24237
Zn, passive film formation in borate buffer polarisation curves, from Mossbauer studies 79−61778
Zn, quadrupole interaction, ^{67}Zn Mossbauer expt. 78−27120
Zn, quadrupole interaction, Mossbauer spectra 78−92004
$ZnCO_3$:Fe^{2+}, electronic relaxation, Mossbauer effect 78−19385
$ZnCo_2O_4$, Mossbauer spectra and cryst. struct. determ. 79−56637
$ZnCrFeO_4$, ferrite spinel, unsupported and SiO_2 supported, structural and catalytic studies 80−44191
$ZnCr_xFe_{2-x}O_4$, Mossbauer spectra, quadrupole splitting, Debye temp. 80−93218
$Zn_xCu_{1-x}Fe_2O_4$, mag. props., Mossbauer spectra 79−87344
ZnF_2, 93.3 keV Mossbauer transition in ^{67}Zn, isomer shifts 80−39978
$Zn_{13}Fe$, ^{57}Fe Mossbauer effect meas. 78−95534
$ZnFeO_4$, ferrite spinel, structural and catalytic studies 80−44191
$Zn_xFe_{3-x}O_4$, collective electron states, ^{57}Fe Mossbauer meas. 77−69748
$Zn_xFe_{3-x}O_4$, cond. mechanism, collective electron description 77−4588
$Zn_xFe_{3-x}O_4$ ferrite, mag. struct., Mossbauer spectra and magnetisation study, 4.2K 80−103818
$Zn_xFe_{3-x}O_4$, Mossbauer exam. of relax. phenomena 77−8479
$Zn_{1-x}Ge_xFe_{2-x}^{3+}Fe_{2x}^{2+}O_4$, double exchange magnetism, Mossbauer study 80−66087
$Zn_{1-x}Ge_xFe_2O_4$, spinel series, obs. by Mossbauer spectroscopy of electron hoppings 78−43754
ZnMn ferrites, prepared by wet chemical and ceramic methods, comparison of struct. and mag. props. *(German)* 79−24470
$ZnMn_{1-x}Cr_xFeO_4$, Mossbauer effect, quadrupole splitting 80−29664
$Zn_{0.8}Mn_{0.2}Fe_2O_4$, spin interaction, neutron diffr. and Mossbauer effect meas. 77−4501
$Zn_xMn_{1-x}Fe_2O_4$, Mossbauer spectra exam. 77−40155
$Zn_{0.3}^{2+}Mn_{0.7}^{2+}Mn_y^{3+}Fe_{2-y}^{3+}O_4$, Mossbauer hyperfine field meas. 77−81033
$Zn_{0.7}Ni_{0.3}Fe_2O_4$ film, epitaxial deposition, comp. and mag. prop. obs. using Mossbauer effect 79−38748
$Zn_xNi_{1-x}Fe_2O_4$, magnetic props. rel. to localised canting model 77−32161
$Zn_xNi_{1-x}Fe_2O_4$, Mossbauer spectra, mag. hyperfine struct. 80−15877
ZnO absorbers, ^{67}Zn isomer shift 80−39920
^{67}ZnO absorber, Mossbauer effect of ^{67}Zn 77−55737
ZnO(S)(Se)(Te), 93.3 keV Mossbauer transition in ^{67}Zn, isomer shifts 80−39978
ZnS, ^{57}Co gamma source, time depend. Mossbauer spectra 80−50245

Mossbauer effect continued
ZnS, time differentiated Mossbauer spectra from ^{57}Co impurities, relaxation processes *(Russian)* 80−34834
ZnS:^{57}Co Mossbauer sources, Fe^{1+} transient charge state 80−108128
ZnS:Co Mossbauer source, Fe^{2+} abnormal populations and vibronic props. 80−15912
ZnS:Fe^{2+}, low temp. Mossbauer spectra, in source and absorber expts. 77−28500
$ZnSnP_2$-$ZnSiP_2$, heterocombination simultaneous crystallisation 78−60560
ZnTe, diamond-like semicond., Mossbauer isomer shift meas. 77−16233
$(ZnTe)_x$-$(ZnSe)_{1-x}$, diamond-type semiconductor, Mossbauer spectra, quadrupole interaction of ^{125}Te 80−44992
ZnTi ferrites, electron exchange between Fe^{2+} and Fe^{3+}, paramag., Mossbauer spectra and susceptibility meas. 77−63327
^{67}Zn spectrometer, double freq. interferometer for absolute velocity calibration of piezoelectric transducer 80−37146
Zr-Fe alloy, Mossbauer spectra parameters of Zr_2Fe particles *(Russian)* 80−29654
Zr-Fe-Cu-W alloy, Mossbauer spectra parameters of Zr_2Fe particles *(Russian)* 80−29654
Zr-H, deposited on carriers, synthesis, structure and catalytic props. 80−29890
Zr-Ir, dil., elec. field gradient at ^{193}Ir, Mossbauer meas. 80−66090
Zr-Nb (20 wt.%), ω-phase form., diffuse Mossbauer scatt. 80−25324
$ZrFe_2$, lattice dynamics, Mossbauer spectra 80−19888
$Zr(Fe_{1-x}A_x)_2$, A=Al or Ni, Laves phase, mag. props. and Mossbauer effect 77−85632
$Zr(Fe_{1-x}Al_x)_x$, transition region, spin glass or long range mag. order 80−44841
$Zr(Fe_{1-x}Co_x)_2$, mag. props. and Mossbauer effects 79−91322
$Zr(Fe_{1-x}Co_x)_2$, mictomagnetism 80−15863
$Zr(Fe_{1-x}Co_x)_y$, transition region, spin glass or long range mag. order 80−44841
ZrH_x:Er, (x=1.5 and 1.85), Mossbauer spectra 80−20527
$(Zr_{1-x}Nb_x)Fe_2$, antiferromag. spin struct., Mossbauer effect study 80−66086
$ZrZn_2$:^{57}Fe mag. props. from Mossbauer effect obs. *(Japanese)* 80−15933

Mossbauer spectra *see Mossbauer effect*
motion picture photography *see cinematography*
motor protection *see machine protection*
motorcoaches
acoustic noise propagation models, railway track 80−48500
noise generation, static and moving tests 80−48498
motors, electric *see electric motors*
motors, hydraulic *see hydraulic motors*
Mott insulator *see localised electron states*
movements, atmospheric *see atmospheric movements*
moving-coil instruments
analogue panel meter, advantages 77−37866
balance indicators *(Polish)* 77−10064
chopping pyrometer for remote meas. below 200°C *(German)* 80−86313
cryogenics, linear variable differential transformer displacement transducer optimisation 80−86323
current and EMF meas. system, vel. control technique 80−98939
galvanometer type, scale charact. alteration method *(Bulgarian)* 77−61081
interchangeable-scale switchboard meters *(German)* 77−82497
light scanners, compensated moving-coil mirror galvanometer 77−58479
linear variable differential transformer for displacement meas. at liquid helium temps. in strong magnetic fields 78−54415
Linicator, heavy duty, physical parameter measured represented by DC current or voltage 77−37868
loudspeaker moving coil temp. meas. systems *(Hungarian)* 80−106698
low inertia scanner performance and selection 79−41429
microelectrode puller, biological appls. 80−30964
microelectrode puller for biological appls. 80−67309
plasma indicator, construction, charact. *(German)* 78−8393
suspensions, compound, for improving sensitivity 79−35707
moving coil microphones *see microphones*
moving-iron instruments
circular-scale 240° moving-iron AC ammeters and voltmeters 77−57360
interchangeable-scale switchboard meters *(German)* 77−82497
low inertia scanner performance and selection 79−41429
moving-magnet instruments
portable instrument for determ. of axes of easy magnetis. of ferromag. single cryst. balls 78−8424
MS SCF calculations *see Xalpha calculations*
MS Xalpha calculations *see Xalpha calculations*
μ-mesons *see muons*
mud *see sediments*
muffin-tin potential
A15 compound trends, self consistent band calcs. 78−79925
A15 compounds, band theory, semiself-consistent band calcs. 78−2406
A15 compounds, linear muffin tin orbital band results by press. calc. 79−65356
A15 compounds, self-consistent LMTO band calcs. 79−37954
A15 structure compounds, electronic struct., electron-phonon interac. and X-ray spectra 78−91613
actinide compounds, band structure and bonding calcs. 80−10871
actinide dioxides, electronic struct. and ionicity 80−10872
actinides, band structure and bonding calcs. 80−10871
actinides, self-consistent relativistic muffin-tin calc., atomic vol. and bulk modulus Ac-Am 78−72065
adsorption of atoms on metals, Green's function formalism for studying electronic struct., local density of states calc. 80−107884
alloy, disordered muffin tin type, coherent pot. approx. appl. 79−15062
alloys, binary disordered, electronic density of states, optical theorem and multiple scatt. theory 79−4500
alloys, disordered, charge density function calculation method 79−42433
alloys, disordered, muffin-tin model, electronic struct. and density of states, theory 80−29301
atomic cluster on metallic surface, density functional calculations 80−44699
atomic cluster total energy, diatomics-in-mol., LMTO calc. pot. curve, Lanczos eigenvalue method 78−9291
muffin-tin potential continued
atomic clusters, muffin-tin potential and SW Xα SCF calcs. for core levels *(German)* 78−82874
atomic clusters, total energy, and muffin-tin orbitals 77−47708
atomic sphere approximation, one electron energy states 77−72811
cluster calculations, scattering theory 78−18940
convergence properties of MS method 78−26803
crystal slab, 3-D, surface states, relativistic Green matrix method, muffin-tin potential 80−80345
crystalline thin films, APW band struct. calc., appl. to Cu monolayers 78−87899
cyclobutane, MS-Xα-MT study 80−52906
decay state interactions, autoionisation bands *(Russian)* 80−75486
diatomic homonuclear molecule, of 1st row, canonical exchange energy modulation parameters, MTXα calc. 79−97997
disordered alloys, electronic density of states in muffin tin model 80−88467
electron-phonon interaction, expt. test of rigid muffin tin approximation 79−65364
films, linearized APW method for electronic band struct., appl. to Fe, Co, Ni, Cu and Al 79−69393
Hamiltonian, density of states 77−28090
HEED, cross-grating, atomic string approx., dispersion surface and Bloch waves 80−49056
inelastic tunnelling cross sections, calc. using self-consistent multiple scatt. 78−90260
inert gas atom photoelectron ang. distribs., theoretical calcs. comparison 79−59412
interband transition probabilities calc. based on muffin tin potential 80−104014
LEED, multiple scatt. of electrons by infinite lattice plane planar scatt. matrix props. 77−76265
liquid metal, electronic structure in muffin-tin model 77−69219
liquid metal, integrated density of states, expression in Roth's effective-medium approx., generalisation of Friedel formula 79−99467
Lloyd formula and muffin-tin CPA local density of states 80−70577
local density of states for an arbitrary array of muffin-tin potentials 80−92805
metal, Fermi surface, effect of nonlocal potential, phase shift parametrisation scheme 78−43289
metal, lattice stability, comparison of BCC and FCC struct. in tight-binding calc. 77−51632
metal, lattice stability, perturbation formalism for comparison of crysts. with different lattices 77−51631
metal, monovalent, impurity potential 79−78039
metal, physisorbed inert atoms, polarisation due to short range interaction with substrate 80−39428
metal, simple, non muffin-tin corrections to eqn. of state *(French)* 80−59906
metal cluster, H site, SCF-Xα-MS calc. 78−47730
metal film, lattice sum, for use in self-consistent warped muffin tin pots 77−15741
metals, amorphous and liq., s-phase-shift model 80−88473
metals, electric properties calc., book 79−28274
metals, non-simple liq., electronic props. 77−47721
metals and alloys, APS, multiple scatt. approach using muffin-tin pot. 80−25490
methane, electronic density, multiple scatt. method, muffin-tin approx. 80−27924
molecular and solid state calcs. 77−409
momentum matrix element calc. using Green's function method 77−1351
multiple scattering eqn. for band theory, for muffin tin potential as special case 79−95309
multiple scattering in condensed media, calc. of density of states for non-crystn. Cu and Fe 78−91578
multiple scattering in condensed media, embedding field and effective medium 78−51867
noble metal alloys, disordered, bulk electronic structure 80−44467
noble metals, liq., muffin-tin pot. model, electronic density of states determ. 77−51645
noble metals, surface electronic structure, calc. method 77−89828
nonsimple metals, calc. of elec. resist. and thermoelec. power 78−19019
oriented orbitals, photoemission cross-sections, surface Green function formalism 80−93453
overlapping muffin tin multiple scattering wave X_α method 79−13638
phaseshift parametrization, position of lowest bound, virtual and reson. states 77−55473
polyacetylene:$ASF_5(AsF_6)(SbF_6)(PF_6)$, metallic, band theory 80−49570
polyacetylene, electronic energy states and charge density contours studied muffin tin orbitals technique 80−80164
polyethylene, electronic energy states and charge density contours studied muffin tin orbitals technique 80−80164
PTFE, electronic energy states and charge density contours studied muffin tin orbitals technique 80−80164
rare earths, liquid, resist. and thermoelec. power, t-matrix calc. 78−26840
relativistic electron-phonon interaction, oscillating rigid muffin-tins 78−47713
relativistic Hartree-Fock-Slater eqns. 77−10607
residual resistivity for electrons scatt. by spin-depend. potentials 77−39829
semi-infinite crystal with surface impurity, electronic states 79−24046
solids, chemical bonding studied using scattering theory concepts 80−103289
superconducting linear accelerator, comparison of short muffin tin structs. *(French)* 78−33330
superconductor, Gaspari-Gyorffy theory, non-local extension 78−80093
surface and film, generalised muffin-tin orbital method 78−95331
surface electronic wave functions in semi-infinite, muffin-tin lattice, spherical-wave method 79−42603
symmetry projection technique, for linear combination of muffin-tin orbitals method 78−2407
thin crystals, surface state calc. 78−14778
transition metal, model potential, generalised APW formulation 78−91579
transition metal, one-electron theory, atomic sphere approx. to KKR and LMTO methods 78−91584
transition metal alloys, disordered, bulk electronic structure 80−44467
transition metal alloys, disordered, elec. resist., force-force correlation function approach 79−51541

muffin-tin potential continued
transition metal carbide, d-band effects in lattice dynamics contrib. to acoustic phonon freqs. 78−2207
transition metal film, energy band calc. by linear combination of muffin tin orbitals method 77−4283
transition metal hydrides, electron-phonon interaction const. calc. 79−65160
transition metal hydrides, electronic states calc. 79−7769
transition metals, 4d, energy band and related props., theory 77−62811
transition metals, band struct., parametrisation via Hubbard's scheme 77−31938
transition metals, electron-phonon coupling, electronic aspects 77−69255
transition metals, interatomic forces, phonon spectra, from band structure charge densities 79−7662
transition metals, liq., electronic struct. and transport props. 80−29314
transition metals, liq., muffin-tin pot. model, electronic density of states determ. 77−51645
transition metals, second series, electronic band Brillouin zone APW calc., electronic config. effects 78−51883
transition metals, surface electronic structure, calc. method 77−89828
transition metals, universal LCAO parameters 80−75503
transition metals and their alloys, amorphous, elec. resist. 78−60103
uranium monopnictides, NaCl struct., band struct. 80−6714
XPS core line asymmetries in muffin tin approximation 79−69953
ZnS:V^{2+}, impurity states by Green's function method 80−92855
A15 compounds, electronic struct., XPS and SXE spectra calc. 79−42437
AgI, FCC and γ phase, electronic struct., relativistic KKR calc. 77−85140
Al (001), surface states between muffin-tin zero and vac. level 79−60894
Al dilute alloys, 3d transition metal impurities, residual resist., influence of multiple scatt. effects 79−19570
Al, energy bands, densities of states and X-ray spectra, superposed self-consistent pots. 78−39010
Al-3d transition metal, dil., localisation of additional screening charge 79−47051
Al-3d transition metal alloy, dil., electronic charge density around impurities 78−34799
Al_2Cu, de Haas-van Alphen effect and LMTO band struct. 79−69396
Ar:H crystalline matrix, Xα scattered wave cluster model 79−73468
β'-Au-Mg, de Haas-van Alphen effect, relativistic LMTO bandstructure, Fermi surface 79−37959
$AuCu_3$, ordered, band struct. and optical props. at 30K 79−60696
BaF_2, F-centres, muffin-tin approx. inadequacy 78−63761
Be, eqn. of state, solid-state models, comparison 80−75332
Be, spin susceptibility, electronic effective mass, spin density functional calcs. 78−43291
Ca, FCC, ground-state props. 78−75989
CaB_6, electronic struct. APW and muffin-tin calcs. 80−29320
CaF_2, F-centres, muffin-tin approx. inadequacy 78−63761
Ce, density functional theory 80−15442
Ce, p core states calc., linear muffin-tin orbitals method 78−91607
Cs, Fermi-surface press. dependence 80−96772
Cs, isostructural transition and lattice vibrs., relativistic LMTO calc. 80−20074
Cu (001) and (110) electronic wave functions by spherical wave method 79−42604
Cu (100) and (111), angle-resolved photoemission and band struct. 79−95904
Cu atom in bulk, local density of states 79−37947
Cu based 3d-transition metal dil. alloys, residual resist., Dingle temp. 77−1409
Cu, Fermi surface orbit integrals, tetrahedron method, Dingle temps. for 3d transition metal impurities 80−44477
Cu, liq., electronic spectrum 77−51646
Cu, partial densities of states, electron-phonon interaction 78−51869
Cu-3d transition metal alloy, dil., electronic charge density around impurities 78−34799
Cu-Ni, alloys, electronic states, KKR-CPA calc. 78−84125
Cu-Ni, disordered muffin tin type, coherent pot. approx. appl. 79−15062
Cu-Ni, soft X-ray emission and local densities of states 79−83059
$Cu_{1-x}Ni$, disordered muffin-tin, electron momentum density in average-t-matrix approx. 79−69390
Cu_2Ni_{1-c}, solutions of KKR-CPA equations for paramagnetic alloys 78−95256
Cu_xNi_{1-x}, bulk electronic structure, comparison of CPA and ATA techniques 80−44467
Cu_xNi_{1-x}, disordered alloy, muffin-tin model, electronic struct. and density of states calc. 80−29302
Cu_xNi_{1-x}, paramag., electronic struct., atomic sphere approx. to KKR-CPA 79−19502
Cu_2Sb, linear muffin-tin calc. for Fermi surface 77−62802
Cu_xZn_{1-x}, disordered alloy, muffin-tin model, electronic struct. and density of states calc. 80−29302
$EuMo_6S_8$, Chevrel phase, RE mag. isolation and supercond. 80−44470
$EuMo_6S_8$, Chevrel phase, mag. interactions, LMTO energy band studies 80−70606
EuO, band struct., linear combination of muffin-tin orbitals calcs. 78−2407
Fe, ferromagnetic, hyperfine fields; SCF calcs. 77−8061
Fe, partial densities of states, electron-phonon interaction 78−51869
FeAl B2 struct., band struct. and density of states, KKR calc. 78−63969
GaAs, electronic density, multiple scatt. method, muffin-tin approx. 80−27924
GaAs, LMTO self consistent band struct. calc. 80−20078
Gd, self consistent relativistic ferromag. band struct. 78−91609
$GdMo_6S_8$, Chevrel phase, RE mag. isolation and supercond. 80−44470
Ge-GaAs superlattice and interface, electronic struct. 78−52065
H_2, ground state, pot. curves, MTXα_R method 80−5482
Hg, expanded liq., electronic props. 77−55477
Hg, expanded liquid, electron density of states calc. using effective medium approx. 79−99468
La, density functional theory 80−15442
La, FCC, ground-state props. 78−75989
La, p core states calc., linear muffin-tin orbitals method 78−91607
LaAg, band calcs., rel. to mag. and electronic props. and martensitic transform. 77−8014
Li, cryst. wave function deter., muffin-tin method 80−65436
Li, lattice stability, comparison of BCC and FCC struct. in tight-binding calc. 77−51632

muffin-tin potential continued
LiH, ground state, pot. curves, MTXα_R method 80−5482
Mg, spin susceptibility, electronic effective mass, spin density functional calcs. 78−43291
β'-MgHg, energy bands and Fermi surface calc. 77−43481
β'-MgTl, energy bands and Fermi surface calc. 77−43481
γ-Mn, antiferromagnetic, self-consistent bandstructure calcs. 80−88475
Mo, (100) and (110) surface density of states 78−52047
Mo, Fermi surface ang. shear deform., rigid muffin tin pot. calcs. 79−77985
Mo ternary chalcogenides, supercond., band struct., muffin-tin orbitals and atomic-sphere approx. 78−51871
Mo_cNb_{1-c}, is the rigid-band model valid? 78−95258
N_2, electronic density, multiple scatt. method, muffin-tin approx. 80−27924
NaH, ground state, pot. curves, MTXα_R method 80−5482
Nb, electron-phonon contrib. to phonon linewidth determ. 78−10146
Nb, electron-phonon interaction, relativistic, APW calc. 80−92837
Nb, electron-phonon spectral function and mass enhancement 78−26988
Nb_3Si, hypothetical, electronic struct., lattice parameters and possible supercond. transition temp. 79−23891
Ni, chemisorption of H, embedded cluster model 80−39427
Ni, liquid, electronic struct. and transport props. 80−29314
Ni-Cr, residual resist., CPA calc. to muffin tin pot. 77−62892
Ni-Cu(Zn)(Ga)(Ge)(As)(Se)(Br)(Kr), dil., ferromagnetic, hyperfine field and relax. time obs. of impurity heavy nuclei 80−75533
Ni-Fe, residual resist., CPA calc. to muffin tin pot. 77−62892
Ni-P, amorphous metallic glass, elec. resistivity 78−91654
Ni-P alloys, amorphous, electrical transport, appl. of extended Ziman theory 77−47787
NiO (100) surface, dynamical LEED calc. 77−62721
$Ni_{13}(O_h)$ cluster, electronic states and X-ray spectra in Xα approx. of multiple scatt. theory 77−28645
Ni(001), reaction of CO and H_2, extended muffin-tin orbital theory 80−76557
Os, correlation effect of crystal pot., RAPW calcs. 78−6265
Pb, Fermi surface and non-muffin-tin energy bands, calc. 80−20072
Pb, supercond. transition temp., theoretical calc. 79−73614
PbS, relativistic electronic mol. struct., calcs. 79−761
PbSe, relativistic electronic mol. struct., calcs. 79−761
Pd, chemisorption of H, embedded cluster model 80−39427
Pd, electron-phonon interaction, expt. test of rigid muffin tin approximation 79−65364
Pd, electron-phonon parameters and supercond. p-state pairing 80−25041
Pd, liq., energy bands and electronic density of states, resistivity 78−34755
Pd, liquid, electrical resist. calc. using muffin-tin pots. 77−69287
Pd, phonon linewidths and electronic mass enhancement, electron-phonon contrib. 79−95099
α-PdH_x, electronic states and Fermi surface props. 80−29310
$PdTe_2$, bandstructure, Fermi surface, LMTO method 78−6264
Pt, chemisorption of H, embedded cluster model 80−39427
Pt_3Sn, electronic struct., calc. using linear-muffin-tin-orbitals method 77−24516
PtTe, electronic struct., self-consistent and non-self-consistent band calcs. 80−44499
Rb, Fermi-surface press. dependence 80−96772
Sc, spin susceptibility, exchange correlation enhancement 77−85167
ScCl, electronic struct., self-consistent and non-self-consistent band calcs. 80−44499
ScH_2, self-consistent bond struct., charge transfer 80−49590
ScH_2, self-consistent energy bands, KKR method with Hedin-Lundqvist approx. 80−49593
ScM, (M=Ru,Rh,Pd,Ag), electronic struct., self-consistent local density functional calcs., LMTO method 79−11059
Si, semi-empirical APW calc. of band structure 80−84424
$SnMo_6S_8$, Chevrel phase, RE mag. isolation and supercond. 80−44470
$SnMo_6S_8$, Chevrel phase, mag. interactions, LMTO energy band studies 80−70606
$SnMo_6Se_8$, Chevrel phase, RE mag. isolation and supercond. 80−44470
SrF_2, F-centres, muffin-tin approx. inadequacy 78−63761
Ta, electron-phonon interaction, relativistic, APW calc. 80−92837
TaN, energy band struct. calc., symmetrised APW method 80−96784
TaN_x metastable FCC, band struct. calc. 79−33231
Tc, Fermi surface, constant-energy-search KKR band theory calc. 77−89689
Th, correlation effect of crystal pot., RAPW calcs. 78−6265
Th, density functional theory 80−15442
Th, electronic states under press. 80−54600
Th, FCC, ground-state props. 78−75989
Th, p core states, linear muffin-tin orbitals method 78−91607
Th, superconducting transition temperature calculation 79−7928
Ti, molten, reson. model calc. of elec. resist. 78−84189
Ti, partial densities of states, electron-phonon interaction 78−51869
TiC, TiC_6^{20-} cluster electron state, MS Xα calculations 77−8037
Tl, band struct. by LMTO method 77−39773
U compounds, NaCl struct. type, relativistic energy bands, LMTO calcs. 80−65442
UO_2^{2+}, relativistic X_α scatt. wave calcs. 78−46268
US, NaCl struct., band struct. 80−6714
V, partial densities of states, electron-phonon interaction 78−51869
V_3Ga, self-consistent APW band struct. calc. 78−47697
V_3In, hypothetical, electronic struct., lattice parameters and possible supercond. transition temp. 79−23891
W, Fermi velocity calc., linear muffin-tin orbital method 79−28272
W, Fermi velocity calc. 79−4504
W, semi-infinite cryst., secondary electron emission, obs. of electronic struct. 79−33871
W, single cryst., coated with ferromagnetic layer, Fermi vel. using band calcs. 79−11307
YH_2, self-consistent energy bands, KKR method with Hedin-Lundqvist approx. 80−49593
ZrBr(Cl), electronic struct., self-consistent and non-self-consistent band calcs. 80−44499

multichannel analysers *see pulse height analysers*
multidimensional digital filters
see also two-dimensional digital filters
nuclear medicine imagery data smoothing 79−25070
phased array US imaging, real-time digital scan conversion and multi-dimensional processing 79−48363
multidimensional systems
2-D polynomial matrices, factorisation and coprimeness 77−64915
ϕ^4 interaction, four-dimensional Green's function model *(Russian)* 78−77725
BWR shutdown margin prediction, multidimensional linear regression model 79−9778
complex multidimensional ball, equivalent projective unitary group of analytic transformations *(Japanese)* 78−12534
complex scan generation by single rotating component 77−58482
diffusion in nonuniform multicomponent system with multidimensional regions *(Russian)* 79−12743
dimer problem, upper bound improvement 78−78607
electromagnet pole-piece design, air gap field computation 79−41295
estuary thermal impact of multiple power plant operations 78−96232
Euler-Lagrange differential in fibred manifolds 78−45469
gas chromatography, advantages of pressure balancing 79−70408
gas chromatography, pressure balancing techniques 80−89576
instability of evolving systems, elastic stability theory and catastrophe theory approaches 78−44442
matrix Riccati eqn., quasi-linearisation, iterative approx. 78−57871
nonlinear wave eqns. in n-dimensional space, periodic solns. 78−93540
nuclear reactor noise analysis, irreversible circulation parameter 78−94069
oscillations of mechanical systems that do not become linear when the parameter vanishes 80−68032
Russian speech automatic recognition, deductive strategy 80−91997
scanning optical sensor signal peak extraction and multiframe correlation methods 79−81380
Schlesinger systems, isomonodromy deformation, integrable Hamiltonian systems 80−22229
stationary random fields, statistical inference 77−64930
multigroup diffusion *see neutron diffusion*
multimeters
AC measurement, using digital instruments 78−93726
analogue and digital, general survey *(German)* 79−44917
automatic, for DC and AC signals *(German)* 77−10044
automatic digital multimeter, PM 2517 80−22347
capacitance meter, using DVM and diode pump cct. 80−62656
combined instruments provide several test functions DMM, oscilloscopes, frequency counters, signal generators 77−34000
combined multimeter/oscilloscope, type D4000, features *(German)* 78−16783
DC current measurement, in-circuit for PCBs 77−18009
digital, accuracy specifications, sources of error 77−116
digital, automatic range selection, HV meas., general discussion 77−41639
digital, Avo DA117, overview of field servicing appls. 80−68210
digital, control functions performed using 4 bit, microprocessor chip *(Slovenian)* 79−181
digital, cost effective design using LSI 77−45858
digital, D 3012 high accuracy multimeter *(German)* 80−22343
digital, design based on Intersil ICL IC series 80−206
digital, design principles, currently available models listed *(German)* 77−34007
digital, Fluke 8500 A microprocessor-based instrum., characts. *(French)* 77−53954
digital, Gould Alpha III, features *(French)* 78−77943
digital, Keithley 172, $4^1/_2$ place display, charge balancing method, remote digital control *(German)* 77−65045
digital, LCD based on Intersil ICL ICs *(German)* 79−6138
digital, LD 130 IC 78−16817
digital, matching true RMS or average-sensing RMS meters to applications 80−47072
digital, Matsushita VP-2500 A 80−212
digital, microprocessor controlled 78−93721
digital, MOS/LSI, mains/battery operated, construction and performance *(French)* 77−61090
digital, resolution and sensing accuracy 77−74428
digital, review of DVMs, DMMs and counter-timers 77−37913
digital, selection criteria 77−45859
digital, technology and future development 77−57345
digital, type Shch68003, with printer output, features 77−74437
digital, using advanced LSI technique, Philips (PM 2517) 79−80640
digital, Weston model 6000, review 77−37908
digital, with LED or LCD display *(French)* 78−57986
digital hand-held instrument with liquid-crystal displays, includes A/D convertor chip 77−74423
digital multimeter conductance function introduction 79−93167
digital multimeter innovation *(French)* 77−10045
digital readout format, new arrangement reduces observational error 77−5822
electronic, using FET and operational amplifier *(Spanish)* 77−37937
enlarger exposure meter, using photodiode and multimeter 80−101857
F-30 digital avometer, MUF-30 control module in CAMAC standard 79−88942
general-purpose digital multimeter design practice 77−57348
high-performance multimeters and voltmeters with microprocessors *(French)* 79−67349
laboratory multimeter with microprocessor, precision *(French)* 79−6139
maintenance, renovation and repair procedures for multimeters including Avo model 8 79−35795
microprocessor controlled multimeter *(French)* 77−74433
nonsinusoidal waveform measurement using analogue multimeters 78−16809
Philips digital multimeter, PM 2517, test report *(German)* 79−49220
portable digital multimeter 79−71427
Quadriovameter MX 737A, 4-digit display *(German)* 78−57988
technology trends *(German)* 79−71437
test instrument survey *(German)* 78−8394
volt-ohm meter, 2.5 digit LED display 78−21162
voltage measurement peak reading RF probe 77−10063
multiperipheral models
absorptive multiperipheralism, geometrical struct. of inelastic diffr. 77−74664
multiperipheral models continued
Adler zero and dual peripheral model 78−78153
baryon+antibaryon annihilation model, high energy, multiperipheral interpretation of dual unitarity diagrams 77−18253
baryonium mass spectrum in planar bootstrap model 78−25020
bootstrap eqns., Pade approx. to dual multiperipheral model 77−30347
cluster model, f-dominance and final-state counting 77−18257
cluster model, multi-Regge, comparison with multiparticle transverse and longitudinal data 80−62952
cluster model based on Bethe-Salpeter eqn., comparison with pp and π^-p data *(Russian)* 77−10230
cluster model study of expt. distribs. of rapidity intervals in π^-p interactions at 60 GeV *(Russian)* 77−34189
clusters, search using rapidity gap method *(Russian)* 78−41517
cosmic ray showers, ang. distrib. and multiplicity 78−36412
cosmic-ray cluster prod. in 1 TeV interactions, comparison with multiperipheral mechanism 77−50036
cross section rise in high energy strong interactions, multipomeron exchange, Mandelstam diagrams 78−41516
cylinder term structure in the topological expansion 79−13093
dual multiperipheral model, Pomeron and Reggeon slopes 78−62379
dual multiperipheral model planar bootstrap 78−4837
dual resonance Pomeron, intermediate mass distribution 78−25026
dual unitarisation, calc. of interference terms in multiperipheral resonance prod. model 77−41829
dual unitarity twist parameter J-depend. 77−26500
eikonal model, particle prod. on heavy nuclei and hadrons 77−71495
elastic scatt. amplitude phase connection with overlapping function *(Russian)* 78−41431
exchange degeneracy breaking, charge conjugation, in s-channel, unitarity, quark diagrams 77−22713
factorization test relations and universality in inclusive and 2-body exclusive interactions 77−79258
Feynman-gas model for semi-inclusive processes, πp appl., multiperipheral model predictions *(Russian)* 78−435
fireball emission, slope of overlap function 77−67637
gluon bremsstrahlung and multiperipheral cluster models 79−22082
hadron+hadron, cluster model, field theoretic, multiperipheral production, Feynman scaling violation 80−57576
hadron-nucleus, rapidity distrib., 22.8, 50, 400 and ≳1000 GeV in emulsion, multiperipheral models 80−91117
hadronic collisions, wave packets and the space-time structure of production processes 79−36048
helicity structure of Pomeron-nucleon-nucleon vertex using multiperipheral model 77−57511
impact parameter amplitudes, overlap slope and multilink interactions 77−38150
inclusive high energy particle-nucleus interactions, A depend. of multiplicity, cross section, rapidity, momenta distrib. 77−79291
inclusive quantity constraints in multiperipheral model 77−30346
intermediate mass distribution of dual resonance pomeron, rel. to multiperipheral processes 78−50020
internuclear cascades and multiple prod. of nuclei *(Russian)* 77−6330
jet analysis, QCD calcs. and phenomenological models 80−52523
KNO scaling and multicomponent cluster models 77−49918
KNO scaling and scaling in the mean for semi-inclusive processes *(Chinese)* 80−22538
many-hadron production at low $P_\perp$, basic concepts and models, review 79−6331
multi-chain model for high energy hadron nucleus collisions 79−59042
multi-Regge model with threshold factor for cluster prod., multiplicity distribs. in pp collisions, 50-400 GeV/c 77−18256
multi-Regge self-consistent model, overlap function and Regge cut 77−49932
multiparticle prod. in hadron-hadron collisions, scaling and multiperipheral model, review *(Russian)* 77−2875
multiparticle production in multiperipheral resonance model complemented by duality 79−36050
multiparticle reactions on deuterons, multiperipheral parton model anal. to rescatt. 79−22154
multiplicative processes, ρ^0 meson formation cross section, pion prod., multiperipheral cluster model *(Russian)* 78−17067
nonlinear reggeon multiple exchanges 77−71496
particle correlations in multiperipheral resonance prod. model, broken SU_3 theory 78−45891
parton model, deep inelastic processes 80−82961
Poincare subgroups, role in high energy physics models, appl. in multiperipheral models 79−97530
Pomeranchuk trajectory in multiperipheral cluster emission model 77−54089
pomeron current model for diffraction dissociation 78−4843
rapidity distribs. of secondary particles prod. at cosmic ray energies 77−22821
rapidity in distrib. in inclusive reacts. *(Russian)* 78−41518
Reggeon calculus, physical basis and implications 77−6101
rising π inclusive cross section as series of threshold effects 78−93918
s-channel helicity conservation multiparticle amplitudes 78−33004
spectral properties of positive operators and j-plane singularities of multiperipheral dynamics 77−79259
superconductive fireball at large p_T, mass, temp. and multiplicity 77−49922
t-channel diffractive scatt., elastic peak and hadron size 79−45083
topological cross-sections for n-particle prod. in NN, $\bar{N}\bar{N}$, $\pi^\pm$N, $K^\pm$N *(Russian)* 77−34141
two-channel, multiplicity distribs. in high energy pp collisions 77−6100
unitarised multiperipheral model and Regge cut exchange 77−57510
unitarity condition and Reggeon theory *(Russian)* 77−30348
vacuum singularities in dual multiperipheral model 77−34140
Zweig rule model for couplings, quark conservation at meson vertices, multiRegge phenomenology 77−82709
e^+e^- annihilation, multiperipheral fireball model, momentum distribs. 77−67665
e^+e^- inclusive annihilation, scaling function in multiperipheral fireball model 77−87985
γρ-Pomeron-Regge vertex function, spin depend. calc., multiperipheral model 78−82223
$K^-p \rightarrow \Lambda X$ or Λ(Pions) or $\Lambda p_{slow} X$, multiperipheral model with heavy clusters *(Russian)* 78−485
$K^-p \rightarrow \Sigma^-\pi^+\pi^-\pi^+$, 4.15 GeV/c, nondiffractive A_1 production, double-Regge model 80−78097
$n \rightarrow p\pi^-\pi^0$, diffractive dissociation induced by 12 GeV K^- 79−40805

multiperipheral models continued
N-N low multiplicity events, scaling and multiperipheral testing at cosmic ray energies 77−18342
NN, 10^{12} eV, rapidity gap distrib., Snider multiperipheral cluster model 80−73757
(P,X), 400 GeV, correlation strength, dependence on target size, multiplicity and cluster size 80−78287
pN, 400 GeV, rapidity gap correlations, Chew-Pignotti multiperipheral model 79−93471
pN, 67 GeV, multiperipheral cluster production 80−73689
pp, 69 GeV/c, two particle correlation functions, multiperipheral cluster model *(Russian)* 79−30762
pp, unitary impact-parameter model for multicluster prod. 78−33091
$\bar{p}p$ annihilation, 0 to 100 GeV/c, statistical and multiperipheral models, π^0 prod. 79−63507
pp inelastic, 28.5 GeV.c^{-1}, particle generation mechanisms, multiperipheral cluster model anal. *(Russian)* 79−9424
pp interactions, many particle correlations, multiperipheral cluster model interpretation *(Russian)* 78−74285
pp→p+X, multiplicity dependence on transverse momentum and missing mass, multiperipheral diagram anal. 79−365
pp→pp+N clusters, multiperipheral process, interference terms in transition, amplitudes, correlation expansions 80−62953
ϕ meson prod. in π^-p→ϕn, OZI rule violation in central region 77−61262
π^-p, 15 and 147 GeV/c, impact parameter anal. of multiparticle prod. 79−30758
π^-p, 40 GeV/c, dispersion of longit. rapidity distribs., multiperipheral cluster model anal. *(Russian)* 78−17063
π^-p→$\pi^-(\pi^0)$X, 40 GeV, three reggeon approach, multiperipheral model evidence *(Russian)* 79−30761

multiphase flow
see also two-phase flow
aerosol particles thermal collection on larger liq. droplets 77−3867
annuli, (non)-uniformly heated, pressure drop during boiling, expt. results 79−81971
annulus, incompressible immiscible fluids, velocity profile 77−62298
boiling, bubble growth at superheated horizontal wall, pure liq. and binary mixtures 79−41719
Brownian motion in shear flow 78−5786
bubble, rising, hydrodynamic interaction with suspended solid particle 78−51221
bubbles in liquid, effect of vibr. in weak gravitational force field *(Russian)* 79−77226
cavitation and polyphase flow, conf., New Orleans, LA, USA, March 1980 80−105430
composite mixture, flow through porous medium, Rayleigh-Taylor instability 80−69912
conference, cavitation and polyphase flow, Niagara Falls, New York, USA (Jun. 1979) 80−4475
curved wall, turbulent boundary layer detachment by perpendicular compressive thrust *(German)* 78−94661
density-wave oscillations, linear stability anal. 80−48775
detonation waves, heterogeneous, propagation and blast wave initiation 80−74915
differential transfer equations for multiphase, multicomponent media 80−14794
diffusion equations 78−94801
disperse system in EM field, hydrodynamics *(Russian)* 77−80222
disperse systems, coagulation, slow, turbulent 78−53259
disperse systems, flotation of fine particles by group of bubbles, kinetics 78−53261
dispersed and heterogeneous systems, mechanics, spatial averaging, cellular scheme 80−48788
dispersed flow, heat and mass transfer, phase transition effect 78−67252
dust entrainment in shock-induced turbulent air flow, dust entrainment 80−43763
Erdogan-Chatwin nonlinear diffusion eqn., asymptotic solns., pipe flow solute dispersion 79−32673
ferrofluid flow in circular pipe, uniform mag. field effects 80−43782
fission reactor multiphase systems, expt. and theoretical review of density-wave oscillations 80−18369
flames, multi-diffusion configurations 77−51134
fluid force on oscillating disc in a still fluid 80−14724
fluid interface problems, simple line interface calculation method 77−58777
fluid-structural interactions, one-dimensional networks, MULTIFLEX code 80−13535
fluidised, open channel flow 80−14826
fluidised bed, fluidisation uniformity, disturbance criterion with uniform coding medium flow distrib. 80−43772
fluidised bed, heat transfer from transverse streamlined cylinder during surface boiling 80−43708
fluidised bed, three-phase, bubble wake solids content 78−42660
fluidised beds, three-phase, heat transfer 79−60056
fluidised solids, open channel flow 80−14826
fog-containing vapour-gas mixture, mass transfer in vapour condensation 77−58772
gas and dust electrocond. flow in elec. and mag. fields *(Russian)* 77−39358
gas-liquid cocurrent flow through packed beds, radial effective thermal conductivity 78−1723
gas-liquid fluidised beds, axial and radial dispersion in dispersed plug flow model 80−10290
gas-liquid fluidised beds, axial liq. dispersion in plug flow model 80−10289
gas-liquid two-phase bubbles in immiscible liq. media, configs. 79−4068
gas-liquid-suspended solid flow, multistage bubble column, residence time 77−84304
gas-radiating particle mixture, shock wave struct. numerical investigation 80−10298
granular material, erosion by airflow, expt. and theory 77−942
granular particles, dynamic flow rates, meas. apparatus 80−14860
hydraulic coal trunk pipeline transport systems, methods of improving economic effectiveness 80−106837
hydraulic resistance of channels with separation or merging of incompressible flows 77−68669
immiscible fluids, continuum mixture theory and integral averaged eqns. 77−2544

multiphase flow continued
laminar, with heat conduction, numerical soln., implicit difference method *(German)* 77−15110
liquid coolant, porous evaporative cooling for subcritical, critical, supercritical coolant parameters 79−55372
liquid-liquid ternary mass transfer in ejectors with cocurrent flow 79−46368
magnetic separation, particle capture and axial filters, theory 78−92516
magnetic sparation, particle capture in axial filters, theory and performance 78−92515
microfluids, linear theory of chemically reacting mixtures 80−14777
model, taking gas compressibility into account 78−83460
moisture transfer, multiphase, in porous media with temp. gradient 80−19497
multicomponent flow through porous media from underground nuclear explosion, flow stability 80−53857
multidomain multiphase fluid mechanics 79−27681
multiphase mixture, two-dimens. nozzle and jet supersonic flows 80−48780
multispecies gas flows, transport eqns. mathematical struct. 78−47084
non-Newtonian systems, rheological props. variation in barotreatment 80−19304
nonsteady multiphase flow through porous media, struct. determ. 78−51237
optical fibre sensors, appls. *(German)* 78−26215
P nabla α term effects in multiphase mechanics 79−90314
packed beds with gas-liquid concurrent upflow mass transport phenomena and hydrodynamics 79−50784
particle flow, gravity-induced, stochastic theories 80−14798
particle separation property of impactor stage with nonstationary flow *(German)* 78−18335
particles in dilute suspension in general flow, mass flow and density meas. 80−101784
particulate matter dynamics in industrial manufacturing processes, appl. of radiotracer techniques 78−41398
perturbed flow, moisture form. kinetics 80−79387
petroleum-water-gas mixture, in inclined stratum, nonstationary filtration, including gravity 78−1729
pipeline flows, measurement of component ratios using γ-ray attenuation 80−38513
pipeline systems, problems in fluid mechanics for hydraulic transport of solid materials 80−106836
porous media, local vol. averaging and distrib. function 77−58780
power system equipment and components, multiphase flow prediction 80−64616
radial solid spread factors in gas-solid packed column at trickle flow, evaluation 79−46363
radiational flame propagation over gas suspension of solid combustible particles 80−53880
reactor blowdown anal., two-phase crit. flow models 77−6531
sedimentation in two-phase flows, kinematic waves *(German)* 77−72310
spheres, deformable contiguous, in incompressible inviscid fluid, hydrodynamics 78−1727
spherical bodies in liquid stream with phase state change, deformation and fragmentation *(Russian)* 79−90308
spherical particles, thermal conductivity determ. 78−71390
steel, liquid, Stokes coagulation model, particle motion according to Boltzmann eqn. *(German)* 80−40357
suspension, fibre, conc., rheology of tube flow, uniform fibre length distrib. 77−58628
suspension, fibre, conc., rheology of tube flow 77−58627
suspension concentrates, physical stability criteria, review 80−45562
suspension of water, air and oil, dynamic behaviour under periodic perturbations *(Russian)* 77−19631
thermoconductive waves, interaction with radiation induced waves *(German)* 78−94803
thermodiffusiophoretic motion, weak solution in binary gas mixture 79−64744
thixotropic-dilatant structures, rheological equations 79−64616
three-phase agitated system, simulation model 77−11241
three-phase fluidised beds, electrocond. technique for meas. of axial var. of holdups 78−67286
torque suppression in mech. stirred liqs. and multiphase systems, additives 77−3864
turbulent, various aspects *(German)* 77−15109
two-dimensional fluid motions induced by motile particles, convection field and geotactic components 77−55080
viscous compressible liquid, bubble behaviour analysis by finite method 77−55072
viscous incompressible liquid, disturbance by small particle stream *(German)* 78−94804
waves, plane, nonlinear viscous multicomponent media 78−51228

multiphonons *see phonons*

multiphoton spectra
see also two-photon spectra
absorption excitation, molecular dynamics 77−29019
acetaldehyde, lowest Rydberg state, multiphoton ionisation spectra 80−83435
acetaldehyde, multiphoton ionisation mass spectra 80−83436
alkaline earth atoms, high Rydberg states 77−68022
alkanes, polycyclic, three-photon ionisation spectra, 3s Rydberg orbital 79−68282
anharmonic molecule, high-order multiphoton excitation features 79−54927
anharmonic molecule, selective multiphoton absorpt. by vibr. mode theory 77−83669
anharmonic molecules, multiple photon absorption in CW laser beams 78−58755
anharmonic molecules, stochastic multiphoton absorpt. processes, classical model 79−45778
anharmonic Morse oscillator, multiphoton excitation, quantum vs. classical treatment 78−5306
atom, deep level X-ray absorption cross section modulation by optical field 77−14399
atom, Doppler-free multiphoton excitation, light shift and saturation 79−76399
atom, multiphoton transition amplitudes, exact summation of higher-order terms 77−18878
atom, multiphoton transitions to continuum, via multiple resons. 77−10650

multiphoton spectra continued
atom, r-photon reson., (r+p) photoionisation rate, theory 79−49998
atom, resonance light scattering, intensity effects 80−91511
atom, selection rules, EM transitions in strong coherent light field 77−447
atom, three-photon ionisation, reson. and non-reson., theory 79−36590
atom, X-ray photoelec. effect in presence of laser radiation 78−37615
atomic photoionisation, in intense radiation and magnetic fields, quasi-energy formalism 79−72284
atomic transition in stochastic field, saturation and Stark splitting 80−9546
atoms, AC Stark effect, multiphoton processes 77−71775
atoms, multiphoton ionisation, reson. cross-section, very-narrow-bandwidth source 78−55150
atoms, multiphoton ionisation, reson. effects, light coherence effects 80−58232
atoms, multiphoton ionisation probability, laser pulse 78−86835
atoms, multiphoton ionisation processes, resonance and laser coherence effects 80−74208
atoms, multiphoton transitions, choice of gauge 79−31488
benzene, multiphoton ionisation mass spectra 80−57420
biacetyl, multiphoton excitation of triplet state, fluoresc. decay 79−31632
biexcitons, nonlinear laser spectrosc., multiphoton transitions 80−84433
biexcitons recombination, polariton effects 78−23033
bound-bound transition rates in hydrogenic atoms 77−23483
trans-butadiene, multiphoton transitions, multiphoton ionisation, thermal lensing spectroscopy 78−33559
capillary waves, active four-photon spectroscopy 79−41699
carbon tetrachloride, intense ps pulse excitation, multiple stimulated Raman spectra 78−66867
chloroform, liq., reson. nonlinear susceptibilities using IR optical parametric oscillator 79−10347
chloropentafluoroethane, isotopically selective multiphoton dissoc., CO_2-laser wavelength, pressure and additives effects 80−78666
coherent four photon Rayleigh scattering *(Russian)* 78−48191
coherent multiphoton intense interactions, convergent perturbation anal. 80−1037
collisionless molecular multiphoton processes, rate eqns. 79−98173
coumarin 1, multiphoton cross-section determination by means of luminescence experiments 80−93377
cyanogen fluoride, fund., hot bands, laser microwave two photon and double reson. spectroscopy 80−32752
cyclopropane-d_0, -d_6, multiphoton ionisation spectra, electronic struct. 78−82803
diatomic molecule, two identical 3-level atoms, excitation spectrum 80−23476
diatomic molecules, model pot. for calc. of multiphoton processes 77−508
diatomic molecules, rot. line strengths in multiphoton transitions 80−48051
2,2-dichloro-1,1,1-trifluoroethane, CO_2 laser multiphoton dissociation, D separation with single step enrichment 79−64112
1,1-difluoroethane, IR multiphoton dissoc., inert gas collision effects 79−16021
1,1-difluoroethylene, IR multiphoton dissoc., inert gas collision effects 79−16021
dimensional quantisation effect, HF characteristics at low temps., multiphoton absorpt., tunnelling *(Russian)* 78−68073
dimethyl POPOP, multiphoton cross-section determination by means of luminescence experiments 80−93377
trans-4-dimethylamino-4′-nitrostilbene, mol. hyperpolarisability in soln., UV dispersion of charge transfer contrib. 79−31986
dirty superconductor, multiphoton absorption *(Russian)* 77−36022
dispersive medium, QED and multiphoton processes at impurity centre *(Russian)* 78−71141
DNMR, multiple-quantum, tickling 80−23446
Doppler free multiphoton spectroscopy, review 77−79707
doubly resonant three-photon spectroscopy, appls. 79−71534
dressed molecule, RF field, saturated absorpt. obs. 80−9648
energy deposition by multiple IR photon absorpt. 80−66833
ethanol, multiphoton absorpt. and dissoc. 80−99530
ethyl vinyl ether, IR multiphoton dissoc., branching ratio and laser pulse duration 78−80772
ethylene, intense IR field multiphoton dissoc., primary products, fluoresc. obs. 79−36715
ethylene, IR multiphoton excitation, optoacoustic meas. 80−1038
ethylene, multiphoton absorption, luminesc. and dissoc. in laser pulse field 78−1040
ethylene, narrow resonances of multiple-photon IR absorpt. 80−99529
ethylenimine, multiphoton ionisation spectra, electronic struct. 78−82803
fifth order atomic optical nonlinearities in multiphoton resonances 80−28275
fluid, molecular, multiphoton Raman scatt. spectra 77−63404
fluoroacetylene, fund. and hot bands, laser microwave two-photon and double reson. spectroscopy 80−32752
fluorobenzene, multiphoton ionisation spectrum in one-photon wavelength region 80−63727
fluorobenzene, multiphoton reson, ionis. spectrum, 51000 cm^{-1} assignment 79−86021
fluoroform-d, laser isotope separation of D multiphoton dissoc. 79−94096
fluoromethane, vel.-tuned multiphoton processes in laser cavity 77−27134
formaldehyde, multiphoton dissoc. using focused DF laser, H-isotope separation 79−94094
four-photon spectroscopy of condensed media, nonlinear spectroscopy developments 80−91860
four-wave mixing spectroscopy in crysts., nonlinear spectroscopy developments 80−91861
free electron laser, multiphoton analysis 80−78826
free-free transitions, mutiphoton, energy absorption laser pulse shape-independ. 80−43184
free-free transitions in quantum electronics 80−28183
gas, resonance four-photon shift, optimal focusing of high-power pumping 80−95574
halogenated hydrocarbon HCl elimination, three and four centre, IR multiphoton dissoc. 79−5137
hexafluoride molecule selective excitation via Doppler free multiphoton process 78−55178
multiphoton spectra continued
hexafluoroacetone, multiphoton absorption and dissociation in strong IR CO_2 laser field 79−98172
trans-hexatriene, multiphoton ionization spectrum in 6.2 eV region 77−27133
inert gas halide lasers, operation and use in photochem. 80−9860
iodomethane, dressed mol., ν_6 band, saturated absorption spectrosc. 79−54844
iodomethane, RF field dressed mol. saturated absorpt. obs. 80−9648
IR laser applications in vibrational photochemistry *(Russian)* 79−5169
IR laser chemistry research using mol. beam *(German)* 80−55683
kinetic equations for collisionless multiphoton excitation of large molecules 79−54914
large molecules, multiphoton excitation models, numerical simulation 80−53078
laser radiation, interaction with free atoms, review 78−13473
laser radiation, selective action on matter, review 80−7832
laser spectroscopy, multiphoton and multistep methods, review 79−35842
laser spectroscopy uses, multiphoton transitions and Doppler effect elimination 77−57398
many-body theory of multiphoton absorption, appl. to Li ionis. 79−22679
metastable atomic or molecular species, multiphoton transition detection 80−58231
methanol, multiphoton absorpt. of intense HF laser radiation 80−23475
methanol, multiphoton decomposition with laser, isotope separation 79−66306
methanol(d_1), multiphoton absorpt. and dissoc. 80−99530
methyl isocyanide photoisomerisation, laser isotope separation, C-isotope enrichment by one-photon vibr. photochemistry 80−81336
methylbenzenes, 3p Rydberg transitions, multiphoton ionis. spectrosc. obs. 80−95644
modelling of multiphoton absorption using SF_6 energy-dependent absorption cross sections 80−32789
molecular gas, model 79−31633
molecular multiphoton processes, reduced eqns. of motion 79−22775
molecular multiphoton processes, stochastic reduction 79−81246
molecular photodissociation, polyatomic mols., dissoc. dynamics 78−82802
molecular spectroscopy, IR laser cavity, Lamb dip and multiphoton techniques, book contrib. 78−9278
molecule, high-order processes, rot. wave approx. 79−59518
molecule, IR collisionless multiphoton excitation, rate equations 79−22774
molecule, IR laser radiation multiphoton absorpt. direct meas. by pyroelec. detector 80−102545
molecule, IR radiation induced vibr. excitation and dissoc. 77−27135
molecule, multiphoton resonances, vibr.-rot. fine struct. effect *(Russian)* 79−86022
molecule, multiphoton scatt. of laser light, review 79−6979
molecule, nonadiabatic multiquantum excitation by reson. radiation 77−19001
molecules, IR laser excitation, exptl. determ. of proportion of captured particles and excitation level *(Russian)* 78−90248
molecules excited by laser IR radiation, excited fraction determ. 80−78661
multi-pulse spectroscopy with Ramsey fringes, resolution and signal strength 78−82869
multifrequency resonance transitions between quasi-energy states 80−43019
multilevel molecular system, coherent pulse propag. effects 80−9968
multilevel molecular system, excitation by laser IR field 78−55212
multilevel systems, nonlinear reson. freq. shifts and saturation effects 78−78675
multimode radiation, many-photon atomic excitation 80−74154
multiphoton ionization spectroscopy extension 79−50163
multiphoton laser assisted excitation transfer, grazing collisions, Heisenberg eqn. of motion 77−57953
multiple quantum transition in NMR, two-dimensional spectroscopy, selective detection 78−23353
N-level system, in strongly saturating oscill. and static fields 78−58639
N-level system in strong monochromatic field 78−29923
n-photon resonance phenomena, finite laser bandwidth effect 80−58230
naphthalene, multiphoton excitation 79−61414
naphthalene, two-photon and mutiphoton excitation, UV fluoresc. spectra 77−88517
naphthalene molecular ion, two and four photon absorpt., dissoc. 80−74210
narrow band gap semiconductors, multiphoton absorption in crossed fields *(Russian)* 80−60553
p-nitroaniline, mol. hyperpolarisability in soln., UV dispersion of charge transfer contrib. 79−31986
nitromethane, multiquantum absorption in intense IR field, isotope shift 77−19000
NMR, multiple-quantum coherence, selective excitation, appl. to benzene 80−23439
nonmonochromatic chaotic field, double optical reson. and reson. fluoresc., AC Stark splitting 80−9547
nonresonant excitation, ensemble of two-level systems, rel. to multiphoton spectra, polyatomic mols. 80−5585
optical Autler-Townes effect, time depend., finite bandwidth laser appl. theory 80−91499
optical triple resonance, semiclassical anal. 79−93963
optically pumped laser three-photon transition theory 80−102690
photoacoustic detection, multiphoton mol. absorpt. in strong i.r. field 77−507
photoionisation, quantum beats, origin 80−52954
photon statistics, influence of multiphoton absorption 79−13931
polyatomic molecule, anharmonic model for mol. photoexcitation 80−9669
polyatomic molecule, collisionless multiphoton dissoc., threshold behaviour, nonthermal theory 80−11905
polyatomic molecule, multiphoton dissoc. dynamics, classical model 80−11904
polyatomic molecule, multiple-photon IR laser pumping, collisional effects 80−9668
polyatomic molecule, quasicontinuum, coherent and mode selective excitation by laser pulse 78−1032
polyatomic molecules, collisionless dissociation by multiphoton IR absorption 77−54580

multiphoton spectra continued
polyatomic molecules, forbidden rotation-vibration transitions *(Russian)* 80−5593
polyatomic molecules, high intensity IR absorpt. 80−14183
polyatomic molecules, intramolecular dephasing processes 78−74695
polyatomic molecules, laser-induced energy distribs. 80−5591
polyatomic molecules, multiphoton absorpt., inverse radiationless transitions detect. *(Russian)* 79−22753
polyatomic molecules, multiphoton IR absorpt., collisional effects 79−41174
polyatomic molecules, multiple-photon absorption, quantitative comparison 80−32790
polyatomic molecules, multistep or multiphoton laser vibr. spectrosc. 78−90151
polyatomic mols., excitation and dissoc., intense IR laser radiation 77−83570
polyatomic mols., laser induced isotope enrichment, selective vibr. excitation mechanisms 77−18994
polyatomic mols., multiple photon IR processes, reviews 80−43125
propynal, rovibronic populations, collisionless IR multiphoton spectra, energy deposition, photoacoustic determ. 80−83354
pyrazine, multiphoton ionisation spectra, circular to linear polarisation ratios, lowest ionisation pot. 78−74716
pyrazine, multiphoton ionisation spectra, of three-photon ionisation region 78−37689
pyridine, multiphoton ionisation spectra, circular to linear polarisation ratios, lowest ionisation pot. 78−74716
pyridine, multiphoton ionisation spectra, of three-photon ionisation region 78−37689
quantum system interacting with nonequilibrium phonons 78−88340
Raman spectroscopy, of IR multiple-photon excited mols. 80−74207
resonance absorption characts., Dyson eqn. 77−61727
resonance interaction of intense light with atoms, review 79−68216
resonance light scattering, spectral props. and photon correls. 80−91510
resonant interactions, canonical description *(Russian)* 77−10714
resonant multiphoton absorption, transients, interference effects 79−85942
resonant multiphoton ionisation by pulsed excitation, Beers-Armstrong model 78−17645
review, multiphoton transitions, perturbation theory, atomic ionisation and intermediate reson., dissoc. 79−41145
RF spectroscopy in laser cavity, pure nucl. quadrupole spectra 78−90320
rotational heating during IR multiphoton excitation, dynamical effects on dissoc. products 80−18892
semiconductor, multiphoton absorption by charge carriers in mag. field 77−28553
semiconductor, multiphoton absorption of intense EM waves 77−1648
semiconductor, nonlinear refractive index under many-photon resonance conditions 78−90449
semiconductor in quantized mag. field, multiphoton Stark effect *(Russian)* 78−72541
semiconductor with non-spherical bands, many-photon magneto-optical absorption 78−19451
semiconductors, four-photon transitions, perturbation theory calc. 80−96786
semiconductors, IR tunable laser *(French)* 80−82836
semiconductors, nonlinear optical props., book contrib. 80−78899
semiconductors with narrow band gap, multiphoton magneto-absorption and electro-absorpt. *(Russian)* 79−19867
solid, intense field effects, multiphoton transition rate 78−10921
solid surface, mol. dynamic processes interaction with laser radiation 80−71943
spherically symmetric molecules, many-photon excitation in IR laser field 80−95596
tetrachloromethane, UV laser photolysis 80−66826
using thermal blooming, applic. to benzene spectroscopy 77−30940
using thermal blooming, theory 77−30939
thermally perturbed systems, impact and separation approxs., interaction theory 77−79593
three-level atom in radn. field, resonance processes *(Russian)* 79−45687
three-level Morse oscillator, sequential and direct multiphoton absorption 79−36714
three-photon absorbers, effect on stabilisation and smoothing for signal intensity correl. characts. *(German)* 77−23709
three-photon absorption: selection rules and line intensities 79−98054
three-photon resonance, Doppler, free power broadening 78−5308
transition probabilities, in intense radiation field, effective Hamiltonian approxs. 77−23482
trichlorofluoreomethane, UV laser photolysis 80−66826
trifluoremethane-d_1, IR photolysis, kinetics of multiphoton dissoc., ^{1}H isotope separation 79−79276
2,2,2-trifluoroethanol, multiphoton absorpt. and dissoc. 80−99530
trifluoroiodomethane, IR multi-photon excited mols. 80−74207
trifluoroiodomethane, multiphoton IR excitation and dissoc. *(Russian)* 80−35562
two level atom, coherent and Raman scatt. spectra, secondary emissions 80−69449
two level model theory, extended, appl. to Doppler-, laser and collision-broadened bound-bound multiphoton absorption 79−3423
two level system, microwave SHG, at. correlations and line shape 77−19219
two level system, microwave SHG, at. correlations and line shape 77−19220
two-level atom, multiphoton reson. fluoresc. in strong low-freq. field 78−55154
two-level atom interaction with EM field, quasi-classical approx. *(Russian)* 77−27031
two-level atoms, multiphoton cooperative radiation, SCF approx. calcs. 80−95856
two-level system in coherent field, reson. scatt., quantum description 79−64053
two-level system in sinusoidal elec. field *(Russian)* 78−58966
unimolecular reactions, laser-induced, by multiphoton IR excitation, theory 80−9664
unimolecular reactions induced by monochromatic IR radiation, intensity and laser energy fluence influence 80−11903
vinyl chloride, IR multiphoton energy deposition and reaction yield, press. and intensity 78−95936
vinyl fluoride, IR multiphoton dissoc., inert gas collision effects 79−16021

multiphoton spectra continued
OsO_4, multiphoton absorpt., inverse radiationless transitions detect. *(Russian)* 79−22753
Ar, electron scatt. in intense IR field, multiphoton free-free transitions 79−81289
Ba, atoms, high-lying levels, optogalvanic detection by laser excitation 79−98055
Ba, bound odd-parity J=1 spectra, multiphoton excitation 79−54795
Ba, even-parity autoionising levels, multiphoton ionisation spectroscopy 79−59417
Ba, laser spectroscopic anal. of Rydberg series, multichannel quantum defect theory 80−18815
Ba, multiphoton ionis. spectroscopy of even- and odd-parity states 78−86973
Ba+Ba(Tl), laser induced collisional and radiative energy transfer 80−53108
CO, $A^1\Pi \leftarrow X^1\Sigma^+$, (2-0) band, three photon excitation, fluoresc. obs. 78−13481
CO, computation of multiphoton IR rovibration spectrum 79−89660
CO, hole burning in single quantum power spectrum due to Autler-Townes splitting 80−9671
CO, rot. line strengths in multiphoton transitions 80−48051
CO, rovibr. multiphoton spectra comput., hole burning effect 80−9672
Ca, bound odd-parity J=1 spectra, multiphoton excitation 79−54795
Ca, laser spectroscopic anal. of Rydberg series, multichannel quantum defect theory 80−18815
Ca, multiphoton ionis. spectroscopy of even- and odd-parity states 78−86973
Ca+Sr, laser induced collisional and radiative energy transfer 80−53108
CdS, linear-circular three-photon dichroism 79−51930
CdS, multiphoton cross-section determination by means of luminescence experiments 80−93377
Cr, multiphoton ionisation and absorpt. 80−95575
CrO_2Cl_2, electronically induced IR multiphoton absorpt., quasicontinuum states, excited singlet radiationless decay 80−48049
Cs, $7^2P_{3/2}$ sublevels, hyperfine struct., multiphoton elec. dipole transitions anal. 80−32692
Cs atoms, exp. multiphoton ionisation through $9D_{3/2}$ resonant level 77−34602
Cs, four-photon ionisation, reson. effects 79−45689
Cs, reson. multiphoton ionisation by pulsed excitation, Beers-Armstrong model 78−17645
Cs_2, $\bar{a}^3A_2$-state detect. by reson. enhanced multiphoton ionis. spectrosc. 80−95551
CsAr, 6dσ states, multiphoton laser spectrosc. obs. 79−85974
CsKr, 6dσ states, multiphoton laser spectrosc. obs. 79−85974
DN_3, IR multiphoton dissoc., form. and reaction of electronically excited ND 78−80771
Ge, saturation of transmitted intensity of CO_2 laser pulses 80−64111
H atom, many-photon excitation spectra, fine structure 79−59419
H, ionisation, by microwave-stimulated multiphoton excitation, resons. obs. 77−68019
H, multiphoton ionisation potential, circularly polarized light 79−27101
H, one-, two- three- and four photon absorpt., truncated model semiclassical calcs. 78−17644
H, Rydberg levels, selective excitation by three-photon absorpt. 80−5518
H, third-order optical harmonic coeffs., R-matrix calc. 77−57955
H-like atoms in intense long wave EM field, multiphoton photoionisation cross sections 79−89652
H_2, electron scatt. in intense IR field, multiphoton free-free transitions 79−81289
HN_3 IR multiphonon dissociation with electronic excitation 80−11934
HN_3, IR multiphoton dissoc. 78−80771
$^2HN_3$ IR multiphonon dissociation with electronic excitation 80−11934
He, metastable, multiphoton transition detection, n^3S-n^3D splitting meas. 80−58231
He, multiphoton ionisation potential, circularly polarized light 79−27101
He, third-order optical harmonic coeffs., R-matrix calc. 77−57955
He_2, three-photon transitions, dichromatic laser field 78−17643
He^+, multiphoton RF reson. meas. 77−448
He+NO, multiphoton ionisation spectra in supersonic expansion, laser entranced collisional effects 80−83459
Hg, four-photon resonance ionis. 77−42289
I_2, 2- and 3-photon absorpt. obs. 80−18864
I_2, coherent multiphoton transitions, nonlinear resonant photoionis. 77−61814
I_2, multiphoton ionis. and dissoc. vibronic/mass spectra method 79−3507
I_2, RF optically heterodyned saturation spectroscopy, reson. degenerate four-wave mixing 80−74211
I_2, reson.-enhanced three-photon absorption, CW intracavity absorption 79−10160
InAs, three-photon absorption, transition effects *(Russian)* 78−35147
K, atomic vapour, resonant interaction with laser, Vavilov-Cherenkov effect *(Russian)* 80−106573
K, reson. three photon ionisation, saturation effects 78−90137
Li, vap., multiphoton absorption, space-charge ion detect. 79−54827
$LiIO_3$, active spectroscopy of polaritons, interf. of direct and cascade processes *(Russian)* 77−38982
MnF_2, two-exciton many photon absorption, effect of statistical props. of light on intensity *(Russian)* 78−95589
N, ionisation, multiphoton absorpt., spectroscopic evidence 80−63726
N_2, multiphoton absorpt., spectroscopic evidence 80−63726
N_2, rot. line strengths in multiphoton transitions 80−48051
NH_3, $\tilde{C}'$-state, 3-photon gas phase spectroscopy obs. 79−89715
NH_3, expansion cooled, mol. photoionisation, rot. struct., rot. predissoc. of excited states 80−91611
NH_3, three photon transitions in gases at microwave freqs. 78−9211
NO, 4-photon ionis. spectrum 2- and 3-photon resons., low temp. assignments 78−70887
NO nonlinear laser spectroscopy, VUV harmonic generation 80−74175
NO, rot. line strengths in multiphoton transitions 80−48051
NO, selectively excited rovibrational states, multiphoton ionisation spectra 80−69202
NO, $v=2\leftarrow1$ absorption band two-and multiphoton spectra, Λ-doubling const. vibr. depend. 77−30942
NO_2 excited, fluoresc. spectrum, IR multiphoton vibr. pumping, photon absorpt. probability distrib. study 80−18854
Na atoms cooling by resonant laser radiation *(Russian)* 80−74155
Na, four- and six-photon resonance spectra *(Russian)* 80−91527
Na, oriented vapour, RF transitions and laser beat reson., expt. technique 77−27005

multiphoton spectra continued
Na, reson. multiphoton ionisation, broadband laser AC Stark splitting 78−70808
Na, two and three photon resonances in strong nonmonochromatic field 77−34908
O_3, multiphoton dissoc. dynamics, classical model 80−11904
OsO_4, multiple IR photon absorpt , rovibr. transitions 79−54926
PbI_2, multiphoton cross-section determination by means of luminescence experiments 80−93377
PbTe, two photon magnetoabsorption *(Russian)* 80−60553
Rb induced radiation in multiphoton excitation above ionisation limit *(Russian)* 79−3425
SF_6 and S_2F_{10}, absorpt. of intense laser radiation, vibr. excitation 80−9667
SF_6 and S_2F_{10}, multiple-photon IR laser pumping, collisional effects 80−9668
SF_6, CO_2 laser excited, optoacoustic meas. of energy absorpt. 77−83667
SF_6, CO_2 laser excited, effect of pulse mode quality 78−66615
SF_6, collisionless multiphoton excitation and V-V energy transfer, coherent versus stochastic theories 78−82804
SF_6, ground state and vibr. heated mols., CO_2 laser pulse absorption 77−46607
SF_6, highly excited, time-resolved IR absorpt. obs. 80−9666
SF_6, IR laser multiphoton excitation, weak transitions in rot. band struct. 78−66614
SF_6, IR laser radiation multiphoton absorpt. direct meas. by pyroelec. detector 80−102545
SF_6, IR multiphoton photolysis, master eqn. anal. 79−47945
SF_6, IR multiple-photon excited molecules, Raman spectroscopy 80−74207
SF_6, laser-irrad., high-resolution double-reson. spectroscopy, collisionless multiphoton dissoc. 80−9623
SF_6, model system, coherent pulse propag. effects 80−9968
SF_6, mulitphoton absorpt., pulsed CO_2 laser radiation absorpt., press., freq., fluence depend. 80−28080
SF_6, multiphoton absorpt. spectrum, temp. depend. calc. 78−86927
SF_6 multiphoton absorpt. meas. by third harmonic generation 80−1036
SF_6, multiphoton absorpt., energy transfer, dissoc. probability, laser field interaction, classical trajectory approx. 80−37730
SF_6 multiphoton dissoc. by mol. beam method, energy distribution meas. by time-of-flight spectra, dissoc. dynamics 80−78670
SF_6, multiphoton excitation and dissociative ionisation, model 78−58754
SF_6, multiphoton excitation due to vibr.-rot. transitions 80−102546
SF_6, multiphoton-excited in mol. beam, photoionsation probe of vibr. energy distrib. 79−76476
SF_6, multiphoton-excited, $\nu_2+\nu_6$ absorption and emission 80−63626
SF_6, multiple photon absorption, thermal enhancement 79−68283
SF_6, multiple photon absorpt., laser pulse intensity and collisions influence 80−95699
SF_6, multiple-photon two-freq. IR laser pumping, optoacoustic spectroscopy 79−36717
SF_6, time-resolved IR absorpt. meas. using injection-locked single mode TEA CO_2 laser 80−9665
SF_6, transmission meas. of multiple photon absorpt. 77−83668
SF_6 type molecule, multiphoton absorption in continuum 78−90247
$^{32}SF_6$, anharmonic splittings, vibr. energy levels, $n\nu_3$ manifold 77−30853
$^{32}SF_6$, multiphoton dissoc. by laser pulse, Ar, N_2 and CF_4 environments 78−73061
S_2F_{10}, IR laser irrad., absorpt., reaction parameters 78−94241
SO_2, IR multiphoton excitation and inverse electronic relax., mol. vibr. and fluoresc. 80−106349
Sr atomic beam, time correlations between two sidebands of reson. fluoresc. triplet, multiphoton processes 80−95570
Sr, bound odd-parity J=1 spectra, multiphoton excitation 79−54795
Sr, laser spectroscopic anal. of Rydberg series, multichannel quantum defect theory 80−18815
Sr, multiphoton ionis. spectroscopy of even- and odd-parity states 78−86973
Te, simultaneous absorpt. of three photons, selection rule, exciton peak on absorpt. edge 78−43303
UF_6, multiphoton irradiation, spectra and modeling of laser induced emission 80−69160
UF_6, multiple photon absorpt. of 16 μm radiation at 300K 79−76475
W, multiphoton ionisation and absorpt. 80−95575
Xe, $^3P_1$ resonance state, three photon excitation, fluoresc. obs. 78−13481
Xe, multiphoton ionisation spectrum, interatomic effects in multiphoton transitions 78−29764
Xe, six-photon ionis., electron energy spectra 79−54824

multiple processor systems *see computer networks*

multiple scattering SCF-X-alpha calculations *see Xalpha calculations*

multiple stars
see also binary stars
ADS 16644, visual multiple system including dwarf or degenerate stars 79−17019
ADS 3358, speckle holography meas. of triple star 78−93120
ADS 7251, photographic obs. in 1962-73 period, orbital motion rel. to invisible satellites *(Russian)* 78−28726
ADS 9476 (Aitken 14), possible astrometric companion *(French)* 79−44553
AN Andromedae, light curve of Am binary systems, possible third body 79−58374
Aquila X-1, binary and triple star models for X-ray outbursts 78−20909
astrometric search for unseen stellar and sub-stellar companions to nearby stars and the possibility of their detection 79−30092
IU Aurigae, eclipsing binary, two-colour photometry rel. to presence of third body 80−36669
IU Aurigae, light curve study of early-type close binaries in triple systems 78−89222
IU Aurigae, massive triple system, obs. 77−64798
α Aurigae (Capella) AB, angular diams. by two telescope interferometry 78−8055
in binaries, undiscovered triples, selection effects *(French)* 79−44546
TZ Bootis, W Ursae Majoris system possible third body 78−69832
SV Camelopardalis, eclipsing binary containing BY Draconis variable, motion round third component 79−67055
ζCancri, occultation by asteroid 15 Eunomia on 1978 January 19, further predictions 78−20714
ζ Cancri, speckle interferometry and holography *(German)* 79−75116
α Canis Majoris (Sirius), possible orbits for third star 78−93312

multiple stars continued
β Capricorni, triple star, fundamental parameters from occultation astrometry and spectroscopy 79−40216
QZ Carinae (HD 93206), massive multiple system in great Carina Nebula, spectral types and orbits 79−97027
QZ Carinae (HD 93206), O-type quadruple eclipsing system, spectroscopic and radial vel. study 80−105275
α and Proxima Centauri, radial vels. and bound state 80−41859
α Centauri, visual multiple system including dwarf or degenerate stars 79−17019
α Centauri and Proxima Centauri, space motions, masses 79−21348
α Centauri C (Proxima Centauri), dMe flare star, quiescent corona, transition region, and chromosphere obs. 80−56850
α Centauri C (Proxima Centauri), EUV flare obs. rel. to flare star scaling theory 77−45453
α Centauri triple system, evolution 78−45356
VW Cephei, evidence for circumstellar matter 77−33563
ξ Cephei, triple system, spectroscopic study 77−22275
VW Cephei, W Ursae Majoris star, third component detect. from rot. line broadening function 80−109494
95 Ceti, visual multiple system including dwarf or degenerate stars 79−17019
close triple systems, orbital evolution, binary eccentricity 79−88699
collisions, by oscill. orbits of second kind 79−35312
CC Comae, contact binary, and visual companion, proper motion 77−74099
contact binary stars, role of third component in producing sudden period changes 80−109497
Cor 197, deviation of residuals in motion 79−44552
CPD −62° 1837 (HDE 308122), long-period variable member of triple 80−105260
α Crucis, improved spectroscopic orbit for α^1 Crucis 80−67792
V389 Cygni, BV photometry of peculiar variable 79−44534
61 Cygni, detect. of three invisible companions to visual binary star 78−28730
V389 Cygni, peculiar binary, spectroscopic obs. and presence of third component 78−85975
SW Cygni, period changes, mass transfer and third body effects 80−62183
61 Cygni, unseen companions, max. entropy spectral anal. of period data *(Russian)* 78−69841
β Cygni, visual obs. of brighter component close companion 80−8663
Cygnus X-1 (HDE 226868) system, search for third star 77−45606
detection by lunar occultation method 79−44542
discovery and observation 79−44541
discovery techniques and spectroscopic meas. 79−44540
dMe-stars, multiplicity 79−44544
doubles, binaries and multiple stars for amateur study 77−17626
BV Draconis and BW Draconis (ADS 9537), W Ursae Majoris stars, photoelectric obs. 79−35296
dynamical evolution from small galactic clusters 79−44568
40 Eridani, triple star, X-ray emission discovery 79−97035
40 Eridani, X-ray and radio images, evidence of corona 80−105282
evolution 77−91571
extra-solar planetary systems, detection by Space Telescope 80−109356
formation, role of ring form. in rotating protostellar clouds 80−56820
formation by dynamical interaction in clusters 79−44567
formation from N-body system decay 79−44569
formation from rotating interstellar clouds 78−93366
1 Geminorum, radial vel. determ. 80−73006
1 Geminorum, spectroscopic triple star, photoelectric radial vels. and orbit of 1 Geminorum B 77−22269
Gliese 815, dMe spectroscopic-visual triple 79−12493
h 3556, triple star, binary orbit and masses and third component relative motion 79−88701
habitable planets in the Galaxy 77−37511
HD 159176, spectroscopic binary, radial vel. obs., triple system possibility 79−25644
HD 165590, spectroscopic-visual triple system 77−67113
HD 165590, visual binary with spectroscopic binary component 78−32519
HD 165590 triple system, spectroscopic obs. 79−84825
HD 188753, close visual binary with spectroscopic binary component 77−57015
Hercules X-1 binary system, possible third star existence 77−33572
AK Herculis, photoelec. obs. and period study, possible visual companion 79−67065
DQ Herculis (Nova 1934), high time resolution spectrophotometry 80−22017
Herschel 2621, intermediate-band photometry rel. to advanced stellar evolution 78−53934
HR 1099, RS Canum Venaticorum variable, visual companion rel. to evolution 77−9754
Hussey 1399, relative motion of AC components rel. to invisible companion 79−44552
IAU Colloquium 33, proceedings (Oaxtepec, Mexico, 13-16 October, 1975) 79−44539
20 Leonis, possible eclipse obs. in triple system 78−12298
20 Leonis, triple system with a δ Scuti variable, spectroscopic obs. 77−49440
δ Librae, evidence for third component unconvincing 78−49475
lunar occultations, limits on undetected companions 79−88642
lunar occultations, photoelec. obs. 78−4079
lunar occultations, photoelec. obs. 79−5819
lunar occultations, photoelectric obs. rel. to multiplicity 78−7982
lunar occultations photoelec. obs. 80−72920
θ Muscae, Wolf-Rayet binary, triple star model 77−22235
nearby stars of Gliese catalogue, additional faint companions data (1969-1978) 80−36513
nonsolar planets, detect. via spinning 78−85977
nonsolar planets, search methods, IR interferometry from Earth orbit 79−53737
origin by condensation in dense nebulae 79−44565
η Orionis, quintuple star, speckle interferometry rel. to mass-luminosity relation 77−71011
η Orionis, quintuple system, spectroscopic orbit from speckle interferometry 77−22276
κ Pegasi, low total mass quadruple system 79−44550
κ Pegasi, radial vel. meas., visual binary with spectroscopic binary component 78−32520
β Persei (Algol), detection of B component, mass determ. 78−65654

multiple stars continued
β Persei (Algol), general problems and history *(Swedish)* 77−22268
β Persei (Algol), hard X-ray obs. 77−13493
β Persei (Algol), orbital inclination and masses determ. from speckle interferometry 80−36668
β Persei (Algol), triple system, long term apsidal motion study 77−87478
perturbation analysis techniques 79−44379
64 Piscium, double line spectroscopic binary, orbit and evidence for third component *(French)* 79−35305
51 Piscium, possible triple star, photoelectric obs. of lunar occultation 77−2331
planetary companions, statistics 77−91572
planetary system formation around MWC 349 newly formed star *(German)* 79−53832
planetary systems, cold satellites searching via speckle interferometry using coherent optical system *(Russian)* 80−12672
planetary systems, computer simulations 79−2559
planetary systems, detection using space-borne interferometers 80−109357
planetary systems, IR interferometric search, cosmic ray Cherenkov radiation effects 80−98523
planetary systems, post supernova survival 80−56860
planetary systems, search strategies 80−46615
planetary systems, spectrographic search of nearby stars 77−78827
planetary systems and stellar multiplicity 79−44564
polarisation by Thomson scatt. in optically thin envelopes, appl. to binary inclinations determ. 78−81655
V Puppis, light curve study of early-type close binaries in triple systems 78−89222
ψ Sagittarii, evolved spectroscopic triple system 79−44551
β Scorpii, lunar occultation astrometry 78−57583
β Scorpii, lunar occultation obs., magnitudes for five components 77−87471
β Scorpii, lunar occultation obs., magnitudes for three components 77−87472
β Scorpii, occultation by Jupiter, turbulent atmosphere obs. 77−37562
41 Sextantis, component A as new metallic line spectroscopic binary 78−53982
sizes and masses rel. to open clusters *(French)* 79−44547
solar type stars, relation between metallicity and multiplicity 77−78788
solar-type stars, fraction having stellar or massive nonstellar companions 78−16463
solar-type stars, multiplicity 77−13386
speckle, interferometric measurements of binary stars 79−71065
speckle interferometric observations, of spectroscopic and visual binary stars 80−90477
SS 433, beam models, energetics anal., possible triple system 80−90433
Stein 2051, orbital motion, evidence for triple system 78−4289
three-body systems disruption, statistical theory for high ang. momentum 77−13220
Trapezia and IR sources 79−44557
Trapezium member stars, space motions *(Chinese)* 80−8654
Trapezium system assoc. with Sharpless 106, compact H II region 79−44566
Trapezium type multiple systems, connection with associations, galactic clusters and emission nebulae 80−67781
Trapezium type multiple systems, relative proper motions *(Russian)* 78−93314
Trapezium type systems, statistical properties 79−44556
Trapezium type systems, UBVRI photometry 79−44558
Trapezium-like multiple systems in molecular clouds 79−101180
Trapezium-like objects, visual and IR photometric obs. 79−92805
Trapezium-type multiple systems, catalogue of 87 systems with O- and B-type primaries *(Russian)* 78−61753
Trapezium-type systems, UBVRI photometry 80−82431
triple close approaches effect on stellar system evolution, one-parameter family appl. 80−17618
triple stars, stability and hierarchy 77−60797
triple stars, stability criterion 77−64801
triple stars, stability of interplay motions 77−60583
triple system decay, numerical expts. 79−44561
triple systems, dynamics, review 79−44559
triple systems, non-rotating, exact mean time of decay *(Russian)* 78−32523
triple systems and close approaches, dynamics, review 79−44560
γ Velorum, photometric obs. 80−90482
DL Virginis, eclipsing binary in triple system, UBV photometry 78−8050
visual binary and multiple stars, micrometer and interferometer meas. 79−35303
visual binary multiplicity 79−44545
visual multiples, parallaxes, and proper motions, Sproul 61 cm refractor astrometric meas. 77−9768
Wolf 630, visual multiple system including dwarf or degenerate stars 79−17019
μ Draconis (ADS 10345), radial vel. var. from spectra in visible 80−17612

multiplex transmission *see multiplexing*

multiplexers *see multiplexing equipment*

multiplexing
see also frequency division multiplexing; time division multiplexing
anthraquinoide, electrochromism, display devices, multiplexing 80−45037
biomedical engineering instruction, microprocessor-based instrumentation system 77−22361
cardiac surgery, data acquisition and processing during operation by multiplexer *(German)* 78−92743
computer holograms, space multiplexing 78−17874
digital laser communication systems, acousto-optical multiplexing and demultiplexing techniques for multigigabits/sec transmission 79−86132
drift chamber and pulse height readout systems using analog multiplexing 77−54490
electron beam patterns using single-crystal thin films 79−89041
emergency medical telemetry standard development and implementation 78−3635
epicardial excitation spread, method for registration *(German)* 80−76845
far IR Michelson interferometry based on fast plasma scanning 77−31513
fibre-optic data bus system design and implementation 77−7017

multiplexing continued
Fourier transform spectroscopy, multiplex advantage, conventions and values 78−32882
Fourier transform spectroscopy, multiplex advantage 78−32883
Hadamard techniques in optics and their relationship to other multiplexing schemes 79−80242
holocinematography, high speed, spatial multiplexing for image separation 77−46704
holographic multiplexing by optical beam coding, applic. to interferometry *(French)* 77−159
holographic multiplexing technique 79−18369
holographic multiplexing technique 79−13925
holographic representations of space-variant optical processors 80−48192
hybrid IR/CCD focal planes, performance, appls. 79−3798
image coding, astronomical IR speckle interferometry appl. *(French)* 80−67580
image correlation in white light by wavelength multiplexing 79−55072
integrated optics for wavelength division multiplexing, review of recent developments 78−38079
low-background astronomical integrated IR detector array development 80−85860
multichannel data logging minicomputer switching program synthesis *(Russian)* 77−9993
multichannel temperature measuring system, thermocouples multiplexing *(German)* 77−53902
multicolour laser light time multiplexing using rotating mirror 78−17999
multiplex holography with chirp-modulated binary phase-coded reference-beam masks 79−27202
nuclear power plant, instrumentation and control, remote multiplexing appl. 80−52752
nuclear reactor multiplex systems, reliability, reliability with repair and availability 79−41012
optical, using phase modulation 80−95830
optical communiation multiplexing, large path-difference white-light interferometry *(French)* 77−10842
optical information processing and transmission in white light 80−95833
optical space-variant processing with polychromatic light 80−87342
optical wavelength division multiplexing systems, use of low-loss optical demultiplexer, 0.8 μm region 79−98463
remote multiplexing for nuclear reactor instrumentation and control circuits 80−57885
scanning interferometric multiplex photometer, airglow appls. 78−62216
simultaneous telephone transmission of four ECG/EEG signals *(Spanish)* 79−62399
single-fibre optical systems, efficient power combiner for multiplexing multiple sources 78−18039
sound, graphical picture transmission, distrib. via domestic satellite, education appl. 80−31463
telemetry system, implantable, multichannel, IC, for animal physiological data recording 77−86661
TRIUMF data interface 77−88304
TV lecturing system using frame multiplexing technique 78−28887
twisted nematic displays, liq. cryst. material deisgn 79−90533
two-dimensional image transmission by wavelength multiplexing 79−27189
Xe laser, high gain, ang. multiplexing for short pulse amplification 79−36924

multiplexing equipment
5 Gbit/s multiplexer, for optical fibre communication system 78−18044
16-channel analog store and multiplexer unit 79−45614
140 Mb/s optical fibre transmission system 78−42436
acousto-optical multiplexer for fibre-optical systems 77−27370
acoustooptical multiplexer/demultiplexer terminals, appl. to laser communication system, expt. results 78−25959
analogue signal multiplexer for multichannel data acquisition system 79−26045
Auger electron spectrometer, microcomputer-based multiplexer for performing depth profiling 79−67435
biomedical recording system, TDM multiplexing system for multichannel signal averaging of visually evoked responses 80−36165
C-CD multiplexer, direct coupling with 5 μm (Hg,Cd)Te photovoltaic detector 77−83987
chirped-grating multiplexers in dielectric waveguides 77−58445
corrugated-waveguide optical demultiplexer mode couplings 80−64194
digital data multiplexer system, for high rate data handling in Spacelab and on ground 79−21138
directional coupler, interference filter all-fibre for wavelength division multiplexing 80−91900
edge interference filters for WDM transmission over multimode opt. fibres 80−83677
EEG analogue multiplexer for FM tape recording 79−34691
EEG recording system, portable pulse-interval modulation telemetry/multiplexing system, home use 80−67261
electro-optic multimode time division multiplex device 77−79958
electro-optic multiplexer system for multimode fibre data communications 79−18510
electro-optical multiplexer for large-numerical-aperture low-loss fibres 77−83993
electrooptical processor, iterative colour-multiplexed 80−23792
fibre-optic communication applications, microoptic grating multiplexers, optical isolators 80−48408
frequency-channel multiplexer and four-channel integrated-optics coupler 80−91936
implantable 8-channel stimulation system for labyrinthine deafness *(German)* 79−16347
linear multiplexer, 14-channel, resolution, efficiency, nuclear spectroscopy appl. 78−33400
LMFBR data multiplexing system 79−76102
micro-optic duplexers for wavelength division two-way fibre optic transmission expt. 78−22194
micro-optic grating for fibre-optic communication systems 79−50423
multimode fibre transmission system, optical multiplexer 77−83960
multireflection optical multi/demultiplexer using interference filters 79−76821
optical access couplers for single strand systems 80−58766
optical channel waveguide arrays coupled to integrated CCD 80−33244
optical data link, single fibre, multimode electro-optic guiding 78−38065
optical demultiplexer, using diffraction grating, for FDM fibre transmission system 80−5845

multiplexing equipment continued
optical demultiplexer for wavelength division multiplexing system 79−64309
optical demultiplexer using concave grating, 0.7 to 0.9 μm, expt. results 80−38099
optical demultiplexer using Si echelette grating 80−53422
optical directional filter structure and characteristics for bidirectional transmission 80−58734
optical fibre communication line with spectral multiplexing in 1.3 μm region 80−74504
optical multiplexer for multimode fibre transmission system 77−88935
optical multiplexer using blazed grating, 1.1 to 1.5 μm, for WDM transmission system 80−38100
optical multiplexer/demultiplexer, low-loss, using interf. filters 80−58728
optical multiplexers/demultiplexers for single-fibre WDM transmission 80−43475
optical subpicosecond gate, velocity-matched directional coupler 80−74512
optical wavelength division multiplexing systems, use of low-loss optical demultiplexer, 0.8 μm region 79−98463
optical wavelength division multiplexing transmission technology 80−58727
optical wavelength-division multiplexer for 1-1.4 μm spectral region 78−55451
optical wavelength-division multiplexing transmission via single fibre, multiplexer design 80−33222
paper tape data transmission, optical fibres 80−43454
physiological response measurement, multiplexing system 80−56292
plasma diagnostics, Thomson scatt. system, analogue data processing circuits 78−87488
remote multiplexing control and safety systems evaluation 79−76109
remote vs. centralised control systems, cost effectiveness, microprocessor band systems, PWR nuclear power plant appl. 78−89971
satellite image sensing and multiplexing system tradeoffs 77−60498
SAW in-line chirp filter applications 78−59207
self-imaging multiplexer and branching couplers 80−106629
temperature multiplexers, types of unit and configurations 80−82757
wavelength division multiplexer using optical fibre pieces 80−91917
wavelength division multiplexing technology status and prospects 80−64203
wavelength multiplexer, single-mode-fibre 80−102816
$LiNbO_3$:Ti phase-matched waveguide electro-optic TE⇄TM mode converter 80−58749

multiplier phototubes *see photomultipliers*

multipliers, electron *see electron multipliers*

multipliers, frequency *see frequency multipliers*

multipliers, voltage *see voltage multipliers*

multiplying circuits
AC polarography, signal components, meas. using multiplier circuitry 78−61119
analogue, p-n junctions capacitance meas. appl. *(Bulgarian)* 78−57977
multiplier unit for acoustic and electronic wattmeters 77−79118
wattmeter, differential, analogue, adiabatic calorimeter and liquid chromatograph appl. *(Czech)* 78−23979

multiprocessing systems
see also distributed processing; parallel processing; pipeline processing
auditory evoked potential data acquisition, dual-processor system 79−79712
CERN computing school, La Grande Motte, France (1976) 77−65414
data acquisition system, design 79−89556
disc based distributed processing data acquisition and anal. system 77−65024
distributed computer system for digitising machines for bubble chamber photographs 78−5110
image processing microprogrammed video display 80−72366
IPNS time of flight neutron scattering instruments system 79−89558
microprocessor-assisted high-precision viscometry 79−50816
multi-microprocessor auxiliary crate controller, data processing in CAMAC 78−46246
multi-microprocessor network, for sonar signal processing algorithms soln. 78−45044
multimicrocomputer system with dynamic variable hierarchy for real-time data acquisition 78−44654
nuclear events picture anal. multiprocessor system *(Italian)* 80−69047
optical waveguide data bus system configurations 79−18544
patient monitoring, multi-microprocessor system *(German)* 78−88752
SMS 201 microprocessor system, weather simulation 79−53500
speech synthesiser implementation 80−96143

multiprogramming
online analysis of large bubble chamber pictures, data acquisition system, CDC 1700 computer *(French)* 77−42223

multivalley semiconductors *see many-valley semiconductors*

multivariable control systems
cancer problem cell kinetic study using digital simulation 77−40639
coupled inverted pendulums, stabilising control *(Japanese)* 79−35545
disturbed cell renewal control system modelling and simulation 79−29510
electrocardiological diagnostic efficiency improvement by cardiovascular system model dynamic optimisation 79−39569
nuclear plant and core power distrib. control 77−67832
nuclear reactor identification, test inputs review 78−41819
reactor spatial control during nuclear station load cycling, multivariable control algorithm 79−13490
Tokamak plasma, construction and simulation study *(Japanese)* 80−100100

multivariable systems
see also multivariable control systems; variable structure systems
acoustic signals, matrix formulation of coherence rel. to unwanted signals removal 77−46831
BWR dynamics, multivariable autoregressive identification 78−94107
complex optical system design, factor analysis methods 79−81509
limit state stability, multicause interaction relationships *(German)* 79−23235
nonlinear coupled dynamic physiological systems, network thermodynamic simulation 79−96504
nuclear reactor multivariable parameter meas. and display microprocessor solution 79−72221
nuclear reactor surveillance, pattern recognition techniques appl. 80−63351

multivariable systems continued
reactor cooling channels, flow anomaly diagnosis, autoregressive model appl. *(Japanese)* 80−83146
river water quality system, recursive estimation techniques appls. 79−5538
visual information processing, multi-input system representation, polynomial algorithm properties 80−101145

multivibrators
see also flip-flops
astable multivibrator freq. control for rapid cond meas. with electrolyte cond. probe 78−37029
automatic coded digital speech transmission, pitch extractor appl. 79−41530
capacitor tolerance measured using astable multivibrator 78−4628
integrated astable optical, Mach-Zehnder interferometric optical switches use 80−87560
Mach-Zehnder interferometric switch for integrated optical multivibrators 80−53479
magnetic core multivibrator, tensile stress measurement appl. 78−9615
monostable, acoustic switch appl., for noise level control *(German)* 77−65649
semiconductor laser two-resonator systems as multivibrators and flip-flops 77−79839
strain gauge transducer, digital output obtained from counter and logic ccts. 79−67281
thermistor, temp. to freq. convertor and bridge for temp. meas. 77−26289
timer, touch controlled, photography appls. *(Spanish)* 80−86478

muon absorption
bremsstrahlung cross-section corrections necessitated by target excitation 78−4931
bremsstrahlung in collisions with nonpointlike nuclei 78−8803
In, muon quadrupolar interaction expansion of crystal lattice *(Russian)* 79−15388
Ta, muon quadrupolar interaction expansion of crystal lattice *(Russian)* 79−15388

muon capture
see also muonic atoms; muonic molecules; radioactivity
A=12, recoil polarisation in muon capture, arbitrary nuclear spin, form factors 79−75978
A=6 to 14 nuclei, muon capture rate calcs. 78−33150
A=6-14, one π exchange currents effect on partial muon capture rates 79−22239
actinide muonic atoms, n emission from radiationless muonic transitions and μ capture 79−3599
anomalous capture and conservation schemes 80−68654
axial current role, possible solns. conserved isovector current hypothesis 79−26401
charged particle emission *(Russian)* 77−50082
closure approximation, appl. to perturbation theory, muon capture and pion electroproduction 78−16680
complex nuclei, a≳20, charged particle emission following μ capture 78−70490
conference on mesonic interface in nuclear struct. Erice, Italy (Sept. 1976) 79−26374
Coulomb capture and atomic radius 79−64124
Coulomb capture in inhomogeneous matter 78−55116
Coulomb capture ratio of muons in oxides of medium and heavy elements 78−8777
exchange current corrections for muon partial capture rates 78−33152
excitation of giant dipole reson. by muon atomic transition 77−26630
excitations and particle emission cascade following muon capture, hydrodynamical model 78−89825
exotic atoms, conf., Erice, Sicily, (1979) 80−67939
heavy atoms, low energy muonic H reactions 77−82871
heavy muonic atom, muon capture by fission fragments, statistical model anal. *(Russian)* 79−9523
heavy nuclei, neutron emission energy and multiplicity distribs. 77−6313
induced pseudoscalar form factor upper bound 77−82872
inert gas binary mixture, μ-capture, near 5 atm., X-ray yield 80−58419
ionic crystals, model requiring const. negative muon Coulomb capture ratios 79−65133
kinematical constraints, linear response theory anal. 79−45210
large energy transfer, inclusive capture rate 77−71590
metallic binary solid solutions, Coulomb capture ratio of muons, Lyman series intensities 77−19985
negative muons, transport properties in matter, energy spectra 77−56239
negative muons, transport properties in matter 77−56238
nonconservation of muon number, models with doubly charged leptons 77−74613
nuclear form factors of 0^+-0^- transition in A=16 system, nuclear struct. effects 80−18246
nuclear radiative muon capture rates, maximum photon energy, sum rule correction calc. 79−6517
nuclear semi-leptonic weak interactions 78−555
nuclear structure aspects of muon capture, naive impulse approx. adequacy 79−26402
radiative μ capture on free p, low energy expansion of two current amplitudes 78−16946
radiative capture, appl. to nuclear spin and isospin doublets 78−82320
radiative muon capture, transition amplitude, PCAC test 80−83076
response tail to high threshold reaction 80−83075
review of present knowledge on nuclear muon capture 77−50090
semileptonic weak and EM interactions, nuclear current operators 79−6515
spin-isospin polarizability of nuclear matter and renormalization of weak currents 79−67697
total capture rates, statistical theory 77−41928
v/c relativistic terms, evaluation 77−30519
virtual pions, Yukawa field and effects on μ-capture, β-decay, mag. moment etc. 79−26379
weak interactions, conf., Bloomington, USA, (May, 1977) 78−414
^{1}H, capture rate of μ^-, meas. by Saclay linac beam *(French)* 79−368
(μ,n), high energy neutron spectroscopy 80−73841
(μ^-, pxn) reaction yields 77−10368
μ^+ localisation in Cu, Al and Al-Mn, temp. depend. 80−44993
$\mu^-+(A,Z)\rightarrow(A,Z-1)+\nu_\mu$, universal V-A interaction, muon capture use for nuclear struct. studies 77−67725
$\mu^-+(A,Z)\rightarrow e^-+(A,Z)$, Z-dependence of coherent μe conversion rate in anomalous neutrinoless muon capture 80−13419

muon capture continued
$\mu^-p \rightarrow \nu_\mu n\gamma$, appl. to nuclear spin and isospin doublets 78−82320
μp+p, elastic scattering cross section of muonic H atoms 80−69278
Π field in nuclei, μ absorpt. and doubly radiative Π absorpt. as probes 77−88063
Ag-Zn, negative muon capture ratios 80−55007
Al, muonic atoms, Lyman series, muon transfer effect 79−7040
Al_2O_3, atomic capture ratio for μ-transferred from μp to Al_2O_3 79−10236
C, μ^- capture, charged particle energy spectra *(Russian)* 78−89828
^{12}C, capture rate of μ^-, meas. by Saclay linac beam *(French)* 79−368
^{12}C, EM and allowed weak transitions, improved impulse approx. treatment 78−41662
^{12}C, muon capture theory 78−553
^{12}C μ capture rate, average nuclear polarisation, elementary particle approach 78−66246
^{12}C, μ^- capture reactions with ^{8}Li prod. *(Russian)* 78−54745
^{12}C, weak hadronic form factor and recoil polarisation in muon capture 78−62508
$^{12}C(\mu,\nu_\mu)^{12}B$, induced pseudo-scalar coupling constant 79−49606
$^{12}C(\mu^-,\nu)^{12}B$, polarisation studies, muon capture, weak interaction aspects 80−68655
$^{12}C(\mu^-,\nu_\mu)^{12}B$, data anal., second-class currents and CVC 77−82874
$^{12}C(\mu^-,\nu_\mu)^{12}B$, Hartree Fock wavefunction, correlations, pseudoscalar coupling constant, capture rates, recoil nuclear polarisation 80−22774
$^{12}C(\mu^-,\nu_\mu\gamma)^{12}B$, appl. of μ^- radiative capture to nucl. spin and isospin transitions 78−86511
$^{12}C(\mu^-,\nu_\mu\gamma)^{12}B$, impulse approx. calc., photon asymmetry and daughter nucleus polarisation 78−37315
$^{12}C(\mu^-,\nu)^{12}B^*$, average polarisation of recoil ^{12}B in direct capture 79−93602
$^{12}C(\mu^-,\nu_\mu)^{12}B$, induced tensor and pseudotensor form factors 77−38253
$^{12}C(\pi^-,\nu)$, polarised π^-, ^{12}B average polarisation, form factors and partial capture rate 79−22263
^{40}Ca, neutron ang. distrib. following polarized muon capture, relativistic corrections 78−13063
^{40}Ca, nucl. effects in radiative muon capture 78−29428
^{40}Ca, polarised muon capture, direct neutron emission 77−38252
$^{40}Ca(\mu,\gamma)$, photon asymmetry, $O(1/m^2)$ and nuclear effects 80−78219
$^{40}Ca(\mu,n\nu_\mu)$, neutron longitudinal polarisation anal. 77−30559
$^{40}Ca(\mu,\nu\gamma)$, ^{40}K,*, 85 MeV/c, radiative capture branching ratio, photon asymm. 77−79365
Cu-Al, negative muon capture ratios 80−55007
H, ^{2}H, ^{3}H, muon capture theory 78−553
H_2, liq., capture rate meas. 80−69275
$^1H+\mu^- \rightarrow \nu_\mu+n$, angular correlations and capture rates, spin and isospin transitions, hyperfine effects 78−70494
$^1H(\mu^-,\nu\gamma)$, radiative capture relativistic calcs., rate and photon spectrum 80−68605
^{2}H and ^{1}H capture, μ-N axial coupling const. *(Russian)* 77−50570
^{2}H, muon capture, kinematics and dynamics 78−33151
$^2H^3H\mu \rightarrow {}^4He+n+\mu^-+17.6$ MeV, muonic catalysis in synthesis reactions *(Russian)* 80−52706
$^2H(\mu,\nu_\mu)$, neutron-neutron off shell interaction differential capture rates 79−71845
$^3H(\mu,\nu)3n$, transitions from bound to continuum three nucleon states 80−5128
^{3}He, muon capture 78−37314
^{3}He, muon capture theory 78−553
^{3}He, total and partial capture rates for μ^- 79−9522
$^3He+\mu^- \rightarrow \nu_\mu+{}^3H$, angular correlations and capture rates, spin and isospin transitions, hyperfine effects 78−70494
$^3He(\mu,\gamma\nu)$, transition amplitude, PCAC tests 80−102152
$^3He(\mu^-,\nu_\mu\gamma)^3H$, appl. to nuclear spin and isospin doublets 78−82320
$^3He(\mu^-,\nu\gamma)$, radiative capture relativistic calcs., rate and photon spectrum 80−68605
KCl-KBr, solid soln., negative muon capture ratios 80−55007
$^6Li+\mu^- \rightarrow \nu_\mu+{}^6He$, angular correlations and capture rates, spin and isospin transitions, hyperfine effects 78−70494
^{7}Li, total muon capture rate 79−6516
Mg, μ^- capture, charged particle energy spectra and asymmetry *(Russian)* 78−89828
N compounds, influence of chemical bond on relative muonic capture rates in elements 78−58874
$^{14}N_{g.s.}$ partial muon capture, mesonic exchange currents, weak process microscopic treatment 80−57742
$^{14}N+\mu^- \rightarrow {}^{14}C+\nu_\mu$, rate calcs. using elementary particle and macroscopic treatments 78−29429
$^{16}N(0^-) \rightleftharpoons {}^{16}O(0^+)\beta$-decay and μ-capture, mesonic exchange correction 78−41673
NaCl-NaBr, solid soln., negative muon capture ratios 80−55007
^{93}Nb, total muon capture rate, quenching of Cabibbo angle 79−22232
Ne, total muon capture rates using HF wave functions 80−63135
^{237}Np muonic, prompt fission, fragment atomic muon capture 80−95312
^{237}Np, muonic atom lifetimes from muon induced fission 80−69269
O, μ^- capture, charged particle energy spectra *(Russian)* 78−89828
^{16}O, capture rate of μ^-, meas. by Saclay linac beam *(French)* 79−368
^{16}O, weak hadronic form factor and recoil polarisation in muon capture 78−62508
$^{16}O+\mu$, total muon capture rate, Skyrme forces, closure approx., sum rule technique 78−54742
$^{16}O(0^+) \rightarrow {}^{16}N(0^-)$, nucl. wave functions and mesonic exchange currents 79−40887
$^{16}O(0^+) \rightleftarrows {}^{16}N(0^-)\beta$ decay and μ capture reactions, mesonic exchange correction 78−58257
^{16}O(e,e), T=1 level form factors, Helm model, pion photoprod. and muon capture appls. 80−52553
$^{16}O(\mu,\nu_\mu)^{16}N^*$, elementary particle treatment 78−8800
$^{16}O(\mu,\nu)$, recoil nucleus odd and even tensor orientations, general expressions 80−13451
$^{16}O(\mu,\nu)^{16}N$ determ. of μ^- partial capture rates 79−45247
$^{16}O(\mu^-,\nu_\mu)^{16}N$, capture rate, A=16 ground and excited states 78−17105
$^{16}O(\mu^-,\nu)^{16}N^*(0^-)$, calculated capture rate 79−59036
$^{208}Pb(\mu^-,\nu)$, RPA calc. of partial and total capture rates 78−74409
Pd, circular polarisation of muonic X-rays, strange μ^- depolarisation 78−25758
^{A}Pu, A=239,242, muonic, prompt fission, fragment atomic muon capture 80−95312
^{A}Pu, A=239,242, muonic atom lifetimes from muon induced fission 80−69269

muon capture continued
^{239}Pu muonic atom, n emission, bound μ influence on fission barrier 78−89845
^{239}Pu, total muon capture rate, quenching of Cabibbo angle 79−22232
^{239}Pu, total muon-capture rate meas. 77−79335
S compounds, influence of chemical bond on relative muonic capture rates in elements 78−58874
S, μ^- capture, charged particle energy spectra and asymmetry *(Russian)* 78−89828
Se compounds, influence of chemical bond on relative muonic capture rates in elements 78−58874
$^{28}Si(\mu^-,\gamma\nu)$, $\gamma-\nu$ ang. correlation, pseudoscalar and tensor form factors, particle-hole model 79−13256
^{232}Th, muonic, μ induced prompt fission, fate of the μ 78−86557
^{232}Th muonic atom, n emission, bound μ influence on fission barrier 78−89845
^{232}Th, μ capture rate in the fission mode, μ lifetime 78−89827
^{232}Th, total muon-capture rate meas. 77−79335
U, A=235, 8, total muon-capture rate meas. 77−79335
^{A}U, A=235,238, muonic atom lifetimes from muon induced fission 80−69269
^{235}U, total muon capture rate, quenching of Cabibbo angle 79−22232
^{238}U, muonic, μ induced prompt fission, fate of the μ 78−86557
^{238}U, μ capture rate in the fission mode, μ lifetime 78−89827

muon decay
$\mu^+ \rightarrow e^+\gamma$, upper limit for decay 78−25030
bound muons, decay characts. 80−42512
conservation of muon number spontaneous breakdown, off-diagonal neutral currents 77−49889
CPT, CP and T invariance from correlations and lifetimes 80−77996
Einstein special relativity test, from H weak decay rate 79−2624
exotic muon and heavy lepton decays in gauge theories 77−49939
inner bremsstrahlung effects and radiative corrections at start of electronic spectrum *(Russian)* 80−37273
lepton mixing and neutrino oscillations, cosmic neutrinos, heavy leptons, μ decay 78−82193
lepton number non-conservation in Weinberg model with two Higgs doublets 77−67585
lepton structure model, muon nonconservation, decay and anomalous mag. moment 77−61250
muon number nonconservation in gauge model with heavy lepton 77−61239
muon number nonconservation postulation 77−87916
muonic atom, lifetime of bound muon, nucl. recoil correction 79−68331
nonconservation of muon number, models with doubly charged leptons 77−74613
processes in supercritical mag. fields *(Russian)* 78−78159
renormalisable theory of pure leptonic weak interaction with induced shadow states 78−37136
review of muon physics, props. and identification 78−82260
scintillation detector system, cosmic ray muon lifetime, undergraduate teaching 78−81752
special relativity, time dilation meas. for relativistic muons 77−71210
$SU(2)_L \times U(1) \times SU(2)_R$ model for lepton decay and neutrino lifetime 78−62331
$SU(2)_L \times U(1)$ theory, radiative corrections, simple renormalisation framework 80−101973
SU(6) exotic gauge model, lepton-quark symm., CP-violation and $\mu \rightarrow e\gamma$ decay 78−12875
SU(6) unified gauge model, mechanism of muon number nonconserving decay 78−12847
total decay rate, decay of polarised muons, electron energy spectrum, book contrib. 78−78161
weak and EM radiative corrections to low-energy processes 80−95274
$\mu \rightarrow 3e$ decay heavy neutral lepton mixing 77−65149
$\mu \rightarrow e^-e^-e^+$, muon number nonconservation 78−8542
$\mu \rightarrow e+\gamma$, SU(2)×U(1) unified gauge theory, mech. for nonconservation of muon number 77−30303
$\mu \rightarrow e+\gamma$ decay and mixing of charged heavy leptons *(Russian)* 78−58178
$\mu \rightarrow eee$, flavour changing neutral current search 80−105836
$\mu \rightarrow ee\bar{e}$, V-A gauge model, muon and electron number nonconservation 77−74667
$\mu \rightarrow ee\bar{e}$, Weinberg-Salam model with neutrino mixing *(Russian)* 77−38114
$\mu \rightarrow e\gamma$, and other rare decays, in SU_6 superunified gauge theory 78−21408
$\mu \rightarrow e\gamma$, decay ang. distribs. and polarisation effects 77−41835
$\mu \rightarrow e\gamma$, decay mode calc. in model with heavy neutral leptons 78−45898
$\mu \rightarrow e\gamma$, gauge theory with lepton mixing, decay probability, neutrino oscillations 77−49940
$\mu \rightarrow e\gamma$, $\mu \rightarrow 3e$, lepton number nonconservation with scalar bosons 78−4798
$\mu \rightarrow e\gamma$, $\mu \rightarrow 3e$, rare decays, natural lepton models, doubly charged leptons 77−34143
$\mu \rightarrow e\gamma$, possible existence of third kind of neutrino *(Chinese)* 78−12896
$\mu \rightarrow e\gamma$, SU(2)×U(1) unified guage theory 78−8643
$\mu \rightarrow e\gamma$, SU(3)×U(1) symmetry, gauge theory 78−58153
$\mu \rightarrow e\gamma$, V-A gauge model, muon and electron number nonconservation 77−74667
$\mu \rightarrow e\gamma$, Weinberg-Salam model with neutrino mixing *(Russian)* 77−38114
$\mu \rightarrow e\gamma$ decay rate in P-symmetric gauge theory 77−49941
$\mu \rightarrow e\gamma$ in Weinberg Salam model, spontaneously broken μ-like charge symm., heavy leptons *(Chinese)* 78−82191
$\mu \rightarrow e\gamma$ or 3e, heavy leptons, CP violation 77−82727
$\mu \rightarrow e\gamma\gamma$, muonic number nonconservation, pole model anal., and decay probability *(Russian)* 79−80817
$\mu \rightarrow e\gamma\gamma$, upper limit, differential decay rates, branching ratio 78−78156
$\mu \rightarrow e\nu\bar{\nu}$, full electron polarisation vector radiative corrections 79−36055
$\mu \rightarrow e\nu\bar{\nu}$, muonic beam with variable helicity, polarisation from electron spectrum 77−6598
$\mu \rightarrow \bar{\nu}_\mu X^+$, hypothetical, search for scalar charged boson, apparatus and theoretical aspects 78−58177
μ-number non-conservation in gauge theories of weak interactions 77−74630
$\mu^- \rightarrow e^-e^-e^+$, decay rate calc. SU(2)×U(1) model 78−8641
$\mu^- \rightarrow e^-\bar{\nu}^-\nu$ model, spiral props. of neutrinos *(Russian)* 78−25031
μ^+ decay from muonium 80−102086
$\mu^+ \rightarrow e^+ + \gamma$, search, lepton number conservation, brief review 77−57516

muon decay continued
$\mu^+ \rightarrow e^+\gamma$, branching ratio upper limit 79−30723
$\mu^+ \rightarrow e^+\gamma$, upper limit for branching ratio 80−78051
$\mu^+ \rightarrow e^+\gamma$, upper limit on branching ratio 78−12897
$\mu^+ \rightarrow e^+\bar{\nu}_e\nu_\mu$, $\bar{\nu}$l search for muon number conservation test, neutrino expt. 80−47270
$\mu^+ \rightarrow e^+\nu\bar{\nu}$, e^+ polarisation, weak interactions and lepton number conservation 80−42444
$\mu^+ \rightarrow e^+\nu\bar{\nu}$, μe universality and μ number nonconservation in rare decays 80−42445
$\mu^+ \rightarrow e^+\bar{\nu}\nu$, pol. meas. 80−73760
μ^+ lifetime, precise meas. by Saclay linac beam *(French)* 79−368
μ^+ polarisation dynamics in mag. mirror field, neutrino emission asymmetry 77−61645
$\mu^\pm \rightarrow e^\pm\gamma$, right-handed ν_μ anal. 78−41525

muon detection and measurement
absolute intensities of medium-energy muons in the vertical and at zenith angles 55°-85° 80−17460
Akenon Air Shower project, e and μ obs., core energy flow, device description 79−72184
calorimeter to study cosmic ray muon interactions 80−37686
CERN neutrino beam monitoring by μ flux in Fe shield meas., Si detectors 78−37523
cosmic ray EAS, search for anomalous muon generation, energy spectra and delay method 78−89026
cosmic ray muons, multiple scattering in mag. spectrometers 80−4215
cosmic rays, coupling functions for muon telescopes at sea level and underground 79−16784
cosmic-ray muons, inelastic scatt. by NaCl nuclei, higher than 300 GeV *(Russian)* 79−22106
deep water muon and neutrino detectors *(Russian)* 78−55109
detector response in EAS 80−63491
drift chambers, construction and test of insensitive regions 79−3304
DUMAND detector, objects in weak interaction studies 79−63463
EAS, single and muon pairs, 20-1000 GeV, showers of 10^4 to 10^7 particles 78−28473
EAS arrival direction distributions 78−28471
energy threshold of cosmic ray muon detectors 80−63489
fast mass depend. trigger design based on ECL integrated ccts. 79−97954
flux measuring system for neutrino spectrum reconstruction at IHEP accelerator 78−21817
hodoscope read-out, fast sparse-data-scan system using CAMAC compatible elements 79−45609
hodoscopes for high intensity muon beam, high-rate photomultiplier-base and precise timing calibration 79−22544
Homestake neutrino detector, mass composition of cosmic ray primaries, muon multiplicities meas. 79−66903
inclined muon monitors, muon spectra, generating functions, rel. to diurnal variation at Kiruna 78−85783
integral μ momentum spectrum, absolute intensity meas. 0.4 to 3.0 GeV/c 79−5720
modular drift-chamber vertex detector at the CERN ISR 79−3302
MUTRON, cosmic ray mag. spectrometer, MWPC trigger system 78−55081
MWPC, external muon identifiers at CERN 78−37488
MWPC, high-flux fast readout system based on new monolithic integrated ccts. 78−37491
proportional and drift chambers, construction of insensitive regions 79−3305
proportional chambers, external muon identifier for Fermilab 15 ft bubble chamber 77−6629
proportional delay line chambers for Fermilab external muon identifiers 78−37489
review of muon physics, props. and identification 78−82260
scintillation detector system, cosmic ray muon lifetime, undergraduate teaching 78−81752
scintillation hodoscope counter for beam meas. in CERN SPS 79−36472
showers underground, multiplicity distribs., local interactions in absorbers 77−5406
XTR-detector, Monte-Carlo simulation, 0.5-5 TeV cosmic ray hadron interactions *(Russian)* 79−49564
μ^+-nucleus 150 GeV deep inelastic scatt. in nuclear emulsions 79−17893
Fe-liquid scintillator multilayer calorimeter, transition effects. muon burst rates 78−90019
LiF thermoluminescent dosimeters, response to ground-level cosmic-ray background 79−59265
Si, defect prod. by GeV muons, thermally stimulated current technique 78−5099
Si detectors and Pb absorber plate, telescope structure, high energy muon flux measurement 80−58061

muon interactions *see lepton-hadron interactions; lepton-lepton interactions; muon-nucleon interactions; muon-nucleus reactions; photon-lepton interactions*

muon-nucleon interactions
see also muon-nucleon scattering
axial coupling const. from ^1H, ^2H muon capture *(Russian)* 77−50570
charged-hadron multiplicities, fractional-prong cross sections, liquid D target 78−74258
cosmic ray μ inelastic scatt., above 300 GeV *(Russian)* 79−22106
deep inelastic μN scatt., EM corrections to asymptotic freedom predictions 78−62403
deep inelastic muon hadron scatt. data, high energy, asymptotically free gauge theories predictions 77−49974
deep inelastic muon scatt. at large Q^2, inconsistency with QCD 79−93374
deep inelastic scatt., asymm., quark proton model evaluation, gauge theories test 78−62408
deep inelastic scatt., heavy lepton mixings, Weinberg-Salam model 80−62992
deep inelastic scattering, appl. of quark parton model 79−30715
deep inelastic scattering, gluon jets 80−105862
deep inelastic scattering in emulsion, 150 GeV, intra-nuclear cascading, existence search 79−75979
dimuon prod. and scale violation 78−62407
EM production of trimuons in deep inelastic muon scatt. 80−22619
hadronic contributions to trimuon prod., quark+antiquark annihilation 78−41551
hadronic final states in deep inelastic scatt. 78−78184
inelastic μN scattering, dimuon events, charm particle prod. and semileptonic decay 77−10260

muon-nucleon interactions continued
ionisation loss formula derivation using covariant method of equivalent photons 78−29337
jet analysis, QCD calcs. and phenomenological models 80−52523
meson electropod. in deep inelast. scatt. from polarised targets 78−25053
multimuon prod. in deep inelast. muon scatt., model calc. 77−13965
nucleon Fermi motion in deuteron, smearing effects, (West β correction), on expt. results. 80−32107
radiative μ capture on free p, low energy expansion of two current amplitudes 78−16946
relativistic corrections to weak exchange currents and μ-p capture 79−75756
scaling deviations in νN, eN, μN inelastic scatt., energy depend. 77−49948
scaling violation, two-component duality model, ν and μ interactions 78−8623
scaling violations in electromagnetic and neutrino charged-current interactions 79−17713
structure functions and charge ratios 78−74264
trilepton production, doubly charged Higgs boson in vectorlike gauge theories 77−61237
trimuon prod. from struct. at lepton vertex 78−8639
weak neutral currents, parity non-conservation in e-N, μ-N forces 77−57484
50-250 GeV EM corrections, *(Russian)* 78−25048
K^-p, π multiplicity and asymmetric fireballs 79−93474
μ^-+nucleus$\rightarrow e^-$+nucleus reaction rate calc. using gauge theory models 77−65157
μ+p, deep inelastic scatt., nucleon struct. functions 78−50036
μd, 147 GeV, inclusive hadron jet behaviour, hadron spectra, quark-parton anal. 79−71757
μd, deep inelastic scatt., nucleon struct. function moments anal., asymptotic freedom critical tests 79−54344
$\mu^-d \rightarrow nn\nu_\mu$, meson exchange currents effect on Λ_d and Λ_q transition rates 79−85256
$\mu^-d \rightarrow nn\nu_\mu$, neutron-neutron off shell interaction differential capture rates 79−71845
μN, 209 GeV, ψ diffractive prod. cross section, $\psi \rightarrow \mu^+\mu^-$ decays 80−102054
$\bar{\mu}$N, deep inelastic cross sections, search for P-nonconservation *(Russian)* 77−245
μN, deep inelastic scattering and asymptotic freedom 80−27511
μn, heavy lepton prod., SU(3)×U(1) model 78−45900
μN, inclusive scatt. 96, 147, 219 GeV, nucleon struct. function determ. 80−42472
$\mu N \rightarrow (x\mu)X$, dimuon and trimuon prod., heavy quark and 4 diffractive prod. 79−93429
μN deep inelast. scatt., inclusive ρ^0 prod. 78−37216
μN deep inelastic reactions, trimuon EM prod., cross sections at 250 GeV *(Russian)* 80−37278
$\mu N \rightarrow eN$, symmetry violation natural suppression, muon and electron lepton number nonconservation 78−8574
$\mu N \rightarrow \mu^-\mu^+ + X$, new bounds for dilepton prod. from heavy neutral leptons 77−46040
$\mu N \rightarrow \mu C\bar{C}$, heavy quark leptoproduction in QCD, charact. 79−17733
$\mu N \rightarrow \mu\Upsilon X$, 209 GeV, Υ muoprod. limits from trimuon final states 80−105909
$\mu N \rightarrow \mu X$, broken colour gauge theory of integer charge quarks 80−13313
$\mu N \rightarrow \mu X$, colour model explanation of νW_2 rise 79−45092
$\mu N \rightarrow \mu X$, nucleon struct. function meas., scaling violation obs. 79−45091
$\mu N \rightarrow \mu X$, scale breaking, modified quark distrib. function for description 77−57543
$\mu N \rightarrow \mu' h + X$, transverse parton momentum meas. 79−13076
$\mu N \rightarrow \mu\mu X/\mu N \rightarrow \mu X$ ratio, charm contrib. 77−57544
$\mu N \rightarrow \mu\psi X$, diffractive and non-diffractive ψ leptoprod. in QCD 80−424
$\mu N \rightarrow x\mu X$, x=2 or 3, charm muoprod. with small angle veto 80−47306
$\mu^-N \rightarrow$hadron shower, charm-pair production effects 80−73748
$\mu^-N \rightarrow \mu^+\mu^-\mu^-N$ in Pb, 10.5 GeV/c, short lived particle search, QED tridents 80−37275
$\mu^-N \rightarrow Ne^-$, muon-electron conversion bounds in ^{32}S 80−91092
μ^+N, 280 GeV/c in Fe, Ψ virtual photoprod. 80−37279
μ^+N in Fe, 280 GeV, dimuon prod. cross sections 80−91094
μ^+N in Fe, 280 GeV, trimuon event cross sections 80−99104
$\mu^\pm N \rightarrow M^0X$, neutral heavy lepton prod., characteristics and possible $M^0 \rightarrow \mu^+\mu^-$ search 79−71751
μp, 147 GeV, diffractive ρ muoproduction and decay into $\pi^+\pi^-$ 77−30391
μp, 147 GeV, inclusive hadron jet behaviour, hadron spectra, quark-parton anal. 79−71757
μp, 219 GeV, proton struct. function determ. 78−82216
μp, deep inelastic scatt., nucleon struct. function moments anal., asymptotic freedom critical tests 79−54344
μp, deep inelastic scattering, scaling deviations, parton model anal. 79−58966
μp, hadron prod. ang. distribs. and transverse momentum, QCD test 80−82980
μp, polarised deep inelastic scatt., energy and y depend. of cross section asymm. 78−45926
μp, semi-inclusive, ang. correl. tests of QCD 79−17735
μp, structure functions in deep inelastic scatt., second-order contributions, QCD predictions 80−13314
μp deep inelastic scatt., charm effects, field theory anal. 78−21435
μp deep inelastic scatt., inclusive cross section, lepton pair EM prod. contrib. *(Russian)* 80−105904
μp high energy data, QCD energy momentum sum rule, gluon fraction of proton 77−49971
μp inelastic scatt., p struct. function determ. 77−61290
$\mu p \rightarrow K_s^0X$, 225 GeV, deep inelastic scatt., strange neutral particle prod. 80−105902
$\mu p \rightarrow \Lambda^0(\bar{\Lambda}^0)X$, 225 GeV, deep inelastic scatt., strange neutral particle prod. 80−105902
$\mu p \rightarrow \mu X$, deep inelastic processes, nucleon struct. function, scale breaking 78−78185
$\mu p \rightarrow \mu n W^+$, current algebra and sum rules high energy W^+ prod. 80−102039
μp semi-inclusive scattering, hadronic fragmentation initiated by pointlike probes 79−49551
$\mu^-p \rightarrow \nu_\mu n$, angular correlations and capture rates, spin and isospin transitions, hyperfine effects 78−70494

muon-nucleon interactions continued
μ^+p inclusive hadron distribs., scaling props., quark-parton fragmentation 77−61296
ψ(3100) prod. cross section from μN in Fe 79−75779
N*(1236) propagator, momentum depend. in N*-excitation current 80−27559

muon-nucleon scattering
see also muon-nucleon interactions
deep inelastic processes, scaling violations, asymptotic free field theory anal. 78−4863
deep inelastic scatt., longit. struct. functions 77−49979
deep inelastic struct. function higher order asymptotic freedom corrections for e, M, γ scatt. 79−93426
deep-inelastic leptoproduction off nucleons, struct. function model in asymptotically free gauge models 79−40786
gauge model of weak and electromag. interactions, polarised lepton scatt. 78−45901
muon scattering at Fermilab, inclusive scatt., quark models, scaling violation 80−5001
nucleon structure functions from quark distrib. functions anal. of μp and μd interactions 78−50035
P-odd asymmetry in l-N scatt., unified model *(Russian)* 77−61300
polarised μ scattering, elastic and deep inelastic, covariant formulation 80−78069
S,P,T-type neutral weak current meas. in μN scatt. 80−32064
$\mu^- + Z \rightarrow Z + \bar{\nu}_\mu + W^+$, anomalous elec. quadrupole moment and cross-section *(Russian)* 77−34148
μN, 270 GeV, multimuon final states, total cross section, associated charm prod. 80−13315
$\mu N \rightarrow 3\mu N$, EM contribution cross section, using radiative quark-parton model 79−40788
$\mu N \rightarrow \mu$+anything, 3.0 to 10.1 GeV muons in nuclear emulsion, cross sections, e comparison 77−46161
$\mu N \rightarrow \mu\mu X$ ($\mu\mu$X), 150 GeV prod. ratios 77−79268
μp, deep inelastic scatt., higher order asymptotic freedom corrections 80−105903
μp, semi-inclusive scatt., quantum chromodynamic predictions 78−29324
μp(d) scatt., nucleon struct. function moments, asymptotic freedom critical test 79−85300
μp deep inelastic scatt., approx. calc. of EM corrections *(Russian)* 79−67558
$\mu^- p \rightarrow \mu^- p$, elastic scatt., polarisation of final lepton *(Russian)* 77−26529
$\mu^+ \rho$ scattering, exclusive vector meson prod. ρ, ρ^0 and ω cross sections 79−49528

muon-nucleus reactions
for inelastic muon-nucleus scattering, see "muon-nucleus scattering"
see also muon capture; muon-nucleon interactions
anomalous interaction rel. to muonic atom energy shift *(Russian)* 78−74804
capture with neutron emission, 3-body decay kinematics 77−67736
CERN School of Physics, Austerlitz-Zeist, Holland (June 1978) 79−30857
charmed particle pair prod. in muon deep inelastic scatt., event location in nucl. emulsion target 80−27906
deep inelastic hadron leptoproduction on nuclei, inclusive hadron final states 78−54741
deep inelastic scattering in emulsion, 150 GeV, intra-nuclear cascading, existence search 79−75979
hadron production in deep inelastic scattering of 150 GeV muons in nuclear emulsions 79−17893
hadronic cascades induced by high-energy muons in iron/plastic calorimeters, calibration calcs. 77−54477
muon capture progress, weak interaction form factors 80−42643
nuclear muon capture, developments in theory and expts. 80−42642
nucleon Fermi motion in deuteron, smearing effects, (West β correction), on expt. results. 80−32107
stopped muons, macroscopic polarisation (Hanle) signals 80−5130
deep inelastic processes, nucleon struct. function, scale breaking 78−78185
e^+e^- pair production cross-section, transferred momentum depend. *(Russian)* 79−54432
(μ,α), reaction probabilities on targets from ^{23}Na to ^{209}Bi 78−29451
(μ^-,e$^-$), reaction rate calc. using gauge theory models 77−65157
($\mu^\pm$,$\mu^\pm$'xN), A=12-203, muodisintegration cross sections, PWBA anal. 80−68650
(μ,n), high energy neutron spectroscopy 80−73841
(μ^-,ν), 1p nuclei M2 giant resonance calcs. 80−22784
(μ,pxn), reaction probabilities on targets from ^{23}Na to ^{209}Bi 78−29451
μ^- to e$^-$ conversion in nuclei, mediation by Majorana lepton 80−22547
$\mu^\pm$ spin rotation, μ relaxation and repolarisation, muonic X-rays 80−42644
μ+atom, e^+e^- pair prod., energy spectrum, screening effects *(Russian)* 78−55250
^{16}O(0$^+$)(μ,ν)^{16}N(0$^-$), one pion exchange current problem for ^{16}O(0$^+$)$\rightleftarrows^{16}$N(0$^-$) 79−85375
Al(μ^-,X), energetic charged particle spectrum, integrated yield 80−18293
^{12}C(μ,γ), exclusive radiative capture, axial currents and induced pseudoscalar form factors 79−97699
^{12}C(μ,ν_μ)^{12}B, induced pseudo-scalar coupling constant 79−49606
^{12}C(μ,ν)^{12}B, polarisation of ^{12}B, weak coupling anal. 77−88116
^{12}C(μ^-,ν)^{12}B(g.s.), qualitative meas. of longitudinal recoil polarisation 79−54429
^{40}Ca($\mu,n\nu$)^{39}K, neutron spectra calc. in simple-pole model 77−71606
Cu(μ^-,X), energetic charged particle spectrum, integrated yield 80−18293
D-T, muon catalysed fusion for pellet ignition 77−3063
Fe cascade showers in ionisation calorimeter 79−84618
Fe, cosmic-ray muons inelastic interaction 79−84616
Fe+μ, 2 to 800 GeV, EM interactions of cosmic ray muons, e^+e^- prod. and knock-on e$^-$ prod. 79−66902
Fe+$\mu\rightarrow$multimuons+X, 150 GeV/c, charmed particle prod. 77−38177
Fe(μ,μ'), small Q^2 and >200 GeV, implications for photonuclear process 77−23001
^{2}H, weak and EM lepton reactions, exchange currents, isobaric excitations and form factors *(German)* 79−93523
^{2}H(μ,ν_μ)nn, differential spectra *(Russian)* 77−82915
^{2}H(μ^-, ν)2n, axial meson exchange currents, a_{nn} and g_ρ extraction 79−97658

muon-nucleus reactions continued
^{2}H(μ^-, ν)2n, hard pions and axial meson exchange current effects 79−40906
^{2}H(μ^+,μ^+)pn, Coulomb break-up amplitude in three-body scatt. theory 79−71844
^{2}H(μ^+,μ^+np), ≤5 MeV, Coulomb break-up of deuteron and n-p off-shell effects 79−75777
^{2}H(tμ,nμ)^{4}He, muon catalysed fusion, neutron yield, muonic molecules 80−106095
^{3}He, μ-capture, total and partial capture rates 79−9522
^{6}Li(H,ν)^{3}H^{3}H, muon capture in ditriton channel by elementary particle model 79−40907
^{6}Li(μ^-,ν_μ)^{3}H^{3}H, total and differential muon capture rates from elementary particle model 79−89297
^{6}Li$\mu^- \rightarrow ^3$H^{3}Hν in ^{6}Li loaded photoemulsion, secondary particles ang. distrib. and energy *(Russian)* 78−89855
^{92,94}Nb production in Earth crust by cosmic-ray muons 77−49045
^{16}O(0$^+$)$\rightleftarrows^{16}$N(0$^-$), beta decay and muon capture rate ratio, mesonic exchange currents 80−42594
^{16}O(μ,γ), exclusive radiative capture, axial currents and induced pseudoscalar form factors 79−97699
^{16}O(μ^-,e$^-$)^{16}O*, shell model anal. of μe conversion rate *(Russian)* 79−89300
Pb(μ^-,X), energetic charged particle spectrum, integrated yield 80−18293
^{242}Pu(μ,f), radiationless muonic transition induced fission, fission dynamics probe, friction coeff. 80−78336
^{32}S(μ^-, e), muon-electron conversion bounds 80−91092
^{32}S(μ^-,e$^+$)-^{32}Si*, muon conversion search, deduced upper limit 79−13285
S(μ^-, e$^-$), upper limit for muon-electron conversion 78−21547
U (M,f), muon excitation probabilities, muonic atoms, Schrodinger eqn. 80−47515
^{A}U(μ,f), A=235,238, prompt and delayed fission, absolute yields and lifetimes 80−78337
^{238}U (μ^-,f), fission product mass distrib., fission probability, radiochem. investigation 78−29514
U(μf), emission of conversion μ in radiation free fission *(Russian)* 78−62587

muon-nucleus scattering
see also muon-nucleon scattering
A dependence of photoabsorpt. processes, from inelastic electron and muon scatt. studies 77−82911
cosmic ray muons, multiple scattering in mag. spectrometers 80−4215
deep inelastic Coulomb corrections 79−89299
deep inelastic multimuon prod., charmed hadron prod. 77−71519
parity nonconservation in elastic scatt. with 0$^+\rightarrow$0$^-$ transition *(Russian)* 77−61402
polarisation of beam, rel. to nucl. recoil effects 79−67738
single and multiple scatt. in continuous media with focusing mag. field 77−24328
$\mu^+ + Z \rightarrow Z + \bar{\nu}_\mu + W^+$, anomalous elec. quadrupole moment and cross-section *(Russian)* 77−34148
$\mu N \rightarrow \mu$+anything, 3.0 to 10.1 GeV muons in nuclear emulsion, cross sections, e comparison 77−46161
NaCl+cosmic ray muons, photonuclear cross section, nuclear muon losses 77−64581
Pb nuclei, multiple scatt. at sea level, Rainwater-Cooper theory, 230 MeV/c muons 78−7850
Pb nuclei, multiple scatt. at sea level, anomalous scatt. distrib. 78−7851

muon probes
alkali metals, muon Knight shift 79−56656
alkali metals, positive muon spin rotation frequency, Knight shift meas. 79−38421
alkaline earth metals, muon Knight shift 79−56656
alkaline earths, positive muon spin rotation frequency, Knight shift meas. 79−38421
antiferromagnet, local field at positive muon 78−92010
capture probabilities of elements in ionic solids, chem. struct. factors 77−50550
cascade depolarisation of negative muons 77−48114
condensed matter, muon spin rot., comparison with Mossbauer spectroscopy *(French)* 80−80667
conference, muon spin rot., Rorschach, Switzerland (Sept. 1978) 79−56652
crystal defects study 79−56700
defect structure, feasibility of using positive muons as probes 79−15389
diamagnetic domains, study by positive muon method 80−60174
diamond type crystals, polarization of μ^+ in muonium atom *(Russian)* 78−39492
diamond-structure crystals, anomalous muonium, μ^+ meson probe appl. *(Russian)* 79−28665
diffusion and trapping in solids 80−71283
diffusion in presence of traps, spin depolarisation, stochastic theory 79−28666
disordered binary alloys of ferromag. crystals, mag. dipole fields at interstitial sites 80−97176
electron gas, spin-polarised, self-consistent screening of positive muon 78−47714
exotic atoms, conf., Erice, Sicily, (1979) 80−67939
ferromagnet, internal fields, positive muon investigation 78−68438
ferromagnet, local field at positive muon 78−92010
ferromagnetic BCC and HCP crystals, anisotropy of dipole fields, at interstitial sites 79−33584
ferromagnetic metal, magnetisation density in vacancies, μ^+ probe, theory 77−28504
ferromagnetic metals, muon spin rotation; freqs., and relax. rates 80−55006
ferromagnets, hyperfine field at positive muon 80−40029
free radical chemistry, μSR appl. 79−57209
interstitial site determ., μSR technique 80−71287
lattice atom displacements near end of implanted μ^+ tracks 78−55890
low temperature physics, appl. of muon spin rotation technique to study of mag. systems 79−65782
magnetic materials, μSR meas. 79−56660
magnetic materials, muon spin relax. 79−56668
magnetic structure, investigation of inhomogeneously magnetised ferromagnetic metals 79−42739
magnetic studies using muon spin rotation, review *(Japanese)* 78−52417
magnetism, state-of-the-art 77−63351

muon probes continued
metal, μ^+ diffusion, μSR linewidths anal. 79−56691
metal, μ^+ relax., theory 77−59501
metal, μ^+ SR, localisation and diffusion, rel. to H 80−50248
metal, electron densities at muons 79−56655
metal, FCC, muon diffusion, theory 78−22883
metal, FCC and BCC, dipole interactions and trapping effects of positive muons 78−47342
metal, H-like impurities electron. struct., μ^+ probes 79−56653
metal, interstitial, quadrupole effect on dipolar field width 78−2457
metal, muon$^+$ spin relaxation, precession freq. and depolarisation *(Russian)* 77−69761
metal, muon macroscopic diffusion 79−56698
metal, muon screening spherical solid model 79−56654
metal, point defects, μSR studies 79−56703
metal, positive muon diffusion 79−19388
metal, positive muon spin depolarisation, defect study 78−47314
metal, quantum theory of light interstitial diffusion 79−56690
metal, spherical solid model for muon and H in metals 79−78601
metal studies by positive probes, review 80−103909
metals, μ^+ diffusion, LAMPF results 80−71285
metals, anomalous temp. depend. of relax. rate of μ^+-meson polaristaion *(Russian)* 78−92012
metals, light interstitials diffusion, multiphonon transition modes classification 80−70448
metals, muon spin rot. diffusion expts. 79−56680
metals, muon trapping by defects and impurities 80−20573
metals, positive muon interactions 80−71284
motion in solids 79−56681
muon spin depolarisation, trap effects 79−56683
muon spin rotation, review, book contrib. 79−22161
muon spin rotation, review of recent advances 79−24252
muonium, bimol. rate consts., Larmor precession relax., kinetic isotope effect rel. to H 77−38752
muonium, existence of quadrupole moment *(Russian)* 78−31143
muonium formation and charged particle tracks 79−57259
muonium-substituted transient radicals observed by muon spin rotation 78−74678
negative muon spin rotation 79−56705
negative muons, transport properties in matter, energy spectra 77−56239
negative muons, transport properties in matter 77−56238
oxide powders, muonium and positronium form. 79−56679
oxides, obs. of slow relax. of spin of negative muons *(Russian)* 78−48105
paramagnet, free electron, muonic and hydrogenic Knight shifts 78−43759
positive muons as light isotopes of H, book contrib. 79−82907
positive-muon spin depolarisation in solids 79−33585
quadrupole moment and relax. of muonium and mesoatom spins 78−19404
quartz, muonic atoms, hyperfine splitting frequency *(Russian)* 79−91332
quartz, muonium EPR transitions by muon-spin rot. 80−29668
quartz, muonium hyperfine splitting meas., muon spin rot. technique 80−50246
α-quartz, muonium precession, quadrupole splitting 79−42879
quartz, muonium precession, quadrupole splitting 79−56678
quartz, quadruple effects in spin precession of muonium 80−75910
rare earth metal, muon spin relax. meas. of Neel temp. and antiferromag. transitions *(Russian)* 79−87369
rare earth orthoferrites, muon states, local mag. fields 80−75911
semiconductors, μSR research 79−56672
solid state materials, struct. and props., appl of μ^+SR 79−65781
spin depolarisation of muons diffusing in presence of traps 79−56682
spin glasses, spin dynamics, EPR, NMR, muon precession, Mossbauer, and neutron scatt. results 79−65689
spin relaxation, zero- and low-field, appl. 80−2680
spin rotation, appl. 78−52415
spin rotation and complementary techniques, EXAFS and Mossbauer effect 80−39912
spin rotation method, review *(Polish)* 80−88901
spin-conversion, by paramag. ions in aq. soln. 79−24251
thymine+muonium, radical form. in aq. soln., spin reson. obs. 78−74679
transition metal silicides, NMR and μSR, microscopic mag. props. *(Japanese)* 78−52368
transition metals, positive muons as light isotopes of H, book contrib. 79−82907
two-frequency precession determ. of hyperfine splitting in matter 77−28505
type II superconductor, positive muon diffusion coeff., determ. from transverse depolarisation 80−25269
μ^- depolarisation, exotic at. orbital ang. momentum alignment effect 80−18946
μ^+ investigation of solids, physics and chemistry of μ^+ and muonium, review *(Russian)* 77−50566
Ag-Zn, negative muon capture ratios 80−55007
Al, defects due to neutron irrad., muon probes study 79−56701
Al, muon diffusion, μSR 79−56696
Al, muon diffusion at low temp., effect of nuclear elec. field gradients 77−52005
Al, μ^+ localisation temp. depend. 80−44993
Al, μ^+ meson diffusion, impurities effect *(Russian)* 78−35077
Al, μ^+SR diffusion, temp. depend. 78−39490
Al, neutron irrad., μ^+ mobility and trapping by vacancies, muon spin rot. meas. 79−4757
Al, positive muon spin rotation meas. 78−10819
Al, proton irradiated, muon spin rotation study at low temps. 78−92011
Al, quenched, muon$^+$ trapping at vacancies, compared with positron annihilation 80−15937
Al, radiation damage due to protons, μSR 79−56702
Al-Ag(Cu)(Mg)(Si)(Zn), dil., μ^+ depolarisation 79−56697
Al-Cu alloys, positive muons diffusion and trapping 79−11372
Al-Mn, dil., coherent propag. and strain-induced localisation of muons 78−95537
Al-Mn, μ^+ localisation temp. depend. 80−44993
Al-Ni, positive muon trapping at vacancies 79−56704
AlGd alloys, μ^+ depolaris. rate 79−56695
$AlMn_x$, muon diffusion, μSR 79−56696
As, muonic Knight shift, temp. and mag. field depend. 79−91331
AuFe spin glass, μ^+ zero-field spin relax. probe for spin dynamics 80−97177
muon probes continued
Be, Knight shift of μ^+ 79−56657
Be, muon location and diffusion, μSR 79−56693
Bi, muonic Knight shift, temp. and mag. field depend. 79−91331
Bi, μ^+ diffusion, spin relax. temp. depend. *(Russian)* 77−48115
Bi, zero field spin relaxation studies as a probe of positive muon diffusion mechanisms 80−34840
Co, crystal hyperfine fields and neutron scatt. 79−56172
Co, dipole field anisotropy, at interstitial sites, lattice-deformation effects 79−33584
Co, ferromag., hyperfine fields at positive muons 78−43758
Co, ferromag., local mag. field at positive muon 77−12295
Co, ferromagnetic, temp. depend. of μ^+ hyperfine field 78−43761
Co host, dil. impurity hyperfine fields, comparison with models 78−14954
Co, interstitial site determ., μSR technique 80−71287
Co, local magnetic fields probed by μ^+ 78−48103
Co, magnetised to saturation, props., positive-muon study 78−6619
Co, muon resonance meas. of local mag. dipole field at interstitials 79−95699
Co, positive muons as light isotopes of H, book contrib. 79−82907
Co, single crystal, muon spin rotation expt. results 77−12294
Cr, antiferromag., muon depolarisation, mag. anisotropy determ. *(Russian)* 79−61290
Cr, antiferromagnetic, muon diffusion, spin relax. and coherent motion 80−71281
Cr, antiferromagnetic, positive muons as light isotopes of H, book contrib. 79−82907
Cr, μ^+ depolarization and diffusion 77−59500
Cr, μSR meas. 79−56667
Cr, spin relaxation of μ^+-mesons *(Russian)* 79−8083
Cr_2O_3, antiferromag., muon spin rotation *(German)* 80−54877
Cr_2O_3, muon spin rotation expts. 80−71282
Cr_2O_3, muon states, local mag. fields 80−75911
Cr_2O_3, μSR meas. 79−56666
Cu, diffusion of muons and protons 79−56689
Cu, elec. field gradient due to interstitial positive muon 78−31142
Cu, lattice relaxation around μ^+ 79−56658
Cu, muon diffusion at low temp., effect of nuclear elec. field gradients 77−52005
Cu, muon localisation and lattice dilation, μSR 79−56694
Cu, muon spin rot., EFG, site of localisation 78−2785
Cu, muon trapping, Knight shift, rel. to H interstitials 80−50247
Cu, μ^+ diffusion data anal., theory of incoherent direct and indirect multiphonon transitions 80−70448
Cu, μ^+ localisation temp. depend 80−44993
Cu, μ^+ meson localisation method *(Russian)* 77−32313
Cu, μ^+ meson spin relax. in cryst. lattices *(Russian)* 79−28664
Cu, μ^+SR diffusion, temp. depend. 78−39490
Cu, positive muon dipolarisation rate 79−56692
Cu, positive muon spin rotation meas. 78−10819
Cu, positive muon spin rotation frequency, Knight shift meas. 79−38421
Cu, positive muons as light isotopes of H, book contrib. 79−82907
Cu, proton irradiated, muon spin rotation study at low temps. 78−92011
Cu, radiation damage due to protons, μSR 79−56702
Cu:μ^+, lattice distortions, microscopic calc. 78−87665
Cu-Al, negative muon capture ratios 80−55007
Cu-Al, positive muon trapping at vacancies 79−56704
CuMn spin glass, μ^+ zero-field spin relax. probe for spin dynamics 80−97177
CuMn, spin glass, random moments time correl., zero field muon spin relax. meas. 80−60335
Dy, crystal hyperfine fields at positive muons 79−56662
Dy, interstitial site determ., μSR technique 80−71287
Dy, μSR in ferro- and antiferromag. phases, local fields 78−43763
$DyFeO_3$, weak ferromagnet, μSR study 80−93226
$ErFeO_3$, weak ferromagnet, μSR study 80−93226
Fe, crystal hyperfine fields and neutron scatt. 79−56172
Fe, ferromag., hyperfine fields at positive muons 78−43758
Fe host, dil. impurity hyperfine fields, comparison with models 78−14954
Fe, hyperfine field and diffusion of μ^+ 77−52006
Fe, magnetised to saturation, props., positive-muon study 78−6619
Fe, muon diffusion, spin relax. 79−78599
Fe, muon diffusion and relaxation studies 80−75913
Fe, muon quantum diffusion 79−78598
Fe, muon$^+$, 40 MeV, traversing magnetised plates, dynamic mag. fields 79−38422
Fe, muon$^+$ diffusion, spin rotation, effect of impurities 80−7249
Fe, muon$^+$ spin precession and relax., hyperfine field temp. depend. 77−63350
Fe, muon$^+$ spin rotation meas., local hyperfine field temp. depend. 77−63349
α-Fe, μ^+ diffusion 79−56687
Fe, μ^+ hyperfine field and relaxation, temp. depend. 78−95538
Fe, μ^+SR, theory of spin depolarisation rate 78−80271
Fe, positive muon diffusion 79−56688
Fe, positive muon diffusion, press. depend. 80−75907
Fe, positive muon spin precession, effect of press. 80−40030
Fe, quantum diffusion of positive muons, 3 to 300K 80−75909
Fe, single crystal, muon spin rotation expt. results 77−12294
Fe, zone-refined, positive muon diffusion at room temp. 79−47377
Fe-Al, hyperfine field meas. using muon-spin-rotation method 80−10933
α-Fe_2O_3, antiferromag., muon spin rotation meas. 78−48106
α-Fe_2O_3, antiferromag., muon spin rotation *(German)* 80−54877
α-Fe_2O_3, muon spin rotation above and below Morin transition 78−43762
α-Fe_2O_3, muon spin rotation expts. 80−71282
α-Fe_2O_3, muon states, local mag. fields 80−75911
α-Fe_2O_3, μSR meas. 79−56666
Fe_3O_4, muon states, local mag. fields 80−75911
FeSi, hyperfine fields about μ^+ 79−56664
Gd, crystal hyperfine fields at positive muons 79−56662
Gd, dipole field anisotropy, at interstitial sites, lattice-deformation effects 79−33584
Gd, ferromag., hyperfine fields at positive muons 78−43758
Gd, ferromag., local mag. field at positive muon 77−85637
Gd, ferromag., temp. depend. of hyperfine field at interstitial positive muon 79−15300
Gd, ferromagnetic, temp. depend. of μ^+ hyperfine field 78−43761

muon probes continued
Gd host, dil. impurity hyperfine fields, comparison with models 78−14954
Gd, interstitial site determ., μSR technique 80−71287
Gd, local magnetic fields probed by μ^+ 78−48103
Gd, positive muons as light isotopes of H, book contrib. 79−82907
Ge, anomalous muonium state 79−56677
Ge, deep donor character of muons and protons 80−10911
Ge, impurity levels of H and muons 79−56162
Ge, muonium relaxation rates 80−75912
n-Ge, μ^+ depolarisation, post muonic stage *(Russian)* 77−48116
Ge, μ^+ meson polarisation, H impurity behaviour 77−20786
Ge, μSR, spin Hamiltonian and anomalous muonium states 80−71286
Ge:As, interaction of muonium with atoms 79−11373
In, muon quadrupolar interaction expansion of crystal lattice *(Russian)* 79−15388
KCl-KBr, solid soln., negative muon capture ratios 80−55007
$LaNi_5H_x$, μ^+ spin relax. and Knight shift 79−56699
MnO, negative muon spin rot., paramag. shift 79−56706
MnO, paramag., μ^- spin rotation at O site 77−20785
MnO, paramagnetic, positive muon longit. spin relax., temp. depend. 78−80268
MnO, positive muon spin relax. 79−56669
$MnO-Al_2O_3-SiO_2$ glass, spin freezing, muon spin depolarisation 78−39491
$MnO-Al_2O_3-SiO_2$ glass, spin freezing, muon spin depolarisation, superparamag. domain model 78−68272
MnSi, μ^+ Knight shift, temp. depend. 78−80270
MnSi, μ^+ probe, itinerant electrons spin fluctuations 79−56671
MnSi, μ^+ spin relax. 79−56670
MnSi, μ^+ spin-lattice relax rate, paramag. phase, near T_c, temp. depend. 79−19825
Na, thermodynamics of light interstitials, rel. to delocalised particles 79−46653
NaCl-NaBr, solid soln., negative muon capture ratios 80−55007
Nb, critical field, muon spin relaxation *(German)* 80−50015
Nb, defects due to neutron irrad., muon probes study 79−56701
Nb, electron irradiated, muon diffusion 80−80668
Nb, muon diffusion, μ^+SR meas. 78−39487
Nb, muon diffusion at low temp., effect of nuclear elec. field gradients 77−52005
Nb, muon diffusion in presence of traps 78−68439
Nb, muon diffusion in presence of traps 79−56684
Nb, muon localisation and lattice dilation, μSR 79−56694
Nb, muon location and diffusion, μSR 79−56693
Nb, muon spin rotation in mixed state 79−56446
Nb, muon trapping, Knight shift, rel. to H interstitials 80−50247
Nb, muon$^+$ depolarisation rate, anomalous temp. depend. 78−48104
Nb, μ^+ meson spin relax. in cryst. lattices *(Russian)* 79−28664
Nb, positive muons, depolarisation rate, anomalous temp. depend. 78−80269
Nb, pure and O doped, muon diffusion and trapping 79−56685
Nb, spin polarised μ^+ meas., localisation and thermal diffusion 78−39489
Nb, zero field spin relaxation studies as a probe of positive muon diffusion mechanisms 80−34840
Nb-V_3Ga mixed state, Meissner effect investigation by muon method *(Russian)* 80−107954
Ni, band structure, μSR Knight shift meas. 79−56663
Ni, crystal hyperfine fields and neutron scatt. 79−56172
Ni, ferromag., hyperfine fields at positive muons 78−43758
Ni, ferromag., hyperfine field of positive muon 79−47378
Ni, ferromag., Knight shift of hyperfine field at positive muon 77−43925
Ni, ferromagnetic, temp. depend. of μ^+ hyperfine field 78−43760
Ni, ferromagnetic zero point motion effect on hyperfine field at interstitial positive muon site 80−2681
Ni host, dil. impurity hyperfine fields, comparison with models 78−14954
Ni, hyperfine field of μ^+, calc. 77−40167
Ni, interstitial site determ., μSR technique 80−71287
Ni, magnetised to saturation, props., positive-muon study 78−6619
Ni, muon hyperfine field, cluster calc. 79−56661
Ni, muon$^+$ spin rotation, hyperfine field determ., 0.12 to 300K 77−24775
Ni, muon$^+$ spin rotation meas., local hyperfine field temp. depend. 77−63349
Ni, paramag., muon spin rot. Knight shift, 637 to 906K 80−75908
Ni, paramag., μ^- relax. 77−24776
Ni, positive muon diffusion 79−56688
Ni, positive muon diffusion, press. depend. 80−75907
Ni, positive muon spin precession, effect of press. 80−40030
Ni, positive muons as light isotopes of H, book contrib. 79−82907
Ni, radiation damage due to protons, μSR 79−56702
Ni-Co, local mag. field on μ^+ 79−56665
Ni-Cr, dil. alloy paramag., μ^- relax. 77−24776
Ni-Cu, local mag. field on μ^+ 79−56665
Ni-H, ferromag., H impurities and μSR, self-consistent calc. 80−84447
NiCr, hyperfine fields about μ^+ 79−56664
Pb intermediate state, Meissner effect investigation by muon technique *(Russian)* 80−107954
Pb, muon angular distrib., Monte Carlo calc. 79−78600
Pb, supercond., internal mag. field meas. by μ^+ method *(Russian)* 79−33391
Pd, metallic, positive muon Knight shift 80−71280
Pd, muon end depolarisation, hyperfine anomaly 77−28503
Pd-Fe, dil. alloy, conduction electron polarisation at 0.1K, μ^+SR 77−20784
Pd-Fe alloy, dil., cond. electron polarisation studied by positive muons 77−28397
Pd-Fe and Pd, muon$^+$ Knight shift, cond. electron polarisation, RKKY oscill. 77−66450
Pd-Rh, dil., hyperfine anomaly between bound negative muon and Rh nucleus 79−56707
β-PdH_x, muon depolarisation rate 77−32312
Sb, muon precession freq., anomalous shift 78−39488
Sb, muonic Knight shift, temp. and mag. field depend. 79−56659
Sb, muonic Knight shift, temp. and mag. field depend. 79−91331
Si anomalous muonium states, time behaviour of μ spin polarisation 79−11371
Si, anomalous muonium state, μSR 79−56674

muon probes continued
Si, deep donor character of muons and protons 80−10911
Si, impurity levels of H and muons 79−56162
Si, muon depolarisation, diamag. and paramag. states obs. *(Russian)* 79−87370
Si, muon depolarisation 79−56675
Si, muon state, muon spin rot. exam. 78−60373
Si, muonium precession freq., form. probability meas. 79−11370
Si, muonium state, anomalous 79−56673
Si, μ^+ spin relaxation in longitudinal mag. fields *(Russian)* 78−88245
Si, μ^+-meson depolarisation, spin relax. *(Russian)* 78−52416
Si, μSR, spin Hamiltonian and anomalous muonium states 80−71286
Si, paramagnetic state (μ^+e^-) at high temp. 79−56676
A-SiC, dimensions of muonium atoms, depolarisation of positive muons 79−11374
SiO_2, fine powder, interstitial vac. thermal muonium production 78−42250
Ta, critical field, muon spin relaxation *(German)* 80−50015
Ta, muon diffusion, μ^+SR meas. 78−39487
Ta, muon location and diffusion, μSR 79−56693
Ta, muon quadrupolar interaction expansion of crystal lattice *(Russian)* 79−15388
Ta, muon spin rotation in intermediate state 79−56446
Ta, muon trapping, Knight shift, rel. to H interstitials 80−50247
Ta, μ^+SR diffusion, temp. depend. 78−39490
Ta, single cryst., positive muon diffusion 78−80267
Te, paramagnetic state (μ^+e^-) at high temp. 79−56676
Te, relaxation of μ^+ meson spin, (μ^+e^-) paramag. state form. *(Russian)* 79−38424
V, diffusion of positive muons 78−47601
V, muon diffusion, μ^+SR meas. 78−39487
V, muon diffusion and trapping 79−56686
V, muon localisation and lattice dilation, μSR 79−56694
V, muon trapping, Knight shift, rel. to H interstitials 80−50247
V, μ^+ meson spin relax. in cryst. lattices *(Russian)* 79−28664
V, μ^+SR diffusion, temp. depend. 78−39490
V_3Ga, supercond., μ^+ probe study *(Russian)* 79−7946
V_3Ga, supercond. μSR meas. 79−56667
ZrH_2, non-secular part of nucl. dipolar broadening detected by μ^+ zero-field spin relaxation 80−7250

muon production
bag model, meson and massive photon production 80−105850
cosmic ray proton atmospheric interactions, direct leptons prod. *(Russian)* 80−12627
cosmic-ray-nucleus reactions, hadron multiple prod., muon time-correl. meas. *(Russian)* 77−14133
di-lepton events in BEBC narrow band beam neutrino expt. 78−41528
dimuon continuum origin and space-time evolution of hadron collisions 77−88015
dimuon continuum production in hadron collisions, nonscaling behaviour 79−22156
dimuon energy asymmetries in neutral heavy lepton decay, ang. momentum constraints 77−38155
dimuon enhancement at 9.5 GeV, vector meson family with hidden 'beauty' *(Russian)* 78−33030
dimuon events, production by heavy lepton decay, appl. to e^+e^- collisions 77−54093
dimuon events with identical sign, signal of creation of heavy leptons in neutrino expts. *(Russian)* 77−82729
dimuon prod., p+Cu, 300, 400 GeV, cross-section meas. 77−6379
dimuon prod. in $\nu(\bar{\nu})$N, possible fifth quark 77−61276
dimuon prod. in proton-nucleus 400 GeV collisions, ψ' and ψ signals 77−10399
dimuon production, QCD and high transverse momentum data reconciliation 79−49478
dimuon production in νN and $\bar{\nu}$N reactions, high energy, quark-parton model with charm 77−57520
dimuon production rate from $\nu(\nu)$ N reactions in steel at 45-205 GeV 78−8646
dimuon resonance obs. at 9.5 GeV in 400 GeV proton-nucleus interactions 77−74847
Dreel-Yan processes, gluon corrections 78−8597
Drell Yan production of intermediate vector bosons, μ prod. in pp, $\bar{p}p$, $\pi^\pm p$ reactions 78−29364
Drell-Yan conjecture in asymptotically free theories 79−17689
Drell-Yan contrib. to lepton pair prod., incident hadron $q\bar{q}$ correlation function 78−89668
Drell-Yan formula in perturbation theory, Abelian gluons 79−30702
Drell-Yan model, hadroprod. of muon pairs 78−45872
Drell-Yan model at measured Q_T: asymptotic smallness of the one-loop corrections 80−105847
Drell-Yan muon prod., QCD correction uniqueness 80−78032
Drell-Yan process as a probe of color excitation 79−36021
Drell-Yan process higher order corrections, QCD and parton model sum rules 80−95251
Drell-Yan processes, A-depend. of valence and sea quark contribs. 80−86684
Drell-Yan processes, asymptotic freedom corrections, Q^2-dependence 80−62933
Drell-Yan processes, nonleading $q\bar{q}$ and qg contribs. 79−85269
Drell-Yan processes, perturbative versus asymptotic freedom convections 79−63446
Drell-Yan trigger, hadronic prod. of dilepton pairs and muons 78−37182
eight quark model, modified left-handed currents, ν reactions and e^+e^- annihilations 78−16982
four-muon prod. by neutrinos 78−29330
hadron interactions, neutral heavy lepton detection probability 78−8612
hadron-hadron collisions, QCD high energy predictions using methods of cut vertices 79−89128
hadron-nucleus collisions, relation between low mass dimuon and meson prods., quark-antiquark interactions 78−41477
hadron-nucleus collisions at 200 GeV, obs. of prompt single muons and dimuons 77−30572
hadronic μ-pair prod., hadron mass corrections and parton transverse momentum 79−36034
hadronic muon pair prod. QCD radiation and mean scaling, longitudinal and transverse momentum 80−42405
hadronic quantum numbers beyond charm as possible source of neutrino induced trimuons 78−12903
heavy lepton hypothesis of μ-e events 78−37195

muon production continued
heavy leptons, weak gauge boson and neutrino trimuon prod. 78−4851
heavy neutral leptons→muon pairs, leptonic cascade decay 78−21407
high-energy cosmic-ray components in atmosphere, scaling features 78−93062
higher-twist effects in QCD, deep inelastic scattering and the Drell-Yan process 80−102020
inclusive hadroproduction of μ pairs, 39.5 GeV/c $\pi^{\pm}$, $K^{\pm}$, p, $\bar{p}$ beams on Cu target 78−62470
lepton+hadron collisions, hadronic contributions to trimuon prod., quark-+antiquark annihilation 78−41551
lepton-hadron, trimuon final states, prod. mechanism model independent study, selection rules 79−93424
longitudinal polarization measurement in NN collisions at 1.9 GeV *(Russian)* 79−3038
low momentum surface beam for LAMPF 78−70672
massive μ pair prod. in hadron collisions, field theoretic parton model 77−30326
massive μ pair prod. in hadron-hadron collisions, asymptotically free parton model 77−13936
massive μ pair prod. in hadronic collisions, ang. distrib, quark-partons+gluons model 77−82706
massive muon pair data, cf asymptotically free parton model 78−8605
Monte Carlo quark-parton model for multiparticle and low mass dimuon prod. 79−30697
multimuon prod. in conjunction with ψ particles in π(p)+nucleus reactions 77−30460
multimuon prod. in deep inelast. muon scatt., model calc. 77−13965
multimuon prod. in neutrino scatt., SU(3) gauge theory 78−58153
multimuon signal in deep inelastic μ-nucleus scatt. 77−71519
neutral current reactions, (V-A) model, mixing between ordinary and heavy leptons 78−41472
neutrino interactions, charm particle prod. and subsequent decay into like-sign dimuons and trimuons 79−63469
neutrino interactions, SU(3)⊗U(1) gauge model of trimuon prod. 77−74671
neutrino produced muons, Fermilab 15 ft bubble chamber, external identifier, proportional chambers 77−6629
neutrino scattering, trimuon event sources 78−25035
pair generation, nucleon cascade role 80−91120
pair production in hadron-hadron collisions, gluon effects, QCD predictions 78−78148
pair production in pp(pp̄), asymptotic freedom and scaling violations 77−26554
pair production in pp and pn interactions, M quiescent mass determ. *(Hungarian)* 79−13163
parton model, asymptotically-free, $W^{\pm}$, Z^0, μ-pair prod. 78−12865
parton model, transverse momentum distrib. determ. 77−71484
photoproduction of relativistic parapositronium, and muonium perturbation expansion *(Chinese)* 79−49432
polarisation of prompt muons prod. at large transverse momenta 77−71542
polarised muonic beam, variable helicity, from π decay 77−6598
polarised prompt muons at high p_T via 400 GeV proton interactions 77−13991
$p\bar{p}\rightarrow\mu^+\mu^-X$, parity violating effects in dilepton production using polarized targets 79−67613
prompt μ production in p-nucleus collisions, multiple prod. model based on lepton-hadron relation 78−29362
proton interactions, beam dump expt. at CERN SPS 78−45979
QCD, $\mu^+\mu^-$ prod. total cross section from Drell-Yan process, large perturbative corrections 80−385
QCD, μ pair transverse momentum distrib. in Drell-Yan processes 78−62374
QCD, leptoprod. and Drell-Yan processes beyond leading approx., Bjorken scaling 79−6323
QCD, transverse momentum distribs. of μ pairs from pN interactions, p-nucleus study 78−62375
QCD calc. of three-jet processes in leptoprod. and hadronic μ-pair prod. 78−21338
QCD hadronic μ pair prod., gluon gauge depend., struct. func. calc. 79−80810
spin dependent photon structure functions from Drell-Yan and e^+e^- reactions 80−82973
SU(3)×U(1) gauge theory of weak and EM interactions 78−70317
sum rules and moments of dimuon prod., valence quark transverse moments 78−54660
super trimuons production, possible evidence of six-fermion interactions 79−71743
transverse momentum of massive muon pairs in QCD 78−45867
trimuon events, heavy lepton prod. in ν interactions 78−41530
trimuon events, probability of production by short lived source of neutrinos 78−37343
trimuon heavy lepton events in ν interactions, $SU(8)_L\times U(1)$ gauge model 77−79242
trimuon prod., EM muon-pair contrib., scaling parton model 78−66106
trimuon prod., heavy-lepton cascade decay, energy ratios 78−66103
trimuon prod., possible new process in ν-N leptonic sector 77−49947
trimuon prod. from neutrino interactions 78−66105
trimuon prod. from struct. at lepton vertex 78−8639
trimuon prod. in ν and $\bar{\nu}$ interactions, EM μ-pair contrib. 78−66107
trimuon prod. mechanism, $\nu(\bar{\nu})$ interactions 78−82199
trimuon production by neutrinos, heavy lepton cascade mechanism using SU(2)×U(1) gauge model 78−58180
trimuon production by neutrinos 77−30362
trimuon production by neutrinos and antineutrinos 78−37198
trimuon production in higher energy ν interactions, rates and properties, cc̄ prod. 79−49508
c-c̄ associated prod., μ^--induced multimuon prod. 79−17707
$ee\rightarrow ee\mu^+\mu^-$, virtual photon-photon collisions, equivalent photon approx. validity 80−5033
$e^-e^-\rightarrow\mu^-\mu^-$, reaction rate in vectorlike gauge model 77−61237
e^+e^-, 27-4, 27.7 GeV/c, hadron prod./muon prod. cross section ratio, thrust distrib., average spherocity 80−426
e^+e^-, 31.57 GeV, $(e^+e^-\rightarrow\text{hadrons})/(e^+e^-\rightarrow\mu^+\mu^-)$ cross section ratio, thrust distrib. and average spherocity 79−89175
$e^+e^-\rightarrow\mu^+\mu^-\gamma$, neutral current effects and hard photon correction 79−13096
e^+e^- annihilation, QCD and semilocal duality $(\text{hadrons}/\mu^+\mu^-)$ cross section ratio 80−78085

muon production continued
e^+e^- annihilation, spin-0 electron or muon pair prod., cross section supersymmetry predictions 80−32092
e^+e^- annihilation at SPEAR, total hadron cross section, ψ prod., μe events 77−57548
e^+e^- anomalous μ prod., heavy lepton spin, decay parameters 77−61267
e^+e^- dimuon and other possible heavy-lepton events, short review 77−30473
$e^+e^-\rightarrow e^+e^-X$, $X=e^+e^-$, $\mu^+\mu^-$, $\pi^+\pi^-$, η′, photon-photon interactions, QED test 79−93425
$e^+e^-\rightarrow e^+e^-(\mu^+\mu^-)$ EM processes, vector resons. cross sections *(Russian)* 77−57517
$e^+e^-\rightarrow e^+e^-(\mu^+\mu^-)(\gamma\gamma)$, 12-31.6 GeV, QED test and Weinberg angle 80−91027
$e^+e^-\rightarrow e^+e^-\mu^+\mu^-$, beam polarisation effects on cross section 77−61269
$e^+e^-\rightarrow e^{\pm}\mu^{\mp}$ anomalous prod., heavy lepton current chirality 77−74668
e^+e^- events, hadron/μ-pair cross-sections, struct. near 4 GeV 77−248
$e^+e^-\rightarrow$hadrons $(\mu^+\mu^-)$, Υ(9.46) muonic branching ratio, total and leptonic width 80−86703
e^+e^- inclusive prod., anomalous muon signal at 7.3 GeV, $n_{ch}\leq 2$, final state multiplicity, cross sections 78−41559
e^+e^- inclusive prod. at 4.8 GeV, anomalous muon events, charm and heavy lepton explanations 77−247
e^+e^- interactions, anomalous eμ and μ events, anal. *(Chinese)* 77−67641
$e^+e^-\rightarrow l^+l^-$, l=3, μ, τ, charged lepton universality test 80−32091
$e^+e^-\rightarrow\mu^+\mu^-$, 30 GeV, charge asymmetry, QED and weak corrections 77−61266
$e^+e^-\rightarrow\mu^+\mu^-$, 40-200 GeV, cross section, one loop corrections in Weinberg model 80−18139
$e^+e^-\rightarrow\mu^+\mu^-$, early weak gauge boson restrictions from PETRA QED cut-off 80−52487
$e^+e^-\rightarrow\mu^+\mu^-$, neutral current anal., weak and radiative asymmetries 79−26320
$e^+e^-\rightarrow\mu^+\mu^-$, polarised e^+,e^-, ψ/J excitation models 79−13095
$e^+e^-\rightarrow\mu^+\mu^-$, radiative corrections around Z^0, Weinberg-Salam model 80−99103
$e^+e^-\rightarrow\mu^+\mu^-$, weak neutral electron current, Lorentz struct. 79−80788
$e^+e^-\rightarrow\mu^+\mu^-$ 6.2-7.4 GeV CM, comparison with QED predictions 78−74194
$e^+e^-\rightarrow\mu^+\mu^-$ at J/ψ energy, ang. distrib. of muon pairs, asymm. parameters 77−2846
$e^+e^-\rightarrow\mu^+\mu^-$ or e^+e^-, EM corrections for μ pair prod. and Bhabha scatt., QED processes 77−18259
$e^+e^-\rightarrow\mu^+\mu^-X$, possible Higgs boson detection in missing mass plot 80−4977
$e^+e^-\rightarrow\mu^+\mu^-\gamma$, large angle final particle emission, energy distribs., Born approx. 79−30722
$e^+e^-\rightarrow\mu^{\pm}$+charged particle(s), 3.8 GeV, anomalous μ prod., new particle pair prod. 78−8637
$e^+e^-\rightarrow\mu$+anything, anomalous prod., 3.9 to 7.8 GeV 77−22722
$e^+e^-\rightarrow\mu 3\pi$, above 6 GeV, inference of τ decay 78−50042
$e^+e^-\rightarrow\mu e$, heavy lepton evidence, new lepton number 77−61268
$e^+e^-\rightarrow\mu e$+anything, longit. polarised beam, asymmetries, props. of heavy leptons 77−10238
$e^+e^-a\mu^+\mu^-\gamma$, virtual electrons bremsstrahlung photon, Feynman diagrams, Weizsacker-Williams approx. 80−52484
$eZ\rightarrow Z\mu\bar{\nu}_{\mu}\nu_e$, muon spectra V-A theory 77−65148
$\eta'\rightarrow\mu^+\mu^-\gamma$, in π^-p interactions at 25 and 33 GeV/c, form factors *(Russian)* 80−4984
$\gamma N\rightarrow\mu^+\mu^-N'$, E_{γ}=20-400 GeV, equivalent photon spectra 77−6129
$\gamma N\rightarrow\mu\bar{\mu}X$, QCD cross sections 80−73715
$\gamma p\rightarrow\mu^+\mu^-$, cross sections, γ struct. function determ. 80−42473
$hh\rightarrow\mu^+\mu^-$+jet+X, QCD anal. of recoiling jets and angular effects in large q_T pair prod. 79−45078
$(K^+,\mu^+\mu^-X)$, on C, W and Cu targets, 225 GeV/c 79−67612
$K_L\rightarrow\mu\mu$, heavy particle decoupling effects in broken symmetry theory 78−82140
$K_L^0\rightarrow\mu^+\mu^-/K_L^0\rightarrow$all branching ratio 77−67647
$K_L\rightarrow\pi^-\mu^+\nu_{\mu}$, transverse polarisation of μ, violation of time-reversal invariance 80−68448
$K_L^0\rightarrow\pi\mu^+\nu_{\mu}$, form factor from μ polarisation meas. 77−38161
$K^-N\rightarrow\mu^+\mu^-X$, K^-/π^- structure function ratio using Drell-Yan process 80−86718
$K^+N\rightarrow\mu^+\mu^-X$, 225 GeV/c, muon pair prod., 2 to 11 GeV/c^2, differential cross section 79−67612
$L^0\rightarrow\nu_L\mu^+\mu^-$, heavy lepton spin, massless spin 3/2 ν four fermion interaction 79−13175
μ pair prod., QCD ang. correl. 78−49976
μ^--induced multimuon prod., phenom. anal. in (V-A) scheme using quark parton model 79−17707
μ^-e^+ pair production in ν_{μ}N interaction *(Russian)* 80−91076
μμ like-sign events in νN interactions, implications for weak gauge models 77−67643
$\mu^-\mu^-$ dimuon events, explanation in $\Delta C\neq 0$ neutral current model 77−54070
$\mu^-\mu^+$ symmetric prod. from ν interactions 77−87969
$\mu^+\mu^-$ anomalous prod. from e^+e^- annihilation, heavy lepton prod. and decay 78−82190
$\mu^+\mu^-$ pair system, meson reson., leptonic decay *(Russian)* 77−67646
$\mu^+\mu^-$ prod. from ν and $\bar{\nu}$ interactions, charm prod. and decay 77−74675
$\mu^+\mu^-$ prod. from vector meson decay, k^0_L+Cu interaction 78−45951
$\mu^+\mu^-$ prod. in Fe+p reacts. at 400 GeV, missing energy obs. 80−22833
$\mu^+\mu^+$ production in hadron-hadron collisions, small transverse momentum distrib., QCD soft gluon bremsstrahlung effects 79−75723
$\mu^-\mu^-\mu^+$ events in ν_{μ} reactions, SU(3) gauge models 77−74674
$\mu^-\mu^-\mu^+$ prod. in neutrino interactions, gauge theory, heavy leptons 77−65085
μN, 209 GeV, ψ diffractive prod. cross section, $\psi\rightarrow\mu^+\mu^-$ decays 80−102054
μN, 270 GeV, multimuon final states, total cross section, associated charm prod. 80−13315
$\mu N\rightarrow(x\mu)X$, dimuon and trimuon prod., heavy quark and 4 diffractive prod. 79−93429
μN deep inelastic reactions, trimuon EM prod., cross sections at 250 GeV *(Russian)* 80−37278
μN deep inelastic scatt., dimuon prod. and scale violation 78−62407
μN inelastic scattering, dimuon events, charm particle prod. and semileptonic decay 77−10260
$\mu N\rightarrow\mu\Upsilon X$, 209 GeV, Υ muoprod. limits from trimuon final states 80−105909

muon production continued
$\mu N \rightarrow \mu\mu X$ ($\mu\mu\mu X$), 150 GeV prod. ratios 77−79268
$\mu N \rightarrow \mu\mu X/\mu N \rightarrow \mu X$ ratio, charm contrib. 77−57544
μN scatt., deep-inelastic, EM production of trimuons 80−22619
$\mu N \rightarrow x\mu X$, x=2 or 3, charm muoprod. with small angle veto 80−47306
$\mu^- N \rightarrow \mu^+\mu^-\mu^- N$ in Pb, 10.5 GeV/c, short lived particle search, QED tridents 80−37275
$\mu^+ N$ in Fe, 280 GeV, dimuon prod. cross sections 80−91094
$\mu^+ N$ in Fe, 280 GeV, trimuon event cross sections 80−99104
NN interactions, longitudinal polarisation of direct muons with $p_\perp$=1.9 GeV/c 79−9411
$NN \rightarrow \mu^+\mu^- X$, (X=system of hadrons) 78−82222
$NN \rightarrow \mu$+anything, 70 GeV, muon polarisation meas. *(Russian)* 77−6185
$\bar{\nu}$ induced dimuon events, V^0 yield, possible beautiful baryon prod. 80−105882
ν interactions, dimuon prod., high y-anomaly, extended minimal Weinberg model 77−26510
ν interactions, trimuon prod., heavy lepton cascade decay 78−25038
$\nu(\bar{\nu})$ high-energy interactions, dimuon distrib. anal., quark-parton model 78−33056
$\nu(\bar{\nu})$ interactions, heavy-lepton interpretation of multimuon events 78−33058
$\nu(\bar{\nu})$ interactions, trimuon events obs. 78−12902
$\nu(\bar{\nu})$-N inclusive same-sign dimuon prod., $c\bar{c}$ creation 77−49946
$\nu(\bar{\nu})$-induced prod. of vector mesons and Higgs boson, muon prod. 78−82198
$\nu(\bar{\nu})$N, high energy dimuon prod., consistency with charm particle prod. 78−89697
$\nu(\bar{\nu})$N, multimuon prod. at FNAL 78−78166
$\bar{\nu}(\nu)$N, opposite sign dimuon props. and rates 79−375
$\nu(\bar{\nu})$N interactions, 7.5-30 GeV, μ pair prod. 78−12904
$\nu(\bar{\nu})N \rightarrow \mu^-\mu^- X$, E>30 GeV, prompt like sign dimuon prod., Fe target, charm prod. 79−93395
$\nu(\bar{\nu})N \rightarrow \mu^+\mu^- X$, dimuon rate and strange quark sea 80−62961
$\nu(\bar{\nu})$+Fe$\rightarrow\mu^-+\mu^-(\mu^+ + \mu^+)$+X, 200 GeV, momentum and ang. distribs. meas. 78−8648
$\bar{\nu}$ trimuon prod., EM and hadronic contrib., $\mu^+\mu^+\mu^-$ rate and distribs. 79−85291
$\bar{\nu}$ trimuon prod., $\mu^+\mu^+\mu^-$ rate, correl. with $\mu^-\mu^-\mu^+$ ν-prod. events 79−85292
ν-induced multimuon prod., phenom. anal. in (V-A) scheme using quark parton model 79−17707
$\nu_\mu(\bar{\nu}_\mu)N \rightarrow \mu(\bar{\mu})$+hadrons, phenomenology, parton model, expt. data, dimuon events *(Russian)* 77−49943
$\nu_\mu(\bar{\nu}_\mu)h \rightarrow \mu^{\pm}1^{\mp}$+X, charm contrib. to prod. of opposite sign dimuons 79−377
$\bar{\nu}_\mu$+N$\rightarrow\mu^+$+X deep inelastic interaction at 2 to 25 GeV *(Russian)* 80−13298
$\bar{\nu}d \rightarrow nn\mu$, virtual nucleon density matrix *(Russian)* 79−26327
$\bar{\nu}_e e^- \rightarrow \nu_e \mu^-$, exotic lepton number violation and neutrino Majorana masses, Higgs sector 80−86615
$\bar{\nu}$N, charged current high energy reactions, μ^+ events scaling-variable distribs. 77−74672
νN, $\mu^- \mu^{prompt}$ events, prod. evidence 78−82196
νN, μ^+ single prod. in inclusive interaction 78−45908
νN, $\bar{\nu}$N interactions muon prod., quark model anal. 78−4850
$\bar{\nu}$N, ratio of μ^+e^- events to μ^+ events, charmed particle prod. model 78−89702
$\bar{\nu}$N, search for μe events 77−26512
νN and $\bar{\nu}$N reactions, dimuon prod. mechanism, coloured quark model 77−22725
$\bar{\nu}$N in Fe, μ^+ polarisation in high energy charged current interactions 79−93399
νN interactions, pair abundance, six quark model without right handed currents 77−6081
$\nu N \rightarrow \mu^- \mu^- X$, charm-pair production 80−22643
$\nu N \rightarrow \mu^- \mu^- \mu^+$, 350-400 GeV, event characts. 79−3011
$\nu N \rightarrow \mu^- \mu^- \mu^+$, high-energy, origin of trimuon events 78−74244
$\nu N \rightarrow \mu^- \mu^- \mu^+$N, 350, 400 GeV, event origin, heavy lepton or quark cascade upper limit 78−89698
$\nu N \rightarrow \mu^- \mu^- \mu^+ X$, internal Drell-Yan mechanism, parton model approach 78−89656
$\nu N \rightarrow \mu^- \mu^- \mu^+ X$ event characts. 79−13105
$\nu N \rightarrow \mu^- \mu^- \mu^+$+anything, explanation in terms of prod. and decay of charmed (or other new quantum number) hadron pairs 77−57527
$\nu n \rightarrow \mu^- p$, total cross-section and differential cross-section, estimation of nucleon mass 80−18128
$\bar{\nu}N \rightarrow \mu^+ e^- X$, relative prod. rate, Vee yield and scaling variable distrib. 79−40768
$\nu N \rightarrow \mu^\pm \mu^\pm$+anything, explanation in terms of prod. and decay of charmed (or other new quantum number) hadron pairs 77−57527
$\nu N \rightarrow \mu\mu X$, dimuon events, D prod., lifetime and fragmentation function 79−93397
$\nu N \rightarrow \mu\mu X$, neutral strange particle prod. in opposite sign dimuon events 80−57584
νN single- and di-muon prod., colour excitation, weak interaction model anal. 78−45906
νN tetramuon prod. sources, heavy quark and lepton cascades, charm prod. 78−70356
ν_μN, charm pair prod. in QCD, trimuon rate 78−45907
$\nu_\mu N \rightarrow \mu^- e^+$, obs. in BEBC 78−78170
$\nu_\mu N \rightarrow \mu^- e^+ X$ in Ne 78−29329
$\nu_\mu N \rightarrow \mu^- e^+$+hadrons, investigation at SCAT chamber *(Russian)* 79−58953
$\nu_\mu N \rightarrow \mu^- e^+$+hadrons, up to 30 GeV, possible heavy neutral lepton prod. 79−36061
$\bar{\nu}_\mu N \rightarrow \mu^+ N$, 2-30 GeV, deep inelastic interactions SKAT preliminary results 80−82963
$\bar{\nu}_\mu N \rightarrow \mu^+ e^- X$ in Ne 78−29329
$(\bar{\nu})\nu N \rightarrow e^- e^- e^+ \mu^+ K^0 + 7\gamma$, exptl. obs. 79−9361
$\nu p \rightarrow \mu^- \Delta^{++}$, 5 to 100 GeV, production, decay distrib. 78−93873
$\nu p \rightarrow \mu^- \Lambda 3\pi^+\pi^-$, E>10 GeV, inclusive 79−376
$\nu p \rightarrow \mu^-$+jet, greater than 10 GeV, jet props. 79−45084
$\nu p \rightarrow \mu^- p\pi^+$, cross section above 1 GeV 79−9362
$\bar{\nu}p \rightarrow \mu^+ X$, deep inelastic scatt., MQM description 80−47305
$\bar{\nu}p \rightarrow \mu^+ + X$, 4.5 GeV^2, p struct. functions x depend., quark distrib. 80−32097
$\bar{\nu}p \rightarrow \mu^+ p\pi^-$, 5-70 GeV, cross section, I=1/2 prod. amplitude 80−62962
$\nu_\mu p \rightarrow \tilde{\mu}\nu_F F^+ X$, $F^+ \rightarrow \mu^+ \nu_\mu \bar{\nu}_F$, total cross section, spectra, unconfined heavy fermion model 77−18269

muon production continued
$(p^\pm, \mu^+\mu^- X)$, on C, W and Cu targets, 225 GeV/c 79−67612
p-nucleus 200-400 GeV interactions, scaling of μ pair prod. 78−82344
p-nucleus reaction at 70 GeV, μ^+ longitudinal polarisation meas. 77−2995
p+Fe$\rightarrow\mu^+\mu^-$+anything, enhancement in μ pair mass spectrum at 9.5 GeV, Υ prod. 79−432
$p+N \rightarrow \mu^- \mu^+ X$, 400 GeV, charged gluon effects, broken colour gauge model study 79−49473
p+nucleus muon yields as W boson search 77−18367
p+nucleus$\rightarrow\mu^+ + \mu^-$+anything, 400 GeV, high-mass dimuon continuum 78−37344
pN, 400 GeV, prompt single muon prod., charm prod. cross section 79−80855
pN, 70 GeV, forward prompt muon yield, μ/π yield ratio *(Russian)* 79−97641
pN, muon pair prod. and new parton radiative processes 79−17766
pN, μ pair prod., QCD predictions for zero and nonzero rapidities 78−89674
pN, $\bar{p}N$, 200 GeV/c, dimuon prod. cross section, Drell-Yan predictions, struct. functions 80−37300
pN in Fe, 400 GeV/c, bottom meson prod. search in multimuon final states 80−47334
$pN \rightarrow \mu^+\mu^- X$, 225 GeV/c, muon pair prod., $q\bar{q}$ annihilation model 79−63552
$pN \rightarrow \mu^+\mu^- X$, determ. of parton sea 78−29304
$pn \rightarrow \mu^+\mu^-$+anything, review of data, explanation using quark models, new quarks 78−74202
$pN \rightarrow \mu X$, 350 GeV p-Fe collisions, prompt muon prod. rate 80−37311
$p^\pm N \rightarrow \mu^+\mu^- X$, 225 GeV/c, muon pair prod., 2 to 11 GeV/c^2, differential cross section 79−67612
pp, prompt μ and $\mu\mu$ prod. 400 GeV, possible charm prod. 78−89750
pp$\rightarrow$charm particles, 400 GeV, evidence for prompt single muon prod. 79−63536
$pp \rightarrow e^\pm \mu^\mp X$, CERN ISR energies, production limits, D(1.87) leptonic decay 77−65186
$pp \rightarrow e^\pm \mu^\mp$+X, charmed meson pair semileptonic decay, inclusive charm prod. cross section 78−89759
pp interactions, effects of hard gluon bremsstrahlung in dimuon and Υ prod., QCD anal. 79−13058
$pp \rightarrow \mu^+\mu^- X$, 62 GeV, ψ and γ cross sections, scaling function 80−105932
$pp \rightarrow \mu^+\mu^- X$, dimuon prod. using polarised beam, Drell-Yan parton model anal. 79−58981
$pp \rightarrow \mu^+\mu^- X$, gluon corrections to Drell-Yan model 79−36037
$pp \rightarrow \mu^+\mu^- X$, muon pair ang. distrib., QCD model study 79−36035
$pp \rightarrow \mu^+\mu^- X$, parity violating effects in dilepton production using polarized targets 79−67613
$pp \rightarrow \mu^+\mu^- X$, polarised p, polarisation direction, structure functions and Drell-Yan parton model test 79−63544
$pp \rightarrow \mu^+\mu^- X$, QCD, parton and dimuon intrinsic transverse momenta 79−13038
$pp \rightarrow \mu^+\mu^- X$, spontaneously broken colour gauge theory effects in Drell-Yan process 79−26344
$pp \rightarrow \mu^+\mu^-$ + anything, review of parton model 77−57498
$pp \rightarrow \mu^\pm e^\mp$+X, possible charmed meson pair prod., $D\bar{D}$ cross section 78−89751
$pp \rightarrow \mu^1 \mu^- X$, large mass, QED calc. with massive photon *(Russian)* 77−30468
pp$\rightarrow$p+μ+X, 200 and 240 GeV, charmed particle forward prod. search 77−22818
$pp \rightarrow \psi X \rightarrow \mu^+\mu^- X$, Drell-Yan mechanism in colour quark model 77−6181
$p\bar{p} \rightarrow Z$+anything, front-back asymmetry differential cross section, $W^\pm$ prod. 79−6352
$(\pi^\pm, \mu^+\mu^- X)$, on C, W and Cu targets, 225 GeV/c 79−67612
$(\pi^-, \psi\, C\bar{C})$, $\psi \rightarrow \mu^+\mu^-$, $C\bar{C} \rightarrow \mu^\pm \nu X$, 225 GeV/c, search for extra μ 80−82967
π, pair production in two-photon e^-e^+ events 77−71523
$\pi^+ \rightarrow \mu^+ \nu_\mu$, at rest, μ^+ momentum meas. 78−45911
π^-+p$\rightarrow$p+μ+X, 200 and 240 GeV, charmed, particle forward prod. search 77−22818
$\pi N \rightarrow \mu^+\mu^- X$, longitudinal photon polarisation from helicity ang. distrib. 80−5025
$\pi N \rightarrow \mu^+\mu^- X$, π-struct. function determ. 79−63553
π^-N, 16, 22 GeV, dimuon prod. parton intrinsic transverse momentum, QCD perturbation 80−63037
π^-N, 217 GeV, dimuon prod., prod. of γ associated with $\chi \rightarrow \psi\gamma$ 79−36081
π^-N collisions 27, 40 GeV/c, low-mass muon pair production *(Russian)* 79−89212
π^-N in Be, 150, 175 GeV/c, high mass muon pair prod., Drell-Yan QCD corrections 80−13343
$\pi^- N \rightarrow \mu^+\mu^- X$, 27, 40 GeV, cross sections and differential distribs. *(Russian)* 78−89919
$\pi^- N \rightarrow \mu^+\mu^- X$, K^-/π^- structure function ratio using Drell-Yan process 80−86718
$\pi^\pm$N, 16 GeV, dimuon prod., $q\bar{q}$ annihilation contrib., exact scaling deviations 79−89196
$\pi^\pm$N, 200 GeV/c, dimuon prod. cross section, Drell-Yan predictions, struct. functions 80−37300
$\pi^\pm N \rightarrow \mu^+\mu^- X$, 225 GeV/c, muon pair prod., $q\bar{q}$ annihilation model 79−63552
$\pi^\pm N \rightarrow \mu^+\mu^- X$, 225 GeV/c, muon pair prod., 2 to 11 GeV/c^2, differential cross section 79−67612
πp, 16-GeV/c, dimuon production and obs. of low-mass continuum 78−37236
$\pi p \rightarrow \mu^+\mu^- X$, quark transverse momentum effect in bag model 80−86668
$\pi^- p \rightarrow \mu^+\mu^-$+hadrons, $\pi^- p \rightarrow$hadrons, quark-parton model 78−74222
π^+p, 11.46 GeV/c, search for new meson resonance prod. in μ channel 80−22641
$\pi^\pm$p, 16 GeV, anomalous prod., f and $A_2{}^0$ tensor mesons as source 78−70411
$\pi^\pm p \rightarrow \mu^+\mu^- X$, 15.5 GeV/c, expt. results from SLAC 78−89748
$\psi \rightarrow \mu^+\mu^-$, search for extra μ in (π^-, ψ $C\bar{C}$), 225 GeV/c 80−82967
$q\bar{q} \rightarrow g\mu^+\mu^-$, large q_T muon pairs ang. distribs. in perturbative QCD 79−85275
$q\bar{q} \rightarrow \mu^+\mu^-$, explanation of obs. p_T distrib. by a proton core of valence quarks 79−17682
Be+n, 300 GeV/c, $\mu^\pm\mu^\mp$ and $\mu^{\pm/\mp}$ events, upper limit for charmed particle prod. 78−37245

muon production continued
Be+p, 150 GeV, inclusive muon pair prod. parameters, statistical interpretation 79−30820
Be+p, direct muon prod. in 70, 50 and 35 GeV collisions 77−2872
Be+π^+, 150 GeV, inclusive muon pair prod. parameters, statistical interpretation 79−30820
C+p, 28.5 GeV, prompt dimuon prod., cross section, atomic number depend., mass distrib. 78−89858
C+p, C+$\pi^\pm$, 225 GeV/c, J/ψ and ψ'(3.7) prod. study using muon pair meas. 77−57694
C+p, props. of prompt muons prod. by 28 GeV protons 79−17906
C+$\pi^\pm$, C+p, massive muon pair prod., test of Drell Yan model 77−57695
C($\pi,\mu^+\mu^-$X), 225 GeV/c, muon pair prod., 2 to 11 GeV/c^2, differential cross section 79−67612
Cu+p, 400 GeV, dimuon and trimuon prod., prompt ν source, D$\bar{\text{D}}$ prod., axions 78−89860
Cu+p, dimuon prod., struct. in Υ region near 9.5 GeV 78−17201
Cu+p, direct muon prod. in 70, 50 and 35 GeV collisions 77−2872
Cu+π^-, 27, 40 GeV, cross sections and differential distribs. for muon pair prod. *(Russian)* 78−89919
Cu+$\pi^-\rightarrow\mu^+\mu^-$X, 16, 22 GeV, quark annihilation model interpretation, scaling 79−36277
e^+e^- annihilation, 30 GeV, inclusive K^0 prod. $K^0K^+/\mu^+\mu^-$ prod. ratio 80−91103
e^+e^-, high energy interactions *(Chinese)* 80−78074
Fe+p, 28.5 GeV, prompt dimuon prod., cross section, atomic number depend., mass distrib. 78−89858
Fe+p, props. of prompt muons prod. by 28 GeV protons 79−17906
νN$\rightarrow$4μX, radiative and hadronic production characts. 79−40771
νN$\rightarrow\mu$3eX, radiative and hadronic production characts. 79−40771
pp$\rightarrow\mu$ pairs, 200, 300, 400 GeV, test of scaling hypothesis 78−4888
$\bar{\text{p}}$p$\rightarrow\mu^+\mu^-$X, scale violating effects in large q_T interactions 79−22125
Pt+p, dimuon prod., struct. in Υ region near 9.5 GeV 78−17201
Pt+p$\rightarrow\mu^+\mu^-$+anything, massive lepton pair prod., Υ family 78−78368
π^-N$\rightarrow\mu^+\mu^-$X, lepton ang. distrib. calc. by QCD 79−26303
Sn+p, Sn+$\pi^\pm$, 225 GeV/c, J/ψ and ψ'(3.7) prod. study using muon pair meas. 77−57694
Sn+$\pi^\pm$, Sn+p, massive muon pair prod., test of Drell Yan model 77−57695
W+p, 28.5 GeV, prompt dimuon prod., cross section, atomic number depend., mass distrib. 78−89858
W+p, 400 GeV/c, dimuon mass spectrum, Υ signals 78−89857
W+p, props. of prompt muons prod. by 28 GeV protons 79−17906

muon scattering *see lepton-hadron scattering; lepton-lepton scattering; muon-nucleon scattering; muon-nucleus scattering; photon-lepton scattering*

muonic atoms
$1s_{1/2}$ levels, self-energy corrections, heavy ats. 78−55262
actinide muonic atoms, n emission from radiationless muonic transitions and μ capture 79−3599
atomic muon repolarisation by polarised nuclei of arbitrary spin 79−94112
capture process, average stopping power 77−88607
charged particle scatt., exact results for three particles 79−81309
conference on high energy physics and nuclear struct. Vancouver, Canada (Aug. 1979) 80−41936
configurational mixing in shell and neutral weak muon-nucl. interaction effects obs. feasibility *(Russian)* 80−32859
conversion Auger transition rate, s-shell electron effects *(Russian)* 77−75349
Coulomb de-excitation of neutral exotic atoms, μ^-p and π^-p H atoms 78−25757
Dirac-Fock method, transition energies, wave functions, charge densities 78−74805
electron screening calculations in O, Al, Fe, In, Ho, Au, Th 78−94339
energy levels, $\alpha^2(Z\alpha)^2$-vacuum polarisation contrib. 79−22867
energy levels, computer calc. codes 79−31743
energy levels 79−76533
energy levels of light hydrogen like and muonic atoms, nuclear size corrections 79−36549
energy shift rel. to anomalous interaction of muons with nuclei *(Russian)* 78−74804
energy shifts and polarisability of deformed nuclei 80−86893
energy-level values, electrodynamic corrections 78−62956
exotic atoms, conf., Erice, Sicily, (1979) 80−67939
fine structure constant determination, atomic metastable beam method 77−68105
fission, distribution of muons among fragments *(Russian)* 78−94040
fragmentation of nucleus caused by decay of bound muon *(Russian)* 79−68333
heavy, polarisation mechanism of parity nonconservation, weak neutral interaction effect *(Russian)* 77−79712
hyperfine splitting frequency in quartz *(Russian)* 79−91332
inert gas binary mixture, μ-capture, near 5 atm., X-ray yield 80−58419
isomer shifts, book contrib. 79−86093
K-shell X-ray transitions in F, Na, Al, Si, P, S, K, nuclear charge radii 78−66195
lepton bound in Coulomb field of nucleus 79−94115
lifetime of bound muon, nucl. recoil corrections 79−68331
light, finite nucl. size corrections to energy levels 79−18321
light muonic atoms, nuclear size effects, energy levels, Lamb shift 80−14254
long range parity violating interaction from γ-Z^0 conversion 80−48108
low-Z elements and their hydrides, muonic X-ray intensities 80−9761
muon capture probability and laser effect on hyperfine level population *(Russian)* 77−75348
muon spin rotation, review of recent advances 79−24252
muon transfer in gas targets 77−42445
muonic K_β/K_α ratios from pure elements 79−68335
muonic X-rays, formation and expts. 80−43215
muonium+Cl_2, gas-phase reaction, muonium spin rot. rate meas. 77−58207
muonium+F_2, exothermic triatomic exchange reactions, dynamics, anal. theory 78−3322
muonium atoms and intraspur reactions in H_2O 79−70358
nuclear and atomic research review 80−43216
nuclear polarisation correction for atoms with deformed nuclei 77−23584
nuclear polarisation energy shifts, phenomenologically extended microscopic calcs. 78−94335

muonic atoms continued
nuclear spectroscopic quadrupole moment extraction from hyperfine structure, polarisability correction 77−18391
nucleus excitation from bound μ^- decay *(Russian)* 79−22869
orbital angular momentum, effect of alignment on depolarisation of μ 80−18946
parastatistics with continuous order, possible description 77−71572
parity violating neutral current effects, E1-E2 interference 79−41254
prompt fission, muon capture by fission fragments, statistical model anal. *(Russian)* 79−9523
prompt fission, muon entrainment by fission fragment, probability *(Russian)* 80−37911
QED, strong and supercritical fields, book contrib. 78−74193
repolarisation of muons in atoms with polarised nuclei 77−61878
review, significance of exotic atoms to particle physics 78−9282
self-energy corrections, Lamb shift 77−75343
transition potential of muonic X-rays, unique parameterisation 79−31745
two bound spheres model, 2p-1s transition energies, muon radius calc. 77−10298
vacuum polarisation, $\alpha(Z\alpha)^3$ correction to energy level shifts 78−21366
vacuum polarisation, test using heavy muonic atom X-ray meas. 78−29287
vacuum polarisation pots. calc. 77−26476
valence nucleons, muonic atom analysis 80−27530
weak interaction effects in transitions 77−13890
X-ray emission, cascade program, calcs. and cataloguing 78−90323
X-ray emission, circular polarisation *(German)* 80−69266
X-ray emission 79−86087
X-ray emission polarisation *(German)* 80−69268
X-ray meas., nucl. charge distrib. determ. 78−54679
X-ray vacuum corrections, nuclear moments, transitions and deformation parameters 80−37912
dμ, spin states in gaseous H_2+7% D_2 mixture exposed to muon beam *(Russian)* 77−10794
(e,e), A$\simeq$60 region, nuclear radius, core polarisation and isotone shifts, muonic X-rays 80−22685
μ number nonconservation 78−45806
μ^- induced instantaneous fission, mesoatomic X-ray radiation *(Russian)* 79−30869
$\mu^\pm$ spin rotation, μ relaxation and repolarisation, muonic X-rays 80−42644
μd+d elastic scatt. cross section for muonic d 79−89811
μ^+e^- atom, hyperfine quadrupole moment of ground state 78−90324
$(\mu^-{}^4\text{He})^+$ ion, meas. of $2S_{1/2}$-$2P_{3/2}$ splitting, QED vacuum polarisation 77−34785
μ^-p, electron scatt. length determ. 79−36801
$(\mu p)_{1S}$ muonic atoms in gaseous H, triplet state lifetime 80−23579
$(\mu p)_{2S}$ and $(\mu p)_{1S}$, muon transfer to heavy atom 77−27209
μp+p, elastic scattering cross section of muonic H atoms 80−69278
μXe muonic atoms, vanishing muon transfer effect 80−9765
π-μ atom prod. in $K_L{}^0\rightarrow\pi\mu\bar{\nu}$ *(Russian)* 78−54629
π-μ Coulomb bound states detection, track correlator as fast trigger 79−45574
$\pi\mu$, production and detection from $K_L{}^0$ decay 79−81306
Al, formed by muon transfer free μp and μd systems, isotope effect on Lyman series 79−86090
Al Lyman series, muon transfer effect 79−7040
Al, muonic X-rays following μ^- transfer from muonic H 78−55259
Au foil array+μ^+ beam, μ^+e^- formation, μ^+ decay spectra 77−75346
B, muonic X-ray transitions, nuclear charge radii 80−99589
Ba 4-3 transitions QED validity test precision meas. 78−33642
Ba, transition energy meas., tests of high-order vac. polarisation corrections 77−71895
Be muonic X-ray transitions, nuclear charge radii 80−99589
^{209}Bi, charge distrib. from elastic electron scatt. and muonic X-ray data anal. 78−54681
^{209}Bi/^{208}Pb isotone pair, charge distrib. polarisation from e^- scatt. and muonic X-ray data consistency 77−22873
C, muonic X-ray transitions, nuclear charge radii 80−99589
Ca, muonic isotope shifts 78−33640
Ca, transition energy meas., tests of high-order vac. polarisation corrections 77−71895
Cl, prod. by muon capture in Ar atom *(Russian)* 79−45869
Cu, in solids, muonic Coulomb capture, ionic charge effect 78−66694
D, initial population of 2S metastable state 77−27207
D muonic atom, μ^- transfer rate to He atoms 77−42447
D-T fusion catalysis for pellet ignition 77−3063
D+Y, muon transfer mechanism from free muonic deuterium 80−69218
Dμ^-, proton scattering, Schwinger variational principle 79−45780
^{161}Dy, E0, E2 and E4 charge moment determ., using muonic atoms 78−21490
F muonic free atom, obs. from Larmor freq. meas. 77−23585
^{A}Fe(e,e), 100-275 MeV, A=54,56,57, cross sections and muonic X-ray meas., charge distrib. systematics 80−86801
H, atomic capture ratio for μ-transferred from μp to Al_2O_3 79−10236
H, collision quenching of 2S-state, distorted waves calc. 77−58211
H, formation at extremely low press. 80−74263
H, initial population of 2S metastable state 77−27207
H, low energy muonic, reaction with heavy atoms 77−82871
H, metastable 2s state fraction at 150 and 600 Torr 78−13631
H muonic formation in low press. targets 78−33639
H, μ^- transfer to Al interfaces, X-rays 78−55259
H+Y, muon transfer mechanism from free muonic hydrogen 80−69218
^{2}H, ^{1}H, μ-N axial coupling const. from muon capture *(Russian)* 77−50570
^{A}H, A=1,2,3, muonic atoms, ground state energy levels from quasipot. eqn. 80−87251
^{165}H muonic X-rays, K- and L-transitions energies meas. 77−79711
He, $2S_{1/2}$-$2P_{3/2}$ level splitting, test of QED predictions on electronic vacuum polarisation 77−3494
He, hyperfine struct., relativistic, radiative and recoil corrections, QED test 80−14256
He, hyperfine structure 80−69273
He, muonic, 3p-3d transitions calcs., energy splittings 80−87253
He neutral muonic atoms, ground state hyperfine splitting 79−68334
He, three-particle system with Coulomb interaction, correl. wavefunctions calcs. 77−68144
^{4}He, Lamb shift calcs. 78−94199
^{4}He, nuclear polarisation corrections 78−22056
$(^4\text{He}+\mu^-)^+$ muonic ion, $2S_{1/2}$-$2P_{1/2}$ energy transition meas. 78−33641

muonic atoms continued
$He\mu^-$, mol. ion formation in liq. He, X-ray intensities, Auger and Stark transitions 78−94338
^{A}Hg, A=198-202,204, muonic X-ray transitions, nuclear state quadrupole moments and charge distrib. 79−41253
H(muonic)+H^+, elastic scatt., cross section 79−871
^{193}Ir, muonic, mag. hyperfine anomaly 77−83768
^{175}Lu, muonic, nuclear spectroscopic ground state quadrupole moments from X-rays 79−98252
^{A}Mo, A=92, 94-98, 100, muonic atom X-ray transitions, nuclear charge radii 80−27545
Mu+H, electron spin exchange cross-sections 80−9685
N, muonic X-ray transitions, nuclear charge radii 80−99589
Na compounds, muonic X-ray intensities, Lyman series 80−23578
Na, muonic, $2s^1/_2$ level decay channel concurrence, neutral current effects observation *(Russian)* 80−83526
Nb-V, negative muon Coulomb capture ratio and Lyman series intensities 80−14255
^{A}Ni(e,e), 100-275 MeV, A=58,60,62,64, cross sections and muonic X-ray meas., charge distrib. systematics 80−86801
^{237}Np muonic, prompt fission, fragment atomic muon capture 80−95312
^{237}Np, muonic atom lifetimes from muon induced fission 80−69269
^{A}Os, A=186, 188, 190, 192, electromagnetic moments from muonic X-rays 78−12972
^{188}Os, muonic resonance spectra, deduced isomer shifts and electric moments 80−18948
^{192}Os, dynamic hyperfine effect, model independ. anal. 78−22057
P allotropic modifications, muonic X-ray intensities, computer analysis 80−23577
P, muonic allotropes muonic Roentgen intensities *(German)* 80−53168
^{31}P, muonic, 3d-2p X-ray transition 80−9764
Pb, 5-4 transition, QED valdity test precision meas. 78−33642
Pb, A=204-208, charge distrib. from elastic electron scatt. and muonic X-ray data anal. 78−54681
Pb, high-lying states transitions, electron screening effects 77−34786
Pb muonic isotopes, A=204, 206, 207, 208, nuclear polarisation energy shifts, RPA calcs. 78−94334
Pb, transition energy meas., tests of high-order vac. polarisation corrections 77−71895
^{204}Pb, muonic, first excited 2^+ state, isomer shift of E2 transition 80−99150
^{207}Pb, muonic, octupole doublet isomer shifts, octupole vibrs. 80−95750
^{207}Pb muonic isomer shifts, neutron hole anomalous moment contribs. 80−78728
^{208}Pb, charge distrib. polarisation from e^- scatt. and muonic X-ray data consistency 77−22873
^{208}Pb, isomer shift of 2.61 MeV gamma transitions 77−38753
^{208}Pb, nucl. polarisation correction 79−64123
Pd, circular polarisation of muonic K_α X-rays 78−9284
Pd, circular polarisation of muonic X-rays, strange μ^- depolarisation 78−25758
^{105}Pd muonic X-rays, nuclear charge parameters, quadrupole moments 78−29377
^{A}Pu, A=239,242, muonic, prompt fission, fragment atomic muon capture 80−95312
^{A}Pu, A=239,242, muonic atom lifetimes from muon induced fission 80−69269
^{239}Pu, highly deformed, muonic X-rays, nuclear charge distrib., elec. quadrupole moment 78−70440
^{239}Pu muonic atom, n emission, bound μ influence on fission barrier 78−89845
^{294}Pu, muonic atom direct electroprod., finite nuclear size effects *(Russian)* 80−69272
Se allotropic modifications, muonic X-ray intensities, computer analysis 80−23577
Se, circular polarisation of muonic K_α X-rays 78−9284
Se, muonic allotropes, muonic Roentgen intensities *(German)* 80−53168
^{28}Si, $3d_{5/2}$-$2p_{3/2}$ muonic X-ray transition, energy, wavelength meas. 78−66695
^{A}Sm, A=144-154, charge distrib. and hyperfine splitting from muonic X-rays 79−40838
^{A}Sm, A=150, 152, muonic, X-ray spectra meas. and anal., charge radii, multipole moments 79−3600
Sn, transition energy meas., tests of high-order vac. polarisation corrections 77−71895
^{181}Ta, X-ray transitions, radial charge parameters, quadrupole moment 77−34226
^{232}Th, highly deformed, muonic X-rays, nuclear charge distrib., elec. quadrupole moment 78−70440
^{232}Th, muonic, μ induced prompt fission, fate of the μ 78−86557
^{232}Th muonic atom, n emission, bound μ influence on fission barrier 78−89845
Tl, A=205,203, charge distrib. from elastic electron scatt. and muonic X-ray data anal. 78−54681
Tl, transition energy meas., tests of high-order vac. polarisation corrections 77−71895
U (M,f), muon excitation probabilities, muonic atoms, Schrodinger eqn. 80−47515
U, A=235, 238, highly deformed, muonic X-rays, nuclear charge distrib., elec. quadrupole moment 78−70440
^{A}U, A=235,238, muonic atom lifetimes from muon induced fission 80−69269
^{235}U, fission studies, target preparation 80−23217
^{238}U, fission and electron decay 77−38754
^{238}U, fission studies, target preparation 80−23217
^{238}U, muonic, μ induced prompt fission, fate of the μ 78−86557
^{238}U, non-axiality effects in quadrupole hyperfine splitting 77−46107
^{238}U, shape isomeric γ-decay 77−34245
^{172}Yb, muonic resonance spectra, deduced isomer shifts and electric moments 80−18948
^{A}Zn(e,e), 100-275 MeV, A=64,66,68,70, cross sections and muonic X-ray meas., charge distrib. systematics 80−86801
^{68}Zn, 2s-2p muonic X-ray transition obs. 80−74264
^{68}Zn muonic atom, dynamical E0 excitation, E0 resonances, muonic X-rays 80−95749

muonic molecules
exotic atoms, conf., Erice, Sicily, (1979) 80−67939
fluorides, muon Coulomb capture ratio 78−62959
free radicals, μSR spectra obs. 80−69279
muon spin resonance frequency spectra, theory 80−1088

muonic molecules continued
muonium-substituted transient radicals observed by muon spin rotation 78−74678
orthopositronium, vac. polarisation corrections in muonic molecules 78−78841
oxides, muonic X-ray spectra, empirical intensity correls. 78−90326
polyethylene, C muonic X-ray spectra, H(D) isotope effects 77−75344
radicals, muon substituted, μSR precession freqs. 79−55004
radicals formation 79−57277
thymine+muonium, radical form. in aq. soln., spin reson. obs. 78−74679
ddμ, rate of formation calc., energy depend. *(Russian)* 77−10795
dtμ, rate of formation calc., energy depend. *(Russian)* 77−10795
dt$\mu\rightarrow{}^4$He+n+μ^-, 2 GeV energy release 78−17250
μH+He, interaction pots. and rot. scatt. calcs. 80−43158
pdμ, fusion reaction rate in gaseous H_2+7% D_2 mixture exposed to muon beam *(Russian)* 77−10794
pdμ, rate of formation calc., energy depend. *(Russian)* 77−10795
ppμ, rate of formation calc., energy depend. *(Russian)* 77−10795
ptμ, rate of formation calc., energy depend. *(Russian)* 77−10795
ttμ_2 rate of formation calc., energy depend. *(Russian)* 77−10795
D_2^+, three-body Coulomb interaction, adiabatic representation 79−31640
$H_{2\lambda}$ liq., capture rate meas. 80−69275
H_2^+, three-body Coulomb interaction, adiabatic representation 79−31640
HBr, isotope chem. shift of μ^+ 79−55005
H_2O (D_2O), O muonic X-ray spectra, H(D) isotope effects 77−75344
^{2}H, ^{1}H, μ-N axial coupling const. from muon capture *(Russian)* 77−50570
^{2}H(pμd, pμt and dμt), ground state energy calc. with correl. wave functions 77−23439
^{2}H(tμ,nμ)^{4}He, muon catalysed fusion, neutron yield, muonic molecules 80−106095
$He_2\mu^-$, mol. ion formation in liq. He, X-ray intensities, Auger and Stark transitions 78−94338
$K_2Pt(CN)_4$, muonic X-ray radiation anisotropy *(German)* 80−69267
PMu_3, (Mu=muonium), $n\nu_2$ vibrational levels, prediction of inversion splittings 78−90146

muonium
bimolecular rate consts., Larmor precession relax., kinetic isotope effect rel. to H 77−38752
bound-state solutions in relativistic two-body formalism 78−13443
chemical reactions, tunnelling effect 79−57276
chemical structure studies with positrons and mesons, review 79−79277
chemistry, isotope effects and collision theory 79−57273
decay rate, taking into account bound electron 80−102086
diamond-structure crystals, anomalous muonium, μ^+ meson probe appl. *(Russian)* 79−28665
exotic atoms, conf., Erice, Sicily, (1979) 80−67939
formation, interaction with radiolysis products in pure water, OH. scavenging by tert-butyl alcohol 79−24806
ground state, hyperfine struct. due to exchange and virtual photons 79−36804
ground state, muon mag. moment and HFS, Zeeman transition obs. 77−75345
ground state splitting, appl. of new relativistic two-body formalism 79−2933
hyperfine quadratic shift in electric field, pressure dependence 78−13442
hyperfine quadrupole moment, orbital mixtures, quarkonium system phenomenology in potential models 79−49496
hyperfine splitting 78−74806
hyperfine splitting correction 78−94336
hyperfine splitting in quartz, precision determ. using muon spin rot. technique 80−50246
hyperfine splitting of ground-state 78−94337
hyperfine structure of ground state, magnetic moments, muonium-antimuonium conversion, excited states 80−69273
hyperfine Zeeman freq. meas. via Ramsey reson. 77−14620
intraspur muonium form. time scale 80−63872
magnetic structure, investigation of inhomogeneously magnetised ferromagnetic metals 79−42739
muon precession freq. shift, temp. depend. *(Russian)* 78−13632
muon spin rotation, review of recent advances 79−24252
muonium+Cl_2, pot. energy surfaces, inversion calcs. 80−93734
oxide powders, muonium and positronium form. 79−56679
photoproduction of relativistic parapositronium, and muonium perturbation expansion *(Chinese)* 79−49432
physics and chemistry of μ^+ and muonium review *(Russian)* 77−50566
polarization of μ^+ in muonium atom in diamond structured crystals *(Russian)* 78−39492
production in fine SiO_2 powder vac. interstices of thermal muonium 78−42250
production in H, low energy struct. of total cross section 77−10792
quadrupole moment, effect on spin precession and relax. *(Russian)* 78−31143
quadrupole moment and relax. of muonium and mesoatom spins 78−19404
quartz, muonium EPR transitions by muon-spin rot. 80−29668
quartz, muonium precession, quadrupole splitting 79−56678
quartz, quadrupolar effects in spin precession of muonium 80−75910
radiolysis effects in muonium chemistry 78−88653
reaction dynamics using surface muons in gas phase 79−57274
reaction in soln., rate const. and effective charge 79−57275
reaction kinetics in liqs., coherent diamag. fraction obs. 79−57278
reaction with DNA and its constituents in water soln., rate constants 79−57210
reactivity in aq. soln. 78−80774
solid, muonium formation and charged particle tracks 79−57259
two-frequency precession determ. of hyperfine splitting in matter 77−28505
μ+$F_2\rightarrow\mu$F+F, isotope effects, quantum mech. and information theoretic calcs. 78−44360
μ^+e^- atom, hyperfine quadrupole moment of ground state 78−90324
($\mu^+\mu^-$) atom, Coulomb disintegration, cross sections and energy spectra *(Chinese)* 80−102589
Ar, muonium formation by positive muons 79−57272
F_2+Mu, impulsive triatomic reaction, vibr. state distrib., impulsive energy release model 78−92456
$F_2(v=0)$+Mu$\rightarrow$MuF($v'\leq3$)+F, (Mu=muonium), quantum mech. calcs. 77−21366

muonium continued
Ge, anomalous muonium state 79−56677
Ge, anomalous muonium states 80−34841
Ge, deep and shallow levels of muonium, electronic struct. 78−39051
Ge, muonium relaxation rates 80−75912
n-Ge, μ^+ depolarisation, post muonic stage *(Russian)* 77−48116
Ge, μSR, spin Hamiltonian and anomalous muonium states 80−71286
Ge:As, interaction of muonium with atoms 79−11373
$H(1s)+\mu^+ \rightleftharpoons Mu(1s)+p$, thermal collision, quantal calc., elastic and transfer cross sections 77−42446
He, muonium formation by positive muons 79−57272
$Mu+F_2(Cl_2)$, isotope effects and collision theory 79−57273
$Mu+F_2 \rightarrow MuF+F$, 300 to 400K in N_2 moderator, reaction rate determ., tunnelling 78−48682
$Mu+F_2 \rightarrow MuF+F$, exchange reaction, quasiclassical dynamics calcs. 79−91942
N_2, muonium formation by positive muons 79−57272
Ne, muonium formation by positive muons 79−57272
O_2+muonium, aq. soln., reaction rate const., spin-conversion 79−100422
OH radical participation in terminal muon spur for muonium prod. 79−57271
Si anomalous muonium states, time behaviour of μ spin polarisation 79−11371
Si, anomalous muonium state, μSR 79−56674
Si, deep and shallow levels of muonium, electronic struct. 78−39051
Si, muonium precession freq., form. probability meas. 79−11370
Si, muonium state, anomalous 79−56673
Si, μ^+-meson depolarisation, spin relax. *(Russian)* 78−52416
Si, μSR, spin Hamiltonian and anomalous muonium states 80−71286
A-SiC, dimensions of muonium atoms, depolarisation of positive muons 79−11374
$X+F_2 \rightarrow XF+F$ (X=Mu, H, D, T), quasiclassical smooth sampling study of threshold behaviour 79−61852

muons
see also cosmic ray muons; muon probes
anomalous mag. moment, eighth-order contribution calc. 78−29261
anomalous mag. moment, finite QED 80−47222
anomalous mag. moment, sixth order, photon-photon contrib. 78−16958
anomalous mag. moment, sixth-order calc. 78−74190
anomalous mag. moment, two-pion contrib. 78−66181
anomalous mag. moment meas. 77−46094
beam channel, 40 GeV/c, Serpukhov, lens, guide reflector, filter 77−18729
catalysis of hot fusion 78−743
characteristic features *(Hungarian)* 79−13180
charge and quark-lepton analogy *(Russian)* 77−219
corrections of the sixth-order anomalous magnetic moment of the muon 79−54371
degenerate muon gas, creation in nuclear matter with neutrinos retention 78−96390
dimensions, mass, elec. and mag. moments *(French)* 80−13305
electric dipole moment meas. of positive and negative muons, new upper limit 78−37209
electron-muon mass ratio in Sp(1,Q)⊗U(1) unified gauge theory 77−61236
electron-muon symmetry of Callan-Symanzik function: two-lepton case 80−73627
flux quantization model, e:μ mass ratio, EM coupling const. 77−79240
fundamental particles in composite hadron model *(Russian)* 77−30312
fusion reactor, catalysis of d-t fusion 80−78438
g−factor, (g-2) expts., review, book contrib. 80−68403
g-2 experiments as a test of special relativity 79−58539
g-factor, anomalous meas. 77−61235
g-factor anomaly, review of theoretical contribs. 77−30384
gyromagnetic ratio, QED consequence 80−22548
heavy muon in minimal gauge scheme as possible cause of eμ, $\bar{\nu}_\mu$ anomalies 77−61241
heavy muons, possible existence of 20 GeV muon *(Russian)* 79−6359
high flux muon channel incorporating a high quality spectrometer field 79−72136
LAMPF linear accelerator muon beam characts., surface and cloud beam polarisation 79−71994
LAMPF stopped muon channel 79−68115
magnetic moment, (g−2) value, second order weak correction in arbitrary gauge models 78−62301
magnetic moment, anomalous, free gluon mass, lower bound in integer-quark-charge model 80−78042
magnetic moment, anomalous in SU(3)×U(1) gauge model 79−3026
magnetic moment, pionic contrib. lower bound 77−26527
magnetic moment, weak correction in gauge models 78−16965
magnetic moment, weak coupling contribution, Weinberg-Salam model 80−22607
magnetic moment form factor 80−18138
magnetic moment of muon, pionic contrib., using exact soln. of Meiman problem 78−78182
magnetic moments, anomalous, QED test 80−77996
mass, QED anal. 78−33011
mass, self-energy formula with grav. self-energy 79−9314
mass formula, chronon in electron theory 80−47224
mass formula of charged leptons 80−13244
mass formulae from EM self energy *(Chinese)* 79−93416
model as $e\bar{\nu}_e\nu_\mu$ (or $\bar{e}\nu_e\bar{\nu}_\mu$) reson. 77−6189
momentum measurements from $\pi^+ \rightarrow \mu^+\nu_\mu$ 80−37253
muon number nonconservation postulation 77−87916
muon-electron mass ratio in a semi-classical model 80−91072
number violation, Weinberg model extension 77−67610
orthomuon mass lower limit from neutrino data anal. 78−62388
physics, review, props. and identification 78−82260
physics and chemistry of μ^+ and muonium review *(Russian)* 77−50566
QED with internal fermion excitations, eμ system 80−9130
quantum electrodynamics review *(Hungarian)* 78−37159
radius, two bound spheres model, 2p-1s transition energies 77−10298
SU(2)×U(1) gauge model, muon anomalous mag. moment, charged Higgs boson contrib. 80−78011
super trimuons production, possible evidence of six-fermion interactions 79−71743
velocity in comparison to neutrinos and antineutrinos 80−9190
weak neutral current couplings of muons 79−85259
e-μ-τ spontaneous symmetry breaking and rare τ decays 79−9301
e μ τ asymmetry, conserved currents *(Chinese)* 79−58904

muons continued
$\mu \rightarrow$e transmutation, failure to observe conversion, reasons and results 79−369
μ:p magnetic moment ratio, discrepancy between direct and indirect determinations 77−18287
μ-e universality, radiative corrections in gauge theory of $\pi^\pm$ decay 77−10244
μ^+, magnetic moment determ. from Larmor precession meas. in liq. Br 78−82259
μ^+, nonadiabatic motion stability in mag. confinement system, numerical simulation 77−61646
μ^+ polarisation dynamics in mag. mirror field, neutrino emission asymmetry 77−61645
$\mu^\pm$, anomalous mag. moment, elec. dipole moment, and test of relativistic time dilation 79−45088
μe problem, mass difference, lepton number and symmetry conservation, forbidden transitions *(Chinese)* 79−13121
μe universality breakdown of neutral weak currents in $SU_2 \times U_1$ gauge *(Russian)* 79−75712
μe universality correction, rare decay mode calcs. 78−45898
μe universality violation in renormalisation theory, neutral leptonic currents *(Russian)* 78−45837
$\mu^+ \rightarrow e^+\gamma$, use in neutrino oscill. length limit theory 77−41838

muscle
abdominal EMG, recording of uterus activity *(German)* 78−92712
acetylcholine-induced current fluctuation in tissue cultured muscle cells under voltage clamp 77−29119
acetylcholine-induced current fluctuation in tissue-cultured muscle cells under voltage clamp 77−29119
acoustic stapedius reflex, human, in industrial noise, fatique and recovery 79−53159
acoustic stapedius reflex growth functions, effect of sensorineural hearing loss 79−16216
action potential of single motor unit, modelling 78−53386
action potentials from a single motor unit, influence of a sustained contract. 78−31801
actions, model for semi-quantitative studies 80−61605
active skeletal muscle, frog, before and after a slow stretch, X-ray diffr. 78−80906
activity patterns of human skeletal muscles rel. to fibre type conposition 78−80869
activity prediction, optimisation method adaptation 79−92273
adaptive control mechanisms for complex motor systems 80−81573
adaptive stiffness control in human movement 80−108947
afferent nerves from muscle spindles, signal interpretation method 80−101188
afterpotentials influence on shape and magnitude of extracellular pots. 80−3625
airway smooth muscle, contracted, hysteresis, dog expts. 80−81634
alpha excitability evaluation by means of muscleforce-freq. curve *(Japanese)* 78−3643
alpha-tropomyosin and its components, thermal denaturing 79−53023
amantadine, neuromuscular blockade by suppression of ionic conductance of the acetycholine receptor 78−64975
ambulatory neuromuscular activation control model 79−57638
AMG-1 myographic analyser 79−57785
amplifier-electrode hybrid module for surface EMG pots. meas. 80−41294
analogue amplifier for mech. recording, myocardium studies 78−40447
anatomical model, internal pressure effects 80−67103
anisotropic nerve-muscle syncytia, elec. props. III. steady form of the excitation front 78−69037
anisotropic nerve-muscle syncytia, electrical props. 78−64971
antagonistic muscles, functional elec. stimulation optimisation, math. modelling, joint motion 80−61730
antagonistic muscles, temporal firing sequences, EMG obs. 80−40984
apparatus for generating controlled ramp movements, studies of spindle afferent acti;vity and tone 78−77121
arbitrary movements control, theory 79−74641
arm and forearm exercise joint force musculoskeletal model 79−92272
arm movements in monkeys, control processes 79−53080
arm posture control, spring model and equivalent neural network 80−101196
arterial smooth muscle, estimates of cellular mechs. 79−16229
artificial arms, muscle- and externally-powered, investigation of freq. of use *(German)* 79−12030
artificial muscle system, load meas. method 77−44852
artificial muscles, deform. props. of contractile polymeric struct. 77−25595
audiomotorial reflex, techniques for provoking and registering *(Croatian)* 79−53162
axolotl muscle, spontaneous release of transmitter from repressed nerve terminals 77−70449
axon conduction velocity modified by reinnervation of mammalian muscle 78−24062
back strength, torso muscular capacity assessment by isokinetic analysis 79−96606
bioenergetics, solitons, muscle contraction mechanism 79−96508
biomechanics, cardiac muscle *(Japanese)* 80−72201
biomedical instrumentation 77−40811
biopsy, semiautomatic image analyser 80−85466
blink reflex, 1st component in rabbit and man 79−74649
blood vessel wall composition analysis with selective histologic staining 79−84067
bowel, rat, adrenalectomy and whole body α-irradiation obs. 79−100676
brachial bicepts, radial decline of the extracellular action pot. 79−16192
cardiac, excitation-contraction coupling 79−96547
cardiac, mathematical contractile model *(Japanese)* 79−57632
cardiac, resting, activation monitored by intensity fluctuation spectroscopy 80−108953
cardiac adaptation and hypertrophy, principle *(Japanese)* 78−31828
cardiac chemical power, derivation of chem. power eqn. and determ. of eqn. consts. 80−16911
cardiac contractile filament and series elastic work and power, mathematical model 80−16981
cardiac contractile filament and series elastic work and power, clinical correls. 80−16982
cardiac contractility *(Dutch)* 78−73171
cardiac energy density function encompassing elastic and contractile props. 79−62279

muscle continued
cardiac fibres, biaxial stress/strain rel. and left ventricular wall stresses 79−29558
cardiac left ventricle, contractile filament stress rel. to wall stress 80−56096
cardiac muscle, frog, aequorin-injected, Ca transients 78−61149
cardiac muscle, passive, viscoelastic theory and obs. 80−94273
cardiac muscle, rat, effects of US on mech. props. 78−96062
cardiac muscle, series elasticity, effects of mech. history and time in twitch 77−37004
cardiac muscle force-velocity relation, anal. in time domain 80−35943
cardiac muscle mechanics ref. to computed zero-load aortic flow 79−29548
cardiac muscle model, numerical study of behaviour of an activation parameter 78−11686
cardiac muscle preparation, isolated, determ. of segment length 77−48982
cardiac muscle stress/strain relationship determ. by computerised tomography 79−92262
cardiac Purkinje fibre relationships 79−43861
cardiovascular system dynamics, characterisation by generation of programmed premature contracts. 79−88113
cell fusion, preceding increased membrane fluidity obs. 77−77873
cell membrane, lateral transport of lipid probe and labeled proteins 77−40646
cell osmotic state and membrane permselectivity repeated microwave irrad. effects quantitation 80−56131
cell surface, heterogeneity of acetylcholine receptor molecules 80−16910
charge movement in the membrane of striated muscle 79−5263
chelonian muscle spindles, model for β motor stimulation 77−44636
chemical power, appl. of power, work and efficiency eqns. to left ventricular energetics in man 80−16912
chemically skinned fibres, rabbit, exponential rate processes study 78−44468
chemomechanical energy transduction, mol. basis 80−72143
cinematographic and bioelectric data, synchronisation device 77−81754
clinical EMGs, computer anal. 78−80985
clinical telemetry of EMG and temporal information during gait 78−80994
colon EMG, use of autoregressive-modelling techniques for anal. 80−101146
colonic contractile activity meas., pharmacological tests in dogs appl. 80−109068
conduction velocity, meas. and recording methods 79−100688
contractile activation in slow and twitch muscle fibres of frog 77−32884
contractile element behaviour as force and shortening generator, Hill's model 80−3681
contractile force in unskinned rat heart fibre 80−30955
contractile machinery of human muscle in health and disease, physiological and metabolic studies 79−39443
contractile properties, effect of successivity of activating pulses 77−25418
contractile proteins relative to eye striated muscle, physico-chemical anal. 77−90819
contractile system, sliding motion anal. 80−67104
contracting muscle, time-resolved studies using small-angle X-ray diffr. 79−12052
contracting or expanding pipe, semi-infinite, unsteady flows 77−86523
contraction, cross-bridge model 78−44475
contraction, mathematical model considering excitability 77−25417
contraction, reciprocal sliding of protofibrils and thick filaments shortening 77−56331
contraction, reliability anal. of the elementary catastrophe theory model 78−44471
contraction, simultation of thermophysical processes 78−96063
contraction, single, high-time resolution X-ray investigation method 80−81777
contraction, time-resolved X-ray diffr., data-collection system *(Japanese)* 80−46108
contraction, voluntary, man, reversal of recruitment order of single motor units obs. 78−40136
contraction kinetics obs., time-resolved X-ray diffr. appl. *(Japanese)* 80−56291
contraction strength of elec. stimulated muscle, control by pulse width and freq. modulation 77−40929
contraction time in skeletal muscles of normal children 78−61163
contraction-relaxation cycle in guinea pig taenia coli, translocation of intracellularly stored Ca 77−86474
contractions, kinetic study 78−48769
control enhancement by use of predictor feedback technology 77−48952
control of upper-limb prostheses, a case for neuroelec. control 78−44704
control system, origin and nature of correls. in the IA feedback pathway 79−24977
controllable force supply for human muscle voluntary reactions meas., design features 79−100801
cricothyroid, response to FM sounds in FM bats 77−21540
cross bridge rotation during contraction, fluctuations in polarised fluoresc. 80−97856
cross bridge slippage in glycerol extracted fibrillar muscle fibres 78−77075
cross-striated, frog, ATP conc. obs. 78−20149
cross-striated fibres, efficiency of light diffr. under stretch and isometric contract 80−85440
cross-striated muscle, reorganisation of sarcomere struct. 77−77895
crossbridge stroke and activity revealed by optical diffr. 78−69021
cultured nerve and muscle, biology 79−2031
current noise parameters in embryonic heart cell aggregates 80−21459
cylindrical cell with a time-variant membrane resistance, meas. of passive parameters 77−29113
data acquisition and anal. of striated muscle diffraction patterns, use of direct memory access microprocessor system 80−89918
deltoid, myoelectric signal rel. to physiological props. 79−70539
diadynamic current therapy, 'tonus-1' apparatus 78−7523
diaphragm, canine, in vivo stiffness props., obs. and meas. system 80−97988
digastric muscles, EMG rel. to mandible opening force 79−74619
digital dynamometry and technical aspects of its development 77−40854
digital EMG processor 79−53283
digital memory recorder in EMG and nerve conduction studies 79−43999
muscle continued
displacement currents in frog skeletal muscle, contrib. of the K conductance channels 79−39409
dolphin, lung collapse and intramuscular circulation during diving 80−81643
duodenal contractility anal. in unanaesthetised dog 79−92207
duodenal slow waves, human, anal. and modelling. 80−72146
dynamic stiffness and crossbridge action 78−48819
dynamic structure, X-ray scatt., time resolved, rapid data collection systems 80−61740
dynamics, digital simulation 78−31807
EEG, filtering of muscle artifact 79−100764
effort monitoring, prototype instrument 77−5092
elastic and viscous props. of resting frog skeletal muscle 77−44700
elastic strain energy, storage in muscle and other tissues 77−16950
elbow joint, moments transmission, isometric tests 80−41083
electric control of human motion 78−27926
electric stimulator for the neuro-muscular system 79−48315
electrical depolarisation and repolarisation obs. 80−3624
electrical properties of a skeletal muscle fibre containing a helicoidal T system, anal. 78−80852
electrical stimulation apparatus 78−36035
electrical stimulation device for leg muscles to correct defective walking 78−36051
electrical stimulator for complex stimulation of leg muscles during walking 79−48377
electrically induced muscle contraction, meas. of suggestion effects *(Slovenian)* 80−81571
electrically stimulated, closed-loop control of force 80−76728
electrically stimulated muscles, cat, control of recruitment and firing freqs. of motor units 78−81092
electrode, screw-in, expt. and clinical evaluation 77−81747
electrodes for sensing EMG pots. 77−90953
electromagnetic stretch, sensorimotor cortex neurons in behaving primates 79−88073
electromyographically EMG triggered photographic technique for recording visual behaviour 78−31919
electron probe, quantitative microanal. of biological thin sections, methods and validity 77−25620
electrophoresis of concanavalin A receptors along embryonic muscle cell membrane 77−29121
electrostatic field resolution due to nerve or muscular spikes, EMG analysis 79−57627
electrostimulation, method and clinical use 79−83877
elliptical nerve and muscle fibres, physico-mathematical anal. 78−11639
EM field effects on isolated nerve and muscle preps. 78−53443
EM fields, direct influence on nerve and muscle cells of man in 1 Hz-30 MHz range 80−51160
EM method for stretching muscles of chronically implanted animals 80−56308
embryonic lobster muscle, synaptic and septate neuromuscular junctions 77−77889
embryonic muscle cell membrane, electrophoretic movement and localisation of acetylcholine receptors 78−85298
embryonic skeletal muscle in culture, props. development during differentiation 78−53363
EMG, analysis of signals, myogram integration, amplitude value determ. 80−40997
EMG, computer anal. of single motor unit pot. parameters 77−9290
EMG, cutaneous trunci muscle in spinal reflexes 80−3635
EMG, diagnostic possibilities 77−44784
EMG, dynamic arm movements data, acquisition and anal. 80−36179
EMG, EEG and unit activity in lateral geniculate, arousal and sleep effect in cats 80−40991
EMG, evoked, evaluation of Wiener filter 80−3747
EMG, filter bank analyser for automatic anal. 80−98162
EMG, freq. response of biceps brachii in isometric contraction to fatigue 80−3621
EMG, human inspiratory diaphragmatic, spectral anal. 79−88071
EMG, instrument for quantitative anal. 78−81041
EMG, instrumentation requirements 80−41301
EMG, integrated, rel. to angular vel. in horizontal elbow flexion 80−3620
EMG, multichannel data acquisition system for the survey of intercostal muscle activity 80−81790
EMG, myographs design and technical requirements 80−40996
EMG, nonstationary model 77−86481
EMG, normalized gait patterns extimation 77−40819
EMG, on-line multifunctional prosthesis control 79−2166
EMG, physiology and mathematics 79−74621
EMG, pulsed integrator for anal. 80−61719
EMG, quantitative, value of automatic anal. 80−8203
EMG, rectified surface, time constant in low pass filtering 80−67266
EMG, selection of electrode-to skin contact area and amplifier input impedance for quantitative surface electrography *(German)* 79−88205
EMG, signal characts. interrelationships at different levels of muscle tension and during fatique 79−34537
EMG, simultaneous recordings of parts of pectoralis major muscles during swimming 80−72147
EMG, single fibre, microcomputer-based jittermeter 80−46078
EMG, single motor unit action pots. identification by computerised anal. 80−72343
EMG, single pots., anal. by means of multivariate methods 80−98170
EMG, stimulated activity from close lying and remote muscles 79−79501
EMG, surface, dT-dL anal. during muscle fatigue, left hand obs. 80−104576
EMG, surface, dT-dL anal. during muscle fatigue, right hand obs. 80−104575
EMG, surface, system for meas., recording and digital anal. *(German)* 80−76848
EMG, surface integrated, rel. to isometric contraction force 79−74618
EMG, sweller-selective gain control along oscilloscope sweep 77−44864
EMG activity during brief isometric contracts, model 77−16922
EMG activity in extraocular muscles visiual display of duration 77−40834
EMG analysis, normal values obtained by automated system 80−3845
EMG analysis of soft tissue lesions affecting shoulder function 78−35828
EMG and EEG sleep telemetry in the rat 78−48947
EMG and muscle force 78−40231

muscle continued
EMG and temporal information during gait, clinical telemetry 78−3638
EMG as a measure of muscular fatigue and its analogue simulation *(Japanese)* 79−8498
EMG bio reeducation of facial palsy 79−34701
EMG biofeedback in hemiplegic patient treatment, comparison of actual and simulated treatment 80−104806
EMG biofeedback in relaxation training, efficacy obs. 77−81636
eMG comparison of quadriceps femoris activity during knee extension and straight leg raises 80−8038
EMG detection by pasteless electrode 79−92413
EMG electrodes, small-size, meas. of uptake area 79−74799
EMG envelopes, spectral anal. and its appl. to study of muscular control processes 79−5390
EMG envelopes spectral anal., appl. to muscle control studies 78−92750
EMG F response, radicular injury evaluation 80−3852
EMG F-wave electrodiagnostic confirmation of upper trunk brachial plexus neuropathies 79−74779
EMG feedback therapy after stroke, efficacy obs. 80−30927
EMG frequency spectrum, recognition of shape 78−40207
EMG generation, quantification using automata theory 77−29132
EMG in alcoholism, nerve conduct. vel. and sensory pot. studies 80−3617
EMG in alcoholism, terminal latencies in superior gluteal, distal peroneal and tibial nerves 80−3618
EMG in human gait description, pattern recognition of multiple signals 77−44795
EMG in quadriparetics and quadriplegics, evoked giant sensory nerve pots. 80−3653
EMG index for localised muscle fatigue 78−57093
EMG investigations of gait 80−8198
EMG investigations of gait in cerebral palsied children 80−72186
EMG jitter effect on single motor unit pots. 79−83960
EMG jitter meas., single fibre, useful device 77−40832
EMG low freq. power spectra, motor units characts. determ. 80−3626
EMG monitor, appl. to electroconvulsive therapy 77−40899
EMG of Vastus medialis, power spectral changes for graded isometric torques 80−3622
EMG operated electronic artificial-leg controller 78−7545
EMG operated prosthesis controller, reliable system 77−48954
EMG pattern of diaphragmatic fatigue 79−88069
EMG period-amplitude analysis, cat locomotion and jumping obs. 80−67057
EMG power deposition in prolate spheroid models of man and animals at resonance 78−31905
EMG power spectra linking to recruitment and rate coding 80−3616
EMG power spectrum, contrib. of individual motor units 77−29129
EMG processing for sleep research 80−67267
EMG recordings, computer editing 78−80999
EMG recordings of muscular contract., estimations of active-state, linear systems muscle model 80−3623
EMG registration of sensory thresholds in the oral mucosa *(Croatian)* 80−108925
EMG shimmer in normal human muscles 79−34538
EMG shimmer in patients with neuropathy and neurogenic atrophy 80−72149
EMG signal, use as a volitional information source for controlling the FES stimulator 78−57128
EMG signal processor, sequential multistate 79−100763
EMG signals, determ. of onset and termination 79−83761
EMG silent period and muscle mechanics in human soleus muscle 80−67060
EMG silent period before voluntary movement rel. to preparatory phase condition *(Japanese)* 79−74622
EMG silent period measurement, automated system 80−89883
EMG spectra, factors affecting interpretation 77−44825
EMG spectral anal. temporal muscle in the rhesus monkey 78−69039
EMG spectrym analysis in neuromotor speech disorders 77−29161
EMG studies of low back mobility and activity levels 80−41059
EMG study of production of Japanese vowels 77−5012
EMG study of production of the Japanese semivowel 77−5013
EMG technique for percutaneous lateral pterygoid muscle 80−3841
EMG telemetry system, wide band 77−90924
EMG wall potentials and sounds of intestine, meas. and computerised anal. *(German)* 78−31944
EMGs, reliable derivation and relation to muscle tension 79−79499
endplate channel characteristics, alteration by permeant cations 78−3467
endplate currents, miniature, effects of Ca^{2+} and Mg^{2+} on decay 78−24064
endplates, acetylcholine-induced channels and transmitter release 78−24063
erythrocyte membrane abnormalities in Duchenne muscular dystrophy 78−96111
evoked muscle potentials, peripheral nerve lesion localisation 78−31802
excitation and contraction processes in muscle 79−5262
excitation spread in smooth muscle and myocardial tissues, fibre interaction 80−51068
excitation-contraction coupling, role of extracellular Ca^{2+} 79−74616
expiratory duration and abdominal muscle responses to elastic and resistive loading 79−100653
extensor carpi radialis, form recognition by EMG freq. spectrum 78−15939
extracellular potentials generated by curved fibres in a vol. conductor, modelling 80−97889
extracellular potentials of a number of muscle fibres in communication, computations 79−43843
extrafusal muscle fibre in spindle capsule of zebra-finches, electron microscope obs. 79−74701
extraocular eye muscle force duction tests after administration of succinylcholine or pancuronium 80−26255
extraocular muscle system, modelling the mechanics for clinical ophthalmology 78−40155
extraocular muscles, relative tensions 79−34554
extraocular muscles in man, single motor unit activity during fixation and saccades 79−16203
extrinsic eye muscles, new and neglected nerve terminals 78−56970
F-actin subunits, struct. non-equivalence 78−64959
F-actin subunits of thin filaments, functional role of struct. non-equivalence 80−76704
fatigue, electrophysiological pattern in healthy humans, effects of artificially induced ischemia 80−97890
muscle continued
fatigue, licalised, during repetitive loading, computerised anal. 78−57103
fatigue characteristics of human gastrocnemius and soleus muscles 78−20169
fatigue in muscular dystrophy, electrophysiological pattern of development 80−97888
fatigued muscle, composition of facuoles and sarcoplasmic reticulum 79−24963
fatigur resistance resulting from electrically induced exercise, alterations in 77−37103
fibre activity, SFEMG studies *(Swedish)* 78−24193
fibre bundle tension development, action of regulatory light chains 80−94270
fibre conduction vel., direct on-line estimation by surface EMG 79−100765
fibre contraction, giant barnacle, increased cyclic GMP levels 77−56369
fibre membrane, post-synaptic, ionophore-mediated Ca influx effects 78−11637
fibre orientation importance in determining the feature of cardiac elec. field 79−39397
fibre resting potential, cricket, influence of ions 78−24046
fibres, computed extracellular pots. 79−74620
fibres, elec. interaction 80−51063
fibres, glycerinated, filament overlap rel. to no. of Ca-binding sites 78−44465
fibres, relaxed, skinned, stretch and radial compression obs., frog 80−30736
fibres, single, isolated, opposite end unequal mech. transients 78−44541
fibres, slow, Ca transients in frog 77−77892
fibres and cylindrical syncytia, elec. pots. induced by current point source 79−74610
fibres examination, example demonstration linear anal. of histologic preparations 78−40443
fibrillar muscle, insects, oscill. contract.-relax. cycles, chemo-mech. coupling rel. 77−48829
filament geometry and the activation of insect flight muscles 79−83750
filtered EMG signal, S/N ratio in isometric contract. *(German)* 77−81490
fine muscular control rehabilitation using ramp threshold feedback 79−83996
firing pattern of single motor units, effect of muscle training 78−7327
flexibility of myosin rod, light meromyosin, and myosin subfragment-2 in sols. 78−53320
flexibility of thin filaments, dynamic light-scatt. evidence 80−41064
flight torque and lift responses of the housefly 78−85311
force development, filament spacing effect on axial forces 80−61597
force development, geometrical factors influencing radial forces 80−67102
force transducer, miniature, for myocardial stimulation and local tension measurements 79−48357
force transients rel. to surface EMG 77−44642
forearm musculature, quantitative anal. 77−36981
frontalis, spontaneous elec. activity as an indicator of surgical patient relax. 78−44686
function stimulation of extremities, its basis, technology rehabilitation 79−34620
gastro-duodenal zone spike activity, stochastic activity 79−79496
gastro-intestinal tract, physiological signals, spectral analysis, autoregressive technique appl. 80−41269
geomagnetic field sensitivity in animals, ferromag. coupling to muscle receptors as basis 80−72185
glycerinated, F-actin conformational changes, polarised UV fluorescence obs. 79−100567
hand, nerve stimulation effects on single motoneurones 79−79511
hand function, normal finger functional strength meas. 79−92276
hart, single muscle cell, Na current 79−43838
heart, contraction variable preload and afterload independence, thermodynamic and clinical consequences 79−79576
heart, excitation contraction coupling, mathematical model 79−96542
heart, isolated, grass-snake, motor reactivity obs. 80−67100
heart Ca^{2+} transients during excitation-contraction coupling 80−97896
heart cells, bivalve mollusc, fine structure 79−92188
heart cells, leaky, heavy water effects 79−62220
heart muscle, modelling of the contractility of the atria and ventricles 79−53079
heart muscle cells, paraffin-embedded, cryofracture 78−57148
heart muscle contractility, animals, analogue computer for calc. *(German)* 78−7378
heart muscle contraction, simulation 77−12954
heart muscle contraction force, rhythm influence modelling, intracellular pool Ca 79−79568
heart muscle staircase phenomenon, behaviour of myosin projections 78−53362
heart relationship between velocity, muscle length, force and contractile state 78−44543
Hill equation, fitting to expt. data 80−89777
hindlimb muscles of cat, coordination in maximal vertical jump 77−40662
Hodgkin-Huxley type electronic modelling of gastrointestinal elec. activity 78−61165
hyperbaric hyperreflexia, tendon-jerk and Hoffman reflexes in Man, soleus muscle 80−61530
hyperemia, new technique for study using ^{133}Xe 79−5351
impulses through a smooth inhomogeneity in an excitable medium 79−79445
innervation-like effect on muscle of axonally moved substances 79−16197
insect fibrillar muscle fibres, stiffness and tension obs. during and after sudden length changes 80−56078
interactive mini-computer system for the anal. of twitch waveforms of human motor units *(Japanese)* 78−28103
intercellular junctions in FANFT-induced carcinomas of rat urinary bladder in tissue culture 80−8230
interlimb coordination, human, expt. obs., two handed movements 79−57636
intestinal motor activity, mathematical model 77−90847
intestinal motor activity, mathematical model 78−77078
intestinal myoelectrical activity model 79−70537
intestinal myoelectrical models, pulse synchronisation expts. 80−67061
intestinal smooth muscle cell, voltage clamp studies of hyperpolarising inactivation 78−80847

muscle continued
intestinal smooth muscle cells, non-cholinergic excitatory transmission 77−77891
intrafusal muscle fibres of Chinese hamster, unusually thick filaments 79−74702
intramuscular nerve action pot. derived from sensory fibres 80−56071
ion channels in development, book contrib. 79−96549
ionic channels, locust muscle, pot.-dependent transition temp. 77−77882
isometric contractile properties of single isolated smooth muscle cells 77−29137
isometric muscle contraction meas., fibre-optic force transducer 79−79715
isometric sustained voluntary contracts., changes in EMG and heart rate 80−3629
isometric voluntary contracts., changes in mech. and bioelec. muscular activity and heart rate 80−3628
isotonic capacitive transducer for length change meas. 79−66585
jaw muscle EMG-activity and static loading of the mandible 79−43951
K-contractures and membrane pot. in mammalian skeletal muscle 77−29117
kinetic model of single muscular contract. 79−57629
laryngeal muscle activity during stuttering 79−57675
laryngeal muscles, reflex activation by sudden induced subglottal press. changes 79−74691
laser beams, active and longterm effects on fibroblasts and smooth muscle cells 78−40268
laser diffraction studies on striated muscle, indication stepwise sarcomere shortening obs. 79−43808
laser irradiated white rats, temp. changes dynamics 79−57594
laser Raman scattering, mol. probe of contractile state of intact single muscle fibres 80−89718
latency time meter model LT 1, operation and use 77−40853
left ventricle active model, deformation by nonlinear finite element anal. 78−35877
left ventricular function and myocardial metabolism prior to and after coronary bypass surgery 77−81646
leg muscle forces during normal human walking, determ. 79−16240
leg muscles, programmed 6-channel elec. stimulator for complex stimulation during walking 77−40923
length reflex control, servosystem simulation 79−57639
limb displacement in man, late EMG response long-loop hypothesis test 79−96544
limb displacement in man, late EMG response muscle and afferent contributions 79−96545
lip muscle contraction for speech, variation in perioral reflex amplitude prior 79−20558
lip muscle EMG during speech, anal., synthesis, manipulation and feature extract. 77−81605
living tissue, NMR 77−77959
local anesthetics, effect of Ph on use-dependent block of Na channels, frog 78−20160
locomotion, functional roles of calf and vastus muscles 77−81488
locomotion, human, dynamic modelling 80−8095
locomotion EMG signals, optimality criterion for processing 78−92612
locomotion studies, simple technique for correlating film and EMG 78−24186
long-latency reflex pathway dynamics, monkey 80−30706
lumbar spine, moments transmission, isometric tests 80−41083
lung airway smooth muscle mech. alterations in canine asthmatic model 79−100648
m. biceps brachii, human, extraterritorial pots. of high-threshold motor units 80−56005
mammalian muscle spindle, mathematical model *(Japanese)* 77−44638
mammalian tissues, shear props. at low MH2 freqs. 77−29174
mass potential, stochastic model *(Japanese)* 78−24056
mechanical efficiency of fast- and slow-twitch muscle fibres during cycling 80−41074
mechanics, thermodynamic model of a biological body 78−80908
mechanics in isometric contract., linear approxs. 77−73535
mechanics in isometric contraction, linear approx. 77−73535
mechanics of muscular organs 77−90836
mechanics study, appl. of acoustic microscopy 78−48952
mechanochemical contractile system as a thermodynamic machine 78−20201
median and ulnar muscle and sensory evoked pots. 79−34530
membrane mechanisms of activation of contracts. of depolarised smooth muscle 79−53071
membrane of insect muscle, permeation of Mn, Cd, Zn and Be through Ca channels 77−56357
membrane potential and active transport, information theory approach 80−35855
membrane potential change in frog muscle fibres treated with eserine 77−56345
membrane protein-lipid complexes, spatial organisation obs. 79−70529
microcomputer aided myoelec. prosthesis control 78−53576
microcomputer system for on-line acquisition of neuromuscular data 78−36015
microprocessor system for multifunctional control of upper limb prosthesis via EMG signal identification 78−3683
microprocessor system for multifunctional control of upper-limb prostheses via myoelectric signal identification 78−88766
microwave dielectric properties of tissue, rotational mobility of tissue water 77−29092
microwave dielectric relaxation in muscle 80−51146
micturition reflex, sequential stimulator for elec. restoration 78−53567
middle-ear muscle contraction, influence on auditory threshold for selected pure tones 78−85319
mitochondria of fish muscle, physiological correls. of Ca accumulating props. 79−20523
models, ultra-relax. in medium with high Ca conc. on exposure to MGATP 77−25388
motor command, extraction from EMG by means of a pulse counting method *(Japanese)* 78−53546
motor coordination and neuromuscular activities in human locomotion 77−44635
motor nerve endings, Ca dependency obs. 77−56368
motor neuron disease, possible mechanisms of spontaneous EMG activity 78−20162
motor output response to applied torque perturbations in man, nonlinearities evaluation 80−76771
muscle continued
motor reactivity, isolated heart of grass snake, pH and temp. effects 80−26219
motor unit, single, recording during strong effort 79−11908
motor unit action potential, study by means of computer simulationa 79−11914
motor unit action potential duration, meas. by means of surface electrode EMG 78−81039
motor unit discharge freq., dependence on isometric muscle tension 77−21510
motor unit surface pots. spectrum and muscle geometry 80−30704
motor units, discharge patterns in tremour states *(Japanese)* 78−31803
motor units, human, dynamic props. in the Hoffmann-reflex and M response 78−7331
motor-unit firing time statistics, effect on EMG spectra 78−31804
motorneurons of different geometry and the sixe size principle 77−36908
multicellular preparations, voltage clamp 77−40955
multifibre preparation, intercellular clefts influence on pot. and current distrib. 80−72145
multistate myoelectric control systems, operator error 78−81076
muscle fibres of Lethocerus maximus, temp. dependance of cross bridge parameters 80−61598
muscle power-density spectrum, effect of electrode bandwidth 79−29517
muscle preparations, viscoelastic props. anal., meas. and model *(German)* 79−83817
muscle stiffness in hypertonic solns. 80−67140
muscle stimulation in cases of spinal injury, exp. study 79−83883
musculo-skeletal shock absorption, relative contrib. of bone and soft tissues at various freq. 79−29549
musculo-skeletal system, complete set of control eqns. for humans 78−40223
musculoskeletal analysis of the pinch action 78−40225
musculoskeletal system, interactive computer modelling 77−40685
myocardial cell, transmembrane action pot., simulation of QRS-I wave *(Japanese)* 77−90740
myocardial contractility, real time meas. by an analog computer *(Japanese)* 79−44015
myocardial damage and high-energy elec. current (defibrillation) 78−57051
myocardial excitability evaluation, strength-interval curves generation under computer control 80−41336
myocardial fibre shortening vel., dependence on inotropic state and haemodynamic conditions 78−31833
myocardial fibres, ionic nature of repeated responses 77−70441
myocardial fibres, mechanism of uncoupling of excitation and contract. obs. 78−15810
myocardial fibres accommodation role of entering currents 77−36898
myocardial infarction in patients with transvenous ventricular pacemakers, ECG diagnosis 77−81624
myocardial inhomogeneity effect on left ventricular circumferential stress distrib. 79−92267
myocardial mitochondrial lipids, composition and phasic transitions obs. 78−53350
myocardial multicellular preps., voltage clamping methods 79−84056
myocardial pacing threshold meas., long term follow-up 77−81730
myocardial perfusion index calculator, device for prediction of subendocardial ischemia 77−40915
myocardial single fibre model, source-field relationships 79−39385
myocardial threshold determ. of degree of pharmacological influence 77−81643
myocardial tissue, shock-frozen, preservation as shown by cryo-ultramicrotomy and freeze-fracture studies 78−53593
myocardium, frog, amplitude of contracts 78−77027
myocardium, frog, effects of temp. on membrane currents 77−52759
myocardium, frog, model of excitation-contraction coupling 79−70541
myocardium, quiescent, anal. of some theological and mech. props., rat 79−74709
myocardium adjacent portions, mutual elec. influence genesis of arrhythmias 79−92202
myocardium contractility determ., anal. of differential quotients 79−34584
myocybernetic control model of skeletal muscle 77−12906
myoelectric aids for hand-prostheses *(Spanish)* 79−84011
myoelectric channel, multistate, signal processing 77−44837
myoelectric control of an artificial hand, sequential movement, tropical climate 80−41323
myoelectric control system, individually adapted, for a multifunctional prosthetic hand 78−57127
myoelectric control system for an above-knee prosthesis, development 78−53575
myoelectric multistate channel, signal processing 78−88768
myoelectric power spectra interpretation, a model and its appls. 77−44641
myoelectric signal, variance parameter 77−29130
myoelectric signal processing, expt. demonstration of optimal myoprocessor performance 80−89882
myoelectric signal processing, optimal myoprocessor derivation 80−89881
myoelectric signals, improved processor 80−104800
myoelectric single motor unit pots., model for generation 77−29131
myoelectrical control and driving system for hand orthoses *(German)* 77−56517
myoelectrically controlled hand which has a sense of touch, experience in fitting 79−12035
myoelectrically controlled systems, five-state, error rate obs. 80−72376
myoelectrically operated artificial hand, dynamically controlled *(German)* 79−8571
myoelectrically operated artificial hand, dynamically-controlled, first practi cal trial *(German)* 79−12029
myoelectrically-controlled prosthesis with sensory feedback 79−57815
myoepithelial cells, scanning electron microscopical image 79−34713
myofibrillar fine structure and cryo-ultramicrotomy 78−53592
myophone for functional rehabilitation *(Spanish)* 78−48924
myoplasm, model of passive 3D anisotropic syncytium as continuous medium 77−16898
myopotential inhibition of the unipolar demand pacer, prevention 77−81709
myoscope, 2-channel, appl. to ophthalmology 77−37085
myosin, column-purified, struct. studies of synthetic filaments 79−92131
myosin, cooperative interaction between the 2 heads, evidence from O_2 exchange meas. 77−32870
myosin, fast and slow, in developing muscle fibres 78−64961

muscle continued
myosin, interaction with a spin-labelled ATP analogue 79−57563
myosin, synthetic, effects of C-protein on filament struct. 79−92132
myosin conformational changes, laser Raman light-scatt. obs. 78−96002
myosin conformational conversions, investigation using 2 types of spin labels 77−52733
myosin filaments backbone, struct. 79−20512
myosin heads, movement during a heart beat 79−48207
myosin heads, return to thick filaments after muscle contract. 78−7319
myosin in chronic cardiac insufficiency, struct. and functional changes 77−36887
myosin molecule, binding to two actin filaments 78−27884
myosin subfragment-1 attachment to actin, expected effect on equatorial reflects. 78−27880
myosin synthesis increased by elec. stimulation of skeletal muscle cell cultures 77−1988
myosin-regulated muscle, changes in cross-bridge attachment 78−53361
myotonia, Ca-induced, computer simulation 79−57633
myotonia and Ca, mathematical model 78−11620
myotonic muscular dystrophy, altered Ca transport in erythrocytes 78−80849
myotubes, cultured, human, acetylcholine-induced conductance fluctuations 78−61157
nerve-muscle preparation, meas. of acoustic props. rel. to physiologic state 77−21673
nerve-muscle syncytia, anisotropic, elec. props. 78−53383
nervous control mechanisms, central and peripheral *(German)* 79−5271
nervous system commands in normal walking, mathematical model of striated muscle *(French)* 80−51071
neuromuscular block indicator, model INMB-1, EMG amplitude meas. 80−104785
neuromuscular blockade, increase of motoneyron survival during normal cell death in the chick embryo 78−27933
neuromuscular blockade monitoring by "twitch box" 78−77132
neuromuscular development, change in synaptic channel gating 79−16195
neuromuscular disorders, biofeedback therapy based on conscious control of motoneurons 79−34702
neuromuscular information transmission, distortion suppression 80−35871
neuromuscular junction, diffusion barrier for acetylcholine, frog 78−7334
neuromuscular junction, frog, Ca-dependent presynaptic action of substance P 77−52773
neuromuscular junction, frog, endplate current fluctuation obs. 77−25416
neuromuscular junction, frog, voltage-dependent effect of curare 77−52775
neuromuscular junction, membrane surface pot. changes effect on drug interactions 80−3631
neuromuscular junction, transmitter release during repetitive stimulation 78−3469
neuromuscular junction continuity, freq. sweep anal. of EMG 79−96686
neuromuscular junction continuity following nondepolarising block sweep freq. anal. 77−52910
neuromuscular junction endplate current simulation 79−62230
neuromuscular mechanism maintaining extrathoracic airway patency 79−100656
neuromuscular model of laryngeal control for pitch change in Japanese word accentuation *(Japanese)* 78−40205
neuromuscular motor structures in man, apparatus for programed multichannel elec. stimulation 77−25585
neuromuscular oscillations, interaction between those centrally and peripherally generated 79−62232
neuromuscular response to ankle rotation simulation with a segmental reflex model 79−8500
neuromuscular synapse, frog, dual action of Er on transmitter release 78−35834
neuromuscular synapses, newly formed, gating props. of acetycholine receptor 78−27934
neuromuscular system, computer simulated, effect of correlated adjacent interspike interval sequences 78−80858
neuromuscular system, human, model for small isometric tensions 77−52771
neuromuscular system, mammalian, energy-optimal controls 77−73522
neuromuscular transmission, evidence for prejunctional role of cyclic nucleotides 77−1987
neuromuscular transmission, modulation by octopaminergic neuron 78−11632
neuromuscular transmission in identified abnormal dystrophic muscle fibres, adequacy 78−27932
neuromuscular unit discharge during muscle fatigue, structural model anal. 80−67066
neurophysiology models and muscle control 78−24057
NMR, transverse resonance relax. in barnacle 77−4989
NMR multiwindow anal. and proton local fields and magnetisation distrib., mouse 80−21444
NMR of mouse muscle, ^{13}C and proton obs. 77−86463
NMR of muscle water, transverse rel. to longitudinal relax. rates obs. 78−35810
NMR relaxation time T, and T_2 rel. to water content 77−12884
oculomotor control system, signal-flow diagram 77−25415
oculomotor control system, synthesis on external feedback loop *(Korean)* 77−90779
oculomotor system, parametero, human, identification, appl. to stratismus 78−3478
oesophageal diaphragmatic EMG in humans, effects of electrode position 80−81753
optimisation techniques, use to predict muscle forces 79−16242
orthotropic elastic moduli for left ventricular mech. behaviour 79−57695
oviduct contractile activity, Si force transducer for extraluminal meas. 77−40805
papillary, diffusional and compartmental models of NA kinetics 77−44617
papillary, rat, stochastic model for characterising dynamic behaviour of 78−35821
papillary fibres, rabbit, effect of preliminary stimulation on repeat responses 78−48768
papillary muscle, rabbit, elec. phenomenon during Ba^{2+} induced contracture 79−83732
muscle continued
papillary muscle selection and testing, some mech. considerations 80−89919
papillary muscles, macroscopic inhomogeneities in mech. response 79−79571
paralysed, μP controlled stimulation, spinal injury appl. 79−83883
paralysed, treatment by elec. stimulation *(Slovenian)* 80−81771
paraplegic patient muscles, provision of functional use by elec. stimulation, review 80−101289
paraspinal, intramuscular stimulation, mapping of activated area 77−29144
paretic skeletal muscle, low freq. bizarre discharges 78−80864
parvalbumins, Ca-binding, lanthamide-substituted, of muscle, ^{13}C NMR obs. 79−96516
pediatric gait biotelemetry, clinical 78−3652
peripheral motor system interaction with CNS 79−8499
peripheral muscle and cerebellar cortex, computational model 78−11629
peristaltic reflex dynamics model 80−56080
peristaltic transport, influence of wave form *(German)* 79−79570
pH, percutaneous micro sensing during haemorrhagic shock and resuscitation 77−52907
phasic muscle stretches, discharge patterns of motorneurons 78−85303
phenylalkylamines, effect on potential dependence of frog muscle-fibre end-plate current 78−31799
phonons and the elastic moduli of collagen and muscle 77−52824
phosphoglycerate kinase, sequence, struct. and activity, hingee-bending enzyme 79−74595
photomotograms, evaluations by special analogue computer *(German)* 78−7465
photosensitive vertebrate smooth muscle, light-induced Ca release 78−64994
physical and biological science conf., Japan (Feb. 1979) 80−12846
physiological factors controlling fundamental voice freq., correl. anal. 78−40201
postural length and strength, control 77−25414
posture maintenance, control mechs. of human muscular activity 79−5306
power flows, bond graph model 79−92260
power produced by maximal velocity elbow flexion 79−57691
proteins, rot. motions, saturation transfer EPR obs. 80−94151
proton NMR spin-lattice relaxation in hydrated collagen and muscle 79−34496
psoas, glycerinated, rabbit, force-length rels. 77−48828
psychological stress evaluators, EMG correl. with voice tremour 77−9214
pulse propagation in muscle 78−92668
Purkinje fibers, delay, block, oneway conduction model 80−21462
quadriceps femoris, function under maximal concentric and eccentric contractions 80−97963
radioactivity of bone and muscle, separation by dermestid ingestion 80−30949
rapid voluntary movement, premotion silent period 77−21511
receptors sensitive to muscle length in the horseshoe crab 80−12167
reflex conditioning effects on motoneuron pool 79−79509
reflex excitability curve assess. using cubic spline function 79−79510
reflex stiffness of man's anti-gravity muscles during kneebends while carrying extra weights 80−61601
regeneration of fibres after transplantation, by electromyographic activity 80−30701
resistance strain gauge-meas. techniques in biomech. expts. *(German)* 80−104819
respiratory muscle EMGs, digital computer technique for anal. 78−28102
rhythmic heart-cell clusters, fluctuations in interbeat interval, membrane voltage noise role 80−30705
rigor cross-bridge patterns in muscle modelling 79−20508
sarcomere length, on-line meas. from diff. patterns 79−48388
sarcoplasmic reticulum of skinned cardiac cells, Ca^{2+}-induced release of Ca^{2+} 80−3612
scanning electromyograph, eight-channel, computer-controlled 79−29674
segmental muscle stretch reflex, partitioning into completely decoupled parallel loops 80−41000
semiconductor force transducer suitable for use with small muscles 80−72395
sensory biosystem, teleological explanation of Weber's law and the motor unit size law 79−96501
sequential muscular contraction 77−48824
shoulder movements, EMG analysis of levator scapulae and rhomboideus major muscles 80−3627
silastic gauge, use as an in vivo muscle force transducer 79−29680
single fibres, Rb^+, Cs^+ and Na^+ localisation, autoradiographic demonstration at 77K 79−96726
single ionic channels obs. in tissue cultures 80−30699
single motor unit pot., recording by monoprlar and bipolar lead 77−81615
single postsynaptic channel currents in tissue cultures 80−30700
skeletal, actin-myosin interaction, quantitative model 77−52753
skeletal, birefringence signals and Ca transients in 78−24041
skeletal, cat, force-vel. and fatiguability obs. 80−81637
skeletal, contracting, simulation studies of mech. stretch 80−94263
skeletal, dependence of energy transduction on time in tension 77−52754
skeletal, dynamic behaviour as unidimensional viscoelastic medium, theoretical study 77−25484
skeletal, dynamic behaviour modelled as unidimens. viscoelastic medium 77−25484
skeletal, effect of stretch on electromotive force 77−36886
skeletal, excitation-contraction coupling blockade by high extracellular concs. of Ca buffers 79−20528
skeletal, exptl. results and modelling of biomech. props. 77−25486
skeletal, frog, active tension changes during and after mech. stimulation 80−94262
skeletal, frog, time resolved X-ray diffr. obs. during isotonic twitch 79−83836
skeletal, general myocybernetic control model *(Japanese)* 78−53385
skeletal, human, conduction vel. estimation in situ by surface electrodes 80−8196
skeletal, human, LF sounds from sustained contract. 80−61751
skeletal, human, mech. simulation 78−35878
skeletal, human, tension development evaluation as a diagnostic meas. 77−40880

muscle continued
skeletal, implanted stimulated electrodes of different materials, threshold meas., cat 80−101297
skeletal, lumped and population stochastic models, implications and predictions 80−76724
skeletal, membranes, ionic radius selectivity 78−24042
skeletal, method for deriving viscoelastic modulus from transient pulse propagation 78−77077
skeletal, red and pale, human, force rel. to fatigability, EMG obs. 80−8076
skeletal, resting frog, elastic and viscous props. 77−44700
skeletal, rhythmic oscill., system anal. of clonus 78−31806
skeletal, single fibres, laser light diffr. theory 80−56110
skeletal, single fibres, sarcomere dynamics, light diffr. studies 78−15797
skeletal, study and modeling of biomech. props. of 77−25486
skeletal, water protons NMR relax. times anisotropy obs. 80−85341
skeletal fibres, endogenous elec. field, dependency on Na^+-K^+ pump 80−108869
skeletal fibres, frog, elec. props. 77−25395
skeletal fibres, frog, helicoids in T system and striations, electron microscope obs. 78−53356
skeletal fibres, guinea pig, force-velocity characts. 77−44643
skeletal fibres, increased optical transparency associated with excitation-contract. coupling 77−29138
skeletal fibres, intramembrane charge, movement and Ca transients 79−66453
skeletal fibres, light diffr. study 80−8096
skeletal fibres, resting, voltage-dependent block of inward K currents 77−52756
skeletal joint tarques method for quantitatively relating to EMG signals 77−48953
skeletal muscle, canine, blood flow and O_2 uptake obs. in acute anaemia 80−45930
skeletal muscle, freq. response characteristics evaluation 79−96594
skeletal muscle, human, in situ meas. of vol. conduct. 77−90755
skeletal muscle, special aspects of IR spectra of mitochondria and endoplasmic reticulum 77−70434
skeletal muscle, spin-echo study of ^{23}Na relax. evidence of sodium ion binding inside a biological cell 78−88698
skeletal muscle, use of implantable stimulators to investigate functional adaptation 77−86721
skeletal muscle and nictitating membrane contractions in expt. animals, new devices for recording 77−48969
skeletal muscle atrophy, influence on needle EMG 80−3853
skeletal muscle bulk specimen, quantitative X-ray microanalysis of diffusible ions 78−57143
skeletal muscle const.-vel. contractions by sequential stimulation of muscle efferents 80−41309
skeletal muscle disease, human, Fourier optical evaluation of histopathological findings 77−37091
skeletal muscle fibre orientation, US attenuation meas. 80−30763
skeletal muscle glucose metabolism, bond graph simulation 77−36894
skeletal muscle mech. props. from in vitro studies of biopsies 80−41098
skeletal muscle motor unit contractile characts. determ. through twitch characts. 80−17159
skeletal muscle motor unit sequential stimulation in cats through peripheral motor nerves 79−57635
skeletal muscle motor units, system for rapid acquisition of surface pot. maps 80−46077
skeletal muscle structure and its model *(Japanese)* 79−66479
skeletal muscle ultrastructure in the baikal grayling, some characts. *(Russian)* 77−29240
skeletal muscle undergoing rhythmic contracts., temp. distrib. 79−11901
skeletal muscles, attachment and composition rel. to function 80−41092
skin-mounted miniature preamplifier for meas. of surface EMG pots. 78−35990
small-angle scattering of biological structures 79−11889
smooth, cell plasma membrane, inhomogenous distrib. of filipin-sterol complexes 79−83720
smooth, contraction in a microwave field, rat obs. 80−56134
smooth muscle, guinea pig, mechs. of change on tone obs. 77−86471
smooth muscle, guinea pig, mechs. of spontaneous relax. 77−86470
smooth muscle cells, effect of a hyperosmolar soln. on the elec. connection between 78−69027
smooth muscle cells, interaction with collagen, in aortic biomechanis 79−43941
smooth muscles of elastic arteries, biophysical props. 78−69011
software support for computerised EMG in clinical dentistry 79−74780
soleus muscle, rat, electrogenic Na^+-K^+ transport obs. 80−21456
sonomotor responses in scalp recorded auditorally evoked pots. 78−3498
soreness, artificially induced, effect of EMG feedback and static stretching 80−12069
source resistance, apparent, of heart and muscle 79−25005
speech production, recruitment and discharge patterns of single motor units 78−65054
speed-force relations in the motor units of the cat tibialis posterior muscle 78−80856
spin-lattice relaxation times for ^{13}C in isotope-enriched glycine accumulated in frog muscle 77−44605
spindle afferents identification during in vivo recordings in man, preamplifier 80−98155
stapedius, reflex thresholds and HF audiometry in juvenile diabetics 80−85411
static isometric muscle force, relative contrib. of motor unit recruitment and rate coding 77−73523
stiffness and tension during and after sudden length changes of glycerinated rabbit psoas muscle fibres 79−25007
stiffness of Ca^{2+}-activated fibres, effect of MgATP at 2 freqs. 78−48822
strapedius, acousticreflex dynamics for pulsed signals 79−20549
strength and movement speed rel. to age and morphology 80−3672
strength gain, neural factors rel. to hypertrophy 80−12168
strength interval curves, computer system for rapid generation 78−40456
strength rel. to level of energy sources 79−11904
stretch and Hoffman reflexes during phasic voluntary contractions of the human soleus muscle 79−16193
stretch reflex system, considerations on mechanisms of focused signal transmission 79−24978
stretch reflex system, math. model *(Japanese)* 80−67067
stretch reflex system in human forearm, adaptive control characts. 79−83758
muscle continued
stretched muscle fibres, mechanical activation and voltage-depend. charge movement 80−3630
striated, analytical soln. to isometric mechanogram of Hill's model 78−73168
striated, contraction, 10 ms time resolution X-ray diffr. 80−61741
striated, frog, pulsed ^{39}K NMR study 77−16920
striated, molecular basis of force development 78−40126
striated, scallop, reversible loss of Ca control of tension obs. 78−53360
striated, vertebrate, thick-filament-linked Ca regulation 78−69020
striated muscle, aspects of intracellular control of force development 79−48228
striated muscle, longitudinal pulse propagation characts. 79−16246
suction capillary for holding moving cells during intracellular elec. recording 79−100793
surface EMG, biopolar recordings, influences on electrode geometry 79−53269
surface EMG, computer anal. during isometric exercise, muscle tension quantification 80−85505
surface EMG, stabilisation of isoelec. line by means of high pass filters 78−31917
surface EMG and fatigue, muscle temp. and blood flow 80−94199
surface EMG use as a measure of dynamic force in human limb muscles 79−34689
surface EMGs, study by means of digital simulation, principles of a model 78−80862
surface EMGs, study by means of digital simulation, spectral anal. 78−80863
surface pH, clinical meas., significance of impedance changes 77−52908
synergy patterns of some lower-limb muscles, variability and biomechanics 79−53175
systemic muscular arterial wall medial smooth muscle orientation obs. 79−70572
telemetered signals from the body *(German)* 77−29220
tendon junction strength, ultrastruct. elements 77−25485
tendon-muscle junction, ultrastruct. elements of strength 77−25485
tension fluctuations during contract. of single fibres 78−20153
tension fluctuations in contracting myofibrils and their interpretation 80−41065
tension transients in fibrillar muscle fibres as affected stretch dependent binding of AMP-PNP 79−20562
tenuissimus muscle, cat dynamic properties 80−8041
therapeutic aid for the disabled using myoelectric feedback 78−36048
thermodynamic cycles problem of muscle 79−53049
three-element model with viscoelastic passive elements 77−32930
tissue, math. models 77−25358
tissue O_2 tensions, short-range telemetry 77−86722
tissue properties, mathematical description 77−25358
torque-velocity relationships and muscle fibre composition, elite female athletes 80−41080
trabeculae of frog atrium, Ca^{2+} incoming current obs. 79−79497
trace elements in animal and human muscle, determ. by neutron activation anal. 78−27869
trachealis muscle, dog, spontaneous mech. activities in vivo 80−101203
transfer function online evaluation by impulse response transformation, rehabilitation test appl. 79−57637
transitter output increases in an identifiable lobster motorneuron with growth of its muscle fibres 78−64974
tremor, normal and alcohol withdrawal, nature and etiology 79−29544
triceps surea, human, linearity between weighted syms of EMGs and total torque 78−20203
tryptophan fluorescence polarisation 80−97877
tubular organs, press. diameter characts. comparison of in vivo and in vitro data 77−36982
twitch muscle fibres, frog, transition temp. of excitation-contraction coupling 79−83751
uniaxial testing apparatus, soft human tissues in vitro 78−61295
upper extremity, eccentric-concentric contract. study 80−85432
upper limb, muscle strengths and musculo-skeletal geometry 79−74699
urethral closing muscles, effects of functional elec. stimulation 77−60286
urinary bladder, pig, active mech. props. of smooth muscle 79−92252
US shear velocity of muscle tissues, mech. props. determ. 80−108930
US-EMG transducer for biodynamic research 78−77164
uterine, isotropy and anisotropy during labour contract. 80−94257
uterine muscle, passive mech. props. of tested in vivo 79−16235
uterine muscle, plane penetration by intrauterine shields 79−29556
uterine smooth muscle in vivo, US induced contracts., mouse 79−25028
Van der Waal's interaction of 2 parallel cylinders, simple interpolation formula 79−92122
vascular smooth muscle, undamped and damped series elastic components 79−83819
vascular tonus model 77−25482
vastus medialis EMG for graded isometric torque tensions, power spectrum distrib. anal. 78−44673
vector EMG investigations on motor units with short, inclined and curved muscle fibres 77−86689
ventricle, canine, discrete zones in elec. connection 77−86460
ventricular muscle, mammalian, slow inward current depression by acetylcholine 79−92210
ventricular muscle, vol. effect for excitation 77−81670
ventricular overloading, conduct. changes in and around the Purkinje-myocardial junction 77−81775
vestibular control of oculomotor and postural mechanisms 80−72151
vibration effect on the F wave in normal man 78−20164
vibration of an elastic rod, appl. to US study of muscles 78−44538
visceral smooth muscles in vertebrates, viscoelastic and plastic props. 78−73169
visco-elasticity of active human muscle, dynamic meas. 77−86667
viscoelastic passive elements of muscle, 3-element description 77−32930
viscoelastic properties, anal. of isolated heart muscle preparations *(German)* 79−53167
volitionally activated low-threshold EDC motor unit, 2 ranges in firing rate 78−20201
volume conducted motor unit pots. in human muscle triceps surae 77−40656
voluntary movements in man, force gradation and motor unit activity 80−97887
water, frog, varied mag. field, multiple-pulse and magic-angle spinning ^1H NMR obs. 80−51135
water, mouse, ^1H NMR anal. above and below freezing 80−56073
water, self diffusion in frog muscle 80−8037

muscle continued
water, study of spin-lattice and spin-spin relax. times of ^{1}H, ^{2}H, and ^{17}O 80−21443
water in muscle, proton and deuteron relax. obs. 77−52740
weight sensation quantification by EMG meas. 77−90940
whitefly, meas. of highest contraction freqs. yet recorded in non-fibrillar flight muscles 79−83835
wideband, isolated amplifier for biological signals 78−57089
work-effort ratio of a large muscle group, theoretical model 80−108949
wrist motion, human, muscular activity model and expt. 79−92285
X-ray diffraction patterns from molecular arrangements with 38-nm periodicities around muscle thin filaments 79−39348
x-ray diffraction studies of the heart, review, book contrib. 80−109079
X-ray microanal. of cultured skeletal muscle cells, calibration 79−100798
Ca diffusion in transient and steady states in muscle 78−3457
Ca^{2+} conductance of acetylcholine-induced endplate channels 79−70546
Ca^{2+} indicator, aequorin luminescence during activation of single isolated smooth muscle cells 79−88064
CdTe/^{133}Xe clearance detector for muscle blood flow studies 78−40305
K^{+} concentration effect on Na^{+} efflux rate obs. 79−79495
O_2, facilitated diffusion in muscle tissues 80−56327

muscovite *see mica*

music
1/f noise, spectral density rel. to computer composition 78−38154
bird song spectrum anal. rel. to Western musical scales 77−50840
course, sound and light in the arts 77−22340
digital coding of high-quality musical sound 80−5883
digital phase shifter using Bell Labs digital filter module 80−5884
digital storage, synthesizing musical tones from stored impulse response 80−48525
frequency perception, colour as a pervading principle over pitch, rhythm, and form 80−56059
high fidelity sound, perception of sound and music 80−42014
keyboard fingering characteristics, CAI *(Japanese)* 78−28889
loudness determ. methods *(French)* 77−34996
melodies pragmatic anal., MACSIM neural network 78−7373
microphone techniques for recording and broadcasting symphonic music, comments and reply 80−53595
microphone techniques for recording or broadcasting symphonic music 80−5885
musical consonance, concept and psychoacoustic foundations *(German)* 77−5007
nonspectral pitch perception 77−9205
perception, appl. of computer program 79−8513
Pfield principle, Hi-Fi music reproduction *(German)* 80−87685
physics of sound of music, book 78−55529
pitch of 2-tone complexes and predictions of modern pitch theories 79−88083
pitch prediction from component freq. ratios, automatic using computer algorithm 79−96574
production and perception, relationship with human communications 80−96110
programmable tone generator presenting melodic and harmonic patterns 77−56381
scale, 12-tone, tempered Fourier transform 80−87671
scales, equal tempered, construction from the harmonic constitution of musical sounds 78−90609
symphonic, practical and aesthetic microphone techniques for recording and broadcasting, comments 80−79073
texts, math. model for anal. and structuring 78−90608
timbre differences between lowpass-filtered harmonic complex tones *(German)* 80−53571
timbre perception, review 78−77068
tone quality, descriptor characts. *(Japanese)* 79−24997
tone quality eval. expts. *(Japanese)* 79−24996
transcription computer program, using melody perception theory 77−5009
visualisation of the even tempered arrangement, logarithmic graph 80−69606

music, electronic *see electronic music*

musical acoustics
1/f fluctuations *(Japanese)* 78−43448
air flow and sound generation in musical wind instruments, book contrib., review 80−19174
annular membrane, vibrating, harmonic props. 79−94425
auditoria, eighth annual Fairey lecture 78−13859
bassoon finite amplitude self-vibration 80−69607
bowed violin strings, investigation of oscillations *(German)* 80−64312
brass instruments, acoustic impedance meas. apparatus 78−1518
brass instrums., acoustic principles and problems of performance 80−74646
cello top and back plates, method of pitch adjustment 77−14859
clarinet, integral equation anal. of self sustained oscillations 78−94490
classic guitar quality correl. with opening transients 79−68516
complex tone classification according to shape of spectrum envelope 80−102939
complex tones, interval-based representations, teaching 80−101684
concert hall, acoustical conditions preferred for ensemble 79−14161
concert hall acoustics, room impression as an overall concept of spaciousness and liveliness *(German)* 78−94484
concert hall design, lateral and ensemble reflection requirements 80−91964
concert hall design for orchestral balance in seats behind stage 80−91963
concert hall problem, coherence length and diffuse reflection formulation 80−91962
concert hall sound system for touring quartet 80−92013
concert halls, hearing impressions of loudspeaker reproductions and orchestras *(German)* 78−94485
concert halls, sound reinforcement system, Nippon Budokan Hall *(Japanese)* 80−64291
concert-hall acoustics, multidimensional description of subjective judgement *(German)* 77−72117
consonance and dissonance of pairs of inharmonic sounds 80−74645
design of music practice rooms, user requirements 80−74606
educational course, for the musician 79−71205
educational course, role of demonstrations, source material 78−49576
electro-piano, cantilever, harmonization of vibration *(Japanese)* 79−18634

musical acoustics continued
figural props. of auditory patterns 79−16214
Fourier analysis of pseudo periodic signals, phase determ. *(French)* 79−90100
frequency fluctuations of musical sounds *(German)* 77−828
guitar, effect of radial ribs on reson. board on nodal lines, holographic study *(French)* 77−80031
guitar body, depend. of natural vibrs. on number and distrib. of ribs. on reson. board *(French)* 77−80030
guitar shaped cavities, prediction and meas. of reson. props. 77−50838
harp, acoustical behaviour of soundboard 77−42669
harp, false gut string displacement meas. 78−75020
harpsichord sounds, time-varying amplitude-freq. structs. in attack transients 77−14858
harpsichords, design and performance anal. 77−42668
Highland bagpipe, acoustics of the chanter and reed 78−94491
Japanese bell, striking rod effect on timbre *(Japanese)* 77−14860
Joseph Haydn concert halls, room acoustics and orchestral sound *(German)* 79−18631
loudspeaker cabinet reflection effects 79−64451
medium-scale live concert sound reinforcement system requirements 80−92012
melodies reproduction and tonal sequences perception 77−36951
mode transitions for sounding modes of flute 80−79072
music stage design 80−74605
non-linear regeneration mechanisms in wind instruments 80−33376
octave synthesizer, teaching appl. 79−44680
orchestra, musical instruments directivity rel. to efficiency of acoust. ref. or absorpt. *(German)* 77−829
orchestral wind instrument physics *(French)* 77−19492
organ flue pipe ranks, scaling rules 77−42667
organ flue pipes, sound prod. 77−7265
organ pipe oscills., edgetones and pipetones 79−23148
organ pipes and edge tones, jet drive mechanisms 77−831
outdoor classical music sound reinforcement systems compared 80−92011
outdoor environment, loudspeakers positioning for assisted reverberation effect 78−13825
perceptual effects of spectral modifications on musical timbres 78−65039
percussion instrument acoustics, multidimens. vibrs., review for teaching 77−57128
percussion instruments, for teaching 77−9838
performed ensemble music, synchronisation 79−98568
Peruvian whistling bottles, acoustic characts. 77−88993
piano notes, anal. Fourier transform methods 78−26009
piano sounds, time-varying amplitude-freq. structs. in attack transients 77−14858
piano strings, coupled motion 79−64452
piano tuning, using dual trace oscilloscope 79−71199
pianos, review of acoustical research *(Japanese)* 80−33375
pitch estimation algorithm for speech and music 79−14173
pitch perception of musical sounds, dependence on degree of training in hearing *(German)* 79−74682
pitch prediction from component freq. ratios, automatic, using computer algorithm 79−96574
psychoacoustic detection threshold of transient intermodulation distortion in recorded music 80−56060
recording studios, shortcomings of apparently improved acoustic designs 80−69601
reproduction in small rooms, acoustic theory *(Spanish)* 78−38155
resonant tubes, definition of quality factor, errors arising 80−69572
retard analysis in motor music 80−106680
reverberation, use of recursive filters 79−72769
review 80−10096
review of recent work on perception, instruments and synthesis 79−76920
rock music sound levels and spectra rel. to hearing damage 79−68517
room impression index, definition on basin of subjective examination *(German)* 78−87202
room reverberation time meas. in musical acoustics course 80−42000
simultaneous notes perception in polyphonic music 78−61191
singer and auditorium interactions 80−74604
singing voice role as musical instrument 77−66818
sound fields and acoustic design in rooms, review of subjective effects *(Japanese)* 80−64293
speed of sound, meas. by clapping technique 80−82620
statistical properties of speech and musical signals 79−76919
statistical props. of music and speech signals, modulated random processes 79−64412
string instruments, body modes calc. 77−7267
string instrums., secondary waves arising from self-excitation *(German)* 79−76918
string vibrations, teaching 77−49536
stringed instruments with soundpost, cavity-assisted resonances 77−19491
stringed musical instruments, acoustics 79−7261
subjective preference tests for musical sound fields with single echo 78−31819
syncopated auditory polyrhythms, discontinuous reversals in meter interp. 78−55528
synthesised musical instrument tones, perceptual evaluation 77−90807
synthetic sound fields, effects of early multiple reflections on subjective preference judgements 79−41517
teaching, to blind student 80−77584
timbre, multidimensional perceptual scaling 77−62113
timbre discrimination in musical patterns 78−88713
timbre recognition, perceptive effects of data reduction *(French)* 80−28387
tonal error, rapid and accurate meas. via digital meter *(German)* 77−830
tone system based on thirteen-step scale *(German)* 78−26008
triads, relationship between beat-rates 78−79172
trombone quality, the subjective assessment 78−83184
trombones, objective and subjective assessment of quality 80−23847
unified sound field anal., effect of room on music rendering *(German)* 77−11092
violin, cavity reson. modified by He or CO_2, for teachers 79−35484
violin, influence of string partials on tone and electronic method of tuning to overtones 77−50839
violin, sound prod. and transmission *(German)* 78−30135

musical acoustics continued
violin instrums., origin of wolf-tone, investigation using functional model *(German)* 79−32149
violin sound post, mechanical admittance meas. rel. to post action 77−23833
violin-shaped cavities, prediction and meas. of reson. props. 77−50838
voice, acoustic props. of timbre types rel. to voice classification 77−90813
warm string tone in concert halls, factors necessary to attainment 80−74603
wave motion experiment, phase vel. meas. using spring 80−8762
wave propag. on acoustically perturbed jet 79−81592
waveform analyser for teaching, evaluation of Pasco Model 9302 77−9842
Western consonance, acoustic component 78−90607
woodwind instrums., significance of formants for vowel quality *(German)* 79−32150
woodwind tone production, effect of reed resonance 80−19172
woodwinds and other vibrating systems, errors associated with resonance curves 79−7255

musical instruments
bass drum, characteristic sound props. 79−14166
bass trombone, timbre and responsiveness, improvement 78−22232
bassoon finite amplitude self-vibration 80−69607
bells, freq. fluctuations *(German)* 77−828
Boehm flute, acoustical anal. 79−41531
bowed string, self sustained oscillations, Hammerstein eqn. 79−98567
bowed string dynamics, general class of models 79−98566
brass, acoustic principles and problems of performance 80−74646
brass, air flow measurements using hot-wire anemometer, calibration at low vels. 79−27724
brass instruments, acoustic impedance meas. apparatus 78−1518
cello, wolf tone charact. 78−51016
cello, wolf tone damping *(German)* 79−18633
cello, wolf tone instabilities *(German)* 79−18632
cello, wolf-tone production *(German)* 79−18630
cello top and back plates, method of pitch adjustment 77−14859
clarinet, functional model of simplified version 80−96147
clarinet, integral equation anal. of self sustained oscillations 78−94490
classic guitar quality correl. with opening transients 79−68516
clavier, tuning, freq. matching using pocket calculator 78−81728
education, vibrating string, tuning guitar by television 80−73134
electronic 80−106682
electronic music, keyboards for pure music, use of consonant chords 78−83183
electronic music, patchable percussion synthesizer 77−68341
electronic music synthesis, using an almost locked oscillator circuit 77−68340
electronic organ Boehm Professional 2000, programmable *(German)* 79−37096
flue organ pipes, voicing adjustments 80−33374
flue-pipes, tone generation and characteristics *(German)* 80−5882
flute, transition between sounding modes 80−79072
four-channel percussion synthesiser using 5700 type modules, construction details 80−106681
guitar, effect of radial ribs on reson. board on nodal lines, holographic study *(French)* 77−80031
guitar, reflex enclosure problem 78−63243
guitar, simple model for LF function 80−106678
guitar, vibr. modes at Helmholtz and first top-plate resonances 77−35003
guitar body, depend. of natural vibrs. on number and distrib. of ribs. on reson. board *(French)* 77−80030
guitar intensity as function of auditory feedback 78−85322
guitar shaped cavities, prediction and meas. of reson. props. 77−50838
guitar strings, correl. of acoustic and subjective quality charact. 80−19173
guitars, tone quality determ. by spectral anal. 77−50841
harmonic generation in organ pipes, recorders, and flutes 80−106679
harp, acoustical behaviour of soundboard 77−42669
harpsichord sounds, time-varying amplitude-freq. structs. in attack transients 77−14858
harpsichords, design and performance anal. 77−42668
Highland bagpipe, acoustics of the chanter and reed 78−94491
Highland bagpipe, pitch changes 79−3864
highland bagpipe, radiation pattern in open air 77−75752
horns, quasi-standing waves, computation of acoustic impedance 80−79071
kettledrum, vibrs. of loaded Indian drums using CRO 78−79173
keyed instruments, musical tone recognition trial using computer *(Japanese)* 78−28889
natural tones, short-time spectral analysis *(Japanese)* 77−88994
nonlinearly excited inharmonic musical oscillators, mode locking 79−14165
oboe, calculation of input impedance using numerical method 79−50538
orchestral wind instrument physics *(French)* 77−19492
organ, pipe oscills., edgetones and pipetones 79−23148
organ flue pipe ranks, scaling rules 77−42667
organ flue pipes, self-sustained oscillations, integral eqn. soln. 78−51015
organ pipes, freq. fluctuations *(German)* 77−828
percussion and harp, use of dynamic support microphones 80−79073
percussion instrument acoustics, multidimens. vibrs., review for teaching 77−57128
percussion instruments, acoustics, for teaching 77−9838
Peruvian whistling bottles, acoustic charact. 77−88993
piano, automatic tuning using freq. generator and deviation detector *(Japanese)* 78−33964
piano, coupled motion of strings 79−64452
piano, multiple rate of tone decay 79−10435
piano, string coupling through bridge admittance 78−30134
piano, string longitudinal vibrations and inharmonic sound box tone *(Japanese)* 78−13865
piano sounds, time-varying amplitude-freq. structs. in attack transients 77−14858
pianos, review of acoustical research *(Japanese)* 80−33375
pipe organ, loudness, plenum combinations 79−18628
pipe organ, loudness, single notes 79−18629
pipes, open ended, end corrects. determ. for fundamental reson. freq., material effects *(Korean)* 77−27443
portable electronic organ 80−96148

musical instruments continued
RE electronic piano, organ pedal cct. construction, tone cct. elements *(Dutch)* 80−99904
review of recent work on perception, instruments and synthesis 79−76920
string instruments, body modes calc. 77−7267
string instrums., secondary waves arising from self-excitation *(German)* 79−76918
stringed, resonant plates, use of synthetic materials 80−102937
stringed instruments with soundpost, cavity-assisted resonances 77−19491
stringed musical instruments, acoustics 79−7261
strings, multiple resonance anal. using electrical transmission line analogy 78−59188
tone analysis using digital processing techniques *(Japanese)* 77−84089
tone filters for electronic organs, tone spectra and source waveforms 80−106683
trombone quality, the subjective assessment 78−83184
trombones, objective and subjective assessment of quality 80−23847
trombones, trombonist's perception 78−90611
violin, bowed string, vibr. demonstrations 77−13532
violin, cavity reson. modified by He or CO_2, for teachers 79−35484
violin, influence of string partials on tone and electronic method of tuning to overtones 77−50839
violin, internal damping, influence of geometry 78−50996
violin, sound prod. and transmission *(German)* 78−30135
violin, timbre and bridge freq. response 78−55527
violin G-string, resonant response and excitation of wolf-note 80−53540
violin instrums., origin of wolf-tone, investigation using functional model *(German)* 79−32149
violin sound post, mechanical admittance meas. rel. to post action 77−23833
violin-shaped cavities, prediction and meas. of reson. props. 77−50838
violins, long time averaged spectra and rated qualities 79−50537
violins, tone quality determ. by spectral anal. 77−50841
wind instrums., nonlinear regeneration mechanisms 80−33376
wolf-tone occurrence criteria in cells *(German)* 80−53570
woodwind, multiphonic tones 78−51017
woodwind and brass, excitation mechanisms 79−90099
woodwind instrums., significance of formants for vowel quality *(German)* 79−32150
woodwinds, effect of reed resonance on tone production 80−19172

N-body problems
see also celestial mechanics; many-body problems
3-body unrestricted problem, distance lower bound estimates *(Russian)* 77−84137
aligned triple collision, new study *(French)* 78−85832
asteroid 108 Hecuba, motion in restricted three-body problem, nonlinear oscills. *(German)* 78−57488
asteroid belt depletion by gravit. forces, numerical calc. of orbits 79−35173
asteroidal three-body problem, long-periodic solns. *(Russian)* 78−49370
axisymmetric rigid body, periodic motions in gravit. field of sphere 78−36446
bifurcation of periodic orbits of the planar circular restricted N-body problem to the three-dimensional general N-body problem 79−16803
bifurcations of straight line oscills., rel. to Stormer and spring pendulum problems 78−71278
billiard ball collisions, max. number of elastic collisions possible 80−12897
binary collisions regularization *(French)* 77−22045
boundary conditions, spherical, for computer experiment 80−105597
celestial mechanics, asymptotic behaviour of solns. as time approaches infinity 77−25918
celestial mechanics, mathematical methods, conf., Oberwolfach, Germany (Aug. 75) 77−25916
celestial mechanics, variation eqns. and eleventh integral *(French)* 77−25921
central configurations 80−41702
central configurations and relative equilib. in Euclidean E^4 space 80−41703
circular and rectilinear motions of axisymm. body under gravit. effect of two spheres 77−13222
circular restricted three body problem, appl. of canonical Kustaanheimo-Stiefel regularisation 77−60586
circular restricted three body problem, soln. method *(Russian)* 77−60588
circular restricted three-body problem, periodic solns. and arcs for zero mass parameter 79−8803
circular restricted three-body problem, props. of solns. for zero mass parameter 79−8804
circular restricted three-body problem, stability of periodic motions close to Lagrangian solns. 78−53804
circular restricted three-body problem *(French)* 78−93084
classical one component Coulomb gas, collective coords., thermodynamic props. 77−5777
close binary stars, form. by two-body tidal capture 77−33556
clusters of galaxies, dynamical evolution 78−12384
clusters of galaxies, gravitationl binding energy, virial discrepancy explanation 77−49484
clusters of galaxies, subclustering, rel. to missing mass 77−45576
clusters of galaxies, velocity dispersion profiles of N-body simulations 80−21908
clusters of galaxies compared with N-body simulations, masses and mass segregation 80−22091
collinear N-body problem, homothetic solns. structural stability 79−75086
conformal props. of exactly solvable problems in space dimens. one 77−60924
continuations existence 79−84652
curvature statistics of some few-body Debye-Huckel and Lennard-Jones systems 80−42051
distribution properties of the channel interactions in N-body scattering and applications 79−45219
double encounter regularization *(Russian)* 80−46367
dynamical systems, effects of integrals on totality of solns. 77−25924
dynamical systems, relation in families of periodic solns. 77−64627
dynamical systems evolution with time-varying gravity, theory 78−24459
Earth-Moon-Sun force function 79−80208
education, Kepler ellipse, some props. 79−97151

N-body problems continued
education, N-body disintegration theory, Maxwellian distrib., nuclear appls. 80−57033
elastic collisions of N billiard balls in three dimens. space 79−30223
elastic rod central collisions soln. from impulse conservation *(German)* 78−22274
electron gas, classical and quantal treatment involving integral eqns. 78−41228
elliptic restricted three-body problem, invariant relation 78−69662
elliptic restricted three-body problem, invariant relation and appl. to asteroids 79−88616
elliptic restricted three-body problem, invariant relation for Trojan asteroids 78−69726
elliptical galaxies, anisotropic vel. distribs. generation 80−36715
Euler's three-body problem, eqns. of motion 80−67953
extended ideal resonance problem, comment 77−22055
families of three-dimens. periodic orbits bifurcating from plane periodic orbits around both primaries 78−57432
force function of two general celestial bodies 78−73620
four body Newtonian problem reduction to 14th order *(French)* 80−21894
four fixed centres problem, new interpretations and appls. 78−28493
four fixed centres problem, real motions qualitative anal. and classification 79−96901
four-body problem, gyrostat near three spherical bodies subject to gravitational forces, motion, orient. *(French)* 77−5422
four-body problem, relative equilib. solns. 79−8805
four-body problem, restricted planetary case 80−41742
four-body problem asymptotic solns., periodic orbits 77−64621
four-body problems, rel. to Titius-Bode law and place for more than ten planets 78−40851
four-body systems, statistical theory for disruption 80−101531
fragmented celestial bodies, particles asymptotic distrib. 78−32326
free interacting rigid bodies, force function *(Russian)* 77−62150
galaxies, flat disc, retrograde stars effect on global bar-forming mode 79−21411
galaxies, rotation and clustering, N-body simulation 80−17670
galaxies and galaxy clusters, relaxation from aspherical initial conditions 78−96538
galaxies distribution, N-body model computations rel. to hierarchical clustering pattern stability 78−86026
galaxy clustering, N-body simulations in expanding Universe 79−44620
galaxy clustering depend. on cosmological density parameter 79−48971
galaxy clustering evolution, cosmological N-body simulations 78−96550
galaxy clustering N-point simulations, covariance function 80−31373
galaxy clusters, missing mass, N-body expts. 80−41904
galaxy clusters, N-body simulations, density profiles 79−35398
galaxy clusters, N-body simulations, set of separation vectors 79−35399
galaxy clusters, vel. dispersion profiles 79−35397
galaxy clusters multiplicity function, self-similar gravitational clustering theory 80−4447
galaxy correlation function evolution, N-body Monte Carlo model 80−62292
galaxy evolution, three-dimens. computer simulation 78−81551
galaxy groups, N-body simulations of clustering 79−44621
galaxy merging, cosmological N-body simulations 80−56922
galaxy merging, N-body simulations rel. to galaxies rot. 80−4439
galaxy models, numerical orbit computation algorithms comparison 79−12497
galaxy pairs, N-body simulation of merging 78−77600
Galaxy-LMC encounter, three-body interaction rel. to galactic plane warping 77−45540
general residual interactions, natural distrib. props., direct proof 79−97262
general three body problem, distances upper estimate *(Russian)* 77−53412
general three body problem, stability of solns. 77−53408
general three body problem, Sundman's inequality and Jacobi's integral derivation *(Russian)* 77−45299
general three-body problem, M_8 manifold topology *(Chinese)* 79−16808
general three-body problem, periodic orbits for Sun-Jupiter-Saturn mass ratio 77−13209
generalised problem of two fixed centres, appl. of motion of point in conservative force field 78−24456
generalised two-dimens. problem of three fixed centres, classification of motions *(Russian)* 78−77465
generalized elliptic restricted three-body problem, libration points 78−53799
generalized three-body problem with force centre term 77−37499
globular star cluster, relax. degree and evolution, appl. of N-body system numerical integration 80−67808
heavy ion collisions at high energy, review of four theoretical methods based on classical approx. 79−89326
Hecuba family resonance asteroids intermediate orbit, three fixed centres generalized problem internal variant 79−84726
Hermite polynomials, zeros of combinations, n-body problems 78−45466
higher order resonances in dynamical systems 79−5738
Hill's curves perturb. due to oblateness of one primary in restricted 3-body problem 79−53705
Hill's equation, new exact method *(Chinese)* 80−105152
infinitesimal librations with variable primary masses, orbit evolution 77−22046
inhomogeneous gravitational systems relaxation, delocalisation effect 79−62877
instability of a three-body system in one dimension 79−35542
integrable system for N particles in one dimension 78−57768
integral bounds for N-body total cross sections 79−75405
interacting particle systems, configuration with min. pot. energy per particle 80−4517
invariant sets and polhodes in the rigid body problem 80−41706
involute set of integrals for completely integrable problems with pair interaction 77−22448
isolated system, ang. momentum flux in higher multipole moments 79−80474
Jacobi's virial equation soln. for nonconservative systems, anal. of depend. on parameters 80−4243
Jacobi polynomials, props. of zeros of polynomial combinations 78−57773
Jupiter-Saturn-Sun system, dynamical stability 77−9679
Kepler problem regularisation 77−64630
N-body problems continued
Keplerian systems, numerical simulations of collisional evolution 80−109342
Keplerian transition matrices for elliptical orbits 78−36442
Lagrangian solutions stability at critical relation of masses *(Russian)* 78−69666
Laguerre polynomials, props. of zeros of polynomial combinations 78−57772
libration points location and stability in restricted problem, effect of perturbs. in Coriolis and centrifugal forces 79−5737
Local Group of galaxies, numerical expts. on gravit. encounters 77−57098
many-body problem solutions, symmetry conservation in moving coordinate system 80−17480
masses for which triple collision is regularizable 80−41704
material test point, statistics of distant perturbs. 78−28494
merging galaxies, numerical simulations 80−36716
microcosm and macrocosm, discrete modelling 80−82643
microscopic charge and current densities in terms of polarisation and magnetisation fields 78−8251
minimally classifying relative equilibria 77−67027
Monte Carlo methods in statistical physics, book 79−80528
Monte Carlo simulation, theory and technical aspects, book contrib. 79−80529
Monte Carlo simulation of Brownian dynamics, new method, convergence props. 79−12719
moving electron in field of two Coulombic ions fixed in space, rel. to H_2^+ line spectrum 80−42083
multibody system equations of motion, computer-aided formulation *(German)* 78−39
n fixed centres problem, particular soln. *(Russian)* 77−17346
N-particle problem, reduced density operators, theory, historical review 79−5945
N-particle scattering, combinatorics 78−24693
Newtonian gravitational systems of specified ang. momentum, improbability of collisions 79−53706
Newtonian problem, relative equilibria and the virial theorem 79−48658
Newtonian stellar dynamics, maximizing functionals, rel. to thermodynamic and dynamical stability 80−12782
non-integrable N-body Hamiltonian systems, variational solns. 78−93524
nonholonomic mech. systems of second order, geometrisation of motion 78−57771
nonholonomic systems of higher order, Mangeron-Deleanu eqns. in Poincare-Chetaev variables 77−33853
nonlinear discrete systems, integrability 80−98858
nonlinear internal wave solitons, Calogero-Moser-Sutherland N-body problem 79−27679
nonrelativistic many boson systems, scatt. theory, classical field limit 79−49103
nonrestricted double-averaged three body problem, Hill's approx. 77−22051
numerical simulation of 3-dimens. gravitating systems of colliding masses 77−9654
numerical solution accuracy 80−21896
one dimensional infinite particle systems with hard core interaction, nonequilibrium dynamics 77−82443
one-dimensional many-body problems, exact results, review *(Russian)* 79−80460
one-dimensional self-gravitating isothermal systems, stability 80−73008
one-dimensional system, time evolution soln. 80−82635
orbit-orbit resonances, appl. of spin-orbit theory to Titan-Hyperion case 78−24451
osculating elements reduction to proper elements for entire solar system 80−21897
particle statistics from induced representations of a local current group 80−57129
periodic orbits around rotating ellipsoid 78−77464
periodic orbits families, proof of existence 78−24449
periodic orbits of second generation and regions of stability, in restricted three-body problem 78−24453
periodic systems dynamical coupling, particular case of homographic soln. 80−36480
permutational symmetry of many particle states 80−57128
perturbed two-body problem, appls. of Pfaff's equations of motion 79−12386
photogravitational restricted circular three-body problem, triangular libration point stability 79−21164
planar elliptic three-body problem, long-period effects at 1/1 reson. 78−85830
planar magnetic binaries problem, areas of motion 78−96386
planar N-body problem, circular-elliptic type periodic solns. 78−93083
planar n-body problem, classifying relative equilibria 77−26169
planar restricted (N+1)-body problem, periodic elliptic motions 78−40806
planar restricted three-body problems, effect of oblateness on triangular solns. at critical mass 79−44339
planar three body problem, bifurcation points 78−24446
planar three body problem, eqn. system adoption for triple collision *(French)* 80−21895
planar three body system, asymptotic solns. 77−49273
planar three- and four-body problem, families of periodic solns. 77−25917
plane circular three-body restricted problem, Hamilton-Jacobi eqn. integrability, separation of variables method *(Russian)* 78−36445
plane elliptic restricted three-body problem, asymptotic soln. for Trojan case 77−60587
plane planetary three body problem, quasi-isosceles movement characterisation *(French)* 80−21893
plane problem of n fixed centres, soln. *(Russian)* 78−24448
plane restricted four body problem, soln. to problem of three fixed centres 77−60584
plane restricted three body problem, asymptotic solns. *(Russian)* 77−22049
planetary disturbing function expansion, convergence of Newton's iteration 77−64629
planetary problem, dynamical coupling of periodic systems, resonance *(French)* 77−73938
Poincare cycles of the linear chain of oscillators 80−4662
Poincare problem in celestial mechanics, soln. 78−28492
post-Newtonian charged n-body problem, centre of inertia and coord. transforms. 79−93025

N-body problems continued
post-Newtonian n-body problem in gravitation with PPN parameters γ and β, centre of inertia 79−17325
post-Newtonian two- and n-body problems with electric charge in general relativity 78−8277
post-post-Newtonian approximation, conditions for static balance 78−12619
potential energy functions, for teachers 79−40318
predictive relativistic mechanics *(French)* 77−45707
quantum dynamics semiclassical approximation 80−12927
quasi-relativistic two particle system, motion integrals, transform. props. *(Russian)* 77−49594
quasiperiodic motions stability in Hamiltonian systems 78−93085
Ray-Reid generalised systems, invariants derivation 80−101710
rectilinear isosceles restricted problem, numerical study 80−4242
regularised numerical method based on Taylor-Steffensen power series *(Russian)* 78−49300
relative motion of noninteracting particles in force field 77−29635
relativistic, direct interaction, Lagrangian formulation *(Russian)* 77−45696
relativistic Kepler problem, field asymptotic behaviour in infinite past 79−88575
relativistic Kepler problem, orbits with gravitational radiation damping, behaviour in distant past 79−88574
relativistic restricted three body problem, appl. of Gauss method to periodic solns. 77−13215
relativistic two body problem, appl. of dynamic confinement from vel. depend. interactions 80−46800
relativistic two-body problem, nonlinear effects 79−8799
renormalised perturbation theory, model of 3-D nonlinear field, free of UV divergences 78−54567
resitricted three-body lunar theory, non-Newtonian corrections *(German)* 77−25960
resonance in the restricted problem of three bodies with short period perturbations in elliptic case 79−25455
restricted averaged elliptical three-body problem, periodic orbits 79−8807
restricted circular three-body problem, appl. of motion of point in conservative force field 78−24456
restricted circular three-body problem, for space vehicles in vicinity of collinear libration point 78−4067
restricted circular three-body problem, stabilisation of collinear libration points 77−64624
restricted elliptic three-body problem, motion near triangular points 79−40064
restricted elliptical three body problem, difference between solns. of exact and averaged problem *(Russian)* 77−45298
restricted elliptical three-body problem, for space vehicle in vicinity of collinear libration point 78−4066
restricted Jupiter orbiter problem, introduction 77−13216
restricted problem, effect of perturbed potentials on libration points stability 80−4241
restricted three body problem; transform. to generalized rot. and pulsating coord. system 78−49298
restricted three body problem, near intermediate orbits of point of small mass 79−62731
restricted three body problem, new connection between families of periodic orbits 78−45204
restricted three body problem, of new kind 78−45210
restricted three body problem, second species periodic solns. with near-Moon passages 77−49271
restricted three body problem, stability limits appl. to Sun-Earth-Moon system 79−75084
restricted three body problem, stability of second species periodic orbits 78−61717
restricted three body problem in three dimensions, axisymmetric periodic orbits 77−64620
restricted three-body, equilib. points in planar mag. binary problem 80−82178
restricted three-body, numerical extrapolation of periodic solutions 78−69663
restricted three-body problem, appl. to asteroidal belt characts. explanation 79−8874
restricted three-body problem, appl. to dynamics of ejecta from satellites close to planets 80−98592
restricted three-body problem, appl. to origin of binary X-ray sources 77−29954
restricted three-body problem, appl. to Trojan asteroids theory 79−12419
restricted three-body problem, asteroid resonance with short-period perturbations 78−53803
restricted three-body problem, asymm. quasiperiodic orbits 79−8801
restricted three-body problem, asymmetric, periodic and asymptotic orbits 79−16807
restricted three-body problem, asymmetric periodic orbits in three dimensions 78−77476
restricted three-body problem, asymptotic solns., plane form and symmetry 79−8814
restricted three-body problem, commensurability induced by oblateness 79−8806
restricted three-body problem, effect of larger primary oblateness on collinear libration points 78−40803
restricted three-body problem, effect of mass ratio on existence of retrograde satellites 77−13210
restricted three-body problem, form. of periodic solns. by appl. of mean schemes 79−25457
restricted three-body problem, higher order stability, appl. to solar system 77−13208
restricted three-body problem, L_4 and L_5 points, stability at pot. maxima 79−7
restricted three-body problem, libration-point capture 77−29636
restricted three-body problem, orbit generation for stable close encounter periodic solns. 78−28489
restricted three-body problem, periodic solns., Sun-Jupiter case 79−25454
restricted three-body problem, periodic solns. in Hill's relativistic problem 78−40804
restricted three-body problem, perturbations of Lagrangian points 78−32327
restricted three-body problem, second species periodic solns. with one near-Moon passage 78−45207

N-body problems continued
restricted three-body problem, solar radiation effects on artificial satellite resonances 79−25456
restricted three-body problem, Sun-Jupiter case, plane symmetric periodic orbits 79−58235
restricted three-body problem, surface fitting of three-dimens. closed solns. 79−8800
restricted three-body problem, symm. of first integrals *(Russian)* 79−21166
restricted three-body problem, theory and appl. 79−58241
restricted three-body problem, three-dimens. branchings of plane periodic solns. 77−64623
rigid bodies, translational-rotational motion eqns. in osculating elements 78−28495
rotating systems, steady motions, computational anal. 80−53618
S-matrix theory, n-body potentials in QED and quantum gravity 78−24969
scattering theory combinatorics, partitions, and many-body physics 80−62504
self-consistent field theory of electrodynamics, many-body scatt. 78−49683
semiconductor, anisotropic, binding energy of exciton complexes 79−15088
sine-Gordon equation solutions, interaction potential between soliton and antisoliton 80−12945
six bodies in cluster, translational-rotational motion *(Russian)* 80−67528
solar system dynamics and long-term stability 79−40095
spin precession in the relativistic two-body problem 79−49118
spin-orbit effect in classical two-body Hamiltonian 77−68386
stability of constant Laplace solutions of the unrestricted three-body problem 80−68030
star cluster models dynamical evolution, early stages 79−8958
star clusters containing massive central black holes, dynamical simulations with self-consistent potentials 80−26915
statistical mechanics, asymptotic commutation problem, correlation weakening principle formulation 79−85070
statistical results validity 78−12084
stellar bar, dynamics, computer model 79−30093
stellar clusters, N-body calculations, statistical results depend. on N 79−80339
stellar collisions, by oscill. orbits of second kind 79−35312
stellar dynamics, two-body tidal dissipation in large N-body systems 78−93329
stellar equilibrium statistical mechanics, steepest-descent techniques for Newtonian clusters 77−45496
stellar gravitating systems, energy transfer 79−40226
stellar systems, relaxation with close encounters 79−48862
stellar systems with continuous mass spectrum, necessary condition for equilib. 78−93328
stellar three-body encounters, probability of binary form. 77−13396
Stormer problem, numerical determ. of asymmetric periodic solns. 77−49270
Sun-Jupiter-Saturn system, stability with bifurcation theory 77−53406
swirling particle fluids, computer studies, evolution of planetary-type bodies 79−35121
terrestrial planets, gravitational N-body problem rel. to accretion 78−53846
thee-body problem, restricted case secular post-Newtonian effects, Treder dynamics 80−72753
three body, generalised twice restricted, appl. to galactic dynamics *(Russian)* 80−51643
three body averaged plane restricted problem, first integrals, computer calc. *(Russian)* 77−56820
three body forces, nonlinear field theories equivalence to action-at-a-distance 77−26181
three body nonrelativistic problem, symmetric elimination of c.m. motion 78−69974
three body problem, generalized circular restricted, triangular libration points *(Russian)* 79−48659
three body problem, Lagrange equilateral triangle, Euler collinear solns., generalisation to nongravit. forces 78−54178
three body problem, planar circular restricted case, stochastic behaviour, reson. overlap criterion 80−105150
three body problems with Coulomb interaction, adiabatic representation, two-level approx. 80−47861
three body restricted problem, stability of generating soln. 77−72146
three rigid bodies problem, particular solns. for translational motion *(Russian)* 80−61999
three spheroidal body problem, stationary motion *(Russian)* 77−64944
three-body, circular plane restricted problem, stable orbits 79−44348
three-body, doubly averaged elliptical restricted problem 80−17479
three-body, elliptic three-dimens. restricted problem, recurrence relations in integration 79−48656
three-body, Hill's lunar problem, literal soln. 79−66909
three-body, Hill's problem in Lunar theory 78−77473
three-body, limited circular, Delaunay-Hill method averaging error estimation *(Russian)* 80−8530
three-body, periodic orbits in small third mass case 78−77467
three-body, planar circular restricted problem, Hill's curves, geometric prop. 78−77474
three-body, planar general problem, isosceles triangle config. 79−48654
three-body, restricted, attitude stability of spinning symmetric satellite in planar periodic orbit 80−4220
three-body, restricted, periodic oscills. around Lagrangian points 79−58236
three-body, unrestricted, Lagrangian solns. stability problem *(Russian)* 80−4245
three-body, unrestricted, Laplace solns. stability *(Russian)* 80−8529
three-body Copenhagen problem, classification of vertical critical periodic orbits 79−75081
three-body gravitational scattering 79−44344
three-body planar elliptic, appl. to long-period effects in Trojan asteroids motion 80−41755
three-body problem, classical restricted, Coriolis asymm. and Jacobian integral 80−61994
three-body problem, colinear positions of relative equilibrium *(French)* 78−36443
three-body problem, conditionally periodic solns., KAMo method 80−109343

N-body problems continued
three-body problem, continuation of periodic orbits, three-dimens. circular restricted to general case 79−44343
three-body problem, doubly-averaged elliptical restricted, trajectories 80−46376
three-body problem, elliptic, Jacobian integral development *(German)* 79−92655
three-body problem, elliptical restricted case, Lagrangian soln. stability *(Russian)* 80−94695
three-body problem, families of 3-dimens. periodic orbits 80−41698
three-body problem, forms of motion qualitative anal. in new model problem 79−62733
three-body problem, general, families of three-dimens. periodic orbits 80−26721
three-body problem, general, regions of motion *(Chinese)* 79−80206
three-body problem, general, three-dimens., biparametric family of symm. periodic orbits 80−61995
three-body problem, general case, families of 3-dimens. periodic orbits 80−41700
three-body problem, general case, topology of M_8 manifold 80−8528
three-body problem, general planar case, families of vertical periodic orbits 80−41699
three-body problem, general planar case, periodic solns. of Poincare's second sort 80−41707
three-body problem, generalised, Lagrangian and Eulerian solns. in absolute axes *(French)* 79−66912
three-body problem, generalized circular restricted, periodic orbits of second genus in 2-D coord. system 79−29980
three-body problem, generalized restricted, zero relative vel. curves 79−84650
three-body problem, model for close encounters in planetary system 78−61718
three-body problem, periodic orbits continuation 79−16806
three-body problem, photogravitational restricted circular case, triangular libration points stability *(Russian)* 80−77272
three-body problem, photogravitational restricted core, Lagrangian points 80−26725
three-body problem, planar case, reduction of eqns., of motion 80−41711
three-body problem, planar case, variational eqn. 80−46371
three-body problem, planar hyperbolic-elliptic motion, central configurations 80−41705
three-body problem, planar restricted, stability of inner planetary systems 79−70975
three-body problem, planar restricted case, lunar capture with variable solar mass 80−56728
three-body problem, planar to three-dimens. general core, periodic orbits 79−66908
three-body problem, plane averaged restricted case, qualitative analysis 80−109345
three-body problem, rectilinear case 80−41708
three-body problem, redundant variables for global regularization 77−25923
three-body problem, restricted, bifurcation orbits, Sun-Jupiter case 79−84647
three-body problem, restricted, families of three-dimens, double-symm. periodic orbits, Sun-Jupiter case 80−26722
three-body problem, restricted, halo orbits in Earth-Moon system 80−36483
three-body problem, restricted, in resisting medium, particular solution *(Italian)* 80−90325
three-body problem, restricted case, Poincare's second species solutions 80−41709
three-body problem, restricted case, Sun-Jupiter case, doubly symm. periodic orbit determ. 80−77269
three-body problem, restricted case, symmetrical solns. 79−96895
three-body problem, restricted case, Titan-Hyperion reson. and close approaches 80−77347
three-body problem, restricted case, u-type families of periodic orbits 80−101530
three-body problem, restricted classical case, generalisation for radiation press. 80−85843
three-body problem, restricted planar elliptic case, stationary solns. 80−46369
three-body problem, restricted plane case, formal integrals 79−96900
three-body problem, restricted three-dimensional, quasi-periodic solns. appl. to reson. asteroids *(Russian)* 79−48727
three-body problem, spatial periodic orbit families 80−77271
three-body problem, stability of interplay motions 77−60583
three-body problem, sufficient conditions for absence of collisions 78−24457
three-body problem, Sun-Jupiter case, axisymmetric periodic orbits 79−58237
three-body problem, Sun-Jupiter-satellite system, three dimens. orbit determ. 80−67526
three-body problem, three-dimens. general case, periodic orbits determ. 80−56696
three-body problem, three-dimens. periodic orbit families, Hill's problem 80−56695
three-body problem, triple collision and tri-parabolic escape 80−67521
three-body resonances in Uranus ring system, quantitative anal. of Dermott-Gold theory 78−4147
three-body system disruption, statistical theory for three-dimens. motion 78−77475
three-body systems disruption, statistical theory for high ang. momentum 77−13220
three-dimens. circular restricted three-body problem, simplified variant 79−8815
three-dimensional general N-body problem, periodic orbits families existence 79−16805
tidal force acting on Moon due to Earth and Sun *(Russian)* 77−78616
time transformations and Cowell's method 78−77466
translatory-rotary motion of three rigid bodies, Euler solns. *(Russian)* 78−53802
triple close approaches effect on stellar system evolution, one-parameter family appl. 80−17618
triple collision in rectilinear three body problem, neighbouring solutions *(French)* 77−13213
triple collision manifold in planar three-body problem *(French)* 79−58238
triple collisions 80−56697
triple rectilinear collision, Siegel matrix, eigenvectors *(French)* 77−70988
triple stars, stability and hierarchy 77−60797
triple stars, stability criterion 77−64801
triple systems, non-rotating, exact mean time of decay *(Russian)* 78−32523
two bodies of variable mass problem, relative orbit 79−62730
two body problem, time transformations and local truncation errors 77−22053
two body problem, time transformations effect on local truncation errors 77−22052
two charged particles problem, Lagrangian and Hamiltonian up to fourth-order terms 80−91736
two finite bodies problem, development of force function *(French)* 77−13218
two gravitating particles system, Lorentz-covariant model 80−8865
two point-masses bound system, influence of weak gravit. wave 80−21903
two solid body problem, force function 80−41701
two-bodies, gravitational parameter inaccuracy consequences computation, for orbits in Earth's gravitational field 78−40460
two-body, general time elements 78−77470
two-body orbital mechanics, solution to Kepler's problem for orbital position 78−73622
two-body problem, first and second isochronous derivatives 80−8527
two-body problem, general case, translating-rotating motion, force function determ. 80−17478
two-body problem, generalisation of Kepler's eqn. 80−105151
two-body problem, intermediate anomaly 78−45209
two-body problem, Kepler initial value problem, geometry, two-circle calcs. 79−71182
two-body problem, new Runge-Kutta algorithms for numerical simulation 79−12387
two-body problem, orbits from Lenz vector, education 78−36763
two-body problem, perturbation theory in rectangular coordinates 79−21158
two-body problem, translational-rotational motion of mutually gravitating rigid bodies 79−96896
two-body problem, with decreasing gravit. const. 77−13219
two-body restricted problem, almost circular orbits in general relativity *(Ukrainian)* 79−101056
two-body variable-mass problem, osculating orbital elements estimation 77−13221
unbounded three body problem estimates with one Hill stable body 79−84946
uniqueness of the N-body Lippmann-Schwinger-Glockle-Tobocman equations 79−54415
unrestricted 3-body problem, Laplace soln. instability *(Russian)* 78−4092
Uranus ring system, two-body and three-body resons. involving tiny Miranda 78−4148
Vlasov dynamics and fluctuations in 1/N limit of interacting classical particles 78−130

N-path filters *see switched filters*

N/D method
baryon resonances and broken SU(4) symm. 77−71455
bound states in baryon-antibaryon systems, NN, N$\bar{\text{N}}$, dispersion method *(Russian)* 78−16933
channel coupling effects and resonance phenomena in pp interactions, N/D eqn. study 79−71765
$e^+e^-\rightarrow\pi^+\pi^-(\pi^0\omega)$, $\rho'(1250)$ description, EM form factors, bound states, N/D method *(Russian)* 80−42465
effective range formula for πN P-wave amplitudes, high-energy contribs. 77−41857
hyperon-nucleon low energy interaction, two-channel separable pot. model, hypernuclei 80−47325
inelastic systems and CDD ambiguity, gap-matching N/D method 80−13234
multichannel problem, coupled, soln. of form factor 78−29277
nonrelativistic models for inelasticities in N/D eqns. many channel scatt. problems 77−49879
Roy eqns., multiple solns., N/D method on finite interval 78−16949
three particle level spectrum, Thomas theorem and Efimov effect, N/D eqns. 80−42562
three particle system, dispersion relations, one channel N/D method, form factors *(Russian)* 79−40689
$K^-{}^4He\rightarrow\pi^-\Lambda^3He$, final state interaction model, Muskhelishvili Omnes eqn. soln., πmomentum distrib. 77−30285
$K\bar{K}\rightarrow K\bar{K}$, dispersion model, matrix N/D method *(Russian)* 78−45954
N$\bar{\text{N}}$, resonances and bound states, multichannel N/D formulation 80−78087
N$\bar{\text{N}}$ cross-sections and resonances in nonstatic OBEP 80−13386
π photoproduction, multichannel N/D model fit, Δ^+ pole parameters 77−10265
πN low energy scatt. amplitudes, partial wave N/D techniques 79−85331
$\pi\omega\rightarrow\pi\omega$, $\rho'(1250)$ meson and two channel $\pi\pi$, $\pi\omega$ problem, N/D method *(Russian)* 80−37297
$\pi\pi$ interaction ρ reson., N/D calc., rebuttal of criticism 77−71462
$\pi\pi\rightarrow K\bar{K}$, dispersion model, matrix N/D method *(Russian)* 78−45954
$\pi\pi\rightarrow\pi\omega$, $\rho'(1250)$ meson and two channel $\pi\pi$, $\pi\omega$ problem, N/D method *(Russian)* 80−37297
$\pi\pi\rightarrow\pi\pi$, dispersion model, matrix N/D method *(Russian)* 78−45954
$\pi\pi\rightarrow\pi\pi$, $\rho'(1250)$ meson and two channel $\pi\pi$, $\pi\omega$ problem, N/D method *(Russian)* 80−37297
$\pi\pi$ scatt., Roy equations, iterative solutions, N/D equations 79−36098
$\pi\pi$ scatt., ρ-meson N/D calc. in Veneziano model 77−67627
ρ meson generation as dynamic $\pi\pi$ resonance, failure, criticism of method 77−10198
ρ reson. prod., N/D calc. 77−71461
$\rho\pi$ scatt. in Bardakci-Halpern model 1^+ channel, N/D anal., A_1 status 79−40688
^{3}H doublet scatt. length, Phillips plot, N/D input parametrisation 80−42672

NAND gates *see logic gates*

narrow band gap semiconductor materials *see narrow band gap semiconductors*

narrow band gap semiconductors
antiferromagnetic excitonic insulator state in strong mag. field *(Russian)* 77−28387
Auger recombination, carrier density depend. 79−38089
Auger transition rate, mag. quantum oscills. 77−69340
band theory, effect of lattice constant variation 80−49596
boundary conditions, energy spectrum, and optical transitions 79−42614
bounded crystal, dispersion law for electrons, Tamm sub-bands *(Russian)* 77−43468
carrier quasienergy spectrum in strong EM wave field 80−92922
chemiluminescence, heterogeneous, ionisation mechanism of excitation 80−50438
conference, Warsaw, Poland (Sept. 1977) 79−82582
conference, Warsaw, Poland (Sept. 1977) 80−49703
cubic, electronic contrib. to dielec. permittivity, calc. 77−59265
current-carrier conc. distrib. nonuniformity, contactless meas. 77−76853
degenerate, band to band radiative recombination *(Russian)* 78−35200
degenerate semiconductors, ferroelec. phase transition, hybridization effect *(Russian)* 79−61319
diamagnetic excitons in two-band Dirac model 80−59888
diamond-like, Auger recomb. calc. 78−63978
electron-hole recombination via plasmon emission 78−39046
electron-phonon interaction, effective mass of carriers determ. 79−11058
electrophotographic processes 80−13169
EM response of electrons, energy depend. relax. time 78−60142
energy spectrum, three band model 77−89699
epitaxial layer, growth, activation by UV and IR radiation 80−71598
EPR line shape, magnetoresist. effect 80−84638
ferroelectric, phase transition, Green's function method 77−52028
ferroelectric phase transition two-channel vibronic mechanism *(Russian)* 79−56745
ferroelectric transition, conductivity band theory rel. to vibronic theory of ferroelectricity 79−19854
ferroelectric transition, quantising mag. field effect 79−87403
ferromagnetic semiconductors, s-f interaction on conduction band, red shift effect theory 80−59872
ferromagnetism of electrons in filled band *(Russian)* 79−78300
film electron-beam microzone refining, in space 78−35325
frequency tripling and self-interaction of strong EM wave in zero-gap semicond. 79−10355
gapless, theory of resonance states in mag. field 80−6773
gapless, transport coeffs. in quantum limit 80−80302
gapless semiconductor, magnetic field resonance states *(Polish)* 80−88508
gapless semiconductor valence band in mag. field 80−49600
gapless semiconductors, screening effects on electron-electron interaction 80−49647
Ge electrode, electon injection in liq. NH_3 80−6977
heavy holes, energy spectrum in mag. field, effect of nonlocal pot. 79−90959
heterojunction, band-edge discontinuities and interface pot. step, two-band narrow-gap approach 80−39665
heterojunctions, between narrow-gap semiconds. interface states 77−55603
high electric field conduction in space and time superlattices 80−49756
hot electron phenomena, I-V curve calc. 80−34457
hot electrons in semiconductor with symmetrical carrier spectra 79−23982
Hubbard model, partly filled narrow band, electron correlation and mag. props. 78−67968
intrinsic, indirect exchange interaction, finite temp., valence bands and energy gaps effect 80−59943
inversion layers in strong elec. field modification of Einstein relation 80−96959
IR devices appls. 80−48464
IR-sensitive, props. and optoelectronic appls. *(German)* 77−20356
IV-VI, fabrication, IR laser and detector appls. 77−77415
IV-VI compounds, impurity levels, intergap interaction effects, T-matrix approx. *(Russian)* 77−31973
IV-VI semiconductor, ferroelec., vibronic model of lattice instability 80−80723
IV-VI semiconductors, crystal binding energy 79−37650
IV-VI semiconductors, mag. susceptibility near ferroelec. transition pt. *(Russian)* 79−95568
IV-VI small gap semiconductor alloys, band edge parameters 80−49594
Kane semiconductor, many photon electron spin orientation, EM wave absorption 80−44506
layered, electron-hole liquid exam. 78−18975
magnetic impurity scatt., contrib. to electron mobility and thermoelec. power 77−15852
magneto-absorption, multiphoton, Dirac eqn. *(Russian)* 79−19867
magnetoresistance, quantum limit behaviour 79−28359
microwave effects, review 79−82618
microwave effects, review 79−95437
MIS devices, large-amplitude hysteresis, model 79−19665
MOS structures of small-gap semicond., capacitance, effect of quantising mag. field 80−84513
multilayers with p-n junctions, relaxation and photocurrent analysis 79−7883
multiphoton absorption in crossed fields *(Russian)* 80−60553
Nernst-Ettingshausen and Hall effects in type I zero-gap state 80−44622
nonparabolic, Monte Carlo transport calcs., acoustic scatt. inelasticity effects 77−51754
one-dimensional with impurities, density of states calc. *(Russian)* 77−39761
optical nonlinearity due to free carriers 79−81491
optical phonon spectrum 79−7794
parametric excitation in Kane's semiconductor 78−52023
photocarrier distrib. and photomagnetoelectric effect near stimulated emission threshold 80−80320
physics, review 77−28112
physics of semiconductors, conf., Edinburgh, Scotland (Sept. 1978) 79−95303
plasma frequency, effect of electron spin, in quantising mag. fields 79−95436
plasma waves parametric amplification 78−43428

narrow band gap semiconductors continued
plasmon-phonon interaction effect on optical phonon dispersion 80−103435
rare earth chalcobismuthites, $RBiTe_3$, prep., elec. props., and crystallographic date 80−59981
recombination, conference, Southampton, England (Aug.-Sept. 1978) 79−38087
recombination instability of electron-hole plasma in narrow-gap semiconductor 80−39621
recombination instability under crossed elec. and mag. fields 80−70712
recombination mechanisms, review 80−96905
resonance two-phonon absorption in zero-gap semicond. 79−55847
resonant scattering, Green's function method and CPA 80−6827
sandwich sample, thermal switching and current-voltage charact., necessary conditions 77−4451
Schottky barrier photovoltaic IR detector using narrow bandgap semiconductor 80−9040
sound absorption in strong EM field of laser 77−55590
stimulated emission charact. 79−31903
stimulated plasmon emission 79−73461
structural transitions associated with morphotropy 77−39675
superlattices, acoustic wave absorpt. and amplification 80−29445
surface states in energy gap 77−69401
$(TCNQ)_2$ benzacridinium, cond. and thermoelec. power meas. 77−35946
TCNQ salts, complex, with aromatic donors, interchain coupling and disorder 78−6314
TCNQ salts, complex, with symmetric and asymmetric donors, transport and mag. props. 78−6315
TCNQ salts, Rb^+TCNQ^-, and TMB^+TCNQ^-, triplet exciton dipolar splitting tensors rel. to mag. susceptibility 77−62839
TCNQ salts organic semiconducting polymers, electron transfer mechanisms 79−42544
ternary diamond-like semiconductors, charact. features of electronic spectrum and stability 79−33230
thin layer zero-gap semicond., dielec. response 80−103635
transition metal borides, electronic density of states, many-electron Hubbard model calcs. 80−20064
transport phenomena electron energy spectrum *(Russian)* 79−51616
two band model with electron-phonon interactions for narrow-gap electron spectra 79−90961
two-dimensional electron spectrum, spin splitting 80−24861
zero gap semiconductor, magnetooptical and impurity effects 80−6721
zero-gap, indirect-exchange interactions 80−29370
zero-gap, magnetophonon oscills. of transverse magnetoresist. in strong elec. fields 80−96916
zero-gap props. correlated to Γ_8 symmetry, review 80−6717
zero-gap semicond., IR absorption coeff., theoretical anal. 80−20641
zero-gap semiconductor, variational approach to resonances 79−82559
zero-gap semiconductors, lattice defects and chemical bonds *(Japanese)* 79−73161
zero-gap semiconductors, reson. states, review 79−82558
zinc blende semiconductors, small-gap, electron scatt. and transport props. 78−95294
zinc blende semiconductors, small-gap, electron scatt. and transport props. 78−95295
zincblende narrow-gap mixed crystals, disorder scatt. 78−51985
zincblende-symmetry narrow-gap semicond., Fermi energy and Fermi-Dirac integrals 80−70604
Ag_2Re films, galvanomag. props. and quantum size effects, obs. 80−70866
Ag_2Te, low temp. thermal cond., thermoEMF 78−43423
$Al_xGa_{1-x}As$, DH, defect generation in active regions at high optical excitation rates 79−23845
As, black phosphorous struct., Raman vibr. spectra and bonding 80−11411
Bi, magneto-thermopower, weak-field, implication for scatt. mech. 80−49790
Bi-Sb narrow gap semiconductor, EM wave propagation in direction parallel to mag. field 78−80014
n-BiSb, cyclotron mass meas., high hydrostatic press. 79−77991
p-$Bi_{0.9}Sb_{0.1}$, Fermi surface anisotropy var. on press. induced transition to gapless state *(Russian)* 77−43483
$Bi_{1-x}Sb_x$, far IR magnetoabsorption, band struct. study 80−50351
$Bi_{1-x}Sb_x$, galvanomagnetic, optical and photoelectric props. galvanomagnetic, optical and photoelectric props. 80−15544
$Bi_{1-x}Sb_x$, narrow band gap semicond., photocond. and photomagnetic effect 79−51630
n-Bi_2Se_3, single cryst., new aspect of carrier scatt. 80−49707
Bi_2Se_3:Hg point defects in crystal lattice, Hall coefficient and IR spectra determ. 80−55129
n-Bi_2Te_3, galvonomagnetic props., influence of hydrostatic press. 79−73536
Cd_3As_2, band struct. and g-factor, Shubnikov-de Haas oscills. meas. 80−49598
Cd_3As_2, band struct. from Shubnikov-de Haas and de Haas-van Alphen effects 80−49597
Cd_3As_2, band structure, pressure dependence of galvano- and thermomagnetic effects 80−6722
Cd_3As_2, effect of annealing on elec. transport props. 80−49739
Cd_3As_2 film, optical absorption edge 80−50450
Cd_3As_2, sp. ht., thermodyn. props. 78−22863
Cd_xHg_{1-x} Te, photodetectors, recomb. processes, photoconductive decay obs. 79−38129
$Cd_xHg_{1-x}Se$ mixed cryst., electron mobility and electron scatt. 78−95296
$Cd_xHg_{1-x}Se$, narrow band gap semicond., electron scatt., and transport phenomena 80−49706
$Cd_xHg_{1-x}Te$, characts. of low temp. transport props. 78−39160
$Cd_xHg_{1-x}Te$ crystals, donor compensation, low temp. cond. study 80−75571
$Cd_xHg_{1-x}Te$, effects of electron heating at low temps. 80−49823
$Cd_xHg_{1-x}Te$, electron mobility and conc. near gapless state, influence of hydrostatic press. 79−65486
$Cd_xHg_{1-x}Te$, influence of nonparabolicity on transverse magnetoresist. near transition to zero gap 80−20228
$Cd_xHg_{1-x}Te$ narrow gap semiconductor, charge transfer device for IR detection appl. *(French)* 79−30563
p-$Cd_xHg_{1-x}Te$ solid soln., thermoelec. effects 79−73538
$Cd_xHg_{1-x}Te$, zero gap semiconductor, interband optical-phonon scattering 80−6846
CeSb, forbidden band gap and electrotransfer parameters 80−39497

narrow band gap semiconductors continued
$Co_{1-x}Fe_xSi$, elec. and optical props. 80−49740
CoS_2, narrow-band ferromag., high press. effect on anomalous elec. resist. 80−70698
$Co(S_xSe_{1-x})_2$, galvanomag. effects, obs. and interpretation 80−70726
CrAl, semicond. solid solns., temp. depend. of elec. resist. at high temp. 78−67941
EuB_6, electronic struct., transport and mag. props. 80−96782
EuB_6, mag. and transport props. 80−54689
$Fe_{0.2}Co_{0.8}S_2$, narrow-band ferromag., high press. effect on anomalous elec. resist. 80−70698
GaAs electrode, electon injection in liq. NH_3 80−6977
$GaAs_{1-x}Sb_x$, narrow-gap film on wide-gap GaAs, energy gap grading, optical transmission meas. 77−20943
GeS(Se)(Te)(O_2), K X-ray spectra, Ge atoms effective charge, energy-gap widths 77−28657
GeSe, galvanomag. meas., anisotropy, metal to semiconductor transition 80−6847
GeTe, concentration of carriers, rel. to stoichiometry 80−6847
GeTe, crystal binding energy 79−37650
GeTe, electron-phonon interactin induced phase transition 79−82338
$Hg_{0.985}Cd_{0.015}Se$, interband $\Gamma_6 \rightarrow \Gamma_8$ magnetoabsorption and band parameters 79−82960
$Hg_{1-x}Cd_xSe$, zinc blende structure, optical and electronic properties 80−6723
HgCdTe, interband magnetoabsorption and band struct. 79−82959
HgCdTe MIS structure, modelling and appl. to CCD IR imagery 78−80058
HgCdTe, Magneto transport anomalies at low carrier densities, Wigner crystallisation 80−20222
HgCdTe, narrow band gap semiconductor IR devices, advances 80−48464
HgCdTe, recomb. effects, mag. quantum oscills. in Auger transition rate 79−82610
HgCdTe, zero gap, unusual high electron mobility and related phenomena 79−82601
$Hg_{0.77}Cd_{0.23}Te$, near reson. spin-flip Raman scatt. 79−82983
$Hg_{0.85}Cd_{0.15}Te$, acceptor states, galvanomagnetic effects study 79−82560
$Hg_{0.86}Cd_{0.14}Te$, spin-flip electron scatt., longit. magnetoresist. obs. 77−43622
$Hg_{1-x}Cd_xTe$, acceptor impurity band form. 80−20119
$Hg_{1-x}Cd_xTe$, avalanche formation, high intensity IR transmission limit 79−78684
$Hg_{1-x}Cd_xTe$, Einstein relation for inversion layers 80−103706
$Hg_{1-x}Cd_xTe$, far IR cyclotron resonance in inversion layer 77−69396
$Hg_{1-x}Cd_xTe$, high intensity IR transmission limit 80−7361
$Hg_{1-x}Cd_xTe$, magnetooptical and impurity effects 80−6721
$Hg_{1-x}Cd_xTe$, magnetoreflection studies 79−82963
$Hg_{1-x}Cd_xTe$, photolum. and optical pumping 80−50424
$Hg_{1-x}Cd_xTe$, quasi-local acceptor levels and electron mobility 78−67974
$Hg_{1-x}Cd_xTe$, semiconducting phase, acceptor states and galvanomagnetic effects 80−11017
n$Hg_{1-x}Cd_xTe$, single-phonon and plasmon recomb. lifetime effect, with magnetically tuned bandgap 79−38098
$Hg_{1-x}Cd_xTe$, zero-gap semicond., reson. states 79−82558
$Hg_{a-x}Cd_xTe$, single-LO-phonon and -plasmon recombination channels narrow-bandgaps 78−91728
n-$Hg_xCd_{1-x}Te$, narrow band gap, Auger effect under high mag. fields 79−82609
$Hg_xCd_{1-x}Te$, photodiode, anomalous noise behaviour in heterodyne and background limited operation 79−69568
$HgCr_2Sd_{4-x}Te_x$, ferromag. semicond., zero bandgap transition 80−96783
$Hg_{1-x}Fe_xTe$ mixed crystals, zero gap, magneto-optical evidence of exchange interactions 80−45045
HgMnTe, interband magnetoabsorption and band struct. 79−82959
$Hg_{1-x}Mn_xTe$, acceptor reson., states in high mag. field 80−49668
$Hg_{1-x}Mn_xTe$, helicon-excited ESR effect 79−95437
$Hg_{1-x}Mn_xTe$, mag. field induced microwave transparency 80−49797
$Hg_{1-x}Mn_xTe$, mag. props., self-consistent two spin cluster model 80−54874
$Hg_{1-x}Mn_xTe$, magnetooptical and impurity effects 80−6721
$Hg_{1-x}Mn_xTe$, Shubnikov de Haas effect and quantum oscills. of thermoelec. power 80−49781
$Hg_{1-x}Mn_xTe$, thermo-oscills. of magnetoresist. 79−56249
$Hg_{1-x}Mn_xTe$, zero-gap semicond., indirect-exchange interactions 80−29370
$Hg_{1-x}Mn_xTe(S)(Se)$, EPR of Mn^{2+}, order-disorder transitions 80−50176
HgSe, dielec. function at 2, 95, and 300K, reflectivity spectra meas. 79−15458
HgSe, Dingle temp. exam. 79−65358
HgSe film, anomalous photocond., electron microscope study 80−65623
HgSe, interband $\Gamma_6 \rightarrow \Gamma_8$ magnetoabsorption and band parameters 79−82960
HgSe, interband $\Gamma_6 \rightarrow \Gamma_8$ magnetoabsorption, temp. study 80−76032
HgSe, magnetooptical and impurity effects 80−6721
HgSe, optical determ. of Γ-point band struct. parameters 79−82523
HgSe(Te), narrow band gap semicond., electron scatt., and transport phenomena 80−49706
HgSe(Te), zero-gap semicond., reson. two phonon absorpt. 79−55847
HgTe, acceptor reson., states in high mag. field 80−49668
HgTe, and ternary compounds, mag. field induced microwave transparency 80−49797
HgTe, contrib. of resonant states to conductivity 79−51577
p-HgTe, far IR reflectivity spectra, experimental and theoretical study of the dynamic dielectric function 78−92069
HgTe, gapless semicond., magnetophonon conc. oscills. *(Russian)* 77−11943
HgTe, magnetooptical study of Γ_8 bands anisotropy 79−82984
HgTe, magnetophonon oscills. of thermoelec. power 80−49789
HgTe, nonlinear effects in transverse quantising mag. fields 77−69353
HgTe, quantum galvanomag. effects 80−49782
HgTe type semiconductors, spin-flip transitions in magneto-optics and magneto-transport 80−50306
HgTe, uniaxially compressed, anomalous magnetoresist. and band crossing 79−65501
HgTe, VPE growth control by EM irrad. *(Russian)* 80−34338
HgTe, vacancy doping, effect on elec. characts. 79−82595
HgTe, zero gap semiconductor, resonant acceptor states 80−6772
HgTe, zero-gap semicond., reson. states 79−82558
HgTe, zero-gap semicond., absorpt. spectrum in mag. field 80−11370

narrow band gap semiconductors continued
HgTe, zero-gap semiconductor, variational approach to resonances 79−82559
HgTe:Mn, impurity scatt. contrib. to electron mobility and thermoelec. power 77−15852
n-InAs, avalanche formation, high intensity IR transmission limit 79−78684
InAs, high intensity IR transmission limit 80−7361
InAs surface accumulation layers, magneto-transconductance study 80−49948
InAs, thermal oxidation, growth rate and chem. comp., temp. depend. 80−108619
InAs(Sb), in MOS struct., electrorefl., band-population effects under heavy surface accumulation 77−48167
n-InSb, acoustoelectric instability, effect of nonparabolic band struct. 79−60875
InSb, Auger recombination, calc. for diamond-like narrow-gap semicond., compared with expt. 78−63978
InSb, avalanche formation, high intensity IR transmission limit 79−78684
InSb, CESR at high mag. fields, scatt. mechanisms 80−93177
InSb, degenerate semicond., surface photo-EMF depend. on bulk consts. 79−69580
InSb, Einstein relation for inversion layers 80−103706
InSb, electron spin relaxation 80−25187
InSb, Ettingshausen effect, influence of surfaces, narrow-gap semicond. characterisation 77−24571
InSb, high intensity IR transmission limit 80−7361
p-InSb inversion layer, magnetotransport 78−64138
n-InSb, Landau-level-electron lifetimes, saturation meas. of magnetoabsorption 78−48150
InSb MOS struct., capacitance of n-channel inversion layers, elec. field effects 80−80393
InSb MOS structure, props. 80−49947
p-InSb, magnetoconductivity and cyclotron reson. in inversion layers 80−49946
InSb, narrow band gap semiconductor, optical nonlinearity due to free carriers 79−81491
n-InSb, narrow gap, appl. of effect of pot. fluctuations induced by cryst. inhomogeneities 80−49780
InSb, parametric amplification of plasma waves 78−43428
p-InSb, stress induced k-linear terms in band struct. 80−49595
InSb, surface, reson. excitation of electron subbands 80−49865
InSb type semiconductor, spin-flip transitions in magneto-optics and magneto-transport 80−50306
InSb:S(Se)(Te), reson. states and reson. scatt., elec. props. 80−49738
Mg_2Sn, Mossbauer effect exam. under press. up to 75 kbar 79−69759
NdSb, forbidden band gap and electrotransfer parameters 80−39497
P, black phosphorous struct., Raman vibr. spectra and bonding 80−11411
(Pb, Sn)Te-type semiconductors, displacive ferroelec. phase transitions, vibronic theory 80−11354
Pb salts, advances in IR device appl. 80−48464
$Pb_{1-x}Ge_xTe$, degenerate semiconducting ferroelectric, structural phase transition temp., mag. field effects 80−45017
$Pb_{1-x}Ge_xTe$, p-n junctions, elec. characts., effect of ferroelec. phase transition 79−33338
PbS, first-principles calc. of eqn. of states 80−49649
PbS(Se)(Te), crystal binding energy 79−37650
PbSe, carrier density depend. of cyclotron mass, Shubnikov-de Haas effect 79−73533
PbSe, polycryst. film, low temp. illumination, residual cond. 77−43756
n-PbSe, pressure induced transition to gapless state 78−2533
n-$Pb_{0.94}Sn_{0.06}Se$ solid solns., Burstein-Moss effect and energy band struct. 80−40118
$Pb_{1-x}Sn_xSe$, band struct. and transport props., hydrostatic press. effects 80−15452
$Pb_{1-x}Sn_xSe$, carrier density depend. of cyclotron mass, Shubnikov-de Haas effect 79−73533
$Pb_{1-x}Sn_xSe$, gapless state and phonon spectrum *(Russian)* 78−30715
$Pb_{1-x}Sn_xSe$, n- and p-type, with band inversion, study of transport phenomena 80−49741
PbSnTe, Magneto transport anomalies at low carrier densities, Wigner crystallisation 80−20222
PbSnTe-like semicond., Auger recomb., nonparabolic approx. 79−15161
$Pb_{0.8}Sn_{0.2}Te$ film, growth in quasi-closed space, single and polycryst. 79−33930
$Pb_{0.8}Sn_{0.2}Te$:Cd, influence of Cd doping on high field magnetoresist. and Hall effect 80−75590
$Pb_{0.8}Sn_{0.2}Te$:In, implanted thin epitaxial films, laser annealing 79−65104
n-$Pb_{0.82}Sn_{0.18}Te$, conduction band struct., determ. by Shubnikov-de Haas meas. 78−2504
$Pb_{0.82}Sn_{0.18}Te$, Hall mobility, scatt. mechanisms, temp. and carrier conc. depend. 77−55548
$Pb_{0.82}Sn_{0.18}Te$, narrow gap semicond., mag. susceptibility meas. *(Russian)* 78−84397
$Pb_{0.82}Sn_{0.18}Te$, narrow-gap, Hall effect quantum oscillations *(Russian)* 77−4377
$Pb_{0.82}Sn_{0.18}Te$, relax. time for Shubnikov-de Haas effect 78−80006
$Pb_{0.82}Sn_{0.18}Te$ solid solution, energy band spectrum characts., Hall effect meas. 77−76737
$Pb_{1-x}Sn_xTe$, ($x<0.35$), permittivity and soft modes, carrier density and comp. effects 80−7256
$Pb_{1-x}Sn_xTe$, displacive phase transition, effect of interband hybridisation 79−33233
$Pb_{1-x}Sn_xTe$, energy band parameters from IR Faraday rotation 78−48154
$Pb_{1-x}Sn_xTe$, epitaxial layers, photolum. in mag. field 79−83033
$Pb_{1-x}Sn_xTe$, far IR magneto-optical meas. 79−61343
$Pb_{1-x}Sn_xTe$, ferroelec. phase transition, hybridization effect *(Russian)* 79−61319
$Pb_{1-x}Sn_xTe$ film, Burstein-Moss effect, absorpt. and photocond. spectra 78−18961
$Pb_{1-x}Sn_xTe$ film, possible applic. as mechanical stress transducers 77−58621
n-$Pb_{1-x}Sn_xTe$, galvanomag. effects, alloy scatt., 4.2K 77−39880
$Pb_{1-x}Sn_xTe$, MBE, O_2 uptake, AES, XPS and UPS expts. 78−95227
$Pb_{1-x}Sn_xTe$, mag. and kinetic props. near ferroelec. transition 80−11160
$Pb_{1-x}Sn_xTe$, Mossbauer investig. of phonon softening at semicond.-semimetal transition 77−43908

narrow band gap semiconductors continued
$Pb_{1-x}Sn_xTe$, narrow gap, many-body interaction effects, Bloch electron scatt. lifetimes, energy renormalisation 80−49637
$Pb_{1-x}Sn_xTe$ narrow gap solid alloys, hole Fermi surface, galvanomag. and oscill. effect obs. *(Russian)* 77−69345
$Pb_{1-x}Sn_xTe$, narrow gap solid solns., mag. susceptibility and energy band spectrum 79−28276
$Pb_{1-x}Sn_xTe$, narrow gap semicond., theory of mag. susceptibility 80−93070
$Pb_{1-x}Sn_xTe$, photoelec. props. 30 to 4.2K, temp. depend. of electron density 80−20246
$Pb_{1-x}Sn_xTe$, Raman scatt., role of soft phonons and interband mixing 77−77209
$Pb_{1-x}Sn_xTe$, soft mode, ferroelec. phase transition crit. temp. and dielec. const. calcs. 77−8530
$Pb_{1-x}Sn_xTe$: Mn, Mn mag. and elec. active states, mag. impurity behaviour 80−44627
$Pb_{1-x}Sn_xTe$:^{119}Sn, symm. breaking of Sn local environment, Mossbauer splitting obs. *(Russian)* 77−40166
$Pb_{1-x}Sn_xTe$:In, with low carrier conc., transport phenomena 80−49783
$Pb_{.87}Sn_{.13}Te$, phonon dispersion, mode softening 79−42175
$Pb_{1-x}Sn_xTe_{1-y}Se_y$, narrow-gap solid soln., lattice parameter, energy gap and Hall mobility of carriers 79−73154
$Pb_{1-x}Sn_xTw$, lattice instability and phonon-width, comprehensive model 79−14906
PbTe, and $Pb_{1-x}Sn_xTe$, VPE growth control by EM irrad. *(Russian)* 80−34338
PbTe, electron-phonon interactin induced phase transition 79−82338
PbTe epitaxial films, carrier recomb. and deep levels, photocond., Hall effect, and luminesc. meas. 79−38024
PbTe epitaxial layers, submillimetre spectroscopy 79−83048
PbTe, ion implantation induced damage and reson. levels 80−49255
p-PbTe, MIS struct. inversion layer sub-bands, IR magnetoreflectance obs. 80−44731
PbTe, Magneto transport anomalies at low carrier densities, Wigner crystallisation 80−20222
PbTe, magneto-optical pinning phenomena 79−82962
PbTe, magneto-optical transitions and band parameters 79−82961
p-PbTe, magneto-optics of free and bound carriers 79−82985
PbTe surfaces, tunnelling spectroscopy in MOS and Schottky barrier junctions 80−49945
PbTe, two photon magnetoabsorption *(Russian)* 80−60553
PrSb, forbidden band gap and electrotransfer parameters 80−39497
Pt complex, bis(1,2-benzoquinonedioximato)platinum(II), intrinsic elec. cond. 78−6377
$PtSb_2$, high field elec. props., impact ionisation 80−96892
Sb_2Te_3, thermoelectric properties and phase transition, under hydrostatic pressure up to 9 GPa 80−65609
SmSb, forbidden band gap and electrotransfer parameters 80−39497
$Sn_xPb_{1-x}Te$ mixed cryst., cryst. growth and assessment 78−80463
SnTe, carrier density depend. of soft TO-phonon, Raman scatt. meas. 78−6684
SnTe, crystal binding energy 79−37650
SnTe, electron-phonon interactin induced phase transition 79−82338
SnTe, ferroelec. transition, quantising mag. field effect 79−87403
SnTe, phase transition at high hydrostatic pressure, Mossbauer study 79−95162
SnTe, softening of TO phonon mode *(Japanese)* 78−2225
SnTe, structural phase transition threshold instability in strong EM field 80−103477
SnTe:Mn, EPR as probe of phase transitions 80−15790
Te, SHG of ps pulses 79−45995
YbB_6, mag. and transport props. 80−54689
YbSb, forbidden band gap and electrotransfer parameters 80−39497
$Zn_xHg_{1-x}Se$, band struct. from Shubnikov de Haas effect and hydrostatic press. meas. 80−49599

natural gas technology
coal gas production using HTR 80−11996
combustion, NO_x and SO_2 form., oxidizing agent excess depend., thermodynamic anal. 78−15677
flowmeter for natural gas industry 78−30392
fluid mixtures, perturbed hard chain theory, thermodynamic props. 79−34343
formation compressibility and edge water encroachment on gas field performance 80−30355
French natural gas industry developments and prospects *(French, English)* 80−21364
gas distribution equipment in hydrogen service 80−97818
gas turbine power stations, off shore, electricity generation, off shore gas utilisation 80−21360
geophysical exploration instruments, implementation guidelines for promotion of electronics in oil and gas sector 79−80039
health risks of high-Btu gas pipeline and electric power transmission systems 80−104520
hydraulic fractures mapping technique 78−69543
liquefied natural gas spilled on water, spreading and evap. investig. 78−26748
liquefied natural gas spills on land and water, dispersion hazard 77−45141
LNG, transport and storage hazards 80−45620
LNG storage and transportation systems, austenitic and martensitic steels 79−70133
low-temp. materials, US/USSR, mechanical and weld props. 79−61736
low-temp. materials, US/USSR, mechanical weld props. 79−61735
marine structures for energy conversion 79−43712
offshore operations, LEO I submersible reliability and safety 77−5373
pipeline compressible flow and heat transfer simulation program 77−19638
simulated natural gas mixtures, enthalpy and phase equil., correl. with modified Starling eqn. 80−61127
sour gas (H_2S in natural gas) plants in Alberta, SO_2 pollution 77−37372
underground coal gasification, potential impacts on groundwater quality 79−87949
underground coal gasification, US Dept. of Energy Program 79−87947
underground coal gasification in steeply dipping beds 79−87948
underground coal gasification program is eastern USA 79−87950
underground coal gasification project 79−87951
underground pipes, excitation of an elastic half-space by a buried line source of conical waves 80−64245

natural gas technology continued
H industrial scale production from natural gas 80−35791
H_2 distribution in natural gas equipment, operating, safety and material problems 80−61468
H_2-methane mixture properties for hydrogen supplementation of natural gas 80−45781

natural resources
see also agriculture; dams; energy resources; mining; water supply
agrometeorological survey, management of resources *(Italian)* 77−81989
asteroids, mining prospects 78−61786
Athabasca oil sands, electrical props. 80−31030
catchment model design and parameter estimation using optimisation method 79−5536
coal, future prospects *(Russian)* 78−32099
coal, surface-mine inventory, LANDSAT imagery appl. 77−91320
coal basin evaluation, appl. of gravity profile across Bonnet Plume Basin, Yukon Territory, Canada 80−76898
conservation, energy analysis approach criticised *(French)* 79−57349
Cornwallis Pb-Zn District, Canada, Mississippi Valley-type deposits controlled by stratigraphy and tectonics 77−91130
critical mineral resources 79−5482
cultivated and natural vegetation mapping 77−56781
depletion of natural resource, man's effect on environment 78−45455
digital image anal. for natural resources inventories 78−96326
digital image processing for resources monitoring 78−96328
Diyala catchment, Iraq, water balance between Derbendikhan and Himrin dams 80−12462
drill hole or sample area-of-influence determ., FORTRAN IV program 77−5327
Earth, imagery data processing techniques *(Italian)* 77−82063
Earth's natural resource obs. from space, present and future 79−5653
Earth's resources and environment obs., satellite meas. capabilities 79−5654
Earth resource satellite attitude meas. and control requirements 78−65482
Earth resource surveying and interpretation 78−24391
Earth Resources Observation System Data Center for Landsat data 78−36289
economics of resource information systems, streamflow data network design 77−73893
education, conservation effects on resource usage, integral expressions 78−69941
energy and mineral resources rel. to plate tectonic research 78−7606
environmental assessment, management system for local development project in Japan 79−57503
environmental information consequences in information systems 79−57500
environmental system modelling, identification and control, conf., Ghent, Belgium (Aug.-Sept. 1977) 79−25250
exploratory drilling exhaustion sequence plot program 78−57334
food and energy shortages, appl. of ocean data and information services 78−69463
forest productivity study using LANDSAT data, computer training, USA 77−78527
Forest Service, digital terrain model appls. 79−84086
free water surfaces mapping methods *(French)* 79−96771
gas, seismic bright spots in Gulf of Oman 78−32057
gas-bearing strata, penetration zone break-up theoretical study *(Russian)* 79−39713
gas-oil-source rock masses, lithogenesis *(Russian)* 80−4006
geophysical equipment for Hungary, prospecting appl. 78−7787
Georges River, Sydney, changes in urban water resource 77−70697
GEOSAT, geological industry reommendations on remote sensing from space 78−69495
geothermal areas in Tuscany, location via geochemical and isotopic methods 77−49049
geothermal energy, heat extraction from hot dry rock masses 78−61378
geothermal energy, technological aspects of exploitation 80−55799
geothermal energy in Holland, prospects *(Dutch)* 80−35634
geothermal heat, extraction by water circulation through crack in dry hot rock mass 79−57355
geothermal heat in Urach region, temp. field investigation at great depths 79−48440
geothermal resources in Nevada, gravity surveys interpretation 80−41365
global problems and energy, nuclear power 78−45454
global problems soln., scientific and social approaches 77−74185
gravimetric sounding, vertical and horizontal gravity gradients relative precision 79−84500
ground water supplies in Himalayan region of Uttar Pradesh, influence of droughts 77−56708
groundwater, extraction potential in W.Uttar Pradesh 78−32130
groundwater, saline water and fresh water zones delineation using resistivity and induced polarisation (IP) survey 80−104867
groundwater and surface water resources, effects of 1975-6 drought on development 78−88869
groundwater occurrence in trappean terrain of Sholapur district, Maharashtra, influence of groundwater divide 79−8649
groundwater teledetection methods *(French)* 79−96776
Hungary, petroleum deposits rel. to sandstone litho-stratigraphy 77−86884
hydrocarbon exploration, seismic signatures of sedimentation models using synthetic seismograms 77−21913
hydrocarbon gases, in sediments of United States Atlantic continental shelf 80−72511
hydrocarbon potential of Palaeozoic onshore Canning Basin, W.Australia 80−46176
icebergs from Antarctica for Saudi Arabia water supply 77−81949
identification of rice-growing land from teledetection data *(French)* 79−96775
image analysis system for Earth resources surveys 79−5644
irrigation detection in the Loire-Britanny river basin *(French)* 79−96774
land use mapping using radar imagery 77−73886
land-use/soil survey data processing for resource planning 78−7804
LANDSAT remote sensing program 78−96330
Lanzarote (Canary Island), geothermal prospects from isotopic comp. of steam samples 77−49048

natural resources continued
limnological ecosystem modelling, real-time estimation methods appl. 79−5541
Lithuanian water resource distrib. optimisation, informational preconditions *(Russian)* 79−92555
management, LANDSAT information, data acquisition by remote sensing *(Italian)* 77−82057
management software system, data analysis, interactive program, equipment 77−82058
mankind's future needs and aspirations in space, conf., Washington USA, 1976 Oct. 78−4078
marine minerals, anal. and exploration by Mobile Initial Condition Indicator 79−5687
Maui offshore gas field, in New Zealand 80−26103
methane outgassing from Earth interior, pot. fuel source 78−92809
metrological servicing in USSR ministry of land reclamation and water management 79−96496
mineral exploration, effect of tropical weathering on elec. and EM meas. 79−88246
mineral resources of Armenian territory foundation, evidence from struct. and age data *(Russian)* 79−74874
mineral resources of USSR, rel. to tectonics *(Russian)* 78−40536
multiband photography for geomorphology, soils and land use study, feasibility 78−12025
multispectral photography from space *(Russian)* 78−16197
nonrenewable resources depletion rate, for teaching 79−62966
ocean, artificial upwelling induced by ocean currents theory and expt. 78−81217
ocean energy potential 80−66956
offshore resources exploration, remote sensing, appls. to oceanography and sea ice 80−77176
oil, exploration and exploitation instrumentation 79−34982
oil, potential of continental margin sediments off N.Brazil 77−21697
oil and gas deposits, N.Michigan detect. by seismic refl. method 77−2265
oil and gas deposits in low amplitude struct., parameters from gravity test data *(Russian)* 79−44271
oil and gas formations, prediction prior to drilling *(Russian)* 79−39970
oil and gas in non-anticlinal traps, reflected wave seismic survey possibilities *(Russian)* 78−12013
oil and gas-bearing structures, seismic exploration *(Russian)* 77−45195
oil well productivity rel. to seismic reflection amplitude 78−69295
ore bodies in Itapicuru greenstone belt, Bahia, Brazil 80−81879
ore reserve estimation, in three-dimensional deposite using FORTRAN IV Function Segment 77−87085
orebodies location in mineworkings, muon hodoscope appl. 79−84491
pegmatite ores in Tanco mine area, SE.Manitoba, in Canada, exploration methods 79−48577
petroleum deposits, screening effect on seismic exploration *(Russian)* 77−44939
petroleum deposits and gas wells, prospecting in W.Caspian Sea area *(Russian)* 77−64281
photointerpretation and photogrammetry teaching in natural resources field 77−74175
planetary resource management, conf. (Toulouse, France, 6-11 March 1978) 79−35015
regional resource appraisal, statistical methods 78−28326
remote sensing, factor analysis approach to spectral interval selection 79−88503
remote sensing, management problems, training 77−82011
remote sensing, study of Earth by astronauts *(Russian)* 78−40795
remote sensing, use of photographic imagery and pattern classification techniques 77−64454
remote sensing by artificial satellites *(Japanese)* 78−16211
remote sensing by Skylab microwave radiometer 78−16273
remote sensing of global phenomena by automatic satellites 77−64457
remote sensing using satellite and aircraft scanner data for Finland 79−100988
remotely sensed data acquisition and processing, developing countries appl. 79−34963
resource management, conf., Alamogordo, NM, USA, 1978 78−69541
satellite data on Earth resources *(French)* 79−53526
satellite monitoring techniques and equipment Conf. on Earth resources electronics Rome, Italy (Mar.77) *(Italian)* 77−82056
satellite on-board processing for Earth resources data 78−61626
satellite remote sensing, issues 78−12022
satellite remote sensing for Earth resources surveying 77−25788
science and world problems 79−80413
sea use plan concepts and criteria 80−46203
Skylab remote sensing data, inflight performance evaluation by ground-based meas. 77−64455
space technology and scientific satellites, conf., Rome, Italy (Mar. 1977) 77−82107
strategy for integration of groundwater resources in regional planning 80−41472
sulphide ore deposits, deep-sea discovery on E. Pacific Rise 79−34799
SE Sumatra coastal environment, remote sensing appls. 79−53556
surface water in India, overall assessment of resources by water balance method 77−56662
survey data, ground receiving systems, facsimile features 77−82012
synthetic aperture radar imaging in geosynchronous orbit 78−65442
teledetection applications *(French)* 79−96769
S.E.Texas counties, Landsat forest and range inventory by administrative boundaries 77−56748
Turkey, karst water resource development 80−61821
undersea, world-wide survey 80−35622
uraniferous materials, disequilib. variability and ^{222}Rn emanation factor 79−62498
USA developments, by means of technological innovations, federal regulations influence 80−16763
visible range spectrometric investigation from Salyut 4, radiation characteristics of environment 80−51638
Volga River, spring floods long-range forecasts, study of effectiveness 78−3837
water, annual flow regulation, appl. of probability and statistical methods *(Chinese)* 79−96778
water, balance in drought years at Masulipatam (Andhra Pradesh) 77−56663
water, balance investigations during drought in England and Wales, 1975-6 period 78−88865
water, discrete representation of storage for stochastic reservoir optimisation 77−64354
water, optimisation model for regional quality model 77−66945
water, pollution due to drought in England and Wales, 1975-6 period 78−88868
water, potential evaporation from soil, water and crop surfaces, eqn. for remote sensing 77−64334
water, preliminary estimation of reservoir storage for Australian streams 77−86947
water, relations between geophysical and hydraulic parameters of alluvial aquifers *(Italian)* 77−53079
water exploration, geophysical methods, International School 1st course proc. (Erice, Italy, 1975 April 15-26) 77−9526
water in Andhra Pradesh, aridity and its fluctuations 77−56661
water power, potential, regional analysis method 79−83557
water resource management, computer-aided solution of linear equation systems, unsymmetric, sparse 77−80210
water resource research using Pennsylvania State Univ. reactor 79−12159
water resource system, time variable, recursive estimation techniques appls. 79−5538
water resources planning, use of multiattribute utility theory 78−11932
water resources policy, scientific and technological considerations 79−8642
water-bearing rock formations, evaluation via DC resistivity sounding method 78−40474
water-resource development project design, optimal apportionment scheme appl. *(French)* 80−77019
wind, energy pattern factor meas., analogue technique appl. 77−81964
Au deposit location in Canton Bousquet, Quebec *(French)* 77−53051
Ge demand evaluation and supply comparison 80−33106
Li concentrations in McDermitt Caldera, in Nevada and Oregon, geological survey 79−48478
Li deposits and potential, Quebec and Atlantic Provinces, in Canada, report 79−48481
Li, estimates of economically recoverable resources for nuclear fusion appls. 80−52788
Li, needs and resources, conf., Corning, USA (Oct. 1977) 79−48473
Li, occurrence in flint clay and related rock types in United States, preliminary survey 79−48475
Li ores in Horse Spring Formation Miocene rocks, Clark County, Nevada, report 79−48474
Li, ores in United Kingdom, brief assessment 79−48476
Li ores resource evaluation, United States Geological Survey role 79−48477
Li pegmatite ores in Western Superior Province, in Canadian Shield, distribution and petrogenesis 79−48480
Li resources, energy reserves of D-T fusion, recovery costs 78−46162
Li resources, Yellowknife area, in NW.Canada, report 79−48482
Li resources and potentials, NW.Ontario, Manitoba, Saskatchewan, in Canada, estimation 79−48483
Li rich brines in SW.Bolivia, chemical composition and distribution 79−48479
Pb-Zn minerals, carbonate-hosted, in NE British Columbia, Robb Lake deposit 79−62494
U borehole logging by prompt fission neutron technique, log interpretation 79−53567
U, Canadian deposits, reconnaissance programme *(French)* 78−88827
U exploration, prompt fission neutron logging technique, computer modelling 79−53566
U, exploration, radiation transport anal. for borehole logging probes 79−53565
U, exploration and assessment technology survey 79−53564
U, exploration and prospecting methods 80−85768
U, geophysical prospecting, ^{222}Rn mapping using mat to avoid hole drilling 80−82087
U in natural waters, meas. by laser beam 78−85705
U, National Uranium Resource Evaluation (NURE) aerial radiometric survey data interpretation via principal components anal. 80−101438
U ore detection, using trace detection sensitive to ^{222}Rn α-particles *(Hungarian)* 78−77339
U, world resources, effect on development of nuclear power 80−55826

natural rubber *see rubber*

natural sciences
see also astronomy and astrophysics; biology; biophysics; chemistry; geology; geophysics; mathematics; physics
education, role in modern society 79−80392
mathematical models, role *(Afrikaans)* 80−8771
popularisation of science problems 80−21
research aspects in society 79−80412
school curriculum, review *(Hungarian)* 79−71167
scientific journals significance, Science Citations Index anal. 77−9831
world problems solution possibilities, due to natural resources shortage 79−80413

natural sciences applications of computing *see natural sciences computing*

natural sciences computing
see also astronomy computing; astrophysics computing; biology computing; chemistry computing; geophysics computing; medical computing; physics computing
air pollution meas. using laser radar data processing system 79−57559
automatic control of photographic analysis precision using minicomputer and meas. engine 77−41710
automatic dimensional analysis using symbolic maths. 77−57173
AUTOPREP, met. office data prep. and telecommunication terminal 79−100923
curve fitting flexible all purpose program 77−2531
differential eqn. soln. methods 78−81820
elliptic boundary value problem, second order, hybrid finite element methods, Dirichlet problem 78−73835
environmental systems control, transient finite element and linear programming method 79−57497
gravitational radiation, anal. of Maryland-Argonne detector 1973-74 data 77−22476
hyperbolic eqns. soln. by method of lines 77−5648
infinite range oscillatory integrals evaluation 77−5652
inner multiplicity of unitary groups, determ. using Gelfand patterns 78−89322
laboratory computer systems, minicomputers, microprocessors, uses 77−79072

natural sciences computing continued
Lie algebras, combinatorial algorithm for generating positive roots 77−2530
mathematics, percentiles of standardised binormal distribution calc., FORTRAN subroutine 78−34
molecular modelling, design of computing systems 77−18814
multidimensional integrals, numerical calc. 78−89323
particulate materials, quantitative three-dimens. characters. using polished sections and computer-controlled SEM system 77−2714
polynomials, series conversion by five term recurrence formula 77−13594
power plant site zone evaluation using computer-aided methods 80−861
spherical Bessel functions j_n and y_n of integer order and real argument 78−89321
turbulent air/water wavy interfaces, statistical anal. 77−924
US atomisation of solns., aerosol dispersion meas., computer appl. *(Russian)* 77−1964
viscosity of fluids at evaluated pressures 80−2191

naval engineering
see also marine systems
computer-aided ship structural design for diploma and undergraduate courses 79−35494
cylindrical shell modal velocities, numerical fluid loading coeffs. 77−5669
deep submergence vehicle development and reliability 77−5376
oceanographic integrated research ship, with data acquisition and processing systems 79−34969
submarine periscope optical test equipment 80−78943
US Naval Observatory clock time scale 78−89460
US Navy fibre-optic technology and systems 77−39063

Navier-Stokes equations
adsorbed polymer layers, hydrodynamic thickness, Navier-Stokes eqn. calcs. 77−65726
advection-diffusion equation, weighted-mean schemes for finite-difference approx. 78−34103
aerodynamically generated sound, extension of Lighthill's theory to non-adiabatic cases, Mach number expansion of Navier-Stokes equations 78−83372
aerodynamically generated sound, extension to relaxing media 78−90567
aerodynamically generated sound, Mach number expansion of Navier-Stokes eqns. 77−62245
aerodynamics, high Reynolds number, global approach and coupling approach 80−48742
aerofoil, oscillating, viscous incompressible flow, finite element anal. 80−38427
aerofoil in unsteady airstream, two-dimens. viscous flow, numerical predictions 78−75166
aerosols, particle-droplet inertial collisions 79−47989
airflow above waves, numerical simulation *(Russian)* 80−4076
airfoils near stall, numerical soln. in optimised boundary fitted curvilinear coordinates 79−77156
anemometry, hot-wire, in very low velocity flow, calibration of probes 80−75008
anisotropic spatially inhomogeneous viscosity fluid, frictional force and torque 79−37367
approximating methods, a rational classification 79−1142
asymptotic results for model eqn. for low Reynolds no. flow 79−14371
autooscillations, azimuthal wave type, rot. Couette flow stability loss 77−75882
axisymmetric, general impossibility of controllable motions 77−51021
axisymmetric cavity flow, viscous, numerical calcs. 79−98737
axisymmetric jet, interaction with plane obstacle, Navier-Stokes eqn. solns. *(Russian)* 80−1659
axisymmetric waves on the surface of viscous fluids 80−96266
axisymmetrical slow motion in half-space, linearised eqns. soln. 78−12572
backward in time, global nonexistence of solns. to Ladyzhenskaya's variants 77−51023
bifurcating periodic solutions at LF 78−16657
bifurcation and stability of nT-periodic solns. branching from T-periodic solns. at resonance 78−69987
bistable wall attachment fluid amplifier, flow field anal. *(Japanese)* 80−53743
blast loading on three-dimensional structures, transient, computational simulation 77−68624
block iterative finite element algorithm 78−20971
blood flow, finite element soln. 80−94269
blood flow in heart, numerical anal. 78−15854
bluff body, laminar incompressible flow, separation, reattachment, eddies, drag 79−59964
blunt body, boundary and wake, supersonic viscous gas flow, numerical soln. 80−38441
blunt body in supersonic flow, Navier-Stokes eqns. numerical computation 80−10263
blunt body problem in nonuniform flow fields 78−5748
Boltzmann eqn., fluid dynamical approx. at level of Navier-Stokes eqn. 80−22308
boundary conditions 79−9124
boundary layer, numerical soln. of linearised Navier-Stokes eqns., effect of cell Reynolds number 80−106780
boundary layer flow, unsteady past wavelike bulge on flat plate, num. soln. of Navier-Stokes eqns. 77−58644
boundary layer growth on spinning sphere, screw motion 77−31315
boundary layer problems, finite difference methods, nonuniform grid generation 80−83780
boundary layer stability, nonlinear effects 78−1636
boundary layers, Navier-Stokes eqns., finite difference model 77−14991
boundary problem, soln. via successive approximations 80−36865
boundary-value problems, a priori estimates *(Russian)* 78−28957
bounded domain, global weak solution to time dependent Navier-Stokes eqns. 80−77621
capillary counter-current system hydrodynamic effects 77−40695
cavity flow motion and heat transfer, fixed and floating boundaries *(Russian)* 77−35144
cavity flows, two and three dimens., multistep technique with implicit difference schemes 79−37398
cavity in viscous liquid, action of press. pulse 79−68769
cell hydrodynamics, information-conserving theory 78−55623
central difference algorithm for high mesh Reynolds nos. 78−46920

Navier-Stokes equations continued
channel, fluid flow behind plate in channel, jet and velocity pulsations *(Russian)* 80−74979
channel flow, semidirect method for two-dimens. incompressible flow 79−7413
channel flows, slowly varying in 3-D 79−92948
chemical laser flows 77−42528
circular cylinder in laminar incompressible viscous flow, finite element anal. 77−84216
circularly polarised inertial wave vectors in rot. fluid 77−3829
Coanda effects, simulation of discontinuous diffusing flow 78−9622
compressible, mixed explicit-implicit splitting method 77−58715
compressible, num. soln. at high Reynolds no., blunt body problems applic. 77−55019
compressible, num. soln. method for hyperbolic systems of eqns. 77−58716
compressible, stability of solns. 77−75874
compressible flow, Navier-Stokes eqns. similarity solns. for large Prandtl number 77−3801
compressible flow, Navier-Stokes solutions using Stetter's method 79−32551
compressible flow in rot. cylinder, linearsed anal., appl. to gas centrifuges 78−71345
compressible gas, heat exchange in free convection condition *(Russian)* 80−28502
compressible Newtonian fluid, laminar flow between rotating discs 77−31320
compressible turbulent flow, kinetic theory, comparison with classical theory 77−3814
concentrical shell system coupled by viscous fluid, dynamics 77−84176
cones at incidence, supersonic viscous flow 80−38439
conference, computation fluid dynamics, Rhode-Saint-Genese, Belgium (March 1977) 77−80134
confined flow, numerical simulation, anal. of higher order methods 80−19316
convection, three-dimensional, natural, in box 78−5743
convection, turbulent, numerical models based on unsteady Navier-Stokes eqns. 80−38415
convection, unsteady combined forced and natural, from circular and elliptic cylinders *(Japanese)* 79−32510
convective diffusion problems, finite element solns., Navier-Stokes eqns. 80−1583
corner, three-dimens., Navier-Stokes eqn. soln., numerical code 78−30314
cosmic turbulence, Navier-Stokes eqns. appl. 77−5604
Couette flow, striated boundary effect on viscous drag 78−59367
creeping flow about sphere, general soln. of linear Navier-Stokes eqn. 78−71307
crystal growth from melt, reformulation of Burton, Prim and Slichter model of segregation 79−4909
crystalline film growth reactor, gasdynamic problems 79−83130
curvature and displacement effects on separation of accelerated flow past cylinder 80−10272
curved jets, deflection due to impact of other jets *(German)* 78−26180
curved semicircular sectors, fully developed viscous flow and heat transfer, Navier-Stokes soln. 80−14814
cylinder, in viscous fluid impulsive translation, numerical computation method 78−5727
cylinder array, 2-dimens. viscous laminar flow field, finite difference method 78−42585
cylinder in incompressible flow, finite element anal., wake development and stability 79−14364
Czochralski bulk flow in the growth of garnet crystals 80−38979
Czochralski crystal-pulling process, digital simulation of flow patterns 78−15304
Darcy's law, theor. deriv. 77−68683
derivation from Euler equation with Brownian motion 79−41650
derivation without stress tensor linearity assumption 77−13542
detached flows past a cylinder with a flat end, subsonic and transonic vels. 80−92187
difference schemes for aerodynamics 77−35160
discontinuities, appl. of distributions *(French)* 80−6022
discrete velocity gas, kinetic theory, boundary conditions, comparison 78−30254
discretisation, splitting of linear operators, iterative methods applied to stationary Navier-Stokes eqn. 80−69755
discs, eccentric, rotating at different speeds, flow between discs, inertia effects 80−92104
disparate-mass gases description, generalised Navier-Stokes eqns. 77−51086
dissipative open system, dynamical transitions 79−64629
domains with non-compact boundaries, soln. of boundary and initial-value problems *(Russian)* 78−30255
driven cavitation flow, Navier-Stokes eqn. soln. numerical stability 80−92147
driven polar cross section cavity, laminar incompressible recirc. flow 78−46988
drop, centrally-located with thin jet in infinite viscous fluid 79−32614
drop, evaporation in vap., slow viscous flow, heat flow asymmetry effect 77−75966
drop, oscillating, immersed in 2nd fluid, induced flow field streaming 78−59454
drop motion in stream of viscous incompressible fluid 77−11252
duct, curved, laminar incompressible viscous flow 78−46932
duct, plane, with sudden expansion, aerodynamics 79−94722
duct flow, laminar, finite element methods compared to Doppler meas. 79−1253
duct of arbitrary cross section, parabolic procedure for three-dimens. compressible viscous flow prediction 79−94716
ducts, axisymmetric, internal viscous flows at moderate to high Reynolds numbers 80−106844
ducts with porous walls, Navier-Stokes exact eqns. 78−67266
dusty gases, fully dispersed wave struct., Navier-Stokes eqns. 80−69875
dynamic flow characteristic determ. of electro-hydraulic servo-valve using laser velocimeter 79−32719
eddies in viscous liquid 79−14412
eddying flow, axisymm., Navier-Stokes eqns. in vectorial form 79−68724
efficiency, finite difference methods for vorticity-stream function form 77−58632
elasticity, iterative solns., depend. on Poisson's ratio 79−1107

Navier-Stokes equations continued
electroosmotic permeability coefficient in charged membrane model 80−108749
electroslag welding, electromechanical and thermal flow phenomena 79−11758
elliptic cylinder about axis perpendicular to flow, autorotation 80−103033
elliptic porous slider, fluid dynamics 79−18952
emulsion, dilute, straining motion, effect of inertia on dynamic viscosity 80−87797
emulsion films, thinning vel., surfactant in continuous and disperse phases 77−84305
equilibrium correlation functions, turbulent flow kinetic theory *(German)* 78−90886
Eulerian and Lagrangian computer codes, pressure iteration, multigrid method 80−53738
exit region central source flow, between finite close parallel rot. discs 77−42849
explicit numerical soln., effects of initial boundary conditions, vorticity 79−81839
external disturbance transformation into boundary layer waves 80−28523
Falkner-Skan boundary layer problem, asymptotic solns. 79−18860
falling horizontal cylinder, low Reynolds number, horizontal plane boundary effect 80−87757
film flow, meniscus shape theory, Navier Stokes eqn. 78−38270
finite difference approx. with second-order accuracy 80−87756
finite difference methods, recent advances 77−80136
finite difference scheme for numerical soln. 78−71306
finite difference schemes, stability anal. 78−89346
finite difference soln., vector and scalar pot. method 77−68558
finite difference soln. errors 80−17807
finite element anal. of nonlinear partial differential eqns., appl. to estuarine flow *(Japanese)* 78−8233
finite element analysis, for steady viscous flow 79−1149
finite element analysis method, 2D unsteady viscous flow 77−89088
finite element and finite difference methods, efficiency comparison 79−1148
finite element approximation, Stokes problem 80−27138
finite element MAC scheme for 2-D incompressible Navier-Stokes flow 80−74824
finite element method smoothing techniques 78−90823
finite element methods for viscous and inviscid incompressible flow 80−17806
finite element soln. for fluid with thermal and buoyancy effects 79−9125
finite element solns., primitive variables versus stream function 79−32443
finite element solution, modal analysis 77−54958
finite elements for numerical simulation, error estimates, Stokes problem 79−1151
finite-difference methods 79−1145
finite-element soln. procedures, for incompressible eqns., using equal order variable interpolation 80−10226
flow between rot. discs, multiple solns. 78−79324
flow between rot. discs, three kinds of solns. 78−79323
flow between rotating and stationary porous discs 78−90914
flow distribution on continuously moving flat plate, Navier-Stokes solns. *(German)* 79−86417
flow field, multiply connected, curvilinear coords. and macro-elements 80−19318
flow fields in plate and cone viscometers with small gap angles 80−19516
flow from noncoaxial rotations of porous disc and fluid at infinity 77−68600
flow in curved tube, finite difference anal. method 80−106846
flow phenomena within vortex sink rate sensor, numerical study 78−63436
flow round circular cylinder at low Reynolds number *(German)* 78−94641
flow with suspended particles, mathematical modelling, numerical simulation 77−72348
fluid, traditional eqns., relation to quantum theory *(French)* 79−9181
fluid bodies, dynamics *(Russian)* 78−12093
fluid dynamics expts. and problems *(French)* 78−9645
fluid flow prlblems, incompressible, free surfaces 80−106774
fluid mechanics, mathematical introduction, book 80−66
fluid motion between two parallel rot. plates, Navier-Stokes eqn. soln. 79−68713
fluid-solid interface, sliding friction coeff., calc. method 77−14987
Fokker-Planck description 78−94632
Fokker-Planck equation, multiple time scale method 79−44861
forward facing step, neutrally stable atmospheric flow, shear layer, separation, vortices 80−48685
free atmospheric convection, rigorous formulation using matched asymptotic expansions *(French)* 77−65740
free-shear plane stationary computer simulated turbulence struct., discretized Navier-Stokes eqns. 78−26111
fundamental problems in general fluid dynamics and hydromag. dynamo theory, book contrib. 77−84213
fundamental triad-interaction system in 3D homogeneous turbulence 79−27623
furrowed channels with pulsatile flow, Navier-Stokes soln. flow patterns, separation 80−33672
gas, dilute, kinetic-hydrodynamic transition obs., Brillouin scatt. 77−7508
gas centrifuge, fluid flow anal., numerical integration of Navier-Stokes eqns. 77−75924
gas mixture, multivel. multitemp., gasdynamic eqns. 79−77052
gas motion in channel with cryogenic walls 78−59487
gas suspension, closed dynamic eqn. system using kinetic theory 80−6190
gas with rot. degrees of freedom macroscopic description of motion 79−86465
gas with rotational degrees of freedom, macroscopic description of motion *(Russian)* 78−46999
gas-solid flow in cylcone, turbulent swirl velocity, particle sizes and concentrations 80−69902
gases with molecular viscosity, flow calc. in large particles method *(Russian)* 80−74826
general finite difference formulation, appl. to vorticity eqns. 77−39269
Navier-Stokes equations continued
generalised representation, of physical situation, appl. to hydrodynamics *(Russian)* 80−69760
grid points condensation in process of solving and using high order schemes in numerical integration of viscous gas flows *(Russian)* 78−59363
group analysis in presence of rot. symmetry and exact solns. 80−8799
Hausdorff measure and eqn. solns. 77−75870
heart valves, blood flow, vortex-grid method 80−41105
heat transfer, cylindrical shrouded cavities, with rot. and coolant through flow 77−72294
heavy viscous liquid forming thin shell on planet in circular orbit *(Russian)* 78−65782
Hermitian finite-difference method 79−1144
Hiemenz flow, pulsatile, struct., and temporal variation of wall shear stress near stagnation point 77−62303
high Reynolds no. flows, finite element method, book contrib. 79−32442
high Reynolds number, vicinity of wall and of initial moment *(French)* 80−74823
highly viscous chemical laser nozzles flow, two dimens. Navier Stokes eqns., implicit marching method 78−63506
holonomic formulation of boundary layer eqns., use of tensors 79−1153
homogeneous turbulence decay from given state at higher Reynolds number 80−1534
horizontal jet penetration in stratified fluid, unsteady laminar flow 77−7430
horizontal parallel plates, unsteady laminar flow of viscous fluid, Navier-Stokes eqn. solns. 80−1683
hypersonic flow, nonequilibrium gas mixtures past blunt bodies, Navier-Stokes equation *(Russian)* 79−18909
hypersonic flow over blunt body, viscous shock-layer eqns. 79−60002
hypersonic flow over cone, large attack angle 79−1210
hypersonic turbulent compression corner flow, numerical simulation 77−62276
hypersonic viscous flows over sphere cones at high angles of attack 79−98746
implicit-explicit solution method 78−83354
incompletely parabolic problems in fluid dynamics 79−44749
incompressible, soln. using primitive variables 80−6017
incompressible flow, eqn. soln. by integro-differential method 77−72266
incompressible flow, three-dimens. problems 77−84211
incompressible flow calcs. by splitting method *(Russian)* 80−74827
incompressible flow cct. large Reynolds number, numerical simulation *(French)* 79−10550
incompressible fluid, fully developed turbulence generated by random stirring, variational approach 79−3991
incompressible Navier-Stokes eqns., soln. by efficient numerical method 78−9619
incompressible three-dimensional internal flows, finite difference soln. of Navier-Stokes eqns. 77−58795
incompressible viscous flow, finite element-anal. by penalty function formulation 79−41651
incompressible viscous flow, restricted rot. invariance 80−92103
incompressible viscous fluid, (2-ε) dimens., long-wavelength non-equilibrium props. 77−61008
inflows, density currents, and fronts 79−10542
inhomogeneous liquid, diffusion model, rel. to correctness of boundary value problems 78−30774
initial value problem approx. soln., incompressible boundary-free flow 78−57788
initial value problem for boundary-free incompressible flow, bounds on solns. 77−11163
instability, post-, in class of smooth functions, mathematical model 80−69649
integration by least squares approx., book contrib. 79−32444
Jeffery-Hamel flow, symmetrical velocity profiles 79−64623
jet, heavy, flowing into nonmixing medium 78−51212
jet, viscous laminar flow, tangential twist eddy flow form., numerical soln. 77−89179
jet interaction in deflecting stream of incompressible liq. 79−81932
jets, laminar, vertical, round, weak buoyancy effects due to temp. differences *(German)* 80−64595
jets, opposing, of viscous incompressible liq., collision, numerical calc. 77−7432
Karman vortex street behind circular cylinder, series truncation method, Navier-Stokes eqns. solns. 78−79325
kinetic theory of dense fluids, generalised Chapman-Enskog soln. 79−54033
laminar duct entrance flow, 2nd order numerical method 78−38407
laminar flow in a channel variable cross-section with movable and porous walls *(Polish)* 79−64768
laminar flow in duct of strong curvature 78−13988
laminar flow in pipes, numerical calc. 78−79376
laminar flow in rotating porous annuli 77−68687
laminar flow with injection in straight duct, vel. distrib. and press. drop 77−11263
laminar forced convection between concentric spheres, num. soln. 77−42831
laminar hypersonic wake of a lifting body, Navier-Stokes solns. *(Russian)* 78−87359
laminar incompressible flow in straight polar ducts 78−22424
laminar liquid film moving along sloping surface, hydrodynamics 77−7365
laminar non-Newtonian flow in porous annulus 77−72333
laminar to turbulent boundary layer transitions, numerical simulation 78−38286
laminar vapor flow calculations in a flat-plate heat pipe 80−23869
laminar viscous incompressible liquid flow in plane channel 80−23985
light induced kinetic effects in gases *(Russian)* 80−92244
limit states for Navier-Stokes eqns. in bounded domain 78−83355
linear, approx. soln. error estimates 78−38268
liquid falling film, surfactant effects 77−89093
liquid leveling, numerical soln. 77−14974
liquid spreading on solid surface, physical regularities *(Russian)* 77−62712
liquid-phase motion in filling of cylindrical channel 77−58791
low Reynolds-number flow in the vicinity of axisymmetric constrictions 80−6147
low viscosity flows, hybrid vortex-ADI soln. of N-S equations 79−68718
magnetohydrodynamic flow between rotating and stationary porous coaxial discs 80−43799

Navier-Stokes equations continued
and mass balanace eqns., conductive additional force density term 78−75411
Maxwellian molecule gas, heat transfer between parallel plates, Navier-Stokes eqns. 80−87839
MHD axisymmetric flow due to current spreading *(Russian)* 77−65810
micro-polar fluid, on flat surface, effect of couple stresses on unsteady drainage 77−14985
micropolar fluid eqns., soln. exist. and uniqueness 77−19583
miscible, viscous, incompressible fluids, oscillatory pressure gradients, anal. 78−38405
mixed finite element method for the Navier-Stokes equations 79−50693
modelling of viscous flow, over mobile base, Navier-Stokes eqns. 78−46921
modified dissipativity for a non-linear evolution equation arising in turbulence 79−94594
molecule, moving in compressible viscous fluid, hydrodynamic drag 79−27732
moving surface, free liquid layer, laminar and turbulent flow, Navier-Stokes anal. 79−94589
multidimensional compressible Navier-Stokes eqn., generalised implicit method 77−68557
multiply connected flow fields, numerically mapped macro-elements 79−1252
natural convection, Navier-Stokes eqn. soln. numerical stability 80−92147
natural convection heat transfer from horizontal ice cylinder, anal. and obs. 77−27521
natural convection in horizontal cylinders, asymmetric boundary conditions, numerical anal. 77−39282
natural laminar convection about isothermal cylinder, Navier-Stokes eqn. soln. 80−92143
Navier-Stokes eqns., bluff body aerodynamics, numerical simulation methods 78−75115
non-cylindrical domains, subdifferential operator theory approach 79−46282
non-Newtonian flow, between two rotating cylinders, nonconcentric 79−68759
noncirculating regions in axial zone of vortex cell 79−14411
nonequilibrium thermally-induced flow fluctuations 80−14661
nonlinear fluid dynamic problems, least squares and finite element method soln. 79−49054
nonreflecting outflow boundary condition for subsonic Navier-Stokes calculations 80−74828
nonselfadjoint operator eigenvalues approx. 77−54952
nonsimilar axisymmetric stagnation flow on a moving cylinder 78−79297
nonstationary, soln., numerical stability of ADI scheme *(French)* 78−87325
nonstationary axial-symmetric suspension flow in viscous liquid 77−39326
nonstationary boundary layer with self-induced press. 78−34164
nonstationary rotating disc flow, Navier-Stokes eqns., analytic and num. results 79−41694
nonstationary Stokes flow in exterior domain, square summability and uniqueness 79−72870
nonstationary suspension flow in viscous liquid 77−39325
nonstationary viscous flow of thermally conductive gas around semi-infinite plate, numerical anal. 80−6104
nozzle, vibr. nonequilib. flow, computational methods comparison 79−60073
numerical downstream continuation, sufficiency 79−77053
numerical method for 2D and 3D viscous flows 77−89082
numerical methods, conf., Swansea, Wales, July 1978 79−1155
numerical solution, fourth+second order method, viscous flow around cylinder *(French)* 77−75869
numerical solution by multi-point finite differences 77−89083
numerical solution methods *(Chinese)* 79−32433
numerical solution using finite difference procedure, unsteady leading edge separation bubble calc. 77−72317
numerical solutions, accuracy of finite difference schemes 79−92946
object in flow, H^{-1} least squares method 79−1143
operator version, convection propagation and convected curl operators, Lie algebra 80−46812
oscillatory free stream flow past rotating disk, Navier-Stokes solns. 79−14416
parallel flow stability, numerical calc. 79−32460
particle oscillation inducing flowfield, in container 79−50770
penalty function solution of steady-state Navier-Stokes equations 80−14648
periodic capillary tube, two phase fluid flow and hysteresis 80−107615
periodic capillary tube, two phase fluid flow and hysteresis 80−107616
peristaltic flow, nonlinear, calc. and expt. 78−9718
peristaltic flow, nonlinear, implicit finite difference method using orthogonal curvilinear coords. 77−39346
photoabsorption convection in horizontal tube, unsteady-state convection, num. investig. 80−33594
pipe, circular, time-periodic flow stability 77−84225
pipe, smooth, entrance regions, laminar flow 79−50696
pipe flow, curved pipes, fully developed oscillatory flow 80−83846
pipe flow, developing, arbitrary curvature 78−79378
pipe flow, low Reynolds number, in vicinity of three dimensional obstacles 80−74981
planar viscous incompressible flow theory counterexample 77−11162
plane Couette flow, transition to turbulence and finite amplitude disturbances 80−33558
plane entry flows and energy estimates for Navier-Stokes eqns. 79−37278
plane incompressible eqns., S-D truncation 79−25863
plane Poiseuille flow, instability caused by nonlinear, nonperiodic and three-dimensional disturbance 78−38291
plane Poiseuille flow, nonlinearity and non-periodicity of two-dimensional disturbance 77−62231
plane Poiseuille flow, transition to turbulence and finite amplitude disturbances 80−33558
plate suddenly accelerated in non-Newtonian fluid 78−90935
Poiseuille flow, at large Reynolds numbers, Navier-Stokes eqn. soln. *(Russian)* 78−59364
Poiseuille flow, plane, horiz., rot., stability, effect of Coriolis force 78−67203
Poiseuille flows, numerical integration, small disturbances as functions of time *(German)* 78−94633

Navier-Stokes equations continued
polymer solns. and suspensions, hydrodynamic interactions *(Russian)* 79−32652
polymer solution, compressible flow about spherical polymer mol. 79−10595
polymer solutions, transport properties, conc. effects 80−64875
porous media, permeability calc. from Navier-Stokes eqns. 77−27593
pressure, capacity, and the Navier-Stokes equations 79−18858
pressure-velocity formulation, incompressible viscous flow 79−1147
pseudo-spectral soln. method for incompressible flow *(French)* 80−52032
pulsatile flow in a tube, effects of suction and wall injection 78−38403
pulsatile flow in furrowed channel, flow pattern calc. 79−23367
PVC rigid, flow and therm. stability 79−64618
random forced flow, ensemble mechanics 77−7363
randomly stirred fluid, large-distance and long-time vel. correls. calcs. 77−89361
randomly-stirred fluid, vel. correlations, variational principle for path-integral functionals 78−81846
rarefied gas, acoustic dispersion, hydrodynamic soln. 77−68630
rarefied gas flow in rectangular groove facing moving wall, eqns. derivation and soln. 77−42874
recirculating flow, numerical methods in Navier-Stokes eqns. 79−1202
rectangular cavity in viscous gas flow, numerical anal. of acoustic resonance 79−64378
relativistic conductive additional terms 77−45746
rocks, hot, dry, hydraulically fractured linearly expanding cracks, eqns. *(Japanese)* 79−34809
rotating concentric spheres, retarding torque in viscous fluid 77−15042
rotating cylinder, source-sink flows, numerical anal. 79−4018
rotating disc in viscous fluid, deceleration 80−28515
rotating flow, finite element anal., upwind scheme 79−1201
rotating flow above rotating disc, non-unique solns. 77−47020
rotating fluid dynamics, review *(French)* 78−30300
rotating sphere, higher order heat transfer 79−4003
rotating square cavity, laminar flow, flow problems with body forces soln. 79−68715
rotational effects avoidance in turbulent flow, numerical solns. *(German)* 80−59057
salt dome evolution, fluid dynamics model 78−77237
second bifurcation of stationary soln. *(French)* 77−68554
second-order boundary-layer effects for large injection or suction, book contrib. 80−1531
secondary flow in plane channel *(Russian)* 78−87394
self-similar soln., appl. to channel flow *(Russian)* 77−42797
separated flows around circular cylinder, numerical solns. 77−3815
separated high Reynolds number flow past a corner, numerical solns. 79−81855
separating flow, fluid-surface interface, static contact line, slip at wall and shape of free surface 80−53737
shock propagation, multidimensional fluid dynamic calcs., artificial viscosity use, Navier-Stokes viscosity 80−92181
shock separated boundary layer, suction effects, compressible Navier-Stokes eqn. solns. 80−24050
shock wave interaction in turbulent boundary layer 79−41711
shock wave propagation, steady state 77−68615
shock wave turbulent boundary layer interaction, numerical simulation, Navier-Stokes eqns. soln. 77−31332
shock waves evolution rel. to dissipative phenomena 77−42857
shock-wave front structure, in liq. 79−64702
simulation, implicit finite-difference procedure, for arbitrary 2-dimens. boundary flow 78−94628
singularities in the three-dimensional Navier-Stokes equations with cylindrical co-ords. 79−90213
slag and metal flow in ESR process, mathematic model 77−73249
slide journal bearing, stationary oil flow, estimation of soln. of N-S and energy eqns. 79−55353
slip flow, developing, vel. distrib. and press. drop, Navier-Stokes analysis 77−55039
smoothing techniques for finite element anal. solns. 80−17804
solid body with cavity containing viscous liq., dynamics 79−18862
solid particles in viscous incompressible fluid, action of gravity, sedimentation *(French)* 77−75964
solution in a time dependent domain 79−18859
solvent, ion migration and frequency-dependent dielectric loss 79−19832
space dimension 4, solns. 78−69988
spatial decay estimate 79−75351
spatial decay estimates, appl. to entry flow 79−14370
sphere motion in fluid-fluid interface, Lorentz soln. method 79−94580
sphere rotating in viscous fluid, induced flow 77−15036
spherical gas bubble in unsteady viscous flow, unsteady boundary layer 79−55357
spherical gas bubble in viscous fluid, initial motion 77−65780
square cavity, recirculating flow, finite element results 79−64764
stability analysis of explicit finite difference schemes for the Navier-Stokes equations 79−46281
stability problems with time-depend. boundary conditions, numerical simulation methods, review 80−19411
stability technique improvement using finite element method 77−72263
stably stratified medium, plane free convection from local heat source 80−96253
stagnation point flow impinging obliquely on wall 79−27617
standing vertex-pair behind flat plate, normal to uniform viscous fluid flow 79−14406
stationary, particular one parameter solns. 79−46283
stationary 2-D eqns. in parabolic form, optimal control *(French)* 77−72321
stationary and periodic solutions, genericity w.r.t. boundary conditions *(French)* 78−28956
stationary evolution approx., numerical method for 2-D viscous flow calc. *(Ukrainian)* 78−65778
stationary Stokes eqns. approx. using penalty-extrapolation method 77−14976
stationary turbulence, path integral functional description, variation principle 79−77083
steady, numerical soln. by highly accurate finite-difference method *(French)* 78−86163
steady flow between a rotating and a porous stationary disc in the presence of transverse magnetic field 78−79382
steady flow past cylinder, num. calc. method 77−54956
steady flow prod. by rot. disc, series soln. anal. 78−71308

Navier-Stokes equations continued
steady incompressible flows in three dimensions, finite-difference methods 80−33554
steady laminar flow through channel with symmetrical constriction in step form 80−100036
steady screw motion, impossibility in Navier-Stokes fluid 79−94627
steady state, numerical method and appl. *(Japanese)* 77−68564
steady state shallow water equations, unified treatment, finite element penalty function approach 79−49056
steady State stefan problem with convection 80−69625
steady streaming flow, cylinder oscillation induced, numerical solns. 79−50711
steady streaming induced between oscillating circular cylinders 80−1602
steady viscous incompressible fluid flow past symmetric cylindrical obstacle, numerical treatment 77−62230
stenosed tube, numerical solns. 80−16975
Stokes eqns., num. soln. using finite element anal. 79−92947
Stokes series, computed extension, circular boundary flow 78−42583
stream function-vorticity finite element solns. for Navier-Stokes eqns. 79−14368
stream function-vorticity formulation incorporating no-slip conditions, variational principle 78−38267
subsonic laminar viscous gas flow in flat channels and in shadow regions *(Russian)* 79−50749
subsonic viscous flow, 3-D unsteady actuator disc theory 79−27615
successive approx. solns. 78−51144
suction effects on shock wave-boundary layer interaction, numerical Navier-Stokes soln. 79−1243
supersonic blunt body flow of viscous perfect gas and nonequilib. gas mixture 80−28578
supersonic cone flow at high angle of attack, numerical simulation, laminar and turbulent flow 79−77178
supersonic flow, parabolic Navier-Stokes equations, implicit finite-difference method using fractional steps technique 80−69866
supersonic laminar flow over backward facing step, numerical soln. at high Reynolds number 77−47040
supersonic trailing edge flow, numerical soln. of 2D laminar and turbulent flows 79−77172
supersonic turbulent compression corner flow, numerical simulation 77−62276
surface mounted obstacles, effects on flow, Navier-Stokes eqns., 3-dimens. integration 79−59960
suspension of particles, wall flow, degeneracy of eqns. 79−1235
swirling flow, non-unique solns. to Navier-Stokes eqns. 79−46321
swirling flow, nonisotropic turbulence model 77−55001
swirling jet from vortex filament, Navier-Stokes eqn. soln. 80−38470
symmetric Couette and Taylor flow between rotating coaxial cylinders, Navier-Stokes eqn. solns. *(German)* 78−94750
Taylor vortex flow, finite difference transient implicit method, stability 79−14404
theory and numerical analysis, book 78−77721
thermally expandable fluid transients, finite difference method 77−79418
thermoplastic recording material, latent image and surface deformation *(German)* 80−42284
thermosphere, dynamics calcs., Navier-Stokes eqns. validity 80−26659
thin films with nondeformable surfaces, generalized equations of hydrodynamics 80−10224
three dimensional laminar flow in curved pipes, Navier-Stokes eqn. numerical soln. technique 79−10611
three dimensional separated turbulent flows at supersonic speeds 80−19435
time dependent, higher order soln. method optimisation and anal. *(French)* 79−37281
time-dependent Navier-Stokes eqn. soln. by finite element method 78−92956
tornado vortex model, appl. to nuclear plant design 78−17444
transformer, oil-cooled, heat exchange anal., network method *(Russian)* 78−83399
transient finite element soln. method 79−3986
transient free convection flow around two-dimensional or axisymmetric bodies 80−69817
transonic flow, unsteady, turbulence modelling, compression waves developing into shock wave 80−74909
transonic flow, viscous effects, Navier-Stokes eqns. soln. method 77−55023
tube banks, heat transfer, viscous flow, numerical anal. 79−55375
tube banks in turbulent flow, heat transfer prediction 79−1080
tube/fluid vibrations, effects of fluid viscosity 79−3967
tubes flow with periodic step changes in diameter, numerical soln. 78−22423
turbulence, amplitude eqn. anal. 78−5731
turbulence, averaged Navier-Stokes eqns. closure, dynamical system approach 78−46941
turbulence, comparison of models 78−46939
turbulence, decay of grid produced turbulence, velocity correlation equations, two- and three-point 80−53741
turbulence, Fourier representation, isolating consts. of motion 77−84235
turbulence, fully developed, origin of intermittency 77−58658
turbulence, homogeneous, three-point method 78−13995
turbulence, isotropic and homogeneous self-similar behaviour *(French)* 80−74838
turbulence, isotropic time-depend. 78−32682
turbulence, kinetic model *(French)* 79−14382
turbulence, Lorenz attractor struct. 78−46944
turbulence, models, two-dimens., vortex and Fourier mode 78−46945
turbulence, numerical simulation, intermittency effects 78−59375
turbulence, observable motions, Navier-Stokes eqns. 80−10230
turbulence, probabilistic nature, closure of Navier-Stokes eqn. 78−1643
turbulence, Ruelle-Takens picture, bifurcations, semiflows and Navier-Stokes eqns. 78−46940
turbulence, two-dimens., ergodic behaviour 80−28494
turbulence and infinite bifurcations, five-mode truncation 80−52031
turbulence dynamical systems approach, Navier-Stokes eqns. and strange attractor 78−46942
turbulence model development expts. with numerical simulations 77−27551
turbulence problem, physical and spectral space methods *(French)* 80−28493
turbulence seminar, theoretical descriptions 78−46938
turbulence universality and scaling, review 79−58548
turbulent and transition flows, num. soln. methods 77−54979
Navier-Stokes equations continued
turbulent convection mode numerical modelling 79−64653
turbulent energy and length scale eqn., mean vel., similar solns. 77−89102
turbulent flow, computational modelling by finite elements 79−1163
turbulent flow, finite element methods 79−1162
turbulent flow, numerical methods in statistical hydrodynamics 77−35121
turbulent flow, numerical simulation 78−94743
turbulent shear flow, computation, phenomenological theories 78−46955
turbulent transonic flow about lifting aerofoil 79−4032
two dimensional, numerical soln. methods *(Russian)* 80−101718
two-dimensional, num. soln. at high Reynolds no. 77−58637
two-dimensional, num. soln. procedure for treating unsteady flow about arbitrary shaped bodies 77−54960
two-dimensional inviscid dynamics, low order model randomness 78−42582
two-dimensional laminar flow between porous walls 79−14477
two-dimensional space isothermal and nonisothermal turbulent flow *(German)* 80−28505
two-dimensional turbulence in square region, inviscid Navier-Stokes eqn. calcs. 78−16656
two-dimensional viscous flow accompanied by stagnation point on plane wall 80−6021
two-phase laminar channel flow, vel. profile 78−9675
U-tube manometers, Navier-Stokes equations solution and expt. verification *(Japanese)* 80−6142
ultracentrifuge, flow, isotope conc. field, numerical model 79−1199
ultracentrifuge, thermally-controlled, for isotopic separation, gasdynamic features 77−54362
unbounded channels and pipes, props. of steady N-S equations 79−27612
unbounded domains, continuous dependence theorems by weight function method 79−77056
uniqueness problem for Navier-Stokes equations in non-limited domains *(Italian)* 79−32432
unsteady 3-dimens. compressible flow, implicit finite difference simulations, transonic appl. 80−64576
unsteady boundary layer on a two dimensional or axisymmetric body with higher order effects 80−92106
unsteady flow analysis in duct with junction, FLIC method 78−18340
unsteady flow in contracting or expanding pipe 77−86523
unsteady squeezing of viscous fluid from tube 79−90296
unsteady stagnation-point flow impinging obliquely on oscillating flat plate 80−6020
unsteady viscous separated laminar flow, numerical modelling 78−46933
variational principle for perfect and imperfect fluids in general relativity 80−90733
variational techniques application 78−89415
velocity distrib. in liq. deposit, response of quartz crystal microbalance 79−30422
velocity-pressure formulation, mixed-interpolation finite elements comparison 78−45486
vertical layers, struct. of laminar-turbulence transition and turbulent convection conditions 80−6040
viscous and potential flow about arbitrary 2-D bodies 77−65730
viscous drainage, over naturally permeable wall, steady-state film profile 77−27509
viscous drainage, over permeable wall, Navier-Stokes eqn. 77−31278
viscous flow, downstream boundary conditions 77−35108
viscous flow, non-Navier Stokes computations, parabolic and thin layer approx. 80−48666
viscous flow, numerical boundary conditions 77−23929
viscous flow, past thin obstacle, boundary layer, iteration method *(Japanese)* 79−94599
viscous flow, unsteady, around elliptic cylinder, heat transfer, finite difference method *(Japanese)* 80−69831
viscous flow between two revolving spheres, unstable motion *(Russian)* 79−32530
viscous flow computations, boundary approx. and accuracy 79−64621
viscous flow equations num. soln. using integral represents. 77−54966
viscous flow of stably stratified fluid over barrier 77−75961
viscous flow of variable viscosity between porous bed and moving impermeable plate 78−90962
viscous flow past circular cylinder, two coord. systems description 77−58643
viscous flow past two-dimensional bluff body, new approx. theory 77−918
viscous flows in unbounded domains, weight function approach to uniqueness 79−46334
viscous flows with no-slip walls, incompressible Navier-Stokes eqn., pseudospectral method 80−69924
viscous fluid, deform. of falling elastic particle 80−79149
viscous fluid, laminar flow, Navier-Stokes eqns., central difference scheme 80−69762
viscous fluid motion *(Ukrainian)* 78−1626
viscous fluid motion in unbounded regions, soln. uniqueness 77−899
viscous fluid squeezing between two plates 77−46991
viscous fluid steady flow, lift and drag of body 77−51027
viscous fluid surface velocity *(Russian)* 79−18856
viscous gas flow, similarity of flows in strongly underexpanded jets 80−6111
viscous gas flow, subsonic and supersonic, simplified Navier-Stokes eqns. 80−31520
viscous incompressible flow problems, two-dimens., Navier-Stokes eqns. soln. and contaminant effects 77−58638
viscous incompressible fluid, two-dimensional turbulence in bounded region 78−30270
viscous laminar jet flow in slipstream calculation *(Russian)* 79−77209
viscous liquid laminar flow in gap, nonstationary Reynolds differential eqn. *(German)* 77−58641
vortex filament with decaying vortical core and axial velocity 79−14415
vortex flow, new exact solution 78−38340
vortex flows, between rotating cylinders, axisymmetric Navier-Stokes equations 80−59044
vortex on viscous fluid surface 79−77123
wake struct. in supersonic gas flow around sphere 79−77119
water at 4°C, unsteady free convection past infinite vertical plate 80−69822
wave generator model, traction force determ., Navier-Stokes liquid motion description 79−77152

Navier-Stokes equations continued
weak nonlinear waves in compressible fluid, higher order approx. 80−92165
weakly-separated zones, numerical prediction *(French)* 77−72276
weather, severe convective event numerical simulation and prediction, Navier-Stokes eqns. initialisation 80−31111
Wedemeyer spin up model, Ekman compatibility conditions, Navier-Stokes eqns. 80−83802
welding arcs, gas velocity fields modelling 80−75039
wetting of a vertical plate by a liquid, model 78−22319
wind-wave interaction, two-layer flow, numerical simulation 78−92823
winds, neutral, in F_2-region, soln. *(French)* 79−35031
AL, shock wave structure, at re-entry speeds 80−43927
CO_2-N_2 downstream mixing gasdynamic laser, Navier Stokes eqns., laminar mixing flows 80−23662
HF laser with flow-through chem. active medium, pulsed-periodic regime realisation 80−106513
^{4}He, liq., positive ions, struct. 79−4440
^{4}He, superfluid, normal fluid heat-exchange drag 80−49441
MHD flow and heat transfer, porous disc eccentric rotations at infinity 79−18965
N_2, cryogenic, shock wave-boundary layer interaction *(German)* 78−71370
NH_4Cl-H_2O, binary dendritic system, exam. of solidification 79−11599

navigation
see also computerised navigation; inertial navigation; radar applications; radionavigation; sonar; tracking
acoustic transponder navigation, for ships 79−32167
acoustic transponder navigation 79−59896
acoustic transponder navigation systems and ATNAV II system 77−70874
aerial photographic equipment developments, aerial survey camera and navigation telescope 77−66997
almanacs for small computers, calculators 79−62726
astro-navigation and positional astronomy computing, new approach using pocket calculator, book 79−12383
astrodynamics conf. (Provincetown, MA, USA, June 1979) 80−82583
celestial, with stereographic projection 77−60866
comet rendezvous, navigation for ion drive 79−35096
deep ocean navigation, acoustic beacon-aided 79−32166
deep ocean navigation by Parametric Array Doppler Sonar 77−3698
depth sounding using airborne laser land profiler, chart production appl. 78−49173
Earth survey satellites, orbit determination 79−25442
galactic inertial-coordinate frame rel. to celestial reference, for starship navigation 78−49346
geodetic positioning convergence with navigation systems 79−25186
geomagnetic secular acceleration, spherical harmonic model 79−88249
gyros appl. to angular velocity meas., precision increase using structural redundancy *(Russian)* 78−49804
gyroscope, fibre optic, phase nulling 79−72719
interstellar relativistic navigation problem, three-dimensional rocket equation 79−21136
marine navigation, remote sensing appls. to oceanography and sea ice 80−77176
maritime navigational aid, numerical models of tide and surge propag. 79−12121
Mars descent vehicle, aerodynamic braking arc control algorithm 79−84629
oceanographic free-fall instruments, position determ. using acoustic navigation system 77−29490
oceanographic microwave remote sensing 80−56612
oceanographic research techniques used in survey ships *(French)* 78−65434
Oceans 1976 conference, Washington (Sept 1976) 77−5241
Pioneer 11 post-Jupiter trajectory midcourse manoeuvre sequence for Saturn targeting options 78−7857
proportional, teaching exercises 80−82611
radar determination of winds at sea 80−26644
satellite navigation, Chebyshev approximations for compression of Ephemerides 80−61993
sea floor relief mapping considerations 80−46169
sea ice cover nonuniform thickness effects on navigability 77−78222
sextant, hand-held SPT-2, construction features 79−32027
ships compass adjustment in fog using atmosphere polarised sunlight cct. 78−24831
short range precision navigation and tracking system using PLL 78−53742
spacecraft, Mariner Jupiter/Saturn 1977 mission 77−5411
spacecraft braking problem in Jupiter atmosphere, ballistic and navigation aspects 80−61981
spacecraft instrum. package reliability enhancement technique 77−29623
spatial pattern recognition by spectral feature classification and coherent optical correlation 80−99644
star tracker error evaluation in optoelectronic direction finders 79−75075
stars and point sources, visibility estimate using visual instruments, search coeffs. 79−7089
stellar direction finder, Cardan point geometry *(Russian)* 80−73312
terrestrial longit. determ., without time, from obs. of lunar altitude 78−85836
TRANSIT satellites' contribution to navigation and geodesy 78−57161
undersea acoustic transponders, locations optimal estimation 79−5684
Venera 9 and 10, flight control 77−78598

NDO calculations
see also CNDO calculations; INDO calculations; MINDO calculations
acetic acid-pyridine, H-bonding, proton transfer, isolated system, solvent effect, MO calc. 80−55629
benzyne, struct. and IR spectrum, MNDO calc. 79−31403
boron trihalides, quadratic potential functions, Coriolis consts. calcs. 79−72239
chemisorption of H on graphite, regular phase, CO-NDO approx. 77−15681
chemisorption of O on graphite CO-NDO calcs. 78−75937
conjugated molecules, conformation, electronic spectra, NDDO calcs. 79−85901
extended Huckel theory, rel. to NDO LCAO theories 80−95536
2-fluoroethyl to ethylene fluoronium ion interconversion, pot. energy surface, MNDO calc. 79−34296
graphite, chemisorpt. of N periodic overlayers, CO-NDO calcs. 79−7745

NDO calculations continued
graphite, chemisorption of H, regular phase, CO-NDO approx. 77−15681
graphite, chemisorption of H,cryst. orbital NDO calcs. 77−7965
hydrides, first row, bending pot. calc. using MINDO approx., force const., equilib. geometry 80−95544
hydrocarbons, dipole moments, NDDO calcs. 80−47894
hyperfine coupling, constants, nucl. spin spin coupling const., NDDO MO calcs. 80−23310
lactam-lactim tautomeric equilibria, quantum chem. calcs. 80−50833
LNDO/S, semiempirical SCF-Cl method for calc. ionis. pot. and electronic transition energies 79−18117
methyl formate($-d_1,d_3,d_4$), mol. vibr. spectrum, struct., beginning with PCILO calc. *(French)* 80−23401
MNDO results for ground-state B-containing mols. 77−88391
MNDO semiempirical calcs. accuracy rel. to current MO methods 80−47893
MO, LCAO method, chem. bond order, ZDO approx. 79−41102
molecular electric polarisabilities, hyperpolarisabilities, nonlinear optical coeffs., MNDO calc. 79−13641
molecule, method of calc. from fragments 79−63905
molecules containing 1st row atoms, K-shell binding energy shifts, NDDO MO calcs. 80−58413
NDDO approximate MO theory, mols. containing first-row atoms 80−32612
poly-ynes, struct., vibr. freqs., ionis. energies, MNDO calc. 77−88390
retinal, proton donor-acceptor isomerisation coupling, bacteriorhodopsin as light driven proton pump 79−79473
S-matrix power series expansion 80−69080
semiempirical MO theory, modified NDO model 80−52887
simple molecules, conformation, electronic spectra, NDDO calcs. 79−85901
third row element mols., general harmonic force field, SCF-MO-MNDO and freq. calc., MOCIC pot. 80−27948
ZDO all valence semiempirical theories, screening effect inconsistencies 80−58154
$C_2H_5O^+$ and $C_2H_5S^+$, stability, proton affinity, ab initio SCF, CEPA PNO, MINDO/3 and MNDO calcs. 79−59357
O-containing compounds, dipole moments, NDDO calcs. 80−47894
$O_3 \rightarrow O_2+O$, MNDO semi-empirical SCF MO calc. 77−44465

nearly-free-electron approximation
Al (001) surface, nearly-free-electron metal, origin of surface reson. states 78−95322
alloy, nearly-free-electron, random, charge transfer rel. to stability 78−6316
alloys, indeterminacy of a priori pseudopots., effects on form factors 80−103608
alloys, local density of states and local environment 79−82509
amorphous superconductor, Eliashberg function, tunnelling and crit. temp. anal. 80−80455
atomic chemisorption on metal surface 78−14588
binary liquid alloy, at. position correls. 77−39529
electrode-insulator boundary, current injection in presence of space charge 79−1619
electron field emission, from high-index crystallographic faces, scatt. approach 77−48323
extended Hartree-Fock Hamiltonian, nearly free electron approx. and pseudopotential method 78−60047
FCC binary alloys, short-range order diffuse scattering, Fermi surface imaging *(Japanese)* 79−7776
Hartree-Fock formalism for solids, appl. to nearly free electron gas 78−30857
ion-ion interaction, third-order contribution, total energy calc. 78−63998
Kronig-Penney model, energy band structure, nearly-free and tightly-bound electron approxs. 78−73792
liquid metals, nonlocal pseudopot. calc. of Knight shifts 78−91965
liquid metals, resistivity as function of press., nearly-free-electron model 78−84192
metal, band induced anisotropy effects in thermoemission 77−32489
metal, H-like impurities electron. struct., μ^+ probes 79−56653
metallic glass, at. position correls. 77−39529
metallic glasses, formation, model based on nearly-free-electron approx. 77−52316
metals, effect of alloying on Fermi surface and Dingle temp. 77−47719
metals, electromigration of weak scatt. impurity in Bloch electron gas 78−6183
metals, holelike Fermi surface, Hall coeff. and magnetocond. tensor 79−4547
metals, nearly-free-electron, secondary electron emission, role of plasmon decay 77−81186
metals, photoemission, theory, book contrib. 78−95670
metals, SHG by surface polaritons, theory 78−9416
Peierls instability in nearly free electron model with nonlinear screening 77−4304
photoelectron spectra of cryst. solids, numerical integration within linear analytic approx. 78−60545
rare earth metallic compounds, indirect multipole interactions 77−4308
RKKY interactions 79−51771
vertex corrections in nearly free electron model 78−72054
Br-graphite, intercalation cpd., magnetothermal oscill. and charge-density waves 80−11199
$Cu_{60}Zr_{40}$, amorphous, elec. resist. calc. and temp. coeff., using t-matrix 78−72130
Ga-M, liq. alloys, mag. susceptibility *(Russian)* 77−24671
Li, analysis of optical consts. 77−40201
Li, liq. and solid states, γ-ray Compton profiles 77−48269
Mg-Bi alloy, liq., far IR reflectivity rel. to possible transport processes 78−2827
Mo, Fermi surface, stress depend., hybridised nearly-free-electron tight-binding model 77−15757
Na (110), surface states in nearly-free-electron approx. *(French)* 79−33326
Na, liq. and solid states, γ-ray Compton profiles 77−48269
Ni-P, metallic glass, elec. resistivity 78−91654
Rb, expanded liq., struct. factor, cond. calc. using NFE model 77−47335
Zn, electromigration, electron wind force calc. 78−6183

nebulae
see also galaxies; planetary nebulae; supernova remnants
AFGL 2789 (V645 Cygni), refl. nebula, perplexing spectrum 80−73066

nebulae continued
AFGL 437, optical and IR obs., young star cluster embedded in nebulosity 78−4394
AO 0235+164, nature of nebulosity assoc. with BL Lacertae object 78−28778
R Aquarii, UV obs. of hot component 80−56854
B361, rotating dust globule, CO obs. 77−33582
Barnard 213 NW, rotation and vel. structure rel. to parent nebula 78−41007
Barnard Loop, Hβ obs. 79−80346
Barnard Loop Nebula, far UV imagery 77−29911
bipolar nebula, new, in Centaurus, discovery, photometry and spectral type 79−84837
bipolar nebulae, study of general phenomenon 78−41026
bipolar reflection nebulae, photoelec. polarization maps 78−28742
Bok globules, collapsing cloud models 80−62216
Bok globules, polytropic models and structure rel. to collapse and evolution 79−84845
bright nebulosities in dust clouds, study of stars in R associations 80−56893
3C 120, Seyfert galaxy, spectrophotometric obs. of assoc. nebulosity 80−67890
3C 249.1, quasar, spectroscopic obs. of assoc. nebulosity 77−33677
3C 48, quasar, nature of assoc. nebulosity 77−13487
California (NGC 1499), visual extinction uniformity across nebula 80−62225
α Canis Majoris (Sirius), search for surrounding nebulosity 78−93242
Carina, recombination line source model, electron temp. and density inhomogeneity 79−92830
Carina, structure and rel. to η Carinae 77−87520
Carina Nebula, extinction determ. from open cluster UBV photometry obs. 80−90513
Carina Nebula, interstellar λ4430 band obs. 78−32555
Carina Nebula, refl. nebula, interaction with η Carinae 77−45433
Carina Nebula and η Carinae, polarimetric study 79−67043
η Carinae, dust condensation 79−17066
η Carinae, evidence for circumstellar disc and asymmetric explosion *(Italian)* 79−53893
η Carinae, high-resolution IR radiation maps of homunculus, spectral and spatial distrib. 80−12767
η Carinae, silicate grains size distrib. in Homunculus Nebula 80−4382
η Carinae nebula, spectral obs. at 4 microns 78−4237
η Carinae nebula, X-ray emission obs., sources identification 80−26876
η Carinae nebulosity, proper motion meas. in complex outer shell 78−28687
Cartina Nebula, O-type stars on line of sight, extinction law, photometry obs. 80−105240
Cassiopeia A, ^{14}N radioemission at 26 MHz 80−41886
SU Cassiopeiae region, reflection nebulae distances rel. to Cepheid pulsation mode 78−89204
catalogue of bright nebulosities in opaque dust clouds 77−64668
S.Celestial Pole region, nebulosity obs. 79−92839
ω Centauri region, faint filamentary nebulosity obs. near globular cluster 80−56914
Cepheus OB3 molecular cloud, obs. of new IR sources 79−67072
Chamaeleon dark cloud, embedded Be-star HD 97048, visible and IR obs. 80−85943
charge transfer of C^+ and S^+ in diffuse nebulae 80−77463
Chu's object in Perseus, refl. nebula assoc. with B-type star 80−62132
CL4, nearby nebula, spurious image in Kron electrographic camera 78−8101
cloud collision and angular momentum in star formation 78−69781
clouds containing magnetic fields, stability 79−5876
S.Coalsack, obs. of IR sources 80−46652
collapsing dark cloud, CO line radiation transfer, Monte Carlo method appl. 79−44357
cometary nebula, remarkable structural change obs. 78−4333
cometary nebula near NGC 7023, brightening, stellar object visual magnitudes 78−20882
cometary nebula near NGC 7023, brightening and spectra 77−74118
cometary nebulae, list of 79 new objects found on Palomar Sky Survey prints *(Russian)* 77−60630
cometary nebulae, shape changes *(Russian)* 77−74125
compact IR sources assoc. with H II regions and molecular clouds, polarimetry 78−41019
condensation in dense nebulae, origin of multiple stars 79−44565
Cone nebula, formaldehyde kinematics and distrib. 80−4418
control stars temperatures, determ. from forbidden O III lines 78−41015
cool gaseous nebulae, electron temps. from radio recomb. lines obs. 79−88726
Corona Austrina dark cloud complex, extinction distrib. 78−54001
Crab, H abundance rel. to H deficiency in Type I supernovae 78−53969
Crab, hard X-ray spectrum 79−62891
Crab, lunar occultation obs. at 114 and 26.3 MHz, small-scale struct. 80−46627
Crab, magnetoparametric instabilities 78−61727
Crab, radio emission from compact source, HF meas. with URAN-1 interferometer 80−31343
Crab Nebula, radiation origin through pulsar magnetosphere cyclotron instability *(Russian)* 80−8645
CRL 2688, bipolar nebula, search for OH emission 78−41016
CRL 2688, Cygnus Egg Nebula, optical spectropolarimetry 77−33602
CRL 2688 (Egg Nebula), 8000-11000 Å spectrum 77−41400
CRL 2688 (Egg Nebula), bipolar nebula, optical and IR polarimetry 78−36658
CRL 2688 (Egg Nebula), bipolar refl. nebula, photoelec. polarization maps 78−28742
γ Cygni, nearby nebula exciting star, UBV photometry 79−97003
V1500 Cygni (Nova 1975), spectroscopic studies, nebular and central binary system 79−62830
γ Cygni nebula, SNR gas collision with dense cloud 79−97055
Cygnus X region, maps of calibrated surface brightness of (Hα+N II) 77−78854
dark cloud complexes in Scorpius and Ophiuchus, extinction distrib. 78−54002
dark cloud evolution, role of magnetic fields 77−67117
dark clouds, $^{13}C^{16}O/^{12}C^{18}O$ double ratio+ isotopic fractionation, evidence 80−73017
dark clouds, C recombination line obs. 79−75260
dark clouds, chemical and thermal equilib. 78−61899
dark clouds, formaldehyde obs., 5 GHz survey 80−73028

nebulae continued
dark clouds, H I 21 cm line obs. 79−21393
dark clouds, H I 21 cm Zeeman effect obs., magnetic fields 79−8977
dark clouds, HCO^+ isotopes, anomalous line intensities 79−17054
dark clouds, NH_3 survey 78−49507
dark clouds, red and nebulous objects, survey, catalogue of 150 objects 80−56904
dark clouds, unsuccessful search for formaldehyde-d_1 79−12500
dark clumpy molecular clouds, dynamic model 80−85980
dark dust cloud model, lifetime of molecules 78−85999
dark globules and star formation 79−58398
dark molecular clouds, dynamic structure 79−5877
dark nebulae, visual extinctions determ. via star counts 78−57612
dark nebulae and globules, star form. regions 78−12347
dark nebulae in M31, catalogue 80−72787
dense clouds, heating by magnetic ion slip, constraint on cloud field strengths 77−45513
dense clouds, ion chemistry and molecular evolution 80−31346
dense clouds, kinematics and dynamics 78−32563
dense clouds and diffuse production of gamma-rays 78−54011
dielectronic recombination through the forbidden levels, in low density and T_e highly ionised plasma 80−43850
diffuse gaseous nebulae, Hα photoelectric photometry *(French)* 80−62240
diffuse nebulae, chemical comp., network of models 79−48900
diffuse nebulae, formaldehyde and H110α recomb. lines obs. towards bright rims 77−87510
disc nebula, interaction with surrounded stellar wind 79−58323
discovery of nebula near radiosource CL4 77−91601
distorted interstellar bubbles discovery around two stars 79−71088
30 Doradus, interstellar and nebular lines towards central object (HD 38268) 80−51839
30 Doradus, nebular complex, photographic obs. 77−33606
30 Doradus, supermassive nebula, motions of neutral and ionised material 77−71137
30 Doradus direction, unique interstellar Ca II K-line profile obs. 80−51850
30 Doradus nebula, in LMC, interstellar Ca II and Na I obs. 80−46643
30 Doradus nebula, surrounding nebulous filaments 79−67076
30 Doradus nebula in LMC, optical obs. of bright core 80−67827
30 Doradus nebular complex, chemical comp. and struct. obs. 80−62226
30 Doradus region, in LMC, radio model 78−96523
30 Doradus region, uvbyR surface photometry 78−81670
double-charge transfer processes in gaseous nebulae 79−30112
DR15, H II region, optical emission assoc. with 408 to 2695 MHz radio sources 80−94881
DR 21/W75 complex, detection of H_2 vibrationally excited 2 μm lines 80−94853
dust cloud complex in Taurus, radio obs. of fragmentation and localised multiple vel. components 78−4308
dust cloud with embedded stars, heating and model 80−26952
dusty nebulae, non on-the-spot (OTS) models 78−85995
dynamical evolution of spherical gas-dust nebulae including diffusion effects 79−80342
element abundances, model anal. of ionisation correction formulae 78−57623
emission, IR obs. 1-1000 μm wavelength 79−67084
emission, with strong S II forbidden lines in LMC 77−29891
emission line spectra, automatic reduction 80−77294
emission nebulae, association with Trapezium type multiple systems 80−67781
emission nebulae, astronomical obs. using optical multichannel analysis of Sao Paulo Univ. 80−26743
emission nebulae in NGC 4449 galaxy 79−84848
emission-line nebulae misclassified as H planetary nebulae, catalogue 80−109378
emission-line stars misclassified as H planetary nebulae, catalogue 80−109378
ESO 210-6A southern globule, nearby star formation 79−21399
evaporation of spherical clouds in hot gas, classical and saturated mass loss rates 77−33583
expanding spherical nebulae with dust, H I Lyman α formation 79−8975
extinction laws from 13-colour photometry 78−81676
filamentary and diffuse nebulosity near giant nonthermal radio loop 78−93445
filaments surrounding RR Pictoris (Nova 1925), spectrophotometry, abundances, ionization 79−40194
formaldehyde absorption and visual extinction in several dark clouds near NGC 2264 79−88715
G206.9+2.3 (PKS 0646+06), supernova remnant, optical nebulosity discovery 78−96518
G292.0+1.8, supernova remnant, optical identification and spectrum 79−84839
galactic, obs. at 5 GHz 78−4327
galactic reflection nebulae, CO obs. 77−53658
Galaxy high latitude nebulosity, as source of enigmatic dark lines crossing (M81) 80−56947
gas cloud, self-gravitating, rotation and Kelvin-Helmholtz instability 79−46287
gas cloud, three-dimens. collapse and fragmentation 78−77552
gas clouds, equilib. states during cooling in gravitational fields 80−94862
gas clouds, stability of self-gravitating magnetized system 79−21170
gas pressure and density *(Danish)* 78−4335
gas properties from spectral line surveys 79−5879
gaseous, star formation sites, radiospectroscopy 79−58408
gaseous nebulae, Fe abundances from Fe III and Fe VI collisional excitation cross sections 78−53806
gaseous nebulae, photoionisation models for third period elements 80−46640
gaseous nebulae, riddle of spectra, history 80−8676
giant and supergiant shell nebulae in Magellanic Clouds, obs. 80−94858
giant molecular cloud near M17, structure and extent from CO 115 GHz obs. 79−71084
giant molecular clouds, H_2 densities and $^{12}C/^{13}C$ ratio from formaldehyde obs. 80−51837
giant molecular clouds, turbulent cores, CS obs. 80−51822
GL 915, 618, 2688, IR sources assoc. with double-lobed refl. nebulae, far IR obs. 78−54009
Gum Nebula, temp. and density vars. *(French)* 80−26951

nebulae continued
H-H 28, H-H 29, large proper motion Herbig-Haro objects, astrometric obs. 79−71022
HD 20722, peculiar nebula surrounding K-type giant 79−58407
HD 44179 (Red Rectangle), bipolar nebula, IR polarimetry 78−36658
Heile's Cloud 2 at SHF cyanohexatriyne detection 78−41018
Heiles 2 cloud collision, assoc. cyanodiacetylene emission at 24 GHz 78−65675
Herbig-Haro object 1, exciting star identified as T Tauri star 80−17633
Herbig-Haro objects, 2 micron search for exciting stars 80−67720
Herbig-Haro objects, new, spectroscopic obs. 79−5763
Herbig-Haro objects, new nearby H_2O masers discoveries 79−21369
Herbig-Haro objects, stellar wind model 79−8912
Herbig-Haro objects, stellar wind model 80−85985
Herbig-Haro objects and surrounding dark clouds, NH_3 23 GHz obs. 80−72934
Herbig-Haro objects in Gum Nebula, spectrophotometry 78−36565
high-latitude reflection nebulae illuminated by the galactic plane 77−17647
Homunculus, evidence for circumstellar disc and asymmetric explosion rel. to η Carinae *(Italian)* 79−53893
RW Hydrae, UV obs. of hot component 80−56854
IC 1318, giant H II region, large-scale line splitting discovery 78−96521
IC 1318 b and c, H_2CO absorpt. 78−16484
IC 1318 nebular complex in Cygnus X region, light extinction 80−51835
IC 1396, bright rims, high resolution 1415 and 4830 MHz obs. 79−71092
IC 1396 (Sharpless 131), 2695 MHz continuum map 80−105310
IC 1795/1805, H II regions IR luminosity compared with exciting star total luminosity 78−96519
IC 2220, refl., surrounding red giant HD 65750, photometric obs. 78−36567
IC 5146 dark cloud complex and cluster, IR obs. 78−89234
intensity ratios of Brackett to Balmer H lines 77−74121
internal dust effects, line transfer, Monte Carlo calcs. 79−48902
interstellar cloud, gravitating plasma polytropes in magnetostatic equilib. 80−94701
ionisation fronts, weak D-type, departures from equilibrium 77−49288
ionisation-shock fronts hydrodynamic linear theory 80−17625
ionization front propag. in inhomogeneous medium 80−46379
IR line emission, airborne obs. 78−93353
IR sources, unidentified emission features, possible mechanism 80−82452
IR sources in AFCRL catalogue, optical, IR and radio studies 78−4393
K3-50, IR obs. of nearby H II regions and dust clouds 77−49457
K3-50, optical nebula, radio obs. of assoc. H II regions 78−16554
Kepler supernova remnant, H abundance rel. to H deficiency in Type I supernovae 78−53969
Kleinmann-Low, interstellar NH_3 excitation 79−5878
Kleinmann-Low, lamellar grating obs. in 100-500 μm region 78−28743
Kleinmann-Low, N_2HD detect. 78−20881
Kleinmann-Low, nature of broad molecular line emission 77−5556
Kleinmann-Low IR nebula, possible ethylene oxide detect. 77−53662
Kleinmann-Low i.r. nebula in Orion, high-vel. gas obs., CO 115 GHz line 77−5554
Kleinmann-Low nebula, ^{12}CO line profile rel. to radially moving cloud model 78−20865
Kleinmann-Low nebula, NH_3 nonmetastable levels obs. 79−25665
Kleinmann-Low Nebula, NH_3 obs. 77−13440
Kleinmann-Low nebula, NH_3 obs. and hot core source 80−73016
Kleinmann-Low nebula, optically thin CO emission 78−4315
Kleinmann-Low nebula, role in new dynamical model of Orion Molecular Cloud 78−93373
Kleinmann-Low nebula, spectrum from 29 to 125 microns 77−33680
Kleinmann-Low Nebula in Orion, far IR polarization 79−12502
Kleinmann-Low nebula in Orion, ice 45μm signature possible identification 79−17068
L134 dark cloud, DCO^+ and HCO^+ obs. 78−65673
L134 dark cloud, detect. of DNC at 152.6 GHz 78−4334
L 43, CO mm wave and near IR obs. of filamentary cloud 79−62886
LF wave propag. in relativistic electron gas, rel. to Crab Nebula *(Chinese)* 78−67356
low-excitation diffuse nebulae, effective temps. of exciting stars 77−13427
Lynds 134, OH emission obs. in dark nebula 80−22062
Lynds 134, optical extinction and surface brightness obs. of dark nebula 80−17627
Lynds 134 dust cloud turbulence, formaldehyde obs. at 6 cm. 80−94845
Lynds 134 N, CO isotope, mapping 79−30108
Lynds 1551, CO obs. of dark cloud and stellar wind driven shocks 80−105318
Lynds 1630 dark cloud, OH 205.1−14.1 IR candidate 80−101630
Lynds 1778/1780, H I and OH emission obs. in dark nebula 80−17628
Lynds 1778/1780, optical extinction and surface brightness obs. of dark nebula 80−17627
Lynds 673 nebula, radiosource obs. at 3.5 and 4 mm *(Russian)* 78−32557
M16, emission nebula assoc. with open cluster NGC 6611, 85α recomb. lines obs. 79−35330
M17, discovery of extended mol. cloud assoc. with star forming complex 77−37635
M17, dusty H II region, stellar optical polarisation meas. 78−45379
M17, far IR obs. rel. to H II region interaction with mol. cloud 80−22053
M17, H I absorpt. lines high resolution mapping 78−81667
M17, high resolution radio and far IR maps compared 79−75263
M17, large-scale vel. components, insect-eye Fabry-Perot obs. 78−93380
M17, Platt particles and spatial temp. fluctuations 78−61907
M1−92, bipolar nebula, OH maser source, UHF spectra obs. 80−90550
M1-78, emission nebula, 15.4 GHz struct. 78−41025
M1-92, bipolar nebula, OH emission obs. 78−41016
M1-92 (Minkowski's Footprint), bipolar refl. nebula, photoelec. polarization maps 78−28742
M3-99, bipolar nebula, search for OH emission 78−41016
M42, far IR polarisation obs. 77−53663
M42 (Orion Nebula), X-ray obs. by Astronomical Netherlands Satellite 78−28852
M42 and M43, optical linear polarisation 78−86004
M43, emission nebula around NU Orionis, radio and IR obs. 78−54012
M43, small diffuse nebulae in Orion complex, optical linear polarization map 80−46644
nebulae continued
M8, IR map 77−64817
M8, new IR-CO source obs. 77−64818
M8, radio recomb. line obs. at 5 and 10 GHz 79−84832
M8 (Lagoon Nebula), far IR obs. 80−4413
M 1-92, Minkowski's Footprint, optical spectropolarimetry 77−33602
Magellanic Clouds, spectrophotometry of nebulae suitable as standards 78−12350
maser emission by nebular regions and stellar atmospheres 78−89242
masses of giant molecular cloud complexes 79−5888
master list of non-stellar objects 77−78668
Merope reflection nebula, near UV photometry of surface brightness 77−29896
Merope reflection nebula, phase function of dust grains in UV 78−32553
molecular abundance variations in interstellar clouds 79−17055
molecular cloud assoc. with NGC 7023, CO obs. at 2.7 mm wavelength 78−41008
molecular cloud complex near M17, detailed obs. 77−33603
molecular cloud complexes, origin, lifetimes and mass 80−82453
molecular clouds, CH radio emission obs. 77−87512
molecular clouds, dust diffusion and sedimentation 79−17062
molecular clouds, embedded supernova, spectra and luminosity, evolution 80−82399
molecular clouds, embedded supernova remnant struct. and emission 80−82450
molecular clouds, expanding H II region effects 79−5880
molecular clouds, line formation, radiative transfer effects 79−5884
molecular clouds, location of newly formed stars 79−58330
molecular clouds, magnetic field 79−67075
molecular clouds 78−32562
molecular clouds eveloping groups of T Tauri stars 79−58400
molecule formation in clouds from singly or multiply ionized atoms 79−17039
Monoceros R1 molecular clouds ring struct., CO obs. 80−12784
Monoceros R2 associations, refl. nebulae and interstellar extinction 77−13409
Monoceros R2 reflection nebula, near IR and mol. obs. of rot. collapsing cloud 77−78840
R Monocerotis, bipolar nebula, optical and IR polarimetry 78−36658
R Monocerotis (NGC 2261 cometary nebula), spectrophotometry *(Russian)* 77−49446
Mz 3 (P-K 331−1°1), obs. of bipolar nebula, possible protoplanetary 78−45376
N51D, bubble-like nebula in LMC, internal motions obs. 80−105295
N70, giant filamentary shell in LMC, dynamics 80−90511
N 59, nebular complex in LCM, filter photography 79−17052
NGC 1333, colliding molecular clouds, star formation, early evolution 80−12757
NGC 1333, detect. of DNC at 152.6 GHz 78−4334
NGC 1435, refl. nebula near Merope, UV surface brightness rel. to interstellar grains phase function 79−97047
NGC 1499, California Nebula, decametric radio emission 79−21385
NGC 1499 (California Nebula), CO obs. along ionisation front 78−24537
NGC 1499 (California Nebula), Hα obs., ξ Persei as exciting star 77−33622
NGC 1999, electronographic imaging polarimetry obs. of reflection nebula 80−26964
NGC 1999, reflection nebula, optical polarisation map and struct. 80−94856
NGC 2023, reflection nebula, far IR study 80−51831
NGC 2024, Cl chemistry as H ionisation source 79−40245
NGC 2024, H II region, near IR obs. 79−58393
NGC 2024, obs. in 40-400 μm range 78−69853
NGC 2024 (Orion B) nebula, CO J=2 to 1 line obs. 80−8673
NGC 2071, H_2O maser source discovery 78−73768
NGC 2175 (S252), galactic H II region, aperture synthesis obs. 77−64828
NGC 2237, Rosette, decametric obs., brightness temp. contours 78−57615
NGC 2237 (Rosette Nebula), H II region obs. in absorption at 12.6 and 25 MHz *(Russian)* 78−41024
NGC 2261, cometary nebula assoc. with R Monocerotis, model 79−21372
NGC 2261, variable refl. nebula assoc. with R Monocerotis, rel. to stellar long period light vars. 80−82350
NGC 2264, detect. of DNC at 152.6 GHz 78−4334
NGC 2264 and 7000/IC 5070, new Hα stars, slitless spectrographic search 80−62120
NGC 2264 and other Bok globules, formaldehyde absorpt. obs. at 6 cm 77−45511
NGC 2359, radial vels. and internal motions in ring-type nebula 78−81678
NGC 2467, H II regions complex, internal motions 77−22304
NGC 3372 (Carina Nebula), embedded open clusters dist. determ. 80−85977
NGC 3603, H II region, interstellar λ4430 band obs. 78−32555
NGC 5367, field stars of cometary globule (reflection nebula) 78−93364
NGC 5367 and associated young cluster, relation to X-ray source (Ariel 1353-40) 77−82294
NGC 6302, direct evidence for energetic stellar wind 80−67835
NGC 6302, line profiles from ionised and neutral gas in peculiar nebula 78−12341
NGC 6334, H_2O masers mapping and star form. 80−73025
NGC 6334, variable far IR source detect. in group of nebulae 80−8671
NGC 6618, polarimetric obs. of nebula and neighbouring stars *(Russian)* 78−49491
NGC 6729, variable refl. nebula assoc. with R Coronae Austrinae, rel. to stellar long period light vars. 80−82350
NGC 6888, around Wolf-Rayet star HD 192163, IUE obs. of absorpt. by hot gas 79−53896
NGC 6888, circumstellar nebula, forbidden N II/Hα ratio 79−8964
NGC 6888, circumstellar nebula, spectroscopic investigations 77−57076
NGC 6888, circumstellar nebula, violet displaced Na I and Ca II lines in Wolf-Rayet star (HD 192163) 80−17640
NGC 6888, filamentary nebula, optical spectra calc. 80−105304
NGC 6888, ring nebula, central Wolf-Rayet star HD 192163, SHF obs. 80−82386
NGC 6888, ring nebula assoc. with Wolf-Rayet star, dust comp. 77−29905

nebulae continued
NGC 6888, ring nebulae around Wolf-Rayer star HD 192163, spectra of filaments and smooth gas *(Russian)* 80−90515
NGC 6914b, surface brightness and UBV colorimetry *(Russian)* 77−13446
NGC 7000, obs. of assoc. Hα emission stars 77−13363
NGC 7000 (North America Nebula), rocket UV imagery 80−82440
NGC 7000/IC 5070 (North America/Pelican) nebular complex, obscuration and excitation 78−36667
NGC 7023, refl. nebula, far UV brightness rel. to HD 200775 reddening and dust albedo and scatt. 80−51832
NGC 7023, refl. nebula, optical and UV extinction of HD 200775 by dust 80−109515
NGC 7023, refl. nebula, radio continuum obs. 79−17048
NGC 7023, refl. nebula, surface brightness study 80−56903
NGC 7023, reflection nebula, optical polarization and IR spectrum of HD 200775 possible protostar 80−85944
NGC 7129, refl. nebula, star form., CO mol. line and far IR obs. 79−17043
NGC 7129, star form. process in mol. clouds 78−32542
NGC 7293, Helix Nebula, O III 5007 Å forbidden line splitting 79−25694
NGC 7538, IR line emission, airborne obs. 78−93353
NGC 7635, Bubble Nebula, line intensities 77−33605
NGC 7822, bright-rimmed mol. cloud, CO obs., heat sources 78−36664
NGC 7822 (W1) optical studies of kinematics rel. to supernova remnant struct. 78−54028
NGC 7822 (W 1), supernova remnant, 2.8 and 6 cm wavelength obs. 78−4383
night sky model for artificial satellite search systems 77−73923
North America and Pelican Nebular Complex, struct., visual extinction map 80−22063
OH 0739−14, M-type giant in reflection nebula, IR obs. 80−46692
OMC-2, detection of H_2 vibrationally excited 2 μm lines 80−94853
Omega, O I 63 μm forbidden emission line obs. 79−25684
Omega, O III 51.8 μm forbidden emission line obs. 79−25685
Omega Nebula (M17, W38, NGC 6618), S III, O III, N III, IR obs. 80−90495
ζ Ophiuchi cloud, Copernicus UV obs. of interstellar C_2 78−41022
ρ Ophiuchi cloud, cosmic ray accel. by stellar winds 80−77512
ρ Ophiuchi cloud, no assoc. with CG 353+16 γ-ray source 80−94896
ζ Ophiuchi clouds, interstellar abundances 79−48875
ρ Ophiuchi dark cloud, formaldehyde abundance 79−71100
ρ Ophiuchi dark cloud, high ang. resolution obs. of far IR source 79−40235
ρ Ophiuchi dark cloud, ice mantles and abnormal extinction 79−21376
ρ Ophiuchi dark cloud, late-type young stars, photometry obs. 80−72942
ρ Ophiuchi dark cloud, new S II and C II regions 78−57617
ρ Ophiuchus dark cloud, IR polarimetry 79−40239
Ophiuchus dark cloud complex, IR study 78−93363
Ophiuchus dark cloud region, IR sources identifications 77−45522
ρ Ophiuchus dark cloud region, soft X-ray obs. 80−26947
Orion, 2.1 μ H_2 emission, high spectral resolution obs. 78−20878
Orion, ^{30}SiO detect. 78−8097
Orion, C abundance from visible and IUE obs. 80−82451
Orion, C I IR forbidden emission lines obs. 78−85987
Orion, chem. comp. from emission line obs. 77−49456
Orion, contraction of star cluster-molecular cloud complex 78−12313
Orion, dimethyl ether emission detect. 79−53862
Orion, double Herbig-Haro object spectrum 77−26006
Orion, ethynyl radical abundance and distrib. 78−65664
Orion, Fabry-Perot high-resolution O I 8446 Å mapping 79−35344
Orion, far-UV rocket survey 77−64762
Orion, forbidden line and optical continuum electron temps. comparison 79−30105
Orion, gaseous depletion unlikely 78−69854
Orion, H_2 2.121 μ emission line vel. and width meas. 79−17061
Orion, H_2 2.12 μm emission, temporal vars. possibility 80−17631
Orion, H_2 emission at 2 microns 78−93351
Orion, H_2 emission from shock-heated region in molecular medium 78−4321
Orion, H_2 IR line emission, shock model 78−8086
Orion, Herbig-Haro objects 80−77397
Orion, high vel. emission object obs. 77−22296
Orion, intracluster dust, circumstellar shells and wavelength depend. of polarisation 77−78839
Orion, IR line emission, airborne obs. 78−93353
Orion, IR obs. by Fourier transform spectroscopy 78−61747
Orion, IR polarisation, preferential extinction in Kleinmann-Low nebula 78−4311
Orion, lamellar grating obs. in 100-500 μm region 78−28743
Orion, large proper motions of nebular features and faint star 78−12349
Orion, linear polarisation obs. 78−45392
Orion, low-luminosity X-ray sources obs., assoc. with star form. 80−26959
Orion, macroscopic motions from atomic line vels. 80−62243
Orion, near IR Fourier spectroscopy of weak lines 79−35328
Orion, nebular condensations found with S20 photocathodes assoc. with Lallemand electronic camera *(French)* 79−44592
Orion, O I 63 μm forbidden emission line obs. 79−25684
Orion, O I 7990 Å and 11287 Å branching ratios, implications 79−41134
Orion, O III 51.8 μ forbidden emission line obs. 78−65510
Orion, optical linear polarisation meas. 77−45536
Orion, photographic obs. in Hα, Hβ and He I 10830 Å lines 78−81669
Orion, photometric study of Orion OB 1 assoc. stars 77−82288
Orion, physical conditions from optical and radio lines obs. 77−45524
Orion, polarisation at 11.1 and 19.6 μm meas., aligned absorbing grains 80−36690
Orion, S III 18.71 μ and O III 88.35 μ forbidden lines obs. 77−5557
Orion, S III 9096 Å forbidden line, Fabry-Perot obs., abundance determ. 78−96515
Orion, S III emission line at 534.37 cm^{-1} 77−73966
Orion, search for vibrationally excited H_2 emission 78−93346
Orion, spectrophotometric obs., ion abundances and thermal balance 77−67121
Orion, spherical model, emission spectrum 77−53666
Orion, struct., radio obs., partially ionized gas 79−21379
Orion, structure and ionized gas 79−67073
Orion, temp. gradients, obs. and model 78−8077
Orion, temps. and abundances in outer part of Great Nebula 79−53868
nebulae continued
Orion, vibrationally excited H_2 78−8076
Orion, X-rays from Trapezium 79−35348
Orion H_2O masers, matter outflow in star formation last stages 78−8091
Orion molecular cloud, 870 μm CO emission 78−12335
Orion Molecular Cloud, $^{15}NH_3$ detection at 23 GHz 79−44590
Orion Molecular Cloud, H_2 2.1 μm emission line vel. profiles 79−71094
Orion Molecular Cloud, H_2 quadrupole line reddening determ. 79−71095
Orion Molecular Cloud, HCN J=4→3 354 GHz transition detection 80−101636
Orion Molecular Cloud 1, cyanoacetylene emission obs. 78−4322
Orion molecular cloud/H II region NGC 1977 interface, radio recombination line obs. 79−25658
Orion molecular clouds, obs. in 40-400 μm range 78−69853
Orion nebula, Becklin-Neugebauer source 3.3 to 5.5 microns spectrum 80−12796
Orion nebula, C and Mg abundances from UV spectrum 80−41882
Orion Nebula, C recomb. line mapping 78−20866
Orion Nebula, far UV imagery 78−4326
Orion Nebula, fine-struct. lines obs. and elemental abundances 80−4410
Orion Nebula, forbidden Cl II and forbidden Fe II near IR high resolution mapping 80−62217
Orion Nebula, forbidden line wavelengths *(French)* 77−64829
Orion Nebula, gaseous depletion *(Italian)* 79−21396
Orion Nebula, H_2 emission interstellar extinction meas. 79−25668
Orion Nebula, H_2O 183 GHz line emission obs. 80−41869
Orion Nebula, He ionisation struct. and abundance, SHF obs. 80−105315
Orion Nebula, high resolution map at 33 μ 78−28757
Orion Nebula, IUE obs. of UV continuous spectrum 80−90499
Orion Nebula, near IR Fourier spectroscopy 77−57071
Orion Nebula, OH masers obs. 78−16493
Orion Nebula, optical evidence for stellar wind bubbles 79−88724
Orion Nebula, radio obs. of nearby H I distrib. and vels. 80−105322
Orion Nebula, search for H_2 ground state S(2) line 79−8961
Orion Nebula, submillimetre emission obs. 80−36685
Orion Nebula, two new methanol transitions obs. in Orion A 79−25667
Orion Nebula (NGC 1976), long-slit spectroscopy in rocket UV 80−105297
Orion Nebula molecular cloud, anomalous var. of $N_2H^+/HCO^+/SO_2$ rel. to ion-molecule reactions 77−26034
Orion Nebula peripheral regions, spectrum obs. rel. to element depletion and ionisation 80−36686
Orion reflection nebulosity, UV photometry from OAO-2 78−65668
Orion region, survey of extremely red stars with Schmidt telescope *(Japanese)* 78−20833
Parsamyan 21, bipolar nebula, search for OH emission 78−41016
Parsamyan 21, colorimetry of cometary nebula *(Russian)* 79−8960
Parsamyan 22, surface brightness and UBV colorimetry *(Russian)* 77−13446
AG Pegasi, symbiotic nova, radio emission rel. to circumstellar nebula 77−22232
Pelican Nebula (IC 5070=W80), CO obs. of expanding mol. shell surrounding H II region 80−105296
ζ Persei cloud model 78−93362
photoelectric spectrophotometry of compact nebulae 78−89236
photoionisation models for gaseous nebulae with optically thin condensations 80−36693
photoionization models for gaseous nebulae 79−21392
Pleiades, filament struct. rel. to interstellar polarisation 77−45500
Pleiades reflection nebulosity, model for filamentary struct. 78−8082
polarisation maps obtained with electronographic camera 77−57081
population of excited atomic states in emission spectra 77−25940
proto-planetary nebulae, props. and comparison with planetary nebulae 80−109538
protosolar nebula, dust grain motion time evolution 80−82234
protostellar cloud, solar-type star form. with spherical symmetry 80−85930
protostellar rotating cloud, two-stage fragmentation 80−22061
R associations, early-type stars in CMa R1 and Vel R2, JHKL photometry 77−45505
R-associations, obs. of free-free emission from embedded B-type stars 80−26851
radio emission, props. of thermal and non-thermal components 77−57101
Red Rectangle, refl. nebula assoc. with HD 44179, spectrum interpretation 77−49462
Red Rectangle (HD 44179), precessing jets model 80−4422
reflection, inhomogeneous, scatt. function for grains of silicates and ice 79−21405
reflection, Mueller scatt. matrices for nonspherical particles 78−90366
reflection, multiple scatt., Monte Carlo approach 78−12320
reflection, scatt. multiplicity 78−12323
reflection, spherical core-mantle dust grains rel. to colour and polarization 79−62896
reflection, with embedded illuminating stars, multiple scatt. 78−12322
reflection, with foreground stars, multiple scatt. 78−12321
reflection nebula, optical colours, polarisation, composite and mixture of nebula grains 78−16502
reflection nebula model, optical colours and polarisation with silicate and graphite grains 78−57622
reflection nebulae, associated mol. clouds, CO emission, EHF obs. 80−82447
reflection nebulae, interstellar grains UV scatt. props. and size distrib. 80−26932
reflection nebulae, scattering props. of interstellar grains 79−53867
reflection nebulae, simplified models 78−96526
reflection nebulae around red supergiants 77−13340
reflection nebulosities, high latitude, as false companions of galaxy (NGC 772) *(Russian)* 80−36723
reflection nebulosity near 20 Tauri (Maia) in Pleiades 78−28734
reflection of light from thick slabs of dust 79−62881
ring-shaped nebulae in LMC, diameter rel. to number of embedded stars 80−77457
Roberts 22, bipolar nebula with OH emission, visual, radio and IR obs. 80−94859
Rosette, internal vels. from Hα emission line profile study 79−53869
Rosette Nebula, far IR emission from compact sources 77−78841

nebulae continued
Rosette Nebula (NGC 2237/2246), new physical parameters from 6.5 GHz obs. 80−4414
rotating clouds, structure and evolution under external pressure 78−61898
rotating interstellar clouds, heating and coronae 79−92837
rotational effects on spectral lines 79−97050
S106, NH_3 obs. of nearby mol. cloud 79−84840
S106 and S235, aperture synthesis obs., star form. regions 78−36672
S140, mol. cloud, continuum emission mapping at 89.6 GHz 80−94842
S140 molecular cloud, energetics, mol. line data, temp., density, abundances 78−36650
S171 (W1), optical supernova remnant radial vel. field 80−62250
S206, galactic nebula, model for struct. 78−12326
S252 (NGC 2175), mol. line obs. of star-forming complex 80−4411
S298, H109α recomb. line obs., core envelope type struct. 79−8965
Sanduleak's star in LMC, candidate symbiotic star, possibly compact high-excitation emission nebula 80−62139
α Scorpii (Antares) emission nebula, high dispersion spectra 79−8916
α Scorpii (Antares) nebula, spectrum 78−41014
self-similar spherical expansion, Rayleigh-Taylor instability 79−8823
Sh 2-158 (NGC 7538), bright high excitation galactic nebula, morphology, excitation and kinematics 79−40241
Sharpless 140, compact source, strong far IR emission obs. 78−36649
Sharpless 155 nebula and Cepheus OB3 association, thermal radio emission obs. 78−96514
Sharpless 235A, optical, radio and IR obs. of H II region 80−4415
Sharpless 254, 255 and 257, triple emission nebula in Orion, obs. 77−13430
Sharpless 88A-B and 106, compact H II regions, optical obs. 79−8969
shell nebulae in Magellanic Clouds, survey in S II, N II and O III forbidden lines and Hα 79−67085
solar nebula, development, chemical and gravitational crystallization *(Hungarian)* 80−72795
solar nebulae, mass transport processes in rotating dust cloud 80−8556
Southern Coalsack, dark nebula, conspicuous globule obs. 77−33614
southern molecular clouds, CS J=1-0 transition at 49 GHz 78−65674
SS 433, associated filamentary optical nebulosity detect. 79−88723
near SS 433, faint, highly-contorted nebular filament discovery 80−94855
stability of magnetic interstellar clouds 79−48885
stability of polytropic gas body, Lane-Emden eqn. 80−12802
star formation, radio obs. 78−32565
star formation regions, IR obs. 78−32564
star formation regions, IR spectroscopy of assoc. lineless objects 79−44586
star formation regions, rel. to galactic spiral struct. in vicinity of Sun *(Russian)* 80−62290
stellar winds and neutral gas in diffuse nebulae 78−28758
superassociations in spiral and irregular galaxies, brightest as distance indicators 80−62260
symmetric nebulae surrounding four luminous stars, IUE low-dispersion spectra 80−46560
T Tauri, ionisation source of emission nebula *(Russian)* 77−49375
T Tauri nebula, ionisation and emission line spectrum calc. 80−67820
T Tauri star, extremely young, and assoc. nebula, fading 78−93236
Taurus Molecular Cloud 1 in Heiles' cloud 2, molecular radio obs. 78−69858
Taurus-Auriga dark clouds, proper motions of T Tauri variables and other stars 80−41821
unidentified 3.3 μ emission feature obs. 77−33601
very-low-excitation compact nebulae in Magellanic Clouds, spectra 78−32556
visible spectra, emission lines due to dust 79−53874
W3(OH), production by moving compact object 78−54064
W50, supernova remnant, optical filaments spectra rel. to SS 433 mass loss rates and lifetime 80−12804
W50, supernova remnant, optical spectrum of faint filamentary nebula 80−90557
W50, supernova remnant, spectrum of optical nebulosity 80−51851
W50, supernovae remnant, associated filamentary optical nebulosity detect. 79−88723
W50 (SS 433), supernova remnant, optical filamentary nebulosity discovery 80−56916
W51, radio recomb. line obs., confirmation of impact broadening theory 78−54019
W75-DR 21 region, structure of CO in molecular cloud complexes 78−89232
Webb Society handbook 80−8743
William Herschel's early investigations of nebulae 80−12876
C II regions assoc. with reflection nebulae, recombination line spectra 78−69857
CH, obs. of 3.3 GHz ground state transitions 78−77592
CH_3^+ ion, radiative assoc. reactions in interstellar clouds 78−41021
CN towards interstellar clouds, EHF emission obs. 79−17037
Fe VI, forbidden emission under nebular conditions 79−8970
H I emission-line spectrum 80−72759
H II regions, anisotropic, with axial symmetry, models rel. to Hα brightness distribs. 78−85993
H II regions, effects of shocks 77−64825
H II regions, weak shocks props. 78−93348
H II regions assoc. with interstellar dark clouds, radio continuum interferometry 80−98699
H I+molecular/H II shells from 1 to 2000 pc dia., wind-driven or supernova remnants 79−25678
H_2 clouds, ionisation by supernovae 78−69856
He H^+, formation and destruction, assoc. IR emission line spectrum 79−44589
He I $2^3S \rightarrow 2^3P$ transition, rate coeff. for electron impact excitation 79−48664
He^+ radio recombination lines, stimulated emission 78−8092
high-velocity clouds, dynamic coronal gas flows 80−56928
N,O abundances in gaseous nebulae 78−8093
N^+ fine structure levels, UV radiative pumping 79−53871
$N^+ + H$, charge transfer reaction in nebulae rel. to ionization struct. 80−46384
NGC 1499, H II region nebula parameters determ. from decametre wavelength obs. *(Ukrainian)* 79−40243
Ne II, III, IV, photoionisation cross sections calc. 80−43014
O II, relative intensities and lifetimes in nebulae, conventional radiation theory 80−109513
nebulae continued
O II and S II forbidden lines as determinant of reddening and electron density 79−30114
OH 0739-14, IR source assoc. with double-lobed refl. nebulae, far IR obs. 78−54009
rho Ophiuchi dark cloud, o-formaldehyde excitation temp. and optical depths 80−51846
ρ Ophiuchi dark cloud complex, gamma-ray sources and particle acceleration 80−31345
SO in dark and molecular clouds, 30 GHz obs. 80−46639

necking
bar, rectangular, necked, void growth, finite element anal. 80−64383
bar, rectangular elastic-plastic, necking in plane tension, boundary value problem 79−50608
biaxially stretched sheets, exam. of void growth and local necking 78−90735
α-brass, with few inclusions, shear mode of ductile fracture 77−36652
corner theories, time-independent incremental behaviour at corner of yield surface 80−64388
creep rupture of specimens with random material props. 79−10491
cylinder, elastoplastic, necking under uniaxial tension 78−63335
cylindrical bar in tension, necking, num. anal. 79−90147
dynamic analysis based on stress wave propagation 80−1440
elastic-plastic circular plates, biaxially stretched, necking calcs. 78−5666
elastic-viscoplastic materials, strain rate effects on necking 80−58918
fuel sheaths, neck growth during high temp. transients in steam 80−78396
loading history depend. 80−5957
metal, fracture under influence of high power US waves *(Russian)* 79−5034
metal, sheet, numerical anal. of tensile tests 77−86101
metal sheets, theories of necking and limit strain calc. 79−29115
metallic shell, explosive expansion, deform. and rupture modes and mechanisms 80−85064
metals, phys. model of process of loss of mechanical stability and neck formation *(Russian)* 78−6969
nylon 6 and 66, necking stress *(Japanese)* 77−56037
1-nylon polymers, stress-strain curve 80−60938
PET, rigid, unoriented, prefracture state study, forced high-elastic deform. 77−59931
plastic instabilities and uniaxial tensile ductilities 80−79180
plastic instability during tensile deform., numerical calc. 78−30203
plastics and reinforced plastics, tabulated data as design guide 77−21087
polycarbonate, ductile, large strain cyclic deform. 80−85000
polycarbonate, neck propag., rel. to dry craze growth mechanism 80−59563
polycarbonate (BPA), thickness depend. of G_c for shear lip propag. from single crack propag. 78−11305
polycarbonate of bisphenol A, neck form. and propag., strain anal. 80−16376
polychlorotrifluoroethylene, necking stress *(Japanese)* 77−56037
polycrystalline wires, small dia., formulation of zero creep method 78−52922
polyethylene, effects of mol. rot. and crosslink on specific draw ratios *(Japanese)* 79−96099
polyethylene, environmental stress cracking, liq. efficiency criteria 80−21134
polyethylene, high density, ductile, large strain cyclic deform. 80−85000
polyethylene, high density, effects of draw rate and temp. on necking stress *(Japanese)* 79−91757
polyethylene, high density, necking stress *(Japanese)* 77−56036
polyethylene, high density, plastic behaviour determ. at const. true strain rate 79−39073
polyethylene, high molecular weight, effect of density on properties 77−90403
polyethylene, high-density, tensile necking, specimen size and loading conditions effects 79−61672
polyethylene, necking stress *(Japanese)* 77−56037
polyethylene, rolled, neck draw *(Japanese)* 77−86090
polyethylene films, oscillatory necking 79−72826
polyethylene glass sphere filled, crack form. and necking *(German)* 78−35452
polyethylene terephthalate, stretching, heat effects, struct. transforms. 79−15735
polyethyleneterephthalate, thermal effects of necking during stretching *(Russian)* 77−32662
polyethymethylene, necking stress *(Japanese)* 77−56037
polymer, crystalline, necking stress, thermodynamically derived equation *(Japanese)* 79−91758
polymer, drawing properties, role of interfibrillar tie mols. 78−76706
polymer, fracture mechanism and surface crazing 77−90446
polymer, plastoelasticity theory 78−75712
polymers, crystalline, oriented, drawing, load elongation behaviour, fibre composite model 79−15691
polyoxymethylene, low-strain deform., transmission electron microscope exam. 79−5013
polypropylene, ductile, large strain cyclic deform. 80−85000
polypropylene, metallic glass filled, mech. props. rel. to temp., strain rate filler content *(Japanese)* 79−15742
polypropylene, microstruct. changes during large strain cyclic deform. 80−66627
polypropylene, necking stress *(Japanese)* 77−56037
polypropylene, oriented, compressive elastic modulus and yield strength 80−16385
polystyrene, plastic fracture near T_g at low strain rate 77−86178
polystyrene-poly(styrene-b-butadiene-b-styrene) polyblends, mech. props. 78−52919
polyterephthalate, necking stress *(Japanese)* 77−56037
pressurised spherical membranes, critical stress for bifurcation into given modes 77−68448
PTFE, necking stress *(Japanese)* 77−56037
punch stretching, localised necking, finite element anal. 80−102971
PVC, plastic behaviour determ. at const. true strain rate 79−39073
PVC, tensile test neck development theory 78−52897
PVC, tensile tests, post-yield phenomena 79−91752
PVC, tensile tests at low strain rate, secondary instability form. *(German)* 77−66727
rotating discs, burst strength and necking 78−79226
round bar, tensile deformation, mathematical description 79−10500
shaped charge jet stability 78−13919

necking continued
sintering, liquid phase, neck growth kinetics, analysis 77−70012
snow, volumetric constitutive law based on neck growth model 80−48595
solidification, gravity level effects, direct obs. 77−36494
spherical powder sintering by surface diffusion, computer simulation 78−48344
steel, alloy, tension test, computer simulation of deform. to fracture 79−11667
steel, austenitic, metastable, micronecking deform. in tension, singularities *(Russian)* 80−30017
steel, C, spheroidized, type 1090, exam. of reverse flow behaviour 78−80610
steel, C, tensile props. in high press. H_2 at room temp. *(Japanese)* 80−108501
steel, deformation and stresses during elongation, application of Ludwig eqn. *(German)* 80−40475
steel, fibrous crack extension, micromechanisms 80−108563
steel, low C, Mn, strain hardening parameters, electron microscope obs. 77−63690
steel, low-C, transformed by cooling in ferritic-pearlitic range, relations between cooling rate, struct. and mech. props. *(French)* 77−32570
steel, maraging, 18 wt.% Ni, tensile props., effect of aged struct. and austenite grain size 77−48511
steel, stainless, clad Al, sandwich sheet material, forming limits 80−3131
steel, structural, influence of deform. heat on the mech. props. *(German)* 78−84904
steel A-106, yield point suppression by H_2 79−8368
strain rate dependent materials, neck development, accuracy of long wavelength approximation 78−56719
strain rate gradient development 79−46219
strain rate sensitivity under uniaxial tension 77−77525
stress distribs. in vicinity of a neck, Bridgman anal. 79−81737
tensile instability in material with strain hardening and strain-rate hardening 78−23717
tensile stability, effect of crack and cavitation generation 77−16659
tensile test piece, profile of contracted part after the beginning of necking *(German)* 77−86269
tension test with neck triaxiality reduction 78−7159
tubular specimens, tensile testing with delayed necking 77−90522
Zircaloy-2, deformation instability and tensile elongation 77−32655
Al alloy, 6061-T6, thickness depend. of G_c for shear lip propag. from single crack propag. 78−11305
Al, circular tube, forming limit of free bulge-forming *(Japanese)* 80−55477
Al-Mg (4 wt.%), enhanced ductility at elevated temps. 77−63740
Al-Zn-Mg, cavitation during superplastic deform. *(Japanese)* 78−15464
Cu, cold worked, grain size effects on short-term strength *(Russian)* 78−56693
Cu, cold-rolled, thickness depend. of G_c for shear lip propag. from single crack propag. 78−11305
Cu, deform. instability and tensile elongation 77−32655
Cu, tensile fracture mech. 77−63782
Cu-Al-Si-C (95, 2.8, 1.8, 0.4 wt.%) fracture characts. of superplastic single phase, exam. 78−48500
Cu-SiO_2 alloy, fracture at elevated temp. 78−39896
Fe, ductile fracture, fractographic characts. SEM exam. of fracture surface necking obs. 78−35506
α-Fe, plastic deform. in neck leading to fracture 78−64655
Fe plastic strain, thermoactivation anal. exam. of method *(Russian)* 79−57164
Fe-Cr-Ni, two-phase ($\alpha+\gamma$), and metastable austenitic, uniform elongation peak 77−77547
Fe-Mn (32.5 and 38.3 wt.%), steel sheet, exam. of form limit diagrams and damage 78−48461
Fe-Ni-C (31, 0.1 wt.%), kinetics of deform. induced martensite, shock loading and grain refinement effects 78−15395
KCl:Ba, γ-irradiation, defect struct., X-ray and chemical etching exam. 77−84793
Mo fibre reinforced Cu with weak interfaces, stability of tensile deform. 80−97533
Ni-Cr machine steel, austenite grain size effects on mech. props. *(Russian)* 77−44292
$Ni_{49}Fe_{29}P_{14}B_6Si_2$ glass, flow and failure 80−40438
$Pd_{80}Si_{20}$, plastic flow, fracture, slanted necking and elongation at high temps. 79−57057
Ti alloy A-75, plastic instability in sheet deformed in uniaxial tension at 300 to 700K 79−47742
Ti-Al-Sn (5, 2.5 wt.%) alloy, fatigue under combined alternating bending and torsional stresses 77−8923
Ti-Al-V (6,4 wt.%), plastic flow instability and multiple necking during superplastic flow 77−8896
Ti-Mo (15 wt.%) alloy, metastable β-phase, deform. characts. 78−6975
V, polycryst., O_2 effects on strength and ductility 77−36529
Zn alloys, deep drawing behaviour, exam. in binary and ternary alloys *(French)* 79−52325
Zn, deep drawing behaviour *(French)* 79−52325
Zn-Al (22 wt.%) superplastic alloy, cavitation and neck form. 80−30022

Neel temperature
actinide dioxides, low temp. lattice parameters, Neel pt. behaviour 77−27867
amorphous magnet, Bethe-Peierls-Weiss approx. 78−76263
anisotropic antiferromagnets, mixture of two, with different easy axis, oblique antiferromag. phase 77−59408
anisotropic pseudo one-dimensional Heisenberg systems, phase diagrams 78−52289
antiferromagnet, cluster approximation, Neel temp. and specific heat calc. 80−54901
antiferromagnetic, spin fluctuation resist. near T_N, theory 77−40071
antiferromagnetic biexcitons in critical temp. range 79−95601
antiferromagnetic Fermi liquid, critical phenomena, neutron scatt., Neel point *(Russian)* 80−71077
antiferromagnets, magnetic susceptibilities in Heisenberg and Ising models 79−24185
1,3-bisdiphenylene-2-phenyl allyl benzene complex, free radical, EPR, antiferromag. long range ordering 79−47335
calcium copper acetate hexahydrate, $CaCu(CH_3COO)_4.6H_2O$ and $CaCu(CD_3COO)_4.6H_2O$, susceptibility meas. 78−2680
copper, benzoate, one-dimens. antiferromag., heat capacity, field-induced crossover of spin-dimensionality 80−97099
Neel temperature continued
copper benzoate, antiferromag. reson. below 1K, Neel temp. determ. 78−39407
copper benzoate, mag. heat capacity and Neel temp. in mag. field 79−61147
copper formate tetrahydrate, antiferromag. phase, neutron diffr. study 80−93085
copper formate tetrahydrate, two-dimens. spin 1/2 Heisenberg antiferromag., phase transition characts. 77−66352
copper formate urea hydrate, two dimens. antiferromagnet, EPR, temp. depend. 80−54937
Cr-Au alloys, dil., elec. resist., 77-700K 78−64035
diammonium layer compounds $(CH_2)_n(NH_3)_2MnCl_4$, quasi-two-dimens. antiferromag., magnetis., spin-flop and crit. exponents 77−66311
dimethylammonium copper chloride, magneto-optical props., 0.03-13.5 eV 77−52132
dimethylammonium iron chloride, two-dimens. antiferromag., ^{57}Fe Mossbauer obs., sublattice magnetis. 77−66443
dimethylammonium manganese trichloride:Cd(Cu), impurities in quasi-one-dimens. Heisenberg systems, anisotropy effect 80−80502
dimethylammonium manganese trichloride, pseudo one-dimens. Heisenberg antiferromag., phase diagrams 79−61148
ferrimagnetic Neel mode with helical mode, coupling energy study *(French)* 80−70999
graphite-$FeCl_{3-x}$ intercalation compounds, Mossbauer spectra 80−20538
Heisenberg antiferromagnet, AFMR freq. temp. depend., integral peak intensities *(Russian)* 80−54951
Heisenberg antiferromagnet, anisotropic, excitations at finite temp., CPA calcs. 79−95562
Heisenberg antiferromagnet, dil., CPA calc. 78−68263
Heisenberg antiferromagnet, disordered, magnetic atom-conc. near percolation threshold, mag. props. *(Russian)* 78−80171
Heisenberg-Ising magnets, random, critical temps., binary mixture, amorphous magnet and spin glasses 80−54911
Hubbard model, FCC, fourth order interaction effects 78−23235
Hubbard model, random one-body approx., higher dimens. lattices 79−37945
Invar, ternary alloys based on Cr-Fe and 4d transition metals, magnetically insensitive 77−28026
Ising model, dipolar antiferromag., negative absolute temp. crit. point determination *(Russian)* 78−43594
Ising model, ferromag. and antiferromag. in mag. field, new perturbation approach 78−56336
itinerant antiferromagnet, paramag. impurity effects on Neel temp., calc. 80−60257
itinerant electron antiferromagnet, effects of paramagnetic impurities 79−4678
itinerant electron antiferromagnetism, effect of mag. field 78−27013
itinerant-electron antiferromagnet elec. resistivity near Neel temp. 79−42742
low-dimensional antiferromagnet Neel temp. in mag. field 77−32200
magnetically ordered metals, possible first order phase transformation 79−95589
manganese formate dihydrate, Zn- and Mg-substituted, anomalous crit. phenomena 80−60316
many-valley semiconductors, antiferromagnetic or atomic ordering effects on conduction electrons 80−2329
metal, with paramag. impurities, impurity conc. depend. calc. 78−68232
metals, Neel temp. and crit. exponents determ. from electronic transport coeffs. 77−69556
mixed valence compounds, dynamic susceptibility, RPA study of Anderson lattice 80−97075
perovskites, ordered, mag. props. *(French)* 78−95434
1,3-propanediammonium tetrachloromanganate(II) mag. props. 4.2-220K 77−20567
pseudo-one-dimensional Heisenberg system, Neel temp. field depend. 78−68277
pyridinium manganese trichloride, pseudo one-dimens. Heisenberg antiferromag., phase diagrams 79−61148
random binary magnetic systems, quenched, Neel temp. calc. 77−89963
random Ising model with transverse field term 79−56545
rare earth alloys, mag. phase diagram 78−10684
rare earth alloys, RFe_4Al_8, mag. props., Mossbauer spectra, ordering effects 77−63179
rare earth heavy binary alloys, press. effect on mag. props. *(Japanese)* 77−43835
rare earth hydrides, props., book contrib. 80−45291
rare earth intermetallic, RCu_4Ag (R=Nd,Sm,Gd,Tb), mag. props. and cryst. struct. 77−20562
rare earth intermetallics, RGa_2, mag susceptibility, 1.5-300K and Neel temp. 78−68184
rare earth intermetallics, RGa_2, ordering and exchange interactions 80−39779
rare earth intermetallics, RM_{12}, mag. interactions, mag. meas. and neutron diffr. 77−63103
rare earth metal, muon spin relax. meas. of Neel temp. and antiferromag. transitions *(Russian)* 79−87369
rare earth orthoferrites, cation depend. *(Japanese)* 77−43834
rare earth palladinides, R_3Pd_4, mag. props. 77−47980
rare earth perovskites, prep. and props. book contrib. 80−44193
rare earth sesquioxides, cubic, indirect exchange interactions Anderson model 79−95585
rare earth tetraborides, mag. and elec. props., metallic character 80−20386
rare earth Y alloys, Neel temps., mag. susceptibility meas. 77−73025
rare earth-gold intermetallics, RAu_2, mag. props., 4.2-300K 79−7972
rare earth-Zn_{12}, mag. props. and structs. 78−84393
rare-earth, light-heavy alloys, resistivity, mag. contrib. to resist. and Neel temp. 78−51971
rare-earth alloy, RSb, (R=Er, Ho, Dy, Tb, Nd, Gd), mag. props., hydrostatic press. depend. 77−80918
rare-earth-Pd alloy, mag. props. 77−20547
semiconductors, magnetic, static magnetic properties, mean field approach 80−7090
spin-1 antiferromagnet, with biquadratic exchange, RPA 77−47953
static properties of spin systems with truncated secular dipolar coupling 78−88130
steel, austenitic stainless, Neel temperature and max. susceptibility calcs. 77−43833
steel, Cr-Mn (13, 19 wt.%), elastic const. behaviour, anomalous, low temp. 80−97521

Neel temperature continued
steel, stainless, Cr-Mn, N strengthened, anomalous low temp. elastic behaviour 77−77524
steel, stainless, Cr-Ni-Mn, N-strengthened, low temp. elastic props., correl. with mag. props. 79−70109
steel, stainless, type 310, antiferromag. ordering, press. depend., Mossbauer meas. 79−73861
TANOL, linear chain antiferromagnet, long-range order, magnetisation, PMR 78−23266
TMMC:Cu(Ni)(Cd), mag. and non-mag. impurity effects on suscept. and Neel temp. 77−66312
TMMC:M, impurity (M) effects on Neel temp. and low temp. mag. susceptibility 78−88113
TMMC, 3d ordering, effect of mag. field, PMR meas. 77−4569
TMMC, effect of impurity spins on three-dimensional ordering 79−24159
TMMC, impurity doped, antiferromag. three-dimensional ordering, proton NMR meas. 79−78414
TMMC, linear antiferromag., mag. phase diagram, expt. and theoretical study 80−71038
TMMC, linear Heisenberg antiferromag., effect of mag. field on 3d ordering and spin correlations 78−68229
TMMC, mag. heat capacity and Neel temp. in mag. field 79−61147
TMMC, Neel temp. in large mag. fields 77−89953
TMMC, quasi-1D antiferromag., mag. phase diagram 80−2573
transition metals, surface- or defect-induced magnetism, nearly half-filled bands 79−1671
trimethylammonium cobalt trichloride, mag. heat capacity and Neel temp. in mag. field 79−61147
two-sublattice magnetic substances, mag. transitions due to exchange-striction mechanism *(Russian)* 77−47995
uniaxial S=1 antiferromagnet, effect of cryst. field anisotropy, Neel temp. calc. 77−28344
weak ferromagnet, with easy plane anisotropy correl. functions and magnetisation, temp. depend. *(Russian)* 80−84581
wustite solid solns., props. connected with localised electron state 80−107734
Au-Mn alloys, equiatomic region of phase diagrams crystallographic and mag. exam. 78−52755
$Ba_2Fe_7O_{11}$, antiferromagnet, exam. of mag. props. by mag. meas., and Mossbauer spectroscopy 78−52256
$BaLaMRuO_6$, (M=Mg, Fe, Co, Ni, Zn), cubic ordered perovskites, Mossbauer and mag. susceptibility meas. 80−75889
$BaMn_{0.99}Co_{0.01}F_4$, magnetoelec. phenomena, dielec. behaviour near Neel temp. 80−71151
$BaMnF_4$, antiferromag., dielec. anomalies at low temp. obs. 77−20791
$BaMnF_4$, spectroscopy near ferroelec. transition, dielec. anomalies near mag. ordering temp. 80−75965
$BaSr_xCa_{1-x}Fe_4O_8$, substituted hexagonal ferrites, mag. split Mossbauer spectra obs. and X-ray struct. data 80−71250
Ba_2XRuO_6(X=La,Eu), ^{99}Ru Mossbauer spectra and other techniques 80−29659
$Bi_2Fe_4O_9$, antiferromag., mag. glass props. *(Russian)* 77−4519
$(CH_3NH_3)_2FeCl_2Br_2$, two-dimensional antiferromag., field depend. of susceptibility meas. 77−63130
$CaCu_3Ti_4O_{12}$, mag. struct. and props. *(French)* 77−69495
$CaCu_3Ti_4O_{12}$, mag. struct., neutron diffr. powder data, 27K T_N 77−69502
$CaFeF_5$, one-dimens. magnetism *(French)* 79−73670
$Ca_xFe_{3-x}O_4$, Ca^{2+}, Mossbauer study 78−10814
$Ca_2LaFe_3O_8$, Fe replacement by diamag. cation, Neel temp. *(French)* 79−73712
$Ca_2LaFe_3O_8$, physico-chemical characterisation, Mossbauer exam. and mag. props. *(French)* 77−28494
$Ca_3Mn_2Ge_3O_{12}$ garnet, metamagnetic transition, high anisotropy peculiarities *(Russian)* 80−60274
$Ca_2Mn_3O_8$, mag. props. 79−78339
$Ca_2Ti_{2-2x}Fe_{2x}O_{6-x}$, antiferromag. phases, Neel temp. variation, vacancy long-range order *(French)* 78−34979
Ca_2XRuO_6 (X=Y,La,Eu), ^{99}Ru Mossbauer spectra and other techniques 80−29659
$Cd_3Cr_2Ge_3O_{12}$, antiferromagnetic ordering of Cd^{3+}, sp. ht. and mag. susceptibility meas. 77−16062
$Cd_2Mn_3O_8$, mag. props. 79−78339
$Cd_{1-x}Ni_xFe_2O_4$, solid soln., mag. and structural characterisation 80−103906
$Cd_xNi_{1-x}Fe_2O_4$, mag. behaviour, Mossbauer meas. 78−52390
β-Ce, susceptibility meas., 2-300K 77−4320
$CeAl_2$, Anderson lattice system, mag. moment reduction, press. effects 80−7093
$CeBi_xSb_{1-x}$, mag. props. and press. effects 80−71026
CeC_2, mag. props. 80−108008
$Ce_xDy_{1-x}C_2$, solid solns., mag. props. 80−108008
$CeIn_3$, Neel temp., hydrostatic press. depend. 80−29549
$Ce_{1-x}La_x$, thermoelectric power, mag. transition temps. 80−20154
$Ce_x(La_{0.76}Y_{0.24})_{1-x}Bi$, mag. phase diagrams 79−56535
$CeMn_2Si_2$, cryst. and mag. struct. and T_N 78−52225
CeSb, mag. phase transitions, zero applied mag. field 78−31070
$CeSb_xAs_{1-x}$, mag. props. and press. effects 80−71026
^{244}Cm, electrical resistivity and mag. ordering 77−80760
$CoAl_xGa_{2-x}O_4$, mag. interactions, susceptibility obs., 4.2 to 300K 79−15294
$Co_3B_7O_{13}Cl$, polydomain ferroelec., magnetoelec. effect below Neel temp. 78−10745
$CoBr_2,6[xD_2O(1-x)H_2O]$, mag. order investig. by neutron diffr. 77−66310
$Co(C_5H_5NO)_6(ClO_4)_2$ $[(BF_4)_2]$, X-Y antiferromagnet, Neel temp., spin correlation functions 80−60345
$CoCl_2$, antiferromag., phase diagram, heat capacity meas. 80−93126
$Co_xNi_{1-x}Cl_2.6H_2O$, calorimetry, γ-type transitions of sp. ht. 78−68256
$CoRh_xGa_{2-x}O_4$, mag. interactions, susceptibility obs., 4.2-1000K 79−15293
$Co_xZn_{1-x}Rh_2O_4$, mag. props., EPR spectra, antiferromag. order 80−75736
Cr alloys, Neel temp. of one dimens. electron gas in spin density wave state 80−65884
Cr, and alloys, surface- or defect-induced magnetism, nearly half-filled bands 79−1671
Cr, elec. resist. near Neel temp. 79−33278
Cr, electronic structure model, Invar effect, antiferromagnetic-non mag. transitions 80−20370
Neel temperature continued
Cr film, size effects on spin density waves, struct. and elec. props. 77−80973
Cr, hyperfine interactions on ^{111}Cd-probe nuclei, TDPAC meas. 80−75904
Cr, magnetic phase diagram in external mag. field, spin reorientation curve, critical point coordinates *(Russian)* 80−29548
Cr, magnetic phase transition at Neel temp. 78−2681
Cr, magnetoresist. meas., Neel temp. independ. of current direction and mag. field 77−85197
Cr, Neel temperature and Fermi energy, nonmag. impurity effects 80−65888
Cr, phase transition at T_N 79−4676
Cr, single Q-state, antiferromag. phase, rel. to band struct. 77−15759
Cr, spin density wave, stress and impurity conc. depend. 77−73029
Cr, spin density wave, temp. depend. of second and third harmonics 77−12094
Cr-Al, antiferromag., transport props., anomalous crit. behaviour 79−61108
Cr-Al, effect of Al concentration and hydrostatic press. on Neel temp. 79−33482
Cr-Al, spin density wave, neutron diffraction studies 79−1664
Cr-Co, spin density wave, neutron diffraction studies 79−1664
Cr-Co (4.0 at.%) alloy, antiferromag., disappearance of resist. min. under press., and press. coeff. of T_N 80−10960
Cr-Co alloys, dil., with local mag. moments, Neel temps. 79−73713
Cr-Fe, antiferromag. sp.ht. around Neel point 79−73750
Cr-Fe (0.6 at.%), antiferromag., anomalous press. effect on resist. minimum 79−15138
Cr-Fe alloys, polycrystalline, antiferromag., elastic moduli and thermal expansion meas. 77−43860
Cr-Fe-Co dilute alloys, Neel temp., thermal expansion rel. to Co content 79−47281
Cr-Fe-Si, spin density wave, neutron diffraction studies 79−1664
Cr-Fe-V, dil., V effect on para- to incommensurate and commensurate transitions 78−68260
Cr-Ga alloys, dil., Neel temp., elec. resist. and thermal expansion meas. 79−51778
Cr-Mo, electrical resistivity, spin density wave gap, Neel temp. 80−88534
Cr-Pd dilute alloys, itinerant antiferromag., neutron diffr. meas. 77−77032
Cr-Pt, dil., effect of Pt on itinerant antiferromagnetism 78−64191
Cr-Re, dil. alloy, mag. susceptibility temp. depend., thermal expansion coeff. *(Russian)* 78−76225
Cr-Si, dilute alloy, mag. susceptibility and Neel temp. meas. 80−71017
Cr-Si, magnetically insensitive Invar-type alloys *(Japanese)* 79−8034
Cr-Si alloys, press. depend. of Neel temp. 77−69555
Cr-Si-V, dil., V effect on para- to incommensurate and commensurate transitions 78−68260
CrAl, semicond. solid solns., depend. of energy gap on AF ordering 78−67941
CrAs, anisotropy of compressibility 79−7648
CrAs, press. depend. calc., volume-striction mechanism of transition 77−24696
CrB_2, crystal growth by floating-zone method, elec. and mag. props. 77−1801
$Cr_xFe_{3-x}O_4$, spin and charge density oscillations due to impurities *(Korean)* 80−20565
$Cr_{1-x}Fe_xOOH$, $0 \leq x \leq 10$, prep., Mossbauer effect, Neel temp. 80−108134
Cr_2O_3, dielec. const. in mag. field, nonlinear magnetoelec. effect in Neel pt. region 80−66006
Cr_2O_3, EPR linewidth, near Neel temp. 78−23327
Cr_2O_3, mag. phase boundaries near bicrit. and Neel points 78−34980
Cr_2O_3, magnetic susceptibility, near Neel temp. 79−56509
Cr_2O_3, specific heat near. Neel temp. 77−63207
CrS, magnetic struct. from neutron diffr. meas., Neel point 77−32164
$CrS_{1-x}Se_x$, antiferromag. props., struct., variations near Neel temp. 78−64199
$CrSb_{1-x}As_x$, exchange striction and press. effect on Neel temp. 77−63189
$CrSb_{1-x}As_x$ press. effect on Neel point 80−71147
Cr_3Se_4, mag. susceptibility and sp. ht. meas. *(French)* 79−56507
$Cr_3Se_xS_{4-x}$, mag. susceptibility and sp. ht. meas. *(French)* 79−56507
$Cr_2Se_{3-x}Te_x$, mag. props. and lattice parameters, comp. depend. 77−66263
$Cr_3Se_{4-x}Te_x$, mag. props. and lattice parameters, comp. depend. 77−66263
Cr_2TeO_6, CC ^{57}Fe Mossbauer spectrum, hyperfine field, Neel temp. 79−56636
$CrVO_4$, Neel temp., mag. susceptibility meas. 80−29550
$CsCoBr_3$, quasi ID Ising antiferromag., polarised Raman scatt. from mag. excitations 80−66182
$CsLi_{0.5}(Al,Fe)_{1.5}F_6$ pyrochlore, Mossbauer contrib. to exam. of cationic order *(French)* 80−93224
$CsLi_{0.5}Fe_{1.5}F_6$ pyrochlore, Mossbauer contrib. to exam. of cationic order *(French)* 80−93224
$CsMnCl_3.2H_2O$:Cu(Co), quasi one-dimens. antiferromag., mag. impurity effect on Neel temp. and spin-flop field 79−61099
$CsMn_{1-x}Cu_xCl_3.2H_2O$, impurities in quasi-one-dimens. Heisenberg systems, anisotropy effect 80−80502
$CsMnF_3$, mag. phase boundaries, XY to Ising crossover, virtual bicritical point 80−50095
$CsMnX_3.2H_2O$ (X=Cl,Br), pseudo one-dimens. Heisenberg antiferromag., phase diagrams 79−61148
$CsNiCl_3$, one-dimens. antiferromag., US attenuation, crit. behaviour 77−66308
$CsNiF_3$, demagnetising effects on antiferromag. reson. 80−15803
$CsNiF_3$, quasielastic neutron scatt. around Neel-point 80−75768
$CsNiFeF_6$ pyrochlore, Mossbauer contrib. to exam. of cationic order *(French)* 80−93224
α-Cs_xVF_3, mag. props. *(French)* 77−80933
$CuBr_2$, NQR freqs. temp. depend., paramag.-antiferromag. transition 79−42867
$CuCl_2.2D_2O$, cryst. struct., mag. and reson. props. 80−60424
$CuCl_2.2H_2O$, antiferromag. reson., HF, press. depend. *(Russian)* 77−36137
$CuCl_2.2H_2O$, high hydrostatic press. effects, NMR obs. 77−40058
$CuCl_2.2H_2O$, influence of high hydrostatic press. on intermediate state associated with spin flopping 78−35020

Neel temperature continued
$CuCl_2.2H_2O$, magnetoelastic props. under press., antiferromagnetic resonance, lattice parameters 80−29598
$CuCr_2{}_xFe_xO_4$, charge transfer, Mossbauer spectroscopy 80−15836
γ-$Cu(IO_3)_2$, cryst. struct. and mag. behaviour 78−79571
$Cu(NH_3)_4SO_4.H_2O$, interface with liq. ^3He, Kapitza resist. anomaly near T_N 77−69139
$Cu(NH_3)_4SO_4.H_2O$, EPR around Neel temp. 78−39390
$Cu_4NiSi_2S_7$, X-ray cryst. struct. determ., mag. props. 80−107172
Dy, anomalous thermal expansion, interferometric meas. 78−52333
Dy, critical exponents and amplitude ratios from elec. cond. data, theoretical model 80−50126
Dy, elec. resist. and mag. struct. near Neel point *(Russian)* 79−47074
Dy, film, thermoreflectance dispersion curves at 315K and 97K 80−7332
Dy-Th, single cryst., mag. susceptibility, transitions, anisotropy 80−54873
Dy-Y paramagnetic-antiferromagnetic transition temp., depend. on Dy conc. 79−69673
$DyAsO_4$, phase transitions obs. 80−70412
DyBi, mag. behaviour 80−71025
DyC_2, mag. susceptibility, temp. depend. 79−87239
Dy_2C_3, cryst. struct., mag. struct. and props., 1.6 to 300K 79−11296
$DyCo_2Si_2$, mag. props. 80−107988
$DyNi_2Si_2$, mag. props., 4.2-200K 80−84602
$Dy_2O_2SO_4$, antiferromag., mag. props. and Zeeman effect meas. 79−33464
$Dy_{1-x}Sm_x$, magnetoresist. of polycryst. specimens in fields up to 44 kOe *(Russian)* 80−92880
$DyVO_4$, phase transitions obs. 80−70412
Er, paramagnetic and antiferromagnetic states, optical absorption *(Russian)* 78−56497
$ErCo_2Si_2$, mag. props. 80−107988
$ErCrO_3$, phonon Raman spectra rel. to mag. ordering 77−52100
$Er_2O_2SO_4$, antiferromag., mag. props. 1.6 to 40K 79−33464
Eu, elec. resist., effect of mag. field near Neel point 77−8073
Eu, elec. resistance anomaly below Neel temp. 77−11889
EuB_6, correlation between mag. struct. and elec. props. 77−63192
$EuMg_2$, cryst. and mag. props., ordering 78−68185
EuS, thermo- and magnetorefl. spectra, dynamical spin fluctuation effect on exciton state 77−52126
$EuS_{1-x}Se_x$, mag. phase diagram, from temp. depend. of magnetisation 80−7105
EuTe, Neel temp. and hyperfine interactions, press. depend. up to 60 kbar, ^{151}Eu Mossbauer obs. 77−63181
$Eu_{1-x}Yb_xTe$, ($0<x<1$), mag. semicond., elec., mag. and optical props. 80−97070
Fe, antiferromag. props., Neel temp. determ. 78−88124
γ-Fe precipitates, antiferromag. ordering, press. depend., Mossbauer meas. 79−73861
Fe-Cr, dil., spin density wave under high press., neutron diffr. study 80−65798
Fe-Cr (70-92 at.%), coexistence of ferro- and antiferromagnetism *(Russian)* 78−47955
Fe-Cr-Ni alloy, austenitic, Neel temp. and max. susceptibility predictions comp. effects 77−43833
Fe-Fe_2O_3-$NaFeO_2$, study of Na-containing wustite region *(French)* 77−73264
Fe-Mn, annealed, α-γ phase transformation obs. 78−75831
Fe-Mn (14.1 wt.%), G14, α-martensite formation in mag. field 79−91648
γ-Fe-Mn alloys, antiferromag., mag. and crystallographic transformations 77−55964
Fe-Mn alloys, mag. susceptibility and conc. depend. of Neel point *(Russian)* 79−47279
Fe-Mn mag. contributions to $\gamma \rightarrow \varepsilon$ phase transformations 80−25694
Fe-Mn-Co-Ni-Cr, antiferromag. props., Neel temp. determ. 78−88124
Fe-Mn-Cr(Ni), mag. and crystallographic transformation depend. on Cr-Ni addition *(Russian)* 79−83334
Fe-Ni(Cr), Invar, exchange interactions between ferromag. and antiferromag. components 80−29545
Fe-Ru(Os), CC hexagonal phase, ^{57}Fe Mossbauer study, saturated hyperfine fields and Neel temp. determ. 79−91321
Fe-Ru(Os) alloys, antiferromag. ordering, hyperfine fields 80−15867
Fe_2As, mag. props., Mossbauer study 80−88897
$FeBO_3$, weak ferromag., mag. field influence on crit. behaviour of susceptibility 78−14942
Fe_3BO_6, weak ferromagnetism and spin reorientation, antiferromag. reson. spectra 78−6580
$Fe_3B_7O_{13}Br$, $Fe_3B_7O_{13}Cl$, polydomain ferroelec., magnetoelec. effect below Neel temp. 78−10745
$Fe_3B_7O_{13}I$, ferroelec., mag. ordering, neutron diffr. meas. 78−72331
$FeBr_2$ metamagnet, unusual phase diagram, theory 80−93119
$FeCO_3$, mag. field drawn destruction of antiferromag. destruction, light depolarisation at mag. transform. *(Russian)* 78−23432
$FeCO_3$, metamagnetic insulator Neel temp. anal. by model including spin fluctuations *(Russian)* 80−15715
$FeCO_3$, vibronic coupling at Neel temp. 80−15491
$FeCl_2$, magnetic phase diagram, optical studies 78−88121
$Fe_{1-x}Cl_2{:}Cd_x$, randomly disordered, tricrit. behaviour, light scatt. 78−68255
$FeCoCrO_4$, Mossbauer study, cation distrib. and Neel temp. determ. 79−33571
$Fe_{1-x}Co_xGe_2$ solid solns., mag. susceptibilities, multiple stages in mag. transitions, effective mag. moment 77−8286
$Fe_xCo_{1-x}Rh_2S_4$, spinel struct., X-ray, mag., elec. and Mossbauer spectra meas. 77−12278
$FeCr_{2-x}In_xSe_4$, struct. and mag. props., comp. depend. 77−66262
$Fe_xCu_{1-x}Rh_2S_4$, mag. tetrahedral intrasublattice interaction, X-ray, magnetisation and Mossbauer expts. 78−52241
FeF_2, mag. sp. ht. near Neel temp. mag. susceptibility meas. 80−60341
FeF_3, amorphous, noncryst. magnet with antiferromag. interactions 79−91228
FeF_3, magnetic susceptibility near Neel point 77−55670
$FeGe_2$, antiferromag., biquadratic exchange 80−2371
$FeMO_2S_4$, Mossbauer investigation, Neel point, superparamag. effects 80−97170
$Fe_{1-x}Mn_xCl_2$, disordered, Raman scatt. from Fe^{2+} and Neel temp. 80−60579
FeMnP, Mossbauer obs. 77−40156
$(Fe_{1-x}Mn_x)_3Si$, sp. ht. at low temps., mag. transitions *(Russian)* 77−32189

Neel temperature continued
Fe_2MoO_4, electron exchange between $Fe^{2+}-Fe^{3+}$ ions on tetrahedral and octahedral sites, Mossbauer spectra 79−78585
$FeMo_2S_4$, cryst. struct., mag. struct. and props., neutron diffr. meas. *(French)* 77−47971
$FeMo_2S_4$, Mossbauer spectra, 79-300K, Neel pt. determ. 78−60360
$FeNb_2O_6$, magnetisation, 1.4-80K, antiferromag. ordering 78−10666
$FeNiBO_4$, mag. and Mossbauer studies 79−65661
$FeNi_2BO_5$, mag. and Mossbauer studies 79−65661
$Fe_{65}(Ni_{1-x}Mn_x)_{35}$, H solid solutions magnetisation behaviour in pulsed mag. fields 79−65674
$Fe_{65}(Ni_{1-x}Mn_x)_{35}$, magnetic struct. and inhomogeneities by neutron scatt. and Mossbauer effect *(Russian)* 77−63122
Fe_2O_3 amorphous film, Mossbauer spectra, mag. props. 80−15851
Fe_2O_3 amorphous RF sputtered thin films, Mossbauer and mag. study 80−34711
α-Fe_2O_3, hematite, high temp. anomalous behaviour of cryst. lattice 77−69087
α-Fe_2O_3, Mossbauer spectra near Neel temp., critical indices, magnetisation *(Russian)* 80−66094
β-FeOOH, ultrafine particles, mag. struct., Mossbauer spectroscopy 78−72372
α-$FeOOH.nH_2O$, hydrogoethite, Mossbauer spectra, Neel point, Fe^{3+} config. 77−32310
$FePS_3$ and $FePSe_3$, mag. props., NMR meas. 79−24223
$FeSO_4$, anhydrous, γ, β and γ-phases, Mossbauer spectra, polymorphism 77−12287
$FeSO_4$, α- and β-forms, magnetic interactions, neutron inelastic scatt. study 80−107980
β-$FeSO_4$, high-temp. polymorph, stability, mag. struct., mag. props. 77−43815
$Fe_{1+\delta}Sb$, nonstoichiometry influence on mag. props. *(Russian)* 80−65813
$FeSn_2$, hyperfine mag. fields at ^{57}Fe, ^{119}Sn nuclei, under press. *(Russian)* 78−39486
Fe_2TeO_6, CC ^{57}Fe Mossbauer spectrum, hyperfine field, Neel temp. 79−56636
$FeTiO_3$, ilmenite, lunar and terrestrial, cell dimensions and antiferromagnetism 77−21764
$FeVO_4$, Neel temp., mag. susceptibility meas. 80−29550
$(Fe_xV_{1-x})V_2S_4$, and $(Fe_xV_{1-x})V_4S_8$, mag. props. 78−27034
$Fe_{1-x}Zn_xF_2$, dil. antiferromag., electronic and mag. props., Raman scatt. and optical absorpt. study 80−108207
$Fe_xZn_{1-x}F_2$, Neel point and short range order, dilution effects, mag. birefr. obs. 80−71019
$Fe_xZn_{1-x}F_2$, Neel temp., CPA calc. 78−68233
$Fe_xZn_{1-x}F_2$, Neel temp. mag. cone depend., CPA calcs. 78−88122
Gd Ni_2Si_2, mag. props., 4.2-200K 80−84602
Gd-Y (40 wt.%) alloy, magnetic phase transitions, elastic consts. meas. 78−14957
Gd-Y alloy, anomalous thermal expansion, interferometric meas. 78−52333
Gd-Y alloys, mag. crit. temp. gap 80−60260
$GdAg_{1-x}In_x$, magnetic transition temp., effect of hydrostatic press. 78−76244
$GdAlO_3$, magnetoelec. susceptibility, mag. struct., mag. phase diagram and crit. coeffs. 77−66303
GdAs(Sb)(Bi), antiferomag., EPR meas., Neel temp. determ. 77−32242
GdB_6 single crystals, mag. behaviour and structure change at low temp. 80−71018
GdC_2, mag. susceptibility, temp. depend. 79−87239
$GdCo_2Si_2$, mag. props. 80−107988
GdCuGe, $Gd_6Cu_8Ge_8$ and $GdCu_2Ge_2$, magnetic props. 77−32180
$Gd_xDy_{1-x}C_2$, solid soln., mag. susceptibility, temp. depend. 79−87239
$GdFe_2Ge_2$, magnetisation, 4.2-273K, and Neel temp. 77−8310
$GdMo_6S_8$, coexistence of antiferromagnetism and superconductivity, neutron diffraction study 79−99685
GdN, and $GdN_{1-x}O_x$, mag. interactions 80−60218
$Gd_2O_2SO_4$, antiferromag., mag. props. 1.6 to 40K 79−33464
GdS, low temp. phase transitions, mag. moment orientation, spin flip 79−99700
GdS(Se), antiferromag., EPR meas., Neel temp. determ. 77−32242
GdSe, low temp. phase transitions, mag. moment orientation, spin flip 79−99700
$GdSn_3$, Neel temp., hydrostatic press. depend. 80−29549
GdTe, low temp. phase transitions, mag. moment orientation, spin flip 79−99700
GeSe, antiferromagnetic behaviour, res. to negative magnetoresistance effect 79−73719
HoAlGa, mag. props. and struct. 78−39302
$HoAu_3$, mag. phase diagram 80−75761
$HoCo_2Ge_2$, crystal and magnetic structure obs. 80−64976
$HoCu_2$, mag. struct. and elec. resist., neutron diffr. obs. 80−60206
$Ho(Ir_xRh_{1-x})_4B_4$ pseudoternary system, supercond. and mag. ordering 80−70876
$Ho_2O_2SO_4$, antiferromag., mag. props. and Zeeman effect meas. 79−33464
$Ho_cY_{1-c}Sb$ system, magnetisation, elec. resist., and sp. ht. meas. 80−60213
$Ho_xY_{1-x}Sb$, mag. props. 80−34634
$KCoF_3$, mag. suscept. and Neel temp. determ. 77−77044
$KCoF_3$, strain sensitive props., Mossbauer spectra obs., Neel temp. distrib. 77−20765
K_2CoF_4, two-dimensional Ising-like antiferromag. birefringence, short-range order effect 77−81081
$KCrO_2$, two-dimens. mag. order, neutron powder diffr. obs. 80−44805
$KFeF_3$, strain sensitive props., Mossbauer spectra obs., Neel temp. distrib. 77−20765
K_2FeF_4, antiferromag., Mossbauer study of mag. ordering 79−28655
K_2FeF_5, Mossbauer spectra, 1D antiferromag. 80−15886
K_2FeF_5, one-dimensional antiferromag. systems, Mossbauer studies 80−71266
$K_{1+x}Fe_xGa_{11-y}O_{17}$, electron hopping and excitation at room temp., ^{51}Fe Mossbauer spectra 80−25257
K_2IrCl_6, sp. ht. meas. at low temp. 80−7119
$KMnCl_3$, magnetic spiral struct., neutron diffr. study 80−39748
$KMnF_3$, mag. props. and struct. transitions, antiferromag. reson. meas. 79−8052
$KMnF_3$, specific heat near Neel temp. *(Russian)* 80−100340
K_2MnF_4, two-dimens. Heisenberg antiferromag., field and temp. depend. of magnetic 77−66272

Neel temperature continued
$K_3Mn_2F_7$, crit. EPR line broadening near Neel temp. 80−71165
$K_2Mn_cMg_{1-c}F_4$, EPR spectra 78−76298
K_2NiF_4, 2D antiferromag., volume depend. of superexchange, US velocity meas. of T_N 78−19237
K_2ReCl_6, sp. ht. meas. at low temp. 80−7119
KVF_3, antiferromag. ordering points, thermal anal. and X-ray diffr. meas. *(French)* 78−84421
α-K_xVF_3, mag. props. *(French)* 77−80933
$LaMnO_3$, orthorhombic lattice distortions, mag. props. rel. to prep. conditions 77−20592
$La_2(MnO_3)_3$, hydrostatic press. effect on mag. struct., neutron diffr. 77−51886
$LaRu_xFe_{1-x}O_3$ perovskites, cryst. struct., elec., mag. and Mossbauer behaviour 77−55274
$LiCrO_2$, two-dimens. mag. order, neutron powder diffr. obs. 80−44805
$Li_xFePS_3(Se_3)$, Li_xMnPSe_3 and $Li_xNiPS_3(Se_3)$, NMR and neutron diffr. obs., mag. props. 80−60433
Li_xNiPs_3, mag. props. and ionic mobility, NMR mag. 79−24223
$(Lu, La, Y, Ca)_3(Ge, Fe)_5O_{12}$, temperature compensated high mobility bubble garnet, LPE and props. 77−20656
$Mg_{1-x}Mn_xTe_2$, random dil. antiferromagnet, mag. props. 80−54870
α-Mn, electronic structure model, Invar effect, antiferromagnetic-non mag. transitions 80−20370
Mn on Ni-Fe (40%), mag. interface effects 77−69638
γ-Mn-Cu, antiferromagnetism, martensitic transformation 79−1673
Mn-Cu, mag. and cryst. struct., neutron and X-ray diffr. meas. *(Russian)* 78−22694
Mn-Cu, shape-memory effect at martensitic transform., cryst. and mag. struct. 77−36610
Mn-Cu (9.3 wt.%), cryst. struct. at FCC to FCT transform. *(Russian)* 80−11643
Mn-Cu alloy, volume effect, paramagnetic-antiferromagnetic and structural transition, lattice consts. 80−39007
γ-Mn-Fe, FCC→FCT transform. temp. and Neel temp., X-ray and neutron diffr. expts. *(Russian)* 78−84797
α-Mn-Fe(Cr), influence of Fe and CR on Neel point *(Russian)* 77−1554
Mn-Ga, Elinvar charact. *(Japanese)* 79−61638
Mn-Ga, mag. and cryst. struct. in conc. region of gamma phase, temp. depend. *(Russian)* 79−65649
Mn-Ni, thermal expansion, mag. susceptibility, lattice consts. 80−100341
Mn-Ni alloys, γ-phase antiferromag., lattice distortion and elastic props., ΔE effect interpret. 77−20671
Mn-Ni alloys, Mn-rich, structural changes associated with antiferromag. ordering 77−69085
Mn-Pt, exam. of Elinvar props., from −150 to 500°C 78−76684
MnAs, struct. and mag. props., temp. depend., neutron study 79−47246
$MnAs_{1-x}P_x$, mixed crystals, metallic magnetically ordered, Hall effect 80−65536
$MnAs_{1-x}P_x$ whiskers, thermoelectric power, 5 to 350K, phonon drag effects and mag. transitions 79−28363
$Mn(Br_{1-x}Cl_x)_24H_2O$, antiferromagnetism, controllable anisotropy 80−93116
$MnBr_2.4H_2O$, high-resolution sp. ht. meas. near Neel temp. 77−28393
$Mn_xCd_{1-x}(NH_3)_2.Ni(CN)_4.2C_6H_6$, Hofmann type mixed cryst., mag. props. 79−4659
$MnCr_2S_4$, substituted, mag. struct. and transitions 80−65795
$(Mn_{0.95}Cr_{0.05})_3Si$, sp. ht. at low temps., mag. transitions *(Russian)* 77−32189
MnF_2, antiferromagnetic phase stability limit near spin-flop boundary 78−10683
MnF_2, local mag. ordering above Neel point, EPR *(German)* 77−36125
MnF_2, mag. susceptibility, crit. behaviour near Neel point 79−91217
MnF_2, specific heat, Heisenberg to Ising crossover near Neel temp. 78−47980
$Mn_{1-x}Fe_xAs$, magnetic transition under high press., exchange striction model calcs. *(Russian)* 80−50096
$Mn_xFe_{3-x}O_4$ ferrite film, exchange interaction depend. on conduction electrons *(Russian)* 80−34621
Mn_5Ge_3-Mn_5Si_3, electrical resistivity meas., order-disorder transition 80−10945
Mn_3In, antiferromag., mag. susceptibility, X-ray and neutron diffr. 79−11314
$Mn(NH_3)_2.Ni(CN)_4.(benzene)_2$, antiferromag. ordering, mag. susceptibility, sp. ht. and Neel temp. meas. 77−12128
MnO, multidomain single cryst. and monodomain cryst., crit. and elastic behaviour, T_N to 300K 77−66407
MnO, neutron diffr. meas., 100 to 700K, spin correls, above and below T_N 77−59390
$Mn_2P_{1-y}As_y$, Mossbauer obs. 77−40156
$MnPS_3$ and $MnPSe_3$, mag. props., NMR meas. 79−24223
MnS_2, first order antiferromag. phase transition 77−8317
$MnS_2(Se_2)(Te_2)$, mag. ordering, 2-cation, 2-anion indirect exchange interactions *(French)* 78−43566
MnSe, mag. suscept., thermal expansion and elec. resist. meas. 78−34964
α-$MnSeO_4$, magnetic interactions, neutron inelastic scatt. study 80−107980
$MnSiN_2$, 180°C Neel temp., mag. struct. and atomic coords., neutron diffr. meas. *(French)* 77−32168
MnTe, effect of press. on Neel temp. and lattice parameter 79−95594
MnTe, pressure dependence, 1 to 4300 bar 78−76247
$MnTiO_3$, quasi-two dimens. antiferromag., mag. crit. behaviour 77−32191
$Mn_xZn_{1-x}F_2$, CPA estimate for Neel temp. 78−76245
$Mn_xZn_{1-x}F_2$, Neel point and short range order, dilution effects, mag. birefr. obs. 80−71019
$Mn_{0.510}Zn_{0.417}Fe_{2.073}O_{4+\delta}$ relationship between magnetic permeability and stoichiometry 79−42799
Mo, single crystal, thermal expansion in magnetically ordered phases 78−2269
$(NH_3)_2FeF_5$, one-dimensional antiferromag. systems, Mossbauer studies 80−71266
NH_4FeF_4, mag. and Mossbauer obs. *(French)* 78−19389
$N_2H_6FeF_5$, Mossbauer spectra, 1D antiferromag. 80−15886
$N_2H_6FeF_5$, one-dimensional antiferromagnetism, Mossbauer study 80−65872
$(NH_4)_2ReCl_6(IrCl_6)$, proton relaxation near antiferromagnetic phase transitions 80−80640

Neel temperature continued
$NaCa_2Mn_2V_3O_{12}$, antiferromag., spin wave contrib. to sp. ht., λ-anomaly at 25.05K T_N 77−77068
$NaCrO_2$, two-dimens. mag. order, neutron powder diffr. obs. 80−44805
$NaFeF_2$, Mossbauer and low-temp. dilatometry study *(French)* 80−80662
$NaMnCl_3$, mag. susceptibility, 4.2-350K, quasi-two-dimens. antiferromagnetism 77−59399
Na_3RuO_4, ^{99}Ru Mossbauer spectra, antiferromag. order, mag. relax. 80−50234
Nd-Dy(Ho)(Tb), HCP struct., mag. props. 77−63177
Nd-Y alloy, mag. character of stable and metastable phases 79−38329
$NdAg_x$, low temp. mag. meas. 80−107989
$NdFeTiO_5$, mag. susceptibility, 4.2-77K, antiferromag. ordering obs. 78−68186
$Nd_{1-x}La_x$, thermoelectric power, mag. transition temps. 80−20154
$NdSn_3$, Neel temp., hydrostatic press. depend. 80−29549
$NdVO_3$-$CaVO_3$ solid solns., mag. props. rel. to cryst. struct. 78−43571
Ni ferrite, quenched, Neel temp. and initial susceptibility 80−75762
Ni-I single crystals, mag. and dielectric props. 80−93095
$Ni(As_xS_{1-x})_2$, mag. elec. and structural props. meas. 77−85447
$Ni_xCd_{(1-x)}(NH_3)_2.Ni(CN)_4.2C_6H_6$, mag. susceptibility meas. 77−63126
$NiCl_2$, Raman spectrum at and below antiferromagnetic ordering temp. 79−99871
Ni_xMn_{1-x} disordered alloy, mag. interactions exam. 77−24687
NiMnGe, crystal and spiral mag. struct., Neel temp., X-ray and neutron diffr. 77−16052
NiMnGe, mag. struct., and mag. phase transitions 77−63187
$Ni(NH_3)_2Ni(CN)_4.2C_{12}H_{10}$, mag. susceptibility, sp. ht., spin arrangements and transition obs. 77−20590
$Ni(NO_3)_26NH_3$, specific heat discontinuity at Neel point 77−51912
$NiNb_2O_6$, antiferromag., principle mag. susceptibility and field induced magnetisation meas. 77−20589
$NiNb_2O_6$, magnetisation and susceptibility, antiferro-paramag. transition, expt. and theory 77−43822
NiO (111) platelets, magnetic anisotropy investigation by torque and mag. susceptibility meas. 80−54885
NiO, adsorption of $CO+N_2O$, catalysed reaction in Neel transition region 78−53258
NiO, antiferromag. ordering, mag. transition-state approach 80−80507
NiO, mag. transition, neutron scatt. exam. 78−56313
NiO, magnetic susceptibility, near Neel temp. 79−56509
NiO:Cr, effect of Cr additives on structure parameters *(Bulgarian)* 80−44319
$NiPS_3$, mag. props., NMR meas. 79−24223
NiS_2, antiferromag. metallic state, neutron diffr. study 79−38325
NiS_2, high press. effect on mag. transition temps. 78−91866
NiS_2, thermal expansion and cryst. distortion below antiferromag. Neel and weak ferromag. Curie temps. 77−15579
$Ni_{0.25}Zn_{0.75}Fe_2O_4$, Mossbauer study, spin fluctuations 80−60471
Np intermetallics, NpM_2Si_2, (M=Cr, Fe, Co, Ni, Cu), Mossbauer and magnetisation expts. 78−31138
$NpCo_2Si_2$, mag. props., high press. studies with $^{237}Np(60)$-resonance 80−39924
$NpFe_{2-x}Co_xSi_2$, mag. and hyperfine props. 80−7247
NpM_2Ge_2 (M=Cr, Fe, Co, Ni, Cu), Mossbauer and magnetisation meas. 77−1555
$NpPd_{3-x}Rh_x$, Mossbauer spectra, hyperfine interactions and mag. ordering 77−20783
$NpSn_3$, band magnetism due to f-electrons, T_N 77−73039
$NpSn_3$, itinerant f-electron antiferromag. obs. 77−8315
$Pb_2Fe_2O_5$, IR absorpt., Mossbauer spectra, Neel temp., cryst. cell *(French)* 79−42759
$PbFe(_{2/3}W_{1/3})O_3$-$Pb(Co_{1/2}W_{1/2})O_3$ solid soln., crystallographic, dielectric, magnetic props., Mossbauer spectra 78−43807
Pb_2MnF_6, antiferromag. and superionic conductor, EPR and NMR meas. 79−99366
Pr-Dy(Ho)(Tb), HCP struct., mag. props. 77−63177
Pr-Nd (5%), impurity modes and mag. ordering 78−84422
$PrCu_2Ge_2$, magnetic props. 77−32180
$PrFe_2Ge_2$, magnetisation, 4.2-273K, and Neel temp 77−8310
$PrSn_3$, Neel temp., hydrostatic press. depend. 80−29549
PuC_x (x=0.8, 1.44, 1.67), low temp. sp. ht., mag. ordering obs. 80−49372
Rb_2CoF_4, critical fluctuations near Neel temp., US attenuation study 80−108013
$Rb_2Co_cMg_{1-c}F_4$, magnetic specific heat, dilution on a two-dimensional Ising-like antiferromagnet 78−91871
$Rb_2Co_xMg_{1-x}F_4$, antiferromag., static critical phenomena, neutron diffr. obs. 79−56528
Rb_2FeF_5, Mossbauer spectra, 1D antiferromag. 80−15886
Rb_2FeF_5, one-dimensional antiferromag. systems, Mossbauer studies 80−71266
$RbMnCl_3$, high-pressure cubic phase, mag. props. 79−47260
$RbMnCl_3$, specific heat near Neel temp. *(Russian)* 80−100340
$RbMn_{1-x}Mg_xCl_3$, dilute pair antiferromag., mag. susceptibility and ESR meas. 79−78338
$RbVF_3$, antiferromag. ordering points, thermal anal. and X-ray diffr. meas. *(French)* 78−84421
α-Rb_xVF_3, mag. props. *(French)* 77−80933
Si-Cr, dil., spin density wave under high press., neutron diffr. study 80−65798
Sm, electrical resistivity, Neel temp., 15 to 300K 80−54672
Sm film, electrical resistivity in 77 to 300K range 77−59339
Sm-Dy (3 wt.%), electrical resistivity, Neel temp., 15 to 300K 80−54672
SmAs, low temp. props. 79−28528
SmBi, low temp. props. 79−28528
$Sm_{1-x}Gd_xS$, metal-insulator transition, induced by temp. and press. *(Japanese)* 79−51488
SmH_2, low temp. sp.ht., antiferromag. ordering and cryst. field splitting effects 78−84439
$SmMg_2$, cryst. and mag. props., ordering 78−68185
SmP, low temp. props. 79−28528
$SmS_{1-x}As_x$ solid solns., intermediate valence phase, lattice const. and mag. susceptibility meas. 79−87245
SmSb, low temp. props. 79−28528
$SmSb_{1-x}S_x$, magnetic ordering and configuration mixing 78−68179
$Sr_{1-x}Ca_xMnO_3$, Neel points, rel. to Curie point of $LaNi_{1/2}Mn_{1/2}O_3$, superexchange interactions 77−77055

Neel temperature continued
$(SrCaR)_3(Cr_xGa_{1-x})O_4$, R=La or Sm, mag. 2-D oxide, phys. props. 78-47974
$SrEuFeO_4$, Neel temp. and spin reorientation, Mossbauer study 80-39934
$Sr_7Fe_{10}O_{22}$, mag. props. and spin order 78-52232
$Sr(Fe_{0.766}W_{0.234})O_3$, cryst. growth, mag. and Mossbauer studies 79-42743
$SrGdFeO_4$, Neel temp. and spin reorientation, Mossbauer study 80-39934
$SrO\text{-}Fe_2O_3$, EMF meas. with solid state cell, Mossbauer effect and magnetic props. *(Korean)* 77-28493
$SrRFeO_4$, R=La, Pr, Nd, Sm, Eu, Gd, Mossbauer effect, Neel temp. and internal mag. field 77-12284
$SrTb_2Fe_2O_7$, Mossbauer spectra, hyperfine parameters, ordering temp. 77-90079
Sr_3YRuO_6, ^{99}Ru Mossbauer spectra and other techniques 80-29659
TMMC, antiferromagneric chain, 3-D ordering temp. controlled by solitons and defects, mag. field depend. 80-60275
Tb, film, thermoreflectance dispersion curves at 315K and 97K 80-7332
Tb, high-pressure phase, mag. field effects *(Russian)* 77-66021
Tb-Cu-Zn(Al), mag. props. *(Russian)* 77-51905
Tb-Ho alloy, influence of internal strain on Neel temp., thermal expansion and elastic const. meas. 77-63176
Tb-Sc(Y)(La)(Lu)(Yb)(Mg)(Th), mag. ordering temps., susceptibility meas. 80-25136
$TbAg_{1-x}In_x$, mag. and transport props. 78-43572
$TbAg_{1-x}Zn_x$ solid solns., mag. props. *(Russian)* 77-77049
TbAlGa, mag. props. and struct. 78-39302
$TbAu_3$, mag. phase diagram 80-75761
$TbFe_2Ge_2$, magnetisation, 4.2-273K and Neel temp. 77-8310
$TbFe_2Si_2$, 5.5K T_N, mag. props. 4.2 to 950K 77-20544
$TbNi_2Si_2$, mag. props., 4.2-200K 80-84602
$Tb_2O_2SO_4$, antiferromag., mag. props. 1.6 to 40K 79-33464
TbP (As)(Sb)(Bi), mag. transitions, quadrupolar interaction effects 80-80512
TbP, singlet-groundstate magnetism, static mag. props. 80-7109
TbSc, crit. scatt. of electrons near antiferromag. transition temp. 79-69505
$(Ti_{1-x}V_x)_2O_3$ spin glass, mag. props., metallic antiferromagnetism 79-82791
$(Ti_{1-x}V_x)_2O_3$, metallic antiferromag. struct., neutron studies 80-65797
$TlMnCl_3$, specific heat near Neel temp. *(Russian)* 80-100340
$Tm_2O_2SO_4$, antiferromag., mag. props. 1.6 to 40K 79-33464
TmSe, mag. ordering under press., neutron diffr. obs. 80-70947
U dipnictides, elec. and mag. props. 78-84399
UGeS(Se)(Te), mag. susceptibility, struct. in temp. range 4.2 to 300K 78-10667
UGeY, (Y=S, Se, Te), mag. ordering, neutron diffr. obs. 78-72329
UN, antiferromag., mag. susceptibility, elec. resist. and elastic consts. meas. 77-69510
UN, mag. susceptibility under press. 80-7086
UN, phonon dispersion relation near Neel temp., neutron coherent inelastic scatt. 78-59900
UN-ZrN, Young's modulus antiferromagnetic anomaly 80-92583
UO_2, crystalline elec. field studies using neutron inelastic scatt. at NRCN 80-10931
UP-PrP (NdP) systems, mag. phase diagrams 78-84424
UPd_2Si_2, magnetic phase transition, neutron diffr. meas. 79-47284
V-Mn-Cr, disordered BCC state, mag. phase diagram, mag. and elec. props. 77-63185
$V_2O_3\text{-}M_2O_3$, M=Ti, Cr, struct. and mag. props. 78-27041
V_3O_5, mag. anisotropy 77-85441
V_3O_5, spin order, one-dimensional, Neel transition 80-39799
V_4O_7, sublattice magnetisation temp. depend., ^{51}V NMR, Neel temp. determ. 79-91301
V_nO_{2n-1} ($3\leq3\leq9$), Magneli phases, mag. susceptibilities at low temp. 80-20389
V_nO_{2n-1}, insulating Magneli phases, mag. susceptibility and sp. ht. meas. 80-34604
V_nO_{2n-1} Magneli phases, elec. and mag. props. 79-37990
$V_2O_{3-x}F_x$ ($0\leq x<0.3$), preparation and physical props. 78-76619
VTe, mag. and elec. transport props. 80-92897
Y-rare earth metal, mag. susceptibility, 4.2 to 300K, Neel temps. 79-19735
YC_2-DyC_2, solid solution, antiferromag. props. 79-91230
$YFe_{1-x}Cr_xO_3$, reorientational transitions, mag. and neutron diffr. exam. 77-12097
$YFeO_3$, induced spin reorientation near Neel point 78-19267
$YFeO_3$ orthoferrite, weak ferromagnet domain struct. near Neel temp. 79-99739
$Y_3Fe_5O_{12}$, amorphous, mag. moments, susceptibility, Mossbauer studies 79-78345
YIG, Neel point behaviour in stoichiometry vicinity 80-88750
Y_5Pd_2, mag. props. 77-20547
$ZnCr_2Se_4$, screw spin struct., neutron diffr. exam. 78-27019
$ZnCr_2Se_4$, screw spin structure, method of controlling the sense, polarised neutron diffr. study 80-70944
$ZnCr_2Se_4$:In, magnetoresist. and elec. resist. above and below Neel temp. *(Russian)* 80-88576

negative feedback *see feedback*

negative feedback control systems *see closed loop systems*

negative ions
3d photoabsorpt. spectra, continuum and discrete states 79-81176
acetate, aq. soln. current-potential curve, influence of NO_3^-, SO_4^{2-}, PO_4^{3-} and Cl^-, obs. *(Japanese)* 78-85172
acetate ion radicals, solns., pulse radiolysis, CIDEP, viscosity depend. 77-75189
acetophenone, enolate anion, electron photodetachment cross-section resons. 78-5298
acetophenone enolate anion radicals, substituted, electron photodetachment cross sections, reson. states 80-1030
air, negative corona low energy humid air ions, etching effect on Al foil 80-40593
air, Trichel corona, negative ion form. 77-35425
air positive point-to-plane corona, continuous and pulse components 79-19119
aliphatic chlorocarbons, electron impact dissoc., $\lesssim$10 eV, negative ion prod. 78-5359
alkali anions, autodetaching sub $^2P_{1/2}$ threshold states 79-22611
negative ions continued
alkali atom+halogen mol., ion pair form., trajectory model 77-16800
(alkali atom)$^+$+(halogen atom)$^-$, recombination 78-7192
alkali metal+$H^+(C^+)(O^+)(S^+)$, negative ion form. 79-50128
alkali metal anions, formation 78-5159
alkali metal atoms and anions, electron affinity, model pot. SCF and CI calcs. 77-38609
alkyl halide and σ^* anion radicals, stability 80-89468
angular distribution, of ions formed by dissoc. attachment 79-81288
anthracene dimer anion, charge reson. transition anal. 80-42931
anthracene ion in liqs., photoelectron emission and photocond. 80-75600
approximate energy relationships, Z^{-1} perturbation expansion 79-13620
atmospheric air simulation, computer, temporal evolution of negative ions *(French)* 77-21869
atmospheric negative ions, electron detachment rates, time lags to breakdown 78-87564
atmospheric negative ions, photodissoc. and photodetachment 78-66609
atmospheric negative ions, photodissoc. and photodetachment 80-69199
atom, electron scattering, correl. effects, Bethe-Goldstone calc. 79-54967
atom, singly-charged, sufficient conditions for finite no. of bound states 79-10047
atom+negative ion, term parameters, electron spectra and scatt. cross sections 77-27148
atom-negative ion collisions, linear approx. in generalised zero-range pot. model *(Russian)* 79-94076
atomic, optimum pot. model used to generate numerical pot., energies and electron affinities determ. 80-99534
atomic, photodetachment, zero core contribution model 79-93961
atomic, Rydberg formula, modified 77-26957
atomic and molecular, quantum chemical calcs. 78-62703
atomic and molecular dynamic polarisability, many-centre short-radius model pots. 78-25735
atomic collisions, negative ion electron detachment, zero range Fermi approach 80-63798
atomic electron scattering, reson. laser induced negative ion production 79-64104
autodetachment, spectroscopy 80-23385
bacterial culture viability under negative ion irrad. in elec. field *(Russian)* 79-83855
beam, positive and negative ion beams nonlinear interaction, math. simulation and expt. 77-595
benzene, negative ion states and π-electron affinity 79-10206
benzyl anion, IR multiphoton electron detachment 79-94043
binaphthyl anion radicals, photoisomerisation, local heating effects 78-85179
1,1′-binaphthyl mononegative ion conformation 77-30774
bromanil, electron affinity, bound and excited negative ion states, lifetimes, electron and alkali metal collisions 79-869
carboxylate, aq. soln. current-potential curve, influence of NO_3^- and SO_4^{2-}, obs. *(Japanese)* 78-85173
charge-exchanging beams, ang. scatt., neutral beam form. 77-46636
chloranil, electron affinity, bound and excited negative ion states, lifetimes, electron and alkali metal collisions 79-869
chlorofluoromethane negative ion products, in 0-10 eV near-monoenergetic electron impact 79-41245
chlorotrifluoroethylene radical anions, EPR spectra and struct. 79-31558
collisions with atoms and molecules, electron detachment for energies near threshold 80-63797
croconate ion, Jahn-Teller coupled vibrs., reson. Raman profiles 77-83602
croconate ion, reson. Raman scatt., Jahn-Teller effect 79-18190
cyanide, on Ag, at electrolyte interface, enhanced Raman effect 79-28767
cyanomethane$^-$, ab initio calcs., electron affinity, stability 77-42239
cyclooctatetraene, anions, in condensed media, electronic spectra 79-22723
cyclopentadienyl ion, electron affinity and Jahn-Teller effect, laser photoelectron spectra 77-88499
3′-cytidylic acid, electron adduct, spin density distrib., INDO calcs. 77-71754
decacyclene anion, photoexcited quartet state, transient EPR 80-78635
diatomic hydrides of first and second row elements, PNO-CI and CEPA calc. 79-768
diatomic negative hydrides, photodetachment 0.5 to 3.0 eV, electron affinities *(German)* 77-61812
DNA-Au (III) interaction, rate consts., activation energies, pH, spectrophotometric obs. 80-30228
duoplasmatron, discharge plasma, negative ion form. and extraction 77-7511
electron density, semi-statistical model 78-21850
electron dissociative attachment of mol. plasma in crossed electric and mag. fields 78-5847
electron impact detachment cross sections, classical scaling theory appls. 80-83492
electron impact ions near threshold, classical approx. *(Russian)* 77-68124
electron stripping in collisions, at. beam form. 77-6926
electronegative gas plasma, negative ion ambipolar diffusion coeffs. 80-44046
electronic structure, stabilisation calcs. using big mol. Gaussian SCF/CI program 79-18121
enolate anion from acetone, gas phase, negative ion chemistry 80-87060
ethylene, and perfluoro derivatives, negative ion states, electron affinities, ionisation pots., overlapping spheres $X\alpha$ calc. 79-26885
Feshbach type reson. scatt., Glauber approx. calcs. 80-102570
fluoranil, electron affinity, bound and excited negative ion states, lifetimes, electron and alkali metal collisions 79-869
formaldehyde anion radical, hyperfine coupling consts., vibr. depend., ab initio calcs. 80-87150
formation by field ionisation 80-89123
formation in high elec. fields 80-2927
formation on sputtering metals and semiconductors with Cs^+, alkali, metal monolayer effect 78-46204
formation processes and props., review *(Japanese)* 80-53127
(formyl-H-F)$^-$, strong H-bond, using recent difinition 79-98240
gaseous dielectrics, electron-molecule interactions and negative ion resonances 78-75480
glycyl anion radical, in α-glycine cryst., struct., ESR obs. 78-33530

negative ions continued
ground state Zeeman splittings, reson. Raman spectra and mag.-optical activity 80−5579
Group IIIA metal tetrahalide ions, vibr. anal. 80−63608
groups II and III, doubly charged negative ions, analytical radial orbitals 77−6668
halide ion+solvated positron, competitive reaction in water, ang. correl. obs. 79−61846
halide ions, recombination, exciplex or excimer form. in plasma 80−75026
halogen, at. ion form. in dissoc. attachment by 0-8 eV electrons 78−74776
halogen ions source 77−41729
halogen molecule negative ion, Cl_2^-, Br_2^-, I_2^-, $ClBr^-$, ClI^-, pot. curve calc. 77−10596
halogens, negative ions, electron spin polarisation in photodetachment 78−25495
halogermane radical anions, ESR spectra and struct. 80−87153
Hartree-Fock-Roothan wavefunctions with 3d and 4d electrons 78−17569
hexafluorides, MF_6, M=S,Se,Te,Mo,W,Re,Ir,Pt ionisation 78−55226
hexafluorobenzene, slow electron attachment obs., π-orbital calcs. 77−6948
hexafluorobenzene anion-radicals in squalane, ESR spectrum optical detection 80−95655
hexafluorobenzene radical anion, ^{13}C hyperfine interaction, EPR obs. 80−83392
hexahalo ions, octahedral, mol. consts. calcs. 80−106317
hexahaloanions of group IV A and V, mol. const. determ. 80−87093
hexaoxy ions, octahedral, mol. consts. calcs. 80−106317
high-temperature chemical processes, review, book contrib. 77−40545
hollow cathode discharge as negative ion source 78−82072
hydrogen maleate ion, electronic spectra, CNDO/S CI calcs. 77−75128
β-iodophenylacetylene radical, PhC_2I^-, from γ-irrad. morpholine β-iodophenylacetylene complex, EPR obs. 77−52652
ion formation and relative yields from laser prod. plasma, mass spectra, appls. *(Russian)* 78−59631
ion production, in reverse polarity field ionis. source 79−92046
ionosphere, EM wave propag. 80−4164
ionospheric D-regions, electron density and energy distrib., due to energetic protons 77−82078
isoelectronic sequence, correlated and HF electron density differences 78−46275
laser induced one-photon transitions between two short-lived negative ion states 80−9731
lifetimes, review, book contrib. 80−9529
mass spectrometry, negative chemical ionis., ionis. techniques, review 78−325
mass spectrometry 80−43211
mass spectrometry detection system 77−29062
mass-analysed ion kinetic energy spectrometry using negative chem. ionis., direct mixture analysis 79−34397
metastable negative ion, electron impact decomp., kinetic energy release 77−6944
methyl anion, geometric struct., electron correlation effects, self-consistent electron pairs 78−22050
methylene anion, electron affinity, $^1A_1$-$^3B_1$ T_0-value, ab initio MRD-CI method calcs. 78−50478
methylene anion, vibronic anal., ab initio CI pot. curves calcs. 78−50479
methylene radical anion and dimer, semiempirical CNDO/2 and nonempirical SCF calcs. 77−79535
MIN, negative ion injector, Na charge exchange cell 80−99386
mixtures, negative chem. ionisation mass analysed ion kinetic energy spectrometric anal. 78−92550
mobility in electronegative gases, new expt. method 78−18372
mobility in O_2 and N_2, temp. depend. 79−14513
mobility in superfluid ^{3}He A and B phases 77−80672
molecular, theoretical calcs., review 78−37552
molecular cations, heats of formation determ. from core electron binding energies 77−86346
molecular ions, gas phase, spectroscopic props, review 78−33501
molecular ions, negative, polar, thermally stable 79−7033
molecular ions, polarisability, mol. orbitals calcs. 77−57860
molecular negative ion, photoelectron ejection ang. distrib. theory 77−491
molecule, polar, slow electron capture and rot. excitation 79−81287
molecule+negative ion, thermochemical data, gas phase acidity scale, mass spectroscopic techniques 80−30234
monothioformate anion, protonation site, ab initio SCF calc. 79−47894
motion at supercritical drift velocities in liquid ^{4}He at low temps. 77−80667
multicomponent polyanions, PMo_9O_{34} model vibr. freqs. 80−23408
naphthalene, photoionis., negative ions role in photoionis. plasma 79−27048
naphthalene anions, electron affinities, transition energy, comparison for gaseous liquid and solid 80−29731
naphthalene radical anion+TCNQ, electron transfer reactions, theory 78−15661
negative ion+molecule, electron detachment *(Russian)* 79−59566
negative ion+neutral atom, autoionisation states investigation by Rydberg series broadening and displacement *(German)* 79−85938
negative ion formation, by sputtering, work function depend. 78−39645
neutralisation in ion-at. collisions, rainbow, interference, and diffr. effects *(Dutch)* 79−50110
nitrobenzene$^-$, positive ion formation energetics by negative ion charge stripping 80−78700
nitromethyl anion, ab initio SCF ab initio MO calcs. of geom. and bond energies 79−31381
orbital functional theory for exchange and correl., local spin density approx., self interaction correction 79−76347
oxocarbon ions, reson. Raman scatt., Jahn-Teller effect 79−18190
oxyanions, in nuclear waste materials, laser Raman spectrometric determ. 78−35743
parabenzoquinone, and perfluoro derivatives, negative ion states, electron affinities, ionisation pots., overlapping spheres Xα calc. 79−26885
Penning source for H^- and $^2H^-$ ions 77−83415
perfluorobenzene, electron attachment, radiative and dissoc., negative ion lifetimes, ion cyclotron reson. spectra 80−74251
perfluorocyclobutane, electron attachment, radiative and dissoc., negative ion lifetimes, ion cyclotron reson. spectra 80−74251
negative ions continued
perfluoromethylcyclohexane, electron attachment, radiative and dissoc., negative ion lifetimes, ion cyclotron reson. spectra 80−74251
perfluorotoluene, electron attachment, radiative and dissoc., negative ion lifetimes, ion cyclotron reson. spectra 80−74251
photoabsorption spectra, long-range field effect 80−91521
photodestruction in elec. field 77−20897
photodetachment 79−52715
photodetachment cross-sections, crossed beam meas. *(German)* 77−42298
photoionisation, expt. techniques, processes, theory, review 77−14402
Plante cell formation using NO_3^- process 79−96437
plasma containing negative ions, thermal equilib. 77−19670
plasma continuum spectra, role of excited and unstable negative ions 77−65842
plasma negative ions, broadening of free-bound radiation threshold, quasistatic theory 80−53941
polar molecule-electron systems, variational method for bound state calc. 78−46261
porphyrins, complex Raman tensors, irreducible tensor method, antisymmetric scatt. 78−37623
positive column, density oscills. due to negative ions, metastable atom model 78−1799
positive corona electrode, negative ion counterflow, elec. field strength meas. 80−38817
positive ion formation energetics by negative ion charge stripping 80−78700
positronium halides, [X^-; e^+], electronic struct., annihilation characts., HF calc. 77−50567
positronium halides, [X^-; e^+], electronic struct., annihilation characts., HF calc. 77−50568
production, in surface plasma source with unclosed electron drift discharge 80−38846
pseudo pot. model Hamiltonian, spin-orbit splitting, intercombination and relativistic orbital reorganisation 78−25424
pyrimidine bases, electron adducts, spin density distribs., INDO calcs. 77−71754
radial correlation incorporation methods 77−42247
resonant electron scatt. by atoms in laser field, negative ion formation, polarisability 77−19089
review 77−27194
rhodizonate ion, reson. Raman scatt., Jahn-Teller effect 79−18190
RX$^-$, radical anion stability conditions, pot. energy diagrams 80−85161
secondary ion mass spectroscopy, negative ion techniques 79−5235
singly-charged, Thomas-Fermi-Amaldi eqn., approx. variational soln. 80−52870
space charge neutralization regions for mixed positive and negative ion beams 79−27159
sputtered from surfaces by Cs^+ impact, energy distrib. 77−81189
sputtering and SIMS analysis, significance of negative ion formation 78−72663
squarate ion, reson. Raman scatt., Jahn-Teller effect 79−18190
stable negative ions instability, Xalpha calcs. 80−99452
trans-stilbene dianion, photolysis, intermediate struct., time-resolved reson. Raman spectra obs. 79−52695
stratosphere, mass spectrometric meas. of negative ions 78−96274
styrene, anions, in condensed media, electronic spectra 79−22723
styrene anions, electron affinities, transition energy, comparison for gaseous liquid and solid 80−29731
TCNQ$^-$, electron affinity, compound states 77−65530
p-terphenyl anion radicals, photoisomerisation, local heating effects 78−85179
tetrafluoroethylene anion, EPR spectra in organic matrix 79−76453
tetrafluoroethylene radical anion, isotropic and anisotropic EPR spectra, conform. 78−13532
thiomethoxyl anion, and deuterate, electron photodetachment, affinities, vibr. freq. and spin-orbit splitting 80−53063
third-row oxyanions, tetrahedral, kinetic and pot. consts. calcs. 77−30951
Thomson scattering, collision-dominated, negative ions effect, ionospheric D-region appl. 78−45118
transition metal complexes, $M(CN)_5X^{n-}$, ^{13}C NMR, chem. shifts 79−51866
transition metal oxyanions, intramol. force fields 79−45693
transition metal oxyanions, tetrahedral, kinetic and pot. consts. calcs. 77−30951
transition metal tetrahalogeno anions, ligand field spectra, MO model 78−17654
triatomic negative ion fragmentation, energy partitioning isotope effects, Monte-Carlo calcs. 77−27126
triatomic negative ions, dissoc. product kinetic energy, classical trajectory method 78−64809
tribenzo [12] annulene, monovalent anion, MCD and absorpt. spectra 78−70859
Trichel corona, negative ion mass spectra 78−87537
Trichel corona negative ion transit times 79−19115
trichlorofluoromethane anion, dissoc. electron attachment, pot. curves calcs. 79−98231
trifluoromethylhalide radical anions, formation, ESR and struct. 77−32809
trihalide anions, VB pseudopot. calcs. on electronic states 77−26984
5-uridylic acid, electron adduct, spin density distrib., INDO calcs. 77−71754
wave function asymptotic coeff. for electron in atom or ion 79−26871
XY_4 oxygenated ions, tetrahedral, mol. consts. 79−36555
XY_4 square-planar type ions, force consts., bond polarizability 78−5201
zinc etioporphyrin I anion radical, photoreduction obs. *(Russian)* 78−23958
$e^+e^-e^-$, two-electron at., three-body problem, binding energy 79−3372
$^{205}TlF_6^{4-}$, radical, prep. and EPR comparison with other hexafluoride radicals 78−68381
Al^-, metastable, electron affinity calcs. 79−31439
Al_2^-, configurations, ab initio study, LCAO, STO, MO-SCF and CI calcs., binding energy *(French)* 80−91447
$AlCl_4^-$, IR spectra in $AlCl_3$-MCl (M=Li, Na, K) melts 79−806
AlF_6^{3-}, octahedral complex, ionis. energy, SCF-Xα study 78−70967
AlF_6^{3-}, SCF Xα SW calcs., ionis. pot. 79−26887
$^{26}Al/^{26}Mg$ isobars, separation via negative ion mass spectroscopy 80−31146
Ar^-, electron capture expts. to search for long lived states 79−72410
Ar^-, free-free radiative absorpt. coeff. calcs. 77−423

negative ions continued
$Ar+H^-$, collisional electron detachment, complete ang. distrib. 78−66650
ArCl, neutral and negative ion states SCF pot. energy curves 78−62745
ArH, neutral and negative ion states SCF pot. energy curves 78−62745
As_2^-, photodetachment cross section, 0.5 to 3.0 eV photon energy *(German)* 77−65518
AsF_6^-, bond order and Raman intensity, delta function eqn. 77−61693
$^{73}AsF_6^{2-}$, radical, prep. and EPR comparison with other hexafluoride radicals 78−68381
$As_4S_4^-$, electronic struct. and vertical electron affinities, INDO-type ASMO SCF calcs. 79−31402
$As_4Se_4^-$, electronic struct. and vertical electron affinities, INDO-type ASMO SCF calcs. 79−31402
B^-, metastable, electron affinity calcs. 79−31439
BF_3^-, geometric struct. of ground state, ab initio calc. 78−5130
BF_4^-, bond order and Raman intensity, delta function eqn. 77−61693
BH_4^-, CNDO/2 calc. of chemical bonding 79−76345
BH_4^-, electron momentum distribution and Compton profiles, FSGO calcs. 80−87032
BH_4^-, pot. energy surfaces and mol. deform. induced by external cation 80−106285
BH_4^-, reduction of $IrCl_6$ by hydrolysis products 78−76854
$B_2H_n^-$, struct., ab initio SCF calcs. *(French)* 79−22598
$B_3H_8^-$ anisotropic motion in powdered tetramethylaminoborane, ^{11}B NMR 77−90045
$B_3H_8^-$, electron momentum distribution and Compton profiles, FSGO calcs. 80−87032
$B_3H_n^-$, struct., ab initio SCF calcs. *(French)* 79−22598
$B_nH_n^{2-}$, n=5-12, localised orbitals, bonding, PRDDO calcs. 78−13431
$B_{10}H_{12}As^-$, ^{11}B NMR 78−90190
BH_3F^-, B-F bond, interference density and kinetic energy 78−74566
BH_3F^-, CNDO/2 calc. of chemical bonding 79−76345
$(B_{10}H_{12})_2Ni^{2-}$, high resolution ^{11}B NMR 79−31553
B(I) hydrides, ab initio calcs., proton and hydride affinities 79−10029
BO^-, ionisation pot. calcs. 77−75076
Be^-, ^2P shape resonances, shift potential calcs. 80−69089
Be^-, $^2P^0$ shape resonance, complex-coord. method calc. 78−74591
BeF_2^-, electron binding, extended basis SCF calc. 79−49944
BeF_2^-, ground state, conform., electron affinity, extended basis SCF calcs. 79−72253
BeO_2^-, electron binding, ab initio calc. 79−45628
BeO(BeO^-), electron affinity and dipole moment, ab initio calc. 78−41938
Bi^-, photodetachment cross-section meas., crossed beam expt. 77−61723
$^{209}BiF_6^{2-}$, radical, prep. and EPR comparison with other hexafluoride radicals 78−68381
Br^-, electron photodetachment cross-section determ., from CsBr dissoc. 77−3330
Br^-, ion mobility in Ar, flow drift tube meas. 77−72405
Br^-, nuclear quadrupole interaction , second-order Stark effect 78−21879
Br^-, plasma, broadening of free-bound radiation thresholds 80−53940
Br^-+He, electron detachment, SCF calcs., $BrHe^-$ and BrHe pots. 80−23503
Br^-+He(Ne)(Ar)(Kr), total electron detachment cross sections, near threshold energies 79−3555
Br^-+K, differential cross-section, small angle scatt. 79−98186
Br^-+methane(fluoromethane), excitation functions, reactive scatt., eV region *(German)* 78−35677
Br_2^-, prod. cross section in K+Br_2 charge exchange reaction 79−20358
Br_2^-(Br^-), formed by electron impact from Sn_4, ionis. efficiency curves 77−61865
$BrCl_2^-$, photodissoc. and photodetachment, pot. curves. 79−64060
$BrHCN^-$, $BrDCN^-$, IR spectra, rel. to mol. geom. 79−22702
$Br(H_2O)_n^-$, geometric and electronic struct., CNDO/2 calcs. 77−79542
$Br(H_2O)_n^-$, geometric and electronic struct., CNDO/2 calc. 79−41113
$Br^-(H_2O)_n$, hydration energies, orientation, ab initio-LCAO SCF MO calcs. 80−27944
BrO^-, electron affinity, formed in Br^-+O_2 reaction 77−63902
BrO_3^- in $NaClO_3$, Raman spectra, fundamental vibr. modes 78−78711
C^-, effective valence shell Hamiltonian, ab initio calcs. 78−82611
C^-, electron impact detachment, cross-section, 10-1000 eV 79−31702
C^-, electron impact detachment cross sections 79−89787
C^-, free-free transitions, continuous absorpt. estimation 78−9098
C^-, near-threshold photodetachment, IR meas. 77−42290
C^-+CO(Mg)(N_2), electron detachment cross-sections, 20-150 keV 78−25690
C_2^-, $A^2\Pi_u$-$X^2\Sigma_g^+$ lines, obs. in carbon stars 80−98661
C_2^-, bound electronic states and electron affinity, IC calc. 79−76349
C_2^-, matrix isolated, vibr. relax., absorpt. spectra 77−75172
C_2^-, matrix isolated, vibr. energy transfer, fluoresc. 78−46382
CF_3O^-, bonding, ab initio calcs. 77−50350
CH_2^-, photodetachment cross section, 0.5 to 3.0 eV photon energy *(German)* 77−65518
CH_3^-, photodetachment cross section, 0.5 to 3.0 eV photon energy *(German)* 77−65518
$CH_3(CH_3^+)(CH_3^-)$, HF, GVB and CI calcs. 77−75063
CH_3OHF^-, IR photodissoc., fluence depend., saturation effects 80−78663
CN, CN^-, HF electron affinity, SCF calcs. 77−67979
CN^-, electron density distrib., theoretical and expt. determ. 77−61683
CN^-, electron density distrib., SCF mol. orbitals calcs. 78−9058
CN^-, electron propagator theory, mol. electron affinities calcs. 80−83521
CN^-, finite field method calc., moments, polarisability, field-induced shifts in mol. props. 78−74561
CN^-, first hyperpolarisability, Hartree-Fock-Slater calc. *(French)* 78−78625
CN^-, ground state pot. curve, CI and coupled pair method calcs. 79−68197
CN^-, ionisation pot., CI and perturbation methods 79−31734
CN^-, ionisation pot. calcs. 77−75076
CN^-, leaches from gasworks site, Kingskettle, Scotland 79−88020
$(CN)^-$, monolayer on Ag, Raman spectra 78−72520
CN^-, proton affinity, enthalpies of form. and soln. 77−47375
CN^-, proton affinity, integral Hellmann-Feynman theorem 78−70767
CN^-, spectrosc. consts. for ground and excited states, ab initio, CI calcs. 80−78551
CN^- transformations by inner source based on $^{10}B(n,\alpha)^7Li$ 79−34341
negative ions continued
(CN^-;e^+)-complex, ab initio LCAO SCF calc., positron affinity and excitation energy 79−49945
$CN^-.H_2O$, redox processes, MINDO/3 calcs. 79−47895
CO, negative-ion resons. associated with inner-shell-excited states, electron impact 77−88580
CO^-, electron impact dissoc., to positive ion states, negative-ion reson. effects 79−54977
CO^- free-free transitions continuous absorption calc. of CO bremsstrahlung 79−63978
CO_2, elec. discharge, negative ions and volt.-current characts. 78−71574
CO_2, negative Van der Waals polymer mols., formed by nozzle expansion 78−90307
CO_2, positive and negative ion reactions 77−40540
CO_2, supersonic jet, $(CO_2)_n^-$ cluster formation and electron attachment 78−5385
CO_2, Trichel corona, negative ions 78−30503
CO_2^-, complex symmetric stretch pot., from CO_2 reson. electron impact data 78−25726
CO_2^-, dissoc., $^2\Sigma_g^+$ state, Wall Porter pot. surface, autodetachment and vibr. level population inversion 80−21275
CO_2-H_2O-O_2, gas mixture, photodetachment and photodissoc., mass spectra meas. 77−500
CO_2-N_2-He, vol. discharge, negative ions effect 80−14956
CO_2-O_2-H_2O, mixture, mol. negative ions, photodissoc. and photodetachment cross section 77−27129
CO_2-O_2-H_2O, photodissoc. and photodetachment of negative ions 80−14182
CO_3^-, form. by photodissociation and ion-mol. reactions in CO_2 and CO_2-O_2 mixtures 78−13558
CO_3^-, formation and dissociation in CO_2 77−60058
CO_3^-, O^- bond dissociation energy 78−7193
CO_3^-, thermally relaxed, photodetachment cross-section and solar detachment rate determ. 77−58094
CO_3^{2-}, electronic struct., X-ray spectra obs. 78−55185
CO_4^-, form. by photodissociation and ion-mol. reactions in CO_2 and CO_2-O_2 mixtures 78−13558
$CO(H,Cl)_3^-$, heats of form., from formyl fluoride gas phase data 77−63900
$CO(H,F)_3^-$, heats of form., from formyl fluoride gas phase data 77−63900
$C^-(^4S^0)$, attachment energies, ab initio calc. 77−30768
C^-(4S)+molecule, spin angular momentum conservation in proton transfer 77−16805
Cd, electron scatt., negative ion form., shape resonances, electron affinity 77−14581
CeI and CeI_2^- formed in CeI_3 by electron irradiation 77−27190
2-chlorothiophene, σ^* anion radical, prod., ESR spectrum assignment 78−11539
Cl^-, atomic core states, antishielding effects calcs. 80−83299
Cl^-, contracted Gaussian basis sets for mol. calcs. 80−83264
Cl^-, electron photodetachment cross-section determ., from CsCl dissoc. 77−3330
Cl^-, far UV spectra in solns. 78−94208
Cl^-, form. in flame by dissoc. electron attachment of HCl, kinetics 78−68872
Cl^-, formation and destruction in ionospheric D-region 78−12049
Cl^-, formation by HCl dissociative electron attachment, differential cross section, Feshbach resons. 80−83508
Cl^- free-bound continuum radiation threshold broadening obs. in plasma 78−71579
Cl^- hydration complexes, gas phase, electrostatic calcs. 80−100055
Cl^-, in alkali chloride aq. solns., relax. rates 77−88471
Cl^-, ion mobility in Ar, flow drift tube meas. 77−72405
Cl^- ion selective electrodes, appl. to biological materials 77−90974
Cl^-, pair polarisability, ab initio SCF MO energies 78−70741
Cl^-, plasma, broadening of free-bound radiation thresholds 80−53940
Cl^- radiative detachment threshold effect of plasma microfield 78−71580
Cl^-, trace determ. by rate controlled coulometric titration 78−11576
Cl^--ionic crystal-metal system, charge transfer mechanism 78−11527
Cl^--Ne(Ar)(Kr)(Xe), longitudinal diffusion coeff., generalised Einstein relation 79−86552
$Cl^-+Ar\rightarrow Cl+Ar+e$, rate const., absolute total cross section, expt. results discrepancy 77−513
$Cl^-+Ar\rightarrow Cl+Ar+e$, rate const., expt. discrepancy 77−514
Cl^-+chloromethane, S_N2 reaction, local orbital description ab initio FSGO method 78−76842
Cl^-+H_2, 4-11 eV, inelastic scatt. 79−98202
$Cl^-+HBr(HI)\rightarrow HCl+Br^-(I^-)$, vibr. product state distribs., IR chemiluminesc. obs. 80−81309
Cl^-+He(Ne)(Ar)(Kr), total electron detachment cross sections, near threshold energies 79−3555
Cl^-+inert gas atom, electron detachment and inelastic processes 78−42208
Cl^-+methane(fluoromethane), excitation functions, reactive scatt., eV region *(German)* 78−35677
Cl^-+Na(K), differential cross-section, small angle scatt. 79−98186
Cl^-+Xe, elastic differential cross-section, 250-500 eV, well depth of 79−86027
Cl^-+Xe^-+Ne, three body ion-ion recombination probability, Monte Carlo simulation 80−85160
Cl_2^-, electron propagator theory, mol. electron affinities calcs. 80−83521
Cl_2^-, gas phase photodissoc. spectrum 77−58098
Cl_2^-, in ion pairs with metals, ESR, in AR matrix, V-centre theory 77−16172
Cl_2^-, photodissoc. and photodetachment, pot. curves. 79−64060
Cl_2^-, pot. energy curves, from Cl_2 dissoc. electron attachment, 0−11.5 eV 77−75312
Cl_2^-, prod. cross section in K+Cl_2 charge exchange reaction 79−20358
$Cl_2^-+HO_2$, reaction in pulse irrad. aq. soln. containing Fe^{2+} and Cl^- 78−20036
Cl_3^-, photodissoc. and photodetachment, pot. curves. 79−64060
Cl_2^-(Cl^-), electron impact total ionis. and electron attachment cross sections 79−3589
Cl_2^-(Cl^-), formed by electron impact from $SnCl_4$, ionis. efficiency curves 77−61865
ClF_2^-, ground and ionised states, Koopman's theorem and Mo relax. in ab initio calcs. 78−1035
$ClHCN^-$, $ClDCN^-$, IR spectra, rel. to mol. geom. 79−22702

negative ions continued
$ClHCl^-$, deuteron quadrupole coupling const., nuclear mag. shielding, geometry depend. 78−58586
ClO^-, electron affinity, formed in $Cl^- + O_2$ reaction 77−63902
ClO^-, photodissoc. and photodetachment, pot. curves. 79−64060
$ClO^- + NO(NO_2)(SO_2)(CO_2)$, rate consts. at 300K 78−76829
ClO_2^-, Cl $L_{II,III}$ fluoresc. X-ray spectra, mol. orbital struct. 78−70848
ClO_3^-, Cl $L_{II,III}$ fluoresc. X-ray spectra, mol. orbital struct. 78−70848
ClO_3^-, in $KClO_4$, detection by EPR of ClO_3 radicals created by X-irrad. 78−76311
ClO_3^- in $NaBrO_3$, Raman spectra, fundamental vibr. modes 78−78711
ClO_4^-, Cl $L_{II,III}$ fluoresc. X-ray spectra, mol. orbital struct. 78−70848
$^{35}Cl^-$, ion mobility in inert gas, drift tube mass spectrometric obs. 79−68896
$^{36}Cl^-$, self-diffusion in NaCl soln., β-active tracer, plastic capillary meas. method 77−50333
Co^-, photoelectron spectra, electron affinity and fine-struct. interval 79−68212
$Co(CN)_6^{3-}$, charge distrib., ESCA, internal standards 78−50585
$Co(CN)_6^{3-}$, electronic struct., ab initio LCAO SCF MO calcs. 79−18112
$Co(CN)_6^{3-}$, electronic struct., photochem. props., MS Xα calcs. 79−22600
$CoCl_4^{2-}$, electronic energy levels calc. by conventional and X alpha Hartree-Fock methods 78−66470
CoO_6^{10-} cluster, valence photoelectron spectrum, relative intensities, limited CI calcs. 79−63918
CoO_6^{10-}, ionisation, electron density relax. effects. ab initio calcs. 78−50466
Cr^-, photodetachment cross-section meas., crossed beam expt. 77−61723
CrC_{n_3-}, clusters, electronic props., mass spectra obs. *(French)* 79−45877
CrF_6^-, multiple scatt. calcs. methods, comparative study 79−6865
CrO_3^- radical in K_2CrO_4 and $KCrO_3Cl$, g-factor anisotropy 78−67994
$Cr_2O_7^{2-}$ centre in lattice, optical props., mol. orbital calcs. 79−15491
Cs, elastic electron scatt., 0.8-20 eV, Cs^- autoionis. state 78−5353
Cs plasma in thermionic converter, mass spectrometric study of positive and negative ions 79−19083
Cs^-, in tetrahydrofuran soln., transient photoelectron nutation 79−3418
Cs^-, multichannel photodetachment 78−42027
$Cs + Cl_2(Br_2)(I_2)(ICl)(IBr)$, negative ion prod. cross sections 77−531
$CsH^-CsH^+(CsH)$, ab initio ground-state pot. energy curves, electron affinities 78−41946
$Cs_2SnCl_6{:}UO_2Cl_4^{2-}$, luminesc., vibronic anal. 79−33767
$Cs_2ZrCl_6{:}UO_2Cl_4^{2-}$, luminesc., vibronic anal. 79−33767
$CuBr_4^{2-}$, ground state Zeeman splittings, reson. Raman spectra and mag.-optical activity 80−5579
$CuCl_4^{2-}$, core ionisation in 3d, 4f and 5f series, rearrangement effects 80−53065
$CuCl_4^{2-}$, electronic energy levels calc. by conventional and X alpha Hartree-Fock methods 78−66470
$Cu_2Cl_8^{4-}$, in Co (III), Cu (II) complex, single cryst. EPR 77−16157
D^-, equilib. yield in Sr vapour 78−17750
D^-, formation in $D^0(D^+) + Cs$ collisions 77−529
D^- ion source for high voltage neutral beams for fusion reactors 80−99379
D^-, neutral beam production for plasma injection heating research 77−76118
D^-, polarised prod. in $^1H + Cs$ atomic collision at 40 keV, 3.1 μA 78−55078
D^-, prod. of 100 keV beam, transport, accel. and diagnostics 77−83440
D^- production by $D^+ + Xe$ double charge exchange *(French)* 79−94080
D^- source using surface ionis., continuous beam prod. 78−9021
D^-, three-particle atomic system, binding energy, Faddeev method calcs. 77−57858
D+Cs, ang. scatt., neutral beam form. via negative ions 77−46636
$D^+ + Rb \rightarrow D^{-,0} + Rb$, equil. fraction of D^- ions, charge transfer cross section 77−65375
D_2^-, collision induced dissoc., positive and negative ions form. 78−50612
D_3^-, collision induced dissoc., positive and negative ions form. 78−50612
D_3^- repulsive state, form. in $D_3^+ + Cs$ electron capture 79−59563
$D(CN)_2^-$, IR spectra, rel. to mol. geom. 79−22702
$D_2O^-(^2A_1)$, obs. in K(Cs) ionis. collisions with D_2O, 100-200 eV 78−17770
F^-, electron impact detachment cross sections, test of classical scaling theory 79−31693
F^-, ion mobility in Ar, flow drift tube meas. 77−72405
F^-, mobility in He, flow-drift tube meas. 80−43831
F^-, near threshold electron detachment cross section, effect of resons. 77−42403
F^-, photodetachment cross section, Stieltjes imaging method 78−55149
F^-, static electric dipole polarisability 79−76332
F^-, Xα method predicting unstable state 78−82640
F^- + atom (Z=10-57), K-shell ionisation, X-ray prod. in transition region, collision symmetry effects 80−43163
F^- + fluoromethane, S_N2 reaction, ab initio LCAO SCF calcs. 77−81402
$F^- + H_2F$, proton transfer reaction, polarisation model 79−39131
$F^- + HF$, proton transfer reaction, polarisation model 79−39131
F^- + He, electron gas model, polarisation inclusion 78−37699
$F^- + Kr^+ + Ar$, three body ion-ion recombination probability, Monte Carlo simulation 80−85160
F^- + methane, MINDO/3-FORCES study, reactant energy, products and paths 78−95926
$F^- + Na(K)$, differential cross-section, small angle scatt. 79−98186
$F^- + X_2^+ \rightarrow [X_2F]^*$, 300K, 50 atm., recombination rates 78−46576
$F^- + X^+ + X \rightarrow XF^* + X$, (X=inert gas), ionic recomb. 78−46574
F^- + Xe, elastic differential cross-section, 250-500 eV, well depth of XeF^- 79−86027
F_2^-, absorption coeffs., shape resonance in e-F_2 scatt. 78−17792
F_2^-, mag. dipole terms evaluation, internucl. distance depend. 78−82864
$(F\text{-}H\text{-}F)^-$, strong H-bond, using recent difinition 79−98240
$F^-(Cl^-)(Br^-)(I^-) + O_2$, 0.2-100 eV, reaction differential cross sections energy depend. meas., exoergicity 77−63902
$FHCl^-$, deuteron quadrupole coupling const., nuclear mag. shielding, geometry depend. 78−58586
FHF^-, deuteron quadrupole coupling const., nuclear mag. shielding, geometry depend. 78−58586
FHF^-, H bonds, vibr. dynamics calcs. 80−23397
negative ions continued
FHF^- end, existence in alkali tetracyanoplatinate complexes, IR spectra 77−77184
$(F^-;e^+)$ complex, ab initio LCAO SCF calc., positron affinity and excitation energy 79−49945
Fe$^-$, electron affinity, nonstatistical fine-struct. detachment intensities at 488 nm, laser electron spectra 79−41144
$FeBr_4^-$, complex Raman tensors, irreducible tensor method, antisymmetric scatt. 78−37623
$FeBr_4^-$, in various solvents, $^4A_1$ ^4E d-d band reson. Raman spectra, solvent depend. 80−55085
$FeCN_6^{4-}$, triplet state quenching agent, in ZnO electrode dye sensitisation obs. 78−76869
$Fe(CN)_6^{4-} \rightleftharpoons Fe(CN)_6^{3-}$, redox pot. in nonaqueous-water mixtures 79−52654
$Fe(CO)_5$, gas phase collisions, negative ion form., struct. 77−6945
$FeCl_4^-$, effective charge, from IR and Raman scatt. intensity obs. 78−62809
FeO^-, UV photoelectron spectra, FeO electron affinity, new ground state assignment, vibr. 77−75212
FeS_6^{10-}, electronic struct., SCF-Xα scatt. wave calcs., rel. to spectra of FeS, FeS_2 78−5138
$Ga_3Br_{10}^-$, vibr. spectrosc., in alkali metal compound crysts. *(French)* 78−6667
GeF_6^{2-}, bond order and Raman intensity, delta function eqn. 77−61693
GeH_3^-, electronic struct., electron affinity, inversion barrier, ab initio SCF Gaussian basis calc. 80−63552
GeO_4^{4-}, normal vibr. freqs. calc. 79−54837
GeX_4, (X=Br,Cl), electron impact dissoc., low-energy reson. capture 78−9263
H, electron elastic scatt. phaseshifts H continuum, frozen-core Hartree-Fock approx. perturbation theory 77−75295
H^-, $^1P_0$-reson., DC Stark effect calcs. 78−42000
H^- affinity radiation, theoretical study of negative absorption 80−38001
H^- and H electron loss in plasma target 78−67371
H$^-$, and isoelectronic sequence, correlated and HF electron density differences 78−46275
H^-, ang. distribs. from H_2 dissociative electron attachment 77−19099
H^-, autoionization states, below N=3 hydrogenic threshold, complex-rot. calc. 77−67966
H$^-$, autoionising states, electric field effect 78−50528
H^- beam, intense, from Penning surface-plasma source, ion-optical characts. 79−13892
H^-, classical many-body collision model incorporating Heisenberg and Pauli principles 80−63511
H^-, DC Stark broadening of $^1P^0$ shape reson. 80−63585
H^-, density meas. by photodetachment 80−48976
H^-, dipole oscillator strength sum, in He isoelectronic series calcs. 78−86821
H^-, dynamic polarisability 79−76526
H^-, dynamic polarisability calc. 77−14599
H^-, elastic form factors, correlated two-electron-core pots., closed form expressions 79−68195
H$^-$, electron affinity, calc. of ion lifetime in elec. field 79−54986
H^-, electron correl. effects, ang. and radial, in momentum space 77−88399
H^-, electron detachment by electron impact, 1s state product, Born approx. 78−78816
H$^-$, electron loss in passing through inert gases 79−13805
H$^-$, electronic structure, stabilisation calcs. using big mol. Gaussian SCF/CI program 79−18121
H^-, energies and widths of $^1P^0(1)$ and $^1S(2)$ resonant states 79−18130
H^-, fluoresc. in γ- and UV-irrad. solvent matrices at 77K 78−70779
H^- form. by surface and vol. processes, neg. ion source appl., review 80−58375
H^-, formation by HCl dissociative electron attachment, differential cross section, Feshbach resons. 80−83508
H$^-$, from H_2^+ ion beam surface interaction, H^- formation by reson. electron capture 80−40691
H^-, generalised quantum defect, energy and radius depend. 80−14067
H$^-$, grazing incidence collision with surface, Balmer radiation, elliptical polarisation 78−86804
H^- ground state, evaluation, failure of local exchange approx. 77−47758
H^-, ground state electron correlation visualisation 79−3367
H^-, H^{2-}, bound states calc. 79−13646
H^-, Hartree-Fock energies, scaled 1/Z expansion, integral eqns. 80−47886
H^-, in solar atmosphere, bound-free electron transitions, review 78−33563
H^-, ion beam bunching with sawtooth voltage 78−4735
H^-, ion beam diagnostics using laser beam 80−95497
H^-, ion source, CW plasma device, current maximisation 79−22521
H^- ion yield from duoplasmatron discharge 78−75382
H^-, magnetron discharge as ion source 77−38528
H^-, many-body perturbation theory with radially restricted basis functions 80−78526
H^-, metastable, electron affinity calcs. 79−31439
H^-, multipole sum rules 77−42257
H^-, numerical Hartree-Fock calc. of $1s^2$ ground state 79−81155
H^-, photoabsorpt. and dispersion profiles, moment theory 77−6709
H^-, photoabsorption spectra, long-range field effect 80−91521
H^-, photodetachment, Feshbach and shape resons. 77−23480
H^-, photodetachment cross sections, one and two electrons, multichannel J-matrix calc. 77−18860
H^-, photodetachment cross section, dynamic polarisability calc., sum rules, basis set depend. 78−17635
H^-, photodetachment cross section, Feshbach and shape reson. elec. field depend. 78−37614
H^-, photodetachment cross section, perturbation-variation method 79−6921
H^- photodetachment cross section, narrow resonances near n=3 threshold 80−27988
H^- polarised ion source, pulse operated, Lamb shift type, for acceleration of polarised protons *(Japanese)* 77−67929
H^-, polarised prod. in $^1H + Cs$ atomic collision at 40 keV, 2.9 μA 78−55078
H^-, prod. from accel. cluster ions for neutral beam plasma injection heating 77−65376
H^-, production by Hall accelerator in Cs vapour, space-charge effects 78−67375

negative ions continued
H⁻, production cross section in e^--H_3^+ collision 80−5628
H⁻ production in foil breakup of H_2^+, inhibition effect 80−99549
H⁻, production in laser-initiated alkali hydride arc 80−32550
H⁻, proof of only one bound state, fixed nucleus approx. 77−30805
H⁻, S autoionising states, appl. of at. reson. theory 80−23329
H⁻, S autoionising states, time stability theory 78−90130
H⁻, S reson. state, appl. of improved line width expression 80−5505
H⁻, shape reson., Stark effect, complex coords., translation and dilatation transforms 79−18141
H⁻ surface ion source, plasma parameters, diagnostics 78−9849
H⁻, surface plasma source, ion form. and secondary electrons *(Russian)* 78−71503
H⁻, surface plasma source, prod. by H atom backscatt. from cesiated W 77−3953
H⁻, three-particle atomic system, binding energy, Faddeev method calcs. 77−57858
H⁻, two-electon photodetachment threshold, blackbody radiation effects 80−91524
H⁻ vac. UV spectra, narrow reson. at 1129.5 Å, H-arc spectra 78−66490
H^{2-}, existence, alternative explanation of results, electron effects 77−19079
H_2^{2-}, existence, expt. evidence 77−19081
H_2^{2-}, metastable, electron affinity calcs. 79−31439
H_2^{2-}, metastable state 77−18805
H_2^{2-}, Z-Z 80−28104
H^{2+}, existence, alternative explanation of results, ion intensities 77−19080
H⁻-like ions, electron correlation and Coulomb hole in momentum space 78−86793
H⁻-positron bound states, CI-Hylleraas calcs. 77−10603
$H+Cs \rightarrow H^- + Cs^+$, low energy cross sections 79−7009
H+positronium→H^++positronium⁻, low energy, field theoretic approach 77−10790
$H^- + {}^4He^{2+}$, electron capture cross sections 79−10198
H⁻+Ar, 0.5 MeV H(H⁻) ionisation comparison 79−41230
H⁻+Ar, electron detachment, 0.5 to 1.0 MeV 78−22021
H⁻+Ar(H_2)(He)(N_2)(Ne), collisional detachment cross-sections, high-energy obs. 77−3442
H⁻+atom, electron loss high energy cross sections 78−13597
H⁻+Cs, fast atom collisions, charge exchange, equilib. fractions calcs. 78−33601
H⁻+H, electron detachment cross-sections, 100 keV-10 MeV 79−59561
H⁻+H_2, electron detachment cross-sections, 100 keV-10 MeV 79−59561
$H^- + H_2^+ \rightarrow H_2^* + H$ recombination react., calcs. *(Russian)* 80−55659
H⁻+H_2(He)(Ar), electron detachment, Born cross sections, Pade approximants 78−17742
H⁻+H_2(He)(Li), 50-150 keV, scatt. angle of neutral H 78−5340
$H^- + H^+$, charge exchange, one or two electrons, symmetry effects *(Russian)* 79−3562
$H^- + H^+$, double charge transfer, 30-200 eV 79−45837
$H^- + H^+$, electron capture, continuum distorted wave calcs. 78−50635
$H^- + H^+$, electron detachment cross sections 79−13818
$H^- + H^+$ charge exchange, quantum transition probabilities calc. 80−9557
$H^- + H^+ \rightarrow H(1S) + H$, level degeneracy effect on charge exchange at term pseudointersection 79−27084
H⁻+HF, reaction, ab initio pot. energy surface calcs. 79−39127
H⁻+H(He), electron detachment cross sections 78−90265
H⁻+H(He), electron detachment in adiabatic regime, mechanisms 80−63800
H⁻+H(He), electron-loss cross-section, double closure calcs. 77−50518
H⁻+He, electron detachment, theoretical obs. 80−63799
H⁻+He, electron detachment cross-sections, 100 keV-10 MeV 79−59561
H⁻+He, electron detachment cross-section, target distortion calcs., 100 keV-100 MeV 79−59562
H⁻+He(Ar), electron detachment cross sections 78−58810
H⁻+He(Ar) low-energy total electron detachment cross-sections, approximation 79−72405
H⁻+inert gas, negative ion detachment cross section determ. 80−63796
$H^- + M^+$ (M=alkali metal atom), ion-ion recombination 78−58779
H⁻+methane→methane+H⁻, nucleophilic substitution, ab initio pot. energy classical trajectory anal. 78−68886
H⁻+methane→methane+H⁻ force decomposition anal. along reaction coord. 78−27741
H⁻+N_2 (inert gas), charge transfer, ejected electron spectra 79−45828
$H^- + N_2 \rightarrow N_2^- + H$, vibr. autodetaching states, excitation and decay 78−33620
H⁻+NH_4^+, substitution and abstraction reactions, ab initio calcs. 77−48624
$H^+ + Cs \rightarrow H^- + Cs^{2+}$, proton conversion, 0.2 to 6.0 keV *(Russian)* 77−1920
$H^+ + H^-$, electron detachment cross-section, crossed beam meas. 77−10728
$H^+ + H^-$, merged beams, double charge transfer cross section 79−22818
H_2^-, autoionising states, complex scaling method calcs. 80−9527
H_2^-, collision induced dissoc., positive and negative ions form. 78−50612
H_2^-, free free absorpt. coeffs. dipole length formulation and two centre close coupling calc. 80−83345
H_2^-, free free absorpt. rel. to opacity in stellar atms. 78−81610
H_2^- resonant states, Feshbach projection-operator calc. 78−5153
H_2^-, variational calcs. of resonant states 79−3571
H_2^++He(Kr)(Xe), collisional dissociation, ion-pair prod., negative ion prod., cross sections 77−14529
H_3^-, collision induced dissoc., positive and negative ions form. 78−50612
H_3^-, dissociating states, lowest singlet and triplet PE surfaces, HF calcs. 79−81160
(H-He)⁻, ab initio calcs. 80−63799
HBr, electron impact ionisation, vibr. excitation spectra threshold peaks, negative ion effects 80−106322
HC_2^-, ground state energy surface, ab initio SCF calc. 78−33446
HCN⁻, ab initio calcs., electron affinity, stability 77−42239
HCN⁻, SCF ab initio ground state pot. energy surface, geometry, rel. to HCN 78−78646
$H(CN)_2^-$, IR spectra, rel. to mol. geom. 79−22702
HCO_3^-(aq), standard enthalpies of solution and formation, standard Gibbs energies of formation and standard entropy 79−57285
HCl⁻, reson. states by electron impact, GO and SCF+CI methods, dissociation channels 77−71883
HCl⁻, resonance states, CI calcs., pot. energy curves 78−29755
HCl⁻, resonance states, interpretation of low energy HCl-electron scatt. 78−17808
HCl+O^-(O_2^-)(NO_2^-)(CO_3^-)(CO_4^-), rate consts. at 300K 78−76829
HD⁻, collision induced dissoc., positive and negative ions form. 78−50612
H⁻(D^-)+He, collisionally induced electron detachment, 0.5 MeV, target effect 80−37858
HD_2^-, collision induced dissoc., positive and negative ions form. 78−50612
HF^- and $(HF)_2^-$, ab initio calcs., electron affinity, stability 77−42239
HF-fluoromethylene anion, in solid Ar, IR spectra, vibr. modes 79−68231
HF_2^-, dipole derivatives, rel. to refl. spectra of Na and K salts 78−80324
HF_2^-, four electron three centre bonding units, ab initio valence bond calcs. 80−27949
HF_2^-, IR spectra and mol. struct. 79−63996
HF_2^-, mag. shielding and susceptibility, finite perturbation mol. orbitals calcs. 77−46513
HF_2^-, matrix isolated, IR spectra and struct. 78−74655
$H_2F_3^-$, struct. H bonding, IR spectra obs. 77−54560
$H_3F_4^-$, struct., H bonding, IR spectra obs. 77−54560
$H_4F_5^-$, struct., H bonding, IR spectra obs. 77−54560
H_3NO^-, ab initio calcs., electron affinity, stability 77−42239
HO^-/H_2O and DO^-/D_2O, ionis. efficiency curves, Feshbach-reson. and dissoc. electron attachment 79−41246
H_2O, Van der Waals polymer mols., negative ions formed in nozzle expansion 78−90296
H_2O^-, ab initio calcs., electron affinity, stability 77−42239
H_2O^-, electron affinity, mol. geom. effects calcs. 78−82618
H_2O^- in flames, electron attachment kinetics 80−3349
H_2O^- in γ-irrad. Y-type zeolite, alternative EPR triplet assignment to NO_3^{2-} 78−11534
HPO_3^{2-}, in NaH_2PO_2-Na_2HPO_3, quantitative anal. by relative Raman intensities obs. *(Japanese)* 78−23991
$H_2PO_2^-$, in NaH_2PO_2-Na_2HPO_3, quantitative anal. by relative Raman intensities obs. *(Japanese)* 78−23991
HPO_4^-(H_2PO_4) radicals + organic compounds, reaction rate consts. 78−15669
HS_n^-, n=1-4, electronic struct., ab initio Hartree-Fock-Slater calcs. 80−74107
HS_n^{2-}, n=1-4, electronic struct., ab initio Hartree-Fock-Slater calcs. 80−74107
$H_2S_2^-$, produced by ns pulse radiolysis of liq. H_2S, optical absorption transients 79−11803
He, electron impact ionisation, decay modes investig. 79−72422
He, He⁻-positron bound states, CI-Hylleraas calcs. 77−10603
He⁻, $3s^23p(^2P)$ obs., electron impact excitation of He(2^3S) 77−50543
He⁻, $(1s2s2p)^4P^0$ metastable state, CI calc. 79−59591
He⁻, binding energy of metastable $1s2s2p\ ^4P^0$ state 80−9524
He⁻, electron impact. post-collision interaction, reson. states 77−10767
He⁻, electron loss in passing through inert gases 79−13805
He⁻, existence in strong mag. field, binding energy, isoelectronic semicond. impurity trapping 78−9097
He⁻, form. by $He^{2+} + H_2$ collisions 78−58811
He⁻, formed in the He+He collisions, decay cross section oscills. *(Russian)* 77−19038
He⁻, inelastic Feshbach resons., quasi projection operator calc. 80−58395
He⁻, ion source, K charge exchange vapour, Pelletron accelerator injector 78−5085
He⁻, isoelectronic sequence, triply excited bound state, variational calc. 80−9526
He⁻, metastable, electron affinity calc. 79−31439
He⁻, purely L^2 method for calculating resonance widths 78−46283
He⁻, reson. calcs. with correlated target state wave functions, complex coord. method 79−26939
He⁻, resonances in post collision interaction 79−13820
He⁻ resons. in 56 to 64 eV electron collisions, autoionising states and spectral line polarisation 80−53145
He⁻, resons. near doubly excited states thresholds, close coupling calcs. 77−54612
He⁻, wave function structure, complex coord. method 78−94190
He +Ar(H_2)(He)(N_2)(Ne), collisional detachment cross-sections, high-energy obs. 77−3442
HeH, neutral and negative ion states SCF pot. energy curves 78−62745
^{3}He, liq., ESR obs. 79−60582
^{3}He, negative ion mobility, theory 80−107598
^{3}He, negative ion structure in normal liq. phase 79−86953
^{3}He, normal and superfluid phase, negative ion motion 78−38900
^{3}He, superfluid, B phase, motion of negative ions 77−11757
^{3}He, superfluid, pair breaking by electron bubbles 79−51352
^{3}He superfluid β-phase, negative ions mobility 79−86956
^{3}He-^{4}He mixtures, quantised vortex lines and lifetime of negative ions trapped by vortices 78−84022
Hg, electron scatt., negative ion form., shape resonances, electron affinity 77−14581
$Hg(CN)_3^-$ ion, CN and HgC stretching vibrations and HgCN bending vibration assignments 80−69140
HgX_3^- (X=Cl,Br), aprotic donor solns., Raman spectra, mol. vibr. and solvent strength 78−29788
HgX_4^- (X=Cl,Br), aprotic donor solns., Raman spectra, mol. vibr. and solvent strength 78−29788
H⁻ source for hollow beams using H_2-Cs 80−23228
I⁻, 3d photoabsorpt. spectra, continuum and discrete states 79−81176
I⁻, $3d^94f$ config., collapse of 4f electron, X-ray spectral obs. *(Russian)* 80−58204
I⁻ and I_2^- formed in CeI_3 by electron irradiation 77−27190
I⁻ beam, duoplasmatron ion source for SIMS, Ar-I_2 medium 77−18123
I⁻ hydration complexes, gas phase, electrostatic calcs. 80−100055
I⁻, in althylamminium iodides, in solns. of low parity, MCD spectra 78−94268
I⁻, ion mobility in Ar, flow drift tube meas. 77−72405
I⁻, plasma, broadening of free-bound radiation thresholds 80−53940
I⁻+CO, endoergic ion-molecule reaction 77−25262

negative ions continued
$I^-+COS(CS_2)(H_2S)$, endoergic reaction, time of flight mass spectral obs. 77−12786
I^-+methane(fluoromethane), excitation functions, reactive scatt., eV region *(German)* 78−35677
I^-+Ne, electron detachment collision, 1-3 keV, differential cross-section 79−72403
I^-+SO_2, endoergic reaction, time-of-flight mass spectral obs. 77−12785
I^-+sulphorhodamine G, physical and chem. kinetics competition, fluoresc. quenching obs. 79−43567
I_2^-, bond stretching depend. in I_2+Na(K)(Cs) ion-pair form. 77−28996
I_2^-, HF and SCF calcs., pot. curves, electron affinity and quadrupole moment determ. 80−95527
I_3^-, geom. and electronic struct., effective pot. calc. 78−74788
I_5^-, geom. and electronic struct., effective pot. calc. 78−74788
$I(H_2O)_n^-$, geometric and electronic struct., CNDO/2 calcs. 77−79542
$I(H_2O)_n^-$, geometric and electronic struct., CNDO/2 calc. 79−41113
$I_2^-(I^-)$, formed by electron impact from SnI_4 ionis. efficiency curves 77−61865
IO^-, electron affinity formed in I^-+O_2 reaction 77−63902
IO_3^-, adsorption desorption by TiO_2 suspension, kinetics, relax. technique 80−93804
IO_3^-, determ. in rainwater by neutron activation anal. 78−76953
IO_3^- in $NaClO_3$, Raman spectra, fundamental vibr. modes 78−78711
$IrBr_6^{2-}$, complex Raman tensors, irreducible tensor method, antisymmetric scatt. 78−37623
$IrBr_6^{2-}$, Raman tensor patterns, vibr. reson. Raman scatt., group theoretical calcs. 78−986
$IrCl_6^{2-}$, complex Raman tensors, irreducible tensor method, antisymmetric scatt. 78−37623
$IrCl_6^{2-}$, ground state Zeeman splittings, reson. Raman spectra and mag.-optical activity 80−5579
K^- and K_2^- form. and decay in discharge plasma *(Russian)* 79−90374
K^-, multichannel photodetachment 78−42027
K^-, photodetachment and at. polarisability 80−91522
$K+Cl_2(Br_2)(I_2)(ICl)(IBr)$, negative ion prod. cross sections 77−531
$K+H_2S(DS)$, collisional ionisation, positive and negative ion energy spectra obs. 80−63775
K+halogenated methane, negative ion form., electron affinities, bond dissoc. energies 78−82827
$KTaO_3$:$OH^-(OD^-)(OT^-)$, IR spectra, spectrosc. consts. 80−100671
Kr, $4p^55s$ state, electron excitation fine struct., neg. on reson. 77−14585
Kr^-, electron capture expts. to search for long lived states 79−72410
Kr-Cl_2 mixture, glow discharge positive column, electron energy distrib. and rates of inelastic processes, negative Cl ions form. 80−19632
LaB_6, negative surface ionisation, intense halogen ion source 79−93850
LaO_4^{7-}, ionisation energies, satellite struct., photoelectron spectra, MS Xα calcs. 78−13425
Li H^-, mol. orbital calcs., diffuse functions for basis sets, electron affinity 78−25436
Li^-, core excited bound states in beam foil expts., CI calcs. 80−78559
Li^-, core-excited bound states 80−91468
Li_2^-, electronic struct., ab initio calcs. 77−34553
Li_3^-, ab initio pseudopotential for FSGO calcs., bond length 77−75043
Li_3^-, electronic struct., SCF and SCF-CI calcs. 80−87044
LiF^-, ground and excited states, ab initio calcs. single config. and multiconfig. SCF calcs. 80−52873
LiF(LiF^-), electron affinity and dipole moment, ab initio calc. 78−41938
LiH, LiH^-, pot. energy curves, electron affinity, spectroscopic consts. 78−5129
LiH (LiH), ab initio ground-state pot. energy curves, electron affinities 78−41946
Li_2O^-, electronic struct. and config., ab initio SCF study 79−85898
$LiOH^-$, electronic struct. and config., ab initio SCF study 79−85898
Mg, electron scatt., negative ion form., shape resonances, electron affinity 77−14581
Mg^-, purely L^2 method for calculating resonance widths 78−46283
Mg^-, shape resonances, shift potential calcs. 80−69089
MgF_2^-, ground state, conform., electron affinity, extended basis SCF calcs. 79−72253
MgO(MgO^-), electron affinity and dipole moment, ab initio calc. 78−41938
$MnCl_4^{2-}$, electronic energy levels calc. by conventional and X alpha Hartree-Fock methods 78−66470
MnO_4^-, aq. soln., O isotope substitution, ^{55}Mn NMR 77−30890
MnO_4^-, bond lengths and coordination numbers, EXAFS meas. 79−51043
MnO_4^-, valence mol. orbital energy, nonempirical pseudopot. 79−22592
Mo, surface, electron-stimulated desorption of negative ions, work function 78−72654
$Mo_2Cl_8^{4-}$, low lying states, weak electronic coupling, Xα valence band theory 79−72237
$Mo_2Cl_8^{4-}$, metal-metal bond energy, SCF-Xα-SW calcs. 80−78538
$Mo_2Cl_9^{3-}$ complexes, cluster exchange coupling consts. SCF-Xα-SW calcs. 80−74120
$Mo_2Cl_8^{3-}(Mo_2Cl_9^{3-})$, electronic struct. and metal-metal bonding, HMO calcs. *(Russian)* 78−1118
MoO_4^-, aq. soln., O isotope substitution, ^{95}Mo NMR 77−30890
$Mo_6O_{19}^{3-}$, in Mo/SiO_2 supported catalyst system, EPR, UV-visible spectra 79−99764
$MoO_{4-n}S_n^{2-}$ in aqueous soln., ^{95}Mo NMR identification 77−48069
$MoO_{4-n}Sn^{2-}$, (n=0-4), $^{17}O(^{33}S)(^{95}Mo)(^{97}Mo)$ NMR investig. 80−53022
MoS_4^{2-}, anharmonicity consts., reson. Raman spectra 77−61754
$MoSe_2$-I^-, photoelectrode, time resolved photocurrent, nanosecond excitation 80−45708
$MoSe_4^{2-}$, anharmonicity consts., reson. Raman spectra 77−61754
N^-, $^3P^e$ shape reson. in absorpt. coeff. 77−424
N^-, appearance pot., form. by electron impact ionisation, mass spectra 77−75320
N^-, continuous absorption coeffs., from elastic e-N scatt. data, target wavefunction effect 78−9128
N^-, form., by double electron transfer, cross-section meas. 78−78806
N^-, free-free absorpt., multichannel theory 77−18816
N^-, Sternheimer valence shielding and antishielding factors 80−18807
N_2 in high press. air plasma, photodissoc. 80−64691
N_2 laser discharge, SF_6 addition, negative ion prod., altered discharge parameters 80−38818
N_2, negative-ion resons. associated with inner-shell-excited states, electron impact 77−88580
negative ions continued
N_2^-, $^2\Pi_g$ resonance effect on N_2 electron impact rot. excitation 77−58184
N_2^-, 2 eV resonance as energy standard in low energy electron scatt 77−71872
N_2^-, first $^2\Pi_u$ state form. and decay 80−58177
N_2^-, free free absorpt. rel. to opacity in stellar atms. 78−81610
N_2^-, resonances in N_2 electron impact excitation *(French)* 78−25723
N_2^-, vibr. autodetaching states, from H^-+H_2, excitation and decay, Franck-Condon factors 78−33620
N_3^- electronic struct., SCF Xα scatt.-wave calcs. 77−50364
N_3^-, high press. IR vibr. spectroscopy *(German)* 80−74170
N_3^-, low-lying excited states 79−31425
NH^-, photoelectron spectra, NH electron affinity and intercombination separation 77−18970
NH_2^-, mol. geom., diffuse functions in SCF calcs. 79−10226
NH_2^-, photodetachment energy, eqn. of motion method 78−5301
NH_3 glow discharge, electron energy distrib. and negative ions *(Russian)* 79−7499
NO^-, $^3\Sigma^-$ and $^1\Delta$ resonances, excitation in electron scatt. 77−31010
NO destruction in collisions with excited molecules 80−14189
$NO^++NO_2^-$ neutralisation reaction, spectroscopic study 79−13819
$NO^++X^-\rightarrow NO+X$ (X=Cl, Br, I), rate const. determ. in flames 78−48633
NO_2^-, ab initio VB wave functions, π-electrons 78−70748
NO_2^-, direct CI calcs. 80−52889
NO_2^-, direct CI method generalised to HF interacting space 79−85908
NO_2^-, electron detachment energy, equations of motion method calcs. 77−50478
NO_2^-, electronic struct., X-ray spectra obs. 78−55185
NO_2^-, heavy cation effect on singlet-triplet intercombination 79−85946
NO_2^-, high press. IR vibr. spectroscopy *(German)* 80−74170
NO_2^- in KI matrix 78−52479
NO_2^-, microwave transition probability in zero field, spin-orbit interaction 78−25518
NO_2^-, $NO_2^-.H_2O$, and peroxy isomers, photodissoc. and photodetachment 3500-8250 Å, rel. to ionosphere 80−35554
NO_2^-, optimisation of diffuse Gaussian exponents 79−3364
NO_2^-, SCF and MC SCF CI calcs. 78−46280
NO_2^-, solvated, in H_2O, ethanol, cyanomethane, and DMF lowest n-π^* transition 79−85960
NO_2^- triplet state lifetimes and fine structs., CNDO-CI calcs. 77−57897
NO_2^-, vertical electronic spectra, ab initio calcs. 78−66538
$NO_2^-+O_2(CO_2)(NO_2)$, photodetachment and de-excitation rates 77−75236
NO_3^-, aq. soln., vibr. width and dephasing, conc. depend. 80−43029
NO_3^-, electronic struct., X-ray spectra obs. 78−55185
NO_3^-, in aq. nitrate solns., vibr. dephasing process, Raman obs. 79−51936
NO_3^-, $NO_3^-.H_2O$, and peroxy isomers, photodissoc. and photodetachment 3500-8250 Å, rel. to ionosphere 80−35554
NO_3^-, triplet state lifetimes and fine structs., CNDO-CI calcs. 77−57897
NO_3^{2-}, in γ-irrad. Y-type zeolite, EPR triplet assignment, instead of H_2O^- 78−11534
$NO_3^-+H_2O$, in aq. NH_4NO_3, H bonding, X-ray diffr. obs., 25°C 78−42881
N_2O, negative Van der Waals polymer mols., formed by nozzle expansion 78−90307
N_2O^-, ground state potential energy surfaces 77−27175
$N_2O_5+CO_3^-(NO_2^-)(F^-)(Cl^-)(Br^-)(I^-)=NO_3^-+XNO_2$, rate consts. 78−56879
$NO_2(NO_2^-)$, ionis. pot. and electron affinity, overlapping sphere MS Xα calc. 78−41948
$NO_3(NO_3^-)$, ionis. pot. and electron affinity, overlapping sphere MS Xα calc. 78−41948
$N^-(^3P)$, energy and width after form. by N_2 and NO dissoc. electron attachment 78−90308
$Na+Cl_2(Br_2)(I_2)(ICl)(IBr)$, negative ion prod. cross sections 77−531
$NaCl^-$, mol. orbital calcs., diffuse functions for basis sets, electron affinity 78−25436
$NaCl^-$, $NaBr^-$, NaI^-, photodetachment cross section resons., 2-2.3 eV 79−54922
NaCl:OH^-, UV and IR absorpt. spectra, colour centres transformation 79−28791
NaF(NaF^-), electron affinity and dipole moment, ab initio calc. 78−41938
NaH^-, mol. orbital calcs., diffuse functions for basis sets, electron affinity 78−25436
NaH^-(NaH), ab initio ground-state pot. energy curves, electron affinities 78−41946
$Nb_2Cl_9^{3-}$, electronic struct. and metal-metal bonding, HMO calcs. *(Russian)* 78−1118
$(NbCl_nBr_{6-n})^-$, ^{93}Nb nucl. spin relax. and mag. shielding 78−58723
Ne, autoionisation region states, differential excitation function resons. obs. 77−6939
Ne, resonant free-free absorpt. by electrons 77−3463
Ne^-, electron capture expts. to search for long lived states 79−72410
Ne^- scatt. electron spectra, distinction from neutral autoionising states 80−83482
$Ne+H^-(D^-)$, electron detachment, dynamical phenomenon 80−106305
Ni^-, photodetachment cross-section meas., crossed beam expt. 77−61723
Ni^-, photoelectron spectra, electron affinity and fine-struct. interval 79−68212
$Ni(CO)_4$, gas phase collisions, negative ion form., struct. 77−6945
O^- and O_2^- ion swarm in O_2, reactions and transport, Monte Carlo calc. 78−59539
O^-, electron impact detachment, cross-section, 10-1000 eV 79−31702
O^-, form. from O_2 adsorbed on reduced Mo_2O_3-Al_2O_3 catalysts 78−85197
O^-, free-free absorpt., multichannel theory 77−18816
O^-, in silicates, XPS quantitative anal. *(Japanese)* 77−48710
O^-, photodetachment, fine struct. transitions, photoelectron spectra 78−55151
O^-, photodissoc. and photodetachment in $O_2/CH_4/H_2O$ mixtures, 3500-8600 Å 79−45776
O^-, spectra in pure O arc plasma, 2000-9000 Å, 9000K 79−32750
O^-, Xα method predicting unstable state 78−82640
$O^-/H_2O(D_2O)$, ionis. efficiency curves, Feshbach-reson. and dissoc. electron attachment 79−41246

negative ions continued
$O^- + CO(Mg)(N_2)$, electron detachment cross-sections, 20-150 keV '78 - 25690
$O^- + CO \rightarrow CO_2^- + e^-$, vibr. chemiluminesc. 78−3340
$O^- + D_2 \rightarrow OD^- + D$, crossed beam studies product ang. and energy distrib. 78−53203
$O^- + N_2$, electron detachment, collision with vibr. excited mols. 79−54961
$O^- + N_2 \rightarrow N_2O + e$, rate studies 78−40036
O^- +Ne(Ar)(Kr), 0.2-1 keV, elastic and inelastic reduced differential cross-sections 80−32829
$O^- + O_2$, electron detachment, collision with vibr. excited mols. 79−54961
$O^- + O_2 \rightarrow O_2^- + O$, cross sections, 0-100 eV *(German)* 77−32785
$O^- + O_2 \rightarrow O_2^- + O$, cross section kinetic energy depend., rate consts. meas. and Monte Carlo calcs. 80−78701
O_2, dissociative attachment coeff. calc. 77−19100
O_2, interactions with slow electrons 79−45848
O_2, Trichel corona, negative ions 78−30503
O_2^-, $A^2\Pi_u$ state pot. energy curve, MCSCF calcs. 80−63565
O_2^-, ab initio pot. curves of $X^2\Pi_g$, $A^2\Pi_u$, $a^4\Sigma_u^-$, $^2\Sigma_u^-$ states 78−66483
O_2^-, EPR in $SrCl_2$ 77−24742
O_2^-, form. on reduced MoO_3-TiO_2 surface 77−90590
O_2^-, generation in CdS aq. dispersion by photolysis, spin trapping detect. 78−11538
O_2^-, in aq. solns. of alkali halides, spectral props. *(Russian)* 78−6766
O_2^- in flames, electron attachment kinetics 80−3349
O_2^-, in ionosphere, effects on EM wave propag. 79−8762
O_2^-, in nonpolar liqs., laser photodetachment, elec. cond. obs. 79−64057
O_2^-, in silicates, XPS quantitative anal. *(Japanese)* 77−48710
O_2^-, photodissoc. and photodetachment in $O_2/CH_4/H_2O$ mixtures, 3500-8600 Å 79−45776
O_2+Na(K)(Cs), negative ion pair form., total cross sections 79−3550
$O_2^- + H_2O_2$, Haber-Weiss reaction kinetics, chain mechanism 79−83444
$O_2^- + N_2$, electron detachment, collision with vibr. excited mols. 79−54961
$O_2^- + O_3$, electron detachment, collision with vibr. excited mols. 79−54961
O_3, radiative electron attachment spectra, vibr. stretching, electron affinity, theory 77−54617
O_3^-, ($O_3^-.H_2O$), photodetachment and photodissoc. cross-sections meas. 79−98170
O_3^-, O^- bond dissociation energy 78−7193
O_3^-, photodissoc, cross section 79−832
O_3^-, photodissoc. and photodetachment in $O_2/CH_4/H_2O$ mixtures, 3500-8600 Å 79−45776
O_3^-, photoelectron, photodetachment and photodestruction spectra 79−64042
O_3+O^-(OH^-)(S^-)(SH^-), associative detachment, rate coeffs. 78−3325
O_3^- +molecule reactions, thermochemistry, electron affinity and rate consts. 78−40040
$O_3^- + X \rightarrow O^- + O_2 + X$, X=He, Ar, CO_2, long-lived excited (or isomeric) state of O_3^- 78−5318
O_4^-, photodissoc. and photodetachment in $O_2/CH_4/H_2O$ mixtures, 3500-8600 Å 79−45776
O_5^{2-}, hypothetical, mol. self-consistent study, possible prep. method *(French)* 80−91717
$O_2^+AsF_6^-$, thermal decomposition, Raman spectra study, free radical mechanism 80−55652
OCN^-, linear mol., Compton profile bond additivity, HF calc. 79−68268
OH^-, and OD^-, photodissoc. and photodetachment in $O_2/CH_4/H_2O$ mixtures, 3500-8600 Å 79−45776
OH^- excitation, cause of laser Raman fluoresc. background at oxide surfaces 78−10875
OH^-, proton affinity, integral Hellmann-Feynman theorem 78−70767
$OH^- + C(N_2)$, electron stripping and breakup, proton spectra 77−83685
OH^- +inert gas, collision-induced dissociation 78−29834
OH^- +methoxybenzene (o-cresol), gas phase reaction, 299-435 K, kinetics and mechanism 78−11515
$OH^- + O_3$, associative detachment, rate coeffs. 78−3325
$O^-(O_2^-)$, optimum pot. model used to generate numerical pot., energies and electron affinities determ. 80−99534
$O^-(^2P^0)$, attachment energies, ab initio calc. 77−30768
O_2−, electron transfer reactions, singlet O_2 form. and quenching 77−29002
O_2^{-*}, vibr. excited, lifetime obs. 77−42422
$O_{2-3}^-.H_2O$, photodissoc. and photodetachment in $O_2/CH_4/H_2O$ mixtures, 3500-8600 Å 79−45776
$O_3^-.H_2O$ and $O_3^-.2H_2O$, photodissoc, and photodetachment 79−833
$OsBr_6^{2-}$, complex Raman tensors, irreducible tensor method, antisymmetric scatt. 78−37623
P^-, contracted Gaussian basis sets for mol. calcs. 80−83264
P^-, metastable, electron affinity calcs. 79−31439
P^-, photodetachment cross-section meas., crossed beam expt. 77−61723
P_2^-, photodetachment cross section, 0.5 to 3.0 eV photon energy *(German)* 77−65518
$PAsO_7^{4-}$, formation in $Mg_2P_2O_7$-$Mg_2As_2O_7$ solid soln., IR absorption spectra exam. 79−1508
PF_6^-, bond order and Raman intensity, delta function eqn. 77−61693
PF_6^-, octahedral complex, ionis. energy, SCF-Xα study 78−70967
$(PMo_{11}O_{39})_7^-$, decomp., in aq. soln., Raman spectra obs. 79−13719
$PMo_{12}O_{40}^{3-}$, vibr. force const. for spectroscopically active freqs. 77−57976
PMo_9O_{34} model vibr. freqs. 80−23408
PO_4^{2-} anion radicals + organic compounds, reaction rate consts. 78−15669
$P^-(^3P_{2,1,0}) + h\nu$, P electron affinity, P^- fine struct. interval 77−79590
$^{207}PbF_6^-$, radical, prep. and EPR comparison with other hexafluoride radicals 78−68381
$PdBr_4^{2-}$, Raman scatt., interference effects 77−68047
Pt complex, $PtCl_4^{2-}$, in chloride-sulphate soln., Pt electrodeposition, galvanostatic transients *(Russian)* 78−31655
$PtCl_4^-$, effective charge, from IR and Raman scatt. intensity obs. 78−62809
Rb^-, in tetrahydrofuran soln., transient photoelectron nutation 79−3418
Rb^-, photodetachment, electron affinity 78−90132
$ReBr_6^{2-}$, IR luminesc. spectra 79−45745
$Re_2Cl_8^{2-}$, in acetonitrile and dichloromethane solns., 300K, emission spectra and lifetimes 79−59447
negative ions continued
$Re_2Cl_8^{2-}$, spectral assignment, metal-metal bonds, SCF Xα SW calcs., relativistic corrections 80−53006
$Re_3Cl_9^-$, electronic struct. and metal-metal bonding, HMO calcs. *(Russian)* 78−1118
$(Re_2OCl_{10})^{3-}$, reson. Raman, IR and electronic spectral studies 79−10118
$RuCl_5NO^{2-}$, polarised Raman and IR spectra, vibr. anal. 77−69819
RuO_4^{2-}, antireson. Raman effect, excitation profile 79−50019
$Ru_4O_{16}^{12-}$ clusters, thermodynamic props., exchange interactions effects 79−24180
S containing small paramag. ions on MgO g-tensors and spin densities 78−46270
S^-, contracted Gaussian basis sets for mol. calcs. 80−83264
S^- ion-selective electrode, sensitivity, surface heterogeneity effects 78−92526
S^-, photodetachment, fine struct. transitions, photoelectron spectra 78−55151
S^-, photodetachment cross section mag. field depend. struct., obs. 78−55148
S^-, photodetachment in mag. field 79−41143
$S^- + O_3$, associative detachment, rate coeffs. 78−3325
S_3^-, photodetachment cross section, 0.5 to 3.0 eV photonenergy *(German)* 77−65518
S_4^{2-}, structure investigation by ab initio calcs. 80−69066
S_4^x, x=2−, 0, 2+, struct. differences explained, SCF Xα scatt. wave MO calcs. 78−74784
S_n^{2-} (n=4-8), vibr. and rot. isomers, Raman spectra *(German)* 78−13504
SCN^-, associated with metallic cations in aq. soln., press. effect, Raman spectra *(French)* 78−80333
SCN^-, electron density distrib., theoretical and expt. determ. 77−61683
SCN^-, linear mol., Compton profile bond additivity, HF calc. 79−68268
$SCN^- + Fe(III)$, reaction kinetics, computer-controlled stopped-flow system 79−15953
$(SCN)_2^-$, and $(SCN)_2$, vibr. anal., bond strengths 80−9582
$SF_5^- + SF_3^+$, ion recombination, flowing afterglow, cross section meas. 77−44473
SF_6, compressed, negative ion drift in applied field 78−87565
SF_6, electron capture, laser radiation influence, possible laser isotope separation appl. 79−22856
SF_6, equilib. electron-transfer reactions in gas phase involving long-lived neg. ion radicals 78−58807
SF_6^-, electron impact, nearly zero energy, probability ratio meas. 79−72433
SF_6^-, matrix isolated, IR spectra, evidence for form. 77−68037
$^{33}SF_6^-$, radical, prep. and EPR comparison with other hexafluoride radicals 78−68381
$SF_6^- + He$, decomposition, SF_5^- form. 78−29833
$SF_6^- + SF_5^+$, ion recombination, flowing afterglow, cross section meas. 77−44473
$S_4N_4^-$, electronic struct. and vertical electron affinities, INDO-type ASMO SCF calcs. 79−31402
SO_2, radiative electron attachment spectra, vibr. stretching, electron affinity, theory 77−54617
SO_2^-, ESR obs., on used hydrodesulphurisation catalysts 77−70342
SO_2-containing ions, photodestruction 80−63722
SO_3^{2-}, SO_4^{2-}, O K-emission spectra, electron struct. 80−87099
SO_4^{2-}, ν_1 Raman linewidth, in acidic aq. soln. 77−65481
SO_4^{2-}, quantitative determ. in aerosol particles 79−20474
$SO_5^{2-} + Tb^{3+}(Dy^{3+})$, in H_2SO_4 soln., electrochemiluminesc. emitters quenching by electrolysis products 79−1794
SO_2XY, (X,Y=Cl,F), positive and negative ion chemistry 78−85140
Sb^-, photodetachment cross-section meas., crossed beam expt. 77−61723
$^{121}SbF_6^{2-}$, radical, prep. and EPR comparison with other hexafluoride radicals 78−68381
SbO_4^{3-}, normal vibr. freqs. calc. 79−54837
$^{77}SeF_6^-$, radical, prep. and EPR comparison with other hexafluoride radicals 78−68381
SeO_3^{2-}, SeO_4^{2-}, O K-emission spectra, electron struct. 80−87099
Si^-, ground state, photodetachment cross section calc., low energy 79−63970
$SiCl_4^-$, ESR of radical in adamantane matrix, γ-irrad. of $SiCl_4$ in adamantane matrix 79−27011
SiF_6^{2-}, bond order and Raman intensity, delta function eqn. 77−61693
SiF_6^{2-}, octahedral complex, ionis. energy, SCF-Xα study 78−70967
SiF_6^{2-}, SCF Xα SW calcs., ionis. pot. 79−26887
SiF_3Cl^-, radical anion struct. and ESR spectrum 78−25571
SiX_4, (X=Br,Cl), electron impact dissoc., low-energy reson. capture 78−9263
$SnCl_4N_2$ ions, force field calc., vibr. amplitude and rot. distortion consts. 79−98245
SnI_3^-, vibr. intensities, forms and freqs. anal. SCF MO LCAO CNDO calcs. 78−9274
SnO_4^{4-}, normal vibr. freqs. calc. 79−54837
SnX_3^-, (X=F, Cl, Br, I), vibr. freqs. and intensities anal. *(Russian)* 77−23492
$SnX_3^-(SnX_2^-)$(X=Cl,Br,I), formed by electron impact from SnX_4, ionis. efficiency curves, structs. 77−61865
$Tc_2Cl_8^{3-}$ ion, visible spectra, electronic struct. 78−5240
Te^-, photodetachment cross-section meas., crossed beam expt. 77−61723
$^{125}TeF_6^-$, radical, prep. and EPR comparison with other hexafluoride radicals 78−68381
TeO_3^{2-}, TeO_4^{2-}, O K-emission spectra, electron struct. 80−87099
TeO_4^{2-}, normal vibr. freqs. calc. 79−54837
TeO_4^{2-}, vibr. props. calcs. *(German)* 79−3431
$Te^-(^2P_{1/2,3/2}) + h\nu$, Te electron affinity, Te^- fine struct. interval 77−79590
$TiCl_5^-$, vibr. anal., force fields and consts. *(German)* 79−45702
$Ti_2Cl_{10}^{2-}$, vibr. anal., force fields and consts. *(German)* 79−45702
$Ti_2Cl_9^-$, vibr. anal., force fields and consts. *(German)* 79−45702
UBr_4O_2 ions, force field calc., vibr. amplitude and rot. distortion consts. 79−98245
UCl_4O_2 ions, force field calc., vibr. amplitude and rot. distortion consts. 79−98245
UF_6^-, electronic struct., ab initio calcs. using relativistic core pots. 79−97987
UF_6^-, form. in U+F surface reactions 77−73465
$UF_6 + e^-$ (K)(Na)(Cs), positive and negative ion formation, electron affinity, bond dissoc. energy 77−75314
$(UO_2Cl_4)^{2-}$, equatorial bonds, MO calcs. 78−82621

negative ions continued
$V(CN)_5NO^{3-}$, struct., FSGO calcs. 78−70736
$V(CN)_6NO^{4-}$, struct., FSGO calcs. 78−70736
VO_4^{-}, charge transfer transition, bond length effects calcs. 77−83721
WF_6^-, formation in WF_6+Na(K) electron transfer reactions 77−19071
WF_6^-, WF_7^-, form. and reactions, WF_6 electron and fluoride affinities, ICR spectra 79−39130
WF_n^-, (n=3,4,5,6) form. by electron impact on WF_6, mass spectra *(German)* 77−88586
WSe_4^{2-}, anharmonicity consts., reson. Raman spectra 77−61754
X^- (X=Cl,Br,I), in atm. press. flames, form. and removal kinetics 77−52642
Xe, $5p^55s$ state, electron excitation fine struct. neg. ion reson. 77−14585
Xe^-, electron capture expts. to search for long lived states 79−72410
$XeCl^-$, well depth of mol., Xe+Cl^- elastic cross-section expt. 79−86027
XeF^-, well depth of mol., Xe+F elastic cross section expt. 79−86027
Zn, electron scatt., negative ion form., shape resonances, electron affinity 77−14581

negative resistance
back diode amplifier, use at low temp. 80−57324
biomembrane electronic cct. model utilising time variant negative res. 78−88696
biopolymer negative resistance, rel. to living cell props. 78−64923
injection field magnetotransistor, operation 79−7888
MIS structure switching charact., theory, appls., expt. 78−68093
MOS structure, instability *(French)* 77−39960
nerve axon, leading edge approx. 77−12903
polyacetonitrile film, in Pt/polymer/metal capacitors, electroforming and elec. cond. 80−54800
polytetrahydrofuran film, in Pt/polymer/metal capacitors, electroforming and elec. cond. 80−54800
semiconductor, complex energy band under optical excitation, high-frequency negative cond. and population inversion 80−107858
semiconductors, differential conductivity with inelastic electron scatt. *(Russian)* 80−2399
unijunction transistor, negative resistance as phase transition, critical exponents *(French)* 80−49746
Al-Al_2O_3-Au device in Cl_2 atmosphere, current-voltage charact., press. depend. 80−65704
Bi_2O_3 film, thermally grown, I-V charact., current controlled neg. resist. 80−15637
n-CdSe, partially illuminated single crystal, current-voltage characteristic and potential distrib. 79−65519
GaAs:Mn(Ni), negative magnetoresist. meas. 77−51768
GaAs-$Ga_{1-x}Al_xAs$, n^+-i-n heterojunction, radiative recombination under double injection *(Russian)* 77−77298
$GaAs_{0.6}P_{0.4}$ p-i-n diode, behaviour of turnover voltage under pulsed conditions 77−20408
n-Si, negative absolute conductance, electrothermal mechanism 79−69518
Si:Ir S-type diodes, charact. 78−56224
Si-SiO_2-SnO_2 structure, switching props. 78−76138
Sn, supercond. film, V-I curve *(Russian)* 77−55639
WO_3 powders, hopping mechanism and Poole-Frenkel effect, elec. props. determ. 80−49734
$ZnIn_2S_4$, S-type negative resist. and switching effects 80−65581
n-ZnSe, long persistent cond. relax. and frozen cond. 80−54735

negative resistance effects
see also Gunn effect
alkali fluoantimonates, dielectric props. and structural phase transitions *(German)* 80−25274
amplifying Gunn diodes, nonlinear effects 79−51622
Anderson localised states, electron correlations effect 79−65499
Anderson localised states, negative magnetoresistance 79−28357
bulk semiconductor, I-V charact. based on impact ionisation, model 77−11925
cetyl alcohol with dipoles, switching and negative resist. phenomenon, quantitative model 78−14769
n-channel MOSFET, Si inversion layer, negative differential resistance 78−30996
charge carrier with anisotropic energy spectrum, cond. oscills. in quantised mag. field *(Russian)* 80−6886
cholesterol film with dipoles, switching and negative resist. phenomenon, quantitative model 78−14769
current instability, hydrodynamic modes, soft modes and fluctuation spectra 79−65491
current instability due to Bragg scatt., travelling dipole domains, fluctuations 78−26874
dielectric diode, Joule instability under space-charge-limited current conditions 80−15618
donors with excited states, non-equilibrium phenomena, theory of kinetics of electron transitions 78−79961
double injection p-i-n diodes, negative resistance charact. 78−30983
EM wave excitation and amplification under negative differential cond. conditions 77−15865
extrinsic semiconductors, negative magnetoresist., Hubbard model *(Russian)* 78−47816
ferrite-semiconductor layer struct., with negative differential cond., spin wave instability 80−25118
graphite, with small-sized blocks, negative magnetoresist. *(Russian)* 80−49779
Gunn devices, negative conductance, temp. and bias voltage depend. 77−51756
HF conductivity of media with inhomogeneous distrib. of mobility in crossed E- and H-fields *(Russian)* 79−1606
history of hot electron physics 78−26869
hot electrons in mag. field, carrier density nonlinearity effect 77−55540
III-V semiconductors, negative resistance and peak velocity in central (000) valley 79−73522
ion/membrane systems, negative resist., current controlled, model 79−34357
metallic thin films and wires, negative temp. coeff. of resistivity 79−78217
MIM diodes, negative differential resistance, stimulated inelastic tunnelling theory 80−49951
MIM junction, tunnelling, tight-binding Green function calc., disorder effect 78−10577
MIS diode, thin-insulator, switching phenomena, current-control-type negative resist. charact. 80−107915

negative resistance effects continued
MOST-transistor struct., breakdown-initiated negative resist. device 80−20314
oxide thin film electroforming, threshold switching and memory effects 77−76940
p^+-π-n^+ structure with low cond. region, double injection, IU charact. of single-level semicond. 79−56296
p^+-i-n^+ structure, double-injection negative differential resist. problem, surface recomb. effects 78−88024
p-n-insulator (tunnel)-metal devices, switching theory; punchthrough mode 79−60926
p-n-p structure, variable-gap, impedance 77−43707
polyphenylene oxide thin films, electrochem. prep., impurity effects on cond., electroforming 80−88655
PVC in metal sandwich struct., switching props., voltage- and current-controlled negative resist. 80−103767
SCLC diode with traps, neg. conductance 79−11221
semiconductor, ambipolar hot-carrier size effect kinetics 80−107799
semiconductor, current instability, bifurcation and stability of dynamical structs. 79−91071
semiconductor, electrical instability, negative differential cond., electron heating by static and alternating elec. fields 79−11165
semiconductor, fluctuation spectra near the threshold of a current instability 79−24037
semiconductor, hopping transport theory for strong elec. field 77−8106
semiconductor, hot electron current voltage curves, transverse mag. field, phonon heating 78−6384
semiconductor, hot electrons in quantizing mag. field and impact ionisation of impurities 78−6386
semiconductor, instabilities of electron-hole plasma under impact ionization and microwave emission 79−65508
semiconductor, magnetoresist. in narrow energy bands, Hubbard model 77−32029
semiconductor, n-type, nonequilibrium photoelectron distribs. and absolute negative cond. in quantising mag. fields 80−65622
semiconductor, negative cyclotron resonance of hot carriers 78−2492
semiconductor, optically stimulated negative conductivity 77−4357
semiconductor, possible apperance of negative differential conductance at microwave freq. 79−11164
semiconductor diode, with deep impurity levels, diffusion effect on negative resist. 78−56217
semiconductor modelling, bulk, negative-cond., transverse spreading of high-field domain 79−1602
semiconductor plasma, with S-like negative resist. region, temp. plasmon oscills. 78−26898
semiconductor structures, s-type switching at high current densities 77−20417
semiconductor tunnelling and negative resistance phenomena, book 78−26947
semiconductor with deep traps, injection filament 77−76837
semiconductor with deep traps, magnetodiode effect 78−6401
semiconductor-insulator-metal system, negative resistance effects 79−11236
semiconductors, due to hot electrons transfer in geometric space *(German)* 78−56150
semiconductors, exhibiting negative photocond., photovoltaic effects 80−96943
semiconductors, n-type, metal-insulator transition and negative resist. effects 79−24026
semiconductors, negative injection conductivity 79−69517
semiconductors with negative differential conductance, surface EM wave excitation, helicon and Alfven waves 79−69543
semiconductors with superlattice, absolute negative resist. *(Russian)* 78−34838
single-valley semiconductor, current instability and domain propag. due to Bragg scatt. 77−28187
Stark-Ladder current theory 78−68035
superconducting microbridges, neg. resist. and hot electrons, model 78−60254
superlattice semiconductor, odd photomagnetoresistance effect 79−95425
thin film heterostructure, energy spectrum study 80−70787
thin wire, negative longit. magnetoresist., kinetic theory 78−34821
tunnel junction, resonance differential negative resistance in the Fredkin-Wannier inhomogeneous field model 80−80355
two-dimensional semiconductor, Gunn instability 78−84305
unijunction transistor transition critical exponents, negative resistance phenomena 80−44713
Ag-CdTe-Ag struct., negative differential resist. 78−19161
Ag-Cr dilute alloys, negative magnetoresist. in pulsed fields up to 35T 77−62899
Ag-SiO-Ag sandwich structures, elec. props. and nonvolatile memory effect 79−87164
(Al,Ga)As DH lasers, superlinear emission charact., negative resist. obs. 80−95895
Al-Al_2O_3 electron transport in very thin multilayers 79−4602
Al-Al_2O_3 triple-barrier structure, negative resist. caused by resonant tunnelling 78−14819
Al-Al_2O_3-Al(Au), thin films, elec. props. *(Czech)* 78−76159
Al-Al_2O_3-Au sandwich conduction props. 78−2580
Al-AlN-Au, voltage controlled negative resist., O_2 press. effect 78−72281
Al-Au couple, electroformed, nonohmic charact. and electron emission 80−60066
Al-BN-Au device, prep. of BN films and IV charact. *(Japanese)* 77−73230
Al-Mn alloys, dil., magnetoresist. meas. 77−62900
Al-Sb_2O_3-In films, negative resistance charact. 80−11103
Al-Si_xNyO_z-Al systems, mechanism of current transfer *(Russian)* 77−69427
$Al_xGa_{1-x}As$, graded-gap crystal, voltage-current characteristics 79−69613
$As_2Se_3Ag_x$ glassy semicond. film, prep. by photodiffusion of Ag, negative photocond. 80−92934
Au film, nonohmic charact. and electron emission 80−60066
Au island films, forming process, I-V charact., and switching 79−11242
Au-Y_2O_3-Y junctions, migration of Au rel. to voltage-controlled negative resist., SIMS obs. 79−91157
Bi, nonequilibrium phonons, negative differential cond., life time oscills. *(Russian)* 78−76117
Bi, stationary I-U curve, falling portion under phonon generation conditions 79−15195

negative resistance effects continued
$Bi_{12}GeO_{20}$, photocond. spectra, current-voltage charact., photoelectret effect 79−69552
Bi_2O_3, film, resist. and current controlled negative resist. 78−39238
$Br_{1-x}Sb_x$, alloy wire, magnetoresistance in high longitudinal fields *(Russian)* 79−87113
C, glassy, negative magnetoresist. 78−23118
C, glassy and fibrous, density of states, magnetoresistance theory appl. 80−44620
$CdCr_2S_4$:In(Ga), resist. and magnetoresist. meas., effect of donor impurities 79−19608
n-$CdCr_2Se_4$, current- and voltage-controlled negative resist. obs. 78−19041
$CdCr_2Se_4$, ferromag. semicond., conc. anomalies rel. to red shift of absorpt. edge 80−70732
$CdCr_2Si_4$:Ga, negative magnetoresist. effects near Curie temp. 79−11152
p-$Cd_xHg_{1-x}Te$-metal contact, negative resist. effects, impact ionisation 77−4440
CdS, domain elec. instabilities, elec. field and temp. distribs., optical meas. 79−11405
CdS-Te-Ge heterojunction, prep. photosensitivity, and negative cond., 77K *(German)* 77−20413
CdSe:Au impurity light absorpt. for current control in negative resistance region 80−11052
CdTe:Ge, negative thermally stimulated cond. 79−19621
Cu-Cr dilute alloys, negative magnetoresist. in pulsed fields up to 35T 77−62899
ErO_x, film, in MIM struct., nonstoichiometry effects on elec. cond. 79−1635
ErO_x, nonstoichiometric film, short-range order charact. and its effect on elec. behaviour 79−99435
$Fe_{1+x}V_{2-x}O_4$ spinels, prep. and charact. *(Korean)* 78−39119
GaAs, compensated, influence of electron gas heating on negative magnetoresist. 77−89778
GaAs, current controlled negative resist. at low temps. 78−39133
GaAs, DC biased, filamentation of laser radiation 80−74428
GaAs diode, reverse-biased, current-controlled negative resist., switching investig. 77−69410
GaAs, epitaxial film, field effect struct., elec. breakdown, negative resist. 77−12030
GaAs, influence of strong transverse mag. field on Gunn effect 80−6854
GaAs ion-irradiated layers switching conduction 78−34868
GaAs n-type, computer study of conditions for absolute negative resistance 77−4358
GaAs, p-n junction, conductance oscillations in a two-dimensional impurity band 79−95477
n-GaAs, rel. to spin wave amplification in n-GaAs-ferrite layer struct. *(Russian)* 77−73016
GaAs:Cr, current voltage characterisation, deep levels and Fermi level determ. 79−7823
GaAs:Cr diode, high magnetosensitivity of negative resist. region 78−26946
GaAs:Cu(Cr) S-type diodes, thermal quenching of injection currents and current-voltage charact. 78−26942
GaAs:Fe, p-π-ν-n struct., photoelec. props. 80−107862
GaAs:Fe LPE layers, negative resist. effects and deep acceptor model 77−72929
n-GaAs:Ni, negative photocond. at low temps., impurity levels 80−6900
GaAs:O p-ν-n structs., injection current and negative photocond., saturation mechanism 80−92967
GaAs-$Al_xGa_{1-x}As$, negative differential resist., real-space electron transfer 80−6958
GaAs-$Al_xGa_{1-x}As$ heterostructures, real-space electron transfer by thermionic emission, analytical model 80−100512
GaAs-GaAlAs, superlattice, subband related anisotropy in negative magnetoresistivity 80−11082
$Ga_xIn_{1-x}Sb$, electron transport in RF field, Monte Carlo simulation 80−96932
$Ga_xIn_{1-x}Sb$, LPE, growth by vertical dipping method and elec. props. 77−85949
GaP, electroluminescent diode, electron irradiated, negative resistance due to impact ionisation 77−15942
GaP LED, negative differential resistance and conductance associated with dielectric losses 77−63468
GaP LED with S-shaped characteristic, negative resist. and red electroluminesc., expt. 78−48237
p-GaSe, single cryst., negative photocond. induced by elec. field 79−19623
Ge, ambipolar hot-carrier size effect kinetics 80−107799
Ge, film, dense electron-hole plasma, negative differential resistance 77−89794
p-Ge, heaviliy doped, anomalous magnetoresist. under uniaxial compression *(Russian)* 79−33302
n-Ge, heavily doped, negative magnetoresistance model, spin-up spin-down electron effective mass variations 79−95423
p-Ge, negative magnetoresist. and Hall effect, press. and field depend. 80−70733
p-Ge, stretched along ⟨111⟩ axis, bulk negative differential cond. and current oscills., 78K 79−19601
Ge, thermal rectification and negative differential cond. 79−42554
n-Ge, uniaxially stretched along [111] axis, negative differential conductance 77−51759
Ge:Au, current-voltage phase shift, impedance of subthreshold domains 77−43609
n-Ge:Au, negative photoconductivity 78−34863
n-Ge:Ni, negative differential conductance of surface channels 79−11134
Ge:Sb, low temp. anomaly of impurity cond. 79−95428
$Hg_{1-x}Cd_xGe$, quantum oscillations of magnetoresistivity *(Russian)* 80−11007
InAs, longitudinal magnetoresistance in extreme quantum limit *(Russian)* 80−11008
n-InAs, negative magnetoresist. in extreme quantum limit 78−64051
n-InAs, negative photocond. and photomemory due to pot. barrier on surface 79−19620
InAs:Mn, NMR, magnetoresist., Hall effect and mag. susceptibility meas. 78−26888
InP:Fe, deep levels 79−56166
InSb, current-voltage characteristics at room temperature and high hydrostatic pressure 80−88560
InSb, hydrostatically pressed, negative differential cond. at room temp. 79−19600
negative resistance effects continued
n-InSb, longitudinal magnetoresistance in extreme quantum limit *(Russian)* 80−11008
p-InSb, magnetoconcentration effect, negative differential conductance 80−70729
n-InSb, negative longit. magnetoresist., carrier conc. and mobility depend., 77K 80−60007
p-InSb, negative magnetoresist. under press. 80−20224
p-InSb, negative photocond. in strong mag. fields 79−82636
p-InSb, negative piezomagnetoresist. and Hall effect meas., antiferromag. order form. 78−19061
n-InSb, reson. excitation of Kondo effect and negative magnetoresist. *(Russian)* 78−56159
InSb, reverse biased diode 78−19129
p-InSb, uniaxially deformed, mag. field induced semicond.-metal transition 79−95457
InSb:Ge, uniaxially compressed, anisotropy of elec. props. 78−19035
p-InSb:In, two-phase polycryst. films, negative magnetoresist. 80−11011
InSb:Mn, NMR, magnetoresist., Hall effect and mag. susceptibility meas. 78−26888
$KTaO_3$, photoconducting, negative differential conductivity 79−65515
La-Gd-Au, amorphous, mag. field depend. of resist. minima 77−59275
Li ferrite, transverse magnetoresistance, temp. depend. 78−19039
MgMn ferrite, transverse magnetoresistance, temp. depend. 78−19039
NH_4SbF_5, dielectric props. and structural phase transitions *(German)* 80−25274
Nb Josephson junctions, excess current anal. 79−28465
Nb_3Ga Josephson junctions, excess current anal. 79−28465
Nd, transport props., low temp., effect of mag. field 80−70679
Pd-Fe(Co)(Ni) dilute alloys, ferromag., magnetoresist. 78−91665
Pr, transport props., low temp., effect of mag. field 80−70679
Pt-polymer-Au capacitor, electroforming, negative resist., electron emission 80−80406
$(SN)_x$, negative magnetoresistance below 4.2K 79−51611
Se, Se:Te, amorphous, negative magnetoresist., doping depend. 78−56161
Se-Ag_2Se, heterojunction, electrically controlled negative differential conductance, mechanism 80−44720
$Se_{60}Te_{30}Ge_{10}$, amorphous, neg. magnetoresist. 79−51603
Si amorphous, ion implantation, negative magnetoresist., localised mag. states 80−70731
n-Si, current instability due to temp.-elec. domain pulsations 77−43608
n-Si, current-voltage charact., static high field domains 78−84223
n-Si, field and current domains, at low temp. 80−6868
n-Si, heavily doped, negative magnetoresistance model, spin-up spin-down electron effective mass variations 79−95423
Si, hot holes negative Hall effect 79−87118
Si inversion layer, negative differential resist. 78−60225
Si MOS inversion layers, negative magnetoresist. 80−49922
Si p^+-i-n^+ diodes, double-injection switching, effect of surface recomb. 78−88025
Si p-n junction diodes, reversed-biased, permanently induced negative resist., expt. 78−56214
Si, p-n-n^+ structure, external resistance effect on current-mode second breakdown 78−56216
Si pin diode, current filament temp. and Au acceptor level capture cross section temp. depend. 78−95351
p-Si, proton irrad. magnetiodiode effect, heat treatment, photocond. spectra 79−69591
Si:Au p^+-i-n^+ diode, I-V charcts., recomb. centre influence 78−19134
n-Si-SiC film junction device, elec. props. 80−15591
p-Si(111) surface inversion layer, Cs covered, negative magnetoresist. in 2D impurity band 78−64135
Sm, transport props., low temp., effect of mag. field 80−70679
SmS, semicond., anomalously high magnetoresist., Hall coeff. and elec. resist. meas. 78−10479
$TaSe_2$:Fe, competition between charge and spin density waves, Landau-Ginzburg theory 79−95352
Te-Ge-As-Si amoprhous film, voltage controlled negative resistance type charcts. 79−69614
TiO_2, polycryst. film, threshold switching 78−14771
$Ti_{0.99}V_{0.01}Se_2$, negative mgnetoresist. and nonlinear cond. 79−87105
U film, condensed on cold substrate, electronic props. *(Russian)* 79−7912
UAsSe, strongly anisotropic ferromag., negative magnetoresist. meas., 77-135K 77−89774
VO_2 film, negative resist. region, applic. as oscillator element and transducer *(Russian)* 77−85359
V_2O_5-As_2O_3-RO, R=Ba, Ca, Pb, semicond. glass, electronic props. 80−88557
V_3O_5, resistivity switching due to phase transition, 154°C 79−19642
Y-Y_2O_3-metal junction, electroforming and conduction 78−26969
$ZnIn_2S_4$ switching investigation, negative resistance state instability, resistivity transitions 80−6920
ZnO, strong accumulation layers, negative magnetoresistance 78−6428
ZnO surface, quantised accumulation layer magnetoresistance, spin scattering model 79−69529
ZnO-Bi_2O_3, heterojunction, current-voltage charcts. 79−56291
ZnS, prebreakdown electrolum., domain form. and negative resist. effects 80−84788
n-ZnSe, impurity band, Hall effect, elec. cond., mobility and magnetoresist. expts. 77−35888
ZnSe:In, heavily compensated, negative magnetoresistance 79−91079
Zr-Pd, metallic glasses, electronic props. and supercond. 79−73486
ZrC-C composite system, negative magnetoresist. 80−60008

negative temperature coefficient thermistors *see thermistors*

nematic liquid crystals
2-naphtoxy α-substituted acetic acid, influence of chiral solute structure on helicity induced by nematic solvent *(French)* 77−68909
4-octyl-4-cyano-biphenyl, nematic to smectic A phase transition texture changes, thermoelectrooptic effect 80−49098
7CB nematic liquid crystal far IR spectra 79−33688
acetic acid-$^{13}C_1$, in nematic phase soln., dipole-dipole couplings, selective spin population transfer investig. 80−60427
4-acetyl-4′-n-alkanoyloxy-azobenzenes, type A, B smectic, nematic phase, solid state polymorphism, preparation, melting behaviour 78−59745
acoustic attenuation anomaly above clearing point 78−75816
acoustic emission, depend. temp. 79−55654
acoustic field response, streaming component and instability 80−80747
acoustic image detector appl. 79−41537

nematic liquid crystals continued
acoustical properties, rotating mag. field study 80−88034
acoustically induced birefringence 78−38126
acousto-optic effect, acoustic streaming 80−88964
acousto-optic effect, birefringence obs., model 77−55767
acousto-optical effect, instabilities generated by US field, review 78−91235
acousto-optical effect due to anisotropic attenuation, new developments and appls. 80−76002
acousto-optical effects, US induced birefringence and opacity 77−28544
acoustohydrodynamic instability 79−94397
acoustooptical modulation assoc. with periodic deform. of liquid crystal layer 78−52471
adjustable access couplers for fibre-optic switching 80−33217
4-alcanoyloxybenzoyloxy-4′-cyanoazobenzene series, influence of substituent on reentrant mesophases 80−88027
4-alcanoyloxybenzoyloxy-4′-cyanobiphenyl series, influence of substituent on reentrant mesophases 80−88027
4-alcanoyloxybenzoyloxy-4′-cyanostilbene series, influence of substituent on reentrant mesophases 80−88027
aligned chiral liquid crystal structure-property relationships 77−76304
aligned monocrystal, elastic neutron scatt. incoherent struct. factor 77−62467
aligned rod system, nematic-smectic transition 79−77729
alignment, produced by RF plasma deposited films on glass or $In_{2-x}Sn_xO_{3-y}$ 77−48350
alignments of director using submicrometre periodicity gratings 78−63666
aliphatic compounds, trans, trans-cyclohexyl cyclohexanoates, synthesis, mesomorphic phases 80−44121
4-n-alkoxy benzoyloxybenzylidene 4′-cyanoaniline series, nematic reentrant mesophases, phase diagrams 80−103467
4-n-alkoxy-4′-cyanodiphenyldiacetylenes, synthesis and mesomorphic props. 79−82148
4-n-alkoxy-4′-cyanostilbenes, synthesis and mesomorphic props. 79−82148
4-n-alkoxy-4′-cyanotoluenes, synthesis and mesomorphic props. 79−82148
trans-p-n-alkoxy-α-methyl cyanophenyl cinnamates, elastic consts. and orientational order parameters 80−44244
n-alkoxy-α-methyl-p′-cyanophenyl cinnamate, orientational order, tricrit. behaviour 79−27907
trans-p-n-alkoxy-α-methyl-p′-cyanophenyl cinnamates, nematic liq. cryst., static dielec. props. 78−60376
alkoxy-benzoic-acids, temp. depend. of Raman spectra of homologous series 77−81098
p,p′-h-alkoxyazoxybenzene homologous compounds, DC Kerr constants 78−27185
alkoxyazoxybenzenes, isotropic-nematic transitions, RI, orientational relax. times 77−24390
p-alkoxybenzal-p′-ethoxyaniline, even-odd effect and chain config. 79−50989
p-n-alkoxybenzoic acic series, nematic liq. crysts., electrooptical props. 79−15438
p-n-alkoxybenzoic acid, elec. cond. anisotropy of nematic structs. 80−1928
p-n-alkoxybenzoic acid, homologs, principal mol. polarisabilities calc., refr. indices of nematic mesophase meas. 78−2004
p-n-alkoxybenzoic acids, mol. arrangement in cryst., nematic, and smectic C phases 79−32889
p-alkoxybenzoic acids, proton spin lattice relax., mol. dynamics 78−34425
4(4′-n-alkoxybenzoyloxy)benzylidene-4″-aminophenols, synthesis and mesomorphic props. 79−90546
4-alkoxybenzoyloxy-4′-cyanotolanes, stable nematic reentrant phase 79−77506
N,N′-bis(p-alkoxybenzylidene)-α,α′-bi-p-toluidines, nematic phase, synthesis, thermodynamic props., gas-liq. chromatographic anal. 79−90763
4-n-alkoxybenzylidene-4′-methylalkylanilines, chiral nematic cryst., mesorphic behaviour and binary systems 78−2000
N-4-n-alkoxybenzylidene-4′-n-butylanilines, elec. cond. in nematic and smectic phases *(German)* 77−15860
p-alkoxybenzylidene-p,n-butylanilines, IR absorpt. spectra, elec. field effects, orientational order parameter determ. by IR dichroism 80−80778
p-alkoxybenzylidene-p-aminocyanoanilines, IR absorpt. spectra, elec. field effect, orientational order parameter determ. by IR dichroism 80−80777
p-alkoxybenzylidene-p-n-alkylanilines, solid state, nuclear spin relax. 78−76337
p-alkoxybenzylidene-p-n-alkylanilines, thermotropic mesophases, proton spin-lattice relax. 78−91968
p-alkoxybenzylidene-p-n-butylanilines, optical and mag. anisotropies in liq. cryst. phase, thermal variations of order parameter *(French)* 79−82149
4-4′-n-alkoxybenzylideneamino-biphenyls, central Schiff's base linkage reversal effect on liq. cryst. props. 80−79683
alkoxylbenzoic acids, orientation in their nematic state 78−42903
6-alkoxynicotinic acid, liq. cryst., prep. and transition temp. 77−27811
4″-n-alkoxyphenyl biphenyl-4-carboxylates, liq. cryst. props. 79−82150
4-alkoxyphenyl-4′-alkylbenzoates, mesomorphic props., terminal alkyl chain length effect 80−88024
p-alkoxyphenylazo-p' phenyl esters, dielec. anisotropy *(French)* 77−80414
p-alkoxyphenylazoxy-p' phenyl esters, dielec. anisotropy *(French)* 77−80414
alkyl cyanobiphenyls, pretransitional behaviour, alkal chain length depend., light scatt. in isotropic phase 80−44301
5-alkyl-2-(4′-cyanophenyl)-1,3-dioxanes, synthesis and electro-optical characts. 80−88029
4,n-alkyl-4′-cyanotolanes, and related compds., homologous series, mesomorphic transition temps. 77−27991
4′-n-alkyl-4-cyanobiphenyls, dielec. dispersion 78−2798
4′-n-alkyl-4-cyanobiphenyls, elasticity, orientational order, and nematic-isotropic transition 77−84643
4-n-alkyl-4-cyanobiphenyls, liq. cryst. of strong positive dielec. anisotropy, static dielec. consts. meas. 78−2790
4′-n-alkyl-4-cyanobiphenyls, nematic, elastic and optical props. 77−11613
4′-n-alkyl-4-cyanobiphenyls, press. effect on liq. cryst. phase transitions 79−95138
alkyl-cyano-biphenyls, nematic to isotropic phase transition, volumetric studies 79−86878

nematic liquid crystals continued
alkyl-cyanobiphenyl homologues, isotropic-nematic phase, optical Kerr effect 80−91866
p-alkyl-p′-cyanocyclohexylcyclohexanes, thermotropic nematics with positive dielectric and negative diamag. anisotropy 78−34435
p-n-alkyl-p′-n-alkoxytolanes, hydrostatic pressure effects, phase transitions *(French)* 78−14448
1-4-n-alkylbenzoyloxyphenyl 2-(4′-cyanophenyl) ethane series, nematic reentrant mesophases, phase diagrams 80−103467
alkylcyano-cyclohexyl-cyclohexanoates, nematic and smectic mesophases 80−19692
alkylcyanobiphenyls, far IR absorpt. in nematic and isotropic phases, order parameter determ. *(French)* 80−50330
trans-4-alkylcyclohexane carboxylic acids, visible and UV spectroscopy transparent matrix 80−45102
alkylcyclohexyl-cyclohexyl-cyclohexanoates, nematic and smectic mesophases 80−19692
trans-4-n-alkylcyclohexylbenzylamines, synthesis and mesomorphic props. 80−44116
4-alkyloxy-4′-cyanobiphenyls (nematic, smectic)-tetrabutylammonium picrate, elec. cond., temp. (conc.) depends. *(German)* 78−55966
4-4-n-alkyloxybenzoyloxy-benzylidene-4′-cyanoanilines, reentrant nematic and smectic phases 80−88308
4-n-alkylphenyl 2′-chloro-4′-(6-n-alkyl-2-naphthoyloxy)benzoates, synthesis and liq. cryst. props. 78−34433
(+)-4-n-alkylphenyl-4′-(4″-methylalkylbenzoyloxy)benzoates, optically active, synthesis and effect on liq. cryst. display props. 78−1997
amphiphilic nematic with optically active compounds, cholesteric states and twisting power 78−63846
p-n-amyloxybenzoic acid, refr. index and orientational order parameter, temp. depend. 79−90537
anamalous stiffness and tilt angle from nonuniform attachment angle 79−86688
anchoring energies determ. from surface tilt angles 79−64986
anisaldazine, nematic liq. cryst., mol. statistical interpretation of viscosity *(Portuguese)* 77−47351
anisotropic crystal interface, influence of second-order elasticity on local Frederiks transitions 78−1982
anisotropic interfacial interactions between nematic liq. cryst. and substrate 78−75532
anisotropic solvents in optical absorpt. spectroscopy, band polarisation determ. 77−42344
anisylidene-p-aminophenyl acetate, nematic liq. cryst., refractive index, density, orientational order 78−76419
anisylidene-p-aminophenyl butyrate, nematic liq. cryst., refractive index, density, orientational order 78−76419
APAPA, nematic liq. cryst., effect of mag. field on US attenuation *(Japanese)* 79−19144
aromatic esters derived from naphthalene, liqs. cryst. props. 78−47235
average orientation in three dimens. parallelepiped model 77−51315
azoxy compound, liquid cryst. mixture, nematic, elec., optical and viscoelastic props. 79−55803
p-azoxyanisole, depend. of phase transition temp. on thickness 78−26669
p-azoxyanisole, directed crystn. in elec. and mag. fields 80−107052
4,4′-azoxyanisole, electronic spectra, influence of order in liq. cryst. struct. 78−71675
p-azoxyanisole, in nonuniform elec. fields, mag.-field stabilisation 79−94901
p-azoxyanisole, neutron scatt. by collective excitations 77−84651
4,4′-azoxyanisole, temp. depend. of refractive indices in nematic phase 79−47410
azoxybenzene, terminally substituted, elastic consts., varying mag. field and temp. 78−18540
azoxybenzenes, nematic, mag. susceptibility, orientational order parameter 78−34426
azoxybenzenes, nematic, refr. index, birefringence, internal field 78−34427
azoxyphenetole, deuterated, cryst. and mol. struct. 79−86782
p-azoxyphenetole, single cryst., deuterated, phonon dispersion curves, inelastic neutron scatt. obs. 80−84261
BBOA, polymorphism, radiothermoluminescence and differential scanning calorimetric study 80−24570
Benard-Marangoni instability *(French)* 78−75538
benzazoles, liq. cryst., prep. and transition temp. 77−27811
benzylidene aniline series, nematic liq. crysts., depolarised scatt. strength, free-energy, coherence length anisotropy 77−62470
benzylidene anilines, nematic phase, dipole coupled ^{13}C NMR technique 79−99073
BEPC, EPR of slowly tumbling VO^{2+} spin probes 79−50985
BEPC, with dissolved KTCNE, ion pairing, EPR obs. 78−73020
biaxial nematics, defect props. *(French)* 77−31587
bicyclohexanes, nematic liq. crysts. with negative diamag. anisotropy, high resolution NMR spectrometry 79−40596
bidimensional coupled evolution eqns., simplified variational model 79−73092
binary mixture, dil., thermodynamic props., statistical model 79−94882
binary mixture, smectic phase form. 78−26670
binary mixtures, phase transitions, entropy, relation to smectic plane tilt angle 80−65203
biopolymers, conditions of liquid crystal formation 80−30642
biphenyl-4-p-n-alkoxybenzoates, nematic liq. cryst., static dielec. props. 78−60376
biphenyl-p-ethylbenzoate, high press. mesomorphic and polymesomorphic transitions 78−18750
biphenylbenzoates, synthesis, mesomorphic, and thermodynamic props. 80−44117
birefringence determ. by new simple method 78−79526
4,4′-bis(heptyloxy)azoxybenzene, nematic liq. cryst., refractive index, density, orientational order 78−76419
4,4′-bis(hexyloxy)azoxybenzene, nematic liq. cryst., refractive index, density, orientational order 78−76419
bis(p-cyanophenyl) terephthalamide, thermotropic liq. cryst. behaviour, optical microscopy obs. 79−32895
bis-4-n-alkylphenyl tetrafluoroterephtalates, synthesis and mesomorphic props. *(French)* 79−86679
bis-4-nalkyltetrafluorophenyl tetrafluoroterephtalates, synthesis and mesomorphic props. *(French)* 79−86679
p-bis-octyloxyazoxybenzene, thermal diffusivity, Rayleigh scatt. obs. 78−94977
BMAOB-cholesteryl caprinate mixture, spiral pitch temp. depend. 78−79529

nematic liquid crystals continued
boundary aligning forces, studied by wall-induced pretransitional birefringence 79−73096
boundary induced cholesteric-nematic phase transition 77−76533
m-bromophenylbenzoyloxybenzoate, nematic phase, freq. depend. of dielec. props. *(French)* 79−91337
bubble domains, struct. and props. in cholesteric-nematic mixture 77−89373
Burgers circuit, Volterra process and homotopy groups 77−62528
p-n-butoxybenzoic acid, refr. index and orientational order parameter, temp. depend. 79−90537
N-(p-butoxybenzylidene)-p-pentylaniline, refr. index and density in nematic and isotropic phases 79−90538
4-butoxybenzylidene-4′-alkylaniline, EHD instabilities in nematic and smectic A phases 79−90530
butoxybenzylidene-aminobenzonitrile, crystalline and liq. cryst. states, low freq. spectra 78−34437
N-n-butoxybenzylidene-n-butylaniline, US propag. near nematic-smectic A transition, mag. field effect 80−39266
N-(p′-butoxybenzylidine)-p-n-octylaniline, order parameters in nematic and smectic phases, X-ray diffr. meas. 79−94874
n′-n-butyl-n-methoxyazoxybenzole, specific heat anomaly and isotropic liquid to nematic liquid cryst. transition *(Russian)* 77−62624
p-n− butyl-p′-methylhydroxyazobenzene/p-n-butylheptanoylazoxybenzene mixture, temp. depend of elec. cond. 80−1925
p-butyloxybenzylidene-p′-octylaniline, thermal diffusivity, Rayleigh scatt. obs. 78−94977
4-butylthiophenol, synthesis 78−51408
caesium perfluorooctanate, thermodynamically independent nematic amphiphilic mesophase obs. 79−95126
cavity interaction with singularity 77−84635
CBNA, nematic-isotropic transition at high press., turbidity meas. 80−92655
CBOOA:nitroxide, liq. cryst. phase transition study by electron spin relax. *(French)* 79−55874
CBOOA, acoustic emission at liq. cryst. transitions prod. by thermo-optically excited defects 79−95137
CBOOA, anisotropic shear viscosity meas. 77−15310
CBOOA, isotropic, nematic, smectic-A phases, Brillouin scatt. 80−11421
CBOOA, liq. cryst. of strong positive dielec. anisotropy, static dielec. consts. meas. 78−2790
CBOOA, liq. cryst.-isotropic transition at high press., P-V-T eqn. of state 79−95135
CBOOA, mag. aligned, smectic A-nematic transition, US absorpt meas. 78−95137
CBOOA, mag. field depend. of laser light scatt., interf. rings 78−26434
CBOOA, nematic phase laser light scatt., mag. field depend., crit. deform. *(Japanese)* 78−2826
CBOOA, nematic to smectic A transition, high resolution X-ray scatt. exam. 78−94984
CBOOA, nematic-smectic transition, singularities, elastic const. var. 77−39537
CBOOA, nonlinear elastic behaviour, near nematic-smectic-A phase transition 77−35679
CBOOA, smectic A, nematic and isotropic phases, surface tension 77−39539
CBOOA, smectic A-nematic transition, X-ray and light scatt. obs. 79−95129
CBOOA, smectic-A-nematic and nematic-isotropic transitions, vol. behaviour 77−39666
CBOOA, temp. depend. of apparent viscosity and density 78−18542
CBOOA, twist viscosity and mech. props. near smectic A-nematic transition 78−95136
CBOOA, US absorpt. and dispersion at nematic-smectic-A transition 79−82287
CBOOA/4-cyanobenzylidene-4′-n-octyloxybiphenyl mixture, reentrant nematic phases 79−41953
cell, with pretilt angle, electro-optical props. *(Japanese)* 78−43837
chiral nematic host, pitch depend. of absorption and optical constrast of dichroic dye guest 77−90164
chiral nematogens, decay time of twist cells of shortened pitch 77−55234
chiral substituted dibenzo[b,f][1,4-diazocines in nematic MBBA, helical twisting power 78−34431
p-chlorobenzylidene-p-n-pentylaniline, metastable phases formed by rapid cooling of mesophase, IR and Raman spectra and DSC obs. 80−34919
cholesteric-nematic liq. cryst. mixtures, electro-optic charact., light scatt. modes *(Japanese)* 78−79527
cholesteric-nematic mixtures, helix inversion 80−24358
cholesteric-nematic soln., thermodynamic props. 79−32903
cholesteryl myristate, density of smectic, cholesteric, blue, isotropic phases 78−42897
circular random walk motion, comparison with neutron scatt. data 77−43146
classical spin system, absence of ordering 78−51402
cluster integral approach, crit. anal. 79−86708
coherent neutron scattering studies, review 79−41956
colloidal solution, flow alignment, transition from isotopic to nematic phase 80−84060
colour effects using birefringent films and pleochroic dyes 80−24353
colour generation, arbitrary, in display device 80−5815
conference, ferroelectric materials and their applications, Kyoto, Japan, Nov. 17-19, 1977 79−19846
constant-coupling theory, cluster variational approach, thermodynamic props., nematic-isotropic transition 77−24265
continuum theory, shear flow 77−68920
continuum theory of crystals subject to EM fields 80−33876
continuum theory of disorder, intermolecular correls. 77−31591
continuum theory of disorder, nuclear magnetic relaxation 77−31592
continuum theory of disorder, order parameters 77−31590
convection, anomalous, temp. gradient critical point *(Russian)* 77−7669
convection, oscillatory convective instability *(French)* 79−1279
convective instability in AC field 77−62475
COOB, acoustic emission at liq. cryst. transitions prod. by thermo-optically excited defects 79−95137
COOB, sheared liq. crystal, near T_{A-N} optical response 79−94895
COOB, smectic A-nematic transition, X-ray and light scatt. obs. 79−95129
COOB-cholesteric liq. cryst. mixtures, helix pitch, temp. depend. 80−64895
copolyazomethine, nematic mesophase, DSC study *(French)* 78−71672

nematic liquid crystals continued
copolyethylene terephthalate-p-oxybenzoate, nematic phase, thermodynamics 78−91427
Couette flow, orientation instability for finite anchoring energies 80−74923
Couette flow, stability 79−32526
CPB, nematic temp. range broadening by nonmesogenic solute 77−47559
CPHB, nematogenic liq. cryst., above T_c, Kerr effect response time, temp. depend. 78−34434
critical dynamics near nematic-smectic A phase transition, renormalisation group approach 80−10646
critical dynamics of smectic A to nematic phase transition 79−1493
critical radius for homeotropic domain 79−19148
critical US absorption 79−65174
cyano biphenyl-substituted benzoates, exhibiting reentrant nematic behaviour, polymorphism and X-ray diffr. 79−94890
cyano compounds, liq. cryst. phases, incommensurate coexistent density fluctuations 80−79691
cyano Schiff bases, high press. reentrant nematic bilayer smectic-*A* transition 79−28087
4-cyano-4′-d_{17}-n-octylbiphenyl, D spin-lattice relax. time, partially averaged quadrupole tensors 77−1076
4-cyano-4′-n-pentyl-d_{11}-2′,3′,5′,6′-tetradeuteriobiphenyl, improved synthesis 79−32893
4-cyano-4′-n-pentylbiphenyl, refr. index meas. and isotropic-nematic phase transition study, surface plasmon technique 80−84282
4-cyano-4′-octylbiphenyl, dielec. props., 1 Hz-1 GHz, in smectic, nematic and liq. phases *(French)* 77−40168
4-cyano-4′-octylbiphenyl, dielectric relax. anal. in nematic and smectic phases 80−108153
4-cyano-4′n-heptyl biphenyl, nematic phase, torsional absorptions 77−48161
4-cyano-4′(n-amyl)-diphenyl, isotropic phase, induced molecular orientation relaxation time, Kerr effect *(Russian)* 80−19699
4-cyano-4′-octyloxybiphenyl, nematic-smetic-A transition, optical birefr. temp. coeff. 78−47505
cyano-biphenyl cpds., mag. susceptibility and order parameters 79−86709
cyano-biphenyl eutectic mixtures, tilt angle meas. of nematic phases 77−80417
cyano-biphenyl LC alignment on obliquely evaporated SiO_2 films 80−79677
cyano-biphenyl series, nematogens and smectogens, props. characterised by even-odd effect 80−107046
cyano-biphenyls, 7-CB and 8-CB director fluctuation quenching by mag. field, optical birefr. obs. *(French)* 78−87613
p-cyano-p′-pentylbiphenyl/p-pentylbenzoic acid, mixture, induced smectic phase, dielec. props. 80−6498
p-cyanobenzilidene p-octyl oxyaniline, nematic, new type of hydrodynamic instability 77−43142
4-cyanobenzoyloxy-4′-pentylstilbene, nematic, smectic A, and orthogonal smectic B phases 80−64890
cyanobenzylidene octyloxyaniline, director bend mode behaviour near nematic to smectic-A phase transition 78−1985
n-pcyanobenzylidene-p-n-octyloxyaniline, liq. cryst., proton FFT of aromatic and alkyl motions 77−15302
N-p-cyanobenzylidene-p-octyloxyanilene, second order nematic-smectic-A phase transition 77−72681
cyanobiphenyl, appl. in fast fluorescent shutter based on guest-host interaction 78−83092
cyanobiphenyl, refr. index, crit. angle meas. 78−60413
cyanobiphenyl, surface tension, meas. near nematic-isotropic transition temp. 78−43219
4-cyanobiphenyl and 4′-alkyl- or 4′-alkoxy-substituted liq. cryst. derivatives, soln., absorpt. and fluoresc. spectra 80−87164
cyanobiphenyl liq. cryst. mixtures, mol. mechanism producing dielec. relax. 78−84521
cyanobiphenyl nematic homologous series, Kerr consts., relax. times, refr. index, dielectric const. 79−19863
4-cyanobiphenyl/4-cyano-p-terphenyl liq. cryst. mixture, order parameters of dissolved dyes 80−100167
cyanobiphenyls, 80CB and its mixtures with 7CB, orientational order and elastic consts. 78−91245
cyanobiphenyls, liq. crysts. flow alignment 79−50988
cyanobiphenyls, nematic, diaelec. consots. and diamag. anisotropies 80−7253
cyanobiphenyls, physical props., appl. to Kerr cells 79−19142
cyanobiphenyls, thermal diffusivity, Rayleigh scatt. obs. 78−94977
cyanobiphenyls molecular conformational mobility study by optical probing method *(Russian)* 80−92459
cyanocyclohexylcyclohexanes, nematic, diaelec. consots. and diamag. anisotropies 80−7253
cyanopentyl-d_{11}-biphenyl-d_4, ordering matrix, proton dipolar coupling obs. 78−63671
p-cyanophenol mixtures, p-alkylbenzoates twisted nematic effect 79−82947
4-cyanophenyl 4-heptyloxybenzoate, nematic and smectic modifications, dielec. relax. meas. 77−69769
4-cyanophenyl 4-n-pentyloxybenzoate, electrical Kerr effect studies 80−25339
p-cyanophenyl p-n-alkylobenzoates, birefringence, polarisability and order parameter 80−100642
4-cyanophenyl-3-methyl-4-(4-n-alkylbenzoyloxy) benzoates, mesomorphic props. 79−94888
p-cyanophenyl-p′-caproyloxybenzoate, charge carrier behaviour, thermal depolarisation current study 80−7283
2-p-cyanophenylazo-S-akloxypyridines, synthesis, phase transition temps., and dielec. props. 79−86876
m-cyanophenylbenzoyloxybenzoates, nematic phase, freq. depend. of dielec. props. *(French)* 79−91337
cyanophenylcyclohexanes, nematic, diaelec. consots. and diamag. anisotropies 80−7253
4-cyanotetrafluorophenyl 4-n-alkylbenzoates, synthesis and mesomorphic props. *(French)* 79−86679
4-cyanothiophenol, synthesis 78−51408
4-cyanphenylene-4′-n-alkoxybenzoates, pulsed NMR Fourier spectroscopy 77−24266
cybotactic nematic mesophase, X-ray scatt. 80−92454
cyclohexane derivatives, low melting nematic cpds., characterisation 79−10798

nematic liquid crystals continued
cyclohexane derivatives, mesophases obs. *(French)* 78−59747
trans-1,4-cyclohexane-di-4′-n-alkoxybenzenes, synthesis and mesomorphic props. 79−94887
cyclohexylcyclohexanes, substituted, anisotropic liq. cryst. solvent for optical absorption spectroscopy 78−45724
DC dynamic scatt. microscopic structure and role of dopants 77−77179
de Gennes model, for nematic to smectic-A transition, anisotropic crit. props. 78−43110
decylammoniumchloride and bromide, lyotropic nematic struct. 78−51410
p-n-decyloxybenzoic acid p-n-hexyloxyphenyl ester, dielec. permittivity in nematic and smectic phases 79−32899
defects, topologically stable, classification in ordered media 77−62516
degree of order of lamellar and hexagonal mesophases rel. to cholesterol additions 77−24260
demonstration experiments 77−60876
deuterated compounds, molecular order and conformation changes in phase transitions 78−47237
DHAB, ordering change due to external DC elec. field, permittivity obs. 78−94990
di-1′,4″-octyloxybenzylidene-1,4-diaminochlorobenzene, nematic with some smectic ordering, EHD instabilities 77−84640
di-(4-n-alkyloxy) benzoic esters, of hydroquinone series, effect of polar substituents on electro optical props. 79−46569
4,4′-di-n-acyloxydiphenyldiacetylenes, synthesis and mesomorphic props. 79−82148
p,p′-di-n-alkoxy-azoxybenzenes, homologous cpds., refr. indices and opt. anisotropy, temp. depend., order parameters 77−16278
p,p′-di-n-butylazobenzene, high press. mesomorphic and polymesomorphic transitions 78−18750
diakyl-cyclohexyl-cyclohexanoates, nematic and smectic mesophases 80−19692
4,4′-dialkoxydiphenyldiacetylenes, synthesis and mesomorphic props. 79−32890
4,4′-dialkyldiphenyldiacetylenes, synthesis and mesomorphic props. 79−32890
dialkyloxyazoxybenzenes, synthesis of ferroelec. smectic B, smectic C, and nematic phases 78−94969
diarylethanes, bromo- or cyano-substituted, mesomorphic props. 79−90535
p-p′-dibutyl-azoxybenzene, DIBAB, light scatt. studies *(Dutch)* 80−33885
p-p′-dibutyl-azoxybenzene, elasticities and viscosities, light scatt. meas. 79−4245
dibutyl-phenyl-benzoyloxy-benzoate, nematic liq. cryst., rot. barrier, PCILO and CNDO/2 calcs. 80−33874
2,3-dichloro-1,4-napthoquinone in EBBA, PMR obs., mol. struct., orientation and solute-solvent interactions 77−27806
dichloromethane in nematic liq. crystal , $A_2(^{12}CH_2Cl_2)$ nuclear relax., dipole-dipole interaction 77−54567
dichroic dye in chiral nematic host, visible absorpt., pitch relationship 78−48193
dicyano compounds, synthesis and dielec. props. 79−86685
dielectric anisotropy, IR spectra, effect of AC elec. field 78−64355
dielectric characteristics obs. *(Russian)* 79−15400
dielectric polarisation, and relaxation, molecular mechanisms 80−34846
dielectric polarisation and relax., mol. mechanisms 80−29673
dielectric properties, of multicomponent mixtures 80−38909
dielectric properties, relaxation process charact. *(Russian)* 78−48116
dielectric properties and dielectric relax. *(Russian)* 79−61301
dielectric relaxation, LF, Freedericksz transition technique meas. 78−1987
dielectric relaxation at phase transitions 79−28090
dielectric-flexoelectric deformations in one dimens. 78−38616
p,p′-diheptylazobenzene, nematic, physical props. 78−79524
4,4-dihexylazoxybenzene, nematic liq. cryst., alignment on surfactant treated obliquely evaporated surfaces 80−49092
p,p′-dihexyloxyazoxybenzene-fluorobenzene, solute orientational order, NMR obs. 77−84627
p,p′-dihexyloxytolan, flexoelec. coeff. in nematic phase, thermal depend. 80−79685
dimer-forming compounds, nematic to isotropic transition 79−28085
4-4′-dimethoxyazoxybenzene-d_{14}, orientational order and internal rot., D NMR obs. 79−50987
1,6diphenyl 1,3,5, hexatriene cholesteryl chlorided cholesteryl laurate mixture, nematic, polarisation fluoresc. meas. 79−78723
director in dielec. regime, dynamical behaviour, EHD instabilities *(Japanese)* 80−59387
disc-like mesogens, nematic optical texture 79−77513
disclinations, control and elimination in twisted nematic displays 77−68912
disclinations, generation process, matrix representation 78−59743
disclinations, rel. to cryst. screw dislocations 77−11477
disorder, continuum theory, comparison with lattice-models 80−54126
display devices with twisted and tilted arrangements, guest-host interactions 80−34891
display technique 78−51419
displays, twisted nematic, review of recent advances 79−99056
p,p′-disubstituted phenyl thiolbenzoates, synthesis and props. 77−15308
p-disubstituted phenylcyclohexane, liq. cryst., investigation of elec. field induced deform. by capacity measurements 79−4234
DMBCA, nematogen, incoherent neutron quasielastic scatt. 79−32887
dodecanate/decyltrimethylammonium micelles, type II mesophase, bilayer struct., NMR spectra study 80−75149
domain instabilities in elec. and mag. fields 79−94875
domain structure, stimulated rearrangement 78−26438
domain structure of new type in dielec. region 77−11480
domains, of 2nd kind, form. with positive dielec. anisotropy *(Russian)* 78−18550
domains due to mag. field 77−58951
domains formed in AC, DC fields, temp. depend. of threshold voltages *(Russian)* 77−39542
dye laser, planar 77−3578
dyes, field-induced colour changes 80−25340
dynamic crit. neutron scatt. obs. near smectic-A nematic phase transition 78−79752
dynamic light scatt., model 80−2730
dynamic scatt. characteristics in mag. field 77−77177
dynamic scattering, material flow due to external electric fields 78−18543

nematic liquid crystals continued
EABAC, liq. cryst., smectic and nematic, distrib. functions by X-ray diffr. 79−99072
EABAC, smectic A, nematic, and isotropic phases, NMR and quasielastic neutron scatt. obs. 80−88022
EBBA: nitroxide, mol. reorientation in nematic and isotropic phases, EPR study *(French)* 79−91297
EBBA, binary systems with non-nematic solutes, phase transition behaviour and ^1H NMR anal. 80−34174
EBBA, containing $FeSnO_3$ particles, Mossbauer study of Brownian motion 79−95691
EBBA, crystallisation and melting of metastable solid crystalline phases 78−2240
EBBA, dielec. permittivity and transmitted light intensity, in DC field 77−12296
EBBA, dynamic light scatt., effect of paramag. iminoxyl radical addition *(Russian)* 77−43131
EBBA, fusion of metastable solid cryst. forms 79−14678
EBBA, in benzene soln., dielec. relax. meas., 4.0, 9.4 and 30.4 GHz 77−40176
EBBA, IR absorpt. spectra, elec. field effects, orientational order parameter determ. by IR dichroism, bend elastic consts. 80−80778
EBBA, IR and far-IR spectra, vibr. assignments 77−16298
EBBA, isotropic phase, order fluctuations, self-diffusion, and rot. motion, proton spin relax. meas. 79−87328
EBBA, linear and nonlinear relaxations of fluid dynamical motion 77−31585
EBBA, liq. cryst., isotropic phase, NMR pulsed field grad. study of self-diffusion 79−90814
EBBA, liq. cryst., Raman and calorimetric evidences for existence of three solid modifications 77−77207
EBBA, macroscopic and microscopic orientations, EPR of nitroxide probe *(French)* 78−75546
EBBA, metastable phases formed by rapid cooling of mesophase, IR and Raman spectra and DSC obs. 80−34919
EBBA, mol. alignment, elec. and mag. field effects, dielec. const. obs. 77−11472
EBBA, mol. and cryst. struct., X-ray diffr. study 80−88134
EBBA, mol. order study by means of C^{13}-H^1 double resonance 79−60275
EBBA, nematic, ordering parameter temp. depend. 79−23517
EBBA, nematic and isotropic phases, dielec. props. 79−87383
EBBA, nematic liq. cryst., effect of mag. field on US attenuation *(Japanese)* 79−19144
EBBA, nematic-isotropic transition, birefringence anomaly at clearing pt. 79−46788
EBBA, nematic-isotropic transition at high press., turbidity meas. 80−92655
EBBA, NMR and Raman scatt. studies in nematic phase 80−100619
EBBA, orientational order, effect of hexa-n-alkoxy-triphenylene disc-like solutes 80−79682
EBBA, orientational order in glassy and nematic phases, IR dichroism meas. 80−64891
EBBA, phase transition enthalpies, 1 bar to 2.5 kbar 78−75814
EBBA, phase transitions, up to 3 kbar, DTA obs. 77−20051
EBBA, polymorphism, radiothermoluminescence and differential scanning calorimetric study 80−24570
EBBA, pVT data and viscosity-press. behaviour 78−94989
EBBA, rapid cooling and mag. field effects on NMR relax. and thermal behaviour 79−82321
EBBA, refr. indices, densities, polarisabilities and mol. order 77−28536
EBBA, RF dielec. props. 79−4238
EBBA, self-focusing, stimulated Brillouin scatt. 77−75625
EBBA, temp. depend. of absorption and fluoresc. of tetracene and perylene-tetracene in liq. cryst. *(German)* 80−18887
EBBA, Tsvetkov parameter, temp. depend. 80−88035
EBBA elec. props solid and liquid states, temp. and freq. depend. *(Russian)* 78−72450
EBBA ordering effect in fluoresc. of perylene and 4-dimethyl-amino-4′-nitrostilbene *(German)* 79−81235
EBBA-aromatic hydrocarbon systems, solute size and shape effect on nematic-isotropic equilib. 79−23710
EBBA-dimethylaminonitrostilbene mixture, nematic, polarisation fluoresc. meas. 79−78723
EBBA-MBBA mixture, differential IR spectroscopy determ. of orientation of molecules 77−7670
EBBA-non-mesogenic binary liq. cryst. system, two-phase premelting, NMR obs. *(Russian)* 78−30743
EBBA/EBCA mixed cryst., mol. alignment, field, temp. freq. depend. 78−75542
EBRA, nematic, EPR investig. 80−108077
effective ion mass and mobility calcs. *(Russian)* 80−79694
EHD, nonlinear effects 77−84642
EHD flow patterns, squint, nonlinear feature 79−94876
EHD instabilities, white noise effect 80−70115
EHD instability, current density 77−80415
EHD instability, nematic liquid crystal in contact with photoconductor 80−79695
EHD instability, phase diagram, for nematic-cholesteric binary mixture 78−1980
EHD instability, temp. depend. 78−1998
EHD instability in dielec. regime 77−27812
EHD instability limits under action of sinusoidal electric fields 77−47342
EHD instability mechanism, liq. cryst. with positive dielec. anisotropy *(Russian)* 77−31594
elastic constants determ. 77−27824
elect. conduct. based on injection-contact phenomena theory *(Russian)* 80−107807
electric and magnetic fields, effect on orientational order in two-dimens. 78−79530
electric field effects on structure and props. *(Russian)* 77−47340
electric field induced nematic to cholesteric transition, transient phenomena of relax. 78−75811
electric field suppression of fluctuations, laser speckle picture 77−7660
electrically controlled transparency based on frustrated total internal refl. 79−32074
electro-optic cholesteric-nematic transition, and memory effect *(Russian)* 77−84911
electro-optic effect, temp. independ. threshold voltage cholesteric-nematic phase change effect 79−91405

nematic liquid crystals continued
electro-optic switch, four-port, for unpolarized fibre light 80−58715
electro-optic valve testing using laser light *(French)* 80−28311
electroconvective flow, vel. and orientation deform. angles *(Russian)* 79−37621
electrode reactions control using dopants, Kerr meas. *(French)* 80−11898
electrohydrodynamic effect, in nematic liq. crysts. in alternating elec. field 79−14676
electrohydrodynamic instability, nematic liq. of positive dielec. anisotropy [illegible]
electrohydrodynamic instability, new type in nematic liq. cryst. ZhK-440 79−14677
electronic spectra, influence of order in liq. cryst. struct. 78−71675
electrooptic cell with asymmetrically treated electrodes 79−55658
electrooptical characteristics of ZhK-440 controllable crystal transparency 80−78996
electrooptical effects in inhomogeneous fields 80−44118
EM wave nonlinear interaction 80−19698
enantiomers, discrimination using liq. crystalline solns., IR rot. dispersion meas. 79−16064
enantiotropic nematic reentrant behaviour at atmospheric pressure in a pure compound 79−69233
enthalpy of fusion of nematogens 78−22645
EPR, mesophase orientation, spinning in weak mag. field, radical probe 77−68913
EPR, spinning in tilted mag. field, lag angle 78−38615
EPR and NMR relax., first-rank tensor component effects 78−14275
EPR of symmetrical three-spin systems undergoing rot. diffusion, slow motional spectra 77−36135
EPR singularities of acetylacetonate in partially ordered liq. cryst. matrix 77−77103
equation of state, anistropic props., perturbation theory 78−67645
equation of state, derivation 77−47560
equation of state, incorporating short-range orient. order 77−55237
equation of state for Maier-Saupe model 77−35474
Ericksen-Leslie continuum theory reformulation 78−30535
trans-4-ethoxy-4′-alkanoyloxyazobenzenes, nematogenic liquid crysts., birefr., order parameters, vol. changes during nematic-isotropic transitions 78−59742
ethoxy-hexyltolane, orientation-statistical props. studies by optical methods *(Russian)* 79−77518
ethoxy-octyltolane, orientation-statistical props. studies by optical methods *(Russian)* 79−77518
p-(p′-ethoxybenzylidene)amino-benzonitrile, cryst. struct. rel. to liq. crystallinity 80−100225
N-p-ethoxybenzylidene-p′-cyanoaniline, nematic, mol. reorientation in DC elec. field, IR ATR spectra study 80−45064
ethoxyhexyltolan, Raman spectra, molecular conformational instability, internal field effects 80−54127
ethoxyoctyltolan, Raman spectra, molecular conformational instability, internal field effects 80−54127
p(p-ethoxyphenyazo)phenyl undecylenate, nematic liq. cryst., refractive index, density, orientational order 78−76419
p(p-ethoxyphenylazo)phenyl heptanoate, nematic liq. cryst., refractive index, density, orientational order 78−76419
p(p-ethoxyphenylazo)phenyl hexanoate, nematic liq. cryst., refractive index, density, orientational order 78−76419
p(p-ethoxyphenylazo)phenyl valerate, nematic liq. cryst., refractive index, density, orientational order 78−76419
p-p-ethoxyphenylazophenyl hexanoate, dielec. relax. in stable and metastable solid phases 80−34851
ethyl-(methoxybenzylidene-amino)cinnamate, low freq. dielec. constant meas. 78−91226
eutectic mixture, glassy nematic phase, complex permittivity tensor 79−91336
eutectic-forming binary system, melting behaviour 77−89526
evolution equations, props. of solns. of a derived system of eqns. *(French)* 77−35471
extensible, micropolar continuum theory 79−4244
ferroelectricity in nematic and smectic liquid crystals *(French)* 78−83729
ferrofluid/lyotropic liq. cryst. combination, ferronematics and ferrocholesterics 80−59378
fibrinogen, liq. cryst., layer, shear orientation 77−27807
field induced twisted structure with quasihomeotropic boundary conditions, electro-optic behaviour 78−60424
field-dependent light scatt. 77−4040
field-induced nematic-cholesteric relax., hysteresis behaviour of texture 77−84900
film, critical splay-bend deform. numerical anal. 77−58957
film, with two free surfaces, mol. orientation 78−47238
flexo-electric domains 78−43792
flexoelasticity in isotropic phases 78−63672
flexoelectric bending, e_{1z}/e_{3x} meas. 77−72555
flexoelectric domains in thin layers *(Russian)* 78−18549
flexoelectric effect in wedgelike layer 79−60264
flexoelectric polar deformations and second order elasticity 78−1979
flexoelectricity 79−77495
flexural elasticity meas. *(Dutch)* 80−34112
flow, book contrib. 78−59531
flow alignment and flow-induced phase transitions 77−15565
flow in flat channel, heat transfer anal. *(Russian)* 77−72397
flow speed of DPM-4 mixed with dye, AC appl. field effect 77−39532
fluorescence using luminesc. impurity, order parameter determ. 79−4240
fluorescent measurement of S_2 and S_4 order parameters 77−24262
Frank elastic constants, statistical mech. theory 80−29104
Freedericksz transition, first-order, second-order elasticity effect 79−99069
Freedericksz transition and anchoring effects for general config. 80−33875
Freedericksz transition and anchoring effects in oblique config. 79−55652
Freedericksz transition in mag. field, domain struct. 80−33880
Freedericksz transitions in twisted nematics with surface tilt 78−71671
gigantic optical nonlinearity, self focusing in oriented mesophase *(Russian)* 80−64120
Ginzburg-Landau equations, vol. solns. disclinations *(Russian)* 77−11762
guest-host interaction properties 78−6007
nematic liquid crystals continued
HAB, dielectric and calorimetric investig. in solid, liq. cryst. and liq. phases 77−84639
haemoglobin, deoxygenated sickle cell, gels, liq. cryst. props. 78−3445
hard rod lattice model, nematic and cryst. ordering, mean field interaction 77−80412
hard rod system, improved lattice model, nematic and isotropic phases 80−33882
hard spherocylinder fluid, mol. dynamics simulation 78−5997
HBAB, temp. depend. of apparent viscosity and density 78−18542
HBAB soln. in CBOOA, re-entrant nematic phase 79−14674
HBBOP and HBH-HBBOP nematic mixtures, relax. freqs. and dielec. anisotropy, binary system behaviour *(German)* 79−33606
HBT, mag. susceptibility and anisotropy, smectic, nematic, isotropic phases 78−18748
HBT, phase transitions, quenching effects, DSC, DTA, X-ray diffr. and microscopic obs. 78−22833
n-heptyl cyanobiphenyl, near IR dichroic spectrum, using unpolarised radiation 78−27201
4-n-heptyl-4′-β-cyanovinylbiphenyl, isotropic mechanism of mol. rot., dielec. permitt. meas. 80−10491
4-n-heptyl-4′-cyanobiphenyl, linear dichroism spectra in nematic and isotropic phases 80−25336
4-heptyl-4′-cyanobiphenyl, liq. cryst., dielec. props. *(French)* 78−10820
4-heptyl-4′-cyanobiphenyl, nematic liq. cryst., alignment on surfactant treated obliquely evaporated surfaces 80−49092
4′-n-heptyl-4-cyanobiphenyl, magnetic field depend. of birefringence and order parameter 77−76534
n-heptyl-4-cyanobiphenyl, nematic phase, dielec. loss, diffusion equations 80−71305
4′-n-heptyl-4-cyanobiphenyl, nematogenic liq. cryst., above T_c, Kerr effect response time, temp. depend. 78−34434
n-heptyl-cyanobiphenyl, dielec. relax. in nematic and isotropic phases 79−82151
p-p′-n-heptyl-cyanobiphenyl-isotropic solute systems, nematic-isotopic phase transformation, volumetric study 80−92653
4-n-heptyl-d_{15}-oxybenzoic acid-d_1, nematic and smectic phases, mol. and relative segmental order 80−96439
heptylcyanobiphenyl, surface and bulk order parameters, refr. index anisotropy 79−90522
4′-n-heptyloxy-4-cyanobiphenyl, 70CB, anomalous mag. field induced birefr. in isotropic phase 78−56461
n-heptyloxy-cyanobiphenyl, dielec. relax. in nematic and isotropic phases 79−82151
4,4′-di-heptyloxyazoxybenzene, diffuse X-ray scatt. near smectic C-nematic transition 79−95139
heptyloxyazoxybenzene, filamentary structures 80−107051
heptyloxyazoxybenzene, liq. cryst., pretransition behaviour, volumetric study 77−69076
4-4′-di-heptyloxyazoxybenzene, liq. cryst.-isotropic transition at high press. 79−95135
4-n-heptyloxybenzylidene-4′-n-hexylaniline, nematic and smectic phases, long mol. axis reorientation, LF dielec. dispersion 80−70124
p-n-heptyloxybenzylidene-aminofluorenone/COOB mixtures, dynamic twist viscosity near polycrit. points 79−95133
p-n-heptyloxybenzylidene-p-aminobenzoic acid, smectic C to nematic transition 79−33076
4-n-heptyloxybenzylideneamino-4′-cyanobiphenyl, reentrant nematic phase and low temp. smectic phases 80−88031
heptyloxylbenzoic acid,.isotropic phase, light scatt., ultrasonic vel. and absorpt. meas. 78−48189
4-n-heptyloxyphenyl 4-n-hexydexybenzoate, freezing polarisation, electret effect *(Polish)* 80−10496
p-n-hexadecyloxycinnamic acid, liq. cryst., radiation stability 78−85184
hexagonal arrays for twist geometry 77−11478
4-n-hexyl-4-cyanobiphenyl, isotropic mechanism of mol. rot., dielec. permitt. meas. 80−10491
hexyl-azoxybenzene, twist viscosity and mech. props. near smectic A-nematic transition 78−95136
4-n-hexyloxybenzylidene-4′-n-hexylaniline, liquid crystal, exam. of orientation order of dissolved molecules 80−44112
4-n-hexyloxybenzylidene-4-n′-hexylaniline, nematic and smectic phases, long mol. axis reorientation, LF dielec. dispersion 80−70124
N-p-hexyloxybenzylidene-p′-toluidene, positron lifetime meas. in solid and liq. cryst. phases 79−61460
p-n-hexyloxybenzylidene-p-aminobenzoic acid, phase transitions, X-ray diffr. and DSC meas. 79−86877
N-p-hexyloxybenzylidene-p-toluidine, optical props., density, and order parameter in liq. cryst. phases 79−55657
p-hexyloxyphenyl-p-pentoxybenzoate, nematic liq. cryst., elec. discharge meas. of persistent internal polarisation 80−10488
high frequency electrohydrodynamic instability, permittivity, elec. cond. *(Russian)* 80−49099
HNBP, statistical mechanics, particle pots. and distrib. functions calcs. 78−2001
HOAB, chain ordering model 80−24357
HOAB, effect of smectic C struct., on dielectric relax. 79−19140
HOAB, liq. cryst., smectic and nematic, distrib. functions by X-ray diffr. 79−99072
HOAB, liq. cryst. phase transitions, specific ht. meas. 79−33075
HOAB, molecular orientatioal order in uniaxial and biaxial phases by NMR 77−84629
HOAB, thermotropic mesophase, DMR chain segments assignment 80−24356
HOAB-cholesteryl benzoate mixture, twisted smectic-C and twisted nematic phases, optical and X-ray investig. 77−84634
HOAOB, isotropic-nematic transition, supercooling and nucleation, interface dendrites 78−42896
HOBA, isotropic phase, Brillouin scatt. spectra, hypersound data determ. 79−91453
HOBHA, thermotropic mesophase, DMR chain segments assignment 80−24356
homeotropic, heated from below, oscillatory convective instability, thermodynamic anal. 79−86690
homeotropic nematic films heated from below, overstability and inverted bifurcation 79−77501
homeotropically oriented, effects of elliptically polarised shear flows, instability patterns obs. 78−14277
homeotropically oriented, spectral studies of acoustooptical interaction 80−88965

nematic liquid crystals continued
homogeneous aligned sample, capacitance response to elec. and mag. fields, appl. to elastic const. determ. 79−90545
homogeneous surface alignment using double SiO deposition, appl. to displays 79−4239
homogeneously aligned, positive dielec. anisotropy, Williams domains as mag. threshold effect 78−26435
homogeneously oriented, neutron small-angle scatt. by dislocations 77−1077
homologous series, even-odd effect in Kerr effect 77−43970
homologous series, molecular polarisability anisotropy, depend. on alkyl chain length 79−23518
hybrid aligned nematic, elec. field induced deform., birefr. 77−4624
hybrid field-effect liquid-crystal light valve, optical data processing performance 80−99860
hydrodynamic correlation functions, propagating modes 78−94988
hydrodynamic instability phenomena and mechanisms, book contrib. *(French)* 77−84229
hydrodynamic theory, near nematic-smectic-A transition, acoustic props. 79−77731
hydrostatics, universal soln. 78−83722
hydrostatics, universal solns. 79−69007
IBPBAC, order parameters in nematic and smectic phases, X-ray diffr. meas. 79−94874
image transducer, performance effects of liquid crystal thickness 80−102838
incompatible nematogens, induced smectic mesomorphism 78−1983
incompressible, two dimens. coupled eqns., flow in mag. field *(French)* 77−84329
induced cholesteric order by chiral 2,2′-spirobiindane derivatives *(German)* 80−64884
induced helical pitch, temp. depend., chiral additives effect *(German)* 79−60277
inelastic light scattering by order parameter biaxial and longitudinal fluctuations *(Russian)* 80−75160
inhomogeneous, with boundary conditions, mol. statistical theory 77−76297
instability, azimuthally-oriented, produced by elec. field *(Russian)* 77−4041
instability threshold in biased rot. mag. field 77−58952
instability when subjected to elliptical shear 79−1393
interaction of injected macromolecules *(Russian)* 78−78848
interface with uniaxial solid, effects of long range van der Waals forces on anchoring 77−7662
intermolecular forces, in anisotropic mean field, hard spherocylinder model 77−35468
internal field, dipole correlation factor 78−34428
internal field anisotropy 79−94898
ionic conduction-induced flow alignment angle, NMR evidence 80−44125
IR absoprtion, strong positive dielec. anisotropy, elastic consts. 78−75545
IR modulator properties 78−25970
isotropic phase, complex shear viscosity 77−39667
isotropic phase, fast ps reorientation, optical Kerr signal 77−15313
isotropic phase, light scatt., ultrasonic vel. and absorpt. meas. 78−48189
isotropic phase, pulse acoustic-optic modulator 80−95993
isotropic phases of nematogens, direct obs. of picosecond mol. reorientation 78−1991
isotropic-nematic liquid crystal phase transition, theory including mol. orientation correlation 78−47508
isotropic-nematic transition, mean-field theory, thermodynamic props. 77−24391
isotropic-nematic transition, model, mol. shape, vol. effects on orientational ordering 78−30741
isotropic-nematic transition, Onsager's orientational order theory 78−79750
isotropic-nematic transition, tricritical behaviour 78−75817
Josephson effect, AC, phase slippage 79−46565
Landau approximation, validity 77−27989
laser breakdown, plasma-acoustic cavitation phenomena *(Russian)* 77−65947
lattice model with attractive isotropic interaction, Wulf Rocco model extension 77−84626
layers, optical phase difference and capacitance, elec. and mag. field depend. 80−28911
LC-440, shear modulus and viscosity relax. near isotropic-nematic phase transition *(Russian)* 77−39543
light deflection by nematic cell structures *(Japanese)* 77−39051
light modulator, scanning mode of operation 80−33200
light scattering, role of order parameter fluctuations *(Russian)* 77−80421
light scattering by nematic cells 77−55772
light scattering centre dimensions, elec. field effect *(Russian)* 78−38619
light scattering quasi-elastic, near instability point, dielec. regime 78−75535
light transmission exam., positive and negative dielectric anisotropy 77−43141
light transmission meas. 80−88025
light transmission through twisted layer 78−68476
low temperature nematic, binary mixture, spin-lattice relax., temp. depend. minima 78−26427
low tilt angle alignment, on evap. SiO layer, compatible with frit sealing 77−68910
low tilt angle nematic alignment with frit sealing 78−38618
lyomesophases, coupling with ferrofluids 79−90526
lyotropic, mag. susceptibility, mol. aggregation meas. 80−19690
macromolecule introduction, interactions 80−30639
magnetic field behaviour when bounded by polished plates, periodic struct. form. 78−51417
magnetic platelets, equil. positions w.r.t applied field 77−11476
magnetic susceptibility temp. depend. *(Russian)* 79−51737
magnetic susceptibility temp. depend. 80−25103
magnetic threshold field, of nematic layers 79−86710
magnetohydrodynamic effect, for 3D model of nematic liquid crysts. 79−41955
Maier Saupe model, soln. in mean field approx., Meyer-Lubensky transition model 80−19694
Maier-Saupe lattice model, stochastic model method simulation 77−43129
Maier-Saupe theory, consistency of mean field theories 77−51316
nematic liquid crystals continued
Maier-Saupe theory, model 77−51317
Marangoni effect in thin droplets 78−6009
material analysis in production quantities 77−76309
matrices, orientating, for UV-visible dichroism meas. *(German)* 77−34668
matrix display, scanning capability improvement 77−55770
matrix for cubic molecules, linear dichroism, distortion and local field contribs. 79−87415
MBAB, liq. cryst., Brillouin-Mandelshtam light scatt. and refr. index 80−55119
MBAB, twist viscosity, temp. depend. 77−35472
MBAB-chiral cpd. mixture, cholesteric, helical screw sense and pitch determ., Grandjean-Cano method *(German)* 77−80609
MBBA: 4-methoxybenzaldehyde, pure and doped, nematic-isotropic transition temps., appl. to purity control 79−55872
MBBA:diacetylferrocene, nematic glass-supercooled nematic transition, Mossbauer temp. obs. 79−95687
MBBA:trichlorobenzene, solute orientation in nematic soln., temp. and conc. depends., NMR obs. 79−46556
MBBA, ^{13}C spin-lattice relax., Fourier-transform NMR, NOE 78−48064
MBBA, acoustic emission rate at nematic-isotropic transition 78−91232
MBBA, acousto-hydrodynamic effects when excited by 20 MHz US surface waves 80−76003
MBBA, aligning props. for Si film surface tension 79−90846
MBBA, alignment on elec. domains of TGS 79−38506
MBBA, and MBBA-EBBA mixtures, determ. of viscosity coefficients by torsional vibrs. 79−14953
MBBA, anisotropic interactions with surface-treated substrates, wall effects on Freedericksz transition 79−99070
MBBA, anisotropic refr. indices from optical interference meas. 77−8538
MBBA, anisotropy of US attenuation 78−43070
MBBA, annihilation of disclinations with Frank index m = +2 77−58955
MBBA, anomalous behaviour of electrical dissipative power 79−4237
MBBA, Brillouin scatt. in isotropic phase 78−2867
MBBA, calc. of order parameter from X-ray diffraction data 79−69009
MBBA, charge carrier drift mobility 78−87801
MBBA, cholesteric struct. induced by chiral sulphoxides 79−86683
MBBA, cylindrical domain struct. thermal excitation, optical obs. 79−73097
MBBA, deflector based on frustrated total internal light refl. 78−50934
MBBA, dielec. permittivity and loss meas., −196 to 0°C 77−59511
MBBA, dielec. permittivity and transmitted light intensity, in DC field 77−12296
MBBA, dielec. relax. in metastable modification of solid phase 80−84689
MBBA, dielec. relax. in nematic phase 79−82153
MBBA, dielec. relax. under shear 79−10794
MBBA, dielectric and calorimetric investig. in solid, liq. cryst. and liq. phases 77−84639
MBBA, dielectric permitt. rel. to molecular props., effect of anisotropy of medium and local field 80−25270
MBBA, diffusion coeff. determ. *(German)* 79−51291
MBBA, doping effect on cond. anisotropy and dynamic scatt. 77−40208
MBBA, dye activated, isotropic phase, induced Raman emission *(Russian)* 78−13766
MBBA, dynamic critical behaviour in NLC above nematic-isotropic transition 80−49096
MBBA, dynamic light scatt., effect of paramag. iminoxyl radical addition *(Russian)* 77−43131
MBBA, dynamic scatt. mode due to electrohydrodynamic instability *(Japanese)* 77−43133
MBBA, dynamically excited, transversal EHD instabilities and umbilics 78−94983
MBBA, effect of elec. field on flow alignment angle 79−10792
MBBA, EHD flow patterns, analogy of instabilities with classical fluid behaviour 77−84335
MBBA, EHD transitions, white noise effects 80−6159
MBBA, elastic consts. determ. 77−27824
MBBA, elec. field effect on optical indicatrix orientation 77−36202
MBBA, electrohydrodynamic instabilities, flow patterns and phase diagrams 77−68915
MBBA, electrohydrodynamic instabilities, power spectra and autocorrel. in flow transitions 77−68914
MBBA, electrohydrodynamic instability, fluctuation of light transmission meas. 77−11468
MBBA, electronic spectra 78−52530
MBBA, electroviscous effect, electrohydrodynamic investigation 78−87804
MBBA, electroviscous effect 79−69010
MBBA, film, nematic-isotropic crit. thickness, Landau-de Gennes theory 77−4189
MBBA, flexibility gradient of fatty acid spin labels, EPR study 80−71181
MBBA, flexoelec. coeff. in nematic phase, thermal depend. 80−79685
MBBA, flexoelectric and dielec. relax. behaviour 78−94979
MBBA, fluorinated analogues, mesomorphic props. 80−70118
MBBA, Frank elastic const. ratio determ. by Rayleigh scatt. 79−99059
MBBA, freq. depend. of proton T_1, rot. diffusional mechanism interpret. 77−12219
MBBA, frozen nematic glass, EPR spectra of copper and cobalt triazene-1-oxide complexes 80−88871
MBBA, HF electrohydrodynamic instability in NLC *(Russian)* 80−54130
MBBA, high freq. EHD instabilities, temp. depend. 79−94879
MBBA, homeotropic nematic layer, torsional shear flow in normal elec. field 79−82155
MBBA, homotropic liq. cryst. growth 78−26439
MBBA, hydrodynamic instabilities and elastic deformation created by US 77−19873
MBBA, hypersonic props., Mandel'shtam-Brillouin spectra obs. 79−4813
MBBA, in alternating elec. field, two-dimens. lattice form. *(French)* 77−11473
MBBA, in benzene soln., dielec. relax. meas., 4.0, 9.4 and 30.4 GHz 77−40176
MBBA, IR absorpt. spectra, elec. field effects, orientational order parameter determ. by IR dichroism, bend elastic consts. 80−80778
MBBA, IR and far-IR spectra, vibr. assignments 77−16298

nematic liquid crystals continued
MBBA, isotropic, depolarised Rayleigh doublet, de Gennes viscosity coeffs. 78−31207
MBBA, isotropic, obs. and anal. of depolarised Rayleigh doublet 78−38184
MBBA, isotropic phase, Brillouin scatt. spectra, hypersound data determ. 79−91453
MBBA, isotropic phase, light scatt., ultrasonic vel. and absorpt. meas. 78−48189
MBBA, isotropic phase, order fluctuations, self-diffusion, and rot. motion, proton spin relax. meas. 79−87328
MBBA, isotropic phase, phase-conjugate refl. by degenerate four-wave mixing 80−43389
MBBA, isotropic-nematic transition, birefringence for tricrit. exponents 79−37816
MBBA, laser radiation transmitted near isotropic transition, spatial coherence 78−18003
MBBA, light modulation by nematic liq. cryst., mech. excitation, response times 79−73094
MBBA, light scatt. by disclinations, spatial coherence props. 77−8544
MBBA, liq. cryst., flexoelectricity and surface polarisation 77−89376
MBBA, liq. cryst., isotropic phase, NMR pulsed field grad. study of self-diffusion 79−90814
MBBA, liq. cryst., light scatt. and birefr. 78−22646
MBBA, liq. cryst., mass diffusion meas., tracer dye-laser method 78−59738
MBBA, liq. cryst.-isotropic transition at high press., P-V-T eqn. of state 79−95135
MBBA, mag. susceptibility and order parameters 79−86709
MBBA, magnetically aligned liq. cryst., highly damped waves studied 79−1277
MBBA, meas. of nonlinear optical susceptibilities in isotropic and nematic phases *(Russian)* 78−74945
MBBA, metastable phases formed by rapid cooling of mesophase, IR and Raman spectra and DSC obs. 80−34919
MBBA, mol. alignment, comparison of exptl. data at high press. with mean field theory predictions 79−99075
MBBA, mol. alignment in elec. and mag. fields 77−58956
MBBA, mol. dynamics near nematic-isotropic liq. cryst. transition *(Russian)* 78−84495
MBBA, mol. order and motion, EPR study 77−76298
MBBA, morphological changes and electro-optical characts. appl. laser light modulation 77−20826
MBBA, nematic, acoustohydrodynamic instability 77−4036
MBBA, nematic, birefringence determ. by new simple method 78−79526
MBBA, nematic, EHD instabilities, director-fluctuation autocorrelation and power spectrum 79−41944
MBBA, nematic, EHD instabilities, director-fluctuation second moment 79−41943
MBBA, nematic, ordering parameter temp. depend. 79−23517
MBBA, nematic, transient elec. current obs. 77−20324
MBBA, nematic, US attenuation anisotropy, temp. depend. 78−43071
MBBA, nematic, viscosity coeffs., Onsager-Parodi relation validity 79−19147
MBBA, nematic and isotropic phases, dielec. props. 79−87383
MBBA, nematic liq. cryst., ^2H NMR, mol. order and reorientation 79−27906
MBBA, nematic liq. cryst., flow patterns and mol. alignment due to elec. fields 77−27825
MBBA, nematic liq. cryst., nonlinear optical processes near Freedericks transitions 79−69011
MBBA, nematic liq. cryst., nonlinear optical suscept. using light combination scatt. *(Russian)* 80−38064
MBBA, nematic liq. cryst., parallel and cross-like domains due to DC and LF electric fields 79−46557
MBBA, nematic liq. cryst., ultrasound produced rolls, spatial coherence props. of scatt. light 78−75534
MBBA, nematic liq. crysts., AC excited, dynamic light scatt., orient. fluctuations 79−1769
MBBA, nematic liquid crystals, wave number spectrum of dissipative structures 80−38904
MBBA, nematic phase, elec. field induced biaxiality, PMR study 79−90532
MBBA, nematic phase, quasielastic and elastic 10 Å neutron scatt. 78−42904
MBBA, nematic twist cells, bi-dimensional struct. in cond. region 79−90542
MBBA, nematic-isotropic transition, birefringence anomaly at clearing pt. 79−46788
MBBA, nematic-isotropic transition, compressibility-press. relations obs. 77−51481
MBBA, nematic-isotropic transition, intermolecular forces, IR N_2O mol. probe obs. 80−29155
MBBA, nematic-isotropic transition, isothermal compressibility and thermal expansion coeff. meas. 79−99301
MBBA, nematic-isotropic transition at high press., turbidity meas. 80−92655
MBBA, NMR and Raman scatt. studies in nematic phase 80−100619
MBBA, nonlinear effects, in elec. and mag. fields 77−24263
MBBA, nonlinear optical amplification above Frederiks transition 80−95937
MBBA, omeotropically aligned thin slice, dielectric permeability *(Italian)* 80−6354
MBBA, one dimens. dielectric-flexoelectric deformations 78−38616
MBBA, order fluctuations, self-diffusion, rot. motion, proton spin T_1 relax. 77−32285
MBBA, order parameters meas. by Raman scatt. 78−6011
MBBA, orientational order in glassy and nematic phases, IR dichroism meas. 80−64891
MBBA, partially deuterated, D spin-lattice relax. 78−48070
MBBA, phase transitions, up to 3 kbar, DTA obs. 77−20051
MBBA, polymorphism, positron annihilation obs. 78−72632
MBBA, positive space charge influence on texture, domain form. factor, polarised light study 80−88037
MBBA, pretransitional effects above phase transition temp., nonlinear dielectric meas. 79−15390
MBBA, proton spin-lattice relax. in crit. regime 80−80631
MBBA, pure and mixed with bezene (chlorobenzene), nematic-isotropic transition, US absorpt., visual hysteresis 80−54355
MBBA, pVT data and viscosity-press. behaviour 78−94989

nematic liquid crystals continued
MBBA, quasi-elastic light scatt. near instability point, conduction regime 77−15306
MBBA, quasihomeotropic orientation induced by PTFE deposited on SiO surface 79−90525
MBBA, Raman spectra in cryst., frozen glassy, and liq. cryst. states 80−60601
MBBA, refr. index, high press. meas. 78−26428
MBBA, refr. index anisotropy, meas. using different methods *(French)* 77−16274
MBBA, refractive index distrib. and mol. alignment in electro-optical effect *(Japanese)* 80−20613
MBBA, relaxation times for formation and break-up of Williams domains 78−34423
MBBA, ring deuterated, dipolar spin system exam. 77−39533
MBBA, secondary dynamic scatt. mode, light transmission and microscopic obs. 79−4246
MBBA, secondary light scatt. in low frequency field, in dielectric state 78−48147
MBBA, shear modulus and viscosity relax. near isotropic-nematic phase transition *(Russian)* 77−39543
MBBA, solid, metastable, wide-line NMR 77−51966
MBBA, solid, NMR and thermal behaviour, cooling and mag. field effects 78−76336
MBBA, solid phase polymorphism, IR and Raman spectra study *(French)* 79−87438
MBBA, solid phase polymorphism and phase transforms., IR spectra obs. 79−8128
MBBA, specific heat anomaly and isotropic liquid to nematic liquid cryst. transition *(Russian)* 77−62624
MBBA, spin thermometric anal. of spin-lattice relax. by order director fluctuation 77−47346
MBBA, statistical mechanics, particle pots. and distrib. functions calcs. 78−2001
MBBA, struct. of flow in cylindrical capillary 77−7671
MBBA, surface alignment using lecithin monolayers, contact angle meas. 79−4247
MBBA, temp. depend. of absorption and fluoresc. of tetracene and perylene-tetracene in liq. cryst. *(German)* 80−18887
MBBA, temp. depend. of apparent viscosity and density 78−18542
MBBA, temp. depend. of EHD instability 78−1998
MBBA, thermal diffusivity, Rayleigh scatt. obs. 78−94977
MBBA, thermal diffusivity meas. by forced Rayleigh scatt. 78−76483
MBBA, tilted alignment induced by short chain surfactants 77−4037
MBBA, transverse electrooptic effect 79−94897
MBBA, Tsvetkov parameter, temp. depend. 80−88035
MBBA, uniaxial, orientational order, polarised fluoresc. meas. 79−55655
MBBA, uniaxial liq. crystalline phase, orientational order, polarised Raman scatt. 77−76296
MBBA, US propag., nonlinear effects 77−59069
MBBA, viewed in transverse elec. field, voltage-freq. thresholds 77−7661
MBBA, volume meas. and phase transitions at high press. 79−90764
MBBA, Williams mode in EHD, applied voltage depend. 79−37620
MBBA, Williams patterns, transverse obs. 77−19869
MBBA as optical attenuator 77−19409
MBBA binary mixtures with a nematogenic or nonmesogenic cpd., dielec. relax. 78−72457
MBBA circumferential surface orientation, in capillary, optical studies 77−47349
MBBA domain pattern changes in electric field 77−1079
MBBA domains, in presence of iminoxyl free radicals, elec. field influence 79−64992
MBBA film, homeotropic nematic cell, subjected to ultrasound, impedance variations 79−41948
MBBA film, optical study of second dynamic scatt. regime *(Italian)* 78−15146
MBBA film, visible interaction of low-intensity US waves 78−10126
MBBA film, with two free surfaces, EHD flow 79−98817
MBBA homeotropic cylindrical boundary, in capillary, cols and noeuds 77−47350
MBBA liq. cryst., free iminoxyl radical addition, domain struct. parameter depend. *(Russian)* 77−58948
MBBA liquid crystal wedge as a polarizing element and its use in shearing interferometry 80−53444
MBBA matrix, polarised fluoresc. of organic mols. 78−90207
MBBA mol. alignment on SiO film, film thickness effects 80−59384
MBBA nematic crystal, EHD instability, damped oscill. of current and flow patterns 79−46562
MBBA nematic liq. cryst. systems, orientational order rel. to solute size, shape 77−4565
MBBA premelting detected by spin probes, effect of spin probe size 79−46563
MBBA-based binary nematic mixtures, dielec. L-relax. 77−40178
MBBA-BBCA mixture, field-induced distortion of mol. orientation 79−99060
MBBA-BBCA-cholesteryl chloride, field induced nematic-cholesteric relax. processes, transient helical pitch 80−38906
MBBA-cholesteryl chloride mixture, mol. orientation during mag. field induced cholesteric-nematic transition 79−28086
MBBA-cholesteryl nonanoate, liq. cryst. mixture, two colour display device 80−70116
MBBA-cholesteryl oleate mixture, memory effect characts., crit. freq. rel. to erase voltage 78−94993
MBBA-CN mixed liquid crystal, dissipative structs. caused by EHD instability 77−80416
MBBA-CPB nematic complex, dielec., elastic and electro-optical props. 77−32350
MBBA-d_{13}, ^1H spin-lattice relaxation, intermol. and intramol. contribs. 80−75873
MBBA-d_{13}, nematic phase, mol. order and director fluctuations, ^2D NMR meas. 79−90529
MBBA-d_{13}, nematic phase, rot. frame spin-lattice relax. 80−84668
MBBA-d_8, H and D spin-lattice relax. 77−59475
MBBA-d_8, mol. order and conformation, ^2D NMR line shape obs. 77−61771
MBBA-EBBA, controllable liq. cryst. transparency, electrooptical characts. 80−78996
MBBA-EBBA, homotropic liq. cryst. growth 78−26439
MBBA-EBBA eutectic mixture, vitrified orientation of Cr(III) acetyl acetonate in liquid cryst. 77−16152

nematic liquid crystals continued
MBBA-EBBA mixture, anisotropic effects in dielec. cond. of thick samples 79−10795
MBBA-EBBA mixture, behaviour in alternating elec. field 78−26440
MBBA-EBBA mixture, nematic layers with homogeneous orientation, acousto-optical props. 77−20824
MBBA-EBBA mixture, nematic liq. cryst., alignment on domains of TGS 79−38506
MBBA-EBBA mixture, transverse electro-optic effect 77−59556
MBBA-EBBA mixtures, thin and mol. films, between Hg electrodes, I-V characts. 79−11253
MBBA-Ge interface, electrorefl., IR transmission and frustrated total internal refl. 78−19513
MBBA-n-heptane, nematic soln., lattice model, thermodynamic functions *(Russian)* 80−64896
MBBA-n-heptane system, thermodynamic functions in lattice model *(Russian)* 80−33887
MBBA/EBBA, mol. interaction energy 80−33881
MBBA/EBBA binary liquid crystal mixture, US absorpt. and vel. dispersion, phase transition and alignment effects *(Korean)* 80−29121
MBBA/n-hexane mixtures, isotropic-nematic transition, transient optical Kerr effect study 79−82323
MBBA/non-mesogenic cpd., binary nematic mixtures, dielec. relax. and intermolecular interaction 79−91350
MBPAA, nematogen, cryst. and mol. struct. 77−72604
Merck 389, polymorphism, radiothermoluminescence and differential scanning calorimetric study 80−24570
Merck 5 and 7a nematic mixtures, EHD ion mobility 79−33104
Merck 5 and Merck 7a mixtures, charge carrier transport 78−51413
Merck phases, ZLI 1052 and ZLI 389, mag. susceptibility anisotropy and order parameter 79−86704
Merck V, oriented iodomethane, longit. NMR, relax. mech. 77−63302
mesogenic compounds with smectic F and nematic phases *(French)* 79−19143
mesogens incorporating trans-1,4-substituted cyclohexane ring system, synthesis and phys. props. 79−90543
mesophase pitch, magnetically-oriented, phys. props., mol. struct. 80−64885
mesophase pitches, synthetic, mag. orientation study 79−94868
mesophase thin layers, boundary effects 79−94903
4-methoxy-4′-azoxybenzene, elasticities and viscosities, light scatt. meas. 79−4245
methoxy-amyltolane, orientation-statistical props. studies by optical methods *(Russian)* 79−77518
p-methoxy-benzoate-p-n-pentylbenzene, isotropic phase nematogen optical Kerr const. 80−78919
p-methoxy-p′-alkyl tolanes, Raman scatt. in isotropic, nematic, and solid phases *(French)* 77−15309
p-methoxy-p′-alkyltolanes, molecular arrangement in solid state *(French)* 77−51364
methoxyamyltolane, nematic phase orientation mol. ordering determ. by Raman scatt. *(Russian)* 79−19153
p-methoxybenzoate-p′-n-pentyl benzene, slow non-critical mol. reorientation in isotropic phase 80−84062
p-(p'-methoxybenzylidene)amino-phenyl acetate, cryst. struct. rel. to liq. crystallinity 80−100225
4-methoxybenzylidene-4′-butylaniline, electronic spectra, influence of order in liq. cryst. struct. 78−71675
p-methoxybenzylidene-cyanoaniline, mol. and cryst. struct., X-ray diffr. study 80−88134
p-methoxybenzylidene-p′-alkyl anilines, Raman scatt. in isotropic, nematic and solid phases *(French)* 77−15309
N-methyl formamide, isotopically enriched, isotropic and nematic phases, NMR spectra 77−32270
methyl iodide, and -d_1, dissolved in nematic phase, C-H bond orientation, ^{13}C NMR 78−46371
MHD effect, high resolution NMR *(Russian)* 78−15040
MHD homogeneous instabilities in nematic liquid crysts. 78−63674
MHD instabilities 77−27828
microdynamics, computer study and models *(Hungarian)* 80−33878
microstructural EHD model, constitutive eqns. 79−10791
mixture, for low voltage dynamic scatt. display 78−27184
mixture, orientational order parameter calc. 77−24259
mixture, ZLI-207, nonideally oriented layers, Freedericksz transition dynamics 80−100163
mixture of hard rigid/flexible mols., unathermal, lattice model *(Russian)* 80−54129
mixtures, binary, induced smectic phases, X-ray diffr. obs. 78−94987
mixtures, dielec. permittivity dispersion 80−88921
mixtures, extended ranges, for appl. in electro-optic devices 78−83728
and mixtures, temp. dependence of density, obs. *(Russian)* 79−14681
mixtures with low-freq. dielec. relax., phase behaviour 78−91246
mixtures with optically active substances, stable inhomogeneities and permanent diffr. gratings 78−1988
mode-coupling theory near clearing point, crit. fluctuations 77−89377
molecular alignment, comparison of exptl. data at high press. with mean field theory predictions 79−99075
molecular alignment on chlorosilane-coated glass 77−11466
molecular alignment using alkoxysilanes, rel. to surface energy 80−100164
molecular conformation and orientational order, NMR studies, review 80−75151
molecular dynamical investigation 78−91252
molecular dynamics, self-diffusion and structure 77−65946
molecular dynamics 79−19141
molecular dynamics in thin films *(Russian)* 79−27903
molecular dynamics method, computer model 78−75544
molecular form and hydrodynamics connection, reactive coeff. *(Russian)* 80−64894
molecular orientation, rel. between meas. and theoretical characts. of ordering in nematics 79−60273
molecular reorientation, incoherent quasielastic, coherent-quasielastic and coherent-inelastic neutron scatt. 78−63640
molecular reorientation in steady mag. field, pulsed NMR Fourier spectra 77−35479
molecular statistical description 77−84650
molecular statistics, random phase approx. 79−41954
molecular structure and elastic consts. 79−77512
molecular structure and var. in nematic-isotropic transition temp. 77−84903
nematic liquid crystals continued
molecular structure effect on mesomorphism, lateral substituents 78−51411
molecular theory, orientation-average pair correlations 79−60272
molecular theory, orientation-averaged pair correlations 78−42905
molecules containing nitrile groups, dipole moments determ. 77−19872
moment singularities at angular corners in linear theory of axial plane reorientation 77−51320
momentum-shell recursion relations in $2+\varepsilon$ dimensions 78−6498
monomer-dimer system with attractive interactions on square lattice, nematic ordering 80−79681
multiple quantum spin-echo spectroscopy in one-deuteron system 80−31832
multiplexed liquid cryst. display, use of cholesteric-nematic phase change 80−107408
multiplexed twisted nematic displays, liq. cryst. material design 79−90533
naphthalene in EBBA, PMR obs., mol. struct., orientation and solute-solvent interactions 77−27806
naphthalene mesophase pitch, thermotropic transformations 79−95127
1,4-naphthoquinone in EBBA, PMR obs., mol. struct., orientation and solute-solvent interactions 77−27806
nematic, material consts., solute effects 77−1072
'nematic' amphiphilic liquid crystalline mesophases, thermodynamic stability 79−95126
nematic bend-splay elasticity near the nematic-smectic-A transition 80−24360
nematic liq. cryst., PMR line breadth temp. depend. 77−8419
nematic liquid cryst., forced light scatt. in interphase *(Russian)* 80−16051
nematic liquid cryst., tricritical behaviour near transition to isotropic fluid *(Russian)* 80−15001
nematic liquid crystal, intermol. forces, in anisotropic mean field, hard spherocylinder model 77−35468
nematic liquid crystals, light diffr. by 3D domain structs. 79−64989
nematic to cholesteric transition, light induced *(Russian)* 78−14452
nematic-chiral mixtures, viscosity and electrooptical characts. 79−86682
nematic-chiral-dye mixture, circular dichroism, selective light scatt. *(Russian)* 80−103944
nematic-cholesteric field-induced relax. time, phase transition temp. depend. 79−86874
nematic-cholesteric liq. cryst. mixture, NMR, reordering, nucleation and growth model 77−72546
nematic-cholesteric mixture, helical pitch, depend. on composition 78−42899
nematic-cholesteric mixture, spiral struct. formation *(Russian)* 77−58953
nematic-cholesteric mixture, surface boundary conditions influence on transition *(Russian)* 79−23705
nematic-cholesteric mixture, with positive dielec. anisotropy, light scatt. in elec. field 77−72548
nematic-cholesteric mixture with positive dielectric anisotropy, light scatt. characts. 78−75537
nematic-cholesteric mixtures, comp. depend. of helical pitch *(Japanese)* 77−72553
nematic-cholesteric mixtures, spiral pitch temp. depend. *(Russian)* 80−19700
nematic-cholesteric mixtures, ternary, comp. depend. of helical pitch *(Japanese)* 77−72554
nematic-isotropic mixture, dielec. props., phase diagram 78−52424
nematic-isotropic phase equilibria, Flory-Huggins theory appl., heat of transition 77−4187
nematic-isotropic phase equilibria in binary mixtures containing rigid rod solutes 79−86873
nematic-isotropic phase transition at high press., thermodynamics *(Russian)* 78−87778
nematic-isotropic phase transition character, molecular bending fluctuations critical growth *(Russian)* 80−79919
nematic-isotropic transition, chain flexibility, flexible chain in rigid rod solvent 79−4400
nematic-isotropic transition, correlation functions, Cotton-Mouton coeffs. 80−15228
nematic-isotropic transition, Landau theory breakdown 79−99302
nematic-isotropic transition, lattice model, semiflexible chain solutes 79−10927
nematic-isotropic transition, lattice model for hard core mols. with flexible tails 78−38818
nematic-isotropic transition, lattice model for hard core mols. with semiflexible tails 78−38819
nematic-isotropic transition, mean-field lattice model, meta- and unstable states 78−38817
nematic-isotropic transition, nature, field renormalisation group formalism study 78−87775
nematic-isotropic transition, permanent dipoles effect 77−20054
nematic-isotropic transition, thermodynamic props. calc. 80−103464
nematic-isotropic transition in mixtures, phase separation and diffusive instabilities 80−29156
nematic-isotropic transition temp. depend. on anisotropy of C-X bond polarisability for terminal substituents 77−20058
nematic-positive, deform. by elec. field between two co-axial cylindrical electrodes 79−50986
nematic-smectic A(C) phase transitions, contribs. to viscosities from order parameter fluctuations 79−60489
nematic-smectic A phase transition, sound attenuation and dispersion 79−82286
nematic-smectic B mesophases, mutual orientation *(French)* 79−55660
nematic-smectic-A phase transition, mean field theory 77−24393
nematic-smectic-C phase transition fluctuations, ring model 77−24392
nematic-smectic-C transition, density and director fluctuations effects 79−55875
neutron diffraction, coherent 78−75550
4-nitrophenyl 4-n-octyloxybenzoate, electrical Kerr effect studies 80−25339
4-nitrophenyl 4-n-pentyloxybenzoate, electrical Kerr effect studies 80−25339
4-nitrophenyl 4-octyloxybenzoate, smectic-A and nematic phases, dielectric meas. 79−23516
4-nitrophenyl-4-octyloxybenzoate, nematic and smectic-A phase, dielec. meas. 78−60392
4-nitrophenyl-4-octyloxybenzoate/cholesteric liq. cryst. mixtures, helix pitch, temp. depend. 80−64895

nematic liquid crystals continued
NMR spectra in solid state 77−16186
nonlinear effects, in elec. and mag. fields 77−24263
nonlinear effects above electrohydrodynamic instability threshold *(Russian)* 78−75551
nonlinear elastic behaviour, near nematic-smectic-A phase transition 77−35679
nonlinear instability in mag. field., Frederiks transition *(French)* 80−49095
nonlinear reversible hydrodynamics, external mag. field influence 80−75156
nonlinear stability of motion, stability criteria *(French)* 77−80410
nonlinear stability of motion *(French)* 77−84623
nonlinear stability of the motion of a nematic liquid crystal 80−83784
nonlinearities and fluctuations at hydrodynamic instability threshold 78−87614
p′-nonylhydroxybenzoic acid, struct. charact., cylindrically symmetrical interatomic-distance function 77−11482
p-n-nonyloxybenzoic acid, nematic, cond. anisotropy, dopant effect 77−7667
p-n-nonyloxybenzylidene-p-aminobenzoic acid, phase transitions, X-ray diffr. and DSC meas. 79−86877
nuclear spin relax., translational self-diffusion 78−43670
nuclear spin relaxation and slow solute motion 79−95662
obliquely oriented, thermal convection *(French)* 78−22643
4n-octyl-4′-cyano-biphenyl, liq. cryst., density, and rel. change at phase transitions determ. 77−80605
4-n-octyl-4′-cyano-diphenyl, appl. in detection of graphite powder particles by optical microscopy 80−9034
4-octyl-4′-cyanobiphenyl, dielec. relax. meas., short range interactions 78−94976
4-n-octyl-4′-cyanobiphenyl, smectic A and nematic liq. cryst., refr. indices and order parameters 78−22644
4′-n-octyl-4-cyanobiphenyl, chain ordering model 80−24357
4′-n-octyl-4-cyanobiphenyl, interlayer elastic const. meas. close to smectic-A to nematic transitions 77−80606
4′-n-octyl-4-cyanobiphenyl, thermotropic mesophase, DMR chain segments assignment 80−24356
octyl-cyano-biphenyl, elastic props. near smectic-A nematic transition 79−23704
octyl-cyano-biphenyl, influence of laser light wave field on nematic phase *(Russian)* 80−92456
octyl-cyano-biphenyl, nematic and smectic-A phase, dielec. meas. 78−60392
octyl-cyano-biphenyl, smectic-A and nematic phases, dielectric meas. 79−23516
octyl-cyanobiphenyl, elastic props. near nematic-smectic A transition 78−59756
octyl-cyanobiphenyl, smectic A-nematic transition, X-ray and light scatt. obs. 79−95129
octyl-cyanobiphenyl nematic cryst., optical and DC Kerr effects 79−7183
4-n-octyl-d_{17}-oxybenzoic acid-d_4, nematic and smectic phases, mol. and relative segmental order 80−96439
octylcyanobiphenyl, crit. heat. capacity near nematic-smectic A transition 80−100323
p-n-octyloxy benzylidene-p-toluidine, mol. order, EPR VAAC probe 80−70114
4-octyloxy-4′-cyanobiphenyl, CN stretching in liq. cryst. phases, vibr. spectra 78−80325
4-octyloxy-4′-heptyl-α-cyanstilbene liquid cryst., mag. props. 78−87615
4-n-octyloxy-4′-cyanobiphenyl, liquid cryst., dielect. polarisation and its dispersion 79−1397
trans-p-n-octyloxy-α-methyl-p′-cyanophenyl cinnamate, mag. and elec. birefr. in isotropic phase 80−80744
p-n-octyloxybenzoic acid, liq. cryst., radiation stability 78−85184
4-n-octyloxybenzoyloxy-4′-cyanostilbene, re-entrant polymorphism, nematic-smectic A-nematic-smectic A, X-ray study 80−34172
4-octyloxybenzoyloxy-4′-cyanostilbene, enantiotropic reentrant nematic behaviour at atmos. press. 79−60490
n-p-octyloxybenzylidene-p-toluidine, dielectric behaviour in nematic mesophase at RF 80−34842
N-p-octyloxybenzylidene-p-toluidine, optical props., density, and order parameter in liq. cryst. phases 79−55657
p,p′-octyloxycyanobiphenyl, flexoelec. coeff. in nematic phase, thermal depend. 80−79685
octyloxycyanobiphenyl, nematic-smectic A transition, heat capacity study 80−88033
octyloxycyanobiphenyl, nematic-smectic-A transition sp. ht. 79−42225
octyloxycyanobiphenyl, twist viscosity and mech. props. near smectic A-nematic transition 78−95136
4-n-octyloxyphenyl 4-n-pentyloxybenzoate, permittivity, microwave dielectric relaxation 80−80671
p-octyloxyphenyl-p′-pentyloxybenzoate, charge carrier mobility and cond. in nematic and isotropic phases 80−44347
p-octyloxyphenyl-p-pentoxybenzoate, nematic liq. cryst., elec. discharge meas. of persistent internal polarisation 80−10488
OEBBA, polarised luminesc. 77−24897
off-state transmission of twisted layer 79−82948
OHMBBA, dielectric behaviour at RF 79−7548
OHMBBA, solid phase dielectric relax. times and strength, mol. rot. 78−72456
oligo methines, thermotropic nematic phase formation, role of molecular mass *(French)* 78−75547
OOAB, liq. cryst., smectic and nematic, distrib. functions by X-ray diffr. 79−99072
OOAB, nematic thermotropic mesophases, end-chain ordering and even-odd effects, deuterium mag. reson. 79−82890
operational principles, display device appl. *(Italian)* 79−46553
optical anisotropy, determ. from NMR and birefringence data *(German)* 77−40205
optical birefringence, for uniform colour generation, cells with special electrodes 77−68911
optically active binary liquid crystal thermometry 79−42952
order parameter fluctuations and anomalous sound propag. just above clearing point, critical dynamics 80−15224
order parameter of dyes in nematic liquid cryst. 77−83614
order parameter temp. depend., diamagnetic susceptibility, refractive index, density and polarisability 77−15315
ordered nonsingular systems, topology appls. 78−10166
ordering, dimer model calcs. 77−27817

nematic liquid crystals continued
organic doublet radicals in nematic and smectic liq. crysts., ENDOR obs. 80−91585
organic dye-nematic liquid cryst. soln., generation of induced radiation *(Russian)* 77−3583
orientation, effect of ultrasound *(French)* 77−59067
orientation causes, on cleavage faces of triglycine sulfate crystal 79−94899
orientation control using organic surfactants 78−91251
orientation fluctuations in high mag. field, quenching, birefringence effects 80−64892
orientation on obliquely deposited SiO film 78−38987
orientation ordering, mol. dynamics obs. 78−91239
orientational acoustic nonlinearity 80−34143
orientational bistability, nematic storage effects 80−70112
orientational electrooptic effects, time charact. 78−27191
orientational fluctuations causing light intensity fluctuations, spectral anal. 80−60618
orientational fluctuations effect on evanescent modes of transmitted EM wave 80−64889
orientational order of molecules, molecular dynamics method study 79−27918
orientational order of surface-aligned crysts. bounded by two parallel substrates 79−32885
orientational order parameter, comparison with cholesteric liquid cryst. 79−27917
orientational relax. calc. 78−75549
orientationally ordered liquids, Helmoholtz free energy, generalised van der Waals theory 80−44119
orientations, twofold, and hysteresis props. 79−82146
oriented, transient behaviour of field induced reorientation 78−30536
oriented film, birefringent stripe pattern generation by ultrasonic waves 77−76301
oriented matrix for $W(CO)_6$ dissolved mol., distortion obs. using linear dichroism 79−95797
oscillatory convective instabilities, Dubois-Violette theory 78−9943
oscillatory instabilities in elec. and mag. fields 80−24361
oxtyloxycyanobiphenyl, nematic-smectic-A transition, high-resolution 80−10649
p-(p-ethoxybenzylidene) amino benzonitrile, positron annihilation exam. 79−19149
PAA, ^{14}N NQR freqs., double-reson. level crossing method 78−6602
PAA, ^{14}N NQR freqs., spectral assignments 78−6602
PAA, adjustable domain struct. in inhomogeneous elec. field, electro-optic props. obs. 80−10494
PAA, collective excitation dispersion, neutron inelastic scatt. data 77−35475
PAA, Couette flow mag. field and boundary condition effects 77−3887
PAA, cryst. phase transitions, intermolecular motion, Raman and inelastic neutron scatt. spectra 80−2164
PAA, deuterated, mol. reorientation, quasielastic neutron scatt. study 79−86705
PAA, effect of mol. struct. on nematic liq. cryst., phase 78−42901
PAA, electric field effects, neutron diffr. study 80−28912
PAA, empirical form for orientation-ordering intermolecular pot. 77−27809
PAA, eqn. of state 77−47560
PAA, equation of state, incorporating short-range orient. order 77−55237
PAA, fluctuations near Rayleigh-Benard instability, real time obs. by neutron scatt. 80−59390
PAA, freq. depend. of proton T_1, rot. diffusional mechanism interpret. 77−12219
PAA, homologous series, isotropic phase, mol. self diffusion by spin echo method 80−44109
PAA, isotropic phase, Brillouin scatt. spectra, hypersound data determ. 79−91453
PAA, isotropic phase, light scatt., ultrasonic vel. and absorpt. meas. 78−48189
PAA, isotropic-nematic phase transition, optical microscopic obs. 79−69230
PAA, isotropic-nematic transition, appl. of integral eqn. for ang. distrib. function *(Russian)* 78−6147
PAA, isotropic-nematic transition, mean-field theory, thermodynamic props. 77−24391
PAA, isotropic-nematic transition, supercooling and nucleation, interface dendrites 78−42896
PAA, light scatt. near cryst. to nematic transition 80−16046
PAA, light transmission in high elec. field grad. 79−19150
PAA, methoxy deuterated, reorientational correl. times, comparison of neutron scatt. and dielec. relax. data 79−7545
PAA, methyl deuterated, dipolar spin system exam. 77−39533
PAA, methyl deuterated, soft-mode dynamics, proton NMR 78−79749
PAA, methyl group rotation in solid and nematic phases, NMR obs. 78−6595
PAA, molecular theory, orientation-averaged pair correlations 78−42905
PAA, nematic, equation of state, anistropic props., perturbation theory 78−67645
PAA, nematic, NMR study of ordering, intramol. mobility 80−100162
PAA, nematic and crystalline phases, NMR and relax. 79−4740
PAA, nematic liq. cryst., effect of magnetic field on US vel. and absorpt. 78−18707
PAA, nematic liq. cryst., elastic consts. determ. 77−27824
PAA, nematic liq. cryst., mol. statistical interpretation of viscosity *(Portuguese)* 77−47351
PAA, nematic liq. cryst., rot. barrier, PCILO and CNDO/2 calcs. 80−33874
PAA, nematic liq. cryst., thermomagnetic behaviour *(French)* 78−87612
PAA, nematic to isotropic liquid cryst. transform. at high press. *(Russian)* 77−4191
PAA, nematic-isotropic phase transition, US meas. 79−90761
PAA, nonlinear effects, in elec. and mag. fields 77−24263
PAA, nonlinear soft mode at Rayleigh-Benard instability, neutron cond. spectrosc. obs. 80−79266
PAA, orientation in thick layers, continuum theory validation 77−15312
PAA, orientation ordering, mol. dynamics obs. 78−91239
PAA, phase transitions, up to 3 kbar, DTA obs. 77−20051
PAA, propagating collective modes, neutron scatt. data 77−35476
PAA, quasielastic neutron scatt., isotope effects 78−83719
PAA, selectively deuterated, proton spin-lattice relax. temp. freq. depend., diffusion 77−43132

nematic liquid crystals continued
PAA, shear flow, effect of mag. fields and boundary conditions 77−7668
PAA, smectic-C and nematic long chain homologues, H-spin-lattice relax. *(German)* 78−87610
PAA, solubilisation of poly-ethylen-oxide chain, effect on twist viscosity 78−67642
PAA, structural and optical anisotropy, NMR spectra 79−14675
PAA, temp. depend. of sp. vol. 77−7665
PAA, Tsvetkov parameter, temp. depend. 80−88035
PAA with deuterated methyls, nematic phase, quasieleastic neutron scatt. study of fast reorientations 78−14280
PAA-d_6, -d_8, H and D spin-lattice relax. 77−59475
PAA-d_8, mol. order and conformation, ^{2}D NMR line shape obs. 77−61771
PAA-di, nematic liquid crystal, NMR data, appl. of Landau-de Gennes theory 80−64893
PAA-PAP, nematic orientational order parameter calc. 77−24259
PAP, cryst. phase transitions, intermolecular motion, Raman and inelastic neutron scatt. spectra 80−2164
PAP, nematic liq. cryst., thermomagnetic behaviour *(French)* 78−87612
PAP, phase transitions, up to 3 kbar, DTA obs. 77−20051
PAP, structural and optical anisotropy, NMR spectra 79−14675
PAP, Tsvetkov parameter, temp. depend. 80−88035
paradiheptyloxyazoxybenzol-d, dynamics of smectic-nematic liq. cryst. phase transiton *(Russian)* 78−55938
parallel and cross-like domains due to DC and LF electric fields 79−46557
paramagnetic, flexomagnetoelec. effects 80−75158
parasubstituted alkyloxybenzoic acids, molecular motion in solid phase 79−61239
PBABA, skewed cybotactic nematic phase, X-ray diffr. obs. 79−77504
PBBA, phase transitions, up to 3 kbar, DTA obs. 77−20051
PCB, nematic, smectic phases, dielec. and optical props. 78−60377
PCB, nematic liq. cryst., US imaging, convertor, acousto-optical effect 78−59218
PCB liquid crystal, conductivity depend. on thickness and electrode molecular orientation 78−91248
PEBAB, nematic, EPR investig. 80−108077
PEBAB, phase transitions, up to 3 kbar, DTA obs 77−20051
PEBAP, nematic liq. cryst., PMR line breadth temp. depend. 77−8419
pentyl cyanobiphenyl, laser and electric field induced Kerr effect 80−84061
pentyl cyanobiphenyl nematogen, depolarised light scatt. 79−95790
p-n-pentyl p′-cyanobiphenyl, anisotropic viscosity, US meas. 77−31581
p-n-pentyl p′-cyanobiphenyl, isotropic phase, viscosity coeffs. 77−31582
p-n-pentyl p-cyanobiphenyl, resolution of acoustic image detector 78−46871
4-n-pentyl-4′-cyanobiphenyl, isotropic, optical and electrical Kerr effect 79−32886
4-n-pentyl-4′-cyanobiphenyl, mol. alignment, comparison of exptl. data at high press. with mean field theory predictions 79−99075
4-n-pentyl-4′-cyanobiphenyl, nematic liq. cryst., refr. indices and order parameters 78−22644
4-n-pentyl-4′-cyanobiphenyl, nematogen, incoherent neutron quasielastic scatt. 79−32887
4-n-pentyl-4′-cyanobiphenyl, refr. index, high press. meas. 78−26428
4-n-pentyl-(4-cyanophenyl)-cyclohexane, surface alignment using lecithin monolayers, contact angle meas. 79−4247
pentyl-cyano-biphenyl, nematic, hydrodynamic parameters meas. with and without applied elec. field 80−100297
pentyl-cyano-biphenyl, nematic phase, transport props. of dissolved ionic species, electrochem. meas. *(French)* 79−90811
p-n-pentyl-p′-cyanobiphenyl, nematic liq. cryst., Raman depolaris. ratios, order parameters 79−28733
p-n-pentyl-p′-cyanobiphenyl, nematic ordering, electric field induced second harmonic generation 79−60263
p-n-pentyl-p′-cyanobiphenyl, nematic phase, mapping of acoustical fields 79−91402
4-n- pentyl-phenylthiol-4′-alkoxybenzoate, homologous series, specific heat meas., nematic-smectic-A tricritical point 80−15227
4-n-pentylbenzenethio-4′-n-octyloxybenzoate, liq. cryst. phase transitions, press. and temp. depend. 79−77730
pentylcyanobiphenyl, elastic and dielec. props. from capacitance-voltage curve 79−32894
4-n-pentyloxy-phenyl-4′-n-octyloxybenzoate, nematic, dielec. relax. and freq. depend. of threshold voltage 80−60497
4,n-pentylphenyl (pentylbenzoyloxy)-3-chlorobenzoate, flexoelec. coeff. in nematic phase, thermal depend. 80−79685
4-n-pentylphenylthiol-4′-n-octyloxybenzoate, sp. ht. and crit. behaviour of liq. cryst. phases 78−67816
phase grating produced by shear flow induced instability 78−9945
phase IV, cholesteric struct. induced by chiral sulphoxides 79−86683
phase transformation, finite crystal SCF method *(Russian)* 77−89528
phase transition, smectic A-nematic, liq. cryst. binary mixture, birefringence study 80−59638
phase transition to smectic C phase, renormalisation group anal. 80−34173
phase transitions and pretransition phenomena, book contrib. 79−60491
phase transitions in Landau's theory 80−29158
phase V, host for porphyrins and zinc, pyrochlorophyllide, oriented photoexcited triplets, EPR study 80−84636
Phase V, transient response to redirected mag. field, EPR study 80−33879
phenyl 4(4-alkylphenyl)cyclohexanecarboxylates, mesomorphism and dielec. props. 77−27810
phenyl 4-alkylbiphenyl-4′-carboxylates, mesomorphism and dielec. props. 77−27810
phenyl 5-alkoxypicolinates, synthesis, phase transition temps., and dielec. props. 79−86876
phenyl 6-alkoxynicotinates, synthesis, phase transition temps., and dielec. props. 79−86876
phenyl benzoate, DC dynamic scatt. and dopant electrochem. props. 77−90130
phenyl benzoate, doping effect on cond. anisotropy and dynamic scatt. 77−40208
phenyl benzoate, dynamic scatt., alignment effects 77−40207
phenyl benzoate and thiobenzoate, 4,4′-disubstituted, mag. susceptibility anisotropy and order parameter 79−86704
4-phenyl n-pentyl ester, Nematel 105, nematogen, isotropic phase, Rayleigh scatt. and mol. reorientation 78−34429

nematic liquid crystals continued
4-phenylbenzylidene-4′-n-alkoxyanilines, central Schiff's base linkage reversal effect on liq. cryst. props. 80−79683
phenylcyclohexanes, alkylamino substituted, synthesis and mesomorphic props. 80−44120
phenylcyclohexanes, low melting pt., for display appl. 77−84652
phenylcyclohexanes, nematic, low melting liq. crysts. with positive dielec. anisotropy, phys. props. 77−43148
phenylcyclohexanes, p-disubstituted, elastic consts. and diamag. anisotropy 79−65639
phenylcyclohexanes, substituted, anisotropic liq. cryst. solvent for optical absorption spectroscopy 78−45724
phenylene derivatives, effect of substitution on liq. crystalline props. 80−70113
p-phenylene-di-p-n-heptyloxybenzoate, liq. cryst., radiation stability 78−85184
phenylpyrimidines, liq. crysts., synthesis and phys. props. 78−1995
phenylthiobenzoate derivatives, thermodynamic and mesomorphic props. 77−11678
photosensitive MIS structure in contact with nematic liq. cryst., light spatial modulation 80−48436
piezoelectric coeffs., Onsager-theory, interparticle pot. and first moment vector 77−24264
piezoelectric effect in curved layer 79−90551
piezoelectric effect use as light modulator 80−83679
piezoelectric instability, threshold charact. *(Russian)* 77−24800
planar, nonlinearities close to thermal threshold 79−99058
planar layers, positive dielec. anisotropy, EHD instability at DC excitation 79−94877
planar texture instability for cholesteric-nematic mixture with negative dielec. anisotropy 78−59739
pleochroic dye solns., guest-host interactions, appl. to electrooptic displays 80−44113
Poiseuille flow, instabilities 77−1073
Poiseuille flow, uniform instability 77−1074
Poiseuille flow instabilities 79−77499
Poisson brackets, nonlinear hydrodynamics eqns. in condensed matter physics 80−54296
polarisabilities, Lippincot δ-function pot. model 80−79686
polarisability anisotropy of nematic homologous series 78−38614
poly(azomethines), thermotropic mesophases *(French)* 79−77507
poly(ethyleneterephthalate)-p-hydroxybenzoic acid copolyester, liquid crystalline, X-ray scatt. obs. 78−9949
poly(n-dodecyl L-glutamate), thermotropic polymorphism, low-angle X-ray diffr. *(French)* 78−34601
poly(paraphenylene terephthalamide), nematic structure by optical and X-ray methods *(French)* 77−31584
poly (γ-benzyl-l-glutamate)-dioxane system, periodic struct. under elec. field 78−47234
poly-γ-benzyl-L-glutamate, soln., liquid crystal transitions anal. 80−65207
poly-γ-benzyl-l-glutamate solns., mesomorphic re-entrance phenomena 79−99074
poly-(p-alkoxy-phenyl-p-acryloylbenzoates), nematic polymer, struct. determ. 79−99064
poly-(phenyl-p-acryloyloxybenzoate), nematic polymer, struct. determ. 79−99064
polyazomethines, thermotropic nematic phase formation, role of molecular mass *(French)* 78−75547
polyazomethines in H_2SO_4, lyotropic nematic phase, threaded textures *(French)* 80−19691
polydisperse solution of rodlike particles, isotropic-nematic phase transition, Onsager theory 80−100324
polymer liquid-crystalline solns., struct. 80−103235
polymer solution, nematic helix-coil transtition model 79−94870
polymer solutions in nematic liquids, dilute, viscosity 80−29199
polymeric, Frank elasticity and light scatt. 77−68916
polymeric liquid crystals structurally related to 4-alkoxyphenyl-4′-alkoxybenzoates, nematic phase 79−60267
polypeptides, electric field-induced phase transition 80−24571
polyribonucleotide complexes, mag. field orientation of nematic liq. cryst. solns., light scatt. and birefr. meas. 79−82152
positive dielectric, pretransitional domains, Kerr effect and orientational relax. 77−77171
potassium laurate-1-decanol-water mixtures, biaxial nematic phase obs. 80−107409
pretilt angle, temp. depend. 78−26432
pretilted cells, Freedericksz transition in mag. field normal to director 79−99071
pretilted nematic structure, colour control by elec. field 77−73127
pretransition effects study, optical method of determ. of crit. indices *(Russian)* 78−63847
pretransitional effects, mol. statistical calc. 77−27990
trans-p-n-propoxy-α-methyl-p′-cyanophenyl cinnamate, high press. mesomorphic and polymesomorphic transitions 78−18750
N-(p-propoxybenzylidene)-p-pentylaniline, refr. index and density in nematic and isotropic phases 79−90538
p-propoxybenzylidene-p-butylaniline, nematic and isotropic phases, dielec. props. 79−87383
N-p-propoxybenzylidene-p-pentylaniline, orientational order in glassy and nematic phases, IR dichroism meas. 80−64891
N-p-propoxybenzylidene-p-pentylaniline, Williams domains, interference study 80−44114
p-quinquephenyl, mag. susceptibility and order parameters 79−86709
p-quinquephenyl, melting data and liq. cryst. transitions 79−55869
Rayleigh disc in aligned nematic liquid crystal for acoustic field detect. 77−11094
Rayleigh scattering, narrow linewidth meas. 77−26408
re-entrant nematic phase, orientational order, electron reson. study 80−103242
reentrant nematic, oriented, capillary shear flow 80−49344
reentrant nematic-smectic A phase transition, Landau theory 79−28084
reentrant-transition, nematic to bilayer smectic-A, under high press. 77−84905
reflection, total internal, review 80−96445
refractive index, appl. to MBBA 77−51313
refractive index, order parameter, density 79−38513
refractive index and birefringence by interference method 80−96440
refractive index meas. by cylindrical cell method 80−11358
refractive index near smectic-A/smectic-C transition, orientational order 80−24572

nematic liquid crystals continued
renormalisation group calc. appl. to nematic isotropic transition 78−59937
reorientation time in magnetic fields, two methods *(German)* 78−59736
reorientation times, in mag. field, optical method determ. *(German)* 78−91240
reversely pretilted cell, conformation of molecular orientation 80−59388
rod system, nematic ordering 79−60271
rotational diffusion and freq. spectra 77−84631
S-effect, growth and decay times 78−2824
Schiff's bases, mesomorphic, two-component system, tricritical nematic-smectic A point 77−51482
Schiff's bases, nematic phase, relation between elasticity and mol. struct. 79−90711
Schiff's bases, phys. props. 79−99057
Schiff base azo dyes in nematic liq. cryst. hosts, order parameters, optical density meas. 80−84055
Schiff base esters, mesomorphic behaviour 78−1993
secondary light scatt. in low frequency field, in dielectric state 78−48147
self diffraction of laser beam by liquid crystal struct. 80−5803
p-sexiphenyl, liq. cryst. phase transitions 79−82322
shear excitation, roll instabilities 78−59737
shear flow, apparent viscosity 77−72549
shear flow, effect of mag. fields and boundary conditions 77−7668
shear flow in presence of electric AC field, elastic and viscous const. determ. 77−43144
shear flow instability, model eqns. 79−41664
shearing, sinusoidal, and temporal sinusoidal standing twist wave 80−84053
shearing flow solns., stability and dissipation 80−49288
SHG, mol. symmetry and macroscopic nonlinearity *(Russian)* 78−90457
SHG potential, phase-matched elec. field induced 79−86214
short range orientational order and nematic-isotropic phase transition 77−27832
smectic-nematic phase boundary, elliptic, thermodynamic anal. 79−99300
sodium decyl sulphate/water/decanol/Na_2SO_4, lyotropic mesophase, mag.-oriented, X-ray diffr. obs. 80−1921
solid phase, ^{14}N NQR, nuclear quadrupole coupling consts. 77−8444
solid-nematic interfaces, reflection and refraction of obliquely incident shear wave 79−86691
solute molecules, orientation and deform., PMR obs. 77−71815
solution, disclinations, thermodynamic treatment 79−32903
solutions, isotropic phase, orientational pair correl. obs. using depolarised Rayleigh light scatt. *(Russian)* 79−90552
solvent-rod mixture, two phase, interfacial free energies, quartic van der Waals theory 80−59377
solvents effects in isomerisation of 2,4,6-trimethoxy-s-triazine 79−91944
solvents for polymer gels, theory 80−11963
sound attenuation, near clear point, microscopic derivation 78−34605
sound propag. near transition to isotropic liquid 79−19320
space charge freezing, electro-optic effect meas. 78−34436
space-time correlation function for scattered light fluctuation 80−19697
specific heat, thermodynamic props. 77−39678
spin-lattice relaxation, orientational depend. 77−84625
spin-lattice relaxation, viscosity effects, theory 77−4574
spin-relaxation, composite Markov process, rot. reorientation and director fluctuations 77−62471
splay nematics, field equation, by minimisation of free energy 79−27914
spontaneous polarisation, rel. to mol. orientation, electro-reflection meas. *(Russian)* 78−55809
statistical mechanics, particle pots. and distrib. functions calcs. 78−2001
statistical model, orientational order parameters 80−28910
statistical theory, correlation 78−75536
stilbene, depend. of phase transition temp. on thickness 78−26669
stress tensor in nematic liquid crystals, micropolar continuum mechanics 78−67647
stress tensor in nematic liquid crystals, micropolar continuum theory 78−67648
stress tensor nonlinearities, viscosity coeffs. 77−27831
striped domain structure in cholesteric-nematic mixture, refr. index distrib. 77−24261
structural parameters and nematic-isotropic transition *(German)* 80−15003
surface, statistical thermodynamics, local order parameter 80−88023
surface, structural crit. point, Landau theory 78−91247
surface, topological singularities *(Russian)* 78−79847
surface alignment, easy axis determ. and temp. depend. of field energy 79−90541
surface alignment, temp. depend. of pretilt angles 79−55656
surface alignment on TGS surface controlled by domain struct. 79−99068
surface and anchoring energies, van der Waals contrib. 80−92455
surface and bulk configurations, topology 80−59381
surface and bulk disclinations, continuum theory 79−86694
surface and interfacial free energy, Van der Waals dispersion force contrib. 79−99399
surface disclination lines rel. to surface-induced homogeneously tilted alignment 77−58950
surface tension, mol. theory 77−1075
surface tension, pre- and post-transitional effects 79−77511
surface tension at interface with vapour or isotropic phase, mol. theory 77−15307
suspended films, electric field effects, vortical and domain structure 77−11470
switching dynamics, with low freq. dispersion of the dielectric anisotropy 79−56708
TBBA, mesophase identification by X-ray diffr., review 80−100166
TBBA, order parameters in nematic and smectic phases, X-ray diffr. meas. 79−94874
TBBA, self diffusion coeffs., neutron diffr. and NMR study 80−19689
TBBA, self-diffusion coeffs., NMR spin echo 77−31789
TBBA, smectic A-nematic transition, cybotactic cluster form., X-ray obs. 78−95138
TBBA, temp. depend. of deuteron NMR splittings in nematic and smectic phases 79−32898
TBBA, US absorpt. and dispersion at nematic-smectic-A transition 79−82287
TBBA mesophases, mol. orientational order 79−37619

nematic liquid crystals continued
temperature dependent material props. correl. to twisted nematic displays 79−32901
terephthal-bis-n-alkylaniline, homologous series, prep. and mesomorphic props. 78−26436
terephthal-bis-p-p'-butylaniline, pretransitional anomaly, US obs. 78−75818
terephthalates, vibr. spectra, vol. struct. 78−18547
terphenyl, thermal diffusivity, Rayleigh scatt. obs. 78−94977
texture, light scatt. determ. in dynamic scatt. regime 79−27913
texture of lyotropic phases of rigid macromolecules *(French)* 79−1394
thermal conductivity anistropy, forced Rayleigh light scatt. meas. 78−94991
thermal instabilities, critical temp. gradient 77−4038
thermal instabilities in layer with oblique orientation at boundaries 80−44110
thermal instabilities in twisted nematic liquid crystals, theory 78−91241
thermal parameters, transition temps. and latent heats 78−22832
thermoconvective instabilities 79−77500
thermotropic, anomalous rheological responses, spectrometer study 80−6358
thermotropic, with negative diamag. anisotropy, appl. to NMR spectrosc. 79−40596
thermotropic liquid cryst., diffusion and nucl. mag. relax. 80−24362
thermotropic systems of rodlike molecules with orientation-depend. interactions 80−33883
thin slab Brownian particle fluid, return to equilib. eqn. *(French)* 77−27829
threshold flexoelectric effect 79−94878
tilt angles of obliquely oriented liq. cryst., total refl. meas. *(French)* 78−79528
tilt bias angle meas. methods 77−58949
tilt control by vacuum deposition alignment 79−10797
tolanes, molecular conformational mobility study by optical probing method *(Russian)* 80−92459
topological instability of singularities at small distances *(Russian)* 78−79531
topological theorem for bounded volume, nematic liq. cryst. appl. 79−67171
topological theory of defects in ordered media 79−93072
trans-p-n-alkoxy-α-methyl p'-cyanophenyl cinnamates, liq. cryst. of strong positive dielec. anisotropy, static dielec. consts. meas. 78−2790
transducers, dynamic scatt., pre-excitation 80−88021
transducers, with nematic liquid crystals, exam. of light absorption behaviour 79−40560
transition temperature, nematic temp. range broadening by nonmesogenic solute 77−47559
transition to isotropic state, static and dynamic behaviour 77−35678
transition to smectic A phase, system of hard rod molecules, effect of orientational fluctuation 80−6496
transverse electro-optic effect in liq. cryst. with negative dielec. anisotropy 77−59556
traversing weak EM wave in static mag. field, electrodynamics 79−14680
trichloromethane in nematic liq. crystal, AX($^{13}CHCl_3$) nuclear relax., dipole-dipole interaction 77−54567
tridimensional variational approximated model, existence, uniqueness and regularity of solns. 80−59379
triradical spin probe, EPR of nematic liq. crystal struct. and mol. dynamics 78−63670
truxene derivatives, temp. inverted nematic-columnar sequence in disc-like mesogens 80−88032
TTF derivatives, smectic and nematic, for liq. cryst. device appl. 80−54124
twist effect dynamics, mol. inclination angles relaxation 79−60276
twist viscosity, planar-model calc. 78−42893
twist waves, accel., effect of material nonlinearity 77−27816
twisted, ang. and voltage depend of light transmission, two-layer model 80−76006
twisted, phase transition like instability in static samples with surface induced tilted alignments 78−26667
twisted cell, off-ninety degree, electro-optical colour effect 77−77172
twisted layer, elastic deform. energies and reverse twist domains 79−37617
twisted nematic cell, dynamic props., voltage depend. 80−70117
twisted nematic cell, Leslie threshold field verification 77−84638
twisted nematic display with cholesteric dopant, transmission characteristic temp. depend. compensation 80−103934
twisted nematic layer, transmission characts. 77−1653
twisted nematic liq. cryst. layer, voltage depend. of capacitance 79−94894
twisted nematic liquid crystal display, capacitative anal. 77−43969
twisted nematic liquid crystal-fibre optic modulator for display 79−72718
twisted nematics, evidence for hexagonal phase 78−34602
two-dimensional, Kosterlitz-Thouless phase transitions 79−7680
two-dimensional, Monte Carlo simulation 80−100168
two-dimensional fluid of overlapping ellipses, nematic ordering 78−34424
uniaxial and biaxial, formed by non-cylindrically symm. mols., computer simulation 80−79680
unified Landau theory, for nematic, smectic-A and smectic-C phases 77−55238
unified model for bulk smectic-A, nematic and isotropic phases 80−79692
US absorption, longitudinal and transverse waves *(French)* 77−51321
US attenuation, elec. field effects 77−15304
US field visualisation by nematic-cholesteric mixed cell 78−1524
US propag. props., review 78−63668
US relaxation time, temp. depend. 78−18712
van der Waals theory, generalised 77−72547
Van der Waals theory, of nematogenic solns. 79−27915
van der Waals theory, self-consistency requirements 78−18541
Van der Waals theory, spherical solutes and rodlike solvents 79−27916
vibrational IR and Raman spectra 79−73913
vibrohydrodynamic instability in liquid crystals, threshold calcs. and mol. reorientation determ. 78−91249
virtual nematic-isotropic transitions, depolarised Rayleigh scatt. 78−51652
viscoelastic properties, Rayleigh scatt. 77−39538
viscoelastic properties, spectral noise intensity of scattered laser light obs. 79−23522

nematic liquid crystals continued
viscometric flow, apparent viscosity 79−60265
viscosity, depend. on order parameter, thermodynamic model 79−77503
viscosity, rel. to order parameter *(Russian)* 78−91242
viscosity, rotational, mol. statistical theory *(Portuguese)* 77−47351
viscous and plastic behaviours 79−86686
volt-ampere characteristic nonlinearity *(Russian)* 79−33292
Williams domain mode, non-linear analysis 77−62472
X-ray and light scattering obs., high resolution 80−92460
X-ray diffr. studies, review 80−100166
xylideneaniline-p′-benzonitri 80−44328
ZLI-207, electro-opt. props. *(Russian)* 77−43967
LC-440, flexoelec. charact. of longitudinal domains 79−46570
MBBA, flexoelec. charact. of longitudinal domains 79−46570
MBBA, nematic, anomalous spectra of current induced noise under high DC field 78−38617
MBBA+optically active substance, pretransition optical rotation in isotropic phase *(Russian)* 80−92657
MBBA(:TEAI), elec. drift mobility, carrier identification *(Korean)* 78−51998
Ni complex, bis-[4-(n-butyl)-styryl-dithiolato] Ni nematic complex, IR absorption 80−49342
Ni complexes, dithienes, nematic and smectic mesophases, synthesis and charact. 80−70120
Ni dithiene complexes, mesomorphic props. 80−88026
PAA, flexoelec. charact. of longitudinal domains 79−46570
4′-n-pentyl-4-cyanobiphenyl, nematogenic liq. cryst., above T_c, Kerr effect response time, temp. depend. 78−34434
Pt complex, bis [4-(n-butyl)-styryl dithiolato] Pt nematic complex with strong IR absorption 80−88305
Pt dithiene complexes, mesomorphic props. 80−88026
SiO_2 glasses surface textures and defects, exam. using liq. crysts. 80−6364

neodymium
see also nuclei with .....
$^{143}Nd/^{144}Nd$ initial ratio in Moon, lunar crust and mantle differential evolution 79−35156
abundance in HD 18474 giant star *(Spanish)* 79−25605
addition to Ni-Cr austenitic stainless steel, effect on heat resist. and comp. of non-metallic inclusions 80−76315
adsorption and absorption of $H_2(D_2)$ 77−4257
atom, L-emission spectrum, new lines obs. 77−79566
atom, L-emission spectrum, new lines obs. 78−86809
atom, new lines, 3930-6450 Å, isotope shifts 80−47929
atom, photon-bound-electron scatt. meas. 77−14394
basalt isotopic abundance, Earth struct. models 80−72475
basalt isotopic and element composition, Reykjanes Peninsula, Iceland 80−21725
borate laser glasses, Cl^-coordinated, Tl^+, Mn^{2+} and Nd^{3+} impurities, absorpt. and X-ray obs. 79−38575
carbon tetrachloride-$GaCl_3$-Nd^{3+} nontoxic liquid phosphor system, synthesis 80−55157
o-chlorobenzoic acid: Nd^{3+}, solid, vibrational spectra 80−84758
crystal structure, P-T phase diagram 78−84776
DMSO:Cr^{3+}, Nd^{3+}, energy transfer and migration, donor-acceptor interaction, phosphoresc. quenching conc. depend. 78−64403
doped (fluoro) phosphate laser glass piezo-optic coeffs. meas. at 0.6328 and 1.15 μm 80−34888
Earth mantle, Nd-Sr isotope correl. and constraints on continental crust comp. and nature of lower crust 80−94498
Earth mantle materials, Nd-Sr isotopic correl. and geodynamic consequences 79−92512
elastic constants, low-temp., mag. field depend. 78−76290
elastic constants, second and third order, calc. 79−51189
elastic constants, single cryst., rel. to mag. struct. changes 77−63249
elastic constants of single cryst., 4.2 to 300K, mag. ordering effects 77−15477
electron and positron multiple scatt. 80−15171
energy transfer between 5d electronic states 80−2808
film, on W(100), struct., electronic and dynamic props. *(Russian)* 77−76702
film, vapour-quenched, unsuccessful search for supercond. above 0.3K 77−12053
fluoride, MF_2:Nd^{3+}, (M=Ba,Ca,Cd), far IR Stark and Zeeman splitting 77−48190
garnet:Nd^{3+}, doped, Schottky specific heat and mag. susceptibility calcs. 79−51759
garnet:Nd^{3+}, spectral, structural regularities, anal. 78−51948
glass:Nd^{3+}, $^4I_{11/2}$ level population, absorpt. and relax. rate meas. 77−36290
glass:Nd^{3+}, line narrowed fluorescence spectra and site dependent transition probabilities 79−38640
glass:Nd^{3+}, nonradiative decay and multiphonon relax. 77−85802
glass:Nd^{3+}, resonantly enhanced four-wave mixing in absorbing media *(Chinese)* 80−102764
glass:Nd^{3+}, spectral props. *(Chinese)* 80−60645
glass:Nd, self-induced transparency effect in two-quantum resonant absorption *(Russian)* 79−3750
glass:Nd, surface struct., laser beam effects, IR spectra appl. 79−95250
glycerol-D_2O:Tb^{3+}, Nd^{3+} soln. and frozen glass, energy transfer 78−60509
granitoid rocks, Nd-Sr isotopic relationship and continental crust development, chemical approach to orogenesis 80−94522
high-power lasers, review 80−32950
internal strain rel. to strain tensor, group theory anal. 79−86835
isotope separation, laser two-step photoionisation 78−46461
isotopes, determ. in nuclear fuels as burnup indicator, separation, mass spectrometric method 77−44553
isotopes conc in ocean floor basalts and ferromanganese deposits 78−61395
isotopic anomalies in Allende meteorite 78−32409
Isua supracrustal rocks, Sm-Nd isotopic investigations and implications for mantle evolution 78−36129
lanthanum nicotinate dihydrate:Nd^{3+} cryst., H coords., EPR and ENDOR determ. 77−59005
laser, disc amplifier, inductive energy source, operational charact. 77−31109
laser, emission freq. conversion by method of reson. pumping of active media 80−1206

neodymium continued
laser, excited stimulated Mendelstam-Brillouin scatt. phase fluctuations *(Russian)* 80−89014
laser, giant nanosecond pulse chain stabilisation 79−13998
laser, miniature, optimum design 79−22966
laser, reproducible active-passive mode locked oscillators 77−88810
laser, second harmonic doubling with $KD_{2x}H_{2(1-x)}PO_4$, 90° synchronism *(Russian)* 77−58386
laser, with mirror plasma-optical Q-switch *(Russian)* 80−33028
laser frequency conversion, resonant pumping of Tm^{3+}, Ho^{3+} activated YAG 78−17944
laser glasses, phosphate and fluorophosphate, Nd doped, piezooptic coeffs. meas. 80−99815
laser material, $Na_3Nd(PO_4)_2$, cryst. struct. 78−79582
laser plasma diagnostics, probing radiation Raman scatt. *(Russian)* 80−19618
laser polarised radiation freq. mixing with ruby laser radiation in $LiIO_3$ cryst. 79−55181
laser rod, glass mech. strength and heat resistance obs. 79−76776
liquid, struct. factors, high temp. X-ray diffr. obs. 79−7544
magnetic form factors, polarised neutron diffr. meas. 80−50057
magnetic structure, 18.6K mag. phase transition 80−65799
magnetic structure, 2D modulated 80−15697
magnetic structure, heat capacity meas., 2 to 10K 79−51788
magnetic structure and crit. behaviour 78−47951
magnetic structures, two-dimens. modulation 79−78317
magnetic-structure, neutron and X-ray diffr. study 80−60197
magnetoresistance, longit., at low temps. and up to 80 kG 77−55515
magnetoresistance, mag. struct., elec. resistance at low temps. *(Russian)* 80−54936
metaphosphate glass: Nd^{3+}, Yb^{3+}, luminesc., energy transmission and migration between Nd^{3+} and Yb^{3+} 80−66297
Nd:glass, high-power laser for fusion reactor appl. 77−7062
Nd:glass multichannel laser with plasma shutter 80−64088
normal spectral emittance above 1000K 77−28028
nuclear fuel, burn-up, chemical separation, ion exchange 80−42746
Oklo natural fission reactors, migration in core sample, appl. to dating of reactions *(French)* 80−21760
orthovanadate:Nd^{3+}, spectroscopic props. 77−16363
phosphate glass:Nd^{3+}, giant laser pulse-induced luminesc., spectral shape temp. depend. *(Russian)* 77−19257
phosphate glass:Nd^{3+}, highly conc., electron energy deactivation and transfer *(Russian)* 80−29802
phosphate glass:Nd^{3+}, nonreson. interaction parameters, luminesc. kinetics obs. *(Russian)* 78−31246
phosphate glass, Nd^{3+} frequency selection by monochromatic laser excitation at resonant transition *(Russian)* 79−78747
photoelectric cross sections at 52.4, 60, 72.2 and 84.4 keV 80−69187
pulsed diode simulators of solid lasers $Al_xGa_{1-x}As$ and $Ga_xIn_{1-x}P_{1-y}As_y$ solid solns. 80−91816
pulsed laser sources using Nd 78−50784
purification, solid-state electrotransport 77−59679
relaxation in weakly ionised expanding plasma 79−41222
sediments of ocean bed, isotopic composition 80−21704
Shiva high-radiance nd-doped disc laser amplifiers 78−59036
silicate glass:Nd^{3+}, electronic excitation spatial diffusion meas. by degenerate four-wave mixing 79−64274
single crystal prep. by solid state electrotransport 78−84709
SL100, commercial Nd laser glass, props. 78−74912
specific heat, 1.5-10K, in applied fields 0-1.3T 79−61158
specific heat anomaly at 773K *(Russian)* 77−28017
spent reactor fuel, burnup determ., isotopic comp. and conc. determ. by mass-spectrometric isotope dilution 79−89373
surface and volume props., flow props.; surface layer thickness *(Russian)* 80−59760
thermal cond., 0.5-8K 78−34819
thermal conductivity at low temps. *(Russian)* 79−11100
thermal conductivity elec. and thermal magnetoresist., at low temps. 77−69301
threshold pot. spectra, $N_{4,5}$ absorpt. widths 79−69578
transition metal intermetallics, ESR of Nd^{3+} 79−87315
transport properties, low temp., effect of mag. field 80−70679
transport properties at high temp., scatt. mechanisms 77−15825
triple-q magnetic structure, neutron and X-ray diffr. investig. 79−73687
triple-q magnetic structure, neutron polarisation and diffr. investig. 79−73686
volcanic rock isotopic composition, Grenada, Lesser Antilles 80−21724
X-ray cross sections, L-shell, proton induced, 1 to 3 MeV range 79−1799
X-ray production surface impact of F^{n+} and Si^{n+}, Lα X-rays 79−69907
α-induced X-ray anal. of Y, La, Ce, Nd content of apatite minerals 79−16084
$BaO-B_2O_3$ glass, $Mn^{2+}\rightarrow Nd^{3+}$ energy transfer, fluoresc. obs. 77−8621
$BaO-B_2O_3$:UO_2^{2+}, Nd^{3+} glass, radiative and nonradiative energy transfer 78−60508
BaR_2O_4:Nd^{3+}, luminesc. 77−52156
BaY_2F_8:Nd^{3+}, ESR spectra and spin-lattice relax. 80−11263
$BeF_2-KF-CaF_2-AlF_3$:Nd^{3+} glass, multiphonon relax., fluoresc. obs. 78−15219
$Bi_4Ge_3O_{12}$:Nd^{3+} and $Bi_4Si_3O_{12}$:Nd^{3+} crysts., absorpt. and luminesc. spectra, 4.2-300K 80−34957
$Bi_{12}SiO_{20}$:Nd, light absorpt. and transmission spectra, photoluminescence spectrum, optical absorpt. coeff. 79−74001
$Bi_{12}SiO_{20}$:Nd, single cryst., photoluminesc. meas. *(Russian)* 78−23519
CaF_2:Md^{3+}, Slater, Racah and Lande parameters, crystal bonding 80−16062
CaF_2:Nd^{3+}, ^{19}F NMR studies 80−60429
CaF_2:Nd^{3+}, cryst. field at O_h sites 77−35899
CaF_2:Nd^{3+}, crystal field splitting 79−65418
CaF_2:Nd^{3+}, crystal field study, absorption spectra 80−20668
CaF_2-YF_3:Nd^{3+}, selective excitation of activator centres, time resolved luminesc. 78−15223
CaF_2-YF_3:Nd^{3+}, spectral migration of electronic excitation, selective laser excitation *(Russian)* 78−80417
$CaLa_4(SiO_4)_3O$:Nd^{3+}, spectra, stimulated emission 77−85755
$CaO-Li_2O-B_2O_3$:Dy^{3+} glass, optical excitation energy transfer from $Dy^{3+}\rightarrow Nd^{3+}$ 79−15515
$Ca_5(PO_4)_3F$:Nd^{3+}, luminesc. and absorpt. spectra, line shift and broadening 77−4678
$Ca_5(PO_4)_3F$:Nd^{3+}, optical fluorescence intensity and cryst. field parameters 78−52570

neodymium continued
$Ca_5(PO_4)_3F:Nd^{3+}$, selective site laser spectroscopy and ESR studies 79−19909
$Ca_5(PO_4)_3F:Nd^{3+}$ site symmetries, EPR and spectral obs. 78−6571
CaS:Nd, Cu, phosphor, electroluminesc., spectral charact. 79−19936
CaS:Nd phosphors, X-ray powder diffr. anal. 80−100204
$CaWO_4:Nd^{3+}$, phase relaxation, electron spin echo spectra 80−29613
$CaWO_4:Nd^{3+}$, phase relax. time rel. to g-factor anisotropy, electron spin echo obs. 80−29615
$CaWO_4:Nd^{3+}$, Slater, Racah and Lande parameters, crystal bonding 80−16062
$CaWO_4:Nd^{3+}$, thermal behaviour of shape and width of 9145 Å laser line 78−6755
$CaWO_4:Nd^{3+}$ $4f^3$ configuration, ground level energy state variation rel. to press. *(Russian)* 77−16358
$CaWO_4:Nd^{3+}$ absorpt. spectra, hypersensitivity of $^4I_{9/2}$ to $^4G_{5/2}$ $^2G_{7/2}$ transition 80−97309
$CaYAlO_4:Nd^{3+}$, absorpt. and luminesc. spectra 77−69901
$CaY_2Mg_2Ge_3O_{12}:Nd^{3+}$, optical absorpt. and fluoresc. intensities 80−29793
$CaY_4(SiO_4)_3O:Nd^{3+}$, absorpt. and luminesc. spectra 77−85755
CdF_2, Nd, ionic cond. investigation by complex admittance method 80−100352
CdF_2:Nd, semicond., symmetry of optical centres, optical and elec. props. 77−59592
$CeM_2:Nd^{3+}$, M=Ru, Rh, Ir, ESR investigation 79−78514
$CsMnBr_3:Nd^{3+}$, nearly 1-dimens. cryst., emission spectrum, extensive energy transfer 79−15516
Ga_2S_3-La_2S_3-Nd_2S_3:Nd^{3+} chalcogenide glass, Nd^{3+} emission and absorption spectra, nonradiative relax. 77−40268
$Gd_3Ga_5O_{12}:Nd^{3+}$, cryst. field anal. 78−64013
$Gd_3Ga_5O_{12}:Nd^{3+}$, optical absorpt. and fluoresc. intensities 80−29793
$Gd_2Gi_2O_7:Nd^{3+}$, spectroscopic props. 77−69866
$Gd_2(MoO_4)_3:Nd^{3+}$, cryst. field parameters 77−66142
$Gd_2(MoO_4)_3:Nd^{3+}$, optical spectrum, free ion wavefunctions, radiative transition probabilities 79−24339
β-$Gd_2S_3:Nd^{3+}$, spectroscopic props. from absorpt., photoluminesc. and excitation spectra 80−34968
K_2O-BaO-GeO_2:Bi^{3+}, Nd^{3+}, absorpt. and excitation spectra, fluoresc. 77−90183
$La_2Be_2O_5:Nd^{3+}$, crystal growth, spectral and laser properties in $^4F_{3/2}\rightarrow{}^4I_{11/2}$ and $^4F_{3/2}\rightarrow{}^4I_{13/2}$ transitions 80−80853
$La_2Be_2O_5:Nd^{3+}$, optical absorpt. and fluoresc. intensities 80−29793
$LaCl_3:Nd^{3+}$, coherent interactions of Kramers doublet system with microwaves in zero static mag. field 77−73078
$LaCl_3:Nd^{3+}$, cryst., appl. to phosphoroscope IR detector 79−49293
$LaCl_3:Nd^{3+}$ radiation upconversion, 1.06 to 0.873 μm 78−19530
$LaCl_3:Pr^{3+}$, Nd^{3+}, single cryst., optical double reson. excitation, energy transfer and transform. 77−69891
LaF_3:Nd, cryst. field anal. of triply ionised ion spectra 80−2796
$LaF_3:Nd^{3+}$, cryst., $4f^3$ config., ground level energy state var. rel. to press. *(Russian)* 77−16358
$LaF_3:Nd^{3+}$, laser-excited fluoresc., self-adsorpt. 78−15210
$LaF_3:Nd^{3+}$, luminesc. decay times 80−2811
$LaF_3:Nd^{3+}$, radiative transition rates of Nd^{3+}, Judd-Ofelt theory 79−33753
$LaF_3:Nd^{3+}$, spin echo envelope modulation exam. 79−61212
$LaF_3:Nd^{3+}$, thermal cond., 300-1450K 80−24686
$LaF_3:Nd^{3+}$, vacuum UV luminesc. *(Russian)* 78−64414
$LaF_3:Pr^{3+}$, Nd^{3+}, fluorescence linewidth and energy transfer 77−8635
$LaM_2:Nd^{3+}$, M=Ru, Rh, Ir, Pt, ESR investigation 79−78514
$La_2Mg_3(NO_3)_{12}.24D_2O$:Nd, dynamic polarisation of deuterons in individual sites 77−59484
$La_2Mg_3(NO_3)_{12}.24H_2O:Nd^{3+}$, polarised neutron diffr. from dynamically and statically polarised protons 80−44078
$LiNbO_3$:Nb, SHG, phase-matching temp., impurity influence 80−69463
$LiYO_2:Nd^{3+}$, absorption and luminesc. spectra, energy level diagram 77−63441
LuAG:Nd^{3+}, cryst. field anal. 78−64013
$LuAlO_3:Nd^{3+}$, spectral-generation charact., expt. and theory *(Russian)* 77−7090
$Lu_3Ga_5O_{12}:Nd^{3+}$, cryst. field anal. 78−64013
ND:glass laser, ultrashort pulse length, passive switch relax. time effect 77−38960
Na borate glass:Sm, Nd, nonradiative energy transfer from $Sm^{3+}\rightarrow Nd^{3+}$ 78−80394
$(NaNO_3$-$Mg(NO_3)_2)$:Nd^{3+}, glass, cryst., absorpt. luminesc. spectra, term struct. of Nd^{3+}, bonding 77−8624
Nd,Cr:Li-La phosphate glass, Nd luminesc. quantum efficiency meas., Nd-Cr nonradiative transfer 80−66296
Nd^{3+},Cr^{3+}:glass, nonradiative energy transfer from Cr to Nd, optical pumping efficiency improvement 80−33001
Nd activated laser glass charact., review 79−27262
Nd Argus 4 TW laser system, damage history 79−18463
Nd garnet ring laser, with return mirror, mode locking 80−99764
Nd glasses, luminesc. obs. by chronospectroscopic technique 79−11467
Nd I, isotope shifts in energy levels of neutral Nd atom 80−69095
Nd I and II, isotope shifts in spectrum, 3900 to 4760 Å, config. mixing 77−30812
Nd IV, 3d and 4f energy level parametrisation, Slater parameters and correl. corrections 80−87041
Nd laser, freq. conversion using rare earth:YAG crystal and reson. pumping *(Russian)* 79−10314
Nd laser glasses, gain coefficient meas. and modelling 79−81436
Nd laser Mikron system, ultimate Xe pump lamp module operating conditions 80−91815
Nd laser produced plasma, nonlinear scattering of laser radiation by fast ion waves in plasma 80−106916
Nd laser pulse irrad. expts., German laser fusion programme 78−63136
Nd laser pumping, Na plasma optical props. 79−4115
Nd, lasers, efficiency enhancement by pump radiation conversion in luminesc. liq. 80−48293
Nd pulsed garnet lasers, pulse repetition frequency, optimal operating regime 80−53303
Nd stoichiometric laser crysts., oscill. props., rate eqns. 78−22135
Nd XIV, UV spectra, 60-600 Å reson. lines 78−33455
Nd^+, spectral branching ratios and transition probabilities, solar abundance 78−9104
Nd^{3+}, $^4F_{3/2}$ level deactivation in $NaCl_3$-$AlCl_3$ vap. complexes 77−61786
Nd^{3+} activated laser matrices, luminesc. quantum efficiency, conc. depend. 79−27263

neodymium continued
Nd^{3+} amino acid complexes, supersensitive transition intensities, spectra *(Russian)* 77−88461
Nd^{3+} auto-extinction, fundamental mechanism and predicative criterion *(French)* 79−59702
Nd^{3+} based stoichiometric laser materials, comparison with GaAs based lasers 77−7088
Nd^{3+}, ESR in cubic intermetallic compounds, AB_2, (A=Y, La, Ce, Lu; B=Ir, Rh) 77−85564
Nd^{3+}, efficient cross pumping by Cr^{3+} in $Nd(Al,Cr)_3(BO_3)_4$ laser 78−59010
Nd^{3+}, $Eu^{3+}\rightarrow Nd^{3+}$ diffusion-limited energy transfer in Na borate glass 78−31238
Nd^{3+}, fluoresc. quenching of organic excited singlet states, rate meas., mechanism 77−38685
Nd^{3+} in $CeRu_2$, $ThRu_2$ and $LaRu_2$ type II supercond., ESR meas. 79−28444
Nd^{3+} in glass and cryst. hosts, fluoresc. branching ratios 78−29956
Nd^{3+} in Nd-Al-Cl complex, vapour phase laser expts. 78−66813
Nd^{3+}, in silica glass, laser-spectroscopic method, for studying solids with nonuniform spectral broadening *(Russian)* 79−40630
Nd^{3+}, intermediate coupling props., relativistic average of config. wavefunctions applicability 78−17574
Nd^{3+} ion miniature phosphate glass lasers with high ion concentration 80−19038
Nd^{3+} ions in solids, anti-Stokes effects 78−80405
Nd^{3+} ions in solids, radiationless decay processes, laser photoacoustic spectroscopy meas. 80−84766
Nd^{3+} laser crystal efficiency 79−50302
Nd^{3+}, local symmetry in frozen aq. solns., EPR and linear electric field effect 77−16169
Nd^{3+} miniature laser principles, materials and integrated optical design 80−33004
Nd: glass laser operating Ge optical switch, picosecond pulse generation at 10.6 μm 79−7159
Nd:AlG, laser, mode locked, output stabilisation 77−61986
Nd:BeF_2 glass lasers for fusion expts. 78−46661
Nd:$CaLa_4(SiO_4)_3O$, laser rod, laser damage initiating inclusions 77−68246
Nd:$CaY_2Ge_3O_{12}$, energy levels and laser action, fluoresc. meas. 79−81438
Nd:$CaY_2Mg_2Ge_3O_{12}$, CW room temp. laser operation, 0.941 and 1.059μm 78−66842
Nd:$CaY_3Mg_2Ge_3O_{12}$, CAMGAR low threshold CW room temp. laser operation at 0.941 μm 78−1234
Nd:$CeCl_3$, diode pumped miniature laser 78−9392
Nd:garnet, freq. axial mode shift, two-mirror resonator synchronisation, stabilisation *(Russian)* 78−22154
Nd:glass, 0.92 μ laser action at room temp. 78−1236
Nd:glass, Argus two-beam laser system, performance 77−88759
Nd:glass, CW SELFOC laser, actively initiated quasi-passive mode-locking 77−19306
Nd:glass, comparative lasing charact. of silicate and phosphate laser glasses 80−74364
Nd:glass, disc laser, using deuterated water as coolant, 1% efficiency 77−23695
Nd:glass, dynamic mode sweep-laser, freq. tuning 78−66851
Nd:glass, fluoresc. decay data from minicomputer-operated spectroscopy equipment 77−74526
Nd:glass, fluorophosphate glass for fusion lasers 78−46660
Nd:glass, Fourier-transform photoacoustic spectroscopy 79−9246
Nd:glass, high efficiency short pulse laser, coaxial flashlamp pumping 77−75558
Nd:glass, large laser effect phosphate and fluorophosphate glasses 78−79021
Nd:glass, laser bulk damage rel. to temp. and conc. 79−14023
Nd:glass, laser material, luminesc., population inversion depend. on pump pulses 77−23679
Nd:glass, laser slot method for radiation extraction 77−50694
Nd:glass, luminesc. greenhouse solar collector 78−13789
Nd:glass, luminesc. quantum yield meas., relative method *(Russian)* 78−35203
Nd:glass, mode locked laser, self-focusing effect on output power 77−751
Nd:glass, oscillator, short laser pulses *(Rumanian)* 79−7165
Nd:glass, ps pulse amplification, self-focusing brightness limitation 77−14725
Nd:glass, pulsed ring laser, quasistationary single-freq. generation *(Russian)* 77−83897
Nd:glass, Q-switched laser, radiation polarisation 77−27293
Nd:glass, self-induced transparency on two-photon reson. line *(Russian)* 79−86221
Nd:glass, silicate and phosphate glass, comparison of gains 80−19039
Nd:glass, stimulated emission cross sections and absorpt. coeffs. at 1.06 μm, calorimetric meas. 77−71987
Nd:glass, stimulated emission cross section by absorpt. meas. from thermally populated $^4I_{11/2}$ levels 78−71107
Nd:glass, subnanosecond pulse oscillator, investigation by high-speed oscillography 80−74411
Nd:glass, thermal distortion induced by optical pumping *(Chinese)* 78−50779
Nd:glass 2 TW laser for fusion expts. 80−33035
Nd:glass amplifier, large aperture, active mirror design 78−46659
Nd:glass amplifier, pump radiation pulse shape influence on stored energy 79−64235
Nd:glass Argus laser system, performance summary 78−55361
Nd:glass composite tunable laser at 1.89, 3.39 and 16 μm 79−72596
Nd:glass conical fibre optics quantum amplifier parameters 78−59024
Nd:glass disc amplifier design 78−46633
Nd:glass disc amplifiers, possibility for efficiency improvement 80−33000
Nd:glass disc laser amplifier with immersion medium 78−1262
Nd:glass fibre optical quantum image amplifier 78−1261
Nd:glass films for integrated optics, RF sputtering and optical charact. 79−46087
Nd:glass high energy laser amplifier, nonlinear pulse propag. 78−50780
Nd:glass laser, blue tunable picosecond pulse generation by synchronous mixing with sideband radiation in $NH_4H_2PO_4$ 80−87431
Nd:glass laser, coaxial digital pulse compression 77−7101
Nd:glass laser, continuous dynamic freq. tuning of pulse radiation 78−29986

neodymium continued
Nd:glass laser, enhanced performance by double doping with Cr 79−31906
Nd:glass laser, Fabry-Perot etalons tuning, narrow linewidth 79−76707
Nd:glass laser, gain coeff. for fusion laser amplifier 77−19261
Nd:glass laser, generation of picosecond light continua depending on various nonlinear processes 80−33095
Nd:glass laser, γ-ray induced absorbing layer form. in optical medium 77−50688
Nd:glass laser, influence of neutron and γ irrad. on generating characts. *(Russian)* 80−69402
Nd:glass laser, line narrowing and tuning using intracavity birefr. filter 77−38916
Nd:glass laser, luminesc. absolute quantum efficiency 77−34893
Nd:glass laser, luminesc. filters efficiency 80−1213
Nd:glass laser, microsecond pulse production, with quadratic loss in laser cavity 77−7147
Nd:glass laser, mode locked, picosec. pulse form., expt. technique 77−38957
Nd:glass laser, mode locking characts. using polymethine dye No. 3955 in solid host 78−17989
Nd:glass laser, mode-locked, ultrashort pulse duration meas., two-photon fluoresc. 79−27302
Nd:glass laser, new rapid-relax. passive trap *(Russian)* 77−54714
Nd:glass laser, optical inhomogeneity cancellation using $LiIO_3$ parametric convertor 80−33049
Nd:glass laser, output spatial characts. using FTIROS material 79−68414
Nd:glass laser, refraction effects and gain meas. 79−31905
Nd:glass laser, repetitively pulsed, high efficiency 77−72005
Nd:glass laser, resonant reflectors in laser cavity, freq. selection 78−55369
Nd:glass laser, short pulse mode-locked, using prisms 80−83617
Nd:glass laser, stable ultrashort light pulses generation *(German)* 80−91823
Nd:Glass laser, sub ns periodically Q-switched 78−17995
Nd:glass laser, TEM_{00} mode operation *(Rumanian)* 78−50798
Nd:glass laser, tunable-wavelength mode-locked, with instant recording of temporal and spectral characts. 77−54732
Nd:glass laser, ultimate power characts. at high pulse repetition freqs. 80−64036
Nd:glass laser, with metallic grating in cavity, Fourier spectrum and periodic mode fields distrib. *(Russian)* 79−31915
Nd:glass laser, with nonlinear absorber, pulsed Q switching 78−9400
Nd:glass laser amplifier, small scale self-focusing effects, exam. 78−55415
Nd:glass laser amplifier, terminal level lifetime effect *(Chinese)* 79−89913
Nd:glass laser amplifiers, self-focusing and suppression by spatial filtering 80−14406
Nd:glass laser and ruby laser placed parallel in cavity, for efficiency increase *(Russian)* 77−10954
Nd:glass laser array, mode locking, spatially coherent beam form. 77−88811
Nd:glass laser array, spatially coherent beam form., mode locking 78−29989
Nd:glass laser cooling and index-matching liquid props. 80−33015
Nd:glass laser development and laboratory work 78−94395
Nd:glass laser in Tl vapour, output conversion from 1.06 micron to 388.1 nm 80−91850
Nd:glass laser irradiated fusion targets, time and space resolved harmonic emission 79−82095
Nd:glass laser materials, intensities of optical transitions 77−689
Nd:glass laser operation, self-focusing influence 79−13997
Nd:glass laser output, passive-mode locked, resonator length effect 78−79044
Nd:glass laser performance and reliability developments 80−78869
Nd:glass laser picosecond pulses, background energy content meas. with saturable absorbers 78−59062
Nd:glass laser prep. and fundamental characteristics *(Japanese)* 79−7133
Nd:glass laser resonator, lasing spectrum singularities and Q-factor, for z-dimens. beam path *(Russian)* 77−88795
Nd:glass laser resonator deform. due to polarisability change of excited Nd ions 79−10313
Nd:glass laser rod, piezoelectric detection of photoacoustic signals 78−54467
Nd:glass laser rod, pumped, thermal relaxation 80−69397
Nd:glass laser rods, pumped in pseudoelliptic cavities, thermal effects 79−76692
Nd:glass laser six beam system, output characts. *(Chinese)* 80−83612
Nd:glass laser system, oscillators operating at 1.054 μm 78−46657
Nd:glass laser system, pulse shaping 78−46658
Nd:glass laser system, Thompson scattering diagnostics of low density plasmas 80−96388
Nd:glass laser system 400 MW, output characts., plasma production appl. 79−41384
Nd:glass laser system for optical wave mixing expts. 78−5521
Nd:glass laser system with parametric freq. conversion 80−1277
Nd:glass laser with active mode locking, ultrashort pulses 80−64087
Nd:glass laser with grid mirror, emission field 79−55142
Nd:glass laser with numerical programmed control *(Russian)* 80−91811
Nd:glass laser with periodic Q-switching, mathematical model 80−33043
Nd:glass laser with US modulated emission 80−48309
Nd:glass laser with US Q-switch 80−64034
Nd:glass laser with unstable resonator and additional feedback, angular divergence 80−48307
Nd:glass laser/parabolic mirror lidar for airborne aerosol mass conc. meas. 77−21937
Nd:glass lasers, optimisation for 1-10 ns pulses operation 78−46651
Nd:glass lasers, performance, Nova system design 78−46652
Nd:glass lasers, periodic monopulse energy output *(Russian)* 78−50787
Nd:glass lasers, status of large JANUS, CYCLOPS, ARGUS and SHIVA systems 77−38929
Nd:glass mode locked ring laser, unidirectional travelling wave operation 77−88812
Nd:glass off-axis multipass laser system 78−50813
Nd:glass passively mode-locked laser, obs. of external feedback influence 80−23729
Nd:glass Q-switched laser, feasibility of tuning range widening 79−59724

neodymium continued
Nd:glass Q-switched laser controlled by external signal, stimulated emission characts. 79−10312
Nd:glass Q-switched laser emitting polarised radiation 79−45974
Nd:glass ring laser, actively mode-locked and Q-controlled, props 79−18445
Nd:glass ring laser, holographic dispersion element *(Russian)* 78−59051
Nd:glass ring laser, mode-locking, unidirectional travelling wave operation 77−61976
Nd:glass ring laser, single synchronizable ps pulse generation 77−14739
Nd:glass rods in Mikron high-power multichannel laser pulse system 80−28249
Nd:glass saturated amplifier, direct meas. of gain recovery 78−71104
Nd:glass Shiva laser system for fusion expts. 78−50820
Nd:glass solid state laser, giant emission pulse prod. 80−91803
Nd:glass telescopic small-signal amplifier with a Brillouin mirror 80−69420
Nd:glass travelling-wave sweep laser, emission spectrum dynamics 78−50829
Nd:glass:CeO_2, TiO_2, lasing action, stabilisation *(Russian)* 78−13715
Nd:glass-YAG composite medium master oscillator, 1.06 μm stable conversion into fourth harmonic 78−46724
Nd:$La_2Be_2O_5$, laser crystal properties 77−19260
Nd:$La_2Be_2O_5$ laser, passive mode locking, ps pulse generation 77−7118
Nd:phosphate glass, high-power laser, design and performance 80−48270
Nd:phosphate glass amplifier for pulse shaping 77−14758
Nd:phosphate glass double pass amplifier with circular polarisation 77−88774
Nd:phosphate glass laser, CW oscillation 79−50311
Nd:phosphate glass laser beam, single ps pulse props. 77−19273
Nd:phosphate glass mode-locked oscillator and amplifier system 79−81446
Nd:phosphate glass oscillator, bandwidth-limited picosecond pulses 77−79830
Nd:silicate glass, resonance laser excitation, inhomogeneously broadended emission spectra 80−66295
Nd:Y_2O_3 single crystal fibre laser, room temp. CW operation at 1.07 and 1.35 μm 78−63121
Nd:YAG, actively AM mode-locked Q-switched laser, pulse compression by liq. Kerr cell 79−22990
Nd:YAG, actively mode locked laser, short pulse generation for fusion 77−88809
Nd:YAG, CW laser gain switching for intracavity pulse amplification 77−88771
Nd:YAG, diode pumped miniature laser 78−9392
Nd:YAG, electro-optical extraction of ps laser pulse *(German)* 80−87416
Nd:YAG, grown from melt, in Mo crucibles, laser props. 80−48261
Nd:YAG, high brightness 1 J freq. doubled laser 77−88776
Nd:YAG, high brightness 1 J freq. doubled laser 78−46615
Nd:YAG, high repetitive picosecond laser system and broad range wavelength tuning *(Japanese)* 79−3698
Nd:YAG, injection locked oscillator, pulse duration var. 77−88772
Nd:YAG, LED end pumped laser, cavity loss, efficiency 77−14740
Nd:YAG, laser, cavity dumping single mode-locked pulses 77−7137
Nd:YAG, laser, semicond. convertor in pump system 77−7129
Nd:YAG, laser amplifier, gain increase by parasitic oscill. suppression 77−14720
Nd:YAG, laser fusion system, short pulse generation, active mode-locking and Q-switching 77−79868
Nd:YAG, laser transition cross sections, modulation *(Chinese)* 78−90418
Nd:YAG, miniaturized laser, end-pumped by superlum. diode, CW operation 77−10938
Nd:YAG, mode locked oscillator, operation at 1.052 μm 80−33017
Nd:YAG, mode-volume matching of oscillating modes of laser containing several active elements *(Chinese)* 79−50325
Nd:YAG, positive branch, unstable oscillator 78−66845
Nd:YAG, ps pulse amplification, self-focusing brightness limitation 77−14725
Nd:YAG, single freq. laser with waveguide resonator 78−1277
Nd:YAG, single mode pulsed oscillator, control of temporal and spectral jitter 78−46629
Nd:YAG, solid-state formation 80−35121
Nd:YAG, unstable resonator, Q-switched laser, operating characts. 79−36928
Nd:YAG, with improved fluoresc. lifetime of $^4F_{3/2}$ state 77−687
Nd:YAG acousto-optically mode-locked CW laser performance and stability criteria 77−38934
Nd:YAG acousto-optically mode-locked CW laser, optical spectra obs. by interferometer 79−7134
Nd:YAG actively mode-locked laser, short pulse generation for laser fusion 78−9404
Nd:YAG CW laser, active stabilisation, laser noise 80−48295
Nd:YAG CW laser, longit. mode number reduction 79−72576
Nd:YAG CW laser, mode locking, 30 W average power 80−87419
Nd:YAG CW mode-locked laser, negative feedback power stabilization 80−69435
Nd:YAG crystal, orientation influence on thermally induced birefringence *(Chinese)* 80−88958
Nd:YAG FM laser, pulse compression in Nd:YAG laser dispersive delay line 77−88815
Nd:YAG fibre laser, self-contained LED-pumped single-crystal 78−1264
Nd:YAG giant pulse lasers, energy characts., superradiance effects 80−64031
Nd:YAG glass clad fibre laser, 1.3 μm operation with LED end pumping 77−7120
Nd:YAG high performance laser system efficiency and beam uniformity 77−19327
Nd:YAG laser, acousto-optic Q-switches 79−7166
Nd:YAG laser, actively modelocked and Q-switched, fusion reactor appl. 79−45980
Nd:YAG laser, appl. in space communications 78−28483
Nd:YAG laser, CW, with high output coupling modulation 80−9917
Nd:YAG laser, CW mode-locked and intracavity freq. doubled, anal. 80−58548
Nd:YAG laser, coherence time meas. of picosecond pulser by light-induced grating method 80−53347
Nd:YAG laser, conductively cooled pulsed design 78−46647
Nd:YAG laser, flash lamp discharge development effects on pumping efficiency 78−71114

neodymium continued
Nd:YAG laser, frequency-doubled, thermooptical instabilities and bistable behaviour 77−71998
Nd:YAG laser, frequency-doubled operation, effects of absorpt. loss in $Ba_2NaNb_5O_{15}$ 79−36957
Nd:YAG laser, hole burning elimination in active medium 77−79851
Nd:YAG laser, influence of birefraction and cooling on output characteristics *(Italian)* 79−50299
Nd:YAG laser, intense fourth harmonic generation, pulse periodic conditions 78−17972
Nd:YAG laser, intracavity modulation, sum freq. mixing, 212.8 nm pulse burst generation 78−74934
Nd:YAG laser, intracavity freq. doubling by $LiIO_3$ long pulse emission 80−102736
Nd:YAG laser, kinematic mode synchronisation *(Russian)* 77−34892
Nd:YAG laser, Kr-pumped for space optical communications 77−19328
Nd:YAG laser, min. amplitude noise for high-sensitivity meas. 79−63317
Nd:YAG laser, mode self locking with combined Q-switching 78−1284
Nd:YAG laser, mode-locked, picosecond pulse parameter meas. 77−19271
Nd:YAG laser, negative feedback, external perturbations effect, spectral depend. 77−83908
Nd:YAG laser, optical pumping, using room temp. CW superluminesc. diode 77−7122
Nd:YAG laser, passive mode-locked, picosecond pulse duration, determ. from luminesc. intensity 78−71134
Nd:YAG laser, passive Q switching at 1.3 μm 79−72610
Nd:YAG laser, phase conjugation using gain saturation 79−64272
Nd:YAG laser, pumped by Kr arc lamp, conductive cooling, for space operation 77−88775
Nd:YAG laser, Q-switched, pulse stretching using Pockels cell 80−95927
Nd:YAG laser, radiation characts. rel. to pumping intensity in long-time operation *(Russian)* 77−68214
Nd:YAG laser, Raman shifted, frequency conversion appl. 80−69451
Nd:YAG laser, reduction of passive Q-switch output jitter 78−46648
Nd:YAG laser, repetitively pulsed, high efficiency 77−72005
Nd:YAG laser, subnanosecond pulse generation at 100K 80−74397
Nd:YAG laser, thermal lens effect on emission stability 80−19064
Nd:YAG laser, unstable resonator oscillator, 12 ns 200 mJ output 77−42548
Nd:YAG laser, using flash lamp pumping source 77−50679
Nd:YAG laser as optical pulse generator, mode locking by acoustooptic loss modulation 79−64260
Nd:YAG laser as source for airborne lidar system for atmospheric expts. *(Italian)* 80−109278
Nd:YAG laser frequency tripling 79−14030
Nd:YAG laser integration into optical systems 80−78887
Nd:YAG laser multipass cell for Raman scatt. diagnostics 80−1231
Nd:YAG laser oscillator, mode-locked, pulse splitting 79−7160
Nd:YAG laser oscillator-amplifier coupled to Nd:glass amplifier, programmable electro-optical pulse form. *(German)* 78−33753
Nd:YAG laser pulse tailoring/synchronization system for laser-plasma interaction expt. 79−98404
Nd:YAG laser pumped $LiNbO_3$, parametric oscillator, picosecond IR pulse generation 78−71151
Nd:YAG laser pumping system, heterostructure spectrum convertor, opaque and sapphire heat sink 79−27272
Nd:YAG laser stabilisation by T-shaped four-mirror resonator *(Russian)* 78−13730
Nd:YAG laser third harmonic pumping a tunable picosecond UV dye laser 79−31927
Nd:YAG laser with internal SHG in coupled resonators, CW coherent UV-source *(German)* 79−98438
Nd:YAG long laser resonator, active and passive mode-locking 78−50832
Nd:YAG long-pulsed laser, resonator config. for relax. oscills. suppression 79−72599
Nd:YAG low power laser, appl. for space communications 77−75567
Nd:YAG master oscillator, spectral comp. form. of high-power laser radiation 78−71115
Nd:YAG mode-locked laser picosecond pulse profile and power meas. 77−7112
Nd:YAG mode-locked laser pulse, quadratic phase evolution direct meas., time resolved interferometry 80−48318
Nd:YAG mode-locked unstable laser, p-branch unstable resonator config. 79−31928
Nd:YAG oscillator, flashlamp pumped, const. gain Q-switching to improve stability 78−50837
Nd:YAG oscillator, output stabilisation by Q-switching 78−83003
Nd:YAG oscillator, Q-switched, generation of high-power ns pulses 80−23730
Nd:YAG passively locked laser, pulse width meas. by SHG method *(Chinese)* 80−87432
Nd:YAG passively mode-locked unstable oscillator 79−45953
Nd:YAG pumped tunable sources, appl. to spectroscopy 80−58576
Nd:YAG regenerative amplifier, variable-duration synchronized pulse generator 79−45967
Nd:YAG regenerative amplifier, expt. studies 80−95909
Nd:YAG repetitively Q-switched laser, fifth harmonic generation for mW 213 nm source 79−55178
Nd:YAG short-pulse oscillator, for Shiva 78−63134
Nd:YAG single crystal fibre laser, self-contained LED pumped 79−59711
Nd:YAG solar pumped laser, freq. doubling 78−59045
Nd:YAG two beam laser irradiation facility for nuclear fusion 77−18705
Nd:YAG unstable resonator design 79−13988
Nd:YAG unstable-resonator oscillator, stable single-axial-mode operation by injection locking 80−53331
Nd:YAG waveguide resonator laser, time characts. 77−58345
Nd:YaG laser reflection resonator with hole coupling 80−58597
Nd^{+3}: glass laser for stimulated Raman scatt. Dewar cell 80−99799
Nd^{3+}: crystal, laser transitions intensities 79−78062
Nd^{3+}: YAG, multiplet splitting, effective ligand point-charge model calcs. 77−76779
Nd^{3+}:Al_2O_3-P_2O_5 glass, high Nd conc., spectroscopy and lasing obs. 78−46609
Nd^{3+}:Ba phosphate and silicate glasses, luminesc. quenching by transition metal and rare earth ions 80−25449
Nd^{3+}:$Ca_3Ga_2Ge_3O_{12}$, stimulated emission at 300K 80−38019
neodymium continued
Nd^{3+}:CaO-Li_2O-Al_2O_3-SiO_2, CaO enriched, laser type glasses, spectroscopic behaviour 78−60497
Nd^{3+}:$CaWO_4$, magnetic, thermal properties in scheelite type crystals 78−91875
Nd^{3+}:$Gd_3Ga_5O_{12}$, growth, stimulated emission, spectral props. 78−95593
Nd^{3+}:$Gd_3Ga_5O_{12}$ pulse-pumped laser action at 1.054 μm 80−64030
Nd^{3+}:glass, ED-2 laser glass, transition probabilities and quantum efficiency 77−58330
Nd^{3+}:glass, fluoresc. line narrowing, hole burning and ion-ion energy transfer 79−89912
Nd^{3+}:glass, inhomogeneously broadened spectra, struct., selective laser excitation obs. *(Russian)* 78−35181
Nd^{3+}:glass, kinetic description of excitation spectra 78−68557
Nd^{3+}:glass, laser induced fluoresc. line narrowing, site depend. 79−33819
Nd^{3+}:glass, laser props., uncorrelated inhomogeneous broadening of 1.06 μm band induced luminesc. quenching 79−31914
Nd^{3+}:glass, multitype opt. centres 78−68558
Nd^{3+}:glass, nonlinear refractive index, two-photon resonant absorption by Nd^{3+} *(Chinese)* 80−43387
Nd^{3+}:glass, oscillator, narrow bandwidth ps. laser operation using Nd^{3+}:YAG as amplifier 78−37894
Nd^{3+}:glass, quantum efficiency for upper laser level, photoacoustic meas. 79−19924
Nd^{3+}:glass, spectral behaviour under narrow-line excitation 79−33747
Nd^{3+}:glass based on alkali metal metaphosphates, luminesc. and lasing *(Russian)* 77−46724
Nd^{3+}:glass energy transfer processes, radiative transitions *(Chinese)* 79−61431
Nd^{3+}:glass laser, analysis of antireflection layers 77−58340
Nd^{3+}:glass laser, Q-switching by exploding PbS film 78−42361
Nd^{3+}:glass laser, stabilised, single-mode, Q-switched, continuous frequency scanning 79−31922
Nd^{3+}:glass laser radiation, 6th and 10th VUV harmonics, cascade generation in Na-Ar and Cd vap. 78−42381
Nd^{3+}:glass luminesc. band profile deform. under free-oscillation conditions 80−71487
Nd^{3+}:inorganic glass, energy transfer processes, nonradiative transitions *(Chinese)* 79−64232
Nd^{3+}:$LaCl_3$, laser-induced fluoresc., hyperfine structs. 80−100677
Nd^{3+}:$LaCl_3$, laser-induced fluoresc. energy transfer effects 80−100678
Nd^{3+}:Li-Nd-La phosphate glass, nonradiative losses, pulse periodic stimulated emission and luminesc. 77−83878
Nd^{3+}:$LiNd_{0.3}La_{0.7}$ phosphate glass, stimulated emission characts. 79−18426
Nd^{3+}:$LiYF_4$, pulsed free running laser action at 1053, 1046 nm, passive mode locking *(French)* 78−79048
Nd^{3+}:NdAlCl vapour complex, optical gain meas. 77−88708
Nd^{3+}:$NdTa_7O_{19}$, fluorescence intensity and lifetime rel. to mini laser prod. *(French)* 77−71988
Nd^{3+}:$POCl_3$-$SnCl_4$, liquid laser material, luminesc. centres conc., temp. depend. 79−50287
Nd^{3+}:$POCl_3$-$SnCl_4$, liquid laser material, luminesc. centres changes, crystn. process effects 79−50288
Nd^{3+}:$POCl_3$-$SnCl_4$ laser, relaxation oscillations with high power spikes obs. 78−42331
Nd^{3+}:$POCl_3$-$ZrCl_4$ free-running liquid laser, design and performance 77−14706
Nd^{3+}:$PbMoO_4$, magnetic, thermal properties in scheelite type crystals 78−91875
Nd^{3+}:phosphate glass, physicochem., spectral, luminesc. and stimulated emission props. 77−54715
Nd^{3+}:phosphate glass laser, brightness enhancement by spatial filtering in amplifying channel 80−48321
Nd^{3+}:quartz fibre, stimulated radiation generation and amplification 77−88729
Nd^{3+}:trifluoride, VUV fluorescence and tunable coherent sources from 1650 to 2600 Å 77−688
Nd^{3+}:YAG, 1.05 to 1.44 μm tunable high-power laser emission on 18 CW transitions 77−88727
Nd^{3+}:YAG, CW laser, 1.05 to 1.44 μm tunability, performance 78−22142
Nd^{3+}:YAG, CW laser with planospherical resonator, freq. degeneracy of modes 79−31953
Nd^{3+}:YAG, laser characts., comparison with Li-Nd-La phosphate glass active elements 80−33002
Nd^{3+}:YAG, Q-switching mechanism by intracavity stimulated Brillouin scatt. 80−106552
Nd^{3+}:YAG, Raman laser with optical-fibre resonator, expt. investigation 79−31913
Nd^{3+}:YAG, stabilised laser with longitudinal mode synchronisation *(Russian)* 77−19315
Nd^{3+}:YAG CW laser, intensity fluctuations in single-freq. mode 80−91802
Nd^{3+}:YAG CW linear laser, longit. mode self-locking 79−72611
Nd^{3+}:YAG CW ring laser, axial mode locking by electrooptic $LiNbO_3$ phase modulator 78−50835
Nd^{3+}:YAG CW ring laser, fluctuation spectrum 80−9914
Nd^{3+}:YAG continuously pumped pulse-periodic laser, stability 80−28241
Nd^{3+}:YAG electro-optically Q-switched pulse-periodic laser 79−45975
Nd^{3+}:YAG electrooptically Q-switched laser pulse duration increase by intracavity SHG 79−94255
Nd^{3+}:YAG fibre laser pumped by single LED, optimum geometry *(German)* 78−55366
Nd^{3+}:YAG laser, analysis of antireflection layers 77−58340
Nd^{3+}:YAG laser, CW operation 77−38901
Nd^{3+}:YAG laser, conc. determ. of ^{137}Cs fission product in coated-particle fuel 80−18416
Nd^{3+}:YAG laser, contrast and configs. of $LiNbO_3$ electrooptic switches 80−33012
Nd^{3+}:YAG laser, high repetition rate electrooptic Q-switching, birefringence 80−69430
Nd^{3+}:YAG laser, improved efficiency with $Al_xGa_{1-x}As$-GaAs LED pump system 79−41396
Nd^{3+}:YAG laser, pumping by alkali metal vapour arc discharge 80−78924
Nd^{3+}:YAG laser, running pulse mode of operation, exptl. obs. 77−7089
Nd^{3+}:YAG laser, spontaneous mode locking necessary conditions, quadratic nonlinearity influence 79−64261

neodymium continued
- Nd^{3+}:YAG laser, stable periodic-pulse, with CW pump 80−74400
- Nd^{3+}:YAG laser, with intracavity SHG, amplitude- and phase-freq. charcts. 78−25884
- Nd^{3+}:YAG laser active element, linearly polarised light depolarisation due to thermally induced birefr. 80−106528
- Nd^{3+}:YAG laser frequency stability improvement using active interferometer *(Russian)* 80−64043
- Nd^{3+}:YAG laser with nonstationary resonator, axial mode synchronisation *(Russian)* 77−75582
- Nd^{3+}:YAG multimode laser radiation noise 80−74366
- Nd^{3+}:YAG Q-switched picosecond laser radiation, pulse duration and energy fluctuations 79−89949
- Nd^{3+}:YAG stabilised single-freq. travelling wave laser 79−18449
- Nd^{3+}:$YAlO_3$ biaxial laser cryst., anisotropy of spectral charcts. 79−50303
- Nd^{3+}:$YAlO_3$ laser, $^4F_{3/2}\rightarrow{}^4I_{13/2}$ transition, stimulated emission wavelength, continuous tuning 77−58334
- Nd^{3+}:$YAlO_3$ laser double-pulse flashlamp trigger cct. 78−55378
- Nd^{3+}:YVO_4, absorption and fluoresc. spectra of laser states 77−38900
- Nd^{3+}:YVO_4, optical absorption intensities 79−24335
- Nd-Sr isotopic var. implications for crustal and mantle chemical evolution 79−66655
- Nd-YAG laser, Q-switched, freq. doubled, 200 kW output 80−33026
- Nd^{3+}-doped trifluorides, vacuum-UV excitation spectra 78−80381
- Nd^{3+}-Yb^{3+}:glass, excitation transfer, selective filling of levels in inhomogeneous contour 77−69898
- $Nd^{3+}+UO_2^{3+}$ solution, nuclear pumped liq. lasers, LASL program 80−64011
- $NdCrOS_2$, single cryst. X-ray diffr. struct. determ. *(French)* 79−23581
- $^{60}Nd+{}^{19}F({}^{28}Si)$, target Lα X-ray prod., projectile charge state depend. 79−47549
- ^{143}Nd, ^{145}Nd, visible spectra, relative isotope shift, odd-even staggering parameters 77−10615
- $^{143}Nd/^{144}Nd$, geochemistry in hydrous mantle nodules and host alkali basalts 80−56420
- $^{143}Nd/^{144}Nd$, in N.Atlantic Tertiary basalts, rel. to magma source regions depletion 79−100821
- $^{143}Nd/^{144}Nd$, ratios in Cretaceous mid-ocean ridge basalt (MORB) from DSDP Holes 417D and 418A 80−94520
- $^{143}Nd/^{144}Nd$ in Bay of Islands ophiolite complex, rel. to midocean ridge basalts source evolution 80−85651
- $^{143}Nd/^{144}Nd$ in calc-alkaline andesites and plateau lavas from S.America 79−29726
- $^{143}Nd/^{144}Nd$ in flood basalts from Siberian Platform 80−56435
- $^{143}Nd/^{144}Nd$ in Kerguelen Islands igneous rocks, inferences on enriched oceanic mantle sources 80−98319
- $^{143}Nd/^{144}Nd$ in mantle xenoliths, equilibrated isotopic comp. meas. with unequilibrated Sr isotopes 80−98321
- $^{143}Nd/^{144}Nd$ in Norwegian eclogites, rel. to crustal origin 80−76978
- $^{143}Nd/^{144}Nd$ in Scottish Caledonian granites, isotopic evidence for crustal provenance 80−109146
- $^{143}Nd/^{144}Nd$ ratio in basalts from Sao Miguel 79−74873
- $^{143}Nd/^{144}Nd$ ratio in Recent continental volcanic rocks 78−53635
- $^{143}Nd/^{144}Nd$ ratios in Scottish continental volcanics, evidence for crustal contamination 79−66693
- $^{143}Nd/^{144}Nd$ vars. in continental and oceanic basalts, rel. to magma sources and mantle struct. 77−21708
- ^{147}Nd, anodic deposition on Pt anode, electrochem. separation 79−91958
- Ni:glass, amplifier module inversion investigation, active element with rectangular cross section 79−27264
- P_2O_5-K_2O-CdO-Na_2O glass:Nd^{3+}, highly doped, spectroscopic props. and CW laser action *(French)* 79−41385
- $POCl_3$:$ZrCl_4$:Nd^{3+}(Er^{3+}), radiative transition probabilities within 4f configs. 77−8617
- $POCl_3$.$SnCl_4$:Nd^{3+}, phosphor, laser parameters and physiochem. props. 77−14709
- $PO(SCN)_3$:Nd^{3+} solns., spectroluminesc. props. 77−16362
- $PbMoO_4$:Nd^{4+}, optical absorpt. intensities, 300, 550 and 4.2K, expt. and Judd-Ofelt theory 77−20894
- PbO-SiO_2 glasses, absorpt. spectra of Nd^{3+} ions and interpret. 78−27277
- $SeOCl_2$:Nd^{3+}, $SbCl_5$ acidified, Racah and Judd-Ofelt parameters in laser liqs. 80−106516
- SiO_2:Nd^{3+} films, cathodoluminesc. 80−20717
- Sm, determination by X-ray fluorescence 78−61127
- $Sr_{1-x}Ba_xNb_2O_6$:Nd, growth of low dislocation density cryst., dislocation struct. 77−40348
- SrF_2:Nd^{3+}, linear dichroism induced by electric field orientation kinetics of Nd^{3+} centres 79−69868
- SrF_2:Nd, far IR spectra 79−33736
- SrR_2O_4:Nd^{3+}, luminesc. 77−52156
- $Sr_2Ta_2O_7$:Nd,Na, SHG, effect of dopants on Curie temp. 79−24267
- $Tb^{3+}\rightarrow Nd^{3+}$, diffusion limited energy transfer in DMSO soln., fluoresc. obs. 79−61428
- $TbAlO_3$:Nd^{3+}, absorpt. and luminesc. spectra 79−91470
- TeO_2-Li_2O glass:Nd^{3+}, highly doped, spectroscopic props. and CW laser action *(French)* 79−41385
- $ThRu_2$:Nd^{3+}, supercond. state, ESR investigation 79−78514
- YAG:Nd,Ce,Cr, effect of γ-rays, fast electrons on optical props., annealing and colour centre destruction 77−8608
- YAG:Nd garnet, heat capacity and thermal diffusivity meas. 80−19956
- YAG:Nd^{3+}, Ce^{2+}, sensitisation, luminesc., absorpt. and emission spectra *(Russian)* 78−10982
- YAG:Nd^{3+}, cryst. field parameters calc., exchange charge model 78−47747
- YAG:Nd^{3+}, cryst. field anal. 78−64013
- YAG:Nd^{3+}, energy transfer between Nd^{3+} ions, laser-excited time-resolved site-selection spectroscopy 79−95839
- YAG:Nd^{3+}, LPE and luminesc. 78−64408
- YAG:Nd^{3+}, many-phonon nonradiative transition probabilities 79−95842
- YAG:Nd^{3+}, nonradiative multiphonon relaxation of isolated impurity level, transition probability calcs. 79−56853
- YAG:Nd^{3+}, photon echo form. 77−23720
- YAG:Nd^{3+} and free Nd^{3+} ion, energy levels, absorption spectra 79−11076
- YAG:Nd^{3+} crystal, zero-phonon linewidths, in $^4I_{9/2}\rightleftarrows{}^4F_{3/2}$ luminesc. band calc. 79−28834
- $Y_3(Al_{1-x}Ga_x)_5O_{12}$:Nd, fluoresc. energy transfer and radiationless relax. 79−38625
- $Y_3(Al_{1-x}Ga_x)_5O_{12}$:$Nd^{3+}$, time-resolved site-selection spectroscopy, energy transfer 80−2814
- $YAlO_3$:Nd, colour centre form. rel. to growth conditions, absorpt. spectra 79−90652
- $YAlO_3$:Nd, refractive index determ. 78−80311
- $YAlO_3$:Nd^{3+}, thermal broadening and shift calcs. of Nd^{3+} energy levels 77−48208
- $Y_3Al_5O_{12}$:Nd^{3+}, one-phonon satellites in luminesc. spectra, rel. to effective phonon density 78−6730
- $Y_3Al_5O_{12}$:Nd^{3+}, single crystal, $^4F_{3/2}$ level splitting and spectra dependence on press. *(Russian)* 77−52183
- YCl_3:$^{143}Nd^{3+}$($^{145}Nd^{3+}$), EPR and ENDOR spectra 79−78515
- YF_3:Nd, Ce, energy transfer between 5d electronic states 80−2808
- YF_3:Tm, Nd, energy transfer between 5d electronic states 80−2808
- $Y_3Ga_5O_{12}$:Nd^{3+}, cryst. field parameters calc., exchange charge model 78−47747
- $Y_3Ga_5O_{12}$:Nd^{3+}, cryst. field anal. 78−64013
- $Y_3Ga_5O_{12}$:Nd^{3+}, energy transfer between Nd^{3+} ions, laser-excited time-resolved site-selection spectroscopy 79−95839
- $Y_3Ga_5O_{12}$:Nd^{3+}, $YGaO_3$:Nd^{3+}, spectroscopic charcts. 77−12427
- YM_2:Nd^{3+}, M=Rh, Ir, Pt, ESR investigation 79−78514
- Y_2O_3:Nd single crystal growth, floating zone method with Xe arc lamp imaging furnace 80−60777
- Y_2O_3:Nd^{3+}, absorpt. spectra, hypersensitivity of $^4I_{9/2}$ to $^4G_{5/2}$ $^2G_{7/2}$ transition 80−97309
- δ-Y_2S_3:Nd^{3+}, spectroscopic props. from absorpt., photoluminesc. and excitation spectra 80−34968
- $Y_3Sc_2Al_3O_{12}$:Nd^{3+}, cryst. field parameters calc., exchange charge model 78−47747
- Y_2SiO_5:Nd^{3+}, EPR and spin-lattice relax. 80−108063
- Y_2SiO_5:Nd^{3+}, stimulated emission 77−52135
- $Y_2Ti_2O_7$:Nd^{3+}, spectroscopic props. 77−69866
- YVO_4:Nd, stimulated emission cross-sections at 1064 and 1342 nm 78−39575
- YVO_4:Nd^{3+}, energy transfer processes, laser-excited time-resolved spectroscopy 80−84765
- YVO_4:Nd^{3+}, fluoresc. lifetime of $^4F_{3/2}$ state 79−87494
- YVO_4:Nd^{3+}, zircon struct., cryst. field analysis 80−80232
- ZnO:Nd, electro- and photoluminesc. 79−83024
- ZnO:Nd, electrolum. brightness waves, 93 to 363K 79−33839
- ZnO:Nd, electrolum. brightness, field strength and freq. depend. 80−100696
- ZnO:Nd, phosphor, electrolum. and photolum. spectra 78−80421
- ZnS:Nd phosphors, optical scintillation mechanism 79−56867
- ZnS:Nd^{3+}, spin-lattice relax. times meas. 78−19324

neodymium alloys
- ESR studies of pseudobinary rare earth intermetallic compounds 80−108064
- misch metal, improvement of Al alloy 51S, for space appl. 80−55466
- mischmetall-Co system, phase relations, microstruct., mag. props. 80−104118
- rare earth intermetallics, RaI_2-Nd, dil., (R=La, Yb, Lu), EPR and mag. susceptibility 80−15797
- steel, austenitic, Cr-Ni-Na(Pr,Ce,La), nonmetallic inclusions modification using rare earth metals *(Russian)* 80−40369
- Ag-Nd, cryst. struct. *(German)* 78−51472
- $Ag_{83.3}Nd_{16.7}$ amorphous alloy, EPR of Nd^{3+} 79−65727
- Al-Sr-Nd phase diagram *(Russian)* 80−20893
- Ba-Nd, phase diagram, microstruct., X-ray, chemical and thermal diffusion anal. *(Russian)* 78−52761
- Ce-Nd, reversible mech. memory effect, α to γ transition *(Russian)* 78−15396
- Ce-Nd-Si, phase diagram, X-ray anal. *(Ukrainian)* 79−38792
- Co-Nd, dilute, magnetic annealing effect, induced anisotropy 77−73054
- $Dy_{50}Nd_{50}$, mag. struct. and ordered moments, neutron diffr. data 77−66252
- $(Gd_{1-y}Nd_y)_{1-x}Fe_x$ amorphous bubble films with good temp. charcts. 79−95616
- $Gd_xNd_{1-x}Zn$, ferromag., mag. susceptibility and magnetisation, temp. depend. 80−70975
- $Ho_{30}Nd_{70}$, mag. struct. and ordered moments, neutron diffr. data 77−66252
- (La,Na)Sn alloys, supercond. transition temp. 79−78254
- (La, Nd)Sn_3, cryst. field effects, normal and supercond. props. 79−60973
- (La,Nd)Sn_3, reverse Kondo effect in presence of crystalline elec. field splitting 80−103684
- (La, Nd)Sn_3, superconducting props. 79−60958
- La alloys, supercond., Nd-doped, crystal field effects, tunnelling within mK range 80−70907
- (LaNd)Sn_3, containing Nd impurities, supercond. and normal state props. 80−49967
- $LuIr_2$-Nd^{3+}, dil., ESR, hyperfine crysts. of $^{143,145}Nd$, g-factor, crystalline field splitting 78−52349
- $LuRh_2$-Nd^{3+}, dil., ESR, hyperfine crysts. of $^{143,145}Nd$, g-factor, crystalline field splitting 78−52349
- Mg-Nd-Zn dilute alloy, metallography and precip. kinetics 80−71655
- Mg-Nd-Zr, phase diagram, Mg rich region, microscopic anal. and elec. resistivity meas. *(Russian)* 78−56619
- Mg-Y-Nd-Zn-Zr (2,2,0.3, 0.7 wt.%), heat treatment effect on casting dimensional stability, alloy mech. props. 78−44146
- Mg-Y-Zn-Nd-Cd alloys, influence of Zr addition on struct. and mech. props. *(Russian)* 80−40370
- Mg-Zn-Zr-Cd-Nd, Lawes phase separation using acetate electrolyte, Cd and Nd effects 79−70237
- Mn-Nd, mag. props. for bulk amorphous deposits *(Japanese)* 79−95971
- $NaAl_2Ga_3$, synthesis, NMR and X-ray absorpt. studies 80−108083
- Nd-Co alloys, NMR of ^{143}Nd and ^{145}Nd 78−19343
- Nd-Co film, amorphous, exam. of domain struct. 78−68336
- Nd-Dy HCP struct., mag. props. 77−63177
- Nd-Dy(Y), elec. resist. temp. depend. 78−2462
- Nd-Fe-B ternary systems, phase equilibria and cryst. struct. *(Ukrainian)* 80−11626
- Nd-Ga, heat of form. and soln., calorimetric meas. *(Russian)* 78−27806
- Nd-Ga, phase diagram *(Russian)* 78−27478
- Nd-Ga alloy, phase diagram, DTA, X-ray and metallographic obs. 79−24494
- Nd-H, possibility of H ordering, DTA meas. 79−52174
- Nd-Ho, HCP struct., mag. props. 77−63177

neodymium alloys continued
- Nd-La, mag. ordering, sp. ht., susceptibility and resist. 78−68238
- Nd-Ni-Al, isothermal section, 600°C, X-ray struct. anal. *(Ukrainian)* 80−33929
- Nd-Pr, Kaufman approach to calc. of intra-rare earth phase diagrams 80−25657
- Nd-Sb, heat of formation meas. 77−90635
- Nd-Sn (0 to 50 at.%), phase equilibria diagram *(Ukrainian)* 79−34001
- Nd-Tb, HCP struct., mag. props. 77−63177
- Nd-Tl phase diagram, intermediate phases 78−60653
- Nd-Y, mag. character of stable and metastable phases 79−38329
- $NdAg_2$, high temp. modification, thermal effects 78−38665
- $NdAg_x$, low temp. mag. meas. 80−107989
- $Nd_{21}Ag_{79}$, and $Nd_{50}Ag_{50}$, amorphous, mag. props. 80−60182
- NdAl, ferromagnetic, extraordinary Hall effect 80−39560
- $NdAl_2$, conduction electron spin and orbital polarisation effects 78−80228
- $NdAl_2$, cryst. field volume magnetostriction calc. 79−8029
- $NdAl_2$, elastic constants, 4.2K to 280K, crystal field effects 77−11615
- $NdAl_2$, ferromag., cryst. field excitations, neutron inelastic scatt. meas. 77−63154
- $NdAl_2$, mag. excitation spectrum, neutron inelastic scatt. 78−10673
- $NdAl_2$, mag. form factor, diffuse moment density, polarised neutron meas. 77−63108
- $NdAl_2$, magnetostriction in high mag. fields 79−99745
- $NdAl_2$, orbital and spin polarisations of cond. electrons 80−65791
- $NdAl_3$, cryst. field effects, inelastic neutron scatt. meas. 77−51710
- $NdAu_{3.6}$, ordering temps. and effective moments 78−60283
- Nd_2Au, mag. props., 4.2-300K 79−7972
- $NdCO_2$:^{57}Fe, easy magnetisation directions, spin rotation like transitions 77−63168
- $NdCo_2$, cryst. field induced spin rot., Mossbauer meas. 77−16227
- $NdCo_2$, elec. resistivity, thermopower, X-ray struct. meas. 80−24874
- $NdCo_2$, magnetocrystalline anisotropic props., torque meas. 80−108003
- $NdCo_2$, sublattice magnetisation, powder neutron diffr. meas. 79−19725
- $NdCo_5$, absorption of H_2, 77-300K 79−23737
- $NdCo_5$, ferromag., thermomag. charact. in mag. field *(Russian)* 78−23273
- $NdCo_5$, mag. moment orientation, anisotropic mol. field model 77−89950
- $NdCo_5$, single ion anisotropy consts. temp. depend. effect of spatial variation of mag. moment 78−91864
- $NdCo_5$, spin reorientation, magnetisation and torque curves, 77-925K 77−4532
- $Nd_{0.35}Co_{0.65}$ film, vac. evaporated, magnetisation ripple struct., TEM and defocused Lorentz microscopy 80−7136
- Nd_2Co_7, mag. saturation and anisotropy, density, lattice parameters 77−85426
- Nd_2Co_7, polymorphism of Ce subgroup alloys, eutectic decomposition *(Russian)* 80−66504
- $Nd_{64}Co_{36}$, amorphous, amg. ordering, susceptibility, magnetisation and hysteresis meas. 78−68190
- Nd_xCo_{1-x} film, amorphous, mag. props. meas. 78−68312
- NdCoAl, mag. props. 78−2659
- $Nd_2Co_{17-x}Al_x$, magnetisation, Curie temp., anisotropy 77−89947
- $Nd(Co_{1-x}Cu_x)_5$, coercive force temp. depend. 79−82823
- Nd_3Co_3Ga, crystal struct., X-ray determ. *(Russian)* 79−27951
- $NdCu_4Ag$, mag. props. and cryst. struct. 77−20562
- $Nd_{1-x}Dy_xCo_5$, rotational type spin reorientation, appl. to thermomagnetic generator 77−85451
- $NdFe_2$, amorphous, magnetization and neutron scatt. meas. 79−78314
- $NdFe_2$, amorphous, small angle neutron scatt. study of mag. order and mag. microstruct. 79−15283
- $NdFe_2$, Curie temp., elec. quadrupole couplings, Mossbauer study 80−39949
- $NdFe_2$, high field Mossbauer study 80−75893
- $NdFe_2$, preparation and mag. props. 80−25259
- Nd_xFe_{1-x} film, amorphous, mag. props. meas. 78−68312
- $NdFe_4Al_8$, mag. props. 78−52250
- NdGa, ferromag., mag. props., 4.2 to 350K 77−63230
- $NdGa_2$, mag susceptibility, 1.5-300K and Neel temp. 78−68184
- $Nd_{11}Hg_{45}$, cryst. struct. determ. 79−77555
- $NdIn_3$, crystalline elec. field parameters, exchange and Coulomb contrib. 77−20278
- $NdIn_3$, magnetisation 80−25106
- Nd_2In, mag. props., 4.2 to 270K 79−56512
- Nd_2In, mag. props. 80−108009
- Nd_3In, mag. props. 80−108009
- Nd_5Ir_2, cryst. struct. 80−96473
- $Nd_{1-x}La_x$ alloy, thermoelectric power 79−78080
- $Nd_{1-x}La_x$, thermoelectric power, mag. transition temps. 80−20154
- $Nd_{0.25}La_{0.75}Mg$, cryst. field, neutron diffr. meas. 78−34810
- $Nd_{0.2}La_{0.8}Zn$, cryst. field, neutron diffr. meas. 78−34810
- $NdNi_5$, H_2 absorption, cell volumes and desorption pressures correlation 78−22860
- Nd_3Os, cryst. struct. 80−96474
- $NdPb_3$, crystalline elec. field parameters, exchange and Coulomb contrib. 77−20278
- $NdPd_3$, crystalline elec. field parameters 77−20278
- $Nd_xPr_ySm_zCo_5$ permanent magnets, coercive force, low-temp. annealing influence *(Russian)* 80−39812
- $NdPt_5$, low temp. mag. susceptibility 80−93075
- Nd_3Pt_2, structure determ., rhombohedral Er_3Ni_2 type 77−80443
- Nd_3Pt_4, mag. props., 4.2 to 160K 79−78343
- Nd_3Rh_2, structure determ., rhombohedral Er_3Ni_2 type 77−80443
- $NdRh_{1.2}Sn_{4.1}$, new supercond./mag. cpds., X-ray powder diffr. data 80−100215
- NdSi mag. struct. and mag. moments, neutron diffr. meas. 77−85424
- $(Nd_xSm_{(1-x)})_2(Co_{0.7}Fe_{0.3})_{17}$, mag. anisotropy 80−34622
- $NdSn_3$, crystalline elec. field parameters, exchange and Coulomb contrib. 77−20278
- $NdSn_3$, elec. cond., cryst. field effect, spin disorder contrib. 80−65540
- $NdSn_3$, magnetoresistance 80−24877
- $NdSn_3$, Neel temp., hydrostatic press. depend. 80−29549
- $Nd_2Y_{1-x}Co_5$, saturation magnetisation and anisotropy, 4.2K-T_c 77−85427
- $Nd_xY_{1-x}Zn$ system, solid soln., mag. susceptibility, 77 to 600K *(Russian)* 80−65776
- Pr-Nd, elec. resist. and magnetisation 77−66367
- Pr-Nd (5 at.%), paramag. excitation spectrum, CPA calc. 80−50043
- Pr-Nd (5%), impurity modes and mag. ordering 78−84422

neodymium alloys continued
- $Sm_{1-x}Nd_xCo_5$ alloys, magnetisation, magnetocrystalline anisotropy, 4.2 to 280K 78−91863
- $Sm_{1-x}Nd_xCo_5$, mag. props., domain boundary pinning on statistical conc. heterogeneities *(Russian)* 79−99728
- $Sm_xNd_{1-x}Co_5$ powders, mag. props. *(Russian)* 79−51812
- $Sm_{0.6}R_{0.4-x}M_xCo_5$ (R=Gd, Dy, M=Pr, Nd), temp. coeff. of magnetisation 80−34688
- Sr-Al-Nd phase diagrams *(Russian)* 78−27480
- Sr-Nd, phase diagram, microstruct., X-ray, chemical and thermal diffusion anal. *(Russian)* 78−52761
- Tb-Nd, antiferromag. state, decrease in stability 77−20556
- Tb-Pr, antiferromag. state, decrease in stability 77−20556
- TbAl-NdAl, existence of high-temperature superconducting phase *(Russian)* 79−42685
- $Tb_{40}Nd_{60}$, mag. struct. and ordered moments, neutron diffr. data 77−66252
- $Y_{0.25}Nd_{0.75}Co_5$, basal plane anisotropy 77−8295
- $Y_{1-x}Nd_xCo_5$, exchange interactions and magnetocrystalline anisotropy 80−34618
- $Y_{1-x}Nd_xCo_5$, ferrimag., magnetisation, exchange interactions, mag. anisotropy 80−80565

neodymium compounds
see also neodymium alloys
- alkali metal neodymium phosphates, $MNdPO_4$, CW laser oscill. near 1.32 μm 77−61957
- alkali silicate:Nd_2O_3, coloured, dichroism *(Polish)* 79−99919
- crystal field and Slater parameters and coordination 78−6771
- ethyl sulphate enneahydrate, mag. susceptibility, 2-27K, appl. as mag. thermometer 79−63224
- glasses, GLS-1 and GLS-22, luminesc. band, forced transition cross sections, laser meas. 80−40152
- laser emission cross sections and fluoresc. quantum efficiency meas. 80−48264
- laser stoichiometric materials, optically pumped miniature, for communication systems 78−50786
- neodymium ethyl sulphate, cryst. c-axis demag. from 25000G, magneto-hydrodynamic props. to 0.01K 77−20599
- neodymium ethyl sulphate, electronic spectra Stark pattern, crystal elec. field and mag. props. 77−12084
- neodymium ethyl sulphate, magnetothermodynamics, absolute temp. scale, mag. moment and magnetization , below 0.5K 78−34984
- oxydiacetate, magneto-optical rotatory dispersion and oxid absorption spectra 79−91409
- perovskite type compounds, electrode catalysts for cathodic reduction of O_2 79−29371
- phosphors, liq., using aprotonic solvents 80−20686
- Al_2O_3-Nd_2O_3, optical absorpt. spectrum and struct. of β-phase *(French)* 77−69848
- Al_2O_3-Nd_2O_3, phase diagram at high temps. *(Japanese)* 77−63649
- Al_2O_3-Nd_2O_3, phase-diagram at 1100°C *(Japanese)* 78−79747
- $(BaF_2)_{1-x}(NdF_3)_x$, crystal growth and struct. 77−12520
- $BaNdMnO_4$, cryst. struct. determ. *(French)* 78−6042
- BaO-Nd_2O_3-P_2O_5 ultraphosphate glasses, Nd^{3+} conc. quenching of luminesc. effect 79−19931
- BaO-Nd_2O_3-TiO_2-Bi_2O_3 system ceramics, high stability low loss dielectric preparation 80−81008
- BaO-TiO_2-Nd_2O_3, exam. of compositional and dielectric props. 79−33601
- $Ca_{0.5}Nd_{0.5}H_n$, H_2 dissociation press., phase behaviour and struct. 78−2260
- $CaNd_{3/2}Nb_{3/2}O_7$, pyrochlore struct., synthesis elec. props. 79−42543
- CaO-Nd_2O_3-Fe_2O_3-Al_2O_3 system, solid-state reactions 80−35173
- CdF_2:NdF_3 films, electroluminesc. meas. *(French)* 79−11471
- $CdNd_4(SiO_4)_3O$, synthesis, cryst. struct. 78−87653
- Cr-$NdAlO_3$, dielectric films, phase composition and structure 80−39464
- $Cs_2NaNdCl_6$, struct. transitions, polarisation optical expts. 79−99318
- α-$CsNd(PO_3)_4$, single cryst. struct. and spectral-luminescent props. 80−96490
- $CsNdP_4O_{12}$, X-ray cryst. struct. anal. 79−7590
- $Eu_{1-x}^{2+}Nd_x^{3+}N_xO_{1-x}$, resist., pressure depend., semicond.-metal transition obs. 79−78104
- $Eu_{1-x}^{2+}Nd_x^{3+}O_{1-x}N_x$, lattice parameters, mag. and elec. props. 80−100578
- Ga_2S_3-La_2S_3-Nd_2S_3:Nd^{3+} chalcogenide glass, Nd^{3+} emission and absorption spectra, nonradiative relax. 77−40268
- HfO_2-Nd_2O_3 solid solns., prep., crystn. 78−42909
- $K_5Bi_{1-x}Nd_x(MoO_4)_4$ solid soln., growth, spectroscopic and laser props. 78−2901
- $K_2CrO_4+Nd_2(NoO_4)_3$, X-ray phase analysis, IR absorption spectra, and thermogravimetric anal. 79−1944
- $K_5NdLi_2F_{10}$ (KNLF), spectroscopy and lasing 80−5737
- $K_5NdLi_2F_{10}$, high yield luminesc., potential miniature Nd laser 79−1784
- $K_5Nd(MoO_4)_4$, Ar^+ laser pumped, quasi-CW laser action 79−18421
- $K_5Nd(MoO_4)_4$, dielec. and optical props. 79−33590
- $K_5Nd(MoO_4)_4$, spectral and struct. props. *(Russian)* 79−52020
- $KNd(PO_3)_4$, cryst. struct. 77−43188
- $KNdP_4O_{12}$, determ. of fluoresc. quantum efficiency and laser emission cross sections 80−48264
- $KNdP_4O_{12}$ epitaxially grown waveguide, laser operation at 1.051 μm 79−18423
- $KNdP_4O_{12}$, laser emission cross sections, fluorescence spectra, radiative lifetimes, quantum efficiency 80−23694
- $KNdP_4O_{12}$, laser waveguide, fabrication by LPE 79−36925
- $KNdP_4O_{12}$ laser waveguide, epitaxial growth 79−91597
- $K_3Nd(PO_4)_2$, synthesis and IR spectra 80−16019
- $K_3NdSi_6O_{15}$, cryst. struct. determ. 78−34493
- $KNd_9(SiO_4)_6O_2$, cryst. struct. determ. 79−90624
- $(La,Nd)P_5O_{14}$, optical props., ferroelastic phase transition induced 79−95731
- $La_{1-x}Nd_xP_5O_{14}$, Nd^{3+} luminesc. anomalously weak quenching 77−75533
- $La_{2-x}Nd_xTi_2O_7$, luminesc. and absorpt. props. 79−65928
- Li-$La_{1-x}Nd_x$ phosphate glasses, stimulated emission spectroscopy of $^4F_{3/2}$ to $^4I_{11/2}$ and $^4F_{3/2}$ to $^4I_{13/2}$ transitions 79−38573
- Li-Nd-La phosphate glass, nonradiative losses, pulse periodic stimulated emission and luminesc. 77−83878
- Li-Nd-La phosphate glass active elements, laser characts., comparison with Nd:YAG 80−33002

neodymium compounds continued
$LiBi_xNd_{1-x}P_4O_{12}$ waveguide laser layer epitaxially grown on $LiNdP_4O_{12}$ substrate 80−23709
LiNd phosphate glass, spectral and generation props. 77−1700
$Li_3Nd_2(BO_3)_3$, cryst. struct., X-ray diffr. meas. 78−10028
$LiNd_{0.5}La_{0.5}P_4O_{12}$ laser, stabilised dual-polarisation oscill. 77−54723
$LiNd(MoO_4)_2$, defect struct. and phase transitions 79−28697
$LiNd(PO_3)_4$, crystallisation from $LiPO_3$ flux, exam. of optical props. *(German)* 79−11401
$LiNd(PO_3)_4$ laser with external and Fabry-Perot resonators, 1.05, 1.32 μm CW oscill. 80−23693
$LiNdP_4O_{12}$ (LNP) laser, optical transmitter appl., properties and LED pumping 79−3712
$LiNdP_4O_{12}$, diode pumped miniature laser 78−9392
$LiNdP_4O_{12}$ efficient miniature laser pumped with GaAlAs laser diode 80−32994
$LiNdP_4O_{12}$ electroluminescent diode pumped miniaturized laser for optical transmission system 79−41395
$LiNdP_4O_{12}$, glass clad, slab waveguide laser 78−46625
$LiNdP_4O_{12}$ glass-clad rectangular waveguide, laser performance 80−32996
$LiNdP_4O_{12}$, grown by top seeded pulling technique, possible laser material 80−25542
$LiNdP_4O_{12}$ laser, fluoresc. and oscill. charact. at 1.317 μm 78−5473
$LiNdP_4O_{12}$ laser, fluctuations in bath of strong Gaussian noise 79−55166
$LiNdP_4O_{12}$ laser, intensity fluctuations due to external perturbations 79−81437
$LiNdP_4O_{12}$ laser, LED and semiconductor laser pumped 77−75552
$LiNdP_4O_{12}$ laser, relaxation oscillations and mode spectra, high density pumping effect 80−69396
$LiNdP_4O_{12}$, laser emission cross sections, fluorescence spectra, radiative lifetimes, quantum efficiency 80−23694
$LiNdP_4O_{12}$ laser material, optical props. and crystal growth *(Japanese)* 79−27259
$LiNdP_4O_{12}$ laser material, crystal growth and optical props. 79−41386
$LiNdP_4O_{12}$ miniaturised lasers for optical communication systems *(Japanese)* 79−27278
$LiNdP_4O_{12}$, simultaneous oscillations of different transitions in lasers 79−22927
$LiNdP_4O_{12}$, single-transverse-mode slab waveguide laser, charact. 79−55141
$LiNdP_4O_{12}$ stable miniature laser with compact resonator, single mode operation 79−50305
$LiNdP_4O_{12}$ substrate, growth of $LiBi_xNd_{1-x}P_4O_{12}$ waveguide laser layer 80−23709
Li_2O-Nd_2O_3-P_2O_5 phase diagram, $LiNdP_4O_{12}$ single crystal growth 80−25668
Li_2O-Nd_2O_3-P_2O_5 ultraphosphate glasses, Nd^{3+} conc. quenching of luminesc. effect 79−19931
MgO-Nd_2O_3-$Al(Cr)_2O_3$, reactions kinetics in mixtures of components and phases 77−40523
$Na_3Nd(AsO_4)_2$, allotropes, prep. and cryst. struct. *(French)* 78−63724
$NaNdP_4O_{12}$, diode pumped miniature laser 78−9392
$NaNdP_4O_{12}$, laser emission cross sections, fluorescence spectra, radiative lifetimes, quantum efficiency 80−23694
$Na_3Nd(PO_4)_2$, laser mat., cryst. struct. 78−79582
$Na_3Nd(PO_4)_2$, synthesis and IR spectra 80−16019
$Na_2NdPb_6(PO_4)_6Cl_2$, self-activated mini-laser material, quantum yield determ. 79−33773
$Na_2Nd_2Pb_6(PO_4)_6Cl_2$, laser material, flux growth *(French)* 78−35288
$Na_2Nd_2Pb_6(PO_4)_6Cl_2$, high-Nd conc. laser material, oscillator strengths and laser effect 79−55140
$NaNd(SO_4)_2$, cryst. struct. by X-ray diffr. *(French)* 78−42990
$NaNdSi_6O_{14}$, cryst. struct., X-ray diffr. meas. 77−15385
$NaNdSi_6O_{13}(OH)_2.nH_2O$, cryst. struct. determ. 78−63738
$(Na_{5-x}Nd_x)(W_{3-2x}Nb_{2x})O_9F_5$, ferroelastic-ferroelectric material *(French)* 79−99834
NbB_4, antiferromag. props. *(French)* 77−20566
$Nb_xY_{3-x}Fe_5O_{12}$, low-temp. magnetocrystalline anisotropy study 79−95586
$(Nd,Ca)_nTi_nO_{3n+2}$, (n=4.5,5 or 6), cryst. struct. determ. *(French)* 79−65039
(Nd, Pb)MnO_3, flux growth 79−83113
Nd complex, $(NdOP(NMe_2)_3)_6(ClO_4)_3$, X-ray struct. determ. 77−31646
Nd complex, Nd^{3+}:ATP, electron spin echo decay envelope anal. 79−54871
Nd, complex, Nd^{3+}-hexakis-antipyrine triiodide single crysts., polarised absorpt. spectra 78−10922
Nd complex, Nd(2,2,6,6-tetramethyl-3,5-heptanedione), vapours, excited-state kinetics and fusion laser media prospects 79−64243
Nd complex, with ortho-phenanthroline and αα′-dipyridyl tris-trifluoroacetate, absorption spectra 79−98113
Nd^{3+} complexes, hypersensitive transitions 79−36620
Nd^{3+} in $Nd(NO_3)_3$(tributylphosphate-d_{27})$_3$, soln. luminesc., stimulated emission *(Russian)* 78−33734
Nd:YAG, pumped laser rod, quantum efficiency 77−88724
Nd-Al-Cl complex, Nd^{3+} vapour phase laser expts. 78−66813
Nd-Cr-B system, phase equil. at 800°C, boride lattice parameters *(Russian)* 78−31388
Nd-Gd-Te alloys of R_2Te_3-T_3Te_4 region, physicochem. props. 78−52017
Nd-H, inelastic neutron scatt. exam. of lattice dynamics 80−29128
Nd-H(D), lattice parameters 80−64982
Nd_2ASe_5, A=Ge, Sn, diffuse refl. spectra and band gaps 79−51963
$Nd(Al,Cr)_3(BO_3)_4$, CW laser action, CR^{3+} cross pumping, Nd^{3+} direct pumping 79−64231
$Nd(Al,Cr)_3(BO_3)_4$, efficient cross pumping of Nd^{3+} by Cr^{3+} 78−59010
$NdAl_3(BO_3)_4$ (NAB) laser, optical transmitter appl., properties and LED pumping 79−3712
$NdAl_3(BO_3)_4$, cw laser action at 1.3 μm 79−27258
$NdAl_3(BO_3)_4$, LPE for thin film miniature lasers 79−74101
$NdAl_3B_4O_{12}$, self-activated mini-laser material, quantum yield determ. 79−33773
$NdAl_{2.07}(B_4O_{10})O_{0.6}$ nonstoichiometric, crystal struct. by X-ray spectral microanalysis 79−77582
$NdAl_3(BO_3)_4$ miniaturised crystals with directly applied mirrors, laser emission 79−22958
$NdAlO_3$, dielectric films, phase composition and structure 80−39464
$NdAlO_3$ films, preparation, electrophys. props. in MIM structs. 77−24956
$Nd_4Al_2O_3$ film, struct. characts., IR spectra 77−48157

neodymium compounds continued
$NdAl_3[BO_3]_4$, luminescence and lasing characts., solubility 79−31910
$NdAl_3[BO_3]_4$, single phase crystallisation region from solvent melt 80−38977
$NdAl_3[BO_3]_4$, thermal stability, X-ray struct. anal., refractive indices 79−4297
$NdAs_2$, single-cryst. struct. refinement 78−63709
$NdAsO_4$, ferroelectricity, dielec. meas. 80−60515
NdB_6, field emission patterns and emission charact. *(Japanese)* 77−85900
$Nd(BO_2)_3$, single cryst., IR absorpt. spectra 80−34903
NdBi, thermal expansion, 20-800°C 79−14942
$Nd(BrO_3)_3.9H_2O$, IR and Raman spectra, vibr. asignments 78−84569
$Nd(BrO_3)_3.9H_20$, single cryst. low-temp. pyroelectricity 79−42906
Nd_2C_3, cryst. struct., mag. struct. and props., 1.6 to 300K 79−11296
$Nd(C_2H_5SO_4)_3.9H_2O$, large single crystal growth 77−4729
$NdCO_3Y^{3-}$, (Y=ethylenediaminetetracetate ion), formation constants *(French)* 80−104458
$Nd_{1-x}Ca_xVO_3$, solid solutions, elec. props. 80−96866
$NdCl_3$, adiabatic susceptibility meas., interaction tensors for Nd^{3+} ions 77−69485
$NdCl_3$, anhydrous, Nd^{3+} absorption spectra and quantum states *(Chinese)* 80−89032
$NdCl_3$, aq. soln., H_2O coordination of metal ion, X-ray diffr. 79−69000
$NdCl_3$, aqueous frozen soln., phase transformations, optical absorpt. spectra, Nd^{3+} Stark splitting 79−1777
$NdCl_3$, Schottky anomalies, ht. capacity meas., 5-350K 77−31784
$NdCl_3$-$AlCl_3$ vap. complexes, Nd^{3+}, $^4F_{3/2}$ level deactivation 77−61786
$NdCl_3$-$AlCl_3$ vapour complex, optical gain at 1.06 μm 78−33742
$NdCl_3$-$SnCl_4$-$POCl_3$, complex formation, struct. and comp. 77−89413
$Nd(ClO_4)_3$, osmotic coeffs. 80−45556
$NdCl_3.6H_2O$:Gd^{3+}, EPR spectra, angular var. calc. 80−54940
$NdCl_3.6H_2O$-$EuCl_3.6H_2O$, in DMSO soln., $Eu^{3+}\rightarrow Nd^{3+}$ radiationless energy transfer 80−5499
$NdCo_4B_4$, and its analogues, struct. determ. *(Ukrainian)* 78−91320
$NdCo(BO_2)_5$, cryst. struct. 78−63735
$NdCoO_3$, ^{59}Co NMR, quadrupolar and hyperfine interactions 79−15366
Nd_2CuO_4, catalytic props., mag. and elec. props. 79−66350
Nd_2CuO_4, magnetic properties obs. 80−70937
$NdCu_3Ru_4O_{12}$, synthesis, cryst. struct., mag. and elec. props. *(French)* 80−107151
$(NdCu_3)(Ti_3Fe)O_{12}$, synthesis, cryst. struct. and Mossbauer exam. 78−84505
$Nd_xEu_{1-x}B_6$ solid solution, mag. susceptibility, lattice parameters, Weiss temp. 80−29535
NdF_3, ^{19}F spin-lattice relax. and mag. couplings 79−65753
NdF_3, bomb calorimetric determ. of enthalpy of formation 80−50879
NdF_3, crystals, shift tensors and F-diffusion, ion interactions, F^- NMR study 80−20471
NdF_3, enthalpy, entropy, heat capacity and Planck function from 5 to 350K 80−15257
NdF_3, enthalpy of formation 80−93789
NdF_3, Faraday rot., paramag. temp. *(French)* 79−65841
NdF_3, gamma-irrad. induced coloration 77−35586
NdF_3, ionisation energies, satellite struct., photoelectron spectra, MS Xα calcs. 78−13425
NdF_3, mag. props. between 2 and 4.2K *(French)* 79−61039
NdF_3, mol. consts., kinetic consts. and L-approx. methods 80−18839
NdF_3, mol. force, compliance and Coriolis consts. 79−31726
NdF_3, Zeeman splitting in mag. fields up to 100 kG 78−52483
$NdFe_3(BO_3)_4$, solubility in Bi_2O_3-B_2O_3 melt and crystallisation 80−19736
$NdFeO_3$, mag. transition, NMR meas. 78−27036
$NdFeO_3$, magnetic struct., time of flight neutron diffr. method 77−8280
$NdFeTiO_5$, mag. susceptibility, 4.2-77K, antiferromag. ordering obs. 78−68186
$NdFeTiO_5$, magnetic props. and crystal growth 78−92185
$Nd(Ga,Cr)_3(BO_3)_4$, cryst. growth by LPE, Nd^{3+} fluorescence, lattice constants 80−29883
$NdGa_3(BO_3)_4$ crystal structure by X-ray spectral microanalysis 79−46621
$Nd_3Ga_2BeO_7$, melilite struct., synthesis 77−81236
$NdGa_5O_{12}$ wafer, dislocations, etch pits and birefr. obs. 78−83818
$Nd_3Ga_5O_{12}$, elastic and thermoelastic consts., US meas. *(German)* 77−59061
$Nd_3Ga_5O_{12}$, floating zone method growth, interface shapes 80−60775
$Nd_3Ga_5O_{12}$:Nd^{3+}, radiationless decay processes, laser photoacoustic spectroscopy meas. 80−84766
Nd_4GeO_8, crystal struct. by X-ray spectral anal., flame photometry, rhombic cell parameters 79−77583
Nd_2GeSe_5, elec. props., 300 to 1100K 79−51585
$NdH_{2.2.7}$, low-temp. sp. ht., mag., elec., and cryst. field splitting effects 80−49379
NdH_2, lattice thermal expansion and point defect form. energy 77−51524
$NdH_{2.57,2.62}$, optical vibr. spectra of H, inelastic neutron scatt. study 80−107391
$NdH_{2.70}$, low temp. phase transition, specific heat meas. 78−14665
$NdH_{2.82}$, high-pressure structural phase transforms. 78−10185
$Nd_4In_5S_{13}$, chalcogenide cryst. struct., diffr. and Patterson function anal. 80−39056
$NdIr_3$, single cryst. X-ray diffr. struct. determ., new tetragonal phase 79−69064
$NdLaP_5O_{14}$, large crystal growth technique *(Chinese)* 79−24418
$Nd_{0.5}La_{0.5}P_5O_{14}$ laser, FM mode-locked 79−86184
$Nd_{0.75}La_{0.25}P_5O_{14}$, miniature laser system bonded mirrors, side pumped by LEDs 78−87058
$Nd_xLa_{1-x}P_5O_{14}$, crystal growth, laser generation charact. 80−38020
$Nd_xLa_{1-x}P_5O_{14}$, large single crystal growth from hot conc. H_3PO_4 and oxide, props. *(French)* 77−4723
$Nd_xLa_{1-x}P_5O_{14}$ laser, pumped by nanosecond pulses, performance 77−38897
$Nd_xLa_{1-x}P_5O_{14}$, laser properties 79−22957
$Nd_xLa_{1-x}P_5O_{14}$, Nd^{3+} stoichiometric materials, luminesc., conc. quenching 78−27315
$Nd_{0.75}La_{0.25}P_5O1_{14}$, laser side-pumped by LED arrays, design procedure and functioning 79−22966
$Nd_xLa_{1-x}TaO_4$, polycryst. optical centres, thermodynamic equilib., 1600-1700K *(Russian)* 77−68970
$Nd_3Mg_3(No_3)_{12}.24H_2O$:$Mn^{2+}$($Gd^{3+}$), EPR spectra, spin Hamiltonian anal. 79−33527

neodymium compounds continued
$Nd(Mn_{1-x}Cr_x)_5Si_2$, mag. and structural props. 79−78342
$Nd_2(MoO_4)_3$, mag. susceptibility, elec. cond. and thermoelec. power '*S* 88091
$Nd_2(MoO_4)_3$, thermo-optical spectroscopy, detection by mirage effect 80−47116
$Nd_2(MoO_4)_3$-$Nd_2(SO_4)_3$ system, sulphatomolybdates and isomorphous substitution 80−19763
Nd_2MoO_6, cryst. struct., IR spectra, elec. and mag. props. 80−33954
NdN, m.p. N_2 press. depend., Pirani-Alterthum meas. 78−43103
NdN, miscibility with UC *(German)* 80−96654
NdN-EuO solid soln., ^{151}Eu Mossbauer spectroscopy 78−6610
NdN-RN systems, (R=La,Ce,Gd), mutual solubilities *(German)* 79−19374
$NdNH_4P_4O_{12}$, isotypism with $PrNH_4P_4O_{12}$ *(French)* 77−24301
$Nd(NO_3)_3$, aqueous soln., single photon absorpt. band struct., electronic resons. coherent ellipsometry 80−90881
$Nd(NO_3)_3$, osmotic coeffs. 80−45556
$Nd(NO_3)_3.6H_2O$, optical absorpt. spectra, 4.2K, single crystal, Stark levels 77−81119
$NdNbO_4$, cryst. growth rel. to investig. of PbO-KF-B_2O_3-PbNdTiNbO$_7$ cross section 77−86004
$NdNbO_4$, ferroelastic, cryst. struct. and twinning struct. 79−27965
$NdNbO_4$, ferroelastic domain wall motion, stress-strain hysteresis curve 77−43271
$NdNbO_4$, room temp. form., symmetry determ. by convergent beam electron diffr. 80−79723
$NdNbO_4$, single cryst. grown by Czochralski method and props. 77−52247
$NdNbO_4$-$CaWO_4$, phase transitions of fergusonite-scheelite *(French)* 80−19942
$Nd_{1/3}NbO_3$, $NdNbO_4$, structural characteristics and residual polarisation 77−15361
Nd_3NbO_7, weberite-type, elec., mag. and opt. props. 77−85212
Nd_2NiO_4, magnetic properties obs. 80−70937
NdO, D_0-state struct., dissoc. energy, mass spectrometric obs., 79−10228
NdO, electronic spectrum, rotational struct. anal. 80−78643
NdO, mag. props., lattice consts., and X-ray absorpt. spectra 80−44798
NdO_2, atomisation energies and stand. ht. of formation 77−54622
Nd_2O_3, A-type, elec. cond. and dielec. const. 4.2-1200K 77−4340
Nd_2O_3, A-type, optical absorpt. spectrum and paramag. susceptibility 79−56811
Nd_2O_3, A-type, thermoelectric power, AC cond. 78−68044
Nd_2O_3, activator in Na_2O-B_2O_3-SiO_2 glass, exam. of distribution by absorption study 79−4832
Nd_2O_3, and oxalate, X-ray fluoresc. spectrometric anal. of trace rare earth impurities 79−24853
Nd_2O_3, cryst. struct., X-ray powder diffr. and electron diffr. study 80−107161
Nd_2O_3, EELS, low loss peak due to plasmon 80−79953
Nd_2O_3, elec. cond., thermoelec. power, dielectric const. 79−69763
Nd_2O_3, electrostatic cryst. field parameters, quickly converging calc. method 77−39809
Nd_2O_3, electrostatic cryst. field parameters including induced dipole contribs. 80−80233
Nd_2O_3, from reactive evaporation, struct. and polymorphic transform. 79−51441
Nd_2O_3, isotopically enriched target preparation using electron gun 80−23226
Nd_2O_3, magnetisation and mag. susceptibility Curie-Weiss behaviour 77−4505
Nd_2O_3, microhardness anisotropy of single cryst. *(French)* 77−52489
Nd_2O_3, neutron diffraction study of high temp. struct. *(French)* 79−65050
Nd_2O_3 powder, piezoelectric detection of photoacoustic signals 78−54467
Nd_2O_3, Raman spectra, lattice vibrs. 79−87440
Nd_2O_3, reaction with liq. Li and liq. Li-N 79−66276
Nd_2O_3 stabilised ZrO_2, refractories prod. and long-term high-temp. behaviour 77−59725
Nd_2O_3, transmission and luminesc. spectra 79−65929
Nd_2O_3-Al_2O_3-SiO_2 glass, exam. of spectroscopic and luminescent props. 78−88364
Nd_2O_3-HfO_2, kinetics of initial stages of formation of cpds. 77−48617
Nd_2O_3-HfO_2 system, phase relationships 80−35169
Nd_2O_3-MoO_2-MoO_3 system, phase equilibria *(French)* 79−52176
Nd_2O_3-SiO_2 glass, exam. of spectroscopic and luminescent props. 78−88364
Nd_2O_3-Y_2O_3 film, segregation obs. by EELS 80−79953
Nd_2O_3-Y_2O_3-As_2O_5 glass, spectroscopic props., rel. to possible appl. in lasers 78−84624
$Nd(OH)_3$, dynamical effects of interaction between 4f electrons and optical phonons 80−108196
$Nd(OH)_3$, heat capacity from 10 to 350K, lattice and Schottky contribs. 80−84300
$Nd(OH)_3$, mol., XPES, satellite phenomena 79−27035
$Nd(OH)_2Br$, hydrothermal phase equilib., cryst. struct. 78−35372
$Nd_7(OH)_{18}Br_3$, hydrothermal phase equilib., cryst. struct. 78−35372
Nd_2O_2S, electrostatic cryst. field parameters including induced dipole contribs. 80−80233
Nd_2O_2S-Ga_2S_3, exam. of preparation and props. *(French)* 78−80504
$Nd_2O_2S_2$, cryst. struct. determ. 79−51087
$3Nd_2O_3.2WO_3$, X-ray charact. and thermal props. 77−43194
$Nd_2O_3.4TiO_2$, growth from soln., struct. 78−83794
$NdOs_4Sb_{12}$, prep. and cryst. struct. 80−100211
NdP-UP solid soln., cryst. field parameters 80−10927
$Nd(PO_3)_2$, vitreous, microhardness 80−25864
NdP_5O_{14} (NPP) laser, optical transmitter appl., properties and LED pumping 79−3712
NdP_5O_{14}, cw laser action at 1.3 μm 79−27258
NdP_5O_{14}, diode pumped miniature laser 78−9392
NdP_5O_{14}, ferroelastic, spectroscopy, ferroelastic/ferroelectric coupling 79−19845
NdP_5O_{14}, ferroelastic, Raman scatt. from soft phonons, 4.2-600K, monoclinic-orthorhombic transition temp. 79−51962
NdP_5O_{14}, ferroelastic, hydrostatic press. effect on phase transition temp. 80−70293
NdP_5O_{14}, fluoresc. decay times meas. 79−8187
NdP_5O_{14}, fluoresc. lifetime meas., IR and photoacoustic spectroscopy 80−60652
NdP_5O_{14}, large crystal growth technique *(Chinese)* 79−24418
neodymium compounds continued
NdP_5O_{14}, large single crystal growth from hot conc. H_3PO_4 and oxide, props. *(French)* 77−4723
NdP_5O_{14} laser, flash-lamp-excited, operation 77−83883
NdP_5O_{14}, laser, flash-lamp excitation, room temp. operation 77−88779
NdP_5O_{14} laser, flashlamp excited, emission cross section at 1.32 μm 79−59701
NdP_5O_{14}, laser material, flux evaporation growth, dislocation etch tunnels 77−35560
NdP_5O_{14}, laser materials, linear conc. quenching of luminesc. 79−31908
NdP_5O_{14}, laser site-selection time-resolved spectroscopy 78−76524
NdP_5O_{14}, luminesc. excited by LED radiation 79−24366
NdP_5O_{14} microlaser pumped by second harmonic of Nd^{3+}:YAG laser 79−98377
NdP_5O_{14}, self-activated mini-laser material, quantum yield determ. 79−33773
NdP_5O_{14} single crystals, fluoresc. decay times, excitation density effect 80−7390
NdP_5O_{14} single crystals grown from polyphosphoric acids, morphology control 80−15395
NdP_5O_{14}, sp. hts. near ferroelastic phase transitions 78−63863
NdP_5O_{14}, spectral line intensity anal. 78−43888
NdP_5O_{14}, thermal cond. and specific heat 79−42325
NdP_5O_{14}, XeF excimer pumping 79−7130
Nd_3PO_7, IR and Raman spectra, vibr. assignments, cryst. struct. charact. 80−97258
Nd_3PO_7, prep. and luminesc. props. 80−34964
$Nd_4P_2O_{11}$, luminesc. props. 80−34964
$Nd_xPb_{1\pm x}Mo_{6+y}S_8$, sputtered supercond. props. 80−50019
$Nd_xR_{1-x}P_5O_{14}$ (R=La, Y: $0.1<x<1$), laser quality cryst. growth, morphology 80−66412
$Nd(ReO_4)_3.4H_2O$, $(ReO_4)^-$ ion vibrs. rel. to static field, Raman investig. *(Russian)* 78−76470
$Nd(ReO_4)_3.4H_2O$, Raman spectra, $(ReO_4)^-$ ion normal vibrs. rel. to static field 79−65858
$NdReSi_2$, cryst. struct. determ. 78−95037
$NdRh_4B_4$, cryst. struct., X-ray diffr. 77−89423
$NdRh_4B_4$, high supercond. transition temp. 77−89893
$NdRh_4B_4$, possible obs. of coexistence of supercond. and long-range mag. order 79−82730
$NdRu_4Sb_{12}$, prep. and cryst. struct. 80−100211
$Nd_{1-x}S$, grown-in defect exam. 78−43014
Nd_2S_3, optical props. and electronic struct. in fund. absorpt. region 80−80817
Nd_2S_3, semimetallic, elec. and thermal transport meas. 78−10442
Nd_2S_3, vibr. spectra, factor-group anal. 80−80793
Nd_3S_4 chem. and mag. structures, neutron diffr. obs., ferromag. long-range order *(German)* 78−10654
$Nd_2(SO_4)_3$, anhydrous, cryst. struct. determ. 78−79598
$Nd_2(SO_4)_3.8H_2O$:Gd^{3+}, EPR, zero field splittings, spin-Hamiltonian parameters 78−91949
NdSb, forbidden band gap and electrotransfer parameters 80−39497
NdSb, mag. excitation spectrum, neutron inelastic scatt. 77−63152
NdSb phonon dispersion curves, lattice dynamics of rare-earth monopnictides 79−37780
NdScFe garnets, mag. props. 77−47979
$Nd_xSm_{1-x}S(Se)$, K X-rays chem. shifts. electronic phase transition, semicond.-metal transition 77−28116
$Nd_{1-x}Sr_xCoO_3$, Anderson transition, elec. cond. meas. 77−51786
$Nd_{1-x}Sr_xCoO_3$, electronic and mag. props., itinerant ferromagnetism obs. 78−10660
$Nd_{1-x}Sr_xVO_{3-0.5x}$, elec. cond. and mag. susceptibility, temp. depend., 77-300K 77−47816
NdT_2, ^{3}He detrapping and release after ^{3}He decay, strain model 77−60101
$NdTa_7O_{19}$:Nd^{3+}($^4F_{3/2}$), fluorescence intensity and lifetime rel. to mini laser prod. *(French)* 77−71988
$Nd_2Ti_2O_7$, crystal struct. and phase transitions, rel. to isomorphous crystals *(Japanese)* 80−49208
$Nd_2Ti_2O_7$, ferroelec., layer type struct., cryst. growth 80−108348
$Nd_2Ti_2O_7$, ferroelec., temp. depend. of SHG intensity 79−24267
$Nd_2Ti_2O_7$, layered ferroelectric, anomalous photovoltaic effect, photovoltaic current 80−75603
$Nd_2Ti_2O_7$, Nd_2TiO_5, paramag. props., mag. susceptibility meas. 1.6 to 70K 78−10649
$Nd_2Ti_2O_7$, transmission and luminesc. spectra 79−65929
$Nd_2Ti_2O_7$-$CaTiO_3$ system, mode of formation and stability of $A_nB_nO_{3n+2}$ phases *(French)* 78−3110
$NdTlO_3$, physicochem. props. 80−25625
$Nd_{1-x}U_xCo_5$, mag. props. and spin-reorientation phase transitions *(Russian)* 78−60284
$NdVO_3$-$CaVO_3$ solid solns., mag. props. rel. to cryst. struct. 78−43571
$NdVO_4$, elastic modes in applied mag. field 79−60423
$NdVO_4$, magnetoelastic interactions, finite strain and rot. effects, elastic consts. 79−87303
$NdVO_4$, monazite struct., IR and NMR spectra 79−78534
$Nd_2V_{10}O_{28}.28H_2O$, cryst. struct. determ. 77−11523
$Nd_2V_{10}O_{28}.28H_2O$, X-ray cryst. struct. anal. 80−39060
$Nd_2(WO_4)_3$, elec. transport and mag. props. meas. 77−24668
$Nd_2(WO_4)_3$, mag. susceptibility, paramag. Curie temp., 300-900K 79−82753
$Nd_2(WO_4)_3$, molar mag. susceptibility, DC elec. cond., thermopower meas. 79−15172
Nd_2WO_6, growth from soln. in melt 77−1806
NdX_3(X=Cl,Br,I) far IR spectra, planar D_{3h} symm. 77−88450
$(NdX_6)^{3-}$, (X=Br, Cl, I), spectral hypersensitive intensity, ligand polarisability contrib. 78−51946
$Nd_{0.14}Y_{0.86}P_5O_{14}$ epitaxial layer an $Gd_{0.33}Y_{0.67}P_5O_{14}$, growth lasing 77−46722
$Nd_{1-x}Y_xP_5O_{14}$, laser emission at 1.32 μm, Ar laser pump source 79−31909
$Nd_xY_{1-x}P_5O_{14}$, conc. quenching 79−61435
$Nd_xY_{1-x}P_5O_{14}$, fluorescence quenching 77−69903
$Nd_xY_{1-x}P_5O_{14}$, fluoresc. conc. quenching, decay rate consts. 78−64404
$Nd_xY_{1-x}P_5O_{14}$, fluoresc. energy transfer and radiationless relax. 79−38625
$Nd_xY_{1-x}P_5O_{14}$, laser material, flux evaporation growth dislocation etch tunnels 77−35560
$Nd_xY_{1-x}P_5O_{14}$:Nd^{3+}, radiationless decay processes, laser photoacoustic spectroscopy meas. 80−84766

neodymium compounds continued
$Nd_2Zn_3(NO_3)_{12}.24H_2O$, EPR of Mn^{2+}, Gd^{3+} doped single crystal 79−24212
$Nd_2Zr_2O_7$-$Nd_2Hf_2O_7$, struct., elec. cond. and melting point 80−54197
$Nd_xZr_{1-x}O_{2-x/2}$, elec. cond. of ceramic solid solutions 80−107554
$Nd_xZr_{1-x}O_{2-x/2}$, fluorite and pyrochlore solid solutions, electrical conductivity meas. 80−65287
P_2O_5-GO_3-Nd_2O_3 system, vitrification regions and physicochem. props. of glasses 77−11673
$Pb_{3-x}Nd_xGe_3O_{11}$, ferroelec. props. 80−75960
$PbNdTiNbO_7$, cryst. growth rel. to investig. of PbO-KF-B_2O_3-$PbNdTiNbO_7$ cross section 77−86004
$Rb_3Nd(PO_4)_2$, synthesis and IR spectra 80−16019
SiO_2-Na_2O-Nd_2O_3 glass, magneto-optical props., absorpt. spectrum 80−88969
$Sm_{1-x}Nd_xSe$, Nd substitution effect on lattice const., resist., and colour 79−56763
$SrNdCrO_4$, mag. struct. determ. by neutron diffr. *(French)* 79−28507
$SrNdFeO_4$, Mossbauer spectra 80−15880
$SrNd_2Fe_2O_7$, mag. struct., neutron diffr. determ. *(French)* 78−52224
$SrO.Nd_{1-x}Sr_xVO_{3-0.1x}$, solid solns., elec. and mag. props. 77−89819
$TlNd(PO_3)_4$, cryst. struct. determ. 79−19216
$U_{1-x}Nd_xS$, mag. phase diagram 80−71027
UO_2-Nb_2O_3, kinetics of initial state of sintering stoichiometric and non-stoichiometric oxide 79−91609
UO_2+Nd_2O_3, sintering, initial stage kinetics, diffusion coeff. 80−2987
UP-NdP systems, mag. phase diagrams 78−84424
YAG:Nd, single crysts., melt growth using heat exchange method 79−52106
$YAl_3(BO_3)_4$-$NdAl_3(BO_3)_4$, substitution of Nd for Y in $YAl_3(BO_3)_4$, exam. 80−11551
$Y_{1-x-e}Gd_xNd_eScO_3$, crystal, absorption, luminescence, stimulated emission spectra 78−15220
Y_2O_3-Gd_2O_3-Nd_2O_3 solution phase diagrams and thermal conductivity *(Russian)* 78−88448
ZnS:Tb^{3+}, NdF_3 film, vac. deposited, electrolum. energy transfer 80−2861
ZrF_4-BaF_2-NdF_3, vitreous phases, network formers, modifiers and stabilisers *(French)* 80−64909
ZrF_4-BaF_2-NdF_3 F^- ion cond. glasses, cond. process 80−107477
ZrF_4-BaF_2-NdF_3 glass, vitreous domain, prep. and optical props. 78−27304
ZrO_2:Nd_2O_3, in contact with $NdCrO_3$, electrical cond. meas. 78−76071
ZrO_2-Nd_2O_3, stabilised, reaction with Cr_2O_3 77−36438
ZrO_2-Nd_2O_3 eutectic, unidirectional solidification, microstruct. and crystallographic characterization 80−35176
ZrO_2-Nd_2O_3 solid solns., prep., crystn. 78−42909
ZrO_2-Nd_2O_3 system, solid solns., evaporation, mass spectroscopy investig., thermodynamics 79−10938
ZrO_2-Y_2O_3-Nd_2O_3, high-temp. thermophys. props. 78−26663
ZrO_2-Y_2O_3-Nd_2O_3, spectral determ. of crystal stabilisation 78−27203

neon
see also nuclei with .....
$1s_5$ level density meas. by fluorescence, effect of dye laser intensity 78−67474
absorber discharge, 3 nsec laser pulse propag., self-induced transparency 77−10986
abundance in gas-rich samples of carbonaceous chondrite meteorites 78−65559
accommodation coeff. meas., on O_2 covered Pt wire, 400-1400K 77−63948
adsorbed on exfoliated graphite, vapour press. meas., 15-30K 79−69350
adsorption on W, potential of He atom above field adsorbed He or Ne atoms 78−35267
adsorption on Xe-plated graphite, virial coeffs. 78−18904
aerodynamic isotope separation technique based on vel. slip in freejet expansions 80−19441
afterglow, 1s atom prod. by recombination, press. depend. 78−59716
afterglow, early, electron temp. at few torr press. *(French)* 77−4013
afterglow, electron energy distrib. meas., Langmuir probe characteristics 77−80350
afterglow, electron-atom bremsstrahlung continuum, afterglow decay *(German)* 78−83626
afterglow, low press. discharge afterglow, dissoc. recombination, microwave diagnostics 78−9876
afterglow, recombination processes, microwave quenching 79−14624
afterglow 78−59715
afterglow plasma, electron energy distrib. function 78−63587
atom, $1s_3$ metastable, velocity-changing collisions, study by time resolved saturated absorption 80−82832
atom, $1s_5$, depopulation effects, dye laser fluoresc. obs. *(French)* 78−41996
atom, 1s and 2s photoionis. cross sections, L^2 calc. 80−951
atom, $2p_1$ level relax. and populations of $1s_2$ and $1s_4$ in afterglow 78−9111
atom, $2p^53p$ config., Lande factors, double reson. meas. *(French)* 78−9113
atom, $2p^53p$ level, stepwise excitation, effective cross section 77−83550
atom, $2p^53p$-$2p^55s$ emission lines, press. broadening, with Ne(He), rel. to repulsive forces 80−9692
atom, $2p^53s^3P_0$ state, optical pumping, g-factor, metastability exchange cross section 80−947
atom, $2p^53s^1P_2$ to ground state, electron collisions of the second kind, rate consts. 79−27090
atom, $2p^53s$ and $2p^53p$ states excitation by slow electrons, H^+, H_2^+, and He^+ 80−43185
atom, $2p^6(^1S_0)$ ground state electron impact excitation cross sections 80−23558
atom, 2p levels prod. by dissoc. recomb. in afterglow, recomb. coeffs., level population 80−43855
atom, 2p-1s transition, time-resolved spectroscopy 78−90103
atom, $3s_2$-$2p_4$ transition relax. consts. using cross saturation of travelling waves in ring laser 79−76374
atom, 40 keV electron scatt. 7-200 mrad, relativistic and electron correlation effects 77−34760
atom, $(2p^53p)$ states, radiative lifetimes, collisional deactivation rate consts. 80−69107
atom, (e,2e) coplanar symmetry reaction, factorised distorted-wave approx., 400-1200 eV 78−55246
atom, absolute photoionis. cross sections for VUV region 77−46547

neon continued
atom, and 1st row ats., Compton profiles, momentum distribs., correlation effects 77−88429
atom, approximate relativistic Hartree-Fock eqns., soln. using Slater-type functions 80−58168
atom, atomic struct. calc., symmetry adapted pair functions, Rayleigh Schrodinger HF variational perturbation theory 80−42944
atom, Auger effect transition energies calc. 79−18168
atom, Auger electron decay, final charge states, beam-foil investig. 77−19060
atom, Auger energies, intensities, for initial K vacancy, many body calc. 77−18869
atom, Auger rates, X-ray transition energies and fluoresc. yield calcs. 77−6714
atom, Auger spectra, correl. effects, energies and wavefunctions, ab initio CI calc. 80−14125
atom, Auger transition rates, KLL, effect of interchannel interaction 77−42301
atom, Autler-Townes effect 78−41998
atom, autoionisation region states, differential excitation function resons. obs. 77−6939
atom, autoionising resons. near 575 Å, ab initio relativistic RPA calc. 80−32681
atom, autoionising states, scatt. electron spectra, post collision interaction effects 78−58819
atom, beam-foil excited ^4P state, delayed coincidence Auger electron lifetime meas. 80−14117
atom, beam-foil populations, charge state distribs., independent electron model 77−19035
atom, below ionisation threshold *(French)* 80−43187
atom, cascade level scheme, optical Autler-Townes splitting 77−3301
atom, CI-Hylleraas variational calc. of ground state 77−18798
atom, closed shell, Jastrow wave functions, var. calcs. 80−83249
atom, clustering of atoms around positron and positive ions 78−55270
atom, collisional transfer coeffs. between 2p levels, in afterglow, laser excitation obs. 80−43856
atom, Compton profile, local density approx., Kohn-Sham self consistent scheme 78−94193
atom, Compton profiles using Gaussian expansion of at. orbitals 80−945
atom, converged $E^{(2)}$ values 78−66479
atom, core ionis., single orbital relax., LCAO MO SCF calcs. 78−29739
atom, correl. contribs. to dipole polarisability, coupled HF-perturbation theory 80−106269
atom, correl. energy, fourth order diagrammatic, many body Rayleigh Schrodinger perturbation theory 80−63556
atom, dipole dynamic polarisabilities and two-photon photoionisation cross section calc., R-matrix approach 80−102444
atom, double ionisation by electron impact, soft X-ray emission *(Russian)* 77−34766
atom, elastic electron scatt., 10^2-10^3 eV, differential and total cross sections calc. 78−42215
atom, elastic electron scattering, crit. point 80−5622
atom, electron and positron elastic scatt., DWBA 77−30995
atom, electron and positron total scatt. cross sections, positronium form. 78−62916
atom, electron binding energies calcs. 78−86768
atom, electron Compton profiles from energy loss spectra 79−7013
atom, electron elastic cross sections, 0.04-1.5 eV 78−42214
atom, electron elastic scatt., differential cross-section meas. 77−3458
atom, electron elastic scatt., phaseshift anal. of ang. distribs. 79−22833
atom, electron elastic scatt., resonance struct. 77−50532
atom, electron impact, fine struct. resolved by reson. free-free radiative absorptions 79−3576
atom, electron impact, near threshold UV-emitting level excitation 78−25711
atom, electron impact, resonances, autoionising states 77−58170
atom, electron impact excitation, multiple-collision diffr. theory 78−82844
atom, electron impact excitation, photon emission, ang. correl. 77−14584
atom, electron impact excitation of $2s2p^63s$ and $2s2p^63p$ configs., energy loss obs. 80−91685
atom, electron impact excitation of autoionising states by fast electrons 79−72425
atom, electron impact ionis., differential cross sections 78−58839
atom, electron impact ionisation, ang. correl., first Born approx. 79−22840
atom, electron impact ionisation, coplanar symm. cross-sections for valence orbitals 79−86072
atom, electron impact ionisation, cross section ratios 78−94326
atom, electron impact ionisation, eikonal approx., shell-averaged, distorted-wave impulse approx. 80−37888
atom, electron impact ionisation cross-section 78−58844
atom, electron impact ionisation yield model 79−45851
atom, electron or photoionisation, electron shake-off, continuum states interaction 78−29766
atom, electron pulse radiolysis, 2p levels formation and decay kinetics 78−31665
atom, electron scatt., effective collision freq. calc. 79−3566
atom, electron scattering, elastic, at low-energy, polarised orbital calc. 78−82840
atom, electron scattering, elastic and inelastic, reson. spectra, R-matrix calcs. 79−72421
atom, electron shadow scattering, cross-sections calcs. 79−59575
atom, electron shake-off following electron or photon bombardment, continuum states interaction 77−14403
atom, electronic struct., perturbation theory, many-body, algebraic approx. 77−18776
atom, electronic struct., universal STO basis sets 79−10021
atom, emission line broadening by He 79−18145
atom, energy analysis, 200 eV-10 keV range 77−83763
atom, energy density functional, gradient corrections 78−25428
atom, energy exchange between scatt. and ejected electrons following $2s2p^63s(^1S)$ state autoionis. 78−46448
atom, exchange energies, Born-Oppenheimer exchange amplitude, Bonham series calcs. 78−29854
atom, excited, reactions in pure afterglow, plasmas using resonance absorpt. spectrometry 80−33835
atom, excited double hole state, single photon decay probability 77−34606
atom, exponential-six pot., new parameters 78−55217

neon continued
atom, Fermi correlation, for parallel-spin electrons in momentum space 77−10602
atom, Feshbach reson. classification, relation to ionis. pots., appl. Ne, Kr, Ar, Xe 77−54519
atom, few-electron states prod. K X-rays obs. 80−9718
atom, fine struct. obs. by beam-gas spectroscopy, level crossing resonances 80−9719
atom, first excited config., intermediate coupling coeff. 80−83450
atom, fluoresc. spectra, mol. bands, 0.1 to 6 atm., 3000-8200 Å 79−3394
atom, foil-excited, KLL-Auger spectrum 77−34604
atom, g-factors meas. by quantum beat spectroscopy 79−93955
atom, gaseous and in solid target, X-ray spectra 77−23452
atom, ground level isotope shift between ^{20}Ne and ^{22}Ne, obs. 79−31451
atom, ground state, configuration interaction, iterative variational method calcs. 78−55127
atom, ground state static polarisability and hyperpolarisability, numerical SCF method 79−36567
atom, ground state wavefunction, SCF HF calc. 78−90070
atom, heavy-ion induced K-shell Auger effect 77−6908
atom, highly-ionised, heavy ion impact, selective electron capture effects 80−14202
atom, impulse Compton profiles, atomic optimised pot. model 78−74618
atom, in magnetised positive column, fluoresc. obs., 4s and 3d levels props. 77−68006
atom, independent particle pots. comparison 80−52846
atom, ionisation potential, KLL Auger energies, SCF transition operator calcs. 78−41925
atom, isoelectronic sequence, excitation energy and oscillator strength, level crossing anomaly, relativistic RPA calc. 80−14077
atom, isoelectronic series, dipole matrix elements derivation 77−83519
atom, isoelectronic series, ionisation pots., Ritz law and Edlen formula 80−32854
atom, isoelectronic series, orbital binding energies within statistical exchange approx. 79−85895
atom, isotopic shift and fine struct. for $2p^5$4d and $2p^5$5s config., Doppler-free two-photon spectroscopy 80−23387
atom, K_α X-ray transition energies 79−98017
atom, K-absorption spectrum, core electron rearrangement effect 80−47880
atom, K-$L_{2,3}L_{2,3}$, post-collision interaction Auger effects 79−45686
atom, kinetic energy functional, gradient expsn. 77−6665
atom, KLL Auger spectrum, new developments, line energies, intensities 77−18868
atom, Koopmans' ionis. pot., relax. correction 79−18308
atom, L-shell photoabsorption cross-section, moment theory and finite basis pseudospectra calcs. 79−63938
atom, laser fluoresc. spectroscopy in microwave discharge 79−36578
atom, laser-induced line shifts and double-quantum Lamb dips 78−86825
atom, Li-like X-ray and Auger populations and line intensities from Cl^{13+} collisions 77−10625
atom, magnetorotation of 6328 Å line, absorpt. coeff. for $3s_2$-$2p_4$ transition 77−71768
atom, metastable, photoionis. cross section calc. 78−33485
atom, metastable, photoionisation rel. to laser development 78−13476
atom, metastable and pseudo-metastable states destruction by electron impact *(French)* 78−9260
atom, metastable electronic states, electron impact excitation, time of flight spectra 80−106411
atom, metastable form. by electron impact *(French)* 78−33611
atom, metastable level deactivation by electron collision in low press. discharge 78−83520
atom, metastable state, Doppler-free linear single-photon spectroscopy 78−50487
atom, metastable state ratio in fast beam, laser-induced fluoresc. obs. 79−54801
atom, min. basis of Slater-transform-Preuss functions 79−59343
atom, near IR spectral lines, transition probabilities 78−13450
atom, noncoplanar symmetric (e,2e) reaction, factorised distorted-wave approx., 0.4-2.5 keV 78−55245
atom, nonempirical calc. of X-ray K-absorpt. spectra 77−88465
atom, nonlinear laser spectroscopy, inside Doppler line *(Russian)* 78−21231
atom, optical oscill. strengths calc. 79−6914
atom, optical pumping of metastable ($2p^5 3s\,^3P_0$) state 78−25486
atom, optical transitions, Doppler broadening, compensation by vel. depend. light shifts 80−52930
atom, optical-optical double reson., $2p_4$ and $2s_2$ level g_J-values by mode crossing 77−50411
atom, orbital relaxation and final-state channel mixing, in Auger effect 78−50520
atom, oscillator strength determ. from resonance radn. self-absorpt. 77−18847
atom, outer 1s, 2s and 2p electron loss cross sections by multicharged ions 78−42185
atom, outer shell photoionisation, relativistic RPA calcs. 80−9571
atom, pair excitation correl. numerical coupled cluster method 80−47906
atom, photoelectron angular distribution β parameters, resonance parameters 78−21886
atom, photoelectron spectra, 21.2-151.4 eV and soft X-ray, ionis. cross-section 78−37683
atom, photoioinisation, expt. techniques, processes, theory, review 77−14402
atom, photoionis. cross-sections, L-subshells, 30-300 eV 79−31483
atom, photoionisation, complex amplitudes at low energy singly and doubly excited resons. 78−78673
atom, photoionisation, relativistic R-matrix theory 78−5184
atom, photoionisation cross-sections, ground state inversion pot. method 78−33481
atom, polarisation transfer collision with Rb atom, NMR of Ne 78−33453
atom, positive column, excited level decay at high electron temp. 77−23442
atom, positron and electron elastic scatt., 100-700 eV, optical model calcs. 77−34761
atom, positron scatt., positronium form. cross-section calcs. 78−9283
atom, positron scatt., total cross sections 78−22031
atom, positron scatt., total cross sections 79−86065
atom, positron scatt. and annihilation 78−33606
neon continued
atom, positron total scatt. cross sections 77−14573
atom, primary ionisation by ~2 MeV relativistic electrons *(Russian)* 77−75309
atom, props. calculation from optimised potential model 79−6895
atom, relax. consts. meas., two travelling waves reson. interaction 77−38644
atom, reson. broadening at low densities 79−31452
atom, reson. four-photon parametric mixing conditioned by multipole relax. rates difference 79−89959
atom, reson. free-free absorpt. by electrons in at. field, negative ion form. 77−3463
atom, reson. interaction of opposite waves, relax. consts. of common level 78−50511
atom, reson. level lifetimes, Zeeman coherence radiative and collisional transfer between excited states 77−23466
atom, reson. obs. in saturated absorpt. spectroscopy 79−89972
atom, reson. transition oscill. strengths, rel. to electron impact 80−27985
atom, scatt. from LiF (001) or W (110) surfaces, sudden decoupling approxs. 78−64437
atom, SCF electron-gas local-spin-density model including correlation 80−9488
atom, second-order correl. energy calcs. 78−33436
atom, self broadening of $2p^5$3p-$2p^5$4d spectral line 79−18144
atom, shake-up energies, Slater transition-state calcs. 79−89651
atom, spectra of metastable states, using Doppler-free spectrosc. with vel. selective pumping 79−81304
atom, spectral line broadening due to reson. interaction 79−22654
atom, statistical model with piecewise exponentially decaying electron densities 78−13408
atom, temp. perturbed Thomas Fermi eqn., variational principle 80−69074
atom, thermalisation of level populations 78−66649
atom, total and differential photoemission cross sections, final state approxs. comparison 77−50414
atom, transition probabilities in const. elec. field 80−37785
atom, triply-excited states contributing to correl. energy, diagrammatic perturbation theory 79−81161
atom, two and three level systems, laser induced dichroism and birefr. 78−79065
atom, two-electron one-photon transition rate 77−71772
atom, velocity diffusion, saturated absorpt. obs. of Hanle effect 77−61716
atom, vertical ionis. pot., many-body Rayleigh-Schrodinger perturbation theory 78−9063
atom, vertical ionis. pot. calc. from one-body Green's function 77−42440
atom, vertical valence ionis. pot., many-body Green's functions 78−22051
atom, weakly ionised, energy transfer at high press. 78−58845
atom, X-ray emission spectrum, multiplet struct. 78−82678
atom, X-ray scattering, anomalous, Kramers-Heisenberg dispersion calc. 79−89628
atom, X-ray spectral line broadening in solid and gas targets 77−6713
atom, X-ray spectrum, Kα satellite lines meas. by soft X-ray spectrometer 78−24911
atom, Zeeman coherence in saturated absorpt., velocity changing collisions study 77−46527
atom, zero-order Hamiltonian, for many-body perturbation theory 80−9483
atom+atom, excitation transfer between 2p levels 78−22006
atom+Cl^{12+}(S^{14+}) soft X-ray emitting slow multiply charged ion prod., recoil ion spectroscopy 77−50516
atom+H^+, ang. and energy distrib. of ejected electrons 79−31668
atom+Li(Na)(K)(Rb), quenching cross sections of alkali n^2P states, 5-100 eV 79−76505
atom broadening of 632.8 nm lasing level line width and shift meas. method 80−37066
atom doubly excited energy levels, subshell ang. momenta coupling, frozen core superposition of config. method 80−52874
atom photoionisation, double-electron, many body perturbation approach 78−17634
atom positron elastic scatt., close-coupling calc. 78−90292
atom with 1s-hole, wave function calcs. using radial orbitals, orthogonality 77−67971
atom-surface scattering, coupled channel calcs., symmetry appls. 78−92156
atomic, selfbroadened collision widths 77−38637
atomic beam, low-energy spectrometry rel. to surface investigations 77−28670
atomic deexcitation effects of X-rays, X-ray preionisation in TEA lasers 79−793
atomic disalignment collision cross sections of $2p_4$, $2s_2$ levels, mode crossing determ. 79−18162
atomic electron scattering, 20-300 eV, total cross sections 79−36778
atomic electron scattering, elastic, 500 eV, differential cross sections optical model 77−30990
atomic impact on W, generalised Langevin theory 77−8701
atomic polarisabilities and shielding factors, coupled HF approx. 78−22048
atomic spectra, Doppler broadening compensated by light shifts 79−41136
atomic structure, Hartree-Fock electron density, kinetic energy functional 79−26879
atomic structure, Thomas-Fermi model with Fermi-Amaldi correction 79−81156
atomic structure determ. by model pot. method 78−86777
atoms, classical many-body collision model incorporating Heisenberg and Pauli principles 80−63511
atoms, Compton profiles, Xalpha wavefunctions 80−106265
atoms, electron energy loss spectra, Compton defect characterised by shift and asymmetry parameters 80−95723
atoms, even-parity levels, double excited energy levels, frozen-core superposition, config. calcs. 80−106273
atoms, high resolution Zeeman spectroscopy by mode crossing 77−71776
atoms, photoionisation, many-body atomic transition theory 77−75111
Auger electron emission due to ion collisions with solid targets *(French)* 80−104031
Auger electron emission from ion-solid collision *(French)* 79−33876
beam source, high-flux 80−58416
biphenyl in Ne or Ar matrix, biphenyl ring torsion by vibronically resolved spectra 79−81228

neon continued
buffer gas line broadening in Cu vapour laser, gas temp. meas. 80−19020
[cc] He-Ne laser scanning system, for video record player, information identification *(German)* 80−106557
Clausius-Mossotti second virial coefficient 80−79426
compressed core density meas. by X-ray continuum edge shift 79−10705
crystal, absolute stability limit *(Russian)* 77−47373
crystal, electron localisation at surface *(Russian)* 79−60893
crystal, exciton exam. 78−51898
crystal, pure and benzene-doped, photoelectron emission, exciton states 77−44116
crystal, vacancy, electronic structure, Green's function theory 80−39525
crystalline, Frenkel exciton calc. 79−23906
crystalline, self-localized exciton, cavity radius, wave function and energy 80−6737
dense, electron injection, comparison with H_2 and He 79−73567
dielectric constant near liquid-vapour critical point 80−50252
diffusion and solubility in PTFE 80−6561
diffusion in RbCl, isotope effects 78−18841
diluent in XeCl laser, performance 79−94212
discharge, 4 MHz, electron energy distrib., probe diagnostics 78−38566
discharge, Boltzmann eqn., numerical study 77−35424
discharge, DC, ionis. wave wavelength, electron gas state depend. 78−1918
discharge, electron energy distrib. meas. in moving striations 77−55191
discharge, excitation mechanisms investig. using radial distrib. of excited atoms 80−38744
discharge, high-freq., excited atoms concentration determ., Ne or Ar, using spectral method *(German)* 80−70053
discharge, high-freq., excited atoms concentration determ., using spectral method *(German)* 80−70053
discharge, hollow-cathode, radiation signals in weak mag. field 78−70789
discharge, ionis. waves coherent nonlinear coupling 79−55497
discharge, ionisation wave, phase instability and disintegration obs. 78−67518
discharge, low-press., atom densities of first excited state 80−38750
discharge, moderate press., visible and UV radiation spectrum 77−31533
discharge, numerical study 79−32838
discharge, plasma column dynamic behaviour, equivalent circuit *(German)* 77−76217
discharge, positive column, axial electric field in transverse mag. field 78−55766
discharge, positive column, travelling strata dispersion 78−14232
discharge, pulsed, spectral charact. *(Russian)* 78−47201
discharge, radial distrib. of line intensities 78−18473
discharge, spectral line intensity radial distrib. 78−5930
discharge, time-resolved population meas. with N_2-laser-pumped dye lasers 77−80362
discharge, wavenumber spectra of turbulent ionisation waves 78−71541
discharge Faraday filter, dye laser freq. locking to absorpt. lines 77−79870
discharge in high press. narrow tube, Kadomtsev-Nedospasov instability 80−107004
discharge lamp, for AAS isotope anal. of B 78−20097
discharge lamp, UV, monochromated, addition to XPS spectrometer 78−89601
discharge plasma, Faraday rot. anomalies in a weak mag. field 80−38659
discharge positive column in longitudinal mag. field, metastable atom radial density distrib. obs. 78−67496
discharge transition, diffuse to contracted state, ionis. waves *(Russian)* 78−30511
discharges, HF and glow, excited atoms concentration determ. *(Russian)* 80−70050
dispersion forces between closed shell atoms 77−88522
Doppler-free two-photon spectra, fine struct. and hyperfine consts. of 4d′ level 77−61725
Doppler-free two-photon spectral line intensities 77−61726
dye laser with modes locked to atomic absorption lines, spectral charact. 80−9881
electric discharge, electron energy distrib. function, Boltzmann eqn. 79−50911
electric discharge, positive column and medium press., calc. 79−50912
electron beam excited states population, press. depend., fluoresc. obs. 78−17802
electron Coulomb profile beyond impulse approx. 80−87083
electron degradation spectra, inner-shell contribs. 77−3474
electron energy distrib. functions in weakly ionised gas under high E/N 80−53916
electron impact excitation, total cross section below ionisation threshold *(French)* 80−43187
electron impact K-shell excitation, EELS 80−106396
electron swarm with anisotropic vel. distrib. function 80−38520
electron transport coeff. calc. in counting gas mixtures 79−32727
electronic Compton profile beyond impulse approx. *(French)* 80−53057
embryo C3H10T1/2 cells, mouse, high-energy neon particle irrad., viral transformation enhancement 80−104668
energy loss straggling for He^{x+}, ion energies of 50-500 keV per nucleon 77−46620
equilibrium K-shell excitation of foil excited Ne-ions 79−22817
excited atom+molecules reactions, electronically excited atoms and alkali metal atoms analogy 80−76490
explosive burning in supernovae 80−94780
frozen gas matrix, laser beam waveguide propag. 80−64168
galactic abundance from Ne/O ratio in planetary nebulae 79−5887
galactic cosmic rays, Ne, Mg and Si isotopes high resolution meas. 80−51631
galactic cosmic rays, Ne isotopes abundances 79−101036
gas, collision-induced light scatt. at low density 77−71765
gas, compressed, Rayleigh-Brillouin spectrum, hydrodynamic region 80−100063
gas, compressed, Rayleigh-Buillouin spectrum, scaling 80−100062
gas, laser induced birefr., polarised light interf. obs. 77−19368
gas, metastable Hg atoms diffusion coeffs., temp. depend. 77−68731
gas, mobility of H^+ and D^+, 300K 77−11303
gas, spherical-source expansion, terminal speed ratio prediction, Monte-Carlo calc. 77−84285
gas, thermal cond., 90-273K 80−48836
gas, thermal cond. meas. using Peltier effect 78−45615
neon continued
gas, thermal conductivity, reduced temp., atmospheric press. 77−84385
gas atoms, electron thermalization time and position distribution meas. 80−93771
gas discharge, laser irrad. and voltage changes 78−63606
gas discharge plasma, electron impact depolarization 80−43847
gas discharge streamer propagation mechanism based on plasma vibrs. *(Russian)* 77−84546
gaseous, positron vel. distrib. at equilib., annihilation decay rate 77−71870
glow discharge, intermediate pressure, voltage-current charact. 79−55604
glow discharge, investigation with cylindrical hollow cathode in Ne and He *(Russian)* 80−28856
glow discharge, ionisation waves, regular and irregular, correlation meas. 78−1917
glow discharge, moving striation modes, numerical calc. 79−1365
glow discharge, Nonlinear mixing of two unstable coherent ionization waves 79−86573
glow discharge, reaction oscills. freq. eqn. derivation, expt. and numerical calc. 77−1027
glow discharge, short, lateral spread 79−46501
glow discharge, travelling striations, controlled by current modulation 79−82118
glow discharge, turbulent ionisation waves, correlation meas. 78−67519
glow discharge, voltage change due to laser irrad., 572-654 nm 78−63605
glow discharge plasma, coherent on-resonance self-focusing of optical pulses 79−41427
He-Ne laser discharge, dynamic charact. 79−98341
He-Ne methane saturated absorpt. stabilised lasers *(Chinese)* 79−59718
HF discharge in inert gas, optical diagnostics, bremsstrahlung 78−9871
HF discharge plasma electron energy distrib. 78−67540
high current discharge, short light pulse form. *(Russian)* 79−27846
hollow cathode discharge, laser induced impedance change, U cathode 79−46500
hollow cathode discharge, role of Penning ionisation of minor species 79−86633
hollow cathode discharge tube, spectral line intensities, rise time 80−103212
hot cathode discharge plasma, second order harmonic surface wave generation 80−38849
impact on W surface, tangential momentum accommodation coeff. meas. by acoustic vel. and absorpt. obs. 80−66867
implantation in Fe, effect on corrosion by H_2SO_4 soln. 80−71793
impurities, in solid D_2, effect on sp. ht. 79−33099
impurities in He quantum magnetometer, influence on signal parameters *(Russian)* 78−82010
impurities in magnetic GdCo and GdCoMo films prepared by RF bias sputtering 77−44163
interatomic potential and transport props. 77−14519
ion, energy and ang. distrib. in passing through C, Cu, Ag films 80−100292
ion, energy of metastable K-LL Auger transition *(Russian)* 78−82704
ion, energy-angle distrib. in C foil, test of Meyer-Klein-Wedell theory 79−49916
ion mobilities in He gas at 82K 80−75023
ionisation waves, state of electron gas 78−14124
ions, isoelectronic series, correlation energy and size, empirical relationship 77−79546
ions, slow, nuclear emulsion track width by photometric meas. 78−94167
ions, two vacancies in K shell, 2 electron 1 photon, and hypersatellite transition probabilities 78−46294
ions in low density plasma, dielectronic recomb., ionization equilib. and radiative energy loss, solar corona appl. 79−68903
isoelectronic sequence, dielectronic recomb. coeffs. 77−27172
isoelectronic sequence, ionisation pot. values 78−5363
isoelectronic sequence, level energies and lifetimes 79−89644
isoelectronic sequence, many-body photoionization calcs. 78−17631
isoelectronic sequence, X-ray spectra 80−87071
isoelectronic series, dielectronic recombination rate, scaling props. 80−32668
isoelectronic series, Koopmans' ionis. pot., virial scaling corrections 79−45655
isoelectronic series, one-electron and two-electron one-photon transitions 78−58775
isoelectronic series, second order correl. energy, Z depend. of irreducible-pair energies 80−91417
isotope separation, HF stationary discharge, travelling mag. field, barodiffusion separation 80−44049
isotope separation, plasma ion cyclotron reson. 77−10787
isotope separation by cataphoresis in DC gas discharge 80−103213
isotope separation by gaseous diffusion transport in regular geometries 79−94099
isotope separation using SIDONIE and PARIS separators 77−14269
isotopes, separation by jet-background interaction 79−54983
isotopes prod. cross sections in natural Mg, Al, Si, by 12-45 MeV protons 77−17310
isotopes prod. in lunar materials by solar cosmic ray protons, rate calc. 77−17311
isotopic compositions meas. in Allende meteorite 77−87344
Lamb-dip structure anal., linear and helicoidal polaris. 78−25852
laser, discharge pumped multiwavelength *(Chinese)* 80−102703
laser, high power, continuous operation 79−22974
laser, induced polarisation anisotropies, direct meas. 77−19234
laser compression of microballoons, explosive-pusher mode, X-ray emission diagnostics 79−54598
laser imploded glass microbubble, compression, X-ray emission 78−18454
laser line, 260 THz, direct freq. meas. 80−53266
laser transition, 6328 Å, homogeneous saturation due to collisions, weak collision model 78−78995
laser transitions, 1.52 μm and 633 nm, mode crossing resonance shape 79−18163
lattice heat capacity, thermal vibrations, Lindeman parameter, lattice dynamic model *(Russian)* 80−29141
Lennard Jones (12,6) pot. distance parameter, transport props. calc. 80−79423
Lennard-Jones potential, equation of state determ., high temp. and pressure, computer expt. 78−75800

neon continued
liquid, Brillouin neutron scatt., limits of classical hydrodynamics for collective motions *(German)* 77−24258
liquid, comparison on interaction induced light scatt. and IR absorption 80−60561
liquid, compressibility, long wavelength limit of liquid struct. factor 78−67633
liquid, effective pair pot. from perturbation approach 77−68908
liquid, electron drift vel., mol. solute effects 77−4338
liquid, higher order struct. functions in long wavelength limit, improved perturbation approx. 79−37606
liquid, higher order structure factors and their inverses 79−55646
liquid, in bubble chamber, Ne-H_2 mixture 77−396
liquid, mol. dynamics calcs. 77−19857
liquid, neutron scatt. determ. of dynamic struct. factor, generalised hydrodynamic anal. 80−54103
liquid, perturbation theory for sound prop. vel. *(Russian)* 77−15500
liquid, principle of corresponding states for viscosity 77−84959
liquid, short range order parameter 78−83712
liquid, struct. factor, improved perturbation anal. of Percus-Yevick eqn. 77−58942
liquid, T_c, P_c, V_c, from eqn. of state 78−2228
liquid, US velocity at 5 MHz *(Russian)* 78−83879
liquid and solid, absorpt. and luminesc. spectra of self-trapped excitons 79−65893
liquid independent structure model, critical point, liquid-vapour equilib., second virial coeff. *(Spanish)* 77−4031
liquid n-H_2, n-D_2, Ne mixtures, deviation from Rao-Wada rule 78−75729
liquid radial distrib. functions and structural parameters 79−55640
liquids, optimised cluster expansion, struct. function evaluation 80−49085
low energy positron scattering 79−89786
low press. discharge, electron free streaming waves expansion 80−79595
low-pressure gas discharges, model 79−37560
luminescent discharge, loss mechanisms *(French)* 78−9877
lunar dust, inert gas conc., separation methods and methods of treatment *(French)* 80−51674
matrix environment effects on PbS molecule vibronic emission systems 77−58070
medium-pressure discharge, electron temp. radial profile meas. by electron-atom bremsstrahlung continuum 78−67497
melting curves, quantum corrections, effective pair pot. calcs. 77−55347
mesic atom, X-ray radiation anisotropy, suppression coeffs. *(Russian)* 78−22058
metastable atom concentration; expts. determ. inside hollow cathode arc discharge *(French)* 77−31540
in meteorites, Ne isotopic comp. rel to Mg(n,α)Ne cross sections 79−96874
methane+methane (He)(Ne)(Ar), dispersion forces 78−13565
microballoon spectra, density-sensitive dielectronic satellite lines 79−72270
microwave breakdown field calc., Monte Carlo method 78−67551
molar volumes and thermodynamic props., 25 to 150°C up to 7 kbar 77−42957
momentum eigenfunctions in complex momentum plane, Hartree Fock functions 80−63517
muonium formation by positive muons 79−57272
Ne IX, electron impact excitation cross section calcs. using nonrelativistic Coulomb-Born approx. 77−42414
negative afterglow, pulse excited, at. spectral lines, microwave quenching 78−63591
negative glow discharge, recomb. at. excitation *(Russian)* 77−76225
negative ions, scatt. electron spectra, distinction from neutral autoionising states 80−83482
normal boiling point reproducibility, cryostat appl. 78−79757
nuclear induced plasma, simulated 80−64786
optical fifth harmonic conversion, 53.2 nm generation 77−10979
Orion Nebula, Ne, S and O abundances from fine-struct. lines obs. 80−4410
Penning ionisation of di/triatomic mols., electron spectra, vibr. transfer 77−14555
Penning mixtures, statistics of gas gain 79−45535
permeability in glass laser targets 77−35367
permeation eccentricities of He, Ne, and D-T, from SiO_2-CaO-Na_2O glass microbubbles 78−47598
phonon dispersion relation, Gruneisen parameters at high press. 79−42179
photoionization mass spectroscopy using synchrotron radiation, reson. width meas. 79−31478
physisorbed on metal, polarisation due to short range interaction with substrate 80−39428
planetary nebulae, Ne V/Ne IV abundance ratios rel. to central stars temps. 79−2565
plasma, 60 MeV ion beam-created, electron props. diagnostics *(French)* 80−10407
plasma, compression, spectra, temp. and density calc. model 78−59663
plasma, electron collision ionisation, electron kinetic behaviour during elec. field perturbation *(German)* 80−64676
plasma, electron energy distrib., relax. process 78−30507
plasma, electron-atom collisions, interaction parameters 100-10000K 79−98857
plasma, EM waves, parametric decay near upper hybrid freq. 78−59590
plasma, generated by 200 MeV protons, electron density and electron temp. 78−22568
plasma, ionisation waves, electron energy distrib. function 78−30421
plasma, laser-imploded target, spatially-resolved X-ray spectra diagnostics 79−37543
plasma, low ionised anisothermal plasma, ionising electron collision kinetics *(German)* 80−33731
plasma, low press. discharge, kinetics and column impedance *(German)* 77−58845
plasma, non-isothermal, low-ionised, influence of HF elec. field on electron ensemble *(German)* 79−77383
plasma, of glow discharge, electron velocity distribution function relax., periodic behaviour in highly modulated elec. field 79−64935
plasma, parametric excitation of backward ion cyclotron wave with a pump in the lower hybrid range 79−37490
plasma, photon reabsorption attenuated radiation emission 80−64776
plasma, reson.-absorpt., of glow discharge positive column, Ne superradiation pulse variation 78−71489
neon continued
plasma, screw instability, wall stabilised arc column in longit. mag. field 78−87551
plasma, temporal decay, electron distrib. function and macroscopic parameters relax. 78−18374
plasma, weakly ionised, photon echo relax. obs. in RF discharge 80−43986
plasma electron velocity distrib. function relax., time depend. electric field *(German)* 77−31424
population inversion mechanism between 4p→3d, laser generation conditions 80−1185
population of $5s'[1/2]_1^0$, $4p'[3/2]_2$ levels interacting with laser radiation 80−23670
positive column, 3S and 3P level populations, rel. theory with recomb. 77−10766
positive column, axial elec. field decrease 79−77439
positive column, axial elec. field in transverse mag. field 78−18472
positive column, electron temp. depend. on transverse mag. field 78−1932
positive column, high-press., optical and probe diagnostics 78−51383
positive column, in low-press. discharge, multistep ionisation 78−75446
positive column, in transverse mag. field, plasma parameter diagnostics 79−19103
positive column, moving striations in longitudinal homogeneous mag. field 78−67523
positive column, radial distrib. of excited atoms *(French)* 78−14237
positive column, wall loss in transverse mag. field 78−55767
positive column, with diffusion loss to wall, axial elec. field effects *(Japanese)* 78−47196
positive column contraction under diffusion-recombination conditions 80−24293
positive column in transverse mag. field, axial electric field 78−30506
positive column plasmas, metastable atom density meas. by improved self absorpt. method 80−87968
positron annihilation in rare gases, Doppler broadening meas., electron mom. distribs. 78−55131
positronium annihilation rate in dense gas 78−55258
pulsed amplified spontaneous emission intensity, spatial and frequency distribs. 79−50270
pulsed amplified spontaneous emission source, statistics and spatial distrib. meas. 78−22102
pulsed transverse discharge, spectrosc. absorpt. investig. with nanosec. time resolution *(Russian)* 80−64782
purification system for Ne circulating in spark chambers 77−14309
recoil ion, highly charged, K X-ray emission 80−91649
resonance excit. of $1s_2$ and $1s_4$ levels via He^+ 100-1000 keV impact 77−10611
RF discharge, emission modulation due to fast electron distrib. time variation 79−41900
ring laser, two-mode, oppositely travelling waves, beat freq. obs. 77−10963
saturated absorption optical Ramsey fringes 79−54204
selective adsorption on LiF(001) during elastic and inelastic scatt. 77−66564
shear viscosity determination under high pressure, using capillary viscometer 78−55708
solar wind, inert gas abundance, 500 Myr ago from lunar dust anal. *(German)* 80−51637
solid, a priori calc. of n=1 valence exciton 78−10364
solid, Brillouin scatt. intensity, elastooptical coefficients 78−10907
solid, bulk and surface excitons, transmission and refl. spectra obs. 79−95340
solid, bulk excitons, expt. 80−92827
solid, bulk excitons, theory 80−92826
solid, cond. band calcs., use of electron atom scatt., phase shifts 77−85139
solid, desorption heat capacity of adsorbed ^4He 80−10736
solid, dielec. const., 4.2-15K 77−8488
solid, doped with Xe and benzene, energy transfer 77−32416
solid, elec. cond. obs., insulating up to 500 GPa 78−95315
solid, energy bands, depend. on choice of exchange-correlation pot. 80−70607
solid, hole band struct., Bratsev wave function calcs. *(Russian)* 80−65437
solid, interface with Cu, thermal boundary resist., 1-3K 77−20178
solid, interface with Cu, thermal boundary resist. meas. above 1K 77−72769
solid, large-gap insulator, valence excitons, integral eqn. method calc. 77−11858
solid, lattice dynamics calc. using energy band theory 80−49320
solid, lattice relax. model of n=1 exciton emission 79−47492
solid, lattice thermal cond. 0.5 to 10K, dislocation densities, average grain sizes 78−79830
solid, lattice vibrs., heat capacities 79−42169
solid, n=1 surface excitons and LO-TO splittings of bulk excitons 79−73445
solid, NMR study of dilute o-H_2 impurity 80−25228
solid, phonon densities of states and dispersion curves, unpaired elastic force model 79−51220
solid, phonon density due to anharmonic effects 77−62597
solid, phonon dispersion, many body pot. assuming variable at. polarisability, mech. props. 79−55840
solid, phonon-dispersion and mode Gruneisen parameters 77−11651
solid, pure and Xe, Kr, Ar doped, photoemission yields and reflectance spectra, exciton dynamics 77−28123
solid, quantum defect theory of excitons 78−51902
solid, quasi-line emission in transitions between excited states *(Russian)* 79−91494
solid, solubility in high press. He 80−10674
solid, thermal cond., 0.5-10K 77−43396
solid, two-phonon scatt. in inelastic neutron scatt. calc. 78−59910
solid, ultraslow diffusion of ^{21}Ne, adiabatic demagnetisation in rotating reference frame 77−73095
solid adsorbed layer, porosity of solid gas layers, appl. to cryosorption pump *(Japanese)* 80−20031
solid and gaseous, excitons 78−23026
spectral line broadening as diagnostic for compressed laser fusion targets 79−98979
spectral line relative intensity, radial depend. in low press. discharge 80−37764

neon continued
stationary discharge with diffuse recombination, limit current and multiple states 78−67498
stony meteorites, light noble gases anal. compilation 78−65574
stopping powers of Z=10 to 18 ions, ^{22}Ne, using DSAM lifetime meas. 78−47456
streamer plasma characts., cond., plasma density and field strength calcs. *(Russian)* 77−47262
superradiation propagation through reson.-absorbing positive column plasma, pulse shape change 79−4117
supersonic radiation waves, excitation by CO_2 laser 79−90433
thermal conductivity, at high press. 80−103099
thermal conductivity, law of corresponding states *(Russian)* 78−87426
thermal conductivity, Lennard-Jones (12-6) pot. parameters calcs. 80−28591
thermal conductivity, near 300K, density depend., 0.8-35 MPa 78−67304
thermal conductivity coeff. meas. 1100-2200K range, differential technique 77−33989
thermosphere, Ne density in situ meas. by AE-C satellite 77−21956
transport properties, exponential 6-pot. model parameters 77−47130
triple point realisation, reference temperature appl. 78−73997
vapour, opto-galvanic effect 79−98013
vapour press., entropy and enthalpy, thermodynamic consistency, two-parameter eqn. 77−80613
vapour press. and triple point, influence of impurities 78−79756
vertical valence ionisation potential calc. by perturbation, CI and CPA techniques 80−69263
volume recombination coeff. meas. method, in Ne positive column, ionis. role 77−51252
X-ray emission, post-foil, Kalpha, correlation with empirical charge state distribs. 78−15252
X-ray line shift for high density laser produced plasma diagnostics 80−64778
Ar ion laser, He, Ne, impurity effects, ignition enhancement and instability suppression 79−13948
Ar:Ne, localised mode due to Ne impurity, Green function technique 77−1201
Ar-Ne, liquid solution, dielectric props., intermolecular interactions *(Russian)* 80−88904
Ar-Ne, mixture, cataphoretic segregation, spectroscopic meas. 79−79261
Ar-Ne gas, positron vel. distrib. at equilib., annihilation decay rate 77−71870
Ar-Ne mixture, thermal conductivity, 400-1500K 79−18987
Ar-Ne mixture in critical region, renormalised one-chain approx. 77−11452
Ar-Ne mixtures, thermal diffusion 80−1726
Ar-Ne(Kr) systems, pot. parameters from binary diffusion coeffs. 78−37700
Ar^{2+}+Ne(Ar)(Kr) single electron capture cross-section 77−88550
atom, correlation energy, many-body Rayleigh-Schrodinger perturbation theory calc. 78−894
atom, oscillator strengths, determ. from self-absorption of reson. radiation 79−89641
atom+Al foil, projectile K-vacancy production cross section, X-ray production rel. to target thickness 77−19059
B+He(Ne)(Ar), ground and excited states interaction, B spectral line breadth 77−68092
Be^++Ne, Be Auger spectra 77−57951
CO-Ne, cryst. at 5K, absorpt. and emission spectra, exciton interpretation 79−87481
CO_2^+, mobility in Ne gas 78−14125
CO_2-N_2-Ne-H_2O mixture IR laser *(Russian)* 79−10323
CO_2+$H_2(CO_2)$(Ne)$(NH_3)(CH_3F)$, rot. transfer collisions, momentum transfer distributions 77−523
Cl^--Ne(Ar)(Kr)(Xe), longitudinal diffusion coeff., generalised Einstein relation 79−86552
Cl+He(C)(O)(Ne), K-shell ionising collisions, average L-shell ionisation probability, K_α spectra 79−72408
Cl^{n+}+Ne$(SiH_4)(H_2S)$(HCl)(Ar), K X-ray cross section, projectile charge depend. 77−19029
Cs^+ in He and Ne gas, ion mobility and longit. diffusion coeff. 78−67308
Cs+Ne, optical pumping, spectral line shape *(Spanish)* 79−22662
Cs_2+He(Ne)(Ar)(Kr)$(N_2)(CH_4)$, collision-induced dissoc., atom-mol.-exchange optical pumping 78−22008
$Cs(6^2P_{3/2})$+He(Ne)(Ar)(Xe), collisional depolaris., nucl. spin depend., by Zeeman scanning 77−19012
Cu-Ne, hollow cathode laser discharge, spectroscopic temp. meas. 79−7490
Cu-Ne CW mW-level laser source at 250 nm 80−43352
Cu-Ne laser, spectral lines emission of gas-discharge pulse plasma 79−31883
Cu-Ne mixture, 3-20 kHz pulse discharge obs. 78−71092
CuCl/Ne discharge, extrema of electron density and output pulse energy 79−10283
D_2 lamps, influence of Ne and Ar on spectral parameters 80−86460
D_2-Ne capillary-arc lamp, optimum parameters 80−95971
DT fusion microballoon, Ne seeded, compression by CO_2 laser 79−22466
F ions+Ne(Ar)(Kr) and C foil and slab, K shell X-ray spectra 78−17599
F+Ne(Ar)(Kr), thermal energy interaction pots., crossed beam study 79−68288
F_2-Ne, mixtures, VUV emissions, mol. F_2 laser at 1575 Å 77−75487
H+inert gas atom, interaction pot. from electron gas model 79−31637
H+Ne^{2+}, ionization model for NGC 7027 planetary nebula 78−36671
H_2-Ne, positron annihilation involving low energy positrons, lifetime spectra 79−94091
H_2-Ne, positron annihilation, positron form. 79−94092
H_2-Ne negative glow discharge, H Balmer line excitations *(Russian)* 77−46516
H_2+Ne, NMR longit. relax., mole fraction depend. 77−61767
H_2+Ne, vibr. excitation effect on dissoc. excitation efficiency 79−76495
H_2^++Ne, vibr. energy effects on kinetics, phase space model 78−11508
HCl+Ne, IR induced vibr. transition, Schrodinger eqn. distorted wave calc. 77−23538
HD+Ne, j=0 to 1 scatt. differential cross section, interaction pot. anisotropy 77−42382
He-^{20}Ne-^{22}Ne, orthogonally polarised laser mode interactions *(Russian)* 77−19235
neon continued
He-CO_2-Xe, supersonic elec. discharge TEA laser, mag. field effects 79−7110
He-Ne, 1.15 μm laser line, 260 THz freq. synthesis using $CdGeAs_2$, Ag_3AsS_3 crysts. 79−64263
He-Ne, 3.39 μm laser, actively mode-locked oscill., modulation freq. depend. 77−61983
He-Ne, 3.39 μm laser with no freq. modulation, freq. stabilisation rel. to methane saturated absorpt. 79−76700
He-Ne, 6328 Å, single-mode collapse 78−94404
He-Ne, 632.8 nm laser, energy characteristics, spatial inhomogeneity effect 77−75483
He-Ne, 632.8 nm line broadening, perturbation energies additivity 79−54941
He-Ne, afterglow of low-press. glow discharge, recombination processes 78−26366
He-Ne, anisotropic ring laser cavity, polarisation characts. 79−59726
He-Ne, complex resonator laser, stabilisation by freq. offset-lock 77−31107
He-Ne, gas discharge laser, stimulated emission, vel. to striation 80−37994
He-Ne, generation by hollow cathode discharge excitation, mechanism *(Russian)* 77−10888
He-Ne, glow discharges, AC cataphoresis meas. using light spectrometry 79−60096
He-Ne, HF discharge, electron energy distrib. 77−34874
He-Ne, I_2 stabilised, freq. stability and reproducibility 78−13726
He-Ne, I_2 stabilised lasers, conf., Germany (Feb. 1977) 78−87069
He-Ne, I_2 stabilised laser design, freq. reproducibility 78−87070
He-Ne, I_2 stabilised laser research 78−87071
He-Ne, I_2 stabilised laser with hot wall I_2 cell 78−87073
He-Ne, I_2 stabilised laser, instrumental freq. offsets 78−87084
He-Ne, I_2 stabilised lasers, international intercomparison meas., hyperfine struct. spacings 78−87088
He-Ne, I_2 stabilised lasers, beat frequency, international comparisons *(French)* 78−87090
He-Ne, internal mirror laser, polarisation props. of output beam 77−46744
He-Ne, LG-75-1 laser 79−94256
He-Ne, laser, Ne absorber induced features in AC response 77−3613
He-Ne, laser, scheme for automatic fine frequency tuning along the Lamb depression 80−74385
He-Ne, laser, short pulses, self mode-locking *(Rumanian)* 79−13995
He-Ne, laser frequency measurements: a review, limitations, extension to 197 THz (1.5 μm) 78−81952
He-Ne, laser pumping transition, mol. beam obs. 77−7064
He-Ne, laser revived by running in He atm. 78−46614
He-Ne, laser single frequency generation model and expt. *(Russian)* 77−58314
He-Ne, laser wavelength measurement using digital interferometer 80−37079
He-Ne, lasers, low-power low-cost design and manufacture 77−19329
He-Ne, lasing spectrum, modulation freq. of resonator losses 77−34902
He-Ne, methane and I_2 stabilised lasers, wavelength intercomparison using Michelson interferometer 78−87089
He-Ne, narrow linewidth frequency scannable 3.39 μm laser, appls. 77−88757
He-Ne, oscills. in laser discharge 78−55339
He-Ne, pulsed atomic Ne laser, time and energy characts. in mag. field *(Russian)* 78−22108
He-Ne, ring laser, difference freq. depend. on active medium gain 77−722
He-Ne, ring laser, rapidly pumped, competition between opposite waves 78−17985
He-Ne, ring laser, Zeeman effect, influence of reson. radiation trapping 77−75574
He-Ne, rotating ring laser, output characts. 78−29982
He-Ne, single mode laser, mode polarisation in transverse mag. fields 78−22107
He-Ne, single mode laser, emission zone nonlinear active lens effect 80−32960
He-Ne, stabilizer two freq. 0.63 μ laser 79−94243
He-Ne, stable laser with methane absorpt. cell, 7 Hz width 3.39 μm line emission 78−17974
He-Ne, thermal diffusion factor, 65 to 300K 78−71418
He-Ne, three-mode laser, total intensity under mode locked conditions, freq. stabilisation 77−83853
He-Ne, two-mode ring laser, stimulated emission regimes 77−657
He-Ne, weakly anisotropic resonator laser, natural polarisation fluctuations of emission 77−79801
He-Ne $^{127}I_2$ stabilised laser source for Michelson interferometer, optical feedback obs. 80−106545
He-Ne 3.39 μm laser, FM eliminated CH_4 locked freq. stabilisation in dual feedback control 80−99772
He-Ne 3.39 μm laser mode-locking for ultrashort pulse generation 77−83909
He-Ne ($^{127}I_2$) laser freq. stability, expt. 77−83915
He-Ne CH_4 locked laser, freq. stability meas. 80−87422
He-Ne CW laser nuclear pumping demonstration 79−13949
He-Ne commercial multimode low power laser, conversion to single mode laser 80−53325
He-Ne compact LG-78 laser 79−7148
He-Ne complex resonator laser, stabilisation 78−55374
He-Ne discharge, 3071, 5665 and 10353 nm. laser transitions 77−54692
He-Ne discharge, gain probing by intracavity dye laser spectroscopy 77−7092
He-Ne discharge, striation oscills., spectral width variations 77−62429
He-Ne discharge, striation parameters, discharge current modulation effect 77−84555
He-Ne discharge laser, stimulated reactive oscills., laser-elec. circuit Q 77−58315
He-Ne discharges, striations in narrow discharges 80−38736
He-Ne double mode laser in axial mag. field. *(Russian)* 79−86160
He-Ne dual mode laser, injection modulation in coupled laser oscillators 80−99773
He-Ne gas laser, anisotropic resonator, linear polaris. freq. depend. 77−10961
He-Ne gas laser, behaviour in nonsynchronous frequency modulation regime *(Russian)* 79−7161
He-Ne gas laser, glow discharge electron irrad. rel. to output characts. 79−64198

neon continued
He-Ne gas laser, modulation method, for relative excitation level, cavity bandwidth and at. temp 80−5771
He-Ne gas lasers, 2 mW and 5 mW, reliability 80−95913
He-Ne gas mixture plasma, role of charge exchange in form. of optical props. 80−28600
He-Ne gas ring laser, unidirectional two-mode lasing, stability region width 79−76721
He-Ne glow discharge, passive freq. charact. 79−50915
He-Ne I_2 stabilised laser, practical approach to design and construction 80−19051
He-Ne IR laser, internal modulation of polarisation 77−19350
He-Ne internal mirror lasers, polarisation in mag. field 78−17907
He-Ne internal mirror laser, degeneration of longitudinal modes and freq. stabilisation *(Japanese)* 78−90426
He-Ne laser, $^{127}I_2$ saturated absorption stabilised, wavelength meas. *(Russian)* 79−22996
He-Ne laser, $^{127}I_2$ stabilised, freq. shifts, limitations 78−90440
He-Ne laser, $^{127}I_2$ stabilised, length or freq. standard 80−106544
He-Ne laser, 0.63 μm emission intensity fluctuations, spectral correl. 78−1212
He-Ne laser, 0.633μm line freq. stabilisation with 3.39μm line locked to CH_4 80−28258
He-Ne laser, 3.39 μm, in-resonator losses, effects on power *(Russian)* 78−5455
He-Ne laser, 60 mW, perturbation spectroscopy *(Rumanian)* 78−50752
He-Ne laser, 6328 Å, output power, using intracavity rot. reflector 79−7113
He-Ne laser, 6328 Å power fluctuations due to striation noise 80−78834
He-Ne laser, anisotropy due to saturating fields 78−55337
He-Ne laser, autodyne effect 79−81404
He-Ne laser, beat freq., high displacement sensitivity meas. 80−95926
He-Ne laser, beat freq. generation between CW dye laser with 80-GHz freq. offset 80−1253
He-Ne laser, cavity losses, phase polarisation method in lasing regime 80−87413
He-Ne laser, compact, transverse microwave discharge, energy charact. 80−64064
He-Ne laser, competitive oscillation mode frequency stabilisation *(Russian)* 79−22962
He-Ne laser, discharge current rel. to optical power, automatic control of radiation level *(Russian)* 77−46716
He-Ne laser, discharge tube design and construction *(Czech)* 79−76702
He-Ne laser, double reson., RF mag. field strength and g-value depend. *(Japanese)* 78−9359
He-Ne laser, doubly resonant intracavity SHG of 1153 nm radiation with stabilization on HFS components of $^{127}I_2$ 80−33077
He-Ne laser, elec. parameters of active element 79−3682
He-Ne laser, field distrib. and spatial coherence of superluminescence at 3.39 μ transition *(Russian)* 78−13682
He-Ne laser, freq. charact. under two-mode generation 80−53264
He-Ne laser, freq. conversion in Na vapour *(Russian)* 78−33776
He-Ne laser, freq. stability improvement with hot wall I cell 77−83914
He-Ne laser, gain, saturation, polarisation and spectral inhomogeneities, relax. consts. 77−50652
He-Ne laser, high stability, single freq., 3.39 μm 78−71121
He-Ne laser, hot wall I cell freq. stabilisation using saturated absorpt. 77−65598
He-Ne laser, I_2 stabilised, wavelength intercomparison 77−19305
He-Ne laser, I_2 stabilised, reproducibility limitations 77−46740
He-Ne laser, I_2 stabilised, freq. shifts 77−50697
He-Ne laser, I_2 stabilised, realisation of length unit 78−87068
He-Ne laser, I_2 stabilised, design construction and performance 79−13978
He-Ne laser, I_2 stabilised, saturated absorpt. lines press. and power broadening 79−76765
He-Ne laser, I_2-stabilised, with long path interferometer, optical feedback effect 77−9544
He-Ne laser, IR lasing lines, anomalous competition effects *(Russian)* 77−68202
He-Ne laser, in axial mag. field, output power dependence of mode locking phenomena 78−71129
He-Ne laser, intensity fluctuations meas., comparison with He-Cd laser 78−71087
He-Ne laser, intensity oscillation spectrum obs. for external modulating signal on discharge plasma 77−7066
He-Ne laser, internal pulse-code modulation, 0.6328 μm at 150 Mbits s^{-1} 79−76725
He-Ne laser, intracavity saturable Ne absorber, response enhancement 77−65602
He-Ne laser, kinetics calcs. using electron distrib. function *(Russian)* 77−61941
He-Ne laser, LG-56, radiation power stabilisation 78−17970
He-Ne laser, laser system for 3.39 μm freq. synthesis 78−18001
He-Ne laser, longit. mode locking using Fabry-Perot etalon 79−50318
He-Ne laser, low noise manufacturing 78−79038
He-Ne laser, mag. polarised performance 77−14750
He-Ne laser, manufacturing problems with low noise specification 78−59047
He-Ne laser, methane stabilised, intercomparisons 77−19304
He-Ne laser, methane stabilised, freq. fluctuation analysis 77−31108
He-Ne laser, methane stabilised, 3.39 μm freq. meas. relative to 10.17 μm CO_2 laser 77−31113
He-Ne laser, methane stabilized, low noise laser tube charact. *(Japanese)* 78−25891
He-Ne laser, methane-stabilized at 88 THz 80−73304
He-Ne laser, microwave pumping advantages 78−50754
He-Ne laser, mode interaction, transition level degeneration effects *(Russian)* 77−61940
He-Ne laser, mode selection and mode locking, effect on two-photon absorpt. efficiency 78−83023
He-Ne laser, mode stabilisation by axial mag. field, long resonator case 77−7143
He-Ne laser, Ne $3s_2$-$2p_4$ transition, relaxation charact. of degenerate states obs. using polarisation spectroscopy *(Russian)* 80−27348
He-Ne laser, near IR emission charact., coupled transitions 77−27275
He-Ne laser, operating on 0.63, 3.39 μm coupled transitions, intensity modulation 80−69365
He-Ne laser, optical freq. standard, freq. stabilised by warm walled I_2 cell *(French)* 78−42343
He-Ne laser, optical heterodyning of spontaneous emission 78−29995
neon continued
He-Ne laser, optimal conditions for microwave pumping 80−32961
He-Ne laser, Original Equipment Manufacturer applics. 78−33765
He-Ne laser, output power, unsaturated gain distrib. 78−50751
He-Ne laser, population changes of Ne levels induced by laser actions in intermed. IR 78−29932
He-Ne laser, population changes of Ne levels, laser action in intermediate IR 78−29933
He-Ne laser, population inversion radial distrib. in active element, excitation conditions effect 78−71079
He-Ne laser, power characteristics obs., with CH_4 cell, at λ=3.39 μ *(Russian)* 78−1207
He-Ne laser, radial profiles of upper and lower level emission 77−31088
He-Ne laser, radiation field spatial distrib. distortions due to multilayer dielectric mirrors 77−38970
He-Ne laser, refl. anisotropy of 6320 Å mirrors 79−98413
He-Ne laser, rejuvenation methods 77−37687
He-Ne laser, self-locked, pulse velocity, power and mode phase 77−61939
He-Ne laser, simultaneous oscillation at 0.63 and 3.39 μm, output power depend. on loss in mag. fields *(Japanese)* 80−32959
He-Ne laser, six new transitions near 1.49 μm 77−38856
He-Ne laser, spatial anisotropy induced by cascade laser transitions 78−29931
He-Ne laser, stabilised by I_2 saturated absorpt., technological principles *(French)* 78−87075
He-Ne laser, stabilised by I_2 saturated absorpt., performance charact. *(Chinese)* 79−59717
He-Ne laser, stabilised by $^{127}I_2$ saturated absorpt., wavelength international comparisons 80−95872
He-Ne laser, thermal effect of penetrating radiation *(Russian)* 78−22109
He-Ne laser, three mode stimulated emission 77−75485
He-Ne laser, transition probabilities of Ne spectral lines at 352, 363, 345 and 543 nm 78−25851
He-Ne laser, two-mode ring laser power resons. 78−1211
He-Ne laser, two-photon amplification on cascade-transitions, power tuning curve meas. 80−48219
He-Ne laser, type 300.1 TEM_{00} *(Rumanian)* 80−9898
He-Ne laser, unmodulated, stabilizing to $^{127}I_2$ hyperfine component, preliminary expt. 79−50328
He-Ne laser, use at 0.63 μm, intensity fluctuations at quantum level 77−27274
He-Ne laser, wavelength meas. appl., reference standard 77−7124
He-Ne laser, wavelength switching using var. methane press. 77−19312
He-Ne laser, with methane absorpt. cell, reson. freq. shift with methane press. 77−50687
He-Ne laser average output power, resonator losses, freq. modulation 77−34901
He-Ne laser beam, intensity fluctuations, spatial distrib. 79−18458
He-Ne laser discharge tubes, design and technology, review *(Czech)* 79−72586
He-Ne laser energy characteristic control, by discharge current modulation 77−79800
He-Ne laser fluctuation spectra of freq. and amplitude 78−82950
He-Ne laser IR applications 79−94275
He-Ne laser light polarisation in transverse mag. field, Zeeman effect *(Dutch)* 78−29997
He-Ne laser mode locking by three-level reson., Zeeman tuning of intracavity Ne absorber 79−89943
He-Ne laser model LG-10, design *(Rumanian)* 80−87407
He-Ne laser near threshold, intrinsic third-order intensity correlation 77−10887
He-Ne laser photon statistics variation with cavity length 80−53265
He-Ne laser plasma, line profiles meas. by optogalvanic spectroscopy 78−62233
He-Ne laser plasma, metastable at. and electron density diagnostics 77−84499
He-Ne laser pulsed internal modulation 77−61985
He-Ne laser radiation intensity rel. to striations and oscillations 77−83852
He-Ne laser reference IR frequency meas. installation 77−79068
He-Ne laser saturation resonance in static magnetic field 77−54693
He-Ne laser simultaneous oscillation at 0.63 μ and 3.39 μ in mag. field, and with Brewster windows 79−68381
He-Ne laser stabilisation, I_2 absorption cell power densities 80−99767
He-Ne laser stabilisation and performance for dimensional meas. 80−19049
He-Ne laser stabilisation by I_2 612 nm saturated absorption 80−99765
He-Ne laser stabilisation by I_2 611.8 nm saturated absorption 80−99766
He-Ne laser stabilised by saturated absorpt. in I_2 at 612 nm 79−59730
He-Ne laser stabilised by methane E-component saturated absorpt., quantum freq. standard 80−9901
He-Ne laser stabilised by methane E-component, reference source freq. reproducibility 80−106507
He-Ne laser status, I_2 vapour stabilised 78−87072
He-Ne laser tube, laser module LGK 7621, construction 80−53314
He-Ne laser tube construction and cost analysis 77−65599
He-Ne laser tube reconditioning 77−78933
He-Ne laser two-beam interferometer phase errors *(Russian)* 79−6166
He-Ne laser unit, factors affecting service life *(German)* 78−90424
He-Ne laser wavelength drift 80−67978
He-Ne laser wavelength stabilisation on I_2 *(Czech)* 78−87061
He-Ne laser wavelength stability, calibration and traceability 80−19050
He-Ne laser with $^{127}I_2$ saturable absorber, high contrast power reson. 78−29976
He-Ne laser with anisotropic cavity, fluctuations of field polaris. 79−27242
He-Ne laser with external optical resonator, SHG 79−27326
He-Ne laser with I_2 absorpt. cell, nonlinear resonances at 0.63 μm *(Russian)* 79−59672
He-Ne laser with internal mirrors, mode polarisation props. 80−23672
He-Ne laser with methane absorber, reson. obs. in output, freq. stabilisation 77−83854
He-Ne laser with methane absorpt. cell, hyperfine struct. influence on freq. reproducibility 78−50864
He-Ne laser with methane nonlinearly absorbing cell, freq. self-stabilisation effect 79−98420
He-Ne laser with transverse microwave discharge, use of secondary electrons 80−9899
He-Ne laser with waveguide resonator, oscill. modes 77−27311

neon continued
He-Ne lasers, discharge reson. props. effect on radiation fluctuations, expt. 78−74883
He-Ne lasers, freq. stabilised by ref. to I and methane absorption transitions 77−83913
He-Ne lasers, I_2 stabilised, saturated absorption signal props. 77−75481
He-Ne lasers, I_2 stabilised, 633 nm line, performance improvement 78−90429
He-Ne lasers, I_2 stabilised, with improved performance 79−22964
He-Ne lasers, in hollow Cu cathode, 632.8 nm output characts. 80−63975
He-Ne lasers, iodine- and methane-stabilised, reproducibility comparison 77−7135
He-Ne lasers, life time depend. on impurity gases *(Chinese)* 79−36881
He-Ne lasers, stabilised by saturation absorpt. in I_2 78−1270
He-Ne lasers, standard wavelength sources 78−74957
He-Ne lasers, transverse microwave freq. gas-discharge pumping 80−74339
He-Ne lasers levels, modulation spectroscopy 78−46572
He-Ne lasing medium, evaluation of population changes of Ne levels 78−25855
He-Ne low-gain laser amplifier, phase control 80−64059
He-Ne methane system, narrow nonlinear resonances in three level system *(Russian)* 80−78898
He-Ne mixture, cataphoretic gas separation in DC glow discharge with end volumes 80−79428
He-Ne mixture, electron beam prod. plasma decay, appl. to laser pumping 79−41847
He-Ne mixture, primary ionisation relativistic growth 79−86554
He-Ne mixtures, disparate mass, double sound propag., theory 80−33724
He-Ne mixtures, spark channel formation 78−1936
He-Ne mixtures, thermal diffusion 80−1726
He-Ne mode-locked binary laser oscillator, bistability induced by optical nutation 79−31958
He-Ne modulated positive column, elec. and optical props. 77−27765
He-Ne multimode and single-mode lasers, phase locking to very high coherence degree 79−76710
He-Ne nuclear-pumped CW lasing 80−48216
He-Ne optical waveguide amplifier, operation 80−43363
He-Ne plasma, HE I 4771 Å line profile 78−67472
He-Ne ring laser, 0.6328 μm, self-pulsing conditions 80−87414
He-Ne ring laser, absorbing medium press. influence on power resonance characts. *(Russian)* 80−23725
He-Ne ring laser, freq. shift of 3.39 μm methane transition 79−27298
He-Ne ring laser, influence of pressure on Zeeman effect 80−19056
He-Ne ring laser, methane absorber narrow nonlinear resonances at low press. *(Russian)* 79−76722
He-Ne ring laser, methane stabilised, nonlinear resonance freq. shift due to back scatt. *(Russian)* 80−78874
He-Ne ring laser, Ne isotopic composition changes during prolonged discharge *(Russian)* 78−22110
He-Ne ring laser, nonlinear polarisation interaction of opposite waves 78−50828
He-Ne ring laser, nonlinear Zeeman effect 78−71123
He-Ne ring laser, nonlinear spectroscopic technique 80−91819
He-Ne ring laser, nonreciprocal effects with transverse mag. field applied to active medium 80−91820
He-Ne ring laser, operating well above lasing threshold Zeeman effect 80−33039
He-Ne ring laser, opposing waves competition at lasing line centre of Ne isotope 80−1187
He-Ne ring laser beat frequency deviation rel. to dispersion and modulation 79−68410
He-Ne ring laser placed in longit. mag. field, nonlinear nonreciprocity effects 80−43377
He-Ne ring laser with methane absorpt. cell, power reson. characts. 80−28255
He-Ne ring laser with nonlinear absorber, competition of orthogonally polarised modes 78−17984
He-Ne rotating ring laser, freq. characts., mode composition effects 77−54741
He-Ne single mode lasers, meas. of intensity of sources of inherent fluctuations 80−32958
He-Ne stabilised transverse Zeeman laser, light source for optical meas. 80−48272
He-Ne stable gas laser with 0.4 Hz line width 80−48294
He-Ne standing wave laser, two-mode locking *(Russian)* 77−79874
He-Ne travelling wave laser, spontaneous emission spectra, 3.39 μm region 80−37995
He-Ne two mode ring laser for interferometry 78−1260
He-Ne two-mode gas laser, strong, coupling, transient 79−55114
He-Ne two-mode laser with methane absorbing cell, freq. stability and reproducibility 79−89934
He-Ne two-mode travelling-wave laser, Zeeman beats 78−50827
He-Ne waveguide laser, discharge plasma theory, max. output intensity depend. on discharge tube radius 79−55110
He-Ne waveguide lasers, HF discharge stability 79−18401
He-Ne waveguide lasers, props. and current-voltage characts. of discharges 78−1208
He-Ne Zeeman laser, two-transitions with common upper level *(Japanese)* 79−55112
He-Ne/CH_4 FM eliminated laser, freq. stability meas. 80−87423
He-Ne/CH_4 laser, IR freq. absolute meas. *(Russian)* 80−9851
He-Ne-Xe, ion laser transitions, hollow cathode excitation 80−1184
He-Ne-Xe ion lasers, hollow cathode, CW operation and excitation mechanism 80−69363
He-Ne-methane ring laser, frequency stabilized, operating charact. 80−14366
He-Ne-methane ring laser, power resonances 80−99761
He-Ne-methane ring laser, freq. synchronisation interval for oppositely directed waves 80−99762
He-Ne-methane stabilised ring laser, freq. stability calcs. *(Russian)* 78−9401
He-Zn-Ne, hollow cathode laser tube, with direct current excitation, Ne addition effect *(Japanese)* 79−76704
^{3}He-^{20}Ne stabilised transverse Zeeman laser, tuning characts., freq. fluctuation 80−48273
He+H_2(He)(N_2)(Ne)(Ar), 25-450 keV, metastable ion beam electron loss and deexcitation cross section 77−34745

neon continued
He+He^+(Ne), tensor polarisabilities of 1snd ^{1}D level, fluoresc. depolarisation obs. 80−69099
He+Mg^+(Ne^+), charge exchange, Rydberg state excitations 77−58159
He+Na, two-photon optical free induction decay meas. by broad-band excitation in unidirectional beams 79−76489
He+Ne, afterglow, metastable state energy transfer, spectra 80−43167
He+Ne, scatt., orbiting reson. total cross-sections 78−5320
He+Ne collisions, MO calcs. for excitation processes 78−25676
He+Ne pot., differential cross section, quantum mechanical inversion 78−70896
He+Ne^{n+} (n=1,2,3,4), excitations, emission cross-sections 77−57914
He+Ne(Ar)(Kr)(Xe), energy transfer, time-resolved VUV spectra 77−19028
He^++He, multicurve-crossing problem, numerical test of semiclassical approx. 78−13590
He^++He(Ne), model pot. for law energy scatt. 78−66642
He^++Ne, 10-150 keV, Rydberg-state total cross section, oscillatory behaviour 77−83716
He^++Ne, $2s^22p^6$-$2s^12p^5$ radiative transition in Ne III, UV spectra 79−6900
He^++Ne, attenuation and single electron charge exchange cross sections, 500-5000 eV 77−34752
He^++Ne*→He*+Ne^+, cross sections 79−22821
He_2^++Ne(Ar)(N_2)(CO)(CO_2)(Ch_4), bimol. and termol. charge transfer reactions, rate coeffs. 77−1910
He(-Ne), electron pair production cross sections, 2.614 MeV, triplet events 77−57580
HeNe, detection in nozzle beam, total collision cross section determ. 77−61826
$HeNe^+$, collisional form., excitation, pot. energy curves calcs. 77−6697
$He_2(^3\Sigma_u)$+Ne(Ar)(N_2)(CO)(C_2)(CH_4), excitation transfer reaction rates 78−5332
^{3}He-^{20,22}Ne/$^{127}I_2$, 0.63 micron laser generated contrasting power resons. *(Russian)* 77−23651
^{3}He-^{22}Ne 0.63 μm laser stabilised with $^{129}I_2$ nonlinear absorpt. cell, freq. characts. 80−53333
^{3}He-^{22}Ne laser, interaction of orthogonally polarised modes with various transverse distribs. *(Russian)* 77−27276
^{3}He-^{22}Ne laser with I_2 absorption cell 77−79867
^{3}He-Ne stabilised by saturated absorption ^{127}I, laser wavelength standard development appl. *(German)* 78−79034
^{4}He stopping cross sections, 1-8.5 MeV 78−58558
He*+Ne, (3^1S, 3^3S, 3^1P, 3^3P) de-excitation cross section temp. depend., time resolved spectra 80−28100
He*(2^1S)+Ne, elastic and reactive scatt., ang. distribs. 77−6919
$He_2(2^3\Sigma_u^+)$+He_2(Ne), reaction rate consts. meas. in afterglow 78−7173
Hg+Ne(Na)(K)(Rb), elastic scatt., interatomic pots. 77−58122
Hg*+Ar(Ne), 6^3P_0 and 6^3P_2 metastable states, interaction pot. parameters 77−79670
I_2+Ne, D-state lifetime and UV laser action 77−14471
K:Ne, ground states and core hole states, self-consistent soln. using density functional formalism 79−69467
K-He(Ne)(Ar)(Kr)(Xe), oscill. strengths, for induced dipole transitions, pot. energy curves 77−75100
KBr*+Ne(Ar)(CO)(N_2)(CO_2), information theoretic anal. 77−521
KrF+He(Ne)(Xe)(NF_3), quenching rate consts. meas. 79−24718
Li+He(Ne), inelastic collisions, Baylis-Gombas pseudopot. appl. 77−58151
Li^++Ne, low energy, ionisation, total cross-section meas. 77−54606
Li*+He(Ne)(Ar), thermal, high-Rydberg Li behaving as ion core 78−22004
Mg^{2+}+Ne collisions, 2p-3p excitation, optical spectroscopy investig. 77−19064
$Mg_{(S)}$+Ne^+, O-dependent photon emission 79−1810
N+Ne, electron excitation, multi-state impact parameter approx. 78−42200
N^++Ne, single electron detachment cross-sections, 35 to 140 keV 77−6909
N_2-Ne, positive column, electron vel. distrib. function *(German)* 78−1885
N_2-Ne glow discharge, energy balance, ionis. collisions *(German)* 78−34263
N_2-Ne glow discharge, kinetic eqn., transport coeff., collision freq., mean energy *(German)* 78−34261
N_2-Ne mixture, gaseous, positronium yields at 77K 79−98254
N_2(-Ne), gas, 77K, positron annihilation lifetime spectra 79−10630
NH_3-N_2(H_2)(Ne)(Ar)(Kr)(Xe), as R(1,1) vibr-rot. line parameters, ν_2 band, using CO_2 laser light 79−3444
N_2O^+, mobility in Ne gas 78−14125
N6d2-Ne discharge lamp, meas. method for partial H_2 press., selective gettering action 77−87775
Na-(Ne)(He)(Ar)(Kr)(Xe), oscill. strengths, for induced dipole transitions, pot. energy curves 77−75100
Na-Ne, gas phase, absorption, D-line profiles, dye laser meas. *(French)* 78−42007
Na-Ne, low press. discharge positive column, multistep ionisation 78−75446
Na-Ne plasma, near-reson. dye laser scatt. and two-photon absorpt. 77−39459
Na-Ne-Ar, low-pressure discharge, AC operated, time-resolved afterglow 77−43099
Na-Ne-Ar AC discharge, positive column 77−39487
Na-Ne-Ar discharge low-press., instability 78−9868
Na+He(Ne), Rydberg states, cross sections for collisional ang. momentum transfer 79−6997
Na+He(Ne)(Ar), Rydberg S and D state relax., trilevel echo effect 79−72409
Na+Ne, electron excitation, multi-state impact parameter approx. 78−42200
Na+Ne, Na(3s→3p) excitation, impact parameter depend. 78−58794
Na+Ne, potential curves from a model potential *(French)* 80−78685
Na+Ne, Rydberg states, collisional angular momentum mixing meas. 77−68093
Na+Ne, Rydberg transitions, excitation transfer cross-section calcs. 77−50520
Na^++Ne, quasimolecular states, coherent population *(Russian)* 77−10718
Na^++Ne collisions, Na KK vacancy prod. 78−17781
NaNe, $X^2\Sigma$, $A^2\Pi$ and $B^2\Sigma$ states, model pot. calcs. 78−78776
Ne $^3P_1$ state, radiative decay time 79−72277

neon continued
Ne 2s, photoelectron ang. distrib., relativistic Dirac-Fock calc. 79−59411
Ne, $3s_2$-$2p_4$ and $3s_2$-$3p_4$ coupled transitions, sensitivity to discharge current fluctuations 77−75484
Ne (II-VI), 209-602 Å, mean lives and oscill. strengths beam-foil spectroscopy 77−79561
Ne, atomic interaction energy, basis set effects in SCF calcs. 77−83678
Ne, charge-state distributions and the population of X-ray emitting states 79−68311
Ne, discharge streamer propagation mechanism based on plasma vibrs. *(Russian)* 77−84546
Ne I, $2p^5 6d$ config. in mag. field, energy levels 79−63955
Ne I, $3d'(3/2)_2$ level, absolute transition probabilities 78−13454
Ne I, at. state densities meas. in Ne-Br_2 mixture 78−62753
Ne I, beam-foil excitation, Rydberg states, relative populations 80−14208
Ne I, isotopic components of spectral line, separation by numerical method 78−21227
Ne I, level crossing in gas laser, at. consts. and collision cross sections determ. 78−50763
Ne I, lifetimes of levels of $2p^5 4d$, $2p^5 5d$, $2p^5 4p$ and $2p^5 5s$ configs. 77−50407
Ne I, transition probabilities for 3p to 4d array 77−437
Ne I, transition probabilities for 3s-4p transitions 77−88415
Ne I, wave functions, weighting factors determ. from g-factors 79−98237
Ne I isoelectronic series, radiative lifetimes calc. 79−98037
Ne I spectra, probabilities of $np^5 n'p \rightarrow np^5 n's$ dipole transitions, two-config. approx. calcs. 77−71779
Ne I to Ne IV, excitation in ion-atom collisions, 100 keV region, emission spectra obs. 80−14205
Ne II, $2p^4 3p$ levels, radiative lifetime by delayed coincidence method 77−83545
Ne II, III, and IV ground state, photoionis. cross sections, close coupling calcs. 80−5513
Ne II, III, IV, photoionisation cross sections calc. 80−43014
Ne II, long pulse UV laser emission, electron beam excited Ne-NF_3 mixture 78−78996
Ne II, radiative lifetime and transition probability calc. 79−3408
Ne II, transition probabilities, lifetimes, intermediate coupling semiempirical calcs. 79−789
Ne II 12.8 μ fine-struct. line in Nova Cygni 1975, contrib. to 10 micron excess 78−93269
Ne II 12.8 μm emission and NGC 253 galactic dynamics 79−92844
Ne II 12.81 μm forbidden line obs. of G333.6−0.2 H II region 80−85983
Ne II forbidden line emission from galactic centre, Sagittarius A-west, IR obs. 78−36680
Ne II high-pressure supersonic flow electronic transition laser, with pulsed blowdown and electron gun facility 79−59723
Ne II IR emission line obs. of NGC 7027, planetary nebula 79−21400
Ne II line Stark broadening in pulsed arc, obs. 78−67469
Ne II lines from pulsed arc plasma, Stark broadening 78−66504
Ne II-VIII L-shell excit. by highly ionised heavy ion impact 78−1074
Ne III, excitation cross-sections, electron impact with simultaneous ionisation 77−68119
Ne III, ion impact excited, branching ratio method for quantum efficiency determ. of UV spectrometer 79−22848
Ne III, O I like ion, solar emission lines density depend. 79−40165
Ne IV, excitation by electron impact, sections of lines meas. *(Russian)* 77−6941
Ne IV, ion impact excited, branching ratio method for quantum efficiency determ. of UV spectrometer 79−22848
Ne isoelectronic series, $2s^2 2p^5 3l$ and $2s^2 2p^6 3l$ configs., excited state energy levels 79−54781
Ne, thermal conductivity, 400-1500K 79−18987
Ne V, excitation by electron impact, sections of lines meas. *(Russian)* 77−6941
Ne V, m-representation approach to atomic structure 79−45645
Ne V forbidden lines, collision strengths for electron impact excitation, astrophys. appl. 79−50138
Ne VI, low lying levels, excitation equilib. and line intensities 79−12401
Ne VI, VII and VIII, total collisional ionis. rates in plasma 77−19102
Ne VII, electron impact excitation cross sections, Coulomb-Born approx. 77−75302
Ne VII, excited states, transaction oscill. states and wavefunctions 79−59367
Ne VII, transition probabilities calcs. 79−54792
Ne VII solar emission line ratios, electron density and temp. determ. 80−17559
Ne VIII, electron impact excitation 77−537
Ne VIII, in plasma, ion electron collisional radiative recomb. coeffs., bottleneck calc. 80−53942
Ne VIII, X, electron ionisation cross sections of excited atoms and ions 80−43186
Ne X Lyman-α line Stark broadening, hot dense laser-produced plasma 77−11402
Ne^-, electron capture expts. to search for long lived states 79−72410
Ne^+, absolute electron impact ionisation cross section 80−83496
Ne^+, converged $E^{(2)}$ values 78−66479
Ne^+, conversion to mol. ions, three body association coeffs. determ. using drift-tube mass spectrometer 80−108699
Ne^+, electron scatt., relativistic R-matrix calc., fine-struct. level transition cross sections 78−13604
Ne^+, excited state, oscillator strengths, core relax. effects calcs. 79−10050
Ne^+ mobility in Ne, fine struct. splitting effect 77−39400
Ne^+, radiating ions, velocity distrib. symm. in hollow cathode discharge, charge and momentum transfer 79−73054
Ne^+, reson. line regularities in plasma Stark widths and shifts 80−43881
Ne^{+++}, prod. from RF sources 79−18070
Ne^{10+}, microdosimetric measurements of pretherapeutic heavy ion beams 80−72337
$^{20}Ne^+$, stopping power in Au at 50-500 eV 77−76478
Ne^{2+}, energy levels of $1s^2 2s^2 2p^N 3d$, (N=2,3,4) configurations 77−46509
Ne^{2+}, mobility in parent gas 79−7439
Ne^{3+}, CI calc. of at. energy levels 80−5624
Ne^{4+}, $2s2p^3$ terms, mean lives, from beam-foil spectra 78−37601
Ne^{4+}, electron impact calcs. using R-matrix and linear algebraic methods 79−59579
Ne^{4+}, electron impact excitation, collision strength calc. 80−5624
Ne^{6+}, Ne^{7+}, production and acceleration in cyclotron *(Japanese)* 78−5084
Ne^{7+}, $1s2l3l'$ config., Auger and radiative deexcitation, intermediate coupling 77−79567
Ne^{7+}, $1s3s3p\ ^4p^0$ state, Hartree-Fock function, third-order energy 78−37569
Ne^{7+}, electron impact, continuum orbital approx., weak coupling theory 78−33417
Ne^{9+} high ionisation-excitation states and mass dependent symmetric collision interactions 77−83720
Ne^{n+} (n=1-4), electron impact ionisation cross-section 78−58844
Ne^{n+}, electron impact inner-shell excitation/ionis. cross sections 77−23564
Ne^{x+}, (x=1-8), electron loss and capture in He, N_2, Ne and Ar *(Russian)* 78−13600
Ne^{x+}, (x=3-7), K-LL Auger transition energies calc. 79−54823
Ne:Ar(Kr)(Xe), luminesc. in vacuum-UV excitation of guest atoms by free and relaxed excitons 79−15519
Ne:H, exciton states and L_α,L_β emission 80−93372
Ne:O_2 (N_2), long-wave UV luminesc. *(Russian)* 78−88347
Ne:Xe, liq., 0.1-0.65 g cm^{-3}, vac. UV absorpt. spectra, Wannier impurity states 77−77232
Ne:Xe film, solid, competition between electronic energy transfer and relax., photoelectron spectra 77−24929
Ne:Xe(Ar), electronic relax. cascades in Wannier and Frenkel type exciton states 79−33759
Ne-Ag, UV ion laser, dominant transition at 318 nm 79−942
Ne-Ag UV laser, spectral range, threshold, power output 78−66809
Ne-Al large diameter hollow cathode discharge, near IR Al II laser transitions 80−102715
Ne-Al^+, hollow-cathode laser, five Al II transitions 358 to 747 nm 77−58316
Ne-Ar, glow discharges, AC cataphoresis meas. using light spectrometry 79−60096
Ne-Ar, high press. mixture, AC discharges, one-dimensional numerical simulation 78−67451
Ne-Ar, mol. force const. from viscosity data, thermal cond. 78−33565
Ne-Ar, solubility in Ar, and related functions, three-body forces 79−10776
Ne-Ar, thermal cond., 90-273K 80−48836
Ne-Ar (He), thermal cond., composition dependence 78−51276
Ne-Ar (0.1%) mixture, AC plasma panel, Paschen breakdown curves 77−11418
Ne-Ar (1%), 250 kV pulsed electron beam-excited, at. line rel. intensities 79−89646
Ne-Ar discharge, transient cataphoresis, time depend. 80−38753
Ne-Ar liquid mixtures, collision induced absorpt. 77−4638
Ne-Ar mixture, cataphoretic segregation, mass spectra obs. 77−52649
Ne-Ar mixtures, glazed electrode AC discharge mode transition obs. 78−67558
Ne-Ar Penning mixture, pulsating discharge, emission spectra, Ne state population 79−55594
Ne-Ar-I_2, low electron beam excitation rates 79−86163
Ne-Ar(-Kr), gas mixtures, thermal cond. meas. in the range 0.5-15 MPa 80−14874
Ne-Ar(He), thermal diffusion factors, (m,6,8) pot. calcs. 79−50835
Ne-Br_2 mixture, at. state densities of Ne I levels, Nf values of Br II levels 78−62753
Ne-CO(CO_2), C nuclear pumped lasers, energy storage 80−63996
Ne-Cu, UV ion laser, dominant transition at 260 nm 79−942
Ne-Cu hollow-cathode laser discharge sputtering obs. 78−66800
Ne-Cu laser, discharge processes, cathode sputtering 78−5463
Ne-Cu pulsed discharge, electron energy distrib., ionis. rate 78−51387
Ne-Cu UV laser, spectral range, threshold, power output 78−66809
Ne-E, anomalous meteoritic Ne component, thermonuclear origin, supernova models 78−45292
Ne-H_2, hollow-cathode discharge, electron energy distrib. 78−71573
Ne-H_2 liq. mixtures, phase equilib. effects, thermodynamic perturb. theory *(Russian)* 80−92663
Ne-H_2 mixture, liquid vapour phase equilib., sound vel., compressibility, thermodynamic perturbation theory obs. *(Russian)* 80−39306
Ne-H-H_2 mixture, positive column characts. and comparison with approx. diffusion theory 80−44025
Ne-HCl mixture breakdown obs. 78−67553
Ne-He, glow discharge, striation current conditions 79−55595
Ne-He and Ne negative afterglows, microwave quenching and recombination processes, Ne spectral emission 77−80307
Ne-He DC glow discharge electron density decay, microwave cavity obs. 78−91167
Ne-He mixture discharges, origin of dark spaces in plasma 78−9881
Ne-Hg RF discharge, atomic ionis. and excitation, spectral line intensities 78−26334
Ne-Kr, gas, diffusion coeffs. meas., 350-1200K 80−14869
Ne-Kr, mol. force const. from viscosity data, thermal cond. 78−33565
Ne-Kr, partially miscible mixture, high press. mol. dynamics using Lennard-Jones pot. 79−41929
Ne-Kr, time-dependent props. near crit. mixing point, 2000 bar, mol. dynamics calcs. 80−24580
Ne-Kr mixture, collision-induced microwave absorpt. 77−88411
Ne-Kr Penning mixtures, Townsend ionisation coeffs. and breakdown pot. meas. 80−19641
Ne-like atoms and ions, gradient expansion of atomic kinetic energy functional 80−95530
Ne-like ions, E1 and M2 transitions, HF calcs. 79−59401
Ne-like ions, Kr-Mo, 2-3 transitions, plasma X-ray spectra classification 79−37544
Ne-like ions, multiply charged, laser plasmas, 1.5-15 Å 78−13462
Ne-methane mixture breakdown obs. 78−67553
Ne-N_2, atomic N nuclear pumped lasers, surface effects 80−63996
Ne-N_2, charge transfer kinetics, weak H^+ beam effects 78−9243
Ne-N_2, energy transfer, H^+ ion beam produced plasma, ion density and temp. 80−38539
Ne-N_2, N_2^+ ($B^2\Sigma_u^+$) state excitation kinetics 78−9239
Ne-N_2 AC discharge, pulse to continuous mode transition, Ne metastable effects *(German)* 80−84011
Ne-N_2 laser, energy pathways by proton excitation 78−5459
Ne-N_2 mixture, cataphoretic segregation in DC discharge, mass spectral anal. 77−32799

neon continued
Ne-N_2 mixture, plasma created by electron beam, spectral composition *(Russian)* 78−30453
Ne-N_2(He), low-ionised plasma, electron kinetics, collision processes influence *(German)* 79−14519
Ne-NF_3, long pulse UV laser emission in electron beam excited supersonic flow 78−66801
Ne-Na, non-Lorentzian spectral line shape 80−106297
Ne-Ne, correl. diagrams, Thomas-Fermi calcs. 80−23294
Ne-Ne, Thomas-Fermi-Dirac model, inhomogeneity corrections 80−23308
Ne-O_2, DC glow discharge, Ne I spectral line intensities 78−74610
Ne-$SF_6(O_2)(CF_4)$ mixtures, viscosity and diffusion coeffs. 77−89225
Ne-Tl hollow-cathode discharge, CW laser generation on Tl II 594.9 nm line 79−76675
Ne-TlCl hollow-cathode discharge, CW laser oscill. on 594.9, 695.1 nm Tl^+ transitions 80−23674
Ne-Xe, equilibrium of coexisting phases 80−87197
Ne-Xe gas discharge, LF oscillations, modulation by gravitation and inertia forces 77−11429
Ne-Xe gaseous mixtures, collision-induced microwave absorpt. 78−78680
Ne-Xe glow discharge, negative flow charge exchange excitation of Xe^+ levels 80−38857
Ne-Xe mixture, microwave absorption, collision-induced 79−22626
Ne-Xe-$F_2(NF_3)$, excited states quenching 79−18406
Ne-Xe-HCl, transient optical absorpt. meas. for XeCl laser 79−55115
Ne^{n+}-Ne, K-shell vacancy prod. cross section, X-ray and Auger electron prod. fluoresc. yield 78−13582
Ne^+-$^3He(^4He)$, $2p_4$ state alignment destroying cross sections 79−89757
Ne^+-$^4Ne^{2+}$, optical transition excitation function and cross sections 80−63787
Ne+acetylene, vibr. relax. study using laser-induced fluoresc. 80−74219
Ne+Al, recoil effects on molecular-orbital X-ray spectra in solid targets 80−25510
Ne+Ar,(Kr), elastic scatt., Monte Carlo averaging of differential cross-section data 78−21997
$Ne+Ar^{12+}(Xe^{24+})(Pb^{40+})$, X-ray transitions 78−66641
$Ne+Ar^{2+}$, charge transfer, energy defect and sealing laws 80−48083
$Ne+Ar^{6+}$, collisional excitation, excitation cross sections 79−98209
Ne+Ar(He)(Kr), thermal diffusion, cond. depend. determ. 77−11300
Ne+Ar(Kr), translation band spectral moments, induced dipole moments 78−55218
Ne+Ar(Kr)(Xe), elastic scatt. absolute total cross section, long range interaction 78−58768
Ne+Ar(Xr)(Xe), total cross section, glory struct. 80−23494
$Ne+B^{5+}(Li^{3+})(H^+)$, K-shell charge transfer cross sections, Bates-Born formalisms 79−45834
$Ne+Be^+$, 180 degree phase jumps for Be^+(2s-2p) excitation amplitudes, coherence obs. 80−63793
$Ne+Be^+$, 2s→2p excitation probability for Be^+, coherence parameters 79−54955
$Ne+Be^+$, Be II 2^2P excitation, alignment and orientation 80−91647
$Ne+Be^+$, charge transfer and excitation, differential cross sections, 2-5 keV 79−36764
$Ne+Be^+(Mg^+)$, high energy, excitation cross section, impact radiation polaris., models comparison 78−1069
$Ne+Be^+(Mg^+)$, ns-np excitation, alignment and orientation, impact, parameter theory 80−91648
$Ne+C^{N+}(N^{n+})(O^{n+})$, charge exchange contribution to K-vacancy production 80−102553
$Ne+C^+$, energy loss collision spectrosc. 79−86037
$Ne+CF_2$, vibr. deactivation of CF_2 first excited single state 79−94061
Ne+CO, intermol. pot. energy surfaces from electron gas model, ang., distance, and vibr. depend. 79−3520
$Ne+CO_2$, energy transfer, anharmonic coupling terms, semiclassical calcs. 80−37861
$Ne+CO_2$, energy transfer rate consts., semiclassical method 80−91640
$Ne+CS_2$, metastable atoms, energy transfer processes 80−83466
Ne+Ca, press. broadening, line shifts 78−5290
Ne+Ca*(Mg*), model pot. curves, including CI 78−42154
$Ne+Cl^-(Br^-)$, total electron detachment cross sections, near threshold energies 79−3555
$Ne+Cl^+$, highly charged low vel. recoil ion time of flight spectra, cross section energy depend. 80−14222
$Ne+Cl^{7+}$, many-electron stripping 77−75277
$Ne+Co_2$, intermol. pot. in repulsive short-range region, ab initio 80−69204
Ne+CsF, sudden, body-fixed and semiclassical approx. calcs. 78−42164
$Ne+D_2$, anisotropic inversion pot., rot. inelastic cross sections 80−78696
$Ne+D_2$, anisotropic potentials, direct inversion methods calcs. 80−69090
$Ne+D_2$, energy-loss scaling in 0.5-3.5 keV 80−63768
$Ne+D_2$, state-resolved $\Delta j=2$ rot. transitions 80−63772
$Ne+e^-(H^+)$(pion), specific primary excitation by fast accelerator particles 80−23559
$Ne+F^{9+}$, double K-shell electron capture, theory 79−68315
$Ne+F^{q+}$, MO X-ray prod. obs. 79−45663
$Ne+F^{q+}$, radiative electron capture X-ray profiles from fast collisions, calcs. 79−49975
Ne+H, 20-500 eV, ion pair and free electron production, integral cross sections 78−46437
Ne+H, electron energy loss 80−87217
Ne+H, low energy elastic scatt. cross section MCSCF calc., van der Waals forces 78−70897
Ne+H, orbiting resons., van der Waals pots., beam scatt. obs. 79−89739
Ne+H_2, gas discharge plasma, H_2 dissoc. excitation, cross section anal. 80−33735
Ne+H_2, metastable state breakdown, temp. depend. 79−98211
Ne+H_2, Van der Waals pot., ab inito SCF model 78−74728
Ne+H_2^+, form. of selected vibr. state H_2^+ beam at high press. by electron impact 77−65547
Ne+H_2^+, reaction pot. energy surface, LCAO-MO-SCF energies 77−1917
$Ne+H_2^+$→NeH^++H, vibr. state distrib. prod. by H_2 vibr. autoionisation cross section depend. 77−48628
Ne+H_2O, hollow-cathode discharge, Ne spectral intensity 79−4202
Ne+$H_2O(D_2O)$, chemi-ionisation and secondary ion reactions, $^3P_{2,0}$ Ne metastables 77−40531
Ne+$H_2O(D_2O)(H_2S)(SO_2)$, Penning ionis. electron spectroscopy, energy peak shifts and shapes 77−42392
Ne+H_2**, collisional deactivation 79−100338
Ne+H_3^+, Petty-Moran ion-impact expt. reinterpretation re vibr. intervals 79−94063
$Ne+H^-$, differential scatt. cross-sections, time of flight spectra 78−42161
$Ne+H^-(D^-)$, electron detachment, dynamical phenomenon 80−106305
$Ne+H^-$(He) , collisional detachment cross-sections, high-energy obs. 77−3442
$Ne+H^+$, electron capture, 4-20 keV, production of highly excited H atom 79−54963
$Ne+H^+$, electron capture, charge-state distrib. 80−32814
$Ne+H^+$, electron capture cross sections 78−62912
$Ne+H^+$, electron capture cross sections 79−86061
$Ne+H^+$, ionisation, projectile energy depend., secondary electron energy distrib. 78−42211
$Ne+H^+$, K-shell capture cross-section 78−33602
$Ne+H^+$ 80−18916
$Ne+H^+(He^+)$, K-shell ionisation, AES meas. 77−10749
$Ne+H^+(He^+)(Ne^+)$, multiple ionisation of Ne 2s and 2p electrons 80−18918
$Ne+H^+(He^{2+})$, K-shell Auger electrons ang. distrib. 79−89756
$Ne+H^+(He^{2+})(Li^{3+})$, inner shell electron capture cross-sections 79−76510
$Ne+H^+(He^{2+})(N^{x+})$, multiply ionised ats. prod. 80−28098
$Ne+H^+(O^{8+})$, K-shell ionisation cross-sections, Glauber approx. calcs. 77−46629
Ne+HD, j=0 to 1 rot. excitation, differential cross sections, time of flight obs. 80−48104
Ne+H(D), free electron production, integral cross-sections determ. 79−89754
Ne+H(2S), metastable atom total quenching 77−46628
Ne+H(2s), 5-25 keV, H(n=3) excitation, Balmer α emission obs. 80−53113
Ne+H(2s), collisional de-excitation, 5-26 keV 79−59546
Ne+He, 2^1s_0-level excitation, rate const., temp. depend. 80−87218
Ne+He, 2p-levels, excitation obs. 80−9712
Ne+He, population transfer between Ne 2p levels *(French)* 77−30975
$Ne+He_2^+$→He+products, surface-hopping trajectory calc. 79−52637
$Ne+He^+$, $He(3^1P)$ level excitation, total emission cross section, fast oscills. obs. 80−58362
Ne+He^+, inelastic scattering data inversion, interaction function recovery 79−89741
$Ne+He^+(Li^+)(Mg^+)(Na^+)(Ne^+)$, autoionising level excitation, electron spectra 77−14554
$Ne+He^+(Ne^+)$, coherent excitation and decay of autoionising states 79−45789
$Ne+He^+$→HeI+Ne^+, HeI3^3P polarisation 79−13813
$Ne+He^{2+}$, electron capture collisions, spin conservation 78−82837
$Ne+He^{2+}(Ar^{2+})$, electron transfer cross-section, <100 eV 78−66654
Ne+HeH^+, collinear reaction, pot. energy surface SCF-LCAO-MO and DIM calc. 78−92467
Ne+He(Ar)(Xe)(N_2)(CO_2), fluoresc. spectra, mol. bands, 0.1 to 6 atm., 3000-8200 Å 79−3394
Ne+He(2^1S, 2^3S), transition probs., pots. 80−58371
Ne+He(2^1S,2^3S), Van der Waals forces, one-electron model pot. calcs. 80−14094
Ne+heavy inert gas, small clusters, beam cluster intensity and collision cross section 77−38711
Ne+heavy ion, highly charged very slow Ne recoil ions, K X-ray transition 80−91649
Ne+highly stripped ion, multiple-ionis. cross sections, Monte Carlo calcs. 79−64091
Ne+I_2*, energy depend. of collision induced intramolecular energy transfer 80−83470
Ne+I^-, electron detachment collision, 1-3 keV, differential cross-section 79−72403
Ne+ion, 100 keV, excited Ne 2s vacancy singlet/triplet population ratio, ion Z depend. 78−37733
Ne+K, K 5^2P level broadening and collisional relax., quantal, semiclassical and expt. comparison 80−18903
Ne+K, photon emission polarisation anal., coincidence studies 80−5614
Ne+K(Zn^+), 0.7-500 keV, K(Zn^+) excitation, reson.-line emission and polaris. 80−18911
Ne+Kr, collision induced microwave absorpt. spectra 80−74216
Ne+Kr, K-L vacancy sharing process, Nikitin two-state model 80−9684
Ne+Kr slow collisions, four-state treatment of K-L vacancy sharing 79−45793
Ne+Kr(Xe) and Ne+Kr+Xe glow discharge, Kr^+ and Xe^+ excitation in negative luminesc. *(Russian)* 77−68883
Ne+Li^+, collisions, vel. dependence of Ne 2s and 2p, vacancy production, electron spectroscopy 80−58344
Ne+Li^+, relative level excitation, orbital ang. momentum quantum number depend. 78−25688
Ne+$Li^{+1,2,3}$, K-shell ionisation depend. on projectile charge state 77−34743
Ne+Li*(2^2P_J), collision induced fine struct. transition 80−74220
Ne+Li(Be^+)(Na)(Mg^+)(K)(Zn^+), collision-induced alignment, reson.-line emission polaris. obs. 80−18912
Ne+Li(Li^+)(Na)(Na^+), autoionising Ne levels excited in 5-10 keV collisions 78−22017
Ne+Li(Na), excitation cross sections, Li I and Na I resonance line emission and polarisation 77−61846
Ne+Li(Na) excitation cross sections, model pot. calcs. 77−58152
Ne+Mg^+, 3^2P differential excitation, alignment and orientation 79−86053
Ne+N_2, K-X-ray spectrum, collisional configuration-rearrangement 78−82816
Ne+N_2, rot. excitation, body-fixed approx. 77−19015
Ne+$N^+(O^+)(Ne^+)$ symmetric collisions, double K-shell ionisation, two-electron-one-photon transitions 77−19067
Ne+N^{2+}, electron capture, product ion energy loss spectra 79−36762
Ne+N^{2+}, electron capture, 0.2-2.4 keV, kinetic energy change 79−59558
Ne+N^{7+}, double K-shell electron capture, theory 79−68315
Ne+NH_3, pure rot. line, press. broadening calcs. 80−78656
Ne+NO, angle depend. intermolecular pot., crossed beams study 80−9682
Ne+Na, 13d-13f transition, collisional dephasing, Ramsey method investig. 79−54791
Ne+Na, 3^2P differential excitation, mechanism 79−86052
Ne+Na, 3^3P-3^2D line broadening obs. 80−78684

neon continued
Ne+Na, D2 reson. linewidth 79−31647
Ne+Na, differential cross section at thermal energy, expt. and theoretical results comparison 80−37851
Ne+Na, inelastic scatt. differential cross-section calcs. 77−10730
Ne+Na, interaction model potential calcs. 79−86036
Ne+Na, Na(3p) excitation 80−1056
Ne+Na, press. broadening coeffs of Na 3S-4D transition 78−25481
Ne+Na_2, collision induced dissoc. rate, vibr. distrib. depend. 79−22791
Ne+Na_2, rot. transitions, state-resolved differential cross-sections 78−62887
Ne+Na^+, excitation and charge transfer, 0.2-12 keV collision 79−68314
Ne+Na($3P_{1/2}$), vel.-changing collisions, effect on 2 photon and stepwise absorpt. line shape 80−87221
Ne+Na(nd), l-changing Rydberg at. collisions, rel. to low-energy electron scatt. 79−50112
Ne+Ne, (He) low pressure broadening and shift of Ne line, Lennard-Jones pot. 80−102554
Ne+Ne, distorted frozen-orbital method for diabatic mol. orbitals 78−41936
Ne+Ne, exchange-repulsion energy, many-orbital cluster expansion 80−18896
Ne+Ne, excitation transfer, coupling coeffs., temp. depend., fluoresc. meas. 78−58620
Ne+Ne, isotropic intermolecular forces evaluation using semi-empirical approach 79−36726
Ne+Ne, pot. curve derived from gas and solid scatt. data, ESMSV pot. 80−1040
Ne+Ne, potential well depth estimation method 79−86034
Ne+Ne, total cross-section, 0.5-1.4 km s^{-1}, long range pot. 79−13787
Ne+Ne collisions, diabatic molecular orbitals 78−62901
Ne+Ne collisions, simultaneous emission of two photons 78−70917
Ne+Ne^+, 2s vacancy prod., coupling state calcs. in mol. basis 79−13806
Ne+Ne^+, coulomb deflection in ion-atom collisions, K-shell excitation 79−94074
Ne+$Ne^{m+}(N^{n+})$, K-shell vacancy prod. cross-section, charge state depend. 78−17751
Ne+Ne^{n+}, (n=1, 2, 3, 4), energy spectra of electrons produced 79−45822
Ne+Ne(Ar), optical emission spectra 77−14551
Ne+Ne(He), 7d′ states, isotope shift, press. shift, press. broadening, two-photon spectra obs. 78−55155
Ne+Ne(He), population transfer from 2p levels *(French)* 79−851
Ne+Ne(He)(Ar), dispersion interaction, series coeffs., variation method 79−3518
Ne+Ne(Ne^+)(Ne^{2+}), 2s vacancy prod. 78−50623
Ne+O^-, 0.2-1 keV, elastic and inelastic reduced differential cross-sections 80−32829
Ne+O^+, pot. energy curves, nonadiabatic coupling matrix elements 80−53110
Ne+O^{8+}, double K-shell electron capture, theory 79−68315
Ne+$O^{n+}(Xe^{n+})(Pb^{n+}+)$, 50 keV, multiple scatt., target at.+energetic ion spatial correlation influence 79−27062
Ne+O^{q+}, electron capture to continuum states, forward ejected electron spectra 79−45831
Ne+OCS, gas, EPR of rot. transitions, T_1 press. depend. 80−9621
Ne+proton, charge transfer, target K-shell electron capture, impact parameter depend. 80−102552
Ne+$SF_6(N_2)$, metastable state de-excitation, rate consts., radiolysis obs. 80−40709
Ne+U, collisional relax. of highly excited states, laser-induced fluoresc. obs. 80−58205
Ne+U^{36+}, radiative charge exchange, 16, 64, 256 MeV/amu 78−55234
Ne+Xe, quenching of excited $Xe^*(^3P_2, ^3P_1, ^1P_1)$ 80−63578
Ne+Xe^++Cl^-, three body ion-ion recombination probability, Monte Carlo simulation 80−85160
Ne+Xe^{10+} depend. of charge transfer on ionisation pot. of atoms 79−64096
Ne^-+$Na^+(K^+)(Li^+)$, electron gas model pots. and collision integrals *(French)* 78−42169
Ne^++2He, three body reaction, rate coeffs., temp. depend., 100 to 300K 80−108703
Ne^++2Ne→Ne_2^++Ne, gas phase reaction rate const. calc. 78−92457
Ne^++Ar, charge transfer reaction rate coefficient 79−91932
Ne^++Ar integral elastic scatt., repulsive potentials derivation 80−63744
Ne^++Ba, 2-1000 eV, spontaneous ionis. mechanisms 79−64090
Ne^++CO_2, CO_2^+ electronically excited states prod. 77−3454
Ne^++Co_2, three dimens. quadrupole ion storage, ion mobility, effect of charge exchange reactions, Monte Carlo calcs. 80−55738
Ne^++Cs, total charge-transfer cross-section meas. 77−50527
Ne^++D_2, elastic scatt. at small angles, 1.3-3.5 keV, scaling law 78−82812
Ne^++$D_2(H_2)$, energy-loss scaling in 0.5-3.5 keV 80−63768
Ne^++ethylene (haloethylenes), 2-stage ion beam mass spectrometric obs. 77−9061
Ne^++H, Penning ionisation, electron energy spectrum 79−72406
Ne^++$H_2(N_2)(CO)(CO_2)(N_2O)(O_2)(NO)(NH_3)(SO_2)(COS)(H_2O)$, thermal energy, reaction rate coeffs. and product distrib. 79−29333
Ne^++He, 10-150 keV, Rydberg-state total cross section, oscillatory behaviour 77−83716
Ne^++He, impact excitation, cascade-fluorescence spectroscopy, level-crossing techniques 80−23357
Ne^++He, multiple ionisation of Ne 2s and 2p electrons 80−18918
Ne^++He, relative level excitation, orbital ang. momentum quantum number depend. 78−25688
Ne^++He(Ne), slow collision, ionis. obs. 79−10194
Ne^++Kr, low vel. collision, enhanced K-L vacancy sharing ratios, X-ray prod. cross section 78−78790
Ne^++Kr(Xe), thermal energy charge transfer reaction rates, mass spectrometric obs. 78−61000
Ne^++methane(chloromethane)(ethylene), thermal energy, reaction rate coeffs. and product distrib. 79−29333
Ne^++N_2, charge exchange, time-resolved emission probe 78−86946
Ne^++N_2O, charge transfer excitation, down to 1 eV 79−45835
Ne^++$NH_3(H_2O)$(Ne) symmetric collisions, double K-shell ionisation, two-electron-one-photon transitions 77−19067
Ne^++Ne, (He^+), gas-phase collisions, intermediate and high velocities, excitation 80−32822
neon continued
Ne^++Ne, coherent excitation and decay of autoionising states 79−45789
Ne^++Ne, multiple ionisation of Ne 2s and 2p electrons 80−18918
Ne^++Ne, quasi-resonant charge transfer at thermal energies 80−48082
Ne^++Ne, reson. transitions, direct and charge-exchange excitation 77−19020
Ne^++Ne collisions, satellite struct. of 2s-subshell ionisation of Ne 77−19065
Ne^++O, K-shell excitation cross sections, variable screening model 77−42387
Ne^++O_2→O^++O+Ne, thermal energy charge transfer, energy disposal determ. 79−64099
Ne^++Zn, charge exchange and Penning ionisation in pulsed discharge afterglow 79−7007
Ne^++fluoromethanes, thermal energy charge transfer reactions mechanism 77−63889
Ne^{10+}+H, charge transfer, total and partial cross-sections calcs. 80−23542
Ne^{2+}+Ar(Kr)(Xe), single electron capture excitation, photon emission, VUV spectroscopy 80−58379
Ne^{2+}+H, charge transfer process, astrophys. plasmas appl. 79−59550
Ne^{2+}+$H_2(N_2)(O_2)(CO)(CO_2)$(methane), charge transfer reactions, rate coeffs. and product-ion distributions meas. 80−104431
Ne^{2+}+He, charge transfer rate coeff. and astrophysical appls. 80−56701
Ne^{2+}+He(Ne)(Ar), electron transfer cross-section, <100 eV 78−66654
Ne^{2+}+He(Ne)(Ar)(Xe)(Kr), cross sections for electron capture, 60 to 200 keV 78−46442
Ne^{2+}+inert gas, low energy reactions, SIFT and drift tube obs. 80−97705
Ne^{2+}+Li, electron capture excitation, VUV spectroscopy 80−63810
Ne^{2+}+Ne, radiative charge transfer coeffs. 79−7010
Ne^{2+}+Xe, electron capture collisions, 15 to 50 keV, excitation 80−102566
Ne^{3+}+Al(Si)(S)(Cl), chem. environment effect on Kα satellites intensity 77−54527
Ne^{4+}+H^+, ^3P_J fine structure transitions 80−37864
Ne^{4+}+Ne, collision, correl. diagram calcs. 80−23504
Ne^{n+}+Ar(He), slow ion and electron prod., VUV radiation 78−5321
Ne^{n+}+$N_2(O_2)$(Ne)(methane), K-shell vacancy prod. cross-section, charge state depend. 78−17751
Ne^{n+}+Ne collisions, n=1 to 4, K-X-ray production, projectile charge state dependence 77−14570
Ne^{z+}+Ar, projectile charge dependence *(Dutch)* 79−50121
Ne^{z+}+$He(H_2)$(Ar), (z=1-4), electron capture into excited projectile states 77−75291
Ne^{z+}+inert gas atom (z=1-4), radiative and non-radiative deexcitation after electron capture 79−7008
Ne^{z+}+Ne(Ar), outer s-subshell vacancy production 79−18275
Ne_2, collision induced Raman spectra and diatom polarisability 80−63647
Ne_2, emission continua in VUV, new oscill. struct. 79−54905
Ne_2, excited state pots., fast calc. 80−9490
Ne_2, near IR absorpt. spectra 78−66547
Ne_2, pair polarisability tensor, extended Gaussian basis set, perturbation coupled HF calc. 77−75058
Ne_2, Raman spectra and polarisability 79−98107
Ne_2, short range interactions between two rare gas atoms 79−26888
Ne_2, total energy MS and LCAO Xα calcs., non-muffin-tin corrections, overbinding 78−46266
Ne_2, van der Waals mol., vibr.-rot. spectrum 79−13698
Ne_2, van der Waals mols., interatomic energy, SCF supermol. ab initio calcs. 77−42370
Ne_2, vibr. spectra, calc. from pot. curve 80−1040
Ne_2^+, $A^2\Sigma_{1/2u}^+$→$D^2\Sigma_{1/2g}^+$ system, theoretical absorption spectrum 80−32734
Ne_2^+, dimer ions, electronic struct., chem. binding 79−31376
Ne_2^+, electronic struct., pot. energy curves, spectroscopic consts. 79−18114
Ne_2^+, formation and destruction in Townsend discharges 80−38747
Ne_2^+, mobility and clustering reaction in Ne 79−10628
Ne_2^+, near UV absorption spectra, config. interaction methods 78−17680
Ne_2^+, photodissoc. mass spectrometric obs. 77−6867
Ne_2^+, photodissociation cross sections, 3500-5400 Å 79−81243
Ne_2+Ar, total integral cross sections for excitation, exchange and dissoc. 80−1044
Ne_2+Kr total integral cross sections for excitation, exchange and dissoc. 80−1044
Ne_2^++atom (molecule), bimolecular and termolecular reaction rate coeffs. 80−81308
Ne_2^++e, in recombination afterglow, line intensity decay complex struct. 79−7503
Ne_2^++He, pot. energy surface, reaction cross sections, ab initio calcs. 80−11881
Ne_2^++Kr(Xe), thermal energy charge transfer reaction rates, mass spectrometric obs. 78−61000
Ne_3, 3-body interactions in binding, semiclassical approx. calcs. 78−21994
Ne_3, 3-body nonadditive interaction, nodal struct. 78−1049
NeAr, detection in nozzle beam, total collision cross section determ. 77−61826
NeH_2, collision-induced dissociation, Monte Carlo quasiclassical trajectory calcs. 79−74357
Ne($^3P_{0,2}$)+Ne, differential cross sections 80−58370
Ne($^3P_2$) elastically scattered, metastable, ang. distrib., conventional rel. to Doppler shift methods 80−58418
Ne(^1S), total X-ray scatt., two-electron density functions 78−70889
NeV, solar emission lines, density dependence 80−21963
NeXe, obs. in Xe-rare gas far UV spectra, press. (temp.) depends. interaction consts. 77−61698
^{1}Ne, A=21, 22 appl. for PWR gas tagging 79−59222
^{A}Ne, A=20, 22, isotope separation by mass-diffusion cascade 79−31218
^{20}Ne, ^{22}Ne, 1.15 μm line isotopic shift, phase-polarisation nonlinear high-resolution spectroscopy in longit. mag. field 79−41423
^{20}Ne $3s_2$−$2p_4$ 6328 Å line wavenumber determ., laser induced line narrowing technique 79−76385
^{20}Ne, Doppler-free two-photon optogalvanic spectroscopy 79−89656
^{20}Ne, high-LET, effects on brain, eyes and other hand structs., mouse 79−66489

neon continued
^{20}Ne in Venus lower atmosphere, abundance from Pioneer Venus 79−48720
^{20}Ne/^{21}Ne/^{22}Ne of energetic flare particles 79−92741
^{20}Ne/^{22}Ne and Ne/O ratios of solar flare-accelerated Ne nuclei 79−92740
^{20}Ne/^{36}Ar ratio in chondrites, abundance pattern established in solar nebula 78−32424
^{21}Ne, $2p^5 3p$ config., hyperfine mag. const. by laser level-crossing technique 78−50509
^{21}Ne, ground state, electronic pumping, alignment transfer with multiple diffusion *(French)* 78−50643
^{21}Ne, hyperfine interaction in 4d subconfiguration, Doppler-free two-photon spectroscopy meas. 80−18944
^{21}Ne in josephinite 78−65313
$^{21}Ne^{n+}$, $5/2^+$ state, hyperfine interactions and mag. moment of 0.350 MeV 78−17583
^{22}Ne anomalous abundance in Orgueil meteorite, evidence for presolar grains 80−41773
^{22}Ne as neutron source for solar systems s-process, difficulty 80−72926
^{22}Ne nucleosynthesis in novae and supernovae outbursts 80−62143
Ne* 5882 Å line, Doppler free spectra, press. broadening and shifts, saturation spectroscopy 80−78565
Ne*-He*, Penning ionisation of metastable He* 80−83472
Ne*+Ar, associative ionisation studied by merging-beams technique 80−91646
Ne*+Ar, Penning and assoc. ionisation, correl. diagrams calcs. 77−50521
Ne*+Ar*, Penning ionisation studied by merging-beams technique 80−91646
Ne*+$Fe(CO)_5$, chemiionisation and chemiluminescence reactions, Penning ionisation and fluoresc. obs. 80−97689
Ne*+H, assoc. ionis., rovibronic struct. in electron energy spectrum 80−106380
Ne*+H_2O, pot. energy surfaces, MO and CI calcs., Penning ionisation electron spectra 80−106376
Ne*+He*→He+Ne^++e, Penning ionisation, merging beams obs. 78−33585
Ne*+Kr, Penning and associative ionisation 77−6910
Ne*+Ne, close coupling calc. 78−66652
Ne*+Ne, differential elastic scatt., rainbow max., mol. states 77−38710
Ne*+Ne, metastability exchange by optical pumping *(French)* 77−61845
Ne*+X, (X=Ar, Kr, Xe, H_2, CO, HCl, F_2Cl_2, NF_3, N_2F_4, N_2O), quenching rate const. for metastable Ne($^3P_2$), flowing afterglow 78−46295
Ne*+Xe, chemiionis. in metastable state collisions 79−68306
Ne_2*, electron impact ionisation cross sections in binary encounter approx. 79−68320
Ne_2*, excimer potential energy curves of several excited states 79−41115
Ne(metastable)+dichloroethylene (dichlorobenzene), mol. ionis., collisional energy depend. 79−54950
O+NO+M→NO_2+M, (M=He, Ne, Ar, Kr), 217-500K, absolute rate consts. 77−16787
$O^{4,5,6,7+}$+Ne(Ar)(Kr)(Xe), 10-30 MeV, charge exchange 77−34757
O(^{5}S)+Ne(Ar)(Kr)(Xe), total cross sections 78−42188
Rb+Ne(Ar), spin relax., van der Waals mols. form. 77−19027
S^{n+}+Ne(SiH_4)(H_2S)(HCl)(Ar), K X-ray cross section, projectile charge depend. 77−19029
Si:Ne, amorphous, implanted, cond. change 78−23097
Si:Ne, amorphous, implanted and sputtered, epitaxial regrowth, influence of noble gas atoms 80−2289
Si:Ne, ion implantation damage, annealing, comparison with Si:Ar and Si:Kr 79−10867
Si:Ne, ion implanted, amorphous, epitaxial regrowth 79−10869
Si:Ne, ion implanted, nature of defect reverse annealing 80−88875
Si:Ne ion implanted, channelling anal. of disorder struct., ^{4}He ions, 0.7 to 2.2 MeV 79−4321
Xe-He(Ne), gas mixture, element and isotope separation in impulse plasma centrifuge *(Russian)* 80−38725
Xe-Ne-He hollow cathode discharge, laser oscill. at 5314 Å Xe II line 79−3679
Xe^{31+}+Ne, 200 MeV collision, Auger emission 77−57952
(Y, Sm, Lu, Ca)$_3$(Fe, Ge)$_5O_{12}$:Ne^+, film, S=1 bubbles dynamic props., temp. depend. 77−20658
ZnS:Ne, implanted single crysts., photolum. and bombardment effect, thermolum. curve obs. 80−55166

neon compounds
D_2Ne, mol. interactions, differential scatt. cross-sections meas. 79−89732
H_2Ne, mol. interactions, differential scatt. cross-sections meas. 79−89732
$NeCN^+$, SCF calcs., dissoc. energies, rot. and hyperfine const. determ. 80−95531
$NeCO_2$, energy transfer, anharmonic coupling terms, semiclassical calcs. 80−37861
NeF, covalent and ionic states, ab initio CI calcs. 78−78634
NeF, low energy state pots. energy curves, fluores. and dipole moment 78−21991
Ne_2F, ab initio diatomics in mols. pot. surface, spin-orbit coupling 79−3519
Ne_2F, energy surfaces, application of molecular electronic struct. theory 78−25452
NeH_2, van der Waals mols., rot. predissoc. 80−63721
NeH_2^+, ab initio potential surfaces, frozen orbital approximation calcs. 78−41927
Ne_nH clusters, ab initio LCAO MO SCF calc., struct. and energy 78−66704
Ne_nH^+ clusters, ab initio LCAO MO SCF calc., struct. and energy 78−66704
$NeHe_2^+$, extended valence bond diatomic calcs., applications to method of diatomics-in-molecules 79−45635
NeO, nonadiabatic coupling matrix elements by Hellmann-Feynman theory and HF 80−83263
Ne.H_2O, excited dimer, first order interaction energy, ab initio calc. 80−32598

nephelometry *see turbidimetry*

Neptune
albedo and brightness temp., 5 μm IR obs. 80−82300
appulses of 12th and 13th magnitude stars (early 1978) 78−16347
astrometry, positions determ. with Odessa meridian circle, (1974 to 1975) *(Russian)* 79−44394
atmosphere, ammonia and water vapour contents 80−90366
atmosphere, evidence for optically thin high-altitude cloud form. 77−53469
atmosphere, IR radiation, review 80−8568
atmosphere, IR refl. spectrum, evidence for weather 77−53468
atmosphere, Raman scatt. 78−28571
atmosphere, review 77−5470
atmosphere, thermal struct. 79−84735
atmospheric thermal profile, supersaturated stratospheric methane 79−40137
atmospheric VHF refraction 80−98608
basic props. 77−45357
brightness changes, solar activity effects 79−75177
brightness temperature at sub-mm wavelengths 79−53743
comet capture duration, simple lower bound 79−2475
contaminant terrestrial microorganisms, limitations to growth 77−41355
effective temperature, from IR photometry 78−32394
far IR obs., temp. determ. 79−12431
figure, hydrostatic equilib. eqn. numerical soln. 79−62773
geometrical and dynamical flattening 79−48734
insolation, latitudinal, seasonal and atmospheric effects 77−60704
ionosphere, model, ionization by galactic cosmic rays and solar EUV radiation 78−4142
IR spectrum from 0.8 to 2.5 microns, obs. 80−21946
limb brightening in 7300 Å methane band, photometry obs. 80−82297
magnetic field, hydromagnetic dynamo in core 80−90365
magnetic field origin 80−36564
methane 6819 Å line interpretation rel. to inhomogeneous scattering models 78−53871
methane 6825 Å band, obs. 77−78715
methane and ethane emission detect. 78−16344
Neptune/Triton system, satellite aided capture of external body 79−75087
Nereid, ephemeris continuation (1977, May-October) 77−49330
Nereid (Neptune II), ephemeris, (1978 May 12 to September 19) 78−53873
Nereid (Neptune II), ephemeris (1980 March 2 to September 8) 80−46481
observations by Galileo, (1612 and 1613) 80−105485
observing in 1977, prospects 77−56874
occultation on 1980 February 10, no event, revised calcs. 80−26805
orbit second-order perturbations, semi-major axis secular vars. *(French)* 79−2474
orbital perturbations by Pluto, representation *(French)* 80−26724
photometric observations for solar luminosity monitoring 77−53500
photometric var. in 1953-76 period 78−85901
polar moment of inertia determ. 80−94694
positions, reduction of 19th century obs., method comparison 80−94691
ring, history of obs. 78−69745
ring, observational evidence in 1846-7 from Lassell and Challis 80−67652
rotation, equatorial flow theory 80−67653
rotation period, correction, photometric and spectroscopic results comparison 80−82301
rotation period, effects of seeing on reflected spectrum 80−46479
rotation period determ. 79−16878
rotation period from IR photometric light curves 78−40869
rotational period from spectral line tilts 78−20726
satellite system and Pluto, origin through encounter with massive body 79−84743
satellites position meas. 78−81573
secular brightness increase, 1972-76 period 78−16346
spectrum in 5-20 micron range, obs. 78−32393
stellar occultation predictions, 1978-80 period 78−40868
stellar reocultation, 1980 August 21, obs. 80−109395
stratosphere, mixing ratios of methane, ethane and acetylene 80−51692
structure and evolution in three-layer interior model 80−72877
thermal evolution, comparison with Uranus 78−85903
Triton, diameter and reflectance, spectral and radiometric obs. 80−17546
Triton, image tube spectra, 6800-9000 Å, search for possible atm., methane upper limit 79−16880
Triton, IR photometry rel. to membership of new class of satellites 78−12146
Triton, narrow band spectrophotometry 79−16879
Triton, satellite with atmosphere, IR spectrum obs. 80−21945
Uranus-Neptune general planetary theory, short-periodic term elimination 79−75153
UV albedo, meas. 80−82295

neptunium
see also nuclei with .....
anion-exchange refinement of Pu and Np separated during extraction refinement of spent fuel elements 78−70624
atom, M-series X-rays, energies and widths 77−75092
atom, UV emission spectra, Fourier transform spectroscopy appl. 78−58060
determination in soln. using automatic controlled-potential coulometer 77−25335
electrolytic stabilisation for separation from nuclear reactor fuels *(German)* 79−3229
hardness and elastic moduli of α-Np 77−20009
ionisation potentials, 2nd-6th, thermochemical calcs. 79−98248
ions, electronic props., Dirac-Fock studies 78−60094
K-shell fluorescence yields from Auger electrons and X-rays, precision meas. 79−31462
long-term environmental behaviour, chemical approaches 79−93765
nuclear fuel reprocessing, displacement re-extraction, math. simulation 77−61586
THTR fuel reprocessing Pu and Np separation from aqueous soln. *(German)* 77−83067
^{241}Am(n,X), Japan Material Testing Reactor, separation of transuranium elements *(Japanese)* 80−52731
CaF_2:Np^{3+}, cryst. field splittings, ab initio MO calcs. 77−20520
Cs_2ZrCl_6:Np^{4+}, EPR obs. 79−33526
Cs_2ZrCl_6:Np^{4+}, EPR data interpretation for octahedral Γ_8 state in cubic cryst. field 80−2634
Cs_2ZrCl_6:Np^{4+}_6, EPR of np^{4+} ground state 80−44903

neptunium continued
$LaBr_3$:Np^{3+}, energy level anal., polarised absorpt. and fluoresc. spectra 80−76056
$LaCl_3$:Np^{3+}, energy level anal., polarised absorpt. and fluoresc. spectra 80−76056
$LaCl_3$:Np^{3+}, phonon-induced relax. in excited optical states, linewidth temp. depend. meas. 80−100688
Np I, first ionisation pot., radiative lifetimes, high-lying energy levels, laser spectroscopy 79−76370
Np I, spectrum, 4000-40000 cm^{-1}, term analysis 77−38629
Np V, absorpt. spectra in aq. solns. 79−65899
Np^{6+}, Sternheimer valence shielding antishielding factor including exchange 77−85182
^{235}Np, radioactive waste, sorption in igneous rocks 80−95367
^{237}Np in invertebrate tissues, uptake from water 79−74765
^{237}Np, lineshape analysis of 60 keV Mossbauer resonance, interference effects 79−28644
^{237}Np migration potential in radioactive waste 80−3537
^{237}Np, Mossbauer isomer shifts, book, contrib. 79−87362
^{237}Np, muonic atom lifetimes from muon induced fission 80−69269
^{237}Np, neutron activation anal., determ. of small amounts in solns. containing U, Pu and fission prod. 78−21682
^{237}Np, sorption on USA subsoils from differing weathering intensity areas 78−16014
^{239}Np, airborne short-lived radionuclides of unknown origin in Sweden (1976) 78−32219
ThO_2:Np^{4+}, cryst. field splittings, ab initio MO calcs. 77−20520
U-^{238}Pu-^{237}Np GCRF fuel cycle to produce isotopically denatured Pu for LWR 80−78427

neptunium compounds
cyclopentadienyl compounds, $(C_5H_5)_3NpX$, (X=F, Cl, Br, I, $(SO_4)_{1/2}$), mag. susceptibility 80−11152
double orthovanadates and orthoarsenates, struct. evolution due to cationic and anionic substitutions 77−19938
in fused salts, redox and chem. props. 77−29038
ternary oxides, electronic and structural props., ^{237}Np Mossbauer spectroscopy 79−33570
$CsNpF_6$, optical spectrum anal. 79−26963
$NpAs_2$, magnetic props., 4.2 to 77K, Mossbauer study 80−39937
$NpBa_6Zr_{12}F_{64}$ glass, Mossbauer spectrum, evidence for charge states 3+ and 4+ *(French)* 78−88231
$NpBa_6Zr_{12}F_x$ glass, Mossbauer spectrum 80−11304
NpC_{1-x}, nonstoichiometric, atomic short-range order obs. by diffuse neutron scatt. 77−24315
NpF_6, electronic struct. and transitions, SCF-Xα-SW calcs. 78−78627
NpF_6, energy levels and bonding, relativistic SCF Dirac-Slater calcs. 77−6691
NpH_x, mag. props., 4 to 700K 79−61075
NpI_4, heat of solution in aq. HCl acid 79−83495
NpO, and NpO_2, electronic struct. and chem. bonding and XPS line shape calcs. 79−33264
NpO_2, cryst. growth by chem. transport 80−16166
NpO_2, IR spectra, values of transverse vibr. frequencies 77−28585
NpO_2, mag. transition at 25K, Kramers doublet as cryst. field ground state 80−59936
NpO_2 single crystal growth, gas phase chemical transport method *(French)* 80−60760
NpO_2, XPS meas. 77−48314
NpO_2, XPS of 5f electrons 77−73216
NpO_2^+, NpO_2^{++} containing compounds, structure and bonding study 77−27868
$NpSe_3$, Np_3Se_5 and $NpTe_3$, magnetis. meas. 77−20542
Np(V)/Np(IV) catalytic redox reactions, kinetics and mechanisms 77−29006
Np(VII) formation in molten salts 77−29039
$Np(VO_3)_4$, crystallographic data *(French)* 78−63725
$Np(VO_3)_4$, X-ray cryst. struct. determ. 79−99133
$^{237}NpO_2$ powder, oxalate based, prep. and charact. 78−11166

Nernst effect *see thermomagnetic effects*

Nernst-Ettingshausen effect *see thermomagnetic effects*

network analysers
automatic, calibration, EM reflection coeff. meas. appl. 78−89463
dual six-port automatic network analyser, performance 80−47074
microwave reflection coeff. meas., calibration error evaluation 79−21768
microwave reflectometers, thru reflect line, improved technique for calibrating dual six-port automatic network analyser 80−47073

network analysis
see also circuit analysis computing; linear network analysis; nonlinear network analysis
biosystems, thermodynamic network anal., book 77−86435
charge sensitive preamplifiers, signal and noise response 78−33404
choke-earthed surgical diathermy circuit analysis 79−20705
circuit with variable mutual inductance, harmonic behaviour determ. *(German)* 77−60901
electrically coupled neurons producing rhythmic activity, snail Helisoma trivolvis 77−40657
epithelium, tight, impedance anal. using distributed resistance model 79−62201
RC double-balanced bridge analysis *(Polish)* 78−89498
reciprocity theorem, calibration of acoustic emission transducers 80−28401
resistance network analogues for multi-level system, relax. and double resonance expts. 77−1583
SQUID magnetometer, enhanced sensitivity using resonant input circuit 79−35799
superposition principle misuse 77−13540
surface acoustic waveguides, microwave network anal., flat overlay guides 77−27411
surface acoustic waveguides, microwave network anal., rectangular ridge guides 77−23790
teaching two-capacitor problem, using circuit self-inductance 79−62960

network analysis (management) *see management science*

network equalisers *see equalisers*

network parameters
see also S-parameters
four-terminal, x-y recorder sweep generator, sweep speed dependent on transfer charact. 80−62649

network synthesis
see also circuit CAD; frequency-domain synthesis; linear network synthesis; nonlinear network synthesis
filter, Kalman, digital, with a priori uncertainty of data, phasemeter appl. 80−98934
magnetic bubble propagation circuits, optimum design 79−78481

network theory *see circuit theory*

network topology
cooperative diffusion in temporary network 78−77820
fibre-optic data bus system design and implementation 77−7017
graph-like state of matter, electrical cond. of random networks, gelation and elasticity 78−65875
macromolecule flexible chain ideal network, contraction effects 77−14625
macromolecule flexible chain ideal networks, contraction 77−14624
rivers, tributary diameter, topologically random channel networks anal. 80−8372

networks *see networks (circuits)*

networks (circuits)
see also specific network and circuit headings e.g. communication networks, pulse circuits, oscillators
capacitive tap weights network, for SAW transducers 77−80041
current notation, positive and negative charges in electronic devices, for teachers 78−12494
education, diffraction grating and interference effects, electronic cct. analogue 79−9052
education, linear programming, introduction and appl. to simple cct. 80−73136
electronics for the physicist with applications, book 80−62403
energy fluctuations power conversion, in diode circuit, thermodynamics 80−17911
multi-microprocessor network, for sonar signal processing algorithms soln. 78−45044
Q-spoiler, sensitivity calibration of marginal oscillators for ion cyclotron reson. spectroscopy 78−21177
seismic recording channel, input cct. parameters matching *(Russian)* 79−39920
thermal conduction and diffusion, electrical circuit analogue, for teachers 78−86089
tilt meters, photoelectric, with negative feedback, block diagrams anal. *(Russian)* 78−88948
transducer, temperature sensing, cct. and charact. *(Polish)* 78−29103
Al_2O_3 circuit substrate, TiO_2 dope PbO-ZnO-B_2O_3 glass corrosion protection 79−29236

Neumann algebra *see algebra*

neural nets
see also brain models
activation and inhibition pattern, rate eqns. 79−92118
active neuron extracellular electric field model 79−62233
adaptation and transient responses due to inhibitory feedback 79−92206
adaptive analogue neural net dynamics, qualitative analysis *(Russian)* 78−27920
adaptive classifier for neuron functional analogue study *(Russian)* 77−40659
aggregation simplifying simulation, neural net appl. 79−8497
algorithms of neuron with extremum control *(Russian)* 77−29133
alpha-rhythm, neural vet model 80−76719
analytic solution based on Ising spin system analogy 80−12074
anthozoans, pennatulacea, colonial coordination 80−94197
arm posture control, spring model and equivalent neural network 80−101196
artificial, competitive and cooperative computation capability 78−92609
artificial, response charact. 78−40137
association and concept-formation theory 77−52763
auditory mechanisms, lower brainstem, book contrib. 79−2084
auditory neural network modelling by computer simulation, spatial firing patterns 79−74686
automaton model I/O characteristic for semi-Markov impulse sequences *(Japanese)* 80−16917
binaural hearing, monaural information processing on short sounds, neuronal model 78−65031
bio- and neurocybernetic models of the living being 79−53018
biocybernetic multilevel system, nervous regulation of internal organs *(Russian)* 78−48779
biosonar signals, moustache bat, auditory information processing 79−11943
brain, math. models of parallel and sequential processes 77−48785
brain cortices large-scale simulation via BOSS system 79−2039
brain function comparison with associative storage system capabilities *(German)* 77−29123
brainstem respiratory activity, math. model of computer-simulated neurons 77−44637
burst generating neurons, FET analogue 77−44630
burst-generating neuron model, field-effect transistor analogue 77−25411
bursting, lobster motor neurons 79−8501
Caianiello type, self-control 78−20167
cat neuronal spike trains, simulation, multiple Markov sequences 77−25413
cat superior colliculus, charact. 78−31808
category detecting nerve cells formation, mathematical theory 78−80859
cell assemblies in the cerebral cortex 79−2033
cells and circuits, insights into construct. by genes 79−39411
central catecholamine neuron systems, anatomy, physiology of dopamine systems, book contrib. 79−2042
cerebellar cortex model, temporal behaviour study 77−86482
cerebellum, neuronal organisation, informational capacity of Purkinje cell and climbing nuclear unit 77−25409
cerebral dynamics model, information sources *(Spanish)* 79−29520
circadian rhythm related to human body temp. 79−70525
cognitron, feedback-type, self-organising neural network with associative memory 78−56962
colour sensing optoelectronic device, neural mechanism modelling 80−12128
communication and control in brain 77−70451
compartmental chain model membrane voltage changes 77−29124
computational cerebellar cortex model, cat appl. 78−11629
computer reconstruction and display, three-dimensional 78−11624
cortex ensemble distribution patterns in different functional states 77−48774
cortical surface interacting neural net model 77−21512

neural nets continued
crayfish stretch receptor neuron excitation and inhibition summation 77−2015
crayfish stretch receptor repetitive firing behaviour nonlinear systems anal. 78−80853
curve crossing problem for Gaussian stochastic processes, appl. 78−85299
dendritic membranes, active vs. passive effects on simulated neuron transfer properties 79−24976
detective quantum efficiency reduction due to lateral neural interactions 78−53395
developing neurons, optimal stimulus distrib. model 77−25419
differential systems with feedback, global convergence conditions 77−40640
diffusion approx. for multi-input model neuron 77−29135
diffusion approximated model neuron firing interval moments 78−96041
diffusion neuron model, parameter estimation 77−40654
digital neuron model *(Russian)* 78−27924
digital simulation of neuron *(Polish)* 79−16189
direction sensitivity in visual cortex, neural net model 79−48248
discrete model synthesis *(Russian)* 77−36910
discrete-time model and applications *(Russian)* 79−2020
double-layer, analysis and simulation with mutually inhibiting interconnections 77−12905
dynamic characteristics of neural network 79−74630
dynamic model of neuronal response in the rat hippocampus 79−34547
dynamical response, effect of boundaries, Limulus retina 80−30717
EEG waves, neural basis 80−108868
electrically coupled neurons producing rhythmic activity, snail Helisoma trivolvis, network anal. 77−40657
electrochemiluminescent cell *(Russian)* 77−40651
electrochemiluminescent cell adaptive properties modelling *(Russian)* 77−40653
electronic model of neuron, ICs, teaching aid appl. 78−85301
electrotonic coupling, effective sign reversal by inhibitory neurons 77−29141
encoders, dynamic charact. in receptors and neurons *(German)* 77−36914
entropic properties of neural signal space, neurodynamic basis of Weber's and Steven's laws 77−73516
epileptic activity modelled as chain reaction within system of interconnecting cells 77−48787
epileptic seizure spatiotemporal patterns, model 77−64019
excitable elements, approx. methods of theroy of networks 77−86479
excitable fibre, steady speeds of spread of stable and unstable impulses, depend. on membrane ionic currents 78−53382
excitation and inhibition structures, integral eqn. models 79−2044
excitation of neurons by electrical synapse, in-phase and antiphase, nonlinear oscillators interaction 80−16918
excitation propagation in neural system model 78−96044
excitatory and inhibitory impulse sequence interactions in math. models of single neurons *(Japanese)* 78−27919
excited and inhibited, stability anal. *(Russian)* 77−40658
expansion-contraction behaviour in sea pen, control by conduction systems 78−53387
external geniculate body receptive field of cat, space-time wt. function 78−64989
external geniculate body receptive fields, neuronal network model 78−64990
finger tapping, human, neutral networks studies by phase transition curves 80−8042
finger tapping by both hands, coordinated, two coupled oscillators as model 80−101163
frequency response characteristics, interactive model implementation and simulation expt. 78−44487
head-neck system mechanics, neuromuscular system model 77−36977
Hebb nets of excitable elements 78−15820
hippocampus CA_3 field model, phasic transition, transfer of spikes in statistical neurone ensembles 78−48781
Hodgkin-Huxley equations for nerve membrane elec. activity, crit. topological test 78−35826
holographic models of neural structs., optical system *(Russian)* 80−76878
homogeneous neural fields, existence and stability of local excitation 80−26220
image number perception in neuron structures 77−44674
image processing algorithm based on neural net props. 80−40993
image size perception in neuron structure, neuron matrices apparatus appl. 77−44673
impulse flows, determ. of quantity of useful information 78−69038
information conversion mechanisms in a nerve cell 79−43862
information processing in neural networks, hierarchically structured model 78−85304
information processing in neuronal synapses, electrical neuronal model design *(Korean)* 80−35865
information transfer in a chain of model neurones 79−74646
inhibition simulation in electrochemiluminescence cell *(Russian)* 78−27925
inhibitory network, probabilistic and stochastic anal. *(Japanese)* 79−39410
Interactive Simulation Language application to nerve cell kinetics 77−21507
interconnected neurons system order development 79−53083
IPFM neural model, input-output anal., spike regularity and record length effects 80−56016
large network models using the brain organisation simulation system 79−8496
lateral-inhibition type neural fields, pattern formation dynamics 77−90761
lateral-inhibitory neural fields, excitation pattern dynamics 79−5270
Leaky-Integrator Neuron Model, input-output relationship 80−72152
leech swimming movement, neuronal generation 79−16198
local neuron population model performance 79−20531
locomotory rhythm generation with recurrent cyclic inhibition, leech 78−35832
lower leg reflex asynchronous control via spinal motor neutron pool 78−27935
M-cells, logic cct. model to account for CNS inhibition features 78−64917
mammalian visual cortex development model 77−44672
neural nets continued
maximum periodic sequence realisable by autonomous threshold element network 78−44489
McCollough effect, synaptic modification associative learning model 77−21531
McCollough effect model 77−16928
membrane two-factor two-mode model 78−7330
memory storage capacity analytic study 79−2023
mixed-system brain dynamics: neural memory as a macroscopic ordered state 79−57622
model equations and envelope eqn. for neural populations 78−31798
modulator-demodulator model, single signed integral PFM and PPM comparison 79−5268
Morishita neurons, modelling networks, cerebellum appl. 80−30703
motoneuron firing rates with strong random synaptic excitation 77−9184
motoneuron optimal control model 77−86486
motorneurons of different geometry and size principle 77−36908
movement detecting neural element in fly visual system, performance 79−43871
multi-input nonlinear system statistical anal. by optimal linearisation *(German)* 78−64918
multilayer, self-organisation 79−83756
multiple Markov sequences of interpoint intervals, inverse density modulation, rel. to removal spike trains 79−20529
music pattern recognition, MACSIM self-learning network 78−7373
myelinated nerve fibre steady-state/dynamic model, threshold comparison 78−27917
neocognitron, self-organising neural network model, pattern recognition mechanism unaffected by shift in position 80−76745
nerve axon, two-factor two-mode model, travelling waves *(Japanese)* 78−20173
nerve conduction model, FitzHugh-Nagumo, repetitive activity and Hopf bifurcation under point-simulation 79−11915
nerve impulse local existence 78−96045
nerve impulses, phase locking of pulse encoders 79−34546
nerve membrane, steady-state finite cable model, complementary variational principles 79−34545
nerve systems, mathematical models *(Hungarian)* 79−39379
nerve-muscle anisotropic syncytia, spread of flat front of excitation 78−53383
nerve-muscle anisotropic syncytia elec. props., steady form of excitation front 78−69037
nervous system, clinical disorders, sensory evoked potentials, book contrib. 79−2029
nervous system perceptual mapping and bionic modelling *(Russian)* 78−27921
neuromathematical concepts of point process theory 78−27916
neuromuscular system deterministic neuron models 79−29523
neuromuscular system output response, effect of correlated adjacent interspike interval sequences of input, computer simulation 78−80858
neuron electronic model *(Spanish)* 80−104580
neuron model, response for density modulated Poisson pulse trains *(Japanese)* 78−35829
neuron model as component of neural network, hardware realisation 80−61534
neuron model using stochastic syncoder 78−15822
neuron populations as information processing system, stochastic properties 78−80860
neuron soma model with high reliability and low power consumption 80−72392
neuronal ensemble principle and epileptic oscillation 79−83739
neuronal interconnection meas., semiautomatic system design 78−44742
neuronal organisation, informational anal. of Brindley's memory scheme 79−53077
neuronal populations, diffusely-connected, computer simulation 78−53384
neurotransmitter dynamic balance, systems and control theoretic anal. 78−44495
nonlinear oscillators transform. to neural eqns. 79−57624
nonlinear system Wiener anal. using Poisson-Charlier crosscorrelation 78−24055
observation methods, US and optical data processing 80−8234
oculomotor control system neurological integrator 77−4993
olfactory bulb model, spatial and temporal charact. freqs. of interactive neural masses 77−25476
olfactory pattern recognition modelling by adaptive spatial filter 78−24080
one-dimensional, uniform, with refractory period, maximum period 79−20530
optic tectum model of various vertebrates *(Spanish)* 78−40144
oscillatory neural networks in the rabbit hippocampus 80−89743
pacemaker phase control 78−11631
pain mechanisms, neural network model 78−85307
pattern generation in lobster stomatogastric ganglion, pyloric network simulation 80−12076
pattern recognition, SYSTEMA approach to cerebral structure *(French)* 77−9164
pattern separability and the effect of the number of connections in a random neural net with inhibitory connections 79−20532
pattern separability in random neural net with inhibitory connections 80−76726
peripheral nervous system, trophic mechanisms, book contrib. 79−2043
phase-locking meas. as test for neural encoding models 79−2036
photosensitive neuron in crayfish caudal ganglion, properties, expt. *(French)* 80−89705
plasticity observations *(Japanese)* 79−57693
potential time relations, 2 pulse series anal., histogram of recurrence time intervals 77−60196
random, experimental studies 80−12077
random pulse generators 78−24189
random threshold element networks with absolute refractory period 77−29143
random topology networks, randomness of generated eigenvalues 80−22291
randomly connected layered, pattern separation considerations 77−44644
recall and recognition in class of adaptive networks 79−48234
recurrent inhibition and afterhyperpolarisation, neuronal discharge effects 79−2035
Renshaw spinal interneuron repetitive firing, model 77−90760
repetitive firing computer models nonlinear systems anal. 78−80854
respiratory rhythm generator, neural network model 77−86485

neural nets continued
retina, interactions between photoreceptors and horizontal cells 78−11648
retina neural networks between cone and photopic L-type horizontal cells 79−83782
retina of cat, neural path real time simulation *(Spanish)* 78−96046
retinal ganglion cells, cat, nonlinear analysis in freq. domain 78−48793
retinal neuronal network of photoreceptors and horizontal cells 78−3482
retinal photoreceptor and horizontal cell synaptic connections 77−90787
reverberation cycles of a single neural equation 79−2022
reverberations and synthesis of a neural network 79−74634
rhythmic movement generation, lobster, leach, book contrib. 79−5273
rod network in turtle retina, elec. spread 78−80874
self-excited oscill. of neuronal circuit with recurrent inhibition and delay *(Japanese)* 78−20172
self-learning network universal element for pattern recognition 77−44621
self-organising multilayered net study 77−40661
self-organising nerve nets, fundamental theory, developmental plasticity anal. 80−67062
self-organising neural net coherent electrochemical emission model *(Russian)* 78−27879
sensory coding, distributed, applied to iconic storage and metacontrast simulations 79−34531
shunting inhibition stochastic modelling 77−9183
signal focusing in segmented stretch reflex system, auxiliary spinal networks 80−40999
simulation method using fast Fourier transform 77−1986
single neural equation, dynamical behaviour 77−56363
somatosensory cerebral evoked potential changes under constant mag. field 79−39383
spike train stochastic model, non-renewal point process properties 77−70447
spike trains, Markov process dependency as estimation measure 77−25357
spike transfer in statistical neuronal ensembles, neurone as nonlinear source of spikes 78−15819
spike-train statistical anal. methods 78−73149
spinal motoneurones refractoriness accumulation and secondary range firing model 77−1985
state variable approach, voltage clamp membrane current description 78−35825
statistical neuronal ensembles, spike transfer 79−57631
stochastic activity models of neurones, book 77−44632
stochastic automaton models for interaction of excitatory and inhibitory impulse sequences in neurons 78−20168
stochastic electronic neuron model 77−48775
stochastic model description of neuronal activity firing pattern evoked by monosynaptic inputs 77−29134
stochastic model for neuron firing sequence 77−4992
stretch receptor array reflex inhibition enhanced contrast 77−2016
superposed processes, serial correlation coefficients of inter-point intervals *(Japanese)* 78−88704
synapse development, selective stabilisation as network specification mechanism 77−16925
synaptic conductance changes, nonlinear effects 79−2045
synaptic facilitation and conditioning, electronic multineural model *(French)* 77−12908
synaptic transmission, nonimpluse-mediated, during cyclic motor program generation 80−51072
synchronous oscillation in idealised neuronal circuit with recurrent inhibition *(Japanese)* 80−101164
syneuristor discrete digital component design 79−96727
temporal oscillations, cortical neurons interactions model 80−3636
thalamic ventrobasal neurone discharges during sleep and wakefulness, computer simulation 79−20533
three-layer random neural net with inhibitory connections, pattern separability 78−44498
tightly coupled two layer random nerve net with inhibitory mechanism, pattern separability 80−61533
toplogical properties of continuous neural networks with analogue neurons 78−48783
two-component model of neuronal circuit with recurrent inhibition *(Japanese)* 77−48784
two-terminal electronic circuit neuron model 80−61526
universal microscopic characts. of neurons, search 79−96546
vestibular nuclei neurons in goldfish, model with ocular proprioception 78−40142
vision, identification of objects by neuronal system with references 77−36919
vision, mental scanning mechanism in foveal vision, expts. 79−5280
vision, neural light intensity analyser model 79−57648
visual behavior, edge and colour discriminations, retinal neurons network 79−48256
visual cortex afferent geometry and neuronal trigger features generation, primates 78−35842
visual cortex direction selectivity development model 79−48251
visual cortex neural circuitry model for orientation sensitivity 79−11927
visual cortex neurons, cat, mechanisms underlying receptive field props. 79−74662
visual foveation system, afferent part, computer simulation model 77−25437
visual hallucination patterns, mathematical theory of neuronal activity 80−35892
visual impedance, nonlinear integral equation 79−100599
visual information processing, primate visual system appl. 80−30722
visual path neuron simulation using analogue and digital electronic circuit *(Spanish)* 78−27942
visual perception of relative motion extraction, neural mechanism model *(Japanese)* 78−56987
visual stimuli equivalence classes, model neural network 78−69064
visual system, cat, neuronal net analysis 79−43872
visual system, human, transient characteristic using masking experiments 80−41009
visual system, inference upon the neural network finding binocular correspondence 79−34557
visual system, quantum fluctuations and adaptive spatial interactions 79−16206
Volterra-like polynomial representation 77−90754
Ba-treated nerve cells, reduced systems, qualitative anal. of model generating long potential waves 80−26213

neuristor networks *see neural nets*

neuron models *see neural nets*

neurophysiology
see also brain; neural nets
40 Hz activity in sigmoid gyrus, nucleus accumbens and amygdala, cross correl. anal. 80−76730
accessory optic projections upon oculomotor nuclei and vestibulocerebellum 80−3643
acetylcholine, diffusion in synaptic cleft of normal and myasthenia gravis human endplates 80−94198
acetylcholine receptor phosphorylation by membrane protein kinase in receptor-enriched T.californica membrane 77−56370
acetylcholine receptor phosphorylation in vitro, E. electricus membrane fragments 77−56371
acetylcholine receptor response to rapid photochem. prod. increases in agonist conc. 77−36909
acetylcholine responses in Aplysia neurons, effect of tris buffer 77−64020
Achilles tendon reflex potentials, shape of T- and H-pots. 77−86480
acoustic biotope, neural representation 80−51116
acoustic biotope neural representation, stimulus event relations for sensory neurons 79−66475
acoustic properties of nerve-muscle prep. as function of physiologic state 77−21673
action pot., lipid bilayer local phase transition 80−89744
action potential, molecular events and energy changes 78−44497
action potential changes associated with proved lumbosacral root compression 80−56006
action potential clamp to probe effectiveness of space clamp in axons 78−40441
action potential propagation, effects of cellular geometry on current flow 80−94196
action potential sources and their volume conductor fields 77−44640
action potentials from cultured neurons, recording by extracellular microcircuit electrodes 80−72382
action potentials from two different sources, distinction using dual channel audio monitor 78−61293
action potentials in single axons, effects of hyperbaric air and hydrostatic press. 80−56007
adaptation and transient responses due to inhibitory feedback 79−92206
adaption model evaluation for vestibulo ocular reflex 79−11931
afferent activity in stellar nerves of Octopus vulgaris 79−66467
afferent elec. nerve stimulation with ref. to prosthesis sensory feedback 77−90962
afferent innervation of heart and great vessels, vagal rel. to sympathetic components 79−83726
afferent nerve stimulation in below-elbow amputees 78−57125
afferent nerves from muscle spindles, signal interpretation method 80−101188
afterpotentials influence on shape and magnitude of extracellular pots. 80−3625
Alopex process: Visual receptive fields by response feedback, trigger features 80−61546
alpha wave amplitude and frequency control, feedback learning system *(Japanese)* 77−44626
alpha-rhythm, neural vet model 80−76719
amacrine cells in Necturus retina, independ. γ-aminobutyric acid- and glycine-releasing neurons 78−35848
amblyopia, human, differences in neural basis, effect of mean luminance 80−72156
ambulatory neuromuscular activation control model 79−57638
amino acid taste and smell, electrophysiological distinctions in catfish 77−44694
animal behaviour, neural control, book contrib. 79−2041
anisometropic amblyopia, expts. on kittens 79−24986
ankle joint reflex response to sinusoidal forces 77−21513
antennal flagellum mechanosensory hair response, lobster 78−27974
antennular chemosensitivity in spiny lobster, amino acids as feeding stimuli 78−53431
anthozoans, pennatulacea, colonial coordination 80−94197
Aplysia, restoration of transmission in synapses inactivated by habituation 80−56009
Aplysia californica, voltage depend. Ca^{2+} current, behavioural sensitization 79−92209
arbitrary movements control theory 79−74641
arm movement control, central integration function model 79−83757
arm movement control processes in monkeys 79−53080
arm movements controlled by peripheral feedback, in humans, simulation 78−80891
arterial smooth muscle, pig, estimates of cellular mechanics 79−16229
arterial system math. model, press.-flow relationships 78−53435
articulation development, possible nonlinear time varying control in feedback path 78−35870
artificial membranes, excitable and ion-selective, review of axon and bilayer membrane props. 77−86451
artificial membranes, excitable and ion-selective, review of non-bilayer lipidic membrane props. 77−86452
artificial neural network response characts. 78−40137
associative information processing structure 78−85300
atrial muscle, cyclic GMP rel. to negative isotropic effect of acetylcholine 77−48781
auditory, neuron receptive fields, owl 78−44512
auditory brain stem potentials, monkey, mapping following monaural clicks 79−16211
auditory brainstem frequency, response to waveform envelope periodicity 80−61590
auditory cortex, amplitude spectrum representation in Doppler-shifted-CF processing area 77−52810
auditory cortex of moustache bat, aural representation in Doppler-shifted-CF-processing area 78−80892
auditory cortex unit response to synthesized formants, cat 80−67098
auditory emitted potentials and temporal uncertainty 79−34575
auditory evoked potentials, averaging and FM 79−34574
auditory evoked response, effects of signal rise time and frequency 79−20552
auditory evoked response, relationship of latency and amplitude with sound intensity 79−20551
auditory evoked response correlate of symbol and significate 79−25000
auditory evoked sustained potentials, nature of response 79−34572
auditory evoked sustained potentials, stimulus relationships 79−34573

neurophysiology continued
auditory frequency measurement based on neural timing 77−5011
auditory function, mathematical model *(Dutch)* 77−9213
auditory hair cells, vertebrate, response latency 79−83794
auditory information, anatomical and physiological basis 79−11944
auditory interneurones, locust, time-intensity trading obs. 80−26238
auditory LF neural and cochlear-microphonic tuning curves in gerbil 78−88718
auditory magnetic evoked fields, human 79−16212
auditory mechanisms, lower brainstem, book contrib. 79−2084
auditory nerve, two-tone suppression, stimulus freq. effect, physiological and psychophysical obs. 78−85317
auditory nerve data appl. to binaural interaction theory, tone detect. in noise 77−36950
auditory nerve discharge rate, two-tone suppression, phenomenological model 77−16936
auditory nerve fibers, stimulus freq. effects on adaptation in auditory nerve fibers 79−43924
auditory nerve fibre, insect, latency shift, neuronal time cue of sound direction 79−48274
auditory nerve fibre bandwidths and critical bandwidths in cat 77−12932
auditory nerve fibre information coding in goldfish 78−40184
auditory nerve fibre model 80−94227
auditory nerve fibre response to cubic difference tone, in cat 79−2081
auditory nerve firing rates, patterns for spoken digits 79−83802
auditory nerve oscillating summed action potential, spike pattern and synchronisation, insect 78−40181
auditory nerve response and brain stem transmission time 80−45917
auditory nerve response from cats raised in low-noise chamber 78−53420
auditory neural interactions, rel. to LF (200 Hz) central masking investigations 77−64040
auditory neural mechanism system properties 78−40200
auditory neuron, characts. of digital model 78−3516
auditory neuron response to pulsed microwave irrad. in cat, microwave hearing 78−40259
auditory neurone phasic sensitivity as function of sound signal freq. 79−57666
auditory neurons, discharge rate density function dynamics for various tone-stimulus intensities 79−88089
auditory neurons of frog mid-brain, discharge rate density function 78−20191
auditory peripheral feedback qualitative model 79−39422
auditory primary neurons, comparative physiology 80−94224
auditory receptive fields, owl brain, centre-surround organisation 79−66476
auditory selectivity, two-stage lateral inhibition 77−56382
auditory space neural map, owl 79−8514
auditory system from middle ear to primary auditory nerve, analogue and computer model 77−29158
auditory system of bat, echo detection and target-ranging neurons 79−62269
auditory system of cricket, directional information coding by descending interneuron 78−77066
auditory system pitch detection mechanism model 77−90811
auditory time shift evoked potentials, generation technique 79−16354
auditory-nerve fibre encoding of 2-tone approximations to steady-state vowels 80−61582
auditory-nerve fibre responses to bandlimited noise, nonlinearities 80−61583
aural combination tones, compatibility between psychophysical and physiological meas. 78−57014
autonomic neuron development 78−77033
autonomic neurotransmitter functions, environmental determ., book contrib. 79−2040
autoradiographic visualisation of rat brain dopaminergic nerve endings, test of technique 80−61742
autorhythmicity and entrainment in excitable membranes 80−108866
average visual evoked response estimation, predictor-subtractor-restorer filter 78−65143
averaged multiple unit activity as estimate of local neuronal activity changes, vol. conducted pots. 80−89917
averager for neuroelec. response meas., operation mode *(German)* 77−77887
axon, giant, Myxicola, internal Cs^+ dialysis, Na inactivation 78−96036
axon, giant squid, current fluctuations obs. 79−24973
axon, squid, Ca buffering, review, book contrib. 79−5267
axon, squid, Na channel gates, interactions with quaternary lidocaine and tetrodotoxin 79−83745
axon, squid, Na channel inactivation, removed by high internal pH or tyrosine-specific reagents 79−20534
axon, squid, physiological role of ATP driven CA^{2+} pump 79−43865
axon, squid giant, compensation of potential changes produced by Er ion with applied potentials 79−16181
axon, squid giant, dispersive structure *(Japanese)* 78−61158
axon, squid giant, exponentiated exponential model g Na^+ and K^+ cond. changes 78−44493
axon, squid giant, poisoned with quaternary strychnine, block of Na conductnace and gating current 79−83746
axon, squid giant, temp. effects on gating currents 78−96037
axon, two-factor two-mode model, travelling waves *(Japanese)* 78−20173
axon adsorption model, action pot. and excitation currents, volt. clamp test 80−56018
axon asymmetry currents and admittance, squid 77−73518
axon cockroach giant, action potential separation by multiunit analysis 79−83760
axon conduction velocity modified by reinnervation of mammalian muscle 78−24062
axon diameter changes concurrent with action pot., crayfish, laser interferometer meas. 77−64029
axon K^+ channel response to time-dependent clamping functions, squid 79−62229
axon membrane, squid, freq. domain anal. of asymmetry current 80−51064
axon membrane, squid, null space in Hodgkin-Huxley eqns., critical test 79−83747
axon membrane admittance change during action pots., squid 79−57621
axon membrane asymm. current, squid, freq. domain anal. 78−44494
axon membrane freq. domain currents 79−62222
neurophysiology continued
axon membrane white noise, stimulation, strength-freq. relationship, squid 78−3466
axon model, ionic distrib., pot. profile and resting pot. 77−12901
axon model, leading edge approx. 77−12903
axon Na conductance and Ca transport, squid, mol. model 78−85305
axon-bearing horizontal cells, teleost retina, functionality obs. 80−51084
axonal branching in brain ascending raphe and nigral projections, fluorescent retrograde double labelling obs. 79−79504
axonal K^+ transport, single-file model for squid giant axon 77−73517
axonal K conductance anal., squid giant axons 79−96543
axonal membrane transport, elec. field distrib., ionic selectivity and permeability 79−34532
axonal transport, components, mechanisms and specificity, book contrib. 79−96551
axonal transport, theoretical approach to anal. 80−67064
axonal transport and microtubules in rabbit tissue after 3.1 GHz pulsed microwave irrad. 77−64097
axonal transport of vasoactive intestinal peptide in sciatic nerve 80−21463
axons, crit. slowing down near transition region from resting to time-ordered states, squid giant axon 78−44486
axons, giant, squid, interaction of Ba^{2+} with K^+ channels 80−85379
axons, squid, effects of internal and external cations and ATP on Na-Ca and Ca-Ca exchange 77−90745
axoplasmic transport, slow, asymm. in branches of bifurcating axons 78−80848
axoplasmic transport along nerve fibres *(German)* 80−45878
axoplasmic transport in mammalian nerve, role of Ca^{2+} 78−24052
axoplasmic transport of proteins, review 80−21464
barbiturate-induced slow outward currents in Aplysia neurones 78−80866
barnacle photoreceptors, initiation of light adaption, intracellular recordings 79−20542
baroreceptor Na sensitivity mediating reflex changes of blood press. and urine flow 77−48818
basilar membrane nonlinear model assessment, spatial differentiation as auditory second filter 77−36949
bat, moustache, target range sensitive neurons in auditory cortex 79−83808
benzodiazepine receptor, coupling to chloride anion channel 79−79486
benzodiazepine receptors in brains of humans and animals, autoradiographic localisation 79−83752
binaural hearing, monaural information processing on short sounds, neuronal model 78−65031
binocular depth perception, model 77−21527
binocular stereopsis perceptual phenomena evidence 77−44671
binocular synchronism monitoring, prolonged monolateral occlusion, electro-oculographic response 79−20543
binocular vision, frog ipsilateral retino-tectal pathways 80−85401
biocybernetic multilevel system, nervous regulation of internal organs *(Russian)* 78−48779
biohолographic models, optical lensless system appl. *(Russian)* 77−40650
biological rhythm phase response curve study, homotopy theory 79−8491
biological system identification, quasi-white random signals optimal use, appl. 77−73528
biomagnetic fields and cellular current flow 80−101192
biomedical engineering applied to neurology 79−96678
Biophysical Society, 23rd annual meeting, conf., Atlanta, USA (Feb. 1979) 79−34468
biopotential recording interference and motion artifact sources and suppression 77−81634
biosonar signals, moustache bat, auditory information processing 79−11943
bipolar cell, catfish, receptive field and input signals 77−12921
blink reflex, 1st component in rabbit and man 79−74649
blink reflex, afferent pathways, human 79−43864
blink reflex, peripheral electrical stimulation inhibitory effect, abolition by naloxone *(French)* 80−35880
brachial biceps, human, extracellular action potential radial decline 79−16192
brain, caudate nucleus, neutotransmitter activity transient alterations after irrad., rat expts. 80−72267
brain, complex visual stimuli representation 78−88709
brain, elec. response rel. to brain functioning in health and neurological disease 80−40998
brain, human, neural generator localisation underlying auditory evoked mag. fields 80−104703
brain, mag. evoked field mapping 80−104705
brain, magnetoencephalogram power spectrum estimation 80−104704
brain, math. models of parallel and sequential processes 77−48785
brain, planning and problem solving mechanisms 80−45877
brain activities, synchronous, spatio-temporal filter approach 80−61503
brain cortices large-scale simulation via BOSS system 79−2039
brain electrical sources, human, 3D localisation, quantitative evaluation 78−92613
brain electrical stimulation in grasshoppers, elicitation of singing and courtship movements 79−83731
brain evoked potentials, rel. to perception mechanisms 78−11627
brain lateralisation, induced by infantile stimulation in rat 79−48239
brain mechanisms of vision 79−96557
brain research, computed transaxial tomography, ring detector positron camera system 80−61739
brain rhythmic activity generation models *(Dutch)* 78−73150
brain stem evoked responses, acoustically depend. wave V latencies 78−85318
brain waves, limit cycle model, Frohlich's model 77−73520
brain waves limit cycle model 78−3464
brainstem auditory evoked responses in man, effect of stimulus rise-fall time and duration 77−12935
brainstem population responses, inhibitory influence 80−104595
brainstem potentials, microwave-evoked, auditory responses, in cats 80−56061
brainstem respiratory activity, math. model of computer-simulated neurons 77−44637
brightness perception and retinal rivalry in binocular vision, integrated model 80−101180
burst firing neurons, prolonged inhibition obs. 79−66469
burst-generating neuron model, field-effect transistor analogue 77−25411
bursting, lobster motor neurons 79−8501

neurophysiology continued
bursting pacemaker neuron, internal Ca^{2+} changes meas. with arsenazo III 77−64021
bursting pacemaker neurons, Ca^{2+} effects modelling 78−44484
callosal neurones selection, effect of visual experience, cat 79−79524
captured nerve fibre multiple single-unit recording by tubular electrode array 77−60321
cardiac ganglion, frog, impulse blockage, partial denervation in changing synaptic organisation 79−53081
cardiac output control mechanism modelling *(Japanese)* 78−69133
cardiac Purkinje fibre, Na current model 79−43861
cardiac slowing, respiratory gating mechanism 77−12902
cardiovascular control dynamic test method evaluation, model considerations *(German)* 77−52813
cat superior colliculus, neuronal network characts. 78−31808
catalytic reaction model, instability and spread of excitation waves, non-trivial modes 78−20161
category detecting nerve cells formation, mathematical theory 78−80859
cell assemblies in the cerebral cortex 79−2033
cell external elec. fields, Fourier transform anal. 79−62223
cell kinetics, appl. of Interactive Simulation Language 77−21507
cell voltage measurement using voltage sensitive dyes 79−57833
cells and circuits, insights into construct. by genes 79−39411
center-surround retinal ganglion cells: receptive field organization with special reference to light-dark adaptation 80−12104
central and peripheral nervous control mechanisms *(German)* 79−5271
central axons, remyelination restores secure conduction 79−83753
central catecholamine neuron systems, anatomy, physiology of dopamine systems, book contrib. 79−2042
central nervous struct. stimulation in invertebrates by focused US 79−20576
central nervous system interaction with peripheral motor system, voluntary human movement 79−8499
cercal system, cricket, const. representation of position of signal source in space 77−25475
cercal system neurones, cricket, const. representation of sound source position 77−70482
cerebellar cortex and peripheral muscle, computational model 78−11629
cerebellar cortical current appl. rel. to underlying cellular activity 77−60195
cerebellar model, spatial freq. characts. *(Japanese)* 80−67068
cerebellar Purkinje cells, synaptic action depression by inferior olive destruct. 79−34544
cerebellar stimulation and eye movement in cats 80−30719
cerebellothalamocortical signals influencing factors anal. 79−16191
cerebral cortex rabbit, contribs. of each layer to EEG 79−57618
cerebral dynamics model, information sources *(Spanish)* 79−29520
cerebral energy metabolism and memory 79−74629
cerebral magnetic field meas. and personnel selection 79−2026
cerebral potential sources location for visual field impairment assessment in humans 80−30922
cerebral potentials preceding unilateral and simultaneous bilateral finger movements 80−26217
cerebral tissue, Ca^{2+} binding rel. to weak oscill. elec. fields 77−1984
cerebral ventricle, intact, site for allografted mature superior cervical ganglion fragments in rats 79−8493
chelonian muscle spindles motor stimulation model 77−44636
chemical synapse, feedback mechanism model through elec. current 78−96043
chemioception, trigeminal mesencephalic nucleus of rabbit, adjacent neuron identity of activation 79−92241
chemoreceptor afferents from aortic and carotid bodies, relative latency of responses 80−101189
chemoreflex responses to hypercapnic stimuli models 79−34578
cholinergic synaptic vesicles, morphological and biochem. heterogeneity 77−64024
chromatic stimuli, duration thresholds 79−57657
chronic sphenoidal electrodes, material improvement 79−16328
cicada singing, neuronal generation 78−7328
ciliary motor responses, intracellularly recorded receptor currents 79−11916
cingulate cortex, monkey, anterior and posterior differentation by afferents 79−66468
circadian pacemaker, transplantation in Drosophila 79−62234
clinical study of neurofunctions, neuropharmacological drug investigation 79−96541
clonus, simplistic model rel. to diagnosis and therapy 77−48786
coaxial depth electrode development 79−29687
cochlea freq. selectivity sharpening models comparison 78−53418
cochlear encoding, reverse correlation technique 78−40183
cochlear fibre responses in guinea pigs with well defined cochlear lesions 80−94226
cochlear inner and outer hair cell selective destruction, freq. discrimination 78−77067
cochlear micromechanics, mechanism for transforming mech. to neural tuning within cochlea 78−11666
cochlear nerve activity rel. to action pot. off-effect in tone-burst electrocochleography 77−56386
cochlear nerve fibres, hysteresis of tuning curves 77−52806
cochlear nucleus, spike rates rel. to perception of phase changes 77−36948
cochlear nucleus neuron tonotopic organisation, evidence from masking of elec. by acoustic stimuli 78−44511
cochlear nucleus neurone response, model of phase struct. of bitonal stimulus 78−80887
cochlear summating potentials, effects of crossed olivocochlear bundle stimulation 77−52800
cognitive neurological functional pattern description *(French)* 77−9186
cognitron, feedback-type, self-organising neural network with associative memory 78−56962
collagen fibre electrode for peripheral neural activity recording *(Japanese)* 77−66879
colliculus of bat, long-latency 'subthreshold' responses to emitted const.-freq. components 79−79562
colour discrimination in domestic cat, neural basis 78−48800
colour sensing optoelectronic device, neural mechanism modelling 80−12128
colour sensitive neural networks, reaction to intensity and colour steps *(German)* 80−76737
colour sensitive neural structures with orientational specificity, chromatic grating detect. 79−96562

neurophysiology continued
colour vision physiological measurement facility, monkey detected responses *(Japanese)* 78−92752
communication and control in brain 77−70451
compound action potentials, volume conductor study, forward problem 79−88067
compound eye, Dipteran, small signal phototransduction 80−35882
computer appl. in clinical laboratories *(Swedish)* 77−44625
conditioning auditory stimuli and the cutaneous eyeblink reflex, human obs. 80−67090
conductance fluctuations in cultured spinal neurones induced by γ-aminobutyric acid 78−80867
conduction times, central and peripheral, in multiple sclerosis, somatosensory obs. 80−89773
conductivity monitor for isolated nerve preparation expts. 80−67301
cone activity, correl. with horizontal cell morphology, goldfish retina 80−45900
cone dark adaption, foveal and parafoveal, effect of background 79−43914
cone light adaption, frog, receptor rel. to ganglion sensitivity changes 79−48253
cone outer segments, light-induced changes in membrane current, tiger salamander and turtle 80−108899
cone sensitivity to flicker, primate, during light and dark adaptation, ERG obs. 79−43900
cone system, attenuation during rapid dark-adaption, frog 79−62253
cone voltage-current relationships, turtle, origin of non-linearity 79−74659
cones, blue, signals in red-green opponent-colour ganglion cells, macaque retina 79−79549
cones, evidence for equivalent-background hypothesis 80−16931
cones, post-receptoral adaption obs. 79−79548
cones, single and double, intraspecific evidence for function in teleost retina 79−62248
contingent negative variation and accuracy of time estimation. A study on cats 80−26216
contraction recorders for animal nictitating membrane and skeletal muscle 77−48969
control system stability properties 77−40640
cornea sensitivity in normal human eyes 80−12093
cortex ensemble distribution patterns in different functional states 77−48774
cortical cells as bar and edge detectors or spatial freq. filters 80−12109
cortical electrical phosphene props. 80−12112
cortical orientation selectivity, of partially visually deprived cats 80−26230
cortical periodic complex cells, cat, spatial freq. selectivity 78−69057
cortical receptive field binocular differences in kittens after rotationally disparate binocular experience 77−90784
cortical spreading depression, math. model 78−80857
cortical surface interacting neural net model 77−21512
cortical visual evoked potential, normal humans, bibliography of research 79−5278
cortical visual evoked potential, normal humans, main chapters of research 79−20537
coupled solitary waves in neurophysics 80−51067
cranio-spinal system, nonlinear, Volterra kernels representation determ. 79−2034
crayfish antenna mechanoreceptor unit sine-wave stimulus response obs. and model 79−57640
crayfish stretch receptor repetitive firing behaviour nonlinear systems anal. 78−80853
crustacean cardiac pacemaker control system, model analysis 77−52766
crustacean cardiac pacemaker control system, simple model 77−52765
crustacean neuromuscular junctions, synaptic facilitation obs. 79−39412
cryoprobe, for medical surgery 80−56274
curve crossing problem for Gaussian stochastic processes, neural modelling appl. 78−85299
cutaneous pressure sensitivity, effect of skin surface temp. on localisation error and two-point threshold 78−77072
cutaneous receptors, multiple unit correl. anal. 79−100638
cutaneous system energy depend. in conditions of simultaneous, residual and reverse masking, humans 78−20196
cyprinid retina, model of function at outer plexiform layer 80−12103
demyelinated mammalian nerve fibres, continuous cond. 77−4995
demyelinated nerve fibre conduction failure, effect of prolonging action pot. 78−73152
dendrite membrane, steady voltage-current characteristic 79−92203
dendritic membranes, active vs. passive effects on simulated neuron transfer properties 79−24976
detective quantum efficiency reduction due to lateral neural interactions 78−53395
diagnosis by sleep EEG 77−60271
difference differential eqns., periodic solns. 77−86489
diffusion approximations to neuronal activity and to the time dependent threshold problem 79−74639
diffusion neuron model, parameter estimation 77−40654
digit-wrist sensory compound nerve action pot. obs. in patients with focal nerve injuries 80−3655
digital simulation of neuron *(Polish)* 79−16189
digital-analogue hybrid 3-channel sequential stimulator 79−92445
Dipteran fly neural superposition eye, rhabdomere visual axis misalignments 77−64032
dipteran giant visual interneurone response props., rel. to optomotor control 78−27940
direction sensitivity in visual cortex, neural net model 79−48248
dolphin, innervation of pectoral fin *(Russian)* 77−64022
dopaminergic feedback regulation, rel. to postsynaptic receptors 77−52774
double-sucrose-gap voltage-clamp method, mathematical model 79−96539
dual input nonlinear system characterisation using impulse trains 78−31761
dynamic characteristics of neural network 79−74630
dynamic model of neuronal response in the rat hippocampus 79−34547
dynamic theory of visual perception 79−74681
dyslexic visual perception and aculomotor performance 79−83769
dystrophic muscle, neuromuscular transmission in abnormal fibres 78−27932
ear, chemical and physical aspects *(Dutch)* 77−9188
ear receptor pattern in herring 79−96579

neurophysiology continued
ECG physiological basis and biomedical apparatus *(German)* 79−100757
echo detecting characts. of inferior colliculus neurons of unanaesthetised bats 77−70484
echo-locating animal, neurocorrelometer model 78−96059
educational course, scientific method illustrated by paraphysical and neuroscience topics 78−24591
EEG, alpha wave asymmetry in coherence and power, effects of task and gender 79−39378
EEG, automated monitoring of long-term implanted electrodes *(Russian)* 80−76857
EEG, cat, computed unit-EEG correls. and laminar profiles of spindle waves 78−11625
EEG, decision P350, waveform and neural mechanism, auditory click and elec. finger stimuli 80−61528
EEG, event-related potential changes in healthy aged females 79−79500
EEG, magnetoencephalogram, current dipole model, central nervous system sisease diagnosis applications 79−48238
EEG, pathological delta waves, cortical electromicrophysiology, cat 78−11626
EEG, pattern-evoked potentials and nerve conduction vel. in family with adrenoleucodystrophy 80−45875
EEG, power spectral density estimates of subcortical spiking frequency 79−24972
EEG, visually evoked responses in children, intermittent photic stimulation *(French)* 79−16201
EEG alpha rhythm, result of corneal-retinal potential modulation obs. 79−34535
EEG automated anal. as prognostic indicator in stroke 77−86699
EEG frequency spectral analysis, physiological aspects 77−25627
EEG of mammalian brains, modulated RF energy effect for acute and chronic irrads. 79−79603
EEG patterns optimal display, relative merits of different montages 77−78004
EEG theta rhythm, dipole-like neuronal sources, anesthetized rat obs. 80−61527
EEG waves, neural basis 80−108868
electrical activity modulation by cholesterol, in Aplysia neurones 78−7329
electrical stimulation remote control device for studying neural mechanism of monkey 77−86719
electrical stimulation with Pt electrodes, exposed electrode area determ. 77−86704
electrical stimulation with Pt electrodes max. surface redox limits 77−86705
electro-oculographic ratio, rod and cone contribution 79−11925
electro-oculographic response, interocular comparison while reading printed material 79−20536
electro-oculography, on-line system for quantitative study of ocular kinetics 79−34699
electrochemical theory, steady and transient pots., in book, for teaching 78−8202
electroconvulsive shock treatment decreases β-adrenergic receptor sensitivity in rat brain 79−79512
electrocutaneous nerve stimulation, humans and toads 79−11909
electrocutaneous nerve stimulation, stimulus waveform selection 79−48236
electrocutaneous stimulus magnitude sensation, effect of pulse height and width *(Japanese)* 78−31998
electrocutaneous tracking, evaluation of sensory feedback codes 79−25004
electrocyte stacks of torpedine ray, assembly for quick-freezing tissues 80−67316
electrode pair, implantable, for recording from intact small nerves 80−36204
electrode stimulation of nervous system, electrochem. safety aspects 77−21659
electrodiffusion, steady-state, scaling, exact. soln. and phase plane 77−25403
electrogenic Na pump, role in slow synaptic inhibition 77−48780
electromotor system of Torpedo, as model cholinergic system 78−53388
electromyograph signal characteristics, various muscle tension levels and during fatigue 79−34537
electromyographic activity during brief isometric contractions, model 77−16922
electromyographic biofeedback, facial palsy treatment 79−34701
electromyographic electrodes, small-size, meas. of uptake area 79−74799
electromyographic recordings, perioral reflex amplitude variation 79−20558
electromyographic shimmer in normal human muscles 79−34538
electronic circuit breaker, recording and stimulation from same electrode 79−34680
electronic feature extractor for action potential parameters 79−84047
electronic neuron model incorporating both active and passive responses 80−8040
electrooculargram recording, single channel method for vertical and lateral eye movements 79−16205
electrophrenic respirator, implantable, Hg battery powered, design, features *(Japanese)* 78−3675
electrophysiological filtered click responses, short-latency, recorded from vertex and external auditory meatus 79−53156
electrophysiological recording from behaving animals, 10-channel commutator 79−84050
electroreceptor-electric organ system, of elephant nose fish, electronic circuit simulation *(Japanese)* 78−40132
electroretinogram, frog, rod and cone generation of wavelets 78−48799
electroretinogram e-wave, frog, rel. to ganglion cell activity and rod responses 79−48254
electroretinographic species difference within the leopard frog complex 79−62254
electrosensory afferent, dogfish, adaptation, neuron discharge regression anal. 78−35833
electrospinogram, human, recorded from intrathecal, epidural and cutaneous levels 79−16182
electrostimulation, stainless steel electrode corrosion control 78−7464
electrostimulator for percutaneous nerve stimulation, chronic pain treatment *(German)* 79−16342
electrotonic coupling, effective sign reversal by inhibitory neurons 77−29141
elliptical nerve and muscle fibres, physico-math. anal. 78−11639

neurophysiology continued
EM fields, direct influence on nerve and muscle cells of man in 1 Hz-30 MHz range 80−51160
EM radiation effects on neuroelec. transmembrane potentials, possible model of mechanisms 80−26259
EMG, cutaneous trunci muscle in spinal reflexes 80−3635
EMG, fatigue characts. of human gastrocnemius and soleus muscles 78−20169
EMG, single fibre, selective gain control along oscilloscope sweep 77−44864
EMG, surface, digital simulation, spectral anal. 78−80863
EMG, surface, model for digital simulation 78−80862
EMG, vector, of motor units with short, inclined and curved muscle fibres 77−86689
EMG in alcoholism, nerve conduct. vel. and sensory pot. studies 80−3617
EMG in alcoholism, terminal latencies in superior gluteal, distal peroneal and tibial nerves 80−3618
EMG in quadriparetics and quadriplegics, evoked giant sensory nerve pots. 80−3653
EMG index for localised muscle fatigue 78−57093
EMG of biceps brachii muscle, single motor unit action pot. model 78−53386
EMG of temporal muscle in rhesus monkey, spectral anal. 78−69039
EMG power spectrum, contrib. of individual motor units 77−29129
EMG power spectrum analysis, in neuromotor speech disorders 77−29161
EMG shimmer in patients with neuropathy and neurogenic atrophy 80−72149
EMG signal generation, quantification using automata theory 77−29132
EMG signal nonstationary model 77−86481
EMG spectra, effect of motor-unit firing time statistics 78−31804
EMG spontaneous activity in paretic skeletal muscle, LF bizarre discharges 78−80864
encephalic receptors, photostimulation in sparrows, induction of Zugunruhe 79−24985
encoder, adaptive model 80−97897
end plate current quantitative description and reconstruction 77−52770
endogenous and exogenous activity in molluscan neurone, identification by spike train anal. 80−89735
endplate acetylcholine-induced channels and transmitter release, humans 78−24063
endplate channel lifetime and cond. alteration by permeant cations 78−3467
entropic properties of neural signal space, neurodynamic basis of Weber's and Steven's laws 77−73516
epidural neurostimulation, percutaneous, histological reaction, short and long term study results 80−67285
epileptic activity modelled as chain reaction within system of interconnecting cells 77−48787
epileptic seizure spatiotemporal patterns, neuronal network model 77−64019
epiphysis, frog, characts. of slow pots. 80−56029
equilibration, physiopathology in aerospace medicine 79−11950
equilibrium reception in an insect, mediation by giant interneurons 80−45925
evoked action potentials, muscular and sensory 79−34530
evoked potential multi-channel data acquisition system, microprocessor controlled 78−11750
evoked potentials in same hand, normal subjects rel. to capral tunnel syndrome patients 79−48231
evoked signals on nerve surface, rabbit, distinguishability 79−57623
evoked spinal cord and nerve root potentials in humans using a non-invasive recording technique 79−39377
excitability, interactions between intrinsic membrane protein and elec. field 78−53377
excitable cell model, numerical method 78−53376
excitable medium wave vel. calc. 77−56366
excitable membrane, rapid transient changes in Na ion conductivity 77−44613
excitable membrane, with asymm. behaviour of inner and outer sides, oligomeric transport model *(Japanese)* 77−44611
excitable membrane analysis, computer calcs. 80−56004
excitable membrane K^+ conductance temp. dependence *(Japanese)* 78−24051
excitable nerve membrane exposed to optical radiation, surface-charge density variation, comment 79−8524
excitation and inhibition structures neural network integral eqn. models 79−2044
excitation detection by real-time detect. of small birefringence change *(Japanese)* 78−15938
excitation of neurons by electrical synapse, in-phase and antiphase, non-linear oscillators interaction 80−16918
excitation propagation in neural system model 78−96044
excitation properties of the squid axon membrane and model systems with current stimulation 80−67054
excitation spread equation boundary conditions for undistorted impulse movement pattern 77−56365
expansion-contraction behaviour in sea pen, control by conduction systems 78−53387
experience neural correlates in single units of cat visual and somatosensory cortex 80−12120
external geniculate body, cat, geometric props. of space of description of images 80−94203
external geniculate body, metric of space of description of images 80−30716
external geniculate body receptive field of cat, space-time wt. function 78−64989
external geniculate body receptive fields, neuronal network model 78−64990
extra-retinal photoreceptor model for Aplysia californica 78−44506
extracellular action potential recording, interference suppression 78−61294
extracellular electric field simulation, hybrid, of neuron with time-dependent surface potential 77−86478
extracellular Na transient meas., appl. of Na liq. ion exchanger microelectrode 77−52949
extracellular potentials generated by curved fibres in a vol. conductor, modelling 80−97889
extraocular motor unit activity, electromyographic recording in man during fixation and saccades 79−16203

neurophysiology continued
extraocular photoreceptors in invertebrates 77−44648
eye, chemical and physical aspects *(Dutch)* 77−9188
eye, electrical phosphene threshold, rel. to Rashbass' model 77−25428
eye, error-correcting mechanisms in large saccades 78−61175
eye, Limulus, circadian rhythm mediation by efferent optic nerve fibres 77−90783
eye, pursuit movements of disappearing moving target 78−61174
eye, retinomotor activity, local control in fish 79−2047
eye, rod outer segments, shedding behaviour under constant light, darkness 79−2050
eye, torsional movements, binocular coordination in cyclofusional response 79−2048
eye 79−83775
eye and hand motor systems, optimal response in pointing at a visual target 80−61567
eye and retina development in kittens 80−12113
eye centrifugal fibres in nonavian vertebrate, source revealed by horseradish peroxidase transport 77−36921
eye extrinsic muscle nerve terminals 78−56970
eye movement, gaze-evoked nystagmus, analogue model 78−27938
eye movement amplitudes, information used by the perceptual and oculomotor systems 80−35885
eye movement control in cephalopods, cerebellar-type system 77−12914
eye movement tracking and regulation test station *(German)* 79−16321
eye movement velocity, constrast effects on smooth-pursuit 79−43891
eye movements, vergence and version, reciprocal innervation model 77−48798
eye movements control, effects of frontal eye field and superior colliculus ablations 80−72154
eye optokinetic movement inversion in anterior visual field, albino rabbit 78−77052
eye pursuit movements in absence of target, perceptual effect 78−73162
eye removal at birth, producing excessive bilateral branching in rat, Co filling method 77−21520
eye tracking movements of acoustic targets, mathematical model 78−80870
eye-specific tecta termination bands, three-eyed frogs 79−62251
F-wave and M-response conduction velocity in diabetes mellitus 80−56015
F-wave in normal man, effect of vibr. 78−20164
fibre membrane analogue-code conversion, ionic mechanisms 80−81575
fibre membrane Na permeab. reversible blockage by increase in temp. of medium above 45°C 80−81576
fiddler crab auditory and vibrational stimuli receptor, Barth's myochordotonal organ 77−77921
field from isolated sciatic nerve in volume conductor 77−21505
file clam mantle edge mechanical and chemical sensitivity 78−53429
fine muscular control rehabilitation using ramp threshold feedback 79−83996
finger tapping, human, neutral networks studies by phase transition curves 80−8042
finger tapping by both hands, coordinated, two coupled oscillators as model 80−101163
finger tapping phase transition curves, human *(Japanese)* 80−56333
fish, lorenzinian ampullae detect. of geomag. variations 79−39381
Fitzhugh nerve conduction equations, appl. of higher order Hopf bifurcation formula 77−86483
FitzHugh-Nagumo equations, perturbation anal. of slow periodic wave soln. 78−24060
Fourier analysis by visual system or by visual investigator determ. 79−53089
fovea, spatial summation, asymmetrical effects of longer and shorter dimensions 79−2061
foveal vision, mental scanning mechanism 79−2066
foveal vision central mechanisms, monkey 80−12108
frequency discrimination capacities in goldfish, phase-locking in saccular nerve fibres 78−88720
frequency selectivity of single auditory nerve fibres in response to broadband noise 77−77906
Frolich's brain wave model, limit cycle collapse and travelling wave onset 78−48780
functional electrical stimulation of motor activity, control, rehabilitation appl. 77−86708
GABA uptake or exchange by synaptosomal fractions 77−12907
gait control, peroneal nerve stimulation sequence effect *(Croatian)* 78−44692
ganglion cell response to far violet light, macaque 78−11656
ganglioside synthesis, chick retina, light stimulation 77−9189
gastrointestinal electrical activity, Hodgkin-Huxley type electronic modelling 78−61165
gating charge immobilisation by inactivation-simulating substance 78−61154
geniculate neurone spatial resolution, impaired by monocular deprivation in kittens 77−21518
giant axon of the squid, gating current and K channels obs. 80−56012
giant axons, axymmetric displacement currents, macromol. gating processes 79−100590
giant axons, time-ordered state, spatially organised struct. obs. in squid 78−53380
glial smooth endoplasmic reticulum acid phosphatase transport into damaged axons, role of microtubules 80−85381
glial-neural interaction demonstrated by Na^+ and Li^+ injection into cortical glia 77−36905
glycolipids, regional synthesis, axonal transport, in neuron of Aplysia californica 79−83755
glycoproteins, fast axonal transport in guinea pig auditory neurons 80−104573
GT-2 gamma scanner, improvement 78−11719
habituation of gill withdrawal reflex, Aplysia californica, synaptic depression 79−83806
hair cell, vertebrate, response to controlled mechanical stimuli 78−15852
hair cell receptor pot., ionic basis in vertebrates, bullfrog obs. 80−26239
hand muscle, nerve stimulation effects on single motoneurones 79−79511
hand tremor differential diagnosis, display system using data compression 77−86697
haptic perception, cerebral lateralisation, interaction of responses to braille and music 78−7374
harmonic-sensitive neurons, mustache bat auditory cortex 79−43933
head-neck system mechanics, for visually triggered head movements 77−36977
neurophysiology continued
hearing, analogue of two-tone suppression in whole nerve responses 78−11671
hearing, binaural processing of information on short sounds, neuronal model 78−80885
hearing, octave enlargement phenomenon and its origin 79−100633
hearing, two-tone suppression in nonlinear model of basilar membrane 77−48811
hearing aids, microelectrode arrays, photolithographic fabrication and neurophysiological performance 79−12034
hearing directionality in amphibia 78−40197
hearing model, cellular approach 78−44515
hearing nonlinearities model described by active processes with saturation at 40 dB 80−56058
heart, electrical activity observability, singular value decomposition 79−11913
heart, frog, possible altered trophic influences during cold acclimation 79−83754
heart control during exercise, computer interpretation of heart rate var. during ergometric test 78−85430
heart natural pacemaker, modelling as pulse-freq. modulator 78−40135
heart pump stimulation, association with positive inotropy in cat 79−16196
hemispheric differential activation during complex visuomotor performance 79−16183
high-pressure neurological syndrome, comparative physiology, compression rate effects 79−88070
hind-limb reflex movements, chelonian, simulation 79−74642
hippocampal afterdischarges in rats, activity spread by ^{14}C method 80−26221
hippocampal burst-firing neurons, slow inward current, voltage clamp obs. 80−94194
hippocampal perforant path, glutamate as transmitter 78−11635
hippocampus pyramidal cells, somatostatin as excitatory transmitter 78−64973
histamine-containing neurones, synaptic responses 77−64027
histological examination of neural structs., Epon block sectioning technique 79−74814
histological section, computer-assisted mapping with the light microscope 80−30963
Hodgkin-Huxley equations, volt. clamped, large amplitude periodic solns. 78−20166
Hodgkin-Huxley equations for nerve membrane elec. activity, crit. topological test 78−35826
Hodgkin-Huxley nerve cond. eqns., bifurcation of periodic solns. 79−5269
Hodgkin-Huxley reduced model, speed of spread of excitation, integral differential eqn. 77−21509
Hodgkin-Huxley standard model, squid axons in reduced external Ca^{2+} 80−94188
holographic brain model for associative memory 79−74640
holographic models of neural structs., optical system *(Russian)* 80−76878
homogeneous neural fields, existence and stability of local excitation 80−26220
homologous displacement resulting from simultaneously applied rostral-caudal tactile stimuli, physiological mechanism 78−20198
human motion bioelectric control transfer functions 78−27926
human motor units EMG spikes and twitch waveforms anal. 77−73519
human vision, Fourier anal. and texture discrimination 78−96051
hybrid neural stimulator for chronic expts. 78−28124
hydra, simple nervous system and behaviour 79−83738
hydrodynamics of neurons, numerical methods for creeping flow investigation 77−5019
5-hydroxytryptamine receptors on visceral primary afferent neurones in rabbit nodose ganglion 77−56364
hypothalamic neurone spontaneous firing over narrow temp. interval 78−56961
ileum, guinea-pig, immediate X-ray induced contractions, localisation of effect by drugs 77−56443
image number perception in neuron structure, multilayer determined neuron network appl. 77−44674
image size perception in neuron structure, neuron matrices apparatus appl. 77−44673
implantable 8-channel stimulation system for labyrinthine deafness *(German)* 79−16347
impulse automatic identification and separation 79−16190
impulse circulation in excitable medium, critical size of closed circuit 79−92200
impulse conduction, modulation along the axonal tree, review, book contrib. 80−108872
impulse conduction along a myelinized fibre, math. model 80−94195
impulse data treatment for comparison with theory 80−97893
impulse density function equations *(German)* 78−92620
impulse flows, determ. of quantity of useful information 78−69038
impulse propagation, subthreshold solns. of Hodgkin-Huxley eqns. 78−77044
impulse spread in medium with non-monotonic function 79−92201
impulse steady speeds of spread depend. on membrane ionic currents, stable and unstable impulses 78−53382
impulses in 2 parallel unmyelinated fibres, induced excitation and synchronisation calcs. 80−56017
inferior colliculus neurons, cat, response to binaural beat stimuli obs. 80−72179
inferior colliculus of immature mouse, plastic reinnervation, autoradiography with ^{14}C-deoxyglucose 79−92233
influx current of edible snail neurons, dependence on Ca^{2+} conc. and membrane pot. 80−108865
information conversion mechanisms in a nerve cell 79−43862
information processing in neural networks, hierarchically structured model 78−85304
information processing in neuronal synapses, electrical neuronal model design *(Korean)* 80−35865
information processing within retina and lateral geniculate nucleus 79−74648
information theory appl. to large information systems 77−56325
information transfer in a chain of model neurones 79−74646
inhibitory network, probabilistic and stochastic anal. *(Japanese)* 79−39410
inhibitory synapse, influence of presynaptic irregularity on action pots., stretch receptor neurons 77−9185

neurophysiology continued
insect mechanoreceptor sensory transduction nonlinear anal. 77−64061
inspiration, graded inhibition, specific effects of flow rate 79−100647
insulin secretion neural control, math. model 78−31796
intellectual activity, classification of normal and anomalous forms, quantised-wave theory of coherent brain appl. *(Russian)* 80−76722
intellectual activity, psychoheuristic relationship of psychotism structs. and giftedness structs. introduction, quantised wave theory of coherent brain appl. *(Russian)* 80−76723
interictal spiking, spontaneous, awake kindled rat 80−67058
interlimb coordination, human, expt. obs., two handed movements 79−57636
interspike interval changes during propagation, quantitative description 77−64023
interspike intervals, meas. teleprocessing, anal. 80−85375
interspike time histograms for random input model 78−40134
intestinal motor activity mathematical model 77−90847
intestinal smooth muscle cells, non-cholinergic excitatory transmission 77−77891
intracellular Ca 79−8495
intracellular recording from pulsating cerebral cortex 77−48960
intracephalic implants of embryonic neural tissue in rats, neuronal interactions study technique 80−30702
intracranial pressure monitoring by passive radiosonde 79−57798
intraspinal nerve fibres, cat, electrical threshold continuous monitoring method 80−46104
ion channels in development, book contrib. 79−96549
ionic channels and gating currents in excitable membranes, review 77−90764
ionic channels in excitable membranes, current problems and biophysical approaches 78−53369
IPFM neural model, input-output anal., spike regularity and record length effects 80−56016
jellyfish electrically-coupled photosensitive neurons controlling swimming 77−90756
laryngeal control for pitch change in Japanese word accentuation, neuromuscular model *(Japanese)* 78−40205
lateral geniculate body, types of receptive fields and freq. characts. 77−25424
lateral geniculate cells, functional organisation after visual cortex removal in newborn kittens 80−81587
lateral geniculate nucleus, cat, electrophysiological classification of X- and Y-cells 78−64996
lateral geniculate nucleus in cat, struct. of identified X and Y cells 80−26231
lateral geniculate nucleus neutron classes, morphological effects of monocular deprivation 77−52781
lateral geniculate nucleus of cat, oscillatory neural activity entrainment 79−92216
lateral geniculate nucleus of cat, periodic stimulation, neural activity transient persistence 80−56021
lateral geniculate nucleus postnatal development in humans 80−12114
lateral geniculate nucleus selective atrophy assoc. with iris coloboma, cat 78−3471
lateral geniculate nucleus X-cell early development, kitten 78−27946
lateral line, onset of neural function in South African clawed frog 80−21480
lateral reticular nucleus neurone activity on scratching 78−24054
lateral-inhibition type neural fields, pattern formation dynamics 77−90761
learning model, for temporal sequences, based on dentate gyrus anatomy 77−21508
leech swimming movement, neuronal generation 79−16198
lens accommodation, interpositus neuron control obs. 80−21469
light adaptation, multiple intracellular contribs., Limulus ommatidia 79−43896
light flash intensity meas. for neurophysiological research 79−49270
light response and kinetics in Aplysia giant neuron 78−53381
light-adapted photoreceptors, sensitivity changing mechanisms evaluation 79−79543
limb tremor, normal and alcohol withdrawal, nature and etiology 79−29544
limbic spindle re-appraisal 78−69036
limbic spindles, cerebral activity or artifact 78−48778
Limulus ommatidia, resonant response of neural model to double freq. stimulation 80−76734
Limulus ventral nerve photoreceptor response height vs. stimulus intensity curve 78−69058
linear spread of nerve potential due to time dependent stimulus 79−24974
living tissue electrical excitation theory development *(French)* 78−88703
living tissue stimulation energy threshold meas. using analogue instrument 79−57745
local neuron population model performance 79−20531
locomotion motor coordination and neuromuscular activities study, humans 77−44635
locomotor, activity circadian rhythm, cockroach, strong phase response curve 78−11630
locomotor disorders of human skeletal muscle using tension development rate 77−40880
locomotory rhythm generation with recurrent cyclic inhibition, leech 78−35832
locus coeruleus neurons, impulse activity in awake rats and monkeys 80−104581
lower leg reflex asynchronous control via spinal motor neutron pool 78−27935
lumbo-sacral motoneuron pools, human, response patterns to distant somatosensory stimuli 80−108924
luminosity-type cells in the turtle retina, short-wavelength input 80−41012
lung irritant receptors and afferent C-fibres, stimulation by prostaglandins 77−12939
lymphatic heart, frog, elec. props. of spinal centre pacemaker 77−56360
M-cells, logic cct. model to account for CNS inhibition features 78−64917
magnetic phenomena, central nervous system, book contrib. 79−5304
magnetoencephalogram genesis mechanisms 78−53432
mammalian nerves, chronic recording, impedance props. of metal electrodes 79−12043
mammalian nervous system, possible microwave mechs. 80−89738
mammalian neuromuscular system energy-optimal controls 77−73522

neurophysiology continued
mammalian neuron connectivity estimate 78−77039
McCollough effect neural network model 77−16928
mechano-sensory receptor of crayfish stretch receptor organ, effect of D_2O 77−44696
median nerve, transient responses to elec. stimulation, SQUID appl. to somatically evoked field meas. 80−104706
median nerve lesion localisation, usefulness of F-wave conduction time, post mastectomy patient 80−56267
medullary interneurons of goldfish, elec. and chem. inhibition in vertebrate central nervous system 77−36911
medullary respiratory neuron activity, rel. to tonic and phasic REM sleep 80−97891
membrane, elec. excitable, phys. model, excitation mechanism 77−36902
membrane admittance, integral representation 78−15811
membrane conductance channels, current-induced coupling, multi-channel interaction and mean field cond. 80−67063
membrane conductance fluctuations and ionic pores, review 77−90752
membrane DC resting pot., automatic offset cct. 77−40940
membrane dynamic equation solving, practical algorithm 78−77038
membrane excitability mechanisms, book contrib. 80−12062
membrane permeability changes, fluctuation anal. 78−11636
membrane process field potentials anal. and synthesis, computer system 80−85374
membrane two-factor two-mode model 78−7330
membranes, excitable, bursting phemomena 79−66455
membranes, excitable, statistical theory nonlinear force-flux reln. and fluctuation 77−9179
membranes, volt.-depend. tetrodotoxin action 77−44620
memory neuron, synapse microchem. for memory component of neuroconnective brain model 80−104579
memory of temporal sequences, model, simulation studies 77−9181
memory rel. to immunological processes, role of microfilaments and microtubuli *(German)* 77−66811
memory storage capacity of neural network, analytic study 79−2023
message operators for expression of information 77−29089
metabolic synapse, comparison of effects of cyclic 3′,5′-AMP and 3′,5′-GMP 78−24058
microcircuits involving dendrites 78−53390
microcomputer-based neurophysiological stimulator, design of and impact on clinical procedures 80−26393
microelectrode current and voltage clamp cct. for central nervous system neurons 78−24191
microelectrode multichannel depth probe fabricated using electron-beam lithography 79−57822
micropipettes of very low resistance for intracellular meas., production method 80−61738
microprocessor−based unit data acquisition and reducing system 80−21598
microtubules in optic nerves of temperature acclimated goldfish, electron microscopy 80−85395
microwave biological effects, overview 80−35964
microwave effects on isolated nerve and muscle preps. 78−53443
microwave irradiation of isolated rat heart after treatment with ANS blocking agents 78−40251
microwave rapid fixation device for inactivation of enzymes in rat brain 77−81761
microwave reception by brain, interaction with nerves 77−12958
microwave response by indivudial Aplysia pacemaker neurons 78−92675
midbrain reticular stimulation, brightness detect., Rhesus monkey 79−43919
mind and brain relationship, a fundamental theory 79−100592
miniature endplate current decay, effects of extracellular Ca^{2+} and Mg^{2+} 78−24064
miniature endplate potential amplitude online meas., programmable calculator conversion 79−84051
minicomputer application for fast expt. data acquisition and processing *(Japanese)* 80−85536
minicomputer system, automatic visual stimuli, hand and eye movement monitoring *(French)* 79−34682
mixed-system brain dynamics: neural memory as a macroscopic ordered state 79−57622
modular gating channel and the Cole-Moore effect 80−30708
Molluscan branched neuron, location of spike-initiating or spike entry zones 80−61536
monitoring system for stroke patients 80−26394
monoamine neutrotransmitters, du channel point, in raphe nuclei of rabbits, elec. stimulation effect *(Chinese)* 78−20170
monoamine-containing neurone connectivity in leech central nervous system 77−44639
monosynaptic potentials onset and propagation, discrete-dynamic equations 78−77040
monosynaptic reflex, influence of visual input 77−60197
Morishita neurons, modelling networks, cerebellum appl. 80−30703
morphognostic coil design for implanted nerve stimulator 79−84014
motion and vision, stabilised spatio-temporal threshold surface 80−16926
motoneuron firing rates with strong random synaptic excitation 77−9184
motoneuron optimal control model 77−86486
motoneuron ventilatory response to added mech. pneumodynamic loads 79−100654
motoneurone cross-correlated firing patterns, recurrent inhibition effects 78−80861
motoneurone model with early inactivation, after hyperpolarisation conductance time-course and repetitive firing 80−40987
motoneurone survival during normal cell death in chick embryo, effect of neuromuscular blockade 78−27933
motoneurone transmitter output rel. to muscle fibre growth, lobster 78−64974
motoneurones excited by phasic muscle stretches, discharge pattern shaping, recurrent inhibitory feedback effects 78−85303
motor axon reflex study after intranervous regeneration 79−43863
motor conduction velocity and H-reflex in infancy and childhood 78−61164
motor control, muscle representation 78−24057
motor nerve conduction vel. and evoked pots. in peripheral nerve lesion localisation 78−31802
motor nerve conduction velocity determ. in normal subjects 77−60275
motor nerve conduction velocity measurement, neuromuscular disorder diagnosis using semiautomatic meter 77−48909
motor nerve endings, hyperosmotic neurosecretion rel. to internal Ca conc. 77−56368

neurophysiology continued
motor nerve impulse, conventional Ca^{2+} channel mediating asynchronous acetylcholine release 78−11638
motor nerve terminals, cyclic nucleotide-mediated Ca flux 77−73524
motor neuron, lower, intranervous regeneration, axon reflexes 79−34541
motor neuron activity patterns of Drosophila, anal. with neural analogues 80−108870
motor neuron disease, mechanisms of spontaneous EMG activity 78−20162
motor neuron firing pattern in Aplysia 79−48244
motor neuron lesions, EMG positive sharp waves and fibrillation potentials 77−60194
motor response of hemiparetic patients, biocybernetic model of hypnosis influence *(Slovenian)* 79−2037
motor systems, eye and hand, optimal response in pointing at visual target 80−56079
motor systems, neurological control of locomotion, book contrib. 79−5272
motor unit action potential, influence of sustained contraction 78−31801
motor unit action potential study using computer simulation 79−11914
motor unit discharge freq. depend. on isometric muscle tension, humans 77−21510
motor unit dynamics, EMG Hoffmann-reflex and M responses, human 78−7331
motor unit potential recording using monopolar and bipolar leads 77−81615
motor unit recruitment and firing freq. control in elec. stimulated muscles of cat 78−81092
motor unit recruitment and rate coding for isometric contractions production 77−73523
motor unit recruitment order reversal by cutaneous stimulation during muscle contraction, man 78−40136
motor unit sequential stimulation in cats through peripheral motor nerves 79−57635
motor units, no preferential activation of fast units in rapid voluntary contractions in man 77−64025
movement detecting neural element in fly visual system, performance 79−43871
movement detection, performance of a wide-field element in the blowfly visual system 80−89763
movement-detecting neurons, fly, contrast sensitivity obs. 80−72163
mu rhythm detect. from human scalp, functional topography 78−48777
multi-microelectrode system for simultaneous recording of closely spaced neurons *(Japanese)* 78−61284
multibarrel microelectrodes, 'piggy-back', simple technique for construction 80−85541
multichannel audio monitor for detecting electrical signals 79−20694
multipath neural systems, statistical anal. 80−101162
multispike train, anal. techniques 77−44868
multiunit signals, educable waveform recognition system for sorting unit discharges 80−51312
multiunit spike train separation techniques evaluation criteria 78−85422
muscarinic suppression of voltage-sensitive K^+ current 80−51070
muscle, cat tibialis posterior, motor units, neuro-mechanical props., speed-force relations 78−80856
muscle, excitation and contraction processes, book contrib. 79−5262
muscle, fast and slow myosin in developing fibres 78−64961
muscle, human, physiological and metabolic studies in health and disease 79−39443
muscle, kinetic model of single contraction 79−57629
muscle, locust, pot.-depend. transition temp. of ionic channels induced by glutamate 77−77882
muscle, of guinea pig, force-vel. characts. for Ca-activated slow- and fast-twitch skeletal fibres 77−44643
muscle, skeletal, contraction time in normal children 78−61163
muscle and nerve fibre electric field resolution for EMG analysis 79−57627
muscle cell cultures biology, book contrib. 79−2031
muscle contraction, effect of successivity of activating pulses 77−25418
muscle contraction, math. model with account of excitability 77−25417
muscle contraction, model using elec. stimulation of cell cultures, myosin synthesis 77−1988
muscle contraction strength control during elec. stimulation, using PWM and FM 77−40929
muscle control system Ia feedback pathway correlations, origin and nature 79−24977
muscle coordination in cat hindlimb during maximal vertical jump, computer model 77−40662
muscle endplate, desensitisation rel. to selective alteration of Na^+ channels 77−77890
muscle fibre end-plate current pot. depend., effect of phenylalkylamines, frog 78−31799
muscle fibre post-synaptic membrane, ionophore-mediated Ca influx effects 78−11637
muscle fibre resting pot. in cricket, influence of ions 78−24046
muscle fibres, computed extracellular pots. 79−43843
muscle fibres, fibrillar, tension transients affected by stretch-dependent binding of AMP-PNP 79−20562
muscle fibres of giant barnacle, cyclic GMP levels associated with contraction 77−56369
muscle innervation-like effect, substances moved by axonal transport, released by nerve stimulation 79−16197
muscle length and strength control, central co-activation of α and static γ motoneurones 77−25414
muscle mechanics thermodynamic model 78−80908
muscle spindle, mammalian, math. model *(Japanese)* 77−44638
muscle strength gain, neural factors rel. to hypertrophy 80−12168
muscle stretch reflex system, multi-channel, focused signal transmission mechanism considerations 79−24978
muscle tension development control by motoneurones 77−66813
muscle training effect on single motor unit firing pattern 78−7327
muscleforce-freq. curve recording from humans, α excitability evaluation *(Japanese)* 78−3643
muslce mass potential, stochastic model, NMV activity *(Japanese)* 78−24056
myelin lattice swelling kinetics study X-ray diffr. obs. 80−21436
myelin swelling and meas. of forces between membranes 79−62204
myelin vesiculation simulated by nerve exposure to Ca ionophore 77−29128
myelinated axon impulse cond. simulation, sensitivity to nodal and internodal parameters 78−35831
neurophysiology continued
myelinated nerve fibre, response to short duration biphasic stimulating currents 80−85373
myelinated nerve fibre simultaneous meas. and counting grid 79−39540
myelinated nerve fibre steady-state/dynamic model, threshold comparison 78−27917
myenteric plexus, mediation of slow synaptic excitation by substance P 78−73153
myoelectric signals, physiology and mathematics 79−74621
myoelectric signals, power spectra interpretation, model and appls. 77−44641
myoelectric single motor unit potential generation model 77−29131
myotonia, Ca induced, computer simulation 79−57633
Myxicola axons, Na tail currents compared with membrane asymm. currents 77−66808
nematode Ascaris, motoneurons physiological activity 79−92208
Nephrops norvegicus (L.), circadian rhythmicity, neurohumoral basis 80−108889
nerve action potential, cybernetic elucidation 79−48243
nerve action potential model 80−30697
nerve bundle conduction velocity distrib. meas. and transfer function anal. 77−44867
nerve bundle magnetic stimulation, capacitive coupling effect 79−48242
nerve cell communication and second messengers role 78−7337
nerve cell cultures biology, book contrib. 79−2031
nerve cell membrane, flow of Na^+ and K^+ through ion channels 79−74644
nerve cell membrane detection of HF EM fields, possibility discussion *(Russian)* 80−76785
nerve conduction eqn. periodic travelling wave solns. stability 79−16194
nerve conduction equation, travelling wave solns. 79−53082
nerve conduction model, FitzHugh-Nagumo, repetitive activity and Hopf bifurcation under point-simulation 79−11915
nerve conduction vel. and refractory period as neurotoxicity parameters 79−83749
nerve conduction velocity, biomagnetic response of lobster circumesophageal connective 78−92619
nerve conduction velocity distribution based on compound nerve action pot. 78−40138
nerve conduction velocity variability, effect of averaging and limb warming 77−60274
nerve evoked pots., sensory and mixed conduction vel. obs. 79−74693
nerve excitable membrane, EM wave effect on surface charge density 78−85334
nerve excitation, gating currents and dipole transitions 80−67056
nerve fibre, active, in finite volume conductor, surface action potentials, model 79−24980
nerve fibre automatic counting using an array processor in a multi-mini computer system 79−79710
nerve fibre conduction vel. distribs., estimation from action pots. 80−3633
nerve fibre conduction vel. distribs., estimation from two compound action pots. 80−8044
nerve fibre counting by pipeline multiminicomputer image processing 80−109013
nerve fibre regeneration passing through nerve suture, stochastic model 79−83740
nerve fibres, myelinated, diffusion of ions 79−24965
nerve fields, topographic maps and columnar microstructure formation 80−56013
nerve fields, topographic organisation 80−89742
nerve impulse electro-diffusion model 79−53078
nerve impulse encoding, elec. processes 80−76718
nerve impulse eqn., periodic solns. 77−66812
nerve impulse equation, dynamic responses of impulse 78−64972
nerve impulse local existence 78−96045
nerve impulse radial decline in restricted cylindrical extracellular space 78−53379
nerve impulse stability theory, Hodgkin-Huxley eqns. appl. 78−48782
nerve impulses, phase locking of pulse encoders 79−34546
nerve ionic permeability of K, Na and Cl, regulation by fixed charges and pH, crayfish 77−66809
nerve membrane, excitable, charge density due to optical irrad. 79−8526
nerve membrane, excitable, surface-charge density when exposed to optical radiation 77−29176
nerve membrane, excitatbility, genetic alteration, temp.-sensitive paralytic Drosophila mutants 80−97895
nerve membrane, steady-state finite cable model, complementary variational principles 79−34545
nerve membrane flicker noise model 77−29125
nerve membrane potential, effect of constant mag. field 79−57679
nerve membranes, cell excitation detect. using birefringency changes *(Japanese)* 77−66876
nerve membranes, protein channels for Na and K ions, mol. mechanisms 77−4994
nerve myelin, phasing the small-angle X-ray diffr. pattern 79−57588
nerve net theories, tentative contributions of neuroanatomy 79−74625
nerve rhythmic excitation conduction, investigation of free-radical processes, frog 79−70543
nerve signal optimal filtering 77−73616
nerve signals derivation from contrast flash data 80−108885
nerve spike trains, Fourier anal. 80−12070
nerve stimulation, contactless, electromagnetic induction technique 77−52779
nerve systems, mathematical models *(Hungarian)* 79−39379
nerve terminal Ca channel selectivity regulation by weak acid site 79−62231
nerve trunk multifibre activity quantitation 80−76853
nerve trunk of squid, ATPase activity changes as function of elec. stimulation freq. 79−57620
nerve trunks, method for determ. of conduction velocity distribs. 79−48241
nerve-muscle anisotropic syncytia, electrotonic membrane pot. distrib. 78−64971
nerve-muscle anisotropic syncytia, spread of flat front of excitation 78−53383
nerve-muscle anisotropic syncytia elec. props., steady form of excitation front 78−69037
nervous activity monitoring in Drosophila by [^{3}H]deoxyglucose 80−56024

neurophysiology continued
nervous system, circadian pacemakers, literature review, book contrib. 79−2028
nervous system, clinical disorders, sensory evoked potentials, book contrib. 79−2029
nervous system, electrical stimulation, laboratory research *(Norwegian)* 78−77096
nervous system disease diagnosis using control characts. in manual control system 79−83990
nervous tissue damage parameters secondary to elec. stimulation 78−44491
nervous tissues, Ca dependent K activation, book contrib. 79−5266
network dynamical response, effect of boundaries, Limulus retina 80−30717
neural coding schemes, integrate-to-threshold anal. 80−35868
neural communication system model, single signed integral PFM and PPM comparison 79−5268
neural feature detectors, coding model 79−74626
neural membrane depolarisation, possible role in work of molecular computer 79−53075
neural network, aggregation simplifying simulation 79−8497
neural network theory, analytic soln. based on Ising spin system analogy 80−12074
neural pulse wave analysis, microprocessor-based instrument 80−104791
neural response evaluation and statistical judgement to sinusoidal stimulation with superimposed drift and noise 79−88068
neural single unit activity recording with photoetched Au multimicroelectrode surface 79−57824
neural spikes amplitude discrimination, histogram computer analysis 77−52778
neural structure bioholographic model investigation using multilayer mask and lens *(Russian)* 77−52769
neural superposition compound eye of male Bibionidae expt. obs. 79−43874
neural system, one-dimensional, numerical investigation of kinetic neuronic equations 80−76725
neural transformations of random signals, Wiener and of functionals of Markov chain 80−76727
neuro-secretion, role of Ca in control mechanism 77−64028
neuroblastoma cells, quiescent, rapid ionic conductance changes, serum induced 79−74612
neuroblastoma tumour, thermal conductivity and diffusivity meas. 79−5252
neuroendocrine effects, microwave-induced, nonspecific stress reaction 80−35969
neurological disorders, closed EEG feedback system 79−34703
neurological function tracking-task instrument, portable, features 77−86678
neuromagnetic fields sources location, using SQUID system, comparison with electrical method 80−101190
neuromagnetic response latency of human visual cortex 78−40151
neuromathematical concepts of point process theory 78−27916
neuromuscular block, sweep frequency technique, conscious, unconscious patient appl. 77−52910
neuromuscular block indicator, model INMB-1, EMG amplitude meas. 80−104785
neuromuscular blockade by amantadine by suppression of acetylcholine receptor ionic cond. 78−64975
neuromuscular blockade monitoring device, twitch box 78−77132
neuromuscular development, synaptic and septate junctions in embryonic lobster muscle 77−77889
neuromuscular development, synaptic channel gating props. changes 79−16195
neuromuscular disorders, biofeedback therapy, conscious control of motor neurons 79−34702
neuromuscular ectopic synapse, gating props. of acetylcholine receptor 78−27934
neuromuscular frequency-depend. block and temp.-induced seizure in ts mutant of Drosophila 78−56963
neuromuscular information transmission, distortion suppression 80−35871
neuromuscular junction, crustacean, ethanol effect on excitatory postsynaptic current duration 77−48777
neuromuscular junction, frog, acetylcholine diffusion barrier 78−7334
neuromuscular junction, frog, Ca-depend. presynaptic action 77−52773
neuromuscular junction, frog, electrostatic screening of neurotransmitter release 80−89741
neuromuscular junction, frog, volt.-depend. effect of curare 77−52775
neuromuscular junction, membrane surface pot. changes effect on drug interactions 80−3631
neuromuscular junction, snake, synaptic channel gating differences at twitch and slow junctions 78−80868
neuromuscular junction channel, in frog, endplate current fluctuations 77−25416
neuromuscular junction continuity, freq. sweep anal. of EMG 79−96686
neuromuscular junction endplate current simulation 79−62230
neuromuscular junction of crab, in vitro action of anaesthetic and convulsant ethers 77−29140
neuromuscular junction transmitter release, effect of α-bungarotoxin 78−44496
neuromuscular junction transmitter release during repetitive stimulation, effect of Sr^{2+} and Ba^{2+} 78−3469
neuromuscular mechanism maintaining extrathoracic airway patency 79−100656
neuromuscular miniature endplate potential online acquisition microcomputer system 78−36015
neuromuscular oscillations, interaction between those centrally and peripherally generated 79−62232
neuromuscular response to ankle rotation, human, simulation with segmental reflex model 79−8500
neuromuscular synapse, frog, dual action of Er^{3+} on transmitter release 78−35834
neuromuscular synapse, response to acetylcholine 77−40660
neuromuscular system deterministic neuron models 79−29523
neuromuscular system electrical stimulator using biopotential amplifier 79−48315
neuromuscular system model for small isometric tensions, human 77−52771
neuromuscular system output response, effect of correlated adjacent interspike interval sequences of input, computer simulation 78−80858
neurophysiology continued
neuromuscular transmission, locust, modulation by octopaminergic neurone 78−11632
neuromuscular transmission, prejunctional role of cyclic nucleotides 77−1987
neuron activity, optical monitoring methods, book contrib. 79−2030
neuron adaptation model allowing for Ca influence on membrane K permeability 79−79508
neuron electronic model *(Spanish)* 80−104580
neuron extracellular electric field model 79−62233
neuron firing rate meas. by freq.-to-voltage converter 79−70715
neuron functional analogue study, adaptive learning system appl. *(Russian)* 77−40659
neuron input current, Helix pomatia, rel. to membrane pot. and extracellular Sr and Ca ion concs. 80−81577
neuron mathematical model, freq. characts. *(Japanese)* 80−35866
neuron membrane, design of a single electrode voltage clamp 80−72385
neuron membrane, electrostatic plasma probe physical analogue 80−79573
neuron membrane Ca channels, displacement currents assoc. with activation of gating mechanism 77−81486
neuron membrane inward Ca current, blocking effect of Cd^{2+} ions 77−81485
neuron model, excitatory and inhibitory impulse sequence interactions in math. models *(Japanese)* 78−27919
neuron model, ICs, teaching aid 78−85301
neuron model, response for density modulated Poisson pulse trains *(Japanese)* 78−35829
neuron model as component of neural network, hardware realisation 80−61534
neuron model using stochastic syncoder 78−15822
neuron multi-input model diffusion approx. 77−29135
neuron populations as information processing system, stochastic properties 78−80860
neuron single-unit pots., multi-microelectrodes system for simultaneous recording *(Japanese)* 79−57826
neuron single-unit pots. recording, multi-microelectrode system characts. *(Japanese)* 80−21581
neuron soma model with high reliability and low power consumption 80−72392
neuronal activity and focal blood flow coupling in experimental seizures 80−40989
neuronal activity firing pattern evoked by monosynaptic inputs, stochastic model 77−29134
neuronal activity model, Ornstein-Uhlenbeck process 80−51030
neuronal average firing frequencies, digital display 77−5117
neuronal cell culture, laser microbeam microscope appl. *(German)* 78−3694
neuronal circuit with recurrent inhibition, two-component model *(Japanese)* 77−48784
neuronal impulse generation, modulation of point processes 80−30698
neuronal mechanism modelling in electrochemiluminesc. cell, adaptation *(Russian)* 77−40653
neuronal mechanism modelling in electrochemiluminesc. cell *(Russian)* 77−40651
neuronal membranes, organisation book contrib. 79−2032
neuronal organisation, informational anal. of Brindley's memory scheme 79−53077
neuronal population density estimation, robust distance method 79−70721
neuronal populations, diffusely-connected, computer simulation 78−53384
neuronal properties underlying visual information processing in barnacle 78−88710
neuronal response analyser with microprocessor *(French)* 79−20730
neuronal spike activity discriminator 77−48966
neuronal spike trains, simulation, multiple Markov sequences 77−25413
neuronal waveforms, optimal recognition 80−56003
neurone activity, simultaneous recording from several neurones in invertebrate central nervous system 77−66880
neurone compartmental chain model membrane voltage changes 77−29124
neurone depolarisation by purine and pyrimidine mononucleotides, in explanted amphibian sympathetic ganglia 78−11633
neurone impulse activity, limiting behaviour of a model 79−57630
neurone local hormonal communication, Aplysia 78−69040
neurone membrane, asymm. displacement currents and effect of internal F anions 77−48773
neurone potentials, 2 pulse series anal., histogram of recurrence time intervals 77−60196
neurone susceptibility to changes in synaptic inflow, evaluation using stochastic model 78−24059
neurones A and B of mollusc, effect of acetylcholine chloride and chlorocholine chloride on resting pot. and membrane resist. 78−53375
neurones of large horse-leech, electrophysiological characts. rel. to intracellular Na^+ conc. 78−53374
neurons, Aplysia, effects of NH_4^+ and HCO_3CO_2 on intracellular Cl^- level 78−44485
neurons, cat, cytoplasmic laminar body identification by phase contrast microscopy 79−48385
neurons, electrical behaviour, general input-output relations 80−85378
neurons, single, rapid killing by irrad. of intracellularly injected dye 80−81795
neurophysiology, computer assisted unit data acquisition/reduction 78−61266
neuroscience, annual review, vol.I, book 79−2027
neuroscience annual review, book 79−96540
neurosecretory cell IR photomicrography 80−30959
neurosecretory structure particle motion, effect of increased K^+ concs. 78−77046
neurostimulation automatic triggering as function of several EEG parameters, apparatus 80−98203
neurostimulator, with improved rectangular pulse cct. *(Rumanian)* 77−21637
neurosurgical cryoprobe, self-contained, with replaceable flask, features 78−7526
neurotransmitter dynamic balance, systems and control theoretic anal. 78−44495
neurotransmitter modulatory actions, book contrib. 79−96550
neurotransmitter release statistics: moment estimates for inhomogeneous Bernoulli trials 79−62228

neurophysiology continued
nexus, evidence for fixed charge, permeability, obs. 80−94193
nicotinic transmission, role of voltage-sensitive receptors 78−44492
node of Ranvier, crit. pot. of repeat responses 79−70538
noise generator for auditory neurophysiological and psychophysical experiments 79−29676
non-stationary neural signals pattern trajectory anal. 78−36082
nonlinear electrotonus problem exact soln. 77−70446
nonlinear system analysis by Wiener kernel estimation in freq. domain 77−1973
nonlinear system Wiener anal. using Poisson-Charlier crosscorrelation 78−24055
nonmyelinated nerve fibre conduction vel. 77−90759
nonprobabilistic measures of information with biological applications *(French)* 77−9160
nonspiking neurones, pharmacological evidence for fast Na channels 78−73151
noradrenaline release during nerve stimulation, regulated by α-adrenoceptor mediated negative feedback 77−29139
noradrenaline-induced hyperpolarisation of spinal motoneurons 80−56010
norepinephrine and epinephrine neuron systems, anatomy and physiology, book contrib. 79−96548
normal and anomalous intellectual activity classification, coherent quantum-wave brain model *(Russian)* 78−27922
nuclei of raphe system, electric stimulation and cooling effects on alertness in cat *(French)* 80−35864
octopus, Eledone cirrhosa, electrophysiology of isolated central nervous system 80−104577
ocular accommodative changes in humans induced by positional ghanges rel. to gravity 77−48789
ocular albinos, human, visual anomalies meas. by evoked pots. 79−43875
ocular dominance, changes induced by stimulation with rotating gratings, lambs 79−34559
ocular dominance shift failure after monocular occlusion in kittens, brain catecholamines 77−1998
ocularity domains and growth behaviour of axon terminals 79−48249
oculomotor control system, expt. set-up for clinical investigation, visual, acoustic, vestibular stimulations 78−80990
oculomotor control system neurological integrator 77−4993
olfaction, bilateral interaction 77−66819
olfactometry, smell intensity meas. *(French)* 80−8073
olfactory bulb, 55 counts/sec rhythm anal. and simulation 80−85422
olfactory bulb, gain mediating cortical stimulus-response relations, nonlinear 80−12165
olfactory bulb, telemetered EEG activity from rabbits 77−86516
olfactory bulb and cortex, spatial props. of EEG event 79−16223
olfactory bulb elec. responses to general and hunger arousal, rat. 79−79565
olfactory cortex of guinea pig maintained in vitro, effects of cooling 78−3525
olfactory pattern recognition modelling by adaptive spatial filter 78−24080
olfactory perception, neurophysiological correlates rel. to amygdalotomy 79−100637
olfactory receptor sites location, inferences from latency meas. 80−56068
olfactory sensitive neurons in lateral hypothalamus, response to gastric distension in rabbits 79−92243
olfactory system and pheromones, telemetered neurophysiological activity, rabbits 77−90816
olfactory tubercle, unilateral lesions, modification of general arousal effects, rat 80−3652
opiate, receptor, synaptosome, EPR study of stereospecific binding of spin labelled morphine 77−9215
optic lobe neurosecretory cells of Poekilocerus pictus, effects of visual stimulation 79−5279
optic nerve fibre arrangement in cat, non-retinotopic 80−30720
optic nerve fibre layer, river lamprey, light- and electron-microscopic obs. 79−43879
optic nerve fibre topography in tectum retinal projection, cichlid fishes 79−48250
optic nerve fine structure in lamprey 77−60201
optic tectum, goldfish, fine struct. 80−85396
optic tectum, IR and visual integration in rattlesnakes 78−69054
optic tectum, pigeon, single cell spatial- and temporal-freq. selectivity 80−41016
optic tectum, pigeon, single-neuron responses to moving sine-wave gratings 80−41015
optic tectum model of various vertebrates *(Spanish)* 78−40144
optic tectum movement detecting cell response to change of wavelength, pigeon 78−7348
optic tract and lateral geniculate neurons, spectral responsiveness and temporal freq. response 77−36923
optic tract fibers, cat, Markov properties of nonstationary spike trains 80−51077
optic tract fibre recordings, lateral spread of light adaptation in rat retina 77−44659
optic tract fibre spike trains, cat, nonstationary anal. on Markov props. *(Japanese)* 77−90780
optic tract fibres, physiologically characterised, projection patterns, cat obs. 80−101167
optic tract fibres, receptive field props., tree shrew 79−48252
optic tract of self-respiring fish, method for obtaining single cell response 77−56545
optic-nerve head, congenital malformations 79−92213
optimal multichannel filtering, simulated nerve signal appl. 79−48233
optimal multichannel filtering for nerve signals, modelling 79−48232
oral motor tasks, stutterers' and nonstutterers' neural response times 79−96585
orbicularis oculi reflex, diagnostic significance of reflex amplitude 79−34540
oscillator, free running, perturbation effect on phase transition curve 79−83737
oscillators, phase locking model 80−21460
oscillatory neural networks in the rabbit hippocampus 80−89743
osmotic stress neuronal adaptation and facultative blood-brain barrier in marine osmoconformer 77−29127
otolith sensitivity assoc. with habituation to linear accels. capable of inducing motion sickness 78−44621
ovipositor receptor, blowfly, monovalent cation sensitive neurones 77−77922
neurophysiology continued
pacemaker neurons, Aplysia, effects of irradiation with 20 MeV electrons 80−17013
pacemaker phase control 78−11631
pacemaker synaptic interactions: modelled locking and paradoxical features 80−51069
pain control by neural augmentation implant, electrophysiological approach 79−29660
pain control in man, medial thalamic permanent electrodes, electrophysiological and clinical study 80−67282
pain mechanisms, neural network model 78−85307
palmar conduction time of median and ulnar nerves in carpal tunnel syndrome 80−12075
paradoxical sleep, occipital spikes and eye movement activity, visually defective children 79−16185
parafascicular neurons, inhibition of nociceptive discharges by elec. stimulation of nucleus centrum medianum 79−29521
parastriate cortex, cat, rabbit, selective response of single units 79−74624
Parkinson tremor generation, linear modelling of possible mechanisms 80−3615
pattern generation in lobster stomatogastric ganglion, pyloric neuron kinetics and synaptic interactions 80−8043
pattern induced flicker colours, sensory process sensitivity to short time delays 78−96048
pattern separability and the effect of the number of connections in a random neural net with inhibitory connections 79−20532
pattern-evoked potential, modifications rel. to stimulated part of visual field 80−26225
peak-detecting window discriminator for neuronal spikes 77−60323
perception space, dimensionality of informational structs. 78−15817
percutaneous elec. stimulation of nervous system for pain relief 78−3668
peripheral motor nerve conduct. studies in lethargic mice 80−3634
peripheral nerve, generation of unidirectionally propagated action pots. by brief stimuli 80−85546
peripheral nerve, single unit detection by real time correlation 79−12047
peripheral nerve biopotential recording by laminated electrodes 78−92760
peripheral nerve conduction velocities distribution estimation 77−90757
peripheral nervous system, trophic mechanisms, book contrib. 79−2043
peripheral nervous system multichannel data anal., frog sartorius muscle mechanoreceptor transducer charact. *(Japanese)* 80−3656
peristimulus time histograms, appl. of cumulative sum technique 79−34536
phase locking in monaural and binaural neurons 78−88717
phase-locked responses in Limulus lateral eye 77−86491
phase-locking meas. as test for neural encoding models 79−2036
phasic pupillary light reflex and visual evokes potentials, simultaneous anal. 80−26226
phenylethanolamine, putative neurotransmitter in Aplysia 77−48783
phonatory initiation, minimal reaction time obs. 79−96583
photic sensitivity of macaque monkey and pulvinar neurons 80−12106
photoelectrode for recording intracerebral cellular Ca^{2+} transients 80−67307
photoreception, transmitter-medicated, diffusion and reaction modelling system 79−70547
photoreceptor, barnacle, conditioning light effect modification by metarhodopsin absorpt. of light 80−8064
photoreceptor, barnacle, effects on prolonged depolarising afterpot. of Mn^{2+}, Ca^{2+} 80−8051
photoreceptor, barnacle, props. of on-transient of intracellular response 80−8052
photoreceptor, barnacle, upper limit on translational diffusion of visual pigment 80−8053
photoreceptor bleaching and adaption reversal by microsecond flashes 79−79542
photoreceptor directional sensitivity, coherence and polarisation obs. 79−100610
photoreceptor membrane interfacial pots., light-induced 80−72161
photoreceptor membrane repair after peroxide oxidation 79−53086
photoreceptor membranes, dynamic aspects of molecular texture 79−79519
photoreceptor noise suppression, rel. to incremental intensity thresholds 79−43895
photoreceptor rod cells, vertebrate, visual transduction, book contrib. 79−96561
photoreceptor synaptic activity in isolated frog retina, Co ion effects 78−48797
photoreceptor transduction, determ. of pigment transition or state coupled to excitation 80−8054
photoreceptors, bullfrog, effect of temp. on rapid dark adaptation 79−43883
photoreceptors of nocturnal gecko, patency in outer segments 78−48796
photoresponse suppression during anoxia, role of Ca^{2+}, Limulus 79−62252
photosensitive neuron in crayfish caudal ganglion, properties, expt. *(French)* 80−89705
photostimulator, LED fibre optic, for research on visual nervous integration 80−67302
phrenic nerve diaphragm, in vitro, elec. stimulator 79−25161
picture distortions compensation of moving patterns typical for time filters 80−76731
pigeon rotation reflex input-output relations and model *(German)* 77−44623
pigmented neurons of pond snail, effect of light on electrogenic processes 77−81528
pineal photoreceptors, evidence for vertebrate visual pigment with two physiologically active states 78−44504
pineal unitary response to light stimulation in frog central nervous system 77−52780
piriform cortex neurons, rabbit, fast and slow inhibitory postsynaptic potentials 79−92244
pitch perception, spatial and temporal cue analysis of complex tones hearing 79−2080
plasticity, effect of early avoidance training on brain development in kittens 79−83734
polyelectrolyte membranes, persistent polarisation in aq. environment, neural model 78−48763
pontine reticular formation neurons, discharge rel. to motor activity 77−66810

neurophysiology continued
ponto-geniculo-occipital waves, correlative evidence for neuronal generation 79−24975
posterior knee joint capsule, cat, receptor neuronal response to stress 79−92212
postsynaptic conductance charge, quantal event at nicotine synapses, numerical reconstruction 79−83748
postsynaptic effects of multiaction gaint interneurone on identified snail neurones 77−70448
potential intervals meas. device, electromechanical, with semiautomatic processing of results 77−5115
premotion silent period in rapid voluntary movement 77−21511
presynaptic Ca^{2+} current rel. to synaptic transmission, in squid giant synapse 77−16926
presynaptic electrical coupling in Aplysia, effects on postsynaptic chem. transmission 77−48782
presynaptic facilitation as mechanism for behavioural sensitisation in Aplysia 77−36912
presynaptic nerve terminals, ATP-depend. Ca storage 77−29126
presynaptic receptors, occurrence and role *(German)* 80−76729
pretectum organisation, cat 80−12107
primary auditory neurons, preferred intervals in spontaneous activity 80−45921
primary visual cortex, orientation selectivity development models, normally and dark reared kittens 80−41007
primary visual cortex orientation selectivity development kinetics, normally and dark reared kittens 80−41006
primate sensory projection spatial mapping, visual perception relevance 77−25436
proprioception and instability of eye in dark 77−86495
proprioceptors with central cell bodies, in locust 80−51132
prosthetics sensory feedback, human tracking performance with afferent elec. nerve stimulation 80−17195
psychogalvanic reflex curve automatic anal. 78−7332
psychophysical laboratory unit organisation and meas. system for persons with impaired locomotor system *(Croatian)* 78−44667
psychophysiological techniques applied to aircraft design and other operational problems 80−26384
pulmonary stretch receptor dynamic response, dog 78−20194
punctuate pressure sensitivity rel. to skin surface temp., cutaneous cross-model interactions 78−3527
pupil, human, normal and diseased, model for computer simulation 77−77895
pupil noise amplitude control, interaction of sensory and motor mechanisms 78−64998
pupil response during mental activity, link with intelligence 80−61532
Purkinje cells of cerebellar cortex, histogram analysis of interpulse intervals 78−96042
quantal size rel. to abrupt changes in nerve terminal vol. 78−31805
queen scallop escape responses, aversive behaviour patterns 78−53430
radial nerve potential recording at wrist in man *(French)* 77−81756
radial nerves branching quotient, determ. in healthy adults 79−34539
random neural nets, experimental studies 80−12077
Random-Access Memory-Interval Timer and buffered storage system 79−84066
Ranvier nodes exposed to DDT, asymm. currents and Na currents 77−48778
ray, Black Sea, electric organ discharge structure 78−64969
reaction times, for functional exploration of sensory, sensory-motor and auditory routes *(French)* 77−37077
reaction times in observation of lunar occultations *(French)* 79−88607
receptive field props. of neurones in visual cortex of cat 80−26227
recurrent inhibition and afterhyperpolarisation, neuronal discharge effects 79−2035
reflex conditioning effects on motoneuron pool 79−79509
reflex excitability curve assess. using cubic spline function 79−79510
refractory period measurements, dependence on conduction distance, computer simulation anal. 80−67065
regenerating neurone in leech, form. of elec. synapse on severed axon segment 77−52776
Renshaw cells dynamic properties, freq. response characts. 78−3462
Renshaw spinal interneuron repetitive firing, model 77−90760
repetitive firing, Hodgkin-Huxley axon modification suggested by crustacean axon results 77−48776
repetitive firing computer models nonlinear systems anal. 78−80854
repetitive firing mechanism excitation parameters, nerve impulse trains statistical evaluation 80−40986
repressed nerve terminals in axolotl muscle, spontaneous transmitter release 77−70449
residual latency techniques and related physiological procedures 79−44001
resonance phenomena in the electrical activity of the brain 79−74627
respiration rhythmogenesis model, Lotka-Volterra equations *(German)* 77−48772
respiratory activity obs. in expt. animals, using automatic reset integrator 79−29683
respiratory control in cats, interactions between central and vagal mechanisms 78−53436
respiratory control system, time series cluster anal. 78−56959
respiratory control system simulation, state-of-the-art 78−53441
respiratory rhythm, synchronisation by electrical stimulation of phrenic nerve 79−11910
respiratory rhythm generation, mathematical model, respiratory neuron classification 80−35873
response regulator model in simple sensory system 77−73534
retardation currents in excitable membranes and models of flicker noise 78−92618
retina, carp, neuronal architecture of on and off pathways to ganglion cells 78−44502
retina, cat, contrast gain control 79−79536
retina, cat, transfer function for spatial freqs. *(Spanish)* 79−62247
retina, cephalopod, dark adaption dynamics 79−79541
retina, cephalopod, extracellularly-recorded photoreceptor pots. 79−62245
retina, developing, transient intraplexiform neuron, histogenesis of inverted amacrine cell, chick 77−90765
retina, excitation and interaction, review, book contrib. 79−5282
retina, frog, GABA and lateral spread and tonic activity 79−74661
retina, frog, morphometric anal. of internal horizontal cells 80−108892
retina, frog, near IR transmission of rods rapid light-induced changes 79−74658
neurophysiology continued
retina, goldfish, X-like and not X-like cells obs. 79−43837
retina, grey squirrel, bipolar and horizontal cells, Golgi morphology and receptor connections 78−48795
retina, Limulus, oscillatory responses 80−101166
retina, Limulus, temp. dependence of dynamic response 79−43866
retina, mammalian, localisation of cholinergic synapses 79−57654
retina, on-centre bipolar cell, effect on polarisation of horizontal cells in carp 79−16207
retina, pigeon, antidromic invasion of ganglion cells 79−43881
retina, pigeon, extensive lateral transmission in inner plexiform layer 77−48794
retina, pigeon, graded pots. accompanying antidromic invasion 79−43882
retina, pigeon, non-directional and directional ganglion cells 79−57655
retina, rat, rod elec. model, early receptor pot. generation 79−57647
retina, roach, post-receptoral neurons, adaption effects in elec. responses 79−79534
retina, serial reconstruct. of adjacent ganglion cells 80−89749
retina, significance of antidromic potentiation and induced activity 80−12092
retina, snapping turtle, mixed rod-cone responses in horizontal cells 79−79533
retina, teleost, enhancement of hyperpolarising S-potentials of surround illumination 79−2051
retina, turtle, modes of chromatic interactions 78−7347
retina chromaticity horizontal cells of turtle, synapse mechanisms 80−51079
retina early receptor potential, quantum mechanical model 79−57644
retina electrical activity and lipid peroxidation 79−43885
retina neural networks between cone and photopic L-type horizontal cells 79−83782
retina of carp, colour coded S-potentials, latency measurement 79−53097
retina of cat, neural path real time simulation *(Spanish)* 78−96046
retina origin from both sides of embryonic brain, optic chiasma crossing problem 79−62250
retina outer plexiform layer lateral interactions after atropine block of horizontal cells, turtle 77−70457
retina physiology, single cell studies on lower vertebrates, book contrib. 79−96558
retina-lamina connectivity, polarisation sensitivity, crustaceae 79−2054
retinal b-wave currents, frog 79−57652
retinal bipolar cells, dogfish, visual signal transmission near absolute threshold 79−79535
retinal bipolar cells, frog, Golgi study 78−56968
retinal bipolar cells, struct. basis for on- and off-centre responses 78−44503
retinal cells of cat, spatio-temporal model 78−92621
retinal chromophore transition dipole moment, orientational changes obs. 80−41023
retinal class IV ganglion cell luminance and chrominance processing in frog 78−40148
retinal degeneration, hereditary, cone inputs to ganglion cells 80−8056
retinal degeneration in RCS rats raised under ambient light levels 79−43887
retinal diffusion, two-stage, rel. to flicker sensitivity 79−74657
retinal ganglion cell activity in ground squirrel under halothane anaesthesia 78−40147
retinal ganglion cell activity induced by ELF mag. fields, method for study 80−56321
retinal ganglion cell firing patterns, implications for separate ON and OFF processes goldfish 77−70458
retinal ganglion cell functional pathways, book contrib. 79−96559
retinal ganglion cell layer, cat, newly identified presumptive microneurones population 80−67077
retinal ganglion cell of cat, refractoriness in maintained discharge 78−64991
retinal ganglion cell on and off processes, spatial distrib., anal. of receptor inputs 79−100606
retinal ganglion cell response props. in Siamese cat 80−12115
retinal ganglion cell response to sinusoidal flicker, mudpuppy 78−48798
retinal ganglion cell responses in dark-reared rats 79−53102
retinal ganglion cell types, of cat, visual resolution and receptive field size 80−56037
retinal ganglion cells, abnormal response in Siamese cats 77−90785
retinal ganglion cells, cat, nonlinear analysis in freq. domain 78−48793
retinal ganglion cells, class I, in the toad, Bufo spinulosus 80−85393
retinal ganglion cells, displaced, projection on accessory optic system, pigeon 77−90781
retinal ganglion cells, goldfish, effects of photic stimulation upon var. of interspike intervals 77−70460
retinal ganglion cells, macaque, macular pigmentation and spectral sensitivity 79−43877
retinal ganglion cells, mudpuppy, hyperpolarising ON/OFF responses 77−25427
retinal ganglion cells, Necturus, responses to stationary and moving stimuli 77−70459
retinal ganglion cells, rat, adaptation pools and excitation receptive fields 78−7356
retinal ganglion cells, responses to stationary and moving stimuli 80−51080
retinal ganglion cells, scotopic increment thresholds 79−79558
retinal ganglion cells, struct. basis for on- and off-centre responses 77−1997
retinal ganglion cells, suppression of maintained activity 79−79537
retinal ganglion cells, surround- to centre-type response transition by receptive field centre darkening 77−44649
retinal ganglion cells in the galago, size and tropographic arrangement 80−67078
retinal ganglion cells of 3 week old kittens, physiological props. 77−36922
retinal ganglion cells of a tree shrew, definition of neural response and incremental sensitivity 80−41011
retinal ganglion cells of cat, response patterns for moving contours 78−69059
retinal horizontal cell reaction to non-uniform illum., model 77−56375
retinal horizontal cells, nonlinear characts. of spatial summation in receptive field, model 80−26232
retinal information processing, computer model 77−66814
retinal L-type horizontal cells, dynamic interaction in receptive field 80−26233

neurophysiology continued
retinal L-type horizontal cells, nonlinearity in dynamic characts. 79 -100603
retinal mechanisms of visual latency in Bufo marinus, electroretinogram obs. 79−48255
retinal model, layered visual processing 80−16925
retinal neuron, variability of interspike intervals during sustained firing, model 77−86492
retinal neuron firing rates, lack of predictability from interspike interval statistics 80−67075
retinal neuron interspike intervals variability, model dynamics 79−24984
retinal neuronal network, interactions between photoreceptors and horizontal cells 78−11648
retinal neuronal network of photoreceptors and horizontal cells 78−3482
retinal neurones, differential labelling by ^{3}H-2-deoxyglucose 79−92447
retinal neurons, catfish, spatiotemporal testing and modelling 80−41005
retinal neurons, spatio-temporal receptive field meas. 79−57649
retinal neurons studies, appl. of white noise anal. *(Japanese)* 79−66471
retinal on-centre bipolar cell, ionic mechanisms of rod and cone signals 78−61177
retinal photoreceptor and horizontal cell synaptic connections 77−90787
retinal pigment epithelium phagocytosis, RCS rat 79−34561
retinal R/G horizontal cells, light intensity and response amplitude relation 79−5281
retinal receptor directional sensitivity, flicker effects 80−8057
retinal rods, thermal activation of visual transduction mechanism 79−74651
retinal sensitivity, monochromatic stimuli, large eccentricities 79−5285
retinal single-photon impulse coding mechanisms *(Russian)* 78−27941
retinal site of transient tritanopia 79−88078
retinal streak, turtle, orientation of horizontal cell axon terminals 79−74653
retinal synaptic transmission effectiveness, neurone regulator model 79−57645
retinas, goldfish, dorsal rel. to ventral areas obs. 79−43880
retino-tectal mapping using microprocessor controller 78−31995
retinotectal pathway, uncrossed, development rel. to plasticity studies, rat 80−56025
retinotectal projection development, Gierer-Meinhardt eqns. appl. 80−56022
retinotectal projection orderly compression following partial tectal ablation, newborn hamster 79−74656
reverberation cycles of a single neural equation 79−2022
rhythmic movement generation, neural nets, lobster, leach, book contrib. 79−5273
rod disc membrane phosphodiesterase control 79−79527
rod network in turtle retina, elec. spread 78−80874
rod outer segment birefringence gradient, struct. interpretation, 3-dielectric layer model 79−83771
rod outer segment phagocytosis obs., rat 79−62249
rod outer segments, intact, GTP hydrolysis rel. to transmitter cycle in visual excitation 79−83773
rod outer segments, spread of activation and desensitisation 80−35881
rod outer segments membrane current fluctuations 79−79530
rod outer segments membrane current obs. 79−79529
rod outer segments pots., frog, local stimulation and adaption obs. 79−79528
rod outer sements, isolated, photoresponses, frog 79−43890
rod photoreceptor membrane, pot. regulation by cyclic GMP 79−74654
rod-cone interaction, spatial patterns 80−16930
rod-cone interaction obs. 79−100607
rod/cone system interactions in goldfish retina 78−35853
rods, frog, bleaching and background adaption 79−79532
rods, role in iconic storage 79−24987
rods, threshold rel. to pigment in Xenopus 79−79526
rods, toad, effects of Ba^{2+} on dark-adapted intensity-response curve 79−79531
rods, toad, effects of Ca^{2+} on intensity-response curve 79−53091
rods, toad, spontaneous quantal events induced by pigment bleaching 80−108895
saccade-related unit activity in monkey superior colliculus 80−12101
saccadic and vergence eye movements, reciprocal innervation model 78−31811
saccadic eye movement, accompanying pots. 80−12102
saccadic eye movement control system, digital analogue simulation 77−44654
saccadic eye movement controller considerations 78−27949
saccadic eye-movement system, processing of direction and magnitude obs. 80−56035
saccadic suppression by corollary discharge in the locust 79−92217
saphenous nerve normal sensory cond. in man 78−61162
Schwann cell layer of squid axon, diffusion models 80−40985
sciatic nerves, frog, isolated, effects of microwave irrad. on vitality 80−108959
scotomata, effect on responses to pattern reversal in one half visual field 79−39417
screening-pigment migration in retinula cells of crayfish, spectral sensitivity 80−72165
section embedding technique for sequential light and electron microscopic exam. 80−67317
seizure discharge autorhythmicity, spike, discharge freq. regulation in focal epilepsy 78−40133
sekeletal muscle dynamics, isometric and isotonic contraction model 78−31807
self-excited oscill. of neuronal circuit with recurrent inhibition and delay *(Japanese)* 78−20172
self-excited wave medium with memory 78−77034
self-organising nerve nets, fundamental theory, developmental plasticity anal. 80−67062
semicircular canal afferent response system identification 78−27927
semicircular canal primary afferents, impulse weight functions, frog 78−69116
sensitivity measurement of neural systems, receiver operating characts. anal 77−44629
sensori-motor spatial development, analytical theory 78−44488
sensorimotor control and learning model 78−69033
sensorimotor cortex neurons in behaving primates, electromagnetic muscle stretch 79−88073
sensorineural hearing loss effect on loudness discomfort level 79−96577
sensory biosystem, teleological explanation of Weber's law and the motor unit size law 79−96501

neurophysiology continued
sensory coding, distributed, applied to iconic storage and metacontrast simulations 79−34531
sensory evoked pots. at the wrist, infants and children 79−79566
sensory fibres, amphibian, spike freq. adaptation due to slow K channels 79−2025
sensory information coding, adaptation and differential sensitivity in system of detectors 77−56367
sensory nerve conduct. vel. of medial antebrachial cutaneous nerve 80−3654
sensory neuron, second order, summation of excitation and inhibition by computer simulation 80−76769
sensory processes, information received by receptors 77−73521
serial section alignment by serial filtering 79−20723
serotonergic excitation, unconventional response in Aplysia 77−86484
short latency potentials from neck and scalp following median nerve stimulation in man 78−31794
shunting inhibition stochastic modelling 77−9183
signal focusing in segmented stretch reflex system, auxiliary spinal networks 80−40999
signal recording using implantable electrode and telemetry system, awake animals *(Japanese)* 80−94427
signal transmission in the nervous system, review of axonal and synaptic transmission 79−100593
signals, dipole theory of interactions 80−81574
single auditory nerve fibres, adaptation, saturation and masking 79−48273
single motor unit, recording during strong effort 79−11908
single optic nerve fibres in Limulus brain, innervation patterns, modified Co staining technique 79−53096
single unit activity, computer program for generating on-line raster dot displays 78−57087
single unit activity from foetal pig brains, recording method 80−67315
skeletal muscle, lumped and population stochastic models, implications and predictions 80−76724
skeletal muscle activity pattern in humans rel. to muscle fibre type composition 78−80869
skeletal muscle general myocybernetic control model 78−53385
skeletal muscle rhythmic oscillation simulation and analysis 78−31806
skeletal muscle structure model *(Japanese)* 79−66479
skeletomotor control system from signal-flow diagram of oculomotor control 77−25415
sleep neuroendocrine phenomena, EEG band anal. 77−9314
sleep-waking process, role of anterior raphe and area postrema 77−36906
slow motor nerve cond. meas. by blocking technique, computer simulation 78−36027
snail giant neurone neurotransmitter 78−15821
snail Helisoma trivolvis, electrically coupled neurons producing rhythmic activity, network anal. 77−40657
soleus muscle, human, stretch and Hoffmann reflexes during phasic voluntary contractions 79−16193
soma potential of interneurone controls tramsmitter release on monosynaptic pathway in Aplysia 78−56964
somatosensory evoked potential, effects of interaction between large and small diameter fibre systems 79−16188
somatosensory evoked potential, scalp-recorded, normal and neurologically disordered patients 79−16186
somatosensory evoked potential in man, far field pots. 77−9182
somatosensory evoked potential measurement and analysis on a small laboratory computer 78−92729
somatosensory evoked potentials, conduct. time in central pathways in man 79−39408
somatosensory evoked potentials, cortical and thalamic activity in cat 79−16187
somatosensory evoked potentials, recovery function of short latency components, cat 79−34534
somatosensory evoked potentials, short latency, stimulus intensity effect 80−35924
somatosensory evoked potentials obs., human and monkey 79−43842
somatosensory evoked response, multiple sclerosis effects, expt. 77−44628
somatosensory pathways, assessment of central conduction 80−97949
somatosensory system afferent signals, modulatory effect of prior input 77−90758
spatial frequency characts. of complex receptive fields 78−20175
spatially distributed neuron response to white noise current injection 79−83728
spectral sensitivyt analysis, math. techniques 77−52786
spectrally-opponent responses in ground squirrel optic nerve 80−35883
speech production, recruitment and discharge patterns of single motor units 78−65054
spike processing instrument for signal detect., based on nonlinear filtering 78−40438
spike recognition and on-line classification by unsupervised learning system 79−57789
spike separation in multiunit records, multivariate anal. 80−26215
spike train data, adaptive filtering 80−67265
spike train processing, data reduction program 77−44861
spike train sampling, implementation of French-Holden algorithm 78−40440
spike train separation by improved time-amplitude window discriminator 77−86726
spike train stochastic model, non-renewal point process properties 77−70447
spike trains, interleaved, in a noisy channel, separation system 80−94424
spike trains, Markov process dependency as estimation measure 77−25357
spike trains, relationship of post-stimulus time and interval histograms to time characts. 78−69032
spike trains rel. to physiology and behaviour, data acquisition system 77−13035
spike unit data acquisition and reduction system 79−79713
spike window discriminator confirmation by analogue delay cct. 77−21664
spike-train statistical anal. methods 78−73149
spinal and sub-cortical evoked pots. following stimulation of posterior tibial nerve in man 78−69034
spinal cord, functional stimulation in multiple sclerosis 79−20606
spinal cord, transient synapses in the embryonic primate 79−74623
spinal cord seizures elicited by high pressures of He 80−12071

neurophysiology continued
spinal cord sensory map, reorganisation after peripheral nerve injury 79−8492
spinal cord to axilla, F-wave conduction vel. 80−97894
spinal evoked potential in man, maturational study 79−79498
spinal motoneurones refractoriness accumulation and secondary range firing model 77−1985
spinal neurones, mammalian, D-α-aminoadipate as selective antagonist. of amino acid-induced and synaptic excitation 78−20171
spontaneous activity of anterior semicircular canal units in anaesthetised pigeon, point process anal. 78−24079
squid giant axon, response of delayed K^+ channels to time-dependent clamping functions 79−39382
squid giant axons, oscillatory subthreshold responses and pot. fluctuation obs. 78−27918
stapedial reflex thresholds with and without anxiety, fluent and disfluent speakers 79−96584
statistical neuronal ensembles, spike transfer 79−57631
stereology conference, Salzburg, Austria (Sep. 1979) 80−22134
stereopsis, review 78−77056
stereoscopic depth channels for position and for motion 80−12146
sterotaxic method for recording from single neurons in the cat eye 80−89913
stick insect leg movement sensory control 77−12904
stimulus artifact suppression, sample and hold amplifier system 78−77163
stimulus-response relation, multivalued, in isolated elasmobranch utricles 79−24979
stochastic activity models of neurones, book 77−44632
stochastic automaton models for interaction of excitatory and inhibitory impulse sequences in neurons 78−20168
stochastic electronic neuron model 77−48775
stochastic neuron models, multi-input-output information transmission 80−30707
stretch receptor neuron excitation and inhibition summation, crayfish 77−2015
stretch receptor organs, crayfish, recurrent inhibition 79−100636
stretch receptor organs, slowly adapting, periodic stimulation with and without perturbations 79−92242
stretch reflex system in human forearm, adaptive control characts. 79−83758
stretch-receptor organs, crayfish, effects of length-steps with and without perturbations 79−25003
striate cortex, cat, movement direction detect. and contrast reversal effects, cell response obs. 80−72155
striate cortex cat, orientation selectivity of single cells 79−2053
striate cortex single cell response, effects of interacting visual patterns, cat 78−7346
striate neurons in area 17 of Siamese cats, response props. 80−12116
striate visual cortex, spatial freq. rows 77−32888
striato-nigral fibres, feedback loop vs. output pathway 77−29136
stuttering, articulatory behaviours, cinefluorographic anal. 80−94240
stuttering model, movement disorder 80−94241
subesophageal ganglion, cricket, descending interneurons, impulse patterns and ventilation 79−29519
superior colliculus, cat, neuron response to stationary and moving visual stimuli 79−43893
superior colliculus and its sensory inputs, primate 80−12100
superior colliculus directional selectivity in hamster rel. to strobe-rearing and dark-rearing 78−69052
supramedullary neurons, in Labridae, number, distrib., and morphological aspects *(Italian)* 79−29515
supraoptic neurons, rat hypothalamus, osmosensitivity obs. 80−104578
surface charge density variation of excitable nerve membrane exposed to optical radiation 79−34542
swimming control in a cubomedusan jellyfish 80−3637
sympathetic ganglia, possible mediation of slow excitatory postsynaptic pot. by cyclic GMP 78−27930
sympathetic ganglia, postsynaptic modulation of excitatory process by cyclic AMP 78−27931
sympathetic ganglia, synaptic potentials and cyclic nucleotides 79−11912
sympathetic ganglia stimulated in vitro, effect of temp. on coated vesicle form. in presynaptic terminals, cat 80−85380
sympathetic ganglion cell in bullfrog, oscill. of $[Ca^{2+}]_i$-linked K^+ conductance 80−35867
sympathetic preganglionic neurons, raphe inhibition 79−92211
synapse formation between parasympathetic neurones deprived of preganglionic innervation, frog heart 77−77888
synaptic action of pentylenetetrazole, selectivity for Cl cond. 78−7336
synaptic active zone functional unity, evidence from quantum and amplitude distribs. 78−3468
synaptic and ephaptic transmission, quantum mech. tunnelling model 77−52772
synaptic cause of neural synergism and antagonism 80−30696
synaptic conductance changes, nonlinear effects 79−2045
synaptic conductivity effect on conditions of spike appearance 79−79507
synaptic facilitation and behavioural sensitisation in Aplysia, role of serotonin and cyclic AMP 77−36913
synaptic facilitation and bursting patterns, modification by hyperbaric air, Aplysia californica 80−56008
synaptic membrane, acetylcholine-activated, interaction of fluoresc. probe 77−90762
synaptic plasticity 79−74643
synaptic potential, release of transmitter from locust nonspiking interneurons 80−3632
synaptic proteins after electroconvulsive stimulation 80−56011
synaptic slow responses, props. and possible underlying mechs., review, book contrib. 80−108873
synaptic terminal, choline transport obs. 79−70544
synaptic transmission, long-lasting potentiation by postsynaptic mechanism 77−32885
synaptic transmission, nonimpluse-mediated, during cyclic motor program generation 80−51072
synaptic transmission modulation and information processing model 77−29142
synaptic transmitter release, modulation by repetitive postsynaptic action pots. 77−4996
synaptic vescles and synaptosomal membranes, electrokinetic props. 80−67055
synaptic vesicle ion content determ. by PIXE 78−61166
neurophysiology continued
synaptosomal preparation, depolarisation-induced ATP release, direct detect. 77−48779
synchronous oscillation in idealised neuronal circuit with recurrent inhibition *(Japanese)* 80−101164
tactile receptor response to stepped and sinusoidal vibrs. of hair, crayfish 77−70481
tactile sensation, mechanoreception physiology and psychophysics *(Japanese)* 80−16962
taste receptors in dolphin tongues, neural struct. and function related to mucous membrane *(Russian)* 79−43937
tectal cells, frog, intracellular recordings 79−79525
tectal units, goldfish, centre-surround organisation and receptive field interactions 79−79538
tectum opticum neuron response characts., Salamandra 79−53092
template-matching mechanism for sensory search with olfactory bulb, anal. 80−56069
temporal oscillations in neural nets, cortical neurons interactions model 80−3636
temporal pattern generation in coupled oscillators, Tritonia mollusc trigger group model 79−96538
temporal stability of solitary impulse solns. of nerve eqn. 78−35830
tendon reflex stimulation threshold meas. device for man 78−7467
tetanus toxin retrograde axonal transport, α vs. γ fibres 77−29120
tetraethylammonium binding sites in crayfish axon membranes 77−64026
thalamic ventrobasal neurone discharges during sleep and wakefulness, computer simulation 79−20533
thalamo-cortical unspecific system, two-freq. oscillatory process investigation 79−53076
thalamocortical interaction model for petit mal seizure pathogenesis 79−83759
thalamocortical non-specific system, auto-oscillatory processes 77−70443
thalamus, cat, stimulus induced and seizure related changes in extracellular K conc. 80−35870
thalamus anatomical and functonal mapping using computer, for stereotaxic surgery 77−37097
thermal regulation, mammals, neural organisation and evolution 79−20535
thermoregulation of rabbit head, facial vein myogenic mech. 80−97869
thermoregulatory system, human, engineering models, review 77−81471
three-dimensional cellular tree structure meas. semiautomatic system 79−70720
threshold model of neuron firing, empirical examination 80−56014
tightly coupled two layer random nerve net with inhibitory mechanism, pattern separability 80−61533
transcutaneous electrical neurostimulation serial/parallel interface system 79−92321
transducer noise in locust photoreceptor, intracellular responses 79−34560
transient polarisation currents in squid giant axon 77−86477
transient tritanopia, expts. in blue cone monochromacy 79−16209
transmitter kinetics model anal. 78−3465
transmitter kinetics model computer simulation results 78−92617
transmitter receptor interactions investigation 79−48240
transmitter release quanta, evidence against subunits 78−77042
transmitter release statistics, applicability of binomial distrib. 77−70450
transmitter synthesis and uptake by isolated sympathetic neurones in microcultures 78−7333
transmitter-specific retrograde labelling in the striato- and raphe-nigral pathways 80−51309
transport of substances in nerve cells 80−89745
tremor state motor unit discharge patterns *(Japanese)* 78−31803
triceps surae motor units, depend. of H-reflex pot. shape on extraterritorial pots. 77−40655
triceps surae muscle, human, vol. conducted motor unit pots. 77−40656
trigeminal motoneuron activity during sleep, intracellular anal., cct. 78−53389
two-terminal electronic circuit neuron model 80−61526
two-tone suppression in cat auditory nerve, rate-intensity and temporal anal. 78−61194
ulna nerve, slowing of motor conduction vel. in sulcus 79−34548
unit activity rel. to movement, photographic technique for anal. 80−67310
unitary discharge automatic recognition *(French)* 77−37072
unitary synaptic potentials rel. to behavioural sequence timing 78−61161
universal microscopic characts. of neurons, search 79−96546
unmyelinated nerve Na channels optimum density, analytic treatment 78−24061
vagus nerve cortical projection area, discharge pattern of neuronal units during hypoxia 77−25407
ventral nerve cords, perfused, ^{31}P-NMR study, crayfish 79−79475
ventral photoreceptors, Limulus, excitation by photons and fluoride ions 80−8065
ventricular action potential, mammalian, analysis 79−62227
vertebrate retina modelling and simulation, extended networks 80−108884
vertebrate retina neuronal activities modelling and simulation 80−85386
vertebrate retinas, outer segment layer, light-induced Ca fluxes 80−94207
vestibular adaptation to long-term stimuli 79−88075
vestibular control of oculomotor and postural mechanisms 80−72151
vestibular mechanisms, rel. to eye movement control, book contrib. 79−96588
vestibular nuclei neurons in goldfish, model with ocular proprioception 78−40142
vestibular system, model of influence on blood press. during sleep 77−25410
vestibulo-ocular reflex gain in monkey at high rot. freqs. 78−56973
vestibuloocular reflex of cat, quick phase generation model 78−56971
visceral function voluntary control, electrophysiological concept 78−35827
vision, apparent brightness rel. to contrast threshold on photopic background 77−9200
vision, binocular grating perception, contrast effects 77−70473
vision, chromatic adaptation effect anal. by linkage model 77−70467
vision, cooperative algorithm for computation of stereo disparity 77−5005
vision, explanation for blue colour of Purkinje's arcs 77−44665
vision, gloss perception, model using binocular cells in lateral geniculate body 80−72167

neurophysiology continued
vision, human, adaptation mechanisms, length-selective and non-length-selective, properties 79−20541
vision, IR nonlinear perception in 800-1355 nm range 80−12123
vision, lateral inhibition as mechanism of movement detect., forward inhibition 78−20176
vision, light intensity analyser model 79−57648
vision, long-lasting afterimages caused by neural adaptation 77−70474
vision, luminance flicker enhancement by colour-opponent mechanisms, monkey obs. 80−61549
vision, magnification in striate cortex and retinal ganglion cell layer of owl monkey 78−40146
vision, masking-induced sensitivity changes in Limulus photoreceptors 80−41024
vision, mental scanning mechanism in foveal vision, expts. 79−5280
vision, pattern recognition functional mechanisms in humans 80−81609
vision, photoconvertible pigment states and excitation, prolonged depolarising afterpot., blowfly 80−8060
vision, photopigment and receptor props. in Drosophila compound eye and ocellar receptors 80−8063
vision, photopigment rapid conversions in blowfly visual sense cells, effect on receptor pot., pupillary response 80−8062
vision, preferred orientation, variability due to methodology 80−56032
vision, prolonged depolarising afterpot., transduction in photoreceptors with bistable pigments 80−8050
vision, psychophysical functions in fish with respecified retinotectal connections 80−12152
vision, receptive fields in area 17 of cat visual cortex, linear and nonlinear properties 80−104583
vision, red-green opponent channel, short-wave cone input obs. 80−41028
vision, relative motion extraction, model 78−48794
vision, spatial frequency channels, inhibition between, complex gratings adaptation 80−72160
vision, spectral sensitivity in goldfish, photochem. and neural correlates 80−81599
vision, transient mechanism in the human system, spatiotemporal characterisation 80−72159
vision, wavelength discrimination near absolute visual threshold, goldfish 79−48264
vision in insects, pathways possibly underlying neural adaptation and lateral inhibition 77−48792
vision lateral inhibition process, semi-group theory appl. 78−65010
vision short-wavelength cone pathways, response saturation, colour opponent mechanisms control 80−41017
vision with moving eyes, microelectrode studies of single neurons *(German)* 78−53397
visual action spectrum, brightness enhancement mechanism 78−69061
visual adaptation 78−15834
visual and nervous systems simulation, straight line recognition algorithm 79−34562
visual areas of mammalian cerebral cortex, book contrib. 79−96560
visual behavior, edge and colour discriminations, retinal neurons network 79−48256
visual cell, proposed role of cyclic GMP 78−64997
visual cells, hierarchical detection structures 79−79523
visual chromatic mechanisms exposed by colour substitution pupil response 79−92221
visual contrast sensitivity 77−25442
visual cortex, altered connections in Siamese cat 80−12091
visual cortex, cat, functionally characterised neurones morphology and intracortical projections 79−74655
visual cortex, cat, neurons selectively sensitive to changing size 79−100608
visual cortex, cat, selectivity for spatial freq. and bar width 78−40152
visual cortex, cat, tuning of receptive fields 79−57646
visual cortex, circuitry changes gated by postsynaptic activity, kitten 79−74652
visual cortex, critical period interaction, kitten 78−56972
visual cortex, neuron specificity acquisition and loss theory 79−83772
visual cortex afferent geometry and neuronal trigger features generation, primates 78−35842
visual cortex cat, effects of alternating monocular occlusion 80−16932
visual cortex changes in uncrossed retinotectal projection after one eye removed at birth 79−57650
visual cortex development, kitten, monocular astigmatism effects 78−7345
visual cortex development model, mammal 78−3483
visual cortex functional specialisation of rhesus monkey 78−80873
visual cortex muscarinic acetylcholine receptor and acetylcholinesterase increase on exposure of dark-reared rats to light 78−24069
visual cortex neural circuitry model for orientation sensitivity 79−11927
visual cortex neurones, rabbit, organisation of background activity 78−69044
visual cortex of cat, neural mechanisms underlying stereoscopic depth perception 80−12147
visual cortex of cat, spectral characts. of stimuli and responses of complex receptive field 77−16927
visual cortex of kittens reared with optically induced squint, neural response and binocularity 79−79556
visual cortex receptive field organisation and spatial freq. characts. 78−69068
visual cortex receptive field spatial freq. characts. rel. to stimulus speed, cat 78−20174
visual cortex simple cells, spatial resolution and nonlinearities, cat 77−9187
visual cortical area 19 of cat, periodic complex cells 78−56974
visual cortical effects of early visual experience 80−12119
visual cortical neurone orientational prop. recovery and ocular motility in dark-reared kittens 78−53396
visual cortical neurone reaction patterns to const. illum. 78−80871
visual cortical neurones, pattern selective adaptation, cats 79−53090
visual cortical neurons, optimality of bar and grating stimuli 80−85391
visual cortical plasticity rel. to local perfusion of noradrenaline 78−35847
visual depth of field, wavelength dependence obs. and calc. 79−62240
visual detection of spatial contrast, influence of visual field location, target extent and illum. 79−2067
visual development, environmental effects 79−11926
visual development in humans, animal models 80−12118
visual discrimination between small objects and large textured backgrounds 78−11652

neurophysiology continued
visual electrophysiological examinations of flying personnel 79−11929
visual event related potentials of the late positive complex in visual discrimination tasks 79−39416
visual evoked human-scalp EEG data monitoring, processing and displaying system 77−90936
visual evoked neural activity intensity and structure, rel. to visual system modelling 77−25426
visual evoked potentials, during hypothermia, prolonged circulatory arrest 79−16204
visual evoked potentials, n-hexane induced changes, ERG of industrial workers 80−45886
visual evoked potentials in monkeys 80−45885
visual evoked potentials in neurological disorders 79−24981
visual evoked response, diagnostic tool in demyelinating diseases 79−20538
visual evoked response, provoked visual impairment in multiple sclerosis 79−16202
visual evoked response meas. using computerised rapid random flash 79−83776
visual flicker-induced asymmetries, separate neural systems for darkness, brightness perception 80−67083
visual foveation system, afferent part, computer model 77−25437
visual global peripheral excitation, local foveal inhibitory effects 79−88076
visual information processing, primate visual system appl. 80−30722
visual information processing, review *(German)* 77−64034
visual metacontrast masking of vernier acuity targets, sustained channels inhibit transient channels 79−53094
visual metacontrast with black and white stimuli, inhibition of on- and off-sustained activity 79−53139
visual monocular space perception, math. model rel. to retinal neurophysiology 80−45910
visual nervous system, human, temporal props. 78−7353
visual neuron receptive field mapping with visual stimulus generator 79−74817
visual neuron-discharges in eye movements 80−12099
visual neurones in dipterous insects, sexual differences 80−41010
visual non-spiking interneurone, spike response 78−11645
visual normalisation with rods and cones 79−100609
visual path neuron simulation using analogue and digital electronic circuit *(Spanish)* 78−27942
visual perception, local organising processes and motion schemas *(Spanish)* 78−69086
visual perception, relative motion induced between stationary lines, velocity sensitive neuron interpretation 79−53149
visual perception of extent, effect of saccadic recalibration 77−48806
visual perception of moving targets, highly specialized nerve circuits 77−81501
visual perception of relative motion extraction, neural mechanism model *(Japanese)* 78−56987
visual photopigments and pseudo-pigments, spectral sensitivity and neural interaction 77−25425
visual pigment processes and prolonged pupillary responses in insect photoreceptor cells 80−8061
visual pigment system kinetics, bistable system measurements appl. 78−92624
visual pigment system kinetics, mathematical anal. 78−92623
visual responses in geniculo-striate and pulvino-extrastriate systems, squirrel monkeys 77−40667
visual sensitivity and adaption, conf., Guildford, England (Sept. 1978) 79−79516
visual shift effect, discovery *(German)* 79−57651
visual single unit recording in pigmented rat, eye movement control 77−81767
visual space, neural representation 77−40670
visual stimuli equivalence classes, model neural network 78−69064
visual stimulus onsets and offsets, response of visual mechanisms 80−16937
visual system, cat, neuronal net analysis 79−43872
visual system, crayfish, coding and decoding of steady state information by patterned pulse trains 80−12105
visual system, entoptic phenomena 79−53106
visual system, goldfish, spatial summation and light adaptation 77−77897
visual system, inference upon the neural network finding binocular correspondence 79−34557
visual system, primate, subdivisions and interconnections 80−12110
visual system, quantum fluctuations and adaptive spatial interactions 79−16206
visual system, signal processing in brain *(German)* 78−48792
visual system development in cat, role of binocular interactions 80−12117
visual system movement processing model 79−66473
visual system neuron response to light stimulus, computer monitored method 77−86725
visual system of crustacean, polarisation sensitivity 78−7350
visual system of fly, giant neuron performance, spike generation 80−108886
visual system spatial and temporal information separation model 78−40167
visual task subjective performance, noise and quality influence 78−53416
visual thalamus, mammalian, neuronal organisation 78−27948
visual tracking, target vel. signals in vermal Purkinje cells, monkey obs. 80−56026
visual Wulst, barn owl, neurons selective for orientation and binocular disparity 77−1996
visual Wulst, owl, effect of monocular deprivation on binocular neurones 77−16929
visual Wulst retinotopic organisation in nocturnal and diurnal raptors 80−12098
visual-neural correlate of speechreading ability 78−64992
visual-vestibular convergence in the vestibular nuclei of the cat 80−85420
visual-vestibular interactions, model of cerebellar influence 78−40156
visually evoked cortical potentials in renal failure, latency changes 79−16200
visually evoked cortical response obs., infants and adults 79−43873
visually evoked potentials, latency and reaction times as power functions of luminance in peripheral field 79−11928
visually evoked potentials and sensory dimensions 80−61548

neurophysiology continued
visuomotor mechanisms of monkey parietal lobe, visual input 78−27943
volitionally activated low-threshold EDC motor units, firing rate response 78−20163
voltage clamp membrane current min. parameter description 78−35825
Volterra-like polynomial representation for neuron models 77−90754
volume conductor principles in scalp EEG recordings, montage design 77−78003
volume-conductor fields of isolated axon, linear filtering problem 78−3463
walking, connections between different legs, quantitative model 80−101161
walking, individual leg control, model 80−101160
walking, mathematical model of muscle commands from nervous system *(French)* 80−51071
walking, nervous command study 79−53184
Wiener filtering, estimation of evoked potentials 79−48235
Ba treated nerve cells, generation of long potential waves 80−56002
C-fibre microelectrodes, neurophysiology appl. 80−67314
Ca conductance, inactivation without facilitation in Cs-loaded Aplysia neurones 78−56965
Ca conduction units in Helix neurones 78−77041
Ca entry in aequorin injected crayfish axon 79−79513
Ca ion levels in squid axons, influence of pCO_2 78−56960
Ca pump driven by ATP in squid giant axons 78−77043
Ca sequestering by endoplasmic reticulum in squid giant axon 79−83733
Ca spike enhancement during neurite in tissue culture 79−70545
Ca^{2+} conductance of acetylcholine-induced endplate channels 79−70546
Ca^{2+} intracerebral transients, photoelectrode for recording 80−30961
Ca^{2+} voltage-depend. facilitated entry into voltage-clamped aequorin injected molluscan neurons 77−90763
Ca-dependent depression of late outward current in snail neurons 78−7335
Co induced chronic epilepsy, secondary ion microanalysis *(French)* 79−62414
K activation associated with intraneuronal free Ca, dorid giant neurons 79−8494
K channel blocking agent, 3,4-diaminopyridine 78−69028
K channel in axonal membrane of mammals (myelinated fibres) 80−61538
K channel ionic interactions, squid giant axon 78−3458
K current components in node of Ranvier membrane frog Rana ridibunda 78−31800
K currents induced by acetylcholine in Aplysia neurones, slow relax. 78−80865
K ion noise currents and inactivation in voltage-clamped node of Ranvier 77−16924
K^+ channels of myelinated nerve, conditioning hyperpolarisation-induced delays 79−88066
K^+ conductance absence in central myelinated axons 80−108871
K^+ currents in squid axons, single channel recordings 80−76721
K^+ ion flux through membrane channels, nerve impulses, random walk anal. 78−77045
K^+ transport of squid axon membrane, internal pH effects 79−62221
Na channel, fully coupled excited state model, conductance in volt. clamped case 78−85297
Na channel, fully coupled transient excited state model, action potential generation, threshold, accommodation and repetitive firing 79−57634
Na channel density in myelinated nerve fibres and nature of axonal membrane 77−52777
Na channel fluctuations, phys. nature, microscopic model 80−35869
Na channels in nerve, evidence for two conductance states 78−11634
Na channels in squid giant axons, n-alkanol potentiation 79−83744
Na conductance in nerve, anomalous temp. dependence of rabbit rel. to frog 79−62235
Na current in cardiac and nervous tissues, validity of dV_{max}/dt as meas. 78−77037
Na permeability inactivation in squid giant nerve fibres, review of exptl. work 78−73154
Na pump activation by external cations in squid axon, effect of ATP levels 78−35818
Na^+ channel gating modifications in Myxicola giant axons 79−88072
Na-channel gating current carriers, electronic model 79−70542
Pb, airborne, effects on children, Steinbuch's Lernmatrix appl. 77−44878

neutral currents
$\Delta C \neq 0$ neutral current model, explanation of $\mu^-\mu^-$ dimuon events 77−54070
$\Delta S = 0$ weak hadron neutral current, quark parton model, νN and e^+e^- interactions 78−12859
annihilations prod. spin-1/2 and spin-0 pairs, weak effects 77−18219
astrophysical role, supernova model of heavy element origin 77−56825
asymptotic freedom predictions for neutral and charged current neutrino interactions 78−8581
atom, contact interactions, parity-violating and parity-conserving, new evaluation techniques 79−26872
atom, metastable, sensitivity and level crossing role in parity nonconservation meas. 80−43005
atom, parity breaking, implications for unification of weak and EM interactions 77−57479
atomic spectra, search for optical rot. induced by weak neutral currents 78−82710
atomic spectroscopy, search for parity-violating weak interaction of electrons with nuclei 79−36571
atoms, heavy, parity non-conservation, relativistic many-body perturbation theory 78−923
atoms, Hiller-Sucher-Feinberg identity, generalisation, accuracy for approx. wavefunctions 80−63512
atoms, parity violation in neutral-weak current interactions, meas. method 79−45670
b-flavour prod. by flavour changing neutral currents, five quark model anal. 79−75720
B-L as fourth colour in an $SU(2)_L \times U(1)_R \times U(1)$ model 79−97589
b-quark, horizontal gauge symmetry, Cabibbo universality and fermion masses 80−22583
baryon-lepton symmetry model, μ-number and flavour nonconserving neutral currents 78−66069
baryon-lepton symmetry model, neutral current test 77−61248
Bethe-Heitler pair prod., neutral currents 78−33022

neutral currents continued
bremsstrahlung evidence for parity nonconservation due to neutral currents 77−6076
canonical neutral-current predictions from the weak-electromagnetic gauge group $SU(3) \times U(1)$ 80−95242
charged heavy lepton production by nondiagonal neutral currents *(Chinese)* 79−17668
charm particle production in weak interactions with diagonal neutral currents *(Russian)* 77−74676
coherent π^0,p^0 meson prod., test for neutral weak currents of exotic space-time struct. 79−75715
colliding e^+e^- beams accelerator expts., 100 GeV, particle prod., weak currents, etc. *(Russian)* 78−58194
coloured quark model of weak interactions 77−18236
compilation of coupling constants and low-energy parameters 79−22159
concepts and effects on weak interaction theory 79−6314
conference on hadron struct. and lepton-hadron interactions, Cargese, France (July 1977) 80−4473
conference on particle physics, Honolulu, Hawaii (Aug. 1977) 79−49485
coupling and structure from Caltech.-Fermilab expt. 77−222
couplings in neutrino-hadron interactions 78−24993
CP violation and off-diagonal neutral currents 79−13008
current induced reactions, conf. 77−34106
deep-inelastic neutral-current cross-sections 78−66074
developments in phenomenology 77−6105
diagonal currents, possible strangeness changing effects 77−49900
discrete symmetries, natural flavor conservation and weak mixing angles 79−49438
droplet model and neutral currents, operator form 80−91043
dual electromagnetism and neutral-current interactions 79−71678
dynamical scaling violations, evidence from neutral current anomalies 79−17664
dynamical scaling violations, slow rescaling discrimination using neutral current anomalies 77−49896
E_7 grand unification, neutral currents problem in $SU(2) \otimes [U(1)]^3$ gauge theory *(Russian)* 80−62913
E_7 grand unification using $SU(3) \times (U(1))^3$ gauge group, neutral currents 80−27444
elastic electron scatt. and atom parity nonconservation caused by nuclear parity violation 80−27427
electromagnetic-like form $\bar{\psi}\gamma^\lambda\psi$, explanation in new formal approach 77−30306
electron, determ. of weak neutral current couplings 79−35994
electron-nucleon interaction, atomic-beam reson. expt., feasibility 77−88602
elementary particle properties from atomic phys. expts., parity violation 77−34578
exclusive one-pion prod., ν-induced neutral current channels 78−54624
factorisation and coupling constant determ. for νe, ed, and ν+hadron 80−27451
five-quark model with right handed current, weak interactions description 77−57485
flavor-changing effective neutral-current couplings in the Weinberg-Salam model 80−86649
flavour changing neutral current search in leptonic and semileptonic decays 80−105836
flavour changing neutral currents with b quarks and/or τ leptons 80−73656
flavour conservation, natural, in neutral weak currents, symm. $SU_2 \times U_1 \times U_{1'}$ model 78−12858
flavour conservation in superheavy quark models 77−49893
flavour mixing in ambidextrous $SU(2)_L \times SU(2)_R \times U(1)$ gauge theory 78−12805
flavour- and muon-number changing in $SU(2) \times U(1)$ model with CP isolation 77−26484
flavour-changing neutral currents 80−22553
flavour-changing neutral-current process in gauge models and strong interactions 78−8541
four-element lepton models, non-diagonal neutral currents *(Chinese)* 78−78132
fundamental constituents of matter and unification of weak and electromagnetic interactions 80−62940
fundamental phys. expts. with reactor neutrons and neutrinos, summary 79−67543
Gargamelle, neutrino physics history, theory and expt. 78−50027
gauge bosons props. in weak interaction theories with natural parity conservation 79−321
gauge models of weak and EM interactions, neutral current constraints 78−45831
gauge models of weak and EM interactions, quantisation and renormalisation of gauge theories, book contrib. 79−30669
gauge theories and neutral currents, review 79−13011
in gauge theories applied to weak interactions, review 77−26479
gauge theories of weak, EM, and strong interactions, book contrib. 79−30694
gauge theories with neutral currents, high-density and high-temp. effects on symmetry breaking 77−22664
gauge theory and neutrino physics, book 79−30726
gauge theory of physical colour, test of nonconfinement by neutral current scatt. expt. 77−46017
gauge theory predictions, obs., neutral currents props., struct. 78−12856
generalised $SU(2) \times U(1)$ gauge model, neutral currents anal. 78−45832
Glashow-Weinberg theorem, neutral currents 78−8582
goldstino couplings and neutral currents, mass relation for lepton and quark superpartners 79−75717
grand unification from neutral currents in gauge models 80−78009
grand unified field theories, two-loop corrections to mixing angle and lifetime of proton 80−13249
hadron decay, ν sources, right hand weak currents and direct neutrinos *(Russian)* 77−82699
hadronic currents in colour $SU(3) \times SU(3)$ model, diagonal neutral currents *(Russian)* 77−49902
hadronic neutral current coupling constants, model independent determination 79−35996
hadronic neutral current in neutrino interactions and single Z-boson hypothesis 79−54295
hadronic neutral current struct. 78−24994
hadronic polarization in neutrino scattering, helicity struct. of weak neutral current 78−74245
heavy atoms, P-odd effect suppression in unified gauge theory, l-N scatt. P-odd asymmetry *(Russian)* 77−61300

neutral currents continued
heavy element nucleosynthesis, current astrophysical theory review 77−29644
heavy lepton decay widths, first-order weak interaction theory 78−45899
heavy lepton model for rare μ and K decay modes 78−45898
heavy leptons as hadron constituents 77−30319
heavy particle decoupling effects in broken symmetry theory 78−82140
Higgs bosons, effects on experimental observables, and fermion mass scale 80−32061
Higgs flavour-changing, suppression in $SU(2)_L \times SU(2)_R \times U(1)$ left-right symmetric gauge theory 80−78016
Higgs induced neutral currents, natural flavour conservation and quark mixing angles 80−42392
Higgs induced neutral currents, symmetries leading to flavour conservation, Cabibbo angle 79−63407
High energy behaviour of weak interactions and renormalisable theories, book contrib. 78−78164
high energy lepton pair prod. with pol. hadrons, P and C violations 80−99068
high energy neutrino interactions, quark parton model anal. 79−30730
high energy neutrino physics, recent expt. results 80−4982
high-energy (>10 GeV) neutrino physics, review of development, book contrib. 78−82201
hyperon semileptonic decay, SU(3) spectrum generation, Cabibbo angle 80−9119
inclusive strangeness changing neutral current interactions 78−8652
intermediate boson decay calcs. using neutral hadronic weak current 77−38118
intermediate boson theory with large dimensionless coupling constant, neutral currents as second order processes 77−61244
isobar prod. by neutral current, polarisation effects 77−18220
isoscalar axial-vector current in neutral-current phenomenology 79−93316
isoscalar neutral current axial vector couplings and nucleon anomalous moments 80−27452
isospin props in ν-p and $\bar{\nu}$-p elastic and quasielastic scatt. 77−2812
L-amino acids, weak neutral currents and biological stereoselection 80−26196
left-right symmetric gauge models, parameter constraints from neutral current data 80−86588
left-right symmetry for $SU_L(2) \times SU_R(2) \times U(1)$ gauge group 78−21375
left-right-symm. unified theory of quarks and leptons 78−41466
lepton pair photoproduction, neutral weak current consequences *(Russian)* 78−12899
lepton structure and neutral currents 77−2788
lepton-nucleus scattering, bremsstrahlung and neutral currents 80−32268
leptonic colour model, expt. evidence 78−62350
leptoproduction, $\mu N \rightarrow \mu X$, broken colour gauge theory of integer charge quarks 80−13313
light-cone algebra anal. of weak currents 79−6311
mesic atom, weak neutral interaction between muons and nuclei, effects impeding obs. *(Russian)* 77−31031
mirror image molecules, parity non-conserving energy difference 79−76366
MIT bag model, static electroweak props., PCAC 80−73645
mixing of states containing heavy quarks 78−422
molecules, parity-violating effects of weak interactions 80−52455
Moller scatt., neutral current effects 77−2786
muon number conservation spontaneous breakdown, off-diagonal neutral currents 77−49889
muon number nonconservation effects in gauge theory with V+A currents and heavy neutron leptons 78−8573
muonic atom, configurational mixing in shell and neutral weak muon-nucl. interaction effects obs. feasibility *(Russian)* 80−32859
muonic atom, heavy, polarisation mechanism of parity nonconservation, weak neutral interaction effect *(Russian)* 77−79712
muonic atoms, long range parity violating interaction from γ-Z^0 conversion 80−48108
muonic atoms, parity violating neutral current effects, E1-E2 interference 79−41254
natural flavour conservation determ. of Cabibbo angle 79−22015
natural flavour conservation in neutral weak interactions, SU(5) and SO(10) unified models 78−4817
neutral transitions, vector-like weak currents, parity violation *(Russian)* 78−24995
neutral-current weak interaction without electroweak unification 80−105835
neutrino + nucleus reactions, using shell model and Weinberg model to describe currents 79−93605
neutrino bremsstrahlung by degenerate electron gas, neutral current effects, stellar interiors appl. 77−13225
neutrino cosmology, open universe with neutrino and graviton dominance 77−17731
neutrino experiments at high energies, total cross sections by currents, review 79−49511
neutrino experiments on neutral currents, expt. verification of theoretical predictions, review 79−89097
neutrino interactions, appl. to weak interaction and nucleon struct. investigations, review 79−80823
neutrino interactions, experimental results for charged and neutral current interactions and multilepton prod. 79−49512
neutrino interactions at high energy, book contrib. 79−30729
neutrino low energy interactions, theoretical aspects 79−67538
neutrino neutral current couplings in $SU(2) \times U(1)$ gauge theories, natural relations, flavour dynamics 79−89095
neutrino physics with Gargamelle bubble chamber, book contrib. 79−30728
neutrino programme at ILL 79−67540
neutrino results at CERN, review 77−34145
neutrino spiral properties using model of the μ decay *(Russian)* 78−25031
neutrino transport, weak neutral currents; supernova model 78−62391
neutrino-bremsstrahlung, neutral current effects in Weinberg model 77−65150
neutrino-nucleus inelast. scatt., test of struct. of weak neutral currents 77−14117
neutrino-nucleus scatt., neutral current struct. 78−8799
neutron stars, cold, neutral currents and neutrino emission 77−45478
neutron stars, neutrino-pair bremsstrahlung in collisions between neutrons and nuclei 77−74789

neutral currents continued
new elementary particles, theoretical predictions, recent expt. results 77−57475
nuclear matter, high-temperature, neutral currents and neutrino Comptonisation 80−21905
nuclear scattering of reactor antineutrinos, neutral current, integrated inelastic cross section 78−29452
nuclear semi-leptonic weak interactions 78−555
nuclear weak and EM interactions, P-violation in e-nucleus scatt. 77−71479
nucleon weak interaction pots. in the Weinberg-Salam model *(Russian)* 80−13258
orthomuon mass lower limit from neutrino data anal. 78−62388
P-violating flavour changing and natural $\Delta S=0$ in vector like theories 77−18217
P-violating neutral currents in L-R symmetric gauge model 77−82698
P-violation and gauge flavours, Weinberg model testing 77−61240
P-violation in nuclear transitions 79−13243
parity conservation in neutral current phenomena, gauge model 79−17656
parity non-conservation in e-N, μ-N forces 77−57484
parity non-conserving processes, weak interaction theory, review 78−50002
parity nonconservation in heavy atoms and weak magnetism in neutral currents *(Russian)* 80−82932
parity nonconserving nuclear interactions and weak neutral currents, review 77−41936
parity violating effects in dilepton production using polarized targets 79−67613
parity violating neutral currents, radiative corrections, Weinberg-Salam and left-right symmetric models 80−52451
parity violating neutral currents in two-photon and autoionisation atomic transitions 80−32034
parity violating nuclear forces, neutral current effects 77−30497
parity violation in atoms induced by radiative corrections 78−78108
parity violation in He and Cs atomic electrons and e-e interaction effects 79−54788
PETRA QED tests, implications for weak neutral current struct. 80−86657
phenomenological model, $\nu_l \mathcal{L} \rightarrow \nu_l$ processes, possible T-violation 77−30359
photoprocesses in few-nucleon systems, exchange meson currents role *(Russian)* 79−22269
pion production by weak neutral currents, gauge theory model predictions 79−13014
polarisation asymm. in charged-lepton-nucleon elastic scatt. 78−33071
purely leptonic processes, hypothesis test, purely diagonal single Z boson neutral currents 79−40713
QCD estimates for associated charm production by weak neutral currents 78−78169
quark and lepton couplings in the weak interactions 79−17665
quark charge origin 78−21373
quark flavour natural conservation in $SU(2) \times U(1)$ theories 77−49899
quark models and unified field theories, review 79−80805
quark-lepton correspondence in neutral current interactions 80−27450
quarks, charged and neutral current coupling 78−89651
quarks and leptons, fermion physics in terms of $SU(2) \times SU(1)$ gauge theory 78−74197
quarks-antiquarks system, effect on neutral currents *(Russian)* 77−6078
reactor neutrino expts., fission fragment ν radiation, neutral currents, inverse β-decay, $\bar{\nu}$ scatt. *(Russian)* 80−42736
review, neutral current effects in nuclei 79−40859
S,P,T-type neutral weak current meas. in μN scatt. 80−32064
scaling violations and neutral currents 78−41529
selections from 1977 Comments on Modern Physics, book 79−30181
semi-leptonic weak interactions, book contrib., strangeness-conserving current, strangeness-changing decays 78−78162
semileptonic neutral currents as higher order effects in Fermi-type charged current theory 78−41474
sequential Weinberg-Salam model, neutral current flavour conservation, fourth generation 79−97561
simultaneous constraints and $s\bar{s}$ effects in neutral-current-coupling determinations 80−37205
$\sin^2\theta_w$, grand unified gauge theories and proton decay 80−73634
single-Z-boson hypothesis, neutral-current processes 77−74639
six-fermion interaction const. and neutral currents *(Russian)* 77−34147
six-quark symmetric model and associated neutral currents 77−18216
Sodium ammonium tartrate, L- and D-mol. energy difference, parity violation 78−25744
standard model neutral current predictions, uniqueness 79−80789
stellar collapse, effect of weak neutral current 78−85964
stellar energy loss rates due to neutrino prod. by neutral currents 77−53577
stellar matter, neutrino opacity, pure neutral vector boson contrib. 78−53928
strange particle production by neutral currents, Gargamelle $\nu,\bar{\nu}$ reactions 78−37201
strangeness changing neutral currents, avoidance in gauge theories of weak and EM interactions 79−22005
strangeness conservation in neutral currents, constraints on vector-like model 78−21374
strength limit at PETRA energies 80−105839
$SU_3 \times U(1)$ gauge models and neutral current reacts. 78−89648
$SU_L(2) \otimes SU(2)_R \otimes U(1)$ and $SU(2) \otimes U_L(1) \otimes U_R(1)$ gauge theories, neutral current constraints 79−277
$SU_L(4) \times U(1)$ four-quark model, lepton quartets and W bosons 77−87934
$SU(2)_I \times (T_3)_R \times U_Y(1)$ gauge unified model, neutral current interactions, ed and ν scatt. 80−18107
$SU(2)_L \times SU(2)_R \times U(1)_L \times U(1)_R$ gauge models, parity violation in SLAC neutral current expt. 79−9305
$SU(2)_L \times SU(2)_R \times U(1) \times U(1)_R$, P violation 79−6308
$SU(2)_L \times SU(2)_R \times U(1)$ based L-R symmetric gauge theory, spontaneous breakdown of parity 79−75681
$SU(2)_L \times SU(2)_R \times U(1)$ gauge group axial-vector isosinglet neutral hadronic current coupling to ν and e 79−63371
$SU(2)_L \times SU(2)_R \times U(1)$ gauge models, neutral currents, P-violation 79−54293
$SU(2)_L \times SU(2)_R \times U(1)$ gauge symm., Higgs particles, parity conservation 78−70305

neutral currents continued
$SU(2)_L \times SU(2)_R \times U(1)$ gauge theory, left-right symm., neutral current struct. 78−41420
$SU(2)_L \times U(1) \times U(1)_R$ model, chiral symmetry and weak neutral currents 80−101980
$SU(2)_L \times U(1)$ gauge group, axial-vector isosinglet neutral hadronic current coupling to ν and e 79−63371
$SU(2)_L \times U(1)$ gauge model with off-diagonal neutral currents, anomalous lepton events 79−2923
$SU(2)_L \otimes SU(2)_R \otimes U(1)$ gauge models confronting neutral current data 79−22013
$SU(2)_L \times SU(2)_R \times U(1)$ gauge models, neutral current sector, natural parity conservation 79−9324
$SU(2) \times SU(2) \times U(1)$ supersymmetric gauge model, atomic parity violation and neutral current predictions *(Russian)* 79−54294
$SU(2) \times U1$ unified theory, symmetry and renormalisation 80−22551
$SU(2) \times U(1)$, gauge theory of weak interactions 78−21328
$SU(2) \times U(1) \times G$ expanded gauge models of neutral currents, propagator momentum transfer 80−47237
$SU(2) \times U(1) \times G$ Weinberg-Salam extension, possible neutral current struct. at PETRA/PEP and LEP 79−89096
$SU(2) \times U(1) \times U(1)$ gauge model, quark-lepton correspondence in neutral and charged current interactions 79−54296
$SU(2) \times U(1) \times U(1)$ gauge models, neutral current struct., parity nonconservation 79−292
$SU(2) \times U(1) \times U(1)$ model, neutral current, quark mass reactors, spontaneous broken Lagrangian 79−97563
$SU(2) \times U(1)$ gauge model and parity violation in atoms 78−4775
$SU(2) \times U(1)$ gauge model predictions for neutral current reactions 77−71424
$SU(2) \times U(1)$ gauge models, with diagonal neutral currents 77−71433
$SU(2) \times U(1)$ gauge theories of weak and EM interactions, neutral current contraints 78−70272
$SU(2) \times U(1)$ gauge theory, lepton struct. 77−82691
$SU(2) \times U(1)$ model, fermion and Higgs multiplet structure, universality 80−62909
$SU(2) \times U(1)$ models, hadronic neutral currents, low energy neutrino reactions, constraints 77−13912
$SU(2) \times U(1)$ symmetry group, μe universality breaking in neutral current weak interactions *(Russian)* 79−58918
$SU(2) \times U(1)$ unified gauge theories, implications of parity violating obs. on heavy atoms 77−46006
$SU(2) \otimes U(1)_y \otimes U(1)_c$ gauge model, neutral current and $\Delta I = 1/2$ rule 79−6257
$SU(2) \otimes U(1)$ gauge group theory tests from neutral current phenomena 78−24992
$SU(2) \otimes U(1)$ gauge models, neutral current couplings 79−40715
$SU(2) \otimes U(1)$ standard and SU(5) grand unification models, neutral current data implications 80−78000
SU(2) gauge invariance, spontaneously broken, $\Delta I = 1/2$ rule, nonleptonic weak interactions model 77−41786
SU(2) x U(1) gauge group, neutral current couplings 77−67567
$SU(3)_L \times SU(3)_R$ as gauge groups of weak and associated charges, symm. breaking 78−74175
$SU(3) \times U(1) \times U(1)$ model, suppression of flavour changing neutral currents 78−21350
$SU(3) \times U(1)$ gauge models, generalised mixing and CP violation in hadron decays 78−41473
$SU(3) \times U(1)$ gauge theory, electro-weak interaction, helicity mixed representation 80−78013
$SU(3) \times U(1)$ gauge theory of weak and EM interactions 78−70317
Su(3)×U(1) unified gauge theory without μ-e universality 79−26274
SU(5), unification of weak, EM and strong interactions, review 80−105814
$SU(5) \times U(1)$ unified theory, neutral current anal. 80−73647
SU(6) grand unification model, hierarchy of symmetry breakings and neutral currents 80−52446
SU(6) model of weak interactions, neutral weak currents at high energy *(Russian)* 78−45836
SU(6) unified gauge group, neutral current coupling to ν_μm and ν_e 78−54626
supernova outburst role of neutral currents of weak interactions *(Czech)* 77−45472
supernovae, neutrino transport in collapsing stellar core model 78−8029
superweak particle cosmological constraints, ν with neutral current interactions, ^{4}He primordial abundance 79−84667
symmetry violation natural suppression, muon and electron lepton number nonconservation 78−8574
three triplet quark model with observable colour, hadron weak current, $\Delta T = 1/2$ rule *(Russian)* 78−74219
torsion potential, coupling strength, experimental bounds 80−73249
two-electron atoms, autoionisable states decay, parity violation effects 79−72231
two-electron ions, autoionisable states decay, parity violation effects 79−72231
$U_3(W)$ gauge models, neutral currents 79−49443
$U_3(W)$-gauge unified EM-weak theory, neutral current neutrino interactions 77−26481
unconfined colour quark models, weak interactions and neutral currents *(Russian)* 80−105841
unified gauge theories, electroweak mixing angle, renormalisation 80−86651
unified gauge theories, electroweak mixing angle, sequential triplets scheme of fermions 80−86650
unified gauge theories of weak currents of hadrons 79−80786
unified gauge theory, low energy neutral current struct. 79−2975
unified left-right symmetric gauge models 79−45044
unified model for atomic parity violation and neutral currents in gauge theories 80−4912
unified SU(3)XU(1) gauge theory with different muon and electron neutral currents 78−58152
unified U_3 gauge theory of weak and EM interactions, six quark flavours and lepton types 77−18215
universal neutral current interactions and urbaryon-lepton correspondence 78−66068
$V_3(W)$ gauge theory, spontaneous symm. breaking, parity violation in atomic physics 77−71476
V+A currents coupling old quarks to new quarks 77−26486
V(e)V(q)+A(e)A(q) neutral currents in $SU(2) \times U(1) \times U(1)$ theory 79−17667

neutral currents continued
(V-A) model, mixing between ordinary and heavy leptons, neutral current reactions 78−41472
vector axial-vector ambiguity in Δ(1236) production 77−74636
vector boson, light neutral, possible exist., quark model construction 77−49898
vectorlike model, parity violation 78−4823
vectorlike $SU(3) \times U(1)$ gauge model of weak interact. $\bar{\nu}$ reactions, neutral currents 77−41805
vectorlike theory with parity violating neutral current and natural symmetry 77−13909
VV+AA gauge model 78−29246
VV+AA type gauge models, effective ν interactions 78−66038
weak, structure, neutrino and antineutrino scattering experiments *(Russian)* 79−49446
weak and EM interactions at high energy [conf. Les Houches, France (July 1976)] 79−80785
weak current interactions, review 80−73654
weak current model with $\Delta C \neq 0$ neutral current 77−54069
weak interaction physics, present status and future prospects, review 79−67492
weak interaction theory, review 78−4822
weak interactions, lepton-hadron symmetry, CP violation and $\Delta I = {}^1/_2$ rule 80−82934
weak interactions, optical experiments as a means of verification 79−6313
weak neutral current, space-time struct., generalised version of confusion theorem 79−75714
weak neutral current coupling const. from νN single pion prod. data anal. 77−13911
weak neutral current couplings calc. of u and d quarks, ν interaction input data 78−54603
weak neutral current couplings of muons 79−85259
weak neutral current struct., ν and $\bar{\nu}$ interactions hadronic energy distrib., Weinberg-Salam model 79−35993
weak neutral currents, internal conversion probe from M1 decay, nuclear matrix elements 79−67712
weak neutral currents, status in weak and EM interactions 79−49444
weak neutral currents displayed in biological isomerism, L- and D-mol. reaction rates 78−415
weak neutral currents unveiled 80−73658
weak quark and lepton chiral symmetries, dynamical breaking gauge interaction 80−47215
weak-EM interference, neutral currents, P-violation, in polarised e-scatt. and e^+e^- interactions 79−63404
Weinberg model, exptl. test *(Russian)* 79−97564
Weinberg-Salam model and extensions, ν EM form factors and mag. moments, neutral currents, astrophysics applics. *(German)* 80−62904
Weinberg-Salam model Yang-Mills theory of electro-weak interactions 80−73638
Weinberg-Salam $SU(2) \times U(1) \times U'(1)$ extension, new neutral current structs. 79−58920
Weinberg-Salam $SU(2) \otimes U(1)$ gauge theory effective Lagrangian, neutral current results 79−35992
Wilson operator formalism, generalised parton model equivalence 78−93855
without gauge theory prejudices 77−34113
y anomaly in $SU(2) \times U(1)$ vector like model, with parity violating neutral current 79−13013
Z-boson and two-boson models 80−18109
b-quark prod. in five quark model by flavour changing neutral currents 79−45073
β-decay, time reversal invariance and second class weak currents, review 78−37309
D^0, $\bar{D}^0$, decays, charm changing neutral current limits, QCD depend., mass differences 80−32062
D^0-$\bar{D}^0$ mixing, flavour-changing Higgs bosons 80−62915
Δ(1236) isomer production, by charged and neutral currents 79−17711
e^-+nucleus parity violating neutral current interaction, gauge theory predictions, radiative corrections 78−86436
ed, polarisation effects in presence of weak neutral current *(Russian)* 77−61291
ed deep inelastic scatt., p-violating asymmetries, neutral current couplings, sea quark contrib. 79−97630
ed elastic scatt., P-odd effects due to neutral weak currents, cross sections *(Russian)* 80−13312
ed elastic scatt., recoil d vector polarisation, p-violation 79−398
ed elastic scattering, neutral weak currents *(Russian)* 78−21434
ed scat., d disintegration, polarised e, neutral weak currents, right-left asymmetry 79−80787
ed scatt., P-violation calc. in weak interaction theory 80−42469
e^-e^- neutral weak currents in atoms and ions, parity nonconservation *(Russian)* 77−46037
$e^-e^+ \rightarrow N^*\bar{N}^*$, weak neutral current effects for polarised e^+e^- pair 80−37287
e^+e^-, annihilation, weak neutral currents of quarks hadron prod. cross section P-odd depend. *(Russian)* 79−93445
e^+e^-, $SU_L(2) \times U(1)$ and $SU_L(2) \times SU_R(2) \times U(1)$ predictions at high Q^2, neutral currents, Z-bosons 80−63029
e^+e^-, weak corrections to three-jet angular distributions 80−22629
$e^+e^- \rightarrow \mu^+\mu^-\gamma$, neutral current effects and hard photon correction 79−13096
$e^+e^- \rightarrow I^{++}$ resonance states, direct production through neutral currents 78−93891
e^+e^- annihilation, neutral weak current effects, gauge model anal. 77−61243
e^+e^- annihilation channel, differential dispersive theory of ψ/J 78−45933
e^+e^- baryon-antibaryon prod. neutral current effects in Weinberg model 77−18310
e^+e^- collisions, weak neutral current effects, unified theories of dimension *(Hungarian)* 79−9326
$e^+e^- \rightarrow F^+F^-$ ($F^+ = \mu^+, p, \pi^+$, etc.), polarised beams, weak neutral currents effects 77−26483
$e^+e^- \rightarrow F\bar{F}$, with polarised particles, weak asymmetries, unified gauge theory anal. 78−8636
$e^+e^- \rightarrow \gamma$+hadrons, high energy, lepton radiation and γ struct. functions, quark parton model 80−32113
e^+e^- →hadron jets, quark helicities, neutral current vector and axial couplings 80−32114
e^+e^- →hadrons, neutral and weak currents anal. 77−26533

neutral currents continued
e^+e^- →hadrons, neutral weak current effects 77−49987
e^+e^- inclusive annihilation, many-hadron final states 78−29339
e^+e^- inclusive hadron prod., neutral weak currents 78−50041
e^+e^- →L^+L^-, test of lepton no. assignment of heavy leptons 77−18266
e^+e^- →l^+l^-, neutral current effects around vector resonances, polarisation 80−105878
e^+e^- →M+X, M=pseudoscalar meson, forward-backward asymmetry from neutral currents 79−71759
e^+e^- →multiple lepton+hadron final states, flavour changing neutral currents 77−30363
e^+e^- →$\mu^+(\tau^+)\mu^-(\tau^-)$, neutral current couplings, lepton polarisation, p violation in SU(2)×U(1) model 80−4975
e^+e^- →$\mu^+\mu^-$, 5.8-7.4 GeV, neutral currents strength limit, pole angle asymm. 78−78157
e^+e^- →$\mu^+\mu^-$, contribution of weak neutral currents *(Russian)* 78−62383
e^+e^- →$\mu^+\mu^-$, contribution of weak neutral currents *(Russian)* 78−62384
e^+e^- →$\mu^+\mu^-$, neutral current anal., weak and radiative asymmetries 79−26320
e^+e^- →$\mu^+\mu^-$, weak neutral electron current, Lorentz struct. 79−80788
e^+e^- →pX, weak neutral current, polarisation effects, asymm. parameters *(Russian)* 78−459
e^+e^- →$p\bar{p}$, asymm. and polarisation of p,$\bar{p}$, neutral weak currents *(Russian)* 78−58195
e^+e^- →$\pi^0\gamma$ or $\eta\gamma$, reaction rate, weak neutral current corrections, 3γ background 77−46069
e^+e^- →$\pi^+\pi^-\pi^0$, neutral current and one-photon graph interf. 77−87990
e^+e^- →$\pi^+\pi^-\pi^0$, weak neutral current effects, asymmetries 77−6139
e^+e^- →$\pi^\pm$X, weak neutral-current effects 77−13968
e^+e^- →$q\bar{q}$→BX, weak-neutral current effects 80−42480
e^+e^- →$q\bar{q}g$, gluon bremsstrahlung, neutral current and beam polarisation effects 80−99106
e^+e^- →$\tau^+\tau^-$, neutral-current effects on ψ-like resonance 78−74239
e^+e^- →$\tau^+\tau^-$ →cascade π and ρ, parity violation from weak and EM interaction interference *(Chinese)* 79−49504
e^+e^- →V($b\bar{q}$ or $\bar{b}q$), $b\bar{q}$ resonance prod. below $b\bar{b}$ threshold via flavour-changing neutral currents 79−89123
eN, pion production, vector-like theories *(Russian)* 78−37221
eN deep inelastic scattering asymmetries, gauge theory predictions 79−22104
eN→eX, SU(2)$_L$×U(1) gauge theory distinguished from SU(2)$_L$×SU(2)$_R$×U(1), neutral currents, z-bosons 80−62908
eN elastic scatt. in nuclei, P violating asymmetry due to weak neutral currents 80−73713
en→enπ, pol. e, P-odd asymmetry and cross sections, SU(2)xU(1), SU(3)xU(1) calcs. *(Russian)* 80−62998
eN scatt., polarised e, testing unified gauge theories prediction 79−17732
e^-N→$e^-\Delta(3/2, 3/2)$, P-odd asymmetry, P nonconserving neutral current interaction 80−57611
e^-N→e^-Nπ, electromag. and weak process from weak neutral current interaction *(Russian)* 78−45928
e^-N elastic scatt., weak interaction model independent anal., e-q neutral current 79−71753
eν_μ scatt., theory of pure leptonic weak interaction with induced shadow states 77−49945
ep, high Q^2, QCD corrections to parity-violating asymmetries 80−22618
ep deep inelastic scatt., p-violating asymmetries, neutral current couplings, sea quark contrib. 79−97630
ep deep inelastic scatt., parity violation and neutral currents 80−22559
e^-p→e^-p, elastic scatt., polarisation of final lepton *(Russian)* 77−26529
eq parity violating neutral current couplings, model independent anal. 79−17737
η, neutral weak current effect on decay mode Weinberg-Salam model, P-violation contrib. 78−86450
η→$\pi^0\nu\bar{\nu}$, presence of second class neutral currents 79−26284
γ circular polarisation, neutral current effect in bremsstrahlung and pair production 80−73655
γN→l^+l^-X, pol. γ, neutral current effect, Weinberg Salam model calcs., p violation 80−5000
γN→l^+l^-X, polarisation effects on P-violating asymmetry in Weinberg-Salam model 80−32055
γN→lepton pairs, weak neutral currents anal. 78−8670
Γ_{pol}N→$\pi^\pm$N, weak neutral interactions, QCD renormalisation 79−93433
γp→p$\nu\bar{\nu}$, energy loss from stellar bodies through ν-prod. by second class weak neutral current 79−35997
K→2π, decay amplitudes in SU(2)×U(1)×U(1) model with new neutral current 80−4986
K^+→$\pi^+e^+e^-$, neutral-current process, strong interaction corrections 80−62968
$K^0\rightleftharpoons\bar{K}^0$, weak neutral current diagonality, mixing amplitude, multi-quark gauge model *(Russian)* 80−68414
l(l̄)N, P-odd asymmetries in deep inelastic scatt. of polarised l and l̄ *(Russian)* 79−49527
$l^\pm$N, deep inelastic scatt., EM corrections to hadronic and neutral currents, systematic effects *(Russian)* 79−49526
μ anomalous mag. moment in SU(3)×U(1) gauge model 79−3026
μ magnetic moment, weak coupling contribution, Weinberg-Salam model 80−22607
μe universality breakdown of neutral weak currents in SU$_2$×U$_1$ gauge *(Russian)* 79−75712
μe universality violation in renormalisation theory, neutral leptonic currents *(Russian)* 78−45837
μN deep inelastic scatt., asymm., quark proton model evaluation, gauge theories test 78−62408
μ^-p→μ^-p, elastic scatt., polarisation of final lepton *(Russian)* 77−26529
neutral current couplings of u and d quarks 78−86435
NN polarised scatt., weak neutral current models 78−41562
ν, EM properties, weak neutral current and form factor *(Russian)* 77−61270
ν, high-energy interactions, neutral-current coupling 78−66104
ν, $\bar{\nu}$, inclusive neutral current interactions 78−25036
ν, $\bar{\nu}$ induced events, SU(2)×U(1) gauge quark models 77−74632
ν,$\bar{\nu}$ experiments at Gargamelle, strange particle production by neutral currents 78−37200

neutral currents continued
ν and $\bar{\nu}$ inclusive processes for neutral currents, sea quark effects, meson prod. 79−22088
ν elastic and inelastic scatt., quark-lepton models 77−18272
ν high energy experimental physics at Fermilab, review 78−50028
ν interactions, parity violations in neutral currents 77−13910
ν interactions involving weak neutral currents, expt., theory, gauge models 77−49901
ν neutral current couplings and νe^- weak neutral current coupling constraint, fermionic assignments 80−4915
ν neutral current data, elastic and deep inelastic, gauge model constraints 79−40718
$\nu(\bar{\nu})$ d, disintegration reactions, helicity flipping neutral currents, tensor coupling 77−49944
$\nu(\bar{\nu})$ inclusive scattering, weak neutral currents with longitudinal cross sections, scaling 78−17007
$\nu(\bar{\nu})$ N interactions, π charge distrib., isospin and V,A struct. of weak neutral currents 77−38157
$\nu(\bar{\nu})$ scatt., Higgs boson prod. by neutral and charged currents 77−18271
$\nu(\bar{\nu})$N, meas. of high-energy neutral current interactions 78−66073
$\nu(\bar{\nu})$N elastic scatt. cross sections in Weinberg model of neutral currents 77−10240
$\nu(\bar{\nu})$N neutral current interaction, charm prod. in quark parton model 77−61246
$\nu(\bar{\nu})$N neutral current interaction cross sections 78−70357
$\nu(\bar{\nu})$N scattering, modified GIM model, scaling violations, naive parton model 78−21414
$\nu(\bar{\nu})$N→$\nu(\bar{\nu})$NNπ^0, charged neutral current ratios with νN→μN″π^0 77−22727
$\nu(\bar{\nu})$N→$\nu(\bar{\nu})$+hadrons, neutral to charged current cross section ratio 78−8651
$\nu(\bar{\nu})$N→$\nu(\bar{\nu})\gamma$N, neutral currents, γ emission cross section *(Russian)* 78−17008
$\nu(\bar{\nu})$N→$\nu(\bar{\nu})\gamma$X, hadron neutral current, parton model *(Russian)* 78−45910
$\nu(\bar{\nu})$N→$\nu(\bar{\nu})\pi$+X, determ. of neutral current coupling consts. 78−8649
$\nu(\bar{\nu})$+N, neutral to charged current inclusive cross-section ratio determ. 77−26511
$\nu(\bar{\nu})$d, scatt., weak hadronic neutral current struct. investig. 80−42438
$\nu(\bar{\nu})$d→np$\nu(\bar{\nu})$, weak neutral currents, (V, A) and (S,T,P) theories 78−12893
$\nu(\bar{\nu})$e, differential cross-section calc. in gauge theories, W-boson exchange 77−82728
$\nu(\bar{\nu})$e, weak neutral electron current, Lorentz struct. 79−80788
$\nu(\bar{\nu})$e→$\nu(\bar{\nu})$e, model examination by diagonal lepton processes anal. 79−6310
$\nu(\bar{\nu})$p elastic scatt., final state polarisations, test for T-invariance and 2nd class currents 79−63466
$\nu(\bar{\nu})$p elastic scatt. and neutral currents, by polarised proton target *(Russian)* 77−26507
$\nu(\bar{\nu})$p→$\nu(\bar{\nu})$p, ν-hadron weak neutral current couplings determ. 78−86435
ν oscillations of neutrinos in matter 78−70358
ν production processes, exclusive, neutral current props., Lorentz struct., internal symm. 77−18267
ν-induced inclusive and semi-inclusive pion reactions, neutral current coupling 77−74673
$\nu_e(\bar{\nu}_e)$e, charged and neutral current interference, test of Weinberg-Salam model 80−42385
ν_e-e scattering, charged- and neutral-current interference 79−89144
ν_e-ν_μ universality corrections for neutral current interactions in Weinberg-Salam model 79−54292
$\nu_\mu(\bar{\nu}_\mu)$p, 2 GeV elastic scatt., charged current/neutral current event ratio 80−57582
$\nu_\mu(\bar{\nu}_\mu)$p→$\nu_\mu(\bar{\nu}_\mu)$p hadronic neutral current, final-proton polarisation 78−82200
$\bar{\nu}$+N inelastic scatt., neutral current evidence for parity nonconservation 77−2815
νd→νd, polarised deuterons, asymmetry in emission of recoil deuterons 77−79264
νd→νnp, photon-neutrino coupling theory, Weinberg-Salam model comp. 79−13102
$\bar{\nu}_e$d→np$\bar{\nu}_e$, axial meson exchange currents 79−85255
$\bar{\nu}_e$d→pn$\bar{\nu}_e$, total cross-section calc. 78−41534
$\bar{\nu}_e$d→pn$\bar{\nu}_e$, weak neutral current reaction, measured cross section 79−80828
ν_μd→pnν_μ, neutral current induced neutrino reactions, differential and total sections 79−17708
νe, elastic scatt., weak neutral currents, space-time struct. *(Chinese)* 79−17715
$\bar{\nu}$e elastic scatt., spin correls., allowance for (S,T,P) interactions of neutral and charged currents 78−12901
$\bar{\nu}$e scatt., single Z boson hypothesis tests, non-diagonal neutral current inclusion 79−40714
νe scattering, weak lepton structure analysis, Weinberg-Salam model *(Russian)* 78−25039
ν_μe (and $\bar{\nu}_\mu$e) scatt., log. order α electromag. corrections 79−63467
$\bar{\nu}_\mu$e→$\bar{\nu}_\mu$e, high energy cross section upper limit, purely leptonic neutron current process search 79−36062
ν_μe→ν_μe, high energy elastic scatt. at Garganelle, neutral current reaction 79−93398
ν_μe→ν_μe, upper limit to cross-section determ. 78−33054
ν_μe→ν_μe, weak vector-like models, induced axial vector coupling 78−50025
$\bar{\nu}_\mu$e→$\bar{\nu}_\mu$e weak neutral leptonic current reaction, high energy search 79−71741
$\nu_\mu e^-$→$\nu_\mu e^-$, high energy, cross section meas. 78−78167
$\bar{\nu}_\mu e^-$→$\nu_\mu e^-$ leptonic neutral current reaction, evidence 77−2814
νN, above W prod. threshold energy, QCD effects, cross sections and neutral currents *(Russian)* 79−67537
νN, charged and neutral current interactions, cross sections and scaling variable distribs. 80−57581
νN, charmed particle prod. due to neutral weak currents *(Russian)* 80−68447
νN, elastic scatt., neutral weak current phenomenology 79−6312
νN, μ^+ single prod. in inclusive interaction 78−45908
$\bar{\nu}$N, neutral current charm particle prod. search 80−22600
$\bar{\nu}$N, single π^0 or π^- prod., neutral current interactions 78−41527
νn→= νpπ^-, neutral current process, excitation function, cross section ratio 80−78053
νN elastic and deep-inelastic scatt., photon-neutrino weak-coupling theory, neutral lepton current 77−30358

neutral currents continued
$\nu N \rightarrow$hadron+hadron neutral current prod. in Weinberg model *(Russian)* 77−6111
νN inclusive interactions, nondiagonal neutral currents, six quark model with slow rescaling 77−49949
νN inelastic scattering, possible soln. with weak neutral currents to ρ-π puzzle 79−17714
$\bar{\nu}$N interactions, semiinclusive π production, charge ratio, Gargamelle freon data anal., weak neutral current 78−12905
$\nu N \rightarrow \nu N\pi\pi$, neutral-current cross sections for double-pion production by neutrinos 79−17712
$\nu N \rightarrow \nu X$, $SU(2)_L \times U(1)$ gauge theory distinguished from $SU(2)_L \times SU(2)_R \times U(1)$, neutral currents, z-bosons 80−62908
$\nu N \rightarrow \nu'$+anything neutral current events, ν' decay modes, upper limits on mass 77−6109
$\nu n \rightarrow \nu n\pi^0$, neutral current induced one-pion production, Weinberg-Salam structure 80−52454
$\nu n \rightarrow \nu p\pi^-$, neutral current induced one-pion production, Weinberg-Salam structure 80−52454
$\nu N \rightarrow \nu\psi X$, neutral current ψ prod., Z^0-gluon fusion model 80−78015
νN single- and di-muon prod. colour changing current 78−45906
$\nu N \rightarrow X$, determ. of all neutral-current coupling constants from inclusive cross sections alone 79−13106
$\bar{\nu}_\mu N \rightarrow$multiple lepton+hadron final states, flavour changing neutral currents 77−30363
$\nu_\mu N \rightarrow \mu^- e^+$, obs. in BEBC 78−78170
$\bar{\nu}$p, 1.1 GeV, charged and neutral current events, strangeness changing currents, charm prod. 80−57583
νp, elastic scatt., weak neutral currents, space-time struct. *(Chinese)* 79−17715
νp, neutral to charged current ratios 79−54333
νP, neutral to charged current cross section ratio, coupling constant 80−27497
νp, $\bar{\nu}$p elastic scatt., tests of flavour-changing neutral currents 78−8653
νp elastic scatt., hadronic neutral current couplings, model independent determ. 79−49448
νp elastic scatt., implications for weak interaction models 77−6108
νp elastic scatt., neutral current struct. anal. 77−61273
νp high energy interactions, vector meson diffr. prod., charged and neutral current 78−54625
νp inclusive interactions, ratio of neutral current to charged current cross sectins 77−79263
$\bar{\nu}$p neutral current, neutral-to-charged current cross-section ratio meas. 78−82197
$\nu p \rightarrow \nu$+vector meson + X, neutral currents, generalised VDM, Regge pole anal. 78−41532
$\nu p \rightarrow \nu n\pi^+$, neutral current induced one-pion production, Weinberg-Salam structure 80−52454
$\nu p \rightarrow \nu p$ elastic neutral current interaction obs. 78−25037
$\nu(\bar{\nu}p)$ elastic scatt., space-time struct. of weak neutral current anal. 77−30365
$\nu p \rightarrow \nu p\pi^0$, neutral current induced one-pion production, Weinberg-Salam structure 80−52454
νp pion prod. by weak neutral currents, PCAC calcs. in various charge modes 77−26508
$\nu p/\nu n$, ratio of neutral current and inelastic cross sections 79−13100
$\bar{p}p$, pp, $SU_L(2) \times U(1)$ and $SU_L(2) \times SU_R(2) \times U(1)$ predictions at high Q^2, neutral currents, Z-bosons 80−63029
$\bar{p}p \rightarrow e^+e^-$ annihilation, weak neutral current effects *(Russian)* 80−105837
$pp \rightarrow \mu^+\mu^- X$, neutral current effects, $SU_L(2) \times SU_R(2) \times U_{L+R}(1)$ theory 78−17060
π inclusive prod., sum rules, π bremsstrahlung 78−45811
π prod. by weak neutral current, comparison of gauge theory models 78−82139
π^0, neutral weak current effect on decay mode Weinberg-Salam model, P-violation contrib. 78−86450
$\pi^0 \rightarrow e^+e^-$, neutral-current anal. 78−8658
π^0 production by ν and $\bar{\nu}$ neutral currents, comparison 79−49509
π^-+emulsion, 200 GeV/c, charm particle decay due to neutral currents *(Russian)* 79−22146
$\psi(3.1) \rightarrow \nu\bar{\nu}$, neutral current decays, possibility of expt. obs. 77−18276
t-quark mass, generalised Cabibbo angle, predictions 79−49447
t-quark mass from discrete symmetries 79−63462
τ-neutrinos, in beam dump expts. 78−50004
u-d quark coupling determ. using ν+n and ν+p deep inelastic cross sections 79−89122
W^0 effects in e^+e^- interactions on a^- resonances 80−42386
Z-mass prediction as test of standard model 80−47239
Bi, neutral current-induced parity nonconserving optical rot., Dirac-HF calcs. 80−47948
Bi, optical transitions, struct. of weak neutral currents *(Russian)* 77−88420
Bi, parity non-conserving optical rot., Weinberg-Salam relativistic central field theory vs. obs. 78−953
Bi, parity nonconserving optical rot. upper limit, obs. vs. Weinberg-Salam theory 78−952
Bi, vapour, optical activity and HFS, neutral weak currents *(Russian)* 79−13660
Bi, vapour, optical rot., parity nonconservation expts. 80−23354
Bi weak charge, SU(2)×U(1) model anal. 79−26281
^{209}Bi, transitions, parity nonconservation due to neutral weak currents 77−13913
$^{12}C+\nu$, neutral current processes in nuclei, elementary particle approach 79−93606
^{12}C(e,e′), 12.71 MeV 0^+ to 1^+ transition, axial isoscalar neutral current, polarisation asymmetry 79−26425
Cs cell, laser beam excitation, multipass, optical pumping and weak neutral current parity violation 80−58207
Cs, optical transitions, struct. of weak neutral currents *(Russian)* 77−88420
$D^0 \rightleftharpoons \bar{D}^0$, weak neutral current diagonality, mixing amplitude, multi-quark gauge model *(Russian)* 80−68414
$\eta \rightarrow \pi^0 e^+ e^-$, presence of second class neutral currents 79−26284
^{18}F, 1.08 MeV γ transition, circular polarisation affected by neutral weak currents 78−41663
H, two-photon transitions, parity nonconservation effects *(Russian)* 78−21892
^{2}H disintegration due to weak neutral currents 79−22273
^{2}H($\bar{\nu}_e$,$\bar{\nu}_e$n)p, neutral current cross section for reactor $\bar{\nu}$ 80−5129

neutral currents continued
^{3}He-B, superfluid, macroscopic parity nonconservation due to neutral currents 77−80671
^{A}Li+ν, (A=6,7), neutral current processes in nuclei, elementary particle approach 79−93606
^{14}N(ν,ν), neutral current struct. 78−66269
Na, muonic, $2s^1/_2$ level decay channel concurrence, neutral current effects observation *(Russian)* 80−83526
Pb, optical transitions, struct. of weak neutral currents *(Russian)* 77−88420
^{42}Sc, weak neutral current props., search for 0^- isomer using ^{42}Ca(p,n) 79−45126
Tl, $6^2P_{1/2}$-$7^2P_{1/2}$ M1 transition, parity violation detection in neutral weak interaction 77−30819
Tl, optical transitions, struct. of weak neutral currents *(Russian)* 77−88420
TlF, P- and T-violating interactions in hyperfine struct., mol. beam reson. expt. 80−53019
^{205}Tl, transitions, parity nonconservation due to neutral weak currents 77−13913
^{46}V, weak neutral current props., search for 0^- isomer using ^{46}Ti(p,n) 79−45126

neutrino detection and measurement
Brookhaven solar neutrino experiment, results and solar model calcs., new solar ν-detectors 79−80286
coherent low energy neutrino detector, design reanal. with neutrino interaction model 80−58096
conference on long distance neutrino detection, Washington, DC, USA (April 1978) 79−80217
Converse hodoscope combined with steamer chamber 80−63455
deep water muon and neutrino detectors *(Russian)* 78−55109
DUMAND array, study of ultrahigh energy neutrino interactions 79−80108
DUMAND detector, neutrinos in the depth of the sea *(French)* 79−75104
DUMAND project, optical acoustic detection, programme status 79−80109
early experiments 79−80408
emulsions, long exposures to high energy neutrinos in severe muon background 79−54744
flash chambers for neutrino detection, construction and performance 80−58026
Gargamelle bubble chamber, neutrino physics, book contrib. 79−30728
hadronic showers, cosmic neutrino induced, acoustic detection 79−76265
high energy neutrino interactions, detection apparatus 79−30730
high energy neutrinos of extraterrestrial origin, possible detection with DUMAND 79−80179
high-energy neutrino astronomy, as probe of galactic nuclei 80−4432
historical review, detection, meas., and interactions with nuclei and nucleons 79−49002
Homestake long-range neutrino detector research program 79−80107
IHEP neutrino beam energy spectra reconstruction *(Russian)* 79−68119
monitoring systems, at the Protvino Institute of High-energy physics 79−9929
neutrino fluctuations, possibility of obs. at nuclear reactor 79−67542
neutrino oscillations, possible and active expts. 79−75759
neutrino programme at ILL 79−67540
proportional drift tube for large calorimeter ν detector 79−13592
proton beam for neutrino experiments, focusing, pulsed power supply 79−9974
proton beam of neutrino experiments facility, particle loss and radiation environment 79−9930
reactor neutrinos, possible practicable use in reactor monitoring 79−67897
solar neutrino detectors, absorpt. cross section rel. to neutrino problem 80−17566
solar neutrino experiments, appl. to cosmological hypothesis testing 79−16918
solar neutrino experiments 79−8902
solar neutrino radiochemical detectors, internal contamination backgrounds 79−16827
solar neutrinos measurement, cosmic ray neutrinos ^{37}Ar prod. rate estimate 79−16837
telecommunication by high energy neutrino beams 79−76266
two-dimensional buffer store based on a multichannel amplitude analyzer 79−26838
undersea detection system, located in deep ocean 80−98522
water Cherenkov neutrino detector, construction and performance 80−91397
ν_τ, beam-dump experiment, observation of ν_τ interactions 80−22601
pN 70 GeV collisions, search for prompt neutrinos 79−13160
^{71}Ga(ν,e$^-$)^{71}Ge, proposed new expt. for solar neutrinos detect. 78−58563
In loaded liq. scintillator for solar neutrino spectroscopy at low energies 78−73639

neutrino-electron interactions
see also neutrino-electron scattering
bremsstrahlung, neutral current effects in Weinberg model. 77−65150
coherent inelastic scatt. by atomic electrons with photon emission *(Russian)* 79−3015
cosmological fluid, lepton era, transport coeffs., Weinberg-Salam model 78−32623
cross section calcs., lepton scatt., book contrib. 78−78161
neutral current processes, factorisation and coupling constant determ. for νe, ed, and ν+hadron 80−27451
scattering angle, Weinberg model *(Russian)* 77−6112
Weinberg-Salam model, transition amplitudes and probabilities for $\nu\nu$, $\bar{\nu}\nu$, $\bar{\nu}\bar{\nu}$, νe, $\nu\bar{e}$, $\bar{\nu}$e, and $\bar{\nu}\bar{e}$ scatt. 78−21415
$e\bar{e}\nu_e\bar{\nu}_e$, reactive mixture, bulk viscosity 78−45565
eν interaction, local conservation law from neutrino massless, gauge invariance 80−42355
$e\bar{\nu}_e\nu_\mu$ (or $\bar{e}\nu_e\bar{\nu}_\mu$) system reson. as muon 77−6189
$\bar{\nu}_e$+e inelast. scatt. total and differential cross sections in Weinberg-Salam theory *(Bulgarian)* 79−85254
$\nu e \rightarrow W^\pm Z^0(\gamma)X$, high energy behaviour and hard photon prod., cosmic rays 80−5028
$\bar{\nu}_e$e annihilation in Weinberg-Salam model, number of quarks and leptons *(Russian)* 80−102041
$\bar{\nu}_e e^- \rightarrow W^-$, intermediate boson prod. by prompt high energy atm. neutrinos 79−3014

neutrino-electron interactions continued
$\bar{\nu}_e e \rightarrow W^- \rightarrow$hadrons, 30 to 100 GeV W-boson underwater detection from cosmic ν *(Russian)* 77−38159
$\nu_\mu e \rightarrow \mu \nu_e$, inverse muon decay rate 80−82965
$\nu_\mu e \rightarrow \mu \nu_e$, exptl. study 79−67536
$\bar{\nu}_\mu e \rightarrow \nu_e \mu^-$, exotic lepton number violation and neutrino Majorana masses, Higgs sector 80−86615
$\nu_e e \rightarrow \nu_e e^-$, SU(2)×U(1) anal. 78−50026
$\bar{\nu}_e e \rightarrow W^- \rightarrow X$, obs. in direct lepton prod. from cosmic ray protons *(Russian)* 80−12627

neutrino-electron scattering
see also neutrino-electron interactions
$\nu^- e^- \rightarrow \nu^- e^-$, reactor data anal., revised antineutrino spectrum 78−21417
dense stellar matter, diffusion approx. to neutrino transport 78−93096
extreme relativistic electron gas, scattered neutrino energy distrib. 78−45215
lectures given at CERN School of Physics (6-19 June 1976) 77−61173
neutral current model examination by diagonal lepton processes anal. 79−6310
neutral current reactions, (V-A) model, mixing between ordinary and heavy leptons 78−41472
neutral weak current, structure *(Russian)* 79−49446
purely leptonic elastic scatt. events, Fermilab data 78−89700
reactor neutrino expts., fission fragment ν radiation, neutral currents, inverse β-decay, $\bar{\nu}$ scatt. *(Russian)* 80−42736
renormalisable theory of pure leptonic weak interaction with induced shadow states 78−37136
spin correls., allowance for (S,T,P) interactions of neutral and charged currents 78−12901
stellar core collapse, neutrino trapping 78−32437
stellar interiors, conservative scatt. and electron scatt. rel. to neutrino thermalisation 79−92659
stellar interiors, neutrino scatt. rel. to transport and equilibration 78−89050
stellar matter, neutrino opacity, pure neutral vector boson contrib. 78−53928
SU(2)⊗U(1) gauge models, neutral current couplings 79−40715
supernovae, neutrino transport in collapsing stellar core model 78−8029
supernovae core collapse, neutrino energy equilibration models 80−105265
weak and EM radiative corrections to low-energy processes 80−95274
weak charge of electron, $SU_2 \times U_1$ theories, $\bar{\nu}_\mu e$ scatt., isospin 78−16974
weak interactions involving neutral currents, expt., theory, gauge models 77−49901
weak lepton streams, structure analysis, Weinberg-Salam model *(Russian)* 78−25039
weak neutral currents, space-time struct. *(Chinese)* 79−17715
Weinberg-Salam model, transition amplitudes and probabilities for $\nu\nu$, $\bar{\nu}\nu$, $\bar{\nu}\bar{\nu}$, νe, $\nu\bar{e}$, $\bar{\nu}e$, and $\bar{\nu}\bar{e}$ scatt. 78−21415
$e\nu_\mu$ scatt., theory of pure leptonic weak interaction with induced shadow states 77−49945
($\bar{\nu}_e$, e), 1.5 to 4.5 MeV, axion search 78−45904
$\nu(\bar{\nu})e$, hypothesis test, purely diagonal single Z boson neutral currents 79−40713
$\nu(\bar{\nu})e$, weak neutral electron current, Lorentz struct. 79−80788
$\nu_e(\bar{\nu}_e)e$, charged and neutral current interference, test of Weinberg-Salam model 80−42385
ν_e-e scattering, charged- and neutral-current interference 79−89144
ν_μ, transition magnetic moment 78−78168
$\nu_\mu(\bar{\nu}_\mu)e$, cross sections and data anal., V or A theory test 78−70355
νe elastic scattering, differential cross section, behaviour in nondiffraction region 79−58952
$\nu e(\bar{\nu}e)$ forward elastic scatt. amplitudes, new sum rules 79−54332
$\nu e \rightarrow \nu e \gamma$, radiational scatt., polarisation effects *(Russian)* 77−46038
$\bar{\nu}e$ scatt., single Z boson hypothesis tests, non-diagonal neutral current inclusion 79−40714
$\nu e^- \rightarrow \nu e^- \gamma$, energy spectra of recoil fermions, Weinberg-Salem model 78−12895
$\nu e^- \rightarrow \nu e^- \gamma$, weak current anomalous interaction with EM field *(Russian)* 77−6104
$\bar{\nu}_e e$, evidence against axions 79−13108
$\bar{\nu}_e e^-$ scatt., fission $\bar{\nu}$ induced reaction cross sections 79−22273
$\nu_\mu e$, scatt. meas., interaction gauge models *(German)* 80−37251
$\nu_\mu e$ (and $\bar{\nu}_\mu e$) scatt., log. order α electromag. corrections 79−63467
$\nu_\mu e \rightarrow \nu_\mu e$, cross section meas. 80−73692
$\bar{\nu}_\mu e \rightarrow \bar{\nu}_\mu e$, high energy cross section upper limit, purely leptonic neutron current process search 79−36062
$\nu_\mu e \rightarrow \nu_\mu e$, high energy elastic scatt. at Garganelle, neutral current reaction 79−93398
$\nu_\mu e \rightarrow \nu_\mu e$, upper limit to cross-section determ. 78−33054
$\nu_\mu e \rightarrow \nu_\mu e$, weak vector-like models, induced axial vector coupling 78−50025
$\bar{\nu}_\mu e \rightarrow \bar{\nu}_\mu e$ SPS energies, upper limit to cross section and mixing parameter 79−71740
$\bar{\nu}_\mu e \rightarrow \bar{\nu}_\mu e$ weak neutral leptonic current reaction, high energy search 79−71741
$\nu_\mu e^- \rightarrow \nu_\mu e^-$, cross section meas. 80−47273
$\nu_\mu e^- \rightarrow \nu_\mu e^-$, high energy, cross section meas. 78−78167
$\bar{\nu}_\mu e^- \rightarrow \nu_\mu e^-$ leptonic neutral current reaction, evidence 77−2814
$\nu_\mu e^- \rightarrow \nu_\mu e^-$, mixing angles of leptons in an extended Weinberg-Salam model 79−71679
$\nu_l \mathcal{L} \rightarrow \mathcal{L} \nu_l$ processes, possible T-violation, phenomenological model of neutral currents 77−30359
W-boson exchange, differential cross section calc. in gauge theories 77−82728

neutrino interactions
see also neutrino-electron interactions; neutrino-neutrino interactions; neutrino-nucleon interactions; neutrino scattering
β-active nuclei, neutrino exchange and long range interactions 80−73826
astrophysics and cosmology, weak interactions 77−25934
asymptotic freedom and parton model appl. to leptonic processes 80−4959
asymptotic freedom predictions for neutral and charged current neutrino interactions 78−8581
b-flavour prod. by neutrinos six quark model anal. 79−75720
bibliography of expts. to 1976 77−22730
bremsstrahlung, neutral current effects in Weinberg model 77−65150
bremsstrahlung in intense mag. field 79−30055
Brookhaven solar neutrino experiment, results and solar model calcs., new solar ν-detectors 79−80286
CERN School of Physics, Austerlitz-Zeist, Holland (June 1978) 79−30857
charged current ν and $\bar{\nu}$ interactions, hadron prod. at high energy, quark parton model 79−36058
charged current ν and $\bar{\nu}$ interactions below 30 GeV/c 78−62389
charged current induced weak one pion prod., form factors from PCAC 80−18129
charged current interactions at 3, 9 GeV, total cross section 79−71739
charm fragmentation, leading particle effects 78−8650
charm model of weak interactions, parton model anal. of hadron leptoproduction 77−6106
charm particle prod. and subsequent decay into like-sign dimuons and trimuons 79−63469
charm particle prod. by neutrino beams and charm particle lifetime 79−63465
charmed baryon prod. and Λ_c^+ decay 79−75770
charmed baryon prod. by neutrinos, quark-model calc. 78−45909
charmed baryons, ground state, production by neutrino interactions 79−93400
charmed D meson production by neutrinos and $D^0 \rightarrow K_S^0 \pi^+ \pi^-$ 78−70354
coherent low energy neutrino detector, design reanal. with neutrino interaction model 80−58096
coloured quark model 77−71482
Comptonisation in high-temp. nuclear matter, neutral current theory 80−21905
conference on hadron struct. and lepton-hadron interactions, Cargese, France (July 1977) 80−4473
conference on long distance neutrino detection, Washington, DC, USA (April 1978) 79−80217
conference on particle physics, Honolulu, Hawaii (Aug. 1977) 79−49485
deep inelastic inclusive neutrino interactions, 2-30 GeV, in SKAT bubble chamber 79−36060
deep inelastic scatt., energy flow, test of perturbative QCD 79−67534
deep inelastic scatt., incusive observables and hard gluon emission 80−99094
deep inelastic scatt., QCD jets, kinematics, thrust and spherocity distrib. 79−75762
deep-inelastic scatt., asymptotic freedom effects 77−79262
diffractive meson prod. 78−21416
dilepton and trilepton production in neutrino experiments *(Polish)* 78−89704
dilepton charge production cross section for ν and $\bar{\nu}$, parton model 80−62966
dilepton events, neutral heavy lepton, rising $\sigma(\bar{\nu})/\sigma(\nu)$ 77−57523
dilepton production in $\nu(\bar{\nu})$ reactions, bottom quark excitation contrib. 80−42439
dimuon events, heavy lepton decay into massive ν with various spin 78−21412
dimuon events with identical sign, signal of creation of heavy leptons in neutrino expts. *(Russian)* 77−82729
dimuon production, high y-anomaly, extended minimal Weinberg model 77−26510
DUMAND array, study of ultrahigh energy neutrino interactions 79−80108
DUMAND project, optical acoustic detection, programme status 79−80109
E7 gauge model, multilepton prod. by ν, heavy leptons 77−74588
early universe, photon-and neutrino diffusion rel. to nonlinear primordial fluctuations 79−25773
Einstein-Dirac eqns., ν radiation in general relativity *(Russian)* 78−49727
errors on ratios of small numbers of events 80−105879
exclusive ν production processes, neutral current props., Lorentz struct., internal symm. 77−18267
exclusive one-pion prod., ν-induced neutral current channels 78−54624
exotic quarks and high gauge groups 77−74583
experimental results, quark parton model anal. 79−30730
experimental results for charged and neutral current interactions and multilepton prod. 79−49512
factorization breaking in deep inelastic neutrino hadron production in perturbative QCD 79−80820
fermion nonminimal gravitational coupling and the solar-neutrino problem 79−75761
five-quark model with right handed current, weak interactions description 77−57485
four-element lepton models, non-diagonal neutral currents *(Chinese)* 78−78132
four-muon prod. by neutrinos 78−29330
fragmentation functions of heavy quarks into hadrons, ν reactions, e^+e^- annihilation appls. 79−3013
fundamental physics with reactor neutrons and neutrinos [conf. ILL, Grenoble, France (Oct. 1977)] 79−59112
Gargamelle, neutrino physics history, theory and expt. 78−50027
Gargamelle bubble chamber, neutrino physics, book contrib. 79−30728
gauge theory and neutrino physics, book 79−30726
hadron final states in deep inelastic processes, parton model 77−34128
hadronic neutral current in neutrino interactions and single Z·boson hypothesis 79−54295
hadronic quantum numbers beyond charm as possible source of neutrino induced trimuons 78−12903
heavy lepton cascade decay 78−25038
heavy lepton prod. and cascade decay 78−33059
heavy lepton search, Pontecorvo oscills., neutrino expts. *(Russian)* 77−87973
heavy leptons, weak gauge boson and neutrino trimuon prod. 78−4851
heavy-lepton interpretation of multimuon events 78−33058
helicity calculation for heavy lepton prod. in ν interactions and cascade decay 78−93870
Higgs boson, charged and trimuon events in neutrino reaction 78−21413
high energy ν experimental physics at Fermilab review 78−50028
high energy neutrino experiments, state of art 79−26322
high energy neutrino physics, recent expt. results 80−4982
high energy neutrino physics, recent results, influence of quark concept on understanding 79−93402
high energy neutrino-hadron collisions, dilepton mass spectrum, V-A and Weinberg interaction calcs. 79−3010
high-energy, obs. of charmed particle decay in nuclear emulsion 77−13953

neutrino interactions continued
high-energy (>10 GeV) neutrino physics, review of development, book contrib. 78−82201
historical introduction, weak interactions, book 78−78133
historical review, detection, meas., and interactions with nuclei and nucleons 79−49002
hot neutron star matter, neutrino transport, opacity 79−75238
inclusive ν+hadron interactions, single-lepton and dilepton prod., test of T invariance 77−34146
inclusive ν deep inelastic scatt. in SKAT bubble chamber, 2-30 GeV 78−62390
Kerr black hole, neutrino wave reflection and transmission 77−9765
leptonic diagonal coupling const. from neutrino data *(Russian)* 77−49950
low and high energy expts. 80−91083
low energies, theoretical aspects 79−67538
low-mass lepton pairs from hadron and neutrino beams, meson annihilation model 79−93401
magnetic field interactions, synchrotron neutrino emission, charge collision emission, star neutrino luminosity 80−41719
mass and mixing in unified model 77−67609
massive neutrinos, radiative decay rel. to cosmic element abundances 79−92668
massive unstable neutrinos, cosmological implications cosmological implications of masses 78−45437
massive unstable neutrinos, cosmological implications of decay modes 78−45437
multilepton production in neutrino expts. 80−91081
muon production in Fermilab 15 ft bubble chamber, external identifier, proportional chambers 77−6629
narrow band beam expts. at SPS 80−91082
nature and production of neutrinos from particle accelerators *(French)* 79−26326
neutral charmed particle decay, direct observation in ν-emulsion interactions 80−9165
neutral current data, elastic and deep inelastic, gauge model constraints 79−40718
neutral current interactions in $SU(2)_L \times SU(2)_R \times U(1)$ gauge models, natural parity conservation, gauge bosons 79−321
neutral current interactions parity violation 77−13910
neutral current processes and $SU(2) \times U(1)$ gauge models 77−74632
neutral current results at CERN, review 77−34145
neutral currents, developments in phenomenology 77−6105
neutral currents, effect of quark-antiquark sea *(Russian)* 77−6078
neutral currents, expt. verification of theoretical predictions, review 79−89097
neutral currents, quark-lepton models 77−18272
neutral currents and six-quark model 77−18216
neutral heavy lepton signatures in ν induced dilepton events, $SU(2) \times U(1)$ model 78−70353
neutral-current coupling, high-energy ν interactions 78−66104
neutrino experiments at high energies, total cross sections by currents, review 79−49511
neutrino oscillation hypothesis and time depend. of Brookhaven solar-ν counting rate 79−80288
neutrino oscillations, effects of matter 79−75760
neutrino oscillations, possible and active expts. 79−75759
neutrino oscillations in ν_e, ν_μ, ν_τ system 80−82964
neutrino reactions, theoretical anal., review 78−82202
neutron stars, neutrino retention rel. to mass and radius 79−62817
new particle search, Brookhaven AGS 79−63468
nuclear semi-leptonic weak interactions 78−555
orthomuon mass lower limit from neutrino data anal. 78−62388
oscillations of neutrinos in matter 78−70358
parton anomalous statistics, deep inelastic ν scatt. *(Russian)* 78−29331
photoneutrino reactions in superstrong magnetoactive plasma, neutron stars appl. 79−35105
physics of neutrino beams 80−91077
probe to investigate weak and strong interactions 77−79261
proceedings of the 1977 CERN-JINR School of Physics, Nafplion, Greece (May-June 1977) 78−81726
prod. and decay of short-living heavy neutral particle 77−87971
QCD anal. of p_T^2 behaviour observed in semi-inclusive neutrino data 79−36015
QCD structure function relation between deep inelastic ν reactions and polarised electroprod. 80−37221
quark charged current tests in neutrino expts. 77−22726
quark distributions and quark jets from the CERN bubble chamber neutrino experiments 79−45085
quark model, renormalisation effects on $\sigma\bar{\nu}/\sigma\nu$ and $\langle y \rangle \bar{\nu}$ 77−18230
quark-parton model, deep inelastic scatt. 77−79270
radiative corrections to high energy inclusive ν scattering, leading log approx. 79−80818
reaction rates and moments, from transform. to centre of mass system 78−45215
reactor neutrino expts., fission fragment ν radiation, neutral currents, inverse β-decay, $\bar{\nu}$ scatt. *(Russian)* 80−42736
reactor neutrinos, appls. in neutrino physics 79−67539
review of 79−80823
right handed neutrino interactions in gauge theories 79−35941
scale breaking parton model for electron and neutrino deep inelastic scatt. 78−66122
scaling violation, two-component duality model, ν and μ interactions 78−8623
scaling violations and $\nu,\bar{\nu}$ cross-sections 77−87970
scaling violations and neutral currents 78−41529
semi-leptonic neutrino interactions at the CERN proton synchrotron and related topics 80−91078
semileptonic decay distribs. of next heavy quark 79−45066
short lifetime charm particles from ν interactions detection in nuclear emulsion 79−22539
short lived particles search in high energy neutrino interactions 79−49510
single pion production in antineutrino induced charged current interactions 79−36063
solar neutrino problem, fermion nonminimal gravit. coupling 78−29294
stable heavy neutrinos, dynamical interactions and astrophys. effects 79−5743
stellar dense cores, time-dependent neutrino transport 80−94783
strange particle production by neutral currents, Gargamelle $\nu,\bar{\nu}$ reactions 78−37201
strange particle production by neutral currents in Gargamelle ν and $\bar{\nu}$ expts. 78−37200
strangeness conservation in neutral currents, constraints on vector-like model 78−21374
$SU(2)_I \times U(1)$ theory, radiative corrections, simple renormalisation framework 80−101973
$SU(2)+U(1)$ gauge models, constraints from neutrino interaction data 77−30251
$SU(2) \times U(1)$ gauge model predictions for neutral current reactions 77−71424
subnuclear physics, review 77−67623
super trimuons production, possible evidence of six-fermion interactions 79−71743
tagging direct neutrinos. A first step to neutrino tagging 79−67532
telecommunication by high energy neutrino beams 79−76266
total cross section meas. using bubble chambers 80−91080
total cross sections for ν_e and $\bar{\nu}_e$ bubble chamber interactions, neutrino oscills. and decay 78−41526
trimuon events, heavy lepton prod. in ν interactions 78−41530
trimuon events, spin-parity selection rules 80−22603
trimuon events obs., $\nu(\bar{\nu})$ interactions 78−12902
trimuon prod., EM muon-pair contrib., scaling parton model 78−66106
trimuon prod. from neutrino interactions 78−66105
trimuon prod. in ν and $\bar{\nu}$ interactions, EM μ-pair contrib. 78−66107
trimuon prod. mechanism, $\nu(\bar{\nu})$ interactions 78−82199
trimuon prod. via heavy lepton, $SU(3) \otimes U(1)$ gauge model 77−74671
trimuon production by neutrinos 77−30362
trimuon production in higher energy ν interactions, rates and properties, $c\bar{c}$ prod. 79−49508
unified model for atomic parity violation and neutral currents in gauge theories 80−4912
V V+AA gauge model 78−29246
V V+AA type gauge models, effective ν interactions 78−66038
weak and EM interactions at high energy [conf. Les Houches, France (July 1976)] 79−80785
weak charmed-baryon resonance prod., neutrino inclusive interactions, scaling behaviour 78−8645
weak interaction model, neutrino-induced multilepton events 78−41533
weak interaction model with 8 quarks and 8 leptons, neutrino experiment heavy leptons *(Russian)* 79−67494
weak interaction physics, present status and future prospects, review 79−67492
weak interaction props. and hadron struct. investigation, book contrib. 79−30727
weak interactions, conf., Bloomington, USA, (May, 1977) 78−414
weak interactions, summer school, Varenna, Italy (Jul. 1977) 80−90597
weak neutral couplings to hadrons in neutrino inclusive, semi-inclusive and elastic reactions 79−36064
weak neutral current, space-time struct., generalised version of confusion theorem 79−75714
weak neutral current couplings calc. of u and d quarks, ν interaction input data 78−54603
weak neutral current struct., ν and $\bar{\nu}$ interactions hadronic energy distrib., Weinberg-Salam model 79−35993
weak neutral currents, light-cone algebra anal. 79−6311
weak production of charmed baryons by neutrinos, relativistic quark model 78−41496
weak selection rules, inclusive prod. of charmed particles and heavy leptons 78−8679
weak-interaction-induced ν oscills., gauge models 78−70359
white dwarfs, neutrino retention rel. to mass and radius 79−62817
Z-boson and two-boson models, neutral current phenomena, μ-e universality 80−18109
b quark prod., left-handed currents and lepton number nonconservation 77−67616
D^0 lifetime from ν and $\bar{\nu}$ interactions 80−105890
$e^+e^- \rightarrow \gamma V \rightarrow \gamma\nu\bar{\nu}$, neutral vector meson radiative prod. and decay *(Russian)* 80−52492
$e\nu_e$ and $e\bar{e}\nu_e\bar{\nu}_e$ mixture, relativistic quantum kinetic theory 79−63140
$\gamma\nu$ weak interaction, spontaneous breakdown of γ and gauge symm. at finite temp. 78−70299
μe prod., heavy lepton decay anal. 78−33057
$\mu^-\mu^+$ symmetric prod. from ν interactions 77−87969
$\mu^+\mu^-$ prod. from ν and $\bar{\nu}$ interactions, charm prod. and decay 77−74675
$\mu^-\mu\ \mu^+$ events in ν_μ reactions, SU(3) gauge models 77−74674
$\mu\ \mu\ \mu^+$ prod. in neutrino interactions, gauge theory, heavy leptons 77−65085
$\nu, \bar{\nu}$, inclusive neutral current interactions 78−25036
$\nu, \bar{\nu}$ charged current induced one pion weak prod., $I=1/2$ resonant contrib. 80−47274
ν and $\bar{\nu}$ 'new physics' data, vectorlike quark-parton model anal. 79−9359
ν and $\bar{\nu}$ charged current interactions total cross sections for 3 to 30 GeV *(Russian)* 78−89705
ν and $\bar{\nu}$ charged-current reactions, Bjorken scaling violations 78−74246
$\bar{\nu}$ anomalies and right-handed currents 78−8654
$\bar{\nu}$ induced dimuon events, V^0 yield, possible beautiful baryon prod. 80−105882
$\bar{\nu}$ interactions, anomalous lepton prod., b-quarks 78−8613
$\bar{\nu}$ interactions, Λ, Σ^0, K^0 prod. 78−8647
$\nu(\bar{\nu})$ charged current induced one π prod., model total cross sections 80−4979
$\nu(\bar{\nu})$ deep inelastic scattering, scaling violations of struct. function moments and perturbative QCD 79−40736
$\nu(\bar{\nu})$ high-energy interactions, dimuon distrib. anal., quark-parton model 78−33056
$\nu(\bar{\nu})$-induced prod. of vector mesons and Higgs boson, muon prod. 78−82198
$\nu(\bar{\nu})$N, meas. of high-energy neutral current interactions 78−66073
$\nu(\bar{\nu})$N, signals for ν_τ interactions in beam dump expt. 79−67535
$\nu(\bar{\nu})$N neutral current interaction, charm prod. in quark parton model 77−61246
$\nu(\bar{\nu})+Fe \rightarrow \mu\ +\mu^-(\mu^+ + \mu^+)+X$, 200 GeV, momentum and ang. distribs. meas. 78−8648
$\bar{\nu}$ trimuon prod., EM and hadronic contrib., $\mu^+\mu^+\mu^-$ rate and distribs. 79−85291
$\bar{\nu}$ trimuon prod., $\mu^+\mu^+\mu^-$ rate, correl. with $\mu^-\mu^-\mu^+$ ν-prod. events 79−85292
ν-N scatt., relativistic quark oscill. model, N* weak prod. *(Russian)* 77−220

neutrino interactions continued
ν_e-ν_μ universality corrections for neutral current interactions in Weinberg-Salam model 79−54292
ν_μ, $\bar{\nu}_\mu$ interactions, pion^0 prod., P violation 77−65151
$\nu_\mu(\bar{\nu}_\mu)h \rightarrow \mu^- l^+ + X$, charm contrib. to prod. of opposite sign dimuons 79−377
ν_τ, charged current interactions, scaling variable distributions 79−378
$\bar{\nu}_e + D \rightarrow \bar{\nu}_e + n + p$, axion search 78−45904
$\bar{\nu} + N$ inelastic scatt., neutral current evidence for parity nonconservation 77−2815
$\nu_\mu \rightleftarrows \nu_e(\bar{\nu}_\mu)(\nu_\tau)$, neutrino oscillation expts. at accelerators 79−67541
$\nu d \rightarrow \mu^- pp_s$, 0.5-6 GeV, total and differential cross-section determ. 78−33055
$\bar{\nu}_e d \rightarrow nne^+$, cross sections, neutrino programme at ILL 79−67540
$\bar{\nu}_e d \rightarrow np\bar{\nu}_e$, cross-section calcs. 80−42440
$\nu\mu \rightarrow \gamma + X$, mass and lifetime exptl. limits 77−50039
$\bar{\nu}_e p \rightarrow ne^+$, cross sections, neutrino programme at ILL 79−67540
$\nu\pi^+$, semi-inclusive deep inelastic scatt., π struct. functions 79−26323
τ lepton, search in neutrino expts., neutrino mixing *(Russian)* 78−54604
Υ (9.5), implications of Υ for ν interactions in weak gauge theories 78−70271
C, thermonuclear combustion neutrino mechanism, form. of neutrino stars and supernova outbursts *(Russian)* 77−87379
Fe-O stars collapse, effects of neutrino radiation and absorpt. 77−87369

neutrino-neutrino interactions
see also neutrino-neutrino scattering
cosmological fluid, lepton era, transport coeffs., Weinberg-Salam model 78−32623
Weinberg-Salam model, transition amplitudes and probabilities for $\nu\nu$, $\bar{\nu}\nu$, $\bar{\nu}\bar{\nu}$, νe, $\nu\bar{e}$, $\bar{\nu}e$, and $\bar{\nu}\bar{e}$ scatt. 78−21415
$\bar{\nu}$ and ν interaction, anomalies and possible dimuon events 77−239
$\bar{\nu}\bar{\nu}$, y-distrib. energy and x-depend., quark right handed coupling 79−26325
$\nu\nu$ effective coupling constant upper limit from high energy beam data *(Russian)* 78−89706
$\nu\bar{\nu}$ system, transport coeffs. 78−93871

neutrino-neutrino scattering
see also neutrino-neutrino interactions
Weinberg-Salam model, transition amplitudes and probabilities for $\nu\nu$, $\bar{\nu}\nu$, $\bar{\nu}\bar{\nu}$, νe, $\nu\bar{e}$, $\bar{\nu}e$, and $\bar{\nu}\bar{e}$ scatt. 78−21415

neutrino-nucleon interactions
see also neutrino-nucleon scattering
$\Delta S=0$ weak hadron neutral current, quark parton model, νN and e^+e^- interactions 78−12859
$\mu^-\mu^{+}$ events, prod. evidence 78−82196
angular correlations of final state leptons and hadrons, quark-gluon dynamics 79−395
associated production, asymm. principles and positivity, Born term model 78−58179
Bjorken scaling law violation, mass dependent, quark-quark interactions 80−9160
Bjorken scaling violation models with new scaling rule 79−26305
charged and neutral current interactions, cross sections and scaling variable distribs. 80−57581
charged current, new phenomena colour-scheme interpretation 77−2817
charged current ν and $\bar{\nu}$ interaction cross sections, bubble chamber expt. 80−62965
charged current high energy νN reactions, μ^+ events, scaling-variable distribs. 77−74672
charged current inclusive interactions in Fe at 30-200 GeV, struct. functions, scaling phenomena 79−75764
charged current inclusive reactions below 6 GeV 77−26515
charged current normalised small-y cross-sections for $\nu,\bar{\nu}$ at 45-205 GeV 77−82733
charged current reacts., appl. of new scaling rule 78−89703
charged spin-1 gluons, integer charged quarks, e- and ν- prod. 77−49894
charged-current total cross-sections for $\nu,\bar{\nu}$ interactions at 20-200 GeV 77−87972
charm and strangeness production, role of gluons 79−13104
charm particle, production in high energy ν-induced reaction, lifetime determ. 79−26426
charm particle production, classification and quark-lepton analogy *(Norwegian)* 77−34137
charm particle production in weak interactions with diagonal neutral currents *(Russian)* 77−74676
cosmic neutrinos, detection and neutrino-nucleon interactions, 1-100 TeV 78−36413
cumulative proton production in neutrino and antineutrino interactions with freon, 2 to 30 GeV *(Russian)* 80−4980
currents and symmetries, theoretical speculations following recent expt. results *(German)* 77−41837
deep inelast. scatt., structure functions, Adler's sum rule and improved scaling variable 77−41843
deep inelastic, review of parton model 77−57498
deep inelastic ν and $\bar{\nu}$ data and four-flavour quark model 77−71505
deep inelastic scatt., quark-parton model with logarithmic scaling violation 80−78071
deep inelastic scatt. and rising $\sigma(\bar{\nu})/\sigma(\nu)$ ratio, neutron-proton structure function difference 77−49978
deep inelastic scattering, appl. of quark parton model 79−30715
dense stellar matter, diffusion approx. to neutrino transport 78−93096
di-lepton events in BEBC narrow band beam neutrino expt. 78−41528
dilepton event anal. 77−30364
dilepton events, extraction of heavy quark and heavy lepton signals 78−74243
dimuon prod. in $\nu(\bar{\nu})$N, possible fifth quark 77−61276
dimuon prod. mechanism, coloured quark model 77−22725
dimuon production at high energy, quark-parton model with charm 77−57520
dimuon production rate from $\nu(\nu)$ N reactions in steel at 45-205 GeV 78−8646
eight quark model, modified left-handed currents, ν reactions and e^+e^- annihilations 78−16982
electromagnetic radiative corrections to deep-inelastic neutrino interactions 80−22602
experimental background to discovery of neutral currents and charm *(French)* 77−38158
field theory phenomenology 79−54304
Glashow-Iliopoulos-Maiani model, charge symmetry violation 77−18194

neutrino-nucleon interactions continued
hadronic contributions to trimuon prod., quark+antiquark annihilation 78−41551
high energy charged current neutrino interactions, spherocity and thrust distribs., jets 79−85293
high energy neutrino and antineutrino beams, excitation of new particles 77−57521
high energy neutrino physics, book contrib. 79−30729
high-energy, deviations from quark-parton models 77−30361
inclusive and exclusive νN weak interactions involving neutral currents, expt., theory 77−49901
inclusive charged current interactions, recent results 79−49506
inclusive interactions, nondiagonal neutral currents, six quark model with slow rescaling 77−49949
inclusive strangeness changing neutral current interactions 78−8652
inelastic scattering, possible soln. with weak neutral currents to ρ-π puzzle 79−17714
jet analysis, QCD calcs. and phenomenological models 80−52523
lectures given at CERN School of Physics (6-19 June 1976) 77−61173
lepton-hadron relation, neutrino induced dimuon and trimuon events 78−25032
meson resonance prod. calc., diffr. VMD model 77−61277
multimuon prod., phenom. anal. in (V-A) scheme using quark parton model 79−17707
Nachtmann moments of $F_2^{\nu N}(x,Q^2)$ and energy momentum sum rule 80−57580
neutral current anomalies, differences between dynamical scaling violations and slow rescaling 77−49896
neutral current coupling and structure from Caltech.-Fermilab expt. 77−222
neutral current coupling from ν-induced inclusive and semi-inclusive pion reactions 77−74673
neutral current couplings in neutrino-hadron interactions 78−24993
neutral current reactions, (V-A) model, mixing between ordinary and heavy leptons 78−41472
neutral lepton current, νN elastic and deep-inelastic scatt., photon-neutrino weak-coupling theory 77−30358
neutral-current quark coupling determination using neutrino-neutron and neutrino-proton deep-inelastic cross sections 79−89122
$O(4)\times U(1)$ gauge model, restrictions from νN expt. data 77−71477
parity violating observables in heavy atoms, implications for $SU(2)\times U(1)$ unified gauge theories 77−46006
PCAC, possible testing in ν-N interactions *(Russian)* 77−61280
pion prod. by weak neutral currents, PCAC calcs. in various charge modes 77−26508
polarised deep inelastic sum rules 77−13952
QCD, ang. asymmetries in hadron distribs. 79−9360
QCD analysis of charged-current structure functions 79−49462
QCD estimates for associated charm production by weak neutral currents 78−78169
quark fragmentation function for new particle ν-production 77−87968
quark model anal. 78−4850
quark properties and existance studies, book contrib. 80−42441
quark-parton model description of neutrino data, particle prod. in $\bar{\nu}$N and νN interactions 77−18270
right hadronic currents in six-quark model, neutrino interaction calcs. *(Russian)* 77−82736
right handed colour octet currents for charm and colour excitation in $\nu(\bar{\nu})$ reactions 78−93874
scaling deviations in νN, eN, μN inelastic scatt., energy depend. 77−49948
scaling violation, quarks with size and excited states 78−74242
scaling violations in electromagnetic and neutrino charged-current interactions 79−17713
second class currents and anomalies in neutrino reactions 77−57522
short-lived heavy neutral particle prod., possible heavy lepton or charmed meson *(Russian)* 77−74677
strange particle production by $\nu(\bar{\nu})$ in quark model 79−13103
straton model, $\Delta(1236)$ prod. by high energy neutrinos *(Chinese)* 78−12900
straton model of $1/2^+$ baryon semileptonic decays and high energy neutrino-nucleon reactions *(Chinese)* 78−12873
structure functions, form factors, negative scaling violation 78−74241
structure functions of deep inelastic scatt., QCD test, high-twist contribs. 80−57579
$SU(2)\times U(1)$ models, hadronic neutral currents, low energy neutrino reactions, constraints 77−13912
$SU(2)\otimes U(1)$ gauge group theory tests from neutral current phenomena 78−24992
t quark, prod. in νN collisions, six quark model calcs. 79−93371
tetramuon prod. sources, heavy quark and lepton cascades, charm prod. 78−70356
total cross-sections, scaling violations, Wilson operator product expansion 77−87967
trimuon heavy lepton events in ν interactions, $SU(8)_L\times U(1)$ gauge model 77−79242
trimuon prod., possible new process in ν-N leptonic sector 77−49947
trimuon prod. from struct. at lepton vertex 78−8639
trimuon production by neutrinos, heavy lepton cascade mechanism using $SU(2)\times U(1)$ gauge model 78−58180
trimuon production by neutrinos and antineutrinos 78−37198
vectorlike model with six quarks, gauge theory, $SU(2)\times U(1)$, νN appl. 77−57480
vectorlike $SU(3)\times U(1)$ gauge model of weak interact. $\bar{\nu}$ reactions, neutral currents 77−41805
weak current model with $\Delta C\neq 0$ neutral current 77−54069
weak interaction studies with the DUMAND detector, 2 to 50 TeV 79−63463
weak neutral current coupling const. from νN single pion prod. data anal. 77−13911
Weinberg model and charm particles, general survey *(German)* 77−22729
y anomaly in $SU(2)\times U(1)$ vector like model, with parity violating neutral current 79−13013
b-quark prod. in five quark model by flavour changing neutral currents 79−45073
b-quark production, $SU(2)\times SU(2)\times U(1)$ gauge group mixing angles 80−68445
$\Delta(1236)$ isomer production, by charged and neutral currents 79−17711
$\Delta(1236)$ production, quark model anal., isovector and axial-vector neutral-current couplings 77−61278

neutrino-nucleon interactions continued

e/μ charged current $\nu(\bar{\nu})$ interaction comparison in Ne-H_2 mixture, μ-e universality 79−9363
γN, deep inelastic scatt., QCD phenomenology 80−42443
K multiple prod., possible semileptonic decay of new charmed meson 77−2819
$\mu^+ \rightarrow e^+ \bar{\nu}_{e} \nu_{\mu}$, $\bar{\nu}$l search for muon number conservation test, neutrino expt. 80−47270
μ^+ single prod. in inclusive interaction 78−45908
$\mu^- e^+$ pair production in neutrino interactions in Gargamelle, associated strange particles 77−61275
$\mu\mu$ like-sign events, implications for weak gauge models 77−67643
$\mu\mu$ pair abundance, six quark model without right handed currents 77−6081
$\mu^- \mu^-$ dimuon events, explanation in $\Delta C \neq 0$ neutral current model 77−54070
μN, deep inelastic struct. function, Nachtmann moments in QCD 80−27510
$\mu^- N \rightarrow \nu t X$, six-quarks model, upper bounds for t-quark production 80−13297
μp charged current interactions, hadron production, quark-parton model comparison 79−40769
$N + \nu \rightarrow M^0$, heavy lepton prod. and decay mechanisms cross section and coupling constant *(Russian)* 79−9365
nν/pν charged current ν cross section ratio, 1-10 GeV, semi-inclusive p prod. rates 79−374
ν and $\bar{\nu}$ inclusive processes for neutral currents, sea quark effects, meson prod. 79−22088
$\bar{\nu}$ anomaly at >50 GeV, anal. using right handed colour octet current scheme 77−30360
ν deep inelastic scatt., four flavour quark model, asymptotic freedom 78−45905
$\nu(\bar{\nu})$ d, disintegration reactions, helicity flipping neutral currents, tensor coupling 77−49944
$\nu(\bar{\nu})$ N interactions, π charge distrib., isospin and V,A struct. of weak neutral currents 77−38157
$\nu(\bar{\nu})$N, 30-100 GeV, invariant-mass struct., possible new hadron prod. 77−2816
$\nu(\bar{\nu})$N, 5-35 GeV, total cross sections via charged current channel, energy depend. *(Russian)* 80−4981
$\nu(\bar{\nu})$N, hadronic system charged particle multiplicities and transverse momentum distribs. 78−78165
$\nu(\bar{\nu})$N, high energy dimuon prod., consistency with charm particle prod. 78−89697
$\nu(\bar{\nu})$N, multimuon prod. at FNAL 78−78166
$\bar{\nu}(\nu)$N, opposite sign dimuon props. and rates 79−375
$\nu(\bar{\nu})$N, pol.N, deep inelastic processes from valence straton distrib. functions *(Chinese)* 80−99095
$\nu(\bar{\nu})$N 2-200 GeV, differential cross section, struct. functions, Bjorken scaling, Callan-Gross ratio 79−392
$\nu(\bar{\nu})$N inclusive interactions, axial vector photon and neutral neutrino processes *(Russian)* 79−30725
$\nu(\bar{\nu})$N interactions, 7.5-30 GeV, μ pair prod. 78−12904
$\nu(\bar{\nu})$N neutral current interaction cross sections 78−70357
$\nu(\bar{\nu})N \rightarrow N'\gamma e(\bar{e})$, current algebras and high energy γ-prod., sum rules 80−102039
$\nu(\bar{\nu})N \rightarrow l^-(l^+)X$, differential cross section in scaling limit, sea quark contribution 78−37196
$\nu(\bar{\nu})N \rightarrow \mu^-(\mu^+)$+hadrons, renormalisable field theory, high energy behaviour 77−61279
$\nu(\bar{\nu})N \rightarrow \mu^- \mu$ X, E>30 GeV, prompt like sign dimuon prod., Fe target, charm prod. 79−93395
$\nu(\bar{\nu})N \rightarrow \mu^+ \mu^- X$, dimuon rate and strange quark sea 80−62961
$\nu(\bar{\nu})N \rightarrow \mu^{\pm} e^+ e^- X$, trilepton event EM and hadronic contrib. 80−409
$\nu(\bar{\nu})N \rightarrow \mu(\mu^+) + c\bar{c} + X$, like sign dimuon prod., and b-quark prod./decay limits 79−85290
$\nu(\bar{\nu})N \rightarrow \nu(\bar{\nu})NN\pi^0$, charged neutral current ratios with $\nu N \rightarrow \mu N'' \pi^0$ 77−22727
$\nu(\bar{\nu})N \rightarrow \nu(\bar{\nu})X$, zero muon channel visible energy distrib., ν_τ test eval. 80−52489
$\nu(\bar{\nu})N \rightarrow \nu(\bar{\nu})$+hadrons, neutral to charged current cross section ratio 78−8651
$\nu(\bar{\nu})N \rightarrow \nu(\bar{\nu})\gamma N$, neutral currents, γ emission cross section *(Russian)* 78−17008
$\nu(\bar{\nu})N \rightarrow \nu(\bar{\nu})\pi + X$, determ. of neutral current coupling consts. 78−8649
$\nu(\bar{\nu})$+N, neutral to charged current inclusive cross-section ratio determ. 77−26511
$\nu(\bar{\nu})$+p interactions, ratio of down to up quarks in proton determ. 77−71504
$\nu(\bar{\nu})d \rightarrow np\nu(\bar{\nu})$, weak neutral currents, (V, A) and (S,T,P) theories 78−12893
$\nu(\bar{\nu})n \rightarrow \mu^-(\mu^+)pX$, semi-inclusive ν-scatt. and π-struct. functions 79−80819
$\nu(\bar{\nu})$p inclusive interactions, flavour symmetry breaking in antiquark distribs. 79−36006
$\nu(\bar{\nu})$p semi-inclusive scattering, hadronic fragmentation initiated by point-like probes 79−49551
$\nu(\bar{\nu})p \rightarrow \mu^-(\mu^+)\Delta^{++}X$, semi-inclusive ν-scatt. and π-struct. functions 79−80819
ν oscillation lengths, number of ν types possible νN expt. 77−41838
ν-N collisions, effects predicted by SU(2)×U(1) unified scheme *(Russian)* 77−218
$\bar{\nu}$-nucleus charged current interactions 79−22275
$\nu_\mu(\bar{\nu}_\mu)$N, charm meson prod. and decay, lepton inclusive distrib., c-quark fragmentation function *(Russian)* 80−52493
$\nu_\mu(\bar{\nu}_\mu)$N, heavy lepton prod. and decay, differential cross sections *(Russian)* 80−105940
$\nu_\mu(\bar{\nu}_\mu)$N, multi muon events, associative charm generation mechanism, D, $\bar{D}$ mesons *(Russian)* 79−89145
$\nu_\mu(\bar{\nu}_\mu)$N, prod. of hadrons with new quantum numbers, quark parton model *(Russian)* 77−82735
$\nu_\mu(\bar{\nu}_\mu)$N charged current total cross sections, (V-A) interactions, nucleon struct. function scaling 78−25033
$\nu_\mu(\bar{\nu}_\mu)$N quasielastic scatt., cross sections, effect of second kind weak hadron currents *(Russian)* 77−82734
$\nu_\mu(\bar{\nu}_\mu)N \rightarrow \mu^-(\mu^+)X$, struct. functions meas., quark-parton model anal. 79−58951
$\nu_\mu(\bar{\nu}_\mu)N \rightarrow \mu^{\mp}$+X, determ. of mass limit of weak boson 79−3012
$\nu_\mu(\bar{\nu}_\mu)N \rightarrow \mu^{\mp}\mu^+ X$, $SU(2)_L \times U(1)$ gauge model with off-diagonal neutral currents 79−2923
$\nu_\mu(\bar{\nu}_\mu)N \rightarrow \mu \mp X$, colour excitation in deep inelastic scatt. 79−13099

neutrino-nucleon interactions continued

$\nu_\mu(\bar{\nu}_\mu)N \rightarrow \mu(\bar{\mu})$+hadrons, phenomenology, parton model, expt. data, dimuon events *(Russian)* 77−49943
$\nu_\mu(\bar{\nu}_\mu)N \rightarrow \nu_\mu(\bar{\nu}_\mu)$+hadrons, gauge theories *(Russian)* 77−49943
$\nu_\mu(\bar{\nu}_\mu)p \rightarrow \nu_\mu(\bar{\nu}_\mu)p$ hadronic neutral current, final-proton polarisation 78−82200
$\bar{\nu}_\mu$ y-distribution anomalies, heavy muon as possible cause 77−61241
$\nu_\tau(\bar{\nu}_\tau)N \rightarrow \tau^{\pm} X$, beam-dump experiment, observation of ν_τ interactions 80−22601
$\nu + N \rightarrow \nu + N + \pi$, six-fermion interaction const. and neutral currents *(Russian)* 77−34147
$\nu + n \rightarrow \nu + p + \pi$, six-fermion interaction const. and neutral currents *(Russian)* 77−34147
$\bar{\nu}_\mu + N \rightarrow \mu^+ + X$ deep inelastic interaction at 2 to 25 GeV *(Russian)* 80−13298
$\nu_\mu + Z \rightarrow Z + \mu^- + W^+$, anomalous elec. quadrupole momentum and cross-sections *(Russian)* 77−34148
$\bar{\nu}d \rightarrow nn\mu$, virtual nucleon density matrix *(Russian)* 79−26327
$\nu d \rightarrow \nu np$, photon-neutrino coupling theory, Weinberg-Salam model comp. 79−13102
$\bar{\nu}_e d \rightarrow np\bar{\nu}_e$, axial meson exchange currents 79−85255
$\bar{\nu}_e d \rightarrow pn\bar{\nu}_e$, total cross-section calc. 78−41534
$\bar{\nu}_e d \rightarrow pn\bar{\nu}_e$, weak neutral current reaction, measured cross section 79−80828
$\nu_\mu d \rightarrow pn\nu_\mu$, neutral current induced neutrino reactions, differential and total sections 79−17708
νFe scattering, comparison of moments from valence struct. function with QCD predictions 79−49521
νH_2, possible new meson or baryon reson. decay 77−240
$\bar{\nu}H_2$-Ne, possible new meson or baryon reson. decay 77−240
$\bar{\nu}$N, 30 to 200 GeV, high-y anomaly 77−82732
νN, charmed particle prod. due to neutral weak currents *(Russian)* 80−68447
νN, deep inelastic scattering and asymptotic freedom 80−27511
νN, high energy, dilepton events, D meson semileptonic decay 80−42446
$\bar{\nu}$N, K^0 and π^- prod. rates, SU(3) symmetry violation in quark jet 80−82966
$\bar{\nu}$N, neutral current charm particle prod. search 80−22600
$\bar{\nu}$N, neutral weak currents at high energy, SU(6) quark vectorlike model *(Russian)* 78−45836
νN, $\bar{\nu}$N, y-distributions, nonscaling and longitudinal struct. function effects 78−33053
$\bar{\nu}$N, ratio of $\mu^+ e^-$ events to μ^+ events, charmed particle prod. model 78−89702
$\bar{\nu}$N, search for μe events 77−26512
$\bar{\nu}$N, single π^0 or π^- prod., neutral current interactions 78−41527
$\nu n \rightarrow = \nu p \pi^-$, neutral current process, excitation function, cross section ratio 80−78053
$\bar{\nu}$N charged-current interactions, semi-inclusive γ prod. 79−71737
$\bar{\nu}$N deep inelastic scatt., net charge in current fragmentation region, quark fragmentation 80−62964
$\nu N \rightarrow \Delta$+leptons, spin-3/2 polarisation density matrix determ. 77−87965
$\nu N \rightarrow e^- N\phi^+$, phi meson as light scalar boson in unified weak and EM interactions 79−17706
νN→hadron shower, charm-pair production effects 80−73748
νN→hadron+hadron neutral current prod. in Weinberg model *(Russian)* 77−6111
$\bar{\nu}$N in Fe, μ^+ polarisation in high energy charged current interactions 79−93399
$\bar{\nu}$N interactions, semiinclusive π production, charge ratio, Gargamelle freon data anal., weak neutral current 78−12905
νN interactions at CERN SPS, search for quarks 78−74240
$\nu N \rightarrow \mu^- e^+ X$, quark fragmentation function 77−87968
$\nu N \rightarrow \mu\ \mu\ X$, charm-pair production 80−22643
$\nu N \rightarrow \mu^- \mu^- \mu^+$, 350-400 GeV, event characts. 79−3011
$\nu N \rightarrow \mu^- \mu^- \mu^+$, high-energy, origin of trimuon events 78−74244
$\nu N \rightarrow \mu\ \mu^- \mu^+ N$, 350, 400 GeV, event origin, heavy lepton or quark cascade upper limit 78−89698
$\nu N \rightarrow \mu^- \mu^- \mu^+ X$, internal Drell-Yan mechanism, parton model approach 78−89656
$\nu N \rightarrow \mu^- \mu^- \mu^+ X$ event characts. 79−13105
$\nu N \rightarrow \mu^- \mu^- \mu^+ + X$, heavy lepton cascade decay 77−57524
$\nu N \rightarrow \mu^- \mu^- \mu^+ + X$, heavy lepton cascade decay 77−57525
$\nu N \rightarrow \mu^- \mu^- \mu^+ + X$, lepton cascade decay, gauge model 77−57526
$\nu N \rightarrow \mu^- \mu\ \mu^+$+anything, explanation in terms of prod. and decay of charmed (or other new quantum number) hadron pairs 77−57527
$\nu N \rightarrow \mu^- \mu^+ X$, quark fragmentation 77−87968
$\nu n \rightarrow \mu^- n\pi^+$, weak current isospin struct. study 79−49507
$\nu n \rightarrow \mu^-$p, bounds on outgoing baryon transverse polarisation , T-odd effects 77−87966
$\nu n \rightarrow \mu^-$p, Higgs boson exchange effects on second-class currents 80−91075
$\nu n \rightarrow \mu^-$p, quasi elastic reactions, cross sections, Gargamelle data anal., V-A theory 77−46039
$\nu n \rightarrow \mu^-$p, total cross-section and differential cross-section, estimation of nucleon mass 80−18128
$\nu n \rightarrow \mu^- p\pi^0$, weak current isospin struct. study 79−49507
$\bar{\nu}N \rightarrow \mu^+ \bar{C}S$, heavy quark leptoproduction in QCD, characts. 79−17733
$\bar{\nu}N \rightarrow \mu^+ X$, left handed weak doublets with mixed quark states 77−26514
$\bar{\nu}N \rightarrow \mu^+$+anything, Tanikawa-Watanabe meson prod. anal. 77−61274
$\bar{\nu}N \rightarrow \mu^+ e^- X$, relative prod. rate, Vee yield and scaling variable distrib. 79−40768
$\bar{\nu}n \rightarrow \mu^+ n\pi^-$, effects of second-class weak currents in $\Delta(1236)$ reson. region 78−8656
$\nu N \rightarrow \mu^{\pm}\mu^{\pm}$+anything, explanation in terms of prod. and decay of charmed (or other new quantum number) hadron pairs 77−57527
νN→μC, C=charmed baryon reson., prod. cross-section in 4-quark model 77−26513
$\nu N \rightarrow \mu N'' \pi^0$, charged/neutral current ratios with $\nu N \rightarrow \nu N' \pi^0$ 77−22727
$\nu N \rightarrow \mu N(\pi\rho)$, diffractive A_1 production 79−89143
$\nu N \rightarrow \mu N\pi$, high energy behaviour, light cone commutators, PCAC calcs. 78−37199
$\nu N \rightarrow \mu N\pi$, PCAC anal. in 1st reson. region 77−82730
$\nu N \rightarrow \mu X$, $\bar{\nu}N \rightarrow \mu X$, (X=system ofhadrons) 78−82222
$\nu N \rightarrow \mu X$, y distrib. changes, modified quark distrib. function for description 77−57543
$\nu N \rightarrow \mu$+anything, or $\mu^+ \mu^-$+anything, quark-parton model, threshold effects of charm prod. 77−46041
$\nu N \rightarrow \mu$+charmed baryon, SU(4) breaking effects, quark parton model 79−40792
$\nu N \rightarrow \mu eV^0$, Gargamelle results, charm search 77−26509

neutrino-nucleon interactions continued
$\nu N \rightarrow \mu\mu X$, dimuon events, D prod., lifetime and fragmentation function 79−93397
$\nu N \rightarrow \mu\mu X$, neutral strange particle prod. in opposite sign dimuon events 80−57584
$\nu N \rightarrow \nu N \pi\pi$, neutral-current cross sections for double-pion production by neutrinos 79−17712
$\nu N \rightarrow \nu X$, broken colour gauge theory of integer charge quarks 80−13313
$\nu N \rightarrow \nu X$, $SU(2)_L \times U(1)$ gauge theory distinguished from $SU(2)_L \times SU(2)_R \times U(1)$, neutral currents, z-bosons 80−62908
$\nu N \rightarrow \nu'$+anything neutral current events, ν' decay modes, upper limits on mass 77−6109
$\nu N \rightarrow \nu l^+ l^-$ (+hadrons), lepton pair production suppression up to 10^5 GeV *(Russian)* 79−36065
$\nu n \rightarrow \nu n \pi^0$, neutral current induced one-pion production, Weinberg-Salam structure 80−52454
$\nu n \rightarrow \nu p \pi^-$, expt. results comparison to theory 80−102038
$\nu n \rightarrow \nu p \pi^-$, neutral current induced one-pion production, Weinberg-Salam structure 80−52454
$\nu n \rightarrow \nu p \pi^-$, threshold pion prod., photon-neutrino weak coupling theory 77−67642
$\nu N \rightarrow \nu \pi X$, scale breaking effects 79−40770
$\nu N \rightarrow \nu \psi X$, neutral current ψ prod., Z^0-gluon fusion model 80−78015
νN single- and di-muon prod., colour excitation, weak interaction model anal. 78−45906
$\bar{\nu} N$ total cross section and ratio $\sigma\bar{\nu}n/\sigma\bar{\nu}p$ 79−22089
$\nu N \rightarrow X$, determ. of all neutral-current coupling constants from inclusive cross sections alone 79−13106
$\bar{\nu} N/\nu N$ cross section ratio rise with energy, modified quark distrib. function for description 77−57543
$\nu_l N$ deep inelastic scatt., radiative correction inaccuracies, quark-parton and Weinberg-Salam theories *(Russian)* 79−93403
$\nu_\mu N$, 4-30 GeV, $\mu^- e^+$ pair production *(Russian)* 80−91076
$\nu_\mu N$, charged heavy muonic lepton production, explanation of Kolar events 79−9364
$\nu_\mu N$, charm pair prod. in QCD, trimuon rate 78−45907
$\nu_\mu N$, $F^+(2030)$ prod. and hadronic decay $F^+ \rightarrow \pi^+\pi^+\pi^-\pi^0$, mass 80−91085
$\nu_\mu N$, heavy lepton prod., $SU(3) \times U(1)$ model 78−45900
$\bar{\nu}_\mu N$, K^0 and Λ inclusive prod., fragmentation function and transverse momentum squared 80−32093
$\nu_\mu N \rightarrow {}^-C_0^+$, ${}^-C_0^+ \rightarrow \Lambda^0 e^+ \nu_e$ Λ polarisation, chiral props. of charmed current 77−61272
$\nu_\mu N \rightarrow 3\mu X$, $SU(2)_L \times U(1)$ gauge model with off-diagonal neutral currents 79−2923
$\nu_\mu N \rightarrow e^+ X$, $SU(2)_L \times U(1)$ gauge model with off-diagonal neutral currents 79−2923
$\nu_\mu N \rightarrow M^0 X$, use of $\Delta\phi$ rule to disprove heavy lepton existence 79−63470
$\nu_\mu N \rightarrow$multiple lepton+hadron final states, flavour changing neutral currents 77−30363
$\nu_\mu N \rightarrow \mu^- {}^-C_0^+$, ${}^-C_0^+ \rightarrow \Lambda^0 e^+ \nu_e$, test of charmed current struct. 77−61271
$\nu_\mu N \rightarrow \mu^- N\pi$, cross sections and invariant mass distribs., inelastic charged current reactions 79−71742
$\nu_\mu N \rightarrow \mu^-$ X, 2 to 30 GeV, characts. of deep inelastic processes *(Russian)* 79−80821
$\nu_\mu N \rightarrow \mu^-$+hadrons, restraint on weak four-fermion interaction constants, quark-parton model *(Russian)* 77−6110
$\nu_\mu N \rightarrow \mu^- e^+$, obs. in BEBC 78−78170
$\nu_\mu N \rightarrow \mu^- e^+$ hadrons, Gargamelle picture anal., strange particles and charm prod. 77−54097
$\nu_\mu N \rightarrow \mu^- e^+$ in heavy Ne, Fermilab results, D^0 prod. and decay 78−89700
$\nu_\mu N \rightarrow \mu^- e^+ X$, anal. of two-lepton events 77−6107
$\nu_\mu N \rightarrow \mu^- e^+ X$, associated K_s^0 production 77−57528
$\nu_\mu N \rightarrow \mu^- e^+$+hadrons, investigation at SCAT chamber *(Russian)* 79−58953
$\nu_\mu N \rightarrow \mu^- e^+$+hadrons, up to 30 GeV, possible heavy neutral lepton prod. 79−36061
$\nu_\mu N \rightarrow \mu^- \mu^+(e^+) + X$, new bounds for dilepton prod. from heavy neutral leptons 77−46040
$\bar{\nu}_\mu N \rightarrow \mu^+ N$, 2-30 GeV, deep inelastic interactions SKAT preliminary results 80−82963
$\nu_\mu N \rightarrow \mu^+ e^- X$ in Ne 78−29329
$\nu_\mu N$ total cross section meas., 2-30 GeV, in SKAT experiment 79−36059
$\nu_\mu N$ total interaction cross section 2-30 GeV *(Russian)* 79−54334
$(\bar{\nu})\nu N \rightarrow e^- e^- e^+ \mu^+ K^0 + 7\gamma$, exptl. obs. 79−9361
$\bar{\nu}p$, 1.1 GeV, charged and neutral current events, strangeness changing currents, charm prod. 80−57583
νp, charged heavy lepton prod. and decay 78−8655
$\bar{\nu}p$, deep inelastic interactions, scaling variable distribs. 79−13101
νp, microcausality, equal-time current commutators, sum rules *(Russian)* 77−74689
νp, multiple production processes regularities, Monte Carlo model 80−102082
νP, neutral to charged current cross section ratio, coupling constant 80−27497
νp, $\bar{\nu} p$ elastic scatt., tests of flavour-changing neutral currents 78−8653
$\bar{\nu}p$, strange particle prod. at CERN PS 78−82195
$\bar{\nu}p$ charged current interaction, inclusive ρ^0 prod. 80−62963
$\bar{\nu}p$ charged current interactions, quark fragmentation, quark-parton model test 80−68444
$\bar{\nu}p$ charged current jet size, comparison with e^+e^- jets 80−22599
$\bar{\nu}p \rightarrow$charm quarks 80−102040
νp high energy interactions, vector meson diffr. prod., charged and neutral current 78−54625
νp inclusive interactions, ratio of neutral current to charged current cross sectins 77−79263
νp inelastic interactions, scaling deviations in secondary hadron energy distrib. 80−9161
νp interactions, 26 GeV, limits on axion prod., cross sections, decay rate 78−62387
νp interactions, charmed meson prod., Regge pole model, cross sections 78−33052
νp interactions, globality prop. of charged multiplicity, pion prod., lepton-hadron relation 77−2813
$\nu p \rightarrow \Lambda_c^+ X$, evidence for $\Lambda_c^+(2260)$ prod. 80−42442
$\nu p \rightarrow \mu^- D^+ X$ or $\mu^- D^{*+} p$, cross sections estimation using V+A form of charm current 77−41839
$\nu p \rightarrow \mu^- \Delta^{++}$, 5 to 100 GeV, production, decay distrib. 78−93873
$\nu p \rightarrow \mu^- K^+ p$, E>5 GeV, cross-section meas. 78−93872
$\nu p \rightarrow \mu^- \Lambda 3\pi^+\pi^-$, E>10 GeV, inclusive 79−376
neutrino-nucleon interactions continued
$\nu p \rightarrow \mu^-$+jet, greater than 10 GeV, jet props. 79−45084
$\nu p \rightarrow \mu^- pD^{*+}$, $D^0(1863)$ and inclusive D^{*+} (2009) prod., mass difference 79−93396
$\nu p \rightarrow \mu^- pk^-\pi^+\pi^+\pi^0$, Σ_c^+ prod. and decay 80−86710
$\nu p \rightarrow \mu^- p\pi^+$, cross section above 1 GeV 79−9362
$\nu p \rightarrow \mu^- p\pi^+$, effects of second-class weak currents in $\Delta(1236)$ reson. region 78−8656
$\nu p \rightarrow \mu^- p\pi^+$, weak current isospin struct. study 79−49507
$\nu p \rightarrow \mu^- \pi^+ p$, E>5 GeV, cross-section meas. 78−93872
$\bar{\nu}p \rightarrow \mu^+ X$, deep inelastic scatt., MQM description 80−47305
$\bar{\nu}p \rightarrow \mu^+ + X$, 4.5 GeV^2, p struct. functions x depend., quark distrib. 80−32097
$\bar{\nu}p \rightarrow \mu^+ n$, Higgs boson exchange effects on second-class currents 80−91075
$\bar{\nu}p \rightarrow \mu^+ n$, quasi elastic reactions, cross sections, Gargamelle data anal., V-A theory 77−46039
$\bar{\nu}p \rightarrow \mu^+ n$ or $\mu^+\Lambda$ or $\mu^+\Sigma^0$, bounds on outgoing baryon transverse polarisation, T-odd effects 77−87966
$\bar{\nu}p \rightarrow \mu^+ \nu$, axial transition form factor determ. 78−8647
$\bar{\nu}p \rightarrow \mu^+ p\pi^-$, 5-70 GeV, cross section, I=1/2 prod. amplitude 80−62962
$\bar{\nu}p$ neutral current, neutral-to-charged current cross-section ratio meas. 78−82197
$\nu p \rightarrow \nu$+vector meson + X, neutral currents, generalised VDM, Regge pole anal. 78−41532
$\nu p \rightarrow \nu n \pi^+$, neutral current induced one-pion production, Weinberg-Salam structure 80−52454
$\nu p \rightarrow \nu p$ observation and comparison with quasi-elastic scatt. 77−238
$\nu p \rightarrow \nu p \pi^0$, neutral current induced one-pion production, Weinberg-Salam structure 80−52454
νp polarised cross sections, new polarised ν sum rules 77−34144
νp production of $\Delta(1236)$, multipole struct. of weak prod. by charged currents 78−29328
$\nu p \rightarrow \Sigma_c^{++} X$, evidence for $\Sigma_c^{++}(2424)$ prod. 80−42442
$\nu p/\nu n$, ratio of neutral current and inelastic cross sections 79−13100
$\nu p^+ \rightarrow \mu^- \Delta^{++}(\nu\Delta^+)$, Δ polarisation, test of T-invariance of weak and charge currents, comment 79−67531
$\bar{\nu} p^+ \rightarrow \mu^+ \Delta^0$, Δ polarisation, test of T-invariance of weak and charge currents, comment 79−67531
$\bar{\nu}_e p \rightarrow n e^+$, Cowan and Reines' expt. 79−80408
$\bar{\nu}_e p \rightarrow n e^+$, interaction cross section, expt. and theoretical discrepancy, discussion *(Russian)* 79−80822
$\nu_\mu p$, Higgs meson prod., possible signals in high energy collisions, gauge groups 78−89649
$\bar{\nu}_\mu p \rightarrow \mu^+ H^0$, props. of neutral hadronic system H^0 anal. 78−41531
$\nu_\mu p \rightarrow \bar{\mu}\nu_F F^+ X$, $F^+ \rightarrow \mu^+ \nu_\mu \bar{\nu}_F$, total cross section, spectra, unconfined heavy fermion model 77−18269
$\bar{\nu}_\mu p(n)$, charged current interactions in Ne, cross section ratio, scaling variables 79−75763
$\bar{\nu}_\mu u \rightarrow \mu^+ b(\rightarrow cX)$, b-quark prod. and decay limits from like sign dimuon prod. 79−85290
π^0 production by ν and $\bar{\nu}$ neutral currents, comparison 79−49509
t-quark production, $SU(2) \times SU(2) \times U(1)$ gauge group mixing angles 80−68445
$\nu N \rightarrow 4\mu X$, radiative and hadronic production characts. 79−40771
$\nu N \rightarrow \mu 3e X$, radiative and hadronic production characts. 79−40771
$\bar{\nu}_\mu p \rightarrow \mu^+ n$, charged current interaction, elastic cross section 79−67533

neutrino-nucleon scattering
see also neutrino-nucleon interactions
charm particle prod., breaking of scaling *(Russian)* 77−46043
collapsing star, neutrino degeneracy and downscatt. effects on neutrino radiation 79−12463
deep inelastic anomalies and longit. struct. functions 77−49979
deep inelastic scatt., N_2 struct., nuclear forces in quark model *(Russian)* 77−61299
deep inelastic struct. function higher order asymptotic freedom corrections for e, M, γ scatt. 79−93426
dense stellar matter, diffusion approx. to neutrino transport 78−93096
E_7 gauge model, lepton assignments and trimuon events in neutrino scatt. 79−17709
elastic and quasi-elastic, determ. of Weinberg angle 77−54064
inclusive charged current scatt., new quark flavours and scaling 77−82731
inclusive same-sign dimuon prod., $c\bar{c}$ creation 77−49946
isoscalar axial-vector current, anal. of elastic νp scatt. 79−93316
leptoproduction, azimuthal depend., parton model calcs. 78−93887
low-energy elastic scattering and supernova explosions 78−89056
neutral current reactions, (V-A) model, mixing between ordinary and heavy leptons 78−41472
neutral lepton current, νN elastic and deep-inelastic scatt., photon-neutrino weak-coupling theory 77−30358
neutral weak current, structure *(Russian)* 79−49446
neutral weak current phenomenology in νN elastic scatt. 79−6312
quark-parton model and QCD description for νN scatt. with charge exchange *(German)* 79−26324
quasielastic and deep inelastic scatt. book contrib. 78−78171
scaling violation in high energy scatt., generalised vector meson dominance 77−67644
stellar interiors, conservative scatt. and electron scatt. rel. to neutrino thermalisation 79−92659
$SU(2) \otimes U(1)$ gauge models, neutral current couplings 79−40715
trimuon event sources 78−25035
valence quark clusters in nucleon structure functions from neutrino scatt. 80−95252
W-boson propagator effects in the neutrino-nucleon scattering 79−13098
weak neutral currents, space-time struct. *(Chinese)* 79−17715
$\nu(\bar{\nu})$N, axial vector photon and neutral neutrino processes *(Russian)* 79−30725
$\nu(\bar{\nu})$N 50-200 GeV, deep inelastic scatt., charged current cross section, Bjorken scaling 78−89699
$\nu(\bar{\nu})$N cross sections in Weinberg model of neutral currents 77−10240
$\nu(\bar{\nu})$N deep inelastic scatt., 45 to 205 GeV, scaling and struct. functions 78−62386
$\nu(\bar{\nu})$N elastic scatt., symmetry relations, current matrix elements 78−54627
$\nu(\bar{\nu})$N inclusive scatt., scaling violation evidence, QCD test 78−89701
$\nu(\bar{\nu})$N scattering, modified GIM model, scaling violations, naive parton model 78−21414
$\nu(\bar{\nu})N \rightarrow \nu(\bar{\nu})\gamma X$, hadron neutral current, parton model *(Russian)* 78−45910

neutrino-nucleon scattering continued
$\nu(\bar{\nu})$p elastic and quasielastic scatt., neutral current isospin props. 77−2812
$\nu(\bar{\nu})$p elastic scatt., final state polarisations, test for T-invariance and 2nd class currents 79−63466
$\nu(\bar{\nu})$p elastic scatt. and neutral currents, by polarised proton target *(Russian)* 77−26507
$\nu(\bar{\nu})$p→$\nu(\bar{\nu})$p, ν-hadron weak neutral current couplings determ. 78−86435
$\nu_\mu(\bar{\nu}_\mu)$p, 2 GeV elastic scatt., charged current/neutral current event ratio 80−57582
νN, above 50 GeV, charge asymmetry rel. to charmed particle generation *(Russian)* 77−10241
νN, above W prod. threshold energy, QCD effects, cross sections and neutral currents *(Russian)* 79−67537
$\bar{\nu}$N(νN) CERN data, inconsistency with e-N in quark-parton model *(Russian)* 77−49951
νN($\bar{\nu}$N) forward elastic scatt. amplitudes, new sum rules 79−54332
νN scatt., QCD effects above W prod. threshold, structure functions 79−71738
νp, implications for weak interaction models 77−6108
νp, neutral to charged current ratios 79−54333
νp, polarised proton, differential cross sections *(Russian)* 77−46042
νp elastic scatt., hadronic neutral current couplings, model independent determ. 79−49448
νp elastic scatt., neutral current struct. anal. 77−61273
νp→νp, energy spectra of recoil fermions, Weinberg-Salem model 78−12895
νp→νp elastic neutral current interaction obs. 78−25037
$\nu(\bar{\nu}$p) elastic scatt., space-time struct. of weak neutral current anal. 77−30365

neutrino-nucleus reactions
for inelastic neutrino-nucleus scattering, see "neutrino-nucleus scattering"
see also neutrino-nucleon interactions
absorption in Coulomb field of nuclei in strong mag. fields, radiation loss by pair prod. 77−14115
C Ne+$\nu_\mu(\bar{\nu}_\mu)$, inclusive distrib. of produced hadrons 78−89854
CERN School of Physics, Austerlitz-Zeist, Holland (June 1978) 79−30857
charm particle prod., lifetime determ. 79−26426
charmed baryon production, mass and F/D ratio, colour magnetic interaction 80−62957
deep inelastic hadron leptoproduction on nuclei, inclusive hadron final states 78−54741
detection and analysis of neutrino interactions in photoemulsion *(Russian)* 78−41900
high energy particle-nucleus interactions, discussion 79−30858
historical review, detection, meas., and interactions with nuclei and nucleons 79−49002
inclusive ν cross section on nuclei, ν_μ representation in SU(6) 78−54626
lepton pair production in ν-nucleus reactions, cross sections, transverse momenta distrib. *(Russian)* 78−54749
multimuon events, QCD predictions for associated prod. of charm 78−25034
radiochemical solar neutrino detectors using (ν,e^-) reaction, (p,n) background from cosmic ray muons 77−61650
right handed colour octet currents for charm and colour excitation in $\nu(\bar{\nu})$ reactions 78−93874
semileptonic weak and EM interactions, nuclear current operators 79−6515
stars, neutrino induced prod. of bypassed elements 77−45408
statistical theory of nuclear ν capture, inclusion of first forbidden transitions, cross sections 78−93990
stellar collapsed core, neutrino prod. of bypassed isotopes, neutrinos role in nucleosynthesis 79−40182
stellar collapsing cores, neutrino prod. and inelastic scatt. by nuclei at extreme temps. 80−36488
supernovae, neutrino-induced nucleosynthesis rel. to D and p-process nuclei prod. 77−87582
transport of neutrinos, weak neutral currents; supernova model 78−62391
e/μ charged current $\nu(\bar{\nu})$ interaction comparison in Ne-H_2 mixture, μ-e universality 79−9363
$\nu(\bar{\nu})$d→np$\nu(\bar{\nu})$, weak neutral currents, (V, A) and (S,T,P) theories 78−12893
$\bar{\nu}$-nucleus charged current interactions 79−22275
$\bar{\nu}$+Ne→p+X, backward proton events, nucleus probe expts. 79−531
ν_μ+Ne→$L^\pm$...., expt. limits on heavy lepton production 78−37197
ν_μ+Ne→μ^-+e^++X, possible charmed particle production 77−67645
ν_μd→pnν_μ, neutral current induced neutrino reactions, differential and total sections 79−17708
π dispersion relation in nuclear matter using ν+nucleus reactions 79−488
^{81}Br+$\nu_{e,\mu}$, 0 to 300 MeV, cross sections, shell model calcs 79−93605
^{81}Br(ν,e)^{81}Kr, solar neutrinos detect. possibility 77−22160
C degenerate core thermonuclear reaction propag., neutrino mech. *(Russian)* 79−5812
^{12}C+ν, neutral current processes in nuclei, elementary particle approach 79−93606
^{12}C+ν_e, 0 to 300 MeV, cross sections, shell model calcs 79−93605
^{12}C(ν,p)^{11}B, occurrence in stellar C layer 80−82337
^{37}Cl neutrino absorpt. cross-sections, rel. to Brookhaven expt. sensitivity to solar neutrinos, collapsing stars and cosmic neutrinos 78−4929
^{37}Cl, ν_e capture, statistical theory, inclusion of first forbidden transitions, cross sections 78−93990
^{37}Cl+ν_e, 0 to 300 MeV, cross sections, shell model calcs 79−93605
^{37}Cl(ν,e$^-$) ^{37}Ar, cosmic ray neutrinos contrib. to solar neutrinos tests 79−16837
^{37}Cl(ν,e$^-$)^{37}Ar, statistical theory calc. of total capture cross section 77−88113
^{37}Cl(ν_e,e$^-$)^{37}Ar, cross-section constraints for ^{8}B solar neutrinos 77−26675
^{37}Cl(ν_e,e$^-$)^{37}Ar, rot. model for mass-37 system, cross section calcs. 77−88114
^{37}Cl(v,e$^-$)^{37}Ar, shell model cross section calc., appl. to cosmic ray and background elimination *(Russian)* 80−5131
^{56}Fe+ν_e, 0 to 300 MeV, cross sections, shell model calcs 79−93605
^{56}Fe(ν_μ, $\mu^-+L^++L^0$)^{56}Fe neutrino-induced heavy-lepton pair production at high energies and multimuon events 79−89298
^{71}Ga+ν_e, 0 to 300 MeV, cross sections, shell model calcs 79−93605

neutrino-nucleus reactions continued
^{71}Ga(ν,e$^-$)^{71}Ge, proposed new expt. for solar neutrinos detect. 78−58563
^{71}Ga(ν,e)^{71}Ge, cross section calc., appl. to solar neutrino expts. interpretation *(Russian)* 77−50119
^{71}Ga(v,e$^-$)^{71}Ge, shell model cross section calc., appl. to cosmic ray and background elimination *(Russian)* 80−5131
^{1}H, inverse β-decay fission $\bar{\nu}$ induced reaction cross sections 79−22273
^{2}H, inverse β-decay, fission $\bar{\nu}$ induced reaction cross sections 79−22273
^{2}H($\bar{\nu}_e$,$\bar{\nu}_e$n)p, antineutrino spectrum 80−102150
^{115}In(νe$^-$)^{115}Sn*, scintillator for solar neutrino spectroscopy at low energies 78−73639
^{A}Li+ν, (A=6,7), neutral current processes in nuclei, elementary particle approach 79−93606
^{26}Mg(ν_e, e$^-$), ^{26}Al prod. cn stellar collapsed core *(Russian)* 80−77285
^{55}Mn(ν,e) ^{55}Fe, cross section calc., appl. to solar neutrino expts. interpretation *(Russian)* 77−50119
Ne+$\nu_\mu(\bar{\nu}_\mu)$, inclusive prod. of hadrons, preliminary data 78−89853
Ne+ν_μ→μ^-e^+, obs. in BEBC 78−78170
Ne($\bar{\nu}$,p), 0.6-25 GeV, backward emitted proton inclusive spectra, short range correlation 80−32281
^{16}O, neutrino absorption cross-sections, <500 MeV, Helm model 77−41956
^{16}O+ν_e, 0 to 300 MeV, cross sections, shell model calcs 79−93605
^{87}Rb(ν,e)^{87}Sr, cross section calc., appl. to solar neutrino interpretation *(Russian)* 77−50119
^{205}Tl(D,e$^-$)^{205m}Pb, ^{205}Pb assay in Tl minerals for solar neutrino flux determ., proposed expt. 77−5447

neutrino-nucleus scattering
see also neutrino-nucleon scattering
collapsing star, neutrino degeneracy and downscatt. effects on neutrino radiation 79−12463
deep inelastic scatt., N_2 struct., nuclear forces in quark model *(Russian)* 77−61299
dense stellar matter, diffusion approx. to neutrino transport 78−93096
elastic scattering of low energy neutrinos by atomic systems *(Russian)* 77−83754
inelastic scatt., test of struct. of weak neutral currents 77−14117
interactions in vertical emulsion target of hybrid apparatus 80−5126
isoelastic processes, one-body density matrix formalism 77−18528
low-energy elastic scattering and supernova explosions 78−89056
neutral current and nuclear scatt. of reactor antineutrinos, integrated inelastic cross section 78−29452
neutral current struct. 78−8799
parity nonconservation in elastic scatt. with 0^+→0^- transition *(Russian)* 77−61402
stellar collapse, neutrino radiation for black hole form. rel. to envelope outburst problem 78−45350
stellar interiors, conservative scatt. and electron scatt. rel. to neutrino thermalisation 79−92659
ν_μ+Z→Z+μ^-+W^+, anomalous elec. quadrupole momentum and cross-sections *(Russian)* 77−34148
^{12}C(ν,ν'), ($\bar{\nu}$,$\bar{\nu}'$), 15.11 MeV state excitation, cross sections, level decay 80−9258
^{12}C(ν,ν'), test of struct. of weak neutral currents 77−14117
^{2}H(ν,ν), polarised deuterons, asymmetry in emission of recoil deuterons 77−79264
^{7}Li ($\bar{\nu}_e$, $\bar{\nu}_e$), antineutrino spectrum 80−102150
^{7}Li(ν,ν)^{7}Li*, fundamental phys. expts. with reactor neutrons and neutrinos, summary 79−67543
^{14}N(v,ν), neutral current struct. 78−66269

neutrino production
astronomical point sources of high energy neutrinos, detect. techniques 79−2484
astrophysical neutrino sources, review 78−77486
beam channel characts., Protvino Inst. 78−37474
beam dump experiments, prompt neutrinos and charm particle lifetime 79−63535
beam dump neutrino experiments, promp neutrino meas. 79−63537
cosmic ray neutrinos, high-energy, prod. spectra and diffuse fluxes 79−44327
cosmic ray proton atmospheric interactions, direct leptons prod. *(Russian)* 80−12627
cosmic ray ultrahigh-energy neutrinos, prod., fluxes and detect. 78−49264
deep inelastic ν prod., QCD and hadronic energy ang. distribs. 80−390
fission prod. β decay in nucl. reactor, $\bar{\nu}$ energy distrib. 79−75924
galaxies active nuclei, high-energy neutrino luminosity and detectability 80−4432
hadron decay, ν sources, right hand weak currents and direct neutrinos *(Russian)* 77−82699
heavy leptons, charged, possibility of new neutrino as decay product 77−10237
Higgs bosons, effects on experimental observables, and fermion mass scale 80−32061
hot neutron star formation, neutrino radiation rel. to envelope outburst problem 78−45350
IHEP neutrino beam energy spectra reconstruction *(Russian)* 79−68119
muon flux measuring system for neutrino spectrum reconstruction at IHEP accelerator 78−21817
nature and production of neutrinos from particle accelerators *(French)* 79−26326
neutrino pair bremsstrahlung and number of lepton generations 80−101978
neutrinos, beam focusing system, Protvino Inst. 78−37477
neutron stars, cold, neutral currents and neutrino emission 77−45478
neutron stars, neutrino emission rel. to cooling 79−101170
nuclear neutrino pair photoprod. in strong mag. field, pulsar neutrino luminosity *(Russian)* 80−68648
pair bremsstrahlung by degenerate electron gas, neutral current effects, stellar interiors appl. 77−13225
parent-child relationship for prompt leptons and neutrinos produced in the forward direction 79−80824
prompt neutrino production in beam dump expt., cluster anal. 79−49556
prompt sources, and axion decays and interactions, pN beam-dump experiment 80−63028
proton+nucleus reactions, neutrino-like particle prod., limits from calorimetry meas. 79−85473
proton beam dump expt. at CERN SPS, obs. of excess ν_e, $\bar{\nu}_e$ events 78−45978
proton interactions, beam dump expt. at CERN SPS 78−45979

neutrino production continued
pulsars, binary, neutrino emission 79−2550
red giant stars, neutrino emission rel. to evolutionary sequences 78−65611
review, of neutrino-generating reactions *(Russian)* 80−13344
stars, neutrino bursts and gravit. waves, proposed search for correl. 78−77567
stellar C-O cores, Urca neutrino loss rates 78−20813
stellar collapse, gravit. radiation and total neutrino losses 78−45317
stellar collapsing core, role of neutrino dissipation 79−101166
stellar collapsing cores, neutrino prod. and inelastic scatt. by nuclei at extreme temps. 80−36488
stellar dense cores, time-dependent neutrino transport 80−94783
stellar energy loss rates due to neutrino prod. by neutral currents 77−53577
supernova neutrino bursts, gravit. radiation generation 78−81642
supernovae, neutrinos emission rel. to gravit. waves generation 78−93092
synchrotron neutrino emission, charge collision emission, star neutrino luminosity 80−41719
target complex at Fermilab, operating experience 80−23230
ultrapressure generation of mesons and neutrinos in plasmas and ion beams *(Russian)* 78−93920
white dwarfs, neutrino cooling rel. to evolution 80−82356
$D^- \rightarrow \tau^- \bar{\nu}_\tau$, charmed mesons, heavy lepton decays, ν_τ neutrino mass depend. *(Russian)* 78−62394
$e^+ + e^- \rightarrow \nu_H$ possibility of production and detection 79−49501
$e^+e^- \rightarrow \gamma\nu\bar{\nu}$, calc. of number N_ν neutrino types 79−26321
$e^+e^- \rightarrow \gamma\nu\bar{\nu}$, neutrino counting, $e^+e^- \rightarrow 3\gamma$ background 80−68441
$e^+e^- \rightarrow \gamma\nu\bar{\nu}$, neutrino type counting possibilities 79−49502
$e^+e^- \rightarrow H\nu\bar{\nu}$, 40-70 GeV, neutrino counting from Higgs boson production 79−97612
$e^+e^- \rightarrow \nu\bar{\nu}$, in strong mag. fields, rate of energy loss 78−29326
$e^+e^- \rightarrow \nu\bar{\nu}\gamma$, formula for differential cross-section, including weak interaction and V-A interaction *(Russian)* 78−62385
$F^- \rightarrow \tau^- \bar{\nu}_\tau$, charmed mesons, heavy lepton decays, ν_τ neutrino mass depend. *(Russian)* 78−62394
$F^\pm \rightarrow \tau^\pm \nu_\tau(\bar{\nu}_\tau)$ beam-dump experiment, observation of ν_τ interactions 80−22601
$\gamma \rightarrow \nu\bar{\nu}$, in strong mag. field, rel. to pulsars and neutron stars *(Russian)* 77−17360
$\gamma \rightarrow \nu\bar{\nu}$ in strong mag. field, absorpt. coeff. and energy loss rate 77−22728
$\gamma e^- \rightarrow e^- \nu\bar{\nu}$, energy spectra of recoil fermions, Weinberg-Salem model 78−12895
$\gamma e^- \rightarrow \nu\bar{\nu} e^-$ in mag. field *(Russian)* 77−26506
$\gamma\gamma \rightarrow \nu\bar{\nu}$, nonzero neutrino mass, early Universe process 78−21483
$\gamma p \rightarrow p\nu\bar{\nu}$, energy loss from stellar bodies through ν-prod. by second class weak neutral current 79−35997
$K^+ \rightarrow \pi^+ \nu\bar{\nu}$, calc. of number N_ν neutrino types 79−26321
$K_L{}^0 \rightarrow \gamma\nu\bar{\nu}$, calc. of number N_ν neutrino types 79−26321
$K_L{}^0 \rightarrow \pi^- \mu^+ \nu_\mu$, transverse polarisation of μ, violation of time-reversal invariance 80−68448
$L^0 \rightarrow \nu_l \mu^+ \mu^-$, heavy lepton spin, massless spin 3/2 ν four fermion interaction 79−13175
$\mu \rightarrow e\gamma$, possible existence of third kind of neutrino *(Chinese)* 78−12896
$\mu^- \rightarrow e^- \nu^- \nu$, model, spiral props. *(Russian)* 78−25031
μ^+ polarisation dynamics in mag. mirror field, neutrino emission asymmetry 77−61645
$\nu\bar{\nu}$ pair emission, stellar plasma in strong mag. field, photon-neutrino coupling theory 77−17548
$\nu\bar{\nu}$ pair emission from electron in superstrong mag. field *(Russian)* 78−49991
pN, 28 GeV in Cu, prompt neutrinos and penetrating particles 80−47336
pN 70 GeV collisions, search for prompt neutrinos 79−13160
$\pi^+ \rightarrow \mu^+ \nu_\mu$, at rest, μ^+ momentum meas. 78−45911
$\tau \rightarrow \nu_\tau e \nu_e$, nature of τ-ν_τ-W coupling, ν_τ mass upper limit and lifetime 79−40824
$^{12}C(\mu^-,\nu_\mu)^{12}B$, Hartree Fock wavefunction, correlations, pseudoscalar coupling constant, capture rates, recoil nuclear polarisation 80−22774
Cu+p, 400 GeV, dimuon and trimuon prod., prompt ν source, $D\bar{D}$ prod., axions 78−89860
Cu+p, 400 GeV, prompt ν prod., axion prod. upper limit 78−89859
Cu+p collisions, 400 GeV, prompt ν prod. 78−46061
^{239}Pu, e and $\bar{\nu}$ energy spectra from fission fragments *(Russian)* 77−23120
^{235}U, e and $\bar{\nu}$ energy spectra from fission fragments *(Russian)* 77−23120

neutrino scattering
see also neutrino-electron scattering; neutrino interactions; neutrino-neutrino scattering; neutrino-nucleon scattering
Bjorken scaling violation models of quarks with substructure 79−26305
chemical potential and heat cond. with allowance for scatt., collapsing stars appl. 79−84657
coherent π^0,ρ^0 meson prod., test for neutral weak currents of exotic space-time struct. 79−75715
deep inelastic structure functions and the quark parton model 80−4992
elastic and inelastic, coherent interaction of neutrinos with dense matter, astrophysics role *(Russian)* 80−68446
elastic scattering of low energy neutrinos by atomic systems *(Russian)* 77−83754
fermion targets, four symmetry relations 79−373
Gargamelle, neutrino physics history, theory and expt. 78−50027
hadronic polarisation, helicity struct. of weak neutral current 78−74245
Higgs boson prod. in $\nu(\bar{\nu})$ scatt., cross-sections for neutral and charged currents 77−18271
high energy ν experimental physics at Fermilab, review 78−50028
high energy neutrino experiments, state of art 79−26322
high-energy (>10 GeV) neutrino physics, review of development, book contrib. 78−82201
inclusive scattering, weak neutral currents with longitudinal cross sections, scaling 78−17007
neutral currents, quark-lepton models 77−18272
neutral currents in $U_3(W)$-gauge theory of unified EM-weak interactions 77−26481
neutral lepton current, lepton-hadron symmetry, CP violation and $\Delta I = 1/2$ rule 80−82934
neutral leptonic currents, μe universality violation *(Russian)* 78−45837
neutron star matter, neutrino scatt. by phonons 79−12488
scale breaking, asymptotically free gauge theory model and phenomenological model 79−13107
semi-inclusive deep inelastic neutrino scatt. QCD effects 79−30724
$SU(2)_L \times (T_3)_R \times U_Y(1)$ gauge unified model, neutral current interactions, ed and ν scatt. 80−18107
$SU(2) \times U(1) \times U(1)$ gauge model, quark-lepton correspondence in neutral and charged current interactions 79−54296
supernova models, multigroup diffusion scheme for collapsing stellar core 79−25590
supernova outburst role of neutral currents of weak interactions *(Czech)* 77−45472
weak elastic scattering 80−91079
$\bar{\nu}$-ν cross-sections, evidence for new quark flavours beyond charm 77−18268
$\nu d \rightarrow \nu d$, polarised deuterons, asymmetry in emission of recoil deuterons 77−79264

neutrinos
see also cosmic ray neutrinos
antineutrino probes for nuclear struct. expts. 79−531
axial EM field source, symm. P-invariant broadened Maxwell eqns. *(Russian)* 78−58141
Bianchi IX model, spectral asymmetry and QFT in curved spacetime 80−56982
Bianchi type-V universes, neutrino viscosity 79−9042
Bianchi-V cosmological space-time, Einstein-Weyl equations, neutrino currents 80−86023
big bang, helium synthesis, neutrino flavors, and cosmological implications 80−73084
Big Bang model, galaxy cluster missing mass from massive leptons, additional ν species 78−81719
black holes, rotating, neutrino fluxes resulting from macroscopic parity violation 80−22034
CERN neutrino beam monitoring by μ flux in Fe shield meas., Si detectors 78−37523
chaotic cosmology, dissipative heating by collisional neutrinos 77−57112
chemical potential and heat cond. with allowance for scatt., collapsing stars appl. 79−84657
chronon in quantum theory of electron, existence of heavy leptons, neutrino spectrum 78−70008
classical ν, gravitational interactions 78−45833
collapsing Fe-O stars with masses of 2 M⊙ and 10 M⊙, neutrino effects 78−20815
collapsing star, neutrino ang. momentum loss by Poynting-Robertson effect 79−16928
collapsing star, neutrino damping of nonradial pulsations 77−56999
cosmological ν sea, EM wave propagation, torsionic background 80−77283
cosmological constraints on numbers 79−62940
cosmological He production and neutrino stability 78−73783
cosmological models, isotropisation of Bianchi spaces due to neutrino viscosity 79−75300
cosmology, primordial neutrino gas 79−53950
CP or T violation effects 78−21349
curved space-time, neutrino fields with geodesic and shear-free rays, zero rest-mass fields 77−17890
curved space-time, propag. of photons and neutrinos 77−79011
decay in gauge theory of weak and EM processes *(Russian)* 79−22087
decay products of charged heavy leptons, possibility of new neutrino 77−10237
dilute systems, kinetic equation 77−33940
Dirac eqn. for massless particles, number of quanta in neutrino field 78−4765
E_6 model of unified interactions, asymptotically free, mass relations and interactions 80−73642
Einstein-Dirac equation, soln., neutrino representation 79−58596
elementary particle physics, information from astronomical observations 80−51935
EM properties, weak neutral current and form factor *(Russian)* 77−61270
emission from blackbody, thermodynamic laws, teaching 80−105451
emission from cylindrically symmetric cluster of many gravitating masses 80−94707
ether as a neutrino sea 77−53728
ether as neutrino sea, materialistic basis for physical explanation 77−53729
excitable ether composed of neutrinos, anomalous structural interactions explained 77−53730
flux from quark matter at core of collapsed stars 80−22028
form factors in 2-D approx. of QED 80−9132
gas in Friedmann universe, statistical model 77−53717
gas of neutrinos and antineutrinos, transport coefficient *(French)* 78−86217
gauge hierarchy and neutrino mass problem 80−90989
gauge theories, EM props., forbidden processes and currents with anomalous Lorentz struct. 78−54599
general relativity, neutrino radiation soln. 78−54261
ghost neutrinos in Einstein Cartan theory 80−52108
Goldstone, mixing of weak and gravit. interactions, massive gravitino 78−8578
Goldstone neutrinos avoidance mechanism, spontaneously broken supersymm. theories limits 77−30279
gravitational indistinguishability of neutrino field and stokesian fluids 79−30159
gravitationally collapsing stars, neutrino processes rel. to mass ejection 77−33534
Hagedorn's big-bang model, strongly degenerate heavy neutrino decay, free quark-baryon ratio 78−16589
heavy, limits on props. of massive neutral leptons from primordial nucleosynthesis 78−57438
heavy lepton, lifetime and mass constraints imposed by big bang nucleosynthesis 79−40308
heavy lepton massive neutrinos in big bang model, mass and number 78−45444
heavy Majorana particles, cosmological and astrophysical implications 80−90331
helicity from ^{12}C μ^- capture 80−68655
historical introduction, weak interactions, book 78−78133
historical review, detection, meas., and interactions with nuclei and nucleons 79−49002

neutrinos continued
historical review 78−89288
horizontal symmetries dynamical symmetry breaking and neutrino masses 80−105830
identification and research at Laue Langevin Institute, Grenoble *(French)* 80−21883
ILL HFR, Grenoble, fundamental phys. expts. with neutrons and ν 79−67932
Jones matrix, appl. in symmetry breaking, SU_2 theory and theory of neutrinos 79−17632
lepton mixing, neutrino oscillations and $\mu \rightarrow e\gamma$ decay 77−49940
lepton mixing and neutrino oscillations, cosmic neutrinos, heavy leptons, μ decay 78−82193
lepton mixing and neutrino oscills. review, 'solar neutrino puzzle' 78−66182
local B-L symmetry of electroweak interactions, Majorana neutrinos, and neutron oscillations 80−73643
magnetic moment calc. in SU(2)×U(1) gauge model 77−18180
mass, four component Dirac particles, perturbation theory model for massless ν 79−435
mass, limitation to less than 30 eV by cosmology 79−6358
mass, second-order effect in Higgs coupling 79−75716
mass and Pontecorvo oscillations of neutrinos using chronon concept in electron theory 78−36879
mass and weak vector current conservation in τ-decay *(Russian)* 79−89215
masses, SO_{10} hierarchical breaking 80−22550
massive neutrinos, mag. moment and spin rotation 80−105895
massive neutrinos, radiative decay rel. to cosmic element abundances 79−92668
massive right-handed neutrino 77−46095
massive supersymmetric pairs, neutrino as massless stable bound state 79−85242
massive unstable neutrinos, cosmological implications 78−45437
massless ν, left-right symmetric gauge models, $SU_{2,L}\times SU_{2,R}\times U_1$ 80−27461
massless fermion representations in grand unified gauge theories 79−97553
minimal O(10) grand unification, ν mass 80−57546
mixing angle between ordinary and heavy leptons in a (V-A) model, constraints 78−4846
neutral current couplings and νe^- weak neutral current coupling constraint, fermionic assignments 80−4915
neutral current couplings in SU(2)×U(1) gauge theories, natural relations, flavour dynamics 79−89095
neutrino+antineutrino system, relativistic kinetic theory, Wigner functions 77−26239
neutrino cosmology, open universe with neutrino and graviton dominance 77−17731
neutrino fields in axially and reflection symmetric space-times 79−40425
neutrino fluctuations, possibility of obs. at nuclear reactor 79−67542
neutrino transport calcs. using neutron transport methods 77−87377
neutrino trapping in rotating matter 79−2673
neutrino types, determ. of total number 78−82258
neutrino-antineutrino gas, transport coeff. values *(French)* 79−30388
neutrino-antineutrino mixture, transport props. 78−93625
neutrino-electron mixture, influence of spin and Weinberg-angle on bulk viscosity 77−61223
neutron star, neutrino-pair bremsstrahlung in hot plasma, strong mag. field 78−61878
neutron star formation, competition between neutrino and gravitational radiation 77−49421
neutron stars, neutrino energy loss rel. to cooling 80−77443
neutron stars, neutrino-pair bremsstrahlung in collisions between neutrons and nuclei 77−74789
neutron stars, neutrinos and gravit. waves emission during form. 78−12266
nonzero rest mass effect on cosmological ^{4}He production 80−105413
nuclear matter with neutrinos retention, eqn. of state and chemical comp. 78−96390
orbital angular momentum 77−50038
oscillation lengths, number of neutrino types, possible νN expt. 77−41838
oscillations, eigenstates of weak interactions 80−105825
oscillations, evidence from Brookhaven solar neutrino expt. 79−16787
oscillations, fundamental phys. expts. with reactor neutrons and neutrinos, summary 79−67543
oscillations, generalised scheme 77−22724
oscillations, Majorana and Dirac mass mixing 80−101969
oscillations, mass and mixing scales 80−105823
oscillations between neutrinos and antineutrinos, conditions for observations 79−17636
oscillations in ν_e, ν_μ, ν_τ system 80−82964
oscillations in weak interaction model 80−78014
oscillations of $\nu_\mu \leftrightarrows \nu_e$, limit determ. in Gargamelle expt. 77−22723
pair prod. in strong mag. field 78−407
parity violation and the masslessness of the neutrino 79−85258
photon double helix struct., 2 intertwined neutrinos, polarisation, helicity props. 78−37255
Pontecorvo neutrino oscillations for Dirac and Majorana masses, CP nonconservation 80−105829
properties and experimental neutrino astrophysics, review, book contrib. 80−72769
properties from low energy interactions, theoretical aspects 79−67538
quark-lepton correspondence, multigeneration $SU(2)_L\times U(2)$-based model, neutrino flavours and masslessness property 80−22584
radiative decay lifetime limits 78−448
radiative stability of finite rest mass neutrinos 79−63568
relativistic Boltzmann eqn., series convergence 78−36949
research installations for investigation of free neutrinos 77−50336
rest mass, effects on Universe density perturbations spectrum and microwave background small-scale fluctuations *(Russian)* 80−109576
rest mass, implications for Universe density perturbations evolution and galaxy clusters hidden mass *(Russian)* 80−105414
rest mass of electron neutrinos, implications for mass density and age of Universe *(Russian)* 80−109575
review, of discovery, production, meas. and appls. *(Russian)* 80−13344
rotating black holes, neutrino emission ang. depend. 79−88696
SO(10) grand unified theory, breaking scheme and neutrino mass 80−47230
neutrinos continued
solar, capture rate problem, role of phion in composite neutron mode 80−41808
solar, detection problem 80−101585
solar neutrino astrophysics, review 79−16917
solar neutrino experiments, appl. to cosmological hypothesis testing 79−16918
solar neutrino flux, quasi-biennial var. and correl. with solar activity 79−44440
solar neutrino flux explanations, nuclear reactions in Sun 77−74035
solar neutrino fluxes, from dirty models with surface contamination resulting from accretion 79−44436
solar neutrino problem, implications of solar oscills. obs. for Sun internal struct. 80−105226
solar neutrino problem, limitations of energy transport by mechanical means 77−17461
solar neutrino problem, theory versus obs. 80−17566
solar neutrinos, influence of interstellar dust accretion 79−12441
species number, rel. to universe lepton number 80−8730
spiral properties using model of μ decay *(Russian)* 78−25031
stable heavy neutrinos, dynamical interactions and astrophys. effects 79−5743
star, spherical, emitting neutrinos, relativistic model 78−73705
stellar collapse, neutrino ang. momentum losses 77−56916
stellar collapsing core, shock struct. and neutrino radiation, rel. to supernova explosions 78−49427
stellar degenerate C ignition, neutrino losses rel. to core implosion 80−77390
stellar dense cores, time-dependent neutrino transport 80−94783
stellar evolved C cores, neutrino energy dissipation rel. to core collapse and C detonation 80−82339
stellar interiors, conservative scatt. and electron scatt. rel. to neutrino thermalisation 79−92659
stress tensor regularisation, two-dimens. space-time 77−67561
$SU(2)_L\times U(1)\times SU(2)_R$ model for lepton decay and neutrino lifetime 78−62331
$SU(2)_L\otimes SU(2)_R\otimes U(1)$ weak model, ν mass and spontaneous P nonconservation 80−62884
SU(2)×U(1) gauge theory, charged heavy lepton and neutrino 78−45794
SU(s) grand unification, neutrino mass and oscillations, B-L nonconservation 80−52449
Sun, exchange current corrections to proton-proton reaction 80−26733
supernovae, effect of core Rayleigh-Taylor convective overturn on neutrino release and explosion 80−77429
supernovae, neutrino mediated shocks 80−94818
supernovae, neutrinos emission rel. to gravit. waves generation 78−93092
supernovae core collapse, neutrino energy equilibration models 80−105265
superweak particle cosmological constraints, ν with neutral current interactions, ^{4}He primordial abundance 79−84667
thermally dissociated matter, neutrino opacity rel. to comp. and eqn. of state 77−33476
total cross sections for ν_e and $\bar{\nu}_e$ bubble chamber interactions, neutrino oscills. and decay 78−41526
trace anomaly for neutrinos in Ricci-flat space-time of six dimens. 78−57847
transport, direct simulation and aspects of equilibration 78−89050
trapping in collapsing stars, effect on nucl. dissoc. 80−90407
unified theories, neutrino number and isotropy of Universe 80−85852
universal lepton mixing and mixing angles in $SU(2)_L\times U(1)$ gauge theory of weak interactions *(Russian)* 79−54298
vacuum neutrino oscillations between ν_e, ν_μ, ν_τ, CP violation 79−291
vacuum neutrino oscills. inhibition by high matter density in stellar core collapse 80−36496
velocity in comparison to muons 80−9190
viscosity in collapsing stellar cores 78−61875
wave equations in conformal space, Dirac theory 78−21364
weak interaction theory review, ν sharing 78−78131
weak neutral current, effects in stellar collapse, review, book contrib. 78−85964
Weinberg-Salam model and extensions, ν EM form factors and mag. moments, neutral currents, astrophysics applics. *(German)* 80−62904
Weyl neutrino, nonlocal position and momentum operators 80−73586
Weyl neutrino, translation props. 79−63392
β-decay, neutrino-free, theory, new aspects 79−13254
$e\bar{e}\nu_e\bar{\nu}_e$ mixture, covariant transport eqns., collision terms from Weinberg Salam theory 77−74315
$e\bar{e}\nu_e\bar{\nu}_e$ mixture, transport eqn. for neutrino component 77−33941
$\mu^\pm \rightarrow e^\pm\gamma$, right-handed ν_μ anal. 78−41525
$\bar{\nu}$, rest mass, upper limit refining using ^{3}H β-spectrum meas. 78−17144
$\bar{\nu} \rightarrow e^+\pi^-$ decays in nuclear matter 77−65209
$\nu \rightarrow \gamma\nu$, in strong mag. field, rel. to pulsars and neutron stars *(Russian)* 77−17360
$\bar{\nu}_e$ mass from ^{3}H β-decay spectrum *(Russian)* 80−91159
ν_e mass from ^{3}H β-spectrum in valine molecule 80−91158
ν_H, possibility of production and detection 79−49501
ν_μ, mass range 100 to 500 keV, discussion 79−63570
ν_μ, rest mass measurements from $\pi^+ \rightarrow \mu^+\nu_\mu$ 80−37253
ν_μ, transition magnetic moment 78−78168
$\nu_\mu \rightarrow \gamma + X$, decay lifetime, mass, expt. limits 77−10234
ν_μ mass limit in absence of muon-lepton-number conservation, unified gauge theories 78−21368
ν_τ, heavy-lepton-associated neutrino, mass calc. 78−4849
ν_τ, mass, lifetime, decay modes and mixing angles 80−445
ν_τ, mass from τ decay 80−63057
ν_τ interactions, signals in beam dump expt. 79−67535
ν_τ spin, suppression of $\tau \rightarrow \nu_\tau\pi$ 78−21410
ν_τ spin determ. from τ-decay branching ratios 79−75757
ν_τ test eval. in zero muon channel visible energy distrib. 80−52489
$\nu' \rightarrow \nu\gamma$, Weinberg-Salam model with neutrino mixing *(Russian)* 77−38114
$\nu_\mu \rightleftarrows \nu_e(\bar{\nu}_\mu)(\nu_\tau)$, neutrino oscillation expts. at accelerators 79−67541
$\bar{\nu}_\mu e^- \rightarrow \nu_e\mu^-$, exotic lepton number violation and neutrino Majorana masses, Higgs sector 80−86615
$\nu\mu \rightarrow \gamma + X$, mass and lifetime exptl. limits 77−50039
$\pi^0 \rightarrow \nu\bar{\nu}$, neutrino mass test 79−93406
τ-neutrinos, in beam dump expts. 78−50004
Fe-O stars collapse, effects of neutrino radiation and absorpt. 77−87369
^{239}Pu(n,f), thermal n, reactor $\bar{\nu}$ and e spectra calc. 79−67791

neutrinos continued
^{239}Pu(n,γ), thermal, fission product $\bar{\nu}_e$ spectrum, β-decay charact. 80−78340
^{235}U(n,f) thermal n, reactor $\bar{\nu}$ and e spectra calc. 79−67791
^{235}U(n,γ), thermal, fission product $\bar{\nu}_e$ spectrum, β-decay charact. 80−78340

neutron absorption
activated metal foil experiments, teaching expts. 79−17165
air, gamma-field from monodirectional neutron source 77−67785
air, luminous emittance of neutron beam 78−86567
attenuation coefficient and total removal cross-section, 14 MeV 79−29427
borosilicate glass, behaviour as control rod in commercial reactor 78−8918
BWR spent fuel element storage, neutron physical aspects 80−68841
CANDU pressurised HWR fuel, bundle end neutron flux peaking effects, plenum use 78−58385
CANDU reactor, Th-fuelled, importance of ^{233}Pa in neutron economy 80−22980
CANDU-PHW, neutron flux regulation by two-phase flow absorber system 79−93799
capture cross sections, expt. determ., fast reactor materials *(Italian)* 78−82355
component reliability tests in thermal neutron environment 78−21787
concretes, normal and ilmenite, energy distrib. of transmitted neutrons 77−23308
criticality of U-Pu aqueous solns., oxides and nitrates, effect of Gd, Gd-B neutron absorbers 77−34393
cross-section absolute meas. method 78−78431
dynamical neutron diffraction and its application, absorpt. effects, book contrib. 79−60231
epithermal 1/V self-shielding of reactor poisons using Nordheim integral method 78−17306
fast test reactor fuel pins in water, critical expts. 79−85726
FFTF, critical expts., with solid neutron absorbers 80−52727
flux distortion in 3-D reactors due to plane absorbers *(German)* 77−6478
FTR fuel pins with solid neutron absorbers, criticality expts. 80−18476
graphite rods, damage by high energy neutrons 80−29070
heavy water, effect of non-1/v absorbers on thermal neutron transport 78−29532
HTGCR, fuel with double heterogeneity, resonance absorpt. 80−32321
HTGR spherical fuel assemblies, resonance integral meas. *(German)* 78−29568
ilmenite concretes, fast neutron attenuation 79−76048
in-reactor measurement of neutron absorber performance 80−73951
industrial neutron radiography using research reactors 79−11757
intermediate resonance method for heterogeneous media, new formulation 77−61490
KERMA values, consistent set for H, C, N, and O for neutrons from 10 to 80 MeV 80−68967
light water, cold neutron interactions, total cross-section meas. 77−67786
linear extrapolation dist. on surface of 2-D absorber 77−6479
LMFBR, elimination of transuranium elements by neutron absorpt. 78−29628
measurement standard for units of absorpt. power 80−102351
monoenergetic neutron transport equation, existence of complex eigenvalues 77−345
multizonal absorbing rod, effectiveness in albedo and diffusion studies *(Russian)* 80−556
neutron escape probability from absorbing body 78−46125
noise, space-depend., induced by vibr. absorber 77−74900
nuclear reactor criticality safety anal., determ. of Dancoff factor for cubic arrays of spherical fuel particles 80−13725
optimisation of absorber distrib. 78−50230
porcelain, neutron-retardation behaviour for continual moisture determ. *(German)* 80−105660
radiometric testing of materials, review 80−71860
radiotherapy shielding, comparison of photoneutron and ^{252}Cf neutron spectra 79−59273
reactor core, independent control of neutron flux using gaseous absorbers 79−71918
reactor physics, control poison optimisation, depletion calcs. 80−57906
regulation, dynamic simulation of two-phase control absorber in nuclear reactor 80−13731
resonance absorpt. in RBMK-type grid 78−664
resonance escape probability, Monte Carlo importance sampling technique 77−61471
resonance escape probability meas. in nuclear fuel 77−71632
resonance heterogeneity effect in vicinity of gross region interface 77−82992
resonance integral calc. in reactor cell lattice, Monte Carlo code, RISO 77−3088
resonance interaction effects, Fourier transform method 77−14207
resonance $J(\theta,\beta)$ function evaluation, comparison of various computational models 77−61483
resonance neutron self shielding factors for Au and Ag, expts. and calcs. 77−42008
self shielding factors, elastic removal cross sections, strong reson. scatt. 79−13374
shielding of 14 MeV neutrons using iron-water combination 77−61614
slow neutron action on glasses and vitreous ceramic and cryst. materials *(Spanish)* 80−57816
soil, neutron moisture meter calibration, neutron absorpt. cross section meas. 77−9545
solid neutron shield development, materials eval. for spent fuel shipping cask 80−13939
solid neutron shield material tests 80−37543
soluble neutron absorber use at ICPP 79−85730
soluble neutron poison use for criticality control at ICPP 79−85727
space depend. spectra in two adjacent moderating media 77−6477
spectra, multiple scatt. corrections and neutron attenuation 77−26928
thermal, energy depend. detection efficiency of cylindrical counter, wall effect, calc. 77−57803
thermalisation of neutrons in solid media calc. 77−50192
thickness measurement using nuclear resonance methods 77−81334
tilted neutron flux distrib., effect of cylindrical absorbing channels 78−13189

neutron absorption continued
tilted neutron flux distrib., influence of small and large absorb. rods 77−79410
TLD, self-shielding factors for TLD-600 and TLD-100 in isotropic flux of thermal neutrons 77−6638
transfer matrix calcs. for thermal neutrons 80−27687
two phase control absorber, results from out-reactor static tests 78−58389
two-different-core system, neutron transit time meas. 78−37414
two-phase control absorber, horizontal absorber elements, expt. study 80−42841
two-phase control absorber development program for CANDU reactors 80−42839
two-phase reactor control, neutron absorber development program 79−97852
ultracold neutrons, lifetime in traps, film-substrate model calcs. 80−106098
ultracold neutrons on strong absorbers, absorpt. coeff. meas. 78−46127
vitreous silica blocks, damage by high energy neutrons 80−29070
water, diffusion length calc. for 1/v and non-1/v absorbers 79−30879
water, effect of non-1/v absorbers on thermal neutron transport 78−29532
water-moderated water-cooled reactor, local control of loop channel energy release profile and magnitude 78−86645
Ag, Doppler factor, comparison between calculated values and measured results 78−54811
Ag-Cu-Pb coin chem. anal. by low energy γ-rays and neutron transmission meas. 80−35591
Al min. activity blanket design for TFTR upgrade 78−58460
Al_2O_3-B_4C, behaviour as control rod in commercial reactor 78−8918
Au, Doppler factor, comparison between calculated values and measured results 78−54811
B, borides, neutron absorbing props., reactor control system, appls., review, book contrib. 78−46154
B_4C, absorber material for fast reactor control appl. 78−8919
B_4C, behaviour as control rod in commercial reactor 78−8918
B_4C, He release correlation during fast-neutron irradiation in fast reactor 78−8965
B_4C, meas. of T retention of fast-neutron-irradiated absorber elements 78−8903
B_4C, neutron absorber material for FBR, in-reactor performance meas. 80−18429
B_4C, thermophysical props. and neutron absorpt. 80−103488
B_4C-graphite, irradiation-induced dimens. changes, rel. to HTGR conditions 78−8905
BF_3-CO_2 mixtures, ang. neutron flux distribs. meas. 77−54276
^{10}B(n,α), n absorption calcs. for activation detectors 78−78434
Be, two group calcs. for neutron wave propagation across an absorption discontinuity 78−89931
^{252}Cf fission neutron, transmission through various shields, dose equivelent meas. 77−61620
^{A}Cr, A=50, 52-54, slow n-interactions, scatt. lengths, absorpt. and scatt. cross-section 78−70539
EuB_6, absorber material for fast reactor control appl. 78−8919
EuB_6, synthesis and hot pressing fabrication for appl. to neutron absorbing core control material 78−8904
Eu_2O_3, absorber material for fast reactor control appl. 78−8919
Eu_2O_3, thermophysical props. and neutron absorpt. 80−103488
$Gd(NO_3)_3$, use in fuel dissolution criticality control 79−85728
Gd_2O_3-UO_2, behaviour as control rod in commercial reactor 78−8918
H_2, neutron energy transfer 30 to 100 MeV 77−52890
H_3BO_3 concentration in primary circuit coolant, method and device for determ. *(Russian)* 77−38331
LiF tile and sheet for thermal neutron shielding *(Japanese)* 78−74510
^{6}Li+n, spin depend. capture and scatt. of slow neutrons 78−46059
^{24}Na, absorption cross-section calc. 77−23075
Pb, reactivity worths of fixed neutron absorbers 78−21654
Pu H_2O solns., Gd poisoned, calc. of sub-critical limits 79−85724
^{45}Sc+n, 0.005 to 22 keV, total neutron cross section for beam filter design 78−78371
Ta, thermophysical props. and neutron absorpt. 80−103488
Th, cross section shape near thermal energy 77−46204
U, reson. absorpt., effect of annular fuel elements 78−666
U water flooded rod lattices, effect of soluble neutron absorbers in criticality prevention 79−85725
U/Pu systems, criticality control by Gd 79−85729
UO_2, ^{235}U enriched lattices, effect of soluble neutron absorbers on criticality 79−80978
UO_2, energy depend. Doppler factor meas. using lead slowing-down time spectrometer 78−17310
UO_2 low enriched fuel rods, storage and transportation, critical separation in water with fixed neutron poisons 80−73918
$UO_2(NO_3)_2$ highly enriched soln. with $Cd(NO_3)_4.4H_2O$ neutron poison, criticality expts. 80−13724
^{235}U-H_2O solns., B poisoned, subcritical limits calc. 79−85723
^{238}U, neutron transmission meas. and anal. 77−26823
^{89}Y, reson. neutron capture cross-section between 2.5 and 100 keV 77−82924
^{90}Zr, neutron absorpt. cross section, optical pot. imag. part 79−9536

neutron activation analysis
$1/E^{1+\alpha}$ epithermal neutron spectra, resonance integral correction, effective resonance energy 80−71978
$1/E^{1+\alpha}$ epithermal neutron spectrum, α-determ. methods, accuracy 80−71977
$1/E^{1+\alpha}$ epithermal neutron spectrum, α-determ. without Cd cover 80−71976
^{252}Cf based nondestructive assay system for fissile material 78−73119
absolute, computer-based system 79−11846
absolute instrumental, consistent set of nuclear parameters 79−11857
absorbing samples, average thermal neutron flux determ. method 78−73112
activation cross section, integral tests in ^{9}Be(d,n) field 80−851
aerosols, urban, characterisation 77−41157
aerosols in atmosphere, detection and measurement 77−41152
air, trace amounts of In, extraction and neutron activation determ 80−12045
air dust, environmental data evaluation problems 80−21425
air particulates in Hong Kong, nondestructive multielement determ. 80−12040
air pollutants 77−25772

neutron activation analysis continued
air pollution, analysis of trace elements in precipitation 77−41154
air pollution, comparison study between city and desert 77−41155
air pollution, emissions from nonferrous plants, neutron-activation anal. 80−21343
air pollution, fast trace element analysis 77−41158
air pollution, particulate matter, analysis 77−41150
air pollution, particulate matter, heavy metal analysis 77−41151
air pollution, particulate matter, statistical control of results 77−41153
air pollution analysis using 14 MeV neutrons, Al, Si, Fe and Pb conc. meas. 77−91257
air pollution control, activation analysis for 14 volatile heavy metals as constituents of aerosol particles 80−16891
air pollution in industrial area, with evaluation of results 77−41156
air pollution meas. in semi-arid zone 78−36317
air samples in UK for 1957 to 1974 period, retrospective analysis 78−3942
Al_2O_3-SiO_2 refractories, using neutron-2 equipment 80−45612
alkaline rocks, neutron activation analysis, destructive and nondestructive methods 78−92573
Allende meteorite, neutron activation anal., isotopically anomalous Xe and $^{184}Os/^{190}Os$ ratio 77−45368
analysis code for automated reduction of gamma ray data 78−23978
ancient Cu alloys, epithermal neutron activation anal. method 78−8490
ancient pottery, characterisation by neutron activation anal., suitable element selection 78−8484
ancient pottery, nondestructive neutron activation anal. 78−12802
andesite, neutron activation analysis, destructive and nondestructive methods 78−92573
annihilation spectra, two-component, resolution using count ratio technique 78−44424
anthropomorphic phantom, assess. of bulk element lacks in patients 79−39497
archaeology, comparison of results from Lawrence Berkeley Lab. and Hebrew University 78−70245
archaeology, trace element neutron activation analysis, pattern recognition techniques 77−40588
atmospheric aerosol, Ankara, trace elements and size distribs. determ. by thermal neutron activation anal. 78−81377
atmospheric aerosol, Pt metals analysis 78−3989
atmospheric aerosol, S.Pole, chem. comp. determ. by instrumental neutron activation analysis 78−3988
atmospheric dust, neutron activation anal. 77−70718
atmospheric dust aerosols, activation analysis experience at Karlsruhe Nuclear Research Center 78−3941
atmospheric particulate material, trace elements analysis by nucl. activation techniques 78−3991
attenuation coefficient and total removal cross-section, 14 MeV 79−29427
automatic channel-width switching in NTA-512B analyzer in multichannel counting mode 79−26840
automobile exhaust pollutants, distrib. of Pb particulate 78−3943
basalts, deep sea, trace element distrib. pattern, neutron activation anal., rel. to genesis 78−11879
bauxite, Si, Al, Fe determ., neutron activation anal. 79−24858
BER II research reactor, transport capsule separation from sample containers at fast pneumatic transport systems for neutron activation analysis 77−74966
biological and environmental samples, cyclic activation and short-lived isotopes meas. 79−88217
biological material analysis, As and Hg determ. 80−36216
biological materials, anal. by monostandard method 80−72398
biological materials, determ. of trace elements 79−12058
biological materials, resonance neutron activation analysis technique 78−3692
biological materials 79−57827
biological samples, device for opening quartz ampoules 78−61121
biological samples, nondestructive proton and neutron activation analysis comparison 78−3691
biological samples, pseudo-cyclic instrumental neutron activation anal. of trace multielement conc. 80−17214
biological samples, Sn analysis at nanogram level by ^{121}Sn liq. scintillation counting 78−3693
biological samples, trace element characterisation, by instrumental neutron activation anal. 78−73116
biomedical methods and applications, in vitro and in vivo *(French)* 77−66834
biosamples, ^{32}P radioactive interference with anal. of trace elements 79−12059
blood analysis, optimal conditions *(Bulgarian)* 78−85280
blood serum, neutron activation anal., sample contamination by quartz container 77−48980
blood serum, neutron activation determ. of Zn, Se, Rb, and Fe concs. 78−20252
body content meas., fate of ^{37}Ar prod. by fast neutron exposure 77−5075
bone, archaeological, Al determ. using neutron activation anal. 79−52847
bone, archaeological, characterisation 78−353
bone, cow femur, mineral comp., neutron activation anal. 78−27859
bone, human hand, CC Ca anal. by local neutron activation 79−83902
bone, short-lived radionuclides, gamma-ray spectrometry, correction for dead-time losses 80−42312
bone F measurement, and F/Ca ratio 77−86592
borehole activation analysis, neutron energy distrib. in low-porosity rock 77−64286
borehole capture gamma-ray anal., optimal size ^{252}Cf neutron source 79−29890
botanic reference materials, candidate standards, homogeneity testing, anal. methods 78−11594
botanical samples, computer-simulated gamma-ray spectra 79−1985
breast tissue exam. using neutron activation and electron microscopy 80−21536
Canadian clay, neutron activation anal. 78−8487
capture cross section meas. using neutron activation anal. 80−32282
clinical in vivo total body anal., neutron uniformity 78−40315
coal, 14 MeV neutron activation analysis ^{16}O and ^{14}N 77−86430
coal, continuous nuclear analyzer development 79−52851
coal, elemental analysis by prompt neutron activation anal. 79−52848
coal, meas. of specific energy ash and moisture by combined neutron and gamma-ray meas. 79−39255

neutron activation analysis continued
coal, quality monitoring, in elec. power generating plant, prompt neutron activation anal. 78−7302
coal, total hydrogen content determ., improved techniques 79−52852
coal 79−48015
coal analytical assembly using capture gamma rays from accelerator neutrons 79−96401
coal and coal derivatives, 14 MeV neutron generator in analysis of ^{16}O 77−86431
coal ash content measurement in moving wagons 80−3431
coal composition determination by ^{252}Cf neutrons, flux level corrections 78−7303
coal conversion products, trace elements determ. 78−85744
coal research, appl. of neutron activation anal. 78−85740
coal research, fast-neutron activation anal. 78−85742
coal research, neutron anal. 78−85265
coal research, prompt-neutron activation anal., system optimisation 78−85743
coastal water pollution, monitoring 77−41068
coins, ancient Greek, neutron activation and at. absorpt. anal. 78−8489
coins, Constantinian, use of ^{252}Cf source 78−350
comparative, computer system 79−11855
complex spectral peaks, computer anal. 78−53302
computer interpretation of spectrometric information in instrumental neutron-activation analysis 79−31351
computer program for multielement analysis with abs. counting 77−21439
computer simulated γ-ray spectra in activation anal. 78−92577
computerised thermal neutron activation anal., correction procedure, detection limit, standardisation 77−44544
concrete, field anal. of plastic state, two source method 77−25352
conference, Munchen, Germany (Sept. 1976) 77−86405
conferences, quantitative study of participants, session titles 80−62361
control software for high throughput system 79−11849
correction for neutron and gamma attenuation effects in 14 MeV anal. 77−81448
cost minimisation 78−48728
cotton plant wilt disease, microelement depend. by neutron activation anal. 77−64165
criticality accidents, dosimetry using activations of blood and hair 80−89857
cross sections for some (n,2n), (n,p) and (n,γ) reactions 79−57335
crude oil, neutron activation anal. for determ. of V 78−20109
cyclic activation analysis, cycle period optimisation 79−66389
cyclic activation using pneumatic shuttling system and switch off and on of source and detector, 14 MeV analysis, short-lived products 79−87908
cyclic activation with flux corrections 79−39253
cyclic instrumental, optimum timing parameters for determ. of short-lived nuclides, computer program 80−61211
cyclotron-produced fast neutrons, applic. to instrumental multielement analysis and radiochem. determ. of F 77−90692
D-T generator, neutron yield control *(German)* 77−23336
data reduction, computer language 78−85241
data reduction, flexibility, MULTELMT program 79−11856
dating of prehistoric Great Basin petroglyphs 78−70243
dead time correction for short and long lived nuclide mix. 80−93825
delayed fission neutron technique, review 79−1979
delayed neutron probe characts. for uranium exploration, field meas. 79−53568
design of apparatus for 14.1 MeV neutron activation anal. *(Spanish)* 77−67531
destructive, automated radiochemical separation systems use 77−90691
determination program, computer ES 1030, algorithm SAND-II *(Russian)* 78−48723
diamond, natural, trace element anal., genetic significance 80−55759
diamond, sub-surface contamination by hot-atom recoil 77−60144
dosimetry film evaluation by neutron activation and X-ray fluoresc. anal. 79−63820
dust samples, rapid characterisation using high-rate loss-free gamma spectroscopy system 78−61129
element anal., advance prediction of spectra 78−85274
element analysis, role of neutron capture γ-rays 80−50926
elemental analysis by neutron inelastic scatter gamma rays with a radioisotope nuetron source 80−30311
elemental sensitivity data modeling for in situ neutron capture gamma-ray experiments 79−61928
environmental, of Cs, Br and As, w.r.t. reliability 78−40106
environmental pollution applications, conf., Vienna, Austria (Mar. 1976) 77−41148
environmental samples, nondestructive analysis using low-energy photon spectrometry 78−3995
environmental samples anal. for U, Th, neutron activation anal. data resolution for high throughput system 79−11848
environmental trace elements, meas. accuracy 78−69509
epidemiologic monitoring, neutron activation analysis of blood and blood components 80−17099
epidemiologic monitoring, trace elements in human skin lesions 80−17100
epidemiological monitoring of human hair, neutron activation trace element anal. 80−17212
epidemiology, determ. of organically-bound chlorine and bromine in biological samples 80−21593
epithermal, comparator technique, errors 77−81441
epithermal, effect of nuclear reactor neutron flux distrib. 79−52833
epithermal neutron fields in nuclear geophysics *(Russian)* 80−85658
equipment with interchangeable irradiation blocks 79−41060
faecal samples, Ca determ. method using instrumental fast neutron activation anal. 80−104733
fast neutron activation analysis in multidisciplinary studies 79−52807
fast neutron spectra, activation technique determ., fusion reactor blanket model appl., unfolding program 77−79500
fast pneumatic transfer systems, time and fluence meas. *(German, English)* 77−38576
fissile material assay, cyclic method of neutron activation and delayed-neutron counting 77−34395
fissile materials, anal. by cyclic activation of delayed neutrons 78−53296
fission reactor core, neutron spectrum evaluation using activation method *(Czech)* 77−65288
fissionable isotopes in aq. soln., assay by pulsed neutron interrogation 78−68966

neutron activation analysis continued
flow meas., asymmetry effects 78−83508
fluence measurement in total body in vivo anal. 77−86613
flux uniformity in in vivo anal. 77−9246
fossil bones from N. Greece, conc. of U and daughter prods., γ-spectroscopy, activation anal. 77−60161
gamma spectra, least squares deconvolution on minicomputer, NAALSQ program 79−11853
gamma spectrometry, data processing system 79−11863
gamma spectrum anal., computer methodology, appl. to geological and environmental samples 79−11867
gamma-ray detection following inelastic neutron scatt. 79−52837
gamma-ray logging K-factors, correction of error 79−84278
gamma-ray peak areas observed with Ge(Li) detectors, least squares spectrum fitting method 79−85854
gamma-ray spectra, rapid reduction via desk-top calculator 77−53870
gamma-ray spectra evaluation, appl. of programmable calculators and minicomputers 79−9956
gamma-ray spectra from Ge(Li) detector, simple computer program (BASIC) for spectra eval. 79−9951
gamma-ray spectra peak shapes observed with Ge detectors, divergence from Gaussian, formula for peak fitting 79−85853
gamma-ray spectra prediction, detection limits, computational procedure 78−85242
gamma-ray spectrometry, automated, original version of neutron activation analysis 79−11861
gamma-ray spectrometry system, automatic, computerised data acquisition, spectral anal. systems, aerosol appl. 77−81442
gamma-ray spectroscopy, instrumental NAA, improvements to basic advance prediction program 80−14042
gamma-ray spectrum analysis program SAMPO, radioisotope identification subroutine IDENT 79−9953
geochemical indicators for genesis of ore deposits *(German)* 80−30301
geological materials, multielemental anal. 80−16747
geological materials, neutron activation anal., coaxial, planar detection comparison appl. 77−81443
geological samples, multielement anal. by sequential instrumental and radiochem. neutron activation 78−7798
geological samples, multielement determ., instrumental neutron activation anal. 79−53550
geological samples, trace element characterisation, by instrumental neutron activation anal. 78−73116
geometric parameters optimisation in 14 MeV anal. 78−95982
Glasgow activation analysis programme 1953-1978, developments 79−87909
glass, ancient samples, trace element anal. by neutron activation, rel. to corrosion and devitrification 78−12801
granulitic rock outcropping, trace elements determination *(Portuguese)* 80−7874
groundwater flow, investig., using In-EDTA tracer and neutron activation anal. 78−11921
hair, biopsy material for trace elements in human body 79−83955
hair, human, multielement neutron activation anal. of trace element concs., Tokyo area 80−45602
halogen content of ultramafic nodules, determ. by gamma-ray spectroscopy and radioactivity meas. 80−76945
high-output generator use of 14 MeV activation analysis 77−90694
high-purity metals, cost effective anal. 77−60162
high-purity substances, analysis methods 79−39241
HTGR fuel refabrication plant, nondestructive fissile assay technique 80−37562
human body, in vivo N meas. by prompt neutron capture γ-ray analysis, body H use as internal standard 79−92441
human body Ca meas. in vivo, effect of size and composition of body 79−92350
human body elemental composition meas., feasibility study 79−70615
human body N meas. by anal. of prompt γs from neutron capture 80−51220
human brain, instrumental NAA of trace element distrib., rel to blood serum conc. 80−17215
human tissue, Br determ. by thermal neutron activation analysis 79−88219
human tissue, Se determ. by thermal neutron activation analysis and atomic absorpt. spectrometry 79−88218
hydrometallurgical plant effluent waters, Mo and W determ. by activation analysis with low-power neutron sources 78−7279
ice cores, from Jungfraujoch, impurity determ. by neutron activation anal. 78−11920
imitation old scientific instrument, identification by neutron activation anal. 78−8491
in vivo, description, need for basic data 77−25553
in vivo, whole body N meas., fractional charge collection technique 77−88345
in vivo total body anal. using 14 MeV neutrons, calibration and evaluation of system 78−53490
in-vivo activation analysis, diagnostic technique 80−56210
inertial confinement fusion target, density in fuel region by activation anal. 80−33807
installation with automatic surface contamination removal 78−88671
instrumental, automated rock analysis appl. 78−3769
instrumental, control and data analysis software 79−11860
instrumental, in US Geological Survey (Reston) 79−11850
instrumental large-scale routine, computer aspects 79−11862
instrumental neutron activation analysis studies of tissues from patients with pulmonary diseases 80−21535
instrumentation and software developments 77−90690
ion exchange preconcentration method 79−52832
Isar River, Bavaria, trace elements distrib. in sediment, suspension and water samples by neutron activation analysis 78−3834
isotope production, identification, teaching appl. 79−44675
Italian chondritic meteorites, Cu, Ir, Pt and Au content by destructive neutron activation anal. 78−12172
kidney, human, PIXE and neutron activation anal., appl. to cancer tissues 80−56199
laboratory and research reactor in Noril'sk mining-metallurgical complex, experience in use 77−23185
liver, bovine, PIXE and neutron activation anal. 80−56199
liver Cd, transportable in vivo meas. system 79−39496
liver matrix, bovine, determ. of bulk and trace elements 78−28050
LMFBR fuel pins, assay with Pb spectrom. 80−37461
neutron activation analysis continued
low activity beta-ray measurements, us Pu-Be neutron source and beta spectrometer 78−73114
low dose concentration profiles in solids, determ. by (n,p) and (n,α) reactions 78−7283
low-energy photon spectra, nonlinear least-squares fitting program 79−1987
lunar regolith samples from Luna-24, element abundance determ., neutron activation obs. 80−67597
lunar samples, primary matter, neutron activation anal. 78−7890
lunar soil samples from Luna-24, N_2 abundance, neutron activation obs. 80−67594
marine sediment, quantitative anal. *(Russian)* 78−92814
marine sediments *(Russian)* 79−29888
metal ion separation, displacement and exchange reactions appl. 79−52834
meteorite, Allende, multielement neutron activation anal. scheme appl. 77−48739
meteorite, Naragh, nondestructive neutron activation anal. 78−77522
methylmercury, determ. in fish, mol. activation anal. 79−24848
milk, trace elements, comparison of cows' milk, infant formulae and human milk 80−61210
milk, trace elements, comparison of cows' milk, infant formulae and human milk 80−71996
milk minerals determ., rapid neutron activation method 79−96717
moisture meas. methods using neutrons *(Chinese)* 79−57342
multi-user computer system 79−11854
multielement standards 79−57332
multielement trace analysis, neutron activation programme using absolute counting 77−77862
Mundrabilla, Fe meteorite, chem. obs. by neutron activation 78−12171
muscle, trace element determ. by radiochem. neutron activation anal. 78−27869
neutron activation analysis meas. of O and N 80−46032
neutron capture γ-ray borehole mineral anal., optimum neutron source size 80−61213
neutron capture γ-rays, practical appls., analytical techniques, PNAA facilities 80−40794
neutron capture cross sections at 14.6 MeV, activation anal. 80−52665
neutron facility of Birmingham radiation centre based on Dynamitron accelerator 77−26887
neutron generator appls., activation analysis, material investigation, radiotherapy *(Czech)* 79−31279
neutron soil moisture meter, design and operation 79−44280
neutron-capture prompt gamma-ray activation analysis: multi-element measurements on various materials 80−40796
NIMROC reference materials, for neutron activation anal. 78−7288
noble metal alloys, determ. of microcomponents, Pt, Pd, Ir, Rh *(Russian)* 77−32858
nonidentical samples and standards, 14 MeV neutrons 79−11858
nuclear oil well logging using 14 MeV neutron-excited gamma-ray spectrometry 79−48581
nuclear reactor fuel element manufacture, process control analysis of ^{235}U in U-Al alloy components, neutron absorpt. method 79−85720
nuclear reactor spent multicomponent fuel mixtures, comp. anal. by delayed-neutron decay 79−71899
nuclear spent fuel, neutron interrogation 80−5307
obsidian, Mayan, source correl. for S.Belize artifacts 78−70244
obsidian sources, chem. characterisation and hydration rates, W.Mexico 78−348
ocean sediments, neutron activated, gamma-ray scanning for elemental profile distribs. 77−17079
oil paintings, neutron activation anal., for teachers 78−81761
optical waveguide materials, radioisotope methods and neutron activation anal. appls. 78−7286
optimisation, computer-selected conditions 78−15740
orchard leaf, multielement anal. by sequential instrumental and radiochem. neutron activation 78−7798
Pacific marine aerosol, continental component identification by combined neutron activation and SEM with X-ray anal. 78−3990
parametric analysis of samples generating complex γ-ray spectra 79−92016
particle accelerator, low energy, chem. anal. appl. 78−85239
particulate matter, conc. on membrane ultrafilters, neutron activation anal. 79−52841
passive activation for environmental transuranic and moisture assay 80−21431
peak areas, analytical results calc. 79−11851
phosphosilicate films, deposited, P conc. meas. 79−69014
photon activation anal. for high energy radiation therapy 80−21534
planetary exploration, neutron-gamma techniques 79−53728
pneumo-tube on vertical channel of thermal neutron research reactor-2000 *(Russian)* 77−38332
polypropylene, film, isotactic, ion injection, space-charge-limited currents 79−69775
potsherds, Melian, instrumental neutron activation anal. 78−8485
potsherds, S.W. African, neutron activation anal. of trace elements, characterisation 78−8486
potsherds, Turkish, neutron activation anal. 78−8487
pottery, sigillated, trace element archaeochem. using neutron activation anal. 78−8488
pottery of Early Bronze Age from Lake Vouliagmeni 77−34063
power plant stack emissions, trace element analysis techniques 78−3938
prompt gamma-ray anal. 77−29084
prompt gamma-ray analysis using 3.29 MeV neutron inelastic scatt. 77−36832
pulse neutron logging, quantitative information analysis *(Russian)* 79−84541
PURNIMA reactor, unfolding of fast neutron spectra 77−74903
quartz, high purity, impurity distrib., neutron activation anal. 80−24485
radiation flux, allowance for fluctuations 78−88688
radioactive waste from leach rate determ. 80−37523
radiochemical neutron activation anal. of environmental matrices for Hg and noble metals 80−16889
radioisotope identification and mass determination, using SAMPO programme with IDENT subroutine 78−48731
radioisotopes, X-ray characteristics in neutron activation anal. at 14 MeV 80−93827
rainwater, multielement anal. 78−69512
rainwater, trace elements determ. by neutron activation analysis 78−3944

neutron activation analysis continued
rare earth metals, neutron activation anal., interference by neutron induced 2nd order nuclear reacts. 77−81444
rare earths, determ. in rocks, by neutron activation anal. 78−27870
rats, in vivo neutron activation anal. 78−73115
reactive metals, neutron activation analysis at 14 MeV for determ. of O_2 conc. 78−11602
reactor fuel anal. using radioactive thermal neutron capture gamma rays 80−61214
reactor neutron distribs. spectral characts., relative meas. by activation ratios method 77−34411
refractories and heat resistant metals, neutron activation anal. using low energy accelerator 77−73499
review 79−66378
river bottom sediments, in situ anal., pollution, mapping and prospecting appl. 77−87115
river water pollution detection, multielement anal. 78−69511
rock, assay-activation analysis, use of Au and Ag standards based on phenol formaldehyde resin 78−3419
rock samples, Sn determ. by modified method 78−85258
rocks, gamma-ray spectra processing with computer graphics 79−2228
rocks, neutron activation analysis, accuracy 78−11589
rocks, optimum method for rare earth elements determ. 79−88491
rocks, Sc determination by neutron activation analysis using ^{46m}Sc 79−79356
rocks, technique for Na/K ratios in fluid inclusions determ. 78−61568
rocks and minerals, rare earth elements determ. 79−88492
sample posture converter for nondestructive activation analysis with neutron generator 80−35497
sample shielding from thermal neutrons in reactor using Cd jacket 77−63991
scalp hair as monitor of population exposure to environmental pollutants, nucl. activation analysis 78−3940
scattering techniques in applied research, medium-flux research reactors 79−13514
screening effect of sample on standard calc. 77−56282
sea water, current vel. determ. via neutron-activation method *(Russian)* 78−77358
sea water chlorinity determ. *(Russian)* 78−77360
seawater, trace element estimation using radioactive ^{14}C *(Dutch)* 77−29459
seawater salt analysis *(Russian)* 79−39898
seawater trace element meas. *(French)* 77−41238
sediment pollution by Hg and As, instrumental neutron activation and atomic abs. spectrometric anal. 80−16890
sedimentary rocks, epithermal neutron activation anal. of Re 77−9153
sediments from Saronikos Gulf, Greece, trace elements analysis 78−3825
self attenuation of neutrons and gammas, Monte Carlo determ. 79−1980
self-shielding by neutron flux 80−93835
semiconductor, impurity determination, multielement analysis with abs. counting 77−21439
serum, human, PIXE and neutron activation anal. 80−56199
short-lived activites use, fast-transfer and deadtime correction systems development 77−90695
short-lived products, rapid anal. using minicomputer based pulse height analyser 79−11866
silicate rocks, multielement anal. by epithermal neutron activation, detector systems 78−20123
silicate rocks and minerals, instrumental neutron activation anal. 78−20548
skeletal Ca, facility for regional in vivo anal. 79−25088
skeletal Ca estimation by exhaled ^{37}Ar meas., fast neutron dose requirement 77−16962
skin lesion Mn, Cu and Zn conc. meas. by neutron activation 80−17063
soil, sample control and identification system, computer operated 79−96402
soils, multielement determ. by computerised instrumental neutron activation anal. 77−44546
solutes in liquids, conc. determ. by (n,α) and (n,γ) reacts., scintallation counting 80−35602
Solvent Refined Coal process, trace element distrib. 78−3421
sphalerites, in-determ. by nondestructive neutron activation anal. 79−87929
spine and forearm Ca changes, meas. apparatus using ^{252}Cf 79−39490
standard reference materials as multielement irrad. standards, appls. 78−80815
standards, nonidentical samples, formalism 80−71980
steel, Al semikilled, $(Fe_xMn_{1-x})O.Al_2O_3$ inclusions, deoxidation, thermodynamic conditions 80−60830
steel, corrosion protection, NAA obs. 78−53038
steel, high alloy, Si determ. 77−1967
steel, high speed, grinding wheel loading meas. using neutron-activated workpieces 79−5070
steel, neutron activation anal. in VVER reactor *(Czech)* 80−5234
steel, O and Al content determ. *(Hungarian)* 78−92586
steel, stainless, fusion blanket structures, NAA 80−23145
steel making slag, F determ. by 14 MeV neutron activation anal. *(Japanese)* 79−20484
stone artifacts, Japanese, trace elements, neutron activation anal., rel. to archaeological provenience 78−8492
stream water, inorganic pollutant analysis 77−41102
sunflower seeds, from Vojvodina, neutron activation anal. 78−20110
surface, bulk anal., neutron activation, radiography, nuclear microprobe techniques, review 78−85238
teaching experiments with 14 MeV neutron generator 77−82353
technological and industrial appl. of neutrons 77−25244
Teflon, F content, determ. by instrumental neutron activation anal. 78−7262
thermal (n,γ) reaction, elemental anal. appl. 80−40795
thermal neutron activation anal., current status in Japan *(Japanese)* 78−35754
thermal neutron induced capture gamma-ray spectrometry 79−52836
thermal-neutron activated samples, CERPL and CEREL codes for γ emitter automatic ident. and determ. 79−11852
tissue biopsies, sampling, storage and anal., evaluation by neutron activation anal. 78−11595
tissue composition measurement by fast neutron activation 77−64131
total body in vivo activation analysis, sealed tube neutron generator system, 14 MeV 79−88162
trace component analysis by radiative neutron capture 79−79358
neutron activation analysis continued
trace element anal. of medical samples, using neutron activation, clinical appl. 80−17101
trace element analysis in sea water and sediment of Northern Adriatic Sea 77−21801
trace element analysis using neutron activation and high-resolution X-ray spectrometry, beta-particle interference elimination 77−90688
trace element determ. in dry biological samples by neutron activation anal. and collection of active C 80−17213
trace element standards, prod. by doping of SiO_2 matrix 78−7289
trace elements, in carbonates, determ. by NAA 78−27858
trace metal distrib. in Atlantic Ocean, neutron activation anal. 78−85745
tree rings, long term environmental pollution histories 79−92107
tree rings, trace element distribs. using neutron activation 78−3939
TRIGA research reactor, instrumental neutron activation analysis pulsed irradiations 79−36450
tumour electrolyte exchange kinetics, meas. using fast neutrons 77−64125
Turkish clay, neutron activation anal. 78−8487
twelve-program package for activation anal. and gamma spectrometry 79−9950
two way scanning method for total body in vivo neutron activation anal. 78−92697
two-phase flow characterisation using neutron techniques, review *(Italian)* 80−19479
undergraduate experiment 78−77651
underground water movement tracing using halogen tracers and NAA 79−88014
urine U analysis by delayed neutrons 80−26331
variable energy fast neutron activation analysis facility 77−30743
water, Cr determ. by activation analysis after preconc. on activated C 78−3993
water, mineral type, Na, Cl, I and S determ. by neutron activation and X-ray fluoresc. analyses 78−3428
water, multielement instrument neutron-activation analysis, ecology appl. 80−40946
water, thermal neutron activation cross-section induced by 42 MeV bremsstrahlung 78−20112
water, trace element anal., role of Ge(Li) high-resolution detector 77−56324
water, trace elements determination using routine neutron activation analysis 78−3992
water pollution, analytical methods comparison 77−90685
water pollution, trace element meas. 77−41103
water pollution by metals monitoring, instrument survey 79−74580
water resource research using Pennsylvania State Univ. reactor 79−12159
whole organs, sampling, storage and anal., evaluation by neutron activation anal. 78−11595
X-ray registration, reduction of background using mag. field 80−16738
zircon minerals, Hf determ. *(Russian)* 77−40615
γ-ray counting, simultaneous use of Ge(Li) semiconductor and NaI(Tl) scintillation spectrometer 80−78485
Ag, air pollutant, trace analysis 77−17215
Ag concentration of coins meas. using small neutron source 79−79332
Al and Si parallel determination, 14 MeV *(Czech)* 79−24862
Al, grinding wheel loading meas. using neutron-activated workpieces 79−5070
Al, simultaneous determ. with Si in atmospheric aerosols by neutron activation anal. 80−72116
Al, trace element removal by vaporisation 79−57309
Al-Sc, dil., thermomigration of Sc 79−69280
Al-Sc, elec. resist. determ. 80−92876
Al-Si alloys, phosphorus content determ. *(Russian)* 77−40614
Am-Be neutron source for anal. of prompt neutron capture gamma-rays *(German)* 77−16879
As, determ. in beef extract, by NAA 78−27856
Au films, thickness meas. standards for Rutherford backscatt. 79−40529
Au, foil, average thermal neutron flux determ. method 78−73112
Au ores, neutron activation and mathematical programming *(Rumanian)* 78−20565
^{197}Au isotopic neutron source, form. cross sections for 3 and 14.1 MeV neutrons 80−32283
BN, O content depend. on heat treatment temp., neutron activation analysis 80−16356
B_2O_3-containing ceramic glaze, neutron probe anal. for control of prep. process *(Polish)* 80−97751
Ba, determ., in biological materials, by thermal NAA 78−27854
Bi, determ. of Hg and Au 79−57336
Bi, impurity content anal. by short lived isotopes *(Russian)* 77−40616
Bi, mapping using ^{210}Po α-particle tracks 78−20129
^{249}Bk determination in samples of transuranium elements by neutron activation analysis 79−100473
Br, determ. in silicate rocks by epithermal neutron activation anal. 78−35741
Br_2 in environmental water samples, determ. by neutron activation, isotope exchange 77−44550
Ca and P determination in small bone biopsies 79−88154
Ca, determination, image vol. samples 78−53308
Ca in vivo meas. by ^{37}Ar method, effect of recirculating breath collection systems on exhalation rate 78−40316
Ca in vivo measurement by ^{37}Ar method, inert gas elimination in humans 78−61247
Ca, total-body meas. by ^{37}Ar method 78−3589
Ca, whole-body, determ. method for rats 80−51302
Cd conc. in kidney and liver, neutron activation anal., organ depth determ. 80−72321
Cd, determ. in beef extract, by NAA 78−27856
Cd levels in kidney and liver, facility for in vivo meas. by neutron capture prompt γ anal. 78−15885
Cd, organ tissue levels, in vivo meas. system 80−67224
Cd trace detection in human liver 79−79632
CdTe, undoped, high-resist.- characterisation, impurity level investig. 77−39801
using Cf source, low intensity, comparison with radioactive X-ray fluorescence analysis 77−16885
^{252}Cf activation facility with ^{235}U fuelled multiplier and low background gamma detectors 77−36843
^{252}Cf neutron assay system for nondestructive assay of enriched U 79−81067

neutron activation analysis continued
^{252}Cf-^{235}U subcritical multiplier, computer-controlled cyclic activation anal. 79−11865
Cl, 14 MeV neutron cross sections 79−52838
Cl determination in small samples of healthy and burnt skin 79−5343
Cl, in aerosols of Otto carburettor engine *(German)* 77−12860
Cr, determ., in biological materials, by NAA 78−27855
Cr, floating zone-refining, activation anal. 80−29875
Cu, determ. in beef extract, by NAA 78−27856
Dy, foil, average thermal neutron flux determ. method 78−73112
Eu_2O_3:Gd, anal. of Gd impurity by activation anal. and cation-exchange 77−16874
F, determ. by instrumental neutron activation anal. 78−7262
F, use of small deuteron accelerator 79−100475
^{19}F, variable energy fast neutron activation analysis facility 77−30743
Fe, purification, recrystn. temp. and elec. resistivity *(Japanese)* 80−100780
Fe utilisation studies by stable tracer ^{58}Fe technique 80−61734
GaAs anodic oxide, quantitative chem. depth profiles 77−72799
GaAs anodic oxide chem. depth profiles, neutron activation analysis and Auger spectroscopy 77−77619
GaAs oxide, plasma grown, semiquantitative chemical depth profiles, Auger spectroscopy and neutron activation anal. 78−53284
Ge(Li) detector, well type, spectrum interpretation problems due to self absorption variations 79−31307
Ge(Li) γ-ray spectrometer for neutron activation anal., modification and appl. of SPECTRA program 78−20107
H_2O, determ. of selected elements and heavy metals 80−76580
Hf, determ. in silicate rocks, meteorites and lunar samples by neutron activation 78−20547
Hg determ. in environmental samples, neutron activation anal. methods, review 77−56284
Hg, determ. in food by neutron anal. 77−36848
Hg in human thumbnails 77−64130
Hg, neutron activation anal. for low levels in water 79−70503
Hg, volatilisation losses during neutron irradiation in a reactor 80−13596
I determination in biological materials by neutron activation anal. 79−57828
I_2 in environmental water samples, determ. by neutron activation, isotope exchange 77−44550
IO_3^-, determ. in rainwater by neutron activation anal. 78−76953
^{129}I, distrib. in irrad. UO_2 pellets, neutron activation anal. *(German)* 77−16880
In, in Sn or Cd by neutron activation analysis, substoichiometric method 78−76954
In-EDTA tracer, for groundwater flow investig., neutron activation anal. 78−11921
K determination in small samples of healthy and burnt skin 79−5343
Li, liq., solubility of Li_2O by neutron activation anal. 78−11601
Li_2O solubility in liquid Li, determ. by fast neutron activation 79−42252
Mg, 14 MeV neutron cross sections 79−52838
Mn determ. in Fe-, Ni-alloys by neutron activation anal., nondestructive, destructive methods 77−63987
Mn determination in environmental waters by neutron activation anal. 79−74584
Mn nodule mining and processing with nuclear meas. 77−4975
MnMgZn ferrites, accurate chemical comp. determ. by instrument-aided neutron activation anal. 79−29438
^{53}Mn, cosmic-ray-produced, in meteorites, anal. 79−30018
^{53}Mn, preparation in cyclotron by target bombard., extraction, anal. 77−61441
Mo-Ni-Fe-Co-Zn alloys, Ni, Fe, Co and Zn distrib. using neutron-activation anal. 79−52531
N human whole body measurement 79−29594
N in vivo determination using neutron capture gamma anal. and Pu-Be sources 77−86606
N, total body meas. by ^{14}N(n,2n)^{13}N, interfering reactions and spatial sensitivity 77−60240
^{14}N, variable energy fast neutron activation analysis facility 77−30743
^{14}N(n,2n)^{13}N reaction for clinical total-body N meas. 79−29589
^{16}N tagging for two-phase mass flow measurement 79−93793
Na, determination in small samples of healthy and burnt skin 79−5343
Na estimation in cotton clothing for use in neutron activation dosimetry 80−47729
Nb, impurity conc. monitoring during single cryst. production 78−31337
Nb, O impurity distrib. determ. by neutron activation anal. *(Russian)* 80−70243
^{237}Np, determ. of small amounts in solns. containing U, Pu and fission prod. 78−21682
O conc. in non-ferrous metals 79−24865
O, determ. in metals, neutron activation anal., sensitivity 78−15742
O whole-body meas. 79−29590
O_2 concentration in metals and semiconds., standardised determ. technique 79−100478
^{16}O, variable energy fast neutron activation analysis facility 77−30743
P in sheep bone, transportable system for determ. 80−109066
P, in urine, 14 MeV neutron activation method *(French)* 78−61254
Pb, in aerosols of Otto carburettor engine *(German)* 77−12860
^{204}Pb(n,n′)^{204}Pb, meas. of lead content of metal fragments 79−52850
Pu borehole assay using delayed-neutron activation anal. 80−21419
Pu, neutron analysis in solid waste 80−42840
^{242}Pu, production in reactor, yield, fractional conc. determ. 77−63986
Ru determ. in silicate rocks, preseparation procedure for neutron activation anal. 77−44547
Sb determ. in biological and environmental samples by neutron activation anal. 79−53008
Se determ. in environmental water by preconc. on charcoal, neutron activation anal. 77−44551
Se, determ. of quantity in human urine 80−36079
Se, in TeO_2, rel. to ^{131}I prod. by TeO_2 irrad. 77−86400
^{75}Se, anal. using coincidence counting, orchard leaves, bovine liver, soot samples *(Japanese)* 80−97750
Si crystal, impurities determ. and resistivity after reactor neutron irrad. 80−65563
Si, impurity determination, by neutron activation analysis 78−11586
Si layer, contamination and cross-contamination in ion implantation 78−83837
Si, MBE growth for semiconductor devices 79−83141
Si, purity for semicond. appls., neutron activation anal. 80−71979

neutron activation analysis continued
Si, simultaneous determ. with Al in atmospheric aerosols by neutron activation anal. 80−72116
Si, solid phase epitaxy, Si⟨100⟩/Pd_2Si system, dissoc. mechanism 77−7980
Si, vacuum deposition, combined with Sb ion implantation *(Japanese)* 78−88428
Si wafers, Au contamination during plasma etching 80−19831
Si:Au, impurity diffusion and distribution obs. *(Japanese)* 77−84787
Si:B, impurity range distrib. determ. by ^{10}B(n,α)^{7}Li reaction 78−11585
p-Si:B, trace determ. of U impurity by fission track method 79−79354
Si:B,P, simultaneous diffusion, radioactivation techniques 77−76622
Si:Ba, Geiger counter determ. of Ba by neutron activation 79−52816
Si:Fe, EPR and neutron activation anal. of thermal defects 78−91355
Si:Fe, solubility study by EPR and neutron activation anal. 80−75361
Si:P, determ. of P content in high-purity Si using meas. of Mo in 12-molybdophosphoric acid by NAA and AAS 80−15148
Si:P, implantation depth distrib. meas. by neutron activation anal., SIMS, junction depth method 77−31693
Si:P, measurement techniques for determining P densities 80−75262
Si:P, SiP precipitation concomitant with P predeposition 77−24326
Si:P implantation profiles, neutron activation anal. 78−7284
Si:Sb, epitaxial film, growth by mol. beam technique 80−2292
Si:Sb, ion implanted doping, isotopic composition shifts on neutron activation determination 80−24487
Si:Sb ion implantation combined with Si vacuum deposition 79−47631
Si-Si_3N_4-SiO_2-Si multilayer structs., impurity distrib., activation anal., autoradiography techniques 77−16881
SiO_2 film, on n-GaAs, Ga content after annealing at 730-940°C neutron activation anal. 78−43255
SiO_2, insulating films, neutron activation anal. and autoradiography 78−92574
SiO_2 wafers, Au contamination during plasma etching 80−19831
SiO_2:Ga film, impurity distrib. after annealing, neutron activation anal. 80−24484
^{28}Si, variable energy fast neutron activation analysis facility 77−30743
Sn, determ. in beef extract, by NAA 78−27856
Sn determ. in rocks by thermal neutron activation anal. 77−44552
Sr, 14 MeV neutron cross sections 79−52838
Ti anode, surface deposit from NaCl electrolysis, elemental anal. 78−73117
$Ti_x(PO_4)_y$, macrocompound determ. *(Russian)* 77−32859
$(U,Pu)O_2$, determ. of O_2 coeff. 80−37457
U, assay of natural samples, meas. of gamma- or neutron activity of short-lived fission products 80−61179
U assay using continuous fast-neutron source 79−52849
U borehole logging system, delayed neutron activation anal. method using ^{252}Cf source 79−53569
U, determ. in environmental samples, neutron activation, neutron assay and fluorometric methods 78−61087
U determination in environmental waters by epithermal neutron activation 79−53010
U determination in sea water by preconc. on Chelex 100 and neutron activation 79−53009
U exploration probes, meas. spatial depend. of delayed neutron signals 79−34989
U in fossil bones, dating 79−52846
U in Hueco and Guadalupe Mountain Indian ceramics, delayed neutron activation analysis 80−85230
U, nondestructive assay of mixed samples 80−18423
U ore assaying by delayed fission neutron process 79−53536
U ore grade direct determ. by photoneutron assay method 79−53570
U, prospecting at exploratory borehole, spatial depend. of delayed-neutron signals 78−7817
U resource evaluation by neutron activation anal. 78−85741
U resource survey, NURAB system for processing neutron activated samples 79−11847
U trace amounts in fossil fuels, determ. by neutron activation anal. 79−83531
U-Al alloy components, process control analysis of ^{235}U during fuel element manuf., neutron absorpt. method 79−85720
^{235}U, anal. by cyclic activation of delayed neutrons 78−53296
^{235}U content in enriched samples, fission track registration technique, solid state detectors 77−56291
V determ. in sea and surface water, preconc. on charcoal, neutron activation anal. 77−44549
V pollution, low level meas. 77−41239
$V_x(PO_4)_y$, macrocompound determ. *(Russian)* 77−32859
Zn, determ. in beef extract, by NAA 78−27856
Zn dust, for O_2 determ. *(Japanese)* 80−11977
ZnS single crystals, O content determ. by fast neutron activation anal 80−15142
Zr, determ. in silicate rocks, meteorites and lunar samples by neutron activation 78−20547
^{94}Zr, in silicate samples, neutron activation anal. 78−76951

neutron angular distribution
see also neutron spectra
14 MeV source in liquid air, ang. neutron spectra meas. 77−3209
accelerator facility, Van de Graaff generator and cyclotron for fast neutron detection and neutron reaction cross-sections 80−47805
Boltzmann equation, eigenvalue precision, influence of boundary conditions 80−27689
Boltzmann equation, eigenvalue precision, influence of boundary conditions 80−27690
critical and non-critical slabs, anisotropic scatt., struct. polynomial soln. of transport eqn. 78−70582
epithermal neutron radial flux distrib. in water, student expt. 79−97146
heavy ion reactors, neutron ang. distrib., compound nucleus decay, fission fragment anisotropy *(Russian)* 80−5160
LWR, outgoing neutron spectrum from H_2O in H_2OV interface 80−27697
organic, neutron response functions, Monte Carlo program 80−14047
random sampling technique for choosing scatt. angle from ang. distrib., dosimetric and shielding calcs. 77−61619
ultra cold neutron extraction from high flux reactor SM-2 77−57787
water, fast neutron angular penetration spectra, comparison with Monte Carlo calcs. 77−23303
(α,xn), 640, 710 MeV, n ang. and energy distribs., intranuclear cascade model 80−83109
nd, backward elastic scatt., 350 to 550 MeV, ang. distribs. 79−75782

neutron angular distribution continued
nd backward elastic scatt., 200 to 800 MeV, ang. distribs. and relativistic momentum transfer variable 79−75783
NN scatt. formalism 78−21463
(p,n), 11.2 MeV reacts. on Cr, Fe, Ni, Zr, Cd, In, Sn, Ta and Au *(Russian)* 79−80940
^{107}Ag(p,n)^{107}Cd, preequilib. emission of neutrons, ang. distrib. 78−62542
Ag(n,n′), 14.1 MeV, precompound processes 78−13093
As(n,n′), 14.1 MeV, precompound processes 78−13093
^{197}Au(p,n)^{197}Hg, preequilib. emission of neutrons, ang. distrib. 78−62542
^{11}B(p,n)^{11}C, 3-49 MeV, cross section, ang. distrib., ^{12}C level spin assignment 78−93996
^{209}Bi(n,2n)^{208}Bi, 14.1 MeV, ang. and spectral distribs. 78−82354
^{209}Bi(p,n)^{209}Po, preequilib. emission of neutrons, ang. distrib. 78−62542
^{13}C(γ,n), 7.6-24 MeV, photoneutron ang. distribs., level scheme and J$^{\pi}$ assignments 80−466
^{13}C(γ,n)^{12}C, 24-26 MeV, photoneutron energy and ang. distribs. 77−30554
^{40}Ca, neutron ang. distrib. following polarized muon capture, relativistic corrections 78−13063
^{48}Ca(p,nx), 45 MeV, preequilib. ang. distrib., generalised exciton model 77−10407
^{252}Cf fission, n angular distrib., 0 to 30° *(Russian)* 78−86564
^{252}Cf spontaneous fission, forward-backward anisotropy of prompt neutron emission 78−25254
^{59}Co(n,n′), exciton model, ang. and energy distribs. of nucl. reaction products *(Russian)* 78−54736
Cu(n,n′), 14.1 MeV, precompound processes 78−13093
^{166}Er+^{86}Kr, 602 MeV, neutron emission in strongly damped collisions 78−82373
Fe, fast neutron spatial ang. distribs. 79−97743
^{56}Fe(n,n′), 14 MeV, ang. distrib., reaction mechanism 77−26756
^{2}H(d,N), 50-85 MeV, ang. distribs., PWBA anal. 79−76005
^{4}He+π^{-}, capture at rest, neutron energy spectrum determ. 79−6702
H(n,n)p, 27.3 MeV, neutron ang. distrib. meas. 78−62532
^{165}Ho(p,xnypγ), 60 MeV, n and γ energies and ang. distribs. 78−89872
^{127}I(n,2n), ^{126}I, 14.1 MeV, ang. and spectral distribs. 78−82354
^{7}Li(p,n)^{7}Be, activation and ang. distrib. meas., absolute neutron yield determ. 78−17199
^{94}Mo(n,n)^{94}Mo, ang. distribs., 5.1 to 8.0 MeV, comparison with coupled channel and spherical optical model calcs. 77−26716
^{96}Mo(n,n)^{96}Mo, ang. distribs., 5.1 to 8.0 MeV, comparison with coupled channel and spherical optical model calcs. 77−26716
^{14}N, 5.0-9.3 MeV neutron scatt., differential cross sections and neutron ang. distribs. 77−23093
^{94}Nb level density, neutron spectra and ang. distribs. nonequilib. processes from ^{94}Zr(p,n) *(Russian)* 80−37376
Nb(n,n′), 14.1 MeV, precompound processes 78−13093
O cross section data test using n spatial distrib. in water 78−74417
O(^{3}He,n), low spin states populated in ^{18,20}Ne 77−14141
^{16}O, 5.0-9.3 MeV neutron scatt., differential cross sections and neutron ang. distribs. 77−23093
^{16}O(γ,n)^{15}O, ang. distrib. asymmetry anal. 78−25172
^{208}Pb(p,nx), 45 MeV, preequilib. ang. distrib., generalised exciton model 77−10407
^{240}Pu-fission, P-odd neutron emission asymmetry *(Russian)* 78−74413
^{A}Sb, A=119,122, level density, neutron spectra and ang. distribs. nonequilib. processes from Sn(p,n) *(Russian)* 80−37376
^{28}Si(n,n), 14.1 MeV, elastic and inelastic scatt., wide angular range, spin orbit interaction 78−89867
^{152}Sm(n,n′γ) spectra and ang. distribs. anomalous excitation *(Russian)* 77−54224
^{120}Sn(p,nx), 45 MeV, preequilib. ang. distrib., generalised exciton model 77−10407
^{181}Ta(n,n′)^{181}Ta, 9.1 MeV, CC neutron spectra and angular distrib. meas. *(Russian)* 78−25198
^{181}Ta(p,n)^{181}W, 10.2 MeV, CC neutron spectra and angular distrib. meas. *(Russian)* 78−25198
^{232}Th(γ,f), fission-neutron and fragment ang. distrib. 77−65239
^{232}Th(n,f), prompt-neutron ang. distrib. 77−65238
^{238}U (n,n), 0.9-3.1 MeV, elastic and inelastic cross-sections meas. 79−26435
^{238}U, neutron elastic and inelastic ang. distribs., 1.1 to 3.1 MeV, to ground state rot. band 77−26717
^{238}U+n, 2.47 MeV, energy spectra and ang. distrib. of neutrons 79−40927
^{238}U(γ,f) fission-neutron and fragment ang. distrib. 77−65239
^{238}U(n,f), prompt-neutron ang. distrib. 77−65238
^{238}U(n,n′), 0.9 to 3.1 MeV ang. distribs. and cross sections 79−9576
^{90}Zr(p,nx), 45 MeV, preequilib. ang. distrib., generalised exciton model 77−10407

neutron beam effects *see neutron effects*

neutron detection and measurement
see also neutron spectrometers
14 MeV neutron spectrum meas. by liquid scintillation spectrum and threshold foil detectors 79−45526
14 MeV source in liquid air, ang. neutron spectra meas. 77−3209
^{10}BF$_3$-paraffin neutron counter calibrated with six neutron sources 79−36474
absolute calibration of detectors, 10-30 MeV range, associated particle method 77−26937
absorption cross-section absolute meas. method 78−78431
accelerator facility, fast neutron research, data acquisition and anal. 80−47806
accelerator facility, Van de Graaff generator and cyclotron for fast neutron detection and neutron reaction cross-sections 80−47805
acetylene, ionisation meas. and $\bar{W}_n$ derivation for neutron irradiation 79−36430
activation analysis, in vivo, total body, neutron uniformity 78−40315
activation detector ave. cross sections in ^{252}Cf benchmark field 78−82598
activation detectors, spectra meas. in range 0.4 eV to 10 MeV 77−42210
activation detectors for fast neutron fluence determ., radiochem. evaluation, reactor appl. *(German)* 77−34510
advanced magnetic confinement fusion, plasma neutron diagnostic techniques with good spatial and energy resolution 79−46478
air, luminous emittance of neutron beam 78−86567
albedo dosimeter response to monoenergetic neutrons 77−90905
albedo dosimeters, for personal neutron dosimetry, thermoluminesc. and track detectors *(Spanish)* 77−37056
albedo neutron dosimetry, advances 80−57982
albedo neutron dosimetry 77−90914
albedo track dosimeter 79−85816
albedo-type neutron dosimeter, description and calibration data 77−65389
alpha recoil gas proportional counter 78−5089
analogue simulation of reactor neutron field, equipment minimisation *(Russian)* 78−74416
Andersson-Braun remmeter modifications for improved directional depend. and thermal neutron sensitivity 78−53499
associated activity method, calibration of flat response neutron detectors 79−9979
associated gamma-ray technique for neutron fluence meas. 79−9978
associated particle methods for flux monitoring 79−9977
associated-particle technique, absolute monitoring of DD and DT fluences 80−99428
automatic power control of IRT-M reactor using in-core detector system 77−50264
bath techniques for neutron source emission rate meas., $MnSO_4$ bath 79−9980
Bayesian deconvolution, appl. and algorithm implementation 78−70103
Benjamin detector unfolding, MATXUF improved on-line uncertainty calc. 79−85876
Benjamin detectors, on-line, real-time neutron spectrum unfolding 79−59297
beta-emission cable-type detector with Ag emitter, sensitivity during long service in reactor 78−86644
betatron, radiation protection meas. 79−29636
black and grey neutron detectors 79−9971
Bonner spheres, calibration using Sb-Be neutron source 78−33394
book, neutron physics 77−67787
BWR, method for detecting bypass coolant boiling 80−571
BWR core flow fluctuation and neutron noise obs. 78−94060
BWR in-core neutron flux instrumentation package 77−71641
BWR neutron noise local component meas., two phase flow study 78−94059
BWR neutron noise source identification, stochastic model data anal. 78−94106
BWR noise, response of neutron detector to local coolant void distribs. 80−683
BWR power plant, neutron noise meas. and analysis 78−94105
BWR power plants, neutron flux monitor 77−14240
BWR power reactor, in-core startup system with neutron flux monitor 80−32405
BWR void effects, stochastic point model and zero-power reactor simulation 78−94061
calibration of neutron detectors, simple recipes for ground scatt. 80−106231
calibration of zero-angle direction for neutron detector 80−91185
calibration using novel source emitting neutrons around 0.5 keV 77−6615
calorimetric dose meas. in cyclotron prod. fast neutron field 77−40787
CANDU self-powered flux detectors, response characts. 80−32404
cellulose nitrate, ^{6}Li enriched, neutron detection props. 80−52828
cellulose nitrate CA8015, calibration for fast neutron dosimetry 79−49907
cellulose nitrate detector, track formation confirmation for ^{7}Li from ^{10}B(n,α)^{7}Li 79−36465
cellulose nitrate film, neutron dosimeter 78−20280
cellulose nitrate film with thin layer of $Li_2B_4O_7$, response to neutrons 78−62677
cellulose nitrate foils, personnel neutron dosimetry meas. by induced molecular wt. changes 79−59269
cellulose nitrate LR115, neutron personnel dosimetry at high energy accelerators 78−20284
coincidence counting, removal of multiplication effects by Monte Carlo method 80−37715
coincidence counting of thermal neutrons, detector and calcs. 80−37716
coincidence methods with thermal neutron, appl. limitations *(Bulgarian)* 79−85874
coincidence system without delay cycle *(Bulgarian)* 79−85873
collimators, Soller slit, comparison of Gd_2O_3 and enriched ^{10}B coatings 78−82564
corrected calibration of Andersson and Braun type rem counter for divergently incident Am-Be neutrons 80−74031
correction for air scattering in front of detector 80−102226
cosmic ray intensity, supermonitor 4-NM-64 with control of long term stability of meas. 78−21808
cosmic ray neutron detector, efficiency determ. by Monte Carlo method 78−21809
cosmic ray neutron supermonitor, neutrons energy and time distribs. 79−84611
cosmic ray spectra at sea level meas. with anthracene scintillator 77−5405
cosmic rays, large underground telescope, Russia *(Russian)* 78−73589
coumarin, aqueous solution, fast neutron irrad., dosimetry appl. 78−44613
coumarin in water and heavy water, fast neutron response 80−845
counter development, electron drift vel. in inert gas mixtures 80−48843
counter with time window, 10 to 1000 μsec, using integrated microcircuits 79−3321
coupled reactor, noise measurement technique *(French)* 77−10462
critical assembly, neutron spectra meas. by activation method 80−32390
CRT neutron flux state indicator 77−79444
data acquisition and expt. control system 79−45589
DC fission chamber, reactor control applications 77−54326
delayed fission neutron technique, review 79−1979
delayed neutron detector assembly design for nondestructive anal. 78−68966
delayed neutron meas. in PWR primary circuit, influence of photoneutrons *(Czech)* 80−5205
delayed neutron measurements with a 3 MV dynamitron accelerator 79−45522
delayed neutron probe characts. for uranium exploration, field meas. 79−53568
delayed neutron spectroscopy with ^{3}He ionisation chamber 77−79501
dePangher long counter, calibration from 2 keV to 19 keV 77−88344

neutron detection and measurement continued
DePangher precision long counter and neutron dose-rate meters, calibration 80−47822
detector calibration, associated particle technique 77−26939
detector efficiency estimation, variational techniques 78−62601
detector for determ. of transuranic element comp. of nuclear fuel cladding hulls 80−63471
detector perturbations to neutron and gamma-ray spectra measurements in liquid air 79−59314
dielectric track detectors appl. *(Czech)* 78−66425
diffractometer, two-axis, use of flexible four detector system 77−65934
discriminator principle, slow neutron counting, scintillation-photomultiplier system 78−29717
dose and quality factor meas. by tissue equivalent proportional counters 80−58079
dose calc., using analytical function, health physics appl. *(Slovak)* 79−25111
dose evaluation, Maxwell method on the basis of activation detector data 78−62664
dosimeter, aq. coumarin soln. response to high LET radiation from $^{10}B(,n\alpha)^{7}Li$ reaction 78−24149
dosimeter and monitoring instrumentation calibration using ^{252}Cf and $^{238}PuBe$ sources 80−13946
dosimeter based on ^{237}Np fission for personnel 79−13539
dosimeter for pulsed neutron dose rate meas., portable, microcomputer-based 80−86991
dosimeter neutron/gamma sensitivity determ., comparison of spectral difference and Pb filtration methods 77−90915
dosimeters, integral, calibration for personal dosimetry *(Czech)* 80−27825
dosimeters, personnel, recent developments 79−63818
dosimeters for personnel monitoring, intercomparison 77−40781
dosimetric meas. using mica and pyrex, fission fragment track technique 78−13347
dosimetric measurements using ^{3}He detects. 79−63819
dosimetry, above 10 MeV, standards 79−13544
dosimetry, basic constants and meas. principles 79−20676
dosimetry, chem. composition of A-150 tissue equivalent plastic 77−21632
dosimetry, comparison of single and multidetector systems *(Russian)* 78−33294
dosimetry, fast pulse reactor, standardisation 79−13543
dosimetry, international intercomparisons 79−20636
dosimetry, neutron dose meas. with B-doped cellulose nitrate film 79−31321
dosimetry, personnel, using cellulose nitrate film and LiF as radiator and TLD 77−64132
dosimetry, standardization, 0.001-14 MeV, description of sources 79−9919
dosimetry, standardized techniques for appl. beyond reactor core 79−9920
dosimetry at JINR synchrocyclotron 80−57983
dosimetry methods for accidental exposures, Czechoslovak intercomparison 78−57075
dosimetry of n and γ from ^{252}Cf source with high emission, safety *(Czech)* 78−33296
dosimetry system, based on fission counter for fuel processing plant 80−57981
dual response albedo neutron personnel dosimeters 79−93885
DUMAND detector, objects in weak interaction studies 79−63463
EBR-II delayed neutron monitor, response to tramp uranium and fission prod. test source 79−67919
electret pulse-detector for fast neutrons 80−23260
energy deposition measurement by thin film resistors 78−29719
energy standards, accuracy 79−13587
EOSCOR: A light weight, microprocessor controlled solar neutron detector 79−101063
equivalent dose and dose rate units, USSR primary standards 77−32955
equivalent-dose measurement with Rossi counter 80−18678
European neutron dosimetry intercomparison project results, recommendations for biological and medical appls. 78−82532
evaporation neutrons in paraffin and lead layers, Monte Carlo methods 79−89346
experimental techniques, reactions below 50 MeV 77−18761
exposure measurement, neutron irrad. of reactor press. vessel steel, safety limitations *(German)* 77−34405
failed fuel element detection, delayed neutrons meas. *(Polish)* 80−73952
fast and thermal flux densities, determ. in intense high-energy photon fields by activation products counting 78−94157
fast neutron contamination in photon beams, determ. using $^{19}F(n,\alpha)^{16}N$ 77−10570
fast neutron contaminations in X-ray beams, determination using activated Al foils 79−6724
fast neutron criticality monitor, response to prompt critical bursts 80−63398
fast neutron detection system, response function and efficiency calcs. 80−14056
fast neutron detector (long counter) absolute calibration by associated activity technique 79−6801
fast neutron detectors and instrumentation, review 77−23378
fast neutron dosimetry techniques 79−20677
fast neutron energy psectra meas. in thermal reactor systems *(German)* 79−3282
fast neutron induced tracks in plastics, comparison using electrochem. etching 80−23154
fast neutron research reactor YAYOI core absorbed dose meas. by chemical dosimeters *(Japanese)* 78−86695
fast neutron spectra, activation technique determ., fusion reactor blanket model appl., unfolding program 77−79500
fast neutron spectrum anal. by threshold detection foil method *(Japanese)* 77−75023
fast neutron spectrum unfolding code MATXUF 78−5091
fast neutron time of flight spectroscopy, multi-angle detector system 80−52810
fast neutrons, energy deposition calc. using adjoint Boltzmann eqn. 79−6723
fast neutrons, monoenergetic, international flux density intercomparison 79−9981
fast pulse reactor at APRF, absolute neutron flux meas., dosimetry, calibration against ^{252}Cf source 77−23389
neutron detection and measurement continued
fast reactor system, eval. of variational method for estim. of neutron detection efficiency 79−80992
fast-neutron detector for use as criticality monitor 77−65391
fast-neutron TLD based on pellets of S-$CaSO_4$:Dy mixture 78−73251
FBR neutron fields, spectral charact. *(Japanese)* 78−46222
fission track method, physical state of fissionable material 78−41899
fissile material conc. in high-activity solns., in-line determ. 77−83066
fissile resistors, appl. to intense neutron flux pulse meas. 79−31326
fission and radiative capture cross sections ratio meas. in reson. region 77−50175
fission chamber, high-speed, with ^{235}U radiators and fast amplifier 77−6620
fission chambers, miniature, for neutron field meas. in critical assemblies 78−82422
fission counter, absolute neutron flux meas. and $^{239}Pu(n,f)$ resonance integral 80−5453
fission counters, high sensitivity, neutron spectroscopy and dosimetry appl. *(French)* 80−58078
fission counters of high sensitivity for use, in high gamma fields 78−8883
fission cross sections and product yields, integral meas. in standard neutron fields 79−13364
fission materials nondestructive analysis development, for EURATOM (CEC) Safeguards Directorate 79−85693
fission reactor, reactivity determination, pulsed neutron source technique, ZR-4 reactor appl. *(Hungarian)* 78−21673
fission reactor core, neutron detector telecontrol device with direct loading *(Russian)* 80−52770
fission reactor core monitoring system accuracy, effect of inoperable in-core detectors 79−93790
fission reactor instrumentation, using self powered detectors, 10^{-12} to 10^{-6} A meter appl., with automatic drift compensation *(Czech)* 78−883
fission track glasses, calibration of fission track dating parameters 77−41207
fission track spark counting method for neutron monitoring 80−58080
fission track technique using mica muscovite for high neutron fluence meas. 80−91395
fluence measurement in total body in vivo neutron activation anal. 77−86613
flux, density measurements for reactor control *(German, English)* 78−17335
flux absolute determ. using associated gamma-ray technique in $^{7}Li(p,n_1\gamma)$ 77−10562
flux density determ., thermal and intermediate energy, using Au foils 78−82536
flux density in nuclear reactors, mixing self-powered detector and current transducer *(Czech)* 77−50328
flux detector system, proton recoil with gas scintillation transmission counter, 1-30 MeV 77−23366
flux measurement techniques for standard cross section meas. 77−23040
flux monitoring and data anal. for neutron standard react. cross sections 78−90039
flux-to-absorbed dose conversion factor 77−90908
foil detector, activation in intermittent flux with multiple decay 79−76314
Fourier time-of-flight diffractometer, computer control 77−26918
Fourier TOF spectroscopy, influence of higher harmonics in chopper modulation function 77−6609
free neutron lifetime measurement using wall and mag. traps of ultracold neutrons 78−5107
FTR, SNEAK, effective delayed neutron fractions, integral meas. on PuO_2/UO_2 77−6497
fuel elements during irradiation, thermal state study using contactless method 80−32392
fuel fabrication and reprocessing plant, radiation protection device based on neutron detection *(French)* 78−66362
fuel fabrication and reprocessing plants, Pu neutron emission checks *(French)* 79−26720
gas counters of slow neutrons, edge effect 78−33384
gas proportional α-recoil spectrum 80−5433
gas scintillation counter with selective level population for high-intensity neutron fluxes detection 80−23253
Geiger counter, neutron calibration technique for detectors with low neutron/high photon sensitivity 79−31344
Geiger-Mueller counter γ dosemeters, fast neutron sensitivities, mixed field dosimetry 78−92705
Geiger-Muller counter, fast neutron sensitivity meas. technique 79−81096
Geiger-Muller gamma dosemeters, fast neutron sensitivities, 14.7 MeV 77−52880
graphite health physics monitor for high energy neutrons 77−83116
graphite ionisation chamber with CO_2 filling, Monte Carlo anal. of fast neutron irradiation 78−82583
graphite radiation damage dosemeter, GAMIN, correlation data 78−29657
Harwell type 95/0075 survey meter, calibration using Sb-Be neutron source 78−33394
high density proportional counter, thermal and epithermal neutrons imaging 79−5399
high energy neutron spectrometry using cellulose nitrate nuclear track detectors 80−91394
high LET radiation therapy beams, expt. microdosimetry 80−12280
high neutron fluence meas. using mica muscovite as track detector 80−106237
high resolution fast neutron spectrometry without time-of-flight using a broad window pulse shape discriminator 79−45523
high-energy (>10 GeV) neutrino physics, review of development, book contrib. 78−82201
HTGR fuel refabrication plant, nondestructive fissile assay technique 80−37562
HTR, fission chamber development 79−76112
hydrocarbon scintillators, Monte Carlo predictions of neutron detection efficiency 79−68150
hydrogenous detectors for reactor spectrum meas. 77−71733
hydrogenous scintillator, fast neutron sensitivity, calibration with ^{252}Cf fission neutrons 77−23376
in-core meas. of energy release, computerised *(Czech)* 78−86637
in-core movable neutron flux mapping computerised console development 78−13308

neutron detection and measurement continued
in-core neutron detection using mag. focused electrons, appl. to fast and thermal reactors 77−50271
in-core neutron detector using magnetically focused electrons 79−45564
Inconel-Inconel coaxial cable self-powered flux detector 80−42842
inelastic rotor spectrom., for high energy vibr. spectroscopy expts. using pulsed neutron source 78−86721
instrument calibration checks, neutron source calibration at NBS 77−38540
integral measurements, shielding cross section test 77−23305
interferometric chopper for neutrons and X-rays 78−82088
intermediate-energy standard neutron field, neutron transport calcs. 79−13588
ion injection type fast neutron dosimeter, fabrication attempts 77−81583
ionisation chamber, C walled CO_2 filled, neutron sensitivity 79−22557
ionisation chamber, tissue-equiv., response to 15 MeV neutrons 77−48874
ionisation chamber design, maximum permissible fluence instrument 79−22556
ionisation chamber mean energy deposition calc., 0.1 to 20 MeV 80−9467
ionisation chambers, development and charact. 79−68157
ionisation chambers, neutron sensitivity energy dependence, C-CO_2, Mg-Ar and TE-TE chambers 79−81134
IRT 2000 reactor in Sofia, neutron spectra and doses in exptl. canals *(Bulgarian)* 78−82489
IVV-2 research reactor, thermal neutron flux distribs. using neutron probes 80−32391
K-emulsion film dosimeter 78−20290
Kodak LR 115 cellulose nitrate films, fast neutron dosimetry 78−20279
LAMPF radiation effects facility, total neutron flux, energy spectrum, meas. and calc. 77−23331
large H-containing detectors, detector efficiency increase by albedo reduction 79−31341
laser detection of scattered neutrons from luminesc. line freq. change 80−23272
leached hull monitor for determ. of transuranic content of spent reactor fuel 79−85606
linear radiation-flux functionals, estimation of local perturbations using Monte Carlo method 80−5457
liquid scintillator containing O_2, selective activation detection of neutrons 78−25392
LMFBR fuel pins, assay with Pb spectrom. 80−37461
LMFBR high-temp. neutron detector test results 77−74909
LMFBR hypothetical accident, use of hodoscopes to obtain tomographic resoln. of fuel motion 79−54537
LMFBR multipin bundles, eval. of hodoscopes for fuel motion meas. 79−93780
local flux density of fast monochromatic neutrons, absolute determ. method 78−5106
LR115 cellulose nitrate detector system for personal dosimetry near high energy accelerators 80−58081
LR115 red cellulose nitrate personnel neutron rem dosimeter, design 80−52826
LWBR delayed-neutron pellet assay gauge 79−54590
LWR, fuel reprocessing plant, NDT control methods 80−5314
LWR irradiated fuel assemblies, nondestructive exam. using γ-ray and neutron techniques 80−66760
LWR spent fuel, non-destructive anal. using inherent and induced neutron radiation *(Russian)* 80−68805
LWR spent fuel, nondestructive meas. and verification for materials safeguards 80−78420
lyoluminescence dosimetry in photon and fast neutron beams, using mannose 78−15902
lyoluminescence dosimetry using saccharides 77−52881
Makrofol, neutron personnel dosimetry at high energy accelerators 78−20284
Makrofol polycarbonate, electrochemical etching of neutron induced tracks, appl. to dosimetry 78−20282
medical dosimetry problems rel. to incorrect composition of tissue-equivalent gas 80−81743
methane-based tissue equivalent gas, W_n and neutron kerma 80−104769
metrological certification of neutron reference sources 77−30682
microprocessor controlled reactivity meter for real time monitoring of reactors 78−33263
miniature thermal neutron detector, flux space distrib. meas. *(Czech)* 77−38549
mixed field, of fast neutrons and γ-rays, Fricke and $Ce_2(SO_4)_3$ dosimeter appls. 78−74514
mixed n-γ field microdosimetry and neutron/gamma discrimination *(French)* 80−12279
mixed neutron-gamma beam from IBR-30 reactor, beam charact., detectors props. *(Russian)* 77−67793
monitor calibration for radiation protection at 24.5 keV and 2 keV 78−89983
Mott-Schwinger scatt. polarimeter for MeV neutrons 79−22571
multi-detector system, using Bonner and threshold fission detectors *(Slovak)* 79−36456
multiaxis neutron diffractometer automation 80−102417
multiple foil activation method for measuring neutron spectra in stopping pion field 78−73248
MWPC, appl. to radiation localisation problems in medicine and biology, review 79−5432
MWPC, pressurised, for neutron imaging, gas density, cathode biasing, effects on resolution 78−37518
NE213 liquid scintallator, light output for electrons and protons 80−32564
NE213 neutron counter, efficiency calibration 80−27877
NE 213, n-γ pulse shape discrimination 77−57816
NE 213 liquid scintillator, decay under neutron and gamma excitation *(German)* 78−55097
NE 213 liquid scintillator, deuterated, decay mode *(German)* 78−55096
NE 213 scintillator, neutron response functions, energy range to 40 MeV *(Japanese)* 80−18756
NE 238 fast liquid scintillator, scintillation decay and n-γ discrimination *(German)* 78−55101
NE-110 scintillation counter, obs. neutron flux meas. 80 to 500 keV 79−735
NE-213 spectrum system for 1.0-20 MeV neutrons 77−88346
neutral beam test facility, D-D neutron meas. 80−37710

neutron detection and measurement continued
neutral particle background, effects in cosmic ray telescopes composed of Si solid state detectors 78−28472
neutron capture absolute yield calibration, saturated resonance technique 79−80935
neutron coincidence, detection of groups of associated pulses in train of random pulses 79−22564
neutron collimated fast beam, radiation quality local distrib. 80−12247
neutron counter (60 element) calibration in energy range 8.5 to 450 MeV 79−6798
neutron counting statistics in subcritical cyclo stationary multiplying system 80−32323
neutron detector efficiency calc. using Monte Carlo computer program 79−63874
neutron dosimetry, appl. of thermoluminescent materials 79−22497
neutron dosimetry, meas. standardisation for biological and biomedical appl. 80−12271
neutron energy spectra at intermediate energy, measuring apparatus 79−54738
neutron energy spectrum in stopping pion field, multiple foil activation method 78−85386
neutron flux distrib. in nonhomogeneous samples, computational model for prompt gamma-ray analysis 80−14060
neutron monitor calibration, standard fields at Physikalisch-Technische Bundesanstalt 80−57999
neutron multiplicity for gamma rays from (particle, xnγ) reacts. 80−37689
neutron standards and appl., conference, Gaithersburg, MD, USA (March 1977) 79−9581
neutron-gamma discrimination in fission chamber *(German)* 77−88357
neutron-gamma pulse shape discrimination, digital technique 77−403
neutron-neutron quasifree scatt. studies using cyclotron 77−34525
non-destructive assay techniques for irradiated fissile material in extended configurations 80−71872
nondestructive assay of highly enriched spent fuel, using Ge(Li) detector and ^{235}U fission chambers 79−89522
nondestructive assay of irradiated nuclear fuel for safeguards, review 78−82495
nondestructive neutron assay for nuclear materials accountability and criticality control 80−66759
nuclear accident dosimetry system, Czechoslovakia 80−57978
nuclear accident dosimetry systems, comparison 79−22496
nuclear accident dosimetry systems, neutron and gamma-ray dose meas. 77−38425
nuclear fuel reprocessing plant, neutron monitors for process and safety control 80−5458
nuclear materials accountability, U and P NDA of crated waste by gamma-ray and neutron coincidence counting 80−83166
nuclear power plants, personnel monitoring concepts 79−85822
nuclear reactor, thermal neutron flux meas. method *(Rumanian)* 78−21670
nuclear reactor noise, specialists' meeting, Gatlinburg, USA, Sept. 1977 78−94057
nuclear ship streaming neutron meas. by two-detector method 77−46408
nuclear track detector, appl. as neutron dosimeter, reponse to standard neutron sources 80−5342
nuclear track emulsion, NTA film, as personnel neutron monitor in criticality accidents 77−29208
on-line calculation of experimental neutron spectra uncertainties 79−59298
on-line reactivity meter, comparison between direct and polarity correlation techniques for projected Gauss Markovian process 79−54528
passive neutron assay of Pu contaminated solid waste streams 79−36373
passive neutron technique for meas. of UF_6 and Pu in sealed containers 77−67954
passive personnel portal detectors for nuclear materials diversion protection using gamma-ray and neutron detectors 80−78389
PBF, temp. sensitivity of Co self-powered neutron detectors under PWR conditions 78−33275
PBHTR, out-of-core instrum. for detection of spatial flux irreg. *(German)* 78−82430
personal dosimeter based on track detector 77−70551
personal dosimetry system, ^{237}Np neutron induced tracks in polycarbonate 78−31908
personnel dosimeter calibration, US NBS standard reference neutron fields 80−9417
personnel dosimeters, European comparisons 80−57980
personnel dosimeters based on film badges and TLDs, appl. *(Russian)* 78−20293
personnel dosimetry, Czechoslovak comparison of methods 77−50302
personnel dosimetry, elec. conductivity meas. method 77−40776
personnel dosimetry in criticality accidents, fast neutron dosimetry system 79−85817
personnel monitoring film, Kodak NTA, energy depend. 79−100753
personnel neutron dosimeters, calibration for use in different neutron fields 80−58001
photodiodes as recoil particle detectors 79−97927
photon dosimeter, fast neutron sensitivity determ., modified Pb attenuation method 79−81095
photoneutron production in neutron detectors in high energy X-ray beams 78−94174
photonuclear reactions, Saclay linac, photon beam prod., 10-100 MeV, giant dipole resonance *(French)* 79−523
Pilot U scintillation response to neutrons, 50 to 120 MeV 77−54453
Pilot U scintillator for 55-225 MeV neutrons 80−18762
plastic detector technique in fast neutron radiography 79−76299
plastic detectors, electrochemical etching of neutron induced tracks using HV 50 Hz supply 78−86738
plastic foils for neutron dosimeters, electrochem. etching prep. techniques 79−76298
plastic neutron scintillation detector efficiency in 80-220 MeV range 78−78568
plastic scintillation counter, time resolution meas. for 16 MeV neutrons 77−83460
plastic scintillator, neutral radiation incident spectrum determ. 77−54398
plastic scintillator of high transparency containing Gd, fission neutron detection efficiency 78−78567
polarimeter, 3-D calibration procedure 80−18770
polarimeter for nucleons between 100 and 500 MeV 78−82599

neutron detection and measurement continued
polarimeters, double scatt. fast neutron, optimisation of geometrical factors 77−54478
polarisation anal., separation of coherent and spin incoherent scatt. from D$_2$O 77−6655
polarisation meas. in (p, n), (α, n) and (d, n) reacts. on light nuclei 78−70726
polarisation meas. with high press. He scintillation counter, Monte Carlo convections 80−14061
polariser-analyser efficiency meas. by spin flip meas. 80−27911
polycarbonate fast neutron dosimeter, development and comparison with conventional emulsion dosimeter 80−86990
polycarbonate track detector, electrochemically etched, meas. of low neutron fluences 80−32577
polyester foil neutron track detection, dosimeter appl. 80−5439
polyethylene-terephthalate track detector, electrochemically etched, meas. of low neutron fluences 80−32577
polymer track detectors, high energy neutron detection 79−26861
portable digital reactivity meter for power reactors PWR, BWR appls. *(German, English)* 77−82999
portable neutron spectrometer/kerma-rate meter, design, performance 78−33361
portable spectrometer/dosimeter for low level neutron radiation meas. 79−49869
position sensitive detectors, electronics, ILL expts. 79−45571
position sensitive detectors for thermal neutrons *(Japanese)* 78−78589
position sensitive gas proportional neutron detectors, microprocessor testing method 78−70692
position sensitive neutron detector using (n,γ) on ^{157}Gd, ^{177}Hf foils, proportional chamber detection of conversion electrons 78−37517
position sensitive proportional detector for thermal and epithermal neutrons 78−25390
position sensitive thermal neutron detector, large area, high precision position readout 80−58063
position-sensitive proportional counter 80−63459
positron sensitive detector for thermal and epithermal neutrons 77−38566
prompt fission neutron logging technique, computer modelling 79−53566
prompt neutron multiplicity distrib. meas. from ^{242}Cm spontaneous fission 80−83131
proportional, methane filled telescopes for fast neutron spectrometry 80−37683
proportional counter, position-sensitive, direct position and time digitizer 80−58090
proportional counter, reactor control applications 77−54326
proportional counters, geom. effects on proton recoil spectra 80−14050
proportional counters, H_2 filled, flux monitors 77−23379
proton recoil data, frequency filtering 78−46240
proton recoil proportional counters, fast monoenergetic neutron fluxes meas. procedure anal. 78−17478
proton-recoil counter technique for measurement of fast neutron spectrum 80−9447
proton-recoil telescope for in-line absolute neutron fluence measurements 79−18079
pulse detector, reactor control applications 77−54326
pulse fission chamber, reactor control applications 77−54326
pulse separation spectrum for detection of fission neutrons and single neutron events 77−6651
pulse shape analyser, effect of pulse pile-up on discrimination between neutrons and gamma rays 80−91402
pulse shape discrimination cct. for n and γ multidetector meas. 78−70709
pulse shape discriminator for n,γ separation, appl. to TOF spectroscopy 79−6786
pulsed accelerator for neutron travel time meas. *(German)* 78−17475
pulsed reactor, fast neutron spectra meas. 77−50222
PWR, 450 MWe, noise obs., analysis and interpretation 78−94072
PWR, core flux meas. by microprocessor based automatic flux mapping system 79−45359
PWR, effect of measurement conditions on the design of delayed-neutron detector units *(French)* 79−97855
PWR, ex-core neutron detectors, calc. of spatial weighting func. 79−36351
PWR, flux monitoring startup and safety system, ex-core, design and qualification 77−65286
PWR, fuel monitoring, by delayed-neutron detectors 80−737
PWR, power monitoring, direct charge detectors appl. 78−17344
PWR, r.m.s. ex-core detector signal to core barrel amplitude scale factor 80−52767
PWR, St. Lucie 850 MWe, neutron streaming meas. and shielding recommendations 78−70608
PWR, system for internal neutron meas. *(French)* 79−76113
PWR, Westinghouse, neutron flux mapping at low power 78−21703
PWR CANDU, thermal neutron flux distribution, meas. and simulation 78−82492
PWR core support barrel motion monitoring by ex-core detectors 79−13446
PWR movable in-core neutron detectors *(Japanese)* 79−26722
PWR multisection ex-core detector spatial weighting functions 79−13481
PWR neutron flux detectors, reliability tests *(French)* 80−32403
Q-factor measurements of Oak Ridge National Labs. Dosimetry Appls. Research Facility 80−83237
quadratic approx. effect on neutron moment and count distrib. in multiplying system 79−89343
quartz, track retaining props. for high temp. in-core neutron fluence meas. 77−75032
quartz resonators appl. for recording intense fluxes 80−23254
quasi-elastic neutron scatt., direct model fitting of uncorrected TOF data 79−31309
radiation quanta, comparison of least-squares and maximum likelihood estimates for counts which follow a Poisson distrib. 79−23487
radiochemical measurement of cosmic ray muon induced neutrons, depth depend. 77−61670
radiometers testing standardisation, Soviet method 80−99405
radiotherapy, high-energy accelerators, mixed photon-neutron field meas. 80−51267
random search algorithm for 2-D data fitting 80−27915
reactivity meters for monitoring extremely subcritical reactors, source analogue 77−71643
neutron detection and measurement continued
reactivity of compact core with two absorpt. reflector, pulsed neutron method *(German)* 77−61500
reactor core, VVER type, neutron noise, diagnostic method of mech. vibrs. *(Czech)* 77−3120
reactor core dosimetry standards 79−9824
reactor dosimetry using TLD and Rh activation techniques 77−50301
reactor in-core flux monitoring 80−5297
reactor material safeguards, unirradiated fuel control in BOR-60 fuel assemblies *(Russian)* 80−68809
reactor neutron, flux meas., calculation of target and detector size in determination of 14-MeV neutron energy flux 79−97829
reactor neutron flux meas., high temp. neutron rad. detectors and cables 79−76111
reactor neutron flux meas., integrated cable detectors for use under flux and/or at high temperature *(French)* 79−76114
reactor neutron flux meas., self-powered neutron detector with enriched-U emitter 79−76115
reactor noise analysis techniques 77−3069
reactor primary coolant flow rate determ. using gamma/neutron ratio near primary line 77−65254
recoil atoms meas. by laser spectroscopy neutron detect. possibility 79−22864
recoil proton counter, ^{1}H(n,n) 180° cross sections 79−36240
relativistic calculations, importance in proton recoil telescope efficiencies 80−102225
REM ratemeter for direct reading of dose equivalent rate 78−53502
rem-dose measurement of mixed p-n radiation using solid state detectors of fission fragments 80−36137
resonance activation neutron detector materials, uni-resonance approx. technique for higher resonance reaction rate 77−75030
response functions of spherically moderated neutron detectors 80−37687
reverse neutron TOF method, appl. to slow-neutron spectrometry with Fourier beam choppers 79−22534
scattered radiation from neutron collimator 77−48870
scattered radiation from neutron collimators 77−40788
scintillating glasses, effects of temp. on pulse height and cond. 77−10547
scintillating glasses, pulse decay time meas. at room temp. 78−46225
scintillating glasses activated by Ce^{3+}, luminesc. 79−38668
scintillation counter, calibration of threshold 80−23258
scintillation counter, liquid time compensated, high efficiency detector for TOF studies 77−23363
scintillation counter, NE213, detection efficiency meas. for 130 MeV neutrons 80−27888
scintillation counter, test of Monte Carlo calcs. by ^{12}C(p,n) and ^{12}C(p,p′) cross section meas. 80−37713
scintillation counter effective solid angle for fast neutrons 77−57819
scintillation counter efficiency, time of flight meas., Monte Carlo method appl. 78−17045
scintillation counter multidetector arrangement for on-line meas. of neutron and γ-ray multiplicities 78−50440
scintillation counters, neutron transit time and interaction coord. determ. 79−26807
scintillation counters, organic, neutron response functions, Monte Carlo program 80−14047
scintillation detector of LiF and ZnS(Ag) vac. coated layers 77−54456
scintillation detectors for neutron physics research 79−72199
scintillation detectors for neutrons from short-lived plasma 80−23263
scintillation detectors with nanosecond time resolution 80−69029
scintillation neutron counter, photomultiplier noise characteristics 80−74077
scintillation pickups with plateau in counting characteristic, review 80−47811
scintillation plastic large area fast neutron detector 78−90022
scintillation spectroscopy, organic, use of logarithmic pulse height and energy scales 80−37690
scintillator containing U, inorganic solid-soln. single-cryst., prototype fission detector, performance 77−54445
scintillator for 250-1000 keV neutron flux meas., >95% efficiency 77−26938
scintillators, thin cylindrical, spectral characteristics for fast neutron spectrom. 79−26806
seawater chlorinity and salinity determ., possible use of neutron methods *(Russian)* 78−65422
secondary standard for total cross sections, BF_3 counters in polyethylene sphere 77−23381
self powered detectors, neutron response, epithermal component 80−58073
self-powered detector with fissile emitter, theoretical evaluation 78−74533
self-powered detectors, beta particle escape efficiency determ. 80−47816
self-powered detectors, reactor in-core monitoring *(Slovak)* 79−31322
self-powered detectors, review 79−45558
self-powered detectors for in-core reactor neutron flux meas., detector signal composition 80−32402
self-powered detectors for incore monitoring 79−45367
self-powered detectors with burn-up, sensitivity anal. 77−75024
self-powered flux detectors, response characts. in CANDU reactors 78−82594
self-powered neutron detectors, calc. of activation component of response to thermal and epithermal neutrons 80−63470
self-powered neutron detectors for incore meas., comparative performance 79−45369
semiconductor counter with ion implantation 80−69030
semiconductor detectors for dosimetry in intense neutron-gamma fields 77−46460
semiconductor detectors for neutron field investigation in critical assemblies 77−54430
sensor performance testing, automatic counting channel and analysis system 79−13612
SIN neutron facility, 150 to 600 MeV, detection and meas. 78−62669
Skylab, spacecraft-produced neutron fluxes meas. 78−28486
slow neutron field in channel of VVR-M-type reactor, measurement of parameters 79−31325
slow neutron fields, meas. of spectral characteristics using Cd ratios of activation detectors 77−67953
slow neutron reaction rate ratio meas. using Cd and Hg prompt gamma reaction 79−30837
small angle neutron scatt. with azimuthal symmetry 78−46212
SNM-57 proportional counter, intrinsic background meas. 77−65399

neutron detection and measurement continued
solid dielectric detectors with breakdown phenomena and their applications in radioprotection 80−91388
solid state nuclear track detector 80−27876
solid state nuclear track detectors, fast neutron dosimetry 78−20278
solid state nuclear track detectors, reactor neutron fluence meas. using Au and In foils 80−69035
solid state nuclear track detectors appl., brief review 78−33299
solid state nuclear track detectors for fast neutron meas. 80−91393
solid state track detector, actinide fission cross section meas., fragment ang. distrib. 79−76300
solid state track detectors, neutron fluence meas., international intercomparison 78−20283
solid state track detectors, use in neutron dosimetry, verification of possibilities *(Czech)* 78−82574
solid-state nuclear track detectors, development and use for reactor phys. expts. 78−41886
solid-state track detectors for mass of temp. of neutron gas 78−66455
solid-state track recorder applications in U.S. nuclear reactor energy programs 80−95506
solutes in liquids, conc. determ. by (n,α) and (n,γ) reacts., scintallation counting 80−35602
spark chamber and time of flight detector for 15-150 MeV neutrons from extended source 77−83447
special nuclear materials, assay and accountability using neutron correlation meas. tech. 80−69015
spectral and intensity distribs. of accelerator prod. neutrons in concrete room 79−49868
spectral meas. of secondary neutrons and photons from 52 MeV proton irrad. of thick targets of C, Fe, Cu, and Pb 78−58282
spectroscopy, new techniques and results 77−23365
spherical survey meter response 80−18679
spontaneous fission low background detection system 79−36475
spontaneously fissioning material, assay using neutron correl. counting 79−85605
spontaneously fissioning material, Monte Carlo neutronic and electronic model for thermal-neutron coincidence counting 80−23165
spontaneously fissioning nuclides, content anal. by neutron counting 79−72206
standard long counter side-on response to fast neutrons 79−22548
standard neutron fields, integral meas. 79−13363
statistical errors of dose estimation in personnel neutron monitoring with albedo dosimeters 79−48344
statistical regularization method for spectra establishment according to threshold detector readings, IBR-30 reactor appl. 78−37483
steam generating channels, volumetric steam content determ. by slow neutron method 79−30903
Stern-Gerlach polarimeter for measuring polarisation of cold neutron beams 80−37679
stilbene, n-γ pulse shape discrimination 77−57816
stilbene crystal, fast neutron counting efficiency 77−71719
stilbene scintillator, ^{239}Pu, capture/fission cross-section ratio meas., 0.007 eV-12 keV 77−54266
subsoil neutron moisture probe, lab. calibration, minimum soil sample size calcs. 77−57333
subthermal neutrons, polarisation meas. by shim and spin reversal methods 77−88363
superdense nuclei, search for neutrons with binding energy >40 MeV *(Russian)* 79−89515
superheated supercond. colloid neutron detector, detection and background rejection tests 78−78580
superheavy elements, search via neutron emission due to spontaneous fission 78−50117
surface barrier spectrometers for fast neutron calibration in MeV range 79−9961
surface of revolution technique, differential elastic cross section absolute meas. 77−23394
temmeter, lack of accuracy considerations 80−42869
thermal, energy depend. detection efficiency of cylindrical counter, wall effect, calc. 77−57803
thermal and epithermal neutron flux densities, self-powered neutron detector sensitivity 80−52817
thermal neutron coincidence counting, correction for variable moderation and multiplication 80−69045
thermal neutron counter for Pu contamination assay in radwaste 79−85716
thermal neutron detection by activation of $CaSO_4$:Dy-KBr 80−32581
thermal neutron distrib. in bone in paraffin phantom, irrad. with 14 MeV neutrons 78−3616
thermal neutron flux density, working standard based on F-1 reactor 78−82410
thermal neutron polarisation anal. experiments, corrections for instrument component inefficiencies and sample multiple scatt. 78−29725
thermal neutron self-shielding factors, Monte Carlo calc. for TLD probes 79−45431
thermal neutron spectra parameter meas. in reactor core 80−9348
thermoluminescence in CaF_2:Dy(Mn) induced by 81 MeV diffr. neutrons 77−52883
thermoluminescent detector for 14.7 MeV neutron-gamma mixed field 77−6625
thermoluminescent detectors, fast neutron sensitivities 80−102413
thermonuclear plasma, pulsed, high-density, neutron diagnostics 79−90462
thin monitors for reactor dosimetry 80−32522
thin-film fission thermocouple detectors for reactors safety expts. 80−22987
time and fluence meas. system at fast pneumatic transfer systems for activation anal. *(German, English)* 77−38576
time of flight coincidence meas. *(German)* 79−18075
time of flight facility with mag. beam swinger, time, energy resolutions 77−57796
time of flight single crystal diffractometer using a position sensitive detector 80−99404
tissue equiv. medium, simultaneous meas. of neutron and gamma ray spectra 78−5058
TLD, energy response of ^{6}LiF, ^{7}LiF to neutrons 77−29210
TLD, neutron dose monitoring using multiple LiF TLD badge 77−90907
TLD, self-shielding factors for TLD-600 and TLD-100 in isotropic flux of thermal neutrons 77−6638
TLD for albedo neutrons, personnel dosimetry system, single- and multi-element devices comparison 78−96099

neutron detection and measurement continued
TLD materials, kerma for monoenergetic neutrons, theory, expt. comparison 77−5086
TLD response to 14.7 MeV fast and thermal neutrons 77−66856
TLD-600, activation and damage effects after neutron pre-exposure 79−13540
TOF high efficiency detectors for high energy neutrons, subnanosec. time resolution 78−37481
TOF meas., rate depend. of counting losses 80−37692
TOF meas. on spectra from N_2 sphere surrounding D-T source 77−38422
TOF neutron detector for meas. with very fast burst source *(French)* 80−14040
track detectors, spectra meas. in range 0.4 eV to 10 MeV 77−42210
track etch detectors, neutron energy depend. and threshold energy 80−61703
track etch imaging, model of directional effects 77−18739
transit-time spectrometry, detector containing ^{3}He 80−63441
TREAT, fast neutron hodoscope perform. tests on 91-pin fuel bundle 79−41005
TREAT facility, pinhole imaging of test fuel element 78−21627
TREAT fast-neutron hodoscope, time and mass resolution of fuel motion, data acquisition system 79−41003
UCN, detection systems, sources, transport, book contrib. 80−22882
ultra cold neutrons, prod., detection, confinement and storage for fundamental phys. expts. 79−63858
ultra-cold neutron scintillation detectors, optimisation 80−74090
ultracold neutron flows, spectra meas. 77−26926
ultracold neutrons, zone mirrors for high resolution image form. 78−87003
variable dead time counters, theoretical response and neutron multiplication effects 79−22570
VIPER reactor, neutron leakage spectrum and dose meas. 79−3243
volumetric steam content determ. by noncontact neutron sensor 79−30904
VVR-SM reactor, neutron flux and dose meas. and evaluation *(Czech)* 80−5252
water moderated reactor, influence of air bubbles on neutron detector response 80−18442
weighting functions for flux and relative speed of change measurement *(Croatian)* 77−10561
yield estimation with solid state nuclear track detectors 77−10544
Λ hyperon polarisation, meas. by hybrid Monte Carlo tech. 80−99431
(n,γ) thermal react. cross section meas. with liquid scintillation spectra 78−25382
n-γ mixed field, dose distrib. meas. on phantoms, TLD, solid-state, photoluminesc. detectors *(Russian)* 78−33297
Ag activation detector, determ. of neutron yield from pulsed neutron sources 79−31332
Ag-activated Geiger counter calibration for neutron yield determ. in Frascati plasma focus expt. 80−99409
Al_2O_3 TLD for dosimetry after accidental gamma radiation release 78−57076
^{241}Am-Be thermal neutron flux standard density variation obs. 77−83409
Ar, liquid, scintillating target, fast neutron polarisation analyser 80−47833
B, liquid scintillation slow neutron detector with n-γ separation cct. 78−862
B neutron capture therapy of brain tumours, simultaneous flux monitoring system 79−92352
^{10}B-loaded liquid scintillator with pulse-shape discrimination 79−59309
BF_3 detector ageing, depend. of temporal distrib. function 79−63872
BF_3 detector assembly for photofission and photoneutron studies 80−63484
BF_3 proportional counter, high press. *(Japanese)* 78−66453
^{10}B, neutron cross section standards, detection techniques 79−9970
^{10}B shields, transport calcs. and transmission factors for activation detectors 78−78434
^{87}Br, prod. by radiochem. separation, for neutron decay obs. 78−70951
C_6D_6, n-γ pulse shape discrimination 77−57816
C_6H_6, n-γ pulse shape discrimination 77−57816
CaF_2, TLD, calc. neutron sensitivities 79−22568
CaF_2:Tm thermoluminescent dosimeters, response to 14 MeV neutrons 79−49867
$CaF_2+Dy_2O_3+KCl$, intermediate neutron detection by thermoluminescence 80−5444
$CaSO_4$:Dy, Cd-covered TLD, thermal neutron dosimetry 77−90912
$CaSO_4$:Dy TLD, thermal neutron and γ-ray meas. in mixed radiation field, activation and capture gamma technique 79−738
$CaSO_4$:Dy TLD meas. of reactor thermal neutrons 78−78441
$CaSO_4$:Dy+Dy_2O_3+KCl, intermediate neutron detection by thermoluminescence 80−5444
$CaSO_4$:Tm, Li, mixed field TLD 77−9263
$CaSO_4$:Tm and nonluminous ^{6}LiF powders mixture, thermoluminesc. response to thermal neutrons 77−73588
$CaSO_4$:Tm composite TLD for γ-rays, X-rays, β-rays, and thermal neutrons 78−28076
$CaSO_4$:Tm/polythene mixture, thermoluminesc. response to fast neutrons 80−5340
Cd covered Au foils, neutron spectra determination by resonance reactions 79−93837
Cd, effective energy cut-off determ., rel. to neutron flux meas. in high-temp. reactor 78−86573
CdTe detector, thermal neutrons 78−17479
CdTe, thermal neutron detection 78−17479
^{144}Ce photoneutron sources, determ. of standard neutron yield, influence of bremsstrahlung 79−72177
^{252}Cf fission, meas. of $\bar{\nu}$ and η, Mn bath systematic effects 77−23132
^{252}Cf neutron source for water-steam mixture void fraction meas. 79−26762
^{252}Cf spontaneous fission spectra, data anal. in TOF meas. 79−26811
^{252}Cf, sub Cd thermal neutron fluxes in H_2O near the source 79−698
Cu as activation detector for thermal neutron meas. 80−52814
DT fast neutrons in blankets and shields, neutrons, associated particle method 77−71690
Dy_2O_3, activation detectors for thermal and fast neutron detection 80−887
Gd, effective energy cut-off determ., rel. to neutron flux meas. in high-temp. reactor 78−86573

neutron detection and measurement continued
Gd loaded large liquid scintillator, neutron radiative capture cross-section meas. 78−25380
Ge(Li) detectors, fast neutron leakage spectrum determ. 80−32565
Ge(Li) diodes, teflon covered for fast neutron detection 78−25384
Ge(Li) surface barrier detectors, fabrication 77−3207
$H(n,n)^1H$, 10 keV-20 MeV, use for neutron flux meas., proton-recoil detectors 79−9960
$^1H(d,n)^4He$, neutron energy meas. with Si detector 80−32566
^1He detector design for transuranic waste assay, low-level, Monte Carl calcs. 79−54542
^1He fast detector with linear energy response 78−25393
^1He gridded fast neutron ionisation chambers, Monte Carlo calc., of energy dependent efficiency 80−99417
^1He ionisation chamber, improved time resolution in n-γ coincidence meas. 80−99416
^1He proportional counter, neutron dose equivalent meas. from thermal energy to 10 keV 79−63875
^1He proportional counters, thermal neutron detection performance, temp. depend. 80−58071
^1He proportional counters in portable detector, calc. and measured efficiency 77−65390
^1He spectrum, meas. of fast neutron streaming through grid plate shield in LMFBR 77−3081
^3He-filled proportional counter, for sensitive dose or dose equivalent meter 79−45427
^{115m}In specific activity, for fast neutron determ. after criticality incident 79−3248
Li glass NE-912, neutron detection efficiency *(Russian)* 80−27901
Li-glass scintillator, pulse height distrib., neutron energy depend. 79−54751
^6Li-loaded liquid scintillators with pulse-shaped discrimination 79−59310
$Li_2B_4O_7$:Ag TLD, fast neutron dosimetry 78−94163
$Li_2B_4O_7$:MN bulb dosimeters, nonuniversality of TL linear energy transfer response 79−97948
LiF TLD, use as thermal neutron detector 78−21821
LiF TLD-700, Harshaw, effect of sample size and batch origin on thermal neutron sensitivity 78−40342
LiF thermoluminescence induced by 13.8 and 81 meV diffr. neutrons 77−56481
Li_2O-MgO-Al_2O_3-SiO_2 glass scintillator for pulsed neutron detection 80−87019
^6Li glass detector, threshold photoneutron spectra meas. 77−88334
^6Li glass scintillators, appl. as neutron detector, problems and consequences 79−9968
^6Li sandwich counter, meas. of neutron spectra in fast neutron systems 80−27884
^6Li semiconductor sandwich neutron spectrometer with background discrimination 78−50431
^6Li-salicylate neutron detectors with pulse shape discrimination 79−97950
^6LiF TLD, response to neutrons, with thermoluminescent-LET dependency 79−13604
$^6Li(n,\alpha)^3H$ reaction, as standard in neutron flux meas., instruments review 79−9969
^7LiF, TLD, calc. neutron sensitivities 79−22568
^7LiF TLD, response to neutrons, with thermoluminescent-LET dependency 79−13604
^7LiF-Teflon disc TLD, determ. of neutron fluence and γ-dose distribs. 79−45434
Mn bath, for intermediate neutron meas., leakage determ. 78−37525
NaI, meas. of fast neutron capture cross sections 78−74530
NaI(Tl), pulse shape discrimination of high-energy neutrons and gamma rays 78−33395
NaI(Tl) scintillator, evaluation as fast neutron monitor 79−45559
Na(Tl) scintillator detectors for neutron-gamma discrimination 80−102386
$^{93}Nb(n,n')^{93m}Nb$, fast neutron flux determ. by ^{93m}Nb disintegration rate meas., X-ray emission *(German)* 77−38579
^{93m}Nb activity measurement, determ of fast neutron fluence in power reactors *(German)* 77−34371
^{227}Np damage track detectors, effects of subthreshold fission on neutron dose meas. 78−33375
^{237}Np dosimeter and spark counting system, for routine personnel monitoring 78−89984
^{237}Np threshold detector, subthreshold phenomena effects on nondestructive assay of reactor fuel 79−22409
$^{16}O(n,p)^{16}N$, utilisation for monitoring 14 MeV neutron generator output 79−3287
polarised neutrons, 2.50 MeV, meas. of small angle scattering (<1°) 80−99432
Pt self-powered detector, neutron sensitivity calc. 78−37449
Pt self-powered detectors, neutron/gamma sensitivity 78−78557
Pt self-powered flux detectors, charact. in HWR 77−65282
Pt-self-powered neutron detector, temp. and radiation tests 79−81132
Pu, determination system by passive neutron counting 79−40985
Pu fallout detection using fission tracks prod. with neutron irrad. spectra 80−95479
Pu in waste, anal. of enhanced variance and twin gate methods 80−5454
Pu, large samples, thermal-neutron coincidence counting 78−82444
Rh self powered neutron detectors, influence of Rh burnup on sensitivity 80−63462
Rh self-powered neutron detectors, reliability anal. 79−41078
Rh-self-powered neutron detector, temp. and radiation tests 79−81132
$^{103}Rh(n,n')^{103M}Rh$ reaction rate, absolute calibration 79−85875
^{106}Ru photoneutron sources, determ. of standard neutron yield, influence of bremsstrahlung 79−72177
Si detectors, fast neutron flux meas. and spectroscopy 77−30709
Si diode as in vivo fast neutron dosimeter 77−73587
Si diode neutron detector for meas. near high-energy accelerator, photon and electron response 78−35963
^{90}Sr photoneutron sources, determ. of standard neutron yield, influence of bremsstrahlung 79−72177
Tm self-powered neutron detectors for power reactors 79−13607
U analysis, in geological samples, delayed neutrons method *(Rumanian)* 79−88507
U, assay of natural samples, meas. of gamma- or neutron activity of short-lived fission products 80−61179
U assay using continuous fast-neutron source 79−52849
U exploration probes, meas. spatial depend. of delayed neutron signals 79−34989

neutron detection and measurement continued
U ore grade direct determ. by photoneutron assay method 79−53570
U ore zone logging, corrections for prompt fission neutron data 79−88353
U, prospecting by active neutron logging, evaluation models 80−98480
^{233}U-^{235}U fuel, nondestructive isotopic meas. using fission neutron counting 80−32385
^{238}U, neutron transmission meas. and anal. 77−26823
W, radiation shielding material, integral tests of ENDF/B-IV high-energy neutron cross-section data 80−23162
$^{64}Zn(n,p)^{64}Cu$, evaluated cross section, neutron flux determ. by foil activation 78−25273
Zr, standard cylindrical calibration sample for long wavelength neutron scatt. meas., proposal 78−29722

neutron diffraction
see also neutron diffraction crystallography; neutron diffraction examination of materials
cold neutrons, diffraction by ruled gratings 79−94139
conference on neutron inelastic scattering, Vienna, Austria (Oct. 77) 79−41912
double monochromator for diffraction studies 78−1957
Fresnel diffr. of slow neutrons, by pointed and square straight-edges, for teachers 77−33794
Harwell backscatt. spectrum for neutron diffraction meas. 77−15288
high pressure sample container for thermal neutron inelastic scattering on fluids 80−37681
interference, gravity and inertial effects, principle of equivalence at quantum level 80−77669
interferometry, proposed expt. as search for nonlinear variants of Schrodinger eqn. 79−92984
interferometry, spin rotation and phase shift, polarisation props. 77−18763
magnetic octupole scatt. of neutrons, quadrupole excitation creation 77−47977
molecule, near-spherical, translational and rotational parameters obtained from neutron scatt. studies 77−61734
monochromator, moving cryst., design and operation 77−74552
non-coherent resonant scattering in crystals *(Russian)* 78−15081
phonon anharmonicity and bound states, effect on inelastic neutron scatt. 77−31739
scattering research, early developments 79−44696
small angle neutron scattering on the Harwell linac 80−19675
solid-state physics aspects of neutron probes 77−27790
spinor wave function, 4π periodicity factor meas. using perfect neutron interferometer 78−45515
ultracold neutrons, diffraction and mirror reflection 78−13193
ultracold neutrons, polarisation and diffr. through monocryst. Fe foils 79−45324
Young's double beam interference experiment with spinor and vector waves 78−89363
zone plate, appl. of diffraction to neutrons imaging and focusing 80−106433
Be monochromator grain identification by neutron topography 79−76244

neutron diffraction crystallography
see also crystal atomic structure
absorption corrections 79−27876
amorphous and gaseous states, philosophical problems in struct. determ. 78−50665
amorphous materials, smoothing and fast Fourier transformation of data 77−58928
amorphous solids, atomic scale determ., direct methods, review 79−37623
amorphous substances, neutron diffr. struct. investigations *(German)* 80−44108
anharmonic crystal, neutron scattering, effect of sublattice displacement 79−77458
anisotropic temperature factors, anharmonic motions 78−9902
aspherical-atom formalism, testing refinements on small molecule data sets 79−7516
automatic neutron diffractometry, development review 79−27879
bent mosaic crystals, preliminary theoretical approach 80−1901
biological structures, X-ray and neutron small-angle scattering 79−11889
biological systems, book contrib. 79−62417
Bloch walls, refraction of cold neutrons 77−26815
book, neutron physics 77−67787
book, with emphasis on technical aspects 79−60225
Bragg peak position, systematic variations 77−19838
Bragg reflection multiplicities for any space group, computer program 77−55213
Bragg reflections, ang. positions calcs. by computer program 80−38863
Bragg-case rocking curves from front and back surfaces of a Si crystal plate 78−91202
charge deformation density refinement, computer program 78−71639
charge density analysis techniques, appl. to s-triazine 78−38578
coherence effects in neutron diffraction and gravity experiments, review 79−58616
coherent scattering, inelastic, influence of refraction 78−87592
cold, and ultracold neutrons, production by a moving cryst. lattice 80−79640
collective modes in classical monoatomic liqs., coherent neutron scatt., book contrib. 77−89371
combined neutron/gamma ray techniques, possibilities 79−46518
combining X-ray and neutron diffr. for charge density distrib. obs., book contrib. 79−60227
computer-controlled CAMAC system *(German, English)* 77−19843
conference, International Crystallography Congress, Warsaw, Poland (Aug. 78) 79−23481
conference on neutron inelastic scattering, Vienna, Austria (Oct. 77) 79−41912
constrained refinement of powder data, program, EDINP 77−19839
copolymer, semicryst. random, characterisation by small angle neutron and X-ray scatt. 80−75189
correlation chopper for TOF neutron scatt., deconvolution, triangular signal function 77−61158
correlation chopper for TOF neutron scatt., deconvolution theory 77−61157
cryorefrigerator, double-stage for cooling to 10K on a 4-circle diffractometer 80−98919

neutron diffraction crystallography continued
crystallography, electron distributions, aspherical-at. least squares refinements combined with Fourier methods 78−71633
crystallography, X-ray neutron, charge deformation, vibr. smearing 78−71634
curved crystals, Laue geometry, theoretical calc. 78−14248
curved monochromators, reflectivity data 79−45515
Debye solid, amorphous and disordered harmonic, struct. factors 78−9954
deformation density and valence density maps, errors, scale factor contrib. 78−38580
detection systems and electronics. ILL expts. 79−45571
diffracting crysts., neutron anomalous flight time 80−87995
diffraction instruments, intercomparison, Commission on Neutron Diffraction work 78−18503
diffraction spectrometer, resolution and luminosity study for liquid on amorphous samples anal. 78−87591
diffractometer, converging beam small-angle, calculated resolution 79−10761
diffractometer, flat-cone, utilising linear position-sensitive detector 78−67624
diffractometer, Multidetector LMT LC 400 CP *(French)* 78−42866
diffractometer, temperature block for 79−94849
diffractometer, time of flight small-angle, for a pulsed neutron source, design study 79−10762
diffractometer, transit-time, for structural investigations of monocrystals 80−64840
diffractometer, two-axis, use of flexible four detector system 77−65934
diffractometer appl. to cation distrib. determ. in nonstoichiometric MnZn ferrite *(Bulgarian)* 78−83656
diffuse scattering, direct methods of anal., review 79−94845
diffusion in crystal, quasi-elastic neutron scatt. laws at finite concs. 79−77829
dilution refrigerator for neutron expts. 77−30151
disordered structures, book contrib. 79−60228
displacive transformation, defect cell and neutron scatt. central peak 77−15531
dynamic scaling theory, tested by temp. shift of neutron crit. scatt. max. of Fe polycryst. 79−50953
dynamic scattering theory, quasiclassical approx., VKB applicability test *(Russian)* 78−71627
dynamical diffraction of neutrons, gravitational and mag. field effects 80−59345
dynamical neutron diffraction and its application, book contrib. 79−60231
dynamical struct. factor for anharmonic oscill. in classical stat. mech. 77−55326
dynamical theory of diffr. in mag. crystals 77−40040
dynamics of mol. crysts., polymers and adsorbed species, book contrib. 77−89505
dynamics of solids and liquids by neutron scatt. book 77−89350
elastic neutron scattering, automatic processing of data obtained with DN-520 neutron diffractometer *(Russian)* 80−54079
electron and magnetisation densities in molecules and crystals, Arles, France (Aug. 1978) 80−105428
electron charge densities, coherent X-ray and neutron diffr., review 77−76260
electron density analysis, exponent refinement, appl. to melamine 78−38579
electron density distrib. in crysts. and mols. from diffr. data 77−7632
electron density distribution, and other densities in crysts., problems of resolution and bias in experimental determ. 79−23490
electron density mapping in mols., cyrsts., conf., Rehovot, Israel, (Apr. 1977) 78−71622
equilibrium and nonequilibrium phonons, excitons, and polaritons, inelastic neutron scatt. 80−84032
extended growth defect characterisation, review 78−30649
extinction, wavelength depend., meas. for UO_2 78−38588
extinction correction, in white X-ray and neutron diffr. 80−100120
extinction corrections, applicability 77−19829
Fankuchen effect, evidence in neutron diffr. of curved crystals 77−55209
Fankuchen effect, existence in Si curved crysts., neutron focusing experiment 79−60224
ferroelectric, displacive, inelastic neutron scatt. cross section 77−36187
ferroelectric domain struct. obs. using TOF neutron diffractometer 79−51923
ferroelectric soft modes, anomalous scatt. 77−59539
ferromagnet, domain struct. and magnetisation determ., vector polarisation techniques 77−63117
ferromagnet, triple dynamic magnetisation fluctuation correl. and feasibility of polarised neutron exam. *(Russian)* 78−88133
fly's eye intensifier-TV neutron counting camera, appl. 79−46519
focusing of neutron Bloch waves in cryst. *(Russian)* 79−32861
FORTRAN software, for mini-computers to control four-circle neutron diffractometer 80−38876
four-circle diffractometer, cooling down to 3.9K 77−27789
furnace, high temp., for neutron diffr. studies 80−19673
furnace design for vertical axis goniometer, diffr. patterns of oxides 77−58926
glass structure, review 77−65954
Grenoble high flux reactor, neutron physics expts., methodical aspects *(German)* 80−554
group theoretical selection rules in inelastic neutron scatt. 77−24247
Heisenberg magnet, random one-dimens., classical, spin dynamics, neutron scatt. cross section 80−60312
high pressure thermal neutron scatt., review 79−37592
horizontally curved analyser crystal, neutron scatt. monochromator appl. 79−50412
incoherent scatt. cross sections by diffuse scatt. techniques 77−24249
incoherent scatt. of slow neutrons, differential cross-section calc., Brownian motion appl. 78−75504
inelastic neutron scatt., use of spin echo property *(French)* 80−64842
inelastic neutron scatt. expts., book contrib. 78−1959
inelastic neutron scattering, uniaxial press appl. 77−35442
inelastic scattering, optimisation of struct. studying conditions *(Russian)* 80−79641
inelastic scattering by one-dimens. defecton *(Russian)* 78−84169
instrumentation and data analysis development, in X-ray and neutron small-angle scattering, review 79−10750
interferometer, perfect crystal, coherent scatt. length meas. 79−46517
interferometer, two cryst. component 79−46512
neutron diffraction crystallography continued
interferometer, with two cryst. components, construction 78−83654
interferometer diffraction pattern, amplitude modulated beam 78−63641
interferometry, comparison of X-ray and neutron interferometry 79−50952
interferometry, determ. of scatt. lengths and magnetic spin rotations 77−24248
interferometry, principles, techniques and appls., book contrib. 78−42862
isotropic system, multiple scatt. correction, Monte Carlo simulation 78−9913
lamellar structures, correction factors for neutron diffr. 77−84590
Laue case rocking curves, oscillatory struct. expt. determ., theoretical analysis 78−9899
Laue diffraction, overcoming 1/2 reflectivity limit 78−79505
Laue scatt. intensity oscills., neutron scatt. using inclination method 78−42867
lineshapes in pulsed neutron powder diffraction 80−64841
liquid metal, up to 1400K and 200 bar, technique and exptl. set-up 77−1064
liquid sample freezing with quartz wool 78−18502
liquid structure, neutron and X-ray diffr. data 79−46538
macromolecular helical wormlike chain statistical mechanics, scatt. function 77−54637
macroscopic bodies, dynamical theory, review 79−4211
macroscopic objects, neutron diffr. expts. 79−23503
magnetic chains, spin 1/2 Ising and classical Heisenberg models with alternating exhange, static props. 79−82737
magnetic domain structure, neutron small-angle scatt. from dynamical theory of diffr. 79−24189
magnetic form factor meas. by inelastic neutron scatt. 78−52221
magnetic inelastic scatt., book contrib. 77−89944
magnetic materials, neutron studies, book contrib. 80−11169
magnetic neutron small angle scattering, using dynamical theory of diffr., determ. of scatt. angle 79−11325
magnetic neutron small-angle scattering, using dynamical theory of diffr., behaviour of neutron intensity after transition through a helical mag. struct. 79−11326
magnetic scattering, relativistic mag. form factors for tripositive rare earth ions 77−40037
magnetic structure determ., book contrib. 79−61064
magnetic structure determ., group theory approach to neutron diffr. pattern interpretation *(Russian)* 79−51749
magnetic structure elastic polarised neutron scatt. atomic mag. moments 80−29531
magnetic structures, neutron diffr., symmetry anal., group theoretical group anal. of exchange Hamiltonian 80−29527
magnetisation density distrib. determ. by polarised neutron beam technique 79−77456
magnetisation density distrib. expt. determs., review 77−77034
melts, neutron diffr. struct. investigations *(German)* 80−44108
Michelson interferometer for ultracold neutrons 80−33858
molecular rotations and diffusion in solids and liquids, book contrib. 77−89573
molecular spectroscopy, recent developments 79−41911
monochromator, bicrystal, of moderate wavelength resolution for use with X-rays or thermal neutrons 77−76254
monochromator, curved, comparison of data with simple model 77−39515
monochromator, multilayer, fabrication and neutron diffr. expts. 77−84589
monochromator material, cryst. growth method for large oriented metal single cryst. plates 77−90267
monochromator with periodically bent single Si crystals 77−58927
monochromators, development of Institut Laue Langevin 79−45514
mosaic crystal, theory of neutron diffr. 77−55211
mosaic crystals, multiple Bragg-reflected neutrons 80−100129
multicomponent profile refinement of time of flight diffraction data 77−1047
multiplane analyser, reflectivity calcs. 79−44984
NBS reactor, summary of activities, (July 1976 to June 1977) 78−82435
nematic liquid crystal, coherent neutron diffr. 78−75550
neutron anal. techniques at Grenoble high flux reactor *(Italian)* 77−15289
non-Arrhenius self-diffusional behaviour effect on quasielastic neutron scatt. and Mossbauer linewidth 78−67853
normal mode calcs. of molecules, crystal phonon dispersion relns. and structure factors for neutron inelast. scatt., computer program 78−91394
on-line ECIL TDC-312 computer-controlled four-circle neutron diffractometer 78−55787
orbital degeneracy, scatt. cross section, operator expression 79−7524
order-disorder transformations, critical scattering of neutrons and X-rays, meas. techniques 79−55609
organic molecular crystals, inelastic neutron scatt., exciton creation 80−70084
orientationally disordered structures, orientation and position correlations of a mol. 80−14966
orientationally disordered structures, positive definiteness of orientational distrib. functions 80−14958
pair distribution functions, non-cryst. material, neutron diffr. data parameter calc. program 79−14652
pair distribution functions, non-cryst. materials, neutron diffr. data calc. program 79−14653
particle-size distribution functions, determ. from SAS data by indirect transformation method 80−38860
perfect and regularly imperfect cryst., diffr. props. and neutron optics appl. 80−24323
phase factor, due to antisymmetric components of density distribs. 79−99033
phase information from anomalous scatt. meas. 79−27875
phase transitions and crit. phenomena, book contrib. 79−60229
philosophic concepts and implementation 79−94932
phonons, anomalous fluctuations, neutron scatt. 78−75743
phonons and neutron scattering, book contrib. 77−89504
phonons and struct. transforms., comparison of neutron and X-ray scatt., book contrib. 77−89518
polarised diffraction, extinction model testing, appl. to YIG 77−1046
polarised neutron diffraction, determ. of magnetic form factors, pioneering work 80−24321

neutron diffraction crystallography continued
polarised neutron diffractometry, method of secondary extinction correction 80−28882
polarised neutron expts., extinction models 80−24322
polarised neutron production and appls., book contrib. 79−58843
polariser, perfect crystal, appl. of mag. prism refraction 79−50950
polariser, supermirror, exptl. evidence 77−39514
polarising monochromator with Fe/Ge multilayers 77−19841
polycrystal cold neutron incoherent inelastic scatt., computation of phonon spectrum 78−34572
polymer, semicrystalline, small-angle neutron scatt. function computation 79−10811
polymers, crystalline, homophase and heterophase, small-angle neutron, X-ray and light scattering, recent developments 79−10751
powder diffractometry, spherical sample container 78−55786
powder least-squares program, POWLS 80−1892
powder neutron diffraction, KSN-2 diffractometer using nucl. reactor 79−86655
powder neutron diffraction, refinement of total pattern 77−76263
powder patterns, LAZY PULVERIX computer program 77−27784
powder patterns, peak shifts and broadening due to finite aperture counters 77−19842
powder reflections, computer program for determining multiplicities, correction for $\bar{3}1m$ Laue symmetry 79−10759
powder reflections, multiplicity determ., computer program 77−39509
principles, book contrib. 79−60226
profile analysis of powder data, review 77−68900
prototype interferometer at Grenoble high flux reactor 79−19127
pulsed source experiments, optimized Monte Carlo simulation 78−9914
pulsed spallation neutron sources 79−76237
quantum theory of neutrons in helical magnetic fields 79−35581
quartz crystal plate, elastically bent, diffr. of pulsed thermal neutron beam 77−43116
radial distrib. anal., computer program 80−28875
random binary alloy, charge and spin struct. factors, CPA theory 77−28374
refinement, modified least-squares formalisms for overcoming the free-atom bias 78−71632
reflection centring algorithm for computer controlled four-circle diffractometer 78−75503
reflection sets, unique, computer program for generation, for all space groups 78−18501
review, role of Fourier transforms in struct. determ. 77−27772
review, X-ray and neutron diffraction techniques, advances, book contrib. 79−67453
Rietveld neutron profile refinement, interactive computer system, POWDER 80−1900
Rietveld profile refinement algorithm, modification for powder data 80−24320
Rietveld profile refinement method, anal. 80−24315
rotating single-crystal slab, secondary extinction 80−14965
scattering, small angle, appl. to materials science 79−10752
scattering amplitude, spin depend. meas. using polarised neutrons 79−45601
scattering by crystals in external alternating fields 79−23502
scattering chamber with high temp. resolution, 370 to 770K, furnace design 77−55212
scattering conference, Gatlinburg, TN, USA (June 1976) 79−41910
scattering facility, small angle, at SAFARI-1 reactor 79−50951
scattering research, early developments 79−44696
scattering techniques in applied research, medium-flux research reactors 79−13514
secondary extinction correction, method in polarised neutron diffractometry 80−28882
secondary extinction free values, determ. for flipping ratio in polarised neutron diffr. 79−50949
secondary extinction in neutron diffraction, Darwin eqn. solns. 79−46514
section topography, cryst. dislocation and planar defect images, book contrib. 78−42863
silicate glass, advantages over X-ray techniques for struct. determ. 78−79533
SIMON, FORTRAN Monte Carlo program for time-of-flight neutron diffractometer simulation 79−50955
slow neutron scatt. by rotating systems of identical nuclei *(Russian)* 80−14968
small angle neutron scatt. expts., high-temp. furnace 77−84591
small angle scatt. depend. on divergence *(French)* 80−49045
small angle scattering, expt. techniques, and appl., review 79−46515
small angle scattering, suitability for alkali silicate glass struct. determ. 78−22663
small-angle neutron scattering instrument, at ORNL using position sensitive area detector 80−79639
small-angle scattering, data evaluation method 77−84580
small-angle scattering, of X-rays and neutrons, (fourth international conf., Gatlinburg, USA (Oct. 77)) 79−10745
spectrometer, crystal-chopper, (Q,ω) transmission function 77−31564
spectrometer, triple-axis, computer-control system with CAMAC interface, program functions 77−19840
spectroscopy techniques and examples *(Dutch)* 80−28884
spin-echo spectrometry and neutron optical polarisers 80−49051
spin-echo to separate inelastic scattering from elastic scattering at high energy resolution 79−32860
spinel structure, space group ambiguity rel. to multiple diffr. 77−84592
spinel structure compounds, cation distrib., neutron diffr., determ., minimum errors 78−1958
static structure factor, non-cryst. material, neutron diffr. data, normalisation, instrument correction program 79−14651
stereographic projections, of expt. electron density distrib. 78−91185
structure factor determs., data processing 78−71631
structure factor equation for structs. consisting of point scatterers 77−55210
texture analysis, quantitative, time of flight vs. conventional method on drawn steel wire 80−81078
thermal diffuse scattering in moving single crystals 79−46521
thermal neutron filter, Si single cryst. 79−45512
thermal neutron scattering theory, book 79−26466
thermal neutrons, (111,$\bar{1}$11) three beam case, general formulation 79−27878
thermal neutrons, dynamical effects in inelastic scattering 79−77459
thermal scattering, incoherent, nonlinear multi-sublattice jump diffusion model 77−28034

neutron diffraction crystallography continued
thermodynamic data determ. by X-ray and neutron scatt. 78−83974
three-beam diffr. from perfect cryst. 79−7523
time of flight spectrometer for elastic neutron scatt. on powdered samples 77−62447
time-depend. phenomena studies using time-of flight neutron diffractometry *(Japanese)* 80−70083
time-of-flight technique, for cryst. struct. investigation 79−19126
topography, domain and cryst. defect studies, results 79−46520
transitional neutron scatt., ambiguity in exptl. results 77−47546
twinned and clustered crystals, method and computer program for intensities meas. on four-circle diffractometer 78−14247
two crystal diffractometer, neutron spectrometer component, luminosity 78−21807
unique phase determination, two-wavelength Bijvoet pair method, reson. neutron scatt. 78−91201
United States national small-angle neutron scatt. facility 79−75670
valence electron distribution, in crysts., diffr. data processing 80−92418
vibrating single crystal, Umweganregung peaks 80−10461
white beam neutron diffr. technique, appl. to Si, KCl and KNO_3 77−31565
X-N maps, room temp., errors due to non correction for thermal diffuse scatt. 78−75487
Cu-Ge neutron monochromator 78−71643
Fe/Ge multilayer neutron polarizing monochromator 79−45513
Fe-Ni (35 at.%), fine coherent effects, neutron diffr. study *(Russian)* 78−75502
Fe_3Mn-Fe_3Si, slow neutron polariser, by single cryst. (111) refl. 80−49052
Si crystal, perfect, meas. ang. deviation of neutrons of order of 10^{-3} sec of arc 79−37593

neutron diffraction examination of materials
see also neutron diffraction crystallography
acetic acid, deuterated, neutron powder diffr. anal. at 4.2 and 12.5K 78−75649
acetic acid, liquid, atomic pair correlation functions 79−7596
acetonitrile, liq., $CD_3C^{15}N$, neutron diffr. 77−11460
acetonitrile, liq., rotational motions, diffusion coeffs., quasi-elastic neutron scatt. study 79−50979
acetonitrile, mol. pair correl. functions, scatt. intensities, statistical mechs. calcs. 79−1382
acetonitrile, mol. pair-correl. function, X-ray and neutron diffr. 78−26420
acetylcholine receptor from Torpedo Californica, struct. anal., low-angle neutron scatt. obs. 80−30651
acetylene, and deuterated derivative, adsorbed on Ag exchanged zeolite, inelastic neutron scatt. 78−6229
actinide compounds, neutron scatt. studies 80−75716
actinide compounds, structure, mag. and related props., review 80−6389
actinide intermetallics, $AnFe_2$, (An=U, Np, Pu, Am), magnetisation, neutron diffr. and Mossbauer expts. 77−63137
adamantane, deuterated single plastic cryst. high-symmetry dispersion curves, coherent inelastic neutron scatt. meas. *(French)* 79−14905
adamantane, Ising, diffuse scatt., hard-core correl., weak-graph method 80−49137
adamantane, plastic cryst., rotational motion, elastic incoherent struct. factor determ. 77−4056
adamantane, plastic cryst. rotational motion, quasielastic neutron scatt. study 79−41991
adamantane, plastic phase, C_4 rot. jumps, existence and uniqueness 80−88067
adamantane, plastic phase, librations, phonon branches, neutron scatt. study *(French)* 79−51222
adamantane-d_{16}, collective librational modes and orientational correlations 79−73266
adsorbed gas films on grafoil, neutron scatt., lattice gas *(Japanese)* 77−47685
adsorbed layers, normal modes of vibr. obs. by neutron scatt. 79−19443
adsorbed molecular, surfaces, and interfaces, neutron scatt., review, book contrib. 80−84394
adsorbed molecules, struct. and dynamics, neutron diffr. and inelastic scatt. 78−87869
adsorbed monolayers, neutron scatt. meas. 79−65306
adsorbed surface structure and dynamics, neutron scatt. studies, review 79−60639
aerosol OT-n-heptane-water, reversed micellar solution; addition of electrolyte, neutron small angle scattering 80−104468
alkali halide:CN^-, internal modes reson. hybridization 79−42194
alkali halides:NH_4^+, inelastic neutron scatt. 78−14407
alkali metal acid oscalates, neutron inelastic scatt. spectra in 2200-200 cm^{-1} range 80−70327
alkali metal dicarboxylates, H bonding and motion, incoherent inelastic neutron scatt. spectroscopy 80−48095
alkali silicate glass, suitability of small angle neutron scatt. for struct. determ. 78−22663
n-alkane chains, pure liq. and solns., small angle neutron scatt., ang. depend. 79−1384
n-alkane mol. config. in melt and cyclohexane soln., small-angle neutron diffr. 78−55800
alloy, binary, magnetic moment determ. from neutron scatt. 77−73011
alloys, concentrated, local atomic arrangements, associated with ordering, review 80−50632
alloys, nearly and weakly ferromagnetic, mag. clusters, unpolarised neutron diffuse scatt. 78−39297
π-allyls, LF vibr. modes of hydrogeneous ligands, incoherent inelastic neutron scatt. 78−6229
4- aminopyridine hemiperchlorate, struct. determ. by neutron diffr. and IR spectra 80−92515
ammonium salts, reorientation of NH_4^+, PMR relax. and inelastic neutron scatt. 79−82167
$^{243}AmO_2$, possible occurrence of antiferromagnetism 79−78332
amorphous ferromagnets, neutron scatt. rel. to elementary excitations, amorphons 80−39494
amorphous magnetic materials, spectral density functions 79−47269
amorphous metals, geometric struct. models and diffraction exam. techniques 80−79700
amorphous solids, inorganic, struct., review 80−15004
anharmonic crystal, neutron scattering, effect of sublattice displacement 79−77458

neutron diffraction examination of materials continued
anharmonic crystals, neutron scatt. cross-section, sublattice displacement effects 79−77460
anthracene, lattice parameters press. depend., elastic consts. 78−38686
antiferromagnet, neutron scatt. by magnons, modulated spin amplitudes 80−75722
atoms diffusing in periodic lattices, quasi-elastic neutron scatt., use of Monte Carlo calcs. 79−60557
p-azoxyphenetole, single cryst., deuterated, phonon dispersion curves, inelastic neutron scatt. obs. 80−84261
BCC crystal, anisotropic spin-pair correlation function, neutron mag. crit. scatt. cross-section 80−60194
benzene, crystal, inelastic coherent neutron scatt., phonon spectra 78−51629
benzene, deuterated, neutron diffraction by electron LINAC 79−50974
benzene, diffusive motion on graphite basal planes, neutron scatt. study 79−42385
benzene, liquid and gaseous, total cross section meas. for cold neutron interactions 79−99055
benzene, total neutron cross sections for subthermal energies 78−74779
benzene chemisorbed on Raney Ni, struct., neutron inelastic spectroscopy study 80−101038
benzene-d_6, intermol. dynamics, neutron scatt. obs. 79−863
benzenetricarbonylchromium, neutron inelastic scatt. spectrum and valence force field 80−48096
Bi, polymorphic transition up to 30 kbar, neutron diffr. investigation 79−14723
binary melts, short-range order, X-ray and neutron scatt. *(German)* 78−14272
biological structure studies, neutron scattering from soln. of macromols. 77−16906
biological systems, book contrib. 79−62417
biology and chemical physics appls. of neutron scatt. spectroscopy, recent advances 77−35445
biphenyl, incoherent inelastic neutron scatt. time of flight spectra, vibr. spectra model calc. 78−63816
biphenyl, incommensurable phases, obs. of excitations, inelastic neutron scatt. 80−49334
biphenyl, incommensurate phases, elastic neutron scatt. study 79−86887
β-bis(ethylammonium)tetrachloromanganate, cryst. struct. refinement, neutron diffr. 78−55858
Bloch wall thickness, neutron small-angle scatt. meas. 80−71092
bone, neutron diffr. of apatite crysts., integrated orientation meas. 77−40952
bone, X-ray and neutron diffr. meas. of apatite cryst. orientation and growth, effect of chem. and heat treatment 79−39431
BPBAC, smectic B phase, neutron diffr. and X-ray obs. 78−94973
α-brass, rolling texture development, dependent on relative stacking fault energy 79−52237
1-bromopentane, low freq. mol. vibrs., neutron inelastic scatt. study 79−46760
butadiene, styrene, 4-vinylpyridine terpolymer, cross-linked by coordination with Fe (III) chloride, ion clustering 78−83748
tert-butanol, mol. dynamics, liq. and cryst. states, neutron inelastic scatt. obs. 78−75599
t-butyl chloride, rotational motions, cold neutron scatt.study 79−51023
t-butyl chloride, solid phases, mol. motion, cold neutron scatt obs. 78−26460
n-butyl-4-(4′-phenylbenzylideneamino)cinnamate-d_9, smectic E, B and A phases, quasielastic neutron scatt. obs. 78−75539
C1q of human complement, neutron scatt. obs., conformational calcs. 80−81537
α-calcium formate, neutron diffr., cryst. struct., 100 and 296K 77−59004
carbamide phosphate, neutron diffr. 77−31652
carbon tetrabromide, disordered phase, neutron, diffuse scatt. 80−79717
carbon tetrabromide, disordered phase, neutron diffuse scattering 80−79716
carbon tetrabromide, plastic phase, orientational disorder 79−73115
carbon tetrachloride, liq. struct. by neutron diffr. 79−73089
carbon tetrachloride, liq. struct. by pulsed neutron diffr. 79−69004
carbon tetrachloride, struct., oscill. amp., neutron diffr. study 79−46544
carboxyl groups, H_2 bonded, C-O vs. O-H length correlation using neutron diffr. data 79−54987
CBOOA, liq. cryst., dynamic crit. neutron scatt. obs. near smectic-A nematic phase transition 78−79752
CBOOA, liq. cryst., smectic A to nematic phase transition, crit. neutron scatt. 78−95135
CDW instabilities, incommensurate struct. phase transitions, neutron scatt. study, review 79−51231
cellulose II, unit cell parameters, neutron diffr. 77−1086
ceramics, local atomic arrangements, associated with ordering, review 80−50632
charcoal, adsorbed H_2 monolayers, H_2 dynamics 79−66341
chemically reactive liquids, container construction 77−35443
chiral molecular systems, differential scatt. of spin $\pm^1/_2$ neutrons, theory 78−33622
chiral molecular systems, differential scatt. of spin $\pm^1/_2$ neutrons, Condon oscillator model 78−33623
chloranil, mol. cryst., soft mode and central peak neutron scatt., struct. transition 79−42209
chloranil, neutron superlattice reflection, soft phonon and central peak scatt., phase transition 78−18732
chloroform. liquid, RIMS calc. of struct., neutron scatt. struct. factor prediction 79−37610
chloroform-d_1, and isotopic forms, liq., neutron diffr. obs. 79−32878
chloroform-d, struct. of mol. in liq. 78−26422
chromatin, low-angle X-ray and neutron diffr., interparticle effects 80−72134
chromatin, neutron scatt. rel. to higher order struct. 79−11894
chromatin subunits, in glycerol/sucrose solns. containing various D_2O/H_2O mixtures, neutron scatt. study 79−11893
clathrate hydrates, containing ethylene, oxide, mol. rot. motion, quasielastic neutron scatt. 78−91274
clathrate hydrates, containing ethylene oxide, mol. rot., inelastic neutron scatt. 78−91275
closed shell chiral molecule, polarised neutron beam interaction, optical activity 79−64111
cobalt formate dihydrate, mag. struct., antiferromag. mode 79−99678
collagen structure in cartilage of intervertebral disc 78−56951

neutron diffraction examination of materials continued
colloids, structure determ. by neutron diffr. and small angle scatt. 80−40748
condensed H-containing media, cold neutron total section data interpretation 80−33857
conference on neutron inelastic scattering, Vienna, Austria (Oct. 77) 79−41912
copolymer solns., small-angle neutron scatt., molecular struct. determ. 77−19863
copolymer solution, small angle neutron scatt., excluded vol. effect *(French)* 79−60259
copper acetate, deuterated, dimeric, single crysts., inelastic neutron scatt. 80−92867
copper formate.$4D_2O$, field-induced antiferromag. order above T_N 78−84389
copper formate anhydrate, cryst. struct. and mag. props. 80−79768
copper formate tetradeuterate, deuterated, paraelec. and antiferroelec. phases, neutron diffr. obs. of struct. 79−87404
copper formate tetrahydrate, antiferromag. phase, neutron diffr. study 80−93085
copper formate tetrahydrate, model two-dimensional ferroelec., short-range order, neutron scatt. 78−68458
copper formate tetrahydrate, short-range order, diffuse neutron scatt. 78−15124
corneal stroma, small angle X-ray and neutron diffr. study 79−11923
critical molecules, neutron scatt., 'optical activity' 80−23567
crystallite orientation distribution function, determ. from isolated axis density values 77−48612
cubic crystals containing substitutional impurities, slow neutron coherent scatt., phonon mass operator 79−28065
cyano derivatives, smectic layer spacings 79−46561
cyclobutadiene iron tricarbonyl, LF vibr. modes of hydrogeneous ligands, incoherent inelastic neutron scatt. 78−6229
cyclohexane, solid, neutron scatt. spectra using inverted geometry, white beam, t. of f. spectrometer 78−34395
cyclohexane fluorinated derivatives, $C_6F_9H_3$, C_6H_{12}, mol. rot. in plastic phases 77−35495
cyclopentane, solid, neutron scatt. spectra using inverted geometry, white beam, t. of f. spectrometer 78−34395
cyclopropane, liq., mol. dynamics, self-diffusion, quasielastic neutron scatt. and NMR spin-echo meas. 78−10201
cyclopropane, liq., molecular motion, incoherent neutron scatt. study 79−50978
cytosine monohydrate, deuterated, neutron diffr. cryst. struct. determ. 80−54215
defective crystals, diffusion processes and multistate diffusion 79−19389
dense fluid, collective modes and neutron scatt. 80−92442
di-(2,2,6,6-tetramethyl-4-piperidinyl-1-oxyl) suberate, nitroxide radical polarised neutron study in paramag. phase 79−47231
di-(2,2,6,6-tetramethyl-4-piperidinyl-1-oxyl)-suberate, spin densities, polarised neutron diffr. meas. 80−50037
dialkylammonium manganese chloride, order-disorder transition mechanism 78−79772
diamond, electron density, neutron diffraction powder data 78−38655
diamond, synthetic, γ-Mn cluster existence, neutron diffr. obs. 77−89464
diatomic molecular fluids, slow neutron scatt., models 80−83463
diatomic molecular fluids, slow neutron scattering, moment expansions 80−87201
diatomic molecular gases, slow neutron scatt., recoil corrections, time of flight, rel. to mol. liq. struct. 79−7028
diatomic molecular gases, slow neutron scatt., recoil corrections, rel. to mol. liq. struct. determ. 79−7027
p-dibromo-tetrafluorobenzene mol. cryst., in commensurate phase, quasielastic neutron scatt. 80−107386
1,5-dibromopentane, low freq. mol. vibrs., neutron inelastic scatt. study 79−46760
p-dibromotetrafluorobenzene, neutron diffr. determ. of struct., constrained refinement 77−19839
2,5dichlorobenzenesulphonic acid trihydrate, neutron diffr. obs. of $H_3O^+.2H_2O$ 78−58855
dichlorodurene, order-disorder phase transition, struct. from neutron diffr. at 70K 78−55825
1,2-dichloroethane, orientationally disordered crystal., mol. orientation 78−34448
dichloromethane, liq. dynamics, neutron inelastic scatt. 78−71664
p-diiodotetrafluorobenzene, neutron diffr. determ. of struct., constrained refinement 77−19839
dilute and moderately dense gases, dynamic and static struct. functions, neutron scatt. study 79−46411
dilute ferromagnet, slow neutron inelastic scatt. by spin excitations, cluster approx. 80−11168
1,4-dimethoxy-2,6-dimethylbenzene, methyl reorientations, NMR relax. and inelastic neutron scatt. obs. 79−61253
dimethyl tin difluoride, solid, methyl group motion, neutron scatt. study 80−10607
dimethyl tin difluoride, solid, methyl reorient., low temp. phase transition, neutron scatt. obs. 79−27932
dimethylacetylene, librational motion, inelastic neutron scatt. obs. 78−75742
dimethylacetylene, tunnel splitting, rot. pot., μeV neutron scatt. study 79−41993
dimethylammonium manganese chloride, neutron diffr., 188K, cryst. struct. 77−47434
dimethylammonium manganese chloride, neutron diffr., 404K, cryst. struct. 77−47435
dimethylammonium manganese tetrachloride, H-bonding, struct. transition, neutron diffr. study 79−42004
dimethylammonium manganese tetrachloride, Heisenberg ferromag., spin wave anal. 79−61237
dimethylammonium manganese tetrachloride, phonon density of states, expt. and calc. 80−54323
dimethylammonium manganese tetrachloride-d_6, structural and mag. phase transitions, neutron scatt. and AC susceptibility meas. 80−44825
dimethyltin difluoride, neutron scatt. exam. methyl group motion 78−59769
dipalmitoyl phosphatidyl choline, deuterated gel phase lipid bilayer, neutron scatt. sudy 79−43829
diphenyl, solid and liquid, total neutron cross sections for subthermal energies 78−74779
diphenylsilanediol, randomised X-ray powder diffraction patterns, adjustable sample holder 80−6317

neutron diffraction examination of materials continued
DMBCA, nematogen, incoherent neutron quasielastic scatt. 79−32887
DNA, oriented films, hydration, slow neutron scatt. obs. 79−57572
DNA pyrimidines, cryst., lattice dynamics 78−75766
DNA-dependent RNA polymerase, determ. of intersubunit distances and subunit shape parameters by neutron small-angle scattering 79−53038
EABAC, smectic A, nematic, and isotropic phases, NMR and quasielastic neutron scatt. obs. 80−88022
EABAC, smectic-A, mol. motions, incoherent quasielastic neutron scatt. obs. 78−59740
electrolytes, aq. solns., X-ray, neutron diffr. data, termination errors, Fourier anal. 77−47299
Elinvar, γ to γ' transformation and γ' phase form. kinetics, lattice consts. 80−35191
emulsion of H_2O-alcohol, percolation mech. and struct. 79−20471
energy dispersive diffractometry for quantitative determination of texture 79−87818
ethane, liquid-vapour coexistence curve, neutron transmission exam. *(Russian)* 78−79758
ethane, solid, mol. reorientational motions, incoherent neutron scatt. studies 80−107070
ethane submonolayer on graphite, struct. and melting, elastic neutron scatt. 80−29266
ethylene, adsorbed on Na zeolite, uniaxial rot., translational dynamics 78−91538
ethylene adsorbed on Ag exchanged zeolite, inelastic neutron scatt. 78−6229
ethylene oxide clathrate, reorientation, residence times, Debye-Waller factors, activation energy, neutron scatt. study 79−41989
ethylene oxide clathrate deuterate, rotational motion, quasi-elastic neutron scatt. study 79−51022
ethylene oxide deuterohydrate, cryst. struct. at 80K 77−72607
ethylene-d_4, phases I and II, struct. determ. by neutron diffr. 77−27870
exciton scattering of neutrons, theory 80−29330
ferrocene, neutron diffr. study of cryst. struct. 79−55728
1,1′-ferrocenedicarboxylic acid, triclinic, X-ray and neutron cryst. and mol. struct. determ. at 78 and 298K 80−29008
ferroelectric, displacive, inelastic neutron scatt. cross section determ. 77−31737
ferroelectric, hydrogen-bonded, incoherent and coherent inelastic neutron scatt. cross sections 77−59524
ferroelectric crystals with modulated struct. neutron scatt. obs. 79−95713
ferroelectric materials, H-bonded, coherent crit. neutron scatt. 79−56742
ferroelectrics, improper and incommensurate phase transitions, neutron scatt. studies 80−75974
ferroelectrics, inelastic neutron scatt., one-phonon differential cross section 80−28883
ferromagnet, amorphous, spin-wave excitations, roton minimum 78−80139
ferromagnet, domain struct. study by time depend. neutron depolarisation 80−50138
ferromagnet, double crit. mag. scatt. in polarised neutron expts. 79−65652
ferromagnet, Heisenberg, Bose-representation correctness of spin operators, anal. 80−15700
ferromagnet, itinerant electron, magnon spectrum just below T_c, theory 80−65833
ferromagnet, neutron crit. scatt., temp. shift of max. in second Born approx. 78−34963
ferromagnet, nuclear spin waves, possible detection by inelastic neutron scatt. 77−85438
ferromagnetic, neutron depolarisation, statistical theory 78−87593
ferromagnetic and antiferromagnetic domains, neutron techniques for obs., review 78−64213
ferromagnetic random binary alloys, elastic neutron scatt. cross section 78−91845
ferromagnetic spin waves above Curie temp., Fisher's droplet model 78−56307
film adsorbed on graphite, two-dimensional phase transitions 80−107653
flexible polymers, in soln., obs. of pair correlation function, temp. and conc. effects small neutron scatt. anal. 79−10780
fluid of diatomic-like mols., with isotropic rot. diffusion quasielastic scatt. cross section 77−47312
fluid sample container for thermal neutron spectroscopy and diffraction 79−46513
fluoroanthene, cryst. struct., X-ray and neutron diffr. meas. 77−47437
2-fluoronaphthalene, disordered form, thermal expansion, neutron and X-ray diffr. study 80−24621
formic acid, deuterated, neutron powder diffr. exam. at 4.5K 78−75650
formic acid, lattice dynamics model to explain neutron scatt. data 79−86856
formic acid, lattice vibr., pot.-function calcs., comp. to neutron scatt. data 79−42168
formic acid, normal and deuterated, dynamic modes, neutron inelastic scatt. study 79−51214
garnet, mag. struct. determ., group theory approach to neutron diffr. pattern interpretation *(Russian)* 79−51749
garnets, neutron diffraction patterns, group theoretical, exchange Hamiltonian symm. anal. *(Russian)* 79−65648
garnets with Fe^{3+} ions in tetrahedral sublattice, mag. ordering and bond geometry 77−32163
gases, coherent neutron scatt. length meas. 79−72435
gels, non-linear behaviour under strong deform. 78−7240
glass ceramic, nucleation and growth studies by small angle neutron scatt. 79−32913
α-D-glucose, further struct. refinement based on neutron diffr. data 79−42043
glycerol, Mossbauer and neutron scatt. 80−20559
γ-glycine, cryst. struct. by neutron diffr. at 83K and 298K 80−35825
α-glycine, deuterated, low freq. intermol. modes, neutron diffr. obs. 80−15086
α-glycylglycine, cryst. struct. and deform. electron density, X-ray and neutron diffr. 79−86777
graphite, adsorbed butane, struct. and dynamics, neutron scatt. study 78−87870
graphite, adsorbed NO monolayer melting and polymorphism 78−84063
graphite, atomic thermal motion comparisons at 300K based on X-ray neutron and phonon spectrum data 79−7657
graphite, coke source inference from neutron small angle scattering meas. 77−74923

neutron diffraction examination of materials continued
graphite, intercalation compound, C_8Rb, elastic and inelastic neutron scatt. 78−30597
graphite, mobility of 2-dimens. hypercrit. fluid methane, neutron scatt. obs. 77−20193
graphite, neutron induced changes, exam. of lattice consts., elastic modulus, elec. cond 79−95053
graphite, neutron irrad., porosity changes, neutron small angle scatt. investig. 78−34544
graphite, nucl. grade, neutron small angle scatt., thermal and radiolytic oxidation effect, porosity size distrib. 79−17977
graphite, phonon dispersion, temp. depend., 4K-1500°C, neutron spectroscopy 78−59906
graphite adsorbed H_2 monolayers, H_2 dynamics 79−66341
graphite adsorption of H_2, dynamics, neutron scatt. exam. 79−60641
graphite with adsorbed butane, intramol. surface vibr. modes, inelastic neutron scatt. obs. 77−72780
graphitised C black, adsorbed methane, rot. tunnelling, neutron scatt. obs. 79−15000
haematite, neutron diffr. exam. of texture, comparison with magnetite 78−52849
haematite, textures and topotactical relationships, neutron diffr. study 79−83229
halomethylsilanes, internal torsion modes, inelastic neutron scatt. 77−19105
halomethylstannanes, internal torsion modes, inelastic neutron scatt. 77−19105
HCP metals, anharmonicity effect on neutron diffr. struct. factor 78−59907
heavy water, collective excitations in 10^8 cm^{-1} momentum range 78−43087
heavy water neutron diffraction by electron LINAC 79−50974
Heisenberg, impure classical chain, dynamic props. using local-moment pair correl. functions 80−15728
helical magnetic structure, Bloch wall effects on small angle neutron scatt. 79−47297
hexabromobenzene, cryst. struct., constrained refinement of neutron powder diffr. data 79−27970
hexachloroethane, orthorhombic, neutron struct. refinement 80−29009
n-hexadecane, pure liq. and solns., small angle neutron scatt., ang. depend. 79−1384
2,4-hexadiyne, solid, methyl group tunnelling and torsion, neutron scatt. 78−18560
hexafluorobenzene, liquid sample freezing with quartz wool 78−18502
n-hexatriacontane, pure liq. and solns., small angle neutron scatt., ang. depend. 79−1384
high pressure chamber for neutron diffraction up to 30 kbar 79−93158
high pressure thermal neutron scatt., review 79−37592
L-histidine.HCl.H_2O, photographic neutron diffr. by modified Laue method 77−66791
holomethylgermanes, internal torsion modes, inelastic neutron scatt. 77−19105
hydration, anionic, press. effect, neutron diffr. obs. of $NiCl_2(^7LiCl)$ heavy water solns. 80−30212
hydrocarbons short-chain, adsorbed on small particles, appl. of neutron scatt. to struct. and dynamics 79−4481
IBPBAC, dynamics of smectic phases, quasi-elastic neutron scatt. meas. 79−86700
IBPBAC, smectic B phase, neutron diffr. and X-ray obs. 78−94973
ice, Ih, elastic diffuse neutron scattering due to D-D correlation functions 80−96493
ice Ih, elastic neutron diffuse scatt., series expsn. calc. 78−2027
imidazole, cryst. struct. at 103K by neutron diffr. 79−37691
impure crystals, vibrs. in average local information transfer approx. 79−46774
incommensurate lattices, optical absorption and neutron scatt., lattice dynamics 79−33039
incommensurate phase transitions, exptl. studies of soft phonons 78−75798
incommensurate structural phase transformations, recent neutron scatt. studies, review 79−42205
Inconel, X-750 and 700, NDT turbine blades by small angle neutron scattering 79−20055
Inconel X750, positron annihilation study of ageing and creep 80−29824
inert gas solids, lattice dynamics, book contrib. 77−47522
inert gas solids, self-consistent phonon theory, book contrib. 77−51460
inhomogeneous media, coherent inelastic scatt. theory 79−50957
intermediate valence compounds, dynamic susceptibilities 80−70653
Invar, Fe-Ni alloy, atomic struct., elastic neutron scatt. obs., phase diagram 79−94964
Invar, ferromagnetic, lattice dynamics 79−55838
Invar, influence of magnetoelastic effects on lattice vibrs., neutron scatt. meas. 78−2722
Invar alloys, mag. struct. small angle neutron scatt. study 79−47249
Invar neutron small angle scatt. magnetocrystalline anisotropy 77−85420
inverse scattering in Rayleigh-Debye approx., length distrib. for thin cylinders 79−24839
ion-water interactions, survey of diffr. studies 80−24347
ionic conductor, quasielastic scatt. of light, neutrons and electrons, Debye-Huckel eqn. *(Chinese)* 78−68521
ionic crystal with vacancies, coherent neutron scatt., calc. 80−59346
ionic direct micellar phase, local order determ. by neutron scatt. *(French)* 79−92013
ionic liquids, struct. determ., summer school lecture series 80−6349
ionic liquids, structural props., review 80−96430
ionic solutions, struct., neutron diffr. technique study 79−10787
Ising spin glass, calc. of wavevector depend. susceptibility 77−63223
itinerant electron system, mag. excitations, neutron scatt. studies 80−44838
itinerant electron systems, mag. excitations, study by inelastic neutron scatt. 79−47264
itinerant oscillator model, anal. for dielectric relax. and incoherent neutron scatt. 79−90509
IV-VI compounds, phase transitions induced by electron-phonon interaction 80−10656
lamellar systems, mol. diffusion, incoherent neutron scatt. function 79−23501
light nuclei liquids, dynamical corrections for structural factor determ. 79−99034
$^6LiH_3(SeO_3)_2$, absolute atomic arrangement rel. to spontaneous polarisation, neutron diffr. study 80−15067

neutron diffraction examination of materials continued
lipid bilayer, site of action of general anaesthetics 78−77008
liquid, neutron incoherent scatt. functions, non-Gaussian corrections 78−42874
liquid, velocity-autocorrelation function from neutron scatt., comparison with Ar, H_2 data 77−1058
liquid, X-ray and neutron diffraction data interpret using statistical mech. models 77−31551
liquid crystal, nematic, homogeneously oriented, neutron small-angle scatt. by dislocations 77−1077
liquid crystal mesophases, aligned monocrystal, elastic neutron scatt. incoherent struct. factor 77−62467
liquid crystals, hydrodynamic instabilities and neutron scattering 79−50990
liquid crystals, inelastic neutron scatt. of motion around director 78−91252
liquid crystals, molecular order and dynamics, high resolution neutron scatt. study 79−50991
liquid crystals, molecular ordering from incoherent quasi-elastic neutron scatt. 79−4241
liquid crystals, struct. and optical props., neutron and X-ray diffr. obs. 80−24323
liquid crystals, structure and dynamics, neutron diffr. studies 78−94972
liquid metal, mol. motions from NQR, viscosity and sound damping 77−1615
liquid structure, TOF pulsed neutron diffraction using electron linac, CCl_4 appl. 78−18504
liquid structure determ., book contrib. 79−60230
liquids, classical, pair pots. from inelastic neutron scatt. data, self-consistent method 78−59728
liquids, longitudinal modes, transverse modes and vel. correls. 79−94858
liquids, neutron diffraction studies at high momentum transfer 79−46525
liquids, neutron scattering, book contrib. 79−60232
liquids, non-mol., individual and collective atomic motion, inelastic neutron scatt. and computer simulation 77−55226
lithium thallium tartrate monohydrate, paraelectric phase structure by neutron diffraction data 79−19238
localised electronic excitation, neutron scatt. theory 79−4539
low-dimensional mag. systems, neutron scatt., review 80−50103
macromolecular aggregates, estimation of locations of subunits from neutron interference data 79−86716
macromolecules, scatt. methods, conf., Prague, Czechoslovakia, (July 1976) 79−1764
macroparticle diffusion, role of inertial effects 80−29196
magnetic critical scattering, static and dynamic scaling theories 79−42783
magnetic crystal, perfect, spin rot. of forward transmitted beam in neutron diffr. 80−50113
magnetic crystal neutron diffr., integrated intensity heats, crystal and mag. struct. determ. 80−44079
magnetic densities and magnetic excitations, neutron studies, book contrib. 80−11170
magnetic domain structure, neutron small-angle scatt. from dynamical theory of diffr. 79−24189
magnetic domain structure studies by neutron depolarisation 79−47299
magnetic film surface, ultracold neutron depolarisation *(Russian)* 78−95493
magnetic neutron scattering, polarisation depend. on generalised susceptibility 79−47255
magnetic phase transition meas. using polarised neutron scatt. 79−87257
magnetic scattering in critical region, differential cross section 78−39294
magnetic soft and hard materials, garnets, magnetic properties and applications, structural props. 80−65760
magnetic structure, neutron diffr. study, symm. anal., polarisation effects 80−93083
magnetic structure, neutron diffraction patterns, group theoretical, exchange Hamiltonian symm. anal. *(Russian)* 79−65648
magnetic structure determ., book contrib. 79−61064
magnetic structure symm. anal. in neutron studies periodicity changes at mag. phase transitions 79−99680
magnetic structures, neutron birefringence meas. 79−47298
magnetic structures, neutron diffr. anal., group theory approach, mag. lattice determ. *(Russian)* 79−47236
magnetic structures, symmetry anal. in neutron studies, phase transition concept 79−99679
magnetic superconductors, mag. scatt. of neutrons 80−103819
magnetic system, solitons near critical point, neutron scattering observation 80−34650
magnetic systems, conference, Julich, Germany (Aug. 79) 80−41934
magnetic systems, one- and two-dimens., review of neutron scatt. studies 77−66254
magnetic systems, polarisation analysis of diffuse neutron scattering 80−25098
magnetic systems, polarized neutron diffractoin in high magnetic fields 79−73684
magnetised solid state plasma, theory of neutron scattering 79−38015
magnetism investig. by neutron scatt., review *(Japanese)* 78−52227
magnetite, neutron diffr. exam. of texture, comparison with haematite 78−52849
magnetite, textures and topotactical relationships, neutron diffr. study 79−83229
manganese acetate tetrahydrate, neutron diffr., cryst. struct. 77−47436
manganese zinc formate dihydrate, two-dimens. antiferromag., anomalous crit. phenomena, neutron scatt. and PMR obs. 80−50104
martensite transformation mechanism, position of C atoms in cryst. lattice *(Russian)* 77−8820
materials problems and basic research needs rel. to energy resources and storage 78−86703
materials science, phys. and mech. props. 80−25538
MBBA, nematic phase, quasielastic and elastic 10 Å neutron scatt. 78−42904
met-myoglobin, struct. determ., neutron crystallography 79−43814
metal, atomic defect config. from X-ray and neutron scattering studies 78−47322
metal, cond. electron polarisation, magnetisation densities, neutron mag. form factors 77−72981
metal, diffusion of H(D), slow neutron scatt. obs., review 80−34248
metal, small angle neutron scattering by surface imperfection 77−51578
metal, textures and collective props. of lattice defects, external surfaces, grain boundaries 77−62543

neutron diffraction examination of materials continued
metal-H alloys, phonon dispersion relation, neutron scatt. studies, review 79−60451
metal-H system, inelastic neutron scattering meas. of optical vibr. freq. distribs. 80−59605
metal-H system, thermal neutron scatt., general multisublattice jump diffusion model 77−66045
metal-H system, thermal neutron scatt., general multisublattice jump diffusion model 77−66046
metal-H system study by neutron scattering, review *(French)* 80−34226
metallic actinide compounds, localised cryst. field states, neutron inelastic scatt. obs. 78−14697
metallic glasses, electronic structure, neutron scatt., elec. resist., Hall coeff., mag. susceptibility and XPS 78−23013
metals, BCC and FCC, H-diffusion and trapping 80−70447
metals, diffusion of H_2, neutron quasielastic scatt. 79−42316
metals, diffusion of H, complex jump diffusion model rel. to quasi-elastic neutron scatt. by H 80−24638
metals, inelastic neutron scatt. cross-section, effect of cryst. field 79−65642
metals, neutron mag. form factors, magnetisation densities, APW wavefunction calcs. 79−47243
methane, adsorbed submonolayer, on graphite, two-dimens. fluid, diffusion coeff. 79−37920
methane, pure and O_2 doped solid, neutron scatt. and proton spin conversion 77−89391
methane-d_1, tunnelling states and nuclear spin conversion 79−10944
methane-d_2, orientational ordering and tunnelling states meas. 79−10963
methane-d_4, adsorbed on graphon, neutron scatt. study 79−60640
methane-d_4, critical behaviour at orientational order-disorder transitions, neutron scatt. 77−43308
methane-d_4, solid, rot. tunnelling, neutron scatt. obs., isotope effect 80−92468
methane-d_4, solid phases I, II, acoustic phonon dispersion curve meas. by neutron inelastic scatt. 78−2212
methane-d_4 monolayer films on graphite, neutron diffr. studies of phases 80−96739
methanes, substituted, internal torsion modes, inelastic neutron scatt. 77−19104
methyl 2,3:4,5-di-O-isopropylidene-α-D-glucoseptanoside, struct. determ., X-ray and neutron diffr. study 79−42050
methyl groups, spin symmetry species, neutron scatt. transitions 80−92470
4-methyl-2,6-ditert-butylphenol, temp. depend. of methyl tunnelling spectrum by inelastic neutron scatt. 79−51015
4-methyl-2,6-ditertiarybutylphenol, methyl group reorientation, classical dynamics, NMR relax. and inelastic neutron scatt. 80−88066
4-methyl-2, 6-ditertiarybutylphenol, tunnelling methyl group, inelastic neutron scatt. study 79−46580
3,5-methyl-pyridine, rot. pot., proton spin-lattice relax., inelastic neutron scatt. study 79−47351
N-methylacetamide, structure, Raman spectroscopy and neutron diffr. obs. *(French)* 80−7343
methylpyridines, rot. tunnelling, NMR relax. and inelastic neutron scatt. 79−4733
micellar solns., small angle neutron diffr., micellar struct. *(French)* 78−11564
microemulsion, struct. description of liq. particle dispersion, ultracentrifugation and small ang. neutron scatt. obs. 79−5184
microemulsions, struct., use of variable-contrast method appl. to neutron scatt. 79−16043
microscopic examination of mag. materials 77−24676
mixture, binary, fluctuations near liq.-liq. crit. point, neutron small-ang. scatt. appl. 79−82347
Mo Co_2, single crystal, polarised neutron diffraction, various temp. and applied fields 78−2650
moderately dense gases, molecular interactions, neutron scatt. 79−50144
molecular and molecular group rotational motion in solid state, neutron scatt. studies 80−24384
molecular crystal, dynamics, neutron spectroscopy appl., review 79−42166
molecular crystals, crit. dynamics of orientational phase transitions 77−7838
molecular crystals, neutron scattering and exciton spectrum due to impurities 78−91622
molecular crystals, rot. excitations and tunnelling, review 79−46579
molecular crystals, rotational and translational dynamics 79−51215
molecular crystals, spectroscopy, bibliography (1977) 80−7317
molecular crystals, spectroscopy, bibliography for 1976 78−72585
molecular dynamics of liqs., neutron scatt. and computer simulation 78−63650
molecular gases and liquids, recoil and detector corrections for slow neutron scatt. 79−41223
molecular liquid, interval normalisation of neutron diffr. data 77−35441
molecular liquids, quasielastic scatt. anal. of scatt. law 78−9938
molecular reorientation, incoherent quasielastic, coherent-quasielastic and coherent-inelastic scatt., data anal. 78−63640
molten salt, possibility of plasmon mode obs., struct. dynamics 80−10477
molten salts, partial struct. factors 79−60258
Mosaic crystals, simple dynamical approach to neutron diffr. 78−83655
multicomponent mixtures, tricritical behaviour, possible exptl. tests 77−47543
myelin, frog nerve, comments on the paracrystalline nature 79−16161
NaCN, lattice dynamics and order-disorder transitions, neutron scatt. expts. 78−14434
naphthalene, lattice dynamics, inelastic neutron scattering 78−79690
naphthalene, lattice parameters, elastic consts., press. depend., neutron diffr. obs. 78−26558
naphthalene, phonon eigenvectors, neutron scatt. intensities determ. 80−44271
naphthalene crystal, external phonon modes, inelastic incoherent neutron scatt. spectra and computer calc. 78−34577
naphthalene-d_8, phonon dispersion meas. and calc. 78−2211
naphthalene-d_8, struct. facators, time of flight neutron diffr. 78−47212
naphthalene-d_8 crystal, dispersion of LF phonons 77−69058
naphthalene-d, press. depend. of lattice freqs. at 100K 79−46768
nematic liquid crystal, circular random walk motion, comparison with neutron scatt. data 77−43146
nematic liquid crystal, coherent neutron diffr. 78−75550
nematic liquid crystals, coherent neutron scatt. studies, review 79−41956

neutron diffraction examination of materials continued
nematic liquid crystals, microdynamics, computer study and models *(Hungarian)* 80−33878
neopentane, comparison with computer simulations of rough sphere fluid 79−99041
neopentane, mol. motion in cryst., liq. and plastic phases, neutron scatt. obs. 78−6021
neopentane, plastic crysts., rot. correlation functions, neutron scatt. obs. 79−46578
neopentane, rotational motions, cold neutron scatt.study 79−51023
neopentane-d_{12}, adsorbed on TiO_2, neutron scatt. study 79−60640
neutron induced X-ray atomic excitation 80−23510
$(Ni_{1-x}Co_x)_{0.98}Mn_{0.02}$, average mag. moment of Mn atoms 79−28509
Ni single crystal near T_c, neutron transmission depolarisation 79−33479
Nimonic 105, temp. and stress depend. of microstruct., small angle neutron scatt. study 79−15726
nitrates of monovalent metals, molten, NO_3^- ion struct., pulsed neutron diffr. obs. 78−22631
t-nitrobutane, phase, II, quasielastic neutron scatt. 78−26458
nitromethane, 1-dimens. reorientation and tunnel splitting in solid 79−99086
non-crystalline materials, pair distrib. functions determ. 77−72522
n-nonadecane, plastic phase, neutron quasielastic scatt. 79−51013
norbornadienes, LF vibr. modes of hydrogeneous ligands, incoherent inelastic neutron scatt. 78−6229
nuclear magnetic ordering, domains, neutron diffr. patterns, theory 80−100577
octafluoronaphthalene, high press. struct., neutron powder diffr. 78−63743
octafluoronaphthalene, struct. phase transition exam. 77−47572
octaphenylcyclotetrasiloxane, mesophase form., neutron diffr. obs. 78−91224
oil films, thickness meas. by neutron imaging, and scattering, exam. of flow props. 79−15815
one-dimensional magnetic systems, obs. of mag. solitons *(Japanese)* 80−2555
organic liquid, simple, struct. exam. and scatt. data interpret. 80−54096
organic molecular crystals, intermolecular interactions, spectroscopic studies, review 80−103958
orientationally disordered cryst., diffuse scatt., hard-core correl., weak-graph method 80−49137
oriented DNA, hydration, neutron scatt. obs. 80−89714
oxides, $RCu_3Mn_4O_{12}$, R=La to Lu, Y, synthesis and mag. props. 80−75717
oxides with perovskite struct., neutron diffr., ferri- and ferromag. props. 78−52214
PAA, cryst. phase transitions, intermolecular motion, Raman and inelastic neutron scatt. spectra 80−2164
PAA, deuterated, mol. reorientation, quasielastic neutron scatt. study 79−86705
PAA, fluctuations near Rayleigh-Benard instability, real time obs. by neutron scatt. 80−59390
PAA, liq. cryst., solid-state polymorphism neutron diffr. meas. 77−4200
PAA, methoxy deuterated, reorientational correl. times, comparison of neutron scatt. and dielec. relax. data 79−7545
PAA, nematic liq. cryst., collective excitation dispersion, neutron inelastic scatt. data 77−35475
PAA, nematic liq. cryst., elec. field effects, neutron diffr. study 80−28912
PAA, nematic liq. cryst., propagating collective modes, neutron scatt. data 77−35476
PAA, quasielastic neutron scatt., isotope effects 78−83719
PAA with deuterated methyls, nematic phase, quasieleastic neutron scatt. study of fast reorientations 78−14280
PAP, cryst. phase transitions, intermolecular motion, Raman and inelastic neutron scatt. spectra 80−2164
parabanic acid, charge density and cryst. struct. redeterm. by X-ray and neutron diffr. 79−46644
paramagnet, classical, static and dynamic response functions 79−47227
paramagnet, neutron polarisation, crit. scatt. above Curie pt. 78−43565
paramagnetic intermediate valence compounds, sum rules and inelastic neutron scatt. 79−61037
paramagnetic metal, polarised neutron inelastic and quasi-elastic scattering 80−50045
paramagnetic metals, polarised neutron studies of field induced magnetisation 80−25084
Pd_3Fe, ferromag. spin wave meas., inelastic scattering of polarised neutrons 78−2665
penninite, one-layer triclinic chlorite, neutron diffraction study 80−84144
4-n-pentyl-4′-cyanobiphenyl, nematogen, incoherent neutron quasielastic scatt. 79−32887
perdeuteronaphtthalene, use of neutron time-of-flight technique for cryst. structs. investigation 79−19126
Permalloy, order-disorder transformations and magnetic properties obs. *(Slovak)* 79−4963
perovskite, Re containing, new seignettomagnets and ferroelectrics 78−19425
perovskite-like oxides, $ACu_3B_4O_{12}$ subseries, synthesis, struct. and mag. props. 77−68960
phonon perturbation by complex defects, expt. studies review 79−42190
phospholipid bilayers, selectively deuterated, neutron diffr. study of mol. struct. 78−24036
physisorbed monolayer on graphite, neutron scatt. studies 80−107655
pivalic acid, orientationally disordered crystal., mol. orientation 78−34448
plagioclase, labradorite, Al/Si distrib. in An_{66}, superstructure in An_{54} 79−94970
plastic crystal, orientational dynamics, neutron scatt. data interpret. using functions derived from group theory 80−107092
PMMA, benzene soln., single chain dynamics by neutron scatt. 79−19136
polarised neutron scattering, appl. 79−46516
polarised neutrons in condensed matter [conference, Zaborow, Poland (Sept. 1979)] 80−22136
polyatomic fluid, local dynamics, spectroscopic studies, summer school lecture series 80−6343
polydimethylsiloxane, benzene soln., single chain dynamics by neutron scatt. 79−19136
polyelectrolyte in solution, variation of contrast, neutron forward scatt. calc. *(French)* 80−54104
polyelectrolyte solution, neutron scatt. 79−77484

neutron diffraction examination of materials continued
polyelectrolytes in soln., conform., small-angle neutron scatt. investigs., review 79−873
polyethylene, chain conform. in solid and melt, low angle neutron scatt. 77−76329
polyethylene, chlorinated, semicryst. random, characterisation by small angle neutron and X-ray scatt. 80−75189
polyethylene, cryst., soln. grown, neutron scatt., mol. dimens. rel. to mol. wt. 79−41258
polyethylene, crystn. at high press., small-angle neutron scatt. 77−55248
polyethylene, molecular clustering in mixtures with polyethylene-d_n, small-angle neutron scatt. 78−26451
polyethylene, protonated and deuterated, neutron scatt. at intermediate Q-values 79−10807
polyethylene, semi-crystn., neutron scattering study 80−38936
polyethylene, solid, heterogeneity investigation by small angle neutron scattering 78−14298
polyethylene, solution crystallized and melt crystallized small angle neutron scatt. 79−14691
polyethylene, uniaxial, deuterated, interchain forces effects on acoustic phonon branches, neutron scatt. study 79−51228
polyethylene oxide, dil. soln., neutron scatt. mol. motion obs. 77−23593
polyethylene oxide, molecular dynamics in conc. soln., quasi-elastic neutron scatt. meas. 78−29870
polyethylene oxide crysts., small-angle neutron scatt. 78−51447
polyisoprene, small angle neutron scatt., single chain form factors 80−107038
polymer, amorphous, bulk, structure models and exptl. methods, review 78−22671
polymer, amorphous, chain conform., small-angle neutron scatt. obs. *(Polish)* 80−10511
polymer, amorphous, segmental distrib., light-, neutron- and X-ray scatt., piezooptical and dielec. meas., review 78−51444
polymer, amorphous, struct. determ. by small-angle X-ray and neutron scatt. 77−84668
polymer, amorphous state struct., conf., Atlantic City, USA (Sept. 1974) 77−76327
polymer, molten or amorphous, chain conform. determ. by diffr. 77−80429
polymer, neutron scatt. studies of chain conform. and dynamics 78−83753
polymer chain, neutron scatt. obs., review 78−14245
polymer chain collapse, in poor solvent, small angle neutron scatt. obs. 78−91215
polymer chain conformation, determ. by neutron scatt. in amorphous polymers 77−76328
polymer chain in bulk and soln., elastic, coherent small-angle neutron scattering 77−80428
polymer chain trapped in suddenly deformed gel, relaxation *(French)* 77−62483
polymer coil, configuration in polymer, polyelectrolyte solns., and hot-stretched polymer samples, neutron scatt. 79−10778
polymer configuration in amorphous and crystalline state, small-angle neutron scatt. *(German)* 77−85398
polymer dilute soln., neutron quasielastic scattering from freely jointed chains 78−18534
polymer glasses and melts, struct., review of expt. results 79−37636
polymer melt, quasielastic incoherent scatt., Q^4-depend. broadening 77−47327
polymer mixtures, thermodynamics, review 79−1506
polymer network, small ang. neutron scatt. 79−90569
polymer network, small-angle neutron scatt. obs. of mol. behaviour 80−37918
polymer protonated and deuterated mixtures, partial miscibility 80−107037
polymer semicrystallised chains, small-angle neutron scatt., mean dimension evaluation 80−43220
polymer solution, dynamical scaling, neutron spin echo obs. 80−14990
polymer solution, partially deuterated, osmotic compressibility from elastic neutron scatt., general formulation 79−90517
polymer solution, semidilute, chain size 78−87607
polymer solution and bulk state, partially labelled chains, neutron scatt. obs. 80−38899
polymer solutions, conformational motions, comp. of neutron and light scatt. expts. 79−41938
polymer solutions, cross-over, pair correlation function, small-angle neutron scatt. meas. 78−22626
polymer solutions, spatial cross-over, obs. in small angle neutron scatt. 79−41937
polymer solutions, tricritical effects, small angle neutron scatt. studies 79−41939
polymers, small angle neutron scattering studies, deuteration effects 79−50956
polymers, structure and molecular dynamics, neutron scatt. meas. 79−51009
polymethacrylic acid semi dilute solutions, conformation and organisation, small-angle neutron scatt. 79−10782
polymethylene, intramol. scatt. function calc. 77−38761
polyolefins, isotropic semicryst., neutron scatt. obs. of struct., radius of gyration 79−94922
polyolefins, semi-crystn., neutron scattering study 80−38936
polyphenyls, inelastic neutron scatt. study of structural phase transitions 79−51255
polypropylene, isotropic, molten and cryst., small-angle neutron scatt., chain-folding 78−63680
polypropylene, molten and cryst., mol. conformation, small angle neutron scatt. study 79−51012
polypropylene, semi-crystn., neutron scattering study 80−38936
polypropylene oxide, rubber and glassy states, conformational motion, neutron scatt. study 79−41259
polystyrene, chain conform. in solid and melt, low-angle neutron scatt. 77−76329
polystyrene, cyclohexane soln., temp. depend. of chain dimensions, small-angle neutron scatt. 78−50671
polystyrene, dil. soln., neutron scatt., quasielastic broadening 77−76286
polystyrene, isotactic, conformation in bulk crystallised state 80−43221
polystyrene, substituted, Raman, IR and neutron spectra of LF vibs. 78−2848
polystyrene, sulphonated, polyelectrolyte solution, correlations and dynamics 80−104446
polystyrene model-networks, structure 77−89385

neutron diffraction examination of materials continued
polystyrene networks, characterisation by small-angle neutron scatt. 77−38765
polystyrene solution, binary and ternary cluster integrals, small angle neutron scattering 79−50975
polystyrene-polyisoprene two-block copolymer soln., conformation, small angle neutron scattering, X-ray diffraction, review *(Rumanian)* 80−6348
polysulphur nitride, Kohn anomalies in phonon dispersion 80−24555
polytetrahydrofuran, dil. soln., neutron scatt., quasielastic broadening 77−76286
polytetrahydrofurane in CS_2, dil. solns. neutron quasielast. scatt. study 79−41935
protein hydration dynamics, quasi-elastic neutron scattering 79−16127
protein solutions, small-angle neutron scatt. using time of flight method, spectrometer 79−1371
protonated samples, rot. states, coherent neutron scatt. 77−84678
pyridine-Ag_5I_6, superionic conductor, dynamical aspects 78−79695
pyridinium pentasilver hexaiodide, solid, incoherent neutron scatt. 78−2291
quantum liquids, neutron scatt. 78−59990
quartz, acoustic activity, inelastic neutron scatt. obs. *(French)* 80−103431
α-quartz and quartz glass, neutron irradiated struct., neutron diffr. meas. 78−22769
quasi-localised spin system, mag. excitations, neutron scatt. studies 80−44838
quasielastic neutron scattering and correlated self-diffusion in cryst. 77−84967
β-quinol, low frequency mode investig. by IR absorpt. and neutron scatt. *(French)* 77−36220
quinuclidine, plastic phase, rot. motion, quasielastic neutron scatt. 79−69038
rare earth alloys, RCo_2 and R_2Fe_{17}, Invar props. 79−56593
rare earth alloys, RZn_{12} and RCu_4Al_8, mag. struct. and interactions 80−25092
rare earth cobaltide, RCo_2, 'as cast', fibre texture 78−3117
rare earth cpds., RRh_4B_4 and RMo_6X_8 (X=S, Se), mag. order and supercond., neutron scatt. studies 80−44807
rare earth intermediate valence systems, neutron scatt., review 80−49674
rare earth intermetallic compounds with Cu_3Au structure, crystal field splitting 80−54663
rare earth intermetallics, mag. struct. 80−15698
rare earth intermetallics, neutron scatt., induced moment magnetism, high press. 80−15699
rare earth intermetallics, RAl_2, orbital and spin polarisations of cond. electrons 80−65791
rare earth intermetallics, RM_{12}, mag. interactions, mag. meas. and neutron diffr. 77−63103
rare earth intermetallics, RPt, (R=Gd, Tb, Dy, Ho, Er, Tm), structs. and mag. props. 80−50069
rare earth metals, mag. excitations, neutron inelastic scatt., review 79−47265
rare earth mixed valence compounds, spin dynamics, mag. neutron scatt., Mossbauer effect, XPS studies 80−39786
rare earth orthochromites, mag. interactions and weak ferromagnetism 78−52220
rare earth orthoferrites, slow neutron elastic scattering, domain boundary observation *(Russian)* 79−82811
rare earth orthovanadites, indirect exchange 78−34977
rare earth orthovanadites, RVO_3, magnetic and cryst. struct., Jahn-Teller effect 77−32169
rare earth systems, mag. excitations, review of neutron scatt. data 80−60227
rare earth systems, magnetic structures and inelastic neutron scattering. review 79−69654
rare earth-Al_2, cubic Laves phases, prep. and phys. props. *(German)* 78−23075
rare earth-cobalt intermetallic, RCo_2 79−19725
rare earth-cobalt intermetallics, R_4Co_3, cryst. field effect on mag. moments direction, neutron diffr. meas. 78−80132
rare earth-Fe alloys, amorphous and crystalline, small angle neutron scatt. study of mag. order and mag. microstruct. 79−15283
rare earth-Ga_2 intermetallics, mag. structs. 78−84394
rare earth-Mg, magnetisation and neutron diffr. meas. 77−63105
rare earth-nonmagnetic metal intermetallic cpds., struct. and props., review 79−95377
rare earth-Zn_{12}, mag. props. and structs. 78−84393
rare earths, spin waves and excitations 78−84407
resonance scattering of neutrons and γ-quanta, high recoil energies *(Russian)* 78−35075
review, time-depend. distribs. 77−43102
ribonuclease A, bovine, cryst. struct. determ. by X-ray and neutron diffr. 80−108841
ribosomal subunit 30 S, of E coli, meas. of location and radii of gyration of proteins by neutron scattering 79−11892
ribosomes, E. coli, contrast variation neutron scattering studies, reassembled subunits 79−20510
ribosomes, E. coli, neutron small-angle scatt., contrast variation study 79−16138
ribosomes of Escherichia coli, partially deuterated subunit, protein and RNA distrib., neutron scatt. 78−77021
rotational tunnelling and diffusion in condensed mol. systems, neutron scatt. 78−63658
rubber, materials props. prediction, elasticity model 80−3113
sapphire, constant phonon energy contours, in bc-plane, inelastic neutron scatt. obs. 77−59083
sapphire container for expts. on liquid metals up to 1900K 79−63215
scattering by associated helical-sonic and spin-helical-sonic waves *(Russian)* 79−24136
screw dislocations, inelastic neutron scatt. 78−75774
screw dislocations, phonon dispersion curves of localised modes, inelastic neutron scatt. 77−72661
silicate glass, advantages over X-ray techniques for struct. determ. 78−79533
silicate minerals, thermodynamics and lattice vibr. props. 79−100830
simple fluids, dynamics, history of inelastic neutron scatt. determ. 79−46539
simple liquid, dynamic properties, neutron scatt. studies, review 79−50972

neutron diffraction examination of materials continued
slow neutron scatt. by rotating systems of identical nuclei *(Russian)* 80−14968
small fluid particles, dynamic props., applicability of neutron scatt. studies 79−41936
smectic A mesophase, self-diffusion and undulation modes, high resoln. neutron scatt. 77−11471
sodium acetate trihydrate, press. depend. of methyl tunnelling motion 80−10603
sodium hydrogen oxalate monohydrate, crystal struct. 78−10032
sodium p-octylbenzenesulphonate ionic micellar solns., neutron diffr. meas. *(French)* 78−44409
solid, rotational tunnelling, neutron scatt. theory 78−18561
spin glass, relaxation times, influence of spectral distrib. on freq. depend. of freezing temp. 80−44848
spin glass, spin freezing, exptl. obs. 77−73032
spin glasses, neutron scattering cross-sections, theory 78−80162
spin glasses, review 77−69578
spin glasses, spin dynamics, EPR, NMR, muon precession, Mossbauer, and neutron scatt. results 79−65689
spin system, mag. excitations, polarised neutron inelastic and quasi-elastic scattering 80−50045
spin-Peierls phase diagrams, obs. and models 80−60330
spinels, diluted, percolation and mag. order 78−68165
spinels, mag. struct., symmetry anal. in neutron diffr. studies 80−25091
squaric acid, antiferroelec., struct. phase transition mechanism 80−75969
squaric acid, cryst., neutron diffr., bond lengths and angles, vibr. modes 77−76384
squaric acid, neutron diffr. mol. and crystal struct. determ. 78−26557
squaric acid, two-dimens., phase transition, elastic neutron scatt. 78−6155
steel, Cr-Mn, metastable constitution diagram and phase transforms. *(Russian)* 80−50590
steel, drawn wire, quantitative texture anal., neutron diffr. studies 80−81078
steel, neutron irradiated press. vessel material, small angle neutron scatt. meas. 79−13428
steel, nuclear reactor press. vessel, radiation induced embrittlement, slow neutron small angle scatt. study *(German)* 77−34390
steel, stainless, maraging, Cr-Co, effect of ageing on microstruct., TEM and neutron diffraction exam. 78−84867
steel, stainless, polycrystalline, elastic consts., inelastic coherent neutron scatt. meas. 80−34122
steel with micro-duplex structure, analysis of rolling texture and its development 80−16327
steels, with micro-duplex struct., neutron diffr. anal. of texture and its development 79−91692
strained polymer networks, neutron scatt. 78−78846
structure factors from integrated intensities of neutron diffr. maxima, accuracy testing 78−47212
succinonitrile, orientationally disordered crystal., mol. orientation 78−34448
succinonitrile, plastic, diffuse scatt., hard-core correl., weak-graph method 80−49137
succinonitrile, plastic phase, mol. motions correlation times, incoherent neutron scatt. 80−49138
succinonitrile, plastic phase, mol. reorientation and rotational isomerization, anal. of elastic incoherent struct. factor 78−22674
succinonitrile, plastic phase, molecular reorientation, rotational isomerism, incoherent neutron scatt. study 79−51021
5-sulphosalicylic acid, dideuterate, $D_5O_2^+$ obs., neutron diffr. 77−35543
superionic conductor, scattering of light and neutrons in diffusion model 78−26719
superionic conductors, struct. and dynamical props., X-ray and neutron scatt. studies, book contrib. 80−24433
surface layer structure, rel. to neutron refl. on boundary *(Russian)* 78−1976
TBBA, biaxial smectic phases, orientational order, neutron scatt. and NQR results 78−91225
TBBA, liq. cryst., orientational order in tilted smectic phases, high resolution neutron quasi-elastic scatt. 77−80413
TBBA, low temp. phase, inelastic coherent neutron scatt. exam. 78−26429
TBBA, phonon dispersion curves in cryst. and smectic phases 79−86863
TBBA, smectic A phase, incoherent neutron quasielastic scatt. exam. of molecular ordering 77−43143
TBBA, smectic C to A phase transition, neutron diffr. exam. 78−91428
TBBA, smectic C to smectic A transition, crit. exponent, neutron diffr. obs. 78−95143
TBBA, smectic liq. cryst., crystalline at liq.-cryst. phases phonon modes, coherent neutron inelastic scatt. study *(French)* 79−51216
TBBA, smectic VI and H phases, orientational order 77−84648
TBBA, smectic-A, self-diffusion, neutron incoherent scatt. law 78−83726
TBBA liquid crystal, self diffusion coeffs., neutron diffr. and NMR study 80−19689
TBBA mesophases, mol. orientational order 79−37619
TCNQ salts, modulated struct., dynamical processes, X-ray and neutron scatt. 79−95155
tendon, calcified, of turkey leg, collagen-mineral axial relationship 77−32872
ternary alloy, metastable miscibility gap determ. by small angle scatt. 77−28780
p-terphenyl, crit. slowing down at struct. phase transition, high resolution neutron spectroscopy 79−82329
o-terphenyl, cryst. struct. determ. by neutron diffr. 79−42046
p-terphenyl, long range order at phase transition, neutron diffr. exam. 77−1228
terphenyl, ortho-, para-, meta-, total neutron cross sections for subthermal energies 78−74779
tetrabromomethane, plastic phase, neutron diffr. obs. and theory 79−77533
tetrahedral molecule, in torsional ground state, total neutron scatt. cross section 79−50954
tetrahydrofuran clathrate, reorientation, residence times, Debye-Waller factors, activation energy, neutron scatt. study 79−41989
tetrahydrofuran clathrate deuterate, rotational motion, quasi-elastic neutron scatt. study 79−51022
tetraiodoethylene, cryst. and mol. struct. at 4K 77−59001
tetraiodoethylene, disorder, neutron powder diffr. data refinement 78−34501

neutron diffraction examination of materials continued
tetramethyl germanium, methyl reorient., lattice vibrs., neutron scatt. obs. 79−51016
tetramethyl silicon, methyl reorient., lattice vibrs., neutron scatt. obs. 79−51016
tetramethyl tin, methyl reorient., lattice vibrs., neutron scatt. obs. 79−51016
tetramethylammonium perfluorooctanoate-water, lamellar lyotropic liq. cryst., neutron diffr. struct. obs. 80−64888
tetramethylammonium tetrachlorocuprate, incommensurate phase, neutron diffr. study 80−79935
tetramethylammonium tetrachlorozincate, ferroelec., incommensurate-commensurate transition, neutron scatt. study 80−40073
tetramethyllead, tunnel splitting, rot. pot., μeV neutron scatt. study 79−41993
texture, evaluation by X-ray and neutron diffr. anal., comparison *(French)* 79−91882
texture, nondestructive investigation by neutron diffr. 79−87795
TGS, crit. behaviour of thermal expansion, neutron diffr. study 80−75371
TGS, cryst., vibr. bands, ferroelec. and paraelec. phase H bonds *(Russian)* 78−15172
TGS, deuterated, paraelec. phase, D atom positions 78−14334
TGS, electrostrictive and dielec. coeffs., neutron diffr. study 80−75943
TGS, ferroelectric transition, neutron diffr. obs. 80−25324
TGS, neutron diffraction enhancement near Curie point with DC field appl. *(Chinese)* 78−68462
TGS, under electrostatic field, mechanism of enhancement of neutron diffr. *(Chinese)* 79−51907
thermal neutron scatt., summer school lecture notes, CRNL 79−14655
thiourea, deuterated, commensurate-incommensurate phase transition, inelastic neutron scatt. 79−28098
thiourea, incommensurate phase, soft modes, condensation of even-order harmonics 80−103313
thiourea, incommensurate phase transition, X-ray and neutron scatt. study 80−75963
thiourea, lock-in phase transform. 80−29698
Tl, time of flight neutron diffraction meas. of c/a ratio and vol. change at transition 77−15335
TMMC:Cu, random one-dimens. Heisenberg antiferromag., spin fluctuations 79−61140
TMMC, 1-D antiferromag., excitation linewidths, temp. depend. 77−20574
TMMC, Cu-substituted, spin dynamics, neutron scatt. cross section 80−60312
TMMC, linear antiferromag., energy gaps in spin-wave dispersion, neutron inelastic scatt. 79−91223
TMMC, one dimens. antiferromag., neutron scatt. exam. of impurity effects 78−43598
TMMC, one-dimens. antiferromag., spin wave line widths, neutron scatt. study 79−51767
TMMC, one-dimensional antiferromag., solitons, neutron inelastic-scatt. meas. 80−44810
TMMC, XY-Ising crossover transition, quasi-elastic neutron scatt. obs. 80−44826
TMMC one-dimens. antiferromagnet, effect of mag. field on correl. length 79−91244
toluenes, substituted, methyl torsion, internal rot., neutron inelastic scatt. 77−43160
tooth enamel, human cryst. struct. refinement, Rietveld method 80−51040
transition, metal nitride, atomic struct. *(German)* 79−90622
transition metal, BCC, neutron spectroscopy of fast H diffusion 80−59731
transition metal 3d alloys, neutron spin wave scatt., itinerancy 77−73018
transition metal alloys, domain struct. of diffuse ω-phase formed in quenching, 1D model 78−27523
transition metal complexes, electron densities, local orbital populations, polarised neutron diffraction 80−88725
transition metal elements and alloys, spin distribution, neutron diffraction expts. 80−25097
transition metal hydride complexes, struct. geometry bonding, neutron diffr. studies 79−46641
transition metal itinerant magnets, neutron scatt. expts. 77−73002
transition metal magnetic clusters, neutron inelastic scatt., review 80−50083
transition metal-H system, exam. of excitation spectra and diffusion mobility of H using neutrons 80−29203
transition metal-metalloid glasses, struct. and plastic flow, review 80−84090
transition metal-nonmetal glasses, with defined local coordination, struct. model 80−84092
translation and rot. dynamics, microscopic Hamiltonian anal., inelastic neutron scatt. elastic consts. 78−38632
n-triacosane, chain axis cryst., quasi-elastic neutron scatt., plastic phase transform 78−6023
s-triazine, transverse elastic mode softening at structural phase transition 79−46777
trichloromethane, liq., radial pair distrib. function determ. 79−77476
trimethylammonium chloride, cation and CH_3 groups rot. diffusion, quasielastic neutron scatt. 77−27840
trimethylammonium chloride, cation and CH_3 groups rot. diffusion, quasielastic neutron scattering 77−27841
trimethylammonium chloride and deuterated forms, cryst., inelastic neutron scatt. H bond vibr. obs. 77−7796
1,3,5-trioxane-1, 3-dioxolane copolymer, semicryst. random, characterisation by small angle neutron and X-ray scatt. 80−75189
n-tritriacontane, C-phase, mol. motion obs., incoherent quasielastic neutron scatt. 79−4260
n-tritriacontane, non periodic molecular motions, neutron scatt. study 79−51024
$(TTF)CuS_4C_4(CF_3)_4$, spin Peierls system, mag. field effects 80−7123
TTF-TCNQ, const. vol. resist., linear temp. depend. 78−51977
TTF-TCNQ, deuterated, compressibility under hydrostatic press., neutron diffr. meas. 78−2197
TTF-TCNQ, deuterated, phase transition exam. by elastic neutron scatt. 77−4194
TTF-TCNQ, elastic neutron scatt. evidence for charge transfer change at high power 80−2163
TTF-TCNQ, elastic scatt. 3D modulated lattice 78−10033
TTF-TCNQ, elastic- and inelastic-neutron scatt. study 79−69208
neutron diffraction examination of materials continued
TTF-TCNQ, inelastic neutron scatt., re-examination 78−30721
TTF-TCNQ, inelastic scattering, Peierls transition exam. 78−10134
TTF-TCNQ, Kohn anomaly, electron-phonon coupling, neutron scatt. 77−7812
TTF-TCNQ, low temp. phase transitions, elastic neutron scatt. obs. 78−14464
TTF-TCNQ, neutron and X-ray diffuse scatt., phase transitions, one-dimens. behaviour and interpret. 78−10381
TTF-TCNQ, phonon dispersion and Kohn anomaly, inelastic neutron scatt. 77−1196
TTF-TCNQ, spin waves, scatt. at $4k_F$, spin-Peierls fluctuations 78−72093
TTF-TCNQ Kohn anomalies, phonon dispersion curves 78−10133
tungsten bronzes, hexagonal, supercond. and special phonons, neutron scatt. obs. 80−15643
type II superconductor, imperfect vortex lattice, small angle neutron scatt. 79−42710
type II superconductor, neutron scatt. from imperfect flux-line lattice 79−56474
type II superconductors, flux-line lattice, small angle neutron scatt. *(German)* 77−85398
ultracold neutron scattering in films 78−9915
uniaxial ferromagnet, neutron depolarisation calc. 78−64192
uniaxial rotator in N-fold cosine pot., correlation functions, neutron incoherent scatt. law 78−9970
velocity selector for neutrons, high resolution, applic. to materials research *(German)* 80−47803
very-slow-neutron transmission, submicroscopic struct. determ. 77−62448
VI_2, mag. structs. and props. 79−61063
void fraction and phase distrib. meas. in transient flow boiling by neutron scatt. 78−94870
water, collective excitations in 10^8 cm^{-1} momentum range 78−43087
water, diffusive motions near 1°C 78−43156
zeolites, type 13X, acetylene adsorption, inelastic neutron scatt. 78−14584
Zircaloy, H diffusion, neutron scatt. and absorpt. study 79−60556
^{6}, Heisenberg ferromagnet, spin dynamics, neutron scatt. expts. 77−20619
AL_2O_3-CoO-SiO_2 glasses, spin correls., neutron diffr. meas. 80−15694
Ag, liquid, neutron diffr. investig. of pair correl. function, coordination numbers 77−35467
Ag, transverse acoustic phonon branch, temp. depend., neutron scatt. *(German)* 78−71808
Ag-Ge, liq. eutectic, neutron diffr. determ. of struct. 77−51302
Ag-Ge, liq. eutectic, struct. by neutron diffr. 78−18537
Ag-Ge, liquid, neutron diffr. investig. of pair correl. function, coordination numbers 77−35467
Ag-Ge liquid alloy, small angle neutron scatt. 79−64982
Ag-Te, liq., struct. and elec. props. 80−49083
$AgBi(CrO_4)$, cryst. struct., neutron diffr. time-of-flight study *(French)* 80−15057
$AgBi(Cr_2O_7)$, cryst. struct. determ. by X-ray and neutron diffr. *(French)* 80−92492
AgBr, Frenkel defects, interstitials, neutron scatt. study 79−42059
AgBr, lattice dynamics, 4.4K 77−39643
AgBr, phonons at elevated temp. 78−79810
AgCl, Frenkel defects, interstitials, neutron scatt. study 79−42059
α-AgI, cation distrib. and anharmonic thermal vib. 77−66005
α-AgI, cond. mechanisms in superionic phases 80−59714
α-AgI, diffusion dynamics, quasielastic neut. scatt. expt. 80−107484
α-AgI, diffusive motion of Ag^+ ions, quasielastic neutron scatt. 77−11726
β-AgI, neutron inelastic scatt., phonon dispersion curves 78−67786
α-AgI, neutron powder diffr. meas. interpretation 80−10533
α-AgI, neutron scatt. expts., Ag^+ ion motion 80−6552
β-AgI, self-diffusion of Ag, quasielastic neutron scatt. study 78−83999
AgI, single cryst. neutron diffr. meas., Ag distrib. determ. 78−10025
α-AgI, superionic compound struct., cation distrib., powder neutron diffr. 77−72595
AgI, superionic cond., cryst. struct., neutron diffr. study 79−42041
AgI, superionic conductor, dynamical aspects 78−79695
AgI type solid electrolytes, expt. props. 78−63877
β-Ag_2S, cond. mechanisms in superionic phases 80−59714
β-Ag_2S, fast-ion conductor, Ag ion density, neutron diffr. study 80−34234
Ag_3SI, superionic conductor, dynamical aspects 78−79695
Ag_3SI, superionic cond., phase transition and cryst. structs., sp. ht., neutron and X-ray diffr. obs. 80−10662
Al, cold neutron small angle elastic scatt., microstruct. exam. 77−84736
Al, liq., calc. of neutron scatt. law 77−47330
Al, liq. and polycryst., density fluctuations, neutron scatt. anal. 80−70349
Al, liq. struct. factor, 680 to 840°C, neutron diffr. study 79−46552
Al, liquid, sapphire container for experiments up to 1900K 79−63215
Al, liquid, structure factor and radial distrib. function, neutron diffr. 77−47334
Al melt, struct. factors, at. distrib. curves, thermodynamic and neutron diffr. study *(German)* 80−19687
Al, melting, existence of before and after effects, neutron scatt. 77−84895
Al, neutron irradiated, phonon dispersion curves, neutron scatt. meas. 77−43290
Al, neutron irradiated, void surface props. determ., anisotropic small-angle neutron scatt. 78−10095
Al, non-pair inter ion interaction through cond. electrons, inelastic neutron scatt. theory *(Russian)* 79−46773
Al, phonon anharmonic response, neutron-scatt. test of computer calcs. 80−44281
Al, phonon density of states by neutron scatt., sp. ht. and Debye temp. 80−2132
Al, phonon scatt. surfaces obs., by neutron film methods 79−46761
Al, polycrystalline, elastic consts., inelastic coherent neutron scatt. meas. 80−34122
Al, reactor irradiated, neutron inelastic scattering meas. of phonon dispersion curves 78−75758
Al, single crysts., total thermal neutron cross sections 80−19672
Al, unpaired ion-ion interaction, transverse phonon branch, neutron scatt. expt. *(Russian)* 78−87751
Al-Ag, resonance splitting of phonons 78−75759

neutron diffraction examination of materials continued
Al-Fe (49 at.%) quenched alloy, neutron diffuse scatt., diffuse ω phase obs. 80−84141
Al-Mg, determ. of distortion field, induced by substitutional defect 80−44536
Al-Mg, dil., form of distortion field produced by Mg substitution, elastic neutron scatt. meas. *(German)* 79−42092
Al-Mg, dil., long-range solute-host interactions 78−95062
Al-Mg, Guinier Preston zone study by neutron diffr. *(French)* 77−28819
Al-Mg (13 wt.%), aged single crysts., small angle neutron scattering 80−1961
Al-Mg supersaturated solid soln., spinodal decomposition at 20°C *(French)* 77−85987
Al-Mg-Zn, neutron small angle scatt. study 79−43255
Al-Mg(-Zn)(-Zn-Cu), exam. of precipitation struct. by neutron scattering 78−92270
Al-Si, neutron small angle scatt. study 79−43255
Al-Si alloys, neutron irrad., precip. processes, neutron small-angle scatt. obs. 77−4131
Al-Si melts, struct. factors, at. distrib. curves, thermodynamic and neutron diffr. study *(German)* 80−19687
Al-Zn, comparison between very-slow-neutron transmission and small-angle neutron scatt. expts. 80−19677
Al-Zn, neutron small angle scattering from above critical point 79−1840
Al-Zn, neutron small angle scatt. study 79−43255
Al-Zn (11.8 at.%), growth and dissolution of metastable precipitates, neutron scatt. study 79−15671
Al-Zn (5.05 at.%), comparison of X-ray and neutron small-angle scatt. 79−15647
Al-Zn (6.8 at.%), neutron small angle scatt., interparticle interference 77−77514
Al-Zn alloy, small-angle neutron scatt. in crit. point regions, 324-435°C *(German)* 77−85993
Al-Zn-Mg, metastable miscibility gap determ. by small angle scatt. 77−28781
$Al_{0.965}Ag_{0.035}$, reson. splitting of phonons 77−59086
Al_3Ce and $Al_{11}Ce_3$, Kondo cpds., mag. behaviour obs. by neutron diffr. 80−50049
$AlCl_3$ aqueous soln., quasi-elastic neutron scatt. study 78−26425
$Al_2Mn_3Si_3O_{12}$, amorphous spin glass, spin relax. 79−65685
$Al_2Mn_3Si_3O_{12}$ amorphous spin glass, spin dynamics, neutron scatt. meas. 80−15741
$Al_2Mn_3Si_3O_{12}$ glass, mag. ordering effects at low temps., Mossbauer and neutron diffr. meas. 77−16047
$Al_2Mn_3Si_3O_{12}$, spin correlations and phase transitions, neturon diffr. exam. 78−84390
β-Al_2O_3-$Ag_2O(D_2O)(NH_4^+)$ 80−107512
β″-Al_2O_3-$Ag_2O(K_2O)(Li_2O)(Na_2O)(Rb_2O)$, single cryst. Raman scatt., cond. mechanism and cryst. struct. 80−66209
β-Al_2O_3-D_2O, anhydrous, prep. and struct. of $DAl_{11}O_{17}$ 80−107187
β″-Al_2O_3-$H_3O^+(Na_2O)$, struct. basis for superionic cond. 80−107498
Al_2O_3-MnO-SiO_2 glasses, spin correls., neutron diffr. meas. 80−15694
β-Al_2O_3-NH_4^+ proton dynamics neutron scatt. study 80−59408
β-Al_2O_3-Na_2O-Li_2O, struct. determ. by powder neutron diffr. 79−46623
β-Al_2O_3-OH_3^+, proton dynamics neutron scatt. study 80−59408
Al_2O_3-SiO_2 glasses, phase decomp., small-angle X-ray and neutron scatt. study 79−14688
γ-AlOOD, boehmite, hydrogen bond, neutron profile refinement of struct. 78−71701
β-Al_2O_3.$(NH_4)_2O$, neutron scatt. study of NH_4^+ motion 78−30785
$Al_{10}V$, well defined local modes, inelastic neutron scatt. study 78−26648
Al_{10}V-Ga, dil., well defined local modes inelastic neutron scatt. study 78−26648
Ar, gas, thermally excited density fluctuations, neutron scatt. 79−23392
Ar, liquid, longitudinal modes, transverse modes and vel. correls. 79−94858
Ar, liquid, neutron incoherent scatt. functions, non-Gaussian corrections 78−42874
Ar, liquid, velocity auto correl. function, 94.4K 78−75504
Ar monolayer film adsorbed on graphite 78−34705
Ar:methane, impurity rotational states, inelastic neutron scatt. study 79−51020
Ar-HCl, liq. density fluctuations, far IR absorpt., neutron scatt. mol. dynamics calc. 78−19461
^{36}Ar, adsorbed film on MnI_2 and PbI_2 cleavage faces, layer-like charact. 79−86994
^{36}Ar, liq. dynamic struct. factor, 120K, press. depend., quasi-elastic NDEMAT 79−50981
As, amorphous, neutron diffr. investig. of local order 77−35480
As, Debye-Waller factors and thermal expansion 78−43089
α-As, neutron scatt. study 79−42178
As_2S_3, crystalline and amorphous, inelastic neutron scatt. spectra 77−24276
As_xS_y vapour deposited film, struct. determ., X-ray and neutron diffr. correl. functions 79−60654
$(As_{0.4}S_{0.6})_{100-x}Cu_x$, glassy, struct. and elec. cond. study 80−59399
As_2Se_3, crystalline and amorphous, inelastic neutron scatt. spectra 77−24276
As_2Se_3, liquid, struct., investigation using neutron diffr. meas. 79−23514
As_2Se_3, vitreous, short-range structure obs. in high momentum transfer region 77−4045
$As_2(Se_{1-x}S_x)_3$, crystal growth and at. struct. 79−60289
As_2Te_3, liq., neutron diffraction study 79−77485
Au-Co melts, struct., compressibility, X-ray and neutron diffr. 77−11614
Au-Fe, dil., local mag. moments, neutron scatt. study 79−61058
Au-Fe, spin glass, mag. moment dynamics, neutron diffuse scatt. meas. 77−69584
Au-Fe, spin glass, spin relaxation rates, neutron scatt. study 79−47235
Au-Fe (14.5 at.%), spin dynamic exam. by diffuse magnetic neutron scatt. 77−8320
Au-Fe (15 at.%), small angle neutron scatt. study 79−47293
Au-Fe (16.2 at.%), cluster glass, mag. small angle neutron scatt. 80−50111
Au-Fe alloy, spin glass, neutron scatt. 78−68265
Au-Fe alloys, spin correlations, neutron diffr. meas. 80−80482
Au-Fe spin glass alloy, neutron scatt. study 79−61179
Au-Pt (60 at.%), solid soln. neutron small-angle scatt. study of phase decomp. 79−15646
$Au_2(Mn,Z)_2$, Heusler alloy, (Z=Al, Cu, Ga, In or Zn), magnetic order and coupling 79−38303

neutron diffraction examination of materials continued
Au_4Mn, atomic short range order and pair interaction, neutron diffr. exam. 78−22695
Au_4V, partially disordered, magnetisation distrib., polarised neutron diffr study 79−47244
p-azoxyanisole, neutron scatt. by collective excitations 77−84651
$Ba_2Bi^{3+}Bi^{5+}O_6$, structure and elec., mag., thermal props. vs. temp. X-ray and neutron powder diffr. study 79−19189
$Ba_2Bi^{V}Bi^{III}O_6$, struct. determ. by powder neutron diffr. 78−34468
$BaCl_2$, molten, struct. determ. by neutron diffr. 78−42883
$BaCl_2.2H_2O$, cryst. struct. determ. by neutron diffr. 78−75639
$BaCl_2.2H_2O$, polycryst. hydrates, librational motion of H_2O mols., neutron diffr. exam. 80−10604
$BaCo_2(AsO_4)_2$, magnetic field effect on mag. ordering neutron diffr. obs. 80−50053
$BaCo_2(AsO_4)_2$, planar X-Y model, mag. ordering 77−66256
BaF_2, anharmonicity vibrs. and correlation effects, neutron diffr. 78−55915
$BaF_{2-x}H_x$, synthesis and struct. determ. using neutron diffr. *(French)* 80−24425
$Ba_3Fe_2TeO_9$, siegnette magnets with hexagonal barium titanate structure 78−76397
$Ba_3Fe_2WO_9$, siegnette magnets with hexagonal barium titanate structure 78−76397
$Ba(H_2PO_4)_2$, antiferroelectric, phonon spectra 77−62592
$BaMnF_4$, mag. and structural phase transitions, neutron scatt. obs. 79−87259
$BaMnF_4$, magnetic neutron scatt. from structurally distorted cryst. 80−93086
$BaMnF_4$, phase transitions review 79−78378
$BaMnF_4$, spectroscopy near ferroelec. transition, dielec. anomalies near mag. ordering temp. 80−75965
$BaMnF_4$, struct. and mag. transitions, magnon dispersion curves, nearest neighbour exchange consts. 79−42760
$Ba_2NaNb_5O_{15}$, incommensurate refls. near ferroelastic transition, neutron and X-ray precession obs. 80−70395
$BaNi_2(PO_4)_2$ and $BaNi_2(AsO_4)_2$, mag. props., neutron diffr. and sp. ht. meas. 80−70948
Ba_2NiReO_6, mag. and cryst. struct. 77−20554
$BaPb_{1-x}Bi_xO_3$, struct. determ., X-ray and neutron diffr. study 79−42039
$BaPt(CN)_4.4H_2O$, cryst. struct., neutron diffr. 77−35521
$Ba_2Sb^{V}Bi^{III}O_6$, struct. determ. by powder neutron diffr. 78−34468
$Ba_3Sb_2NiO_9$, 6H, cation ordering, powder neutron diffr. obs. 78−55852
$BaTiO_3$, cubic, optical modes meas. by neutron scatt. 79−69213
$BaTiO_3$, phonon scatt. surfaces obs., by neutron film methods 79−46761
$BaTiO_3$, polarisation reversal and surface neutralisation 78−27169
$BaVS_3$, annealing influence on lattice constants, neutron diffr. profile anal. 80−1976
$BaVS_3$, mag. transition and hyperfine interaction, neutron spin-flip scatt. obs. 80−97093
$BaVS_3$, magnetisation and neutron study 80−84588
$BaWO_4$, slow neutron inelastic scatt. spectra, Debye temp. calcs. *(Russian)* 80−59347
$Ba[Pt(CN)_4Br_2]4.5H_2O$, single crystal neutron diffr. struct. exam. 78−2082
Be, phonon spectrum from inelastic coherent scatt. of cold neutrons 80−10617
Be, single cryst., mean square atomic displacement and antisymmetric atom vibrations, neutron data 80−49180
Be_4TeO_7, cryst. growth by solid-state reaction and struct. *(German)* 78−18603
Bi, Debye-Waller factors and thermal expansion 78−43089
Bi, liq., collective motions, cold neutron scatt. obs. 78−67639
Bi, phonon density of states by neutron scatt., sp. ht. and Debye temp. 80−2132
Bi, single crysts., total thermal neutron cross sections 80−19672
Bi-Cu alloys, molten, struct., thermal neutron diffr. meas. 77−39526
Bi-Cu alloys, molten, struct., cold neutron scatt. in region of small momentum transfer 77−39527
Bi-Cu melts, struct., neutron scatt., conc. of segregated regions calc. 77−39528
$BiFeO_3$, ferroelec., antiferromag., cryst. and mag. struct., neutron diffr. study 80−65786
$Bi_2Fe_4O_9$, mag. struct., neutron diffr., transition 78−52217
$Bi_2Fe_4O_9$, mag. struct., neutron diffr. meas. 78−91844
Bi_2Te_3, lattice vibrs. coherent inelastic neutron scatt. meas. 78−34576
$BiVO_4$, cryst. growth and struct. 80−35078
Br_2, liq., evaluation of effective pair pot. 78−75527
Br_2, liq. struct. factor by neutron diffr., wavelength depend. 77−89370
CBOOA, smectic A order parameter meas. and crit. scatt. near smectic A⇄nematic phase transition 77−84649
CD_4, adsorbed film on PbI_2 cleavage faces, layer-like charact. 79−86994
CO myoglobin struct. determ., neutron crystallography 79−43814
C_2O_3, liq., mol. conform. and orientation correlation 79−32877
C_3O_2, liq., neutron diffraction studies at high momentum transfer 79−46525
$C_{24}Rb$, intercalated graphite, order struct. determ. by neutron scatt. 80−107143
CS_2, liq., S partial struct. factor, 20°C, from X-ray and neutron diffr. data 77−80407
CSe_2, liq., partial struct. factor, neutron diffraction meas. 80−79672
$CaCl_2$, aqueous soln., ion hydration 80−35518
$Ca(Cu_{0.78}Mn_{0.22})_3Mn_4O_{12}$, mag. structure, neutron diffr. powder data, 350K ferromag. T_c 77−69502
$CaCu_3Ti_4O_{12}$, mag. struct. and props. *(French)* 77−69495
$CaCu_3Ti_4O_{12}$, mag. struct., neutron diffr. powder data, 27K T_N 77−69502
CaD_2, neutron diffr., NMR 77−15378
CaF_2, anion motion at high temps., quasielastic nuetron scatt. obs. 80−59715
$CaF_{2-x}H_x$, solid soln. prep. and struct. determ. *(French)* 78−51505
$CaHPO_4$, monetite, cryst. struct. refinement, H bonding, neutron diffr. meas. 77−47389
$CaHPO_4$, monetite, low-temp. ordering of H atoms, X-ray and neutron diffr. study at 145K 80−39022
$Ca_3Mn_2Ge_3O_{12}$, antiferromagnetic garnet, neutron diffr. study in mag. field 80−50060
$Ca_3Mn_2Ge_3O_{12}$, highly anisotropic garnet, neutron diffr. obs. of mag. struct. 78−68168
$Ca_3Mn_2Ge_3O_{12}$, mag. struct. study 80−2554

neutron diffraction examination of materials continued
- $Ca_3Mn_2Ge_3O_{12}$, neutron diffr. in mag. field, metamagnetism, antiferromag. ordering 79−65651
- $Ca_3Ti_{2-x}V_{1+x}Fe_{1+x}O_{12}$, garnet, mag. and neutron diffraction investigation 77−16044
- $CaWO_4$, slow neutron inelastic scatt. spectra, Debye temp. calcs. *(Russian)* 80−59347
- Cd, electron-phonon interactions, inelastic neutron scatt. meas. 79−99285
- Cd, phonon density of states calc. from neutron diffr. data 77−24369
- $Cd_{1-x}Zn_xCr_2Se_4$, mag. semicond., neutronographic obs. *(Russian)* 79−11297
- γ-Ce, FCC, localised vibration of interstitial H impurities 80−75322
- γ-Ce, field induced mag. form factor 78−68151
- Ce, inelastic neutron scatt. under press. near first order γ-α phase transition 77−63102
- Ce, inelastic neutron scatt. cross-section, effect of cryst. field 79−65642
- γ-Ce, lattice and spin dynamics, inelastic neutron scatt. obs. 79−86859
- Ce, liq., 4f electron susceptibility temp. depend. 80−20378
- Ce, liq. struct., neutron diffr. meas. 77−51305
- Ce-H(D), inelastic neutron scattering exam. of lattice dynamics 80−29128
- CeAg(Mg)(Zn), magnetic struct. and cryst. field, neutron diffr. exam. 78−72328
- CeAl, mag. props. and mag. struct. 78−6517
- $CeAl_2$, dynamic Jahn-Teller effect, neutron energy loss obs. 79−78060
- $CeAl_2$, low temp. mag. behaviour, neutron diffr. 78−84395
- $CeAl_2$, mag. behaviour 2.5 to 300K, neutron scatt. meas. 77−63110
- $CeAl_2$, mag. ordering, neutron diffr. meas. 78−6518
- $CeAl_2$, mag. ordering and anomalous ground state, neutron diffr. obs. 79−78331
- $CeAl_2$, multiple q mag. struct. 79−78330
- $CeAl_2$, multiple-q mag. struct. 80−25100
- $CeAl_2$, multiple-*q* structure or coexistence of different mag. phases, neutron diffr. study 80−107985
- $CeAl_2$, neutron diffr. at low temp., magnetism 80−20383
- $CeAl_3$, cryst. field effects, inelastic neutron scatt. meas. 77−51710
- $CeAl_3$, inelastic neutron scatt. meas. 79−47066
- CeBi, phase diagram in mag. field, hydrostatic press. effect 80−25132
- $CeCu_2Si_2$, local mag. moments, neutron scatt. study 79−61058
- $CeD_{2.12}$, lattice vibrs., coherent neutron scatt. meas. 77−62598
- $CeD_{2.12}$, neutron cryst.-field spectroscopy 80−14967
- $CeD_{2.12}$, phonon dispersion relations 78−30716
- CeD_x, $1.94 \leq x \leq 2.74$, Ce^{3+} ground state crystal field splitting from inelastic neutron scattering 79−99517
- CeD_x, (x=1.94 to 2.75), phonon dispersion, crystal field splitting, neutron scatt. study 79−60452
- $Ce_{0.73}Ho_{0.27}Ru_2$, superconductors, mag. correlations and crystal-field levels 80−34547
- $(Ce_{1-c}Ho_c)Ru_2$, superconducting, mag. props., neutron scatt. study 80−44808
- $CeIn_3$, mag. struct., neutron diffr. study 80−80481
- $Ce_x(La,Y)_{1-x}Sb$, and $Ce_x(La,Y)_{1-x}Bi$, antiferromag. spin arrangement, neutron diffr. obs. 77−63106
- $(Ce_xLa_{1-x})Al_2$, inelastic neutron scatt. cross-section, effect of cryst. field 79−65642
- $Ce_{1-x}La_xSn_3$ (x=0 to 1), mag. susceptibility and magnetisation, lattice parameters, X-ray and neutron diffr. meas. 80−49675
- $Ce_{0.9-x}La_xTh_{0.1}$, mixed valence state, static and dynamic mag. response 80−103816
- $Ce_x(La_yY_{1-y})_{1-x}Al_2$, local mag. moments, neutron scatt. study 79−61058
- $CeMn_2Si_2$, cryst. and mag. struct. determ. 78−52225
- CeP(As)(Sb), compressibility, room temp., from neutron diffr. meas. of lattice parameter variation up to 41 kbar 77−27940
- $CePd_3$, dil., local mag. moments, neutron scatt. study 79−61058
- $CePd_3$, intermediate valence system, mag. neutron scatt. cross-section meas. 77−20552
- $CePd_3$, magnetic neutron scatt. cross-section and linewidth, temp. depend. 77−63080
- $CePd_3$, mixed valence cpd., theory of inelastic mag. neutron scatt. 79−15284
- $CePd_3$, neutron scatt., spontaneous relax. of 4f magnetisation, interconfig. fluctuations 77−77025
- $Ce_{1-x}Pr_xAl_2$, mag. struct., comp. depend., neutron diffr. and mag. susceptibility meas. 80−50054
- CeSb, antiferromag., first-order transitions, mag. phase diagram 80−60252
- CeSb, ferromag., mag. excitation spectrum, inelastic neutron scatt. obs. 79−78352
- CeSb, mag. excitations dispersion 80−25121
- CeSb, mag. phase diagram and mag. struct. determ. 77−63182
- CeSb, mag. phase diagram for mag. field applied along ⟨111⟩ direction 79−33458
- CeSb, mag. phase transitions, zero applied mag. field 78−31070
- CeSb, mag. transition, effect of applied mag. field 78−43590
- CeSe, mag. ordering, ε expansion predictions, neutron diffr. obs. 79−61060
- $CeSn_3$, field induced form factor, temp. depend. 79−78308
- $CeSn_3$, induced magnetic form factor, polarised neutron studies 80−25078
- $CeSn_3$, intermediate valence cpd., search for phonon anomalies, inelastic neutron scatt. 80−100317
- $CeSn_3$, polarised neutron study of induced magnetisation 80−34594
- CeTe, mag. ordering, ε expansion predictions, neutron diffr. obs. 79−61060
- $Ce_{0.736}Th_{0.264}$, induced mag. form factor 79−78307
- $Ce_{0.74}Th_{0.26}$, mixed valence alloy, spin dynamics 78−10708
- $Ce_{0.74}Th_{0.6}$, induced magnetic form factor, polarised neutron studies 80−25078
- $Ce_{0.8}Th_{0.2}$, inelastic neutron scatt. meas. 79−47066
- $Ce_{1-x}Th_x$, mixed valence systems, spin dynamics and mag. ordering 78−68162
- $CeTl_3$, mag. susceptibility, magnetisation, neutron diffr., elec. resist., and sp. ht. meas. 80−75733
- CeX (X=P, As, Sb, Bi), neutron inelastic scatt. expts. 80−19674
- $Ce_{0.08}Y_{0.92}Sb$, dilute f-electron system in cluster regime, crystal field and exchange splittings 80−97062
- CeZn, cryst. field and exchange effects, inelastic neutron scatt. study 80−24855
- CeZn, mag. struct. and cryst. field effects 78−52223

neutron diffraction examination of materials continued
- ClF_5, condensed phases, structural study by vibr. spectroscopy and X-ray and neutron diffr. 79−1405
- ClO_2F, cryst. struct., X-ray and neutron diffr., Raman spectra *(French)* 78−83788
- Cm, mag. structure, neutron diffr. meas., antiferomag. below 52K 77−63101
- CmO_2, lattice parameter, neutron diffr. meas. 77−63101
- Co complex, $Co(II)(1,2,4\text{-triazole})_2(NCS)_2$ quasi two-dimens. canted S=1/2 antiferromag. 80−70976
- Co, crystal hyperfine fields and neutron scatt. 79−56172
- Co, ferromag., domain struct., small-angle neutron scatt. 77−66382
- Co fine particles in Cu, interface magnetisation 80−88858
- Co, itinerant ferromag., Fermi surface and single particle excitations 80−34350
- Co, martensitic HCP-FCC transition, neutron scatt. obs. 79−51252
- Co, molten, mag. small-angle scatt., persistent spin fluctuations 79−11288
- Co, small-angle crit. neutron scatt. 78−31087
- Co, spin fluctuations above Curie temp., diffuse mag. neutron scatt. obs. 80−50102
- Co^{2+}, mag. form factors, spherical and aspherical parts 79−78315
- Co-Al, mag. struct. of Co rich intermetallic cpd., neutron scatt., cluster model 78−80130
- Co-Ga, binary alloy, small-angle neutron scatt. from superparamag. behaviour 78−19217
- Co-Ga alloys, ferromag., local configuration studies, neutron scatt. and spin echo NMR 77−63114
- Co-Ga-Mn, small-angle mag. neutron scatt., states of mag. order study rel. to Mn and Fe substitution 79−11292
- Co-Mn alloys, FCC, mag. moments of Mn atoms 78−76226
- Co-P alloys, geometric struct. models and diffraction exam. techniques 80−79700
- $Co_3B_7O_{13}I$, neutron diffr. investig. of mag. and cryst. struct., ferro- and paraelec. phases 77−32170
- $CoBr_2.6[xD_2O(1-x)H_2O]$, mag. order investig. by neutron diffr. 77−66310
- $CoBr_2$, magnetic excitations, neutron scatt. investigation 80−39761
- $CoBr_2.6D_2O$, crystallographic and mag. struct. determ. 77−8278
- $CoBr_2.6(0.48D_2O, 0.52H_2O)$ spin-flop system, intermediate phase existence, sublattice magnetisation reorientation 80−80510
- $CoBr_2.6[(D_2O)_{0.48}(H_2O)_{0.52}]$, antiferromag. ordering, quasi-elastic neutron scatt. study 79−61068
- $CoBr_2.6[(1-x)H_2O.xD_2O]$, mag. intermediate phase, magnetisation and neutron scatt. meas. 80−60195
- $CoCO_3$-LiCl-H_2O system, complexing during cryst. growth, of spherocobaltite, electron diffr., neutron diffr. and spectroscopic obs. 77−44144
- $CoCl_2$, acoustic phonon dispersion determ. from neutron scatt. 77−39645
- $CoCl_2$, antiferromag., mag. excitations, mag. neutron inelastic-scatt. meas. 77−85437
- $CoCl_3$, interlayer force constants 78−14406
- $CoCl_2.2H_2O$-$FeCl_2.2H_2O$, random mixture with competing spin anisotropies, tetracrit. transition, neutron diffr. obs. 80−2575
- $CoCl_2.6D_2O$, crystallographic and mag. struct. determ. 77−8278
- $CoCl_2.6D_2O$, neutron diffr. study, cryst. and mag. struct. *(French)* 78−42946
- CoF_2, antiferromag. crit. props., neutron scatt. obs. 80−88749
- CoF_2, domain formation in staggered field induced by uniaxial stress, neutron diffr. exam. 78−76289
- $Co_{0.92}Fe_{0.08}$, lattice dynamics by neutron scatt., FCC phase 77−51463
- $Co_{0.92}Fe_{0.08}$, phonon dispersion and Debye temp. temp. depend., neutron inelastic scatt. 79−33047
- Co_2FeGa, alloy, site preference of Co and Fe, Mossbauer and neutron study 79−78577
- CoGa, onset of ferromag., diffuse mag. neutron scatt. meas. 77−63113
- $Co_2Ga_{2-x}Cr_x$, ferromag., local configurational studies, neutron scatt. and spin echo NMR 77−63114
- $Co_2Ga_{2-x}Cr_x$, ferromag., site selecting and moment distrib. 77−77031
- $Co_2Ga_{2-x}Cu_x$, mag. and struct. phases from magnetisation, neutron, X-ray diffr. techniques 78−52253
- $Co_2Ga_{2-x}M_x$ (M=V, Cr, Mn, Fe), mag. props. and order 77−12093
- $Co_2Ga_{2-x}Ni_x$, mag. and struct. phases from magnetisation, neutron, X-ray diffr. techniques 78−52253
- Co(GaTiV) alloys, ferromag. onset, electron conc. depend. 80−60203
- $Co_2Ga_{2-x}V_x$, ferromag., local configuration studies, neutron scatt. and spin echo NMR 77−63114
- $Co_2Ga_{2-x}V_x$, ferromag., site selectivity and moment distrib. 77−77031
- CoMnP, cryst. mag. struct., neutron diffr. study *(French)* 80−59439
- CoMnP, ferromagnetism and metamagnetism, polarized neutron diffr. study 80−44809
- $CoNb_2O_6$, magnetic struct., neutron diffr. and mag. susceptibility meas. 80−15693
- $Co_xNi_{1-x}O$, antiferromagnet, neutron diffr. study of mag. struct. 80−34595
- CoO, antiferromag. mag. excitations, spin wave model, neutron scatt. study 79−51766
- CoO, collinear antiferromag., equiv. type-II mag. struct. 78−56296
- CoO, mag. excitations, neutron scatt. expts., 13K 79−61092
- Co_4P, amorphous, mag. excitations and static struct., neutron scatt. obs. 78−68204
- $CoS_{2-x}Se$, magnetism and metamagnetic transition, neutron diffr. and NMR meas. 80−15717
- CoU_2S_5, mag. struct., exchange energy, magnetisation and neutron diffr. expts. 78−68170
- $CoWO_4$, mag. struct. refinement, neutron diffr. meas. *(German)* 77−16049
- $Co_{1-x}Zn_xF_2$, antiferromag. crit. props., neutron scatt. obs. 80−88749
- $CoZrD_3$, polycrystn., neutron and X-ray diffr. anal. of struct. 79−65061
- Cr, antiferromagnetic spin-density-wave domain and size and behaviour, X-ray and neutron topography 79−42793
- Cr, antiferromagnetic transition, first order, crit. neutron scatt. obs. 79−33480
- Cr complex, dinuclear, exchange interactions, neutron inelastic scatt. obs. 77−55502
- Cr complex, trivalent dimer, mol. electronic excitations, neutron inelastic scatt. 77−47985
- Cr, incoherent neutron scatt. cross section, neutron polarisation anal. 79−24137
- Cr, incommensurate antiferromag., inelastic neutron scatt. meas. 80−25088
- Cr, inelastic neutron scatt. expts., spin density waves 80−44818

neutron diffraction examination of materials continued
Cr, mag. struct., effect of mag. field direction, neutron diffr. obs. 77−63121
Cr, magnetic excitations of incommensurate spin density wave 80−11183
Cr, paramag., mag. form factors, neutron diffr. study 79−47234
Cr, single cryst., mag. hysteresis, neutron diffr. obs. 79−15327
Cr, single modulation state, temp. limits of cryomagnetic method 78−72374
Cr, transverse spin-density-wave phase, absence of neutron diffr. line broadening due to polarisation domains 77−24677
Cr^{3+} clusters in mol. complexes, interference effects in neutron scatt. 77−85544
Cr-Al, elementary excitations, exchange stiffness const., inelastic neutron scatt. study 79−47294
Cr-Al, mag. excitation, neutron spectrometry 79−4654
Cr-Al, spin density wave, neutron diffraction studies 79−1664
Cr-Al alloys, antiferromag., charge and spin density, neutron and X-ray diffr. 77−31971
Cr-Co, spin density wave, neutron diffraction studies 79−1664
Cr-Fe, antiferromag. phase boundary, neutron diffr. meas. 78−95437
Cr-Fe, dil., spin correlations and neutron scatt. near crit. conc., theory 80−60327
Cr-Fe, disordered, polarised neutron diffuse scatt. meas., 4.6-110K 80−34592
Cr-Fe (14 wt.%), spin density wave and spin glass ordering coexistence at low temps. 79−61059
Cr-Fe alloy, dil., antiferromag., mag. incoherent elastic neutron scatt. 79−73678
Cr-Fe-Si, mag. excitation, neutron spectrometry 79−4654
Cr-Fe-Si, spin density wave, neutron diffraction studies 79−1664
Cr-Fe(2.8 at%), antiferromag., meas. of incoherent elastic neutron scatt. cross section 79−19723
Cr-Ge system, XPS, X-ray and neutron diffr. and mag. meas. to study chem. bonding and electronic struct. 80−60749
Cr-Mn alloy, strain wave and spin density wave intensities, neutron diffr. 78−60266
Cr-Mo-Fe (2, 14 wt.%), spin density wave and spin glass ordering coexistence at low temps. 79−61059
Cr-Pd dilute alloys, itinerant antiferromag., neutron diffr. meas. 77−77032
Cr-Pt, dil., effect of Pt on itinerant antiferromagnetism 78−64191
Cr-Pt alloys, neutron diffraction study, (100) magnetic peak, magnetic structure transitions 79−56506
Cr-Re, mag. excitation, neutron spectrometry 79−4654
Cr-Re, mag. excitations in commensurate antiferromag. phase 80−50079
Cr-Re (0.18 wt.%), mag. excitations in longitudinal and transverse SDW phases 80−70946
Cr-Si alloys, antiferromag.-ordering, neutton diffr. 77−69492
Cr-V alloy, strain wave and spin density wave intensities, neutron diffr. 78−60266
CrB_2, helical mag. struct., neutron diffr. meas. 77−85425
$(CrF_6)^{3-}$ 6a AR→AT complexes, electron densities, local orbital populations, polarised neutron diffraction 80−88725
CrFe, mag. correls. and onset of ferromag., neutron scatt. study 80−50105
$(Cr_{1-x}Fe_x)_{1+\delta}Sb$, interstitial occupancy, Cr:Fe distrib., X-ray and neutron diffr. study 79−42012
$Cr_{0.6}Mn_{0.4}$, mag. moment, neutron diffr. study 79−33459
$Cr_{0.98}Mn_{0.02}$, spin dynamics and spin wave form factor, neutron scatt. expt. 77−40047
$(Cr_4(OH)_6(NH_3)_{12})Cl_6.4H_2O$, exchange interactions in Cr^{3+} clusters, inelastic neutron scatt. obs. and Heisenberg Hamiltonian calc. 79−78359
$Cr_4(OH)_6(NH_3)_{12}Cl_6.4H_2O$, exchange coupled mol. Cr^{3+} tetramers, inelastic neutron scatt. 80−65792
β-CrOOH, neutron diffr. exam., cryst. and magnetic struct. *(French)* 78−2654
β-CrOOH(D), crystal struct., isotope effects on bond lengths 77−15371
α-CrOOH(D), isotope effects in bond lengths 77−80488
$Cr_{0.995}Pt_{0.005}$ alloy, mag. struct., neutron diffr. study 80−60198
CrS, magnetic struct. from neutron diffr. meas., Neel point 77−32164
CrS_xTe_{1-x} (x=0 to 0.2), magnetic props. study 80−11194
Cr_3Se_4, mag. susceptibility and sp. ht. meas. *(French)* 79−56507
$Cr_3Se_xS_{4-x}$, mag. susceptibility and sp. ht. meas. *(French)* 79−56507
Cr_3Si, single cryst. growth by floating zone method, X-ray and neutron diffr. study 79−74084
CrTe, mag. ordering under high-press., ferromag. transition, ESR and neutron diffr. *(French)* 78−31053
CrTe, neutron diffr. at high press., mag. transition *(Russian)* 79−38326
$Cr_{1-x}Ti_xN$, cryst. and mag. struct., at low temps. *(French)* 80−29005
$CrUSe_3$, mag. struct. and delocalized moments, powder neutron diffr. obs. 77−69496
$Cr_{1-x}V_xN$, solid soln., mag. struct. *(French)* 78−6519
Cs, accurate struct. factor determ. by X-ray and neutron diffr. 79−51046
Cs, liquid, neutron diffr. struct. anal., density and viscosity temp. depend. 80−6352
Cs_2, liq. struct. factor determ. rel. to short-range correlations 77−1060
CsB_3H_8, IR, Raman and inelastic neutron scatt. spectra 79−42966
CsCN, inelastic neutron scatt. by coupled rotational and translational modes 80−70333
$CsCoCl_3$, anisotropic antiferromag., inelastic neutron scatt. study 78−60274
$CsCoCl_3$, Ising-like antiferromag., spin dynamics 79−42747
$CsCoCl_3$, Ising-like antiferromag., instantaneous spin correlations 79−42746
$CsCoCl_3$, mag. excitation spectrum, spin-wave response, neutron scatt. study 80−50080
$CsCoCl_3$, mag. struct., neutron diffr. meas. 78−43563
$CsCoCl_3$, one-dimensional antiferromag., neutron scatt. investig. of spin waves 77−47982
$CsCoCl_3$ spin dynamics, neutron scatt. study 80−80493
Cs_3CoCl_5, neutron diffr. struct. at 4.2K 80−54176
$CsCoCl_3.2D_2O$, crit. behaviour along metamag. phase transition 77−59409
$CsCoCl_3.2D_2O$, metamag., thermodynamic props. near multicrit. pt. 77−66305
$CsCrCl_3$, mag. structure and excitations, neutron diffr. and susceptibility meas. 80−44806
$CsCrI_3$, neutron diffr. expts. at 300, 77 and 1.2K 80−107163
$CsCuCl_3$, helical mag. struct., neutron diffraction study 80−107983

neutron diffraction examination of materials continued
$Cs(D_xH_{1-x})_2AsO_4$, cryst. struct. in ferroelec. and paraelec. phases neutron diffr. meas. 77−7694
CsD_2PO_4, neutron scatt. study of ferroelectric phase transitions 77−59538
CsD_2PO_4, one dimens. ordering, ferroelec. transitions, neutron scatt. study 80−25316
$CsFeCl_3$, pseudo-one-dimens. singlet ground state ferromag., mag. excitations, neutron scatt. study 80−97064
$CsFeCl_3.2D_2O$, cryst. and mag. struct., neutron scatt. and NMR expts. 79−7969
Cs_2FeF_5, mag. struct. and one-dimens. antiferromagnetism 80−60209
$CsGa_{1-x}Fe_xS_2$, tetrahedrally coordinated Fe atoms in low spin state, mag. props. and neutron diffr. study *(German)* 80−88714
CsH_2AsO_4, ferroelec., temp. depend. of shear angle, neutron scatt. meas. 77−8524
$CsHCl_2$, H bond bending vibrs., inelastic neutron scatt. obs. 79−89800
CsHClBr, H bond bending vibrs., inelastic neutron scatt. obs. 79−89800
$CsH(NO_3)_2$, inelastic neutron scatt. spectra, H bonds bending vibrs. 79−14893
CsH_2PO_4, cryst. struct. of paraelectric material 78−79592
CsH_2PO_4, ferroelec. transition, neutron diffr. study 80−93247
CsH_2PO_4, one dimens. ordering, ferroelec. transitions, neutron scatt. study 80−25316
CsH_2PO_4, paraelectric phase, struct. exam. by neutron diffr. 79−37679
$CsH_3(SeO_3)_2$, paraelec. phase, struct. determ. by neutron diffr. 78−34472
$Cs_2KFe(CN)_6$, single cryst. neutron diffr. struct. determ. 80−28972
$CsMnBr_3$, quasi-one-dimens. antiferromagnet, inelastic neutron scatt. 78−14929
$CsMnBr_3.2D_2O$, extended scaling in spin flop system 79−73737
$CsMnBr_3.2D_2O$, mag. phase diagram near bicrit. point 79−15302
$CsMnBr_3.2D_2O$, spin-flop systems, neutron scatt. expts. 79−61109
$CsMnBr_3.2D_2O$, spin-flop system, extended scaling near bicrit. pt. 79−51752
$CsMnF_3$, spin-wave dispersion relations, neutron inelastic scatt. obs. 77−51895
$CsMnF_4$, planar ferromag., cryst. and mag. struct., Jahn-Teller effect 80−75715
$CsMnFeF_6$, mag. short-range ordered, neutron scatt. meas. 77−16048
$CsMnFeF_6$, neutron scatt. and magnetisation meas. 77−66258
Cs_2MnNiF_6, cation distrib. and mag. struct. *(French)* 78−14935
$CsNiF_3$, 1-dimens. ferromag., evidence for solitons, inelastic neutron scatt. study 79−78430
$CsNiF_3$, crit. exponent crossover, quasielastic neutron scatt. around Neel point 77−24693
$CsNiF_3$, in mag. field, spin wave dispersion, inelastic neutron scatt. 77−77046
$CsNiF_3$, nonlinear excitations, 1D-ferromag., neutron scatt. 80−70949
$CsNiF_3$, one dimens. ferromag., spin wave dynamics, inelastic neutron scatt. study 79−47270
$CsNiF_3$, one-dimens. ferromag., solitons in external mag. field 79−19724
$CsNiF_3$, one-dimens. ferromag. phonon dispersion surfaces 79−42180
$CsNiF_3$, one-dimens. ferromag., solitons as gas of quasiparticles, inelastic neutron scatt. obs. 79−73679
$CsNiF_3$, quasielastic neutron scatt. around Neel-point 80−75768
$CsNiF_3$, solitons in one-dimens. ferromag., inelastic neutron scatt. 78−95450
$CsNiF_3$:Mg, ferromag. chain system, temp. depend. of correlation length, quasi-elastic neutron scatt. meas. 77−16046
$CsPbBr_3$, struct., Debye-Waller factor, neutron diffr. study 79−90609
$CsPbCl_3$, high-resolution elastic neutron diffr. study 80−28984
$CsPbCl_3$, nucl. smearing functions, multipole analysis 80−88097
$Cs_2PbCu(NO_2)_6$, α-modification, Jahn-Teller induced α to β transition, neutron diffr. obs. 79−1498
$Cs_2PbCu(NO_2)_6$, incommensurate Jahn-Teller transition, Huang scatt. 80−70401
$Cs_2PbCu(NO_2)_6$, low-temp. γ-modification, struct., powder neutron diffr. study, 160K 80−84151
$Cs_2PbCu(NO_2)_6$, successive Jahn-Teller phase transitions, neutron and X-ray diffr. 78−95154
$CsPbX_3$, (X=Cl,Br), anharmonic thermal vibrs., neutron diffr. study 80−29125
$Cs_2Pt(CN)_4.H_2O$, cryst. struct., neutron diffr. meas. 77−47393
Cs_2SiF_6, lattice dynamics from neutron scatt., Raman and IR absorpt. meas. 79−60449
$CsUOF_5$, struct. obs. using neutron diffr. and NMR 79−32962
$Cs_2(VOF_4(H_2O))$, neutron and X-ray diffr. struct. determ. 79−90613
$Cs_9(XeO_3Cl_2)_4Cl$, neutron and X-ray diffr. struct. determ., Xe-Cl bonding 78−30591
$Cs_2[Cu(H_2O)_6](SO_4)_2$, Tutton's salts, stereochem., neutron struct. determ. 78−18609
Cu (220), mosaic single cryst., neutron integrated reflectivities 79−86656
Cu, cold neutron small angle elastic scatt., microstruct. exam. 77−84736
Cu, defect-phonon perturbations after neutron irrad., neutron scatt. study 80−44278
Cu, high purity, small-angle neutron scatt. from pores in high temp. fatigue 79−14795
Cu, liquid, saphhire container for experiments up to 1900K 79−63215
Cu, liquid, struct. factor, neutron diffr. meas. and Monte Carlo calc. 80−38903
Cu, polycrystalline, elastic consts., inelastic coherent neutron scatt. meas. 80−34122
Cu, single crystals, deformed, extinction, γ-ray diffractometry and neutron struct. refinement 77−84588
Cu, single crysts., deformed and annealed, neutron small angle scattering 79−82127
Cu, single crysts., total thermal neutron cross sections 80−19672
Cu, zero to first sound transition, inelastic-neutron scatt. data 77−31738
α-Cu-Al, single crysts., deformed and annealed, neutron small angle scattering 79−82127
Cu-Al-Ni, struct. anal. of stress induced β_1'' martensite by neutron diffr. 79−60308
Cu-Be solid solutions, local oscill. conc. depend., impurity bands *(Russian)* 80−75318
Cu-Co, superparamagnetic, mag. aftereffects, dynamic neutron depolarisation study 80−50147
Cu-Fe, dil., local mag. moments, neutron scatt. study 79−61058
Cu-Fe, dil. alloy, spin relaxation rates, neutron scatt. study 79−47235

neutron diffraction examination of materials continued
Cu-Fe (1.2 at.%), Fe moment and lattice distortion, neutron scatt. meas. 79−24133
Cu-Ga, disordered, phonon dispersion curves, inelastic neutron scatt. study 79−51223
Cu-Ge, disordered, phonon dispersion curves, inelastic neutron scatt. study 79−51223
Cu-Ge (5 at.%), single crystal, Bridgman growth, neutron diffraction topographic obs. of layer substructure 79−27938
Cu-Mn, dil., local mag. moments, neutron scatt. study 79−61058
Cu-Mn, spin glass alloy, magnetic excitations, neutron scatt., diffuse mag. scatt. 78−10695
Cu-Mn (15 at.%), mictomagnetic, short-range ordering, neutron scatt. polarisation anal. 80−50110
Cu-Mn (4.7 at.%), spin glass, spin correlations, neutron scatt. cross section meas. 79−51790
Cu-Mn (8 at.%), spin glass, neutron scatt. and susceptibility investig. of spin dynamics 77−40076
Cu-Mn (8 to 75 at.%), spin correl., neutron polarisation anal. study 80−65905
Cu-Mn alloy, spin glass, neutron scatt. 78−68265
Cu-Mn spin glass alloy, neutron scatt. meas. of Edwards-Anderson order parameters 79−11323
Cu-Mn spin glass alloy, spin correl. function, combined neutron spin echo and polarisation anal. 80−50107
Cu-Mn spin glass neutron diffr. expts. *(French)* 78−43593
Cu-Mn spin glasses, spin dynamics, neutron scatt. meas. 79−8002
Cu-Ni, disordered ferromag., spin density asphericity, neutron diffr. study 79−47251
Cu-Ni (20-80 at.%), clustering, diffuse neutron scatt. study, conc., temp. depend., miscibility gap location 78−47529
Cu-Ni alloys, mag. diffuse scatt. 78−14931
Cu-Pt system, phonon dispersion relations, force constant disorder effect 80−84263
Cu-Te, liq., struct. and elec. props. 80−49083
Cu-Zn-Al martensite, lattice dynamics, neutron scatt. meas. 80−88286
Cu_3Au, heterophase fluctuations near order-disorder transform., X-ray and neutron diffr. 77−73272
Cu_3Au, X-ray and inelastic neutron scatt. investig. of spinodal ordering 77−77473
CuBr, Debye-Waller factors and Debye temp., powder neutron diffr., 295K 78−91407
CuBr, neutron scatt. investig. of anharmonic effects on Debye-Waller factor 77−11658
β-CuBr, phonon spectra, dispersion curves parameter calc. from zinc blende zone boundary conditions 78−51632
CuBr, superionic cond., cryst. struct., neutron diffr. study 79−42041
$CuBr_2(Cl_2)$, aq. soln., structural transition, neutron diffr. study 80−64872
CuCl, difference Fourier maps, effects of phase errors 79−99033
CuCl, inelastic scattering, phonon dispersion curve determination at 4.2K 78−6132
CuCl, neutron scatt. of TO phonon at 5K 79−60446
$CuCl_2.CuCl_2.2D_2O$, neutron scatt. aspherical effects, mag. form factor 78−27017
$CuCl_2.2D_2O$, staggered magnetisation, neutron diffr. obs. 78−39296
$CuCl.2N(C_5D_5)$, one-dimens. antiferromag., mag. excitation line-shape, field depend., neutron study 79−38314
$CuCr_2S_4$, neutron diffr. study of mag. struct. *(Russian)* 79−95580
$CuCr_2Se_4$, electronic state, polarized neutron diffr. obs. 79−56501
$CuCr_2Se_4$, mag. moment distrib. by neutron diffr., Goodenough model 80−70945
Cu_2FeGeS_4, crystallographic and magnetic structure *(French)* 80−28998
$CuFe_2O_4$-$CuGa_2O_4$, physicochem. props. *(French)* 77−44233
$CuFe_2S_3$, cubanite, spontaneous magnetisation, polarised neutron obs. *(French)* 78−23245
$Cu_{0.5}Ga_{0.5}Cr_2S_4$, mag. struct. determ. 77−8272
CuI, superionic cond., cryst. struct., neutron diffr. study 79−42041
$Cu_{1/2}In_{1/2}Cr_2S_4$, transition from long-range to short-range mag. ordering 77−36087
r-CuMn, annealing ordered phase study by neutron diffr. 80−89265
CuMn, spin glass, mag. correls., neutron scatt. study 80−50105
$Cu_{0.95}Mn_{0.05}$, spin glass, inelastic neutron scatt., time-of-flight and three-axis techniques 80−50108
$Cu_{0.95}Mn_{0.05}$, spin glass, low temp. mag. excitation spectrum, inelastic neutron scatt. obs. 80−50109
γ-$Cu_{15}Mn_{85}$, antiferromag., neutron diffr. 80−2550
Cu_3Mn, atomic short-range order, TOF neutron diffraction 79−10831
Cu_2MnAl, ferromag. Heusler alloy, polarised neutron study of mag. moment density 78−84391
Cu_2MnAl Heusler alloy, inelastic magnon scatt. of neutrons 77−4509
Cu_2MnAl, Heusler alloy, spin waves, neutron inelastic scatt. meas. 77−80921
Cu_2MnAl-Pd_2 MnAl mixed Heusler alloys, mag. props. 80−60269
$Cu_2Mn_{0.863}Al_{1.057}$, Heusler alloy, mag. moment distrib., polarised neutron study 79−47247
$CuMn_2O_4$, comment on cryst. struct. determs. by neutron diffr. 79−23585
$CuMn_2O_4$, crystallographic props. 78−14329
$Cu_2Mo_6S_8$, phonon density of states, mode softening correl. with supercond. transition temp. 79−51714
$Cu(NO_3)_2.2.5\ D_2O$, magnetic ordering, neutron diffr. meas., 0.08-0.25K 80−39749
$Cu_{0.435}Ni_{0.565}$, clustering, temp. depend., diffuse neutron scatt. study 79−42013
Cu_6PS_5Br, cryst. struct. at 293 and 473K, thermal parameters 80−59450
$Cu_{1-x}Pd_xMnSb$, mag. phase transition 80−60268
$CuSO_4.5H_2O$, EXAFS, rel. between Debye-Waller factor and thermal parameters meas. by neutron diffr. 80−84803
$Cu_{66}Ti_{34}$, metallic glass, neutron diffr. meas. of struct. factor 80−24367
$Cu_{0.57}Zr_{0.43}$, amorphous, partial struct. factor, TOF pulsed neutron 79−14684
$Cu_{0.57}Zr_{0.43}$ amorphous alloy, neutron diffr. obs. of struct. 80−88060
$Cu_{46}Zr_{54}$, metallic glass, dynamical struct. factor and freq. distrib. meas. 80−54136
$Cu_6[Si_6O_{18}].6H_2O$, dioptase, cryst. struct. refining by X-ray and neutron diffr. methods 79−23586
t-cyanobutane, solid, uniaxial molecular reorientation, quasielastic neutron scatt. 78−42927

neutron diffraction examination of materials continued
$DAl_{11}O_{17}$, anhydrous, cryst. struct. from powder neutron diffr. 80−1983
DCN, phonons meas. by neutron coherent inelastic scatt. 79−95097
D_2O, atom pair correlation functions, X-ray, electron and neutron diffr. data 77−80406
D_2O bond length, angle, high momentum transfer liq. phase neutron scatt. 77−27195
D_2O, molecular dynamics anal. by inelastic neutron scatt. 77−35462
D_2O, struct., temp. effects, neutron diffr. obs. 77−72544
D_2O, struct. at press. 79−60253
D_2O_2, lattice dynamics, neutron scatt. study 79−42176
D_2O_2, lattice phonons by neutron scatt., covalent force model 78−67782
$D_3O.ClO_4$, solid, neutron powder diffr. study 80−107176
D_xTaS_2, struct., form. by cathodic reduction, neutron diffr. obs. 79−73150
dimethylammonium manganese tetrachloride, 2D Heisenberg antiferromag., spin wave anal. 80−54879
Dy-Pr(Nd) alloys, mag. struct. and ordered moments, neutrons diffr. data 77−66252
Dy-Sc, magnetic relax. phenomena 79−33579
DyAg, neutron diffr. expts. in external mag. field, temps. below 1.2K 79−61067
DyB_4, cryst. and mag. struct., neutron diffr. meas. 80−15692
$DyCrO_4$, determ. of mag. struct. by neutron diffr. 79−51753
$Dy_3Ga_5O_2$, induced staggered mag. fields, neutron diffr. study 80−60196
DyMg, mag. props., neutron diffraction and magnetisation meas. 77−16045
$DyMo_6S_8$, long range mag. order in supercond. state 79−65653
$DyMo_6S_8$, supercond. and antiferromag. coexistence, neutron study 78−95401
$DyMo_6S_8$, superconductor, neutron scatt. exam. of mag. phase 79−73680
$Dy_{1.2}Mo_6S_8$, long-range mag. order and supercond., neutron diffr. obs. 79−78320
Dy_2Ni_{17}, magnetic struct. by neutron diffr. and Mossbauer spectra *(French)* 77−32165
$DyPO_4$, mag. transitions under hydrostatic press., neutron diffr. study 80−71030
$DyPO_4$, metamagnet, mag. phase transitions, elastic neutron scatt. study 79−78371
Er-La, HCP, mag. phase diagram, neutron diffr. meas. 80−70950
$ErAl_2$, crystal field study rel. to $La_{0.9}Er_{0.1}Al_2$ 78−76036
ErB_4, cryst. and mag. struct., neutron diffr. meas. 80−15692
ErB_4, mag. phase diagram, neutron diffr. study 80−50091
$Er_cCe_{1-c}Pd_3$, cryst. field spectra, neutron scatt. study 80−50047
$ErCo_2$, amorphous, mag. correlations, neutron exam. 79−73682
$ErCo_2$, amorphous, mag. correlations, neutron exam. 79−73683
$ErCo_2$, mag. excitation spectrum, neutron inelastic scatt. obs. 79−78351
$ErCo_{5.6}$, easy magnetisation direction 78−84415
$ErCo_2(Fe_2)$, mag. excitations, RPA theory 80−65830
ErCu, cubic antiferromag., mag. excitations inelastic neutron scatt. meas. 78−72341
$ErFe_2$, Czochralski growth, and cryst. quality determ. 77−8742
$ErFe_2$, effect of H on sublattice magnetization, elastic neutron scatt. obs. 79−78327
$ErFe_2$, excited state spin waves inelastic scatt. meas. 78−76234
$ErFe_2$, Laves phase, cryst. field effects on spin wave dispersion relations 78−84408
$ErFe_2$, spin excitations, neutron scatt. obs. 77−63153
$ErFe_2$, spin waves, exchange interaction, neutron scatt. study 79−47267
$ErFe_3$, mag. struct. 78−2651
$ErFe_4Al_8$, neutron diffr. exam., mag. struct. 78−10656
$ErFeO_3$, temp. depend. of neutron depolarisation factor meas. near spin reorientation transition 77−16053
ErMg, mag. props., neutron diffraction and magnetisation meas. 77−16045
$ErMo_6S_8$, long range mag. order in supercond. state 79−65653
$ErMo_6Se_8$, crystal field excitations, inelastic neutron scatt. obs. 79−78321
$ErMo_6Se_8$, mag. ordering and supercond., neutron diffr. 78−68125
$ErMo_6Se_8$, mag. supercond., neutron scatt. obs. 80−70952
Er_2Ni_{17}, magnetic structure by neutron diffr. 77−73000
$ErNi_{0.6}Cu_{0.4}$, sp. ht. and modulated mag. struct. 77−32167
$ErRh_4B_4$, reentrant supercond., mag ordering, neutron diffr. obs. 78−14879
$ErRh_4B_4$, superconductor, neutron scatt. exam. of mag. phase 79−73680
$ErRh_{1.1}Sn_{3.6}$, synthesis, supercond. and mag. props. 80−100547
$ErTiO_3$, magnetic structure determination, neutron scatt. study 80−65809
$(Er_xY_{1-x})Al_2$, cryst. field splitting, inelastic neutron scatt. data 80−44551
$Er_xY_{1-x}Al_2$, mag. props. meas. and neutron diffr. data 80−7126
EuO, Heisenberg ferromagnet, exchange interactions, neutron scatt. expts. 77−20579
EuO, Heisenberg ferromagnet, static crit. props., neutron scatt. expts. 77−20618
EuO, mag. form factor of Eu^{2+}, solid state effects 78−2653
EuS, Heisenberg ferromagnet, exchange interactions, neutron scatt. expts. 77−20579
EuS, Heisenberg ferromagnet, static crit. props., neutron scatt. expts. 77−20618
$Eu_{0.4}Sr_{0.6}S$, spin glass, spin dynamics, neutron scatt. study 80−65907
$Eu_xSr_{1-x}S$, ferromagnet-spin glass transition, mag. ordering, mag. susceptibility and neutron scatt. meas. 80−50135
$Eu_xSr_{1-x}S$, insulating spin glass, mag. props. 80−2589
$Eu_xSr_{1-x}S$, non-metallic spin glass system 79−61175
$Eu_xSr_{1-x}S$, onset of ferromagnetism for x near 0.5 neutron diffr. obs. 79−24181
$Eu_xSr_{1-x}S$, spin glass to ferromag. transition, neutron scatt. and susceptibility meas. 80−60254
$(Fe,Mn)WO_4$, mixed cryst., magnetically disordered system, Mossbauer and neutron diffr. meas. 77−16225
Fe, band theoretic interpretation of neutron scatt. expts., spin wave modes 80−44791
Fe complex, $Fe(1,2,4\text{-triazole})_2(NCS)_2$, quasi-2-dimens. $S=^1/_2$ antiferromag., mag. props., hidden canting 80−107986
α-Fe crystal, phonon spectrum, slow neutron inelastic scatt. meas. 77−80592
Fe, crystal hyperfine fields and neutron scatt. 79−56172
Fe, double critical magnetic scattering in polarised neutron expts. 79−65652
Fe, ferromag., domain struct., small-angle neutron scatt. 77−66382

neutron diffraction examination of materials continued
Fe, ferromag., dynamic susceptibility calc., neutron scatt. intensity calc. 80−80488
Fe, itinerant ferromag., Fermi surface and single particle excitations 80−34350
Fe, mag. anisotropy in crit. region, neutron polarisation-vector analysis 78−31065
Fe, magnetisation, spin wave and Stoner contribs. 77−73017
Fe, molten, mag. neutron scatt. at small momentum transfer caused by spin fluctuations 77−47968
Fe monocrystal, neutron crit. scatt. anisotropy 77−66327
Fe, neutron critical scatt., above T_c, polaris. asymmetry 78−34994
Fe, neutron critical scattering, temp. shift 78−38589
Fe, neutron magnetic critical phenomena, review of new effects 79−56534
α-Fe, phonon spectrum, cold neutron inelastic scatt. obs. 77−7811
Fe polycrystal, temp. shift of neutron crit. scatt. max., test of dynamic scaling theory 79−50953
Fe powder, Debye-Waller factor by neutron diffraction 79−95113
Fe, spin correlation function 79−78334
Fe, spin fluctuations above Curie temp., diffuse mag. neutron scatt. obs. 80−50102
Fe^{2+}, mag. form factors, spherical and aspherical parts 79−78315
Fe^{3+} clusters in mol. complexes, interference effects in neutron scatt. 77−85544
Fe-Al, local ordering, neutron scatt. study 78−64193
Fe-Al, low energy Stoner excitations, spin wave obs. in neutron scatt. study 79−51770
Fe-Al, magnetic moment determ. from neutron scatt. 77−73011
Fe-Al alloy, short range order, neutron scatt. meas. 77−19907
Fe-B, amorphous alloys, compositional study on short-range struct. 80−84095
Fe-based system, concentration ferro-antiferromag. transitions *(Russian)* 79−99699
Fe-C alloys, liq., struct., neutron and X-ray diffr. meas. 77−51306
Fe-C melts, short-range order, neutron scatt. obs. *(German)* 78−71669
Fe-Co, long range order, neutron powder diffr. meas. 79−42243
Fe-Co, mag. moment of Cr and Mn atoms, polarised neutron scattering 79−11290
Fe-Co (30-70 at.%), order-disorder transition, comp. depend., neutron diffr. expts. 78−15393
Fe-Co alloy, atomic ordering phenomena obs. *(Russian)* 77−81254
Fe-Co-Cr, magnetic, phase transform. obs. *(French)* 79−47676
Fe-Co-Ni, at. mag. moments, neutron scatt. and Mossbauer meas. 79−42744
Fe-Co-Si, BCC solid soln. interchange energies, high temp. neutron diffr. 80−29166
Fe-Co-Ta for semipermanent magnets *(French)* 79−47675
Fe-Cr, dil., spin density wave under high press., neutron diffr. study 80−65798
Fe-Cr, spin waves by neutron spectrometry 80−44819
Fe-Cr-Al alloys, localised mag. moment determ. and electron struct. 77−66268
Fe-Cr-Co hard-mag. alloys, fine cryst. struct. *(Russian)* 77−66706
Fe-Cr-Ni, Fe-Co-Mn, Fe-Cr-Co and Fe-Ni-Mn alloys, BCC, atomic mag. moments determ. 77−59396
Fe-Cr-(Co), decomposition of solid soln. in mag. field, neutron and X-ray diffr. study *(Russian)* 78−68694
Fe-Cu alloys, mag. moment distrib., elastic neutron scatt. obs. 79−78340
Fe-Ge, amorphous, atomic struct., neutron diffr. study 80−59392
Fe-Mn, dil. alloy, mag. moment distrib., temp. depend., diffuse polarised neutron scatt. study 79−47250
Fe-Mn-Ni antiferromag. alloy, neutron scatt. exam. of antiferromagnons 77−66283
Fe-Ni, local ordering, neutron scatt. study 78−64193
Fe-Ni (31 at.%), austenitic, ageing, absence of at. order 77−11502
Fe-Ni (32.3 at.%), mag. struct. in commensurable approx., neutron diffr. study 80−60212
Fe-Ni (33-38 at.%), low-angle neutron diffr., anomalous crit. scatt. *(Russian)* 80−60193
Fe-Ni (35 at.%), fine coherent effects, neutron diffr. study *(Russian)* 78−75502
Fe-Ni Invar alloy magnetic inhomogeneous struct. model 79−56503
Fe-Ni system, ferro-antiferromag. transition, γ phase mag. struct. 79−91231
Fe-Ni-Al alloys, ordering X-ray and neutron diffr. obs. *(Russian)* 79−20038
γ-Fe-Ni-Cr, mag. struct., neutron scatt. study *(Russian)* 78−68160
γ-Fe-Ni-Cr, magnetic phase diagram *(Russian)* 78−39292
Fe-Ni-Cr-Ti-Al Elinvar alloys, dispersion-hardened, structural transform. *(Russian)* 79−1872
Fe-Ni(-Al)(Mn) Invar alloys, mag. heterogeneities *(Russian)* 77−66251
Fe-Ni(-Mn)(Cr)(V), concentration ferromag. antiferromag. phase transition and mag. state diagram. *(Russian)* 80−20401
Fe-Ni(Pt), Invar alloy, magnetic excitation exam. by neutron diffr. 79−56521
Fe-Pd alloy, mag. struct. determ., neutron scatt., Mossbauer and mag. meas. *(Russian)* 78−2648
Fe-Pd alloys, spin density radial distrib. determ. 79−73685
Fe-rare earth alloys, amorphous, magnetoelasticity and moment rot., US vel. calc. and neutron scatt. meas. 80−65992
Fe-Rh alloys, spin wave spectrum in antiferromag. and ferromag. phases, inelastic neutron spectrometry 77−63158
Fe-Si (2.5%), Bloch wall zig-zag struct., neutron small angle scatt. 77−16099
Fe-Si (3 wt.%), ferromag. domains, imaging by neutron interferometry 80−71087
Fe-Si (3%), spikn related contrast effect, visibility of 180° ferromag. domain walls 78−43612
Fe-Si (3.5 wt.%), dynamic neutron depolarisation meas. of ferromag. domain struct. 79−82812
Fe-Si (3.5 wt.%), magnetisation reversal and domain walls 78−84451
Fe-Si (3.5 wt.%), static neutron depolarisation meas. of ferromag. domain struct. 78−14978
Fe-Si (3.5 wt.%) picture frame cryst. , domain wall bowing dynamic neutron depolarisation 78−56344
Fe-Si (4 at.%), Bloch wall thickness determ. by neutron small-angle scatt. 80−15754
Fe-Si (4 wt.%), neutron crit. scatt., experimental anisotropy 78−38590
Fe-Si (7.5, 14.3 at.%), mag. moments and form factors, neutron diffr. obs., d-band electron redistrib. 79−51751

neutron diffraction examination of materials continued
Fe-Si plate, ferromag. domain structure obs. by neutron diffr. topography 77−69645
Fe-SiO multilayer film, interface magnetisation, neutron Bragg refl. 78−56355
Fe-SiO multilayer film, interface magnetisation 80−7135
Fe-SiO multilayer films, interface magnetisation 80−88858
Fe-Tb dilute alloy, amorphous, small angle mag. scatt. 78−27021
Fe-Ti, BCC, mag. moment distrib. 79−47240
Fe-Ti, D storage, desorption isotherm and struct. study by neutron diffr. 79−1549
Fe-Ti, mag. moment distrib. and environmental effects around Ti impurity 80−7092
Fe-V, conc. depend. of mag. moment distrib., polarised neutron diffr. meas. 78−19218
Fe-V alloys, BCC, ferromag., polarised neutron diffr., appl. of multiband CPA theory 77−77033
Fe-V(Cr)(Mn), dil., local mag. moments, polarised neutron elastic diffuse scatt. 80−50088
Fe_2-Mn-Al alloys, Fe-rich, disordered, local moments on Fe and Mn 77−43811
Fe_3 Pt, ordered ferromagnetic alloy, magnetic excitation obs. 80−70978
$Fe_{0.7}Al_{0.3}$, local environment effects and magnetic clustering 78−10658
Fe_3Al, order-disorder transition effect on low energy spin waves 79−47271
Fe_3Al, partly disordered B2 struct., spin wave dispersion relation 78−64201
$Fe_{80}B_{20}$, amorphous, cold neutron scatt., local and extended defects 80−84089
$Fe_{83}B_{17}$ metallic glass, struct. from neutron diffr. study 80−6363
$Fe_3B_7O_{13}I$, ferroelec., mag. ordering, neutron diffr. meas. 78−72331
$Fe_{83}B_{16.5}Si_{0.5}$, amorphous, spin waves, inelastic neutron scatt. meas. 79−73701
$FeCO_3$, mag. neutron scatt., spin orbit coupling effects 77−85419
$Fe_2Ca_3Si_3O_{12}$ glass, mag. ordering effects at low temps., Mossbauer and neutron diffr. meas. 77−16047
$FeCl_2$, interlayer force constants 78−14406
$FeCl_2$, magnon-phonon hybridisation, inelastic neutron scatt. study 79−47272
$FeCl_3$ aq. soln., quasi-elastic neutron scatt. 79−37607
$Fe_{1-x}Co_xCl_2.2H_2O$, random mixture with competing spin anisotropies, tetracrit. behaviour 80−60324
Fe_2CoGa, alloy, site preference of Co and Fe, Mossbauer and neutron study 79−78577
$(Fe_{0.5}Co_{0.5})Si$, weak itinerant ferromag., polarised neutron scatt. exam. 77−4503
$Fe_{3-x}Co_xSi$, structural, mag. moment, and hyperfine field behaviour, local environment model 79−65762
Fe_xCr_{1-x}, spin-wave evolution crossing from ferromag. to spin-glass regime 80−97080
$FeGa_2O_4$, magnetic props. by Mossbauer effect, neutron diffr. and magnetisation meas. 77−43918
FeGe, hexagonal, low-temp. mag. struct., neutron diffr. meas. 78−95418
FeI_2, neutron inelastic scatt. from mag. excitations 80−50078
$FeMgBO_4$ and $FeMg_2BO_5$, mag. props., spin glass behaviour 79−61145
γFeMn alloys, itinerant antiferromag., spin dynamics, neutron scatt. meas. 77−12105
FeMn, dil., diffuse scatt. cross sections, polarized neutrons 78−43567
$(FeMn)_3$ Si alloys, L2,A struct. of single phase alloy 77−59393
$(Fe_{1-x}Mn_x)_3Al$ alloys, disordered, mag. moments and distrib. on lattice sites 77−63112
$(Fe_{1-x}Mn_x)_3Al$, local Mn moment distrib., neutron scatt., nucl. spin echo *(Russian)* 77−12091
$(Fe_{1-x}Mn_x)_3Al$, mag. moments determ. from magnetisation and neutron and electron diffr. expts. 79−56520
$(Fe_{1-x}Mn_x)_{75}P_{15}C_{10}$, amorphous pair radial distrib. functions, neutron scatt. study 80−49128
$Fe_xMn_{1-x}Pt_3$, ferro-antiferromag. transform. at 4.2K *(Russian)* 78−88117
$(Fe_{1-x}Mn_x)_3Si$, $(Fe_{1-x}Co_x)_3Si$, order distrib., hardening effect *(Russian)* 77−89410
Fe_2MnSi, antiferro- and ferromag. props. 77−12104
$(Fe_{93}Mo_7)_{80}B_{10}P_{10}$, amorphous, neutron scatt. investig. of spin waves, magnetisation 77−47984
Fe_2MoO_4, magnetic struct. of low and room temp. by neutron diffr. 77−63100
$FeMo_2S_4$, cryst. struct., mag. struct. and props., neutron diffr. meas. *(French)* 77−47971
$(Fe_{0.45}Nb_{0.53})O_2$, rutile, cation distrib. and mag. ordering *(German)* 80−107116
$Fe_{0.66}Ni_{0.34}$ Invar alloy, magnetic form factor 79−56504
$Fe_{65}Ni_{35}$ ferromagnetic alloy, zero sound anomaly, inelastic neutron scatt. 79−46764
$Fe_{65}Ni_{35}$, ferromagnetic Invar alloy, lattice vibrations 78−91403
$Fe_{65}Ni_{35}$, mag. cluster structs., 25-422°C 77−69493
$Fe_{65}Ni_{35}$, quasi-localised spin system, neutron scatt. 78−68194
$Fe_{65}{}^{60}Ni_{35}$, electron irradiated, small angle neutron scatt. 78−52218
$Fe_{70}Ni_{30}$, short range order, diffuse elastic neutron scatt. study 78−52219
$Fe_{70}{}^{60}Ni_{30}$, small angle neutron scatt., magnetisation inhomogeneity 78−52218
$Fe_{20}Ni_{60}B_{19}P_1$, amorphous, spin waves, inelastic neutron scatt. meas. 79−73701
$Fe_{65}(Ni_{1-x}Mn_x)_{35}$, anomaly of subcrit. neutron scatt. and depolarisation effects at antiferro- to ferromag. transition *(Russian)* 77−47996
$Fe_{65}(Ni_{1-x}Mn_x)_{35}$, magnetic struct. and inhomogeneities by neutron scatt. and Mossbauer effect *(Russian)* 77−63122
$Fe_{65}Ni_{28}Mn_1$, disordered, mag. struct. near ferro-antiferromagnetic transition 80−60211
$Fe_{40}Ni_{40}P_{14}B_6$, amorphous ferromag., spin wave excitations 80−97079
$(Fe_{0.3}Ni_{0.7})_{0.75}P_{0.16}B_{0.06}Al_{0.03}$, amorphous, spin wave spectrum, neutron scatt. 77−16064
$(Fe_{65}Ni_{35})_{75}P_{16}B_6Al_3$, amorphous ferromag., high temp. spin dynamics 78−47965
$(Fe_{65}Ni_{35})_{75}P_{16}B_6Al_3$, amorphous ferromagnet, mag. excitations 79−7984
$(Fe_xNi_{1-x})_{75}P_{16}B_6Al_3$, amorphous, spin wave excitations and low temp. magnetisation 79−33468
FeO, lattice dynamics, coherent inelastic neutron scatt. 78−59899
FeO, wustite, lattice dynamics, inelastic neutron scatt. meas. 77−84867
$Fe_{1-x}O$, low-energy mag. excitation dispersion curves 79−4665

neutron diffraction examination of materials continued
$Fe_{1-x}O$, wustite, cryst. dynamics, mag. excitations, neutron scatt. study *(French)* 79−51740
$Fe_{1-x}O$, wustite, defect struct. 80−107216
$Fe_{1-x}O$, wustite, phonon and magnon props., inelastic neutron scatt. 78−52236
$Fe_{1-x}O$, wustite, vacancy and interstitial ion order, equilib. conditions, neutron diffr. obs. *(French)* 78−14336
$Fe_{1-y}O$, wustite, struct. evolution, mean isotropic thermal agitation factor, depend. on equil. temp. and comp. *(French)* 77−68947
$Fe_{1-y}O$, wustite, struct. at high temp., neutron diffr. obs. *(French)* 79−86754
$Fe_{1-y}O$, wustite, struct. at high temp., neutron diffr. *(French)* 80−1982
α-Fe_2O_3, H-T phase diagram 79−87258
Fe_2O_3, haematite, mag. domain distrib., appl. of mag. Laue neutron diffr. method 78−95455
α-Fe_2O_3, haematite, substituted, Morin transition, neutron diffr. study 80−54897
α-Fe_2O_3, hematite, field-induced domain struct., neutron diffr. meas. *(German)* 77−16101
α-Fe_2O_3, neutron Laue diffr. investig. of domain distrib. 77−24712
α-Fe_2O_3:Al^{3+}(Ga^{3+})(Cr^{3+})(In^{3+}), substitution effect on Morin transition, neutron diffr. study 80−44827
Fe_2O_3-P_2O_5 system, vitreous, struct. obs. using neutron scatt. 78−22667
Fe_3O_4, crit. exponents meas. by polarized neutron scatt. 80−44828
Fe_3O_4, mag. crit. scatt., neutron spectroscopy 77−20614
Fe_3O_4, magnetite, reduced A-site moments, polarised neutron study 79−47253
Fe_3O_4, neutron diffuse scatt. due to mol. polarons 80−15460
Fe_3O_4, neutron diffuse scatt. due to molecular polarons 80−88488
Fe_xO, non-stoichiometric, mag. struct., neutron diffr. exam. 79−42737
$FeOHSO_4$, mag. structure, modulation of moments, neutron diffr. meas. 77−69499
FeOOH, high-pressure phase, neutron diffraction study 78−52212
ϵ-FeOOH, synthesis, mag. struct. 78−34961
Fe_2P, mag. moments and form factors, polarised neutron diffr. study 79−65650
Fe_2P, mag. struct., neutron diffr. study 78−23246
$Fe_{0.75}P_{0.15}C_{0.10}$, amorphous, mag. excitations and static struct., neutron scatt. obs. 78−68204
$Fe_{75}P_{15}C_{10}$, amorphous, mag. excitations, inelastic neutron scatt. 78−10674
FeP(Ga)(As)(Sb), dil., short-range order, neutron diffuse scatt. and spin echo NMR 80−50106
$Fe(Pd_{1-x}Au_x)_3$, mag. struct. ferro-antiferromagnetism coexistence *(Russian)* 79−82759
$FePt_3$, neutron scattering study of spin waves 78−91856
Fe_3Pt, quasi-localised spin system, neutron scatt. 78−68194
$Fe_{72}Pt_{28}$, ferromagnetic Invar alloy, lattice vibrations 78−91403
FeS, zinc blende type, mag. struct. *(French)* 78−91846
$Fe_{0.996}S$, antiferromag., energy dispersion of spin waves, inelastic neutron scatt. meas. 77−69522
$FeSO_4$, α- and β-forms, magnetic interactions, neutron inelastic scatt. study 80−107980
β-$FeSO_4$, high-temp. polymorph, stability, mag. struct., mag. props. 77−43815
FeSi, (110), Neel cryst., refr. of neutrons in Bloch walls using double cryst. arrangement 79−24191
FeSi, domain struct. and magnetisation reversal, time depend. neutron depolarisation 80−50138
FeSi picture frame single cryst., domain wall motion and magnetisation reversal, time-depend. neutron depolarisation study 80−88782
FeSi, single cryst., orientation of pieces of zigzag Block walls, neutron small-angle scatt. determ. 79−24190
Fe_3Si-based alloy, dil., cond. electron polarisation and moment perturbations 78−68224
Fe_3Sn_2, mag. props., neutron diffr. and magnetisation meas. 79−11294
$(Fe_{0.5}Ta_{0.5})O_2$, rutile, cation distrib. and mag. ordering *(German)* 80−107116
$FeTh_2S_5$, mag. struct. and props., neutron diffr. and mag. meas. 80−60201
FeTi-D(H), γ-phase, neutron and electron diffr. 80−84156
β-FeTiD, neutron diffr. exam. of struct. 78−47282
α-$FeTiD_{0.057}$, solid soln., interstitial D, neutron diffr. study 80−39071
$FeTiD_x$, γ-phase struct., neutron diffr. study 79−51085
$FeTiD_x$($O \leq x \leq 1.9$), neutron diffr. struct. anal. 80−75447
$FeTiH_x$, (x=0.65 to 1.03) diffusion of H, neutron scatt. exam. 79−65243
Fe_2TiO_4, cooperative Jahn-Teller effect, neutron scatt. study 80−49678
Fe_2TiO_4, cooperative Jahn-Teller phase transition, crit. diffuse scatt. 80−59930
Fe_2TiO_5, anisotropic spin glass behaviour 79−99707
Fe_2TiO_5, anisotropic spin glass type behaviour 80−60296
FeU_2S_5, mag. struct., exchange energy, magnetisation and neutron diffr. expts. 78−68170
Fe_2WO_6, neutron diffr. patterns and mag. struct. 77−66250
Ga, liq., neutron diffr. room temp. to 1303K, struct. model 78−51405
n-GaAs, magnetised semiconductor, coupled LO phonon-plasmon modes inelastic neutron scatt. 79−73459
$Ga_{0.67}Cr_2S_4$, semiconducting thiospinelide, spin glass type mag. ordering *(Russian)* 80−50123
α-GaOOD, powder neutron diffr. cryst. struct. exam. 78−2081
GaS, anisotropic phonon dispersion 77−84864
GaS_xSe_{1-x} layered system, neutron diffr., IR and Raman scatt. 79−87443
Gd, ferromag., domain struct., small-angle neutron scatt. 77−66382
Gd, mag. short range order, 80 to 425K 79−42784
^{160}Gd, ferromagnetic, isotopically enriched single crystals short-range order 79−4653
$GdCu_{1-x}Zn_x$, mag. struct. determ. 79−87238
GdMg, canted mag. struct. in S-ion compound, neutron diffr. obs. 78−34962
$GdMg_3$, mag. props., Mg conc. depend. 78−84392
$GdMg_3$, mag. props. 78−72346
$GdMo_6S_8$, coexistence of antiferromagnetism and superconductivity, neutron diffraction study 79−99685
$GdMo_6S_8$, long range mag. order in supercond. state 79−65653
$Gd_{1.2}Mo_6Se_8$, coexistence of supercond. and long range antiferromag. order 80−84534
Ge (111), mosaic single cryst., neutron integrated reflectivities 79−86656
Ge crystal, Laue scatt. intensity oscills., neutron scatt. using inclination method 78−42867
Ge melt, tetrahedral concs., neutron diffr. study *(German)* 80−19688
Ge, single crysts., total thermal neutron cross sections 80−19672
$GeCl_4$, liq. struct., oscill. amp., neutron diffr. study 79−46544
$GeCl_4$, liq. struct. by neutron diffr. 79−73089
Ge_2N_2O, pressure induced tetrahedral tilting and deform. 80−24415
Ge_2N_2O, time-of-flight neutron diffr. study 79−19200
GeO_2, α-quartz structure, compression mechanism 79−23673
GeO_2, vitreous, neutron diffr. obs. using Harwell linac 78−22666
GeS, phonon dispersion relations, neutron scatt. study 79−42182
$GeSe_2$, liquid, struct., investigation using neutron diffr. meas. 79−23514
GeTe, liq., neutron diffraction study 79−77485
$Ge_{0.5}Te_{0.5}$, strucutral anal. by neutron diffr., radial distribution functions 80−15010
H position in metals, determ. method using neutron quasi-elastic scatt. 79−42042
H storage materials, H diffusion in $Ti_2NiH_2(FeTiH)(LaNi_5H_6)$, neutron diffr. obs. 80−51013
H-bonded species, in soln., vibr. relax. model 78−84559
H_2, adsorbed on Al_2O_3, diffusive motion, neutron scatt. study 79−42394
H_2, adsorbed on Ni, inelastic neutron scatt. 78−18898
H_2 adsorbed on Pd black, vibr. spectrum assignments, inelastic neutron scatt. obs. 78−71942
H_2 adsorbed submonolayer, ortho-para separation coeff., mol. alignment and rot. levels 77−7971
H_2, dense gas, self-diffusion, quasielastic incoherent neutron scatt. obs. 78−22451
H_2, gaseous, high density, enhanced self diffusion, incoherent neutron scatt. study 79−46417
H_2, liq. slow neutron scatt. rel. to intermol. excitations, analyt. model 77−58941
H_2, solid, inelastic neutron scatt., theoretical analysis 78−34569
p-H_2, solid, neutron diffr. studies up to 5 kbar 80−59436
H_2, solid, neutron scattering expts. 78−79693
H_2, solid, orientationally disordered and ordered state, rot. transition J=1 to J=0 79−23543
H_2, solid collective excitations observed by incoherent neutron scatt. 79−23690
H_2, solid ortho-para mixtures, incoherent neutron scatt. 77−47304
H_2, states velocity auto-correl. function, relax time, neutron scatt. obs. 80−58401
H_2-Ar, states velocity auto-correl. function, relax time, neutron scatt. obs. 80−58401
HCl, intermol. partial struct. factors, isotopic substitution and neutron diffr. obs. 80−53157
HCl, solid, incoherent neutron scatt. of proton motions 78−75600
$H_3Co(CN)_6$, strong NHN hydrogen bond, vibr. lattice and mol., incoherent inelastic neutron scatt. 80−39232
H_xMoO_3 ($0.3<x<2.0$), synthesis and phase characterisation 79−1416
H_xMoO_3, structural anal. by neutron diffr. 79−65043
$HNO_3.H_2O$ glassy form, stochastic rot. motions 79−7551
H_xNbS_2, struct., form. by cathodic reduction, neutron diffr. obs. 79−73150
H_2O, liq. struct. factor, neutron diffr. meas. 79−46547
H_2O, molecular dynamics anal. by inelastic neutron scatt. 77−35462
H_2O-organic aerosol-n-heptane reverse-type micellar soln., neutron small-angle scatt. *(French)* 80−26059
$(H_5O_2^+)_3(PW_{12}O_{40}^{3-})$, struct. of Keggin's 'pentahydrate' from X-ray and neutron diffr. data 77−47382
$(H_5O_2^+)_3(PW_{12}O_{40}^{3-})$, struct., X-ray and neutron diffr. study 79−42037
$H_3PW_{12}O_{40}.21H_2O$, cryst. struct. 78−42977
H_xTaS_2, nonstoichiometric, incoherent neutron spectra, X-ray diffr. 78−42998
$H_{0.4}WO_3$, inelastic neutron spectra 77−15287
He, adsorbed monolayer struct., superfluid film excitation spectrum 77−7942
He, condensed phases, neutron scatt. techniques and results, book contrib. 80−2230
He, FCC, lattice dynamics at high press. 78−10255
He II, superfluid, single atom neutron scatt. and two roton connected state branches *(Russian)* 80−44381
He II-^{3}He, roton lifetime from neutron inelastic scatt. meas., 1.27-2.15K 79−56011
He, liq., multiphonon boundary of excitation spectrum, neutron and inelastic light scatt. 80−92740
He, solid, theory and thermodynamic props., book contrib. 77−47646
He, superfluid, inelastic neutron scatt. spectra, roton-roton interactions 78−95194
^{2}He, liq., 0.015K, elementary excitations, neutron scatt. study 79−46874
^{3}He dilution refrigerator for neutron diffr. exam. of nucl. antiferromag. order 79−58701
^{3}He, dynamic props., neutron scatt. studies, review 79−50972
^{3}He, liq., dynamic form factor, particle density, spin density correlation, RPA calcs. 79−46873
^{3}He, liq., inelastic neutron scatt., 10 and 20 bars, wavevector transfers 78−71899
^{3}He, liq., neutron inelastic scatt. studies of elementary excitations 79−65275
^{3}He, liq., neutron scattering, dynamical form factor, RPA calc. 77−7938
^{3}He, liq., pressure cell for neutron scatt. 78−14246
^{3}He, liq., spin fluctuation peak obs. by inelastic neutron scatt. 80−49447
^{3}He, liquid, low-energy spin fluctuation peak, theoretical anal. of neutron obs. 80−6584
^{3}He liquid, zero sound lifetime, neutron inelastic scatt. study 80−65329
^{3}He, neutron inelastic scattering, zero sound and spin-fluctuation peaks 78−79836
^{3}He, neutron scatt. meas. 79−46860
^{3}He under pressure, inelastic neutron scatt., zero sound mode nature 79−55998
^{3}He-^{4}He mixtures, excitation spectrum, exptl. studies using neutron inelastic scatt. 77−59170
^{3}He-^{4}He mixtures, excitation spectrum, neutron inelastic scatt. study 79−46877
^{3}He-^{4}He mixtures, neutron inelastic scatt. studies of elementary excitations 79−65275
^{4}He, FCC, inelastic neutron scatt., phonon spectra, dispersion curves 78−51785

neutron diffraction examination of materials continued
^{4}He, FCC high-density cryst., lattice dynamics by inelastic neutron scatt. 79−1539
^{4}He film, adsorbed, few atomic layers, excitations, two-dimensional roton. 80−39381
^{4}He, HCP, Debye-Waller factor by inelastic neutron diffraction 78−43206
^{4}He, liq., dynamic struct. factor, 2.5K, inelastic neutron scatt. study 79−55647
^{4}He, liq., dynamic structure, neutron diffr. determ. 77−11749
^{4}He, liq., effective pair potential, 4.2K, from inelastic neutron scatt. data 79−50980
^{4}He, liq., inelastic neutron scatt., observability of Beliaev terms 78−51764
^{4}He, liq., nonsuperfluid, dynamic struct. factor, neutron scatt. meas. 79−46545
^{4}He, liq., nonsuperfluid, low momentum transfer neutron scatt. study 79−46546
^{4}He, liq., phonon temp. depend. above and below T_λ, neutron scatt. meas. 79−55973
^{4}He, liq., quasiparticle model, finite temp. 77−39715
^{4}He, liq., static struct. factor and pair correls., neutron diffr. study, 1.00 to 4.27K 80−80010
^{4}He, liq., static structure factor and pair correlation function, at saturated vapour press. 80−64878
^{4}He, liq., vortex rings, neutron elastic scatt. cross section calc. 79−4443
^{4}He, nonsuperfluid liq., neutron scatt. dynamic struct. factor, saturated vap. press. 78−42878
^{4}He, normal liq., collective excitations, neutron inelastic scatt. study 80−107590
^{4}He, superfluid, bound 2-roton state by neutron scatt. meas. *(Russian)* 79−86951
^{4}He, superfluid, condensate fractions and pair correlations 80−39375
^{4}He, superfluid, elementary excitation line shapes, energies and linewidths, neutron scatt. obs. 79−60572
^{4}He, superfluid, elementary excitations, μeV resolution study by neutron spin echo 80−65327
^{4}He, superfluid, neutron inelastic scatt. studies of elementary excitations 79−65275
^{4}He, superfluid, neutron scatt. and thermodynamic quantities, need for more precise data 78−22916
^{4}He, superfluid, neutron scattering, role of two roton bound state 79−4446
^{4}He, superfluid, neutron spin-echo study of excitations 80−80014
^{4}He, superfluid, phonon dispersion, neutron scatt. study 79−51336
^{4}He, superfluid, phonon dispersion 80−10722
^{4}He, superfluid, roton energy determ. from neutron diffr. exam. 77−24458
^{4}He, superfluid, roton lifetime, inelastic neutron scatt. meas. *(Russian)* 79−7723
^{4}He, superfluid, roton-roton interactions and excitations at large wavevectors, neutron scatt. meas. 77−28058
^{4}He, superfluid, roton-roton interactions, neutron scatt. meas. 79−46860
^{4}He, superfluid, singular f-sum rule, applicability to inelastic neutron scatt. 80−6577
^{4}He, superfluid, thermodynamic versus neutron meas. at low temp. 79−51327
^{4}He superfluid film, neutron scatt., surface effects 78−10251
Hf-O, phase props. 77−40415
HfV_2D_4, disordered solid solution, order-disorder transition 80−88321
Hg, solid, phonon dispersion curves, neutron inelastic scatt. 78−14410
$Hg_{3-\delta}AsF_6$, dynamical props., Hg chain behaviour, neutron scatt. study 79−95103
$Hg_{3-\delta}AsF_6$, one dimensional phonons and chain ordering 80−24544
$Hg_{3-\delta}AsF_6$, one-dimens. phonons and phase-ordering phase transition, neutron scatt. expts. 78−26644
$Hg_{3-\delta}AsF_6$, one-dimens. fluctuations and chain ordering transform., neutron scatt. calc. 78−59923
$Hg_{3-x}AsF_6$, energy gap in phonon dispersion of linear Hg chains 79−42172
$Hg_{3-x}AsF_6$, phase-ordering phase transition, elastic neutron scatt. obs. 79−33087
Hg_2Cl_2, neutron and Raman scatt. studies, ferroelastic transitions 80−76015
Hg_2Cl_2 prototype phase, soft mode, inelastic neutron scattering, Raman effect 78−91411
$HgCr_2S_4$, spinel, mag. struct., symmetry anal. in neutron diffr. studies 80−25091
α-HgI_2, inelastic neutron scatt. selection rules 78−79503
HgI_2, red, phonon dispersion, inelastic neutron scatt. obs. 78−75756
$HgSO_4.H_2O$, X-ray and neutron diffr. study of struct. 80−33936
$HgSeO_4.H_2O$, cryst. struct. determ. by neutron diffr. 78−55838
HgTe, phonon dispersion relations, neutron study 80−70340
Ho, low field susceptibility and helical-ferromag. field induced phase transition 78−47975
Ho, magnetic phase transition, second order, order parameter in mag. field, neutron diffr. 79−61104
Ho-La, HCP, mag. phase diagram, neutron diffr. meas. 80−70950
Ho-Pr(Nd) alloys, mag. struct. and ordered moments, neutron diffr. data 77−66252
$HoAl_2$, Ho moment reorientation, polarized neutron diffr. study 79−42761
$HoAl_2$, magnetisation and neutron diffr. meas., cryst. field and exchange 77−63163
$HoAl_2$, single cryst., redeterm. of Ho neutron scattering length 79−99032
HoAlGa, mag. props. and struct. 78−39302
$HoAlO_3$, 0.04K, antiferromag. ordering *(French)* 78−10653
$HoCo_2$, ground state spin excitations, inelastic nneutron scatt. study 80−50077
$HoCo_2$, mag.excitations, neutron inelastic scatt. meas. 80−60231
$HoCo_2$, paramag. and ordered phases, Pauli type Co susceptibility, polarised neutron diffr. obs. 77−63077
$HoCo_2Ge_2$, crystal and magnetic structure obs. 80−64976
$HoCrO_3$, cryst. field levels and mag. interactions, inelastic neutron scatt. study 77−69277
$HoCrO_3$, Ho^{3+} mag. form factor meas. by inelastic neutron scatt. 78−52221
$HoCrO_3$, mag. form factor of Ho^{3+}, inelastic neutron scatt. meas. 77−16050
$HoCu_2$, mag. struct. and elec. resist., neutron diffr. obs. 80−60206
neutron diffraction examination of materials continued
HoF_3, crystal structure by powder neutron diffr. study 80−15077
$HoFe_2$, Czochralski growth, and cryst. quality determ. 77−8742
$HoFe_2$, effect of H on sublattice magnetization, elastic neutron scatt. obs. 79−78327
$HoFe_2$, mag. struct., polarized neutron diffr. study 79−78326
$HoFe_2$, spin wave and cryst. field excitations, neutron scatt. 78−68196
HoFeMn, Laves phase, mag. moment on Ho, neutron diffr. obs. 77−63107
$Ho_{12}Fe_{32}O_2$, struct. and ferrimag. props., neutron diffr. obs. 79−78319
HoGa garnet, mag. ordering induced by hyperfine interaction, neutron diffr. meas. 77−66265
$Ho_3Ga_5O_{12}$, hyperfine interac. induced antiferromag. order *(French)* 77−59392
Ho_5Ge_4, mag. struct., neutron diffr. study 80−25093
$Ho_{1.15}Lu_{0.05}Mo_6S_8$, long range mag. order in supercond. state 79−65653
$HoMn_2$, Laves phase, mag. moment on Ho, neutron diffr. obs. 77−63107
$HoMo_6S_8$, long range mag. order in supercond. state 79−65653
$HoMo_6S_8$, reentrant supercond., direct. obs. of long range ferromag. order 78−76190
$HoMo_6S_8$, superconductor, neutron scatt. exam. of mag. phase 79−73680
$HoMo_6S_8(Se_8)$, mag. supercond., neutron scatt. obs. 80−70952
$Ho_{1.2}Mo_6Se_8$, crystal field excitations, inelastic neutron scatt. obs. 79−78321
HoN type conducting magnets with singlet ground state, inhomogeneous ferromagnetism *(Russian)* 77−63118
Ho_2Ni_{17}, ferrimag. struct., neutron diffr. expt., cryst. field calcs. 77−73001
$HoNi_{0.5}Cu_{0.5}$, sp. ht. and modulated mag. struct. 77−32167
Ho_2O_3 powder, redeterm. of Ho neutron scattering length 79−99032
Ho_2O_2S powder, redeterm. of Ho neutron scattering length 79−99032
HoP, flopside mag. struct. to ferromag. transition, elastic neutron scatt. obs. 80−50058
$HoPO_4$, metamagnet, mag. phase transitions, elastic neutron scatt. study 79−78371
$HoRh_4B_4$, ferromag., mag. struct., neutron diffr. obs. 79−78323
Ho_xTe, mag. ordering, neutron diffr. meas. 78−2649
$HoTiO_3$, magnetic structure determination, neutron scatt. study 80−65809
$HoVO_3$, antiferromag., at. and mag. struct., neutron diffr. meas. 79−24142
HoZn, mag. excitations near spin rot. temp., neutron scatt. study 79−19731
I_2 liq., static structure factor, neutron diffraction 80−103236
$In(OH)_3$, cubic, cryst. struct., X-ray and neutron diffr. obs. 79−77568
K, accurate struct. factor determ. by X-ray and neutron diffr. 79−51046
K, CDW, detection attempt by neutron diffr. 80−49634
K, lattice parameter determ. by neutron scatt. 79−7576
K, mode Gruneisen parameters, neutron scatt. obs., 4.5K, 0.001-4.1 kbar 77−4179
K, phonon frequencies, normal mode Gruneisen parameters, pseudopot. calcs. 79−42184
K, search for anomalous phonons, coherent inelastic neutron scatt. meas. 77−47525
K solution, in KBr, conc. fluctuations, neutron small-angle scatt. study in electrolyte-metal transition range 79−14668
KAg_4I_5, superionic phase transition, dynamical and crit. pt. props. 80−107535
KBr, Debye-Waller factors at 4.2 and 295K 79−7667
KBr, liquid inelastic neutron scatt. obs. from short wavelength charge fluctuations 78−47487
KBr, mode Gruneisen parameters, acoustic phonon dispersion relations 79−42201
KBr, molten, charge fluctuations, neutron diffr. anal. 79−42198
KBr, molten, solutions of K, conc. fluctuations, small angle neutron scatt. study 80−92448
KBr:CN^-, neutron scatt. studies of $(CN)^-$ defects 80−92620
KBr:CN^- 80−49316
$KBr_{1-x}(CN)_x$, mixed mol. cryst., coupled rot. and translational modes 80−84267
KCN, cryst., struct., phase transition, 6-300K, neutron diffr. obs. 77−76347
KCN, inelastic neutron scatt. by coupled rot. and translational modes 80−79895
KCN, lattice dynamics and order-disorder transitions, neutron scatt. expts. 78−14434
KCN, phase transition at 168K, neutron inelastic scatt. line shapes for phonons obs. 78−38840
KCN, phonon freq. distrib., cubic and monoclinic phases 78−22800
$(KCN)_{0.25}(KBr)_{0.75}$, rot.-translation interactions, neutron scatt., 0-300K 78−67783
$(KCN)_{0.5}(KBr)_{0.5}$, lattice dynamics neutron scatt. obs., glass phase formation 80−15207
$KCaF_3$, struct. phase transitions, DSC, birefr., and neutron powder diffr. obs. 80−70149
KCl, γ-irrad. and doped, lattice relax., cold neutron scatt. obs. 77−7715
KCl, white beam diffr. technique 77−31565
KCl:CN^-, phonon-internal mode hybridisation, neutron scatt. 78−2217
KCl:CN^-, coherent admixtures of phonons with impurity libronic excitations, neutron scatt. study 80−49316
KCl:Tl, neutron scattering from localised electronic excitation, theory 79−4539
$KCrO_2$, two-dimens. mag. order, neutron powder diffr. obs. 80−44805
$KCuF_3$, nearly 1-D spin-$^1/_2$ antiferromagnet, spin wave energy dispersion 80−2551
$KCuF_3$, one-dimens. antiferromag., spin waves, neutron scatt. study 80−65848
K_2CuF_4, magnon condensation 79−91220
K_2CuF_4, magnon condensation obs. in quasi-2D planar ferromag. phase 80−60232
K_2CuF_4, quasi two-dimens. Heisenberg ferromag., spin wave spectrum lineshape, neutron scatt. obs. 77−66286
K_2CuF_4, spin wave meas. in low energy range, inelastic neutron scatt. 78−88105
K_2CuF_4, two-dimensional ferromag., spin-wave lineshape, neutron scatt. data 77−16065
K_2CuF_4, two-dimensional planar ferromagnet, giant fluctuation of spins *(Japanese)* 80−54894

neutron diffraction examination of materials continued
$K_2Cu_{1-x}Mn_xF_4$ system, ($0 \leq x \leq 0.2$), prep., cryst. chem., and ferromag. props., X-ray and neutron diffr. study 79−24162
$K_2Cu_{1-x}Zn_xF_4$, two-dimens., ferromag., spin wave excitations 78−80140
$K_2Cu_xZn_{1-x}F_4$, two-dimens. ferromag., spin correls. near percolation limit 80−44840
KD_2PO_4, ferroelec., tetragonal⇄monoclinic transition, neutron powder diffr. meas. 77−7693
KD_2PO_4, ferroelec. domain struct. obs. using TOF neutron diffractometer 79−51923
KD_2PO_4, neutron scattering from coupled polar-elastic waves 80−92623
KD_2PO_4, para- and ferroelec. phases spatial distrib. during first order phase transitions 79−42923
KD_2PO_4, phase transitions study, role of cryst. struct. determ. 80−75197
KD_2PO_4, struct. at high press. in rel. to effect of press. on T_c 79−42915
$KD_3(SeO_3)_2$, phase transition, neutron diffr. 80−2158
$KD_3(SeO_3)_2$, phase transition, neutron scatt. study 80−75351
$KF.2H_2O_2$, cryst. struct., X-ray and neutron diffr. meas. 77−39569
K_2FeF_4, two dimensional easy plane antiferromag., neutron scatt. expts. 80−65838
K_2FeF_5, mag. struct. and one-dimens. antiferromagnetism 80−60209
K_2FeF_5, one-dimensional antiferromag., neutron diffr. and mag. meas. *(French)* 79−47241
$KFeO_2$, cryst. and mag. struct., neutron and X-ray powder diffr., and Mossbauer effect meas. 77−84722
$K_{10}(Fe_3O(SO_4)_6(H_2O)_3)_2.12H_2O$, mag. exchange interaction of trinucl. Fe^{3+} complex *(German)* 78−14947
$KFeS_2$, cryst. struct. and mag. ordering, neutron diffr. and mag. susceptibility meas. 80−54867
$KFeS_2$, spin analogue of active sites of ferrodoxins, mag. struct., neutron diffr. exam. 79−73688
$KHCO_3$, inelastic neutron scatt. spectra, H bonds bending vibrs. 79−14893
KH_2PO_4, ferroelec., tetragonal cryst. struct. determ., neutron diffr. meas. 77−7693
KH_2PO_4, ferroelectric transition, neutron diffr. obs. 80−25324
KH_2PO_4, KD_2PO_4, high-press. struct. rel. to dynamical models 78−80307
KH_2PO_4, neutron critical scatt. in struct. transition due to homogeneous crystal deform. 79−42922
KH_2PO_4, phase transitions study, role of cryst. struct. determ. 80−75197
KH_2PO_4, shear angle and order parameter of ferroelec. transition by neutron diffr. 77−12339
KH_2PO_4, single crystal neutron diffraction study at high pressure 80−92497
KH_2PO_4, struct. at high press. in rel. to effect of press. on T_c 79−42915
KH_2PO_4, tricrit. point, γ-ray and neutron diffr. 78−39516
KH_2PO_4, tricrit. point, neutron diffr. study under high press. 79−33624
KH_2PO_4-type ferroelectrics, inelastic neutron scatt. theory 78−48122
$KIO_3.HIO_3$, I atom electronic struct. in X-ray-neutron difference synthesis 79−90595
$KMnCl_3$, magnetic spiral struct., neutron diffr. study 80−39748
$K_2Mn_{1-x}CoF_4$, mag. and neutron scatt. exam. 79−33466
$KMnF_3$ lattice parameters, temp. depend., 21°C to MP 77−76583
K_2MnF_4, two-dimensional antiferromag., crit. behaviour, quasielastic neutron scatt. 77−85468
$K_3Mn_2F_7$, double-layer antiferromag., mag. ordering, neutron scatt. meas. 79−61062
$K_3Mn_3F_7$, Heisenberg double-layer antiferromag., neutron scatt. 79−61065
$K_2Mn_{0.987}Fe_{0.022}F_4$, antiferromag., mag. field induced transitions, neutron scatt. meas. 79−82782
$K_2Mn_{1-x}Fe_xF_4$, anisotropy on two and three dimens. mag. order 77−66259
$K_2Mn_{1-x}Fe_xF_4$, layered antiferromag., anisotropy effects on mag. ordering, neutron diffr. study 79−47254
$K_2Mn_{1-x}Fe_xF_4$, mag. and neutron scatt. exam. 79−33466
$K_2Mn_{1-x}Fe_xF_4$, tetracrit. line in x-H-T phase diagram, neutron scatt. exam. 78−47977
$K_2Mn_{1-x}Fe_xF_4$, vs. transition temperature, phase diagram, critical lines crossing tetracritical point, discussion 78−39326
$KMn_{1-x}Ni_xF_3$, antiferromag. crit. props., neutron scatt. obs. 80−88749
$KMn_{0.1}Zn_{0.9}F_3$, exchange interaction determ. by neutron scatt. 79−47274
$KMn_{0.18}Zn_{0.82}F_3$, excitation of Mn^+ clusters, neutron scatt. 78−68200
$KMn_xZn_{1-x}F_4$, three dimens. Heisenberg antiferromag., fluctuations near percolation threshold 79−78390
KND_2, neutron diffr. anal. of librations of amide ion *(German)* 77−27788
KND_2, neutron diffr. exam. 31K *(German)* 77−62506
α-KNO_3, lattice dynamics, inelastic neutron scatt. 79−4383
KNO_3, phase II, lattice dynamics, coherent neutron inelastic scatt. 78−59897
KNO_3, white beam diffr. technique 77−31565
$KNa[Pt(CN)_4].3H_2O$, neutron diffr. cryst. struct. exam., refinement by least squares 78−2079
$KNbO_3$, acoustic modes near orthorhombic-tetragonal phase transition, temp. depend. 79−28058
$KNbO_3$, one-dimens. ferroelectric, phonon dispersion surfaces 79−42180
$KNbO_3$, orthorhombic, anharmonic effects 78−79721
$KNbO_3$, tetragonal phase, inelastic neutron scatt. 80−19676
K_2NiF_4, two-dimensional antiferromag., crit. behaviour, quasielastic neutron scatt. 77−85468
K_2O-TiO_2-SiO_2 system, vitreous, struct. obs. using neutron scatt. 78−22667
K_2OsCl_6, soft rotary mode near phase transition, inelastic neutron scatt. obs. 79−60472
K_2OsCl_6, ferrorotative transition, neutron scatt. expt., consistency with displacive and order-disorder models 78−51673
$K_2PbCu(NO_2)_6$, incommensurate Jahn-Teller transition, neutron scatt. meas. 77−69065
$K_2PbCu(NO_2)_6$, incommensurate Jahn-Teller phase transition 78−79730
$K_2PbCu(NO_2)_6$, incommensurate Jahn-Teller transition, Huang scatt. 80−70401
$K_2PbCu(NO_2)_6$ Jahn-Teller phase transitions, X-ray and neutron measurements 78−91438
$K_2Pt(CN)_4$, quasi-one-dimens. Peierls system, phonon dispersion and neutron scatt., calc. 80−24550
$K_2Pt(CN)_4Br_{0.3}\times 3H_2O$, struct., neutron determ., Peierls distortion 79−46640

neutron diffraction examination of materials continued
$K_2Pt(CN)_4Br_{0.3}.2.7D_2O$, under hydrostatic press., compressibility, neutron diffr. 79−46742
$K_2Pt(CN)_4Br_{0.3}.3.2D_2O$, Kohn anomalies, phonon dispersion curve 78−10133
$K_2Pt(CN)_4Br_{0.3}.3.2D_2O$, lattice dynamics, neutron scatt. expts. 78−14412
$K_2Pt(CN)_4Br_{0.3}.3.2D_2O$, dynamic struct. factor, inelastic neutron scatt. study 79−42185
$K_2Pt(CN)_4Br_{0.3}.xH_2O$, dynamical props. near Peierls instability, neutron scatt. 78−14436
$K_2Pt(CN)_4Cl_{0.3}(Br_{0.3}).3H_2O$, struct., single cryst. neutron diffr. expts. 78−14321
$K_{1.75}Pt(CN)_4\times 1.5H_2O$, struct., neutron determ., Peierls distortion 79−46640
$K_{1.75}Pt(CN)_4.1.5H_2O$, struct., single cryst. neutron diffr. expts. 78−14321
$K_{1.6}Pt(C_2O_4)_2\times 1.2H_2O$, struct., neutron determ. 79−46640
K_cRb_{1-c}-alloys, lattice dynamics of substitutional alloys, force constant disorder 78−75786
$K_{0.5}Rb_{0.5}I$, mixed cryst., phonons. inelastic thermal neutron scatt. 77−1192
$K_xRb_{1-x}I$, Debye temp. conc. depend. 79−90746
K_2ReCl_6, structural phase transition, soft rotary mode, obs. by triple-axis neutron scatt. 79−1483
K_2SO_4, longitudinal-acoustic soft mode in phase transition 80−75326
K_2SeO_4, improper ferroelec., struct., phase transform. and lattice instability neutron scatt. meas. 77−63379
K_2SeO_4, incommensurate lattice instability, ferroelec. transition, neutron scatt. study 79−42210
K_2SeO_4, incommensurate to ferroelec. transition, hydrostatic press. effects, neutron scatt. study 80−108166
K_2SnCl_6, elastic consts., inelastic neutron scatt. and US meas. 80−59553
K_2SnCl_6, phase instabilities and mode softening X-ray and neutron diffr. 77−7830
K_2SnCl_6, structural phase transition exam. by neutron powder diffr. 78−55940
$K_{0.33}WO_3$, hexagonal, phonon dispersion curves, neutron scatt. obs. 78−14411
K_2ZnCl_4, incommensurate phases, neutron scatt. 79−38501
$K_2[M(H_2O)_6](YO_4)_2$, Tutton's salts, M=Cu, Ni, Zn, Y=S, Se stereochem., neutron struct. determ. 78−18609
$K[(OH)_{0.42}(O_2)_{0.50}]$, cubic solid soln., structural and mag. study *(French)* 80−107177
$K_2[Pt(CN)_4]X_{0.3}.3H_2O$, X=Br, Cl, X-ray and neutron diffr., 31K-room temp. 78−42964
$K_3[SO_3ON(SO_3)_2].3/2H_2O$, struct. determ., X-ray and neutron diffr. 79−42038
Kr gas structure, three-body-contrib., neutron diffr. obs 80−43820
Kr, gas structure by neutron diffr., three-body pot. contrib. 79−90358
Kr mono- and bilayers on graphite, two-dimens. struct., neutron diffr. study 79−42393
Kr on graphite, neutron diffr. obs. 77−72789
Kr:methane, impurity rotational states, inelastic neutron scatt. study 79−51020
$(La,Er)Al_2$, cryst. field parameters, inelastic neutron scatt. study 79−23937
(La,Na)Sn alloys, supercond. transition temp. 79−78254
La, DHCP and FCC phases, phonon density of states 78−67791
La, liq. struct., neutron diffr. meas. 77−51305
La-H(D), inelastic neutron scattering exam. of lattice dynamics 80−29128
LaAg, Tb and Pr substituted, superconductors, cryst. field transitions linewidths 80−24854
$LaAg_xIn_{1-x}$, crystal struct., neutron diffr. obs. 80−49187
$LaAg_xIn_{1-x}$, phonon dispersion, elastic consts. and struct. instability, soft mode behaviour 80−103436
$LaAl_2$, inelastic neutron scatt. 80−11165
$LaAl_2$, Tb and Pr substituted, superconductors, cryst. field transitions linewidths 80−24854
$La(Co_{1-x}Ni_x)_5$, distrib. of Co and Ni atoms, neutron diffr. obs. *(Russian)* 80−64954
LaD_3, stoichiometric, structural phase transform., neutron diffraction evidence 80−88319
$La_{0.9}Er_{0.1}Al_2$, crystal field study rel. to $ErAl_2$ 78−76036
$La_2Li_{0.5}Co_{0.5}O_4$, neutron diffraction data 80−80226
$La_2Mg_3(NO_3)_{12}.24D_2O$, use of neutron time-of-flight technique for cryst. structs. investigation 79−19126
$La_2Mg_3(NO_3)_{12}.24H_2O$, neutron diffr. obs. 78−18598
$La_2Mg_3(NO_3)_{12}.24H_2O:Nd^{3+}$, polarised neutron diffr. from dynamically and statically polarised protons 80−44078
La_2MnFeS_5, antiferromag., mag. props. and mag. struct., neutron diffr. and magnetisation meas. 80−65801
$LaMnO_3$, ferromag.-paramag. phase transition, neutron diffr., calorimetric investigs. 78−31072
$LaMnO_3$, monoclinic and cubic perovskite struct., mag. props., neutron diffr. meas. 78−27022
$LaMnO_3$, orthorhombic lattice distortions, mag. props. rel. to prep. conditions 77−20592
$LaMnO_3$, phase diagram, mag. moments, neutron diffr. study 80−108414
$La_2(MnO_3)_3$, hydrostatic press. effect on mag. struct. 77−51886
La_2MnZnS_5, antiferromag., neutron diffr. study 80−25099
$LaNi_5$, crystal field investigation from inelastic slow neutron scatt. expts. 80−39538
$LaNi_5D_6$, cryst. struct., neutron diffr. obs. 79−19221
$LaNi_5H_6$ sponges, Al or Mn substitution, neutron diffr. 80−24427
$LaNi_5H_{\geq 3.0}$, H diffusion coeff., neutron scatt. obs. 80−24643
$LaNi_5H_x$ hydrogen storage system, ($0 \leq x \leq 6$), neutron scatt. obs. of static and dynamic props. 78−14323
$LaNi_5H_6(D_6)$, low energy excitations of H and D 79−77699
La_2O_3, fast ionic O_2 diffusion, neutron scatt. evidence 79−99357
La_2O_3, neutron diffraction study of high temp. struct. *(French)* 79−65050
$La_2O_2S_2$, cryst. struct. determ. 79−51087
$LaPb_3$, Tb and Pr substituted, superconductors, cryst. field transitions linewidths 80−24854
$La_{1-x}Pr_3(Sn_3)$, superconducting, cryst. field excitations, inelastic neutron scatt. obs. 80−15653
$La_{1-x}Pr_xSn_3$, supercond., 0.6 meV cryst. field transitions, neutron spectroscopy 78−67991

neutron diffraction examination of materials continued
$La_{1-y}Pr_ySn_3$, neutron spectroscopy of 0.6 meV cryst. field transitions 78−30894
$LaSn_3$, inelastic neutron scatt. 80−11165
$LaSn_3$, Tb and Pr substituted, superconductors, cryst. field transitions linewidths 80−24854
$La_{1-x}Sr_xCrO_3$ system, phase relationships, cryst. struct. 77−69073
$La_{1-x}Tb_xAg$, supercond., 0.6 meV cryst. field transitions, neutron spectroscopy 78−67991
$La_{1-y}Tb_yAg$, neutron spectroscopy of 0.6 meV cryst. field transitions 78−30894
$La_{1-x}Tb_xAl_2$, supercond., 0.6 meV cryst. field transitions, neutron spectroscopy 78−67991
$La_{1-y}Tb_yAl_2$, neutron spectroscopy of 0.6 meV cryst. field transitions 78−30894
$La_{1-x}Tb_xSn_3$, supercond., 0.6 meV cryst. field transitions, neutron spectroscopy 78−67991
$La_{1-y}Tb_ySn_3$, neutron spectroscopy of 0.6 meV cryst. field transitions 78−30894
Li, anharmonicity and low temp. phase struct., neutron diffr. study 80−107105
Li-Ag, liq. alloy, density, compressibility and diffr. data 77−47336
Li-ND_3, near liq.-liq. crit. point, conc. fluctuations, neutron diffr. long wavelength thermodynamic limit 79−10948
Li-Na, liq., short-range order, neutron diffr. obs., near crit. composition 78−22639
$Li_2Ag_{2-x}In_x$, optical props., struct., energy bands, interband transitions 78−72539
$LiAlSiO_4$, β-eucryptite one-dimens. fast ion cond., temp. depend. of cryst. struct. 80−107191
β-$LiAlSiO_4$, eucryptite, one-dimensional ionic conductor, neutron scatt. study 80−49361
Li_5B_4, cryst. struct., X-ray and neutron diffr., and NMR 79−23571
$LiBa_3Nb_3(Ta_3)(Sb_3)Ti_5O_{21}$, insertion of Li, X-ray and neutron diffr. study *(French)* 78−91324
$Li_2Cd_{2-x}In_x$, optical props., struct., energy bands, interband transitions 78−72539
$LiCrO_2$, two-dimens. mag. order, neutron powder diffr. obs. 80−44805
LiF, γ-irradiated, Huang diffuse scattering of neutrons 80−10544
$Li_{0.13}Fe_{2.87}O_4$, acoustic spin wave dispersion branch, exchange const., neutron scatt. study 79−47266
$Li_{0.5}Fe_{2.5}O_4$, temp. depend. of mag. moments, neutron diffr. data *(Russian)* 77−28371
$LiFePO_4$, cryst. struct. by neutron diffr. 78−43003
$Li_xFePS_3(Se_3)$, Li_xMnPSe_3 and $Li_xNiPS_3(Se_3)$, NMR and neutron diffr. obs., mag. props. 80−60433
$Li_{0.5}Ga_{0.85}Cr_{1.625}O_2$ spinel, tetrahedral coordination of Cr^{3+} ion, electronic spectra, X-ray and neutron diffr. *(French)* 79−65031
LiH, antiferromagnetism, neutron diffraction study, appl. to polarised targets 79−68065
LiH, mag. domains and nucl. mag. ordered phases, antiferromag. and ferromag. neutron diffr. obs. 80−50051
LiH, mag. ordering in nucl. antiferromag. state, neutron diffr. obs. 79−65654
LiH, neutron diffr. evidence of nuclear antiferromagnetism 79−61066
LiH, nucl. antiferromag. struct., neutron diffr. and dynamic polarisation *(French)* 78−88226
LiH, nuclear antiferromagnetism studied by neutron diffr. 79−11358
LiH, nuclear ordered ferromag. and antiferromag. phases, neutron diffr. study 80−50052
$LiH_3(SeO_3)_2$, ferroelec., absolute atomic arrangement and spontaneous polarisation, neutron diffr. study 80−59442
α-$LiIO_3$, neutron diffr. intensity enhancement under DC field, investig. 80−10462
$LiIO_3$ single crystal, DC field effect, neutron diffr. enhancement *(Chinese)* 80−44077
$LiNO_3.3H_2O$, neutron diffr. studies at 120 and 295K, H bond studies 80−88099
$(Li_{0.63}Na_{0.37})_2O.2SiO_2$, short range struct. by pulsed neutron scatt. 80−59396
$LiNbO_3$, ferroelec., phonon dispersion relations, neutron inelastic scatt. meas. 78−56435
Li_2O-Al_2O_3-SiO_2, phase separation of initial stages of sitallisation 80−88053
Li_2O-LiX-B_2O_3 glass, X=halogen, high anionic cond. of new solid electrolytes 80−107546
LiOH, electron distrib. of OH^- 78−75973
$Li_2O.2SiO_2$, short range struct. by pulsed neutron scatt. 80−59396
Li_2SO_4 based solid electrolytes, FCC phase transport mechanism studies and uses 80−107525
Li_2SO_4, fast ion conductors, X-ray diffr., neutron diffr., and Brillouin scatt. study 80−107170
Li_2SO_4, high temp. fast ion cond. phases, neutron diffr. obs. of struct. 80−107512
M-$LiTa_3O_8$, neutron diffr. obs. 78−18599
$LiTbF_4$, ferromag., susceptibility, sp. ht., renormalisation group theory test 77−16087
LiTi, substituted ferrite, cation distribution, Mossbauer, X-ray, neutron diffr. study 80−28975
Li_xTiS_2, struct. determ. by neutron diffraction 80−54196
LiZn, substituted ferrite, cation distribution, Mossbauer, X-ray, neutron diffr. study 80−28975
$Li_{0.5(1-x)}Zn_xFe_{2.5-0.5x}O_4$, cryst. struct., neutron and X-ray diffr. obs. *(Russian)* 77−31645
$Li_{0.5(1-x)}Zn_xFe_{2.5-0.5x}O_4$, canted spin struct., neutron diffr. study 78−68175
^7Li, lattice dynamics, temp. depend., 110-424K 77−20033
$Ls_6Fe_4S_{14}$, antiferromag., neutron diffr. study 80−70954
Lu, mag. form factor, field-induced, polarised neutron technique meas. 77−72998
Lu-rare earth, dil. alloy cryst. field determ. 78−10651
Lu-rare field, dil. alloy, cryst. field parameter determ. 78−10650
$LuCo_2$, paramag., field induced mag. density localisation 77−72999
$LuFe_2$, ferromag., magnetisation density, neutron diffr. study 80−60217
Ma-Cu (10 at.%), antiferromag. defect scatt., neutron polarisation anal. 78−2652
Mg, phonon density of states calc. from neutron diffr. data 77−24369
Mg, phonon spectrum and thermodynamic functions, inelastic coherent cold neutron scatt. *(Russian)* 78−55917
Mg-Bi (30 at.%), molten, short range order and partial struct. factor, neutron and X-ray diffr. 78−9941

neutron diffraction examination of materials continued
Mg-Bi melt; X-ray and neutron diffr., conc. depend., correl. number and nearest neighbours 80−49091
Mg-Cd melts, atomic struct., short range order and melting *(German)* 78−14273
$MgAl_2O_4$ spinel, low energy phonon obs. by inelastic neutron scatt. 78−43084
$MgCl_2$ aq. soln., quasi-elastic neutron scatt. 79−37607
$MgCr_2O_4$, magneto-electric splitting of crystal field Γ_2-level of Cr^{3+} ion, neutron spectroscopic obs. 79−19562
$MgCu_{2-x}Ni_x$, X-ray and neutron diffr. investigation of Laves phases of $MgCu_2$-type *(German)* 80−15050
$MgCu_{2-x}Zn_x$, X-ray and neutron diffr. investigation of Laves phases of $MgCu_2$-type *(German)* 80−15050
$Mg_{1-x}Er_x$, dil., cryst. field interactions, neutron scatt. spectra 80−50048
MgF, single crysts., neutron diffr. study, least squares refinement 79−73147
MgF_2, rutile structure, dielectric props., neutron and Raman scatt. exam. 78−79684
$MgGa_xFe_{2-x}0_4$, spinel struct., neutron diffr. exam. 77−12096
Mg_2GeO_4 spinel, struct. refinement, neutron diffr. 77−72590
$MgMn_2O_4$, cation migration, neutron diffr. investig. 77−7896
$Mg(NH_3)_6(ClO_4)_2$, solid, mol. rot., Raman contour, quasielastic neutron scatt., and PMR obs. 79−87444
$MgNi_{2-x}Zn_x$, X-ray and neutron diffr. investigation of Laves phases of $MgCu_2$-type *(German)* 80−15050
MgO, neutron irradiated, Huang diffuse scattering of neutrons 80−10544
MgO, radiation induced O interstitials, EPR meas. 78−55866
MgO:Co^{2+}, weak dynamic Jahn-Teller coupling, neutron inelastic scatt. obs. 80−59934
MgO:Cr^{2+}, critically coupled spin-phonon mode 78−67779
MgO:Cr^{2+}, paramag., spin-phonon coupling, inelastic neutron scatt. obs. 79−60441
$Mg_{0.82}Pt(C_2O_4)_2\times5.3H_2O$, struct., neutron determ. 79−46640
MgV_2O_4, spinel, mag. struct., symmetry anal. in neutron diffr. studies 80−25091
Mn ternary carbides, Mn_3MC, M=metal, mag. props. 77−63116
Mn ternary nitrides, Mn_3MN, M=metal, mag. props. 77−63116
γ-Mn-Au(Pd), magnetic struct. for compositions near onset of antiferromag. ordering 77−63111
γ-Mn-Cu, antiferromag. defect neutron scatt. study 79−47252
γ-Mn-Cu, antiferromagnetism, martensitic transformation 79−1673
γ-Mn-Cu, changes in cell dimensions at martensitic transform. 78−19750
Mn-Cu, mag. and cryst. struct., neutron and X-ray diffr. meas. *(Russian)* 78−22694
γ-Mn-Cu, metastable, structural aspects of decomposition 79−1871
Mn-Cu, mictomagnetic props., neutron diffr. obs. 80−65906
γ-Mn-Cu (10 at.%), spin wave studies using neutron diffraction 80−70991
Mn-Cu alloy, plastic deform. mechanism and shape-memory effect, mag. struct. obs. *(Russian)* 78−60705
Mn-Cu alloys, spinodal decomp. at 380°C, neutron diffr. anal. *(Russian)* 79−20023
Mn-Cu alloys, stressed, diffuse neutron scatt. exam. 78−47950
γ-Mn-Fe, FCC→FCT transform. temp. and Neel temp., X-ray and neutron diffr. expts. *(Russian)* 78−84797
Mn-Ga, mag. and cryst. struct. in conc. region of gamma phase, temp. depend. *(Russian)* 79−65649
γ-Mn-Ni (15 at.%), antiferromag. defect scatt., neutron polarisation anal. 80−50056
γ-Mn-Ni-C, elastic anomalies, martensitic transformation in Mn rich alloys 78−84807
Mn-Ni(Pd), atomic and mag. order, neutron diffr. exam. 79−73697
γ-Mn-Pd, antiferromag. defect neutron scatt. study 79−47252
Mn-Pd (10 at.%), antiferromag. defect scatt., neutron polarisation anal. 78−2652
Mn-Pt alloys, mag. struct., neutron diffr. study 79−91210
β-Mn-Sn, Mossbauer and neutron diffr. exam. 77−66253
Mn-ZnF_2, crit. neutron scatt. 78−52249
$Mn_{1.11}Al_{0.89}$, crit. behaviour, neutron diffr. meas. 78−34982
$Mn_{1.11}Al_{0.89}$, neutron diffr. investig. of mag. struct., degree of order 77−55662
$Mn_3Al_2Ge_3O_{12}$, garnet, mag. ordering, neutron diffr. patterns 78−19220
MnAs, estimation of ionic states through neutron form factor meas. 77−63115
MnAs, high spin state electron config. *(Japanese)* 77−43812
MnAs, struct. and mag. props., temp. depend., neutron study 79−47246
$MnAs_{0.925}P_{0.075}$, estimation of ionic states through neutron form factor meas. 77−63115
$MnAs_{0.925}P_{0.075}$, low spin state electron config. *(Japanese)* 77−43813
$MnAs_{1-x}P_x$, high spin-low spin transition 77−20591
$MnCrF_5$, antiferromag., mag. struct. *(French)* 78−52211
$Mn_3Cr_2Ge_3O_{12}$, magnetically ordered Mn^{2+} and Cr^{3+} ions *(Russian)* 77−8281
$Mn_{2.5}Cr_{0.5}O_4$, mag. struct., neutron diffr. obs. 79−33460
$Mn_xCr_{3-x}O_4$, cubic and tetragonal structs., neutron diffr. obs. 79−19369
$Mn_xCr_{3-x}O_4$, mag. struct. determ. by neutron diffr. 77−40035
$Mn_{1.88}Cr_{0.12}Sb$, antiferromag.-ferrimag. transition, neutron crit. scatt. and crossover effect 80−71023
γ-MnCu, antiferromag., stressed, mag. defects meas. by neutron polarisation anal. 80−50076
γ-MnCu crystals, antiferromag. Czochralski growth 80−97420
γ-MnCu, Mn-rich, inclined spin axis, neutron diffr. study 80−75723
MnCu, neutron scatt. near crit. comp., effects of stress and ageing 79−19722
MnD_x, synthesized at high pressures, neutron diff. anal. of struct. 80−28977
MnF_2, antiferromag. and piezomag. domain struct., neutron topography study 80−71088
MnF_2, antiferromag. domains, obs. using neutron technique 78−64213
MnF_2 lattice parameters, temp. depend., 21°C to MP 77−76583
MnF_2, spin-flop transition obs. by neutron diffr. 79−73734
Mn_4F, non-collinear component in mag. struct. 80−25089
$MnFe_2O_4$, exchange splitting of ionic S-state, neutron spectra 78−52240
$Mn_{1-c}Fe_cPt_3$, noncollinear mag. structs., neutron diffr. anal. *(Russian)* 80−25087
$Mn_3Ga_{1-x}Mn_xN$, perovskite struct., phase transformations *(French)* 80−81048

neutron diffraction examination of materials continued
- $Mn_3GaN_{1-x}C_x$, perovskite struct., phase transformations *(French)* 80 - 81048
- Mn_3In, antiferromag., mag. susceptibility, X-ray and neutron diffr. 79 - 11314
- $Mn_2N_{0.86}$, crystal struct. determ. by neutron and X-ray diffr. *(French)* 77 - 80461
- Mn_4N, mag. struct. non-collinearity, neutron diffr. obs. 80 - 65796
- $Mn(Nb_{0.5}Ta_{0.5})_2O_6$, non-uniaxial spin-flop magnet, crit. exponents, neutron diffr. meas. *(German)* 77 - 16086
- $Mn(Nb_{0.5}Ta_{0.5})_2O_6$, nonuniaxial spin-flop magnet, bicrit. lines, crossover 78 - 14973
- $Mn(Nb_{0.5}Ta_{0.5})_2O_6$, random and spin-flop magnet, neutron crit. scatt. 79 - 24169
- $Mn(Nb_{0.5}Ta_{0.5})_2O_6$, spin flop magnet, four dimens. phase diagram and multicrit. phenomena 79 - 15304
- $Mn_{73}Ni_{27}$, generalised susceptibility, spin wave contrib., inelastic mag. neutron scatt. 79 - 47262
- MnO, antiferromagnetic-paramagnetic phase transiton at high press. 80 - 39778
- MnO, lattice dynamics, coherent inelastic neutron scatt. 78 - 59899
- MnO, lattice vibrs., phonon dispersion curves, neutron scatt. study 79 - 42177
- MnO, neutron diffr. meas., 100 to 700K, spin correls, above and below T_N 77 - 59390
- MnO, order-disorder mag. transition, press. or stress induced, neutron scatt. obs. 80 - 65880
- MnO, paramag., neutron scatt., spin-wave-like excitations, obs. 78 - 68146
- MnOOH, mag. ordering, fine struct. and crit. behaviour, neutron diffr. meas. 80 - 65800
- MnP, ferro-spiral transition, neutron scatt. studies 80 - 65876
- MnS, crit. behaviour, neutron diffr. exam. 78 - 80169
- $MnSO_4$, mag. struct. and phase transitions, neutron diff. study 80 - 60208
- MnSb, electronic state, neutron diffr. study 78 - 87906
- MnSb, interstitial cations, mag. and crystallographic study 79 - 55698
- MnSb-CrSb, NiAs-type system, single crystals, neutron diffr. studies 80 - 60200
- $Mn_{1+\delta}Sb$, ferromag., mag. disturbance around Mn interstitials 80 - 54868
- $Mn_{1+\delta}Sb$, Mn electronic state, neutron diffr. study 80 - 65806
- Mn_2Sb, spin-wave dispersion relations, exchange interactions, neutron inelastic scatt. 80 - 65832
- β-$MnSeO_4$, mag. interactions 79 - 78361
- α-$MnSeO_4$, magnetic interactions, neutron inelastic scatt. study 80 - 107980
- MnSi, itinerant electron system, neutron scatt. 78 - 68194
- MnSi, weak itinerant ferromag., mag. excitations, neutron scatt. obs. 78 - 34969
- MnSi, weak itinerant ferromagnet, mag. excitations 79 - 7985
- MnSi, weak itinerant magnetic compound, paramagnetic response function, polarised neutron scattering 80 - 107982
- Mn_5Si_3, polycrst., mag. struct., 66-100K *(Russian)* 78 - 68161
- $Mn_5(Si_{1-x}Ge_x)_3$, magnetic and cryst. struct., ferromag. props. 77 - 59391
- $Mn_5(Si_xGe_{1-x})_3$ solid solution, mag. ordering, magnetisation and neutron scatt. meas. 78 - 27023
- $MnSiN_2$, 180°C Neel temp., mag. struct. and atomic coords., neutron diffr. meas. *(French)* 77 - 32168
- Mn_3SnN, perovskite type struct., mag. props., neutron and Mossbauer meas. 77 - 32159
- Mn_2SnS_4, cryst. struct. refinement and mag. struct. determ. *(French)* 80 - 107131
- α-$MnSo_4$, mag. interactions 79 - 78361
- Mn_2TeO_6, magnetic structure, stability of mag. modes, neutron diffraction study *(French)* 80 - 39744
- $MnTiO_3$, quasi-two dimens. antiferromag., mag. crit. behaviour 77 - 32191
- MnZn ferrite, nonstoichiometric, neutronographic determ. of cation distrib. *(Bulgarian)* 78 - 83656
- MnZn ferrites, neutron diffr. exam. of influence of technology on mag. and cryst. parameters 79 - 42741
- $Mn_xZn_{1-x}F_2$, crit. neutron scatt. near percolation threshold 78 - 2693
- $Mn_xZn_{1-x}F_2$, three dimens. Heisenberg-Ising antiferromag., fluctuations near percolation threshold 79 - 78390
- $Mn_{1-x}Zn_xFe_2O_4$, prepared by wet method, neutron diffr. and high field Mossbauer expts. 80 - 75719
- Mo powder, struct. facators, time of flight neutron diffr. 78 - 47212
- MoO_2, cryst., neutron diffr., mag. props. 77 - 16038
- Mo_6Se_8, Chevrel phase supercond., phonon spectra, neutron scatt. meas. 79 - 42174
- Mo_6X_8 (X=S, Se), phonon density of states, mode softening correl. with supercond. transition temp. 79 - 51714
- β-N_2, dynamical struct. factor $S(Q,\omega)$, digital simulation 77 - 76502
- N_2, liq., struct. factor, short-wavelength neutron scatt. obs. 80 - 44105
- N_2, liq. struct., thermal neutron diffraction 79 - 46542
- N_2, neutron diffraction patterns at room temp., correls. and struct. factor 78 - 82810
- N_2 overlayer on graphite, orientational ordering, neutron scatt. meas. 80 - 10783
- α-N_2, solid, librational motion, neutron scatt. 77 - 43304
- ND_3, adsorbed on graphon, neutron scatt. study 79 - 60640
- ND_3, cryst. struct. between 2-180K, neutron powder profile refinement 79 - 73134
- $(ND_4)_2BeF_4$, incommensurate-commensurate phase transition and spontaneous polarisation 77 - 40192
- β-ND_4Br, ND_4^+ orientational fluctuations, neutron scatt. obs. 79 - 7557
- ND_4Br, neutron diffr. exam. of P-T phase diagram 77 - 7861
- $(ND_4)_2D_3IO_6$, neutron diffr. study 80 - 88098
- ND_4NO_3, cubic, mol. orientation determ. by multipole anal. 79 - 73136
- NH_3, adsorbed on silica gel, neutron scatt. investig., mol. vibrs., rots. 77 - 51608
- $NH_4Ag_4I_5$, superionic phase transition, dynamical and crit. pt. props. 80 - 107535
- $(NH_4)_2BeF_4$, paraelec. phase, X-ray and neutron diffr. cryst. struct. anal. 80 - 84159
- NH_4Br, NH_4^+ rot. motion, quasielastic neutron scatt. obs. 80 - 96492
- NH_4Br, neutron diffr., exam. of P-T phase diagram 77 - 7861
- N_2H_5Br, mol. ion motion and barriers to rot., PMR and neutron scatt. meas. 79 - 24226

neutron diffraction examination of materials continued
- NH_4Cl, NH_4^+ dynamics in disordered states, neutron scatt. exam. 78 - 26459
- NH_4Cl, NH_4^+ ion rotation, near order-disorder transition, quasielastic neutron scatt. obs. *(German)* 77 - 84679
- NH_4Cl single crystals, quasielastic neutron scattering expts. near order-disorder phase transition 79 - 4410
- N_2H_5Cl, mol. ion motion and barriers to rot., PMR and neutron scatt. meas. 79 - 24226
- $NH_4Cl_{1-x}Br_x$, phonon dispersion 78 - 75760
- NH_4ClO_4, instantaneous jump reorientations, neutron scatt. study 79 - 41990
- NH_4ClO_4, NH_4 ion rot. tunnelling splitting, inelastic neutron scatt. 77 - 15325
- NH_4FeF_4, two-dimens. antiferromagnetism 77 - 66444
- $NH_4H_2AsO_4$, H positions, paraelectric phase 79 - 19210
- $(NH_4)_2H_3IO_6$, neutron diffr. study 80 - 88098
- NH_4I, $(NH_4)_{0.16}K_{0.84}I$ and $(NH_4)_{0.16}K_{0.84}Br$, reorientation motion of NH_4^+ 78 - 79542
- NH_4I, coexisting phases and NH_4^+ dynamics, neutron scatt. exam. 79 - 42158
- NH_4I, reorientation dynamics of NH_4 ions, quasielastic neutron scatt. obs. 77 - 31610
- NH_4I, reorientational motion of ammonium ions in octahedral environments, neutron scatt. exam. 79 - 42159
- $(NH_4)_{0.16}K_{0.84}I(Br)$, reorientation motion of ammonium ions in octahedral environments, neutron scatt. exam. 79 - 42159
- $((NH_4)_{0.16}K_{0.84})_2SO_4$, reorientational relax. times, quasielastic neutron scatt. obs. 78 - 55821
- $((NH_4)_xK_{1-x})_2SO_4$, NH_4^+ dynamics, neutron scatt. study 79 - 42167
- NH_4N_3, cryst. struct. determ. by neutron diffr. 78 - 79574
- NH_4NO_3, phase II, cryst. struct., neutron diffr. study, profile refinement method 79 - 60314
- NH_4NO_3, phase III, cryst. struct., neutron powder diffractometer study 80 - 107134
- $(NH_4)_2PbCl_6$, inelastic neutron scatt. and pot. shape 80 - 1946
- $(NH_4)_2PdCl_6$, inelastic neutron scatt. and pot. shape 80 - 1946
- $(NH_4)_2PtCl_6$, inelastic neutron scatt. and pot. shape 80 - 1946
- $(NH_4)_2ReCl_6$, neutron diffr. study of cryst. struct. 79 - 55701
- NH_4SCN, charge distrib., deform. density, cryst. struct. determ. by X-ray and neutron diffr. 77 - 47415
- $(NH_4)_2SO_4$, NH_4^+ dynamics, neutron scatt. study 79 - 42167
- $(NH_4)_2SO_4$, reorientational relax. times, quasielastic neutron scatt. obs. 78 - 55821
- $(NH_4)_2SnCl_6$, inelastic neutron scatt. and pot. shape 80 - 1946
- $(NH_4)_2SnCl_6$, NH_4^+ ion rot. states, inelastic neutron scatt. obs. 78 - 30552
- $(NH_4)_2TeCl_6$, inelastic neutron scatt. and pot. shape 80 - 1946
- NH_4ZnF_3, rot. motion of NH_4^+ in lattice, neutron scatt. 79 - 37773
- $(NH_4)_2[Pt(CN)_4]Cl_{0.42}.3H_2O$ quasi one dimensional conductor, physical props., cond. freq. depend. 79 - 95393
- $(Na,K)NbO_3$ solid solns., struct. transitions, neutron powder diffr. 78 - 38649
- Na, accurate struct. factor determ. by X-ray and neutron diffr. 79 - 51046
- Na, atomic jump processes, quasi-elast. neutron scatt. study 80 - 84317
- Na, liq., inelastic thermal neutron scatt., interatomic pots. calc. 78 - 42891
- Na, martensitic transform. obs. neutron scatt. meas. 77 - 15581
- Na, self-diffusion, quasielastic neutron scatt. obs. 79 - 90818
- Na-K liquid alloys, struct., X-ray and neutron diffr. meas. 80 - 107041
- $Na_2B_4O_5(OH)_4.8H_2O$, borax, neutron diffr. cryst. struct. determ. 79 - 14740
- $NaBr.2H_2O$, polycryst. hydrates, librational motion of H_2O mols., neutron diffr. exam. 80 - 10604
- $NaBr.2H_2O$, single cryst. struct. anal. by neutron diffr. 79 - 77561
- NaCN, cryst., struct., phase transition, 6-300K, neutron diffr. obs. 77 - 76347
- NaCN, diffuse scatt., hard-core correl., weak-graph method 80 - 49137
- Na_2CO_3, disordered struct., 400°C neutron and X-ray powder diagrams 79 - 46625
- Na_2CO_3, incommensurate structural phase transform., neutron diffr. obs. 79 - 86886
- $Na_2CO_3.1.5D_2O_2$, neutron profile refinement and deuterium positions 79 - 90602
- NaCl, γ-irrad. and doped, lattice relax., cold neutron scatt. obs. 77 - 7715
- NaCl, phonon freqs. in off-symm. directions, neutron inelastic scatt. 79 - 46767
- NaCl solution, ionic hydration for cations 77 - 62460
- $NaClO_3$, acoustic activity, inelastic neutron scatt. obs. *(French)* 80 - 103431
- $NaClO_3$, lattice vibrations and sp. ht., neutron spectroscopic study 80 - 107388
- $NaCrO_2$, two-dimens. mag. order, neutron powder diffr. obs. 80 - 44805
- $Na_{0.6}(D_2O)_2VX_2$, X=S,Se, struct., chem. reactions, and hydration/dehydration process 79 - 46616
- NaF, anharmonicity of lattice vibrations, neutron scatt. study, rel. to melting 77 - 84862
- $NaFeF_4$, two-dimens. antiferromagnetism 77 - 66444
- $NaH_3(SeO_3)_2$, ferroelec., proton motion within H bonds, neutron scatt. study 80 - 75986
- $NaH_3(SeO_3)_2$, paraelec., neutron diffr. refinement of struct. 77 - 72584
- $NaH_3(SeO_3)_2$, proton behaviour in H-bonding, neutron spectroscopy obs. *(German)* 78 - 22816
- NaI:Cl^-, local vibr. exam. by neutron scatt. 77 - 24373
- $NaMnCl_3$, mag. struct. and spin-flip transition, powder neutron diffr. exam. 80 - 60210
- $NaMnCrF_6$, mag. struct., neutron Laue diffr. method 80 - 70951
- $NaMnCrF_6$, magnetic struct., neutron Laue diffr. study *(French)* 79 - 99682
- Na_2MnFeF_7, trigonal weberite variant, X-ray and neutron diffr. *(German)* 78 - 51508
- $NaND_4C_4H_2D_2O_6.4D_2O$, ferroelec. phase, incommensurate satellite refls. 78 - 84531
- $NaNH_4SeO_4.2H_2O$, neutron-diffr. investigation 79 - 46638
- $NaNO_2$, antiferroelec. phase, struct. anal. by neutron diffraction 80 - 24410
- $NaNO_2$, ferroelec., electron distrib., X-ray and neutron diffraction study 80 - 24411

neutron diffraction examination of materials continued
$NaNO_2$, rot. behaviour of NO_2 radicals in order-disorder transition, Fourier synthesis study of neutron data 79−56739
$NaNO_3$, lattice vibration neutron diffusion study *(French)* 80−103429
$NaNbO_3$, cubic to tetragonal transition, inelastic neutron scatt. study *(French)* 79−60469
Na_2O-GeO_2 glasses, neutronographic study of Ge^{4+} struct. state 80−19711
NaOD solution in D_2O, collective excitations in liquid and amorphous state, 77 to 300K 80−92636
NaOH, cubic, reorientational motion of OH^- ion, neutron scatt. 79−51017
$Na_2O.2SiO_2$, short range struct. by pulsed neutron scatt. 80−59396
Na_3PO_4, high temp. fast ion cond. phases, neutron diffr. obs. of struct. 80−107512
$Na_2Pt(CN)_4Br_2.2H_2O$, cryst. struct. determ. 77−24296
Na_2S, phonon dispersion curves, inelastic neutron scatt. obs. *(German)* 78−14414
NaSCN, cryst. struct. and electron density determ., X-ray and neutron diffr. meas. 77−47414
$Na_2SO_4.10H_2O$, Glauber's salt, neutron diffr. cryst. struct. determ. 79−14740
$Na_2S_2O_3.5H_2O$, cryst. struct. determ. by neutron diffr. 78−63714
$Na_3SbS_4.9D_2O$, Schlippe's salt, H bonds and cryst. struct. refinement, by neutron diffr. 79−19191
$NaTaO_3$, high temp. structs. neutron powder diffr., comparison with $SrZrO_3$ and $NaNbO_3$ 80−88094
Na_xVSe_2, mag. and elec. props. rel. to struct. transitions 78−91848
Na_xVSe_2, synthesis and struct. determ. 78−26537
$Na_2[Pt(CN_4)].3H_2O$, cryst. struct. 77−58990
$Na_8[Si_6Al_6O_{24}](OH)_2.1{:}7H_2O$, hydrosodalite, cryst. struct. by neutron diffr. 78−95039
Nb complex, $NH_4[NbO(C_2O_4)_2(H_2O)].3H_2O$, cryst. struct. 77−24306
Nb, Debye-Waller factor and H_2 diffusion, neutron spectroscopy study 79−37881
Nb, diffusion constant of H, anomalous temp. depend., quasielastic neutron scatt. 77−43381
Nb, electron-phonon contrib. to phonon linewidth determ. 78−10146
Nb, fluxoid lattice, eqn. props., small-angle neutron diffraction measurements 80−34573
Nb, fluxoid-line lattice in intermediate mixed state, small-angle neutron scatt. 77−63042
Nb, paramag., mag. form factors, neutron diffr. study 79−47234
Nb, pure and N doped, neutron diffuse-scatt. intensities 80−59597
Nb pure single crystal, low-κ type II superconductors, determ. of low field critical parameters 79−11278
Nb pure single crystals, anisotropy in flux-line lattice symmetry of low-κ type II superconductor, neutron diffr. study 79−11279
Nb, supercond. fluxoid line lattice neutron scatt. study 79−42712
Nb, type II superconductor, equilibrium misalignment, fluxoids and appl. mag. field, anisotropy interaction 79−24112
Nb, with Nb_2N precipitates, flux pinning, magnetization, bulk flux density gradient, and neutron scatt. meas. 79−56472
Nb, X-ray and neutron diffuse scatt. intensities comparison, thermal vibrs. 77−43294
Nb-B, atomic order, stability, supercond. *(French)* 80−50021
Nb-D, density fluctuations, small angle neutron scatt. study 79−60359
Nb-D, Huang diffuse scattering of neutrons 80−10544
Nb-D, stability curve for phase separation of D, neutron small-angle scatt. study 79−15672
Nb-H, BCC, tetrahedral interstitial site H band modes, neutron scatt. obs. 79−55852
α-Nb-H, thermal neutron scatt., general multisublattice jump diffusion model 77−66046
Nb-H(D), H ordering, review 80−60850
Nb-H(D) system, single cryst. prep. and characterisation 79−95910
Nb-N, diffusion of H, incoherent neutron scatt., interstitial effects 79−60558
Nb-Ta, supercond., transport current distrib., neutron small angle scatt. study 79−42711
Nb-Ta (13 wt.%) alloy, flux line bending by transport currents, neutron diffr. 77−8247
Nb-Zr, acoustic phonon anomalies and superstructure, neutron inelastic scatt. meas. 80−19892
Nb-Zr, diffuse neutron scatt. 78−71816
NbC_x, phonon density of states and dispersion relations 79−42173
NbC_x, static distortions and Debye temp. determ., neutron diffr. exam. *(Russian)* 77−80482
$NbD_{0.04}$, neutron scatt. exam., press. depend. of superstruct. reflection 78−22696
β-$NbD_{0.75}$, phonon dispersion curves 78−67792
$NbD_{0.85}$, localised D vibrs., temp. depend., neutron inelastic scatt. study 80−107395
$NbD_{0.85}$, phonon dispersion of α' and β phases, neutron scatt. 78−91398
NbD_x, λ-phase struct., neutron and electron diffr. meas. 79−94962
$NbH_{0.02}$, diffusion of H, neutron scatt. study 79−60550
$NbH_{0.02}$, jump models for H diffusion, quasielastic scatt. of slow neutrons 79−95208
$NbH_{0.11}$, incoherent struct. factor of H, neutron scatt. exam., quasielastic energy spectrum 79−99186
$NbH_{0.15}$, dispersion step in $[\zeta\zeta 0]T_1A$ branch at $\zeta=0.03$, neutron scatt. study 79−60453
$NbH_{0.73}$, multiple wavelength neutron powder diffr. data, Rietveld profile refinement algorithm 80−24320
$NbH_{0.82}$, localised H vibrs., temp. depend., neutron inelastic scatt. study 80−107395
$NbH_{0.82}$, phonon dispersion of α' and β phases, neutron scatt. 78−91398
NbH_x, diffusion of H atoms, quasielastic neutron scatt. obs., book contrib. 79−82383
NbH_x, HF phonons, neutron spectral obs. 80−49317
$NbH_x(D_x)$, acoustic and optic phonons, neutron diffr. obs., book contrib. 79−82296
$NbH_x(D_x)$, H conc. detect. by neutron interferometry, precipitation effects 78−67735
$NbH_{0.004}N_{0.007}$, H-diffusion, interstitial trapping, quasielastic neutron scatt. study 79−42298
δ-NbN, phonon dispersion curves, anomalies 79−99284
NbN single crystal preparation, zone melting and nitriding techniques 80−60776
NbN_x, phonon density of states and dispersion relations 79−42173
NbO, single cryst. with 25% vacancies, neutron damage 77−15459

neutron diffraction examination of materials continued
NbO_2, structural fluctuations at high temps., inelastic neutron scatt. 78−55947
NbO_2, structural phase transform., neutron scatt. obs. 78−14458
NbO_x, interstitial O, diffuse neutron scatt. 78−83809
$NbS_2.(pyridine)_{1/2}$, intercalation complex, vibr. spectra 77−59076
$NbSe_2$ (2H), charge density wave transitions, neutron diffr. exam. 77−89515
$Nb_{1-x}Sn_x$, sp. ht., supercond. T_c and martensitic transform. *(French)* 78−43508
Nb_3Sn, effect of coupling between thermal and elastic variables 77−1203
Nb_3Sn, phonon softening in $[\zeta\zeta\zeta]$ transverse modes, neutron scatt. obs. 79−33062
Nb_3Sn, supercond. props. and struct., neutron irrad. dose depend. 77−15985
Nb_3Sn(Al), phonon density of states, temp. depend. 79−42183
Nd, mag. struct., 18.6K mag. phase transition 80−65799
Nd, magnetic form factors, polarised neutron diffr. meas. 80−50057
Nd, magnetic structure and crit. behaviour 78−47951
Nd, magnetic-structure, neutron and X-ray diffr. study 80−60197
Nd, triple-q magnetic structure, neutron polarisation and diffr. investig. 79−73686
Nd, triple-q magnetic structure, neutron and X-ray diffr. investig. 79−73687
Nd, two-dimensionally modulated mag. struct. 79−78317
Nd-H, inelastic neutron scatt. exam. of lattice dynamics 80−29128
Nd-H, possibility of H ordering, DTA meas. 79−52174
$NdAl_2$, ferromag., cryst. field excitations, neutron inelastic scatt. meas. 77−63154
$NdAl_2$, mag. excitation spectrum, neutron inelastic scatt. 78−10673
$NdAl_2$, mag. form factor, diffuse moment density, polarised neutron meas. 77−63108
$NdAl_3$, cryst. field effects, inelastic neutron scatt. meas. 77−51710
$(NdCu_3)(Ti_3Fe)O_{12}$, synthesis, cryst. struct. and Mossbauer exam. 78−84505
$NdFe_2$, amorphous, magnetization and neutron scatt. meas. 79−78314
$NdFeO_3$, magnetic struct., time of flight neutron diffr. method 77−8280
$Nd_{0.25}La_{0.75}Mg$, cryst. field, neutron diffr. meas. 78−34810
$Nd_{0.2}La_{0.8}Zn$, cryst. field, neutron diffr. meas. 78−34810
Nd_2O_3, neutron diffraction study of high temp. struct. *(French)* 79−65050
$Nd_2O_2S_2$, cryst. struct. determ. 79−51087
NdP-UP solid soln., cryst. field parameters 80−10927
Nd_3S_4 chem. and mag. structures, neutron diffr. obs., ferromag. long-range order *(German)* 78−10654
NdSb, mag. excitation spectrum, neutron inelastic scatt. 77−63152
NdSi mag. struct. and mag. moments, neutron diffr. meas. 77−85424
Ne, Brillouin scatt. of neutrons, limits of classical hydrodynamics for collective motion *(German)* 77−24258
Ne, liq., neutron scatt. determ. of dynamic struct. factor, generalised hydrodynamic anal. 80−54103
Ne, phonon dispersion relation, Gruneisen parameters at high press. 79−42179
Ne, solid, phonon-dispersion, mode Gruneisen parameters and elastic consts. 77−11651
Ne, solid, two-phonon scatt. in inelastic neutron scatt. calc. 78−59910
Ni (100), Bloch wall meas. by enutron small-angle meas. 80−15753
Ni alloys, mag. moment distrib., analysis of diffuse neutron scatt. data 77−32178
Ni, band theoretic interpretation of neutron scatt. expts., spin wave modes 80−44791
Ni catalyst, H_2+CO, adsorption, co-adsorption, reaction, neutron inelastic spectroscopy method 79−99408
Ni catalysts, chemisorption of $H_2(H_2O)$, dynamics, neutron spectrosc. obs. 80−59778
Ni, cold neutron small angle elastic scatt., microstruct. exam. 77−84736
Ni, crossover phenomena, stress induced above Curie point, neutron scatt. study 79−61113
Ni, crystal hyperfine fields and neutron scatt. 79−56172
Ni electrodeposit, mag. domain struct., neutron depolarisation 78−2716
Ni, electrodeposited sheet, mag. domain struct. obs. by neutron depolarisation 77−69605
Ni, ferromag., domain struct., small-angle neutron scatt. 77−66382
Ni, ferromag., dynamic susceptibility calc., neutron scatt. intensity calc. 80−80488
Ni, ferromag., exchange integral maximisation, neutron scatt. obs. and ten-fold degenerate Hubbard model comparison 80−71004
Ni, ferromagnetic domain struct., static neutron depolarisation meas. 79−82812
Ni, forbidden magnon scatt., polarized neutron meas. 79−78350
Ni, itinerant ferromag., Fermi surface and single particle excitations 80−34350
Ni, liq., neutron scatt. and atomic dynamics 77−55233
Ni, liquid, neutron scatt. and atomic dynamics 78−22637
Ni, liquid, sapphire container for experiments up to 1900K 79−63215
Ni, liquid, structure factor at 1873K 79−77490
Ni, mag. densities, spin and orbital contrib., neutron diffr. meas. 79−78316
Ni, mag. layer, domain struct., neutron depolarisation study 79−47299
Ni, magnetic neutron scattering by dislocations, temp. depend. 80−103820
Ni, magnetic susceptibility, generalised, neutron scatt. meas. 80−34606
Ni, magnetisation spin wave and Stoner contribs. 77−73017
Ni, multiple wavelength neutron powder diffr. data, Rietveld profile refinement algorithm 80−24320
Ni, neutron depolarisation near Curie point *(German)* 78−14934
Ni, plastically deformed, dislocation struct., mag. small angle scatt. of neutrons *(German)* 78−22730
Ni powder, neutron diffr. study of Debye-Waller factor using reverse Fourier time-of-flight method 80−49050
Ni, Raney, chemisorpt. of H_2, neutron inelastic spectroscopy investig. 77−48686
Ni, rolling texture development, dependent on relative stacking fault energy 79−52237
Ni, surface, chemisorption of H_2O, neutron inelastic spectroscopy 79−69353
Ni, texture nonhomogeneity during rolling 79−91670
Ni, thermal expansion anomaly near Curie temp. 77−85474
Ni, Voigt function fit, of X-rays and neutron powder diffr. profiles 79−86651

neutron diffraction examination of materials continued
Ni^{++}, mag. form factors, spherical and aspherical parts 79−78315
Ni-Co, elementary excitations, exchange stiffness const., inelastic neutron scatt. study 79−47294
Ni-Co, FCC, spin wave stiffness const., neutron scatt. study 79−51769
Ni-Co, rolling texture development, dependent on relative stacking fault energy 79−52237
Ni-Co alloy, stiffness const., interpretation within band model 79−42748
Ni-Co alloys, FCC, spin wave stiffness, inelastic neutron scatt. 77−63156
Ni-Cr, elementary excitations, exchange stiffness const., inelastic neutron scatt. study 79−47294
Ni-Cu, electron-irrad., neutron-scatt. studies 80−75268
Ni-Cu alloy, ferromag. polarised neutron scatt., evidence for mag. environment effect 77−40039
Ni-Fe, elementary excitations, exchange stiffness const., inelastic neutron scatt. study 79−47294
Ni-Fe, FCC, Invar behaviour, spin waves stiffness consts., neutron scatt. study 79−51769
Ni-Fe (67.7 at.%), noncommensurate atomic struct., neutron diffr. exam. *(Russian)* 77−84701
Ni-Fe-Cu, Mu-metal, mag. aftereffects, dynamic neutron depolarisation study 80−50147
Ni-Ge, amorphous, atomic struct., neutron diffr. study 80−59392
Ni-Mn, dil., mag. moment distribs. and environmental effects, neutron scatt. obs. 80−60247
Ni-Mn, mag. moment and asphericity of spin density distrib., polarised neutron scatt. obs. 80−44813
Ni-Mn, spin wave stiffness const., low temp. neutron scatt. meas. 79−51768
Ni-Mn (17-27 at.%), low-angle neutron diffr., anomalous crit. scatt. *(Russian)* 80−60193
Ni-Mn alloy, disordered FCC, stiffness const., single cryst. neutron inelastic scatt. meas. 77−20558
Ni-P amorphous alloys, electrodeposited and melt-quenched atomic and electronic structures 80−88062
Ni-Pd, mag. form. factor, polarised neutron diffr. meas. 80−29525
Ni-Pd alloy, disordered, local environment effects, neutron scatt. expts. 78−68172
Ni-Pt, magnetic moment distrib., diffuse neutron scatt. meas. 80−34593
Ni-Pt alloys, magnetic-moment distrib. neutron study 80−97066
Ni-Rh alloy, disordered, local environment effects, neutron scatt. expts. 78−68172
Ni-Rh alloys, ferromag., local-environment effects, mag. diffuse neutron scatt. cross-section meas. 77−55664
Ni-Rh ferromagnetic alloy, mag. moment spatial distrib. 77−66275
Ni-Ru, environmental effects and mag. moment distrib., magnetisation and neutron scatt. meas. 79−91211
Ni-SiO multilayer film, interface magnetisation 80−7135
Ni-SiO multilayer films, interface magnetisation 80−88858
Ni-Te, liq., struct. and elec. props. 80−49083
Ni-Ti, mag. moment distrib. and environmental effects around Ti impurity 80−7092
Ni-Ti (2wt.%) alloy, polarised neutron diffuse scatt. 77−36057
Ni-V, elementary excitations, exchange stiffness const., inelastic neutron scatt. study 79−47294
NiAl, quenched and annealed, void formation 79−46652
Ni_3Al based alloys, mean square atomic displacements 79−28053
Ni_3Al, itinerant ferromag., Fermi surface and single particle excitations 80−34350
Ni_3Al, unpaired spin density distrib., polarised neutron diffr. 78−10659
$NiBr_2$, commensurate and incommensurate mag. struct., neutron diffr. study 80−97067
$NiBr_2$, low-temperature magnetic phase, incommensurate spin structure 80−93082
$NiCl_2$ aq. soln., quasi-elastic neutron scatt. 79−37607
$NiCl_2$, aq. soln., structural transition, neutron diffr. study 80−64872
$NiCl_2$, mag. struct. at 4.2K, neutron diffr. *(French)* 77−63097
$NiCl_2$ solution, ionic hydration for cation 77−62460
$NiCl_2$-D_2O solution, hard-sphere model 77−62461
$NiCl_2$-heavy water solution, inelastic neutron scattering 78−91203
$NiCo_2O_4$, ferrimagnetic spinel, neutron diffr. study 79−99681
$Ni_{1-x}Co_xO$, LF magnons, inelastic neutron scatt. exam. 77−66288
$Ni_{0.89}Cr_{0.11}$, phonons with disorder caused by force consts., neutron diffr. obs. and CPA calc. 80−96602
NiD_x synthesized at high pressures, neutron diffraction anal. of struct. 80−28977
NiF_2, press. induced strain transition obs., neutron powder diffr. meas. 78−55948
$Ni_{0.75}Fe_{0.25}$, influence of atomic ordering on spin waves, inelastic neutron scatt. 77−69516
Ni_3Fe, short range order determ. after heat treatments 79−96044
Ni_3Fe, short-range order, diffusive elastic neutron scattering 80−24400
$NiFe_{2-t}Al_tO_4$, cryst. and mag. props. 78−14940
NiI_2, antiferromagnetic, neutron diffr. and sp. ht. meas. 77−55663
$Ni_3(Mn, Al)$, ordering process mechanism by neutron diffr. *(Russian)* 77−55961
$Ni_3(Mn,Cu)$, ordering kinetics, neutron diffr. and elec. resist. meas. *(Russian)* 77−47379
Ni_3Mn, partially ordered, spin-wave dispersion relation, inelastic neutron scatt. meas. 80−20394
NiMnGe, crystal and spiral mag. struct., Neel temp., X-ray and neutron diffr. 77−16052
NiMnGe, mag. struct., and mag. phase transitions 77−63187
$NiMnGe_{1-x}Si_x$, mag. props., neutron diffr. and magnetometric meas., 80-600K 80−65793
$Ni_2Mn(Mn_xSn_{1-x})$, Heusler alloy, antiferromagnetic order, X-ray and neutron diff. 78−64189
$Ni(NH_3)_6(ClO_4)_2$, stochastic NH_3-rotation, neutron incoherent scatt. 77−51331
$Ni(NH_3)_6I_2$, phase transition and rot. excitation 80−96642
$Ni(NH_3)_6X_2$, X=Cl,Br,I, rotational tunnelling by inelastic neutron scatt. 78−30553
$Ni_{62}Nb_{38}$, metallic glass, struct., neutron diffr. study 80−54148
NiO, antiferromag. domains, obs. using neutron technique 78−64213
NiO, antiferromag. domains exam. by magnetic neutron Laue diffr. 79−51806
NiO, bulklike powder, sp. ht., 14-280K 79−69260
NiO, lattice dynamics, coherent inelastic neutron scatt. 78−59899
NiO, mag. struct., neutron Laue diffr. method 80−70951
NiO, mag. transition, neutron scatt. exam. 78−56313

neutron diffraction examination of materials continued
NiO, phonon dispersion relations, neutron scatt. meas. 79−42181
NiO, thin plate, antiferromag. domain obs. by neutron diffr. topography 77−32209
$Ni_{1-x}Pt_x$, disordered, phonon dispersion relations using neutron inelastic scatt. 79−69212
$Ni_{1-x}Pt_x$, disordered phonon dispersion relations, neutron inelastic scatt. 78−43085
$Ni_{0.97}Ru_{0.03}$, mag. form factor and moment distrib., obs. using polarised neutrons 78−68171
$Ni_{0.97}Ru_{0.03}$, mag. moment distrib. polarised neutron study 79−42738
NiS, high energy spin waves, neutron scatt. study 79−51765
NiS_2, antiferromag. metallic state, neutron diffr. study 79−38325
NiS_2, mag. struct. at 5K, polarised neutron study 78−80131
NiS_2, neutron diffr. anomaly at Curie temp., antiferromag. refl. 78−76260
NiS_2, pyrite type, mag. struct., antiferromag. refl. of neutron diffr., susceptibility meas. 77−69497
NiS_2, spin struct. and mag. props. 78−39300
NiS_2, weak ferro- and antiferromag., magnetisation and neutron diffr. meas. 80−65794
$Ni_{0.991}S$, sublattice magetisation temp. var. 77−40077
$Ni_{1-x}S$, and $Ni_{1-x}S_{1-y}O_y(Se_y)$, mag. state in metal-semicond. transition region *(Russian)* 77−89926
$Ni_{1-x}S$, metal-semimetal transition, lattice dynamics and thermodynamic props. 80−29324
Ni_2Sc_2W, mag. order 77−63120
$NiTe_2$, acoustic phonon dispersion, inelastic neutron scatt. meas., elastic consts. and sound vels. 79−95098
$Ni_{40}Ti_{60}$, amorphous, chem. short-range-order, X-ray and neutron scatt. obs. 80−96447
$NiWO_4$, mag. struct. refinement, neutron diffr. meas. *(German)* 77−16049
$Ni_{0.25}Zn_{0.75}Fe_2O_4$, structural phase transition, X-ray and neutron diffr. study 80−79735
$Ni_{0.32}Zn_{0.68}Fe_2O_4$, mag. props. and neutron damage 77−47973
NpC_{1-x}, nonstoichiometric, atomic short-range order obs. by diffuse neutron scatt. 77−24315
$NpCo_2Si_2$, mag. struct., neutron diffr. determ. 80−93084
$NpCu_2Si_2$, mag. struct., neutron diffr. determ. 80−93084
$NpFe_{2-x}Co_xSi_2$, mag. and hyperfine props. 79−51887
$NpFe_{2-x}Co_xSi_2$, mag. and hyperfine props. 80−7247
O_2 adsorbed monolayers, antiferromag. struct. obs. by neutron diffr. 77−66257
O_2, liq. struct., thermal neutron diffraction 79−46542
p-oD_2, solid, slow neutron scatt. into external radiation field *(Russian)* 80−59348
P, black allotrope, orthorhombic bonding, up to 26.6 kbar, neutron diffr. obs. 79−99106
$PD_{0.75}Ni_{0.25}$, spin wave excitations, neutron inelastic scatt. meas. 77−47983
Pb (220), mosaic single cryst., neutron integrated reflectivities 79−86656
Pb, effect of supercond. transition on phonon energies and lifetimes 79−28432
Pb, liq., collective excitations, neutron inelastic scatt. obs. 80−75148
Pb, liq., dynamic scatt. functions, 300 and 600°C, neutron scatt. study 79−50983
Pb, liq., dynamic struct. factor, slow neutron scatt. obs. 80−28908
Pb, liq., struct. factors 78−18538
Pb, liquid, neutron diffr. meas. of pair and direct correl. functions 77−55229
Pb melt, struct. factors, tetrahedral concs., neutron diffr. study *(German)* 80−19688
Pb, melting, existence of before and after effects, neutron scatt. 77−84895
Pb, phonon softening, neutron scatt. at high press. 78−80091
Pb, single crysts., total thermal neutron cross sections 80−19672
Pb, transverse acoustic phonons, freq. and damping, supercond. transition temp. effects 79−42687
Pb-Bi (4.1 at.%) solid soln., tetragonal distortion field for substitutional Bi atoms, neutron scatt. 78−51568
$Pb_{1-x}Bi_xF_{2+x}$, solid soln., struct. and ionic cond. correl., neutron diffr. study *(French)* 80−84324
$PbCO_3$, neutron diffr. topographic study of growth defects 78−91282
PbF_2, acoustic phonon modes up to high temps., neutron scatt. meas. 79−33052
PbF_2, anion disorder at high temps. 80−59614
PbF_2, fast ion conductor, phonon freq. distrib., temp. variation 80−84264
PbF_2, inelastic neutron scatt. study of phonon dispersion relation 78−30712
PbF_2, lattice dynamics 78−79697
PbF_2, phonon temp. depend., neutron scatt. study 79−60450
$Pb_5Ge_3O_{11}$, struct. of paraelec. phase, neutron diffr. meas. 77−84720
$PbHPO_4$, neutron diffr. exam. of struct. at room temp. 79−38490
$PbHPO_4$, phase transitions study, role of cryst. struct. determ. 80−75197
PbI_2, 2H polytype, optical mode inversion hear M-critical point, neturon scatt. mass 80−103432
PbI_2, phonon dispersion surfaces, low dimensional features 79−42180
$PbMo_6S_8$, Chevrel phase supercond., phonon spectra, neutron scatt. meas. 79−42174
$Pb_{1.2}Mo_6Se_8$, Chevrel phase supercond., phonon spectra, neutron scatt. meas. 79−42174
$PbMo_6X_8$ (X=S, Se), phonon density of states, mode softening correl. with supercond. transition temp. 79−51714
α-$Pb(N_3)_2$, cryst. struct. determ. 78−10006
$Pb_3(NO_4)_2$, press. induced ferroelastic phase transition, neutron diffr. study 79−73308
Pb_3O_4, cryst. struct., 5-240K, symm. change at 170K *(French)* 78−34618
$Pb_3(PO_4)_2$, ferroelastic transition, soft modes, inelastic neutron scatt. obs. 77−31772
$Pb_3(PO_4)_2$, ferroelastic transformations and struct. as function of temp., neutron diffr. study 79−19188
$Pb_3(PO_4)_2$, ferroelastic phase transition, inelastic neutron scatt. *(French)* 80−24584
$Pb_3(P_{0.95}V_{0.05}O_4)_2$, ferroelastic transition, soft mode, inelastic neutron scatt. study 80−70357
PbSe, lattice dynamics, slow neutron inelast. scatt. 77−31740
Pb_xSe_{2-x} melts, viscosity and radial distrib. function for stoichiometric and peritectic comp. 80−1916

neutron diffraction examination of materials continued
$Pb_{1-x}Sn_xSe$, band inversion effect on phonon spectra 78−79699
$Pb_{1-x}Sn_xSe$, gapless state and phonon spectrum *(Russian)* 78−30715
$Pb_{1-x}Sn_xTe$, lattice instability and phonon lifetimes, neutron scatt. 78−55932
$Pb_{.87}Sn_{.13}Te$, phonon dispersion, mode softening 79−42175
$PbTiO_3$, neutron powder profile refinement, temp. depend. 78−51476
$Pb(Zr,Ti,Ge)O_3$, antiferro-ferroelectric transition 78−95565
$PbZrO_3$, ferroelec. solid solns., atom shifts, polarisation and Curie temps. 80−100636
$PbZrS_3$, cryst. struct. refinement using neutron diffr. powder data 79−4294
$PbZr_{0.9}Ti_{0.1}O_3$, neutron powder profile refinement, temp. depend. 78−51475
Pd, paramag., mag. form factors, neutron diffr. study 79−47234
Pd, phonon linewidths, inelastic neutron scatt. meas. 79−95100
Pd-Fe alloys, dil., anisotropy of neutron polarisation near ferromag. phase transition 77−32234
Pd-Fe(Mn), dil., depend. of neutron small-angle scatt. intensities on appl. mag. field and temp. 79−11291
Pd-Gd (1 at.%), lattice distortion around impurities determ. by polarised neutron method 79−1372
Pd-H(D) alloy, low temp. ordering 79−14654
Pd-Mn, dilute, paramag. diffuse neutron scatt. 77−63094
Pd-Mn (10 at.%), spin glass, inelastic neutron scatt. exam. 79−61170
Pd-Mn alloy, spin glass, neutron scatt. 78−68265
Pd-Mn dilute alloys, mag. moment distrib., polarised neutron diffuse scatt. meas. 77−80914
Pd-Mn(Fe), mag. ordering phenomena, neutron scatt. obs. 80−44812
Pd-Pt, resonant modes, rel. to CPA predictions 78−75757
Pd-Si, amorphous, compositional study on short-range struct. 80−84095
Pd-Si, amorphous metallic glass, with defined local coordination, struct. model 80−84092
$Pd_{0.96}Ag_{0.04}$, phonon dispersion curves at 296K 80−24546
$Pd_{70}Ag_{30}$, force-const. disorder system, obs. of reson.-like phonon mode 79−90745
γ-PdD, struct. determ. by neutron diffr. 79−7593
$PdD_{0.63}$, inelastic neutron scatt. line shapes, Pd-D, D-D force consts. 78−47481
$PdD_{0.63}$, phonon lineshapes Debye-Waller factors, 80K, inelastic neutron scatt. study 79−42187
$PdD_{0.64}$, neutron scatt. exam. of 50K transition 78−55942
$PdD_{0.73}$, (1, 1/2, 0)-superlattice reflection splitting near 50K, neutron diffr. studies 80−70168
PdD_{1-x}, deuteron density modulation of D atoms 79−99101
β-PdD_x, (1, 1/2, 0) superlattice reflection, neutron diffr. exam. 79−65038
β-PdDx (x=0.710, 0.742, 0.754, 0.780), structural changes in temp. region of 50K anomaly 80−100131
$Pd_{0.5}Fe_{0.5}$, disordered, spin wave dispersion relation, neutron inelastic scatt. 79−61090
$Pd_{0.98}Fe_{0.01}$ $Gd_{0.01}$, Pd-Gd exchange const., neutron diffuse scatt. meas. 80−71002
Pd_3Fe, itinerant ferromagnet, neutron inelastic scatt. 79−7970
Pd_3Fe, spin wave dispersion relation at 4.2K, neutron inelastic scatt. meas. 77−63157
Pd_3Fe, spin wave dispersion, neutron inelastic scatt. meas. 78−14943
$Pd_{0.98}Fe_{0.01}Gd_{0.01}$, ferromag., Pd-Gd exchange const. and Pd polarisation, neutron scatt. meas. 80−25122
$PdH_{0.73}$, 50K transition, γ-ray and neutron diffr. study 79−14932
β-PdH_x diffusion of H, high resolution neutron scatt. meas. 79−60551
PdH_x, diffusion of H atoms, quasielastic neutron scatt. obs., book contrib. 79−82383
α-PdH_x, H-motions, conc., temp., momentum transfer, annealing depend., neutron scatt., study 79−42197
α-PdH_x, impurity motion, neutron scatt. obs. 80−24682
PdH_x, inelastic neutron scattering meas. of optical vibr. freq. distribs. 80−59605
PdH_x, local, soft modes, superconductivity thermal neutron inelastic scatt. *(Chinese)* 80−70331
α-PdH_x, local mode intensity var. with conc., temp., direction and annealing 77−11653
α-PdH_x, next-neighbour jumps of H in quasi-elastic neutron scattering 78−91487
PdH_x, optical phonon spectra, inelastic neutron scatt. study 79−42186
PdH_x, PdD_x, ordering, resistivity, annealing and neutron diffr. obs. 79−34030
$PdH_x(D_x)$, acoustic and optic phonons, neutron diffr. obs., book contrib. 79−82296
Pd_3Mn, disordered, mag. correls., neutron scatt. study 80−50105
$Pd_2MnIn_{1-y}Sb_y$, Heusler alloy, mag. order obs. 80−29528
$Pd_2MnIn_{1-x}Sn_x$ and $Pd_2MnIn_{1-y}Sb$, Heusler alloys, mag. order, disorder effects 80−88723
$Pd_2MnIn_{1-x}Sn_{1-x}$, mag. order exam. 77−40036
$Pd_{2-x}MnSb$, struct., appl. as improved neutron polariser 80−60199
$Pd_2MnSn_{1-x}Sb_x$, mag. order exam. 77−40036
$Pd_3P_{0.8}$, pure and deuterated, cryst. struct., neutron diffr. study 80−84152
$Pd_{0.9}Rh_{0.1}$, lattice dynamics, inelastic neutron scatt. meas. at 296K 80−29135
$Pd_{0.95}Rh_{0.05}$, exchange-enhanced, phonon dispersion relations exam. 77−84868
a-$Pd_{0.8}Si_{0.2}$ alloy, struct. factor determ. rel. to short-range correlations 77−1060
$Pd_{0.8}Si_{0.2}$, amorphous ribbon, struct. factor anisotropy, pulsed neutron diffr. study 78−87619
$Pd_{80}Si_{20}$, amorphous alloy, partial struct. functions, X-ray, electron and neutron diff. studies *(Japanese)* 80−88050
$Pd_{80}Si_{20}$ metallic glass, vibrational spectrum, inelastic neutron scatt. meas. 79−60465
o-pH_2, solid, slow neutron scatt. into external radiation field *(Russian)* 80−59348
polystyrene in CS_2, dil. solns., neutron quasielast. scatt. study 79−41935
Pr, central peaks and soft modes, quasi-elastic mag. scatt. obs. 77−66377
Pr, liq. struct., neutron diffr. meas. 77−51305
Pr, magnetic excitations, exchange, crystal field and magnetoelastic interactions 80−2563
Pr, magnetic form factors, polarised neutron diffr. meas. 80−50057
Pr, magnetic ordering due uniaxial stress, mag. excitons by neutron scatt. 78−84467

neutron diffraction examination of materials continued
Pr-H, inelastic neutron scatt. exam. of lattice dynamics 80−29128
PrAl, annealed, mag. props. and mag. struct. 78−6517
$PrAl_2$, cryst. field interpretations of inelastic neutron scatt. meas. and mag. props. 79−56174
$PrAl_2$, cryst. field splitting of Pr^{3+}, inelastic neutron scatt. exam. 77−20275
$PrAl_2$, crystal field splitting, inelastic neutron scatt. study 79−47067
$PrAl_3$, crystal field splitting of Pr^{3+}, inelastic thermal neutron scattering 78−67996
$PrAl_3$, crystal-field effects, inelastic neutron scatt. meas. 77−8268
Pr_3Al, crystal field splitting, inelastic neutron scatt. study 79−47067
Pr_2C_3, cryst. struct., mag. struct. and props., 1.6 to 300K 79−11296
$Pr_{0.9}Ca_{0.1}MnO_3$, mag. struct. neutron diffr. and magnetisation study 79−61061
$Pr_{1-x}Ca_xMnO_3$, struct. and magnetisation study 80−65804
$PrCo_2Ge_2$, cryst. and mag. struct., neutron diffr. study 79−69059
$PrCo_2Ge_2$, crystal and magnetic structure obs. 80−64976
$PrCu_2$, cryst. field transitions near cooperative Jahn-Teller transition 78−84178
$PrCu_2$, mag. excitations and cooperative Jahn-Teller transition 79−65196
PrD_2, neutron scatt. and cryst. fields 78−79970
$PrD_{2.5}$, neutron scatt. and cryst. fields 78−79970
PrF_3, crystal field split levels, inelastic neutron scatt. study 79−47065
PrF_3, Pr^{3+} mag. form factor meas. by inelastic neutron scatt. 78−52221
$PrFeO_3$, crystal field splitting, inelastic neutron scatt. study 79−47067
$PrFeO_3$, magnetic struct., time of flight neutron diffr. method 77−8280
$PrGaO_3$, crystal field splitting, inelastic neutron scatt. study 79−47067
$Pr_xLa_{1-x}Al_3$, cryst. elec. field 80−24856
$Pr_{0.25}La_{0.75}Mg$, cryst. field, neutron diffr. meas. 78−34810
$Pr_{0.25}La_{0.75}Zn$, cryst. field, neutron diffr. meas. 78−34810
$PrMg_3$, cryst. field study, inelastic neutron scatt. and sp. ht. meas. 80−59939
$PrNi_5$, crystal field investigation from inelastic slow neutron scatt. expts. 80−39538
$Pr_2O_2S_2$, cryst. struct. determ. 79−51087
PrSb, mag. excitations, press. depend., inelastic neutron scatt. meas. 78−10699
PrSb, magnetic to nonmagnetic transition, press. or stress induced, neutron scatt. obs. 80−65880
PrSb, neutron scatt., press. induced antiferromag. 80−15699
PrSb, pressure-induced antiferromag., neutron scatt. study 80−39750
PrSi, mag. struct. and mag. moments, neutron diffr. meas. 77−85424
$PrSn_3$, inelastic neutron scatt. spectra, cryst. elec. field effects 78−43336
Pr_3Tl, critical fluctuations temp. depend. 80−25160
Pr_3Tl, exchange-coupled singlet-groundstate system, central model 77−77060
Pr_3Tl, singlet-ground state system, central mode, in ferromag. transition, neutron scatt. obs. 77−66317
$PrVO_3$, neutron diffr. exam. of first order mag. transition 78−2685
Pt, chemisorption of H_2, incoherent inelastic neutron scatt. exam. 79−60642
Pt, mag. field induced conduction electron , polarisation, magnetisation density, and neut neutron mag. form factor 78−18945
Pt-Co alloys, crit. neutron scatt. in crit. conc. region for onset of ferromagnetism 78−72347
Pt_3Cr, ferrimag., magnetisation density, polarised neutron diffr. meas. 80−60204
Pt_3Mn, cryst. dynamics at 80K 79−23688
Pt_3Mn, mag. excitation dispersion relation 80−25090
cis-$Pt(NH_3)_2Cl_2$, torsions, metal-metal interactions, inelastic neutron scatt. study 79−46581
$(Pt(NH_3)_4)[PtCl_4]$, torsions, metal-metal interactions, inelastic neutron scatt. study 79−46581
$PuFe_2$, ferromag. mag. cross section, form factors, saturation magnetisation values, polarized neutron study 79−47245
PuP, electronic ground state 77−15789
PuP, ferromag. mag. cross section, form factors, saturation magnetisation values, polarized neutron study 79−47245
Rb, liq., pair interaction pot., thermodynamic, neutron diffr. calcs. 77−11463
Rb, liq., struct. factor determ. by neutron diffr. up to 1400K and 200 bar 77−1064
Rb, liquid model, derivation of vel. autocorrelation function from incoherent scatt. function 79−77491
Rb-K, lattice vibrs. in CPA, comparison to neutron scatt. meas. 79−42165
$RbAg_4I_5$, single particle excitations, inelastic neutron scatt. obs. 80−59599
$RbAg_4I_5$, solid electrolyte, neutron scattering study 78−79696
$RbAg_4I_5$, superionic phase transition, dynamical and crit. pt. props. 80−107535
RbBr, phonon freqs. at 80, 290, 370K, neutron inelastic scatt. study, comparison to Gruneisen parameters 78−51631
$RbCaF_3$, 193K phase transition, crit. neutron scatt. obs. 78−10161
$RbCaF_3$, cubic to tetragonal phase transition, neutron diffr. obs. 79−23730
$RbCaF_3$, cubic to tetragonal phase transform., X-ray, neutron, Mossbauer diffr. study 80−49360
$RbCaF_3$, neutron scatt. central peak rel. to soft mode 78−75794
$RbCaF_3$, struct., phase transitions, neutron diffr. study 80−33918
$RbCaF_3$, structural phase transition, superlattice points, neutron diffr. obs. 80−19944
$RbCoCl_3.2D_2O$, metamagnetic phase transition, crystallographic and mag. struct., neutron diffr. meas. 80−44174
$RbCoF_3$, antiferromag., anisotropic exchange, dispersion relations of mag. excitations 77−69532
Rb_2CoF_4, two dimens. Ising like antiferromag., spin wave excitations 78−72342
$Rb_2Co_cMg_{1-c}F_4$ mag.-nonmag. two-dimens. antiferromag. Ising system, spin fluctuations 80−80545
$Rb_2Co_cMg_{1-c}F_4$, random 2D antiferromag., neutron inelastic scatt. 79−28505
$Rb_2Co_cMg_{1-c}F_4$, random two-dimens. Ising antiferromag., unstable mag. long-range order, neutron scatt. obs. 80−44839
$Rb_2Co_xMg_{1-x}F_4$, antiferromag., static critical phenomena, neutron diffr. obs. 79−56528
$Rb_2Co_xMg_{1-x}F_4$, neutron scatt. exam., obs. of two dimens. mag. long range order 78−56295
$Rb_2Co_xMg_{1-x}F_4$, two-dimens. Ising antiferromag., fluctuations near percolation threshold 79−78390

neutron diffraction examination of materials continued
Rb_2CrCl_4, 2D-ferromag., renormalisation of long wavelength spin waves, neutron scatt. 80−60229
Rb_2CrCl_4, spin wave temp. depend. 79−4662
Rb_2CrCl_4, two-dimens. easy-plane ferromag., cryst. and mag. struct., temp. variation of moment 77−66255
$RbD_3(SeO_3)_2$, incommensurate nature of intermediate phase, neutron diffr. obs. 80−50276
$RbD_3(SeO_3)_2$, phase transform., inelastic neutron scatt. study 78−39514
$RbF.H_2O_2$, X-ray and neutron diffr. struct. determ. 78−67698
$RbFeCl_3$, pseudo-one-dimens. singlet ground state ferromag., mag. excitations, neutron scatt. study 80−97064
Rb_2FeF_5, mag. struct. and one-dimens. antiferromagnetism 80−60209
RbH_3PO_4, phase transitions study, role of cryst. struct. determ. 80−75197
RbH_2PO_4, tetragonal phase disordered struct. 78−42980
$RbH_3(SeO_3)_2$, improper ferroelectric phase transformation, neutron scattering study 78−80302
$RbH_3(SeO_3)_2$, ferroelec., location of H atoms in cryst. struct., neutron diffr. meas. 78−2093
$RbH_3(SeO_3)_2$, low temp. struct., neutron diffr. 78−38669
$RbH_3(SeO_3)_2$, order parameter 77−66460
$RbH_3(SeO_3)_2$, paraelec. phase, H bonding, neutron diffr. 77−47420
RbI, elastic constants determ. by inelastic neutron scatt. 78−79659
RbI, NaCl to CsCl phase transition by elastic diffuse and inelastic neutron scatt. 80−2162
RbI, phase transition, diffuse neutron scatt. in metastable press. region 78−67825
$Rb_{1-c}K_c$, local mode exam. by neutron diffr. 79−37781
Rb_2MnCl_4, 2D Heisenberg antiferromag. spin wave analysis 80−54879
Rb_2MnCl_4, Heisenberg antiferromag., spin wave anal. 79−61237
$Rb_3Mn_2Cl_7$, two dimens. double layer antiferromag., neutron diffr. exam. 77−8277
$RbMnF_3$, Heisenberg antiferromagnet, spin diffusion below T_N 78−34968
$Rb_2Mn_cMg_{1-c}F_4$, dil. antiferromag., mag. correlations, neutron scatt. meas. 77−66356
$Rb_2Mn_cMg_{1-c}F_4$, two-dimens. antiferromag., spin fluctuations, neutron diffr. study 80−44846
$Rb_2Mn_xMg_{1-x}F_4$, random magnetic-nonmagnetic 2-dimens. antiferromag., spin fluctuation dynamics 77−63147
$Rb_2Mn_xMg_{1-x}F_4$, two dimens. Heisenberg-Ising antiferromag., fluctuations near percolation threshold 79−78390
$Rb_2Mn_{0.5}Ni_{0.5}F_4$, site-random two-dimensional antiferromag., crit. behaviour, quasielastic neutron scatt. 77−85468
$RbNO_3$, struct., high temp. phases, neutron diffr. study 80−79756
$RbNiF_3$, neutron scatt., automatic data processing *(Russian)* 80−54079
$Rb_2PbCu(NO_2)_6$, incommensurate Jahn-Teller transition, Huang scatt. 80−70401
Rb_xWO_3, low lying phonon dispersion curves, neutron scatt. study 80−92622
$Rb_9(XeO_3Cl_2)_4Cl$, neutron and X-ray diffr. struct. determ., Xe-Cl bonding 78−30591
Rb_2ZnBr_4, average struct. determ. from neutron diffr. diagrams 79−32955
Rb_2ZnBr_4, incommensurate phase transition, neutron-scatt. obs. 79−4390
Rb_2ZnBr_4, incommensurate phases, neutron scattering study 79−15417
Rb_2ZnBr_4, incommensurate and commensurate phases, neutron scatt. meas. 79−82936
Rb_2ZnBr_4, modulation phase transitions, neutron scatt. 79−95712
Rb_2ZnCl_4, incommensurate phases, neutron scatt. 79−38501
$Rb_2[C_2O_4].D_2O_2$, neutron profile refinement at 5K 80−88103
$Rb_2[Cu(H_2O)_6](SO_4)_2$, Tutton's salts, stereochem., neutron struct. determ. 78−18609
$Rb_2[Pt(CN)_4Br_2]$, neutron diffr., cryst. struct. 77−35522
RuF_5, mag. props. 80−15707
SF_6, plastic phase, neutron diffr. obs. and theory 79−77533
SF_6, plastic phase, orientational disorder 79−73115
$(SN)_x$, acoustic phonons, inelastic neutron scatt. obs. 78−6136
$(SN)_x$, acoustic phonons 78−79698
$(SN)_x$, cryst. struct. by neutron diffr. 78−34488
$(SN)_x$ film and crystal, acoustic and optical phonons, Raman, i.r. and transmission spectra 77−4642
Sb, Debye-Waller factors and thermal expansion 78−43089
$SbCl_3$, liquid, neutron X-ray diffraction pattern and models 80−38893
$SbCl_3$ liquid, X-ray and neutron diffraction study at 80°C 79−4230
α-Sb_2O_4, cryst. struct., neutron diffr. study 77−47391
SbSI, cryst. struct. and thermal vibr. parameters, −185, 16 and 100°C obs. 77−43180
SbSI, ferroelec. transition, inelastic neutron scatt. 77−40189
SbSI, paraelectric-ferroelectric transition, low freq. phonon branches, neutron scatt. obs. 79−61313
Sb_2Se_3, liq. struct. anal., neutron diffr. study 78−79519
Sc, paramag., mag. form factors, neutron diffr. study 79−47234
Sc-rare earth, dil. alloy, cryst. field parameter determ. 78−10650
Sc-rare earth, dil. alloy, cryst. field determ. 78−10651
Se, liq. and amorphous, struct. by pulsed neutron diffr. using an electron LINAC 77−51307
Se, liq. struct. factor determ. rel. to short-range correlations 77−1060
Se, liquid, chain molecule struct. exam. by time-of-flight pulsed neutron diffr. 77−55228
Se, trigonal, vitreous and red amorphous, phonon density of states comparison 80−54329
$Se_{1-x}Te_x$ systems, amorphous and liq. states, short range order, neutron scatt. study 80−49124
Si, amorphous, hydrogenated and deuterated, struct. 80−103245
Si crystal, perfect, meas. ang. deviation of neutrons of order of 10^{-3} sec of arc 79−37593
Si curved crystal, evidence for Fankuchen effect 77−55209
Si curved crystal, neutron diffr., existence of Fankuchen effect 79−60224
Si, curved crystals, comparison with theory, for Laue geometry 78−14248
Si, Gruneisen coeff. from stress-induced phonon energy meas., inelastic neutron scatt. 79−82298
Si melt, struct. factors, at. distrib. curves, thermodynamics, neutron diffr. study *(German)* 80−19687
Si melt, struct. factors, tetrahedral concs., neutron diffr. study *(German)* 80−19688
Si, neutron diffraction by perfect cryst., mag. field effects 79−73071
Si, neutron irrad., small angle neutron scatt. meas. 80−29073

neutron diffraction examination of materials continued
Si, single crysts., total thermal neutron cross sections 80−19672
Si, twinned, neutron diffr. topographic obs. 78−38727
Si, vibrating single crystal, Umweganregung peaks 80−10461
Si, white beam diffr. technique 77−31565
Si:H film, amorphous, plasma-deposited, small angle X-ray and neutron scatt. studies 80−59826
Si:P, As, chem. etching, thick epitaxial layers prod. for dopant conc. investigations by neutron activation anal. 79−37728
Si-Cr, dil., spin density wave under high press., neutron diffr. study 80−65798
Si-Ge solid solution, thermal neutron monochromators 80−49053
$SiCl_4$, liq. struct., oscill. amp., neutron diffr. study 79−46544
$SiCl_4$, liq. struct. by neutron diffr. 79−73089
$SiCl_4$-$TiCl_4$, liq. struct., oscill. amp., neutron diffr. study 79−46544
SiH_4, plastic phase, rotational motion, quasi-elastic neutron scatt. study 79−51022
SiH_4, plastic phases I and II, neutron inelastic scatt. 79−7558
Si_3N_4, amorphous, CVD prep., struct. characts. by pulsed neutron diffr. 80−33891
α-Si_3N_4, lattice and atomic position parameters, neutron diffr. study 79−42040
Si_2N_2O, high-press. neutron diffr. exam. 77−51357
SiO_2, adsorption of water, neutron scatt. exam. 79−60643
SiO_2, amorphous, phonons, neutron, IR and Raman spectra calcs. 78−10150
SiO_2, α-quartz structure, compression mechanism 79−23673
SiO_2 gel, irrad., adsorpt. of NH_3, neutron scatt. 79−33194
SiO_2, glassy, small-angle neutron scatt. obs. 77−7677
SiO_2, hydroxylated amorphous, small-particle dynamics, neutron scatt. 80−79899
$SmAl_2$, exchange and cryst. field effects 80−24857
$SmCo_5$, exchange and cryst. field effects 80−24857
$SmCo_5$, temp. depend. of Sm mag. form factor, polarized neutron expts. 79−78329
$SmMn_3C$ noncolinear mag. struct., mag. transition *(French)* 77−69494
SmN, magnetic props., neutron diffr. and mag. susceptibility meas. 80−50036
SmS, high-pressure mixed-valence phase, diagram and electronic entropy, neutron diffr. obs. 79−33267
SmS, induced magnetic form factor, polarised neutron studies 80−25078
SmS, mixed valence, induced mag. form factor 78−68163
$Sm_{0.75}Y_{0.25}S$, intermediate valence system, mag. excitations 79−60771
$Sm_{0.75}Y_{0.25}S$, intermediate valence compound, phonon investigation by neutron scatt. 80−6476
$Sm_{0.76}Y_{0.24}S$, mixed valence, induced mag. form factor 78−68163
SmZn, ferromag., cond. band antiparallel polarisation exceeding 4f moment 80−60207
SmZn, unusual form factor, polarised neutron scatt. 79−99684
Sn melt, struct. factors, tetrahedral concs., neutron diffr. study *(German)* 80−19688
Sn, molten, struct. investig. by neutron diffr. 79−4233
Sn-Zn, molten, struct. investig. by neutron diffr. 79−4233
$SnCl_4$, liq. struct., oscill. amp., neutron diffr. study 79−46544
$SnCl_4$-$TiCl_4$, liq. struct., oscill. amp., neutron diffr. study 79−46544
$SnCl_2.2D_2O$, order-disorder transition, neutron diffr. study, lattice statistical model 80−24558
SnF_2, second order $\beta \rightleftarrows \gamma$ transition, neutron diffr. and NMR obs. 80−107095
$SnHPO_4$, hydrogen-bonded dimers 77−15357
SnI_4, mol. solid, dynamics, press. and temp. depend. 78−79691
$SnMo_6S_8$, Chevrel phase supercond., phonon spectra, neutron scatt. meas. 79−42174
$SnMo_6S_8$, phonon density of states, mode softening correl. with supercond. transition temp. 79−51714
$SnNbS_2$, intercalate, cryst. struct. determ. 78−26534
$SnSe_2$, layer struct., acoustic phonon dispersion curves, propag. modes 77−51462
$SnTaS_2$ intercalate, cryst. struct. determ. 78−26534
$Sr_xBa_{1-x}Nb_2O_6$, neutron and light scatt. in phase transition region 78−64336
$SrCl_2$, anion disorder at high temps. 80−59614
$SrCl_2$, anion motion at high temps., quasielastic nuetron scatt. obs. 80−59715
$SrCl_2$, high temp. powder neutron diffr., transition to highly conducting phase 78−47586
$SrCl_2$, specific heat anomaly and sublattice disorder, neutron diffr. meas. 79−42238
$SrCl_2$, superionic, quasielastic neutron scatt. 78−79504
$SrCoO_{3-x}$, mag. and neutron diffr. study 80−65805
$SrF_{2-x}H_x$, synthesis and struct. determ. using neutron diffr. *(French)* 80−24425
$SrFeO_{3-x}$, neutron diffr. exam. of mag. struct. 77−20553
$SrGa_2$, layered, dispersion of acoustic phonons, inelastic neutron scatt. 78−47484
$SrLaCoO_4$, struct. and mag. props., electronic struct. of trivalent Co *(French)* 79−86760
$SrLaFeO_4$, mag. and cryst. struct. determ. *(French)* 80−54866
$SrMCrO_4$, M=La, Nd, mag. struct. determ. by neutron diffr. *(French)* 79−28507
$Sr(ND_2)_2$, neutron diffraction exam. 31 to 570K, temp. depend. of lattice parameters *(German)* 79−69085
$SrNd_2Fe_2O_7$, mag. struct., neutron diffr. determ. *(French)* 78−52224
$SrR_2Fe_2O_7$ series, mag. struct. and spin reorientation, neutron diffr. and Mossbauer meas. 77−69503
$SrTiO_3$, anharmonic motion rel. to struct. transition 78−79718
$SrTiO_3$, central peak in spectrum of ferroelec. mode fluctuations and dielec. losses, 4.2K 78−19432
$SrTiO_3$, effect of coupling between thermal and elastic variables 77−1203
$SrTiO_3$, H_2 reduced, neutron scatt. study of structural phase transition, central-peak enhancement 78−30755
$SrTiO_3$, heavily reduced, soft mode behaviour 80−71409
$SrTiO_3$, neutron quasi-elastic scatt. above structured phase transition 79−27877
$SrTiO_3$, neutron spectroscopy of central peak energy width 77−32334
$SrTiO_3$, semiconductor, soft modes, zone boundary mode 80−71357
$SrTiO_3$ under [111] uniaxial stress, neutron scatt. 78−67798
$SrWO_4$, slow neutron inelastic scatt. spectra, Debye temp. calcs. *(Russian)* 80−59347

neutron diffraction examination of materials continued
$SrZrO_3$, high temp. phases, struct. determ., soft mode transitions 78−42942
$SrZrO_3$, struct. determ. 77−15351
TTF-TCNQ, high press. structural transitions, neutron scatt. study 80−96647
TTF-TCNQ, transverse acoustic mode, inelastic neutron scatt. meas. 77−47526
Ta, Debye-Waller factor and H_2 diffusion, neutron spectroscopy study 79−37881
Ta-D, stability curve for phase separation of D, neutron small-angle scatt. study 79−15672
Ta-H, BCC, tetrahedral interstitial site H band modes, neutron scatt. obs. 79−55852
Ta-H(D), H ordering, review 80−60850
Ta-H(D) system, single cryst. prep. and characterisation 79−95910
TaC_x, static distortions and Debye temp. determ., neutron diffr. exam. *(Russian)* 77−80482
Ta_2D, neutron diffr. meas. of disorder-order phase transitions 80−29947
$TaH_{0.13}$, diffusion of H, neutron scatt. study 79−60550
TaH_x, diffusion of H atoms, quasielastic neutron scatt. obs., book contrib. 79−82383
$TaH_x(D_x)$, acoustic and optic phonons, neutron diffr. obs., book contrib. 79−82296
ε-TaN, cryst. struct. determ. by neutron diffr. exam. 78−26522
β-Ta_2N, growth by annealing Ta in N_2, cryst. struct. 77−35533
β-Ta_2N-εTaN, prep. by exothermic reaction and by zone melting, cryst. struct. 77−35533
TaS_2, $1T_2$ phase, Kohn anomaly, neutron scatt. meas. 77−69056
TaS_2 (2H), intercalation with deuteropyridine, neutron diffr. meas. 79−90612
TaS_2, kinetic study of NH_3/ND_3 exchange by neutron diffr. 79−29350
TaS_2:NH_3, mol. motion, neutron quasielastic scatt. obs. 79−90827
TaS_2-2H electrodes, topotactic reduction nechanism, neutron diffr. obs. and intercalation cpd. form. 80−108748
$TaS_2(NH_3)$ and $TaS_2(NH_3)_{1/3}(H_2O)_{2/3}$, incoherent inelastic neutron spectra 80−84163
TaS_2·(pyridine)$_{1/2}$, intercalation complex, vib. spectra 77−59076
$TaSe_2$ (2H), charge density wave transitions, neutron diffr. exam. 77−89515
Ta_2WO_8, neutron powder diffr. study of cryst. struct., profile anal. 79−55706
$Ta_{1-x}Zr_xSe_2$ (1T), CDW stacking order, interlayer interactions and impurity effects 77−7699
Tb, magnon lifetimes at 4.2K 80−15710
Tb, neutron elastic scattering, high-angle, anal. 80−80480
Tb-Er alloy, magnetisation process of helical spin struct., neutron diffr. and magnetisation meas. 77−43850
Tb-Pr(Nd) alloys, mag. struct. and ordered moments, neutrons diffr. data 77−66252
Tb-Tm alloys, mag. struct., neutron diffr. 77−8273
Tb-Y, spin wave dispersion, spiral mag. struct., neutron scatt. study 79−47268
TbAlGa, mag. props. and struct. 78−39302
$TbAl_xGa_{2-x}$, mag. props. and phase transitions 80−25133
$TbAsO_4$, cryst. struct. refinement at 77K and 5K by profile anal. from neutron diffr. powder data 79−37677
$TbAsO_4$, mag. ordered, neutron diffr. study 79−47238
TbB_2, mag. props. and neutron diffr. 78−84401
TbB_2, mag. struct., ferromag. ordering, neutron diffr. study 80−15692
TbB_4, ferromag. ordering, neutron scatt. meas. 78−10655
$TbBe_{13}$, mag. struct., neutron diffr. meas., 4.2K 78−47953
$TbBe_{13}$, magnetic structure at low temps., antiferromagnetic, neutron diffraction study *(French)* 80−39743
$TbCo_2$, polarised neutron diffr. exam. of mag. struct. 79−73681
$TbCo_5$, mag. state of Tb sublattice neutron diffr. meas. *(Russian)* 77−80915
$TbCo_{5.1}$, singularities of mag. transition *(Russian)* 77−77053
$TbCo_{5.1}$, sublattice magnetisation, temp. depend., neutron diffr. anal. *(Russian)* 80−103815
$TbCu_2$, collinear mag. struct., neutron diffr. meas. 79−87242
TbD_2, mag. struct., neutron diffr. study 77−85421
TbD_2, sublattice magnetisation, cryst. elec. field effects 78−39295
TbD_x, non-stoichiometric, complex antiferromag. struct., neutron diffr. study 80−50061
TbF_3, crystal structure by powder neutron diffr. study 80−15077
$TbFe_3$, ferrimag., mag. struct., powder neutron diffr. determ. 79−78328
$TbFe_4Al_8$, commensurate-incommensurate modulated mag. struct., neutron diffr. obs. 79−95576
$TbFe_4Al_8$, neutron diffr. exam., mag. struct. 78−10656
TbGa garnet, mag. ordering induced by hyperfine interactions, neutron diffr. meas. 77−66265
$TbGa_2$, mag. props. and struct., neutron diffr. patterns at 4.2, 300K 77−63109
$Tb_3Ga_5O_{12}$, hyperfine interac. induced antiferromag. order *(French)* 77−59392
Tb_5Ge_4, mag. struct. and mag. transitions, neutron diffr. expts. 78−43564
$Tb_{0.5}Ho_{0.5}$, ferromag. and helical phase, spin wave dispersion relations 79−24149
TbIG, neutron depolarisation near mag. compensation point 77−24709
$(Tb_cLa_{1-c})Be_{13}$, mag. struct., cryst. field effects, neutron diffr. study 80−65789
TbMg, mag. struct. and mag. props. 77−8275
$TbMg_3$, antiferromagnetic struct. 78−14930
$TbMg_3$, mag. props., Mg conc. depend. 78−84392
$TbMg_3$, mag. props. 78−72346
$TbMnO_3$, mag. struct., ordering of Mn^{3+}, Tb^{3+} moments, neutron diffr. expt. 77−69500
$TbMo_6S_8$, long range mag. order in supercond. state 79−65653
$TbMo_6S_8$, superconductor, neutron scatt. exam. of mag. phase 79−73680
$Tb_{1.2}Mo_6S_8$, long-range mag. order and supercond., neutron diffr. obs. 79−78320
$Tb_{1.2}Mo_6Se_8$, crystal field excitations, inelastic neutron scatt. obs. 79−78321
Tb_2Ni_{17}, magnetic structure by neutron diffr. 77−73000
$Tb(OH)_3$, neutron diffr. struct. exam. 78−2077
Tb_2O_2S, tunnelling effect and mag.-cryst. transition, neutron diffr. expts. 77−63180
TbP, mag. excitations above antiferromag. ordering temp., inelastic neutron scatt. obs. 80−50112
neutron diffraction examination of materials continued
TbP, magnetic Γ_1-Γ_4 exciton, inelastic neutron scatt. study 80−11159
TbP, singlet-groundstate magnetism, static mag. props. 80−7109
Tb_xS, mag. ordering, neutron diffr. meas. 78−2649
Tb_xTe, mag. ordering, neutron diffr. meas. 78−2649
$Tb_{0.26}Y_{2.74}Fe_5O_{12}$, anomalous props., 200-250K 79−28527
$Tb_xY_{3-x}Fe_5O_{12}$, spin-reorientation phase transitions, neutron depolarisation factor 78−27037
Tc, paramagnetic form factor, polarised neutron diffr. study 80−39745
TeO_2-Fe_2O_3 glass, atomic arrangement 78−83743
TeO_2-Li_2O glassy system, struct. recomb. model 80−19707
TeO_2-P_2O_5 system, glass struct., neutron diffr. study 80−70128
$ThC_{0.063}$, cryst. struct. and lattice dynamics 80−88088
$ThCo_5$ itinerant electron metamagnetism, polarised neutron study 80−39742
$(ThCu_3)(Mn_2Fe_2)O_{12}$, synthesis, cryst. struct. and Mossbauer exam. 78−84505
$ThCu_3Mn_4O_{12}$, mag. structure, neutron diffr. powder data, 430K ferrimag. T_c 77−69502
$ThCu_3Mn_4O_{12}$, mag. struct. of new perovskite-type ferrimag. 78−52222
ThC_{1-x}, nonstoichiometric, atomic short-range order obs. by diffuse neutron scatt. 77−24315
Th_4D_{15}, cryst. struct. meas. by neutron diffr. with spallation neutron source 77−43190
$ThFe_5$, mag. props., ferrimag. moment arrangement 79−33475
Th_4H_{15}, H vibr. modes, neutron scatt. study, phonon density of states 79−42195
$ThSn_3$, inelastic neutron scatt. 80−11165
$\{Th[(CH_3)_5C_5]_2H(\mu\text{-}H)\}_2\text{-}C_6H_4CH_3$, molecular structure by neutron diffraction 79−89801
Ti alloys, domain struct. of diffuse ω-phase formed in quenching, 1D model 78−27523
Ti, paramag., mag. form factors, neutron diffr. study 79−47234
α-Ti, solubility of H, neutron diffr. study 80−15254
Ti, Ti recrystallisation texture from neutron diffr., cf X-ray diffr. *(French)* 77−84593
Ti-Fe-H system, H diffusion, neutron scatt. obs. *(German)* 79−56963
$TiBe_2$, neturon diffr. study of mag. ordering 80−44811
$TiBe_{1.8}Cu_{0.2}$, ferromag., magnetisation density 80−103817
TiC, lattice dynamics, inelastic neutron scatt. 78−55918
TiC_x, comp. determ. by neutron diffr. 77−40411
TiC_x, phonon density of states and dispersion relations 79−42173
TiC_x, static distortions and Debye temp. determ., neutron diffr. exam. *(Russian)* 77−80482
TiC_xN_y, neutron diffr. investig. 77−51355
$TiCl_4$, liq. struct., oscill. amp., neutron diffr. study 79−46544
$TiCl_4$, liq. struct. by neutron diffr. 79−73089
$TiCl_4$-$SiCl_4$($SnCl_4$), liq., beat effects, neutron diffr. studies 80−38897
$TiCuD_{0.90}$, neutron powder diffr. study for cryst. struct. refinement 78−95018
TiD_x, α- and β-phases, D-site occupancy, neutron diffr. study 79−42014
TiFeD, cryst. struct., Mossbauer and neutron diffr. obs. 80−34839
$TiH_{1.92}$, thermal neutron inelastic scatt. phonon spectra determ. *(Chinese)* 79−10906
TiN, phonon dispersion curves, soft-mode behaviour, inelastic neutron diffr. 78−43083
TiN_x, phonon density of states and dispersion relations 79−42173
$TiN_{0.32}H_{0.19}$, cryst. struct., neutron diffr. anal. *(Russian)* 80−64965
Ti_2Ni, determ. of H diffusion coeff., quasielastic neutron scatt. 78−30781
$Ti_{50}Ni_{47}Fe_3$, premartensitic phases, neutron scatt., sp. ht. and electron microscopy obs. 79−96025
$TiO_{0.42}$, diffuse X-ray and neutron scatt. due to out-of-step configurations of O atoms 77−62518
$TiSe_2$ (1T), lattice dynamics and phase transitions 78−79727
$TiSe_2$ (1T), phonons and CDWs, inelastic neutron scatt. meas. 79−28059
$TiSe_2$, phonon dispersion surfaces, low dimensional features 79−42180
$TiSe_2$, semimetal, electronic props., superlattice form. 77−15532
$TiSe_2(S_2)$ (1T), electronic and vibronic struct. 80−44500
$TiTe_2$, struct. refinement by neutron diffr. 79−27967
$(Ti_{1-x}V_x)_2O_3$, metallic antiferromag. struct., neutron studies 80−65797
TlCl, Debye-Waller parameter by powder elastic neutron diffr. 80−29140
TlCl, phonon dispersion relations, neutron scatt. exam. 78−51628
$TlMnCl_3$, weak ferromag. and mag. struct., temp. depend. 78−19219
Tl_3PSe_4, phonon dispersion temp. depend. 80−96600
$Tl_2PbCu(NO_2)_6$, incommensurate Jahn-Teller transition, Huang scatt. 80−70401
Tl_2Te-Tl liquid system, conc. fluctuation, time-of-flight quasielastic neutron scatt. obs. 80−88324
$(Tm,La)Al_2$ disordered alloys, cryst. field transitions, inelastic neutron scatt. obs. 80−50055
$TmAl_2$, ferromagnetic structs., elastic neutron scatt. obs. 80−50055
$TmCo_2$, paramag. and ordered phases, Pauli type, Co susceptibility, polarised neutron diffr. obs. 77−63077
$TmCo_5$, easy magnetisation direction 78−84415
$TmCu_5$, crystal field level scheme, neutron inelastic scatt. and specific heat meas. 79−51536
$TmFe_2$, amorphous, neutron scatt. at transition, spin diffusion, magnetisation meas. 78−68174
$TmFeO_3$, temp. depend. of neutron depolarisation factor meas. near spin reorientation transition 77−16053
Tm_2Ni_{17}, magnetic structure by neutron diffr. 77−73000
TmS, antiferromag. struct. below 8.9K, neutron diffr. obs. 79−78318
TmSe, intermediate valence compound, mag. neutron scatt. 78−68164
TmSe, mag. neutron scatt. 80−25096
TmSe, mag. ordering under press., neutron diffr. obs. 80−70947
TmSe, mag. props. and struct. 80−25109
TmSe, mixed valence systems, spin dynamics and mag. ordering 78−68162
TmSe, mixed-valent, field-depend. mag. phase transitions 78−10657
TmSe, spin dynamics, neutron scatt. study 79−24178
TmZn, cooperative Jahn-Teller effect 78−67998
α-U, charge density wave, first order transition 80−10664
α-U, induced magnetisation density 78−47952
α-U, lattice dynamics 79−95101
α-U, spin density determ. by polarised slow neutron scatt. 77−28375
α-U, superstruct. neutron scatt. obs. near 43K 79−95116
U-Ga system cpds., mag. struct. 77−20559
UAl_2, dynamical susceptibility, diffuse neutron scatt. study 79−24138

neutron diffraction examination of materials continued
UAl_2, elastic consts., temp. and mag. field depend. 80−55450
UAl_3, inelastic neutron scatt. 80−11165
UAs and UPd_4, localised cryst. field states, neutron inelastic scatt. obs. 78−14697
UAs, magnetic struct. in high mag. fields, neutron diffr. study 80−34597
U_1As_4, mag. struct. 77−20559
UBr_3, cryst. field levels, neutron scatt. determ. 80−65509
UBr_5, cryst. struct. investig., powder neutron diffr. 78−91321
$UC_{0.60}N_{0.40}$ optical phonon splitting 78−71810
$UC_{1-x}N_x$, nonstoichiometric, atomic short-range order obs. by diffuse neutron scatt. 77−24315
UCl_4, cryst. field transitions obs. by neutron spectroscopy 77−47780
UD_3, crystalline elec. field studies using neutron inelastic scatt. at NRCN 80−10931
UF_4, crystalline elec. field studies using neutron inelastic scatt. at NRCN 80−10931
UGe_3, induced magnetisation density and f-d bonding, polarised neutron diffr. study 80−50063
UGe_3, magnetisation density, neutron scatt. meas. 80−50038
UGeY, (Y=S, Se, Te), mag. struct. and ordered moments 78−72329
UH_3, hyperfine splitting of proton determ. by inelastic neutron scatt. 77−43814
UMn_2, cubic to monoclinic struct. transition obs. 78−75833
UN, cubic antiferromag., anisotropic critical neutron scatt. behaviour 79−61112
UN, mag. inelastic scatt. 80−7079
UN, phonon dispersion relation near Neel temp., neutron coherent inelastic scatt. 78−59900
U_2N_2Te, mag. struct. 77−63119
$UO_{2\text{ and }2.11}$, temperature factor determ. by powder elastic neutron diffraction 78−10152
UO_2, crystalline elec. field studies using neutron inelastic scatt. at NRCN 80−10931
UO_2, extinction, wavelength depend. 78−38588
UO_2, lattice shear distortions 79−99221
UO_2 powder, temp. depend. of atomic thermal displacements, Rietveld profile-refinement procedure 80−49190
UO_2, reanal. of neutron diffr. data 80−15084
UO_2, single crysts., nucl. neutron diffr. intensity meas. analysis, extinction 79−27957
UO_2, single-cryst. neutron diffr. data, reanal. using third cumulants 80−100130
γ-UO_3, neutron powder profile obs. 77−15337
α-UOF_4, neutron diffraction study 78−14327
$UO_2(NH_2O)_2.2(NH_3O).2H_2O$, neutron diffr. cryst. struct. determ. 79−19206
$UO_2(NH_2O)_2.3H_2O$, low temp. neutron anal X-ray diffr. exam. 78−2068
α-$UO_2(NH_2O)_2.4H_2O$, low temp. neutron diffr. exam. 78−26518
β-UO_2SO_4, X-ray and neutron powder diffr. cryst. struct. anal. 79−14760
UO_2SeO_4, α- and β-phases 79−14760
UP-PrP (NdP) systems, mag. phase diagrams 78−84424
UPb_3, crystal field energy levels, magnetisation and susceptibility, neutron spectra obs. 80−50064
UPd_3, crystalline elec. field studies using neutron inelastic scatt. at NRCN 80−10931
UPd_3, crystalline electric field levels of U, neutron scatt. exam. 78−60267
UPd_3, U^{4+} mag. form factor meas. by inelastic neutron scatt. 78−52221
UPd_2Si_2, magnetic phase transition, neutron diffr. meas. 79−47284
US, phonon anomalies 79−7663
US-UC_2, solution studies 77−21120
$US_xN_yO_z$, neutron diffraction exam. of structure 78−79777
USb, antiferromag., neutron diffr. exam. of ordered state 77−20557
USb, collective elementary magnetic excitation, neutron inelastic scatt. obs. 79−24141
USb, crit. neutron scatt. 77−24674
USb, neutron inelastic scatt. from collective excitation 80−7080
USb, neutron inelastic scatt. meas., phonon spectra, mag. response, anisotropy 80−50065
USb, short-range spin correlations, neutron study 78−39293
$USb_{0.8}Te_{0.2}$, magnetisation and polarised neutron studies 79−56515
$USb_{0.8}Te_{0.2}$, magnetisation and neutron meas., mag. moments 80−15703
$USb_{0.9}Te_{0.1}$, multiaxial mag. ordering, magnetisation and neutron scatt. meas. 79−51750
$USb_{0.9}Te_{0.1}$, multiaxial mag. structure 80−15696
$USb_{1-x}Te_x$, mag. struct. and mag. phase diagram, neutron diffr. study 80−50059
U_3Si, crystalline elec. field studies using neutron inelastic scatt. at NRCN 80−10931
USn_3, crystalline elec. field studies using neutron inelastic scatt. at NRCN 80−10931
USn_3, inelastic neutron scatt. 80−11165
UTe, crit. exponents, neutron and magnetisation meas. 80−88823
UTe, critical mag. fluctuations near T_c 80−7122
UTe, ferromag., negative electron spin polarisation in photoemission 79−19967
UTe, magnetisation and neutron meas., mag. moments 80−15703
$(U_xTh_{1-x})S$, mag. props. rel. to elec. struct., 1.5-300K 77−1557
V, Debye-Waller exponent, 4.2 to 296K, incoherent elastic neutron scatt. 79−4382
V, Debye-Waller factor and H_2 diffusion, neutron spectroscopy study 79−37881
V, neutron diffraction determ. of O, N, C interstitial sites 77−19944
V, neutron multiple scatt. calcs., expt. verification using polarisation anal. technique 78−42865
V, paramag., mag. form factors, neutron diffr. study 79−47234
V polycrystalline plate, struct. facators, time of flight neutron diffr. 78−47212
V, search for antiferromagnetism, neutron diffr. meas. *(Russian)* 78−6516
V-H, BCC, tetrahedral interstitial site H band modes, neutron scatt. obs. 79−55852
V-H(D), hydrogen ordering, review 80−60850
V-H(D) system, single cryst. prep. and characterisation 79−95910
V-Mn-Cr, disordered BCC state, mag. phase diagram, mag. and elec. props. 77−63185
V-N system, phase formation *(Russian)* 78−39739

neutron diffraction examination of materials continued
V-Pt, dilute, inelastic neutron scatt. and quasilocal vibrs. *(Russian)* 77−80595
VC_x, static distortions and Debye temp. determ., neutron diffr. exam. *(Russian)* 77−80482
VC_xN_y, superstructure induced by ageing, neutron diffr. obs. *(Russian)* 80−49195
VCl_4, liq. struct. by neutron diffr. 79−73088
$V_{3-x}Cr_xSi$, x=0 to 3, struct., supercond. and mag. props. 80−1962
α-$VD_{0.7}$, interstitial vibr., coherent neutron scatt. study 79−42196
α-$VD_{0.7}$, vibrations of interstitial D, coherent neutron scatt. 80−96612
$VD_{0.8}$, antiphase domains during ordering, neutron diffr. 77−90348
V_4D_3, multistage ordering process, neutron diffr. obs. 77−59114
V_3Ga, long-range order parameter variations determ. and correls. with supercond. T_c 77−11504
V_3Ga, superconducting transition temp. and electron density of states 77−32105
V_3Ge, superconducting transition temp. and electron density of states 77−32105
$VH_{0.07}$, diffusion of H, neutron scatt. study 79−60550
$VH_{0.51}$, optic modes study by neutron spectroscopy 80−19891
VH_x, diffusion of H atoms, quasielastic neutron scatt. obs., book contrib. 79−82383
$VH_x(D_x)$, H conc. detect. by neutron interferometry, precipitation effects 78−67735
VI_2, mag. superlattice, neutron oscill. and Weissenberg photography 80−65802
$V_{3-x}M_xGa$, M=Ti, Cr, Mn, Fe, Co, Ni, cryst. struct. and microhardness meas. 79−86740
β-V_2N, neutron powder profile-refinement cryst. struct. determ. 80−15060
VO_2, metallic, magnetisation distribution and band structure 78−76223
$V_{0.97}O_{0.03}$, lattice dynamics exam., neutron scatt. 79−23689
α-$V_{0.97}O_{0.03}$ solid soln., impurity vibrs., inelastic neutron scatt. study 80−92635
V_2O_3, high-temp. transition domain, small angle diffuse neutron-scatt., 400-600K 77−69231
V_2O_3, lattice parameter anomalies at high temp. 78−47522
V_2O_3:Cr, pure and doped, sound vels. and elastic consts. from phonon dispersion curves 79−55844
V_2O_{3+x}, nonstoichiometric, microscopic mag. props., NMR and inelastic-spin-flip neutron scatt. 79−38323
V_2O_5-TeO_2 system, vitreous, struct. obs. using neutron scatt. 78−22667
V_3O_7, hyperfine interactions, inelastic spin flip neutron scatt. 77−28372
$VOCl_3$, liq. struct. by neutron diffr. 79−73088
V_3Si, d-spacing fluctuations above Martensitic phase transition 80−7570
V_3Si, lattice dynamics, inelastic coherent neutron scatt. 78−26645
V_3Si, neutron irrad., neutron diffraction studies 78−88076
$V_3Si(Ge)(Ga)$, phonon density of states, temp. depend. 79−42183
$V_{0.97}U_{0.03}$, phonon spectrum, quasi-local vibrs., inelastic incoherent neutron scatt. 77−15519
VUS_3, mag. struct. and delocalised moments, powder neutron diffr. obs. 77−69496
V_2WO_6, magnetic structure, stability of mag. modes, neutron diffraction study *(French)* 80−39744
Va_2D, neutron diffr. meas. of disorder-order phase transitions 80−29947
W single crystal, ^{156}W enriched, nucl. and mag. scatt. of polarised neutrons 79−87234
WC, microcrystalline, mol. dynamics, motion of H_2O and H_2 mols. adsorbed on surface, catalytic activity 78−71941
WO_2, struct. refinement by powder neutron diffr., profile anal. 79−99139
Xe:methane, impurity rotational states, inelastic neutron scatt. study 79−51020
$(Y,Er)Al_2$, cryst. field parameters, inelastic neutron scatt. study 79−23937
Y, diffusion of H, neutron scatt. and absorpt. study 79−60556
Y, paramag., mag. form factors, neutron diffr. study 79−47234
Y-rare earth, dil. alloy, cryst. field parameter determ. 78−10650
Y-rare earth, dil. alloy, cryst. field determ. 78−10651
YAG, neutron diffr. determ. of O coordinates 77−1117
YAG, phonon spectrum, incoherent inelastic neutron scatt. meas. 77−66006
$(Y_{3-x}Ca_x)(Fe_{2-x}Sn_x)(Fe_3)O_{12}$, long and short range magnetic order 79−38419
YCo_5, substituted, magnetocryst. anisotropy, different contribs. of two Co sites 77−8301
$Y(Co_{1-x}Cu_x)_5$, neutron diffr., thermal expsn. *(French)* 80−19749
$Y(Co_{1-x}Cu_x)_5$, neutron diffraction study *(Chinese)* 80−39000
$Y_2(Co_{0.31}Fe_{0.69})_{19.2}$, statistical site occupancy deviations, neutron diffr. investig. 77−7717
$Y(Co_{1-x}Ni_x)_5$, distrib. of Co and Ni atoms, neutron diffr. obs. *(Russian)* 80−64954
$Y(Co_{1-x}Ni_x)_5$, mag. heterogeneities and coercive force, neutron scatt. study 80−2553
$YD_{1.96}$, cryst. struct. by neutron diffr. 80−70179
$Y_{1-x}Er_x$, dil., cryst. field interactions, neutron scatt. spectra 80−50048
YFe_2, amorphous concentrated spin glass, susceptibility, Mossbauer and neutron scatt. meas. 80−39783
$Y(Fe_xAl_{1-x})_2$, mag. order in pseudobinary systems down to millikelvin temps. 78−19251
$YFe_{1-x}Co_xO_3$, reorientation transitions, neutron diffr., mag. behaviour *(Russian)* 77−24678
$YFe_{1-x}Cr_xO_3$, reorientational transitions, mag. and neutron diffr. exam. 77−12097
$YFe_{4.5}Ga_{0.5}O_{12}$ domains, neutron dpolarisation and Faraday rotation study 80−93137
$Y_6(Fe_xMn_{1-x})_{23}$, mag. order in pseudobinary systems down to millikelvin temps. 78−19251
YFe_2O_4, two-dimensional spin ordering, neutron diffr. study 80−29530
$YH_{1.98}$, cryst. struct. by neutron diffr. 80−70179
YIG, magnetisation density, polarized neutron expts. 78−52215
YIG, polarised neutron expts., extinction models 80−24322
YIG, polariser neutron study of covalency effects 80−2552
YIG, spinwave dispersion curves 78−19230
Y_6Mn_{23}, ferrimag., mag. interactions, polarized neutron diffr. meas. 79−78322
YNi_2 amorphous alloy, at. struct. 80−19704
YNi_3, magnetism resurgence, neutron diffr. and mag. props. study 80−65819

neutron diffraction examination of materials continued
Y_2Ni_{17}, ferromag. struct., neutron diffr. expt., cryst. field calcs. 77−73001
YS, soft-mode behaviour in phonon dispersion, inelastic neutron scatt. meas. 78−38807
YS, supercond., phonon anomalies, inelastic neutron scatt. 78−59901
$Y_{1-x}Tb_xPd_3$, magnetisation, magnetostriction, and inelastic neutron spectra 80−65998
YbCuAl, mixed valence cpd., dynamic susceptibility, neutron inelastic scatt. 80−65807
$YbCu_2Si_2$, local mag. moments, neutron scatt. study 79−61058
$YbCu_2Si_2$, mag. 4f Zeeman-level power spectrum using diffuse mag. neutron scatt. 79−60775
$YbFeO_3$:Co, mag. struct. factors, neutron diffr. study 79−47248
Zn (0002), mosaic single cryst., neutron integrated reflectivities 79−86656
Zn, anharmonicity of lattice vibrs., elastic neutron scatt. 77−51454
Zn, liquid, structure factor, 460 to 650°C, by neutron diffr., elec. resist. temp. coeff. 77−47333
Zn, mean square displacement of atoms in cryst. lattice, rel. to sp. ht. *(German)* 80−79902
Zn, molten, struct. investig. by neutron diffr. 79−4233
Zn, phonon density of states calc. from neutron diffr. data 77−24369
Zn single crystals, antisymmetric atomic vibrs. from elastic neutron scattering data 79−33046
Zn, single crysts., total thermal neutron cross sections 80−19672
Zn, site symmetrized Fourier invariant treatment of anharmonic temperature factors 79−33040
$ZnCl_2$, aq. soln., structural transition, neutron diffr. study 80−64872
$ZnCr_2O_4$, mag. phase with short range order *(French)* 77−63203
$ZnCr_2Se_4$, screw spin struct., neutron diffr. exam. 78−27019
$ZnCr_2Se_4$, screw spin structure, method of controlling the sense, polarised neutron diffr. study 80−70944
$Zn_{0.005}Fe_{2.995}O_4$, phase transitions, neutron elastic scatt. and resist. meas. 77−28000
$Zn(HSeO_3)_2.2H_2O$, neutron diffr. cryst. struct. determ. 80−33983
$Zn_{0.8}Mn_{0.2}Fe_2O_4$, spin interaction, neutron diffr. and Mossbauer effect meas. 77−4501
$Zn_{0.75}Ni_{0.25}Fe_2O_4$, mixed ferrite-spinel, helicoidal struct. 79−47242
$Zn_xNi_{1-x}Fe_2O_4$, magnetic props. rel. to localised canting model 77−32161
ZnS, cubic, thermal vibr. temp. depend., anharmonic models 80−92618
$Zn_4Si_2O_7(OH)_2.H_2O$, X-ray and neutron diffr. study 79−99159
Zr alloys, domain struct. of diffuse ω-phase formed in quenching, 1D model 78−27523
Zr, BCC, lattice dynamics, 1400K, phase transform. 79−19337
Zr, HCP, normal vibr. modes, temp. depend. 79−19339
Zr, HCP, temp. depend. of C-axis phonon dispersion curves 78−59884
Zr, magnetic form factor, field-induced, polarised neutron scatt. meas. 80−50044
Zr, phonon density of states, scatt. law in thermal neutron field 77−72663
α-Zr:H, energy of interstitial H calc. 79−23596
Zr-Nb (20 wt.%) ω-phase transform., structural model, intensity distrib. in neutron diffr. 77−77472
ZrC_x, static distortions and Debye temp. determ., neutron diffr. exam. *(Russian)* 77−80482
$Zr(Ca)O_{2-x}$, internal, external distortion mechanisms, neutron diffr. study 78−83946
$Zr(Ca)O_{2-x}$, lattice shear distortions 79−99221
$ZrCr_2D_x$, site occupation modes and cryst. struct., neutron diffr. study 80−59440
$ZrD_{1.82}$, and $ZrD_{1.96}$, struct. and phase equilib., neutron diffr. obs. *(Russian)* 78−92244
$Zr(Fe_xCo_{1-x})_2$, mag. order in pseudobinary systems down to millikelvin temps. 78−19251
$ZrH_{1.92}$, total neutron cross section of protons at 77.4K 79−60444
ZrH_2, H positions by neutron quasi-elastic scatt. 79−42042
$ZrMn_2D_3$, deuterated hexagonal Laves-phase, D atoms interstices and diffusion paths, positional disorder 79−73334
ZrN, phonon dispersion curve anomalies, inelastic neutron scatt. obs. 79−86858
ZrNb, ω-phase, diffuse neutron scatt. meas. 78−14311
Zr_2Ni, search for soft phonon modes, neutron scatt. 79−23686
$ZrV_2D_{4.5}$, deuterated cubic Laves phase, D atom distrib., neutron diffr. anal. 80−29006
$ZrV_2D_x(H_x)$, site occupation modes and cryst. struct., neutron diffr. study 80−59440
$Zr(Y)O_{2-x}$, internal, external distortion mechanisms, neutron diffr. study 78−83946

neutron diffusion
see also neutron flux; neutron transport theory
albedo on vacuum-liq. H_2 boundary for exponentially damped neutron flux, exptl. determ. 78−4977
analytical angular integration technique for generating multigroup transfer matrices 80−68722
angular effects in toroidal diffusion, one-group homogeneous diffusion model 79−22351
asymmetric weighted residual methods, high-order schemes 77−82985
asymptotic approximations to neutron transport eqn. 79−9663
asymptotic multigroup approx. for critical radius of sphere *(Russian)* 77−57702
benzene vapour, slow neutron scatt., effect of pressure total interaction cross section 78−17273
black sphere linear extrapolation distance, energy depend. and anisotropic scatt. effects 77−54270
Boltzmann equation, derivation of diffusion equation by Hilbert expansion equation 79−17368
breeder reactor piles, instantaneous neutron kinetics in cavities 80−32393
Brownian motion theory viewpoint *(French)* 77−61473
buckling approximation, assessment of DB^2 transverse leakage predictions in neutron transport computations 80−13529
BWR, neutron noise field, two-group diffusion theory 80−18461
BWR core, three dimens. calcs., new brief neutron diffusion scheme 77−42014
BWR core calculations using improved coarse mesh methods 80−68849
channel power meas. correlation with lattice consts. 79−13380
checkerboard pool core, series of two group calcs. 78−74424
coarse mesh 3-D diffusion code, ROCS 77−46252

neutron diffusion continued
coarse-mesh nodal method based on response matrix considerations 77−65262
code comparison for LMFBRs 80−95337
coefficient adjustment using transport theory results 79−22359
cold neutrons and applications of quasielastic scattering *(Japanese)* 80−27685
collision probability method, development and applications 80−27706
complex buckling modes in asymmetric cell lattices 79−30881
computer codes for neutron transport calcs., MARC, PN, user's guide 77−3068
consistent homogenization procedure to obtain few-group cell parameters 79−85586
coupled-core reactors anal. with method of moderator region response function 78−58331
critical reactor calc., AGA two-sweep iterative methods 79−36298
criticality safety anal. at Oak Ridge 80−37431
DELILAH correlation code for param. adjustment of 1 group diffusion eqns. 79−13413
discontinuous variational approx., neutron diffusion and transport theory 78−46129
discrete-ordinates neutron transport equations in slab geometry, convergence rates of spatial difference equations 80−27688
double criticality of uniform-power-reflected reactors 80−57828
energy dependent transport theory, exact solns. 80−32319
evaporation neutrons in paraffin and lead layers, Monte Carlo methods 79−89346
fast breeder reactors, core burnup props., modified on-group calc. method for 3-d anal. *(Japanese)* 79−49645
fast neutron albedo for Fe, concrete and Fe-covered concrete radiation shields 79−76151
fast neutron transport through laminated Fe-H_2O shield 80−13931
fast reactor, physical studies of large heterogeneous core concept 78−17307
fast reactor finite difference diffusion theory codes, optimised iteration strategies and data management 77−83005
fast reactor power distribution calc., effective one-group coarse mesh method 79−63717
fast reactor SDX cell homogenization code, validation results for pin geometry 79−80997
fast reactor shields, relative accuracies of transport theory approximations 77−61481
FBR, 2-D power distrib. calc. by appl. of Askew coarse mesh method 79−22372
FBR, multigroup 1-D diffusion program MED 78−78456
FBR, neutron-physical calc., multi-group diffusion equation solution *(Czech)* 78−66332
FBR, nonstationary prompt-neutron diffusion, multigroup treatment 80−86956
FBR, three-dimens. diffusion calcs., spatial mesh effects 79−13515
FBR analysis, general multigroup nodal procedure based on response matrix principles [for FBR analysis] 80−57827
few-group diffusion theory, one-group coarse mesh technique 79−26495
few-group diffusion theory model for VO_2 and MO_2 assembly anal. 77−46273
finite difference method approx. by coarse mesh method 77−88185
finite element anal. with space depend cross sections 77−82986
finite element code, neutron flux computation 78−50449
finite element energy depend. method for 2-D diffusion 77−82987
finite element soln. technique for 2-D equations 79−89347
finite medium age-diffusion kernels in source-sink theory 77−67782
fission reactor, one-group model, convergence acceleration in perturbation theory problems 78−37406
fission reactor theory, relationship among the various anisotropic diffusion coefficients for periodic lattices 80−57826
fission reactors, fluidised bed concept, diffusion theory 80−68729
fission reactors, homogeneous reactor cells, few-group cell parameters 80−27696
fission reactors, seed-blanket calcs., 2-D, one-channel synthesis method, transport and diffusion 80−73876
flux calc., use of Aitken extrapolation method 79−13379
flux distribution from microtron convertor in graphite moderator with water reflector *(Russian)* 77−82979
flux synthesis, single channel, finite element trial functions for 3-D reactor calcs. 80−42734
flux synthesis program KASY, consideration and appl. to reactor design problems 77−88184
flux-distortion factor for a foil in a exponentially varying flux 78−89930
Fourier expansion for xyz-geometry 80−9326
fuel storage pool criticality calc., transport-consistent diffusion algorithm 79−9721
functional anal. of multigram neutron diffusion problem 78−58317
fusion reactor radiation protection, shield integral expts. at ORNL 80−47709
gadolinia-based fuel pins, efficient diffusion theory parameterization 79−67840
Galerkin-type spectral synthesis of neutron diffusion eqn., asymptotic error estimates 77−82989
GCFR, Argonne, calc. of void streaming in critical expts. 77−83007
GCFR lattice, Monte Carlo and diffusion theory calcs. of steam worth 79−80991
generalized rebalance, common framework for transport acceleration methods 79−22356
graphite, pulsed neutron wave propagation expt. using electron LINAC *(Japanese)* 80−78345
graphite pebble bed system, meas. of neutron wave propagation *(German)* 77−6481
Grenoble high flux reactor, neutron physics expts., methodical aspects *(German)* 80−554
heat release distribution random component determ. method 77−54289
heterogeneous media, neutron drift 78−29528
heterogeneous reactor, neutron distrib. determ. by 1-D multiregion cylindrical cell 79−26488
heterogeneous reactor eqns., difference eqn. approach to soln. 77−61485
homogenisation, appl. to neutron diffusion in spatially periodic medium 79−49644
homogenised diffusion theory parameters, rigorous calc. 79−85587
homogenized group parameter computation 79−26493
HWR, multidimens. space time kinetics studies 78−29547
HWR, multidimensional space time kinetics, TRIMHX code 80−47538
implicit nonstationary iteration, appl. to 3D neutron diffusion 79−63712

neutron diffusion continued
infinite cylinders, critical and subcritical, n multiplication factor, nuclear criticality safety 78−78442
inlet coolant temp. fluctuations transfer function, space-depend. global component 79−30887
integral coarse mesh diffusion method appl. to reactor transients with feedback 79−85585
effective neutron isolation thickness values from reflector savings data 78−669
iterative soln. of transport eqn. 78−29534
Larmor precession, spin echo, memory effects and polarized neutrons, pulsed source efficiency improvements 79−45323
lattice cell diffusion coefficients, unified derivation of definitions 78−58332
linear eqns., soln. by method of implicit non-stationary iteration 78−70581
liquid air, transport of neutron and secondary γ-rays from 14 MeV source 78−50234
LMFBR, anisotropic diffusion effect on criticality of plate lattice fast assembly 79−26463
LMFBR, appl. of BWR simulator to neutronics calc. tool 79−40987
LMFBR, bubble collapse reactivity increases in boiling fuel/steel pools 79−31025
LMFBR, comparison of neutron diffusion computer codes 77−88188
LMFBR, effect of mag. field on operating characts. 79−71885
LMFBR, neutron streaming through control rod followers, diffusion coeff. by numerical integration 80−13636
LMFBR benchmark calcs. by 2 and 3 dimens. diffusion methods 78−74432
LMFBR simulated meltdown configs., integral physics parameter meas. 80−13698
LMFBR small core disruptive accidents, transport/diffusion comparisons 79−31022
Los Alamos density exponent formula, integral version, comparisons using multigroup theory 78−74425
LWR, thermal neutron steady state spectra in pure and poisoned water 79−36306
LWR core, few group 2-D diffusion eqns. in hexagonal geometry, HEXAB-II-30E code *(Bulgarian)* 80−68765
mixed-lattice multidimensional reactor calcs., coarse mesh finite difference method 77−34375
monatonic liquid, slow neutron scatt. law 77−30647
monopole and dipole response coefficient theory comparison with expt. 78−13188
multichannel synthesis approximation, basis functions for finite element formulation 80−47528
multidimensional, nodal Green's function method 79−59106
multidimensional calculations using a nodal Green's function method 80−47547
multidimensional reactor calcs., interface current techniques 77−88193
multigrid iteration strategy appl. to neutron diffusion eqn. 79−85577
multigroup charged-particle transport calcs., temp. effects on cross sections 80−57818
multigroup cross section calculation, self-shielding, subgroup method *(Rumanian)* 78−46140
multigroup cross sections, GGTC-ENEL computer code using intermediate resonance method 78−58323
multigroup diffusion eqn. finite element soln., appl. of natural coordinate system 77−54278
multigroup diffusion eqns., soln. methods *(Czech)* 77−38312
multigroup diffusion equation, synthesis-finite element method 80−27699
multigroup diffusion equations, solution methods *(Czech)* 77−46202
multigroup diffusion program EMA-II-30, two dimens., flux distrib. *(Russian)* 77−38318
multigroup diffusion theory, current weighted total cross section determ. in unresolved energy region 80−18365
multigroup diffusion theory, optimum boundary condition 78−41801
multigroup neutron diffusion equation, time-integrated method of soln. 80−27695
multigroup theory, functional analysis 80−13525
multigroup transfer coeffs., efficient eval. for shielding appls. 80−47747
multigroup transport theory, finite slab inverse problem 78−74418
multigroup-multipoint diffusion operator spectrum with delayed n 78−74430
multigroup-multipoint diffusion operator with delayed neutrons, spectrum 77−54274
multizonal absorbing rod, effectiveness in albedo and diffusion studies *(Russian)* 80−556
neutron diffusion modelisation, optimal design and eigenvalue problems 78−66329
neutron importance meas. by dynamic method in subcritical reactor core 79−17956
neutronics code, CONIFERS for reactors with channels 78−25281
nodal fluxes determination using approx. analytical method 77−65261
nodal methods for solving time depend. group diffusion eqns. 77−82988
non-multiplying homogeneous slab assembly, time depend. multigroup P1 eqn. soln. 78−17267
nonlinear diffusion system in reactor dynamics, bifurcation anal. 79−97741
nonmultiplying two-zone cylindrical medium, asymptotic neutron distribs. 77−46203
nuclear fuel performance and radiation enhanced neutron diffusion *(Japanese)* 79−30914
nuclear reactor cylindrical models, diffusional approx., finite element anal. *(Russian)* 80−18414
nucleate pool boiling, meas. of void frequency distribs. and profiles using neutron beams 80−27691
one-group equations, finite element soln. tech. using imaginary nodal points and element subdivision 80−68721
optimal iteration strategies, geometric interpretation 79−22358
PBR fission reactors, neutron flux distribs. in multisphere configs., diffusion-theoretical model *(German)* 80−73875
PDQ-8 neutron diffusion-depletion program 79−71876
Pickering reactor, simulation of wire activation expts. with SORGHUM code 78−25310
plate lattice, diffusion coeff. anisotropy meas. 78−17268
plate lattice fast assembly, anisotropic diffusion, criticality correction estimation method 78−29523
power reactor parameter identification in Xe oscillation model using maximum likelihood method 80−18466
pulsed neutron die-away in fast multiplying assemblies 80−18366
neutron diffusion continued
PWR, improved water density feedback model for neutron diffusion calc. 79−67890
PWR core, large, appl. of coarse-mesh finite difference eqns. for k_{eff} and peak power factors 78−17305
PWR core, Xe oscillation model, neutron diffusion eqn., nonlinear system 78−58322
PWR core analysis, transport-to-diffusion theory for gadolinia-loaded fuel pins 80−57908
PWR design, higher order nodal depletion program MEDIUM-2, exptl. verification 79−26492
PWR neutronic predictions with improved water density evaluation model 77−46272
quantum neutron diffusion eqn., Boltzmann eqn. classical limit 80−13524
radiation protection, benchmark shielding problems obtained from integral tests of neutron cross sections 80−47740
reactivity measurement by inverse kinetic method 79−63752
reactor core, uniform infinite lattice eigenvalue as function of buckling 79−609
reactor core pin power distribution det. based on nodal coarse mesh calcs. 77−88195
reactor design and anal., numerical methods 77−79427
reactor dynamics, finite element analysis for two dimensional eqn. *(German)* 77−88190
reactor operation and control simulator ROCS, extension to two energy groups 79−81034
reactor physics, grid-coupling methods for the multigrid solution of the neutron diffusion equation 80−47555
reactor physics, three dimensional calcs. with finite element method *(German)* 77−88189
recursive Monte Carlo method, geometrical imaging and surface sources 79−85578
removal-diffusion shielding code SHREDI, bidimensional, fundamentals and results 78−70645
rethermalization of neutrons in water-graphite system 79−97806
S_N calculations, modified transport formulation compatible with anisotropic diffusion theory using ANL DIF3D diffusion code 80−47526
scattering research, early developments 79−44696
simulated meltdown experiment, modified diffusion coeffs. for neutron streaming 78−33278
slowing down time in hydrogenous multiplying system 77−61472
source importance factor in reactor kinetics, adiabatic approx. 78−46137
spatially depend. spectrum, expansion about local Maxwellian 78−29537
spheres, soln. of basic problems by method of elementary solns. and F_N method 79−40981
static multigroup diffusion equation, three dimens., MULTIPOL code for coarse mesh approx. *(German)* 77−88186
steam generating channels, volumetric steam content determ. by slow neutron method 79−30903
subsoil neutron moisture probe, lab. calibration, minimum soil sample size calcs. 77−57333
symmetric SOR and SIP methods, numerical soln. of multigroup diffusion eqn. 78−74431
thermal neutron diffusion eqn. in medium with cylindrical hole, soln. 80−51548
thermal reactor assemblies, effective neutron diffusion parameters 80−73874
thermalisation in hydrogenous moderators 77−65253
time depend. diffusion eqn. for neutronic calcs., use of exterior differential forms 78−54871
time-dependent continuous-energy equation, weak solns. 77−65244
time-lethargy equivalence relations for infinite plane geometry problems 77−61470
transfer matrix calcs. for thermal neutrons 80−27687
transport codes DOT and TWOTRAN as standards for diffusion in pebble bed reactors 80−68750
transport problem, 2-D, diffusion synthetic acceleration method 79−22357
two-dimensional neutron diffusion eqn. for triangular region, finite Fourier transform soln. 78−78432
two-group diffusion calc. by spatial synthesis algorithm 78−13200
ultracold neutron diffusion along guide tube 78−33237
ultracold neutrons (UCN) transmission through moving goffered foils 79−17955
variational culculus calc. methods in rectangular and cylindrical coordinates 79−17949
volumetric steam content determ. by noncontact neutron sensor 79−30904
water, diffusion length calc. for 1/v and non-1/v absorbers 79−30879
water assemblies, Cd, Sm, Gd, poisoned, absorption discontinuity effect 78−13191
water assemblies, neutron diffusion across absorpt. discontinuity 78−21620
water slabs, fast neutron penetration spectra 78−29535
water vapour, slow neutron scatt., effect of pressure total interaction cross section 78−17273
wave propag. in multi-region systems, delayed neutron effects 78−50229
ZPPR modification (1977), neutron diffusion calcs. 79−9662
Al-graphite two-dimensional shield, neutron penetration meas. 79−3245
Be assembly, space- and angle-depend. steady state thermal neutron spectra 77−67783
Be, fusion reactor blanket material, neutron multiplication meas. 79−59255
Be, neutron diffusion in finite blocks, flux synthesis method for 3D multigroup eqn. 77−34366
Be, two group calcs. for neutron wave propagation across an absorption discontinuity 78−89931
H_2 solid-liquid mixture, nonstationary diffusion of neutrons 79−4212
Na void reactivity anal., applicability of Benoist's diffusion coeff. 77−14218
Ni single crystal near T_c, neutron transmission depolarisation 79−33479
^{233}Pa, calc. of critical mass and radius by three group diffusion theory 79−13419
^{239}Pu, criticality of thin flat foils versus spherical shells, two-group diffusion anal. 79−26530
Th fuelled thermal reactor, model for estimating flux distribs. 77−61482
UO_2-PuO_2 fuelled lattice, reactivity predictions using multigroup transport theory 78−89957

neutron economy *see neutron flux*

neutron effects
see also irradiation induced creep
A15 compounds, neutron irrad., X-ray scatt. theory 79−37740
A15 superconductors, radiation induced Tc, gap anisotropy effects 78−52125
A-15 compounds, radiation induced damage, TEM and heat capacity meas. 79−56349
acetylene, ionisation meas. and $\bar{W}_n$ derivation for neutron irradiation 79−36430
activation cross section meas. for fusion reactor wall and blanket materials 77−26881
activation cross sections meas. for generalised intermittent irradiation, fusion machines appl. 78−58283
air, luminous emittance of neutron beam 78−86567
alkaline earth fluorides, F-centre annealing and intrinsic luminesc. 79−65937
alloy, substitutional solid soln., irradiated creep rate enhancement theory 77−63739
alloy constituents, segregation during irradiation 79−55791
alloys, austenitic, neutron irradiation induced embrittlement, review 79−65120
alloys, neutron irradiated, enhancement by implanted He 79−28016
amoeba, combined effects of thermal neutrons and agents which interact with DNA 78−20219
amorphous medium, atomic cascades, time-energy distribs. 77−1156
Araldite, neutron irradiation, elastic moduli effects, hardener conc. depend. 79−55804
atomic displacement rates in collision cascade, appl. of HV electron microscope 77−24330
austenitic steel neutron-irradiated weld toughness rel. to ferrite content 79−83327
biological, evaluation criteria for neutron contamination of 25 MV photon therapy beam from Varian Clinac-35 77−86628
biological, neutron radiotherapy, review 77−5076
biological, OER of high-energy neutrons prod. by 80 MeV deuterons on Be 77−81538
biological acute and late reactions, mice, comparison of heavy particles for therapy 78−85338
biological tissue, calc. of spectra and linear energy transfer 79−100659
blood cell permeability to K^+, Na^+ repair after X-ray, fast-neutron damage 79−57615
bone marrow, effect of a 600 MeV neutron beam, mouse 79−96630
bone marrow cell-culture, RBE of different-energy neutrons 79−34508
BOR-60 reactor shim-rod sockets, Kh18N9 steel 79−46716
BR-5 Soviet reactor, effect of operating conditions of vacancy porosity of austenitic stainless steel 79−32990
brain tumour, rat, RBE of cyclotron fast neutrons rel. to ^{60}Co γ-rays 80−76797
α-brass, dezincified specimen, effect of voids on positron annihilation 79−15553
bronchial tumour reaction to combined neutron-telecobalt therapy 79−20642
BWR, control blade worth depletion meas. 80−719
cancer treatment using neutron 77−40733
CANDU, stress anal. of fuel channel interaction with end shields 79−59161
capillary blood flow, long-term effects of ^{60}Co gamma and fission spectrum neutrons, mouse 78−80927
carbonaceous matrix materials for HTGK fuel rods, irradiation-induced dimensional changes 80−65052
carcinogenesis by fission neutrons, RBE rel. to γ-rays 79−70588
cardiac ultrastructural effects, aged mouse, fission spectrum neutrons rel. to γ-rays 80−41138
cell neoplastic transformation and dose fractionation, role of damage repair 80−72242
cell nucleoside effect, dependence on LET 80−35980
cell radiosensitivity, neutron relative biological effectiveness in different exptl. tumours, 15 MeV neutrons 79−20591
cell survival, OER and RBE, comparison of heavy particles for therapy 78−85337
cell survival vs. depth, comparison of heavy particles for radiotherapy 78−85336
cells, repair of radiation damage due to cyclotron-produced neutrons 80−3740
ceramic nuclear fuels, irrad. induced rare gas diffusion 80−59524
ceramic nulcear fuel, irradiation induced creep 77−42056
ceramics, applications in fusion systems, neutron effects 80−32473
ceramics, ion beam irradiation techniques for simulation of 14 MeV neutron irradiation 80−10584
cervical spinal cord, rhesus monkey, effects of 50 MeV (d→Be) neutron irrad. 80−101228
Chinese hamster ovary cells, response to fast neutron radiotherapy beams 80−21497
chromosomally aberrant cells, Japanese A-bomb survivors, dose-response relationship of neutrons and γ-rays 80−94295
cladding dilatation, influence of radial temp. gradient 77−46287
component reliability tests in thermal neutron environment 78−21787
composition changes in neutron-irradiated materials, calculation methods 77−62565
compound superconductors, radiation effects on critical currents 78−52175
coronary arteries and aorta, late ultrastruct. changes after irradiation, mouse 79−57725
creep and growth, radiation induced, fundamental mechanisms 80−92596
creep testing, high energy neutron irradiated materials, apparatus 79−79200
creep testing ampoule for materials subject to reactor irradiation and dissociating coolant 78−3301
creep testing machine using torsion, in radiation zone of nuclear reactor 78−11480
cryopumps, neutron irrad. effects on pumping characts. appl. to fusion reactors 79−44915
CTR first wall spectrum effects on atom displacement and He prod. 78−46168
cyclohexane, neutron irradiation, radical distribution, ESR study *(Japanese)* 80−44920
cyclotron applications, radiation damage, radioisotope dating, and large-scale radioisotope prod. 79−54692

neutron effects continued
damage, solid-state physics 77−27790
damage correlation with heavy ion effects, predicted temp. shift on swelling with radiation dose rate change 79−7630
damage function anal., computer simulation 78−87721
defect diffusion, radiation effects 78−87827
Demokritos research reactor, fast neutron irrad. facility 80−99270
dentin, human, effects of irradiation on wear resistance, microhardness and acid solubility 79−96634
deoxyribonuclease I in aq. soln., inactivation by thermal neutrons 80−104664
diacel solid state track detector 79−750
diamond, natural, topography of impurity distrib. and neutron-induced colouring 77−39613
diamond, sub-surface contamination by hot-atom recoil in neutron activation anal. 77−60144
diamond, synthetic and natural, neutron irrad., optical and elec. props. *(Russian)* 78−59841
diamonds, natural, paramagnetic centres with S=5/2 79−47334
diffusion in solids *(Japanese)* 77−59048
dilute alloys, defect trapping and solute segregation in irradiated alloys 80−13603
discrete ordinate codes, discrete cross section expansion 79−69162
dislocation bias and point defect relaxation volumes 79−99248
displacement damage anal., program DISPKAN 79−14854
displacement spike annealing, Mont Carlo method computer expteriments 78−30672
DNA, double strand breaks, protein cross-links, induced by fast neutrons, γ-rays 79−66446
DNA strand breaks, lymphoma cells, detected by hydroxyapatite chromatographic technique 79−43819
doped-silica optical fibres, nuclear radiation effects 80−33172
dose measurements in a dummy for test animal irradiation in a reactor 78−61218
dose-response relationship of neutrons and γ-rays to leukemia incidence, atomic bomb survivors 80−36148
dosimetry, above 10 MeV, standards 79−13544
dosimetry, international intercomparisons 79−12014
dosimetry, neutron dose meas. with B-doped cellulose nitrate film 79−31321
E. coli, value of photoreactivable component after exposure to ionising radiation 80−72224
E. coli strains differing in DNA repair capability, survival after fission-spectrum neutrons irrad. 80−98031
EBR-II, fabrication of in-reactor creep capsules using previously irradiated cladding tubes 79−54478
EBR-II, mixed-oxide fuel pins, results from expt. F11A after cladding break 79−67861
EBR-II irradiation subassembly and creep specimen container design 79−54479
elastomer, radiation mechanical props., creep *(Russian)* 77−16641
electron accelerator, shielding for high energy neutron dose 79−54609
epoxy resin, low temp. irradiation effects on mechanical props., use in superconducting magnets 78−60737
experimental radiation transport to large distances from a bare reactor 79−59275
Fabry-Perot interference filters, neutron irrad. effects 80−14437
fast neutron and photon therapy, randomised clinical trials 79−20638
fast neutron exposure, risk of leukemia 80−30782
fast neutron facility in CP-5 reactor, neutron flux, energy spectrum, primary recoil distribution 79−41056
fast neutron fluence meas. technique, uses neutron irrad. effect on light absorption of cellulose acetate 78−13345
fast neutron induced DNA strand breaks and repair obs., cultured mammalian cells 80−61651
fast neutron sublethal damage and cell division delay expts. 79−20588
fast neutron teletherapy, preliminary clinical results 79−20639
fast neutron therapy, radiobiological bases 80−35995
fast neutron therapy history 79−20634
fast neutrons in normal tissue, early and late damage obs. 79−20590
fast reactor materials, fast neutron damage 78−10093
fast reactor peripheral fuel element shells, radiational swelling circumferential nonuniformity 79−19289
fast reactor steels and alloys, neutron damage development, irradiation conditions, chemical composition 80−34082
fast reactor subassemblies, irrad. swelling induced bow 79−93724
FBR fuel cladding alloys, phase instabilities and swelling behaviour 79−54500
FCC metals, high dose neutron irrad. effects, 4.6K 78−34548
ferroelectric ceramic, polycryst., elasticity props., neutron bombardment effects 80−79856
ferroprobe performance under neutron irradiation 78−60960
FFTF irradiation test program 79−67928
fibroblast cells, human, comparative response to 50 MeV neutrons 79−34512
fission reactor materials, intrareactor facility for physicomechanical props. investig. by pulsed US spectroscopic method 78−70591
fission reactor materials, radiational growth due to diffusional anisotropy 79−71897
fission reactor welded pressure components, effect of material property changes on operating conditions 79−20197
free plant cell, suspension-cultivated, survival after X-ray and fission neutron irrad. 79−92296
Frenkel pair stability in HCP lattice 79−60353
fuel element, diametral evolution meas. during irradiation, medina service 77−42062
fuel element modelling, interpreting and predicting irradiation creep 77−42058
fuel form and cladding carbide distrib. on fuel-clad interaction during irrad. 79−85618
fuel pins, fast breeder, fuel-cladding mech. interaction, obs. and anal. 80−86959
fuel rod, simulated, for HTGR, pre- and postirradiational thermal transport and thermal expansion 79−6742
fusion devices, controlled, surface effects, conf., San Francisco, USA (Feb. 1976) 77−30659
fusion materials, damage parameters spatial variations, implications 80−34065
Fusion Materials Irradiation Test Facility 80−91361
fusion neutron induced nuclear recoil emission probabilities 78−15256

neutron effects continued
fusion reactor, MFTF, intense neutron environment, test cell side wall design, shielding materials 80−102318
fusion reactor, neutron irradiation effects on organic insulators at 5K for superconducting magnets 80−107336
fusion reactor, radiation-induced degassing of cryopumps 79−85780
fusion reactor alloy damage effects, simulation of likely neutron environment 78−8972
fusion reactor electrical insulators 78−95082
fusion reactor first wall, prod. of H, D and He by 15 MeV neutrons 79−93831
fusion reactor first wall material, mobile He inclusion in void swelling rate theory model 80−34069
fusion reactor first wall materials, mechanical, corrosion and irrad. behaviour requirements 77−67875
fusion reactor first wall materials development evaluations, fatigue crack growth testing optimisation 80−35444
fusion reactor first wall radiation damage, H and He gas prod. from stainless steel 78−82512
fusion reactor first-wall program, appl. ORR fission reactor for simulation of neutron environment 78−8973
fusion reactor insulators, radiation damage calcs. using MORSE code 80−34061
fusion reactor materials, microstruct. development in simulated irrad. 80−34072
fusion reactor materials, primary damage, energy depend. 80−34064
fusion reactor materials, range calculations using multigroup transport methods 80−34070
fusion reactor metals, He embrittlement, grain boundary cavity model 80−34075
fusion reactor metals and alloys, microvoid form., gaseous impurity atom effects, positron annihilation study 80−49275
fusion reactor potential materials, He generation by 14.8 MeV neutron 79−67944
fusion reactors, neutron irradiation damage *(Japanese)* 79−31180
n-GaAs, neutron irrad. and thermally induced defects, annealing stages 77−51409
gamma radiation field induced in air by fast neutrons, intensity and absorbed energy calc. method 77−50310
gas atoms per bubble of inert gas in solid 77−76468
gas bubbles growth, during irradiation, stress effect 80−49277
GCFR, prototypic grid-plate shield confirmation experiment 79−54562
GCFR claddings, neutron-induced He implantation, calc. of total flux 80−42773
gerbil, Mongolian, radioresist. to fast neutrons 77−48844
glass, to promote colouring 77−8961
glassy semiconductors, neutron irradiated, paramag. centres 79−82872
glassy-C, irradiation induced dimensional changes 80−65052
graphite, chem. rate theory applic. to fast neutron irrad. damage 77−27913
graphite, creep irradiation expt., design, operation, initial results 77−42067
graphite, cyclic fatigue, influence of stress cycle and neutron irrad. 79−52335
graphite, development and irradiation program for PBHTR appls. 80−5245
graphite, electron-spectroscopic analysis of neutron-irradiated pyrographite 80−63261
graphite, EPR, effect of motional averaging, anisotropy, skin effect rel. to heat treatment and neutron irradiation *(French)* 80−34752
graphite, fast neutron flux effect on irradiation damage 78−22768
graphite, fast neutron irrad. damage, chem. rate theory applic. effect of annealing and thermal equilib. defect concs. 77−67804
graphite, fast neutron irrad. damage theory and modifications 77−67805
graphite, fusion reactor first wall appl., radiation damage 79−86822
graphite, heat strength calc. for power reactors 79−36331
graphite, irradiated, stored at room temp., neutron damage annealing and C_{44} shear modulus 80−2080
graphite, irradiated ultimate tensile bending and compressive strength charact. 78−15479
graphite, irradiation creep 77−42066
graphite, irradiation induced creep, UKAEA reactor group studies 77−42065
graphite, irradiation-induced temp.-change effects, semiempirical model calc. 80−42775
graphite, isotropic nuclear, neutron irrad. behaviour 78−18683
graphite, material properties, neutron irrad. effects, model 79−10880
graphite, microhardness changes, effect of annealing and neutron irradiation 77−8861
graphite, neutron damage at 1200°C, fusion reactor first-wall appl. 79−93829
graphite, neutron effects on shrinkage 80−37456
graphite, neutron induced changes, exam. of lattice consts., elastic modulus, elec. cond 79−95053
graphite, neutron irrad., annealing of radiation damage 79−1465
graphite, neutron irrad., microporosity, elec. resist., length, struct. changes 78−43051
graphite, neutron irrad., porosity changes, neutron small angle scatt. investig. 78−34544
graphite, neutron irradiated, effect on quantum limit Shubnikov-de Haas oscills. 78−95304
graphite, neutron irradiated, thermoelec. and thermomag. effects 77−59296
graphite, neutron irradiation, electron transport, annealing study 80−39165
graphite, neutron irradiation effects on thermal shock resist. and fracture toughness *(Japanese)* 80−66622
graphite, neutron-irradiated, EPR, rel. to electronic struct. *(Japanese)* 78−19326
graphite, nucl. grade, unirrad. and neutron irrad., compressive stress effect on Young's modulus 77−61503
graphite, polycryst., neutron irrad., low temp. sp. ht. anomalies, spin-spin interactions 79−15307
graphite, polycryst., reactor-grade, isothermal annealing obs., by ESR *(Japanese)* 77−43254
graphite, pyrolytic, galvanomag. effects, effect of fast neutron irradiation 80−34465
graphite, pyrolytic, neutron irrad., Raman spectra, point defects 77−69834
graphite, pyrolytic, neutron irrad. at low temp., thermal cond. recovery *(French)* 77−62566
neutron effects continued
graphite, pyrolytic doped with B^{11}, neutron irrad. damage at 60°C 79−90702
graphite, radiation alteration over wide range of neutron flux and irradiation temp. 80−29072
graphite, radiation creep 77−42064
graphite, reactor-grade, permeability, effect of neutron irradiation 79−71900
graphite, reloadable creep facility for tensile or compressive expts. 77−42070
graphite, structural, impact toughness, reln. to compressive strength 78−88605
graphite, synthetic materials, radiation defects, review 77−47494
graphite, uniaxial tensile creep capsules with continuous strain registration 77−42071
graphite damage function in neutron irrad. up to 15 MeV 80−34059
graphite radiation damage dosemeter, GAMIN, correlation data 78−29657
graphite reflectors in PBR with OTTO fueling, neutron effects, stress anal., cooling measures *(German)* 77−34368
graphite rods, damage by high energy neutrons 80−29070
graphite structures in PBR, neutron radiation damage, mech. props., stress fields *(German)* 77−34387
gustatory function, radiation-induced changes, neutrons rel. to photons 80−12184
haematopoietic microenvironment, progenitor cells radiosensitivity, mouse expts. 80−45983
heavy ion simulation of neutron radiation damage 80−29071
heavy-ion simulation of neutron radiation damage, HT ultra-high facility for potential reactor materials 77−57786
heteroallelic reversion induction, in diploid yeast fission neutron O_2 enhancement ratio 79−88139
hollow sphere exposed to radiation, thermoelastoplastic problem 77−14928
HTGR Biso coated fuel particles, neutron induced permeability 77−42100
HTGR fuel elements, neutron irradiation behaviour of graphitic matrix materials 79−19283
HTGR fuel rods with diluted thermosetting matrices, irradiation performance 77−83038
HTGR pyrocarbon coated fuel, neutron effects in range 1273-1773K 77−79434
HTGR pyrocarbon coated particles, neutron induced permeability 77−79435
HTR annular compacts, creep strain limit expt. 77−42069
HTR compact and matrix material, uniaxial creep meas. under tensile load at 900°C 77−42068
HTR fuel, high neutron flux, high temp., post irradiation exam. 78−58360
HTR fuel specimens, neutron irradiated, post irradiation exam., microradiography, metallography, burn-up determ. 78−58361
III-V semiconductors, radiation-induced defects, review 77−80544
Inconel 600, Neutron irradiation using HFIR for evaluation as fusion reactor material 78−13324
Inconel X750 springs, in-reactor stress relaxation 78−11256
inert gas release from irradiated solids 78−22767
insulators, neutron activated β-emitters, hyperfine interactions 78−39070
interstitial cluster nucleation at the onset of irradiation 78−79635
intestinal cell sublethal damage after mixed treatment with X-rays and fast neutrons, mouse 77−64086
intestine, mouse, response to 14 MeV neutrons 79−66490
ion accelerators for fusion ignition, neutron resistant ceramic insulator development 80−37639
ion injection type fast neutron dosimeter, fabrication attempts 77−81583
iron oxalate, γ-ray and neutron irrad. effects, Mossbauer spectra obs. 79−65778
irradiated material in elastoplastic region, systems of remote meas. of forces and deform. in cyclic tests 77−90546
irradiation creep, temp. depend. 77−43252
irradiation facility in WR-1 organic-cooled research reactor, corrosion testing 78−89945
Kapton (polyimide), insulators for superconducting magnets, effect of low temp. irradiation 80−25817
knock-on reactions, Kinchin-Pease model 77−27912
lens opacification in mice exposed to 14 MeV neutrons 78−65097
leukemia risk from neutron exposure 79−39509
leukemia risk from neutrons 79−70589
life shortening in RFM and BALB/c mice as function of radiation quality, dose and dose rate 80−41134
liver, RBE of cyclotron fast neutrons and γ-rays for late hepatic injury in rats 80−108975
LMFBR, effect of cracks in fast neutron embrittled hexagonal subassembly ducts 78−74446
LMFBR, in-reactor irrad. creep expt., thermal anal. 79−67854
LMFBR core design, irradiation creep data 77−46211
LMFBR core materials, effect of swelling and creep on performance 78−13261
LMFBR permanent reactor structures, design, irradiation effects 78−21623
low and intermediate energy radiation physics 80−19845
lung, canine, relative effectiveness of fast neutron and ^{60}Co γ-ray irradiation 80−3737
lung epithelial cells, type 2, proliferative response after X-rays and fission neutrons 80−108974
lung tumour induction in RFM mice after localised X- or neutron irrad. 80−72260
LWR, fission product activities, fuel survey 80−736
LWR controlled porosity fuels, short term irradiation behaviour 79−49686
LWR high-power rods under irradiation, chemical state 79−97809
LWR pressure vessels, radiation embrittlement, role of ASTM 79−22435
lymphocyte, hog, energy metabolism effect of ionising radiation 79−92301
lymphocyte chromosome aberrations and the Poisson distrib. 79−100675
lymphocytes, human, RBE for d(42 MeV)-Be neutrons based on chromosome-type aberrations 80−104663
lymphocytes, human, variation in neutron RBE values compared to X-rays 80−101229
lymphoma, murine, effect of synchrony on survival of L5178Y cells after neutron irrad. 80−72227

neutron effects continued
malignant melanoma, thermal neutron capture therapy, in vitro radiobiological anal. 80−104657
mammalian cells, influence of radiation quality on effectiveness of small doses 80−30785
mammalian cells, lethally damaged, proliferation obs. after irrad. by various particles 80−108971
martensite ageing, influence of neutron irradiation *(Czech)* 78−84859
material irradiation facility in the WR-1 research reactor, structural material development 78−54868
materials research by low temp. neutron irrad. *(Japanese)* 77−72637
medical neutron dosimetry, standards 79−12013
metal, anelastic study of intrinsic point defects, irradiation effects 78−47323
metal, anisotropic, inelastic deform. under complex loading conditions and high neutron flux, equation 78−80598
metal, BCC, neutron irradiated, spontaneous recombination volumes of Frenkel defects, rel. to compressibility 78−71765
metal, creep, point defects 78−48462
metal, FCC, investigation of stage-I_E interstitial nature by TEM 78−47329
metal, heavy irradiation damage at high temps., void swelling problems *(Japanese)* 77−59049
metal, ion and neutron irrad., low temp. defect prod. and stage 1 recovery 78−79637
metal, irrad., peak void swelling temp. 77−72608
metal, irradiated, triangular Frank loop dissociation 77−11599
metal, irradiated, void nucleation theory 79−1464
metal, irradiation creep and swelling, cascade damage effect 77−19991
metal, low temp. neutron irrad., dose depend. of recovery peaks 78−71767
metal, positron annihilation study of neutron damage, review 78−71769
metal, radiation damage effects, neutrons and heavy ions, rel. to reactor technology, review 77−43255
metal, radiation stimulated diffusional flow, neutron irrad. *(Russian)* 79−29132
metal, vacancy defect mobilities and binding energies obtained from annealing studies 78−47325
metal, void swelling and dislocation loop growth on fast particle irrad. *(Russian)* 77−59047
metal surface, 14.8 MeV neutrons, radionuclide product ejection range 78−15257
metallic mirrors for laser fusion reactors, neutron and gamma irrad. response calc. 80−23121
metals, effect of neutron irrad. on plasticity characts. 78−64607
metals, fast neutrons, simulation by accelerated multiply charged ions, $^{56}Fe^{3+}$ expts. 77−30651
metals, FCC, very high dose reactor neutron irrad. at low temp. 78−71766
metals, general rate theory model of void swelling 79−23655
metals, irrad., mechanism of formation of vacancy dislocation loops *(Russian)* 80−65053
metals, irradiation creep strain, produced by vacancy loops, calc. of magnitude 78−72815
metals, radiation effects, ion beam study, review 79−10883
metals, radiation effects on elasticity and elastic moduli, yield stress 80−2078
metals, swelling during pulsed irrad., model, void growth exam. 78−47436
metals, vacancy porosity kinetics at high irradiation doses of fast neturons 79−28018
metals and alloys, irradiated, solute segregation and precipitation effects on void swelling 78−67741
metals in nuclear reactors, thermo-elasto-visco-plasticity 77−3111
metals irradiated, heavily, exam. of percolative mass transfer 78−79639
metals under stress, thermally and radiation induced creep, constitutive relns. 77−90413
methylbenzene, solid, pulsed cold neutron source, moderation props., radiation decomp. 77−83407
mixed fluoride crystals, nucl. radiation effects 80−80831
mixed oxide fuels, SEM obs. of gas bubble morphology 80−57843
mixed-oxide fuel, irradiated, microstruct. charact. and radial distrib. of retained fission gas 79−59188
momentum transfer and damage energy gradient effects on He permeability 78−10102
MOS capacitor, neutron damage mechanisms in CCDs 79−19672
multiple neutron fractions, RBE for late spinal cord injury 79−25051
MX type reactor fuels, microscopic swelling meas., effects of grain boundary migration 78−66348
Mylar (polyester), insulators for superconducting magnets, effect of low temp. irradiation 80−25817
NBS reactor, summary of activities, (July 1976 to June 1977) 78−82435
neutron irradiated, positron annihilation at temps. 350 to 1000°C 78−55894
neutron radiography, industrial applications in USA, review of data and neutron effects 78−60891
neutron-irrad., void annealing, positron annihilation obs. 77−76469
Nimonic PE16, neutron irradiated after heat treatment, solute segregation to pt.-defect sinks 79−78976
Nomex (nylon paper), insulators for superconducting magnets, effect of low temp. irradiation 80−25817
nonfissile metals and alloys, irradiation creep 77−42072
nonmetallic crystals, collapse of tracks formed by fission fragments 80−24510
nuclear fuel, MX type, self diffusion in- and out-of-pile 78−82457
nuclear fuel, transport phenomena under severe temp. gradient 80−615
nuclear fuel cladding, slightly oval cylindrical shells, creep anal. 78−78468
nuclear fuel restructuring and relocation under irrad., COMETHE code calcs. 77−46235
nuclear fuels, radiation enhanced kinetics in the fuel lattice 80−59522
nuclear reactor component, fluence limits anal., damage function methods, computer simulation 77−18668
nuclear reactor material, neutron energy spectrum depend., damage function *(German)* 77−34386
nuclear reactor pressure vessel material surveillance capsule, neutron radiation, limiting condition 80−47572
nuclear reactor pressure vessels, radiation embrittlement, allowable crack size, unstable fracture 77−10465
nucleation of defect clusters in crystalline solids 79−42051
neutron effects continued
oil, lubricating, radn. effects and radn. dosimetry appl. 80−2069
optical fibre, neutron and gamma induced transient absorpt. and luminesc. 80−58763
optical fibre, step-index, pulse dispersion, neutron irrad. effects 80−91897
optical fibre attenuation and pulse dispersion 80−58730
optical fibres, glass and plastic, neutron irradiated, optical absorpt. spectra 0.7 to 1.1 μm 80−58762
organic scintillator, captured γ quanta yield, fast neutron irrad. 77−46457
oxide fuel in reactor creep, LMFBR design aspects 77−42057
oxide nuclear fuel, fission gas release and swelling, simple operational model 80−92565
p^+-n diode under forward bias, effects of radiation-induced deep levels on admittance 78−23157
PAN fibres, neutron irradiated, struct. and props. *(Russian)* 80−25763
pathologic effects of neutron and photon exposures of lung and spinal cord, rabbit expts. 80−41126
personnel dosimetry, Czechoslovak comparison of methods 77−50302
personnel dosimetry, need for improved standards 79−12012
phase stability of sigma phase, irrad. effect 78−11200
PMMA, neutron and gamma irradiation effects 80−66839
PMMA, neutron irradiation, radical distribution, ESR study *(Japanese)* 80−44920
PMMA, reactor irrad., growth of macroscopic radiolytic gas bubbles, diffusion model 80−65058
point defect distrib. in bounded media under irradiation 77−7712
point defect nucleation and growth, rate theory model for simultaneous clustering 80−13604
point defect precipitation near grown-in dislocations during neutron irradiation 78−26600
point defect sink strength in irradiated materials 77−51368
point defects of rad. damage to construction materials, math. modelling 79−90703
polycarbonate, insulators for superconducting magnets, effect of low temp. irradiation 80−25817
polyethylene, neutron irradiation, radical distribution, ESR study *(Japanese)* 80−44920
polyethylene, welded, exam. of neutron irrad. effects on tensile characts. *(Japanese)* 78−84918
polypropylene, insulators for superconducting magnets, effect of low temp. irradiation 80−25817
polypropylene, neutron irradiation effect on weldability and adhesion *(Japanese)* 79−60405
polysytene, neutron and gamma-irradiation effects 80−66839
precession in mag. field, equivalence principle test *(Norwegian)* 77−64986
precipitation stability under irradiation, point defect effects 77−21148
pressure vessel, Oconee nuclear station, surveillance capsule results 79−18019
pressure vessels for PWR, BWR, safety calcs., design, operation control *(German)* 77−34404
pulmonary metastases of mouse fibrosarcoma, RBE of neutrons prod. by 50 MeV deuterons on Be 77−81536
PWR, KWU 1300 MWe facility, neutron flux computer calcs., radiation damage 77−34370
PWR, reactor cavity shield system, design and anal. 79−59225
pyrocarbon, irradiation-induced dimensional changes 80−65052
pyrocarbon coated particles, influence of fast neutrons on transport behaviour of solid fission products *(German)* 79−13427
pyrocarbon coating, isotropic, gas permeability, neutron irradiation effect *(French)* 80−63260
pyrocarbon coating of Biso fuel, neutron effects on stress and strain 77−79437
pyrocarbon coating of Biso fuel, neutron effects on stresses and strains 77−79436
pyrocarbon coatings, deposition in fluidized bed, TEM, changes by irradiation 80−34084
pyrocarbon nuclear fuel coating, props. and neutron irrad. behaviour *(German)* 77−67816
pyrocarbons, EPR, effect of motional averaging, anisotropy, skin effect rel. to heat treatment and neutron irradiation *(French)* 80−34752
pyrographite, initial stress state, neutron irrad. effect 80−97555
quartz, comparison of different radiation effects 78−26596
quartz, crystal structure rearrangement due to neutron irrad. 80−64981
quartz, effect of neutrons on electr. characts. *(Russian)* 77−48119
quartz, fast neutron irradiated, saturation of 9.4 GHz hypersonic attenuation 79−23682
quartz, fast neutron irradiated, spin-lattice relax., 0.1 to 4.2K 79−78519
α-quartz, Gruneisen constants for optical modes, neutron irrad. and press. effects *(Russian)* 78−22815
quartz, irrad., annealed optical absorpt. power *(Russian)* 77−36273
quartz, neutron irradiated, annealing effect on optical props. *(Russian)* 77−32381
quartz, neutron irradiated, thermal spikes 78−38757
quartz, neutron irradiated, X-ray cryst. struct. anal. 79−14853
quartz, radiation stimulated Ag diffusion *(Russian)* 77−39694
α-quartz, Raman spectral lines, radiation and temp.-induced changes in width and intensity 78−2859
quartz, surface damage by X-rays, γ-rays, neutrons, SEM study 80−79837
quartz, surface quality determ. using Ag diffusion and neutron-activation method 79−51401
quartz, TFTR diagnostic windows, radiation damage 80−34063
α-quartz and quartz glass, neutron irradiated struct., neutron diffr. meas. 78−22769
quartz crystal, oscillating characts., nucl. and X-irrad. effects 79−78626
quartz radiation defects, effect of annealing on absorpt. spectrum *(Russian)* 77−47495
radiation damage computer simulation system, WINERY 78−30675
radiation induced solute segregation, kinetic model, GEAR package of subroutines 78−30673
radiation induced solute segregation and precipitation study by means of Johnson-Lam kinetic model 79−43252
radiation testing of materials in reactors, measure of radiation effect, dosimetric information 78−79640
radiation therapy, cyclotron biological intercomparisons 79−20589
radioactivation of shielding materials Fe, Benelex by fast neutrons, γ-ray spectra, decay rates 79−682
radiobiology, OER of Fermilab high energy neutrons 77−70500

neutron effects continued
radiotherapy planning and radiation quality definition 80−12246
rate equations, irrad. induced voids, swelling, creep 80−49274
reactor graphite, stress and strain determ. depend. of mech. charact. on temp. and fluence 79−40998
reactor irradiations facility, 70-400°C 80−6439
reactor materials, fast breeder and fusion reactors, review *(Japanese)* 79−81011
reactor materials, radiation-induced embrittlement and swelling due to void form, ASTM research 78−13231
reactor radiation damage, neutron metrology for irradiation parameters 79−46717
reactor structural materials, alloy phase thermochemical stability, calc. of radiation effects 79−60406
recoil T atoms+H_2O, neutron effects, apparent phase effect 77−63935
refractory fusion reactor materials, neutron irrad., microstruct., voids, nucleation TEM study 80−29065
rice, M_1 damage, RBE of thermal neutrons 80−104649
root meristem cells, Vicia faba, subnuclear chromosome aberrations rel. to neutron energy deposition 80−26280
rotating target neutron souces, appl. to high energy neutron induced effects on fusion reactor materials 79−45493
Sandia Laboratories nuclear weapon neutron environment simulation, hardening tests 79−22448
sapphire, 14.8 MeV neutron damaged, optical vibronic absorption spectra 80−50384
sapphire, F-centre, fluorescence decay below 75K 80−60664
sapphire, neutron bombard., F-centre fluorescence, photoluminescence 80−100676
scintillation screen containing Li for neutron introscopy 79−76302
seed radiosensitivity of winter hexaploid triticale 79−20583
seedlings, Vicia faba, effects of different radiation types on growth *(German)* 79−43961
semiconductor, neutron transmutation doping, damage-energy distrib. 80−15137
semiconductor, neutron transmutation doping 80−15133
semiconductor doping, computer controlled neutron irrad. system 80−19851
semiconductor doping by nuclear transmutation method *(German)* 78−95066
semiconductor p-n junctions voltage-current charact., fast neutron irrad. effects *(Russian)* 80−65659
semiconductors transmutation doping, conf., Columbia, USA (April 1978) 80−12849
silicate glasses, effect of high dose X-rays and reactor radiation 80−19838
silicone-clad silica low-loss fibre radiation response obs. 78−1397
simulation, reliability of use of ^{235}U fission fragments 79−42113
simulation by the implantation, uniform conc. injection 78−79648
simulation of neutron damage, using HVEM, state-of-the-art 77−51417
sink strength of dislocation loops, growth in irradiated materials 79−99246
skin, X-ray and fast neutron damage, relationship between OER, RBE and no. of fractions 80−35978
skin γ and neutron responses, dose fractionation effects 79−20593
skin injury, pig, relative biological effectiveness of neutrons and γ-rays 79−34605
skyshine from nucl. facilities *(Japanese)* 79−18054
slow neutron action on glasses and vitreous ceramic and cryst. materials *(Spanish)* 80−57816
SNR-300 fuel rods, postirradiation examinations of RAPSODIE-1 expt. 77−46219
solids, defect form. due to fast neutron bombardment, influence of temp. *(Russian)* 77−65992
solute segregation, under irradiation 78−48407
spermatogonial stem cell survival in mouse, split dose neutron and X-irrad. 78−28012
spermatogonial stem cells, mouse, survival after split-dose irrad. with fission neutrons 80−72244
sputtering at 14 MeV, models for ejection of micron-sized chunks 77−36318
sputtering measurement 78−95621
squamous-cell carcinoma, spontaneous, in mice, comparison of neutron- and X-irrad. effects 80−98033
stainles steel, type 316, irrad. in simulated environment, tensile props. 80−34076
stainless steel, 18Cr-11Ni, for nuclear reactors, mech. props., neutron effects 77−34383
stainless steel, ferritic SUS 410 type, coated with organometallic complexes and Ti alkoxides 80−34078
stainless steel, He prod., cross section determ. 79−22282
stainless steel, neutron dose determ., from isotope abundance ratio, mass spectra obs. 80−61220
stainless steel, type 304, stress free swelling at high neutron fluences 77−42093
stainless steel, type 316, neutron irrad., microstruct. and tensile props. 80−34077
stainless steel in fusion reactors, effect of pulsed radiation on swelling 79−31190
stainless steels, type 304, fast-neutron swelling behaviour 79−67864
steel, 0Kh16N15M3B, irradiation effects on resistance to cyclic elastoplastic deformation 79−91767
steel, 3.5% Ni neutron irrad. effects on tensile props., microstructure effects 77−69005
steel, A302B, neutron damage, ductile-brittle transition temp. 77−3109
steel, additivity deviations in thermal and radiation induced embrittlement 77−73348
steel, AISI 316, fast reactor irradiated, solution treated, struct. 77−69008
steel, alloy A533B1, neutron irrad., flow growth charact. by acoustic monitoring 80−100918
steel, austenite, γ and neutron irradiation, Mossbauer spectra anal. 78−692
steel, austenitic, ASTM A533B and A542, H_2 embrittlement behavior of unirrad. steels for nuclear reactor press. vessels 79−8340
steel, austenitic, cold worked, derivation of simple void-swelling equation 79−7631
steel, austenitic, fracture toughness meas. by Charpy impact testing, welding, heat treatment, neutron irrad. effects 79−5062
steel, austenitic, high content of low melting additives, high temp. neutron irradiation embrittlement *(Russian)* 79−73218
neutron effects continued
steel, austenitic, neutron irrad., He release kinetics 78−79638
steel, austenitic, neutron irradiated, He absorption 77−51414
steel, austenitic, Ni-Cr, neutron-irradiated solute segregation and void swelling 79−60407
steel, austenitic, X6CrNi1811 and X6CrNiMo1713, crack growth under Na cooled fast breeder reactor conditions *(German)* 78−56798
steel, austenitic stainless, Cr-Ni, resist. damage rate during neutron irrad. at 23K 80−96571
steel, austenitic stainless, Cr-Ni (16, 16 wt.%), in-pile rupture strength, cold work and soln. annealing effects 77−63687
steel, austenitic stainless, creep, rel. to radiation swelling and stacking fault energy *(Russian)* 78−27562
steel, austenitic stainless, effect of irrad. and other factors on fatigue crack propagation 79−20194
steel, austenitic stainless, fast neutron irrad., effect on mech. props. 78−92309
steel, austenitic stainless, fatigue crack propagation, effect of neutron irradiation 80−97583
steel, austenitic stainless, fatigue crack propagation, influence of neutron irradiation 80−97584
steel, austenitic stainless, fusion reactor first-wall and blanket material, mech. props. 80−34074
steel, austenitic stainless, He role in neutron induced microstruct. evolution 80−29064
steel, austenitic stainless, mech. props. correl. methodology development for fusion environments 80−29068
steel, austenitic stainless, multiaxial creep equations for nonlinear and volume-nonconservative in-reactor creep 79−59164
steel, austenitic stainless, neutron dose rate depend. of swelling in fission reactors 80−104233
steel, austenitic stainless, neutron irrad., mag. props. 80−29067
steel, austenitic stainless, neutron irrad. effects on fatigue crack propag. 80−29069
steel, austenitic stainless, neutron irradiated OKh16N15M3B, reactor structural material, low-cycle fatigue study 79−91793
steel, austenitic stainless, neutron-irradiated, gamma-alpha transformation 79−96027
steel, austenitic stainless, radiation-induced swelling in BOR-60 reactor 79−97814
steel, austenitic stainless, type 316, D-T fusion neutron and Ni^{2+} ion damage 78−14388
steel, austenitic stainless FV548, neutron irradiated, Si-rich phase occurrence of M_6C phase 80−15156
steel, austenitic type 316, continuous gas generation effects in neutron and simulation environments 80−34068
steel, austenitic-ferritic stainless, radiation swelling in fission reactors 80−65063
steel, crack propagation stress wave obs. of brittle fracture *(German)* 77−56110
steel, CT specimens, irradiated in FRJ-1 research reactor, neutron flux densities, temp. fields meas. 77−83029
steel, Cu, fission reactor vessels, neutron embrittled, exam. of technique for in situ thermal annealing 79−29114
steel, damage function for mech. props. 78−13228
steel, ferritic alloy and martensitic stainless, void swelling response after fast reactor irradiation 80−6437
steel, for PWR press. vessels, RT_{NDT} shift of ductile-temp. curve, correl. with neutron dose *(German)* 77−34388
steel, high speed, irradiated, absolute tool wear determ. by γ-γ coincidence counting of radiotracers 77−73352
steel, irrad. effects at high temp., simulation by HV electron microscope 77−1153
steel, irradiated, liberation of He in uniform heating 77−50248
steel, irradiation induced swelling, empirical relationship with dose and temp. 77−50247
steel, low alloy, 15Kh2MFA and 15Kh2NMFA, neutron irrad. embrittlement, effect of P, Sb and Sn impurities 80−85055
steel, low alloy, radiation embrittlement, heat treatment effects 78−19893
steel, low alloy, reactor pressure vessel, effect of Mn and C content on irrad. response 79−20196
steel, low-alloy hydrogenation and embrittlement under neutron irrad. in contact with water *(Russian)* 77−52529
steel, low-alloy structural, radiation hardening, rel. to embrittlement *(Russian)* 77−21243
steel, LWR pressure vessel, neutron radiation effects on material props., review *(German)* 77−34382
steel, martensitic, delayed fractures suppression *(Czech)* 78−67743
steel, mass spectrometer system for He assay 77−34397
steel, mild, yield point, effect of neutron irrad. and N_2 conc. 80−45365
steel, Mn-Ni-Mo, PWR pressure vessel, irrad. induced embrittlement, chemical composition effect *(French)* 79−20195
steel, neutron irradiated 15KhMFA, H_2 induced delayed fracture *(Russian)* 78−35476
steel, neutron irradiated press. vessel material, small angle neutron scatt meas. 79−13428
steel, NiMoCr waterquenched, for BWR press. vessel, fast neutron fluence evaluation, irrad. behaviour *(German)* 77−34369
steel, nuclear reactor material irrad. effects, neutron energy depend., damage model *(German)* 77−34385
steel, nuclear reactor press. vessel, neutron exposure, safety limitations *(German)* 77−34405
steel, nuclear reactor press. vessel, radiation induced embrittlement, slow neutron small angle scatt. study *(German)* 77−34390
steel, reactivity meas., determination method *(Russian)* 80−664
steel, reactor pressure vessel failure and radiation damage *(Czech)* 80−619
steel, reactor pressure vessels, positron annihilation as nondestructive monitor of radiation damage 77−4130
steel, reactor vessel, neutron irrad. effect on brittle fracture charact. *(Slovak)* 78−50254
steel, stabilised, pressurised capsules in-pile creep meas. 77−42077
steel, stainless, 20% cold worked 316, in-reactor stress relaxation in bending 77−42079
steel, stainless, 20% coldworked 316, irradiation creep, depend. on temp. and atom displacements 77−42075
steel, stainless, 304, bend test ductility of irrad. specimens for LMFBR appls. 80−104235
steel, stainless, 304L, irrad. induced creep and swelling 79−93723

neutron effects continued
steel, stainless, 316, neutron irradiation embrittlement, pre-irradiation treatment and composition modification 80−3171
steel, stainless, 316, sputtering by fusion neutrons meas. 77−36321
steel, stainless, cladding, irradiation enhanced creep 77−42074
steel, stainless, dose rate and cascade collapse effects on swelling 79−23656
steel, stainless, EBR-II reflector assembly irrad. induced bowing, implications for core restraint design 80−104234
steel, stainless, effect of He preinjection on swelling during neutron radiation damage simulation 80−44236
steel, stainless, fatigue props. of low-fluence neutron irrad. samples 80−97585
steel, stainless, FBR cladding stress distrib., effect of irradiation-induced swelling 80−19850
steel, stainless, fusion reactor shield, neutron induced activity and γ-ray source investigation 78−54872
steel, stainless, in-pile irrad. effect simulation by Ni ion bombardment, dislocation density, swelling 77−347
steel, stainless, in-reactor deformation and fracture behaviour of EBR-II driver fuel cladding 80−42769
steel, stainless, irradiated, vacancy loop effect on swelling 79−14852
steel, stainless, irradiation creep and swelling, microstructural modelling 77−52407
steel, stainless, irradiation creep in bending 77−42078
steel, stainless, irradiation induced creep in BR2 reactor using resonant cavity method 77−42080
steel, stainless, Kh18N10T, long-term strength under in-pile irrad. conditions 78−6940
steel, stainless, low-cycle fatigue characteristics of neutron irrad. samples 80−97586
steel, stainless, neutron irrad., point defect cond. and void radius change, appl. of model for void growth 78−47436
steel, stainless, neutron irrad., pore annealing kinetics 77−72638
steel, stainless, neutron irrad., solution-annealed and cold-worked, swelling 78−13229
steel, stainless, neutron irradiated, stress effects on microstruct. 77−47490
steel, stainless, neutron irradiation and N_2O_4 corrosion effects *(Russian)* 80−52741
steel, stainless, neutron irradiation effect on low cycle fatigue and tensile props. at 298K 80−30059
steel, stainless, sintered Kh18N10T, friction and corrosion props. for frictional units of nuclear plants 78−60845
steel, stainless, solution annealed 304L, in-reactor deform. 77−42076
steel, stainless, swelling, neutron induced, neutron flux and irrad. temp. dependence 78−79636
steel, stainless, type 304L, neutron irradiated, in-reactor precipitation and ferritic transformation 79−77644
steel, stainless, type 304L, neutron irradiated, TEM study of ferrite formation 79−42112
steel, stainless, type 316, cold worked, precipitation response to neutron irrad. 80−34073
steel, stainless, type 316, influence of preirrad. thermal-mechanical treatment on phase stability and swelling 79−55792
steel, stainless, Type 316, irrad. effects on tensile props. and microstruct. 80−65059
steel, stainless, type 316, modelling effects of fast neutron irradiation in mech. behaviour 80−84234
steel, stainless, type 316, neutron irrad. damage simulation using HVEM, surface effect on void swelling 78−29572
steel, stainless, type 316, neutron irradiated, ferrite formation, study by mag. meas. and TEM 79−37742
steel, stainless, type 316, stress-free swelling at high neutron fluence, rel. to LMFBR core environment 78−13239
steel, stainless, type 316, struct. life anal. for fusion reactor first-wall appl. 78−13326
steel, stainless, type 4301, radiation enhanced permeation of H_2 80−59732
steel, stainless, used as reactor cladding material, void swelling obs. by HV electron microscope *(Japanese)* 79−42108
steel, stainless 304, previously irradiated, irradiation induced stress relaxation in fast flux environment 77−25104
steel, stainless 304 and 308 and weld material, fatigue crack propag. in neutron irradiation 78−23815
steel, stainless 316, 20% cold worked, swelling increase due to inreactor temp. reduction 78−34547
steel, stainless 316, carbide precipitation rel.-to in-reactor deform. 79−8302
steel, stainless 316, cladding failure during thermal transients 79−8316
steel, stainless 316, dislocation substruct. prod. by elev. temp. fatigue crack propag., TEM obs. 78−19863
steel, stainless 316, fatigue behaviour of materials containing significant amounts of irrad.-induced He 80−100917
steel, stainless 316, irradiated void swelling incubation period, stress effects 78−6105
steel, stainless 316, irradiation induced swelling, stress effects 78−34545
steel, stainless AISI 316, fast neutron void swelling simulation dose and dose rate effects 77−15457
steel, stainless AISI 316, neutron irradiated, rel. between irradiation induced swelling and shear modulus 80−15157
steel, stainless AISI 316, Si and Ti effect in phase stability and swelling behaviour 79−78972
steel, stainless austenitic, neutron irrad., swelling due to gamma prime and $M_{23}(C,Si)_6$ form. 78−51590
steel, stainless M316, neutron irradiated, occurrence of ordered FCC phase 77−51411
steel, stainless type 316, irrad. induced nuclear cladding swelling, empirical development of design equation 80−59527
steel, stainless type 316, neutron irradiated, or themally aged diamond-cubic η phase formation, TEM study 79−99249
steel, stainless type 316, neutron irradiated, transient mech. response prediction 79−74207
steel, stainless types 361 and 304, He and He prod. cross sections for 15 MeV neutrons 77−50291
steel, tubular, type 0Kh16N15M3B, reactor irradiated, creep resist. *(Russian)* 80−25762
steel, type 1Kh18N9T, neutron irradiated, microstruct. and mech. props. *(Russian)* 80−24503
steel, type 316 stainless, Neutron irradiation using HFIR for evaluation as fusion reactor material 78−13324

neutron effects continued
steel 0Kh16N15M3B, neutron irradiated, kinetics of nucleation and growth of vacancy pores and dislocation loops *(Russian)* 77−51408
steel for nuclear reactor press. vessels, criteria for brittle fracture *(German)* 77−34389
steel for nuclear reactor pressure vessels, irrad. and post-irrad. examination equip. and techniques *(German)* 77−36696
steel pearlitic, statistical anal. of joint effect of Ni, Cu, P on irradiation embrittlement 78−71770
steels, austenitic and type 316, neutron irradiation induced embrittlement, review 79−65120
steels, irradiated pressure vessel, reference fracture toughness curves 80−100921
steels for nuclear reactor pressure vessels, neutron irrad. embrittlement, temp. effects, annealing *(German)* 77−34384
stopping power data, air/nitrogen gaps, graphite-tissue and polythene tissue interfaces 80−26353
strongly neutron-absorbing material, neutron irrad., self-shielding and burnout effects 79−28017
superconducting compounds 78−52121
superconducting fusion magnets, radiation effects 78−50294
superconducting magnet epoxy fracture after low-temp. irradiation 79−34147
superconducting magnet materials and components for high energy, phys. appl. 77−69012
superconductor, A-15, irrad. effects on supercond. transition temp. 78−6472
superconductor, fast neutron irrad. effects on T_c, comparison for C-15 Laves phase, A-15 and Chevrel phases 77−55633
TCNQ salt, N-propyl-quinolinium$(TCNQ)_2$, defect conc. depend. phase transition 80−44577
TCNQ salt, NPQn $(TCNQ)_2$, neutron irrad. induced defect concentration depend. phase transition 80−29449
TCNQ salt, Qn$(TCNQ)_2$, defect depend. of dielec. permeability and cond. 79−78608
TCNQ salt, Qn$(TCNQ)_2$, defect depend. of dielec. permeability and conductivity 79−91340
TCNQ salt, Qn $(TCNQ)_2$, configurational entropy, thermoelec. power meas. 80−34432
TCNQ salts, TSF-TCNQ, and HMTSF-TCNQ, low temp. fast neutron irradiation, elec. cond. meas. 80−59964
TCNQ-HMTSF, irrad. effects on resist. 21K 78−60113
technological and industrial appl. of neutrons 77−25244
testes, mice, comparative effects of various radiations on weight loss and spermatogenic stem-cell survival 80−108976
testis weight loss following high energy neutron or γ irrad., mouse expts. 80−35985
TFTR coil materials, neutron irrad. effects 80−34060
therapy beams, radiobiological intercomparisons 80−3739
thermo-plasticity of irradiated metals 77−4146
thermocouples in nuclear reactor radiation *(Russian)* 77−82515
thermoluminescent dosimeter, neutron damage, displacement and ionis. fractions of fast neutron kerma 78−30669
tissue and equivalent material recoil spectra 80−17022
tissue neutron and gamma-ray response function, mid-head, military appl. 80−8185
TLD-600, activation and damage effects after neutron pre-exposure 79−13540
toroidal fusion magnet systems, radiation damage effect on max. attainable magnetic field 78−50295
transition metals, implantation of He^+, range profiles and thermal release 80−39138
TTF-TCNQ, and related compounds, low temp. irrad. effects 80−24906
TTF-TCNQ, low temp. fast neutron irradiation, elec. cond. meas. 80−59964
TTF-TCNQ low temp. mag. susceptibility, neutron irrad. effects 80−60311
$TTT_2I_{1.5-x}Br_x$, chem. impurities and neutron irrad. induced defects, effects on DC cond. 80−49699
TTT_2I_3, chem. impurities and neutron irrad. induced defects, effects on DC cond. 80−49699
tumour incidence and longevity in neutron and γ-irrad. rabbits, RBE assess. 80−104661
tumour response to neutron radiation therapy, animal expts. 79−20594
type II superconductor, neutron irradiation effects *(Rumanian)* 78−52144
ultracold neutron heating 77−76470
Vicia faba bean root growth, effects of π^- and neutrons 78−28003
Vicia faba growth reduction, RBE of d(50)-Be neutrons and 650-MeV He^{2+} 80−98025
vitreous silica blocks, damage by high energy neutrons 80−29070
void densities, interpretation from critical radius arguments 79−23657
void growth, rel. to intrinsic point defect properties 78−47315
void nucleation, heterogeneous 77−51415
void size distribution during irradiation and annealing, time depend. computation 78−30674
void swelling, effect of recombination of sink strengths in rate theory 79−14851
void swelling, rel. to in-pile precipitation 78−70595
void swelling, transition from gas bubbles 78−14383
void swelling and irradiation induced creep 77−44297
void swelling simulation, effect of self ion injection 78−22772
voids, radiation induced, in US and in 80US-10UC-10UC_2 79−50951
weld metal, submerged arc irradiated, reference fracture toughness curves 80−100921
Zircaloy, annealed, neutron irradiated, inhomogeneous deform. behaviour 80−85014
zircaloy, H diffusion, effect of reactor irradiation 77−14231
Zircaloy, in-pile temp. depend of yield strength and growth, under neutron irrad. 79−73219
Zircaloy, in-reactor creep meas. appl. in design of PWR fuel 77−42073
Zircaloy, post irradiation recovery of growth 79−46711
Zircaloy cladding, irrad., tensile props., effects of temp., strain rate and annealing 77−48463
Zircaloy cladding tubes, under internal and external overpressure in FRG-2 in-pile creep 77−42082
zircaloy cladding tubes of irrad. fuel, flattening test *(Japanese)* 77−42054
Zircaloy fuel cladding, irrad. capsule design for continuously monitoring creepdown 79−54513

neutron effects continued
Zircaloy fuel cladding, irradiation-induced in-reactor corrosion in CANDU reactors 80−104352
Zircaloy-2, annealed, neutron irradiation growth 79−42109
Zircaloy-2, cold worked, temp. cycling effects on irradiation growth 80−2079
Zircaloy-2, interstitial/vacancy nature of neutron induced dislocation loops, TEM study 79−42110
Zircaloy-2, irrad. damage, TEM characts. 80−107332
Zircaloy-2, irradiation growth, reaction rate theory calcs. 80−88212
Zircaloy-2, irradiation growth, shape and volume changes 80−92562
Zircaloy-2, neutron irrad., low temp. deform. studies 79−47757
Zircaloy-2, neutron irradiated, inhomogeneous deformation behaviour 80−50679
Zircaloy-2, radiation and isotope effects on corrosion in H_2O/D_2O mixture 77−21314
zircaloy-2 cladding tubes, post neutron irrad. ring-tensile props. pre-hydriding effect 77−42053
Zircaloy-2 irradiation growth at 353 and 553K, texture and temp. cycling effect 79−46709
Zircaloy-2 pressure tube elongation, neutron induced creep and growth, meas. and anal. 80−93628
Zircaloy-4, stress relaxation specimens, thermally induced strain recovery causing microstruct. changes 77−25057
Zircaloy-4 cladding, irrad. growth prediction using crystallographic texture model 77−46300
Ag, cascade energy density effect on isochronal recovery 78−47431
Ag, gas bubble embrittlement mechanism 78−60824
Ag, neutron irradiation, low temp. recovery, effect of plastic deform. 78−51588
Ag, recovery and formation of mixed dumbbells after thermal neutron irradiation 79−69161
Ag-Zn, vacancy prod. rate by displacement cascades, anelastic meas. during neutron irrad. 80−19794
Ag-Zn (30 at.%), neutron irrad., at. mobility enhancement, Zener relax. meas. 77−1157
AgAu, recovery and formation of mixed dumbbells after thermal neutron irradiation 79−69161
AgCl, colloid bands induced by reactor irradiation at low temps. 78−26567
AgCl, colloid centres induced by reactor neutrons at 20K 78−72560
Al alloy, dil. 78−22766
Al alloys, neutron irradiation effects on microstruct., mech. props. and swelling 79−65121
Al alloys, neutron irradiated, suppression of radiation damage microstruct. by trace impurities 79−77643
Al, annealed and neutron irrad., exam. of positron lifetimes in voids and other defects 78−47426
Al, creep, rel. to radiation swelling and stacking fault energy *(Russian)* 78−27562
Al, defects due to neutron irrad., muon probes study 79−56701
Al, electron and neutron irrad., Doppler broadened positron annihilation meas. *(German)* 77−62563
Al, fast neutron irradiated, struct. of defect cascades, diffuse X-ray scatt. study 80−39167
Al film, neutron irradiated, increase of elec. resist. 78−26973
Al, He injected, tracing bubble evolution by positron annihilation 77−19992
Al, high purity, neutron irradiated, void annealing kinetics 80−44234
Al, irradiation defects, intrinsic thermal expansion meas. 79−95186
Al, neutron activation analysis, trace element removal technique 79−57309
Al, neutron damage, positron annihilation 80−65056
Al, neutron irrad., μ^+ mobility and trapping by vacancies, muon spin rot. meas. 79−4757
Al, neutron irradiated, direct obs. of radiation induced coated cavities 77−47493
Al, neutron irradiated, phonon dispersion curves, neutron scatt. meas. 77−43290
Al, neutron irradiated, void surface props. determ., anisotropic small-angle neutron scatt. 78−10095
Al, neutron irradiation, mobile interstitials production 80−34080
Al, positron annihilation, effects of quenching, annealing and neutron irrad. 80−20732
Al, quenched, irradiated, anisotropic electron scatt. on defects 79−95397
Al, quenched, irradiated, and quenched plus irradiated, grain boundary hardening 80−3162
Al, reactor irradiated, neutron inelastic scattering meas. of phonon dispersion curves 78−75758
Al, rigidity modulus, neutron irrad. and quenched, point defects 78−27546
Al, shock compression at high press., neutron irrad. *(Russian)* 80−88264
Al, stabiliser for fusion reactor supercond. mag., neutron irrad. effects on magnetoresistance 80−34062
Al, struct. metal, effective damage levels in neutron radiation environment 79−36236
Al, vacancy distribution, interbonding atoms, heat peaks in scattered cascades *(Russian)* 80−39169
Al-Co, dil., electron and neutron irradiation, interstitital atom clustering at ^{57}Co impurity, Mossbauer meas. 78−30607
Al-Co alloy, dil., fast neutron radiation damage, interstitial trapping, Mossbauer spectra and elec. resist. meas. 77−27914
Al-Cr, neutron irrad., Cr atom distribution NMR study 80−54957
Al-Cu (4 wt.%), effect of semicoherent precipitation on void swelling, when neutron irradiated 79−42115
Al-Cu (4 wt.%) alloy, irrad., weak-beam dark-field obs. of dislocations near θ' precipitates 80−107333
Al-Cu (up to 0.5 at.%), neutron damage rate, interpretation of results 78−63794
Al-Cu alloy bicrystals, neutron irrad. effects on grain boundaries, intergranular fracture and precip. 77−48520
Al-Ga, dil., neutron irrad., 4.2K, defect prod., recovery 77−1155
Al-Ge, galvanomag. transport coeffs., Hall effect 79−91029
Al-Ge, internal friction and shear modulus after neutron irrad. at 80K 79−1468
Al-Li, cold worked neutron irrad. alloys, He bubble behaviour, microstruct. changes 77−54359
Al-Mg, dil., neutron irrad., 4.2K, defect prod., recovery 77−1155
Al-Mg 0.1 at.%, neutron-irradiated, dislocation loop characterisation by TEM 79−23614

neutron effects continued
Al-Mg (0.1 at.%), neutron damage, positron annihilation 80−65056
Al-Se-Ag switching element, neutron irradiated, role of Ag in switching effect and diffusion of Ag 78−19163
Al-Si, neutron small angle scatt. study 79−43255
Al-Si alloys, neutron irrad., precip. processes, neutron small-angle scatt. obs. 77−4131
Al-Si-Al contact current response to 100 keV neutron irrad. *(Russian)* 80−49956
Al-SiO_xN_y-Al structure, effect of fast neutrons on elec. strength *(Russian)* 77−85343
$Al_xGa_{1-x}As$ epitaxial diode, neutron and γ-irrad. effects on cathodolum. in SEM 79−11473
Al_2O_3, electron slowing-down flux spectrum, due to β-decay of neutron-activated ^{164}Dy 78−10108
α-Al_2O_3, neutron damage, fusion/fission ratio 80−34066
Al_2O_3, neutron irrad., EPR spectra, F^+-centres 77−4558
Al_2O_3, neutron irradiated, electron centres, optical spectra exam. 77−63440
Al_2O_3, optical props. of F-centre 79−43003
α-Al_2O_3, polarised luminescence in neutron- and proton-irradiated single crystals 80−66271
Al_2O_3 void formation by fast neutron irradiation, TEM exam. 78−51591
Au, electron and neutron irrad., quenched, Doppler broadened positron annihilation meas. *(German)* 77−62563
Au, fast neutron sputtering 77−36316
Au, neutron activation cross sections meas. for generalised intermittent irradiation, fusion machines appl. 78−58283
Au, neutron damage, defect clusters 80−34067
Au, neutron damage calc., deuteron break-up source, sputtering appl. 77−35593
Au, neutron sputtering yield determ. 77−36319
Au, scattering and radiation damage for 14 MeV neutrons and 10 to 20 MeV protons 77−15458
Au, sputtering by fast neutrons 79−61470
Au-Fe (17 at.%) alloy, fission fragment irrad., simulation of neutron effects 77−80549
B, neutron irradiated, quantitive anal. using cellulose nitrate solid state track detectors 78−56937
B_4C, effect of fast neutron irradiation on struct. 78−26597
B_4C, FBR control rod elements, neutron damage and post-irrad. annealing 80−13581
B_4C, used as control rods in FBR, irradiation effects 78−67742
B_4C-Al(silicone)(graphite), neutron shielding materials, long term radiation effects 80−9413
Ba hexaferrite, irradiated by fast neutrons, mag. props. 80−97116
BaF_2, thermoluminesc. and F-centre annealing, after neutron irrad. 80−7422
BaF_2, undoped, H-centre prod. by reactor neutron irrad., optical absorpt. meas. 77−59010
BaF_2, undoped and U-doped, neutron irrad., absorpt. band attributed to F_2- centres 80−7380
BaF_2:U, absorption band spectra following neutron irrad. 80−29763
$BaSO_4$, single cryst., neutron bombard. effect on struct. 78−63793
$BaTiO_3$ type perovskite ferroelectric, neutron irradiated, amplification of freq. dispersion of permittivity *(Russian)* 78−52419
Be, neutron irradiated, annealed, tensile props. and swelling, effect of He bubbles 78−22765
Be, neutron irradiated, gas porosity, Brownian motion 79−73222
Bi and Bi:Te, neutron radiation defects 78−47430
C and graphite cloths and fibres 78−78496
C, heat-treatment and neutron irrad. effects on US atten. and Young's modulus 79−11644
C, modulus of elasticity, interrelationship with crystalline struct., heat and irradiated effects 77−21210
C, pyrolytic, fast neutron flux effect on irradiation damage 78−22768
C resistors as low temp. sensors in low temp. reactors, gamma, neutron irrad. investig. 77−45848
C, soft and hard, sp. ht. anomalies and spin-spin interactions, review 79−69261
C-C composite material, syntactic-foam type properties 78−44169
C-fibres, irradiation-induced dimensional changes 80−65052
CO_2, ionisation meas. and $\bar{W}_n$ derivation for neutron irradiation 79−36430
$CaCO_3$ calcite, colour changes, micropits, hardness lattice distortion, absorption spectra 77−39617
CaF_2, (n,γ) induced lattice defects, struct., polarised ^{20}F NMR 77−20724
CaF_2, (n,γ) induced lattice defect annealing, polarised ^{20}F NMR 77−20725
CaF_2, (n,γ) induced point defects, struct. and annealing 78−59842
CaF_2, F-centre growth by neutron irrad. 79−55788
CaF_2, thermolum., F-centre annealing after neutron irrad. at 20K 79−55787
CaF_2, thermoluminesc. and F-centre annealing, after neutron irrad. 80−7422
CaF_2, undoped, H-centre prod. by reactor neutron irrad., optical absorpt. meas. 77−59010
CaO, MCD, optical absorpt. lines 77−77255
$CdAl_2O_4$, LWR burnable poison, irradiation and corrosion beahviour *(German)* 79−67846
$CdCr_2Se_4$, reactor radiation influence on ferromagnetic phase transform. *(Russian)* 80−75760
CdS, irrad. with high doses of fast reactor neutrons, self-healing of radiation damage 79−73221
CdS, neutron and fast electron irrad., local centre form., TSC and photoluminesc. meas. 78−87719
CdS, neutron irradiated, photoelectric props. 77−35962
CdS, neutron irradiated, intrinsic defects 78−51599
CdTe-HgTe, neutron irrad. rel. to elec. props. 79−15141
CdTe-HgTe, semicond. solid solns., effect of reactor irrad. on electrophys. props. 77−51744
$CeAl_3$, effect of disorder on cond. transition into ground state 77−89755
Co, neutron sputtering yield determ. 77−36319
Co-Cu(Ti)(Fe), neutron radiation stimulated diffusion, electrical resistivity exam. *(Russian)* 79−14959
CoO-containing glass, effects of γ-rays, electron beam and neutron flux on transmissivity *(Japanese)* 77−73156
Cr, neutron irradiated at 24.5K, elec. resist. exam. of radiation damage *(French)* 78−30671

neutron effects continued
Cr_2O_3-stainless steel system under fusion reactor first wall condition, oxide dispersoid stability 80−40374
Cu, cascade energy density effect on isochronal recovery 78−47431
Cu, damage production by high energy d-Be neutrons, elec. resist. meas. 77−62564
Cu, defect-phonon perturbations after neutron irrad., neutron scatt. study 80−44278
Cu, dislocation decoration, damage clusters, after irrad. at 200 to 400°C 77−24332
Cu, dislocation pinning rate, neutron and electron irrad., meas. by internal friction method 80−96570
Cu, electron and neutron irrad., Doppler broadened positron annihilation meas. *(German)* 77−62563
Cu, fusion reactor shield, neutron induced activity and γ-ray source investigation 78−54872
Cu, inertial confinement reactor first wall response to thermonuclear radiation 79−76133
Cu, inhomogeneous clustering of radiation damage after neutron irradiation between 200 and 400°C 80−15161
Cu, irradiated, small edge dislocation loops, electron microscope image contrast, Burger's vector determ. 77−76410
Cu, isochronal recovery of high energy d-Be neutron damage 78−51592
Cu, neutron and electron irrad., interstitial formation, dislocation pinning, internal friction meas. 80−100284
Cu, neutron damage, defect clusters 80−34067
Cu, neutron damage and gas prod. spatial variation in Li(d,n) radiation damage facility 77−42207
Cu, neutron damage calc., deuteron break-up source, sputtering appl. 77−35593
Cu, neutron irrad., replacement sequences, calcs. using ADDES and COMENT codes 79−46714
Cu, neutron irrad. cryst., edge and screw dislocation groups, mean vel. 79−7607
Cu, neutron irradiated, effect on internal friction 78−15445
Cu, neutron irradiation, mobile interstitials production 80−34080
Cu, neutron irradiation damage inhomogeneous clustering, TEM obs. 79−73223
Cu, neutron irradiation induced dislocation loops and point defects, temp. depend., 316 to 483K 77−51410
Cu neutron production of free interstitials 80−34071
Cu normal metal in composite superconductor, neutron irradiation effects 79−38049
Cu, scattering and radiation damage for 14 MeV neutrons and 10 to 20 MeV protons 77−15458
Cu single crystals, neutron irradiated, secondary slip 80−88161
Cu, single crystals, neutron irradiated, stresses and secondary slip between overlapping and dislocation arrays 80−88162
Cu, stabiliser for fusion reactor supercond. mag., neutron irrad. effects on magnetoresistance 80−34062
Cu, thermal neutron irrad., stage II recovery 77−31695
Cu, thermal neutron irradiated, isochronal resist. recovery, 30-400K 79−19287
Cu, thermal-neutron damaged, I_D and I_E recovery substages 77−35590
Cu, X-ray studies of fusion energy neutron damage 78−51593
Cu-Al (11.47 wt.%), high temp. phase transforms., effect of pre-exposure to neutrons 79−20045
α-Cu-Al (15 at.%) alloys, low temp. neutron irrad. induced point defects behaviour 77−43251
Cu-Au, dil., thermal neutron irradiated, isochronal resist. recovery, 30-400K 79−19287
Cu-Au, dose depend. of recovery after thermal neutron irrad. 77−69011
Cu-Cr, dil. alloys, Frenkel defects, effects on anomalous resistivity and thermopower 77−8084
Cu-Fe (1.5 wt.%) alloy, void form. during irrad. in HVEM, reactor irrad. simulation and ageing effects 80−107327
Cu-Ni, neutron irradiation, enhanced diffusion, elec. resist. meas. 80−6440
Cu-Ni, neutron radiation stimulated diffusion, electrical resistivity exam. *(Russian)* 79−14959
CuAu, thermal-neutron damaged, I_D and I_E recovery substages 77−35590
Cu_3Au, atomic rearrangements during fast and thermal neutron irradiation 79−42114
Cu_3Au, fast neutron irrad., displacement cascades 78−83852
Cu_3Au, heavy-ion or neutron bombardment, disordered zone form., TEM diffr. contrast 77−11600
Cu_3Au, irrad., displacement cascades, direct obs. method 80−107335
$Dy_2Ti_2O_7$, neutron irrad., structural and volume changes 77−51416
Eu_2O_3, for controlling fast reactor, irrad. behaviour 78−37409
Fe alloys, swelling, correlation with number of bonding d electrons 77−47491
Fe and Fe alloys, fast neutron irradiated at high temps., mech. props. 79−51157
Fe, BCC, neutron-irradiated, Frenkel defect spontaneous recomb. volumes 79−60355
Fe base superalloy, type A-286, elevated temp. fracture toughness testing of thin section irrad. materials 80−61063
Fe, fast neutron irrad., elec. resist. *(French)* 79−51159
α-Fe, high purity, neutron and electron-irrad., interstitial migration at 200K 79−55920
α-Fe, internal friction peaks from dislocation relax. in plastically deformed and/or neutron irrad. sample 78−48438
α-Fe, irradiation induced void swelling, Cr additions effect 80−55408
Fe, irradiation softening in single crystal, temp. and orientation depend. 77−86113
α-Fe, low temp. mag. relax. 79−8022
α-Fe, mag. aftereffect after neutron irrad. at 77K 78−2705
α-Fe, magnetic aftereffect correlations with internal friction after low temp. neutron irradiation 78−10733
α-Fe, magnetic aftereffect disaccommodation between 30 and 300K after low-temp. neutron-irrad. 80−29585
α-Fe, magnetic aftereffect spectrum after low temp. neutron irradiation 78−10732
Fe, magnetic disaccommodation, low temp. in neutron-irrad. sample, Bordoni relax. 77−4542
α-Fe, neutron irradiated, mobile C atom trapping, anelastic and magnetic relaxations 80−100306
α-Fe, plastically deformed and/or irrad., high purity, internal friction peaks due to dislocation relax. 77−86075

neutron effects continued
Fe, pure, neutron irrad. and H_2 absorption effects on mech. props. 78−34546
Fe, radiation-induced swelling in BOR-60 reactor 79−97814
Fe, reliability of use of fission fragments to simulate neutron irrad. 79−42113
Fe, scattering and radiation damage for 14 MeV neutrons and 10 to 20 MeV protons 77−15458
Fe struct. metal, effective damage levels in neutron radiation of environment 79−36236
α-Fe, vacancy migration, annealing expt. study, irradiation induced defects 78−6956
Fe, vacancy recovery stage, radiation doping, elec. resistivity meas. 79−51102
α-Fe, void swelling response after fast reactor irradiation 80−6437
Fe:C, neutron irradiated at low temp., mag. disaccommodation 80−44881
Fe-(Mo)-CaF_2, sintered, friction and corrosion props. for frictional units of nuclear plants 78−60845
Fe-Al (38.5-47 at.%), type B_2 ordered alloys, elec. resist. recovery stages *(French)* 77−69010
Fe-Al (40 at.%), ordered, plastically deformed, neutron irrad. damage and recovery, resist. meas. 77−19993
Fe-Al (40 at.%) and Fe-Al (50.5 at.%) ordered alloys, 20K neutron irrad. effects, stoichiometry depend., resist. obs. *(French)* 80−84215
Fe-Al (50.5 at.%), ordered, neutron irrad. enhanced defect diffusion, resist. meas. 77−11598
Fe-B amorphous alloy, fast neutron and ^{235}U fission fragment irrad. 80−100288
Fe-C-Cu (0.21, 0.2 wt.%), neutron-irradiated, resolution of C atoms, internal friction meas. 78−31442
Fe-C-Cu (0.21, 0.2 wt.%), neutron irradiated, torsional props. effect of Cu additions and annealing temp. 78−56699
Fe-Co-V, neutron irradiated, damage rates 79−77646
Fe-Co(-V) alloys, neutron irradiated, influence of dislocation doping on recovery 79−46715
Fe-Co(Al), B_2 superlattices, point defect investigations 78−47357
Fe-Cr, irradiation induced void swelling, Cr additions effect 80−55408
Fe-Cr-Ni, neutron irradiated, rel. between irradiation induced swelling and shear modulus 80−15157
Fe-Cr-Ni based alloys, Ni^+ ion and neutron irradiated, γ′ particle redistrib. and phase stability 79−78977
Fe-Cu (0.34 wt.%), neutron irradiated, field-ion microscope detection of ultra-fine defects 79−42116
Fe-Cu (1.77%) alloy, influence of neutron irrad. on electric resist. *(Russian)* 79−38041
Fe-Cu-Ti, improvement of irradiation-enhanced Cu embrittlement by Ti addition 79−43393
Fe-N, neutron irrad. effects on mech. props. 79−4338
Fe-Ni, dil., point defect relax. after low temp. neutron irrad. 78−52316
Fe-Ni alloy, disordered, short-range order study by time-depend. PAC method 78−6618
$Fe_{80}B_{20}$, amorphous, fast neutron and fission fragment irrad., effect on elec. resist. 80−19846
$Fe_{80}B_{20}$ amorphous alloy, low field magnetic props. 77−55690
FeCo, neutron irradiated, damage rates 79−77646
FeCo, ordered and disordered alloy, annealing of point defects created by neutron irrad. at 20K *(French)* 79−1467
$Fe_{50}Co_{50}$, neutron irradiation, close pair recombination *(French)* 80−39162
$FeCo_2V$, ordered and disordered alloys, annealing of point defects created by neutron irrad. at 20K *(French)* 79−1467
$Fe_{49}Co_{49}V_2$, neutron irradiation, close pair recombination *(French)* 80−39162
$Fe_{78}Mo_2B_{20}$, amorphous, fast neutron and fission fragment irrad., effect on elec. resist. 80−19846
GaAS, semi-insulating and n-type, doping by neutron transmutation 80−96553
GaAs, carrier lifetime, radiation induced changes, edge luminesc. spectra 77−8664
GaAs, defect clusters induced by γ-rays and neutrons, effect on elec. props. 80−29408
GaAs, electroluminescent study of irrad. induced struct. damage, athermal annealing 80−108280
GaAs, electron and neutron irrad., defect clusters 80−2077
GaAs, fast neutron irrad., effect on cryst. lattice period, X-ray diffr. meas. 79−37743
GaAs, irradiated with fast neutrons, IR vibrational absorpt. 78−75776
GaAs MIS Schottky barrier diodes, radiation effects 79−24078
GaAs, neutron irradiated, change in lattice period during annealing 77−55307
GaAs, neutron transmutation doping, shallow donors magneto-optical effects 80−20255
GaAs, reactor irrad., opt. props. 77−90137
GaAs, reactor-irradiated, anisotropy in diffuse small angle neutron scatt. 78−51598
GaAs Schottky barrier diode, under high neutron fluence, current transport 80−65679
GaAs, transmutation doping by thermal neutrons 80−10581
GaAs:B, electron or neutron irradiated, low symmetry interstitial B centre 78−79605
GaAs:Si, neutron irrad., strain detection by local mode IR absorpt. meas. 77−69828
GaP, light emitting diode structure, effect of neutron irradiation on cathodoluminesc. 79−28843
GaP:Zn, O LED, irrad. effects on capacitance, I-V and electrolum. charcts. 77−66543
Ge, As impurity precipitation from solid soln., neutron irrad. effect 80−29177
Ge coaxial detectors with reverse electrode, radiation damage resistance 79−41076
Ge, defects, radiation effects 80−29016
Ge detector, high purity, fast neutron damage 80−59526
Ge detector, high purity, fast neutron damage, hole trapping and detrapping 80−63463
Ge, dislocation ensembles motion in neutron irradiated covalent crystals *(Ukrainian)* 80−10579
Ge, doped, electron or neutron irradiated, vibrational absorption 78−6718
Ge, irradiation at about 6K, low temp. annealing of defect 78−2162

neutron effects continued
n-Ge, lightly doped, compensated by disordered regions, conductivity and Hall mobility 80−11016
Ge, lightly doped, heavily compensated by fast neutrons, electrical props. 77−89766
Ge, n- and p-type, fast neutron irrad. at low temp., resistivity, annealing characts. 77−89481
Ge, neutron irrad., absorpt. edge 80−93320
Ge, neutron irrad., Hall effect and magnetoresist. meas. 80−6883
Ge, neutron irrad., substitution of impurity atoms by self-interstitials, Ge(n,γ) reaction 80−39166
p-Ge, neutron irrad. quenched sample, lattice defects 79−19284
Ge, neutron irradiated, capture of positrons by radiation defects 78−38756
Ge, neutron irradiated, positron annihilation, ESR and resist. meas. 80−15160
Ge, neutron-irradiated, positron lifetime 80−97374
Ge, reactor irrad., opt. props. 77−90137
Ge, transmutation-doped, impurity cond., 1.5-4.2K 77−89758
Ge:Ga, cryst. defects due to neutron irrad., elec. cond. and annealing 79−55789
Ge:Sb, cryst. defects due to neutron irrad., elec. cond. and annealing 79−55789
n-Ge:Sb, fast neutron irrad. effects on donor conc., and annealing 78−56107
Ge:Sb, neutron irrad., carrier mobility theory and expt. 78−56166
Ge:Sb, neutron irradiated, hopping cond. between shallow defect levels 77−4347
n-Ge:Sb, neutron-irradiated, paramag. defects, analysis of EPR spectra 77−55703
Ge:Sb, thermal defects, influence on radiation defect formation and annealing 77−55281
Ge(Li) detector, fast neutron damage 80−59525
GeS_{11} glass, neutron irrad., thermal and elec. props. 79−19286
$GeS_{1.35}$ glass, neutron irrad., AC elec. cond. 80−24924
GeS_8 glass, activation energies after neutron irradiation, elec. cond. and transmission coeff. 78−83850
GeS_x amorphous semiconductor, neutron irrad. effects on thermal parameters 77−11597
GeS_x, neutron irrad., thermal and elec. conductivity and heat capacity 78−2165
H_2O, neutron irradiation and mag. field effects on cavitation and nuclei spectra 77−62568
He accumulation fluence dosimetry for fusion materials neutron irrad. testing 80−32479
Hg, volatility in NAA from samples and standards *(Russian)* 80−41128
HgI_2, soft γ-ray detector fabrication and props. 77−3208
I, neutron activation cross sections meas. for generalised intermittent irradiation, fusion machines appl. 78−58283
InAs, defect formation processes, effect on physical props. 78−2163
InAs, neutron bombarded, optical absorption, struct. defect form. and nuclear alloying *(Russian)* 78−31206
InGaAs, LED, 1.06 μm range, neutron and γ-irrad. effects 79−97433
InP, defect formation processes, effect on physical props. 78−2163
InP_xAs_{1-x}, defect formation processes, effect on physical props. 78−2163
n-InSb, high-resist., prep. using radiation compensation 80−34016
InSb, neutron bombarded, optical absorption, struct. defect form. and nuclear alloying *(Russian)* 78−31206
InSb, neutron irrad., defect cluster form., effect on elec. props. 80−65062
In_2Te_3, photosensitivity on γ- and neutron-irrad., γ-ray dosimeter mat. applic. 77−85258
KCl, phonon scattering on small radius colloids 78−38798
KCl single crysts., thermal stability of neutron induced damage 78−79634
KCl(:LiF), radiative Q-centres, opt. absorpt. and thermal conductivity 77−47450
LiCl, neutron irradiated, EPR exam. 78−76309
LiF crystals, in pile irradiation, nucl. reactions 78−29463
LiF, influence of neutron irrad. temp. on F-aggregate centre form. 78−72561
LiF, irrad. at pile temp., higher F aggregate centres produced during thermal annealing 77−43212
LiF, irradiated at 20K, deformation under stress *(French)* 79−90715
LiF, NMR exam. of point defects generated in (n,γ)-reaction *(Russian)* 78−60347
LiF, neutron irrad., F-centres prod., hyperfine structure constants *(Japanese)* 77−69729
LiF, neutron irradiated, ESR of Li metals *(Japanese)* 79−82858
LiF, neutron-irrad., X-ray diffr. profiles 77−84803
LiF, radiation induced voids, formation on dislocations 80−15159
LiF, single crystal, neutron and gamma irradiation, SEM and Bragg profile anal. 80−15158
LiF single crystal, void disappearance 78−55864
LiF single crystals, exam. of void morphology effects on their disappearance kinetics 79−10843
LiF, slip anisotropy under neutron irrad. and external stress, orientation of defects 77−31674
LiF:H, neutron irrad., ENDOR meas. 79−11356
LiF:OH, neutron irrad., interstitial H-centres, ESR obs. 80−93175
$Li_{0.5}Fe_{2.5}O_4$, neutron-irrad., mag. spectra *(Russian)* 77−44092
LiI crystal, irradiated at low temps., optical absorption spectra 80−45123
LiI, reactor irrad., absorpt. spectra 79−65902
$LiNbO_3$, radiation induced heating by thermal neutrons, meas. of temp. 79−4337
LiO_2 sintered pellets, neutron irradiated, T release 78−5014
Li_2O, neutron irrad. effects, optical absorpt. spectra 80−75271
Li_2O, neutron irradiated, ESR of F^+, O^-, H^0 and colloidal Li centres 78−2737
Li_2O pellets, neutron irrad., microstruct. and Vickers mircohardness meas. 79−8339
Li_2O pellets, neutron irradiated, temp. distrib. 80−86968
Li_2O pellets, sintered, neutron irradiated, ESR study 80−92566
Li_2O_1 fund. optical absorpt. edge, number of displaced atoms from $^6Li(n,\alpha)^3H$ reaction 78−51594
^6LiD sphere, T prod. under 14 MeV neutron irradiation 79−59254
Mg alloys, neutron irradiation effects, on microstruct., mech. props. and swelling 79−65121
Mg, dislocation loops induced by neutron irrad., TEM obs. 79−51113
neutron effects continued
Mg, neutron irrad. damage, TEM obs. 79−46713
$MgAl_2O_4$, faulted defect aggregates prod. by neutron-irrad. 80−107331
$MgAl_2O_4$, radiation damage, optical absorpt., F-centres 80−64994
MgF_2, gamma- or neutron irradiated, ESR meas. on hole centres 77−12201
MgO, defect centres, thermolum. examination 78−15235
MgO, MCD, optical absorpt. lines 77−77255
MgO, neutron irradiated, Huang diffuse scattering of neutrons 80−10544
MgO, radiation induced O interstitials, EPR meas. 78−55866
MnZn ferrites, initial mag. permeabilities under low temp. reactor irrad. 77−36093
Mo, 14 MeV neutron damage 77−15460
Mo alloys, dil., HVEM bombarded, neutron damage simulation, defect cluster and dislocation obs. 80−107330
Mo alloys, fusion reactor first wall and blanket material, props. for struct. appl. 80−30071
Mo alloys, fusion reactor first-wall and blanket material, mech. props. 80−34074
Mo, BCC, neutron-irradiated, Frenkel defect spontaneous recomb. volumes 79−60355
Mo, effect on microcracks *(Ukrainian)* 79−77639
Mo, elastic aftereffect after fast neutron irrad. at 5K 77−89431
Mo, fusion neutron induced radioactive emissions from surfaces 77−36321
Mo, fusion reactor shield, neutron induced activity and γ-ray source investigation 78−54872
Mo, hardened sub-structure, high-temp. radiation resist. *(Russian)* 78−56654
Mo, high-temp. neutron irradiated, annealing study by positron lifetime 77−51413
Mo, inertial confinement reactor first wall response to thermonuclear radiation 79−76133
Mo, irrad. between 425 and 1000°C, ductility in bending 80−39164
Mo, irradiated, small edge dislocation loops, electron microscope image contrast, Burger's vector determ. 77−76410
Mo, irradiated with fission fragments, creep, 20-30K *(French)* 77−48493
Mo, irradiation induced voids, irrad. temp. determ. from void lattice const. 77−46289
Mo, irradiation temp. determ. by electrical resistivity meas. 78−58354
Mo, neutron bombard., radiation damage, electron microscopy obs. *(Russian)* 80−44235
Mo, neutron dose depend. of elec. resist., vacancy-interstitial recomb. *(Russian)* 77−80546
Mo, neutron irrad., radiation anneal hardening mechanism 80−71678
Mo, neutron irradiated, influence on X-ray diffr. patterns *(Russian)* 78−22764
Mo, neutron irradiated, radiation softening and hardening 80−34083
Mo, neutron irradiated, relationship between void size and positron lifetime 77−15454
Mo, neutron irradiated, small angle X-ray scatt. and TEM study of voids 79−14849
Mo, neutron irradiated, void swelling and shrinkage, TEM study 80−34079
Mo, neutron irradiated extended low temp. annealing 79−79014
Mo, neutron irradiated single crystals, vacancy reactions in III recovery 79−73220
Mo, neutron irradiation induced length change, 40 to 450 degrees C 78−47433
Mo, neutron low energy interaction cross sections, gravitational spectrometer meas. 80−24521
Mo, neutron radiation-induced shrinkage of voids 79−51158
Mo, neutron-bombarded, diffuse X-ray scattering *(Russian)* 80−92560
Mo, neutron-irradiated, high-temp., positron annihilation characts. meas. 77−89480
Mo, neutron-irradiated, positron lifetime study 79−23654
Mo, point defect migration, stage III annealing 77−80548
Mo, positron investig. of neutron irrad. induced voids 77−8679
Mo, positron lifetime meas. of neutron irrad. induced voids 77−7766
Mo, vacancy diffusivity from width of grain boundary void denuded zone 77−47615
Mo, vacancy recovery stage, radiation doping, elec. resistivity meas. 79−51102
Mo, void containing, positron annihilation characts. 80−80898
Mo-Ti, irrad. between 425 and 1000°C, ductility in bending 80−39164
Mo-Ti (1 wt.%), fast neutron irradiated, direct obs. of solute segregation to voids 79−78971
Mo-Ti-Zr alloy, neutron radiation-induced shrinkage of voids 79−51158
Mo-Ti-Zr alloy TZM, fatigue and plastic flow, irradiation effects 77−52466
Mo-Zr-B, porosity and mech. props. after neutron bombard., 780-1080°C *(Russian)* 80−24502
Mo-Zr-B alloy, neutron irrad. at 780-1080°C, porosity, hardening and embrittlement *(Russian)* 80−29062
Mo_3Os, effect of high energy neutron irradiation on supercond. transition temp. 77−36012
$(Mo_{0.6}Ru_{0.4})_{82}B_{18}$, supercond. metallic glass, neutron irrad. effects 80−29060
NaCl, effect of annealing and neutron irrad. on block struct. 80−29061
NaCl, interrupted neutron irrad. expts. involving dislocations 79−99208
NaCl, neutron irradiated, induced flow stress and optical absorpt. 77−62569
$NaReO_4$, EPR spectra of paramag. centres and free radicals 80−108072
Nb, 14 MeV neutron sputtering, ion microprobe, SEM, He^+ backscatt. anal. 77−36317
Nb, 15 MeV and fission neutron displacement dqmage, TEM anal. 77−35592
Nb alloys, fusion reactor first wall and blanket material, props. for struct. appl. 80−30071
Nb alloys, fusion reactor first-wall and blanket material, mech. props. 80−34074
Nb based alloys, He and simultaneous damage production simulation 80−32480
Nb carbide interstitial phases, elec. and mag. props., neutron radiation effects 79−77640
Nb, creep induced by neutron irrad. 79−74221
Nb, damage production by high energy d-Be neutrons, elec. resist. meas. 77−62564
Nb, defects due to neutron irrad., muon probes study 79−56701

neutron effects continued
Nb, embrittlement, yield stress, fracture stress and strain *(Japanese)* 77−76472
Nb, fast neutron sputtering 77−36316
Nb, fast neutron sputtering 78−15255
Nb, flux pinning by voids during neutron irrad. 77−40008
Nb, fusion neutron damage effects on mech. props., simulation by 16 MeV protons 78−71768
Nb, fusion neutron induced radioactive emissions from surfaces 77−36321
Nb, irradiated superconductor, fluxoid defect interactions 78−52166
Nb, isochronal recovery of high energy d-Be neutron damage 78−51592
Nb, low temp. neutron irradiation 77−27915
Nb, neutron bombarded, defect size distrib. influence on hardening *(Russian)* 80−10580
Nb, neutron damage and gas prod. spatial variation in Li(d,n) radiation damage facility 77−42207
Nb, neutron damage and sputter yields 77−57742
Nb, neutron damage calc., deuteron break-up source, sputtering appl. 77−35593
Nb, neutron induced defect structs., TEM exam. 77−84802
Nb, neutron irrad., microstruct. and tensile props. 80−34077
Nb, neutron irrad., positron annihilation, microvoid form. 78−88381
Nb, neutron irrad., yield stress and activation vol. 77−90418
Nb, neutron irrad. effects on mech. props. 78−91361
Nb, neutron irradiated, radiation anneal hardening *(Japanese)* 80−89243
Nb, neutron irradiated, TEM obs. of interstitial clusters 79−19288
Nb, neutron irradiation, low temp., 15 MeV, effect on superconducting props. 78−52179
Nb, neutron sputtering yield determ. 77−36319
Nb, neutron-irradiated, positron annihilation ang. correl. meas. 80−93430
Nb, radiation damage in fusion reactors, computer expts. 80−13839
Nb, radiation hardening and yield strength correlations for 16 MeV H^+ and (D,T) neutron effects 78−14389
Nb, recovery and recrystallisation, fast neutron irradiation effects 77−70069
Nb, scattering and radiation damage for 14 MeV neutrons and 10 to 20 MeV protons 77−15458
Nb, simulation expts. for sputtering by 14 MeV neutrons 77−36320
Nb, superconductor, neutron irradiation, low temp., effect on critical current 78−52180
Nb wires, neutron irrad., radiation anneal hardening 200 to 700°C 79−70077
Nb-Cu, neutron radiation stimulated diffusion, electrical resistivity exam. *(Russian)* 79−14959
Nb-O, effect of neutron irradiation damage on low temp. deformation characts. TEM study 79−42117
Nb-Ti, radiation effects on critical currents 78−52175
Nb-Y and Nb, mech. props., neutron irrad. and Y scavenging effects 77−90394
Nb-Zr (3 wt.%), neutron-irradiated, positron annihilation ang. correl. meas. 80−93430
Nb-Zr(Nf)(Mo)(W)(Rh), dil., neutron irradiation at 4.6K, influence of impurities on defect prod. 79−55790
Nb_3Al, neutron irrad. effects on transition temp. *(Japanese)* 79−82707
Nb_3Al, supercond. props. and lattice parameter, comp. and neutron irrad. effects 80−70880
NbC, supercond. critical temp., neutron irrad. effect 80−80433
NbC, thermal stress cracking 79−77641
NbC_x, reactor irrad. effects on elec. resist. and supercond. props. *(Russian)* 78−47895
Nb(CN), supercond. critical temp., neutron irrad. effect 80−80433
Nb_3Ge, low temperature electron, neutron irrad. effects on critical temp. *(French)* 80−75669
Nb_3Ge, neutron irradiated, A15 compound, recovery of T_c by annealing 78−52132
NbO, ion channelling, neutron and deuteron radiation damage 79−65131
NbO, single cryst. with 25% vacancies, neutron damage 77−15459
Nb_3Pt, neutron irrad. effects on supercond. props. 79−38224
Nb_3Si, supercond. props., effect of neutron irrad. 79−38211
Nb_3Sn, A-15 struct. Nb based superconductors, irrad. type influence on radiation defects 80−15093
Nb_3Sn, crit. current density, low dose fast neutron irrad. effect 78−14910
Nb_3Sn, crit. current enhancement by low temp. fast neutron irradiation 77−40014
Nb_3Sn, critical current density 78−52176
Nb_3Sn, critical current enhancement by low temp. fast neutron induced flux pinning centres 78−52177
Nb_3Sn, degradation mechanism of superconducting transition temp. under high energy neutron irradiation 78−52124
Nb_3Sn, fast neutron irradiation, effect on critical current density 78−19197
Nb_3Sn, highly disordered, elec. resist. and supercond. T_c 78−52142
Nb_3Sn, low temp. neutron irrad. expts., E_n=14 MeV 79−33424
Nb_3Sn, neutron irrad., crit. current change rel. to temp. and metallurgy 78−80109
Nb_3Sn, neutron irrad., elec. resist., temp. depend. 79−91024
Nb_3Sn, neutron irrad., X-ray scatt. theory 79−37740
Nb_3Sn, neutron irrad. effect on upper crit. field and crit. current 77−72954
Nb_3Sn, neutron irrad. effect on supercond. fusion magnet props. 78−52128
Nb_3Sn, neutron irrad. effects on transition temp. *(Japanese)* 79−82707
Nb_3Sn, neutron irradiation at 8K, supercond. crit. current and crit. temp. meas. 77−28334
Nb_3Sn, supercond. props., effect of neutron irrad. 80−80463
Nb_3Sn, supercond. props. and struct., neutron irrad. dose depend. 77−15985
Nb_3Sn, superconducting props., effect of radiation induced atomic disorder 78−52133
Nb_3Sn, TEM of radiation damage 79−65122
Nb_3Sn, X-ray study of fission fragment induced structural damage 78−51589
Nb_3Sn(Al), neutron irradiated, A15 compound, recovery of T_c by annealing 78−52132
Nb_3(SnGa), wire, neutron effect on T_c, I_c and flux pinning 79−38216

neutron effects continued
Nb_3Sn(Ge), resistivity and T_c measurement after low temp. neutron irradiation 78−52123
NbTi, neutron irrad. effect on supercond. fusion magnet props. 78−52128
Nd:glass laser, influence of neutron and γ irrad. on generating characts. *(Russian)* 80−69402
Ni alloy, radiation-induced swelling in BOR-60 reactor 79−97814
Ni alloys, swelling, correlation with number of bonding d electrons 77−47491
Ni binary alloys, constituent segregation during irradiation 79−55791
Ni, creep, rel. to radiation swelling and stacking fault energy *(Russian)* 78−27562
Ni, creep, volumetric, irradiation induced, stress effect on swelling 77−43253
Ni, fusion neutron damage effects on mech. props., simulation by 16 MeV protons 78−71768
Ni, irrad., slip bands, TEM and SEM obs. 78−51596
Ni, neutron and heavy ion damage correlation, dose rate and He injection effects 79−7629
Ni, neutron irrad., microstruct. and tensile props. 80−34077
Ni, neutron irrad., void formation, C interstitial effects 77−76471
Ni, neutron irradiation, low temp. recovery, effect of plastic deform. 78−51588
Ni, radiation hardening and yield strength correlations for 16 MeV H^+ and (D,T) neutron effects 78−14389
Ni, radiation-induced swelling in BOR-60 reactor 79−97814
Ni, scattering and radiation damage for 14 MeV neutrons and 10 to 20 MeV protons 77−15458
Ni, vacancy diffusivity from width of grain boundary void denuded zone 77−47615
Ni, void swelling caused by neutron and self-ion bombardment, 573 to 873K 78−14387
Ni:^{235}U (0.1 at.%), exam. of saturation defect conc. and elec. resistivity meas., for neutron irrad. at 7K 78−47435
Ni-Al, neutron irradiated, rel. between irradiation induced swelling and shear modulus 80−15157
Ni-base alloys, Nimonic PE-16, type 718 and type 625, neutron irrad. effects on fatigue crack propag. 80−29069
Ni-Be (2 wt.%), high-temp. radiation embrittlement, mechanical tests and TEM *(Russian)* 77−44331
Ni-Be alloys, struct. and phase stability in neutron bombardment field *(Russian)* 77−76467
Ni-Cr (0-35 at.%), neutron irrad. at 25K, damage, elec. resist. obs. *(French)* 80−54286
Ni-Cr Nimonic alloys, mech. props., high-temp. irrad. effects 80−100885
Ni-Cr-Fe-Ti alloy KhN77TYuR, long-term strength under in-pile irrad. conditions 78−6940
Ni-Fe, 79 NM alloy, gamma and neutron influence on mag. susceptibility comparative study *(Russian)* 80−39751
Ni-Pd(Cu)(Cr), directional order anisotropy energy induced by neutron irradiation, temp. depend. 77−66294
Ni-Ti(Fe), neutron irradiated, thermally activated deform. 80−6438
Ni-Zn ferrite, neutron irrad., mag. spectra, domain wall behaviour 77−48006
Ni-Zn ferrites 600 NN and M450 NNI, Curie point radiative shift due to neutron irrad. *(Russian)* 80−39775
Ni_2Cr, neutron irrad., point defect prod. and annealing 78−87718
Ni_3Fe, disaccommodation meas. after low temp. electron and neutron irrad. 80−88832
$NiFe_2O_4$, ferrite, mag. anisotropy compensation under neutron irrad. 80−75807
$NiFe_2O_4$ ferrite, mag. props., neutron irrad. 80−103858
Ni_3Mn, anal. of irrad. disordering data 79−1466
Ni_3Mn, atomic rearrangements during fast and thermal neutron irradiation 79−42114
Ni_3Mn, fission neutron disordering at 5K, exam. 78−47434
Ni_3Mn, neutron irradiated, disordering by replacement collision sequences, saturation magnetisation meas. 77−47492
NiZn ferrite, effect of reactor radiation on mag. props. 77−32215
$Ni_{0.32}Zn_{0.68}Fe_2O_4$, mag. props. and neutron damage 77−47973
$Ni_{0.85}Zn_{0.15}Fe_2O_4$, ferrite, mag. anisotropy compensation under neutron irrad. 80−75807
Pb, neutron irrad. effect on cyclotron reson. *(Russian)* 77−69216
Pb, reactor radiation-induced hardening, computer modelling *(Russian)* 79−37738
Pb superconducting junction, neutron irradiated, tunnel spectroscopy 78−10618
PbF_2, gamma-ray and neutron irrad. at low temps., EPR of Pb^{3+} ions 77−63262
Pb(Zr,Ti)O_3, piezoelectric ceramics, low fluence neutron irrad. effects 80−92564
$Pb(Zr_{1-x}Ti_x)O_3$, electrical conductivity and I-V charact., neutron effects 78−47781
Pd, localised vacancies produced by thermal neutron capture recoil 78−26598
Pd/Al_2O_3 catalyst, contact poison 2-methylthiophene damage reduction by neutron irrad. *(Russian)* 79−20467
Pd-Ni, neutron radiation stimulated diffusion, electrical resistivity exam. *(Russian)* 79−14959
Pd-Si, amorphous, neutron irradiated, small angle X-ray scatt. study 79−14850
Pd-Si amorphous alloy, neutron irradiation effects *(Japanese)* 77−84806
PdO, irrad., black form., adsorpt. props. 77−11796
$Pd_{80}Si_{20}$, amorphous, structural changes by neutron irradiation, X-ray scatt. meas. 78−6104
$Pd_{80}Si_{20}$, amorphous, structural changes with neutron irrad., X-ray scatt. obs. 80−33898
Pt, crowdion conversion to dumbbell, two-interstitial model, thermal neutron irrad. 80−33992
Pt, damage production by high energy d-Be neutrons, elec. resist. meas. 77−62564
Pt, isochronal recovery of high energy d-Be neutron damage 78−51592
Pt, neutron damage, positron annihilation 80−65056
Pt, neutron irradiation, low temp. recovery, effect of plastic deform. 78−51588
Pt, point defect properties, damage curve anal. 78−47359
Pt, recovery of thermal-neutron-irradiated samples 78−95081

neutron effects continued
Pt, recovery spectrum after thermal neutron irrad., resist. obs., Au addition effect and defect conc. depend. 80−65057
Pt, thermal and fission neutron produced defect configurations 78−47432
Pt-Mn-Sn alloy, mag. hyperfine fields 79−1737
Pt_3Fe, collision cascades, neutron induced superparamagnetism *(Russian)* 78−2166
PtO, irrad., black form., adsorpt. props. 77−11796
Pu, liq., enthalpy and heat capacity meas. using neutron heating 77−20078
δ-PuSc (5, 12, 18 at.%), f.c.c., contraction by self irradiation at 4.2K *(French)* 77−4129
S, allotropic modifications and activity distrib. 80−70255
$(SN)_x$, neutron and heavy ion bombard., effect on elec. cond. along chain axis 78−56136
sapphire, TFTR diagnostic windows, radiation damage 80−34063
Se, damage expts. review, defect interactions 77−84800
Se, single crystals, fast neutron irradiated, annealing expts., dark conductance, reflectivity spectra 77−85266
Si, annealed, neutron-irradiated, EPR centre (S=1), charcts. 80−71177
Si crystal, impurities determ. and resistivity after reactor neutron irrad. 80−65563
Si, defect storage kinetics during neutron irrad. 80−24505
Si depletion regions, radiation damage coeffs. for fission neutron and gamma-ray irrad. 80−34058
Si, dislocation ensembles motion in neutron irradiated covalent crystals *(Ukrainian)* 80−10579
Si, divacancy charge states, photoconductivity spectra 77−15899
Si, doping by neutron transmutation doping, detect. and identification of potential impurities activated 79−42090
Si doping by nuclear transmutation 77−84782
Si doping by thermal neutron irrad., annealing charcts. of bulk electron traps obs. 80−49244
Si dosimetry diode, irrad. by γ-rays and fast neutrons, lattice defect annealing *(Czech)* 79−45570
Si, ESR in neutron transmutation doped samples 80−20462
p-Si, energy spectrum and thermal stability of radiation defects, impurity photocond. spectra 77−4406
Si, fast neutron and ion irradiation, radiative recombination centres 77−81152
Si, floatzone, P doping by thermal-neutron irradiation 78−22750
Si, heavily disordered, fast neutron irrad., IR absorption following heat treatment 78−2448
Si, homogeneous epitaxial layers, production, appl. of neutron transmutation doping 78−38737
Si, homogeneous n-type doping by thermal neutrons 80−2051
n-Si, interaction of disordered regions with point defects 79−19296
Si, interstitials in radiation defect formation 77−15461
Si, irrad., displacement damage for monoenergetic neutrons 78−30670
n-Si, irrad., elec. props., in strong elec. fields 79−95416
Si, irrad., internal friction obs. of defects 78−51597
n-Si, irradiated with large neutron doses, defect annealing 80−19849
Si, junction FET, annealing of neutron induced defects, transductance meas. 78−43052
Si, minority carrier lifetime in neutron doped samples 80−20218
Si monocrystals, neutron irradiation installation for power thyristor production 77−65993
Si, neutron and electron bombard., radiation defect recomb., photoelec. props. meas. 80−60039
n-Si neutron and electron irrad., isochronous annealing influence on edge absorpt. 80−11449
Si, neutron bombarded homogeneous (NBH) P doping, power device appls. 77−1138
Si, neutron damage, displacement and ionis. fractions of fast neutron kerma 78−30669
Si neutron displacement cross section, radiation effects intercalibration, damage coeff. 79−23653
Si, neutron doped, γ-irrad. influence on elec. props. 80−6845
Si, neutron irrad., EPR, ⟨100⟩ split di-interstitial, positive charge state 77−20698
Si, neutron irrad., Hall effect and magnetoresist. meas. 80−6883
Si, neutron irrad., point defects photopopulation and photoionis., IR spectra meas. 80−25423
Si, neutron irrad., residual radioactivity meas. 80−19829
Si, neutron irrad., small angle neutron scatt. meas. 80−29073
p-Si, neutron irrad. effects, admittance meas. of n^+-p diode 78−51587
Si, neutron irrad. effects on lattice parameter and anomalous X-ray transmission 79−86821
n-Si, neutron irradiated, annealing behaviour characterisation by electrochem. meas. 80−19847
Si, neutron irradiated, changes in lattice period, X-ray meas. 77−7767
Si, neutron irradiated, charcts. of defect form. 78−14382
n-Si, neutron irradiated, charcts. of changes in mobility 78−39135
Si, neutron irradiated, direct band gap transition, IR absorpt. 79−73980
p-Si, neutron irradiated, elec. props. 78−51939
Si, neutron irradiated, influence of defects and temp. on positron annihilation 77−4699
Si, neutron irradiated, intrinsic defect exam. by IR spectra 78−52534
Si, neutron irradiated, resistivity and minority carrier lifetime, radial inhomogeneity *(Russian)* 78−26881
Si, neutron transmutation doped, zero-bias resist. of grain boundaries 78−76072
Si, neutron transmutation doping, photoluminesc. characterisation 80−11453
Si, neutron transmutation doping, impurities 80−15134
Si, neutron transmutation doping, radioactivity form. 80−15135
Si, neutron transmutation doping for IR detector material 80−15136
Si, neutron transmutation doping in Harwell reactors 80−15138
Si, neutron transmutation doping, irrad. facilities 80−15139
Si, neutron transmutation doping, General Electric test reactor 80−15140
Si, neutron transmutation doping, automated irrad. facility 80−15141
Si, neutron transmutation doping, annealing, lattice damage 80−15163
Si, neutron transmutation doped, highly compensated, resistivity fluctuations 80−15531
Si, neutron transmutation doped, elec. props. 80−15532
Si, neutron transmutation doping, irrad. techniques 80−19827
Si, neutron transmutation doped, isochronal annealing of resistivity 80−19828
Si, neutron transmutation doping, ^{31}P conc. meas. 80−19833
neutron effects continued
Si, neutron transmutation doping, at. displacement effects 80−19852
Si, neutron transmutation doping, annealing, deep defect levels 80−20123
Si, neutron transmutation doping using nuclear reactor thermal neutron irrad., review 80−39161
Si, neutron transmutation doping, impediments to use in power device fabrication 80−96560
Si neutron-prod. defects, investigation by transcond. meas. of JFETs 77−15455
Si, neutron-produced defects, deep level transient spectroscopy 79−47047
Si, neutron-transmutation doped, annealing behaviour, EPR obs. 79−86804
Si, O impurity precipitation from solid soln., neutron irrad. effect 80−29177
Si, p^+-n diode, neutron irrad., defect levels, G-T and C-T curves obs. 77−62986
Si, p-n junctions, neutron transmutation doping, breakdown process 80−15600
Si, p-n junctions, voltage-current charcts., fast neutron irrad. effects *(Russian)* 80−65659
Si, phonon-phonon relaxation investigation for conventional and neutron doped crystals 80−96927
Si, photodiode, 1.06 μm range, neutron and γ-irrad. effects 79−97433
Si, piezospectroscopic effect on zero phonon luminescence lines 80−50406
Si, radiation-doped and annealed, carrier density and mobility meas. 78−56145
Si, subthreshold irrad., migration of Sn, Mossbauer obs. 77−15462
Si transistor damage charcts. by neutron displacement cross section 79−42118
Si transistors, damage by fast burst reactor neutrons, Pb, paraffin shields 77−23172
Si wafer, thermal neutron irrad., charge carriers behaviour obs. *(Japanese)* 79−42484
Si:As, neutron damage mechs. in IR detectors 78−30668
Si:Au, neutron irradiated, penetration of Au into Si 78−59984
Si:B, irrad. with fast neutrons true profiles of impurity photocond. bands from piezodichroisms 79−91103
Si:Ga, neutron irrad., Hall effect meas. of shallow donor levels 80−20124
p-Si:Ga, neutron transmutation counterdoped, shallow defect levels, Hall effect and photocond. obs. 79−87055
Si:Gd, radiation defect form., effect of Gd impurities, elec. and optical meas. 78−71764
Si:Gd, radiation defects effect on elec. props. 77−28184
Si:In, neutron irrad. to compensate for residual B, photocond., IR focal plane array 78−67727
Si:In extrinsic detectors, compensation of residual B by neutron transmutation 78−281
Si:In extrinsic IR detector material with high responsivity compensated by neutron transmutation, float-zone growth 80−75597
Si:Li P/N type solar cells, irradiation obs. 79−66406
Si:Ni(Co)(Mn), influence of neutron irradiation as elec. props. 78−55895
Si:P, Au, neutron irradiated, distrib. of P and Au determ. 78−79627
Si:P, Cu(Au) radiation-doped, influence of growth defects on elec. props. 79−69144
Si:P, doped by neutron transmutation, electron traps 78−84164
Si:P, doped by neutron transmutation, lattice defects 80−34018
Si:P, doping by neutron transmutation, residual radioactivity 79−33009
n-Si:P, fast neutron irrad., defect clusters and defect build-up kinetics 79−33019
Si:P, homogeneous nuclear transmutation technique, thyristors appl. 80−70236
Si:P, neutron irrad. crysts., qualitative distrib. of P using autoradiography 80−24486
Si:P, neutron irradiated, influence of growth defects on change in cond. 78−39117
Si:P, neutron transmutation doped, electron trap annealing, deep level transient spectra 78−14368
Si:P, neutron transmutation doped, radiation damage exam., elec. props. 78−95080
Si:P, neutron transmutation doped, EPR obs. of annealing behaviour 79−1453
Si:P, neutron transmutation doped, EPR, electron trapping 79−73179
Si:P, neutron transmutation doping, elec. props. rel. to neutron fluence 80−96555
Si:P, neutron transmutation doping, resist. homogeneity rel. to compensation ratio 80−96556
Si:P Czochralski crystal donor homogenisation by thermal neutron irradiation 78−6108
SiC, fusion reactor first wall appl., radiation damage 79−86822
SiC, pyrolitic coating for nuclear fuel particles 77−79465
SiL, neutron damage at 1200°C, fusion reactor first-wall appl. 79−93829
Si_2N_2O, fast neutron irradiation, variation of lattice parameters 80−24504
SiO_2, amorphous, very small angle X-ray scatt. before and after thermal neutron irrad. 80−75270
SiO_2, amorphous and cryst., neutron irrad. and unirrad., intrinsic defect photolum. 80−50401
SiO_2, fused, irrad., O_2^- radical defect centres, ESR obs. 79−61222
SiO_2 gel, irrad., adsorpt. of NH_3, neutron scatt. 79−33194
SiO_2, vitreous, effect of neutron irrad. on low temp. dielec. susceptibility 79−73878
SiO_2, vitreous, fast neutron irrad. effect on struct., interstitials role 78−26599
SiO_2, vitreous, fast neutron irrad., low temp. US meas., two-level systems role 78−30703
SiO_2, vitreous, irradiated, EPR exam. of H_2 hyperfine spectra 79−28611
SiO_2, vitreous, neutron irrad. effects on heat capacity, thermal cond., US velocity temp. depend. 78−83851
SiO_2, vitreous, neutron irrad., luminescence nature and ESR signals correl. 79−43038
SiO_2, vitreous, radiation behaviour of optical props. 78−21655
SiO_2, vitreous, valence-attenuation pair defect, states, IR and Raman spectra 79−91442
SiO_2, vitreous and neutron irrad., thermal cond., heat treatment effect 79−90837
SmS:P, neutron irrad., semiconductor-metal transition 80−24975

neutron effects continued
Sn, tetragonal β-phase, neutron-irradiated, Frenkel defect spontaneous recomb. volumes 79−60355
SnO_2 film, reactor irrad. induced changes in elec. props. 77−28267
SrF_2, neutron irrad., role of F-centres in thermoluminesc. 79−19941
SrF_2, thermoluminesc. and F-centre annealing, after neutron irrad. 80−7422
SrF_2, undoped, H-centre prod. by reactor neutron irrad., optical absorpt. meas. 77−59010
$Sr_{0.3}La_{0.7}MnO_3$, neutron-irrad. induced phase transition 77−89952
SrO, neutron- or proton-irrad., F^+ centre fluoresc. yield and lifetime, 5 to 140K 80−55181
SrO, neutron-irradiated single cryst., F^+ centres, ENDOR obs. 80−15824
$SrO-Li_2O-Al_2O_3-SiO_2:Tb^{3+}$ glass, energy transfer, luminesc. efficiency under UV, neutron and charged-particle excitation 79−95822
TCNQ salts, Qn(TCNQ)$_2$ and N-propyl-Qn(TCNO)$_2$, low temp. mag. susceptibility, neutron irrad. effects 80−60311
TTT_2I_3, neutron irrad. induced defects and chemical impurity effects on DC cond. 80−39565
TZM, irrad. between 425 and 1000°C ductility in bending 80−39164
Ta, BCC, neutron-irradiated, Frenkel defect spontaneous recomb. volumes 79−60355
Ta, neutron irradiated, microstruct. and swelling 77−69006
TaS_2, 1T and 1H polytypes, fast neutron irrad., defect prod., effects on resist. and charge density waves 80−65060
Te, damage expts. reviews, defect interactions 77−84800
tetrafluoromethane+C react. in ionising radiation of nuclear reactor 77−63934
ThO_2 sintered pellets, ^{131}I release at low temps. 78−21650
ThO_2-UO_2 (0.1 wt.%), ^{133}Xe release after low dose irradiation 77−74919
Ti alloys, fusion reactor first-wall and blanket material, mech. props. 80−34074
Ti based alloys, He and simultaneous damage production simulation 80−32480
Ti, characterization of dislocation loops 80−88155
Ti, fast neutron irrad., twinning deform. at room temp. 80−65061
Ti, irradiated and cold worked, internal friction pdaks 77−86074
Ti, neutron irrad., low temp. deform. studies 79−47757
Ti, neutron irradiated, relation between microstructure and recovery behaviour 77−15456
Ti, neutron low energy interaction cross sections, gravitational spectrometer meas. 80−24521
Ti, thermally activated tensile props. 77−62567
Ti, twinning deformation, neutron irradiation effects 80−75236
Ti-Al-Mo, type Ti-6242S, irrad. induced creep 80−39163
Ti-Al-Sn, type Ti-5621S, irrad. induced creep 80−39163
Ti-Al-V, irrad. induced creep 80−39163
Ti-V-Cr, type Ti-15-333, irrad. induced creep 80−39163
TiB_2, low temp. radiation damage, calorimetric investigation 77−27916
TiB_2, low-temp. neutron irrad., electrical resistance and stored energy 78−67744
TiC, low-temp. reactor irrad., calorimetric investig. 77−80547
TiC_x, effect of structural vacancies on neutron radiation damage 77−35591
TiN, supercond. critical temp., neutron irrad. effect 80−80433
(U,Pu)CNO irradiated fuel, electron microprobe anal. 78−70601
$(U,Pu)O_2$ 316 stainless steel clad rods for GCFR, high temp. fast flux irrad. tests 77−18666
$(U,Pu)O_2$, in pile creep 77−42060
$(U,Pu)O_2$, irradiated fuel, O_2 pot. meas. using galvanic cell 79−49689
$(U,Pu)O_2$, mixed oxide fuel elements, Pu redistribution 78−78463
U abundance in Himalayan plants, fission track determ. 80−101305
U conc. in blood meas. by thermal neutron induced fission, chem. etching, conc. rel. to leukaemia 80−21532
U, irradiation growth during fission fragment and proton bombard. 80−92568
U, liq., enthalpy and heat capacity meas. using neutron heating 77−20078
U, reactivity meas., determination method *(Russian)* 80−664
U-Al (0.78 at.%), behaviour of metastable phases under neutron irrad., application of model 78−48408
U-Cr-Al (0.2, 0.1 at.%) fuel elements with high swelling resistance for KS-15O reactor 78−78471
U-Si-Al fuel rods, Zr-Nb cladding, irradiation behaviour with peripheral voidage 78−54835
UAl_x-Al dispersion fuel for thermal high flux reactors, irradiation 77−18660
UC, effect of porosity on fission-gas-induced swelling 78−8959
UC, fission dose depend. of lattice parameter changes 77−24333
UC, low temp. reactor irradiation 80−39168
UC, MX-type LMFBR fuels, TEM exam. of microscopic swelling 78−70596
UC, nuclear fuels, irrad. induced kinetics, diffusion and fission gas resoln. 80−59523
UC+UC_2, neutron irradiation, U_2C_3 deposition 78−33253
UC_2 and (8Th, 1U)O_2 fuel kernel, experimental containing CVD ZrC coatings, irradiation behaviour 77−3103
U_2C_3+UC, MX-type LMFBR fuels, TEM exam. of microscopic swelling 78−70596
$U_6Fe_{0.98}$ supercond. transition temp. reduction by neutron irradiation 77−63020
UN, fission enhanced creep and swelling, in-pile meas. 77−42061
UO_2 and UC, creep props. under irradiation 77−42059
UO_2, effect of point defects on nonequilibrium bubble behaviour 79−93722
UO_2 equiaxed grain growth modelling 80−13589
UO_2, high burnup nuclear fuels, relation between fission product release and fuel microstruct. 80−57845
UO_2, high temp. irradiation, effect on microstruct. and unstable fission products 78−33250
UO_2 irradiated, grain edge porosity growth 79−19285
UO_2, irradiated, spacing of intergranular fission gas bubbles 78−66340
UO_2, irradiation induced lattice defects 78−33251
UO_2, irradiation induced vol. change 78−67740
UO_2, microstructure in rods operated above critical heat flux 77−42098
UO_2, mobility of intragranular bubbles during irradiation 77−6520
UO_2, monocrystalline, fission gas release charact. during irradiation 78−4985
neutron effects continued
UO_2, neutron and electron irradiated, imperfect dislocation loops *(French)* 79−7606
UO_2, neutron irradiated, diffusion of fission product T 78−67866
UO_2, neutron irradiated, thermal recovery of defects 79−45348
UO_2 neutron transmission temp. depend. 79−82265
UO_2 nuclear fuel, sputtering by thermal neutrons, depend. of ejection coeff. on neutron flux 80−83157
UO_2 nuclear fuels, distribution and size of intragranular fission gas bubbles 80−57840
UO_2 nuclear fuels, irrad. induced kinetics, diffusion and fission gas resoln. 80−59523
UO_2 pellet fuel, radiation induced densification 77−6519
UO_2 pressurised rods, He fill-gas absorpt. during irradiation 80−37454
UO_2 pyrocarbon-coated HTR fuel particles, fast neutron influence on fission product transport 80−42777
UO_2, quenched and neutron irrad., recovery processes, vacancy migration 77−28048
UO_2, radioactive gas release during irradiation 77−74922
UO_2, transfer of fission gas between grain faces and edges 78−79815
UO_2 volatization pot. of metallic inclusions in irrad. nuclear fuel during LOF overheating transients 80−57895
$UO_2:Cr_2O_3$, fission gas release and swelling 80−47567
UO_2-PuO_2, irradiated fuel pins with various initial stoichiometries, radial O_2 distrib. *(German)* 77−46285
UO_2-PuO_2, mixed oxide fast reactor-fuel pin, fission gas bubble distrib. 78−78459
UO_2-PuO_2 fuel pin, hyperstoichiometric, post irradiation examination 80−63258
$UO_2-U_3O_8$ thin films, sputtering under influence of fission fragments at low irrad. doses 77−48282
UO_{2+x}, elect. cond. and thermoelectric power 78−52020
UO_2(Li) pellets, T release on heating after neutron irradiation 78−40071
$U_{0.8}Pu_{0.2}C_xN_{1-x}(0\leq X\leq 1)$, MX-type LMFBR fuels, TEM exam. of microscopic swelling 78−70596
V,V-Zr (2 wt.%), internally oxidised, neutron irradiated, annealing effect on mech. props., elec. cond. and electron microscope obs. *(Japanese)* 79−15701
V alloys, fusion reactor first wall and blanket material, props. for struct. appl. 80−30071
V alloys, fusion reactor first-wall and blanket material, mech. props. 80−34074
V based alloys, He and simultaneous damage production simulation 80−32480
V, fusion neutron induced radioactive emissions from surfaces 77−36321
V, He preinjected, void swelling on neutron irradiation 77−7765
V, high purity, neutron irradiated effect, comparison of high purity with V-O 77−84805
V, neutron irrad., yield stress and activation vol. 77−90418
V, neutron irradiated, saturable trap anal., of solute segregation applied to O_2 trapping 79−77645
V, neutron irradiated, void swelling, O_2 effect 78−6106
V, neutron low energy interaction cross sections, gravitational spectrometer meas. 80−24521
V, purification and plastic props. 80−25810
V, radiation hardening and plastic instability *(Russian)* 78−39842
V, sputtering under 14.1 MeV neutron impact 77−48281
V, superconductor, neutron irradiation, low temp., effect on critical current 78−52180
V surface, particle release by neutrons 80−25493
V:O, neutron irrad., void form., 673-1073K 80−29066
V-H, effect of neutron irrad. on electrical resistance, magnetic susceptibility 80−29063
V-O, neutron irradiated effects, comparison with high purity V 77−84805
V-Zr-C, radiation hardening and plastic instability *(Russian)* 78−39842
VC, damage sustained during neutron irradiation 77−1841
$V_{0.75-x}Ga_{0.25+x}$ ^{51}V, nucl. spin-lattice relax. time, annealing and neutron effects 79−82710
V_3Ga, high current density multifilament wire, neutron effects on equilibrium and transport props. 78−52126
V_3Ga, neutron irrad. effect on upper crit. field and crit. current 77−72954
V_3Ga, neutron irrad. effects on transition temp. *(Japanese)* 79−82707
V_3Ga, neutron irradiation and annealing 78−52130
V_3Ga, supercond., neutron-induced disorder revealed by isochronal annealing 77−72938
V_3Ga superconducting multifilamentary wires, effect of low temp. neutron irrad. 77−32132
$V_2O_5-P_2O_5$ based glasses, specific heat effect of fast neutron irradiation 77−69096
V_3Si, low fluence neutron irradiation, behaviour of supercond. transition temp. 78−43509
V_3Si, neutron irrad., elec. resist., temp. depend. 79−91024
V_3Si, neutron irrad., grain boundary pinning, field-depend. change of crit. current density 80−65759
V_3Si, neutron irrad., neutron diffraction studies 78−88076
V_3Si, neutron irrad., sound velocity, magnetic susceptibility and upper critical field 78−88074
V_3Si, neutron irrad., volume pinning force, summation and saturation behaviour 79−95554
V_3Si, neutron irrad. effects on transition temp. *(Japanese)* 79−82707
V_3Si, neutron irradiated, A15 compound, recovery of T_c by annealing 78−52132
V_3Si, neutron irradiated single crystal, superconducting transition temp. widths, resistivity and heat capacity meas. 78−91802
V_3Si, neutron-irrad., ht. capacity and resistivity 78−88075
V_3Si, normal state resistivity as function of neutron irrad. 79−56194
V_3Si, supercond. props., effect of neutron irrad. 80−80463
W, BCC, neutron-irradiated, Frenkel defect spontaneous recomb. volumes 79−60355
W, defect recovery following neutron irrad., annealing effect 79−77642
W, irradiation temp. determ. by electrical resistivity meas. 78−58354
W, neutron irrad., at thermal energies, annealing exam. of recovery 78−47355
W, neutron irrad., recovery of defects, isochronal and isothermal annealing 79−46712
W, neutron irradiated, FIM obs. of radiation damage 79−7632
W, neutron low energy interaction cross sections, gravitational spectrometer meas. 80−24521

neutron effects continued
W, stacking faults, microstress relax. effects, field ion images 77−89453
W, structural defect recovery after irradiation and cold work 78−47429
W, thermal neutron irradiated, radiation damage and stage III defect annealing 78−51586
W, thermal neutron irradiated, recovery processes 80−19848
W, vacancy recovery stage, radiation doping, elec. resistivity meas. 79−51102
W-Re, neutron irrad. effects on phase stability free energy changes 79−11566
zircalloy-2, annealed, neutron irradiated, 573 to 923K, damage struct. 79−99247
Zn, electron momentum distrib., neutron-induced defects, positron annihilation study, for single cryst. 80−71508
Zn, neutron irradiated, recovery of c-axis spacing and elec. resist. 80−34081
$ZnFe_2O_4$, cation distrib., preference energy determ. by neutron irrad. method 77−15384
$ZnFe_2O_4$, neutron damage effects, superparamag. state replacement cascades 77−16051
ZnS, additively coloured or neutron irradiated, near IR emission 77−90199
ZnS-Na_3AlF_6 Fabry-Perot interference filter, neutron irrad. effects on props. 79−76867
ZnS-O, single cryst., fast neutron irrad., optical props. 78−27331
ZnSe, reactor irrad., opt. props. 77−90137
Zr alloy, neutron irradiated, in-pile dimensional changes 77−24331
Zr alloys, irradiation growth, influence of microstructure and test conditions 80−92561
Zr alloys, neutron irrad., yield strength changes and radiation hardening, damage annealing *(Italian)* 77−65269
Zr alloys, thermal capture cross-section var. with time, calc., mech. and corrosion props. var. 77−61505
Zr and alloys, irrad. at 573 to 923K, damage struct. 80−107334
Zr, annealed, neutron irradiated, 573 to 923K, damage struct. 79−99247
Zr base alloys, irradiation growth, dislocation model 78−51595
Zr carbide interstitial phases, elec. and mag. props., neutron radiation effects 79−77640
Zr, deformed at 77K, effect of fast-neutron irradiation on deformation twinning, TEM and optical microscopy obs. 79−37741
Zr, displacement damage anal., program DISPKAN 79−14854
Zr, foil bending by in situ ion irrad., neutron damage simulation, room temp. oxide growth 80−107342
Zr, HCP, neutron-irradiated, Frenkel defect spontaneous recomb. volumes 79−60355
Zr hydride interstitial phases, elec. and mag. props., neutron radiation effects 79−77640
Zr, irradiation growth, influence of microstructure and test conditions 80−92561
Zr, irradiation growth, reaction rate theory calcs. 80−88212
Zr, neutron irrad., low temp. deform. studies 79−47757
Zr, neutron irradiated, dislocation loop nature 77−47489
Zr neutron irradiated, faulted loops 78−10094
Zr, neutron irradiated, twinning deformation 79−14848
Zr, neutron irradiated, yield point phenomenon 79−52304
α-Zr, point defect props., effect on irradiation behaviour of Zr alloys 78−30609
Zr, scattering and radiation damage for 14 MeV neutrons and 10 to 20 MeV protons 77−15458
Zr, single crystal, irradiation creep 77−42081
Zr, TEM obs. of irradiation damage, critical review 79−10879
Zr, tensile deformation behaviour, neutron irrad. effects, dislocations, twinning inhibition 77−90393
Zr-Al (8.0 wt.%), tensile props. and fracture toughness after fast neutron irradiation 80−3198
Zr-Al (8.6 wt.%), dimensional stability struct. and mech. props, effects of neutron irrad. 80−92563
Zr-Al (8.6 wt.%), effect of fast neutron irradiation on irradiation growth of Zr_3Al 78−55896
Zr-Al (8.6 wt.%), fast neutron irradiated, tensile props. and fracture toughness 80−84994
Zr-Al (8.6 wt.%), neutron irradiation effect on tensile props., swelling 77−7768
Zr-Al(8.6 wt.%), mech. props., corrosion and fast neutron irrad. influence 78−84948
Zr-Al(8.6 wt.%), neutron irradiated, irradiation growth and recovery, annealing 80−15162
Zr-B (1.3 wt.%), investigation of swelling due to neutron irrad. *(Russian)* 79−60404
Zr-base alloy as reactor core material, microstruct., deform. and fracture 78−4988
Zr-base alloys, annealed specimens, irradiation growth 80−49276
Zr-Cr-Fe, irradiation damage, metallurgical struct. effect 77−51412
Zr-H, effect of neutron irrad. on electrical resistance, magnetic susceptibility 80−29063
Zr-Nb, fracture resistance, atomic reactor material *(Russian)* 77−25140
Zr-Nb (2.5 wt.%), annealed, irradiation growth at 353K 79−46710
Zr-Nb (2.5 wt.%), annealed and quenched-and-aged, neutron irradiated, 573 to 923K, damage struct. 79−99247
Zr-Nb (2.5 wt.%), effect of irradiation on stability of precipitates 77−69007
Zr-Nb (2.5 wt.%), fuel cladding, anisotropy after creep and irradiaton 78−7001
Zr-Nb (2.5 wt.%), nuclear fuel channels, neutron effects on ultimate fracture strength, 293 to 573K 80−85054
Zr-Nb (2.5 wt.%) neutron effects on oxidation kinetics 78−690
Zr-Nb(2.5 wt.%) alloy, effect of pre-irradiation on oxidation 78−88580
Zr_3Al, hyperperitectoid, tensile strength, effect of fast neutron irrad. 77−52408
Zr_3Al, neutron irrad. effect on tensile props. 80−3156
Zr_3Al, ordered, notch sensitivity, neutron suppression 78−23779
Zr_3Al, ordered, strengthening by fast neutron irrad. 78−84838
ZrC, low-temp. reactor irrad., calorimetric investig. 77−80547
ZrC, thermal stress cracking 79−77641
$ZrH_{1.8}$, radiation-induced defects in hydrogen sublattice 79−37739
$ZrH_{1.9}$, neutron irrad. induced defects, nature and thermal stability 77−50246
ZrH_x, two-phase ($\delta+\epsilon$), homogenisation during neutron bombard. *(Russian)* 78−18684
ZrO_2, neutron irrad., monoclinic to cubic transform. 78−87720
ZrO_2, Y_2O_3 stabilized, neutron irrad. damage 77−84804

neutron flux
$1/E^{1+\alpha}$ epithermal neutron spectra, resonance integral correction, effective resonance energy 80−71978
$1/E^{1+\alpha}$ epithermal neutron spectrum, α-determ. without Cd cover 80−71976
γ-spectrographic anal. of neutron fluxes and depleted fuel fission products 79−97933
absolute determ. using associated gamma-ray technique in $^7Li(p,n_1\gamma)$ 77−10562
absorbed dose conversion factor 77−90908
absorbing samples, average thermal neutron flux determ. method 78−73112
acceleration technique for iterative methods in diffusion equation *(Japanese)* 79−80971
accelerator facility, fast neutron research, data acquisition and anal. 80−47806
accelerator-breeder target neutronics, neutron leakage 79−81060
activation analysis, in vivo, total body, neutron uniformity 78−40315
activation analysis, radiation flux, allowance for fluctuations 78−88688
activation analysis in vivo, neutron flux uniformity 77−9246
activation detector ave. cross sections in ^{252}Cf benchmark field 78−82598
activation detectors for determination 77−71727
analogue simulation of reactor neutron field, equipment minimisation *(Russian)* 78−74416
angular effects in toroidal diffusion, one-group homogeneous diffusion model 79−22351
anisotropic scattering treatment using improved comput. code *(Japanese)* 80−13526
Argonaut reactors, coupled core, neutron wave propagation, Be, graphite and D_2O as internal reflectors 80−27752
associated particle counting tech. for abs. monitoring of DD and DT neutron fluences 80−99428
associated particle methods for flux monitoring 79−9977
bath techniques for neutron source emission rate meas., $MnSO_4$ bath 79−9980
beam experiments *(Japanese)* 80−27684
beta-emission cable-type detector with Ag emitter, sensitivity during long service in reactor 78−86644
black and grey neutron detectors 79−9971
Bonner sphere spectrometer, least-squares technique for extracting neutron spectra 78−33366
bounded flux-at-a-point estimators, Monte Carlo methods 79−587
BRUCE A Unit 1 reactor, flex distrib. meas. for various reactivity control configurations 78−25317
Bruce core, ZED-2 mockup, responses of Pt, V and Co self powered flux detectors 78−58391
burnup equations, determination of neutron flux and isotopic changes in reactor cell 78−58340
BWR, effect of multiple boiling channels on void fluctuation spectra 80−18464
BWR, fast moderator feedback effects during severe press. transients 78−4990
BWR, global noise identification by spectral and parametric methods 79−63730
BWR, in-core investigation of two-phase flow using neutron-noise techniques 79−54530
BWR, neutron image anal. by one-dimens. core model 77−61478
BWR, neutron noise field, two-group diffusion theory 80−18461
BWR, noise anal. model 78−50237
BWR, noise sources of neutron flux, coherence anal. 77−88199
BWR, operational stability monitoring by reactor noise polar correlation 79−93761
BWR, Quad Cities 1, localized cold critical expt. 79−81001
BWR, shield design against neutron streaming in pressure vessel vicinity 80−13678
BWR, transactinide buildup in nuclear fields, sensitivity anal. rel. to neutron flux and spectra *(Italian)* 79−45356
BWR, void fraction profile determ. by neutron noise anal. 78−46150
BWR boiling noise, local and global component obs. and calc. 78−94066
BWR diagnostic anal. using multivariate autoregressive processes 77−23220
BWR fluctuations, in neutron flux, due to steam bubbles 80−47534
BWR in-core neutron flux instrumentation package 77−71641
BWR neutron noise source identification from existing instrumentation 79−13483
BWR noise, response of neutron detector to local coolant void distribs. 80−683
BWR noise anal., identifiability of dynamics using autoregressive modelling 79−45340
BWR parameter estimation, multivariate anal. of neutron noise signals 80−18465
BWR power distribution analysis, three-dimensional calc. program 79−9674
BWR power plants, monitoring instrum. 77−14240
BWR power reactor, in-core startup system with neutron flux monitor 80−32405
BWR stability monitoring using time series anal. of neutron noise 80−47625
BWR stochastic neutron flux fluctuation obs. and modelling, thermohydraulic parameters 78−94065
BWR-4 neutron noise anal. of incore instrum. tube vibr. and impacting 79−36353
BWR-4 neutron noise analysis spectra characterisation 79−13482
CANDU pressurised HWR fuel, bundle end neutron flux peaking effects, plenum use 78−58385
CANDU reactor, integral transport code PEAKAN for flux peaking anal. 79−59135
CANDU reactor, Th-fuelled, importance of ^{233}Pa in neutron economy 80−22980
CANDU self-powered flux detectors, response characts. 80−32404
CANDU-PHW, neutron flux regulation by two-phase flow absorber system 79−93799
CANDU-PHW, thermal neutron flux-mapping system 80−792
CANDU-PHW reactor online spatial control, flux mapping appl. 77−88266
checkerboard pool core, series of two group calcs. 78−74424

neutron flux continued
chopper for neutron pulse propagation experiments 78−13362
CIRENE LWCHW reactor, two-phase flow rods for neutron flux control, computer anal. 79−59217
Clinch River Breeder Reactor primary coolant pipe chaseway neutron streaming analysis 79−9661
coarse-mesh nodal method based on response matrix considerations 77−65262
collision probability integrals, annular geometry, evaluation using analytic expansions 80−32317
collision probability integrals, props. in annular geometry-11 evaluation 79−67812
compatible product ang. quadrature for transport in x-y geom. 77−82981
complex heterogeneous reactor cells, neutron flux calculation by imbedding element method *(Russian)* 78−58321
core pin power distribution det. based on nodal coarse mesh calcs. 77−88195
cosmic ray neutrons, Ames collaborative study on mid-latitude flights 78−53538
counting-Campbelling channel for in-core and out of core meas. 80−32406
coupled cores, calc. of buckling variation and neutron flux, Green's function method 78−74421
coupled-core reactors anal. with method of moderator region response function 78−58331
critical assembly, Big Ten, ^{235}U enriched U (10%) 80−823
critical assembly, rapid calc. of neutron fluence and dose 77−38317
critical point reactor, response to inherent reactivity noise input 79−45336
critical slab, isotropic and anisotropic scatt., asymptotic solution, strained coords. method 80−42733
cross section adjustment in anal. of benchmark expts. 79−63718
cross-section adjustments, sensitivity to uncertainties 80−47531
cyclotron, variable energy, shielding calcs., concrete and earth shield design 77−61622
deep-penetration transport calculations and neutron transport eqn. forms 78−8868
density determ., thermal and intermediate energy, using Au foils 78−82536
density fluctuations in on-off controlled reactor, exact stochastic anal. 79−36308
density measurements for reactor control *(German, English)* 78−17335
depression factor determ. by integral transform method 78−50233
detection using self-powered Inconel-Inconel coaxial cable 80−42842
detector calibration associated particle technique 77−26939
detector system, proton recoil with gas scintillation transmission counter, 1-30 MeV 77−23366
diffusion equation, Fourier expansion for xyz-geometry 80−9326
diffusion flux calc., use of Aitken extrapolation method 79−13379
discrete ordinates calc., weighted-difference formulation 79−9660
distribution at fuel element surface meas. *(Czech)* 79−36344
distributions in nuclear reactors, improved response matrix method calcs. 77−34363
dosimetry, comparison of single and multidetector systems *(Russian)* 78−33294
dosimetry, fast pulse reactor, standardisation 79−13543
dosimetry, standardization, 0.001-14 MeV, description of sources 79−9919
dosimetry, standardized techniques for appl. beyond reactor core 79−9920
dosimetry techniques for accelerator-based irradiation facilities 79−41041
effective neutron resonance cross sections, calc. in energy and space 79−17954
energy dependent transport system in slab geometry, positive solns., subcriticality 77−50185
epithermal neutron field for ^{10}B neutron capture therapy, prod. using FBR 80−61692
epithermal neutron flux distrib., effect on neutron activation anal. 79−52833
epithermal neutron radial flux distrib. in water, student expt. 79−97146
explicit iterative technique for FX2 reactor analysis computer code 78−17302
explosion induced conical system, internal break even possibilities 79−94811
fast, determ. by ^{93m}Nb disintegration rate meas. *(German)* 77−38579
fast and thermal flux densities, determ. in intense high-energy photon fields by activation products counting 78−94157
fast flux, approximated space-energy resolution 77−82991
fast monoenergetic, international comparison of meas. 80−83138
fast neutron contaminations in X-ray beams, determination using activated Al foils 79−6724
fast neutron facility in CP-5 reactor, neutron flux, energy spectrum, primary recoil distribution 79−41056
fast neutron fluence determination by activation detectors, radiochem. evaluation, reactor appl. *(German)* 77−34510
fast neutron fluence meas. technique, uses neutron irrad. effect on light absorption of cellulose acetate 78−13345
fast neutron generator, LiOD-D_2O thermal-to-14 MeV convertor, evaluation 79−9928
fast neutron generator, LiOD-D_2O thermal-to-14 MeV convertor, evaluation 79−13567
fast neutrons, monoenergetic, international flux density intercomparison 79−9981
fast pulse reactor at APRF, absolute neutron flux meas., dosimetry, calibration against ^{252}Cf source 77−23389
fast reactor, plate lattice heterogeneity effect with course group consts. 77−3075
fast reactor adjoint neutron spectrum calc. using bilinear weighted cross sections 77−83003
fast reactor boiling detection by noise analysis 79−13449
FBR, multigroup 1-D diffusion program MED 78−78456
FBR, neutron physical characts. calcs. *(Bulgarian)* 79−85602
FBR, neutron-physical calc., multi-group diffusion equation solution *(Czech)* 78−66332
FBR, nonstationary prompt-neutron diffusion, multigroup treatment 80−86956
FFTF irradiation test program 79−67928
filtered neutron beam facility, 2, 24 keV neutron beams prod., filter comps. and configs. 77−6597
filtered neutron beams, 2 and 24.5 keV, current density profiles and high energy background *(German)* 78−58529
fission counter, absolute neutron flux meas. and ^{239}Pu(n,f) resonance integral 80−5453
fission foils of ^{235}U, ^{238}U, ^{237}Np used for neutron fluence meas. 78−13177
fission fragment track and activation detectors, neutron fluence and reactor core centre flux mapping 78−13346
fission reactor, automatic diagnosis of abnormal phenomena 78−17330
fission reactor, one-group model, convergence acceleration in perturbation theory problems 78−37406
fission reactor, reactivity determination, pulsed neutron source technique, ZR-4 reactor appl. *(Hungarian)* 78−21673
fission reactor thermal power determ. using neutron flux density meas. 80−73955
fission reactors, homogeneous reactor cells, few-group cell parameters 80−27696
fission reactors, reactivity reserve and K_{eff} estimation *(Russian)* 80−73913
fission track glasses, calibration of fission track dating parameters 77−41207
fissionable nuclei A=232 to 252, systemization of relative yields of retarded neutrons 79−40974
fluctuation-type reactor power and period meter, errors 77−54292
fluence measurement in total body in vivo neutron activation anal. 77−86613
flux depression factors for scatt. and absorbing media 78−4976
flux distortion in 3-D reactors due to plane absorbers *(German)* 77−6478
flux interpolation for elastic down scatt. 78−29560
flux peaking anal., nuclear fuel bundle ends, program PEAKAN 78−82493
flux synthesis program KASY, consideration and appl. to reactor design problems 77−88184
flux-distortion factor for a foil in a exponentially varying flux 78−89930
foil detector, activation in intermittent flux with multiple decay 79−76314
FPR neutron spectrum in presence of experimenter's tahle 78−21676
FTR, calc. of resonant reaction rates near region interface 79−80993
fuel element rod bundle, neutron field calc., surface pseudosource method 80−27772
fuel rod malfunction, neutron noise as information carrier for early detection 77−14242
full flux covariance matrix calc. for NBS intermediate-energy standard neutron field 80−5348
fusion reactor, Tokamak type, released energy in blanket 77−34447
fusion reactor materials, nuclear response functions library, MACKLIB-IV 79−67950
fusion reactors, molten-salt blanket, effect of Pb and Bi neutron multiplication zones on the fission rates of ^{232}Th and ^{235}U 80−99272
gamma-ray laser pumping, Mossbauer effect in magnetised plasma 80−28186
gas target neutron source for radiotherapy, generation by ^{3}H(d,n), energy spectra, flux 78−92698
GCFR benchmark shielding expts. 79−9902
graphite-Th assemblies for fusion blankets, neutronic calcs. using 14 MeV source 79−59262
gravitational interaction *(Russian)* 78−36901
Grenoble high flux reactor, neutron physics expts., methodical aspects *(German)* 80−554
heterogeneous computer program for square fuel rod lattices in cylindrical tank 78−58346
heterogeneous critical assemblies with strongly blocked absorber, reactivity temp. effects 80−32395
heterogeneous reactor, homogenization, finite difference eqns. of neutron distrib. 79−40992
heterogeneous reactor, neutron thermalisation effects on physical characts. 79−26487
HFIR, dimensionality reduction of reactor noise signatures, improved automated noise anal. 77−6499
HFR test reactor, HIP-TEDDI code for neutron flux calcs. 79−3223
high n flux fusion heating, ^{6}Li(n,t)^{4}He use 78−89975
high neutron fluence meas. using mica muscovite as track detector 80−106237
high-power reactor, conditions for nonuniform field production 78−37405
higher order perturbation methods, implicit and explicit, for reactor anal. 78−78444
homogenized-cell diffusion parameters from transport codes 78−17300
HTGR, large pebble bed, Xe oscillations detection 80−22988
HTPBR, neutron and physical aspect calcs. *(German)* 80−22941
HTR cores, comparison of energy group models for Xe transients determ. 77−67803
Hungarian research reactor, reconstruction and modifications *(Hungarian)* 77−50205
HWGCR, KS-150, in-core instrumentation, neutron flux, temp. distrib. 77−83050
HWR, multidimens. space time kinetics studies 78−29547
HWR TV-O, active core neutron spectrometry using Bonner spheres *(Czech)* 80−73948
hybrid reactor, reaction rate sensitivity to fission spectrum changes 80−47712
ICRU phantom neutron fluence to dose index conversion factors 79−9909
imbedded neutron flux calc., reconstruction of original material struct. of fuel bundle 77−88196
in-core movable neutron flux mapping computerised console development 78−13308
inert gas plasmas, prod. by U fission fragments in nucl. reactor props. 77−76147
infinite homogeneous multiplying system, joint factorial moments of neutron and count bivariate distrib. 79−76062
intermediate-energy secondary spectrum system, determ. of neutron characteristics, ΣΣ-ITN *(Rumanian)* 79−22355
IRT 2000 reactor in Sofia, neutron spectra and doses in exptl. canals *(Bulgarian)* 78−82489
IRT-2M reactor with loop channels in active area, physical parameters *(Russian)* 79−31067
IVV-2 research reactor, thermal neutron flux distribs. using neutron probes 80−32391

neutron flux continued
k_∞ measurements, RB-2 reactor, null reactivity oscill. method 79−9665
Kalman filter technique, neutron flux distrib., optimal allocation of in-core detectors 78−54839
KEMA Suspension Test Reactor neutron flux and Dodewaard BWR temp. noise 79−3193
kerma factors for H, C, N, O and tissue, 20-70 MeV 77−73584
kinematics of neutron producing reactions 80−86862
LAMPF radiation effects facility, total neutron flux, energy spectrum, meas. and calc. 77−23331
laser detection of scattered neutrons from luminesc. line freq. change 80−23272
leakage spectra from critical assemblies, depth dose, dose equiv. and quality factor 78−58504
linear accelerator used in high-energy photon radiotherapy, 10 MV, neutron prod. 77−16995
linear radiation-flux functionals, estimation of local perturbations using Monte Carlo method 80−5457
LMFBR, compact Na cooled reactor, KNK-1, total and fast neutron flux meas. *(German)* 78−62591
LMFBR, comparison of neutron diffusion computer codes 77−88188
LMFBR, distrib. on core support grid plate 78−21675
LMFBR, fast neutron streaming through grid plate shield 77−3081
LMFBR, Na boiling detection, power spectral density surveillance systems 80−68740
LMFBR, neutron streaming through control rod followers, diffusion coeff. by numerical integration 80−13636
LMFBR ex-vessel low level flux monitor neutron source strength determ., appl. of nuclear data 77−26865
LMFBR fuel pin bundle, wire-spaced, three-dimens. deflection modes 78−13301
LMFBR meltdown cores, exptl. study of integral physics parameters 80−13664
LMFBR Na-heated steam generator, flow instability detection by noise anal. 79−97854
LMFBR PHENIX vibration-induced neutron noise obs. 79−13453
local flux density of fast monochromatic neutrons, absolute determ. method 78−5106
LWBR detection of thermal shield motion using ex-core neutron detectors 79−59220
LWFBR, neutron balance in chain reaction, delayed neutrons role, reactor safety *(German)* 79−26726
LWR, core reactivity changes, influence of axial flux distrib. 77−46365
LWR, feasibility of reactivity determ. from neutron noise spectral density with ^{252}Cf in initial loading 79−81002
LWR, large cores, anal. of space-time effects using coarse mesh flux expansion method 77−67794
LWR, reactor cavity neutron flux calc. 79−89362
LWR, thermal neutron disadvantage factors for PuO_2-UO_2 and UO_2 lattices 80−73945
LWR, zero power coupled core, cross power spectral densities, core separation distance effects 79−54469
LWR neutron flux distrib. in hexagonal geom., appl. of transmission probability method 79−93680
LWR parameter sensitivity to uncertainties in thermal neutron data 78−29561
LWR sensitivity coeffs. depend. on macroscopic spatial flux variation 79−80988
measurement, calculation of target and detector size in determination of 14-MeV neutron energy flux 79−97829
measurement by Mn bath method, expt. determ. of neutron leakage 79−97744
measurement system at fast pneumatic transfer systems for activation anal. *(German, English)* 77−38576
measurement techniques for standard cross section meas. 77−23040
microexplosion reactor neutronics, adjoint transport eqn. technique 80−47713
Millstone Unit No.2 neutron spectra and fluence determ. 79−9907
moderation, quasi-asymptotic neutron flux attenuation constant in a moderator with a cylindrical cavity *(Bulgarian)* 80−68725
monitor, H_2 filled proportional counter, for cross section meas. 77−23379
monitoring and data anal. for neutron standard react. cross sections 78−90039
monitoring by in-core detectors 80−5297
monitoring during reactor refuelling and start-up, instrum. *(Polish)* 80−42792
monoenergetic fast neutrons, international intercomparisons *(Japanese)* 78−29521
monopole and dipole response coefficient theory comparison with expt. 78−13188
Monte Carlo shielding calcs., biased selection of particle flight directions as variance resolution technique 78−29653
Monte Carlo track rotation estimator, calc. of total flux at point 79−71385
multi-group transport eqn., time-independ., soln. using spherical harmonics 78−37386
multidimensional neutron transport equation, spherical harmonics soln. by finite Fourier transform. 78−17269
multigroup diffusion equation, synthesis-finite element method 80−27699
multigroup diffusion program EMA-II-30, two dimens., flux distrib. *(Russian)* 77−38318
multigroup neutron flux calcs. with MURLAB program 78−29541
multilayered reflector region, neutron diffusion codes, analytic treatment 79−93683
multizone reactor neutron flux profile optimisation program *(Russian)* 79−13412
NE-110 scintillation counter, obs. neutron flux meas. 80 to 500 keV 79−735
neutral beam injector penetrations, limiting neutron streaming, neutron flux calc. 80−95400
neutron diffusion 3-D coarse mesh code, ROCS 77−46252
neutron flux density for irradiation of human tissue, max. permissible dose calc. 79−43992
neutron multiplier, criticality studies 77−34503
neutron source, 14 MeV, skyshine anal., Monte-Carlo computer code 78−66429
neutron standards and appl., conference, Gaithersburg, MD, USA (March 1977) 79−9581
neutronic analysis of the NBS intermediate-energy standard neutron field (ISNF) 80−27692
neutron flux continued
neutronic noise, relations with coolant temp. fluctuation and control rod vibr. at KUR 78−58327
nodal fluxes determination using approx. analytical method 77−65261
noise analysis in PWR and BWR power reactors 80−86964
noise studies in BWR and PWR 80−557
nonlinear reactor noise anal., appl. of Langevin eqn. with system-size expansion 80−68727
nonmultiplying two-zone cylindrical medium, asymptotic neutron distribs. 77−46203
NRU, NRX reactors, homogeneous cell parameters for 2-D reactor codes by axial averaging of 3rd parameter 79−54577
nuclear power plants, diagnostic system using noise anal. 78−50279
nuclear pumped lasers, thermal neutron traps description 80−64041
nuclear reactor, thermal neutron flux meas. method *(Rumanian)* 78−21670
nuclear reactor level CRT state indicator 77−79444
nuclear reactor pressure vessel material surveillance capsule, neutron radiation, limiting condition 80−47572
nuclear reactor pressure vessel steel irradiation, neutron flux densities neutron spectra and temp. fields in large specimens 77−74924
nuclear ship streaming neutron meas. by two-detector method 77−46408
number fluctuations in nuclear reactor, appl. fluctuation theory *(Hungarian)* 77−49679
Oklo natural fission reactor, computer calc. of neutron balance and flux distrib. *(French)* 80−21767
one-group neutron transport equation and angular flux separability 79−17952
optimum control during nuclear station load following 79−9761
optimum design for subcritical neutron multiplier 79−59290
p-cell homogenization, transient flux effects, incorporation into 2-D iteration scheme 78−17301
particle collision method in spherical geometry by escape probabilities, flux transport eqn. 78−78433
PB-HTGR, control-rod induced flux perturbations, numerical anal. using out-of-force instrumentation *(German)* 80−83179
PBHTR, out-of-core instrum. for detection of spatial flux irreg. *(German)* 78−82430
PBR fission reactors, neutron flux distribs. in multisphere configs., diffusion-theoretical model *(German)* 80−73875
perturbation due to NE213 scintillation spectrometer in a LiF assembly 79−85855
photon beam 18 MV, from Philips SL/75-20 linear accelerator, fast and slow neutron contamination 78−65127
plane geometry neutron transport theory, general anisotropic energy depend. scatt., phys. interpretation 78−4973
point neutron flux, Monte Carlo schemes evaluated 79−586
point reactor without delayed neutrons, moments of probability distrib. calc. 77−57705
portable digital reactivity meter for power reactors PWR, BWR appls. *(German, English)* 77−82999
power and temp. fluctuations for reactor with temp. feedback, exact statistical anal. 79−36309
power reactor noise analysis, nonlinear kinetics effects and new techniques 79−13454
pressure vessel, Oconee nuclear station, surveillance capsule results 79−18019
Princeton large Tokamak, obs. of electrodisintegration neutron prod. 78−5029
prompt gamma-ray anal. of neutron flux distrib. in nonhomogeneous samples, computational model 80−14060
proton recoil proportional counters, fast monoenergetic neutron fluxes meas. procedure anal. 78−17478
proton-recoil counter technique for measurement of fast neutron spectrum 80−9447
proton-recoil telescope for in-line absolute neutron fluence measurements 79−18079
pulsed neutron research, book 80−22146
pulsed source, maximum density and capture rate of neutrons moderated 80−13522
PWR, calcs. of neutron environment inside containment 80−13676
PWR, effect of measurement conditions on the design of delayed-neutron detector units *(French)* 79−97855
PWR, fast-neutron dose rate meas. inside containment shell 80−13674
PWR, fixed in-core gamma thermometer for neutron flux meas. 80−717
PWR, flux monitoring startup and safety system, ex-core, design and qualification 77−65286
PWR, KWU 1300 MWe facility, neutron flux computer calcs., radiation damage 77−34370
PWR, neutron density noise variation during core life 80−99201
PWR, neutron noise diagnostics of 2-D control rod vibrs. 80−68840
PWR, Westinghouse, neutron flux mapping at low power 78−21703
PWR CANDU, thermal neutron flux distribution, meas. and simulation 78−82492
PWR core anal. using 3-D spatial neutronics codes 79−89360
PWR internal vibrations, neutron noise monitoring 79−13445
PWR movable in-core neutron detectors *(Japanese)* 79−26722
PWR neutron flux detectors, reliability tests *(French)* 80−32403
PWR neutron noise increase with operating time 79−13447
PWR neutron noise meas. and modelling 79−13443
PWR neutron noise sources 78−94108
PWR noise analysis using multivariate autoregressive time series modelling 80−23028
radiation effects in fission reactor materials, energy spectrum depend., damage function *(German)* 77−34386
radiotherapy 25 MV X-ray beam, fast and thermal neutron profiles 78−73246
radiotherapy betatron, 25 MeV, fast neutron component and patient dose 78−3592
radiotherapy shielding, comparison of photoneutron and ^{252}Cf neutron spectra 79−59273
radiotherapy with pions, nucl. emulsion studies 78−73219
rare earths, isotopic analysis, Oklo natural fission reactor fluence distrib. meas. *(French)* 80−21759
reaction and neutron leakage rates for a large thorium metal assembly surrounding a DT neutron source 80−106099
reactivity and neutron density noise excited by random rod vibr. 77−50203
reactivity coefficients, perturbation effects from point-kinetics model *(Hungarian)* 80−78346

neutron flux continued
reactivity effect of cross-section processing for moist bulk-oxide criticals 80−37493
reactivity functions generation by use of Cd rod 77−57709
reactivity insertion, unexpected, rapid detection 78−58370
reactivity meters for monitoring extremely subcritical reactors, source analogue 77−71643
reactor, core power and flux distribs., BITNOD large-mesh code appl. 78−17304
reactor, dice games to illustrate probability, teaching 78−12515
reactor control by neutron flux, expt. investigation of optimal processes 77−3139
reactor core, effect of ENDF/B-IV cross sections on design parameters 78−13219
reactor core, independent control of neutron flux using gaseous absorbers 79−71918
reactor core, VVER type, neutron noise, diagnostic method of mech. vibrs. *(Czech)* 77−3120
reactor core critical assemblies, neutron flux depend. on moderators 79−71879
reactor core dosimetry standards 79−9824
reactor critical facility, fast neutron spectrum meas. using (n, α) and (n, p) reactions 80−78403
reactor dynamics optimal control, exact closed-form soln. for terminal cost problem 79−54472
reactor lattice epithermal neutron spectra, spherical harmonics anal. 78−21619
reactor malfunction detection by Dynamic Data System methodology 79−622
reactor neutron field fluctuations, energy distrib. and reactor power 80−32396
reactor neutron flux instrumentation commissioning, EM compatibility 79−89466
reactor neutron flux meas., high temp. neutron rad. detectors and cables 79−76111
reactor neutron flux meas., integrated cable detectors for use under flux and/or at high temperature *(French)* 79−76114
reactor neutron noise theory, role of factorial cumulants 79−63711
reactor neutrons, high level field stability, iterative calc. method 79−63714
reactor noise, AR-MA anal. hidden state variables 80−73944
reactor noise, neutron multigroup theory, calc. of second order correl. functions *(German)* 79−89390
reactor noise in presence of vibrating control plate, at-power measurement 77−61491
reactor noise monitor, real time calc. of RMS values, av. freq. and peak freq. 79−76079
reactor noise theory as a Markov process 78−74420
reactors, ex-core detector neutron noise to core barrel amplitude scale factor 80−27779
regulator horizontal shift, effects 79−71877
relativistic calculations, importance in proton recoil telescope efficiencies 80−102225
resonance escape in slab lattices, variational method 79−85572
response matrix doubling equations for particle distribs. calcs. improved formulations 77−6480
RFSP-JUL, program for unfolding n spectra from activation data 78−82570
S_N transport method for calc. of anisotropic transmission problems 80−68720
scintillator for 250-1000 keV neutron flux meas., >95% efficiency 77−26938
self shielding factors, elastic removal cross sections, strong reson. scatt. 79−13374
self-powered detectors for in-core reactor neutron flux meas., detector signal composition 80−32402
self-powered flux detectors, response characts. in CANDU reactors 78−82594
shape factors of non-critical small fast assemblies and their use in k_{eff} calculations 79−89351
shielding, in 3-D direct-coupled-ray method 78−21785
single channel flux synthesis, finite element trial functions for 3-D reactor calcs. 80−42734
Skylab, spacecraft-produced neutron fluxes meas. 78−28486
slab geometry and neutron density, transport soln. props., piecewise polynomial variational approx. 77−54269
slow neutron flux distribution from microtron convertor in graphite moderator with water reflector *(Russian)* 77−82979
slow neutron reaction rate ratio meas. using Cd and Hg prompt gamma reaction 79−30837
slowing down length in hydrogenous moderators calc. by Fick's law 79−22352
solid state nuclear track detectors, reactor neutron fluence meas. using Au and In foils 80−69035
spatial approximation using coarse mesh methods QUABOX and CUBBOX, and higher order polynomials *(German)* 77−88192
spatial fluctuations of neutron and powder distribution in critical reactor 79−71917
spatially depend. spectrum, expansion about local Maxwellian 78−29537
spectral uncertainties in ENDF/B dosimetry cross section file benchmark spectra 77−23306
standard installation improvement for reproducing unit of thermal-neutron flux density 78−74524
standard neutron spectrum field *(Japanese)* 79−9562
standardisation in nuclear radiation meas. technology with SINUPERM system 78−50410
stationary monoenergetic neutron transport equation for slabs, power series solns. comparison 78−13190
steel, CT specimens, irradiated in FRJ-1 research reactor, neutron flux densities, temp. fields meas. 77−83029
stochastic point reactor kinetics eqn. soln., 79−63719
streaming through ducts in shields, Albedo-Monte-Carlo method usefulness 79−89345
subcritical core assembly, neutron physical parameters 79−63738
surface barrier spectrometers for fast neutron calibration in MeV range 79−9961
terphenyl, partially hydrogenated, neutron thermalisation spectrum 77−67812
TFTR, isodose contour map construction using DOT 3.5 computer code 79−67949
thermal, absolute determ., $4\pi\alpha$-γ coincidence meas. 79−85576
neutron flux continued
thermal and epithermal neutron flux densities, self-powered neutron detector sensitivity 80−52817
thermal neutron acceleration in medium with reson. excitation by EM wave *(Russian)* 78−37394
thermal neutron distrib. in bone in paraffin phantom, irrad. with 14 MeV neutrons 78−3616
thermal neutron flux, determ. accuracy 77−342
thermal neutron flux density, working standard based on F-1 reactor 78−82410
thermal neutron fluxes prod. in water by isotope and accelerator neutron sources 78−55077
thermal spectra calcs. using synthetic scatt. kernel 77−14206
thin monitors for reactor dosimetry 80−32522
threshold foil meas. of reactor neutron spectra, radiation damage appl. 78−29691
tilted neutron flux distrib., effect of cylindrical absorbing channels 78−13189
tilted neutron flux distrib., influence of small and large absorb. rods 77−79410
time depend. neutron transport solns. in infinite media, multiple collision technique 77−82982
Tokamak Fusion Test Reactor diagnostic penetrations, neutron streaming calc. 79−9877
toroidal geometry effects in neutron transport eqn., discrete ordinate S_N method 78−13327
TR-1 reactor, thermal spectrum using neutron radiography of wedge shaped absorber 78−74439
transient space-time simulation, computer code 77−18644
transmission probability method for calculation of neutron flux distributions in hexagonal geometry 80−106101
transuranic neutron flux meas. in radwaste using leached hull monitor 79−85606
TRIGA-reflector regions, spatial variation of fast neutron spectra 77−46422
TRIUMF thermal neutron facility, design, experience, fluxes and activation levels 79−76222
Twin Beam Mirror, effect of hot beam injection angle 80−48939
two-dimensional response matrix doubling eqns. for currents calc. in infinite rod 77−65263
two-phase control absorber, horizontal absorber elements, expt. study 80−42841
two-phase control absorber development program for CANDU reactors 80−42839
two-phase reactor control, neutron absorber development program 79−97852
ultracold neutron gas obtained on pulsed reactor of IIN type 78−13194
ultracold neutrons, heating and anomalous confinement times *(Russian)* 78−33358
ultracold neutrons, transmission through moving pot. barrier 78−8867
unfolding from activation data 79−13375
VIPER reactor, neutron leakage spectrum and dose meas. 79−3243
VVER reactors, neutron fields in ionisation chamber channels 79−71878
VVER-1000 reactor, neutron axial field stabilisation 79−63741
VVR-SM reactor, neutron flux and dose meas. and evaluation *(Czech)* 80−5252
water moderated reactor, local and global effects of gas bubbles 78−17328
water shield, neutron transport, 2-D benchmark expt. 78−58318
water-moderated water-cooled reactor, local control of loop channel energy release profile and magnitude 78−86645
weighting functions for flux and relative speed of change measurement *(Croatian)* 77−10561
WWER fuel assembly, thermohydraulic evaluation, program module BIPR-5K *(Bulgarian)* 79−85695
WWER-440 reactors, neutron-physical characts. calc. by BIPR 5K programme *(Bulgarian)* 79−85601
ZPPR, loading error simulations and control worth meas. 80−27777
ZPPR critical expts. for radial parfait heterogeneous reactor concept 78−13224
ZPPR mockup critical assembly for Clinch River reactor, source level flux monitor expts. 77−54337
(α,n) thick target yields for Li, ^{9}Be, B, Pb^{19}F$_2$, Zn^{19}F$_2$, Mg, ^{27}Al, Si, and ^{28}SiO$_2$ 79−71860
D plasma, explosion fusion, optimisation of Ar admixture 79−41031
(n, p) and (n, 2n) neutron flux meas. 14-19 MeV 79−13291
Al-graphite two-dimensional shield, neutron penetration meas. 79−3245
Am-Be source, in paraffin, neutron thermalisation anal. *(Spanish)* 77−67781
^{241}Am-Be thermal neutron flux standard density variation obs. 77−83409
Au, foil, average thermal neutron flux determ. method 78−73112
B neutron capture therapy of brain tumours, simultaneous flux monitoring system 79−92352
BF_3-CO_2 mixtures, ang. neutron flux distribs. meas. 77−54276
Be, neutron diffusion in finite blocks, flux synthesis method for 3D multigroup eqn. 77−34366
Be+d neutron source, material damage study, He prod. and neutron fluence per neutron obs. in irrad. material 78−86710
Be(^{3}He,n) fast neutron generation in cyclotron 77−88311
Cd, effective energy cut-off determ., rel. to neutron flux meas. in high-temp. reactor 78−86573
^{252}Cf spontaneous fission spectrum irrad. facility for neutron reaction rate meas. 77−14294
^{252}Cf, sub Cd thermal fluxes in H_2O near the source 79−698
D-D fusion reactor blanket, nucl. characts., summary 78−89973
D-T concentric plasma compression, optimum output of fusion neutrons 79−41030
D-T explosion induced compression, neutron yield 79−67940
D-T explosion induced compression, neutron yield, thermal conduction effects 79−67941
D_2O thermal column irradiation facility Penn State Breazeale Reactor 80−9339
Dy, foil, average thermal neutron flux determ. method 78−73112
Fe+H shield, neutron flux meas., comparison with Monte Carlo calcs. 77−23349
^{56}Fe(n, p), 14-19 MeV, cross section meas., neutron flux, secondary standard 79−13291
Gd, effective energy cut-off determ., rel. to neutron flux meas. in high-temp. reactor 78−86573

neutron flux continued
$^{1}H(n,n)^{1}H$, 10 keV-20 MeV, use for neutron flux meas., proton-recoil detectors 79−9960
$^{1}H(d,n)^{4}He$, neutron fluence and energy transfer standard 80−102194
$^{3}He(n,p)^{3}H$, plasma form by reaction prods. in nuclear reactor 77−76146
Li sphere, neutron spectra and T prod. meas. 78−62604
Li_2O pellets, thermal neutron flux distrib. inside and outside 80−47700
^{7}LiD enriched capsule, prod. of 14 MeV neutrons in reactor 78−55072
$^{6}Li(n,\alpha)^{3}H$ reaction, as standard in neutron flux meas., instruments review 79−9969
Mn bath, for intermediate neutron meas., leakage determ. 78−37525
Mn bath, neutron field topography from directed sources with E_n=230 keV 79−76054
Na cooled power reactor noise analysis for malfunction diagnosis 79−13450
Na, neutron flux integral meas., interactive graphic techniques 78−62590
$^{24}Na(\gamma,n)$, 42 MeV, photoneutron flux determ. from induced activity meas. in water 78−20112
^{93m}Nb activity measurement, determ of fast neutron fluence in power reactors *(German)* 77−34371
O cross section data test using n spatial distrib. in water 78−74417
Pu, determination system by passive neutron counting 79−40985
Pu fuel lattice, cluster-type, thermal-neutron behaviour 77−61477
PuO_2-UO_2, light water moderated lattices, critical expts. 79−6728
Si detectors, fast neutron flux meas. and spectroscopy 77−30709
^{159}Tb, neutron resonances, time-of-flight spectra 80−27633
Th fuelled thermal reactor, model for estimating flux distribs. 77−61482
Tm self-powered neutron detectors for power reactors 79−13607
U radiation contour, effect of neutron flux distrib. in active zone 77−54291
U-graphite lattice, spectrum structure near a resonant absorption line 77−50221
UO_2 cylindrical fuel rods, thermal neutron flux depression meas. 79−81010
UO_2 nuclear fuel, sputtering by thermal neutrons, depend. of ejection coeff. on neutron flux 80−83157
^{235}U fission cross section for Na-Be photoneutrons 77−23159
^{238}U, energy-depend. Doppler effect calc. using collision probability method 77−57714
$^{64}Zn(n,p)^{64}Cu$, evaluated cross section, neutron flux determ. by foil activation 78−25273

neutron flux density *see neutron flux*

neutron interactions *see kaon-nucleon interactions; lepton-nucleon interactions; neutron-nucleus reactions; nucleon-nucleon interactions; photon-nucleon interactions; pion-nucleon interactions*

neutron moderation
see also neutron transport theory
absorption resonance controlled reactor *(Spanish)* 78−8872
albedo cell calculations in the thermal region taking into account thermalisation *(Russian)* 80−52710
anisotropy effects on differential cross sections in CM frame *(Portuguese)* 80−18364
anticipated transients without trip, effect of moderation coefficient 77−50273
black and grey neutron detectors 79−9971
BWR channels, void fraction meas. by fast neutron moderation 77−34380
Candu reactor moderator effectiveness as LOCA heat sink 79−81021
cold moderator, considerations for pulsed neutron source 79−76219
cold pulse from methane at 20K, time dependence 77−67928
continuous slowing down theory, appl. to reson. 77−26822
continuous slowing down theory for fast neutron spectrum 77−50190
energy dependent transport theory, exact solns. 80−32319
energy deposition calc., role of adjoint Boltzmann eqn. 78−4974
epithermal neutron radial flux distrib. in water, student expt. 79−97146
epithermal neutron radiation field development for cerebral tumour therapy *(Japanese)* 78−88742
evaporation neutrons in paraffin and lead layers, Monte Carlo methods 79−89346
fast systems, stochastic method for calc. of Rossi-α parameter 77−61502
finite medium age-diffusion kernels in source-sink theory 77−67782
finite water assemblies, steady state thermal neutron spectra, space and ang. depend. 77−50187
fissile materials, moderation control, risks and benefits evaluation 79−26671
fission reactors, fluidised bed concept, diffusion theory 80−68729
fission reactors, integral experiments for testing Th and ^{233}U data 80−27707
fluctuation problem, probability balance eqn. 77−37829
flux distribution from microtron convertor in graphite moderator with water reflector *(Russian)* 77−82979
flux measurement by Mn bath method, expt. determ. of neutron leakage 79−97744
Fourier-transformed neutron slowing-down kernel moments, MAGGIE code 78−29540
fusion reactor, pellet neutron moderation on blanket neutronics 80−836
graphite, pulse propagation interf. effect of cold neutrons in graphite 77−54273
graphite assemblies pulse propagation, effect of transverse stack dimensions 77−54272
graphite assembly, pulse propagation, dispersion and diffusion parameters 77−54271
graphite moderator structure design and manufacturing specification 80−23110
graphite pebble bed system, meas. of neutron wave propagation *(German)* 77−6481
Harwell 136 MeV electron linac, slow neutron production, optimisation calcs. 79−41048
heavy gas moderator, neutron spectrum joining function, series methods, Runge Kutta integration 77−34365
heavy water, spectra determ. by TOF methods 79−85582
heterogeneous reactor, neutron thermalisation effects on physical charcts. 79−26487
heterogeneous system with large spherical cavity, average velocities of neutron distrib. 78−29539
HFBR, safety features of cold neutron moderator 80−23114
hybrid fusion, fission blanket, ^{238}U fueled, data deficiencies, weighting functions, neutron source effects 77−23295
neutron moderation continued
inertial confinement fusion pellets, neutron moderation, effects on damage and radioactive inventory 80−47704
intermediate resonance method for heterogeneous media, new formulation 77−61490
low-enrichment uranium systems, regulatory perspective 77−65317
LWR, thermal neutron steady state spectra in pure and poisoned water 79−36306
methylbenzene, solid, pulsed cold neutron source, moderation props., radiation decomp. 77−83407
monopole and dipole response coefficient theory comparison with expt. 78−13188
multigroup neutron slowing down codes, resonance treatment modification 78−82412
neutron moderation, linear Boltzmann operator, in various geometries, contributions to spectral theory *(Rumanian)* 78−46128
nuclear fuel preparation, moderation control in large-capacity process unit 77−65316
polycrystalline scatterers in open tangential reactor channel, intense monochromatic longwave neutron beam prod. 77−71712
pulsed neutron wave propagation expt. using electron LINAC *(Japanese)* 80−78345
pulsed source, maximum density and capture rate of neutrons moderated 80−13522
pulsed spallation neutron source, accelerator, target and moderator design 77−67930
PWR fuel storage, criticality eval. of low-density moderation 79−26667
PWR neutronic predictions with improved water density evaluation model 77−46272
quasi-asymptotic neutron flux attenuation constant in a moderator with a cylindrical cavity *(Bulgarian)* 80−68725
reactor core critical assemblies, neutron flux depend. on moderators 79−71879
reactor theory for nuclear power engineering 77−18645
regulator horizontal shift, effects 79−71877
resonance capture of neutrons, light or heavy atom moderators 80−14310
resonance interaction effects, Fourier transform method 77−14207
response functions of spherically moderated neutron detectors 80−37687
rethermalization of neutrons in water-graphite system 79−97806
shielding of 14 MeV neutrons using iron-water combination 77−61614
showing of neutrons, linear eqn. solns. *(French)* 79−76047
slow neutron fields, meas. of spectral characteristics using Cd ratios of activation detectors 77−67953
slowing down length in hydrogenous moderators calc. by Fick's law 79−22352
slowing down of resonance neutrons in matter 77−50191
slowing down particles, spatial depend. of energy spectrum 79−65129
slowing down spectra, Placzek discontinuities 77−51423
slowing down time in hydrogenous multiplying system 77−61472
slowing-down density in finite height cylindrical shell, exact boundary conditions in age theory 78−54812
slowing-down density in spherical symmetry 78−50235
space craft thermionic reactors, reflector drums as control mechanism 80−42784
space depend. spectra in two adjacent moderating media 77−6477
spatially depend. spectrum, expansion about local Maxwellian 78−29537
spent nuclear fuel storage, supercriticality through optimum moderation 80−57896
thermal neutron coincidence counting, correction for variable moderation and multiplication 80−69045
thermal neutron scatt. in water, cylindrical graphite-water system with temp. discontinuity 79−71925
thermal reactor, homogeneous, critical size calc. 77−23171
thermal spectra calcs. using synthetic scatt. kernel 77−14206
thermal-neutron transfer from pulse source in moderator with large cylindrical cavity 78−37392
thermalisation in hydrogenous moderators 77−65253
thermalisation of neutrons in solid media calc. 77−50192
thermalization, appl. of invariant imbedding technique 79−67811
thermalization of neutrons, review of Soviet research 79−36300
THERMOS spectrum code, accurate reduced mesh model for neutron thermalisation 80−57829
time-energy distrib. of slowing down neutrons 77−50184
transfer matrix calcs. for thermal neutrons 80−27687
two-phase reactor control, neutron absorber development program 79−97852
ultracold neutrons, multilayer ferromag. shutter 80−91354
water, diffusion length calc. for 1/v and non-1/v absorbers 79−30879
wave interference pattern obs. 77−74901
wave propagation across temp. discontinuity in infinite graphite assembly 77−38314
Weapons Neutron Research Facility initial target/moderator configuration 79−9933
Wigner-Wilkins scattering kernel computation 79−36296
Be, anisotropy in thermal neutron scatt., anal. 80−552
Be assembly, space- and angle-depend. steady state thermal neutron spectra 77−67783
Be, finite assemblies, thermal neutron wave propagation 78−58320
Be, neutron diffusion in finite blocks, flux synthesis method for 3D multigroup eqn. 77−34366
BeO, finite assemblies, thermal neutron wave propagation 78−58320
D_2O, neutron scatt. cross section determ. by DEUKER computer code 79−54468
Fe, ns. slowing down time, expt. obs. 78−58319
LiF, ns. slowing down time, expt. obs. 78−58319
Pb reflector in small Fe pile, material group consts. meas. 79−6738
Pu, unmoderated, criticality safety practices for handling in glove boxes 79−26669
UF_6, ^{235}U enriched, moderation control 77−65315
UO_2 low enriched fuel rods, storage and transportation, critical separation in water with fixed neutron poisons 80−73918
UO_2 rods, 2.35 wt.% ^{235}U enriched, in water with fixed neutron poisons, benchmark calcs. for subcritical clusters 79−26674
UO_2 rods, 2.35 wt.% ^{235}U enriched, in water with fixed neutron poisons, critical separation between subcritical clusters 79−26673
$^{233}UO_2/ThO_2$ water-moderated lattice analysis with ENDF/B-IV data 79−9800

neutron moderation continued
^{235}U-Al castings in water moderated lattices, pulsed reactivity meas. 79−26529
ZrH rethermaliser for IVV-2 reactor hot neutron flux increase 80−37676

neutron-nucleus reactions
for inelastic neutron-nucleus scattering, see "neutron-nucleus scattering" see also neutron radiative capture; nucleon-nucleon interactions
0.13 to 7.0 MeV neutrons, fission cross section ratio meas. 79−97738
2 keV filtered beam facility applications 77−23346
^{238}U(n,f), reactor n, shoulders in very asymmetric mass distrib., cumulative yields 79−59005
$\sigma_f(^{239}Pu)/\sigma_f(^{235}U)$ meas., neutron energies 0.27-9.85 MeV 78−660
$\langle\Gamma_n^0\rangle$ for isotonic groups, dependences *(French)* 77−3005
absolute cross section meas. using fixed energy neutron sources 79−13365
actinide series neutron-induced-fission systematics in MeV region 77−67778
actinides, neutron fission cross section meas., fragment ang. distrib. using solid state track detector 79−76300
activation cross section meas. for fusion reactor wall and blanket materials 77−26881
activation detector ave. cross sections in ^{252}Cf benchmark field 78−82598
Adler-Adler cross section formalism, improved resonance formula for fissile elements 78−74358
average activation cross sections in ^{252}Cf spontaneous fission neutron field 79−30830
benchmark experiments for nuclear data validation 77−23203
Breit-Wigner single-level formula for cross sections, multilevel correction 78−29441
capture cross sections at 14.6 MeV, activation anal. 80−52665
cascade reactions, statistical theory 77−26699
charged particle reaction cross section facility 77−26917
charged particle reactions, experimental techniques, applications 77−23031
compound neutron absorption processes, optical pots., one particle vibr. state effects *(Russian)* 80−105956
compound nucleus formation, level densities, K-band positions 77−22855
continuous slowing down theory, appl. to low-energy neutron resonances 77−26645
cross section needs for fission reactor design 77−23193
cross section representation in unresolved resonance region 77−23051
cross section requirements of CTR program model calcs. 77−23292
cross sections up to 20 MeV, updated empirical-statistical model code THRESH 77−23046
cross-section standards, status report 77−23017
cryonuclear physics for radioactive decay and neutron+nucleus reaction studies *(Dutch)* 78−29416
Csikai-Peto effect, reevaluated by statistical model calc. method 78−25180
delayed fission produced in synthesis induced by heavy-ion beams and neutron currents *(Russian)* 79−89341
doorway states reln. to optical model *(Russian)* 77−6213
effective neutron resonance cross sections, calc. in energy and space 79−17954
evaluated nuclear data, estimated uncertainties 77−23169
evaluated nuclear data files in unresolved resonance region, data representation 78−29459
experimental techniques, reactions below 50 MeV 77−18761
Faddeev approach to neutron scatt. from protons in heavy hydrocarbons in eV range 78−54728
fast neutron dose to the human body, contrib. for ^{39}K, ^{35}Cl and ^{32}S 80−51263
fast neutron induced nonelastic reaction cross section data, $E_n \geq 14$ MeV 77−23058
fast reactor physics, assessment of JAERI fast group constants set version 2 80−602
fission, near thermal, effects of phonon transfer on cross sections 78−50221
fission, neutron induced, double humped fission barrier concept 78−29443
fission, role of double humped barrier, review 77−26659
fission cross section trend, 3-5 MeV, statistical model description 77−23126
fission cross sections, parameter testing in statistical model *(Russian)* 80−52653
fission product nuclear data evaluation, cross sections up to 15 MeV, resonance parameters 77−23044
fission product yields, tabulation 78−25253
fission products, neutron cross sections for 27 nuclides important in fast reactor calcs. 77−67741
fission products, neutron cross-sections data for ENDF/B-IV library 78−25290
fission products, transmutation by spallation and neutron reactions using linear accelerator 78−13268
fission reactor, nuclear yields, production of transuranium elements by multi-step neutron irradiation *(Japanese)* 80−52729
fission resonances, spin determ. using polarised beam and target, review 77−26796
fusion reactor first wall, prod. of H, D and He by 15 MeV neutrons 79−93831
heavy isotope reactivity coeffs., in fast neutron critical assemblies 79−63742
high-energy reactions in astrophysics, comparison of methods for cross-sections calc. 78−28505
inclusive charged particle prod., A-depend. 78−33179
inclusive charged particle prod. in high energy collisions 79−89308
isotope producing reactor, accumulation losses of transuranium isotopes 77−61595
light nuclei, three and four nucleon low energy scatt. expts., review 79−80945
light-nuclei, neutron resonance reactions using Kapur-Peierls formalism 77−50136
multigroup cross sections, GGTC-ENEL computer code using intermediate resonance method 78−58323
multigroup cross sections, nuclides from ^{242}Pu to ^{253}Es 77−26754
multigroup neutron data production from ENDF/B-IV, survey of codes 77−23170

neutron-nucleus reactions continued
multigroup time-dependent delayed γ-spectra from fission and activation 78−13184
(n,2n) reaction, induced in fission neutron spectrum, effective threshold energies 78−25181
(n,α) reaction and α-decay of nuclear compound states *(Russian)* 78−29472
(n,γ) cross sections meas. for 22 elements between Z=3 and Z=82 77−26681
n-process of neutron capture, alternative to r-process 77−2336
neutron capture cross sections, expt. determ., fast reactor materials *(Italian)* 78−82355
neutron cross-sections for reactor dosimetry, status 77−23304
neutron differential cross section data generation, appl. to resonances and neutron transport *(German)* 78−82414
neutron emission spectra from 14 MeV neutron reaction, precompound model calc. 79−36235
neutron expts. at LAMPF for n-p interaction determ. 77−18557
neutron gas, highly rarefied, non-equilibrium thermodynamics under creative and destructive reactions 79−12747
neutron interactions with nuclei, conf. 77−23015
neutron physics, recent advances 77−26640
neutron radiography, physical processes and math. methods review, neutron-nucleus interaction effects 78−60888
neutron resonance parameters, neutron energies 1-30 eV range, ^{245}Cm 78−17167
neutron spectroscopy, new techniques and results 77−23365
neutron standard cross section expts., flux monitor, source, data acquisition and anal. 78−90039
neutron standards and appl., conference, Gaithersburg, MD, USA (March 1977) 79−9581
neutron strength function fluctuations 77−22858
neutron-rich nuclei, search for prod. using fast neutrons 77−23011
nuclear reactor fuel breeding using independ. neutron sources 77−26840
nucleon knockout, off-shell effects, momentum-space wavefunctions 77−88122
polarised neutron expts., review 77−26700
R-matrix anal. of reactions in ^{7}Li system below 10.5 MeV 77−26751
R-matrix resonance cross-section expressions, new Kapur-Peierls type expansions 77−30528
radioactive waste, actinide elimination by nuclear transmutation 77−61569
rare earth nuclei, (n,2n) cross sections analysis at 14.7 MeV 78−17194
RCPL1 program, calc. of Doppler broadened neutron resonance cross-sections 79−67810
reaction survey 77−26702
reactor materials, fission cross sections meas. in YAYOI reactor, fast neutron spectrum 77−42013
reactor structural material transmission meas. using TOF spectrometer 80−18440
recent advances in neutron physics, prod., handling, detection, nuclear reactions, resonances 77−26686
resonance analysis of neutron transmission data, least square fitting program REFIT 80−22840
resonance escape probability meas. in nuclear fuel 77−71632
resonance widths Γ_γ anal. for several nuclei *(Russian)* 77−30561
s-wave neutron reduced widths 77−22850
SAIPS information determination system, algorithms for spectra determ. w.r.t. measured reaction rates *(Russian)* 80−102416
self shielding factors, elastic removal cross sections, strong reson. scatt. 79−13374
semiconductor doping by nuclear transmutation method *(German)* 78−95066
standard cross sections, uncertainties and correls. in evaluated data sets 77−23196
standard neutron spectrum field *(Japanese)* 79−9562
thermonuclear reaction rate data for intermediate mass nuclei 80−31427
time reversal invariance present evidence 79−63386
total neutron cross section meas. on gross fission products, 1 eV-240 eV 77−23064
total reaction cross sections of metals and gases for very cold neutrons 78−86566
UCN, quasibound states in matter, reson. positions and widths 80−73833
Voigt functions analysis, appl. to neutron cross sections 80−22879
Wigner's random matrix model, time reversal violation 77−30542
yrast isomer prod., pulsed beam meas. using plastic scintillation spectrum 80−27871
$D^0(1865)$ prod. from neutron interactions at 300 GeV/c 78−37244
γ-ray emission, neutron-induced interference in proton-induced anal. method 78−27868
(n,2n), 14 MeV, empirical formulae for cross sections 78−13103
(n,2n), 14 MeV cross-section calcs. 77−30601
(n,2n), 14.7 eV, isomeric cross-section ratios, statistical theory, moment of inertia 79−97701
(n,2n), 14.7 to 24.0 MeV, cross sections on ^{45}Sc, ^{59}Co, ^{89}Y, ^{93}Nb, ^{103}Rh, ^{169}Tm, ^{165}Lu, ^{181}Ta, ^{197}Au, ^{209}Bi 78−25192
(n,2n), 14.8 MeV, isomeric states prod. cross-sections 77−26744
(n,2n), A=45 to 209, threshold to 20 MeV, evaporation mechanism 79−30842
(n,2n), activation cross sections 79−57335
(n,2n), on Y, In, Hf, Tl, Pb, Bi, 14 MeV, isomeric state formation cross section, half-lives, gamma-ray spectra 77−30604
(n,2n), ΣΣ spectrum, integral cross section meas. 80−68672
(n,2n), two-particle emission in terms of exciton model *(Russian)* 77−304
(n, 2n) and (n, 3n) cross-sections anal., level-density parameters of A>150 nuclei 79−30824
(n,2n) cross sections, 14.1 MeV, on Zn, Ga, Ge, As and Se isotopes *(Spanish)* 77−30563
(n,2n) cross sections, 14.7 to 24.0 MeV, various nuclei from ^{9}Be to ^{209}Bi 77−26730
(n,2n) cross sections, statistical theory 77−26699
(n,2n) cross sections around 14.5 MeV, integrated preequilibrium-cum-statistical model approach 79−6609
(n,2n) excitation functions, reactions with two particles emission *(Russian)* 77−61427
(n,2n) reaction cross sections in precompound emission model *(Russian)* 77−34304
(n,2n) reactions, ang. distribs. and energy spectra, evaporation model, Monte Carlo calc. 79−45271

neutron-nucleus reactions continued
(n,2n) reactions at 14.8 MeV, isomeric ratios in 107<A<143 mass range 78−13073
(n,2n) reacts. on ^{45}Sc, ^{58}Ni, ^{59}Co, ^{93}Nb, ^{175}Lu, and ^{197}Au, statistical model anal. 77−26655
(n,2n)reaction mechanisms, threshold to 15 MeV, statistical model 77−26729
(n,3n) cross sections, 14.7 to 24.0 MeV, various nuclei from ^{9}Be to ^{209}Bi 77−26730
(n,3n) reacts. on ^{45}Sc, ^{58}Ni, ^{59}Co, ^{93}Nb, ^{175}Lu, and ^{197}Au, statistical model anal. 77−26655
(n,α), 14 MeV, empirical formulae for cross sections 78−13103
(n,α), 14 MeV, total cross sections, pre-equilibrium model anal. 78−58272
(n,α), fast n, ^{3}He emission cross sections for A=27-115 80−13475
(n,α), integral data meas. in ΣΣ neutron field 78−70537
(n,α), light element profiling and lattice localisation using neutron induced reactions 79−5205
(n,α), ΣΣ spectrum, integral cross section meas. 80−68672
(n,α), total α-widths of neutron resonances, nuclei from ^{64}Zn to ^{177}Hf 77−26708
(n,α) cross sections, 14 MeV, empirical formulae 79−63662
(n,α) cross sections, 14.1 MeV, on Zn, Ga, Ge, As and Se isotopes *(Spanish)* 77−30563
(n,α) for Fe group elements, Hauser-Feshbach theory, He prod. in fusion reactors 77−23100
(n,α) reactions on 36≤Z≤83 targets, tables of cross sections and reaction rate factors 77−46162
(n,α) reactions on light nuclei, review 77−26697
(n,α) resonance neutron reactions, α-widths from statistical relationships, deviations 78−33173
(n, α) with resonance neutrons, properties of highly-excited states of nuclei *(Russian)* 80−106053
(n,d), 2.48, 3.28 MeV, elastic differential cross section 79−45266
(n,d) reactions, 800 MeV, light nuclei, d quasifree and quasielastic cross sections 78−70534
(n,d) reactions on ^{6,7}Li, ^{12}C, ^{14}N, ^{16}O, ^{20}Ne, ^{27}Al, ^{209}Bi, proton hole states study 77−26726
(n,d) reactions on light nuclei review 77−26697
(n,e), odd-n actinides, vibr. band systematics, excitation energies and rot. parameters 79−36137
(n,e) reactions study using internal target β-spectrometer with transport solenoid, background suppression 77−6612
(n,e$^-$) high precision spectroscopy, internal conversion coeffs. for nuclear struct. 80−37353
(n,f), 3-5 MeV, cross section predictions 78−29513
(n,f), integral data meas. in ΣΣ neutron field 78−70537
(n,f), intermediate struct. line fitting, subthreshold fission resonances 80−102214
(n,f), parity violation in compound nuclei 80−47368
(n,f), themal, parity violation from opposite parity rot. states 80−95303
(n,f) cross sections from (^{3}He,df) and (^{3}He,tf) reactions 77−23128
(n,f) simulated cross sections for exotic actinide nuclei 80−544
(n,f) sub-barrier fission, intermediate structure, cross sections, widths 77−34357
(n,^{3}He), fast n, ^{3}He emission cross sections for A=27-115 80−13475
(n,^{3}He) activation cross sections, 14.6 MeV, comparison with Hauser-Feshbach calcs. 77−26721
(n,n′α), fast n, ^{3}He emission cross sections for A=27-115 80−13475
(n,n′γ), 14.8 MeV, isomeric states prod. cross-sections 77−26744
(n,n′γ), A=28-152, spherically doubly even nuclei, level excitation cross sections, statistical anal. *(Russian)* 79−67707
(n,n′γ), excitation of low levels of ^{48}Ti, ^{56}Fe, ^{58}Ni, ^{92}Zr and ^{94}Zr isotopes, 1.57 to 2.8 MeV inelastic neutron scatt. *(Russian)* 78−41722
(n,n′γ) cross section, effect of intensive EM wave on γ decay *(Russian)* 79−59070
(n,nγ), A=19-207, neutron scattering resonance radiative widths 80−99146
(n,nγ) and (n,γ) reactions producing ^{105}Pd, level scheme 77−82849
(n,np), 14 MeV cross-section calcs. 77−30601
(n,p), 14 MeV, empirical formulae for cross sections 78−13103
(n,p), 14 MeV, total cross sections pre-equilibrium model anal. 78−58272
(n,p), 14 MeV cross sections, empirical formulas 78−70517
(n,p), 14.8 MeV, isomeric states prod. cross sections 77−26744
(n,p), activation cross sections 79−57335
(n,p), integral data meas. in ΣΣ neutron field 78−70537
(n,p), light element profiling and lattice localisation using neutron induced reactions 79−5205
(n,p), ΣΣ spectrum, integral cross section meas. 80−68672
(n, p) absolute cross section at excitation function maximum 79−45272
(n,p) at 14.7 MeV, on 48 stable nuclides 77−61417
(n, p) charge exchange scatt., 190-590 MeV, differential cross section and ang. distribs. 80−57775
(n,p) cross sections, 14.1 MeV, on Zn, Ga, Ge, As and Se isotopes *(Spanish)* 77−30563
(n,p) excitation functions, meas. and calc. for nuclei with Z≥48 and E_n of 10 to 20 MeV 77−41970
(n,p) excitation functions for Z≥48 nuclei, 10 to 20 MeV *(Russian)* 77−34305
(n,p) reactions on ^{6,7}Li, ^{12}C, ^{14}N, ^{16}O, ^{20}Ne, ^{27}Al, ^{209}Bi, isovector analogue giant resonances study 77−26726
(n,p) reactions on 36≤Z≤83 targets, tables of cross sections and reaction rate factors 77−46162
(n,p) reactions on light nuclei, review 77−26697
(n,p) scatt. observables, R-matrix calc., 20-140 MeV 77−57668
(n,pn), 14 MeV cross-section calcs. 77−30601
(n,pπ$^-$), 100 to 300 GeV, coherent neutron dissociation on nuclei 78−29465
(n,pπ$^-$) reactions on nuclei, 8 to 24 GeV/c, coherent diffractive prod., cross sections 78−41711
(n,t), 14 MeV, cross sections, fast neutron reaction excitation function calc. 79−45267
(n,t) activation cross sections, 14.6 MeV and 22.5 MeV, comparison with Hauser-Feshbach calcs. 77−26721
(n,t) reaction, 14.6 MeV medium and heavy mass nuclei, production cross sections 79−49629
(n,t) reactions on light nuclei, review 77−26697
(n,x) reactions on medium and heavy nuclei, models 77−26698
(n,X) X=p,2n,3n, precompound and compound emission mechanisms 80−102176
neutron-nucleus reactions continued
(n,xn) x=2,3 cross section meas., 6 to 15 MeV, various nuclides 77−23083
(n,Zα), fast n, ^{3}He emission cross sections for A=27-115 80−13475
n+C→(n*→Λkπ)X, 45 GeV, production cross section 77−82795
nd break-up, quasi-free scattering, peripherical nature 78−89726
t emission in fast neutron interactions with nuclei 78−29462
^{235}U(n,f), thermal to 1.75 MeV, energy spectra and yields of alpha-particles 77−26805
^{64}(n,α)^{61}Fe, 14.3 MeV, decay scheme for ^{61}Fe 78−46053
^{64}(n,p)^{64}Co, 14.3 MeV, decay scheme for ^{64}Co 78−46053
^{238}(n,xn), x=2,3, sensitivities of secondary neutron energies to fusion blanket neutronics 77−23295
^{28}A(n,p)^{28}Mg, reactor neutron irrad., product yield 79−538
^{37}A(n,α), thermal, cross-sections meas. 78−94012
^{37}A(n,p), thermal, cross-sections meas. 78−94012
^{107}Ag(n,2n), 14.6 MeV, cross-section meas. 79−59055
^{107}Ag(n,e$^-$), ^{108}Ag transition multipolarity and conversion electrons 80−52627
Al, (n,xp), (n,xd) and (n,xα) reactions, 14 MeV, sub-Coulomb barrier protons 77−30597
Al+n, total cross section for 6 to 14 Å neutrons 77−88148
^{26}Al(n,p)^{26}Mg, stellar reaction rate, rel. to ^{26}Al prod. during C burning 79−70948
^{27}Al (n,np), 14.6 MeV, differential cross sections, statistical model calcs. comparison *(Russian)* 78−78385
^{27}Al+n, 15 MeC, cross sections for emission of sub Coulomb barrier charged particles 77−23007
^{27}Al(n,α), 14.7-19.0 MeV, excitation functions relative to ^{56}Fe(n,p), n flux independent ratio 79−3142
^{27}Al(n,α), 14.8 MeV, expt. and statistical model determ. of α-prod. in fusion reactors 80−95397
^{27}Al(n,α), 4.5-18.3 MeV, cross sections and excitation curves *(Chinese)* 79−49601
^{27}Al(n,α) 14.8 MeV, isomeric state formation cross section, half-lives, gamma-ray spectra 77−30604
^{27}Al(n,α)^{24}Na, recoil escape efficiency, evaporation model, Monte Carlo calc. 79−45271
^{27}Al(n,α)^{24}Na threshold reaction cross section, ^{252}Cf source 77−23039
^{27}Al(n,d), 56.3 MeV, spectroscopic factors, ^{26}Mg levels 78−4935
^{27}Al(n,n′), (in)elastic scatt. cross sections, duration of collision process *(Russian)* 79−80942
^{27}Al(n,p), 14.7-19.0 MeV, excitation functions relative to ^{56}Fe(n,p) 79−3142
^{27}Al(n,p)^{27}Mg, 12.9-15.9 MeV, reaction cross section meas. 78−37337
^{27}Al(n,p)^{27}Mg, Al content in steel determ. *(Hungarian)* 78−92586
^{27}Al(n,p)^{27}Mg, ave. neutron activation cross sections for ^{241}Am-Be source 79−31282
^{28}Al radioisotope source, activation expt. 79−31
Al(n,X), 14.8 MeV, γ-prod. cross section 79−49622
Am (A-241, 243), neutron induced fission rate meas. in Zebra 77−57698
^{A}Am(n,f), thermal, sub-barrier fission fragment energy correlations for A=241, 243 80−42715
^{241}Am (n,f), 2.5 MeV neutrons, absolute cross section meas. (1.98±0.07 b) 80−73872
^{241}Am, neutron cross sections, 1 keV to 15 MeV, optical and stat. model calcs. 77−57655
^{241}Am, total and fission cross sections in resonance region, resonance parameters 77−23160
^{241}Am, total cross-section in resonance region 77−26746
^{241}Am, total neutron cross section and neutron reson. parameters, 0.004 to 30 eV 77−50135
^{241}Am-Be neutron spectrum, (n,p) reaction average cross-sections 80−22827
^{241}Am(n,X)Cm, Japan Material Testing Reactor, separation of transuranium elements from fission products and cladding *(Japanese)* 80−52731
^{241}Am(n,f), 14.8 MeV, cross-section meas. using mica track detectors 80−95330
^{241}Am(n,f), 14.8 MeV, mass yield distrib., and absolute fission yield, isomer ratios 80−18352
^{241}Am(n,f) 100 eV to 5.3 MeV, fission cross-section meas. rel. to ^{235}U 79−85567
^{243}Am, total neutron cross section and neutron reson. parameters, 0.4 to 35 eV 77−46171
^{243}Am(n,f), thermal neutron induced fission cross section 80−37403
^{36}Ar, neutron low energy total cross-section, bound level parameters 77−23071
^{36}Ar(n,d), 14.1 MeV, absolute ang. distrib. meas. 78−595
^{40}Ar(n, ^{3}He)^{38}S, ^{38}S producting using compact cyclotron 77−90894
^{40}Ar(n,d)^{39}Cl, 14.5 MeV, charge state study in liquid Ar ionization chamber *(Russian)* 80−9298
^{40}Ar(n,p)^{40}Cl, 14.5 MeV, charge state study in liquid Ar ionization chamber *(Russian)* 80−9298
^{197}Au, 14.7 MeV neutron capture cross-section measurements with activation technique 80−32282
^{197}Au+n, strength functions and scatt. lengths from total and scatt. cross sections 77−26706
^{197}Au(n,2n) average activation cross sections in ^{252}Cf spontaneous fission neutron field 79−30830
^{197}Au(n,2n)^{196}Au, cross-section ratio of isomeric states of ^{96}Au, spin-cut-off factor calc. 78−13096
^{197}Au(n,γ), ^{198}Au energy level spins 79−457
^{197}Au(n,xn), 20.6 MeV, neutron yield cross sections and spectra *(Russian)* 80−91188
^{A}B+n, A=10,11, 1.0 to 14 MeV, total cross-section meas. using ^{9}Be(d,n)^{10}B neutron source 79−22280
^{10}B, four-body breakup induced by 18 MeV neutrons, double final state interaction 78−17192
^{10}B, total neutron cross section, 90 to 420 keV 79−40913
^{10}B+n, l_n5 to 14 MeV total cross-section meas. 77−26742
^{10}B(n, α)^{7}Li, tumour dose enhancement in fast neutron therapy 78−73249
^{10}B(n,α$_0$)^{7}Li, 1-1500 keV, cross section meas. 77−26755
^{10}B(n,α$_1$)^{7}Li*, 0.1 to 2.0 MeV, cross section meas. 79−36237
^{10}B(n,α$_1$)^{7}Li*, 1-1500 keV, cross section meas. 77−26755
^{10}B(n,α), 2 and 24 keV, ang. distribs., branching ratio 79−54440
^{10}B(n,α), n absorption calcs. for activation detectors 78−78434
^{10}B(n,α) cross section standard, status 77−23040
^{10}B(n,α) cross section standard, R-matrix anal. 77−23041
^{10}B(n,α)^{7}Li, 10 keV to 1 MeV, review of cross section meas. 79−9587

neutron-nucleus reactions continued
^{10}B(n,α)^{7}Li, 13.9 MeV, differential cross sections meas. 78−78387
^{10}B(n,α)^{7}Li, appl. to anal. of fusion reactor materials, archeometry, and nuclear spectroscopy 80−61200
^{10}B(n,α)^{7}Li, for neutron activation anal. of Si:B, range distrib., IBR-30 expts. 78−11585
^{10}B(n,α)^{7}Li, ionizing radiation and cavitation threshold, calc. of dose rate cavitation threshold 78−94774
^{10}B(n,α)^{7}Li, neutron cross section standards, detection techniques 79−9970
^{10}B(n,α)^{7}Li, radiation chemical transform. of CN^- by inner source 79−34341
^{10}B(n,α)^{7}Li, recoil particles, radiolysis of aq. solns., intrajectory reacts. *(French)* 77−12812
^{10}B(n,α)^{7}Li, thermal neutron flux, determ. accuracy 77−342
^{10}B(n,α)^{7}Li, thermal polarised n capture, P-odd asymmetry meas. *(Russian)* 80−13452
^{10}B(n,ααd)n, review 77−26697
^{10}B(n,ααt), review 77−26697
^{10}B(n,αγ)^{7}Li, 0.1 to 2.2 MeV, cross section determ. 79−45248
^{10}B(n,αγ)^{7}Li, 5 to 700 keV, relative cross section, ^{11}B $^{5}/_{2}^{-}$ level 78−89866
^{10}B(n,αγ)^{7}Li, relative cross section, 5 to 800 keV 77−26727
^{11}B+n, 1.5 to 14 MeV total cross-section meas. 77−26742
^{11}B(n,α)^{8}Li, 14.4 MeV, ang. distrib., total cross sections 79−89303
^{11}B(n,α)^{8}Li, 14.4 MeV, spectra and ang. distribs., recoil nucl. transitions 78−17193
Ba, A=134-138, average neutron cross sections, statistical and optical model calcs. 78−29458
^{136}Ba(n,2n)^{135}Ba^{m}, 14.2 MeV, neutron activation cross sections 80−91180
^{138}Ba, 14.7 MeV neutron capture cross-section measurements with activation technique 80−32282
^{138}Ba(n,2n)^{137}Ba^{m}, (14.2±0.2) MeV, activation cross sections, Ge(Li) meas. 79−22278
^{138}Ba(n,α)^{135}Xe^{m,g}, 14.2 MeV, neutron activation cross sections 80−91180
^{138}Ba(n,p), 14.2 MeV, neutron activation cross sections 80−91180
Be, integral test of cross section, neutron leakage spectra, spherical assembly 77−23033
Be+n, 250 GeV/c, search for charm prod. 78−41712
Be+n, 300 GeV/c, $\mu^{\pm}\mu^{\mp}$ and $\mu^{\pm\pm}$ events, upper limit for charmed particle prod. 78−37245
^{9}Be+n, 1.0 to 14 MeV, total cross-section meas. using ^{9}Be(d,n)^{10}B neutron source 79−22280
^{9}Be+n, 1.5 to 14 MeV total cross-section meas. 77−26742
^{9}Be(n, p) and ^{9}Be(n, t), 18.3 MeV, ang. distribs. 77−18539
Be(n,p̄pX), narrow struct. in p̄p mass spectrum, threshold to 2700 MeV/c^2 79−63511
^{209}Bi (n, xnf), fission high energy neutrons *(Russian)* 80−106091
^{209}Bi (n,3n)^{207}Bi, 14 MeV, cross section determ. 78−50177
^{209}Bi, reson. parameters for s and p-wave levels 78−37322
^{209}Bi(n,^{3}He)^{207}Tl, 14 MeV, cross section determ. 78−50177
^{209}Bi(n,2n), 14.1 MeV, pre-equilib. contributions, neutron yields and energy spectra, statistical model calcs. 77−50126
^{209}Bi(n,2n)^{208}Bi, 14.1 MeV, ang. and spectral distribs. 78−82354
^{209}Bi(n,α), 14 MeV, excitation of ^{206}Tl 12$^-$ isomeric state 78−70453
^{209}Bi(n,α)^{206m}Tl, 14 MeV, cross section determ. 78−50177
^{209}Bi(n,n), 16-18 MeV differential cross section resonant characters 79−75952
^{209}Bi(n,xn), 20.6 MeV, neutron yield cross sections and spectra *(Russian)* 80−91188
^{209}Bi(n_{th}, α), cross section 78−66284
^{249}Bk neutron total cross-section obs., 0.005 to 1000 eV 79−9577
^{249}Bk(n,f) cross section between 0.7 and 3.0 MeV 77−50170
^{76}Br(n,p)^{76}Se, thermal energy, ^{77}Br proton branches 78−89878
^{80}Br(n̄,X), annihilation, 1.4 GeV/c, $\pi^{\pm}$, p emission angles, momentum and multiplicity distribs. 80−532
^{87}Br, prod. by radiochem. separation, for neutron decay obs. 78−70951
C, integral test of cross section, neutron leakage spectra, spherical assembly 77−23033
C, natural, total and elastic scatt. cross sections for neutron energy <5 MeV, 8.5-15 MeV, use as standard 79−9588
C+n, 200 GeV, multiplicity distribs., target thickness effects, appl. to air shower obs. 77−50127
c+n in cellulose nitrate plastic detector, spallation products 78−17198
CC ^{93}Nb(n,2n), 14 MeV, cross section compilation 80−91181
^{A}C+n, A=12,13, 1.0 to 14 MeV, total cross-section meas. using ^{9}Be(d,n)^{10}B neutron source 79−22280
^{12}C, four-body breakup induced by 18 MeV neutrons, double final state interaction 78−17192
^{12}C+n, 18.2 MeV, multiparticle breakup, three-α correl. spectra 77−6364
^{12}C+n, 1.5 to 14 MeV total cross-section meas. 77−26742
^{12}C+n, matrix and shell model unification 78−54699
^{12}C+n, total and elastic cross sections in few MeV region 79−59057
^{12}C(n, X), compound resonance decay based on bound and metastable single nucleon states *(Russian)* 80−5107
^{12}C(n̄,X), annihilation, 1.4 GeV/c, $\pi^{\pm}$, p emission angles, momentum and multiplicity distribs. 80−532
^{12}C(n,2α), 60 kev-20 MeV, average energy per ion pair, calc. 80−22841
^{12}C(n,2n), 60 kev-20 MeV, average energy per ion pair, calc. 80−22841
^{12}C(n,2n)^{11}C, 23 to 34 MeV, excitation functions, statistical model anal. 77−23082
^{12}C(n,3α)n, review 77−26697
^{12}C(n,α)^{9}Be, ionizing radiation and cavitation threshold, calc. of dose rate, cavitation threshold 78−94774
^{12}C(n,n′), (in)elastic scatt. cross sections, duration of collision process *(Russian)* 79−80942
^{12}C(n,n′)3α, 60 kev-20 MeV, average energy per ion pair, calc. 80−22841
^{12}C(n,n′α), 60 kev-20 MeV, average energy per ion pair, calc. 80−22841
^{12}C(n,n′p), 60 kev-20 MeV, average energy per ion pair, calc. 80−22841
^{13}C+n, 1.5 to 14 MeV total cross-section meas. 77−26742
^{40}Ca, Hauser-Feshbach code for cross section evaluation 77−23045
^{40}Ca+n, 14.1 MeV neutrons, estimated dose to bone and whole body 79−53256
^{40}Ca(n,X), local approximation to a non-local potential 80−91182
^{40}Ca(n,α)^{37}Ar, body Ca reaction due to fast neutrons, fate of ^{37}Ar 77−5075
^{40}Ca(n,α)^{37}Ar, radiochemical measurement of cosmic ray muon induced neutrons, depth depend. 77−61670
^{40}Ca(n,α)^{37}Ar in fission reactor material Ca impurity, ^{37}Ar form. 77−83048
^{40}Ca(n,t)^{38}K, 14.6 MeV neutrons, activation cross section meas. 79−45254
^{42}Ca(n,p)^{42}K, 14.7 MeV neutron cross sections 78−70520
^{43}Ca(n,p)^{43}K, 14.7 MeV neutron cross sections 78−70520
^{44}Ca(n,α)^{41}Ar, 14.7 MeV neutron cross sections 78−70520
^{44}Ca(n,p)^{44}K, 14.7 MeV neutron cross sections 78−70520
^{48}Ca(n,Zn)^{47}Ca, 14.7 MeV neutron cross sections 78−70520
^{48}Ca(n,2p2n), ^{45}Ar β-decay scheme and half life, K deduced energy levels 78−78319
^{48}Ca(n,2pn), ^{46}Ar β-decay scheme and half life, K deduced energy levels 78−78319
Ca(n,γ), E>2.5 keV, reson. parameters, odd-even effects 77−34299
^{A}Cd(n,nγ) A=114,116, energy levels, spins, and gamma-ray multipole mixing ratios investig. 80−52580
^{106}Cd, total neutron cross section meas. below 1.5 keV 77−26743
^{109}Cd(n,α), thermal, cross-sections meas. 78−94012
^{112}Cd(n,2n), 13-18 MeV, compound nucleus and precompound emission models 77−74841
^{112}Cd(n,p)^{112}Ag, 13-17 MeV, cross section meas. by activation method 78−46057
^{114}Cd, total neutron cross section meas. below 1.5 keV 77−26743
^{114}Cd(n,t)^{112}Ag, 14.6 MeV neutrons, activation cross section meas. 79−45254
Cd(n,n′γ), A=114,6, E=2.67 MeV, ang. distribs. meas., 3$^-$ octupole states anal. 77−38275
Ce (n,2n) react cross sections at 14.8 MeV 78−74355
^{140}Ce+n, 20-240 keV total cross section, resonance multilevel shape anal., level spacings 79−3148
Cf, neutron irradiation separation and α-spectra identification of ^{253}Es 78−17435
^{249}Cf(n,f), thermal., yields of isotopes of Nb, I and Cs, charge distrib. 78−41789
^{249}Cf(n,f) thermal n, ^{139}Ba and ^{142}La fractional independent yield and γ-activity 79−89337
^{252}Cf(n,f), fast reactor neutrons, effective cross section meas. 77−23119
Cl isotopes, effect of isotopic abundance on kerma 78−29536
^{35}Cl(n,α), thermal, negative energy resonance parameters 77−23025
^{35}Cl(n,d), 14.1 MeV, absolute ang. distrib. meas. 78−595
^{35}Cl(n,p), thermal, negative energy resonance parameters 77−23025
^{37}Cl(n,d), 14.1 MeV, absolute ang. distrib. meas. 78−595
Cl(n,X), 14.8 MeV, γ-prod. cross section 79−49622
^{A}Cm(n,f), A=224,246, 0.3-45 MeV, near threshold fission cross section, energy depend. *(Russian)* 80−37406
^{243}Cm(n,f), thermal neutron fission cross section and fission-resonance integral 80−86942
^{244}Cm, fast neutron cross-sections 78−21556
^{244}Cm, neutron induced fission rate meas. in Zebra 77−57698
^{245}Cm (n,f), thermal, charge distrib., ^{135}I and ^{190}Ba fractional cumulative yields 80−63074
^{245}Cm(n,f), cross section, 0.01 to 35 eV 78−21612
^{245}Cm(n,f), neutron yield dependence on fragment mass 79−67787
^{245}Cm(n,f), thermal neutron fission, kinetic energy distribs. determ. 78−658
^{245}Cm(n,f), thermal neutron induced fission, mass yield obs. 80−32309
C(n,xα), thick target corrections for charged particle spectra 80−37714
Co isotopes, E_n=14 MeV, cross sections for charged particle prod., data compilation 80−9289
^{59}Co (n, n′γ), 1.3-3.9 MeV, energy level structure and decay scheme 79−45164
^{59}Co, neutron resonance spectroscopy, R-matrix anal. 78−21555
^{59}Co+n, 16-22 MeV, cross sections for prompt γ, compound statistical model calcs. 79−543
^{59}Co+n, 8-31 MeV, spin-spin depend. of total cross section 78−17172
^{59}Co+n, calc. using pre-equil. statistical model code GNASH 78−4946
^{59}Co(n,2n), 14 MeV, cross section compilation 80−91181
^{59}Co(n,2n), (n,np), (n,d), 16.2 to 21.8 MeV, γ-ray prod. cross sections 78−13080
^{59}Co(n,2n), isomeric cross-section ratio and excitation function, mixed-powder method and gamma-ray spect. 80−47472
^{59}Co(n,2n) direct process contrib., cross section and secondary n spectrum *(Russian)* 78−78386
^{59}Co(n,α), excitation function, mixed-powder method and gamma-ray spect. 80−47472
^{59}Co(n,n′γ), level transitions, deexcitations and lifetimes 80−18222
^{A}Cr, A=50, 52-54, slow n-interactions, scatt. lengths, absorpt. and scatt. cross-section 78−70539
^{A}Cr(n̄,X), A=50, 52-54, 14 MeV, X=p,n′p,α,n′α,^{3}He, production cross-sections 80−42648
^{A}Cr(n,X), A=50,52, 14.8 MeV, charged particle emission, cross section, Hauser-Feshbach anal. 79−67750
^{A}Cr(n,2n), A=50, 52, 54, 14 MeV, cross section compilation 80−91181
^{52}Cr(n,p)^{52}V, ave. neutron activation cross sections for ^{241}Am-Be source 79−31282
Cr(n,X), 14.8 MeV, γ-prod. cross section 79−49622
^{132}Cs radioactive target, search for (n_{th},p) and (n_{th},α) reactions 77−23010
^{132}Cs(n,d), thermal, cross-sections meas. 78−94012
^{133}Cs, nuclear resonance parameters, 1 to 400 eV, calc. by shape and area methods 79−30789
^{133}Cs+n, CsI crystal bombardment, p and α emission spectra, yields, preequilib. mech. 77−50139
^{133}Cs(N,γ)^{134}Cs, exciton model, γ spectra calc. 78−62539
^{134}Cs, nuclear resonance parameters, 1 to 400 eV, calc. by shape and area methods 79−30789
Cu, total neutron cross-section meas. 77−74839
^{A}Cu(n,X), A=63,65, 14.8 MeV, charged particle emission, cross section, Hauser-Feshbach anal. 79−67750
^{A}Cu(n,α), A=63,65, 14.8 MeV, expt. and statistical model determ. of α-prod. in fusion reactors 80−95397
^{63}Cu+n, 30-150 keV, resonance parameters from total cross-section meas. 77−26739
^{63}Cu(n, 2n), 14-19 MeV, cross section meas., neutron flux, ^{62}Cu half life 79−13291
^{63}Cu(n,2n)^{62}Cu, 12.9-15.9 MeV, reaction cross section meas. 78−37337
^{63}Cu(n,α)^{60}Co, 14 MeV, cross section by activation relative to ^{27}Al(n,α)^{24}Na 78−74359

neutron-nucleus reactions continued
^{nat}Cu+n, 30-150 keV, resonance parameters from total cross-section meas. 77−26739
^{nat}Cu(n, 2n), 14-19 MeV, cross section meas., neutron flux 79−13291
^{nat}Cu(n, nα), 14-19 MeV, cross section meas., neutron flux 79−13291
^{nat}Cu(n, p), 14-19 MeV, cross section meas., neutron flux 79−13291
^{243}Cu, thermal neutron capture and fission cross sections, resonance integrals 77−67744
Cu(n,X), 14.8 MeV, γ-prod. cross section 79−49622
Cu(n,n), A=63, 65, E=10-150 keV, total cross-sections and reson. parameters 77−38273
DT fast neutrons in blankets and shields, neutrons, associated particle method 77−71690
DT-Pu plasma, neutron induced fission, fission fragment slowing down 79−26749
DT-Pu plasma, neutron induced fission, enhancement of neutron prod. and fusion rate 79−26750
D(n,2n)p, review reactions on light nuclei, review 77−26697
^{164}Dy+n, capture cross section meas. in Triton reactor *(French)* 80−18308
Dy(n,α)Gd, A=161, 163, at 14.1 and 18.2 MeV, α-emission energy spectra 77−65224
Er+n (A=162-170), (n,α), (n,t), (n,np), (n,nd), (n,p), (n,2n) reaction cross sections 78−82350
^{x}Er+n, (A=166-170), strength functions and scatt. lengths from total and scatt. cross sections 77−26706
^{167}Er(n,p)^{167}Ho, (14.2±0.2) MeV, activation cross sections, Ge(Li) meas. 79−22278
^{254}Es(n,f), neutron yield dependence on fragment mass 79−67787
Eu, enriched isotopes, EBR-II irrad., integral cross sections 79−67843
^{x}Eu (n,X), A=153, 154, 155, total neutron cross sections, effect on reactor characts. 80−32284
^{x}Eu+n, (A=151, 153), strength functions and scatt. lengths from total and scatt. cross sections 77−26706
^{151}Eu(n,α)^{148}Pm, α spectra and ang. distribs. calc., statistical knock-on-model 77−79371
^{153}Eu+n, capture cross section meas. in Triton reactor *(French)* 80−18308
^{152g}Eu, neutron resonance obs. by time of flight spectroscopy, cf. ^{151}Eu and ^{153}Eu *(Russian)* 78−25120
F, differential cross sections for prod. of low energy photons 77−23068
^{9}F+n, 16-22 MeV, cross sections for prompt γ, compound statistical model calcs. 79−543
^{19}F, Hauser-Feshbach code for cross section evaluation 77−23045
^{19}F(n, α)^{16}, average cross sections in ^{235}U fission neutron spectrum 80−22828
^{19}F(n, α)^{16}N, determ. of fast neutron contamination in photon beams 77−10570
^{19}F(n, α)^{16}N, reactor neutron, source of ^{16}N γ-rays to activation of elements in (γ, γ′) reaction 78−88689
^{19}F(n, p)^{19}O, average cross sections in ^{235}U fission neutron spectrum 80−22828
^{19}F(n̄,X), annihilation, 1.4 GeV/c, $\pi^{\pm}$, p emission angles, momentum and multiplicity distribs. 80−532
^{19}F(n,2n), 14.7-19.0 MeV, excitation functions relative to ^{56}Fe(n,p) 79−3142
^{19}F(n,α)^{16}N, 13.9, 15.6 MeV, differential cross-sections meas., statistical model calc. 77−41972
Fe, and Fe:Na mixtures, neutron shielding benchmark expts. 78−29655
Fe assembly, meas. of absolute fission rates/source neutron using solid state track detectors 78−58559
Fe, gamma fields induced by ^{252}Cf neutrons 78−50240
Fe, integral test of cross section, neutron leakage spectra, spherical assembly 77−23033
Fe isotopes, E_n=14 MeV, cross sections for charged particle prod., data compilation 80−9289
Fe, natural, neutron total cross section minima 78−37387
Fe, total neutron cross-section, thick sample transmission meas. and resonance anal. 77−23066
Fe+n, A=54, 56, 1-70 keV, total cross section, resonance parameters *(Russian)* 78−17210
^{x}Fe(n,X), A=54,56, 14.8 MeV, charged particle emission, cross section, Hauser-Feshbach anal. 79−67750
^{x}Fe(n,X) A=54, 56, 57, transmission and capture meas. 80−18313
^{x}Fe(n,2n), A=54, 56, 14 MeV, cross section compilation 80−91181
^{54}Fe, high resolution total neutron cross section meas. 77−23065
^{54}Fe(N,α)^{51}Cr, 6-10 MeV, cross-sections meas. 79−93613
^{54}Fe(n, 2n), 14-19 MeV, cross section meas., neutron flux 79−13291
^{54}Fe(n,2n), 14.7-19.0 MeV, excitation functions relative to ^{56}Fe(n,p), ^{53}Fe half life 79−3142
^{54}Fe(n,2n) direct process contrib., cross section, DWTA and DWBA anal. *(Russian)* 78−78386
^{54}Fe(n,γ) 2.5-500 keV, valence neutron capture, reson. parameters 77−57659
^{54}Fe(n,p)^{54}Mn, 6-10 MeV, cross-sections meas. 79−93613
^{54}Fe(n,p)^{54}Mn threshold reaction cross section, ^{252}Cf source 77−23039
^{54}Fe(n,t)^{52m}Mn, 14.6 MeV neutrons, activation cross section meas. 79−45254
^{56}Fe, Hauser-Feshbach code for cross section evaluation 77−23045
^{56}Fe, high resolution total neutron cross section meas. 77−23065
^{56}Fe+n, 16-22 MeV, cross sections for prompt γ, compound statistical model calcs. 79−543
^{56}Fe+n reactions in man, dose from 14.8 MeV 78−20275
^{56}Fe(n, p), 14-19 MeV, cross section meas., neutron flux, secondary standard 79−13291
^{56}Fe(n,2n), direct process contrib., cross section, DWTA and DWBA anal. *(Russian)* 78−78386
^{56}Fe(n,2nγ), (n,n′γ), 14.6 MeV, γ-ray ang. distrib. *(Russian)* 77−88147
^{56}Fe(n,γ), 2.5-870 keV, resonance neutron capture study 77−2990
^{56}Fe(n,p)^{56}Mn, 12 to 18 MeV, cross section meas. *(Chinese)* 79−22297
^{56}Fe(n,p)^{56}Mn, 14.8 MeV, absolute cross-section meas. using on-line neutron flux monitoring system 77−34300
^{56}Fe(n,p)^{56}Mn, 14.8 MeV, cross section determ. 78−37347
^{56}Fe(n,p)^{56}Mn, 6-10 MeV, cross-sections meas. 79−93613
^{56}Fe(n,p)^{56}Mn, ave. neutron activation cross sections for ^{241}Am-Be source 79−31282
^{56}Fe(n,p)^{56}Mn, for ^{56}Mn(2.58 hr) preparation 78−50178
^{56}Fe(n,p)^{56}Mn threshold reaction cross section, ^{252}Cf source 77−23039
^{57}Fe(n,X) transmission data up to 400 keV, J^{π} value for resonances 80−18311
neutron-nucleus reactions continued
^{58}Fe+n, total cross section from 7 to 325 keV, resonance struct. anal. 78−74357
Fe(n,X), 14.8 MeV, γ-prod. cross section 79−49622
Fe(n,X), 3 eV-1 MeV transmission meas., resonance anal. 80−18316
Fe(n,xn), 20.6 MeV, neutron yield cross sections and spectra *(Russian)* 80−91188
^{x}Fm(n,f), A=253, 255, 257, 259, fission mass distrib. transition, liquid drop and shell model calcs. 80−32310
^{69}Ga(n,n′γ), fast n, levels, J^{π}, transitions and mixing ratios, statistical anal. *(Russian)* 80−13382
^{158}Gd+n, capture cross section meas. in Triton reactor *(French)* 80−18308
^{160}Gd(n,2n), 14.6 MeV, activation cross section 77−88128
Ge isotopes, activation cross-sections for 14.7 MeV neutrons 77−6367
^{1}H(n̄,X), annihilation, 1.4 GeV/c, $\pi^{\pm}$, p emission angles, momentum and multiplicity distribs. 80−532
^{1}H(n,d), 1.88 GeV/c, neutral missing mass, ABC effect obs., cross section 78−74364
^{1}H(n,d)π^{0}, 459, 648, 802 MeV, relative diff. cross section and ang. distrib. 80−52671
^{1}H(n,γ)^{2}H, 2200 m/s neutrons, capture cross section 77−74849
^{1}H(n,π^{0})^{2}H, differential cross sections for 470-590 MeV, ang. distribs. 80−57628
^{1}H(n,π^{0})^{2}H, nuclear forces charge symmetry test 80−5071
^{2}H disintegration, energies up to 50 MeV *(Russian)* 78−89848
^{2}H+n, deuteron breakup reaction, Reid soft-core pot. calcs. at 22.7 and 46.3 MeV 77−74860
^{2}H(n, nn)p, 25 MeV, neutron-neutron effective range 80−83041
^{2}H(n, np)n, 130 MeV, Faddeev eqn. multiple scatt. series anal. 79−97707
^{2}H(n,Nπ)^{2}H, deuteron spectra 78−62669
^{2}H(n,2n)p, 21.5 MeV, quasi-free scatt. 79−75993
^{2}H(n,2n)p, in thick targets, n-n scatt. length determ., computer expt. 80−57776
^{2}H(n,n′)pn, polarised n, 14, 30 MeV, neutron analysing power 79−71835
^{2}H(n,n), (n,p), 24 MeV, quasifree scatt., n-n effective range, Monte Carlo anal. 80−68554
^{2}H(n,n) scattering length determination, using NN interaction radius approx. 79−6426
^{2}H(n,nn), 14.1 MeV, n-n quasifree scatt. obs. 78−82337
^{2}H(n,nn)p, 21.5 MeV, cross section, nn effective range parameter 79−67669
^{2}H(n,nn)p, neutron-neutron quasifree scatt., 14.1 MeV 77−23018
^{2}H(n,np), at ϑ_n=0°, collinearity effect 78−82356
^{2}H(n,np)n, <27 MeV, n-n scatt. length 79−17904
^{2}H(n,p2n), 120 MeV, n-n scatt. length determ., Watson-Migdal model anal. 78−82339
^{2}H(n,p)2n, 13.98 Mev, proton spectra and n-n scatt. lengths 77−88141
^{2}H(n,p)nn, 13.95 MeV, proton spectrum, neutron-neutron scatt. length 77−26704
^{2}H(n,pn)n, 22.7, 46.3 MeV, perturbation calcs. for realistic pots. 79−45265
^{2}H(n,pnn), 794 MeV, quasielastic charge exchange, modified impulse approx. 78−50173
^{2}H(n,π^{-}), 400-580 MeV, differential cross sections and ang. distribs. 80−86906
^{2}H(n,π^{-})^{3}He, 400 to 580 MeV at backward pion angles 80−73847
^{2}H($\bar{\nu}_e$,$\bar{\nu}_e$n)p, neutral current cross section for reactor $\bar{\nu}$ 80−5129
^{3}H+n, 14 MeV, spectra meas. 77−18558
^{x}H(n,X), 60 keV-80 MeV, A=1,2,3 total cross section and scatt. length 80−99176
^{3}He(n,p) cross section standard, status 77−23040
^{3}He(n,p)^{3}H, for direct nucl. pumping of ^{3}He-Xe laser 77−71972
^{3}He(n,p)^{3}H, plasma form by reaction prods. in nuclear reactor 77−76146
^{3}He(n,p)^{3}H direct nuclear pumped laser 77−83851
^{3}He(n,p)^{3}H react., direct nuclear pumped lasers 79−31863
^{3}He(n,p)T, appl. to anal. of fusion reactor materials, archeometry and nuclear spectroscopy 80−61200
^{4}He+n, pole positions of ^{5}He resonances, models calcs. 78−70530
^{4}He+n, separable pot. fits to reson. parameters 78−8822
^{4}He(n,X), local approximation to a non-local potential 80−91182
^{x}Hf(n,nγ), 2.75 MeV, A=180,178,176, levels and excitation cross sections 79−75839
^{177}Hf(n,γ), 1-165 eV, γ-ray spectra obs., level scheme determ. 77−50130
^{178}Hf(n,α), 14.8 MeV, energy spectra, statistical model anal. 77−10396
^{180}Hf(n,α), 14.8 MeV, energy spectra, statistical model anal. 77−10396
^{180}Hf(n,α), thermal cross-sections 78−4932
^{180}Hf(n_{th}, α), cross section 78−66284
Hg, total neutron cross section meas., 4.5×10^{-4} to 10 eV, TOF method 77−14120
^{165}Ho+n, polarised projectile and target, spin depend. of total cross section *(Russian)* 78−17211
^{165}Ho+n, strength functions and scatt. lengths from total and scatt. cross sections 77−26706
^{127}I, 14.7 MeV neutron capture cross-section measurements with activation technique 80−32282
^{127}I neutron resonance parameters, 20 eV to 2 keV 77−22897
^{127}I+n, CsI crystal bombardment, p and α emission spectra, yields, preequilib. mech. 77−50139
^{127}I(n,2n), ^{126}I, 14.1 MeV, ang. and spectral distribs. 78−82354
^{127}I(n,2n), 4.5-18.3 MeV, cross sections and excitation curves *(Chinese)* 79−49601
^{127}I(n,n′γ), fast n, γ-ang. distribs., level ang. momenta 80−18224
^{115}In, thickness depend. of total and capture cross section 77−26747
^{191}Ir(n,γ), development of high intensity ^{192}Ir gamma-ray radiographic source 77−2715
^{39}K(n,α)^{36}Cl, ionizing radiation and cavitation threshold, calc. of dose rate, cavitation threshold 78−94774
^{84}Kr+n, capture cross section meas. in Triton reactor *(French)* 80−18308
^{86}Kr(n_{th},γ)$_2$, Q-value, ^{87}Kr levels 77−74798
^{139}La(n,t)^{137m}Ba, 14.6 MeV neutrons, activation cross section meas. 79−45254
Li, activation by fusion plasma neutrons 79−13521
^{6}Li, ^{7}Li, two and three body neutron reactions, 14.6 MeV 77−26725
^{6}Li neutron inelastic scatt. cross-sections and partial widths, calc. 78−78370
^{6}Li, total cross section meas., 10 eV to 10 MeV 77−23037

neutron-nucleus reactions continued
^{6}Li-n, R-matrix calc. of total elastic, (n,α) differential cross-sections and polarisation 77−57669
^{6}Li+n, spin depend. capture and scatt. of slow neutrons 78−46059
^{6}Li+n total cross-section meas., 0.1 to 3.0 MeV 77−26740
^{6}Li(n, d)^{5}He, 6.77, 6.57 MeV, two body breakup, ang. distrib., DWBA, optical model anal. 77−18539
^{6}Li(n, p)^{6}He, 6.77-4.71 MeV, ang. distrib. excitation function, DWBA, optical model, anal. 77−18539
^{6}Li(n, t)^{4}He, 7.25-4.71 MeV, ang. distrib., excitation function, DWBA optical model anal. 77−18539
^{6}Li(n,^{3}H)^{4}He, polarised neutrons, 0.2-2.4 MeV, analysing power meas. 77−38268
^{6}Li(n,α), 2-10 MeV, total cross section, ^{7}Li 3/2^{-} state 80−18297
^{6}Li(n,α), 2-800 keV, cross section meas. 78−70516
^{6}Li(n,α), importance in in-pile irradiation of LiF crystals 78−29463
^{6}Li(n,α) absolute cross section meas., 964 keV 77−23035
^{6}Li(n,α) cross section standard, status 77−23040
^{6}Li(n,α) cross section standard, R-matrix anal. 77−23041
^{6}Li(n,α) T, mechanism for driving ^{6}LiD pellet to fusion temp. 79−93823
^{6}Li(n,α)^{3}H, 1-1500 keV, cross section meas. 77−26755
^{6}Li(n,α)^{3}H, 10 to 14 MeV, cross sections 77−26724
^{6}Li(n,α)^{3}H, 23 keV cross section, absolute meas., ang. distribs. 80−18305
^{6}Li(n,α)^{3}H, 25 keV, angular anisotropy, s-p wave interf. 77−23036
^{6}Li(n,α)^{3}H, 2.7 MeV triton recoil range, reaction in Li_2O single cryst. 80−63372
^{6}Li(n,α)^{3}H, 3 to 600 keV, new meas. of cross section 77−26723
^{6}Li(n,α)^{3}H, 3-800 keV, cross section meas. 78−89865
^{6}Li(n,α)^{3}H, below 100 keV, differential cross section, angular anisotropy 79−9583
^{6}Li(n,α)^{3}H, eV and keV energy range, ang. anisotropy 77−26722
^{6}Li(n,α)^{3}H, in Li_2O, fund. optical absorpt. edge, number of displaced atoms 78−51594
^{6}Li(n,α)^{3}H, low energy, deuteron exchange mechanism, S-matrix theory 79−30840
^{6}Li(n,α)^{3}H, radiolysis of Co III-EDTA soln. 80−93788
^{6}Li(n,α)^{3}H, use in quantitative microlocation of Li in the brain 80−41353
^{6}Li(n,α)^{3}H cross section, exptl. data base for ^{7}Li system 79−9584
^{6}Li(n,α)^{3}H reaction, as standard in neutron flux meas., instruments review 79−9969
^{6}Li(n,α)T, appl. to anal. of fusion reactor materials, archeometry, and nuclear spectroscopy 80−61200
^{6}Li(n,α)T cross section from 70 to 3000 keV from the ^{235}U(n,f) calibration of a thin glass scintillator 79−85471
^{6}Li(n,α)t, 2-10 MeV, absolute cross section meas., ang. distribs. 77−23059
^{6}Li(n,d)^{5}He, 56.3 MeV, ang. distrib. meas., spectroscopic factors determ. 77−88140
^{6}Li(n,dα)n, review 77−26697
^{6}Li(n,t), 2 and 24 keV, ang. distribs. 79−54440
^{6}Li(n,t)^{4}He, 0-3.9 MeV, ^{7}Li, energy of first 3/2^{-} excited state from S-matrix anal. 79−473
^{6}Li(n,t)^{4}He, 0.2-1.4 MeV polarised neutrons, analysing powers meas. 77−23074
^{6}Li(n,t)^{4}He, meas. review, differential, angle integrated and neutron total cross sections 79−9582
^{6}Li(n,t)^{4}He, R-matrix anal. of ^{7}Li system 79−9585
^{6}Li(n,t)^{4}He, thermal polarised n capture, P-odd asymmetry meas. *(Russian)* 80−13452
^{6}Li(n,t)^{4}He, use in high n flux fusion heating 78−89975
^{7}Li+n, elast. and inelast. scatt. of 9.1±0.2 MeV neutrons, double differential cross section meas. 79−30838
^{7}Li(n,α)^{4}He, ionizing radiation and cavitation threshold, calc. of dose rate, cavitation threshold 78−94774
^{7}Li(n,d)^{6}He, 56.3 MeV, ang. distrib. meas., spectroscopic factors determ. 77−88140
^{7}Li(n,n'α)T, three body sequential reactions, kinetics modelling 80−37371
^{7}Li(n,n'α), cross section, appl. to fusion reactor neutronics 78−62604
^{7}Li(n,tαn), review 77−26697
^Li(n,x), A=6, 7, 14.6 MeV, ang. distribs. and cross sections for ^{6,7}Li, ^{6}He products 80−42650
^{6,7}Li(n,p)^{6,7}He, 800 MeV, cross-sections 77−61423
^{24}Mg(n,α)^{21}Ne, near 14 MeV, differential cross sections compared to compound-nucleus theoretical results 78−37350
^{24}Mg(n,p), 14.8 MeV, isomeric state formation cross section, half lives, gamma-ray spectra 77−30604
^{25}Mg(n,α)^{22}Ne, near 14 MeV, differential cross sections compared to compound-nucleus theoretical results 78−37350
^{26}Mg(n,α)^{23}Ne, near 14 MeV, differential cross sections compared to compound-nucleus theoretical results 78−37350
Mg(n,α)Ne reaction, cross sections at 14.1 and 14.7 MeV and implications for meteorites 79−96874
Mg(n,γ), A=24, 25, 26, E=0.1-1800 keV, determ. of isobaric analogue impurities 77−6386
Mg(n,x) transmission meas., determ. of isobaric analogue impurities 77−6386
^{55}Mn, 14.7 MeV neutron capture cross-section measurements with activation technique 80−32282
^{55}Mn, neutron resonance spectroscopy, R-matrix anal. 78−21555
^{55}Mn(n,X), 14 MeV, X=p,n'p,α,n'α,^{3}He, production cross-sections 80−42648
^{55}Mn(n,2n), 14 MeV, cross section compilation 80−91181
^{55}Mn(n,α)^{52}V, neutron activation anal., Ge(Li) and NaI(Tl) detector γ-ray spectrometer 80−78485
Mo stable isotope eval., 5 keV-5 meV neutrons, rel. to reactor structural steel 80−13620
Mo+n, 1.6×10^{-3} to 10 eV, total cross section, raactor structural material 78−46052
^Mo, A=92, 95, 96, 97, 98, 100, (n,p), (n,n'p), (n,α), (n,n'α), (n,^{3}He) prod. cross sections at 14 MeV 80−93829
^Mo(n,2n), A=92, 100, 14 MeV, cross section compilation 80−91181
(n,3n), 14.7 to 24.0 MeV, cross sections on ^{45}Sc, ^{59}Co, ^{89}Y, ^{93}Nb, ^{103}Rh, ^{169}Tm, ^{165}Lu, ^{181}Ta, ^{197}Au, ^{209}Bi 78−25192
(n,pπ^{-}), neutron coherent dissociation using nuclear targets, comparison of expt. data with Deck model 79−89309
N, neutron air transport sensitivity to nitrogen cross section uncertainties 77−23165
N+n in cellulose nitrate plastic detector, spallation products 78−17198
neutron-nucleus reactions continued
^{14}N, four-body breakup induced by 18 MeV neutrons, double final state interaction 78−17192
^{14}N(n,2n), 14.7-19.0 MeV, excitation functions relative to ^{56}Fe(n,p) 79−3142
^{14}N(n,2n)^{13}N, meas. of total body N, interfering reactions and spatial sensitivity 77−60240
^{14}N(n,2n)^{13}N reaction for clinical total-body N meas. 79−29589
^{14}N(n,3α)t, 18.2 MeV, correlation spectra meas. 77−2992
^{14}N(n,3αt), review 77−26697
^{14}N(n,α)^{11}B, 12-18 MeV, pickup of three nucleons, distorted wave approx. 80−22793
^{14}N(n,α)^{11}B, 13.9 MeV, differential cross sections meas. 78−78387
^{14}N(n,p$_0$), (n,α_0), (n,α_1), 0.5 to 15 MeV, cross section meas. 79−54437
^{14}N(n,p)^{14}C, subsurface production of ^{14}C, groundwater dating 80−85690
^{15}N+n, continuum shell model calcs. of particle emission threshold effects, cross section, line shape of resonances 78−46014
Na, neutron cross sections, ENDF/B-IV assessment and evaluation 78−25291
^{23}Na, 14.7 MeV neutron capture cross-section measurements with activation technique 80−32282
^{23}Na(n, α)^{20}F, average cross sections in ^{235}U fission neutron spectrum 80−22828
^{23}Na(n, p)^{23}Ne, average cross sections in ^{235}U fission neutron spectrum 80−22828
^{23}Na(n,Xγ), 0.2 to 20 MeV, reaction cross sections 80−99172
^{23}Na(n,2nγ), (n,n'γ), 14.6 MeV, γ-ray ang. distrib. *(Russian)* 77−88147
^{23}Na(n,α)^{20}F, 14.1 MeV, cross-section meas. *(Spanish)* 77−67738
^{24}Na(n,np), 14.6 MeV, differential cross sections, statistical model calcs. comparison *(Russian)* 78−78385
^{24}Na(n,pn), 14.6 MeV, differential cross sections, statistical model calcs. comparison *(Russian)* 78−78385
Na(n,X), 14.8 MeV, γ-prod. cross section 79−49622
Nb integral test of cross section, neutron leakage spectra, spherical assembly 77−23033
^{93}Nb, (n,p), (n,n'p), (n,α), (n,n'α), (n,^{3}He) prod. cross sections at 14 MeV 80−93829
^{93}Nb(n,2n), 13-19 MeV, neutron excitation functions, meas. by activation techniques 79−30825
^{93}Nb(n,2n), 14.8 MeV, ^{92}Nb^{g}, cross-section and half-life 78−70491
^{93}Nb(n,2n)^{92m}Nb react. cross section meas., 14-19 MeV 78−93992
^{93}Nb(n,d), 15 MeV, cross-section meas. 78−50171
^{93}Nb(n,γ)^{94}Nb, exciton model, γ spectra calc. 78−62539
^{93}Nb(n,xα), 15 MeV, cross-section meas. 78−50171
^{93}Nb(n,xp), 15 MeV, cross-section meas. 78−50171
Nd (n,2n) react. cross sections at 14.8 MeV 78−74355
Nd, enriched isotopes, EBR-II irrad., integral cross sections 79−67843
^Nd+n, A=143,145, capture cross section meas. in Triton reactor *(French)* 80−18308
^{145}Nd(n,α), studied with intense neutron spectrometer 77−23364
^{143}Nd(n,α), thermal cross-sections 78−4932
^{143}Nd(n,α)^{140}Cd, thermal neutrons, partial cross-section 78−608
^{143}Nd(n,α)^{140}Ce, reaction mechanism 79−9558
^{143}Nd(n,$\gamma\alpha$)^{140}Ce, thermal neutrons, partial cross-section 78−608
Nd(n,2n) A=142, 148, 150, 14.6 MeV, activation cross section 77−88128
Ni isotopes, (n, particle) cross section data base construction, MeV range, statistical models 77−26728
Ni isotopes, E$_n$=14 MeV, cross sections for charged particle prod., data compilation 80−9289
^Ni(A=58, 59, 61), thermal neutron induced charged particle spectroscopy 77−71611
^Ni(n,X), A=58,60, 14.8 MeV, charged particle emission, cross section, Hauser-Feshbach anal. 79−67750
^Ni(n,X) A=58, 60, transmission data, resonance anal. 80−18317
^{58}Ni(n,X), transmission and capture data up to 120 keV 80−18311
^{58}Ni(n,2n), 13-19 MeV, neutron excitation functions, meas. by activation techniques 79−30825
^{59}Ni(n,2n), 14 MeV, cross section compilation 80−91181
^{58}Ni(n,2n)^{57}Ni, cross sections determ. 79−49624
^{58}Ni(n,p)^{58}Co, 3-4.8 MeV, cross section meas. 77−26738
^{59}Ni, neutron cross-sections and resonance integrals 77−23072
^{59}Ni(n,2n), 14 MeV, cross section compilation 80−91181
^{59}Ni(n,α)^{56}Fe, 0.029 to 0.042 eV, cross section for He prod. 77−23079
^{59}Ni(n,α)^{56}Fe, cross section determ. for He prod. in stainless steel 79−22282
^{60}Ni+n, total and differential cross-sections, optical-statistical and coupled-channel models 80−13472
^{60}Ni(n,p), 14.7 MeV, cross section meas. and ENDF/V IV evaluation 79−85458
^{62}Ni(n,α), 14.7 MeV, cross section calc., and ENDF/V IV eval. 79−85458
^{64}Ni(n,d)^{63}Co, 14.3 MeV, decay scheme for ^{63}Co 78−46053
Ni(n,X), 14.8 MeV, γ-prod. cross section 79−49622
Ni(n,α), cross section for 2 step reaction 77−6368
N(n,γ), 14 MeV neutron source, electron recoil spectra from gamma-rays anal. 77−26683
^{237}Np (n,f), 3 eV to 2 MeV, cross-section meas. 77−3058
^{237}Np fission and capture cross sections in GCFR neutron spectra 80−37404
^{237}Np neutron resonance parameters 8 to 204 eV 79−54436
^{237}Np(n,f), 14.7 MeV, Xe relative cumulative yields, fine struct. peak *(Russian)* 79−30868
^{237}Np(n,f), ave. no. of neutrons/fission meas. 78−41792
^{237}Np(n,f), cross section, barrier heights, widths, intermediate structure theory 77−34357
^{237}Np(n,f), thermal neutron sub-barrier fission ^{134}I and ^{135}Xe yields 80−86935
^{237}Np(n,f), thermal to 14.7 MeV, statistical theory calcs. 77−23137
^{237}Np(n,f), thermal-neutron sub-barrier fission 77−74891
^{237}Np(n,f) cross section in ^{252}Cf spectrum, integral test for evaluated data 77−23134
^{237}Np(n,f) cross section standard, status 77−23040
^{237}Np(n,f) integral cross section ratio meas. using ^{235}N(n$_{th}$,f) neutron spectrum 77−23130
^{237}Np(n,f)/^{239}Pu(n,f), 0.13 to 7.0 MeV neutrons, fission cross section ratio meas. 79−97738
^{237}Np(n,γ), meas. of delayed $\gamma\gamma$ coinc., search for ^{238}Np shape isomer *(Russian)* 77−324

neutron-nucleus reactions continued
Np(nth, f), sub-barrier fission, fragment energy correl. meas
[illegible]-10.4
^{238}Np(n,f), subthreshold fission, fine struct. resonances anal. 78−652
^{238}Np(n,f) near threshold cross-sections 77−65240
O cross section data test using n spatial distrib. in water 78−74417
O + n in cellulose nitrate plastic detector, spallation products 78−17198
^{16}O(n,2n)^{15}O, ^{15}O recoils, labelled mol. O_3 form. 78−3359
^{16}O(n,αγ), 7 to 10.5 MeV, γ-ray prod. cross-section meas. 77−34315
^{16}O(n,αγ), 7-10.5 MeV gamma-ray prod. cross sections meas. 78−37338
^{16}O(n,n′γ), 7-10.5 MeV, gamma-ray prod. cross sections meas. 78−37338
^{16}O(n,p)^{16}N, meas. and calc. ^{16}N activity in water of nuclear powered ship 78−13192
^{16}O(n,p)^{16}N, neutron activation anal. of metals 78−15742
^{16}O(n,p)^{16}N, O content in steel determ. *(Hungarian)* 78−92586
^{16}O(n,p)^{16}N, utilisation for monitoring 14 MeV neutron generator output 79−3287
^{16}O(n,p)^{1}u6N, 14.1 MeV, cross-section meas. *(Spanish)* 77−67738
^{17}O(n,α)^{14}C, subsurface production of ^{14}C, groundwater density 80−85690
O(n,X), 14.8 MeV, γ-prod. cross section 79−49622
^{189}Os(n,e^{-}), thermal and reson. energies, levels and γ-ray transitions 79−36189
^{190}Os(n,γ), energy levels and spectra of ^{191}Os determ. 77−41917
^{192}Os(2n,γ)^{194}Os, level transitions, prolate-oblate transition 78−62540
^{192}Os(n,2n), 13-18 MeV, compound nucleus and precompound emission models 77−74841
^{192}Os(n,3n), 13-18 MeV, compound nucleus and precompound emission models 77−74841
^{31}P+n, 14.1 MeV neutrons, estimated dose to bone and whole body 79−53256
^{31}P(n,2n)^{30}P short-lived positron emitter production obs. 79−76236
^{31}P(n,α)$_{28}$Al, 14.7 MeV neutron cross sections 78−70520
^{31}P(n,α)^{28}Al, 14 MeV neutron activation anal. of urine samples *(French)* 78−61254
^{231}Pa spontaneous fission, prediction of fission-product mass yields and related parameters 79−30862
^{231}Pa(n,f), fission spectrum averaged cross section 78−70576
^{231}Pa(n,f), thermal to 14.7 MeV, statistical theory calcs. 77−23137
^{231}Pa(n,f), thermal-neutron sub-barrier fission 77−74891
^{231}Pa(n,f) sub-barrier fission, fragment mass and kinetic energy distribs. 79−17942
^{231}Pa(n,f) thermal neutron-induced fission cross-section 79−30859
^{233}Pa(n,f), cross sections, semi-empirical formula 80−22864
Pb target, inelastic screening and total nuclear cross-sections 78−8824
^Pb(n,γ), A=204, 206-8, sub- and super-barrier fission, results interpretation 79−67784
^{206}Pb+n, 3-50 KeV, neutron resonances, J^{π} assignments, decay scheme 79−36217
^{206}Pb(n,p), ^{207}Pb isobar-like isospin forbidden state excitation *(Russian)* 79−75855
^{206}Pb(n,p), energy dependence, 13.4-20.3 MeV rel. to exciton model calc. 79−75989
^{207}Pb+n, obs. of ^{208}Pb giant mag. dipole states, spin parity assignments 77−57666
^{207}Pb+n resonances, d+s admixture 77−22899
^{207}Pb(n,γ), primary E2 transitions to ^{208}Pb ground state 78−58284
^{207}Pb(n,p) reaction, isobar analogue state excitation *(Russian)* 80−102124
^{208}Pb (n,Zn) direct process contrib. n angular correlations *(Russian)* 78−78386
^{208}Pb (n,p), energy dependence, 13.4-20.3 MeV rel. to exciton model calc. 79−75989
^{208}Pb(n,n′γ), 5.2-8.5 MeV, E1 excitations, collective states and spin assignments, statistical model anal. 79−54405
^{208}Pb(n,n), 16-18 MeV differential cross section resonant characters 79−75952
Pb(n,X), 14.8 MeV, γ-prod. cross section 79−49622
Pb(n,n), 13.7-15 MeV, differential cross section energy depend., meas. and optical model 80−18304
^{102}Pd(n,2n), 13-18 MeV, compound nucleus and precompound emission models 77−74841
^{105}Pd(n,p)^{105}Rh, 13-17 MeV, cross section meas. by activation method 78−46057
^{110}Pd(n,2n), 13-18 MeV, compound nucleus and precompound emission models 77−74841
^{147}Pm, 0.02 to 250 eV, neutron total cross section and neutron resonance parameters 79−97709
^{147}Pm, neutron total cross sections and resonance parameters up to 400 eV 77−23020
^{141}Pr+n, spherical optical model anal., fast neutron differential elastic scatt. and total cross sections 78−46051
Pu (A=239-242), neutron induced fission rate meas. in Zebra 77−57698
Pu (n,F) thermal, rare gas yields, odd-even effect *(French)* 77−50172
Pu, A=239, 241, fission probability, Γ_n/Γ_f ratio struct. 78−37382
Pu isotopes, ENDF/B-4 cross sections, integral data 77−23200
Pu, multigroup time-dependent delayed γ-spectra from fission and activation 78−13184
^Pu(n,f) A=239,242,244, 14.8 MeV, cross-section meas. using mica track detectors 80−95330
^Pu, A=239, 241, 2200 m/s and 20°C Maxwellian neutron data 79−9651
^Pu/^{235}U, A=240, 242, fission cross section ratio meas. 0.127 to 7.4 MeV 80−5180
^Pu(n,f), A=238 to 242, prediction of fission-product mass yields and related parameters 79−30862
^Pu(n,f), A=239, 242, 0.1 to 10 MeV fission cross section rel. to ^{235}U 79−13354
^Pu(n,f), A=239.241, nuclear constants eval. for heavy fissile nuclei using nuclear models *(Russian)* 79−59100
^Pu(n,f), A=240, 242, 244, 0.1 to 30 MeV, cross-sections rel. to ^{235}U 78−50217
^Pu(n,f), fission product decay heat calc. by summation method, appl. to FBR 79−30863
^Pu(n,f) A=240,241, 14.8 MeV, meas. of reaction parameters using solid state nuclear track detectors 80−91201
^{240}Pu(n,f), fission-fragment yields of neutron fission in FBR 80−83102
^{239}Pu, ^{241}Pu cross sections, third IAEA evaluation of Maxwellian neutron data 77−23136

neutron-nucleus reactions continued
^{239}Pu, 14 MeV interactions, neutron and γ-ray spectra meas. 79−93612
^{239}Pu (n,f), 10 eV-100 keV, fission cross section 80−27681
^{239}Pu, deformation effects on neutron total cross-sections, adiabatic coupled-channel calc. 79−17896
^{239}Pu, infinite multiplication factors, neutron captures and fission, rel. to GCFR parameters 78−33245
^{239}Pu neutron data evaluation for ENDF/B-V 78−25288
^{239}Pu neutron data reevaluation for Nuclear Data Library KEDAK-3 77−23042
^{239}Pu, prompt-neutron fission spectrum, Maxwellian and Watt distribs. 77−50177
^{239}Pu, σ(n,γ)/σ(n,f) estimate based on expt. data up to 1977 79−89312
^{239}Pu, thermal neutron-induced fission, ^{96}Nb and ^{98}Nb yields 78−54807
^{239}Pu/^{235}U, (n,f) ratio meas. in range 1 keV-30 MeV 78−46118
^{239}Pu+n, 13.9, 14.6 MeV, absolute neutron fission cross sections, associated particle method 78−89926
^{239}Pu+n, ratio between capture and fission cross sections up to 30 keV 78−70538
^{239}Pu(n, f), 0.024 to 7.4 MeV fission cross section ^{235}U/^{239}Pu ratio 79−40975
^{239}Pu(n, f), undisturbed resonance integral determ., and neutron flux meas. 80−5453
^{239}Pu(n,X), nuclear reaction statistical model parameters *(Russian)* 80−18280
^{239}Pu(n,X), thermal n, gamma spectra from capture, fission and fission products 80−37352
^{239}Pu(n,f,), 0.10-2.07 MeV, meas. of prompt fission neutron spectra 77−23146
^{239}Pu(n,f,) slow polarised neutrons, product separation asymmetry *(Russian)* 80−106088
^{239}Pu(n,f), 0.005-0.4 eV, fission fragment average kinetic energies in resonance region 80−18358
^{239}Pu(n,f), 0.1-1 Mev, light charged particle emission, saddle point states 79−22343
^{239}Pu(n,f), 0.3 eV resonance energy, mass distrib. of products 78−70578
^{239}Pu(n,f), 1 keV to 1 MeV, cross-section meas., ratio to ^{235}U 77−23144
^{239}Pu(n,f), 100 keV-1 MeV, light charged particle yields 77−71631
^{239}Pu(n,f), 2-144 keV, cross-section meas. 77−26813
^{239}Pu(n,f), 2-144 keV, cross-sections meas. 77−26814
^{239}Pu(n,f), 35 to 1500 keV, near equilib. delayed neutron energy spectra 77−34354
^{239}Pu(n,f), abs. meas. of fission cross-sections with photoneutron sources 79−30860
^{239}Pu(n,f), absolute yields and group constants of delayed neutrons in fast fission 77−54261
^{239}Pu(n,f), cross section, parameter testing in statistical model *(Russian)* 80−52653
^{239}Pu(n,f), cross sections for ^{252}Cf neutrons 78−25258
^{239}Pu(n,f), cross-section, 2, 24, 55, 144 keV neutron 78−17262
^{239}Pu(n,f), cumulative yields of Ru and Pd isotopes 79−576
^{239}Pu(n,f), fission cross-section averaged over ^{252}Cf neutron spectrum 79−30861
^{239}Pu(n,f), low energy, fission widths, channel characts. 78−29515
^{239}Pu(n,f), mass distribution of fragments *(Russian)* 78−29517
^{239}Pu(n,f), meas. of α-values in BOR-60 reactor core 79−97830
^{239}Pu(n,f), P-odd asymmetry obs. *(Russian)* 77−82977
^{239}Pu(n,f), polarised thermal neutrons, parity nonconservation *(Russian)* 78−33232
^{239}Pu(n,f), sub MeV neutrons, equilib. delayed neutron energy spectra meas. 77−38308
^{239}Pu(n,f), thermal, correlation for independent fission yield uncertainties 78−50216
^{239}Pu(n,f), thermal n, fission fragment energy correlation meas., fine struct. and deformation 79−13355
^{239}Pu(n,f) 80−37405
^{239}Pu(n,f) 0.009-0.6 eV cross-section, Westcott factor 80−546
^{239}Pu(n,f) cross section in ^{252}Cf spectrum, integral test for evaluated data 77−23134
^{239}Pu(n,f) cross section meas., fragment ang. distrib. using solid state track detector 79−76300
^{239}Pu(n,f) integral cross section ratio meas. using ^{235}U(n_{th},f) neutron spectrum 77−23130
^{239}Pu(n,γ), thermal, fission product $\bar{\nu}_e$ spectrum, β-decay characts. 80−78340
^{239}Pu(n,n′), 3-5 MeV, fission isomer prod. 77−61462
^{239}Pu(n,t), absolute yields of ^{99}Mo, ^{111}Ag, ^{140}Ba, ^{147}Nd, ^{153}Sm 77−50167
^{239}Pu(n_{th},f), fission product mass distribs. 77−74896
^{239}Pu(n_{th},f), yields of Cd and Sn isotopes, symm. region 77−34358
^{240}Pu-fission, P-odd neutron emission asymmetry *(Russian)* 78−74413
^{240}Pu(n,2n), ^{239}Pu fission isomers, half lives 77−30641
^{240}Pu(n,f), 14.8 MeV, products from ^{66}Ni to ^{169}Er, mass distrib., total chain yields 78−25255
^{240}Pu(n,f), 500-10000 eV, subthreshold fission structure 77−23143
^{240}Pu(n,f), cross section, barrier heights, widths, intermediate structure theory 77−34357
^{240}Pu(n,f), mass yield distrib. and absolute fission yields 79−13356
^{240}Pu(n,f) 10 to 250 keV, subthreshold neutron fission cross section meas. 79−22344
^{241}Pu, evaluation of neutron cross sections in region 10^{-5} eV to 15 MeV 78−17254
^{241}Pu, multilevel resonance parameters for 0.01 to 100 eV neutrons 79−36154
^{241}Pu, neutron capture and fission cross sections, 0.01 eV-30 keV 78−29512
^{241}Pu resonances, probability table method and correlated data 79−36284
^{241}Pu, statistical anal. of reson. neutron fission cross section 77−38305
^{241}Pu(n, f) thermal-neutron fission, determ. of cumulative fission yields 79−54462
^{241}Pu(n,f), 0.01-50 eV, fission cross-section, Westcott g_f factors 77−23153
^{241}Pu(n,f), thermal, correlation for independent fission yield uncertainties 78−50216
^{241}Pu(n,f), thermal neutron fission, kinetic energy distribs. determ. 78−658
^{241}Pu(n,f) 1 keV to 30 MeV neutrons, cross section meas. rel. to ^{235}U 79−36286
^{241}Pu(n,f) fission cross section meas., 8 eV to 70 keV 77−50168
^{242}Pu, neutron capture cross-section, 5-70 keV 77−23055

neutron-nucleus reactions continued
^{242}Pu+n, 10 keV-20 MeV, ENDF/B-V cross sections 80−22837
^{242}Pu(n,f), cross section, barrier heights, widths, intermediate structure theory 77−34357
^{243}Pu(n,f) near threshold cross-section calcs. 77−65240
^{244}Pu fast neutron fission cross-section 77−18636
^{244}Pu(n,2n)^{243}Pu, E_n=14 MeV, search for finite isomer 77−54222
Pu(n,f), 0-18 MeV, prompt neutron spectrum, evaporation model *(Chinese)* 80−42721
Pu(n,f), A=240, 241, 242, cross-sections meas. in range 0.001-30 MeV 77−26809
Pu(n,f), A=241, 243, subthreshold fission, fine struct. resonances anal. 78−652
Pu(n,f), delayed neutron spectra from thermal- and fast-neutron fission, reactor calcs. 77−34355
Pu(n,f), thermal to 14.7 MeV, statistical theory calcs. 77−23137
^{226}Ra (n_{th},f), upper bound to cross-section determ. *(Russian)* 77−14201
^{226}Ra, total enutron cross-section up to 1 keV 77−26745
Rb (n,2n) react. cross sections at 14.8 MeV 78−74355
Rb (n,α) 14.8 MeV, cross section 79−49600
^{84}Rb radioactive target, search for (n_{th},p) and (n_{th},α) reactions 77−23010
^{85}Rb(n,2n), 14.6 MeV cross-section meas. 79−59055
^{85}Rb(n,2n), 14.8 MeV, CC Rb cross sections and decay props. 79−49600
Rb(n,p), 14.8 MeV, cross section 79−49600
^{32}S (n,pn), 14.6 MeV, differential cross sections, statistical model calcs. comparison *(Russian)* 78−78385
^{32}S(n,np), 14.6 MeV, differential cross sections, statistical model calcs. comparison *(Russian)* 78−78385
^{32}S(n,t)^{30}P short-lived positron emitter production obs. 79−76236
^{A}Sb(n,2n), A=121,123, 12.8-18.1 MeV, activation cross sections 80−47477
^{A}Sb(n,2n) A=121, 123, 14 MeV neutron activation cross sections meas. c.f. statistical theory estimates 79−13300
^{A}Sb(n,p), A=121, 123, 14 MeV neutron activation cross sections meas. c.f. statistical theory estimates 79−13300
^{45}Sc, 0.4-22 keV neutron total cross section, deep minima 79−9591
^{45}Sc, total cross section, parametric fit, bound level parameters, spin 77−23048
^{45}Sc+n, total cross section, neutron resonances, thermal scatt. parameters 78−8821
^{45}Sc(n,2n), 13-19 MeV, neutron excitation functions, meas. by activation techniques 79−30825
Si, natural, neutron total cross section minima 78−37387
^{A}Si(n,α), 14.8 MeV, A=28-30, cross section determ. for threshold detectors 79−17907
^{A}Si(n,p), 14.8 MeV, A=28-30, cross section determ. for threshold detectors 79−17907
^{28}Si, binary and tertiary reactions, energy distribs. of secondaries 77−23043
^{28}Si(n,n′γ), 13.9 MeV, spin flip probability from 1.78 MeV state, direct theory 80−9234
^{28}Si(n,p), 21.6 MeV, cross sections, proton spectra, ^{28}Al analogue dipole state 77−30571
^{28}Si(n,p)^{28}Al, 14.1 MeV, cross-section meas *(Spanish)* 77−67738
^{28}Si(n,p)^{28}Al, ave. neutron activation cross sections for ^{241}Am-Be source 79−31282
^{28}Si(n,p)^{28}Al*, obs. of analogue dipole state 77−30596
^{30}Si+n→^{31}Si, residual radioactivity meas. 79−33009
^{30}Si(n,^{3}He)^{28}Mg, ^{28}Mg producting using compact cyclotron 77−90894
^{30}Si(n,^{3}He)^{28}Mg, ^{28}Mg production with 50 MeV neutrons 77−90895
^{30}Si(n,β)^{31}P transmutation doping 78−6107
^{30}Si(n,β)^{31}P transmutation doping and electrical characterisation 78−10071
Si(n,α)Mg, A=28,29, 14.1 MeV, cross sections determ. 78−37348
Si(n,γ), A=28.9, E=31.7-67.7 keV, gamma-ray spectra, single particle effects obs. 77−6372
Sm (n,2n) react. cross sections at 14.8 MeV 78−74355
Sm, enriched isotopes, EBR-II irrad., integral cross sections 79−67843
^{A}Sm(n,nγ), 2.75 MeV, A=150,152,154, levels and excitation cross sections 79−75839
^{147}Sm+n, capture cross section meas. in Triton reactor *(French)* 80−18308
^{147}Sm(n, α)^{144}Nd, 12 to 18 MeV, energy and angular distribution of α-particles, statistical, pre-equilibrium and knock-on models 80−13477
^{147}Sm(n,α), 2 keV, ^{148}Sm compound states partial α-widths, α-spectra 80−47392
^{147}Sm(n,α)^{144}Nd, 12.4 to 18.2 MeV, energy spectra, ang. distrib., statistical, preequilib., knock-on models anal. 77−26731
^{147}Sm(n,α)^{144}Nd, 2 keV, statistical model anal. 80−102186
^{149}Sm, neutron total cross sections and resonance parameters up to 400 eV 77−23020
^{154}Sm(n,2n), 14.6 MeV, activation cross section 77−88128
Sn, solid and liquid, neutron cross sections, Doppler effect meas. 80−22933
^{120}Sn+n, transmission and capture γ-ray meas., ^{121}Sn props. 77−3004
^{124}Sn(n,Zn)^{123}Sn^{m} γ-ray, X-ray and electron spectra, ^{123}Sb transitions 77−88073
So(n,2n), A=121,3, cross-section meas., isomeric ratio calc. *(Spanish)* 77−67739
^{86}Sr(n,t)^{84}Rb, 14.6 MeV neutrons, activation cross section meas. 79−45254
^{88}Sr(n,γ) valence neutron capture, 3-400 keV, ^{89}Sr resonance parameters 77−2989
Ta, differential cross sections for prod. of low energy photons 77−23068
^{181}Ta resonances, probability table method and correlated data 79−36284
^{181}Ta(n,2n), 14.6 MeV, cross-section meas. 79−59055
^{181}Ta(n,2n)^{180}Ta^{m}, 14.68 MeV, cross section 80−68659
^{181}Ta(n,2n)^{180}Ta^{m}, (14.2±0.2) MeV, activation cross sections, Ge(Li) meas. 79−22278
^{181}Ta(n,α), 270-875 keV, ^{178}Lu isomeric states and spins, transition probability 80−52582
^{181}Ta(n,total), 15 to 2030 eV resonances, time of flight spectroscopy 78−41716
^{181}Ta(n_{th}, α), cross section 78−66284
^{159}Tb(n,γ), resonance parameters *(Russian)* 77−74850
^{46}Tc(n,p)^{46}Sc threshold reaction cross section, ^{252}Cf source 77−23039
^{99}Tc+n, capture cross section meas. in Triton reactor *(French)* 80−18308

neutron-nucleus reactions continued
^{130}Te(n,t)^{128g}Sb, 14.6 MeV neutrons, activation cross section meas. 79−45254
Th, fast neutron total cross section, 0.1 to 5.0 MeV 78−58278
Th, neutron total cross-section meas. near 24 keV 78−29456
^{212}Th(n,f), 1 eV-100 keV, subthreshold fission widths 77−26798
^{230}Th, total neutron cross-sections in thermal energy region 77−26745
^{230}Th(n,f), 0.68-1.10 MeV, fission fragment ang. distribs., resonance and moment of inertia 80−102219
^{230}Th(n,γ), 680-1050 keV, fission barriers and cross sections, fragment ang. distribs. 80−18357
^{230}Th(n,γ) 720 keV, fission barrier third minimum, ^{231}Th, asymmetrically deformed, rot. bands 79−3068
^{232}Th, 14 MeV interactions, neutron and γ-ray spectra meas. 79−93612
^{232}Th cross sections, optical and statistical model calcs., reactor appls. 77−54227
^{232}Th, deformation effects on neutron total cross-sections, adiabatic coupled-channel calc. 79−17896
^{232}Th fast fission yield of tritium, implications for FBRs 77−46195
^{232}Th, induced fission in natural systems, radiochem. obs. 78−4966
^{232}Th, neutron cross section meas. 80−526
^{232}Th+n, 0.1-18 eV, neutron total cross section determ. 80−22838
^{232}Th+n, strength functions and scatt. lengths from total and scatt. cross sections 77−26706
^{232}Th(n, 2n), cross sections calc. 79−30829
^{232}Th(n,2n), 13-18 MeV, cross sections, pre-equilibrium contrib. 79−45258
^{232}Th(n,2n), ratio to (n,γ) in fast reactor, direct meas. 80−102233
^{232}Th(n,2n)^{231}Th, testing of ENDF/B-IV Th data in GCFR lattice 79−67836
^{232}Th(n,2pn), ^{230}Ra and Ac prod. 78−54724
^{232}Th(n,e), ^{233}Th excited levels, using thermal and average reson. neutron capture 79−45166
^{232}Th(n,f), 0.1-30 MeV, subthreshold cross-section meas. 77−74894
^{232}Th(n,f), 1 eV to 20 keV, cross section meas. 79−67794
^{232}Th(n,f), 14.8 MeV, peak to valley ratio of mass distribs. 77−26801
^{232}Th(n,f), 1.35-2.1 MeV, $\bar{\nu}_p$ values 77−74893
^{232}Th(n,f), 1.38 MeV, prediction of fission-product mass yields and related parameters 79−30862
^{232}Th(n,f), 1.55-3 MeV, mass asymm., ang. anisotropy of fragments *(Russian)* 78−17265
^{232}Th(n,f), 2-8 MeV, fission product yields and mass distribs. 80−86939
^{232}Th(n,f), 35 to 1500 keV, near equilib. delayed neutron energy spectra 77−34354
^{232}Th(n,f), barriers of emitted fragments, fission asymm. *(Russian)* 77−10459
^{232}Th(n,f), cross section up to 6 MeV, rotational states obs., fragment ang. anisotropy 77−23161
^{232}Th(n,f), cross sections, semi-empirical formula 80−22864
^{232}Th(n,f), fast neutrons, delayed neutron spectra, reactor calcs. 77−34355
^{232}Th(n,f), fast neutrons, fission product mass distribs. 77−74896
^{232}Th(n,f), fission fragment ang. distribs., triplet-humped fission barrier 77−74892
^{232}Th(n,f), fission spectrum averaged cross section 78−17253
^{232}Th(n,f), thermal to 14.7 MeV, statistical theory calcs. 77−23137
^{232}Th(n,f), thermal-neutron sub-barrier fission 77−74891
^{232}Th(n,f), yield meas. of Kr, Xe, Sn, Sb, proton odd-even and neutron shell effect 77−82976
^{232}Th(n,f) cross-section meas., rotational bands 77−26803
^{232}Th(n,f) Kr and Xe isotope yields 78−74410
^{233}Th cross sections, optical and statistical model calcs., reactor appls. 77−54227
^{233}Th(n,f), 1.2-2.3 MeV, transition state effect on fragment KE *(Russian)* 78−661
Ti isotopes, capture and transmission meas., 1 to 100 keV 77−26712
Ti+n, 1-4.5 MeV, elastic inelastic, total cross sections, optical-statistical, coupled-channels models 79−539
^{A}Ti(n,X), A=46-50, 14 MeV, X=p,n′p,α,n′α,^{3}He, production cross-sections 80−42648
^{46}Ti, ^{48}Ti, (n,xp), (n,xd) and (n,xα) reactions, 14 MeV, sub-Coulomb barrier protons 77−30597
^{46}Ti+n, 15 MeV, cross sections for emission of sub Coulomb barrier charged particles 77−23007
^{46}Ti(n,2n), 14 MeV, cross section compilation 80−91181
^{46}Ti(n,p), 4.5-18.3 MeV, cross sections and excitation curves *(Chinese)* 79−49601
^{47}Ti(n,p)^{47}Sc, carrier-free radiopharmaceutical prep. with epithermal neutrons 79−79652
^{48}Ti+n, 15 MeV, cross sections for emission of sub Coulomb barrier charged particles 77−23007
^{48}Ti(n,γ)^{49}Ti, T violation test, γ-ray directional correlation 78−62330
^{48}Ti(n,p), 4.5-18.3 MeV, cross sections and excitation curves *(Chinese)* 79−49601
^{205}Tl(n,t)^{203}Hg, 14.6 MeV neutrons, activation cross section meas. 79−45254
Tl(n,n′γ), 1.03-2.26 MeV, ang. distribs. meas., intermediate coupling model 77−38276
^{169}Tm+n, strength functions and scatt. lengths from total and scatt. cross sections 77−26706
^{235,238}U(n,f), fast neutrons, fission product mass distribs. fission product mass distribs. 77−74896
U, A=233, 5, statistical anal. of reson. neutron fission cross section 77−38305
U FBR fission yield, burnup determ. in mixed oxide fuels 77−23138
U isotopes, ENDF/B-4 cross sections, integral data 77−23200
U, Pu fission by thermal neutrons, HIAWATHA, fission-fragment recoil mass spectrometer 78−16892
^{A}U, A=233, 235, 238, deformation effects on neutron total cross-sections, adiabatic coupled-channel calc. 79−17896
^{A}U(n,X), A=233, 235, thermal n, gamma spectra from capture, fission and fission products 80−37352
^{A}U(n,f), A=233,235, ejection fission products angular depend. on thermally polarised neutron capture *(Russian)* 80−86941
^{A}U(n,f), A=235, 238, fission-fragment yields of neutron fission in FBR 80−83102
^{A}U(n,f), A=235, 238, meas. of α-values in BOR-60 reactor core 79−97830
^{A}U(n,f), A=235,7,8, cross section meas., fragment ang. distrib. using solid state detector 79−76300

neutron-nucleus reactions continued
^{233}U(n,f) A=232 to 236, 238, prediction of fission-product mass yields and related parameters 79−30862
^{233}U(u,f), A=233, 235, cumulative yields of Ru and Pd isotopes 79−576
^{233}U(n,f), fission product mass distrib. 79−67789
^{233}U(n,f), reactor neutron fission, kinetic energy distribs. determ. 78−658
^{233}U, ^{235}U cross sections, third IAEA evaluation of Maxwellian neutron data 77−23136
^{233}U cross sections, evaluation of ENDF/B-IV and Hansen-Roach cross sections 78−29550
^{233}U cross sections, optical and statistical model calcs., reactor appls. 77−54227
^{233}U fission by polarised neutrons, P odd asymmetry of emitted fragments *(Russian)* 80−18354
^{233}U neutron-induced reaction, data eval. including $\bar{\nu}_p$ and fission spectrum 79−67795
^{233}U, thermal neutron-induced fission, ^{96}Nb and ^{98}Nb yields 78−54807
^{233}U, total neutron cross section meas., 40 keV to 4.5 MeV 79−13293
^{233}U/^{235}U, (n,f) ratio meas. in range 1 keV-30 MeV 78−46118
^{233}U+n, strength functions and scatt. lengths from total and scatt. cross sections 77−26706
^{233}U(n,f), energy depend. of η^{233}U in 0.02 to 1.00 eV region 77−23118
^{233}U(n,f), thermal polarised neutrons, neutron emission P-odd asymmetry *(Russian)* 80−78338
^{233}U(n,f) slow polarised neutrons, product separation asymmetry *(Russian)* 80−106088
^{233}U(n,t), thermal, Mn bath meas. of η_{2200}, Monte-Carlo anal. 77−23142
^{233}U(n_{th},f), fission neutrons per absorption, Monte Carlo anal. of meas. 77−23141
^{234}U(n, f), 3 eV to 8.9 MeV, intermediate struct. 77−74895
^{234}U(n,f), cross section rel. to ^{235}U in 2-3 MeV region 78−21613
^{234}U(n,f), intermediate struct. anal. 77−79408
^{235}U, 14 MeV interactions, neutron and γ-ray spectra meas. 79−93612
^{235}U (n, f), thermal neutron fission, time-depend. delayed neutron group yields 79−54463
^{235}U, capture to fission ratio determ. from low energy gamma-ray meas. 77−23152
^{235}U, capture to fission ratio in range 10-500 keV 77−26804
^{235}U, fission and activation by fusion plasma neutrons 79−13521
^{235}U fission cross section for Na-Be photoneutrons 77−23159
^{235}U, fission probability, Γ_n/Γ_f ratio struct. 78−37382
^{235}U, fission to capture ratios in range 0.2-15.0 keV 77−3057
^{235}U, neutron induced fission cross section, 0.008 eV to 30 keV 77−50165
^{235}U, thermal n induced ternary fission, α energy and ang. distribs. 79−22345
^{235}U, thermal neutron-induced fission, ^{96}Nb and ^{98}Nb yields 78−54807
^{235}U, thermal-neutron induced fission, scission point configuration determ. 77−82973
^{235}U, thermal-neutron-induced microscopic approach to statistical theory *(Chinese)* 78−86559
^{235}U to ^{239}Pu fission cross-section ratio from 0.001-30 MeV 77−26807
^{235}U+n, 13.9, 14.6 MeV, absolute neutron fission cross sections, associated particle method 78−89926
^{235}U(n, f) 0.024 to 7.4 MeV fission cross section ^{235}U/^{239}Pu ratio 79−40975
^{235}U(n, f) thermal 3 MeV, ^{136}I isomeric ratio *(French)* 80−68709
^{235}U(n, γf), X-ray prefission yield depend. on fission width 77−10453
^{235}U(n,2n), threshold to 13 MeV, cross section meas. by Gd loaded liquid scintillator 80−52669
^{235}U(n,α), thermal, α-particle spectra 78−78425
^{235}U(n,α), thermal fission neutron spectrum 80−42712
^{235}U(n,e$^-$), ^{236}U low lying levels from 4$^-$ isomer decay 80−47396
^{235}U(n,f), ^{132m}I and ^{134m}I isomer yield ratios 77−38306
^{235}U(n,f), 0.001-25 keV, polarised n, spin separated cross sections, resonance struct. 79−3126
^{235}U(n,f), 0.1 to 10 MeV fission cross section rel. to ^{239}Pu and ^{242}Pu 79−13354
^{235}U(n,f), 0.1-20 MeV neutron fission cross section 79−9655
^{235}U(n,f), 0.10-2.07 MeV, meas. of prompt fission neutron spectra 77−23146
^{235}U(n,f), 0.2 to 1.4 MeV, average number of prompt neutrons 77−23140
^{235}U(n,f), 0.3-10 MeV, cross-section meas. 77−26806
^{235}U(n,f), 0.3-12.5 MeV, fission cross-sections meas. 78−46117
^{235}U(n,f), 0.3-1.4 MeV, energy depend of fission fragment anisotropy 79−80962
^{235}U(n,f), 0.5 MeV, prompt neutron spectrum meas., TOF techniques 77−34356
^{235}U(n,f), 0.52 MeV, prompt neutron spectra meas. 77−23158
^{235}U(n,f), 1 keV to 30 MeV neutrons, cross section meas. rel. to ^{241}Pu 79−36286
^{235}U(n,f), 2-144 keV, cross-section meas. 77−26813
^{235}U(n,f), 2-144 keV, cross-sections meas. 77−26814
^{235}U(n,f), 6-9 MeV, fission product yields 78−66324
^{235}U(n,f), abs. meas. of fission cross-sections with photoneutron sources 79−30860
^{235}U(n,f), absolute yields and group constants of delayed neutrons in fast fission 77−54261
^{235}U(n,f), ang. distrib. of fission fragments 78−37383
^{235}U(n,f), cross sections for ^{252}Cf neutrons 78−25258
^{235}U(n,f), cross-section, 2, 24, 55, 144 keV neutrons 78−17262
^{235}U(n,f), cross-section below 1 keV 78−4969
^{235}U(n,f), energy depend. of cross section, 0.8-20 MeV 77−23156
^{235}U(n,f), fission cross-section averaged over ^{252}Cf neutron spectrum 79−30861
^{235}U(n,f), fission fragment average kinetic energies in resonance region 80−18358
^{235}U(n,f), fission fragments with high KE, mass separation based on TOF spectra 78−46209
^{235}U(n,f), intermediate struct. in keV cross-section 77−23154
^{235}U(n,f), light particle yields and spectra 77−50173
^{235}U(n,f), mass distribution of fragments *(Russian)* 78−29517
^{235}U(n,f), neutron spectrum of thermal fission 79−97736
^{235}U(n,f), nuclear constants eval. for heavy fissile nuclei using nuclear models *(Russian)* 79−59100
^{235}U(n,f), polarised thermal neutrons, parity nonconservation *(Russian)* 78−33232
^{235}U(n,f), quantum numbers of low-lying resonances 77−23148

neutron-nucleus reactions continued
^{235}U(n,f), reconciliation of $\bar{\nu}_p$ meas. 77−67776
^{235}U(n,f), spins of resonances below 150 eV 77−23147
^{235}U(n,f), subthreshold fission, fine struct. resonances anal. 78−652
^{235}U(n,f), symmetric fission, proton scatt. by fission fragments in neck area 80−83130
^{235}U(n,f), thermal, appl. of $\bar{\nu}$ constraint to fission product yields 80−22874
^{235}U(n,f), thermal, α-particle spectra 78−78425
^{235}U(n,f), thermal, charge and mass yields of light fission products 77−23122
^{235}U(n,f), thermal, charge distrib. of fission products 77−23123
^{235}U(n,f), thermal, correlation for independent fission yield uncertainties 78−50216
^{235}U(n,f), thermal, discrete neutron emission probability 78−25257
^{235}U(n,f), thermal, fission product decay spectra calcs., comparison with expt. results 79−93674
^{235}U(n,f), thermal, fragment ionisation, charge distribs., stat. and instant perturbation theory *(Russian)* 80−63219
^{235}U(n,f), thermal, Rb and Cs relative and independ. fission yields 80−27679
^{235}U(n,f), thermal fission, fission product decay heat evaluation by least-squares method 79−30865
^{235}U(n,f), thermal n, fission fragment energy correlation meas., fine struct. and deformation 79−13355
^{235}U(n,f), thermal n, fission product isobaric charge distrib., parity effects 79−17791
^{235}U(n,f), thermal n, max. energy dissipation 79−89338
^{235}U(n,f), thermal polarised n capture, P-odd asymmetry meas. *(Russian)* 80−13452
^{235}U(n,f), thermal to 15 MeV, total delayed neutron yield calcs., energy depend. 77−34353
^{235}U(n,f) 3.5 MeV fragment X-rays 77−18638
^{235}U(n,f) absolute cross section, ^{252}Cf neutron source 77−23133
^{235}U(n,f) cross section, 1 keV to 1 MeV 77−23139
^{235}U(n,f) cross section, thermal normalization technique for meas. of neutron cross section vs. energy 79−9590
^{235}U(n,f) cross section in ^{252}Cf spectrum, integral test for evaluated data 77−23134
^{235}U(n,f) cross section in range 0.2-8.2 MeV 78−654
^{235}U(n,f) cross section standard, status 77−23040
^{235}U(n,f) fission rates, interlaboratory comparison in Mol-ΣΣ field 77−23131
^{235}U(n,f) integral cross section ratio meas. using ^{235}U(n_{th},f) neutron spectrum 77−23130
^{235}U(n,f) near threshold cross-section calcs. 77−65240
^{235}U(n,f) self-shielded fission rates, 0.464-2150 eV 79−59096
^{235}U(n,f) standard reaction, Monte Carlo simulation of cross section fluctuations 77−61461
^{235}U(n,f) sub-barrier fission, fragment mass and kinetic energy distribs. 79−17942
^{235}U(n,f) up to 36 keV, statistical anal., cross sections, intermediate struct. 78−653
^{235}U(n,γ), 10-500 keV, capture to fission ratio, double humped fission barrier parameters 79−89336
^{235}U(n,γ), thermal, d, t, He emission probabilities from stable core model *(Russian)* 80−68713
^{235}U(n,γ), thermal, fission product $\bar{\nu}_c$ spectrum, β-decay characts. 80−78340
^{235}U(n,γ), thermal, shape isomer in ^{236}U, isomeric/prompt fission ratio 77−323
^{235}U(n,γf), X-ray yield fluctuations, γ-transitions in ^{236}U 80−106085
^{235}U(n,t), thermal, Mn bath meas. of η_{2200}, Monte-Carlo anal. 77−23142
^{235}U(n_{th},f), fission fragment yield distribs., excitation energy depend. 78−50218
^{235}U(n_{th},f), fission neutrons per absorption, Monte Carlo anal. of meas. 77−23141
^{235}U(n_{th},f), fragment-mass depend. of fission neutron spectrum, TOF method 78−82398
^{235}U(n_{th},f), investigation of conversion electrons in range 150 to 1500 keV *(Russian)* 77−10458
^{235}U(n_{th},f), Maxwellian reference description of fission spectrum shape 77−23129
^{235}U(n_{th},f), neutrons ang. correl., multiplicity 79−3187
^{235}U(n_{th},f), statistical approach to scission mechanism 77−18631
^{235}U(n_{th},f), yields of Cd and Sn isotopes, symm. region 77−34358
^{235}U(n_{th},f) ionic charge distrib., effect of internal conversion 78−78428
^{235}U(n_{th},f) mass yields, direct physical meas. using recoil mass spectrometer 77−50178
^{235}U(nth, f), above-the-barrier fission, fragment energy correl. meas. 78−21614
^{236}U, 30-1800 eV, total cross section meas. 77−23061
^{236}U(n,f), cross section rel. to ^{235}U in 2-3 MeV region 78−21613
^{236}U(n,f), fast n, fragment mass and kinetic energy distribs. *(Russian)* 80−5181
^{236}U(n,f), P-odd asymmetry in neutron emission *(Russian)* 79−89339
^{238}U, 14 MeV interactions, neutron and γ-ray spectra meas. 79−93612
^{238}U delayed fission cross-section for 14 MeV neutrons, shape isomer excitation 77−26808
^{238}U fast fission yield of tritium, implications for FBRs 77−46195
^{238}U fast-neutron fission, calculated fission product yields 79−67796
^{238}U, fission and activation by fusion plasma neutrons 79−13521
^{238}U, infinite multiplication factors, neutron captures and fission, rel. to GFR parameters 78−33245
^{238}U, neutron capture cross-section below 100 eV meas. 77−26680
^{238}U neutron cross sections evaluation for incident neutron energies up to 4 keV 80−5146
^{238}U neutron data reevaluation for 77−23042
^{238}U, neutron induced fission rate meas. in Zebra 77−57698
^{238}U, neutron resonance parameters, transmission meas. on natural U 77−23063
^{238}U, neutron resonance parameters, time-of-flight spectroscopy 80−47375
^{238}U, neutron transmission, resonance meas. and anal. 79−26436
^{238}U neutron transmission meas. and resonance analysis 79−9575
^{238}U pulsed sphere meas., neutron emission spectra rel. to fusion-fission blanket calcs. 77−23298
^{238}U resonances, probability table method and correlated data 79−36284
^{238}U total neutron cross section, ENDF/B-IV representation 77−2983

neutron-nucleus reactions continued
^{238}U, Weale expt. calc. using modified ENDF/B-IV cross sections 79−17908
^{238}U/^{235}U (n,f) cross-section ratio meas., 600 keV-22 MeV 77−23145
^{238}U/^{235}U fission cross section ratio, 2 to 25 MeV, high resolution meas. 77−50176
^{238}U+n, 13.9, 14.6 MeV, absolute neutron fission cross sections, associated particle method 78−89926
^{238}U+n, Doppler effect meas. at 24 and 144 keV 79−97704
^{238}U+n, resolved resonance energies, 100 eV-170 keV 78−37339
^{238}U(n,2n), 13-18 MeV, cross sections, pre-equilibrium contrib. 79−45258
^{238}U(n,2n), E_n=14.9 MeV, effect of Fe shielding, hybrid reactor situation 77−50122
^{238}U(n,2n)^{237}U, 13 to 18 MeV, excitation functions, statistical model anal. 77−23082
^{238}U(n,2n)^{237}U, meas. of average cross section by anion exchange method 79−30828
^{238}U(n,2nf), 13.5-17.5 MeV, fragment anisotropy 77−54263
^{238}U(n,αn′), 14.7 MeV, cross section, possible contrib. to (γ,α) 79−85458
^{238}U(n,f), 0.10-2.07 MeV, meas. of prompt fission neutron spectra 77−23146
^{238}U(n,f), 0.3-10 MeV, cross-section meas. 77−26806
^{238}U(n,f), 0.3-12.5 MeV, fission cross-sections meas. 78−46117
^{238}U(n,f), 14.5 MeV, neutron emission, mass distrib. and energetics 80−47512
^{238}U(n,f), 1.5-7.7 MeV, mass yield curves 78−41788
^{238}U(n,f), 1.52 MeV, mass yield distrib. meas. 77−67777
^{238}U(n,f), 1.8-16.8 MeV, fission fragment energy spectra using glass sandwich detectors 78−82399
^{238}U(n,f), 4.9-7.5 MeV, ^{239}U second-chance fission decay times from crystal blocking 79−85568
^{238}U(n,f), 5 eV-2.5 MeV, fission cross section, fission barrier second well parameters, resonances 80−63217
^{238}U(n,f), 5 eV-5 keV, sub-barrier fission 77−23151
^{238}U(n,f), 6-9 MeV, fission product yields 78−66324
^{238}U(n,f), absolute yields and group constants of delayed neutrons in fast fission 77−54261
^{238}U(n,f), cross section up to 6 MeV, intermediate struct. obs., fragment ang. anisotropy 77−23161
^{238}U(n,f), fission product decay heat calc. by summation method, appl. to FBR 79−30863
^{238}U(n,f), second well gamma decay if subthreshold fission resonances 77−26800
^{238}U(n,f), subthreshold cross-section, high resolution meas. 77−26799
^{238}U(n,f) cross section in ^{252}Cf spectrum, integral test for evaluated data 77−23134
^{238}U(n,f) cross section meas., 3 eV-100 keV 77−26793
^{238}U(n,f) fast neutron fission yield determ. 79−40970
^{238}U(n,f) fission rates, interlaboratory comparison in Mol-ΣΣ field 77−23131
^{238}U(n,f) integral cross section ratio meas. using ^{235}U(n_{th},f) neutron spectrum 77−23130
^{238}U(n,n′α), 14.7 MeV, cross section upper limit 79−85457
^{238}U(p,xn), 800 MeV, neutron spectra meas., check on flux calcs. 77−23349
U(n,X), Japan Material Testing Reactor, U and Pu isolation and isotopic ratios *(Japanese)* 80−52730
U(n,f), 0-18 MeV, prompt neutron spectrum, evaporation model *(Chinese)* 80−42721
U(n,f), 1 to 7 MeV, ratio of ^{238}U and ^{235}U cross sections 79−30867
U(n,f), A=233,235,238, 35 to 1500 keV, near equilib. delayed neutron energy spectra 77−34354
U(n,f), A=233-238, cross-sections meas., 0.1-30 MeV 77−23150
U(n,f), A=234,6,8, 0.1-30 MeV, fission cross-sections relative to ^{235}U 77−61463
U(n,f) A=235,238, sub MeV neutrons, equilib. delayed neutron energy spectra meas. 77−38308
U(n,f), delayed neutron spectra from thermal- and fast-neutron fission, reactor calcs. 77−34355
U(n,f) fission cross section ratio of ^{235}U to ^{238}U for 0.1 to 25 MeV neutrons 79−36285
U(n,f), thermal to 14.7 MeV, statistical theory calcs. 77−23137
U(n_{th},f), A=233,5, isomeric yield ratio of ^{148}Pm meas. 77−82975
^{51}V, neutron resonance spectroscopy, R-matrix anal. 78−21555
^{51}V(n,X), 14 MeV, X=p,n′p,α,n′α,^{3}He, production cross-sections 80−42648
^{51}V(n,α), 4.5-18.3 MeV, cross sections and excitation curves *(Chinese)* 79−49601
^{51}V(n,d), 15 MeV, cross-section meas. 78−50171
^{51}V(n,p)^{51}Ti, neutron activation anal., Ge(Li) and NaI(Tl) detector γ-ray spectrometer 80−78485
^{51}V(n,xα), 15 MeV, cross-section meas. 78−50171
^{51}V(n,xp), 15 MeV, cross-section meas. 78−50171
^{A}W(n,nγ), 2.75 MeV, A=182,184,186, levels and excitation cross sections 79−75839
^{186}W, 14.7 MeV neutron capture cross-section measurements with activation technique 80−32282
^{124}Xe(n,2n)^{123}Xe, ^{123}I prod. in nucl. reactor, for nucl. medicine 77−2051
^{125}Xe(n,d), thermal, cross-sections meas. 78−94012
^{127}Xe radioactive target, search for (n_{th},p) and (n_{th},α) reactions 77−23010
^{127}Xe(n,α), thermal, cross-sections meas. 78−94012
^{132}Xe+n, capture cross section meas. in Triton reactor *(French)* 80−18308
Y isotopes, Hauser Feshbach calcs., of neutron cross sections 80−22839
^{88}Y(n,2n)^{87}Y cross sections, spin dependence and preequilibrium emission 77−30598
^{89}Y, 14.7 MeV neutron capture cross-section measurements with activation technique 80−32282
^{89}Y, high resolution neutron total cross section meas., 27-240 keV 78−25193
^{89}Y, total neutron cross section, 0.3 to 9.0 MeV 78−70519
^{89}Y, total neutron cross-section, 0.3-9.0 MeV, fluctuation anal. 77−23030
^{89}Y(n,2n)^{88}Y, preequilibrium emission effects 77−30598
^{89}Y(n,t)^{87m}Sr, 14.6 MeV neutrons, activation cross section meas. 79−45254
^{171}Yb(n,α), α-decay of highly excited states of deformed nuclei *(Russian)* 79−9526

neutron-nucleus reactions continued
^{176}Yb(n,2n), 14.6 MeV, activation cross section 77−88128
^{64}Zn(n,p)^{64}Cu, evaluated cross section, neutron flux determ. by foil activation 78−25273
Zr (n,2n) react. cross sections at 14.8 MeV 78−74355
Zr isotopes, Hauser Feshbach calcs., of neutron cross sections 80−22839
^{90}Zr neutron absorption, multipole giant resonance contrib. to optical pot. imaginary part 80−18263
^{90}Zr(n,X), 10-20 MeV, multipole giant resonance contrib. to optical pot. imaginary part 80−78241
^{91}Zr, 292.4 eV neutron resonance parameters, radiative and neutron widths, spin assignments 77−6369
^{94}Zr(n,α)^{91}Sr, fast n, fission spectrum averaged cross section 80−63177
Zr(n,X), A=92,94, total cross section meas. 77−2986

neutron-nucleus scattering
see also nucleon-nucleon scattering
A=24 to 209, 7 to 26 MeV, neutron scattering and isospin dependence of the optical model potential 79−45250
absorption cross-section absolute meas. method 78−78431
anisotropy effects on differential cross sections in CM frame *(Portuguese)* 80−18364
coherent parity-violation experiments with neutron beams 79−59073
coherent scattering with parity-violating pots., weak interaction probe 77−71599
coupled channels method, separable, neutron-nucl. scatt. 77−2954
cross section width fluctuation factor, neutron capture, elastic and inelastic scatt. 77−34294
Cross sections for gamma-ray production by 14-MeV neutrons 78−21552
cross-section standards, status report 77−23017
differential cross section meas. for fast neutrons using spheroidal scatterer 77−54479
Doppler free- and recoil free resonance neutron spectroscopy 77−26924
elastic, ang. distrib. meas., study of optical model spin orbit term 77−30599
elastic, ang. distrib. meas., study of optical model spin-orbit term 77−30600
elastic, angular distrib. of diff. cross sections, recording and anal., Legendre polynomial expansions 80−91185
elastic, isospin depend. of N-nucleus optical pots. 77−34311
elastic and inelastic, 4 to 8.5 MeV, summary of ORNL programme 77−23090
elastic and nonelastic scatt. on nuclei of rock-forming elements in borehole-layer system 78−61582
elastic back angle scatt., spin-orbit effects, Fe,Co,In,Bi targets 77−67746
elastic neutron and proton, cross sections, microscopic optical model pot. calcs. 78−593
elastic neutron scattering, probability density function approach 80−13480
elastic scattering, 11 MeV, isospin depend. of neutron-nucleus optical pot. 77−14126
elastic-removal cross sections, spectral corrections, reactor cores 77−46278
EM wave field effect on scatt. spectrum, field quanta absorpt. and emission *(Russian)* 77−41971
fast neutron induced nonelastic reaction cross section data, $E_n \geq 14$ MeV 77−23058
fast neutron scatt., reaction mechanisms and nucl. struct. 77−26696
fast scatt. from medium mass nuclei, i-spin depend., review 77−26695
fluctuation enhancements of compound cross-sections for elastic, directly coupled and weakly absorbed channels 77−26653
fusion reactor materials, 14 MeV neutron scatt. in extended samples of LiF and ^{56}Fe 77−57739
high-energy scattering, review 77−79283
imaginary inelastic transition form factor, microscopic theory 78−50175
inelastic, 14.2 MeV, optical model anal. 77−54225
inelastic, EBR-II energy depositions by nuclear recoil 77−46277
inelastic cross sections, 2 to 4.5 MeV, for Al, Ti, V, Mn, Fe, Ni, Nb, Pb, Bi 77−23087
microscopic optical model anal. of (n,n) and (p,p) cross sections 78−29434
multigroup scattering matrices, processing of ENDF/B data 79−26464
neutron cross-sections for reactor dosimetry, status 77−23304
neutron elastic removal cross sections, interference effect of strong scattering resonances in LMFBR 80−68658
neutron electric moment information from scatt. *(Russian)* 79−5998
neutron interactions with nuclei, conf. 77−23015
neutron optical potl. from sub-Coulomb (p,n) data on ^{51}V, ^{54}Cr, ^{55}Mn, and ^{59}Co 77−26649
neutron physics, recent advances 77−26640
neutron stars, neutrino-pair bremsstrahlung in collisions between neutrons and nuclei 77−74789
neutron-photon multigroup cross sections for neutron energies ≤60 MeV 79−30880
neutron-trinucleon scattering lengths, four-body model with separable NN interaction *(Ukrainian)* 77−30495
non-elastic scatt. cross section at 14.2 MeV meas. method 80−73843
optical model pot. in 4 to 100 MeV range, shell effects 77−54197
optical model spin-orbit pot. for spin $^1/_2$ particles 79−97686
p-wave neutron-reduced widths, anal. 79−36242
parity violation effects in neutron scattering and capture 80−105808
parity violation in forward scatt. amp. 79−67482
polarised neutrons, expt. determination of parity violation 79−59048
random sampling technique for choosing scatt. angle from ang. distrib., dosimetric and shielding calcs. 77−61619
resonance theory of potential scatt., phase shift parameters 78−16685
shell and isotope effects in neutron-nucleus interactions, review of Soviet research 79−36168
small-angle scatt., possible test of neutron electric polarisability 77−22674
spin ± 1/2 polarised neutrons, differential scatt. by chiral systems, coupled oscill. model 80−102177
spin dependent nuclear scatt. lengths of slow neutrons 79−75982
thermal neutron scatt., shell model formalism 78−13095
thermal neutron scatt. parameters for light nuclei (A=12 to 27) 79−93628
total cross section fluctuations, shell model approach using Greens function, resonances 79−22283
two-channel Hamiltonians and the optical model of nuclear scattering 79−59043

neutron-nucleus scattering continued
width fluctuation correction to reacts. involving continuum level excitations 78−46124
(α,n,p) elastic scatt., ^{6}Li structure three body model 79−75875
^{1}H(n,n)^{1}H at 16.9 MeV, analysing power meas. 78−4941
^{1}H(n,n), 2.48 and 3.28 MeV, elastic differential cross section and related phase shift analyses 79−75992
(n,d) elastic differential cross section at 2.48 and 3.28 MeV 78−89862
(n,n), A=90 region, elastic, inelastic and total cross section, statistical model calcs. 80−68674
(n,n), cross section and polarisation, Lane model extension to light nuclei 79−85449
(n,n), elastic and inelastic scatt. on various isotopes, cross sections meas. and calcs. 78−13081
(n,n), microscopic optical model pot. 78−54729
(n,n), pol. n, 16.1 MeV, differential cross section, optical model fit 80−32259
(n,n), single particle bound state, energy independ. optical model, asymmetry term 80−37316
(n,n) compound scatt. and optical model polarisation 77−2971
(n,n) resonance TOF spectroscopy at Nevis Lab. 77−23073
(n,n′), 14 MeV, continuous spectra, multi-step direct reaction anal. 80−78258
(n,n′), 14 MeV, cross-sections calc. using Blanns geom. depend. hybrid model 77−26749
(n,n′), 14 MeV, pre-equilibrium anal., geom. depend. effects and direct component 77−23026
(n,n′), 14.6 MeV, ang. distribs., preequilib. and equilib. neutron emission, unified model 80−86891
(n,n′), 9-14 MeV, anal. of twice differential cross-sections 77−30590
(n,n′), integral data meas. in ΣΣ neutron field 78−70537
(n,n′), odd mass nuclei, 2-4.5 MeV, level excitation functions, Hauser-Feshbach-Moldauer model test 79−36238
(n,n′), two-particle emission in terms of exciton model *(Russian)* 77−304
(n,n′) cross sections for nuclei of A=77 to 197, statistical model calcs. 77−14119
(n,n′) cross sections meas. from 160-375 GeV/c 80−13474
(n,n′) scatt. on N=50 and Z=50 nuclei, isospin dependence of expt. nuclear deformations 77−82817
(n,n′γ), 14.2 MeV, meas. of gamma-ray production cross-sections 77−23070
(n,n′γ) cross section meas. using electronic collimation of 2.7 MeV neutrons 77−6591
nd scatt., at d breakup energy, boundary condition method 79−22127
^{2}H(n,p)n, 63.1 MeV, differential cross section 80−63186
^{152}(n,n) elastic and inelastic 1.7, 2.75 MeV, cross sections 79−75839
^{107}Ag(n,n), 0.25-4.5 MeV, total, elastic and inelastic cross sections, optical-statistical anal. 80−27639
Ag(n,n′), 14.1 MeV, precompound processes 78−13093
Al, sensitivity of displacement per atom cross sections rel. to in-group weighting schemes 79−36236
^{27}Al (n,n′γ), 14.6 MeV, differential cross sections, statistical model calcs. comparison *(Russian)* 78−78385
^{27}Al(n,n′γ)^{27}Al, γ-ray prod. cross-section meas. 79−26434
^{27}Al(n,n), (in)elastic scatt. cross sections, duration of collision process *(Russian)* 79−80942
^{241}Am, 0.5 to 25 MeV, total neutron cross section determ. 79−30831
^{75}As(n,γ), J, 3-2.8 MeV, ^{75}As levels determ. 77−26611
^{75}As(n,n′γ)^{75}As, deexcitation gammas, energy levels, branching ratios, spins, parities, excitation function meas. 78−89869
^{75}As(n,n), slow n coherent scatt. length, free cross section, bound states 80−86909
As(n,n′), 14.1 MeV, precompound processes 78−13093
^{197}Au(n,n′)^{197m}Au, E_n=3 and 14.1 MeV, form. cross sections of short-lived isomer, cyclic activation technique 80−32283
^{197}Au(n,n′)^{197}Au, pre-equilib. and evaporation model anal. 77−6366
^{197}Au(n,xn), 20.6 MeV, neutron yield cross sections and spectra *(Russian)* 80−91188
^{A}B+n, A=10,11, 1.0 to 14 MeV, total cross-section meas. using ^{9}Be(d,n)^{10}B neutron source 79−22280
^{10}B, total neutron cross section, 90 to 420 keV 79−40913
^{10}B(n,n), 4-8 MeV, differential cross section meas., struct. determ. 77−23016
^{10}B(n,n), cross sections for neutrons of 4 to 8 MeV 78−21553
^{11}B(n,n), 2.6-8 MeV, ^{12}B levels, J$^{\pi}$ and diff. cross sections, R-matrix anal. 80−78151
^{11}B(n,n), 4-8 MeV, differential cross section meas., struct. determ. 77−23016
Ba, A=134-138, average neutron cross sections, statistical and optical model calcs. 78−29458
Be, double differential neutron cross sections at 5.9, 10.1, and 14.2 MeV 77−67743
^{8}Be(n,n)^{8}Be elastic scatt. generalised optical potentials, three-body approximation *(Russian)* 79−13313
^{9}Be+n, 1.0 to 14 MeV, total cross-section meas. using ^{9}Be(d,n)^{10}B neutron source 79−22280
^{9}Be+n, differential elast. and inelast. scatt. 7 to 15 MeV 79−36234
^{9}Be(n,2n) pseudolevel eval. validation 80−22697
^{9}Be(n,n), 2-5 MeV polarised neutrons, analysing power, R-function and phase-shift anal. 77−23088
^{9}Be(n,n), 7-15 MeV elast. and inelast. scatt. 77−34314
^{9}Be(n,n), cross sections and polarisation from Lane model anal., multichannel constraints 79−80914
^{209}Bi coherent scattering of polarised thermal neutrons, parity violating effects 78−29461
^{209}Bi, elastic and inelastic differential scatt. cross sections, 1.5-3.0 MeV *(Russian)* 77−26688
^{209}Bi(n,n), 0.6 to 1.0 MeV, optical model params. 78−21557
^{209}Bi(n,n), 1.2 to 4.5 MeV total and differential cross sections 80−86903
^{209}Bi(n,n), 50, 100, 200 MeV, eikonal scatt. by complex pots., cross sections 80−27643
^{209}Bi(n,n), direct scatt., polarised thermal neutrons, empirical parity-violating potentials and neutron optical activity 79−59074
^{209}Bi(n,n), TOF transmission spectroscopy, strength functions 77−23077
^{209}Bi(n,xn), 20.6 MeV, neutron yield cross sections and spectra *(Russian)* 80−91188
Bi(n,n), 10 MeV, neutron polarisation meas. at small angles 77−3014
Bi(n,n), 10.4 MeV, polarised neutrons, analysing power 77−30545
Bi(n,n), 2.5 MeV, small angle scatt., cross section, asymm. 78−74361
C, elastic and inelastic cross sections, 8 to 14.5 MeV 77−23091
neutron-nucleus scattering continued
C, elastic and inelastic scatt. cross sections, 9 to 15 MeV 77−23086
C, natural, total and elastic scatt. cross sections for neutron energy <5 MeV, 8.5-15 MeV, use as standard 79−9588
^{A}C+n, A=12,13, 1.0 to 14 MeV, total cross-section meas. using ^{9}Be(d,n)^{10}B neutron source 79−22280
^{12}C+n, resonances, appl. of unified model 78−29437
^{12}C+n, total and elastic cross sections in few MeV region 79−59057
^{12}C(n,n′)C* 15.85 MeV polarised neutrons, analysing power meas. 77−2969
^{12}C(n,n′γ)^{12}C, ^{12}C gamma line Doppler broadening at 4438 keV 80−91147
^{12}C(n,n), 0.2-5.0 MeV, unified weak coupling model 77−82930
^{12}C(n,n), 14.2 MeV, elastic, inelastic, backscatt. meas., optical model test 78−58275
^{12}C(n,n), 15 to 18 MeV, resonance effects 77−30591
^{12}C(n,n), 15.85 MeV polarised neutrons, analysing power meas. 77−2969
^{12}C(n,n), 8 to 14.5 MeV, differential elastic and inelastic cross-sections 78−29455
^{12}C(n,n), (in)elastic scatt. cross sections, duration of collision process *(Russian)* 79−80942
^{12}C(n,n), <17 MeV, resonating group calcs., phase shifts and differential cross sections 80−32275
^{12}C(n,n), multichannel quasi-separable pot. approach 78−37320
^{12}C(n,n), spin-flip probability to first 2^{+} level 80−78288
^{12}C(n,n)^{12}C, 1.8-4.0 MeV, R-matrix anal. 77−23038
^{12}C(n,n)^{12}C, polarised neutron scatt. 77−26734
^{40}Ca(n,n′), 11 MeV, isospin effects cf. with direct reaction theory 77−34312
^{40}Ca(n,n′), excitation of low-lying collective states 78−17205
^{40}Ca(n,n′)^{40}Ca, imaginary inelastic transition form factor, microscopic theory 78−50175
^{40}Ca(n,n), 10 and 50 MeV, optical model real potential 78−58274
^{40}Ca(n,n), 11-26 MeV, differential cross sections, global optical model anal. 80−18298
^{40}Ca(n,n), 2-3 MeV neutrons, cross section meas. using associated particle TOF spectrometer 79−45255
^{40}Ca(n,n), optical-model real pot., nuclear matter compressibility, effect 77−74823
^{40}Ca(n,n) 2-3 MeV neutrons studied using assoc. particle TOF spectrometer 80−13468
Ca(n,n) 20, 26 MeV, Coulomb correction term to optical model pot. 77−38280
Ca(n,n)Ca, 11-26 MeV, optical model fit 77−79372
^{110}Cd(n,n′γ), fast reactor neutrons, γ-ray ang. distrib. 77−6287
^{111}Cd(n,n′)^{111m}Cd, 13-17 MeV, cross section meas. by activation method 78−46057
^{112}Cd(n,n′γ), fast reactor neutrons, γ-ray ang. distrib. 77−6287
Cd(n,nγ), γ spectra and ang. distrib., ^{114,116}Cd energy levels, spins, particles 77−88070
Ce(n,n′) 1.8 meV to 1.8 eV, total neutron cross-section meas. using TOF spectrometry 79−85466
Cl isotopes, slow neutron scatt. 77−71610
^{35}Cl(n,n), thermal, negative energy resonance parameters 77−23025
^{244}Cm, fast neutron cross-sections 78−21556
C(n,n), 7-15 MeV elast. and inelast. scatt. 77−34314
C(n,n) cross section standard, status 77−23040
C(n,n), differential elast. and inelast. scatt. from 9-15 MeV, cross-section meas. 77−2984
C(n,n), total cross sections below 2 MeV, R-matrix fits to data 80−13466
^{59}Co, neutron resonance spectroscopy, R-matrix anal. 78−21555
^{59}Co, radiative transitions from unbound states obs. in neutron inelastic scatt. *(Russian)* 78−41664
^{59}Co(n,n′), 14.6 MeV, ToF spectra meas. *(Russian)* 78−41721
^{59}Co(n,n′), exciton model, ang. and energy distribs. of nucl. reaction products *(Russian)* 78−54736
^{59}Co(n,n′), exciton neutron inelastic scatt. model *(Russian)* 78−33189
^{59}Co(n,n′γ), 1.1-3.3 MeV, level inelastic scatt. cross section, decay γ-rays, spins, branching ratio 79−6605
^{59}Co(n,n), compound nucl. effects in spin-spin cross-sections 77−10402
^{59}Co(n,n), spin-spin cross-section for polarised neutron and target, 0.4 to 30 MeV 77−26656
^{60}Co, neutron scatt. cross section meas., parameters of neutron levels 80−5147
^{69}Co(n,n), deformation effect in aligned target 80−47364
Co(n,n′), 9.1 MeV, equilib., pre-equilib., direct process anal. *(Russian)* 77−46172
^{A}Cr, A=50, 52-54, slow n-interactions, scatt. lengths, absorpt. and scatt. cross-section 78−70539
^{A}Cr(n,n′γ), A=50-54, 0.84-3.97 MeV, neutron inelast. scatt. cross-sections determ. 78−62529
^{50}Cr(n,n)^{50}Cr, 1.5-3.0 MeV elast. and inelast. scatt., differential cross section *(Russian)* 78−25199
^{52}Cr(n, n), 1.77 to 3 MeV, validity of Wick's inequality in the calculation of the lower limits of the differential elastic cross sections 80−5137
^{52}Cr(n,n′γ), 0.5-10 MeV, γ-ray production cross sections 77−26762
^{52}Cr(n,n)^{52}Cr, 1.5-3.0 MeV elast. and inelast. scatt., differential cross section *(Russian)* 78−25199
^{54}Cr(n,n)^{54}Cr, 1.5-3.0 MeV elast. and inelast. scatt., differential cross section *(Russian)* 78−25199
Cr(n,n′γ), 3-6 MeV, γ-ray prod. cross sections 77−26767
^{133}Cs(n,n′γ), level scheme and deexcitation of excited ^{133}Cs levels 78−13004
Cu (n,X) 80−68673
Cu(n,n), 14.2 MeV, polarisation in forward angle scatt. 80−18282
Cu(n,n), 16.1 MeV, 2.9 MeV, differential cross section and polarisation meas. 77−3013
Cu(n,n), 16.1 MeV, polarisation meas., optical model anal. 79−22264
Cu(n,n) 2.9 MeV, elastic differential cross section and polarisation ang. depend., statistical anal. 79−45264
Cu(n,n), fast neutrons, differential cross sections, optical model calcs. *(Chinese)* 79−9572
Cu(n,n′), 14.1 MeV, precompound processes 78−13093
Cu(n,nγ), 0.67-19.6 MeV, prod. cross sections, discrete and continuum γ rays 365 to 6620 keV 77−34293
^{162,164}Dy(n,n′γ) 1.5-2.4 MeV, ang. distribs., Dy levels, J$^{\pi}$, γ-branching 77−74768
^{162}Dy(n,n′γ), study of ^{162}Dy levels up to 2 MeV 77−6285
^{164}Dy(n,n′γ), γ spectrum, level populations 77−61406

neutron-nucleus scattering continued
$^{152}Eu^{m}$ (n,n′), thermal neutron acceleration by isomeric nuclei *(Russian)* 80−52680
^{153}Eu(n,X), gamma transitions and band levels *(Russian)* 79−67700
Fe, high resolution fast neutron gamma-ray prod. cross sections 77−67745
^{54}Fe, elastic and inelastic differential scatt. cross sections, 1.5-3.0 MeV *(Russian)* 77−26688
^{56}Fe, 0.4-1000 keV neutron total cross section, deep minima 79−9591
^{56}Fe, elastic and inelastic differential scatt. cross sections, 1.5-3.0 MeV *(Russian)* 77−26688
^{56}Fe, radiative transitions from unbound states obs. in neutron inelastic scatt. *(Russian)* 78−41664
^{56}Fe+n, 0-2.2 MeV, doorway state struct. 77−88143
^{56}Fe(n, n′), transmission of neutrons at 24.37 keV 79−54435
^{56}Fe(n, n), 1.77 to 3.0 MeV, validity of Wick's inequality in the calculation of the lower limits of the differential elastic cross sections 80−5137
^{56}Fe(n, n), up to 1 MeV, cross section by coupled channels method, simple vibrational model 78−70535
^{56}Fe(n,2nγ), (n,n′γ), 14.6 MeV, γ-ray ang. distrib. *(Russian)* 77−88147
^{56}Fe(n,n′), 14 MeV, ang. distrib., reaction mechanism 77−26756
^{56}Fe(n,n′), 14 MeV, γ competition in decay of unbound states 78−8811
^{56}Fe(n,n′γ), 14 MeV, ratio of γ to neutron width 77−30593
^{56}Fe(n,n′γ), 14.6 MeV, maximum excitation state γ-decay, cross section *(Russian)* 80−68586
^{56}Fe(n,n′γ), up to 14.6 MeV, radiation and neutron widths for highly excited levels *(Russian)* 78−605
^{57}Fe(n,n), high resoln. scatt. meas. 80−18311
^{58}Fe+n, total cross section from 7 to 325 keV, resonance struct. anal. 78−74357
^{58}Fe(n,n), 0.03-500 keV, total cross section, resonance parameters and level spacings 79−6603
Fe(n,2n), displacement per atom cross section, sensitivity rel. to n ang. distrib., energy spectra 79−36236
Fe(n,2n), primary knock-on spectra, sensitivity rel. to secondary n spectra, ang. distrib. 79−36236
Fe(n,n), 2.9 MeV, differential cross section and polarisation meas. 77−3013
Fe(n,n) 2.9 MeV, elastic differential cross section and polarisation ang. depend., statistical anal. 79−45264
Fe(n,n), 500 to 3000 keV high resolution differential cross-section meas. 77−30592
Fe(n,n), MeV elastic and inelastic cross sections meas. 80−32277
Fe(n,n′ unresolved), displacement per atom cross section, sensitivity rel. to n ang. distrib., energy spectra 79−36236
Fe(n,n′ unresolved), primary knock-on spectra, sensitivity rel. to secondary n spectra, ang. distrib. 79−36236
Fe(n,n′γ), 8.5 to 14.2 MeV, differential cross section for prod. of 0.847 MeV γ-ray 77−23080
Fe(n,xn), 20.6 MeV, neutron yield cross sections and spectra *(Russian)* 80−91188
^{76}Ge(n,n′γ)$_{2^+}$ 2.0 to 4.1 MeV, level and decay schemes 77−23092
Ge(n,n′), 2^+ level excitation cross sections, intermediate resonances, optical model with coupled channels *(Russian)* 79−40897
^{1}H(N,N), 180° cross-sections 77−26737
^{1}H(n,n), 14.2 MeV, polarised n, analysing powers 79−71832
^{1}H(n,n), 16.9 MeV, anal. power, F-wave contribs. 80−63158
^{1}H(n,n), 180° cross sections for fast neutron meas. with counter telescopes 79−36240
^{1}H(n,n), pol. n, 13.5-16.9 MeV, anal. power and spin-orbit phase parameters 80−78269
^{1}H(n,n)$_1$ pol. n, 50 MeV, anal. power 80−68639
^{1}H(n,n)^{1}H, 10 keV-20 MeV, use for neutron flux meas., proton-recoil detectors 79−9960
^{1}H(n,n)^{1}H, 325 MeV, phase shift anal. and mixing parameters 77−79277
^{1}H(n,n)^{1}H, 50 MeV polarised neutrons 77−26732
^{1}H(n,n)^{1}H, differential cross section below 30 MeV, phase shift anal. 79−9586
^{1}H(n,n)^{1}H, polarised neutron scatt. 77−26734
^{1}H(n,n)^{1}H analysing power, 14.5 MeV, Hamburg polarised neutron facility, initial expts. 77−26946
^{1}H(n,n)^{1}H, 14 MeV polarised neutrons, analysing powers 77−54210
^{1}H(n,n)p, 210-495 MeV, free elastic scatt., phase shift anal. 80−52676
^{1}H(n,p), pol. n and p, 220-495 MeV, free elastic scatt., D_t and P parameters 80−52674
^{1}H(n,p), pol. n and p, 220-495 MeV, free elastic scatt., Wolfenstein parameters R_t, A_t 80−52675
^{1}H(n,p)n, pol. n,p, 50 MeV, spin correlation parameter $A_{yy}(\theta)$, phase shift anal. 80−68530
^{2}H+n scattering, 14.4 MeV, parity nonconserving asymm. 78−21449
^{2}H(n, np)n, 17 to 27 MeV, neutron-neutron scattering length determination, Monte Carlo analysis 80−13476
^{2}H(n,2n)p, inelastic scatt. mechanism at moderate energy *(Russian)* 78−41723
^{2}H(n,n), 10 MeV, differential cross section, (p,p) comparison for Coulomb force 79−71793
^{2}H(n,n), 30 MeV, plarisation asymm., analysing power 78−62538
^{2}H(n,n), 794 MeV, extreme back angle scatt. 78−50174
^{2}H(n,n), 8.05 MeV, elastic differential cross-section meas. by recoil technique 78−17207
^{2}H(n,n), (n,p), 24 MeV, quasifree scatt., n-n effective range, Monte Carlo anal. 80−68554
^{2}H(n,n), Amado model, NN exchange cuts in second Born amplitude 77−2790
^{2}H(n,n), backward scattering, 200 to 800 MeV search for bump in 180° excitation function 78−62445
^{2}H(n,n), elastic scatt., perturbation calcs., Faddeev eqns., Reid soft core pot. 78−33177
^{2}H(n,n), ghost states and Pauli principle for many-body scatt. 79−76001
^{2}H(n,n), local soft core NN pots., quasiparticle formalism 79−6529
^{2}H(n,n), nonlocal nonsymmetric pot., treatment of Schrodinger eqn. 78−82325
^{2}H(n,n), polarisation effects in 3-body system 79−80946
^{2}H(n,n), polarised n, anal. power predictions 79−85445
^{2}H(n,n), precise low energy cross section meas. with polyethylene targets 78−82342
^{2}H(n,n), quantum theory evolution law approach appl. *(Russian)* 79−80866

neutron-nucleus scattering continued
^{2}H(n,n), scattering amplitudes, 14.4 MeV Faddeev eqns. variational soln. *(Russian)* 79−85321
^{2}H(n,n), virtual state in three nucleon system, partial wave dispersion relations 79−40920
^{2}H(n,n) 14.2 MeV, polarised n, analysing powers 79−71832
^{2}H(n,n) backward elastic scatt., 350 to 550 MeV, ang. distribs. 79−75782
^{2}H(n,n) backward elastic scatt., 200 to 800 MeV, ang. distribs. and relativistic momentum transfer variable 79−75783
^{2}H(n,n) backward scatt., relativistic effects 77−18519
^{2}H(n,n) scatt. length in $J=1/2^+$ three-N state calc. with super-soft core 77−71570
^{2}H(n,n)^{2}H, 12 MeV, polarised neutrons, analysing power meas. 78−33193
^{2}H(n,n)^{2}H, 14 MeV polarised neutrons, analysing powers 77−54210
^{2}H(n,n)^{2}H, 2.45 MeV, polarised n, depolarisation factor ang. distrib., phase shifts 78−78358
^{2}H(n,n)^{2}H, 2.6 MeV polarised beam, ang. variation of polarisation 77−26733
^{2}H(n,n)^{2}H, 50 MeV polarised neutrons 77−26732
^{2}H(n,n)^{2}H, polarised n, 12 MeV, analysing power, similarity with (p,p) scatt. 78−70514
^{2}H(n,n)^{2}H, polarised neutron scatt. 77−26734
^{2}H(n,n)^{2}H, sum rules linking doublet and quartet phase-shifts with ^{3}H binding *(Russian)* 77−74831
^{2}H(n,n)^{2}H, up to 14 MeV, elastic and inelastic cross sections phase shift anal. 77−22996
^{2}H(n,n)^{2}H analysing power, 14.5 MeV, Hamburg polarised neutron facility initial expts. 77−26946
^{3}H(n,n), scatt. length, 4-nucleon problem, integral eqn. approach 80−91183
^{3}H(n,n), thermal n_1 coherent scatt. length, four body problem relation 79−75997
^{3}H(n,n), zero energy total cross section and scatt. lengths 80−57778
^{3}H(n,n) coherent scatt. length meas. by neutron interferometry 79−59113
^{3}H(n,n) differential cross section, nonrelativistic theory of four nucleon systems *(Russian)* 79−80881
^{3}H(n,n) four-nucleon integral eqn. solns. using effective UPA 79−71794
^{3}H(n,n)^{3}H, four-body model of the four-nucleon system 79−63643
^{3}H(n,n)^{3}H, possible anomaly in backward scatt. cross section near 14 MeV 77−6363
^{3}H(n,n)^{3}H, possible anomaly in backward elastic scatt. cross section near 14 MeV 78−13088
^{3}H(n,n)^{3}H, up to 14 MeV elastic and inelastic cross sections, phase shift anal. 77−22996
^{3}He(n,n), ^{4}He continuum microscopic calcs. cross sections and levels 80−57702
^{3}He(n,n), 1-24 MeV optical model anal. 77−23027
^{3}He(n,n), 2.43, 3.0 MeV, analysing power ang. distrib. 77−30568
^{3}He(n,n), 2.63 MeV polarised neutrons, asymmetry 77−26736
^{3}He(n,n), 3.7-15.3 MeV, polarised n, analysing power, A=4 system neutron channels 79−75965
^{3}He(n,n), 8 to 17.1 MeV, cf. proton polarisation in ^{3}H(p,p) 78−25171
^{3}He(n,n), coherent scatt. length meas. by neutron interferometry 78−13098
^{3}He(n,n), scatt. length, 4-nucleon problem, integral eqn. approach 80−91183
^{3}He(n,n) coherent scatt. length meas. by neutron interferometry 79−59113
^{3}He(n,n) differential cross section, nonrelativistic theory of four nucleon systems *(Russian)* 79−80881
^{3}He(n,n) thermal n_1 coherent scatt. length, four body problem relation 79−75997
^{3}He(p,p)^{3}He, 0.02-2 eV, scatt. lengths *(Russian)* 77−61430
^{4}He, multiple scatt. effects in fast neutron polarisation expts., Monte Carlo anal. 78−13052
^{4}He+n, 20 MeV, phase shift, resonating group method 78−50159
^{4}He+n, below 15 MeV, R-function anal. 77−23028
^{4}He(n,n), 2-5 MeV polarised neutrons, analysing powers, R-function and phase shift anal. 77−23088
^{4}He(n,n)^{4}He, below 21 MeV, R-function and physical-state parameters 77−88105
Hf(n,n′γ), 2.75 MeV, direct excitation of some collective levels 77−26720
Hg(n,n), 2.5 MeV, small angle scatt., cross section, asymm. 78−74361
Hg(n,n) 2.9 MeV, elastic differential cross section and polarisation ang. depend., statistical anal. 79−45264
H(n,n), A=2,3, differential scatt. rate distribs., multigroup rate coeffs. determ. 77−61476
H(n,n) cross section standard, status 77−23040
H(n,n)p, 27.3 MeV, neutron ang. distrib. meas. 78−62532
H(n,p)n, 25.8, 50.9 MeV, differential cross-sections 78−600
Ho+n, neutron spin states amplitudes and scatt. cross sections 77−23019
^{165}Ho(n,n), 1 and 2 MeV, oriented nuclei, deformation effect meas., coupled-channel calc. 77−65218
^{165}Ho(n,n), polarised n and target 0.4-2.5 MeV, total cross section spin-spin effect 79−17899
Ho(n,n), 2.5 MeV, small angle scatt., cross section, asymm. 78−74361
^{127}I(n,n′γ), 3, 14 MeV, 57 and 202 keV γ-ray prod. cross section 79−67706
I(n,n) 2.9 MeV, elastic differential cross section and polarisation ang. depend., statistical anal. 79−45264
In, A=113m, 115m, cross-section of inelastic neutron acceleration 78−17196
^{A}In(n,n′), A=113,115, average activation cross sections in ^{252}Cf spontaneous fission neutron field 79−30830
^{115}In(n,n′), cross section meas. using proton recoil detector with CsI(Tl) scintillator 79−54433
^{115}In(n,n′)^{115m}In, 0.335 to 14.74 MeV, excitation curve 77−23084
^{115}In(n,n′)^{115m}In, threshold to 4.1 MeV, excitation function by activation technique 78−78372
^{115}In(n,n′)^{115m}In integral cross section ratio meas. using $^{235}U(n_{th},f)$ neutron spectrum 77−23130
In(n,n), 2.5 MeV, small angle scatt., cross section, asymm. 78−74361
K(n,n), 14 MeV, differential cross-section meas. 77−88130
^{6}Li, ^{7}Li, two and three body neutron reactions, 14.6 MeV 77−26725
^{6}Li (n,n), 4-7.5 MeV, differential scatt. cross sections meas. 79−26437

neutron-nucleus scattering continued
^{6}Li neutron inelastic scatt. cross-sections and partial widths, calc. 78−78370
^{6}Li-n, R-matrix calc. of total elastic, (n,α) differential cross-sections and polarisation 77−57669
^{6}Li+n, 12 and 20 MeV, resonating group method exam., effective internuclear potential 78−50159
^{6}Li+n, spin depend. capture and scatt. of slow neutrons 78−46059
^{6}Li(n,n), 0.1 to 3.0 MeV, cross-section meas. 77−26740
^{6}Li(n,n), 2-5 MeV polarised neutrons, analysing powers, R-function and phase shift anal. 77−23088
^{6}Li(n,n), 4-7.5 MeV, differential cross section meas. 77−34313
^{6}Li(n,n), 4-8 MeV, differential cross section meas., struct. determ. 77−23016
^{6}Li(n,n), 7 to 14 MeV, differential cross sections of elastic and inelastic scatt. 79−22279
^{6}Li(n,n), 7-15 MeV elast. and inelast. scatt. 77−34314
^{6}Li(n,n), differential scatt. rate distribs., multigroup rate coeffs. determ. 77−61476
^{6}Li(n,n), resonating group calcs. of phase shifts and cross sections 78−50168
^{6}Li(n,n)^{6}Li, meas. review, differential, angle integrated and neutron total cross sections 79−9582
^{6}Li(n,n)^{6}Li, R-matrix anal. of ^{7}Li system 79−9585
^{6}Li(n,n)^{6}Li cross section, exptl. data base for ^{7}Li system 79−9584
^{7}Li (n,n), 4-7.5 MeV, differential scatt. cross sections meas. 79−26437
^{7}Li+n, elast. and inelast. scatt. of 9.1±0.2 MeV neutrons, double differential cross section meas. 79−30838
^{7}Li(n,n′)^{7}Li, triton-alpha disintegration of ^{7}Li 77−38279
^{7}Li(n,n′γ), 0.57-4 MeV, cross-section meas. 77−2985
^{7}Li(n,n′γ)^{7}Li*, threshold to 5 MeV, absolute meas. of cross section 79−67751
^{7}Li(n,n′γ)^{7}Li* (0.478 MeV) cross-section meas. from 0.5 to 5.0 MeV 80−68661
^{7}Li(n,n), 4-7.5 MeV, differential cross section meas. 77−34313
^{7}Li(n,n), 4-8 MeV, differential cross section meas., struct. determ. 77−23016
^{7}Li(n,n), 7 to 14 MeV, differential cross sections of elastic and inelastic scatt. 79−22279
^{7}Li(n,n), 7-15 MeV elast. and inelast. scatt. 77−34314
^{7}Li(n,n) elastic and inelastic, calc. excitation functions and integrated cross sections 78−86534
^Li(n,x), A=6, 7, 14.6 MeV, ang. distribs. and cross sections for ^{6,7}Li, ^{6}He products 80−42650
Li(n,n), 14 MeV, differential cross-section meas. 77−88130
^{55}Mn, neutron resonance spectroscopy, R-matrix anal. 78−21555
^{55}Mn(n,n′γ), 1.0-3.6 MeV, γ-branching meas. 77−79310
^{55}Mn(n,n′γ), 2.2-3.2 MeV energy level J^{π} assignments, transition branching and mixing ratios 79−40881
^{55}Mn(n,n′γ), populations of half integer spin mag. substates 77−30493
^Mo(n,n) A=92,96,98,100, E_n=7 to 26 MeV, determ. optical model pot. parameters 79−22286
^{92}Mo(n,n′), 11 MeV, isospin effects, cf. with direct reaction theory 77−34312
^{92}Mo(n,n′), isospin dependence of expt. nuclear deformations 77−82817
^{92}Mo(n,n), 7-26 MeV, differential cross sections, global optical model anal. 80−18298
^{94}Mo(n,n)^{94}Mo, ang. distribs., 5.1 to 8.0 MeV, comparison with coupled channel and spherical optical model calcs. 77−26716
^{96}Mo(n,n)^{96}Mo, ang. distribs., 5.1 to 8.0 MeV, comparison with coupled channel and spherical optical model calcs. 77−26716
^{100}Mo(n,n′γ), fast n, gamma transitions, level energies and scheme 80−73822
Mo(n,X), 2 keV-20 MeV cross sections, coherent optical and statistical model calcs. 80−18318
Mo(n,n), unified optical model anal., Lane model breakdowns 79−17873
^{14}N, 5.0-9.3 MeV, differential cross sections and neutron ang. distribs. 77−23093
^{15}N(n,n) elast. and inelast. scatt. shell model anal. of threshold effects *(Russian)* 77−287
^{15}N(n,n)^{15}N, reson. struct. in continuum shell model, heavy-ion implications 77−54243
^{15}N(n′,n)^{15}N, continuum random phase approx. 80−27635
Na, neutron flux integral meas., interactive graphic techniques 78−62590
^{23}Na(n,2nγ), (n,n′γ), 14.6 MeV, γ-ray ang. distrib. *(Russian)* 77−88147
^{23}Na(n,n′γ), 0.52-4.23 MeV, cross-sections, ang. distribs., mag. substate populations meas. 78−13100
^{23}Na(n,n′γ), cross-section near threshold 78−8808
^{23}Na(n,n′γ), populations of half integer spin mag. substates 77−30493
^{24}Na(n,n′γ), 14.6 MeV, differential cross sections, statistical model calcs. comparison *(Russian)* 78−78385
Na(n,n), 500 to 3000 keV, high resolution differential cross-section meas. 77−30592
^{93}Nb, (n,n), 14.6 MeV, radiation widths and particle widths of highly excited states, γ-transitions 79−6409
^{93}Nb(n,n′), exciton neutron inelastic scatt. model *(Russian)* 78−33189
^{93}Nb(n,n′)^{93m}Nb, fast neutron flux determ. by ^{93m}Nb disintegration rate meas., X-ray emission *(German)* 77−38579
^{93}Nb(n,n′γ), 1.3-2.7 MeV, energy levels, decay scheme, de-excitation gammas 78−41710
^{93}Nb(n,n′γ), (n,γn′), 14.6 MeV, differential cross sections from nγ coincidence spectra anal. *(Russian)* 78−17209
^{93}Nb(n,n′γ), up to 14.6 MeV, radiation and neutron widths for highly excited levels *(Russian)* 78−605
Nb(n,n′), 14.1 MeV, precompound processes 78−13093
Nb(n,n′), 9.1 MeV, equilib., pre-equilib., direct process anal. *(Russian)* 77−46172
^Nd(n,n) A=142,144,146,148,150, 7 MeV, optical pot. and deformation, cross sections 79−89230
^{146}Nd, 7 MeV elastic and inelastic scatt., diff. cross sections, deformation effects 77−26768
Nd(n,n) elastic and inelastic scatt. on even-A isotopes, 4.08 MeV, deformation effects 77−26715
^Ni, A=58,60,62, elastic and inelastic neutron scatt., 1.5-3 MeV *(Russian)* 77−26689
^Ni(n,n′γ), A=58-64, <4 MeV, gamma prod. and inferred cross sections 80−525
^Ni(n,n), A=58,60,62,64, 5 MeV, differential cross sections, optical, statistical and coupled channel anals. *(Russian)* 80−37377
neutron-nucleus scattering continued
^{58}Ni(n, n), 1.77 to 3.0 MeV, validity of Wick's inequality in the calculation of the lower limits of the differential elastic cross sections 80−5137
^{58}Ni(n,n′γ), 0.5-10 MeV, γ-ray production cross sections 77−26762
^{60}Ni+n, total and differential cross-sections, optical-statistical and coupled-channel models 80−13472
^{60}Ni(n,n′γ), 0.5-10 MeV, γ-ray production cross sections 77−26762
^{64}Ni, elastic and inelastic scatt. of 1.5-3.0 MeV neutrons *(Russian)* 77−61428
Ni(n,n′γ), 3-6 MeV, γ-ray prod. cross sections 77−26767
^{237}Np, neutron resonance params., 8 to 250 eV 77−26709
^{237}Np neutron resonance parameters 8 to 204 eV 79−54436
^{16}O, 5.0-9.3 MeV, differential cross sections and neutron ang. distribs. 77−23093
^{16}O(n,n′γ), 7 to 10.5 MeV, γ-ray prod. cross-section meas. 77−34315
^{16}O(n,n), 2-5 MeV polarised neutrons, analysing power, R-function and phase-shift anal. 77−23088
^{16}O(n,n), elastic cross section, microscopic calc. 80−531
^{16}O(n,n), totally microscopic description, optical pot. and many-body theory 79−546
^{16}O(n,n)^{16}O, complex-generator−corrd. technique in resonating-group calcs. 77−67705
^{17}O(n,n′)^{17}O, imaginary inelastic transition form factor, microscopic theory 78−50175
^{190}Os(n,n′)^{190m}Os, 13-17 MeV, cross section meas. by activation method 78−46057
Pb, 7-14 MeV, absolute cross sections for small-angle elastic scatt. 77−26769
^{204}Pb(n,n′)^{204}Pb, meas. of lead content of metal fragments 79−52850
^{204}Pb(n,n′γ), 1.5-3.1 MeV, levels, J^{π}, excitation functions and mixing ratios 80−102123
^{206}Pb(n,n), 15-18 MeV, total cross section 79−75990
^{206}Pb(n,n), 25-600 keV, ^{207}Pb doorway resonances, M1 ground state radiative strength, level density 79−93589
^{206}Pb(n,n) 25-700 keV, ^{207}Pb parity assignments and M1 radiative strength 80−52614
^{207}Pb+n, 3-485 keV, ^{208}Pb resonance parameters, s-, p- and d-wave entrance channel doorway states 79−470
^{207}Pb(n,n)^{207}Pb, 265 keV, (s+d)-wave mixing 77−46167
^{208}Pb, elastic and inelastic cross sections, 2.5 MeV, comparison with optical model 77−30595
^{208}Pb, fast neutron scatt. and capture, microscopic isovector optical pot. test 80−52682
^{208}Pb(n, n), ^{209}Pb excited states and 3/2^{-} resonances, shell model, calcs. 80−18262
^{208}Pb(n,n′), 26 MeV, isospin effects, cf. with direct reaction theory 77−34312
^{208}Pb(n,n′), excitation of low-lying collective states 78−17205
^{208}Pb(n,n), ^{209}Pb reson. parameters calc., shell model 77−82920
^{208}Pb(n,n), 7-26 MeV, differential cross sections, global optical model anal. 80−18298
^{208}Pb(n,n), (n,n′), 7-26 MeV, optical model anal. 78−37340
Pb(n,n) 0.6-2.2 MeV small angle scatt., differential cross sections ang. depend. 79−85472
Pb(n,n), 10 MeV, neutron polarisation meas. at small angles 77−3014
Pb(n,n), 10.4 MeV, polarised neutrons, analysing power 77−30545
Pb(n,n), 14.0-17.4 MeV, neutron polarisation, ang. depend. diffraction struct. 80−18283
Pb(n,n), 14.2 MeV, polarisation in forward angle scatt. 80−18282
Pb(n,n), 16.1 MeV, polarisation meas., optical model anal. 79−22264
Pb(n,n), 2.9 MeV, elastic differential cross section and polarisation ang. depend., statistical anal. 79−45264
Pb(n,n), A=206,207,208 0.6 to 1.0 MeV, optical model params. 78−21557
Pd(n,n′), near threshold energy for first 2^{+} collective levels excitation, statistical model test 77−61408
^{208}Pn(n,n), ^{209}Pb excited states, 3/2^{-} resonances from shell model 80−78240
polarised neutrons, 2.50 MeV, meas. of small angle scattering (<1°) 80−99432
Pr+n, neutron spin states amplitudes and scatt. cross sections 77−23019
^{141}Pr+n, spherical optical model anal., fast neutron differential elastic scatt. and total cross sections 78−46051
^{241}Pu, evaluation of neutron cross sections in region 10^{-5} eV to 15 MeV 78−17254
^Rb(n,n′γ), 550-2100 keV, A=85,87, levels, excitation functions, J^{π}, Hauser-Feshbach anal. 80−105982
^{103}Rh, elastic and inelastic cross sections up to 1500 keV, γ-ray transitions, 40 keV isomeric state 77−23089
^{103}Rh(n,n′)^{103M}Rh reaction rate, absolute calibration 79−85875
^{103}Rh(n,n(γ)), 0.2-2 MeV, ^{103}Rh level scheme, branching ratios, spins, parities, cross sections 78−78374
Ru(n,n′), near threshold energy for first 2^{+} collective levels excitation, statistical model test 77−61408
^S, A=32,33,34, 0.51 to 51.9 eV neutrons, determ. of neutron scatt. lengths, absorpt. and free cross sections 79−30841
^{32}S (n,n), 0.6 to 3.6 MeV, excitation functions meas., optical model anal. 78−58280
^{32}S, neutron scatt. obs., 1-3 MeV, ang. distrib., optical model anal. 77−50125
^{32}S(n,X), 2.5-1100 keV, resonance struct. from total and capture cross sections 80−42620
^{32}S(n,n′γ), 13.9 MeV, 2^{+} (2.23 MeV) excitation, spin flip probab., deexcitation γ-rays 80−86853
^{32}S(n,n′γ), 14.6 MeV, differential cross sections, statistical model calcs. comparison *(Russian)* 78−78385
^{32}S(n,n′γ) 14.2 MeV, spin-flip probability from 2.23 MeV state 77−14123
^{32}S(n,n), 14.2 MeV, elastic, inelastic, backscatt. meas., optical model test 78−58275
^{32}S(n,n), 2-3 MeV neutrons, cross section meas. using associated particle TOF spectrometer 79−45255
^{32}S(n,n), 2-3 MeV neutrons studied using assoc. particle TOF spectrometer 80−13468
^{32}S(n,n), 21.5 MeV, optical model and coupled channel calcs. 77−26714
^{32}S(n,n), 25-1100 keV, total cross section, multilevel anal., strength functions, optical parameters 80−78298
^{32}S(n,n), 5 MeV, elastic and inelastic scatt., differential cross-sections, model anal. *(Russian)* 80−42668
^{32}S(n,n), spin-flip probability to first 2^{+} level 80−78288

neutron-nucleus scattering continued
^{32}S(n,n) and ^{32}S(n,n′) 21.5 MeV reaction, differential cross-sections, deform. parameters 77−57658
Sb(n,n′γ), 1.5-2.7 MeV, ^{A}Sb, A=121,123, levels below 2 MeV, spins, transitions and mixing ratio 80−32191
^{45}Sc+n, 0.005 to 22 keV, total neutron cross section for beam filter design 78−78371
Se enriched even isotopes, diffr. cross sections for elastic and inelastic scatt., symmetry effects 77−26757
^{A}Se(n,n), A=76-78, 80, 82, slow n coherent scatt. length, free cross section, bound states 80−86909
Se(n,n)Se, A=76, 78, 80, 82, 6-10 MeV, isospin and strong coupling effects 77−6383
Se(n,n′) 2^{+} level excitation cross sections, intermediate resonances, optical model with coupled channels *(Russian)* 79−40897
Se(n,n′γ), 2.0 to 4.1 MeV, even A=76-82 isotopes level struct. 77−34233
Se(n,n′γ), even-A isotopes, 2.0 to 4.1 MeV, level and decay schemes 77−23092
^{A}Si, A=28,29,30, 0.51 to 5.19 eV neutrons, determ. of neutron scatt. lengths, absorpt. and free cross sections 79−30841
^{28}Si+n, isobaric analogue resonances from total and differential elastic cross sections 78−41715
^{28}Si(n,n′γ), 1.96-4.15 MeV, prod. cross section for 1780 keV transition 79−59058
^{28}Si(n,n), 0.6 to 3.6 MeV, excitation functions meas., optical model anal. 78−58280
^{28}Si(n,n), 14.1 MeV, elastic and inelastic scatt., wide angular range, spin orbit interaction 78−89867
^{28}Si(n,n), 5 MeV, elastic and inelastic scatt., differential cross-sections, model anal. *(Russian)* 80−42668
^{28}Si(n,n), core-parricle doorway states calc. 77−23003
^{28}Si(n,n), spin-flip probability to first 2^{+} level 80−78288
^{28}Si(n,n), to 4.5 MeV, s- and p- wave reson. struct., R-matrix interpretation 77−23002
Si(n,n), 20, 26 MeV, Coulomb correction term to optical model pot. 77−38280
Si(n,n), 500 to 3000 keV high resolution differential cross-section meas. 77−30592
Si(n,n)Si, 11-26 MeV, optical model fit 77−79372
Sm isotopes, deform. effects in neutron scatt. 77−74758
^{A}Sm, A=148, 150, 152, 154, 7 MeV elastic and inelastic scatt., diff. cross sections, deformation effects 77−26768
^{A}Sm(N,N′) A=152,154, deformed nuclei struct., rot. model with optical pot., coupled channel formalism 79−3146
^{152}Sm (n,n), 2.4-7.2 MeV, inelastic and elastic optical model and deformation parameter depend. *(Russian)* 80−13481
^{152}Sm(n,n′γ), 1.0-2.75 MeV, statistical model deviations *(Russian)* 77−26690
^{152}Sm(n,n′γ), 2.5 MeV, direct excitation of rotational levels 77−30594
^{152}Sm(n,n′γ), 2.75 MeV, direct excitation of some collective levels 77−26720
^{152}Sm(n,n′γ) spectra and ang. distribs. anomalous excitation *(Russian)* 77−54224
^{152}Sm(n,n′γ), 2.5 MeV, rot. level direct excit. 77−14127
Sm(n,N′), 7 MeV, A=148,150,152,154, differential cross sections, coupled channel anal., deform. effects 77−54219
Sm(n,n), (n,n′), (n,n′γ), A+148,150,2, E=2.47 MeV collective excitations obs. 78−33187
Sm(n,n) elastic and inelastic scatt. on even-A isotopes, 4.08 MeV, deformation effects 77−26715
S(n,n), 14.8 MeV, differential cross section absolute meas. by surface of revolution technique 77−23394
S(n,n) 20, 26 MeV, Coulomb correction term to optical model pot. 77−38280
S(n,n)S, 11-26 MeV, optical model fit 77−79372
Sn, neutron cross section, filtered neutron beam technique, Doppler effect 80−52670
^{A}Sn(n,n′), A=116, 118, 120, 122, 124, 11 MeV, levels, deformation parameters, isospin effects, optical parameters 80−57679
^{A}Sn(n,n′), A=116, 118, 120, 122, 11 MeV, octupole vibr. states, diff. cross section, deformation length, DWBA anal. 80−102092
^{A}Sn(n,n′γ), even A=116-124, $2_2^{+}\rightarrow 2_1^{+}$ transitions, pairing interaction effect *(Russian)* 79−3114
^{A}Sn(n,n), 11-26 MeV, A=116, 118, 120, 122, 124, differential and total cross sections, optical pots. 80−78293
^{A}Sn(n,n), A=116,118,120,122,124, isovector deformation parameters and core polarization 79−67642
^{A}Sn(n,n) A=116, 124, 11, 24 KeV, differential cross sections, global optical model anal. 80−18298
^{112}Sn, determ. of multipole mixture values in $2_2^{+}\rightarrow 2_1^{+}$ transitions *(Russian)* 79−89268
^{114}Sn, determ. of multipole mixture values in $2_2^{+}\rightarrow 2_1^{+}$ transitions *(Russian)* 79−89268
^{124}Sn(n,n), pol. thermal, parity violation near resonance, DWBA calcs. 80−68528
^{124}Sn(p,p), threshold enhancement of parity violation, Born approx. 80−18191
Sn(n,n′) (A=118,120,122,124), isospin dependence of expt. nuclear deformations 77−82817
^{88}Sr(n,n′), 11 MeV, octupole vibr. states, diff. cross section, deformation length, DWBA anal. 80−102092
^{88}Sr(n,n), elastic and inelastic, 11 MeV, isospin effects, optical and deformation parameters 79−17794
^{181}Ta(n,n′)^{181}Ta, 9.1 MeV, CC neutron spectra and angular distrib. meas. *(Russian)* 78−25198
Ta(n,X), slow and ultracold total and inelastic cross sections 80−68673
Tb+n, neutron spin states amplitudes and scatt. cross sections 77−23019
^{159}Tb polarised target, transmission of polarised resonance neutrons, 20 eV to 100 keV, spins *(Russian)* 77−50138
^{159}Tb, transmission of polarised resonance neutrons through polarised target, 20-100 keV 77−26657
Te(n,n′), A=124-130, scattering cross sections and optical model 78−4944
Te(n,n′γ), A=124-130, gamma-ray ang. distribs. 77−34316
^{232}Th level structure and decay parameters from (n,n′) and (n,n′γ) meas. 77−30494
^{232}Th, neutron cross section meas. 80−526
^{232}Th, neutron elastic and inelastic cross sections, 2.5 MeV, comparison with optical model 77−30595

neutron-nucleus scattering continued
^{232}Th(n, N′), cross sections calc. optical model calcs. 79−30829
^{233}Th(N,N′), deformed nuclei struct., rot. model with optical pot., coupled channel formalism 79−3146
^{48}Ti, elastic and inelastic differential scatt. cross sections, 1.5-3.0 MeV *(Russian)* 77−26688
Ti(n,n), 1-4.5 MeV, elastic inelastic, total cross sections, optical-statistical, coupled-channels models 79−539
Tm+n, neutron spin states amplitudes and scatt. cross sections 77−23019
Tm(n,n′) 1.8 meV to 1.8 eV, total neutron cross-section meas. using TOF spectrometry 79−85466
U, 7-14 MeV, absolute cross sections for small-angle elastic scatt. 77−26769
^{236}U(n,n), 30-1800 eV, cross section meas. 77−23061
^{238}U, 0.9-2.7 MeV, elastic and inelastic diff. cross sections for scatt. from ground, 45, 148 keV states 77−26770
^{238}U (n,n), 0.9-3.1 MeV, elastic and inelastic cross-sections meas. 79−26435
^{238}U, elastic and inelastic ang. distribs., 1.1 and 3.1 MeV, to ground state rot. band 77−26717
^{238}U, elastic and inelastic cross section meas., 100 to 150 keV 77−26718
^{238}U, neutron cross section integral meas., interactive graphic techniques 78−29457
^{238}U, neutron elastic and inelastic cross sections, 2.5 MeV, comparison with optical model 77−30595
^{238}U, neutron resonance params. and cross sections, 9 eV to 4 keV 77−26710
^{238}U, neutron transmission, resonance meas. and anal. 79−26436
^{238}U+n, 2.47 MeV, energy spectra and ang. distrib. of neutrons 79−40927
^{238}U(N,N′), deformed nuclei struct., rot. model with optical pot., coupled channel formalism 79−3146
^{238}U(n,n′), 0.3 to 3.0 MeV, ground state rot. band excitation 77−23085
^{238}U(n,n′), 0.9 to 3.1 MeV ang. distribs. and cross sections 79−9576
^{238}U(n,n′), cross section param. from optical model anal. 78−21557
^{238}U(n,n′γ), 1.06 MeV, cross sections and γ spectra for various energy levels *(Russian)* 79−40883
^{238}U(n,n′γ) cross section estimates 77−57675
^{238}U(n,n′γ) technique for study of levels near 1 MeV 77−26719
^{238}U(n,n), 0.6-2.2 MeV small angle scatt., differential cross sections ang. depend. 79−85472
^{238}U(n,n), elastic and inelastic scatt. cross sections at 144 keV 78−21554
^{238}U(n,n), sensitivities of secondary neutron energies to fusion blanket neutronics 77−23295
^{238}U(n,n)^{238}U, differential elastic and inelastic cross sections at 144 keV 78−4945
U(n,n), 2.5 MeV, small angle scatt., cross section, asymm. 78−74361
V, fast-neutron total cross-sections, 1.0-5.5 MeV 77−82923
^{51}V, neutron resonance spectroscopy, R-matrix anal. 78−21555
^{51}V(n,n′)^{51}V, 14.1 MeV, pre-equilib. and evaporation model anal. 77−6366
^{184}W (n,n′γ), fast n, level struct. and populations, γ-transitions 79−75841
^{186}W(n,n′γ), fast n, level struct. and populations, γ-transitions 79−75842
W(n,n′γ), 2.75 MeV, direct excitation of some collective levels 77−26720
^{89}Y, high resolution neutron total cross section meas., 27-240 keV 78−25193
^{89}Y(n,n′), calc. of fluctuation compound nucleus cross sections 77−23029
Y(n,n′), 9.1 MeV, equilib., pre-equilib., direct process anal. *(Russian)* 77−46172
Zn even isotopes, fast neutron elastic and inelastic scatt. cross sections *(Russian)* 77−74853
^{A}Zr(n,n′γ) 2.2-3.7 MeV, A=92, 94, level and decay scheme, J^{π} assignments 79−17850
^{A}Zr(n,n′γ), A=92, 94, 3-6 MeV, γ-ray prod. cross sections 77−26767
^{90}Zr, neutron reson. parameters below 300 keV 78−8805
^{90}Zr(n,n′), 11 MeV, isospin effects, cf. with direct reaction theory 77−34312
^{90}Zr(n,n′), 11 MeV, octupole vibr. states, diff. cross section, deformation length, DWBA anal. 80−102092
^{90}Zr(n,n′), isospin dependence of expt. nuclear deformations 77−82817
^{90}Zr(n,n), 11 MeV, differential cross sections, global optical model anal. 80−18298
^{91}Zr, high resolution neutron transmission and capture 78−8806

neutron polarisation
absolute polarisation in elastic scatt. from light nuclei 77−23088
coherent scattering with parity-violating pots., weak interaction probe 77−71599
cold neutron beam polarising supercond. hexapole magnet 79−31300
crystal, magnetically-ordered, polarisation of incident neutron 79−7524
depolarisation meas., exptl. set up and process program 80−18771
eikonal description of nucleon-nucleon elastic polarisation data 77−13948
electric and magnetic dipole moments 80−4993
electric polarisability, expt. determ. and degree of precision, review 79−58961
EM polarisabilities from γN scatt., $\pi^{0}\rightarrow 2\gamma$, $\eta^{0}\rightarrow 2\gamma$ decay rates 77−18289
fast neutron beam sources, status report 77−23343
ferromagnetic domain structures, neutron depolarisation studies 80−25155
filter, cryogenic, construction 77−23341
free neutron lifetime measurement using wall and mag. traps of ultracold neutrons 78−5107
Hamburg polarised neutron facility, initial expts. 77−26946
HF magnetic chopper for polarised neutrons 77−14293
interferometry, determ. of scatt. lengths and magnetic spin rotations 77−24248
Larmor precession, spin echo, memory effects and polarized neutrons, pulsed source efficiency improvements 79−45323
lepton-nucleon isobar prod. by neutral current, polarisation effects 77−18220
magnetic scattering of neutrons on excited atoms or mols., cross sections, neutron polarisation *(Russian)* 78−55249
magnetic texture meas. with polarised neutrons 79−95577
matter current density and R parameter meas. 77−30544
measurements and facilities for reactions between light nuclei 77−18764

neutron polarisation continued
monochromatic thermal neutron polarisation crossed mag. field method 80−78477
monochromatisation by spatial spin reson. technique *(Russian)* 77−79497
monochromator with Fe/Ge multilayers 77−19841
monoenergetic polarised neutron beam from 200-500 MeV prod. at TRIUMF 77−83413
multilayer monochromator-polariser *(Russian)* 80−27854
multiple reflection effects on polarisation of nonmonochromatic beams *(Russian)* 78−41883
multiple scatt. effects in fast neutron polarisation expts., Monte Carlo anal. 78−13052
neutron stars, spin alignment, spin-torsion forces and strong-gravity interactions 80−56870
nonhomogeneous magnetic field, semiclassical solns. of Pauli equation *(Russian)* 79−22365
nuclear and neutron polarisation expts., spin depend. of neutron cross-sections, mag. moments, radiation capture of neutrons *(Russian)* 80−52654
nuclear struct. expts., review 77−26700
optical activity in helicoidal antiferromagnetic materials 78−74419
polarimeter, 3-D, critical spin dynamics in ferromagnets meas. 79−18098
polarimeter, 3-D calibration procedure 80−18770
polarimeter for threshold photoneutron spectroscopy 77−30739
polarisation meas. with high press. He scintillation counter, Monte Carlo convections 80−14061
polarised neutron diffraction, determ. of magnetic form factors, pioneering work 80−24321
polarised neutrons in condensed matter [conference, Zaborow, Poland (Sept. 1979)] 80−22136
polarised powerful neutron beam, in vertical reactor channel 78−5082
polariser, perfect crystal, appl. of mag. prism refraction 79−50950
polariser, supermirror, exptl. evidence 77−39514
polariser-analyser efficiency meas. by spin flip meas. 80−27911
production and appls. of polarised neutron beams, book contrib. 79−58843
production of polarised beam using ferromag. doubly bent neutron guide *(Russian)* 77−46446
recent advances in neutron physics, prod., handling, detection, nuclear reactions, resonances 77−26686
scattering amplitude, spin depend. meas. using polarised neutrons 79−45601
scattering of polarised neutrons, appl. 79−46516
secondary neutron polarization via penetration through a ferromagnetic shielding wall 80−47742
slow neutron polarisation by polarised proton filter using ethylene glycol 78−90046
slow neutrons, using polarised proton filter 79−63238
spectrometer, separation of coherent and spin incoherent scatt. from D_2O 77−6655
spin rotation and phase shift in neutron interferometry, polarisation props. 77−18763
Stern-Gerlach polarimeter for measuring polarisation of cold neutron beams 80−37679
subthermal neutrons, polarisation meas. by shim and spin reversal methods 77−88363
thermal neutron polarisation anal. experiments, corrections for instrument component inefficiencies and sample multiple scatt. 78−29725
thermal neutrons, spin-flipping methods for polarised beams 78−25370
TRIUMF neutron beam, monoenergetic polarised, 200 to 500 MeV 79−13573
tuneable polarisers for neutrons 80−315
ultracold neutron polarisation 78−29681
ultracold neutron storage in magnetic traps 77−23344
ultracold neutrons, polarisation and diffr. through monocryst. Fe foils 79−45324
β-decay, polarisation effects in intense EM field *(Russian)* 79−22243
$\gamma n \rightarrow \pi^- p$, 700 MeV, polarised neutrons, target asymmetry meas. 77−13967
n-p analysing power, polarised neutrons in $^3H(d,n)^4He$ reaction 78−62544
n-p spin-correlation parameter at 50 MeV 77−49993
NN scatt. formalism 78−21463
NN spin-polarisation meas. 78−74272
$np \rightarrow pn$, charge exchange models, polarisation 77−30444
np scatt., analysing power meas. at 14 MeV, multiple scattering effects 77−10572
np scatt. at 1.03 GeV 78−82245
pn, elastic, inelastic, inclusive reactions, polarisation studies with effective mass spectrometer 77−30412
$^{11}B(p,n)^{11}C$, analogue reaction at 16.3 to 26.5 MeV, polarisation transfer meas. 77−26735
$^9Be(\alpha, n)_0$ 100 MeV, neutron polarisation meas. 78−70726
$^9Be(d,n)^{10}B$, polarised 4.5 MeV neutron source 77−57790
$^{40}Ca(\mu,n\nu_\mu)$, neutron longitudinal polarisation anal. 77−30559
$Fe_{2.45}Mn_{0.05}Si$, slow neutron polariser, by single cryst. (111) refl. 80−49052
$^1H(n,p)n$, 50 MeV, polarisation parameter meas. 78−50148
$^2H(\alpha, n)_0$, 100 MeV, neutron polarisation meas. 78−70726
$^2H(d,n)^3He$, 35-275 keV, neutron polarisation determ. 77−41942
$^2H(p, n)_0$, 50 MeV, neutron polarisation meas. 78−70726
$^3H(d,n)^4He$, 700 keV, n polarisation meas., scintillation + TOF technique 78−86538
$^3H(p,n)^3He$, coupled channels anal. of neutron polarisation 77−18560
$^3He(d,n)^4He$, 14 MeV polarised neutron facility 79−85851
$^3He(n,n)$, 8 to 17.1 MeV, cf. proton polarisation in $^3H(p,p)$ 78−25171
$^4He(d, n)_0$, 50 MeV, neutron polarisation meas. 78−70726
$^4He(t,n)$, R-matrix anal. of polarisation effects in ^7Li system 77−2968
$^{165}Ho+n$, polarised projectile and target, spin depend. of total cross section *(Russian)* 78−17211
$Li_{0.5}Fe_{2.5}O_4$, slow neutron polariser, by single cryst. (222) refl. 80−49052
^6Li+n, polarised slow neutrons, spin depend. capture and scatt. 78−46059
$^7Li(p, n)_0$, 50 MeV, neutron polarisation meas. 78−70726
$^{55}Mn(p,n)^{55}Fe$, neutron polarisation at isobaric analogue resonances 78−54759
Ni single crystal near T_c, neutron transmission depolarisation 79−33479
$^{208}Pb(\gamma,n_0)$, 170-320 keV, search for collective M1 resonance 77−46103
neutron polarisation continued
$^{208}Pb(\gamma,n)$, polarimeter for threshold photoneutron spectroscopy 77−30739
$^{208}Pb(\gamma,n)$, s-d wave admixture in $^{207}Pb+n$ system 77−30555
$Pd_{2-x}MnSb$, struct., appl. as improved neutron polariser 80−60199
$^{51}V(p,n)^{51}Cr$, neutron polarisation at isobaric analogue resonances 78−54759

neutron production
1-MJ plasma focus expt., neutron yield, current distrib., scaling law 77−74991
actinide muonic atoms, n emission from radiationless muonic transitions and μ capture 79−3599
cold, and ultracold neutrons, production by a moving cryst. lattice 80−79640
cyclotron, small, applications *(Hungarian)* 78−70656
electron linear accelerators appl., bremsstrahlung and (γ,n) processes *(Japanese)* 78−78532
fission, method for predicting $\bar{\nu}(Z,A,E_n)$ 77−26792
fission and neutron evaporation widths, statistical formula correction *(Russian)* 79−13281
focus, current sheath struct. diagnostics, fast particle beams, deuterated polyethylene fusion 77−76206
fusion neutron generation using explosive implosion of polyethylene shell in D_2-filled cone 78−82510
fusion reactor scheme, relativistic electron beam energy deposition, solid target 78−5894
laser fusion DT target, conical, for implosion studies with CO_2 laser 79−41849
linear acceleration reactors, anal. of neutron yield produced by high-energy protons 80−22895
Maxwellian D ion plasma, ion temp. diagnostics appls. 80−49005
neutral beam source of neutrons for shielding design criteria for fusion program 80−99387
nuclear neutron producing reaction kinematics 80−86862
photoneutron production in neutron detectors in high energy X-ray beams 78−94174
photoneutron yield from electron-irradiated thick targets in giant-resonance region, calc. of photon track length 80−82983
plasma, dense focus, neutron production 77−74989
plasma, in Alcator Tokamak high-density discharge, parameters for D_2, neutron emission 78−18438
plasma focus, low-energy, neutron yield props., filling press. depend. 77−74992
plasma focus, Mather type, neutron emission 79−19084
plasma focus, mechanisms for neutron production 79−90435
plasma focus, neutron and X-ray sources space-time struct., scintillator diagnostics 77−74993
plasma focus, nonthermal processes, neutron spectra 78−42804
plasma focus device, neutron emission meas. 79−90475
plasma focus device dynamics, 120 and 20 kV, neutron and X-ray emission diagnostics 77−74990
recent advances in neutron physics, prod., handling, detection, nuclear reactions, resonances 77−26686
red giants, ^{14}C and neutrons prod. during He shell flashes 77−26005
single neutron emission induced by stopped π^- in 1p shell nuclei 79−59089
stellar gravitational collapse, neutronisation and lepton escape rel. to hydrodynamics 80−77388
thermonuclear neutron production of action of laser on conical target *(Russian)* 78−13320
Tokamak, nonaxisymmetric, reduced fusion neutron production 78−63577
Tokamak, PLT, photo-neutron prod. 77−30668
total cross section meas., secondary standard, BF_3 counters in polyethylene sphere 77−23381
ultra-cold neutrons, review of prod., transport and appl. 79−40982
ultracold neutrons, extraction, transportation and storage 77−26826
ultracold neutrons, review of Soviet expt. research on prod. and storage 79−97923
(α,n), mixture and compound neutron yield from separate component thick target yields 80−37414
d-d neutral beam facility neutron yield meas., shielding and diagnostics 79−9878
DD reaction for neutron generation in thermonuclear reaction initiation *(Russian)* 80−42848
ed, 2.3 GeV, inclusive electroprod. cross sections for final state nucleons 77−34159
$e^{\pm}d \rightarrow e^{\pm}np$, polarised, parity violating asymmetry 80−78080
e^+e^- annihilation, 4 and 7 GeV, $\bar{n}$ and $\bar{\Sigma}^+$ prod., cross sections 79−63494
$e^+e^- \rightarrow n\pi$, jet struct., lightlike (zero mass) quarks anal. 79−63496
(γ,n), 45-160 MeV, cross sections in quasi-deuteron model for direct reactions 80−63170
(γ,n), neutron focus in radiation field of relativistic channelled particles 79−85852
$\gamma d \rightarrow np$, 300 MeV, dibaryon resonance manifestation, pseudoindependent amplitude elimination *(Russian)* 80−57612
$\gamma d \rightarrow pn$, 250 to 800 MeV, differential cross-section and proton polarisation, theoretical models 80−78081
$\gamma d \rightarrow pn$, proton polarisation energy depend., 400-700 MeV *(Russian)* 80−63000
$\gamma p \rightarrow n\pi^+$ section asymmetry, pion-proton twin birth contribution *(Russian)* 80−47308
K^-p, neutral channel cross section meas., 1470 to 1560 MeV CM energy 78−82237
pd, 350-1000 MeV, neutron prod. double differential cross section in meson generation reactions *(Russian)* 80−42490
pp, 350-1000 MeV, neutron prod. double differential cross section in meson generation reactions *(Russian)* 80−42490
$pp \rightarrow nX$, baryonium exchange, triple-Regge couplings 80−86763
$pp \rightarrow nX$ or ΛX_t, 12, 24 GeV/c, n/Λ ratio, cross sections 78−58213
$\bar{p}p \rightarrow \bar{p}p\pi^0(\bar{p}n\pi^+)(\bar{n}p\pi^-)$, 8.8 GeV/c, one pion prod. cross sections, Deck model anal. 80−105919
$\pi^-d \rightarrow nn$, mechanism, cross-sections, EM form factors 79−89181
$\pi^-d \rightarrow \pi^-pn$ final state interactions and d breakup for 438 MeV/c π^- impulse *(Russian)* 80−18145
π^-N, in C, 5 GeV/c, π^0 and n inclusive spectra, cascade model *(Russian)* 80−68490
π^-p and π^-Ne inclusive reactions, 200 GeV, n and $\bar{n}$ prod. 77−18349
$\pi^-p \rightarrow \eta n$, 15 to 40 GeV/c, study of $\eta \rightarrow 2\gamma$ 79−58978

neutron production continued
$\pi^-p \rightarrow \pi^0 n$ reaction for large transmitted momenta, 40 GeV/sec *(Russian)* 78−12934
$^{241}Am(\alpha,n)$, neutron yield in AmO_2 79−17912
$^{197}Au+^{132}Xe$, 7.5 MeV/amu ions, neutron multiplicities as func. of total energy loss 78−21606
$^{197}Au(^{63}Cu,X)$, 400 MeV, neutron multiplicity in deep inelastic collisions 80−18324
$^{197}Au(n,n')^{197}Au$, pre-equilib. and evaporation model anal. 77−6366
$Be+p(\bar{p})(K^-)(\pi^-)$, 200 GeV/c, forward inclusive prod. spectra, of K_s, Λ^0, $\bar{\Lambda}^0$, n 78−82393
$^9Be(d,n)^{10}B$ use of neutrons for meas. of full cross sections *(Russian)* 80−69008
^{209}Bi (n, xnf), fission high energy neutrons *(Russian)* 80−106091
$^{209}Bi(n,2n)$, 14.1 MeV, pre-equilib. contributions, neutron yields and energy spectra, statistical model calcs. 77−50126
^ACf, A=250, 252, 254, spontaneous fission fragment kinetic energy and neutron multiplicity meas. 80−42717
^{242}Cm, spontaneous fission, prompt neutron multiplicity distrib. meas. 80−83131
$C(\pi^-,X)$, 3 GeV/c, n inclusive spectra, neutron yield *(Russian)* 80−13510
$Cu(\pi^-,X)$, 3 GeV/c, n inclusive spectra, neutron yield *(Russian)* 80−13510
D plasma neutron generation by CO_2 laser implosion of polyethylene shell into conical region 78−87468
D, shell target compression on laser heating *(Russian)* 80−47718
D_2 gas target implosion 78−54869
D_2 plasma, compression by microfusion explosion, expt. biconical system 80−13783
$^{166}Er(^{86}Kr,X)$, 5.1-7.9 MeV/N, deep inelastic neutron emission, pre-equilibrium effects search 80−63200
^{257}Fm, spontaneous fission fragment kinetic energy and neutron multiplicity meas. 80−42717
$^2H(d,n)^3He$, 6 to 17 MeV, n prod. absolute differential cross sections 78−74373
$^2H(\pi^-,n)n$, mechanism, cross-sections, EM form factors 79−89181
$^3H(d,n)^4He$, 6 to 17 MeV, n prod. absolute differential cross sections 78−74373
$^3H(p,n)^3He$, 6 to 17 MeV, n prod. absolute differential cross sections 78−74373
$^4He+\pi^-$, capture at rest, neutron energy spectrum determ. 79−6702
$^6Li(d,n)^7Be$, 0.2-0.9 MeV, differential and total cross sections for neutrons 77−23096
$^{150}Nd(\alpha,n)^{153}Sm$, 14 to 22 MeV, theoretical and expt. study of ^{153}Sm 79−58999
$^{16}O(\gamma,n_0)$, 21.6-25.7 MeV, ground state photoneutron polarisation ang. distrib. 80−57765
(p,n) for A between 27 and 238, 800 MeV, n prod. systematics, π associated cross section 79−3153
$Pb(\pi^-,X)$, 3 GeV/c, n inclusive spectra, neutron yield *(Russian)* 80−13510
Ta(p, xn), 23 MeV, n energy distribs. *(Russian)* 78−86537
Ti-T target system for production of 14 MeV neutrons, improvements 80−63433
U(Ne,n)X, 337 MeV/N inclusive double differential neutron prod. cross sections 80−32294
UO_2, burnup determ. in PWR and BWR using NDA of neutron emission rates 80−83148
$^{233}U(n,f)$, thermal polarised neutrons, neutron emission P-odd asymmetry *(Russian)* 80−78338
$^{235}U(n_{th},f)$, fragment-mass depend. of fission neutron spectrum, TOF method 78−82398
$^{235}U(n_{th},f)$, neutrons ang. correl., multiplicity 79−3187
$^{238}U(p,f)$ 12 MeV, estimation of neutron yield from individual fragment in medium-excitation fission 80−542
$U(\pi^-,X)$, 3 GeV/c, n inclusive spectra, neutron yield *(Russian)* 80−13510
$^{51}V(n,n')^{51}V$, 14.1 MeV, pre-equilib. and evaporation model anal. 77−6366
W-D_2O with 10 MeV electron beams 80−83231
Z-pinch, noncylindrical, dynamics and particle accel. mechanism 77−76170

neutron-proton interactions
see also neutron-proton scattering
2n-2p system of mirror nuclei, charge exchange part, linear binding energy relation 77−22901
bremsstrahlung, effects of nonminimal currents and role of various couplings 78−70394
charge exchange cross sections, Regge pole and cut behaviour of Fermilab. energies 78−441
charge exchange reactions, 150 to 800 MeV, reaction cross sections 79−67572
charge exchange scatt., ang. distribs., 300 to 800 MeV 78−62434
charge exchange scatt., proton spectra, π prod. 78−62669
charged-particle multiplicity distribs. at 400 GeV/c 80−13337
correlations between potentials and observables in the NN interaction 79−67577
D-transfer effect on phase shift anal. near 325 MeV 78−82294
diffractive dissociation of 200 GeV/c protons, 4 and 5 particle final states *(Russian)* 77−34188
diffractive dissociation of neutrons, pn reactions at 37 GeV 77−2873
effective target mass distribution in relativistic proton-nucleon inelastic interactions 78−66162
elastic charge exchange, 200 to 600 MeV, differential cross section meas. 79−67571
EM effects in precision anal. of low-energy np interaction data 78−93896
EM phase shift calc. within relativistic model, isospin non-conservation 78−62438
exclusive double diffraction dissociation at CERN ISR 79−9412
heavy long lived particles, 4 to 10 GeV/c, search 78−78380
inclusive, nucleon charge exchange, reggeized one pion exchange model *(Russian)* 77−2888
inelastic Δ and N* production, polarisation studies with effective mass spectrometer 77−30412
inelastic charge exchange, quark interchange 80−86759
lepton direct prod. in pN via hypothetical hadron and heavy lepton prod. *(Russian)* 77−46074

neutron-proton interactions continued
Lorentz-invariant method, 24 and 70 GeV/c interactions, including pionisation 79−80848
multiparticle final states at 195 GeV/c, charge struct. and correlation features 78−58208
muon pair prod. and new parton radiative processes 79−17766
$n+p \rightarrow p+n$, charge exchange, energy depend., possible explanation, Regge exchange 78−21465
nuclear emulsion, pp and pn inelastic interactions, 69 GeV/c 78−66161
nucleon, diffractive 19.2 GeV/c excit., 2- and 3-particle decays *(Russian)* 78−473
parton-parton interaction in high transverse momentum collisions, phenomenological description 77−57574
pion prod. at 800 MeV, model tests 77−18316
quark parton model, total cross sections 78−45859
semi-inclusive and exclusive, 19.2 GeV/c, cross sections, spectra *(Russian)* 77−6179
statistical bootstrap model anal. of $\bar{N}N$ annihilations 78−37224
total cross sections, 20 to 140 MeV 77−22761
K prod. in nN interactions, effect on μ charge ratio 77−18363
$n+p \rightarrow (p\pi^-)+p$, 35-65 GeV/c, diffr. dissoc. 77−13988
$\bar{n}p$, 1.44 GeV, comparison with empirical model 78−25060
$np \rightarrow (p\pi^-)p$ diffraction dissociation, Deck model with absorption 77−26548
$np \rightarrow (p\pi^-)p$ diffractive dissociation, struct. in momentum transfer 77−13992
$\bar{n}p$ annihilations, 0.5-0.8 Gev/c, multiprong reactions anal. 78−66141
np bremsstrahlung, struct. depend. of interaction current 79−63510
np capture, total cross section between 38 and 73 MeV 79−67581
$np \rightarrow d2\gamma$, theoretical prediction of cross section 79−58961
$np \rightarrow d(\pi\pi)^0$, 800 MeV, d momentum spectrum meas., two nucleon exchange model 78−70384
$np \rightarrow d(\pi\pi)^0$, threshold to 3 GeV/c, effective Hamiltonian for ABC effect 77−65168
$np \rightarrow d(\pi\pi)^\circ$, ABC effect, effective Hamiltonian formalism 78−17042
$np \rightarrow d\gamma$, d relativistic effect on photon circular polarisation 78−93900
$np \rightarrow d\gamma$, γ-polarisation, NN weak pot. in simple gauge model 78−54644
$np \rightarrow d\gamma$, parity nonconservation effects due to $\rho^- \rightarrow \pi^-\gamma$, short dist. contrib. to γ circular polarisation 77−41855
$np \rightarrow d\gamma$, parity-nonconserving nucl. force 77−10333
$np \rightarrow d\gamma$, photon circular polarisation, d P-state, Dirac spinor 78−70390
$np \rightarrow d\gamma$, photon polarisation and weak EM transition $\rho^\pm \rightarrow \pi^\pm\gamma$ 77−22758
$np \rightarrow d\gamma$, sum rules for weak NNπ amplitudes and theoretical descriptions of nonleptonic hyperon decays 79−17663
$np \rightarrow d\gamma$ process, weak interaction between nucleons *(Russian)* 79−63513
$np \rightarrow d\gamma$ radiative capture, relativistic effects, parity violation, Weinberg-Salam model *(Russian)* 80−32120
$np \rightarrow d\pi^0$, 350-550 MeV, d ang. distrib. 79−75784
$np \rightarrow d\pi^0$, 795 MeV, test of isospin invariance 79−75786
$np \rightarrow d\pi^0$, charge asymmetry effects of nuclear forces 77−10332
$np \rightarrow d\pi^0$, nuclear forces charge symmetry test 80−5071
$np \rightarrow d\pi^+\pi^-$, 1.73 GeV, $\pi^+\pi^-$ effective mass spectrum anomaly *(Russian)* 79−67570
$np \rightarrow d\pi^+\pi^-$, 1.73GeV/c effective mass spectrum ($\pi^+\pi^-$), narrow enhancements 80−86741
$np \rightarrow \gamma d$, gamma polarisation due to weak parity violating effects 77−41851
$np \rightarrow \gamma d$, photon circ. polarisation calc. using relativistic d wave function 79−67582
$np \rightarrow nn\pi^+$, 790 MeV, deviation from T=1 matrix element, π centre of mass ang. distrib. 78−70392
$np \rightarrow np$, high energy collisions, EM-hadronic interference, spin depend. phenomena 79−422
$np \rightarrow p\Delta_{33}^0$, 1.39 to 1.90 GeV/c, corrections to one pion exchange amplitudes 78−41560
$np \rightarrow pX$, 800 MeV, proton spectra, πN(1232) resonance 78−62437
$np \rightarrow p+$anything, inclusive charge exchange, parameter-free model 77−18336
$np \rightarrow pn$, 150-800 MeV, charge exchange cross section 79−409
$np \rightarrow pn$, 5-25 GeV/c, charge exchange scatt., πNN vertex function, one pion exchange 80−37291
$np \rightarrow pn$, 8 GeV/c, Regge anal. of charge exchange scatt. 77−22756
$np \rightarrow pn$, charge exchange models, polarisation 77−30444
$np \rightarrow pn$, energy depend. of np charge exchange, phenomenological anal. 78−25082
$np \rightarrow pn$ charge exchange amplitudes, energy dependence, up to 60 GeV/c 77−6171
$np \rightarrow pp\pi^-$, 11.9 GeV/c, differential cross section 77−22805
$np \rightarrow pp\pi^-$, 790 MeV, deviation from T=1 matrix element, π centre of mass ang. distrib. 78−70392
$np \rightarrow p\pi^-+p$, neutron dissociation reaction, 50 to 300 GeV/c 79−17765
$np \rightarrow p\pi^-\pi^+\pi^-\pi^-n$, 5.1 GeV/c, $p\pi^+\pi^+(n\pi^-\pi^-)$ combination effective mass distrib. singularity *(Russian)* 79−67569
$np \rightarrow px$, baryonium exchange, triple-Regge couplings 80−86763
$np \rightarrow \pi^0 d$, differential cross sections for 470-590 MeV, ang. distribs. 80−57628
$\bar{n}p$ reactions in Gargamelle, charged and neutral pion prod. 78−462
np thermal radiative capture, cross section calc. including meson exchange 79−67583
p-nucleus interactions, 20 to 200 GeV/c relativistic particle angular distribs. *(Russian)* 78−46065
p-nucleus interactions, energy dependence of two particle rapidity correls. 77−34292
$p+Be \rightarrow \phi+X$, 400 GeV/c, ϕ decay modes, OZI rule 78−599
$\bar{p}n$, 1.6 GeV/c, search for direct single electron production 77−49994
$\bar{p}N$, charm-pair production 80−22643
$\bar{p}n$, charmed meson prod. at 12.4-15.0 GeV/c 77−6176
$\bar{p}n$, mean charged multiplicity, energy depend., modified Heisenberg calcs. 79−40806
$\bar{p}n$, resonance in cross section, rescatt. effect in d, annihilation product 78−62431
$\bar{p}n$, S-resonance anal. 79−63509
$\bar{p}n \rightarrow 3\pi^-2\pi^+$, 1.0 to 1.6 GeV/c, like pion interference 77−26538
pN collision, 200 GeV/c, production of long-lived hadrons and leptons, antinuclei production 80−13342
$pn \rightarrow d(\pi\pi)^0$, effective two body interaction Hamiltonian, missing mass, ABC effect 78−70388
$\bar{p}n$ interactions in flight, beam target reversed symm. 78−41566

neutron-proton interactions continued
pn→$\mu^+\mu^-$ +anything, muon pair production, M quiescent mass determ. *Hungarian)* 79−13163
pn→$\mu^+\mu^-$ +anything, review of data, explanation using quark models, new quarks 78−74202
pn→nKΛ, field current relations *(Chinese)* 79−22126
pN→N*N coherent dissociation via p+A→p$\pi^+\pi^-$+A 22.5 and 15.3 Gev, Glauber anal. 77−22809
pn→np, charge exchange processes, baryonium trajectories, Regge pole description 80−9180
pn→p_{slow}+x, 195 GeV/c, triple Regge model anal., dominant π exchange 78−54657
pn→pX, 100 to 400 GeV/c, slow-proton prod., Regge trajectory 80−22646
pn→pX, 19 GeV/c pion exchange model of neutron fragmentation 79−63549
pn→ppπ^-, 19 GeV/c, neutron dissociation 79−36106
p̄n→p̄pπ^-, 2.98 GeV/c, $\bar{\Delta}^{--}$ prod. in additive quark model framework 80−52529
pn→ppπ^-, N diffractive dissociation into Nπ system, near threshold calcs. *(Russian)* 78−54623
p̄n→$\pi^-\pi^-\pi^+$, 0.40-0.92 GeV/c, partial-wave analysis 78−66147
p̄n→$\pi^+\pi^-\pi^-$, 1.09 to 1.43 GeV, spin-parity function, Veneziano model anal. 79−13148
p̄n→$\pi^+\pi^-\pi^-$, 2.98 GeV/c, Dalitz plot 79−80835
pn→πX, central region, Regge Mueller approach, inclusive cross sections *(Russian)* 78−58218
pn sphericity distribution, in 70 GeV/c inelastic collisions, multiplicity depend. 79−80852
p̄n strong interaction effects on antiprotonic atoms X-rays of light nuclei 78−29867
p̄n→xπ, temperature parameter for thermal-like emission spectra, fluctuations 80−68482
p̄n:p̄p annihilation ratio, low energy and stopped p̄ in C, p̄N system resonance 77−18313
p^-n, high-energy, react. differences and annihilations 78−74279
π prod. in pp, np, πp interactions, mass quantisation *(French)* 78−25059
π^+ prod. in 460-580 MeV interactions 79−75785
^{2}H(p,pp)n, 6.4 to 25.8 MeV, pn final state interaction, cross sections 78−54757

neutron-proton scattering
see also neutron-proton interactions
$^1S_1$-$^3D_1$, $^3D_2$ phase parameters and deuteron quadrupole moment, pot. reconciliation 79−67575
amplitude parameter determ. with Glauber model for 50 GeV scatt. 79−75798
analysing power, precision, meas. in 14 to 17 MeV region using polarised neutrons 78−70393
analysing power meas. at 14 MeV, multiple scattering effects 77−10572
analysing power meas. of np scatt. at 16.9 MeV 78−4941
asymmetry meas. with polarised beams and targets 78−62459
charge exchange reaction, Regge parametrization of NN differential cross sections and polarizations 79−17746
Coulomb interaction effects on calc. of scatt. characts. 79−9529
cross section meas., 70-400 GeV/c 78−82244
differential cross section and logarithmic slope parameter determ., 70 to 400 GeV/c 79−30751
differential cross section meas. 78−62421
differential cross-sections at 25.8 and 50.0 MeV 78−600
dipole pomeron model, 70 to 400 GeV/c 80−105927
dispersion approach to the inverse scattering problem *(Russian)* 79−22128
dual absorptive model and np elastic scatt. at high energies 80−102072
elastic scattering, relativistically invariant scaling law 77−13986
Faddeev approach to neutron scatt. from protons in heavy hydrocarbons in eV range 78−54728
forward scatt. amplitude and charge exchange, 1.5-60 GeV/c 78−4867
free elastic scatt., 220-495 MeV, Wolfenstein parameters and polarisation, I=0 phase shifts 79−67594
high-energy scattering, review 77−79283
large angle, 5 to 12 GeV.c^{-1}, differential cross section meas. 79−3036
large angle np elastic scatt., 5-12 GeV/c, ang. distribs. 77−57565
large transverse momentum, spin-spin forces 78−78216
large transverse momentum processes, np elastic scattering data, comparison with theory 77−57566
measurement status and phase shift analyses near 50 MeV 79−67595
nuclear forces, charge symm. breaking, test by np elastic scatt. 78−89798
phase shift anal., K-matrix at low energies 77−57634
phase shift anal. 78−62425
phase shift anal. and mixing parameters at 325 MeV 77−79277
phase shift analyses, 0 to 425 MeV 77−54115
phase shift analyses, 50, 325 MeV, single energy and energy depend. solns. 77−54116
phase-shift anal., 50 MeV, spin-correlation parameter meas. 78−62424
polarisation asymmetry in pn elastic scatt., effective mass spectrometer study 77−30412
polarisation expts., Regge and diffraction descriptions 77−57564
polarisation in 1.03 GeV scatt. 78−82245
polarisation parameter for pn and pp elastic scatt. at 11.8 GeV/c 78−66158
polarisation phenomena in close-to-forward scatt., intermediate energy region 80−78086
polarized proton-neutron total cross sections from proton-deuteron data 80−22633
preasymptotic effects in large angle elastic scatt. amplitudes, quasipot. scatt. *(Russian)* 80−57631
spin dependent EM hadronic interference, pn and Λp elastic scatt. amplitudes 78−12923
spin-correlation parameter at 50 MeV 77−49993
spin-spin forces in 6 GeV polarised elastic scatt. 80−433
triple scatt. parameters meas. 78−62420
two-channel Jost matrix construction on second-order S-matrix *(Russian)* 79−9294
n-hadron amplitudes from p-hadron and d-hadron amplitudes in Glauber-model 77−22803
n-p phase shift data and pot. model for inverse scatt. and T-matrix 79−6431
nd scatt., at d breakup energy, boundary condition method 79−22127

neutron-proton scattering continued
np analysing power, 14.5 MeV, Hamburg polarised neutron facility, initial expts. 77−26946
np bremsstrahlung at 200 MeV 78−66144
np elastic scatt., 70-400 GeV/c, cross sections, simple Regge pole model 80−63032
np forward angle elastic cross section meas. at 790 MeV 79−6345
np→np, high energy, polarisation, spin correls., s-channel helicity amplitudes 77−30435
np→pn, 8 to 23.5 GeV/c, test of Veneziano-type πNN form factor in fitting dσ/dt data 79−17725
np→pn charge exchange scatt., 60 to 300 GeV/c 77−6172
np→pn charge exchange scatt., 60 to 300 GeV/c, anal. 77−6173
pn elastic scatt., 24 GeV/c, polarisation and anal. power 79−63528
virtual scatt. from ^{4}He+p two pronged events 79−3152

neutron radiative capture
36≤Z≤83 targets, tables of cross sections and reaction rate factors 77−46162
^{181}Ta(n,γ), γ-ray spectral shape depend. on n energy diverging interval size 78−78373
γ-ray angular distrib., radiative capture of fast nucleons 77−41964
ΣΣ spectrum, integral cross section meas. 80−68672
A=10-58, neutron separation energies, self consistent set from (n,γ) reaction 80−52563
A=40 to 60, valence capture model, appl. to total photon widths *(French)* 77−34291
A=45 to 200, mass dependence for radiative capture of 14.1 MeV neutrons 78−13087
A=90 to 160 fission product neutron capture cross-section adjustment based on integral meas. 79−9578
absolute yield calibration, saturated resonance technique 79−80935
abundance peak, A≈252, due to subshell effect of N=164 77−2993
activation cross sections for (n,γ) reactions 79−57335
anomalous M1 capture in mass region A=20-40, non-statistical effects 77−30582
average resonance neutron capture, completeness in nuclear spectroscopy 80−106006
average resonance parameter eval. and calcs., statistical model for capture process 80−18271
borehole capture gamma-ray anal., optimal size ^{252}Cf neutron source 79−29890
cancer therapy in mice, long range effects, dose effect 78−48877
chondrite Yamato-74191, inert gas composition and neutron capture effects 80−46504
coal analysis by neutron-capture gamma-ray meas. in boreholes 79−52853
collective excitations, role in fast capture 77−23024
collective M1 excitation, nucleon radiative capture model 78−58276
common doorway resonance, decay amplitude phase relation from (n,γ) reactions 80−57758
compound nucleus decay, failure of statistical theory 77−54213
conference on neutron capture gamma ray spectroscopy, Upton, USA. (Sep. '78) 80−36780
coupled channel calc. of direct and collective cross sections of deformed nuclei 77−26748
cross section meas. using large Gd loaded liquid scintillator 78−25380
cross section measurement techniques, review 77−26932
cross section width fluctuation factor, neutron capture, elastic and inelastic scatt. 77−34294
cross sections above 2.5 keV for light and closed shell nuclides, mechanisms, resonance parameters 77−23049
cross sections at 24 keV, statistical theory 79−26430
cross sections for fission product nuclides in fast reactors *(Japanese)* 80−521
direct and resonance capture, giant dipole and quadrupole resonances 80−37385
dissipation in 1-dimens., time depend. HF calc. for slow neutron capture 79−63613
DSD capture model, for γ-ray ang. distrib. 78−89861
dynamical r-process, nuclei far from β-stability 77−26004
E1-E2 direct-semidirect model for fast nucleon radiative capture, γ ang.-distribs. 78−62536
element analysis, role of neutron capture γ-rays 80−50926
ENDF/B prompt γ-ray evaluations, models and data 77−26753
explosive r process cooling process 78−69791
fast, 5 to 15 MeV, validity of direct-semidirect capture theory, review 77−26694
fast neutron capture, refined direct-semidirect model 77−18541
fast neutron gamma ray detection system 77−26925
fast neutrons, higher-order processes, coupled channel treatment 77−61431
fission and radiative capture cross sections ratio meas. in reson. region 77−50175
fission products, cross sections from anal. of integral meas. 77−23032
fission products, effects of neutron capture on decay power in nuclear reactors 77−6500
fission products in fast-thermal critical facility STEK, adjustment methods, error evaluation for capture cross sections 77−6498
gamma-ray lasers, direct pumping by resonance capture of neutrons 80−14310
gamma-ray production cross sections for reactor materials 77−23067
giant dipole resonance intermediate struct. using (n,γ) and (γ, n), Brink hypothesis test 80−63150
giant dipole resonance region radiative nucleon capture, expt. ang. distrib. coeffs., direct-semidirect theory 78−74354
heavy and neutron-rich elements synthesis by rapid neutron capture process 78−77488
high spin state studies, heavy ion reaction complementarity 80−37381
in-beam gamma-ray spectroscopy, book 77−83449
induced capture by nuclei in laser radiation field *(Russian)* 80−13479
isotopic anomalies from neutron reactions during stellar explosive C burning 80−12651
l=1, near 24 keV, gamma-ray spectra, width correlations 77−26765
long neutron capture chains, abundances evaluation method 78−45216
M1 capture, correlations as evidence of semi-direct mechanism 78−8814
multigroup time-dependent delayed γ-spectra from fission and activation 78−13184
(n,γ) cross sections meas. for 22 elements between Z=3 and Z=82 77−26681

neutron radiative capture continued
neutron capture γ-rays, practical appls., analytical techniques, PNAA facilities 80−40794
neutron capture cross sections, 25 keV, evidence for slow nucleosynthesis 79−45259
neutron capture cross sections, MeV region, using activation technique 78−86535
neutron capture gamma and electron spectroscopy, instruments and techniques 80−37695
neutron interactions with nuclei, conf. 77−23015
neutron space-energy spectrum in inhomogeneous medium, allowing for neutron capture 77−23163
neutron-capture prompt gamma-ray activation analysis: multi-element measurements on various materials 80−40796
nonfissile nuclei, inherent inaccuracy in capture cross section calc. reactor appl. 80−22836
nonstatistical effects in neutron capture γ-ray spectra from target elements Ca to U 77−30569
nuclear struct. anal. from capture data, review 77−26701
organic scintillator, captured γ quanta yield, fast neutron irrad. 77−46457
P-wave neutron capture, statistical model radiation widths for 75<A<130 78−33161
parity violating terms in nuclear EM operators and struct. effects 79−6482
parity violation effects in neutron scattering and capture 80−105808
parity violation in nuclear forces, neutron capture γ-ray expts. 80−37322
polarised neutron expts., spin depend. of neutron cross-sections, mag. moments, radiation capture of neutrons *(Russian)* 80−52654
polarised thermal neutron capture, prod. of polarised β-active nuclei 77−30695
polarised/unpolarised neutrons, expt. determination of parity violation 79−59048
prompt gamma-ray activation anal. 77−29084
prompt gamma-ray spectra in keV region, rel. to reactor shielding 77−26761
prompt neutron capture γ-ray analysis of in vivo N, body H use as internal standard 79−92441
pulsed source, maximum density and capture rate of neutrons moderated 80−13522
quadrupole isoscalar and isovector capture of 5-50 MeV nucleons 77−2994
r-process nucleosynthesis of superheavy nuclei, beta-delayed fission 77−23012
r-process seed nuclei prod. at low densities and temps. 77−64742
radiative nucleon capture, pure resonance model, direct-semidirect model, pure semidirect model 80−78257
reaction survey 77−26702
reactor decay spectra, absorption effects on decay heat and spectral pulse kernels 80−22931
recoil reactions in mixed crystals, effects on chem. processes 77−90632
resonance activation neutron detector materials, uni-resonance approx. technique for higher resonance reaction rate 77−75030
resonance capture anal. 77−26693
resonance capture reactions with a total energy detector 80−37694
resonance neutron self shielding factors for Au and Ag, expts. and calcs. 77−42008
s-process, pulsed neutron flux effects 78−20812
s-process element prod. in deeply mixed convective envelopes of red giant stars 77−33470
s-process isotopes, nonthermal isomeric branching, importance of long-lived states 78−7983
s-process nucleosynthesis, neutron capture time scale from s-process Kr in meteorite 80−73080
sea water, gamma-radiation appl. to chlorinity determ. under natural conditions *(Russian)* 78−77360
semi-direct model calcs., 6-15 MeV 77−23047
slow neutron capture cross-section data, critical anal. 77−30578
slow neutron reaction rate ratio meas. using Cd and Hg prompt gamma reaction 79−30837
spherical even nuclei, role of doorway states in gamma decay of highly excited states 77−30581
spin assignments using polarised beams and gamma spectroscopy 80−37323
spin assignments using polarised neutrons and oriented target nuclei 78−29724
stellar interiors, s-process during thermal pulses of He shell burning 78−28668
thermal (n,γ) reaction, elemental anal. appl. 80−40795
thermal neutron capture γ-ray meas. using neutron guide tube 80−58099
total 14 MeV cross sections, meas. and anal. with statistical and direct reaction models 77−54226
total radiative width and degree of freedom, statistical model calcs. 80−57732
total radiative width of neutron resonances *(Russian)* 79−13270
trace component analysis by radiative neutron capture 79−79358
triplet state effect on radiative np capture, γ-ray circular polarisation meas. *(Russian)* 77−23009
valence model, mass range 40<A<70 79−45256
valency doorway model, appl. to Mo isotopes 77−23021
variable energy linearly polarised photon beam prod. 79−76248
cross section, statistical theory anal., radiative strength functions, In, Ta, Au, Sm, Eu *(Russian)* 78−17212
γ source generation and properties, review 80−14029
γ-ray resonant scattering, solid state properties of target 80−18060
(n,e⁻) high precision spectroscopy, internal conversion coeffs. for nuclear struct. 80−37353
(n,γ), (n,γγ), recent experiment review, future experiment suggestions 80−37382
(n,γ), A=20 to 240, E1 and M1 strength functions 80−52625
(n,γ), A=75 to 103, γ-strength functions and stat. model cross section calcs. 80−52612
(n,γ), A=94-190, resonance capture, low lying level population fluctuations, γ-rays 80−52619
(N,γ), ang. distribs. from direct-semidirect model 79−71852
(n,γ), E1 and M1 strength functions, A- and energy-depend., giant dipole resonances 80−37348
(n,γ), Fast n, gamma rays in giant dipole region, review 80−37351
(n,γ), γ-rays, QED test review 80−37199
(n,γ), integral data meas. in ΣΣ neutron field 78−70537
neutron radiative capture continued
(n,γ), interacting boson and Nilsson model tests, Pt-Os transition region 80−37380
(n,γ), mechanism in 3s size resonance, s-wave radiative width partition 80−37387
(n,γ), mechanism in 3s size resonance, radiative width statistical and valence effects 80−37388
(n,γ), non-spherical even-even nuclei, energy gap from γ-transitions 80−47395
(n,γ), odd-n actinides, vibr. band systematics, excitation energies and rot. parameters 79−36137
(n,γ), on-line gamma anal. using Ge detector 80−52624
(n,γ), parity violation in compound nuclei 80−47368
(n,γ), polarized space parity nonconservation, optical pot. and GDR parameters *(Russian)* 80−86803
(n,γ), resonance TOF spectroscopy at Nevis Lab. 77−23073
(n,γ) gamma ray spectra calc. 80−52620
(n,γ) gamma ray study at Tehran nuclear research centre 80−57735
(N,γ) reactions in giant dipole resonance region, role of exchange forces 77−88126
(n,γ) reactions with polarised thermal neutrons, spin state determ. *(Dutch)* 79−22290
(n,γ) spectroscopy, nuclear struct. investigation, review 80−37379
(n,γ) thermal react. cross section meas. with liquid scintillation spectra 78−25382
(n,γ) total cross sections of 14 MeV neutrons, from activated nuclei β-ray counting 79−3156
(n,γα), (n,γf), low energy γ-transitions between compound states, statistical theory 80−57737
(n,γα), thermal n, systematic search, γ-spectra and selective state population 80−37390
(n,γp), thermal n, systematic search, γ-spectra and selective state population 80−37390
(n,xγ), cross section meas., threshold to 20 MeV 77−23069
np capture, parity violation in nucl. anal. 77−46165
np doubly radiative capture, M1-M1 transitions and cross section calcs. 79−13292
np→γd, gamma polarisation due to weak parity violating effects 77−41851
^{181}Ta 79−40910
^{208}(N,γ), pol. N, anal. power and giant multipole resonances, direct-semidirect model 80−18265
^{52}(n,γ), thermal, ^{53}Cr levels, J$^{\pi}$, γ-transitions and 1626 eV resonance 80−42610
Ag, cross-sections determ. by Fe filtered beam TOF method 77−23078
^{107}Ag (n,γ), ^{108}Ag low-lying states and state distrib. 78−50084
^{107}Ag(n,γ), 16.3 eV, ^{108}Ag levels and γ-transitions, population-spin correlation 80−63097
^{107}Ag(n,γ), cross sections for prod. of ^{108}Ag^{m} 79−29625
^{107}Ag(n,γ)^{108}Ag, coincidence meas. of low-lying states of 215.38 keV 78−12975
^{107}Ag(n,γ)^{108}Ag^{m}, in stainless-steel structure of high-power nuclear reactors 80−42747
^{109}Ag(n,γ), ^{110}Ag 118.718 keV isomer, low lying states and transitions, coincidence study 80−73806
^{109}Ag(n,γ), ^{110}Ag low lying states, decay scheme and $T_{1/2}$ 80−47393
^{109}Ag(n,γ), ^{110}Ag low-lying levels obs. 80−47422
Al, γ-ray energies and intensities 78−89876
^{27}Al(n,γ), pol. Al and n, 0.017 eV, ^{28}Al levels, transitions and spin 80−78153
^{27}Al(n,γ), pol. thermal, ^{28}Al levels, spins and γ-rays, multipole mixing 80−47398
^{27}Al(n,γ), resonance capture, ^{28}Al E1 transitions and partial radiative widths 80−52618
Al(n,xγ)Al, E_n=5.3 MeV, γ prod. cross-section obs. 78−89863
Am, A=241,3, neutron capture cross-sections 77−61469
^{241}Am, thermal cross sections and resonance integrals of fission and capture 77−71629
^{241}Am(n,γ) cross section meas., thermal to 350 keV 77−23034
^{241}Am(n,γ)^{242m}Am, γ-quanta in population of spontaneously fissile isomer *(Russian)* 79−30835
^{243}Am, thermal cross sections and resonance integrals of fission and capture 77−71629
^{36}Ar(n,γ), valence neutron capture in s-wave capture 77−23076
Au, 0.02-3.0 MeV fast neutron cross sections 77−26758
Au, activation cross sections meas. for generalised intermittent irradiation, fusion machines appl. 78−58283
^{197}Au(n,γ)^{198}Au integral cross section ratio meas. using ^{235}U(n_{th},f) neutron spectrum 77−23130
^{197}Au, effective cross section dependence on thermal neutron temp. 80−547
^{197}Au, 10-500 keV, absolute cross sections 77−26772
^{197}Au, 24.3 keV activation cross sections with Fe filter technique 77−26763
^{197}Au, cross-sections determ. by Fe filtered beam TOF method 77−23078
^{197}Au, neutron capture cross section ratios in range 10 to 90 keV 78−50163
^{197}Au, neutron capture cross sections, 0.5 to 3.0 MeV 79−40912
^{197}Au(n,γ), ^{198}Au level spin assignments from γ ang. distrib. and circular polarisation 80−52570
^{197}Au(n,γ), 0.5-3.0 MeV, ^{198}Au gamma-ray strength functions from spectrum fitting method 80−52616
^{197}Au(n,γ), absolute yield calibration, saturated resonance technique 79−80935
^{197}Au(n,γ), average activation cross sections in ^{252}Cf spontaneous fission neutron field 79−30830
^{197}Au(n,γ), cross section meas. using large Gd loaded liquid scintillator 78−25380
^{197}Au(n,γ) ^{198}(n,γ)^{199}Au, high energy transitions 80−22878
^{197}Au(n,γ) standard reaction, Monte Carlo simulation of cross section fluctuations 77−61461
^{198}Au(n,γ), 0.5-3.0 MeV, γ-spectra strength functions 80−32240
Au(n,γ) cross section standard, status 77−23040
Au(n,γ), cross section standards, review 79−9589
^{10}B(n,γ)^{11}B, ionizing radiation and cavitation threshold, calc. of dose rate, cavitation threshold 78−94774
^{138}Ba(n,γ), 30 keV, capture cross sections, stellar nucleosynthesis 80−42663
^{138}Ba(n,γ), resonance n capture cross section meas. 3 to 100 keV 79−93610

neutron radiative capture continued
^{209}Bi, 4.9-8.0 MeV, γ-ray prod. cross-section meas. 77−38264
^{209}Bi(n,γ), 2.6-901 keV, cross-sections, resonance peaks, radiative widths 77−3002
^{209}Bi(n,γ), TOF transmission spectroscopy, strength functions 77−23077
^{249}Bk, thermal cross sections and resonance integrals of fission and capture 77−71629
^{79}Br(n,γ), thermal, ^{80}Br level struct. determ. 78−41667
^{81}Br(n,γ), thermal, ^{82}Br level struct. determ. 78−41667
^{12}C + n, TOF transmission meas. of neutron resonances 80−37374
^{12}C(n,γ)^{13}C, ground state γ-ray energy using ^{13}C n separation energy 78−70434
^{12}C(n,γ)^{13}C, ionizing radiation and cavitation threshold, calc. of dose rate, cavitation threshold 78−94774
^{13}C(n,γ)^{14}C, subsurface production of ^{14}C, groundwater dating 80−85690
^{40}Ca(n,γ$_0$)^{41}Ca, 6 to 13 MeV quadrupole radiation, direct-semidirect model calcs. 79−545
^{40}Ca(n,γ$_0$)^{41}Ca, 8,12 MeV γ-ray ang. distrib. 78−66279
^{40}Ca(n,γ), 10 MeV polarised neutrons, ^{41}Ca giant dipole resonance 79−93620
^{40}Ca(n,γ), 8-12 MeV, fast neutron gamma ray detection system 77−26925
^{40}Ca(n,γ), direct-semidirect and compound nucleus contribs. to cross sections 80−68662
^{40}Ca(n,γ), fast n, ^{41}Ca E2 resonance, cross sections and γ spectrum 80−57759
^{40}Ca(n,γ)^{41}Ca, up to 15 MeV, higher-order processes, coupled channel treatment 77−61431
^{43}Ca(n,γ), ^{44}Ca gamma ray spectra 77−38278
^{48}Ca(n,γ)^{49}Ca, neutron activation meas. of F/Ca ratio 77−86592
Ca(n,γ), A=42, 44, γ circular polarisation meas. 78−62533
Cd covered Au foils, neutron spectra determination by resonance reactions 79−93837
Cd stable even-A isotopes 106-116, neutron capture resonance parameters and cross sections 78−50161
^{109}Cd, production in nuclear reactors by neutron irrad. of ^{107}Ag 80−52798
^{111}Cd (n,γ), meas. of absolute partial p-wave capture cross-section 77−34307
^{113}Cd(n,γ), meas. of absolute partial p-wave capture cross-section 77−34307
^{114}Cd(n,e$^+$e$^-$), thermal 77−26624
Cd(n,γ), facility for in vivo meas. of kidney and liver Cd 78−15885
Ce, fast neutron capture and the microscopic isovector optical potential 79−63668
^{A}Ce(n,γ), A=140, 142, 30 keV, capture cross sections, stellar nucleosynthesis 80−42663
^{140}Ce, 6.2-15.6 MeV, gamma-ray spectra, cross-section meas. 78−33176
^{140}Ce(N,γ$_0$), 2-10 MeV, giant M1 resonance in direct-semidirect model 79−17898
^{140}Ce(n,γ), ^{141}Ce collective M1 excitation effects on γ-ang. distribs., direct semidirect model 80−57733
^{140}Ce(n,γ), resonance n capture cross section meas. 3 to 100 keV 79−93610
^{249}Cf, thermal cross sections and resonance integrals of fission and capture 77−71629
^{252}Cf(n,γ), neutron capture gamma expt. equipment designs 80−52832
Cl, γ-ray energies and intensities 78−89876
^{35}Cl(n,γ), ^{36}Cl anomalous M1/E1 strength ratio and doorway states 80−57730
^{35}Cl(n,γ), slow n, 398 eV resonance J^π determination 79−36147
^{35}Cl(n,γ), thermal, negative energy resonance parameters 77−23025
^{35}Cl(n,γ)^{36}Cl, E1 and M1 radiative strength functions 78−4940
^{37}Cl(n,γ), spectroscopic factors calc. using potential capture model 77−30583
^{37}Cl(n,γ)^{38}Cl, recoil energy spectrum calcs. 78−86531
^{245}Cm, thermal cross sections and resonance integrals of fission and capture 77−71629
^{248}Cm(n,γ), ^{249}Cm excited and single particle states, γ-transitions 80−47399
^{250}Cm(n,γ), ^{251}Cm beta decay, ^{251}Bk level struct. 79−36200
Co, 0.02-3.0 MeV fast neutron cross sections 77−26758
^{59}Co, neutron capture cross section meas. 80−5147
^{59}Co(n,α), thermal, isomer state excitation, relative probabilities 79−75814
^{59}Co(n,γ), 2.5 keV-1 MeV, TOF capture cross-section meas. 77−30586
Cr, absolute cross sections in keV range 77−26771
Cr, neutron capture cross sections intermed. energy region, method and exptl. facility 78−21637
Cr(n,γ), up to 600 keV, cross sections, resonance parameters, point-wise evaluation 77−23050
^{133}Cs(n,γ), ^{134}Cs 176.403 keV isomer, populating γ-rays, low lying levels 80−78200
^{133}Cs(n,γ)^{134}Cs, E$_n$=14.1 MeV, γ emission exciton model *(Russian)* 79−13302
Cu, 0.02-3.0 MeV fast neutron cross sections 77−26758
Cu, determ. of recoil energy and effective mass from narrow resonance line shapes 77−57660
^{243}Cu, thermal neutron capture and fission cross sections, resonance integrals 77−67744
Cu(n,γ), 63, 5, cross-section meas., reson. parameters determ. 77−38274
Cu(n,xγ)Cu, E$_n$=5.3 MeV, γ prod. cross-section obs. 78−89863
^{163}Dy(n,γ), thermal, ^{164}Dy multipole mixing in γ to ground bands 80−52615
^{164}Dy(n,γ), thermal, isomer state excitation, relative probabilities 79−75814
Dy(n,γ), thermal, ^{162,164}Dy gamma to ground band transitions, γ-γ directional correlations 80−68579
^{A}Er,A=166,168,170, fast neutron radiative capture cross sections, 5 to 350 keV *(Russian)* 78−33188
^{167}Er(n,γ), thermal, CC ^{168}Er high intrinsic excitation levels, γ-decay props. 80−52588
^{A}Eu(N, γ), A=151, 153, cross sections, time of flight spectra, scintillation detectors 80−27634
^{151}Eu, ^{153}Eu, 20 eV to 200 keV capture cross section 77−26759
^{151}Eu, capture cross section, E$_n$=0.1-100 keV, reson. parameters 77−50121
^{151}Eu(n,γ), ^{152}Eu 89.8488 keV isomeric state feeding, delayed coincidence meas., level scheme 80−63126
^{151}Eu(n,γ), ^{152}Eu transition probabilities and deformations 79−97680
neutron radiative capture continued
^{151}Eu, capture cross section, E$_n$=0.1-100 keV, reson. parameters 77−50121
^{153}Eu(n,γ), ^{154}Eu low lying levels, bands, transitions 80−57694
^{153}Eu(n,γ)^{154}Eu, thermal, ^{154}Eu level scheme 77−61374
Eu(n,γ), separated isotopes, integral capture cross section meas. in CFRMF 77−26760
^{19}F(n,γ)^{20}F, neutron activation meas. of bone F content 77−86592
Fe, 24-160 keV, multigroup capture cross section and self shielding factor 77−26773
Fe, absolute cross sections in keV range 77−26771
Fe, determ. of recoil energy and effective mass from narrow resonance line shapes 77−57660
Fe, γ-ray energies and intensities 78−89876
Fe, integral neutron capture cross sections in GCFR lattices 78−13246
Fe, neutron capture cross sections intermed. energy region, method and exptl. facility 78−21637
^{A}Fe(n,X) A=54, 56, 57, transmission and capture meas. 80−18313
^{A}Fe(n,γ), A=54,56,58, resonance capture, ^{55,57,59}Fe level schemes 79−547
^{54}Fe (n,γ), valence neutron capture in s-wave capture 77−23076
^{54}Fe neutron capture, asymmetric s-wave reson., background interf. 78−21563
^{54}Fe(n,γ), 1-18 keV, ^{55}Fe resonances, levels, J^π, valence capture γ-ray spectrum 80−86852
^{54}Fe(n,γ), cross section, resonance and background interference 80−18310
^{56}Fe partial radiation widths from neutron capture resonances, valency model calcs. 77−26707
^{56}Fe(n,γ), ^{57}Fe anomalous M1/E1 strength ratio and doorway states 80−57730
^{56}Fe(n,γ), 6-150 keV, shape anal. and width correlations 77−26766
^{56}Fe(n,γ), anal. of gamma decay of ^{57}Fe 1.167 keV p$_{1/2}$ resonance 77−30585
^{56}Fe(n,γ), resonance state, partial radiation widths of high energy transitions 78−13104
^{56}Fe(n,γ)^{57}Fe, high energy γ-ray transitions of ^{56}Fe resonances, E$_n$=7 to 70 keV 77−23081
^{57}Fe, (n,γ), cross section, 2.5-200 keV, s-wave resonances 80−18309
^{58}Fe(n,γ), ^{59}Fe resonances, primary γ-intensities, E1-M1 correlation 80−57740
^{58}Fe(n,γ) capture and total cross section meas. below 325 keV, resonance parameters 80−18314
^{58}Fe(n,λ), resonance capture cross section s- and p-wave radiative widths 80−47476
Fe(n,γ), A=56, 58, γ circular polarisation meas. 78−62533
Fe(n,γ), cross-section meas. principal resonance parameters 80−18312
Fe(n,γ), thermal, ^{57,59}Fe levels, J^π and transition branching ratio 80−105976
^{A}Gd, A=156,158,160, fast neutron radiative capture cross sections, 5 to 350 keV *(Russian)* 78−33188
^{A}Gd(n,γ), A=154,156-8, 2, 24 keV, resonance averaged γ-spectra, level and J^π appls. 80−37347
^{152}Gd(n, γ), ^{153}Gd levels and γ-ray spectra 80−57736
^{154}Gd(n,γ), thermal, ^{155}Gd, vibr. state, level scheme, γ and conversion electron spectra 80−57696
^{155}Gd, K X-ray intensity following thermal neutron capture 77−26691
^{156}Gd(n,γ), up to 2.24 keV, n resonances, spectra fluctuation, statistical theory test 79−36188
^{157}Gd(n,γ), γ and conversion electron spectra, ^{158}Gd collective bands 78−89819
^{1}H(n, γ)^{2}H, 37 to 72 MeV, total cross section meas. 79−49627
^{1}H(n,γ), ^{2}H γ-energy and binding energy 80−52564
^{1}H(n,γ), polarised neutrons, calc. of P-violating asymmetry 77−18565
^{1}H(n,γ), thermal, γ-ray energy, ^{2}H neutron binding energy and n mass excess 80−47362
^{1}H(n,γ), thermal, photon circular polarisation in parity violating capture 77−6375
^{1}H(n,γ), thermal calc. of γ-circular polarisation, p-nonconservation effects 77−18564
^{1}H(n,γ)^{2}H, exchange current contribs. to parity violating elec. transitions 78−29383
^{1}H(n,γ)^{2}H, exchange current and interaction effects using unitary equivalent transforms. 79−9566
^{1}H(n,γ)^{2}H, relativistic effects 77−18519
^{1}H(n,γ)^{2}H, relativistic invariant approach, parity violation 79−3147
^{1}H(n,γ)^{2}H, repulse core effect 77−38259
^{1}H(n,γγ), branching ratio meas. 77−30579
^{1}H(n,γγ), cross-section calc. 77−6385
^{1}H(n,γγ), thermal, consistency between pion exchange currents and NN pot., cross sections 80−68556
^{1}H(n,γγ), thermal n, cross section for two-quantum n capture 79−54439
^{1}H(n,γγ)^{2}H, cross section upper limit 80−52683
^{1}H(n,γγ)^{2}H, thermal, upper cross-section limit 77−3001
^{2}H(n, γ), slow neutrons, mesic interaction current, isobaric resonance *(Italian)* 78−25179
^{2}H(n, γγ), thermal, cross-section meas. 77−26703
^{2}H(n,γ)^{3}H, existence of excited states of A=3 nuclei 79−9553
^{2}H(n,γγ), thermal, calc. of cross-sections and branching ratios 77−14131
^{2}H(n,γγ), three-particle calc. 77−50131
^{3}He, 1-70 keV, effective cross sections *(Russian)* 79−30836
^{3}He(n,γ), thermal, effective cross section *(Russian)* 80−37378
^{3}He(n,γγ), thermal, calc. of cross-sections and branching ratios 77−14131
^{3}He(n,γγ), thermal neutrons, cross section and branching ratio 79−45263
^{199}Hg, K X-ray intensity following thermal neutron capture 77−26691
H(n,γ), parity violation study, high-rate counting circuitry for γ-rays 78−62527
H(n, γγ), thermal, cross-section meas. 77−26703
Ho, 0.02-3.0 MeV fast neutron cross sections 77−26758
^{165}Ho, 0 to 2 keV, neutron strength function of states with selected spin 77−26705
^{165}Ho, 24 keV neutron capture cross section meas. with Fe-filtered neutron beam 79−40910
^{165}Ho, cross-sections determ. by Fe filtered beam TOF method 77−23078
^{165}Ho(n,γ), <2 keV, spin depend. of s-wave neutron strength function 78−21562
^{165}Ho(n,γ), polarised neutron capture by polarised nucleus, assignment of spins to ^{166}Ho levels 79−59062

neutron radiative capture continued
^{115}I(n,γ), average activation cross sections in ^{252}Cf spontaneous fission neutron field 79−30830
^{127}I, 24 keV neutron capture cross section meas. with Fe-filtered neutron beam 79−40910
^{127}I, 24.3 keV activation cross sections with Fe filter technique 77−26763
^{127}I, cross-sections determ. by Fe filtered beam TOF method 77−23078
^{127}I(n,γ) cross section 77−23032
^{127}I(n,γ)^{128}I in fast reactors, effective cross sections calc., from expt. results *(Dutch)* 79−537
In, activation cross sections meas. for generalised intermittent irradiation, fusion machines appl. 78−58283
^{115}In, 24 keV neutron capture cross section meas. with Fe-filtered neutron beam 79−40910
^{115}In, 24.3 keV activation cross sections with Fe filter technique 77−26763
^{115}In, effective cross section dependence on thermal neutron temp. 80−547
^{115}In, thickness depend. of total and capture cross section 77−26747
^{115}In(n,γ), population of ^{116}In low-lying levels 77−30589
^{115}In(n,γ)^{116m}In, 14.7 MeV, cross-section meas. with improved activation technique 77−50133
^{191}Ir(n,γ), resonance, ^{192}Ir levels, resonances and low energy γ-rays 80−47397
^{191}Ir(n,γ), thermal, isomer state excitation, relative probabilities 79−75814
^{193}Ir, neutron capture cross sections, 0.5 to 3.0 MeV 79−40912
^{39}K(n,γ)^{40}K, ionizing radiation and cavitation threshold, calc. of dose rate, cavitation threshold 78−94774
^{138}La, thermal neutron capture cross section and reson. integral 77−6365
^{139}La(n, γ), 10-70 keV, gamma-ray transitions 78−17185
^{139}La(n, γ), 2.5-90 keV, s- and p-wave resons. 78−17186
^{139}La(n,γ), non-statistical capture, radiative widths, γ-ray doorway state model 80−37389
^{139}La(n,μ), 14.1 MeV, gamma emission from pre-equilibrium exciton model 79−75960
^{6}Li(n,γ), cross section and spectroscopic factors from direct capture pot. model 80−99171
Li(n,γ)^{8}Li, ionizing radiation and cavitation threshold, calc. of dose rate, cavitation threshold 78−94774
^{A}Lu(n,γ), A=175,176, 30 keV, capture cross sections, stellar nucleosynthesis, ^{176}Lu cosmic clock 80−42663
^{175}Lu(n,γ), reson. spins, secondary γ-transition intensity 78−21512
^{176}Lu, effective cross section dependence on thermal neutron temp. 80−547
^{176}Lu, K X-ray intensity following thermal neutron capture 77−26691
^{176}Lu(n,γ), reson. spins secondary γ-transition intensity 78−21512
^{27}Mg(n,γ)^{28}Mg, reactor neutron irrad., product yield 79−538
^{55}Mn, absolute cross sections in keV range 77−26771
^{55}Mn(n, γ) cross-section meas., ^{56}Mn gamma intensity, k_0 factors calcs. 79−26433
^{55}Mn(n,γ), pol. Mn and n, 0.017 eV, ^{56}Mn levels, transitions and spins 80−78154
^{55}Mn(n,γ)^{56}Mn, 2.5-600 keV, total cross section, resonance energies and capture area 79−6607
Mn(n,γ), primary transitions using focused 24 keV filtered neutron beam 80−63436
Mo, determ. of recoil energy and effective mass from narrow resonance line shapes 77−57660
Mo isotopes, valency doorway model 77−23021
Mo stable isotope eval., 5 keV-5 meV neutrons, rel. to reactor structural steel 80−13620
^{A}Mo(n,γ) A=98, 100 resonance parameters, capture Γ-rays and reaction mechanism 80−18272
^{93}Mo(n,γ), levels and gamma decay scheme of ^{99}Mo 77−30580
^{99}Mo effective activation cross section from (n,γ) reaction *(Japanese)* 79−97702
^{100}Mo resonances, search for valence neutron capture in 3p neutron giant resonance 77−30587
^{100}Mo(n,γ), ^{101}Mo levels, γ-rays and p-wave resonance partial radiative widths 80−57739
^{100}Mo(n,γ), 0.1-26 keV, ^{101}Mo resonances, levels, J^{π}, level spacings, cross section 79−89278
^{100}Mo(n,γ), levels and gamma decay scheme of ^{101}Mo 77−30580
Mo(n,X), 2 keV-20 MeV cross sections, coherent optical and statistical model calcs. 80−18318
Mo(n,γ), 24 keV cross-sections meas., A=92-98 77−57671
Mo(n,γ), 3-90 keV, neutron reson. parameters, capture cross-sections meas. 77−6371
Mo(n,γ)^{93,99}Mo, 0-3 MeV, valence doorway model for radiative capture 77−79368
^{14}N(n,γ), gamma-field from monodirectional neutron source in air 77−67785
^{14}N(n,γ), γ-ray energies, calibration standards 80−52613
^{14}N(n,γ)^{15}N, in vivo N determ. using Pu-Be sources 77−86606
^{64}N(n,γ), γ circular polarisation meas. 78−62533
^{23}Na, 24-160 keV, multigroup capture cross section and self shielding factor 77−26773
^{23}Na, 2.8 keV and thermal neutron capture gamma-ray spectra 77−38263
^{23}Na, absolute cross sections in keV range 77−26771
Na(n,γ), thermal, ^{24}Na^{m}, polarised, β-decay asymmetry and mag. moment 80−91157
Nb, 0.02-3.0 MeV fast neutron cross sections 77−26758
^{93}Nb, 24 keV, neutron capture cross section meas. with Fe-filtered neutron beam 79−40910
^{93}Nb, cross-section determ. by Fe filtered beam TOF method 77−23078
^{93}Nb neutron resonances, spin and parity assignments from (n,γ) meas. 77−26569
^{93}Nb(n,γ), 14.1 MeV, gamma emission from pre-equilibrium exciton model 79−75960
^{93}Nb(n,γ), cross-section below 3 MeV, coherent optical and statistical model calcs. 77−26713
^{93}Nb(n,γ) ^{94}Nb, E_n=14.1 MeV, γ emission exciton model *(Russian)* 79−13302
^{94}Nb(n,γ)^{95m,g}Nb, isomeric cross section ratio 79−49623
^{95}Nb(n,γ)^{95}Nb, ^{95m}Nb, cross section meas. rel. to fusion reactor design probs. 77−23060
^{A}Nd, A=142,144,148,146,150, fast neutron radiative capture cross sections, 5 to 350 keV *(Russian)* 78−33188
neutron radiative capture continued
^{142}Nd(n,γ)^{143}Nd, E=thermal, ^{143}Nd levels, J, π 77−10320
^{143}Nd(n,γ)^{144}Nd, ^{144}Nd excited states, level scheme extension 77−6231
^{143}Nd(n,γα), ^{144}Nd capture states partial α-decay widths 80−37328
^{143}Nd(n,γα), thermal n, ^{140}Ce γ-spectra, E1 and M1 hindrance factors 80−37386
^{144}Nd(n,γ), 0.04 to 11 keV, reson. γ-ray anal. 78−8823
^{148}Nd(n,γ)^{149}Nd→^{149}Pm, energy levels 80−27592
^{150}Nd(n,γ), ^{151}Nd rot. states, spin, parity, γ-rays, conversion electrons meas. 77−6196
Nd(n,α), struct. of A=147, 149, and 151 levels 77−34232
Ni, 0.02-3.0 MeV fast neutron cross sections 77−26758
Ni, absolute cross sections in keV range 77−26771
Ni, neutron capture cross sections intermed. energy region, method and exptl. facility 78−21637
^{A}Ni(n,γ), A=58, 60, 61, 6-150 keV, shape anal. and width correlations 77−26766
^{A}Ni(n$_{th}$,γ)$^{A+1}$Ni (A=58, 60, 62, 64), γ-ray spectra, level schemes, M1 and E2 strength functions 77−57674
^{58}Ni, ^{60}Ni partial radiation widths from neutron capture resonances, valency model calcs. 77−26707
^{58}Ni(n,X), transmission and capture data up to 120 keV 80−18311
^{58}Ni(n,γ), direct-semidirect and compound nucleus contribs. to cross sections 80−68662
^{59}Ni(n,γ), thermal, ^{60}Ni level scheme and γ-rays 80−63099
^{65}Ni(n,γ)^{66}Ni, cross sections determ. 79−49624
Ni(n,γ), A=58, 60, resonance state, partial radiation widths of high energy transitions 78−13104
Ni(n,γ), cross-section meas. principal resonance parameters 80−18312
Ni(n,γ), primary transitions using focused 24 keV filtered neutron beam 80−63436
^{237}Np fission and capture cross sections in GCFR neutron spectra 80−37404
^{237}Np, neutron resonance params., 8 to 250 eV 77−26709
^{237}Np neutron resonance parameters 8 to 204 eV 79−54436
^{237}Np(n,γ), thermal, ^{238}Np levels, resonances and transitions 80−52589
^{237}Np(n,γ) 25 to 650 keV and 2600 to 5500 keV, ^{238}Np energy level scheme determ. by Nilsson model 79−26370
^{16}O+n, 3-30 MeV, TOF transmission meas. of neutron resonances 80−37374
^{16}O(n,γ), thermal n, total cross section 79−54439
^{16}O(n,γ), total cross-section meas. 77−50131
^{16}O(n,γγ), single-particle direct-capture calc. 77−50131
^{16}O(n,γγ), thermal, calc. of cross-sections and branching ratios 77−14131
^{17}O(γ,n), cross section, Lane-Lynn radiative capture mechanisms 80−52660
^{17}O(n,γ), thermal cross section, ^{18}O level gamma decay 80−52623
^{A}Os(n,γ), A=186-188, 2.6-800 keV, capture Maxwellian cross sections, galactic nucleosynthesis 80−42664
^{186}Os, ^{187}Os cross section ratios, E_n=25 keV, age of universe 77−6384
^{188}Os(n$_{th}$,γ), ^{189}Os spectroscopy, Nilsson model, triaxiality 77−14035
^{189}Os(n,γ), thermal and reson. energies, levels and γ-ray transitions 79−36189
^{190}Os(2n,γ), ^{191}Os capture cross section, ^{192}Os level scheme and rot. bands 79−6413
^{190}Os(n,γ), ave. reson. capture, Nilsson model strength fragmentation 77−74844
^{192}Os(n,γ), 2 keV, ^{193}Os level scheme and transitions, Coriolis coupled Nilsson states 80−57698
^{192}Os(n,γ)^{193}Os, ^{193}Os energy levels, neutron separation energy 78−41642
^{192}Os(n,γ)^{193}Os, energy levels and spin assignments 79−36161
Os(n,γ), 5-350 eV for A=187, 189, neutron reson. and spin-state determ. 77−6224
^{141}P(n,γ), resonance parameters, s-wave radiative and reduced neutron widths 80−47471
^{206}Pb(n,γ), 25-600 keV, ^{207}Pb doorway resonances, M1 ground state radiative strength, level density 79−93589
^{206}Pb(n,γ), 3-50 keV, ^{207}Pb neutron separation energy and resonances, decay transitions 79−36217
^{206}Pb(n,γ), <50 keV, ^{207}Pb p-wave resonances, enhanced primary M1 transitions 80−57728
^{206}Pb(n,γ), direct-semidirect and compound nucleus contribs. to cross sections 80−68662
^{207}Pb(n,γ), ^{208}Pb M1,E1,M2,E2 localised γ-ray strengths 80−37350
^{207}Pb(n,γ), up to 1 MeV, obs. of ^{208}Pb giant M1 fine struct. 77−79347
^{208}Pb, 4.9-8.0 MeV, γ-ray prod. cross-section meas. 77−38264
^{208}Pb, fast neutron capture and the microscopic isovector optical potential 79−63668
^{208}Pb, fast neutron quadrupole radiative capture, direct-semidirect model 77−26711
^{208}Pb, fast neutron scatt. and capture, microscopic isovector optical pot. test 80−52682
^{208}Pb(N, γ$_0$), γ-ray ang. distribs., giant E3 resonances, direct-semidirect model 79−67727
^{208}Pb(N,γ$_0$), 2-10 MeV, giant M1 resonance in direct-semidirect model 79−17898
^{208}Pb(n,γ), 6 to 40 MeV, dipole/quadrupole interference, direct-semidirect model, γ ang. distrib. 78−93994
^{208}Pb(n,γ), fast, direct-semidirect and pure resonance model calcs. 80−47486
^{208}Pb(n,γ), pure resonance model for fast nucleon capture 79−80936
^{208}Pb(n,γ)^{209}Pb, 11 MeV, gamma-ray spectra, role of two-particle one-hole states 77−26764
^{208}Pb(n,γ)^{209}Pb, dipole centre and giant quadrupole capture, cross sections calc. 77−10398
^{208}Pb(n,γγ), thermal, calc. of cross-sections and branching ratios 77−14131
^{A}Pd (n,γ), A=104, 105, 106, 108, 110, cross sections above 2.6 keV 79−80933
^{105}Pd, 20 eV to 200 keV capture cross sections 77−26759
^{107}Pd fission product neutron capture and total cross-section obs. 79−9573
^{107}Pd(n,γ) and transmission meas., level parameters 78−58277
^{108}Pd(n,γ), ^{109}Pd low spin odd parity states, rot. aligned model, Coriolis calc. 80−57695
^{108}Pd(n,γ), thermal, resonance, ^{109}Pd low spin odd parity levels, γ-rays, particle-rotor comparison 80−73805
^{108}Pd(n,γ), thermal and resonant, ^{109}Pd levels, J^{π}, transitions, unique parity states, and spectroscopic factors 80−42547

neutron radiative capture continued
^{141}Pr, neutron capture cross section and transmission TOF meas. 79−67752
^{141}Pr(n,γ), circular polarisation, ang. distrib. meas. 80−32285
^{141}Pr(n,γ), non-statistical capture, radiative widths, γ-ray doorway state model 80−37389
^{195}Pt(n,γ), ^{196}Pt negative parity states in partially decoupled bands, γ-transitions 80−47360
^{195}Pt(n,γ), thermal-2 keV, ^{196}Pt level struct. and J^{π} assignments, interacting boson approx. O(6) limit 79−75853
^{195}Pt(n,γ)^{196}Pt, low spin positive-parity states struct., O(6) limit of IBA model 78−33110
^{196}Pt(n,γ), ^{197}Pt states from ang. distribs. and spectroscopic factors 78−78267
Pu, multigroup time-dependent delayed γ-spectra from fission and activation 78−13184
$^{\wedge}$Pu, A=240, 242, neutron capture cross section ratios in range 10 to 90 keV 78−50163
^{239}Pu, capture/fission cross-section ratio meas., 0.007 eV-12 keV 77−54266
^{239}Pu, integral neutron capture cross sections in GCFR lattices 78−13246
^{239}Pu, σ_c/σ_f ratio meas. in BFS critical assemblies 79−97737
^{239}Pu, $\sigma(n,\gamma)/\sigma(n,f)$ estimate based on expt. data up to 1977 79−89312
^{239}Pu+n, ratio between capture and fission cross sections up to 30 keV 78−70538
^{239}Pu(n,X), thermal n, gamma spectra from capture, fission and fission products 80−37352
^{239}Pu(n,α), meas. of α-values in BOR-60 reactor core 79−97830
^{239}Pu(n,γ), comparison of exptl. cross section meas. methods 77−23157
^{240}Pu, 50 to 250 keV, cross-section ratios c.f. ^{197}Au 79−22281
^{240}Pu resonance capture in reactor cell codes, parametric description 79−13384
^{240}Pu(n,γ), average cross section from 200 eV to 350 keV 77−50129
^{240}Pu(n,γ) cross section meas., thermal to 350 keV 77−23034
^{241}Pu, evaluation of neutron cross sections in region 10^{-5} eV to 15 MeV 78−17254
^{241}Pu, multilevel resonance parameters for 0.01 to 100 eV neutrons 79−36154
^{241}Pu, neutron capture and fission cross sections, 0.01 eV-30 keV 78−29512
^{241}Pu(n,γ) cross section meas., thermal to 350 keV 77−23034
^{242}Pu, 50 to 250 keV, cross-section ratios c.f. ^{197}Au 79−22281
^{242}Pu, cross section for fast neutrons 78−82351
^{242}Pu(n,γ)^{243}Pu, populating Nilsson and rot. levels 77−6202
^{244}Pu(n,γ) resonance integral meas. 80−73846
^{187}Re(n,γ), thermal, isomer state excitation, relative probabilities 79−75814
^{103}Rh, 20 eV to 200 keV capture cross section 77−26759
^{103}Rh, absolute cross sections in keV range 77−26771
^{103}Rh, neutron capture cross sections, 0.5 to 3.0 MeV 79−40912
^{103}Rh(n,γ), cross-sections above 2.6 keV 80−32276
^{104}Rh(n,γ), 0.5-3.0 MeV, γ-spectra strength functions 80−32240
$^{\wedge}$Ru(n,γ), A=100-104, cross-sections above 2.6 keV 80−32276
^{102}Ru(n,γ), levels and gamma decay scheme of ^{103}Ru 77−30580
^{104}Ru(n,γ), levels and gamma decay scheme of ^{105}Ru 77−30580
Ru(n,γ), $^{\wedge}$Ru, A=99, 101, neutron resonance mean spacings and strength functions *(Russian)* 79−40895
Ru(n,γ) cross sections for ^{101,102,104}Ru 77−23032
^{32}S(n,X), 2.5-1100 keV, resonance struct. from total and capture cross sections 80−42620
^{32}S(n,γ), doorway structs. 79−532
^{32}S(n,γ), fast n, doorway structs. and single particle resonances, microscopic treatment 80−52646
^{32}S(n,γ), non-statistical effects in shell model calcs. 80−32274
^{32}S(n,γ), single particle resonances and doorway states, K matrix formalism 80−37384
Sb, determ. of recoil energy and effective mass from narrow resonance line shapes 77−57660
^{121}Sb(n,γ), ^{122}Sb, low-lying state props., coupled neutron quasiparticle-proton model 77−61378
^{121}Sb(n,γ), γ and conversion electron spectra, ^{122}Sb energy level scheme 78−54721
^{124}Sb(n,γ)^{125}Sb, reactor neutron capture cross section of 60.3-day ^{124}Sb 80−13469
^{45}Sc+n, 0.005 to 22 keV, total neutron cross section for beam filter design 78−78371
^{45}Sc(n, γ), 2.5-100 keV, s- and p-wave radiative widths 78−17187
^{45}Sc(n,γ), ^{46}Sc energy levels, resonances, spin and parity 80−52673
^{45}Sc(n,γ), ^{46}Sc level deexcitation, E1 and M1 absolute radiative widths 80−52622
^{45}Sc(n,γ), pol. n, ^{46}Sc transition polarisation, levels and spin assignments 80−52656
^{28}Si(n,γ), 2.7-6.2 MeV, ^{29}Si doorway state neutron capture, levels and γ-spectra 80−57729
^{28}Si(n,γ), 565, 813 keV, ^{29}Si neutron resonance, γ-spectra, partial and total radiative widths 80−42578
^{28}Si(n,γ), 565, 813 keV, resonance γ, spectra, valence model test 80−63124
^{28}Si(n,γ), calc. of neutron and gamma widths for ^{29}Si $3/2^{-}$ doorway resonances 77−26587
^{28}Si(n,γ), doorway structs. 79−532
^{28}Si(n,γ), fast n, doorway structs. and single particle resonances, microscopic treatment 80−52646
^{28}Si(n,γ), n and γ width correlation, valence, optical and shell model comparison 79−6606
^{28}Si(n,γ), single particle resonances and doorway states, K matrix formalism 80−37384
^{29}Si(n,γ), evidence for neutron capture through doorway states 79−17909
^{30}Si (n,γ)^{31}Si, thermal neutron cross-section determ. 80−95321
Si(n,γ), ^{28}Si p3/2 neutron resonance γ-decay, partial rad. widths 80−52617
Si(n,γ), 3.2-15 MeV, cross-sections determ. 77−41962
$^{\wedge}$Sm, A=144,148,150,152,154, fast neutron radiative capture cross sections, 5 to 350 keV *(Russian)* 78−33188
^{144}Sm(n,γ), ^{145}Sm primary γ-rays, direct capture and neutron separation energy, (d,p) correlation 80−57738
^{144}Sm(n,γ), resonance and thermal n, γ-spectra, recent expt. review, non-statistical effects 80−37383
neutron radiative capture continued
^{145}Sm(n,γ), 3-7.2 MeV, ^{145}Sm neutron separation and level exciton (n,γ) and (d,p) correlations 80−22756
^{149}Sm(n,γ)^{150}Sm, neutron capture γ-ray spectra calcs. 78−94006
^{150}Sm(n,γ), ^{151}Sm low energy levels from expt. and Coriolis mixing calcs. 80−57697
S(n,γ), 3.2-15 MeV, cross-sections determ. 77−41962
Sn, simple configurations in capture states 77−22939
$^{\wedge}$Sn(n,γ) A=114,116,118, ^{115,117,119}Sn resonance meas., weak coupling model calc. for levels, J^{π} assignments 79−6416
^{115}Sn(n,γ), thermal, ^{116}Sn levels, J^{π} and transitions 80−52587
^{117}Sn(n,γ)^{118}Sn, disturbance of parity in ^{118}Sn gamma decay *(Russian)* 77−3008
^{117}Sn(n,γ)^{118}Sn, parity violation obs. 78−8820
^{120}Sn+n, transmission and capture γ-ray meas., ^{121}Sn props. 77−3004
^{122}Sn(n,γ)^{123}Sn^{m}, γ-ray, X-ray and electron spectra, ^{123}Sb transitions 77−88073
Sn(n,γ), up to 20 keV, ^{123,125}Sn level schemes, spin-parity assignments, neutron separation energies 77−54215
^{87}Sr(n,γ), 2, 2A keV, level of ^{38}Sr 77−30584
^{88}Sr(n,γ_1), ang. distrib. anal. in generalised direct-semidirect model 77−23023
^{88}Sr(n,γ), 2, 24 keV level struct. of ^{89}Sr 77−30584
^{88}Sr(n,γ), 7-11 MeV ang. distrib. from fast capture 78−54758
Ta, 0.02-3.0 MeV fast neutron cross sections 77−26758
^{181}Ta(n,α), thermal, isomer state excitation, relative probabilities 79−75814
^{181}Ta(n,γ), 2-3 eV, γ-spectra, energy levels, J^{π} 78−602
^{181}Ta(n,γ), 30 keV, capture cross sections, stellar nucleosynthesis 80−42663
^{181}Ta(n,γ), thermal, ^{182}Ta rot. bands, bandheads and decay data 79−93491
^{182}Ta, configuration mixing in positive parity states 77−22854
Ta(n,γ), separated isotopes, integral capture cross section meas. in CFRMF 77−26760
^{159}Tb, neutron resonances, time-of-flight spectra 80−27633
^{159}Tb(n,γ)^{160}Tb, E_n=14.1 MeV, γ emission exciton model *(Russian)* 79−13302
^{99}Tc, neutron capture cross section meas. up to 80 keV 78−25197
^{99}Tc(n,γ), thermal, ^{100}Tc level scheme, transitions and J^{π} values, n binding energy 79−63590
^{100}Tc, struct. anal. by (n,γ) reactions in Grenoble High Flux Reactor 77−34310
^{123}Te(n,γα), ^{124}Te capture states partial α-decay widths 80−37328
^{123}Te(n,γα), thermal n, ^{120}Sn γ-spectra, E1 and M1 hindrance factors 80−37386
^{125}Te(n,γ), 2, 24 keV, ^{126}Te level struct. 77−34308
^{130}Te(n,γ), resonance and thermal n, γ-spectra, recent expt. review, non-statistical effects 80−37383
^{130}Te(n,γ), thermal, ^{131}Te γ-transitions, spectroscopic factors and reduced transition intensities 80−91143
Th, metal rods, neutron capture, effective resonance integral meas. 77−71653
^{159}Th(n,γ), 2.6-700 keV, cross-sections and resonance parameters 78−50172
^{230}Th(n,γ), ^{231}Th excited states and bands, spins, γ-transitions 80−57699
^{232}Th, 24 keV neutron capture cross section meas. with Fe-filtered neutron beam 79−40910
^{232}Th, effective cross section dependence on thermal neutron temp. 80−547
^{232}Th, neutron cross section meas. 80−526
^{232}Th/^{238}U neutron capture cross section ratio, direct determ. for reactor lattices 77−50137
^{232}Th-^{238}U containing lattices, direct meas. of relative capture rates 77−61403
^{232}Th(n, γ), cross sections calc. optical model calcs. 79−30829
^{232}Th(n,e^{-}), ^{233}Th vibrational states determ. 77−30514
^{232}Th(n,γ), ^{233}Th excited levels, using thermal and average reson. neutron capture 79−45166
^{232}Th(n,γ), cross-section from 2.6-800 keV 78−8807
^{232}Th(n,γ), ratio to (n,2n) in fast reactor, direct meas. 80−102233
^{232}Th(n,γ) uncertainty file, for sensitivity anal. of fast reactor system 79−67835
^{232}Th(n,γ)^{233}Th, testing of ENDF/B-IV Th data in GCFR lattice 79−67836
Ti isotopes, capture and transmission meas., 1 to 100 keV 77−26712
$^{\wedge}$Ti(n,γ), A=46 to 50, thermal capture, gamma ray spectra 79−93629
$^{\wedge}$Ti(n,γ) A=46, 47, 49, 50, 45 MeV, cross section meas., resonance parameters 80−18315
^{46}Ti(n,γ), γ circular polarisation meas. 78−62533
^{169}Tm, neutron capture cross sections, 0.5 to 3.0 MeV 79−40912
^{169}Tm(n,γ), 0.5-3.0 MeV, ^{170}Tm, gamma-ray strength functions from spectrum fitting method 80−52616
^{169}Tm(n,γ), capture cross section from 10^{-5} eV to 2×10^{7} eV, statistical model 80−63189
^{170}Tm(n,γ), 0.5-3.0 MeV, γ-spectra strength functions 80−32240
Tn, absolute cross sections in keV range 77−26771
$^{\wedge}$U(n,X), A=233, 235, thermal n, gamma spectra from capture, fission and fission products 80−37352
$^{\wedge}$U(n,α), A=235,238, meas. of α-values in BOR-60 reactor core 79−97830
^{234}U(n,γ), thermal n, ^{235}U vibrational and single particle states 79−36123
^{234}U(n,γ)^{235}U, 5-49 MeV, low-spin states 78−512
^{235}U, capture to fission ratio determ. from low energy gamma-ray meas. 77−23152
^{235}U, capture to fission ratio in range 10-500 keV 77−26804
^{235}U, σ_c/σ_f ratio meas. in BFS critical assemblies 79−97737
^{235}U(n,γ), ^{236}U low lying levels from 4 isomer decay 80−47396
^{235}U(n,γ), 10-500 keV, capture to fission ratio, double humped fission barrier parameters 79−89336
^{235}U(n,γ) resonance capture, primary γ-transitions, parity assignments 77−26619
^{235}U(n,γ)^{236}U, gamma-ray spectra study *(Russian)* 77−6392
^{236}U(n,γ), 30-1800 eV, cross section meas. 77−23061
^{236}U(n,γ), 5-125 eV, ^{237}U levels, bands and J^{π} assignments, n binding energy 80−5041
^{238}U, 0.02-3.0 MeV fast neutron cross sections 77−26758
^{238}U, 24 keV, neutron capture cross section meas. with Fe-filtered neutron beam 79−40910

neutron radiative capture continued
^{238}U, 24.3 keV activation cross sections with Fe filter technique 77−26763
^{238}U, absolute cross sections keV range 77−26771
^{238}U, capture width of 6.67 eV neutron resonance 78−50162
^{238}U, cross-sections determ. by Fe filtered beam TOF method 77−23078
^{238}U, effective cross section dependence on thermal neutron temp. 80−547
^{238}U, energy-depend. Doppler effect calc. using collision probability method 77−57714
^{238}U, meas. of Cd ratio of neutron capture rates in slightly ^{235}U enriched fuel, systematic errors 78−8901
^{238}U, neutron capture cross section representation, TRX-2 lattice param. sensitivity 78−25275
^{238}U, neutron capture cross section ratios in range 10 to 90 keV 78−50163
^{238}U, neutron capture cross-section below 100 eV meas. 77−26680
^{238}U neutron cross sections evaluation for incident neutron energies up to 4 keV 80−5146
^{238}U, neutron resonance params. and cross sections, 9 eV to 4 keV 77−26710
^{238}U, stat. model calcs. of neutron capture gamma-ray spectra 77−67742
^{238}U(N,γ), neutron capture rate, absolute meas. 79−63678
^{238}U(n,γ), 2, 24 keV, resonance averaged γ-spectra, level and J^{π} appls. 80−37347
^{238}U(n,γ), 20-550 keV, cross section meas. 77−23056
^{238}U(n,γ), 5-20 MeV, direct and collective capture, excitation curve, γ-spectra 78−94001
^{238}U(n,γ), coupled channel calc. of direct and collective cross sections of deformed nuclei 77−26748
^{238}U(n,γ), cross section and resonance shape, gas molecule vibr. effects 80−42661
^{238}U(n,γ), cross section meas. using large Gd loaded liquid scintillator 78−25380
^{238}U(n,γ), L100 eV cross-section and resonance parameters 77−34309
^{238}U(n,γ), p-wave assignment of resonances 77−23062
^{238}U(n,γ), statistical anal. of intermediate struct. in cross-section 77−23057
^{238}U(n,γ), thermal, ^{239}U vibr. states 78−41627
^{238}U(n,γ) cross section, 5-100 keV, doorway state detection, statistical tests 79−93590
^{238}U(n,γ)^{239}U resonance capture self-indication obs. at 77, 293 and 873K 79−9574
^{239}U, struct. anal. by (n,γ) reactions in Grenoble High Flux Reactor 77−34310
^{50}V, γ-ray spectrum from thermal neutron capture 78−21568
^{51}V(n,γ), 2.6-215 keV, ^{52}V capture area, resonance parameters and mean level spacings 79−6608
^{51}V(n,γ), circular polarisation, ang. distrib. meas. 80−32285
^{52}V(n,γ), sputtering yields from V metal surface 80−25493
^{136}Xe(n,γ), resonance and thermal n, γ-spectra, recent expt. review, non-statistical effects 80−37383
^{136}Xe(n,γ), thermal, Lane-Lynn theory of direct neutron capture verification 79−36218
^{136}Xe(n,γ)^{137}Xe, determ. of neutron binding energy of ^{137}Xe 77−41879
^{136}Xe(n_{th},γ)^{137}Xe, spectra meas., ^{137}Xe level and decay scheme 78−13102
^{59}Y(n,γ), thermal, isomer state excitation, relative probabilities 79−75814
^{89}Y, fast neutron capture and the microscopic isovector optical potential 79−63668
^{89}Y, 6.2-15.6 MeV, gamma-ray spectra, cross-section meas. 78−33176
^{89}Y, reson. neutron capture cross-section between 2.5 and 100 keV 77−82924
^{89}Y(n,γ), 7-11 MeV ang. distrib. from fast capture 78−54758
^{89}Y(n,γ), direct-semidirect and compound nucleus contribs. to cross sections 80−68662
^{170}Yb(n,γ), 10-70 keV capture cross-section 80−27631
^{173}Yb(n,γ), search for non statistical effects 77−30588
^{173}Yb(n,γ)^{174}Yb, width correlation, primary transition intensities for resons. 77−79370
Yb(n,γ), ^{A}Yb A=172, 174, electric monopole transitions from excited $K^{\pi}=0^{+}$ levels 79−6486
Zn, 0.02-3.0 MeV fast neutron cross sections 77−26758
^{64}Zn(n, γ) cross-section meas., ^{65}Zn gamma intensity, k_0 factors calcs. 79−26433
Zr alloys, thermal capture cross-section var. with time, calc., mech. and corrosion props. var. 77−61505
^{A}Zr(n,γ), A=64, 66, 67, 68, 70, 2.8-500 keV, capture cross sections 80−57780
^{90}Zr(n,γ), thermal cross section, ^{91}Ze primary γ-rays and binding energies 80−52566
^{90}Zr(n,γ)^{91}Zr, thermal neutron reactions, γ-ray line obs. 78−17190
^{91}Zr, high resolution neutron transmission and capture 78−8806
^{92}Zr(n,γ)^{93}Zr, thermal neutron reactions, γ-ray line obs. 78−17190
^{94}Zr(n, γ) cross-section meas., ^{95}Zr gamma intensity, k_0 factors calcs. 79−26433
^{94}Zr(n,γ)^{95}Zr, thermal neutron reactions, γ-ray line obs. 78−17190
^{96}Zr(n, γ) cross-section meas., ^{97}Zr gamma intensity, k_0 factors calcs. 79−26433
^{96}Zr(n,γ)^{97}Zr, thermal neutron reactions, γ-ray line obs. 78−17190
Zr(n,γ), 2-24 keV, ^{A}Zr, A=91, 92, 94, binding energy and primary γ-ray intensities 80−52565
Zr(n,γ), A=92,94, cross section meas. 77−2986

neutron radiography
see also nondestructive testing
accurate dimensional meas. 78−60926
albedo method, local nonuniformity monitoring obs. 80−35482
autoradiography, visualisation of fissionable radionuclides in rat lung 78−28055
autoradiography for accurate localisation of ^{239}Pu in bone 77−40773
Birmingham dynamitron accelerator appl. to nuclear fuel radiography using Be target 77−81452
cardiac pacemaker batteries, investigation of electrolyte, USA National Bureau of Standards 80−56179
computed axial tomography, using filtered neutron beams 80−101258
computerised axial tomography, nucl. fuel anal. 78−82529
contrast enhancement using gaseous ^{3}He penetrant 80−93707
contrast enhancement using Gd_2O_3 additive, ordnance appl. 80−30177
contrast reduction factor evaluation 78−82067

neutron radiography continued
conversion efficiency enhancement in neutron radiography 78−7444
crack detection in TRIGA fuel rods 77−50229
detail improvement by indirect method *(German)* 79−100309
diffusion of H in β-Ti, V, Nb and Ta, neutron radiographic meas. 77−39696
edge enhancer, active differentiation cct. 79−24706
electron linear accelerator *(German)* 78−7150
electronic piece parts reliability evaluation 78−31610
equipment and methods review, beam production, sources and image recording 78−60889
fast neutron radiography for extended objects using Kodak CA 80-15 plastic detector 78−20267
fast neutron radiography of extended biological and medical objects *(German)* 78−15880
fast neutrons, disadvantages as medical diagnostic method 77−25554
fast neutrons, prod. of shadowgraphs of fast events 78−41400
graphite fibre reinforced epoxy resin, radiographic technique for resin content meas. 78−3286
Hanford Engng. Development Lab. facility 79−96255
HFEF/N, handling equipment for neutron radiography facility 79−45443
high-speed-motion neutron radiography system, modulation transfer functions 78−7158
highly specialised applications, useful references 78−60893
hot fuel examination, neutron radiography facility 79−9725
image improvement with 14.5 MeV 77−52594
image quality 77−81347
imaging systems, MTFs and resolution capabilities 80−66758
industrial applications in USA, review of data and neutron effects 78−60891
industrial neutron radiography using research reactors 79−11757
irradiated fuel pins, coupled fast reactivity measurement facility 79−93720
Kodak CA 80-15 plastic detector, fast neutron radiography for extended objects 78−20267
materials testing, radionuclide methods, in West Germany, industrial use impetus *(German)* 79−96231
microneutronographic and neutron-induced autoradiographic techniques, review of appl. in metallurgy 78−60892
mixed oxide reactor fuel, possible Pu particle detection 77−71637
mobile equipment using ^{252}Cf source 79−43534
NBS reactor, summary of activities, (July 1976 to June 1977) 78−82435
NDT in triton reactor, industrial appls. *(French)* 79−61826
neutron facility of Birmingham radiation centre based on Dynamitron accelerator 77−26887
neutron radiography facility handling equipment 79−9726
nondestructive materials testing, review of radiographic principles and methods 78−53065
nondestructive testing, nuclear engineering appl. *(Slovak)* 80−76430
nuclear fuel inspection review and facility description 78−60890
nuclear materials safeguards reference measurement system utilizing resonance neutron radiography for nondestructive assay meas. 80−78377
nuclear methods of NDT, review 77−32756
painting and artist identity, autoradiography and gamma-ray spectroscopy appl. 80−26073
physical processes and math. methods review, neutron-nucleus interaction effects 78−60888
plastic detector technique in fast neutron radiography 79−76299
polyurethane, void detection by neutron gauging 78−23910
polyurethane foam, fast-neutron gauging for void detection 78−7157
reactor materials at HFEF/N 79−45442
reactor test facility, fast flux 80−18371
resonance energy neutron radiography techniques 78−82528
resonance energy neutron radiography using dynamitron accelerator 79−52480
resonance neutron radiography using a position-sensitive proportional counter, appl. to meas. of nuclear fuel 80−13597
review of application in industrial analysis 79−52609
simulated neutron tomography for nondestructive assays 80−99218
skarns, B distrib. as mineralisation test, (n,α) radiography 77−17091
solid state nuclear track detectors 80−97671
steel:B, brittle rupture, (n,α) radiography method *(Russian)* 78−48491
surface, bulk anal., neutron activation, radiography, nuclear microprobe techniques, review 78−85238
technique and appls. to aerospace industry 79−79198
technological development review, neutron props. and history 78−60887
Texas A and M Nuclear Science Centre, neutron radiography facility, development and utilisation 80−9401
thermal neutron fluxes prod. in water by isotope and accelerator neutron sources 78−55077
thermal neutron radiography, using ionographic process 79−11734
thermal neutron radiography facility on IRT-2000 reactor 78−17286
thin coatings, thickness monitoring using slow-neutrons 77−71297
tomography investigation using research reactor 78−23915
TR-1 reactor, thermal spectrum using neutron radiography of wedge shaped absorber 78−74439
transient gas density meas. using neutron radiography 78−47076
TREAT, neutron radiography equipment improvements 79−45462
TREAT facility, pinhole imaging of test fuel element 78−21627
trends, review *(German)* 77−32745
void reconstruction in 2-D, using neutron transmission 78−22605
water determ. in scrap metal 77−56177
B burnable poison in reactor fuel side plates, identification by neutron radiography 79−54492
^{252}Cf, use of TV imaging techniques 78−60922
D_2O-H_2O mixing, diffusion meas. using neutron radiography 77−15605
Fe-C-B, exam. of phase diagram using neutron autoradiography 79−8279
Gd neutron radiographic amplifying screen sensitivity 78−7448
Gd, neutron radiography uses 77−66722
Gd_2O_2S scintillation convertor screen characterisation for portable system 77−40510
H and water transport studies review 78−59961
H embrittlement in metals, assessment of techniques for local detection 78−3439
H_2 diffusion in metals, conc. profile meas. 77−24438
Li-I_2 pacemaker battery electrolyte exam. 80−30940
Mo-B alloys, B distrib. in welds, nuclear track autoradiography study 79−43282

neutron radiography continued
Si-Si_3N_4-SiO_2-Si multilayer structs., impurity distrib., activation anal., autoradiography techniques 77−16881
^{235}U-fission track micromapping, exam. of U mobilisation processes in Precombrian sediments 80−98477

neutron reflection
Argonaut reactors, coupled core, neutron wave propagation, Be, graphite and D_2O as internal reflectors 80−27752
Bloch walls, refraction of cold neutrons 77−26815
BWR/6 axial reflectors, Monte Carlo modelling 80−22939
charge determination, expt. using ultraslow neutrons 79−9370
concrete, differential characts. of current number albedo 77−71633
concrete, effect of azimuthal angle on fast neutron albedos 78−8866
concrete interfaces, Monte Carlo Spectra calc. 80−27686
critical slab reactor with finite reflector problem soln. 77−65251
diphenyl, cold neutron interaction cross-sections, 353-653K 79−93682
enriched, water-reflected, critical measurements 79−26569
fast reactors, effect of neutron reflection from walls of room on pulse parameters 77−23187
fissile material critical arrays, effects of packaging materials 79−26567
fissionable highly-compressed pellets, neutron kinetics 77−38315
flux distribution from microtron convertor in graphite moderator with water reflector *(Russian)* 77−82979
guide tubes, effect of sharp bend on transmission 77−385
homogeneous slabs, dosimetric quantities and neutron spectra 77−38319
image formation with ultracold-neutron waves 80−78752
neutron bottles, surface physics and chem. rel. to storage time anomaly 79−85575
neutron charge, upper limit determination method using neutron reflection *(Russian)* 80−32316
neutron generation time for reflected systems 80−563
neutron source, 14 MeV, skyshine anal., Monte-Carlo computer code 78−66429
PWR spent fuel storage pools, graphic method for neutron multiplication factor comparison 79−26566
reactor control rods, influence of neutron trap on critical loading and efficiency *(Russian)* 80−37474
reflected cylindrical reactor, eigenfunction and numerical solns. to critical problem 78−58326
scattering materials effect on average neutron energy, spectral index, hardness parameter 77−26816
shields, homogeneous slabs, computer calcs. of transmitted, reflected spectra 77−3067
slab with finite reflectors, bounds for critical length 78−82409
Soller collimators, appl. to small angle neutron scatt., Monte-Carlo simulation 78−29701
space craft thermionic reactors, reflector drums as control mechanism 80−42784
spin rotation and phase shift in neutron interferometry, polarisation props. 77−18763
super mirrors, reflectivities calc. 79−45320
ultra cold neutron production, by Bragg reflection from moving crystal, Monte Carlo simulation 79−701
ultra cold neutrons, axial peaking in conical guide tube 77−14295
ultra-cold neutrons, review of prod., transport and appl. 79−40982
ultracold, storage on horizontal plane with restrictive walls 77−23345
ultracold neutron reflection from one-dimens. pot. barrier, reson. struct. *(Russian)* 78−37393
ultracold neutrons, diffraction and mirror reflection 78−13193
ultracold neutrons, extraction, transportation and storage 77−26826
ultracold neutrons, neutron-optical image formation *(Russian)* 80−5193
ultracold neutrons, reflection from diffused pot. threshold *(Bulgarian)* 78−82411
ultracold neutrons, transmission through moving pot. barrier 78−8867
ultracool neutrons, mirror refl. in multilayer struct., interference methods *(Russian)* 77−34367
$Fe_{2.45}Mn_{0.05}Si$, slow neutron polariser, by single cryst. (111) refl. 80−49052
$Li_{0.5}Fe_{2.5}O_4$, slow neutron polariser, by single cryst. (222) refl. 80−49052
Ni-Mn multilayer for monochromators and supermirrors, neutron reflectivities 80−22880
Ni-Ti multilayers for monochromators and supermirrors, neutron reflectivities 80−22880
Pb reflector in small Fe pile, material group consts. meas. 79−6738
UO_2 rods in water with U or Pb reflecting walls, critical expts. 80−32331

neutron scattering *see kaon-nucleon scattering; lepton-nucleon scattering; neutron-nucleus scattering; nucleon-nucleon scattering; photon-nucleon scattering; pion-nucleon scattering*

neutron scattering (crystallography) *see neutron diffraction; neutron diffraction crystallography; neutron diffraction examination of materials*

neutron sources
0.5 keV-centred spectrum, use in calibration of neutron sensitive instruments 77−6615
3 ns pulsed beam-target, thermonuclear neutron burst simulation 80−87008
14 MeV, for non-destructive analysis, density distribution radiation effects *(German)* 77−25349
14 MeV intense source facility using T ion beam and D jet target 77−83428
14 MeV neutron generator, concrete shielding dose transmission factors 77−71702
14 MeV neutron generators for radionuclide prod. 80−3811
25 keV filtered beam facility, monoenergetic calibration of dosimeters and spectrometers 77−23348
absorption medium random, neutron source mean strength *(French)* 80−74057
accelerator-based pulsed cold neutron source *(Japanese)* 80−47796
activation calc. and exptl. comparison for 14 MeV neutron source, fusion technique validation 79−9657
anisotropic neutron emission from lab. sources 78−90009
Argonne intense pulsed neutron source, commissioning 79−67997
bath techniques for neutron source emission rate meas., $MnSO_4$ bath 79−9980
beam experiments *(Japanese)* 80−27684
beam for cancer radiotherapy 77−81567
BNL high flux beam reactor, neutron beams 77−30693
Bratislava 14 MeV source, design concept 80−99362
Brookhaven Accelerator-based Neutron Generator 77−38465

neutron sources continued
burst source, TOF meas. *(French)* 80−14040
calibration at NBS for calibration checks of neutron radiation instruments 77−38540
chopper for neutron pulse propagation experiments 78−13362
clinical neutron source engineering problems and dose distributions 79−20635
cold moderator, considerations for pulsed neutron source 79−76219
cold neutrons, 5 to 6 Å, polarised, prod. methods and existing systems 79−68120
cold neutrons, experimental reactor low temp. facilities *(French)* 77−131
cold neutrons and applications of quasielastic scattering *(Japanese)* 80−27685
cold pulse from methane at 20K, time dependence 77−67928
conference on neutron capture gamma ray spectroscopy, Upton, USA. (Sep. '78) 80−36780
conference on neutron inelastic scattering, Vienna, Austria (Oct. 77) 79−41912
CTR blanket design *(Japanese)* 78−46164
CTR blanket design and associated problems *(Japanese)* 77−50286
cyclotron, neutron production by 25-55 MeV protons on Be, spectra and yield 77−70539
cyclotron beams, spectra at 0° from 83.7 MeV deuterons and 100.2 MeV protons on Be 77−73593
cyclotron-produced beams, energy spectra and dose distrib. spectra 77−70554
D-T generator, neutron yield control, meas. method *(German)* 77−23336
dense plasma focus devices matching with fission reactors 78−37436
dense plasma focus Julich I, neutronics, fusion plasma investigation 77−35396
deuteron accelerator, two freq., for high power neutron generator, expt. 78−78540
deuteron linac, for high intensity neutron source 77−38464
deuteron linac as neutron generator for materials irradiation and fusion reactor investigation 77−34486
deuteron stripping intense source for fusion reactor materials anal. 77−83423
direct current accelerator for 14 MeV neutron prod., thermal-mech. design 78−66383
dosimetry, standardization, 0.001-14 MeV, description of sources 79−9919
dosimetry techniques for accelerator-based irradiation facilities 79−41041
Drabkin neutron monochromator optimisation 79−22518
Dynagen IV, compact high intensity neutron generator 77−86603
electrostatic 160 kV, 200 mA dc accelerator for high 14 MeV neutron yield 77−83421
electrostatic low energy, high current accelerator for 14 MeV neutron production 80−99353
engineering test facility as an intense pulsed neutron source or time-of-flight neutron source 80−57831
epithermal neutron field for ^{10}B neutron capture therapy, prod. using FBR 80−61692
epithermal neutron radiation field development for cerebral tumour therapy *(Japanese)* 78−88742
facility for polarised and unpolarised monoenergetic neutrons 77−30694
fast neutron beam for medical use, production and definition *(French)* 80−69003
fast neutron facilities for radiobiological irrad. 80−109064
fast neutron facility in CP-5 reactor, neutron flux, energy spectrum, primary recoil distribution 79−41056
fast neutron fields produced by Kyoto University Cyclotron 80−27840
fast neutron filter of liquid O_2, effect of antiresonance of 2.37 MeV beam prod. 77−79494
fast neutron generator, LiOD-D_2O thermal-to-14 MeV convertor, evaluation 79−9928
fast neutron generator, LiOD-D_2O thermal-to-14 MeV convertor, evaluation 79−13567
fast neutron generator tube, Haefely-GFK, for radiotherapy 79−20652
fast neutron prod. cross sections at Louvain la Neuve isochronous cyclotron 78−29682
fast neutron pulse reactor, IBR-2, 4 MW 79−699
fast neutron radiotherapy unit, AEG/RDI 79−20653
fast neutron sealed-tube radiotherapeutic installations, characteristics 79−20650
fast neutron therapy equipment trials 79−20657
fast neutron therapy history 79−20634
fast neutron therapy system using cyclotron beam, beam optics and shielding 79−57756
fast neutron therapy with medical cyclotron, clinical results 79−20643
Filippov dense focus, time and space resolved neutron emission meas. 77−58896
Filippov plasma focus apparatus fundamental characteristics *(Japanese)* 77−51244
filtered 2 keV beam facility 77−23346
filtered beams, 2 keV, 24 keV, 144 keV, calibration and use 79−9937
filtered beams at NBS reactor 2 keV, 25 keV and 144 keV 77−38539
filtered neutron beam facility, 2, 24 keV neutron beams prod., filter comps. and configs. 77−6597
filtered neutron beams, 2 and 24.5 keV, current density profiles and high energy background *(German)* 78−58529
fission reactor research, pulsed-neutron sources for flow measurement 79−93695
fixed energy, absolute cross section meas. 79−13365
flux monitoring and data anal. for neutron standard react. cross sections 78−90039
FMIT neutron source, energy spectra and yields, fusion reactor mat. development appl. 80−32552
Frascati Tokamak, 1MJ plasma focus dynamics, neutron production scaling 80−24220
fusion, plasma focus as large fluence neutron source 77−88315
fusion materials development studies, irradiation sources 80−32478
Fusion Materials Irradiation Test Facility, high flux neutron source for material development 80−32551
Fusion Materials Irradiation Test Facility 80−91361
fusion plasma focus as high intensity neutron source 77−83433
fusion plasma source, PROMETHEUS, potential mirror concepts for materials testing 77−83431

neutron sources continued
future nuclear power technology, impact of nuclear research in India 80−95345
gas jet target with electron beam heating, plasma density meas. 77−39457
gas target, high pressure, liquid N cooled, intense fast-neutron prod. by $^{3}H(d,n)$ reaction 77−3201
gas target neutron generator, Canadian research 77−83427
gas target neutron source for radiotherapy, generation by $^{3}H(d,n)$, energy spectra, flux 78−92698
generator appls., activation analysis, material investigation, radiotherapy *(Czech)* 79−31279
generator facility with alternative 30° target 80−9444
GLEEP reactor neutron thermal and epithermal flux calibration 79−93856
guide tubes, effect of sharp bend on transmission 77−385
Harwell 136 MeV electron linac, slow neutron production, optimisation calcs. 79−41048
HFBR, safety features of cold neutron moderator 80−23114
HFR at Grenoble, neutron beam installations 77−26864
high intensity, high energy source for fusion reactor developments *(Japanese)* 79−31179
high intensity neutron sources in thermal, resonance and fast ranges 80−37677
high-intensity, with rotating and gaseous targets, characts. and appl. *(Slovak)* 79−68114
high-output generator use of 14 MeV activation analysis 77−90694
ILL ultra and very cold neutron source performance 79−45519
in-core fast neutron generator using LiOD thermal neutron convertor 77−10511
intense high-energy sources for fusion reactors and radiotherapy 77−83419
intense neutron generators 77−75018
intense neutron source (INS) prototype tests 79−76220
intense neutron source facility, skyshine anal. methods comparison 80−5349
Intense Neutron Source Facility skyshine analysis 79−9931
Intense Pulsed Neutron Source (IPNS-1) accelerator 500 MeV fast kickers 79−72131
Intense Pulsed Neutron Source (IPNS-1) accelerator RF system 79−67998
intense pulsed spallation source, UCN production 80−14024
intense sources of fast neutrons, review, book contrib. 79−22161
intense sources of fast neutrons, review 79−22522
ion pulse stacking for prod. of intense current pulses 80−23209
isochronous cyclotron sector magnet field calc., integral eqn. method 79−41053
jet target intense neutron source 78−66384
JINR synchrophasotron, neutron prod. by deuteron stripping 78−33340
LAMPF radiation effects facility, total neutron flux, energy spectrum, meas. and calc. 77−23331
Larmor precession, spin echo, memory effects and polarized neutrons, pulsed source efficiency improvements 79−45323
laser solenoid radiation test facility 77−83430
linac, Chalk River high-current 100% duty factor accelerating columns 77−38468
linear electron accelerator for neutron prod. using bremsstrahlung and (γ,n) processes *(Japanese)* 78−78532
low-power, use in activation determ. of Mo and W in hydrometallurgical plant effluent waters 78−7279
mechanical interrupter-monochromator with changeable rotors for slow neutron beam, 3 to 60 MeV 77−46442
methylbenzene, solid, pulsed cold neutron source, moderation props., radiation decomp. 77−83407
metrological certification of neutron reference sources 77−30682
monochromatic intense beam of longwave neutrons, prod. by polycryst. scatterers in open tangential reactor channel 77−71712
monochromatic thermal neutron polarisation crossed mag. field method 80−78477
monoenergetic beams from sector focusing isochronous cyclotron 77−26917
monoenergetic polarised neutron beam from 200-500 MeV prod. at TRIUMF 77−83413
negative reactivity reactor expts. using controlled intensity neutron sources 79−17967
neutron capture γ-ray borehole mineral anal., optimum neutron source size 80−61213
neutron curved monochromators, reflectivity data 79−45515
neutron focus in radiation field of relativistic channelled particles 79−85852
neutron monochromator, development of Institut Laue Langevin 79−45514
neutron multiplier, criticality studies 77−34503
neutron multiplier, criticality studies for ^{252}Cf source 78−25367
neutron radiography, equipment and methods review, beam production, sources and image recording 78−60889
neutron standards and appl., conference, Gaithersburg, MD, USA (March 1977) 79−9581
neutronic analysis of the NBS intermediate-energy standard neutron field (ISNF) 80−27692
NISUS facility, sensitivity anal. for secondary intermediate energy standard neutron field 79−36451
non-fission, fuel supply enhancement for converter reactors 79−17960
nuclear NDT methods, sensitivities and detection limits 77−32756
nuclear reactor fuel breeding using independ. neutron sources 77−26840
output of 14 MeV neutron generators, meas. using $^{16}O(n,p)^{16}N$ 79−3287
particles and radiation therapy, conference, Berkeley, USA (1976) 79−20619
photoneutron target design for fast-neutron spectrum measurements 80−23232
plasma focus devices, neutron emission parameters 80−24221
polarised, use in light nuclei reactions 77−18764
polarised beam prod. using ferromag. doubly bent neutron guide *(Russian)* 77−46446
polarised fast neutron beam sources, status report 77−23343
polarised generator, intensity increase of polarized deuterium by using a short compressor magnet 80−18732
polarised powerful neutron beam, in vertical reactor channel 78−5082
polarising neutron guide using laminated mirror 78−9012
polarising Soller guides for cold neutrons 78−54501
neutron sources continued
primary beam and shielding radiation quality and absorbed dose obs. 80−12281
proton linac as source for radiotherapy 77−81569
pulsed, appl. of neutron spin echo 79−81115
pulsed, cooled polyethylene moderator 78−70666
pulsed, for nucl. consts. meas. 77−50321
pulsed, inelastic rotor spectrom., for high energy vibr. spectroscopy expts. 78−86721
pulsed, mechanical velocity selector for small angle scatt. instrument 79−13586
pulsed, neutron guides, geometry optimisation and simulation 80−47802
pulsed, neutron installations and facilities 77−23317
pulsed, research trends in neutron physics 77−22825
pulsed, TOF, spectroscopy with 1 GeV proton synchrocyclotrons 77−26927
pulsed neutron, from spallation target, Rutherford Laboratory 78−29208
pulsed neutron generator, ING-2 80−23204
pulsed neutron generator with laser deuteron source 80−27844
pulsed neutron physics facility, remote operation and maintenance 79−9934
pulsed neutron research, book 80−22146
pulsed neutron source, proton synchrotron 77−83191
pulsed neutron source creation by laser/relativistic-electron-beam plasma heating 78−74527
pulsed neutron sources by accelerators, appl. to neutron scatt. *(Japanese)* 77−383
pulsed neutrons from spallation source, thermal neutron scatt. 77−83350
pulsed power appl. to intense neutron source development 77−83432
pulsed source, small angle scatt., low-Q spectrometer appl. 78−55083
pulsed spallation neutron source, accelerator, target and moderator design 77−67930
pulsed spallation neutron sources 79−76237
pulsed spallation neutron sources 80−27852
pulsed spallation neutron sources for slow neutron scatt. 77−83426
pulsed spallation source for neutron scattering research 77−83351
pulsed thermonuclear sources, book contrib. 80−23235
pulsed UCN source, meas., produced by Doppler-shifted Bragg refl. 80−32556
pulses sources for epithermal neutrons, review 79−45516
radiation therapy, cyclotron biological intercomparisons 79−20589
radiotherapeutic source developments at Cyclotron Corporation 79−20651
radiotherapy, linear accelerator neutron sources and characts. 80−51239
radiotherapy beams prod. by protons and deuterons on Be and Li, dosimetry 78−24141
recent advances in neutron physics, prod., handling, detection, nuclear reactions, resonances 77−26686
remote handling design for the intense pulsed-neutron source 80−69006
review and development, neutron production processes, particle accelerator appl. *(Dutch)* 79−81108
rotating target dc 14 MeV source 77−83422
rotating target neutron souces, appl. to high energy neutron induced effects on fusion reactor materials 79−45493
RTNS-II neutron sources: status report 79−76221
sealed tube generator system, 14 MeV, for total body in vivo activation analysis 79−88162
SIN neutron facility, 150 to 600 MeV, detection and meas. 78−62669
skyshine analysis of 14 MeV neutron source, Monte-Carlo computer code 78−66429
slow neutron polarisation by polarised proton filter using ethylene glycol 78−90046
spallation neutron source, alternative π, μ and ν beam prod. and uses 78−66442
spallation neutron source, LASL, neutral beam injection for proton storage ring 79−76156
spallation neutron sources for neutron beam research 79−9926
spallation source, synchrotron magnets 79−68039
spiral deflector of a neutron generator target 79−76247
stainless steel, reduction of H by Ar glow discharge, rel. to ultra cold neutron storage 80−104459
standard fission neutron irradiation facility 79−31285
subcritical cyclostationary nuclear reactor, neutron counting statistics, sinusoidally modulated neutron source 80−99203
subsonic gas target neutron generator 80−5424
superconducting cyclotron neutron source for radiotherapy 79−20655
synchrocyclotron, Leningrad Institute of Nuclear Physics 80−87003
synchronisation of neutron beam, ultracold neutron spectrometer 79−721
synchrotron, intense pulsed neutron source, vacuum system 79−63261
target, for neutron production, by electron accelerator 3 to 10 MeV *(Rumanian)* 79−63855
target design for intense pulsed neutron source 80−23233
thermal, pulsed, from multiplying media, anal. and interpretation of experimental data *(Rumanian)* 78−46203
thermal neutron filter, Si single cryst. 79−45512
thermal neutron fluxes prod. in water by isotope and accelerator neutron sources 78−55077
thermal neutron standard field with Maxwellian distrib. using KUR heavy water facility 78−33342
thermal neutrons, 2 to 3 Å, polarised, prod. methods and existing systems 79−68120
thermal-neutron-driven 14-MeV neutron generator 80−95496
theta-pinch, linear, 14 MeV neutron source appls. 77−23332
THTR 300 MW(e) Schmehausen station, anal. of non-central neutron source 77−67802
Tokamak, neutron source and toroidal geometry neutronics effects 77−34457
Tornado traps, rotating plasma operation 77−15226
transformer septum magnet for intense pulsed neutron source 79−68102
transuranics for industrial and medical appl. *(French)* 77−42206
TRIGA Mk.II reactor for $B(n,\alpha)$ therapy, remodelling and dosimetry 80−56200
TRIGA research reactor, instrumental neutron activation analysis pulsed irradiations 79−36450
TRIGA-II Musashi reactor, neutron irradiation facility for medical purposes *(Japanese)* 77−56459
TRIUMF neutron beam, monoenergetic polarised, 200 to 500 MeV 79−13573
TRIUMF thermal neutron facility, design, experience, fluxes and activation levels 79−76222
twinned neutron monochromator 78−840

neutron sources continued
UCN, detection systems, sources, transport, book contrib. 80−22882
UCN, gravitation influence on lifetimes on traps 80−18750
UCN, storage in pulsed aperiodic-action reactor 80−18749
UCN (VCN) sources, beam tubes and neutron guides, for fundamental phys. expts. at ILL Grenoble 79−67932
UCN conservation in Al and Cu walled vessels *(Russian)* 80−14034
UCN container materials, reduction of surface H by ion bombardment 80−9446
UCN prod. using Doppler shifted Bragg scatt. and intense pulsed neutron spallation source 80−14024
UK pulsed spallation neutron source 79−45517
ultra cold neutron extraction from high flux reactor SM-2 77−57787
ultra cold neutron prod. rate in external liq. He source 78−70678
ultra cold neutron production, by Bragg reflection from moving crystal, Monte Carlo simulation 79−701
ultra cold neutron source, expt. current status and results 80−37678
ultra cold neutron source, using down-scatt. of 10 Å neutrons in liquid He 79−68121
ultra cold neutrons, prod., detection, confinement and storage for fundamental phys. expts. 79−63858
ultra cold neutrons, production and storage *(Russian)* 79−45518
ultra cold neutrons, super thermal source 80−52807
ultra-cold and cold neutrons, interaction with superfluid ^{4}He 77−83434
ultra-cold neutrons, storage in pulsed reactor *(Russian)* 77−3204
ultracold, neutron storage bottles, shortening of storage time, surface contamination 78−17461
ultracold, storage on horizontal plane with restrictive walls 77−23345
ultracold low energy neutron storage in vessels with condensed metal walls *(Russian)* 78−78542
ultracold neutron accumulation, above-barrier neutron effects, lifetime determ. 80−102227
ultracold neutron beams from ultracold neutron gas 77−26913
ultracold neutron diffusion along guide tube 78−33237
ultracold neutron flows, spectra meas. 77−26926
ultracold neutron polarisation 78−29681
ultracold neutron storage in mag. trap *(Russian)* 78−29538
ultracold neutron storage in magnetic traps 77−23344
ultracold neutron storage ring supercond. magnet design 79−31266
ultracold neutrons, ferromagnetic gates 77−46440
ultracold neutrons, heating and anomalous confinement times *(Russian)* 78−33358
ultracold neutrons, review of Soviet expt. research on prod. and storage 79−97923
ultracold neutrons, upscattering detected as main reason for anomalous loss in storage expts. 78−46205
ultrahigh flux reactor, Grenoble, neutron-physical expts. *(German)* 80−5209
USA National Bureau of Standards reactor utilisation 79−9693
variable energy fast neutron activation analysis facility 77−30743
very cold neutrons from linac-cold moderator system 80−27842
water-cooled target for the 14 MeV neutron source, design and experiment 80−47795
Weapons Neutron Research Facility initial target/moderator configuration 79−9933
ZING-P prototype pulsed spallation neutron sources for slow neutron scatt. 77−83426
ZING-P pulsed neutron source prototype, inverted geom. TOF spectrom. 77−83448
(d,n) reactions on T, D, NA-2 neutron generator, fast neutron spectrum, stilbene scintillation spectrometer meas. *(Czech)* 77−71710
π factories, use as neutron sources 78−21791
Am-B, neutron fluence-to-dose conversion factors 79−6771
Am-Be neutron probe, underestimation of radiation exposure by film badges 78−15900
Am-Be neutron source for anal. of prompt neutron capture gamma-rays *(German)* 77−16879
^{241}Am-Be, 100 mCi source for student expt. on neutron moderation in water 79−97146
^{241}Am-Be, determ. of ave. neutron activation cross-sections 79−31282
^{241}Am-Be neutron spectrum, (n,p) reaction average cross-sections 80−22827
^{241}Am-Be thermal neutron flux standard density variation obs. 77−83409
^{241}Am(n,α) sources, characteristic gamma-ray spectra from light elements within sources 79−3269
^{197m}Au, for neutron activation analysis, form. cross sections for 3 and 14.1 MeV neutrons 80−32283
B_4C filtering of FBR spectra for generation of neutron reference source 80−42884
Be, absolute neutron yield meas. for protons from threshold to 3 MeV 77−79498
Be compact target, fast neutron prod. by 30 MeV deuteron irradiation 77−83424
Be, neutron focus in synchrotron radiation *(Russian)* 78−33344
Be, neutron spectra from p,d, ^{3}He collisions 80−524
Be+d, 14-40 MeV, Monte Carlo calc. of neutron yields 79−49887
Be+d, dosimetric props. 79−12009
Be+d, low-energy spectrum, rel. to neutron prod. for radiotherapy 78−40319
Be+d neutron source, material damage study, He prod. and neutron fluence per neutron obs. in irrad. material 78−86710
Be+p beams, 30 and 40 MeV, polyethylene filtration 78−53494
Be(^{3}He,n) fast neutron generation in cyclotron 77−88311
^{9}Be(α, n), 100 MeV, neutron polarisation meas. 78−70726
^{9}Be(d,n), 14-23 MeV, thick target neutron yields 77−57791
^{9}Be(d,n), 14.8-23 MeV, thick target neutron yields 77−26752
^{9}Be(d,n), 40 MeV deuterons from ORIC, intense neutron source 77−83425
^{9}Be(d,n) neutron field, integral tests of activation cross sections 80−851
^{9}Be(d,n)^{10}B, polarised 4.5 MeV neutron source 77−57790
^{9}Be(d,n)^{10}B use of neutrons for meas. of full cross sections *(Russian)* 80−69008
^{9}Be(d,n)^{10}Be, neutron distrib. from bombardment of thick Be target 77−83408
^{9}Be(p,n), 14-23 MeV, thick target neutron yields 77−57791
^{9}Be(p,n), 14.8-23 MeV, thick target neutron yields 77−26752
Be(d,n), activation cross-section, integral tests, dosimeter appl. 80−32553
Be(d,n), planar, used for high-energy neutron irradiation induced creep testing 79−79200
neutron sources continued
Be(d,n), stripping-theory anal. of thick-target neutron prod. 77−6600
Be(p,n), 26, 35 and 45 MeV protons, neutron beam dosimetry 78−28083
Be(p,n), 26 MeV fast neutron therapy beam, dose meas. 78−28054
^{13}C(α,n), n and 6.13 MeV γ-ray emission for Ge(Li) detector calibration 79−13572
^{144}Ce photoneutron sources, determ. of standard neutron yield, influence of bremsstrahlung 79−72177
^{252}Cf activation facility with ^{235}U fuelled multiplier and low background gamma detectors 77−36843
^{252}Cf fission source, undergraduate laboratory expts. 77−382
^{252}Cf for interstitial radiotherapy implantations, clinical study 78−11722
^{252}Cf, heavy metal shielding 79−9892
^{252}Cf, high-intensity, remote fabrication and calibration equipment and techniques 77−54388
^{252}Cf, medical and industrial sources and applications 77−26915
^{252}Cf, neutron activation anal. of Constantinian coins 78−350
^{252}Cf, neutron energy spectra and doses in liquid air 77−67901
^{252}Cf neutron source, dosimetry meas. technique tests 79−68113
^{252}Cf neutron source for water-steam mixture void fraction meas. 79−26762
^{252}Cf neutron sources, appls. of activation anal., review 80−18728
^{252}Cf, neutron sources for calibration of personnel dosimeters 80−13946
^{252}Cf, optimal size source for borehole capture gamma-ray anal. 79−29890
^{252}Cf, optimum design for subcritical neutron multiplier 79−59290
^{252}Cf radiotherapy source dosimetry, appl. of liq.-dielec. ionisation chamber 77−13009
^{252}Cf shuttling source for nuclear fuel reactivity monitoring 79−9813
^{252}Cf source fabrication 77−26916
^{252}Cf, source for industrial and medical appl. *(French)* 77−42205
^{252}Cf source in tissue-equivalent phantom, neutron absorbed dose obs. 80−12278
^{252}Cf source projector for plesiocurietherapy 77−29197
^{252}Cf source with high emission, n and γ dosimetry, safety *(Czech)* 78−33296
^{252}Cf spontaneous fission neutron source, enhancement by ^{238}U surrounding cylinder, determination of $\nu\sigma_f$ 77−6594
^{252}Cf spontaneous fission neutron field, ave. activation cross sections 79−30830
^{252}Cf spontaneous fission spectrum irrad. facility for neutron reaction rate meas. 77−14294
^{252}Cf spontaneous fission spectra, data anal. in TOF meas. 79−26811
^{252}Cf, standard spectrum, status report 77−23017
^{252}Cf, status, application and prospects 77−26914
^{252}Cf, sub Cd thermal neutron fluxes in H_2O near the source 79−698
^{252}Cf, use for brachytherapy 78−20272
^{252}Cf, use in neutron activation anal. 77−29084
^{252}Cf wire neutron source distrib. meas. by autoradiography 77−61643
^{252}Cf-^{235}U subcritical multiplier, computer-controlled cyclic activation anal. 79−11865
^{252}Cf-based borehole logging system, delayed neutron activation anal. method for uranium 79−53569
^{242}Cm-Be, neutron spectra calc. 77−30687
^{244}Cm-Be, neutron spectra calc. 77−30687
Co, absolute neutron yield meas. for protons from threshold to 3 MeV 77−79498
Cu, absolute neutron yield meas. for protons from threshold to 3 MeV 77−79498
^{244}Cu, source for industrial and medical appl. *(French)* 77−42205
D gas target with compact medical cyclotron, dosimetry of neutron field 77−73592
D ion accelerator, design and operation 79−49883
D-Ar mixture, effect of Ar admixture on plasma temp. 79−37446
D-D fusion reactor blankets and shields, effect of neutron source ratio on nuclear characts. 79−41033
D-D sources for medical appl., survey 77−25547
D-T mixed beams driven into solid targets 77−83420
D-T neutron source design for radiotherapy 79−20656
D-T sources, accelerator prod. neutrons of high flux rate, review 77−23342
D-T sources for medical appl., survey 77−25547
D+d, low-energy spectrum, rel. to neutron prod. for radiotherapy 78−40319
D+d reaction, 6.8 to 11.1 MeV, beam dosimetry 78−53509
o-D_2, liq. convertor for ultra cold neutrons 79−45520
D_2O, secondary photoneutron effects on thermalisation experiments 80−99364
D_2O thermal column irradiation facility Penn State Breazeale Reactor 80−9339
DT, 14 MeV neutron generator therapy facility 77−81568
DT miniature target assembly, neutron yield calib. with associated particle monitoring 79−45505
DT plasma in biconical system, neutron generation by shell implosion 79−37524
D(d,n), source of neutrons for quasifree scatt. obs. on D_2O 77−34525
Fe pile with Pb reflector, material-group consts. meas. 79−6738
Fe/Ge multilayer neutron polarizing monochromator 79−45513
^{72}Ga half-life determ. by ^{56}Mn activation and decay obs. 79−26398
H_2 cold neutron source construction 79−45521
^{1}H(t,n), signal to background ratio for 10 to 14 MeV neutron prod. 77−30683
^{2}H(α,n), 100 MeV, neutron polarisation meas. 78−70726
^{2}H(d,^{3}He)n, 2-20 MeV collimated monoenergetic neutron beam prod. using associated particle technique 77−83418
^{2}H(d,n), signal to background ratio for 10 to 14 MeV neutron prod. 77−30683
^{2}H(d,n)^{3}He, 6 to 17 MeV, n prod. absolute differential cross sections 78−74373
^{2}H(p, n), 50 MeV, neutron polarisation meas. 78−70726
^{3}H(d, n)^{4}He, meas. of mean d interaction energy in tritiated Ti layer 79−31281
^{3}H(d,n)^{4}He, 6 to 17 MeV, n prod. absolute differential cross sections 78−74373
^{3}H(d,n)^{4}He, in nanosecond associated particles time of flight system 77−6604
^{3}H(d,n)^{4}He, neutron energy meas. with Si detector 80−32566
^{3}H(p,n), signal to background ratio for 10 to 14 MeV neutron prod. 77−30683
^{3}H(p,n)^{3}He, 6 to 17 MeV, n prod. absolute differential cross sections 78−74373

neutron sources continued
^{3}He(d,n)^{4}He, 14 MeV polarised neutron facility 79−85851
^{4}He, superfluid, purification technique from ^{3}He, for neutron source bottle 78−17823
^{4}He(d, n), 50 MeV, neutron polarisation meas. 78−70726
^{140}La half-life determ. by ^{56}Mn activation and decay obs. 79−26398
Li (p,n), 26, 35 and 45 MeV protons, neutron beam dosimetry 78−28083
Li, absolute neutron yield meas. for protons from threshold to 3 MeV 77−79498
Li-free sources for source driven breeding thermal power reactors 79−13383
^{6}LiD, new material for polarised targets for pol. neutron prod. *(French)* 80−68987
^{6}LiD enriched capsule, prod. of 14 MeV neutrons in reactor 78−55072
^{7}Li(d,n), 14-23 MeV, thick target neutron yields 77−57791
^{7}Li(d,n), 14.8-23 MeV, thick target neutron yields 77−26752
^{7}Li(d,n), neutron spectra and yields from thick targets 77−30602
^{7}Li(p, n), 50 MeV, neutron polarisation meas. 78−70726
^{7}Li(p,n), 14-23 MeV, thick target neutron yields 77−57791
^{7}Li(p,n), 14.8-23 MeV, thick target neutron yields 77−26752
^{7}Li(p,n), 77−30602
^{7}Li(p,n)^{7}Be, activation and ang. distrib. meas., absolute neutron yield determ. 78−17199
^{7}Li(p,n)^{7}Be as therapy neutron source especially for small cyclotrons 80−26335
^{7}Li(p,n)^{7}Be source of fast neutrons for small cyclotrons, neutron therapy appl. 79−57755
Li(d,n), neutron spectra from thick target bombardment for therapy 78−28049
Li(d,n) radiation damage facility, spatial variation of damage and gas prod. 77−42207
Li(p,n), neutron spectra from thick target bombardment, for therapy 78−28049
Mn bath, neutron field topography from directed sources with E_n=230 keV 79−76054
Na-D photoneutron sources, construction, yield 77−23347
^{24}Na half-life determ. by ^{56}Mn activation and decay obs. 79−26398
^{22}Ne(α,n)^{25}Mg neutron source effects in red giants and planetary nebulae 78−49430
O_2 filtered neutron beam of 2.35 MeV 80−27848
^{207}Pb(γ,n), new 86 keV neutron source 79−704
Pu-Be, for in vivo N determ. using neutron capture gamma anal. 77−86606
Pu-Be neutron source, for activation anal., β-ray meas. 78−73114
^{238}Pu, neutron source for medical use *(French)* 77−42205
^{238}PuBe, neutron sources for calibration of personnel dosimeters 80−13946
^{239}Pu-Be source, neutron spectra calc. 77−18725
^{228}Ra-Be (α,n) source, neutron spectrum calc. from angular distrib. and cross-section data 78−41882
^{106}Ru photoneutron sources, determ. of standard neutron yield, influence of bremsstrahlung 79−72177
^{45}Sc+n, 0.005 to 22 keV, total neutron cross section for beam filter design 78−78371
^{45}Sc(p,n), source of monoenergetic 10-50 keV neutrons 77−54387
^{149}Sm polarising filter for thermal neutrons 78−54502
^{90}Sr photoneutron sources, determ. of standard neutron yield, influence of bremsstrahlung 79−72177
T gas target as intense 14 MeV neutron source 77−83429
T, low-temp. gas target fast neutron prod. facility 77−30691
T-D sources, natural U booster 77−42208
^{181}Ta(γ,n) photoneutron absorpt. cross section meas. 20.9 to 837.8 keV *(German)* 80−5122
T(d,n), LLL 14 MeV neutron source facility 77−38491
Ti, tritiated self supported target prep. 80−23211
TiT targets, prod. of DT neutrons by d^+ beam irradiation analysed 77−18727
U borehole logging by prompt fission neutron technique, log interpretation 79−53567
U, exploration, radiation transport anal. for borehole logging probes 79−53565
U ore grade direct determ. by photoneutron assay method 79−53570
U shell, fission rate distrib. thermal neutron sources 78−62584
^{A}U, A=235, 238, fission and activation by fusion plasma neutrons 79−13521
^{238}U filtered beam of 186 eV neutrons, development 77−88318
^{238}U(p,xn), 800 MeV, neutron spectra meas., check on flux calcs. 77−23349
W-D_2O with 10 MeV electron beams 80−83231
ZrH rethermaliser for IVV-2 reactor hot neutron flux increase 80−37676
^{88}Zr, spallogenic, radiochem. separation for photoneutron source 77−14296

neutron spectra
see also neutron spectrometers
$1/E^{1+\alpha}$ epithermal neutron spectra, resonance integral correction, effective resonance energy 80−71978
$1/E^{1+\alpha}$ epithermal neutron spectrum, α-determ. methods, accuracy 80−71977
$1/E^{1+\alpha}$ epithermal neutron spectrum, α-determ. without Cd cover 80−71976
14.8 MeV neutrons, pulse-height spectrum prod. in NE-102A plastic scintillation counter 78−845
14 MeV neutron spectrum meas. by liquid scintillation spectrum and threshold foil detectors 79−45526
14 MeV source in liquid air, ang. neutron spectra meas. 77−3209
^{10}B(π^-,2n), stopped pion absorption 78−25243
^{12}C(π^-,2n), stopped pion absorption 78−25243
^{9}Be(π^-,2n), stopped pion absorption 78−25243
absolute neutron spectrum determination, by S and II code from reaction rates in ΣΣ-ITN facility *(Rumanian)* 79−63862
absorber rod vibr. induced neutron density fluctuations, QMC reactor expt. 80−37469
activation detectors for determination 77−71727
analysis, informational-computer system *(Russian)* 79−89514
atmosphere, secondary nucleon spectra, 2-component model *(Russian)* 78−41612
atmospheric cosmic rays, 50 MeV≤E≤100 GeV, Monte Carlo simulation *(German)* 77−13197
neutron spectra continued
background determ. in neutron transmission meas. with linac 78−17270
Benjamin detectors, on-line, real-time neutron spectrum unfolding 79−59297
biological tissue, calc. of spectra and linear energy transfer 79−100659
BWR, transactinide buildup in nuclear fields, sensitivity anal. rel. to neutron flux and spectra *(Italian)* 79−45356
BWR in-core instrument tube vibration obs. by reactor noise techniques 78−94064
BWR-4 neutron noise analysis spectra, instrument tube flow-induced vibr. 78−94063
calculating module of pin-cell burnup code BETTY 77−71634
concrete, effect of azimuthal angle on fast neutron albedos 78−8866
cosmic ray neutrons, Ames collaborative study on mid-latitude flights 78−53538
coupled core reactor, space depend. neutron fluctuation spectra, HF struct. 80−37468
critical assembly, neutron spectra meas. by activation method 80−32390
CTR, model blanket expt., neutron spectra sensitivity analysis 78−29648
cyclotron, neutron production by 25-55 MeV protons on Be, spectra and yield 77−70539
cyclotron, variable energy, shielding calcs., concrete and earth shield design 77−61622
cyclotron beams, spectra at 0° from 83.7 MeV deuterons and 100.2 MeV protons on Be 77−73593
cyclotron-produced beams, energy spectra and dose distrib. spectra 77−70554
(d,n) on Be, C, Al, Ni, Cu, Mo, Ta and Pb, secondary neutron emission characts. 79−30843
dead time distortions in reverse Fourier TOF spectrometry 79−6789
delayed neutron energy spectra from fast fission of ^{235,238}U, ^{239}Pu 77−38308
delayed neutron energy spectra of fast fission in ^{233,235,238}U, ^{232}Th, ^{239}Pu 77−34354
delayed neutron fractions in SNEAK fast critical assembly, integral meas. on PuO_2/UO_2 77−6497
delayed neutron spectra, gross props. 78−78327
delayed neutron spectra from neutron induced fission of U, P and Th, reactor calcs. 77−34355
delayed neutron spectra from precursors with A=79-130 77−82884
delayed neutron spectra from separated fission products with A=88-144 77−34268
delayed neutron theoretical pulse height spectra 78−78328
dense plasma focus Julich I, neutronics, fusion plasma investigation 77−35396
depth dose, dose equivalent, quality factor for various reactors and shields 78−94143
differential neutron spectra estimation using foil activation data and IUNFLD code 78−29690
differential spectra from ^{2}H muon capture *(Russian)* 77−82915
Doppler broadening of resonance levels, substantial reduction during cooling 79−97932
Doppler effect, nuclear, meas. technique 77−50232
Doppler free- and recoil free resonance neutron spectroscopy 77−26924
dosimeter-based adjustments of fast-neutron spectra 79−54611
dosimetry, comparison of single and multidetector systems *(Russian)* 78−33294
dosimetry techniques for accelerator-based irradiation facilities 79−41041
efficiencies and light curves for meas. using NE-213 80−878
electron beam fusion, pellet and pellet-blanket neutronics and photonics 80−74006
electron linear accelerators produced neutrons, bremsstrahlung and (γ,n) processes *(Japanese)* 78−78532
emission spectra from 14 MeV neutron reaction, precompound model calc. 79−36235
energy transfer spectra, linear, in chemical nuclear reactor *(Russian)* 78−46130
evaluation by iterative method, computer-aided, using multisphere response meas. *(Slovak)* 77−83444
fallout observation, Chinese A-tests 80−27820
fast neutron beams in clinical use, low energy component 79−49899
fast neutron energy psectra meas. in thermal reactor systems *(German)* 79−3282
fast neutron facility in CP-5 reactor, neutron flux, energy spectrum, primary recoil distribution 79−41056
fast neutron induced nonelastic reaction cross section data, E_n≥14 MeV 77−23058
fast neutron pulses, time distrib. of doserate behind polyethylene/Fe layers *(German)* 77−26886
fast neutron spectra, activation technique determ., fusion reactor blanket model appl., unfolding program 77−79500
fast neutron spectra transmitted through iron and sodium slabs 80−73873
fast neutron spectrum anal. by threshold detection foil method *(Japanese)* 77−75023
fast neutron spectrum unfolding code MATXUF 78−5091
fast neutron transport through laminated Fe-H_2O shield 80−13931
fast pulse reactor ^{237}Np/^{238}U and ^{239}Pu/^{237}Np spectral index meas. and calc. 79−9804
fast reactor adjoint neutron spectrum calc. using bilinear weighted cross sections 77−83003
fast reactor neutron energy spectra for dosimetry 79−3219
fast spectrum unfolding with MATXUF on-line real-time derivative method 78−74553
FBR, neutron spectra in the MeV range in fast critical assemblies 80−83210
FBR neutron fields, spectral charact., expts. and calcs. *(Japanese)* 78−46222
finite water assemblies, steady state thermal neutron spectra, space and ang. depend. 77−50187
fission fragment deexcitation, statistical model anal. of spin influence 79−17941
fission neutron spectra, light water-moderated, depth-dose characts. 80−106205
fission neutron spectra degraded through low Z shields, depth-dose distrib. 79−39516
fission neutrons, for cross section validation and flux transfer 77−23129
fission reactor core, neutron spectrum evaluation using activation method *(Czech)* 77−65288

neutron spectra continued
fissionable nuclei A=232 to 252, systemization of relative yields of retarded neutrons 79−40974
flux detector system, proton recoil with gas scintillation transmission counter, 1-30 MeV 77−23366
flux spectral uncertainties in ENDF/B dosimetry cross section file benchmark spectra 77−23306
FPR neutron spectrum in presence of experimenter's tahle 78−21676
full flux covariance matrix calc. for NBS intermediate-energy standard neutron field 80−5348
fusion neutrons from beam driven toroidal plasma 78−5034
fusion reactor, first wall neutron spectra prod. around 14 MeV point source, feasibility study 79−54597
fusion reactor radiation protection, shield integral expts. at ORNL 80−47709
gas target neutron source for radiotherapy, generation by $^{3}H(d,n)$, energy spectra, flux 78−92698
GCFR, Pu fuelled, fission products and secondary gamma-ray spectra 78−676
graphite, thermal-neutron spectra calc. 77−26824
graphite high temp. bulk, B poisoned, thermal neutron spectra meas. 79−54465
Hauser-Feshbach calculation of the fission neutron spectrum 80−22801
health physics research reactor, neutron spectra meas., various shielding conditions 80−63396
high energy neutron spectrometry using cellulose nitrate nuclear track detectors 80−91394
homogeneous slabs, dosimetric quantities and neutron spectra 77−38319
hydrogenous neutron deectors for reactor spectrum meas. 77−71733
infinite homogeneous multiplying system, joint factorial moments of neutron and count bivariate distrib. 79−76062
intermediate-energy secondary spectrum system, determ. of neutron characteristics, ΣΣ-ITN *(Rumanian)* 79−22355
intermediate-energy standard neutron field, neutron transport calcs. 79−13588
IRT 2000 reactor in Sofia, neutron spectra and doses in exptl. canals *(Bulgarian)* 78−82489
LAMPF radiation effects facility, total neutron flux, energy spectrum, meas. and calc. 77−23331
laser fusion reactor targets, energy partition and neutron spectra 78−58451
leakage neutron spectrum meas. in light water using time of flight technique 78−62592
leakage spectra from critical assemblies, depth dose, dose equiv. and quality factor 78−58504
leakage spectra from Fe, Nb, Be, polythene spheres, integral test of cross sections 77−23033
linear accelerator, 25 MV X-ray, Bonner spectrometer neutron meas. in intense photon field 78−24133
lineshapes in pulsed neutron powder diffraction 80−64841
liquid air, calc. of neutron and gamma-ray energy spectra 78−29529
liquid air, energy spectra and doses of ^{252}Cf neutrons 77−67901
liquid air, transport of neutron and secondary γ-rays from 14 MeV source 78−50234
liquid N_2, calc. of neutron and gamma-ray energy spectra 78−29529
LMFBR, fast neutron streaming through grid plate shield 77−3081
LMFBR core design, benchmark tests of JENDL-1 for structural materials 80−13616
LWR, fuel utilisation, spectral shift control methods 80−47586
LWR, outgoing neutron spectrum from H_2O in H_2OV interface 80−27697
Millstone Unit No.2 neutron spectra and fluence determ. 79−9907
mixed neutron-gamma ray field, γ contrib. to proton recoil counter spectrum 77−88337
molecular spectroscopy book 80−27052
muon capture in heavy nuclei, neutron emission energy and multiplicity distribs. 77−6313
natural nuclides from meteorites, spontaneous fission neutron multiplicity *(Russian)* 79−40977
NE213 organic scintillators, effect of light output efficiency of charged particles on unfolded neutron spectrum 78−29700
neutron collimated fast beam, radiation quality local distrib. 80−12247
Nimonic PE16, irradiation creep data obtained in fast and thermal neutron spectra correlation with displacement cross-sections 80−84993
nuclear far from β-stability, delayed neutron energy spectra, structure effects 80−78226
nuclear fission fuel, delayed-neutron spectra characterisation 77−79345
nuclear isotopes far off stability line, production, props., review *(Hungarian)* 79−9927
nuclear reactor, two-phase flow characterisation by neutron noise techniques 78−94058
nuclear reactor pressure vessel steel irradiation, neutron flux densities neutron spectra and temp. fields in large specimens 77−74924
on-line calculation of experimental neutron spectra uncertainties 79−59298
overlapping, multigroup collision prob. method 80−52718
PAA, nonlinear soft mode at Rayleigh-Benard instability, neutron cond. spectrosc. obs. 80−79266
photoneutron spectra of fission products from U, Pu 77−23127
photoneutrons, spectral and intensity distribs. of accelerator prod. neutrons in concrete room 79−49868
plasma focus, 1 kJ, neutron-, ion-, and electron-energy spectra determ. 77−35404
plasma focus, nonthermal processes, neutron spectra 78−42804
primary beam and shielding radiation quality and absorbed dose obs. 80−12281
prompt fission neutron spectra calc., nucl. evaporation theory 80−22870
prompt fission neutron spectra for ENDF/B-V 80−22869
prompt fission spectrum uncertainties, implications for integral data testing 80−22871
prompt-neutron lifetime meas. in MARIUS III critical facility 79−67841
pulsed reactor, fast neutron spectra meas. 77−50222
PURNIMA reactor, unfolding of fast neutron spectra 77−74903
PWR, 450 MWe, noise obs., analysis and interpretation 78−94072
PWR, survey of neutrons inside containment 80−13675
PWR neutron noise interpretation by vibration analysis 78−94073
Q-factor calcs. for spectra below 4 MeV, dosimetry appls. 79−79654
Q-factor for charged particle recoils rel. to neutron energy 80−63397
quasi-elastic neutron scatt., direct model fitting of uncorrected TOF data 79−31309
radiation effects in fission reactor materials, energy spectrum depend., damage function *(German)* 77−34386
radiation effects on nuclear reactor steel, neutron energy depend., damage model *(German)* 77−34385
radiation protection, benchmark shielding problems obtained from integral tests of neutron cross sections 80−47740
radiation shielding materials, benchmark radiation transport data, air-over-ground neutron and gamma spectroscopy 80−23161
radiotherapy beams prod. by protons and deuterons on Be and Li, dosimetry 78−24141
radiotherapy shielding, comparison of photoneutron and ^{252}Cf neutron spectra 79−59273
radiotherapy sources energy spectra, d(49)-Be and p(41)-Be 79−62347
radiotherapy with pions, nucl. emulsion studies 78−73219
reactor core dosimetry standards 79−9824
reactor critical facility, fast neutron spectrum meas. using (n, α) and (n, p) reactions 80−78403
reactor lattice epithermal neutron spectra, spherical harmonics anal. 78−21619
reactor neutron distribs. spectral charcts., relative meas. by activation ratios method 77−34411
reactor radiation damage, neutron metrology for irradiation parameters 79−46717
reconstruction from activation meas. using method of effective cross sections 79−59105
reflection of neutrons between plane-parallel concrete interfaces, Monte Carlo calc. 80−27686
reverse Fourier TOF anal. with mech. beam choppers 79−6788
RFSP-JUL, program for unfolding n spectra from activation data 78−82570
SAIPS, information determination system, algorithms for spectra determ. w.r.t. measured reaction rates *(Russian)* 80−102416
scattering materials effect on average neutron energy, spectral index, hardness parameter 77−26816
shielding effects of thickness and geometry on neutron spectra 78−33300
single neutron emission induced by stopped π^- in 1p shell nuclei 79−59089
space depend. spectra in two adjacent moderating media 77−6477
space-energy spectrum in inhomogeneous medium, allowing for neutron capture 77−23163
spectroscopy, new techniques and results 77−23365
stainless steel, neutron group constants, meas. of energy and space distribs. 77−26829
standard installation improvement for reproducing unit of thermal-neutron flux density 78−74524
standard neutron spectrum field *(Japanese)* 79−9562
stationary transport eqn. formulations 79−13378
statistical regularization method for spectra establishment according to threshold detector readings, IBR-30 reactor appl. 78−37483
steel, austenitic, types M316, FV548, 304, irradiation creep data obtained in fast and thermal neutron spectra correlation with displacement cross-sections 80−84993
stopping pion field, multiple foil activation method 78−85386
superdense nuclei, search in reactor active zone 79−75824
terphenyl, partially hydrogenated, neutron thermalisation spectrum 77−67812
TFTR neutral beam injectors, neutronics calcs. 79−59253
thermal neutron scatt. in water, cylindrical graphite-water system with temp. discontinuity 79−71925
thermal neutron standard field with Maxwellian distrib. using KUR heavy water facility 78−33342
thermal spectra calcs. using synthetic scatt. kernel 77−14206
thermalisation in heavy water, meas. and calc. of spectra using TOF methods 79−85582
thermalization, appl. of invariant imbedding technique 79−67811
thermalization of neutrons, review of Soviet research 79−36300
threshold foil meas. of reactor neutron spectra, radiation damage appl. 78−29691
tissue, calcs. of charged particle recoils, slowing down spectra, LET, event-size distribs. 79−25040
tissue neutron energy deposition spectra from improved cross-section values 80−26300
TOF meas., rate depend. of counting losses 80−37692
TOF spectra, multiple scatt. corrections and neutron attenuation 77−26928
TOF spectra effects of imperfect beam modulation using mechanical correlation choppers 77−57798
Tokamak test reactor, neutron activation code REBATE 79−49852
TR-O reactor, neutron spectrum meas., oscillation techniques *(Czech)* 80−52754
transmitted, reflected neutron spectra from homogeneous slab shields, computer calcs. 77−3067
TRIGA Mk.II reactor core, thermal neutron spectra parameters meas. 80−9348
TRIGA-reflector regions, spatial variation of fast neutron spectra 77−46422
ultracold neutron flows, spectra meas. 77−26926
unfolded neutron spectrum and foil reaction rate computation and meas. 79−9904
unfolding , optimised smoothing, FERDOR method 80−27860
unfolding from activation data by variational techniques 79−13375
unfolding from meas. p spectra 79−63860
VIPER reactor, neutron leakage spectrum and dose meas. 79−3243
water, fast neutron angular penetration spectra, comparison with Monte Carlo calcs. 77−23303
water shield, neutron transport, 2-D benchmark expt. 78−58318
Zebra 8 assemblies, neutron spectra meas. with proton recoil counters 77−38393
Zebra Pu fuelled assembly, neutron TOF spectra meas. 77−38333
(α,n) cross-sections and α-stopping power in light elements 77−74862
(α,n) thick target yields for Li, ^{9}Be, B, $Pb^{19}F_2$, $Zn^{19}F_2$, Mg, ^{27}Al, Si, and $^{28}SiO_2$ 79−71860
(α,xn), 640, 710 MeV, n ang. and energy distribs., intranuclear cascade model 80−83109
(d,n) diagnostic neutron spectra from deuterons 2.5, 3.0, 3.5 MeV on ^{12}C, ^{27}Al, ^{19}F, CH_2, CD_2, Teflon 79−40933
(γ,n), preequilibrium exciton model with evaporative component, photoneutron spectra, giant resonances 80−57762
(n,2n) reacts. on ^{45}Sc, ^{58}Ni, ^{59}Co, ^{93}Nb, ^{175}Lu, and ^{197}Au, statistical model anal. 77−26655

neutron spectra continued
(n,3n) reacts. on ^{45}Sc, ^{58}Ni, ^{59}Co, ^{93}Nb, ^{175}Lu, and ^{197}Au, statistical model anal. 77−26655
(n,n′), 14 MeV, continuous spectra, multi-step direct reaction anal. 80−78258
(p, n), 22.2 MeV, A=27-197, neutron spectra, direct and equilib. processes *(Russian)* 80−52648
(p,n), high resolution neutron spectroscopy in near threshold region 79−45251
$pp \rightarrow np\pi^+$, 647-805 MeV, neutron momentum spectra obs. 77−30417
^{109}Ag(p,n)^{109}Cd, 6 and 7 MeV, neutron spectra meas. *(Russian)* 78−54764
Ag(n,n′), 14.1 MeV, precompound processes 78−13093
Al+π^-, 0.75 GeV/c, neutron energy spectra meas. 79−67777
Ar(^{3}He,n)Ca, A=36, 38, 40, 11.5 MeV, neutron ang. distrib. and energy spectra 77−65227
^{85}As, investigation of beta-strength functions by neutron and γ-spectroscopy 79−45209
^{85}As, neutron and gamma-ray spectroscopy of delayed neutron emission 77−22973
As(n,n′), 14.1 MeV, precompound processes 78−13093
^{197}Au(^{132}Xe,X), neutron multiplicities 80−57797
^{197}Au(π^-, xn), single and correlated n spectroscopy, nuclear temp. 79−6713
B concentration profiling in solids by neutron TOF using ^{11}B(p,n)^{11}C 79−51131
^{10}B(π^-,2n), neutron-pair emission characts., excitation energy spectra 78−13159
^{12}B* neutron decay in ^{12}C(π^-, γ)^{12}B*, shell model 80−22652
^{138}Ba(γ,n), E1 and M1 radiative strength functions 77−22999
Be assembly, space- and angle-depend. steady state thermal neutron spectra 77−67783
Be, neutron spectra from p,d, ^{3}He collisions 80−524
Be+d, 14-40 MeV, Monte Carlo calc. of neutron yields 79−49887
Be+d, low-energy spectrum, rel. to neutron prod. for radiotherapy 78−40319
Be+p beams, 30 and 40 MeV, polyethylene filtration 78−53494
Be(^{3}He,n) fast neutron generation in cyclotron 77−88311
^{6}Be+^{7}Li, 2 MeV neutron energy spectrum meas. using nuclear emulsion technique 78−62574
^{9}Be(d,n),(p,n), 14-23 MeV, thick target neutron yields 77−57791
^{9}Be(d,n) 83.7 MeV, 0° neutron spectra, comparison with Serber model calcs. 77−6400
^{9}Be(d,n)^{10}Be, neutron distrib. from bombardment of thick Be target 77−83408
^{9}Be(p,n), comparison of expt. obs. 79−59056
^{9}Be(π^-,2n), neutron-pair emission characts., excitation energy spectra 78−13159
^{9}Be(t,n), 1.1-1.7 MeV, neutron spectra and ang. distribs. meas. *(Russian)* 77−50140
Be(d,n), stripping-theory anal. of thick-target neutron prod. 77−6600
^{209}Bi, reson. parameters for s and p-wave levels 78−37322
Br, A=87-89, delayed neutron energies delayed neutron energies 77−74816
Br, A=87-89, delayed-neutron emission probabilities 77−74817
^{87}Br, investigation of beta-strength functions by neutron and γ-spectroscopy 79−45209
^{87}Br, neutron and gamma-ray spectroscopy of delayed neutron emission 77−22973
^{12}C, π^- capture reactions, neutron spectra determ. by 2 and 4 nucleon cluster expansions 79−6703
^{12}C(^{16}O, n)^{27}Si, 12.8 MeV resonance investig. by time-of-flight spectra and n-γ coincidence 79−9627
^{12}C(π^-,2n), neutron-pair emission characts., excitation energy spectra 78−13159
^{12}C(π^-,n), stopped pion, neutron energy spectra, mean energies and multiplicities 80−9311
^{13}C(α,n), n and 6.13 MeV γ-ray emission for Ge(Li) detector calibration 79−13572
^{13}C(γ,n), threshold to 25 MeV, photoneutron cross-section 77−14113
^{13}C(γ,n)^{12}C, 24-26 MeV, photoneutron energy and ang. distribs. 77−30554
Ca(^{3}He,n)Ti A=40, 42, 13 MeV, neutron ang. distrib. and energy spectra 77−65227
^{40}Ca(μ,nν)^{39}K, neutron spectra calc. in simple-pole model 77−71606
^{48}Ca(p,nx), 45 MeV, preequilib. ang. distrib., generalised exciton model 77−10407
Cd covered Au foils, neutron spectra determination by resonance reactions 79−93837
Cd+π^-, 0.75 GeV/c, neutron energy spectra meas. 79−67777
^{110}Cd, n spectra of isobaric analogue resonance decay from ^{109}Ag(p,n)^{109}Cd *(Russian)* 78−89841
^{140}Ce(γ,n) E1 and M1 radiative strength functions 77−22999
^{232}Cf spontaneous fission neutron spectrum 77−50166
^{252}Cf, fission neutron spectra Maxwellian temp. 77−26811
^{252}Cf fission neutron TOF spectrum fine struct. 77−88182
^{252}Cf fission-neutron spectrum unfolding experiment 80−13514
^{252}Cf, measured neutron and γ spectra in a tissue equivalent medium 80−3805
^{252}Cf, neutron emission 80−37405
^{252}Cf spontaneous fission, meas. of fission neutron spectra 80−22873
^{252}Cf, spontaneous fission, neutron spectra and no. depend. on fragment mass and kinetic energy *(Russian)* 77−46197
^{252}Cf spontaneous fission, prompt neutrons and fission fragments *(Russian)* 79−40976
^{252}Cf, spontaneous fission neutron spectrum meas. using ^{6}Li spectrom. 78−17477
^{252}Cf spontaneous fission neutron spectrum meas. 79−9653
^{252}Cf spontaneous fission spectra, data anal. in TOF meas. 79−26811
^{252}Cf, standard spectrum, status report 77−23017
^{242}Cm-Be, neutron spectra calc. 77−30687
^{244}Cm-Be, neutron spectra calc. 77−30687
^{59}Co(n,n′), 14.6 MeV, ToF spectra meas. *(Russian)* 78−41721
C(π^-,n) spectrum obs. and calc. 79−17933
Cs, A=141-145, delayed-neutron emission probabilities 77−74817
Cu fusion + hybrid reactor materials, neutron spectra meas. and calcs. 80−23142
Cu+p, 52 MeV, spectral meas. of secondary neutrons and photons from thick targets 78−58282
Cu(n,n′), 14.1 MeV, precompound processes 78−13093
D-T plasma, Monte Carlo anal. of particle spectra 79−72992
neutron spectra continued
D+d, low-energy spectrum, rel. to neutron prod. for radiotherapy 78−40319
D+d reaction, 6.8 to 11.1 MeV, beam dosimetry 78−53509
D(γ,n), photoneutron energy spectra meas. *(Dutch)* 79−3281
^{152g}Eu, neutron resonance obs. by time of flight spectroscopy, cf. ^{151}Eu and ^{153}Eu *(Russian)* 78−25120
Fe, an assessment of ENDF/B-IV based on integral meas. 77−50194
Fe, group consts., neutron spectra of small pile surrounded by Pb reflector 79−6738
Fe, neutron group constants, meas. of energy and space distribs. 77−26829
Fe shield, meas. of neutron and gamma ray penetration 80−47730
Fe+p, 52 MeV, spectral meas. of secondary neutrons and photons from thick targets 78−58282
Fe+π^-, 0.75 GeV/c, neutron energy spectra meas. 79−67777
^{254}Fm spontaneous fission, distrib. of mass, KE and neutron yield 78−17257
Ge(Li) detectors, fast neutron leakage spectrum determ. 80−32565
^{3}H(d, n)^{4}He, meas. of mean d interaction energy in tritiated Ti layer 79−31281
^{3}H(d,n)^{4}He, neutron fluence and energy transfer standard 80−102194
^{4}He+π^-, capture at rest, neutron energy spectrum determ. 79−6702
Ho-Ag(Cu)(Mg)(Zn), crystal field parameters from neutron spectra, ordered state mag. props. 77−43546
^{165}Ho(^{56}Fe, xn HI), 8.5 MeV/u, damped collision α- and n-emission, n multiplicities 79−93653
^{165}Ho(p,xnypγ), 60 MeV, n and γ energies and ang. distribs. 78−89872
^{137,138}I, delayed-neutron emission probabilities 77−74817
^{137}I, delayed neutron energies 77−74816
^{137}I, investigation of beta-strength functions by neutron and γ-spectroscopy 79−45209
^{137}I, neutron and gamma-ray spectroscopy of delayed neutron emission 77−22973
^{115}In(p,n), 5 to 9 MeV, neutron spectra of ^{115}Sn, TOF meas. *(Russian)* 79−9579
Li sphere, neutron spectra and T prod. meas. 78−62604
Li+d, 40 MeV, target system neutron spectra 79−9595
^{6}Li sandwich counter, meas. of neutron spectra in fast neutron systems 80−27884
^{7}Li+^{7}Li reaction, 2 MeV, neutron energy spectrum meas. using nuclear emulsion technique 78−62573
^{7}Li+n, elast. and inelast. scatt. of 9.1±0.2 MeV neutrons, double differential cross section meas. 79−30838
^{7}Li(d,n), neutron spectra and yields from thick targets 77−30602
^{7}Li(d,n),(p,n), 14-23 MeV, thick target neutron yields 77−57791
^{7}Li(p,n) 77−30602
^{7}Li(p,nα), 7-10 MeV, neutron spectra meas. 77−26741
^{7}Li(p,np), 7-10 MeV, neutron spectra meas. 77−26741
Li(d,n), neutron spectra from thick target bombardment for therapy 78−28049
Li(p,n), neutron spectra from thick target bombardment, for therapy 78−28049
Mn bath, neutron field topography from directed sources with E_n=230 keV 79−76054
N, neutron scatt. and gamma-ray prod., Monte Carlo anal. 77−26682
^{14}N(π^-,2n), neutron-pair emission characts., excitation energy spectra 78−13159
^{14}N(π^-,n), stopped pion, neutron energy spectra, mean energies and multiplicities 80−9311
Na-D photoneutron sources, construction, yield 77−23347
Nb fusion + hybrid reactor materials, neutron spectra meas. and calcs. 80−23142
^{A}Nb, A=90,91,94 neutron spectra, level density, direct processes from Zr(p,n) *(Russian)* 79−67666
^{93}Nb(n,n′γ), (n,γn′), 14.6 MeV, differential cross sections from nγ coincidence spectra anal. *(Russian)* 78−17209
Nb(n,n′), 14.1 MeV, precompound processes 78−13093
^{59}Ni(n,α)^{56}Fe, cross section determ. for He prod. in stainless steel 79−22282
^{237}Np(n,f), ave. no. of neutrons/fission meas. 78−41792
^{16}O(γ,n), photoneutron energy spectra meas. *(Dutch)* 79−3281
^{16}O(π,γn), direct and resonance reaction unified shell model, n, γ spectra 80−52696
^{16}O(π^-,γ), one and two neutron emission, decay channels 79−45300
^{16}O(π^-,n), stopped pion, neutron energy spectra, mean energies and multiplicities 80−9311
^{17}O, delayed neutron emission following ^{17}N β-decay 77−18481
O(π^-,n) spectrum obs. and calc. 79−17933
Pb+p, 52 MeV, spectral meas. of secondary neutrons and photons from thick targets 78−58282
Pb+π^-, 0.75 GeV/c, neutron energy spectra meas. 79−67777
^{208}Pb(p,nx), 45 MeV, preequilib. ang. distrib., generalised exciton model 77−10407
^{235}Pu, prompt fission neutron spectra 79−9654
^{239}Pu, prompt-neutron fission spectrum, Maxwellian and Watt distribs. 77−50177
^{239}Pu thermal fission, prompt neutrons and fission fragments *(Russian)* 79−40976
^{239}Pu-Be source, neutron spectra calc. 77−18725
^{239}Pu(n,f), fission neutron spectra, TOF meas. 78−17476
^{239}Pu(n,f) 80−37405
Pu(n,f), 0-18 MeV, prompt neutron spectrum, evaporation model *(Chinese)* 80−42721
^{228}Ra-Be (α,n) source, neutron spectrum calc. from angular distrib. and cross-section data 78−41882
Rb, A=92, 97, delayed-neutron emission probabilities 77−74817
Rb, A=92-97, delayed neutron energies 77−74816
^{135}Sb, investigation of beta-strength functions by neutron and γ-spectroscopy 79−45209
^{135}Sb, neutron and gamma-ray spectroscopy of delayed neutron emission 77−22973
^{28}Si(n,n), to 4.5 MeV, s- and p- wave reson. struct., R-matrix interpretation 77−23002
^{28}Si(π,nγ), neutron spectra from coincidence expts. 79−85499
^{152}Sm(n,n′γ) spectra and ang. distribs. anomalous excitation *(Russian)* 77−54224
^{120}Sn(p,nx), 45 MeV, preequilib. ang. distrib., generalised exciton model 77−10407
^{93}Sr excited state depopulation γ-rays, n coincidence from ^{94}Rb β-delayed n decay 80−52631

neutron spectra continued
^{181}Ta(n,n')^{181}Ta, 9.1 MeV, CC neutron spectra and angular distrib. meas. *(Russian)* 78−25198
^{181}Ta(p,n)^{181}W, 10.2 MeV, CC neutron spectra and angular distrib. meas. *(Russian)* 78−25198
Ta(p, xn), 23 MeV, n energy distribs. *(Russian)* 78−86537
^{159}Tb, neutron resonances, time-of-flight spectra 80−27633
ThO_2, spherical pile, neutron spectrum meas. and analysis 78−17311
^{232}Th, fusion + hybrid reactor materials, neutron spectra meas. and calcs. 80−23142
Ti:T, depth profiling by neutron TOF spectroscopy 77−73500
TiT targets, prod. of DT neutrons by d^+ beam irradiation analysed 77−18727
U-graphite lattice, spectrum structure near a resonant absorption line 77−50221
U-light water slab, meas. of space depend. ang. thermal neutron spectra 77−14208
U-ZrH system, neutron spectrum in critical pile 79−45322
UO_2, energy depend. Doppler factor meas. using lead slowing-down time spectrometer 78−17310
^{233}U neutron-induced reaction, data eval. including $\bar{\nu}_p$ and fission spectrum 79−67795
^{233}U, prompt-fission-neutron spectra 79−67793
^{233}U(n,f), fission neutron spectra, TOF meas. 78−17476
^{235}U, delayed neutron groups from thermal fission 79−30864
^{235}U, prompt-fission-neutron spectra 79−67793
^{235}U, quantitative determ. of unauthorised removal of nuclear materials, using changes in spectral indices *(Russian)* 80−63294
^{235}U(n,α), thermal fission neutron spectrum 80−42712
^{235}U(n,f), 0.5 MeV, prompt neutron spectrum meas., TOF techniques 77−34356
^{235}U(n,f), 0.52 MeV, prompt neutron spectra meas. 77−23158
^{235}U(n,f), 0.6, 7 MeV, fission neutron spectra meas. 80−22872
^{235}U(n,f), fission neutron spectra, TOF meas. 78−17476
^{235}U(n,f), neutron spectrum of thermal fission 79−97736
^{235}U(n,f), thermal, discrete neutron emission probability 78−25257
^{235}U(n_{th},f), fragment-mass depend. of fission neutron spectrum, TOF method 78−82398
^{238}U, fusion + hybrid reactor materials, neutron spectra meas. and calcs. 80−23142
^{238}U, integral neutron spectrum meas. to test ENDF/B-IV data 77−26825
^{238}U, neutron resonance parameters, time-of-flight spectroscopy 80−47375
^{238}U prompt fission, prompt neutron multiplicity distribs. *(Russian)* 77−340
^{238}U pulsed sphere meas., neutron emission spectra rel. to fusion-fission blanket calcs. 77−23298
^{238}U+n, 2.47 MeV, energy spectra and ang. distrib. of neutrons 79−40927
^{238}U(α,xnf), 50 MeV, post and prefission neutron meas. 79−76042
^{238}U(n,f), 7 MeV, fission neutron spectra meas. 80−22872
^{238}U(p,xn), 800 MeV, neutron spectra meas., check on flux calcs. 77−23349
U(n,f), 0-18 MeV, prompt neutron spectrum, evaporation model *(Chinese)* 80−42721
^{181}W, level absolute density from n spectra, statistical anal. of ^{181}Ta (p, n) *(Russian)* 79−97657
^{181}W level density, n spectra and ang. correls., direct and nonequilib. processes from ^{181}Ta(p,n) *(Russian)* 80−68631
^{90}Zr(p,nx), 45 MeV, preequilib. ang. distrib., generalised exciton model 77−10407

neutron spectrometers
accelerator facility, fast neutron research, data acquisition and anal. 80−47806
accelerator facility, Van de Graaff generator and cyclotron for fast neutron detection and neutron reaction cross-sections 80−47805
activation detectors, spectra meas. in range 0.4 eV to 10 MeV 77−42210
alpha recoil gas proportional counter 78−5089
analyser crystal, with automatically variable curvature, for three-axis spectrometer, construct., calibration 77−57797
Astacus, a time focussing neutron diffractometer based on the reverse Fourier principle 79−77457
Benjamin detector unfolding, MATXUF improved on-line uncertainty calc. 79−85876
Benjamin detectors, on-line, real-time neutron spectrum unfolding 79−59297
Bonner spectrometer, spectral meas. in intense photon field of high-energy X-ray therapy machine 78−24133
Bonner sphere spectrometer, least-squares technique for extracting neutron spectra 78−33366
calibration and testing using moderator spheres *(Czech)* 80−47804
cold neutron time of flight spectrometer at Studsvik, Sweden 80−63444
combined, with Bonner and thresold fission detectors *(Slovak)* 79−36456
constant-Q-spectrom. for pulsed neutron sources 78−58532
control using microprocessors *(German)* 79−49363
correlation chopper for TOF neutron scatt., deconvolution, triangular signal function 77−61158
correlation chopper for TOF neutron scatt., deconvolution theory 77−61157
cosmic ray neutron supermonitor, neutrons energy and time distribs. 79−84611
cosmic ray variations, Elbrus spectrographic system appl. 79−84605
crystal-chopper spectrometer, (Q,ω) transmission function 77−31564
diffraction spectrometer, resolution and luminosity study for liquid on amorphous samples anal. 78−87591
diffractometer, transit-time, for structural investigations of monocrystals 80−64840
diffractometer, two-axis, use of flexible four detector system 77−65934
diffractometers using position sensitive BF_3 counters 77−35444
DIN-2K double slow neutron spectrometer *(Russian)* 79−45528
fast, based on electrostatic charge-exchange accelerator 80−63440
fast neutron scattering expts., associated particles time of flight system 77−6604
fast neutron spectrum unfolding code MATXUF 78−5091
fast neutron time of flight spectroscopy, multi-angle detector system 80−52810

neutron spectrometers continued
fission counters, high sensitivity, neutron spectroscopy and dosimetry appl. *(French)* 80−58078
Fourier time-of-flight spectroscopy, higher-harmonics contamination in slow-neutron spectra, theory 80−74072
Fourier TOF spectroscopy, influence of higher harmonics in chopper modulation function 77−6609
fusion reactor, TFTR, neutron spectrometer mech. design 80−95498
gas counters of slow neutrons, edge effect 78−33384
gas proportional α-recoil spectrum 80−5433
Harwell, neutron diffractometers, spectrometers and ancillary equipment 79−45527
Harwell backscatt. spectrum for neutron diffraction meas. 77−15288
Harwell linac II total scatt. spectrometer, calibration using Ni diffr. data 78−86725
HFR at Grenoble, neutron beam installations 77−26864
high press. appl. 78−49852
high resolution fast neutron spectrometry without time-of-flight using a broad window pulse shape discriminator 79−45523
high-resolution neutron gravity spectrometer 78−78554
hydrocarbon scintillators, Monte Carlo predictions of neutron detection efficiency 79−68150
inelastic rotor spectrom., for high energy vibr. spectroscopy expts. using pulsed neutron source 78−86721
inelastic spectrometer using resonance detector, energy transfer values in the order of 1 eV 80−74067
liquid scintillator cell for fast neutron beams in clinical use 79−49899
low-angle spectrometer, using 2D position-sensitive counter, for molecular biology 79−12053
mechanical velocity selector for small angle scatt. instrument on pulsed source 79−13586
mixed n-γ field portable scintillation spectrometer with pulse shape discrimination 77−77992
modular minicomputer multiparameter data system 77−23396
MWPC at LAMPF, neutron physics programme 77−26951
NE213, detection efficiency meas. for 130 MeV neutrons 80−27888
NE213 liquid cylindrical neutron spectrom., anisotropy of response 80−5434
NE213 liquid scintallator, light output for electrons and protons 80−32564
NE213 organic scintillators, effect of light output efficiency of charged particles on unfolded neutron spectrum 78−29700
NE213 scintillator in LiF assembly, Monte Carlo calc. of neutron flux perturbation 79−85855
NE 213, pulse shape discrimination 80−27862
NE 213 liquid scintillator, decay under neutron and gamma excitation *(German)* 78−55097
NE 213 liquid scintillator, deuterated, decay mode *(German)* 78−55096
NE 238 fast liquid scintillator, scintillation decay and n-γ discrimination *(German)* 78−55101
NE-213, continuous functional representation of response surface 79−81116
NE-213, proton recoil data, neutron spectrum unfolding with MATXUF 78−74553
NE-213 spectrum system for 1.0-20 MeV neutrons 77−88346
NE-213 system, 1-15 MeV, Pu-Be and ^{252}Cf neutron spectra meas. 77−26930
neutron and γ-ray spectra meas. on radial shielding model of KS-150 reactor *(Slovak)* 78−21624
neutron beam charged particle spectrometers, appl. of drift chambers 79−3278
neutron energy spectra at intermediate energy, measuring apparatus 79−54738
neutron ionization chambers, development and characts. 79−68157
neutron spin echo appl. on pulsed neutron sources 79−81115
neutron spin-echo attach. for three-axis neutron spectrometer, theory 79−3270
neutron totally absorbing TOF spectrom. 78−850
organic, neutron response functions, Monte Carlo program 80−14047
PANSI, polarisation anal. neutron scattering instrument, description and appls. 80−23280
photodiodes as recoil particle detectors 79−97927
Pilot U scintillator for 55-225 MeV neutrons 80−18762
plastic scintillation counter NE-102A, pulse-height spectrum prod. by 14.8 MeV 78−845
polarimeter for threshold photoneutron spectroscopy 77−30739
polarisation anal., separation of coherent and spin incoherent scatt. from D_2O 77−6655
polarised neutron diffraction, determ. of magnetic form factors, pioneering work 80−24321
polarised neutrons in condensed matter [conference, Zaborow, Poland (Sept. 1979)] 80−22136
portable microprocessor controlled neutron spectrometer, NE213 organic scintillator 80−58022
portable neutron spectrometer/kerma-rate meter, design, performance 78−33361
portable spectrom./kerma-rate meter, microprocessor system 77−54485
portable spectrometer/dosimeter for low level neutron radiation meas. 79−49869
position sensitive detector, appl. to small angle neutron scatt. with azimuthal symmetry 78−46212
precision automatic angular-displacement control system 78−186
pulse shape analyser, effect of pulse pile-up on discrimination between neutrons and gamma rays 80−91402
pulsed spallation neutron sources for slow neutron scatt. 77−83426
quasi-elastic neutron scatt., direct model fitting of uncorrected TOF data 79−31309
reactor structural material transmission meas. using TOF spectrometer 80−18440
Rensselaer intense neutron spectrometer system 77−23364
resolution function of constant Q spectrometer 80−63443
reverse neutron time of flight method, slow neutron spectrometry with Fourier beam choppers 80−106230
reverse neutron TOF method, appl. to slow-neutron spectrometry with Fourier beam choppers 79−22534
scintillating glasses, pulse decay time meas. at room temp. 78−46225
scintillation, NE213 organic liquid, response functions to high energy neutrons 77−6634
scintillation, with stilbene crystal, separation of neutron and gamma-ray spectra in mixed field *(Czech)* 77−50327

neutron spectrometers continued
scintillation associated particle TOF system for d(n,n) scatt. meas. 78−58535
scintillation counter, liquid time compensated, high efficiency detector for TOF studies 77−23363
scintillation counter, NE 213, Munich pulse shape discrimination cct., low energy performance 78−46233
scintillation counter effective solid angle for fast neutrons 77−57819
scintillation counter multidetector arrangement for on-line meas. of neutron and γ-ray multiplicities 78−50440
scintillation counter with pulse-height discrimination against γ-ray background, calibration and energy scale stabilisation 78−13378
scintillation counters, neutron transit time and interaction coord. determ. 79−26807
scintillation liquid (NE 224) high-efficiency time-compensated neutron spectrom. 78−17468
scintillation plastic large area fast neutron detector 78−90022
scintillation spectrometers, with LED and PIN photodiode, stabilising system 80−47821
scintillation TOF meas. with very fast burst source *(French)* 80−14040
scintillator, organic, meas. of $^{16}O(\gamma,n)$ and $D(\gamma,n)$ spectra *(Dutch)* 79−3281
scintillator for 250-1000 keV neutron flux meas., >95% efficiency 77−26938
scintillators, thin cylindrical, spectral characteristics for fast neutron spectrom. 79−26806
shielding of analyzer crystal of neutron spectrometer 80−42887
small angle neutron scattering on the Harwell linac 80−19675
small-angle neutron scatt. using time of flight method, spectrometer, appl. 79−1371
solid-state tandem telescope, for 3-20 MeV neutrons 77−3206
Soller collimators, appl. to small angle neutron scatt., Monte-Carlo simulation 78−29701
spark chamber and time of flight detector for 15-150 MeV neutrons from extended source 77−83447
spin-echo integral transform spectroscopy 80−4748
spin-echo spectrometry and neutron optical polarisers 80−49051
stilbene scintillation fast neutron spectrom. with pulse shape discrimination 78−55084
stilbene scintillation spectrometer, meas. of fast neutron spectrum from NA-2 generator *(Czech)* 77−71710
superposition spectral recording method 78−78548
surface barrier detectors, fabrication techniques for fast neutron spectrometry 79−18074
SV5-C time of flight spectrometer 79−45529
synchronisation of neutron beam, ultracold neutron spectrometer 79−721
system for nuclear fuel rod inspection 80−47669
tetralin based scintillator, appl. in neutron spectrometry 77−30723
thermal, energy depend. detection efficiency of cylindrical counter, wall effect, calc. 77−57803
time coder with variable channel width for time-of-flight expts. 78−33403
time of flight, pseudostatistical modulation method *(Russian)* 78−33360
time of flight, review of operation and circuitry 77−6605
time of flight, use with 1 GeV proton synchrotron 77−26927
time of flight facility at Manitoba cyclotron lab. 79−81114
time of flight facility with mag. beam swinger, time, energy resolutions 77−57796
time of flight spectrometer facility for 8UD Pelletron tandem accelerator 79−85856
time of flight spectrometer for elastic neutron scatt. on powdered samples 77−62447
time of flight spectrometer in expts. with DD neutrons 77−65383
time of flight spectrometers, historical review of developments 79−72179
time-of-flight, cold-neutron, resolution function determ. 78−78030
time-of-flight, fast neutron cross section facility for CTR program 77−26931
TKSN-420, triple axis neutron spectrometer, resolution functions 80−69011
TOF, control and data processing system 78−25385
TOF associated particle spectrum based on $D(d,n)^3He$ 79−45255
TOF large time compensated scintillation counters for high energy neutrons 78−55085
TOF low-Q spectrom. appl. to small angle scatt. with pulsed neutron source 78−55083
TOF meas. of direct react. spectra, resolution improvement 80−18753
TOF spectra effects of imperfect beam modulation using mechanical correlation choppers 77−57798
TOF spectrom., Monte Carlo scatt. simulation 77−34509
track detectors, spectra meas. in range 0.4 eV to 10 MeV 77−42210
transit-time, detector containing ^3He 80−63441
triaxial crystal, automatic 79−97925
triple axis spectrom., energy resolution function 80−9449
triple-axis, computer-control system with CAMAC interface, program functions 77−19840
two crystal diffractometer, neutron spectrometer component, luminosity 78−21807
ultracold neutron spectrometer 79−720
velocity selector for neutrons, high resolution, applic. to materials research *(German)* 80−47803
B, liquid scintillation slow neutron detector with n-γ separation cct. 78−862
CdTe, thermal neutron detection 78−17479
Ge(Li) detectors, fast neutron leakage spectrum determ. 80−32565
Ge(Li) diodes, teflon covered for fast neutron detection 78−25384
Ge(Li) surface barrier detectors, fabrication 77−3207
He scintillation counter use in neutron time of flight spectrometer for 0.4-4 MeV range 79−68134
^3He ionisation chamber, delayed neutron spectroscopy 77−79501
^3He proportional counter for fast reactor neutron field spectral charact. *(Japanese)* 78−46222
LiF:Mg,Ti TLD based passive neutron spectrometer and dosimeter 77−54394
^6Li sandwich counter, meas. of neutron spectra in fast neutron systems 80−27884
^6Li sandwich surface barrier spectrometers for fast neutron calibration in MeV range 79−9961
^6Li semiconductor sandwich neutron spectrometer with background discrimination 78−50431
^6Li-salicylate neutron detectors with pulse shape discrimination 79−97950
^6Li-semiconductor spectrometer, meas. of neutron spectra in thermal reactor systems *(German)* 79−3282
NaI(Tl), pulse shape discrimination of high-energy neutrons and gamma rays 78−33395
$^{16}O(n,p)^{16}N$, utilisation for monitoring 14 MeV neutron generator output 79−3287
Si sandwich surface barrier detector with ^6LiF radiator 77−57807

neutron stars
see also pulsars
1 M⊙ neutron star penetrating 16 M⊙ companion, double core evolution 78−53980
$^3P_2$ pairing near transition temp. in dense neutron matter 78−57571
abnormal, structure, stability and normal-abnormal transition 79−71063
abnormal phase in dense neutron star matter 78−20849
abnormal state transformation and metastable states *(Chinese)* 78−85967
accreting compact object in binary system, magnetosphere theory, X-ray sources 80−46394
accreting matter, nuclear γ-ray line emission 78−4403
accreting neutron star, magnetopause struct. 78−65647
accreting neutron stars, cyclotron line emissivity 80−90463
accreting neutron stars, nuclear burning and X-ray bursts 78−36724
accreting rotating neutron star, X-ray burst source model, burst energy histograms 79−35428
accretion by rotating mag. neutron stars, torques rel. to pulsating X-ray sources period changes 80−31320
accretion disc, interaction with rot. mag. field 80−62173
accretion disc interaction with stellar mag. field, plasma diffusion across Alfven surface 78−93461
accretion environment, photon pair prod. in transrelativistic plasma 78−20632
accretion magnetospheres, general solns. 77−45400
accretion onto magnetised neutron stars, fate of sinking filaments 80−51798
accretion onto magnetised neutron stars, normal mode anal. of interchange instability at magnetopause 77−13376
accretion onto magnetised rot. neutron stars, possible instabilities 77−13377
accretion process giving rise to X-ray emission 80−90459
Alfven surface in accreting X-ray source, role in X-ray pulses form. 77−78899
anisotropic models, stability against radial and nonradial pulsations 77−13378
asymmetric nuclear matter, compression modulus, neutron excess effects, neutron stars 79−36182
asymptotic freedom and dense baryonic matter 79−62738
axisymmetric accretion two-dimensional gas-dynamic theory 77−33334
bimetric theory of gravitation, viability, gravitational radiation from neutron star binaries 79−35611
binary neutron stars, evolution, gravit. radiation and mass transfer 77−78821
binary stars with single optical component, ellipsoidality effect on light vars. 79−92806
in binary systems, accretion disk flux distrib. and colours 80−94778
binary systems formation rel. to gravit. radiation 79−35291
binary X-ray pulsars, review 77−29869
binary X-ray pulsars, rot. history 79−62871
binary X-ray sources, review 77−17631
binary X-ray systems, accretion flows 78−12432
binding energy and stability of cold neutron star 79−17006
Cassiopeia A, supernova remnant, evidence for illumination by binary neutron star 77−33615
Centaurus X-3, neutron star characts. from correlated spin-up and X-ray luminosity meas. 80−101648
Centaurus X-3, stellar wind vel. change during transition 80−12829
CG 195+4 (Geminga) pulsating γ-ray source, neutron star models 78−4402
characteristics and evolution, from radio, X-ray, and γ-ray obs. 77−37611
charged particle motion in an electromagnetic field on Kerr background geometry 79−9167
close binary systems, neutron stars tidal disruption by black holes 77−13387
close binary systems containing neutron stars, X-ray source model *(German)* 79−84814
close binary systems in quiet stage, detect. from γ-ray emission 79−67058
close binary systems with neutron star components, evolution *(Italian)* 79−21354
cold dense star with frozen-in mag. field, degeneracy removal, ideal electron gas approx. *(Russian)* 77−87365
cold matter at super-nuclear densities including pion condensates 78−17128
cold neutron star matter, decompression 77−33544
cold relativistic neutron gas, study of massive neutron cores 79−35292
compact X-ray sources, masses 78−12430
composition and struct. 77−29872
composition of outer crust, influence of mag. field 80−101610
Compton scattering by unmagnetised electrons in ambient mag. field, vacuum polarisation effects 80−86631
conference, 11th Masurian school in nuclear physics, Mikolajki, Poland (Aug.-Sept. 1978) 79−63605
conservation of energy equation from scale covariant gravitation theory 80−73216
cooling, effects of pion condensate form. 80−77443
cooling, vacuum polarisation effects *(Russian)* 77−17360
cooling and possible temp. determ. 78−40984
core, phase transition between nucl. and quark matter 80−67771
cosmic exploration by X-rays, 1978 Bakerian lecture 79−48964
Crab Nebula, central mag. dipole rot. neutron star theory for supernova remnant 80−51834
Crab pulsar, electron-positron flux at neutron star surface 77−64789
Crab pulsar, magnetized cracks in crust rel. to matter flow, radio, X-ray and optical emissions 80−72990
critical accretion flow of gas into compact stars, rel. to X-ray sources 78−20817
crust, correl. between speeds of fast and slow magnetoelastic modes 79−8942
crust, torsional oscills., period determ. 80−90464

neutron stars continued
crust superfluid, pinning and threading of quantized vortices 77−45475
crystalline physiology, model for non-chemical form of life 77−90978
cyclotron line emissions meas. with Ge(Li) balloon borne spectrom. 80−41721
cyclotron self-absorption in accretion columns of magnetic degenerate stars, X-ray sources appl. 80−12760
Cygnus X-1, model of neutron star surrounded by massive disc 80−36736
Cygnus X-1 (HDE 226868) system, search for third star 77−45606
Cygnus X-3, gamma-ray emission from mag. accretion disc 77−78894
degenerate electron-neutron plasma, energy release mechanism 77−74790
degenerate matter, pionisation *(Russian)* 77−91558
degenerate relativistic electron gas, electron collisions, thermal conductivity 80−109355
dense hadronic matter, in asymptotically free gauge theory, neutron stars eqn. of state 78−36627
dense matter, transport props., neutron stars appl. 79−67236
dense neutron matter, ferromag. transition, pure hard core gas model 78−70478
dense neutron matter physics, implications for neutron star props. 80−77277
dense neutron star matter eqn. of state, QCD instanton effects 79−92796
dense nucleon matter, density and isospin waves 79−93540
disc accretion onto magnetised compact objects, theory *(Russian)* 79−44467
disc accretion onto magnetised neutron star, fate of matter and ang. momentum 78−28715
disk accretion, transition zone radial and vertical structure 80−4393
dynamics and structure 79−97017
e^+e^- spontaneous creation in inhomogeneous magnetic fields 80−22540
Eddington luminosity limit and supercritical accretion, time-independ. calcs. 80−67768
effective temperatures, from search for EUV thermal radiation from nearby pulsars 77−22259
Einstein-Cartan theory, static fluid spheres, field eqn. analytic solns., neutron stars 79−2688
elastic medium, gravit. and acoustic waves, relativistic eqns., neutron star appl. 78−24712
electrically conducting rot. sphere behaviour in time-independ. homogeneous external mag. field 78−49309
electrodynamics in curved space, theory 80−90465
electrodynamics of disk accretion onto magnetic neutron star 80−85973
electron-positron annihilation in mag. field, γ-production 77−10236
electron-positron pair annihilation in strong mag. field *(Russian)* 79−17705
EM radiation near black holes and neutron stars 78−53978
episodic accretion of gas and cosmic γ-ray bursts 78−69824
equation of state and bounds on mass of nonrotating neutron stars 77−45477
equation of state of ideal neutrons in intense mag. field 78−89401
equations of state from Thomas-Fermi model 79−48840
equilibrium configuration of neutron matter, allowing for nuclear and gravit. interactions *(Russian)* 77−18462
evolution, terminal stages in quantum chromodynamics 77−78773
evolution of neutron star immersed in blue supergiant envelope 80−98689
expansion of neutron star matter and its final nuclear composition 80−67769
extended Fermi-hypernetted chain scheme, Landau parameters calc., transport coeffs., Jastrow theory 77−41529
Fermi quantum crystals, melting curves low temp. anomalies 78−24757
force-free magnetic fields, existence in neutron star interiors 78−40983
force-free magnetic fields in degenerate stars, stability 78−49425
formation, competition between neutrino and gravitational radiation 77−49421
formation, from evolution of mass-accreting white dwarfs 80−77281
formation, gravit. radiation burst 77−53571
formation, hydrodynamics of stellar collapse 78−45318
formation, neutrinos and gravit. waves emission 78−12266
formation, role of stellar degenerate C ignition 80−77390
formation, stellar collapse triggering by thermonuclear burning in degenerate C core 78−65608
formation following stellar collapse and explosion, massive star core hydrodynamics 79−16995
formation from core collapse, electron neutrino and antineutrino emission, spectral calcs. 80−109454
formation of neutron stars and black holes *(Swedish)* 78−69823
formation rate in Galaxy, estimation from stellar statistics 79−40208
formation rate in galaxy, upper limit 78−49471
formation rate in stellar systems 78−28674
formation through stellar core collapse, effects of eqn. of state on mass 80−85928
free precession, role of vortex pinning 77−49420
G127.1+0.5, optical counterpart of compact radio source assoc. with supernova remnant 78−16555
gas accretion, origin of cosmic gamma-ray bursts 77−5600
general relativistic stellar evolution code 79−58317
globular cluster X-ray source formation by collisions of compact and normal stars 78−28854
gravitational collapse, neutrino damping of nonradial pulsations 77−56999
gravitational collapse of core of massive star, neutrino trapping 78−32437
gravitational collapse of stellar core, secondary indications 80−62177
gravitational equilib. of a massive neutron core, relativistic treatment 78−57570
gravitational lens effect, EM wave diffr. in Schwarzschild space-time 80−90750
gravitational lens effect, focusing by slowly rotating relativistic spherical mass 80−105155
gravitational radiation, from neutron stars and white dwarfs 78−65646
gravitational radiation of dipole sources, Maxwell's eqns. analogue, appl. astrophysics 77−13536
gravitational wave, relfection from compact stars 78−49314
gravitational wave amplitudes and asymptotic eigenfrequencies distrib. for even modes 79−17300
gravitational waves emission, theory and astronomical appls. 79−92664
hadron plasma theory *(Russian)* 78−37148
neutron stars continued
hadronic matter components, leptons and baryons *(Polish)* 79−88587
HD 153919 (=4U 1700−37), supergiant-neutron star, optical variability 80−82419
HD 49798, strange composite sdO star, possible existence of collapsed companion 78−49435
HD 50896, WN5 star, emission-line spectrum vars. rel. to possible neutron star companion 80−51791
HD 77581 (=Vela X-1), supergiant+neutron star, stellar wind mass transfer, spectral obs. 80−94892
Hercules X-1, cyclotron line form. by reson. Compton cyclotron scatt. 80−8711
Hercules X-1, cyclotron self-absorpt. in accretion column of mag. degenerate star 80−12760
Hercules X-1, mag. neutron star, cyclotron emission and beaming mechanisms 78−36726
Hercules X-1 (HZ Herculis), X-ray continuum and Fe line emission during X-ray low state 80−105393
Hercules X-1 (HZ Herculis) mass determ. 77−78891
HZ Herculis (Hercules X-1), Ariel V X-ray spectra 80−90580
HZ Herculis (Hercules X-1), hard X-ray spectrum, strong cyclotron line emission 78−41085
high density matter, relativisitc quantum many-body problem 78−4909
homogeneous ellipsoidal stars, evolution 77−33333
hot neutron star formation, neutrino radiation rel. to envelope outburst problem 78−45350
hot neutron star matter, neutrino transport, opacity 79−75238
hot perfect fluid relativistic stars, asymptotic eigenfrequency distrib. for even parity perturbations 78−49668
ideal Fermi gas, thermodynamics and eqn. of state 77−30117
inner crust nuclear compositions 80−31322
instantons in a quark plasma, superheavy hadrons and neutron stars *(Russian)* 79−36039
instantons in quark plasma, multibaryon hadrons and neutron stars 79−40733
interacting neutron gas at high density and temp., supernova models appl. 77−33330
interacting neutron matter model at postsupernova temps. 77−45399
interior plasma, mag. field rel. to pulsar periods long-term changes 80−22029
interiors, MHD eqns 79−35288
international school proc. (Varenna, Italy, 1975 July 14-26) 79−80334
isothermal neutron star core, eqns. of state 79−62864
liquid neutron matter, pion condensation and the linear σ-model 79−59027
LMC X-4, spectroscopic obs. rel. to secondary identification as neutron star 79−9028
luminosity enhancement following X-ray bursts 78−32502
in M15, globular cluster, dynamical models with neutron stars 78−32536
magnetic, accreting, light scatt. in strongly mag. plasma 79−62739
magnetic, accretion flow, magnetospheric struct. and stability 78−4269
magnetic, vacuum birefringence effects on X-ray polarisation 79−40209
magnetic fields, effect of vacuum birefringence on X-ray emission polarisation 78−4408
magnetic fields, strengths and props. of stellar condensed matter 80−82187
magnetic fields and related effects 80−72991
magnetic fields in superdense stars, cyclotron reson. emission 79−75207
magnetic neutron stars, disc accretion model 78−93294
magnetic poles, pair formation and electric field boundary conditions 80−101613
magnetised neutron star, cyclotron line form. in atmosphere 79−48839
magnetised neutron stars, thermal radiation 80−56869
magnetism in superdense stars, quantum theory 79−92753
magnetospheres, charged particle distribs. 77−13379
magnetospheres, laboratory modelling 79−75240
magnetospheres, pair annihilation in superstrong magnetic fields 80−85847
magnetospheres, Thomson scatt. rel. to hard X-ray spectra of Centaurus sources 77−2493
magnetospheres of accreting compact stars possessing multipole magnetic fields 79−97020
mass limit in bimetric gravit. theory 77−78813
mass upper limit, Brans-Dicke theory 77−33543
mass upper limit for stability against black hole form. 78−96498
mass-radius relation, obs. constraints, dense matter eqn. of state 80−46597
mass-radius relations for cold spherical body, relativistic effects 80−26730
masses, evidence from X-ray astronomy 77−71154
masses, observational constraints 77−5543
masses, upper limit determ. from dense stellar matter physics 80−101611
massive cold spherical stars, rest-mass density and redshift 80−56859
massive neutron star, fermionic matter, coupled Dirac-Einstein eqns., self consistent soln. 78−73731
massive spheres with an isothermal core 80−82405
materials motion around a source whose luminosity changes 79−12394
maximum mass, theory 77−33545
MHD processes near compact superdense objects 79−40206
MHD relativistic processes 78−12280
micropulses, drifting subpulses and nonradial oscills. 80−67766
model, quantum statistical mechanics treatment 77−49418
model with trapped neutrinos, implications for stellar collapse 80−90407
model within general relativity, mass evaluation 80−101612
MXB 1730−333, rapid X-ray burster, accreting rot. magnetised neutron star model 79−84866
MXB 1730−335, accreting neutron star model of rapid burster 79−30145
MXB 1730−335, comparison with dwarf novae rel. to neutron star model 78−12410
N49, vibr. neutron star as source of March 1979 γ-ray burst 80−105270
n-vertex loop diagrams in superstrong calc. field, calc. method 77−71472
neutral currents and neutrino emission of cold stars 77−45478
neutrino angular momentum loss by Poynting-Robertson effect 79−16928
neutrino cooling in pion-condensed phase 78−45351
neutrino emissivities 79−97016
neutrino luminosity, contribution of crust 79−97018
neutrino opacity, pure neutral vector boson contrib. 78−53928

neutron stars continued
neutrino radiative lifetimes, limits from supernovae 79−16785
neutrino retention, influence on stellar mass and radius 79−62817
neutrino scattering by phonons in dense matter 79−12488
neutrino-pair bremsstrahlung in collisions between neutrons and nuclei 77−74789
neutrino-pair bremsstrahlung in hot plasma, strong mag. field 78−61878
neutron $^3P_2$ superfluidity under π^0 condensation in neutron star matter 80−47417
neutron matter, energy per particle and effective mass 77−30499
neutron-rich nuclei, energy density mass formula appl. 79−35290
neutronization kinetics in superdense matter with frozen-in mag. field *(Russian)* 78−46019
Ni's theory of gravity for massive neutron stars 78−4273
nonequilibrium shells, role in X-ray emission and nucleosynthesis, review 80−67774
nonlinear electrodynamics in generalised gravitational theory 77−5727
nonrotating, bounds on moment of inertia calc. 77−41387
nonrotating, integral eqns. for even parity perturbations 78−36628
nonrotating, mass and moment of inertia bounds 79−2551
nonstationary accretion of stellar wind, rel. to X-ray bursters *(Russian)* 78−69825
nonuniformly rotating neutron stars, struct. and mass *(Russian)* 77−91559
nuclear and neutron matter with isobars, transition pot. model, neutron stars 80−68573
nuclear energy release in neutron star envelopes as sources of X-ray emission 77−78814
nuclear fusion and C flashes, theory 78−93293
nuclear matter, phase transitions at finite temperatures 79−6468
nuclear matter at high temp. and density, bulk props. 78−89812
nuclear matter equation of state, relativistic quantum field theory of neutron stars 80−5088
nuclear physics of neutron stars, review 79−92797
nuclei excitation energies in hot matter, limits 80−56703
null radiation gravitation deflection by relativistic spherical masses 79−58600
opacity, electron scatt. in strong mag. field, approx. formulae 79−92662
oscillations, junction conditions across perturbed contact discontinuities 80−94787
outer crust, electron solid in superstrong mag. field, bifurcation theory approach 80−4640
particle acceleration at magnetic poles 78−93295
ϕ Persei, binary Be star, HE II emission rel. to compact secondary component 80−12768
X Persei, photometric behaviour, 1964 to 1979, and binary star model 79−53820
photoneutrino reactions in superstrong magnetoactive plasma, neutron stars appl. 79−35105
pion condensation and star dynamics 79−67047
pion condensation in dense nuclear and neutron matter 80−37333
pionisation, appl. to superdense celestial bodies *(Russian)* 79−96907
pionization in superdense degenerate matter *(Russian)* 78−46020
plasma accretion, interaction with mag. field and accretion flow hydrodynamics 80−109452
plasma coupling, boundary conditions 80−94823
plasma interface, physical processes in strong gravit. field, electron-positron pair prod., γ-ray emission *(Russian)* 79−80333
plasma processes, space-time curvature 79−84873
polar-cap sparking model, rel. to synchronised drift of pulsar radiation patterns 77−57005
positronium annihilation in strong magnetic fields 79−17007
positronium decay, in strong mag. fields, 10^{12} Gauss 79−88578
postglitch behaviour of quantum plasma 79−35289
potential drops above pulsar polar caps, nonneutral beam accel. 78−4267
propeller spindown of rotating magnets, torque calc., neutron stars appl. 79−8831
properties, general description *(Danish)* 77−67106
pulsar, dynamics of differential rotating sphere 77−37609
pulsar, quasar and X-ray source obs. 80−36657
pulsar constrained atmosphere, min. energy state 79−25622
pulsar electron cap, electrons accel. in internal zone 80−46592
pulsar magnetosphere, generalised Ohm law 77−37610
pulsar magnetosphere, magnetoactive plasma equilib. in gravit. field *(Russian)* 80−26895
pulsar magnetosphere model, cylindircal, with particle inertia but no dissipative forces 80−51796
pulsar magnetosphere models, interior and exterior struct., pair prod. 80−46594
pulsar NP 0531, distrib. model of press., density, ang. vel., matter rot., grav. field *(Ukrainian)* 80−12775
pulsar polar caps as foil-less diodes, nonneutral relativistic beam accel. 80−17604
pulsar radio emission, generation in neutron star mantle *(Russian)* 79−101168
pulsars, emission regions location, obs. limits 78−65637
pulsars, radio and X-ray, review 78−69820
pulsars and compact X-ray sources, gravit. redshifted γ-rays, neutron star mass constraints 78−4274
pulsars emission mechanism, AC Josephson effect hypothesis 80−82404
pulsating X-ray binaries, spindown by EM friction with stellar wind 78−12431
pulsating X-ray sources, secular period changes 77−45613
pulsating X-ray sources period vars., torque vars. and stellar response 79−9029
pulsation damping due to interior weak interaction processes 80−77439
QCD and superdense matter, quark and gluon plasma, hadronic structure, neutron stars, hadron collisions, review 80−73683
QCD of highly condensed matter 78−70267
QCD of quark matrer to nuclear matter transition at neutron star density 78−54608
quark beta decay and cooling 80−82406
quark gas, nonAbelian gauge field theory 78−21341
quark matter, phenomenological equation of state, neutron star appl. 79−63424
radial perturbations of slowly rotating neutron stars, stability 80−98685
radiating accretion column, X-ray pulsar model 77−53710
radiation pressure effects on spherical accretion 78−61725
radiation source form. mechanism, mag. annihilation *(Chinese)* 80−77440
neutron stars continued
radiative transfer, in surface layers of neutron stars with mag. fields 80−94826
radio pulsars, model *(Russian)* 78−40982
redshift determ. of X- and γ-ray lines rel. to strong principle of equivalence 78−40814
relativistic accretion on X-ray pulsars 79−9032
relativistic dense matter, statistical mechanics using phenomenological quantum field model 78−89814
relativistic elasticity, one dimensional nonlinear motion 79−84953
relativistic elasticity appl. to neutron stars 78−12267
relativistic fluid spheres rel. to neutron star models 79−5855
relativistic many-body theory, quantum chromodynamics and neutron stars/supernova 79−40752
relativistic quantum mechanical model for solid core of neutron star 77−33546
relativistic slowly rotating stars 79−21321
relativistic star, rotating shell model 79−88650
relativistic superdense matter 78−12091
rotating, elec. field anal., effect on accretion and radio pulsar model 80−109453
rotating, general relativity, exact solns. for slow rot. 79−75239
rotating magnetic, accretion flow inside magnetosphere rel. to rot. rate 78−8037
rotating neutron star, mag. configuration of plasma-sphere 79−75241
rotating neutron star, stress-deformed state *(Russian)* 77−37612
rotating neutron stars, form of quantum vortex filaments 80−67770
rotating neutron stars, props. in bi-metric theory of gravitation 80−90466
rotating permanently magnetised sphere, EM field in inertial and comoving reference frames 79−71316
rotating relativistic neutron star, interior MHD struct. 79−71062
rotating stars, existence of ergoregions 78−24523
rotating stars stability and gravit. radiation 78−93210
rotational energy loss, slowing down index and time derivs. 80−67762
Schwarzschild electrodynamics, rel. to black holes and neutron stars 78−77480
secular instabilities of rigidly rotating stars in general relativity, theoretical formalism 80−4341
secular instabilities of rigidly rotating stars in general relativity, numerical results 80−4342
secular instability in rotating stars, resulting from thermal cond. 80−21986
sigma model in mean-field approx., pion condensation 77−88069
slow rotation in collapsed stars, effects of mass loss 78−49426
slowly rotating neutron stars, appl. of bimetric theory of gravit. 79−85042
slowly rotating stars, gravit. collapse, supernova explosion, neutron star or pulsar remnant 78−96472
SMC X-1, observational constraints on mass 77−29957
SMC X-1, spin-up rate of X-ray pulsar 77−29956
SMC X-1, VBLUW photometry, evidence for accretion disc 78−12409
solar companion star, neutron star in hyperbolic orbit 78−12198
sources of gravitational radiation, conf. proceedings (Seattle, 24 July-4 Aug. 1978) 80−36778
spectra of magnetic dense stars, theoretical anal. of atomic spectra 80−105160
spherical accretion, X-ray spectra and luminosity 77−82271
spherical multicomponent fluid, hydrostatic equilib., thermodynamic interpretation, 3-component neutron star 79−49135
spherically symm. accretion near Eddington limiting luminosity 79−16809
spin alignment, spin-torsion forces and strong-gravity interactions 80−56870
spin down rel. to X-ray sources in binary stars *(Chinese)* 78−28857
spindown rates, of neutron stars in close binary systems 79−40210
SS 433, accreting mag. neutron star model *(Russian)* 80−36647
SS 433, beam models, energetics anal., possible triple system 80−90433
SS 433, early-type star plus neutron star model 80−56843
SS 433, massive black hole and pulsar models rel. to precessional motion origin of 164^d period 80−62138
SS 433, Of star orbited by neutron star, model 80−22025
SS 433, spectral features interpreted a precessing neutron star with jets, possible binary 80−90447
stability criterion for stellar cores *(Russian)* 78−93214
state equation and two nucleon nuclear interaction for nuclear matter *(Russian)* 79−40879
static plasma polarisation in Schwartzschild gravitation field *(Russian)* 79−16825
stellar collapse to neutron stars and black holes, computer generation of spherical spacetimes 80−46385
stress tensor of cosmic and lab. type-II superconductors 78−6485
structure, baryon to quark matter transition 77−5424
structure, determ. from pulsars and compact X-ray sources 80−77442
structure, microscopic interpretation 77−64790
structure, physics of matter at high density 79−84815
structure and evolution, general relativistic eqns. 77−33471
structure and physics 79−67046
structure from X-ray timing obs. of pulsating X-ray sources 79−5917
Sun possible companion, mass, vel., and luminosity 79−2490
superconducting props. of π condensates 78−32993
supercritical accretion discs winds struct. and appearance, numerical models 80−21984
supercritical time-dependent accretion, theory 80−85967
superdense celestial bodies, theory 80−67773
superdense magnetised astrophysical objects, interiors physical conditions 80−17603
superdense matter, hydrodynamic model, nonlinear pion+pion chiral Lagrangian, $e^+ + e^-$ and p+p collisions 78−32966
superdense matter eqn. of state, nuclear size correction to relativistic Thomas-Fermi model 78−29413
superdense matter state *(Japanese)* 77−29643
superdense neutron matter, relativistic theory and eqn. of state 78−45349
superdense quark core, spontaneous magnetisation possibilities 80−8646
superdense stars in quantum limit of ultrastrong frozen-in mag. fields 77−53620
superfluid dynamics, rotating, lab. expts. 78−49469
superfluid interiors, relax. processes between superfluid and crust 78−65645
superfluid mechanics for high density of vortex lines 78−54290

neutron stars continued
superfluid neutron matter, $^3P_2$ pairing, mag. field effects, vortices 80 62174
superfluid phase transition for neutron star matter 80−101607
superfluid phase transition in neutron star matter 79−59025
superfluidity in neutron stars, theory 80−77441
supergiant stars with degenerate neutron cores, equilib. models struct 77 33472
supernuclear matter, test of quark bags and interacting neutron models 77−78812
supersonic accretion, radiative effects 78−40978
surface, nuclear crystals form. *(Polish)* 77−17355
surface layers, Coulomb collisions in degenerate plasma in quantising mag. field, photon absorpt. *(Russian)* 78−55715
thermal properties and detectability, cooling and heating processes 80−31323
thermal X-ray emission, review of theory 80−41849
thermal/timing instability, rel. to pulsar timing obs. and X-ray transients 79−92795
thermonuclear bursts assoc. with chromosphere flares 80−98684
thermonuclear flashes, model for X-ray bursts 78−12417
thermonuclear flashes in degenerate envelope *(Russian)* 79−35294
thermonuclear flashes in envelope of accreting neutron star, theory rel. to X-ray burst sources 80−109455
thermonuclear flashes in envelopes of accreting objects 80−67772
thermonuclear flashes on accreting neutron stars 80−31321
thermonuclear runaways on neutron stars, theory 80−22032
Thomson scattering in strong mag. field, vacuum polarisation effects 80−86632
transformation between two kinds of neutron stars *(Chinese)* 79−80332
triple close approaches effect on stellar system evolution, one-parameter family appl. 80−17618
two-body problem in Rosen's bimetric gravitational theory 77−37796
4U 1223−62 (GX 301−2, WRA 977), binary star orbit determ. from X-ray obs. 80−90570
4U 1626−67, 7.7-second X-ray pulsar, simultaneous X-ray and optical obs. 80−51914
4U 1700−37 (=HD 153919), eclipsing binary, secondary neutron star, X-ray obs. 80−86016
4U 1700−37 (HD 15319), high-energy X-ray obs. rel. to neutron stars accretion 80−86014
ultrahigh density neutron star matter, props. 77−91560
ultrahigh energy neutrino flux from galactic neutron stars, calc. 79−53851
Universe, high density matter, many body treatment, pulsars 80−26738
unmagnetized, supercritical accretion rel. to galactic bulge X-ray sources 79−80331
upper mass limit, accounting for differential rotation 78−4272
variable rest masses, black hole solutions and neutron star models 79−30162
viscous neutron matter, differential rot. 77−60788
warm neutron degenerate matter, eqn. of state 79−84810
weak interactions, conf., Bloomington, USA, (May, 1977) 78−414
X-ray and soft γ-ray radiation mechanism during plasma accretion 77−87468
X-ray binaries, anomalous periastron positions rel. to neutron star masses 79−25756
X-ray binaries, double core evolution 79−84816
X-ray binary sources, pulsating, spin-up due to accretion from Keplerian disc 80−67904
X-ray burst source model, He flashes on accreting neutron star 79−17008
X-ray burst sources, accreting compact objects models 78−12427
X-ray burst sources, matter accretion from magnetopause 77−49419
X-ray burst sources, model, substorm process at accreting neutron star 79−17132
X-ray burst sources, neutron star accretion model 78−49566
X-ray burst sources, persistent emission rel. to nature of galactic bulge X-ray sources 79−84871
X-ray burst sources, simple physical model 77−29960
X-ray burst sources in globular clusters, neutron stars hypothesis *(Russian)* 78−16480
X-ray bursting sources, time dependent accretion by magnetic neutron stars 78−4401
X-ray bursts during passage through dense clouds 77−78896
X-ray emission lines Zeeman splitting by mag. field 78−4275
X-ray emission models 80−62175
X-ray pulsar as accreting neutron star in compact binary 78−49470
X-ray reflection from surfaces, appl. to Hercules X-1 78−28716
X-ray source, intensities from stellar wind flow past compact object 80−22116
X-ray sources, compact, radio emission origin 80−62317
X-ray sources, pulsating, accretion disc mag. field calc. for oblique mag. dipole configuration 80−94895
X-ray sources, strongly magnetised plasma collisional relax. of ion beam 80−33785
X-ray sources of galactic bulge, highly compact binary model 79−35430
X-ray sources with repeating bursts, magnetospheric accretion model 77−5597
X-ray spectra from accretion column, optically thick region inc. 80−67767
X-ray stars in globular clusters 78−20916
X-rays from accretion as signals from extraterrestrial civilisations 77−53432
Yang-Mills gauge theory of gravity, gravit. field of spherically symm. matter distribs. 78−4773
zero sound propagation in dense neutron matter, Landau theory 78−53977
zero-temperature degenerate stars with subnuclear densities, radial oscills. 78−12219
β-decay of π condensates as cooling mechanism 78−4271
$e^+e^- \rightarrow \nu\bar{\nu}$, in strong mag. fields, rate of energy loss 78−29326
γe Compton and Thomson scatt. in strong magnetic fields, differential cross sections, neutron star appl. 79−67530
$\nu(\bar{\nu})$ emission from supernovae, form. and cooling of neutron stars 78−8038
ν transport in π condensed matter 78−4270
π fields in nucl. matter 78−58246
π^- condensation, nonrelativisitc treatment, mean field method 77−30500
π^- condensation in neutron star matter 77−53420

neutron stars continued
π^0 condensation in symmetric nuclear matter and pure neutron matter 79−3108
Fe atoms and condensed matter in strong mag. fields, var. calc. ground-state energy 77−75046
H, transition probabilities and expectation values, in intense mag. field 79 10066
H_2-He plasma interface in strong gravit. field, bremsstrahlung, neutron stars and pulsars appl. *(Russian)* 79−67048
He burning shell evolution in accreting stars 80−85968

neutron transport theory
see also neutron diffusion; neutron moderation
absorption cross section of fission product aggregate, energy dependence 79−76075
acceleration technique for iterative methods in diffusion equation *(Japanese)* 79−80971
activation calc. and exptl. comparison for 14 MeV neutron source, fusion technique validation 79−9657
activation cross sections meas. for generalised intermittent irradiation, fusion machines appl. 78−58283
air transport benchmark calcs., sensitivity anal. of cross section and method uncertainties 77−23168
air transport sensitivity to nitrogen cross section uncertainties 77−23165
air-over-ground calcs. for various cross sections, weapon effect studies 77−23164
albedo cell calculations in the thermal region taking into account thermalisation *(Russian)* 80−52710
albedo method for single group calculations of multiband spherical cells *(Russian)* 80−52709
American Nucl. Soc. winter meeting 1977 78−58315
American Nucl. Soc. Winter Meeting 1977 78−82408
AMPX code for coupled multigroup n-γ cross section sets 80−68741
analogue simulation of reactor neutron field, equipment minimisation *(Russian)* 78−74416
analytical angular integration technique for generating multigroup transfer matrices 80−68722
angular effects in toroidal diffusion, one-group homogeneous diffusion model 79−22351
anisotropic computations, selection of angular quadrature 77−37828
anisotropic media, discrete ordinates method 79−85579
anisotropic Milne's problem, soln. using H-functions 77−53840
anisotropic multigroup transport cross sections, low order approx. 77−34364
anisotropic neutron transport anal. 78−50227
anisotropic neutron transport eqn., n-dimens. time independent, fundamental soln. 79−45321
anisotropic scatt. effect, critical slab problem, neutron transport theory 77−88187
anisotropic scattering media, neutron transport formulae 79−17959
anisotropic scattering of monoenergetic neutrons from spheres, slabs, cylinders, extrapolation length determ. 79−45318
anisotropic scattering treatment using improved comput. code *(Japanese)* 80−13526
anisotropic source flux iteration techniques, interpolation schemes 80−99200
anisotropy of scatt. and fission 78−8865
Argonaut research reactors, effect of atmos. press. variation on reactivity *(German)* 80−5199
asymptotic expansion method in reactor calcs. 77−23181
asymptotic solutions, large critical systems, mono- and polyenergetic cases 77−23179
Bell-Pal fundamental eqn. for n stochastic behaviour in Boltzmann continuum model 78−78436
benchmark testing of anisotropic diffusion coefficients, void-worth calcs. for finite lattices 80−47546
bilinear functionals, upper-bound estimations 77−67796
Boltzmann eqn., P_1 and diffusion eqn. asymptotic equivalence 80−95334
Boltzmann equation, derivation of diffusion equation by Hilbert expansion equation 79−17368
Boltzmann equation, eigenvalue defn. and use 77−54275
Boltzmann equation, eigenvalue precision, influence of boundary conditions 80−27689
Boltzmann equation, eigenvalue precision, influence of boundary conditions 80−27690
Boltzmann equation, in parallelepiped, functional methods use 77−57701
Boltzmann equation, two-vector, analytical solns. in nonplanar geom. 77−65246
Boltzmann equation with average force field caused by anisotropic momentum changes 77−13714
Boltzmann neutron transport operator, dominant eigenvalue determ. for inhomogeneous body 79−13377
boral shielding material, neutron transmission calc. 80−854
bound neutrons in matter, transmission coeff. *(Russian)* 78−13199
bounded flux-at-a-point estimators 79−587
bounded Monte Carlo estimator for reaction rates in finite volume elements 79−85571
buckling approximation inclusion in finite element calcs. 78−17276
BWR, input neutron noise, stochastic variables quantisation 79−85573
BWR in-core neutron detector sensitivity to control rod vibr. using neutron noise anal. 80−57910
BWR lattice geometries, comparative study of two-dimens. transport methods 77−61484
C_N method, appl. to cylindrical geom. 78−29533
C_n method in spherical geometry, appl. to transport problems 79−22362
C_N method of transport eqn. soln., appl. to plane geom. 78−29524
CACTUS, a characteristics solution to the neutron transport equations in complicated geometries 80−95336
CANDU, LOCA, space-time neutronic anal. 80−13663
CANDU reactor, integral transport code PEAKAN for flux peaking anal. 79−59135
CANDU-PHW, neutron group cross sections in resolved resonance region calcs. 80−13573
capture probabilities for thick samples at resonance energies 78−46123
capture probability, linear Boltzmann eqn., Pade approximants, appl. to spherical geometry 80−52143
Chandrasekhar H-equation, Banach space anal. 77−13224
Chandresekhar's H-equations in multigroup neutron transport, iterative solns. 78−37389
Chandresekhar's operator valued H-function, analytic continuation 78−37388

neutron transport theory continued
CHART program, eqn. soln. in cylindrical and spherical geometries 80−5197
Clinch River Breeder Reactor primary coolant pipe chaseway neutron streaming analysis 79−9661
coarse-mesh eqns. for the numerical soln. of 2nd-order transport eqn. 80−47527
coarse-mesh nodal methods, generalized approach 79−80987
collision probability integrals, annular geometry, evaluation using analytic expansions 80−32317
collision probability integrals in annular geometry, properties 79−22361
collision probability method, development and applications 80−27706
collision probability program for uniform slab lattices 79−89350
compatible product ang. quadrature for transport in x-y geom. 77−82981
complex buckling modes in asymmetric cell lattices 79−30881
complex particle transport problem soln., general-purpose Monte Carlo codes 79−583
complex relaxation lengths, existence in absorbing medium 79−589
conjugate gradient solution to discrete ordinates equation 78−21622
conservative medium, one-speed and multigroup eqns. 77−33960
constant cross-section model of transport eqn., validity test 78−66327
constrained finite elements and response matrices 77−61475
continuous energy Monte Carlo code VIM, cross section preparation 77−23166
continuous slowing down theory params. in highly absorbing media 78−29559
contribution Monte Carlo, exponential biasing model 80−5195
contribution Monte Carlo technique, variational derivation 80−5194
contribution transport, deterministic approaches 80−555
contributions, volumetric distrib. Monte Carlo calc. 79−36295
convolution and H-equations for operator-valued functions 77−50186
convolution integral calculations for neutron transport in reactors 80−47561
correlation technique for resonance calculations 79−71875
coupled neutron-nuclide problems, time depend. generalised perturbation theory 80−32322
critical and non-critical slabs, anisotropic scatt., struct. polynomial soln. of transport eqn. 78−70582
critical assembly, rapid calc. of neutron fluence and dose 77−38317
critical problem solution, sufficient conditions 79−58657
critical radius of sphere, asymptotic multigroup approx. *(Russian)* 77−57702
critical reactor calc., AGA two-sweep iterative methods 79−36298
critical slab, isotropic and anisotropic scatt., asymptotic solution, strained coords. method 80−42733
critical slab reactor with finite reflector problem soln. 77−65251
critical systems design, algorithm of Monte Carlo methods 79−40501
criticality calculations by source-collision iteration technique for cylindrical system 77−65268
criticality of neutron transport in a slab with finite reflectors 79−17950
criticality problem for highly anisotropic scattering 79−58658
cyclotron radiation transport in plasmas by neutron transport techniques 80−38660
cylinder, homogeneous infinite, isotropic scatt., one vel. approx. 79−582
data covariance estimation methods for sensitivity-based data assessment 78−13400
deep penetration problems, rebalance methods, effectiveness 80−47533
deep penetration shielding problems, calc. of contribution flux and current spatial distrib. 79−59283
deep-penetration radiation transport, event and point value in Monte Carlo importance sampling 78−8869
deep-penetration transport calculations and neutron transport eqn. forms 78−8868
deep-penetration transport problems, appl. of contributon Monte Carlo methods 80−47530
density distribution functions moments 77−30645
density fluctuations, statistical anal. by Fokker-Planck method 77−26818
design calculations for A 14-MeV neutron collimator 79−59257
diamond scheme approx. to neutron transport eqn. 79−36299
diffusion acceleration, modified approach 80−13528
diffusion coefficient adjustment using transport theory results 79−22359
diffusion eqn. asymptotic approximations to neutron transport eqn. 79−9663
diffusion synthetic acceleration methods for diamond differenced discrete ordinates eqns. 77−82983
direct coupled-ray method for design oriented 3-D anal. 77−83111
discontinuous variational approx., neutron diffusion and transport theory 78−46129
discrete angle finite element formulation of radiation transport 78−13197
discrete eigenvalues of transport eqn. with anisotropic scatt. 80−553
discrete integral transport methods, modified source interpolation scheme 77−57699
discrete ordinate eqn., weighted-residual method soln. 79−6725
discrete ordinates calc., weighted-difference formulation 79−9660
discrete ordinates calculations of the importance factor of a neutron source using ANISN code 80−68723
discrete ordinates transport problems on large scale, numerical methods efficiency 79−85099
discrete time decay constants above Corngold limit for infinite slabs 77−50212
discrete-ordinate transport eqn., variational difference schemes 77−65250
discrete-ordinates eqns., linear continuous triangular-mesh difference scheme 79−59134
discrete-ordinates neutron transport equations in slab geometry, convergence rates of spatial difference equations 80−27688
dispersion function, consequences in anisotropic scattering 80−27241
dose and LET distributions due to neutron and photons from stopped pion 77−52878
double P_L eqns. for sphere, series soln. 78−13187
doublet fusion reactor, neutron wall loading, two-dimens. calc. 78−66407
Dragon reactor zero energy expts., further n energy group and transport calcs. 78−78445
DWR core global power distrib. calcs. equivalent, Homogenized, and condensed nuclear parameters 80−655
earth, radiation transport for neutron and γ-ray point sources above air-ground interface 80−32526
effective neutron resonance cross sections, calc. in energy and space 79−17954
eigendistributions in linear transport theory 80−13523

neutron transport theory continued
eigenvalue eqns., appl. to fast and thermal neutron systems 78−50231
eigenvalue spectrum of homogeneous multiplying systems for monoenergetic neutrons with anisotropic scattering 79−22353
elastic n scatt. from n, d, t, ^{6}Li, differential scatt. rate distribs., multigroup rate coeffs. determ. 77−61476
elastic-removal cross sections, spectral corrections 77−46278
electron beam fusion of D-T pellets, neutronics and photonics 80−52781
electron-beam fusion coupled pellet-blanket neutronics 80−47717
electronuclear fuel production, medium-energy nucleon-meson transport calcs. 79−81061
elementary neutron slowing down equation, infinite series soln. 79−17951
empirical relation for variation of k_{eff} 77−74902
ENDF/B-V cross section data for shielding appls., Monte Carlo MCNP integral calcs. 80−47744
ENDF/B-V nuclear data for shielding appls., energy balance anal. 80−47745
energy dependent transport system in slab geometry, positive solns., subcriticality 77−50185
energy independent transport equation, soln. method with anisotropic fluxes *(Russian)* 79−17958
energy spectra, stationary transport eqn. formulations 79−13378
energy-dependent albedo calc. for neutron scatt. 79−9659
epithermal few-group cross sections, unit cell with neutron leakage 77−50199
epithermal-neutron field in medium with inhomogeneous water distribution 79−17957
escape probability, Boltzmann linear eqn., Pade approximants 80−551
escape probability from absorbing body, approx. for slab and cylinder 79−30883
escape probability from absorbing body, approx. for slab and cylinder 79−30882
escape probability from absorbing body, polynomial expression 80−47523
ESP-TIMOC modular code for neutron transport problems, in FORTRAN IV 78−50236
estimated uncertainties in evaluated nuclear data 77−23169
even-parity transport eqn., complex trial functions 79−59108
explicit iterative technique for FX2 reactor analysis computer code 78−17302
F_N method, appl. and numerical results 79−30878
F_N method, theory and appl. 79−30877
factorised kernels and DKPL soln. to transport eqn. in rectangular parallelepiped 79−80968
fast liner reactor conceptual design, nucleonics 80−13790
fast neutron spectra transmitted through iron and sodium slabs 80−73873
fast neutrons, energy deposition calc. using adjoint Boltzmann eqn. 79−6723
fast pulse reactor ^{237}Np/^{238}U and ^{239}Pu/^{237}Np spectral index meas. and calc. 79−9804
fast reactor, effective cross section preparation from multigroup cross sections *(Rumanian)* 80−47543
fast reactor design data adjustments 79−9695
fast reactor neutron noise analysis, energy-dependent formalism 79−13489
fast reactor physics, assessment of JAERI fast group constants set version 2 80−602
fast reactor shields, relative accuracies of transport theory approximations 77−61481
fast reactor space-depend. depletion anal. continuous slowing down theory 79−80990
fast reactor spectrum calculation by space-depend. continuous slowing down theory 77−54293
fast reactor three-dimensional hexagonal-Z systems anal. using THREETRAN (hex,z) 79−80994
fast reactors, generalized treatment of heterogeneity effects for the shielding factor method 79−40990
FBR, few group constants for reactivity calcs. errors *(Czech)* 77−71639
FBR, multiplication factor evaluation of bare and reflected small fast assemblies using variational method 79−85583
FBR, nonstationary prompt-neutron diffusion, multigroup treatment 80−86956
FBR, optimisation of burnup characteristics, nonlinear programming method 77−14239
FBR analysis, general multigroup nodal procedure based on response matrix principles [for FBR analysis] 80−57827
FFTF, delayed-neutron parameters 79−80999
fictitious anisotropic fission and scattering kernel with vanishing critical thickness 79−590
field charact. calc., beyond Fe barrier, effect of scatt. indicatrix approx. and consts. representation 78−17272
finite element analysis, modified method for neutron transport eqn. 80−47529
finite element diffusion and P_1 eqns. soln. by iteration 77−50188
finite element method, theoretical considerations 79−13372
finite element method, two-dimens., one-group test problems 80−37412
finite element methods for radiation transport calcs. 78−13196
finite element solns. of neutron transport eqn., appl. to strong heterogeneities 77−26820
finite moments algorithm for particle transport problems 79−67237
finite slabs, orders-of-scatt. anal. 77−22502
fission reaction rate standards and applications 79−9650
fission reactor, coupled cores, neutron transit time determ. by noise anal. method 78−37413
fission reactor neutron gas, nonequilibrium thermodynamics *(Japanese)* 78−62595
fission reactor reactivity perturbation calc. by difference iterations in the Monte Carlo method 80−5210
fission reactor theory, reduced three-dimensional transport equation with anisotropic scattering 80−18368
fission reactor theory, relationship among the various anisotropic diffusion coefficients for periodic lattices 80−57826
fission reactors, ω mode transport eqn., asymptotic soln. 80−102231
fission reactors, fluidised bed concept, diffusion theory 80−68729
fission reactors, seed-blanket calcs., 2-D, one-channel synthesis method, transport and diffusion 80−73876
fissionable highly-compressed pellets, neutron kinetics 77−38315
fluctuating cross sections in Monte Carlo calcs. 77−65265

neutron transport theory continued
flux calculation in complex heterogeneous reactor cells by imbedding element method *(Russian)* 78−58321
flux depression factor determ. by integral transform method 78−50233
flux depression factors for scatt. and absorbing media 78−4976
flux distortion in 3-D reactors due to plane absorbers *(German)* 77−6478
flux distributions in nuclear reactors, improved response matrix method calcs. 77−34363
flux interpolation for elastic down scatt. 78−29560
flux perturbation due to a 5 cm×5 cm NE213 scintillation spectrometer in a LiF assembly 79−85855
flux synthesis, single channel, finite element trial functions for 3-D reactor calcs. 80−42734
Fokker-Planck eqn., quantum dynamical semigroups 77−61034
fuel assembly spectrum code verification based on integral transport theory 79−80996
fuel enrichment and neutron density problems 80−27693
functional analytic treatment of transport eqn. 77−14209
fusion blankets, comparative anal. of neutron multipliers 79−18049
fusion reactor, blanket temp. variation with slab geometry 78−78495
fusion reactor, neutron activation of struct. components 78−74476
fusion reactor blanket, response matrix formulation for particle transport 77−34458
fusion reactor blanket with synthetic fuel prod., neutronics and heating analyses 80−13812
fusion reactor duct neutron streaming simulations, perturbation and variational corrections 80−23143
fusion reactor inertial confinement pellets, neutronics modelling 80−37593
fusion reactor Li blanket models, Monte-Carlo and discrete ordinates calcs. *(German)* 77−83096
fusion reactor materials, neutronics analysis using ENDF/B-V cross-section covariance data 80−47710
fusion reactor materials, nuclear response functions library, MACKLIB-IV 79−67950
fusion reactor neutronics, anisotropic neutron transport calc. using scatt. kernel without polynomial expansion 79−67936
fusion reactor neutronics, higher-order variational functional derivation 79−9880
fusion reactor neutronics simulation using low energy neutron source 78−5030
fusion reactor shielding experiment, cross-section sensitivity calcs., one- and two-dimensional models 80−27799
fusion-fission Tokamak, T breeding, optimisation with geom. program 78−74477
Galerkin type methods for approx. soln. 77−87706
gaseous core reactor neutronics, proliferation potential, and resource utilisation 79−9716
Gaussian type quadrature formula, appl. to the Milne problem 78−86565
GCFR, design of deep penetration integral expt. for ThO_2 blanket and radial shield mockup 80−23167
generalized quadrature technique for transport eqn. soln. 79−22363
generalized rebalance, common framework for transport acceleration methods 79−22356
GETRANS, two-dimens. integral neutron transport code 79−22366
group constants for Fe and steel, energy and space distribs. 77−26829
group cross sections, adjustment of fitting integral meas. 80−86951
group cross sections fitting integral meas., adjustment 79−93679
H-matrix calculations, incorporation of linear constraints 79−30394
Haywood's model test, U-light water slab, meas. of space depend. ang. thermal neutron spectra 77−14208
heavy water, effect of non-1/v absorbers on thermal neutron transport 78−29532
Hermite-Sοο theory soln. to neutron transport eqn., one-group shielding problem 79−97746
heterogeneous fuel pin cells, nodal method in 2-D calcs. 78−21631
heterogeneous lattices, unified theory 80−37428
heterogeneous reactor, neutron importance function 77−50216
historical review 79−58659
homogeneous cylinder, numerical soln. of integral transport eqn. by analytical methods 79−17953
homogeneous slabs, dosimetric quantities and neutron spectra 77−38319
homogenization methods to obtain group-diffusion parameters for reactor calculations 80−670
homogenized diffusion approximations to the neutron transport equation 80−47522
homogenized-cell diffusion parameters from transport codes 78−17300
HTGCR, fuel with double heterogeneity, resonance absorpt. 80−32321
HTPBR, neutron and physical aspect calcs. *(German)* 80−22941
hybrid anal., separation technique and sensitivity theory 80−37632
hybrid fusion-fission blanket design, Th based, nucleonic performance aspects 80−47714
hybrid reactor analysis, separation technique for transport eqn. and sensitivity theory 80−57823
ICRU phantom neutron fluence to dose index conversion factors 79−9909
importance concept in Markov processes, generalised neutron physics method 78−4471
infinite homogeneous multiplying system, joint factorial moments of neutron and count bivariate distrib. 79−76062
inhomogeneous medium with cavity, transport operator spectrum *(Chinese)* 78−16756
inhomogeneous transport eqn., optimal choice of initial flux for iterative solns. 77−26819
inlet coolant temp. fluctuations transfer function, space-depend. global component 79−30887
integral and integro-differential transport theory 78−50228
integral eqn., iterative and direct approaches to critical dominant eigenfunction 77−38313
integral eqn. soln. in x-y geom. by numerical method 77−3066
integral transport eqn. approx. soln. by collision probability methods 77−82984
integral transport theory, 3-D appls., criticality calculations for a finite prism 80−18367
integrals, quadrature sums, Gaussian, orthogonal polynomial method 80−83139
integro-differential coupled-core reactor models, asymptotic stability 80−13531
neutron transport theory continued
intermediate-energy standard neutron field, neutron transport calcs. 79−13588
invariant imbedding eqns. in general geometries 79−76050
inverse albedo problem for finite medium 79−17366
inverse eigenvalue problem for a finite multiplying slab 80−86228
inverse problem, infinite medium with azimuthally depend. plane source 78−57872
inverse problem, two-term. scatt. law 79−75479
irreversible circulation of fluctuation 80−27700
isotropically scattering homogeneous slab, criticality problems in energy depend. neutron transport theory 79−54466
iterative methods, restrained acceleration 78−29530
k_{eff} of metallic assemblies, sensitivity to fission and inelastic scatt. spectra 77−23198
Kalman filter technique, neutron flux distrib., optimal allocation of in-core detectors 78−54839
laminated slab system, j_n formulation simplification method *(Czech)* 79−6722
large core hexagonal assembly, triangular-mesh neutron transport calc. 79−9720
laser driven fusion reactor, Monte Carlo study of asymmetric effects of LiO_2 blanket 78−74464
laser fusion blanket, neutronics and photonics 78−5025
laser-driven fission-fusion microexplosions, nuclear and thermohydrodynamic calcs. 80−47696
lattice cell calc. in cylindrical geometry, cosine current approx. 78−50226
lattice parameters for CANDU-type reactor, correction to HAMBUR resonance integral 77−46275
lattices, uniform, homogenisation, small buckling approx. 80−52721
leakage effects in self-shielding factor methods, consistent treatment 77−50227
linear Boltzmann equation, scattering matrix 77−18643
linear extrapolation dist. on surface of 2-D absorber 77−6479
liquid air, calc. of neutron and gamma-ray energy spectra 78−29529
liquid N_2, calc. of neutron and gamma-ray energy spectra 78−29529
LMFBR, appl. of BWR simulator to neutronics calc. tool 79−40987
LMFBR, benchmark calcs. by diffusion methods 77−79414
LMFBR, heterogeneous core design, neutron and γ-transport effects 78−8893
LMFBR, physics problems of fast reactor shielding 79−67873
LMFBR, SNR-300, criticality prediction 79−40989
LMFBR, value function, reson. struct., reactivity coeff. 79−76069
LMFBR critical assembly, neutron diffusion calc., DB^2 transverse leaking predictions 80−13529
LMFBR small core disruptive accidents, transport/diffusion comparisons 79−31022
LWR, large cores, anal. of space-time effects using coarse mesh flux expansion method 77−67794
LWR, neutronic thermohydrodynamic interaction model *(French)* 79−89349
LWR, reactor cavity neutron flux calc. 79−89362
LWR, thermal neutron steady state spectra in pure and poisoned water 79−36306
LWR anal., CASMO fast transport theory assembly depletion code 78−25278
LWR concrete shielding, ANS coupled cross-section standards 79−59281
LWR cones, computation of cell group consts. 80−566
LWR core transient anal. using coupled neutronics and thermal hydraulic models 80−715
LWR kinetic anal. with feedback, hypothetical accident transients 80−13697
LWR neutron flux distrib. in hexagonal geom., appl. of transmission probability method 79−93680
LWR parameter sensitivity to uncertainties in thermal neutron data 78−29561
LWR sensitivity coeffs. depend. on macroscopic spatial flux variation 79−80988
LWR shielding, neutron transport anal. comparison of several multigroup libraries 80−23168
matrix methods for radiation transport 78−13198
maximal variational principle for transport theory 78−62166
medium of const. cross section, neutron slowing down and transport 78−33235
microexplosion reactor neutronics, adjoint transport eqn. technique 80−47713
Milne problem for two half spaces in two group transport theory 77−67784
Milne-problem for isotropic scatt. with backward leak 78−8870
minimizing splitting costs in Monte Carlo particle transport 80−47532
mixed-mesh method description of highly anisotropic scattering 79−26494
monoenergetic multiregion transport eqn., soln. using $S_{\infty}{}^0$ semianalytic method *(German)* 79−30885
monoenergetic neutron systems, quadratically anisotropic scatt., influence on decay const., transport eqn. eigenvalues 78−46122
monoenergetic neutron transport, periodic boundary conditions 77−343
monoenergetic neutron transport equation, existence of complex eigenvalues 77−345
Monte Carlo biased transport calcs. optimisation, prediction of statistical error 79−58654
Monte Carlo calcs., variance anal. 79−93079
Monte Carlo calculations, error prediction 79−59109
Monte Carlo calculations, state-space splitting 77−65264
Monte Carlo code, reduction of computational time for point detector estimator 80−68724
Monte Carlo deep penetration calcs., appl. of fictitious scatt. transport model 78−29526
Monte Carlo elastic angular data, equal probability steps 78−668
Monte Carlo error prediction from track length estimator theory 78−29527
Monte Carlo heat conduction solution using transport theory approx. 77−65260
Monte Carlo method, applicability of sampling technique *(Spanish)* 79−6721
Monte Carlo method, new approach to adjoint Boltzmann eqn. 78−21618
Monte Carlo neutronic and electronic model for thermal-neutron coincidence counting 80−23165

neutron transport theory continued
Monte Carlo shielding calcs., biased selection of particle flight directions as variance resolution technique 78−29653
Monte Carlo simulation for design studies and integral expt. anal. 77−26828
Monte Carlo solution of equation, influence of group averaging of consts. *(Russian)* 77−65242
Monte Carlo track rotation estimator, calc. of total flux at point 79−71385
Monte Carlo tracking technique for slab cells 79−85580
Monte Carlo transport calcs., error anal. 79−80548
MR research reactor, fast neutron space-energy distrib. 79−40983
multi-group transport eqn., time-independ., soln. using spherical harmonics 78−37386
multi-group two-dimensional eqn., cylindrical geometry, finite element method appl. 78−29522
multidimensional, transverse leakage approx. 78−29531
multidimensional inverse problem in transport theory 80−174
multidimensional neutron transport computation 77−82980
multidimensional neutron transport equation, spherical harmonics soln. by finite Fourier transform. 78−17269
multidimensional reactor dynamics equation, fast factorization and exponential transform. procedures 78−17303
multigroup, Chandrasekhar H-eqns., comparison of iterative methods 80−47521
multigroup albedo eqns. for cylindrical rod 78−667
multigroup calculations for TRIGA-type reactor analysis 79−30876
multigroup charged-particle transport calcs., temp. effects on cross sections 80−57818
multigroup collision prob. method, applied to overlapping neutron spectra theory 80−52718
multigroup criticality condition for a space-independent multiplying assembly via the Chapman-Kolmogorov equation 80−86949
multigroup cross section calculation, self-shielding, subgroup method *(Rumanian)* 78−46140
multigroup cross sections, GGTC-ENEL computer code using intermediate resonance method 78−58323
multigroup diffusion process in a fixed or variable set *(French)* 79−93678
multigroup diffusion theory, current weighted total cross section determ. in unresolved energy region 80−18365
multigroup discrete ordinates transport eqns., computational efficiency of numerical methods 79−80970
multigroup formalism for evaluation of continuous slowing down theory params. 78−37391
multigroup integral transport theory code, thermal reactor lattice studies 78−50225
multigroup Monte Carlo calcs. 78−4570
multigroup neutron data production from ENDF/B-IV, survey of codes 77−23170
multigroup neutron flux calcs. with MURLAB program 78−29541
multigroup neutron slowing down codes, resonance treatment modification 78−82412
multigroup one-dimens. transport with anisotropic scatt. 77−3064
multigroup scattering matrices, processing of ENDF/B data 79−26464
multigroup shielding calc., subgroup approx. of spatial distrib. of unscatt. and singly scatt. neutrons 79−59104
multigroup theory, functional analysis 80−13525
multigroup transfer coeffs., efficient eval. for shielding appls. 80−47747
multigroup transfer cross-sections for elastic and discrete level inelastic neutron scatt. 80−42732
multigroup transport problems, Monte Carlo game, moments method 80−52720
multigroup transport theory, finite slab inverse problem 78−74418
multigroup transport theory, inverse problem 77−38316
multiplication factors, temp. depend., reactor fuel lattices, comparative evaluation HTGR, HTLTR 78−29557
multiregion problems in plane geometry, half range orthogonality relations 78−21621
multiregion problems in plane geometry 78−17274
N-group, criticality problem in slab geom. 77−65243
negative reactivity determ. by rod-drop, correction for time of fall 77−46222
neutron bursts in matter, time-depend. linear transport eqn. 79−26462
neutron density fiuctuations in on-off controlled reactor, exact stochastic anal. 79−36308
neutron differential cross section data generation, appl. to resonances and neutron transport *(German)* 78−82414
neutron diffusion in water containing 1/v and non-1/v absorbers 79−30879
neutron escape probability from absorbing body 78−46125
neutron leakage in presence of voids, Monte Carlo anal. 77−38324
neutron moderation, linear Boltzmann operator, in various geometries, contributions to spectral theory *(Rumanian)* 78−46128
neutron multigroup transport operator spectrum for bounded spatial domains 79−97742
neutron spectrum reconstruction from activation meas. 79−59105
neutron trasnfer with anisotropic scattering 79−54467
neutron weapons, physical and military problems *(Norwegian)* 79−81091
neutron-photon multigroup cross sections for neutron energies ≤60 MeV 79−30880
neutronic data base generation for transient reactor calcs. 77−83004
nodal codes, efficient coarse mesh rebalancing method 77−14211
noise analysis of power reactor, simulation using nucleate boiling noise generator 78−54840
noise studies in BWR and PWR 80−557
non-multiplying homogeneous slab assembly, time depend. multigroup P1 eqn. soln. 78−17267
nonanalogue Monte Carlo games, conditions concerning nonanalogue transition kernels and estimators 78−62594
nonlinear reactor problems. appl. of successive overrelaxation method 79−59133
nonlinear transport, initial value problem, integro-differential equations 77−61474
nonstationary transport in systems with large spherical cavities book contrib. 80−22881
nonuniform lattice problems, 2-D constrained finite element anal. 80−86952
nonuniform transport problems, estimation of perturbation in solving by Monte Carlo methods 78−17271

neutron transport theory continued
Nordheim integral treatment for resonance processing, proper use 80−37427
N.S. Mutsu, primary shield, mock-up experiments, analysis 78−21782
N.S. Mutsu, radiation streaming, repair plan 78−21781
nuclear constants, determ. as an inverse problem in radiation transport 80−83140
nuclear reactors, HCDA, neutronics and hydrodynamics equations, energy release, DISCAL code 80−68842
numerical code, automated approach to quantitative error anal. 77−67788
numerical methods, recent work at LASL 78−13195
numerical solution of time-dependent two-dimensional P_1 equation of neutron transport 79−40980
one group, integral transport eqn. for homogeneous sphere, neutron scatt., classical diffusion, anal. 78−62589
one-dimensional discrete ordinates, theoretical properties 79−76053
one-dimensional transport equation soln., local separation of angle and energy 77−65248
one-group criticality in infinite rectangular prism, S_N-method 77−14205
one-group diffusion equations, finite element soln. tech. using imaginary nodal points and element subdivision 80−68721
one-group neutron transport equation and angular flux separability 79−17952
one-group transport theory, benchmark solns. of multimedia problems 79−85581
operator for medium with central spherical cavity, spectral props. *(Chinese)* 77−26817
optimal iteration strategies, geometric interpretation 79−22358
optimisation of absorber distrib. 78−50230
optimum biasing of integral equations in Monte Carlo calculations 79−54078
orders-of-scattering invariant imbedding-type eqns. for internal particle distribs. 79−59111
P_N approx., modified form with exact asymptotic roots, change in Marshak free surface boundary conditions 80−52717
P_N approximation in spherical geometry, time depend. 79−80967
P_N approximations, front behaviour of monoenergetic neutron pulses 79−59107
p-cell homogenization, transient flux effects, incorporation into 2-D iteration scheme 78−17301
Pal-Bell stochastic equations for particle transport scattering theory 79−45319
PALLAS discrete ordinates transport code, improvement 79−76052
particle collision method in spherical geometry by escape probabilities, flux transport eqn. 78−78433
particle transport phenomena, theory, book 79−63176
PBF reload core cell calc., failure of Wigner Seitz approx. 78−25264
PBHTR, space-shielding cross sections 78−25274
PBR fission reactors, neutron flux distribs. in multisphere configs., diffusion-theoretical model *(German)* 80−73875
PDX Tokamak, neutron skyshine Monte Carlo calcs. 80−47711
perturbation computation with correlated sampling, nuclear reactor neutron transport 79−588
perturbation higher order time depend. theory, appl. to nuclear reactors 78−58333
phase space time evolution technique-neutron transport eqn., mathematical relationship 79−162
plane geometry, general anisotropic energy depend. scatt., phys. interpretation 78−4973
point kinetics, smoothing and extrapolation method 77−65252
point kinetics on asymptotic representation of space-, energy-, angle-depend. reactor kinetics 79−80985
point neutron flux, Monte Carlo schemes evaluated 79−586
point-like nuclear reactor neutron kinetics solns. using numerical method *(Italian)* 78−58324
polynomial solns. to tensorial differential eqns. for monoenergetic neutrons in slab and sphere geom. 78−50232
power and temp. fluctuations for reactor with temp. feedback, exact statistical anal. 79−36309
power reactor, neutron density fluctuations, stochastic nonlinear model, Fokker-Planck eqn. 78−58316
power reactor nodal anal., albedo conditions 79−80989
probability table method extension 79−584
prompt fission neutron logging technique, computer modelling 79−53566
prompt gamma-ray anal. of neutron flux distrib. in nonhomogeneous samples, computational model 80−14060
pulsed neutron die-away in fast multiplying assemblies 80−18366
pulsed neutron reactivity meas., approx. of kinetic distortion correction factor 77−54268
pulsed neutron research, book 80−22146
pulsed neutron source, use of perturbation theory for exptl. study 78−66328
pulsed neutron source on multiplying media, anal. and interpretation of experimental data *(Rumanian)* 78−46203
PWR, KWU 1300 MWe facility, neutron flux computer calcs., radiation damage 77−34370
PWR, neutron streaming in upper reactor cavity, dose rate calc. 79−89365
PWR, Pu isotope calcs. for steady-state core anal. 79−59126
PWR, shielding against neutron and gamma streaming, computational methods 78−21783
PWR cavity shield design, radiation streaming, calc., appl. of Monte Carlo and discrete-coordinates technique 79−89364
PWR core anal. using 3-D spatial neutronics codes 79−89360
PWR core analysis, transport-to-diffusion theory for gadolinia-loaded fuel pins 80−57908
PWR reactor cavity shield system, design and anal. 79−89366
quadratic approx. effect on neutron moment and count distrib. in multiplying system 79−89343
quantised diffusion eqn. contracted to linear Boltzmann eqn. 77−17926
quasilinear reactor system subject to white Gaussian multiplicative noise, moment stability anal. 79−22373
radiation dose deposition calcs. in human marrow 80−26365
radiation protection studies expt. and theoretic results comparison 80−47750
radiation shielding, cross section sensitivity analysis 78−21778
radiation streaming, shield design problems 78−21780
radiation transport calc., Monte Carlo approach for engineers 79−585
radiative transfer calculations, appln. of multiband method 80−95333

neutron transport theory continued
radiography, physical processes and math. methods review, neutron-nucleus interaction effects 78−60888
random sampling of scattering angle in neutron transport 79−85574
ray-effect mitigation methods for two-dimens. neutron transport theory 77−26821
RCP01 Monte Carlo program, neutron capture and photon heating rates 79−71912
RCPL1 program, calc. of Doppler broadened neutron resonance cross-sections 79−67810
reactivity calc., cross-section library inadequacy 79−9697
reactor cavity radiation streaming, albedo Monte Carlo methods 79−89363
reactor core and shield calc., radiation transport program benchmark tests 78−78440
reactor dynamics, localised, P, approx. to Boltzmann eqn. 80−78347
reactor kinetics, computer assisted learning package 77−33809
reactor kinetics digital simulation 77−88216
reactor lattices, functional estimation using first-order perturbation 80−27698
reactor neutron noise anal. techniques, unified theory 79−30886
reactor noise, neutron multigroup theory, calc. of second order correl. functions *(German)* 79−89390
reactor noise theory, adjoint space applic. 78−13202
reactor parameter estimation using empirical criticality eqn. 79−17965
reactor physics, grid-coupling methods for the multigrid solution of the neutron diffusion equation 80−47555
reactor physics, transport theoretic P_N approximation 80−57830
reactor radiation streaming anal. using spherical harmonics expansion of albedo data 79−89367
reactor reson. absorpt charact. 80−86955
reactor shielding, current status and future prospects 78−25328
reactor shielding methods, development in USA 78−21776
reactor theory for nuclear power engineering 77−18645
reactor transients, approximation methods, range of validity 77−54304
recursive Monte Carlo method, geometrical imaging and surface sources 79−85578
recursive Monte Carlo technique for generating importance functions 79−59272
reflected critical reactor problem, slab geometry, improved P-L soln. 77−23178
reflected critical slab, asymptotic soln. using invariant embedding principle 80−27683
reflected reactors, two-group theory of noise, appl. to vibr. absorbers 79−26468
resolvent integration techniques for generalized transport equations 79−76051
resonance escape in slab lattices, variational method 79−85572
resonance heterogeneity effect in vicinity of gross region interface 77−82992
response matrix doubling equations for particle distribs. calcs. improved formulations 77−6480
response matrix eqns., properties 77−67795
response matrix finite element soln. 80−13527
response matrix method with linearly anisotropic ang. distrib., one-dimens. anal. of fast reactors 77−14215
rethermalization of neutrons in water-graphite system 79−97806
rocks, neutron slowing props. in water bearing containers *(Russian)* 77−73720
S_N calculations, modified transport formulation compatible with anisotropic diffusion theory 80−47526
S_N methods, exponential supplementary eqns., one-dimens. case 77−50189
S_N transport method for calc. of anisotropic transmission problems 80−68720
second order transport eqn., variational formulation and projectional methods 80−164
secondary neutron polarization via penetration through a ferromagnetic shielding wall 80−47742
self shielding factors, elastic removal cross sections, strong reson. scatt. 79−13374
self-shielded cross-section generation in complex multiregion cells 79−9718
self-shielding factors, discrepancies between ETOX and TIMS codes 80−68744
semi-infinite medium, time depend. monoenergetic neutron transport eqn. soln. 80−95335
SHETAN−a three-dimensional integral transport code for reactor analysis 80−63238
shielding, in 3-D direct-coupled-ray method 78−21785
shielding, Monte Carlo calcs., event-value path-length biasing 77−38421
shielding benchmark calcs. by Discrete Ordinates and Monte Carlo methods 80−73886
shields, homogeneous slabs, computer calcs. of transmitted, reflected spectra 77−3067
showing of neutrons, linear eqn. solns. *(French)* 79−76047
singularities of soln. in cylindrical symm. 77−23162
skyshine analysis of 14 MeV neutron source, Monte-Carlo computer code 78−66429
slab criticality and Milne problem, finite element computation 77−57700
slab geom., subcriticality and supercriticality of energy depend. transport 78−33236
slab geometry, monoenergetic neutron transport eqn., analytic solns. 79−97745
slab geometry, reflection and transmission functions 78−74415
slab geometry and neutron density, transport soln. props., piecewise polynomial variational approx. 77−54269
slab reactor neutron transport, finite element method, practical considerations 79−76046
slab reactor with finite reflectors, criticality 79−26475
slab with finite reflector, critical problem, F_N method 80−63221
slab with finite reflectors, bounds for critical length 78−82409
slabs and spheres, criticality problems 80−57817
slow neutron scattering, microscopic cross section, gas imperfection effects 79−40984
slowing down and propagation in gravity field, approx. theory 80−99199
slowing down in highly anisotropic scatt., statistical fluctuations of collision energy losses 77−62572
slowing down of resonance neutrons in matter 77−50191
slowing-down equation, with inelastic scatt., infinite media 79−26465
slowing-down problem, comparison of VIM and MC^2-2 codes 77−23167
neutron transport theory continued
smoothness of solution of 2D neutron transport equation 79−89344
SNR-300, coolant outlet duct design from neutron transport experiments *(German)* 78−29566
SOLASE-H hybrid reactor, blanket neutronics calc. for blanket design 80−13805
solid-angle subtended at point by cylinder, eval. method 79−59110
source biasing optimisation technique using Monte Carlo calc. 79−26005
space craft thermionic reactors, reflector drum control mechanism, fuel and moderator 79−17988
space craft thermionic reactors, reflector drums as control mechanism 80−42784
space depend. spectra in two adjacent moderating media 77−6477
space dependent stochastic neutron kinetics with Gaussian parametric excitation 80−63223
space independent low power model, multigroup energy formalism for reactor stochastic eqns. 80−63224
space-energy-angle depend. theory 77−14204
spatial approximation methods for the S_N equations in x, y geometry 80−47525
spatial differencing schemes for slab transport eqns., linear characteristic and quadratic methods 80−47524
spatial fluctuations of neutron and powder distribution in critical reactor 79−71917
spectra unfolding from activation data 79−13375
spectral fine-structure effects on material and Doppler reactivity worths 79−26473
spectrum calculating module of pin-cell burnup code BETTY 77−71634
spheres, soln. of basic problems by method of elementary solns. and F_N method 79−40981
spherical geom., semi-analytic soln. to transport eqn. 78−37390
spherical geometry, density transform method extension 77−54277
spherical harmonics approximations 77−3065
stainless steel, reduction of H by Ar glow discharge, rel. to ultra cold neutron storage 80−104459
standard variance reduction techniques in Monte Carlo transport problems, leakage estimator 78−78443
stationary monoenergetic neutron transport equation for slabs, power series solns. comparison 78−13190
stationary nonlinear transport problem 80−27242
stochastic transport, functional theory 80−37413
streaming ray technique for particle transport calculations 80−47716
subcritical limits for special fissile actinides 80−52708
subcritical reactor, neutron joint factorial moments and count bivariate distribs. 79−59120
suboptimal control of reactors with distributed parameters, computer model, singular perturbation theory 77−6530
symmetrised neutron transport eqn., fast Fourier transform method solns. 78−78435
temperature-dependent nonlinear neutron transport problem 80−47520
TFTR, isodose contour map construction using DOT 3.5 computer code 79−67949
TFTR neutral beam injectors, neutronics calcs. 79−59253
TFTR neutral-beam injectors, shielding calcs. 80−23172
thermal lattice leakage calcs. using modified B_1 method 80−47545
thermal neutron acceleration in medium with reson. excitation by EM wave *(Russian)* 78−37394
thermal neutron monochromators, Monte-Carlo simulation of mechanical velocity selectors 78−24886
thermal neutron scattering theory, book 79−26466
thermal neutron transport in moving media 79−63713
thermal reactor assemblies, effective neutron diffusion parameters 80−73874
thermal spectra calcs. using synthetic scatt. kernel 77−14206
thermal-neutron transfer from pulse source in moderator with large cylindrical cavity 78−37392
thermalization, appl. of invariant imbedding technique 79−67811
thermionic reactor, ^{233}U fuel and Be moderator, neutron physics analysis 77−50281
thermodynamics and distrib. function of neutron gas system in stationary power reactor with decoupling 80−86950
three dimens. integral monoenergetic, initial value problem, inhomogeneous isotropically scatt. body 77−344
three-dimensional, integro-differential equations discrete ordinate solution 80−63222
three-dimensional neutron transport eqn., boundary value problem 79−67809
THTR 300 MW(e) Schmehausen station, anal. of non-central neutron source 77−67802
time depend. neutron transport solns. in infinite media, multiple collision technique 77−82982
time depend. transport, discrete transfer cross section expansion 79−80969
time dependent, multigroup equation solutions 78−29542
time-depend., multigroup-P_L-approx. 77−74904
time-dependent continuous energy eqn., generation of benchmark solns. 79−22364
time-dependent neutron transport in spherical geometry 80−13530
time-energy distrib. of slowing down neutrons 77−50184
time-lethargy equivalence relations for infinite plane geometry problems 77−61470
tissue-equivalent material, freq. of occurrence of nucl. reactions due to neutrons up to 50 MeV 77−9243
Tokamak, 2-D neutronics model for major penetrations 78−5027
Tokamak, expt. power reactor, neutronic and photonic calcs., blanket and shield design 78−29644
Tokamak, neutron source and toroidal geometry neutronics effects 77−34457
Tokamak divertor slot design to enhance mag. shielding 78−5028
Tokamak hybrid blanket, neutronics and thermal hydraulics 78−66406
Tokamak reactor blankets, effects of neutral beam injection tubes, shielding calcs. 80−23173
toroidal geometry, computational method 78−22538
toroidal geometry effects in neutron transport eqn., discrete ordinate S_N method 78−13327
track length estimator, efficiency for reaction rate estimation 78−46126
track length estimators, comparison 78−82413
transfer matrix calcs. for thermal neutrons 80−27687
transient state initialization of quasi-static neutronics treatment 79−59192

neutron transport theory continued
transmission probability method for calculation of neutron flux distributions in hexagonal geometry 80−106101
transport acceleration methods, generalised rebalance 78−29525
transport effects on nodal coupling parameters 78−29558
transport equations for contributons 79−22354
transport-equation, with anisotropic scatt. in finite slab geometry 79−17364
transverse buckling effects in 2-D calcs. 80−32318
TREAT reactor, computational method for predicting neutron hodoscope performance 79−80995
two-dimens. kinetic calc. by finite-element anal. 78−665
two-dimensional, appl. of constrained finite elements 79−22360
two-dimensional, comparison of rebalance stabilization methods 80−5220
two-dimensional eqns. in curvilinear coordinates, numerical soln. *(Russian)* 77−30646
two-dimensional problems, diffusion synthetic acceleration method 79−22357
two-dimensional reactor sensitivity analysis using discrete-ordinates transport theory 79−9706
two-group integral eqn., asymptotic solns. 77−14203
two-group problems with anisotropic scatt., closed-form solns. 78−4569
two-group tranport transforms, comput. merit in finite nonplanar media 77−65247
two-media Milne problem in two-group neutron transport theory 78−17275
two-media problems in two-group neutron transport theory 79−36297
two-phase flow void fraction determ., simulation of neutron scatt. method 79−90321
UCN, detection systems, sources, transport, book contrib. 80−22882
UCN, gravitation influence on lifetimes on traps 80−18750
UCN, storage in pulsed aperiodic-action reactor 80−18749
ultra-cold neutrons, review of prod., transport and appl. 79−40982
ultracold, neutron optics, gravitational effects and applicability of Fermat's principle *(Russian)* 79−13376
ultracold neutron accumulation, above-barrier neutron effects, lifetime determ. 80−102227
ultracold neutron storage in plane, quantum effects *(Russian)* 79−9658
ultracold neutrons in scatt. medium, optical potential *(Russian)* 77−34362
unified neutron transport theory for reactor analysis 80−63246
upper atmosphere, Monte Carlo calcs. 80−8468
variational coarse-mesh method based on constrained ang. trial functions 77−65245
variational method for neutron stochastics 79−13373
void reconstruction in 2-D, using neutron transmission 78−22605
Voigt functions analysis, appl. to neutron cross sections 80−22879
VVER reactors, neutron physics calcs. programs *(Russian)* 79−30884
VVER-100 LWR reactor core theory, calc. of physical parameters 79−63735
water, effect of non-1/v absorbers on thermal neutron transport 78−29532
wave propag. in multi-region systems, delayed neutron effects 78−50229
wave propagation across temp. discontinuity in infinite graphite assembly 77−38314
wave propagation in heavy H_2O, scattering kernel, molecular mode contrib. 80−52707
waves in subcritical assemblies, transport calcs. 77−82990
weak solution and approximate methods for the transport equation 79−76049
Weale expt. calc. using modified ENDF/B-IV cross sections 79−17908
weapon physics, appl. of space angle synthesis to 2-D transport 77−83107
weighting functions for flux and relative speed of change measurement *(Croatian)* 77−10561
width fluctuation correction to reacts. involving continuum level excitations 78−46124
Wiener-Hopf factors of L_1 matrices 78−8871
ZEPHYR code for general two-dimens. geoms. 77−65249
zero-variance multigroup Monte Carlo quadratures 80−5196
ZPPR critical expts. for radial parfait heterogeneous reactor concept 78−13224
Au, neutron activation cross sections meas. for generalised intermittent irradiation, fusion machines appl. 78−58283
^{10}B shields, transport calcs. and transmission factors for activation detectors 78−78434
BeO, neutron wave propag., space and angle depend. study 80−106096
Cl isotopes, effect of isotopic abundance on kerma 78−29536
D-D fusion reactor blanket, nucl. characts., summary 78−89973
D-D fusion-fission hybrid reactor, energy multiplication and fissile prod. 79−36409
D-D fusion-fission hybrid blankets, neutronics anal. 80−13809
DT fast neutrons in blankets and shields, neutrons, associated particle method 77−71690
Fe, an assessment of ENDF/B-IV based on integral meas. 77−50194
Fe, fast neutron penetration, cross section characts. effect, Monte Carlo study 77−23216
Fe, fast neutron spatial ang. distribs. 79−97743
Fe radiation shielding, computational benchmark for deep penetration 80−47738
Fe-Ni-Co-V alloys, effects on fusion reactor neutronics performance 80−47705
$^{56}Fe(n, n')$, transmission of neutrons at 24.37 keV 79−54435
^{3}H breeding ratio maximisation by geometric programming 79−9879
I, neutron activation cross sections meas. for generalised intermittent irradiation, fusion machines appl. 78−58283
Li, T breeding performance eval., multigroup neutron and photon transport calc. 80−13831
LiO_2, T breeding performance eval., multigroup neutron and photon transport calc. 80−13831
Li_7Pb_2, T breeding performance eval., multigroup neutron and photon transport calc. 80−13831
N, neutron scatt. and gamma-ray prod., Monte Carlo anal. 77−26682
^{16}N activity in water of powered ship 78−13192
Na, multigroup and point energy transport calcs. 77−50193
$Pu(NO_3)_4$, slab tanks for criticality control, neutron multiplication calc. 80−13606
^{239}Pu direct enrichment of LWR assemblies in a fusion hybrid 80−37604
^{240}Pu, effect on neutron lifetime in nuclear explosives 79−13531

neutron transport theory continued
U, exploration, radiation transport anal. for borehole logging probes 79−53565
U mineral deposits, criticality study using ore model *(Spanish)* 77−70655
UH_3 critical mass calc. by Monte Carlo methods as function of ^{238}U enrichment 79−36320
$UO_2(NO_3)_2$ highly enriched solns., benchmark critical expt. calc. study, KENO-IV code 79−18026
$^{\Delta}UO_2(NO_3)_2$, a=233, 235, slab tanks for criticality control, neutron multiplication calc. 80−13606
$^{235}U+BeO$ nearly homogeneous multiplying systems, pulsed neutron study, age-diffusion model 80−37442
^{238}U, meas. of Cd ratio of neutron capture rates in slightly ^{235}U enriched fuel, systematic errors 78−8901
W, radiation shielding material, integral tests of ENDF/B-IV high-energy neutron cross-section data 80−23162

neutrons
see also cosmic ray neutrons; delayed neutrons
anomalous magnetic moment in struct. model using phions 80−18134
beam characterisation by radioactivation image transfer technique 79−88196
behaviour in magnetic field of linear current, system with latent symm. 0(3) *(Russian)* 77−67588
beta decay characteristics 79−6338
book, neutron physics 77−67787
bound multineutron system, 8 and 20 neutrons, existence probability 80−68570
charge, upper limit determination method using neutron reflection *(Russian)* 80−32316
charge determination, expt. using ultraslow neutrons 79−9370
charge distrib., NΔ mass difference, quark model anal. 77−67653
charge form factor, new data anal. 79−67549
charge form factor zeros 80−413
charge radius, quark-parton model, deep inelastic e-N struct. functions 77−71488
charge radius and deep inelastic struct. functions 78−70334
charge radius and quark-parton model 77−22694
charge struct., form factor in quark-parton model 77−54106
charge structure, Clemental-Villi model 77−2830
clinical beams, light-ion flux mixed with collimated fast-neutron beams 80−81723
cold pulse from methane at 20K, time dependence 77−67928
cold relativistic neutron gas, study of massive neutron cores 79−35292
composite, containing proton+low-mass scalar meson, decay mechanism 77−2948
cross-sections and kerma values for C, N and O from 20 to 50 MeV 80−101217
decay, weak interaction meas., coincidence type ion electron converter detector obs. 80−58100
delayed, from heavy isotope photofussion, kinetic functions 79−63709
dipole moments and spin rot. meas. 79−36080
dipole moments and spin rotations 78−74296
disintegration, concepts of leptons and quarks, unified field theory *(French)* 80−91038
electric and magnetic dipole moments 80−4993
electric charge, optical instrument for determining upper limit 80−63501
electric dipole moment, CP violation in gauge theories 80−91041
electric dipole moment, expt. search 77−26555
electric dipole moment, quark and gluon corrections 80−4994
electric dipole moment, search using ultra cold neutrons 79−67551
electric dipole moment, ultracold neutron technique *(Russian)* 79−75775
electric dipole moment in Kobayashi-Maskawa model 79−93417
electric dipole moment in $SU(2)\times U(1)\times SU_F(2)$ gauge symmetry 79−89091
electric dipole moment search with ultra-cold neutrons, expt. set-up 80−37270
electric dipole moment using ultra cold neutron source, expt. current status and results 80−37678
electric dipole moment using ultracold neutrons 80−82974
electric form factor determ. in $^{2}H(e,e'p)n$ 79−3138
electric moment prediction in six-quark model *(Russian)* 79−93379
electric polarisability, from photoabsorption cross-section 80−57597
EM form factors from MIT bag model 79−93419
EM structure functions from electron scatt. data 80−13306
finite energy sum rule for nucleon polarizabilities difference *(Russian)* 79−58905
form factors, studied by $^{12}C(d,p)^{13}C^*$ reactions leading to unbound states 77−26775
fundamental physics with reactor neutrons and neutrinos [conf. ILL, Grenoble, France (Oct. 1977)] 79−59112
grand unification, neutron oscillations and massive neutral Majorana leptons, baryon number 80−91033
half life meas., p registration method *(Russian)* 78−93879
interferometry, Earth rot. affecting wave function phase 79−54012
lifetime, expt. determ. 79−58958
lifetime, expt. determ. using storage of decay protons 79−58959
local B-L symmetry of electroweak interactions, Majorana neutrinos, and neutron oscillations 80−73643
magnetic moment, expt. determ. using meas. of ratio of p/n Larmour frequency 79−58962
magnetic moment meas., Bloch-Siegert effect in Ramsey separated oscill. field technique 79−3063
magnetic moment meas., fundamental phys. expts. with reactor neutrons and neutrinos, summary 79−67543
magnetic moment meas. 78−8719
magnetic moment meas. separated oscillatory-field magnetic resonance technique 80−22613
mass, ratio to Planck's constant *(German)* 79−6077
matter, equilibrium config. allowing for nuclear and gravit. interactions *(Russian)* 77−18462
matter at supernuclear densities, neutron star test of interacting neutrons models 77−78812
ME-EM field model of free electron state 78−49988
mean lifetime meas. using EM trap 80−73703
medical accelerator high energy X-ray beams, neutron dosimetry 79−83942
naive three-point-quarks model, deep inelastic data and n charge radius contradiction 79−355

neutrons continued
neutron electric dipole moment, expt. determ. of non-zero value employing ultra cold neutron storage methods 79−58963
neutron spinor rotation and the neutron few-body interaction 79−59113
neutron-antineutron oscills., proton instability *(Russian)* 80−101948
neutron-proton mass difference, classical electrodynamic model 77−6123
nuclei, search for ^{3}n' and ^{4}n' in ^{7}Li+π^- capture reactions *(Russian)* 77−74889
oscillation phenomenology in gauge model with spontaneously broken B-L symmetry 80−90996
polarised, false effects in decay triple correlation, time-parity violation search *(Russian)* 78−78180
polarised, spin-electron correlation coeff., G_A/G_V ratio *(Russian)* 79−97625
properties, expt. determ. and degree of precision, review 79−58961
properties of free neutrons, review of possible future experiments 79−58994
proton-neutron mass difference, Cottingham formula simplification with causality conditions 77−61286
proton-neutron mass difference, higher intermediate hadronic states 78−45920
QCD, neutron electric dipole moment, chiral estimate, current algebra, CP violating reactions 80−27471
quantum mechanical phase shift in Earth's gravitational field, obs. 79−45000
quantum theory of neutrons in helical magnetic fields, Schrodinger eqn. solns. 79−35581
quasibound states in matter, reson. positions and widths 80−73833
recent advances in neutron physics, prod., handling, detection, nuclear reactions, resonances 77−26686
relativistic, ultra-degenerate, non-interacting gas, Fermi energy and eqn. of state in intense mag. field 78−89401
scaling behaviour of struct. functions in parton model 78−16988
Soller slit collimators for thermal neutrons 77−45916
spin rotation by precession during interferometry 80−32584
spinor rotation, search using Fresnel interferometer *(German)* 79−9376
spinor wave function, 4π-periodicity factor using perfect cryst. interferometer 78−45515
storage, for very slow neutrons in superconducting mag. storage ring 79−59293
storage in superfluid ^{4}He 79−86948
structure function nonsinglet moments from deep inelastic lepton scatt., QCD 80−62980
SU(5) invariant theory, B-L nonconservation and neutron oscillation 80−78005
trapped neutrons in graphite systems, pseudo decay consts. meas. at 77, 194K 77−42007
ultra cold, thermomagnetic gates, accumulation in closed vessels 80−87005
ultra cold neutrons, prod., detection, confinement and storage for fundamental phys. expts. 79−63858
ultra-cold, storage in pulsed reactor *(Russian)* 77−3204
ultra-cold neutrons, review of prod., transport and appl. 79−40982
ultracold, coherent inelastic scatt. by trap walls 78−5086
ultracold, damping of quasistationary wave functions, in traps 78−9013
ultracold, magnetic traps for storage 77−23344
ultracold, one-phonon scatt. in Cu 77−61480
ultracold, reflection from diffused pot. threshold, Cu chamber storage *(Bulgarian)* 78−82411
ultracold, storage and experimental uses 77−61479
ultracold, storage and investigation of fundamental props. 80−447
ultracold, storage on horizontal plane with restrictive walls 77−23345
ultracold, use for lifetime meas., collision loss calcs. *(Russian)* 80−52504
ultracold neutron accumulation, above-barrier neutron effects, lifetime determ. 80−102227
ultracold neutron storage in mag. trap *(Russian)* 78−29538
ultracold neutrons, extraction, transportation and storage 77−26826
ultracold neutrons, interaction with time-depend. pot., nonstationary quantum effects obs. *(Russian)* 77−9913
ultracold neutrons, review of Soviet expt. research on prod. and storage 79−97923
ultracold neutrons, supergravitation and gravitino 3/2 investig. 79−85047
unpolarised, Young's double beam interference expt., spinor wave function sign reversal interpretation 78−89363
n→$\bar{n}$ oscillations in nuclei, detectable annihilation rate, grand unification 80−101966
n→pe$\bar{\nu}$, expt. determ. of correlation coefficients in neutron β-decay 79−58960
p-n mass difference, quark-parton model anal. 78−93859
pn mass difference, effects of EM mixing, $\Lambda \rightleftharpoons \Sigma^0$, $\eta \rightleftharpoons \pi^0$, $\omega \rightleftharpoons \rho^0$ *(Russian)* 78−74255

Newtonian fluids *see fluids*

nickel
see also nuclei with .....
(001) surface, electronic struct. of ordered S overlayers 80−84835
(001) surface N adsorption due to ion beam irrad., surface struct. LEED study *(Chinese)* 80−84364
(001) surface states, surface magnetisation, electron spin polarisation 80−88612
(100) oxidised surface structure anal., extented appearance potential fine struct. study. 80−75411
(111), chemisorption and reaction of NH_3, LEED, desorption and photoemission expts. 80−59799
absorbed Na(Te), core-level photoelectron diffraction 78−95659
absorbed on W(111), surface site geometry diffusion charact. 78−75944
absorbers, deuteron distrib., depend. on direction of implantation *(German)* 77−4123
absorption of H_2, demagnetisation of surface due to absorption 77−80990
absorption spectrum anomalies, 2-3 eV, optical anisotropy *(French)* 78−43893
accommodation coefficients, of Na, Rb and Cs on Ni, 658-1095K 77−47666
acoustic emission during magnetisation, stress effects 79−82854
acoustic hardening, influence of US treatment temps. and material purity *(Russian)* 80−11656
activator in Mo sintering, grain size effects 77−63590

nickel continued
adosrbed H on (111) surface, angle-resolved and variable impact energy electron vibr. excitation spectroscopy 80−76119
adsorbed benzene on (111) surface, vibr. loss spectra 79−23838
adsorbed c(2×2) Na overlayer, core level excitation effects, synchrotron radiation UPS study 80−40234
adsorbed c(2×2)-CO on (001), struct. by LEED, self-consistent scatt. pot. 80−70536
adsorbed c(2×2)CO on (100) surface, photoemission orientation determ. 79−19974
adsorbed C on Ni (100), LEED struct. anal., substrate distortion 80−6637
adsorbed chalcogen, structure, force consts., binding energies and photoemission, importance of final state multiplet splitting 78−71966
adsorbed CO, angle-resolved polarisation-dependent photoemission, adsorbate orientation 77−4716
adsorbed CO, core level spectrum, satellite struct., ab initio HF-LCAO calc. 80−40233
adsorbed CO, on (100) surfaces, LEED study of c(2×2) struct. 79−86983
adsorbed CO c(2×2) on (001) face, surface geometry determ. by deep-core-level XPS 80−40224
adsorbed CO low energy electron scatt. 79−56896
adsorbed CO on (111) face, CO stretching vibr., high resolution electron loss spectroscopy 78−14605
adsorbed CO on stepped surface, vibrs. from electron energy loss spectra 79−73406
adsorbed H_2, CO, and methanol, interaction on (100) surface, temp. programmed desorption study 80−66876
adsorbed layers of CO, dissociation 77−31875
adsorbed layers of CO, molecular desorption anal. 77−31874
adsorbed methoxy species, photoelectron spectra, electronic struct. and orientation 80−83420
adsorbed Na and Te on (001), photoelectron diffr. effects in core-level photoemission 80−76144
adsorbed O_2 layer on (001) surface, angle-resolved UPS 77−40333
adsorbed O, order-disorder transition of O 79−82447
adsorbed on W (111) surface, surface site geometry and diffusion charcts. of Ni atoms 78−71953
adsorbed S, crystallography by LEED, appl. of iso-intensity map method 79−19128
adsorbed S(Se), surface bonding mechanism for ang. resolved photoemission 79−69360
adsorbed S and O on (110), surface struct. anal. using hybridisation model 80−44423
adsorbed S on surface, oxidation studied by AES 79−83505
adsorbed Se and Te on (001) surface, photoelectron diffr. obs. 80−40223
adsorption, of CO on stepped surface, adsorpt.-desorpt. behaviour, LEED, AES, thermal flash desorpt. study 78−71984
adsorption, of O_2, oxidation 80−108730
adsorption and decomp. of hydrocarbons on (111) surface, high resolution EELS study 80−40739
adsorption and decomposition of formic acid, obs. using combined SIMS-FDS-AES system 78−40076
adsorption isotherms for H 77−11776
adsorption of acetic acid and ethylenediamine, XPS study 80−76132
adsorption of acetylene, on (111) surface 78−95952
adsorption of acetylene and ethylene, angular resolved UPS exam. 78−72685
adsorption of acetylene on (111) surface, chemisorbed O_2 effects, CH formation 78−18902
adsorption of acetylene on (111) surface, identification of CH species by electron energy loss spectra 79−15022
adsorption of alkali metals, depend. of electron state of adatom on conc. 78−72001
adsorption of C on (100) surface, substrate reconstruction, LEED constant momentum transfer averaging study 80−39445
adsorption of chalcogens, orbital identification in INS and UPS spectra 77−43427
adsorption of chalcogens on (111) surface, angle-resolved photoemission 80−40230
adsorption of Cl on (111) surface 77−85069
adsorption of CO, absolute coverage determ., AES and LEED 77−76661
adsorption of CO, adsorbed mol. bond config. and orientation, ang. resolved photoemission 77−44506
adsorption of CO, binding and energy level shifts, NiCO and Ni_2CO electronic struct. 78−34882
adsorption of CO, high press., low temp. Raman spectra 78−6219
adsorption of CO, mol. orientation, ion scatt. 78−71949
adsorption of CO, on (100) surface, UPS study 79−76473
adsorption of CO, on Ni (001) surface, XPS for adsorbate geometry 79−65314
adsorption of CO on (001), orbital energy spectrum 78−2369
adsorption of CO on (100), bonding struct., vibr. excitations 77−15687
adsorption of CO on (100) surface, EELS and concomitant surface anal. 80−7453
adsorption of CO on polycryst., SIMS 78−14585
adsorption of ethylene and acetylene, vibr. spectra from electron energy loss *(French)* 78−34696
adsorption of ethylene at room temp., surface complex vibr. from electron energy loss spectroscopy 79−73404
adsorption of ethylene on (110) face, decomp. 77−85071
adsorption of ethylene on (111) surface, dehydrogenation, thermal desorption and AES study 80−29274
adsorption of H_2, activation mechanism, extended Huckel calc. *(French)* 79−42379
adsorption of H_2, inelastic neutron scatt. 78−18898
adsorption of H_2 on Ni (111), LEED intensity spectra, 173K 79−28192
adsorption of H_2S and S on (100) surface, ang. distrib. of S Auger emission 77−32475
adsorption of H, extended Huckel theory 78−10286
adsorption of H, on (110) surface, structural investig. by He diffraction 79−86984
adsorption of H on (110) surface, substrate reconstruction, LEED constant momentum transfer averaging study 80−39445
adsorption of N_2, photoemission and electronic struct., cluster calcs. 80−97403
adsorption of N_2 on (001) surface, c(2×2) struct. form 80−80083
adsorption of Na, hybridisation between adatom s and p resons., jellium model 80−6932

nickel continued
adsorption of O_2, Se, S and Te on (111) surface, bonding geometry and electronic struct. 79−77909
adsorption of O_2 on (100) surface and reduction of surface oxide by H_2 80−108741
adsorption of O_2 on (110) surface, obs. by electron microscopy, AES and LEED *(French)* 77−62732
adsorption of O, electronic struct. and UPS 78−15281
adsorption of O, sputtering by low energy ions 77−62758
adsorption of O(Se)(Te), photoemission intensities from core states 78−95654
adsorption of O on {100} surface, low energy ion scatt. study 80−39420
adsorption of S, diffusion, multiple binding sites, photoelectron spectra, LEED struct. 77−66569
adsorption of S, Se, photoelectron diffr. data 80−29851
adsorption of S(O)(N)(C), internal and external sources of electrons 77−44097
adsorption of Se on (001) surface, resonancelike peaks in angle-resolved UPS 79−69955
adsorption of W, average work function change 79−28190
adsorption of water $(O_2)(H_2)$(CO), combined XPS/LEED/SIMS exam. 79−83075
adsorption residual C removal by electron beam irrad. and heat treatment *(Chinese)* 80−88421
adsorption site of Se layers, photoelectron intensity modulation 79−47589
AES meas. 77−36323
AES meas. of soft X-ray emission threshold potential *(Russian)* 79−33866
AES of (110) surface *(Dutch)* 79−1802
air contamination effect on compatibility with liquid Li in stainless steel vessels at 600°C 78−25285
air electrode, bifunctional, for Fe-air batteries 80−72028
alpha particle energy loss straggling 80−42902
alpha-particle bombardment, He liberation during tempering 77−46290
alpha-particle impact, exfoliation depth and damage energy distrib., range 80−29075
alpha-particle irrad., Mossbauer study of nucl. reaction aftereffects 80−40015
aluminisation, soln. of binary multiphase diffusion problem allowing for variable diffusivity 77−16744
aluminisation in Al packs, for protective coating form., kinetic diffusion theory 77−32727
amorhpous and liquid states, electronic states and transport 79−99474
amorphous, elec. cond. calc., t-matrix approach 77−55510
amorphous, elec. resist. calc. 78−60103
amorphous film, getter sputtered at 25K, resistivity, Curie temp. 78−52673
amorphous film, getter sputtering at 25K 79−38741
angle resolved photoemission spectra 78−43986
angle-resolved photoemission, band struct. 78−95680
angular forces and normal vibration 79−73270
anisotropic magnetisation meas., 4-250K 80−65862
anisotropy energy in (100) plane, temp. dependence 78−2674
annealed and cold worked, H diffusivity and solubility *(Japanese)* 78−51739
annealing twins, density, effect of recrystallisation temp. and electron microscope resolution *(French)* 78−31423
annealing twins density, photoemission microscopy 80−35208
anode spot form., in vac. arc, threshold current time depend. 78−87515
anodic dissolution into silicate glass melt, exam. 78−88582
anodic oxidation, cathodic reduction, arrest struct. 77−12735
anodic oxidation, role of oxide defects 80−76403
anodic oxidation in 1N H_2SO_4 soln. 79−91849
anodic oxidation in neutral electrolyte, ellipsometric obs. 78−27673
anodic passive film form. in NaOH soln., refl. and ellipsometric study 80−104447
anodically oxidised, 100 keV proton channelling investig. of oxide layer struct. 77−84820
anomalous resistivity near Curie temp., band theoretical calc. 78−56127
APS and band theory of magnetism 77−40303
atmospheric corrosion, moisture adsorption and indoor corrosion rates 80−71799
atom, doublet open-shell restricted SCF eqns. 79−59350
atom, electron bombard., 300 to 600 keV, K_α/K_β X-ray intensity ratios, K-shell ionis. cross sections 78−37747
atom, from Ni(CO)$_4$+inert gas, chemiluminesc. 80−55647
atom, ionisation potential, term value, correlation energy by vertical anal. 78−41964
atom, $K\alpha^h$ hypersatellite spectra and double photoionisation cross-section 79−85922
atom, $K\alpha\alpha^h$ emission, method for L-shell config. calc. 77−42269
atom, Kα and Kβ X-ray spectra induced by 84 MeV N^{4+} 77−50517
atom, K-shell hole production by light ions, hydrogenic and Hartree-Fock model of target 77−83715
atom, Lα and Lβ_1 emission spectra structure 77−27013
atom, $M_{III,IV}$ spectrum, ab initio calculation 80−83276
atom, $O^{2+,3+,4+,5+}$ induced K-shell X-ray production cross section, 7 to 24 MeV 77−61850
atom, orbital energies, ab initio rel. to pseudopot. calcs. 78−82613
atom, photoelectric cross sections, 5-40 keV photons, X-ray emission spectra 77−18866
atom, pseudopotential calculations, parameter fitting scheme appls. 78−41928
atom, rel. at. transition probabilities, by flame at absorption spectroscopy 79−89642
atom, reson. X-ray Raman scattering, IR divergence of Compton effect 78−21873
atom, UV matrix freq. shifts, ionis. pot., assignments appl. to Ni_2, Ni_3 77−75178
atom, Xα theory appls. approximations 80−9510
atom, X-ray transitions in laser produced plasma 80−100093
atom+$H^+(D^+)$, K shell ionisation, nuclear Coulomb effect 80−91650
atom+ion collisions, K X-ray transition energies, two electron-one-proton mechanism 77−18828
atomic and metallic 3p excitation 79−22633
atomic cluster, EXAFS study of bond length and binding energy 79−81317
atomic layers, Pauli paramagnetism to band ferromagnetism transition thickness depend. 78−72377
atomic magnetic moments comparison to values of ferromagnetic metal 78−52244
atoms, Xe matrix isolation, photoemission 80−27987
attenuated total reflection minima, correlation with surface polariton modes, computational study 78−31265
Auger effect, K→M^2 radiative, low energy satellites meas. 80−45174
Auger emission clean and gas-adsorbed surfaces, ang. distribs. 78−39636
Auger emission from (100) surface, ang. resolved meas., compared with electron multiple scatt. calc. 77−32476
Auger energy calc. using XPS, effect of 3d-4s admixed screening on relax energies 77−1782
band electron momentum distributions calc. 78−18950
band model, effective Coulomb interaction momentum depend. 79−78298
band model of high temp. magnetism 78−26809
band struct., angle-resolved photoemission meas. 80−71569
band struct., cryst. pot. anisotropy effect *(Russian)* 80−88474
band structure, μSR Knight shift meas. 79−56663
band structure, and temp.-depend. mag. exchange splitting, angle resolved photoemission obs. 78−60546
band structure, correlation effects 79−60697
band structure, parametrisation via Hubbard's scheme 77−31938
band structure, rel. to lattice const., spin polarised APW calc. 80−20073
band structure and multielectron excitations, angle-resolved photoemission determ. 80−76147
band theoretic interpretation of neutron scatt. expts., spin wave modes 80−44791
Barkhausen and magnetoplastic effect, simultaneous obs. 79−28583
BCC and FCC struct., X-ray absorption spectra, Mossbauer spectra, comparison *(Russian)* 78−64299
beam-foil collisions, X-ray transitions between correl. many electron quantum states 77−79689
black, solar collector selective coatings, optical and thermal props. 79−62028
black Cr and Ni electrodeposit spectral selective props. for solar absorbers 79−62036
blistering, He^+ ion energy and irradiation temp. effects 80−34103
blistering by $^4He^+$ bombardment temp. depend. 78−43967
blistering model, correlation between blister diameter and skin thickness 78−95067
Bloch wall meas. by enutron small-angle meas. 80−15753
bombardment by 1 to 30 keV ions, emitted radiation spectral comp. *(Russian)* 77−81159
bonding of O to (100) surface 78−79889
borate glass: Ni, absorption spectra, mag. props., coordination behaviour *(German)* 80−40147
bound hole pairs, XPS study, satellite peaks 80−40218
bright, rest potential meas. and interpretation in NaCl and dil. H_2SO_4 *(French)* 78−85056
Brillouin spectra, light scatt. cross section for surface ripples 80−71434
Brillouin-Mandelstam scattering from thermal and excited magnons 80−70980
bulk modulus and thermal expansion coefficient, mag. contributions 79−8039
calcium tartrate tetrahydrate:Ni^{2+}, optical absorpt. spectrum 78−84610
candidate current collector for Li-FeS_x battery, anodic corrosion rate in LiCl-KCl eutectic 79−100513
carbonyl powder, dislocation density sintering 80−108372
carbonyl powder, sheet filtration materials with metallic gauze backing layers, bending strength and ductility 78−60613
carburized single crystal sheets, lattice strain during interstitial diffusion *(Japanese)* 78−10220
catalyst, Al_2O_3 supported, CO adsorpt. in H_2-He, effect of H_2S on IR spectrum 78−71945
catalyst, alumina supported, porous pellets, thermal cond. 79−86936
catalyst, chemisorption of ethylene(-d), Raman and vibr. spectra 80−108747
catalyst, diamond synthesis by graphitisation of carbon materials at high press. and temp. 80−60795
catalyst, effect on crystallization of amorphous C film 79−14683
catalyst, formic acid decomp. kinetics and mechanism, mol. beam relax. spectroscopy 77−70340
catalyst, in diamond synthesis, growth mech. *(Japanese)* 77−60122
catalyst, magnetooptical investigation of mag. props. 79−69858
catalyst, polycryst. ribbon, methane formation, CO hydrogenation kinetics 78−40078
catalyst in diamond synthesis, intermed. phases of Ni-C system, satellite structures *(German)* 77−32538
catalysts, chemisorption of $H_2(H_2O)$, dynamics, neutron spectrosc. obs. 80−59778
catalysts for fuel cells, thermoanalytic investigation *(German)* 79−74420
catalytic effect on ZrC whisker CVD 78−51865
catalytic graphitisation, three-phase, of phenolic resin C by Ni particles 78−68922
cathode spots on vac. arc discharge electrodes, model 78−91179
cathodic charging of H_2, positron annihilation Doppler broadening obs. 79−83055
cathodic polarisation in alakaline earth metal salt solns., surface changes 79−61869
cathodically H charged, isothermal ageing 79−15703
cavitation-erosive wear in surface-active media, dislocation struct. and fracture study by FMR *(Russian)* 79−52384
cavity coalescence following $^4He^+$ irrad. 80−70272
cavity evolution in 500 keV $^4He^+$ irrad. 80−29082
channelling and blocking of proton beam, target magnetisation effect 77−69022
channelling of Si ions, transient mag. fields rel. to bound s electron polaris. 79−33023
chemical plating of glass ceramic with Ni and Cu 77−44379
chemisorbed acetylene on (111) surface, ind. vibrs., high resolution electron energy-loss meas. 79−90877
chemisorbed CO, adsorption sites and long range order, vibr. spectra 79−46946
chemisorbed CO, orientation of CO from angle resolved photoemission 77−8721
chemisorbed H_2, desorption kinetics, rate equations 79−82448
chemisorbed H_2 on (111) face, geometry, LEED anal. 79−28200
chemisorbed H_2 photoemission spectrum, Anderson model parameterisation 77−40334

nickel continued
chemisorbed O_2, angle resolved photoemission from chemisorption induced states and LEED spectra 77−85898
chemisorbed overlayers of O and S, A-vector orientation depend. of angle-resolved photoemission 77−59671
chemisorbed Si, P and Cl on (100) surfaces, LEED and angle-resolved AES obs. 79−95258
chemisorption, competitive, on metallic films, IR spectra, oil matrix technique 77−9118
chemisorption, dissoc. of $CO(H_2)(N_2)$, on cryst. surface *(German)* 78−53257
chemisorption, dissociative, and mol. adsorption of NO 80−65373
chemisorption, of CO, CNDO calcs. *(German)* 78−29751
chemisorption, of CO, SIMS, AES, desorpt. meas. 78−87875
chemisorption, of H_2, isothermal desorption near Curie temp., rate meas. 80−29268
chemisorption, of O, S and Se, struct. and energy levels calc. 77−47663
chemisorption and magnetisation, book 77−25311
chemisorption bonding of H on surface (111), UPS obs. 77−76671
chemisorption geometry of H on (111) surface, LEED, thermal desorption, and work function meas. 80−39433
chemisorption of benzene on (100) and (111) faces, LEED and high resoln. electron energy loss spectra 78−6224
chemisorption of benzene on (111) and (100) faces, vibr. EELS study 80−39436
chemisorption of CO, (100) surface, mol. cluster theory 77−69174
chemisorption of CO, ab initio LCAO MO SCF calc. for NiCO 78−62712
chemisorption of CO, C-O bond lengths, electronic struct. 78−6210
chemisorption of CO, carbonylation rate mag. field depend. 79−24828
chemisorption of CO, catalytic activity, SCF-Xα-SW calcs. 78−15711
chemisorption of CO, N_2, NO, semiempirical calcs. 78−14611
chemisorption of CO, on {001} surface, LEED study of mol. orientation in c(2×2) struct. 79−86982
chemisorption of CO, on (001) face, electronic struct. of $(M)_5CO$ clusters 78−95948
chemisorption of CO, on (100) surface, mol. levels, angle depend. calcs. 78−90069
chemisorption of CO, Raman spectra 80−2755
chemisorption of CO, vibr. spectra from electron energy loss spectra *(French)* 78−22951
chemisorption of CO and C_2H_2, final state mol. relax. 77−62752
chemisorption of CO and its methanation 77−56250
chemisorption of CO on (001) surface, back donation in chemisorption bond, UPS study 80−107642
chemisorption of CO on (100) and polycrystalline surfaces, low energy SIMS and AES 80−34309
chemisorption of CO on (100) surface, possibility of reduced bond length 79−28202
chemisorption of CO on surface (100), c(2×2) struct., dynamical LEED expts. 78−34710
chemisorption of CO on surfaces (100)p(2×2)O and (100)c(2×2)O, LEED and energy loss spectra 78−2375
chemisorption of cyclohexane and ethylene, C-H stretch vibration, broadened and softened, dehydrogenation 78−47666
chemisorption of ethylene, adsorption and decomposition exam. 77−55459
chemisorption of H_2, interaction between adsorbates, model Hamiltonian calc. 79−46964
chemisorption of H_2, molecular complex model 77−1314
chemisorption of H_2, neutron inelastic spectroscopy investig. 77−48686
chemisorption of H_2, periodic surface model calc. 78−30822
chemisorption of H_2, Raman spectra, vibr. bands 79−61368
chemisorption of $H_2(D_2)(HD)$, vibr. excitation and struct., electron energy loss spectra 78−47660
chemisorption of H_2 and O_2 on (110), LEED 77−24470
chemisorption of H, bond nature 80−34297
chemisorption of H, electronic struct. of H using angle-resolved photoemission 79−69573
chemisorption of H, embedded cluster model 80−39427
chemisorption of H, model, comparison with UPS data 79−46932
chemisorption of H, O and CO on (001) surface, localised orbital approach 77−69166
chemisorption of H, surface magnetism 78−95510
chemisorption of H, Xα cluster calcs. *(Japanese)* 78−72002
chemisorption of H and O, (001) surface, localised orbital approach 78−14587
chemisorption of H on (111) surface, order-disorder transition, cluster-variation method 80−15372
chemisorption of H on large cluster, bonding energy, HF calc. 79−39204
chemisorption of hydrocarbons, C 2s levels, initial state shift 78−34703
chemisorption of methanol, UPS and flash-desorption exam. 77−55455
chemisorption of methanol on (111) surface, methoxy species, electron energy-loss spectra 79−29391
chemisorption of N_2 on (110) surface, mol. and dissociative mechanisms 80−39431
chemisorption of N_2-containing gases at high-press., XPS 77−20990
chemisorption of NO, (110), LEED, AES and thermal desorption meas. 77−15695
chemisorption of NO on (100), LEED, AES, UPS, and thermal desorption study 80−39449
chemisorption of O_2, MSXα total energy calcs. with non-muffin-tin corrections 77−72795
chemisorption of O_2 and CO, ion bombard., particle ejection, SIMS obs. 79−78810
chemisorption of O_2 and H_2 on (100) surface, and their interaction, UPS 77−51600
chemisorption of O_2 on (110) surface and initial oxidation, AES, EELS, and work function meas. 80−54523
chemisorption of O, electronic struct., KKR model calcs. 78−56200
chemisorption of O, S, Se, NO and O_2, cluster theory 80−29264
chemisorption of O(S), geometry of overlayers 78−2373
chemisorption of O(S)(Se)(Te), orbital energy spectrum of chemisorbed electrons 78−2542
chemisorption of O and S on (001) surface, angle-resolved UV photoemission calc. 77−85890
chemisorption of O on (111), adlayer phases and binding sites 80−80069
chemisorption of S, ang. depend. of multicentre Auger matrix element for Ni (100)-c(2×2)S 78−92151
nickel continued
chemisorption of S and CO, surface struct. from ang. resolved UPS 78−31303
chemisorption of S and Se, Xα cluster model calcs. 79−65313
chemisorption of S on (001) surface, thermodynamics, AES study 79−82452
chemisorption of S on Al_2O_3-supported surface, thermodynamic parameters meas. 80−88424
chemisorption of S-containing alkanes on clean Ni 78−14595
chemisorptive binding of O, CNDO calc. of potential energy curves *(German)* 80−44431
cluster approach to single H atom in single crystal 78−47334
clusters, chemisorption of H, macroscopic 79−82445
clusters, electronic struct. and mag. props., MO calc. 77−20219
clusters, FCC and icosahedral structs., relax. and stability, cohesive energy minimization 79−42479
clusters, valence band and core binding energies, UPS meas. 79−38721
coadsorption of CO and H_2S on (110), (100) and (111), surface coverage meas. by SIMS 79−90876
coated Armco Fe, heat resistance assessment at varying temps. *(Russian)* 77−25189
coated C fibre, coating struct., SEM study 80−97605
coated Mo and W filaments, creep and recrystn. *(Russian)* 78−19822
coating, electron beam evaporated, ductility and struct. 78−11439
coating, heat treated, as plated, electrochemical study of corrosive wear 80−16536
coating, self lubricating containing oxides, carbides and borides on steel 80−21189
coating, sliding wear resistance 77−12708
coating hardness rel. to sulphamate electrolyte selection *(Bulgarian)* 78−88552
coating on Al alloy substrates, adhesion strength, meas. using microindentation method 80−40640
coatings, detonation powder spray deposition 80−61028
coatings, nondestructive testing, holographic interferometry appl. *(German)* 79−79186
cohesive properties 79−94952
cold rolled, influence of impurities on recovery and recrystallisation, positron annihilation meas. 79−15696
cold rolled, positron annihilation examination of recrystallisation *(German)* 77−70252
cold swaged, unidirectional recrystallisation over range of temp. gradients *(Japanese)* 78−48424
cold worked, annealed, exam. of anelastic relaxation at low temp. 78−84877
cold-rolled anomalous effects during X-ray stress meas. *(German)* 80−104184
cold-worked, Bordoni peaks activation parameters 79−82282
cold-worked, impurity-induced vacancy clustering 79−99972
compact, on H_2 permeated backing, precipitation *(Russian)* 78−27520
compressive deformation, single crysts., strengthening, tested at 293 and 77K *(German)* 80−50689
concentration determ. in atm. and rainwater in Vizcaya, Spain *(Spanish)* 78−57264
concentration in atmospheric sedimentable powder, in Vizcaya, Spain *(Spanish)* 78−57265
contact interaction with graphite at high press. and temp. *(Russian)* 79−11722
contact junction formation by ion evaporation 77−90285
contact to GaAs, effect on minority carrier diffusion length 78−72260
contacts for low cost Si solar cells 80−94017
content in Cu alloy of Mayfield chondritic meteorite 80−67671
core level excitation effects, synchrotron radiation UPS study 80−40234
core-electron excitation edges 80−66345
correlation effects, perturb. treatment within Hubbard model 80−70582
correlation effects, perturbation treatment 80−59897
corrosion, high temp., SO_4 induced, studied at 900°C in O_2+4.2% SO_2 80−97639
corrosion, indoor, rate meas. 80−76404
corrosion, model for cond. mechanism in oxide, rel. to basic atomic processes of metal corrosion 77−25198
corrosion, monitoring using polarisation resistance meas., techniques and correlations 77−16711
corrosion and electrochem. behaviour in NaOH soln. containing ClO_3^- *(Japanese)* 78−72928
corrosion and passivation in phosphate soln., pH depend., ellipsometric study 80−104448
corrosion by molten alkali metal hydroxides and liquid Li 77−44414
corrosion due to V_2O_5 melts *(Japanese)* 80−93691
corrosion HCl, thiourea and derivatives effect 79−96179
corrosion in 0.1 N $HClO_4$, Cl^- effect 79−39020
corrosion in atmosphere, environmental test 79−66205
corrosion in LiCl-KCl eutectic melt containing nitrate ions *(Japanese)* 78−92398
corrosion in molten Na_2SO_4 at 1173K, E-pO^{2-} diagram 78−44247
corrosion in SO_2, high temp. 79−20281
corrosion mechanism, localized, in alcoholic H_2SO_4 77−86218
corrosion of electrolytic coatings in 40% wt. KOH 80−30175
corrosion resistance in 1M $LiAsF_6$/THF, suitability for organic electrolyte Li secondary batteries 79−100387
corrosion susceptibilities in synthetic geothermal brines 77−86223
creep, effect of AC mag. field, 1.5-4.2K *(Russian)* 79−11657
creep, irrad. induced with 17 MeV deuterons 80−93607
creep, mag. field effect, 4.2K *(Russian)* 77−90000
creep, rel. to radiation swelling and stacking fault energy *(Russian)* 78−27562
creep, single crystals, 1.5-50K, orientation effects *(Russian)* 79−15757
creep, struct. and activation characts., effective stress, electron microscopy and resistometric obs. *(Russian)* 80−40427
creep, substruct. and internal stresses *(Russian)* 80−97527
creep, transient stage stress depend. at $T<T_{0.2MP}$, dislocation struct. *(Russian)* 77−48482
creep, variation in dislocation density, determ. by X-ray diffr. analysis *(Russian)* 80−76302
creep, volumetric, irradiation induced, stress effect on swelling 77−43253
creep at 77, 295K, formation of five struct. 80−60926
creep parameters, high temp. 80−50685
creep rate at low stresses, effect of grain size 80−71707
creep rates, stress depend. and activation energies, constant stress tests, comparison with dislocation creep theory 80−71708
critical exponent β for hyperfine fields, PAD techniques 78−19403

nickel continued
critical exponent meas. by PAC in $Ni^{100}Rh$ 77−20774
crossover phenomena, stress induced above Curie point, neutron scatt. study 79−61113
crossover phenomena, stress-induced above Curie point 77−4543
crystal growth, oriented, by vacuum intake method *(Russian)* 77−4732
crystal hyperfine fields and neutron scatt. 79−56172
crystal spectroscopy to small quantum energies, $M_{2,3}$ spectrum 77−69938
crystallites, vacancy diffusion and vacancy lattices, semi-empirical mol. orbital calcs. 77−1121
crystals, thick, imperfect, dynamical X-ray diffr. topographic effects 77−68898
crystals in strong magnetic field, EM excitation and vel. dispersion of sound *(Russian)* 80−39837
cubic crystals, anisotropic, dislocation loops, electron microscope image contrast 80−39101
cubic single crystal misorientation angle determ. by US speed meas. 80−54315
Curie point, thermal expansion anomaly 77−85474
Curie temperature, press. depend., using press. cell developed for meas. with cubic-anvil press 80−13109
Curie temperature calc. using model containing five bands 79−56536
cyclic creep in single crystals 79−66129
cyclic deformation, high temp. 80−16429
cyclic flow stress and microstructural changes during multiple step testing at elevated temperatures 79−91746
Czochralski grown single crystal, crystal perfection 78−47252
Czochralski growth conditions rel. to cryst. imperfections, mag. domain walls 77−68937
de Haas van Alphen signal anal. by linearly recursive approx. 78−91603
de Haas-van Alphen effect, absolute amplitude, Fermi surface neck 77−85134
Debye Waller determ. from modified Cheveau model 78−59918
Debye Waller factor by mol. dynamics simulation 77−80598
Debye-Waller factor, using reverse Fourier time-of-flight method, neutron powder diffr. study 80−49050
Debye-Waller factor temp. parameter 78−30725
Debye-Waller factors, modified ang. force model 77−66013
decarburisation rate, resistivity relaxation measuring system, for surface reaction meas. 80−55718
defect cluster evolution, ion implanter adaption on 100 kV electron microscope 79−2888
defect electronic struct., strength characteristics relation by positron annihilation 79−91526
defect removal, obs. by positron annihilation 78−84677
defect structure, formation kinetics, work hardening and resistivity study *(Russian)* 80−10557
defect symmetry, time differential PAC meas. 78−15069
defects at thermal equilib. and melting, positron annihilation meas. 77−76391
deformation, cyclic, at high temps. of alloy 200 80−21055
deformation hardening by shock front, quasiisentropic compression, front width effects 79−100209
deformation in const. mag. field, 4.2K *(Russian)* 80−29591
deformation twins contribution to yield stress, Hall-Petch law for inter-twin spacing 79−24588
deformed, coercivity and remanence anisotropy 78−31093
deformed, cyclically, polarisation stress field, dislocation shuttling, computer calcs. 79−96095
deformed, magnetic susceptibility anisotropic changes 78−27025
deformed, struct. form. during annealing, Ni_3Al type ordered phase precipitation *(Russian)* 80−45325
deformed, work-hardening, dislocation and mosaic struct., X-ray and electron microscopy 77−35625
deformed bars, cold rolled, exam. of microstruct. by thin foil TEM 78−88502
deformed by filing, fine struct. obs. *(Russian)* 77−21309
deformed by hydrostatic extrusion, drawing or drawing under press., dislocation struct. obs. *(Russian)* 77−21213
dendrites, on Al, CV, selective solar photothermal absorber 78−52683
density of states, photoemission expts. above and below T_c, rel. to magnetism model 77−20536
deposition on stress-annealed pyrolytic graphite, binding 77−59210
depth distrib. of self-ion damage, TEM 77−51419
depth profiling of ^3He ion implantation 78−59830
desorption, associative from mixed adlayers of O and N 80−54512
desorption of CO, on (111) preexponential factor 80−49515
desorption of CO due to ion bombard., comparison of surface anal. methods 79−8213
desorption of H_2, HD and D_2, vel. distribs. 77−43431
desorption of N and O, from Ni on SiO_2 200 to 400K *(German)* 78−30835
determ. in vitreous silicates by ESCA *(Japanese)* 80−40787
determination, in heavy crude oil, by at. absorpt. spectroscopy 77−52681
determination, in hydrodesulphurisation catalysts, by at. absorpt. spectroscopy 77−9145
determination, in serum, matrix effects in graphite furnace AAS 78−85230
determination, in steels, by spectrographic method using combined discharge 79−57327
determination by intracavity at. emission spectroscopy 79−52830
determination in soln. using at. emission anal. with exploding foil excitation 77−12840
determination using laser excited atomic fluoresc. spectrosc. 80−93811
deuteron diffusion obs. by D(d,p)T reaction *(German)* 77−59150
deuteron irradiation-induced creep mechanisms 80−39171
deuteron range profiles in 100 to 400 keV region, expt. and computer simulation 77−51422
diamond:N_2, Ni, spin-spin interaction of N_2 and Ni centres, temp. effects 78−88177
diamond:Ni, synthetic, X-ray absorpt. fine structure study of impurities 80−55133
diamond containing electroless Ni coatings, fabrication and props. 79−47795
diamond surface interaction with gases and metals 77−72758
dielectric matrix, analytic model 80−75512
diffusion, in HgTe single crystals 79−77818
diffusion, of In, temp. depend. *(Russian)* 78−75880
diffusion and electrotransport in Th, 965-1625°C 79−90828
diffusion and solubility of S *(Russian)* 80−70465

nickel continued
diffusion bonding with Cu 77−62687
diffusion coefficient in Al, resistometric determ. 79−51313
diffusion coefficients calc. for H and D *(Russian)* 78−91483
diffusion in Ag, resistometric technique 78−38880
diffusion in Au, rate rel. to Cu 77−80652
diffusion in $LiNbO_3$, and its effect on acoustic velocity 77−84847
diffusion in Nb, radiotracer and electron microprobe meas. 77−76615
diffusion in Si below 475° role of defects 79−51319
diffusion in Th at 500 to 800°C *(German)* 79−28157
diffusion into Cu and Cu-Ni, resistometric meas. 80−29222
diffusion of Ag, volume and grain-boundary, diffusion parameter temp. depend. meas. *(Russian)* 78−67863
diffusion of Cs, AES, SIMS depth profile study *(German)* 78−84008
diffusion of D, isotope effect, elec. resistivity meas. 79−86928
diffusion of H_2 in single- and polycrystals at 60°C grain boundary effects *(German)* 80−2211
diffusion of H, book contrib. 79−82390
diffusion of H, trapping and mobility near vacancies, dislocations and cracks 80−49426
diffusion of H and trapping 80−70447
diffusion of H in H_2 quenched sample, elec. resist. recovery 78−2299
diffusion of H in imperfect lattices 80−49425
diffusion of Mn, radiation-enhanced, effect of point defect fluxes 77−89588
diffusion of positive muons 79−56688
diffusion of Si, ion radiation effect on redistrib. 78−34551
diffusion welding, migration of oriented intergranular boundary with pores *(Russian)* 80−84943
dilute impurity hyperfine fields, comparison with model 78−14954
dislocation core energy, core tension, Peierls model 79−27984
dislocation dynamics, HVEM in situ obs. 78−83822
dislocation intersection and solution strengthening, effect of solute on obstacle profiles 80−7590
dislocation struct. formed by C diffusion in single crystals, electron microscope obs. *(Japanese)* 78−10053
dislocation structure evolution after hydroextrusion *(Russian)* 80−96530
dislocation structure parameter determ. due to plastic deformation *(Russian)* 80−54242
dislocation substructure formation under hydrostatic extrusion 78−56696
dislocations gliding on (001) planes, bright field and weak-beam images 80−107266
dispersed, K_β emission spectra, cluster effects 77−28650
dispersion curves from deLaunay angular force model 79−33054
dispersion strengthened, high-temp. cyclic deformation 80−21056
dispersions, semi-amorphous, on Al_2O_3-graphite, mag. characterisation 80−44876
dissolution and passivation, role of adsorbed S 79−66340
dissolution and passivation in acid environment, effect of P *(French)* 80−45440
dissolution and passivation in acid medium, effect of S in solid solution *(French)* 78−64771
dissolution in methanolic soln. *(Rumanian)* 79−74283
dissolution kinetics and diffusion coefficients in molten Al 80−59666
distribution coefficient of Ir, Os, Ru between liquid and solid phase, zone fusion *(French)* 77−77374
distribution in alloy steel welds, laser emission microanal. method 78−61110
domain patterns and dislocations, effect of annealing in cyclically deformed crysts. 78−71740
domain walls, 109 and 71°, stable orientations, theory and X-ray observations *(Japanese)* 80−60359
Dorn relationship for creep prediction, introduction of force factor *(Russian)* 78−18185
ductile, electrolytic, densification of particulate materials, general law 78−19692
ductility and fracture, nonmetallic inclusions effect 80−104221
dynamic exponent, crossover obs., TDPAC meas. 80−108021
dynamic rearrangement of atomics in large cluster using Frohlich-Raimes method 78−30586
dynamic strength and logarithmic modulus of plasticity 77−16655
dynamical spin susceptibility, noninteracting spin band model 78−31059
effective exchange parameter, q-depend, intra-atomic interaction 79−4542
electrical resistance and H solubility at high press. *(Russian)* 79−91018
electrical resistance in DC mag. field after ultrasonic deform. *(Russian)* 80−54671
electrical resistivity and stress amplitude change during push-pull fatigue 79−91792
electrical resistivity anomaly near Curie point, effects of grain size *(French)* 77−4318
electrochemical behaviour, in molten V_2O_5 *(Japanese)* 80−89498
electrochemical overgrowths, role of substrate dislocations and grain boundaries in nucleation and growth 79−51454
electrochemically prod. emitters, field ionis. props. 77−90254
electrocrystallisation, inhibiting factors study 79−74105
electrocrystallisation, reaction mechanism, appl. of impedance meas. *(French)* 80−103597
electrocrystallisation noise, phenomenological model 78−51845
electrode, adsorption of O_2 in KOH soln. 79−61871
electrode, appl. in rotating multipolar wiper-blade cell 79−43751
electrode, electrochem.-ellipsometric studies of oxide films formed during O_2 evolution 79−16007
electrode, smooth, potentiodynamic investig. 77−21395
electrode reactions with molten glass 80−85186
electrodeposit, change in twin faults during growth, X-ray study 79−65334
electrodeposit, crystallite morphology *(French)* 77−32535
electrodeposit, linear defect obs., TEM study 79−4304
electrodeposit, mag. domain struct., neutron depolarisation 78−2716
electrodeposit on Cu, defects and their effect on props. 80−39474
electrodeposit structure, rel. to electrochem. noise 78−67916
electrodeposited, oxidation 78−64756
electrodeposited, role of stacking fault energy 77−29016
electrodeposited coating on Fe membrane, effect on H permeation, proposed catalytic mechanism 78−53252
electrodeposited film, appl. of stereomicroscopic method for obs. of organic molecule incorporation 80−2288
electrodeposited film, saturation magnetisation and perpendicular anisotropy meas. 78−76277

nickel continued
electrodeposited film, thermal anal., occlusion of gases rel. to mag. props. 80−59823
electrodeposited in sulphamate bath, cyclic stress, meas. appl. in high temp. range 80−19295
electrodeposited monocrystals, struct., effect of stress applied during electrodeposition 78−26777
electrodeposited sheet mag. domain struct. obs. by neutron depolarisation 77−69605
electrodeposition, chemical factors 80−16207
electrodeposition, on to $Al_xGa_{1-x}Sb$ solid soln. 80−93505
electrodeposition, structure-internal stress relationship 80−70561
electrodeposition cathode polarisation, influence of unsaturated sulphates *(Russian)* 79−91963
electrodeposition from alkaline citrate electrolytes, cathodic process rate *(Russian)* 79−8440
electrodeposition from alkaline citrate electrolytes, coating impurity quantities and props. *(Russian)* 79−8252
electrodeposition from alkaline citrate electrolytes, Ni/electrolyte interaction *(Russian)* 79−11796
electrodeposition from alkaline citric electrolytes, cathodic processes *(Russian)* 78−48338
electrodeposition in sodium thiocyanate soln., kinetics study using rotating disc electrode method *(Spanish)* 78−92486
electrodeposition on B single crystals to form ohmic contacts 77−44177
electrodeposition on Cu, growth and microstruct. 77−11823
electrodeposition on Cu (001), three-dimens. epitaxial crystallites, TEM image contrast 80−88457
electrodeposits, influence of Ni sulphamate operating parameters on impurity content and props. 79−28971
electrodeposits, struct., electrolyte anions influence 80−20056
electrodeposits on (001)Cu films, growth and mag. anisotropy 79−42810
electroless Ni, plating application, brief report 77−70290
electroless Ni deposits from Ni/P and Ni/B plating solutions, solderability by contact angle meas. study 79−88910
electroless plating, effect of ultrasonic irrad. 79−33953
electroless plating, oxidation kinetics 78−95847
electroless plating, Schottky barrier solar cell fabrication 79−83591
electroless plating process and props. for diamond turning optical surfaces 80−1375
electrolessly deposited, structural comparison with electroplated films 79−23869
electrolytic, O, H, N liberation during vacuum heating, Mossbauer spectra *(Russian)* 80−35594
electrolytic and carbonyl grades, sintered sheet material, stopping power and pore size relationship 78−19693
electromigration in Pb, steady-state method 78−87820
electromigration of H_2, effective valency effects *(French)* 79−23781
electron beam irradiated, influence of created pulsed press. on struct. and props. *(Russian)* 78−34539
electron bombardment of Ni substrate in residual gas containing hydrocarbons, secondary electron yield *(German)* 77−40315
electron field emission, electron spin polarisation determ. 77−32508
electron field emission, energy distribution, effect of adsorption of CO 79−8231
electron field emission, positive spin polarisation and band model of magnetism 77−52226
electron field emission, spin polarisation, positive sign 77−73220
electron inelastic mean free paths and energy losses, electron gas statisitcal model 79−46733
electron irradiated, temp. depend. positron trapping 78−91360
electron irradiated in HVEM, interstitial loop growth 80−107326
electron mean free paths and stopping powers calc. using statistical model 77−19996
electron microscopic observation of {220} planes 80−18047
electron spectroscopy, energy loss and photoemission 78−72682
electron spin polarisation in field emission, surface magnetism 78−68607
electron spin polarised tunnelling from superconductors 79−78263
electron tunnelling into ferromagnetic metals 80−60104
electron-phonon coupling, point contact spectroscopy obs. *(Russian)* 80−70342
electronic and magnetic props., spin split energy band dispersions 79−78829
electronic energy loss of protons (deuterons), 80-800 keV 79−23666
electronic structure, influence of temp. X-ray photoelectron study 77−28681
electronic structure, photoelectron spectra, theory 80−80168
electronic structure and optical consts. by inelastic electron scatt. 80−7451
electronic structure of nontransition element impurity atoms 77−73023
electroplated, fuchsin additive effect on low-temp. annealing characts., resist. meas. 77−32725
electroplated coatings internal stresses, theory and meas. review *(German)* 78−56049
electroplated layer, field ion microscope study 79−28246
electroplated layers, internal friction and ΔG effect, rel. to bath comp. and annealing 78−19296
electroplating method for high-temp. stress meas., applications *(Japanese)* 78−15617
electroplating method for high-temp. stress meas., fundamentals *(Japanese)* 78−15616
electropolishing in alcoholic soln. of H_2SO_4 77−16718
electrospark machining, spreading and form. of surface layer, in solid-alloy-liquid-metal systems, kinetics *(Russian)* 78−27668
EM and acoustic energy attenuation in many-domain magnets 80−7140
emissitivty and reflectivity, oxide film thickness effect 79−82364
emitter characts. for field desorption mass spectrometry of salts 77−63980
energy band dispersion and mag. exchange splitting, angle-resolved photoemission meas. 80−71567
energy band structure, investigating near-Fermi part from PES 80−2328
energy loss of heavy nonrelativistic ions in matter, semiclassical theory 80−84224
energy loss spectra of C^{2+} ions in Ni targets 80−65114
energy-band dispersions and exchange splitting, angle-resolved photoelectron spectroscopy 79−69402
entropy of fusion, local spin disorder 77−47601
epitaxial electrodeposition, surface-stress phenomena at start 80−35542
epitaxial film on NaCl, struct. and purity 78−72047
epitaxial films, even magneto-optical effects 80−76007
epitaxial films (110), uniaxial anisotropy, expt. 77−20648

nickel continued
epitaxial growth, on NiO(100), by low pressure hydrogen reduction *(French)* 80−11578
epitaxial monocrystal structure rel. to externally applied stress 77−76708
epitaxy on W (001) 78−60041
erosive wear mechanisms, combined TEM and SEM obs. 80−108601
evaporated coating on Al single crysts., surface strengthening effects 77−8972
evaporated metal nuclei on C, SiO_2 films, atm. contamination, AES meas. 77−4264
evaporation onto graphite, formation and decomposition of Ni_3C 79−15055
EXAFS in photoelectron yield spectra 80−16123
exchange splitting of 3d bands, angle-resolved photoemission meas. 80−71568
exploding wire, elec. resist. at high temp., submicrosec. pulse heating meas. 77−89747
exploding wire, elec. resistivity in fast RCL circuit 77−31995
exploding wire, plasma prod., X-ray diagnostics 78−5909
explosive compaction of metal powders 78−64501
extraction equilirbium, with versatic acid 911 79−43620
Faraday rotation in X-ray region 79−82958
fast reactor structural material, integral expts. 80−13612
fast reactor structural materials, activation, (n,p), (n,α) cross sections 80−13624
fast reactor structural materials, nuclear data 80−13611
fatigue crack propag. qualitative stereoscopic fractography obs. 79−96143
fatigue crack propagation mechanism, quantitative stereoscopic fractography study 79−74238
fatigue cracks, use of SEM in quantitative stereofractographic anal. 78−80645
FCC, electrodeposition of HCP Co layer 79−11527
FCC, H impurity self-consistent electronic screening charge density, cluster calc. 79−33255
FCC, high-angle (001) CSL twist boundaries, struct. 79−46677
FCC, polycrystalline, deformation-strain curve description using substruct. parameters *(Russian)* 79−87690
FCC, props. of vacancies and divacancies 80−10545
FCC, rolling texture development 79−87657
FCC, stacking fault, antiphase boundary energies, investig. methods, review *(French)* 79−42080
FCC(111) substrate, orientation relationship with Fe vac. deposits 80−59836
Fermi surface under press., de Haas-van Alphen effect meas. 80−75499
ferromagnet, dynamic susceptibility calc. 80−80488
ferromagnet, itinerant, spin waves, surface effects, RPA calc. 80−60226
ferromagnet, magnetic anisotropy energy, symmetrical polynomials, appl. to Ni 77−66293
ferromagnet, static and dynamic magnetoelastic coupling 77−20665
ferromagnetic, anomalous transmission of microwave power at FMR at 4.2K 79−82877
ferromagnetic, calc. hyperfine fields and their press. derivations 80−6796
ferromagnetic, chemisorption of H, spin-spin interactions, UPS spectra calc. 80−6630
ferromagnetic, critical NMR obs. near mag. transition 77−81026
ferromagnetic, de Haas-van Alphen effect, press. effects *(Russian)* 78−2413
ferromagnetic, diffusion and orientation aftereffects 80−88830
ferromagnetic, effect of pressure on electron struct. *(Russian)* 79−77987
ferromagnetic, electromagnetically excited acoustic waves at low temp. 77−77081
ferromagnetic, electron spin polarised photoemission spectrum for (111) surface 80−25525
ferromagnetic, electron-magnon interactions 78−68205
ferromagnetic, electronic struct. and hyperfine field of nonmag. impurities, calc. 80−70658
ferromagnetic, electronic struct. by real space approach 80−65432
ferromagnetic, EMF generation by pulsed laser irrad. 78−68021
ferromagnetic, exchange integral maximisation, neutron scatt. obs. and ten-fold degenerate Hubbard model comparison 80−71004
ferromagnetic, exchange splitting, angle-resolved photoemission meas. 78−43985
ferromagnetic, Fermi surface and band struct. 78−6267
ferromagnetic, Fermi surface determ. 77−11843
ferromagnetic, Hall effect, anomalous, rel. to scatt. processes 80−44572
ferromagnetic, hyperfine field and relax. time obs. of impurity heavy nuclei 80−75533
ferromagnetic, hyperfine field of positive muon 79−47378
ferromagnetic, hyperfine fields at positive muons 78−43758
ferromagnetic, hyperfine fields on ^{12}B, NMR obs., near T_c 77−28476
ferromagnetic, hyperfine mag. fields at ^{67}Ge, TDPAC meas. 78−43701
ferromagnetic, itinerant, Fermi surface and single particle excitations 80−34350
ferromagnetic, Knight shift of hyperfine field at positive muon 77−43925
ferromagnetic, phonon assisted magnon transmission at 24 GHz 79−82878
ferromagnetic, photoemission spectra and band struct., spin polarisation of bulk photoemission 79−78843
ferromagnetic, positive muons as light isotopes of H, book contrib. 79−82907
ferromagnetic, self-consistent calc. of energy bands 77−39774
ferromagnetic, struct. in nucl. spin echoes 80−60453
ferromagnetic, temp. depend. of μ^+ hyperfine field 78−43760
ferromagnetic, temp. depend. of hyperfine fields for F 80−20141
ferromagnetic antiresonance transmission at 24 GHz, temp. depend., g-factor and magnetisation 77−51959
ferromagnetic domain struct., small-angle neutron scatt. 77−66382
ferromagnetic domain struct., static neutron depolarisation meas. 79−82812
ferromagnetic film, ion plating prep., coercive force and magnetoresist. 77−12546
ferromagnetic film, surface states, surface magnetisation and electron spin polarisation 80−65648
ferromagnetic metals, spin fluctuation theory, Curie temp., mag. susceptibility 80−65937
ferromagnetic metals, ultrasound attenuation, EM generation 80−108046
ferromagnetic properties, book contrib. 80−75724
ferromagnetic reson. damping, one electron model 77−8409

nickel continued
ferromagnetic resonance, expt. data used to explain asymmetry of reson. curves *(Russian)* 79−4728
ferromagnetic resonance, linewidth, single crystal 78−2744
ferromagnetic rods, direct and inverse electromagnetic conversion 79−52569
ferromagnetic single cryst., transmission of 24 GHz radiation, effect of diffuse surface scatt. of carriers, calc. 80−34780
ferromagnetic state, energy bands, self-consistent calcs. 79−19509
ferromagnetic zero point motion effect on hyperfine field at interstitial positive muon site 80−2681
ferromagnetic-paramagnetic transition, angular resolved photoemission 78−68603
ferromagnetism, itinerant electron model, spin quantization direction fluctuations, short range order. 80−34582
ferromagnetism, Stoner model, mol. field coeff., temp. and field depends. 77−72975
ferronickel, thermoelec. determ. of Ni content 78−40096
fibres, magnetisation reversal 77−69625
fibres, porous, permeable material production 77−12580
field emitted electrons, spin polarisation 77−40337
field ion appearance spectroscopy, ion generating processes at field emitter surface 79−52086
field ion emitter, calibration using energy distrib. of free space field ionisation 77−69971
field-emitted electron spin polarisation by tunnelling through surface pot. 80−29861
field-emitted electrons, spin polarisation, theory 77−44134
filings, interrelation between dynamic and static distortions, X-ray diffr. meas. *(Russian)* 77−43305
film, 618 MHz SAW attenuation rel. to mag. field 77−40110
film, (001), electronic struct. by self-consistent numerical-basis-set LCAO discrete variational method 79−60938
film, (110), strain effects on mag. anisotropy 77−80972
film, adsorbed $H_2(CO)$, ferromag. reson. exam. 78−15028
film, adsorption of CO, effect on resist., negative p-values 77−85083
film, amorphous layer covered, target prep. for channelled ion stopping power meas. 80−63431
film, chemisorption induced mag. dead layers, ferromag. reson. obs. 79−91261
film, CO adsorption effect on galvanomagnetic and magnetic props. 78−43490
film, damping and vel. of longit. elastic waves at 9.4 GHz 80−10596
film, deform. meas. in UH vacuum system by Michelson interferometer 77−2650
film, deposited by cylindrical magnetron sputtering, internal stresses, optical reflectance and elec. resist. 77−43449
film, deposition by ion beam sputtering, composition and stress state 77−89674
film, double layer with Pt on Si substrate, silicide formation 78−84010
film, EELS, anomalous L_3/L_2 white-line ratios 80−93444
film, effect of He ion implantation on domain struct., Lorentz electron microscopy 77−20654
film, effects of finite size on crit. phenomena, resistivity anomaly 79−38192
film, electrodeposited, recrystallisation kinetics, X-ray scatt. *(Russian)* 78−60045
film, epitaxial growth on (001) diamond, TEM exam. 77−66098
film, evaporated, adsorbed acetylacetone, XPS study 80−76133
film, evaporated, chemisorpt. of CO, ellipsometric investig. *(German)* 80−61156
film, evaporated, elec. resist. and galvanomagnetic props. 80−80411
film, evaporated, for use as variable delay SAW device, magnetostrictive effects 80−71144
film, evaporated, galvanomag. and mag. props., thickness depend. 78−23181
film, evaporated, galvanomag. and mag. props. 78−23180
film, evaporated, galvanomag. props., oscill. due to CO adsorption 77−1496
film, evaporated, hydrocarbon chemisorptions, IR refl. study 79−69343
film, evaporated, interaction with BCl_3, HCl, adsorpt. 78−75945
film, evaporated, uniaxial mag. anisotropy 77−51929
film, evaporated on cold substrate, temp. depend. of elec. resist. 78−19166
film, even magneto-optical transmission effects 77−32354
film, excess (1/f) voltage noise 79−42598
film, ferromag., light scatt. from surface acoustic spin waves 79−33719
film, ferromag., magnetoresistance parameter meas. *(Spanish)* 80−2485
film, ferromag. reson., thermodynamical anal. 79−42840
film, ferromagnetic, transverse Kerr magneto-optical, effect, thickness depend. 77−59559
film, ferromagnetic (100) and (110), energy bands 79−1630
film, few atomic layers thick, transition from Pauli paramag. to band ferromag. 80−44885
film, five atomic layers, electronic band struct. using linearised APW method 79−69393
film, granular, tunnelling of spin-polarised electrons and magnetoresist., exchange effects 77−12024
film, growth on amorphous C, electronic props., UPS and XPS obs. 79−82476
film, H at. recombination coeff. calc., catalysis appl. 77−48634
film, hexagonal phase identification, electron microscopy *(Russian)* 77−15711
film, implanted with C ions, HCP struct. formation, electron diffr. study *(Russian)* 79−82469
film, inelastic electron scatt. 79−15570
film, inelastic electron scattering 78−92155
film, interaction with O_2, AES, EELS, work function, and gravimetric meas. 80−75433
film, ion beam sputtering prep., struct. and mag. props. 80−35085
film, ion bombarded, porosity 77−66099
film, kinetic electron emission when penetrated by H^+ ions with 0.3 to 30 keV energy 79−91554
film, laser CVD 79−78897
film, laser induced reactions with Si 79−70365
film, laser-induced reaction with Si, surface struct. obs. 79−19471
film, layer mode growth on Fe (001) surface, AES study 80−49540
film, linear mag. birefr. dispersion 77−69807
film, low-angle grain boundary struct. *(Russian)* 79−42807
film, mag. field depend. surface acoustic wave attenuation meas. 77−20674
nickel continued
film, mag. susceptibility correlation with SAW attenuation 79−47310
film, magnetoelastic excitations, phonon spectroscopy and forbidden transitions 79−82853
film, magnetooptic Kerr effect meas. near crit. point 77−69811
film, microstructure of charged boundary between ferromag. domains 79−69705
film, multi- and single-layer, reson. curves subjected to tangential mag. reversals *(Russian)* 80−50195
film, on (001) Ag, FCC and BCC metal-on-metal epitaxy, geometric factors, electron microscopy 78−22980
film, on Si, formation of Ni_xSi_y, effect of substrate nature 77−15703
film, phonon transport into SrF_2 substrate, diffusive scatt. at impurities 80−49487
film, polycryst., singularities of recrystallisation *(Russian)* 78−2382
film, polycrystalline, resist., conduction electrons and s-d exchange interaction 78−19021
film, precise temp. meas. using combination of Pt resistor and Au-Pt thermocouple 79−49227
film, RF sputtered on $LiNbO_3$, SAW delay variation obs. 79−56102
film, self consistent calc. of surface phenomena 79−73560
film, single cryst., domain width from ferromag. reson. 80−39879
film, solar collector coating, microstruct., FIM and SEM obs. 80−26166
film, spin polarised photoemission, surface magnetism 79−52083
film, spin wave resonance 79−33542
film, sputter deposited on Cu, induced stresses 80−24774
film, sputtered, on Si, annealing effects on transmission electron diffr. patterns, silicide form. 78−91562
film, strained and strain-free, ferromag. reson. meas. 78−95525
film, struct., oxidation, and exoelectron emission rel. to bulk samples *(Russian)* 79−37927
film, surface magnetisation, electric field effect 78−14991
film, surface magnetoplasma waves, ATR meas. 77−69639
film, surface properties and photoelectron spin polarisation 78−14782
film, temp. depend. of magneto-optical effects 77−81167
film, thickness dependence of perpendicular mag. anisotropy 77−80974
film, thickness meas., using nondestructive radioisotopic technique 80−68179
film, transition from Pauli paramagnetism to band ferromagnetism 79−61192
film, transverse Kerr magneto-optical effect enhancement by surface magnetoplasma waves 77−52056
film, ultrathin, field effect meas., influence of CO adsorption 80−11108
film, vac. deposited, hexagonal phase *(French)* 78−63944
film, vacuum deposited, ethylene adsorption and reactivity with adsorbed H, surface pot. meas. 79−86995
film, vacuum deposited on liquid-He-cooled sapphire, galvanomag. props. 79−95519
film, work function change during water adsorpt. *(German)* 79−42365
film, work function changes upon water contamination 80−44705
film (111), ferromag., energy bands and planar densities of states, LCAO calc. 79−4509
film and foil, surface IR wave propag. distance 77−28641
film and foil corrosion and water adsorption 78−7099
film characterisation technique, APFIM, time-of-flight spectroscopy 80−75138
film coating of optical fibres, magnetron sputtering, mechanical props. improvement 79−72723
film coatings for Mo tips, film characterisation by atom probe FIM atomic clusters, voids 80−33863
film crystallisation on C fibres and sapphire crystals *(Russian)* 80−75455
film deposit on (001)Fe substrate, misfit twin crystals 77−4273
film for resistor appls., props. and prep. *(Hungarian)* 77−4737
film growth on graphite and amorphous C, electronic struct. by photoemission and Auger obs. 79−77947
film on Fe foil, EM excitation of sound, Mossbauer study *(Russian)* 79−99795
film on leucosapphire, island growth on annealing in Ag vapour *(Russian)* 78−51830
film on Si, ion implanted, inert-gas-bubble form., TEM and Rutherford backscatt. anal. 79−90682
film on Si substrate, ion-beam induced silicide form. 79−46718
film on steel, type AISI 316, thermal passivation in controlled vacuum 80−76276
film on W (110), field ion microscope exam. 78−34731
film presence effect on NiSi dissoc. 79−47892
film pulse biased sputter deposited, Kr entrapment 79−28255
film thickening in aqn. soln., rel. to anion type and conc. 79−96180
films, (100), spin density by self-consistent linear APW method 80−65710
films, adhesion on graphite 80−80141
films, adsorption of ethylene, decomposition, coverage depend. meas. 80−96743
films, CO covered, adsorpt. of H, isotherms, resist., work function changes 78−75926
films, electrodeposition, current modulation, pulse freq. rel. to struct., props. *(German)* 79−11528
films, electronic struct. calc., effects of chemisorption; contact pot. and surface magnetisation 80−103734
films, evaporated, effect of CO adsorption on galvanomag. and mag. props. 79−33363
films, evaporated, effect of CO adsorption on galvanomag. and mag. props. 79−33364
films, Faraday rotation effect dispersion 80−40092
films, ferromagnetic reson., photoacoustic detection 80−80613
films, HCP and amorphous, RF sputtered, O_2 incorporation, ESCA obs. 80−10832
films, oriented, hypersound excitation at 8.9 GHz by exploiting mag. anisotropy 77−85541
films, self-supporting, electroplating method of prep. 80−66436
films, sputtered, hexagonal and amorphous, O incorporation, ESCA and electron diffr. meas. 79−11046
films on Pyrex, AES, purity 77−8755
fine particles, positron annihilation meas. 79−61461
fine particles, prep. by gas evaporation technique, crystal habit 77−52239
fine particles, prep. by vacuum evaporation, crystal habits 78−88437
fission reactor structural material, resonance data eval. below 300 keV, Doppler effect calc. 80−13618
fission reactor structural material data eval. for JENDL-1 80−13617

nickel continued
Flade potential as thermodynamically reversible pot. 79−5159
flameless atomisation, effect of interfering metals on absorption 77−90675
fluid bed electrolysis, deposition 80−55672
foil, 20 keV $^4He^+$ irrad., depth distrib. of bubbles 79−69166
foil, critical exponent β determ. by microwave transmission 77−69575
foil, crystal struct. as function of substrate temp. during deposition 80−18742
foil, direct extraction determ. of urinary ^{210}Po and ^{210}Bi 79−100707
foil, electron bombard., impurity redistrib. during third stage of annealing, residual resist. meas. 80−6434
foil, hydrogenated, surface states of chemisorbed H_2 and elec. cond. 77−69399
foil, hydrogenated, thermoelectric and Hall effects 79−65559
foil, microwave transmission, parallel RF and mag. fields 77−59462
foil, oxidation to produced NiO for elec. cond. meas. at 1000°C 78−10451
foil, phase transition to NiH_B, mag. study 78−71860
foil, polycryst., channelling micrographs using accelerators, defects investig. 77−11445
foil, push-pull straining device for h.v. electron microscope in-situ deform. 77−4875
foil, sputtering with ^{252}Cf fission products, desorbed secondary ions 78−68596
foil electrolytic perforation, surface film phase composition obs. *(Russian)* 80−61004
foil solar collector selective surface performance 79−62078
foil substrate with Ag island film, elec. props. 77−43745
foils, cyclotron beam intensity monitors 77−38578
foils, hydrogenated, thermoelec. and Hall effect 78−43364
forbidden magnon scatt., polarized neutron meas. 79−78350
force field 79−33051
forced magnetostriction at 4.2K 80−50155
fracture, 1.6 to 300K, electron fractography obs. *(Russian)* 77−90437
fracture map for Ni deformed in uniaxial tension 78−56764
fracture under influence of high power US waves *(Russian)* 79−5034
Frank loops, growth kinetics and 'preference factor' during electron irradiation 78−22723
friction props. of surface films in air and high vacuum 78−60850
frictional behaviour, effect of mechanical properties 80−55548
fusion neutron damage effects on mech. props., simulation by 16 MeV protons 78−71768
fusion reactor material, stress distrib. from He ion irrad., vol. expansion, calcs. 77−35599
galactic cosmic rays, isotopic composition, balloon meas. 78−89024
galvanic oxidation in borate buffer soln. 80−100948
galvanic plating, stressed condition effect on magnetic thickness gauge reading 78−88611
geometrically induced structure on SXAPS and Auger electron appearance potential spectra 79−38695
grain boundaries mobility, effect of impurities *(Polish)* 79−96073
grain boundary defect structure, hardening effects, TEM 80−103365
grain boundary diffusion in γ-Fe *(Japanese)* 78−18837
grain boundary diffusion in γ-Fe 79−23787
grain boundary internal friction, B solid solubility as function of grain size 80−60903
grain boundary ledge density, effect on flow stress 78−48465
grain boundary ledges, contrast phenomena identification 78−51555
grain boundary migration during recrystallisation after cold drawing 77−73289
grain boundary sliding and deformation mechanism maps 80−3128
graphitisation of pyrolytic C, activation energy and graphitisation rates 79−57010
growth direction orientation effect on impurity distrib. 78−47261
growth of single crysts. by recrystallisation 78−68626
Gruneisen parameters, low temp. 79−23694
hardness after-effect studied by anelastic relaxation 80−66570
heat capacity temp. depend. meas., internal energy and entropy, anharmonic theory calcs. *(Russian)* 80−54402
heat diffusivity and heat cond. near Curie point 77−24706
heat transfer during cooling with water *(German)* 80−23873
heavy ion irradiated, dendritic void growth 78−14386
heavy ions with energy 0.4-0.9 MeV/A, stripping by C foils, straggling, foil behaviour 78−33351
Hopkinson effect, mag. field depend. *(Russian)* 79−4657
Hubbard model, photoemission spectrum, effect of electron correlation 79−78828
HVEM obs. of irrad. damage 77−35589
hydrogen, and liquid Hg-embrittlement 80−25862
hydrogenated foil, surface states and thermo EMF 78−91674
hydrogenation rel. to fine struct. 78−59950
hyperfine field and magnetisation, press. and temp. depend. 80−6795
hyperfine field at positive muon 80−40029
hyperfine field of μ^+, calc. 77−40167
hyperfine fields for ^{12}B and ^{12}N 77−8418
hyperfine interactions on implanted ^{12}B, crit. behaviour near T_c 78−43663
immiscible picritic liquids, Ni partitioning 78−32069
implantation of He ions, TEM exam. of He gas bubble lattice 79−46726
implanted, ^{155}Tb sources produced by recoil implantation, ^{155}Gd Mossbauer transition 80−40009
impurity hyperfine fields 79−99518
Incoloy-800, creep-fatigue interaction 77−70113
interatomic electron interactions, effect of electron correl. 79−38010
interatomic pair potential, phonon spectra 80−33927
interatomic potentials from experimental phonon spectra 78−75621
interband optical conductivity, self energy correction 80−2792
intercalation compound with TaS_2, NbS_2, microstructure 77−84729
interdiffusion with Zircaloy-4 79−42320
interface with polymer, electronic struct., XPS study 80−45204
intergranular corrosion in dil. H_2SO_4 solns., S segregation effects 80−30152
intergranular precipitation after annealing, ion imaging microanalysis *(French)* 79−61594
internal fields, positive muon investigation 78−68438
internal friction, and rigidity modulus, strain amplitude-depend. *(Japanese)* 80−92606
internal friction, instantaneous, depend. on phase of torsional oscills. *(Russian)* 80−71142
internal friction near Curie temperature 78−44163
nickel continued
internal friction peak, H-induced in cold worked Ni 80−107368
internal magnetic pressure and compressibility anomalies, itinerant model 77−16034
interstitial diffusion of C in single crystals, stress distrib. changes 77−47626
interstitial site determ., μSR technique 80−71287
interstitials, displacement field calc. using discrete lattice model 77−1122
intrinsic stacking fault energy, effect on cyclic hardening 79−11638
ion+Ni target collisions, quasimol. KX-ray spectra, Doppler shift 77−19044
ion backscattering, charge states of 1.5 to 15 keV backscatt. He and Ne ions 79−4882
ion bombard., ion and photon yields, CO adsorption effect 80−89098
ion bombarded, He gas-bubble superlattice form. 80−2086
ion bombardment, energy distrib. of positive secondary ions and sputtered atoms 77−32485
ion impact desorption of atoms and molecules by low energy ion scattering 79−4883
ion implantation produced crystalline phase transitions 80−7558
ion implanted, ranges of implanted 10-30 keV D^+ 78−83858
ion implanted with Dy, annealing study by Rutherford backscatt., TEM, and total current spectroscopy 79−4343
ion irradiated, Auger electron spectra struct., possible surface diagnostic methods 79−69946
ion irradiated, cavity depth distrib. determ. technique 79−51161
ion irradiated with 20 and 500 keV $^4He^+$, depth distrib. of cavities and dislocation damage 80−107346
ion irradiated with heavy ions, defect cluster obs. 80−107341
ion irradiated with rare gas ions, in situ electron microscopy obs. of cluster creation 80−107343
ion plated onto Nb and Ta, prep., H_2 absorption and desorption rate *(Japanese)* 80−108358
ion stopping power systematics, Z_1-oscills. 79−65130
ions, beam-foil spectra from 20 to 238 MeV energy, 5 to 60 nm, lifetime meas. problems 80−9722
ions, two vacancies in K shell, 2 electron 1 photon, and hypersatellite transition probabilities 78−46294
ions in Tokamak plasmas, spectroscopy and atomic physics 80−53938
irradiated, numerical simulation of void nucleation 79−73208
irradiated with Cu and Ni ions, depth depend. damage profile 79−14857
irradiated with He^+, bubble depth distrib. meas. by TEM and blister form. mech. 78−95088
irradiation creep during 4 MeV proton bombardment 77−43256
irradiation induced creep, D bombardment, 22 MeV at 224°C 78−80597
irradiation-induced creep, mechanism for large transient strains 78−14391
irradiation-induced creep following 4 MeV H^+ bombardment 78−14390
Ising-type system, impurities, local crit. behaviour 77−48001
island film, cond. of two-layer metal systems *(Russian)* 79−51693
isothermal desorption of CO, UPS study, time-resolved approach 80−39440
isotopic composition of primary cosmic rays 79−70937
itinerant electron ferromagnet, magnetovolume effects 80−60397
itinerant electron ferromagnetism, local exchange model 77−72994
itinerant electron ferromagnetism, press. effects on mag. props. 77−66241
itinerant ferromagnet, neutron inelastic scatt. 79−7970
itinerant ferromagnet, spin-wave dispersion and linewidth 79−4668
itinerant strong ferromagnetism, effect of electron correlations 79−7962
K shell photoelectric cross section, at 74.409 keV 79−72288
K shell prod. cross section of Ti, Cr, Fe, Ni, Cu, Zn for 75 to 150 keV p and e excitation 79−47552
K-shell X-ray prod. by $^{14}N^+$ bombardment 80−91482
Kapitza resistance of interfaces with liq. ^3He and ^4He, 0.3-1.4K 77−24475
kinetic friction re-examination using modified pin and disc machine 80−55547
kinetics of C deposition from adsorbed CO on (100) surface 80−76553
Landau-Lifshitz damping, wave no. and temp. depend. 80−34779
laser, cataphoretic at. distrib. in chloride-He discharge 77−31092
laser irrad., elec. cond. recovery *(Russian)* 77−55512
laser irradiation effect, virgin and ion-implanted Ni 80−108306
lattice and force consts., pairwise atomic repulsions in cluster model 79−32939
lattice atom displacements near end of implanted μ^+ tracks 78−55890
lattice dimensions, difference between vacuum condensates and massive specimens *(Russian)* 77−31912
lattice dynamics, phonon dispersion curves, θ-T curves 78−26642
lattice images, obs. with a field emission electron microscope 79−14659
lattice isolation of impurities from hyperfine interaction and channelling results 78−43731
lattice vibrations at (111) surfaces and stacking faults 79−86974
layer, vol. composition of sharp filamentary textures, elec. cond. meas. *(German)* 78−22978
layers, fibre texture volume part determ. by quantitative X-ray diffr. *(German)* 77−48595
layers, thickness determ. by laser microprobe and flame atomic absorpt. 80−27355
LEED, phase of diffracted wave calc. 78−71647
LEED, spin polarisation effects 77−43696
light ion (H, D, He, Li) irrad., defect prod. and electronic stopping power 80−34088
light scattering from surface and bulk thermal magnons 80−45087
liquid, absorption of gaseous O_2 78−51686
liquid, contact reaction with B_4C-Ti(V)(Cr) 80−55707
liquid, coordination numbers, calc. in microinhomogeneous struct. model *(Russian)* 80−38902
liquid, crystallographic orientation relationships in coalescing sintered W spheres 80−45249
liquid, effective interionic pots. determ. from expt. data 77−47338
liquid, electrical transport 79−38040
liquid, electronic density of d-states, hard-sphere model and tight-binding approx. calc. 79−15065
liquid, electronic struct. and transport props. 80−29314
liquid, Hall effect, band struct. and exchange scatt. 80−80250
liquid, multiple scatt. calcs. of resist. 78−76039
liquid, N activity coeff. 77−72699
liquid, N solubility depend. on added elements, mechanism *(Russian)* 80−65223

nickel continued
liquid, neutron scatt. and atomic dynamics 77−55233
liquid, neutron scatt. and atomic dynamics 78−22637
liquid, neutron scattering experiments up to 1900K using sapphire container 79−63215
liquid, O_2 diffusivity, meas. by EMF method 78−14494
liquid, soft X-ray band spectra 77−52199
liquid, spreading over α-SiC single crystals 79−86962
liquid, struct. factor and isothermal compressibility 77−11462
liquid, struct. factor and radial distrib. curves, X-ray determ. *(Russian)* 77−31580
liquid, surface tension meas. with levitated metal droplets, influence of oscill. amplitude 78−51798
liquid, thermoelec. power meas. 77−35928
liquid, viscosity, up to 2100K, vibr. method 78−38866
liquid, viscosity calc. using microinhomogeneous struct. model *(Russian)* 80−15284
liquid diffusion of O_2, Ar, H_2 *(Russian)* 77−55369
localised moments, detection by electron energy loss spectra 77−69949
low temperature lattice parameter, Gruneisen parameter 77−76357
luminescence characteristics of pure surfaces acted on by flux of field emission electrons 80−100695
magmas, Ni content rel. to tholeiitic rocks 79−88318
magnetic aftereffect reactivation of single crystal by plastic deform. 79−65697
magnetic aftereffects of H isotopes, book contrib. 79−82835
magnetic anisotropy, effective const., magnetoelastic contrib. 78−14951
magnetic anisotropy, $X_{2spin\ down}$ hole pocket in Fermi surface 78−39314
magnetic anisotropy constants fitting to torque curves 79−7989
magnetic anisotropy consts., first three, ferromag. reson. determ. 77−8414
magnetic anisotropy consts., K_3 and K_1, determ. 77−4512
magnetic anisotropy energy 77−28382
magnetic densities, spin and orbital contrib., neutron diffr. meas. 79−78316
magnetic domain structure, neutron small-angle scatt. from dynamical theory of diffr. 79−24189
magnetic domain structure of single crystal 79−65695
magnetic domain walls, oblique, obs. by X-ray topography 78−6540
magnetic domain walls in Czochralski-grown single cryst., X-ray topography 77−20630
magnetic domains, μ^*-tensor method, temp. and surface orientation depend. 77−16098
magnetic domains, Czochralski grown single cryst., X-ray topography 77−12147
magnetic excitations, variation of de Haas-van Alphen frequency 79−8019
magnetic ground state props., simple one-electron theory 77−63063
magnetic hyperfine field at ^{140}Ce, TDPAC meas. 79−11363
magnetic hyperfine fields of Zr, DPAD meas. 80−39901
magnetic impurity in β'-NiAl, self consistent embedded cluster model 80−2549
magnetic internal friction peak bifurcation in rot. mag. field *(Russian)* 78−39380
magnetic layer, domain struct., neutron depolarisation study 79−47299
magnetic neutron scattering by dislocations, temp. depend. 80−103820
magnetic permeability, effect of ion implantation 77−28414
magnetic permeability, reversible, deform. and ion implantation effects 77−48013
magnetic properties of single-domain powders after plastic deform. *(Russian)* 78−6554
magnetic reversals, US induced stroboscopic electron microscope obs. 77−48026
magnetic surface anisotropy 77−1553
magnetic surface anisotropy of transition metals, model calc. 80−34625
magnetic surface states, photoelectron spectra, surface Brillouin zones 80−6928
magnetic susceptibility, generalised, neutron scatt. meas. 80−34606
magnetically ordered state, softening with varying mag. field *(Russian)* 78−35017
magnetisation, hydrostatic press. effect, Procopiu effect and hysteresis meas. 77−48023
magnetisation, spin wave and Stoner contribs. 77−73017
magnetisation and relative vol. temp. depend. near Curie point *(Russian)* 78−14962
magnetisation curves in high mag. fields above Curie point 77−66386
magnetisation in high mag. field, Arrott-Noakes plot 80−54919
magnetisation in pulsed field up to 320 kOe, 283 to 693K, band theory *(Russian)* 77−80920
magnetisation measurements by rotating sample magnetometry 77−69514
magnetisation process in high mag. fields in crit. region 77−85498
magnetisation temp. depend. exam. using ^{61}Ni NMR 77−73089
magnetised mono- and polycryst., activation vol. var. during low temp. deform. *(Russian)* 78−3178
magnetised to saturation, props., positive-muon study 78−6619
magneto-optic Kerr effect at (100) platelet surface 78−15151
magneto-optical Kerr effect spectra in UV region using synchrotron radiation 77−52127
magneto-optical near UV reflection-spectra, meridional and polar intensity effects *(Russian)* 78−39572
magneto-volume effects calc., rel. to itinerant electron model 78−43621
magnetocrystalline anisotropy consts., determ. from magnetisation perpendicular to applied field 78−68219
magnetocrystalline anisotropy energy, temp. and magnetisation depend. 78−6525
magnetocrystalline anisotropy energy in (100) plane, 13.8 to 258K 77−63171
magnetoelastic contribs. to US vel., elastic consts., and susceptibility 80−75829
magnetoelastic effect on longitudinal compression, weak field spin rotation model 79−82851
magnetoelastic effects, ΔE-effect and macroeddy current damping, internal friction meas. 78−64253
magnetoelastic excitations and ferromagnetic resonance 79−82879
magnetoplastic effect and eddy current heating *(Russian)* 77−43858
magnetostriction, lattice parameter changes, direct X-ray obs. 78−15001
magnetostriction and rolling texture, effect of alloying additions *(Russian)* 77−32229
magnetostriction and texture, effects of rolling, oxidation and alloying 77−36671
nickel continued
magnetostriction constant, effects of compression 77−40109
magnetostrictive vibr. obs. by laser interferometric technique 80−66000
magnetostrictive vibration meas., appl. of laser interferometric technique 80−37059
magnon relaxation, spin-orbit interaction, itinerant electron ferromagnets 80−11179
mass transfer parameters, lattice defect effects under laser pulse action *(Ukrainian)* 80−6537
mean excitation energies from α-particle stopping power meas. 79−13615
mean excitation energy based alpha particle stopping power meas. 78−30678
Medicus matrix cathode, surface characts. 80−66378
melt, diffusion of N_2 *(Russian)* 78−18812
melt, struct. charact. time depend. in X-ray studies *(Russian)* 80−24350
metal cluster, adsorption of CO, mol. orbital calc. 78−18895
metallic coated, produced by electrospark alloying, corrosion behaviour in Cl saturated NaCl solns. *(Russian)* 79−39026
metallic particles, stability and electronic struct. *(French)* 80−80155
metallised coating on polyethylene terephthalate film, fracture under laser irrad. *(Russian)* 80−76333
microcrack propagation and plastic strain 80−81187
microcrystals, H_2 chemisorption effect on superparamagnetic relax. time, Mossbauer meas. 79−61284
microparticle, 38 at truncated octahedron, electronic spectrum fluctuations 79−19501
microscopic elastic limit, effect of preliminary plastic strain *(Russian)* 77−76485
microstructure inhomogeneities, cold neutron small angle elastic scatt. 77−84736
microvoid form., gaseous impurity atom effects, positron annihilation study 80−49275
modulus defect due to internal strain 78−76286
molten, contact reaction with graphite 80−15342
molten, mag. small-angle scatt., persistent spin fluctuations 79−11288
molten, migration into WC-Ni hard alloys sintered, with uneven binder metal distrib. 78−35336
molten, near-order struct., X-ray scatt. meas. 77−55231
monolayer and submonolayer films, on ZnO, UPS study 80−7472
multilayer Ni deposits, simultaneous thickness and electrochemical potential determination for individual layers 80−71813
multiple scattering, relativistic cross section for double scatt. 79−69898
multiple wavelength neutron powder diffr. data, Rietveld profile refinement algorithm 80−24320
muon$^+$ rotation meas., local hyperfine field temp. depend. 77−63349
muon$^+$ spin rotation, hyperfine field determ., 0.12 to 300K 77−24775
muon$^-$ relaxation in paramagnetic metal 77−24776
muon hyperfine field, cluster calc. 79−56661
muon probe expts. 77−63351
muon spin rotation; freqs., and relax. rates 80−55006
n=2-2 transitions in XUV spectra, anal. 80−102472
neutron and heavy ion damage correlation, dose rate and He injection effects 79−7629
neutron depolarisation near Curie point *(German)* 78−14934
neutron irradiated, microstruct. and tensile props. 80−34077
neutron irradiated, slip bands, TEM and SEM obs. 78−51596
neutron irradiated, void formation, C interstitial effects 77−76471
neutron irradiated, void swelling, role of divacancies, calcs. 79−99236
neutron irradiation, low temp. recovery, effect of plastic deform. 78−51588
neutron transmission depolarisation by single crystal near T_c 79−33479
neutron yield calcs., electron beam incidence 78−95622
Ni powder 2JJ, porous, effect of sintering conditions in struct. and strength 80−20823
nickeliferous limonites, pressure leaching for Ni extraction, using H_2SO_4 78−39717
NMR study of metal precipitated onto a cathode *(Russian)* 80−93185
nuclear material, neutron capture cross sections in intermed. energy region, method and exptl. facility 78−21637
nuclear spin relaxation and Knight shift of ^{61}Ni in paramag. solid and liq. phases 78−76327
optical absorption in near IR 79−38539
optical components, electroless Ni coated Be, comparison with glass 80−69473
optical constants, 5461 and 6328 Å, nearly ideal surface 77−36192
optical constants, influence of temp. and relation to bandstruct. 80−25403
optical constants 12 to 24 μm, anomalous skin effect region 77−20842
optical constants at high temp. 79−24281
optical elements, US cleaning, deleterious effects 77−42631
optical spectrum, anomalous temp. depend. around T_c, band struct. 80−40128
order-disorder transitions on (111) surface, LEED observation 78−47668
oriented bicrystal, sintering prod. technique 80−108371
oxidation, (100) face, O-Ni system vibrs. rel to struct. 77−66089
oxidation, chemisorption and oxide nucleation stages, low-energy SIMS and AES obs. 79−43083
oxidation, combination anal. using ESCA, AES and SIMS 78−72924
oxidation, diffusion enthalpy and entropy 78−7084
oxidation, electron beam influence, disappearance potential spectroscopy obs. 77−1766
oxidation, high temp., effect of C on cavity form., SEM study 80−97638
oxidation, reflectance IR study rel. to component of stainless steel 79−47811
oxidation, role of grain growth 77−81337
oxidation, staged flow of O_2 interaction process, secondary ion emission obs. 78−11386
oxidation at Curie temp. 79−29279
oxidation in air, 50-150°C, film growth obs. using AES and contact resist. 80−3242
oxidation kinetics, influence of intermediate annealing treatment 80−89412
oxidation kinetics near Curie temperature 78−88578
oxidation mechanism in composite atmos. *(Polish)* 79−79142
oxidation of (110) and (111) surfaces at room temp., combined SIMS-AES/LEEDS exam. 79−20241
oxidation of (110) surface, initial stage kinetics, RHEED and X-ray emission 78−15588
oxidation rate transition, at Curie temp. 78−27685

nickel continued
oxidation study by X-ray photoelectron spectroscopy 79−61787
oxidation transport processes using tracers in growing NiO scales 80−25913
oxide covered, tensile deform. in high vac., particle and photon emission 78−39672
oxide dispersion strengthened, creep and tensile props. 77−86042
oxide dispersion strengthened materials, effect of prior creep at 1365K on room temp. tensile props. 78−39857
oxide film form. by electropolishing or anodising, open circuit breakdown 77−90495
oxide films, metal and O_2 transport, AES and inert marker, techniques 80−97641
oxide scale, high temp., metallographic obs. of inner layer 80−3240
oxide surface layer, TOF atom probe anal. 78−64766
oxidised surface, adsorbed amines and hydrazines identification by surface ionis. 77−21456
oxidised surface, oxidising conditions effect on thermally stimulated exoelectron emission *(Japanese)* 80−89127
N.Pacific, trace metal vertical profiles 80−67381
pack aluminisation process kinetics 77−32718
pair potentials calc., appl. to point defect props. 80−19798
pallasite meteorites, olivine ion microprobe anal. for Ni 79−58304
paramagnetic, μ^- relax. 77−24776
paramagnetic, Fe and Co impurity effects on susceptibility, Faraday obs. *(Russian)* 80−88731
paramagnetic, mag. form factors in Stoner-like model 80−97061
paramagnetic, model calc. of dynamical spin susceptibility 77−69489
paramagnetic, muon spin rot. Knight shift, 637 to 906K 80−75908
paramagnetic, temp. depend. of spin susceptibility 79−4651
paramagnetic state, itinerant electron model 80−65769
particle formation by evap., electron microscopy obs. of interaction processes 80−104053
particles, vibrations associated with twins 80−100253
partitioning between forsterite and aluminous silicate melts, pressure depend. 79−44176
partitioning between magma and cryst. phases of komatiitic lavas 77−49061
partitioning between olivine and silicate melt, comments 79−88319
partitioning eqns. for basalt crystallisation temp. determ. 79−88343
passivation, film form., stability and breakdown 78−19937
passive film, XPS study 79−100469
passive surface, anodic process kinetics 79−15861
permeability, of D thermal ats., anomalously high transmission, 20 to 520°C *(Russian)* 77−72752
permeability and diffusivity of hydrogen *(Japanese)* 78−66345
permeability of H, pressure and sample thickness depend. *(Japanese)* 78−51740
permeation of H, D and T 79−77823
β-phase form., H enriched, at surface and grain boundaries during H_2 absorption *(Russian)* 78−31410
phase layer growth during aluminide coating 78−27682
phase transformations and vacancy form. by positron annihilation 80−2155
phonon density of states determ. from thermodynamic functions 80−96616
phonon dispersion, model pseudopotential approach 77−11646
phonon dispersion relations, 5-parameter model calc. 78−75748
phonon dispersion relations and Debye-Waller factor calcs. 78−51630
phonon generation and attenuation at FMR 80−39875
phosphate glass: Ni, absorption spectra, mag. props., coordination behaviour *(German)* 80−40147
photoacoustic effect from thermally thin solid 80−75304
photoelectric cross sections at 52.4, 60, 72.2 and 84.4 keV 80−69187
photoelectric effect in paramag. and ferromag. states, Auger spectra 78−95649
photoelectron spectra, threshold Auger emission 80−29849
photoelectron spectra of (100) surface, pure and S-covered *(French)* 77−36360
photoelectron spectroscopy, one-electron energy investig. 80−55263
photoelectron spin polarisation 77−32501
photoemission, angle-resolved, from clean surface 78−15294
photoemission, d-band, resonance enhancement by coupling to 3p excitation 80−20766
photoemission, exchange-split energy-band dispersions 80−35059
photoemission, spin polarisation of reson. two-hole bound state 79−83099
photoemission from chemisorbed c(2×2)O, c(2×2)S and CO on Ni (100) 77−32502
photoemission near Curie temp. 79−78841
photoemission spectra, core-level satellite struct. 80−29855
photoemission spectra, valence band and core level satellite due to excitation of d electron 80−97408
photoemission spectra of d-band, bound hole pairs 79−47590
photon emission due to Ar^+ ion bombard., adsorbed and recoil-implanted O effect 80−80872
photoneutron yields released by incident electrons, improved calc. 80−27630
pigmented anodic Al_2O_3, for selective absorpt. of solar energy, optical and struct. props. 80−55892
pinned domain wall motion, magnetic damping studies 80−65956
plane shock wave loading, microdistortion X-ray anal. *(Russian)* 77−52399
plasma, Tokamak-produced, $2s^22p^k$-$2s2p^{k+1}$ transitions in F I to Be I isoelectronic sequences 80−37765
plasma, X-ray transport 79−64837
plasma arc srapying, chem. reaction with plasma gases 80−66427
plasma frequency, temp. depend. 78−56100
plasma impurity, flux on wall of DITE Tokamak 80−28688
plasma oscillations, Fermi level position effect on excitation energies for band transitions 79−99493
plasma sprayed coating, effect of Si substrate surface conditions and impact velocity of sprayed particles 80−21145
plastic deform., accelerated, evolution of H_2 77−36594
plastic deform. build-up during low cycle fatigue *(Russian)* 77−25207
plastic deformation, cyclically deformed, HVEM in-situ study 80−103339
plastic deformation, effect on H transport rates 80−21044
plastically deformed, dislocation struct., mag. small angle scatt. of neutrons *(German)* 78−22730
plastically deformed, positron trapping rate, temp. depend. 80−71507
nickel continued
plastically deformed, recovery stages III and IV investig. by positron annihilation 77−31715
plastically deformed, volume fraction of recrystallised material determ. from positron annihilation 77−1760
plastically deformed at room temp., glide on {001} planes, TEM obs. 79−19257
plasticity, athermal and thermal *(Russian)* 79−11685
plated aspheric metal mirror fabrication for IR optical systems 80−14497
plated Fe single crystal, deformed at 77K, surface obs. 78−19916
plated film, magnetisation and mag. interface anisotropy 77−85510
plated Nb(Ta), H absorption rate, metallic film effect 80−49525
plated WC powder, detonation spray deposited hard alloy coating, electrical conductivity 77−12025
platelet, transmission reson. meas. 77−20710
plates, thin, helicon-Doppleron effect on spin wave propag. 77−66394
plating, electroless, of Fe powder 80−61026
plating C steel nails, barrel plating efficiency 80−100964
plating on Fe, surface film softening in single slip orientation 77−32719
plating surface props. of Ni after each step of activation process 78−95243
PLEED results for W (100) using appl. of GaAs spin-polarized electron source 80−69000
point contacts between ferromag. metals, singularities depend. in d^2V/dI^2, phonon spectra 79−60457
point defect estimation from specific heat and volume in plastically deformed pure metals *(Russian)* 80−54223
point defect-dislocation loop interaction, effect on dislocation loop growth kinetics 78−47415
point defects and planar defects, computer simulation 78−43013
polarisation-dependent angle-resolved photoemission for band structure studies 78−95678
polarised, ferromag., evidence for K-shell polarisation of ^{12}C ions via mol. orbital promotion 80−71273
polarised, precession meas. on nucl. excited C-, O- and F-ions recoiling 78−37285
polishing for optical appl. 78−5587
polycrystal, mech. behaviour in microplastic strain region *(Russian)* 78−39838
polycrystalline, magnetoresistance anisotropy, planar Hall effect 79−23947
polycrystalline, strain hardening, dislocation link length model 80−84953
polycrystalline foil, deposition of columnar and laminar forms of C 78−63943
polycrystalline foils, methanation reaction, kinetic information 78−73081
polygonisation, high press. grain growth, dislocation, electron microscopic obs. 77−16613
porosity, effect of 2 MeV Xe^+ ion irradiation on pore distribution and size 79−71898
porosity depth distrib. of annealed samples following bombardment by 1 MeV Ar^+ ions 80−5333
porous, internal friction and effective elasticity modulus, temp. depend. *(Russian)* 79−29118
porous layer, on Cu surface, accel. heat transfer, to boiling n-octane 77−85056
positive muon diffusion, press. depend 80−75907
positive muon spin precession, effect of press. 80−40030
positron annihilation, Doppler broadened lineshapes, prevacancy lattice expansion 78−27349
positron annihilation ang. correl., trapping by mono- and multi-vacancies 77−32466
positron capture by dislocations, vacancies, rel. to temp. *(German)* 78−30606
positron lifetime meas., 4.2 to 1700K, monovacancy form. enthalpy 80−97370
positron trapping, defect specific temp. depend. 78−47336
positron trapping, temp. depend., vacancy form. energy 77−90215
positron trapping by vacancies using ^{19}Ne source 78−47341
positronium form. in two-photon positron annihilation 79−61462
powder, atomisation of melt, charact. of metal powder 78−19688
powder, correlation between specific surface area and technological props. 78−64503
powder, hot pressing on steel substrate, densification kinetics 80−40290
powder, light scatt., close particle packing 78−1161
powder, magnetic resistance changes 77−1411
powder, nonspherical, mean pore size of sheet material 77−28757
powder, porous, relationships between mech., physical, and microstructural characts. 80−20846
powder, positron annihilation, interaction with defects in grain and pores *(Russian)* 77−16520
powder, recrystallisation, effect of sintering atmosphere 77−12573
powder, resist.-sintability *(Japanese)* 80−16228
powder, sintered, use of extruded porous materials as fuel cell electrodes 80−40853
powder, spark erosion prep. 78−27452
powder, subjected to vibratory milling, exam. of plastic deformation, recrystallisation, sintering 80−16234
powder charact. effects on sintering 77−1828
powders, prep. of spherical starting particles, for suspension electrolysis 78−60689
precipitated in decomposing β-NiH, Bitter powder pattern 79−28104
precipitates, isothermal annealing influence on structural state, X-ray diffr. anal. *(Russian)* 80−100849
preoxidised, reaction with SO_2 at high temp. 79−39047
production from reduction of $(Ni_{1-x}Mg_x)_2SiO_2$ *(Russian)* 78−44043
protective coating on Al powder *(Russian)* 78−60881
proton energy straggling 79−77652
proton stopping power meas. at 100 keV, using ion induced X-ray emission 78−48725
proton-induced L-shell ionisation cross-sections 80−100707
pseudodiffusion of Ni in single crystal Si during RF sputtering 78−2396
pure, anomalous grain growth 80−20984
pure, reaction with sintered Li_2O pellets 79−39137
pure, X-ray study of occluded H_2 77−16586
pure and doped, mech., mag. relax. meas. dumb-bell self-interstitial reorientation *(German)* 78−52879
push-pull fatigued polycrystals, point defects, elec. excess resist. meas. 80−100910
quadrupole interaction of vacancy associated with Te impurity, β-γ TDPAC meas. 78−43730

nickel continued
quasi-particle energies, two-hole XPS satellite 80−66399
quasiatomic, resonant photoemission at 3p-core threshold, in Ni phthalocyanine 79−78847
quasiatomic excitation, causing energy loss peak, UPS 78−72691
quenched vacancies, effect of oxidation *(French)* 78−27686
quenching experiments 78−48432
radiation damage and diffusion 80−24645
radiation damage due to protons, μSR 79−56702
radiation damage from 16 MeV protons, effect on microstruct. and mech. props. 79−46721
radiation hardening and yield strength correlations for 16 MeV H^+ and (D,T) neutron effects 78−14389
radiation-induced swelling in BOR-60 reactor 79−97814
Raney Ni surface, chemisorbed benzene struct., neutron inelastic spectroscopy study 80−101038
Raney nickel, use as hydrogen electrode *(French)* 78−27766
range and range straggling of heavy radioactive ions 78−22776
range distributions for 25-200 keV $^{14}N^+$ ions 80−103405
range of $^{27}Al^+$ ions, meas. by (p,γ) reson. broadening 79−46729
range of Ni^+ ions in Cu, increase due to ion bombardment induced crystalline reorientation 78−26611
rapid melting and solidification of surface layer, exam. using computer heat flow model 78−83228
reaction kinetics of liquid with B_4C 80−84344
reactor structural material transmission meas. using TOF spectrometer 80−18440
recovery from nickeliferous pyrrhotite, by thermal upgrading 77−60034
recovery of single crystal after varying amounts of cold work 79−100162
recrystallisation kinetics, high press. effects *(Russian)* 77−48453
rectilinear screw dislocation, magnetisation distrib., mag. moment anal. 80−44897
recycling, effect on comp. 80−66455
reflection of H, D and He ions 78−95640
reinforced with W fibres, fabrication, heat treatment, and mag. and mech. props. 77−40408
resistivity, thermal and elec., spin disorder scatt. anal. 78−76063
resonant photoemission exam. 78−27371
roadside soil and plants in Alexandria district, Egypt, contamination with Cd, Ni, Pb and Zn 78−81171
rod, polycryst., demagnetising factor of polycryst. rod 77−73046
rod, spontaneous vibr. modes excited by reversible magnetostriction 79−56587
rolled, annealing texture *(Russian)* 77−21159
rolled, dislocation struct. and recovery during annealing *(Russian)* 79−29084
rolling texture, athermal softening *(Russian)* 77−66655
rolling texture development, dependent on relative stacking fault energy 79−52237
rotating cylinder electrodes, mass transfer investigation 79−43589
rubbing of cast Fe, surface temperature effect on dry sliding wear 80−60983
Saguenay fjord sediments, distrib. and partition of Co, Ni, Cr and V 77−33100
SAW attenuation coeffs. and wave speeds 79−46903
scattering and radiation damage for 14 MeV neutrons and 10 to 20 MeV protons 77−15458
seawater, predominance-area diags. and equilib. ratios for Co and Ni inorganic forms 78−3819
secondary electron emission, effect of ion implantation with K^+ and Ba^+ ions 79−91544
secondary electron emission coeffs. for multiply charged ion bombard. 78−11051
secondary electron emission under Ar^+ ion bombard. near Curie point 80−29838
secondary ion emission, energy spectra, 0-55 eV, contamination levels 79−15573
secondary negative ion emission, effect of adsorbed O_2 *(Russian)* 79−28881
self implantation damaged, crit. behaviour, perturbed ang. distrib. meas. anal. 80−60476
self interstitial migration and crowdion conversion, dislocation pinning expts. 77−84762
self ion bombardment, dislocation loop growth and void swelling 78−6110
self-diffusion, expt., 813-1193K 77−15618
self-diffusion and vol. diffusion coeffs. of Co and W, 1050 to 1400°C *(Russian)* 79−28147
self-diffusion in NiO, 700-1400°C, rel. to oxidation mechanism 78−27681
self-ion irradiated, defect clusters, annealing 78−18687
self-ion irradiated, He effect on void form. 78−6112
self-sputtering yields, low energy 78−56553
sheared crystal, magnetocrystalline anisotropy torque meas. 78−24830
sheet, surface, adsorbed ^3H, ethylene-^{14}C determ., autoradiography method 77−63989
shock hardening, anomalous residual, at short pulse duration 80−20942
shock loaded, work hardening and press. depend. of dislocation arrangement and density 78−48429
shock loaded, work softening 78−27537
shock loading parameter effect on substruct. and mech. props. 79−52360
shock-loaded, residual strengthening, effect of grain size, dislocation cell size and deform. twin spacing 79−91744
simultaneous sulfidation-oxidation at 603°C in Ar-SO_2 atmospheres 79−8389
single crystal, compressed, strengthening and dislocation cells *(German)* 80−66536
single crystal, preferred growth direction in floating zone method 80−25555
single crystal, stretched, electron microscope exam. of deformation cell structure during polygonization *(German)* 80−7651
single phase FCC, cyclic deform. long range stress changes 80−54308
single-crystal films, spin wave reson. spectra 79−11350
single-domain particles, LF mag. susceptibility, 2K up to Curie point 80−29582
sintered, pressed, plasticity as function of porosity *(Russian)* 80−75290
sintered carbonyl type and with dispersed ZrO_2 inclusions, struct. effect on high-temp. ductility 77−63757
sintered permeable materials with bidisperse structure, pore-forming additions effect 80−84885
sintering, isothermal, surface area reduction 77−8779
nickel continued
sintering kinetics, metallographic study 80−93519
sliding charact., friction and wear *(Japanese)* 78−56778
slip band theory, model for creep based on dislocation climb at grain boundaries, comparison with expt. data 79−37756
slip character, H effect 80−89287
small clusters, local densities of states 80−88466
softening of strained single crystals *(Russian)* 80−40499
solar selective black coatings, electrochem. deposition on Zn surfaces 80−29885
solid, Kα hypersatellite spectrum, double K ionis. 77−18829
solidified from supercooled condition, Si conc. influence on struct. *(Russian)* 77−16567
solubility in liq. Li, impurity effects of O_2, N_2 and C 79−77760
solubility of C *(Czech)* 79−77757
solubility of H_2, 500 to 1000°C *(Japanese)* 78−38845
solutions, conc. changes, proton induced X-ray emission obs. 77−25325
sound attenuation anomaly near mag. transition temp. 78−15004
specific heat, 0-100 kbar, press. depend. 77−51512
specific heat, temp. depend. *(Russian)* 78−56341
specific heat of high purity single cryst. near crit. temp. 78−64212
specific heat rounding near mag. crit. temp. 79−95595
spheres in glass matrix, brittle composites, fracture 79−66141
spin polarised electron emission, review 77−73215
spin polarised low energy electron scatt., elastic and magnon-inelastic 78−34970
spin polarised tunnelling expts. 78−39372
spin-elastic wave three freq. interactions, parameters, excited wave amplitudes *(Russian)* 79−91276
spin-wave exchange stiffness const. 77−4510
splat quenched, gaseous impurities effect on struct. 77−4042
spontaneous magnetisation, temp. depend. 77−63141
spontaneous magnetisation data up to 0.98 T_c, reanalysis 78−47959
spontaneous magnetostriction determ. method, molecular field theory study *(Russian)* 80−50157
spreading kinetics of Al 80−24717
sputter deposit, thick, microstruct., tensile props. 77−40461
sputtered, ionisation probability, energy dependence 80−35041
sputtered coating microstructure on mechanically activated cathode *(Russian)* 79−91586
sputtering by low energy H^+, Rutherford backscattering technique 80−40198
sputtering in inert atm., with uncooled cathode, oxidation of metallic coatings, X-ray diffr. obs. 78−3041
sputtering of adsorbed layers 77−36335
sputtering rate on Ar ion bombard. 80−55245
sputtering yield as function of incident ion masss 79−74042
sputtering yields, ang. distrib. and differential, for low-energy light-ion irrad. 80−71527
sputtering yields for light ions 79−87537
stability under various stresses of perfect Ni crystal 80−104208
stacking fault energy, by electron microscope obs. of dissoc. edge dislocations and faulted dipoles 77−72627
stacking fault energy and delamination wear, single phase FCC 78−3239
stacking fault energy eval. from twinning stress of Ni-Ge (1 to 9 at.%) *(Japanese)* 78−59820
static strain ageing, 373 to 473K 77−36558
steel, maraging, 0Kh6N8M7S, effect of Cr, Ni and Mo on hardness 80−21093
steel, mild, conc. profile of implanted Ni and Cr 77−81339
steel, residual stress determ. by X-ray integration *(German)* 79−52551
steel/Ni, roll bonded clad plate, fatigue crack growth *(Japanese)* 79−61706
stepped surface, morphology exam. by LEED and AES 78−71913
stepped surface, secondary electron emission, diffraction features 79−83068
stopping of 3-7 MeV α-particles and 4-6 MeV protons *(Russian)* 79−51181
stopping power for 0.3-1.5 MeV protons 79−55801
stopping power for 28 MeV α-particles, re-evaluation 78−79651
stopping power for ^{107}Ag, ^{109}Ag and ^{150}Sm 80−70284
stopping power meas. for 4-5 MeV/N ^{16}O, ^{40}Ar, ^{65}Cu, and ^{84}Kr 78−70720
stopping power meas. of 0.3 to 2.6 MeV ^4He ions 79−3329
stopping power of 0.5-2.0 MeV ^4He ions, elastic backscatt. meas. 78−87730
stopping powers, low energy, determ. by TOF techniques 79−45594
stopping powers, projectile range for Z=8-20, 0.0125-12.0 MeV/nucleon 78−83856
stopping powers for 28.8 MeV α-particles 77−80556
stopping powers for 8.78 MeV α-particles 77−80557
strain tempering by rapid heating and cooling of cold drawn wires *(Japanese)* 78−84863
stray mag. fields above stripe domains, electron microscope and μ^*-tensor determ. 80−71089
strength differential effect, temp. and strain rate sensitivity in saturation cycling 79−66094
stress corrosion susceptibility, S segregation effect, Auger spectrosc. study 80−61019
stress induced cross-over effect near Curie point *(German)* 80−103873
stress induced crossover effect near Curie point *(German)* 80−103874
stress relaxation, in-reactor study at low temps. 80−93588
structural changes, creep mechanism, multiple dislocation cross slip *(Russian)* 80−59476
structural singularities of plastic deform. at localised flow stage, TEM obs. *(Russian)* 78−6968
structure factor at 1873K 79−77490
substrate, interface with Cr film prep. by evap. and ion plating, AES determ. of comp. profiles 77−89675
substrate, kinetics, Ni_2Al_3 layers growth by cementation *(French)* 80−35127
substrate, Sn autocatalytic deposition 80−100965
substrate for C deposition, surface effects 77−28721
substrate for polystyrene film, electrode effect on carrier injection, TSC, I-V characts. 80−34463
substrate for solar selective surfaces, graphite coating props. 78−74952
sulphidation in H_2S-H_2 mixtures, 450-600°C 78−3257
sulphidation kinetics, in H_2S-H_2 550 to 600°C mixture 78−64780
sulphidation of single crystal, Ni_3S_2 initial growth, electron microscope obs. *(Japanese)* 77−52670
supercooled, struct. refinement mech. *(Russian)* 80−20975

nickel continued
surface, {100} and {100} with O overlayer, crystallographic effects in low energy ion scatt., local ion-atom neutralisation 80−84377
surface, (001), adsorbed c(2×2)CO layer, struct. 80−88428
surface, (001), Ar ion bombarded, enhancement of oxidation, AES study 80−97644
surface, (001), c(2×2) Se overlayer, angular resolved UPS 78−76584
surface, (001), chemisorbed O_2, electronic struct. and overlayer struct. theory 79−28391
surface, (001), chemisorption bonding c(2×2)O, self-consistent electronic struct. 79−78146
surface, (001), H_2 dissociative adsorption, calc. 80−101036
surface, (001), initial oxidation, RHEED and X-ray emission meas. 77−31885
surface, (001), intensity profiles, barrier reson. features, LEED 78−64089
surface, (001), p(2×2) and c(2×2) O superstructure, angle resolved photoemission from adsorbate 78−23585
surface, (001), reaction of CO and H_2, extended muffin-tin orbital theory 80−76557
surface, (001), spin polarised photoemission theory 79−15584
surface, (001) and (001)c(2×2)S adsorbed, electronic surface resonances by LEED 79−24051
surface, (100), (111) clean and H_2S S-adsorbed, ang. distrib. of Auger electron emission *(Japanese)* 78−43963
surface, (100), adsorbed Na, photoelectron diffr. aximuthal patterns, struct. sensitivity 80−107644
surface, (100), adsorption of H_2, LEED, work function meas. and thermal desorpt. obs. 79−23843
surface, (100), adsorption of Xe, UPS obs. 79−33897
surface, (100), bonded Se, electronic orbitals 78−72224
surface, (100), c(2×2) O overlayer, angle-resolved photoemission study 79−33903
surface, (100), catalysis of CO+H_2, reaction rate, AES and UPS obs. 79−79290
surface, (100), chalcogen adsorption, UPS study 80−6648
surface, (100), chemisorption of O_2, SIMS and XPS 79−15019
surface, (100), clean and gas-covered, electron energy loss spectra 79−47570
surface, (100), CO ordered overlayers, angle resolved, UV photoemission 78−56570
surface, (100), core levels in adsorbed Cs, electron binding energies 78−18896
surface, (100), electronic struct. of c(2×2) and p(2×2) O overlayers 79−47144
surface, (100), model, bonding of S 78−56027
surface, (100), reson. behaviour of interband excitations in photoelectron spectra 80−104043
surface, (100), Se overlayers, normal photoelectron diffr. of Se 3d level 79−11501
surface, (100), secondary electron spectra, adsorbed elements effects 80−50480
surface, (100) and (110), effect of depassivation on state of activation 79−61777
surface, (100) and (110), S saturated, UPS 77−32500
surface, (100) and (111), overlayer covered systems, angle-resolved UPS, substrate effects 78−84694
surface, (110), adsorbed H, adatom configuration, He diffr. study 80−103569
surface, (110), adsorption and decomp. of formic acid, modulated mol. beam scatt. anal. 79−89032
surface, (110), Ar^+ refl. at grazing angles, computer simulation 79−87549
surface, (110), effect of surface O on catalytic and chemisorptive behaviour, ligand effects and oxide states 77−85066
surface, (110), ferromag., surface magnetisation, polarised LEED expt. 80−97118
surface, (110), graphitic monolayer, oxidation mechanism 80−101037
surface, (110), ion impact desorption of O_2 by ion scatt. 77−35805
surface, (110), kinetics of surface C oxidation, AES meas. 79−79291
surface, (110), mag. exchange splitting of electronic surface states 80−88610
surface, (110), methane interaction kinetics, AES-LEED-ellipsometry 77−62756
surface, (110), O_2 adsorption, LEED and ion scatt. study 80−84386
surface, (110), polarised LEED study of magnetism 80−71102
surface, (110), positive spin polarisation in field emission and demagnetisation by H_2 adsorption 78−52646
surface, (110), S adsorbed layer struct. from anal. of LEED pattern 79−73407
surface, (110), theory of ion scatt. 80−7458
surface, (110)(2×1)C, kinetics of D_2 desorption, LEED and AES meas. 77−47683
surface, (110) and (111), two-photon photoemission 80−76150
surface, (110) clean, low energy ion scatt. 80−104026
surface, (111), ^{57}Co vacuum deposited, Mossbauer effect emission 79−80735
surface, (111), adsorption of H_2 at low temps., LEED meas. 78−56045
surface, (111), adsorption sites of CO, LEED, AES, thermal desorption, work function, and IR system meas. 79−77903
surface, (111), C monolayer phase condensation, LEED and AES obs. 79−46960
surface, (111), chemisorbed CO, bond energies 80−100398
surface, (111), chemisorption of H, geometry, order and disorder 79−65311
surface, (111), clean and with CO absorbed layer, angle-resolved photoemission meas. 77−16463
surface, (111), CO, CO_2 carburisation, AES meas., electron beam-induced effects 77−48588
surface, (111), coadsorption of CO and H_2, surface carbide influence, vibr. electron energy loss obs. 79−52772
surface, (111), proposed struct. of adsorbed H, order-disorder transition 79−60628
surface, (111), pyrazine physisorbed, UV spectroscopic ellipsometry obs. 79−86997
surface, (111), S free and covered, D_2 desorption, ang. depend. of flux, mean energy and speed ratio 79−86993
surface, (111), scatt. of mol. and atomic H ions 79−69943
surface, (111), with adsorbed CO, H_2 and O_2, Raman spectra 79−28769
surface, (111) Λ_1-symmetry surface state, angle resolved photoelectron spectra 78−80034
nickel continued
surface, (111) and (100), desorption of H, preexponential factors 79−46918
surface, adsorbed C^+ layer removal, by 20-30 keV Ar^+ bombardment, in plasma 77−76103
surface, adsorbed CO, intermediate UPS/XPS synchrotron radiation study 78−52633
surface, adsorbed CO, N_2, valence band photoemission, SCF MO CNDO calc. 80−100754
surface, adsorbed CO and H_2 layers laser induced desorption expt. 79−1548
surface, adsorbed formic acid decomp., dipole interactions effects 80−61143
surface, ang. distrib. of electrons photoemitted from benzene mols. 77−69968
surface, blistering due to 20 keV He ion irradiation, temp. depend. 79−73228
surface, bremsstrahlung isochromat, incident electron energy and final-state symm. effects 79−69909
surface, C interaction, monolayer form. and struct. stability 80−10756
surface, charged-particle emission caused by laser beam scanning 80−11518
surface, chemisorption of CO, tight-binding theory 77−20395
surface, chemisorption of NO, XPES meas. 79−77922
surface, chemisorption of water, neutron inelastic spectroscopy 79−69353
surface, clean and S saturated, directional UV photoemission 78−15295
surface, clean and with adsorbed Na, photoemission, directional memory effects 80−100753
surface, CO chemisorpt., mol. cluster calc. 80−100407
surface, coadsorption of Pb or Sn with P or C, AES study 80−54521
surface, contact angs. meas., aq. ethanol (glycerine) solns., 20-70°C 78−56025
surface, coverage and desorption of CO flash desorption spectrum 80−49493
surface, Cs and K coated, survival probabilities of emerging H^- ions 80−45187
surface, d-band narrowing, obs. using angle-resolved XPS 80−11062
surface, desorption of H_2, activation barrier with holes model 77−80697
surface, electron spin polarisation, effect of H_2 adsorption, electron capture spectroscopy 78−14933
surface, electron spin polarisation, electron capture spectroscopy 78−95645
surface, electron stimulated interaction of H_2O, AES obs. 77−31902
surface, electronic surface resonances of crystals, Ni(001) and oxygenated Ni(001) 79−95464
surface, H^+ impact of grazing incidence, polarised fluoresc. of reflected H atoms 79−63951
surface, H ion impact, elliptic polarisation in Balmer radiation 80−35039
surface, HMO study of H and H_2 adsorption 77−15682
surface, interaction with He metastable atoms 79−91558
surface, laser induced ionic desorption, mechanism 77−15686
surface, Li ion scatt. expts. and computer simulation 77−63511
surface, location of adsorbed atoms, surface channelling meas. 80−84373
surface, magnetic order 78−95439
surface, mech. for reflection of protons at kilovolt energies 79−8215
surface, Ni (100)-c(2×2)CO, surface struct., LEED meas. 80−6647
surface, O_2 layer thickness, reson. α-scatt. from ^{16}O 78−64778
surface, O monolayer, angle-resolved UV photoemission calc. 77−24927
surface, oxidation, structural changes, low energy ion scatt. study 80−35423
surface, photoemission 78−52619
surface, polycryst., interaction with O_2, SIMS and flash filament meas. 79−47829
surface, polycryst., mol. beam scatt. 79−95895
surface, polycryst. and single cryst., ang. distribs. of CsCl restituted to gas phase 80−6626
surface, polycrystalline, adsorbed S, H_2^+ ion induced desorption 78−84069
surface, polycrystalline, O_2 and S covered, initial sticking coeff. of H_2 78−63937
surface, positronium emission 80−80897
surface, reson. band struct., lateral surface struct. 78−68067
surface, self-diffusion of singel atom, in (331) plane, field-ion microscopy 78−67895
surface, single-atom self-diffusion FIM study 80−103548
surface, SiO_2-supported, chemical composition of hydrocarbon chemisorbed layers *(German)* 79−92002
surface, small angle backscattering of H_2, D_2, He and Ne from single and polycrystalline surfaces 79−24404
surface, spin distribution of electrons, electron capture spectroscopy 78−14932
surface, stay time meas. for physisorbing Xe, Kr and CO_2 78−56044
surface, stepped, acetylene dehydrogenation 79−52752
surface, Te c(2×2) overlayer, 4d levels, angle resolved photoemission cross section, atomic and solid-state effects 80−29853
surface, transformed into hydride and decomposed, dislocation density and dislocation profile depth, positron annihilation and X-ray estimation 78−38711
surface, twinning in crystallised Cu layers 77−24495
surface, with chemisorbed CO, ion-bombarded, molecular cluster ejection, model 79−87543
surface (001), adsorbed N_2, p(2×2) struct., LEED and AES study 80−54515
surface (001), azimuthal anisotropies of ejected dimer ions, SIMS expt. 80−60730
surface (001), barrier struct., LEED anal. 80−20023
surface (001), c(2×2) Se overlayer, angle resolved UPS, resonancelike peaks 79−87562
surface (001), chemisorption site determ. for S and CO, angle-resolved UPS 78−71970
surface (001), clean and S-covered, angular resolved Auger emission, expt. results and predictions from simple model 78−39635
surface (001), electronic struct., matching Green function calc. 78−88013
surface (001), local density of states, asphericity of pot. and charge transfer, ab initio self-consistent calcs. 79−15064
surface (001), Na c(2×2) overlayer, surface struct. effects via photoexcited core electron diffr. 79−74063
surface (001), Ne^+ scattering and neutralisation on first and second layers 80−35045

nickel continued
surface (001), overlayer struct. of O, theory of electronic struct. 79−65319
surface (001), structural parameters and interplanar spacing by LEED averaging 77−11771
surface (001), surface electron struct., matching Green function method calcs. 78−88014
surface (001) with Te overlayer, surface sensitivity of MeV He ion scatt. 79−56904
surface (100), adsorbed CO vibr. EELS, large-ang defl. 80−44405
surface (100), adsorption of CO, SIMS and XPS meas. 79−42378
surface (100), ang. resolved Auger emission and LEED Kikuchi intensities at 850 eV 80−66340
surface (100), angle resolved photoemission, final-state effects 78−56565
surface (100), bonding of chalcogen overlayers, photoemission expts. 77−35819
surface (100), chemisorption and decomp. of formic acid -d_1 79−34361
surface (100), chemisorption of CO, Hartree-Fock-Slater mol. cluster calcs. 79−51650
surface (100), chemisorption of first row atoms, molecular cluster theory 77−1309
surface (100), chemisorption of unsaturated hydrocarbons, LEED and AES obs. 77−31904
surface (100), clean and chalcogen-covered, electron ejection by metastable He atom impact 79−8217
surface (100), clean and with chemisorbed O, rapid LEED intensity meas. 80−44420
surface (100), coadsorption of Sn on Pb, P or O contaminated surface, AES study 80−88437
surface (100), electronic struct., self-consistent local orbital calc. 80−65649
surface (100), initial oxidation, electron energy loss spectra, LEED, AES, and work function meas. 79−61795
surface (100), initial oxidation process, angle-resolved AES and LEED obs. 79−52463
surface (100), interaction with methane, diffusion of deposited C, AES-LEED study 79−99418
surface (100), mag. props. 80−44861
surface (100), O and S chemisorption, surface vibrs., electron energy loss spectra 79−33173
surface (100), oxidation study using low energy ion scatt. technique 79−49338
surface (100), segregation isosteres for C 77−1282
surface (100), spectroscopy by He metastable beam 77−36334
surface (100), spin polarised photoemission 80−45221
surface (100), with adsorbed O_2 monolayer, surface EXAFS, secondary electron yield meas. 79−47544
surface (100) and (110), reaction of acetylene, room temp., UPS expts. 80−61151
surface (100)-p(2×2)C, decomposition of formic acid and adsorption/desorption of H_2, CO, and CO_2 79−91995
surface (101), light emission by scattered 195 keV He^+ ions after focusing and channelling interactions 78−35240
surface (110), adsorption of CO and CO_2, electron bombard. effects, AES and electron stimulated ion desorption obs. 79−51430
surface (110), chemisorption of O, 2D lattice gas model 79−69357
surface (110), clean and S covered, atomic struct., medium energy ion scatt. 79−61483
surface (110), damage induced by bombard. with 3-30 keV noble gas ions 80−60728
surface (110), dissolution of C, 615-660K, AES, LEED 78−63932
surface (110), dissolution of C adlayer, 600-913K 80−49504
surface (110), electron energy loss spectra and AES obs. 79−47826
surface (110), O_2 coverage effects on surface relax., medium energy ion scatt. obs. 79−28181
surface (110), relax., LEED results and anal. by convolution-transform method 77−89624
surface (110), self diffusion, temp. depend. directional anisotropy 78−87851
surface (110), struct. anal. during O_2 adsorption, low energy ion scatt. meas. 79−82424
surface (110), surface relaxation and composition, medium energy ion scatt. spectra 78−63916
surface (110), surface self-diffusion, sinusoidal profile decay technique 79−99404
surface (111), adsorption of acetylene and ethylene, surface structs., LEED and AES obs. 79−60636
surface (111), adsorption of CO and O, LEED and low-energy ion scatt. investigation 79−65324
surface (111), adsorption sites of CO using IR reflection-absorption spectroscopy 79−69355
surface (111), chemisorpt. of CO, surface optical excitations, reflectance spectra, electron energy loss meas. 78−84064
surface (111), coadsorption of CO and hydrocarbons, C≡O bond weakening 79−90863
surface (111), H_2 adsorption, UPS obs. 77−1786
surface (111), Mossbauer effect emission spectroscopy and AES 79−91329
surface (111), photoyield near theshold negative-positive spin polaris. crossover 80−2922
surface (111), single crystal, spin polarisation of emitted photoelectrons 80−45215
surface (111), VUV photoyield, electron spin polaris. enhancement 79−74054
surface (111), with submonolayer of O, H or C_2H_2, surface phonons obs. by EELS 80−39403
surface (111)(110)(100), H adsorption, model 80−50889
surface (111) and (110), laser-induced charge transfer to adsorbed CO, photoemission expts. 80−59798
surface analyses, quantitative, by collision spectroscopy of backscatt. medium energy ions 77−8704
surface analysis, medium energy ion backscatt. expts., solid state detector 79−4456
surface channelling of Ar ions at (110) face 79−73233
surface coverage by CO, backscatt. coeff. from ^{14}C radiation 78−30824
surface damage due to two component He^+ and D^+ ion beam 79−49880
surface decarburisation rate in dry H_2, soft mag. material manufacture 78−60882
surface density of states in simple model 77−47874
surface diffusion effect on sintering 79−74117
nickel continued
surface dopant in Mo, effect on fatigue *(Russian)* 80−7660
surface electronic structure, rigid exchange splitting model 77−11977
surface hyperchannelling, scatt. of low energy Ar ions, computer simulation 80−34110
surface interaction, of O_2, SIMS and flash desorption obs. 78−76568
surface phonons due to O_2 adsorption on (100) surface 78−2359
surface reaction of H_2 and O_2, SIMS and thermal desorption meas. 80−40742
surface self-diffusion; directional anisotropy 77−43367
surface self-diffusion in presence of adsorbed halogens *(French)* 80−24723
surface subjected to friction, wear, exoelectron emission, rel. to O_2, H_2O, gaseous adsorpt. 79−1816
surface vibrations, chemisorbed O influence 80−84361
surface with adsorbed CO, vibr. modes, anal. of electron-energy loss data 79−82461
surfaces, adsorption, chemisorption of atomic, mol. H_2, semi-empirical CNDO MO calcs. *(German)* 79−95465
surfaces, Au-coated and polished, EUV reflection efficiencies 79−14073
surfaces (100), (110), and (111), interaction with O_2, 295 and 485K, photoemission obs. 77−72784
suspension, determination of dielectric constant 77−40579
tarnishing in air, 23-200°C, relative humidities from ambient to 95% 78−19940
tellurite glass, Cu^{2+} and Ni^{2+} doped, band-pass filters for 550 to 616 nm, transmission characts. 78−71166
TEM exam. of ion damage in FCC metals 78−87727
temperature magnetic hysteresis near Curie temp. 79−56567
tensile tests, 77 to 873K 77−32649
tensile-deformed single crystal glide step heights, latex sphere and SEM obs. *(German)* 77−59018
texture nonhomogeneity during rolling 79−91670
textured galvanic layers, grain size determ., matrix and twinning orientations *(Russian)* 77−43461
thermal acoustic magnons, Brillouin scatt. meas. 78−95424
thermal desorption of ^3He, low temp. release 80−34294
thermal emission, magneto-optic circular polarisation obs. 80−70435
thermal emissivities and diffusivities, expt. transient technique and theory for foils 78−43353
thermal expansion, 300-1000K, and power law consts. near Curie temp. 78−38858
thermal expansivity, simple eqn. of state appl. 77−27970
thermal softening, influence of alternating mag. field *(Russian)* 78−23312
thermotransmission spectrum, $M_{2,3}$ edge, temp. depend. 80−50463
thickness meas. of Au and Ni layers on Cu substrates simultaneously 80−13041
thin film, chemical cpd. form. by N_2^+ and Ar^+ ion bombardment *(Russian)* 79−73225
thin film, size depend. electronic cond., annealing effects 79−47174
thin film *(French)* 80−44446
thin film resistor, rare earth alloying effects *(Russian)* 79−78211
thin films, surface demagnetisation due to chemisorption, ferromagnetic reson. study 80−80616
thin foil thickness meas. using ^{148}Gd and ^{241}Am alpha-particles 79−30417
thin plate, Young's modulus meas. by composite vibrator method *(Japanese)* 78−11463
thin-walled cylinder, elongation upon torsion 80−64386
TMMC:Ni, mag. and non-mag. impurity effects on suscept. and Neel temp. 77−66312
trace element anal. by (pX,X) expt. 78−61128
transduction efficiency using magnetostrictively coupled meander-coil EM transducers 79−46144
transient magnetic field discontinuity seen by O(F) ions 80−24515
trapping and release of inert gases, thermal evolution mass spectrometry 78−95077
tunnel currents, spin polarisation, simple band theory interpretation 79−78451
tunnelling electron spin polarisation rel. to band struct. 78−68095
twisted tubular polycryst. sample in axial mag. field, circular magnetisation 77−32230
two-dimens. ⟨110⟩ domain wall 77−69648
ultrafine particles for solar energy photothermal conversion 79−100538
ultrafine particles prepared by vacuum evap. on running oil substrate, mag. behaviour 79−28565
UPS, angle-resolved, in modified LEED system 78−15293
UPS, density of states determ. 78−52623
UPS, two-electron reson. at 3p threshold, rel. to Cu (100) expt. 80−25522
UPS measurements, occupied d-band width obs. 77−20234
US attenuation, mag. field and temp. depend. 77−90008
US attenuation and magnetisation, mag. field depend., for single cryst. *(Russian)* 78−6559
US deform., electron microscope exam. *(Russian)* 78−35447
US deformation at low temps. *(Russian)* 79−11656
US torsional vibrations in metals, measurement of absorpt. 80−58856
US wave attenuation, phonon viscosity and dislocation drag coeffs. 80 and 298K 77−76491
V-Ni interface, diffusion above 500°C *(German)* 79−28156
vacancy and divacancy diffusion 79−82377
vacancy diffusion along single edge dislocations, computer modelling *(Russian)* 77−47612
vacancy diffusivity from width of grain boundary void denuded zone 77−47615
vacancy micropore form. during bombardment by 300 keV Ni ions 78−2172
vacuum condensate, Mo-Ni, prod. by simultaneous condensation from 2 sources, growth direction *(Russian)* 77−21026
vacuum deposited epitaxial layer on Fe (001) substrate, orientation relationship 80−65415
vacuum-condensed film, structural changes under glow discharge *(Russian)* 79−15852
valence-band photoemission spectra, self-energy corrections effect 80−11534
vapour deposited on polystyrene, core-level spectra 79−56911
vapour deposition on O-treated polystyrene, microscopic interactions 80−3407
vapour laser, operation by dissoc. of metal complex 77−54702

nickel continued
vapour press. above different crystallographic planes *(Russian)* 78−18762
void annealing and void formation energy 77−68962
void swelling and defect microstructs., ion irradiation induced, TEM obs. 79−51164
void swelling caused by neutron and self-ion bombardment, 573 to 873K 78−14387
void swelling rates in self-ion irrad. sample 80−29081
voids and swelling following $^{56}Fe^{3+}$ bombardment fast neutron effects simulation 77−30651
Voigt function fit, of X-rays and neutron powder diffr. profiles 79−86651
volume changes and defect healing due to plastic deform. *(Russian)* 80−81139
volume diffusion of Ag, In, Sn, and Sb, activation energies, expt. and by Le Claire method *(Russian)* 79−99369
volume strained, sintered, porous, physicomechanical props., electrical resistivity 77−12572
volume-strained sintered porous, physicomech. props., u.s. vibration propag. velocity 77−1823
VPE on W (110), alignment of (111)FCC-(110)BCC epitaxial metal pairs 79−19488
wear, atmos. press. effect, rel. to fatigue 77−70189
wear, recrystallisation as controlling process, FCC metal 77−56117
wear in unlubricated sliding, mechanical aspect 77−12706
wear tracks, TEM obs., tested in simulated face seal 77−52508
whiskers, diffusion parameters of Zn, 750 to 950°C 77−66101
wick, sintered, effective thermal cond. meas. 78−94582
wire, bamboo struct., plastic deform. *(French)* 77−28877
wire, high purity, elec. resist. determ. 77−39817
wire, internal friction, influence of orientation of mag. field *(Russian)* 79−24559
wire, polycryst., magnetoelastic hysteresis with torsion, inverse Wiedemann effect *(Spanish)* 77−73064
wire, polycrystalline, inverse Wiedemann effect for low torsional stress 79−11332
wire in Ag matrix, coercivity meas. 77−20642
wire plasma sputtering with W particles, coagulation, struct. and particle size *(Russian)* 80−40260
wires, debonding and pull-out from epoxy resin and cement paste matrices 79−29142
wires, in epoxy resin matrix, crack propagation 79−29188
work hardening, grain size effects 77−16605
work hardening tendency in pure and W fibre reinforced state, at elevated temps. 77−52353
X-ray absorption and emission K and L spectra, APW calc. 78−68579
X-ray Debye-Waller factors, CGW vs. DAF models 79−37794
X-ray emission spectra, L_l and L_η 78−39631
X-ray emission spectra, low energy plasmon satellites 79−65957
X-ray emission spectra, rel. to TiNi alloy struct. 77−44091
X-ray intensity reson. near 2p threshold 80−60717
X-ray K-absorpt. edge shifts, plasmon energies correlation 80−20734
X-ray K-absorpt. spectra, depend. on composition and temp. changes *(Russian)* 80−55226
X-ray K-emission satellites, quasi-stationary states and origin 80−80903
X-ray photoemission spectroscopy of $1S_{1/2}O$, $1S_{1/2}C$ and $2P_{3/2}Ni$ states, Ar ion implanted Ni 80−16149
X-ray resonant Raman scatt. and fluoresc. near K-absorpt. edge 79−52042
X-ray spectra, L_{III}-binding energy, absolute determ. from self-absorpt. meas. 80−71519
X-ray stress meas., anomalous effects in cold-rolled specimen *(German)* 80−104184
XPS escape depths and relative photoionisation cross section for 3p subshell 77−73212
XPS for band struct. 79−33889
XPS line intensity ratios for outer electron shells 79−100018
XPS valence band spectra 77−21007
yield point, effect of alloying elements *(Russian)* 80−50670
Young's modulus and shear modulus, temp. depend. 78−27553
Ag-Ni, composite, fibre and layer structs., anomalous props. caused by internal phase boundaries 78−72754
AgBr:Ni^{2+}, low-temp. EPR 77−77091
AgCl:Ni, double quantum EPR transition, superhyperfine struct. 80−7154
AgCl:Ni, optically detected double resonance, radiative recombination electron traps 80−20518
AgCl:Ni^{2+}, low-temp. EPR 77−77091
Al bronze, O free, annealing in photoemission electron microscope, twin density recrystallised grain size relation *(German)* 78−52850
Al_2O_3:Ni, gamma-irrad., low temp., induced absorpt. spectra 79−56820
Al_2O_3:Ni, γ-irrad., thermoluminesc. 78−2925
Al_2O_3:Ni, heat transfer at low temp. 78−38888
Al_2O_3:Ni anodised films, electrolytically coloured, spectrally selective surface 80−11490
Al_2O_3:Ni^{2+}, corundum, phaser production of transverse phonons by impurity centres *(Russian)* 78−91390
Al_2O_3:Ni^{3+}, effect of uniaxial stress on EPR spectra 79−82862
Al_2O_3:Ni^{3+}, Jahn-Teller effect for Ni^{3+}, EPR 79−82564
Al_2O_3:Ni^{3+}, phonon-spin interaction study by thermal cond. meas. 79−82395
Al_2O_3:Ni^{3+}, thermally detected EPR meas. 77−63273
β-Al_2O_3-Ni, absorpt. and emission spectra, mag. susceptibility 79−87471
Al_2O_3-Ni cermets, prep. and props. *(French)* 80−20877
As:Ni film, amorphous, chemical modification of props. 80−49250
Au plated Ni powder for electroplating conductive pastes 79−95957
Au/Ni, interdiffusion, backscatt. study 80−79991
Au-Ge/Ni ohmic contact to GaAS, solid phase epitaxy formation 79−60658
(Au-Ge)-Ni film, for contacts to n-GaAs, metallurgical investigation using inert substrate 77−85313
B diffusion layer, multicomponent, formation *(Russian)* 77−44400
B diffusion layer formation *(Russian)* 77−48570
BP:Ni pillar crystal growth from vapour 80−60758
$BaTiO_3$:Ni, annealed in H_2 and O_2, valence change in phase stability 80−20600
C content determ., isotope-spectral method *(Russian)* 80−55766
C diffusion in α-phase, high temp. vacuum metallography investigation *(Russian)* 77−72718
C fibre, Ni coated, high-temp. compatibility 78−19829
nickel continued
C fibre penetration, ZrN (TiC) diffusion barrier effectiveness 78−60624
C fibre reinforced, hot pressed and electrodeposited, strength 79−38898
C fibre reinforced Ni, struct. and strength change at high annealing temp. *(Russian)* 79−66076
C precipitation 80−29958
C:Ni, X-ray photoemission studies 80−76138
CO_2 reaction, interfacial kinetics, $^{14}CO_2$-CO exchange reaction, S effect 79−47978
CaF_2: Ni crystals, X-irradiated, EPR study of Ni^+ and Ni^{3+} 80−75849
CaF_2:Ni, X-irrad., impurity effects on defect prod. 80−92525
CaF_2:Ni, X-irrad., optical absorpt. spectra and dichroism meas. 80−108239
CaF_2:Ni, X-irrad., thermolum. 80−60686
CaF_2:Ni, X-irradiated, optical and EPR meas. 80−108235
CaO:Ni^{2+}, vibronic splitting, effect of including higher vibronic states in calc. 79−55851
$Ca(OH)_2$:Ni^{2+} single cryst., X-irrad., Ni^+ EPR, g-factors and point-charge model 80−2626
$CdBr_2$:Ni^{2+}, charge transfer near UV spectra, 4.2K, mag. circular dichroism 78−80378
$CdCl_2$:Ni^{2+}, charge transfer near UV spectra, 4.2K 78−80378
CdI_2-Ni^{2+}, absorption and mag. circular dichroism, spectra, phonon density of states of CdI_2 deduced 79−19913
$Cd(NH_3)_6(BF_4)_2$:Ni^{2+}, EPR of $[Ni(NH_3)_6]^{2+}$, temp. depend. at phase transition 77−20685
CdS:Ni, dark cond. and photoconductivity 78−76110
CdS:Ni, elec., photoelec. and luminesc. props. *(Russian)* 78−84259
CdS:Ni, elec., photoelec. and luminesc. props. 79−95828
CdS:Ni, exciton reflection spectra 78−72557
CdS:Ni, impurity to band electronic transitions, photocond. and dark cond. obs. *(Russian)* 77−8150
CdS:Ni, nonradiative recomb., photocond. spectra 80−70764
CdS:Ni, recomb. parameters, photocond. spectra meas. *(Russian)* 80−49820
CdS:Ni^{2+}, config. interaction and cryst. field theory 77−39811
CdS:Ni^{2+}, Zeeman effect at Ni impurities 80−60633
CdTe:Ni, exciton refl., photoluminesc. and mag. suscept. meas., influence of impurities 77−39787
CdTe:Ni, luminesc. and refl. spectra, high temp. annealing effects 80−24472
Cl_2O_3:Ni^{3+}, EPR spectra anal. using dynamic Jahn-Teller model 79−82863
Co alloys, determination of Ni and Co by flameless atomic absorption spectrophotometry 77−90674
Co-Ni, interdiffusion coeffs. and conc. penetration curves, electron microprobe meas. 77−66047
Co-Ni interface, intrinsic interdiffusion coeffs. and activation enthalpies 77−84998
Co-Ni sandwich system, interdiffusion, Kirkendall effect 77−69121
Co-Ni system, interdiffusion zone growths *(Czech)* 78−84009
CoO:Ni^{2+}, far IR absorpt. by impurities and collective antiferromag. reson. mode 77−8576
Cr_3C_2(-Ni-Cr), self-weldability in high temp Na *(Japanese)* 80−89392
Cu coated, thickness monitoring by back scattering of single energy electrons, density meas. 79−97362
Cu, determination of Ni and Co by flameless atomic absorption spectrophotometry 77−90674
Cu:Ni, Dingle temps. calcs., tetrahedron method 80−6699
Cu/Ni coherent modulated structures, electronic struct. and magnetism 80−103620
Cu/Ni double layer evaporated film, misfit dislocation effect on strength *(Japanese)* 79−42425
Cu/Ni film counter, surface counting method for diffusion study 79−42321
Cu/Ni interface, diffr. studies of conc. variations 79−42322
Cu/Ni multilayer films, electron beam induced diffusion during AES depth profiling 80−19993
Cu-Ni, bimetallic film, exam. of diffusion by electrical resistivity meas. *(Russian)* 79−14970
Cu-Ni, interface, ferromagnetic and cond. spin reson. mode coupling 79−78521
Cu-Ni bicrystal, misfit dislocation config., moire patterns, interdiffusion effects 78−84110
Cu-Ni bicrystals, epitaxial growth, chemical interdiffusion, X-ray diffr. line profile anal. 79−1527
Cu-Ni bilayer system, optical mechanical and corrosion props. 77−32707
Cu-Ni bimetallic film, Moire patterns, interdiffusion effects 77−51621
Cu-Ni bimetallic films, dislocation wall form. during interdiffusion, TEM obs. 78−51856
Cu-Ni bimetallic thin film, effect of microstructre on interdiffusion 79−77840
Cu-Ni evaporated thin film couple interdiffusion obs. 78−43187
Cu-Ni film system, time depend. diffusion coeffs., grain boundary and dislocation effects 77−80656
Cu-Ni system, X-ray diffr. line broadening from small subgrains containing gradients of spacing 78−67612
Cu-Ni thin film couples, interfacial reactions, contact resistance meas. 78−63882
Cu-Ni thin thin film couples, polycryst., interdiffusion singularities, Frenkel and Kirkendall effects *(Russian)* 77−24447
Cu-Ni-CuCl-KCl/NaCl system, isothermal chem. metal transport *(German)* 77−63569
Cu+Ni foil target, 50-65.5 MeV, K-vacancy production, impact parameter depend. 79−54958
diffusion of As, 970-1360°C *(Russian)* 80−29218
electroless plating on Zn-Al alloys, baths and activating solns. *(Japanese)* 80−71604
Fe base alloy:Ni, amorphous, effect on corrosion resistance 77−4869
Fe, ferromagnetic transmission resonance, nonlinear phenomena 77−81016
Fe-Cr-Mn-Ni, influence of Ni on defect conc. energy *(Russian)* 80−54241
Fe-Ni, bimetallic molecule, matrix isolated, Mossbauer spectrum 78−68425
Fe-Ni, bimetallic molecule, matrix isolated, Mossbauer spectrum 78−88233
Fe-Ni system, interdiffusion zone growths *(Czech)* 78−84009
Fe-Ni-C (19.5, 0.73 wt.%), banded struct. formed by deform., TEM and optical obs. 78−39869

nickel continued
ferromagnetic, anomalies in thermal expansion and heat capacity 79−73744
GaAs:Ni, behaviour of Ni impurity in $3d^8$ state, optical absorption and photocond. meas. 78−47737
GaAs:Ni, intra d-shell excitations of acceptors 80−84757
GaAs:Ni, negative magnetoresist. meas. 77−51768
n-GaAs:Ni, negative photocond. at low temps., impurity levels 80−6900
GaAs:Ni, substitutional impurity elec. struct. 80−88513
n-GaAs:Ni, VPE, deep-level transient spectroscopy 80−34383
GaAs:Ni,O_2 effects on opt. props. 77−16350
GaAs:Ni^{3+}, EPR assessment of $3d^7$ transition metal impurity state 78−48031
GaAs:Ni^{3+}, mag. and optical props. 78−10763
GaAs/Au-Ge/Ni, Schottky barrier energy var. with interdiffusion 77−20435
GaN:Ni, lattice parameters, variation with stoichiometry and doping 79−73153
GaP:Cu-Ni, Schottky barrier, TSC meas., trap levels 78−91709
GaP:Ni, absorpt. and luminesc. spectra 79−42996
GaP:Ni, deep traps, near IR luminesc., polarised spectra meas. 80−16077
GaP:Ni, electron-hole recombination via deep state 79−99560
GaP:Ni, Hall effect and absorpt. spectrum investig. of acceptor level 77−44033
GaP:Ni, multivalence impurity, EPR and optical absorpt. meas. 80−75844
GaP:Ni, Ni contaminant, detection through IR photoluminescence 78−15212
GaP:Ni, optical and EPR study of two-electron-trap state 79−73806
GaP:Ni, photolum. excitation spectroscopy 80−80841
GaP:Ni, positron annihilation meas. rel. to deep levels study 80−60712
GaP:Ni, whisker growth on surface 79−33212
GaP:Ni^{2+}, d→d luminesc. spectra 80−7414
GaP:Ni^{3+}, EPR assessment of $3d^7$ transition metal impurity state 78−48031
Ge:Ni, gamma ray effects on impurity states 80−96822
n-Ge:Ni, negative differential conductance of surface channels 79−11134
n-Ge:Ni, quasi-surface conduction effects on photocond. spectrum and IR quenching 77−1452
n-Ge:Ni, recomb. waves, current instabilities obs. 77−1431
n-Ge:Ni, recombination of hot electrons on Ni impurity centres 80−44612
Ge:Ni, Sb 80−96906
n-Ge:Ni,Sb, transient response at 4K, nonequilib. carrier recomb. 77−43659
Ge:Ni compensated, hot electron recomb. anisotropy 78−39125
n-Ge:Ni p^+-n-n^+ structs., double-injection current-voltage charact. 80−60074
Ge-Au-Ni trilayer film, interdiffusion obs., on annealing 78−2308
Ge-Au-Ni trilayered film, annealing, interdiffusion 78−22902
Ge-Ni contacts, surface electron state spectrum, surface treatment effects *(Russian)* 80−34497
H assisted cracking, mechanisms, review 80−50721
H diffusion in electrolytic Ni, coeff. determ. *(Russian)* 79−8441
H^++U(Ni)(Au)(Sn), 4.88 GeV, K-vacancy production cross sections 77−19036
H_2 embrittlement *(Japanese)* 77−48526
H_2 induced deform. during thinning, electron-optical obs. in single crystal foils 79−57059
HIO_3:Ni, growth and struct. perfection, effect of impurity ions 77−12514
InI:Ni, impurity behaviour during directional crystallisation, partition coeffs. 77−16491
InP:Ni^{3+}, EPR assessment of $3d^7$ transition metal impurity state 78−48031
InSb-anodic oxide-Ni, energy band diagram, internal photoemission meas. 79−33356
$KMgF_3$:Ni, Co, emission from Ni-Ni and Ni-Co pairs, exchange coupling const. 79−33788
$KMgF_3$:Ni, Ni-Ni pair optical spectra 80−45042
$KMgF_3$:Ni^{2+}, absorpt., MCD and emission spectra 79−51953
$KMgF_3$:Ni^{2+}, acoustic Faraday and Cotton-Mouton effects, theory 80−65987
$KMgF_3$:Ni^{2+}, EPR meas., g-factor, spin-orbit coupling const. and mag. moment determ. 77−80999
$KMgF_3$:Ni^{2+} high energy absorption spectra interpretation 78−6716
K_2MnF_4:Ni, mag. effects of impurities 80−65869
K_2MnF_4:Ni^{2+}, and undoped, magnon spectra, Raman and far IR spectra meas. 77−20573
K_2MnF_4:Zn(Mg)(Ni), local magnetisation, NMR and Green's function study 80−65870
K_2SO_4-$ZnSO_4$ glass:Ni^{2+}, visible spectra 79−51990
$KZnF_3$:Ni^{2+}, absorpt., MCD and emission spectra 79−51953
$KZnF_3$:Ni^{2+}, mechanism of conc. quenching of fluoresc. from T_{2g} of Ni^{2+} 77−59605
$KZnF_3$:Ni^{2+}, Mn^{2+}, interference transition electric dipole mechanism 80−34896
$KZnF_3$:Ni^{2+}, temp. depend. of luminesc. 79−83016
$LaMg(NO_3)$:Ni^{2+}, pressure depend. of zero-field splitting of two mag. centres *(Russian)* 77−32249
$La_2Zn_3(NO_3)_{12}.24H_2O$:$CO^{2+}$, Mn^{2+}, Ni^{2+}, mag. exchange interactions, EPR 77−36118
LiCl:Ni, electron transfer absorption bands 79−95810
LiCl:Ni^{2+}, EPR meas. of Ni^{2+} vacancy dipoles 79−28594
LiCl:Ni^{2+}, first order induced Raman scatt. from Ni^{2+} and cation vacancies 77−48169
LiCl(Br):Ni^{2+}, optical absorpt., charge transfer spectra 80−2797
LiF:Ni, dislocation behaviour in diffusion zone, Cottrell clouds *(Russian)* 80−70212
LiF$_2$:Ni^+, compressed D_{4h} cluster, g_{zz}-g_0 value 77−80756
α-$LiIO_3$:Ni^{2+}, absorption spectra, impurity environments 78−27275
$LiNbO_3$:Ni optical absorpt. spectra 80−71450
MgF_2:Ni, growth by vertical gradient freeze method, in self-sealing graphite crucibles 78−31334
MgF_2:Ni electronic transition laser, tunable IR emission 78−59030
MgF_2:Ni^{2+}, temp. depend. of luminesc. 79−83016
MgO:Ni, heavily doped, defect characterisation, rel. to use as laser material 80−65000
MgO:Ni, optical absorpt. spectrum in mag. field, and 2p-3d charge transfer 77−52141
nickel continued
MgO:Ni, X-ray stimulated luminesc. 79−28802
MgO:Ni^{2+}, config. interaction and cryst. field theory 77−39811
MgO:Ni^{2+}, elastic interaction of mag. centres, EPR line width meas. 78−19315
MgO:Ni^{2+}, near IR luminesc. from isolated and exchange-coupled Ni^{2+} ion pairs, temp. depend. 80−93382
MgO:Ni^{2+}, next-nearest-neighbour ion effects on impurity 2p levels 77−20987
MgO:Ni^{2+}, single crystal, thin film, near IR luminescence *(Russian)* 79−28807
MgO:Ni^{2+}, temp. depend. of luminesc. 79−83016
$MgSiF_6.6H_2O$:Ni^{2+}, EPR meas., low temp. phases 77−63269
$MgTiF_6.6H_2O$:Ni^{2+}, EPR meas., low temp. phases 77−63269
Mg_2TiO_4:Ni, ESR of Ni^{3+} 80−97131
$MnCO_3$ crystals, gel. grown, Ca^{2+}, Ni^{2+} impurity influence, SEM study 80−20778
MnF_2:Ni^{2+}, IR fluoresc., field depend., exchange energy 78−68543
Mo, determination of Ni and Co by flameless atomic absorption spectrophotometry 77−90674
Mo, recrystallisation kinetics, deform. degree effects *(Russian)* 78−6943
Mo-Ni film system, diffusion reaction, phase form. 77−84999
Mo-Ni thin film junction, phys. vap. deposition parameters effect on thermoelec. power 77−39922
N IX to Ni XII, wavelengths of transitions between lower configurations 80−99474
NH_4Cl:Ni^{2+}, EPR spectrum, spin Hamiltonian, zero-field splitting effects 80−97135
$(NH_4)_2Zn(SO_4)_2$:Ni^{2+}, optical absorpt. spectrum, room and liq. air temp. 79−15499
NI:MgF_2, laser, broadly tunable CW operation, output powers, optical pumping 80−32995
NI+H^+, 4 MeV beam-foil X-ray production cross-section 79−7003
Na^++Ti(Ni)(Zn)(Fe), 0.2-3.0 MeV, united-at. limits, mol.-orbital continua 77−19030
NaCl:Ni, elec. cond. and distrib. of Ni^{2+} ions 79−33010
NaCl:Ni single crystals, VUV spectrum, ionic conductivity, X-ray diffr. 78−92097
NaCl:Ni^{2+}, kinetics of impurity precipitation 77−69090
NaCl:Ni^{2+}, Z_4-like centre, absorpt. spectra obs. 78−76498
Na_2O-B_2O_3-SiO_2 glass-Ni compact, indented, strength and fracture toughness 80−93636
$Na_2Zn(SO_4)_2.4H_2O$:Ni, optical absorpt. and EPR. obs. 78−76501
(Ni,Mo)/Al_2O_3, hydrodesulphurisation catalyst, prep., props. and appls. 77−86360
Ni 200, C interstitial effect of yield point develop. during static strain ageing, model 78−88498
Ni (VIII), semiempirical investigation of spectra 78−33434
Ni (001)/CO(O) system, adsorbate geometries determ. from final state scattering in X-ray photoemission 80−54488
Ni (100)-c(2×2)-O system, adsorbed monolayer, RHEED study 79−77912
Ni, (100)p(2×2)O and (100)c(2×2)O surfaces, struct. and vibrs. of adsorbed CO 78−2375
Ni alloys, thermionic electron emission into Cs vapour 78−60540
Ni based powders, determination of entrapped Ar content, using vacuum fusion tech. 79−5193
Ni catalyst, chemisorption of benzene, Raman and vibr. spectra 80−108747
Ni catalyst, H_2+CO, adsorption, co-adsorption, reaction, neutron inelastic spectroscopy method 79−99408
Ni cluster-H, electronic struct. calc., H-metal bonding 77−89823
Ni, cold-worked, rel. between dislocation and ferromag. damping 80−107369
Ni, corrosion rates in SO_2-O_2-SO_3 atmospheres under simultaneous sulfidation-oxidation 79−79162
Ni, deposition of layers from carbonyl vapour 77−4727
Ni, dispersed catalyst on Al_2O_3 and SiO_2, epitaxial and textural effects, ferromag. reson. 78−23963
Ni electrodeposits, fibre textures before and after thermal treatment 79−91693
Ni, grain boundary cavities growth under applied stress and internal pressure 80−29032
Ni I, in solar spectrum, effect of parity of spectral terms on curve of growth 77−53539
Ni I, UV lines, oscillator strengths from hook method and absorpt. meas. in furnace 80−83319
Ni I 1.3968 μm laser transition in hollow cathode discharge 79−81409
Ni I isotope shift for stable isotopes, nuclear charge radii 80−99484
Ni I solar photosphere from oscillator strength obs. 80−98625
Ni II, laser oscill. at 796.24, 797.54 nm in hollow cathode discharge 79−86161
Ni II, oscillator strengths, near UV lines, wall-stabilized arc meas. 78−42003
Ni III-VI, struct. and transition probabilities, ab initio calc. using Thomas-Fermi central pot. 79−3360
Ni IV spectrum anal., energy level classification 77−61700
Ni, intermodulation generation in RF mag. field, field interaction with domain walls 79−56600
Ni ion+Ni(Fe) collisions, X-ray spectra, two-electron transitions 77−19050
Ni, magnetoelastic and magnetostrictive sensitivities, reversible and irreversible components *(Russian)* 80−25172
Ni passivation, S influence study by Auger and electron spectroscopy 80−65347
Ni powders, stereological appl. in study of compacting process, elec. and mech. props. *(French)* 80−40286
Ni, tubular sample, basic EM theory 78−43620
Ni V spectrum, 990 to 1400 Å, ionisation pot. 77−30811
Ni XI, Ni XII, forbidden transitions, solar coronal spectrum appl. 78−77537
Ni XII, XIII, XIV, XV, 3s-3p and 3p-3d transitions, oscillator strength and energy levels calcs. 80−83251
Ni XII-XVIII solar $3s^23p^n$-$3s3p^{n+1}$ transition arrays, UV spectra classification 80−63570
Ni XIX, mag. quadrupole lines, in TFR600 Tokamak plasma, 10-20 Å 79−13662
Ni XIX, spectrum in solar corona 77−2390
Ni XVII solar coronal EUV line intensities 80−51731
Ni XVII transition probabilities and collision strengths 80−78562

nickel continued
Ni XVIII solar XUV flare lines, oscillator strength meas. 79−5796
Ni XX, spectra and energy levels of F isoelectronic series 79−93948
Ni XXI, X-ray spectra in laser plasma, $2p^6\ ^1S_0 \rightarrow 2s2p^5\ ^1P_1$ 79−1340
Ni XXI, XXIII, spectral energy levels, relativistic corrections, config. superposition method 80−32616
Ni XXIV, spectra calcs., fine struct., transition energies 77−42260
Ni XXV, Ni XXVI, line classifications in laser-produced spectra 79−81175
Ni XXV and XXVI resonance lines in Tokamak discharges 79−68941
Ni XXVI, CC Li I-like spectra, energy struct., accurate semiempirical formulae 79−49970
Ni XXVII, He-like ion, oscillator strengths of transitions between low-lying S and P states 78−13470
Ni^-, photodetachment cross-section meas., crossed beam expt. 77−61723
Ni^-, photoelectron spectra, electron affinity and fine-struct. interval 79−68212
Ni^+ bombardment of stainless steels, effect on stress corrosion cracking and microhardness 80−85087
Ni^+, generation by laser ionis. source for ICR spectroscopy, chem. appls 80−45597
Ni^{2+}, complex formation with carboxylic acids in aqueous soln., thermodynamic parameters *(Italian)* 77−48669
Ni^{2+} dopant in CaF_2, CdF_2, BaF_2 78−27265
Ni^{2+}, fluoresc. quenching of organic excited singlet states, rate meas., mechanism 77−38685
Ni^{2+}, in zeolites, reduction, UV spectroscopic obs. 77−77738
Ni^{2+}, mag. form factors, spherical and aspherical parts 79−78315
Ni^{2+} partitioning in olivine and silicate melts 79−66683
Ni^{2+}, Rayleigh and Compton scatt., differential cross section determ. 80−52912
Ni^{4+}, Sternheimer valence shielding antishielding factor including exchange 77−85182
Ni:^{111}In, ion implantation damage, DPAC obs. 77−59052
Ni:^{116}Er, hyperfine interaction of impurities, Mossbauer spectra 77−48105
Ni:^{119}Sn, 78−52382
Ni:^{129m}Xe, Mossbauer obs. of mag. hyperfine field 77−8460
Ni:^{129}Te, implanted atom sites, Mossbauer obs. 77−20756
Ni:^{172}Yb, hyperfine mag. field, TDPAC meas. 78−52394
Ni:^{192}Ir, NMR/ON, resonant freq. shift with applied field 77−28462
Ni:^{235}U (0.1 at.%), exam. of saturation defect conc. and elec. resistivity meas., for neutron irrad. at 7K 78−47435
Ni:^{57}Fe, Mossbauer meas. near Curie temp. 78−10817
Ni:^{83}Rb, implanted atom sites and hyperfine interactions, Mossbauer obs. 77−24765
Ni:^{86}Y, mag. hyperfine field determ. by DPAC 77−8458
Ni:B, impurity electronic struct. calc., ^{12}B NMR data anal., magnetisation decrease 79−47046
Ni:B(N), hyperfine interactions, recoil-implanted β-NMR method *(Japanese)* 79−51865
Ni:Bi, impurity site distrib., channelling and nucl. orientation obs. 77−15447
Ni:C, bulk-to-surface precip. and surface diffusion, AES meas. 77−11784
Ni:C, bulk-to-surface precip. and surface diffusion of C, AES data interpretation 78−34713
Ni:C, H(D), isotope effects of C-H and C-D complexes 77−20129
Ni:Cr, He^+ radiation-enhanced diffusion and segregation effects of point-defect trapping 79−77824
Ni:D, diffusion study using D(d,p) reaction 79−5202
Ni:F, ion-implanted, mag. hyperfine field, anomalous temp. depend., PAC meas. 79−4754
Ni:F, lattice location of implanted F rel. to mag. hyperfine fields 77−59041
Ni:H, energy and electron density of states 78−51929
Ni:H thin plate, recovery of quenched-in solute H 77−62673
Ni:He, defect props., quantum-chemical and lattice-defect hybrid approach 79−4528
Ni:He, implanted, profile meas. technique 77−80524
Ni:In_3, He, lattice defect struct., PAC meas. 80−70190
Ni:K^+(Ba^+), ion implantation, effect on inelastic refl. and energy losses of fast primary electrons 78−55900
Ni:Kr gas trapping and release, thermal evolution mass spectrometric study 80−34026
Ni:Lu, nuclear orientation meas., hyperfine field 77−32308
Ni:MgF_2, efficient CW optically pumped laser, 1.63 to 1.75 μm operation 79−18425
Ni:MgF_2, tunable transition-metal-doped solid state lasers 80−58549
Ni:MgO, tunable transition-metal-doped solid state lasers 80−58549
Ni:N, difference in conc. distribs. between implanted N^+ and N_2^+ ions 77−80529
Ni:O, single crystal, $^{18}O^+$ ion implantation in channelling directions, expt. conditions and range profile obs. 80−65022
Ni:O single crystal, $^{18}O^+$ ions implantation in channelling directions, stopping power meas. from max. range 80−65078
Ni:Ra, hyperfine field determ. 77−85622
Ni^{2+}:MgO laser system, optical parameters 80−48260
Ni/Al_2O_3, sintered catalysts, mag. and catalytic props. for methanation reaction 79−79296
Ni/Al_2O_3 catalysts, coprecipitated methanation type, metal-support interaction, XPS obs. 80−80936
Ni/Al_2O_3 composite film, optical props., rel. to solar collector appls. 78−72622
Ni/Al_2O_3(SiO_2) methanation catalysts, nonreduced, IR spectra 78−88288
Ni/Au film on silicon vacuum deposited, electron impact mass spectrometric exam. of surface contaminants 78−75957
Ni/Au-Ge/GaAs contact system, alloying behaviour, microprobe AES and X-ray diffr. 80−54548
Ni/Cr multilayers, AES depth profiling by sputtering with N_2^+ ions 79−95881
Ni/Fe interfaces sputter profiling, by AES 79−15572
Ni/Fe layers, interdiffusion, Auger sputter profiling obs. 79−46848
Ni/GaAs film contact system, alloying reaction 80−96747
Ni/NiO, relative chemical potential of oxygen *(German)* 78−31642
Ni/Ni(II) electrode reaction in LiCl-KCl eutectic melt, impedance meas. *(Japanese)* 79−100392
Ni/Pt/Si(111) Schottky diodes, current-voltage characts. and comp. profiles 80−84508

nickel continued
Ni/SiO_2, adsorption of CO, scavenging effect of H_2, in situ Fourier transform IR spectra obs. 80−39410
Ni/ThO_2, adhesive energy, meas. techniques 80−50803
Ni/ZrO_2-Y_2O_3, sputtered multilayered ceramic/metal coatings, props. 80−40620
Ni-7070 pyrex glass boundary, 9 MHz Stoneley wave generation 79−82433
Ni-Ag, thin-film, elec. cond. depend. on substrate film thickness and condensation temp. 79−7911
Ni-Al_2O_3, composite coating, electrodeposited, exam. of particle-cathode adhesion during formation 79−33954
Ni-Al_2O_3, composite solar selective absorbers optical props. 79−52037
Ni-Al_2O_3 cermet, fabrication and mech. characts. 79−38781
Ni-Al_2O_3 composite film, selectively absorbing, optical props. 78−6798
Ni-Al_2O_3-Al superconductor, spin polarisation of tunnelling electrons, band model 77−72947
Ni-Cd, with plastic bonded Ni oxide electrodes, basic electrochemical parameters 80−50951
Ni-Cd accumulators, plastic bonded electrodes, active layer composition influence on galvanostatic and potentiostatic discharge curves 80−55834
Ni-Cd all with MnO_2 doped positive electrodes 79−96439
Ni-Cd batteries, button and cylinder types, self discharge behaviour during storage *(German)* 80−66960
Ni-Cd cell lifetime prediction, computerised pattern recognition 80−3504
Ni-Cd sealed battery electrode performance meas. 80−66962
Ni-ceramic coating structure, influence of micropowder inclusion *(Russian)* 80−59820
Ni-Cr, movement and dislocations using SEM and diffr. contrast method *(Chinese)* 79−51110
Ni-Cr multilayer structs., sputter profiling, depth resolution and surface roughness effects, AES obs. 77−76694
Ni-Cu conductor system for Si solar cells 80−93991
Ni-Cu diffusion couple surface, epitaxial, AES, CO chemisorption and LEED 77−31891
Ni-Cu interface, diffusion coeff. using method of nets 78−22903
Ni-Eu_2O_3, specific resistivity and emissivity, 1000 to 1500K 77−43675
Ni-Fe thermocouple, appl. to surface temperature measurement 80−62668
Ni-Fe_3O_4 system, interdiffusion 79−69301
Ni-ferrite powders, form. in presence of Li_2SO_4-Na_2SO_4 molten salts, prep. and characts. 80−84869
Ni-Ge planar interface, first phase to nucleate 77−62764
γ-Ni-γ'-Ni_3Al-TaC fibre reinforced eutectic, oxidation protection 77−40475
Ni-H, ferromag. disappearance obs. 77−43824
Ni-H, implanted film, resistivity and TDPAC meas. 78−39229
Ni-H interaction, 0.75 Å$\leq$R$\leq$5 Å, NiH form. effect of inner orbitals *(German)* 78−29752
Ni-H system, energy and electron density of states, improvements to theory 80−70636
Ni-H system, phase diagram and thermodynamic properties calcs. 80−66480
Ni-H_2 sealed storage battery, characts., charging, transient, stationary regimes 77−63930
Ni-$LiNbO_3$, layered structure, mag. control of surface elastic waves 77−20666
Ni-like ions, multiply charged, laser plasmas, 1.5-15 Å 78−13462
Ni-Mn multilayer for monochromators and supermirrors, neutron reflectivities 80−22880
Ni-Mo, multilayer films, depth resolution determ. in Auger depth profiling meas. 79−78800
Ni-n-GaP:Si(Ge) contacts, doping effect in elec. props. 80−6983
Ni-Na-di-2-ethylhexyl phosphoric acid-H_2O system, droplet phenomena 77−48697
Ni-NiO composite mixture, preferential sputtering, XPS expts. 79−87544
Ni-NiO_x-NiS_y, black Ni, struct.-depend. thermal and optical props., rel. to solar thermal conversion 79−79404
Ni-NiO-Ni, integrated MOM junctions, characts. at DC and optical freqs. 78−41349
Ni-O system, oxidized polycryst. Ni films, H_2 reduction, AES 77−12472
Ni-P undercoat, effect on struct. form. in sintered electrophoretic Cr_3C_2 alloy coatings 80−61027
Ni-polymer contacts, charge transfer and contact charge spectroscopy 79−56305
Ni-sapphire interface, effect on shear strength of adsorbed species 80−49485
Ni-Se interface, reactive diffusion, electronic struct., UPS study 78−51748
Ni-Si film struct., silicide form. He^+ back scatt. and X-ray diffr. obs. 79−51442
Ni-Si film system, silicide first phase form., reaction kinetics 78−79821
Ni-Si film-wafer interface, marker motion in Ni_2Si formation 77−89593
Ni-Si interface, NiSi formation from Ni_2Si, Pt marker study 78−87830
Ni-Si structure, contact resist. and bulk resist. of Si, pulse method 78−52083
Ni-Si surface barrier struct., surface electronic states, annealing effects *(Russian)* 78−6441
Ni-SiC coating adhesion to Al alloy, metal interdiffusion *(Russian)* 80−66697
Ni-SiC composite coatings, phase composition calc., wear resistance *(Russian)* 79−11709
Ni-SiO cermet film, elec. resist., percolation effects 77−76954
Ni-SiO composite film, acoustic damping capacity and struct. *(Russian)* 77−59070
Ni-SiO multilayer film, interface magnetisation 80−7135
Ni-SiO multilayer films, interface magnetisation 80−88858
Ni-SiO_2, granular film, hopping cond., magnetoresist. 78−56240
Ni-SiO_2 composite film, influence of hardening phase on yield stress *(Russian)* 79−5001
Ni-SiO_2 granular metal films, minimum metallic cond. 78−56241
Ni-SiO_2 supported catalysts, particle size, H_2 chemisorption, Mossbauer study 80−7219
Ni-Si(111), interface, reactivity and struct., ion channelling meas. 80−92788
Ni-thoria dispersed (2 vol.%), meas. and eval. of H_2 trapping by permeation technique 79−60555
Ni-Ti film system, interdiffusion, phase growth kinetics *(Russian)* 77−72722

nickel continued
Ni-Ti multilayers for monochromators and supermirrors, neutron reflectivities 80−22880
Ni-TiO_2 electrochem. composite coating phase composition and microhardness factors *(Russian)* 79−91598
Ni-V system, interdiffusion, kinetics of phase growth *(Russian)* 80−29230
Ni-W surfaces in contact, deform. and adhesion at very low loads 80−39457
Ni-$ZnSiP_2$ Schottky contact, production and props. 79−7901
Ni-ZrO_2, dispersion-strengthened condensate, density and mech. props. 77−44196
Ni-ZrO_2, thin layers, vapour deposited, dispersion strengthened, exam. of struct., mech. props. 78−80554
Ni+Cl^{n+}, 35 MeV, K-shell vacancy sharing, impact parameter depend., X-ray obs. 77−71858
Ni+Cl^{x+}, K-shell ionization probability in energetic nearly symmetric heavy-ion collisions, 35 MeV 79−27078
Ni+Fe, two electron one-photon X-ray transitions, Dirac-Fock calcs. 78−17600
Ni+H^+, K-shell ionisation calcs. 80−23534
Ni+H^+, K-shell ionisation cross-sections calcs. 80−43165
Ni+H^+($^4He^{2+}$)(O)(Li), K-shell ionis., impact parameter depend. 77−83707
Ni+H(D)(He)(Li)(C)(O)(F) ions, K-shell ionis., universal cross sections 78−62895
Ni+Mn(Pb), inner shell vacancy prod., impact parameter depend. 77−6906
Ni+N^+, X-ray production cross section, $K\beta/K\alpha$ ratio, 0.5-2.5 MeV/amu 77−54526
Ni+Ni, 12-90 MeV, molecular orbital K X-rays ang. distrib. 79−10125
Ni+Ni, 39 MeV, X-ray emission spectra, nonLorentzian shape of atomic line tail 78−21872
Ni+Ni, continuum X-ray radiation, collision broadening 80−9539
Ni+Ni, exchange interactions and exchange integrals 80−37849
Ni+Ni, recoil effects on molecular-orbital X-ray spectra in solid targets 80−25510
Ni+Ni interaction, ab initio HF and CI calcs. 79−59535
Ni+Ni symmetric collisions, molecular-K-X-ray anisotropy spectra, discrete struct. 77−14560
Ni+Ni^+, with nuclear sticking, molecular orbital and compounds nucleus X-ray emission 80−1048
Ni+Ni^{x+}, K X-rays, two-electron-one-photon excitation 78−13589
Ni+Ni(Nb), Doppler shift of continuum X-rays from quasimols. 79−22808
Ni^++Fe(Ni), 25, 40 MeV K-shell double ionis., $K\alpha\alpha$ and $K\alpha\beta$ obs. 77−57918
Ni^++H_2(HD)(D_2), endothermic reactions, investig. 80−97692
Ni^{14+}+H^+, collisional excitation of fine struct. transitions in ground state 77−19017
Ni^{16+}+Ne, highly charged very slow Ne recoil ions, K X-ray transition 80−91649
Ni^{2+}+MoO_3 catalyst on Al_2O_3, Raman spectrum 80−108742
Ni_2, A→X system, Ar matrix isolation fluoresc. spectrosc. obs. 80−9628
Ni_2 and Ni_2^+, lowest electronic states, GVB and POL-CI calcs. 79−31409
Ni_2, extended basis set LCAO Xalpha treatment 80−95537
Ni_2, Hartree-Fock-Slater calcs., using pseudopot. method 77−57859
Ni_2, UV Ar matrix spectra theory 77−75178
Ni_3, in solid Ar, reson. Raman spectra 80−63638
Ni_3, linear system, energy based integral repulsion method calcs. 78−82606
Ni_3, UV Ar matrix spectra theory 77−75178
Ni_5, and Ni_9 clusters, Hartree-Fock-Slater model calcs. 77−72899
Ni_n clusters, Ar matrix, UV-visible spectra pot. energy curves 77−65552
Ni(II), selective separation from rare earth elements on chelate ion exchangers 78−58861
Ni(IX), resonance transitions, classification 80−42985
$Ni_{13}(O_h)$ cluster, electronic states and X-ray spectra in $X\alpha$ approx. of multiple scatt. theory 77−28645
NiVI, sixth spectrum analysis 220-335 and 890-1325 Å regions 80−95565
^{58}Ni+p, K-shell X-ray photon proton coincidences, nucl. time delay 79−18281
^{59}Ni, management of radioactive waste produced on dismantling PWRs 80−27756
^{59}Ni, thermal neutron cross sections for He prod. 77−23079
^{61}Ni, $3d^94p\ ^3D_2$ level, hyperfine struct., level crossing obs. *(French)* 78−41997
^{61}Ni, Mossbauer isomer shift, book contrib. 79−87354
^{63}Ni applications in biological research 80−12321
^{63}Ni, management of radioactive waste produced on dismantling PWRs 80−27756
Ni(100), with adsorbed K^+, He^+ impact, Auger deexcitation spectrosc. 79−100010
$_{28}{}^{58}Ni^{n+}$+$_{25}$Mn($_{50}$Sn)($_{82}$Pb), 45, 94, and 138 MeV Ni inner shell vacancy production, impact parameter depend. 79−41130
Pb impregnated porous Ni, porous, internal friction and effective elasticity modulus, temp. depend. *(Russian)* 79−29118
Pb:Ni, paramag. impurity effect on work hardening at superconducting transition *(Russian)* 77−47915
PbS-Ni, phase diag., cpd. formation and electrophys. props. 77−85997
Pd/Ni/Cr layered catalyst for H_2-O_2 recombination in BWR coolant 80−18504
Pd-Ni bilayers, on single cryst. Si, vacuum annealing, silicide form. 79−51444
plasticity, high temp., oxide inclusions effect 80−50681
Pt-Ni bilayers, on single cryst. Si, vacuum annealing, silicide form. 79−51444
$RbMnF_3$:Ni, antiferromag., exchange splitting of $^3T_{2g}E$ state, fluorescence meas. 77−12419
$RbMnF_3$:Ni, thermal cond., spin wave and mag. impurity contribs. 77−40046
S penetration of NiO scales 78−64776
^{32}S ions+Be(C)(Ni), radiative electron capture, X-ray ang. distrib. 77−38729
Se-Ni-Mylar multilayered struct., interfacial bonding effect on adhesion, ESCA obs. 79−95274
Si (111)$\sqrt{19}\times\sqrt{19}$ Ni surface struct., RHEED 77−62452
Si:Ni, (111) surface impurity, ESCA obs. 78−52640

nickel continued
Si:Ni, amorphous, vac. evaporated, doping, transport and optical props. 80−49715
Si:Ni, capture probabilities of two deep impurity levels by photocond. decay 80−49799
Si:Ni, electronic states of impurities 77−43531
Si:Ni, γ-irrad., interaction of deep-level impurity atoms with radiation defects 77−76457
Si:Ni, low temp. annealing effect on behaviour of Ni 79−10862
Si:Ni,O, interaction of Ni with O, influence of heat treatment, IR absorption meas. 77−4667
Si:Ni amorphous films, ESR and elec. cond. 80−50171
Si:Ni deep impurity levels, electron capture probabilities rel. to temp. 78−2523
Si:Ni p^+n and n^+p diodes, thermally stimulated capacitance obs. of Ni acceptor levels 78−19137
Si/Ni, Stoneley waves at (001) interface between cubic symm. cryst. 80−100388
Si-Ni, influence of neutron irradiation on elec. props. 78−55895
n-Si-Ni, Schottky barrier, thermal annealing effect on props. 79−69596
n-Si-Ni, Schottky-barrier, I-V characts. of elec. contact 79−19662
Si-Ni Schottky barriers, thermionic field emission at room temp. 78−6445
Si-Ni Schottky diode, type II localised interface states, Si surface prep. effects 78−39210
Si-TiO_x-Ni, MIS amorphous solar cell, increase in open-circuit voltage and short-circuit current on addition of TiO_x layer 79−57425
SrF_2:Ni, X-irrad., optical absorpt. spectra and dichroism meas. 80−108239
SrO:Ni, EPR of Ni^+, two-stage increase in symmetry, reorientation of cryst. field axes 78−27085
SrO:Ni, optical absorption spectra in visible and near IR region 80−45119
SrO:Ni^+, noncentral Jahn-Teller ion, energy minimum localisation, ESR study 80−25198
SrO:Ni^{2+}, EPR line splitting rel. to Jahn-Teller coupling and soft localised mode 80−66022
SrO:Ni^{2+}, ionic thermocurrent meas. 80−108148
SrO:Ni^{2+}, linear Stark effect for zero-phonon optical absorpt. line 80−80830
$SrTiO_3$:Ni, photochromism, optical absorption spectra and EPR meas. 77−1708
$SrTiO_3$-Ni, electrochromism, optical and elec. meas. 79−95732
TaC fibre reinforced eutectic superalloy, creep and rupture 77−63744
TiC-Mo_2C-Ni cermets, influence of anomalous phases on strength 78−92228
TiC-Ni, grain growth kinetics *(French)* 77−44252
TiC-Ni, reaction kinetics under simulated liq.-phase sintering 78−52746
TiC-Ni composite coating, activated reactive evaporation prep., structure 77−44393
TiC-Ni composite coatings, form. and wear resistant props. 77−63602
$TiCrB_2$-Ni, interphase reactions, electron probe anal., metallography and hardness exam. 80−2990
TiO_2:Si(Fe)(Ni)(Mn)(Cr), anodes, performance in photoelectrolysis of water 79−74407
TiO_2-Ni (100) interface, electronic props., struct., comp., chemical bonding 80−84499
VC-Ni, fracture mode determination, using Auger electron spectroscopy 80−7680
W, chemically driven grain growth during sintering in liquid Ni 79−61532
W fibre reinforced, alloy by effect on struct. stability, mech. props., metallographic exam. 78−56600
W fibre reinforced, high temp. strength 79−70021
W fibre reinforced Ni, high temp. stability 77−48372
W, fibre reinforced Ni, produced by liquid infiltration 77−48371
W fibre reinforced Ni composite, study at high temp. in O_2 and combustion gases 77−48567
W fibre reinforced Ni composites, high temp. tensile and creep props. 77−52444
W, sintering, Ni activated, grain boundary diffusion mechanism 79−91606
W:Ni compacts, optimum conc. of Ni for activated sintering, optical microscopy obs. 79−38758
W-Ni point contact diode, IR antenna characts. 77−49772
W-Ni point contact diode, rectifying props. in CO_2 laser radiation 77−76942
W-Ni point contact diode detectors at 10.6 μm, mech. and props. 78−24861
W-oxide-Ni high speed submicron junction, electron tunnelling spectra 79−99635
Y-Ni-Al ternary system, 800°C isothermal section in range 0 to 33.3 at.% Y *(Russian)* 77−70028
$Zn(BF_4)_26H_2O$:Ni, phase transition study, EPR of diluted Ni^{2+}, 98-298K 80−75846
$ZnCl_2$-KCl-NaCl, molten system, containing Ni^{2+} ions, appl. to electrorefining, polarographic study 80−66810
$ZnIn_2S_4$-Ni diode, electric and photoelectric characts. 77−12005
ZnO:Cu O:Ni, photocond., electron escape probabilities and trap depths 77−32041
ZnO:Ni^{2+}, Zeeman effect at Ni impurities 80−60633
ZnO:Ni^{2+} tetrahedral ion config. interaction and crystal field spectra intensity 78−43335
ZnS:Ag,Ni scintillator, effects on light decay time 77−42217
ZnS:Cu, O, Ni, photocurrent spectral distrib., killer impurity effects 77−8135
ZnS:Cu,O,Ni photoconductors, killer impurities effect on electron escape probabilities and trap depths 77−4392
ZnS:Ni, IR luminesc. and absorpt. spectroscopy 80−108261
ZnS:Ni, impurity-induced Raman scatt., central force const. reduction 77−32379
ZnS:Ni, vibr. modes of transition element impurities 78−76472
ZnS:Ni^{2+}, Zeeman effect at Ni impurities 80−60633
ZnS-CdS:Ag, Ni, Co, thermoluminesc. glow curves 78−95611
ZnS-CdS:Ag, Ni, Co phosphor, thermoluminesc. 77−66547
ZnS-CdS:Ni, electron-irradiated phosphors, void formation mechanism 79−55780
ZnS-CdS:Tm,Ni, recomb. centre interaction, luminesc. quenching 78−10946
ZnS(Se):Ni, optical absorpt., impurity ionisation, optical phonon coupling 80−88505

nickel continued
ZnSe:Ni, evidence for exciton binding at Ni impurity sites, photolum. excitation spectrum 80−45135
ZnSe:Ni, photocapacitance meas. of impurity level 77−69372
ZnSe:Ni, photolum. excitation spectroscopy 80−80841
$ZnSiF_6.6H_2O$, spin-phonon interaction between Ni^{2+} ions, phonon bottleneck effects, splitting parameters *(Russian)* 80−15796
$ZnSiF_6.6H_2O:Ni^{2+}$, EPR 77−59451
$ZnSiF_6.6H_2O:Ni^{2+}$, cryst. field, uniaxial compression method *(Russian)* 78−35027
$ZnSiF_6.6H_2O:Ni^{2+}$, spin-lattice relax. at press. up to 6.5 kbar 78−48033
$ZnWO_4:Ni^{2+}$, luminescence rel. to Ni concn. 79−24352
ZrC-Ni, refractory-liquid metal, interfacial reactions, C effect, electron microprobe analysis 77−12829

nickel alloys
see also Elinvar; Invar; nickel compounds; Permalloy
adhesive wear under unlubricated conditions 80−108593
age hardened, stress corrosion cracking resistance, plastic deform. and microstruct. relation 77−63829
Alinco 5, thermal treatment in mag. field, mag. props. 78−91905
ALLOY 713LC, corrosion kinetics and products under low oxygen partial pressures *(German)* 79−87764
Alnico, 5 and 8, spinel type permanent magnet, magnetic aftereffect 77−16118
Alnico, domain struct., variation under influence of heat treatment *(Russian)* 78−23292
Alnico, high-energy magnetic materials technology developments and props. *(Italian)* 80−54914
Alnico 5 alloy, S and Ti additions effect rel. to non-metallic inclusions, coercive force and grindability 80−89375
Alnico 5 and 8, spinodally decomposed magnetic alloy, magnetic flux temp. coeff. *(Japanese)* 78−35006
Alnico 8, permanent magnetic alloy, topography of precipitate phase *(Chinese)* 80−66512
Alnico alloy, C addition effects on struct. and mag. props. 78−23835
Alnico alloys, effect of Ce addition on mag. props. 78−2699
Alnico type YuNDK25DA alloy permanent magnets, thermal mag. hysteresis 80−75818
alumel, B versus H measurement from 25 to 180°C 78−23297
Alumel, thermocouple alloy, heat treatment effects on thermoEMF and mag. flux 77−63235
alumel thermocouples, decalibration, quantitative SIMS anal. 80−4705
aluminide coating, spontaneous form. of diffusion barrier *(German)* 78−71886
amalgam, anodic polarisation in alkaline soln. 80−11823
amorphous, corrosion characteristics, book contrib. 79−66225
amorphous, liq. quenched, struct., thermal stability and mech. props. 80−88059
amorphous metal-metalloid alloys production by ion implantation, TEM study 80−15128
anodic charact. meas. by AC impedance method *(Japanese)* 79−70224
anomalous Hall effect, contribution from skew scattering and side displacement of two-current model 79−56198
Astroloy, grain coarsening by critical strain annealing 79−47711
austenitic alloy GAB 286, energetic particle bombardment, thermodynamic and dimensional stability 77−27904
austenitic alloys, corrosion performance in automobile exhaust environments 78−7091
Bi-Ni base alloys, heterogeneous, supercond., magnetisation meas. *(French)* 78−6477
binary, constituent segregation during irradiation 79−55791
binary, magnetic resist. anisotropy, two-current model 77−20295
binary alloy, irrad. with heavy ions, non-equilib. segregation phenomena 80−19950
binary alloys, solute segregation and precip. under heavy-ion bombard. 79−11623
binary substitutional solutions, thermodynamics 80−44336
boride coatings on Ni alloy, thermal stability, exam. of coating 78−44271
Brightray S, lattice contraction during ageing 80−3030
Carpenter 20 Cb-3 alloy, pitting resist. in low salinity geothermal brines 80−93681
chemically stabilised, sensitisation and corrosion resist., heat treatment depend., precipitation steel, stainless, Cr-Ni 79−38827
Chromel, thermocouple alloy, heat treatment effects on thermo EMF and mag. flux 77−63235
Chromel alloy, influence of elastic strain on oxidisability *(Russian)* 79−70116
chromel thermocouples, decalibration, quantitative SIMS anal. 80−4705
coated with Cr_3C_2 (Cr_7C_3) based coatings, detonation deposited, wear resist., 20-1000°C 80−11843
Colmonoy, friction behavior in high temp. Na environment *(Japanese)* 80−40546
Colmonoy, self-weldability in high temp Na *(Japanese)* 80−89392
Colmonoy hardfacing materials, friction characts. in high temp. Na *(Japanese)* 80−89356
compatibility with Si_3N_4, solid-solid reactions 79−28151
composite, Cr_3C_2 fibre reinforced, oxidation and creep, Y additions effect 80−66685
computer prediction of long term strength by generalised diagram method 77−70133
Constantan, fatigue, grain size effect 77−21260
Constantan single wire, thermal expansion +20 to −60°C, strain gauge use 77−67427
constitution changes due to radiation effects 80−34048
constructional, KhN56VMKYu, creep, viscosity, resist. to inelastic deform. 80−89309
correl. between void swelling and thermodynamic stability 80−641
corrosion, monitoring using polarisation resistance meas., techniques and correlations 77−16711
corrosion behaviour in reducing environment of coal fired MHD generator 80−104322
Coulomb and exchange scatt. amplitudes, spin dependent residual resistivities 78−64033
crack growth behaviour at 425°C of type 718 79−61731
creep, corrosion, and fatigue testing for appl. in nucl. process heat system 78−13237
creep, effect of preliminary heat treatment on struct. and props. of alloy EI617 77−21195
creep crack growth in alloy 718 77−63776

nickel alloys continued
creep transients, friction stress and recovery, dislocation substruct. 80−60933
crevice corrosion by water vapour, CO, methane in HTR coolants, model 77−25202
crevice corrosion in marine conditions 77−56135
Cu_cNi_{1-c}, soft X-ray emission spectra 78−95620
Cu_xNi_{1-x}, magnetism of surface 78−95511
Cu-Ni, dil., local mag. moments and Kondo effect, theoretical model 79−69651
Cunial MNA13-3, Mn addition effect on props. 80−21035
CVD Al coating, transport agent comparison 78−11429
cyclic creep of heat resistant alloys *(Russian)* 78−19845
cyclic oxidation, Ni base alloys, role of thermal shock 80−97640
cyclic oxidation, static and dynamic, high temp. alloys 78−88576
damping, logarithmic decrement meas. by torsion pendulum *(German)* 79−74195
defect buildup and solute segregation, in alloys under pulsed irradiation, Ni model material 78−71757
dilute, factors affecting high-temp. oxidation behaviour, alloying effects 77−77638
dilute, hyperfine field at positive muon 80−40029
dilute, hyperfine field distribs., DPAC meas. 80−93222
dilute, implant profiles modification by radiation enhanced diffusion and segregation 80−88217
dilute, impurity effects on grain boundary mobility *(Polish)* 79−96073
dilute, near surface composition, effect of irradiation and sputtering 79−33168
dilute metastable alloy formation by ion implantation 80−15130
directionally solidified, fatigue crack propag. 77−36639
directionally solidified Mar M200, Hf additions, effect of vol.% γ' on creep rupture 78−27526
distillation deoxidation during electron beam melting *(Russian)* 79−70306
$DyNi_{3.4}$, magnetisation data 77−32177
earth reentry exposure, simulated, effect on mech. props., oxidation of ThO_2 dispersion hardened alloys, Haynes 188 and Hastelloy X 79−5086
electrical resistivity at low temp. *(Russian)* 79−23941
electrolytic deep etching 78−31604
electronic specific heat, near and weak ferromagnetics 78−80158
embrittlement in high-pressure hydrogen, protection by Cu electroplating, aerospace engine appl. 80−76416
eutectic alloys, unidirectionally solidified, solidification and morphology relationship 80−25684
eutectic alloys in gas turbines, Ni-Cr-Al coatings, use of diffusion barrier 79−24673
fatigue and cyclic plasticity rel. to struct. inhomogeneity 80−81184
fatigue and heat resistance of alloy EhI867, annealed, effect of structural state *(Russian)* 79−34140
fatigue crack growth at 298 and 823K, frequency and wave form effects, in alloy 718 78−64636
fatigue crack propag. kinetics *(Russian)* 77−70146
fatigue crack propagation, kinetics 78−68804
fatigue strength, temp. depend. of high temp. alloys 77−56100
$Fe_{40}Ni_{40}P_{14}B_6$, amorphous, tape wound core, fluctuations of driving field 78−10726
$Fe_{40}Ni_{40}P_{14}B_6$, $Fe_{32}Ni_{36}Cr_{14}P_{12}B_6$, amorphous Hall effect, press. and temp. depends. 77−66155
ferromagnetic, hyperfine fields of 4d and 5d impurities 78−31133
ferromagnetism, Stoner model, mol. field coeff., temp. and field depends. 77−72975
filamentary crystal prep. from brittle high-strength mats., mech. props. *(Russian)* 77−59712
glassy, continuous-biased sputter-deposited Kr entrapment 80−24603
Hall effect, anomalous, two current model 77−62906
Hall effect, normal, at 4.2K, two-spin current model interpretation 77−15829
Hastealloy X, relations between weld heat affected zone cracking and microstruct., Gleeble test *(Japanese)* 78−52858
Hastelloy, C-276, H transport rel. to ageing treatment 80−75384
Hastelloy, C-276, H-induced crack growth 80−71747
Hastelloy, H_2 embrittlement in H_2S environments, impurity segregation effects 80−71724
Hastelloy, thermionic electron emission into Cs vapour 78−60540
Hastelloy alloy, G and C-276, pitting resist. in low salinity geothermal brines 80−93681
Hastelloy B-2, corroded surface, electron bombardment effect during Auger electron anal. 80−61014
Hastelloy B-2, decomposition of metal oxide films under electron bombardment 78−19928
Hasteiloy C, stress corrosion cracking in high temp. caustic soln. 77−59964
Hastelloy C-276, cold worked, annealed, surface segregation, Auger spectroscopy study 79−83204
Hastelloy C-276 and C-4 cold worked high alloy material, factors affecting H_2 embrittlement in H_2S environments 78−31502
Hastelloy C-276 and G, accelerated H_2 charging in aq. H_2SO_4 at 0.2% yield stress 80−30144
Hastelloy C-276/Bi_2Te_3 contacts, elevated temp. compatibility, appl. to radioisotopically powered thermoelec. generator 79−49680
Hastelloy C-4, loaded at high temp., useful life 80−40523
Hastelloy N, air contamination effect on compatibility with liquid Li in stainless steel vessels at 600°C 78−25285
Hastelloy N, Si additions, comp. of eta carbide after ageing 78−52816
Hastelloy X, carburisation and dimens. stability in HTGR, He environment 80−45366
Hastelloy X, corrosion behaviour in simulated HTGR He environment 79−54495
Hastelloy X, creep, effect of He environment and grain size *(Japanese)* 77−48488
Hastelloy X, creep and creep rupture props. in air and helium at 900°C *(Japanese)* 77−52405
Hastelloy X, creep props. and appl. to structural design *(Japanese)* 77−59862
Hastelloy X, grain size effect. creep and creep-rupture *(Japanese)* 80−16382
Hastelloy X, H permeability using permeation method, effects of heat treatment *(Japanese)* 78−51740
Hastelloy X, heat resistant superalloys, for nuclear plants in He, creep props. *(Japanese)* 79−83263

nickel alloys continued
Hastelloy X, high temp. low cycle fatigue strength *(Japanese)* 77−59910
Hastelloy X, high temp. low cycle fatigue tests, ductility, fracture 77−90523
Hastelloy X, mech. props. effect of solidification substruct. 77−25040
Hastelloy X, thermal fatigue props. 80−21071
Hastelloy X-R, reaction with sintered Li_2O pellets 79−39137
Hastelloy-X, carbonisation and carburisation in high press. He environment *(Japanese)* 79−26516
Hastelloy-X, electron irrad., void swelling 79−14822
Hastelloy-X, fatigue crack propag. at elevated temps. in solid solution strengthened superalloys 78−39895
Hastelloy-X, low cycle fatigue crack propagation at 25°C and 760°C 80−104270
Hastelloy-X, Ni-Cr-Fe-Mo, cyclic oxidation resist. improvement by high temp. etching treatment 80−97627
Hasteloy B, equilibrium surface bombarded with high dose He^+ ions 78−95091
Hayes alloy no.716, Fe-Cr-Ni-Co-W-Mo-Si-C-B (26, 22, 12, 3.5, 3, 1.2, 1.1, 0.4 wt.%), hardfacing alloy 80−100802
Haynes alloy 188, fatigue crack propag. at elevated temps. in solid solution strengthened superalloys 78−39895
Haynes alloy 188, H_2 permeability 77−46399
Haynes alloy 188, SEM exam. of fracture surface, due to low cycle fatigue at 700°C *(Japanese)* 78−52963
Haynes alloy 20 Mod, pitting resist. in low salinity geothermal brines 80−93681
heat resistance, thermal fatigue, type VZhL-12U 79−20179
heat resistant, creep resistant deform. 79−100234
heat resistant, cyclic determ. at elev. temps. 79−66125
heat resistant, determ. of sub-ppm levels of Ag by graphite furnace atomic absorption spectrometry 78−48730
heat resistant, EI867, mech. props., effect of prolonged elevated temp. 77−21194
heat resistant, fatigue limit comparison in torsion and tension-compression 80−81181
heat resistant, high temp. plasticity at different strain rates 77−21233
heat resistant, optimum alloying 77−55904
heat resistant alloy EhP539L, heat treatment effect on props. and hardening phase morphology 80−29995
heat resistant alloy KhN60MKBYuT, plasticity, precipitation 77−70120
heat resistant alloys, atomic absorption spectrometry with heated graphite atomizer, Bi and Pb trace quantities 78−15749
heat resistant alloys, orientational correspondence between γ solid solution, and $\gamma+\gamma'$ eutectic precipitation *(Russian)* 79−11621
heat resistant casting alloy, fatigue resistance, microstruct. obs. 79−66159
heat resistant charact. extrapolation by temp.-time methods, creep data 78−15477
heat resistant EI437B and EI929, surface condition, air stream effect 80−76409
heat resisting, types EhI598, ZhS6KP, and 1, fatigue under mech. and thermal stress 79−66164
heat-resistant, EP742 type, variation in struct. during thermomechanical treatment *(Russian)* 79−52250
heat-resistant composite materials, creation of matrices with operating temp. of 1100°C *(Russian)* 77−55913
heat-resisting alloy, EP199, creep-rupture strength in NH_3 and decomp. products *(Russian)* 77−52534
high heat resistant, industrial appl. and comp. *(Korean)* 79−24716
high-temperature materials, technological requirements, R and D, report 80−45222
hot corrosion in coal conversion system atmos. 79−96200
hot hardness and oxidation resistance meas. 78−31588
HYCSOS chemical heat pump, low grade heat enhancement using $LaNi_{5-x}Al_x$ 80−61467
hydrogen permeation charact. 79−67948
Iconel, oxide film quantitative anal. by XPS and rastered ion bombardment 77−40604
In 519 high temp. low-cycle fatigue behaviour for nuclear process heat appl. 80−628
IN-100, fatigue crack growth retardation at elevated temp. 80−3158
Incaloy 623, cold worked, factors affecting embrittlement in H_2S 78−31502
Incaloy 800, for LMFBR steam generators 77−3108
Incaloy IN 738, dispersion hardened superalloy 78−11156
Inco 718, fatigued specimens, plastic zone size 77−25150
INCO 901, fatigue crack propag. theory 78−5692
Incoloy, 800 and 807, heat resistant superalloys, for nuclear plants in He, creep props. *(Japanese)* 79−83263
Incoloy, alloy 800, $M_{23}C_6$/austenite phase boundary defect struct. resolution by weak beam microscopy 80−3046
Incoloy, evaluation for use in nuclear process heat appl. 78−13234
Incoloy, oxide-dispersion-strengthened, pulsed YAG laser welding 79−70075
Incoloy, stress corrosion cracking in high temp. caustic soln. 77−59964
Incoloy 600, H_2SO_4 vapour corrosion, in general atomic S-I thermochem. water-splitting cycle 80−45449
Incoloy 600 and 800, surface film in hot conc. NaOH, XPS study 80−11824
Incoloy 600 vacuum heat treatment for improved corrosion resistance of PWR steam generator tubing 80−5246
Incoloy 800, 600 and 718, press. vessel, fatigue design criteria 78−60758
Incoloy 800, and 800 H, low cycle fatigue behaviour comparison 79−43438
Incoloy 800, and 800H, proposed specification changes 79−43298
Incoloy 800, appl. 79−43553
Incoloy 800, austenitic, creep fatigue interaction at 600°C 78−64672
Incoloy 800, austenitic, fatigue at elevated temps., second phase form. effect 77−36637
Incoloy 800, cast, microstruct. evolution during creep, TEM obs. 79−43366
Incoloy 800, chem. behaviour and mech. performance in HTR He at high temps. 79−47842
Incoloy 800, clean and steam oxidised, T_2 permeation 80−88364
Incoloy 800, contamination and decontamination of samples from KFA experimental duct of DRAGON reactor 79−45600
Incoloy 800, corrosion and carburization in liquid Na up to 973K 79−47841

nickel alloys continued
Incoloy 800, corrosion fatigue crack propagation in pure water at 85°C *(Japanese)* 79−43472
Incoloy 800, corrosion resist. props. in high temp. steam, review 79−47839
Incoloy 800, cracking in NH_3 at 600°C 79−70207
Incoloy 800, creep and fatigue props. in high temp. gas cooled reactor He environment 79−47776
Incoloy 800, creep crack growth, age hardening effect 79−43436
Incoloy 800, creep rupture, creep strength and tensile data, 500 to 800°C 79−43371
Incoloy 800, creep rupture ductility, 500 to 600°C, hardness and metallurgic exam. 79−43435
Incoloy 800, creep rupture props. at 525°C 79−43437
Incoloy 800, design codes and lifetime prediction aspects for nuclear and non nuclear appls. 79−47778
Incoloy 800, design problems in steam generators of high temp. reactors 79−45352
Incoloy 800, eddy current testing *(German)* 79−96257
Incoloy 800, effect of liquid Na on creep and rupture props. 79−47775
Incoloy 800, exam. of caustic stress corrosion cracking, comparison with type 304 stainless steel 79−29261
Incoloy 800, exam. of mech. and microstructural props. 79−5022
Incoloy 800, fatigue crack behaviour in bending and pull-push modes 77−81315
Incoloy 800, from KFA experimental duct at 700°C and 480 d in DRAGON reactor, mech. props. before and after contamination 79−47777
Incoloy 800, high temp. corrosion and mech. props. in Na environment 79−47840
Incoloy 800, high temp. gaseous corrosion in sulphidising environments 79−47838
Incoloy 800, high temp. oxidation in low O_2 pressures, SEM obs. of oxide morphologies 79−47844
Incoloy 800, intergranular precipitation, predicted behaviour 79−100148
Incoloy 800, mech. props. above 600°C 79−43370
Incoloy 800, mechanical props., heat treatment and appl., conf., Petten, Netherlands (March 1978) 79−43296
Incoloy 800, mechanisms of corrosion in He 79−47843
Incoloy 800, microstruct. effect on mech. props. 79−43367
Incoloy 800, nuclear grade boiling tubing superalloy, Co and C content anal. 80−78397
Incoloy 800, oxidation resistance, alloy depletion effect 77−8989
Incoloy 800, pretreatment potential effect on pit generation *(Japanese)* 79−43474
Incoloy 800, reaction with sintered Li_2O pellets 79−39137
Incoloy 800, review of mech. props. up to 600°C 79−43368
Incoloy 800, review of structural charact., heat treatment and comp. effects 79−43297
Incoloy 800, review on high temp. gaseous corrosion in carburising and oxidising environments 79−47837
Incoloy 800, solution annealed, low and high cycle fatigue correlation 79−43439
Incoloy 800, steam oxidised, oxide coating anal. 80−89399
Incoloy 800, stress corrosion cracking and anodisation during straining in boiling NaOH soln. 80−30140
Incoloy 800, stress corrosion cracking in contaminated aq. media at high temp. *(French)* 79−20273
Incoloy 800, stress corrosion cracking in NaOH solns., electrochem. aspects, peening treatment 80−97618
Incoloy 800, thin wall tubing, creep-rupture testing in steam under constant and cyclic load 79−47774
Incoloy 800, use up to 550°C, creep ductility 79−43369
Incoloy 800 and 802, influence of carburisation on mech. props. 79−20254
Incoloy 800 Fe base heat resistant alloy oxidation 77−86231
Incoloy 800 for HTR appls., correlation of carburization behavior, mechanical property degradation, and exposure conditions 80−5244
Incoloy 800 H, 617, high temp. low-cycle fatigue behaviour for nuclear process heat appl. 80−628
Incoloy 800 in 50% NaOH, stress corrosion cracking, slow strain rate method *(Japanese)* 80−55575
Incoloy 800H, carburisation and dimens. stability in HTGR, He environment 80−45366
Incoloy 800H, H_2SO_4 vapour corrosion, in general atomic S-I thermochem. water-splitting cycle 80−45449
Incoloy 800H, high temp. low cycle fatigue, ageing and cold working effect 79−43277
Incoloy 800H, high temp.-low cycle fatigue, ageing and cold working effect on initial stress/strain curve 79−47720
Incoloy 825, corrosion resistance as structural material for denitrification vessel 77−36685
Incoloy 901, foil prep. for TEM exam. 80−88001
Incoloy 903, H_2 permeation and diffusion 78−26730
Incoloy 903, microstruct. and effect of H_2 charging 77−86143
Incoloy MA956E, mechanical alloying for high temp. appl. 78−44046
Incoloy-800, annealed, mech. behaviour anal. for elevated-temp. LMFBR appl. 80−18428
Incoloy-800, meas. of H and D permeation for reactor safety anal. 79−77822
Inconel, 617 and 625, heat resistant superalloys, for nuclear plants in He, creep props. *(Japanese)* 79−83263
Inconel, caustic stress corrosion cracking resistance, processing variables effect 80−71796
Inconel, chloride corrosion in hot acidic media 78−35552
Inconel, compact ductile fracture toughness specimens, load line displacement measurement method at elev. temps. 78−27700
Inconel, corrosion in acidic chloride soln. at 25°C 77−70202
Inconel, D trapping in fusion reactor materials, temp. dependence 80−37577
Inconel, fatigue crack growth rate in high temp., high purity oxygenated water 80−40622
Inconel, fusion reactors Li cooling system, corrosion inhibition by Al additions 80−108646
Inconel, ion plating using alumina 77−40476
Inconel, pressure vessel bottom, subcritical crack growth in ligament between instrumentation rods 79−22428
Inconel, sputtering and blistering from H^+ and He^+ bombardment 78−79649
Inconel, steam generator tubing, mag. probe inspection 80−85119
Inconel, stress corrosion cracking in high temp. caustic soln. 77−59964

nickel alloys continued
Inconel, type 706, precipitation and creep rupture behaviour, optical and TEM study 79−74158
Inconel, X-750 and 700, NDT turbine blades by small angle neutron scattering 79−20055
Inconel 600, atomic S diffusion *(French)* 79−74307
Inconel 600, corrosion fatigue crack propag. at 85°C in 50% NaOH, potential effect *(Japanese)* 80−11834
Inconel 600, corrosion fatigue crack propagation in pure water at 85°C *(Japanese)* 79−43472
Inconel 600, Cr diffusion 77−20110
Inconel 600, effects of ageing and misorientation on intergranular corrosion *(Japanese)* 79−79158
Inconel 600, equilibrium surface bombarded with high dose He^+ ions 78−95091
Inconel 600, exam. of caustic stress corrosion cracking, comparison with type 304 stainless steel 79−29261
Inconel 600, fusion reactor vac. vessel, air, N, adsorpt., thermal desorpt., heat treatment effects 78−54880
Inconel 600, mechanisms of dynamic strain ageing and jerky flow 79−79024
Inconel 600, Neutron irradiation using HFIR for evaluation as fusion reactor material 78−13324
Inconel 600, nuclear grade boiling tubing superalloy, Co and C content anal. 80−78397
Inconel 600, oxide layer, mechanical impedance meas. method 80−45444
Inconel 600, PWR primary corrosion products 80−13578
Inconel 600, reaction with sintered Li_2O pellets 79−39137
Inconel 600, S penetration leading to sulphide form. *(French)* 79−74306
Inconel 600, small bore tubing, crevice corrosion 80−60999
Inconel 600, stress corrosion cracking and anodisation during straining in boiling NaOH soln. 80−30140
Inconel 600, stress corrosion cracking in NaOH soln. 79−66196
Inconel 600, stress corrosion cracking in NaOH solns., electrochem. aspects, peening treatment 80−97618
Inconel 600, stress corrosion cracking in primary water 79−93728
Inconel 600, surface composition depend. on H atom influx, AES 79−5192
Inconel 600, thermal outgassing after various surface preparations 79−67952
Inconel 600, thermal treatment, grain boundary microstruct. and SCC resistance 80−71675
Inconel 600, thermionic electron emission into Cs vapour 78−60540
Inconel 600, XPS exam. of initial growth of oxide films 79−20240
Inconel 600 alloys, stress corrosion cracking, prediction in 10% NaOH soln. at 315°C 80−97616
Inconel 600 and 601, films deposited by cylindrical magnetron sputtering, internal stresses 80−24773
Inconel 600 and 601, influence of carburisation on mech. props. 79−20254
Inconel 600 and 718, gas desorption coeffs., electron- and ion-induced, bakeout temp. effect 79−65329
Inconel 600 and 718 in liquid Na environment, fatigue crack propag. 80−40624
Inconel 600 in 50% NaOH, stress corrosion cracking, slow strain rate method *(Japanese)* 80−55575
Inconel 600 safe-end cracking failure at Duane Arnold reactor 80−104295
Inconel 606, discontinuous creep process 79−66124
Inconel 617, 800, corrosion behaviour in simulated HTGR He environment 79−54495
INCONEL 617, corrosion kinetics and products under low oxygen partial pressures *(German)* 79−87764
Inconel 617, creep, morphological changes of carbides, affect on creep props. 80−108509
Inconel 617, mass spectrometric study, high temp. reactor system appl. 79−43663
Inconel 617, microstruct., mech. props., thermal ageing effect 77−36557
Inconel 625, accelerated H_2 charging in aq. H_2SO_4 at 0.2% yield stress 80−30144
Inconel 625, creep rupture behaviour in Ag environment 80−25853
Inconel 625, creep rupture strength and corrosion in HTC in He *(German)* 77−77557
Inconel 625, electron yields under ion bombardment for clean and oxidised surfaces 80−66368
Inconel 625, nitriding in N_2-H_2 glow discharge 80−16590
Inconel 625, organic contamination removal by plasma cleaning and etching 80−97645
Inconel 625, pitting resist. in low salinity geothermal brines 80−93681
Inconel 625, plasma nitriding, hardness meas., Rutherford backscatt. surface anal. 80−45442
Inconel 625, secondary ion emission due to H ion bombardment 79−8216
Inconel 625, surface treatment of plane and hollow components in glow discharges 79−1923
Inconel 675, wall and limiter material for Tokamaks, induced desorption diffusion and gas production by 100 eV electrons and ions 79−675
Inconel 706 and 718, relations between weld heat affected zone cracking and microstruct., Gleeble test *(Japanese)* 78−52858
Inconel 718, blistering by 2 MeV He^+ ions, optical microscopy and SEM obs. 79−42119
Inconel 718, creep fracture characts. 79−52339
Inconel 718, environment effect on high temp. fatigue crack growth 80−30090
Inconel 718, grain growth during sintering 80−97449
Inconel 718, H_2 permeation and diffusion 78−26730
Inconel 718, H plasma effects on fusion device vacuum vessel 80−21111
Inconel 718, heat capacity 313 to 1053K 79−10964
Inconel 718, high temp. fretting fatigue, fatigue and fretting wear 80−3197
Inconel 718, low cycle fatigue at 298 and 823K 77−86151
Inconel 718, plastic deform., accelerated evolution of H_2 77−36594
Inconel 718, superalloy, wear of superhard tool during cutting, SEM and metallographic obs. 78−64720
Inconel 718, surface flawed tensile bars, utility in cyclic life studies 77 21342
Inconel 718 cladding possibility for gas-cooled fast breeder reactor fuel 77−18667
Inconel 738, SEM and electron beam analyser study *(German)* 79−20056
nickel alloys continued
Inconel 750, volatilisation of oxides during oxidation at 1200°C 78−23873
Inconel 800, simulated, steam oxidation 80−76405
Inconel 82, discontinuous creep process 79−66124
Inconel alloy 600, precipitation effect on corrosion 77−25180
Inconel alloy 600 in 10% NaOH soln. at 315°C, influence of thermal treatment 79−91841
Inconel alloy 600 steam generator tubing, effect of C content and thermal treatment on SCC behaviour 79−91844
Inconel alloy 718, exam. of struct., properties and continuum synthesis of ductile fracture 78−76736
Inconel alloys for VHTR heat exchangers, material criteria and selection 78−13232
Inconel hardfacing materials, friction characts. in high temp. Na *(Japanese)* 80−89356
Inconel MA754, mechanical alloying for high temp. appl. 78−44046
Inconel X750, positron annihilation study of ageing and creep 80−29824
Inconel X750 springs, in-reactor stress relaxation 78−11256
Inconel X, X-ray study of stress meas., elastic const. *(Japanese)* 79−66092
Inconel X-750, deform. and fracture characts., 24-816°C 80−108551
Inconel X-750 foil, surface pretreatment for improved coating adherence 79−15877
Inconel-625, hydrogen permeation characts. 79−69295
Inconel-718, blistering and exfoliation by 2 MeV He^+ beam 79−46722
Inconel-sheathed MgO-insulated $Pt_{90}Rh_{10}$/Pt thermocouple, decalibrations during 1200°C use, ion microprobe obs. 78−57957
inelastic cyclic deform. and fatigue 77−63795
interatomic interaction by XPS 80−7474
intermetallic compounds, containing d-transition metal, hydrogenated, magnetism 80−34609
intermetallic second phase obs. using electrolytic extraction and SEM 79−34074
Kovar, effect of magnetic electrons on atomic interactions 77−43820
Kovar, thermostress treatment of thin-rolled sheets 79−52273
Kovar substrate, TiB_2 coating prep. by CVD and interaction with substrate 79−24680
Kovar-silicon oxynitride-aluminium cathode, local electron emission and electroluminescence patterns obs. 80−108327
liquation cracking during welding, comp. influence 80−66645
low C 80 A, TEM obs. of cellular transformation products 80−3045
magnetic moment distribution 77−32178
magnetic props. at freq. up to 1 MHz *(Russian)* 77−8330
magnetically-soft materials, mag. characts. determ. methods, review 79−40593
magnetostriction and rolling texture, effect of alloying additions *(Russian)* 77−32229
magnetostriction and texture, effects of rolling and oxidation 77−36671
Magnico alloy, with Si, Nb, Ti and La, low-temp. thermomag. treatment 77−63812
Magnico alloy, with Si, Nb, Ti effect of Ub on mag. props. and grindability 77−63811
manganin foil like gauge calibration in planar shock wave expts. 80−95091
manganin resistance gauge for high pressure meas. 77−10036
mathematical-physical considerations rel. to metal powder prod. 80−11595
metallic glasses, ductile-brittle transition 77−4847
metallic glasses, elastic const. 77−66671
metalloid-transition metal amorphous surface alloys formed by ion implantation, TEM study 78−67730
metallurgical stability and corrosion in impure He atmospheres, HTR appl. 79−36329
metastable alloy form. by ion implantation 79−82252
metastable alloy formation by ion implantation 79−14828
Metglas 2826 ribbon, saturation magnetostriction meas. by small-angle magnetisation rot. 80−60391
Metglas 2826 ribbon, voids formation during crystallisation 80−108428
Metglas 2826-A, anomalous magnetisation, critical effects, superparamagnetism 77−8328
Metglas 2826A, direct meas. of decomp. on crystn. by X-ray microanal. in STEM 79−48025
mischmetal-$Ni_{5-x}Al_x$ ternary alloys, Al addition effects on structural and H_2 absorpt. props. 79−52761
Mischmetal-Ni, $MMNi_5$ substituted hydrides for H storage appls. 80−45791
Mischmetal-Ni alloy, H_2 adsorption and desorption *(Japanese)* 77−47668
mischmetal-Ni-Al alloys, H_2 absorpt.-desorpt. characts. 79−95168
Mo-Ni powder mixtures, form. using electric discharge sintering 77−12563
Monel, in thermoluminesc. dosimeter, low dose meas. *(Japanese)* 78−86696
Monel, Ni-Cu-Fe-Mn, resistance spot weld quality evaluation, using stress wave emission technique 78−53066
Monel 400, corrosion susceptibilities in synthetic geothermal brines 77−86223
Monel 400, stress corrosion cracking in high temp. caustic soln. 77−59964
Monel 400, stress corrosion cracking in NaOH soln. 79−66196
Monel K-500, environmental fatigue crack growth in H_2 79−5084
Monel K-500, fatigue crack growth rates in vacuum and O_2 environment 79−5083
Monel metal, cast, electrochemical behaviour in NaCl soln. 79−87763
Multimet, fatigue crack propag. at elevated temps. in solid solution strengthened superalloys 78−39895
mutual alloying behaviour of the elements straddling the line Li-Mg-Cu-Au in the long periodic table 78−84769
N31, martensitic point lowering by microplastic deform. and room temp. ageing *(Russian)* 77−25049
$(Ni_{1-x}Co_x)_{0.98}Mn_{0.02}$, average mag. moment of Mn atoms 79−28509
Ni_3Al-Ni_3Nb eutectic alloy, aluminide coating microstruct. exam. 78−15593
β_1-Ni-Al, premartensitic transformation 78−76645
Ni-base alloy 713LC, creep rupture strength and corrosion in HTR in He *(German)* 77−77557
Ni-Co, H_2 embrittlement, heat treatment and impurities effect 80−76331
Ni-Cr alloy Kh20N80, sintered sheet material, stopping power and pore size relationship 78−19693

nickel alloys continued
Ni-Cr-Mo-Ti-Al, quenching and ageing effects on props. of type 36NkhTYuM8 79−52275
Ni-Fe atomic and mag. ordering, cluster variation calc. *(Russian)* 78−15391
Ni-Pd-P, metallic glass, electronic structure, pulsed NMR study 80−75869
Ni-Zn ferrites, mag. param. 78−35005
Nichrome, alloyed with refractory metal borides, mech. props., rel. to appl. as electrodes in electrospark machining 80−21174
Nichrome, Kh20N80, varying porosity, effective thermal cond., 373-1400K, meas. method 78−75053
Nichrome, oxidation resistant coating, electrophoretic deposition on Mo *(Japanese)* 79−20270
nichrome, oxidised surface, adsorbed amines and hydrazines identification by surface ionis. 77−21456
Nichrome, volatilisation of oxides during oxidation at 1200°C 78−23873
Nichrome based dispersion hardened material, Ti, Y, Zr addition effects on crystallisation *(Russian)* 79−74143
Nichrome wire, porous, strength charact. 78−6997
Nichrome-silicate glass-CaF_2 multicomponent self-lubricating coating, prep. by plasma spraying, and props. 80−40604
Nichrome/steel, porous metal-thread sheet materials, filteration, permeability and strength props. *(Russian)* 79−78915
nickeliferous materials, properties and appls. *(German)* 79−79182
Nicralloy-coated 80−40611
Nicrosil-Nisil, thermocouple appl. for digital furnace control system 78−49831
Nilomag alloy 771 coloured, X-ray photoelectron spectroscopy of surface film 78−64899
Nimanic 80A, inhomogeneity effect of cyclin strain on crack initiation 78−48532
Nimocast, diffusion of Cs, AES, SIMS depth profile study *(German)* 78−84008
Nimomic PE-16, equilibrium surface bombarded with high dose He^+ ions 78−95091
Nimonic, ageing, roie of quenched-in vacancies 77−52363
Nimonic, IN100, γ' precipitates, casting conditions effect on morphology 80−7548
Nimonic, irradiated, void nucleation, numerical evaluation 80−70252
Nimonic 105, creep and stress rupture props., trace elements influence 80−66602
Nimonic 105, friction stress meas. during creep 79−61665
Nimonic 105, overaged, creep and fatigue crack growth 77−86138
Nimonic 105, quantitative STEM chem. anal. using standard and standardless programs 79−17578
Nimonic 105, temp. and stress depend. of microstruct., small angle neutron scatt. study 79−15726
Nimonic 115, superalloy, critical strain model for creep fracture 77−32648
Nimonic 75, crevice corrosion by water vapour and methane in Ar at 1 and 25 atm. 77−25203
Nimonic 80 A, TEM obs. of cellular transformation products 80−3045
NIMONIC 80A, corrosion kinetics and products under low oxygen partial pressures *(German)* 79−87764
Nimonic 80A, creep in tension and torsion 77−25113
Nimonic 80A, creep rapture under non-proportional loading 80−108518
Nimonic 80A, creep rupture strength and corrosion in HTR in He *(German)* 77−77557
Nimonic 80A, intergranular creep fracture under const. cavity density 78−60825
Nimonic 80A, lattice contraction during ageing 80−3030
Nimonic 80A, order hardening, comparison between revised theory and expt. 80−93565
Nimonic 80A, rapidly solidified, struct. and initial precipitation, field-ion and TEM study 79−78982
Nimonic 80A, stress dip creep tests 79−74223
Nimonic 80A, struct., fracture charcts. 80−3071
Nimonic 80A superalloy, contrast from cavities in HVEM 80−79780
Nimonic 90, creep rate stress exponents and friction stress, comparison with Lagneborg particle by-passing model 80−55481
Nimonic 90, dispersion hardened, friction stress rel. to initial and secondary creep 80−11711
Nimonic alloy, effect of annealing on hardness, carbide phase strengthening *(Russian)* 79−34137
Nimonic cylinder, stress redistribution obs. 77−4831
Nimonic EhI437B, heat resistant, true breaking stress in rapid air stream 79−66163
Nimonic PE16, abnormal grain growth after cold working and annealing 79−74176
Nimonic PE16, creep rupture props. in CO_2, air and vacuum environments at 700°C 79−74248
Nimonic PE16, fatigue crack growth rate, temp. effect 77−77568
Nimonic PE16, grain boundary carbide precipitation kinetics 77−52332
Nimonic PE16, He injected, bubble-void transitions in Ni ion bombard. 80−34095
Nimonic PE16, irradiation creep data obtained in fast and thermal neutron spectra correlation with displacement cross-sections 80−84993
Nimonic PE16, neutron irradiated after heat treatment, solute segregation to pt.-defect sinks 79−78976
Nimonic PE16, Ni ion irradiated, Ni segregation to voids 79−28020
Nimonic PE16, oxidation in Ar-H_2O-H_2 atmosphere 78−35584
Nimonic PE16, precipitation and growth kinetics of γ' 78−64546
Nimonic PE 13, mass spectrometric study, high temp. reactor system appl. 79−43663
Nimonic PE 16, γ' particle dispersion rel. to yield stress 79−29153
Nimonic PE 16, corrosion behaviour in high temp. impure He gas 80−76402
Nimonic PE-16, damage in high energy fluence D plasma 77−34427
Nimonic PE-16, electron irrad. in HVEM, void growth, vacuum environment influence 80−107323
Nimonic PE-16, neutron irrad. effects on fatigue crack propag. 80−29069
Nimonic type, elastic interphase strains on ageing effects on extinction *(Russian)* 77−66646
Nimonic type PE-16, irradiated, numerical simulation of void nucleation 79−73208
Nitinol memory material for solid-state engine 78−59288
NK, thermocouple alloy, heat treatment effects on thermoEMF and mag. flux 77−63235
nuclear fusion reactor materials development trends 77−46401

nickel alloys continued
Numonic 80A, grain boundary crack diffusional growth, high temp. rupture possibility 78−47471
overaged, creep and fatigue crack growth in IN 738 LC 77−86138
oxidation reaction investigation by X-ray diffr. and fluorescence *(German)* 79−57345
oxidation resistance at elevated temps., effect of various alloying additions 77−56134
oxide film isolation and obs. method 77−52563
oxide spallation, influence of ΔT (oxidising temp. minus cooling temp.) 77−52551
particle erosion meas. 77−66703
Permalloy-type sputtered film, structuring rel. to laser sputtering method *(Russian)* 77−59689
phosphor bronzes, surface Cs^+ impact, 5.5 keV negative secondary ion emission obs., rel. to Cu *(French)* 77−66562
plasma spraying of self-fluxing alloys, interaction with oxygen 79−61774
plasticity, heat treatment effect 80−76277
powder, crystallised by supercooling methods, struct. props. *(Russian)* 80−54483
powder, hot hydrostatic pressing of disk, capsule design 80−20839
powder alloy ZhS6U, US method of porosity detection 80−71828
precipitation hardening, effect on dynamic strain ageing and jerky flow 80−20945
precipitation identification by electron probe microanalysis *(German, English)* 77−77857
production methods, review of powder metallurgy methods, mathematical-physical considerations 79−95970
pseudoelastic single crystal fatigue 79−52364
radiation-induced swelling in BOR-60 reactor OKh17N40B, OKh20N60B, KhN77TYu 79−97814
rare earth alloys, $R_{69}Ni_{31}$, amorphous, Curie temp., mag. susceptibility and coercive force, 4.2 to 300K 80−93092
rare earth alloys, $RAuNi_4$, (R=Gd, Tb, Dy, Ho, Tm, Yb and Er), mag. props. 77−20595
rare earth alloys, $RGe_{2-y}Ni_y$ phases with AlB_2-type struct., lattice parameters 77−24292
rare earth intermetallic, $R_2Fe_{17-x}Ni_x$, mag. anisotropy and hyperfine interactions 77−8298
rare earth intermetallic, $RCo_{5x}Ni_{5-5x}$, narrow Bloch walls, magnetisation, 4.2K 77−8333
rare earth intermetallics, $R_{0.2}La_{0.8}Ni_5$, H_2 storage appl., desorption isotherms dependence on d-bandfilling 78−18912
rare earth intermetallics, $RFe_{5-x}Ni_x$, giant intrinsic mag. hardness 78−56354
rare earth intermetallics, RNi_3, amorphous alloys, mag. and transport props. 79−42513
rare earth intermetallics, $RNiSi_3$, mag. susceptibility, 80-1200K *(Russian)* 77−66281
rare earth-$(Co_{1-x}Ni_x)_5$, single cryst., mag. props., mag. reversal 77−85489
rare earth-Co-Ni alloys, $R(CoNi)_5$ type, mag. props. and mag. reversal phenomena *(Russian)* 77−51924
rare-earth-Ni alloy, RNi_2 (R=Gd, Tb, Dy, Ho or Er), Mossbauer effect of ^{57}Fe 77−69743
recrystallisation after hot deformation *(German)* 80−25716
recrystallisation and grain growth, influence of alloying *(Russian)* 80−81071
recrystallised grain boundary inheritance and props. 77−59816
Rene 41, Ni-Cr-Co-Mo-Ti-Al-Fe (18.96, 11.09, 9.65, 3.06, 1.59, 0.89 wt.%) formation of Cr_2O_3 monocrystals on heat treatment 79−52455
Rene 41, volatilisation of oxides during oxidation at 1200°C 78−23873
Rene 80, dislocation behaviour during plastic deform. *(Japanese)* 80−108504
Rene 95, as hot isostatically pressed (HIP) and HIP+forged, low cycle fatigue 80−25854
Rene 95, Ni based superalloy, effect of grain size and gamma prime size, on fatigue crack propag. 78−64686
resistivity anisotropy 77−39821
resistivity magnetoresistance, s,p impurities in ferromag. host 78−68008
Rheocast high performance superalloy, solid-liquid phase charact. 77−28803
rolled, annealing texture *(Russian)* 77−21159
SA, thermocouple alloy, heat treatment effects on thermoEMF and mag. flux 77−63235
Sanicro 30, stress corrosion cracking in NaOH soln. 79−66196
Sanicro 31, T permeation 80−88364
semiquantitative anal. with SIMS, AES and wet chemical anal. 77−48291
short-time and long-time strength of hot worked KhN55VMTFKYu produced by powder metallurgy 77−28752
solidification, method for evaluating influence of each element on microsegregation *(French)* 79−74159
solidified from supercooled condition, Si conc. influence on struct. *(Russian)* 77−16567
spin polarised tunnelling 78−95494
spin waves, mag. props. of alloys, review 80−44823
spring alloys, microplastic deform. and endurance limit 80−81197
sputter induced surface composition changes, in alloys 80−49470
steel, 18% Ni maraging, fatigue strength, effect of soln. treatment and inclusions 78−23805
steel, 18Ni-maraging, SCC, subcritical flow growth, comparison of aircraft alloys in NaCl soln. 78−53028
steel, alloy, cluster formation susceptibility in 40 KhN, influence of isothermal working in H_2 *(Russian)* 78−56643
steel, alloy, Fe-Cr-Ni-Mo-Al, (13, 8, 2, 1, wt.%), H_2 effects on fracture, exam. 78−60809
steel, alloy, Fe-Ni, effect of metallurgy on stress corrosion cracking, and hydrogen embrittlement 78−60885
steel, alloy, Fe-Ni-Cr-Mo-V-C, H_2S stress corrosion cracking, effects of overload, exam. 78−60886
steel, alloy, Fe-Ni-Cr-Mo-V-C, HY130, effect of H_2 and impurities on brittle fracture, review 78−60765
steel, alloy, Fe-Ni-Cr-Sb-C effect of Ni, Sb, on temper embrittlement 78−60813
steel, alloy, Fe-Ni-Mn-Si-Cr-Ni-Mo, effect of metallurgy on stress corrosion cracking, and hydrogen embrittlement 78−60885
steel, alloy, maraging, 250-grade, ductility and toughness of hot isostatically pressed powder 78−52925
steel, alloy, martensitic transforms. during deform. of types N28, N29, N30 and N31 78−56639

nickel alloys continued
steel, alloy, Ni (1 to 9 wt.%), Mossbauer, X-ray and electron microscope studies of martensite 78−56621
steel, alloy, Ni-Cr-Mn, type 4340 intergranular brittle fracture, exam. by impact testing and Auger spectroscopy 78−52978
steel, alloy, Ni-Cr-Mo, alloys SNCM8, SAE 4161, heat treated, residual stress at fatigue fracture surface *(Japanese)* 78−64622
steel, alloy, Ni-Cr-Mo, SNCM8, mech. stre-ngth under combined alternating strength 78−64690
steel, alloy, softening process in deformed type 15GYuT, metallographs *(Russian)* 78−52840
steel, alloy, YuNDK24, magnetisation direction in interaction domains *(Russian)* 79−99720
steel, alloy low, Ni-Cr, tempered martensite embrittlement 80−7669
steel, alloy type N24M5, martensitic transform. microkinetics 78−56637
steel, austenitic, cold worked 10Kh11N23T3MR, structural transformations, aging effect, electron microscope obs. 80−40402
steel, austenitic, Cr-Ni, anomalous stress-depend. of creep rate 80−11712
steel, austenitic, Cr-Ni, bulk and intergranular autodiffusion of ^{59}Fe *(French)* 79−55921
steel, austenitic, Cr-Ni, nonmetallic inclusions modification using rare earth metals *(Russian)* 80−40369
steel, austenitic, Cr-Ni (18,12 wt.%), containing coarse grain boundary precipitates, thermomechanical treatment 78−27545
steel, austenitic, Cr-Ni (18, 11 wt.%), creep rupture *(German)* 78−11297
steel, austenitic, Cr-Ni (18, 15 wt.%), oxidation resist., metallic alloying additions effect 79−52419
steel, austenitic, CrNi, high Mo, corrosion, effect of struct. *(German)* 77−90481
steel, austenitic, martensitic transform. temp., singularities in 50Kh2N22 *(Russian)* 78−68689
steel, austenitic, mechanical props. of DIN X8 CRNIMONB 1616 and DIN X2 CRNI 189, FBR safety anal. 78−60966
steel, austenitic, Mn-Ni-Cr, Mn effects on cracking *(German)* 77−59889
steel, austenitic, Ni alloy, stacking fault energy of austenite, high resolution electron microscopy *(Russian)* 80−44219
steel, austenitic, Ni-Cr, precipitation strengthened, anelasticity, plastic creep limit, 823K 79−1899
steel, austenitic, Ni-Cr high alloy, N_2, P and Ni effect on stress corrosion cracking and stacking fault energy *(Czech)* 78−60875
steel, austenitic (03KH18N10T), heat treatment for fission reactor appls. 80−66454
steel, austenitic stainless, biphase, ferritic, ageing and thermomech. treatment effects on struct. and props. 80−35226
steel, austenitic stainless, bulk and grain boundary diffusion of Fe, Cr, Ni, effect of Si content 78−38875
steel, austenitic stainless, Cr-Ni (18, 10 wt.%), ^{59}Fe self-diffusion in ferrite/austenite interface *(French)* 80−19975
steel, austenitic stainless, Cr-Ni-Mo (21,6,9 wt.%), N_2-strengthened, surface segregation of B, Auger and XPS spectra 79−90854
steel, austenitic stainless, Cr-Ni-Mo-Mn, Mo, Mn and ageing effects 78−35413
steel, austenitic stainless, Cr-Ni-Ti, creep deform. effects on intergranular TiC dispersion stability 78−84912
steel, austenitic stainless, hot plasticity, Y additions effect 79−83270
steel, austenitic stainless 12Kh18N10T and 15Kh17N2, corrosion cracking in chloride and alkaline solutions 80−55576
steel, austenitic stainless Cr-Ni, ^{51}Cr tracer diffusion coeffs. 80−34225
steel, austenitic stainless Ni-Cr, heat resist. and comp. of non-metallic inclusions, effect of La, Nd, Pr and Ce 80−76315
steel, C, diffusion of H_2, SCC via martensite form. cooling rate changes on Mn and Ni addition *(Russian)* 78−56813
steel, C-Mn-Cr-Mo (0.4, 0.8, 1.1, 0.25 wt.%) C, Ni, Mo, Cr addition effects on toughness of bainite 78−11327
steel, CC Cr-Ni, rock-like fracture *(Chinese)* 78−31497
steel, CC Cr-Ni, soaking at forging temp., effect on struct. and mech. props. *(Czech)* 78−64628
steel, Co-Cr-Ni-Mo-Mn (39.65, 20.25, 15.33, 7.08, 1.9 wt.%) carbide formation during tempering after plastic deformation 80−16330
steel, Cr, and Cr-Mo-Ni, austenite decomposition, deform. effects, ferrite reaction 79−1842
steel, Cr-C-Ni, struct. prop. rel., design of struct. steels for high strength and toughness 80−97491
steel, Cr-Mo and Cr-Ni-Mo, V effects on recrystallisation *(Russian)* 77−66654
steel, Cr-Mo-Nb-Ni, low alloy, material selection for LMFBR steam generator tubes 78−54834
steel, Cr-Ni, bainitic habit plane determ. 79−1927
steel, Cr-Ni, martensite defect identification by positron annihilation 78−39867
steel, Cr-Ni, microstructural distrib. of cathodic H_2, autoradiography *(French)* 79−99234
steel, Cr-Ni, pendant drop melt extracted, struct. and props. 80−76242
steel, Cr-Ni (14, 5 wt.%), 00Kh14N5M, tempering resistance, mech. props., Cu addition effect 79−79012
steel, Cr-Ni (18,10 wt.%)-Ti stabilized, corrosion fatigue strength, inhibitor BA-6 effect *(Russian)* 77−16727
steel, Cr-Ni (18%, 12(8)%), martensite formation and reversion, effect on void swelling 80−11641
steel, Cr-Ni-(Mo) (25, 28, 2 wt.%), lattice dilation by N_2 77−16592
steel, Cr-Ni-Cu (14, 5, 2 wt.%), phase transform. and props., preliminary heat treatment effect 79−79011
steel, Cr-Ni-Mo, 'light spots', fractographic anal. 79−29204
steel, Cr-Ni-Mo, dynamic and static softening behaviour at hot forming temp. *(German)* 80−25728
steel, Cr-Ni-Mo, for boiler tubes, austenisation conditions effect obs., on structure and mechanical props. 80−3151
steel, Cr-Ni-Mo, handbook data for type 34KhN1M 79−78960
steel, Cr-Ni-Mo-Mn, wetting of TiC, expt. planning investigation 80−60822
steel, Cr-Ni-Mo-V, magnetic induction, struct. dependence *(Czech)* 80−50141
steel, Cr-Ni-Mo-V, Mossbauer austenitometry and mag. props. 80−40003
steel, Cr-Ni-Mo-V-Nb (12,8,1,1.5,0.4 wt.%) Ce addition effects on strength and hardness *(Russian)* 78−15454
steel, Cr-Ni-Nb, containing controlled particle dispersions, creep strength 77−52425
nickel alloys continued
steel, Cr-Ni-Ti-B, grain size effect on mech. and struct. props. *(French)* 80−45361
steel, Cr-Ni-W(Mo), W and Mo addition effect on carbide form., X-ray obs. *(Russian)* 79−87639
steel, CrMoNi, cantilever beam method to determ. J_{Icc} and J_{Iscc} *(Chinese)* 78−15488
steel, Cu-Ni-Mo (2, 2, 0.25 wt.%), sintering, kinetic characts. 80−60805
steel, fatigue and tensile props., of heat resisting bars, type SUH 660-B and SUH 310-B at elevated temps. 79−38979
steel, fatigue crack growth data, three component model anal. 80−3161
steel, Fe-Cr-Ni (17.20, 7.34 wt.%), transform.-induced plasticity 78−23774
steel, Fe-Ni-Cr mag. susceptibility and magnetoresistance, temp. depend. *(Ukrainian)* 77−73004
steel, high Ni, medium C, impact fatigue strength 79−79104
steel, high Ni, orientational variations of martensite transform. during deform of metastable austenite 78−84805
steel, high Ni (19 wt.%), thermal stabilisation of austenite 78−15397
steel, high-strength, fatigue, interaction effects between trace impurities and environment 80−66651
steel, low alloy, Ni, exam. of stress corrosion cracking in S environment 79−20256
steel, low C, Cr-Ni (25, 25 wt.%), σ phase form., prestrain effects *(Japanese)* 78−92260
steel, low C, tempered, lath martensite, Ni (5 wt.%), microstruct./yield strength relationship 77−21234
steel, low C Cr-Ni, temper embrittlement by antimony, Ti addition effects 77−32683
steel, low-temperature behaviour, mechanical, electrical and magnetic props. *(German)* 80−3081
steel, maraging, 18 wt.% Ni, tensile props., effect of aged struct. and austenite grain size 77−48511
steel, maraging, 18Ni300, ageing, electron diffr. and microscope obs. *(Polish)* 79−34070
steel, maraging, α to γ transform. and austenite stabilisation *(Russian)* 79−52212
steel, maraging, Cr-Ni-Ti, effect of Ti addition on hardness and energy scatt. 79−15687
steel, maraging, grain refinement due to cyclic heat treatment 78−52971
steel, maraging, heating of thin samples with brief ageing, N6G4M, ON18K9M5T 78−52866
steel, maraging, investigation with lower Ni and Co contents *(Chinese)* 78−84812
steel, maraging, Ni, stress corrosion cracking 78−35563
steel, maraging, Ni-Co-Mo (18,10,5 wt.%) precipitation *(Japanese)* 78−15402
steel, maraging, type 200, effect of freq. on cyclic crack growth in salt water environment 78−64680
steel, maraging 250-grade, fatigue crack growth model, notch analysis of fracture approach 78−52984
steel, maraging low-Ni, isothermal martensitic transformations *(Russian)* 78−88465
steel, maraging Ni-Co-Mo, precipitation, elec. resist. meas. *(Japanese)* 78−11228
steel, martensitic, Cr-Co-Ni-Mo, notch toughness, rel. to sensitivity to stress conc. 78−31532
steel, martensitic, Cr-Ni, grain refining and phase transforms. effect on plasticity *(Russian)* 78−39837
steel, martensitic, Cr-Ni deform., effect of phase composition and struct. *(Russian)* 77−25102
steel, martensitic, Cr-Ni-Co-Mo-Ti, Kh12N8K5M3TYu, ageing of C free martensite *(Russian)* 79−1884
steel, martensitic, Ni-Cr-Mo, fatigue crack initiation and propag. in water 77−9000
steel, martensitic 07Kh16N4B, corrosion cracking in chloride and alkaline solutions 80−55576
steel, Mn-Cr-Ni-N, N effect on relaxation behaviour, internal friction temp. depend. *(Russian)* 78−52872
steel, Mn-Mo-Ni, embrittling effects of residual elements 80−66655
steel, Mn-Ni-Al, nonmagnetic, carbide-intermetallic strengthening 79−83208
steel, Mn-Ni-Cr, diffusion of Fe, Mn, Si, V and W *(Czech)* 77−59148
steel, Mn-Ni-Mo low alloy steels for nuclear appl., toughness and heat treatment 80−5239
steel, MnMoNi(Cr), pressure vessel, stress relief cracking 79−43404
steel, N32, $\alpha \rightarrow \gamma$ transform., struct., texture conc. var. depend. on plastic deform. *(Russian)* 79−66050
steel, Ni, cross girder connections, fatigue strength, design stress 78−64700
steel, Ni, cryogenic fracture toughness enhancement through grain refinement 77−36651
steel, Ni, high-strength, impact fatigue strength, heat treatment conditions effect 80−76285
steel, Ni, low alloy, low strength, stress corrosion cracking in sulphide environment 79−47812
steel, Ni, N22, X-ray diffr. study of austenite lattice near martensitic transform. *(Russian)* 79−1868
steel, Ni, sintered, relation between microstruct., microchemistry and mech. props. 78−64504
steel, Ni (17 wt.%), martensitic deform. temp., cryst. struct. effect *(Russian)* 80−66576
steel, Ni (19 and 24 wt.%), austenite thermal stabilisation at sub-zero temps. 77−52324
steel, Ni (21 wt.%), ageing, nitrided case struct. investigation 80−35416
steel, Ni (5 wt.%), corrosion fatigue 78−27683
steel, Ni (9 wt.%), effect of repeated tempering on notch strength *(Japanese)* 79−43280
steel, Ni (9 wt.%) static and dynamic fracture toughness 77−36664
steel, Ni ion implanted, corrosion behaviour 80−11840
steel, Ni-B, B effect on temperability and microstructure 79−15710
steel, Ni-C, martensitic, microstructural distrib. of cathodic H_2, autoradiography *(French)* 79−99234
steel, Ni-Co-C (9, 4, 0.2 wt.%) enthalpy, sp. ht. to 2000K 79−10960
steel, Ni-Co-Cr, high-strength medium C, Cr effect on props. 80−76339
steel, Ni-Co-Cr-Mo-C (10,14,2,1,0.16 wt.%), stress corrosion cracking at 22°C in 3.5% NaCl 79−8390
steel, Ni-Cr, (4,1, wt.%), isothermal embrittlement, AES exam. of grain boundary segregation 78−60814
steel, Ni-Cr, anodic dissoln. in NaCl solns. at high current densities *(Russian)* 80−76396

nickel alloys continued
steel, Ni-Cr, case-hardened, surface durability in rolling contact fatigue testing 77−63684
steel, Ni-Cr, corrosion on N_2O_4 flow 520-890K and 8-9 MPa *(Russian)* 80−3256
steel, Ni-Cr, cyclic re-austenitizing 80−35222
steel, Ni-Cr, long-time exposure to N_2O_4, effect on mech. props. *(Russian)* 78−48573
steel, Ni-Cr, P induced temper embrittlement, Mo effect 77−86148
steel, Ni-Cr, temper embrittled, electron microscope and X-ray micros-truct. obs. 79−38870
steel, Ni-Cr, temper embrittlement by Sb, Ni, Cr effects 77−36628
steel, Ni-Cr, temper embrittlement by Sn 77−86149
steel, Ni-Cr and Ni-Cr-Mo, quenched and tempered struct. effect on H diffusion coeff. and solubility *(Japanese)* 78−52857
steel, Ni-Cr temper embrittlement by P 77−40448
steel, Ni-Cr-Mo, cleavage fracture toughness, temperature and notch sharpness influence *(German)* 80−35291
steel, Ni-Cr-Mo, exam. of delayed fracture using fracture mechanics *(Japanese)* 78−52961
steel, Ni-Cr-Mo, fracture toughness determ. from yield strength and cleavage fracture strength *(German)* 80−35292
steel, Ni-Cr-Mo, Ni effect on fracture toughness, heat treatment effect *(Korean)* 79−91781
steel, Ni-Cr-Mo, quenched and tempered, nothced bar tensile tests *(German)* 80−35247
steel, Ni-Cr-Mo, weld, stress corrosion cracking, metallurgical effects 79−43468
steel, Ni-Cr-Mo (11, 5, 3 wt.%), maraging, corrosion cracking in chloride and alkaline solutions 80−55576
steel, Ni-Cr-Mo (2.5 wt.%), elevated temp. fatigue, effect of zero load rest period 77−8943
steel, Ni-Cr-Mo and Ni-Cr, impact strength, effect of modified ausforming *(Japanese)* 79−11692
steel, Ni-Cr-Mo increase of crack initiation time in delayed fracture by fatigue accumulation *(Japanese)* 78−11312
steel, Ni-Cr-Mo-V, stress corrosion cracking 77−52542
steel, Ni-Cr-Mo-V, turbine rotor shaft, fracture toughness, validity criterion for K_{IC} 78−72861
steel, Ni-Cr-Mo-V low-alloy, additive remedy for temper brittleness 80−66659
steel, Ni-Cr-P (0.06 wt.%), influence of intercritical heat treatment on temper embrittlement susceptibility 78−52863
steel, Ni-Cr-Ti, thin bands, cold working, props. and struct. of 36NKhTYu 79−78994
steel, Ni-Cr-Ti-P, Ti and P solubility effect on free surface segregation 79−11628
steel, Ni-Mn (16, 2 wt.%), 40N16G2, single crystal, stabilisation and destabilisation mechanisms *(Russian)* 78−23732
steel, Ni-Mn-C, austenitic, proof stress change meas. by internal friction with martensitic transform. 78−56638
steel, Ni-Mo, powder forged, as-forged props., effect of process variables 77−59715
steel, Ni-Mo, powder forged, fracture processes and fracture toughness 78−72870
steel, Ni-Mo-C (2.0, 0.2, 0.4 wt.%) sintered, struct. transforms. and mech. props. after quenching 80−66557
steel, Ni-Mo-Cr, embrittling effects of residual elements 80−66655
steel, Ni-Mo-V, fracture toughness data, comparison with equivalent energy and energy per unit area data 78−52965
steel, Ni-S-(Mn), ferrite to austenite transform. effect on sulphide precipitation 77−86025
steel, Ni-Sn temper embrittled, interaction detect. by Mossbauer spectroscopy 77−86176
steel, Ni-Ti, high-alloy, precipitation hardening, fatigue strength 79−79103
steel, Ni-Ti-Al, 36NTYu, heavily deformed, subgrain struct. due to discontinuous precipitation of γ' phase *(Russian)* 79−52218
steel, NiCr, random load fatigue crack propag. 78−64692
steel, NiCrMoV, stress corrosion cracking, cold work effects 78−11383
steel, Si (6.5 wt.%) Mn, Ni and Al additions influence obs., on mech. and magnetic props. *(Slovak)* 79−5064
steel, Si-Mn-Ni-Cr-Mo, acoustic emission during stress corrosion cracking appl. to materials testing 78−53042
steel, sintered, Ni-Cr-Mo additions, struct., props., thermomechanical treatment effects 77−12657
steel, stainless, 304, weld decay, precip. of $M_{23}C_6$ during thermal cycles *(Japanese)* 79−52468
steel, stainless, austenitic, CC Ni-Al, γ-phase, fracture mechanical aspects of abrasive friction, wear, chip formation 78−72865
steel, stainless, austenitic, Cr-Ni-Mn-Si-Mo-C alloy, 13Khi8N10G3S2M2, elastic moduli exam. after thermomechanical treatment *(Russian)* 79−24558
steel, stainless, Cr-Ni, low temp. plastic deformation, in mag. field 79−83256
steel, stainless, Cr-Ni (18,10 wt.%) Ti stabilised, cavitation failure, relationship of corrosive and erosive factors *(Russian)* 77−16722
steel, stainless, Cr-Ni (18, 10 wt.%), long-term strength in H at high pressure 80−55485
steel, stainless, Cr-Ni (18, 8 wt.%) average inclusion size and contents exam. measurements using optical microscopy and Br-Methanol methods *(Korean)* 79−66080
steel, stainless, Cr-Ni (18, 9 wt.%), cold rolled, struct. 79−83214
steel, stainless, Cr-Ni-Mn, N strengthened, low-temp. elastic props. 79−70109
steel, stainless, Cr-Ni-Mo (16, 14, 3 wt.%), corrosion resist., vacuum heat treatment effect 79−87754
steel, stainless, Cr-Ni-Mo-N, phase diagrams 80−35161
steel, stainless, Cr-Ni-Nb stabilised, Te vapour effect on creep and tensile props. 79−24583
steel, stainless, Cr-Ni-Ti, metallographic detection of $(Ti,Ni)_6C$ 80−66721
steel, stainless, Ni-Cr-Mo, two-phase, compositional charge of ferrite and austenite *(Japanese)* 79−4948
steel, stainless, Ni-Cr-Mo-W (29, 13, 3, 2 wt.%), long-term strength in H at high pressure 80−55485
steel, stainless, stabilised with Cr-Ni-Nb, reaction with Te vapour 77−8986
steel, stainless, surface cleaning by H^+ bombard., AES study 78−53022
steel, stainless, type 430, Ni^+-implanted, struct., comp. and electrochem. anal. of surface alloy 80−16603
nickel alloys continued
steel, stainless, type Kh17N13M2T, strengthening by plastic deformation and cold working *(Russian)* 78−52839
steel, stainless complex alloy, hot ductility, B effect 80−30038
steel, stainless type 316, fusion reactor Li cooling system, corrosion inhibition by Al additions 80−108646
steel, struct. change of hot-worked austenite during post-deform. holding 80−35228
steel, type 1Kh17N2, alloying element redistrib. during friction *(Russian)* 77−81326
steel, WC reinforced surface layer, serviceability improvement by Ni, Cu-Ni, V alloying additions 77−21290
steel, X5CrNiTi26.6, ferrite-austenitic struct., optical and electron microscopy 78−84848
steel austenitic Cr-Ni-Be, cellular precipitation *(Japanese)* 78−11229
steel austenitic stainless, Cr-Ni 316 type, electron irradiated, void swelling 79−42104
steel Ni (9 and 5 wt.%), for liquefied natural gas appls., material and weld props. 79−61736
steel Ni (9 and 5 wt.%), liquefied natural gas appls., material and weld props. 79−61735
steel Ni-Cr, Sb doped, temper embrittlement susceptibility, intercritical heat treatment effect 78−64570
steels Ni-rich, tetragonality anomalies of martensite 77−77478
STEM microanal. of precipitates and their nuclei 80−81067
STEM microanalytical techniques comparison for precip. comp. determ. 78−35790
strength properties, dispersity of struct. effect, alloy KhN45Yu 80−55486
strengthening by modified ausforming 78−76665
stress corrosion cracking control measures 77−90509
stress corrosion cracking test machine, design and construction, appl. to Fe-Cr-Ni alloys 80−97649
stress relaxation, in-reactor study at low temps. 80−93588
superalloy, γ' precipitate size determ. technique 79−34221
superalloy, γ'-precipitation influence on recrystallisation 80−29955
superalloy, ⟨111⟩ monocrystals under compression, inhomogeneous deformation 77−63736
superalloy, aluminite coating, improvement by sputtering *(French)* 79−29278
superalloy, cast, microstruct. and microanalysis 78−35393
superalloy, coated with Ni-Co-Cr-Al-Y, fatigue cracking in coating 78−11438
superalloy, conventional and powder-metallurgical, σ-phase precip. 80−11646
superalloy, directionally solidified, struct. and props. *(Chinese)* 80−20918
superalloy, dispersion strengthened, creep stress component rationalization *(Korean)* 79−66115
superalloy, electroless codeposition of Si and Ti 77−16513
superalloy, fatigue crack opening load variation with meas. location 80−16425
superalloy, IN 718, acoustic emission interpretation of ductile fracture processes 80−35300
superalloy, IN-100, aluminised, microstruct. degradation, influence of corrosioin protective coating 80−40611
superalloy, IN-738, microstruct. changes during isochronal heat treatment, 773-1467K 78−27531
superalloy, instrumental anal., use of HF induction melting and centrifugal casting *(Japanese)* 77−56280
superalloy, internal stresses due to dislocation walls around second phase particles 79−99210
superalloy, laser melted, epitaxial resolidification 77−90491
superalloy, microscopic inhomogeneity of plastic strain influence on fatigue cracks *(German)* 80−40470
superalloy, phase extraction *(German, English)* 77−52599
superalloy, preparation for instrumented anal., HF induction melting, casting 78−48607
superalloy, rapid solidifcation, use in gas turbine engines 80−84888
superalloy, single crystal, apparent and effective creep parameters, incubation period 77−63715
superalloy, STEM microanalysis of precipitates 80−104492
superalloy, transient liq. phase diffusion bonding and mechanism *(Japanese)* 78−2279
superalloy IN713LC, hot corrosion, thermal cycling effects 77−70204
superalloy IN 100, corrosion resistant intermetallic coating, microstruct. effect on mech. props. 78−85058
superalloy IN-738, γ' precipitate coarsening during ageing and creep 79−52271
superalloy Mar-M200, slow fatigue crack propagation rate meas. using high freq. resonant technique 78−52983
superalloy Nimonic 80A, microstruct. anal. by high-resolution electron microscopy 80−76459
superalloy powder, thinning technique for microstruct. obs. using analytical electron microscopy 78−48587
superalloy powders, removal of interstitial contaminants 78−84735
superalloys, corrosion by O_2 containing H_2O and gaseous NaCl, volatile products 78−27674
superalloys, hot workability, effect of S, Ca, Mg, Y and Zr minor elements 80−66552
superalloys, low temp. hot corrosion, Na_2SO_4-induced, mechanism, burner rig tests 80−40610
superalloys, mechanical integrities of surface oxides, oxidation 78−95844
superalloys, mechanical integrities of surface scales, contaminant corrosion 78−95845
superalloys, powder metallurgical, creep-rupture at intermediate temps. 80−97568
superalloys, Si-based coatings for high temp. appl., process development and props. 80−40614
superalloys, sigma phase prediction techniques 80−7567
superalloys, SIGMA-SAFE, phase diagram approach to sigma phase problem 78−64547
superalloys *(French)* 79−43339
Supermalloy, 24 GHz ferromagnetic antiresonance transmission 77−51957
Supermalloy, 9, 24 and 38 GHz ferromagnetic reson. absorpt., line shapes 77−51958
supermalloy, foil, microwave transmission, parallel RF and mag. fields 77−59462
superplastic deformation, effect on struct. of heat-resistant alloy ZhS6KP 79−96090

nickel alloys continued
superplastic superalloy IN-738 load relaxation testing 77−40507
surfaces, electron emission in Cs vapour, plasma anode meas. 77−90235
swelling, correlation with number of bonding d electrons 77−47491
taenite, cloudy, origin in meteorites, TEM study of Santa Catharina anomalous Fe meteorite 79−66968
Ti-Ni, electron emission and shape memory effect 80−50687
Ticonal, domain struct., variation under influence of heat treatment *(Russian)* 78−23292
Ticonal, effect of rare earth metals on mag. props., struct., and phase transformations 79−99732
ticonal, grindability improvement, thermomagnetic and heat treatments 77−16625
Ticonal, two- and one-dimens. modulated struct. after thermomag. treatment and water quenching *(Russian)* 80−29983
Ticonal strength, effect of thermal stresses and phase transforms. 79−87721
Ticonal with magnetic texture, struct. damages during ageing 77−16626
Ticonal with Sm, magnetic props., phase transform. after thermomagnetic treatment 78−3155
Ticonal-type alloys, struct. after quenching from 800-850°C *(Russian)* 77−59822
Tokamak fusion reactor, blanket structural material selection and development *(Japanese)* 79−97901
trace element anal., at. absorpt. spectrometer performance appl. 77−77825
transition metal alloy, ferromag., H-impurity complex obs. by magnetic aftereffect 78−72373
Tribaloy 700, hard surfacing in Na, friction, wear and corrosion 79−24628
tunnel currents, spin polarisation, simple band theory interpretation 79−78451
tunnelling electron spin polarisation rel. to band struct. 78−68095
type 625, neutron irrad. effects on fatigue crack propag. 80−29069
type 718, neutron irrad. effects on fatigue crack propag. 80−29069
Udimet 500, microstructural instability in industrial gas turbine engine vane 77−28833
Udimet 520, γ' distribution in slip plane, dislocation loop form. during creep *(Japanese)* 79−42075
Udimet 520, γ' phase composition variation with ageing 77−8866
Udimet 520, Nicralloy-coated, microstruct. degradation, influence of corrosioin protective coating 80−40611
Udimet 520, precipitation hardening *(Japanese)* 79−43259
Udimet 700, creep, rupture, grain size effects 77−21229
Udimet 700, creep crack growth 78−48517
Udimet 700, high temp. fatigue crack growth, fracture mech. approach 79−52340
Udimet 700, microstruct. of resolidified zones formed by laser melting single crysts. 79−78953
Udimet 700, Ni-Co-Cr-Al-Ti (18.8, 15.2, 4.5, 3.39 wt.%) exam. of high temp. creep 79−61684
Udimet 700, Ni-Co-Cr-Al-Ti (18.8, 15.2, 4.5, 3.39 wt.%) exam. of high temp. creep, viscoplastic flow 79−61685
Udimet 700, Ni-Co-Cr-Ti, hold time effects on high temp. fatigue crack growth 79−5036
Udimet 700 superalloy, laser melt quenching and alloying 79−69919
unipolar arc damage in hot, dense D plasma 79−3235
US vibration during crystallisation, effect on mech. props. *(Russian)* 78−19827
wear resistance, struct. effect 79−29229
welding crack resist. during welding, heating, stress reduction by hardening 79−24618
work hardening tendency, at elevated temps. 77−52353
ZhS6K, diffusion layer form. on Nb addition, struct., comp. *(Russian)* 78−56814
Zircaloy, H absorption, Sn(Fe)(Cr)(Ni) effect 80−49527
Zircaloy cladding, stress corrosion cracking due to I and Cs redistrib. in LWR fuel rods 80−32343
Zircaloy-2, neutron irradiated, inhomogeneous deformation behaviour 80−50679
Zircaloy-2, tritium diffusion 80−32341
Zircaloy-4, anomalous oxide growth during transient temp. oxidation 80−50773
Zircaloy-4, microstrain and particle size meas. by Warren-Averbach method 80−55420
Zircaloy-4 tubes, texture influence on anal. of thermoelastic/plastic anisotropy and initial yielding 80−35260
β'-NiAl, Ni rich, electron diffr. pattern anomalies, rel. to martensitic transform. and short range ordering 78−6926
Ag-Cd-Ni, internally oxidised, oxide particle size control *(Japanese)* 80−89480
Ag-Cu-Ni, phase diagram determ. 77−63634
Ag-Ni, composite powder mixtures, compressibility and sinterability 77−63592
Ag-Ni, two ductile phase, exam. of rolling deformation 78−72819
Ag-Ni, two ductile phase alloy, exam. of softening behaviour after cold rolling 78−72847
Ag-Ni (10 wt.%) wire, plastically deformed, fracture struct. *(German)* 80−71744
Ag-Ni solid solution, reversible surface segregation, radioactive tracer, LEED, and AES expts. *(French)* 77−69155
Ag-Ni supersaturated metastable solid solns. formed by ion beam mixing 80−107425
Ag-Pd-Ni, corrosion in marine atm., potentiometric technique, appls. 79−24693
AgNi, dil., mag. susceptibility of isolated Ni atoms 80−65777
Al/NiSi/Si system, high temp. interaction study, elec. and struct. charcts. 79−24075
Al-A_3Ni eutectic, effect of some thermal parameters on the directional solidification process 78−88456
Al-Al_3Ni, aligned, eutectic alloy, mech. behaviour at high strain rates 78−39855
Al-Al_3Ni, eutectic, creep model 77−36588
Al-Al_3Ni, eutectic composite, directionally solidified, thermal cycling induced distortion 78−39899
Al-Al_3Ni, eutectic composite, abrasive fragmentation *(Czech)* 80−30110
Al-Al_3Ni directionally solidified eutectic, microstructural degradation in temp. gradient 78−3145
Al-Al_3Ni directionally solidified eutectic alloy, struct. and mech. props. *(Korean)* 80−29944
nickel alloys continued
Al-Al_3Ni eutectic, cryst. struct., orientation, electron microscopy, computer calcs. *(German)* 77−72582
Al-Al_3Ni eutectic, temp. gradients, microstructural changes 80−84971
Al-Al_3Ni eutectic, thermal stability in temp. gradient 79−61611
Al-Al_3Ni eutectic alloy, electrolytic prep. of Al_3Ni fibres, SEM and anodic polarisation studies 80−100817
Al-Al_3Ni eutectic composite, substructural matrix hardening *(Russian)* 77−21162
Al-Al_3Ni eutectic composite, structural response to shape variations 79−83190
Al-bronze, input energy, hysteresis, and fracture in low cycle buckling fatigue, superelastic range 78−31527
Al-bronze, single crystal rod, energy dissipation, deformed by cyclic buckling in superelastic range 78−31479
Al-Cu-Mg-Fe-Ni, Hiduminium RR58, crack propag. rates in air and salt soln. 80−21063
Al-Cu-Mg-Ni-Fe alloy RR 58, creep resistance at elevated temps., thermomechanical treatment effects 77−59836
Al-Cu-Ni, alloy RR 350, θ'-hardened, deform. induced microstructural instability, high temps. 80−16321
Al-Cu-Ni, directionally solidified, exam. of struct. of two phase alloys 78−80537
Al-Cu-Ni, vacancy ordering, electron microscope and electron diffr. obs. 79−27954
Al-Fe-Ni, influence of strain path on mech. props., orthogonal tensile paths 80−30035
Al-Fe-Ni, oxidation in hot water, electron microscope obs. of initial stages 79−11718
Al-Mn-Ni, permanent magnetic materials, grain struct. effect *(Rumanian)* 79−73773
Al-Ni, composite, paramagnetic resonance and electron-positron annihilation *(Russian)* 79−87314
Al-Ni, couple phase diagrams and thermochemical data 79−66037
Al-Ni, dil., core and valence band spectra, XPS study 80−84837
Al-Ni, dil., electronic states, XPS meas. 77−44117
Al-Ni, ingots, solidified, formation of equiaxed eutectic grains *(Japanese)* 78−39756
Al-Ni, interdiffusion and intrinsic diffusion in NiAl δ phase 79−10988
Al-Ni, liq., dissoln. and diffusion of alloying components, 700-1000°C *(Russian)* 80−15275
Al-Ni, liquid, thermodynamic props. 79−91619
Al-Ni, liquid alloys, thermodynamic charact. calc. *(Russian)* 78−27475
Al-Ni, optical emission spectrographic analysis of some binary alloys by a glow discharge of Grimm lamp *(Japanese)* 79−99015
Al-Ni, positive muon trapping at vacancies 79−56704
Al-Ni, rapid quenching, struct. and decomp. 80−76244
Al-Ni, solidification in mag. field, crystallite obs. *(Russian)* 77−4770
Al-Ni, thermoelastic phase transform., acoustic emission 80−3039
Al-Ni (10 to 70 at.%). NMR of ^{27}Al *(French)* 77−51974
Al-Ni (2 at.%), rapidly quenched from melt, vacancy loops and precipitates, TEM 77−59769
Al-Ni (3-18wt.%), gun-quenched from melt, struct. 80−76225
Al-Ni (3.6 at.%), quenched from melt, distortion of matrix caused by coherent precipitates, electron diffr. meas. 77−59791
Al-Ni (6 wt.%), fine-grained, deform. in tension and torsion 80−85008
Al-Ni (6 wt.%) misorientation between subgrains, second-phase particles role, STEM microdiffr. obs. 80−104415
Al-Ni (63.6 at.%), elastic softening and electron diffr. anomalies prior to martensitic transform. 77−86078
Al-Ni alloys, solid and liq. mag. susceptibility, 600-1650°C *(Russian)* 80−15685
Al-Ni eutectic, mechanism of lamellar spacing adjustment 78−31395
Al-Ni eutectic alloy, directional solidification using electroslag remelting 79−61578
Al-Ni foil, vapour deposited, multiply twinned particles, electron microscopy 77−28083
Al-Ni mixed-powder-based plasma-sprayed coatings, strength characts. 77−12548
Al-Ni multiphase system, simultaneous diffusion in cylindrical symm. *(Russian)* 80−100357
Al-Ni solid, liquid mixture, diffusion processes *(Russian)* 80−107563
Al-Ni system, Knight shift, NMR line widths determ. *(French)* 77−77113
Al-Ni with multiple layer plasma coating, exam. of cohesion strength *(Russian)* 80−7714
Al-Ni-Co, directionally solidified ternary eutectic morphology *(Czech)* 77−59772
Al-Ni-Co(Si), directionally solidified eutectic, morphological and mech. props. *(Russian)* 80−30057
Al-Ni-Si, eutectic, unidirectional solidification 77−16565
Al-Ni-Si sintered SAS-1 alloy, struct. *(Russian)* 79−52135
Al-Ni-Ti, calc. of phase equilibria using thermodynamic values from different models 78−60646
Al-Ni-(Mg) (6, 0.3 wt.%), fine grained, Luders' band deform. 77−77527
Al-Ni(Cd)(Fe)(Si), cold worked, struct. and props. 80−71666
Al-Ni(Pt)(Zn), rapidly solidified, twinned dendrites 80−70572
Al-Pt_2Ni_{1-x}-n-Si system, Schottky-barrier height 80−34520
Al-Pt_xNi_{1-x}Si-Si system, diffusion, compound form., and microstructure 80−34253
Al-Si-Cu-Mg-Ni, piston, depend. between min. creep rate and time of beginning of secondary creep *(Czech)* 80−35267
Al-Si-Cu-Mg-Ni cast alloy, fractography *(German, English)* 79−87809
Al-Si-Cu-Ni alloy casting, thermal props. 78−95814
AlCu-NiCo (5 at.%), Θ' hardened, creep mechanism 80−85013
Al_4(Ni, Co)$_3$ ternary phase in Al-Ni-Co system, cryst. struct., vacancy controlled phase *(Chinese)* 80−70164
Al_3Ni, cryst., theoretical morphology and comparison with observed habits *(French)* 80−79732
Al_3Ni dendrite facets, determ. cryst. direction by SEM *(French)* 78−87893
Al_3Ni-Al two-phase matrix, Al electrolytic etching in $AlCl_3$ molten salts 78−3280
Al_2O_3-NiCr composite, plasma sputtering of electroheating coatings, elec props. *(Russian)* 80−108350
Au/Ni-P, interdiffusion, backscatt. study 80−79991
Au-Cu-Ni, computer characterisation, exam. of phase equilibria and miscibility gap 79−11561
Au-Cu-Ni, phase precipitation on domain boundaries, effect of Ni *(Russian)* 78−39777

nickel alloys continued
- Au-Cu-Zn-Ni (13, 3.4, 8.5 wt.%), white gold, metallographic structure after cold rolling, effect of heat treatment, recrystallisation *(French)* 79−52238
- Au-Fe-Ni layer coating, Fe and Ni conc. meas. by X-ray diffr. *(German, English)* 80−34330
- Au-Ge-Ni/GaAs metal-semiconductor thermoelectric coolers, effects of contact resist. and dopant conc. 80−81481
- Au-Ni, composition modulated foils, layer struct. and mech. props. 79−95300
- Au-Ni, dil., valence and core level spectra, XPS study 80−84838
- Au-Ni, elec. resist. in liquid and solid state *(Russian)* 79−51549
- Au-Ni, fast liq. quenched, anomalous sp. ht. near ferromag. crit. comp. 77−80947
- Au-Ni, heat capacity, 1.5 to 15K 78−95452
- Au-Ni, liquid alloy system, determ. of thermodynamic props. using Knudson effusion method, phase diagram calc. *(German)* 78−51707
- Au-Ni, mag. clustering 79−7977
- Au-Ni, magnetisation and sp. ht., ferromag., paramag. and crit.-conc. regions 79−38330
- Au-Ni, modulated struct. form. by spinodal decomp., lattice imaging electron microscopy obs. 79−95996
- Au-Ni, preferential sputtering 79−83080
- Au-Ni, supermodulus effect, one-dimens. modulated structs. 79−95068
- Au-Ni, surface segregation, strain effects 80−80042
- Au-Ni, UPS study, localised states 80−93449
- Au-Ni (15 at.%) film, evidence of modulated struct., TEM exam. 78−87887
- Au-Ni (30 at.%), singularities of struct. state, diffuse electron and X-ray scatt. *(Russian)* 79−4945
- Au-Ni bimetallic cluster, segregation and short range order props. at boundaries 79−29071
- Au-Ni foil, composition-modulated, elastic modulus enhancement 77−52382
- Au-Ni solid soln., creep 78−15475
- Au-Ni surface composition determ. 79−69328
- Au-Ni-Cu phase diagrams, thermodynamic calc. *(Korean)* 78−68672
- Au-Ni-Cu-Zn, white gold, metallographic struct., heat treatment and plastic working effect 80−40403
- Au-Ni-O surface, quantitative Auger analysis using relative sensitivity factors 78−7295
- Au-SnNi-Au ohmic contacts on n-GaAs 78−35319
- $Au_{35}Ni_{65}$, vapour quenched amorphous alloy, atomic arrangements 80−100173
- B-Ni, form by Ni doping of zone-refined B, elec. conductivity 77−31682
- $BaNiSn_3$, cryst. struct. rel. to $ThCr_2Si_2$ type *(German)* 78−51470
- Be depth profiling by d and α detection in $^9Be(p,d)$ and $^9Be(p,\alpha)$ 79−5203
- Be-Co-Ni, phase relations *(German)* 79−43209
- Be-Ni, plastic deform., flow stresses, fracture *(Russian)* 80−108496
- BeNi, dil., electronic struct., NMR study 80−108085
- CC Fe-Ni-Cr (35, 15 wt.%): Nb(Ti)(Mo), corrosion in HTGR He environment 80−61021
- CC Ni_3Al, refractory transition metal alloying effects on ht. capacity 78−26691
- $CaNi_5$, Haucke compounds, low temp. heat capacity, Debye temp. 80−96663
- Cd-Ni, dil., mag. and supercond. props. 79−38237
- Ce-Mn-Ni, cryst. struct. determ. 77−11508
- Ce-Mn-Ni system, phase diag. 77−52283
- Ce-Ni, hydriding characts., applicability for H_2 storage material 78−83955
- Ce-Ni liq., X-ray diffr. exam. of struct. 77−62465
- Ce-Ni-Si, thermoelectromotive force and electrocond. *(Ukrainian)* 80−54670
- Ce-Ni-Si system, mag. props. in 77-300K rar ge *(Russian)* 78−56290
- $Ce(Cu,Ni)_2$, pseudobinary phases, struct. and mag. props. rel. to Ce valence 78−6032
- $CeNi_2$-$CePt_2$ system, structural and mag. studies on valence behaviour of Ce 80−103809
- $CeNi_3$, and ternary hydride, mag. props. 80−108007
- $CeNi_x$, sorption at press. up to 1500 atm. 80−97819
- $Ce_{4.5}Ni$, absorpt. of D, heats of reaction and equilib. press., T-getters for CTR 78−51683
- $CeNi_4Al$, mag. susceptibility, H adsorption-desorption cycle effects 80−107990
- $CeNi_{8.5}Si_{4.5}$, X-ray cryst. struct. determ. 80−88089
- (Co,Cr,Ni)-TaC, eutectic alloy, directionally solidified, struct. defects, autoradiographic investig. *(Russian)* 77−25038
- (Co,Ni)-$Cr_{23}C_6$ eutectic, microstruct. effect on fracture energy 80−7662
- Co-Cr-Mo-Ni-Fe-Si-Mn-C, protective coatings by B diffusion, microstruct. and mech. props. 78−11427
- Co-Cr-Ni, phase diagram calc. 79−1848
- Co-Cr-Ni alloy FSX 414, electrochemical corrosion meas. in molten sulphate 79−96178
- Co-Cr-Ni superalloy Mar-M509 standard and Mo modified, phase anal. 77−63675
- Co-Cr-Ni-Ta-Al-Y (25, 10, 5, 3, 0.5 wt%), exam. of hot corrosion 79−20251
- Co-Cr-Ni-TaC, directionally solidified eutectic, mech. props. and sruct., thermal cycling effects *(Russian)* 78−92282
- Co-Cr-Ni-W-Ta-C, alloy Mar M-509, TEM exam. of thermal fatigue crack propag. in cast alloy 78−76740
- Co-Cr-Ni-W-TaC (15.7, 9.5, 3, 12.77 wt.%) alloy Co50B3W, temperature cycling effect on rupture strength 78−39898
- Co-Cr-NiTaC eutectic, directionally solidified, microstructural stability 79−38815
- Co-Cr-Nr-TaC eutectic alloys, fatigue, microstructure effects 78−23803
- Co-Fe-Ni semi-hard mag. alloy, 3-D Barkhausen effect meas. 77−69623
- Co-Fe-Ni semihard magnetic alloy, directional distrib. of magnetisation changes connected with Barkhausen effect 78−14985
- Co-Fe-Ni-Si-B glasses, soft mag. props. 79−73774
- Co-Fe-V-Ni, mag. and mech. props., heat treatment and stress effects 80−60363
- Co-Mn-Ni-Fe-Si-B amorphous alloys, mag. props., low magnetostriction 80−75832
- Co-Ni, (10 at.%), magnetisation in high mag. field, Arrott-Noakes plot 80−54919
- Co-Ni, cryst. struct. and stacking fault influence on mag. props. *(Russian)* 80−25164

nickel alloys continued
- Co-Ni, deformed and isochronally annealed, positron lifetimes, annihilation at dislocation trapped monovacancy 80−55221
- Co-Ni, dendritic segregation 80−76260
- Co-Ni, dil., effective mag. field at ^{59}Co, impurity conc. depend., spin echo expts. 78−48080
- Co-Ni, electrodeposition, mag. props. *(French)* 78−64488
- Co-Ni, ferromag. film, ion plating prep., coercive force and magnetoresist. 77−12546
- Co-Ni, liq., thermoelec. power and elec. resist. meas. 77−51719
- Co-Ni, liquid, solubility of H, 1400 to 1800°C 77−1231
- Co-Ni, magnetic anisotropy induced by magnetic and stress annealing 78−35010
- Co-Ni, magnetic anisotropy induced by mag. annealing and cold rolling, expt. 80−7695
- Co-Ni, magnetic anisotropy induced by mag. annealing and cold rolling, calc. 80−7696
- Co-Ni, magnetocrystalline anisotropy consts. meas., 77-700K 78−43582
- Co-Ni, selective catalytic surface behaviour, tight-binding approx. calcs. 78−76924
- Co-Ni, surface chemical comp. changes due to ionic bombardment *(Russian)* 77−1776
- Co-Ni, temp. depend. of asphericity of mag. moment distrib. 77−20538
- Co-Ni (0.45 to 7.23 wt.%) theoretical analysis of cation distrib. in (Co, Ni)O scale 77−12747
- Co-Ni (32 wt.%), FCC, rolling texture development 79−87657
- Co-Ni (33 wt.%), FCC deform. twinning kinetics, relationship to stress-strain behaviour 78−52887
- Co-Ni (5 to 95 at.%), paramag. props., 800-1800°C *(Russian)* 77−55660
- Co-Ni alloy, electrodeposition of cylindrical thin films 80−29886
- Co-Ni alloy, slip charact., and fatigue, FCC twinning and FCC to HCP martensite transform. effect 80−35182
- Co-Ni alloy surfaces, oxidation, APS 79−87755
- Co-Ni alloys, electrodeposited, struct., internal stress, and mag. props. 78−95471
- Co-Ni alloys, electropolishing in alcoholic soln. of H_2SO_4 77−16718
- Co-Ni fine particles, anhysteretic growth of exchange fixed remanent states 77−16116
- Co-Ni/steel/Co-Ni three layer composite, high strength with increased damping capacity 77−1850
- Co-Ni-Cr (20,20 wt.%), internal oxidation, improvement of mech. props. *(French)* 77−16521
- Co-Ni-Cr superalloys, γ'-precipitation-strengthened, yielding 77−8894
- Co-Ni-Cr-Al-Ta, S-57 alloy hot corrosion, cyclic oxidation, depth of attack determinations 80−11837
- Co-Ni-Cr-B, centrifugally cast metallurgical coatings for wear resistance in plastics molding machines 79−29285
- Co-Ni-Cr-B, X-306 centrifugally cast cylinder lining alloy, compatibility with hardfacing alloys 77−32726
- Co-Ni-Cr-C, carbide precipitation 79−29065
- Co-Ni-Cr-Mo, mech. props., effect of twinning and FCC to HCP transform. 77−4779
- Co-Ni-Cr-Mo (35, 20, 10 wt.%), MP35N, TEM study of phase transformations 80−81054
- Co-Ni-Cr-Nb, effect of Fe addition on precipitation behaviour 80−29962
- Co-Ni-Cr-Nb (40, 18, 1.8 wt.%), precipitation behaviour of NbC, effect of ageing temp. on morphology 80−89227
- Co-Ni-Cr-Nb FCC alloy, electron microscope obs. of deform. twins 79−60380
- Co-Ni-Cr-Ta-C (10, 10, 14, 1 wt.%), aligned eutectic, directionally solidified, fatigue crack propag. 78−27624
- Co-Ni-Cr-W-Fe, HA-188 alloy, hot corrosion, cyclic oxidation, depth of attack determinations 80−11837
- Co-Ni-Fe, metallic glasses, mag. props. *(German)* 79−51813
- Co-Ni-Fe, semi-hard magnet, irreversible magnetisation changes, directional distrib. 79−24196
- Co-Ni-Fe-Si(B), amorphous ribbon, magnetostriction meas. 80−15778
- Co-Ni-Mo-C, amorphous alloys, med. props. and thermal stability *(Japanese)* 80−85049
- Co-Ni-P, film, props. independent of mag. hysteretic and anhysteretic remanences *(French)* 80−2604
- Co-Ni-P electrolytic layers, partial anhysteretic remanent magnetisation, additivity prop. *(French)* 80−44882
- Co-Ni-Zn, diagram of state, crystalline lattice consts., microhardness *(Russian)* 80−66479
- (Co-Ni)-$Cr_{23}C_6$ eutectic alloy, directionally soldified, microstruct. and crystallography 78−48390
- Co(Cr,Ni)-TaC fibrous eutectic, deformed, thermal stability of microstruct. *(Russian)* 79−1895
- $Co_{57}Fe_5Ni_{10}(Si,B)_{28}$, amorphous, soft mag. props., switched-mode power supply appls. 80−88850
- $(Co_{1-x}Fe_xNi_y)_{80}(Si_{1-z}B_z)_{20}$, amorphous films, spin wave spectra 80−34777
- $Co_2Ga_{2-x}Ni_x$, mag. and struct. phases from magnetisation, neutron, X-ray diffr. techniques 78−52253
- $Co_{1-x}M_xSi$ (M=Fe, Ni), elec. field gradient, quadrupole splitting of ^{59}Co 80−29641
- $Co_{2-x}(Ni,Fe)_xTiSn$, Heusler alloy, positive contribs. to hyperfine fields, magnetisation and NMR meas. 78−43654
- CoNi, Hall effect, anomalous, residual coeff. calcs. using coherent pot. method *(Russian)* 80−80249
- $Co_{0.65}Ni_{0.35}$, precursory phonon obs. of FCC to HCP transition 78−43082
- $Co_{20}Ni_{80}$, oxidation study by Auger electron spectroscopy *(Ukrainian)* 80−7711
- $Co_{1-x}Ni_xAl$, Knight shift and mag. susceptibility study, electron struct. peculiarities *(Russian)* 80−15814
- CoNiB, corrosion-resistant amorphous mag. thin films 80−54923
- $Co_{40}Ni_{40}B_{20}$, magnetostriction, temp. depend. 78−91921
- $Co_{40}Ni_{40}B_{20}$, spontaneous Hall effect and resistivity 79−19576
- CoNiCrMo, artificial hip joints, fatigue strength 79−48375
- $Co_{50}Ni_{20}Fe_6Si_{12}B_{12}$, amorphous, mag. props., effects mech. deform. 80−39840
- CoNiP, cylindrical amorphous electrodeposited layers, mag. props., torsion influence 80−88848
- CoNiP film, amorphous electrolytic, prep. and magnetic props. *(Slovak)* 79−51823
- $(Co_{1-x}Ni_x)_{75}(PBAl)_{25}$, amorphous, high-field magnetoresist. meas. 80−34423
- $Co_{1-x}Ni_xSi$, IR refl. spectra in plasma refl. region 78−27233

nickel alloys continued
- $Co_{1-x}Ni_xSi$, solid solution optical props. 78−72556
- $Co_{2-x}Ni_xTiSn$, mag. ordering, ^{119}Sn Mossbauer spectroscopy and magnetisation meas. 78−43753
- $Co_{0.9}P_{0.1}$ noncrystalline ferromagnet, electroless deposited, struct. and microscopic mag. props. 80−88063
- 25Cr-20Ni stainless steel dendritic solidification, growth morphology and solute redistrib. *(Japanese)* 80−81045
- Cr-Co-Ni hard film on Mo substrate for magnetic recording 80−2608
- Cr-Fe-Ni, cryst. struct. and defects, high resolution electron microscopy obs. 79−94961
- Cr-Fe-Ni, γ-solid soln., thermodynamic activity determ. at 1500K 80−108397
- Cr-Fe-Ni, phase diagram calc. 79−1848
- Cr-Fe-Ni alloys, claddings, chemical compatibility with UC nuclear fuels, thermodynamic model 80−63263
- Cr-Fe-Ni alloys, interface with Th carbide fuels, basic chemical compatibility, thermodynamic calcs. 79−93727
- Cr-Fe-Ni-Si, ternary phase equilibria for Cr-Fe-Ni rich portion, lattice stabilities 80−71628
- Cr-Mi-W-(-Mo), heat resistant weld seam metal, tensile strength, thermophysical characts. 79−91769
- Cr-Mo-Ni-Ti alloy A-286, stress-rupture data correlation 77−44346
- Cr-Ni, Ar ion bombard., O_2 flooded, secondary ion yield as function of original conc. *(French)* 78−39643
- Cr-Ni, blistering after 40 keV He ion bombard. 80−39175
- Cr-Ni, dil., mag. susceptibility, 77 to 400K *(Russian)* 80−50066
- Cr-Ni, fatigue, low cycle, test results, least square deviation method 77−63796
- Cr-Ni, fusion reactor first wall materials, compatibility with impure He 80−32469
- Cr-Ni, H_2 penetration from N_2-H_2 mixtures *(Russian)* 77−69117
- Cr-Ni, high temp. strength, interatomic bonds ionic component correlation *(Russian)* 79−15761
- Cr-Ni, Inconel, first wall material thermal response 80−32456
- Cr-Ni, Inconel 718, fusion reactor blanket materials for Argonne Experimental Power Reactor 80−32450
- Cr-Ni alloy, 01Kh18N40M5, blistering under high He^+ irradiation 80−29095
- Cr-Ni alloy, He blistering at high irradiation doses 79−51167
- Cr-Ni alloy NK40, thermal fatigue life *(Japanese)* 78−19880
- Cr-Ni austenitic steel, Ti stabilised, nuclear reactor pipeline appl. *(Hungarian)* 77−18658
- Cr-Ni compressor disk, surface plastic deform., optimal method 80−60924
- Cr-Ni steel, austenitic, effect of Si on carburising mechanism at 930°C 77−56155
- Cr-Ni steel, carburised, effect of atm. during heating to quenching temp. on austenite decomp. 77−56157
- Cr-Ni steel, low-temperature behaviour, mechanical, electrical and magnetic props. *(German)* 80−3081
- Cr-Ni steel, strengthening by elastic deform. at −196°C 77−55987
- Cr-Ni VKh-4 alloy, deformation and fracture mechanism investigation *(Russian)* 80−11738
- Cr-Ni-Fe, Inconel 625, plasma chamber material for power generating Tokamak, suitability tests 80−32449
- Cr-Ni-Fe, ternary phase diagrams, interactive computer program 80−71629
- Cr-Ni-Ga, phase equilibria diagrams at 800 and 600°C *(Ukrainian)* 78−92236
- Cr-Ni-Mo-Cr_xC_y wear resistant coating prep. by laser beam melting, and props. 80−40607
- Cr-Ni-Mo-Cu-Nb steel, martensitic precipitation hardenable, corrosion-resistant, heat treatment, structure and props. 79−74169
- Cr-Ni-Nb steel, oxidation in CO_2, charged-particle nuclear techniques 80−61022
- Cr-Ni-Ti alloy and steel, emissitivty and reflectivity, oxide film thickness effect 79−82364
- CrC-Ni alloys, exam. of activated sintering 80−16241
- CrC-Ni-(P), hard alloys, sintered, fracture props., P addition effects 78−60610
- Cr_3C_2/Ni-Cr, self-weldability in high temp Na *(Japanese)* 80−89392
- Cr_3C_2/Ni-Cr hardfacing materials, friction characts. in high temp. Na *(Japanese)* 80−89356
- Cr_3C_2-(WC)-Ni, sintered, cavitation erosion resistance *(Japanese)* 77−52500
- Cr_3C_2-Ni, friction and wear, 20-1000°C 80−30112
- Cr_3C_2-Ni alloys, electrophoretic deposition from conc. suspensions for P/M prep. of hard alloys 77−63575
- Cr_xC_y-(Ni-Cr) sprayed coatings, for gas cooled reactor heat exchangers, factors affecting performance 80−40609
- $CrNi_2$ type alloys, ordering, influence of static stresses *(Russian)* 78−56631
- Cu/Sn-Ni/Au tricouples, electrodeposited, interdiffusion obs. 80−84331
- Cu-Al-Ni, duplex shape memory effect after nonuniform plastic deform. *(Russian)* 80−25759
- Cu-Al-Ni, elastic const. behaviour near Ms 77−12623
- Cu-Al-Ni, formation of martensitic phases during deform. by extension 79−20048
- Cu-Al-Ni, habit plane for SIM $\gamma' \rightleftarrows \beta_1'$ transform. 78−56640
- Cu-Al-Ni, heredity of martensitic transformations 79−47688
- Cu-Al-Ni, hypereutectic, martensitic transform., effect of β_1-phase decomposition *(Russian)* 78−23705
- Cu-Al-Ni, mixed powder compacts, Ni content influence in sintering behaviour *(Japanese)* 80−35130
- Cu-Al-Ni, phase diagram associated with stress induced martensitic transform. 79−8272
- Cu-Al-Ni, positron annihilation study of vacancies before and after martensitic transform. 79−99971
- Cu-Al-Ni, quenched, complex martensite form. 79−56977
- Cu-Al-Ni, rubber like behaviour 77−86114
- Cu-Al-Ni, single variant twinned martensites, pseudoelasticity 77−28849
- Cu-Al-Ni, sintered, internal friction after heat treatment *(Japanese)* 80−11686
- Cu-Al-Ni, stress induced martensite 77−36500
- Cu-Al-Ni, struct. anal. of stress induced β_1'' martensite by neutron diffr. 79−60308
- Cu-Al-Ni (13.8, 7.9 wt.%), cooling rates effect on internal friction *(Japanese)* 80−39217
- Cu-Al-Ni (14, 2.5 wt.%). thermodynamics of thermoelastic martensitic transform. 79−61585

nickel alloys continued
- β-Cu-Al-Ni (14, 3 wt.%), single cryst., thermal effect due to stress induced martensite formation 80−81059
- Cu-Al-Ni (14, 4.5 wt.%), premartensitic alterations 77−12655
- Cu-Al-Ni (14, 8 wt.%), γ′-martensitic, sintered high damping 80−50577
- Cu-Al-Ni (14.0 4.2 wt.%), two stage superelasticity, successive martensite to martensite transform. 77−8826
- Cu-Al-Ni (14.1, 3 wt.%), autooscillations and nonlinear anelasticity 80−70307
- β_1-Cu-Al-Ni (14.2, 4.3 wt.%), quenched, metastable 2H type phase characts., TEM and electron diffr. study 79−74149
- Cu-Al-Ni (14.3, 4 wt.%), ω-phase form. during quenching and ageing *(Russian)* 80−25686
- Cu-Al-Ni (14.5, 3 wt.%), polycrystalline, pseudoelastic, cyclic stress strain response 77−86144
- Cu-Al-Ni (14.5, 3 wt.%), fatigued, polycrystn., pseudoelastic, dislocation and martensite substructs. 79−82223
- Cu-Al-Ni alloy, thermoelastic transformation hysteresis loop width strain rate depend. *(Russian)* 79−100138
- Cu-Al-Ni alloy single crystals, anomalous elasticity orientation depend., martensitic phase struct. during strain 79−87634
- Cu-Al-Ni alloys, deformed, fine struct. of martensite *(Russian)* 78−6923
- Cu-Al-Ni alloys, successive stress-induced martensitic transformations and associated transformation pseudoelasticity 79−43245
- Cu-Al-Ni Marmen alloys, rapid solidification and ageing 80−76245
- β-Cu-Al-$Ni_3(DO_3)$, nonradial diffuse streaks and complex diffuse scatt. patterns of electrons 79−7527
- Cu-Al-Ni-Fe, (10, 5, 5 wt.%), cast microstruct. 78−80535
- Cu-Al-Ni-Fe system, corrosion behaviour in sea water 80−45421
- Cu-Al-Ni-Fe-Mn, cast Ni-Al bronze, fracture metallography 78−27597
- Cu-Au, elastic modulus and internal friction during plastic deform., dislocation props. determ. 80−35244
- Cu-Be-Ni-Ti-Mg (2, 0.3, 0.2, 0.02 to 0.4 wt.%), multiple step ageing *(Russian)* 78−19786
- Cu-Be-Ni-Ti-Mg bronze, alloying element influence on minimum thermo EMF, cold working *(Russian)* 80−34426
- Cu-Be-Ni-Zr, anodic behaviour of intermetallic phase 78−72895
- Cu-Mn-Ni, thin film, vacuum deposited, struct., elec. cond. *(Russian)* 78−19668
- Cu-Mn-Ni alloy, Manganin, elec. resist. under static pressures up to 110 kbar, pressure gauge appl. 79−1594
- Cu-Ni, (1-1.3 at.%), elec. cond. exam. in solid and liquid phase *(Russian)* 77−62895
- Cu-Ni, (10 at.%), magnetisation in high mag. field, Arrott-Noakes plot 80−54919
- Cu-Ni, AES analysis of protective oxide film 79−39035
- Cu-Ni, adsorption of H_2+CO on (110) surface, TDS and UPS obs. 80−80052
- Cu-Ni, alloys, electronic states, KKR-CPA calc. 78−84125
- Cu-Ni, annealing effect on oxidation kinetics, reduction in vacancy level 80−50760
- Cu-Ni, cast, strength and hot ductility, alloying and residual elements effect 80−66595
- Cu-Ni, chemical emission by Ar^+ ion bombardment *(French)* 77−86410
- Cu-Ni, chemisorpt. of CO, SIMS, AES, desorpt. meas. 78−87875
- Cu-Ni, clean surface, surface segregation and growth process of altered layer *(Japanese)* 80−24720
- Cu-Ni, coating on Ti alloy VT9, plastic deform. and diffusion annealing effect on props. *(Russian)* 78−35425
- Cu-Ni, cold worked solid solution, flow stress and activation volume 80−16393
- Cu-Ni, comp. modulated alloy films, transport props., 10 to 300K 79−95515
- Cu-Ni, composition modulated foils, layer struct. and mech. props. 79−95300
- Cu-Ni, corrosion, performance for condenser tube 79−39046
- Cu-Ni, critical concentration for ferromagnetism 78−14969
- Cu-Ni, crystal growth from melt Monte-Carlo method modelling, surface roughness *(Russian)* 79−77536
- Cu-Ni, crystallisation temp., overcooling temp. *(Russian)* 80−97472
- Cu-Ni, Cu rich, chemical and intrinsic diffusion coeff. determ. 79−28130
- Cu-Ni, cyclically deformed, electrical resistance changes 79−57096
- Cu-Ni, density of states of d-electrons, tight binding approx. calcs. 80−59863
- Cu-Ni, diffusion of Ni, resistometric meas. 80−29222
- Cu-Ni, diffusional homogenisation in compacted powder blends, X-ray diffr. line profile analysis 78−80491
- Cu-Ni, dil., dislocation damping, 95-297K, at high strain amplitudes 78−39824
- Cu-Ni, dil., electronic struct., virtual bound state due to s-d hybridisation 78−75990
- Cu-Ni, dil., far IR absorptivity meas. using multireflection cell 77−18075
- Cu-Ni, dil., impurity electron struct., self-consistent KKR Green's function calc. 79−78040
- Cu-Ni, dil., screening charge density round $\Delta Z = -1$ impurities, vacancies, NQR study 80−103897
- Cu-Ni, dil., valence and core level spectra, XPS study 80−84838
- Cu-Ni, dil. alloy, optical reflectivity meas. virtual bound state model analysis 78−2873
- Cu-Ni, dilute solid soln., exam. of recrystallisation and stored energy 78−52836
- Cu-Ni, disordered ferromag., spin density asphericity, neutron diffr. study 79−47251
- Cu-Ni, disordered muffin tin type, coherent pot. approx. appl. 79−15062
- Cu-Ni, effect of alloying and residual elements 78−85033
- Cu-Ni, elastic modulus and internal friction during plastic deform., dislocation props. determ. 80−35244
- Cu-Ni, electrolytic plating 80−35425
- Cu-Ni, erosive wear by impinging SiC particles, surface hardness and material props. effect 77−66705
- Cu-Ni, evaporation limited segregation 80−70513
- Cu-Ni, film, compositionally modulated, enhanced magnetisation density 78−84460
- Cu-Ni, film, preferential sputtering due to altered layer struct., AES meas. 78−76573
- Cu-Ni, foils, supermodulus effect, one-dimens. modulated structs. 79−95068

nickel alloys continued
Cu-Ni, galvanic corrosion in sulphide modified seawater 80−100953
Cu-Ni, in 0.1 M NaCl, electric pot. and pH meas., crevice corrosion 78−31564
Cu-Ni, initial oxidation study by microprobe-AES method *(Japanese)* 79−15867
Cu-Ni, liq., surface conc. profile and surface energy 80−84350
Cu-Ni, liquid, surface tension *(Japanese)* 79−19431
Cu-Ni, long and short range electronic effects in bonding of CO and H_2 77−7974
Cu-Ni, mag. ordering temp. depend. on atomic short-range order from susceptibility meas. 79−61159
Cu-Ni, melt, accel. by shock wave treatment, crystallisation *(German)* 77−86022
Cu-Ni, microconductors, cast, struct. and physical props. exam 78−44232
Cu-Ni, microvoid form., gaseous impurity atom effects, positron annihilation study 80−49275
Cu-Ni, neutron irradiation, enhanced diffusion, elec. resist. meas. 80−6440
Cu-Ni, neutron radiation stimulated diffusion, electrical resistivity exam. *(Russian)* 79−14959
Cu-Ni, Ni effect on stainless steel embrittlement during soldering 79−47773
Cu-Ni, nucleation and growth of oxidation zones during diffusional creep *(Russian)* 79−52431
Cu-Ni, optical absorption and photoemission spectra 80−45216
Cu-Ni, oscills. in composition depth profile, UPS meas. 78−71919
Cu-Ni, parametric eval. of susceptibility to sulphide induced corrosion in sea water 80−16560
Cu-Ni, Portevin-Le Chatelier effect, during tensile deform. *(German)* 79−8330
Cu-Ni, powder, sintered, effect of cold and hot dynamic pressing, upon structure and props. 79−33970
Cu-Ni, powder mixture electric discharge sintering, struct. changes 77−77446
Cu-Ni, powder mixtures, form. using electric discharge sintering 77−12563
Cu-Ni, preferential sputtering Auger electron spectra obs. 79−33880
Cu-Ni, preferred crystallographic orientation of unidirectionally solidified polycrystals *(Czech)* 79−43233
Cu-Ni, quantitative AES anal. of M_1 VV transition, computer simulation 79−91542
Cu-Ni, random ferromag. alloy, local mag. moment calc. 80−70974
Cu-Ni, rubbing contact with cast Fe, surface temperature effect on dry sliding wear 80−60983
Cu-Ni, sintered, props. and degree of nonhomogeneity 80−20848
Cu-Ni, sintering, Kirkendall effect 80−93518
Cu-Ni, soft X-ray emission and local densities of states 79−83059
α-Cu-Ni, solid soln., ductility, comp. effect *(Japanese)* 79−43334
Cu-Ni, sputter-induced subsurface segregation, Auger electrons obs. 80−10757
Cu-Ni, sputtered and sputter-deposited surfaces, in-situ AES meas. 77−48296
Cu-Ni, sputtering yield, surface binding energies 80−50503
Cu-Ni, strength and substruct., strain point influence *(Russian)* 79−52233
Cu-Ni, sulphidation between 653 to 770K, exam. of scale morphologies, using X-ray diffr., and electron microprobe anal. 78−88559
Cu-Ni, surface comp. and catalysis, AES and thermal desorption meas. 79−46898
Cu-Ni, surface comp. calc. by regular soln. theory, surface relax. effects 79−42355
Cu-Ni, surface composition cluster size distrib., Monte Carlo method calc. 78−63915
Cu-Ni, surface layer, effect of Ar^+ bombardment, AES and SIMS 80−25504
Cu-Ni, surface segregation and in-depth profile, AES 77−31856
Cu-Ni, surface segregation, comparison of low-energy ion-scatt. results with theory 78−38923
Cu-Ni, UPS, surface and bulk density of states, comp. depend. 77−44125
Cu-Ni (10 at.%), creep, substruct. and internal stresses *(Russian)* 80−97527
Cu-Ni (10 at.%), hardening, recovery, and struct. changes during high temp. creep *(Russian)* 80−89288
Cu-Ni (10 at.%), struct. changes during deform. *(Russian)* 78−19818
Cu-Ni (10 at.%) alloy, creep, dislocation density variation *(Russian)* 79−96101
Cu-Ni (10 wt.%), deformed bars, cold rolled, exam. of microstruct. by thin foil TEM 78−88502
Cu-Ni (10 wt.%), supercooled melt, dendrite growth morphology *(Japanese)* 78−11216
Cu-Ni (100), UPS spectra, direct transition and matrix element effects 80−55268
Cu-Ni (110), adsorption of CO and H_2, UPS, thermal desorption, AES,and LEED study 80−80087
Cu-Ni (20 and 50 wt.%), sulphidation, exam. of scale growth kinetics 78−88560
Cu-Ni (20 wt.%) contour plate, for relay appl. creep characts. obs., use of Larson-Miller method *(Japanese)* 80−55454
Cu-Ni (20-80 at.%), clustering, diffuse neutron scatt. study, conc., temp. depend., miscibility gap location 78−47529
Cu-Ni (30-90 wt.%), elect. resist. rel. to cold working and heat treatment 80−71765
Cu-Ni (4 at.%), anneal hardening mechanism 80−60879
Cu-Ni (40 at.%), grain boundary migration, intergrain liq. layer effects *(Russian)* 77−15633
Cu-Ni (50 wt.%), preferential sputtering, thickness and in-depth comp. profile of altered layer, AES 78−39649
Cu-Ni (50 wt.%) alloys, estimation of sublimation energy of Cu atoms, evaporation rate and surface composition, AES meas. *(Japanese)* 80−49352
Cu-Ni (70 at.%), mech. behaviour in microplastic strain region *(Russian)* 78−39838
Cu-Ni alloy, α-phase, lattice sp. ht. calcs. 80−65246
Cu-Ni alloy, dislocation density during deform., comparison of electron microscopy and X-ray diffr. *(Russian)* 79−5002
Cu-Ni alloy, sputtered altered layers, in-depth profile, model 78−19613
Cu-Ni alloy prep. by sulphide-oxide reactions 77−48366
nickel alloys continued
Cu-Ni alloy surfaces, chemisorption of CO, LEED, AES, thermal desorption, and work function meas. 79−90879
Cu-Ni alloys, activity of most oxidizable element *(French)* 79−61868
Cu-Ni alloys, alloying additions effect on thermal conductivity, 20-400°C *(Russian)* 77−59159
Cu-Ni alloys, artefacts in thin foil images 80−3056
Cu-Ni alloys, chemical interdiffusion under uniaxial stress 80−65307
Cu-Ni alloys, density of states determ. by continued fraction method 78−47690
Cu-Ni alloys, dislocation climb sources activated by 1 MeV electron irradiation 77−89443
Cu-Ni alloys, electron irradiated, dissociated struct. of dislocation loops with Burgers vector a⟨100⟩ 77−89444
Cu-Ni alloys, magnetic diffuse neutron scatt. 78−14931
Cu-Ni alloys, sulphide induced corrosion 79−91836
Cu-Ni alloys, XPS apparatus appls. *(Dutch)* 79−1982
Cu-Ni alloys 706 and 715, corrosion in flowing seawater, O_2 effect 79−43460
Cu-Ni alloys 706 and 715, corrosion in flowing sea water, dissolved sulfide effect 80−35379
Cu-Ni bimetallic cluster, segregation and short range order props. at boundaries 79−29071
Cu-Ni clusters, electronic states and mag. props., MO calc. 77−20219
Cu-Ni composite formation by electric discharge sintering 77−63594
Cu-Ni crystals, growth, H_2 reduction of CuI-$NiBr_2$ mixture, habit study by X-ray difr., optical and SEM 79−60665
Cu-Ni diffusion couple, diffusion bonding process, fracture surface exam. *(German)* 77−35762
Cu-Ni dil. mag. alloy, NMR of ^{63}Cu around impurities 77−16187
Cu-Ni dil. paramagnetic alloys, sp. elec. resist., effect of Ni clusters *(German)* 78−95293
Cu-Ni electrode, photopotentials, rel. to corrosion 79−24648
Cu-Ni film, (001), in situ oxidation, TEM obs. 78−23874
Cu-Ni film, coevaporated, AES anal. and ion sputtering effects 79−15044
Cu-Ni film, ferromag. mag. susceptibility meas., 30-130°C 79−95615
Cu-Ni film, struct. and mag. order effects on electron transport props. 78−6460
Cu-Ni films, compositionally modulated, magnetic anisotropy, magnetisation curves 80−88840
Cu-Ni films, thickness depend. of Curie temp., resist. meas. 78−6545
Cu-Ni oxidised with NO, surface comp., AES obs. 77−20176
Cu-Ni single phase alloy, sputter yields 79−87546
Cu-Ni sulphidised alloys, Ru and Os behaviour during carbonylation *(Russian)* 80−40584
Cu-Ni system, composition depend. of third-order elastic consts. 77−62579
Cu-Ni textured alloys, grain boundary effusion of Ni to surface 79−90680
Cu-Ni thin films, ferromag., Hall effect meas. 80−80428
Cu-Ni tubing, viscoplastic bending 78−35464
Cu-Ni:polyethylene, surface, obs. at very low accel. voltage (200 V-1 kV) by SEM 80−10764
Cu-Ni/Au-Ni multilayer films, ohmic behaviour, use as strain gauge 80−65713
Cu-Ni/Au-Ni multilayers obtained by co-evaporation in UHV, ohmic stability and TCR 79−78226
Cu-Ni-Al, ageing charact., optical TEM, X-ray, hardness obs. 79−29079
Cu-Ni-Al, grain boundary reaction under isothermal ageing at 623 to 973K *(Japanese)* 79−70090
Cu-Ni-Al, review 80−7564
Cu-Ni-Al (5, 2.5 at.%), precip. hardening *(Japanese)* 80−71663
Cu-Ni-Be (30, 0.5 wt.%), grain boundary reaction after ageing and quenching, obs. *(Japanese)* 79−70089
Cu-Ni-Be-(Al) (30,0.5,(0.2-2) wt.%), Al addition effect on grain boundary reaction *(Japanese)* 80−54254
Cu-Ni-Co, alloy pre-form prep. through reduction of sintered oxides 80−40284
Cu-Ni-Co, mag. props. of system of disperse ferromag. particles, 73 to 673K *(Russian)* 80−65968
Cu-Ni-Cr, lattice imaging and optical microanalysis of spinodal decomp. 78−52754
Cu-Ni-Cr, microstruct. behaviour and mechanical hardening 78−47281
Cu-Ni-Cr (28, 2.8 wt.%), spinodal alloy, microstruct. and tensile props. 78−39858
Cu-Ni-Cr system, coarsening in the ($\gamma_1+\gamma_2$) region, metallographic study 78−84762
Cu-Ni-Fe, age hardenable, dislocation interactions with internal coherency stresses 77−36528
Cu-Ni-Fe, age hardened, yield strength correlation with internal coherency strains 77−44254
Cu-Ni-Fe, alloy pre-form prep. through reduction of sintered oxides 80−40284
Cu-Ni-Fe, corrosion resistant, SCC, crevice corrosion in seawater 79−96177
Cu-Ni-Fe, magnetic properties, heat treatment and compressive stress effects 80−60367
Cu-Ni-Fe, permanent magnet, temp. effect 80−34701
Cu-Ni-Fe, quenched and aged, deformed, low-temp. elec. resist. meas. *(Russian)* 77−52514
Cu-Ni-Fe, spinodal alloy, heat treatments for improved mech. props. 79−5024
Cu-Ni-Fe, spinodally decomposable, densification using four different powder methods 80−40283
Cu-Ni-Fe, synergistic effect of Ni and Fe on sea water corrosion 78−35561
Cu-Ni-Fe (14, 7 wt.%), solid soln., decomposed, magnetostatic interaction between ferromag. particles *(Russian)* 77−80967
Cu-Ni-Fe (26,8 wt.%), microduplex struct. form., hardness meas., optical and electron microscopy *(Japanese)* 78−76659
Cu-Ni-Fe alloys superparamag. early stages of decomp. *(Russian)* 78−6890
Cu-Ni-Fe solid solution, after precip., susceptibility of interacting superparamag. grains 79−99733
Cu-Ni-Fe tube, stressed, corrosion failure caused by cooling water, denickelation *(German)* 79−29286
Cu-Ni-Mn (20,20wt.%), structural transform., X-ray and hardness study *(French)* 78−39760
Cu-Ni-Nb (30, 0.9 at.%), precipitate free zones, X-ray microanal. 80−108768

nickel alloys continued
Cu-Ni-Nb (30,1 wt.%), precipitation 77−86035
Cu-Ni-Nb-Al, correlation of γ' and γ'' precipitates phase stability 80−25704
Cu-Ni-Nb-Al, formation of γ' and γ'' precipitates 78−76655
Cu-Ni-O, liquid alloy, thermodynamic study by EME method *(Japanese)* 78−15367
Cu-Ni-O system, distrib. of Ni between Cu and Cu_2O *(Russian)* 77−16540
Cu-Ni-P, precipitation hardening 77−12633
Cu-Ni-S, molten, thermodynamic props. 80−104122
Cu-Ni-Sn, liq. alloy, calc. and anal. of mixing enthalpies *(German)* 80−44325
Cu-Ni-Sn, liq. alloy, mixing enthalpies determ. using a SETARAM high temp. calorimeter *(German)* 80−44324
Cu-Ni-Sn, thermal decomposition after prior cold work 78−15427
Cu-Ni-Sn (10, 6 wt.%), spinodal decomposition, X-ray and electron diffr. study 80−81063
Cu-Ni-Sn (10, 6 wt.%), temp. depend of yield stress and work hardening 80−21026
Cu-Ni-Sn (15, 8 wt.%), prior deform. effect on spinodal age hardening 80−108465
Cu-Ni-Sn (15, 9 wt.%), age hardening accompanying phase transition 78−64551
Cu-Ni-Sn (4,4 wt.%) resistance spot weld quality evaluation, using stress wave emission technique 78−53066
Cu-Ni-Sn (4-15, 4-8 wt.%), strip strengthened by spinodal decomp., stress relax. in bending 80−7616
Cu-Ni-Sn (9, 2 wt.%), surface comp., Auger electron spectroscopy study, manufacture and storage influence 80−65348
Cu-Ni-Sn (9, 6 wt.%), decomposition, initial stages, TEM study 80−2992
Cu-Ni-Sn spinodal substitute for Be-Cu alloy 80−35217
Cu-Ni-Su alloy, flat spring, mechanical props. in bending, stress relax. test, 23 to 232°C 78−72806
Cu-Ni-Ti, ordering within precipitates, TEM obs. 80−108461
Cu-Ni-Ti system, phase equilibria in Cu rich region and Cu-T quasi-binary constitution *(Japanese)* 80−89203
Cu-Ni-Ti system, reactions with melt in Cu-rich region *(Japanese)* 80−89202
Cu-Ni-W melt, solubility of W, primary solidification 78−19726
Cu-Ni-Zn, Cu rich, penetration tendency model for diffusion 77−39701
Cu-Ni-Zn, diffusion couples, zero-flux planes and flux reversals 80−15313
Cu-Ni-Zn, microduplex, superplastic deform., cavitation and fracture 78−64640
Cu-Ni-Zn, multiphase couples, diffusion paths and struct. at 775°C 77−62666
Cu-Ni-Zn (18, 27 wt.%), surface comp., Auger electron spectroscopy study, manufacture and storage influence 80−65348
Cu-Ni-Zn alloy, at 775 degrees C, diffusional and thermodynamic interactions 78−38883
Cu-Ni-Zn alloy, FCC, cold-worked, microstruct., X-ray obs. 78−3143
Cu-Ni-Zn alloy, surface comp., outdoor exposure influence 80−59770
Cu-Ni-Zn system, tie lines in a two phase region 80−24404
Cu-Ni-Zn-Mn fine grained precipitation-hardenable alloy, high strength and ductility 80−100805
α-Cu-Ni-Zn-Pb, fire cracking and ordering *(German)* 78−60760
α-Cu-Ni-Zn-Pb, fire cracking, effect of pores and impurities 79−29207
Cu-$NiAl_2O_4$, internally oxidised, orientational relationships of precip. oxide phase 77−4783
Cu-Ni, preferential sputtering, Auger meas. 78−27358
Cu-Ni(10 (30) wt.%), seawater corrosion rate meas., electrochem. method validity 80−45426
Cu-Si-Ni, undercooled, grain refinement 79−34079
Cu-Sn alloy, surface comp., outdoor exposure influence 80−59770
Cu-Sn-Ni, mech. props. after thermomech. treatment 79−79009
Cu-Ti-Ni, wetting of Al_2O_3, alloying effects 80−107617
β-Cu-Zn-Ni (47.5, 4.7 and 9.9 wt.%), order-disorder transformation temperature effect on quench hardening 78−95745
Cu_3Au-Ni, antiphase domains morphology 80−108460
CuNi alloys, electronic theory of surface segregation 79−23819
$Cu_{0.435}Ni_{0.565}$, clustering, temp. depend., diffuse neutron scatt. study 79−42013
$Cu_{0.85}Ni_{0.15}$, liq., 3d bandwidths, photoelectron spectrum 77−4286
$Cu_{1-x}Ni_x$, mag. transition, NMR meas. by spin-echo technique 77−32267
Cu_2Ni_{1-c}, solutions of KKR-CPA equations for paramagnetic alloys 78−95256
Cu_cNi_{1-c}, Fermi surface of concentrated paramag. alloys 78−95257
Cu_xNi_{1-x}, bulk electronic structure, comparison of CPA and ATA techniques 80−44467
Cu_xNi_{1-x}, disordered alloy, muffin-tin model, electronic struct. and density of states calc. 80−29302
Cu_xNi_{1-x}, low-temp. elec. resist. meas. *(Russian)* 77−52514
Cu_xNi_{1-x}, paramag., electronic struct., atomic sphere approx. to KKR-CPA 79−19502
Cu_xNi_{1-x} random alloy, angle-resolved photoemission 78−95683
CuNiCr, IN838, heat treatment effect on fatigue and corrosion fatigue behaviour 80−20982
Cu_2NiSn, Heusler alloy, elec. resist., 4.2 to 300K 80−75547
$Cu_{3-x}Ni_xSn$, one-dimens. long period superstructs. with Zn and Ni additions 78−83777
β(CuNi)Zn alloys, effect of normal stress on {112} ⟨111⟩ slip 79−47760
α-CuNiZn alloys, Zener-relaxation effect 80−3121
β-(CuNi)Zn, anomalous strengthening 77−48503
β-(CuNi)Zn, cross slip 78−26576
Cu_2NiZn, atomistic approach to ordering 79−94944
Cu_2NiZn, characterisation of superlattice dislocations by TEM 79−55748
Cu_2NiZn, comparison between different theories predicting stacking fault energy from extended nodes 80−75240
Cu_2NiZn, separation of partials of superlattice dislocations, anisotropic elasticity theory, ordering 79−65082
Cu_2NiZn, stacking fault energy determ. from extended nodes 80−107280
Cu_2NiZn, superlattice dislocations 78−83816
Dy-Fe_xNi_{1-x} system, mag. hyperfine field, influence of lattice struct. and substituent 77−8058
$Dy(Co,Ni)_2$, intrinsic mag. aftereffect obs. 77−63237

nickel alloys continued
$Dy(Co,Ni)_2$, intrinsic mag. aftereffect meas., domain wall motion 80−71121
$Dy(Fe_xNi_{1-x})$, mag. interactions, mol. field model 77−73010
$Dy(Fe_xNi_{1-x})_2$, mag. behaviour, susceptibility and Mossbauer expts., 4.2-1300K 78−52235
$Dy_2(Fe_{1-x}Ni_x)_{17}$, Mossbauer spectra, hyperfine field interactions 78−6614
$Dy_{1-x}Ho_xNi_2$, cryst. field quenching of Dy^{3+} 4f shell, Mossbauer effect meas. 78−39480
$DyNi_2$, H_2 absorpt., Mossbauer study 80−44987
$DyNi_2$, single cryst. mag. props. 77−24684
$DyNi_3$, amorphous, mag. struct. and moments 77−66260
$DyNi_3$, amorphous, resist. meas., 1.2-290K 78−19015
$DyNi_{3.4}$, amorphous, mag. props. 77−72985
$DyNi_5$ crystal, basal plane anisotropy, torque meas. 80−65857
Dy_2Ni_{17}, hyperfine interactions and cryst. field effects, Mossbauer spectra 80−2369
Dy_2Ni_{17}, magnetic struct. by neutron diffr. and Mossbauer spectra *(French)* 77−32165
$DyNi_2Si_2$, Mossbauer spectra 80−20558
Er-Co-Ni, cryst. struct. and H_2 capacity 77−89543
$ErCo_{5-x}Ni_x$ ferrimagnetic series, magnetisation, coercive field meas. 78−91896
$Er_2(Co_{1-x}Ni_x)_{17}$, mag. anisotropy and intersublattice exchange interactions 78−31066
$Er_2Co_{17-x}Ni_x$, effect of substitution on mag. props. 79−78363
$Er_2Co_{17}Ni_x$, magnetisation, Curie temp., anisotropy 77−89947
$Er_6Ga_{1.5}Ni_{2.5}$, struct. determ. by X-ray powder method *(Ukrainian)* 80−39001
$ErNi_5$, cryst. field parameters in ferromag., paramag. states, susceptibility meas. 77−63139
$ErNi_x$, sorption at press. up to 1500 atm. 80−97819
Er_2Ni_{17}, magnetic structure by neutron diffr. 77−73000
$ErNi_{0.6}Cu_{0.4}$, sp. ht. and modulated mag. struct. 77−32167
$Eu(Ni_{1-x}Cu_x)_5$, mixed valency, isomer shift temp. depend. 78−84511
$EuNi_xCu_{5-x}$, mixed valency of Eu, Mossbauer expts. 78−52407
$EuNi_5H_x$, Mossbauer effect exam. 78−48094
$EuNi_xZn_{5-x}$, mixed valency of Eu, Mossbauer expts. 78−52407
(Fe,Co,Ni)-Si(B), amorphous mag. alloy, magnetostriction rel. to soft mag. props. 80−84633
(Fe, Co, Ni)$_3$V, control of ordered struct. and ductility 80−21029
(Fe, Ni, Co)-Si-B, amorphous, compositional effect on struct. changes, after heating up to 700°C, exam. *(Japanese)* 78−48433
(Fe,Ni,Co)$_3$V, long-range ordered alloy for fusion reactor appl. 80−32481
$(Fe,Ni)_{83}B_{15}C_2$, amorphous alloy, mag. props., possible appl. to power transformers 79−28558
$(Fe,Ni)_{80}(P,B)_{20}$, quenched alloy ribbon, mag. moments, Curie temp. 77−40041
$(Fe,Ni)_{80}P_{14}B_6$ amorphous alloy, mag. props., possible appl. to power transformers 79−28558
Fe base melt, thermodynamic props. *(Russian)* 77−55363
Fe, cast, Ni resist alloy, austenitic type ChN15D7Kh2, struct. stability 79−87633
Fe, cast-Mg, 78−44149
Fe, cast-Ni, 78−44086
Fe-(Ni), cast, influence of Ni content on corrosion props. *(German)* 80−35370
Fe-Al-Co-Ni, Alnico alloys, irreversible remagnetisation processes in rotating fields *(Russian)* 79−8015
Fe-Al-Ni-Co-Cu alloys, Ti alloying and deoxidising addition *(Russian)* 78−80181
Fe-B-Ni, amorphous alloy, anelastic relaxation 79−4997
Fe-C-Cr-Ni, white cast, effect of abrasion on carbide microstructure *(German)* 78−88540
Fe-C-Ni-Cr, athermal alloy, exam. of martensite transformation kinetics 78−80545
Fe-C-Ni-Cr(Cu), dynamically hot pressed, mech. props., additives effect 78−60620
Fe-Co-Ni, at. mag. moments, neutron scatt. and Mossbauer meas. 79−42744
Fe-Co-Ni Perminvar, mag. props. singularities in region of mag. anisotropy *(Russian)* 80−84614
Fe-Co-Ni powder, video recording appl. *(Russian)* 77−55910
Fe-Co-Ni-Al, Si alloying of mag. hard alloys *(Russian)* 79−73765
Fe-Co-Ni-Al (35, 14.5, 7.2 wt.%), high-coercivity, substructure and texture change during bending and upsetting 80−21037
Fe-Co-Ni-Al-Cu, polycryst. hard mag., C diffusion 79−77827
Fe-Co-Ni-Al-Nb (15-20, 14, 9, 0.1-5.5 at.%), Nb effect on magnetic props., lattice parameter *(Russian)* 77−55689
Fe-Co-Ni-Al-Zr magnetically hard alloys, reduction *(Russian)* 78−43614
Fe-Co-Ni-C, activity coeff. of C at 1273K 80−96667
Fe-Co-Ni-Si-B amorphous alloy, magnetostriction and permeability, effect of annealing 79−1701
Fe-Co-Ni-W alloy, 45KKhVN, plastic deform., electron microscope obs. *(Russian)* 78−80584
Fe-Co-V-Ni, annealing effect on microstruct. rel. to mag. and mech. props. 80−89267
Fe-Cr-Ni, AES investigation of corrosion and growth nature of surface layers 77−77330
Fe-Cr-Ni, analysis and synthesis of phase diagrams 79−11563
Fe-Cr-Ni, appl. of computational techniques for treatment of thermodynamic data, phase diagram calc. 78−10172
Fe-Cr-Ni, austenitic, oxidation behaviour on addition of Si 77−12740
Fe-Cr-Ni, austenitic, self-diffusion and swelling under irradiation 80−39343
Fe-Cr-Ni, α-particle induced precip. and phase instability 79−1470
Fe-Cr-Ni, cold-rolled foils, dilatometric study 80−21033
Fe-Cr-Ni, corrosion behaviour in hot conc. NaOH soln. *(Japanese)* 80−85082
Fe-Cr-Ni, corrosion by coal char at 871° and 982°C 80−3237
Fe-Cr-Ni, electron irradiated, resistivity during annealing, 4.2-1300K 78−87962
Fe-Cr-Ni, Fe-rich, melting equilibria *(German)* 77−52282
Fe-Cr-Ni, foil, in situ oxidation in HVEM 80−104354
Fe-Cr-Ni, irradiated, Ni segregation to sinks 78−91472
Fe-Cr-Ni, mag. state at low temps. *(Russian)* 78−56298
Fe-Cr-Ni, melting and solidification *(French)* 77−66635

nickel alloys continued
Fe-Cr-Ni, neutron irradiated, rel. between irradiation induced swelling and shear modulus 80−15157
Fe-Cr-Ni, shock loading effect on phase equilib. *(Russian)* 79−29017
Fe-Cr-Ni, single crystal anomalies in curve of critical shear stress versus temp. at low temps. 77−16656
Fe-Cr-Ni, solid soln. strengthened and precipitation hardened, in-reactor creep 79−43327
Fe-Cr-Ni, spin system, relaxation props. at low temp. 79−82758
Fe-Cr-Ni, stable and metastable, thermal expansion, 4.2-290K *(Russian)* 78−47537
Fe-Cr-Ni, stress corrosion cracking in high temp. caustic soln. 77−59964
Fe-Cr-Ni, textured ($\alpha+\gamma$) alloy, α' lath martensite formation 78−95749
Fe-Cr-Ni, thermodynamic prediction in coal gasifier environment 79−43206
Fe-Cr-Ni, two phase ($\alpha+\gamma$) alloys, transformation-induced plasticity 77−63721
Fe-Cr-Ni, two-phase ($\alpha+\gamma$), and metastable austenitic, uniform elongation peak 77−77547
Fe-Cr-Ni (12, 15 wt.%) austenitic alloy, Ni^{6+} irradiated, void swelling and phase stability, Si and Ti effects 80−65055
Fe-Cr-Ni (18, 14 wt.%), single strain induced γ to α' cryst. transform. *(Japanese)* 78−11221
Fe-Cr-Ni (18,14 wt.%), γ to ε to α martensitic transform., external stress effect, double tensile deform. exam. 80−108438
Fe-Cr-Ni (19, 13 wt.%), austenitic, Ni^+ ion irradiated, multiple dislocation loops *(French)* 80−65064
Fe-Cr-Ni (20,15 wt.%), low cycle fatigue life under hold time conditions, grain size effect 77−77577
$\alpha+\beta$-Fe-Cr-Ni (23.19, 4.91 wt.%), orientation relationship between austenite and lath martensite 78−39775
Fe-Cr-Ni (25, 20 wt.%), single crystal, stress corrosion cracking 78−35553
Fe-Cr-Ni alloy, austenitic, Neel temp. and max. susceptibility predictions comp. effects 77−43833
Fe-Cr-Ni alloy, deforming stresses anomalous temp. depend. *(Russian)* 77−81296
Fe-Cr-Ni alloy, dual-ion-irradiated, swelling anal. 78−86600
Fe-Cr-Ni alloy, quantitative anal. method based on ion bombardment induced secondary ion and photon emission 79−19963
$\alpha+\gamma$Fe-Cr-Ni alloy, stress-induced α'-martensite occurrence 78−23704
Fe-Cr-Ni alloy 800, sensitization times for intergranular corrosion 77−16746
Fe-Cr-Ni alloys, linear expansion, 4.2-300K rel. to antiferromag. rearrangement 78−43146
Fe-Cr-Ni alloys, oxidation-sulphidation in gas mixture, parabolic kinetics, thermochem. diagram 78−72932
Fe-Cr-Ni and Fe-Ni-Mn, BCC, atomic mag. moments determ. 77−59396
Fe-Cr-Ni austenitic alloys, environment sensitive cracking, metallurgical variables effect 80−35391
Fe-Cr-Ni austenitic alloy, cold deformed, α-γ transition, calorimetric study *(Russian)* 80−55390
Fe-Cr-Ni based alloys, Ni^+ ion and neutron irradiated, γ' particle redistrib. and phase stability 79−78977
Fe-Cr-Ni based alloys, surface oxides at high temps., backscattering Raman spectroscopy 80−93291
Fe-Cr-Ni liquid alloy, N_2 soln. and TiN precipitation 78−6931
Fe-Cr-Ni melts, S solubility and solid soln. precipitation *(Russian)* 80−15251
Fe-Cr-Ni system, austenitic, energetic particle bombardment, thermodynamic and dimensional stability 77−27904
Fe-Cr-Ni system, diffusion coeff. consts. calcs. for multi-component systems *(Russian)* 79−90815
Fe-Cr-Ni system, isothermal diffusion *(Russian)* 79−69300
Fe-Cr-Ni-Al alloys, 25 keV ion implanted, metallic corrosion behaviour 79−52447
Fe-Cr-Ni-C (17.2, 7.34, 0.2 wt.%), twin related laths, fracture elongation, TEM study 79−29192
Fe-Cr-Ni-C (23.19, 4.91, 0.025 wt.%), two phase alloy, effect of prestrain above Md temp. on Ms temp. 78−80543
Fe-Cr-Ni-Cu-Sn, Cu and Sn effect on Cr and Ni segregation *(German)* 78−72777
Fe-Cr-Ni-Mn-Mo, liquid, N_2 solubility 78−44087
Fe-Cr-Ni-Mo, liquid, N solubility, AlN precipitation 79−11630
Fe-Cr-Ni-Mo-V, Mo and V effects on segregation *(German)* 77−55942
Fe-Cr-Ni-P-C, amorphous, stress corrosion cracking 77−25123
Fe-Cr-Ni-Si, sintered, carbide coated, crack propag. energy in impact bending 79−66162
Fe-Cr-Ni-Ti-Al, superalloy, Ti, Ni, Al, H_2 variations effect on mech. props. 78−3188
Fe-Cr-Ni-(Mo), AES using peak-to-peak value *(Japanese)* 79−20485
Fe-Cr-Ni(Ni-Mn)-C, carbide-austenite equilibria, 1173 to 1373K, microscopic and X-ray obs. 78−44085
Fe-Cu-Ni, austenite to ferrite+precipitate reaction, TEM/STEM study 80−3075
Fe-Cu-Ni, Ni effect on austenite decomposition 80−3048
Fe-Cu-Ni (2, 5 wt.%), interphase precipitation obs. in assoc. with Widmanstatten ferrite lateral growth 80−40365
Fe-Cu-Ni (2,2 wt.%), isothermally transformed, precipitate orientations 80−50640
Fe-Cu-Ni-Cr_3C_2-C based sintered friction material, wear, surface geometry and struct. effects 80−25875
Fe-M, dil., M=transition metal, impurity electronic struct., multiple scatt. approach 80−92856
Fe-Mn (3 wt.%), Sn diffusion along grain boundaries, micro-Auger spectroscopy 77−11740
Fe-Mn-Co-Ni-Cr, antiferromag. props., Neel temp. determ. 78−88124
Fe-Mn-Mi, martensitic, morphology and substruct. study 77−70059
Fe-Mn-Ni, age hardenable, struct. and strength 77−52339
Fe-Mn-Ni, fracture toughness, thermomechanical treatment effects 78−60794
Fe-Mn-Ni, mag. and crystallographic transformation depend. on Cr-Ni addition *(Russian)* 79−83334
Fe-Mn-Ni antiferromag. alloy, neutron scatt. exam. of antiferromagnons 77−66283
Fe-Mn-Ni base maraging alloys, age hardening 79−74170
Fe-Mn-Ni-C, age hardenable, struct. and strength 77−8844
Fe-Mn-Ni-V-C (0.5, 3.0, 1.0, 0.2 wt.%), austenite decomp., isothermal transform. characts. 80−97477

nickel alloys continued
Fe-Mo-Ni-C, carbide-austenite equilibria, 1173 to 1373K, microscopic and X-ray obs. 78−44085
Fe-Ni, (10 at.%), magnetisation in high mag. field, Arrott-Noakes plot 80−54919
Fe-Ni, alloy, composition determination using secondary ion emission *(French)* 77−86409
Fe-Ni, alloy 20N24, martensitic, exam. of structure after laser treatment, and recrystallisation *(Russian)* 79−11608
Fe-Ni, and Fe-Ni-Cr alloys, preferential sputtering, XPS expts. 79−87544
Fe-Ni, Ar ion bombard., O_2 flooded, secondary ion yield as function of original conc. *(French)* 78−39643
Fe-Ni, arc electrode processes, thermodynamic approach *(Russian)* 77−27755
Fe-Ni, atomic valence states, ferromag. props. *(Ukrainian)* 78−2656
Fe-Ni, austenite formed from martensite during annealing in ($\alpha+\gamma$) region, crystallographic study 78−19782
Fe-Ni, austenitic, precipitation of AlN *(French)* 78−23711
Fe-Ni, α to γ transformation, changes in Young's modulus and electrophysical props. *(Russian)* 79−20042
Fe-Ni, $\alpha\rightarrow\gamma$ conversion, electron microscope and X-ray spectral microanal. 79−78966
Fe-Ni, $\alpha\rightarrow\gamma$ transform., role of grain boundary diffusion, Mossbauer obs., homogenisation effect *(Russian)* 79−52197
Fe-Ni, BCC, cyclic cleavage crack growth model for fatigue 80−55519
Fe-Ni, BCC, ferromag., spin wave stiffness constant 78−91851
Fe-Ni, brittle transgranular and intergranular fatigue crack growth rate, yield strength effect 78−68786
Fe-Ni, coercive force depend. on grain struct. and inclusions 77−20635
Fe-Ni, cryst. growth from melt, distrib. of growth directions 79−33924
Fe-Ni, crystallisation temp., overcooling temp. *(Russian)* 80−97472
Fe-Ni, crystallization texture, rolling, effect of impurities 78−15425
Fe-Ni, DC arc plasma, meas. of conc. ratio of component atoms *(Russian)* 77−27754
Fe-Ni, deposition of layers from carbonyl vapour 77−4727
Fe-Ni, dil., high freq. induction melting and centrifugal casting, working curve sample prep. photoemission anal. *(Japanese)* 78−53050
Fe-Ni, dil., point defect relax. after low temp. neutron irrad. 78−52316
Fe-Ni, dilute, irradiation softening effect on yield stress 80−76319
Fe-Ni, dissolution rate into molten Al, convection mass transfer *(Japanese)* 78−71858
Fe-Ni, effect of alloying additions on magnetoelastic effects 78−43624
Fe-Ni, effect of electron irradiation and deform. on martensitic transform. 77−16581
Fe-Ni, effect of plastic deform. and martensitic transformation on Fe atom mobility *(Ukrainian)* 78−55974
Fe-Ni, elect. phenomena rel. to martensitic avalanche *(French)* 78−68691
Fe-Ni, electrical resist., 1000 to 1700°C *(Russian)* 77−85193
Fe-Ni, electrodeposition, mag. props. *(French)* 78−64488
Fe-Ni, electrolytic film, coercive force depend. on electroplating conditions *(French)* 77−55691
Fe-Ni, electron state density and elec. resist. 80−39558
Fe-Ni, electronic struct., XPS study 80−29842
Fe-Ni, elinvar comp., props. of materials used in electromechanical filter resonators *(Czech)* 80−76318
Fe-Ni, enthalpy of transform. of γ to α' and α' to γ transforms. *(French)* 79−47683
Fe-Ni, exam. of mech. adhesion, with vitreous coating 79−20336
Fe-Ni, FCC, anomalous props. at high temp. and new phase *(Japanese)* 78−80520
Fe-Ni, FCC, elastic props. and stability near martensitic transform. temp. *(Russian)* 78−6921
Fe-Ni, FCC alloy, magnetovolume instability 79−8031
Fe-Ni, FCC alloy, thermoelec. power, anomalous conc. depend. at high temp. 79−4548
Fe-Ni, FCC and BCC lattices, X-ray characteristic temp. *(Russian)* 78−67797
Fe-Ni, fatigue crack propag., low temp. 80−35311
Fe-Ni, fcc alloys, spin wave energy calc. 79−87247
Fe-Ni, $Fe_{65}(Ni_{1-x}Cr_x)_{35}$, low-temp. elec. and galvanomag. props. rel. to mag. boundaries *(Russian)* 77−35910
Fe-Ni, ferro-nickel oxidation, appl. of mag., thermomag. methods *(French)* 79−20318
Fe-Ni, ferromag., high-field susceptibility 80−7083
Fe-Ni, ferromagnetic films, domain boundary creep relaxation effects *(Russian)* 79−82840
Fe-Ni, film, depth profiles, sputter etching obs. 79−83079
Fe-Ni, first order displacive transformations, localized soft modes and US effects 79−73281
Fe-Ni, fracture mechanism in various temperature and stress intervals *(Russian)* 79−24600
Fe-Ni, fracture toughness at cryogenic temp. 78−72878
Fe-Ni, grain boundary segregation, X-ray microanal. by STEM 80−66740
Fe-Ni, Hall effect, anomalous, residual coeff. calcs. using coherent pot. method *(Russian)* 80−80249
Fe-Ni, hardening by plastic deform. during polymorphic transform., struct. mechanics for γ-phase form. *(Russian)* 77−90344
Fe-Ni, hardening by plastic deform. during polymorphic transform., mechanical props. *(Russian)* 77−90345
Fe-Ni, hot shortness *(Japanese)* 78−84998
Fe-Ni, hydrogenated, Mossbauer effect meas. 78−92002
Fe-Ni, hyperfine field distrib., temp. and press. depend. 78−91651
Fe-Ni, influence of hydrogen press. on temp. of martensitic transform. *(Russian)* 78−27514
Fe-Ni, interference microscopy, for colour development and phase separation 80−100976
Fe-Ni, internal friction study, tempering effects *(French)* 77−81286
Fe-Ni, Invar alloy, explanation of phys. anomalies *(Russian)* 78−88112
Fe-Ni, ion-implanted, depth profile and diffusion coeff. 80−54277
Fe-Ni, itinerant electron ferromagnet, magnetovolume effects 80−60397
Fe-Ni, layers formed by reaction with molten Al, X-ray, EPMA and hardness meas. *(Japanese)* 78−72926
Fe-Ni, lenticular martensite growth by transformation wave propag. 80−81055
Fe-Ni, liq., thermodynamic characts. calc. *(Russian)* 80−15264
Fe-Ni, liq. alloy, electrochem. meas. of O, thermodynamic props. at 1873K 80−30244

nickel alloys continued
Fe-Ni, liquid, activity meas. by transportation method *(Japanese)* 79−4949
Fe-Ni, liquid and solid, thermochem. props. 77−59755
Fe-Ni, liquid diffusion of H_2 *(German)* 78−14487
Fe-Ni, local environment effect on at. mag. moment 79−82763
γ-Fe-Ni, local magnetisation of Fe atoms, Mossbauer effect meas. 80−75891
Fe-Ni, local ordering, neutron scatt. study 78−64193
Fe-Ni, low frequency power losses 78−95466
Fe-Ni, low-noise, for cores of ferromag. probes and mag. modulators 79−8017
Fe-Ni, mag. aftereffect meas., phenomenological description 80−88835
Fe-Ni, magnetic ordering, effect on diffusibility, penetrability and solubility of H_2 *(Russian)* 77−24435
Fe-Ni, magnetisation calc. method based on moments of density of states 80−65770
Fe-Ni, martensite burst transformation, supercooling 78−84806
Fe-Ni, martensitic transform. dynamic, quasi-static atomic displacements, NGR, X-ray and electron scatt. meas. *(Russian)* 78−68688
Fe-Ni, martensitic transformation, microscopic mechanism *(Russian)* 79−34036
Fe-Ni, mechanisms of EM generation and detection of US Lamb waves 78−39382
Fe-Ni, metallic glasses, mag. props. *(German)* 79−51813
γ-Fe-Ni, Mossbauer exam. 79−56640
Fe-Ni, N27T2 and N28, internal friction peaks after reverse martensitic transform. *(Russian)* 78−92287
Fe-Ni, optical and electronic characts., 20-1750°C, comp. depend. *(Russian)* 78−84601
Fe-Ni, ordered, low temp. $\alpha \rightarrow \gamma$ transform. *(Russian)* 78−19740
Fe-Ni, ordered, tetragonal, identification with clear taenite in meteorites 80−8604
Fe-Ni, ordered phase, Llo superstruct., Mossbauer spectrum, Debye-Scherrer pattern from LL-chondrite 80−50241
Fe-Ni, oxidation, Mossbauer spectroscopy, metallography, SEM and X-ray diffr. anal. 78−15577
Fe-Ni, permeability and coercive force, effect of thermomag. treatment in rotating field *(Russian)* 77−21294
Fe-Ni, point defect form. at high temps. *(Russian)* 79−86787
Fe-Ni, powder mixture, effect of granulometric distrib. on importance of Kirkendall effect during calcination *(French)* 77−11721
Fe-Ni, quenched irreversible alloy, zero or negative thermal dilatation, para-process mag. susceptibility 79−4419
Fe-Ni, reactive metal alloy, effects of thermomechanical processing on strength and toughness 79−70112
Fe-Ni, recrystallisation under laser irradiation *(Russian)* 78−35396
Fe-Ni, reference material for determ. of C activity, interaction parameter *(Czech)* 79−42278
Fe-Ni, reverse martensitic transform., prior deform. effect 77−63668
Fe-Ni, reverse martensitic transform., shape deform. reversibility 80−66506
Fe-Ni, reversibility of crystal orientation in reverse martensitic transformation 79−83199
Fe-Ni, secondary recrystallization *(Czech)* 79−70080
Fe-Ni, secondary recrystallisation singularities *(Russian)* 80−66528
Fe-Ni, secondary recrystn. and mag. props. 80−89247
Fe-Ni, segregation of ^{121}Sb, Mossbauer spectroscopy 79−47698
Fe-Ni, segregation of inhomogeneities during crystallisation *(Russian)* 78−27521
Fe-Ni, shape memory effect *(Russian)* 78−38771
Fe-Ni, sintered, porosity determ. by US attenuation and sound vel. meas. *(German)* 80−76437
Fe-Ni, slip and twinning, SEM and optical obs. 79−71209
Fe-Ni, solid and liq., paramag. susceptibility and electron struct., 800-1800°C *(Russian)* 80−25081
Fe-Ni, solid and liquid, determ. of activities for temp. range 1500-1900K, using mass spectroscopy 79−11558
Fe-Ni, solid soln., cyclic stress-strain props., depend. of fatigue crack growth rate 77−4853
Fe-Ni, sputtered using Hg^+ and Ar^+ beams, variation as function of ejection angle, AES exam. 77−44105
Fe-Ni, strain energy controlled shape of cryst. forming due to martensite transform. or decomposition 78−38648
Fe-Ni, strain hardening and rate-sensitivity, effect on ductile-brittle transition temp. 78−39900
α-Fe-Ni, struct. after polymorphic transform. under press. *(Russian)* 80−29946
Fe-Ni, struct. defects effect on interdiffusion 80−15314
Fe-Ni, surface comp. obs. by AES 78−10266
Fe-Ni, taenite, superstruct. in Fe meteorites 78−61820
Fe-Ni, thermal diffusivity during martensitic and austenitic transform. *(French)* 77−59781
Fe-Ni, thermal expansion, ferromagnetic-paramagnetic transition *(Russian)* 80−54412
Fe-Ni, thermodynamic props., anomalous 80−39313
Fe-Ni, unlimited component solubility, intercrystallite internal adsorption *(Russian)* 80−39294
Fe-Ni, XPS obs. of Fe 2p states 78−52625
Fe-Ni, XPS of valence electrons *(Russian)* 77−77340
Fe-Ni, yield stress, temp. depend. *(Russian)* 78−56691
Fe-Ni (1 to 5 at.%), mech. props. below 300K *(French)* 79−8314
Fe-Ni (1 wt.%), machine induced residual stress contrib. to pitting susceptibility 79−61784
Fe-Ni (15, 25 at.%), longitudinal forces in the hot torsion test *(German)* 79−38889
Fe-Ni (18 wt.%), martensitic transform., external stress effect *(French)* 78−23707
Fe-Ni (19wt.%), oxidation in CO_2, 700 to 1000°C, kinetics study 78−72931
Fe-Ni (20 to 100 wt.%), exam. of C diffusion coeff., in temp. range 950 to 1100°C 78−51747
Fe-Ni (20 to 31 wt.%), exam. of martensitic transform. and reverse transform. using differential and thermomagnetic resistance analysis *(French)* 79−52214
Fe-Ni (23 wt.%), struct., composition changes during α to γ transform., martensite plastic deformation influence *(Russian)* 80−11642
Fe-Ni (23-35 at.%), cooled below 70K in mag. field, uniaxial anisotropy *(Russian)* 78−19244
Fe-Ni (23.1 wt.%), α to γ transformation, struct., conc, changes, heating rate, residual austenite influence *(Russian)* 79−83194

nickel alloys continued
Fe-Ni (24 wt.%), isothermal decomp., mag. determ. of austenite content 80−20886
Fe-Ni (25 to 50%), FCC, meteorites and thermodynamic equilib., Mossbauer and X-ray diffr. study 80−88087
Fe-Ni (25 wt.%), and single phase, solidified from undercooled melt, mech. props. 77−48540
Fe-Ni (25%), solidification of powder or large ingot, heat losses 77−12612
Fe-Ni (28 at.%), martensitic transformations, Mossbauer scattering evidence of soft modes 80−93223
Fe-Ni (28 wt.%), martensitic reversion, effect of internal stresses *(French)* 77−21142
Fe-Ni (29 at.%), calc. of elastic interaction between locally transformed regions with screw and edge dislocations 78−83844
Fe-Ni (29 wt.%), martensite nucleation at dislocations, elasticity model 80−55393
Fe-Ni (29.3%), N29, martensitic tranform. kinetics and morphology, ordering role 77−63673
Fe-Ni (29.58 wt.%), acoustic absorpt. and emission associated with martensitic transform. 79−34035
Fe-Ni (29.5at%), martensitic transform., pisition lifetime spectra meas. 77−36498
Fe-Ni (3 wt.%), embrittled, microanalysis of grain boundary segregation using STEM 78−35633
Fe-Ni (3 wt.%), grain boundary segregation of Sn and P embrittling additions, STEM microanal. 78−76654
Fe-Ni (3 wt.%), influence of temper embrittlement, on stress corrosion susceptibility 78−85023
Fe-Ni (3 wt.%), low temp. softening *(German)* 79−29081
α-Fe-Ni (3-12 wt.%), structure and $\gamma \rightarrow \alpha$ polymorphic transform. kinetics 80−71645
Fe-Ni (30 wt.%), Ni segregation singularities during dendrito-cellular solidification *(Russian)* 80−7542
Fe-Ni (31 at.%), austenitic, ageing, absence of at. order 77−11502
Fe-Ni (31 wt.%), thermoelastic martensite obs. 80−3052
Fe-Ni (31 wt.%) alloy, Bridgman grown, cellular to dendritic crystn. transition, morphology and microstruct. *(Russian)* 79−14709
Fe-Ni (31%), deformed by slip, misaligned zones in $\{259\}_A$-martensite crysts. *(Russian)* 77−59850
Fe-Ni (32 at.%), exam. of streaming due to intrinsic fluctuations 79−11602
Fe-Ni (32 wt.%), EMF appearance during $\gamma \rightarrow \alpha$ transform. *(Russian)* 80−89215
Fe-Ni (32 wt.%), electrohydraulic effect and struct. changes *(Russian)* 78−23783
Fe-Ni (32 wt.%), martensitic transform., study by fast electronic amplification *(French)* 77−86028
Fe-Ni (32.3 at.%), mag. struct. in commensurable approx., neutron diffr. study 80−60212
Fe-Ni (32.86, 30.65 wt.%), characts. of quenched struct. formed in textured sheets, TEM and optical microscopy study 79−34084
Fe-Ni (33-38 at.%), low-angle neutron diffr., anomalous crit. scatt. *(Russian)* 80−60193
Fe-Ni (33.7 wt.%), γ-phase stability near martensitic transform., shear modulus obs. *(Russian)* 79−4966
Fe-Ni (35 at.%), fine coherent effects, neutron diffr. study *(Russian)* 78−75502
Fe-Ni (35 to 100%), magnetoelastic attenuation of torsional vibr. and shear modulus defect *(Russian)* 77−80982
Fe-Ni (4 wt.%), extrinsic grain boundary dislocations, low C content influence 80−107273
Fe-Ni (47 to 65 wt.%), soft magnetic alloy with crystallographic texture and field induced anisotropy, pulse permeability and excursion rate *(German)* 79−73779
Fe-Ni (50 to 94 wt.%), FCC, form. and migration energy of vacancies, induced magnetic anisotropy *(French)* 78−2110
Fe-Ni (50 wt.%), obs. in Santa Catharina meteorite 79−30024
Fe-Ni (50 wt.%), surface comp. and oxide film thickness after various surface treatments, AES study 80−66693
Fe-Ni (6-8 wt.%), solution of ^{119}Sn, study by Mossbauer spectroscopy 80−75888
Fe-Ni (8 wt.%), monocrystal, thermodynamics of growth, model *(French)* 78−87635
Fe-Ni (9.21 wt.%), oxidation in CO_2 at 700-1000°C 78−44265
Fe-Ni alloy, anisotropic hyperfine interactions, Mossbauer spectra 80−15854
Fe-Ni alloy, anodic oxide film formed in H_3BO_3-$Na_2B_4O_7$ soln., exam. of in depth profile by AES and sputter etching 79−20247
Fe-Ni alloy, α to γ slow transformation mechanism, Ni content influence *(Russian)* 80−7569
Fe-Ni alloy, cellular-dendrite struct., effect of temp. gradient and crystallisation rate on morphological singularities *(Russian)* 78−3115
Fe-Ni alloy, cold work stored energy effect on mag. moment vs. temp. curve 78−95419
Fe-Ni alloy, detection in Santa-Catharina meteorite *(French)* 79−16895
Fe-Ni alloy, diffusivity, heat capacity and thermokinetic behaviour, simultaneous meas. *(French)* 77−1235
Fe-Ni alloy, disordered, short-range order study by time-depend. PAC method 78−6618
Fe-Ni alloy, electropolishing in alcoholic soln. of H_2SO_4 77−16718
Fe-Ni alloy, FCC, high-field susceptibility and spin wave spectrum 79−56493
Fe-Ni alloy, martensitic transform., influence of thermal and electron irrad. treatment of austenite *(Russian)* 80−66509
Fe-Ni alloy, positron lifetime 80−2891
Fe-Ni alloy, rod-shaped martensite→austenite transform, struct. mech. *(Russian)* 77−66636
Fe-Ni alloy, solid solution, vibr. analogue of Bain deform. and morphology of martensite in 78−2224
Fe-Ni alloy, surface decarburisation rate in dry H_2, soft mag. material manufacture 78−60882
Fe-Ni alloy, X-ray microanalysis in scanning transmission electron microscope, limitations 78−20122
Fe-Ni alloy near crit. conc., Mossbauer γ-rays small angle scatt. 80−7217
Fe-Ni alloy toroidal core, magnetic noise *(Russian)* 78−60308
Fe-Ni alloy type YuNDK25B, anomalous magnetocaloric effect 80−60278
Fe-Ni alloys, cold rolled, exam. of phase composition using Mossbauer spectroscopy 80−21204

nickel alloys continued
Fe-Ni alloys, diffusivity of N_2 79−46845
Fe-Ni alloys, electrodeposit on Cu, texture investig. 77−11818
Fe-Ni alloys, electronic struct. by XPS obs. 79−33226
Fe-Ni alloys, FCC, mag. props. calc. 79−65659
Fe-Ni alloys, graim growth texture 79−91687
Fe-Ni alloys, γ- and α-phase struct. in supercooled austenite *(Russian)* 77−66642
Fe-Ni alloys, heat treatment variations effect on surface conditions and on Hg wetted switch behaviour 80−66547
Fe-Ni alloys, influence of hydrostatic press. on γ to α′ transform. during plastic deform. *(Russian)* 79−15663
Fe-Ni alloys, mag. state of austenite and γ→α transform. *(Russian)* 80−40350
Fe-Ni alloys, qualitative analysis of order-disorder structure by secondary ion-ion emission *(Ukrainian)* 77−69950
Fe-Ni alloys, reverse martensite start temp., heating rate effects *(Russian)* 78−6924
Fe-Ni alloys, shape memory effect, martensite fine struct. effect *(Russian)* 79−52215
Fe-Ni alloys, struct. of γ and α-phases near martensitic transform. point *(Russian)* 78−64541
Fe-Ni alloys, thermal expansion rel. to X-ray emission spectra *(Russian)* 77−32470
Fe-Ni alloys, thermal props., let. review *(Russian)* 78−18805
Fe-Ni and Fe-Co-Ni, liquid, solubility of H, 1400 to 1800°C 77−1231
Fe-Ni austenite, α→γ transform and stabilisation, Mossbauer and electron microscopy obs. *(Russian)* 78−23703
Fe-Ni austenite, precipitation hardened, transform. strengthening 79−24531
Fe-Ni austenitic, effect of Al and Ti on relaxation resist. 80−20993
Fe-Ni base alloy, precracked specimen, K_{Ihcc} threshold value under const. load at high temp. *(Chinese)* 78−31499
Fe-Ni base amorphous alloy, crystallisation 77−84660
Fe-Ni base amorphous alloys, effect of annealing on Curie temp. 80−34632
Fe-Ni base metallic glass, annealing embrittlement 78−64635
Fe-Ni base metallic glasses, microhardness charact. of stability under annealing 79−57011
Fe-Ni based alloy, amorphous rapidly quenched, mag. props. 77−66269
Fe-Ni based alloys, amorphous, amorphous, thermopower meas., Nordheim-Gorter relations 79−99535
Fe-Ni based amorphous alloys, Hall and ohmic resistivities 79−91013
Fe-Ni based metallic glasses, hydrostatic press. effect on mag. props. 78−19300
Fe-Ni based metallic glasses, nonisothermal crystallisation kinetics, DSC anal. 79−27927
Fe-Ni based metallic glasses, search for Invar-like magnetoelastic behaviour 79−56596
Fe-Ni based metallic glass, Metglas 2826 MB, Mossbauer study 80−75897
Fe-Ni binary alloy, specific heat temp. depend., α to γ transformation *(Russian)* 79−83198
Fe-Ni electrodeposit, sectional analyses and impurities *(Japanese)* 80−21350
Fe-Ni electrodeposited coatings, packing defects 79−60662
Fe-Ni evaporated films with perpendicular anisotropy, magnetoresistance obs. 78−2585
Fe-Ni film, amorphous, martensite form. time and struct. 80−104159
Fe-Ni film, α→γ transition, Mossbauer effect *(Russian)* 77−40154
Fe-Ni film, mag. and struct. props., effect of O_2 partial press. during deposition 79−90903
Fe-Ni film, vacuum-deposited, internal stresses, thickness and comp. effects *(Russian)* 77−80713
Fe-Ni films, dynamic domains and pulse mag. reversals *(Russian)* 79−28571
Fe-Ni films, lattice constants rel. to mag. moments *(Russian)* 77−32218
Fe-Ni films, on glass substrate, thermoelec. effect 80−107769
Fe-Ni films, scatt. of homogeneous spin waves by anisomeric oriented plane, ferromag. reson. 78−19336
Fe-Ni fluorination kinetics and fluoride film form., chem. nature obs. 80−101035
Fe-Ni heterogeneous alloys, ferrite, martensite and austenite phase distrib., effect on mech. props. 80−45363
Fe-Ni liquid alloy, physical and chemical props. deviations from Raoult's law *(Russian)* 78−95729
Fe-Ni martensite, TEM of passivity layer 77−36689
Fe-Ni martensite, twin struct. 79−77607
Fe-Ni martensites, deform. twinning for crystals with transform. twin microstruct. 77−31677
Fe-Ni martensitic alloys, age hardening 79−47736
Fe-Ni melt, short-range order, m.p. to 1750°C *(Russian)* 78−94966
Fe-Ni metallic glass wide strips, low-field mag. props. 79−51822
Fe-Ni metallic glasses, crystallisation 77−43157
Fe-Ni Metglas type, ohmic and Hall resist., 100-700K, mag. behavour obs. 80−80254
Fe-Ni mixed powders, effect of Ni particle size and unequal interdiffusion, on sintering process *(Japanese)* 78−84728
Fe-Ni ordered phase in meteorites, Mossbauer studies 80−41776
Fe-Ni ordering on annealing and electron irrad., mech. props. change *(Russian)* 80−29981
Fe-Ni powder, Ni clad Fe grains, exam. of electrochemical formation process 79−33974
Fe-Ni single crystal, lattice strain induced by anisotropic distrib. of M_2 *(Japanese)* 80−35262
Fe-Ni single crystal, pseudo-Kossel study of fibrous substruct. 77−1835
Fe-Ni single crystals, stress induced martensite 77−8827
Fe-Ni solid soln., thermodynamic study 78−6904
Fe-Ni solid solution, deformation mechanism, softening phenomena, dislocation-solute atom interactions *(French)* 80−45344
Fe-Ni superstructure in metal particles in chondrites 80−12713
Fe-Ni surface alloy formed by ion implantation, anodic polarisation 78−48562
Fe-Ni surface alloys, corrosion resistant, formation by ion implantation 79−28009
Fe-Ni system, constant modulus alloys for mech. oscillators 79−61641
Fe-Ni system, ferro-antiferromag. transition, γ phase mag. struct. 79−91231
Fe-Ni system, Ni addition effects on activated sintering of Fe powder compacts 77−4756

nickel alloys continued
Fe-Ni two-phase films, alloy component redistrib. during annealing, electron diffr. anal. *(Russian)* 79−20053
Fe-Ni/Fe, bimetal film, exchange const. determ. from hysteresis loops *(Russian)* 77−48015
$Fe-Ni_3$, hyperfine field, variation with atomic order 79−7953
Fe-Ni/pure Fe exchange coupled films, mag. reversals, hard layer thickness effects *(Russian)* 78−56359
Fe-Ni-Al, correlation of microscopic features, with macroscopic crack propagation 78−60800
Fe-Ni-Al, Curie temp. depend. on ordering, antiferromag. ordering *(Russian)* 79−61101
β_2-Fe-Ni-Al, diffusion 77−24449
Fe-Ni-Al, liq. alloys, N solubility and AlN precipitation 80−11648
Fe-Ni-Al, magnetic anisotropy form. and struct. changes by annealing, Mossbauer obs. 80−39994
Fe-Ni-Al, Mossbauer spectra, strong elastic stress effects 77−90084
Fe-Ni-Al, oxidation in O_2 at 600 to 800°C 79−83376
Fe-Ni-Al, struct. of aged austenite *(Russian)* 77−52357
Fe-Ni-Al, type YuN14DK25BA, thermomag. treatment 80−16512
Fe-Ni-Al (10, 0.1 wt.%), clustering of Al_2O_3 inclusions 79−83205
Fe-Ni-Al (18.2 wt.%) aged, fracture toughness and mode, grain size depend. 77−12700
Fe-Ni-Al (30, 4wt.%), ageing, peculiarities of struct. state *(Russian)* 79−57008
Fe-Ni-Al alloy, metastable equilib. in its high-coercivity state *(Russian)* 79−52161
Fe-Ni-Al alloys, ordering X-ray and neutron diffr. obs. *(Russian)* 79−20038
Fe-Ni-Al alloys, phase diagram, miscibility gap, DTA meas. 78−92237
Fe-Ni-Al system, multiphase diffusion at 1000°C, diffusion structs. and props. 80−19995
Fe-Ni-Al system, multiphase diffusion at 1000°C, interdiffusion coeffs. for β and γ alloys 80−24684
Fe-Ni-Al-C, form. of ductile Ni_3Al by split quenching, mech. props. 79−100197
Fe-Ni-Al-Co-Cr-Ti, YuNDK35T5BA, exam. of hypodissociation process *(Russian)* 79−11547
Fe-Ni-Al-Co-Cu alloy, sintered single-crystal mag. prod., props. 77−66709
Fe-Ni-Al-Co-Cu-Sn alloy YuNDK35T5, Sn addition effects on physicomechanical and magnetic props. and workability *(Russian)* 77−70101
Fe-Ni-Al-Co-Cu-Ti, 38 to 40 wt.% Co, 8 to 8.5 wt.% Ti, alloy YuNDKT tempering and thermomagnetic treatments 78−3154
Fe-Ni-Al-Co-Cu-Ti alloy YuNDKT, nature of X-phase heat treatment effect on microstruct. 77−90380
Fe-Ni-Al-Co-Cu-Ti magnetic alloy electrolytic treatment with programmed pulse current *(Russian)* 79−100282
Fe-Ni-Al-Co-Cu-Ti YuNDK type, S effect on mech. props. 80−60927
Fe-Ni-Al-Co-Ti base alloys, highly coercive, phase comp., Mossbauer meas. 80−39996
Fe-Ni-Al-Cu (25, 14, 4 wt.%), alloy YuND4, effect of Ti addition on structure, mag. props. 80−15714
Fe-Ni-Al-Ti, N27Yu2T2, aged austenite, diffuse electron scatt. distrib. during martensitic deform. *(Russian)* 78−60669
Fe-Ni-Al-(Cu) (12, 0.5, 0.5 to 3 wt.%), Cu addition strengthening at 77K, mech. props. 80−60875
Fe-Ni-Al(Ti)(Nb)(V), cryogenic toughness, strength, rel. to reactive metal addition 78−39885
Fe-Ni-Al(2.5, 7.5 at.%), fracture surface morphology, ageing temp. effects 77−16600
Fe-Ni-B, chemical ordering, crystallisation and glass transition temp. 79−90563
Fe-Ni-B, metallic glass, Mossbauer investigation of electronic struct. 78−92009
Fe-Ni-B glassy ribbons melt spinning, gas boundary layer effects 80−76217
Fe-Ni-B metallic glass, X-ray diffr. meas., semi-empirical struct. model 80−107059
Fe-Ni-B-Mo, crystn. temp. and elec. cond. correl., Mo effect 80−75179
Fe-Ni-B-Si, amorphous, mag. props., heat treatment effects 80−89370
Fe-Ni-B(-P), ferromag., magneto-optical spectra in amorphous and cryst. states *(Russian)* 80−84749
Fe-Ni-B(-P) amorphous alloys, mag. annealing mechanism, induced anisotropy 78−95484
Fe-Ni-C, atomized, O/C ratio effect, particle size on annealing kinetics, physicotechnological props. 80−20832
Fe-Ni-C, ausformed, ductility of martensite *(Japanese)* 77−48490
Fe-Ni-C, austenite cryst. volume effect on martensitic transformation temp. 80−40352
Fe-Ni-C, C effect on recrystallisation and reversion *(French)* 77−81282
Fe-Ni-C, calc. of activity data, and exam. of phase equilibria 79−10912
Fe-Ni-C, cast, spheroidal graphite, metallography of solidification 78−19737
Fe-Ni-C, couplings of thin plate martensites 79−24492
γ-Fe-Ni-C, electromigration of C, effect of Ni addition 78−6184
Fe-Ni-C, FCC, effect of two gamma states on C activity 78−6897
Fe-Ni-C, Fe rich portion of phase diagram determ. 79−24497
Fe-Ni-C, HVEM study of strain induced martensite 79−20047
Fe-Ni-C, intercrystalline embrittlement in tempered martensite, elimination by reaustenitization *(Slovak)* 80−108548
Fe-Ni-C, internal friction anomaly with reheat transform. 79−100204
Fe-Ni-C, lattice parameters of cementite, annealing effect 80−29007
Fe-Ni-C, lenticular martensitic alloy, fractured at liquid N_2 temps., crack propag. mode *(Japanese)* 77−48524
Fe-Ni-C, martensite nucleation, tensile prestraining effect 77−8828
Fe-Ni-C, martensitic, deformed, stress induced C distrib. *(Czechoslovakian)* 77−32641
Fe-Ni-C, martensitic, H_2 effect on fracture charact. *(Czech)* 78−60746
Fe-Ni-C, martensitic, internal friction 77−16633
Fe-Ni-C, martensitic, mech. charact., effect of ageing and tempering *(Slovak)* 78−19791
Fe-Ni-C, martensitic, mech. and fracture charact., effect of starting austenite heterogeneity *(Slovak)* 78−19792
Fe-Ni-C, martensitic, modulation of local C atom cumulation during ageing *(Slovak)* 78−19790
Fe-Ni-C, martensitic delayed fracture *(Slovak)* 79−43401
Fe-Ni-C, martensitic transform., Mossbauer obs. *(Russian)* 78−6927
Fe-Ni-C, martensitic transform., new investigation method *(French)* 79−91881

nickel alloys continued
Fe-Ni-C, mech. and structural props. under cathodic H_2 at elevated temps. *(French)* 77−59920
Fe-Ni-C, model alloy, intercrystalline brittleness caused by segregation and precipitation in austenite *(Slovak)* 79−70073
Fe-Ni-C, N31, austenite state in premartensitic temp. interval *(Russian)* 78−56634
Fe-Ni-C, phase diagram determ. 79−24495
Fe-Ni-C, plastic deform. effect on austenite stabilisation *(Korean)* 80−21021
Fe-Ni-C, quenched martensite, annealing during cathodic hydrogenation, 200°C *(French)* 80−93573
Fe-Ni-C, Redlich-Kister eqns., activity coeffs., phase equilib. 78−23664
Fe-Ni-C, role of strain in deform. induced martensitic transform. *(Japanese)* 78−92263
Fe-Ni-C, self-diffusion processes during homogenisation of heterogeneous systems *(Russian)* 79−60539
Fe-Ni-C, single crystal, form. and strength of strain-induced martensite 79−100225
Fe-Ni-C, splat-quenched martensite formation obs. 77−44247
Fe-Ni-C, thin foil, high voltage TEM exam. of martensitic form. 78−92264
Fe-Ni-C (0.15, 0.05 wt.%) pore formation kinetics during crystallisation, FORTRAN study *(Russian)* 80−54158
Fe-Ni-C (10, 0.6 wt.%), effect of austenite yield strength on martensitic transformation 78−39772
Fe-Ni-C (19 to 30, 0.04 to 0.8 wt.%) alloys, transformation of martensite in austenite, optical and electron microscopic exam. *(Russian)* 78−35382
Fe-Ni-C (21, 0.6 wt.%), stress assited and strain induced martensite morphologies 78−3187
Fe-Ni-C (23, 0.39 wt.%), austenitic or martensitic structs., corrosion faces anal. *(French)* 80−21181
Fe-Ni-C (24, 0.45 wt.%), martensites, TEM observation of double twinning 78−76651
Fe-Ni-C (24, 0.45 wt.%), single crystal, plastic deform. effect on martensitic burst transform. 79−15695
Fe-Ni-C (24, 0.5 wt.%), struct. of burst and isothermal martensites 79−38825
Fe-Ni-C (25, 0.02 wt.%), thermal stabilisation role in martensitic transformations 80−25697
Fe-Ni-C (25, 0.2 wt.%), strain-induced martensite *(Korean)* 80−71646
Fe-Ni-C (26.4, 0.24 wt.%) martensite, partially twinned, slip lines obs. 78−84913
Fe-Ni-C (26.4, 0.24 wt.%), austenitic single crysts., effect of prior deformation on martensite burst transformation, SEM obs. 79−38823
Fe-Ni-C (27, 0.23 wt.%), work hardening and martensitic transform. at 263K 79−100143
Fe-Ni-C (30, 0.5 wt.%) single cryst., stress induced martensitic transform. 80−60860
Fe-Ni-C (30.59, 0.02 wt.%), effect of loading on transformation of retained austenite to martensite 79−47686
Fe-Ni-C (31, 0.1 wt.%), kinetics of deform. induced martensite, shock loading and grain refinement effects 78−15395
Fe-Ni-C (31, 0.1 wt.%), metastable austenite, fractography 77−59919
Fe-Ni-C (31, 0.1 wt.%), pre-deformation and temp. effect on transformation-deformation behaviour 80−3127
Fe-Ni-C (31, 0.28 wt.%), crossings of thin plate martensites, TEM obs. 80−25756
Fe-Ni-C (31.1, 0.02 wt.%), coarse grained, microstructural aspects of martensitic transform. 79−56978
Fe-Ni-C (31.1, 0.02 wt.%), kinetics analysis of temp. rate of nucleation of a thermal martensitic transformation 79−78965
Fe-Ni-C (31.24, 0.21 wt.%) effect of deformation and ageing after deformation, on martensitic transformation temp. 78−76650
Fe-Ni-C (31.9, 0.02 wt.%), metallographic study of austenite grain size effect on martensite kinetics 79−1863
Fe-Ni-C (31.9, 0.02 wt.%) alloy, hardness of martensite-austenite mixtures 80−60959
Fe-Ni-C (31.9,0.02 wt.%), determ. of number and size distrib. of martensitic plates 80−76255
Fe-Ni-C (32.7, 0.01 wt.%), athermal marrtensitic transition investigation by acoustic emission *(Russian)* 79−91645
Fe-Ni-C (9, 0.1 wt.%), effect of intercritical tempering on impact energy, exam. of mech. props. 78−52861
Fe-Ni-C alloy, austenitic, pre-deform. effects on TRIP *(Japanese)* 77−8890
Fe-Ni-C alloy, external stress effects on equilibrium morphology, thermodynamic model *(Russian)* 78−52804
Fe-Ni-C alloy with single-component martensite texture, $\alpha \rightarrow \gamma$ transform., changes in shape *(Russian)* 80−104152
Fe-Ni-C alloys, obs. of banded struct. formed by deformation 79−79050
Fe-Ni-C austenite, effects of strain rate grain size, temp., on yield stress 78−72821
Fe-Ni-C austenite, metastable, influence of prior deform. on yield stress 78−15461
Fe-Ni-C austenitic alloy, banded struct. formed by deform. 80−71713
Fe-Ni-C austenitic single crysts., deform. props., martensitic transformation, SEM study 79−29143
Fe-Ni-C martensite, autoradiographic evidence of C clustering 79−83203
Fe-Ni-C martensite morphology, butterfly-lenticular transition temp., Cr addition effect *(Japanese)* 80−81053
Fe-Ni-C-B, and Fe-Ni-Co-B-C-Si, amorphous, room-temp. saturation induction 78−95476
Fe-Ni-C-Mn (3.56, 3.25, 0.6 wt.%), solid soln., quenched, changes during annealing to crystal structure, mech. props. *(Russian)* 79−34076
Fe-Ni-C-Sb, Sb additions effect on fracture charact. of martensite *(Czech)* 77−70162
Fe-Ni-Co, diffusion controlled phase growth 78−30782
Fe-Ni-Co, magnetic permeability, effect of ion implantation 77−28414
Fe-Ni-Co, phase diagram redeterm., Fe-rich portion 77−44219
Fe-Ni-Co, rel. between induced uniaxial anisotropy and coercive force 78−91904
Fe-Ni-Co, texture form. after cold working and annealing *(German)* 80−3089
Fe-Ni-Co alloys, struct., appl. of mag., thermomag. methods *(French)* 79−20318
Fe-Ni-Co base alloys, composition changes during electron radiation melting *(Russian)* 78−19718

nickel alloys continued
Fe-Ni-Co coating electrodeposition optimum conditions *(Russian)* 79−83292
Fe-Ni-Co film, electron-nucl. mag. reson. 78−35063
Fe-Ni-Co foils, mag. reversals of mag. domains in low-coercivity channels *(Russian)* 79−42813
Fe-Ni-Co-B-P soft magnetic metallic glasses, status report 78−64226
Fe-Ni-Co-C, substruct. effect in mech. props. 80−30086
Fe-Ni-Co-C (29.6, 10.7, 0.009 wt.%), thermal stabilisation role in martensitic transformations 80−25697
Fe-Ni-Co-Cu-Ti YuNDKT alloys, impaired mag. props. with C and S additions 80−60368
Fe-Ni-Co-Mo alloys, struct. transform. produced during tempering 77−86058
Fe-Ni-Co-Mo phase diagram and structure *(Russian)* 80−20899
Fe-Ni-Co-Mo-Ge alloy 40NKM, excess mag. noise after various thermomag. treatments *(Russian)* 80−29575
Fe-Ni-Co-Ti, coherent particles effect inherited by martensite on $\alpha \rightarrow \gamma$ transformation *(Russian)* 80−108443
Fe-Ni-Co-Ti, martensite cryst. lattice tetragonality, $\gamma \rightleftharpoons \alpha$ transform. *(Russian)* 79−61587
Fe-Ni-Co-Ti, shape memory effect after appl. of bending moment *(Russian)* 80−45305
Fe-Ni-Co-V, effects on fusion reactor neutronics performance 80−47705
Fe-Ni-Co-W(Mo) (18.65, 8.99, 4.87 wt.%), ageing charact., 380-530°C 80−60876
Fe-Ni-Co(Cu) alloy components, dynamics of arrival to arc discharge during roasting *(Russian)* 77−16895
Fe-Ni-Cr, at. distrib. effect on mag. props. *(Russian)* 78−2657
Fe-Ni-Cr, austenitic, creep strength and ductility, effect of γ' precipitation 77−36597
Fe-Ni-Cr, austenitic, dispersion-hardened alloys, thermomechanical working *(Russian)* 77−66659
Fe-Ni-Cr, austenitic with dispersed phases, oxidation 80−16540
Fe-Ni-Cr, carbide form. by C diffusion, precip. distrib. and morphology 80−104164
Fe-Ni-Cr, compatibility with Li_2O pellets, mass spectrometric study of Li_5FeO_4 evaporation 79−8385
Fe-Ni-Cr, diffusion in Th at 500 to 800°C *(German)* 79−28157
Fe-Ni-Cr, heavy ion irrad., defect cluster obs. 80−107341
Fe-Ni-Cr, high Ni content, intergranular corrosion, effect of Cr *(French)* 80−7708
Fe-Ni-Cr, mag. props. in weak mag. fields *(Russian)* 80−75771
γ-Fe-Ni-Cr, mag. struct., neutron scatt. study *(Russian)* 78−68160
γ-Fe-Ni-Cr, magnetic phase diagram *(Russian)* 78−39292
Fe-Ni-Cr, oxide film form., combination anal. using ESCA, AES and SIMS 79−16092
Fe-Ni-Cr, pulsed HVEM irrad., effect on microstruct. evolution 80−34053
Fe-Ni-Cr, vapour-deposited film, effect of condensation temp. on form. of metastable phases and mag. props. 79−65700
Fe-Ni-Cr (10, 6 to 14 wt.%), electrochemical polarisation in high temp. water *(Japanese)* 79−15868
Fe-Ni-Cr (20, 15 wt.%), fusion reactor struct. alloys, dual-ion irrad, effects 79−45403
Fe-Ni-Cr (20, 15 wt.%), single and dual ion irrad., microstruct. studies 80−29077
Fe-Ni-Cr (23, 5 wt.%), martensite orientation formed under uniaxial stress alloy [001] 77−77475
Fe-Ni-Cr (25, 15 wt.%), high temp. creep, dispersed γ'-Ni_3(Al, Ti) effects *(Czech)* 78−64590
Fe-Ni-Cr (25, 15 wt.%), mobile dislocation density in steady state creep, strain transient dip test, TEM exam. 80−7650
Fe-Ni-Cr (30.6, 21.3 wt.%), Alloy 800, high temp. oxidation at low O_2 press., SEM, AES and electron probe microanal. study 80−93688
Fe-Ni-Cr (35, 15 wt.%), high temp. alloys, for HTR primary components, alloying additions for carburisation protection 80−5243
Fe-Ni-Cr (35, 15 wt.%) superalloy, stress rupture and tensile props., C and B additions effect *(Chinese)* 80−104244
Fe-Ni-Cr (40, 15.8 wt.%), precipitation and creep ruputure behaviour, optical and TEM study 79−74158
Fe-Ni-Cr (40, 20 wt.%), Kh20N40 alloys, phase composition after quenching, tempering 78−60650
Fe-Ni-Cr (44, 17 wt.%), nuclear microprobe methods for investigating oxidative corrosion 80−71787
Fe-Ni-Cr (45,25 wt.%), surface oxide layers, compar. study of comp. and struct. by secondary ion emission and electron microprobe *(French)* 77−56286
Fe-Ni-Cr alloy, cast, etching methods for determ. of primary struct. 78−23888
Fe-Ni-Cr alloy 800, creep ductility decline 77−48502
Fe-Ni-Cr alloy 800, minor alloying element effect on creep, ageing microstruct. 78−27572
Fe-Ni-Cr alloy electrodeposition from sulphate electrolyte with cystine and Na citrate additives *(Russian)* 78−48336
Fe-Ni-Cr alloys, stacking fault energies calc. 79−60387
Fe-Ni-Cr alloys, X-ray fluorescence anal., interelement correction, models, computer program 77−56315
Fe-Ni-Cr austenitic alloy, homogeneous and dispersion strengthened, internal stresses and high temp. creep 78−19841
Fe-Ni-Cr austenitic steel, martensitic transform. kinetics, metastability criterion *(French)* 78−68690
Fe-Ni-Cr base alloy, oxidation and hot corrosion *(Chinese)* 80−21149
Fe-Ni-Cr based alloy, KhN35VTYu, temp. depend. of energy of fracture, influence of γ' phase *(Russian)* 80−81147
Fe-Ni-Cr coating, electrodeposited, exam. of passivity 78−80655
Fe-Ni-Cr corrosion protective coating on steel 78−48572
Fe-Ni-Cr film, ferromag. reson. meas. *(Russian)* 77−1601
Fe-Ni-Cr melts, O solubility *(Russian)* 80−15250
γ-Fe-Ni-Cr solid soln., thermodynamic activities determ. in Ni rich corner at 1500K 77−32561
Fe-Ni-Cr system, absolute partial pressures and chem. activities of component metals 80−50600
Fe-Ni-Cr vapour deposited film metastable phase formation *(German)* 78−38984
Fe-Ni-Cr-Al-Ti-W-Mo (35, 15, 2.4, 2.3, 2.2 wt.%) wrought superalloy, freckles *(Chinese)* 80−104137
Fe-Ni-Cr-Al-Y, oxidation mechanism, Y addition effect on kinetics and oxide adherence 80−97623
Fe-Ni-Cr-B, X-101 centrifugally cast cylinder lining alloy, compatibility with hardfacing alloys 77−32726

nickel alloys continued
Fe-Ni-Cr-C, effect of austenite yield strength, stacking fault energy, on martensite morphology 78−80546
Fe-Ni-Cr-C, ferritic, P segregation to free surface, 723 to 823K, AES 78−48411
Fe-Ni-Cr-C, martensitic transform. effect of austenite prestrain above M_d temp. 78−15398
Fe-Ni-Cr-Mn-Al-Ti Incoloy 800, exam. of scale morphology, alloying element distrib. after oxidation 78−80677
Fe-Ni-Cr-Mo superalloy, mech. props., η-phase form. effect *(Chinese)* 80−20925
Fe-Ni-Cr-P-B, Metglas 2826A, TEM of shear bands 78−48483
Fe-Ni-Cr-P-B, Metglas 2826A, hardness, elastic moduli, density, cryst. temp., mech. props., for flywheel appl. *(Dutch)* 78−52878
Fe-Ni-Cr-P-B amorphous alloy, localized corrosion 80−16559
Fe-Ni-Cr-S, phase relations rel. to sulphidation of austenitic stainless steel 79−38800
Fe-Ni-Cr-Si, superalloy, Cr and Si effect on mech. props. and microstruct. *(Chinese)* 79−100207
Fe-Ni-Cr-Si (35, 18, 2 wt.%), heating element wire, failure and oxidation 79−83378
Fe-Ni-Cr-Si alloy 800, Si effect on creep and age hardening 77−48444
Fe-Ni-Cr-Ti, superalloy A286, powder, exam. of microstruct. and mech. properties 78−52979
Fe-Ni-Cr-Ti based alloy, 36 NKhTYu, high temp. deform. characts., superplastic behaviour *(Russian)* 77−63719
Fe-Ni-Cr-Ti-Al, ausaging alloy, cellular precipitate indentification *(Chinese)* 78−11225
Fe-Ni-Cr-Ti-Al, Ti and Al effect on microstruct. and mech. props. *(Chinese)* 79−74130
Fe-Ni-Cr-Ti-Al, with thermoelastic control coeff., comp. and heat treatment influence on props. *(French)* 80−81074
Fe-Ni-Cr-Ti-Al Elinvar alloys, dispersion-hardened, structural transform. *(Russian)* 79−1872
Fe-Ni-Cr-Ti-Mn-Mo, (25.8, 14.04, 2.17, 1.27, 1.30 wt.%), superalloy A-286, precipitation hardening, exam. of fracture toughness and mech. props. 78−92355
Fe-Ni-Cr-Y, oxidation at 800 to 1300°C, Y addition effects, comparison with Ni-Cr-Y alloy *(French)* 79−43481
Fe-Ni-Cr-Y, Y addition effect on selective oxidation/diffusion phenomena relationship *(French)* 80−108623
Fe-Ni-Cr-base superalloys, characterisation of PNP components 80−5242
Fe-Ni-Cu-C-O powder, atomized, reduction and decarburizing annealing parameters 80−25603
Fe-Ni-Ge, liquid alloy, H_2 thermodynamic interaction, solubility *(Russian)* 78−11202
Fe-Ni-M alloys, (M=C, Ti,Mn), habit plane and morphology of lath martensites 77−8823
Fe-Ni-Mn, BCC, mag. state of Mn, NMR and saturation magnetisation meas. 78−39442
Fe-Ni-Mn, dil. alloys, NMR freq. temp. depend., spin echo meas. 78−64296
Fe-Ni-Mn, martensite, aged, grain boundary embrittlement 79−96144
Fe-Ni-Mn, martensitic transforms., expt. investigation *(French)* 78−84803
Fe-Ni-Mn, temp. coeff. of linear expansion *(Russian)* 77−80634
Fe-Ni-Mn (20, 5 wt.%), rel. orientation between adjacent martensite laths 80−76254
Fe-Ni-Mn (20, 5 wt.%), surface martensite, crystallography and morphology 80−40354
Fe-Ni-Mn alloy, martensitic transform. kinetics *(Russian)* 77−81262
γ-Fe-Ni-Mn alloys, spin glass state, short and long range order investigation 80−65808
Fe-Ni-Mn martensitic alloy, precipitation 77−12630
Fe-Ni-Mn melt, thermodynamic dissolution of O_2 *(Russian)* 78−27473
Fe-Ni-Mn-C (5.9, 4.4, 0.48 wt.%) alloy, elastic moduli near martensitic transform. 80−7619
Fe-Ni-Mn-H, ferromag., magnetisation curves 78−88144
Fe-Ni-Mn(Mo) alloys, two-stage martensitic transformation kinetics, depend. on austenite initial state *(Russian)* 79−74151
Fe-Ni-Mo, ferrite plus martensite structures, exam. of mech. props. 78−56709
Fe-Ni-Mo, high-strength ferritic, for cryogenic service, mech. characteris. 77−70143
Fe-Ni-Mo, inhomogeneous solid solns., annealed and work hardened states, X-ray K-absorption spectra *(Russian)* 78−56544
Fe-Ni-Mo, martensitic transformation, annealing, influence on struct. of austenite *(Russian)* 80−81057
Fe-Ni-Mo, phase relations in system at 1100°C 80−108392
Fe-Ni-Mo, small angle X-ray scatt. study, pre-precipitation phenomenon obs. *(French)* 78−19757
Fe-Ni-Mo (16.4, 8.1 wt.%), effect of substituting Mo by W during ageing 80−29991
Fe-Ni-Mo-C, amorphous alloys, mech. props. and thermal stability *(Japanese)* 80−85049
Fe-Ni-Mo-C, Mossbauer investig. of secondary hardening, carbide form. *(Russian)* 77−44260
Fe-Ni-Mo-C, sintering 78−35333
Fe-Ni-Mo(Si), austenite, annealing effect on atom redistrib., Mossbauer anal. *(Russian)* 80−66529
Fe-Ni-Mo(Ti)(Si), ordered, low temp. $\alpha \rightarrow \gamma$ transform. *(Russian)* 78−19740
Fe-Ni-Mo(13,3wt%), welded alloy, fracture and strength for cryogenic service 79−38930
Fe-Ni-P, interface composition during diffusion controlled precipitate growth 77−36513
Fe-Ni-P, segregation kinetics, theory, and temper brittleness 80−11649
Fe-Ni-P-B, amorphous, crystn. and struct. 80−75175
Fe-Ni-P-B, amorphous, magnetically induced anisotropy 77−89948
Fe-Ni-P-B, amorphous ferromag. alloys, mag. struct., Mossbauer study 80−39746
Fe-Ni-P-B, amorphous paramag. alloys, hyperfine field distrib., Mossbauer study 80−39958
Fe-Ni-P-B, metallic glasses, fracture toughness, shear rupture failures, critical thickness 79−52365
Fe-Ni-P-B, metallic glasses, struct. relax., annealing effects on mag. props. 80−89261
Fe-Ni-P-B amorphous ribbons, form. by melt spin technique 80−76215
Fe-Ni-P-B metallic glass, crystallisation temperature values from isothermal transformation times 80−59397
nickel alloys continued
Fe-Ni-P-B(C), amorphous alloy, anelastic relaxation 79−4997
Fe-Ni-Pt system, ordered phase fields of equilibrium diagram 78−48373
Fe-Ni-S, exam. of liquidus surface and tie lines, using electron probe analysis 79−11557
Fe-Ni-Sb (4, 0.0087 at.%), surface segregation 79−96031
Fe-Ni-Sb-S, S/Sb surface site competition in segregation 80−40366
Fe-Ni-Si, double spontaneous reversible deformation during thermal cycling 78−84942
Fe-Ni-Si-B, amorphous paramag. alloys, hyperfine field distrib., Mossbauer study 80−39958
Fe-Ni-Si-Mn-Cr(Co-Mo), effect of prolonged aging on mag. props. 80−16513
Fe-Ni-Ta (-Co), alloys, Co effect on martensite ageing at 300-600°C *(Russian)* 80−20972
Fe-Ni-Te alloy system, first-order phase transformation obs. 78−64533
Fe-Ni-Te alloys, magnetisation 79−7975
Fe-Ni-Ti, ageing mechanism, neutron diffr. expts. *(Russian)* 78−48403
Fe-Ni-Ti, martensite, tetragonality, X-ray obs. 77−63665
Fe-Ni-Ti, preaged martensite, shear strain magnitude, X-ray diffr. method 80−93592
Fe-Ni-Ti, shape recovery depend. on hardening *(Russian)* 79−83259
Fe-Ni-Ti, undeformed metastable alloy, cellular decomposition of austenite during ageing *(Russian)* 79−100178
Fe-Ni-Ti (25.9, 2.15 wt.%), exam. of effect of inhomogeneous solid soln., on martensitic transformation *(Russian)* 79−34034
Fe-Ni-Ti (27.4, 2 to 3 wt.%), aged, stress induced martensitic transform., mech. props. *(Russian)* 79−87632
Fe-Ni-Ti (30, 3 wt.%), reverse martensitic transform. and memory effect *(Russian)* 79−87627
Fe-Ni-Ti (30, 6 wt.%), austenitic, discontinuous coarsening of lamellar cellular precipitates, morphology 79−78967
Fe-Ni-Ti (30, 6 wt.%), austenitic, discontinuous coarsening of lamellar cellular precipitates, growth kinetics 79−78968
Fe-Ni-Ti (31.2, 5.3 wt.%), γ-phase ageing effect on martensitic transform. *(Russian)* 77−28814
Fe-Ni-Ti alloys, high pressure effect on martensite crystal nucleation and growth *(Russian)* 78−39769
Fe-Ni-Ti martensitic alloy, γ' particle effect on crystallisation struct. *(Russian)* 78−44129
Fe-Ni-Ti-Al, martensite, nature of tetragonality 79−32936
Fe-Ni-Ti-Al-Nb, struct. mechanism for inverse $\alpha \rightarrow \gamma$ transform. *(Russian)* 80−40351
Fe-Ni-Ti-C (31, 4, 0-18 wt.%), coherent precipitates in austenite, effect on martensite substruct. 77−52327
Fe-Ni-Ti-(Cu) (12, 0.25, 2 wt.%), Cu addition strengthening at 77K, mech. props. 80−60875
Fe-Ni-V, austenite, martensite elec. cond. depend. on heating *(Russian)* 79−70177
Fe-Ni-V, effect of low temp. ageing on props. during high temp. ageing *(Russian)* 78−39811
Fe-Ni-V, nitrided austenitic alloys, modulated substitutional interstitial solute atom clustering 79−74160
Fe-Ni-V alloy, ageing of martensite *(Russian)* 78−39808
Fe-Ni-V-C alloy, reverse α to γ transformation, previous deformation influence on struct. and props. *(Russian)* 79−100139
Fe-Ni-V-Co, Co influence on age hardening *(Russian)* 78−68703
Fe-Ni-V-(CO) alloy, lattice parameter variation during ageing *(Russian)* 78−39812
Fe-Ni-V-(Cu) (12, 2, 2 wt.%), Cu addition strengthening at 77K, mech. props. 80−60875
Fe-Ni-WC hard alloy, struct. and props. 79−79007
Fe-Ni-(C), substruct. of ausformed martensite 77−36548
Fe-Ni-(C), thin foil martensite, TEM obs. 77−51378
Fe-Ni-(Cr)(Ti)(Al) austenite, high N content, cryst. struct. electron diffr. and electron miscroscope anal. *(Russian)* 79−24490
Fe-Ni-(Cu) (12, 0.5 to 3 wt.%), Cu addition strengthening at 77K, mech. props. 80−60875
Fe-Ni-(P), phase diagram determ., 700 to 300°C 80−108399
Fe-Ni(-Mn)(Cr)(V), concentration ferromag. antiferromag. phase transition and mag. state diagram. *(Russian)* 80−20401
Fe-Ni(-Mo), formation of austenite structure in relation to α to γ transformations 79−100142
Fe-Sb-Ni, dil., interactions and precip., Mossbauer study 80−39997
Fe-Sb-Ni, dil., short range order, NMR study 80−71237
Fe-Sb-Ni, interactions and segregations, Mossbauer and X-ray diffr. study 80−70415
Fe-Si-Al-Ni alloy, Super Sendust, Ni content and thermomag. treatment effects 77−4861
Fe-Si-Ni, ductility and mag. props., Ni addition effects 78−76704
Fe-Si-Ni (6.5 wt.%, up to 2 wt.%), elongation, cold workability and mag. permeability meas. 77−12667
$Fe_{40}Ni_{40}B_{20}$, amorphous alloy, ductile-brittle transition temp., relation to composition 78−52972
$(Fe\text{-}Co\text{-}Ni)_{78}Si_8B_{14}$, amorphous, low coercivity and zero magnetostriction 78−23299
$(Fe\text{-}Ni\text{-}Mo)_{80}(P\text{-}B)_{20}$, amorphous, mag. aftereffects and struct. instabilities 80−88833
$(Fe\text{-}Ni)_{1-x}(SiO)_x$, cermet film, internal strsses *(Russian)* 78−75951
Fe_3Al-Ni, ternary ordered solid soln., formation by substitution 77−43177
$(FeCoNi)_8B_{20}$, glass, evidence supporting split-band model from magnetostriction 78−95509
$(Fe_xCo_yNi_{1-x-y})_{78}Si_8Bi_{14}$ amorphous ribbons, saturation magnetostriction and vol. magnetostriction 77−85538
$Fe_{36}Cr_{12}Ni_{14}B_{12}B_6$, amorphous X-ray absorpt. spectra, effective coordination charges 80−84805
FeNi amorphous films, fast phase transition investigation by TEM method 80−107029
FeNi, enrichment to 90% Ni 77−28749
FeNi, itinerant electron model, spin wave stiffness const. calc. 80−34613
FeNi-Cu, composite fibre and layer structs., anomalous props. caused by internal phase boundaries 78−72754
$(Fe_{0.5}Ni_{0.5})$-Co, solid and liq., paramag. susceptibility and electron struct., 800-1800°C *(Russian)* 80−25081
$Fe_{1-x}Ni_x$ ($x<29$at.%), γ-phase dispersion, Mossbauer spectra 78−52399
$Fe_{1-x}Ni_x$, elec. resist., anomalies in temp. depend. 79−23942
$Fe_{1-x}Ni_x$, FCC, anomalies in sp. ht. and thermal expansion 79−19739
$(Fe_{1-x}Ni_x)_{78}Si_{10}B_{12}$, amorphous, Hall effect and magnetoresist. *(Japanese)* 77−85199

nickel alloys continued
$Fe_{40}Ni_{18}Mo_4B_{18}$ amorphous alloys, compatibility of DC and AC mag props. 80−34695
$Fe_{65}Ni_{35}$, mag. cluster structs., 25-422°C 77−69493
$Fe_{65}Ni_{35}$, quasi-localised spin system, neutron scatt. 78−68194
Fe_xNi_{1-x} amorphous film, growth stress and structure factor, stabilisation by conduction electrons 80−38920
Fe_xNi_{1-x}, amorphous films, crystallisation, effect of codeposited O_2, N_2 or Kr gases 80−10807
$Fe_{1-x}Ni_xAl$, Knight shift and mag. susceptibility study, electron struct. peculiarities *(Russian)* 80−15814
FeNiB, amorphous alloy, high resolution imaging by electron microscopy 79−99039
$(FeNi)_{80}B_{20}$, glass, elastic consts. 79−83249
$(FeNi)_{80}B_{20}$, metallic glass, saturation moments and Curie temp. 77−1542
$(Fe_{0.6}Ni_{0.4})_{100-x}B_x$ and $(Fe_{100-x}Ni_x)_{80}B_{20}$ amorphous alloys, X-ray diffr. struct. determ. 80−64906
$(Fe_{1-x}Ni_x)_{75}B_{25}$, amorphous and cryst., short range order, Mossbauer study 80−39961
$(Fe_{1-x}Ni_x)_{83}B_{17}$, amorphous alloys ferromagnetic resonance 80−108080
$(Fe_{100-x}Ni_x)_{100-y}B_y$, metallic glass, embrittlement and crystn. 80−7685
$(Fe_{100-x}Ni_x)_{83}B_{17}$, amorphous, crystn. 80−75176
$(Fe_{100-x}Ni_x)_{83}B_{17}$ glassy alloys, Ni content influence on crystn., and bend ductility changes, during annealing 79−73103
$Fe_{38}Ni_{38}B_{24}$, amorphous, magnetisation and FMR expts. 79−95607
$Fe_{40}Ni_{20}B_{20}$, metallic glassy ribbon, casting conditions *(Japanese)* 80−55386
$Fe_{40}Ni_{40}B_{20}$ alloys, crystalline and amorphous, resistivity minimum, X-ray, Mossbauer studies 79−73489
$Fe_{40}Ni_{40}B_{20}$, amorphous, induced mag. anisotropy, reorientation kinetics 77−43829
$Fe_{40}Ni_{40}B_{20}$, amorphous, hyperfine field distrib., Mossbauer effect meas. 79−4755
$Fe_{40}Ni_{40}B_{20}$, amorphous, hyperfine field distrib., Mossbauer study 79−28657
$Fe_{40}Ni_{40}B_{20}$, amorphous, anomalous thermal dilatation 79−55668
$Fe_{40}Ni_{40}B_{20}$, amorphous, resist. min. disappearance on annealing 79−60786
$Fe_{40}Ni_{40}B_{20}$, amorphous, processing conditions effect on mag. props. 79 73775
$Fe_{40}Ni_{40}B_{20}$, amorphous, mag. loss meas. 79−73776
$Fe_{40}Ni_{40}B_{20}$, amorphous, high-field magnetisation curve, spin wave spectrum and microstructural inhomogeneities 80−15702
$Fe_{40}Ni_{40}B_{20}$, amorphous, casting conditions effect on mag. props. *(Japanese)* 80−34698
$Fe_{40}Ni_{40}B_{20}$, amorphous, mag. props., effects mech. deform. 80−39840
$Fe_{40}Ni_{40}B_{20}$, amorphous, phase transforms., resistometric anal. 80−75538
$Fe_{40}Ni_{40}B_{20}$, amorphous, RF annealing effects 80−108037
$Fe_{40}Ni_{40}B_{20}$, amorphous ribbon prod., apparatus parameters effect on dimens. 77−12570
$Fe_{40}Ni_{40}B_{20}$, amorphous ferromag., resist. and galvanomagnetic props., rel. to magnetisation 78−14712
$Fe_{40}Ni_{40}B_{20}$, amorphous and crystalline, resist. minimum 79−47079
$Fe_{40}Ni_{40}B_{20}$, amorphous ferromag., resistivity down to 60 mK 79−60783
$Fe_{40}Ni_{40}B_{20}$, amorphous ribbon, anal. of casting conditions 79−95965
$Fe_{40}Ni_{40}B_{20}$, amorphous ribbon, power loss variation with freq. and applied stress 80−88849
$Fe_{40}Ni_{40}B_{20}$ and $Fe_{40}Ni_{40}P_{14}B_6$, amorphous, mag. aftereffect spectra and annealing props. 80−88831
$Fe_{40}Ni_{40}B_{20}$ glass, ^{10}B self-diffusion, meas. by SIMS 80−49406
$Fe_{40}Ni_{40}B_{20}$ glass, phase transform. during isochronal annealing 78−14451
$Fe_{40}Ni_{40}B_{20}$, metallic glass, embrittlement kinetics and crystn., quenching influence 78−68766
$Fe_{40}Ni_{40}B_{20}$, metallic glass, low temp. specific heat, metalloid effects 80−34654
$Fe_{40}Ni_{40}B_{20}$, molten, jet streaming, planar and cylindrical, instabilities rel. to glassy alloy casting 80−35129
$Fe_{50}Ni_{30}B_{20}$, crystallisation of amorphous alloys, TEM and X-ray diffr. exam. of struct., growth characts. 78−79539
$Fe_{80-x}Ni_xB_{20}$ and $Fe_{80-x}Ni_xP_{14}B_6$ amorphous alloys, microhardness correl. with mag. props. 80−88826
$Fe_{80-x}Ni_xB_{20}$, $Fe_{80-x}Ni_xP_{14}B_6$, amorphous, microhardness meas., dependence on mag. props. *(Croatian)* 79−11688
$Fe_{80-x}Ni_xB_{20}$, ferromag. metallic glass, saturation magnetostriction meas. 77−36108
$Fe_{80-x}Ni_xB_{20}$, spontaneous Hall effect and resistivity 79−19576
$(Fe_{1-x}Ni_x)_{80}B_{20}$ amorphous soft magnetic films 79−82836
$(Fe_xNi_{1-x})_{80}B_{20}$, $(Fe_xNi_{1-x})_{80}P_{14}B_6$, new soft amorphous ferromagnetic glasses *(Croatian)* 79−11298
$(Fe_xNi_{1-x})_{80}B_{20}$, amorphous alloys, engineering mag. props. 79−51832
$(Fe_xNi_{1-x})_{80}B_{20}$, amorphous, Mossbauer spectra, mag. props. 80−15843
$(Fe_xNi_{100-x})_{80}B_{20}$, glassy, elec. resist. at elevated temp. 79−73484
$Fe_xNi_{80-x}B_{20}$, amorphous ferromag., low temp. resistivity 79−56181
$Fe_xNi_{80-x}B_{20}$ and $Fe_xNi_{80-x}P_{14}B_6$ metallic glasses, low temp. resist. and galvanomag. effects, mag. state influence 80−84461
$Fe_xNi_{80-x}B_{20}$, $Fe_xNi_{80-x}P_{14}B_4$, amorphous Hall effect voltage meas. *(Croatian)* 79−11102
$Fe_xNi_{80-x}B_{20}$, $Fe_xNi_{80-x}P_{14}B_6$, amorphous ferromag., galvanomag. props. 79−56196
$Fe_xNi_{80-x}B_{20}$ glass, resist., magnetoresist., and thermoelec. power 80−70681
$Fe_xNi_{80-x}B_{20}$, quenched ferromag. ribbon, Brillouin spectra 80−2776
$(Fe_yNi_{1-y})_{80}B_{20}$, mag. anneal anisotropy in amorphous alloys 77−16069
$(Fe_{1-y}Ni_y)_{0.8}B_{0.2-x}P_x$, amorphous, hyperfine fields and local mag. moments, Mossbauer study 80−75895
$Fe_{1.6}Ni_{78.4}B_{10}P_{10}$ metallic glass, superparamag. behaviour, chem. inhomogeneities role 80−84625
$Fe_{20}Ni_{60}B_{19}P_1$, amorphous, spin waves, inelastic neutron scatt. meas. 79−73701
$Fe_{40}Ni_{40}B_{20-x}P_x$, amorphous, mag. saturation, spin wave stiffness, temp. depend. 80−75741
$Fe_{40}Ni_{40}B_{20-x}P_x$ metallic glasses, local struct. and dynamic disorder of Fe and Ni, EXAFS obs. 80−89088
$Fe_{80-x}Ni_xB_{20-y}P_y$, amorphous, Rayleigh region and coercive force 80−88806
$(FeNi)_{80}Bi_{17.5}Al_2Si_{0.5}$, stress-induced variation in magnetisation and dynamic magnetostrictive charact. 80−88855
$(Fe_{0.5}Ni_{0.5})_{1-x}Co_x$, paramag. susceptibility, solid and liq. phases 1000-1800°C *(Russian)* 77−16040

nickel alloys continued
$Fe_{65}(Ni_{1-x}Cr_x)$, microhardness and specific heat, depend. on Cr content *(Russian)* 79−100240
$Fe_{65}(Ni_{1-x}Cr_x)_{35}$, mag. viscosity and anomalies near Curie temp. 79−73781
$Fe_{65}(Ni_{1-x}Cr_x)_{35}$, remanent magnetisation, temp. depend., anomalies near Curie temp. *(Russian)* 78−60310
FeNiCrAlLi alloy, γ' hardened, noncellular mech. for form of lamellar η phase morphology 77−28824
$Fe_{32}Ni_{36}Cr_{14}P_{12}B_6$, Metglas 2826 A, ferromag. reson. for g-values and relax. parameters, 77 to 430K 77−63289
$Fe_{32}Ni_{36}Cr_{14}P_{12}B_6$, metallic glass, changes in Curie temp., physical dimensions and mag. anisotropy during annealing 77−85446
$Fe_{32}Ni_{36}Cr_{14}P_{12}B_6$, Metglas 2826A, Hall resistivity, effect of thermal cycling and annealing 78−56125
$Fe_{32}Ni_{36}Cr_{14}P_{12}B_6$, shear band form. 78−68756
$Fe_{32}Ni_{36}Cr_{14}P_{12}B_6$ metallic glass, dynamic mechanical props. 79−10894
$Fe_{32}Ni_{36}Cr_{14}P_{12}B_6$, elastic, magnetoelastic and thermal props. 79−19759
$Fe_{32}Ni_{36}Cr_{14}P_{12}B_6$, glassy, ferromag. anisotropy of resistivity 79−23939
$Fe_{32}Ni_{36}Cr_{14}P_{12}B_6$, METGLAS 2826A, metastable crystallization phases, TEM obs. 79−55671
$Fe_{32}Ni_{36}Cr_{14}P_{12}B_6$, amorphous ferromagnet, long and short range exchange interactions, Mossbauer spectra and interpretation 79−56526
$Fe_{32}Ni_{36}Cr_{14}P_{12}B_6$, amorphous mag. solids, Mossbauer exam. 79−61281
$Fe_{32}Ni_{36}Cr_{14}P_{12}B_6$, Metglass 2826A, mag. props. under high press., Mossbauer meas. 79−73860
$Fe_{32}Ni_{36}Cr_{14}P_{12}B_6$, Metglas 2826A elec. resist. during crystn. 79−91014
$Fe_{32}Ni_{36}Cr_{14}P_{12}B_6$ glass, thermal expansion, glass transform. and crystn. temps. 80−2183
$Fe_{32}Ni_{36}Cr_{14}P_{12}B_6$, metallic glass, high-resolution XPS study, electronic state struct. 80−29846
$Fe_{32}Ni_{36}Cr_{14}P_{12}B_6$, metallic glass, Doppler broadening of positron annihilation γ-radiation and elec. resist. 80−66321
$Fe_{32}Ni_{36}Cr_{14}P_{12}B_6$ metallic glass, crystn. kinetics by TEM 80−75186
$Fe_{32}Ni_{36}Cr_{14}P_{12}B_6$, Metglas 2826A, EPR at 20 GHz 80−75848
$Fe_{32}Ni_{36}Cr_{14}P_{12}B_6$ Metglas, bending deform., shear band form., high-speed cinematographic obs. 80−89322
$Fe_{32}Ni_{36}Cr_{14}P_{12}B_6$, Metglas amorphous films, corrosion resist. and ion plating use 80−89423
$Fe_{32}Ni_{36}Cr_{14}P_{12}B_6$ metallic glass, effect of pre-ageing on glass transition temp. 80−100326
$Fe_{0.5}(Ni_xMn_{1-x})_{0.5}$, elec. resist., anomalies in temp. depend. 79−23942
$Fe_{0.5}(Ni_xMn_{1-x})_{0.5}$, FCC, anomalies in sp. ht. and thermal expansion in paramag. temp. range 79−19739
$Fe_{65}(Ni_{1-x}Mn_x)_{35}$, anomaly of subcrit. neutron scatt. and depolarisation effects at antiferro- to ferromag. transition *(Russian)* 77−47996
$Fe_{65}(Ni_{1-x}Mn_x)_{35}$, magnetic struct. and inhomogeneities by neutron scatt. and Mossbauer effect *(Russian)* 77−63122
$Fe_{65}Ni_{28}Mn_1$, disordered, mag. struct. near ferro-antiferromagnetic transition 80−60211
$Fe_{40}Ni_{40}(Mo,Si,B)_{20}$, amorphous, soft mag. props., switched-mode power supply appls. 80−88850
$Fe_{0.49}Ni_{0.415}Mo_{0.095}$, Vibralloy, high-temp. vibrating reed meas. 79−55811
$Fe_{40}Ni_{38}Mo_4B_{18}$ amorphous ribbons, magnetoelastic effects in as-quenched and stress-relieved states 80−80588
$Fe_{40}Ni_{38}Mo_4B_{18}$, amorphous, crystallization, heat treatment and irradiation effects *(French)* 79−90558
$Fe_{40}Ni_{38}Mo_4B_{18}$, amorphous, mag. anisotropy, Mossbauer study 80−65864
$Fe_{40}Ni_{38}Mo_4B_{18}$, amorphous, reversible enhancement of mag. directional ordering rate 80−103829
$Fe_{40}Ni_{38}Mo_4B_{18}$ glassy alloy, high permeability, low field mag. characts. 78−68301
$Fe_{40}Ni_{38}Mo_4B_{18}$ metallic glass, reorientation kinetics of magnetization 79−24155
$Fe_{40}Ni_{38}Mo_4B_{18}$, metallic glass, mag. and transport props. 80−39752
$Fe_{40}Ni_{38}Mo_4B_{18}$ ribbon, magnetic characterisation 80−34680
$(Fe_{1-x}Ni_x)_2P$, mag. props. 78−23248
$(Fe_{1-x}Ni_x)_{80}P_{20}$, amorphous, ferromagnetic alloys, mag. anomalies of Invar type *(Russian)* 80−93089
$Fe_{40}Ni_{40}P_{20}$, amorphous alloy, ductile-brittle transition temp., relation to composition 78−52972
(FeNi)PB amorphous wires, surface oxidation and annealing influence on induced anisotropy 80−100957
$(Fe_{0.04}Ni_{0.96})_{80}P_{10}B_{10}$, amorphous, mictomagnetic to ferromag. transition 78−34981
$(Fe_{0.04}Ni_{0.96})_{80}P_{10}B_{10}$, amorphous magnetisation, field and temp. depend. 80−39755
$(Fe_{1-x}Ni_x)_{80}P_{10}B_{10}$, amorphous, magnetostriction meas. by ferromag. reson., induced anisotropy 77−32232
$(Fe_{1-x}Ni_x)_{80}P_{10}B_{10}$, amorphous microwires, magnetisation reversal and anisotropy 78−91885
$Fe_{20}Ni_{60}P_{14}B_6$, $Fe_{30}Ni_{50}P_{14}B_6$, amorphous ferromags., thermoelec. power and resistivity near Curie temp. 79−56200
$Fe_{27}Ni_{53}P_{14}B_6$, amorphous, Hall resist. and mag. props., short range order effects 80−34422
$Fe_{27}Ni_{53}P_{14}B_6$, metallic glass, changes in Curie temp., physical dimensions and mag. anisotropy during annealing 77−85446
$Fe_{40}Ni_{40}P_{14}B_{06}$, amorphous, strip domains, anisotropy const. effects 80−29571
$Fe_{40}Ni_{40}P_{14}B_{20}$, Metglas 2826, amorphous ferromag., resistivity down to 60 mK 79−60783
$Fe_{40}Ni_{40}P_{14}B_6$, (Metglas 2826), ferromag. Curie temp. determ. 78−64206
$Fe_{40}Ni_{40}P_{14}B_6$, amorhpous ribbon, influence of torsion on mag. props. 80−7138
$Fe_{40}Ni_{40}P_{14}B_6$, amorphous ribbon, cold rolling, annealing mag. props. 77−8958
$Fe_{40}Ni_{40}P_{14}B_6$, amorphous, deform. and annealing effects on mag. and mech. props. 77−12717
$Fe_{40}Ni_{40}P_{14}B_6$, amorphous, magnetoelastic props. 77−16136
$Fe_{40}Ni_{40}P_{14}B_6$, amorphous alloy, small angle X-ray scattering 77−65953
$Fe_{40}Ni_{40}P_{14}B_6$, amorphous, thermal stress effect on mag. easy axis 77−80928
$Fe_{40}Ni_{40}P_{14}B_6$, amorphous, domain struct. 78−10719
$Fe_{40}Ni_{40}P_{14}B_6$, amorphous tape wound cores, mag. props. *(German)* 78−10727
$Fe_{40}Ni_{40}P_{14}B_6$, amorphous, mag. props. 78−10728
$Fe_{40}Ni_{40}P_{14}B_6$, amorphous alloy, structural relaxation kinetics, X-ray diffr. exam. 78−38627

nickel alloys continued
$Fe_{40}Ni_{40}P_{14}B_6$, amorphous alloy, ductile-brittle transition temp., relation to composition 78−52972
$Fe_{40}Ni_{40}P_{14}B_6$ amorphous ribbon, mag. anisotropy distrib. near surface 78−95430
$Fe_{40}Ni_{40}P_{14}B_6$, amorphous toroidal core, switching characts. and domain structs. 78−95477
$Fe_{40}Ni_{40}P_{14}B_6$, amorphous, energy dispersive X-ray diffr. study of structural relaxation 79−14689
$Fe_{40}Ni_{40}P_{14}B_6$, amorphous, annealed and unannealed, temp. depend. of flow stress and ductility 79−29119
$Fe_{40}Ni_{40}P_{14}B_6$, amorphous ferromagnet, domain struct., Rayleigh region and coercive field 79−28559
$Fe_{40}Ni_{40}P_{14}B_6$, amorphous alloy sheet, fabrication by gas melt spraying method 79−24466
$Fe_{40}Ni_{40}P_{14}B_6$, amorphous, stress-induced mag. easy axis 79−33516
$Fe_{40}Ni_{40}P_{14}B_6$, amorphous, continuous versus discrete hyperfine field distrib., Mossbauer spectra 79−33583
$Fe_{40}Ni_{40}P_{14}B_6$, amorphous, transverse magnetoresist., stress effect 80−15501
$Fe_{40}Ni_{40}P_{14}B_6$, amorphous, mag. props., effects mech. deform. 80−39840
$Fe_{40}Ni_{40}P_{14}B_6$, amorphous, resistometric study of short-range ordering rel. to heat treatment 80−70140
$Fe_{40}Ni_{40}P_{14}B_6$, amorphous ferromagnet, Mossbauer hyperfine fields, mag. struct. 80−75894
$Fe_{40}Ni_{40}P_{14}B_6$ amorphous alloy, temper embrittlement 80−76295
$Fe_{40}Ni_{40}P_{14}B_6$, amorphous, mag. polarisation in approach to ferromag. saturation 80−80560
$Fe_{40}Ni_{40}P_{14}B_6$, amorphous, steady-state creep rate, cryst. effect 80−81102
$Fe_{40}Ni_{40}P_{14}B_6$, amorphous, mag. permeability aftereffect during annealing 80−88834
$Fe_{40}Ni_{40}P_{14}B_6$, amorphous ferromag., spin wave excitations 80−97079
$Fe_{40}Ni_{40}P_{14}B_6$ amorphous ribbon, mag. domains and anisotropy distrib. 80−108029
$Fe_{40}Ni_{40}P_{14}B_6$, elastic, magnetoelastic and thermal props. 79−19759
$Fe_{40}Ni_{40}P_{14}B_6$, $Fe_{29}Ni_{49}P_{14}B_6Si_2$ glasses, internal friction and shear modulus 79−52287
$Fe_{40}Ni_{40}P_{14}B_6$, $Fe_{35}Ni_{32}Cr_{15}P_{12}B_6$, amorphous ferromagnets, Barkhausen noise and core losses 77−69618
$Fe_{40}Ni_{40}P_{14}B_6$, ferromagnetic metallic glasses, Brillouin scattering 78−92085
$Fe_{40}Ni_{40}P_{14}B_6$ glass, low temp. heat capacity meas., electronic, phonon contributions exam. 78−10689
$Fe_{40}Ni_{40}P_{14}B_6$ glass, crystn. kinetics, DSC expts. 78−26444
$Fe_{40}Ni_{40}P_{14}B_6$ glass, positron lifetimes in as-received, cold-rolled, embrittled and crystallized samples 79−74177
$Fe_{40}Ni_{40}P_{14}B_6$ glass, struct. relax., ferromag. reson. and X-ray scatt. 79−90566
$Fe_{40}Ni_{40}P_{14}B_6$ glass, thermal expansion, glass transform. and crystn. temps. 80−2183
$Fe_{40}Ni_{40}P_{14}B_6$ glass, viscosity near T_g, using rapid heating, and fusion characts. 80−70438
$Fe_{40}Ni_{40}P_{14}B_6$, glassy metal fabric for mag. shield 77−8347
$Fe_{40}Ni_{40}P_{14}B_6$, glassy, mag. props. and hyperfine interactions, Mossbauer obs., 4.2-1000K 78−10812
$Fe_{40}Ni_{40}P_{14}B_6$, glassy, ferromag. anisotropy of resistivity 79−23939
$Fe_{40}Ni_{40}P_{14}B_6$, hardness, elec. cond., photo emission, and mag. props. *(Norwegian)* 79−32909
$Fe_{40}Ni_{40}P_{14}B_6$, high-field suscept. and spin wave spectrum 78−10662
$Fe_{40}Ni_{40}P_{14}B_6$, induced anisotropy energy and saturation magnetisation temp. depend., torque magnetometer meas. 78−10680
$Fe_{40}Ni_{40}P_{14}B_6$, irradiation swelling 78−30682
$Fe_{40}Ni_{40}P_{14}B_6$, metallic glass, acoustic emission generated during viscous flow 78−39853
$Fe_{40}Ni_{40}P_{14}B_6$, metallic glass, cryst., isothermal annealing behaviour 80−6367
$Fe_{40}Ni_{40}P_{14}B_6$ metallic glass, ferromag. reson., spin waves, thermal ageing and long-range order effects 80−25214
$Fe_{40}Ni_{40}P_{14}B_6$, metallic glass, high-resolution XPS study, electronic state struct. 80−29846
$Fe_{40}Ni_{40}P_{14}B_6$ metallic glass, isothermal viscosity and crystn. 80−49395
$Fe_{40}Ni_{40}P_{14}B_6$ metallic glass, crystn. 80−70127
$Fe_{40}Ni_{40}P_{14}B_6$, metallic glass, glass transition, viscous flow and differential scanning calorimetry meas. 80−96635
$Fe_{40}Ni_{40}P_{14}B_6$, metallic glass, bending tests, evidence of ideal elastic-plastic deform. 80−97543
$Fe_{40}Ni_{40}P_{14}B_6$, Metglas 2826, ferromag. reson. for g-values and relax. parameters, 77 to 430K 77−63289
$Fe_{40}Ni_{40}P_{14}B_6$, Metglas 2826, ferromag. antireson. transmission at 24 GHz, 26 to 270°C 77−69696
$Fe_{40}Ni_{40}P_{14}B_6$, Metglas 2826, magnetising processes 78−10725
$Fe_{40}Ni_{40}P_{14}B_6$, Metglas 2826, acoustic emission during viscous flow 78−42915
$Fe_{40}Ni_{40}P_{14}B_6$, Metglas 2826, stability, crystallisation, ductility meas. 78−47246
$Fe_{40}Ni_{40}P_{14}B_6$, Metglas 2826, amorphous ribbon core, appl. in force transducer 78−93669
$Fe_{40}Ni_{40}P_{14}B_6$, metglas 2826, amorphous, Hall resistivity, thermal cycling and annealing effects 79−38050
$Fe_{40}Ni_{40}P_{14}B_6$ Metglass, spontaneous vibr. modes excited by reversible magnetostriction 79−56587
$Fe_{40}Ni_{40}P_{14}B_6$, Metglas 2826, hot forming 80−84980
$Fe_{40}Ni_{40}P_{14}B_6$, Metglas 2826, amorphous ribbon under tension, mag. domain walls and pulsed magnetisation reversal 80−88825
$Fe_{40}Ni_{40}P_{14}B_6$, quenched amorphous, high field susceptibility and microstructure 77−69506
$Fe_{40}Ni_{40}P_{14}B_6$, amorphous, kinetics of induced mag. directional order 80−44824
$Fe_{40}Ni_{40}P_{20-x(B)}B_{x(B)}$, ferromagnetic metallic glass, thermal and mech. stability 77−66698
$Fe_{40}Ni_{40}P_yB_{20-y}$, amorphous, mag. props. effect of metalloid elements 79−28658
$Fe_{44}Ni_{40}P_{14}B_6$, homogeneous deformation effect on crystn. and Curie temp. 80−21045
$Fe_{46}Ni_{40}P_{16}B_6$, ferromagnetic amorphous alloy, even magneto-optic effects 77−55776
$Fe_xNi_{80-c}P_{14}B_6$, amorphous, annealing effects on mag. props. 79−78383
$Fe_xNi_{1-x}P_{14}B_6$, amorphous, spin-glass regime, magnetoresist. meas. 80−34418
nickel alloys continued
$(Fe_xNi_{1-x})_{80}P_{10}B_{10}$, amorphous, weak itinerant ferromag., Arrott plots 77−73007
$(Fe_xNi_{1-x})_{80}P_{10}B_{10}$, amorphous, magnetisation reversal and domain boundary configs. 80−88809
$(Fe_xNi_{1-x})_{80}P_{14}B_6$, Mossbauer spectroscopy, mag. hyperfine interaction, Curie temps. 78−6617
$(Fe_xNi_{100-x})_{80}P_{10}B_{10}$, amorphous, elec. resist., 2 to 300K, composition depend. 80−44562
$Fe_xNi_{80-x}P_{14}B_6$ (x=0, 20, 40, 60, 80), metallic glass, low temp. sp. ht. 80−2588
$Fe_xNi_{80-x}P_{14}B_6$, amorphous, sp. ht. and susceptibility meas., spin glass and mictomag. props. 78−68274
$Fe_xNi_{80-x}P_{14}B_6$, amorphous ferromag., resistivity, mag. contrib., 1.5-50K 79−56182
$Fe_xNi_{80-x}P_{14}B_6$, amorphous ferromag., T^2 saturation in resist. below 0.3K 79−60785
$Fe_xNi_{80-x}P_{14}B_6$, and $Fe_xNi_{80-x}B_{20}$ glass, microhardness, correl. with mag. props. 79−57085
$Fe_xNi_{80-x}P_{14}B_6$ glass, resist., magnetoresist., and thermoelec. power 80−70681
$Fe_xNi_{80-x}P_{14}B_6$ metallic glasses, low temp. resistivities 78−91659
$Fe_xNi_{80-x}P_{14}B_6$, metallic glass, low temp. sp. ht. for spin-glass and spin-cluster-glass regime 80−71071
$(Fe_yNi_{100-y})_{79}P_{13}B_8$, metallic glass, low temp. sp. ht. for spin-glass and spin-cluster-glass regime 80−71071
$(Fe_{0.3}Ni_{0.7})_{0.75}P_{0.16}B_{0.06}Al_{0.03}$, amorphous, spin wave spectrum, neutron scatt. 77−16064
$(Fe_{0.5}Ni_{0.5})_{75}P_{16}B_6Al_3$ glass, struct. relax. as origin of Curie temp. ageing 78−84418
$(Fe_{1-x}Ni_x)_{75}(PBAl)_{25}$, amorphous, high-field magnetoresist. meas. 80−34423
$(Fe_{1-x}Ni_x)_{75}P_{16}B_6Al_3$, amorphous alloy, low temp. elec. resist. saturation 78−68005
$(Fe_{1-x}Ni_x)_{75}P_{16}B_6Al_3$, amorphous, low temp. elec. resist. 79−56183
$(Fe_{1-x}Ni_x)_{75}P_{16}B_6Al_3$, amorphous, saturation magnetisation, temp. depend., ferromag. reson. meas. 79−73818
$(Fe_{65}Ni_{35})_{75}P_{16}B_6Al_3$, amorphous ferromag., high temp. spin dynamics 78−47965
$(Fe_{65}Ni_{35})_{75}P_{16}B_6Al_3$, amorphous ferromagnet, mag. excitations 79−7984
$(Fe_{65}Ni_{35})_{75}P_{16}B_6Al_3$, amorphous, crystn. temp., press. and heating rate depend. 80−70132
$(Fe_xNi_{1-x})_{0.75}P_{0.16}B_{0.06}Al_{0.03}$, metallic glass, thermal expansion 78−43151
$(Fe_xNi_{1-x})_{75}P_{16}B_6Al_3$, amorphous, spin wave excitations and low temp. magnetisation 79−33468
$(Fe_xNi_{1-x})_{75}P_{16}B_6Al_3$, magnetisation temp. depend., spin wave theory 80−44927
$Fe_xNi_yP_{14}B_6(S_2)$, coiled ribbons, stress relaxation 79−29120
$Fe_{29}Ni_{49}P_{14}B_6Si_{12}$, Metglas fibre reinforced mortar, fracture props. 79−70159
$Fe_{29}Ni_{49}P_{14}B_6Si_2$ glass, crystn. kinetics, DSC expts. 78−26444
$Fe_{29}Ni_{49}P_{14}B_6Si_2$, Metglas 2826 B, paramag. reson. for g-values and relax. parameters, 77 to 430K 77−63289
$Fe_{29}Ni_{49}P_{14}B_6Si_2$, metallic glass, changes in Curie temp., physical dimensions and mag. anisotropy during annealing 77−85446
$Fe_{29}Ni_{49}P_{14}B_6Si_2$, Metglas 2826B, Hall, elec. resist., magnetisation and heat capacity meas. 78−68019
$Fe_{29}Ni_{49}P_{14}B_6Si_2$, Metglass 2826B, saturation magnetisation, temp. depend., ferromag. reson. meas. 79−73818
$Fe_{72}Ni_8P_{13}C_7$ glass, erosion craters produced by spark machining, scanning microscopy obs. 78−44268
$(Fe_{1-x}Ni_x)_{80}PyB_{20-y}$, local struct. disorder and crystallisation, Mossbauer exam. 79−1728
$Fe_{3-x}Ni_xSi$, limits of solubility, mag. props. and electron conc. 78−10670
$(Fe_{1-x}Ni_x)_{77}Si_{10}B_{13}$, amorphous magnetic alloys, density meas. 80−1934
$(Fe_{1-x}Ni_x)_{77}Si_{10}B_{13}$ amorphous alloy system, saturation mag. moment, Curie temp., mag. susceptibility 80−39753
$(Fe_{1-x}Ni_x)_{77}Si_{10}B_{13}$, amorphous, Landau-Ginzburg theory, magnetisation and Curie temp. 80−75700
$(Fe_{1-x}Ni_x)_{78}Si_{10}B_{12}$ amorphous alloys, cold rolled and as-quenched, mag. anisotropy 80−97089
$Fe_{62.4}Ni_{15.6}Si_7B_{15}$ amorphous ferromagnetic alloy, anomalous magnetisation possible reasons, Mossbauer spectra *(Russian)* 79−78441
$Fe_{1-x}Ni_xSn$, transferred hyperfine fields at ^{119}Sn, Mossbauer spectroscopy 79−33582
FeNiTe alloys, disordered, polycrystalline, elec. resist., temp. depend. 80−49692
Fe_3Si-Ni, dil., cond. electron polarisation and moment perturbations 78−68224
GCFR fuel pin claddings, oxidation behaviour in He environment 80−16594
Ga-Ni-R, (R=Dy, Ho, Er, Tm, Lu), struct. determ. by X-ray powder method *(Ukrainian)* 80−39001
Gd-Co-Ni series intermetallics, induced moments, magnetisation meas. 77−63138
Gd-Ni, amorphous, mag. and elec. props. 80−80499
Gd-Ni, amorphous, mag. props. and ferromag. reson. 80−75862
Gd-Ni, amorphous, Mossbauer spectra 80−25262
Gd-Ni, amorphous film, galvanomag. effects, Hall detector 77−89882
Gd-Ni, amorphous film, Kerr and Hall effect meas. 77−24722
Gd-Ni, CPA calcs., moments and transition temps. 78−52252
Gd-Ni, ferromag., elec. resist. temp. depend. 80−96843
Gd-Ni-Al, (Gd<33.3 at.%), isothermal section, 800°C, X-ray and microscopic anal. *(Russian)* 79−27950
$Gd(CO_xNi_{1-x})_2$, mag. interactions, effects on moments *(Rumanian)* 79−15296
$Gd(Co_{1-x}Ni_x)_2$ compounds, NMR and thermal expansion 80−66070
$GdCo_{5c}Ni_{5-5c}$, intrinsic coercivity, anisotropy, exchange and cryst. field interactions 80−75806
$Gd(Co_xNi_{1-x})_2$, EPR exam. 79−28600
$Gd(Co_xNi_{1-x})_2$, mag. props., composition and temp. depend. 79−15289
$Gd(Co_xNi_{1-x})_2$, Mossbauer spectra, mag. props. 80−20563
$Gd_{1-x}Dy_xNi$, FeB-CrB type stacking variations, cryst. struct. 80−64952
$Gd_{18}Fe_{82-x}Ni_x$, amorphous film, mag. and galvanomag. props. 77−24715
$Gd_2(Fe_{1-x}Ni_x)_{17}$, Mossbauer spectra, hyperfine field interactions 78−6614
$Gd_{0.9}La_{0.1}Ni_2$, Ni contrib. to ordering, ^{139}La NMR spin echo 77−63317
$Gd_{0.1}La_{0.9}Ni_5H_x$, ^{155}Gd Mossbauer spectra 77−63340

nickel alloys continued
$Gd(Ni,Cu)_2$, spin disorder resist. evaluation, influence of antiferromagnetic order 77−73035
GdNi, single cryst., magnetocrystn. anisotropy 80−88746
$GdNi_2$, H_2 sorption props. 79−86980
$GdNi_5$, anomalous behaviour near Curie point 78−91880
$GdNi_5$, Gd_2Ni_{17}, Mossbauer effect 77−85635
$GdNi_x$, (x=3, 3.5, 8.5), ferrimag., mag. reson. above and below Curie temp. 80−97148
$Gd_{1-x}Ni_x$, CPA calcs., mean mag. moments 77−72997
$Gd_{1-x}Ni_x$, temp. depend. of magnetisation 77−77043
$Gd_{68}Ni_{32}$, amorphous ferromag., mag. and transport meas. 77−89930
Gd_xNi_{1-x} sputtered amorphous films, mag. props. and Hall meas. 78−95488
$Gd_2Ni_{17-x}Al_x$, cryst. struct., X-ray obs. 79−65034
$Gd_2Ni_{17-x}Al_x$, EPR of Gd^{3+} ions 80−97139
$Gd_2Ni_{17-x}Al_x$, mag. behaviour in paramagnetic region 79−73675
$GdNi_2H_4$, effect of absorbed H_2 on struct. and mag. behaviour 78−2682
$GdNi_2H_4$, effect of H_2 absorption on struct. and mag. behaviour 78−10685
$(Gd_{1-x}R_x)(Co_{1-x}Ni_y)_5$, origin of hyperfine fields acting on Gd, Mossbauer study 80−44967
$(Gd_{0.5}Y_{0.5})Ni$, FeB struct., cryst. field effects on mag. struct. 78−52226
$Gd_{1-x}Y_xNi$, FeB-CrB type stacking variations, cryst. struct. 80−64952
Ge-Ni, amorphous, struct., EXAFS study 80−49110
Ge-Ni, liq., enthalpy of formation meas. 80−30267
Ge-Ni, smooth and continuous ohmic contact to n-GaAs 78−68086
GraNi-rare earth intermetallics, struct. by X-ray powder method *(Ukrainian)* 80−10529
H assisted cracking, mechanisms, review 80−50721
H solubility in binary alloys, 850-1150°C, conc. depend. *(Russian)* 77−59120
Hf-Ni, amorphous, formation, decomposition and elec. transport props. 80−20143
Hf-Ni, oxidation of intermetallic phases 79−100298
Hf-Ni (65 to 80 at.%), phase diagram and cryst. struct. of intermediate phases 79−52170
Hf-Ni-H, catalytic activity, exam. by conversion of toluene, and bicyclic aromatic hydrocarbons 80−30276
Hf-Ni-H, catalytic props. 80−30274
Hf-Ni;Ga, alloys, phase diagrams and cryst. struct. *(Russian)* 80−25658
HfNi, hyperfine critical exponents, TDPAC meas. of bulk meas. 77−8465
$HfNi_3$, α and β modifications, X-ray cryst. struct. determ. 79−7578
Hf_3Ni_7, X-ray cryst. struct. determ. 79−4270
Hf_xNi_{21}, single-cryst., X-ray cryst. struct. determ. 79−4269
$Hf_3Ni_2Si_3$, struct., lattice consts., space group, X-ray Weissenberg camera data 78−47284
Ho-Ga-Ni (60, 30 wt.%) cryst. struct., isostructural compound structural study 80−33930
$HoCo_{5-x}Ni_x$, lattice parameters and mag. props. 79−82817
$HoCo_{5.5-x}Ni_x$, cryst. struct. and mag. props. 80−75800
$Ho(Fe_xNi_{1-x})$, mag. interactions, mol. field model 77−73010
$Ho(Fe_xNi_{1-x})_2$, mag. behaviour, susceptibility and Mossbauer expts., 4.2-1300K 78−52235
$Ho_{0.01}Gd_{1-x}Y_xNi_2$, spin echo meas. on ^{165}Ho, limited quenching of Ho moment by cryst. field 79−73851
$HoNi_3$, amorphous, resist. meas., 1.2-290K 78−19015
$HoNi_5$, ferromag., magnetisation and paramag. susceptibility 80−25082
Ho_2Ni_{17}, ferrimag. struct., neutron diffr. expt., cryst. field calcs. 77−73001
$HoNi_{0.5}Cu_{0.5}$, sp. ht. and modulated mag. struct. 77−32167
$HoNi_{0.7}Cu_{0.3}$, mag. behaviour 79−99688
$Ho_{1-x}Y_xNi$, ferromag. behaviour, struct., Curie temp. 79−99677
In-Ni, liq., spreading kinetics on Cu surface 80−10742
La-Ni, D_2 absorption, 500-700°C 79−23736
La-Ni, hydriding characts., applicability for H_2 storage material 78−83955
La-Ni-H, catalytic props. in hydrogenation of propylene, dehydrogenation of propane 80−30277
La-Ni(-Ce)(-Co), H absorption for storage appls. 80−45790
$La_{1-x}Ca_xNi_5$, H_2 sorption props. 78−91533
LaB_6-Ni-WC(TiC)(NbC)(TiB_2), thermionic emission 77−28678
$La(Co_{1-x}Ni_x)_5$, distrib. of Co and Ni atoms, neutron diffr. obs. *(Russian)* 80−64954
$La_{0.9}Eu_{0.1}Ni_{4.6}Mn_{0.4}$, absorption-desorption props. of H_2, degradation mechanism, Mossbauer study 80−88431
$LaNi_4$, absorption and desorption of H_2 77−81400
$LaNi_5$, absorption of H_2, kinetics, diffusion consts. 78−14508
$LaNi_5$, absorption of H_2, 77-300K 79−23737
$LaNi_5$, activated, slow step for H_2 absorpt. (desorpt.) 78−18894
$LaNi_5$, adsorption and desorption charact. of H_2 *(Japanese)* 77−47667
$LaNi_5$, aspects of electrochem. storage of H 79−24917
$LaNi_5$, crystal field investigation from inelastic slow neutron scatt. expts. 80−39538
$LaNi_5$, H storage using metal hydrides, self restoring of active surface 80−45815
$LaNi_5$, H_2 absorpt. kinetics *(Chinese)* 80−103561
$LaNi_5$, H_2 absorption in thin film hydriding alloys 80−65238
$LaNi_5$, H_2 sorption kinetic studies using high-accuracy volumetric device 79−56071
$LaNi_5$, H_2 storage appl. 78−18785
$LaNi_5$, Haucke compounds, low temp. heat capacity, Debye temp. 80−96663
$LaNi_5$ hydrides, 4.2K paramag. susceptibility 80−70934
$LaNi_5$ hydrogen storage capacity, intermetallic compounds research results 77−7843
$LaNi_5$, magnetism and H_2 storage 80−70941
$LaNi_5$ metal hydrides, numerical physical property data for H storage 80−40929
$LaNi_5$, Pauli paramagnet, adsorption of H, proton and ^{139}La NMR 79−78535
$LaNi_5$, self restoring of active surface, photoemission, mag. susceptibility study 78−48280
$LaNi_5$, surface segregation induced by O_2, LEED and AES exam. 79−11009
$LaNi_5$ surface segregation, influence of O_2, H_2, H_2O, SO_2 *(German)* 80−51008
$LaNi_5$ type ternary alloys, H_2 sorption/desorption reaction kinetics 80−45813

nickel alloys continued
$LaNi_5$:Gd, ESR, exchange induced g-shift, H_2 uptake effect 77−4556
$LaNi_5$/H system, thermodynamics of H trapping 80−107444
$LaNi_5$/Ti-Zr-Cr-Mn hydriding alloy mixtures for H storage 80−45788
$LaNi_5$-Gd, dil., ESR spectra, fine struct. and random stresses 80−25203
$LaNi_5$-H, thermodynamics of solution of H at small content 77−21104
$LaNi_5$-H, with small Cr additions, NMR parameters *(Russian)* 80−29637
$LaNi_5$-H system, rel. partial absorption (desorption) enthalpies 80−50881
$LaNi_5$-type ternary alloys, H_2 absorption and desorption kinetics 80−55932
$LaNi_5+3H_2 \rightleftarrows LaNi_5H_6$ reaction, absorpt. capacity and reaction kinetics 79−43626
$LaNi_x$, sorption at press. up to 1500 atm. 80−97819
$LaNi_4Al$, solubility and sorption props. of H_2, effect of Al 80−103482
$LaNi_{5-x}Al_x$, Al addition effects on structural and H_2 absorpt. props. 79−52761
$LaNi_{5-x}Al_x$, use in hydride conversion and storage system chemical heat pump 80−72077
$LaNi_{5-x}Al_x$, versatile alloy system for metal hydride appls. 77−86308
$LaNi_{5-y}Al_y$ alloys and related hydrides, thermodynamic and struct. props. for H_2 storage appl. 80−16847
$LaNi_{5-y}Al_y$ alloys and their hydrides, for H storage appls. 80−45816
β-$LaNi_{5-y}Al_y$ hydrides, H diffusion, NMR studies 80−15298
$LaNi_{4.4}B_{0.6}$, H_2 absorpt. props. 80−88432
$La(Ni_{1-x}Cu_x)_5$, H_2 sorption props. 78−91533
$LaNi_4Cu$, H_2 absorption, cell volumes and desorption pressures correlation 78−22860
$La_7Ni_3D_2$ storage material, neutron, X-ray diffr. study 78−83954
$LaNi_4Fe$, H_2 absorpt. cracking, acoustic emission characts. *(Japanese)* 80−66631
$LaNi_{5-x}Fe_x(Cr_x)$, Fe and Cr electron hydride formation, X-ray and SEM obs. *(Japanese)* 79−43202
$LaNi_2H_{4.6}$, effect of synthesis, heat treatment, on comp. stability, chemical props. 80−29985
$LaNi_3H_x$ (x=4.7, 4.9), NMR line width, spin-lattice relaxation time temp. depend., H self-diffusion *(Russian)* 79−61248
$LaNi_5H_6$, H storage material, H diffusion, neutron diffr. obs. 80−51013
$LaNi_5H_{6.6}$, $LaNi_5H_{6.2}$, H diffusion NMR spectra *(Russian)* 78−2287
$LaNi_5H_{\geq 3.0}$, H diffusion coeff., neutron scatt. obs. 80−24643
β-$LaNi_5H_x$, H_2 diffusion, NMR meas. 79−82378
$LaNi_5H_x$ hydrogen storage system, ($0 \leq x \leq 6$), neutron scatt. obs. of static and dynamic props. 78−14323
$LaNi_5H_x$, μ^+ spin relax. and Knight shift 79−56699
$LaNi_6H_6$, solar energy storage by metal hydride 80−61455
$La_2Ni_7H_y$ (x=9.9, 11.4), NMR line width, spin-lattice relaxation time temp. depend., H self-diffusion *(Russian)* 79−61248
$La_xNi_yH_z$, thermokinetics of H evolution 80−30593
$LaNi_5H_6(D_6)$, low energy excitations of H and D 79−77699
$LaNi_{4.6}In_{0.4}$, H_2 absorption props., desorpt. pressure calc., and decomp. pressures 79−24827
$LaNi_4M$, M=transition metal, H_2 storage appl., desorption isotherms dependence on d-bandfilling 78−18912
$LaNi_{4.6}Sn_{0.4}$, H_2 absorption props., desorpt. pressure calc., and decomp. pressures 79−24827
Mg-Mg_2Ni eutectic alloy and Mg_2Ni, catalytic effect in hydrogenation, surface analysis 80−30283
Mg-$MgNi_2$-Zn, diagram of state, Zn solubility, initial phase precipitation *(Russian)* 80−66478
Mg-Ni, binary system, nonstoichiometry, of Laves phases, $MgNi_2$ *(French)* 78−52770
Mg-Ni (0 to 40.41 wt.%), damping capacity 77−48474
Mg-Ni-S, electroforming, mech. props. rel. to heat treatment 80−35133
Mg-Ni-W-Co-Al-Cr alloy KhN56VMKYu, Al effect on excess Mg phase 80−29926
Mg_2 Ni metal hydrides, numerical physical property data for H storage 80−40929
$MgCu_2$-$MgNi_2$, electronic sp. ht. 1.5 to 4.2K, Fe impurity effects *(German)* 77−59125
$MgCu_{2-x}Zn_x$, X-ray and neutron diffr. investigation of Laves phases of $MgCu_2$-type *(German)* 80−15050
$MgNi_2$, four-layer, Friauf-Laves phases, stacking variants 80−96468
Mg_2Ni, magnetism and H_2 storage 80−70941
Mg_2Ni sorption capacity, grain size distrib., and compactness for H_2 storage appl. 79−74547
Mg_2NiH_4, solar energy storage by metal hydride 80−61455
Mg_2NiH_x, PMR exam. of motion of H 78−56383
$MgNi_{2-x}Zn_x$, X-ray and neutron diffr. investigation of Laves phases of $MgCu_2$-type *(German)* 80−15050
MgO/Ni-Cr (80, 20 wt.%) cermets, sintered, elec. resist. temp. effect 80−3206
Mn determ. by neutron activation anal., nondestructive, destructive methods 77−63987
Mn-Cu-Ni-Bi, magneto-optic film for storage appl. 77−12165
Mn-Ni, atomic and mag. order, neutron diffr. exam. 79−73697
Mn-Ni, γ-phase antiferromag., lattice distortion and elastic props., ΔE effect interpret. 77−20671
Mn-Ni, melt, solubility and activity of S *(Russian)* 77−25012
Mn-Ni, shape memory effect 78−35386
Mn-Ni, single cryst. or polycryst., elastic anomalies at antiferromag. transition 78−14972
Mn-Ni, spin fluctuations effect on sp. ht. 79−82788
Mn-Ni, thermal expansion, mag. susceptibility, lattice consts. 80−100341
γ-Mn-Ni (15 at.%), antiferromag. defect scatt., neutron polarisation anal. 80−50056
Mn-Ni alloys, Mn-rich, structural changes associated with antiferromag. ordering 77−69085
Mn-Ni antiferromag., Invar-like thermal expansion and spontaneous volume magnetostriction 77−69654
Mn-Ni-Al, phase stability 77−48397
γ-Mn-Ni-C, elastic anomalies, martensitic transformation in Mn rich alloys 78−84807
Mn-Ni-C system, pressure effect on melting diagram *(Russian)* 77−55943
Mn-Ni-Ti (Zr) systems, and mech. props. thermal expansion for different heat treatments *(Japanese)* 79−29123
Mn-Ni-Ti(Zr), non-ferromagnetic Elinvar-type alloys 79−24566
Mn-Ni-V(Nb)(Ta), nonferromagnetic Elivar type, mech. props. meas. 77−48473

nickel alloys continued
$Mn_{0.6}Ni_{0.4}$, liq., soln. enthalpies of C and Mn, enthalpy determ. for graphite-diamond transform. and Mn_5C_2 form. 78−59945
$Mn_{73}Ni_{27}$, generalised susceptibility, spin wave contrib., inelastic mag. neutron scatt. 79−47262
$Mn_{0.6}Ni_{0.4}B_{0.02}$, liqs., enthalpy of formation of B_4C at 1320K 79−11814
MnNiGe, coupled nature of mag. and struct. transition under press. 79−8033
$Mn_xNi_{1-x}Sb$, spin glass state and synthesis in high temp. and press. atmospheres 78−23277
β-$Mn_{66}Ni_{20}Si_{14}$, X-ray crystal struct. refinement 79−14735
$MnNiSi_{1-x}Ge_x$, mag. props. 77−12118
Mo-B-Ni, microalloying influence on mechanical props., cold rolling, plasticity *(Russian)* 80−40502
Mo-Hf-C-Ni, electrochemical phase composition anal., precip. of HfC phase *(Russian)* 80−20901
Mo-Ni (40 at.%), exam. of ion transfer *(Russian)* 79−28127
Mo-Ni film system, diffusion reaction, phase form. 77−84999
Mo-Ni sputter deposited, amorphous and crystn., Ni^{++} ion irradiation effects, TEM study 79−65128
Mo-Ni two phase alloys, elec. and mass transport *(Russian)* 78−76044
Mo-Ni-Fe-Co-Zn alloys, Ni, Fe, Co and Zn distrib. using neutron-activation anal. 79−52531
Mo-TiC-Ni phase equilibria, subsolidus temp., metallographic and X-ray anal. 80−16278
Monel, Norton-Bailey parameters, from creep rupture data 80−30098
NI_3Al, structural order and homogeneity, X-ray, mag. susceptibility and Mossbauer meas. 77−63663
Nb-Ge-Ni, phase composition and superconducting props., influence of Ni *(Russian)* 80−20898
Nb-Nb-Al-(Cr), γ/γ'-δ type eutectic, fatigue, effect of composition and microstruct. 78−48520
Nb-Ni, alloying element influence on strength, ductility, surface and grain boundary energies *(Russian)* 79−74234
Nb-Ni, amorphous, synthesis by vapour quenching, and struct. 78−11111
Nb-Ni, amorphous, thermal stability, crystn., DSC and elec. resist. study 80−107060
Nb-Ni, amorphous thin film, vapour quenched, elec. resistivity and thermoelectric power 79−33275
Nb-Ni, cathodic polarization in conc. KOH soln. 80−16591
Nb-Ni, glassy alloy, struct. anal. using X-ray diffr. 79−51004
Nb-Ni amorphous alloys, glass transition and ductility, O additions effect 80−75168
Nb-Ni glass, photoemission spectra meas. 77−55867
Nb-Ni glasses, struct. factor temp. depend. 80−28920
Nb-Ni metallic glass, hardness, elastic moduli, density, cryst. temp., mech. props., for flywheel appl. *(Dutch)* 78−52878
Nb-Ni metallic glass, temp. depend. of resistivity 78−47759
Nb-Ni-Al, cryst. struct. and defects, high resolution electron microscopy obs. 79−94961
Nb_3Al-Ni, mag. impurities effect on supercond. props. 77−1524
$Nb_{0.4}Ni_{0.6}$, amorphous, pair distrib. function, temp. depend., rel. to glass transition 80−24368
$Nb_{40}Ni_{60}$, 3 MeV Ni^+ ion implantation, electron microscope exam. of ion damage 78−91365
$Nb_{40}Ni_{60}$, amorphous, produced by Ni^+ implantation, damage distrib. 80−107062
$Nb_{60}Ni_{40}$, metallic glass, obs. of temp. depend. of struct. factor 78−87624
$Nb_{50}Ni_{50-x}Fe_x$, amorphous, mag. ordering and local random anisotropy 78−68273
$Nb_{50}Ni_{50-x}Fe_x$, amorphous alloy, mag. interactions 78−95432
$Nb_{50}Ni_{50-x}Fe_x$, magnetically dil. glass, 3d moments, mag. susceptibility and magnetisation meas. 79−95574
NbTi-Al-(Cu-Ni) multifilamentary composite supercond. wire, stability, AC losses 77−76998
Nd-Ni-Al, isothermal section, 600°C, X-ray struct. anal. *(Ukrainian)* 80−33929
$NdNi_5$, H_2 absorption, cell volumes and desorption pressures correlation 78−22860
$(Ni,Co)_3Ge$, Co effect on temp. depend. of yield stress 78−31487
$(Ni,Fe)_3Ga$, magnetovolume effects near crit. conc. for ferromag. 79−56591
$(Ni,Co)_3Ge$, single cryst., Co effects on temp. depend. of yield stress 77−4812
$Ni_{75}Si_8B_{17}$, amorphous alloy, crystallisation study *(Japanese)* 78−9959
Ni 201, stress corrosion cracking in high temp. caustic soln. 77−59964
Ni alloy, precipitation strengthened compositions with oxide particles, condensed, struct. criteria and thin layer possibilities *(Russian)* 80−89236
Ni alloy EI617, cyclic temp. variation, loading parameter effect on laws governing distortion 77−16627
Ni alloy EhI698, new etchant for revealing microstructure 80−25934
Ni alloy IN-738, Y_2O_3 (1.5 wt.%) addition, mechanical alloying 77−40427
Ni alloy-Al_2O_3-Al superconductor, spin polarisation of tunnelling electrons, band model 77−72947
Ni alloys, aluminising, thermodynamic anal. of phase transforms. 80−76413
Ni base alloy IN792, carbide morphology 77−36508
Ni base alloys EhI607A and EhI929VD, fatigue strength, temp. depend. 79−15791
Ni base superalloy, rupture life, prior temperature cycling effect 78−60840
Ni base superalloys, recrystallisation 77−16616
Ni based porous metals, exam. of volume change under high pressure 78−52906
Ni based Rene 80 superalloy, initial stages of pack aluminisation 80−76188
Ni based superalloy, interaction of annealing twins in fcc metals and alloys 78−68712
Ni based superalloys 713C and Mar-M200, Si effect on oxidation, hot corrosion and mech. behaviour 78−39950
Ni dilute alloys, mechanisms of radiation induced segregation 79−77649
Ni Ga, defect struct. 78−30608
Ni steel, neutron irrad. effects on tensile props., microstructure effects 77−69005
Ni/Cr-Fe-C, Inconel, dislocation intersection and solution strengthening, effect of solute on obstacle profiles 80−7590
Ni/Ni_3Al-Ni_3Nb, directionally solidified lamellar eutectic alloy, deform. anisotropy and fracture 77−36604

nickel alloys continued
Ni/Ni_3Al-Ni_3Nb eutectic, directionally solidified, plastic deformation *(Russian)* 78−39843
Ni/Ni_3Al+Ni_3Nb, directionally solidified eutectic alloy, crack growth rate under creep fatigue conditions 79−52361
Ni-3d metal, ferromag., spin polarised tunnelling expts. 78−39372
Ni-(Co)-Cr, aluminide coating, microstruct. and chem. 80−76189
Ni-(W,Cr)C, corrosion and corrosive wear in sea water 78−92408
Ni-A-Ti (6,1 wt.%), γ' phase precip., deform. effects *(Russian)* 78−48404
Ni-Ag, corrosion in marine atm., potentiometric technique, appls. 79−24693
Ni-Ag alloy, metallographic struct. and formability *(German, English)* 80−30201
Ni-Al, (2 and 6 wt.%), oxidation, α-Al_2O_3 growth, microstruct., precip. 80−108626
Ni-Al, B2 type, vacant sites on Ni sublattice and p-d stabilization energy 79−60357
Ni-Al, band model of high temp. magnetism 78−26809
Ni-Al, band struct. and density of states, KKR method and X-ray meas. 80−10863
Ni-Al, CC Ni-Al (42 at.%), Al_2O_3 growth, morphology and spalling model 78−53030
Ni-Al, cohesive props., augmented-spherical-wave calcs. 79−94952
Ni-Al, dil., oxidation mech. at 800 to 1200°C 77−90483
β_2-Ni-Al, elastic consts., supersaturated thermal vacancy effects 80−54298
β_1-Ni-Al, elastic softening and electron diffr. anomalies prior to martensitic transform. 77−8825
Ni-Al, electronic, mag., and cohesive props. 80−44491
Ni-Al, ferromag. solid sol., electronic struct., X-ray absorpt. spectra meas. 79−69653
Ni-Al, grain boundary diffusion in migrating boundaries 79−46830
Ni-Al, intercrystalline creep rupture *(Czech)* 77−86135
Ni-Al, ion irradiated, dendritic growth of voids 77−11605
Ni-Al, liquid, diffusion coeff. differences, rotating-disc determ. 80−39330
Ni-Al, melt, short-range order and microinhomogeneity, rel. to NiAl form. 77−35466
Ni-Al, neutron irradiated, rel. between irradiation induced swelling and shear modulus 80−15157
Ni-Al, order hardening, comparison between revised theory and expt. 80−93565
β'-Ni-Al, precipitation studies 80−3067
Ni-Al, Raney nickel catalyst, surface texture studied by N_2 adsorption and ESCA *(French)* 79−69348
Ni-Al, solid soln., rheological study of crystallographic order on creep *(French)* 80−97548
Ni-Al, solid soln. and solid soln. hardened, stead state creep 78−27578
Ni-Al, spinodal decomposition, atom probe field ion microscopy study 80−3028
Ni-Al, transition metal group VIII aluminide, NMR near equiatomic composition *(Russian)* 80−20479
Ni-Al, with large volume fraction of γ', precipitation hardening 77−36524
β-Ni-Al, X-ray absorpt. spectra meas., Fermi level location 80−35005
Ni-Al (0.5 wt.%), microstruct. formation during internal oxidation, effect of additional microalloying *(Russian)* 77−80650
Ni-Al (12.8 at.%), irradiation enhanced coarsening 79−66060
Ni-Al (12.8 at.%) foil, ion irrad., surface effects on precip. morphology 80−104168
Ni-Al (12.8 wt.%), Ni^+ ion irradiation, precipitate restructuring, mechanisms and kinetics 79−77650
Ni-Al (14 at.%), two stage ageing effect on spatial distrib. of γ'-phase particles *(Russian)* 78−39805
Ni-Al (15 wt.%) single crystals, morphological changes of γ' precipitates during uniaxial stress-annealing 79−83236
Ni-Al (1.18 wt.%), substruct. hardening effect, depend. on mechanism controlling creep rate, 700°C 79−20144
Ni-Al (36 at.%) martensite, ordering obs. *(Russian)* 77−80446
β_2-Ni-Al (47.6 to 60.5 at.% Ni), elastic stiffnesses −196 to 400°C 78−27556
Ni-Al (51 to 55 at.%), vacancy defective, TEM exam. of structure 78−76677
Ni-Al (6.05 wt.%), prediction and meas. of precipitate number density 78−19756
Ni-Al (6.2 wt.%), high temp. creep *(Czech)* 77−63727
Ni-Al (6.3 at.%), influence of localised order on thermo-EMF and Hall-EMF *(Russian)* 78−6951
Ni-Al (6.35 wt.%) foil, radiation-induced precipitate redistrib. 78−30681
Ni-Al (6.35 wt.%) precipitate coarsening, redistribution and renucleation during ion irradiation 78−23709
Ni-Al (7.2 wt.%), fatigue crack propag., plastic work role 79−79070
Ni-Al alloy, solid phase reaction kinetic parameter calcs., defect formation *(Russian)* 80−54399
Ni-Al alloys, effects of electron irradiation in precipitation, nucleation and dislocation loop growth, TEM study 79−42106
γ,γ'-Ni-Al alloys, irrad. effects on precip. 77−8829
Ni-Al alloys, XPS for band struct. 79−33889
Ni-Al base ageing alloys, single cryst., deform. and hardening 78−23716
Ni-Al bronze, fracture resistance of tubes 78−19867
Ni-Al bronze, fracture toughness 77−81312
Ni-Al coating, low temp. hot corrosion, Na_2SO_4-induced, mechanism, burner rig tests 80−40610
Ni-Al film, co-evaporated, comp.-depend. struct. and morphological changes 79−87020
Ni-Al film, high-temp. condensed, electron diffr. and elec. resist. *(Russian)* 79−4485
Ni-Al films, evaporated, grain size and microstruct. 80−15423
Ni-Al solid solns., N_2^+ irrad., void ordering 78−79644
Ni-Al solid solutions, Ni-rich, phase transforms. during quenching 77−32577
Ni-Al spraying powders, alumina and aluminide formation 80−25920
Ni-Al system, calculating interdiffusion coefficient in case of cylindrical symmetry *(Russian)* 79−69297
Ni-Al system, Mossbauer spectroscopy investigation *(Russian)* 80−20523
Ni-Al system, ordering and instability of β phase near martensitic transform. *(Russian)* 80−45304
ζ Ni-Al system, solid soln., interdiffusion *(Japanese)* 80−70476

nickel alloys continued
Ni-Al thermally reactive powder, particle heating dynamics during plasma deposition 80−16179
Ni-Al_2O_3, dispersion strengthened, thick vacuum condensate, control of struct. and mech. props. 80−16324
Ni-Al_2O_3 alloy, electron beam evaporated, struct. and mech. props. 78−11114
Ni-Al-Cr, ageing kinetics and γ'-phase particles spatial distrib. under applied load *(Russian)* 77−32598
Ni-Al-Cr, IN-100, growth geometry of carbides in dendritic monocrystals, solidification effects 79−11597
Ni-Al-Cr, precipitation-strengthened, mechanical props. 78−84968
Ni-Al-Cr, strain hardening, participation of various slip systems *(Russian)* 79−24536
Ni-Al-Cr alloy Ehi 826 77−86120
Ni-Al-Cr alloy IN 100 powder, rapidly solidified, effect of high melt superheat on microstructure 79−52195
Ni-Al-Cr CO alloy, IN 100 protective Ni-Al coating, Ti content influence on oxidation behaviour *(French)* 78−3258
Ni-Al-Cr superalloy IN-100, crack retardation at elev. temp., hold time effect of single overload 79−79068
Ni-Al-Cr_3C_2, eutectic, directionally solidified, high-temp. oxidation 80−50775
Ni-Al-Cr_3C_2, eutectic, Al_2O_3 coatings for oxidation resist. 80−50776
Ni-Al-Cr_3Cr_2, eutectic alloy, directionally solidified, oxidation resistance, influence of Y 80−89409
Ni-Al-Cr-Co-Ti, Waspaloy, exam. of dislocation-precipitate interaction, cyclic stress-strain behaviour 78−84925
Ni-Al-Cr-Mo-Ti-W-(Co) alloys EhI 826 and EhI 929, reverse elastic after effect under loading 78−39829
Ni-Al-Cr-Ti-W-Mo, US vibration applied during solidification, improved strength, corrosion resistance *(Russian)* 78−15382
β'-Ni-Al-Fe, mag. impurity states, resist. meas. 77−55519
Ni-Al-Fe system, order-disorder phase transform., Gorskii-Bragg-Williams approx. *(Russian)* 79−29048
Ni-Al-Fe(Co), electrical and mag. anomalies due to substitutional atoms 77−15839
Ni-Al-Mn alloy system, oxidation resist. 79−24661
Ni-Al-Mo, eutectic form., struct. and mech. props. *(Russian)* 77−21129
Ni-Al-Mo (12.7, 21.6 wt.%), directionally solidified eutectic composite, precipitation 80−108454
γ-αNi-Al-Mo eutectic, γ' precipitation 77−12629
γ/γ-Ni-Al-Nb, aligned eutectic alloy, H_2 embrittlement 77−8951
Ni-Al-Nb, eutectic form., struct. and mech. props *(Russian)* 77−21129
Ni-Al-Nb ternary system, electron microprobe analysis of nickel-rich region at 1473K 80−71631
Ni-Al-Si, β-phase stability *(Russian)* 78−39738
Ni-Al-Ta, solvus surface determ. using precipitation method 79−15674
Ni-Al-Ta (7.5, 2.0 wt.%), dendritic monocrystal, microsegregation and nonhomogenisation 79−37940
Ni-Al-Ta dendritic monocrysts., directionally solidified, coarsening kinetics 80−108425
Ni-Al-Ti, ageing kinetics and γ'-phase particles spatial distrib. under applied load *(Russian)* 77−32598
Ni-Al-Ti, eutectic alloy charact. by melting temp., composition and oxidation resistance 78−52771
Ni-Al-Ti, soln. temp. of hardening intermetallic phase in heat resistant alloys 78−52865
Ni-Al-Ti cast superalloy, eutectic transform. on ageing *(Chinese)* 79−100110
Ni-Al-Ti ferromagnetic non-homogeneous alloy, composition determination by Curie temp. meas. 80−11196
Ni-Al-Ti protective coating, on Ni-Al alloy IN 100, Ti content influence, oxidation behaviour *(French)* 78−3258
Ni-Al-Ti-Cr superalloys, estimation of conjugate γ and γ' compositions 79−8282
Ni-Al-Ti-(W) (Cr) (Co) (Mo) (Ta) (Nb), heat resist., solidification range 80−35177
Ni-Al-Ti(Nb), heat-resisting dispersion-hardening alloys, props. and struct., γ'-phase comp. influence *(Russian)* 80−20943
Ni-Al(-Si), diffusion, lattice parameter, microhardness, and constitution, effect of Si additions *(Russian)* 80−84316
Ni-Al(Cr)(Ti), ion irradiation induced void swelling and defect microstructs., TEM obs. 79−51164
Ni-Al(Pd)(Cu) itinerant electron ferromagnet, magnetovolume effects 80−60397
Ni-Al(Ti)(Mo)(Si), effect of solute misfit and temp. on irradiation induced segregation 78−72779
Ni-As, dil., temp. depend. of hyperfine field, TDPAD meas. 78−43700
Ni-Au, amorphous film, ferromagnetic, anomalous Hall resist. 77−15832
Ni-Au, dil., orientation depend. of surface segregation, AES and SEM obs. 78−71908
Ni-Au, electronegativity and core electron binding energy shifts of Au 77−15346
Ni-Au, local environment effects, magnetisation decrease 79−65664
Ni-Au, oxidation in air, 50-150°C, film growth obs. using AES and contact resist. 80−3242
Ni-Au alloys, surface segreg., surface energy and solute strain energy effects 77−72760
Ni-Au film, amorphous, magnetoresist., in fields up to 80 kG 77−39823
Ni-Au-Fe, liq., activity of iron at 1573K 77−70328
Ni-B, amorphous alloys, phase diagram 79−96002
Ni-B, film crystallisation on C fibres and sapphire crystals *(Russian)* 80−75455
Ni-B, grain boundary internal friction, B solid solubility as function of grain size 80−60903
Ni-B, hydrogen embrittlement, effect of B additions *(Japanese)* 78−84973
Ni-b, hyperfine interactions from 6 to 730K, ^{12}B NMR 80−29372
Ni-B (3 at.%), columnar alloys, metallographic obs. of eutectic struct. *(Russian)* 78−27469
Ni-B alloy film, magnetisation-temp. charact., order-disorder transform. *(Japanese)* 78−76279
Ni-B amorphous alloy film, atomic and electronic transport *(French)* 78−84325
Ni-B amorphous films, electronic transport and crystn. activation energies *(French)* 80−6807
Ni-B electroless-plated amorphous films, anomalous mag. temp. charact. 80−96757
Ni-B glass, X-ray obs. of struct. 79−1399
Ni-B thin film glasses, mag. props. and corrosion resist. 80−80576

nickel alloys continued
Ni-B-Cr, composite, wear resistant coating on steel 45 78−11420
Ni-base alloy, screening studies for evaluation for nucl. process heat system 78−13236
Ni-base cost multicomponent alloy, γ', carbide, boride phases, quantities, composition *(Russian)* 78−75627
Ni-base superalloy, effects of grain boundary carbides on creep and back stress 80−3130
Ni-base superalloys, emission spectral anal. with fixed time integration technique *(Japanese)* 80−71974
Ni-base superalloys, technique for replication of γ' 80−79648
Ni-base wear resistant dispersion hardened electrolytic coating, annealed and sintered 78−35593
Ni-based alloys, binary, ternary, complex, TiC additions, effects 78−92305
Ni-based heat resisting alloys, strain resistance under complex loading program conditions 79−57073
Ni-based TaC eutectic, directionally solidified, elastic moduli 80−84984
Ni-based-Ta(Cn,N) hard metals, isostatic hot pressing influence on mechanical properties 78−92219
Ni-Be, annealed under load, spatial distrib. of precips. *(Russian)* 77−59790
Ni-Be (2 wt.%), high-temp. radiation embrittlement, mechanical tests and TEM *(Russian)* 77−44331
Ni-Be alloy, precip. sequence 78−80549
Ni-Be alloys, struct. and phase stability in neutron bombardment field *(Russian)* 77−76467
Ni-Be bronze, Fe and Si alloying addition effect on phase composition *(Russian)* 78−15360
Ni-Be system, radiation induced solute segregation and precipitation study by means of Johnson-Lam kinetic model 79−43252
Ni-C, coupled phase diagrams and thermochemical data 79−66036
Ni-C, dil., ferromag., electronic struct. of interstitials 77−62867
Ni-C, ferromag. prep. by splat-quenching, obs. of electronic struct. of interstitial C 77−62868
Ni-C, graphite nucleation on surface *(Russian)* 80−40360
Ni-C, magnetic aftereffects of H isotopes, book contrib. 79−82835
Ni-C, supersat. solid soln., decomposition and graphite surface energy determ. *(Russian)* 77−15677
Ni-C (1.8 at.%), precipitation of graphite and NiC TEM obs. 77−52334
Ni-C interstitial alloys, electronic struct. 77−35886
Ni-C interstitial alloys, electronic struct. and ordering of sp defects 78−91639
Ni-C solid solns., surface graphite layer form., high-temp. metallography investig. 79−29306
Ni-C-Ce, overmodification *(Russian)* 80−40432
Ni-C-W-Cr(-Mo), Vickers hardness and crystallisation temp. 80−16361
Ni-C. exam. of metastable phase diagrams, at high temp. and pressure *(Russian)* 79−56955
Ni-Cd, dil., ferromagnetic dynamic crit. exponent, hyperfine interaction vs. neutron scatt. expts. 78−84437
Ni-Ce-Fe-Ti (77, 20, 4, 2.5 wt.%), long-term strength in H at high pressure 80−55485
Ni-Co, cryst. growth from melt, distrib. of growth directions 79−33924
Ni-Co, dil., optical absorpt., electronic struct. 80−108227
Ni-Co, dislocation intersection and solution strengthening, effect of solute on obstacle profiles 80−7590
Ni-Co, electrical resistance and H solubility at high press. *(Russian)* 79−91018
Ni-Co, elementary excitations, exchange stiffness const., inelastic neutron scatt. study 79−47294
Ni-Co, FCC, spin wave stiffness, inelastic neutron scatt. 77−63156
Ni-Co, FCC, spin wave stiffness const., neutron scatt. study 79−51769
Ni-Co, fatigued, struct. and cyclic stress strain, influence of stacking fault energy and atomic size-module-interactions *(German)* 79−42082
Ni-Co, ferromag. films, magnetoresistance effect, crystal struct. 78−68017
Ni-Co, ferromagnetic resonance, surface anisotropy 78−95526
Ni-Co, high-field susceptibility, spin-wave spectrum, CPA calc. 80−65818
Ni-Co, liquid, activity meas. by transportation method *(Japanese)* 79−4949
Ni-Co, local mag. field on μ^+ 79−56665
Ni-Co, low temperature lattice parameter, Gruneisen parameter 77−76357
Ni-Co, mag. props. of single-domain powders after plastic deform. *(Russian)* 78−6554
Ni-Co, oxide scales, cation distrib. calc. by approx. analytical method 77−48594
Ni-Co, plasticity, athermal and thermal *(Russian)* 79−11685
Ni-Co, platelets, FMR field and linewidth, room temp. 77−4563
Ni-Co, recovery of single crystal after varying amounts of cold work 79−100162
Ni-Co, rolling texture development, dependent on relative stacking fault energy 79−52237
Ni-Co, solid and liq., paramag. susceptibility and electron struct., 800-1800°C *(Russian)* 80−25081
Ni-Co (10 wt.%), cast single phase, solidified from undercooled melt, mech. props. 77−48540
Ni-Co (25 at.%), polycrystalline, mech. damping 77−28850
Ni-Co (25 wt.%), short range order parameters from Mossbauer data 79−56645
Ni-Co (25 wt.%), single crysts., mag. annealing effect on magnetostriction and magnetisation *(Japanese)* 80−34744
Ni-Co (25 wt.%), single crysts., mag. annealing effect on magnetostriction and magnetisation at high temps. 80−108047
Ni-Co (5(66) wt.%), internal stresses during creep 80−3142
Ni-Co alloy, stiffness const., interpretation within band model 79−42748
Ni-Co amorphous alloys, magnetostriction 80−34738
Ni-Co electrodeposit, strength, heat treatment and comp. var. effects 77−32660
Ni-Co film, magnetisation induced uniaxial anisotropy 77−48016
Ni-Co film, spin wave resonance 79−33542
Ni-Co film, spin-wave reson. exam. 78−2746
Ni-Co films, electron-beam evaporated, magnetoresist. anisotropy, deposition temp. effect 80−34528
Ni-Co plate, surface anisotropy from ferromagnetic reson. 78−48049
Ni-Co thin films, spin-wave reson. obs., exchange stiffness const. 80−44924
β-Ni-Co-Al, martensitic transform., metallographic, X-ray diffr., and elec. resist. obs. *(Russian)* 78−19748

nickel alloys continued
Ni-Co-Al (1, 35.2 at.%), tempered martensite, new ordered phase 79−11560
Ni-Co-Al alloys, continuous precip., SEM, TEM, X-ray diffr. study 80−89220
Ni-Co-C solid solution, C precipitation, Ni_3Co ordering, Ni-Co lattice parameter meas. *(Czech)* 80−60867
Ni-Co-Cd alloys, electrodeposition from acetate bath 78−68637
Ni-Co-Cr, type E1929VD, effect of stress conc. on fatigue strength at elevated temps. 79−57115
Ni-Co-Cr alloys IN 738, Pt plated, aluminization 78−31583
Ni-Co-Cr superalloy, powder produced, necklace struct. development 80−40395
Ni-Co-Cr system, heats of formation and of transformation 80−50599
Ni-Co-Cr TEM foils, white band contrast 80−75134
Ni-Co-Cr/Al_2O_3 catalyst, IR spectra of adsorption and interaction with pyridine 80−71946
Ni-Co-Cr-Al-Ti-Mo superalloy IN738, casking porosity removal using hydrostatic press. sintering 80−55322
Ni-Co-Cr-Al-Y, plasma-arc-sprayed, metallurgical characts. and oxidation behaviour 80−40618
Ni-Co-Cr-Al-Y coating, electron beam evap., low press. gas scatt. 77−40474
Ni-Co-Cr-Al-Y coating, electron beam deposited, for Ni-base superalloy, fatigue crack initiation and propag. 78−11438
Ni-Co-Cr-Al-Y protective coating for combustion turbines, hot corrosion evaluation 80−40608
Ni-Co-Cr-Mb-W-Ta, Cr, Mb, W, Ta effects on σ phase occurrence 77−36507
Ni-Co-Cr-Mo-Al, Astroloy, extruded powder metallurgy superalloy, recrystallisation study 79−4976
Ni-Co-Cr-Mo-Al-Ti (17.5, 15.1, 4.9, 4.15, 3.25 wt.%), creep and stress rupture behaviour in air and vacuum 80−60918
Ni-Co-Cr-Mo-Ti-Al Nimonic 105, loading frequency and environmental effects on high temp. fatigue crack growth 78−64675
Ni-Co-Cr-Ta-Al-W-Mo-Ti, cast, phase volume fraction determ. using manual point count practice 78−53052
Ni-Co-H, solid soln., Curie points and spontaneous magnetisation behaviour 80−50093
Ni-Co-H system, phase transform. under high H_2 press., Co additive effects *(Russian)* 78−60645
Ni-Co-Mn, dil. alloys, NMR freq. temp. depend., spin echo meas. 78−64296
Ni-Co-Mn, dil. ferromag. alloy, mag. moment, saturation magnetisation meas. 78−64195
Ni-Co-Mo, phase relations in system at 1100°C 80−108392
Ni-Co-Mo alloys, electrodeposition, struct. 79−28970
Ni-Co-Mo-Al-Cr, melt, effect of Al, Cr on O_2 activity, electrochemical determ. 79−11556
Ni-Co-Mo-Ti, maraging, electron diffr. obs. of second phase *(Chinese)* 80−11655
Ni-Co-P, amorphous alloy, electrical and mag. props. 78−95281
Ni-Co-P, amorphous electrodeposited films, domain wall motion, Kerr effect 78−60322
Ni-Co-P, ferromag. film, amorphous to cryst. transition, diffr. and resistivity meas. 78−60587
Ni-Co-W, electrodeposition, surface morphology and cryst. struct. 80−71602
Ni-Co(Fe) film, anal. of main component by atomic absorpt. spectrophotometry 77−70381
Ni-containing alloys, hot workability after reheating using S-containing fuel 80−108483
Ni-Cr, (30 wt.%), collective dislocation movements, in situ study 80−100243
Ni-Cr, alloy, composition determination using secondary ion emission *(French)* 77−86409
Ni-Cr, anodic dissoln. in NaCl solns. at high current densities *(Russian)* 80−76396
Ni-Cr, austenitic alloy, oxidation mechanism, adhesion of Cr_2O_3 scale *(Polish)* 79−79143
Ni-Cr, corrosion resistance of dental casting alloys 78−31561
Ni-Cr, creep-fatigue failures, damage concept appl. 80−40535
Ni-Cr, deformed, struct. form. during annealing, Ni_3Al type ordered phase precipitation *(Russian)* 80−45325
Ni-Cr, degradation after exposure to 1% H_2S/H_2 gas mixture at 1000°C 80−89408
Ni-Cr, dil. alloy paramag., μ^- relax. 77−24776
Ni-Cr, dispersion strengthening, prep. from powder, mech. props. 79−91658
Ni-Cr, ERNiCr-3 weld metal, strain-rate effects on high temp. behaviour 79−93726
Ni-Cr, elementary excitations, exchange stiffness const., inelastic neutron scatt. study 79−47294
Ni-Cr, film, quantitative anal. by DC arc optical emission spectroscopy 78−68940
Ni-Cr, heat resistant cast and wrought for petrochemical industry, creep rupture *(German)* 77−36618
Ni-Cr, heat resisting, dispersion hardened, electrical resistance meas. *(Russian)* 77−66708
Ni-Cr, heat-resist., high-temp. ductility and embrittlement 80−76314
Ni-Cr, heavy ion irrad., defect cluster obs. 80−107341
Ni-Cr, high temp. thermomech. treatment effect on tensile diagrams of KhN77TYuR *(Russian)* 80−60884
Ni-Cr, high temp. wire resistance strain gauges 77−53896
Ni-Cr, interband absorpt. and refractive index, photoconductivity dispersion function 77−36263
Ni-Cr, low short-term creep resist. at 700°C 80−76313
Ni-Cr, low temp. sp. ht. near ferro-paramag. transition 77−63218
Ni-Cr, mag. moment distrib. 77−32178
Ni-Cr, microstruct. effects in low-cycle fatigue tests 77−56108
Ni-Cr, Ni rich, discontinuous precipitation *(German)* 79−91653
Ni-Cr, O transport, during fatigue crack growth, exam. 78−52981
Ni-Cr, ordering by nucleation and growth and by spinodal decomposition *(French)* 78−27471
Ni-Cr, ordering in the vicinity of Ni_2Cr 79−38819
Ni-Cr, partial dislocation, stacking fault TEM study *(Chinese)* 80−84174
Ni-Cr, phosphidation in P vapour, 700°C, phosphide layer struct. and kinetics 80−25906
Ni-Cr, residual resist., CPA calc. to muffin tin pot. 77−62892
Ni-Cr, self-weldability in high temp Na *(Japanese)* 80−89392

nickel alloys continued
Ni-Cr, solid soln., exam. of back stress role in creep behaviour of particle strengthened alloys 78−52889
Ni-Cr, solid soln., lattice parameter meas. rel. to conc. and temp. depend. *(Czech)* 80−28949
Ni-Cr, solubility limit determ., X-ray method 79−43199
Ni-Cr, solubility of H_2, 500 to 1000°C *(Japanese)* 78−38845
Ni-Cr, surface oxide characterisation by Raman spectroscopy 80−50308
Ni-Cr, variation in absolute thermoelec. power under heat/treatment *(Ukrainian)* 79−38051
Ni-Cr, wrought, fatigue at high temp., microstruct. assessment 79−29208
Ni-Cr (Mo), solid soln., US deform., electron microscope exam. *(Russian)* 78−35447
Ni-Cr (Mo)(W) melts, N_2 diffusion *(Russian)* 78−18812
Ni-Cr (0-35 at.%), neutron irrad. at 25K, damage, elec. resist. obs. *(French)* 80−54286
Ni-Cr (2 wt.%), role of hydrostatic pressure on sintering of creep cavities 79−28980
Ni-Cr (20 wt.%), Al and Ti containing, oxidation, effect of dispersal oxides 77−44404
Ni-Cr (20 wt.%), CC W fibre reinforced, alloy by effect on struct. stability, mech. props., metallographic exam. 78−56600
Ni-Cr (20 wt.%), high temp. frictional characts. 80−21118
Ni-Cr (20 wt.%), Norton-Bailey parameters, from creep rupture data 80−30098
Ni-Cr (20 wt.%), oxidation, 800 to 1300°C, effect of volume and intergranular diffusion *(French)* 77−86228
Ni-Cr (20 wt.%), oxidation, O_2 press. effects *(Japanese)* 78−15578
Ni-Cr (20 wt.%), oxidation in humid air, 800 to 1250°C *(French)* 79−79165
Ni-Cr (20 wt.%), plasma-sprayed coating, on steel 79−96222
Ni-Cr (20 wt.%), reinforced by coated Mo filaments, effect of coating on composite strength 78−56710
Ni-Cr (20 wt.%), surface oxide layers, compar. study of comp. and struct. by secondary ion emission and electron microprobe *(French)* 77−56286
Ni-Cr (20 wt.%), volume and grain boundary diffusion of Ni and Cr, C effect *(French)* 79−95203
Ni-Cr (20 wt.%) alloy LNKh, room-temp. friction characts. 80−25874
Ni-Cr (20 wt.%) based composite, use of SiC fibres with protective Al_2O_3 coating, IR investigation 78−60623
Ni-Cr (20wt.%), powder, nonspherical, mean pore size of sheet material 77−28757
Ni-Cr (23 and 33 wt.%), kinetic and morphological study of sulphidation in S_2, H_2S and H_2S/H_2 79−52424
Ni-Cr (25 to 40 wt.%), transport numbers of alloy components determ. 77−62667
Ni-Cr (27.4 and 40.2 wt.%), compositional changes, in underlying alloy produced by oxidation 79−8395
Ni-Cr (33 at.%), plastic deformation, HVEM study *(French)* 80−66605
Ni-Cr (33 at.%), US deform. effect on short range order form. *(Russian)* 78−39839
Ni-Cr (33.3 at.%) alloy, ordering after US deform., microhardness and elec. resist. meas. *(Russian)* 79−20113
Ni-Cr (44 to 50 wt.%), oxidation 79−43483
Ni-Cr (70 wt.%), oxidation behaviour, 1073-1473K 80−89416
Ni-Cr alloy, cast, etching methods for determ. of primary struct. 78−23888
Ni-Cr alloy, dispersion-hardened, prod. by mech. alloying 78−15345
Ni-Cr alloy, EI 437B, vibrocreep at normal and high temps. 77−4824
Ni-Cr alloy, KhN70VMTYu, gas turbine blades, thermocyclic strength characts., exam. 78−60743
Ni-Cr alloy, Kh20N80, inclusions and plasticity, crystn. conditions influence *(Russian)* 80−20923
Ni-Cr alloy, structural changes, during thermal stress cracking, X-ray and microhardness meas. *(Russian)* 78−35496
Ni-Cr alloy EhI617, thermocyclic treatment effect on struct. and thermal fatigue resistance 78−7045
Ni-Cr alloy Ehi 617, equation of condition for creep, expt. checking 77−86120
Ni-Cr alloy KhN70MVYu wire, recrystn., optimum heat treatment 80−76278
Ni-Cr alloy KhN70VMTYu, heat resistant, explosive loading effect on struct. and mech. props. *(Russian)* 78−39787
Ni-Cr alloy submerged arc weld surfacing using metal powder filler additions 79−57157
Ni-Cr alloys, creep crack growth, environmental sensitivity 80−85030
Ni-Cr alloys, crystallisation anomalies *(Russian)* 78−19719
Ni-Cr alloys, low temp. transform. mechanism, electrophys. props. obs. *(Russian)* 77−59777
Ni-Cr alloys, method of etching in Br-methanol reagent 77−90516
Ni-Cr alloys EHI437B and VZh98, tension tests in high speed gaseous streams 77−63761
Ni-Cr austenitic alloy, oxidation mechanism, intergranular diffusion effect *(French)* 80−81229
Ni-Cr base alloy, strain relaxation, effect of grain size, particle size, γ' vol. fraction 79−47741
Ni-Cr based coatings, hot corrosion resist. 79−24674
Ni-Cr coatings on steel, standardisation 79−57139
Ni-Cr complex alloy with good creep resistance, friction stress/flow stress relation 79−8337
Ni-Cr electrochem shaping in nitrate and chlorate, hardening γ'-phase concentration influence *(Russian)* 77−8979
Ni-Cr film, electrical props. rel. to AES conc. depth profile 77−32092
Ni-Cr film, electron spin polarisation, meas. using supercond. tunnel junction 77−69637
Ni-Cr film, long range order 79−60657
Ni-Cr film, RF sputtered, Seebeck coeff. 77−63004
Ni-Cr film, resistance stabilisation by surface oxide formation 79−78214
Ni-Cr film, struct. transforms. induced during annealing, resist. obs. 79−77965
Ni-Cr film, vac. deposition, elec. props. and comp. struct. 79−77966
Ni-Cr films, vac. deposited, comp. and temp. coeff. of resist., AES obs. 79−91161
Ni-Cr films implanted with N ions, electric properties *(Russian)* 80−107927
Ni-Cr foldfoil strain gauge, for cryogenic anal. of supercond. structs. in high mag. fields, fusion reactors 78−54947
Ni-Cr Nimonic alloys, mech. props., high-temp. irrad. effects 80−100885

nickel alloys continued
Ni-Cr plasma spray coated Ti substrate, interface interaction 77−21323
Ni-Cr powder mixture, dispersion hardened, homogenisation 77−12638
Ni-Cr resistor layers, ESCA meas., expt. *(Hungarian)* 77−4951
Ni-Cr solid soln., Ni rich, thermodynamic activity of components 79−70043
Ni-Cr superalloy, interactions between creep and low cycle fatigue *(Chinese)* 80−66572
Ni-Cr surface, chemisorption, appl. of vac. UV photoelectron spectrometer *(Japanese)* 78−62264
Ni-Cr thin film production by HF cathode sputtering *(Bulgarian)* 79−19992
Ni-Cr thin film resistors, α-particle elastic scatt., and PIXE anal. 79−48022
Ni-Cr thin film resistors using jumping electron beam, expt. *(Hungarian)* 77−4738
Ni-Cr thin films, resistor appls., props. and prep. *(Hungarian)* 77−4737
Ni-Cr type alloys, Co surface pretreatment to attain pore-free aluminised coatings 80−40612
Ni-Cr wires, added metals effect on sublimation behaviour in vac. *(German)* 79−90775
Ni-Cr/Au films, interdiffusion processes and oxidation phenomena 80−59735
Ni-Cr/$MgSiO_3$, methanation catalysts, S resistant, XPS characterization 79−83506
Ni-Cr/ThO_2, adhesive energy, meas. techniques 80−50803
Ni-Cr/ZrO_2-Y_2O_3 sputtered multilayered ceramic/metal coatings, props. 80−40620
Ni-Cr-Al, comparison of cyclic oxid. resist. with Co-Cr-Al 78−88572
Ni-Cr-Al, hot corrosion resist. of Na_2SO_4 cooled specimens 78−44264
Ni-Cr-Al, oxidation, NaCl vapour effects on microstruct. 78−44274
Ni-Cr-Al, oxidation at 850°C in air containing HCl gas 79−8396
Ni-Cr-Al, protective coating, exam. of interdiffusion kinetics, development of analysing procedure 79−5085
Ni-Cr-Al, resist. to cyclic oxidation at 1100 and 1200°C 77−77641
Ni-Cr-Al, shape of γ'-precipitates on surface after sublimation *(German)* 77−81266
Ni-Cr-Al (15, 5 wt.%), oxide dispersion strengthened, effect of dispersoids on oxidation 78−80679
Ni-Cr-Al (17.83, 2.85 wt.%), under ion irradiated, modification of precipitate interface and effect of precipitates stability 79−77651
Ni-Cr-Al (20, 4 wt.%), tensile stress effect on high temp. oxidation *(Japanese)* 80−89393
Ni-Cr-Al (40, 4 wt.%), γ' and α-Cr duplex precipitation, TEM *(Japanese)* 77−25061
Ni-Cr-Al alloy, Al_2O_3 adherence, improvement by addition of Pt and Rh 77−8995
Ni-Cr-Al alloy, scale behaviour in carbonaceous gas atmos. 77−36693
Ni-Cr-Al aluminised coating, diffusion paths for formation and degradation of oxidation resistant coatings 78−11431
Ni-Cr-Al coatings, corrosion and thermal shock resist. in diesel engines 79−24675
Ni-Cr-Al coatings Ni eutectic alloys in gas turbines, use of diffusion barrier 79−24673
Ni-Cr-Al sintered alloy, hot vac. pressure, fracture and mech. characts. 80−66667
Ni-Cr-Al_2O_3 powder targets for plasma-ion spray deposition of resistance films 80−84897
Ni-Cr-Al-Cr-Hf-Zr-C, directionally solidified eutectic with (Hf,Zr)C reinforcement, precipitation, and thermal cycling 78−44057
Ni-Cr-Al-Cu, Evanohm, Kapitza conductance meas. using superconducting current comparator 77−41645
Ni-Cr-Al-TaC, eutectic composite, microstructure, fatigue props. 80−85038
Ni-Cr-Al-ThO_2, hot corrosion, cyclic oxidation depth of attack determinations 80−11837
Ni-Cr-Al-Ti, KhN78TYu, heavily deformed, subgrain struct. due to discontinuous precipitation of γ' phase *(Russian)* 79−52218
Ni-Cr-Al-Ti, stress corrosion cracking, factors influencing susceptibility 80−97617
Ni-Cr-Al-Ti (Ti-Co), exam. of back stress role in creep behaviour of particle strengthened alloys 78−52889
Ni-Cr-Al-Ti alloy type ZhS6U, effects of heat treatment in high vel. gas streams on props. 79−57025
Ni-Cr-Al-Ti-Mo, low temp. mech. behaviour, precipitation 78−39860
Ni-Cr-Al-W-Ti alloy MA 6000E, mechanical alloying for high temp. appl. 78−44046
Ni-Cr-Al-Y coating for oxidation protection of Ni base TaC eutectics 77−40475
Ni-Cr-Al-Y/ZrO_2-Y_2O_3, NASA two-layer thermal barrier coating, for gas turbine engines, test results 80−40617
Ni-Cr-Al-Y_2O_3 superalloy, recrystn. and texture development 80−16328
Ni-Cr-AlPt, exam. of phase diagram 79−8276
Ni-Cr-B-Si, hard faced with WC, exam. of abrasion and wear props. 79−34202
Ni-Cr-B-Si-Fe alloy, Cr content by X-ray fluoresc. 79−43654
Ni-Cr-Ce, Ce effect on oxidation 79−43484
Ni-Cr-Co, Mo, Ti, Y and R alloying additions influence on oxidation *(Russian)* 80−40587
Ni-Cr-Co, Nimocast alloy 738, γ'' precipitate morphology and creep rupture, thermal stress crack effect 78−11318
Ni-Cr-Co alloy IN738, electrochemical corrosion meas. in molten sulphate 79−96178
Ni-Cr-Co alloys, relax. resist. exam. by bending and tension 79−24564
Ni-Cr-Co base superalloy APK1, hot isostatically pressed, heat treatment, fracture props. 77−73251
Ni-Cr-Co based alloy, IN-738 turbine blades, hot isostatically pressed investment castings, effect of heat treatment on grain boundary struct. 80−89270
Ni-Cr-Co superalloy, combined TEM, FIM, atom probe microanalysis of precipitates and carbide phase comp. 80−100844
Ni-Cr-Co superalloy, σ-phase effect on mech. props. *(Chinese)* 79−74229
Ni-Cr-Co superalloy IN-792, crack growth resistance, metallurgical effects 77−36655
Ni-Cr-Co-Al alloy IN-738, uniaxial damage accumulation law for time depend. loading with creep-fatigue interaction 79−83324
Ni-Cr-Co-Al super alloy, IN-738, creep failure criteria 80−65150
Ni-Cr-Co-Al-Ti-W-Ta-Mo, IN 738 LC, loading frequency and environmental effects on high temp. fatigue crack growth 78−64675
Ni-Cr-Co-Al-W-Mo-Ti-Ta, heat resist. and struct., Ta effect 80−76312

nickel alloys continued
Ni-Cr-Co-Mo, long-term corrosion stability rel. to use in joint endoprostheses 78−36059
Ni-Cr-Co-Mo alloy MP35N alloys, cold worked, factors affecting embrittlement in H_2S environments 78−31502
Ni-Cr-Co-Mo alloy MP35N, accelerated H_2 charging in aq. H_2SO_4 at 0.2% yield stress 80−30144
Ni-Cr-Co-Mo-Al, IN-67 alloy, hot corrosion, cyclic oxidation, depth of attack determinations 80−11837
Ni-Cr-Co-Mo-Al-Ti (10, 15, 3, 5.5, 4.5 wt.%), superalloy, exam. of creep and fracture behaviour 78−48464
Ni-Cr-Co-Mo-Al-Ti alloys, Waspaloy, Astroloy, exam. of microstruct. effect on crack growth 78−52977
Ni-Cr-Co-Mo-Ti-Al, powders, HCl surface treatment to prevent TiC precipitation, fracture props. 79−8397
Ni-Cr-Co-Ti, superalloy sintering thermochemical surface treatment 80−25617
Ni-Cr-Co-Ti-Mo-W-Al (14, 9.8, 5, 4, 3.9, 3 wt.%), low cycle fatigue, prior heat treatment effect 80−60962
Ni-Cr-Co-W (47.5, 25, 12, 8.75 wt.%), vaporization of IN-643, high-temp. mass spectrometry 79−7685
Ni-Cr-Co-(Se), oxidation resistance 77−21320
Ni-Cr-Fe, high temp. corrosion and creep in carburizing and oxidising atmos. 79−11727
Ni-Cr-Fe, Inconel, effects of heat treatment on surface segregation, Auger spectroscopic exam. 80−7602
Ni-Cr-Fe, Nimonic-75, electroless siliconization 78−27679
Ni-Cr-Fe, radiation enhanced precip. and dissolution of precipitates, point defect kinetics and dislocation obs. 80−108467
Ni-Cr-Fe, stress corrosion cracking, factors influencing susceptibility 80−97617
Ni-Cr-Fe (15.7, 7.63 wt.%), Inconel 600, anal. of pit generation by 3.5% NaCl, by stochastic theory *(Japanese)* 78−85038
Ni-Cr-Fe (75, 35, 12 wt.%), electron and α-particle irrad., positron annihilation and elec. resist. meas. 79−83054
Ni-Cr-Fe Alloy 600, acid intergranular corrosion rel. to caustic stress corrosion cracking stress relieving effect 77−66712
Ni-Cr-Fe Alloy 600, stress corrosion cracking in high purity water, effect of microstruct. 77−66713
Ni-Cr-Fe steam generator tubes, stress corrosion susceptibility, heat treatment effect 79−20258
Ni-Cr-Fe-Mo-Co (21.41, 19.28, 8.64, 2.16 wt.%), Hastelloy alloy X, exam. of thermal stability 78−84865
Ni-Cr-Fe-Si-B wear-resist. and corrosion-resist. coatings by furnace melting 80−35428
Ni-Cr-Fe-Ti alloy KhN77TYuR, long-term strength under in-pile irrad. conditions 78−6940
Ni-Cr-Fe-W, type EHI868, loading history effect on resist. to cyclic elastoplastic strain 80−16398
Ni-Cr-HfO_2, dispersion-strengthened, hot rolling effects on props. *(Russian)* 77−59797
Ni-Cr-M alloys, M=minor alloying addition Y, La, Ce, Sm, Th, U, Zr, V, corrosion rates 77−16750
Ni-Cr-Mg alloy, KhN70VMTYu, Mg effect on grain boundary struct., props. 79−19261
Ni-Cr-MgO system, elec. resist. variation with comp. and prep. method 78−60637
Ni-Cr-Mn alloy solidification, effects of Si, Mo and Co alloying 79−83193
Ni-Cr-Mn-Fe-Nb (20,3,3,2.5 wt.%), short-range order effects on tensile behaviour 80−25793
Ni-Cr-Mo (74, 20, 4 wt.%), long-term strength in H at high pressure 80−55485
Ni-Cr-Mo steel, corrosion and cavitation-erosion resist. *(Russian)* 78−11395
Ni-Cr-Mo-C hardfacing alloy, hardness and abrasive wear resistance 79−79117
Ni-Cr-Mo-Fe-Mn, Kh12M23, intermetallic phases exam. *(Russian)* 78−39740
Ni-Cr-Mo-Mn alloy 02KhN40MB, corrosion-resist, heat-resist., phys. and mech. props. 80−35411
Ni-Cr-Mo-Ti (19,11,3 wt.%) for TiC reactively sputtered coatings, adherence, XPES and wear study 80−25565
Ni-Cr-Mo-V steel disc, rolling contact fatigue and residual stress on contact surface 77−32671
Ni-Cr-Mo-W-Al-Ti, heat-resist., phase comp. 80−76250
Ni-Cr-Nb-Al eutectic alloys, sulphidation/oxidation at high temps., corrosion mechanism 78−72934
Ni-Cr-NbC eutectic composite, unidirectional solidification, thermal cycling, temp. range effect on microstructural degradation 80−89272
Ni-Cr-P, amorphous, corrosion behaviour, immersion tests and electrochem. meas. *(Japanese)* 80−85085
Ni-Cr-P thin films deposited by electroless plating, resist. characts. 79−4607
Ni-Cr-Si, corrosion and failure mechanisms of coatings for gas turbine applications 79−29284
Ni-Cr-Si (10, 1.8 wt.%), Zr, Hf, La or Sm alloying additions effect on oxidation resist. 77−63831
Ni-Cr-Si alloy system, oxidation resist. 79−24661
Ni-Cr-Si thermocouple alloy, props. and thermoelec. reference data 79−26057
Ni-Cr-Ta alloy, precipitation hardening, 650 to 800°C 77−59798
Ni-Cr-Ta system, phase equilib. of Ni rich region at 1523 and 1273K 80−93541
Ni-Cr-Ta-Ti-Si, EP557 precipitation hardening alloy, mech. props., heat treatment effect 80−60877
Ni-Cr-TaC directional eutectic, high-strength, interphase boundaries *(Russian)* 79−38812
Ni-Cr-TaC eutectic-like composite, obs. of interfacial diffusion by high resolution TEM 79−4432
Ni-Cr-ThO_2 (20, 2 wt.%), dispersion hardened, model for high temp. deform. based on struct. obs. 78−19809
Ni-Cr-ThO_2(20, 2 wt.%), dislocation struct. after high temp. deform. 77−52393
Ni-Cr-Ti, type EHI698, loading history effect on resist. to cyclic elastoplastic strain 80−16398
Ni-Cr-Ti (19.51, 4.2 wt.%), quench-ageing and fracture *(German)* 77−70088
Ni-Cr-Ti rapidly solidified superalloys, surface segregation 80−76263
Ni-Cr-Ti-Al, precipitation of γ' phase during single and combined ageing treatment *(Russian)* 77−52328

nickel alloys continued
Ni-Cr-Ti-Al (20, 2.4, 1.4 wt.%), under ion irradiated, modification of precipitate interface and effect of precipitates stability 79−77651
Ni-Cr-Ti-Al/Au-Ni brazed joint, high temp., AE under elev. temp. and loading *(German)* 78−31597
Ni-Cr-Ti-Al-Fe-Co (19.65, 2.40, 1.37, 0.78, 0.52 wt.%), strength of γ' hardened alloy, ageing exam. 78−88501
Ni-Cr-Ti-Al-Mo-Nb-Fe (13-16, 2.35-2.75, 1.3-1.7, 2.8-3.2, 1.8-2.2, 2.0 wt%), heat resistant props, mech props. struct., stepwise ageing effects *(Russian)* 78−76666
Ni-Cr-Ti-Co-W-Al-Mo alloys AF-115 and AF2 1DA, superalloy powder compacts, fatigue origins 78−48521
Ni-Cr-Ti(Al), effect of ultrasound on crystallisation, dendritic structure, and plasticity *(Russian)* 80−11637
Ni-Cr-Ti(Nb)(Zr), eutectic alloy charact. by melting temp., composition and oxidation resistance 78−52771
Ni-Cr-W, oxidation behaviour in air at 1000-1250°C 80−89407
Ni-Cr-W (20, 10 to 40 wt.%), phase composition, struct. and props. 80−21034
Ni-Cr-W (20, 3 wt.%), high temp. creep, atmospheric effect on anomalous behaviour 78−80617
Ni-Cr-W-C(-Si), struct. and props. of corrosion and wear resistant alloys 79−24627
Ni-Cr-W-C(Si) hardness, corrosion resistance, wear resistance tests in 10% HCl *(German)* 78−92368
Ni-Cr-W-Co granules type ZhS6U, EP741, hot hydrostatic pressing 80−60796
Ni-Cr-W-Co-Ti, thermal fatigue, effects of inclusions 80−81183
Ni-Cr-W-Co-Ti heat resistant alloy ZhS6K, fatigue resistance, heat treatment and protective coating effects 77−81320
Ni-Cr-W-Co-(Al)(Ti)(Mo), high-temp. sulphide corrosion 80−76408
Ni-Cr-W-Mo-Al-Ti (15,6,3,2,2, wt.%), wrought, Si effect on transition brittleness *(Chinese)* 80−55491
Ni-Cr-W-Mo-Ti-Al, heat-resist., recovery and recrystn. 80−76268
Ni-Cr-W-Mo-Ti-Al alloy KhN67MVTYu, heat treatment effect on mech. props. 77−70082
Ni-Cr-W(Mo)(Ti)(Al), long range ordering of matrix of complex heat resistant alloys *(Russian)* 77−77509
Ni-Cr-Y, oxidation at 800 to 1300°C, Y addition effects, comparison with Fe-Ni-Cr-Y alloy *(French)* 79−43481
Ni-Cr-Y, Y addition effect on intergranular and volumetric diffusion, oxidation reduction *(French)* 79−83382
Ni-Cr-Zr, degradation after exposure to 1% H_2S/H_2 gas mixture at 1000°C 80−89408
Ni-Cr-ZrO_2, dispersion hardened, sintered, rupture 77−21272
Ni-Cr-(Al), oxide dispersion strengthened, creep and tensile props. 77−86042
Ni-Cr-(Al), oxide dispersion strengthened materials, effect of prior creep at 1365K on room temp. tensile props. 78−39857
Ni-Cr-base superalloys, characterisation of PNP components 80−5242
Ni-Cr-type alloys, theory of ordering, superstruct. form. *(Russian)* 77−81256
Ni-Cr(-Fe), blackness change in air, 1-8 micron, 1200°C, film props. depend. 77−66033
Ni-Cr(-Mo), creep parameters, high temp. 80−50685
Ni-Cr(-W), heat-resistant, integrated hemispherical degree of blackness, specific elec. resist., oxidised surfaces 79−86912
Ni-Cr(Al) gas corrosion, in composite atmospheres *(Polish)* 79−79142
Ni-Cr(Co)(Fe), liquid, N activity coeff. 77−72699
Ni-Cr(Fe)(Cu) alloy, matrix effect in SIMS anal. using O_2^+ primary beam 80−76576
Ni-Cr(Mo), oxidation effect on magnetic props. *(Russian)* 78−23868
Ni-Cr(Mo), solid soln., US effect on mech. props. *(Russian)* 78−23819
Ni-Cr(Mo), wear tracks, TEM obs. tested in simulated face seal 77−52508
Ni-Cr(V)(Co)(Mn)(Mo)(Ru)(Fe), spin wave stiffness consts., RPA CPA band model 79−61088
Ni-Cr(20 wt.%), oxidation at elevated temps., struct. effects *(French)* 77−59994
Ni-Cr(20 wt.%), oxidation in pure O_2, 800 to 1200°C, secondary ion emission exam. of oxide film *(French)* 77−59995
Ni-Cu, chemisorption of CO, inhibition by Cu *(French)* 77−1295
Ni-Cu, crystal growth, oriented, by vacuum intake method *(Russian)* 77−4732
Ni-Cu, electron-irrad., neutron-scatt. studies 80−75268
Ni-Cu, ferromag., mag. moment, local environment effects, HF CPA cluster calc. 80−65817
Ni-Cu, ferromag., polarised neutron scatt., evidence for mag. environment effect 77−40039
Ni-Cu, ferromagnetic, Hall effect, anomalous, rel. to scatt. processes 80−44572
Ni-Cu, ferromagnetic and spin glass transition, DC magnetisation meas. 79−78369
Ni-Cu, high temp. compatibility with pyrolytic C 79−65261
Ni-Cu, high-field susceptibility, spin-wave spectrum, CPA calc. 80−65818
Ni-Cu, hydrogenated, Curie point, cluster magnetism 78−14960
Ni-Cu, implantation damaged, crit. behaviour, perturbed ang. distrib. meas. anal. 80−60476
Ni-Cu, liq., activity meas. of O_2 by EMF method *(Japanese)* 80−54408
Ni-Cu, local environment effects, magnetisation decrease 79−65664
Ni-Cu, local mag. field on μ^+ 79−56665
Ni-Cu, low field magnetisation meas., mag. props. comp. depend. 78−91879
Ni-Cu, mag. anisotropy, temp. and conc. depend. 77−63172
Ni-Cu, mag. moment distrib. 77−32178
Ni-Cu, magnetoresistivity anisotropy, spin mixing 80−88538
Ni-Cu, nearly ferromag., heat capacity meas. in mag. field 0.3 to 4K, superparamag. clusters 77−69579
Ni-Cu, nearly ferromag., spin-glass-like distrib. of interaction fields 79−91243
Ni-Cu, Ni rich alloys, magnetic phase transition, elec. resistivity meas. 300-700K 79−82781
Ni-Cu, Ni-rich, temp. depend. resist. 80−10943
Ni-Cu, protective coating on Al powder *(Russian)* 78−60881
Ni-Cu, short-range atomic clustering, residual resist. meas. 80−29386
Ni-Cu, sp. ht. in mag. field, 1.2-15K 78−68262
Ni-Cu, spin fluctuations effect on temp. depend. of elec. resistivity 78−47776
Ni-Cu, sputtered using Hg^+ and Ar^+ beams, comp. variation as function of ejection angle, AES exam. 77−44105

nickel alloys continued
Ni-Cu, sputtering rate, radiation-induced segregation and preferential sputtering effects, kinetic model 80−40199
Ni-Cu, surface composition, AES 78−14558
Ni-Cu, surface segregation using atom-probe FIM 79−77883
Ni-Cu, surface segregation, computerised atom-probe FIM study 80−75412
Ni-Cu, thermal conductivity, data anal. and synthesis 78−95284
Ni-Cu, tunnelling electron spin polarisation 77−73058
Ni-Cu, W fibre reinforced, liquid phase sintering under press. 78−19695
Ni-Cu (30 at.%), H(D) penetration, reversed kinetic isotope effects 77−43387
Ni-Cu (30 wt.%), cast cold- and warm-worked, recrystallization 79−29092
Ni-Cu (30 wt.%), cast single phase, solidified from undercooled melt, mech. props. 77−48540
Ni-Cu alloy, asymmetry of XPS of shell electrons *(Russian)* 78−76579
Ni-Cu alloy, magnetoresistance anisotropy, planar Hall effect 79−23947
Ni-Cu alloy, optical absorpt. meas. 78−19518
Ni-Cu alloy, surface comp. and catalysis 80−54489
Ni-Cu alloys, spontaneous resist. anisotropy 77−89752
Ni-Cu film, deposited by cylindrical magnetron sputtering, internal stresses 80−24773
Ni-Cu semiconducting cast ingots, effect of EM stirring on struct. *(Russian)* 78−6915
Ni-Cu-Al(Si), spinodal decomposition, morphology of microstructure, elastic strain energy anisotropy effect 78−15354
Ni-Cu-H systems, Curie temp. during phase transitions under high press. H_2 80−71029
Ni-Cu-Mn, dil. alloys, NMR freq. temp. depend., spin echo meas. 78−64296
Ni-Cu-Mn, mag. and galvanomag. meas. 77−89928
Ni-Cu-Si, Si effect on structural changes during ageing, TEM and X-ray obs. 78−15438
Ni-Cu-Si (38,5 at.%), changes in modulated struct. during ageing early stages *(Japanese)* 79−100183
Ni-Cu-X (X=Sn, Nb, Ti), spinodal decomp. alloys, linear expansion coeff. influence on morphological anisotropy *(Japanese)* 80−70431
β-Ni-Cu-Zn, electron microscopy of premartensitic state 79−66059
Ni-Cu(Co,Al,Cr,Si,Ti,Zr,Mo,W,K) powder based composite high temp. strength of W reinforcing fibres 79−70021
Ni-Cu(Pd)(Pt)(Rh), ferromag., press. effect on Curie temp. 79−51781
Ni-Cu(Zn)(Ga)(Ge)(As)(Se)(Br)(Kr), dil., ferromagnetic, hyperfine field and relax. time obs. of impurity heavy nuclei 80−75533
Ni-Cu(5%), absolute composition depth profile, surface segregation, field-ion microscope obs. 79−33166
Ni-Dy, annealing behaviour of implantation damage, Dy outdiffusion, TEM obs. 77−77505
Ni-Dy, dil., implanted impurity hyperfine interaction 78−68417
Ni-Fe, 79 NM alloy, gamma and neutron influence on mag. susceptibility comparative study *(Russian)* 80−39751
Ni-Fe, (100) surface, O interaction, LEED and XPS studies 79−82437
Ni-Fe, activity of iron at 1573K 77−70328
Ni-Fe, adsorption of O_2, oxidation 80−108730
Ni-Fe, alloy pre-form prep. through reduction of sintered oxides 80−40284
Ni-Fe, chemical emission by Ar^+ ion bombardment *(French)* 77−86410
Ni-Fe, Curie points, mag. props. of H solutions FCC metal sublattice parameter behaviour 79−69671
Ni-Fe, dil., hyperfine mag. fields, press. effect, Mossbauer meas. 80−71277
Ni-Fe, dil., optical absorpt., electronic struct. 80−108227
Ni-Fe, dil., temp. depend. of Mossbauer absorpt. near Curie point *(French)* 80−11305
Ni-Fe, disordered alloy, CPA treatment, elec. resist. 77−1408
Ni-Fe, disordered FCC, local densities of states calc. 77−59244
Ni-Fe, electronic struct. calc., effects of chemisorption; contact pot. and surface magnetisation 80−103734
Ni-Fe, elementary excitations, exchange stiffness const., inelastic neutron scatt. study 79−47294
Ni-Fe, epitaxial thin film, mag. structures and stresses, ferromag. resonance 78−72375
Ni-Fe, FCC, H_2 embrittlement *(Japanese)* 77−48526
Ni-Fe, FCC, Invar behaviour, spin waves stiffness consts., neutron scatt. study 79−51769
Ni-Fe, fatigued, struct. and cyclic stress strain, influence of stacking fault energy and atomic size-module-interactions *(German)* 79−42082
Ni-Fe, film, anomalous Hall and Nernst-Ettingshausen effect, contribution of phonon and impurity scatt. *(Russian)* 78−64145
Ni-Fe, film, domain struct., effect of biaxial stresses 78−88153
Ni-Fe, film, magnetisation induced uniaxial anisotropy, substrate temp. depend. 77−8367
Ni-Fe, film, magnetisation reversal, magnetoresistance meas. 77−16132
Ni-Fe, high-field susceptibility, spin-wave spectrum, CPA calc. 80−65818
Ni-Fe, high-permeability alloys developments *(Slovak)* 79−4694
Ni-Fe, IR spectra, cond. electron charcts. *(Russian)* 77−48173
Ni-Fe, influence of atomic ordering on spin waves 79−7987
Ni-Fe, magnetic aftereffects of H isotopes, book contrib. 79−82835
Ni-Fe, magnetisation curling in superparamagnetic spheres 77−8363
Ni-Fe, magnetostrictive vibr. meas., appl. of laser interferometric technique 80−37059
Ni-Fe, new soft magnetic material for pulse transfer and choking in power electronics *(German)* 79−28555
Ni-Fe, orientation aftereffect 80−88830
Ni-Fe, power losses at extremely low freqs. 80−88815
Ni-Fe, residual resist., CPA calc. to muffin tin pot. 77−62892
Ni-Fe, soft mag. props. rel. to metallurgical aspects 80−88810
Ni-Fe, split bands rel. to sp. ht., g-factor and magnetostriction data 77−72977
Ni-Fe, thermal conductivity, data anal. and synthesis 78−95284
Ni-Fe, thermal fluctuation aftereffect meas. by pulse field method 80−88837
Ni-Fe, W-fibre reinforced, fabrication, heat treatment, and mag. and mech. props. 77−40408
Ni-Fe, X-ray study of occluded H_2 77−16586
Ni-Fe (15%) film, evaporated, uniaxial mag. anisotropy 77−51929
Ni-Fe (19 wt.%), mag. anisotropy induced by cold rolling *(Russian)* 80−84595
Ni-Fe (2 wt.%) oxidation, 800 to 1000°C 77−36686

nickel alloys continued
Ni-Fe (20 wt.%), thin film ferromagnetic band, magnetisation under domain creep conditions *(Russian)* 79−91262
Ni-Fe (20%) film, condensed, struct. from electron diffr. 77−59222
Ni-Fe (20at.%), vacancy-C interaction, Lomer's model insufficiency *(French)* 77−76456
Ni-Fe (36 to 50 wt.%), initial permeability, domain struct. model 80−88811
Ni-Fe (40%), Mn coating, mag. interface effects 77−69638
Ni-Fe (40%) (111) film with C coating, surface magnetism 77−73056
Ni-Fe (50%), slow mag. domain wall motion 77−69597
Ni-Fe (67.7 at.%), noncommensurate atomic struct., neutron diffr. exam. *(Russian)* 77−84701
Ni-Fe alloy, continuous electrodeposition 80−16208
Ni-Fe alloy, extraordinary viscous magnetic wall motion 78−84465
Ni-Fe alloy, FCC, density, lattice parameters, X-ray diffr. and hydrostatic weighing 78−55904
Ni-Fe alloy, Ni base cathodes, powder metallurgy technique 80−29903
Ni-Fe alloy, oxidation, diffusion enthalpy and entropy 78−7084
Ni-Fe alloy film electrodeposition, modification of soln. composition 80−16209
Ni-Fe alloys, electrodeposited, electron microscope investig. *(Russian)* 77−43442
Ni-Fe alloys, pulse permeability and loss in toroidal core pulse current transformers 78−43615
Ni-Fe based metallic glasses, Curie pt. anomalies 80−60256
Ni-Fe conductor, EM pulse shielding, magnetisation curves 80−28143
Ni-Fe epitaxial films (110), uniaxial anisotropy, expt. 77−20648
Ni-Fe film, Barkhausen noise spectra meas. 77−16131
Ni-Fe film, differential susceptibility, struct. const. and losses 79−91271
Ni-Fe film, domain struct., uniaxial stress effects 78−10740
Ni-Fe film, effect of tensile stress on mag. domain struct. 78−68332
Ni-Fe film, electrodeposition, role of buffers and anions 80−25583
Ni-Fe film, electron spin polarisation, meas. using supercond. tunnel junction 77−69637
Ni-Fe film, ferromag. reson. under weak influence of eddy currents *(German)* 77−8412
Ni-Fe film, Kerr magnetooptic effect, appl. to waveguide type optical modulator, theory 77−11015
Ni-Fe film, low field domain wall mobility 80−25167
Ni-Fe film, mag. and hyperfine field exam. of uniaxial anisotropy 77−66391
Ni-Fe film, oligatomic, ferromag. reson. and torsion magnetometry, 123-373K 77−59461
Ni-Fe film, relax. effects in domain boundary creep *(Russian)* 77−24723
Ni-Fe film, thermally activated domain wall motion 80−88777
Ni-Fe film, unidirectional anisotropy by exchange coupling, appl. to biasing of magnetoresist. read head 78−91907
Ni-Fe films, coercivity control for single-level masking bubble devices using surface modification and intermediate layers 79−51816
Ni-Fe films, energy change of Bloch wall with angle to easy axis, calc. *(Slovak)* 80−103863
Ni-Fe films, in state of undersaturation in perpendicular fields, micromagnetic struct. *(Russian)* 79−61193
Ni-Fe films, magnetisation reversal in narrow strips, TEM study 80−34720
Ni-Fe films, US generation by ferromag. reson. 78−88155
Ni-Fe films, viscous magnetic domain wall motion anal. 79−95617
Ni-Fe metallic glass, METGLAS 2826, creep props. 79−15746
Ni-Fe microelectrode array probe for electrophysiology 79−84049
Ni-Fe multilayered films, mag. domain structures 79−82847
Ni-Fe narrow stripes, mag. props. and domain struct. 79−82843
Ni-Fe overlay, influence on bubble device performance 79−78466
Ni-Fe oxidised film, extraordinary viscous wall motion at extreme vel. 78−14997
Ni-Fe oxidised films, easy-axis switching 79−91266
Ni-Fe polycrystalline film cross-tie memory for shipborne radar/sonar 80−42204
Ni-Fe powder, effect of vibration and current pulses on shaping 79−95973
Ni-Fe protective coatings on Al powder *(Russian)* 78−60881
Ni-Fe reed contact, Au-plated, submicron Auger spectroscopy exam. 79−15027
Ni-Fe soft magnetic alloys, developments and components *(Hungarian)* 78−48000
Ni-Fe solid soln., precip. hardened, paramag.-ferromag. transition on ageing 78−52255
Ni-Fe wire, hard-drawn, increased Barkhausen noise at low temps. 77−16114
Ni-Fe/Mn interface, mag. surface effects, dead layers and exchange anisotropy 77−24718
Ni-Fe-Al type B2 lattice alloys, Fe atom distribution, Mossbauer study *(Russian)* 79−99796
Ni-Fe-C, 20 at.% Fe, vacancy-C interaction, induced mag. anisotropy *(French)* 79−55775
Ni-Fe-Cd, ternary alloy, electrodeposition from acetate bath 79−95950
Ni-Fe-Ce superalloy, vacuum melted, Ce effects on microstruct. 77−36552
Ni-Fe-Co, alloy with step hysteresis loops *(German)* 79−42806
Ni-Fe-Co (17,3 wt.%), thin film ferromagnetic band, magnetisation under domain creep conditions *(Russian)* 79−91262
Ni-Fe-Co film, domain wall energy meas., by domain tip propag. method 77−55692
Ni-Fe-Co film, magnetoelastic vibr. generation during high freq. mag. reversals *(Russian)* 78−60320
Ni-Fe-Co film, nonmagnetostrictive, mag. props., effect of deposition parameters of Al underlayer 77−77078
Ni-Fe-Co films, for logic devices, mag. switching vel., anisotropy field and coercive force *(Korean)* 77−51930
Ni-Fe-Co films, nonmagnetostrictive, magnetoresistance effects 78−35013
Ni-Fe-Co films, saw tooth magnetic domains investigated 78−14994
Ni-Fe-Co-Ti, electron microscopy and mag. meas. 80−71097
Ni-Fe-Cr, extraordinary Hall effect, elec. and mag. meas. at 77 and 300K 80−34421
Ni-Fe-Cr, PE 16, thermally activated domain wall motion 79−95603
Ni-Fe-Cr (18, 18 wt.%) superalloy, mech. props., 4-295K 77−44327
Ni-Fe-Cr alloy, PE 16, coercivity of picture frame cryst. 78−14988
Ni-Fe-Cr base superalloy, addition effect on mech. props. *(Chinese)* 80−20998

nickel alloys continued
Ni-Fe-Cr film, hysteresis loop meas. using magnetooptical system 79−69707
Ni-Fe-Cr PE 16, Bloch wall motion, thermally activated 78−43610
Ni-Fe-Cr soft magnetic film plating bath 79−43465
Ni-Fe-Cr superalloy type 718, heat treatment effect on room temp. and elevated temp. fracture toughness response 80−100922
Ni-Fe-Cr-Mo-Ti-Al, PE 16, thermally activated domain wall motion 80−88777
Ni-Fe-Cr-Nb-Ta-Mo alloy, fatigue crack growth, stress ratio and hold-time effects 80−40531
Ni-Fe-Cu, Mu-metal, mag. aftereffects, dynamic neutron depolarisation study 80−50147
Ni-Fe-Cu, thermodynamic activities of components in pseudobinary section Ni_3Fe-Cu at 1520K 77−59752
Ni-Fe-H and Ni-Co-H, hydride formation in high press. range 80−65235
Ni-Fe-Ho film strips, domain struct. and new rot. processes 77−85533
Ni-Fe-Mn, ferromag. reson. linewidth and saturation magnetisation 78−72418
Ni-Fe-Mn alloy, NMR signals due to Mn atoms with antiparallel moments 78−27113
Ni-Fe-Mn ferromagnetic alloy, magnetic state of Mn atom, local environment effect 77−66298
Ni-Fe-Mo, K-effect, Mossbauer study 80−39998
Ni-Fe-Mo-Cu (79, 16, 4.3, 0.7 wt.%) K-state formation, physical props. exam. 78−47761
Ni-Fe-Mo(Cr), determ. of preferential locations of Mo or Cr on Fe and Ni sublattices, by X-ray intensity study 79−37662
Ni-Fe-Nb, Hardperm, origin of high magnetic permeability 77−8362
Ni-Fe-Nb, hardperm alloy, effect of sheet thickness and heat treatment on magnetic props. *(Japanese)* 78−31095
Ni-Fe-Nb, Hardperm alloy, sheets, effect of sheet thickness, and annealing, on mag. props. 78−76772
Ni-Fe-Nb, mag. props. and struct. *(Chinese)* 78−84450
Ni-Fe-Nb (Mo), magnetic alloy, TEM and X-ray obs. *(Chinese)* 80−24401
Ni-Fe-Nb-Al, mag. props. and struct. *(Chinese)* 78−84450
Ni-Fe-Nb-Al (11.2, 8.09, 79.66 wt.%), modulated struct. growth process rel. to ageing *(Chinese)* 80−66541
Ni-Fe-Nb-Al(-Mo), wear resisting mag. head material, mag. props. and struct. 80−35350
Ni-Fe-Nb-Mo (11.42, 6.92, 1.54 wt.%), Hardperm, high magnetic permeability alloys 77−8361
Ni-Fe-Nb-Mo-Al, head material for mag. recording, DC and AC mag. props. 80−88812
Ni-Fe-Nb(Ta)-W, high magnetic permeability alloys, Hardperm 77−48012
Ni-Fe-Pd thin films, mag., surface and corrosion props. 80−34707
Ni-Fe-Rh films, mag. and corrosion props. 80−34702
Ni-Fe-W alloy, electrodeposition, SEM and optical obs. 79−66018
Ni-Fe(Co), local ordering effect on spin wave stiffness const. 77−66282
Ni-Fe(Pd)(Pt)(Cu), ferromag., influence of local ordering on spin wave stiffness const. 77−89937
Ni-Ga, band model of high temp. magnetism 78−26809
Ni-Ga, phase diagrams and cryst. struct., DTA, X-ray diffr. and microprobe anal. *(French)* 79−47660
Ni-Ge, amorphous, atomic struct., neutron diffr. study 80−59392
Ni-Ge, band model of high temp. magnetism 78−26809
Ni-Ge, liq., density and surface energy, temp. depend., 1000-1700°C *(Russian)* 77−15662
Ni-Ge, liq. alloy, thermodynamic activity, mass spectrometric determ. *(German)* 78−20052
Ni-Ge , defect-solute interactions and radiation-induced segregation 80−25705
Ni-Ge (1 to 9 at.%), twinning stress used to eval. stacking fault energy of pure Ni *(Japanese)* 78−59820
Ni-Ge (2 at.%), vacancy cluster form. during deform. positron lifetime meas. 79−56882
Ni-Ge (2 wt.%), positron annihilation, photon ang. distrib. meas. effect of deformation, annealing temp. *(Russian)* 78−35220
Ni-Ge alloys, liq., integrated emissivity, electric resistivity 78−43155
Ni-Ge binary system, phase diagram rel. to that of Co-Ge *(French)* 80−97463
Ni-Ge-Au evaporated contacts on GaAs, TEM obs. 80−75449
Ni-Ge-Au/GaAs cathode struct., with enhanced injection efficiency, contact resist. 77−20431
γ-Ni-γ'-Ni_3Al-TaC fibre reinforced eutectic, oxidation protection 77−40475
Ni-H, ferromag., H impurities and μSR, self-consistent calc. 80−84447
Ni-H, ferromag. disappearance obs. 77−43824
Ni-H, implanted film, resistivity and TDPAC meas. 78−39229
Ni-H, in high press. H conditions, published results anal., atomic ratio calcs. 79−69254
Ni-H, system, melting temp., effect of H_2 *(Ukrainian)* 79−52153
Ni-H system, cluster calc. of electronic struct. of interstitial H 78−43326
Ni-H system, energy and electron density of states, improvements to theory 80−70636
Ni-HfO_2 (3 wt.%), dispersion hardened alloy VDU-2, thermal and mech. treatment 77−90376
Ni-HfO_2(2.14 wt.%), dispersion hardened, HfO_2 particle size effect on struct. and mech. props. *(Russian)* 80−20944
Ni-Hf(Zr)(Ti), wetting of AlN, effect of alloys exam. 78−80710
Ni-In, dil., symmetry of lattice defect, DPAC meas. 78−43729
Ni-In, dil., uncorrelated radiation damage, TDPAC meas. 78−43343
Ni-In, elec. field gradient, at ^{111}Cd probes, temp. depend. 79−28643
Ni-In, FCC, cellular precipitation kinetics 78−52823
Ni-In, FCC crystals, exam. of volume transform. kinetics of cellular precipitation 79−11625
Ni-In, implantation damaged, crit. behaviour, perturbed ang. distrib. meas. anal. 80−60476
Ni-In, ion-implanted, impurity defect interaction and diffusion, Rutherford backscatter and TDPAC expts. 80−34039
Ni-In, protective coating on Kovar, vacuum seal for borosilicate glass appl. *(Italian)* 80−40621
α-Ni-In, solid solution, lamellar microstructure, influence of grain boundaries on thermal stability 78−72795
Ni-In, thermodynamic props., phase diagram 77−55949
Ni-In(Sn), electrical cond. and magnetic susceptibility of B 8_2-compounds *(German)* 79−42520

nickel alloys continued
Ni-M, dil., high field susceptibility 78−52230
Ni-maraging weld metal, increasing fracture toughness by heat treatment 78−72871
Ni-Mn, dil., mag. moment distribs. and environmental effects, neutron scatt. obs. 80−60247
Ni-Mn, disordered, disordered, exchange-anisotropy field, magnetisation curves 78−72365
Ni-Mn, disordered, mag. struct., high field twist deform. 78−68166
Ni-Mn, disordered FCC, stiffness const., single cryst. neutron inelastic scatt. meas. 77−20558
Ni-Mn, equilib. ordered, high field magnetisation 77−85491
Ni-Mn, hydrogenation kinetics, magnetisation, interstitial H influence 80−35528
Ni-Mn, low temp. anomalies of elec. resist. *(Russian)* 79−60788
Ni-Mn, low temp. kinetic props., 4.2-77.3K *(Russian)* 79−19568
Ni-Mn, mag. moment and asphericity of spin density distrib., polarised neutron scatt. obs. 80−44813
Ni-Mn, ordered and disordered, press. effect on Curie temp. 80−71148
Ni-Mn, ordering by nucleation and growth and by spinodal decomposition *(French)* 78−27471
Ni-Mn, permeability, diffusion and solubility of H 80−107573
Ni-Mn, remanent magnetisation reversal, local environment model 79−33507
Ni-Mn, spin wave stiffness const., low temp. neutron scatt. meas. 79−51768
Ni-Mn, tunnelling electron spin polarisation 77−73058
Ni-Mn (10∼40 wt.%), γ solid soln., interdiffusion 80−100366
Ni-Mn (17-27 at.%), low-angle neutron diffr., anomalous crit. scatt. *(Russian)* 80−60193
Ni-Mn (5%), magnetisation curve reduction 78−31096
Ni-Mn (up to 32 at.%), Curie temp., press. depend., using press. cell developed for meas. with cubic-anvil press 80−13109
Ni-Mn alloy, NMR signals due to Mn atoms with antiparallel moments 78−27113
Ni-Mn alloys, ferromagnetism-to-spin glass phase transition and strong mag. field effect 80−75773
Ni-Mn base polynary alloys, magnetic and elect. props. *(Japanese)* 78−15551
Ni-Mn base polynary alloys, magnetic, and elec. props., composition and heat treatment effects 79−11710
Ni-Mn disordered alloys, mag. moment and Curie point 78−76243
Ni-Mn ferromagnetic alloy, magnetic state of Mn atom, local environment effect 77−66298
Ni-Mn film, magnetic properties obs., heat treatment influence *(German)* 77−56118
γ-Ni-Mn solid soln., interdiffusion 1073 to 1323K *(Japanese)* 79−99374
Ni-Mn-Al-Si-Co, Alumel, Ettingshausen-Nernst coeff. and transport props. from 200 to 473K 80−44573
Ni-Mn-Co(Fe), low temp. anomalies of elec. resist. *(Russian)* 79−60788
Ni-Mn-Cu, interdiffusion at 1173K *(Japanese)* 79−99375
Ni-Mn-H, hydride phase form. and decomposition in hygh-press. gaseous H_2, magnetisation meas. 79−56953
Ni-Mn-H solid solutions, mag. props. 80−88753
Ni-Mo, and Ni-Mo-V, struct. changes on annealing *(Russian)* 77−21145
Ni-Mo, discontinuous precipitation as internal sulphidation mode 77−8835
Ni-Mo, eutectic form., struct. and mech. props. *(Russian)* 77−21129
Ni-Mo, off-stoichiometric, ordering 78−52752
Ni-Mo, phase boundary motion kinetic during interdiffusion *(Russian)* 79−60559
Ni-Mo, powder mixture, electric discharge sintering, struct. changes 77−77446
Ni-Mo, short range order considerations and development of long range order 77−16574
Ni-Mo, sintering limited solid solubility, peritectic diagram 77−28754
Ni-Mo, solubility of H_2, 500-1000°C *(Japanese)* 78−38845
Ni-Mo, sputtering rate, radiation-induced segregation and preferential sputtering effects, kinetic model 80−40199
Ni-Mo, variation in absolute thermoelec. power under heat/treatment *(Ukrainian)* 79−38051
Ni-Mo (10.7 wt.%) alloy, ordering energy calc. 80−10522
Ni-Mo (14.4 wt.%) single crystals, ordered phase precipitates influence on deformation character, mechanical props. *(Russian)* 79−74155
Ni-Mo (17.5 at.%), discontinuous precipitation reaction *(German)* 79−87643
Ni-Mo (20.8 wt.%), order, heat treatment effects 80−40406
Ni-Mo (5.8-24 at.%) solid soln. struct. and strength characts. *(German)* 79−4975
Ni-Mo alloy electrodeposits, codeposited impurities rel. to H_2 permeation, props. 79−19493
Ni-Mo binder of binary carbide hard alloy, physicomech. props. 77−90461
Ni-Mo-Al and Ni-Mo-Al-V, high-resist., struct. transforms., TEM *(Russian)* 78−19762
Ni-Mo-Al eutectics, unidirectional solidification 77−4769
Ni-Mo-B metallic glass ribbons, tensile strength, crystn. temp. 80−89173
Ni-Mo-C(-Cr)(W), Vickers hardness and crystallisation temp. 80−16361
Ni-Mo-Cr, type E1867, effect of stress conc. on fatigue strength at elevated temps. 79−57115
Ni-Mo-Cr-Si, plasma and detonation coatings, Laves- and carbide-strengthened, comparative props. 78−15562
Ni-Mo-MoS_2 composite, Mo alloying effect on physicochem. interactions 80−7692
Ni-Mo-W, diagram of state, W solubility, dispersion hardening *(Russian)* 80−66477
Ni-Mo-W, type N55M20V25, quenched at various cooling rates, phase transformations *(Russian)* 79−66052
Ni-Nb (5, 10 at.%), initial oxidation process at high temps., appl. of high energy ion backscattering anal. for O oxidation *(Japanese)* 79−24651
Ni-Nb (5 to 45 at.%) alloys, free energy and thermodynamic props. investigation using EMF method *(Russian)* 79−52160
Ni-Nb alloys, oxidation at high temp., high energy ion backscattering anal. *(Japanese)* 80−35405
Ni-Nb amorphous alloy, transformation to crystalline state, ion emission microscope study *(Russian)* 79−82158
Ni-Nb_2O_5, fibrous composite, aligned in situ growth by preferential internal oxidation 78−6879

nickel alloys continued
Ni-Nb-Al, eutectic, thermal cycling effect on strength and ductility *(Russian)* 79−24601
Ni-Nb-Al, unidirectionally solidified γ/γ′-δ eutectic, fatigue crack propag. 79−29184
Ni-Nb-Al (21,2.5 wt.%), eutectic aligned alloy, mech. behaviour at high strain rates 78−39855
Ni-Nb-Al (25, 2.5 wt.%), directionally solidified γ/γ′-δ eutectic, growth conditions on struct. 80−11639
Ni-Nb-Al-Cr, directionally solidified, exam. of growth and morphology 79−11601
Ni-Nb-Al-(Cr), eutectic, mech. props., high press. H_2 effects 77−63779
Ni-Nb-C, obtained by liq. quenching, superconductivity 80−75699
Ni-Nb-Cr-Al, directionally solidified eutectic superalloy, high temp. oxidation resistant coatings 78−39937
γ/γ′-δ-Ni-Nb-Cr-Al (20, 6, 2.5 wt.%), growth kinetics of γ′ precipitates 77−40424
Ni-NbC (10 wt.%) eutectic alloy, directional solidification and struct. *(Russian)* 80−84922
Ni-NbC eutectic, microstructure and strength depend. on composition and crystallisation conditions *(Russian)* 79−100128
Ni-Ni_2B eutectic, high temp. X-ray anal. 80−71639
Ni-Ni_3Al-Cr_3C_2 eutectic composite, creep 77−40431
Ni-Ni_3Al-Ni_3Nb, directionally solidified, role of twinning in cyclic stress strain behaviour 78−80605
Ni-Ni_3Ti eutectic alloys, solidification 77−70042
Ni-Ni_4Mo, strengthening by ordered precipitates 77−86041
Ni-NiAl solid soln., high temp. transforms *(Russian)* 79−56973
Ni-$NiAl_2O_4$, internally oxidised, orientational relationships of precip. oxide phase 77−4783
Ni-Nichrome, MOM diode, breakdown effect in visible and near-IR regions 80−6999
Ni-O, liquid alloys, surface tension and wettability of Al_2O_3 *(Japanese)* 79−99398
Ni-Os, short-range order parameters, ordering energy on first coordination sphere *(Russian)* 79−69058
Ni-P, amorphous, elec. resist. calc. 78−60103
Ni-P, amorphous, electrical transport, appl. of extended Ziman theory 77−47787
Ni-P, amorphous, low P, struct. study using high-angle X-ray diffr. 80−107055
Ni-P, amorphous, NMR expts. and interpretation 79−8060
Ni-P, amorphous, prod. by ion implantation 80−75257
Ni-P, amorphous, reversible effects of temp. on struct. 78−34442
Ni-P, amorphous, struct., X-ray scatt., rel. to Cu-Zr alloys 77−51324
Ni-P, amorphous alloys, low temp. mag. props., comp. depend. 77−66387
Ni-P, amorphous electrodeposited alloys, phase-separation *(Japanese)* 80−54140
Ni-P, amorphous magnetisation, NMR and coercive force meas. 77−32187
Ni-P, amorphous metallic, sound attenuation and rel. meas. 77−31722
Ni-P, amorphous metallic, logarithmic temp. depend. of sound vel. 77−31725
Ni-P, amorphous metallic glass, elec. resistivity 78−91654
Ni-P, coating onto $BeFe_{12}O_{19}$ and $SrFe_{12}O_{19}$ 80−25593
Ni-P, electrodeposited film, thermal anal., occlusion of gases rel. to mag. props. 80−59823
Ni-P, electroless deposition on Al, X-ray and SEM obs. 79−90907
Ni-P, metallic glass, acoustic wave vel. log. temp. depend. *(French)* 77−72659
Ni-P, molten alloy, struct., X-ray scatt. 78−22640
Ni-P, struct. obs. by X-ray diffr., low temp. annealing and deform. effects 79−56995
Ni-P (8 wt.%), protective coating for wear and corrosion resistance of steel 77−21329
Ni-P alloy, electrodeposited, heat induced struct. changes *(Japanese)* 78−15433
Ni-P amorphous alloy, positron annihilation exam. of crystallisation 79−43061
Ni-P amorphous alloy prep. by ion implantation 78−22748
Ni-P amorphous alloys, electrodeposited and melt-quenched atomic and electronic structures 80−88062
Ni-P amorphous thin films, crack networks of voids 78−2399
Ni-P electrodeposit, magnetisation coercivity and magnetostriction 78−68338
Ni-P film, amorphous, ion implanted, struct. and domain struct. obs. 79−91272
Ni-P metal metalloid glass forming alloys, gram atomic volumes 78−38628
Ni-P metallic glasses, crystn. kinetics by differential scanning calorimetry 78−91257
Ni-P-B, amorphous, giant moments and short-range order 77−4499
Ni-P(B), amorphous, thermal anal. and X-ray diffr., solidification struct. development *(French)* 78−91253
Ni-Pb, conc. profiles across solid-liq. interfaces 80−55382
Ni-Pd, anodic behaviour, potentiodynamic current density and impedance potential meas. *(German)* 80−25925
Ni-Pd, disordered, local environment effects, neutron scatt. expts. 78−68172
Ni-Pd, FCC disordered polycryst. alloy, magnetisation, band ferromag. 78−80180
Ni-Pd, high mag. field effects, mag. isotherms near Curie point, exchange splitting energies 80−60272
Ni-Pd, mag. form. factor, polarised neutron diffr. meas. 80−29525
Ni-Pd, mag. moment distrib., one-mag.-species model calc. 80−65788
Ni-Pd (1 at.%), surface comp. and surface segregation, AES obs. 79−51404
Ni-Pd alloy, magnetostriction and mag. anisotropy meas. 79−4713
Ni-Pd surfaces, electrochem. passive film form. and comp. determ. by SEM, SIMS, XPS 80−39401
Ni-Pd-Ge, phase relationships and struct. 77−36451
Ni-Pd-H, film, struct. and phases formed, when Ni, Pd are sputtered in H 80−29289
Ni-Pd-Mn, ternary FCC solid soln., saturation magnetisation and Curie temp., medical appl. *(Japanese)* 79−61114
Ni-Pd-Mn ternary alloys, mag. characts., use for thermoseed 80−107995
Ni-Pd-P, metallic glass, amorphous and electronic structs., NMR Knight shifts and linewidths meas. 78−68400
Ni-Pd-P amorphous alloys, tensile deform. 77−32646

nickel alloys continued
Ni-Pd-Si, amorphous, low-field mag. susceptibility meas., 4.2-580K 79−61057
Ni-Pd-Si, phase composition, isothermal section at 800°C *(German)* 77−16544
Ni-Pd(Cu)(Cr), directional order anisotropy energy induced by neutron irradiation, temp. depend. 77−66294
Ni-Pd(Pt), renormalisation of spin wave stiffness 79−51764
Ni-Pd(Pt) mag. props., average and local density of states, CPA calc. 77−59242
Ni-Pt, disordered, extension of Taylor's theory of lattice vibr. 79−4387
Ni-Pt, itinerant ferromagnet. magneto-volume expts. 77−66404
Ni-Pt, local environment and mag. props. effect of disorders 77−63085
Ni-Pt, magnetic moment distrib., diffuse neutron scatt. meas. 80−34593
Ni-Pt, magnetovolume effects near crit. conc. for ferromag. 79−56591
Ni-Pt, short range order, many electron effects, pseudopotential method 78−79954
Ni-Pt, short-range order parameter calc. in pseudopot. approx. *(Russian)* 80−49183
Ni-Pt alloys, mag. props. under hydrostatic press. 78−6556
Ni-Pt alloys, magnetic-moment distrib. neutron study 80−97066
Ni-Pt alloys, thermal expansion, mag. contribs. 77−43355
Ni-Pt disordered alloy, off-diagonal, T-matrix itinerant electron ferromagnetism calcs. 80−25067
Ni-Pt spin susceptibility, temp. variation, band model calc. 77−28365
Ni-Pt-P, metallic glass, amorphous and electronic structs., NMR Knight shifts and linewidths meas. 78−68400
Ni-Pt-P, metallic glass, electronic structure, pulsed NMR study 80−75869
Ni-Pu, dil., effective mag. fields, temp. depend. *(Russian)* 78−43587
Ni-Re, dil. alloys, two-band Mott conductivity *(Russian)* 78−60118
Ni-Re, sintering, limited solid solubility, peritectic diagrams 77−28754
Ni-refractory metal/Si interactions, phase separation 80−65303
Ni-Rh, disordered, local environment effects, neutron scatt. expts. 78−68172
Ni-Rh, disordered, vol. paramagnetostriction calc. 77−80985
Ni-Rh, ferromag., local-environment effects, mag. diffuse neutron scatt. cross-section meas. 77−55664
Ni-Rh, local environment and mag. props. effect of disorders 77−63085
Ni-Rh, mag. moment distrib., one-mag.-species model calc. 80−65788
Ni-Rh, thermal EMF, elec. resist., mag. susceptibility, mag. moment and Curie temps., 18-500°C *(Russian)* 77−20288
Ni-Rh ferromagnetic alloy, mag. moment spatial distrib. 77−66275
Ni-Ru, environmental effects and mag. moment distrib., magnetisation and neutron scatt. meas. 79−91211
Ni-Ru (3.3 at%), magnetisation, magnetocrystalline anisotropy, magnetostriction and elastic consts., thermal variations 79−28563
Ni-Ru (≤4 at.%), influence of alloying on mag. anisotropy 80−71010
Ni-Ru peritectic alloys, rapidly cooled, crystn. peculiarities *(Russian)* 80−20922
Ni-S, defect control by heat-treatment in S atmos. 79−43293
Ni-S, dil. alloy, AES of grain boundaries *(French)* 80−50477
Ni-S, electrodeposited film, thermal anal., occlusion of gases rel. to mag. props. 80−59823
Ni-S, phase diagram calc. and thermodynamic props. of liq. phase 80−108401
Ni-S, S atom redistribution under high temp. electron irrad., residual elec. resist. reduction *(Russian)* 79−82256
Ni-S solid solns., residual elec. resist. *(Russian)* 80−70465
Ni-Sb, dil., vacancy-impurity binding enthalpy, positron annihilation 79−91525
Ni-Si, band model of high temp. magnetism 78−26809
Ni-Si, Cs ion-bombarded, surface Cs concs., AES meas. 79−83073
Ni-Si, defect-solute interactions and radiation-induced segregation 80−25705
Ni-Si, intergranular segregation of Si, electron energy loss spectrometers, X-ray anal. *(French)* 79−8388
Ni-Si, ion beam irradiation induced Ni_3Si surface film segregation 78−38761
Ni-Si, liquid, surface tension model using surrounded atom concept 77−15665
Ni-Si, magnetoresistivity anisotropy, spin mixing 80−88538
Ni-Si, proton irrad., γ' precipitation, early stages 80−34096
Ni-Si (1 at.%), dose depend. of ion irradiation induced segregation 79−42123
Ni-Si (12.7 at.%), heterogeneous precipitation at internal and external surfaces during Ni ion irradiation 79−77647
Ni-Si (12.7 at.%) foil, ion irrad., surface effects on precip. morphology 80−104168
Ni-Si (12.7 wt.%) Ni^+ ion irradiation, precipitate restructuring, mechanisms and kinetics 79−77650
Ni-Si (6.32 wt.%), under ion irradiated, modification of precipitate interface and effect of precipitates stability 79−77651
Ni-Si (up to 3.7 wt.%), supercooled, struct. refinement mech. *(Russian)* 80−20975
Ni-Si film system, silicide first phase form., reaction kinetics 78−79821
Ni-Si liquid alloys, thermodynamic props., enthalpy of mixing *(Russian)* 80−34207
Ni-Si melt, ultra acoustic study *(Russian)* 78−15613
Ni-Si melt refining by electric fields, ionic conduction of Ni, Si *(Russian)* 80−65273
Ni-Si solid soln., radiation, induced precipitation dose rate effects 78−6936
Ni-Si solid soln., radiation-induced solute redistribution and precipitation, model 79−19277
Ni-Si solid solution alloys, γ phase precipitation under irrad. 77−1839
Ni-Si:Cr, He^+ radiation-enhanced diffusion and segregation effects of point-defect trapping 79−77824
Ni-Si-B, amorphous, thermal stability of ductility 80−76327
Ni-Si-B, embrittlement by crystallisation *(Japanese)* 78−48513
Ni-Si-B amorphous alloys with metalloid elements, embrittlement/crystn. relationship *(Japanese)* 79−96134
Ni-Si-B powder, oxidation at 850°C, SEM, ESCA, and elec. cond. meas. 80−7717
Ni-Si-Mg thermocouple alloy, props. and thermoelec. reference data 79−26057
Ni-Si-Mn(Al) alloy systems, oxidation resist. 79−24661
Ni-SiC, electrodeposited, oxidation 78−64756
Ni-SiC coating, heat treated, as plated, electrochemical study of corrosive wear 80−16536

nickel alloys continued
Ni-SiC(WC), dispersion hardened coating, chemically deposited using electroless baths, exam. of protection props. 79−34208
Ni-Sn, spectral determ. of comp. using UHF plasmotron as source 79−52812
Ni-Sn intermetallic phase growth kinetics at liq. Sn-solid Ni interface 80−71638
Ni-Sn intermetallics, Ni_3Sn_4, Ni_3Sn_2 and Ni_3Sn, oxidation, AES obs. 77−48575
Ni-Sn system intermetallic formation rate, H_2 adsorption effect 79−90819
Ni-Sn(Sb), dilute ferromagnetic alloy, resistivity and magnetoresist. anisotropy 79−11106
Ni-Ta, dil., crit. behaviour, ^{181}Ta PAC expt. 78−43723
Ni-Ta, dil., crit. behaviour of local magnetization, PAC and magnetisation meas. 78−48098
Ni-Ta (70, 30 wt.%) metallic glass, struct. and crystn. *(Russian)* 80−70136
Ni-Ta system, phase diagram diffusion relation *(Russian)* 77−52287
Ni-Ta-Al system, phase equilibria and diagram, electron probe, X-ray diffr. anal. 80−29927
Ni-Ta-Al-Fe, Al and Fe effect on precipitation kinetics 79−20054
Ni-Ta-C, composites of γ+TaC 77−85965
Ni-TaC, eutectic alloy, fibre reinforced, directionally solidified, anisotropic yielding behaviour 79−11675
Ni-Ta(Sn)(Er)(La) ion implanted surface alloys, solid solubility and radiation-induced disorder, backscatt. obs. 79−46692
Ni-Ta(7 at.%), short-range order, pseudopot. calc. and diffuse X-ray scatt. *(Russian)* 77−28008
Ni-Te, liq., struct. and elec. props. 80−49083
Ni-Th (1 at.%), surface comp., temp. and O_2 exposure effects, AES study 80−80914
Ni-ThO_2, dispersion hardened, fracture mechanism map 78−60823
Ni-ThO_2, dispersion strengthened, high temperature cyclic deformation 80−16430
Ni-ThO_2, irradiated with 5 MeV Ni^{++}, ThO_2 redistrib. 78−71771
Ni-ThO_2 (2.51 wt.%), dispersion hardened, high temp.-strength, deform. method and annealing effects 79−1882
Ni-ThO_2 dispersion strengthened, high temp. strength, grain size and shape effects 77−48447
Ni-ThO_2(HfO_2) dispersion hardened alloys, recrystallisation during annealing, O_2 partical press. effects *(Russian)* 78−3140
Ni-Ti, Curie temp. determ. using deviation from Mattheisen's rule 79−15306
Ni-Ti, dil., optical absorpt., electronic struct. 80−108227
Ni-Ti, heavily doped, linear expansion meas. 80−103501
Ni-Ti, mag. moment distrib. and environmental effects around Ti impurity 80−7092
Ni-Ti, martensitic phase transformation effect on low cycle fatigue behaviour 80−7666
Ni-Ti, near equiatomic, pretransform. lattice instability, TEM and electron diffr. 79−11616
Ni-Ti, near equiatomic alloy, TEM exam. of austenite-martensite interface 78−51401
Ni-Ti, Ni-rich, temp. depend. resist. 80−10943
Ni-Ti, Nitinol memory material heat engine, comment on efficiency 80−3529
Ni-Ti, Nitinol memory material heat engine, reply to comments on efficiency 80−3530
Ni-Ti, shape memory effect, criteria for efficiency assessment *(Russian)* 80−21015
Ni-Ti, shape-memory effect, intermetallic compounds 20-years research results 77−7843
β-Ni-Ti, struct. changes during annealing, TEM and selected area diffr. 79−34081
Ni-Ti, structural instability, deform. effects on electron energy spectrum 80−39284
Ni-Ti, tunnelling electron spin polarisation 77−73058
Ni-Ti, with shape memory effect, working medium in heat engine *(Russian)* 78−48449
Ni-Ti (0-1.5 at.%), elec. cond., mag. phase transition, 300-750K 78−2678
Ni-Ti (1 wt.%), serrated yield, 77 to 873K 77−32649
Ni-Ti (10 wt.%), X-ray study of ageing of plate and powder 77−1847
Ni-Ti (12 wt.%), dil. alloys, transform. early stages 78−3096
Ni-Ti (12 wt.%), early stages of transformation 80−76251
Ni-Ti (1.6, 7.64 wt.%), monophase high temp. scaling, metallography study 80−21159
Ni-Ti (2wt.%) alloy, polarised neutron diffuse scatt. 77−36057
Ni-Ti (3 wt.%), C precipitation 80−29958
Ni-Ti (48 at.%), annealed and rolled electron microscope and probe analysis of structure 79−100189
Ni-Ti (51.5 at.% Ni) metallide, thermal cond., elec. resistivity, 90-450K 78−68009
Ni-Ti (60 at.%) alloy, high stress effects on struct. and props. *(Russian)* 78−19838
Ni-Ti (8 and 10 wt.%) alloy, aged, precipitation behaviour at 550 to 950°C, X-ray and electron microscopy exam. 78−39785
Ni-Ti (9.6 wt.%), mag. study on phase decomposition *(Japanese)* 80−15758
Ni-Ti alloy, shape memory effect mechanism 77−28865
Ni-Ti alloy, struct. and props., self-propagating high temp. synthesis *(Russian)* 78−26492
Ni-Ti mech. memory alloys, tensile props. *(Korean)* 77−63724
Ni-Ti shape memory alloy processing and medical applications *(German)* 80−17203
Ni-Ti shape memory alloy trigger for space satellite boom latch and release mechanism 80−7575
Ni-Ti thin film, phase growth kinetics due to diffusive processes *(Russian)* 77−72722
Ni-Ti/Cu composite, plastic deform. influence on internal friction *(Russian)* 80−100871
Ni-Ti-Al, martensitic, coherent γ'-phase particles and influence on $\alpha \rightarrow \gamma$ transformation *(Russian)* 79−29056
Ni-Ti-Al superalloy, pendant drop melt extracted, struct. and props. 80−76242
Ni-Ti-Co, Co effect on martensitic transform. temp. and low temp. props. *(Korean)* 78−11224
Ni-Ti-P, amorphous, corrosion behaviour, immersion tests and electrochem. meas. *(Japanese)* 80−85085
Ni-Ti(Fe), neutron irradiated, thermally activated deform. 80−6438

nickel alloys continued
Ni-transition metal, deviation from Matthiessen's rule in elec. resist. 77−4319
Ni-V, del. alloy, anisotropy consts., K_3 and K_1, determ. 77−4512
Ni-V, dil., optical absorpt., electronic struct. 80−108227
Ni-V, dil., oxidation behaviour at 1200°C 77−77636
Ni-V, elementary excitations, exchange stiffness const., inelastic neutron scatt. study 79−47294
Ni-V, ferromag. reson. meas., anisotropy consts. determ. 78−39410
Ni-V, interdiffusion coeffs. in phase transform. range, 810-1175°C *(Russian)* 78−91490
Ni-V, low temp. sp. ht. near ferro-paramag. transition 77−63218
Ni-V, magnetocryst. temp. and conc. depends., rel. to resistivity 77−40052
Ni-V, solid and liq., mag. susceptibility and electronic struct. 80−39738
Ni-V, solid soln., diffusion and thermodynamic props. 80−65278
Ni-V system, conc. depend. of interdiffusion coeff., 810-1175°C, rel. to phase diagram *(Russian)* 79−4429
Ni-V system, interdiffusion, kinetics of phase growth *(Russian)* 80−29230
Ni-V(Mo)(Ru)(Cr), weak ferromag., stiffness const., low-temp. meas., rel. to RPA-CPA theories 78−31063
Ni-V(Nb)(Ta)(Si)(Ge), dil., mag. props. at elevated temps. 77−63089
Ni-W, eutectic form., struct. and mech. props. *(Russian)* 77−21129
Ni-W (2%), Mg diffusion meas., 970-1330K, appl. of vapour collect and AES method 78−75876
Ni-W (20 to 50 at.%), phase distrib. var. with annealing time, metastability of hexagonal phase *(Russian)* 77−8851
Ni-W (45.5 wt.%), eutectic, mech. props., high press. H_2 effects 77−63779
Ni-W directionally solidified eutectic composite, foil prep. for TEM 78−53072
Ni-W sintered powder pressings, intermetallic phases *(Russian)* 80−55349
Ni-W-B, superalloy, M_5B_3 type boride 78−44131
Ni-W-C, X-800 centrifugally cast cylinder lining alloy, compatibility with hardfacing alloys 77−32726
Ni-W-C(Nb) system, γ to (γ+W) phase boundary calcs. using Wigner method *(Russian)* 80−54346
Ni-W-Co-Cr, superalloy MAR 200, with Hf, cellular composite prod. by isothermal dendrite ripening 78−44150
Ni-WC, dispersion hardened, centrifugally cast metallurgical coatings for wear resistance in plastics molding machines 79−29285
Ni-Y, amorphous, elec. resist., press. depend. 80−96841
Ni-Y, amorphous, resist. and magnetoresist. meas., weak itinerant ferromagnet 78−68018
α-Ni-Zn, continuous precipitation kinetics *(Russian)* 78−76652
β-Ni-Zn, eutectoid decomposition kinetics *(German)* 77−8819
Ni-Zn, γ-phase region, X-ray and electron diffr. obs. 79−61562
Ni-Zn, implantation damaged, crit. behaviour, perturbed ang. distrib. meas. anal. 80−60476
γ-Ni-Zn, inversion antiphase domains, formation and stabilisation, electron conc. effect 78−14363
Ni-Zn, physical-chemical metallurgy *(German)* 80−108390
α-Ni-Zn, solid soln. diffusion annealing effect *(Japanese)* 80−34255
Ni-Zn alloy electrodeposition from acetate bath 77−52257
Ni-Zn alloys, XPS for band struct. 79−33889
Ni-Zn diffusion couple, annealing and reaction diffusion *(Japanese)* 78−51749
Ni-Zn liquid alloys, Zn activity obs., 1100 to 1300K 78−40072
Ni-Zn melt, Zn activity determ. *(German)* 78−19715
Ni-Zn solid soln., lamellar spacing in discontinuous precipitation, expt. proof of Gaussian distrib. *(German)* 77−36517
α'_2-Ni-Zn-Cu martensite, thermoelastic, microscope obs., TEM 77−55966
Ni-Zn-Mn-Fe spinel, crystn. from soln. in melt 80−2945
Ni-Zr, amorphous phase form. in Zr-poor region, hardness and fracture strength *(Japanese)* 80−84914
Ni-ZrO_2, dispersed inclusions, effect on recovery and recrystallisation 77−25064
Ni-ZrO_2, dispersion strengthened, thick vacuum condensate, control of struct. and mech. props. 80−16324
Ni-ZrO_2, electron-beam-evaporated condensate, cold deform. and annealing effects on microstruct. 80−16331
$Ni_{0.95}$ S Fe, spin glass, spin flop in exchange field 80−34640
Ni_2 (Al, Nb) single crystals, orientation and temp. depend. of yield stress 80−25791
Ni_2-rare earths, H_2 reaction, thermal anal. 79−100434
Ni_3 (Al.Ti), flow stress and work hardening, exam. of temp. depend. by tensile tests 78−84839
Ni_x Cu_{1-x} paramag., coherent pot. approx. for nonoverlapping muffin tin potentials 78−2451
NiAg, dil., disordered, virtual bound states, reson. model pot. theory 79−23934
Ni_3(Al, Nb) single crystal, yield stress, orientation and temp. depend. 80−108511
Ni_3(Al,Ti), deformation characts., temp., strain rate and orientation depend. 77−44320
γ'-Ni_3(Al,Ti), single crystal, dislocation movement, HVEM obs. *(Japanese)* 80−108503
Ni_3(Al,W), yield strength, temp. and orientation depend. 77−28857
Ni_3(Al,W), yield stress, orientation depend. 78−39830
β-NiAl alloy, elastic soft modes preceding martensitic phase transition 79−4388
β_2-NiAl alloys, Young's modulus, −196 to 800°C, effect of martensitic transforms. 79−83253
NiAl, annealed near stoichiometric, elec. resist. meas. 77−8071
β'-NiAl B2 phase, mag. aftereffect 80−34700
NiAl, bonding, self-consistent energy bands 78−91610
NiAl coating on Ti alloy, electrospark applied, friction and wear resistance obs. *(Russian)* 79−1916
NiAl, compositional depend. of oxidation rates 79−8393
β'-NiAl, density of states, XPS meas. 78−48284
β'-NiAl, dislocation climb, hot stage TEM 77−24318
NiAl, electronic struct. by cluster calc., comparison with self-consistent APW method 77−69209
β'-NiAl, electronic struct. and optical props. 80−97228
NiAl, kinetics, Ni_2Al_3 layers growth by cementation *(French)* 80−35127
NiAl martensite, Ni-rich, precip. of Ni_3Al, mechanism 77−86033
NiAl, nonstoichiometric, interstital defect cluster obs. 80−107226

nickel alloys continued
β-NiAl, omega-like structural defects, diffuse X-ray scatt. obs. 79−95005
β'-NiAl, ordered, hardness after-effect studied by anelastic relaxation 80−66570
β-NiAl, oxidation, α-Al_2O_3 growth and microstruct. 80−108627
NiAl, oxidation, effect of gaseous NaCl 78−95853
β-NiAl, oxide films, metal and O_2 transport, AES and inert marker, techniques 80−97641
NiAl precipitation hardening of medium C steel, fatigue behaviour 78−84983
NiAl, quenched and annealed, void formation 79−46652
β'-NiAl, self consistent embedded cluster model for Fe, Co, Ni mag. impurities 80−2549
β'-NiAl, self-consistent embedded-cluster model for mag. impurities 78−67973
β'-NiAl, single cryst., quenched and annealed, ω-like diffr. effects, TEM and X-ray diffr. study 79−60216
NiAl, sputtered in vacuum, struct. *(Russian)* 77−69986
NiAl, thermal defects, dilatometric study *(Japanese)* 80−15092
NiAl, vapour phase mass spectra, correl. between bond strengths in liq. and gas phases 77−35466
NiAl, X-ray spectra, electronic structure 79−78793
NiAl-Cr, eutectic, directionally solidified, temp. behaviour of misfit dislocations *(German)* 78−3119
NiAl-Cr eutectic alloy, directional solidification singularities *(Russian)* 78−68678
NiAl-V join, phase relations and eutectic directional solidification 78−31396
$NiAl_3$, quantitative STEM chem. anal. using standard and standardless programs 79−17578
$Ni_{1-x}Al$ solid solution, vacancy ordering exam. by electron diffr. after annealing 78−3123
β-$Ni_{1\pm x}Al_{1\mp x}$, defect struct. and Debye Waller factors vs. composition 77−31658
Ni_2Al_3 layers, growth on Ni, NiAl substrates by cementation, kinetics, interdiffusion *(French)* 80−35127
γ'-Ni_3Al and β-NiAl, pure and alloyed environmental resistance 77−59962
Ni_3Al and Ni_3(Al, Ti), S segregation to grain boundaries 78−48410
Ni_3Al, at. displacements, characteristic temp. and lattice spacing, temp. depend. *(Russian)* 79−90598
Ni_3Al based alloys, mean square atomic displacements 79−28053
Ni_3Al, cold-worked, substruct., X-ray diffr. obs. 77−59806
Ni_3Al, deformation characts., temp., strain rate and orientation depend. 77−44320
Ni_3Al, dissociation of superdislocations and plastic deform. mech. *(Russian)* 78−52909
Ni_3Al, ductility, tensile and compressive tests *(Japanese)* 77−52414
Ni_3Al, ductility in poly- and single crystals, compressive and tensile tests 78−56715
Ni_3Al, elastic moduli changes at Curie point 77−66406
Ni_3Al, film, deposition by ion beam sputtering, composition and stress state 77−89674
Ni_3Al, itinerant ferromagnet, magneto-volume expt. 77−66404
Ni_3Al, itinerant ferromag., Fermi surface and single particle excitations 80−34350
Ni_3Al, long-range order parameter, temp. depend. 77−27849
Ni_3Al, magnetovolume effects near crit. conc. for ferromag. 79−56591
Ni_3Al, Mossbauer experiments on homogeneity 78−48395
Ni_3Al, Mossbauer spectra, exam. of struct., superlattice population anal. 78−88240
Ni_3Al, noncoherent second phase particle effect on strain-hardening parameters *(Russian)* 79−47703
Ni_3Al, off-stoichiometric alloy, inverse mag. susceptibility rel. to defect conc. 80−60216
Ni_3Al, overshooting while testing in tension 78−44189
Ni_3Al, room temp. ductility improvement by ternary trace element addition *(Japanese)* 79−52315
Ni_3Al, substitutional soln. and defect hardening mechanisms 77−21155
Ni_3Al, thermal expansion, mag. contribs. 77−43355
Ni_3Al, unpaired spin density distrib., polarised neutron diffr. 78−10659
Ni_3Al/Ni_3Nb, DSC-1 and DSC-2 lattices, coincident and near coincident cells for two lattices 77−84746
Ni_3Al-B, $L1_2$ type intermetallic cpd. room temp. ductility improvement by B addition *(Japanese)* 80−35263
Ni_3Al-Fe, Fe effect on Mossbauer effect study 77−32298
Ni_3Al-Fe (10 at.%), activation anal. of plastic deform. 79−1900
γ'-Ni_3Al-Fe (10 at.%) alloy, steady-state creep 78−15460
Ni_3Al-Ni_3Nb, directionally crystallised, thermal and electric cond., emissivity 77−43556
Ni_3Al-Ni_3Nb, directionally crystallised eutectic, influence of prolonged annealing on microstructs. and props. *(Russian)* 79−74182
Ni_3Al-Ni_3Nb, eutectic, temp. and thermal cycling influence on oxidation 80−45417
Ni_3Al-Ni_3Nb, eutectic alloy, crack development, failure energy capacity *(Russian)* 80−40480
Ni_3Al-Ni_3Nb directional eutectic, oxidation and interaction with protective coatings *(Russian)* 77−52526
Ni_3Al-Ni_3Nb eutectic, directionally solidified, high-temp. oxidation mechanism 80−16544
Ni_3Al-Ni_3Nb eutectic alloy, ^{63}Ni diffusion rate rel. to struct. defects *(Russian)* 78−2288
Ni_3Al-Ti(Cr)(Fe)(Zr)(Mo)(W), powder, X-ray spectral analysis exam. 80−16239
β'-$Ni_{48}Al_{52}$, 3d transition metal impurities, elec. resist. meas. 77−69295
$(NiAl)_{1-x}M_x$, M=3d transition metal, elec. resist. and magnetoresist. 77−43580
Ni_3(Al.Ti), single crysts., flow and fracture behaviour tested in tension 79−79075
$Ni_3Al(\gamma')$-$Ni_3Nb(\delta)$, directionally solidified, deformation substruct. and slip systems 79−8326
NiAu, dil., disordered, virtual bound states, reson. model pot. theory 79−23934
$Ni_{1-x}Au_x$, amorphous, elec. resist., temp. depend., spin wave contrib. and resist. minimum 78−51961
$Ni_{1-x}Au_x$-Co, dil., hyperfine field and isomer shift, precip. process, Mossbauer expts. 80−25267
$Ni_{1-x}Au_x$-Co, dil., Mossbauer effect, mag. hyperfine field 80−20528
$Ni_{1-x}B_x$ amorphous film, crystn., TEM obs. 79−87019
$Ni_{100-x}B_x$, amorphous, mag. struct., mag. susceptibility meas. 80−80485

nickel alloys continued
$Ni_{100-x}B_x$, rapidly quenched, mag. moment, temp. and comp. depend. 78−47957
$Ni_{66}B_{34}$, morphological, structural and phys. props. *(French)* 80−44444
NiC, electronic structure of interstitials 79−1583
Ni_3C films, form. by carburisation, characterisation 80−34337
NiCo film, crit. angle meas., pinning mech. 79−1719
NiCo, itinerant electron model, spin wave stiffness const. calc. 80−34613
(NiCo)-Cr-Al-Y/ZrO_2-Y_2O_3 plasma sprayed ceramic coating for turbine engine components 80−40616
$Ni_{62}Co_4Al_{34}$, fine struct. of martensite, electron microscopy obs. *(Russian)* 79−46672
$(Ni_xCo_{1-x})_3Ge$ single crysts., $L1_2$ struct., cross-slip 80−40459
$(Ni_{1-x}Co_x)_{0.78}P_{0.14}B_{0.08}$, amorphous, mag. props., local environment model 77−12119
NiCoPd, anodic dissolution, SFE effect *(German)* 80−25924
NiCr film, resistive, electron beam deposition, evaporation, gas phase analysis *(Polish)* 79−20492
NiCr, hyperfine fields about μ^+ 79−56664
NiCr, sputtered, detection by electron probe microanal., substrate depend. 80−35607
NiCr thin film resistor, 'clean vacuum' deposition equipment suitability obs. *(Polish)* 79−15611
Ni(Cr)/Ni_3Al-Ni_3Nb directional eutectic, oxidation and interaction with protective coatings *(Russian)* 77−52526
NiCr-AlY sintered fibre metal struct. abradable seal material, friction and wear 78−56785
NiCr-Ge, amorphous, junction, current-voltage charact. 80−44725
NiCr-MoAl-ThO_2 (13,3 wt.%), powder, mech. alloying 78−84744
$Ni_{0.89}Cr_{0.11}$, phonons with disorder caused by force consts., neutron diffr. obs. and CPA calc. 80−96602
Ni_2Cr, fine-domain ordered alloy, early deform. stages, dislocation struct. and motion *(Russian)* 77−81291
Ni_2Cr, neutron irrad., point defect prod. and annealing 78−87718
Ni_2Cr ordered alloy, mech. twinning *(French)* 77−72624
NiCrAlY, mechanically alloyed, maintaining elongated grain struct. after deform. 77−36534
NiCu, dil., disordered, virtual bound states, reson. model pot. theory 79−23934
NiCu molecule, electronic states determ. by ab initio HF and CI methods 80−69087
$Ni_{1-x}Cu_x$ (x=0.03, 0.16, 0.24), photoemission study, surface, bulk electronic struct. 78−48281
$Ni_{1-x}Cu_x$+CO, $Ni(CO)_4$ form. activation energy, mag. phase depend. 80−3409
$Ni_{23}Cu_{77}$ random substitutional alloy, (001) surface, angle resolved photoemission 77−85895
$(Ni_xCu_{1-x})_2MnSn$, mag. props. and lattice parameter, composition depend. 77−80916
$Ni_{0.7}Cu_{0.3-x}Si_x$, magnetic props., 4.2 to 800K 77−8290
$(Ni_{1-x}Cu_x)Ti$, martensitic, shape memory effect kinetics and thermodynamics 80−3021
Ni(Fe,Cr), electron states density model and mag. characts. calcs. *(Russian)* 80−92804
Ni_3(Fe,Cr), electron states density model and mag. characts. calc. *(Russian)* 80−92804
Ni_3(Fe,M), M=Cr,Mo,W, elec. resist., temp. depend. anomalies, Hall and Nernst-Ettinghausen effects *(Russian)* 80−10942
Ni_3(Fe,M), M=Cu, Cr, Mo, W, kinetic phenomena rel. to ordering and electron struct. *(Russian)* 78−76043
NiFe alloy, ion-beam sputtering, excitation efficiency of atoms 78−19623
NiFe alloys, spin-wave exchange stiffness const. calcs., weak ferromagnetism 77−4510
NiFe disordered alloys, Mossbauer spectra, hyperfine mag. field distrib., Curie temp. 80−7198
NiFe film, domain wall mass and relax. time from forced oscills. 80−71133
NiFe film, ferromag. reson., thermodynamical anal. 79−42840
NiFe film, sputtered, physical props. 79−77938
NiFe film, stationarity and behaviour of Barkhausen noise 79−24198
NiFe, film deposition, sputter gun system, bubble device appls. 77−12532
NiFe, grain oriented, mag. domain wall slow motion, tunnelling mechanism 77−32210
NiFe, itinerant electron model, spin wave stiffness const. calc. 80−34613
NiFe, mag. hysteresis, departure from Rayleigh law in low mag. fields 77−40086
NiFe, magnetic surface anisotropy of transition metals, model calc. 80−34625
NiFe, magnetising energy, anisotropic effects 80−88743
NiFe, single and multilayer thin films, strip domains, inplane magnetisation 80−103866
NiFe soft magnetic alloys, magnetic props., effect of annealing and fabrication *(German)* 78−53004
NiFe, sputter etching in Ar-O plasma, implications for mag. bubble device fabrication 79−83347
NiFe stripes, mag. props. and domain struct. 80−44886
NiFe tape, rapid surface and vol. magnetisation, eddy-current-limited domain wall motion 77−12159
NiFe thin films, magnetoresistance, quasi-static characts. 80−107766
NiFe, US induced mag. reversals, stroboscopic electron microscope obs. 77−48026
NiFe-Ho film strips, curling-type mag. domains 77−48020
$Ni_{0.75}Fe_{0.25}$, influence of atomic ordering on spin waves, inelastic neutron scatt. 77−69516
$Ni_{0.83}Fe_{0.17}$ films, reson. oscills. of mag. domain walls and Bloch lines, stroboscopic electron microscopy 80−54931
$Ni_{1-x}Fe_x$, short range order exam. allowing for formation of structural domains *(Russian)* 78−6888
Ni_3Fe alloy, step-like deformation *(Russian)* 78−27559
Ni_3Fe, atomic order, Mossbauer effect obs. 77−69736
Ni_3Fe, change of H_2 diffusivity with order-disorder transformation 80−59729
Ni_3Fe, compression induced mag. anisotropy and superlattice dislocations, annealing effect 78−31067
Ni_3Fe, compression induced magnetic anisotropy, annealing effect 80−93112
Ni_3Fe, Debye temp. determ. from elastic consts. and X-ray meas., effect of configurational order 78−30727
nickel alloys continued
Ni_3Fe, disaccommodation meas. after low temp. electron and neutron irrad. 80−88832
Ni_3Fe, dislocations, rate of piling up, rel. to average length of slip lines *(Russian)* 77−76416
Ni_3Fe disordered alloys, Mossbauer spectra, hyperfine mag. field distrib., Curie temp. 80−7198
Ni_3Fe, disordered single crysts., thermo-activated mechanism of plastic deform. *(Russian)* 78−84909
Ni_3Fe, domain struct. after tensile deform., dislocation effects 80−71083
Ni_3Fe, electronic structures, order effect 79−90938
Ni_3Fe, influence of order on Mossbauer spectra of ^{119}Sn 79−42876
Ni_3Fe, low-temperature specific heat, long and short range order effects 80−100339
Ni_3Fe, magnetocryst. anisotropy, annealing temp. depend. 80−103828
Ni_3Fe, mono- and polycrysts., strain hardening, test temp. effects *(Russian)* 80−66531
Ni_3Fe, Mossbauer spectra, long range order 78−10810
Ni_3Fe, Mossbauer spectra, order-disorder transition 78−10811
Ni_3Fe, non-linear local environment effect, Mossbauer effect of ^{57}Fe 80−39909
Ni_3Fe, nondislocation origin friction stress in alloys, deformation hardening 80−21050
Ni_3Fe, order-disorder transition phase diagram, Mossbauer meas. 80−39995
Ni_3Fe, ordered, monocrystals, thermally activated deform. processes 80−50684
Ni_3Fe, ordered and disordered states, strain hardening characts., temp. depend., multiple slip case *(Russian)* 78−15421
Ni_3Fe, polycrystalline alloy evolution of slip-line pattern during straining 80−107362
Ni_3Fe, roll magnetic anisotropy and dislocations *(Japanese)* 77−80930
Ni_3Fe, short range order determ. after heat treatments 79−96044
Ni_3Fe, short-range order, diffusive elastic neutron scattering 80−24400
Ni_3Fe, short-range order parameter calc. in pseudopot. approx. *(Russian)* 80−49183
Ni_3Fe, single cryst. ordered and quenched, stress relax. *(Russian)* 77−44282
Ni_3Fe single crystals, longitudinal magnetoresist. meas. 80−70675
Ni_3Fe, single crysts., long range order degree influence on strain hardening *(Russian)* 80−11660
Ni_3Fe, superlattice dislocations, compression induced mag. anisotropy 77−85442
Ni_3Fe, superlattice dislocations, compression induced mag. anisotropy 77−85443
Ni_3Fe, transport props. and magnetisation, effect of alloying with Cr, Mo, W or Cu *(Russian)* 78−39095
Ni_3Fe, X-ray diffraction investig. of order-disorder transform. *(Russian)* 77−70043
Ni_3Fe:C, mag. anisotropy depend. on C content, magnetometric study *(Russian)* 80−54887
Ni_3Fe-Sn, dil., atomic order detection by ^{119}Sn spectroscopy 80−39993
$Ni_{73}Fe_{27}$, order-disorder transition, Mossbauer study 79−95163
$Ni_{40}Fe_{40}B_{20}$ glass alloy, rapidly quenched, explosive welding to A516-70 steel and to itself 78−39954
$Ni_{50}Fe_{30}B_{20}$, magnetostriction, temp. depend. 78−91921
$Ni_xFe_yCr_{1-x-y}$ films, struct., mag. props., and corrosion resist. 80−34706
$Ni_{35}Fe_{30}Cr_{15}P_{14}B_6$, amorphous, anodic polarisation and localised corrosion 77−21310
$Ni_{36}Fe_{32}Cr_{14}P_{12}B_6$, metallic glass, crystallisation 79−77520
$Ni_{36}Fe_{32}Cr_{14}P_{12}B_6$, amorphous, electrochem. corrosion in chloride solns. 80−50763
$Ni_{36}Fe_{32}Cr_{14}P_{12}B_6$ metallic glass, mech. props. and thermal stability 80−76362
$(Ni_{1-x}Fe_x)_{99}Mn$, ferromagnetic, NMR study of local environment effect, relaxation mechanism 80−7193
$Ni_3(Fe_{1-x}Nb_x)$, temp. and conc. depend. of anomalous Hall effect *(Russian)* 80−70674
$(Ni_{100-x}Fe_x)_{79}P_{13}B_8$, amorphous dil. alloys, spin glasses, magnetisation meas. 79−61178
$Ni_{40}Fe_{40}P_{14}B_6$, amorphous alloy, microstruct. study of crystallisation 77−86062
$Ni_{40}Fe_{40}P_{14}B_6$ metallic glass alloy, US spot welding to Cu 79−21730
$Ni_{80-x}Fe_xP_{14}B_6$, amorphous alloy, resistivity variations near critical temp. 79−73488
$(Ni_{99}Fe_1)_{79}P_{13}B_8$, amorphous, low temp. sp. ht., mag. contribs. 80−80552
$(Ni_xFe_{1-x})_{80}P_{10}B_{10}$, amorphous, Curie temp., press. effect 80−75833
$Ni_{49}Fe_{29}P_{14}B_6Si_2$ glass, flow and failure 80−40438
NiFr, mag. film, pulse switching at low temp. 80−103868
Ni_3GA single crystals, anomalous temp. depend. of strength, dislocation struct., optical and TEM 79−74228
NiGa, defect struct. model 79−46648
NiGa, point defects, lattice parameter determ. 78−38695
NiGa, vacancy conc. in B2 phase exhibiting triple defects 79−42058
Ni_3Ga, form. mech. of superlattice intrinsic stacking faults 77−27897
Ni_3Ga, off-stoichiometric alloy, inverse mag. susceptibility rel. to defect conc. 80−60216
Ni_3Ga, stacking fault form. in situ obs. by stretching thin foils in electron microscope 77−62547
Ni_3Ga, strongly enhanced itinerant paramag., theory of anomalies in field depend. of magnetisation 77−69488
Ni_3Ga, with $L1_2$ struct., dissociated struct. of superlattice dislocations 79−37706
NiGe, and Ni_2Ge, amorphous film, electron diffr. exam. of struct. 77−35828
NiGe, Ni_2Ge and Ni_3Ge, X-ray spectrum analysis energy band struct. *(Ukrainian)* 77−52200
$Ni_{0.625}Ge_{0.375}$, amorphous film, crystn. mechanism *(Russian)* 77−51623
Ni_3Ge, amorphous film, electron diffr. exam. of struct. 77−35827
Ni_3Ge single crystal, cleavage fracture 79−61694
Ni_3Ge single crystal, yield stress, temp. and orientation depend. 77−90432
Ni_3Ge single crystals, orientation and temp. depend. of flow stress 79−5008
Ni_3Ge-Fe_3Ge solid soln., flow stress, transition from positive to negative temp. depend. 80−60906
Ni_5Ge_3, amorphous and cryst. films, opt. props. in interband absorpt. region 80−66315

nickel alloys continued
Ni_5Ge_3, amorphous film, elec. resist., microstruct. and annealing 77−85188
Ni_5Ge_3, amorphous-crystalline transition, opt. and elec. characts. *(Russian)* 77−85191
Ni_5Ge_3, solid and liquid, physicochemical props. and structure 80−39548
$Ni_{74}Ge_{26}$, ordered BCC phases at high temp. 79−32948
Ni_xGe_{1-x}, liq., ang. distrib. of positron annihilation 77−55848
NiH_x, desorpt. of H_2, fine struct. 78−59950
NiH_x, electronic band struct. and interatomic bond 78−43295
NiH_x, formation and decomp. studies 80−71626
NiH_x, magnetization, elec. resist., and non-occurrence of supercond. 79−56195
$Ni_{98}M_2$, M=impurity metal, formation of MH(D)-complexes 80−65236
$Ni_{78-x}M_xSi_{10}B_{12}$ (M=refractory metal), glass form. and thermal stability 80−79703
Ni_3(Mn, Al), ordering process mechanism by neutron diffr. *(Russian)* 77−55961
Ni_3(Mn,Cu), ordering kinetics, neutron diffr. and elec. resist. meas. *(Russian)* 77−47379
NiMn, high field magnetisation 80−2557
$Ni_{1-x}Mn_x$, ferromagnetic, NMR study of local environment effect, relaxation mechanism 80−7193
$Ni_{1+x}Mn_{1-x}$, martensite nucleation 77−59787
Ni_3Mn, antiphase domain struct. *(Russian)* 78−39814
Ni_3Mn, at. ordering during annealing, mag. field effect 78−15394
Ni_3Mn, atomic rearrangements during fast and thermal neutron irradiation 79−42114
Ni_3Mn, change of H_2 diffusivity with order-disorder transformation 80−59729
Ni_3Mn, dislocation struct. after heat treatments, TEM *(Russian)* 77−8848
Ni_3Mn, dissociation of superdislocations and plastic deform. mech. *(Russian)* 78−52909
Ni_3Mn, elec. resist., relax. time near order-disorder transition 78−87788
Ni_3Mn, ferromagnetic reson. field and line width temp. depend. 3-300K 79−95651
Ni_3Mn film, anomalous behaviour of Hall effect *(Russian)* 77−28262
Ni_3Mn, fission neutron disordering at 5K, exam. 78−47434
Ni_3Mn, mag. domains perpendicular to AC demagnetising field 77−20632
Ni_3Mn, magnetic phase exam. 77−20631
Ni_3Mn, neutron irradiated, disordering by replacement collision sequences, saturation magnetisation meas. 77−47492
Ni_3Mn, nonstoichiometric, order-disorder transition, A1 to $L1_2$ *(French)* 79−1861
Ni_3Mn, order-disorder transform. *(Russian)* 77−59776
Ni_3Mn, ordered at below Kurnakov temp. then deform., a/2⟨110⟩ dislocations and deform. antiphase boundaries *(French)* 77−51384
Ni_3Mn, partially ordered, field induced uniaxial anisotropy at low temp. 77−40053
Ni_3Mn, partially ordered, remanence reversal 77−69619
Ni_3Mn, partially ordered, spin-wave dispersion relation, inelastic neutron scatt. meas. 80−20394
Ni_3Mn, thermoremanent magnetisation and blocking temp. 80−34601
Ni_3Mn thin films, transmission spectra, structural order depend. 80−66318
Ni_xMn_{1-x} disordered alloy, mag. interactions exam. 77−24687
$Ni_2Mn_{0.9}Fe_{0.1}Sn$, Fe site hyperfine field and mag. moment, Mossbauer effect meas. 78−76365
NiMnGe, crystal and spiral mag. struct., Neel temp., X-ray and neutron diffr. 77−16052
NiMnGe, mag. struct., and mag. phase transitions 77−63187
$NiMnGe_{1-x}Si_x$, mag. props., neutron diffr. and magnetometric meas., 80-600K 80−65793
Ni_2MnIn, Heusler alloy, order-disorder phase transitions, X-ray diffr. meas. 77−66640
$Ni_2Mn_xM_{1-x}Sn$ (M=Ti,V) mag. hyperfine fields, ^{119}Sn Mossbauer spectra study 80−55003
$Ni_2Mn(Mn_xSn_{1-x})$, Heusler alloy, antiferromagnetic order, X-ray and neutron diff. 78−64189
NiMnSb, hyperfine mag. field at Cd impurity, TDPAC study 80−39906
$Ni_{1+x}MnSb$, mag. hyperfine field on ^{111}Cd, TDPAC obs. 78−43709
$(Ni_{0.75}Mn_{0.25})_{82}Si_{10}B_8$, amorphous, exchange anisotropy, mag. susceptibility meas., 4.2K to room temp. 80−11186
NiMnSn, Heusler alloy, hyperfine field at ^{111}Cd, TDPAC meas. 78−43705
Ni_2MnSn alloy, ionic spin distribution and RKKY interactions 78−27028
Ni_2MnSn, ferromag. Heusler alloy, electronic struct., spin polarisations, theory 80−54598
Ni_2MnSn, Heusler alloy, mag. interactions and cond. electron polarisation, spin echo NMR meas. 77−77125
Ni_2MnSn, itinerant ferromagnet, neutron inelastic scatt. 79−7970
Ni_2MnSn, large single cryst. growth by Czochralski and Kyropoulous method 79−47613
Ni_2MnSn(In)(Sb), Heusler alloy, hyperfine field at ^{111}Cd, TDPAC meas. 78−43705
$Ni_2Mn_xT_{1-x}Sn$, (T=Ti, V or Cr), Heusler alloy, mag. moment exam. 77−24682
$Ni_2Mn_xT_{1-x}Sn$, T=Ti(V)(Cr), ferromag., magnetisation, susceptibility 77−12102
$Ni_2Mn_xTi_{1-x}Sn$, Mossbauer spectra, mag. hyperfine field 80−15857
$Ni_2Mn_{1-x}V_xSn$, large single cryst. growth by Czochralski and Kyropoulous method 79−47613
Ni_3(Mo,Ta), quenched alloys, DO_{22} type ordered phase form. 78−95768
Ni_3Mo, modulated struct. phenomena, survey 79−95033
Ni_4Mo alloy, high temp. oxidation, oxide layer growth, struct., mech. behaviour 78−44269
Ni_4Mo, antiphase domains growth kinetics, TEM and electron diffr. *(Russian)* 77−32557
Ni_4Mo, coherent phase form. at stress concentrators *(Russian)* 80−49356
Ni_4Mo, domain struct. on annealing, and dislocation struct. during deform. *(Russian)* 77−16640
Ni_4Mo, electron irrad. in electron microscope, radn. ordering 79−86818
Ni_4Mo, ionisation states of field evaporated ions 77−81200
Ni_4Mo, order-disorder phase transform., X-ray diffr. *(Russian)* 79−1855
Ni_4Mo, ordered, electrical resistivity and thermal EMF, temp. depend. *(Russian)* 77−55513
nickel alloys continued
Ni_4Mo, ordering near Kurnakov point, form. of coherent phase in stress concentrators 79−7691
Ni_4Mo, quenched, short-range order, electron diffraction study 77−39560
Ni_4Mo, statistically homogeneous ordering, computer-simulated field ion images 78−9991
Ni_4Mo, stoichiometric and quenched, short range order and order-disorder transform. 79−78955
$Ni_{65}Mo_7Fe$, O_2 effect on secondary recrystallisation and mag. props. 80−35201
Ni_3Nb intermetallic compound, oxidation kinetics in 500-1000°C range *(Russian)* 77−56144
Ni_3Nb platelet reinforced Ni base alloy 77−36635
Ni_3Nb/Ni_3Al, DSC-1 and DSC-2 lattices, coincident and near coincident cells for two lattices 77−84746
$Ni_{60}Nb_{40}$, stability, crystallisation, ductility meas. 78−47246
$Ni_{62}Nb_{38}$, metallic glass, struct., neutron diffr. study 80−54148
NiP, amorphous, electrical transport 79−38040
NiP amorphous alloy, heat treatments influence on opt. props., struct. and DC resist. obs. 80−80892
$Ni_{1-x}P_x$, electrodeposited, amorphous, mag. and transport props. 78−52106
$Ni_{76}P_{24}$, cryst. and amorphous, thermopower and resist. meas. 80−20145
$Ni_{77}P_{23}$ metallic glass, struct. relax., X-ray expts. 79−1400
$Ni_{78}P_{22}$, amorphous metallic alloy, US attenuation 78−75789
$Ni_{80}P_{20}$, amorphous, struct. factor temp. depend., X-ray diffr. study *(Japanese)* 79−51005
$Ni_{80}P_{20}$ amorphous alloy, liquid-quenched structure 77−1082
$Ni_{80}P_{20}$ glass, mag. props. 77−63125
$Ni_{81}P_{19}$, amorphous alloys, electronic struct., γ-ray Compton scatt. study *(Japanese)* 80−84422
NiPB amorphous alloys, ^{31}P and ^{11}B NMR near paramag.-ferromag. transition 79−33558
$Ni_{78}P_{14}B_8$, amorphous, local symmetry around glass-former sites, elec. quadrupole effects, NMR 80−80618
$Ni_{78}P_{14}B_8$, $Ni_{80}P_{12}B_8$, amorphous mag. clusters, sp. ht. meas. 78−68274
$Ni_{80}P_{14}B_6$ glass, low temp. heat capacity meas., electronic, phonon contributions exam. 78−10689
NiPBAl, metallic glass, viscous flow, alloying effect 78−79793
$Ni_{0.98}Pd_{0.02}$, dil. ferromag., nucl. mag. relax. meas. 77−16198
$(Ni_{0.5}Pd_{0.5})_{82}P_{18}$ amorphous alloy, liquid-quenched, crystn. kinetics, effect of thermal history 80−100175
$(Ni_{0.5}Pd_{0.5})_{82}P_{18}$ amorphous alloy, liquid-quenched, crystn. kinetics, nucleation 80−100176
$(Ni_5Pd_5)_{82}P_{18}$, amorphous alloy, crystallisation 77−89382
$(Ni_5Pd_5)_{82}P_{18}$ amorphous alloy, glass transition temp. 77−84909
NiPt, quenched, ordering kinetics and domain struct. form. during isothermal tempering *(Russian)* 80−66502
NiPt, short-range order, effect of plastic deform., electron diffr. anal. *(Russian)* 80−24403
$Ni_{1-x}Pt_x$, disordered, phonon dispersion relations using neutron inelastic scatt. 79−69212
$Ni_{1-x}Pt_x$, disordered phonon dispersion relations, neutron inelastic scatt. 78−43085
$Ni_{1-x}Pt_x$, disordered system, phonon dispersion relations using pseudo unit cell model 79−28066
Ni_3Pt, change of H_2 diffusivity with order-disorder transformation 80−59729
Ni_xPt_{1-x} disordered alloy, itinerant system, induced magnetism 78−52191
$NiPt_NGe_{N'}$, cryst. struct. *(German)* 80−44171
$(Ni_xPt_{1-x})_{75}P_{25}$ metallic glass system, ^{31}P and ^{195}Pt NMR 77−12211
$(Ni_{1-x}Rh_x)_{99}Mn$, ferromagnetic, NMR study of local environment effect 80−7192
$(Ni_{1-x}Rh_x)_{99}Mn$, ferromagnetic, NMR study of local environment effect, relaxation mechanism 80−7193
$Ni_{0.97}Ru_{0.03}$, mag. form factor and moment distrib., obs. using polarised neutrons 78−68171
$Ni_{0.97}Ru_{0.03}$, mag. moment distrib. polarised neutron study 79−42738
$(Ni_{1-x}Ru_x)_{99}Mn$, ferromagnetic, NMR study of local environment effect 80−7192
NiSb, at. struct. and mag. susceptibility 77−39561
NiSb, dilute alloy, impurity-induced vacancy clustering 79−99972
NiSb, resist., susceptibility and thermopower rel. to electronic struct. 78−67935
$Ni_{0.96}Sb_{0.04}$, surface segregation, XPS and AES obs. 80−76135
Ni_5Sb_2, cryst. struct. *(German)* 78−83775
NiSi, dissociation in presence of Ni film 79−47892
NiSi, NMR and μSR, microscopic mag. props. *(Japanese)* 78−52368
NiSi, partial sputtering yields 77−8696
NiSi-Si:As(Sb), implanted dopant redistrib. after silicide form., appl. to ohmic contacts 79−37729
$NiSi_2$, epitaxial film on Si, ^{4}He ion channelling meas. and RHEED anal. 80−10834
$NiSi_2$, layer, on Si, ion implantation damage, channelling obs. 78−30676
$NiSi_2$ layer, on Si, struct. modelling, using axial and phase channelling techniques 79−4489
$NiSi_2$, substrate ion implantation, channelled, through metal silicide film 80−70231
$NiSi_x$, cryst. struct. of phase *(German)* 79−99119
$Ni_{1-x}Si_x$, electronic states of Si NMR study 80−50216
Ni_2Si formation at Ni film/Si wafer interface, marker motion obs. 77−89593
Ni_2Si formation from Ni-Si sample, obs. by ^{31}Si tracer and Rutherford backscatt. methods 79−4431
Ni_2Si-Si, and NiSi-Si interfaces, chemical state, AES expts. 78−91767
Ni_3Si coatings, form. and stability during high temp. irrad. 80−35088
Ni_3Si precipitation in irradiated Ni-Si solid soln. alloys 77−1839
$Ni_{76}Si_{24}$, ordered BCC phases at high temp. 79−32948
Ni_xSi contact for n-type Si, current load capacity meas. *(Czech)* 77−89846
$Ni_{78}Si_{10}B_{12}$, amorphous, struct. factor temp. depend., X-ray diffr. study *(Japanese)* 79−51005
$Ni_xSi_yB_z$, $(Fe,Ni)_{78}Si_{10}B_{12}$ and $(Ni,Co)_{78}Si_{10}B_{12}$ ternary and quaternary amorphous alloys, effect of comp. on crystn. *(Japanese)* 79−94910
NiSn, thermally prepared Mossbauer spectroscopy 79−61269
Ni_3Sn_2, single cryst. embrittlement and subboundary hardening via interstitial segregation *(Russian)* 77−12679
Ni_3Sn_2, thermally prepared Mossbauer spectroscopy 79−61269
Ni_3Sn_4, thermally prepared Mossbauer spectroscopy 79−61269

nickel alloys continued
NiTa, exam. of oxidation 79−96221
NiTaC, eutectic alloys, chem. incompatibility of ceramic nitrides for directionally solidifying 80−81046
NiTaC eutectic superalloy, casting, furnace atm. effects 80−84880
NiTaC eutectics, high cycle fatigue at room temp. 80−16459
NiTaC-13, directionally solidified eutectic alloy, chem. compatibility with ceramic materials 79−87623
$Ni_{1-x}Te_2$, long period superstructs. rel. to partial ordering, electron diffr. 79−51056
$Ni_2(Ti,Mn)Sn$, Heusler alloy, mag. meas. 79−47261
NiTi alloy single cryts., ferromag. reson., g-value and linewidth 80−71186
NiTi based alloys, plastic deform. mechanism 79−11676
NiTi equiatomic alloy, single cryst. elastic consts. near martensitic transform. 80−75283
NiTi martensite, shape memory effect, struct. characts., TEM $2^1/_2$ D imaging obs. 80−108446
NiTi, martensitic, shape memory effect kinetics and thermodynamics 80−3021
NiTi, martensitic transform. rel. to low frequency internal friction peaks 79−96024
NiTi, premartensitic transformation of B2 phase, shape memory 80−84931
NiTi, reversible martensitic transformations 78−27516
NiTi, search for electronic phase transition, soft X-ray appearance potential spectra 79−24391
NiTi shape memory alloys, mech. fatigue 79−29166
NiTi shape memory effects, substitution of Cu for Ni 79−61661
NiTi, stacking faults prod. by martensite transition, lattice imaging electron microscopy obs. 79−96026
$Ni_{1-x}Ti_x$, ferromag. props., Ti conc. effect 80−54872
Ni_3Ti, electronic struct., Xα calc., photoelectron and AES spectra 80−20769
Ni_3Ti-Ni eutectic alloy, directional solidification singularities *(Russian)* 78−68678
$Ni_{40}Ti_{60}$, amorphous, chem. short-range-order, X-ray and neutron scatt. obs. 80−96447
NiTiCu, shape memory alloys, electron microscope and X-ray diffr. study of struct. 79−82179
$Ni_3Ti_{0.5}Ta_{0.5}$, conservative domain struct., TEM study 80−79776
$Ni_{62}Ti_{29}Zr_9$, amorphous, H-sorption, X-ray and DSC obs. 80−49526
Ni_3V, dissociation of $^1/_2\langle 112\rangle$ perfect dislocations and nature of slip dislocations 78−43022
Ni_3V, ordered, domain size effect on mech. props. 79−79027
Ni_3V, stacking faults, twinning deform., electron microscopy obs. 78−6070
Ni_4W, order-disorder phase transition, X-ray struct. exam. *(Russian)* 78−64532
Ni_4W_9 ionisation states of field evaporated ions 77−81200
$(Ni_{1-y}Y_y)_3Al_{1-x}Sc_x(Ti)_x$, quarternary gamma prime ($L1_2$) pseudobinary props. revealed by ionicity modified pair model 78−19725
NiZn β- and γ-intermetallic compounds, thermodynamics *(German)* 78−92242
NiZn with γ-brass struct., superstructures and defect obs. 80−107284
$Ni_{1-x}Zn_xFe_2O_4$, statistical model and phase transform. *(German)* 77−85473
$Ni_{100-x}Zr_x$, (x=34-40) metallic glass, cryst., isothermal annealing behaviour 80−6367
$Ni_{11}Zr_9$, cryst. struct., X-ray obs. 79−65035
Ni_3Zr, cryst. struct. and stability 79−90597
$Ni_{64}Zr_{36}$, amorphous and cryst., H-sorption, X-ray and DSC obs. 80−49526
Ni_xZr_{1-x} metallic glass, crystallisation kinetics, elec. resist. and mag. susceptibility meas. 80−103659
Nichrome, plasma spray coatings, relaxation phenomena 80−19876
No-Ni alloy, integral emissivity in range 1200 to 1700°C 77−43357
$NpNi_2$, lattice distortions in ferromag. phase, X-ray obs. 80−15774
$NpNi_2Si_2$, Mossbauer and magnetisation expts. 78−31138
Nr-Cr-ThO_2 (20, 2 vol.%), Orowan stress/creep threshold stress comparison 77−8901
$PD_{0.75}Ni_{0.25}$, spin wave excitations, neutron inelastic scatt. meas. 77−47983
Pb-$Cu_{91}Ni_9$-Pb superconducting junction, crit. currents 79−69633
Pb-Ni, creep, low-temp., thermal heating and quantum mechanisms, supercond. transition effects 80−79868
Pb-Ni, strength loss in supercond. transition, nonmag. and paramag. impurities influence *(Russian)* 80−70875
Pb-Ni-Si, metallic glass, electron irrad., positron annihilation radiation, angular correlation study 78−84678
Pd Ni, effect of hydrogenation on thermopower 80−39562
Pd-Ni, Auger sensitivity factors 78−43964
Pd-Ni, dil., ferromag., magnetoresist. 78−91665
Pd-Ni, dil., ferromagnetism, local moments, susceptibility, magnetisation and Curie temp. *(Russian)* 78−88115
Pd-Ni, dil., local orbital moment evidence 77−20299
Pd-Ni, dil., resist. min. 80−11050
Pd-Ni, dil., Zeeman splitting of cond. electrons 77−11884
Pd-Ni, dil. paramag. alloy, local moments, rel. to nearly mag. impurities in nonmag. host 78−2647
Pd-Ni, dilute ferromagnets, press. effect on Curie temp. 80−65873
Pd-Ni, disordered alloy, onset of ferromagnetism, effect of press. 79−61111
Pd-Ni, liquid alloys, enthalpy of form. *(Russian)* 77−56244
Pd-Ni, local susceptibilities, ^{61}Ni Mossbauer spectroscopy 78−95536
Pd-Ni, magnetovolume effects near crit. conc. for ferromag. 79−56591
Pd-Ni, melt, struct. and physical-chemical props., thermodynamic props. *(Russian)* 78−18536
Pd-Ni, NMR of ^{27}Al meas. 77−12215
Pd-Ni, nearly ferromag., quasiparticle picture for de Haas-van Alphen effect 78−91592
Pd-Ni, neutron radiation stimulated diffusion, electrical resistivity exam. *(Russian)* 79−14959
Pd-Ni, normal Hall effect *(Russian)* 80−103676
Pd-Ni, onset of ferromagnetism 78−23270
Pd-Ni, spin fluctuation alloy, thermopower peak diffusion origin 80−88542
Pd-Ni, surface comp. and catalysis, AES and thermal desorption meas. 79−46898
Pd-Ni, thermal expansion and magnetostriction meas. near crit. conc. for ferromagnetism 80−65881

nickel alloys continued
Pd-Ni, thermopower and crit. conc., spin fluctuation system 78−30909
Pd-Ni (15-90 at.%), thermo EMF at 4.2-300K *(Russian)* 80−92881
Pd-Ni alloy, dil., magnetothermopower meas. 79−78079
Pd-Ni alloy, paramag. giant moments 78−56291
Pd-Ni alloys, kinetic props., transverse magnetoresistance *(Russian)* 77−76790
Pd-Ni alloys, kinetic props., anomalous Hall coefficient *(Russian)* 77−76791
Pd-Ni alloys, onset of ferromag. 79−56533
Pd-Ni disordered alloy, Landau model for mag. props. 77−66276
Pd-Ni-H, hydride formation in high press. range 80−65235
Pd-Ni-H alloys, hydrogenation under high press., superconducting crit. temp. 78−88058
Pd-Ni-H alloys hydrogenised under high press., supercond. crit. temp. 77−51834
Pd-Ni-P, amorphous, elec. resistivity negative temp. coeff., CAP calcs. 79−42515
Pd-Ni-P, metallic glass, viscous flow, alloying effect 78−79793
Pd-Ni-P metallic glass, energy loss spectra and Auger spectra 78−23563
Pd-Ni-Si amorphous alloys, crystn. process during isothermal ageing 80−89275
PdAl-Ni, phase diagrams, eutectic points and solubility *(Russian)* 80−40333
PdNi (4.7 at.%), effect of alloying on activation energy of H_2 diffusion 80−107571
$Pd_{48}Ni_{32}P_{20}$, metallic glass, viscosity meas. from rates of thermal transformations 78−26713
$(Pd_{99}Ni)_{1-x}Pt_x$, spin-fluctuation thermopower 79−60802
$Pd_{60}Ni_{20}Si_{20}$, amorphous, struct., high resolution electron microscopy 80−1969
$(Pd_{95}Rh_5)_{1-x}Ni_x$, low-temp. spin-fluctuation resist., effect of pot. scatt. 77−15840
Pr-Ni, amorphous, thermal stability, crystn., DSC and elec. resist. study 80−107060
Pr-Ni-Al system, Pr (0 to 33.3 at.%), isothermal section at 800°C *(Ukrainian)* 79−34002
$PrNi_5$, crystal field investigation from inelastic slow neutron scatt. expts. 80−39538
$PrNi_5$, crystal-field effects, comparison of calcs. with expts. 79−87071
$PrNi_5$, hexagonal, cryst. field effect in thermal expansion 80−49390
$PrNi_5$, LF dynamics and ^{141}Pr thermal relax., coupling parameter and RKKY exchange mechanism 80−103812
$PrNi_5$, metallic Van Vleck paramag., nucl. interactions, NMR meas. 80−44953
$PrNi_5$, nucl. cooling agent, relax. and exchange, EPR and NMR study 80−25237
$PrNi_5$, nucl. demagnetization, end temps., nucl. entropy 79−19718
$PrNi_5$, nuclear demagnetisation, cooling of ^{3}He to 1 mK 77−65037
$PrNi_5$, powder, in contact with liq. ^{3}He, thermal relaxation and heat capacity, mag. susceptibility 79−44909
$PrNi_5$, two stage nuclear demagnetization experiments 79−65644
$PrNi_5$-Gd, dil., single crystal, ESR study 80−75850
$PrNi_x$, sorption at press. up to 1500 atm. 80−97819
Pt-Ni, dil., surface segregation, equilib. surface composition, AES meas. 77−85039
Pt-Ni, disordered, vol. paramagnetostriction calc. 77−80985
Pt-Ni, mag. inhomogeneity, low field DC susceptibility meas. 78−56301
Pt-Ni, XPS d bands and core levels 77−32498
Pt-Ni (42 wt.%) relationship between mag. saturation flux and tensile strength 79−15819
Pt-Ni alloys, onset of ferromag. 79−56533
Pt-Ni disordered alloy, Landau model for mag. props. 77−66276
Pt-Ni vacuum condensates on Si and SiO_2, thermally treated, X-ray anal. *(Russian)* 80−70559
Pt-Ni-P, metallic glass, viscous flow, alloying effect 78−79793
$Pt_{0.7}Ni_{0.3}Fe$, magnetically hard, cryst. morphology and mag. domain struct. 77−69615
$Pt_{45}Ni_{30}P_{25}$, metallic glass, viscosity meas. from rates of thermal transformations 78−26713
Rh-Ni alloy, onset of ferromag. 79−56533
Rh-Pd-Ni, dil. alloy, mag. moment 78−95416
Rh_2NiSn, Heusler alloys, hyperfine mag. field at Sn 78−39482
Sc-Ni, phase diagram determination, using X-ray diffr., metallography and DTA techniques *(Russian)* 79−34004
Sc-Ni-Ga, phase equilibria, diagrams of state, X-ray, microstructural study *(Russian)* 80−55356
Si-containing deposit layers on Ni alloys, appl. methods *(German)* 78−85025
Si-Ni, (LMM) Auger electron emission by keV Ar^+ bombardment 79−95880
Si-Ni, liquid alloys, thermodynamic charact. calc. *(Russian)* 78−27475
SiC fibres reinforced Ni complex alloy, influence of TiN coating on fibre matrix interaction *(Russian)* 78−95820
SiC-Ni based superalloy reaction, at elevated temps. 80−3287
$Si_{1-x}Ni_x$ film, metastable impurity band, conductivity meas., semiconductor-metal transition 77−76884
$SmCo_{5-x}Cu_y$, giant intrinsic magnetic hardness, high field meas. 78−68289
$SmCo_2Ni_3$-Y(Pr)(Gd)(Tb)(Er), giant intrinsic magnetic hardness 78−56347
$SmCo_{2.5}Ni_{2.5}$, mag. after effect *(Russian)* 78−6544
$SmCo_{5-x}Ni_x$, giant intrinsic mag. hardness, temp. and time depend. 77−69627
$SmCo_{5-x}Ni_x$, giant intrinsic magnetic hardness, high field meas. 78−68289
$SmCo_{5-x}Ni_x$, giant intrinsic magnetic hardness analysis 78−88146
$SmCo_{5c}Ni_{5-5C}$, exchange fluctuations and giant intrinsic mag. hardness 78−56310
$Sm_2Co_{17-x}Ni_x$, effect of Ni on mag. props. 78−68296
$Sm_2Co_{17-x}Ni_x$, effect of substitution on mag. props. 79−78363
$SmNi_2$, hyperfine interactions and exchange fields acting on Eu^{3+}, Mossbauer obs. 77−63338
$SmNi_{5-x}Cu_x$, giant intrinsic mag. hardness due to randomised cryst. field interactions 78−68208
$SmNi_4M$, M=Fe, Cu, Al, intrinsic mag. hardness 77−85506
Sn-Ni, electrodeposit, Mossbauer meas. 80−39990
Sn-Ni, electrodeposited, thermal stability 77−52319
Sn-Ni, electroplated, passive layer, ESCA study 78−23867
Sn-Ni, equiatomic, metastable, transformation kinetics, Avrami parameters calc. method 78−92239

nickel alloys continued
Sn-Ni alloys, electrodeposited Mossbauer spectroscopy 79−61269
Sn-Ni electrodeposit, contact resist. corrosion effect 78−47847
Sn-Ni electrodeposit, metastable, transform. kinetics, X-ray and SEM meas. 78−38979
Sn-Ni electrodeposited equatonic alloy, cryst. struct., X-ray, electron diffr. anal. 80−79748
Sn-Ni electrodeposits, metastable, transform. kinetics 78−43262
Sn-Ni electrodeposits, worn, and Au coated, corrosion resist. 77−77633
Sn-Ni electroplated alloy, etch rates using quartz cryst. microbalance, contact resist. 77−59981
Sn-Ni equiatomic electrodeposited alloy, surface comp. 78−47649
Sn-Ni metastable alloy, surface film comp., time depend., XPS 78−60870
Sn-Ni metastable equiatomic alloy, sputter deposition 78−3043
Sn_3Cu_6Ni, γ-brass struct., F-cells, X-ray diffr. 77−19903
SnNi electroplate, anal. by SIMS, ion scatt. spectrometry, and Rutherford backscatt. 78−95979
SnNi, metastable, oxidation, AES obs. 77−48575
$SrNiSn_3$, cryst. struct. rel. to $ThCr_2Si_2$ type *(German)* 78−51470
steel, austenitic stainless, 18 Cr-11 Ni, effect of boron on nucleation of $M_{23}C_6$ carbides *(Polish)* 78−84808
Ta-Ni amorphous metal films, struct. and elec. characterisation 79−87017
Ta-Ni film, amorphous, UHV deposited, elec. and struct. props. obs. 78−6233
Ta(C,N)-Ni-HfC(HfN)(Mo_2C)(VC), sintering, prod. of hard metals 78−11155
Ta(C,N)-Ni-VC, sintering behaviour, VC effect 80−93520
TaC-NiC, powder for plasma arc spray coating appl. 78−15591
TaC-Ni(-W) alloys, oxidation resistance 77−60000
Tb-Ni, amorphous film, Kerr and Hall effect meas. 77−24722
$TbNi_5$, ferromag., magnetisation and paramag. susceptibility 80−25082
Tb_2Ni_{17}, magnetic structure by neutron diffr. 77−73000
$TbNi_{2-x}Cu_x$, elec. resist. and mag. props. 78−72348
$ThNi_5$, Haucke compounds, low temp. heat capacity, Debye temp. 80−96663
$ThNi_5$, methanation catalyst, AES and characteristic energy loss spectra 78−56915
Th_7Ni_3, effect of absorbed H_2 on mag. behaviour 80−60184
$ThNi_{5-x}Al_x$, absorption of H, form. of hydride 77−84932
$ThNi_{5-x}Mn_x$, struct. and magnetisation exam., temp. depend. 78−2662
Ti-CrB_2-Ni-Mo, interphase reactions, electron probe anal., metallography and hardness exam. 80−2990
Ti-Cu-Ni-Au metallisation systems, in 85°C 78% RH SO_2 contaminated environment, performance 79−74304
Ti-Fe-Ni (67, 30, 3 wt.%), reversible shape alteration *(Russian)* 80−71647
Ti-Hastelloy-N, homogenization 79−61606
Ti-Ni, effect of alloying on crit. points and martensitic transform. hysteresis 80−20935
Ti-Ni, electron phase transition XPS, optical spectra and mag. susceptibility meas. 80−19943
Ti-Ni, energy band structures, X-ray spectra obs. *(Ukrainian)* 77−32469
Ti-Ni, eutectoid decomposition, effect of interphase boundary struct. on mech. 79−4952
Ti-Ni, eutectoid decomposition 79−24491
Ti-Ni, first order displacive transformations, localized soft modes and US effects 79−73281
Ti-Ni, H_2 diffusion at room temp. *(Japanese)* 80−19987
Ti-Ni, hysteresis-free 'memory' effects 78−35385
Ti-Ni, internal friction and US props. *(Russian)* 80−84247
Ti-Ni, laser melting and splat quenching to form foils for TEM obs. 80−29986
Ti-Ni, martensite transform. B2-B19′, optical props. and electron struct. *(Russian)* 80−34878
Ti-Ni, martensitic transform., monoclinic to triclinic phase *(Russian)* 80−81058
Ti-Ni, multiplicity of structural transitions, phase diagrams, elec. cond. meas. 80−71649
Ti-Ni, oxidation, high temp., comparative study with Ti *(French)* 79−20285
Ti-Ni, oxidation of intermetallic phases 79−100298
Ti-Ni, passive surface, anodic process kinetics 79−15861
Ti-Ni, reversible shape changes during martensitic transform., dislocation struct. stability *(Russian)* 77−63666
Ti-Ni, thermoelastic phase transform., acoustic emission 80−3039
Ti-Ni, vacuum pressure seal with thermomechanical drive 80−31773
Ti-Ni (48 to 53 at.%), heat treatment and deviation from stoichiometry 80−104192
Ti-Ni (50.4 wt.%), thermal conversion efficiency of ideal thermoelastic marmem cycle 79−66057
Ti-Ni (51 at.%), martensitic transformation, thermoelastic, hysteresis, exothermic and endothermic effects *(Russian)* 78−19749
Ti-Ni (51 at.%), plastic deform., two reversible form change effects *(Russian)* 77−8881
Ti-Ni alloy, effect on $[Cu(NH_3)_4.(H_2O)]^{2+}$ solns. on drilling *(Russian)* 78−53017
Ti-Ni alloys, absorpt. of H_2, press.-composition-temp. relationships, enthalpy, entropy 80−2267
Ti-Ni alloys, absorpt. of H_2, thermodynamic parameters calc. 80−2268
Ti-Ni amorphous alloys, glass transition and ductility, O additions effect 80−75168
Ti-Ni-Al-(Ga), Th_6Mn_{23} type struct., mag. susceptibility *(Russian)* 79−42736
Ti-Ni-Co, constitution diagram, isothermal section, interdiffusion coeffs. *(Russian)* 80−89200
Ti-Ni-Co cubic B_2 alloys, phonon enhancement of electronic sp. ht. near martensitic transform. 79−60522
Ti-Ni-Co(Fe), shape memory temp., alloying effect 79−38912
Ti-Ni-Cu (44.5, 10 wt%), opposing stress effect on shape memory and martensitic reversion 78−44185
Ti-Ni-Cu system, phase relations at 800 and 870°C 78−27481
Ti-Ni-Fe, multiplicity of structural transitions, phase diagrams, elec. cond. meas. 80−71649
Ti-Ni-Fe, plasticity, tensile stress-strain diagrams, ultimate tensile strength, elec. resist. depend. on temp. *(Russian)* 79−61652
Ti-Ni-H, catalytic props. 80−30274
Ti-Ni-Mo (1.5, 2 wt.%), Mo effect on microstructure 77−36536
Ti-Ni-Si metallic glass, prep., thermal and mech. props. 78−64497

nickel alloys continued
Ti-Pd-Cu-Ni-Au metallisation systems, in 85°C 78% RH SO_2 contaminated environment, performance 79−74304
TiB_2-Ni (20 wt.%), initial stage sintering under high press., lattice strain 77−55905
TiC-(Mo-Cr-Ni-Mn) steel alloy, optimum comp. and manufacture conditions, Mn effect 80−84896
TiC-Ni, particle growth quantitative anal. by metallography and stereology 77−77684
TiC-Ni powder compact, wetting problems in sintering 80−11596
TiC-Ni-Co-Cr, sintered, mech. props. effect of processing factors 78−11159
TiC-Ni-Cr(Mo) hard alloy mixtures, pressing 77−63596
TiC-Ni-Mo hard alloy, wear resistance under end face friction cond. 78−60846
TiC-Ni-Mo hard alloys, use in hard layer prod. by electrospark alloying 77−59998
TiC-Ni-Mo sintered hard alloy TN-20, fracture surfaces 80−7684
TiC-Ni-Mo(W), cemented carbides, grain growth, metallographic obs. 77−24982
TiN-Ni mixed powder compact, phase relations and denitrification during sintering *(Japanese)* 79−43167
TiN-Ni powder compacts, sintering, gas atm. and vac., shrinkage, solid solubility *(Japanese)* 78−72750
TiNi alloys, structural transform., physical props. and memory effects *(Russian)* 79−1856
TiNi, imperfect elasticity, elastic after-effect on basis of martensitic transformation theory *(Russian)* 79−100198
TiNi, shape memory effect, spontaneous EMF generation 77−32637
TiNi, soft X-ray spectra, electronic struct. 77−44091
TiNi, strain recovery, memory effect, in martensite phase *(Russian)* 77−4806
TiNi-H system, thermodynamic rels. and struct. transformations 80−49385
TiNi-TiCu, exam. of shape memory effect, specific work 79−100216
$Ti_{0.60}Ni_{0.40}$ metallic glass, Young's modulus meas. by impulse induced resonance technique 80−40411
$Ti_{1-x}Ni_x$, electronic struct. and anomalies of elec. and mag. props. 80−6710
Ti_2Ni, determ. of H diffusion coeff., quasielastic neutron scatt. 78−30781
$Ti_{70}Ni_{20}B_{10}$, amorphous alloys, crystn. behaviour, TEM study *(Japanese)* 80−84087
$Ti_{50}Ni_{47}Fe_3$, premartensitic phases, neutron scatt., sp. ht. and electron microscopy obs. 79−96025
Ti_2NiH_3, H storage material, H diffusion, neutron diffr. obs. 80−51013
Ti_2NiO_x (x=0 to 0.5), hydrogen characts., thermogravimetry/DTA meas. 79−52760
Ti(V,Ni)/Al bimetal film structure, macroscopic defects *(Russian)* 79−1555
Tm_2Ni_{17}, magnetic structure by neutron diffr. 77−73000
U-Ni dilute alloy fission product source design and use at EBR-II 79−9932
U-Ni metallic glasses, glass form. and thermal stability 80−75183
U-Ni-B, isothermal section of phase diagram, X-ray obs. 79−52157
UAl_2-UNi_2, phase relationships, thermal, microscopic and X-ray exam. *(German)* 78−88447
$U(Co_xNi_{1-x})_2$, cryst. struct. and mag. props. at 4.2K 80−54175
UNi_2, mag. phase transition, elec. resist. meas. 80−97094
UNi_5, core and valence band spectra, XPS obs. 80−50530
$UNi_{0.5}Cu_{4.5}$, core and valence band spectra, XPS obs. 80−50530
$UNi_{5-5x}Cu_{5x}$, NMR and press. effects 80−25230
$UNi_{5-x}Cu_x$, thermoelectric power, 5-300K 79−65444
$U_3Ni_3Sb_4$, and related compounds, X-ray diffr. cryst. struct. determ. 79−42009
$U_3Ni_4Si_4$, X-ray cryst. struct. determ. 80−33931
UO_2 pellets-graphite-Zircaloy cladding, evaluation of graphite lubrication 80−32342
V-Ni, ion bombard., void form. 80−34097
V-Ni alloy, onset of ferromag. 79−56533
V-Ni sigma phase alloys, NMR and electric-field gradients 80−108109
V-Ni-Al, phase equilib., elect. cond., hardness *(Russian)* 77−66627
V-Ni-Mo, structure in alloy crystallisation region, peritectic equilibria *(Russian)* 80−50622
V-Ni-Mo alloy, annealed at 1150°C, isothermal section *(Russian)* 79−52154
$V_{77}Ni_{23}$, nuclear spin-lattice relax. time, electronic density of states 77−59354
$V_{3-x}Ni_xGa$, cryst. struct. and microhardness meas. 79−86740
$V_{75-x}Ni_xGa_{25}$, supercond. transition temp. and electron-phonon coupling parameter 79−60952
V_3Si-Ni solid soln., supercond. T_c and paramag. susceptibility *(Russian)* 77−59348
W fibre reinforced Ni alloy, high temp. composite development 77−48370
W fibre reinforced Ni-Cr (20 wt.%), hot pressing kinetics 78−35334
W-Co-Ni, contact materials, activated sintering, Ni effects 79−95967
W-Cu contact materials with Ni and Co dopants, sintering 77−55908
W-Cu-Ni, electrical contact material, comparison of Ni and Co effects *(Korean)* 78−10539
W-Cu-Ni powder, liquid phase sintering, stabilisation of porous structure and control of volume changes 79−95974
W-Ni, liquid phase sintering, microstruct. meas. 78−44054
W-Ni, liquid phase sintering 80−16232
W-Ni, liquid phase sintering 80−25613
W-Ni, MBM diode, resist. depend. of detected signals 80−2482
W-Ni, MOM diode, breakdown effect in visible and near-IR regions 80−6999
W-Ni, surface barrier influence on C diffusion in stainless steel type 1Kh18N9T *(Russian)* 80−54434
W-Ni (0.5, 2 and 5 wt.%), Ni effect on shrinkage anisotropy during sintering 77−21056
W-Ni compact, sintering behaviour and workability *(Japanese)* 80−20822
W-Ni liquid alloys, sintered, coarsening of W grains, exam. 78−56598
W-Ni powder compacts and wires, recrystallisation, influence of omnidirectional press. *(Russian)* 77−8849
W-Ni sintered alloy, etching 79−29323
W-Ni system, grain growth and densification during liquid phase sintering 79−38760

nickel alloys continued
W-Ni system, liq. phase sintering, 1640°C, solubility and vol. diffusion of Ni in W 79−86895
W-Ni-Cr, high-temp. phase diag. *(French)* 77−48393
W-Ni-Cu(4, 2 wt%), radionuclide calorimeter for liquid He range 4.2 to 8K 79−18093
W-Ni-Fe, W-Ni-Fe-Mo (Mn), sintering and mechanical props. *(Japanese)* 80−21086
W-Ni-Fe (5(2), 5(2) wt.%) pore formation, effect on mech. props. 80−45396
W-Ni-Fe system, reduction kinetics and alloy form. 80−60801
W-Ni-Fe(Co)(Cr), structural characterisation *(French)* 77−56074
W-Ni-Fe(Cu), liquid phase sintered, interfacial embrittlement 79−57101
W-Ni(Co) point-contact diodes as harmonic generators and mixers, DC bias dependence 80−75653
W-Re fibre-reinforced Ni-base refractory alloy, struct. and props. *(Russian)* 77−59721
W-ThO_2 fibre reinforced Ni base alloys, powdered matrices, fibre/matrix interaction above 1300°C, alloying effects *(Russian)* 78−95755
WC-Ni (10 wt.%), room temp. transverse rupture strength *(Japanese)* 77−63774
WC-Ni detonation sprayed coating, wear resistant 78−35594
WC-Ni hard alloy composite, sintered, void healing 80−60821
WC-Ni hard alloys, sintered, with uneven binder metal distrib., molten Ni migration 78−35336
WC-TiC(TaC, NiC)-Co, hard, homogeneity and wear resistance estimation, by magnetic method 77−90558
Y-Ni, liquid alloys, enthalpy struct. *(Russian)* 78−27474
Y-Ni amorphous alloy, spontaneous magnetisation, Curie temp. and paramag. susceptibility 78−68189
Y-Ni-B, X-ray and microstruct. anal., phase composition 77−16539
$Y(Co_{1-x}Ni_x)_5$, distrib. of Co and Ni atoms, neutron diffr. obs. *(Russian)* 80−64954
$Y(Co_{1-x}Ni_x)_5$, mag. heterogeneities and coercive force, neutron scatt. study 80−2553
$Y(Co_{1-x}Ni_x)_5$, magnetocryst. anisotropy, different contribs. of two Co sites 77−8301
$Y(Co_{1-x}Ni_x)_5$, spontaneous magnetisation mag. anisotropy, spin reorientation transformation *(Russian)* 80−7082
$Y_2Co_{17-x}Ni_x$, effect of Ni or mag. props. 78−68296
$YFe_{3-x}Ni_x$, electronic sp. ht., saturation magnetisation and lattice parameter meas. 78−68261
$Y_2(Fe_{1-x}Ni_x)_{17}$, Mossbauer spectra, hyperfine field interactions 78−6614
YNi_2 amorphous alloy, at. struct. 80−19704
YNi_2, density of states, mag. props. 79−90936
YNi_3, loss of ferromagnetism after H_2 absorpt., Pauli paramag. props. 80−34588
YNi_3, magnetism resurgence, neutron diffr. and mag. props. study 80−65819
YNi_5, Haucke compounds, low temp. heat capacity, Debye temp. 80−96663
YNi_5, solubility of H_2 *(Russian)* 78−15356
$Y_{0.22}Ni_{0.78}$ amorphous alloy, low temp. sp. ht. 79−65680
Y_2Ni_{17}, ferromag. struct., neutron diffr. expt., cryst. field calcs. 77−73001
Y_3Ni_2, crystal struct., tetragonal type 78−14309
Y_xNi_{1-x}, amorphous, high press. magnetisation and Curie temp. 80−20442
$YNi_{5-x}Al_x$, Al addition effects on structural and H_2 absorpt. props. 79−52761
$YbNi_2$-$YbCu_2$ system, valency state, Yb behaviour *(French)* 80−45277
$YbNi_2Ge_2$, intermediate valence cpd., mag. susceptibility expts., 4.2-280K 78−39288
Zircaloy-4, vapour transport of Zr and Si 80−55437
Zn-Cd liquid/Fe-Ni-Al mag. powder, effective viscosity of composites *(Russian)* 80−54424
Zr-Nb (2.25 wt.%), oxidation kinetics in flowing CO_2, 873 to 1173K 80−16596
Zr-Nb-Sn (3.0, 1.0 wt.%), oxidation kinetics in flowing CO_2, 873 to 1173K 80−16596
Zr-Ni, amorphous and crystalline, d-band struct., alloying effects 80−59862
Zr-Ni, diffusion of H_2, 900 to 1080°C *(Korean)* 80−19988
Zr-Ni, energy spectra of valence electrons *(Ukrainian)* 78−6814
Zr-Ni, oxidation of intermetallic phases 79−100298
Zr-Ni, surface layer, segregation of ferromag. Ni, magnetooptic investigation 80−2256
Zr-Ni (65 to 80 at.%), phase diagram and cryst. struct. of intermediate phases 79−52170
Zr-Ni alloy, H_2 storage in form of capsules *(French)* 79−92091
Zr-Ni alloys, energy spectra, X-ray emission obs. *(Russian)* 78−19604
Zr-Ni amorphous alloy, thermal stability and electronic props. 79−73487
Zr-Ni metallic glasses, glass form. and thermal stability 80−75177
Zr-Ni-Cu-H, catalytic activity, exam. by conversion of toluene, and bicyclic aromatic hydrocarbons 80−30276
Zr-Ni-Cu-H, catalytic props. 80−30274
Zr-Ni-Ga, mag. susceptibility in phases of structural type Th_6Mn_{23} *(Russian)* 79−24130
Zr-Ni-H, catalytic activity, exam. by conversion of toluene, and bicyclic aromatic hydrocarbons 80−30276
Zr-Ni-H, synthesis at high H pressure exam. of props. 80−29924
Zr-Ni-H_x(x=2.8 to 3), surface layer, segregation of ferromag. Ni, magnetooptic investigation 80−2256
Zr-Sn-Fe-Ni (1.5, 0.1, 0.15 wt.%), electron irradiation damage, direct obs. 80−84212
Zr-Sn(Fe)(Ni) (0.15 wt.%), electron irradiation damage, direct obs. 80−84212
$Zr_3Co_{1-x}Ni_x$, phase stability and supercond. T_c 78−80519
$Zr_{50}Co_{50-x}Ni_x$, transform. and deform. studies 79−1864
ZrNi, surface segregation of Ni, influence on catalytic activity 80−30275
$ZrNi_5$, methanation catalyst, AES and characteristic energy loss spectra 78−56915
Zr_2Ni, search for soft phonon modes, neutron scatt. 79−23686
Zr_2Ni, spin-pairing state investig. via Josephson current between weakly-coupled superconductors 77−47942
$Zr_{70}Ni_{30}$ amorphous alloys, struct. factors and radial distrib. functions 80−84096
$Zr_{70}Ni_{30}$, metallic glass, low temp. resist., supercond. T_c 79−38235

nickel compounds
see also nickel alloys
bis-tetraethylammonium tetrachloronickelate, heat capacity, structural transitions 79−65209
calcine, reactivity, contact I-V meas. 77−85975
chloride layered compound with graphitised PAN fibre, struct. and elec. cond. 79−91600
complexes, quenching of single O_2 79−94028
dimethyl nickel, equilib. geometry, orbital energies, ab initio rel. to pseudopot. calcs. 78−82613
ethylenediammonium nickel chloride, struct. and mag. props., vibr. spectra 79−10842
etioporphyrin, reson. Raman spectra, excitation profiles, nucl. distortion and Jahn-Teller effects 77−58018
ferrite, gas phase fluorination for improved props. 78−52306
ferrite, quenched, Neel temp. and initial susceptibility 80−75762
ferrite, spinel type catalytic oxidation of CO, role of mag. exchange interactions 78−56916
ferrites, internal friction and modulus defect at US freqs. 79−19762
ferrites, polycryst., X-ray diffr. struct. anal., chem. anal. *(German)* 77−72598
halides, XPS, multiplet struct. and multielectron excitations, in 3 p and 2p shells 80−78649
hexapyridol perchlorate, $Ni(C_5H_5NO)_6(ClO_4)_2$, sp. ht., mag. ordering transition 77−48004
intercalation, electron microscopy 80−84164
methylene nickel, equilib. geometry, orbital energies, ab initio rel. to pseudopot. calcs. 78−82613
Ni complex, dimethylglyoxymate film, prep. and physical props. 79−90923
nickel acetate tetrahydrate:Mn^{2+}, EPR spectra, angular var. calc. 80−54940
nickel phthalocyanine iodide, single-cryst. elec. cond., low-dimens. mol. metals 78−76057
$NiWO_4$, antiferromag., low symmetry exhibited during spin-flop phase transition 80−60263
oxalate, decomposition kinetics, in polymeric medium, thermogravimetry and DTA 78−52749
oxalate, electronic struct. from Huckel calcs., optical props. and reactivity 77−89741
oxalate hemihydrate, photographic props. eval. for use as high-speed photographic materials 77−44497
oxide, interatomic interaction by XPS 80−7474
oxide reduction by electron cyclotron reson. plasma of H, model study on discharge cleaning 80−76548
oxide surface layer, TOF atom probe anal. 78−64766
oxides, AES meas. 77−36323
perovskites, ordered, mag. props. *(French)* 78−95434
3p photoelectron spectra, light-inuced changed in multiplet satellites 80−80946
phthalocyanide, cryst. struct. sensitivity of band struct. 79−42444
phthalocyanine, ohmic and space-charge-limited currents in vacuum ambient 77−20323
phthalocyanine, resonant photoemission at 3p-core threshold from quasiatomic Ni 79−78847
phthalocyanine film, surface photovoltage, central ligand effect 79−78231
piston engine using $LaNi_5H_x$ as energy conversion medium, prototype 79−70458
polyphosphinate, bulk compressibility meas. to 30 kbar 80−76306
reduced Ni oxide, H absorption 80−76529
rubrene fluorescence, quenching by Ni complexes 79−94028
silicides, formation in double layers of Ni and Pt films on Si substrate 78−84010
sulphide ores from Kambalda, W.Australia, sulphide fabrics 78−77229
sulphides, surface oxidation studied by AES 79−83505
systems Ni ions anal. by ESCA *(Japanese)* 80−40787
triple orthoarsenates, $KNiCr_2(AsO_4)_3$ and $NaNiCr_2(AsO_4)_3$, prep. by high temp. synthesis, and cryst. struct. 79−66028
$(TTF)_2(NiS_4C_4H_4)_3$, disordered solid soln. and struct. modulation obs. 79−94986
Tulton salts, cryst. field spectra in visible and near IR regions, solid dilution effect 80−100666
vanadates, elec. and mag. props., stoichiometry 78−51991
$[Ni(NH_3)_6](ClO_4)_2$, X-ray powder diffr. exam. of enantiomorphic transitions 78−2054
Al_2O_3-Nb_2O_5-NiO, isothermal phase sections, 1100, 1250, 1400°C *(Italian)* 79−20032
$Ba_2Ni_3F_{10}$, cryst. struct. and antiferromag. props. 80−107153
$BaNi_2(PO_4)_2$ and $BaNi_2(AsO_4)_2$, mag. props., neutron diffr. and sp. ht. meas. 80−70948
$BaTiO_3$-Ni(Co, Mn)Fe_2O_4, ceramic, exam. of prep. and physical props. 78−68655
$C_{11.3}NiCl_{2.13}$ intercalation compounds, cryst. struct. *(French)* 80−33947
Ca-Mg-Ni hydrides, water form. on O_2 exposure 80−97727
$Ca_xNi_{1-x}Fe_2O_4$, initial permeability and Curie temp. 80−25130
$Ca_xNi_{1-x}Fe_2O_4$, X-ray struct. anal., determ. of lattice constant and interplanar distances *(French)* 80−96487
$Ca(No_3)_2.3.91H_2O$-$NiCl_2$ melts, glass forming, transport behaviour 78−59963
CaO-SiO_2-NiO melt, viscosity and elec. cond., effect of NiO conc. *(Japanese)* 79−23760
CaO-SiO_2-NiO-MgO glass melt, interaction of NiO and MgO, elec. cond. and IR spectra obs. *(Japanese)* 80−24632
CdNi ferrite, quadrupole interaction, cation distrib. influence 78−2776
$Cd_{0.8}Ni_{0.2}Fe_2O_4$ ferrite, Fe spin relaxation Mossbauer study, mag. hyperfine struct. *(Russian)* 80−15932
$Cd_{1-x}Ni_xFe_2O_4$, solid soln., mag. and structural characterisation 80−103906
$Cd_xNi_{1-x}Fe_2O_4$, mag. behaviour, Mossbauser meas. 78−52390
CdS-$NiCl_2$ interface, elec. props. using SAW techniques 79−56302
$CeNiC_2$, struct. determ. using X-ray diffraction *(Ukrainian)* 80−33949
$Ce_6Ni_6P_{17}$, synthesis and cryst. struct. 78−75634
Co complex, (4-methylpyridine)$_4Ni(NCS)_2$, porosity 77−76364
$Co_{0.08}(Ni,Cu)_{0.92}Fe_2O_4$ sphere, rotational hysteresis, mag. field strength and orientation depend. *(Russian)* 77−16110
$Co_xNi_{1-x}Cl_2.6H_2O$, calorimetry, γ-type transitions of sp. ht. 78−68256
$Co_xNi_{1-x}Cl_2.6H_2O$, solid solution, mag. props. and phase diagram, calc. 80−7104
$Co_x(Ni_{0.5}Cu_{0.5})_{1-x}Fe_2O_4$ ferrite, relation between elec. cond. and mag. anisotropy 80−75548

nickel compounds continued
- $Co_xNi_{1-x}Fe_2O_4$, induced mag. anisotropy consts., conc. and temp. depend. 80−108001
- $(Co_{1-x}Ni_x)O$, single crysts., morphology change during compressive creep testing 79−29144
- $Co_{3-x}Ni_xO_4$, $0 \leq x \leq 1.1$, struct., semicond.-semimetal transition, Seebeck coeff. 78−87972
- $Co_xNi_{1-x}O$, antiferromagnet, neutron diffr. study of mag. struct. 80−34595
- $(Co_yNi_{1-y})_{1-x}O$ and O_2 prep. props., and reactions 77−12569
- CoNiZn ferrites, Fe excess, complex permeab. var. with annealing temp. 77−89979
- CoP-NiCoP, composite ferromag. film, exchange coupling between soft and hard layers, FMR obs. 79−78448
- $Co_{0.0031}Zn_{0.5676}Ni_{0.4293}Fe_2O_4$, single phase ferrite powder, from solid solution of schoenite-type salt 77−16524
- $(Co_{0.001}Zn_{0.189}Ni_{0.143}Fe_{0.667})SO_4.(NH_4)_2SO_4.6H_2O$, schoenite-type salt, formation of single phase ferrite powders 77−16524
- Cr-Ni-O, computer-assisted anal. and calcs. of phase diagrams 80−25667
- $Cr_{1-x}Ni_xSi_2$, prep., elec. cond. and thermoelec. props. 80−49697
- $CsNiBr_3$, double ordering in mag. linear chain system, sp. ht. and NMR data 79−28545
- $CsNiCl_3$, antiferromag. coupling in linear chains, molecular orbital approach 78−52239
- $CsNiCl_3$, double ordering in mag. linear chain system, sp. ht. and NMR data 79−28545
- $CsNiCl_3$, linear chain antiferromag., mag. props., 1.1 to 7K 79−61076
- $CsNiCl_3$, mag. props. 79−73736
- $CsNiCl_3$, noncollinear magnetic order and spin wave spectrum in presence of competing exchange interactions 80−65834
- $CsNiCl_3(Br_3)$, quadrupole interaction meas. by NMR spin-echo modulation 77−85615
- $CsNiF_3$, 1-dimens. ferromag., evidence for solitons, inelastic neutron scatt. study 79−78430
- $CsNiF_3$, anisotropic Heisenberg chain, nonlinear excitations 80−70927
- $CsNiF_3$, field depend. mag. behaviour, mag. linear dichroism 79−73903
- $CsNiF_3$, NMR and relax. exam. 78−52371
- $CsNiF_3$, one-dimens. anisotropic paramagnet, EPR meas. 79−73799
- $CsNiF_3$, one-dimens. ferromag., solitons as gas of quasiparticles, inelastic neutron scatt. obs. 79−73679
- $CsNiF_3$, one-dimens. ferromag., collective excitations in mag. field 80−44822
- $CsNiF_3$, solitons in one-dimens. ferromag., inelastic neutron scatt. 78−95450
- $CsNiFeF_6$ pyrochlore, Mossbauer contrib. to exam. of cationic order *(French)* 80−93224
- Cu-Ni ferrite films, LPE growth 80−96752
- CuCoNi ferrite magnetoacoustic oscills. rel. to microstruct. 77−85536
- $Cu_xNi_yO_z$, protective oxide film on Cu-Ni alloy, AES 79−39035
- $(Cu_xNi_{1-x})S_2$, XPS of valence band meas. 77−85885
- Cu_2O-NiO-SiO_2, equilibrated with liquid Cu, Pb and Ni distrib. 77−28790
- Cu_2S-Ni_3S_2, melt viscosity 77−51536
- $Dy_3Ni_7B_2$, struct., space groups, X-ray study *(Ukrainian)* 80−39029
- $DyNi_2Si_2$, mag. props., 4.2-200K 80−84602
- $ErNi_2Si_2$, mag. props., 4.2-200K 80−84602
- $(Fe,Ni)O_4$, magnetostriction calcs. *(Dutch)* 80−2619
- Fe-Co-Ni-O, mag. powder prod. by reduction of oxalates 77−63582
- Fe-Ni sulphides in Murchison meteorite, props. and rel. to phase Q1 79−58303
- Fe-Ni-Cr-S-O compounds, occurrence in Allende chondrite *(French)* 78−32411
- Fe-Ni-O, computer-assisted anal. and calcs. of phase diagrams 80−25667
- FeC_x-CrC_y-NiC_z, stainless steel carbide, solar selective surface, fabrication, magnetron sputtering system description 80−80967
- FeC_x-CrC_y-NiC_z, stainless steel carbide, graded solar selective surface, magnetron sputtered 80−81485
- FeC_x-CrC_y-NiC_z, stainless steel carbide, sputtered solar selective surface, grading profile 80−81486
- $FeNiBO_4$, $FeNi_2BO_5$, Mossbauer spectra, mag. relax. 80−15889
- $Fe_{40}Ni_{40}C_{14}P_6$ amorphous film, dislocation and mag. struct., neutron diffr. study 80−70956
- $(Fe_{1-x}Ni_x)_2O$, yH_2O crystal growth, characterisation by Mossbauer spectroscopy, mag. meas. and electron microscopy *(French)* 80−80655
- $Fe_{3-x}Ni_xO_4$, low temp. Mossbauer spectra, electron transfer and spin density distribution 78−52404
- $Fe_{3-x}Ni_xO_4$, Mossbauer spectra, effect of Fe^{2+} conc. 77−69754
- $(Fe_{1-x}Ni_x)_2P$, Curie temp., press. depend. meas. 80−97091
- $(Fe_{1-x}Ni_x)_2P$, magnetisation, susceptibility, thermal expsn. 79−11302
- $(Fe_{1-x}Ni_x)_3P$, cryst. struct. and mag. props. 78−19222
- $Fe_{2-x}Ni_xP_{1-y}As_y$, band model of mag. props. 77−40029
- $Fe_{2-x}Ni_xP_{1-y}As_y$, mag. props. Mossbauer obs. 77−40156
- $(Fe_xNi_{1-x})_{80}P_{14}B_6$, amorphous, hyperfine field distrib., ^{57}Fe Mossbauer spectra 79−11367
- $Fe_{0.5}Ni_{0.5}S_2$, hyperfine field at ^{57}Fe, Mossbauer effect *(Japanese)* 77−43916
- $Fe_{1.985}Ni_{0.975-x}Zn_xCo_{0.04}O_{4+y}$, elementary coupling energy of Co^{2+} to lattice 77−1549
- Fe_xNi_{1-x}(1,10-phenanthroline)$_2$(NCS)$_2$, spin crossover, Mossbauer and magnetism study 80−44980
- Fe_2O_3-MgO-NiO, tie-lines between solid solns. of oxide and spinel at 1273K *(French)* 79−100124
- Fe_2O_3-NiO-Na_2O-Li_2O-B_2O_3-SiO_2 glass, EPR meas. of exchange interactions 77−32243
- Fe_2O_3-NiO-ZnO-CoO (15.1, 17.6, 0.6 wt.%) ferrite, effect of electron beam machining on surface layer 79−34178
- Fe_3O_4-Cr_2O_3-Ni_2O mixture, reduction by gases heated by electric arc discharge *(Russian)* 78−15704
- Fe_3O_4-$NiFe_2O_4$, solid soln., activities determ. from EMF of galvanic cell 80−16290
- FeS-Ni_3S_2, melt viscosity 77−51536
- FeS-Ni_3S_2-Cu_2 S melt, enthalpy *(Russian)* 78−95730
- $Fe_{1+x}Sb$-NiSb solid soln., mag. props., Mossbauer spectra, solubility limits, and lattice consts. *(Russian)* 77−59394
- Gd Ni_2Si_2, mag. props., 4.2-200K 80−84602
- $Ge_xNi_{1-x}O$, crystallographic and elec. props. 77−32011
- $(Ge_{1/3}Se_{2/3})_{100-x}Ni_x$, ESR, rel. to elec. cond. 80−7155
- $(Ge_{0.32}Se_{0.32}Te_{0.32}As_{0.4})_{100-x}Ni_x$, ESR, rel. to elec. cond. 80−7155
- $HoNi_2Si_2$, mag. props., 4.2-200K 80−84602

nickel compounds continued
- InSb:NiSb, size reson. scatt. from hard cylindrical pot. obs. in magnetoresist. 79−95421
- InSb-NiSb, 8 mm band noise generation *(Russian)* 78−39175
- InSb-NiSb, eutectic, intraband magneto-optical studies, far IR transmission spectra 79−61371
- InSb-NiSb, eutectic alloy, Te-doped, electrophys. props. 77−35955
- InSb-NiSb, longit. thermomag. amplifier 77−47838
- InSb-NiSb, photovolt. effects rel. to theory of semicond. with internal elec. short circuits 80−65620
- InSb-NiSb eutectic, struct. and optical props., IR polariser appl. 80−45078
- InSb-NiSb plate, nature of transverse photo-EMF 79−15186
- InSb-NiSb plate, transverse EMF due to modulated illumination 77−55572
- InSb-NiSb system, anisotropic, acoustomagnetoelec. effect, theory 79−24021
- InSb-NiSb two-phase system, photomag. effect, orientational depend., 90-300K *(Russian)* 78−2524
- InSb-NiSb two-phase system, electron scatt. mechanism *(Russian)* 78−6373
- $K(Ni(CN)_2HN_2S_2)$, cryst. struct. determ. 78−63715
- $KNiCl_3$, disorder as observed by electron diffr. 80−75213
- $KNiF_3$, ^{19}F spin-lattice relaxation 80−93211
- K_2NiF_4, antiferromag., one-magnon light scatt. from spin-flop and paramag. regions, effect of anisotropy 79−33677
- K_2NiF_4, antiferromag., one-magnon light scatt., effect of anisotropy 79−33676
- K_2NiF_4, quadratic layer antiferromag., field induced two magnon nuclear spin-lattice relax. 79−61258
- $KNi_xMn_{1-x}F_3$, mixed antiferromagnet, light scatt. meas. 80−16025
- $K_2Ni(MoO_4)_2$, paramag. props., 90-800K *(French)* 80−39734
- $K_2Ni(MoO_4)_2$, X-ray cryst. struct. determ. 79−14782
- $K_2Ni_2(SO_4)_3$, cubic langbeinite struct., low temp. mag. susceptibility 78−56299
- $K_xNi_{x/2}Ti_{8-x/2}O_{16}$, ionic cond. meas. 78−67856
- $LaNi_{1-x}Fe_xO_3$, UPS, XPS, X-ray absorpt. spectra, band struct. study 79−56885
- $LaNiC_2$, struct. determ. using X-ray diffraction *(Ukrainian)* 80−33949
- $LaNi_{1-x}Co_xO_3$, mag. props. 77−85411
- $LaNi_{1-x}Co_xO_3$, UPS, XPS, X-ray absorpt. spectra, band struct. study 79−56885
- $LaNi_5D_6$, cryst. struct., neutron diffr. obs. 79−19221
- $LaNi_5H_x$ (x=4.7, 4.9), NMR line width, spin-lattice relaxation time temp. depend., H self-diffusion *(Russian)* 79−61248
- $LaNi_5H_6$ sponges, Al or Mn substitution, neutron diffr. 80−24427
- $La_2Ni_7H_x$ (x=9.9, 11.4), NMR line width, spin-lattice relaxation time temp. depend., H self-diffusion *(Russian)* 79−61248
- $LaNi_{1-x}Mn_xO_3$, ^{55}Mn NMR study, magnetisation meas., ferromag. and Pauli paramag. components 80−7191
- $La_6Ni_6P_{17}$, synthesis and cryst. struct. 78−75634
- $Li_{0.45}Ni_{0.1}$, $Fe_{2.45}O_4$, sintering, mag. props., rare earth oxide additive effects *(Japanese)* 77−66602
- $Li_2Ni_2(MoO_4)_3$, paramag. props., 90-800K *(French)* 80−39734
- $Li_2Ni_2Mo_3O_{12}$, cryst. struct. and struct. type systematics 77−72587
- Li_xNiPS_3, antiferromag., mag. props. and ionic mobility, NMR meas. 79−24223
- $Li_xNi_{1-x}0$ (x=0 to 0.03), solid soln. effect of Li on densification during sintering 80−25638
- Mg-Cu-Mn-Ni-Fe-O, UHF ferrites, synthesis, physicochem. state, mag. and dielec. parameters 79−11536
- Mg_2NiH_x, PMR exam. of motion of H 78−56383
- $Mg_xNi_{1-x}(NO_3)_2.6H_2O$, crystal structure changes due to substitution of Mg^{2+} *(German)* 80−24428
- MgO-NiO, STEM microanal., absorpt. effects 80−80902
- MgO-NiO, solid soln. formation, initial stage obs. 77−81243
- (Mn,Ni,Zn) ferrite single cryst., flame fusion cryst. growth, conc. change 77−77369
- $Mn_xCd_{1-x}(NH_3)_2.Ni(CN)_4.2C_6H_6$, Hofmann type mixed cryst., mag. props. 79−4659
- $Mn_{3-x}Ni_xB_4$, mag. props. *(Russian)* 77−51923
- $Mn_{3-x}Ni_xB_4$, with onset of spontaneous magnetisation below T_N, singularities of mag. props. *(Russian)* 77−59427
- $Mn_xNi_{1-x}Cl_2.nH_2O$, antiferromag., sp. ht. meas. 79−91226
- N_2 complex, $NiC(C_6H_5NO)_6(NO_3)_2$, singlet ground-state systems, field induced mag. long range order 80−60266
- NCl_2, phase transition of adsorbed Xe 78−56040
- NH_4Cl:$NiCl_2$, TSC obs. of polarisation 79−78618
- $(NH_4)_2Ni(CrO_4)_2.6H_2O$, X-ray single cryst. struct. determ. 79−19207
- $(NH_4)_{0.8}Ni_{1.1}PO_4.xH_2O$, ion exchange props., Cs^+ ion sorpt., struct., IR spectra 77−9121
- $(NH_4)_2Ni(SeO_4)_2.6H_2O$:$Mn^{2+}$, EPR spectra, spin quenching 78−2732
- $NaAl_2O_4$-$MgAl_2O_4$ spinel solid solns., activities rel. to cation distrib. 77−15377
- NaCl-KCl-$NiCl_2$ system diagram investig. *(Russian)* 79−96014
- NaH_2PO_4-NH_4Cl-$NiCl_2$, soln., Ni yield, factors affecting, pot. use as radiographic media 79−52702
- $NaNiF_3$, cryst. struct. 77−76362
- $Na_{2.4}Ni_{0.8}(MoO_4)_2$, paramag. props., 90-800K *(French)* 80−39734
- Na_5NiO_4, crystallographic data *(German)* 78−63736
- $Na_2NiTi_7O_{16}$ bronze, synthesis in $NaBO_2$, growth conditions *(French)* 78−43998
- $Na_2Ni_2Ti_6O_{14}F_2$, characterisation and mag. props., 90-800K, $Na_xTi_4O_8$ bronze isotypes *(French)* 80−39735
- Na_2O-Al_2O_3-SiO_2-TiO_2-NiO glass, paramagnetic centres, form. during crystn., ESR study 79−65710
- Na_2O-B_2O_3-NiO melts, NiO activity and solubility meas. by EMF method *(Japanese)* 80−92677
- Na_2O-BaO-NiO_2-SiO_2 glass, ion-bombarded, optical time intensities 80−35037
- Na_2O-SiO_2-NiO melt, viscosity and elec. cond., effect of NiO conc. *(Japanese)* 79−23760
- Na_2O-SiO_2-NiO systems Ni ions anal. by ESCA *(Japanese)* 80−40787
- Na_3PO_4-$Ni_3(PO_4)_2$ system, phase equilibrium diagrams, crystallographic study, double orthophosphates *(French)* 80−93546
- $Na_4[M^{II}(NH_3)_4][M^I(S_2O_3)_2]_2.L$, ($M^{II}$=Cu, Ni), ($M^I$=Cu, Ag), (L=$H_2O$, NH_3), IR spectra, vibr. anal. *(French)* 78−52477
- Ni bi-univalent cpds., soln., activity coeffs., osmotic coeffs., water activity, Gibbs energy, molality depend. 80−51963
- Ni cermet selective absorbers, photothermal conversion appls. 80−21413

nickel compounds continued
Ni complex, ^{57}Ni-bleomycin synthesis from cyclotron prod. ^{57}Ni 77−86629
Ni complex, 1,2-benzoquinonedioximates, refl. spectra, 0.5-2.5 eV, Young's modulus and internal friction 78−39562
Ni complex, 1-(2-thiazolylazo)-2-naphtholato Ni (II), cryst. struct. 77−11536
Ni complex, 2,6-N,N-diacetyldiaminopyridine-Ni(II) elec. cond., γ dose and temp. (303-363K) effects 80−103696
Ni complex, 2,6-N,N-dibenzoyldiaminopyridine-Ni(II) elec. cond., γ dose and temp. (303-363K) effects 80−103696
Ni complex, $(Ni(C_2H_5NO)_6)(NO_3)_2$, field induced level crossing and cryst. struct. 79−47070
Ni complex, (1,4,5,8,9,12,13,16-octamethyltetradbenzporphinato nickel)$^{+y}$ $(I_3^-)_y$, atomic limit of Hubbard model and polarons 80−39860
Ni complex, $(4\text{-methylpyridine})_4Ni(NCS)_2$, porosity 77−76364
Ni complex, $[Ni(OCH_3)\ (acac)\ (CH_3OH)]_4$, sp. ht., 0.4-285K, methyl group internal rotation 78−47531
Ni complex, $[Ni(en)_2Cl]_2Cl_2$, heat capacity, X-ray diffraction and mag. meas., phase transition 78−47515
Ni complex, $[Ni(niox)_2]$, ^{61}N Mossbauer spectrum, quadrupole splitting 79−76456
Ni complex, BDN II in tetrahydrothiophene-1,1-dioxide, saturation behaviour, Q-switching appl. 80−48354
Ni complex, bis-4-dimethylaminodithiabenzyl nickel, tetrachlorethane soln., photochem. and thermal stability 80−16708
Ni complex, bis-(1,2-benzoquinonedioximato)$_2$Ni.05I, X-ray scatt. 77−1101
Ni complex, bis-[4-(n-butyl)-styryl-dithiolato] Ni nematic complex, IR absorption 80−49342
Ni complex, bis(L-isoleucinato)NiII dihydrate, struct. 78−18604
Ni complex, bis(N-benzylsalicylaldiminato) Ni (II), lattice consts. and space group 79−37680
Ni complex, bis[3,4,-benzo-N-(S)-sec butylsalicilaldiminato] nickel (II), stereochemistry, De Voe theory 77−14600
Ni complex, β-diketonate complexes, CNDO calcs. 79−59358
Ni complex, cis-dichloro-bis(1,2,cyclohexadionedioxime) cryst. and mol. struct. 80−44198
Ni complex, di-(trichloroacetate).4n-para-anidine crystal struct., bond angles 79−86774
Ni complex, diaquo-bis-(acetylacetonate) nickel (II), cryst. struct. 80−100205
Ni complex, hexa(pyridine 1-oxide) di-perchlorate, S=1 ground state, mag. props. in external field 80−11157
Ni complex, $hexa(pyridine\text{-}N\text{-}oxide)(ClO_4)_2$, field-induced mag. ordering in S=1 singlet ground-state 78−23288
Ni complex, hexamethylphosphorotriamide Ni (II), paramagnetic, pulsed NMR, substitution reaction *(French)* 78−10793
Ni complex, in $Na_2O\text{-}K_2O\text{-}SiO_2$ glass, optical absorption complex coordination change, annealing effects 79−69870
Ni complex, linear chain type, synthesis 78−6047
Ni complex, Ni (II)-substituted ethylenediamines and monocarboxylates, cryst. and mol. struct., X-ray diffr. obs. 79−82182
Ni complex, Ni acetylacetonate-alkylamine coordination cpd., ^{1}H and ^{13}C NMR hyperfine coupling const. 79−41187
Ni complex, Ni-hexamethylenetetramine, reflectance spectra 78−31218
Ni complex, $Ni(C_5H_5NO)_6(ClO_4)$ field-induced mag. phase transition obs. 77−36072
Ni complex, $Ni(C_5H_5NO)_6(ClO_4)_2$, field induced antiferromag., magnetocaloric effect 80−29551
Ni complex, $Ni(NH_3)_6(ClO_4)_2$, high-press. phase, EPR meas. 78−38842
Ni complex, $Ni(S_2C_2(CN)_2)_2^{2-}$, elec. cond. 79−73505
Ni complex, $Ni(5\text{-methylpyrazole})_4X_2$, (X=Cl, Br, I), mag. props., EPR, ligand field calcs. 77−62880
Ni complex, $Ni(detc)_2$, spin-lattice relax. of Cu^{2+} 77−59453
Ni complex, Ni(l-spartein)Cl_2, IR circular dichroism spectra, vibr.-electronic interaction 80−55074
Ni complex, nickel di-(trichloroacetate).4n-toluidene complex, crystal struct., bond angles 79−82189
Ni complex, nickel di-(trichloroacetate).(aniline)4 complex, crystal struct., bond angles 79−82190
Ni complex, nickel-bis-dithiolene, pseudopot. MCSCF and limited CI calcs. 80−83292
Ni complex, octaethylporphyrinato-Ni(II), meso-deuterated and ^{15}N substituted derivs., reson. Raman spectra 79−13726
Ni complex, octaethylporphyrinato-Ni(II), meso-deuterated and ^{15}N substituted derivs., reson. Raman spectra 79−13725
Ni complex, S_4N_4 with $NiCl_2$, mass and IR spectra, config. 78−13494
Ni complex, tetrathiotetracene nickel bis-(ethylene-1,2-dithiolene) quasi-one-dimensional cond., cryst., mag. and elec. props. 78−10424
Ni complex, tris(ethylenediamine)nickel(II) nitrate, mag. props. from susceptibility and sp. ht. meas., 0.3-3.0K 78−91877
Ni complex, with 1,2,4-triazole, mag. susceptibility, 2-300K, struct., antiferromag. props. 77−77045
Ni complex soln., BDN II, saturable absorber for 1.315 I laser 79−27297
Ni complex:Cu^{2+}, Ni(II)bis(diethyl-dithiocarbamate):Cu^{2+}, electron spin-lattice relax. 77−1589
Ni complexes, $[Ni(NH_3)_6](ClO_4)_2$ and $[Ni(ND_3)_6](ClO_4)_2$, phase transitions, Raman spectra meas. 77−66501
Ni complexes, dithienes, nematic and smectic mesophases, synthesis and characts. 80−70120
Ni complexes, dithiolato complexes, smectic C phase, synthesis, isobaric phase diagrams 78−94970
Ni complexes, Ni(II) porphyrins, picosec. flash photolysis, transient absorpt. 80−52976
Ni complexes, $Ni(PX_3)_4$ (X=F, OCH_3, Cl, CH_3, H), CNDO/2 calc. of magneto-optical props. and electronic content of metal-ligand bonds 77−23430
Ni complexes, Ni(glycinate)$_2$(pyrazine) and Ni(glycinate)$_2$(pyridine)$_2$, and isotopic forms, IR band assignments 79−22710
Ni complexes, quenching of singlet O_2 79−94028
Ni complexes, solid-state polymerisation 79−74380
Ni complexes, with CO, O_2 and NO ligands, in NiCa-Y zeolite, EPR, UV obs. 77−63949
Ni complexes hexamethylamine nickel halides, Ni^{2+} EPR in high pulsed mag. field, zero field splitting parameters 80−71160
Ni complexes of N,N,N′,N′-tetramethylethylenediamine, cryst. struct. 78−34467
Ni compound, $[Ni_3(CO)_6]_n^{2-}$, n=1,2, one-electron states in polynuclear carbonyls 79−95358

nickel compounds continued
Ni dithiene complexes, mesomorphic props. 80−88026
Ni ferrite with domain struct., FMR absorpt. line intensity and shape 77−90041
Ni ferrite-$BaTiO_3$, piezomagnetic-piezoelectric sintered two-phase composite, magnetoelec. conversion 77−12181
Ni II acetylacetonate, XPS 80−74196
Ni oxide-based electrode, air hydrophobically treated, electrochem. characts. 79−61876
Ni porphin, reson. Raman excitation profiles, simulation, vibronic coupling consts. 77−65471
Ni^{2+} aqueous complex, EPR, PMR and spin-spin relax. 79−69713
Ni/NiO, relative chemical potential of oxygen *(German)* 78−31642
Ni-benzene, second order two-spin cross-relax. 79−95632
Ni-Ca-B, Ni-B side of ternary diagram 77−59766
Ni-Cl boracite, chem. vapour transport, appl. of flux function method 79−52091
Ni-Co-Zn ferrite, exam. of electromag. characteristics 79−1409
Ni-Fe-O ferrite system, thermodynamic stability, dissociation and phase relations *(Japanese)* 80−55378
Ni-Fe-Ti-O spinel phase, single-phase region and cryst. chem. characts. 77−52301
Ni-ferrite, ultrafine powder, prod. by cryochemical, freeze drying, spray drying or soln. techniques 80−55336
Ni-Ge-SiO, solar selective absorber surfaces, optical behaviour at high temp. 80−101130
Ni-I single crystals, mag. and dielectric props. 80−93095
$Ni\text{-}NiO_x\text{-}NiS_y$, black Ni, struct.-depend. thermal and optical props., rel. to solar thermal conversion 79−79404
Ni-N_iO-Ni, integrated MOM junctions, characts. at DC and optical freqs. 78−41349
Ni-O system, oxidized polycryst. Ni films, H_2 reduction, AES 77−12472
Ni-P, electrodeposited films, amorphous and crystalline, electron microscopy, in-situ crystallisation 79−11043
$Ni\text{-}P\text{-}Al_2O_3$ (SiC), composite deposit electrodeposition *(Russian)* 78−35326
Ni-Pd-H, film, struct. and phases formed, when Ni, Pd are sputtered in H 80−29289
Ni-Pt silicide Schottky diodes, current-voltage characts. and comp. profiles 80−84508
Ni-S, thermodynamics and phase relations 79−47666
Ni-S incongruently subliming system, SEM and TEM obs. of high temp. transitions, temp.-comp. diagrams 80−104136
Ni-S melt, thermodynamic props. 80−19957
Ni-S mixtures, binding of phases, two-correl. model 77−80438
Ni-S system, Knudsen effusion and thermodynamics 78−79759
Ni-Se mixtures, binding of phases, two-correl. model 77−80438
Ni-Te mixtures, binding of phases, two-correl. model 77−80438
Ni-W-O system, phase relations in dioxide-trioxide region, 1373K 78−11212
Ni-W-O system, phase relns. and Gibbs' free energy of formation of $NiWO_4$ 77−73262
Ni-Zn ferrite, elastic moduli temp. and composition depend. 78−26617
Ni-Zn ferrite, electrical cond., Seebeck coeff. and saturation magnetisation 77−20315
Ni-Zn ferrite, grain size depend. of grain boundary sliding *(Japanese)* 80−15120
Ni-Zn ferrite, high temp. behaviour of grain boundaries under bending stress *(Japanese)* 77−1875
Ni-Zn ferrite, neutron irrad., mag. spectra, domain wall behaviour 77−48006
Ni-Zn ferrites, comp., lattice imperfections, sintering 78−3080
Ni-Zn ferrites, hot-pressed, key props. 78−15348
Ni-Zn ferrites, mag. recording head props. rel. to manuf. from schoenite-type solid solns. 77−85496
Ni-Zn ferrites, polycrystalline, grain boundary slip *(Japanese)* 77−63764
Ni-Zn ferrites 600 NN and M450 NNI, Curie point radiative shift due to neutron irrad. *(Russian)* 80−39775
Ni-Zn-Co ferrites, synthesis from solid solns. of schoenite-type salts 80−93511
Ni-ZrO_2 compact cermet cathode for high temp. water vapour electrolysis *(French)* 79−74399
$NiAl_tFe_{2-t}O_4$, Kerr effect, magneto-optical refl. spectra 79−82954
$NiAl_2O_4$, entropy of form. determ. using solid electrolyte twin thermocell 78−27812
NiAs, optical props., 0.05-5 eV 77−48194
NiAs, structure types, coordination 77−19913
NiAs type structure, Mossbauer line broadening due to diffusion 77−12281
$Ni(As_xS_{1-x})_2$, mag. elec. and structural props. meas. 77−85447
$Ni(BF_4)_2.6H_2O$, EPR, cryst. field symmetry 79−28593
$Ni_3B_7O_{13}Br$, boracite single cryst., nucleation control density growth 80−80955
$Ni_3B_7O_{13}Br$, cubic, approx. nonlinear optical susceptibility 80−78904
$Ni_3B_7O_{13}Br$, ferroelec. 43m-mm2 phase transition, molar heat capacity meas. 80−93249
$Ni_3B_7O_{13}Cl$, boracite, on Cr-Cl boracite, gas phase synthesis of epitaxial layers 79−60650
$Ni_3B_7O_{13}Cl$, specific heat anomaly at F43c→$Pca2_1$ transition 79−28690
$Ni_3B_7O_{13}I$, 10K mag. transition and accompanying struct. transition 77−69565
$Ni_3B_7O_{13}I$, cubic, Raman spectrum, 88-295K, vibr. anomalies 78−76479
$Ni_3B_7O_{13}I$, dynamics of ferroelec. phase transition, Raman spectra obs. 79−33630
$Ni_3B_7O_{13}I$, magnetoelectric tensor component detection 79−95625
$Ni_3B_7O_{13}I$, nonlinear magnetoelec. and dielec. props. 79−65704
$Ni_3B_7O_{13}I$, phase transition, X-ray diffr. obs., 77-300K, rel. to mag. susceptibility anomaly 77−47573
$Ni_3B_7O_{13}I$, Raman spectra in paraelec. phase 78−60434
$Ni_3B_7O_{13}I$, shear modulus anomalous temp. depend. 78−43061
$Ni_3B_7O_{13}I$, struct. and mag. transitions, light scatt. study 79−24308
$Ni_3B_7O_{13}I$, unit cell parameters and struct. transitions, 20 to 293K, X-ray diffr. study 80−24431
$Ni_3B_7O_{13}X$, X=Cl, Br, I, ferromag. ferroelectrics *(Japanese)* 79−65804
NiBr, band system in near UV, vibr. analysis 80−32733
NiBr boracite single crystals, dielectric, pyroelectric props., vapour phase transport growth 80−80673
$NiBr_2$, ^{1}Eg spin-forbidden transition, temp. depend. and magnetoabsorpt. 78−48151
$NiBr_2$, aq. solns., EXAFS meas. 80−60714

nickel compounds continued

$NiBr_2$, commensurate and incommensurate mag. struct., neutron diffr. study 80−97067
$NiBr_2$, low-temperature magnetic phase, incommensurate spin structure 80−93082
$NiBr_2$, mag. model, 0K phase diagram, spin wave spectrum 79−87273
$NiBr_2$, photoconductivity spectrum meas. using rate of charge method, transport props. 78−60160
$NiBr_2$, self consistent band struct., intersecting spheres model 79−37985
$NiBr_2$, thermoreflectance meas. 77−24866
$NiBr_2$, two-phonon vibronic progressions, Raman obs. 80−29742
$NiBr_2$, vibr. struct. in cryst. field electronic transitions 78−59895
$NiBr_2$, XPS, satellite of Br 4s line 78−56556
$Ni(BrO_3)_2.6H_2O$, low temp. EPR meas. 77−81001
$NiBr_2.6H_2O$, antiferromag. transition, susceptibility and sp. ht. meas. 77−69587
$NiBr_2.6H_2O$, antiferromag. ordering and paramag. behaviour 78−14941
NiC, colour change on replacement of PbO in glaze *(German)* 79−91813
Ni_3C film, thermal decomposition, AES meas. 78−56056
Ni_3C films, on graphite, thermal decomp., AES lineshape study 79−79293
Ni_3C formation and decomposition during evaporation of Ni onto graphite 79−15055
$Ni(C_5H_5NO)_6(ClO_4)_2$, susceptibility and magnetisation meas., field, freq. and temp. depend. 77−66279
$Ni(CN)_2$-dodecylamine, lamellar paraffinic system, phase transitions, wide-line NMR obs. *(French)* 80−44929
$Ni(CN)_4^{2-}$, mol. vibrs. and reaction pathways, min. energy coords. and compliance consts. 77−57966
NiCO, and core ionised, binding and relax. energy ab initio LCAO MO SCF calc. 78−62712
NiCO, hypothetical mol., adsorbate bond geometry, determ. using photoemission 78−71951
NiCO, linear, ab initio RHF-MO calcs., rel. to adsorption 79−26883
NiCO, liquid interactions, ab initio LCAO MO SCF calcs. 79−18256
$NiCO_3$, crystal growth by counterflow diffusion and temp. drop hydrothermal synthesis 77−4731
$NiCO_3$, impurity in $SrCO_3$ dissoc. 78−27425
$Ni(CO)_4$, back donation, multiple scatt. Xalpha calcs. 79−36527
$Ni(CO)_4$, back donation, multiple scatt. Xalpha calc. 79−63913
$Ni(CO)_4$, bonding, IR intensity anal. 78−25526
$Ni(CO)_4$, bonding, shakeup energies, and shakeup intensities for photoelectron spectra 80−50528
$Ni(CO)_4$, form., ion migration, in NaCaX zeolite 79−33522
$Ni(CO)_4$, form. on single Ni cryst., reaction kinetics and induced surface facetting 80−71948
$Ni(CO)_4$, form. reaction rate, substrate mag. phase depend. 80−108737
$Ni(CO)_4$, gas phase collisions, negative ion form., struct. 77−6945
$Ni(CO_4)$, ionisation energies, approx. SCF Hartree-Fock-Slater calcs. 77−75334
$Ni(CO)_4$, mol. struct. by gaseous electron diffr., quadratic force field refinement 79−64115
$Ni(CO)_4$ monitoring using Fourier IR technique 79−16106
$Ni(CO)_4$, ppb in air meas. by chemiluminesc. detector 80−40692
$Ni(CO)_4$, valence orbital energies, pseudopot. calcs. 78−37546
$(Ni_3(CO)_6)_n^{2-}$, n=1,2, one-electron states in polynuclear carbonyls 79−95358
$Ni_{1-x}Cd_xFe_2O_4$, mag. props. rel. to ionic struct. 80−75756
$Ni_xCd_{(1-x)}(NH_3)_2.Ni(CN)_4.2C_6H_6$, mag. susceptibility meas. 77−63126
$NiCl_2$, aq. soln., diffusion and struct. 78−14488
$NiCl_2$, aq. soln., Ni^{2+} coordination from extended X-ray absorption fine struct. 80−1913
$NiCl_2$, aq. soln., partial struct. factors in long wavelength limit 78−47231
$NiCl_2$ aq. soln., quasi-elastic neutron scatt. 79−37607
$NiCl_2$, aq. soln., Raman spectrum, local order 78−84563
$NiCl_2$, aq. soln., structural transition, neutron diffr. study 80−64872
$NiCl_2$, aq. soln., viscosity meas., struct. props. 78−75863
$NiCl_2$, aq. solns., EXAFS meas. 80−60714
$NiCl_2$ aqueous solution, hydration of Ni^{2+} 78−79518
$NiCl_2$ aqueous solutions, autocorrelation spectroscopy 77−36796
$NiCl_2$, cryst., self-consistent band struct., intersecting spheres model 80−75505
$NiCl_2$, heavy water soln., anionic hydration, 1 bar and 1 kbar, neutron diffr. obs. 80−30212
$NiCl_2$, mag. struct. at 4.2K, neutron diffr. *(French)* 77−63097
$NiCl_2$, Raman spectrum at and below antiferromagnetic ordering temp. 79−99871
$NiCl_2$, self consistent band struct., intersecting spheres model 79−37985
$NiCl_2$, soln., activity coeffs., osmotic coeffs., water activity, Gibbs energy, molality depend. 80−51963
$NiCl_2$ solution, ionic hydration for cation 77−62460
$NiCl_2$, spin orientation of mag. impurity atom 77−59403
$NiCl_2$, thermoreflectance meas. 77−24866
$NiCl_2$, two-phonon vibronic progressions, Raman obs. 80−29742
$NiCl_2$, vibr. struct. in cryst. field electronic transitions 78−59895
$NiCl_2$, zone sublimation 78−52664
$NiCl_2$-CdS interface, transverse acoustoelec. voltage spectroscopy 80−49828
$NiCl_2$-$Cd(NO_3)_2$4.1H_2O, melt viscosity, equivalent conductivity, glass transition temp. 78−75855
$NiCl_2$-D_2O solution, hard-sphere model 77−62461
$NiCl_2$-He discharge, cataphoretic Ni distrib. 77−31092
$NiCl_2$-heavy water solution, inelastic neutron scattering 78−91203
$NiCl_2$-tetra-n-butylammonium iodide melts, densities and kinematic viscosities 79−77793
$NiCl_4^{2-}$, charge distrib. and ligand field splitting calc. 77−62879
$NiCl_2(Br_2)$, polymorphic phase changes of adsorbed NO 77−31900
$NiCl_2(Br_2)(I_2)$, prep. using chem. transport via gas complexes *(German)* 79−15599
$NiClO_4$, neutron activated, radiation annealing 80−93569
$Ni(ClO_4)_2$ $6H_2O$, sp. ht. between 2 and 17K 78−47532
$Ni(ClO_4)_2$, soln., activity coeffs., osmotic coeffs., water activity, Gibbs energy, molality depend. 80−51963
$Ni(ClO_4)_2$, solution, dielectric relaxation studies 78−84519
$Ni(ClO_4)_2.2H_2O$, ion solvation enthalpies in various solvents *(French)* 79−69264
$Ni(ClO_4)_2.6H_2O$, EPR and IR spectra, 98-298K, phase transition at 224K 78−84477
$NiCl_26NH_3$, low temp. sp. ht. and mag. ordering 80−75784
$NiCl_2.2H_2O$, mag. phase diagram and exchange parameters 77−77054
$NiCl_2.6H_2O$, antiferromag., phase diagram, low temp. canted paramag. boundary, bicritical point 79−47282
$NiCl_2.nH_2O$, cryst. struct. *(German)* 80−1987
NiCo ferrite, induced mag. anisotropy, hysteresis loops, Barkhausen effect *(Russian)* 78−64203
$Ni(Co)_4$+inert gas, dissoc. energy transfer, chemiluminesc. 80−55647
$Ni_{2-x}Co_xBaFe_{16}O_{27}$, ferromagnetic reson., anisotropy and g-factor, spin-orbit interactions 77−24749
$Ni_xCo_{1-x}Cl_2.6H_2O$, mixed uniaxial planar antiferromag., magnetisation process 80−88788
$Ni_{1-x}Co_xF_2$, Raman scatt. by mag. excitations 77−55775
$NiCo_2O_4$, ferrimagnetic spinel, neutron diffr. study 79−99681
$Ni_{1-x}Co_xO$, LF magnons, inelastic neutron scatt. exam. 77−66288
$Ni_{1-x}Co_xO$ mixed crystal, lowest mag. excitation, antiferromag. reson. meas. 77−69704
$Ni_xCo_{3-x}O$, composition depend antiferromagnetic-ferrimagnetic ordering, mag. susceptibility meas. 80−70973
$Ni_{50}Co_{40}P_{10}$ amorphous film, spin wave excitation, ferromagnetic resonance study 80−50198
$Ni_{1-x}Co_xS_2$, anomalous elec. props., polaron transport in highly correl. narrow bands 77−85222
$Ni_{1-x}Co_xS_2$, elec. cond., thermoelec. power and optical meas. 80−59986
$Ni_{1-x}Co_xS_2$, elec. transport and semicond.-metal transition 80−10985
$Ni_{1-x}Co_xS_2$, Mott transitions, temperature induced, Hubbard model theory 80−29326
$Ni_{0.5-x}Co_xZn_{0.5}Fe_2O_4$ ferrospinal solid solutions, cryst. lattice defects and props. 80−19796
$NiCr_{0.5}Al_{1.5}O_4$, thermal expansion 79−73327
$NiCr_xFe_{2-x}O_4$, magneto-otpical refl. spectra by equatorial Kerr effect *(Russian)* 77−32400
$NiCr_2O_4$, ^{61}Ni Mossbauer effect studies of hyperfine interactions, mag. dipole and elec. quadrupole 78−43746
$NiCr_2O_4$, acoustic props. rel. to cooperative Jahn Teller effect and structural phase transform 80−24538
$NiCr_2O_4$, cooperative Jahn-Teller phase transition, channelling obs. 78−38839
$NiCr_2O_4$, plasma-sprayed coatings, props. 77−59999
$NiCr_2O_4$, sign of net mag. hyperfine field, ^{61}Ni Mossbauer study 80−39946
$NiCr_2O_4$ single crystal, appl. of particle channelling to the study of a cooperative Jahn-Teller phase transition 79−4413
$NiCr_2O_4$, thermal expansion 79−73327
$NiCr_2O_4$:Fe, Mossbauer effect 80−15874
$NiCr_2S_4$, thermal stability, thermochemical, thermodynamic and crystallochemical props. of chalcogenide spinels 77−51519
$Ni_{1-x}Cr_xS$, elec. transport, mag. susceptibility and DTA meas. 80−96954
NiD_x synthesized at high pressures, neutron diffraction anal. of struct. 80−28977
NiF $^2\Delta$-$^2\Pi$ system, rot. anal. 79−98115
NiF_2, antiferromag. reson., Lagrange and nonequilib. thermodynamics descriptions 79−15357
NiF_2, crystal growth from melt in enclosed graphite crucible 77−4735
NiF_2, ESCA, charge transfer satellite struct., hole state localisation intensity depend., MS-MO calc. 77−66139
NiF_2, electronic UV laser excited Raman, scatt. by mag. excitons 78−68492
NiF_2 film preparation and characterisation 80−59815
NiF_2, high temp. polymorphism and thermal props. 80−75199
NiF_2, magnetisation and antiferromagnetic resonance freq. in mag. field *(Russian)* 80−34781
NiF_2, melting curve, press. up to 40 kbar, rel. to high press. melting systematics 77−51475
NiF_2 powder, preferred orientation, X-ray intensity corrections 80−1880
NiF_2, press. depend. of elastic moduli to 10 kbar 77−35619
NiF_2, press. induced strain transition obs., neutron powder diffr. meas. 78−55948
NiF_2, tetragonal to orthorhombic transition at high press., possible mag. ordering 78−18765
NiF_2, thermal expansion and magnetostriction, 55K to room temp. 80−80586
NiF_2, two-spin light scattering, disordered phase rutile antiferromags. 78−80336
NiF_2, valence-electron density of states, XPS meas. 77−69963
NiF_2, weak ferromag., antiferromag. reson., phenomenological theory 78−60339
NiF_2-BaF_2-CrF_3, X-ray crystallography study, phase identification at 700°C, cryst. symm. *(French)* 78−95733
NiF_2+CO, react., Ar matrix isolated, ab initio MO calcs. 78−92458
$(NiF_6)^{4-}$ complex, open-shell cluster calcs., semiempirical LCAO-MO method 80−54583
NiF_6^{4-}, electronic excitation energy calc., correl. energy correction 78−17576
NiF_6^{4-}, spectra, cryst. field least squares fitting interpretation 80−44548
NiFe ferrite, prep. of single crystal by chem. transport with $TeCl_4$ 80−104051
$Ni_{1-3x}^{2+}Fe_{2+2x}^{3+}Vac_xO_4^{2-}$ (Vac=cation vacancy), solid solns., cryst. lattice imperfections 80−39069
$NiFe_{2-t}Al_tO_4$, cryst. and mag. props. 78−14940
$NiFe_{2-x}Al_xO_4$, ^{57}Fe and ^{61}Ni Mossbauer spectra 80−39940
$NiFe_{2-x}Al_xO_4$, cation distrib. calc. from equilib. conditions 78−22701
$NiFe_{2-x}Al_xO_4$, stress-induced anisotropy in LPE grown single cryst. films, domain struct. 79−28238
$Ni_{0.6}Fe_{2.4}B_7O_{13}I$, boracite, orthorhombic-trigonal transition region, Mossbauer investig. 79−87342
$Ni_{0.6}Fe_{2.4}B_7O_{13}I$, boracite, mag. hyperfine interactions, Mossbauer study 80−39935
$NiFeF_5.7H_2O$, thermal decomp. 77−81394
$Ni_{0.51}^{2+}Fe_{0.46}^{2+}Fe_{1.95}^{3+}O_4^{2-}$, elec. resistivity above 300K 79−78099
$Ni_{0.89}^{2+}Fe_{0.13}^{2+}Fe_{2.11}^{3+}O_4^{2-}$, elec. resistivity above 300K 79−78099
$NiFe_{2-x}Mn_xO_4$, cell dimens. determ. 78−26526
$NiFeO_4$, induced ferrimagnetism, temp. depend. of sublattice magnetisation, Mossbauer study 77−66280
$NiFe_2O_4$, core line X-ray photoelectron spectra 78−7263
$NiFe_2O_4$, domain wall size and mag. losses in freq. spectra 77−85481
$NiFe_2O_4$, effect of sintering in air in range 1373-1773K on lattice parameter 79−19208
$NiFe_2O_4$, electronic phase transition 80−65640

nickel compounds continued

$NiFe_2O_4$ epitaxial film on NdGG, structural and ferromagnetic reson. meas. 77−1574
$NiFe_2O_4$, exchange integrals from magnetisation meas. 79−47273
$NiFe_2O_4$, ferrite, mag. anisotropy compensation under neutron irrad. 80−75807
$NiFe_2O_4$ ferrite, mag. props., neutron irrad. 80−103858
$NiFe_2O_4$ ferrite form. mechanism in mixture of metallic oxide powders 77−63609
$NiFe_2O_4$, hysteresis and other mag. props. rel. to microstruct., TEM investig. 77−20636
$NiFe_2O_4$, LPE growth, film quality, mag. meas. 78−11136
$NiFe_2O_4$ mag. fluid particles, comp., struct., and mag. props. 80−60374
$NiFe_2O_4$, microstruct. and magnetic props., electron microscope obs. 79−87290
$NiFe_2O_4$ milled ferrite powder, substruct. and sinterability 80−84894
$NiFe_2O_4$, parametric excitation of spin waves in samples with regular domain struct. *(Russian)* 77−32183
$NiFe_2O_4$ precipitation process from silicate glass, ESR study, effective g value, transition temp. 80−25194
$NiFe_2O_4$ precipitation from silicate glass, Mossbauer study 80−54998
$NiFe_2O_4$, prep. by double decomp. reaction, mag. charcts. *(French)* 79−33463
$NiFe_2O_4$, single cryst. prep. by chem. transport 78−23589
$NiFe_2O_4$, soft ferrite, squareness ratio and max. induction 79−99730
$NiFe_2O_4$, solid state formation, exam. of kinetics for formation at 700 to 1400 degrees C 78−48648
$NiFe_2O_4$, superexchange interactions, three-sublattice anal. 79−61095
$NiFe_2O_4$, thermally induced surface chemistry and struct., XPS 78−22939
$NiFe_2O_4$:Ir^{4+}, mag. anisotropy, single ion contrib., octahedral sites 77−4511
$NiFe_2O_4$-$BuTiO_3$, in situ composite growth, phase diag., melting relns. 77−21132
$NiFe_2O_4$-Fe_2O_3, effects of excess Fe_2O_3 on mag. props. 77−85495
$NiFe_2O_4$+ZnO, powders, cation mutual diffusion coeffs. calc. 77−15635
$Ni_{0.33}Fe_{2.33}O_4$, {001} ⟨110⟩ glide system, room temp. TEM obs. 79−90660
$Ni_{1-x}Fe_{2+x}O_4$, mag. anisotropy constant, contrib. of Fe^{2+} ion 79−33476
$Ni_{1-x}Fe_2O_4$ ferrites, mag. thermal expansion anomaly 77−69595
$Ni_{2/3}Fe_{7/3}O_4$, precipitation of α-Fe_2O_3, optical microscopy, SEM and TEM studies *(French)* 80−11650
$Ni_xFe_2O_4$ series, chem. and mag. transformation, X-ray diffr. and mag. susceptibility study 79−51774
$Ni_xFe_{3-x-\Delta}O_4$, mag. aftereffects 79−56572
$Ni_xFe_{3-x}O_4$, DC and low freq. cond. and influence of microstruct. 80−70699
$Ni_xFe_{3-x}O_4$, magnetostriction, 80 to 300K, depend. on comp. and electron ordering on octahedral sites 80−65995
$Ni_xFe_{3-x}O_4$, solubility in high-temp. aqueous soln., appl. to PWR 78−4987
$Ni_xFe_{3-x}O_4$, spinels, fine particles, magnetic properties obs. 80−71031
$Ni_xFe_{3-x}O_4$, x<1, anomalous microwave loss 79−69540
$Ni_{0.98}{}^{57}Fe_{0.02}S_{1.0}$, quadrupole splitting and ground state, Mossbauer spectra 80−29657
$(Ni_{1-x}Fe_x)S$, solid solns., electronic props., X-ray, thermal and Mossbauer study 79−78376
$(Ni_{1-x}Fe_x)_{1-\delta}S$, anisotropic spin glass, mag. props. 80−39793
$(Ni_{1-x}Fe_x)_{1-y}S$, anomalous thermal hysteresis in metal-semicond. transition 80−39640
$Ni_{1-x}Fe_xS_2$ (x=0 to 0.075), weak ferromag. exam. 79−51755
$NiFe_2Se_4$, thermal cond., temp. depend., 100 to 400K 77−35764
$Ni^{2+}Fe_{0.75}{}^{3+}V_{1.25}{}^{3+}O_4$, acoustic props. rel. to cooperative Jahn Teller effect and structural phase transform 80−24538
$NiGe_x$, Ni X-ray emission spectra *(Russian)* 78−21942
$NiGeO_3$, HP phase transform. 80−19941
βNiH, decomposing, α-phase precipitate detection by Bitter powder pattern 79−28104
NiH, extended basis set LCAO Xalpha treatment 80−95537
NiH, gaseous, dissociation 79−91925
NiH, pot. energy curves, Hartree-Fock and valence bond methods 78−41958
NiH solid solutions, H impurity screening, lattice deformation, dipole force tensor component calcs. 79−77611
NiH_2, pot. energy curves, Hartree-Fock and valence bond methods 78−41958
NiH_4, electronic structure, ab initio calcs. 79−89601
NiH_n thin film, X-ray phase analysis *(Russian)* 77−59124
NiH_x, desorpt. of H_2, fine struct. 78−59950
NiH_x, electronic band struct. and interatomic bond 78−43295
Ni_2H, hexagonal type, cryst. struct. determ. by electron diffr. 79−55724
$Ni(H_2O)_6(ClO_4)_2$, specific heat meas., 90 to 376K, phase transitions 78−83970
$Ni(H_2O)_6SiF_6$, $Ni(D_2O)_6SiF_6$, Raman spectra, vibr. modes 79−61369
$Ni(H_2V)_2(H_2O)_2$, synthesis and characterisation *(French)* 80−45225
NiI_2 anhydrous, magnetic phase transition, neutron diffr. study 80−71033
NiI_2, antiferromagnetic, neutron diffr. and sp. ht. meas. 77−55663
NiI_2, far IR study of lattice dynamics 78−80359
NiI_2, Mossbauer spectrum, electronic and mag. props. 77−32302
$Ni_7I_2B_{16}O_{30}$, isomorphous phase transition ~120K 78−79764
$NiI_2.6H_2O$, disordered linear chain mag., ESR, mag. susceptibility and NMR meas. 77−20688
$NiK_4(P_3O_9)_2.7H_2O$, cryst. struct. determ. *(French)* 78−79568
Ni_5La, connected storage of H *(Russian)* 80−55937
$NiLa_2O_4$ electrochemical electrodes, kinetics of O_2 evolution, appl. to electrolytic H energy prod. 80−30430
$Ni_{1-x}Li_xO$, $0.01 \leq x \leq 0.08$, mag. susceptibility in region 80 to 800K *(Russian)* 78−2664
$Ni_xMg_{1-x}O$, EPR in magnetoconcentrated solid solution *(Russian)* 80−39856
$Ni_pMg_{(1-p)}(OH)_2$, random magnet, AC susceptibility 79−47258
$Ni_xMg_{1-x}(OH)_2$, random magnet, magnetisation 79−24195
$(Ni_{1-x}Mg_x)_2SiO_2$, reduction to Ni *(Russian)* 78−44043
Ni_3Mn, anal. of irrad. disordering data 79−1466
$Ni_xMn_{1-x}Cl_2$, sp. ht., 2-28K, anomalies *(Russian)* 77−89970
$NiMoO_4+TeO_2$, solid state reaction 80−108709
NiMoP, cryst. struct. determ. 77−80468
$NiMo_2Re_2S_8$, cubic structure, mixed tetrahedral cluster *(French)* 77−15372

nickel compounds continued

$Ni(Mo_2Re_2)S_8$, synthesis and electrical props. of mixed tetrahedral cluster phases 80−2971
$Ni_2Mo_6S_6O_2$, O-containing Chevrel phases, synthesis and props. 80−108368
$Ni(NH_3)_6(BF_4)_2$, enantiomorphic transition, X-ray powder diffr. meas. 78−30574
$Ni(NH_3)_8(BF_4)_2$, phase transition, group theoretical anal. 80−65218
$Ni(N_2H_4)B_xH$, development, effect on photosensitivity of paper *(Russian)* 80−73509
$Ni(NH_3)_6(ClO_4)_2$, EPR determ. of phase transition temp., line shape anal. 77−20063
$Ni(NH_3)_6(ClO_4)_2$, phase transition, group theoretical anal. 80−65218
$Ni(NH_3)_6(ClO_4)_2$, stochastic NH_3-rotation, neutron incoherent scatt. 77−51331
$Ni(NH_3)_6(ClO_4)_2$, structural phase transition, X-ray diffr. obs. 79−65023
$Ni(NH_3)_6(ClO_4)_2$, thermal expsn., phase transitions 79−60525
$Ni(NH_3)_6I_2$, EPR of Ni^{2+} ion near structural phase transformation 80−11248
$Ni(NH_3)_6I_2$, phase transition and rot. excitation 80−96642
$Ni(NH_3)_6(NO_3)_2$, jumpwise vol. change in structural phase transition 79−42233
$Ni(NH_3)_6(NO_3)_2$, Raman spectra exam. of orientational phase transitions 78−31184
$Ni(NH_3)_2Ni(CN)_4.2C_{12}H_{10}$, mag. susceptibility, sp. ht., spin arrangements and transition obs. 77−20590
$Ni(NH_3)_6(PF_6)_2$, EPR investig. of struct. transition 77−20679
$Ni(NH_3)_6SO_4$ solution, dielectric relaxation studies 78−84519
$Ni(NH_4)_2(SO_4)_2.10H_2O$, precipitation, supersaturation, cryst. size distrib. changes 77−72573
$Ni(NH_4)_2(SO_4)_2.6H_2O$, electron density distrib., X-ray diffr. 78−95035
$Ni(NH_4)_2(SO_4)_2.6H_2O$, precipitation from equimolar aqueous solns., kinetics study 80−7848
$Ni(NH_4)_2(SO_4)_2.6H_2O$, Mn^{2+} doped, EPR study 80−34763
$Ni(NH_3)_6X_2$, (X^-=Cl^-, BF_4, $ClO_4{}^-$) spin dynamics at struct. phase transition 79−15309
$Ni(NH_3)_6X_2$, (X=Cl, Br, I, ClO_4, BF_4) and d, far IR, Raman spectra, 80-300K 78−31190
$Ni(NH_3)_6X_2$, X=Cl,Br,I, rotational tunnelling by inelastic neutron scatt. 78−30553
$Ni(NH_3)_6{}^{++}$, photographic developer, potentiodynamic polarisation curves for Ag-less development *(Russian)* 80−90921
NiNO, ground and core hole states, config. depend. HF LCAO SCF calc., relax. and binding energy 80−29453
$Ni(NO_3)_2$, aq. electrolyte, apparent molar heat capacity and volume, of 298.15K 79−65208
$Ni(NO_3)_2$, soln., activity coeffs., osmotic coeffs., water activity, Gibbs energy, molality depend. 80−51963
$Ni(NO_3)_26NH_3$, specific heat discontinuity at Neel point 77−51912
$0.5Ni(NO_3)_2 \times 1.5Ni(OH)_2$ form., X-ray parameters 77−16519
$Ni(NO_3)_2.4H_2O$, two spin ordered states under mag. field 79−15308
β-$Ni(NO_3)_2.4H_2O$, X-ray cryst. struct. determ. 80−28958
$Ni(NO_3).6H_2O$, Ni(II) coordination in aq. soln., EXAFS 77−85837
$Ni(NO_3)_2.6H_2O$, rhombic cryst. field, spin ordering in mag. field 77−77058
$Ni(NO_3)_2.6H_2O$, susceptibility and specific heat meas., spin ordering, antiferromag. spin pair coupling 80−7084
$NiN_4S_4H_2$, vibr. anal. 78−90148
$NiNa_2H_8(PO_4)_4.4H_2O$, cryst. struct. determ. *(French)* 78−26504
$NiNa_6(SO_4)_4$, vanthoffite cryst. struct., lattice parameters and thermal behaviour 77−19929
$Ni_3NbB_3O_{15}$, flux growth and chem. charcts. 78−23595
$NiNb_2O_6$, antiferromag., principle mag. susceptibility and field induced magnetisation meas. 77−20589
$NiNb_2O_6$, bonding characterisation 78−38680
$NiNb_2O_6$, flux growth 77−21015
$NiNb_2O_6$, force fields rel. to cryst. struct. *(French)* 80−107104
$NiNb_2O_6$, magnetisation and susceptibility, antiferro-paramag. transition, expt. and theory 77−43822
$Ni_3Nb_2O_8$, flux growth and chem. charcts. 78−23595
$Ni_{0.34}NbS_2$, intercalation compound, struct. and photoemission meas. 77−16453
$Ni_{1/3}NbS_2$, intercalate, metallic, cond., Hall effect and mag. props. 77−76789
Ni_xNbS_2 vacancy ordering, transition state cluster model, electron diffr. 77−47547
NiO, ^{18}O conc. profile, secondary emission of negative or positive ions *(French)* 79−60395
NiO (001), diffr. of monoenergetic He atoms 79−61487
NiO (001), surface layers, sublattice magnetisation temp. depend., LEED exam. 78−27018
NiO (001) surface, chemisorption of H, surface and second-layer defect effects 80−65369
NiO (100), ang. depend. of Auger electron emission 79−61474
NiO (100), antiferromag., LEED calcs. of exchange refls. 78−14949
NiO (100), electron energy loss spectra exam. 78−72652
NiO (100), surface struct., LEED study 80−39396
NiO (100) surface, dynamical LEED calc. 77−62721
NiO (100) surface, electronic states, electronic energy loss spectroscopy 78−6426
NiO (100) surface, LEED expt. and calc. down to 60 eV 80−92767
NiO (100) surface, sulphurisation by H_2S, AES, LEED, RHEED structural study *(French)* 78−64888
NiO, (100) surface interaction with SO_2, electron diffr. and Auger spectrosc. obs. *(French)* 80−97728
NiO (111) platelets, antiferromag. S domains, optical obs., spin-flop 80−54915
NiO (111) platelets, magnetic anisotropy investigation by torque and mag. susceptibility meas. 80−54885
NiO (111) surfaces, antiferromag., mag. scattering by polarised LEED, spin polarisation effect in theory 80−29529
NiO, ⟨001⟩ tilt boundary relative energy 80−29033
NiO, ⟨100⟩ coincidence twist boundaries energy 80−107270
NiO, ab initio SCF and CI calcs. on d-d transitions, $NiO_6{}^{10-}$ d-electron delocalisation 77−35896
NiO, absorption spectrum temp. depend. 77−48162
NiO, adsorption of CO+N_2O, catalysed reaction in Neel transition region 78−53258
NiO, amorphous, charge transport in band tails 78−76026

nickel compounds continued
NiO and lithiated NiO, thermally grown, electrochemical capacitance variations 80−29475
NiO, antiferromag., one-magnon light scatt. from spin-flop and paramag. regions, effect of anisotropy 79−33677
NiO, antiferromag., one-magnon light scatt., effect of anisotropy 79−33676
NiO, antiferromag., two magnon reson. Raman scatt. 79−33703
NiO, antiferromag. domains, obs. using neutron technique 78−64213
NiO, antiferromag. domains exam. by magnetic neutron Laue diffr. 79−51806
NiO, antiferromag. ordering, mag. transition-state approach 80−80507
NiO, Auger quantitative anal. 78−73104
NiO based pigments, willemite struct., synthesis 80−20855
NiO, bulk props., initial state MO Ni_4O_4 and $Ni_{13}O_{14}$, cluster model, lattice and force consts., photoemission and CT absorpt. spectra 80−84828
NiO, bulklike powder, sp. ht., 14-280K 79−69260
NiO catalyst, superparamagnetic, elec. props. 79−65506
NiO, catalytic decomp. of methanol, mol. beam relax. spectrometry using surface temp. modulation 79−29401
NiO, catalytic oxidation of CO, activated complex struct., rate consts. 78−80786
NiO, chemical diffusion of Ga^{3+}, influence on reaction rate of $NiGa_2O_4$ spinel form. *(German)* 78−22894
NiO, chemical diffusion 79−60544
NiO, cluster model, unrestricted Hartree-Fock calcs. 77−85125
NiO, colorant, bandpass filter glass, 550-616 nm, transmission characts. 78−66919
NiO, cryst., Debye characteristic temp. calcs. 79−37796
NiO, cryst. growth using $K_2S_2O_7$ as flux material 80−71582
NiO, cubic NaCl-type cryst., Debye temp. 80−54333
NiO, dielec. behaviour, Dick and Overhauser shell model calcs. 80−45001
NiO, diffusion obs., RF sputtering as microsectioning technique 78−14499
NiO, diffusion of ^{35}S 77−15629
NiO, diffusion of ^{35}S by two different modes 80−59720
NiO, diffusion of Cr_2O_3, spinel formation via solid state reaction, kinetic parameters calc. 78−34644
NiO, diffusion of ion-implanted ^{18}O 80−107494
NiO, diffusion of Ni in bulk and along dislocations 79−82381
NiO, dipole orientation from bound polaron hopping 80−84437
NiO disc, reduction with CO 77−4936
NiO, doped and pure single crystals, plastic deform. 77−36578
NiO, doped and undoped, elec. props. and surface characts. 80−65571
NiO doped glass, improved band-pass characts. 78−42394
NiO, effect of addition on crystallisation of Na_2O-Al_2O_3-SiO_2-TiO_2 glass 78−87626
NiO, elec. cond. and chem. diffusion coeff. at high temps. 79−23962
NiO, elec. cond. meas. at 1000°C 78−10451
NiO, elec. cond. under low O_2 press. 78−64041
NiO, elec. cond. variation with temp. *(French)* 79−60829
NiO electrode for photolysis 80−40696
NiO electrodes, effect of $Co(OH)_2$ on self-discharge, IR spectra obs. 80−21295
NiO, electron correls., defects, metal-insulator transition 78−63960
NiO, electronic cond., rel. to basic processes of Ni corrosion 77−25198
NiO, electronic polarisability of ions 77−40175
NiO, electronic states, VB and CI calcs. 78−62728
NiO, electronic struct. calc. 78−43297
NiO, entropy of form. determ. using solid electrolyte twin thermocell 78−27812
NiO, equilib. geometry, orbital energies, ab initio rel. to pseudopot. calcs. 78−82613
NiO, evaporation curve struct. from AC arc electrodes *(Russian)* 78−3051
NiO, exchange striction 78−56309
NiO films, on Ni (100) electrodes, oxide defect sites role in breakdown 79−43587
NiO fine particles, mag. props. rel. to physicochem. props. 78−52315
NiO, fine struct. in elastic-electron-yield spectra at transition-metal core energies 79−69938
NiO, formation on Ni (110), initial stage kinetics, RHEED and X-ray emission 78−15588
NiO, grain boundary thermal grooving, mass transport, self-diffusion coeffs. 80−44217
NiO, H chemisorption, cluster model, bonding 78−38939
NiO, H chemisorption, perfect surfaces, cation vacancies, self-consistent HF-VB calcs. 79−69351
NiO, Hall effect anomaly, sign reversal at 600K 80−100471
NiO impurity in MgO-Al_2O_3-SiO_2 glass, gamma ray irrad. exam. of ESR spectrum of Ni(I) 79−4719
NiO impurity in silicate melt, effect on elec. cond. *(Ukrainian)* 77−69104
NiO, interface for xerographic Se photoreceptor on flexible Ni foils 78−29184
NiO, isoelectric point meas. 80−88609
NiO, L_l and L_η X-ray emission spectra 78−39631
NiO, lattice dynamics, coherent inelastic neutron scatt. 78−59899
NiO, lattice dynamics calc. 79−46769
NiO, lattice dynamics using three body force shell model 77−76506
NiO, lattice parameters, microstrains, non-stoichiometry, comparison between mosaic microcrysts. and quasi-perfect single microcrysts. 80−24414
NiO, linear birefringence in S-domains near antiferromag. phase transition 80−60261
NiO, lithiated, semicond. oxide O_2 electrode characts. 79−24073
NiO, localised charge carrier transport, Seebeck, resistivity meas. 78−72152
NiO, mag. struct., neutron Laue diffr. method 80−70951
NiO, mag. transition, neutron scatt. exam. 78−56313
NiO, magnetic neutron Laue diffr. study of domain struct. and distrib. 78−95455
NiO, magnetic susceptibility, near Neel temp. 79−56509
NiO, matrix isolated IR spectra, ground state vibr. freqs. 80−28015
NiO, meas. of standard molar free energy of form. by EMF method of high temps. *(Japanese)* 78−11546
NiO, microwave cond. and DC cond. meas., 803-1873K 77−43638
NiO, multidomain mat., opt. anisotropy meas. at T_N 77−16279
NiO, nonstoichiometric, near-surface and bulk chem. diffusion 80−80035

nickel compounds continued
NiO, on Ni, particle and photon emission during tensile deform. 78−39672
NiO, optical absorpt. spectrum interpretation by comparison with MgO:Ni 77−52141
NiO ore, reduction of Ni in segregation roasting process *(Japanese)* 80−71908
NiO, oriented bicrystal growth by floating zone and Verneuil's method *(French)* 78−92186
NiO, paramag. shifts of ^{19}F at O 78−43719
NiO, phonon dispersion, calc. using extended three-body force shell model 77−27964
NiO, phonon dispersion relations, neutron scatt. meas. 79−42181
NiO, physicochem. props. at high temps. *(French)* 80−39582
NiO, plasma reduction melting *(Russian)* 78−31359
NiO, plasmochemical synthesis, oxidised from metals, exam. of props. 80−2984
NiO, polycryst., crystallite size distrib., X-ray diffr., mean squares smoothed Fourier transforms 77−27777
NiO, polycrystalline, high temp. deform. 78−3174
NiO powder, IR active modes in large clusters of spheres 79−42964
NiO powder, mixed with graphite, reduction mechanism *(Korean)* 78−11555
NiO, powder pressed disc, oxidising conditions effect on thermally stimulated exoelectron emission *(Japanese)* 80−89127
NiO, prepared by thermal decomp. of $Ni(OH)_2$, microporosity and irreversible water vapour adsorption 80−80060
NiO promoted $CuAl_2O_4$ catalyst, surface oxidation state and comp., XPS study 80−76134
NiO reaction with Fe_2O_3, microstruct. 79−87834
NiO, relax. valence averaging, Mossbauer spectra evidence 77−1626
NiO samples, colour difference, X-ray line broadening study 80−100206
NiO scale on Ni, elec. cond. 77−48568
NiO, self consistent energy band calc. 78−23022
NiO, self-diffusion of Ni, 700-1400°C, rel. to Ni oxidation mechanism 78−27681
NiO, single cryst., of S 78−95186
NiO, single cryst. cleavage plane, oxidising conditions effect on thermally stimulated exoelectron emission *(Japanese)* 80−89127
NiO single crystals, ang. distrib. of X-ray photoelectrons anal. of satellites *(German)* 79−11497
NiO single crystals, growth by material transfer in DC arc, and X-ray anal. 79−52113
NiO, single crysts., annealed, dislocation arrays in low angle tilt boundaries, TEM study 79−37707
NiO single crysts., creep along ⟨100⟩, stresses 50 MPa-120 MPa, 950-1200°C *(French)* 79−20121
NiO, single crysts., TEM of dislocations 79−4306
NiO, solubility of FeO at 1273K *(French)* 79−33089
NiO, solubility of S at 1000°C 78−63858
NiO, stress relief and plastic flow in temp. range 1323-1473K 80−89302
NiO, strong mag. field effect on reduction 77−4868
NiO, superexchange interactions, models, prospects for ab initio calcs. 77−69281
NiO, surface layer spacing relax., electrostatic argument 79−46901
NiO, surface sublattice magnetis., temp. depend., determ. using low energy electron exchange scatt. *(Japanese)* 77−55700
NiO, temp. depend. of thermal expansion and IR lattice vibrational mode 77−84950
NiO, thermal expansion, birefringence, AC susceptibility, temp. depend. 78−10664
NiO, thermodynamic study of point defects, anal. of elec. cond. results 79−23963
NiO, thin films with spinel-type defect structure, FMR study 80−39877
NiO, thin plate, antiferromag. domain obs. by neutron diffr. topography 77−32209
NiO, transient photocond. 78−60163
NiO, transport number and cationic cond. *(French)* 80−15297
NiO, transport props., temp. and stoichiometry depend., antiferromag. T-domain influence 77−8332
NiO, under controlled atmosphere, exam. of composition and temp. dependence, of lattice parameter *(French)* 79−19214
NiO, undoped and Al doped, Ni self-diffusion, vacancy-impurity complex effects 80−107493
NiO, undoped and Li_2O doped, surface reequilibration kinetics 77−55449
NiO, with spinel-type defect struct., ferromagnetic reson. meas. 78−43647
NiO, X-ray determ. of electron density distribs., atomic scatt. factors 80−15078
NiO:^{67}Zn, perturbed ang. correl. 78−95535
NiO:C, surface charge, O(1s), C(1s) and Ni(2p) XPS 80−45196
NiO:Cr, effect of Cr additives on structure parameters *(Bulgarian)* 80−44319
NiO:Fe, estimation of 4s covalent bonding of Fe^{2+} and Fe^{3+} ions, Mossbauer spectra 78−72441
NiO:Fe, exchange anisotropy of Ni-ferrite precipitates 79−28520
NiO:Li_2O-ZnO p-n heterojunction, contact resist., effects of water vapour 80−34506
NiO:$Li^+(Na^+)$, finely divided catalyst, low-temp. doping 79−51128
NiO:Mn, microhardness, plasticity, ageing effects 79−43291
NiO/SiO_2, catalyst, XPS for surface struct. and composition 79−43093
NiO-Al_2O_3, Verneuil-grown crysts., phase comp. 77−66586
NiO-Al_2O_3 powders, coprecipitated particle-size distrib. meas. 78−39726
NiO-Al_2O_3 reaction at film-substrate interface, Rutherford backscatt. obs. 80−59733
NiO-Al_2O_3 system, concurrent meas. of vol., grain boundary and surface diffusion coeff. 77−55399
NiO-CaF_2 two-phase material, press. sintering, activation energy and compaction mechanism 79−47651
NiO-CdO-Fe_2O_3 system, phase equilibria 79−11582
NiO-Cr_2O_3-$MgSiO_3$ methanation catalyst, S-resistant, IR and Raman spectra 80−93290
NiO-CuO, equilibrium relations 80−55375
NiO-Fe_2O_3, isoelectric point meas. 80−88609
NiO-H_2, interaction with surface, quantum chemical study 80−45549
NiO-MgO, crystalline soln., microstrain rel. to lattice energy and strain energy 77−24411
NiO-MgO, ESR and refl. spectra, Ni^{2+} distrib. 79−33745
NiO-MgO solid solns., surface comp. study by XPS 80−104035
NiO-MgO-ZnO, solid soln. form and colour *(Japanese)* 77−63647

nickel compounds continued
NiO-Ni composite mixture, preferential sputtering, XPS expts. 79−87544
NiO-$NiAl_2O_4$-Al_2O_3, heterogeneous solid state reactions, role of phase boundaries, dynamic equilib. at interfaces 78−71848
NiO-P_2O_5 glass, ESR of VO^{2+} ions 80−100610
NiO-TiO_2, solid soln. series, between rocksalt and spinel structure 78−51513
NiO-WO_3, phase relns. 78−3106
NiO-ZnO, solid solution, exam. of mechanism and kinetics of reaction with Fe_2O_3 ferrite formation 80−3309
NiO_2, elect. cond. under low O_2 press., kinetics interpretation 79−82587
NiO_2, $Ni(O_2)_2$, coordination of mol. O_2 with Ni, EHT calcs. 77−18795
NiO_2 single crystals, welding, optical and SEM study 79−65097
NiO_x, O(1s) XPS energies, oxidised metal surfaces, powders 77−16457
NiO_x-valve metal oxide interface, electron injection and reactions 77−76936
$Ni_{1-x}O$, electronic cond. at high temp., vacancies and interstitials effect *(French)* 78−79990
Ni_5O, ionisation energies, self-consistent-charge Hartree-Fock-Slater calcs. 77−6687
Ni_xO, film, thermoelec. power, activation energy variation with electrode spacing in DC sputtering 78−76099
Ni_xO_y, and $Ni_x(OH)_y$ surfaces, chem. changes induced by Ar^+ bombardment, XPS obs. 79−83084
NiO(:Li), dielec. dispersion and polarozation 78−2803
NiO−CaF_2, hot-pressed, mech. props., thermal expansion rel. to CaF_2 additive 79−43321
$Ni(OH)_2$, adsorption props. of surface, gas-chromatographic investigation 79−66343
$Ni(OH)_2$ electrodes, charged, reversible potentials meas. 80−55669
$Ni(OH)_2$, electrolytic precipitation, prep. of Ni-Cd battery plates *(Chinese)* 79−57237
$Ni(OH)_2$, quasi-two-dimensional antiferromagnet, specific heat 79−11317
$Ni(OH_2)$-α-$Mn(OH_2)$ system, precip. and ht. treatment 77−85916
$Ni(OH_2)_6(NO_3)_2$:Mn^{2+}, EPR spectra, crystal field symm. and strength 77−69674
$Ni(OH_2)_6(SiF_6)$, phase transitions, spectrometric exam. *(French)* 78−88291
NiOOH, sintered plate electrodes, residual capacity cause expts. 80−55745
NiO(S), spectrally selective EM wave absorber, solar energy collector material, props. *(Dutch)* 78−50872
$(NiO)_nV_2O_5$, (n=1, 2, 3), elec. and mag. props. 79−78094
NiO(100), low-energy secondary electron emission, 8 and 12 eV peaks 77−28668
NiO(100) surface, rumpling calc. 78−14559
NiP, valence electron energy spectrum, deduced from X-ray spectra and XPS 79−99984
Ni_2P, CVD on Mo plate, microhardness and resist. to chem. attack 79−66009
Ni_xP_{1-x} surface, laser produced ripple patterns 77−79878
$Ni(PF_3)_4$, force fields, mean vibr. amplitude calcs. 77−54552
NiP_4O_{11}, formation in phosphoric acid melts 78−27394
$Ni_2P_2O_7$, new variety, crystalline struct. *(French)* 79−65051
$Ni_2P_2O_7$-$H_4P_2O_7$-H_2O system, solubility isotherm at 0°C 77−25027
$Ni_2P_2O_7$-$K_4P_2O_7$-H_2O solubility at 25 degrees C, double phosphates formation 80−54381
$NiPS_3$, antiferromag., mag. props., NMR meas. 79−24223
$NiPS_3$, layered semiconductors, optical and electronic props. 80−70761
$NiPS_3$-Li, chemical and electrochemical intercalation *(French)* 78−38679
$(Ni_5Pd_5)_{82}P_{18}$, phase separated, exam. of crystallisation by differential thermal analysis 78−87623
$NiPtCl_6.6H_2O$, S=1 ground state, mag. props. in external field 80−11157
$NiPtCl_6.6H_2O$, singlet-ground-state magnets, ESR at low temps. 80−97132
$Ni(Rh_{1-x}Cr_x)_2S_4$, ferromag. spinel system with metallic conduction 79−56513
$Ni_{1-x}Rh_xS$, nonvolume effect of Rh substitution on paramag. metal-antiferromag. nonmetal transition 79−28277
NiS, antiferromag., press. effect on metal-nonmetal transition 77−69229
NiS, electrodeposition, using nonaqueous solvents 80−76200
NiS, electronic struct. from X-ray emission spectra 77−28661
NiS film, electrolytically deposited, mag. props., S content influence 80−44884
NiS, high energy spin waves, neutron scatt. study 79−51765
NiS inclusions in glass, microcracking, fracture mech. description 80−89333
NiS, metal-nonmetal transition under press. 77−69228
NiS, semiconductor-metal transition, UPS and XPS 79−23896
NiS, spin polarons exam. and metal-insulator transition 78−10377
NiS, struct. mechanism of low-temp. phase transition in hexagonal modification 78−71855
NiS, thermodynamic study of $\alpha \rightleftarrows \beta$ transition *(French)* 80−60854
NiS, X-ray diffr. obs., high press., diamond anvil camera method 77−4082
NiS_2 80−15832
NiS_2, anomalous magnetoresist. 79−78121
NiS_2, antiferromag. metallic state, neutron diffr. study 79−38325
NiS_2, antiferromag. struct., effects of four spin interactions 77−51885
NiS_2, core-level and valence-band XPS 80−93450
NiS_2, electron correls., defects, metal-insulator transition 78−63960
NiS_2, high press. effect on mag. transition temps. 78−91866
NiS_2, hyperfine parameters and quadrupole splitting determ., ^{57}Fe Mossbauer spectra 77−77131
NiS_2, mag. props. rel. to Hubbard model 79−78373
NiS_2, mag. struct. at 5K, polarised neutron study 78−80131
NiS_2, mag. torque curve 79−47305
NiS_2, model for weak ferromag. 79−65632
NiS_2, neutron diffr. anomaly at Curie temp., antiferromag. refl. 78−76260
NiS_2, pure and Co doped, ferromag. props. 79−91227
NiS_2, pyrite type, mag. struct., antiferromag. refl. of neutron diffr., susceptibility meas. 77−69497
NiS_2, Raman scatt., optical phonon peaks obs. 77−85728
NiS_2, spin struct. and mag. props. 78−39300
NiS_2, thermal expansion and cryst. distortion below antiferromag. Neel and weak ferromag. Curie temps. 77−15579

nickel compounds continued
NiS_2, weak ferro- and antiferromag., magnetisation and neutron diffr. meas. 80−65794
NiS_2, weak ferromagnet, galvanomagnetic effect 79−11148
NiS_2, weak ferromagnetic semiconductor single crystal, elec. and magnetic props. 77−85226
NiS_2-$NiSe_2$(CoS_2)(FeS_2), ^{57}Fe isomer shift, quadrupole splitting, Mossbauer study 80−15832
$Ni_{0.991}S$, sublattice magnetisation temp. var., neutron diffr. 77−40077
$Ni_{1-x}S$, and $Ni_{1-x}S_{1-y}O_y(Se_y)$, mag. state in metal-semicond. transition region, neutrnon diffr. obs. *(Russian)* 77−89926
$Ni_{1-x}S$, metal-semimetal transition, lattice dynamics and thermodynamic props. 80−29324
$Ni_{1-x}S$, oxidation, TG/DTA/MS obs. 78−31745
β-Ni_3S_2, defect struct. 78−63754
Ni_3S_2, exam. of vaporisation kinetics, using a levitation technique 78−51658
β-Ni_3S_2, formation during Ni sulphidation in H_2S-H_2 mixtures 78−3257
β-Ni_3S_2, formed during sulphidation of Ni, defect struct. and chemical diffusion 78−2115
Ni_3S_2, hazelwoodite, X-ray cryst. struct. determ. 80−88105
Ni_3S_2, heazlewoodite, dissolution in acidic ferric chloride soln. at 25°C 79−95172
Ni_3S_2, initial growth on Ni single crystal, electron microscope obs. *(Japanese)* 77−52670
Ni_3S_2, oxidation 79−83354
Ni_7S_6, alternative transform, behaviour, direct obs. by TEM 77−1227
Ni_xS_y, interaction with Pd *(Russian)* 79−52758
Ni_xS_Y, role of adsorbed S in dissolution and passivation 79−66340
$NiS_4C_4(CF_3)_4$.TTF, 1-dimens. mag. props. 77−66271
$Ni(S_2N_2H_2)_2$, cryst. struct. determ., new β modification 78−63716
$NiSO_4$, aq. soln., UV transmission filter characts. 77−3679
$NiSO_4$, photographic developer, potentiodynamic polarisation curves for Ag-less development *(Russian)* 80−90921
$NiSO_4$ soln. in H_2O, methanol-H_2O, US dispersion, 3-60 MHz *(German)* 78−59862
$NiSO_4$, solution, dielectric relaxation studies 78−84519
$NiSO_4$, spirals, growth and dissolution from liq. state 80−15027
$NiSO_4$:Li (10 at.%), powder, semiconducting, exam. of freeze drying rate in cryochemical prep. method 78−52706
$NiSO_4.H_2O$, hydrate librational modes in IR spectra 78−48161
$NiSO_4.H_2O$, IR spectra, H_2O external modes temp. depend. 78−58683
$NiSO_4.6H_2O$, uniaxial crysts., circular dichroism and optical activity 80−45029
$NiS_2O_3.6H_2O$, cryst. data and mag. susceptibility 77−76368
$NiS_2O_3.6H_2O$, p-p vector orient., PMR obs. 78−52361
$NiS_2O_3.6H_2O$, X-ray diffr. study, cryst. struct. determ. 79−4286
$NiSO_4.7H_2O$, Mn^{2+} doped, EPR study 80−34763
$NiS_{2-x}Se_x$, elec. cond., thermoelec. power and Hall effect meas. 80−65561
$NiS_{2-x}Se_x$, elec. resistivity temp. depend., pressure depend., paramagnetic-antiferromagnetic transition 78−10690
$NiS_{2-x}Se_x$, first-order Raman scattering 80−108206
$NiS_{2-x}Se_x$, mag. struct., ^{57}Fe Mossbauer study 78−56409
$NiS_{2-x}Se_x$ phase diagram, intermediate valence effects 80−103834
$NiS_{2-x}Se_x$, sp. ht. and elec. resist. in metallic regime 77−69589
$NiS_2(Se_2)$, electronic struct., UPS and XPS study 80−80935
NiS_yTe_{1-y}, mag. susceptibility, correl. with metal-insulator transition data 79−24145
NiSb, bandstructure and density of states calc. 80−70580
NiSb, cryst. growth from nonstoichiometric melt, and cryst. chem 78−35286
NiSb, electronic struct., XPS meas. 78−2990
NiSb, optical props., 0.05 to 5 eV 77−48194
NiSb-PbS(Se)(Te) eutectic system, crystn. 79−52190
$Ni_{1.1}Sb$, temperature effect on lattice consts., Mossbauer spectra and density 80−88124
$NiSb_2O_6$, force fields rel. to cryst. struct. *(French)* 80−107104
Ni_2Sc_2W, mag. order 77−63120
β-NiSe, d-electron deficit model, electrochem. meas. of free enthalpy *(French)* 78−30605
NiSe film, vac. deposited, phase transformation, electron microscope studies 80−2302
NiSe, thin film phases, struct. and resist. 78−39236
$NiSe_2$ 80−15832
$NiSe_2$, core-level and valence-band XPS 80−93450
$NiSe_2$, hyperfine parameters and quadrupole splitting determ., ^{57}Fe Mossbauer spectra 77−77131
$NiSe_2$, mag. props. rel. to Hubbard model 79−78373
$NiSe_2$, paramag. props., NMR, mag. susceptibility 80−60175
$NiSi_x$ formation from Ni_2Si at Ni-Si interface, Pt marker study 78−87830
NiSi, parallel contacts, Schottky barrier height meas. 80−96965
$NiSi_2$, amorphous, crystallisation by energy beam annealing 79−69012
Ni_2Si, chemical composition of Earth's inner core 80−8266
Ni_3Si, homogeneity region 78−23678
$NiSiF_6$, 6%, second order two-spin cross-relax. 79−95632
$NiSiF_6$, dilute, single-spin cross-relax. calcs. 80−97129
$NiSiF_6.6H_2O$, and hexadeuterate, optical absorption spectrum, 300 and 80K 79−73966
$NiSiF_6.6H_2O$, dielec. loss and relax., 100-270K, reorient. mech. 78−35088
$NiSiF_6.6H_2O$, dynamical props. of H_2O below 300K, Raman spectroscopic obs. 79−8140
$NiSiF_6.6H_2O$, EPR spectrum at low temp. 78−43632
$NiSiF_6.6H_2O$, EPR line shape, Tanaka-Kondo method 80−29602
$NiSiF_6.6H_2O$, ESR spectra at low temperatures and high pressures 78−52339
$NiSiF_6.6H_2O$, ferromag. ordering, susceptibility and heat capacity obs. 79−61080
$NiSiF_6.6H_2O$, non-Kramers system, spin-lattice relaxation at strong fields 80−100612
$NiSiF_6.6H_2O$, paramag., nucl. and electron spin lattice relax. 78−84494
$NiSiF_6.6H_2O$, single cryst., EPR, 77-300K, Debye temp. 77−85551
$NiSiF_6.6H_2O$(.$6D_2O$), near IR spectrum, 80K, assignments 78−48164
Ni_2SiO_2, elec. cond. under defined thermodynamics activities, up to 20 kbar, 340-1100°C 80−6832
Ni_2SiO_4, reaction with Fe to produce Ni *(Russian)* 78−15332
Ni_2SiO_4, single crystals, chem. transport prod. mechanism and thermodynamics *(German)* 77−36383

nickel compounds continued
$NiSnCl_6.6H_2O$, singlet-ground-state magnets, ESR at low temps. 80−97132
$NiSnCl_6.6H_2O$, ESR line shift at very low temps. 78−56375
$NiSnF_6.6H_2O$ anisotropy of probability of Mossbauer effect 79−42874
$NiSnF_6.6H_2O$, ferromag. ordering, susceptibility and heat capacity obs. 79−61080
$NiTO_3$, sintering additive for $SrZrO_3$ 78−23638
$NiTa_2O_6$, force fields rel. to cryst. struct. *(French)* 80−107104
$Ni_{1/3}TaS_2$, Hall coefficient and resistivity 80−39610
$Ni_{1/3}TaS_2$, magnetic susceptibility, function of temp. 80−39756
$NiTe_2$, acoustic phonon dispersion, inelastic neutron scatt. meas., elastic consts. and sound vels. 79−95098
$NiTe_2$, layer type dichalcogenides, reflectivity, 6 to 40 eV, electronic deep level excitation 77−55801
$Ni_{1-x}Te$, fluctuating localised mag. moments, d band motion, Mossbauer study 80−65768
$Ni_{1-x}Te_2$, mixing energies of Ni atoms and vacancies 79−27975
$Ni_{3\pm x}Te$, two-layer system, diffr. features 79−82187
$Ni_{3\pm x}Te_2$, long period superstruct., electron microscopy 79−86761
$Ni_{3\pm x}Te_2$, modulated struct. phenomena, survey 79−95033
$NiTiF_6.6H_2O$, mag. and struct. transitions 78−68257
$NiTiO_3$, antiferromag., mag. anisotropy, magnetisation meas. 80−65856
$NiTiO_3$, HP phase transform. 80−19941
$NiTiO_3$, photoacoustic spectra, spectrometer sample cell design investig. 77−74520
$NiTiO_3$, synthesis from products of soln. spray drying, kinetics 77−16519
$Ni(UO_2AsO_4)_2.8H_2O$, prep. cryst. struct. characterisation 78−30589
$Ni_2V_2O_7$, V-O-V bridge stretching freq. correl. with bond angle 78−74636
$Ni_3(VO_4)_2$, Neel temp., mag. susceptibility meas. 80−29550
$Ni_3(VO_4)_2$ temp. depend. of heat capacity, 60-1080K, Debye temp. 77−7869
$Ni_3V_2O_8$, flux growth and chem. characts. 78−23595
$(NiV_2O_4)_c(MgFe_2O_4)_{1-c}$, struct. parameters, IR spectra, cluster-component analysis 77−47425
$Ni_2V_2PbO_8$, flux growth and chem. characts. 78−23595
$NiWO_4$, AC elec. conductivity, thermoelec. power and dielec. const. 80−70736
$NiWO_4$, mag. struct. refinement, neutron diffr. meas. *(German)* 77−16049
$NiWO_4$ monoclinic antiferromagnet, orientational phase transition and intermediate state *(Russian)* 80−15725
$NiWO_4$, monoclinic antiferromag., domain struct. induced by strong mag. field 80−44856
NiZn complexes with hydrazine, X-ray diffr. expts. *(Rumanian)* 79−73149
NiZn ferrite, dielec. props., Jahn-Teller ion effects 80−97181
NiZn ferrite, effect of reactor radiation on mag. props. 77−32215
NiZn ferrite, exchange integrals, magnetisation data and mol. field theory 78−19241
NiZn ferrite, laser drilling and cutting, anal. of results using computer model 79−70180
NiZn ferrite, mag.-mechanical-microstruct. interactions 77−1578
NiZn ferrite, magnetic props., porosity and grain size effects 77−36095
NiZn ferrite, magnetic field effect on Rayleigh wave attenuation 78−6557
NiZn ferrite, prep. of single crystal by chem. transport with $TeCl_4$ 80−104051
NiZn ferrite, wall topography change induced by external press. 80−34734
NiZn ferrite, ZrO_2 additions influence on sintering and physicochem. props. 80−108369
NiZn ferrite quarter wave type absorber 79−38386
NiZn ferrites, comp., X-ray diffr. and saturation magnetisation obs. 78−18617
NiZn ferrites, density and mag. props., isostatic pressure effect 80−60816
NiZn ferrites, internal friction and ΔE effect depend. on demagnetisation method 80−80584
NiZn ferrites, mag. head props., technical possibilities and limitations 80−88803
NiZn ferrites, mag. susceptibility freq. spectrum, effect of pressure 78−95420
NiZn ferrites, Mossbauer effect and IR spectra 78−64300
NiZn ferrites, nonstoichiometric, initial susceptibility and microstruct. 80−84591
NiZn ferrites, substituted ferrospinel, spin configuration determ. *(Russian)* 77−32162
NiZn ferrites, V_2O_5induced mag. aftereffects 80−60379
NiZn ferrites under high press., grain growth *(Chinese)* 78−52825
NiZnCo ferrite, excess Fe type, saturation magnetostriction meas., oxidation effects 79−82852
NiZnCo ferrite, model of photomagnetic effect 77−43853
NiZnCo ferrite, quantitative anal., using X-ray fluorescence 78−40090
NiZnCo ferrites, switching time and coeff., hydrostatic press. effect 80−88802
NiZnCo ferrites, temp. stability, effect of Fe content and processing conditions 79−28993
NiZnCo ferrites, voltage response under sinusoidal and pulse magnetisation effected by hydrostatic press. 80−88846
$Ni_{0.25}Zn_{0.75}Fe_2O_4$, Mossbauer study, spin fluctuations 80−60471
$Ni_{0.25}Zn_{0.75}Fe_2O_4$, Mossbauer study, noncollinear spin struct. 80−60472
$Ni_{0.25}Zn_{0.75}Fe_2O_4$, structural phase transition, X-ray and neutron diffr. study 80−79735
$Ni_{0.32}Zn_{0.68}Fe_2O_4$ ferrites microstructure and magnetic props., effects of silica content, sintering temp. and sintering time 79−87746
$Ni_{0.32}Zn_{0.68}Fe_2O_4$, mag. props. and neutron damage 77−47973
$Ni_{0.36}Zn_{0.64}Fe_2O_4$, normal grain growth 78−72796
$Ni_{0.38}Zn_{0.62}Fe_2O_4$, preparation, Mossbauer study 80−50231
$Ni_{0.4}Zn_{0.6}Fe_2O_4$, conditions for max. resistivity 77−21065
$(Ni_{0.47}Zn_{0.53})_{1-x}Fe_{2+x}O_4$, recording head medium 77−86187
$Ni_{0.5}Zn_{0.5}Fe_2O_4$ coarse grain polycryst. ferrite, diffusional creep *(Japanese)* 80−104238
$Ni_{0.5}Zn_{0.5}Fe_2O_4$, Hall mobility, elec. cond. and carrier conc., 30 to 180°C 77−51765
$Ni_{0.685}Zn_{0.177}Fe_{2.138}O_{4+\gamma}$, phase diagram, therm. anal. 79−78945
$Ni_{0.71}Zn_{0.29}Fe_2O_4$ and $Ni_{0.57}Zn_{0.43}Fe_2O_4$, form. kinetics 79−83159
$Ni_{0.8}Zn_{0.2}Fe_2O_4$, twisted tubular polycryst. sample in axial mag. field, circular magnetisation 77−32230

nickel compounds continued
$Ni_{0.85}Zn_{0.15}Fe_2O_4$, ferrite, mag. anisotropy compensation under neutron irrad. 80−75807
$Ni_{1-x}Zn_xFe_2O_4$, LPE growth, film quality, mag. meas. 78−11136
$Ni_{1-x}Zn_xFe_2O_4$, polycryst., domain wall energy rel. to anisotropy 80−71090
$Ni_{1-x}Zn_xFe_2O_4$ spinel, low-temp. transitions and spin configurations, Mossbauer study 78−27144
$(Ni_xZn_{1-x})_{0.5}Fe_2O_4$, spontaneous vibr. modes excited by reversible magnetostriction 79−56587
$Ni_xZn_{1-x}Fe_2O_4$, catalytic oxidation of CO, mag. props., kinetic parameters and composition depend. 80−16723
$Ni_xZn_{1-x}Fe_2O_4$, crystal growth from BaO-B_2O_3-ZnO-NiO-Fe_2O_3 melt, exam. of crystal props. 80−40249
$Ni_xZn_{1-x}Mn_2O_4$, mag. props. 78−43573
$Ni_{1-x}Zn_xO$, solid soln., reaction with Fe_2O_3, microstruct. 79−87834
$NiZrF_6.6H_2O$, uniaxial ferromagnetism 78−80143
Ni_xZrS_2, ($0<x\leq0.50$), intercalation compounds, ordered phases obs. 80−33962
Ni_xZrS_2, fundamental optical absorption edge 79−99904
$Ni[B_6O_7(OH)_6].5H_2O$, cryst. struct. determ., X-ray diffr. 78−26546
$Ni_2[Fe(CN)_6]$, and $Ni_3[Fe(CN)_6]$, mag. susceptibility, reflectivity spectra and cryst. field 79−56808
$(Ni[NH_3]_6)(ClO_4)_2$, reorient. correlation times of NH_3 and ClO_4 groups, Raman obs. 79−28748
$Ni[UO_2(SO_4)_2].4H_2O$, revision of crystallographic data 78−22699
Ni(s, 1)+NiO(s)+NiX_2O_4 (X=Al, Ga), chem. potential and solubility of O_2 80−92679
Pb_2NiReO_6, new seignettomagnets and ferroelectrics 78−19425
PbO-NiO-SiO_2 system, melt, viscosity meas. in temp. range 950 to 1250°C *(Japanese)* 79−77663
PbO-SiO_2-NiO-MgO glass melt, interaction of NiO and MgO, elec. cond. and IR spectra obs. *(Japanese)* 80−24632
$Pb_{0.94}Sr_{0.06}(Ti_{0.47}Zr_{0.53})O_3$-NiO, modified, dielec. and piezoelec. props. 80−11342
$PrNiC_2$, struct. determ. using X-ray diffraction *(Ukrainian)* 80−33949
$Pr_6Ni_6P_{17}$, synthesis and cryst. struct. 78−75634
Pt compound, $[Pt_3(CO)_6]_n^{2-}$, n=1,2, one-electron states in polynuclear carbonyls 79−95358
$RbCl_2$-$NiCL_2$, impurity ion and vacancy aggregation, thermally stimulated depolarisation exam. 78−18678
$RbNiCl_3$, cryst., ^{35}Cl and ^{87}Rb NMR down to 1.3K 79−42848
$RbNiCl_3$, mag. props. 79−73736
$RbNiCl_3$, noncollinear magnetic order and spin wave spectrum in presence of competing exchange interactions 80−65834
Rb_2NiF_4, obs. of short range order by optical birefringence 79−11318
Rb_2NiF_4, planar antiferromagnet, cluster-Bethe-lattice method 80−22306
$RbNi_xMn_{1-x}F_3$, powder, mag. props. 80−2560
S-Ni-Fe system containing monosulphide solid soln., elec. and struct. relations 80−90038
ScNiSi, X-ray determ. of struct., new representative of struct. type TiNiSi 78−79595
$ScNiSi_3$, cryst. struct., X-ray diffr. meas. 78−10027
$ScNi_{0.25}Si_{1.75}$, X-ray determ. of struct., new representative of struct. type $ZrSi_2$ 78−79595
SnO_2-NiO, activated sintering mechanism 80−60810
Sr_2NiReO_6, new seignettomagnets and ferroelectrics 78−19425
$TbNi_2Si_2$, mag. props., 4.2-200K 80−84602
TeO_2-NiO system, phase diagram and vitrification 79−83182
TiO-NiO solid soln., lattice thermal cond. 79−23791
TiO_2-NiO-Sb_2O_3 phase equilibria 78−44098
$TmNi_2Si_2$, mag. props., 4.2-200K 80−84602
UO_2-Ni, surface, grain boundary and interfacial energies 78−21649
UO_2-Ni, surface, grain boundary and interfacial energies 78−71905
V_xO-Ni_yO, solid solutions, exam. of thermal conductivity 78−79827
WO_3-$NiCO_3$-Fe_2O_3, reduction alloy form. 80−60801
$ZnFe_2O_4$+NiO_2(MgO) powders, cation mutual diffusion coeffs. calc. 77−15635
$Zn_{1-x}Ni_xCr_2S_4$, spin struct., mag. props. meas. 77−85428
$Zn_{0.7}Ni_{0.3}Fe_2O_4$ film, epitaxial deposition, comp. and mag. prop. obs. using Mossbauer effect 79−38748
$Zn_{0.75}Ni_{0.25}Fe_2O_4$, mixed ferrite-spinel, helicoidal struct. 79−47242
$Zn_{1-x}Ni_xFe_2O_4$, heat treatment and sintering effect on porosity 80−25610
$Zn_xNi_{1-x}Fe_2O_4$, magnetic props. rel. to localised canting model 77−32161
$Zn_xNi_{1-x}Fe_2O_4$, Mossbauer spectra, mag. hyperfine struct. 80−15877
Zr-Ni-H, surface segregation of Ni, influence on catalytic activity 80−30275
ZrN-NiO, solid-phase reactions 79−11774

night airglow *see nightglow*

night sky
see also nightglow; twilight
artificial satellite search systems, night sky model 77−73923
atmospheric extinction, effect on electrophotometric obs. 79−96825
auroral zone, UBV photometry at geographic latitude 69°22′ north 79−44376
brightness, calibration using direct sensitometer, astronomical photographic photometry appls. *(French)* 77−13246
brightness, effects of urban lighting 77−73853
brightness, Mitaka, Japan *(Japanese)* 80−82067
brightness spatial var. obs. using intensified vidicon camera 77−70832
dark night sky paradox, expansion and hierarchical struct. of the universe 78−86055
dark sky paradox and origin of universe 79−25770
darkness, variation of duration with latit. 77−25632
extragalactic background light, upper limit 79−17142
extragalactic background light at 5115 Å, upper limit 79−101225
extragalactic background light intensity at 5100 Å wavelength 78−4414
galactic Hα background emission, high spatial and spectral resolution pictures 80−56897
heat engine using clear night sky as heat sink for teaching 80−27082
integrated starlight, synthetic spectrum between 3000 and 10000 Å, discussion 80−62200
interstellar UV radiation field, obs. from S2/68 sky-survey telescope 80−77523
IR sky background, 2.4 μm meas. 78−81715
light pollution and possible measures 78−49139
light pollution over Jena, night sky brightening at Karl-Schwarzschild Observatory 80−51533

night sky continued
lunar eclipses, visibility of Earth umbra against sky background 78−61770
Mt. Majdanak (1976 June-July), atmospheric extinction and night sky brightness *(Russian)* 79−39856
natural illumination measurement in 0.4 to 1.2 μm spectral region, photometer 78−57367
Olbers' paradox, comment 78−86070
'Olbers' paradox', history and resolution 77−33758
Sacramento Peak Observatory, night sky brightness conditions 80−12545
Sacramento Peak Observatory night sky conditions, cloud cover, seeing and precipitable water 80−51653
Simkin effect and Hg I 4047 Å night sky contamination effect on galaxy redshift determ. 78−41032
sky background, microwave emission spectra 79−48967
spectrum, distortion of galaxies radial vels. meas. 77−41406
starlight, integrated, synthetic spectrum between 3000 and 10000 Å, calc. method and results 80−46536
Toronto, city light pollution and night sky spectra 79−16668
urban light pollution, interference filters for nebulae observations 79−88599
zenithal brightness monitoring, light pollution rel. to astronomical observations 78−49141
He I, interstellar, UV emission, obs. and implications 80−62234

nightglow
auroral zone, UBV photometry at geographic latitude 69°22′ north 79−44376
balloon obs., intensity distribution over sky *(Japanese)* 77−82075
balloon obs., intensity distribution over sky *(Japanese)* 77−82076
continuum between 0.8 and 1.1 μ, Soviet obs. 78−81483
continuum near 8500 Å, intensity meas. 78−49195
E-region, diffuse Lyman alpha and beta and O I 5577 Å line radiation 79−66853
F-region nighttime dynamics from airglow features mapping 78−88980
Fabry-Perot pressure-scanned interferometer for nightglow meas. 77−9510
high-latitude airglow, near IR spectrum, comparison with auroral spectrum 77−53272
intensity fluctuations during stratospheric warmings 80−4162
IR emission meas. (0.9-2.3 μm) using interferometer-spectrometer 80−12583
lower thermosphere, emissions vars. rel. to thermal tides 77−78550
lower thermosphere and upper mesosphere, seasonal and long-term vars. and dynamics 77−33237
meteoric night-glow, origin 77−91488
meteoric nightglow, review of historical obs. 80−94761
multislit spectrometer for the night airglow observation 78−73542
near IR nightglow, meas. rel. to galactic centre and Aquila region mapping 79−12514
near IR nightglow continuum 77−78551
O I nocturnal 6300 Å luminesc., profiles from incoherent scatt. radar and photometry *(Portuguese)* 80−41591
optical emission features in aurora and nightglow, satellite obs., ground scatt. effect 78−77385
Pc 1 pearl event correl. with 4278 Å nightglow, Antarctic obs. 80−72664
photographic observations from Skylab 77−60505
photometer for nightglow studies, filter-tilting type 77−73889
sky model for artificial satellite search systems 77−73923
temperatures, internal gravity wave effects 78−45066
tropical UV airglow, mag. storm effects 77−45214
twilight visibility function of near-Sun astronomical objects, nightglow effects 77−5321
upper atmosphere emission at night and twilight horizons, Salyut 4 obs. 77−9590
visible spectra using field compensated interference spectrometer 80−36424
VLF wave events at L=4 correl. to optical emission 80−101468
N I 5200 Å forbidden line, ground-based meas. contamination by OH emissions 78−4020
N I (^{2}D) 5200 Å emission obs. in nightglow rel. to prod. in auroral zone 79−21090
N_2^+ 4278 Å band intensity meas. at Arecibo 77−64504
N_2^+ 4278 Å emission and electron flux comparison in auroral zone 77−87151
N_2^+, first negative band system correl. to mag. storm 80−72665
Na density correl. to Na I, OH and O I emissions 80−41585
Na enhancement and nightglow, spaced lidar obs. 80−101466
Na I 5893 Å line emission meas. with zenith photometer 79−53601
Na I 5893 Å nightglow and Na atoms distrib. in mesosphere, simultaneous obs. 78−88961
Na I D doublet, excitation, Na abundance 80−98497
Na I D-line profiles, interferometric studies 78−36353
Na I nightglow intensity vars. rel. to Na photochem. 79−70905
Na winter nightglow, correl. with radio absorpt. 77−33239
NaD, nightglow spectral intensity changes, correl. with O_2 spectra 80−61932
NaI night airglow, D-line excitation mechanism 79−84562
O I, 6300 Å nightglow enhancements by high powered HF radiowaves *(Portuguese)* 80−41592
O I 5577 A emission rel. to lower thermosphere interaction with stratosphere 77−70899
O I 5577 Å, Na and OH emissions var. during stratospheric warmings 77−53270
O I 5577 Å, night sky emission rel. to occurrence of nighttime E-region *(Russian)* 77−45223
O I 5577 Å and 6300 Å forbidden line emissions meas. with zenith photometer 79−53601
O I 5577 Å forbidden line rel. to O_2 and OH band spectra 78−61639
O I 5577 Å green line, nighttime var. of 2-15 min fluctuations 78−49193
O I 5577 Å line, intensity var., related to solar tides *(Russian)* 80−12585
O I 5577 Å line intensity latit. var., Chapman's mechanism 77−37474
O I 5577 Å line profiles, thermospheric temp. vars. determ. 77−9584
O I 5577 Å nightglow, meas. via two-channel rocket photometer 78−45078
O I 5577 Å nightglow obs., evidence for vertical transport latit. var. near mesopause 79−70903
O I 557.7 nm line, excitation 79−75008

nightglow continued
O I 557.7 nm nightglow in central polar cap 77−33238
O I 630 nm line profiles, thermospheric temps. and winds 79−58143
O I 6300 Å Doppler shifts, equatorial F-region neutral winds determ. 78−81473
O I 6300 Å emission, line profiles and Doppler shifts rel. to thermospheric winds and temps. 78−32263
O I 6300 Å emission, nighttime vertical distrib. models 79−53602
O I 6300 Å emission assoc. with F-layer irregularity zone 78−12038
O I 6300 Å forbidden emission at mag. equator, rel. to vertical E×B plasma drift vel. 80−36435
O I 6300 Å forbidden line, ground-based meas. contamination by OH emissions 78−4020
O I 6300 Å line, ground meas. for exospheric temp. determ. 77−67003
O I 6300 Å line correl. with electron content in nighttime F-region 77−67007
O I 6300 Å line meas. of O(^{1}D) quenching coeff. by molecular collision, optical meas. 79−2419
O I 6300 Å mid-latitude fluctuations rel. to F-region 78−49194
O I 6300 Å nightglow, Doppler shifts rel. to thermosphere midlatit. winds at 105°W and 79°W 79−16727
O I 6300 Å nightglow, obs. rel. to neutral comp. vars. at F-region heights *(Portuguese)* 80−41584
O I 6300 Å nightglow intensity rel. to Arecibo backscatter radar data 78−77401
O I 6300 Å pre-dawn emission and super-thermal ions from conjugate points 77−9589
O I 6300 Å red emission, first obs. in Guinea 79−58146
O I 7774 Å multiplet obs. over Arecibo during magnetic storm 80−72663
O I airglow emission rate, midlatitude maximum characts. obs. 79−84561
O I and N I forbidden lines emission in nightglow, historical review 79−5699
O I EUV and far UV emissions obs. in tropical ionosphere 77−2297
O I green line (5577 Å) in nightglow 79−48596
O I UV nightglow obs. at midlatit. 78−81482
O_2 7620 Å band, rocket-borne photometry 77−13128
O_2 (0,0) 7619 Å emission band, altitude distrib. from rocket obs. 77−29530
O_2 A-band in nightglow 79−48596
O_2, $A'^3\Delta_u$ state, inversion, presence in nightglow and discharges 80−63616
O_2 and [O I] intensity var. 77−73899
O_2 atmospheric system, rocket meas. of 7619 Å band *(Japanese)* 80−94631
O_2 Herzberg bands, emission rates 77−70901
O_2 Herzberg bands, excitation 79−75008
O_2, IR bands excitation mechanism, reaction rate consts. 78−65448
O_2, nightglow spectral intensity changes correl. with NaD spectra 80−61932
O_2, UV nightglow emission meas. 80−41590
O_3 electronically excited state, role in stratospheric chemistry and nightglow 78−20472
O(^{1}D) production by O_2^+ dissociative recomb. 77−41251
OH (6-2) and (8-3) bands, rotational temps. and intensities 79−58147
OH (7,2) Meinel 6861 Å emission band, altitude distrib. from rocket obs. 77−29530
OH (8-3) Meinel band in nightglow 79−48596
OH airglow, spectrum rel. to atmosphere warming at 90 km during 1976-77 winter *(Russian)* 79−88518
OH band emission diurnal and seasonal vars., correl. with O I 5577 Å 77−64506
OH band emissions, equilib. nature of rot. temp. 77−64508
OH band emissions, rot. temp. calc. 77−64507
OH emission, intensity meas. during 1969 NASA airborne auroral expedition 77−29529
OH emission, photometric obs. to find mesosphere neutral temp. 80−82121
OH emission IR photographs, evidence for wave systems 77−45212
OH Meinel bands, rocket meas. of 6863 Å band *(Japanese)* 80−94631
OH Meinel bands intensity var. at Poona, rel. to O_3 conc. 79−5698
OH, Na D-line and O I 5577 Å emissions, correl. 79−80067
OH, obs. using balloon-borne IR telescope 78−36453
OH($X^2\pi$) emissions, theory and meas. in (9-3) band 78−88960
OH(8-3) 7274 Å band rel. to O_2 and forbidden O I spectra 78−61639
OI, F-region neutral temp. by 630 nm spectra, during spread-F activity 80−41587
O_2(0-1) 8645 Å band rel. to OH and forbidden O I spectra 78−61639

Nilsson's model *see nuclear shell model*

niobium
see also nuclei with .....
(001) ideal surface, self-consistent pseudopot. calcs. 77−76894
absorption rate of H, metallic film effect 80−49525
adhesive interaction with siliconised Mo 77−48569
adsorbed H distrib., electron-stimulated desorption ion imaging 80−103572
adsorption of CO, AES obs. 77−35818
adsorption of H, sticking coeff. calc. 80−59803
adsorption of O_2, continuous meas. of surface pot. variations using mirror electron microscope 77−47680
adsorption of O_2, electron-stimulated desorption study 79−11017
adsorption of O_2 and N_2, on (100) planes, LEED-AES obs. 77−69186
adsorption on W (100), effect on surface reson. 79−65983
air contamination effect on compatibility with liquid Li in stainless steel vessels at 600°C 78−25285
alloy addition to hot rolled medium C steel, effect on transformation and strength 80−7607
alloying addition to low-alloy steel, role in austenitic grain growth 77−44255
annealing, of single crysts. for tunnel meas., ultra high vac. device *(German)* 80−89169
anodic oxidation, open circuit transient anal., dielec. and elec. props. of oxide film 80−3245
anodic oxide coating effects on mechanical behaviour 77−32659
anodic oxide films, space charge, TSC obs. 77−32326
anodic oxide layers, depth profiling by sputtered neutral mass spectroscopy 77−77833
anodised layer, structure and stoichiometry, thickness effects 77−77634
anomalous slip of single crystal, obs. 77−8900

niobium continued
atom, in niocalite, study of 4d excited states 77−26989
atom, integral K-shell Compton scattering, cross-section, for 1250 keV photons 78−90128
atom, Lα X-ray spectra, $_{40}$Zr to $_{48}$Cd, linewidths 79−41131
atoms, $N_2N_3N_{45}$ super Coster Kronig processes 80−106303
band effective mass, Animalu TMMP theory 80−29312
band structure, deformation potentials calc. by Green's function method 79−1568
band structure, self-consistent pseudopot. calc. 77−43487
band structure, X-ray emission bands, self-consistent calc. 77−28104
band structure and X-ray emission spectra calcs. 77−28105
BCC, electronic struct., appl. of fast self-consistent cluster calc. for large systems 79−82513
BCC, interaction energy between self-interstitial and screw dislocation, calc. 80−70248
BCC, stress-induced interaction and ordering 79−42057
BCC, structural singularities rel. to solid soln. behaviour *(Russian)* 77−11696
BCC, void nucleation following electron irrad. 80−29054
BCC crystal, elastic constants, thermal expansion and bulk modulus 80−6452
BCC lattice, optical prop. in range λ=0.265−18 μ, polarimetric meas. 79−15075
bicrystals, impact strength at 20° and −190°C *(Russian)* 80−45379
bimetal Nb-steel Kh18N10T with Cu interlayer, cyclic heating effect 77−16687
binding energies and surface layer identification following ion bombardment *(French)* 77−44541
blister diameter and blister skin thickness correl. under He ion irrad. SEM obs. 79−82266
blister form. on single crystal under Ne^+ ion bombardment 78−71772
blistering by 5-15 keV He ions, dose rate and temp. effects 77−35595
blistering by He^+ bombardment at thermonuclear reactor energies 80−34104
blistering by He atoms, (10-20 keV), exam. of skin structure, thickness, He distribution and swelling 79−60412
blistering under He ion irrad. *(Russian)* 78−18686
blisters due to He irrad., proton backscatt. study 80−75273
borosilicate cladding compatibility *(Russian)* 77−66741
bremsstrahlung spectra for 1 GeV electrons and positrons, planar and axial channelling *(Russian)* 77−32465
bulk granular supercond., thermal fluctuations compared to Josephson weak link array 78−43520
catastrophic slip bands, fine struct. *(Russian)* 78−38718
cathodic sputtering by Hg^+ ions, mech. of positive ionisation of atoms 78−27363
channelling study of $^4He^+$ irradiation damage, effect of dissolved O_2 79−82270
channelling study of $^4He^+$ irradiation damage, effect of irradiation temp. 79−82271
charge density distortions and lattice dynamics 78−30714
chemical vapour deposited, kinetics and microstruct., pressure and temp. depend. 80−11569
chemisorption of H, photoemission studies 80−76145
chemisorption of H, two-state model kinetics 80−75438
chemisorption of O_2 and initial oxidation on (110) and (750), LEED, AES, SIMS, and EELS obs. 80−44408
clusters, scattered wave Xα calcs. 79−15068
coated system, Nb on Mo, Ti, evaporation, carburisation and diffusion behaviour 77−44410
cold plastic deform., oriented microdistortions *(Russian)* 78−39840
cold-rolled, deform. zone geometry and texture gradients 77−48452
Compton profile anisotropy, electronic struct. of hydride 77−73182
Compton profile meas. 77−4698
core level binding energies 80−71564
corrosion by molten alkali metal hydroxides and liquid Li 77−44414
corrosion kinetics in sulphidizing atm. 80−35396
corrosion resistant pure metal, passivity and pitting in chloride solutions 78−44258
corrosion susceptibilities in synthetic geothermal brines 77−86223
coupled fields in one dimension: cross-over from a continuous symmetry to a discrete one 78−87821
creep induced by neutron irrad. 79−74221
creep rate in vacuum, grain size effect 80−108514
critical current density, deviation from critical state model 80−84578
crystal growth rate, influence on degree of perfection of single cryst. *(Russian)* 77−43162
cubic crystals, anisotropic, dislocation loops, electron microscope image contrast 80−39101
CVD coatings on graphite, grain struct. depend. on temp. 80−25574
damage production by high energy d-Be neutrons, elec. reist. meas. 77−62564
defect annealing in 7 MeV-irrad. samples, positron annihilation obs. 80−24497
defects due to neutron irrad., muon probes study 79−56701
deformation at 77-158K, slip and dislocation struct. 79−83277
deformed, α′-peak in internal friction spectra 80−16368
deformed, temp. effects on ageing, interstitial conc. depend. *(French)* 77−21182
deformed polycrystalline, γ-peak obs. and interpret. in internal friction, 300-500K 80−81098
density, rel. to elastic const. calc. from US meas. 77−86079
desorption kinetics of halogens, pulsed ion beam method 80−34300
desorption of O_2 in a vacuum, thermodynamic props. calcs. *(Russian)* 80−54501
determination, in Mg alloy, emission spectrographic DC arc-powder technique 78−48713
dielectric function and energy loss function, APW band struct. calc. 77−62850
diffuse electron scatt. *(Russian)* 80−103438
diffusion and solubility in Be 77−35757
diffusion and trapping of H(D) at ion implantation induced defects 77−47622
diffusion and trapping of O_2 79−77816
diffusion anomalies, vacancy model *(French)* 77−43366
diffusion coefficient calc. of O and N from internal friction meas. 77−89586
diffusion constant of H, anomalous temp. depend., quasielastic neutron scatt. 77−43381
diffusion in pyrolytic graphite, 1450 to 1950°C 77−39693
niobium continued
diffusion of ^{95}Zr in bulk crystal, diffusion coeff., effect on Nb self diffusion isotope effect 78−47602
diffusion of Fe, Co and Ni, and self-diffusion investig. 77−76615
diffusion of Fe, effect on self diffusion 77−84992
diffusion of Fe and self-diffusion 78−47590
diffusion of H_2, in single crystal, Debye-Waller factor, neutron spectroscopy 79−37881
diffusion of H_2, isotope effects, crystal field stabilisation 80−59728
diffusion of $H_2(D_2)$, quantum rate theory for symmetric double well pot. 78−55970
diffusion of H_2 *(Japanese)* 78−10221
diffusion of H, book contrib. 79−82390
diffusion of H, expt. compared with theory for light interstitial diffusion *(Russian)* 77−15632
diffusion of H, influence of H-H pairing, jump model 78−75878
diffusion of H, neutron radiography meas. 77−39696
diffusion of H(D), role of tunnelling, reson./nonreson. approaches 80−59718
diffusion of H and D at high conc. 78−26731
diffusion of H and D in Nb, low temp., from quenching and annealing study 80−6555
diffusion of H and trapping 80−70447
diffusion of interstitial O_2, sink/barrier phenomena 79−60553
diffusion of N, alloying additions and struct. defects effect 79−55938
diffusion of O_2 78−2298
diffusion of O and N, statistical calcs. on Arrhenius lines 80−59722
diffusivity of O, N, exam. 78−51741
dislocation damping, amplitude depend. 80−59469
dislocation etching of single crystal 78−14352
dislocation struct. after tensile creep test under reactor radiation conditions *(Russian)* 80−45348
dislocation substruct. in deformed and recovered single crystal 77−8897
dislocation-free single crystal, deformed at 180K, X-ray topographic obs. 79−24587
ductile fracture, low temp. annealing effect, precip. of Nb_2O_5 *(Russian)* 77−52456
elastic constants, 0K to melting point 79−38882
elastic constants up to melting point, US meas. 77−86081
elastic properties, at high temp. 80−30007
elastically deformed, quadrupole effects, NMR line intensity *(Russian)* 78−56400
electrical resistance, 200-2700K 78−39088
electrical resistivity, high temp., supposed failure of Boltzmann eqn. 77−72849
electrical resistivity changes with plastic deformation 77−89749
electrical resistivity due to interstitial H (D) 80−96848
electrode, surface changes induced by strong cathodic polarisation 79−100388
electrodeposition onto W 77−59704
electromigration measured by resistance method, for H and D impurities 79−23783
electromigration of grain boundaries *(Russian)* 77−7909
electron beam irradiation, 2.3 MeV, positron annihilation exam. of radiation defects *(Russian)* 78−34542
electron bombardment, high-energy, secondary electron emission 80−80917
electron diffraction axial channelling Kossel patterns, Bloch wave model, obs. 78−42869
electron diffraction Kossel pattern anal. 78−83676
electron drag on mobile dislocations, flow stress meas. 79−91197
electron energy losses due to H, obs. by scanning TEM 80−79850
electron irradiated, energy and orientation depend. of at. displacement 79−99244
electron irradiated, muon diffusion 80−80668
electron-coupled phonon spectrum, effects of strain 79−7943
electron-phonon interaction, calc. using APW band struct. calcs. and measured phonon spectra 78−14869
electron-phonon interaction, relativistic, APW calc. 80−92837
electron-phonon interaction electronic contrib. 77−15524
electron-phonon spectral function and mass enhancement 78−26988
electronic and optical properties 78−91612
electronic density of states, optical mass and DC elec. resist., Slater-Koster interpolation 77−15731
electronic specific heat calculations 79−73323
electronic structure, APW calcs., self-consistency and exchange effects 77−66109
electronic structure, self-consistent mixed-basis approach 79−69394
electronic structure, thermoreflectance studies 80−76047
electronic structure with non-muffin-tin pot., self-consistent relativistic APW calc. 77−66108
electrotransport in Th, 1370-1665°C 78−59979
electrotransport of H(D) at high H concs. 80−34246
embrittlement, slow strain rate by O_2 77−28902
emittance at 400 to 850K and normal spectral reflectance at room temp. 77−20813
enthalpy and heat capacity determ., 1650-2707K 78−71866
enthalpy meas., by levitation calorimetry 80−103499
etching, selective plasma 78−39940
evaporated film, adsorpt. of CS_2 and H_2S, 195 to 473K 79−33197
fabrication by carbothermic reduction-electron beam melting combination *(Japanese)* 79−100075
Fermi surface, electron mass enhancement, orthornormal function enhancement 80−96777
Fermi surface, Fermi velocity, electron-phonon interaction parameter 79−7778
fibre glass composite, new technique for producing fine metal fibres 80−108384
field emission anomalies in mag. field *(Russian)* 80−93462
field evaporation, search for high ionic charges 78−35269
film, BCC, optical props. 79−78781
film, bias sputtering prep. 79−1826
film, critical currents due to microwave field 80−25058
film, critical mag. fields and currents, temp. depend. *(Russian)* 80−103798
film, deform. in electron microscope, dislocation mechanism 79−82227
film, deposited in quasi-closed vol., supercond. props. 79−91180
film, electron beam evaporated film, struct., supercond., purity *(German)* 77−52253
film, electron beam evaporator for in situ deposition studies in UHV electron microscope 80−40264

niobium continued
film, epitaxy, struct. and supercond. props., on (001) surface of fluorophlogopite *(Russian)* 80-80101
film, evaporated, adsorpt. of SO_2, corrosion 78-79897
film, evaporated, interaction with BCl_3, HCl, adsorpt. 78-75945
film, evaporated, optical props., rel. to struct. 80-55211
film, far IR reflection and transmission spectra, room temp. 77-55792
film, influence of target texture on backscatt. yield of 2 MeV ^4He particles 79-4875
film, ion bombardment with N_2^+, Ar^+, struct. changes, chemical compound formation *(Russian)* 78-95084
film, laser induced reactions with Si 79-70365
film, low temp. internal stresses *(Russian)* 79-11036
film, magnetron-sputtered, intrinsic stresses and supercond. props. 80-24772
film, optical absorption meas. using synchrotron radiation, 20-250 eK 77-12457
film, props. control, bias sputtering model 78-72720
film, sputter-deposited on stainless steel, electron microscopy and ESCA 77-52554
film, sputtered, tunnelling characts. 79-4621
film, struct. and electrophys. props. at 4.2K 80-80436
film, superconducting tunnelling, meas. of annealing characteristics 79-7944
film, superimposed Ta film, cation-transport processes during anodic oxidation, Rutherford backscatt. and nucl. microanal. 79-20264
film, thin, microbridge, video detection of far IR radiation *(Japanese)* 80-97038
film microbridge, fabrication and I-V characts. 79-87198
film on sapphire substrate, orientational growth, epitaxial textures, nucleation textures *(Russian)* 80-75454
film on Si, Ar ion bombard., $NbSi_2$ form. 80-10709
film on Si substrate, intermixing, ion induced silicide formation 80-34101
film sputtered onto Cu substrate, microstruct. and supercond. props. 77-85370
films, oxidation, XPS study 80-80944
films, vac. evaporated, optical cond. 80-76100
films electron beam evaporated, struct. defects *(German)* 77-76684
flaking and blistering due to He and Ne ion bombardment 80-29092
flow stress, depend. on magnetic fields 77-73311
flow stress temp. depend., effect of interstitial atom clustering and embrittlement *(Russian)* 78-34538
flux pinning by proton irradiation damage 77-47947
flux pinning by voids during neutron irrad. 77-40008
fluxoid lattice, eqn. props., magnetisation measurements 80-39725
foil, electron energy loss spectra 80-7452
foil, oxidized, electron irradiation damage, AES study 79-28015
foils, coated with thin H-permeable Pd film, AES and SIMS 79-52467
foils, polycryst., proton irrad., diffusion of nuclear react. products *(German)* 77-35756
friction, He environment 4.2-80K 78-48543
Friedel's theory of amplitude depend. damping 78-27552
fusion neutron damage effects on mech. props., simulation by 16 MeV protons 78-71768
fusion reactor blanket struct. material, low cycle fatigue behaviour 80-30073
fusion reactor first wall material, cyclic deform. tests 80-30074
fusion reactor material, 10 to 1500 keV $^4He^+$ irrad., blister skin thickness, meas.-calcs. correl. 77-35597
fusion reactor material, neutron damage and sputter yields 77-57742
fusion reactor material, stress distrib. from He ion irrad., vol. expansion, calcs. 77-35599
fusion reactor wall, microexplosion of pellet, energy deposition 78-54890
fusion reactor wall material, surface behaviour under ion irrad., E_i=1 and 10 keV 77-57740
glissile dislocation interactions, TEM obs. 77-31666
grain boundary faceting, high purity samples 78-83826
grain boundary orientation in pure, cubic, lattice *(Russian)* 77-11567
granular films, ratio of supercond. transition temps. 80-84529
granulated film, critical current temp. depend. *(Russian)* 80-103803
graphite/epoxy laminates, with Nb powder filler, stress meas. by X-ray diffr. from fillers 79-43331
growth by pulling from a melt on a pedestal, charact. arrangement of dislocations 79-4911
Hall and Nernst-Ettingshausen effects, temp. depend. *(Russian)* 77-85198
He trapping, temp. depend. 77-31685
heat of sublimation, Knudsen effusion mass spectrometric determ. 79-81297
heteroepitaxial layers on sapphire, residual mechanical stress and strain influence on superconductivity 80-15644
high field de Haas van Alphen spectroscopy 79-73425
high frequency cyclotron resonance study 79-11057
high temp. radiative props., expt. determ., spectral emissivities 80-74718
high-temperature nonlinear electrical resistivity, supposed failure of Boltzmann eqn. 78-91664
hole ellipsoid scatt. rate temp. dependence, magnetoacoustic obs. 79-51472
hydrogen embrittlement, deformation behaviour of Nb-H alloys 79-11687
implantation of He, replacement of implanted ^3He by subsequent ^4He bombardment, and vice versa, using $^3He(d,\alpha)$ 79-4325
implanted with He, TEM of tensile specimen 77-51398
impurity concentration monitoring during single cryst. production 78-31337
impurity distribution, O determ. by neutron activation anal. *(Russian)* 80-70243
interaction with gases, H_2, N_2, O_2, CO, water vapour and hydrocarbons *(German)* 79-74296
interatomic forces, phonon spectra, from band structure charge densities 79-7662
interatomic pair potential, phonon spectra 80-33927
internal friction, meas. between 90 and 300K 79-100205
internal friction, of high purity single crysts., after plastic deformation, dislocation relaxation 79-38876
internal friction and elastic constants, reson. vibrs. of metal spheres 78-15443
internal friction peaks, induced by work hardening, low temp. relax. spectra *(French)* 77-1844
niobium continued
interstitial diffusion, theory of Gorsky effect for low interstitial H conc. 79-10896
interstitial impurity effects on strength 78-3194
ion+Nb target collisions, quasimol. KX-ray spectra, Doppler shift 77-19044
ion bombard. by 5 keV Ar^+, sub-surface damage 80-103399
ion bombardment, sputtering, re-emitted kinetic energy ang. distrib. 80-2910
ion implanted, He blistering, large swelling meas., gas press. model 80-88218
ion irradiated, void ordering 78-22770
ion plated with Pd and Ni, prep., H_2 absorption and desorption rate *(Japanese)* 80-108358
ion prod. in hollow cathode source 78-74525
ion-implanted bridge with thick Pb banks, fabrication and characterisation of film parameters 80-100569
irradiated superconductor, fluxoid defect interactions 78-52166
isochronal recovery of high energy d-Be neutron damage 78-51592
isotope effect for H diffusion 78-6182
ISSEC selection for fusion reactor 80-57950
Josephson junctions, excess current anal. 79-28465
Josephson junctions, submicron, fabrication by evaporation 79-28920
Josephson point-contact far IR detector props. 79-30543
K shell photoelectric cross section, at 74.409 keV 79-72288
kinetics and thermodynamics of reaction with N_2 *(German)* 79-74415
laser microprobe emission spectroscopy, matrix effects 77-16870
lattice atom displacements near end of implanted μ^+ tracks 78-55890
lattice distortion, due to O and N di-interstitial clusters 78-71726
lattice dynamical models, phonon dispersion curves 77-89506
lattice dynamics, local frequency spectrum, mean thermal displacement of H 80-59604
lattice dynamics, microscopic theory 79-7664
lattice dynamics, modified Sharma-Joshi model 79-51221
lattice location measurements of O, using $^3He/^{16}O$ and $^1H/^{18}O$ prompt. nucl. reactions, in irrad. effects 79-86813
layer, ion bombarded, supercond. props. and struct. 80-88671
liquid, exam. of O_2 solubility using thermodynamic analysis *(Russian)* 79-55889
liquid, spectral emissivity and brightness-temp. meas. at MP 77-43356
liquid Nb, enthalpy meas. by levitation calorimetry 80-103499
local heating during abrupt strain, catastrophic slip band formation 80-7652
lower critical field anisotropy 78-76201
luminescence characteristics of pure surfaces acted on by flux of field emission electrons 80-100695
magnetic form factors, neutron diffr. study 79-47234
magnetic surface barrier breakdown by O diffusion, permeability meas. 79-56601
mechanical properties neutron irrad. and Y scavenging effects 77-90394
mechanical props. and dislocation struct., mag. field effect 80-54935
mechanical props. and dislocation struct., mag. field effects *(Russian)* 79-42818
membrane, H permeation *(Japanese)* 80-100363
microhardness and charact. hardness 79-52376
mixed state, Abrikosov vortices orientation depend. of elastic props. *(Russian)* 77-40007
mixed state, muon spin rotation 79-56446
mixed state, sp. ht., 0.03-0.3K, electronic and nucl. contribs. 78-10621
mobile interstitials after electron irrad., resistivity recovery meas. 79-55783
momentum dependence of electron-phonon interaction 79-7665
$muon^+$, depolarisation rate, anomalous temp. depend. 78-80269
$muon^+$ depolarisation, localisation and thermal diffusion 78-39489
$muon^+$ depolarisation rate, anomalous temp. depend. 78-48104
muon diffusion, μ^+SR meas. 78-39487
muon diffusion, LAMPF results 80-71285
muon diffusion and trapping in pure and O doped samples 79-56685
muon diffusion at low temp., effect of nuclear elec. field gradients 77-52005
muon diffusion in presence of traps 78-68439
muon diffusion in presence of traps 79-56684
muon localisation and lattice dilation, μSR 79-56694
muon location and diffusion, μSR 79-56693
muon spin depolarisation, trap effects 79-56683
muon trapping, Knight shift, rel. to H interstitials 80-50247
nanobridge, Josephson effect, quasiparticle diffusion time, inelastic scatt. time 80-34556
Nb, pure, production by carbothermic reduction-electron beam melting combination method 80-89177
neutron damage, 15 MeV and fission neutrons, TEM anal. 77-35592
neutron damage and gas prod. spatial variation in Li(d,n) radiation damage facility 77-42207
neutron damage calcs., deuteron break-up source, sputtering appl. 77-35593
neutron diffuse-scatt. intensities 80-59597
neutron dispersion relation measurement using automatic triaxial crystal neutron spectrometer 79-97925
neutron induced defect structs., TEM exam. 77-84802
neutron irrad., microvoid form., ang. correl. and yield strength meas., TEM obs. 78-88381
neutron irrad., yield stress and activation vol. 77-90418
neutron irrad. effects on mech. props. 78-91361
neutron irradiated, embrittlement, yield stress, fracture stress and strain *(Japanese)* 77-76472
neutron irradiated, microstruct. and tensile props. 80-34077
neutron irradiated, positron annihilation ang. correl. meas. 80-93430
neutron irradiated, radiation anneal hardening *(Japanese)* 80-89243
neutron irradiated, TEM obs. of interstitial clusters 79-19288
neutron irradiation, low temp., 15 MeV, effect on superconducting props. 78-52179
neutron irradiation, low temp. 77-27915
neutron irradiation induced creep, high-energy, using in situ apparatus 79-79200
neutron spectra for fusion + hybrid reactor materials 80-23142
neutron sputtering yield determ. 77-36319
nitriding, high-temp., kinetics and mechanism *(Russian)* 79-74300
nitriding, kinetics 80-35415
NMR study up to 1700K, Knight shift and spin-lattice relax. time 80-2653
nonlinear resistivity, failure of Boltzmann equation 77-11893

niobium continued
nuclear fusion reactor materials development trends 77−46401
O_2 getters for LMFBR fuel pins 78−74437
optical emission, broadband, due to heavy ion bombardment 77−28635
optical properties and electronic props. 79−42439
optical properties of bulk Nb, 6.6 to 23 eV 79−4815
optical spectroscopy, for investigation of electronic struct. 78−91611
oxidation, AES and low-energy SIMS meas. 79−47832
oxidation, ESCA *(French)* 77−36361
oxidation, heterogeneous reaction kinetics, microcalorimetric and thermogravimetric curve comparison 77−21359
oxidation, staged flow of O_2 interaction process, secondary ion emission obs. 78−11386
oxidation at high temp. and low O_2 pressure, ESCA study *(French)* 77−25179
oxidation in H_2 atmospheres, TEM exam. of precipitated phase morphology and struct. 78−76790
oxidation in imperfect vac., solute O_2 level change and ductility loss 79−52452
oxidation kinetics, abnormal, at high temp. 79−29289
oxidation mechanism, 673 to 823K 80−108644
oxide film characterisation, using low energy electron induced X-ray spectroscopy *(French)* 78−41386
oxide growth and oxide coatings, XPS and AES studies 80−50765
phonon density of state determ. from thermodynamic crystal functions *(Russian)* 79−82291
phonon dispersion, anomalous struct., tight-binding calcs. 78−10137
phonon dispersion curves, charge fluctuation model 77−84869
phonon dispersion curves, extended du Launay model 77−4162
phonon dispersion curves, extended screened-shell model 80−96601
phonon frequencies, seventh-neighbour tensor force model 78−91402
phonon linewidth, electron phonon contrib. determ. 78−10146
phonon linewidths and electron-phonon interaction 79−73273
phonon spectra, self-consistency condition for force const. models 80−44264
plastic deformation, Shubnikov phase penetration, Faraday effect obs. 79−82731
plastic deformation effect on positron annihilation and supercond. transition *(Russian)* 77−39993
plastic deformation effects on superconducting specific heat transition 80−20352
plastic deformation under H_2 loading, cold worked exam. of α internal friction peak, 78−92307
plastic relaxation of internal stresses during mech. twinning at 4.2K, optical and SEM study *(Russian)* 79−66108
plastically deformed, changing lattice dynamics 78−67793
plastically deformed, flux density gradients and pinning forces, Faraday effect obs. 79−61010
plastically deformed, hydrostatic pressure effect on dislocation relaxation, US exam. 78−76696
plastically deformed single crystal, foil, damage free prep. for TEM and X-ray topography *(German, English)* 80−30200
plastically deformed single crystal, low temp. thermal cond. 79−28336
point contact, far IR freq. depend., of AC Josephson effect 79−33407
point contact Josephson junctions, thermally recyclable, as low-noise mixers 78−62224
point contact junction, supercond. weak couplings, high-freq. props. 78−68122
point contacts, AC Josephson effect meas. at 604 GHz 77−80876
point contacts, Josephson effects in far IR, high freq. behaviour 79−1643
point contacts as low-noise Josephson mixers, 115 GHz meas. 79−26123
polycrystalline, low energy H^+ scatt., computer study 77−36338
positive muon diffusion mechanisms, zero field spin relax. studies as probe 80−34840
positron annihilation and vacancy formation 80−16119
positron trapping and annihilation at vacancies 80−29823
precipitation from gaseous phase, Ta behaviour during H_2 reduction of $NbCl_5$ and $TaCl_5$ *(Russian)* 78−44017
preparation by electromagnetic levitation in ultrahigh vac. 80−29899
projected range distrib. of 5-25 keV $^4He^+$ 80−65094
protective coating form. by reaction with Sn-Al melt *(Russian)* 79−70221
proton diffusion, NMR obs., 120-480K 80−34812
proton irradiated, dislocation loops and mag. flux pinning 79−56463
proton irradiated, simulation of 14 MeV neutrons 79−1469
proximity effect of Cu-clad wire as temp. sensor below 1K 79−85139
proximity electron tunnelling spectroscopy 80−107964
pure, reaction with gas residual in vacuum, physicomech. props. effect 80−16587
purification, using hot extraction of gases, from refractory metals under vacuum elec. cond. meas. *(Russian)* 79−56940
quantitative anal., for D, by ion microanalysis 78−56945
quark detection using Nb balls *(Czech)* 79−26850
quasiparticle velocity, anisotropic many-body effects 79−33223
radiating power, integral normal, high-temp. meas. technique 77−65667
radiation anneal hardening of neutron irrad Nb 200 to 700°C 79−70077
radiation blistering by $^4He^+$ ions implanted sequentially at different energies, 3 to 500 keV 77−35594
radiation damage from 16 MeV protons, effect on microstruct. and mech. props. 79−46721
radiation damage in fusion reactors, computer expts. 80−13839
radiation hardening and yield strength correlations for 16 MeV H^+ and (D,T) neutron effects 78−14389
radioisotopic X-ray fluorescence determ. in industrial samples 77−52702
reactive, trapping of energetic 18 keV deuterons 78−10096
recovery and recrystallisation, fast neutron irradiation effects 77−70069
reflection of H 77−36336
reinforced Cu and Al based composites, fatigue strength, surface layer effects 77−12697
relaxation from room temp. to 114°C, computer optimisation of elastic aftereffect curves 77−90390
relaxation intensity due to interstitial O, temp. effect *(French)* 77−86080
residual resistivity, effect of interstitial atoms of O, N and C *(German)* 77−11895
resistivity recovery following low temp. electron irrad. of high-purity sample 77−27909
resistivity studies of interstitial He mobility 79−14800
resistivity variations caused by H and D interstitials, isotope effects 77−89750

niobium continued
RF superconductivity, appl. to particle acceleration, overview 79−31244
rotational magnetisation and torque meas. in mag. field 78−43515
scattering and radiation damage for 14 MeV neutrons and 10 to 20 MeV protons 77−15458
scattering rate temp. depend. from magnetoacoustic expts. 79−65522
secondary electron emission, on proton and deuteron irrad., 0.5-2.5 MeV 77−63512
self diffusion, 1353 to 2693K, diffusion coeff. 78−47576
self diffusion, up to 2570K 78−47564
separation from fission products, fast chem. methods 77−16856
single crystal growth by plasma heating 78−60569
slip localisation during discontinuous plastic flow of single cryst. at 4.2K *(Russian)* 77−69029
Snoek-Koster relaxation transient period, in cold worked Nb 79−34086
solubility of O_2, temp. depend. 79−99326
solute trapping of H, symmetry of O-H pair 80−108488
sphere, expt. determ. of fractional charge $^1/_3e$ 79−21694
spheres, residual resistivity ratio, prep. method effects *(German)* 79−8372
spray coating form. in pure Ar atm. 77−32709
spreading of Sn-Cu alloy films in vacuum, 700 to 800°C *(Russian)* 77−80680
sputter deposited film, O contamination, Auger anal. 78−52669
sputtered, angular depend. of energy spectra of sputtered ions 78−68595
sputtered film, analysis by X-ray diffr., electron diffr. and AES *(Czech)* 79−51448
sputtered film, compressive stress transition 78−10310
sputtered film interface with stainless steel, for supercond. AC cables 79−74089
sputtering by 10 keV inert gas ions, angular distrib. 79−52061
sputtering by 14 MeV neutrons, ion microprobe, SEM, He^+ backscatt anal. 77−36317
sputtering by 14 MeV neutrons, simulation expts. 77−36320
sputtering by energetic neutrons and protons, round robin expt. 78−11052
sputtering by fast neutrons 77−36316
sputtering by fast neutrons 78−15255
sputtering by fusion neutrons meas. 77−36321
sputtering yield, SEM and scanning Auger microprobe obs. 79−87545
SQUID, granular supercond. characterisation 79−28489
SQUID, low-noise DC type, with 1 μm tunnel junctions 80−80450
SQUID, oxidised Nb granules as three-dimens. Josephson junction array 79−67362
SQUID using thin film microbridge *(Japanese)* 80−31816
steady state O_2 solubility *(German)* 78−38851
steel, martensitic, age hardening with Cu, Nb additions, exam. of hardness 80−7681
steel, stainless/Nb interaction in vacuum percussion welding, Ni interlayer effect 79−29061
strain profile of plastic zone in dislocation-free single cryst. by X-ray topography 79−14876
strength differential effect, temp. and strain rate sensitivity in saturation cycling 79−66094
stress differential in surface oxide softening of single crystals 77−86116
stress induced interaction of point defect pairs, in BCC solutions 78−79608
substrate, contact angle with low melting metals 79−77864
super-Schottky and Josephson-effect devices, using Nb on thin Si membranes 79−28469
superconducting, AC losses surface effects 77−28313
superconducting, amorphous film, conductivity and transition temp., ion bombardment effects *(Russian)* 80−49969
superconducting, anisotropy in flux-line lattice symmetry 79−11279
superconducting, anisotropy of crit. field, magnetisation meas. 79−78260
superconducting, anisotropy of generalised Ginzburg-Landau parameters 79−4630
superconducting, deformed, oscillation in current-voltage characts. near H_{c2} 79−28491
superconducting, determ. of low field critical parameters 79−11278
superconducting, field history effect of flux gradient 78−91828
superconducting, fluctuation contrib. to sound attenuation near H_{c2} 79−33397
superconducting, flux density gradient determ. by Faraday effect 79−24113
superconducting, flux pinning, magnetization, bulk flux density gradient, and neutron scatt. meas. 79−56472
superconducting, flux-line lattice, dielastic interaction with internal stresses of cryst. imperfections 78−56270
superconducting, fluxoid line lattice neutron scatt. study 79−42712
superconducting, fluxoid-line lattice in intermediate mixed state, small-angle neutron scatt. 77−63042
superconducting, fluxoid-void interaction 79−7950
superconducting, hypersonic attenuation near critical field H_{c1} 77−77005
superconducting, hysteresis in time depend. fields up to 3 kOe 77−24637
superconducting, magnetoresist. and mag. breakdown in field up to 175 kOe *(Russian)* 77−20492
superconducting, muon spin relaxation *(German)* 80−50015
superconducting, nonequilib. mixed state, with pinning centres, mag. flux interactions *(Russian)* 78−39275
superconducting, O_2 diffusion profiles in surface layer 79−24101
superconducting, optical props. and electron-phonon interactions 80−2510
superconducting, peak effect due to vortex pinning in subsurface layer *(Russian)* 80−93060
superconducting, pure, fluctuations and sound attenuation near $T_{c2}(B)$ 77−15996
superconducting, single crysts., fluxoid pinning by small nitride precips. 80−70913
superconducting, spin fluctuations effect on T_c, from sp. ht. and mag. suscept. 80−7030
superconducting, state of art of tunnelling 79−69634
superconducting, strong-coupling microscopic parameters, electron tunnelling obs. 78−14888
superconducting, surface effect on crit. current density 79−61014
superconducting, surface effect on critical current density 79−65627
superconducting, surface resistance derivative meas. for annealed and unannealed crysts. supercond. 79−33395
superconducting, thermodynamic props. 80−107955
superconducting, torque anisotropy due to defects, flux line pinning 77−20509

niobium continued
superconducting, US attenuation, hysteresis near and below H_{c1} 80−75676
superconducting and normal state, thermal cond. meas., 0.05-23K 77−63025
superconducting bicrystal, flux pinning by grain boundaries 79−24114
superconducting bridges, variable thickness, microwave mixing 77−85390
superconducting bridges by electron beam lithography and ion implantation Josephson effect 80−20355
superconducting C-band cavities for linear accelerator appl. 79−36432
superconducting cavities, AES depth profile meas. on oxide layer 77−8984
superconducting cavity, RF, expectations and limitations 79−1648
superconducting crit. temp., functional derivative with electronic density of states, Eliashberg eqns. 79−56368
superconducting critical magnetic field and crit. temp. 79−7947
superconducting critical temperature, enhancement by radiation damage 78−2609
superconducting cylinder, hollow, flux-flow voltages during guided flux collapse 77−16012
superconducting cylindrical specimen, vol. pinning forces, Faraday effect obs. 77−24651
superconducting Eliashberg eqns. soln. 77−43776
superconducting film, supercond. relax. phenomena at microwave freqs. *(Russian)* 79−47187
superconducting film, surface impedance 79−24110
superconducting film, switching, storage and erasure effects 77−8253
superconducting film, transition temp. and crit. current, Gd ion implantation effects 77−39986
superconducting film, transition temp. and transition width, impurity effects *(Russian)* 77−66222
superconducting film, vac. deposited, deposition parameter effects on crit. temp. 80−2514
superconducting film prod. by electron beam sputtering *(Russian)* 78−15308
superconducting films, crit. depairing currents, temp. and mag. field depend. 80−7058
superconducting films, penetration depth measured with Nb-NbO_x-PbIn Josephson junctions 79−42691
superconducting films, supercond. props. and electronic density of states *(Russian)* 79−28439
superconducting foil, cross correlation measurements on moving vortex arrays 79−24117
superconducting foil, flux flow noise cross-correl. functions 77−36034
superconducting foil, time behaviour of local flux flow noise 79−24116
superconducting granular films as weak link in Josephson devices 80−88685
superconducting inclusions in Cu alloy wire, resist.-temp. meas., percolation theory 79−28490
superconducting inhomogeneity detection by penetration depth meas., proximity theory 77−28288
superconducting microbridges, heating and flux flow, I-V curves and microwave mixing 79−28474
superconducting microbridges, vertical type, fabrication and DC characts. 80−103788
superconducting microwave cavity appl., secondary electron emission and AES meas. 79−56895
superconducting mixed state, hysteresis of US attenuation 80−84549
superconducting mixed state, low temp. sp. ht. meas. 77−24638
superconducting mixed state, US attenuation meas. near B_{c2} 78−64167
superconducting muffin-tin type microwave cavity for accelerator use 77−26905
superconducting parameters, tunnelling meas. 79−91192
superconducting phonon struct. obs. in proximity tunnelling 77−77008
superconducting point contact, 9 GHz complex impedance 77−28303
superconducting point contact, high freq. props. in far IR 80−54840
superconducting point contact, singularities of I-V curve and voltage fluctuations 80−93044
superconducting point contacts, cond. mechanism 79−56440
superconducting point contacts, DC and HF behaviour 78−31021
superconducting point contacts, freq. and voltage depend. in noise background 79−58796
superconducting point junctions, I-V characts. *(Russian)* 79−51727
superconducting RF cavities for high energy storage rings, 700 MHz meas. 79−68059
superconducting solid resonators, high stability oscillators, appl. to fundamental physics, metrology 79−26034
superconducting state influence on dislocation motion *(Russian)* 80−70208
superconducting surface layers, O enrichment, penetration depth and resist. meas. 78−19180
superconducting T_c and H_{c2} effect of purity and alloying with Ta, Cr, Mo or Re 77−85375
superconducting T_c control by N ion implantation 78−2606
superconducting thin film, devitrified glass or ruby substrate, elec. props. 77−55635
superconducting transition effect on electronic work function 77−47928
superconducting transition temp., correl. with resist. anomalies and defect struct. 77−47920
superconducting transition temp. from Eliashberg eqns. 79−51709
superconducting transition temperature, ab initio calc. 80−25036
superconducting tunnel junction, temp. dependent props., 2-9K 77−24642
superconducting variable thickness bridges, mm wave response 79−28463
superconducting weak link, props. 79−38262
superconducting weak link fabrication, electron beam lithography, ion implantation 78−47913
superconducting wire, Cu clad, Meissner effect in Cu meas. 78−64166
superconducting wire, Cu clad, proximity effect, Meissner screening length meas. 79−60996
superconducting wire, helical propag. of flux jumps 78−14901
superconductive fixed points for temperatures above 0.5K 79−63221
superconductive transition point as reference temp. 80−107943
superconductive tunnelling, at thermally oxidised junctions, supercond. parameters determ. 79−19699
superconductive tunnelling meas. on single cryst. 79−47203
superconductivity, dynamic destruction 77−69461
superconductivity, influence of plastic deform. 77−85378
superconductivity and phonon softening, between electron bands and phonons 78−14859
niobium continued
superconductor, deformational twinning, mag. props. *(Russian)* 79−95543
superconductor, determination of surface and bulk props. 79−61011
superconductor, dielastic interaction of flux line lattice with internal stresses of cryst. imperfections 78−14906
superconductor, effect of changes in $\alpha^2(\Omega)F(\Omega)$ on the zero-temp. energy gap 80−97025
superconductor, Eliashberg eqns., numerical solns., Fermi surface calcs. 77−1514
superconductor, flux pinning under heavy ion irradiation 78−52167
superconductor, high crit. flux density gradient near surface 79−87221
superconductor, two-band, attenuation of longitudinal ultrasound 77−51847
superconductor, upper crit. field, temp. depend. and anisotropy 80−80462
superconductor energy gap determ. by pt. contact tunnelling 78−19185
surface, (001), low energy H^+ and He^{++} ion refl., computer simulation 80−11524
surface, adsorbed C^+ layer removal, by 20-30 keV Ar^+ bombardment, in plasma 77−76103
surface, adsorption of O_2, variation in work function, retarding field and thermionic emission meas. *(French)* 79−78823
surface, clean and oxidised, electronic struct., UPS meas. 78−95682
surface, coverage of O atoms as function of adsorption sputtering and diffusion rates 79−69354
surface, scatt. H^{2+}, polarised Balmer radiation, adsorbed O_2 effects 80−99569
surface, secondary ion emission mechanism, under Hg^+ ion bombardment 79−100013
surface blister bursting, 20 keV He ion irrad., 700 to 800K 77−36349
surface blistering, SEM and TEM obs., ion energy, dose and target temp. depends., review 77−43261
surface carburisation with propane 79−8382
surface damage caused by He^+ ion bombard. 80−39177
surface deformation, He implanted, integrated lateral stress 77−31697
surface electron states on (001) surface, pseudopot. calc. 77−8167
surface geometry and emission parameters, changes during directional mass transport 78−2344
surface oxide covered, primary electron beam effect on secondary emission coeff. *(French)* 79−47563
surface oxide softening, anisotropy 78−60716
surface oxide softening in single crystals, TEM obs. 77−40462
surface reflection and penetration of 25 eV to 10 keV He, T and H atoms 77−59657
surface topography formation due to elec. transfer processes *(Russian)* 80−54482
swelling correlation with local gas concentration following He irrad. 80−70271
thermal and elec. cond., 9-50K in cryst. and films 79−87078
thermal and electrical conductivity, temp. depend., 900-2100°C, additive effects *(Russian)* 77−15816
thermal conductivity, 0.3-20K, temp. and impurities effects 78−14883
thermal expansion, 1200-2000K 79−55905
thermal expansion, influence of plastic strain *(Russian)* 79−65220
thermal expsn., 1261-2289K 78−43150
thermo EMF and mag. breakdown *(Russian)* 77−80884
thermophysical meas. above 2500K, apparatus 77−45845
thermopower, 200-1600K 79−65446
thick layer vapour deposition by photoresist stripping 79−83135
thin film microbridges, fabrication and characts. 79−19705
thin-film Josephson tunnel junctions, fabrication and props., in situ ellipsometric meas. 80−65749
thin-film SQUID working at 4.2K, fabrication and characterisation 80−100570
third-order elastic consts. using nonlinearity parameter 78−75733
transport of H, study by neutron radiography, review of results 78−59961
type II superconductor, equilibrium misalignment, fluxoids and appl. mag. field, anisotropy interaction 79−24112
type II superconductor, inductive response to trapezoidal magnetic field 78−39277
unipolar arc damage in hot, dense D plasma 79−3235
US anomalous attenuation, single cryst. at low temps. 78−43076
US flaw detection sensitivity enhancement by focusing system 78−53113
vacuum condensate, Mo-Nb, prod. by simultaneous condensation from 2 sources, growth direction *(Russian)* 77−21026
vacuum heat treatment effects on gas content and elec. and mech. props. *(Russian)* 79−43281
vacuum technology appl., melt processing and appl. *(Hungarian)* 80−55318
vaporisation, influence of inert gases on losses *(Russian)* 79−55878
vapour deposition onto hot strip, mathematical model *(Russian)* 78−80476
variable thickness bridges on GaAs substrates, props. 79−28464
voids, TEM, elastic side band imaging 80−75219
volt ampere characteristics during electron melting process *(Russian)* 80−75336
VPE on sapphire, highly oriented film prod. 77−66097
W fibre reinforced Nb, plastic deform. and fracture 77−40438
weak link SQUID 79−38258
wetting by Cu-Ag-P alloy 79−82417
wire, interaction with stationary gases in high vacuum, HF fields effects *(Polish)* 79−34394
wire drawing, $NbFe_2$ layers form. by diffusion 79−28153
X-ray and neutron diffuse scatt. intensities comparison, thermal vibrs. 77−43294
X-ray emission L-spectra, influence of temp., liq. N_2 temps. *(Russian)* 80−80907
X-ray $L\beta_2$ emission bands of pure Nb and metal-like compounds, room and liquid N temps. 77−28654
X-ray $M\zeta$ energy, revised values 80−14102
X-ray reflection intensities, charact. temps. and Debye-Waller factors, 100-370K 78−18731
yield point and dislocation struct. temp. depend. for single cryst. *(Russian)* 77−81290
μ^+ meson spin relax. in cryst. lattices *(Russian)* 79−28664
Al/Nb superimposed layer anodic oxidation, ion movement study by O^{18} and MeV ion beam techniques 78−15604
Al-Al_2O_3-Nb, quantitative proximity tunnelling spectroscopy 79−91193

niobium continued
Al_2O_3/Nb, fracture mech. parameter determ. at high temps. *(German)* 79−70136
Al_2O_3/Nb laminates, metal to ceramic joints, adherence props. 80−45386
Al_2O_3/Nb/Al_2O_3 joint, solid state bonded, exam. of bond fracture strength 78−76826
Al_2O_3-Nb, cermet thin film, electrical transport and thermoelectric power 77−20462
Al_2O_3-Nb composites, influence of gas impurities on solid-state bonding on annealing 80−11739
Ar ion surface erosion 77−36342
$BaTiO_3$:Nb, elec. props., contact material influence 80−70848
$BaTiO_3$:Nb, ferroelec. and paraelec. phases, props. 79−42919
$Ca_{0.2}Ba_{0.8}TiO_3$:Nb, conductive single cryst. growth by Verneuil method 77−85928
Cr coated, prior thermal working effect on coating quality *(Russian)* 78−23820
Fe-Ni-Nb, cryogenic toughness, strength, rel. to reactive metal addition 78−39885
H uptake rates, enhancement by thin surface overlayers of Pd or Pt 79−82345
H_2 diffusion, low temp. recovery 79−73342
H_2 embrittlement, macroscopic behaviour at low temps. 77−32665
H_2 embrittlement, microscopic obs. at low temps. 77−32666
H_2 isotope release 80−37580
He depth distrib. 77−30665
He^+ bombardment, high dose 800 to 1400°C 77−36344
$La_2Mg_3(NO_3)_{12}.24H_2O$:$Nd^{3+}$, proton raser, self-radiating nuclear spin system *(German)* 80−53298
Li ion depth profiling using $^7Li(p,n)$ reaction 77−80534
Mo/Nb welded joints in sheet metal, detect. and exam. of cracks, initiation, development 77−73385
Mo-Al_2O_3, vaporis. at elevated temp., mass spectrometric obs. 79−29388
Mo-Si protective coating against oxidation *(Russian)* 79−39029
$MoSe_2$:Nb(Re), layered, elec. props., semicond.-metal transition 77−11922
NB-H(D), lattice expansion due to interstitially dissolved impurity 77−39600
Nb complexes, F-containing, X-ray K absorption edges, chem. interpretation 78−74676
Nb, de Haas-van Alphen study of Fermi surface, cyclotron effective masses, mag. breakdown effects, KKR calcs. 78−43288
Nb, effect of electron irradiation on low temp. deform., tensile stress-strain curves 79−55784
Nb films, ion beam sputtered, supercond., laser annealing effects 80−97024
Nb, fluxoid lattice, eqn. props., small-angle neutron diffraction measurements 80−34573
Nb IX (X), 4p-5s transitions 77−23453
Nb, mono- and polycrystn., crystallographic orientation, etching technique determ. 80−71814
Nb, neutron bombarded, defect size distrib. influence on hardening *(Russian)* 80−10580
Nb, of H, lattice distortion and migration energy of H impurities 78−30796
Nb single cryst., He ion implantation, depend. of blister deckeldicke and depth profiles on incidence angle 79−73226
Nb, superconducting film, thickness depend. of electrophys. parameter *(Russian)* 78−10590
Nb thin foils, surface segregation during sputtering at elevated temps., Auger study 80−54386
Nb V, $4p^64d$-$4p^54d5s$ transitions, level assignments 79−22631
Nb VIII, 4p-5s transition 77−27010
Nb VIII, energy levels, $4s^24p^4$ to $4s4p^5$ transitions obs. 77−3288
Nb VIII, IX, X, 4p-4d transitions obs. 78−82669
Nb XIII, energy levels, spectrum obs. 80−63571
Nb XXXII, XXXIII, XXXIV, transition identification X-ray spectra 80−32648
Nb XXXIX and XL, X-ray spectrum weak line detection 80−5497
Nb^{39+}, ^1P and ^3P energy levels, relativistic RPA calc. 80−47913
Nb:He, implant saturation and annealing, effect on struct. and supercond. props. *(Russian)* 78−43538
Nb:He, mech. props. and microstruct. 80−85003
Nb:N, deviations from Matthiessen's rule 78−39092
Nb:N, H, atomic tunnelling of interstitial pair, specific heat meas. 78−47600
Nb:N, H_{c2} anisotropy, impurity and temp. dependence 78−43533
Nb:N, neutron diffuse-scatt. intensities 80−59597
Nb:N, non-pure supercond., Ginzburg-Landau parameter 77−76997
Nb:N,H(D), thermal cond., 0.07 to 1.5K, influence of N interstitials 79−65601
Nb:O, $^4He^+$ irrad.-induced lattice site change 79−99252
Nb:O, type II supercond., radiation-induced flux pinning 78−80106
Nb/Cu, layered ultrathin coherent structs., supercond. props. 80−84525
Nb/Cu layered ultrathin coherent struct. 80−80122
Nb/In composite superconductor, transport props. 80−88658
Nb/Ta thin film proximity effect bridge 79−82712
Nb-Al, tunnelling expts. on normal metal backed by Al 80−65751
Nb-Al proximity sandwiches, supercond. transition temp. and tunnelling meas. 80−7045
Nb-Al superimposed metallic layers, ionic movements during anodization, Rutherford backscatt. and nuclear microanal. 80−71913
Nb-Al_2O_3 cermet-type film, thermoelec. power and annealing effects 77−47911
Nb-Al_2O_3 composite, semicond. films, cond. on localised states 77−24628
Nb-Al_2O_3 heterophase film, elec. props. rel. to Al_2O_3 content 77−15969
Nb-Cu bilayers used in refractory lift-off process, appl. to high Tc supercond. circuits 79−47626
Nb-Cu-Nb junctions, Josephson effect meas., critical current, temp. depend. 80−93041
Nb-D, Huang diffuse scattering of neutrons 80−10544
Nb-epoxy, interface, Kapitza resist. in supercond. and normal states 77−66085
Nb-Ga-Ir system, phase equilib. at 1000°C and supercond., Nb-rich portion 77−36480
Nb-H, acoustic phonon anomaly at small wavevectors 78−59882
Nb-H, $\alpha+\alpha'$ region, precipitation morphology investigation by gamma ray diffr. 77−52333

niobium continued
Nb-H, BCC, tetrahedral interstitial site H band modes, neutron scatt. obs. 79−55852
Nb-H, incoherent spinodals, meas. by Gorsky effect 78−19712
Nb-H, interstitial position of H from entropy of soln. 77−65989
Nb-H, spinodals and diffusion coefficients of H, sample shape depend. 78−19713
α-Nb-H, thermal neutron scatt., general multisublattice jump diffusion model 77−66046
Nb-H interstitial alloy, props. and synthesis 79−69265
Nb-H interstitial alloys, prep. and props. 78−23669
Nb-H single crystal, shear moduli, temp. and H conc. depend. 78−39823
Nb-H single crysts., critical current and flux pinning *(Russian)* 77−47946
Nb-H system, Huang diffuse scatt. of X-rays from displacement field 77−15446
Nb-H system, screening of H impurity and lattice distortion *(Russian)* 79−1577
Nb-H system, temp.-stimulated acoustic emission, hydride precip. 80−3044
Nb-H systems, supercond., H conc. depend. *(Russian)* 77−47932
Nb-H(D) system, incoherent phase transition 79−73304
Nb-H(D) system, solubility, entropy and enthalpy, isotope effects 77−20069
Nb-I-Pb junction, double-peak structure *(Russian)* 79−82716
Nb-I-Pb junctions, fine struct. of current-voltage curves *(Russian)* 79−19693
Nb-N, diffusion of H, incoherent neutron scatt., interstitial effects 79−60558
Nb-N (0.3 to 300 at. ppm), deform. 77−48477
Nb-N system, ion-implanted, supercond. crit. temp., effect of implantation conditions 78−19176
Nb-Nb Josephson junctions, submicron, thermally recyclable, fabrication and characts. 80−100566
Nb-Nb_2O_5-Nb structure, Schottky barrier effects on capacitance and loss tangent 77−8203
Nb-Nb_2O_5-Pb Josephson junction formed on Nb film edge 80−107960
Nb-Nb_2O_5-Pb(In) Josephson junctions, props. of Nb_2O_5 thermally grown tunnel barriers 80−100568
Nb-Nb_3Al superconductor, fabrication by quench-age method 77−40403
Nb-Nb_3(Al,Ge) multifilamentary supercond., fabrication and props. 77−20480
Nb-Nb_xO_y-Pb, tunnelling junction, current-voltage characts., knee struct. 79−38261
Nb-Nb_xO_y-Pb, two-dimens. Josephson junction, supercurrent vs. mag. field characts. 80−34562
Nb-Nb_xO_y-Pb Josephson tunnel junction form. and ageing, adsorbed gas effect *(Russian)* 78−14899
Nb-Nb_xO_y-Pb Josephson junction current-biased on Fiske steps, mag. field depend. 80−84567
Nb-Nb_xO_y-Pb junction, thin Al layer effect on tunnelling characts. 77−85393
Nb-Nb_xO_y-Pb(In) Josephson junctions, preparation and props. *(Russian)* 79−91188
Nb-Nb_xOy-Cu/Pb supercond. proximity junction, max. DC Josephson current, thickness depend. 79−82719
Nb-NbO system, single- and two-phase, sputtering yield, SEM and scanning Auger microprobe obs. 79−87545
Nb-NbO_x-Al/Pb supercond. proximity function, production by RF sputtering and photolytographic techniques 77−43787
Nb-NbO_x-Pb Josephson junction, self-reson. modes 78−64169
Nb-NbO_x-Pb Josephson junctions with high current densities, critical current 80−100552
Nb-NbO_x-Pb Josephson tunnel junctions, fabrication using FR glow discharge oxidation 80−34559
Nb-NbO_x-Pb junction, static charact. of tunnelling cryotrons 79−28480
Nb-NbO_x-Pb superconductive tunnel junctions, oxide tunnelling barriers, ESCA characterisation 80−65745
Nb-NbO_x-Pb tunnel junction, crit. Josephson currents, temp. depend. 78−2629
Nb-NbO_x-Pb tunnel junctions with high normal resists.,, crit. currents 79−56399
Nb-NbO_x-Pb tunnel junctions at 4.2K, conductance of oxide barrier 80−7046
Nb-NbO_x-Pb tunnel junction, temp. depend. of effective Nb energy gap 80−80454
Nb-NbO_x-PbIn tunnel junctions with ultra-thin Nb electrodes 79−56398
Nb-NbO_x-PbIn window type junctions, critical Josephson current depend. on magnetic field 79−65607
Nb-NbO_x-Sn long Josephson junctions, flux-flow voltage, dynamic vortex motion 79−4620
Nb-NbO_xPb tunnel junctions, current density distrib. 80−39717
Nb-Nb(Nb_3Sn) supercond. point contacts, crit. currents, effect of laser radiation *(Russian)* 79−28484
Nb-O, effect of O_2 on penetration of Li at 400°C 79−11719
Nb-O, Snoek mechanism and long distance diffusion under strain ageing *(French)* 77−81279
Nb-oxide-Pb Josephson junctions, anomalous microwave-induced voltages 78−39266
Nb-oxide-Pb Josephson tunnel junction, capacitance and ellipsometrically determined oxide thickness 77−4469
Nb-Pb supercond. tunnel junction proximity effect, theory 80−65752
Nb-Pb tunnel junction, crit. Josephson current, proximity effect model 80−93047
Nb-PbSn, Josephson tunnel junction, 3rd yr undergrad. expt. 78−54126
Nb-Si, bridge, crit. current 80−20359
Nb-stainless steel bimetallic strip Cu interlayer struct. during thermal fatigue *(Russian)* 78−15498
Nb-Ta bimetallic loop, supercond., thermoelec. flux effects due to penetration depth changes 77−24636
Nb-Ta superimposed metallic layers, ionic movements during anodization, Rutherford backscatt. and nuclear microanal. 80−71913
Nb-Te-Pb Josephson junctions, prep. and props. 80−65754
Nb-Ti superconductor, for fusion facility, cold-pressure-welded joints 78−62630
Nb-Ti-O system, phase equilib., microstruct., thermal, and X-ray anal. 77−8806
Nb-Ti-Ti_3O system, phase analysis, struct. stabilization 77−90330
Nb+Mo, K-shell vacancy prod., impact parameter depend. 80−14225

niobium continued
Nb+Nb, selected MO X-ray coincidence with separated at. K X-rays 80−43148
Nb+Nb, X-ray ang. distrib., 35-75 MeV 2 pΣ MO calc. 79−76380
Nb+Nb symmetric collisions, MO-2pσ radiation anisotropy, quasimolecular nature 78−70924
Nb+O_2, high temp. interaction kinetics and mechanism 79−100432
Nb_6 clusters, electronic struct., scattered wave-Xα calc. 79−11053
$NbD_{0.04}$, neutron scatt. exam., press. depend. of superstruct. reflection 78−22696
$NbD_{0.6}$, Compton profile meas. 77−4698
NbD_x, acoustic phonons conc. depend. 77−15515
$NbH_{0.026}$, nucl. acoustic reson. of interstitial H 79−51867
$NbH_{0.29}$, Compton profile and electron momentum distrib. anisotropy 77−44079
NbH_x, proton Knight shift and mag-suscept., high resolution meas. 77−55716
$NbH_x(D_x)$, H conc. detect. by neutron interferometry, precipitation effects 78−67735
Nb_3Sn, effect of O ion irradiation on supercond. 78−52131
^{93}Nb, in RTPR blanket, Bondarenko formalism to account for resonance self-shielding effects 77−23300
^{95}Nb, beta decay, K-shell electron ejection 77−18888
^{95}Nb inhalation in beagle dogs, deposition and retention, dosimetry 78−35959
Nb_2(g), dissoc. energy, heat of form., Knudsen effusion mass spectrometric determ. 79−81297
Ng-Pb Josephson junctions, magnetic field behaviour of zero field steps 80−100561
Ni/Ni_3Al-Ni_3Nb, directionally solidified lamellar eutectic alloy, deform. anisotropy and fracture 77−36604
Ni+Ni(Nb), Doppler shift of continuum X-rays from quasimols. 79−22808
O interstitial diffusion coeff., effective charge *(German)* 77−35759
Pb-Nb-Pb bridged, variable thickness, ion implant, coherent vortex motion props. obs. 80−100562
$Pb_{0.94-x/2}Ba_{0.6}Nb_xZr_{1-x}O_3$, Nb dopant morphology effect on microstructure 80−81005
Pb(Zr,Ri)O_3:Ni-silicon rubber flexible composite pyroelectric, dielectric props. 80−80704
Pb(Zr,Ti)O_3:Fe(Nb) ceramic, elec. and electromechanical props., depend. on dopants 80−81212
Pb(Zr,Ti)O_3:Nb ceramic, stress effects on ferroelec. hysteresis, macroscopic strain, US vel. 79−4778
SnO_2:Nb^{4+}, direct mechanism in supertransferred hyperfine interaction 79−23936
$SrTiO_3$:Nb, Fermi surface meas., oscillatory magnetothermal effect study 79−65357
$SrTiO_3$:Nb, heat treated, Hall effect, electrical cond., optical absorpt., defect states 78−47812
$SrTiO_3$:Nb, reduced sample, optical absorpt., effect of impurity-O vacancy complex *(Korean)* 79−8163
Ta-Nb-Ta sheet, interface topology, exam. method 77−72797
Ti coated, reduction of void number density and size by ion irradiation 78−51600
n-TiO_2 photoelectrochemical electrodes, effect of Nb doping on quantum efficiency 80−101121
TiO_2:Nb, rutile, elec. cond., 1273-1623K, O_2 press. depend., charge compensation mechanism 77−85217
TiO_2:Nb, rutile, low temp. sp. ht. 78−55957
TiO_2:Nb, rutile, Seebeck effect, 90-300K 78−43427
TiO_2:Nb, Seebeck coeff., Fermi level temp. depend. 79−11161
TiO_2:Nb, thermoelectric power meas. at high temp., point defect model 77−32030
TiO_2:Nb semicond. electrodes, electroreduction process kinetics, cathodic dark current meas. 80−66807
V, superconductor, neutron irradiation, low temp., effect on critical current 78−52180
YAG:Nd laser pulses, mutual exchanges with plasma *(German)* 80−48918
YIG:Nb, tetrahedral Fe^{2+} detect. by induced anisotropy ang. variation 79−11311
ZrB_2-SiC-C-Nb, refractory cermets hot pressing and oxidation resist. 80−3231
ZrO_2:Nb, thermoluminescence, traps and emission centres 79−24373

niobium alloys
see also niobium compounds
A15 compounds, mode softening and high supercond. crit. temp. 78−14851
A15 compounds, preferential order-disorder 77−84702
A15 compounds, self-consistent LMTO band calcs. 79−37954
A15 superconductors, high press.-high temp. treatment, phase props. 77−28746
A-15 compounds, irrad. effect on supercond. transition temp. 78−6472
ageing, high-temp., ageing struct. and morphology of hardening phases *(Russian)* 80−40390
ageing, high-temp., struct. and morphology of hardening phases *(Russian)* 80−40390
BCC, solid solution hardening, crystal resolved shear stress depend. on dislocations 80−40373
BCC ternary, solid soln. hardening model, compared with expt. results 77−44262
chemically stabilised, sensitisation and corrosion resist., heat treatment depend., precipitation steel, stainless, Cr-Ni 79−38827
cold worked, chemicothermal strengthening, internal oxidation 80−35229
creep, high temp. estimation and long term strength charact. 78−3195
dilute, diffusion and trapping of O_2 79−77816
film, sputtered, high press. induced shifts in supercond. transition temp. 77−85374
film, superconducting props. 79−38215
fusion reactor first wall and blanket material, props. for struct. appl. 80−30071
fusion reactor first-wall and blanket material, mech. props. 80−34074
fusion reactor materials, He and simultaneous damage production simulation 80−32480
heat resistance and brittleness, influence of nitriding in alloy VN2AE *(Russian)* 79−8380
Inconel, sputtering and blistering from H^+ and He^+ bombardment 78−79649

niobium alloys continued
Inconel 625, electron yields under ion bombardment for clean and oxidised surfaces 80−66368
Inconel 718, grain growth during sintering 80−97449
Inconel alloy 600, precipitation effect on corrosion 77−25180
Inconel alloy 718, exam. of struct., properties and continuum synthesis of ductile fracture 78−76736
interstitial impurity effects on strength 78−3194
lattice dynamical models, phonon dispersion curves 77−89506
low-alloy, strength and ductility at high temp. and different strain rates 80−16401
magnetic susceptibility and Knight shift meas., d-metal alloys 80−66055
Magnico alloy, with Si, Nb, Ti and La, low-temp. thermomag. treatment 77−63812
Magnico alloy, with Si, Nb, Ti effect of Ub on mag. props. and grindability 77−63811
Ni_3Al-Ni_3Nb eutectic alloy, aluminide coating microstruct. exam. 78−15593
non-metallic inclusion form. during quenching from liquid state 78−95766
oxidation protection from $MoSi_2$ coating, diffusion-slip casting appl. method 80−21187
Recalloy, Fe-Nb, semihard magnetic alloy, magnetic props., hardness, microstruct. 78−56660
steel, Al-Ti-(Mo), Al-Ti-V-(Mo), Al-Ti-Nb-(Mo) and Al-V-(Mo) low-alloy, toughness improvement through Ti additions 80−66525
steel, austenitic, DIN X8 CRNIMONB 1616 mech. props., FBR safety anal. 78−60966
steel, austenitic, Kh17N13M3T, activation charact. of rupture, 630-730°C, Sb and Nb microalloying effects *(Russian)* 79−5033
steel, austenitic, phase composition of Kh14N16 with Zr, Ti, Nb and N additions after quenching and tempering 77−90378
steel, C-Mn-Nb, Nb microalloying, weldable, structural, recrystallization and precipitation induced by high temp. deform. *(French)* 79−61632
steel, C-Mn-Nb, weldable, high temp. thermomechanical treatment 79−15709
steel, Ce, Nb, addition effects on hot plasticity *(Russian)* 77−66680
steel, cold-formed, low pearlite, Nb alloyed, Nb effects, precipitation, recrystallisation *(German)* 77−8832
steel, Cr-Mo-Nb-(Ni)(Ti), low alloy, material selection for nuclear steam generator tubes 78−54834
steel, Cr-Mo-Ni-Nb, Nb effect on mech. props. *(German)* 80−30012
steel, Cr-Ni-Mo-V-Nb (12,8,1,1.5,0.4 wt.%) Ce addition effects on strength and hardness *(Russian)* 78−15454
steel, Cr-Ni-Nb, containing controlled particle dispersions, creep strength 77−52425
steel, emission spectrochemical analysis of Nb, effect of Mn, interference for Nb II 3194.977 Å 77−21457
steel, high Nb, HSLA, low temp. fatigue props. 80−40490
steel, high strength, Nb(C, N) precipitation in austenite, effect on mech. props. *(Japanese)* 77−21186
steel, high-speed tool, Nb addition effect on hardening 79−34048
steel, high-strength, fatigue crack growth rate and crack tip shapes, cyclic bending *(Russian)* 80−71740
steel, low C, Mb-Nb, reheated, quenched, tempered, microstruct. 77−36550
steel, microalloy V-Nb, V, Nb effects on strength and formability of cold rolled sheets 77−55979
steel, microalloyed, hot-rolled, Nb(C,N) precip. and austenite recrystn. 80−97513
steel, Mn-Mo-Nb, high strength, ductile, acicular ferrite struct. 77−21191
steel, Mn-Nb-Al-C, crack progag. and hot ductility during straightening concast strand 80−66646
steel, Mo-Nb (2.5, 0.035 wt.%) Mo content effect on sulphide stress cracking resistance 80−21157
steel, Nb,(V),(Al), hot-rolling, laboratory simulation, recrystn. of austenite 80−97512
steel, Nb, high and medium C, austenite grain growth 78−11249
steel, Nb-stabilised, orientation depend. of cell size and recrystallisation texture development 79−91682
steel, Nb-V, cold rolled, HSLA, prod. by precipitation hardening, annealing 78−88471
steel, Nb-Va microalloyed, mech. props. *(French)* 80−35252
steel, R6M6, micro-alloying effect 78−6939
steel, stainless, Cr-Ni-Nb stabilised, Te vapour effect on creep and tensile props. 79−24583
steel, stainless, oxidation effect of Nb 80−35394
steel, stainless, stabilised with Cr-Ni-Nb, reaction with Te vapour 77−8986
steel, V-Nb, supercooled austenite isothermal decomp., struct., strength and fracture charact. 80−60966
steel, weld metal, contrib. to mechanism of Nb(C,N) precip. *(Slovenian)* 78−84816
steel precipitation, low C, precipitation of Nb and V, critical temperature identification, by meas. electric resistance *(Slovak)* 77−4781
superconducting, A-15 type, universal defect behaviour, transition temp. rel. to lattice parameter 77−69440
superconducting, electron probe comp. meas. 77−12852
superconducting, metallurgical factors influencing T_c 79−38225
superconducting, technical requirements and props. *(Slovak)* 78−88069
superconducting and normal phases, electron scatt. and lattice thermal cond. 77−77001
superconducting film, multisource deposition rate control using mass spectrometer as sensing element 78−72730
superconducting magnets, energy transfer applications, Nb alloys, construct., stabilisation methods, mech. and elec. props. *(Dutch)* 78−49871
superconductivity, dynamic destruction 77−69461
superconductor, flux pinning under heavy ion irradiation 78−52167
surface blister bursting, 20 keV He ion irrad., 700 to 800K 77−36349
zircaloy-4, Nb additions, corrosion behaviour 77−40469
Ag-Nb, optical props., DC resist. and thermoelec. power 77−85824
Ag-Nb-Ga, phase relations, A15 phase diffusion layer formation 78−52764
Al-Cr-Nb, calc. of phase equilibria 79−11569
Al-Nb, struct. and props. of alloys obtained from granules 80−50717
Al-Nb-R system, R=rare earth, X-ray diffr. obs. of phase equil. *(Ukrainian)* 77−32560
Al-NbTi solenoid magnet for high energy particle detector, conductor and cryostat design 79−31319

niobium alloys continued
Au-Nb, dil., Friedel d-reson. scatt. and elec. resists. 80−44566
Be-Nb-Zr, glassy and partially crystalline, supercond. T_c and struct. props. 78−60239
CC NbTi, pool cooling superconducting test coil, Japanese design for fusion reactor large coil task 80−99340
Co-Al-Nb, monovariant directionally solidified eutectics, struct. and mech. props. *(Russian)* 78−92254
Co-Fe-Nb, heavily cold worked, magnetic hardening 79−20073
Co-Fe-Nb (12, 3 wt.%), semihard magnetic alloy, relationship between precipitation and coercivity 77−8839
Co-Fe-Nb alloy, mag. precipitation-hardening and Bloch wall pinning 78−80173
Co-Fe-Nb alloys, effect of cold working on mag. props., and precipitation morphology 78−39803
Co-Fe-Nb semihard mag. alloy, mag. precip. hardening 77−8960
Co-Fe-Nb-Mo, semihard magnetic alloy, magnetic props. 78−95469
Co-Nb, dil., NMR-ON meas., mag. hyperfine splitting const. of ^{90}Nb 78−43651
Co-Nb alloys, segregation of Nb to stacking faults, field ion microscopy investigation 77−8816
Co-Nb-C, obtained by liq. quenching, superconductivity 80−75699
Co-Nb-Si, directionally solidified eutectics 79−61575
Co-Ni-Cr-Nb, effect of Fe addition on precipitation behaviour 80−29962
Co-Ni-Cr-Nb (40, 18, 1.8 wt.%), precipitation behaviour of NbC, effect of ageing temp. on morphology 80−89227
Co-Ni-Cr-Nb FCC alloy, electron microscope obs. of deform. twins 79−60380
Co-Si(Al)(Cr)-Nb, eutectic alloys, charact. by melting, oxidation resistance and composition 78−52768
Co_2Nb, Laves phase, elec. resist. rel. to mag. props. 77−59282
Co_2Nb, mag. susceptibility, 77-500K *(Russian)* 77−80911
Co_2NbSn, ferromag., hyperfine fields meas. by NMR 77−63315
Cr-La-V-Nb-Ta, La, V, Nb Ta effect on hardness and strength *(Russian)* 79−34050
Cr-M, optimum alloying with rare earth metals, Ti, Zr, Hf, Nb, Ta 78−68651
Cr-Mo-V-Nb, supercooled austenite isothermal decomp., struct., strength and fracture charact. 80−60966
Cr-Nb, dislocation cell growth kinetics by TEM during annealing *(Russian)* 79−65084
Cr-Nb, Invar alloys, thermal expansion, plasticity *(Russian)* 79−55907
Cr-Nb-Mo system, comp. and temp. depend. alterations in mech. props., phase diagram interpret. *(Russian)* 80−85045
Cr-Ni-Mo-Cu-Nb steel, martensitic precipitation hardenable, corrosion-resistant, heat treatment, structure and props. 79−74169
Cr-Ni-Nb steel, oxidation in CO_2, charged-particle nuclear techniques 80−61022
Cu-Nb, exam. of monotectic reaction, using chill casting technique 78−68679
Cu-Nb, formation of two phase microstructure, during volumetric, and directional cyrstallisation *(Russian)* 79−29040
Cu-Nb, supercond. wire, directional solidification of melts, supercond. ionisation temp. *(Russian)* 78−76596
Cu-Nb (0,4 at.%), splat quenched, aged, superconductivity *(Japanese)* 77−63018
Cu-Nb (17 wt.%) multifilamentary wires, fabrication and supercond. characts. 79−56476
Cu-Nb (7 wt.%), solidification microstruct., SEM 77−12611
Cu-Nb alloy, chill casting, consumable arc melting, ingot prep. techniques 80−84879
Cu-Nb alloys, origin of superconductivity 77−47918
Cu-Nb alloys for superconducting wire, casting of dendritic structure 80−2976
Cu-Nb composite superconductor produced by rapid quenching 78−48351
Cu-Nb filamentary composites, powder metallurgy prod., supercond. props. 79−56477
Cu-Nb multifilamentary composites, in situ formed, anomalous strength increase 79−43323
Cu-Nb multifilamentary composite, dislocation resistivity 80−70671
Cu-Nb_2Sr, multifilamentary supercond. composites, in situ formed, critical currents 79−65625
Cu-Nb_3Sn, in situ formed multifilamentary composite, supercond. and mech. props. 78−39279
Cu-Nb_3Sn composite wires, powder metallurgically produced, supercond. props. 78−31026
Cu-Nb_3Sn multifilamentary tapes, in situ formed, crit. current density anisotropy 80−84576
Cu-Nb_3Sn superconducting composite, crit. props., AC hysteretic losses 80−50014
Cu-Nb-Sn, multifilamentary supercond. composite wires, fabrication on laboratory scale and mech. props. 80−29897
Cu-Nb-Sn composites, cold-powder-metallurgy processed, supercond. critical currents 79−78279
Cu-Nb-Sn dil. alloys containing Nb_3Sn precipitates, superconductivity 78−43507
Cu-Nb-Sn system, phase equilibria and supercond. props. *(Russian)* 80−50589
Cu-Nb-Sn(Ge), phase relations and diffusion layer form. 77−36458
Cu-Nb(Nb_3-Sn) composite wires, powder metallurgy prod., supercond. props. and annealing 79−33428
Cu-Ni-Nb (30, 0.9 at.%), precipitate free zones, X-ray microanal. 80−108768
Cu-Ni-Nb (30,1 wt.%), precipitation 77−86035
Cu-Ni-Nb-Al, correlation of γ' and γ'' precipitates phase stability 80−25704
Cu-Ni-Nb-Al, formation of γ' and γ'' precipitates 78−76655
Cu-Sn-Nb multifilamentary alloy, high field crit. current density 78−27004
$Cu_{40}Nb_{30}X_{30}$ (X=Ti, Zr, Hf), superconductors with metastable ordered structs. 80−108484
Cu(Sn)/Nb(Al), composite superconductor fabrication and charact. 77−81242
Fe-Al-Nb (36.2, 4.65 wt.%) fatigue deform. 77−44350
Fe-C-Mo-Nb-Al-Ti-B (0.015, 5.75, .7, 1.6, 2.5, 0.1 wt.%), TZM sheet, wear resistance, effect of surface hardening 77−59985
Fe-Co-Mo-Nb semihard mag. alloy, mag. props., thermal expansion, elec. resistivity and hardness *(Japanese)* 80−88789
Fe-Co-Ni-Al-Nb (15-20, 14, 9, 0.1-5.5 at.%), Nb effect on magnetic props., lattice parameter *(Russian)* 77−55689

niobium alloys continued
Fe-Cr-Co-Al-Nb, phase equilib., X-ray diffr. meas. *(Russian)* 79−47658
Fe-Cr-Nb-C, X-ray microanal. of carbide phases rel. to Nb conc. *(Russian)* 78−88467
Fe-Mn-Nb, struct. and props., Nb alloying effects *(Russian)* 77−90360
Fe-Mn-Nb-V, high Mn, dispersion strengthening 77−16602
Fe-Nb, dil., high freq. induction melting and centrifugal casting, working curve sample prep. photoemission anal. *(Japanese)* 78−53050
Fe-Nb, mag. and Mossbauer meas. 77−63133
Fe-Nb, split bands evidence from sp. ht. and elec. transport data 77−24515
Fe-Nb (3.1 wt.%), semihard mag. alloy, Recalloy, mag. props., elec. cond. *(Japanese)* 78−10723
Fe-Nb creep resistant alloy, precipitate free zones elimination 80−16312
Fe-Nb internally nitrided, mech. props. 77−44307
Fe-Nb-C (0.04, 0.02 wt.%), strengthening, hot rolling *(Chinese)* 79−100154
Fe-Nb-Co, Recalloys, semihard mag. alloys, mag. and elec. props., hardness, thermal expansion *(Japanese)* 79−5066
Fe-Nb-N, precipitation study, 550 to 600°C *(German)* 77−90350
Fe-Nb-V-C-N, equilibrium comp. and solubility in steels, model of ideal solns. *(Russian)* 80−60832
Fe-NbC, exam. of phase diagram, and mech. props. *(Russian)* 79−20028
Fe-NbN-C-Mn-Si, dispersion hardening effect on mech. props. 78−3137
Fe-NbN-(C), dispersion hardening effect on mech. props. 78−3137
Fe-Ni-Ti-Al-Nb, struct. mechanism for inverse $\alpha \rightarrow \gamma$ transform. *(Russian)* 80−40351
Fe-Si-Nb, eutectic alloy, exam. of eutectic temp., composition, and oxidation resistance 78−52767
Fo-Fe-Nb, cold-worked and aged, mag. props. and microstruct. 80−34690
Gd-Nb amorphous films, spontaneous Hall effect and elec. resist. 80−80251
Hf-Nb (30 to 50 at.%) exam. of beta phase decomposition processes 78−76674
Hf-Nb-Ga, phase equilibria X-ray study at 800°C *(Ukrainian)* 79−95998
$Hf_{0.65}Nb_{0.35}$, superconducting alloy, transition temp. and flux line pinning 77−43772
$(Hf_xZr_{1-x})_{80}Nb_{20}$, influence of Hf additions to $Zr_{80}Nb_{20}$, beta decomposition anal. 79−8304
LaB_6-Ni-NbC, thermionic emission 77−28678
Mn-Ni-Nb, non-ferromagnetic Elivar type 77−48473
Mo-Mb, thermoelectric alloy for in pile temp. meas. *(French)* 79−67894
Mo-Nb, binary continuous solid solution, elec. resist. and thermoelec. power behaviour 79−69492
Mo-Nb, impurity diffusion and vacancy-impurity binding energy 80−15307
Mo-Nb, thermoelec. power, 4.2 to 300K 80−70683
Mo-Nb alloy, secondary electron emission coefficient 77−77333
Mo-Nb solid solutions, enthalpy of soln. of H meas. 80−2166
Mo-Nb-C, mech. props., effect of alloying and Mo cryst. orientation *(Russian)* 80−71706
Mo-Nb-Ti-N alloy, with dispersed second phase, ductile-brittle transition 80−93653
Mo-Nb-TiN, dispersion hardened with strong interface, fracture mechanism 79−5058
Mo-Si protective coating against oxidation *(Russian)* 79−39029
Mo-W-Mo (4.74, 2.17 wt.%), creep resistance in ultrahigh vacuum 79−5027
Mo-Zr-Nb-C, carbide precip. hardening kinetics, ageing singularities *(Russian)* 77−25059
Mo-Zr-Nb-C, polythermal sections *(Russian)* 78−15365
Mo-Zr-Nb-C alloys, phase diagram and comp., Zr and Nb influence *(Russian)* 79−52167
Mo_cNb_{1-c}, is the rigid-band model valid? 78−95258
NB-H(D), lattice expansion due to interstitially dissolved impurity 77−39600
Nb alloys, long-term ageing effects on ductility and microstructure 77−44348
Nb/Cu-Sn-Mg, superconductor, effect of Mg addition to Cu-Sn matrix 80−25028
Nb/H, heat capacity and supercond. between 1.5 and 16K 80−2521
Nb-Al, A-15 struct., influence of composition on supercond. transition temp. 77−20486
Nb-Al, A15 and σ-phases, supercond. and normal state electronic props. 77−43765
Nb-Al, couple phase diagrams and thermochemical data 79−66037
Nb-Al, prep. from gaseous phase *(Russian)* 78−27451
Nb-Al (20 at.%), diffuse scatt. before Nb_3Al phase form., unstable phase *(Russian)* 78−3131
Nb-Al film, Josephson junction, tunnelling exam. 79−38257
Nb-Al σ- and A15-phases, Knight shift and supercond. 77−15984
Nb-Al-C, phase diagram and lattice constants, X-ray diffr. method 80−89207
Nb-Al-Ge-Cu, rapidly quenched, comp. and phase equilib. 80−76235
Nb-Al-Ir A-phase, crystal struct. determ., $MgZn_2$-Laves C14 type 77−1099
Nb-Al-Si, supercond. transition temp., Si conc. depend. 78−84339
Nb-Al-(Ge) film, superconductor, high rate sputter deposition and heat treatment 77−36399
Nb-Al(Ga, Si, Ge, Su)-Cu, rapidly quenched, comp. and phase equilib. 80−76235
Nb-Al(Ga)(Ge), fast quenching of A15-phases *(German)* 77−36014
Nb-B, atomic order, stability, supercond. *(French)* 80−50021
Nb-C, coupled phase diagrams and thermochemical data 79−66036
Nb-C, phase comp. and precip. after heat treatment 79−57020
Nb-Co, X-ray emission spectra investigation of electron struct. of Laves phases *(Russian)* 78−23554
Nb-Cr, diffusion of N, effect of Cr and struct. defects 79−55938
Nb-Cr(Mn)(Mo)(Zr), internal impurity adsorption effect on bond type of intercrystallite zones 77−16684
Nb-Cu, neutron radiation stimulated diffusion, electrical resistivity exam. *(Russian)* 79−14959
Nb-Cu (0.02 wt.%), Cu electron Nb_5Si, $NbSi_2$ and NbB_2 form. *(Russian)* 78−15400
Nb-Cu-Sn, cast supercond. alloy, crit. current, degradation resistance 78−76203

niobium alloys continued
Nb-D, density fluctuations, small angle neutron scatt. study 79−60359
Nb-D, stability curve for phase separation of D, neutron small-angle scatt. study 79−15672
Nb-D system, phase equilibria study *(Japanese)* 79−78936
Nb-Fe, formed on laser irradiation of Nb-Fe interface, Mossbauer spectra *(Russian)* 79−60560
Nb-Fe, X-ray emission spectra study of electron struct. of Laves phases *(Russian)* 78−23555
Nb-Fe(Co)(Ni)(Os), alloying element influence on strength, ductility, surface and grain boundary energies *(Russian)* 79−74234
Nb-Ga, A15 phase, chem. deposition on Hastelloy substrate, for superconducting tape *(German)* 80−104071
Nb-Ga, A15 type, melt produces specimens, supecond., homogeneity, transition temp. *(German)* 78−2608
Nb-Ga, phase system form. and stability of A15 phase 77−90347
Nb-Ga, superconductor, phase diagram determ. using various methods up to temp. of 2200°C 79−8414
Nb-Ga (16 to 28 at.%), transition temp., upper critical field and magnetisation curves 77−80866
Nb-Ga-Cu, fast quenching of A15-phases *(German)* 77−36014
Nb-Ga-Cu, phase diagram, metallographic and X-ray study, annealed and as-cast supercond. crit. temp. *(Russian)* 78−56617
Nb-Ga-Fe ternary system, phase equilib. at 1000°C, supercond. transition temp. 80−35158
Nb-Ga-Ir, phase equilib. at 1000°C, cryst. data for intermediate phases 78−52763
Nb-Ga-Sc, superconducting transition temp., X-ray, microscopic and microprobe anal. *(Ukrainian)* 80−75667
Nb-Ga-Y, X-ray and microprobe anal., isothermal section and supercond. transition temp. *(Ukrainian)* 79−38793
Nb-Ge, A15 struct. superconductor, high field transport props. TEM study 80−34574
Nb-Ge, amorphous supercond. alloy, resistivity, transition temp. 80−60126
Nb-Ge, compounds with A15 structure, films, TEM study *(French)* 80−80135
Nb-Ge, supercond. A-15 phase, supercond. transition temp. after ion implantation 80−49972
Nb-Ge, supercond. film, prep. and props. *(Russian)* 77−66218
Nb-Ge, superconductivity film prod. by electron beam sputtering *(Russian)* 78−15308
Nb-Ge, supersuperconducting transition temp., correl. with resist. anomalies and defect struct. 77−47920
Nb-Ge, thermal anal. of levitation-heated samples 79−2772
Nb-Ge, transition metal atom stabilised superconductivity 79−7924
Nb-Ge alloys, stoichiometry and phase equilibria, X-ray diffr. study *(French)* 79−70040
Nb-Ge film, CVD and sputter deposited, critical current density and stability 77−28327
Nb-Ge film, coevaporated, supercond. critical temp. and struct. 77−28275
Nb-Ge film, phase transformations due to annealing, electron diffr. study 80−54551
Nb-Ge film, supercond., TEM expts., correl. of struct. and elec. props. 78−14628
Nb-Ge film, supercond., two-phase, tetragonal Nb_5Ge_3 phase identification by electron diffr. 77−89665
Nb-Ge film, supercond. transition temp., rel. to prep. conditions 77−36009
Nb-Ge supercond. thin film characterisation by ion scatt., ion-induced X-rays, and ion resonance 77−40617
Nb-Ge system, phase diagram determ. 79−38796
Nb-Ge system, reaction diffusion, electron probe anal. 79−28152
Nb-Ge vapour deposited films with T_c of ~20K, preps. *(Japanese)* 77−12048
Nb-Ge-Cu, phase equilib. and supercond. props. *(Russian)* 80−40332
Nb-Ge-Fe, effect of Fe on supercond. and mag. props. 79−56351
Nb-Ge-Ni, phase composition and superconducting props., influence of Ni *(Russian)* 80−20898
Nb-Ge-Si, A15 struct. superconductor, high field transport props. TEM study 80−34574
Nb-Ge-Si, compounds with A15 structure, films, TEM study *(French)* 80−80135
Nb-Ge-Si, Si effect on raising superconducting transition temp. in pelicular specimens *(Russian)* 78−23188
Nb-Ge-Si, supercond. state transition temp., influence of Si on alloy constitution *(Russian)* 79−78244
Nb-Ge-Si film, CVD, struct., comp., stability and homogeneity 80−15421
Nb-Ge-Sn A15 cpds., CVD, superconductivity 79−38222
Nb-Ge-Sn(Pt)(Ir), A15 cpds. prod. by liq. quenching, phase stability and supercond. props. 79−95538
Nb-Ge(Si), amorphous supercond. alloy, produced by coevaporation, struct. and supercond. 79−91179
Nb-Ge(Si) and Nb-Ge-Si, A15 cpds., CVD prep. and supercond. crit. temp. 79−60949
Nb-H, acoustic phonon anomaly at small wavevectors 78−59882
Nb-H, BCC, quasimolecular Jahn-Teller reson. states 80−44550
Nb-H, BCC, tetrahedral interstitial site H band modes, neutron scatt. obs. 79−55852
Nb-H, coherent, surface spinodal decomposition and quasiperiodic β-precip. 77−73257
Nb-H, coherent α-α' phase transition, sample shape depend. 79−34005
Nb-H, elastic interaction and phase transition, book contrib. 79−83178
Nb-H, electron work function, 300 to 600 degrees C, contact potential difference meas. 80−29462
Nb-H, fatigue 79−11695
Nb-H, fusion reactor first wall material, cyclic deform. tests 80−30074
Nb-H, incoherent spinodals, meas. by Gorsky effect 78−19712
Nb-H, interstitial position of H from entropy of soln. 77−65989
Nb-H, lattice strains, book contrib. 79−82202
Nb-H, modulated ordering, elastic free energy theory 79−94945
Nb-H, ordering of hydride phases 77−19902
Nb-H, spinodals and diffusion coefficients of H, sample shape depend. 78−19713
α-Nb-H, thermal neutron scatt., general multisublattice jump diffusion model 77−66046
Nb-H, thermokinetics of H_2 generation from transition metal-H compounds 79−74421
Nb-H (30 at.%), specific heat at $\varepsilon \rightarrow \zeta \rightarrow \beta$ phase transition 77−12616

niobium alloys continued
Nb-H alloys, evidence of internal friction peak 78−52881
Nb-H interstitial alloy, props. and synthesis 79−69265
Nb-H interstitial alloys, prep. and props. 78−23669
Nb-H single crystal, shear moduli, temp. and H conc. depend. 78−39823
α-Nb-H solid soln., BCC, const. vol. thermodynamic functions 79−61561
Nb-H system, accommodation effects during hydride precipitation, TEM 80−89218
Nb-H system, enthalpy and entropy changes for non-stoichiometric hydride formation 79−52741
Nb-H system, Huang diffuse scatt. of X-rays from displacement field 77−15446
Nb-H system, phase diagram and transforms., struct. obs. of various phases 80−104125
Nb-H system, phase equilibria studies *(Japanese)* 79−78935
Nb-H systems, supercond., H conc. depend. *(Russian)* 77−47932
Nb-H(D) system, anelastic behaviour, 0.5-15K 80−49300
Nb-H(D) system, incoherent phase transition 79−73304
Nb-H(D) system, single cryst. prep. and characterisation 79−95910
Nb-H(D)(T) system, BCC, US vel. changes caused by H isotope dissolution 80−65117
Nb-Hf, single cryst. elastic consts. 77-298K 78−84879
Nb-Hf (26 at.%), mixed state, ultrasonic velocity meas. 79−60974
Nb-Hf (38 at.%) superconductor, peak effect, summation problem, mag. history flux pinning force 80−20362
Nb-Hf(26 at.%), mixed state, magnetoacoustic attenuation 77−4473
Nb-Ir, A 15- and σ-phases, supercond. 79−73645
Nb-Ir-O, H-phase, cryst. struct. 78−38664
Nb-Ir-O, phase struct., supercond. H-phase 78−39246
Nb-Ir(Rh) system glasses, form., crystn. and microhardness, resist. obs. 80−89178
Nb-Mo, BCC, press. derivatives of elastic moduli, Fermi surface topological changes, band struct. 79−61639
Nb-Mo, BCC, struct. singularities rel. to solid solution behaviour *(Russian)* 77−11696
Nb-Mo, diffusion of N, effect of Mo and struct. defects 79−55938
Nb-Mo, elastic moduli of single crystals 77−31712
Nb-Mo, electronic density of states, temp. depend. of elec. resist. and mag. susceptibility 77−11891
Nb-Mo, electronic struct., thermoreflectance meas. 0.5-5.0 eV 80−45050
Nb-Mo, optical props., 0.1-25 eV, band models 78−10892
Nb-Mo, prod. by simultaneous carbothermic reduction of oxides/electron beam melting method *(Japanese)* 80−11590
Nb-Mo, resistivity due to H incorporation 80−70666
Nb-Mo, specific heat enhancement and electron-phonon interaction 80−65242
Nb-Mo, superconductivity and phonon softening, between electron bands and phonons 78−14859
Nb-Mo alloy, single crysts. slip geometry on straining in tension *(Russian)* 77−66678
Nb-Mo alloy, solubility of H_2 77−89542
Nb-Mo alloys, phonon dispersion, anomalous struct., tight-binding calcs. 78−10137
Nb-Mo monocrystal, elastic moduli, 4.2 to 300K *(Russian)* 77−52381
Nb-Mo solid soln., single cryst., yield point and dislocation struct., temp. depend. *(Russian)* 77−81290
Nb-Mo steel, HSLA, low temp. fatigue props. 80−40490
Nb-Mo system, electron-phonon coupling const. and supercond. transition temp., average T-matrix approx. 80−39707
Nb-Mo-Al-(Cr) eutectic directionally crystallised alloy, heat resistance, alloy struct. *(Russian)* 80−40481
Nb-Mo-C, phase comp. and precip. after heat treatment 79−57020
Nb-Mo-Fe, dil., local environment and mag. props. 78−64187
Nb-Mo-Fe, dil., local moment formation 78−43562
Nb-Mo-Tc alloys, supercond., point-group symmetry 78−64163
Nb-Mo-Ti-Zr, influence of C content on creep charact. and creep-rupture strength *(Russian)* 77−48483
Nb-Mo-Ti-Zr-C, work function temp. and phase depend. *(Russian)* 80−2449
Nb-Mo-Zr, erosion coeff., temp. depend. reactor wall swelling due to He ion bombardment 78−17418
Nb-Mo-Zr-Ti, Zr and Ti effects on struct. and mech. props. 77−70061
Nb-Mo(Ru)(Re), kinetics and thermodynamics of reaction with N_2 *(German)* 79−74415
Nb-Mo(Ti)(Zr), nitriding, diffusive saturation, lattice spacing and activation coeffs. *(Russian)* 80−21168
Nb-Mo(Zr) alloys, vacuum heat treatment effects on gas content and elec. and mech. props. *(Russian)* 79−43281
Nb-Mo(Zr) film, amorphous, temp. stability 78−63948
Nb-N, BCC, solution hardening and softening 77−12635
Nb-N, dil., low temp. interstitial hardening 79−20060
Nb-N system, ion-implanted, supercond. crit. temp., effect of implantation conditions 78−19176
Nb-N(O)(C) system, specimen prep. for metallography *(German, English)* 80−89439
Nb-Nb_2C, directional crystn. using plasma heating 78−60569
Nb-Nb_2C eutectic composites, directionally solidified, growth crystallography and lamellar to rod transition 77−32569
Nb-Nb_3Al superconductor, fabrication by quench-age method 77−40403
Nb-Nb_3Sn supercond. point contacts, crit. currents, effect of laser radiation *(Russian)* 79−28484
Nb-Nb_3(Al,Ge) multifilamentary supercond., fabrication and props. 77−20480
Nb-Nb-Al-(Cr), γ/γ'-δ type eutectic, fatigue, effect of composition and microstruct. 78−48520
Nb-Ni, amorphous, synthesis by vapour quenching, and struct. 78−11111
Nb-Ni, amorphous, thermal stability, crystn., DSC and elec. resist. study 80−107060
Nb-Ni, amorphous thin film, vapour quenched, elec. resistivity and thermoelectric power 79−33275
Nb-Ni, cathodic polarization in conc. KOH soln. 80−16591
Nb-Ni, glassy alloy, struct. anal. using X-ray diffr. 79−51004
Nb-Ni amorphous alloys, glass transition and ductility, O additions effect 80−75168
Nb-Ni glass, photoemission spectra meas. 77−55867
Nb-Ni glasses, struct. factor temp. depend. 80−28920
Nb-Ni metallic glass, hardness, elastic moduli, density, cryst. temp., mech. props., for flywheel appl. *(Dutch)* 78−52878
Nb-Ni metallic glass, temp. depend. of resistivity 78−47759

niobium alloys continued
Nb-Ni-Al, cryst. struct. and defects, high resolution electron microscopy obs. 79−94961
Nb-O, BCC, Snoek type reordering during strain ageing *(French)* 79−8312
Nb-O, cyclic creep, effect of O_2 conc. and temp. 78−48466
Nb-O, exam. of surface segregation equilibrium and kinetics, by Auger spectroscopy *(Russian)* 79−56981
Nb-O system, solid soln. hardening and softening 80−71665
Nb-Os, phase diagram exam. 77−21103
Nb-Pd constitution diagram, metallographic and X-ray diffr. anal. 80−89204
Nb-Pt, A15 phase, comp. and order effects on supercond. props. 77−85372
Nb-Pt, A15- and δ-phases, Knight shift of ^{195}Pt meas. 78−19350
Nb-Pt alloy, superconducting parameters of A15- and σ-phases 78−39242
Nb-Pt-O system, phase equilibria, diagram, unit cell parameters, supercond. 80−55352
Nb-Re-(Ru)-N system, N_2 solubility and solubility limit *(German)* 77−4205
Nb-Re(Ru)-N, α-solid soln., thermodynamics *(German)* 77−12600
Nb-Re(Ru)-N system, spectral emissivity, lattice parameter, initial rate of N_2 absorption *(German)* 77−4204
Nb-Rh, radiation disorder model of phase stability 80−16297
Nb-Rh, σ-phase alloy, superconductivity and resistance behaviour 80−70882
Nb-Ru(Pd), dil., impurity diffusion and vacancy-impurity binding energy 80−15307
Nb-Ru(Re)(Os), dil., impurities effect on elec. resist. at 0.4 and 77.3K *(Russian)* 79−91196
Nb-Si, compounds with A15 structure, films, TEM study *(French)* 80−80135
Nb-Si amorphosamorphous thin film tunnel junctions 79−28473
Nb-Si compounds, CVD, struct. and supercond. props. 79−24447
Nb-Si diagram of state, melting temp., polymorphic transform. temp. *(Russian)* 80−50594
Nb-Si film, superconductivity close to A15 stoichiometric phase 79−95540
Nb-Si liquid quenched alloy, metastable A-15 and amorphous phases, interstitials 80−54394
Nb-Si-Cu, struct. and supercond., Cu influence 80−50592
Nb-Si-Sn(Pt)(Ir), A15 cpds. prod. by liq. quenching, phase stability and supercond. props. 79−95538
Nb-Si(−V)(Zr)(Mo)(Ta)(W)(C)(B)(Ge), ductile amorphous, superconductivity 80−60131
Nb-Sn, A15 compounds, Hall coeffs. 79−33281
Nb-Sn, depend. of supercond. transition temp. on composition *(Russian)* 78−19173
Nb-Sn, diffusion couple, phase equilibria, effect on T_c and H_{c2} 79−56462
Nb-Sn, reactive diffusion *(Russian)* 77−20133
Nb-Sn, supercond. foils, phase anal. by Mossbauer spectra 78−64305
Nb-Sn alloys, stoichiometry and phase equilibria, X-ray diffr. study *(French)* 79−70040
Nb-Sn filamentary composite, supercond. crit. current and temp., as function of reaction conditions 77−28330
Nb-Sn sinter material, for superconducting tubes for magnetic shielding 79−67446
Nb-Sn-Cu, Cu effect on Nb solubility and peritectic transform. temp. in Sn bath *(Czech)* 77−59754
Nb-Sn-Si(As), ternary A15 phase regions, solubility 77−44215
Nb-Sn(Al)(Ga)(Ge)(Si)-C, phase equilib. and supercond. 80−50593
Nb-Sn(Ge), A-15 compound formation by ion implantation 78−51572
Nb-T alloy, effect of T on low temp. yield stress of Nb, comparison with Nb-H alloy behaviour 78−39863
Nb-Ta, resistivity due to H incorporation 80−70666
Nb-Ta, supercond., transport current distrib., neutron small angle scatt. study 79−42711
Nb-Ta, supercond. theory of upper crit. field, shift of Fermi level 77−63038
Nb-Ta, terminal solubility of H and characts. of solid solns. 79−86894
Nb-Ta (13 wt.%) alloy, flux line bending by transport currents, neutron diffr. 77−8247
Nb-Ta (20.at.%), optical props., 0.1-25 eV, band models 78−10892
Nb-Ta (54 at.%) cylinder, superconducting mag. and resistive behaviour 77−8252
Nb-Ta alloys, electron-phonon interaction and supercond. transition temp. *(Russian)* 79−28426
Nb-Ta alloys, H diffusion at 296K 80−84329
Nb-Ta system, short-range order exam. by diffuse X-ray scatt. *(Russian)* 77−31644
Nb-Ta type II supercond., defect-free, AC permeab. 77−8250
Nb-Ta-O solid soln., thermodynamic props. 78−31386
Nb-Th, eutectic composition 80−100828
Nb-Ti, annular superconductor, field replication and flux shielding 77−28286
Nb-Ti, electrical resist. at low temp., enhancement due to short-range supercond. order 77−28157
Nb-Ti, film, composition determ. by ^{3}He elastic scatt. 78−76974
Nb-Ti, Helmholtz coils, optimisation, critical current rel. to mag. induction 79−67353
Nb-Ti, metallurgical treatment, effects on props. 79−38846
Nb-Ti, multi-filamentary superconducting wires, mag. field dependence of AC losses 78−60256
Nb-Ti, multifilament composite technical superconductors, development and manufacture 79−19707
Nb-Ti, multifilament superconductor, metallurgical design 79−33434
Nb-Ti, multifilament wire, superconducting magnet system, development for physical experiments 80−9008
Nb-Ti, multifilamentary, Mirror Fusion Test Facility, superconductor core manufacturing and quality 80−93521
Nb-Ti, pinning curves, high field J_c and scaling behaviour 80−93064
Nb-Ti, radiation effects on critical currents 78−52175
Nb-Ti, resistivity due to H incorporation 80−70666
Nb-Ti, sheet, flux trapping, appl. to mag. shielding and levitation 80−31806
Nb-Ti, single core conductor, carrying DC transport current, alternating field losses 80−34550
Nb-Ti, supercond., optimised pinning struct., crit. data 1.8-4.2K 77−89913

niobium alloys continued
Nb-Ti, supercond. and mag. props., anisotropy *(Russian)* 77−59361
Nb-Ti, supercond. Helmholtz coils, optimisation 79−2795
Nb-Ti, supercond. low-temp. plasticity 77−15992
Nb-Ti, superconducting, pinning mechanism at high mag. fields 79−95555
Nb-Ti, superconducting solenoid wire appl. 79−93174
Nb-Ti, superconductive materials and magnet systems developed at Intermagnetics General Corp. 79−58699
Nb-Ti, superconductivity after heavy ion irradiation at low temps. and high fluence 77−69437
Nb-Ti, superconductor optimisation for 12 Tesla toroidal field coils 80−91272
Nb-Ti, thermal conductivity in low temp. range 78−39259
Nb-Ti, type II supercond., hysteresis losses for round cross section with collective interaction 78−43513
Nb-Ti, void volume fraction reduction, Ni^+ ion irradiation 79−51162
Nb-Ti, wire drawn and hydrostatically extruded supercond., crit. current density 79−38275
Nb-Ti 10 kA conductor development for Tokamak toroidal coil 79−31217
Nb-Ti (46%) composite superconductor, fabrication 77−24989
Nb-Ti (50%), supercond., cryostat design for magnetisation study *(Spanish)* 80−75673
Nb-Ti (60 at.%), aged, TEM exam. of precipitation process *(Japanese)* 78−48409
Nb-Ti alloy, supercond. and high mag. fields 79−87215
Nb-Ti alloy strip, crit. current anisotropy 78−10624
Nb-Ti alloys, crit. current density, scaling law 78−31027
Nb-Ti alloys, oxidation, ESCA *(French)* 77−36361
Nb-Ti filamentary superconductor critical current density rel. to thermal treatment 79−33440
Nb-Ti films, ion beam sputtered, study by ^{4}He backscattering and nucl. reaction microanal. 79−42400
Nb-Ti in Cu, composite supercond. field replication and flux shielding 77−28286
Nb-Ti in Cu matrix composite superconductor, cyclic stress effects on transport props. 77−28336
Nb-Ti multifilamentary cable magnet, quench development 77−26351
Nb-Ti multifilamentary supercond., AC losses, mag. field depend. of loss-freq. charact. 79−33384
Nb-Ti multifilamentary superconducting composite, subjected to rotating mag. induction, losses 79−33386
Nb-Ti multifilamentary supercond., commercial, crit. current density 79−38274
Nb-Ti multifilaments, effect of mech. and thermal treatments of supercond. props. 80−104197
Nb-Ti superconducting alloy, critical current density, heat treatment effects *(Japanese)* 78−14909
Nb-Ti superconducting coils, for thermonuclear fusion *(French)* 80−95399
Nb-Ti superconducting composites, crit. current changes and fatigue damage after 4.2K strain cycling 77−28323
Nb-Ti superconducting cylinders, dynamically stabilised, differences in shielding versus trapping behaviour 77−47933
Nb-Ti superconducting magnet system, for short sample test on Tokamak superconductor 80−9010
Nb-Ti superconducting multifilamentary composites, high current, effect of matrix on losses 77−24649
Nb-Ti superconducting multifilamentary wires, high B losses 77−24650
Nb-Ti superconducting multifilamentary composites, high current, crit. current degradation 77−24659
Nb-Ti superconducting multifilamentary wires, mechanisms for crit. current degradation 77−28324
Nb-Ti superconducting single layered multifilamentary coil, eddy current loss depend. on demagnetisation 80−97040
Nb-Ti superconducting wire, Cu clad, Meissner effect in Cu meas. 78−64166
Nb-Ti wires, microplastic behaviour, acoustic emission, appl. to training effect in supercond. magnets 77−26356
Nb-Ti/Cu composite disc, crit. state model for crit. current determ. 79−99665
Nb-Ti/Cu sheet composite, flux trapping and shielding capabilities in transverse fields 80−15667
Nb-Ti-Al alloy, effect of heat treatment on strength and elastic props. 77−55976
Nb-Ti-C, phase comp. and precip. after heat treatment 79−57020
Nb-Ti-Ta, pinning curves, high field J_c and scaling behaviour 80−93064
Nb-Ti-Ta, superconductor optimisation for 12 Tesla toroidal field coils 80−91272
Nb-Ti-Ta alloys, metallurgical anal. and crit. current densities 79−38286
Nb-Ti-Zr, electrical resist. at low temp., enhancement due to short-range supercond. order 77−28157
Nb-Ti-Zr, supercond. wire, anomalous increments of AC losses due to flux jumps 77−28289
Nb-Ti-Zr, superconducting, ageing effect on critical current density *(Japanese)* 79−61747
Nb-Ti-Zr, superconducting, critical current density and microstruct. correlation *(Japanese)* 79−61748
Nb-Ti-Zr, superconducting wire, coil simulation, class and instability meas. 79−71487
Nb-Ti-Zr, superconducting wire, coil simulation meas. of losses and instabilities 80−37050
Nb-Ti-Zr, wire, anomalous crit. AC 77−16014
Nb-Ti-Zr ternary alloy wires, flux jumping 79−60965
Nb-Ti-Zr ternary system, high-field supercond. 80−97045
Nb-Ti-Zr wire, supercond., longit. critical currents in AC mag. field 77−72958
Nb-TiN(HfN)(ZrN), BCC solid soln., nitride solubility, alloying effects *(Russian)* 79−51262
Nb-Ti(Mo), AC loss minimum, pinning, flux distribution 80−84574
Nb-Ti(Zr), type II superconductor, mech. behaviour and stress effects 77−86083
Nb-Ti(Zr)(Hf)-N, exam. of phase equilibrium using electron microscopy and X-ray analysis *(Russian)* 79−15654
Nb-V, binary continuous solid solution, elec. resist. and thermoelec. power behaviour 79−69492
Nb-V, negative muon Coulomb capture ratio and Lyman series intensities 80−14255
Nb-V, resistivity due to H incorporation 80−70666

niobium alloys continued
Nb-V, valence bands, X-ray M- and L-emission bands obs. *(Russian)* 78−19602
Nb-V (20 at.%), optical props., 0.1-25 eV, band models 78−10892
Nb-V alloys, electron-phonon interaction and supercond. transition temp. *(Russian)* 79−28426
Nb-V oxidation in air, rate determining process *(Russian)* 80−21170
Nb-V system, H_2 absorpt. 80−59808
Nb-V system, short-range order exam. by diffuse X-ray scatt. *(Russian)* 77−31644
Nb-V_3Ga mixed state, Meissner effect investigation by muon method *(Russian)* 80−107954
Nb-V-Cr, Nb-V, and Nb-Cr, oxidation resist., Cr and V effects *(Russian)* 80−40585
Nb-V-O solid soln., thermodynamics of O_2 78−68673
Nb-V(Mo), thermopower composition depend. 79−65445
Nb-W, cold plastic deform., oriented microdistortions *(Russian)* 78−39840
Nb-W, diffusion of N, effect of W and struct. defects 79−55938
Nb-W, single cryst. elastic consts. 77-298K 78−84879
Nb-W-Mo-Zr, 5MVTs, reaction with gas residual in vacuum, physicomech. props. effect 80−16587
Nb-W-Mo-Zr, long-term strength props., vac. level effect 80−55484
Nb-W-Mo-Zr (5, 2, 1 wt.%), surface-layer struct. and mech. props., effect of O_2 diffusion saturation 79−5087
Nb-W-Mo-Zr (5, 2.1, 0.92 wt.%), creep resist., high temp. ageing in vacuum 80−71716
Nb-W-Mo-Zr-C, strength and ductility, prolonged high-temp. soaking effect 80−55483
Nb-W-Mo-Zr-C(5,2,1,0.02 wt.%) alloy 5 BMTs, short-time tensile strength in liquid Bi and Li *(Russian)* 77−25186
Nb-W-Ta-Zr, 5VTT, reaction with gas residual in vacuum, physicomech. props. effect 80−16587
Nb-W-X-C, X=Ti, Zr, Hf, quenched from liquid state, formation of non-metallic inclusions *(Russian)* 79−57007
Nb-W-Zr-N alloy, with dispersed second phase, ductile-brittle transition 80−93653
Nb-W-Zr-Ta, long-term strength props., vac. level effect 80−55484
Nb-W-Zr-Ta (90, 4.5, 3.5, 2 wt.%) creep and creep limit in super vac. at 1100°C, heat treatment effect 80−81133
Nb-Y, cold plastic deform., oriented microdistortions *(Russian)* 78−39840
Nb-Y mech. props., neutron irrad. and Y scavenging effects 77−90394
Nb-Zn-N alloys, Zr-N complex formation, internal friction temp. depend. *(Russian)* 80−54311
Nb-Zr, (10 at.%), optical props., 0.1-25 eV, band models 78−10892
Nb-Zr, acoustic phonon anomalies and superstructure, neutron inelastic scatt. meas. 80−19892
Nb-Zr, BCC phase, elastic consts., 4.2-300K 77−81285
Nb-Zr, cold plastic deform., oriented microdistortions *(Russian)* 78−39840
Nb-Zr, crit. current, flow-flow resist. depend., allowance for superheating *(Russian)* 80−93061
Nb-Zr, deformed, α-peak, internal friction meas. between 90 and 300K 79−100205
Nb-Zr, deformed strip, pinning force, widely varied j_c, temp. and mag. field variations *(Russian)* 79−7948
Nb-Zr, diffuse neutron scatt. 78−71816
Nb-Zr, diffusion of N, effect of Zr and struct. defects 79−55938
Nb-Zr, diffusion of O_2 78−2298
Nb-Zr, effect of band structure on elastic constants and superconductivity 79−8313
Nb-Zr, elastic constants, 0K to melting point 79−38882
Nb-Zr, fusion reactor first wall materials, compatibility with impure He 80−32469
Nb-Zr, single cryst. elastic consts. 77-298K 78−84879
Nb-Zr, thermoelec. power, 4.2 to 300K 80−70683
Nb-Zr, type II supercond., radiation-induced flux pinning 78−80106
Nb-Zr (1 at.%), annealed, TEM study of ion implanted irregular He bubbles 80−15164
Nb-Zr (1 wt.%), corrosion behaviour in high temp. impure He gas 80−76402
Nb-Zr (1 wt.%), D_2 diffusion coeffs., 923-1148K 77−84991
Nb-Zr (1 wt.%), fusion reactor blanket struct. material, low cycle fatigue behaviour 80−30073
Nb-Zr (1 wt.%), He bubble growth, α-particle effects 78−67749
Nb-Zr (1 wt.%), high temp. creep, under O_2 stream pressure *(Russian)* 77−52404
Nb-Zr (1 wt.%), internal oxidation state of O_2, dispersion hardening by diffusion alloying, X-ray diffr. and internal friction *(Russian)* 79−70102
Nb-Zr (1 wt.%), ion irradiated, void ordering 78−22770
Nb-Zr (1%), He bubbles and voids with ringed images SEM and TEM exam. 78−51529
Nb-Zr (1.5 wt.%) alloy, field ion microscopy investigation, surface struct. 80−45220
Nb-Zr (3 wt.%), neutron-irradiated, positron annihilation ang. correl. meas. 80−93430
Nb-Zr alloy, 5VMTs1, thermal expsn., 1261-2289K 78−43150
Nb-Zr alloy, BCC-ω phase transition, electronically driven nature 80−103433
Nb-Zr sputtered films on Ta, struct. and supercond. props. *(Japanese)* 78−52138
Nb-Zr-Al superconductor, struct. determ. by optical microscopy and electron diffraction *(Russian)* 77−16628
Nb-Zr-C, (1, 0.1 wt.%) alloy, mech. characts. structral sensitivity in strained state *(Russian)* 79−52301
Nb-Zr-C, dispersion-hardened with carbide phase, influence of hydrostatic extrusion on struct. and props. *(Russian)* 77−52338
Nb-Zr-C, effect of ageing on high temp. strength *(Ukrainian)* 79−52249
Nb-Zr-C, erosion coeff., temp. depend. reactor wall swelling due to He ion bombardment 78−17418
Nb-Zr-C, phase comp. and precip. after heat treatment 79−57020
Nb-Zr-C, plastic deform. and annealing, dislocation struct. *(Russian)* 80−20951
Nb-Zr-C, strengthening phase struct. and morphology after prolonged high temp. stress in vacuum *(Russian)* 77−25065
Nb-Zr-C, structural depend. of elasticity limit fracture features *(Russian)* 79−29171

niobium alloys continued
Nb-Zr-C (0.1, 0.01 wt.%) plastic deform. influence on electronic state of Nb atoms 80−40463
Nb-Zr-C alloy, creep in vacuum, prolonged high-temp. ageing effects *(Russian)* 78−56692
Nb-Zr-C alloy, long term strength rel. to carbide precipitate geometry *(Ukrainian)* 78−92266
Nb-Zr-C alloy, long term loading at high temps. effect on struct. and morphology of carbide phase 79−15754
Nb-Zr-C alloy, strengthening phase, struct. and morphology after stress ageing *(Russian)* 78−31454
Nb-Zr-C alloy, strengthening phase, particle distrib. anal. *(Russian)* 79−15685
Nb-Zr-C alloy, struct. changes during stressed and unstressed ageing at 900, 1100°C *(Russian)* 79−29064
Nb-Zr-C welding solid solutions, ageing kinetics, influence of inclusion elements *(Russian)* 80−100853
Nb-Zr-N, deformed and annealed, internal friction, rel. to structural state *(Russian)* 78−6957
Nb-Zr-N biphase alloy, recrystallization annealing 80−104180
Nb-Zr-O, corrosion resistance in molten Li *(Russian)* 78−31567
Nb-Zr-Ti, needle field emitter, ion bombardment effects, field emission microscope obs. 77−55869
Nb-Zr-Ti alloys, scale formation 77−44229
Nb-ZrN alloy, high temp. hardness and short duration tensile strength *(Russian)* 77−44266
Nb-Zr(Nf)(Mo)(W)(Rh), dil., neutron irradiation at 4.6K, influence of impurities on defect prod. 79−55790
Nb_3/Sn-Cu composites, in situ processed, supercond. props. 80−75698
Nb_3(Al,Ge) and Nb_3(Al,Si), liq. quenched, supercond. props. 80−84580
Nb_3(Al,Ge) supercond., diffused layer critical current depend. on Cu before and after annealing *(Russian)* 79−69643
Nb_3(Al,Ge) superconducting wire, improved fabrication method 77−28763
Nb_3(Al, Ge) tape, effect of thermal treatment on superconducting props. 79−61016
NbAl, α phases, lattice parameter and order 77−76359
Nb_2Al, $NbAl_3$, supercond. and mag. props. 77−47922
Nb_3Al, A-15 struct., converted from cold worked BCC struct., crit. currents 80−75697
Nb_3Al, A15 cpd., normal state, low temp. resist. 80−107762
Nb_3Al, and $Nb_3Al_{0.76}Ge_{0.22}$, supercond. props. of cold worked core wires an basis of A15 phases 77−85369
Nb_3Al, anomalous resistivity, insight from band theory 78−60106
Nb_3Al, BCC struct., cold working and converting to A-15 struct. 78−64553
Nb_3Al, band struct. and density of states from self-consistent pseudopotentials 79−69401
Nb_3Al base ternary solid solns., supercond. T_c, dopant depend. 77−1510
Nb_3Al based ternary solid solns., supercond. transition temp., paramag. susceptibility and lattice parameters meas. *(Russian)* 77−43766
Nb_3Al, bonding, electronic charge distribs. and struct. transform. from self-consistent pseudopotentials 79−69054
Nb_3Al, complex refractive index meas. 80−93264
Nb_3Al core wires and pressed powder compacts, supercond. transition 80−34541
Nb_3Al, electron energy loss spectra, AES and HEED investig. of surface 77−24635
Nb_3Al film, electron-beam coevaporated, prep. and characts. 80−76187
Nb_3Al film, quasiamorphous, supercond. phase formation by heat pulse 77−63017
Nb_3Al, high-T_c supercond., apparent T^2-depend. of normal-state resist. and lattice sp. ht. 77−47921
Nb_3Al, liq.-quenched, crit. current density and T_c 77−72957
Nb_3Al, mechanical and supercond. props. 79−38214
Nb_3Al, metallic bonding, electronic states calcs. 78−79916
Nb_3Al multifilamentary composite, metallurgy, fabrication and supercond. props. 77−28764
Nb_3Al, multifilamentary wires, supercond. props. 78−64175
Nb_3Al, NMR of ^{93}Nb and spin-lattice relax. time at low temp. 77−85388
Nb_3Al, neutron irrad. effects on transition temp. *(Japanese)* 79−82707
Nb_3Al, nuclear magnetic relaxation, near T_c *(Russian)* 79−42852
Nb_3Al, obs. of shear struct., electron microscopy *(Russian)* 78−6938
Nb_3Al, phonon density of states, temp. depend. 79−42183
Nb_3Al, prep. by reduction of Nb_2O_5 and Al_2O_3 by CaH_2, thermodynamic calc. 80−100809
Nb_3Al, quantum interference and Josephson effect *(Russian)* 78−56259
Nb_3Al, quasi-one-dimensional supercond., giant enhancement of nucl. relax. rate near T_c 78−56257
Nb_3Al, supercond., fast neutron irrad. effects on T_c 77−55633
Nb_3Al, supercond. props. and lattice parameter, comp. and neutron irrad. effects 80−70880
Nb_3Al, superconductivity, crit. temp., paramag. susceptibility comp. depend. *(Russian)* 77−66219
Nb_3Al superconductors, sputter deposited, BCC to A15 transition, microstruct. investig. 78−27512
Nb_3Al tape, effect of thermal treatment on superconducting props. 79−61016
Nb_3Al, temp-depend. of elec. resist. 80−103675
Nb_3Al:^{93}Nb, NQR spectra, NQR signal disappearance in supercond. state 78−19369
Nb_3Al-Nb_3Ge-Nb_3Ga system, supercond. crit. temps. 77−8218
Nb_3Al-Ni(Cr)(Fe) mag. impurities effect on supercond. props. 77−1524
Nb_3Al(Ga), NQR freq. temp. depend., supercond. transition temp. 80−93207
Nb_3Al(Ga)(Si)(Ge)(Sn), electronic struct. calcs. 79−47005
Nb_3Al(Ga)(Si)(Ge)(Sn), electronic struct., electron-phonon interactions, and low temp. anomalies 79−60701
$Nb_3Al_{0.8}Ge_{0.2}$, supercond., sp. ht. meas. 77−28296
$Nb_3Al_{0.83}Ge_{0.21}$, A-15 phase, sp. ht. meas. 79−19689
$Nb_3Al_{1-x}Ge_x$, RF sputtering synthesis, supercond. transition temp. variation 77−81216
NbAlIr A′ phase, struct. 78−18587
Nb_3(AlSi), electronic characts. from thermomodulation spectra 79−87421
Nb_3(AlSi) film, thermomodulation spectra, 1.1-2.8 eV 78−48250
Nb_3(AlSi), ternary supercond. alloy films, T_c, props. *(Russian)* 78−88055
$Nb_3Al_{0.2}Si_{0.8}$, A-15 alloy synthesis by ion implantation 78−80489

niobium alloys continued
$Nb_3Al(Sn)$, electron-phonon coupling and supercond. crit. temp. 79−33379
Nb_3As, structural and supercond. props. press. effects 80−39700
Nb_3Au, A-15 struct. supercond., microhardness, bonding 78−76199
Nb_3Au, BCC, density of states, comparison with A-15 78−80095
Nb_3Au, supercond. diffusion layer prep. 79−1834
$Nb_{-3}Au$, upper crit. field 79−82729
$NbBe_{12}$, by diffusion saturation in vacuum, resistance to heat 78−44259
Nb(C,N), superconducting diffusion wires, high field expts. on press. effects up to 15 kbar 79−61006
Nb_4CoP, new ternary phosphide with Nb_4CoSi type struct. *(Russian)* 77−55262
$NbD_{0.04}$, neutron scatt. exam., press. depend. of superstruct. reflection 78−22696
$NbD_{0.6}$, Compton profile meas. 77−4698
NbD_x, acoustic phonons conc. depend. 77−15515
NbD_x, λ-phase struct., neutron and electron diffr. meas. 79−94962
$NbFe_2$ layers form. by diffusion during Nb wire drawing 79−28153
$Nb_{40}Fe_{40}P_{14}B_6$, metallic glass, explosive compaction, mech. props. 80−89176
$NbFe_{2-x}Si_x$, crystalline struct., electron microscopy determ. *(French)* 80−54174
$Nb_{78}Fe_{40}Si_{80}$, X-ray cryst. struct. determ. *(French)* 80−15048
$Nb_{0.75}Ga_{0.25}$, A 15 phase high transition temp., sp. ht. determ. 80−60140
Nb_3Ga, comp. and LRO effects on supercond. T_c 77−39992
Nb_3Ga, critical data, under hydrostatic pressure to 15 kbar 79−47217
Nb_3Ga, Debye temp., determ. from elec. resist. meas. *(French)* 77−4322
Nb_3Ga film, quasiamorphous, supercond. phase formation by heat pulse 77−63017
Nb_3Ga film, RF sputtered, supercond. and struct. props. 77−28274
Nb_3Ga Josephson junctions, excess current anal. 79−28465
Nb_3Ga, supercond. crit. temp. and struct., heat treatment and stoichiometry effects 77−43769
Nb_3Ga, temp-depend. of elec. resist. 80−103675
Nb_3Ga, thermodynamic and expt. study of CVD 79−24441
Nb_3Ga with structure A15, apparatus for rapid hardening from liquid state 80−76275
Nb_3Ga:^{93}Nb, NQR spectra, NQR signal disappearance in supercond. state 78−19369
Nb_3Ga-Nb_3Pt, supercond. crit. temp., comp. depend. *(Russian)* 77−59347
Nb_4Ga_5, cryst. struct. and homogeneity range 78−42957
$Nb_{78}Ga_{22-x}Mn_x$, supercond. props., influence of Mn mag. impurities 80−54825
$Nb_{80}Ga_{20-x}Mn_x$, supercond. props., influence of Mn mag. impurities 80−54825
Nb_3Ga(So)(Ir)(Pt)(Au), X-ray $M_{IV,V}$ emission bands *(Russian)* 80−45170
Nb_3(Ge,Si) A15 film, supercond. and structural props. 79−87177
Nb_3(Ge, X), X=Si, Ga, CVD tapes, supercond. props. at high mag. fields 79−38279
NbGe, thin superconducting films, high field expts. on press. effects up to 15 kbar 79−61006
$NbGe_2$ single crysts., elec. resist. and superconductivity 79−38233
$NbGe_2$, superconducting transition temp. meas. of sputtered films and bulk 80−7019
$Nb_{0.82}Ge_{0.18}$, structural and supercond. props. press. effects 80−39700
$Nb_{1-x}Ge_x$, supercond., mag. field props. 80−54822
Nb_3Ge, A-15 diffusion layers, influence of additions of growth and supercond. props. *(German)* 80−11130
Nb_3Ge A15 cpd., bulk modulus 80−7611
Nb_3Ge, A15 cpd., normal state, low temp. resist. 80−107762
Nb_3Ge, A15 superconductor, rel. between transition temp. and density of states 79−15247
Nb_3Ge, amorphous and crystalline A-15 phases 78−83896
Nb_3Ge, amorphous film, supercond., flux flow resist., vortex pair dissoc. 80−88701
Nb_3Ge amorphous films, microstruct. X-ray small angle scatt. study 79−14685
Nb_3Ge, amorphous films, thermally-activated internal friction peaks, structural obs. 80−80147
Nb_3Ge amorphous films, X-ray diffr. analysis of microstruct. 78−72035
Nb_3Ge, amorphous nongranular thin superconducting film, thermodynamic and resistive transitions 80−34571
Nb_3Ge, anomalous resistivity, insight from band theory 78−60106
Nb_3Ge, α-particle irrad., supercond. transition width 78−23193
Nb_3Ge, α-particle irrad., relationship between density of states and supercond. transition temp. 79−42684
Nb_3Ge, band struct. and density of states from self-consistent pseudopotentials 79−69401
Nb_3Ge, bonding, electronic charge distribs. and struct. transform. from self-consistent pseudopotentials 79−69054
Nb_3Ge, bridge contact, Josephson effect 80−70906
Nb_3Ge, CVD, AC losses, temp. depend., 4-20K 77−28311
Nb_3Ge, CVD, hysteretic losses, precipitates and deposition temp. effects 77−28319
Nb_3Ge, CVD, impurity doping effect on supercond. crit. props. 78−52174
Nb_3Ge CVD tapes, supercond. props. at high mag. fields 79−38279
Nb_3Ge, CVD-prepared, high field props. and scaling 79−56455
Nb_3Ge coevaporated film, high supercond. transition temp., nucleation and growth 80−76185
Nb_3Ge composite filament, continuous, high-strength, prep. and supercond. props. 77−28765
Nb_3Ge continuous supercond. tape, prep. by CVD 77−80893
Nb_3Ge, crit. current density temp. depend. 77−47951
Nb_3Ge, DC sputtered films, annealing and mech. deform. effects on struct. and supercond. props. 79−38217
Nb_3Ge, density of states from critical field meas. 79−42690
Nb_3Ge, disordered superconductor, T_c depression by acoustic plasmon overdamping 80−7020
Nb_3Ge, effect of ^{16}O and ^{32}S ion irrad. and thermal recovery on T_c, residual resist. and slope of crit. field 79−56348
Nb_3Ge, electron energy loss spectra, AES and HEED investig. of surface 77−24635
Nb_3Ge, electron-lifetime effects on props. 80−10951
Nb_3Ge, epitaxial growth of polycryst. films with high supercond. transition temp. 77−63015

niobium alloys continued
Nb_3Ge film, CVD, thermal expansivity, X-ray diffr. meas. 78−6166
Nb_3Ge film, CVD fabrication of supercond. tape for high-field magnets 78−95698
Nb_3Ge film, CVD on inside of Cu tube, AC losses 77−28312
Nb_3Ge film, critical current density and flux pinning 77−20510
Nb_3Ge film, EXAFS meas. 78−2935
Nb_3Ge film, electron beam co-deposited, prep. and supercond. crit. temp. 78−15310
Nb_3Ge film, far IR reflection and transmission spectra, room temp. 77−55792
Nb_3Ge film, growth by co-evaporation in O_2, critical temp. enhancement 77−28273
Nb_3Ge film, high-temp. supercond. phase stabilisation w.r.t. prep. conditions *(Russian)* 80−70871
Nb_3Ge film, in supercond. proximity sandwich, energy gap struct., appl. to electron-phonon spectra 79−56401
Nb_3Ge film, low temp. sputter deposition 78−48315
Nb_3Ge film, nucleation of high-T_c phase in presence of impurities 78−88054
Nb_3Ge film, prep. by coevaporation, supercond. props. 78−91830
Nb_3Ge film, prepared by cosputtering, supercond. props. 79−4634
Nb_3Ge film, sputtered, chemical composition versus lattice parameter a_o and supercond. transition temp. relations 77−43771
Nb_3Ge film, sputtered and evaporated, transition temp., critical field and current anisotropy 77−28328
Nb_3Ge film, supercond., intercorrelations between composition, lattice parameter a_0 and T_c 77−8217
Nb_3Ge film, supercond., electron beam codeposition in O_2, Cl_2 or air, phase diagram 77−28728
Nb_3Ge film, supercond., TEM obs. of microstruct. foil prep. method 77−55642
Nb_3Ge film, supercond., epitaxial growth on Nb_3Ir and Nb_3Rh substrates 78−80473
Nb_3Ge film, superconductive, crit. temp., resistivity, structure depend. on comp. 78−6470
Nb_3Ge film, superconducting, A-15 type, getter-sputtering with controlled additions of O 78−88427
Nb_3Ge film, superconductivity, relevance of mag. interactions, EPR study 80−100545
Nb_3Ge film, T_c var. with ^4He irrad. induced defects 77−8220
Nb_3Ge films, correl. between crit. current density and microstruct. 79−38277
Nb_3Ge films, form. of A15 phases by DC sputtering 79−38740
Nb_3Ge films, prep. by DC sputtering and solid state diffusion, supercond. props. and struct. 79−38212
Nb_3Ge, granular supercond., simple model for resistive-nonresistive transition 78−72298
Nb_3Ge, high pressure and temp. treatment effect on supercond. props. *(Russian)* 77−1512
Nb_3Ge, high T_c, development as high field supercond. 79−61015
Nb_3Ge, high T_c film with impurity expanded lattice, form. and stabilisation 79−56099
Nb_3Ge, high T_c films, electron tunnelling and AES anal. 79−28471
Nb_3Ge, high T_c supercond., anal. of X-ray traces 79−56098
Nb_3Ge, high-T_c supercond., apparent T^2-depend. of normal-state resist. and lattice sp. ht. 77−47921
Nb_3Ge, hysteretic losses in parallel AC and DC mag. fields 79−87217
Nb_3Ge, inhomogeneous superconductor, scaling laws for pinning forces 79−47214
Nb_3Ge, low fluence alpha irradiation, behaviour of supercond. transition temp. 78−43510
Nb_3Ge, low temperature electron, neutron irrad. effects on critical temp. *(French)* 80−75669
Nb_3Ge, metallic bonding, electronic states calcs. 78−79916
Nb_3Ge, metallic glass, internal friction peak obs. 78−79666
Nb_3Ge, neutron irradiated, A15 compound, recovery of T_c by annealing 78−52132
Nb_3Ge, ordered and disordered A15 phases, energy gaps, tunnelling 77−8235
Nb_3Ge, RF and DC sputtered films comparison, O content effect 78−72022
Nb_3Ge, RF sputtered film, high superconducting transition temp. 77−59346
Nb_3Ge, sputter-deposited, superconducting T_c and phase relationship 79−56344
Nb_3Ge sputtered and evaporated, struct.-depend. anisotropy of supercond. crit. currents 79−38292
Nb_3Ge sputtered film, struct. and superconducting props. 77−28337
Nb_3Ge sputtered films, Ge surface segregation exam. by AES 79−56084
Nb_3Ge, sputtered on Cu, film-substrate interface obs. by electron microscopy 80−65398
Nb_3Ge, structural and supercond. props. press. effects 80−39700
Nb_3Ge, supercond., elec. resist., phenomenological model 77−43775
Nb_3Ge, supercond., projected upper limits to crit. current density 77−36037
Nb_3Ge, supercond., single phase, sp. ht. meas., 4-29K 78−72307
Nb_3Ge, supercond. film, amorphous content, X-ray diffr. study, rel. to transition temp. 80−75668
Nb_3Ge, supercond. film, CVD, crit. temp., crit. current density 78−76204
Nb_3Ge, supercond. film, electron beam codeposition, synthesis and props. 78−72296
Nb_3Ge supercond. film, of high transition temp., US attenuation 80−49991
Nb_3Ge, supercond. film, prep. by chem. transport reaction, critical props. 79−47635
Nb_3Ge, supercond. sputtered film, ion scatt., AES, depth profiling 77−11806
Nb_3Ge, supercond. tape, growth technique via amorphous state 78−84708
Nb_3Ge supercond. thin films, He- and Ar-irradiated, X-ray diffr. studies 80−29503
Nb_3Ge, superconducting, high crit. temp., prep. *(Japanese)* 79−78914
Nb_3Ge, superconducting A-15 type compounds, transition temp., radii ratio and structure *(Chinese)* 80−44752
Nb_3Ge superconducting film, α-particle induced defects and stoichiometry 77−32101
Nb_3Ge superconducting films, tunnelling obs., X-ray and electron diffr. obs. 77−32123

niobium alloys continued
Nb_3Ge superconducting film, CVD deposited, second phase (tetragonal Nb_5Ge_3) rel. to critical current 77−32131
Nb_3Ge superconducting film preparation and props. 79−11515
Nb_3Ge superconducting films, role of O_2 in form. of struct. *(Russian)* 79−60950
Nb_3Ge superconducting film, crit. temp. correl. with resist. relations and film struct. *(Russian)* 80−15646
Nb_3Ge superconducting films, high critical temp., optimum sputtering conditions 80−15647
Nb_3Ge superconducting films, quantitative Auger anal. 80−55740
Nb_3Ge, superconducting hybridisation and bonding, XPS exam. 78−2988
Nb_3Ge superconducting long tapes, CVD prepared, high current densities at 20 T 79−33436
Nb_3Ge, superconducting thin films, energy gaps from tunnelling meas. 80−25050
Nb_3Ge superconductivity film, Nb_5Ge_3 and NbO content, X-ray diffr. obs. 80−2515
Nb_3Ge tape, prepared continuously by CVD, props. 78−60257
Nb_3Ge tape, supercond., prep. by continuous CVD process 78−11121
Nb_3Ge tape conductors, strain depend. of crit. current density 79−38278
Nb_3Ge:H film, sensitivity of supercond. transition temp. to H content 78−47894
Nb_3Ge-based superconducting alloys, upper critical field temp. depend. *(Russian)* 78−10622
Nb_3Ge-Mo(Ti)(Zn), synthesis from thermalised sputtering and changes in Tc and depend. of H_{c2} on temp. 79−56350
Nb_5Ge_3, 0.30K supercond. transition temp. meas. with 0.14K transition width 78−6468
Nb_xGe_y, film deposition by ion beam methods 78−72728
$Nb_3Ge_xAl_{1-x}$, ternary supercond. alloys, comp. variations 80−97022
$Nb_3Ge_{1-x}Ga_x$ CVD films, supercond. transition temp. depend. on lattice parameter 79−38219
$Nb_2Ge_{1-x}Ga_x(Sn_x)$ CVD films, supercond. props., 4.2 to 19K 79−42713
$Nb_3Ge_{1-x}M_x$ (M=Ga,Sn), pseudo-binary, scaling laws for supercond. crit. currents 79−24118
$Nb_3Ge_{0.8}Nb_{0.2}$, A-15 type struct. and order parameter 79−77552
Nb_3Ge(Si), RF sputtered films, amorphous atomic scale struct. 80−84064
Nb_3Ge(Sn), electron irradiation at cryogenic temps., effect on T_c and transport props. 78−52122
Nb_3Ge(Sn) plasma energies, tight-binding energy-band model 78−84159
Nb_3Ge(Sn), superconducting, optical props. and electron-phonon interactions 80−2510
$Nb_{78}Gn_{22-x}Fe_x$, $Nb_{80}Ga_{20-x}Fe_x$, A15 phase supercond. 79−87181
$NbH_{0.02}$, jump models for H diffusion, quasielastic scatt. of slow neutrons 79−95208
$NbH_{0.11}$, incoherent struct. factor of H, neutron scatt. exam., quasielastic energy spectrum 79−99186
$NbH_{0.29}$, Compton profile and electron momentum distrib. anisotropy 77−44079
$NbH_{0.3}$, α-α' phase transition, sp. ht. anomaly 78−39764
$NbH_{0.453}$, influence of H on bulk band struct., optical absorptivity spectra obs. 77−89692
β $NbH_{0.82}$, fracture, TEM obs. 80−108519
NbH_2, harmonic and anharmonic elastic props. 80−10589
NbH_x, coherent α-α' phase transition 80−71641
NbH_x, proton Knight shift and mag-suscept., high resolution meas. 77−55716
NbH_x, supercond. T_c and low temp. resistivity, morphology 77−72940
NbH_x, thermopower, role of phonon dynamics 79−33284
NbH(D), ordered, TEM obs. of anisotropic lattice distortions 79−7579
α-NbH_xD_y, H diffusion, NMR spin echo obs. 80−34228
$NbH_{0.004}N_{0.007}$, H-diffusion, interstitial trapping, quasielastic neutron scatt. study 79−42298
Nb_3In, thin films with A-15 struct., prep. 78−80478
$Nb_{0.55}Ir_{0.45}$ metallic glass, Young's modulus meas. by impulse induced resonance technique 80−40411
Nb_3Ir, A-15 struct. ^{93}Nb NQR spectra 80−20496
Nb_3Ir, A-15 struct. supercond., microhardness, bonding 78−76199
Nb_3Ir, polycryst. substrate for epitaxial growth of Nb_3Ge films 77−63015
Nb_3M, M = Si, Sn, Ge, Ga, Al, electronic struct., electron-phonon interactions and X-ray spectra 78−91613
$Nb_{0.5}Mo_{0.5}$, soft X-ray spectra, theoretical considerations 80−11511
$Nb_{80}Mo_{20}$, $Nb_{75}Mo_{25}$, supercond., phonon cond. below 1k 78−14881
$NbMo_2Be$, predicted A15 struct. and T_c=30K 78−76182
$(Nb_{0.99}Mo_{0.01})_{1-x}Ge_x$, supercond. transition temp. and crit. field 79−38220
$(Nb_{1-x}Mo_x)_3Ge$ system, composite transition metal atom supercond. 77−39984
$Nb_{1-x}Mo_xSe_2$, supercond. transition temp. and mag. susceptibility 77−12043
$Nb_3Nb_{1-x}Si_x(Ge_x)$, impurity stabilised A15 supercond., transition temp., lattice consts., specific heat 80−93026
$Nb_{0.4}Ni_{0.6}$, amorphous, pair distrib. function, temp. depend., rel. to glass transition 80−24368
$Nb_{40}Ni_{60}$, 3 MeV Ni^+ ion implantation, electron microscope exam. of ion damage 78−91365
$Nb_{40}Ni_{60}$, amorphous, produced by Ni^+ implantation, damage distrib. 80−107062
$Nb_{60}Ni_{40}$, metallic glass, obs. of temp. depend. of struct. factor 78−87624
$Nb_{50}Ni_{50-x}Fe_x$, amorphous, mag. ordering and local random anisotropy 78−68273
$Nb_{50}Ni_{50-x}Fe_x$, amorphous alloy, mag. interactions 78−95432
$Nb_{50}Ni_{50-x}Fe_x$, magnetically dil. glass, 3d moments, mag. susceptibility and magnetisation meas. 79−95574
Nb_3Os, A-15 struct. ^{93}Nb NQR spectra 80−20496
Nb_3Os(Ir)(Pt)(Au), XPS of valence electrons meas. 77−21003
Nb_3Pt, A-15 struct. ^{93}Nb NQR spectra 80−20496
Nb_3Pt, neutron irrad. effects on supercond. props. 79−38224
Nb_3Sb, 4 to 294K, magnetic susceptibility meas. 79−99675
Nb_3Sb, de Haas-van Alphen effect and Fermi surface 78−6262
Nb_3Sb, NMR of ^{93}Nb and spin-lattice relax. time at low temp. 77−85388
Nb_3Sb, NQR study, ^{93}Nb nuclear relax. 78−88073
Nb_3Sb, resist. charcts. in normal state 78−51963
$NbSe_2$ nonstoichiometry, electrical props. *(Japanese)* 78−10593
$NbSe_2$-Fe, dil. alloy, magnetotransport and superconductivity 77−55516

niobium alloys continued
$NbSe_3$, electronic props. variation with struct. 79−42438
$NbSe_3$, freq. depend. conductivity 80−107838
$NbSe_x$, nonstoichiometric, thermodynamic props. and crystal struct. *(Japanese)* 78−11206
$NbSi_2$, superconducting transition temp. meas. of sputtered films and bulk 80−7019
$NbSi_2$-Si interfaces, chemical state, AES expts. 78−91767
Nb_3Si, A-15 diffusion layers, influence of additions of growth and supercond. props. *(German)* 80−11130
Nb_3Si A15 phase from amorphous Nb-Si alloys, high-press. synthesis 80−93516
Nb_3Si A15 struct., high press. synthesis *(Chinese)* 80−70917
Nb_3Si, A15 struct., synthesis at high press., preferable conditions *(Chinese)* 77−48363
Nb_3Si, amorphous films, thermally-activated internal friction peaks, structural obs. 80−80147
Nb_3Si epitaxial layers, ion implantation synthesis, supercond. transition temp. optimization 79−38218
Nb_3Si film, quasiamorphous, supercond. phase formation by heat pulse 77−63017
Nb_3Si film, supercond., obtained by vaporisation in vacuum, props. 78−14865
Nb_3Si films, form. of A15 phases by DC sputtering 79−38740
Nb_3Si, high press. phase, prod. by recrystn. of metastable sputter deposits, struct. and supercond. props. 78−60571
Nb_3Si, high T_c, supercond. props. from extrapolation of sp. ht. meas. on A-15 Nb-Si 80−25045
Nb_3Si, high T_c supercond., anal. of X-ray traces 79−56098
Nb_3Si, hypothetical, electronic struct., lattice parameters and possible supercond. transition temp. 79−23891
Nb_3Si, metastable A-15 struct. synthesis by ion implantation, supercond. transition temp. 80−55319
Nb_3Si, structural and supercond. props. press. effects 80−39700
Nb_3Si, substituted, splat cooling influence on supercond. T_c and stoichometry 80−80439
Nb_3Si, supercond., A15 film, electron beam evaporation 80−29284
Nb_3Si, supercond. phase, formation by explosive compression 79−82701
Nb_3Si, supercond. props., effect of neutron irrad. 79−38211
Nb_3Si, superconducting, high transition temp., sputtering 78−15309
Nb_3Si, superconducting A-15 type compounds, transition temp., radii ratio and structure *(Chinese)* 80−44752
Nb_3Si type with A15 struct., supercond. transition temp., depend. on stoichiometry *(German)* 77−69444
Nb_3Si, universal defect behaviour, transition temp. rel. to lattice parameter 77−69440
Nb_4Si, Nb_5Si_3 and $NbSi_2$, ultrasoft X-ray emission bands, empirical band schemes 78−15249
Nb_5Si_3, supercond. props. and cryst. struct. 79−78245
NbSn multifilamentary superconducting composites, micromechanics 79−38878
$Nb_{1-x}Sn_x$, sp. ht., supercond. T_c and martensitic transform. *(French)* 78−43508
Nb_2Sn, filamentary segments, flux pinning, proximity effects, percolation thresholds 78−56269
Nb_3Sn, 2-MeV proton-irradiated, Mossbauer effect studies 79−69757
Nb_3Sn, [111] transverse acoustic phonon softening near martensitic transform. 79−73283
Nb_3Sn, A-15 compounds, interlattice displacements, elastic consts. 78−55906
Nb_3Sn, A-15 cubic phase, band calc. using APW method 79−56120
Nb_3Sn, A-15 struct. Nb based superconductors, irrad. type influence on radiation defects 80−15093
Nb_3Sn, A-15 struct. supercond., microhardness, bonding 78−76199
Nb_3Sn, A-15 supercond. cpd., martensitic transform. 79−60499
Nb_3Sn, A-15 superconductor, dHvA effect 78−75985
Nb_3Sn, AC losses, surface effects 78−64171
Nb_3Sn A15 composite superconductors, hydrostatic extrusion *(French)* 80−104090
Nb_3Sn, A15 compound, exam. of deformation processing, review 78−39864
Nb_3Sn, A15 cpd., normal state, low temp. resist., disorder effects 80−107762
Nb_3Sn, acoustic soft modes in high mag. fields, soft sound vel. meas. 77−43482
Nb_3Sn, alloying agent influence on struct. and supercond. props. *(Russian)* 80−39698
Nb_3Sn, anisotropic thermal parameters of Nb 79−99282
Nb_3Sn, annular superconductor, field replication and flux shielding 77−28286
Nb_3Sn, atomic displacements induced by radiation damage, X-ray study 80−2085
Nb_3Sn, α-particle irrad., relationship between density of states and supercond. transition temp. 79−42684
Nb_3Sn based multifilamentary superconductors, bronze process fabrication, voids growth obs., via hot stage SEM 80−70089
Nb_3Sn bronze process, flux pinning scaling law depend. on strain 80−75696
Nb_3Sn cable for TESPE superconducting toroidal coil used for Tokamak fusion plasma containment 79−54223
Nb_3Sn, cavities, quasiparticles in energy gap corresponding to weak spots 79−56386
Nb_3Sn, coherence parameter, nonlinear high temp. supercond. elements with A-15 lattice *(Russian)* 80−60127
Nb_3Sn composite, superconducting transition depend. on non-hydrostatic stress 80−107948
Nb_3Sn composite processes with Cu-Sn-Zn matrix, superconducting props. 78−84370
Nb_3Sn, composite superconductor, sp. ht., 4-24K, calorimetry 77−32116
Nb_3Sn composite supercond., current transfer, theory 78−72315
Nb_3Sn composite supercond., current transfer, expt. results 78−72316
Nb_3Sn, composite supercond., powder metallurgical prep. 80−2981
Nb_3Sn, composite superconducting wire, critical current-bend strain relationships 80−93063
Nb_3Sn, composite wire, boundary resistance and cryogenic stability 79−69629
Nb_3Sn composite wires, supercond., degradation mech. under tensile strain at 4.2K 79−38284
Nb_3Sn composites, crit. currents and microstruct. 79−38280
Nb_3Sn conductor, bronze-process fine-filament, development and props. 79−33426

niobium alloys continued
Nb_3Sn conductors for toroidal-field coils, forced-flow, flow characts. 79−58741
Nb_3Sn, crit. current ang. depend., prep. conditions effect 77−47949
Nb_3Sn, crit. current density, low dose fast neutron irrad. effect 78−14910
Nb_3Sn, crit. current enhancement by low temp. fast neutron irradiation 77−40014
Nb_3Sn, critical current density 78−52176
Nb_3Sn, critical current enhancement by low temp. fast neutron induced flux pinning centres 78−52177
Nb_3Sn, critical currents, ang. depend., prep. conditions effects 77−43793
Nb_3Sn, critical data, under hydrostatic pressure to 15 kbar 79−47217
Nb_3Sn, cryostabilised conductor cooling system for Large Coil Program 78−50393
Nb_3Sn cryotron, thermally controlled, used in transformer-rectifier flux pump for superconducting magnet 80−4727
Nb_3Sn, Cu admixture in Sn bath effect on critical current and stability temp. 80−7059
Nb_3Sn, current carrying capacity increase by Hf addition 80−7056
Nb_3Sn, de Haas van Alphen meas. of Fermi surface for $H \leq 40$ T 79−73424
Nb_3Sn, de Haas-van Alphen oscills. in normal state 79−56116
Nb_3Sn, Debye temp., determ. from elec. resist. meas. *(French)* 77−4322
Nb_3Sn, Debye-Waller factor temp. depend. 79−14907
Nb_3Sn, degradation mechanism of superconducting transition temp. under high energy neutron irradiation 78−52124
Nb_3Sn, delayed flux entry and surface barriers, tunnelling obs. 77−59355
Nb_3Sn, density of states from critical field meas. 79−42690
Nb_3Sn, dependence of max. trappable field on supercond. cylinder wall thickness 77−72952
Nb_3Sn diffusion layer material, characterisation 79−38213
Nb_3Sn, diffusion-processed layer, texture meas. 79−82726
Nb_3Sn, distrib. of mag. field of transport current in type II supercond. 79−51730
Nb_3Sn, effect of changes in $\alpha^2(\Omega)F(\Omega)$ on the zero-temp. energy gap 80−97025
Nb_3Sn, effect of diffusion couple Sn content on superconductivity 79−61009
Nb_3Sn, effect of O ion irradiation on supercond. 78−52131
Nb_3Sn, effect on critical temp. for supercond. of disorder, induced by α-particles 78−47897
Nb_3Sn, elastic instability in cubic to tetragonal phase transitions 78−39767
Nb_3Sn, electron beam deposited, microstruct., rel. to supercond. props. 79−37935
Nb_3Sn, electron energy loss spectra, AES and HEED investig. of surface 77−24635
Nb_3Sn, electron-lifetime effects on props. 80−10951
Nb_3Sn, electronic props. calc. 79−7780
Nb_3Sn, electronic struct., APW method 78−72066
Nb_3Sn, electronic struct. from three-dimens. k.p model 78−84139
Nb_3Sn, fast neutron irradiation, effect on critical current density 78−19197
Nb_3Sn fatigue effects in unidirectional composites, computer simulated model 80−35289
Nb_3Sn filament, crit. current stress induced degradation 77−24658
Nb_3Sn, filamentary, fatigue tests on small coils 78−64652
Nb_3Sn, filamentary conductors, type-II, low temp. 30 GeV proton effects on critical props. 78−52178
Nb_3Sn, filamentary supercond., mech. props. and crit. current 77−24657
Nb_3Sn, filamentary superconducting composite, TEM 77−80887
Nb_3Sn filamentary superconducting composites, mechanical properties and microstructure 79−57054
Nb_3Sn filamentary wires, fabricated by infiltration method, supercond. props. 77−28761
Nb_3Sn, filaments in Cu matrix, thermal strain effects on superconducting critical temp. 80−93032
Nb_3Sn film, electron beam evaporation, growth morphology 77−44167
Nb_3Sn film, electron beam codeposited, growth morphology and tensile props. 78−10301
Nb_3Sn film, growth by high-rate magnetron sputtering, transition temp. and crit. currents 77−28718
Nb_3Sn film, high T_c, high-rate magnetron sputtering, supercond. transition temp. meas. 77−43770
Nb_3Sn film, quasiamorphous, supercond. phase formation by heat pulse 77−63017
Nb_3Sn film, SQUIDs for operation above 14.5K 77−66226
Nb_3Sn film, T_c var. with ^4He irrad. induced defects 77−8220
Nb_3Sn film contacts, quantum interference at H_2 temp. *(Russian)* 77−12041
Nb_3Sn film formation, solubility, precipitating processes *(Russian)* 80−92792
Nb_3Sn film on insulating substrate, crit. mag. fields *(Russian)* 79−11277
Nb_3Sn films, deposition by quasi-closed vol. method, supercond. crit. temp. 80−15645
Nb_3Sn, flux density gradient determ. by Faraday effect 80−107969
Nb_3Sn, flux trapping and shielding capabilities in transverse fields 80−15667
Nb_3Sn, for supercond. microwave cavities, secondary electron emission and AES meas. 79−56895
Nb_3Sn forced flow superconductor design considerations for Large Coil Program 78−50394
Nb_3Sn forced flow superconducting test coil, Westinghouse design for fusion reactor large coil program 80−99337
Nb_3Sn, forced flow toroidal field coil, Westinghouse Electric conceptual design for test coil 78−50392
Nb_3Sn, gap anisotropy, electron irrad. effect on transition temp. 78−10599
Nb_3Sn, grain size in A15 reaction layers 78−14911
Nb_3Sn, helicon-phonon interaction for parallel wave propagation 78−64054
Nb_3Sn, high-T_c supercond., apparent T^2-depend. of normal-state resist. and lattice sp. ht. 77−47921
Nb_3Sn, high-current A-15 microcomposite material 80−44781
Nb_3Sn, high-rate sputter-deposited, effect of oxygen on microstruct. 80−20343
niobium alloys continued
Nb_3Sn, high-temp. supercond., tunnelling spectra, electron pairing anal. 79−87205
Nb_3Sn, highly disordered, elec. resist. and supercond. T_c 78−52142
Nb_3Sn, hot isostatically pressed, plastic deform. 80−108510
Nb_3Sn in bronze, supercond. props. thermally induced matrix stresses 77−32134
Nb_3Sn in Cu matrix composite superconductor, cyclic stress effects on transport props. 77−28336
Nb_3Sn, inhomogeneity detection by penetration depth meas., proximity theory 77−28288
Nb_3Sn, irrad. effects on supercond. transition temp. 78−6472
Nb_3Sn, irradiated, critical current density 79−38293
Nb_3Sn, lattice dynamics at 300K 79−65155
Nb_3Sn, lattice microstrain induced metastable phase, low temp. struct. and props. 77−8482
Nb_3Sn, low field microwave props., H_{c1} 77−28317
Nb_3Sn, low fluence alpha irradiation, behaviour of supercond. transition temp. 78−43510
Nb_3Sn, low temp. irrad. with 20 MeV S ions, effect on supercond. props. 79−38223
Nb_3Sn, low temp. neutron irrad. expts., $E_n = 14$ MeV 79−33424
Nb_3Sn, martensitic transform. coupling with supercond. transition 78−44126
Nb_3Sn, martensitic transition, lattice anharmonicity 79−8300
Nb_3Sn microfilamentary superconducting composite, critical currents, fracture props. 80−107970
Nb_3Sn monofilament wires, supercond. props., effect of Be alloying additions to bronze matrix 79−87222
Nb_3Sn monofilamentary wires, supercond. crit. current density, bending effects 80−50018
Nb_3Sn, monofilaments, radiation-enhanced diffusion growth, crit. current density 80−65758
Nb_3Sn, multifilament composite technical superconductors, development and manufacture 79−19707
Nb_3Sn, multifilament conductors, strain-crit. current meas. 78−64174
Nb_3Sn multifilament conductors, strain effect on crit. props. 78−80108
Nb_3Sn multifilament conductors, fabrication and props. 79−33427
Nb_3Sn, multifilament conductors appl., production and props. *(German)* 80−3081
Nb_3Sn multifilament supercond. wire, hydrostatic extrusion processing 79−33976
Nb_3Sn multifilament superconductors, designed for high B appl., losses 79−33414
Nb_3Sn multifilament superconducting composites, alternative technologies for fabrication 79−38756
Nb_3Sn, multifilament superconductor, metallurgical design 79−33434
Nb_3Sn multifilament superconductors produced by ECN technique, prep. and props. 79−33975
Nb_3Sn multifilament superconductors, AC losses 79−60979
Nb_3Sn, multifilament superconductor, pulsed mag. field losses and critical current densities 80−54853
Nb_3Sn, multifilamentary, optimization of high field crit. current density 79−38288
Nb_3Sn, multifilamentary and cabled superconductors, cryogenic stability anal. 79−59260
Nb_3Sn, multifilamentary composite wires, critical current strain depend. 77−20511
Nb_3Sn multifilamentary conductor, crit. current, tensile stress effects 77−28329
Nb_3Sn multifilamentary conductor, for fusion research magnets, manufacture and props. 77−28760
Nb_3Sn multifilamentary conductors, crit. current under tensile stress 77−89912
Nb_3Sn multifilamentary conductors, enhancement of supercond. crit. current by tensile stress 78−6490
Nb_3Sn multifilamentary conductors for large-scale magnets, crit. currents, stability, and stress effects 79−38291
Nb_3Sn multifilamentary composite superconductor, effect of heat treatment on supercond. props. 79−33376
Nb_3Sn multifilamentary composite superconductor, reaction treatment, crit. current, transition temp. and bend props. 79−33430
Nb_3Sn multifilamentary conductor for fusion research 79−35797
Nb_3Sn multifilamentary composite wires, supercond. crit. current density, temp. and mag. field depend. 79−33425
Nb_3Sn, multifilamentary conductors, production using solid state diffusion technique 79−56454
Nb_3Sn multifilamentary composites, supercond. destruction by current, long N-S interfaces 79−56480
Nb_3Sn, multifilamentary conductors, effect of bronze on compression 79−61012
Nb_3Sn, multifilamentary conductors, stress-induced enhancement of critical currents 79−69644
Nb_3Sn multifilamentary composites, crit. currents, flux pinning, and crit. field 79−78280
Nb_3Sn, multifilamentary coils for Lawrence Livermore Laboratory superconducting High Field Test Facility 80−90834
Nb_3Sn multifilamentary composite supercond. wires, transverse sections prep., ion milling, TEM obs. of grain size 80−101000
Nb_3Sn multifilamentary dipole magnet, construction and performance 77−28758
Nb_3Sn multifilamentary dipole magnets, supercond. props., 4.2 to 15K 79−31275
Nb_3Sn multifilamentary hollow superconductor and magnet, fabrication and crit. currents 79−38289
Nb_3Sn, multifilamentary high-field superconductor, status of development 79−61004
Nb_3Sn, multifilamentary supercond., flexibility and elec. characts. 77−24990
Nb_3Sn, multifilamentary supercond., crit. current, bend tests 77−28335
Nb_3Sn multifilamentary supercond., Cu-stabilised, recent developments 77−28759
Nb_3Sn, multifilamentary supercond., prod. by ECN powder metallurgy method and props. 77−28762
Nb_3Sn, multifilamentary supercond., stress effects 77−32133
Nb_3Sn multifilamentary superconductors crit. current up to 18 T 77−47950
Nb_3Sn multifilamentary stranded compd. supercond., design, processing, mech., supercond. props. 77−76999
Nb_3Sn multifilamentary superconductor, stress induced normal⇄supercond. transition 79−33377

niobium alloys continued
Nb_3Sn multifilamentary superconducting wires, crit. current density in high mag. field 79−38281
Nb_3Sn multifilamentary superconducting wires, improved high-field props. 79−47215
Nb_3Sn multifilamentary supercond. composites, crystallographic texturing 80−71669
Nb_3Sn, multifilamentary superconductor preparation by 'in situ' and cold powder methods, review 80−93522
Nb_3Sn multilayered supercond. power line conductors, elec. props. and growth morphology 77−28325
Nb_3Sn, NMR of ^{93}Nb and spin-lattice relax. time at low temp. 77−85388
Nb_3Sn, neutron irrad., crit. current change rel. to temp. and metallurgy 78−80109
Nb_3Sn, neutron irrad., elec. resist., temp. depend. 79−91024
Nb_3Sn, neutron irrad., X-ray scatt. theory 79−37740
Nb_3Sn, neutron irrad. effect on upper crit. field and crit. current 77−72954
Nb_3Sn, neutron irrad. effect on supercond. fusion magnet props. 78−52128
Nb_3Sn, neutron irrad. effects on transition temp. *(Japanese)* 79−82707
Nb_3Sn, neutron irradiation at 8K, supercond. crit. current and crit. temp. meas. 77−28334
Nb_3Sn neutron scatt. data, coupling between thermal and elastic variables 77−1203
Nb_3Sn, nonstationary Josephson effect, 13-18.3K, 9-10 GHz, 20 MW *(Russian)* 78−2631
Nb_3Sn, normal state, Fermi surface, APW band calc. and de Haas-van Alphen oscills. 79−65369
Nb_3Sn, O^{4+} bombarded, Mossbauer studies 80−2672
Nb_3Sn, on $LiNbO_3$ substrate, US attenuation of SAW in applied mag. field 80−75678
Nb_3Sn patterned film, appl. to refractory lift-off process using Nb-Cu bilayers 79−47626
Nb_3Sn, phonon density of states, temp. depend. 79−42183
Nb_3Sn, phonon softening and T_c, strong electron-phonon coupling 78−31009
Nb_3Sn, phonon softening in [ζζζ] transverse modes, neutron scatt. obs. 79−33062
Nb_3Sn, powder metallurgically produced, microstruct. characts. 80−89233
Nb_3Sn, produced by Sn implantation, supercond. and Mossbauer effect 79−4612
Nb_3Sn, proton and γ-irradiated, lattice dynamics from ^{119}Sn Mossbauer studies 78−39458
Nb_3Sn, proton irradiated, Mossbauer effect at 78K 78−19394
Nb_3Sn, quasi-one-dimensional supercond., giant enhancement of nucl. relax. rate near T_c 78−56257
Nb_3Sn, radiation damage effect on superconducting props. 78−52127
Nb_3Sn, resist. characts. in normal state 78−51963
Nb_3Sn, softening of surface phonons in (100) plane 80−107627
Nb_3Sn, stabilized multifilamentary superconductor, internal Sn diffusion process 79−61749
Nb_3Sn strip, made by diffusion method, crit. curent anisotropy, Zr alloying addition effects *(Russian)* 78−47921
Nb_3Sn, supercond., AC losses, low field behaviour morphology depend. 77−24655
Nb_3Sn, supercond., crit. fields Pauli paramag. limiting and material parameters 79−78277
Nb_3Sn, supercond., dielastic interaction of flux line lattice with internal stresses of cryst. imperfections 78−14906
Nb_3Sn, supercond., dielastic interaction of flux line lattice with internal stresses of cryst. imperfections 78−56270
Nb_3Sn, supercond., effect of trapped mag. flux on AC losses 79−33420
Nb_3Sn, supercond., elec. resist., phenomenological model 77−43775
Nb_3Sn, supercond., fast particle irradiation effects, using anti-site defect model, electronic state influences 79−56346
Nb_3Sn, supercond., production of high current carrying strip *(Russian)* 79−33435
Nb_3Sn, supercond., projected upper limits to crit. current density 77−36037
Nb_3Sn, supercond., thin film, US attenuation of SAWs 80−49988
Nb_3Sn, supercond. and high mag. fields 79−87215
Nb_3Sn, supercond. composite, residual stress state, crit. currents 80−80468
Nb_3Sn, supercond. crit. temp. and transition width, 25 MeV O ion irrad. effects 77−69439
Nb_3Sn, supercond. crit. temp., functional derivative with electronic density of states, Eliashberg eqns. 79−56368
Nb_3Sn, supercond. diffusion layer, Zr content and Nb cold working effects 77−16015
Nb_3Sn, supercond. film, electron beam codeposition, synthesis and props. 78−72296
Nb_3Sn, supercond. props., effect of neutron irrad. 80−80463
Nb_3Sn, supercond. props. and struct., neutron irrad. dose depend. 77−15985
Nb_3Sn, supercond. props. of cold worked core wires an basis of A15 phases 77−85369
Nb_3Sn, supercond. props. and appls., state-of-the-art 79−33413
Nb_3Sn, supercond. tape, crit. current, effect of Sn-Nb phase, annealing 79−24119
Nb_3Sn, supercond. thermodynamics 79−42693
Nb_3Sn, supercond. transition temp., deform. effects 77−12051
Nb_3Sn superconducting, formed from Cu-Sn alloy, props. 79−42709
Nb_3Sn, superconducting, inelastic scattering of light 79−33390
Nb_3Sn, superconducting accelerating struct., high field exam. 79−36439
Nb_3Sn superconducting bridge junction, crit. current temp. depend. *(Russian)* 78−34938
Nb_3Sn superconducting composite, bronze process, metallurgy 80−3004
Nb_3Sn superconducting film, α-particle induced defects and stoichiometry 77−32101
Nb_3Sn, superconducting filament formation near edge dislocation *(Russian)* 79−4635
Nb_3Sn superconducting layers, crit. currents, struct. and prep. *(Slovak)* 78−56273
Nb_3Sn superconducting microwave resonator for measuring dielectric loss in polymeric solids 79−67316
Nb_3Sn superconducting multifilamentary wires, mechanisms for crit.current degradation 77−28324

niobium alloys continued
Nb_3Sn superconducting multifilamentary conductors, AC losses 79−33394
Nb_3Sn superconducting multifilamentary wire, stress effects 79−33431
Nb_3Sn superconducting multifilamentary composites, strain depend. of crit. current and crit. field 79−33432
Nb_3Sn superconducting multifilamentary conductors, localisation of defects by inductive procedure 79−33433
Nb_3Sn superconducting props. and structural transition *(Russian)* 77−12052
Nb_3Sn, superconducting props., effect of radiation induced atomic disorder 78−52133
Nb_3Sn, superconducting thin films, energy gaps from tunnelling meas. 80−25050
Nb_3Sn, superconducting toroidal field coils for Tokamaks 78−50388
Nb_3Sn, superconducting transition temp., crit. parameters 77−28280
Nb_3Sn superconducting wires, in situ multifilamentary, mech. props. 79−47746
Nb_3Sn superconducting wire, fabrication from Cu-Nb-Sn alloy using controlled high temp. gradient 80−25056
Nb_3Sn, superconductive fixed points for temperatures above 0.5K 79−63221
Nb_3Sn, superconductive materials and magnet systems developed at Intermagnetics General Corp. 79−58699
Nb_3Sn superconductor, bronze processed, effect of third element additions 77−28333
Nb_3Sn superconductor, low temp. deuteron irradiation 78−52182
Nb_3Sn, superconductor for Large Coil Program, low temp. stability, joints, design method 80−106195
Nb_3Sn superconductors, bronze-processed, effect of Ta additions 78−95404
Nb_3Sn superconductors, Kirkendall voids, effects on mech. and supercond. props. 79−33429
Nb_3Sn superconductors, mech. behaviour, diffusion *(German)* 78−39880
Nb_3Sn, TEM of radiation damage 79−65122
Nb_3Sn tapes, appl. of method for continuous meas. of crit. current 77−24656
Nb_3Sn tapes, transition temp. meas. using Si linear thermometer 77−57330
Nb_3Sn, ternary additions effect on upper crit. field at 4.2K 77−28316
Nb_3Sn, thick walled tube, calc. of transverse dipole mag. field distributions *(French)* 79−47209
Nb_3Sn thin film bridges, AC Josephson effect 79−42702
Nb_3Sn, thin film weak-links SQUIDs, localised region radiation damage, fabrication and properties 78−47912
Nb_3Sn, thin superconducting films and diffusion wires, high field expts. on press. effects up to 15 kbar 79−61006
Nb_3Sn tunnel junctions, tunnelling density of states and electron-phonon spectral function 79−65618
Nb_3Sn, vap. deposited supercond. film, effect of N_2 and tape heating 78−34939
Nb_3Sn, vapour deposited, supercond., surface resist. and penetration depth 79−33392
Nb_3Sn wires used in He cryostat for superconducting magnet 79−58733
Nb_3Sn, X-ray study of fission fragment induced structural damage 78−51589
Nb_3Sn, Young's modulus, 4.2-300K, behaviour near martensitic transition 80−66564
Nb_3Sn, Zr alloy element effect on growth kinetics *(Chinese)* 79−90579
Nb_3Sn-Al_2O_3 composite, electron beam deposited, microstruct., rel. to supercond. props. 79−37935
Nb_3Sn-Au, supercond. tunnel junction with microshort circuit, nonlinear phenomena 78−14898
Nb_3Sn-Cu, high-current A-15 microcomposite material 80−44781
Nb_3Sn-Cu composite superconductors, in-situ, AC losses 79−38283
Nb_3Sn-Cu multifilamentary wires, in situ prep., supercond. and mech. props. 79−38768
Nb_3Sn-Cu multifilamentary composite wire, Nb_3Sn filament morphology and grain size 80−100855
Nb_3Sn-Cu superconducting composite, electron beam co-evaporated, TEM study 79−28247
Nb_3Sn-Cu superconducting composite with submicrometer filaments, fabrication and props. 79−38282
Nb_3Sn-Cu superconducting composites, produced by cold extrusion of fine powders 79−38767
Nb_3Sn-Fe(Co)(Mn), mag. impurities effect on supercond. props. 77−1524
Nb_3Sn-Nb_3Sn supercond. point contacts, crit. currents, effect of laser radiation *(Russian)* 79−28484
Nb_3Sn-Pb tunnel junction, Josephson props. 79−7937
Nb_3Sn-V_3Ga concentric solenoid magnet system, 17.5 T operation 77−26353
Nb_3Sn-Zr (0.8%), supercond. tape, crit. current, two stage annealing effect *(Russian)* 77−63046
Nb_3Sn_4 film, critical currents due to microwave field 80−25058
Nb_3(Sn-Al) system, X-ray spectroscopic studies of electronic struct. of A15 cpds. 80−2900
Nb_3Sn(Al), neutron irradiated, A15 compound, recovery of T_c by annealing 78−52132
Nb_3Sn(Al)(Ga)(Ge)(Si), supercond. transition temp., rel. to A15 phase stability 78−52137
Nb_3(SnGa), wire, neutron effect on T_c, I_c and flux pinning 79−38216
$Nb_3(Sn_{1-x}Ga_x)$, bronze processed wires, critical current densities in fields up to 23.5 T 78−47922
Nb_3Sn(Ge), resistivity and T_c measurement after low temp. neutron irradiation 78−52123
Nb_3(SnIn) tapes, diffusion processed, high field props. 79−38266
Nb_3(SnIn) wires, prep. by ductile fabrication process and props. 79−38265
NbSnSb, synthesis and struct. *(French)* 79−90596
Nb_3Su-Cu supercond. composites, fabrication, magnet appl. 80−11602
$Nb_{30}Ta_{70}$, microwave props. of 8.6 GHz supercond. cavity 77−28297
$Nb_{53}Ta_{47}$, effects of hydrostatic pressure on changes in elastic consts. caused by addition of H 80−75287
$Nb_{53}Ta_{47}$, pure and hydrogenated crysts., effect of pressure on elastic consts. 80−7614
$Nb_{73}Ta_{27}$, supercond., flux density distrib. meas. 77−32129
$Nb_{73}Ta_{27}$, supercond., flux pinning by precipitates 77−47948
$Nb_{80}Ta_{20}$, supercond., phonon cond. below 1k 78−14881

niobium alloys continued
NbTi, 7 T multipurpose split-coil superconducting magnet system for Mossbauer spectroscopy and susceptibility measurements, 2 to 300K 79−58746
NbTi cabled and soldered superconds. with low losses, for fusion research magnets, development 79−35796
NbTi, chemical comp., supercond. films and bulk surfaces 78−76973
NbTi composite supercond., current transfer, theory 78−72315
NbTi composite supercond., current transfer, expt. results 78−72316
NbTi, composite wire, boundary resistance and cryogenic stability 79−69629
NbTi composites, cryogenic stability due to boundary resistance between filament and matrix 79−58748
NbTi, dynamic stress effects, supercond. magnet training problems 78−49870
NbTi filament reinforced Cu, superconducting composite, elastic const., temp. depend. 78−68717
NbTi, filamentary conductors, type-II, low temp. 30 GeV proton effects on critical props. 78−52178
NbTi filaments for position-sensitive superconducting detector of ionizing particles 80−63460
NbTi films, effect of Ar- and N-ion bombardment on texture *(Russian)* 80−107338
NbTi, forced flow superconducting test coil, EURATOM design for fusion reactor Large Coil Task 80−99339
NbTi forced flow superconducting test coil, Swiss design for fusion reactor Large Coil Task 80−99341
NbTi, General Dynamics Convair conceptual design test coil 78−50389
NbTi, General Electric test coil conceptual design 78−50390
NbTi in Al composite superconductor, AC losses and crit. current 77−28310
NbTi, monocore and filament conductors, crit. current densities and anisotropy factors, heat treatment effects 79−38285
NbTi monofilamentary wire in current sharing state, supercond. temp. sensor use 80−57288
NbTi multifilament superconductor, AC loss reduction by low twist rates 77−12057
NbTi multifilament supercond. wire, hydrostatic extrusion processing 79−33976
NbTi, multifilamentary composite wires, critical current strain depend. 77−20511
NbTi multifilamentary composite, appl. of method for continuous meas. of crit. current 77−24656
NbTi multifilamentary composite wires, supercond. crit. current density, temp. and mag. field depend. 79−33425
NbTi multifilamentary superconductor, production samples, performance 77−40012
NbTi multifilamentary wires, 30 GeV proton irradiated, effect on crit. currents 77−89911
NbTi, neutron irrad. effect on supercond. fusion magnet props. 78−52128
NbTi, RF magnetoresistance, flux flow resistivity 79−61002
NbTi solenoid, operating at 9 T in He gas 77−74461
NbTi, solid soln. supercond., crit. current anisotropy 79−38273
NbTi split coil superconducting magnet system, for Mossbauer spectroscopy and susceptibility meas. 79−71486
NbTi, supercond., measurement of thermal conductivity 79−58682
NbTi, supercond., processing parameter optimisation for high mag. field appls. 79−38290
NbTi, supercond., thermal cond. meas 79−60970
NbTi, supercond. critical temp., appl. of cryogenic calorimetry 79−40577
NbTi supercond. threads in Cu matrix, struct. composition and props. *(French)* 79−73649
NbTi, superconducting, orientation effects on magnetisation 77−28287
NbTi, superconducting, serrated yielding meas. via dynamic stress test facility 77−77698
NbTi, superconducting multifilamentary conductors, crit. current density, bending effects *(German)* 80−39727
NbTi superconducting state, stability under localised heat pulses 79−73611
NbTi superconducting tapes, mag. field profiles 77−28326
NbTi, superconducting test coil, General Dynamics Convair Division, Intermagnetics General Corp. design for fusion reactor Large Coil Program 80−99338
NbTi superconducting test coil, General Electric design and manufacture program, for fusion reactors 80−102319
NbTi, superconducting toroidal field coils for Tokamaks 78−50388
NbTi superconducting wire, Cu clad, proximity effect, Meissner screening length meas. 79−60996
NbTi, superconductor, acoustic emission during flux jump 80−39724
NbTi wire, supercond., magnetisation rel. to field orient. 78−52151
NbTi/In composite superconductor, transport props. 80−88658
NbTi/In granular composite, resistivity mag. field depend. 80−15654
NbTi-Al-(Cu-Ni) multifilamentary composite supercond. wire, stability, AC losses 77−76998
NbTi-Cu, composite superconductor, acoustic emission 80−84546
NbTi-Cu, cryostatic influence of formvar coatings on sizing of stabilizer 79−61633
NbTi-Cu, supercond. composite, use in temp. and heat transfer coeff. meas. 80−77780
NbTi-In granular supercond. composites, mag. field-induced dissipation 80−84545
$(Nb_{0.99}Ti_{0.01})_{1-x}Ge_x$, high T_c, resist. meas. 80−88531
$(Nb_{0.99}Ti_{0.01})_{1-x}Ge_x$, supercond. transition temp. and crit. field 79−38220
$(Nb_{0.99}Ti_{0.01})_{1-x}Ge_x$, supercond., mag. field props. 80−54822
$Nb_{1-y}Ti_ySe_2$, supercond. transition temp. and mag. susceptibility 77−12043
NbV-VO_x-Pb Josephson tunnel junction, VO_x effect on props. 79−87203
$Nb_{1-xv}V_xv_Hx$, interaction between interstitial H and V, NMR meas. 77−59471
Nb_3X, X=Ge, Gu, Al, Sn, Pt, composition effects on T_c 77−76993
NbZr, energy anal. of diffuse ω-reflections, Mossbauer, X-ray scatt. 78−60369
NbZr, thermally activated flux creep, effect on AC response 79−33416
$Nb_{0.75}Zr_{0.25}$, effect of force constant, disorder on Eliashberg function 80−29504
$Nb_{0.75}Zr_{0.25}$, supercond. energy gap, proximity tunnelling method determ. 79−56404

niobium alloys continued
$Nb_{1-x}Zr_x$, supercond., McMillan-Rowell tunnelling spectroscopy 79−60985
$(Nb_{1-x}Zr_x)_3$ Sn, bronze-processed tape, AC losses between 5 and 16K 79−82727
$Nb_{20}Zr_{80}$, supercond., US attenuation 80−44766
$Nb_{20}Zr_{80}$, supercond. and normal, sp. ht. meas., 2-20K 80−70893
$(Nb_{0.99}Zr_{0.01})_{1-x}Ge_x$, supercond. transition temp. and crit. field 79−38220
$(Nb_{0.99}Zr_{0.01})_{1-x}Ge_x$, supercond., mag. field props. 80−54822
NbZr(Hf)-C(N) alloys, phase comp. after casting and annealing, precip. 79−56983
$(Nb_{0.99}Zr_{0.01})_3Sn$, AC power losses in parallel AC and DC mag. fields 80−97041
Ni alloy, ZhS6K, diffusion layer form. on Nb addition, struct., comp. *(Russian)* 78−56814
Ni superalloy Mar-M200, slow fatigue crack propagation rate meas. using high freq. resonant technique 78−52983
Ni/Ni_3Al-Ni_3Nb eutectic, directionally solidified, plastic deformation *(Russian)* 78−39843
Ni/Ni_3Al+Ni_3Nb, directionally solidified eutectic alloy, crack growth rate under creep fatigue conditions 79−52361
γ/γ-Ni-Al-Nb, aligned eutectic alloy, H_2 embrittlement 77−8951
Ni-Al-Nb, eutectic form., struct. and mech. props *(Russian)* 77−21129
Ni-Al-Nb, heat resist., solidification range 80−35177
Ni-Al-Nb, heat-resisting dispersion-hardening alloys, props. and struct., γ′-phase comp. influence *(Russian)* 80−20943
Ni-Al-Nb ternary system, electron microprobe analysis of nickel-rich region at 1473K 80−71631
Ni-Cr-Mn-Fe-Nb (20,3,3,2.5 wt.%), short-range order effects on tensile behaviour 80−25793
Ni-Cr-Nb, eutectic alloy charact. by melting temp., composition and oxidation resistance 78−52771
Ni-Cr-Nb-Al eutectic alloys, sulphidation/oxidation at high temps., corrosion mechanism 78−72934
Ni-Cr-Ti-Al-Mo-Nb-Fe (13-16, 2.35-2.75, 1.3-1.7, 2.8-3.2, 1.8-2.2, 2.0 wt%), heat resistant props, mech props. struct., stepwise ageing effects *(Russian)* 78−76666
Ni-Cu-X (X=Sn, Nb, Ti), spinodal decomp. alloys, linear expansion coeff. influence on morphological anisotropy *(Japanese)* 80−70431
Ni-Fe-Cr-Nb-Ta-Mo alloy, fatigue crack growth, stress ratio and hold-time effects 80−40531
Ni-Fe-Nb, Hardperm, origin of high magnetic permeability 77−8362
Ni-Fe-Nb, hardperm alloy, effect of sheet thickness and heat treatment on magnetic props. *(Japanese)* 78−31095
Ni-Fe-Nb, Hardperm alloy, sheets, effect of sheet thickness, and annealing, on mag. props. 78−76772
Ni-Fe-Nb, mag. props. and struct. *(Chinese)* 78−84450
Ni-Fe-Nb, magnetic alloy, TEM and X-ray obs. *(Chinese)* 80−24401
Ni-Fe-Nb-Al, mag. props. and struct. *(Chinese)* 78−84450
Ni-Fe-Nb-Al (11.2, 8.09, 79.66 wt.%), modulated struct. growth process rel. to ageing *(Chinese)* 80−66541
Ni-Fe-Nb-Al(-Mo), wear resisting mag. head material, mag. props. and struct. 80−35350
Ni-Fe-Nb-Mo (11.42, 6.92, 1.54 wt.%), Hardperm, high magnetic permeability alloys 77−8361
Ni-Fe-Nb-Mo-Al, head material for mag. recording, DC and AC mag. props. 80−88812
Ni-Fe-Nb-W, high magnetic permeability alloys, Hardperm 77−48012
Ni-Nb, dil., mag. props. at elevated temps. 77−63089
Ni-Nb (5, 10 at.%), initial oxidation process at high temps., appl. of high energy ion backscattering anal. for O oxidation *(Japanese)* 79−24651
Ni-Nb (5 to 45 at.%) alloys, free energy and thermodynamic props. investigation using EMF method *(Russian)* 79−52160
Ni-Nb alloys, oxidation at high temp., high energy ion backscattering anal. *(Japanese)* 80−35405
Ni-Nb amorphous alloy, transformation to crystalline state, ion emission microscope study *(Russian)* 79−82158
Ni-Nb_2O_5, fibrous composite, aligned in situ growth by preferential internal oxidation 78−6879
Ni-Nb-Al, eutectic, thermal cycling effect on strength and ductility *(Russian)* 79−24601
Ni-Nb-Al, unidirectionally solidified γ/γ′-δ eutectic, fatigue crack propag. 79−29184
Ni-Nb-Al (21,2.5 wt.%), eutectic aligned alloy, mech. behaviour at high strain rates 78−39855
Ni-Nb-Al (25, 2.5 wt.%), directionally solidified γ/γ′-δ eutectic, growth conditions on struct. 80−11639
Ni-Nb-Al-Cr, directionally solidified, exam. of growth and morphology 79−11601
Ni-Nb-Al-(Cr), eutectic, mech. props., high press. H_2 effects 77−63779
Ni-Nb-C, obtained by liq. quenching, superconductivity 80−75699
Ni-Nb-Cr-Al, directionally solidified eutectic superalloy, high temp. oxidation resistant coatings 78−39937
γ/γ′-δ-Ni-Nb-Cr-Al (20, 6, 2.5 wt.%), growth kinetics of γ′ precipitates 77−40424
Ni-NbC (10 wt.%) eutectic alloy, directional solidification and struct. *(Russian)* 80−84922
Ni-NbC eutectic, microstructure and strength depend. on composition and crystallisation conditions *(Russian)* 79−100128
Ni-Nb(-Cu)-C, NbC dispersed supercond. tapes, fabrication and charcts. 78−19773
Ni-Ni_3Al-Ni_3Nb, directionally solidified, role of twinning in cyclic stress strain behaviour 78−80605
Ni-W-Nb system, γ to (γ+W) phase boundary calcs. using Wigner method *(Russian)* 80−54346
Ni-Zr-C (1, 0.1 wt.%), safe-life testing strengthening phases evolution and influence on heat resist. *(Russian)* 79−52476
Ni-ZrB_2 powders, densification by hot pressing 80−25604
Ni_2 (Al, Nb) single crystals, orientation and temp. depend. of yield stress 80−25791
Ni_3(Al, Nb) single crystal, yield stress, orientation and temp. depend. 80−108511
Ni_3Al-Ni_3Nb, directionally crystallised, thermal and electric cond., emissivity 77−43556
Ni_3Al-Ni_3Nb, directionally crystallised eutectic, influence of prolonged annealing on microstructs. and props. *(Russian)* 79−74182
Ni_3Al-Ni_3Nb, eutectic, temp. and thermal cycling influence on oxidation 80−45417
Ni_3Al-Ni_3Nb, eutectic alloy, crack development, failure energy capacity *(Russian)* 80−40480

niobium alloys continued
Ni_3Al-Ni_3Nb directional eutectic, oxidation and interaction with protective coatings *(Russian)* 77−52526
Ni_3Al-Ni_3Nb eutectic, directionally solidified, high-temp. oxidation mechanism 80−16544
Ni_3Al-Ni_3Nb eutectic alloy, ^{63}Ni diffusion rate rel. to struct. defects *(Russian)* 78−2288
$Ni_3Al(\gamma')$-$Ni_3Nb(\delta)$, directionally solidified, deformation substruct. and slip systems 79−8326
Ni(Cr)/Ni_3Al-Ni_3Nb directional eutectic, oxidation and interaction with protective coatings *(Russian)* 77−52526
$Ni_3(Fe_{1-x}Nb_x)$, temp. and conc. depend. of anomalous Hall effect *(Russian)* 80−70674
Ni_3Ga, temp. depend. of mech. props. *(Russian)* 79−38895
Ni_3Ge, temp. depend. of mech. props. *(Russian)* 79−38895
Ni_3Nb intermetallic compound, oxidation kinetics in 500-1000°C range *(Russian)* 77−56144
Ni_3Nb platelet reinforced Ni base alloy 77−36635
Ni_3Nb/Ni_3Al, DSC-1 and DSC-2 lattices, coincident and near coincident cells for two lattices 77−84746
$Ni_{60}Nb_{40}$, stability, crystallisation, ductility meas. 78−47246
$Ni_{62}Nb_{38}$, metallic glass, struct., neutron diffr. study 80−54148
P+Nb, dil. alloy, NMR obs. of ^{93}Nb 80−71203
Pd-Nb, dilute, low temp. sp. ht. and mag. susceptibility 77−62650
$Pd_2Mn_{1-x}Nb_xSn$, Heusler alloy, NMR and mag. coupling 78−43676
Pt-^{95}Nb, nuclear orientation meas. 79−65644
Pt-Nb dil. alloy, 0.5 at.%, ^{195}Pt NMR for local mag. susceptibility 78−84484
Ru-Nb alloy, mag. suscept. of HCP transition metal alloys *(Russian)* 78−80138
$Sm_2(Co, Cu, Fe, Nb)_{17}$, permanent magnet, improved props. 77−89978
steel, Nb, deform., recrystn. and precip. interaction 80−97515
Ta-Nb, kinetics and thermodynamics of reaction with N_2 *(German)* 79−74415
Ta-Nb (50 at.%), with N_2, spectral emissivity, N_2 absorption rate, N_2 solubility, thermodynamic data *(German)* 77−25026
Ta-Nb-V, solid solutions, superconductivity and charge transfer 79−7926
Ta-Nb-V BCC solid solutions, supercond. and normal state, sp. ht. meas. 78−84347
$Ta_{70}Nb_{30}$, Abrikosov vortex formation kinetics *(Russian)* 80−93055
Ti-Al-Nb-Ta-Mo (6, 2, 1, 0.8 wt.%), elevated temp. flow strength, creep resist., diffusion welding characts. 80−30033
Ti-Cu-Nb, heat treatable alloys, effect of alloying on strength, tensile props. 78−56671
Ti-Nb, cold strained, exam. of ω and α phases, precipitated during ageing *(Russian)* 79−11620
Ti-Nb, diffuse electron scatt. *(Russian)* 80−103438
Ti-Nb, in Cu matrix, ductile failure at low temps. of superconducting composites 79−57119
Ti-Nb, influence of different factors on supercond. transition width *(Russian)* 79−1636
Ti-Nb, phase transformation due to shock wave treatment *(Russian)* 79−91641
Ti-Nb, plastic deformation and thermal cond., 2.5 to 10K, dislocation pinning 77−35629
Ti-Nb, sintered, manufacture and exam. of props. 79−95975
Ti-Nb (4.32 wt%), high temp. oxidation kinetics under 1 bar pressure, 1255-1471K 80−89410
Ti-Nb alloys, Fe, Mo, V, Ta alloying additions on microstruct. after combined treatment *(Russian)* 77−59826
Ti-Nb BCC alloys, diffusion coeffs. of Ti and Nb, 950 to 1511°C 79−73333
Ti-Nb superconducting alloys and cmpds. with A15 struct., H_2 effect on supercond. props 79−28438
Ti-Nb system, high-temp. oxidation *(Russian)* 79−74301
Ti-Nb-Al, decomposition during isothermal annealing 80−25653
Ti-Nb-Ge foils, β phase decomposition, electron microscopy struct. investigation *(Russian)* 79−83172
Ti-Nb-H, proton spin-lattice relax. time, conc. depend., diffusion effects 77−4576
Ti-Nb-H system, quadrupole interaction, ^{93}Nb NMR *(Russian)* 77−24761
Ti-Nb-Mo(V)(Ta)(Al)(Zr), BCC struct., tetragonal phase form. by cold deform. *(Russian)* 78−88462
Ti-Nb-Na (4 to 31, 8 to 38 at.%), with uniform distribution of refractory metal, prep. *(Russian)* 77−28747
Ti-Nb-Si, amorphous alloy, supercond. props. and crystn. behaviour, TEM and DTA study *(Japanese)* 80−84536
Ti-Nb-Ta-Ge (40,20,0.8 wt.%) foil, dispersion hardening, TEM and electron diffr. obs. *(Russian)* 79−1873
Ti-Nb-V-Zr, superconductor, struct. determ. by optical microscopy and electron diffraction *(Russian)* 77−16628
Ti-Nb-V(25 wt.%, 15 wt.%), precipitation of β and ω phases during ageing at 350°C 77−8838
Ti-Nb-W, 20 to 1000°C, isothermal section, X-ray anal., microstruct., hardness, cond., transform. *(Russian)* 77−55947
Ti-Nb-Zr (35, 3 wt.%), martensitic τ phase, X-ray diffr. obs. 80−16300
Ti-Nb-Zr-Fe, supercond. and paramag. props., effect of Fe additions *(Russian)* 80−65730
Ti-Nb-Zr-Fe-Mo-V, cold worked, struct. and phase transform. during ageing 78−3153
Ti-Nb-Zr-Ta, superconducting props. comp. depend., stress effects and precipitation behaviour, X-ray scatt. 80−93059
Ti-Nb(40 at.%), regions of maximum stability of β lattice 77−8838
Ti-Zr-Nb-Si, Nb and Si surface alloying effects on wear and corrosion resistance *(Russian)* 77−25191
Ti_3Al-Nb, ordering transform. and mech. props. 78−31402
Ti_3Al-Nb (10 wt.%), dynamic elastic moduli 77−86070
$Ti_{55}Nb_{45}$, supercond., anomalous phonon thermal resist. 77−69451
$Ti_{1-x}Nb_xH_{1.94}$, electronic struct. MNR meas. 80−15439
$Ti_{1-x}Nb_xH_{1.94}$, x=0.25, 0.50, low temp. specific heat meas. 80−2179
$Ti_xZr_{1-x70}Nb_{30}$, ω phase precipitation 79−34042
U-Mo-Nb-Zr-Ti (0.75, 0.75, 0.75, 0.5 wt.%), heat treatment effect on microstruct. and mech. props. 78−23729
U-Nb, absolute thermoelec. power values 77−20303
U-Nb (14 at.%), exam. of shape memory effects 78−76694
U-Nb (14 at.%), martensitic and polymorphic transformations 80−60861
U-Nb (4.5 wt.%), correlation between oxidation and stress corrosion cracking 79−20253
U-Nb and U-Nb-Zr, shear martensitic transform. during quenching, plastic deform. and annealing 77−28815

niobium alloys continued
U-Nb-C system, phase equilibrium exam. *(German)* 78−23670
U-Nb-Zr (16.6, 5.6 wt.%), stability of BCC phase 79−66039
U-Nb-Zr (7.5, 2.5 wt.%), elastically bent, ageing induced shape instability 77−16622
U-Nb(2-3, 4.5, 6.0 and 8.0 wt.%), SCC in air 77−73363
U-$Q^4(Q^5)$, Q^4=quad, Q^5=quint, stress corrosion cracking in moist air, salt water, salted moist air 78−35562
UO_2-(Zr−Nb) system, high-temp. reaction 78−66344
$(V,Nb)_3Ga$, $(V,Nb)_3Ge$ and $(V,Nb)_3Si$ solid solns., supercond. T_c, absolute thermal EMF, microhardness 77−36006
$(V,Nb)_3Si$ type with A15 struct., supercond. transition temp., depend. on stoichiometry *(German)* 77−69444
V-Hf-Nb, multifilamentary, superconducting props. improvement 79−38267
V-Nb, diffusion in H_2 *(Japanese)* 78−10221
V-Nb, effects of heat treatment on mech. props. 77−21176
V-Nb, mech. props., −196-1000°C, comp. depend. 78−39847
V-Nb, supercond. T_c and H_{c2}, effect of purity and alloying with Ta, Cr, Mo or Re 77−85375
V-Nb, vacuum deposited supercond. films, T_c chem. comp. depend. *(Russian)* 78−19174
V-Nb, X-ray K-emission spectra *(Russian)* 77−55851
V-Nb-Mo(Cr), corrosion in liquid Na, O_2 effects 77−8987
V-Nb-Ta, supercond., elec. resist. and electron-phonon interaction parameters 78−14862
V-Nb-Ti-N alloy, dispersion hardened, fracture characts. 79−15794
V-Nb-Ti-N alloy, with dispersed second phase, ductile-brittle transition 80−93653
V-Zr-Nb alloy, rel. between density of states and martensitic and superconducting phase transition temps. 78−10594
VNb-NbO_x-Pb Josephson tunnel junction, compared with VNb-VO_x-Pb 79−87203
$V_{2-x}Nb_3Hf$, NMR of ^{51}V and mag. susceptibility, 20-300K *(Russian)* 80−93192
V_3Si-Nb solid soln., supercond. T_c and paramag. susceptibility *(Russian)* 77−59348
W-C-Nb, vacuum melted, phase composition, struct. and props. 78−31403
W-Nb (0-30 at.%), average thermal expansion coeff., 500-1200K 78−14483
WC-Co-Ta-Ti-Nb, cemented carbide, deformation, high temp., stress relaxation, and strain rate depend. 78−39854
WC-Co-TaC-TiC-NbC cemented carbide, microstructure, high temp. deformation, uniaxial plastic compression 80−40451
WC-NbC-Co, TiC and TiN coating by ion plating, and cutting tests 79−24678
WC-TiC-NbC-Co, CVD and activated reactive evaporation of TiC, AES obs. of substrate-layer interactions 79−24679
Zr,Nb (2.5 wt.%), interaction of hydride, stress, and crack growth at 600K, metallographic obs. 77−12695
Zr-Mo-Nb-V-Sn (1,2,2,2 wt.%), heat treatment, transform. reactions and mech. props. 79−24545
Zr-Nb, (2.5 wt.%), cold-worked pressure tubing for CANDU reactors, slit burst testing 79−26532
Zr-Nb, effect of Nb addition on corrosion resistance of Zr alloys 79−97813
Zr-Nb, fracture resistance, atomic reactor material *(Russian)* 77−25140
Zr-Nb, phase transformation sequences, prediction using free energy composition diagrams 79−4951
Zr-Nb, pressure tube alloy, initiation COD as fracture criterion 78−72862
Zr-Nb, role of oxide plasticity in oxidation behaviour 77−36680
Zr-Nb, singularities of $\beta \rightarrow \omega$ transform. in alloy, with high content of β-stabiliser *(Russian)* 78−76644
Zr-Nb, stacking solitons in ω-phase systems and quasielastic scatt. 79−38822
Zr-Nb, structure associated with BCC to omega transform. *(Russian)* 80−108432
Zr-Nb (0.1, 2.5 wt.%), foil, dislocation loop nucleation and growth during 1 MeV electron irrad. 80−88152
Zr-Nb (1 and 2.5 wt.%), annealed, thermal expansion, α/β transition *(Russian)* 78−26702
Zr-Nb (1 at.%), high-temp. nitriding, chemical and metallographic anal., disintegration test 79−24668
Zr-Nb (1 wt.%), corrosion in water at 285°C 77−56161
Zr-Nb (1 wt.%), static strain ageing between 295 to 773K, TEM obs. of plastic strain 79−38855
Zr-Nb (1 wt.%), stress drop expt. during creep 79−29152
Zr-Nb (1 wt.%), TEM study on intermetallics in Zr alloys 79−11622
Zr-Nb (1 wt.%), tensile props., 295 to 773K 79−8318
Zr-Nb (1 wt.%) exam. of creep behaviour, 373 to 773K 78−80599
Zr-Nb (1 wt.%) high-temp. reaction with UO_2 78−66344
Zr-Nb (20 wt.%), ω-phase form., diffuse Mossbauer scatt. 80−25324
Zr-Nb (20 wt.%) ω-phase transform., structural model, intensity distrib. in neutron diffr. 77−77472
Zr-Nb (20%), low-j_c supercond. vortex pinning *(Russian)* 77−80885
Zr-Nb (2.3 and 5.5wt.%) martensite, precipitation 77−8836
Zr-Nb (2.5 at.%), thermal neutron capture cross-section var. with time, calc. 77−61505
Zr-Nb (2.5 wt.%), annealed, irradiation growth at 353K 79−46710
Zr-Nb (2.5 wt.%), annealed and quenched-and-aged, neutron irradiated, 573 to 923K, damage struct. 79−99247
Zr-Nb (2.5 wt.%), channel tubes, in-reactor creep and irrad. growth 80−93604
Zr-Nb (2.5 wt.%), cold worked, in reactor oxidation of crevices and cracks 78−23865
Zr-Nb (2.5 wt.%), cold worked, press. tubes, secondary cracking obs. 78−80630
Zr-Nb (2.5 wt.%), cold-worked, pressure tubing, metallography and mech. props. 80−89269
Zr-Nb (2.5 wt.%), crack resistance, influence of ZrH_x fracture toughness 80−16444
Zr-Nb (2.5 wt.%), effect of irradiation on stability of precipitates 77−69007
Zr-Nb (2.5 wt.%), effect of pre-irradiation on oxidation 78−88580
Zr-Nb (2.5 wt.%), fractographic aspects of H_2 induced delayed cracking 79−47767
Zr-Nb (2.5 wt.%), fuel cladding, anisotropy after creep and irradiaton 78−7001

niobium alloys continued
Zr-Nb (2.5 wt.%), H_2 induced subcritical crack growth meas., application of potential drop method 78−27645
Zr-Nb (2.5 wt.%), heat treatment effects on slow crack growth, cold working effects 77−28836
Zr-Nb (2.5 wt.%), high temp. oxidation in flowing O_2, 873-1173K 80−93687
Zr-Nb (2.5 wt.%), hydride forming materials, H_2 induced delayed cracking 78−27623
Zr-Nb (2.5 wt.%), hydride TEM obs. in pressure tubing 79−8338
Zr-Nb (2.5 wt.%), hydride induced crack growth, effect of stress, temp. and H_2 content 80−3178
Zr-Nb (2.5 wt.%), hydride precipitation and growth at crack tips, electron optical obs. 80−108449
Zr-Nb (2.5 wt.%), meas. of crack growth at elevated temp. by holographic interferometry 79−38933
Zr-Nb (2.5 wt.%), memory effect in hydride precipitation 78−11227
Zr-Nb (2.5 wt.%), neutron irrad. at 573 to 923K, damage struct. 80−107334
Zr-Nb (2.5 wt.%), nuclear fuel channels, neutron effects on ultimate fracture strength, 293 to 573K 80−85054
Zr-Nb (2.5 wt.%), oxidation kinetics appl. to loss of coolant accidents, data review 78−19958
Zr-Nb (2.5 wt.%), pressure tubes, irrad. creep and growth, anisotropy factors 80−97536
Zr-Nb (2.5 wt.%), seam welding tubing, microstruct. in weld region 79−61621
Zr-Nb (2.5 wt.%), strain ageing 77−77511
Zr-Nb (2.5 wt.%), superplasticity 77−12669
Zr-Nb (2.5 wt.%), superplastic and strain rate depend. plastic flow, 873 to 1373K 80−30052
Zr-Nb (2.5 wt.%), tensile specimen, stress corrosion cracking by stray contamination 77−70215
Zr-Nb (2.5 wt.%), transforms. during annealing of welded joint, after thermal cycling *(Russian)* 80−29984
Zr-Nb (2.5 wt.%) alloys, microstruct investigation by electron microscopy using oxide films 79−70243
Zr-Nb (2.5 wt.%) neutron effects on oxidation kinetics 78−690
Zr-Nb (2.5 wt.%) pipe, fracture resistance, hydrogenation effect 80−104279
Zr-Nb (2.5 wt.%) pressure type rel. between stess intensity factor, crack opening displacement and J-integral 80−100920
Zr-Nb (97.5, 2.5 wt.%) nuclear reactor pressure tube material, H embrittlement study by TEM 80−76363
Zr-Nb alloy, direct imaging of point defects using TEM 77−35453
Zr-Nb alloy, isothermal decomposition at elevated temp. 78−27470
Zr-Nb microduplex alloys, struct. and props. 78−3170
Zr-Nb pressure tubes of PWR reactor, cracks identification and avoidance 78−82472
Zr-Nb solid solutions, BCC, direct imaging of linear defect using diffuse scatt. 78−22726
Zr-Nb-Fe (13 wt.%, 5 wt.%), struct. changes during decay of BCC β solid solution 79−15669
Zr-Nb-Fe(Mo) alloys, decomp. of β solid soln., metastable and equilib. phases 79−11632
Zr-Nb-Ga, phase equilibria 800°C *(Ukrainian)* 80−35157
Zr-Nb-Ge, singularities of $\beta \rightarrow \omega$ transform. in alloy, with high content of β-stabiliser *(Russian)* 78−76644
Zr-Nb-H_2, exam. of phase diagram, using modified format 79−8280
Zr-Nb-Mo, phonon spectra anomalies, lattice dynamics calculations, superconductivity parameters 79−7655
Zr-Nb-Mo-Re, alloying effect on dislocation core struct., determ. by discrete lattice modelling 78−30618
Zr-Nb-Sn (3,1 wt.%), corrosion resist. depend. on mech. and heat treatments 80−653
Zr-Nb-Sn (3.0, 1.0 wt.%), high temp. oxidation in flowing O_2, 873-1173K 80−93687
Zr-Nb-Sn(3 wt.%, 1 wt.%), oxidation kinetics in flowing CO_2 at high temp. 80−47575
Zr-Nb-V-Fe (12 wt.%, 6 wt.%, 4 wt.%), struct. changer during decay of BCC β solid soln. 79−15669
Zr-Nb-V-Si superconductor, struct. determ. by optical microscopy and electron diffraction *(Russian)* 77−16628
β-Zr-Nb(Cb) alloys, anneal hardening and flow softening 79−78993
Zr-Nb(2.5 wt.%), oxidation kinetics in flowing CO_2 at high temp. 80−47575
Zr-Nb(2.5 wt.%), tensile props., strain rate and temp. effects 77−73307
Zr-Sn-Mo-Nb, creep and creep fracture, 623 to 823K *(Czech)* 77−59916
Zr-Sn-Mo-Nb, fracture in creep 77−36581
Zr-Sn-Mo-Nb, steady state creep 77−36580
Zr-Sn-Mo-Nb (3,1,1, wt.%), creep and creep fract. at 623 to 823K *(Czechoslovakian)* 77−32643
ZrB_2-Nb, reactions between components 80−100812
ZrC-NbC-MoC_{1-x} alloys, physicomech. props., comp. depend. 79−66097
ZrNb, ω-phase, diffuse neutron scatt. meas. 78−14311
ZrNb, pressure tube, fragmentation on failure 78−72863
ZrNb, supercond. thermal cond. meas. 79−60970
$(Zr_{1-x}Nb_x)Fe_2$, antiferromag. spin struct., Mossbauer effect study 80−66086
$(Zr_{1-x}Nb_x)Fe_2$, magnetovolume effects and Invar characters 80−15773
$Zr_{1-x}Nb_xZn_2$, microscopic mag. props., NMR investigation 80−15807

niobium compounds
see also niobium alloys
anodised layer, structure and stoichiometry, thickness effects 77−77634
borides, chemical vapour deposition *(French)* 77−36406
carbide interstitial phases, elec. and mag. props., neutron radiation effects 79−77640
carbides, diffuse, production and superconductive props. *(Bulgarian)* 80−80467
carbides, nonstoichiometric, elastic props., 20-2000°C 77−12661
chalcogenides, layered, soln. mechanism of metals 79−42249
chalcogenides and chalcogenide halides, geometrical struct. and metal-metal bonding 80−80172
complex, $NbOCl_3.2L$ (L=Ph_2SO, Ph_3PO and $(Me_2N)_3PO$), prep. and characterisation 78−30592
KKR calc. of energy bands 80−34355
minerals, cryst. struct., X-ray powder diffr. study 80−107169
mixed oxides, cryst. struct., electron microscopy study 78−91310

niobium compounds continued
niobate based ceramics, synthesis, struct., elec. cond., mag. props. *(Czech)* 80−45259
niobate flux growth, MNb_2O_6, M=Ni, Co, Mn,Fe 77−21015
nitrides, diffuse, production and superconductive props. *(Bulgarian)* 80−80467
oxides, XPS study, electron binding energies, spin orbit splittings, exchange splittings 79−78839
oxides formed on metal at high temp. and low O_2 pressure, ESCA study *(French)* 77−25179
PbO-Nb_2O_5 system, X-ray and electron microscopic phase and struct. determ. *(French)* 80−92508
pyrochlore, high temperature chlorination 78−11180
rare earth oxide (R_2O_3)-Nb_2O_5 glassy systems 78−52856
refractory carbides, borides and nitrides, wetting by and interactions with liq. metals 80−54473
strength of nonlinear interaction between collinear surface acoustic waves 80−33295
synthesis, structs. *(French)* 78−51519
tungsten bronze, tetragonal, type structure cpds, transition sequences *(French)* 77−89538
X-ray Lβ_2 emission bands of pure Nb and metal-like compounds, room and liquid N temps. 77−28654
$Ag_2Nb_2O_5F_2$, cryst. struct. determ. from single cryst. diffr. data *(French)* 78−95030
$Al_2Nb_2O_7$, new phase of mixed oxide 78−59787
Al_2O_3-Nb, dielectric cermet, thermophysical props. 77−51557
Al_2O_3-Nb_2O_5-NiO, isothermal phase sections, 1100, 1250, 1400°C *(Italian)* 79−20032
B_2O_3-Nb_2O_5 complexes, phase equilib. high resolution TEM obs. 78−35378
B_2O_3-Nb_2O_5 system, phase equil. and phase struct. obs. by high resolution TEM 80−108419
$Ba_4NbRu_3O_{12}$ $(Ru_3O_{12})^{13-}$ cluster obs. in presence of orbital degeneracy and spin-orbit coupling *(French)* 80−70655
$Ba_3Nb_6Si_4O_{26}$, IR spectra and cryst. struct. *(French)* 79−11418
$Ba_3(Nb_4Ti_4)O_{21}$, effects of Sb substit., synthesis and cryst. chemistry 77−76379
Bi-NbO_2-Bi system, Schottky barrier effects in transport and dielec. props. 80−29486
Bi_2O_3-Nb_2O_5, sintered, high oxide ion cond. meas. 78−14503
Bi_2O_3-TiO_2-Nb_2O_3, subsolidus phase equilibria 77−55954
$Cd_2Nb_{2-2x}Sn_{2x}O_{7-2x}F_x$, solid soln., X-ray diffr. and Mossbauer study *(French)* 78−87659
$CeNbO_{4+x}$, oxidation-reduction reactions 78−39930
CeO_2:Nb_2O_5, sintered, elec. cond. and solid solubility, 800 to 1329°C 79−99546
$CoNb_2O_6$, magnetic struct., neutron diffr. and mag. susceptibility meas. 80−15693
$Co_{0.32}NbS_2$, intercalation compound, struct. and photoemission meas. 77−16453
$Co_{1/3}NbS_2$, intercalate, metallic cond., Hall effect and mag. props. 77−76789
Cr-Ti/MgO-NbC dispersion-strengthened, high temp. wear and oxidation resist. 80−25877
Cr-Ti/NbC dispersion-strengthened, high temp. wear and oxidation resist. 80−25877
$Cr_{8-x}Nb_{3+x}Si_8$, cryst. struct. *(French)* 78−38675
Cu-NbTi, composite conductor, acoustic emission 80−97032
Cu_xNbS_2, $0.8<x<1$, order-disorder transitions and incommensurate superstruct. 77−15587
CuO-Nb_2O_5, phase anal., density determ. 78−10015
Cu_2O-Nb_2O_5, phase anal., density determ. 78−10015
Fe-NbC, dispersion strengthened, thick vacuum condensate, control of struct. and mech. props. 80−16324
Fe-NbC condensate, struct. and mech. props., disperse particle content depend. *(Russian)* 78−19772
$Fe_{0.33}NbS_2$, intercalation compound, struct. and photoemission meas. 77−16453
$Fe_{0.33}NbS_2$, lattice dynamics and hyperfine interactions, Mossbauer spectra study 80−108135
$Fe_{1/3}NbS_2$, intercalate, metallic cond., Hall effect and mag. props. 77−76789
Fe_xNbS_2, ordering of Fe atoms 78−38650
Fe_xNbSe_2 (2H), mag. susceptibility meas., 1.3-300K 80−39740
Fe_xNbSe_2, transport props. and mag. ordering 80−65527
$Fe_xNb_xV_{2-2x}O_4$, complex solid solns., synthesis and phase diagram, semicond.-metal transition temp. 79−43214
$Fe_xNb_xV_{2-2x}O_4$, NMR analysis of semiconductor transitions 78−52367
$Ga_2Nb_2O_7$, and $Ga_2Nb_2O_{7.25}$, new phase of mixed oxide 78−59787
H_xNbS_2, struct., form. by cathodic reduction, neutron diffr. obs. 79−73150
$HbSe_2$:Mn layered superconductor, crit. temp. and fields 77−51836
$KNbO_3$, complex electronic dielectric const. from tight binding energy bands 78−60054
$K_{10}(Nb_8O_{21})_2.Nb_6X_4O_{26}$, X=Si, Ge, cryst. struct. *(French)* 77−76378
K_2O-Al_2O_3-P_2O_5-Nb_2O_5 glasses, struct. singularities, IR spectra *(Russian)* 78−2861
K_2O-Al_2O_3-P_2O_5-Nb_2O_5 glasses, struct. role of Nb 78−67653
K_2O-SrO-Nb_2O_5 system, selective delineation of dislocations by etching 77−72617
$KTa_{1-y}Nb_yO_3$, quantum ferroelec., elastic compliance, impurity effects 79−99835
$LiBa_3Nb_3Ti_5O_{21}$, insertion of Li, X-ray and neutron diffr. study *(French)* 78−91324
Y-Z $LiNbO_3$, acoustic effects of filamentary defects 80−75314
Y-Z $LiNbO_3$, filamentary defects visualisation at wafer inspection stage 80−75315
Y-Z $LiNbO_3$, radiation patterns of bulk acoustic modes from finite interdigital transducer 80−43491
$LiNbO_3$, SAW reflection from conducting strips 80−5853
$LiNbO_3$, temp. coeff. of freq. determ. 80−75316
$LiNbO_3$:3$Li_2O.Nb_2O_5$ eutectic, dielectric props. 79−1743
$Li_x(NbO)_4Nb_{30}O_{90}$, struct. and ionic cond. 79−65246
$Li_x(WO)_4W_{30}O_{90}$, struct. and ionic cond. 79−65246
$Mn_{0.25}NbS_2$, mag. anomaly rel. to struct. disordering 78−43557
$Mn_{0.26}NbS_2$, intercalation compound, struct. and photoemission meas. 77−16453
$Mn_{1/3}NbS_2$, intercalate, metallic cond., Hall effect and mag. props. 77−76789

niobium compounds continued
$(Na,Li)NbO_3$ ceramic, optimum prep. conditions and characterisation 78−3079
$NaNbTiO_5$, high temp. chlorination kinetics 79−61765
Na_2O-SrO-Nb_2O_5 system, solid state equil., 800°C *(Italian)* 77−47549
$NaYb(WO_4)_2$, thermal expansion, X-ray determ. 80−39323
(Nb,Ta)As, X-ray cryst. struct. determ. 79−69078
$(Nb,Ta)_8N_9$, cryst. struct. determ. *(German)* 80−107145
$(Nb,Ti)N_x$, metastable supercond. phase, effects of rapid quenching on transition temp. 78−2611
Nb anodic oxide films, reversible optical changes 78−35580
Nb complex, $NH_4[NbO(C_2O_4)_2(H_2O)_2].3H_2O$, cryst. struct., neutron diffr. obs. 77−24306
Nb complex, $NbCl_5$ complex with O- and S-containing ligands, prep., and characterisation 79−14729
Nb complex, prep. by halide reaction with tetramethylurea and tetramethylthiourea, and characterisation 79−15972
Nb complexes, ^{93}Nb quadrupole coupling tensors form EPR meas. 80−88866
Nb-C-N-O-H, solid solns. of H, exam. of props. 80−29172
Nb-D-H, equilib. H/D separation factors 80−59668
Nb-H, behaviour of H in Nb, relation to mech. props. 78−80572
Nb-H, electron work function, 300 to 600 degrees C, contact potential difference meas. 80−29462
Nb-H, exam. of electron structure 80−29306
Nb-H system, NMR evidence for low temp. pseudo-cubic phase 78−80526
Nb-H system, temp.-stimulated acoustic emission, hydride precip. 80−3044
Nb-H(D), H ordering, review 80−60850
Nb-H(D) system, single cryst. prep. and characterisation 79−95910
δ-Nb-N, plates and powder, oxidation *(French)* 79−66184
Nb-N, superconducting layers, sputtering in high vacuum apparatus *(German)* 80−89147
Nb-N system, disordered, hopping cond., expt. evidence for electron correl. effects, low temp. 78−14729
Nb-N_x, disordered thin films, thermometrical props., appl. as temp. sensors *(French)* 79−65558
Nb-N(-H) system, electrophys. props. of nitrides and hydronitrides 77−85215
Nb-Nb_2O_5-Pb Josephson junction formed on Nb film edge 80−107960
Nb-Nb_2O_5-Pb(In) Josephson junctions, props. of Nb_2O_5 thermally grown tunnel barriers 80−100568
Nb-Nb_xO_y-Pb, tunnelling junction, current-voltage characts., knee struct. 79−38261
Nb-Nb_xO_y-Pb, two-dimens. Josephson junction, supercurrent vs. mag. field characts. 80−34562
Nb-Nb_xO_y-Pb Josephson junction current-biased on Fiske steps, mag. field depend. 80−84567
Nb-Nb_xO_y-Pb(In) Josephson junctions, preparation and props. *(Russian)* 79−91188
Nb-Nb_xOy-Cu/Pb supercond. proximity junction, max. DC Josephson current, thickness depend. 79−82719
Nb-NbO system, single- and two-phase, sputtering yield, SEM and scanning Auger microprobe obs. 79−87545
Nb-NbO_x-Al/Pb supercond. proximity function, production by RF sputtering and photolytographic techniques 77−43787
Nb-NbO_x-Pb, miniature tunnel junction, gap voltage determ. 79−7939
Nb-NbO_x-Pb Josephson junctions with high current densities, critical current 80−100552
Nb-NbO_x-Pb Josephson tunnel junctions, fabrication using FR glow discharge oxidation 80−34559
Nb-NbO_x-Pb junction, static charact. of tunnelling cryotrons 79−28480
Nb-NbO_x-Pb superconductive tunnel junctions, oxide tunnelling barriers, ESCA characterisation 80−65745
Nb-NbO_x-Pb tunnel junction, crit. Josephson currents, temp. depend. 78−2629
Nb-NbO_x-Pb tunnel junctions with high normal resists.,, crit. currents 79−56399
Nb-NbO_x-Pb tunnel junction, temp. depend. of effective Nb energy gap 80−80454
Nb-NbO_x-PbIn tunnel junctions with ultra-thin Nb electrodes 79−56398
Nb-NbO_x-PbIn window type junctions, critical Josephson current depend. on magnetic field 79−65607
Nb-NbO_xPb tunnel junctions, current density distrib. 80−39717
Nb-O, effect of neutron irradiation damage on low temp. deformation characts. TEM study 79−42117
Nb-O solid solution, interaction with O_2 at low press., segregation equilib. and chemisorpt. *(French)* 77−24483
Nb-O solid solutions, desorpt. of oxides *(French)* 78−14610
Nb-O(N), dislocation pinning, impurity interactions, strengthening *(Russian)* 80−92532
Nb-S system, phase relations at high temp., elec. and mag. props. 80−29932
Nb-Ta-N sputtered films and their anodic oxides, elec. props. of resist. and dielec. films 80−11126
Nb-Ti-O, phase equilibria 80−96624
Nb-V-Mo-Au, gaseous AuV obs. and dissoc. energy by high-temp. mass spectrometry 79−45860
Nb_3As, electronic and supercond. props. 77−16011
$Nb_5(B,Si)_3$, stability of heatproof coating 77−86201
NbB_2, hot pressing 80−25635
NbB_2, single crysts., hardness anisotropy and slip 80−21085
NbB_2, superconductivity below 1K 80−20342
NbB_2, vapour transport in temp. gradient in presence of iodine 79−19997
NbC, abrasive action, X-ray investig. 77−52497
NbC, additions to sintered high-speed steel, effect on hardness and cutting performance 77−66608
NbC, adsorption, of Cs(K), adsorpt. energy. thermionic emission 77−7978
NbC, band struct. and X-ray emission spectra, APW and Xα calc. 80−70605
NbC, bond energy and ionization efficiencies from SIMS 79−24400
NbC, C implanted, channelling crit. angle and min. yields 78−47458
NbC, chemical bonding and X-ray emission spectral analysis 77−44088
NbC coated emitters, thermionic emission props. *(Japanese)* 77−40322
NbC coating, vapour deposition, phys. and chem. props. 77−40456
NbC coating on C steel and Armco Fe, deposition, struct. and props. 79−52462
NbC crystals, electron energy spectra 80−49568

niobium compounds continued
NbC, deformation behaviour during rubbing in wide temp. range 80−16486
NbC, deposition with vapour-gas phase circulation in closed circuit 77−55927
NbC, determ. in cementite by annealing in moist H_2 *(German)* 79 39231
NbC dispersion strengthened Fe condensates, struct., mech. props. 77−90361
NbC, elastic modulus, porosity factor 77−21207
NbC, electronic struct. of vacancies, effect on supercond. transition temp. 80−29347
NbC electronic structures calc. and obs., by APW method and X-ray photoelectron spectroscopy *(Japanese)* 79−15074
NbC, electronic structure, PES study 80−70594
NbC, electronically driven lattice instabilities, role of p-d hybridisation 78−63835
NbC, etchant for revealing microstructure 80−85097
NbC, exam. of temp., and composition effects, on diffusion coeff. in its homogeneity range 79−33115
NbC, generalised susceptibilities and electronically driven phonon anomalies 79−42208
NbC, high temp. supercond., role of electronic struct. on obs. phonon anomalies 77−24363
NbC, high-temp. plastic deform. effects on elec. props. 77−44370
NbC, microhardness and charact. hardness 79−52376
NbC, micropowder, abrasive props. 77−63821
NbC micropowder surface finishing of metals, surface struct. 80−11842
NbC micropowders, abrasive lapping of refractory metals 77−44391
NbC, NbC-ArC, right-through sat. prep., strength and plasticity, temp. depend. 77−40432
NbC, nonstoichiometric, simple shell model for phonon dispersion 77−24370
NbC, nonstoichiometric, simple model for phonon dispersion, rel. to C vacancies 78−30718
NbC particles, growth and dissolution, in aged and deformed austenitic stainless steel 78−39782
NbC, phonon anomalies rel. to superconductivity 77−12055
NbC, phonon anomaly rel. to Fermi surface 77−11853
NbC, phonon dispersion relations, modified 3-body force shell model 77−55332
NbC, physicomechanical props. within the homogeneity range 77−1848
NbC, prep. by impregnation, strength, surface submicrocracks 77−16661
NbC, pressing regime influence on high-temp. creep *(Russian)* 80−100852
NbC, recrystallisation 78−11251
NbC, refractory micropowder, geometric parameters of grains 77−16529
NbC, rock salt struct., surface energy bands, Shockley surface states, bonding 80−92956
NbC, self consistent APW-Xα calc., electronic struct. 77−20237
NbC single cryst., Vickers microhardness, slip mechanism 80−71732
NbC single crystals, synthesis and impurities 80−55329
NbC, solid-phase reacts., effect of nonstoichiometry, thermodynamic evaluation 78−60632
NbC, supercond., phonon anomalies, microscopic theory 78−14867
NbC, supercond. critical temp., neutron irrad. effect 80−80433
NbC, supercond. transition temp. and lattice dynamics 79−56361
NbC, superconductor, appl. of non-local extension to Gaspari-Gyorffy theory 78−80093
NbC, thermal stress cracking, neutron radiation effects 79−77641
NbC, true heat capacity meas. by pulse method 80−19953
NbC, ultrafine powders and sintered compacts, prep. and supercond. props. 77−40015
NbC, vacuum condensate, struct. and mech. props., second phase effect *(Russian)* 80−71705
NbC, valence band struct. *(Russian)* 78−6268
NbC, valence band XPS meas., comparison with X-ray emission spectra and band struct. spectral calcs. 80−50535
NbC weak link SQUID 79−38258
NbC, X-ray emission band exam. and electronic struct. 77−8689
NbC, X-ray emission spectra, interpretation in terms of relativistic elec. dipole transition probabilities 79−3459
NbC-NbB_2, phase relns. 78−23677
NbC-VC, phase diag. calc. 77−90329
$NbC_{0.86}$, single crystal work function, thermionic emission and contact pot., microhardness and binding 79−19649
$NbC_{0.89}$, implantation or diffusion of C rel. to supercond. transition temp. 77−69442
$NbC_{0.98}$, single crysts., creep, 1800-2700°C *(Russian)* 79−5005
NbC_x (x=0.868, 0.834, 0.766), single crysts., thermomech. behaviour during annealing 80−3104
NbC_x, complex phases with NaCl struct., microhardness rel. to electronic structure 77−90438
NbC_x, creep-comp. curves for homogeneous region 78−52911
NbC_x, monocrystal, work function anisotropy of electrons *(Russian)* 79−73568
NbC_x, phonon density of states and dispersion relations 79−42173
NbC_x powders, nonstoichiometric, sintering kinetics 79−100099
NbC_x, reactor irrad. effects on elec. resist. and supercond. props. *(Russian)* 78−47895
NbC_x, self diffusion, near surface effect 79−42303
NbC_x, static distortions and Debye temp. determ., neutron diffr. exam. *(Russian)* 77−80482
NbC_x, stoichiometric and defective phases, electronic energy spectrum and physical props. *(Russian)* 77−35868
NbC_x, supercond. transition temp., light element implantation effect 80−107951
NbC_x, thermophys. props. 77−89600
NbC_x, thermophysical props. at high temp., thermal vacancies form. 78−43141
NbC_x, x=0.868, 0.834, 0.766, self-diffusion of ^{14}C 80−29206
NbC_x+Be→Be_2C layer, limiting stage investig. 77−36786
Nb_xC powders, plastic deform. characts. on vibratory milling 78−11183
NbC(N), critical temp. enhancement, surface effect on phonon spectrum and electronic state density *(Chinese)* 80−2507
NbCN, preparation methods and supercond. properties *(French)* 79−73618
Nb(CN), supercond. critical temp., neutron irrad. effect 80−80433
NbCN superconducting films, high field critical current densities and resistive transition 79−61018

niobium compounds continued
NbC_xN_{1-x}, obs. of phonon anomalies, sp. ht. meas. and supercond. transition temp., 1.5-90K 77−39985
NbC_xN_{1-x}, s.p. ht., 4.2-100K, phonon anomaly rel. to supercond. transition 78−14880
NbC_xO_y, x+y=0.73 to 0.88, thermal expansion coefficients 80−103502
$Nb_xC_yO_z$, H solubility 80−34191
$NbCl_4$, high press. elec. resistivity 80−29404
$NbCl_5$, anomalies of ^{93}Nb and ^{35}Cl NQR, 4.2-480K 79−99789
$NbCl_5$ in chloroaluminate melts, Raman spectral study 80−34915
$NbCl_5$, mol. struct., vibr. assignments, barries to pseudorotation 78−29858
$NbCl_5$, nuclear electric hexadecapole interactions of ^{93}Nb 79−1722
$NbCl_5$, nuclear electric hexadecapole interactions 80−65513
$NbCl_5$, photoelectron spectra 79−821
$Nb_2Cl_9^{3-}$, electronic struct. and metal-metal bonding, HMO calcs. *(Russian)* 78−1118
$(NbCl_nBr_{6-n})^-$, ^{93}Nb nucl. spin relax. and mag. shielding 78−58723
$(NbCl_nBr_{6-n})^-$ complexes in acetonitrile soln., ^{93}Nb spin relax. and mag. shielding 80−44944
$NbCl_5OPCl_3$, vibr. amplitude and normal coord. anal. *(German)* 78−66536
$NbCl_5.CD_3CN$, Raman spectra and Teller-Redlich product rule 79−69817
$NbCl_5.CH_3CN$, Raman spectra and Teller-Redlich product rule 79−69817
$NbCl_5.POCl_3$, Raman spectra, normal coordinate treatment 77−46568
NbCn, superconducting film, high field critical current densities and resistive transition 79−73648
$Nb_xCr_{1-x}O_2$, (x≥0.5), cryst. growth by chem. transport and phase transitions 78−35281
$Nb_xCr_{1-x}O_2$, cryst. prep. and struct., mag. props. 78−52198
NbD, orthorhombic β phase, ^{93}Nb Knight shift and quadrupole coupling parameters 78−19352
NbD, structs. phase diagrams, morphologies, prep. methods, book contrib. 80−25675
β-$NbD_{0.75}$, phonon dispersion curves 78−67792
$NbD_{0.85}$, localised D vibrs., temp. depend., neutron inelastic scatt. study 80−107395
$NbD_{0.85}$, phonon dispersion of α′ and β phases, neutron scatt. 78−91398
α-NbD_x, under hydrostatic press., γ ray diffr., Bragg refls. 78−75726
NbD_x, x=0.55 to 0.88, deuteron and ^{93}Nb mag. resonance, β-α transitions 77−20721
NbF_5, nuclear electric hexadecapole interactions of ^{93}Nb 79−1722
$(NbF_5)_4$ mass spectra, vel. distrib. effects, mol. beam inlet method, mol. dissoc. 77−54627
$NbGa_2O_x$, O stabilised cpd., struct. determ. 80−103301
Nb_3Ge, projected critical current, comparison with $PbMo_6S_8$ 79−69642
Nb_3Ge, superconducting transition temp. 78−47898
NbH, internal friction 78−6962
NbH, orthorhombic β phase, ^{93}Nb Knight shift and quadrupole coupling parameters 78−19352
NbH solid solutions, H impurity screening, lattice deformation, dipole force tensor component calcs. 79−77611
NbH, structs. phase diagrams, morphologies, prep. methods, book contrib. 80−25675
$NbH_{0.02}$, diffusion of H, neutron scatt. study 79−60550
$NbH_{0.11}$, incoherent struct. factor of H, neutron scatt. exam., quasielastic energy spectrum 79−99186
$NbH_{0.15}$, dispersion step in $[\zeta\zeta 0]T_1A$ branch at ζ=0.03, neutron scatt. study 79−60453
$NbH_{0.3}$, α-α′ phase transition, sp. ht. anomaly 78−39764
$NbH_{0.73}$, multiple wavelength neutron powder diffr. data, Rietveld profile refinement algorithm 80−24320
$NbH_{0.76}$, Compton profile anisotropy, electronic struct. 77−73182
$NbH_{0.82}$, localised H vibrs., temp. depend., neutron inelastic scatt. study 80−107395
$NbH_{0.82}$, phonon dispersion of α′ and β phases, neutron scatt. 78−91398
NbH_x, diffusion of H atoms, quasielastic neutron scatt. obs., book contrib. 79−82383
NbH_x, HF phonons, neutron spectral obs. 80−49317
NbH_x, structural transform. rel. to order-disorder transform. 80−60858
$NbH_x(D_x)$, acoustic and optic phonons, neutron diffr. obs., book contrib. 79−82296
$NbH_x(D_x)$, cryst. struct., phase diagrams, order-disorder transition 78−55836
NbI_4, metallic state, resistivity anomaly 79−15136
NbI_4, NbI_5, Nb_3I_8, elec. cond., temp. and press. depend. 79−60830
NbI_4, quasi-one dimens., press.-induced metal-insulator transition 78−43447
$Nb_zM_{11-z}Ge_8$, M=V, Cr, Mn, cryst. struct. *(French)* 78−38675
$Nb_xMo_6S_8$ Chevrel phase, synthesis, stability and charact. 80−71608
NbN, 2-dimens. supercond. phase transition, universal current scaling in crit. region 79−28429
NbN, band structure, nonorthogonality and tight-binding fit 80−59852
NbN, chemical bonding and X-ray emission spectral analysis 77−44088
NbN, critical data, under hydrostatic pressure to 15 kbar 79−47217
NbN diffusion wires, crit. currents and supercond. crit. field under high press. 79−38287
NbN embedded in resin, composite supercond., high transition temp. 80−88660
NbN film, supercond., upper crit. field 78−64172
NbN film, ultrathin granular, zero dimensionality and Josephson coupling 78−10612
NbN, for supercond. microwave cavities, secondary electron emission and AES meas. 79−56895
NbN granular films, crit. current behaviour 80−15672
NbN granular films, supercond., crit. props. 80−88661
NbN granular microbridges, Josephson effects 80−84556
NbN, granular superconductor, simple model for resistive-nonresistive transition 78−72298
NbN, granular thin film, phase transition between incoherent and coherent supercond. states 79−56394
NbN, granulated film, critical current temp. depend. *(Russian)* 80−103803
NbN, γ- and δ-forms, cryst. growth and supercond. transition temp. 80−107946
NbN, interatomic interactions from XPS 80−49171
NbN, opt. consts. and physicochem. spectra 77−85677
NbN, optical props. and charact. electron energy loss spectra 79−52056
δ-NbN, phonon dispersion curves, anomalies 79−99284
NbN preparation, by precip. from gaseous NgF_5-N_2-H_2 mixture 80−20857
NbN, Raman spectra and superconductivity of various phases 78−68506
NbN, self consistent APW-Xα calc., electronic struct. 77−20237
γ-NbN, single crystal growth by annealing, NbN in nitrogen gas pressure 79−8246
NbN single crystal preparation, zone melting and nitriding techniques 80−60776
NbN, supercond. granular films as weak link in Josephson devices 80−88685
NbN, supercond. props., SQUID behaviour 78−72311
NbN, supercond. RF reactively sputtered films, deposition parameter effects on props. 80−80972
NbN, supercond. transition temp. and lattice dynamics 79−56361
NbN superconducting reactively sputtered film, Auger anal. 78−72297
NbN, ultrafine powders and sintered compacts, prep. and supercond. props. 77−40015
NbN weak links, granular, Josephson behaviour 80−75681
NbN, X-ray emission band exam. and electronic struct. 77−8689
NbN-NbN point-contact Josephson junction, fabrication and charact. 78−19189
NbN-V_3Ga point-contact Josephson junction, fabrication and charact. 78−19189
NbN_x, phonon density of states and dispersion relations 79−42173
NbN_x, solid soln, strain ageing, internal friction, elec. cond. kinetics *(Russian)* 78−76667
Nb_2N, supercond. props. and structural phase transform. induced by C^+ and N^+ implantation 80−107942
$NbN_{0.7}C_{0.3}$, cryst. growth and supercond. transition temp. 80−107946
NbN_xHy, diffusion of H, PMR obs. 79−69287
NbN_xO_y, solid soln, strain ageing, internal friction, elec. cond. kinetics *(Russian)* 78−76667
NbO and NbO_2, H solubility 80−34191
NbO binding energies, and surface layer identification following ion bombardment *(French)* 77−44541
NbO chemical bonding and X-ray emission spectral analysis 77−44088
NbO, cryst. growth and microstructure 79−95913
NbO, electronic struct. from photoelec.- and X-ray emission spectra and X_α calcs. of NbO_6^{-10} cluster 79−23892
NbO, high press. elec. resistivity, semiconductor to semiconductor transition 80−29404
NbO, ion channelling, 1 MeV deuterons 79−60416
NbO, ion channelling, neutron and deuteron radiation damage 79−65131
NbO, photoemission and X-ray emission spectra 78−64442
NbO, single cryst. growth by chem. transport reactions 77−12508
NbO, single cryst. with 25% vacancies, neutron damage 77−15459
$4NbO_{0.76}$ thin film, FCC cell struct. investigation 80−92796
NbO_2, binding energies and surface layer identification following ion bombardment *(French)* 77−44541
NbO_2, chemical transport with $TeCl_4$, exam. of deposition and crystal morphology 79−52093
NbO_2, continuous coating crystallite, electrocrystallisation from molten fluorides containing oxide contamination 79−24423
NbO_2, cryst. growth and microstructure 79−95913
NbO_2, electronic band struct., optical props., generalised susceptibility, struct. transition 79−95328
NbO_2, high press. elec. resistivity, phase transition 80−29404
NbO_2, high-speed high-current field switching 77−80816
NbO_2 hollow needles, electrocrystallisation from molten fluorides containing oxide contamination 79−24423
NbO_2, IR dispersion 79−65854
NbO_2, Lifshitz point behaviour 80−70402
NbO_2, low temp. elastic consts. and Debye temp. 78−47463
NbO_2, low temp. sp. ht. and Debye temp., role of phonon-like CDW excitations 77−80632
NbO_2, on-state decay rel. to recomb. and nonlinear props. 80−84492
NbO_2, photoelectron spectra, X-ray and UV polycrystalline 79−28889
NbO_2, rutile phase, energy levels, momentum density, and Compton profile, embedded cluster model 80−50453
NbO_2, semicond., thermal expansivity 80−34213
NbO_2, semicond. cryst., elastic props. 79−19308
NbO_2, semiconducting, elastic const., press. depend. at 296K 79−23672
NbO_2, slightly substoichiometric, microstructure 77−47584
NbO_2, structural fluctuations at high temps., inelastic neutron scatt. 78−55947
NbO_2, structural phase transform., neutron scatt. obs. 78−14458
NbO_2, sustaining and decaying of the high conductance on state 79−95454
NbO_2, threshold switching recovery curve, distribution trapped carrier lifetime 80−20258
NbO_2, vapour phase molecular struct., high temp. electron diffr. 79−68330
NbO_2-Na_2O-SiO_2, amorphous films, characteristics of monostable switching 77−80817
$NbO_{2.417}$, chemical transport with $TeCl_4$, exam. of deposition and crystal morphology 79−52093
$NbO_{2.417}$ to $NbO_{2.5}$, equilib., chem. transport with $TeCl_4$ 80−2934
NbO_4^{3-}, normal vibr. freqs., force consts. calc. *(Russian)* 77−6759
NbO_x, AES depth profile meas., prep. of supercond. cavities from Nb 77−8984
NbO_x, interstitial O, diffuse neutron scatt. 78−83809
NbO_x, phase comp. on heating 2000-4000K 80−21267
NbO_x, solid soln, strain ageing, internal friction, elec. cond. kinetics *(Russian)* 78−76667
$Nb_{10}O_{28}^{6-}$, mol. config. from cryst. structs. 77−71886
$Nb_{12}O_{29}$, cryst. growth and microstructure 79−95913
$Nb_{12}O_{29}$, high resolution lattice image, by HV electron microscope 77−15292
$Nb_{12}O_{29}$-Nb_2O_5, oxide defect structures of stable and metastable phases, 800 to 1100°C 79−46651
Nb_2O_3 in MIM structure, space charge density *(Russian)* 78−10579
Nb_2O_5 amorphous film, in Nb-Nb_2O_5-MnO_2 sandwich, elec. cond. variation during heat treatment 79−82593
Nb_2O_5, amorphous film in MIM struct., Schottky barrier effects on dielec. props. 77−8203
Nb_2O_5 amorphous films, switching phenomena and dielec. breakdown 77−24594
Nb_2O_5 and Al_2O_3 simultaneous reduction by CaH_2, Nb_3Al prep. 80−100809

niobium compounds continued
Nb_2O_5 anodic coatings, refr. index and spectral phase change, reflectance meas. 79−43052
Nb_2O_5, B-form single crysts., ESR of Mo^{5+} and W^{5+}, site symmetry 80−54946
Nb_2O_5 binding energies and surface layer identification following ion bombardment *(French)* 77−44541
Nb_2O_5, carbothermal reduction in N_2 intermediate phases 79−11773
Nb_2O_5, chemical effect, influence on stopping power 80−47830
Nb_2O_5 containing aluminosilicate glasses, paramagnetic defect formation, ESR study during crystn. 79−65739
Nb_2O_5, cryst. growth and microstructure 79−95913
Nb_2O_5, dielec. dispersion and polarisation 78−2803
Nb_2O_5, diffusion of O_2, solid-gas isotope exchange method *(French)* 78−34650
Nb_2O_5, effect on sintering and stability of ZrO_2-based solid solns. 77−40410
Nb_2O_5 electrodes, in aq. and acetonitrile solns., electrochromism 80−50298
Nb_2O_5, electron energy spectrum by optical and thermal methods 79−69418
Nb_2O_5, electron irradiation damage, AES study 79−28015
Nb_2O_5, for supercond. microwave cavities, secondary electron emission and AES meas. 79−56895
Nb_2O_5, hydrated gel, prep. conditions on pore struct., adsorpt. meas. 78−3068
Nb_2O_5, partially reduced, electrical conductivity 77−15918
Nb_2O_5, partly reduced, mag. and elec. props. 77−43593
Nb_2O_5, polycryst. film, switching processes, dielec. breakdown 77−39981
s-Nb_2O_5, prep. by high temp. chlorination of pyrochlore mineral 78−11180
α-Nb_2O_5, reduction in H_2 discharge, AES and SEM anal. 77−59708
Nb_2O_5, single cryst. growth by chem. transport reactions involving $TeCl_4$ 77−36382
Nb_2O_5 waveguide, in-plane scatt. and loss mechanisms 80−33216
Nb_2O_5-MgO-Al_2O_3, solid state equilibria at 1400°C phase diagram *(Italian)* 78−23671
Nb_2O_5-PbO, acoustooptic props. from comp. and density 80−76000
Nb_2O_5-TiO_2, splat cooled, crystallization and ordering 77−68953
Nb_2O_5-TiO_2-ZrO_2, quasiternary system 77−44229
Nb_2O_5-V_2O_5-P_2O_5, glasses and glass ceramics, elec. cond., struct. 80−84466
Nb_2O_5-WO_3, solid-state reactions, electron microscopic obs. 77−16818
Nb_2O_5-WO_3 system, TEM study of intergrowth of ReO_3 and tetragonal-type structs. 79−7580
Nb_2O_5-WO_3 system complex cpds. with TTB type subcells, HV superhigh resolution electron microscopy obs. of struct. 80−103311
Nb_2O_5-ZrO_2 sputtered thin layer structure and optical props. 79−28851
$Nb_{28}O_{70-x}$, O diffusion, rel. to Nb_2O_5 nonstoichiometry *(French)* 78−47583
Nb_xO_y, lattice imaging 78−30522
Nb_xO_y structures, dislocations and related defects 77−7724
$NbOAsO_4$ and $NbOAsO_4$ $4H_2O$, crystal growth, composition, struct. and crystallographic charact. 80−54198
$NbOI_2$, cryst. struct., X-ray determ. 79−14770
$NbOPO_4$, cation ordering effect on Raman spectra 78−43850
$Nb(OR)_2Cl_3.L$, halo-alkoxide complex, prep. and props. 78−18605
$3Nb_2O_5.8WO_3$, circular diffuse scattering studied by 1 MV high resolution electron microscopy 80−59350
Nb_8P_5 precipitates, obs. in austenitic stainless steel *(Japanese)* 80−89221
Nb_3Pb superconducting film, prep., vac. deposition 80−89149
Nb_5Pt_3O, R phase of Nb-Pt‖O system, cryst. struct. 80−96495
NbS, supercond. props. at press. up to 20 kbar 79−24111
NbS_2, 2H layer cpd., electronic susceptibility and CDWs 78−39040
NbS_2, 2H layer cpd., tight-binding fit to bond struct. 78−39000
NbS_2 (2H), anisotropy of upper critical field 78−76200
NbS_2 (3R), Raman spectra, vibr. modes 79−87449
NbS_2, enthalpy and specific heat, temp. depend. 80−54406
NbS_2, high pressure polymorphs 78−51459
NbS_2 intercalate with tetraalkylammonium hydroxide, prep. and struct. 80−79752
NbS_2, intercalation compounds, octahedral, microstructural study 77−84729
NbS_2 intercalation complexes with 3d transition metals, mag. and metallic transport props. 80−44814
NbS_2, intercalation cpd. with pyridine, nucl. spin-lattice relax. meas. 80−54962
NbS_2, nucl. spin-lattice relax. meas. 80−54962
NbS_2-$(pyridine)_{1/2}$ intercalation complex, superlattice struct., NMR meas. 80−70180
NbS_3, cryst. struct., X-ray diffr. obs. 79−1412
NbS_3, electronic struct. and predicted cond. props. 80−92815
NbS_3, Peierls distortion, chain polytypism and dislocation coupling 78−79589
NbS_3, Peierls distortion, electron diffr. obs. 80−39503
NbS_3, phase transitions and elec. props. 80−20178
NbS_3, transport props. 80−20175
Nb_3S_4, anisotropic superconductor, critical field and specific heat meas. 80−44779
Nb_3S_4, electronic struct. and predicted cond. props. 80−92815
Nb_3S_4, supercond., prep. and transition temp. 78−84341
$NbSCl_3$, prep. and characterisation 77−59705
$NbS_2Cl_2(Br_2)(I_2)$, absorpt. edge spectrum, fine struct. 80−66219
$NbS_2Cl_2(Br_2)(I_2)$, prep., struct. and props. 80−28994
$NbS(Se)_2$, polymorphism at high press. and temps., T_c and band struct. 78−26528
$NbS_{1.6}Se_{0.4}$, layered supercond., fluctuation induced diamag. and dimensionality 77−77006
$Nb_3S_{1.7}Se_{2.3}$, supercond., prep. and transition temp. 78−84341
$NbS_2.Sn$, $NbS_2.Sn_{1/3}$ intercalation cpds., lattice dynamics, hyperfine interactions 79−61273
$NbS_2.(pyridine)_{1/2}$, intercalation complex, vibr. spectra 77−59076
$NbSbS_3$, synthesis and single cryst. growth and struct. 77−52234
$NbSc_5HfO_{12}$, cryst. struct. determ., powder X-ray diffr. exam. 77−4083
$Nb_{1.5}Sc_{5.5}O_{12}$, cryst. struct. determ., powder X-ray diffr. exam. 77−4083
$NbSc_6O_{11}F$, cryst. struct. determ., powder X-ray diffr. exam. 77−4083
NbSe (2H), scattering effects on CDW transition temperature 80−107720
$NbSe_2$, 2H layer cpd., electronic susceptibility and CDWs 78−39040
$NbSe_2$, 2H layer cpd., tight-binding fit to bond struct. 78−39000
niobium compounds continued
$NbSe_2$, 2H phase, layered type II supercond., NMR meas. 77−36024
$NbSe_2$, 2H polytype, effect of incipient CDW on second-order Raman spectra 78−80357
$NbSe_2$, 2H polytype, Fermi surface and CDWs 77−51641
$NbSe_2$, 2H polytype, layered cpd., thermal props. at CDW transitions 77−47750
$NbSe_2$ (2H), CDW amplitudes determ. by ^{77}Se NMR 77−77116
$NbSe_2$ (2H), charge density wave transitions, neutron diffr. exam. 77−89515
$NbSe_2$ (2H), charge density waves state, NMR meas. 78−39421
$NbSe_2$ (2H), effect of CDW fluctuations on Raman active optic phonon freq. 78−87750
$NbSe_2$ (2H), electronic response function including electron-phonon matrix elements 79−28300
$NbSe_2$ (2H), incommensurate and commensurate struct., Raman scatt. 79−95739
$NbSe_2$ (2H), intercalated with TCNQ, elec. resistivity temp. behaviour anomaly *(Russian)* 80−10953
$NbSe_2$ (2H), layered, anisotropy and electron-phonon coupling effects on sp. ht. 77−51844
$NbSe_2$ (2H), metallic layer cpd., angle-resolved photoemission spectra 79−47593
$NbSe_2$ (2H), metallic layer cpd., reconstructed band struct. and Fermi surface 79−95312
$NbSe_2$ (2H), pure and Fe doped, layer supercond., anisotropy and temp. depend. of H_{c2} 77−51857
$NbSe_2$ (2H), Raman scatt. from supercond. gap excitations 80−93340
$NbSe_2$ (2H), Raman scatt. by supercond. gap excitations, coupling to CDWs 80−103956
$NbSe_2$ (2H), supercond., thermodynamic props., exhibiting anisotropy and strong-coupling effect 77−12062
$NbSe_2$ (2H), surface struct. determ. by dynamical LEED 77−43415
$NbSe_2$ (2H), surface struct. and interplanar separation by LEED 77−59191
$NbSe_2$, adsorption of Cs and O_2, 200-300K 78−26767
$NbSe_2$, charge density wave state, NMR meas. 77−8430
$NbSe_2$, experimental data, upper critical field theory fit 80−75692
$NbSe_2$, high pressure polymorphs 78−51459
$NbSe_2$, I_2 vapour phase transport kinetics *(French)* 78−11092
$NbSe_2$ intercalated with Rb, EXAFS 80−2897
$NbSe_2$, intercalated with Rb, EXAFS meas. 80−40185
$NbSe_2$ intercalation complexes with 3d transition metals, mag. and metallic transport props. 80−44814
2H-$NbSe_2$, layer struct. supercond., H_{c2} temp. and ang. depend. 77−8248
$NbSe_2$, layer type dichalcogenides, reflectivity 6 to 40 eV, electronic deep level excitation 77−55801
$NbSe_2$, layered dichalcogenide, US vel. rel. to CDW 77−76490
$NbSe_2$, layered supercond., fluctuation induced diamag. and dimensionality 77−77006
$NbSe_2$, $NbSe_3$, comparison of elec. cond. 78−14715
$NbSe_2$, origin of CDW, elec. susceptibility calc. from band structure 77−51679
$NbSe_2$ pure and intercalated with ethylenediamine, positron annihilation study 80−84801
$NbSe_2$ solid lubricant, antifriction and elec. props. depend. on oxidation temp., dopant influence 80−108584
$NbSe_2$, supercond., upper crit. field 77−15994
$NbSe_2$, supercond. and normal state, thermal cond., temp. and mag. field depend. 78−26992
$NbSe_2$ superconducting microbridges, current-voltage curves, hysteresis of crit. current *(Russian)* 77−69452
$NbSe_2$, thermal dissociation 78−44370
$NbSe_2$, thermal expansion, lattice parameter meas. 78−18804
$NbSe_2$, upper crit. fields and reduced dimensionality 80−70910
$NbSe_2$:Fe, local moment form., mag. susceptibility meas. 79−82756
$NbSe_2$:Fe (2H), pure and doped, magnetoresist. and elec. resist. temp. depend. rel. to CDW form. 80−44574
$NbSe_2$:Mn, Kondo effect, mag. ordering and superconductivity 77−62915
$NbSe_2$:Mn, supercond., anomalous flux flow and matching 77−12069
$NbSe_3$ and $Nb_{1-x}Ta_xSe_3$, thermoelec. power meas., 10-300K 80−20177
$NbSe_3$ and related cpds. bands, bonds and charge density waves 79−95327
$NbSe_3$, CDW, cryst. struct., X-ray and electron diffr. studies 79−14768
$NbSe_3$, CDW condensate, soliton pair creation by elec. fields 77−69309
$NbSe_3$, CDW form., direct electron diffr. 78−30877
$NbSe_3$, CDW form., non-linear props., temp. and press. depend. 80−49753
$NbSe_3$, CDW form., supercond. and Fermi surface determ., press. study 80−70891
$NbSe_3$, CDW linear chain metal, two band model in ohmic region 79−38056
$NbSe_3$, CDW noise, temp. and freq. depend. 80−103681
$NbSe_3$, CDW transitions *(Japanese)* 78−30880
$NbSe_3$, chain-like compound, low temp. phase transition 78−80088
$NbSe_3$, chemical bonding and dimensionality 78−75992
$NbSe_3$, cond., Frohlich mode motion *(Russian)* 79−95395
$NbSe_3$, conductivity anisotropy and transverse magnetoresistance 79−38055
$NbSe_3$, depinning props. of lower CDW, weak pinning model *(French)* 80−70630
$NbSe_3$, elec. field depend. thermopower 79−56204
$NbSe_3$, elec. resist. anomalies down to 7 mK associated with CDWs 79−60811
$NbSe_3$, electronic struct., chem. interpret. of geom. deform., oxidation state formalism 80−107690
$NbSe_3$, Fermi surface, press. effects, Shubnikov-de Haas effect meas. at 1.5K 80−20068
$NbSe_3$, Frohlich sliding mode, nonlinear resist. and noise 79−60808
$NbSe_3$, incommensurate CDW, X-ray scatt. and elec. field studies 79−42471
$NbSe_3$ interference effects of CDW motions 80−88544
$NbSe_3$, linear chain metal, anomalous transport props. 78−14718
$NbSe_3$, linear-chain metal, Hall effect meas. 78−76058
$NbSe_3$, mag. anomalies at CDW transitions 80−11158
$NbSe_3$, mag. susceptibility, CDW effect 80−88716
$NbSe_3$, metallic, non-ohmic cond., CDW pinning 80−39563
$NbSe_3$, non-Ohmic conduction, depinning of charge density waves 79−65459

niobium compounds continued
$NbSe_3$, non-ohmic transport props. near phase tranistions 78−72213
$NbSe_3$, oscillatory magnetotransport, Fermi surface anisotropy, Hall effect, g-factor, Dingle temp. 78−51975
$NbSe_3$, Peierls distortion, electron diffr. obs. 80−39503
$NbSe_3$, phase transitions, phys. props. meas. 77−8005
$NbSe_3$, phase transitions and elec. props. 80−20178
$NbSe_3$, phonon study of chemical bonding 80−20645
$NbSe_3$, quantum oscillation, Fermi surface exam. 78−60049
$NbSe_3$, quasi one-dimens. conductor, CDW phase transform., X-ray scatt. study 80−24594
$NbSe_3$, satellite electron diffr. below 59K, Fermi surface features 78−84136
$NbSe_3$, Shubnikov-de Haas oscills. 78−2502
$NbSe_3$, superconducting transitions and diamagnetism 80−84526
$NbSe_3$, superconductivity under press. 77−76995
$NbSe_3$, thermoelectric power 79−28362
$NbSe_3$, transport props. 80−20175
$NbSe_3$, two band model and galvanomagnetic study 80−20176
$NbSe_3$, two charge density wave locking 79−95350
$NbSe_3$, Young's modulus meas. 78−48443
$NbSe_3$:Ta, elec. cond., anomalous, and microwave absorpt. 79−42527
$NbSe_3$:Zr, dopant effect on supercond. transition temp. rel. to CDW 80−39699
$NbSe_x$, x=1.48-2.0, nonstoichiometric, elec. props., supercond. transition temps. 79−73624
$NbSe_x$, x=1.48-2.0, nonstoichiometric, press.-comp.-temp. rel. determ. by annealing 79−74139
Nb_2Se_9, cryst. struct. from twin-crystal data 79−90599
Nb_3Se_4, supercond., prep. and transition temp. 78−84341
$Nb_3Se_5Cl_7$, preparation, struct. and props. 79−65040
$NbSe_2Cl_2(Br_2)(I_2)$, prep., struct. and props. 80−28994
$NbSe_2Cu_x$, ordering study using electron diffr. and microscopy 80−39043
$NbSe_2$(2H), CDW layered cpd., phase diagrams 79−69243
$NbSe_2$(2H), CDW onset temp. and supercond. crit. temp., press. effects up to 20 kbar 77−39987
$NbSe_2$(2H), CDW phase transition, effect of electron-phonon scattering 78−95265
$NbSe_2$(2H), elastic consts., from dispersion curve and linear compressibility data 77−11618
$NbSe_2$(2H), I-free, anomalous resist. 77−51732
$NbSe_2$(2H) intensity vars. of angle-resolved photoemission spectra 79−83104
$NbSe_2$(2H), layered metallic magnetoresist. and Fermi surface above and below CDW onset temp. 79−19578
$NbSe_2$(2H) layered supercond., effect of Fe impurities on sp. ht. 79−60972
$NbSe_2$(2H), low field magnetoresist. and anomalous transport props. 80−65602
$NbSe_2$(2H) microscopic theory of charge density wave instability 78−79732
$NbSe_2$(2H), Raman spectra of soft modes at CDW transition 77−16301
$NbSe_2$(2H), specific heat and critical field, anisotropy and strong coupling effects 77−36021
$NbSe_2$(2H)-hydrazine, intercalation cmpd., kinetic studies by transmittance meas. at 1600 nm 78−71981
$NbSi_2$, formation by Ar ion bombard. of Nb-on-Si system 80−10709
$NbSi_2$, self-propag. high-temp. synthesis 80−2988
Nb_3Si, A-15 struct. stability, atomic radii ratio *(Chinese)* 80−54393
Nb_3Si, A-15 type, growth by levitation melting, transition temp. meas. *(Chinese)* 79−24424
Nb_3Si, electronic and supercond. props. 77−16011
Nb_3Sn filamentary composite conductor design 79−30515
Nb_3Sn filamentary hexapole magnet construction and testing 79−30503
Nb_3Sn flux exclusion tube for mag. field shielding in particle spectrometers 79−13578
Nb_3Sn high field superconductors, filamentary, manuf. and appl. limits *(German)* 77−55647
Nb_3Sn monofilamentary composite superconductor, tensile stress influence on critical current 80−97046
Nb_3Sn multifilament conductor critical current rel. to mech. strain 79−31215
Nb_3Sn multifilamentary superconductor AC hysteresis losses 79−33437
Nb_3Sn supercond. tape substrate structural changes 79−33373
Nb_3Sn, thin film, TEM microanalysis 80−104491
$(Nb_{1-x}Ta_x)_2C$, modulated structs., periodic antiphase domains 79−94969
$Nb_{0.95}Ta_{0.05}Se_3$, resist 0.5K to room temp., supercond. transition temp. and crit. field 79−82704
$Nb_{1-x}Ta_xSn_2$, supercond. transition temp. and upper crit. field 80−39723
$NbTe_2$, CDW and accompanying periodic structural distortions 78−72094
$NbTe_2$, high pressure polymorphs 78−51459
$NbTe_2$, layer cryst., dislocations and domain struct. 80−39102
$NbTe_2$, phase transformations and domain structures *(French)* 78−27509
Nb_3Te_4, supercond., prep. and transition temp. 78−84341
$Nb_{1-x}Ti_xO_2$, X-ray struct. anal. 80−28954
$Nb_{1-x}V_xSe_2$, elec. and mag. anomalies at CDW transition 80−107722
$Nb_{0.87}V_{0.13}Se_2$(4Hb), stacking layer study, appl. of convergent beam electron diffr. 80−39116
$Nb_nW_{6-n}O^{(n+2)-}$, config., IR and Raman spectra 77−42324
$Nb_{1-x}W_xSe_2$ x=0 to 0.15, elec. resist., mag. suscept., heat capacity, structural, supercond. transition *(Russian)* 78−31006
NbO_2F, strain energy due to {001} crystallographic shear planes 79−99223
$nbSe_2$ (2H) single crystal, elec. resistivity, effect of hydrogen intercalation *(Russian)* 78−84338
Nd:YAG lasers, sun-pumped and lamp-pumped, for space communications 79−86194
$Ni_{0.34}NbS_2$, intercalation compound, struct. and photoemission meas. 77−16453
$Ni_{1/3}NbS_2$, intercalate, metallic, cond., Hall effect and mag. props. 77−76789
NiO, stress appl. high temp. creep and point defects, creep rate obs. 80−49297
$PbNb_2O_6$-$NaNbO_3$, DTA *(French)* 77−44234
$Pb_{0.99}Nb_{0.02}(Zr_{0.95}Ti_{0.05})_{0.98}O_3$, ferroelec. ceramic, stress effects 80−2119
$Pb_{0.95}Sr_{0.05}(Zr_x, Ti_{1-x})O_3$-$Nb_2O_5$, phase coexistence range, lattice consts. 80−92680

niobium compounds continued
$Pb(Zr,Ti)O_3$:Nb_2O_5 elec. cond. study 79−11120
$PbZr_{1-x}Ti_xO_3$:Nb_2O_5 ceramic, ferroelec. transitions, polarisation meas. *(French)* 80−66124
rare earth oxide-Nb_2O_5 system, phase formation thermodynamics 77−86348
$RbCrCl_3$ crystals, $\beta \rightarrow \gamma$ structural phase transition, lattice dynamical anal. 80−84291
$Rb_{12.20}Nb_{33.56}O_{90}$, tunnel cryst. struct., X-ray diffr. 78−18611
Rb_2O-Nb_2O_5, phase equilib. relns. and crystal chemistry, structs. useful as ionic conductors 79−20033
Rb_2O-Nb_2O_5 mixed oxides, cryst. struct., electron microscopy study 78−91309
Rb_2ZnBr_4, incommensurate phase, ^{87}Rb NMR lineshape 80−93191
$SbCl_5$-$NbCl_5$, melt and solid-soln. Raman spectra, $SbNbCl_{10}$ dimer *(German)* 77−4645
$SnNbS_2$, intercalate, cryst. struct. determ. 78−26534
SnO_2-Nb_2O_5, activated sintering mechanism 80−60810
$Sr_3NbO_{5.5}\square_{0.5}$, $Sr_2CaNbO_{5.5}\square_{0.5}$, $LaNb_{2.6}Zr_{0.4}O_{8.8}\square_{0.2}$, ionic conductivity 77−20119
Th-Nb-C, phase diagram *(German)* 77−48413
TiC-NbC, prod. and props. 77−28772
TiN-Nb(Ta)N, microcomposite film prod. for radio resistors 78−3052
$Ti_{1-x}Nb_xH_{1.94}$, x=0.25, 0.50, low temp. specific heat meas. 80−2179
TiO_2, anatase-rutile transform., inhibition by Nb_2O_5 addition 79−78948
TiO_2:Nb_2O_5, conduct. rel. to defect structure, obs. 77−76392
TiO_2:Nb_2O_5, preparation method, effect on semiconductive props. and sintering temp. 77−16527
TiO_2:$Ta_2O_5(Nb_2O_5)$, rutile, defect struct. and elec. cond. at 1273K 80−44604
TiO_2-Nb_2O_5 sputtered thin layer structure and optical props. 79−28851
TiO_{2-x}:Nb_2O_3, defect struct. and thermodynamic props. 79−86790
TiO_{2-x}:Nb_2O_5, defect struct. and thermodynamic props. 79−90650
$TlNbO_3$ and $Tl_3Nb_{16}O_{41}$, new phase of mixed oxide 78−59787
UC-NbC and UC-ZrC-NbC, solid soln. strengthening rules, physicomech. prop. changes 77−28826
V-H(D), anelasticity due to long-range diffusion 80−60904
VNb-NbO_x-Pb Josephson tunnel junction, compared with VNb-VO_x-Pb 79−87203
$(V_{1-x}Nb_x)_2C$, modulated structs., periodic antiphase domains 79−94969
$V_{1-x}Nb_xO_2$, metal-semicond. transition, polarised Raman scatt. 77−90151
$V_{1-x}Nb_xSe_2$, CDW anomalies, Nb substitution effects, mag. susceptibility, 16-300K 79−38005
V_2O_5-P_2O_5-Nb_2O_5 glasses, switching 80−88604
$(V_{1-x}Ta_x)_2$ C, C ordering formation of varieties 80−38968
$W_xNb_yO_z$ ordering of atom string, cluster model 77−68959
$W_{1-x}Nb_xSe_2$, packing defects, correl. with diffr. pattern changes 77−15429
WO_3-$N6_2O_5$ system, strain energy due to {001} crystallographic shear planes 79−99223
WS_2-NbS_2 system, compds., elec., antifriction props. 79−38066
Y_2O_3-Nb_2O_5, solid state reactions, 1275 to 1350°C, electron microscopy, EPMA, X-ray diffr., dilometry *(Japanese)* 78−63883
ZnO-Nb_2O_5 system, Czochralski growth, phase relations and cryst. data 78−9975
ZrC-NbC, kinetic characteristics, review 78−47613
ZrC-NbC, prep. by impregnation, strength, surface submicrocracks 77−16661
ZrC-NbC-MoC_{1-x} system, thermal expansion coeff. up to 2500°C 79−69267
ZrC-NbN, mag. susceptibility, zone struct., conc. and temp. depends. 77−8788
$ZrC_{0.97}$-$NbN_{0.93}$, $Zr_{0.5}Nb_{0.8}C_xN_{0.98-x}$, solid solns., elastic props. expansion and hardness 77−52380
ZrN-NbC solid solns., mag. susceptibility and elec. resist. in 300-1300K range 77−24670
$Zr_{0.5}Nb_{0.5}C_xN_{1-x}$, mag. susceptibility, zone struct., conc. and temp. depends. 77−8788
$4.26ZrO_2.Nb_2O_5$, elec. cond. meas. 80−100463

nitrogen
see also nuclei with .....
^{14}N II ground state hyperfine structure quantum beats via ion-beam surface interaction at grazing incidence 79−10233
absorption by $LaCo_5$ at low temps. 80−24599
absorption during plasma melting of C steel, combined effect of C and O_2 *(Russian)* 79−39193
absorption in liquid Cr at high temps. *(Japanese)* 79−43201
absorption of activated N_2 on Pt single cryst. faces 77−85070
abundance and isotopic comp. in stony meteorites 78−65558
abundance anomalies in QSO Q0353−383, UV and visible spectral obs. 80−82532
abundance enhancement in planetary nebulae 78−93376
abundance in B-type stars in associations and general field 80−67702
abundance in globular cluster NGC 6752 first giant branch 80−67719
abundance in H II regions 80−46680
abundance in H II regions from Hα/[N II] ratio *(Italian)* 79−21395
abundance in lunar soil samples from Luna-24, neutron activation obs. 80−67594
abundance in red giant stars in 47 Tucanae cluster 79−97000
a.c. discharge, stability *(Russian)* 78−26358
activation analysis by photonuclear reaction *(Japanese)* 78−76945
active, heterogeneous atom recomb. on glass Langmuir-Rideal mechanism 80−7853
active condensed, thermolum. meas. *(French)* 80−11484
addition to austenitic stainless steel, effect on yield strength, solid soln. hardening 77−52430
adsorbed dense monolayer on graphite cleavage face, phase transition 78−56034
adsorbed layer, inelastic low energy electron scatt. 78−72653
adsorbed layer (1×1), on Ti (0001), underlayer geometry, electronic struct. calcs. and UPS meas. 80−54751
adsorbed layer on Cu(100), electronic props., UPS, XPS and Auger spectra 77−66088
adsorbed layer on Cu (110) surface, temp. depend. evolution, Auger line shape 78−2376
adsorbed layer on W (001) clean surface, long-range inhibition of displacive phase 80−2266
adsorbed layers, on W (210), surface struct., LEED obs. 79−82449

nitrogen continued
adsorbed on α-cyclodextrin surface, effects on positron annihilation 79−65952
adsorbed on graphite, Mossbauer obs. 80−18060
adsorbed on Kr-plated graphite, order-disorder transition classification, realisation of four-state Potts model 77−51605
adsorbed on metal-sapphire interface, effect on shear strength 80−49485
adsorbed on Ni, valence band photoemission, SCF MO CNDO calc. 80−100754
adsorbed on Ni (001) surface, p(2×2) struct., LEED and AES study 80−54515
adsorbed on W, effect of SIMS sputtering induced recomb. anal. 80−55243
adsorbed on W(100), vibr. spectra, bonding struct., LEED study 80−84387
adsorbed on W(210), surface struct., rel. to adsorbed CO 79−15009
adsorbent mesopores, capillary evaporation and struct. 80−107614
adsorption, by new high-efficiency polymer cryovacuum adsorbent 79−63249
adsorption, on activated wood charcoal 79−28973
adsorption, on montmorillonite, specific surface area 79−29406
adsorption and cryogenic refrigeration systems 79−58722
adsorption isotherm, determ. of porous texture of solids 79−77897
adsorption of N_2 on Kr-plated graphite, order-disorder transition classification, realisation of four-state Potts model 77−51605
adsorption on $CaHPO_4$ powder and granules with starch mucilage binder, surface area obs. on compression 80−80998
adsorption on Cu (100), LEED, data averaging 77−15668
adsorption on Fe, 80-290K, XPS and UPS obs. 77−31901
adsorption on Fe, temp. controller for filament heating appl. *(Japanese)* 77−51603
adsorption on Fe (110), UPS and LEED/Auger meas. 77−72773
adsorption on GaAs (110), UPS and EELS study, tight-binding calcs. 80−49496
adsorption on Ge surface, adsorption potentials and trapped electrons role 79−90872
adsorption on graphite, monolayer two-dimensional phase change, calorimetric investig. 77−47669
adsorption on graphite, surface homogeneity changes on gasification 79−51396
adsorption on Ir, field emission exam. of effect of steps on surface potential 78−30829
adsorption on Ir (110) surface 78−38961
adsorption on Ir and Pt, field emission meas. 77−24479
adsorption on MgO powder, 77 to 150K, mol. motion anal. 78−84051
adsorption on microporous C 78−22956
adsorption on MnO_2 coated Al_2O_3 and SiO_2 powder supports, dispersion mode obs. 80−81363
adsorption on MnO_2 porous powders, Al_2O_3 and SiO_2 coated, surface free energy changes 80−84363
adsorption on Mo, surface coverage 78−60036
adsorption on NaCl, electrostatic interaction energies 79−23831
adsorption on Nb and W (100) planes, LEED-AES obs. 77−69186
adsorption on Ni(Al)(Mg), internal and external sources of electrons 77−44097
adsorption on Ni (001), c(2×2) struct. form 80−80083
adsorption on Ni-Al, Raney nickel catalyst, surface texture *(French)* 79−69348
adsorption on North Ray Crater lunar soil (Apollo 16), rel. to soil maturity 77−87287
adsorption on PAN-based C fibres, surface characts. 78−35536
adsorption on Pd surface, hydrogenation, AES meas. 77−1315
adsorption on polycryst. W, α and β adsorption states 80−100404
adsorption on Pt, thermal desorption meas., α and β-states 77−15696
adsorption on pure and SiO_2-coated TiO_2, 77.4K, microcalorimetry obs. 80−80062
adsorption on Ru (0001) surface, AES, LEED and thermal flash desorption meas. 78−38954
adsorption on Sc and Lu surfaces, effect on reflection EELS 80−20742
adsorption on vacuum-deposited Ta film photoelec. props. 78−15298
adsorption on W, thermal desorption and pulsed time of flight mass spectra anal. 80−30285
adsorption on W{100}, disorder effects on work function change 77−20192
adsorption on W(100) surface, adsorbate density determ 77−1320
adsorption on W(110) vicinals, step sites as dissoc. centres 80−6642
adsorption on W (001), effect on LEED electron spin polarisation and intensity profiles 80−65377
adsorption on W (110), 300K and 100K, XPS, UPS and XAES 79−28203
adsorption on W (110), thermal desorpt. and work function meas. 77−1294
adsorption on ZnO, 76.8 to 87.3K, expt. isotherms 77−31869
adsorption on Zr, dissoc. and diffusion 80−80085
adsorption onto Al film 77−24486
adsorption-desorption kinetics on Si and Ge surfaces 77−47684
adsorption/desorption isotherm on meso-porous SiO_2 gel 77−4941
aerosol particles, size-fractionated, C, N and O determ. by particle elastic scatt. anal. 78−81466
afterglow, catalysis and quenching by SF_6 78−51376
afterglow, Lewis-Rayleigh afterglow, spectrum 77−61757
afterglow, Lewis-Rayleigh type, spectrum 79−64938
afterglow, light intensity radial distrib. current and press. depend. *(German)* 77−11434
afterglow, short-lived, electron and ion density enhancement obs. 78−63625
afterglow decay, diffusion and recombination, microwave cavity expts. 79−90479
afterglow decay, radiation escape kinetics, radiation captured by plane optically thick layer 80−95593
afterglow laser, recombination-pumped 77−50657
afterglow plasma, interaction with glass, Cu, steel walls, calorimetric method obs. 78−14177
afterglows, Rayleigh-Lewis and pink types, mechanisms 78−63622
airglow solar activity effect on (0,0) second positive band 77−70902
alkali metal+N_2, thermal ionis. rate coeff. 77−30982
alloying addition to low-alloy steel, role in austenitic grain growth 77−44255
Antarctic ice sheet, nonbiogenic fixed N, ecological implications 78−32129

nitrogen continued
antiprotonic atoms of light nuclei and isotopes, p̄-n strong interaction effects 78−29867
Arabian Sea, inorganic N system equilib. 77−41060
arc, axial flow stability, cathode emission mechanism change effect 78−83638
arc, high intensity, anode region temp., current density, flow field, numerical anal. 78−9827
arc, laminar flow, equilib. composition deviation 80−24274
arc, plasma parameters determ. by laser scatt. 79−32812
arc, radiation transport 78−79486
arc, spectroscopic meas. w.r.t. LTE 77−19786
arc jet enthalpy meas. by fast miniature total calorimetric probe 78−67486
arc plasma, recombination with gas flow, spectroscopic diagnostics 77−7626
arc plasma, stabilised by gas injection, thermochem. nonequil., particle excitation, vibr. temps. 80−19634
arc vacuum UV radiation loss calc. 78−71581
arcs, spectroscopic meas. rel. to LTE 77−76200
association, on metal surface, chemical energy accommodation, flow reactor obs. 79−24816
atmospheric, rot. Raman and elastic scatt. for temp. profiles 77−9515
atmospheric chemistry, history *(German)* 79−53415
atmospheric gases condensation on cold metal surfaces, nucleation barrier 78−22838
atom, $3p^4S^0$-state quenching in low-press. glow discharge 80−23355
atom, $^4S^0$ ground state, photoionisation calcs. 79−85909
atom, $(^4S_{3/2})$, kinetic study by time resolved atomic resonance fluorescence 80−95557
atom, $(2p^3\ ^2P^0)$ state, form. and depletion in N afterglow 79−49951
atom, ab initio effective valence shell Hamiltonian for neutral and ionic valence states 80−74117
atom, and 1st row ats., Compton profiles, momentum distribs., correlation effects 77−88429
atom, associative ionisation, merging beams experiment 80−63789
atom, beam-foil populations, charge state distribs., independent electron model 77−19035
atom, bremsstrahlung by electrons, configuration interaction 78−13483
atom, CNDO/S nucl. screening const. calcs. 78−86787
atom, coherent radn. excited by external field 79−81184
atom, dipole oscill. strength distribs., sums 78−21975
atom, dipole properties and dispersion energies additivity, using atoms and small mol. models 80−53091
atom, elastic electron scatt., low energy, linear algebraic method 77−88562
atom, electron affinity, modified variational approx. 78−66679
atom, electron and proton interaction cross sections 77−50538
atom, electron attachment, low energy electron elastic scatt., review of theory 77−68111
atom, electron elastic scatt. resonance, neutral bremsstrahlung 77−46639
atom, electron impact excitation, near threshold, cross-sections for $(2s^22p^23s)^4P$ and $(2s2p^4)^4P$ states 80−91684
atom, electron impact ionis., 7-1000 eV, cross-section 78−86956
atom, electron impact ionis. cross-section, accuracy of fast at. beam method 79−81283
atom, electron scatt. and photoionis., correlation effects 78−58842
atom, electron scatt. Bethe-Goldstone and pseudostate approx. 77−68112
atom, electrons effective collision freq. calc. 79−3567
atom, energy levels of $1s^22s^22p^N3d$, (N=2,3,4) configurations 77−46509
atom, ground and excited states, atomic polarisability calc. 77−83756
atom, ground state, second virial coeffs. calcs., 6000 to 20000K 77−14524
atom, ground state energy, HF calc., second-order correction 78−86784
atom, ground state static polarisability and hyperpolarisability, numerical SCF method 79−36567
atom, HFS and g_J factor, precision meas. ground state 77−88412
atom, high Rydberg states, radiative decay rates, TOF meas 78−46302
atom, intermediate coupling props., relativistic average of config. wavefunctions applicability 78−17574
atom, ionis. cross-section, accuracy of crossed at. beam method 79−81284
atom, many electron autoionisation states, perturbation theory Z-expansion, numerical results 80−52863
atom, mean lifetimes of astrophysically important excited levels 77−46528
atom, min. basis of Slater-transform-Preuss functions 79−59343
atom, model pots., STO calcs. 77−408
atom, $np^2(n+1)s$ excited-state config. quadrupole moments, Sternheimer shielding factor 80−37755
atom, nucl. quadrupole coupling const., relativistic many-body perturbation theory 78−37566
atom, oscillator strength calc. for $^4S^0$ to ^4P sequences 78−25485
atom, oscillator strengths for 18 resonance lines 79−5741
atom, outer 1s, 2s and 2p electron loss cross sections by multicharged ions 78−42185
atom, photoionis. cross section, many-channel quantum defect method 78−17638
atom, polarisation functions for Gaussian basis sets 78−5126
atom, pseudospectral dipole oscillator strength distribs. 78−50503
atom, radiative lifetimes of visible and near IR transitions, solar abundance 78−50506
atom, real STOS, parameter optimisation method 78−41929
atom, reson. line shapes determ. by Zeeman scans 77−6723
atom, Rydberg-valence mixing, oscillator strengths 79−31492
atom, s-shell spin polarisation calcs. 77−75318
atom, SCF electron-gas local-spin-density model including correlation 80−9488
atom, spectra in Ar inductively coupled plasma 80−91474
atom, spherical ground state nuclear quadrupole interaction, Breit interaction, relativistic perturbation theory 80−42939
atom, spin magnetic moment densities, spin density functional method calcs. 77−67969
atom, Stark broadened VUV lines in wall-stabilised arc, 1100-1800 Å 78−90107
atom, triple-dipole energy calcs. using pseudo spectral theory 78−46418
atom+organic molecule, rate const., discharge flow-reson. fluoresc. meas. 78−7178
atom recombination, Smith side tube method obs. 78−68881
atom-atom pot. parameter in azabenzene, dispersion energy calcs. 80−23489

nitrogen continued
atomic periodic overlayers, chemisorption on graphite, CO-NDO calcs. 79−7745
atomic spectra of aurora, UV obs. of N(^{2}P) metastable state 80−77185
atoms, far vac. UV spectra, oscillator strengths for 3s, 4s, 5s, 3d and 4d ^4P_J-$2p^3\ ^4S_{3/2}{}^0$ 80−74178
atoms and molecules, dispersion energy consts., dipole oscill. strength, refractivity 77−50492
aurora, near IR spectrum obs. 77−53272
auroral collision processes of metastable N(^{2}P) 80−72658
bare nucleus+He, electron capture to excited states, X-ray cross-sections 77−71814
benzene-H_2N_2 gas ternary diffusion coefficient obs. *(Japanese)* 79−10626
birefringence of boundary layer of rarefied heat conducting gas 77−80265
body N measurement by $^{14}N(n,2n)^{13}N$, interfering reactions and spatial sensitivity 77−60240
body storage, man, dynamic model 78−27997
boiling, press. effect on internal charact., bubble growth 77−15568
boiling 80−53770
boiling curve, by unsteady-state quenching method 79−14232
boiling heat exchange, surface roughness influence, press. depend. *(Russian)* 79−68562
boiling heat transfer from stainless steel surface, surface roughness effect 80−48705
boiling heat transfer from structured surfaces to liquid nitrogen *(German)* 80−99919
boiling in high centrifugal accel. fields, peak nucleate boiling heat flux 79−59907
boiling in tubes, heat transfer, cryogenic stabilisation 78−30162
breakdown formative time lag rel. to gap geometry, pressure, and overvoltage 79−18994
breakdown in crossed elec. and mag. fields, modified Paschen's law 80−24121
breakdown in superimposed DC and HF electric fields 78−67571
breakdown voltage and voltage-current charact. obs., up to 2400°C 78−87510
breakdown voltages, from normal to cryogenic temps. 78−59692
broad beam ion source used for sputtering and etching 80−69002
bubble formation in sodium carboxymethylcellulose at single submerged orifice, model 79−32640
iso-butane+Cd($^1P_1$), laser excitation, absolute quenching cross sections and branching ratios 79−49979
capillary condensation and evap., apparatus and calc. method 80−2150
capillary condensation and evap., scanning curves within B-type hysteresis loops 80−2151
carbothermal reduction, of Nb_2O_5, intermediate phases 79−11773
CdS:N, Mn, ion implanted, anomalous enhancement of EPR signal of Mn^{++} 78−27080
chemisorbed layer on Cu, self-consistent electronic struct. calc. 78−2544
chemisorbed on Ag film, reflectance and elec. resist. changes 80−11495
chemisorbed on Cu (100) film, electronic struct. 77−59315
chemisorbed on transition metals at high pressures, XPS 77−20990
chemisorption, electronically-activated, on Cu (100) surface 79−66348
chemisorption, on Cu(100), bonding, MO theory 77−76659
chemisorption, on Rh and W perfect surfaces 79−86979
chemisorption in steel, saturation kinetics for high-temp. carbonitriding *(Russian)* 79−52450
chemisorption of Cr, Mo and W, SXAPS obs. 79−52048
chemisorption of W (110), surface diffusion, scanning Auger spectroscopy exam. 77−55452
chemisorption on Au film on W substrate, effect on crystallite growth, FEM obs. 79−46976
chemisorption on Cu (001), electronic struct. of Cu_5N cluster, Xα scattered-wave calcs. 79−60902
chemisorption on Fe{111} clean single crystal surface, of N_2, NH_3, H_2, photoelectron spectroscopy, LEED studies 77−66087
chemisorption on LaB_6, time of flight atom-probe FIM study 80−6652
chemisorption on Ni, Cu, Pd, and Ag, semiempirical calcs. 78−14611
chemisorption on Ni (100), molecular cluster theory 77−1309
chemisorption on Ni (110), mol. and dissociative mechanisms 80−39431
chemisorption on polycryst. Ti, secondary electron yield spectrum obs. 78−38933
chemisorption on polycryst. Ti surface, secondary electron yield obs. 78−71971
chemisorption on Pt {111}, refl.-absorpt. IR spectroscopy 77−47676
chemisorption on Ti{0001}, at. underlayer form. 77−15693
chemisorption on Ti (0001), valence band struct., XPS and UPS study 80−35062
chemisorption on Ti film, changes in work function 77−59221
chemisorption on W(100) surface, α and β states, AES and electron energy loss spectra 77−1313
chemisorption on W {110}, underlayer mechanism 80−39432
chemisorption onto Fe, dissociative, during catalytic synthesis of NH_3, promoter action of K 79−29390
chloroform-N_2, gaseous compressed mixture, mol. reorientation, Raman spectra 80−23422
circulation in human organism, model *(Russian)* 79−2093
Clausius-Mossotti function, exam. of variation with gas density 78−52418
CO_2-N_2, highly efficient gas for nanosecond pulse CO_2 laser system *(Japanese)* 80−48214
coadsorption with O_2 or C, on W {100}, AES obs. 77−35821
coal, 14 MeV neutron activation analysis ^{16}O and ^{14}N 77−86430
coating, on Al thin film, effect on supercond. 80−7026
combustion products, appl. in CO_2 gasdynamic laser 79−27240
compressed, breakdown at cryogenic temp., obs. *(Russian)* 78−67448
compressed, depolarised light scatt., different contributing processes calc. *(French)* 78−79406
compressed, elec. breakdown at cryogenic temps. 78−51368
concentration in thermosphere, depend. on solar activity 80−77178
concentration meas. by $^{14}N(d, p_5)^{15}N$ 80−42671
condensation pump with preevacuation 77−74414
condensed gas films, thermal radiation absorpt. 78−32824
continuum rel. to atm. absorpt. spectra near 2400 cm^{-1} 78−11968
cooled discharge plasma electron energy distrib. function 78−63633
corona discharge, force exerted on electrode 77−19803
critical heat flux in horizontal tube, up to critical press. *(German)* 80−99921
crossed-beam phase-matched CARS generation 78−50850
nitrogen continued
cryogenic, shock wave-boundary layer interaction *(German)* 78−71370
cryogenic vapour columns, improved natural convection heat transfer 79−59986
cryostat for −195 to +150°C range with sample heating 77−74406
crystal, screened nucl. pot. and lattice dynamics., pseudo-atom approx. 78−34575
crystal, X-ray structure factors, mapping of electrostatic props. 79−94841
crystallisation, theory based on metallic cond. of porous network 79−59903
crystals, luminesc. and biexcitons 79−69893
cyclobutane-t, chemically activated by nuclear recoil, vibr. energy transfer 77−66763
DC low press. positive column, electron distrib. function superelastic electron collision depend. 79−46498
dense vapour, electron localisation 80−87840
density measurement up to 1800K and 8 kbar, procedure 78−81947
desorption, from Fe, surface anal., XPS appl. 79−24875
determination, combustion-gas chromatographic method, data processing 80−40762
determination, in nonferrous metals by nucl. reaction method, surface treatment effects 78−11596
determination, in steel, by nuclear methods *(French)* 77−60160
determination, in steel, using Rutherford backscatt. and (α,p) reaction anal. 79−5216
determination, in Ta film on Corning glass, nondestructive method *(German)* 78−43272
determination by activation anal. (α,n), (α,p) reacts. investig. 80−61206
determination in Lake Ontario tributary waters 79−79418
determination in metals, by deuteron irrad., nucl. microprobe anal. 78−7285
determination in thin steel sheets by internal friction meas. *(German)* 78−27715
determination in vivo using neutron capture gamma anal. and Pu-Be sources 77−86606
determination of Zr, chem. analysis by photon and proton activation *(French)* 79−43666
diamond: N, plastically deformed, EPR of two N atom centre 78−72408
diamond:N_2, Ni, spin-spin interaction of N_2 and Ni centres, temp. effects 78−88177
diamond:N^+, high temp. ion implantation 79−23623
diamond:N, effect of displacement upon impurity levels, pseudopotential calc. 77−39803
diamond:N, electronic struct. of deep levels, LCAO, SCF method 79−82555
diamond:N, imaging of paramag. N centres by EPR 79−65732
diamond:N, N9 and ND1 energy levels, electron irrad. photocond. obs., thermolum. 78−6324
diamond:N, paramagnetic centres, exchange interaction, spin density delocalisation 80−39847
diamond:N, photocond. in N2 absorpt. band 79−91102
diamond:N, spin-lattice relax. of Jahn-Teller N centre 77−66412
diamond:N, substitutional impurities 79−87056
diamond:N, synthetic, impurity effect on strength charact. and thermal stability 80−11726
diamond:N, type Ib, electron irradiated, migration of N, optical absorption meas. 78−56505
diamond, N, vacancy enhanced aggregation of N 80−70245
diamond, transformation of type IB dispersed N into type IA aggregate N 78−6089
diamond surface interaction with gases and metals 77−72758
diatomic mols., internal partition functions for O_2, N_2, NO and their ions, max. summation indices 80−27995
dibutyl sebacate diffusivity, from aerosol drop evap. obs. 79−43639
dielectric strength, bubble-phase equilib., high press., low temp. *(Russian)* 77−20798
diffusion, anomalous, in microporous graphite compact 78−34655
diffusion and surface distrib. in Ta, probed by (p,γ) resonance broadening method 78−38918
diffusion approx. of Boltzmann eq. for slow electrons 79−82044
diffusion in austenitic stainless steel 77−62677
diffusion in BCC Fe 77−4222
diffusion in Fe, Fe_4N growth kinetics *(Korean)* 80−93540
diffusion in fluid Fe alloy, effect of Si, P, Al and B *(German)* 77−20099
diffusion in group V refractory metals, statistical calculations on Arrhenius lines 80−59722
diffusion in liquid Fe based solns. 78−75862
diffusion in liquid Ni and Ni-Cr (W) (Mo) *(Russian)* 78−18812
diffusion in Nb, alloying additions and struct. defects effect 79−55938
diffusion in Nb, internal friction meas. 77−89586
diffusion in Si during annealing, effects on ion implanted layers 77−24436
diffusion in Ta, internal friction meas. 78−75888
diffusion in Ti and Zr fibres, high-temp. nitriding kinetics *(Russian)* 80−21166
diffusion in Ti-TiN phase system 77−39699
diffusion in V, least squares computer technique 78−38881
diffusion in water, laser interferometric study 77−76584
diffusion rate in Au thin layers 80−100359
diffusion through graphite powder compacts, time-lag analysis 78−2301
diffusion with CO in chamber and formed coke *(German)* 80−100356
diffusivity and solubility in complex liquid Fe alloys at 1600°C 77−39684
diffusivity in Nb, exam. 78−51741
discharge, anomalous heating *(Russian)* 80−1866
discharge, combined, in average press. gas using two HV pulse sources, gas laser development 80−44027
discharge, effect of Cs additive on I-V charact. 79−32813
discharge, elec. and optical props. calcs. *(Russian)* 79−10741
discharge, electron beam sustained high press., time behaviour of recomb. coeff. 80−10447
discharge, excitation efficiency of rot. and vibr. levels, heating due to collisions and relax. 80−38751
discharge, externally maintained, instability growth time, associative ionisation 80−6254
discharge, flowing, electron-beam maintained, cathode shape effects 79−27850
discharge, high-current, with inductive storage bank, exploding wire-initiated 80−10450

nitrogen continued
discharge, high-pressure, quasi-stationary stage characts. *(Russian)* 77−27756
discharge, HV diffuse, gas stream temp. inlfuence 79−32842
discharge, ionisation current increase, metastable mol. induced cathode secondary electron emission 80−38830
discharge, non-Boltzmann vibr. level populations, CARS determ. 78−5968
discharge, overvolted 77−19780
discharge, overvolted and homogeneous, electron density evolution 79−1359
discharge, streamer, spatial and temporal spectroscopy 78−5971
discharge plasma, ionic comp., mass spectra meas. *(Russian)* 78−22571
discharge plasma, radial distrib. profile of atom conc., Lewis-Rayleigh afterglow radiation 77−89312
dissolution in metallurgical slags, $CaO-SiO_2-Al_2O_3$ 77−21109
dissolved in ethyl ether, effect on nucleation press. 77−51486
dissolved organic, automated rapid system for anal. of natural waters 78−93014
electric breakdown, vol. discharge with external photoionisation, plasma focus spark channel *(Russian)* 80−38738
electric breakdown between coaxial cylinders in crossed elec. and mag. fields 78−5963
electric breakdown gas discharge, Paschen curve double minima 80−44036
electric breakdown in filled diodes, electrode temp. depend. 80−1735
electric breakdown in long high-voltage gaps with gamma and alpha particle irrad. 79−18993
electric breakdown voltage, 300-2100K *(Russian)* 78−51370
electric breakdown waves 77−31542
electric discharges, formative time lags, expt. 77−1025
electrical and optical discharge parameters at moderate press. 80−6300
electrical breakdown at high press. and field strengths, steady-state expts. 78−79488
electrical current, bipolar, in dense gas without volume ionis. 80−6208
electron backscattering coeffs., 100 eV to 5 keV 80−9750
electron beam sustained discharge, electron neutral inverse bremsstrahlung 78−63604
electron beam sustained discharge, performance 78−75365
electron drift velocity, density dependence, high press., quantum mech. theory 79−1285
electron drift velocity and longit. diffusion coeff. time-of-flight meas. 77−80264
electron drift vels., time-of-flight meas. 80−28855
electron energy distrib. and transport coeffs., in E×B fields 78−51277
electron spectra, valence momentum distribs. and config. interaction from (e,2e) reaction 77−19101
electron swarm develop., Boltzmann eqn. anal. 78−79487
electron swarm development, Boltzmann eqn. method 80−43832
electron swarm parameters for high E/N, Monte Carlo simulation 80−19548
electron transmission function and mean energy per ion pair, obs. 80−23566
electron transport coeffs. in crossed fields at low E/p 77−24050
electron-beam-sustained discharge stability model 78−71608
electrotransport behaviour in Sc 77−11738
electrotransport in La 80−24674
emission from Ir(111) surface, following decomp. of hydrazine, ang. struct. 80−97731
energy levels, position orbital calcs., electron repulsion integrals, teaching appl. 78−93494
energy loss straggling for He^{x+}, ion energies of 50-500 keV per nucleon 77−46620
enrichment in planetary nebulae 79−35326
EPR of N atoms in multiple trapping sites in N_2 matrix 78−56367
equation of state, perturbed-hard-sphere, applicable to sub- and supercritical temps. 79−19350
ethyl ether-N_2, bubble homogeneous nucleation in gas-liq. soln., press., expt. and theory 78−91430
ethylene + N_2, gaseous, excess enthalpy, determ. by flow calorimetry 78−91057
ethylene-O_2-N_2-Al particle mixture, two-phase detonation and combustion *(French)* 80−61097
evaporation of N_2O_4 in enclosed containers, N_2 medium, 1.12-4.96 gauge atm 77−47564
extraction from Ta powder, by vacuum hot extraction method, effect of graphite *(Japanese)* 78−84729
F ions recoiling in gases, hyperfine interactions 78−74735
in F- and G-type stars, abundances 77−91530
fast electron beam, transition from non-selfmaintained volume discharge to spark discharge *(Russian)* 79−23466
filament lamps, Kr-Ag-N gas mixture, thermal conduction coefficient calculational methods *(Russian)* 80−96335
film, condensed, UPS linewidths 78−31294
film, on metal or sapphire substrates, luminescence and nonradiative energy transfer to surfaces 80−97350
film boiling, heat-exchange intensification, nitrogen in pipes 79−81876
filtering gases, mixing zone in different porous media *(Russian)* 77−51112
fixation, semiempirical INDO study 80−16898
fixation in Atlantic deep-sea and coastal sediments 78−81211
fixation in prebiotic atmosphere 79−58096
fixation using fusion energy heat source 80−32510
fixed N in fertilizers, effect on stratospheric ozone 78−28288
flame consistuent, laser Raman spectrum, for temp. meas. appl. 77−5833
flame gas, electron-neutral energy exchange in AC field 77−42519
flow, alkali metal vap. condensation, heat and mass transfer 78−75192
flow, pipe, local heat transfer to turbulent flow, superposition principle, expt. 78−83479
flowing N spark gaps, electric breakdown study, improved method 80−64821
fluid, high density behaviour, extrapolated $P\rho T$ surfaces and critical density 80−87834
fluid, structure and dynamics 80−38889
freon-N_2 low-pressure mixture prebreakdown current obs. 79−18995
freons in nitrogen, interdiffusion coefficient, calc. and obs. *(Russian)* 77−76017
gas, μ, ρ and T-surfaces, global behaviour, rel. to catastrophe theory 78−26226
gas, collision-induced microwave absorpt. 77−42312
nitrogen continued
gas, compressed, stimulated Raman scatt., multimode radiation conversion to coherent Stokes wave 79−89971
gas, density up to 2000K and 6 kbar by displacement method 78−51266
gas, electron energy degradation, Monte Carlo study 80−69969
gas, eqn. of state, second virial coeffs., intermol. pot. at low temp. 79−46416
gas, heating in combined discharge 77−84387
gas, in crossed elec. and mag. fields, elec. strength calcs. 78−87568
gas, in water, cavitation, gas supersaturation thresholds under high press. 77−16861
gas, ionisation current growth, Townsend swarm coeffs. 78−59541
gas, lateral diffusion to electron mobility ratio 79−1284
gas, low press., relativistic electron beam propag. 79−76569
gas, P, ρ, T surfaces and Riemann-Hugoniot catastrophe theory 79−6066
gas, picosec. pulse CARS obs. 79−6942
gas, pure rotational CARS obs. 80−99511
gas, Rayleigh and Raman depolarised light scatt., density evolution 78−58706
gas, refr. index and Lorentz-Lorenz functions, 944 cm^{-1} and 15803 to 22002 cm^{-1} 78−59543
gas, rot. relax. in viscous shock layer *(Russian)* 77−89162
gas, stimulated Raman scatt. on rotational and vibrational transitions 79−27330
gas, total ionization created by completely stopped H^+ ions 79−46419
gas, two-stage expansion in gasdynamic CO_2 laser using supersonic nozzle 78−71076
gas, up to 50 atm, refr. index, 328, 3103 MHz *(French)* 78−14129
gas, vibr. energy diffusion coeff., 900-2000K 78−26227
gas, virial coeffs., from theory of system of nonpolar mols. of arbitrary symmetry 78−9743
gas, viscosity rel. to ionis., skin friction of wetted oscill. disc 78−34252
gas, weakly ionised, electron transport coeffs., Boltzmann eqn. anal. *(Japanese)* 80−59183
gas breakdown threshold meas. using pulsed HF(DF) laser 77−11423
gas breakdown threshold using laser radiation 79−1283
gas discharge, low press., emitted photon probe for electron swarm parameters 80−43839
gas discharges, electron swarm motion, computer simulation 77−89339
gas filled chamber, passage of low current electron beam 80−38523
gas flow through cracks 79−98693
gas laser, at. and mol. vibr. and electronic metastable states, book contrib. 77−50653
gas refractive index meas., 150 GHz to 6 THz 77−5892
gaseous, light scatt., effects of correlation between mol. and intermolecular axis 79−50844
gaseous, positronium yields at 77K 79−98254
glassy state, spin density and current correl. functions, computer simulation 79−14661
glow discharge, characts. depend. on initial conditions 78−51378
glow discharge, DC, low-press., translational/rot. temps. relation 78−38454
glow discharge, DC, metastable atoms prod. 80−38758
glow discharge, DC, nitridation of Mg surfaces, 0.3-5 torr, mechanism 78−3370
glow discharge, decay instability and contraction, interferometric and photographic obs. *(Russian)* 78−59696
glow discharge, high press., collision freq. 77−55184
glow discharge, ion flow mass-energy relations, near hollow cathode 77−84563
glow discharge, ionis. mechanism 78−13613
glow discharge, neutral components comp., mass spectroscopy study *(Russian)* 80−10439
glow discharge, non-self-maintained, ionisation instability, vibr. states excitation calc. 77−19805
glow discharge, RF plasma, gas rotational temp. determ. 79−90458
glow discharge, semi-self maintained, stability *(Russian)* 79−27845
glow discharge, variable current penetration mechanism 79−55584
glow discharge, volt-ampere charact. in gas flow *(Russian)* 80−106991
glow discharge instability in afterglow 80−6313
glow discharges surface coronas and photopreionisation stability, demonstration 80−105475
grain boundary migration rate during secondary recrystallisation, in steel, N_2 effect *(Czech)* 77−59812
grain boundary segregation, in α-Fe 78−72778
heat of vaporisation measurement, Dewar for student expt. 77−9840
heat transfer during boiling in field of centrifugal forces 79−60493
heat transfer during nucleate boiling, heating wall and metallic coating thicknesses depend. 79−32210
heat transfer in boiling on surface of vertical cylindrical rod 80−48706
high intensity arcs, anode contraction region modeling 80−103210
high power discharge laser excited through high dielectric constant ceramic materials 80−58572
high temp. elec. breakdown characts., theory and obs. 78−87581
hollow cathode discharge, ion mass composition 79−68969
human, body, in vivo N meas., by prompt neutron capture γ-ray analysis, body H use as internal standard 79−92441
human body N meas. by anal. of prompt γs from neutron capture 80−51220
human whole body measurement, using neutron activation anal. 79−29594
hypersonic flow, in shock tunnel, mass spectrometric analysis 77−31328
hypersonic shock layer at moderate Reynolds number, oscillatory-dissoc. relax. *(Russian)* 77−39311
impurity determ. by atm. press. ionisation mass spectrometer anal. technique 77−56263
impurity determination in group VA metals, from internal friction meas. 79−39246
impurity in CoGd, H_2 and N_2 contaminated amorphous films, mag. props. 79−1690
impurity in FeGd, H_2 and N_2 contaminated amorphous films, mag. props. 79−1690
impurity in W and Mo, struct., mech. props. and purification 79−52277
inductively coupled plasma discharge, temp. and vel. profiles 77−4004
injection into liquid through porous plate, squeezing out of liq. 80−64622
intermolecular force, orientation depend., using charge density and dispersion force data 77−50487
interstellar abundance from XUV absorption line obs. 79−5741
interstellar N bearing molecules, gas phase reactions 78−28754

nitrogen continued
interstellar neutral ^{14}N, search for radioemission 80−41886
interstitial in V, neutron diffr. determ. of site 77−19944
interstitials, in transition metals, electronic structure 79−1583
ion+Ar, Kα X-ray satellites prod. 80−9541
ion backscattering, technique for metal impurities anal. in Tokamak plasma 79−4182
ion implantation in $GaAs_{1-x}P_x$, characterisation by photolum. and channelling 80−54262
ion implantation of N^+ and N_2^+ in Au, Fe, Ni, and Zr, conc. distrib. meas. 77−80529
ion impurity in linear Z-pinch He plasma, outer 2s-shell electron excitation emission 78−22113
ion laser, travelling wave excitation 80−91774
ion pair creation by high-energy ions, meas. of average energy required 80−103105
ion source, HF, proton yield increase, influence of various admixtures to H_2 obs. 80−57422
ion source, saddle-field type, gas depend. characts., at. spectroscopy appls. 78−78039
ion stimulated sorption onto Ti film, TiN_x form., sorption ratio, capture coeff. anal. 80−39411
ionisation, energy dependence of $\bar{W}$ for alpha particles 79−6999
ionisation, radial dose, LET and energy per ion pair for ^{18}O ions 78−7452
ionisation by high-energy C^{6+} ions, W-value rel. to dosimetry 77−66849
ionisation path formation by laser beam with retractable focus 79−18992
ionisation potential, calc. by equations-of-motion, Green's function method, critical analysis 77−30762
ions, beam-foil excitation, relative initial populations, lifetime curves 80−14210
ions, collective acceleration 80−5406
ions, energy loss in tissue-equivalent gas for elastic nuclear collisions 78−86759
ions, in plasma, spectral line intensity rel. to composition *(Russian)* 77−36851
ions, ionisation equilib. and radiative energy loss rates in low-density plasmas 78−87430
ions, two vacancies in K shell, 2 electron 1 photon, and hypersatellite transition probabilities 78−46294
ions and neutral atoms in Venus daytime thermosphere 80−17517
isotope enrichment, laser isomerisation of ethyl and methyl isocyanide 79−27096
isotope fractionations in Fischer-Tropsch and Miller-Urey reactions, appl. to carbonaceous chondrites 80−46496
isotope ratios in C stars, spectral analysis 79−30057
isotope separation, microwave reson., triplet state photochem. technique 77−32818
isotopes, origin and $^{15}N/^{14}N$ ratio evolution 78−93201
isotopic composition, spectrosc. determ. in systems below natural ^{15}N levels *(Russian)* 77−68130
isotopic composition determ. using RMO-4S omegatron mass spectrometer 78−5368
jet, free, streamlines and local velocities in rarefied atm. 77−42884
jet, freely expanding, quantum effects in rot. relax. 80−58355
jet, mixing zone in continuous to free mol. transition 79−32605
jet, molecular rot. level population during condensation 79−86481
jet flow, free expansion of N_2, expt. tests of energy balance eqn. 79−98777
jet interaction, with liq. Pb and Sn streams in metal powder prod. 79−43170
jets, single and multiple free, CW laser Raman spectroscopy 80−32727
K-shell, excitation and ionisation, vibr. struct., electron energy loss spectra obs. 80−18943
KERMA values, consistent set for H, C, N, and O for neutrons from 10 to 80 MeV 80−68967
Lake McIlwaine, Rhodesia, distrib. in sediments 77−33114
laser, 3371 Å, fringe visibility curve 78−46695
laser, 337.1 nm emission, high specific power, high pulse repetition freq. 79−45932
laser, 3371 to 1124 Å conversion by nonresonant freq. tripling in compressed Kr gas 79−64279
laser, 406 nm emission on C→B band 80−64047
laser, ω→a, a→a′ electron transitions, strong near IR generation *(Russian)* 79−76676
laser, appl. of pulsed transversally excited discharge *(French)* 80−107009
laser, capacitor modification 77−14735
laser, coherent radiation from unstable resonator 77−71994
laser, compact high-power TEA, superradiant laser pulses 78−90427
laser, compact LEA, for sub-nanosecond pulse generation 79−76708
laser, construction and properties, axial or cross-field discharge 80−69418
laser, development of miniature high-power high-press. UV and IR lasers 78−46642
laser, double-channel 80−19046
laser, dynamic characts. of discharge, power supply circuit 79−18446
laser, effect of SF_6 on lasing characts. 77−65591
laser, electrode configuration for high peak powers and high repetition rates 78−55379
laser, electron beam excitation 77−711
laser, employing electron seeding technique, performance 77−71997
laser, first positive system, for optical fibre meas. 78−59020
laser, helical TE, tube geometry simplification 80−69406
laser, helical TE, with circular beam cross section 80−33023
laser, high power tunable liq. Raman type, for spectroscopy 80−48277
laser, high power UV travelling wave excitation via low-impedance high-voltage pulsers 77−3608
laser, high-power, practical design 77−42545
laser, high-power pulsed laser manufacture and reliability 77−19331
laser, high-press., effect of SF_6 addition 78−25859
laser, high-press., UV *(Japanese)* 78−55346
laser, home-built, design improvements 78−46612
laser, LG-21 serial, org. dye accessory invertor 77−68224
laser, long pulse UV, from N_2-CF_4 mixture 78−63067
laser, miniaturised, for operation at atmospheric press. 77−54733
laser, multi-stage TEA type 80−95912
laser, multichannel Blumlein type, elec. and optical characts. 79−59719
laser, new struct. *(French)* 77−61971

nitrogen continued
laser, oscillator-amplifier system using press.-depend formative time lag of discharge 80−14354
laser, oscillatory circuit with current breaker for discharge excitation 77−14759
laser, photopreionisation stabilised, high-power, ultraminiature 79−22977
laser, photostabilised UV, gain, fluoresc., and energy extraction characts. 79−7118
laser, power investig. using Crookes radiometer 79−62978
laser, pulsed, interfacing with higher freq. electro-optic instrumentation 77−50698
laser, pulsed with damping capacitors, dynamics *(German)* 77−10957
laser, pump for dye laser, conversion to UV radiation in nonlinear crysts. 77−743
laser, pumped by relativistic electron beam, numerical model 77−75492
laser, pumping 0.915 to 1.04 μm of IR dye laser 77−61969
laser, reliable, high-power, design 77−706
laser, rotational struct. variation in 337.1 nm transition 80−78836
laser, Schenck-Metcalf, capacitor modification 79−18439
laser, sealed system with 10 kHz pulse repetition freq. 77−58344
laser, sealed-off miniature high-power, transverse excitation 78−22143
laser, segmented equiv. circuits and rate eqns. *(Chinese)* 79−50282
laser, simple and reliable atm. press. 79−55150
laser, simple and reliable UV emitting, with H_2 thyratron switch 79−27290
laser, simple high-power TEA, operating in UV 79−94251
laser, single freq. emission, superradiance line splitting 77−75495
laser, stimulated emission kinetics under pulse-periodic conditions, theory 79−59689
laser, stimulated emission kinetics under pulse-periodic conditions 79−64212
laser, superrad., inexpensive construction *(Korean)* 78−22147
laser, superradiant, fast helical pin discharge, 4.5 mJ 77−23660
laser, superradiant UV, method for brightness increase 79−36917
laser, TE, anal. of time variation of discharge channel voltage by Pockels effect 78−90412
laser, TEA, for sub ns spectroscopy, modified elec. field 78−17964
laser, TEA, pump for dye laser amplifier system 78−82984
laser, TEA high-power, using modified Marx generator 80−1229
laser, TEA system, coherent UV generation, synchronisation technique 78−17949
laser, time shape of laser pulse 79−7120
laser, transient discharge stage calcs. 77−666
laser, transverse excited $C^3\Pi_u$-$B^3\Pi_g$ (0-0) UV laser band, spectroscopic analysis 79−76671
laser, travelling wave, pump for short resonator tunable dye laser 80−48291
laser, travelling wave pulsed 79−59685
laser, using discrete capacitors in Blumlein type circuit 77−660
laser, UV, discharge-excited, improvement in efficiency *(Japanese)* 78−33724
laser, UV *(Russian)* 77−83859
laser, UV multichannel, short duration pulse generation 79−969
laser, UV TEA, with Blumlein pulse generator, fabrication *(Japanese)* 80−69417
laser additive effects on pulsed CO TE and CS_2/O_2 chemical lasers 79−31876
laser cell for high temp. transverse discharge 77−38914
laser channel dynamic behaviour, spontaneous emissions obs. *(German)* 78−25867
laser discharge emission model and meas. 78−71093
laser for pumping dye lasers with spectral narrowing 78−25903
laser induced gas breakdown threshold at 1.06 micron 80−28594
laser induced tunnelling, avalanche initiating electron prod. 77−39441
laser interference-free coaxial system, construction and operational anal. 77−38918
laser near-threshold IR enhancement by He additive *(Japanese)* 80−14324
laser oscillator-amplifier system, in 337 nm N_2 band 77−14748
laser pulsed, construction and theoretical explanation *(Slovak)* 80−95874
laser pump for tunable dye laser oscillator-amplifier system *(Japanese)* 79−68406
laser pumped dye laser, construction and performance of laser and pumping source *(Japanese)* 77−58341
laser spark in dense gas near metallic target *(Russian)* 80−38682
laser transition, IR, excitation process 80−87383
laser UV-IR pulse time lag theory *(Japanese)* 80−14325
laser with discrete ceramic capacitors in Blumlein-type circuit 77−19330
late-type supergiants, C, N and O abundances for G AND K Ib stars 78−24509
liberation from electrolytic Ni during vacuum heating, Mossbauer spectra *(Russian)* 80−35594
liquefaction systems, optimum operating conditions 77−61075
liquefied, prebreakdown mechanism, intermittent electron emission obs. 77−32325
liquid, absorpt. of high energy electrons 78−882
liquid, anemometrical technique for flow rate meas. 77−31409
liquid, ang. distrib. of stimulated Raman scatt. following excitation by two coherent beams 80−106571
liquid, atmospheric pressure, pool boiling heat transfer from horizontal plates *(Japanese)* 78−67016
liquid, atom pair pots., X-ray diff. 80−100158
liquid, automatic level controller, transfer system for cold traps 78−24805
liquid, automatic level monitoring, in Dewar flasks 80−57309
liquid, boiling, critical heat fluxes, effect of cylindrical heater dimensions 79−35756
liquid, boiling, cryogenic, heat transfer rel. to sinusoidal elec. field 77−72135
liquid, boiling on water, initial water temp. effect 77−19606
liquid, breakdown strength, in mm gap range, press. effects 79−91357
liquid, Brillouin scatt. obs., US vel. and absorpt. 80−45085
liquid, bubble chamber fluid, thermal turbulence, optical distortion effect 77−3221
liquid, collision-induced microwave absorpt. 77−42312
liquid, cryogenic, elec. breakdown, time lag 80−29684
liquid, cryogenic refrigeration system, computer design and optimization 79−58750
liquid, cryostat for obtaining temps. −195 to 150°C and forced heating of specimen 77−74403

nitrogen continued
liquid, decanting siphon using self-opening valve 80−57310
liquid, delay of broadband-pumped stimulated Raman gain 79−50351
liquid, dephasing of mol. vibr. related to correl. functions 78−75523
liquid, dielec. breakdown, press. depend. of polarity effect 80−75936
liquid, dielectric breakdown, using discharge figures 80−11338
liquid, diffusion, free vol. theory, Macedo-Litovitz eqn. 77−51530
liquid, discharge development in nonuniform elec. field 79−91358
liquid, elec. breakdown by field induced microbubbles 79−91365
liquid, elec. breakdown characts. 79−91364
liquid, electric strength determination 79−38451
liquid, evpoarating in horizontal tube, local heat transfer coeff. 77−23959
liquid, falling film rewetting 78−75906
liquid, filling system, automatic 77−41620
liquid, film boiling heat transfer, orientation effect 80−48554
liquid, film boiling heat transfer coeff. for vertical surfaces 80−48556
liquid, for cryogenic equipment for freezing and in-transit temp. control, food and medical appls. 79−58714
liquid, for use in reclamation industry 79−58712
liquid, heat transfer from heated plate 79−63235
liquid, high repetition rate stimulated Raman scatt., thermal blooming 80−91865
liquid, high-field carrier transport at pre-breakdown and breakdown regions 80−25305
liquid, impurity separation, laser thermal method *(Russian)* 77−7859
liquid, in cryostat dewars, appl. to microwave thermal noise source 79−58700
liquid, in gas-controlled cryogenic heat pipe, performance anal. 78−75034
liquid, in Kr, methane, and CO, Raman scatt. parameters, high-resolution coherent active spectroscopy 80−66207
liquid, investigations on heat transfer during pool boiling 79−60494
liquid, IR Raman laser with unstable resonator 79−31957
liquid, laser action due to stimulated Raman scatt., nonmonochromatic pump radiation 79−64284
liquid, laser sonolum. at elevated hydrostatic press. 80−71498
liquid, magnetic field-induced temperature changes 78−57960
liquid, mol. correl. functions, effective pair pot. evaluation 80−10476
liquid, near **BP**, vibr. reson. energy transfer and dephasing, Raman spectra 77−6790
liquid, nucleate boiling heat transfer at reduced pressures 80−48557
liquid, nucleate boiling heat transfer from PTFE coated surface 78−34000
liquid, nucleate boiling in centrifugal accel. field, heat transfer and flux 78−94538
liquid, nucleate pool boiling in N_2 and Ar-N_2 mixtures 79−60495
liquid, partial discharge, cryogenic insulators 78−1920
liquid, photoacoustic and photorefractive detect. of small absorpts., electrostrictive limits 80−108171
liquid, photoelectric determ. of conduction state energies and electron ranges 77−89487
liquid, possible active media in high-power Raman lasers 80−19028
liquid, powerful tunable IR and far IR Raman sources 80−5787
liquid, pressure transmitting medium in low-temperature optical chamber 80−57358
liquid, principle of corresponding states for viscosity 77−84959
liquid, PTC thermistor P310-C11 level sensor 80−52247
liquid, pure vibr. Raman spectra 80−97262
liquid, Raman lineshape 80−11384
liquid, Raman Q branch temp. depend., interferometric obs. 77−43987
liquid, second virial coeffs., 77.3 to 90.1K 79−90754
liquid, sensor using domestic incandescent gas lighter element 79−63201
liquid, shock compression temp., detonation front glow 80−43737
liquid, short-term elec. insulating characts. of some immersed polymeric materials 79−85145
liquid, simulation of atomic and quadrupole interactions, predictions 77−11457
liquid, solubility of light alkanes, IR spectroscopy obs. 80−59654
liquid, solubility of light olefins 80−39286
liquid, solubility of solidified hydrocarbons and halogen-hydrocarbons, calc. by Preston-Prausnitz method 78−26686
liquid, solubility of solidified toluene 79−37843
liquid, spectral splitting of stimulated Raman scatt. 78−50860
liquid, spin density and current correl. functions, computer simulation 79−14661
liquid, spontaneous Raman scatt., vibr. dephasing, review 77−28568
liquid, stimulated Raman scatt., creation of laser source, near IR to submillimetric waves *(French)* 79−31993
liquid, stimulated Raman scatt., parametric generation 77−741
liquid, stimulated Raman scatt., tunable millijoule radiation output 15 to 18 μm 77−88859
liquid, stimulated Raman scatt. excited by picosecond light pulses 79−14034
liquid, stimulated Raman scatt. of excimer laser wavelengths for new lines in UV 79−59755
liquid, struct. factor, short-wavelength neutron scatt. obs. 80−44105
liquid, supply to vacuum installations 80−31762
liquid, surface tension and density profile from expression for excess free energy 77−80681
liquid, thermodynamic perturbation theory, equilib. props. 79−64976
liquid, thermodynamic props., perturbation theory with hard dumbbell reference system 80−14991
liquid, thermosiphon, flow oscills. 77−23960
liquid, tunable anti-Stokes Raman scatt. by light mixing 78−18007
liquid, tunable Raman laser based on third Stokes component 78−50859
liquid, two level controller 80−52241
liquid, US absorpt., bulk viscosity and relaxation 77−35639
liquid, use as cooling agent in industry 79−58709
liquid, used in cryogenic fuelled power packs for operating pneumatic tools 79−58715
liquid, used in cryosurgical instrument for proctological and gynaecological operations for malignant tumours 79−70699
liquid, vibr. dephasing calc., diatom anharmonicity 78−94959
liquid, vibr. line broadening, Zwanzig-Mori theory and quasi-elastic processes 78−27221
liquid, vibrational dephasing, computer simulation, Raman spectra, pair potential effect 80−63863
liquid, viscosity, density depend., theory 77−20105
liquid, wavefront restoration during stimulated Raman scatt. 78−18013
liquid computer-simulated ang. correlations and rot. motion 77−11461
nitrogen continued
liquid internal discharge initiation, expt. 77−24220
liquid N_2 level detector for storage Dewar, teaching labs. 78−41125
liquid N_2 thermosiphon, effects of heater geometry on flow stability 79−58728
liquid N level control in nonvacuum X-ray cryostat 77−41624
liquid Raman laser with slowly relaxing active medium, radiation divergence 79−98352
liquid stimulated Raman scatt. gain under spatially inhomogeneous pumping 77−58389
liquid structure, thermal neutron diffraction 79−46542
liquid surface, floating insulation beads effect on evaporation rate 77−30164
liquid-vapour surface, computer simulation 80−54478
Lithuanian lake catchment area soil N and P distrib. *(Russian)* 79−96780
low pressure discharge, gas temp., laser interferometric meas. *(German)* 79−68951
low threshold breakdown, near target, by pulsed laser radiation *(Russian)* 78−22594
low-pressure DC discharge positive column, vibration temp. radial distrib. 78−67499
lung emptying patterns, multiple breath N_2 washout data 78−92666
Mars atmosphere, N_2 dayglow prediction 77−53452
mass identified ions in O, N, CO and CO_2, transport properties, obs. and calc. 79−50837
matrix for O_3+Zn(Cd) matrix reactions, IR, Raman and visible spectra 80−87110
matrix N-N stretching vibr., IR activation, guest mol. depend. 80−60570
mesic atom, X-ray radiation anisotropy, suppression coeffs. *(Russian)* 78−22058
methane+N_2, rot. line width of vibr. bands 78−33552
methane and N_2 counter diffusion through porous solids 77−80649
methane-Cd($^1P_1$), laser excitation, absolute quenching cross sections and branching ratios 79−49979
methane-N_2-H_2 gas mixtures, RF discharge, vibr. and rot. anal. of CN, N_2 and C_2 78−5241
methane-N_2-isobutane gas mixture composition by Raman spectra 80−87124
methane-O_2-N_2 mixtures, prediction of propagating laminar flames 79−52663
methane-O_2-N_2 premixed flat flame, ruby laser-induced gas breakdown thresholds 79−1951
microwave discharge at high press., vibr. excitation *(French)* 78−14239
migration in Fe-Ti, rel. to mag. permeability disaccommodation *(Polish)* 79−95611
mixing ratio in Saturn troposphere 80−94748
mixtures, marginal comp., thermal diffusion column performance evaluation *(German)* 80−59157
mobility of Li^+ in N_2 gas, obs. using injected-ion drift tube mass spectrometer 78−1784
moist, sound tube meas. of relaxation freq. 78−1058
molar volume measured by adiabatic compression 78−51267
molecular, electron density distrib., electron correl. effects, approx. HF-CI calcs. *(German)* 78−33439
molecular, photoelectron spectra, valence region strong shake-up bands, Koopman's theorem breakdown 79−72354
molecular adsorption and dissociative chemisorption on Fe, XPS obs. 79−99427
molecular beam generation, parameters rel. to stream perturbation before skimmer 79−86468
molecular beams, nozzle-formed, energy parameter determ., time-of-flight method 79−64122
molecular charge density contours for cryst. struct. 78−38645
molecular cluster formation, in rarefied nozzle flowfield 80−5639
molecular constants and collision cross sections, level crossing in gas laser 78−50763
molecular electron elastic scatt., computer anal. of differential cross sections 77−58160
molecular electron scattering, 50-500 eV, two-pot. approach 79−41242
molecular electron scattering, local-exchange approx. for intermediate-energy-differential cross sections 80−48094
molecular excitation, in glow discharge and afterglow 78−63623
molecular ion mobility in N_2, flow drift tube obs. 77−19663
molecular liquid, mean squared torque and mean squared force, interaction energy spherical harmonic expansion 80−54093
molecular oscillator, in liq. ang. freq. autocorrelation function 79−90511
molecular overlayer on graphite, orientational ordering, neutron scatt. meas. 80−10783
molecular photodissoc. ionis., 16-41 eV 77−18995
molecular photoionisation cross sections, at. extrapolation, ground state inversion method appl. 80−18787
molecular polarisability, internuclear depend. of α_0 and α_2 78−58866
molecular sieves, adsorpt. of atmospheric gases, comparison of 13X and 4A at low temp., press. *(German)* 80−88423
molecule, 0-10 eV photoelectron spectra obs., new differential retarding field analyser characts. 77−41735
molecule, I^- system bands, line broadening and shift 80−87138
molecule, 250 MW 0.53 micron laser pulse scatt. spectra, vibr.-rot. transitions *(Russian)* 77−46570
molecule, $3\sigma_g$ photoionis., shape-reson.-induced non-Franck-Condon vibr. intensities 80−43120
molecule, 400 eV core-excited valence states, limited CI calc., transition energies and oscillator strengths 79−68196
molecule, $^5\Pi_u$-$^5\Sigma_g^+$ transition, MC-SCF calcs. 79−76412
molecule, $a^1\Pi_g$, Doppler free two-photon excitation 78−17641
molecule, adsorption on graphite, orientational ordering, theory 80−2262
molecule, angular distribution He I (Ne I) photoelectron spectra 79−31606
molecule, asymmetry parameter, angle resolved photoelectron spectra, multiple scatt. method 80−63708
molecule, asymptotic expansion for Morse-Pekeris oscillators, band strength factors, electronic transition moment 78−78755
molecule, $B^3\pi g$ state excitation and deactivation in positive column 77−3482
molecule, B^3PI_g state, Hanle effect on rot. level 77−58090
molecule, B^3pi_g state vibr. levels, obs. in Lewis-Rayleigh afterglow 77−6797
molecule, $B'^3\Sigma_u^- \rightarrow B^3\Pi_g$ (0,0) emission band 78−58690

nitrogen continued
molecule, B-state collisional transfer, press. effects, oscillator strengths, time resolved spectra 79−36744
molecule, bonding, spin density functional theory 78−17558
molecule, $C^3\Pi_u$ state, electron impact excitation function approx. 79−7022
molecule, $C^3\Pi_u$-state, electron impact excitation, low energy 80−9746
molecule, $C\ ^3\Pi_u$ state, vibr. levels radiative lifetime, transition moment internucl. distance depend. 78−1027
molecule, CARS, optical Stark effect on vibr., and rot. transitions 80−99512
molecule, collision induced far IR absorption at high press. 78−5161
molecule, collision-induced absorpt. at 4.6 cm^{-1} 78−78679
molecule, collision-induced far IR absorpt., quadrupole moment 77−27163
molecule, computer controlled CARS spectra of Q branches 78−62241
molecule, core ionisation, single orbital relax. energy contrib. calcs. 78−82637
molecule, core-ionised, core-valence excited and shake-up states, all electron MRD CI calc. 78−21858
molecule, correlated electron density using AHF GTO wavefunctions 80−23313
molecule, correlation energy, quadruply excited configs. effects 79−54773
molecule, diagrammatic perturbation theory, using universal even-tempered basis set 80−58131
molecule, differential photoelectron cross sections, energy depend. 79−10149
molecule, dipole oscill. strength distribs., sums 78−21975
molecule, dipole properties and dispersion energies additivity, using atoms and small mol. models 80−53091
molecule, dissoc. by electron impact and EUV photoabsorpt., rel. to aurora and airglow 78−58847
molecule, dissoc. chemisorption on Fe(Ni) *(German)* 78−53257
molecule, dissociation, weak bias and anharmonicity effects 78−82661
molecule, dissociative electron attachment, $N^-(^3P)$ form. 78−90308
molecule, elastic and inelastic electron scatt., state to state cross section 80−78708
molecule, elastic and inelastic electron scatt. differential cross section, obs. and calc., struct., binding energy 80−28109
molecule, elastic electron scatt., 50 eV, centrifugal-dominant channel decoupling, INDOX polarised SCF model 80−32831
molecule, elastic electron scatt., eigenphase sums 77−42407
molecule, elastic electron scatt., low-energy, static exchange in R-matrix 78−13601
molecule, elastic electron scatt., total cross-section, 0-1000 eV 78−17795
molecule, elastic electron scatt. from 0 to 1000 eV, energy dependent exchange pots., continuum multiple scatt. method 80−43182
molecule, elastic low energy electron scattering, ab initio pseudostates calcs. 78−9247
molecule, elec. and mag. props., equations of motion method calcs. 77−83513
molecule, elec. field gradient electronic contrib., using generalised X-ray scatt. factors 77−75321
molecule, electrical discharge excitation, vibr. level population distrib., electron beam fluoresc. obs. 80−48031
molecule, electron Compton profiles from energy loss spectra 79−7013
molecule, electron elastic scatt., differential cross-section meas. 77−3458
molecule, electron elastic scatt., discrete basis static exchange approx. calcs. 78−42219
molecule, electron elastic scatt., free-electron-gas model exchange pot. 78−58824
molecule, electron elastic scatt. cross-sections calcs. 80−48088
molecule, electron elastic scatt. differential cross section 79−86067
molecule, electron energy-loss spectra, dipole-forbidden states 79−59588
molecule, electron excitation, collisional deactivation and energy transfer 77−10774
molecule, electron excitation of Birge-Hopfield bands ($b^1\pi_u$-$X^1\Sigma_g^+$) 80−95731
molecule, electron impact, absolute emission cross-sections meas., calibration appls. 79−85996
molecule, electron impact, differential cross-section, converged close-coupling calcs. 78−90290
molecule, electron impact, electron distrib. function in laser radiation field, vibr. excitation influence 80−28112
molecule, electron impact, reson. vibr. excitation, ab initio R matrix calc. 80−32842
molecule, electron impact, rot. excitation 77−58184
molecule, electron impact energy degradation, spatial yield spectra, microplume model 79−98235
molecule, electron impact enhanced vibr. excitation, continuum multiple scatt. model with Hara exchange approx. 80−43196
molecule, electron impact excitation, energy transfer, source of $O(^1S)$ in aurora 79−48598
molecule, electron impact excitation, rate coeffs., momentum transfer cross-section 78−78819
molecule, electron impact excitation, resonances in metastable and UV emitting levels 78−25727
molecule, electron impact excitation, to high Rydberg states, by threshold energy collision 80−83509
molecule, electron impact excitation, $x^1\Sigma_g^-$ and $y^1\Pi_g$ states lifetimes meas. 78−17806
molecule, electron impact excitation cross section of rot. states in glow discharge plasma 77−43092
molecule, electron impact excitation cross-sections for $B^3\Pi_g$, $C^3\Pi_u$ and $E^3\Sigma_g^+$ states 80−1073
molecule, electron impact excitation of electronic states, 10-50 eV 78−13619
molecule, electron impact excitation of electronic states, 10-50 eV 78−17810
molecule, electron impact excitation of electronic states, 12.5-14.2 eV energy loss region 78−17811
molecule, electron impact excitation total cross sections, oscill. strengths, independent particle model calcs. 77−61856
molecule, electron impact ionis., differential cross sections 78−58839
molecule, electron impact reson. dissoc., intermediate negative ion form. 79−36783
molecule, electron impact reson. excitation of new valence state 79−36785
molecule, electron impact resonant scattering, absolute cross sections from boomerang model 79−89798
molecule, electron impact rot. and vibr. excitation, elastic scatt., close coupling and Born approx. 80−28108
molecule, electron impact spectroscopy, high energy, Compton defect 77−88578
molecule, electron ionisation, N_2^{2+} form., decay to N^+, coincidence detect. 77−79695
molecule, electron multiple scatt. method, scatt. cross section calc. 80−63816
molecule, electron resonant scatt., total cross section function 77−50548
molecule, electron scatt., absolute total cross-sections 80−83486
molecule, electron scatt., effective pot. calcs. 80−53131
molecule, electron scatt., elastic and inelastic, Glauber approx. 80−91695
molecule, electron scatt., Glauber eikonal approx. calcs. 80−53130
molecule, electron scatt., iterative static-exchange calc. 79−18290
molecule, electron scatt., local exchange pot. comparison 80−78707
molecule, electron scatt., low energy, multichannel variational calcs., static exchange approx. 80−83483
molecule, electron scatt., reson. excitation and dissoc. attachment, vibr. state depend. 80−78717
molecule, electron scatt., total cross-sections, meas. apparatus 77−54628
molecule, electron scatt., vibr. excitation, rot.-vibr. close-coupling calcs. 77−6947
molecule, electron scatt., vibr. struct. in resonances 78−17813
molecule, electron scatt. cross sections, 0.04-3.7 eV 79−54978
molecule, electron scatt. ground state vibr. levels population 78−1093
molecule, electron scattering, 13.6 eV, coupled channel treatment calcs. 79−64106
molecule, electron scattering, charge polarisation effects, SCF treatment 79−50132
molecule, electron scattering, iterative static exchange method 80−53155
molecule, electron scattering, total cross section 80−37881
molecule, electron-mol. adiabatic polarisation pots. and ab initio SCF polarisabilities 80−9499
molecule, electronic density, multiple scatt. method, muffin-tin approx. 80−27924
molecule, electronic ground state correl. energy, many-body diagrammatic perturbation theory calc. 78−917
molecule, electronic states calc. using five-parameter pot. function *(Russian)* 77−3270
molecule, electronic states excitation and population in glow discharge 77−487
molecule, electronic struct., binding energy and interatomic distance, SCF variational cellular calc. 80−9498
molecule, electrostatic interaction energies for point charge and NaCl (100) surface 78−74592
molecule, energy band calc. by linear combination of muffin tin orbitals method 77−4283
molecule, energy levels, low lying triplet states, infrared emission analysis 78−58691
molecule, ESCA spectra from YMζ radiation source, 132.3 eV 77−4958
molecule, excitation energies, eqn. of motion-Green's function calcs., 3rd order contribs. 77−65417
molecule, excited kinetic investigation of vibr. distrib. function, Raman scatt. *(Russian)* 78−66557
molecule, finite field method calc., moments, polarisability, field-induced shifts in mol. props. 78−74561
molecule, first positive system, electronic transition probabilities 80−78603
molecule, fission fragment excitation, delayed coincidence spectroscopy 77−24189
molecule, fixed-location, spectral variation of photoelectron ang. distribs. 77−14489
molecule, flame temp., CARS spectra diagnostic investigation 80−43404
molecule, fluid, light scatt. orientational memory function at moderate density 80−102521
molecule, formation of $C^3\Pi_u$ and $B^3\Pi_g$ in early afterglow 79−34305
molecule, Franck-Condon factors, semiempirical three-parameter pot. functions 77−18986
molecule, gas, electron impact ionisation, electronic fluoresc. spectra 80−95664
molecule, gaseous, collision-induced absorpt., temp. depend., rel. to atm. far IR transmission 79−62584
molecule, geometry optimisation, using bond function augmented basis sets 78−905
molecule, ground state ionis. pots., generalized Mo theory 80−52907
molecule, ground state MNDO calcs. 78−911
molecule, ground state potential energy, non-muffin tin MS Xα calcs. 77−14355
molecule, ground state props., coupled cluster and MBPT methods appl. 80−47881
molecule, HF calcs., compared with optimised LCAO results 78−5139
molecule, high resolution absorpt. in VUV 77−61762
molecule, high-resolution electronic emission spectrum, 15300 Å 78−66549
molecule, high-speed Raman spectroscopy, condensed discharge vibr. excitation, vibr. temp. 78−82740
molecule, HP collision-induced translational-rotational for IR absorption obs. 77−38628
molecule, in β-quinol clathrate, guest-host interaction, mag. reson. spectra 78−76346
molecule, in Ar matrix, luminesc. lifetime 79−36690
molecule, in solid N_2, phonon-assisted v-v transfer rates 79−10901
molecule, in upper atmosphere, electron impact cross-section 78−28398
molecule, in upper atmosphere, electron impact yield spectra 78−28401
molecule, in zeolitic matrix, IR active fundamentals obs. 77−71800
molecule, inner shell $(2s)^{-1}(\pi 2p)^1\Pi$ state, energy, vibr. struct., electron impact investig. 78−13611
molecule, inner-shell ionisation, relax. effects calcs. 77−42351
molecule, inner-valence ionisation, correl effects calcs. 78−9198
molecule, integrated CARS power, press. depend. 78−59081
molecule, internal partition function calc. 78−55159
molecule, intracavity laser spectroscopy, transient absorption 78−1293
molecule, ionisation by UV radiation from CO_2 laser produced Cu plasma 78−17624
molecule, ionisation pot., Koopman's theorem, corrections using energy shifted perturbation theory 79−6845
molecule, ionisation potential, Green's function-eqns. of motion calcs., third order terms 78−41926
molecule, ionisation pots. and excitation energies, correl calcs. 77−26986

nitrogen continued
molecule, isotopic forms, visible spectra, rovibronic, and rot. anal. $C'\,^3\Pi_u$ and $C\,^3\Pi_u$ interaction 77−18933
molecule, K-shell photoabsorpt. spectra using synchrotron radiation 78−74711
molecule, K-shell photoabsorption spectrum, mol. effects 77−27124
molecule, K-shell photoionis. cross section 77−88505
molecule, K-shell photoionisation, symmetry breaking hole localisation 79−829
molecule, large angle elastic and inelastic electron scatt. differential cross section, exchange corrections 80−28111
molecule, light polarisability parameters, Raman scatt. ang. meas. 80−37814
molecule, line broadening, short range force effects, semiclassical calcs. 79−98085
molecule, liq. and gas, induced absorpt. spectral moment, mol. calcs. 80−63737
molecule, low energy electron (positron) collisions, ab initio adiabatic polarisation pots. 80−14240
molecule, low energy electron impact dissociative ionis., N^{2+} form. and energy distrib. 80−5626
molecule, low energy electron scatt. phaseshifts 77−31011
molecule, low-energy electron scatt., calcs. 77−31013
molecule, low-energy electrons elastic scatt. cross sections 78−42213
molecule, master eqn. theory, dissoc. rate consts. 77−77742
molecule, matrix HF calcs. using universal basis sets 79−59354
molecule, matrix isolated, fundamental vibr. Raman spectra 80−272
molecule, mean energy expended per ion pair by electron impact, Fowler eqn. 77−71882
molecule, metastable level electron impact excitation, resonances *(Russian)* 80−43198
molecule, metastable state mol. ion form. by electron impact 77−14594
molecule, mol. struct. 2-electron integral evaluation by Multipole Expansion of Diatomic Overlap 78−908
molecule, MRD CI calc., lowest dissoc. limits 78−21859
molecule, MSXα calc., partial wave expansion, binding energy and orbital energy 80−37738
molecule, multi-config. SCF super-CI calc., density matrix formulation 80−78547
molecule, multiphoton absorpt., spectroscopic evidence 80−63726
molecule, multiphoton ionisation, EM field gradient forces 78−66608
molecule, multiphoton ionization, nonlinear interaction order and kinetic energy 79−45771
molecule, multiple moments, polarisabilities and anisotropic long range interaction coeffs. 80−43206
molecule, multipole moments, far IR spectrum determ., pot. function effects 77−50435
molecule, N K-shell excitation, high-resolution electron energy loss spectra 80−53152
molecule, nonadiabatic coupling matrix elements by Hellmann-Feynman theory and HF 80−83263
molecule, nonequilibrium dissociation rates in electrical discharges, temp. depend. 78−33447
molecule, nonlinear optical polarisability meas. 79−54991
molecule, one-electron properties, basis set contraction effects 77−88383
molecule, one-electron props., polarisabilities and polarisability derivatives, SCF and CI calcs. 80−37746
molecule, orientated, (e,2e) spectra, electron momentum density 79−98236
molecule, oscill. strengths for shape resonances near K edges 77−75224
molecule, partial photoionisation cross-section determ. using synchrotron radiation 77−75243
molecule, PE curve, spectroscopic consts., perturbation theory appl. 80−23341
molecule, photoabsorpt. cross section, 10 to 50 nm 77−61797
molecule, photoabsorpt. cross-section, 50-340 Å, as sum of empirical at. cross-sections 78−58718
molecule, photoabsorpt. cross-section, photoionis. continuum 77−68029
molecule, photoabsorption, moment anal. 78−46321
molecule, photoabsorption and photionisation, UV region meas. 78−42087
molecule, photoelectron ang. distrib., energy depend. 79−22760
molecule, photoelectron ang. distrib., photon energy depend., 16-25 eV 80−53046
molecule, photoelectron ang. distrib. asymmetry parameter for 30.4 nm photons 79−98151
molecule, photoelectron asymmetry parameters 80−95684
molecule, photoelectron spectra, 21.2-151.4 eV and soft X-ray, ionis. cross-section 78−37683
molecule, photoionis., transition probabilities at threshold, to $X(^2\Sigma_g{}^+)$, $A(^2\Pi_u)$ and $B(^2\Sigma_u{}^+)$ vibr. levels 78−94294
molecule, photoionis. and photoabsorpt. cross sections for aeronomic calcs., data tables 80−41599
molecule, photoionis. cross section calc. for YMζ and ZrMζ lines, HF vs OPW methods 77−42353
molecule, photoionisation cross section and asymmetry parameters calc. in UV region using static pot. 80−95692
molecule, photoionisation of π-shell, discrepancies due to π-π^* transition, modified static-exchange calcs. 79−98163
molecule, polarisabilities, quadrupole and dipole moments, nucl. geom. effects 79−63899
molecule, polarisability derivatives, SCF and CI calcs. 79−59348
molecule, polarisability tensor anisotropy, Raman spectra differential scatt. cross section 80−18860
molecule, pot. curves, binding and ionisation energies and config. variational cellular method 80−32597
molecule, preionis. and predissoc., rel. to spectral line shape 80−63724
molecule, proton affinity determ. from N_2H^+ appearance pot. from N_2H_2 78−58869
molecule, pseudospectral dipole oscillator strength distribs. 78−50503
molecule, pulsed H^+ excitation, fluoresc. decay and press. depend. 77−14483
molecule, Q-branches, high resolution pulsed CARS 78−17676
molecule, quadrupole moments calcs. from line broadening collision with acetaldehyde 80−28065
molecule, radiation chem., primary neutral dissoc. excitation, isotopic exchange mechanism 78−48670
molecule, Raman intensities calcs., ab initio method 80−52993
molecule, Raman intensity, ab initio calc. 80−1028
molecule, Raman spectra, intermol. torques and orientational correlation times 80−48006
nitrogen continued
molecule, relative ionisation energies, Tamm-Dancoff approx. calcs. 80−83243
molecule, relax. time in presence of water vap. *(Russian)* 78−74741
molecule, rot. excitation by electron impact 1-4 eV 78−55248
molecule, rot. line strengths in multiphoton transitions 80−48051
molecule, rot. perturbed Morse oscillator, eigenfunctions and Franck-Condon factors 77−42309
molecule, rot. Raman linewidths, self broadening calcs. 77−42356
molecule, rot. relax. classical trajectory computation, using Lennard-Jones pot. 78−62880
molecule, rot. temp. meas., rocketborne electron beam fluoresc. meas. 77−29519
molecule, rot. temps. determ. in diffusion flames using CARS 79−29358
molecule, rotational Raman calibration of Thomson scatt. 80−1844
molecule, SCF calcs. using cusped Gaussian basis sets, polarisation effects 80−74118
molecule, second virial coeffs. 80−83440
molecule, static polarisabilities, ab initio SCF HF calcs., internucl. separation depend. 78−9073
molecule, statistical correlation energies 78−78637
molecule, stimulated scattering investigation, 1-4 atm press. range 80−91568
molecule, structural second virial coeff., intermol. pot. and mag. scatt. 80−78678
molecule, supersonic mol. beam, CARS rot. temp. meas. 80−23423
molecule, TFDW eqn., energies calc. 79−59355
molecule, three-body electron attachment 80−24245
molecule, total and partial photoionis. cross sections, threshold to 100 Å 77−58092
molecule, total Xα energy, LCAO calc., rel. to local density models 80−32607
molecule, transition moments between excited electronic states 78−5204
molecule, triple-dipole energy calcs. using pseudo spectral theory 78−46418
molecule, triplet state electronic energy delocalisation 77−3478
molecule, triplet-triplet transitions, Einstein-A coeffs., oscill. strengths, lifetimes, theory and experiment comparison 80−47876
molecule, UV spectra, new band, $^3\pi_u$ state lower vibronic levels 78−17682
molecule, V-V and V-T/R energy transfer rate coeffs. by semiclassical collision model 80−9694
molecule, valence electron spectra, excited by Y Mζ and Al Kα ESCA sources 78−53301
molecule, vertical electronic spectrum, MRD-CI method calcs. 78−42033
molecule, vertical ionisation pots., CI calcs. 79−13645
molecule, vertical valence ionis. pot., many-body Green's functions 78−22051
molecule, vertical valence ionis. pot. calc. by perturbation, CI and CPA techniques 80−69263
molecule, vibr. excited, form. in charge transfer reactions 77−3455
molecule, vibr. intensity meas. in photoelectron spectra for ionic ground states 77−18972
molecule, vibr. struct., core and valence ESCA spectra, Franck-Condon and HF anal. 80−32602
molecule, vibr. struct. of K_α emission spectra 78−86886
molecule, vibr. temp. meas. in CO_2 fast flow laser 80−32955
molecule, VUV absorpt. spectrum, homogeneous perturbation between $c_4'(0)\,^1\Sigma_u{}^+$ and $b^1(1)\,^1\Sigma_u{}^+$ levels 77−83618
molecule, Xα theory appls. approximations 80−9510
molecule, X-ray and electron scatt., first Born approx. calcs. 77−61867
molecule, X-ray K-absorpt. spectra, reson. obs., near fine struct. 80−37817
molecule, X-ray K-absorpt. spectra, vibr. fine struct., ab initio restricted HF calc. 78−86883
molecule, Xe matrix-isolated and solid, UPES obs. 79−45762
molecule, zeolite matrix isolated, induced IR spectra 78−46333
molecule+H^+, electron capture and loss cross-sections, 1-20 keV *(French)* 77−38728
molecule+H(2S), collisional quenching, mass spectral obs. 78−25685
molecule electron impact dissociation rel. to O_3 generation in air-fed ozonisers 80−3323
molecule first negative system, Deslandres table 79−98118
molecule photoelectron spectra ang. distrib. asymmetry parameter, vibr. state depend. 77−75218
molecules, ab initio MO-LCAO-SCF and Gordon-Kim intermolecular pot. for seven different orientations 80−95522
molecules, collisional destruction of singlet He I states in low press. glow discharge 80−49030
molecules, excitation efficiency for rot. states 80−102557
molecules, gaseous, density behaviour of rototranslational spectrum, IR spectra obs. 80−28002
molecules, isoelectronic sequence, Rydberg transitions, term value-ionisation pot. correl. 80−58276
molecules, Lennard-Jones 12:6 parameters calc. from viscosity data 77−46612
molecules, structure factor 80−43137
monolayer, adsorbed on graphite, lattice dynamics 78−75946
monolayer on graphite, phonon dispersion curves for postulated four sublattice struct. 78−47667
monolayer on graphite, sp. ht. and u.p., size and steric effects 77−85073
mud volcanoes, Copper River Basin, Alaska, composition of emitted gases 79−84308
muonic X-ray transitions, nuclear charge radii 80−99589
muonium formation by positive muons 79−57272
α-N_2, computer-simulation with atomic pair pot., plastic cryst., phonon dispersion 77−7679
β-N_2, cryst. struct. at 25 kbar and 296K 80−10528
N_2+Li^+, differential cross-sections, classical trajectory calcs. 78−29841
N_2*+NO(H_2O), vibr. excited quenching temp. depend., flowing afterglow 77−54595
nebulae, N and O abundances 78−8093
negative ion mobility in O_2 and N_2, temp. depend. 79−14513
neutron activation analysis meas. of O and N 80−46032
neutron diffraction patterns at room temp., correls. and struct. factor 78−82810
neutron kerma factors for H, C, N, O and tissue, 20-70 MeV 77−73584
NGC 5236, spiral galaxy, N abundance radial var. and central N overabundance 80−82497
NGC 6720 (Ring Nebula), strong forbidden N II emission and element abundances 77−26035

nitrogen continued
nitridation of Mg in HF discharge, temp. effect 80−3399
nitridation of Ta by ionised glow-discharge to form FCC Ta_xN_y 77−52266
nitriding of steel through ionic bombardness 80−45414
non-LTE, pulsed discharge, I-V characteristic obs. 78−71618
nonequilibrium plasma, thermocouple diagnostics 80−103188
nuclear pumped lasers, electron impact cross section meas. 80−63985
nuclei in molecules, isotope shifts calcs. 78−86917
optogalvanic spectroscopy in discharge, 570 to 620 nm 79−54862
oriented molecules, vibrationally inelastic electron scatt. 78−67907
origin and abundances in terrestrial planets and meteorites 78−28559
overabundance in nucleus of NGC 6946 spiral galaxy *(French)* 78−89257
oxidation, in atmosphere, relativistic electron beam stimulation by collective effects *(Russian)* 77−77763
oxidation in intense electron beam maintained glow discharge 79−32841
oxidation resistance improvement of low-alloy steel 80−66706
P ρ T surfaces, butterfly catastrophe 79−86546
pair potential, 2nd virial coeff., nonproduct integration algorithm calc. 77−47128
γ Pavonis, C and N abundances 77−91531
permeability in hard elastic polypropylene films, extension effects 80−40412
permeation through metal barrier, adsorpt. processes 78−63879
permeation through Mo, monocryst. and polycryst. specimens *(Russian)* 79−60554
photoelectron spectra, partial cross sections depend. on photon energy, 16 to 40 eV 78−1025
photoreduction, to NH_3, by desert sand 79−83483
physisorbed monolayer on graphite, neutron scatt. studies 80−107655
pink afterglow, ionisation and ion conversion mechanisms 78−63624
pion energy loss, W-value 77−56473
pionic, Auger electron emission *(Russian)* 80−69271
piston pumps, double-acting, for cryogenic N_2 79−58716
in planetary nebula in irregular galaxy NGC 6822, abundance and nucleosynthesis 80−41867
planetary nebulae, abundances of He, Ne, Ar, N, and Cl 80−109532
planetary nebulae in Magellanic Clouds, He, N and O abundances, effects of excitation class 80−109519
plasma, 10000-13000K, VUV continuum radiation 78−91152
plasma, 18000-45000K, continuum emission coeff., laser spark temp. meas. 77−31527
plasma, absorpt. of energy from large amplitude electromag. pulse 79−90412
plasma, beam and glow discharge type, macroscopic props., kinetic eqns. 80−43864
plasma, charge exchange in collisions of multi-charged ions *(Russian)* 79−98859
plasma, DC glowing discharge rel. to microwave discharge, electron energy distrib., probe meas. *(Russian)* 77−47280
plasma, dense molecular gas, breakdown due to laser radiation, numerical simulation 80−38686
plasma, diffuse, population densities of triplet states, correl. with electron impact processes 80−43966
plasma, electron beam energy distrib., excitation and ionisation model, Monte Carlo method *(Russian)* 79−27790
plasma, electron beam produced, energy distribution of electrons 77−3959
plasma, electron binding to O_2, mechanism 79−55452
plasma, electron kinetics *(German)* 78−91171
plasma, electron temp. and conc. meas., complete LTE 77−65908
plasma, electron transport coeffs. at high E/N values 79−94836
plasma, electron-atom collisions, interaction parameters 100-10000K 79−98857
plasma, electronic excitation levels in gas-discharge 80−24280
plasma, in graphite reactor, temperature distribution *(Russian)* 77−51241
plasma, ionis. and radiation characts. 78−71459
plasma, laser-produced electron temp. and spontaneous mag. field meas. 77−84469
plasma, low-temp., low-power laser radiation scatt. diagnostics *(Russian)* 79−98975
plasma, LTE, radiation emission, theory 77−39410
plasma, mol. vibr. excited, electron distrib. function, temp., drift vel., kinetic coeffs. *(Russian)* 79−7445
plasma, non-equilib., excited species, vibr.-rot. anal. fluoresc. obs. 80−54034
plasma, non-self sustained discharge current, gas purity effects 80−38845
plasma, of theta pinch, $N^{+,2+,3+}$ lines Stark broadening, He(II) line diagnostics 80−24249
plasma, pulse discharge, electron conc. *(Russian)* 77−27753
plasma, pulsed discharge, component conc. radial distrib. determ. *(Russian)* 77−21462
plasma, spatial distrib. in transverse-discharge supersonic stream, continuum theory and probe meas. 80−48866
plasma, Stark broadening, photoelec. obs. 77−23463
plasma, surface treatment of polyester fabric, effect on surface struct., props. 78−95831
plasma created by electron beam, spectral composition *(Russian)* 78−30453
plasma decay under constant voltage *(Russian)* 80−106988
plasma discharge stream, rarefied, diagnostics using sounding and UHF interferometry 79−41872
plasma electron-impact ionis. rate coeffs. obs., Li-like N and O 79−41878
plasma heating in electrodeless RF capacitative discharge, mechanism, impurity effect 80−59312
plasma impurity, high-temp. ionis. equilib. and radiative cooling 78−42712
plasma jet, atomiser, thermal characteristics 77−51246
plasma jet, heat transfer to rotating water-cooled cylindrical wall *(French)* 80−28850
plasma jet, normally-impinging, heat transfer rates to flat plate 80−75061
plasma jet, spectroscopic obs., electron temp. 77−31512
plasma jet anode root behaviour rel. to hollow-anode thermal insulation 78−71554
plasma jets, temperature distrib. by spectroscopic meas. *(Korean)* 77−80355
nitrogen continued
plasma stream of vortical plasmatron, HF temp. fluctuations, holographic interferometry obs. 77−43068
polymer degradation products, chem. anal. by UV photoelectron spectroscopy 78−53300
pool boiling, transient, premature transition to stable film boiling 79−81709
POPOP-Ar-N_2, electron beam pumped, intense laser emission at 381 nm 78−74898
positive column, flowing, visible spectrum obs. 80−49026
positive column, gas temp., interferometric diagnostics, heat cond. calc. 79−32834
positive column, superelastic collisions and electron distrib. function 80−1858
positive corona discharge, current oscills. 77−11431
positronium + N_2 (inert gas), fine struct. interval, collisional density shifts 77−34788
preionisation effect on discharge characts, for CO_2 laser 77−61938
premixed H_2-O_2-N_2 laminar flames, temp. profile, comparison of spectroscopic meas. 80−42227
premixed H_2-O_2-N_2 laminar flames, temp. profiles, Raman, absorpt. and line reversal obs. 80−42227
pressure in vacuum system determ., by mass spectrometry 78−70133
primary origin and N/O abundance ratio in galaxies 80−8686
propane + $Cd(^1P_1)$, laser excitation, absolute quenching cross sections and branching ratios 79−49979
pulmonary function testing, continuous distribution of specific ventilation from N_2 washout 78−92665
pulse discharge regime, time-depend. of radiation *(Russian)* 77−84548
pulsed electrical breakdown at high temps. *(Russian)* 78−34379
pulsed laser, with plane parallel plates 79−86170
pulsed laser stroboscopic fluorimeter 80−35593
pure gas, enthalpy, Carlson-Thodos van der Waals eqn. calcs. 80−83878
purification, using 2.5 m^3/h equipment *(Polish)* 79−12782
PWR, N_2 bubble appl. to eliminate solid water plant evolutions 80−18557
Raman laser, liq., tunable high power systems and appls. 77−27302
Raman scattering for turbulent flame diagnostics 77−72368
rare earth-transition metal alloy thin films vapour deposition, influence of gaseous phase on mag. props. *(Polish)* 80−39820
rarefied fluid dynamics, flow meas. by electron beam-body interactions 80−6186
rarefied gas, rotational relax. in shock layer 79−64703
Rayleigh scattering at 10.6 μm 77−38674
reaction with Al powder, in low-temp. plasma 80−16257
reactive N in unpolluted troposphere, stratospheric source 80−94561
recombination, in transient plasma 78−83521
recombining atomic plasmas, population inversion 80−32679
red giant stars, meridional circulation and CNO anomalies 79−48786
relativistic electron beam transport at low pressures 78−75373
removal from Fe, by dry H_2 method *(Japanese)* 78−11234
River Main, County Antrim, N and P loads meas. by discrete and intensive sampling 79−44213
rotational collision number from thermal cond., 700-2500K 80−23526
rotational temp., determ. in unipolar HF discharge in air *(German)* 77−1033
saturation in steel, gas carbonitriding 79−57152
scattering, inelastic and trapping desorpt., from W, elementary steps in chemisorpt. 80−60737
seawater concentration, rel. to Al, control by biological activity 78−61437
segregation in Fe, equilib. and struct. *(German)* 79−47690
shock activation of supersonic nozzle with overexpansion, jet form. 78−18330
shock tube, three dimens. wave struct. of nonstationary gas outflow 77−55068
solar quiet corona, X-ray spectrum of highly ionised O and N 78−45297
solid, α- and γ-forms, Raman spectra, vibron and lattice freq. shifts, libration 80−16020
solid, α- and γ-phases, Raman intensities of internal and external modes 79−33706
solid, α-form, coherent loss of vibr. and librational excitations 79−86852
solid, α-phase, anharmonic lattice vibrations calcs. 78−71812
solid, α-phase, librational motion, spin-lattice relax. 78−15047
solid, α-phase, mol. dynamics simulation 77−47519
solid, α-phase, NQR meas. 77−12252
solid, α-phase, nuclear spin-lattice relax., mag. field depend., theory 78−68407
solid, α-phase, time-resolved CARS, disorder effects on coherent vibr. states 80−93342
solid, β-phase, for IR absorption spectra 80−11385
solid, adiabatic demagnetisation of stabilised N atoms *(Russian)* 79−82412
solid, anisotropy of chem. shift tnesor, ^{15}N NMR obs. 77−90053
solid, cathodoluminesc. 77−28634
solid, electron impact excited, luminesc. spectra 77−48252
solid, exciton-phonon coupling in strong coupling limit, temp. depend. 80−92616
solid, far IR 4.2K absorption apparatus 79−30583
solid, gamma-phase, anharmonic lattice vibr. 79−33705
solid, interaction of 1-3 keV electron beam, range and secondary emission 79−15568
solid, lattice dynamical calcs., use of anisotropic at.-at. pot. functions, α-γ transition 78−71811
solid, lattice vibrs., group theoretical anal. by computer 77−80590
solid, low-press. diffusion of vapour 78−22842
solid, luminesc., multiphonon-assisted energy transfer 79−47498
solid, melting curves, Lennard-Jones Devonshire theory 80−65201
solid, mol. libration and α-γ phase transition, Kihara pot. calcs. 80−44312
solid, mol. libration in α and γ phases, core pot. calcs. 79−86849
solid, N atoms visible photoluminesc. 79−19939
α-solid, NQR echo envelope modulation due to intramol. dipole coupling 77−48083
solid, porous, contact heat transfer in sublimation 77−31767
solid, Raman spectra vibron and lattice freq. shifts, librational force consts., α- and γ-phases 78−19460
solid, Raman spectroscopy up to 374 kbar 80−7353
solid, refl. spectra, 500-1300 Å 79−33724
solid, self-localisation of high frequency triplet excitations *(Russian)* 79−8176

nitrogen continued
solid, semimicroscopic approach to lattice dynamics of mol. crystals 78−75765
solid, simulation of dynamical props. of molecular solids 78−30710
solid, stimulated Raman scatt. and CARS 78−13752
solid, surface excitation prod. by at. beam deposition, stimulated emission 79−99911
solid, UV spectra, phonon induced exciton fine struct. 79−15477
solid, vacuum UV luminesc., 8K 78−10958
solid and matrix isolated mol., triplet state spectra *(Russian)* 80−5574
solid matrix, ^{57}Fe Mossbauer spectra, Fe_xN mol. form., IR spectra confirmation 77−59496
solid-state α-β transition obs., thermometric fixed point applicability 80−13076
solubility in CaO-Al_2O_3 melt in presence of graphite 78−38850
solubility in electroslag remelting type slag CaO-Al_2O_3-CaF_2 78−44110
solubility in Fe-Cr alloys *(Russian)* 80−92675
solubility in Fe-Cr-Mn alloys above 1000°C, effect of Cr and Mn *(Bulgarian)* 79−65203
solubility in liquid Fe-Cr-Ni containing Mn and Mo 78−44087
solubility in liquid metals, droplet weighing method 79−86889
solubility in liquid MN, exam. 78−51685
solubility in Mn, 650-1030°C, 13-25 at.% N range 79−90783
solubility in Mo, determ. using high-pressure autoclaves 77−15592
solubility in molten polyethylene, statistical thermodynamical method, sorption data 78−71859
solubility in plasticized PVC *(Polish)* 79−69252
solubility parameters, calc. from eqn. of state 77−11660
sorption by Ti, gas-discharge device appl. 80−10796
sorption on ThO_2 sol-gel for nucl. applics. 77−4940
space charge limited current in N_2 and air, high pressure effect 79−32735
spark gap resistance and elec. pulse rise time 77−31538
stable N^- prod. in sputter ion source, design implications for tandem for sensitive C anal. 78−33350
stationary beam discharge plasma, electron kinetics 80−38775
steel, 30N9K4, effects of Mo, V, and N on grain growth, tempering, hardenability, strength and toughness 78−44202
steel, austenitic, Cr-Mn-N, plastic deformation influence on internal friction, relaxation processes *(Russian)* 80−100870
steel, austenitic stainless, influence of varying Cr, Mo, N contents on resist. to pitting corrosion 78−80668
steel, austenitic stainless, N-alloyed 80−108490
steel, austenitic stainless, stacking fault energy, effect of N 80−107279
steel, ferritic, with interstitial N, continuous precipitation and clustering 80−7585
steel, low C sheets, effect of N_2 content on recrystn. texture 79−83233
steel, unkilled deep drawing sheets, influence of N content on recrystn. *(German)* 80−40376
steel structural strengthening, stainless, austenitic, N_2 influence on phase transition obs. *(Rumanian)* 77−55973
steels, ferritic and martensitic, C and N migration at low temps., monograph 80−22149
sticking probability and coverage determ. on W{411} and W{320} 80−54528
superfluorescent UV laser, demonstration 80−105475
supersaturated solns. of nitrogen and water, bubble nucleation, contact angle effects 79−94702
supersonic molecular beam source, simple calibration method 80−82845
TEA pulsed UV laser 77−68228
tektites and natural glasses, N concs. 80−41446
Texas impoundments, critical levels of P and N_2 78−11929
thermal accommodation coeff. on W, gas saturated system 77−70335
thermal conductivity, 400 to 1500K, vibr. internal energy calc. 79−18986
thermal conductivity, corresponding states model 80−69964
thermal conductivity, law of corresponding states *(Russian)* 78−87426
thermal conductivity, simple relation, 1000-3000K 77−24048
thermodynamic and transport props., consistent correlation using Lennard-Jones (12-6) and Buckingham (exp-6) pots. 78−91045
thermodynamic perturbation theory 80−14985
thermomagnetic effect, Knudsen gas between Au surfaces, low temp. 78−30405
thermosphere, at. N composition, seasonal and diurnal variation 80−85782
thermosphere, N_2 density profiles meas. between 90 and 220 km altitude 78−77383
thermosphere, N densities at high altitudes 79−16729
thermosphere, N density, global empirical model 77−33232
thermosphere, N density diurnal variability 77−78549
thermosphere, temperature-depend. model 78−16226
thermosphere N_2 composition, seasonal-latitudinal tidal struct. and mass density 80−101467
threshold photoelectron spectra by electron attachment, autoionisation to high J-levels 77−75211
tissue composition measurement by fast neutron activation 77−64131
tissue inert gas washout, diffusion limited obs. 79−84069
Titan, N_2 atmosphere evolution 79−30005
trace analysis in water, by isotopic dilution and optical spectroscopy 77−5253
track autoradiography for N detect. 80−100979
translational energy transfer rate, after pulsed discharge, interferometric obs. *(Russian)* 78−26322
triple point realisation, reference temperature appl. 78−73997
47 Tucanae stars, N anomaly anal. 79−48867
twinning of single crystals, electron microscope and diffr. exam. 77−35574
two-dimensional freezing, on differently graphitised carbon 79−77896
upper atmosphere, far UV N and N_2 emissions in dayglow 78−28361
UV laser, travelling-wave corona excitation 77−7121
vapour columns, cryogenic, complex flow 78−34119
vapour from solid N for temp. production in 20-63K range 78−221
vapour pressure, effect of high mag. fields 78−38825
venous gas bubble prod. by transient deep isobaric counterdiffusion of He against N_2 78−11790
vibration and electronic excitation results obtained with magnetically collimated electron impact spectrometer 79−49334
vibration stimulated Raman scatt., four photon parametric effects 80−33087
vibrational excitation by electron impact at 30-75 eV, quantum mech. and crossed beam studies 77−34767

nitrogen continued
vibrational excitation calculation, in gas mixture discharge 79−77442
vibrational temps. at 40 to 140 km altitude 77−70762
viscomagnetic heat flux, in a Burnett regime 78−71400
viscosity determ. up to 2000K 79−32730
viscosity meas., capillary method *(Japanese)* 77−35301
viscosity measurement using capillary-type closed viscometer, effect of unsteady flow 78−9736
viscosity measurements using oscillating disc type viscometer 78−51273
viscosity near liquid-vapour transition 79−77799
W50, supernova remnant, N overabundance from optical spectrum 80−90557
water vapour-N_2, absorption at CO_2 laser frequencies 79−50011
water vapour-N_2, nonstationary rarefaction wave, nonequilib. condensation obs. 77−75937
X-ray production, K-shell, on N^+ impact on Ge, Rb, Y, Zr and Ag targets 77−75090
$^{15}N_2$ monolayer, adsorbed on Grafoil, reson. photon scatt. 80−34832
Al:N, positron annihilation, detection of N impurities 79−65777
Al-C-silaceous sand mixture in N_2 atmos., weight loss during heating, compaction *(Japanese)* 80−35151
$Al_xGa_{1-x}As$:N, indirect band-gap, visible laser oscill. at 77K 77−79820
$Al_xGa_{1-x}As$:N, ion implantation, in situ annealing photoluminesc. obs. 80−10567
$Al_xGa_{1-x}As$:N, luminescent material, appl. in optically pumped lasers and electrolum. diodes *(Japanese)* 77−44069
$Al_xGa_{1-x}As$:N, photolum. excitation spectra 77−63451
$Al_xGa_{1-x}As$:N, photoluminesc. and optical absorpt. spectra of N impurity bound-excitons 79−47496
$Al_xGa_{1-x}As$:N^+, (x=0.58), laser annealing of optically active impurities, photolum. charact. 80−20682
Ar plasma jet, surrounded by Ar, He, N_2, H_2 gases, recombinations in decaying jet 78−9753
Ar:N_2, long wave UV luminesc. *(Russian)* 78−88347
Ar-N_2, electron-beam-excited laser lines at 337.1, 357.7, and 380.5 nm, gain conditions 79−86166
Ar-N_2, proton beam pumped, laser actqn at 3577 Å 80−9861
Ar-N_2 electron beam pumped laser characts. at 25-350°C 78−58984
Ar-N_2 gas mixture, vapour-liq. equilib. data *(German)* 77−84915
Ar-N_2 gas scintillation MWPC for high-intensity 5-10 keV X-rays 78−82575
Ar-N_2 interaction, electron gas pot. calc., Gordon-Kim model, ang. orientation depend. 78−70893
Ar-N_2 laser, electron beam excited, gain measurements using amplified spontaneous emission 80−37986
Ar-N_2 laser, intense proton beam pumping 78−78998
Ar-N_2 laser, UV emission, 100-500K, kinetic model 77−58321
Ar-N_2 liquid soln., selective adsorption by plane homogenous surface and C atoms, mol. dynamics calc. 80−59806
Ar-N_2 mixture, adsorption on chabazite, test of eqns. for gas mixture adsorption on heterogeneous surface 78−60030
Ar-N_2 mixture, electrodeless RF discharge, discharge current harmonics obs., conc. depend. 80−44029
Ar-N_2 mixture, electron beam pumped, lasing obs. at 337, 358, 380 and 406 nm 80−102700
Ar-N_2 mixture, fission fragment energy deposition kinetics, rel. to nucl. pumped laser 77−23652
Ar-N_2 mixture, lasing at four lines 80−99713
Ar-N_2 mixtures, DC arc, energy balance of electrons 78−42797
Ar-N_2 plasma, diffusion separation N_2 dissociation 77−76036
Ar-N_2-H_2 plasma equilibrium compositions and thermodynamic props. 78−71433
Ar-N_2(CO), non-self-sustained discharge instability, negative differentiated cond. *(Russian)* 80−38740
Ar-$N_2(Cl_2)(F_2)(H_2O)$ laser, energy pathways by proton excitation 78−5459
Ar+N_2, atomic 1s states deactivation 77−50398
Ar+N_2, bimol. and three body quenching, reson. state $^1P_1$, $^3P_1$ and excimer Ar atoms 79−3540
Ar+N_2, IOS opacities and integral cross sections, partial wave parameter identification effects 77−38719
Ar+N_2, pulsed microwave discharge, early afterglow and radiative transitions, Penning ionisation 78−9874
Ar+N_2, quantual cross-sections, j_zCCS and statistical j_z approx. surprisal anal. 77−14513
Ar+N_2, rot. excitation, classical transition probabilities calc. 77−88533
Ar+N_2, rot. excitation, planar trajectory approx. calcs. using body-fixed coords. 77−75267
Ar+N_2, rot. inelastic collision cross section, centrifugally decoupled exponential distorted wave approx. 79−842
Ar+N_2, rot. inelastic cross section, classical trajectory calc. surprisal anal., pot. energy surface depend. 77−14542
Ar+N_2, rotational excitations, close-coupling calcs. 77−27157
Ar+N_2, vibr. cross-section, exponential distorted wave and effective Hamiltonian 78−37709
Ar+N_2, vibr. excitation of N_2(C) and N_2(B), reaction rate and branching ratio determ. 78−25662
Ar^++$(N_2)(H_2)(O_2)$, charge exchange reaction rates 77−86295
Ar^++N_2, charge transfer cross sections 77−34751
Ar^{x+}+Kr(N_2), (x=2-7), electron capture cross sections, 10-110 keV 77−6923
$Ar^+(Ar^{2+})$+N_2, reaction rate consts. 78−48613
ArN_2, interaction potential, modified electron gas model potential 79−72385
Ar($^3P_{0,2}$)+N_2, rate consts. and N_2(C):N_2(B) branching ratio 78−5327
$Ar_2(^3\Sigma_u^+)$+N_2, quenching, fast absorption spectrophotometry 79−54940
Ar*+N_2, 3371 and 3577 Å laser emission, kinetic model 78−5465
Ar*+N_2, excitation transfer collision, vibronic energy partitioning 77−75264
Ar*+N_2, metastable mol. form., emission spectra 77−19019
Ar*+N_2→Ar+N_2*, electronic to vibr. energy transfer, time depend. theory 80−23514
atom, UV, visible spectra in Ar plasma, 230-620 nm 78−13456
BN, ^{15}N zero point vibr. energy from nuclear photon scattering 80−59593
Bi:N film, ion-implanted, struct., X-ray obs. 77−76692
C-H-O(-N) gas mixtures, high temp. emissivity, 4.8 μ region, shock waves 77−76027
C-N bond in methylamine, nucl. mag. isoscreening line diagrams 80−78555
C+N_2 reaction, CNN radical prod., matrix isolation study 78−86880

nitrogen continued
CNO anomalies in spectra of OB stars 77−29835
CO-N_2, liq., polarised vibr. Raman scatt. lineshapes 78−27199
CO-N_2 and CO lasers, energy and spectral characteristics 80−14327
CO-N_2 dil. liq. solns., resonant IR third harmonic generation 77−31116
CO-N_2 discharge, energy balance influence of N_2 rot. level reson. excitation 78−17903
CO-N_2 discharge, plasma characts. and vibr. kinetics anal. 80−59331
CO-N_2 plasma mixture decay, effective recombination coeffs. *(Russian)* 77−47144
CO-N_2-Ar mixture, supersonic expansion, CO vibr. level populations, gasdynamic laser appl. *(French)* 77−23659
CO-N_2-He glow discharge, CO loss rate 77−19788
CO-Xe-N_2-He gas laser power rel. to mixture composition *(Russian)* 79−7114
CO_2:N_2:He plasma, lasing action, gain limiting attainment possibility 79−89884
CO_2-CO-N_2-He in CO_2 lasers, ionisation wave, slow changes, dispersion curves 80−38822
CO_2-He-N_2, absorpt. coeff. for 10.6 μm CO_2 laser radiation, 295 to 650 K 80−92252
CO_2-He-N_2, gas dynamic laser, gain coeff. numerical estimates, book contrib. 80−1183
CO_2-N_2, CW gasdynamic laser, qualitative comparison with N_2O-N_2 laser 78−25856
CO_2-N_2, CW mixing gasdynamic laser, saturation parameter and small signal gain 79−45923
CO_2-N_2, gasdynamic laser mixture, vibr.-nonequilib. nozzle flows, numerical and approx. solns. 78−74881
CO_2-N_2, gasdynamic laser, gain-optimisation, theory 79−76664
CO_2-N_2, gasdynamic laser, theoretical gain-optimisation, parametric study 79−76665
CO_2-N_2, gasdynamic mixing laser, performance for various injection techniques 77−38917
CO_2-N_2, glow discharge instability, non self sustained ionisation source, mechanism 80−38819
CO_2-N_2, high temperature gas diagnostics by spectral remote sensing, 700-1350K 78−74002
CO_2-N_2, hot gas mixture, spectral and integral emission capacities calcs. *(Russian)* 77−68054
CO_2-N_2, ionisation current growth, Townsend swarm coeffs. 78−59541
CO_2-N_2, kinetic cooling effect by CO_2 laser radiation, temp. dependence 80−10347
CO_2-N_2, non self sustained repetitively pulsed discharge instability obs. 80−38820
CO_2-N_2 electroionisation laser mixture, ionisation instability of semi self maintaining discharge 80−63971
CO_2-N_2 fast-flow laser with unstable resonator, self-oscillation instability 80−95870
CO_2-N_2 gas mixture, kinetic cooling by CO_2 laser radiation *(Russian)* 77−89229
CO_2-N_2 gasdynamic laser, amplification coeff. rel. to water vapour content *(Russian)* 77−7057
CO_2-N_2 gasdynamic laser, thermal nonequilibrium heating of active medium by elec. arc 80−53258
CO_2-N_2 laser, high-pressure, numerical optimisation 77−10882
CO_2-N_2 mixture, strongly excited, vibr. relax. 80−102555
CO_2-N_2 mixture, temperature measurement by spectrum line reversal 80−73358
CO_2-N_2 mixture gasdynamic laser, energy characts. 80−69362
CO_2-N_2-^{3}He, laser, plasma diagnostics of media capable of lasing in nucl. reactor environment 79−10279
CO_2-N_2-H, laser discharge circuit parameters, effect on energy imput mode 77−75476
CO_2-N_2-H_2, non-self-maintained glow discharges at atm. pressure, elec. characteristics and energy exchange 78−71606
CO_2-N_2-H_2 electron beam controlled laser, efficiency and output energy depend. on H_2 78−58978
CO_2-N_2-H_2O fast flow discharge laser, output power time depend. 80−99697
CO_2-N_2-H_2O gasdynamic laser, small signal gain and vibr. wall accomm. 79−98340
CO_2-N_2-H_2O mixture, unstable-oscillatory expansion *(Russian)* 78−1637
CO_2-N_2-He, coefficient of optical amplification behind an axisymmetric shock wave *(Russian)* 77−89153
CO_2-N_2-He, non-self-sustained plasma discharge instability, electron collisions *(Russian)* 77−76050
CO_2-N_2-He, pulse-periodic operation of electron-beam-controlled discharges, energy characts. changes 80−102695
CO_2-N_2-He, transverse combined discharge laser, 10-20 kW *(Russian)* 77−54703
CO_2-N_2-He, vol. discharge, negative ions effect 80−14956
CO_2-N_2-He (H_2O) gas mixture, method for obtaining vibrational population inversion 79−94210
CO_2-N_2-He CW gasdynamic laser, closed-cycle, construction and operating parameters 80−23717
CO_2-N_2-He discharge, voltage drop, impedance 77−47291
CO_2-N_2-He discharge, energy balance, influence of N_2 rot. level reson. excitation 78−17903
CO_2-N_2-He discharge, electron distrib. relax., numerical study 80−54070
CO_2-N_2-He electroionisation laser, freq. mode, lasing conditions 80−63970
CO_2-N_2-He gas mixtures, fluorescent IR radiation from glow discharge 78−94386
CO_2-N_2-He gas mixtures, time-of-flight meas. of electron transport parameters 78−94387
CO_2-N_2-He gasdynamic laser, effect of weak flow perturbations on gain 80−14316
CO_2-N_2-He laser, civr. temp. approx. for N_2, applicability limit 78−5452
CO_2-N_2-He laser, pulsed microwave discharge pump, skin effect and gain 79−13945
CO_2-N_2-He laser, vibr. population distrib. of N_2, vibr. temp. determ. 77−14688
CO_2-N_2-He laser media excitation by electron beams admitted through gasdynamic windows 80−99694
CO_2-N_2-He laser mixtures, self-sustained glow discharges, low ionisation pot. organic additives effects *(French)* 77−88694
CO_2-N_2-He laser mixtures, electron swarm parameters, Boltzmann eqn. anal. 79−18396

nitrogen continued
CO_2-N_2-He laser mixture in nonself-sustained discharge, direct heating mechanism 80−28195
CO_2-N_2-He mixture, ionisation and attachment coefficients 78−42706
CO_2-N_2-He mixture in gas-dynamic system with independent thermal excitation, population inversion in two-step mixing 79−89888
CO_2-N_2-He mixture supersonic adiabatic expansion, population inversion and gain 80−19017
CO_2-N_2-He mixture volumetric glow discharge formation at atm. pressure 78−71615
CO_2-N_2-He nozzle flows with boundary layer, gain coefficients 80−14312
CO_2-N_2-He pulsed transverse discharge, investigation of gain 80−9855
CO_2-N_2-He system, CO_2 TEA laser discharge development, high-speed-camera investigation 79−55109
CO_2-N_2-He volume discharge, self-sustained, with UV preionis. 79−60211
CO_2-N_2-He-O_2 discharge mixture, three body electron attachment to O_2 80−64779
CO_2-N_2-He(H_2) laser mixtures, composition effect on excitation efficiency in dicharge 78−5453
CO_2-N_2-Ne-H_2O mixture IR laser *(Russian)* 79−10323
CO_2-N_2-O_2 mixtures, thermalisation under reson. excitation by laser radiation *(Russian)* 78−26231
CO_2+N_2, broadening of $30^0 01_{II} \leftarrow 00^0$ band 78−86865
CO_2+N_2, near IR absorpt., collisional broadening 77−30872
CO_2+N_2, semiclassical energy transfer method, Coriolis coupling 78−90266
CO_2+N_2+He, glow discharge positive ion species identification *(Russian)* 80−84014
$CO_2+O_2(N_2)$(air), bending mode vibr. deactivation rate, 1500-350K, shock tube meas. 77−38714
$CO_2(01^10)+N_2(CO)(O_2)$, collisional deactivation rate const., 160-375K, photoacoustic obs. 79−10179
$C^3\Pi_u$ effective lifetime 80−102704
CS_2-N_2 gas binary diffusion coeff. obs. *(Japanese)* 79−10627
$CS_2+He(Ar)(N_2)$, perturbed rot. diffusion of CS_2, IR spectra 78−75245
$Cd+N_2$, vap., creation of inverse population of atomic Cd 6^3S and 5^3P_2 levels 80−58219
CdS:N, P, As, Sb, Bi photoluminescence obs. 78−10965
CdSe:N, implanted, electroreflection obs. 80−40089
CdSe:N, single crystals, luminesc. 79−87493
$Cl+NO+N_2 \rightarrow NOCl+N_2$, rate const. temp. depend. 78−76828
Cl_2+N_2 mixture, Raman laser optical excitation, electron phototransition theory *(Russian)* 80−99711
Co_2:He:N, glow discharge instability in afterglow 80−6313
Co_2-N_2-He, pulsed discharge with temp. and density gradient in cathode sheath 79−41899
Cr particle nitrogenation, metallographic obs. *(Bulgarian)* 78−15712
Cs-N_2 discharge, Cs_2^+ form. rate, mass spectra obs., N_2 press. depend. 79−27853
Cs-N_2 plasma, collision recomb. of charged particles *(Russian)* 77−80373
Cs-N_2 plasma, excited atomic state inversion obs. 78−71460
Cs-N_2 system, optically pumped, spin relax. 79−59420
$Cs+N^+(N_2)^+$, total charge-transfer cross-sections meas. 77−50527
$Cs_2+He(Ne)(Ar)(Kr)(N_2)(CH_4)$, collision-induced dissoc., atom-mol.-exchange optical pumping 78−22008
Cs^*+N_2, excited states quenching 78−5330
Cu, adsorbed mol. monolayers, UV-visible spectra 78−72619
Cu-N mixture, partially ionised, transport and thermodynamic props. 77−80276
Cu-N_2, effect of Cu vapour on wall stabilised arc extinguishing times 78−87548
$D_2^+ + N \rightarrow ND^+ + D$, product kinetic energy distrib. obs. 77−46619
$D^{**}+N_2$ fast collisions, impulse approx. 80−106281
$F+N^{4+}$, bonding effect on Kα satellite struct. 79−59392
F_2-N_2 mixtures, electron attachment rate to F_2, elec. cond. meas. 79−7019
Fe, liquid, N solubility depend. on added elements, mechanism *(Russian)* 80−65223
Fe surface hardening, ion-carbo-nitriding in CO-N_2-H_2 gas mixtures, expt. *(Japanese)* 80−71670
Fe:C,N, mag. relax. due to C and N meas., 210 and 410K 77−36102
Fe:C(N), small concs. determ., mag. and mech. relax. methods 80−7879
Fe:N, ion implanted foil, Mossbauer effect study, nitride form. 78−27149
α-Fe:N, mag. field depend. of reverse permeability 77−80969
α-Fe:N, valency effect of interstitials 80−65502
Fe:O,N, bonding of Al, growth of intermediate phases, effect of O and N impurities 78−27680
Fe-CR (26 wt.%), role of C and N in brittle fracture 80−16456
Fe-Cr-Mn-N, influence of N on defect conc. energy *(Russian)* 80−54241
α-Fe-N, supersaturated solid solns., N atom precip. kinetics, resist. meas. 80−60864
Fe-N (10 at.%), structural transforms., expt. investig. *(Russian)* 77−12613
α-Fe-N solid soln., N precipitation kinetics, defects effect 77−59789
Fe-Ni alloys, diffusivity of N_2 79−46845
GAP:N LED, acoustic emission study of defects 79−86799
$Ga_{1-x}Al_xP$:N epitaxial films, ion implanted, cathodoluminescence study 80−60684
Ga(As,P):N, intermediate range model of N states 79−73467
Ga(As,P):N, isoelectronic impurity states, long-range, short-range model 80−75524
Ga(As,P):N, theory of bound states induced by disorder and isoelectronic pots. 77−35889
GaAs:N, extended Huckel theory appl. 80−59916
$GaAs_{0.6}P_{0.4}$:N, isoelectronic tape by ion implantation and CO_2 laser annealing 80−24464
$GaAs_{1-x}P_x$, N trap bound state, Hall effect determ. 78−19055
$GaAs_{1-x}P_x$, N^+ implantation photoluminesc. props. 77−68987
$GaAs_{1-x}P_x$, N^+ implantation, annealing props. 77−68988
$GaAs_{1-x}P_x$:N, $0.6<x<1$, photoluminesc., comp. depend. 78−52546
$GaAs_{1-x}P_x$:N, film, optical absorpt. from photoluminesc. meas. 78−92134
$GaAs_{1-x}P_x$:N, Koster-Slater model and N-states 78−47732
$GaAs_{1-x}P_x$:N, LED, external quantum efficiency, press. effect 77−8655

nitrogen continued
$GaAs_{1-x}P_x$:N, N isoelectronic trap, model calc. of N_Γ and N_x electronic states 78−10398
$GaAs_{1-x}P_x$:N, photoluminesc. and optical absorpt. spectra of N impurity bound-excitons 79−47496
$GaAs_{1-x}P_x$:N, photolum. and electrolum. study of N isoelectronic traps 80−89061
$GaAs_{1-x}P_x$:N, upper branch of N isoelectronic trap., photo- and electrolum. expts. 77−63462
$GaAs_{1-x}P_x$:N epitaxial layers, absorption and photolum. spectra meas. 77−24894
$GaAs_{1-x}P_x$:N heterojunction, N_x and N_Γ bound states, high-press. effects on electroluminesc. meas. 77−11870
$GaAs_{1-x}P_x$-SiO_2:N,Zn ion-implanted multiple layers, ion range distribs., secondary ion microprobe meas. 79−42129
$Ga_xIn_{1-x}P$:N, Delta lattice parameter model, correl. with electronic props. 78−91560
$Ga_xIn_{1-x}P$:N layers, LPE growth, luminesc. and direct exptl. obs. of band struct. effects 77−52157
GaP:Bi,N, photoluminesc., electroluminesc., 4.2 to 300K, excitons and hole traps 80−108275
GaP:N, appl. of temp. modulated photolum. induced by photoexcitation technique 78−95605
GaP:N, bound exciton absorpt. line asymmetry, electroabsorption spectra 80−71459
GaP:N, bound excitons, low temp. photoluminesc. thermal quenching 77−48228
GaP:N, Cd(Zn),(C), interimpurity recomb., acceptor binding energies 78−34796
GaP:N, electron binding by N pairs 79−90990
GaP:N, electron charge distrib. in vicinity of substitutional N 77−24531
GaP:N, electron-hole liq., luminesc. obs. 80−25438
GaP:N, electronic energy levels calc., optimisation 79−28315
GaP:N, epitaxial layer, determination of nitrogen concentration from cathodoluminescence spectra 78−38744
GaP:N, epitaxial layer doping 77−51396
GaP:N, epitaxial layers, N concentration determination by two independent methods 80−39142
GaP:N, excited states of excitons bound to NN_i pairs, fluoresc. obs. 77−44039
GaP:N, extended Huckel theory appl. 80−59916
GaP:N, luminesc. decay kinetics 79−38646
GaP:N, luminesc. from electron-hole drop 79−33813
GaP:N, N doping profiles in GaP grown by LPE, cathodoluminesc. data 79−23631
GaP:N, phonon satellite intensity distrib. in luminesc. spectrum 77−55832
GaP:N, photoluminesc., temp. depend., exciton recombination mechanism 78−88355
GaP:N, photoluminescence, temp. modulated 79−38623
GaP:N, piezo-modulated spectroscopic investigation of N and N-N pairs 77−66474
GaP:N, radiative recomb. from electron-hole drops, impurity induced transition 78−19547
GaP:N, radiative recomb. of electron-hole liq. 79−73442
GaP:N, spin dependent exciton recombination at N_2 isoelectronic traps 77−69734
GaP:N, temp. modulated photoluminesc. 77−55818
GaP:N, temp.-modulated photoluminesc., phonon assisted tunnelling process 78−23511
n-GaP:N,O,S,C end, dielec. const. from S-C donor acceptor pair spectra 79−65788
GaP:N LED, acoustic emission, NDT of dislocation motion 78−91759
GaP:N LED, deep level studies, growth by time difference method at controlled vapour pressure 80−39522
GaP:N LED structures, local dopant conc. determ. using SEM cathodolum. spectra 80−101057
GaP:N p-n structure yellow light emitting source 77−69412
GaP:N VPE LED, deep level centres, DLTS studies 79−42493
GaP:N VPE layers, thermal emission energies, trapping, and carrier lifetimes, deep level capacitance spectroscopy 79−42487
GaP:N(N,O) epitaxial struct., luminesc. study of degradation during heat treatment 80−45139
GaP:N(Te), ion implanted at 40 keV, refl. spectra, 210-2000 nm, annealing *(Russian)* 78−80386
GaP_xAs_{1-x}, N doped, alloying induced shift between excitation and luminesc. of N bound exciton 79−52013
GaP_xAs_{1-x}:N, impurity electron states, binding energies and wavefunctions 79−42488
GaP_xAs_{1-x}:N, luminesc. of N bound state excitons, local-environment effects 80−100691
$H+B^{q+}(C^{q+})(N^{q+})(O^{q+})$, ($2 \leq q \leq 4, 5$), cross sections at keV energies 80−78705
$H+C^{2+}(C^{3+})(N^{2+})$, radiative charge transfer, rate coeffs., pot. energy curves 77−88554
$H+H^+(Arq^+)(Kr^{q+})(B^{q+})(C^{q+})(N^{q+})(O^{q+})$ charge transfer and impact ionis. cross sections calcs. 77−88555
H+N, stripping cross-sections, binary encounter approx. theory 78−50618
$H+N_2$, charge prod. cross sections and differential scatt. calcs. 78−94313
$H+N_2$, excitation of Hα and Lα emissions, rel. to aurora 79−68309
$H+N^+(N^{2+})$, ionization model for NGC 7027 planetary nebula 78−36671
H^0+N^{3+}, electron loss cross section 80−63805
H^++He(Ar)(Kr)$(O_2)(H_2)(N_2)$, 2.2-8.2 keV, H(n=3) form., absolute cross sections 77−34755
$H^+ + N_2$, visible band emission cross-sections 77−16847
$H^+ + N_2$ collision, binary encounter calcs. of proton energy deposition 78−74746
H_2-N_2, liquid-vap. equilib., 63-110K and up to 57 MPa 79−55881
H_2-N_2 glow discharge, positive column, electron energy-distrib. spatial variation 77−47294
H_2-N_2 mixtures, 300K, proton spin relax., single relax. time approx. 77−61766
H_2-N_2-Ar, two-phase flow film boiling, in vap. generator, heat transfer 78−75190
H_2-N_2(Ar) gas mixture, correl. between kinetic theory of thermal cond. and expt., 90 to 300K, 1 bar 79−81707
H_2-O_2-N_2 flame, photochem. reactions involving Na*, laser saturated conditions 78−80762
nitrogen continued
H_2-O_2-N_2 flames, diffusion coeff. meas. for CO, Br, I and Tl 78−51272
$H_2+D_2(N_2)(HCl)(CO_2)$, V-V transfer, pulsed fluoresc. obs. 77−14540
H_2+Ne^+, thermal energy, reaction rate coeffs. and product distrib. 79−29333
$H_n^+ + N_2$, (n=2 to 27), 250-900 eV collisions, fragmentation 77−88525
HBr-nN_2 aggregates, near IR spectra in monatomic matrix 78−21921
HCl-N_2 mixture, electron swarm, Cl^-.HCl cluster formation, dissoc. attachment, drift tube mass spectra 78−68884
HCl-nN_2 aggregates, near IR spectra in monatomic matrix 78−21921
$H^{35}Cl+N_2$, collision broadened vibr.-rot. linewidths, and shifts in fund. band, low temp. obs. *(French)* 77−68076
$HF+H_2(D_2)(N_2)$, 200K and 295K vibr. relax. rates 80−63766
$H_2{}^{16}O$, $HD^{16}O$, $H_2{}^{18}O$, mol. diffusivities in N_2, isotope effects 79−1282
$HO_2NO_2+N_2 \rightleftarrows HO_2+NO_2+N_2$ react., kinetics, RRKM theory appl. 78−73032
H_2S+N_2, press. broadening of spectral linewidth, calcs. 77−30932
He-N mixture, RF discharge, mass spectroscopy, floating double probe meas. 80−84016
He-N_2, de excitation rate consts., energy transfer, pulse radiolysis obs. 80−30303
He-N_2, pulsed atomic N laser, time and energy characts. in mag. field *(Russian)* 78−22108
He-N_2 gas mixture, correl. between kinetic theory of thermal cond. and expt., 90 to 300K, 1 bar 79−81707
He-N_2 laser, energy pathways by proton excitation 78−5459
He-N_2 mixture, plasma created by electron beam, spectral composition *(Russian)* 78−30453
He-N_2 mixtures, mutual diffusion coeff. meas. depend. on cell geometry 77−3911
He-N_2 mixtures, thermal diffusion 80−1726
He-N_2 plasma, N_2 $B^3\Pi_g$ state excitation, role of long lived states, luminesc. 80−37829
He-N_2-CO_2 mixture, IR laser output from elec. discharge after X-ray preionisation 79−64205
He-N_2-CO_2 mixture in supersonic nozzle, shock activation with overexpansion, jet form. 78−18330
$He+B^{3+}(C^{4+})(N^{5+})(O^{6+})$, electron transfer 78−13598
$He+H_2(He)(Ar)(N_2)$, fast metastable at. collisional destruction cross section 78−74760
$He+H_2(He)(N_2)(Ne)(Ar)$, 25-450 keV, metastable ion beam electron loss and deexcitation cross section 77−34745
$He+N_2(O_2)(HCl)$, Pennin ionis. electron spectra, new differential retarding field analyser characts. 77−41735
$He^+ + N_2$, ≲0.1 eV, charge exchange, UV and visible luminesc. spectra 77−83722
$He^+ + N_2$, low energy collisions, vibronic excitation model 77−83689
$He^+ + O_2$, (N_2), charge transfer reactions, product ion distribs. 77−73445
$He^{2+} + N_2$, 200-600 eV, 0-20°, comparison with He^{2+}+Ne(Ar) 78−74732
$He_2^+ + Ne(Ar)(N_2)(CO)(CO_2)(Ch_4)$, bimol. and termol. charge transfer reactions, rate coeffs. 77−1910
$He^+(He_2^+)+N_2(CO)(CO_2)(H_2S)$, charge transfer Penning ionis. 78−17784
$He_2(^3\Sigma_u)+Ne(Ar)(N_2)(CO)(C_2)(CH_4)$, excitation transfer reaction rates 78−5332
^{4}He stopping cross sections, 1-8.5 MeV 78−58558
Hg-N_2, optical pumping, vibr. excitation, laser theory 78−66517
Hg-N_2, optically pumped pulsed 546.1 nm laser emission 79−13952
$Hg+N_2$, inelastic collision, 6^3D_1 population transfer to other 6s6d Hg levels, fluoresc. obs. 78−78791
$HgBr_2+N_2(A^3\Sigma_u^+)$, dissoc. excitation 80−63774
$In_{1-x}Al_xP$:N, radiative recombination at isoelectronic centres 79−52027
$In_{0.3}Ga_{0.7}P$:N ion implanted, photoluminescence study 80−97322
$In_{1-x}Ga_xP$:N, composition depend. of bound state luminesc. transitions 78−39595
$In_{1-x}Ga_xP$:N, radiative recombination at isoelectronic centres 79−52027
$In_{1-x}Ga_xP$:N_2, N-trap bound states, photoluminesc. and absorption data 77−1719
KBr*+Ne(Ar)(CO)$(N_2)(CO_2)$, information theoretic anal. 77−521
Kr-N_2 gas mixture, vapour-liq. equilib. data *(German)* 77−84915
Kr-N_2 plasma, afterglow ion prod. and loss processes 77−11401
$Kr+N_2$, reaction rate constants in afterglow 77−427
$Li^+ + N_2$, (0.5 to 1.0 keV) energy loss spectra, ionisation, electronic and vibro-rot. transitions 77−14541
$Li^+ + N_2$, rot-vibr. transitions, semiclassical calc. of cross sections 79−22798
$Li^*+H_2(N_2)$, thermal, high-Rydberg Li behaving as ion core 78−22004
liquid N_2 for stimulated Raman scatt. Dewar cell, 1.06 to 1.4 μm Q-switched laser pulse conversion 80−99799
Mn-N, liquid, N soln. 79−99321
Mo, cast state, interaction nature between C, O_2 and N_2 *(Russian)* 79−70114
Mo:N, ion implanted proton-irradiated, annealing behaviour 78−91362
Mo:N film, high T_c amorphous phase stabilisation by interstitial nitrogen 78−23622
Mo:N film, implantation effect on supercond. and struct. transform. 77−4462
Mo:N single cryst., interaction of N with vacancies 79−82261
Mo-N solid solution, exam. of enthalpy of solution, variation with temp. 79−10947
Mo-N solid solution, thermodynamic props., 1618 to 1883K 80−65230
Mo-Zr, nitride form. in N_2 atmos. *(Russian)* 78−19938
Molecule discharge excited vibr.-rotation states meas. by CARS *(Russian)* 79−3429
molecule, fission fragment excitation of optical radiation, quenching by UF_6 77−23665
molecules in nonequilibrium gas-dynamic current, vibr.-level populations determ. by Raman scatt. 80−99509
N and N_2 in thermosphere, annual var. from Aeros Nims data 80−12578
N, bubble formation during injection, system pressure and thermophysical effects *(German)* 79−41745
N, detect. in Venus upper atmosphere 80−77310
N I, forbidden radiative transition probabilities rel. to NGC 7027 low-excitation emission 77−64823
N I, laser transition obs. at 9064 Å in He-N_2 afterglow 78−74891
N I, resonance line broadening in low press. He discharge lamps 78−9123

nitrogen continued
N I, weighted oscillator strengths for elec. dipole and forbidden transitions, data tables 80−37779
N I 1.04 μm forbidden multiplet relative intensity, auroral forms mean height indicator 79−70909
N I 5200 Å airglow, anal. of consistency of ground-based obs. with satellite results 80−98496
N I 5200 Å forbidden line nightglow, ground-based meas. contamination by OH emissions 78−4020
N I (^{2}D) 5200 Å emission in auroral zone, prod. 79−21090
N I forbidden lines in nightglow, historical review 79−5699
N I interstellar absorption in γ Cassiopeiae direction, UV obs. 80−51823
N I plasma jet, spectroscopic diagnostics, Stark broadening and shift, study 80−38727
N I transition probabilities and absolute oscillator strengths, rel. to H I regions 77−49448
N II, electron impact excitation cross sections, rel. to solar corona abundance 80−58391
N II, m-representation approach to atomic structure 79−45645
N II, N III, interstellar, fine struct. levels population ratios 79−35351
N II, optical oscill. strengths 79−98032
N II 2144 Å, emission feature obs. in UV aurora 78−88963
N II 6584 Å forbidden line profiles of giant H II regions 79−67081
N II homologous ions series, Stark broadening trends 80−105157
N II lines contrib. to auroral 2150 Å spectral feature 78−61645
N III, electron impact excitation cross sections, generalised oscillator strengths, Born approx. 80−18928
N III, electron impact width of plasma lines, approximative semiclassical formula 80−43972
N III, low lying levels, excitation equilib. 79−12401
N III, optical oscill. strengths meas. 79−98031
N III, VUV spectrum *(Chinese)* 80−42974
N III forbidden lines in Omega Nebula (W38, M17, NGC 6618), IR spectral obs. 80−90495
N III intersystem multiplet as density indicator for solar plasmas 80−31264
N III lines for solar diagnostics 79−30031
N IV, 2s3p $^3P_1$-2s^2 $^1S_0$ intercombination line transition probabilities 80−18823
N IV, absorption spectra, 4f electron localisation effects in collapsing shell 77−3290
N IV, dipole lengths, dipole vels. and transition probabilities 79−35113
N IV, electron impact excitation cross sections, Coulomb-Born approx. 77−75302
N IV, electron-impact excitation calcs. 79−81286
N IV, excited states, transaction oscill. states and wavefunctions 79−59367
N IV, intercombination lines, transition probabilities determ. 79−89645
N IV, N V, electron impact ionisation 78−70941
N IV, transition probabilities calcs. 79−54792
N IV solar emission line ratios, electron density and temp. determ. 80−17559
N IV+H charge exchange cross section rel. to intercloud gas 77−45514
N, in upper atmosphere, prod. by meteoroids 79−2404
N in upper thermosphere, impact of gas-surface reactions on mass spectrometric meas. 79−66849
N ion+Au, L-shell X-ray production and subshell ionisation cross sections meas. 80−91637
N, ionisation, multiphoton absorpt., spectroscopic evidence 80−63726
N ions+B(C), 10-40 MeV, soft X-ray spectra 77−75089
α-N, low freq. absorpt. spectra, libration modes *(Russian)* 80−55078
N V, absorption spectra, 4f electron localisation effects in collapsing shell 77−3290
N V, beam-foil decay curves, mean lives determ. 80−9553
N V, beam-foil spectra assignment, compared with HF energies, isoelectronic sequence 79−31424
N V, electron ionisation cross sections of excited atoms and ions 80−43186
N V, hot interstellar gas diagnostic, IUE obs. 80−101634
N V, ionis. rate meas. in theta-pinch plasma, VUV obs. 78−26254
N V, optical oscillator strength 80−47941
N V, plasma impurity UV emission, poloidal asymmetry obs., grad B drift 78−26331
N V, VI, laser produced plasma, satellite spectra 78−5165
N VI, electron impact excitation cross sections calc. using nonrelativistic Coulomb-Born approx. 77−42414
N VII, and isoelectronic series, in laser-produced plasma, Balmer fine struct. (broadening) 80−48860
N^-, appearance pot., form. by electron impact ionisation, mass spectra 77−75320
N^- autoionisation from N_2 electron impact dissoc., EELS 80−106397
N^-, continuous absorption coeffs., from elastic e-N scatt. data, target wavefunction effect 78−9128
N^-, form., by double electron transfer, cross-section meas. 78−78806
N^-, free-free absorpt., multichannel theory 77−18816
N^-, reson. in i.r. spectrum 77−424
N^-, Sternheimer valence shielding and antishielding factors 80−18807
N^+, acceleration by intense relativistic electron beam in spatially periodic mag. field *(Russian)* 79−10255
N^+, amorphous target impact, 800 keV, electronic stopping power, models comparison 78−2180
N^+ and N_2^+, beam-foil and beam-gas excitation, Coulomb explosion effects, Auger spectra obs. 80−14220
N^+, beam-foil excitation, absolute Auger yield meas. 80−14203
N^+, beam-foil excitation; absolute Auger yield meas. 79−45685
N^+, beam-tilted C foil interactions, charge-state distrib., photon emission, 100-400 keV 79−22814
N^+, electronic stopping power in solids, range distrib. energy depend. 80−92575
N^+, expt. results on W-values for heavy particles 79−7000
N^+ fine structure levels, UV radiative pumping in nebulae 79−53871
N^+, from exploding fast mol. ions, Auger spectra 80−32781
N^+, N_2^+, distribs. in auroral arc. 77−2292
N^+ photochemistry in thermosphere 79−96847
N^+, reson. line regularities in plasma Stark widths and shifts 80−43881
N^+ sources and sinks in thermosphere 79−96848
N^+, stark broadening of high orbital ang. momentum states 79−22650
^{14}N II, 2p3p $^1P_1$, hyperfine struct. after ion beam surface impact at grazing incidence 80−58403
^{14}N II-2p3p^{3}D-state, hyperfine structure 77−42396
nitrogen continued
^{14}N III, hyperfine struct. of quadruplet levels *(French)* 77−19103
$^{14}N^+$, stopping power in Au at 50-500 eV 77−76478
^{15}N, isotopic anal., collector sensitivity error source 77−42441
^{15}N, self-diffusion in Si_3N_4, isotope exchange meas. 77−11724
N^{2-}, parameters for analytical radial orbitals, total and binding energies 77−6668
N^{2+}, spectral line breadth in molecular nonequilibrium plasma *(Russian)* 80−48044
N^{3-} ion, in crysts., X-ray scattering factors using Xα method 79−7521
N^{4+}, 1s3s3p $^4P^0$ state, Hartree-Fock function, third-order energy 78−37569
N^{4+}, 2s-2p excitation absolute cross sections by electron impact, rate coeffs. temp. depend. 79−94087
N^{4+}, electron impact, inner shell excitation cross-sections 79−59580
N^{4+}, electron impact ionis. cross sections 79−22845
N^{4+}, fine struct. and lifetimes, doubly excited quartet system 78−78827
N^{4+}, ionisation cross-section, excitation autoionisation effects 79−45850
N^{4+}, N^{5+}, production and acceleration in cyclotron *(Japanese)* 78−5084
N^{5+}, electron impact excitation, cross-sections, modified Oppenheimer approx. 78−82843
N^{5+}, few-parameter two-electron wavefunction of ground state 77−75051
N^{6+}, resonant coherent excitation of channeled ions 79−51178
N^{7+}, prod. in electron-beam superconducting ion source 77−23333
N^{n+}, electron impact inner-shell excitation/ionis. cross sections 77−23564
N^{n+}, n≤5, extracted from ECR plasma ion source, charge state distrib. 80−24268
N^{x+}, (x=1-7), electron loss and capture in He, N_2, Ne and Ar *(Russian)* 78−13600
N/C ratio determination in atmospheres of C stars, peculiar red giants 80−17580
N/S gradient in M33 galaxy, supernova remnant evidence 80−56929
N-Fe solid soln. in equilibrium with N_2 gas, partial molar enthalpy and excess entropy 80−60838
N-H bond in methylamine, nucl. mag. isoscreening line diagrams 80−78555
N-N, correl. diagrams, Thomas-Fermi calcs. 80−23294
N-O mixtures, positive glow corona in quasi-uniform fields 80−100104
N+Al(Sn), inner-shell multiple ionisation systematics, X-ray obs. 80−63790
N+alkene (1,3-butadiene)(acetylene), reaction rate consts., pulse radiolysis obs. 80−35508
N+Bi, BiN form., IR matrix spectra, comparison with group V nitrenes 80−18853
N+BrCn(CH_4)(C_2H_2)(CCl_4)(CH_2Cl_2)($CHCl_3$), CN quartet state production, fluoresc. anal. 78−68888
N+H_2^+, triplet state ab inito CI pot. energy surfaces 78−74729
N+H_2SO_4, atmosphere chemistry, collisional reaction probabilities 80−90168
N+H_2→NH+H, pot. surface, HF calc. 80−16669
N+H^+, electron capture cross sections 78−62912
N+H^+(He^{2+}), K-shell Auger electrons ang. distrib. 79−89756
N+H(2S), excitation and ionisation contributions to sum-rule Born cross sections 80−99551
N+Li^+(Co^+)(Au^+), cross-section, closure-Born approx. 78−66630
N+N, K-shell excitation, Auger electron spectrosc. obs. 80−9714
N+N_2O, NO($B^2\Pi_r$) form., quenching 79−64038
N+NF_2, electronically-excited free radical reactions 80−97707
N+NO, ^{4}(S) state reaction rate, discharge flow and photolysis reson. fluoresc. method 79−5142
N+NO_2→N_2O+O, crossed beam study, produce ang. distrib. 79−34311
N+N→N_2, recombinational afterglow spectra, 10-300K 78−44355
N+Ne, electron excitation, multi-state impact parameter approx. 78−42200
N+O, endoergic chemiionisation, semiclassical theory 79−98208
N+O_2F→N_2(NF), lasing potential of excited fluorides 78−63106
N+OH, direct rate meas. 80−30217
N+O(^{3}P), endoergic assoc. ionisation, merged beam obs. 79−100348
N+O(C), K-shell excitation, Auger electron spectrosc. obs. 80−9715
N+one-electron ion, sum-rule Born cross sections, excitation and ionis. contribs. 79−22812
N+transition metal clean surface, 10^{-3} to 10^{-10} mbar, 77 to 370K, reactions 78−64889
N+U^{36+}, radiative charge exchange, 16, 64, 256 MeV/amu 78−55234
N^++Ar(H_2)(N_2)(O_2)(CO)(NO)(CO_2), charge exchange, 1-3 keV, N^+(^{3}P) and (^{1}D) states 79−36760
N^++Ar(Kr)(Ne), single electron detachment cross-sections, 35 to 140 keV 77−6909
N^++CO, integral reactive cross-section calcs. 78−27750
N^++CO(CO_2) (methane)(NO), product distribs., rate consts., ion cyclotron reson. obs. 77−52618
N^++elements Ca to Zn, X-ray production cross section, Kβ/Kα ratio, 0.5-2.5 MeV/amu 77−54526
N^++H, charge transfer reaction in astrophys. nebulae rel. to ionization struct. 80−46384
N^++H_2, electron capture and ion-loss cross-section, 2.4-24.3 keV 80−58373
N^++H_2, reaction dynamics, low energy mol. beam obs. 77−9064
N^++H_2, triplet state ab inito CI pot. energy surfaces 78−74729
N^++H_2 (hydrocarbons), rotational-vibrational product excitation 79−47901
N^++H_2(DH), >6 eV reaction dynamics 77−32779
N^++H_2(N_2), reactant ion electronic states, effect on charge transfer cross sections 80−63809
N^++H_2→NH^++H, classical trajectory calc. 79−100337
N^++H^+, ^3P_j fine structure transitions 80−37864
N^++H(H_2), 0.1-13 keV electron capture cross-sections meas. 79−36761
N^++H(hydrocarbons), chemiluminescence, total reaction cross sections dependence on collision energy 79−47530
N^++He(Ne), slow collision, ionis. obs. 79−10194
N^++inert gas, electron capture (loss) by metastable (ground-state) ions, 2-30 keV 78−25695
N^++Kr, charge exchange cross-sections *(German)* 77−10753
N^++methane, charge transfer reaction, dissoc., isotope effects, mass spectra 77−21382
N^++N, 35-200 keV, K MO X-rays, production mechanism, spectral distrib. 78−42183

nitrogen continued
$N^+ + N_2$, 35-200 keV, X-ray spectrum, rel. to $N^+ + N$ mechanism 78−42183
$N^+ + N_2$, luminescent charge transfer, metastable and ground state ions 78−42202
$N^+ + N_2$, X-ray emission ang. distrib., MO calc. 79−54803
$N^+ + N_2$ collisions, 2.0 MeV ion energy, electron capture and loss cross section 77−34754
$N^+ + N_2(H_2)$, total charge transfer cross section, 5-100 keV 79−3561
$N^+ + NH_3(H_2O)(Ne)$ symmetric collisions, double K-shell ionisation, two-electron-one-photon transitions 77−19067
$N^+ + O_2$, branching ratio kinetic energy depend. 80−97703
$N^+ + O_2$, drift tube mass spectra, rate coeffs. and prod. distrib. 77−77746
$N^+ + O_2$, electron capture and ion-loss cross-section, 2.4-24.3 keV 80−58373
$N^+ + O_2$, $NO^+(a^3\Sigma^+)$ ion prod. 80−7784
$N^+ +$ Th, charge transfer cross-section, 1-500 eV 78−82835
$N^+ +$ U, charge transfer cross-section, 1-500 eV 78−82835
$N^{2+} +$ B(F), K Auger electron spectra 79−89758
$N^{2+} +$ He, electron capture, 0.2-2.4 keV, kinetic energy change 79−59558
$N^{2+} +$ He, electron transfer cross-section, <100 eV 78−66654
$N^{2+} +$ He(Ne)(Ar), electron capture, product ion energy loss spectra 79−36762
$N^{2+} +$ inert gas target, 60-200 keV single electron capture 80−43172
$N^{2+} +$ Ne, electron capture, 0.2-2.4 keV, kinetic energy change 79−59558
$N^{2+} +$ O, collision, correl. diagram calcs. 80−23504
$N^{3,4,5+} + H_2$ single and double electron capture cross sections, (0.3-1.2) 10^8 cm s^{-1} 77−34756
$N^{3+} +$ H, charge exchange, assoc. reaction, rel. to interstellar gas 80−7763
$N^{3+} +$ H, charge exchange collisions, quantal calcs. 79−94079
$N^{3+} +$ H, multicharged ion thermal charge exchange reaction, rel. to astrophysics 80−63815
$N^{4+} +$ Ti, ratio of single K-shell ionisation cross section to double K-shell ionisation cross section 80−53119
$N^{5+} +$ Ti, ratio of single K-shell ionisation cross section to double K-shell ionisation cross section 80−53119
$N^{7+} +$ He, electron capture and impact-ionis. cross sections, Monte Carlo calcs. 79−27083
$N^{7+} +$ Ne, double K-shell electron capture, theory 79−68315
$N^{n+} +$ Al, X-ray prod. and electron transfer cross-section 79−45790
$N^{n+} +$ C, 4 to 40 MeV, beam-foil K-shell X-ray prod. cross sections 78−33461
$N^{n+} +$ H, charge transfer cross sections, oscillatory behaviour in low-energy collisions 80−63806
$N^{n+} +$ H, electron capture cross-sections, He- and Li-like ions 79−59559
$N^{n+} + H_2$, electron capture cross-sections, He- and Li- like ions 79−59559
$N^{n+} +$ Ne, charge exchange contribution to K-vacancy production 80−102553
$N^{q+} + H$,(q=1 to 7), electron capture and impact ionisation cross sections 77−75290
$N^{q+} + H(H_2)$, q=1-5, single electron capture cross sections 78−55233
$N^{x+} +$ He, electron capture, K X-ray emission ang. distrib. 77−57919
$N^{x+} +$ He(Ne), multiply ionised ats. prod. 80−28098
N_2, N_2^+, first positive and Meinel systems in aurora 77−13144
N_2 3371 Å dayglow emission, excitation by photoelectron impact 77−33236
N_2 ($^1\Sigma_g^+$) charge density, X-ray scatt. factors, gas phase electron diffr. 78−930
N_2, ($C^3\Pi_u$) state, radiative lifetime, collisional quenching, pulse radiolysis meas. 78−29813
N_2, ($C^3\Pi$) nonequilibrium rotational level distrib. in gas discharge *(Russian)* 78−86796
N_2, (N_2^+), Franck-Condon factors, isotope effects calcs. 78−1031
N_2, ab initio calcs. of the derivative of the static polarisability 79−3597
N_2, absorpt. spectrum, using vacuum UV storage ring source 77−7165
N_2, adsorption on Ni, photoemission and electronic struct., cluster calcs. 80−97403
N_2 afterglow, chem. reactions rel. to plasma props, appl. to toluene polymerisation 80−3346
N_2, anharmonic molecules in disturbed thermosphere, vibr. relaxation rel. to NO conc. 79−12322
N_2 arc, magnetically stabilised cross-flow, temp. and flow fields meas. 80−54054
N_2, α-particles stopping cross-section determ. 79−49917
N_2 bands in proton-induced poalr cap aurora, intensities 78−77389
N_2, bond order values, ab initio calcs. and basis set depend. 80−32605
N_2 bubbles coalescence in dil. aq. solns. 79−4062
N_2, $C^3\Pi_u$ excited state, lifetime determ. by phase-shift and delayed-coincidences methods 77−18988
N_2 $C^3\Pi_u$-$B^3\Pi_g$ second positive system, transition probabilities, transition moment 78−50593
N_2, canonical exchange energy modulation parameters, MTXα calc. 79−97997
N_2 collisions with O^{2+} ions, reaction rates 79−16726
N_2, continuum, energy loss cross sections for 300, 400 and 500 eV electrons 79−94090
N_2 continuum absorpt. contrib. to atm. transmission, 4.0 to 5.3 μm 79−92589
N_2, core photoelectron line shape, localisation role 79−59512
β-N_2 cryst., vibr. Raman spectra 80−60558
α-N_2, crystal dynamics at 15K 77−24366
N_2 dayglow intensity from photoelectron impact 80−46331
N_2, desorbed after N atom recomb. on Fe, vibr. energy, electron beam induced fluoresc. 80−61149
N_2 discharge, electron shock wave formation, numerical simulation 80−38777
N_2, dissoc. of nonequilib. gas, two-quanta V-V exchange 79−3547
N_2 dissociation role in plasma positive column Mg nitridation 78−63628
N_2 dissolved in Ar, mol. orientation, Raman spectrosc. obs. 80−52994
β-N_2, dynamical struct. factor S(Q,ω), digital simulation 77−76502
N_2, electron correl., quadrupole excitation in correl. energy theories 79−36538
N_2, electron impact dissoc., EELS, N^- autoionisation 80−106397
N_2, electron impact excitation cross-sections meas. *(Spanish)* 79−98230
N_2, electron impact excited, broadband photon yield meas. *(French)* 78−25723
nitrogen continued
N_2, electron impact ionis., rot. energy distrib. of $N_2+(X^2\Sigma_g^+)$ 79−76520
N_2, electron impact vibr. excitation, adiabatic approximation, energy-modified 79−59523
N_2, electron scatt., adiabatic polaris. pots. 79−10203
N_2, electron scatt., differential elastic cross-section, 0-30 eV 78−78815
N_2, electron scattering, low energy, R-matrix calc. 79−59571
N_2, electron scattering excited, hybrid theory results for 5 and 10 eV 77−27191
N_2, electronic structure calcs., self-consistent, accelerating convergence of iterative process 80−87037
N_2, flow, cold gas, through porous-tube, heat-transfer, suction effect 78−59474
N_2, fluoresc. efficiencies of electrons, 4900-10500 Å wavelength range 77−61870
N_2, Franck-Condon factors, rot. quantum number effect 79−31613
N_2 free jet expansion, rot. level population kinetics, electron-beam diagnostics 78−5776
N_2 gas, domains and boundaries of non-stationary oblique shock wave reflexions 79−68746
N_2, gas with clusters, free expansion, upper rot. levels population *(Russian)* 78−33581
N_2, gas-liquid surface of mol. fluids, mol. dynamics computer simulations 80−39387
N_2 glow discharge, non-self-sustained, cathode spots annular structure investig. 80−24281
N_2, high average power and longitudinal discharge laser 79−94244
N_2, high energy electron spectroscopy techniques 80−62740
N_2, hypersonic nozzle flow, supercooling and spontaneous condensation 78−1549
N_2, identified as source of 2150 Å auroral emission feature rather than NO 78−45083
N_2 in aurorae, vibrational distrib. 79−80068
N_2, in auroral upper atmosphere, vibr. excitation rel. to IR emissions 77−33247
N_2, in CO_2 laser, electron beam-ionis. optical pumping characts. 77−75477
N_2 in diffuse interstellar clouds, Copernicus search, upper limits 79−25661
N_2 in high press. air plasma, photodissoc. 80−64691
N_2 in premixed laminar methane-air flame, Raman scatt. meas. of vibr. temp. 79−80622
N_2 in UV aurora, spectrum between 2100 Å and 2300 Å 78−88963
N_2 in upper atmos., vibr. level distrib., theory 80−41576
N_2, in upper atmosphere, as source of 1027 Å auroral emission 79−80064
N_2 in upper atmosphere, effects of soft electron precip. on vibr. energy distrib. 77−33261
N_2 influence on photodissociation of UF_6 80−95698
N_2, ionisation by electron bombard., empirical and semi-empirical calcs. 79−36784
N_2 laser, high-power, TE, UV, using Blumlein transmission line, construction characts. *(Korean)* 79−22971
N_2 laser discharge, SF_6 addition, negative ion prod., altered discharge parameters 80−38818
N_2 laser pumped DFB dye laser, tunable single ps pulse generation 79−55147
N_2 laser transitions, $Ar(^3P_2)+N_2(C^3\Pi_u)$ excitation transfer cross section, radiative lifetime 79−27246
N_2 laser-pumped dye laser, generation of tunable ultrashort light pulses *(German)* 79−27275
N_2 lasers, pulsed operation, characteristic data comparison 79−10287
α-N_2, lattice energies, non-additive three body contributions, triple-dipole term 80−54168
N_2, liquid, Q-band position, width in cryogenic mixtures *(Russian)* 78−46401
N_2 liquid high-power tunable Raman lasers and applications 77−54709
α-N_2, mol. cryst., theory of time evolution of exciton coherence 80−65455
N_2, mol. spectra, 500-1300 Å, matrix isolated 79−33724
N_2, molecular fluid, Rayleigh and Raman light scatt. props., orientational and collision induced effects 80−63644
N_2, N_2-He, barrier discharge, struct., spectral anal. *(Russian)* 77−21463
N_2, N_2^+, airglow emissions from cometary inner comas 78−45282
N_2, N_2^+, discharge pumped multiwavelength lasers *(Chinese)* 80−102703
N_2, N_2^+, MO correlation diagrams 77−61689
N_2, N_2^+ auroral bands, excitation studies from airborne spectroscopy 77−29533
N_2, N_3, spectroscopic data review 77−38680
N_2, negative-ion resons. associated with inner-shell-excited states, electron impact 77−88580
N_2, non self sustained repetitively pulsed discharge instability obs. 80−38820
N_2, non-self-maintained discharge, high press., ionisation instability, pulse discharge train *(Russian)* 77−47282
N_2, nonempirical calc. for molecules in electric field 78−25459
N_2, nucl. spin-spin coupling, scanning MO HF LCAO calc. 79−50045
β-N_2, orientational order, model 78−67667
N_2, oscill. strengths of $W^3\Delta_u$-$X^1\Sigma_g^+$ band system 79−59486
N_2, photoelectron ang. distrib., multiple scatt. calc. 79−81238
N_2, photoionis., shape-reson. enhanced nucl. motion effects 80−1031
N_2 plasma, microwave discharge, electron energy distrib. function *(Russian)* 77−11415
N_2, plasmochemical action of relativistic electron beam, calc. by degradation spectrum method *(Russian)* 79−37536
N_2, polarisability anisotropy derivative determ. from relative Raman intensities 78−55177
N_2 positive corona into spark, prebreakdown phase, spectroscopic anal. 80−38790
N_2, press.-density depend. at high density, functional depend. using osculating curves 79−93109
N_2, pressure broadening of HNO_3 linewidth, 200 and 300K 78−46399
N_2, quadratic vibr. force const., from X-ray scatt. factors 79−45864
N_2, rarefied flow, visco-magnetic heat flux 79−98844
N_2, reaction with O^+, nonthermal rate coeffs. in ionosphere 78−57375
N_2 reduction in solar nebula, kinetic inhibition 80−85875
N_2, rotational Raman intensities and polarisability anisotropy change meas. with internuclear distance 80−63641

nitrogen continued
N_2, self-consistent electron pairs with higher order effects, quadruple iteration convergence 78−46276
N_2, shake-up peak positions and intensities calcs. using eqns. of motion Green's function method 78−86910
N_2 single and multiple free jet conc. meas., CW laser Raman spectroscopy 79−97447
α-N_2, solid, librational motion, theory 77−43303
α-N_2, solid, librational motion, neutron scatt. 77−43304
α-N_2, solid, Raman spectra vibron bands, a priori calcs. 78−31181
α-N_2, solid, thermal expansion and Gruneisen coeff. *(Russian)* 79−10969
α-N_2, solid, $w^1\Delta_u$-$X^1\Sigma_g^+$ intensity and band shape 79−47427
N_2, spatial yield spectra for electron energy degradation 79−100992
α-N_2, temp. depend. of IR spectra, Gruneisen parameters determ. 80−84730
N_2, thermal cond. meas. at room temp., and pressures up to 35 MPa 79−86551
N_2, thermosphere composition, temp. and turbulence, 1967-75 obs. 80−51588
N_2, threshold photoelectron spectra, 15-20 eV 79−54912
N_2, total scatt. cross sections for intermediate-energy positrons 80−91692
N_2, transverse excited $C^3\Pi_u \rightarrow B^3\Pi_g$(0-0) UV laser band, spectroscopic rot. anal. 79−7115
N_2, two-phase flow in horizontal tube, heat transfer and pressure drop over extensive pressure range 79−58747
N_2 UV lasers, performance and operation *(Polish)* 79−55124
N_2 UV TEA lasers 79−41388
N_2, valence excitation energy and UV spectra, HAM/3 calc. 78−25453
N_2, valence-shell MO calc. with pseudopot. 78−907
N_2 Vegard Kaplan bands in bright auroral displays, ground-based photometry 77−33245
N_2, vibr. and rot. anal. of vis., UV spectra, RF discharges in N_2, H_2, CH_4 mixtures 78−5241
N_2, vibr. excitation using steady state chemical reaction between CO and N_2O 80−50851
N_2, vibr. populations of excited states under auroral conditions 78−42035
N_2, X-ray and high-energy elastic electron scatt., vibr. averages 79−81279
N_2, X-ray spectra, K-photoabsorpt. cross-section, 400-450 eV 78−94257
N_2, Xα-SW MO projection of LCAOC MOs 78−25422
N_2^-, $^2\Pi_g$ resonance effect on N_2 electron impact rot. excitation 77−58184
N_2^-, 2 eV resonance as energy standard in low energy electron scatt. 77−71872
N_2^-, first $^2\Pi_u$ state form. and decay 80−58177
N_2^-, free free absorpt. rel. to opacity in stellar atms. 78−81610
N_2^-, vibr. autodetaching states, from $H^- + H_2$, excitation and decay, Franck-Condon factors 78−33620
N_2^+ 1 NG emissions from proton aurora, anomalous vibr. distrib. 80−67448
N_2^+, 1NG: $B^2\Sigma_u^+ \rightarrow X^2\Sigma_g^+$, 3800 to 4750 Å spectra, mol. consts. 78−42081
N_2^+, 1s hole satellite spectrum, large-scale CI calc. 77−65428
N_2^+ 3914 Å, auroral emission rel. to instantaneous particle energy deposition rate 78−81491
N_2^+, 3914 Å band spectra, fluoresc. efficiency 79−81226
N_2^+ 3914 Å emission in dayside cleft aurora 77−2294
N_2^+ 4278 Å auroral emission, calc. from electron flux meas., comparison with obs. 77−9592
N_2^+ 4278 Å band nightglow intensity meas. at Arecibo 77−64504
N_2^+ 4278 Å bands in meteor spectra, quantitative anal. 78−45290
N_2^+ 4278 Å emission and electron flux comparison in auroral zone 77−87151
N_2^+ 4278 b auroral intensity in DMSP data calibration 80−8443
N_2^+ ($B^2\Sigma_u^+$) state in Ne-N_2 mixture, excitation kinetics 78−9239
N_2^+, A- and B-states interactions, time-resolved obs. 80−18862
N_2^+, active ion bombardment of pyrolytic graphite or Si (100), SIMS obs., 79−16034
N_2^+, auroral Meinel band excitation rel. to pulsating structs. extreme thinness 80−72667
N_2^+, $B^2\Sigma_u^+$ excited state, lifetime determ. by phase-shift and delayed-coincidences methods 77−18988
N_2^+ bands, appl. to temp. meas. by spectroscopy using ICP plasma source 79−12858
N_2^+, $C^2\Sigma_u^+$-$B^2\Sigma_u^+$ homogeneous predissoc.; perturbations calcs. 79−86020
N_2^+, deperturbation of first negative group, $B^2\Sigma_u^+$-$X^2\Sigma_g^+$ 79−59481
N_2^+ discharge laser, superluminosity, spatial-spectral struct. 79−55116
N_2^+, dissociative recombination rates 77−86295
N_2^+, dissociative recombination in ionosphere, rate cont. 80−17435
N_2^+, electron impact, rate coeff. in thermosphere, AE satellite meas. 79−48594
N_2^+, electron impact dissociative recomb. coeffs. inferred from Atmosphere Explorer meas., objections 78−86957
N_2^+, electron impact dissociative recombination, ion-beam expt. 79−54981
N_2^+, electron impact excitation, ionisation, rel. to auroral spectral intensities 79−84563
N_2^+, electron impact excitation cross-sections meas. *(Spanish)* 79−98230
N_2^+, electronic transition moment, internucl. separation depend., semiempirical calc. method 78−9199
N_2^+, emission in $Ne^+ + N_2O$ charge transfer excitation, down to 1 eV 79−45835
N_2^+, excitation in RF discharges *(French)* 77−61868
N_2^+, excitation of 3914 Å band by proton impact 77−68101
N_2^+, exploding fast mol. ions, Auger spectra 80−32781
N_2^+ first negative (0-1) band temp. height profile in auroral arc 78−40725
N_2^+, first negative spectra excited by N_2 electron impact, modelling 77−61758
N_2^+, fission fragment excitation of optical radiation quenching by UF_6 77−23665
N_2^+, fluoresc. and production cross-sections by photoionis. of N_2 78−9204
N_2^+, fluoresc. quantum yields and lifetimes, meas. method, ion form. 77−6815
N_2^+, Franck-Condon factors, rot. quantum number effect 79−31613
nitrogen continued
N_2^+ high-pressure laser, superradiance spatial structure 79−64215
N_2^+ in ionosphere mid-latit. F_1-layer, mean diurnal var. 79−96856
N_2^+, in rarefied plasma stream, energy accommodation coeffs. meas. by thermoanemometric sounding 80−16722
N_2^+, interaction with Si, SiO, and SiO_2 surfaces, XPS and UPS obs. 78−48265
N_2^+ ion laser, gain and saturation 78−79001
N_2^+ laser, charge transfer pumping, high press. pulsed glow discharge 77−14691
N_2^+ laser, elec. discharge pumped 77−7069
N_2^+ laser, regenerative power amplifier operating on blue-green line 79−7139
N_2^+ Meinel system, high resolution spectrum to 11 250 Å 80−99497
N_2^+, mol. orbital calc., localised treatment of hole states 79−54765
N_2^+, partial photoionisation cross section and photoelectron angular distribution for $X^2\Sigma_g^+$ state determ. 80−83429
N_2^+, perturbation of $B^2\Sigma^+$ rotational levels by $^4\Sigma^+$ level, lifetimes meas. *(French)* 77−88437
N_2^+, produced by threshold ionis., $X(^2\Sigma_g^+)$, $A(^2\Pi_u)$ and $B(^2\Sigma_u^+)$ vibr. struct. and mol. parameters 78−94294
N_2^+, radiative lifetime of $B^2\Sigma_u^+$ state 78−90220
N_2^+ recombination, effect on aeronomic determ. of $O^+(^2D) + N_2$ charge exchange rate coeff. 78−88954
N_2^+, reson. absorpt., 1st negative band, in irrad. air, calcs. 77−30850
N_2^+, spectroscopic consts., remeas. 77−58197
N_2^+, spectrum, appl. air arc temp. meas. 80−59314
N_2^+, sputtering of multicomponent film, in AES depth profiling 77−16889
N_2^+, UV spectral line width in rarefied free jet, for rot. temp. 80−6184
N_2^+, vibr. intensity distribs. for electronic states prod. by photoionis. 78−25614
N_2^+ $X^2\Sigma_g^+$-state, vibr. states asymmetry parameter and photoelectron spectrum 80−95591
$^{14,15}N_2$, Fourier spectrometry and IR emission spectra 80−83368
N_2^{2+}, auroral ionosphere spectral emission process 80−41577
N_2^{2+}, low-lying electronic states, pot. energy curves calcs. by SCF technique, vibr. and ionisation consts. 80−69091
N_2^{2+}, recomb. energy determ. from pot. curves 80−58335
N_2^{n+}, Coulomb explosion following heavy ion impact, ab initio SCF calc. 79−18277
N_2:CO, IR and Raman spectra, vibron band, vibron-phonon combination bands 78−68495
N_2:CO_2(N_2O)(methane-d_4), liq., vibr. relax., Raman scatt. obs. 78−92061
N_2:N, dynamically induced electronic transitions of matrix isolated atom 78−63825
N_2/Ar ratio vars. in fault zone groundwater air bubbles for earthquake prediction 78−88803
N_2/CCl_4, inhomogeneous broadening of Morse oscillator, temp. depend. 77−61803
N_2/SF_6 positive-point corona phenomena, breakdown voltage/press. characts. 80−38859
N_2-Ar, detection gas suitability for proportional scintillation counter *(German)* 78−41901
N_2-Ar, laser high power, energy and power output *(Russian)* 77−7065
N_2-Ar, liq. mixture, isotropic Raman line shape theory 78−88298
N_2-Ar, thermal diffusion factors meas. 80−10344
N_2-Ar, visomag. diffusion flux theory 78−47087
N_2-Ar corona dishcharge, convection and mixing, atm. press., mass spectra obs. 80−1853
N_2-Ar equimolar mixture, transverse Dufour effect 80−6194
N_2-Ar laser, stimulated emission obs. at 337.1, 357.7 and 380.5 nm 78−17925
N_2-Ar liq. mixtures, coherently excited mol. vibrs., dephasing time 78−62813
N_2-Ar mixture, picosecond dephasing of coherently excited vibrations 78−22172
N_2-Ar mixture non-self-sustained discharge instability obs. 78−71612
N_2-Ar mixtures in 300-1050K range, rot. energy relaxation 78−50617
N_2-Ar plasma, coupled thermal-chem. relax., thermodynamic nonequilib. 78−34265
N_2-Ar-O_2, liq. vap. equilib. prediction using cubic eqn. of state 78−18737
N_2-Ar-O_2 system, vapour-liq. equilib. 80−54358
N_2-Ar(Kr)(O_2)(CO)(CH_4), liquid, high resolution CW CARS spectra 80−63635
N_2-Ar(methane)(ethane) binary and ternary mixtures, dielec. const., excess vol. 80−7254
N_2-BCl_3 mixture, thermodiffusion props., effect of resonant excitation of mol. vibr. by laser, isotope separation 80−100047
N_2-CO, angularly resolved CARS 80−22453
N_2-CO, electrical discharge excitation, vibr. level population distrib., electron beam fluoresc. obs. 80−48031
N_2-CO mixed cryst., librational motion, Raman obs. 78−6661
N_2-CO pulsed non self sustained discharges, peculiarities 80−38811
N_2-CO_2, expanding stream of CO_2 laser, effect of H_2 addition on gain coeff. *(Russian)* 77−27271
N_2-CO_2, N_2 non-self-maintained discharge, high press., ionisation instability, pulse discharge train *(Russian)* 77−47282
N_2-CO_2 laser mixture, electron drift vels., time-of-flight meas. 80−28855
N_2-CO_2 mixture non-self-sustained discharge ionisation instabilities, obs. 78−71610
N_2-CO_2 nonequilibrium aerosol flux mixing, inverse population of vibrational levels *(Russian)* 77−10743
N_2-CO_2-H_2O gasdynamic laser mixture, electron beam diagnostics 77−83845
N_2-CO_2-He, vol. discharge with UV preionisation by capillary discharge, ionis. pots. depend. 80−44065
N_2-CO_2(-He) volume discharge, N_2 vibr. levels, stepwise excitation, effect on electron energy balance 80−54071
N_2-CO-^{3}He, nucl. reactor active zone, plasma and sustained discharge props. 80−5729
N_2-CO-Ar, C_2 and CN form. by optical pumping, room temp. 80−16701
N_2-CO-OCS, liq. mixture, vibr. energy relax. and exchange, laser induced fluoresc. obs. 78−70905
N_2-chloromethane mixture, binary diffusivities, 25-110°c 79−23391
N_2-Cs plasma, decay, Cs level population inversion 79−55455
N_2-Cu arc plasma, transport coeffs. 80−96344

nitrogen continued
N_2-ethane(propane)(n-butane) mixtures, viscosity, diffusion coeffs. 80−1722
N_2-ethylene, liq., Zwanzig perturbation expansion convergence, free energy 77−76274
N_2-F_2 mixture, fast Blumlein discharge excited, intense 3371 Å laser emission 79−41365
N_2-H_2, high-temp. plasma, transport coeff. calcs. 77−62340
N_2-H_2, mixed plasma, elastic collision energy loss *(German)* 79−41793
N_2-H_2 arc, bent and rot., flow mechanism 80−70047
N_2-H_2 mixture, glow discharge, ionisation and excitation obs. 78−67505
N_2-H_2 plasma, transport coeffs. and collision processes *(German)* 79−23395
N_2-H_2O plasma state, partial equilib. with reaction invariants *(French)* 79−52739
N_2-H_2O-CO_2 gas mixture, oscillatory nonequilib. in planar supersonic nozzle flow 78−1758
N_2-He, binary diffusion coeffs., press. depend., 300 and 323K, Thorne's eqn. 80−1724
N_2-He, heat of mixing, 2-15 bar *(French)* 79−7436
N_2-He ion nuclear pumped lasers feasibility study and quenching 80−64001
N_2-He laser, charge transfer pumping at atm. press., in elec. avalanche discharge 79−10286
N_2-He mixture, film condensation, appls. to condensers for cryogenic installations 78−59941
N_2-He mixture, speed of sound, temp. depend. at high press. 77−84388
N_2-He plasma, laser produced, high press. amplified stimulated emission 80−78843
N_2-He-CO_2, discharge ionisation growth, diffusion coeffs. 78−83636
N_2-hydrocarbon mixtures, phase equilib. calcs., modified Soave eqn. of state 79−19353
N_2-Kr gas mixtures, separation using silicone rubber, cellulose acetate membranes, separation factor 77−36791
N_2-Kr-Xe, liquefaction, retention of ^{85}Kr from fission exhaust gases, separation technique *(German)* 80−27753
N_2-methane, gas, vibr. relax. time by US meas. 79−98852
N_2-methane, rapidly developing discharge, streak camera records interpretation 80−59280
N_2-methane mixture, binary diffusivities, 25-110°c 79−23391
N_2-methane mixture, US propag. vel. up to 40 kbar, additivity deviation 77−42959
N_2-N_2 anisotropic interaction pot. model, comparison with solid state data 77−34712
N_2-N_2O mixture, conc. depend. of thermodiffusion const. 77−7503
N_2-NF_3, electron attachment coeffs. using swarm techniques 80−53915
N_2-NH_3 mixture, viscosity measurements using oscillating disc type viscometer 78−51273
N_2-NO thermal cond., mag. field effect 79−94764
N_2-NO(He), discharge ionisation growth, diffusion coeffs. 78−83636
N_2-Na-H_2 jet, ignition and extinguishment in simulated LMFBR accident conditions 78−8932
N_2-Ne, charge transfer kinetics, weak H^+ beam effects 78−9243
N_2-Ne, positive column, electron vel. distrib. function *(German)* 78−1885
N_2-Ne glow discharge, energy balance, ionis. collisions *(German)* 78−34263
N_2-Ne glow discharge, kinetic eqn., transport coeff., collision freq., mean energy *(German)* 78−34261
N_2-Ne mixture, gaseous, positronium yields at 77K 79−98254
N_2-Ne(H_2), low-ionised plasma, electron kinetics, collision processes influence *(German)* 79−14519
N_2-O_2, electron impact dissoc. ionisation, N^- form., mass spectra 77−75320
N_2-O_2, vap.-low. equilib., mag. field effect 78−91429
N_2-O_2 gas mixture, weakly ionised, electron transport coeffs. anal. *(Japanese)* 80−59184
N_2-O_2 gas mixtures, elec. breakdown voltage, 113-293K 79−1363
N_2-O_2 mixture, impulse breakdown processes at low press. 80−44021
N_2-O_2 mixture, moist, electron beam irrad., SO_2 oxidation, appl. to exhaust gas treatment 78−80766
N_2-O_2 mixture, NO synthesis, reactions of vibr. excited N_2 in nonequilib. plasmachem. system 77−86310
N_2-O_2 mixture transient discharges, RF techniques 80−70067
N_2-O_2 nonselfsustaining discharge plasma, current establishment/relax. processes, rel. to CO_2 laser *(Russian)* 79−99011
N_2-O_2-Ar saturated air vapour mixture, film, mixed condensation, comparison with water vapour 77−11780
N_2-O_2^+(NO^+), temp.-dependent ion mobilities 79−86553
N_2-propane mixture, total emissivity, press. depend. 78−90673
N_2-SF_6, AC particle initiated breakdown, compressed gas mixture 78−87556
N_2-SF_6, elec. breakdown and corona stabilisation obs. 78−87582
N_2-SF_6 laser, UV, discharge-excited, improvement in efficiency *(Japanese)* 78−33724
N_2-SF_6 mixture, breakdown voltage and discharge extension of long gaps 77−84550
N_2-SF_6 mixtures, effective ionisation coeff. and static breakdown voltage meas. 80−19549
N_2-SF_6 pulsed discharge laser with CW X-ray preionisation 80−95910
N_2-SF_6(CF_4) mixtures, viscosity and diffusion coeffs. 77−89225
N_2-Xe afterglow, $6s_{12}$ metastable atom density decay rate 78−63612
N_2+^{20}Ne(^{22}Ne), isotope separation by jet-background interaction 79−54983
N_2+Al^+, reaction cross sections 77−29000
N_2+alkali metal atom, temp. depend. of vibr. relax. time 77−34725
N_2+Ar, 0.06-0.41 eV, metastable at. electronic excitation transfer 79−64071
N_2+Ar, binary diffusion coeff. pressure depend. meas. 80−43826
N_2+Ar, collinear collision, vibr.-translation energy transfer, model calc. 78−66634
N_2+Ar, cross sectional factorization expressions, close coupling input tested in sudden approximation 79−43571
N_2+Ar, form-factors, l-dominant, analytical formulae 80−1052
N_2+Ar, inelastic scatt. exponential perturbation theories 80−74217
N_2+Ar, intermolecular pots. from Thomas-Fermi-Dirac functional 77−19009
N_2+Ar, metastable atom excitation of $C^3\Pi_u$ state, symmetry, propensity rules and alternation intensity, rot. spectrum 80−87135
N_2+Ar, molecular fluid mixtures, equilibrium props. 80−64867
N_2+Ar, polarisation in elastic scatt., close-coupling calcs. 78−25650
nitrogen continued
N_2+Ar, proton excited, time-resolved, VUV, UV and vis. photon emission 77−14547
N_2+Ar, repulsive pot. energy surface, approx. calc. and differential scatt. expt., comparison 79−22788
N_2+Ar, rot. and vibr. inelastic mol. collision cross section calc. 79−59542
N_2+Ar, rot. energy transfer, power scaling law 79−54942
N_2+Ar, rot. inelastic collision, orientation depend., close coupling calcs. 78−9232
N_2+Ar, rot. inelastic cross-section, IOS calcs., partial wave parameters 78−50616
N_2+Ar, rot. relax., approx. treatments 79−76494
N_2+Ar, rotational cross-sections, energy depend., modified exponential model 79−50115
N_2+Ar, scatt., l_z-conserving sudden approx. calcs. 78−66628
N_2+Ar, short-range intermol. pots., combined interatomic pots. calcs. 80−87198
N_2+Ar, total differential cross section, diffr. oscills. quenching 78−66625
N_2+Ar, triplet state excitation *(French)* 77−83704
N_2+Ar rotational excitation, differential cross sections and orientation effects, classical trajectory method 80−23523
N_2+Ar^+, energy transfer, vibronic excitation, emission spectra 78−66578
N_2+Ar^+(He^+)(Ne^+), charge transfer, thermal energy, product distrib. obs. 78−25656
N_2+Ar^+(Kr^+)(Xe^+), near-resonant charge transfer, 4-45 keV 77−27176
N_2+Ar^{12+}, N K-shell Auger effect 77−6908
N_2+Ar+POPOP, electron beam excited, energy transfer mechanisms 80−23497
N_2+Ar*, de-excitation processes, pulse radiolysis, rate consts., optical obs. 77−65529
N_2+Ar*($^3P_{0,2}$), rot. and vibr. energy transfer, relative reaction rates 78−9233
N_2+Ar*(He*), sensitised fluoresc., vel. depend. 77−10744
N_2+Ar(Xe), $A^3\Sigma_u^+$ state energy pooling in flowing afterglow, Herman IR system 80−83503
N_2+BA, radiation quenching of metastable Ba (5d ^{1}D) in gas 79−85932
N_2+BP, dissoc. reacts. 79−43627
N_2+BaCl, intermultiplet energy transfer 79−27063
N_2+BaCl($C^2\Pi$), collisional quenching, laser induced fluoresc. decay meas. 79−27075
N_2+Br^-, total electron detachment cross sections for energies around threshold 80−99550
N_2+C^-(O^-), electron detachment cross-sections, 20-150 keV 78−25690
N_2+C^+ collisions, luminesc. 80−1055
N_2+C^{+*}, charge transfer cross-sections, 0.7-2.4 keV, C^+(^2P) and C^+(^4P) 78−58806
N_2+C^+(N^+)(CO^+), total charge transfer cross section, 5-100 keV 79−3561
N_2+C^+(N^+)(O^+), luminescent charge transfer, metastable and ground state ions 78−42202
N_2+CF_2, vibr. deactivation of CF_2 first excited single state 79−94061
N_2+CO, adsorption on ZrC-W eutectic alloy 79−69951
N_2+CO, electronically inelastic collision, distorted wave calc. and pot. energy curve 80−9709
N_2+CO, line broadening, short range force effects, semiclassical calcs. 79−98085
N_2+CO_2, 301_{III}-000 band, intensities, press.- and self-broadening coeffs. meas. 78−78695
N_2+CO_2, CO_2 1st vibr. levels collisional deactivation, photoacoustic study 79−98187
N_2+CO_2, energy transfer, semiclassical calc. 79−86042
N_2+CO_2, vibr. energy transfer, time-resolved laser induced fluorescence 78−29842
N_2+CO_2, vibr. relax., optoacoustic obs. *(French)* 78−42178
N_2+CO_2+benzene, electronically excited, mol. fluoresc., vibr. relax. cross sections and equilibration rates determ. 80−87205
N_2+CO_2(O_2)(N_2), IR spectral absorpt. induced by press. in atmos. *(Russian)* 80−56600
N_2+CO(N_2)(O_2)(NO)(CO_2)(methane), ionis. at low energy 78−58791
N_2+Cd, electronic-vibrational process, state-resolved products distrib. determ. 79−6956
N_2+Cd($^1P_1$), laser excitation, absolute quenching cross sections and branching ratios 79−49979
N_2+Cd(Zn)(Sr), $A^3\Sigma_u^+$ state, vibr. excitation 80−1054
N_2+Cd($5^3P_{0,1}$), absolute quenching cross sections 80−5604
N_2+Cl^-, total electron detachment cross sections for energies around threshold 80−99550
N_2+Cl^{4+}(I^{5+}), 20 MeV, electron loss cross sections, pot. model data anal. 79−27082
N_2+Co_2, spectral line breadth in CO_2 15 μm band 79−22765
N_2+Cs, collisional relax. and population quenching of Cs 78−25467
N_2+CsF, rot. inelastic collisions, mol. beam meas. 80−1049
N_2+Cu, preferential energy transfer from N_2 to specific Cu energy levels 80−43152
N_2+D, fast collision, electron scatt. resons., ionisation, deexcitation 79−81268
N_2+DF, vibr. relax., laser-induced fluoresc. obs. 79−64028
N_2+ethane, system, vapour-liq. equilib. data 78−83929
N_2+ethene, system, vapour-liq. equilib. data 78−83929
N_2+FCN, rot. spectra and geom. struct. of FCN 78−82725
N_2+Fe (atomic), interaction mechanism via clusters 77−25263
N_2+Fe interaction, chemical species formed studied by Mossbauer effect 80−43080
N_2+Fe^{4+}, 20 MeV, gaseous targets, electron loss, charge state yields 79−54957
N_2+H, collisional coherent excitation, meas. of Lyman α-photons 80−99552
N_2+H, stripping cross-section, 0.3 to 3 keV 78−78807
N_2+H_2, (oriented), total collision cross-sections, anisotropic pot. parameters calcs. 78−13568
N_2+H_2, cross sections, for electron stripping of fast H_2 meas. 77−83705
N_2+H_2, N_2 dissoc. rates, nonequilib. vibr. populations, elec. discharge conditions 77−88535
N_2+H_2, rot. excitation, fixed nuclei approximation calcs. 79−6990
N_2+H_2^+→N_2^++H_2, rot. energy distrib., 10 and 25 keV 79−76507

nitrogen continued
N_2+H_2O, collision broadened H_2O absorpt. line, laser radiation intensity effects 77−83661
N_2+H_2O, vibr.-translation relax. cross section in glow discharge plasma 77−43092
N_2+H_2O 78−66631
$N_2+H_2O+SO_2$, condensation nuclei form., ion polarity and age depend. 79−39220
$N_2+H_2+N_2H_4$, mixtures with nonthermal vibr. excitation of mol. N_2 80−76545
$N_2+H_2(D_2)$, vibr. relax. in liquid phase 79−847
N_2+H^-, 1 to 5 keV, production cross sections for 3d,3s,4s,5s states of H 78−33603
N_2+H^-, charge transfer, ejected electron spectra 79−45828
$N_2+H^-(He)^-$, collisional detachment cross-sections, high-energy obs. 77−3442
$N_2+H^-\rightarrow N_2^-+H$, vibr. autodetaching states, excitation and decay 78−33620
N_2+H^+, 5-100 keV, secondary electron energy and ang. distrib. 80−14223
N_2+H^+, electron ejection, energy distrib. binary encounter approx. calcs. 77−30971
N_2+H^+, energy transfer, dissoc., cross section calcs. 77−50522
N_2+H^+, excitation process, N_2 and N_2^+ light emission *(Japanese)* 78−25678
N_2+H^+, K-shell capture cross-section, Auger effect 78−33602
N_2+H^+, spatial distrib. of excited moles. induced by 100 and 150 kev proton beams 78−58793
N_2+H^+, vibr. excitation, differential scatt., low energy meas. 79−89749
N_2+H^+ collision, total ionis. cross section and stopping power for protons 80−69228
$N_2+H^+(He^+)$, 1 MeV, dissoc. ionis., time-energy spectra 77−34744
$N_2+H^+(He^+)$, K-shell ionisation, AES meas. 77−10749
$N_2+H^+(He^+)$, N_2^+ 3914 Å emission cross sections, 0.5-34 keV 77−54598
N_2+H^+(e), vibrational N_2^+ excitation *(Russian)* 80−53156
N_2+HCN (001), relax. rate consts., using Cs vap. IR source 80−9696
N_2+HCl, HCl linewidth, impact parameter calcs. 79−89714
N_2+HCl, HCl ν_0-ν_1 band perturbations, linewidth and shifts calcs., IR spectra obs. *(French)* 80−58251
N_2+HF, HF(v=3) relax. and rate consts. 80−61069
N_2+HF, vibr. relax., laser fluoresc. obs. 77−14484
N_2+HF, vibr. relax. laser induced fluoresc. obs. 79−64037
N_2+H(He), vibr. state distrib., charge exchange 150-2400 eV 78−42195
N_2+H(2s), 5-25 keV, H(n=3) excitation, Balmer α emission obs. 80−53113
N_2+He, anisotropic intermol. pots., crossed beam expts. 79−31639
N_2+He, collisionally excited neutral and ionic emission, flowing afterglow 77−51248
N_2+He, Penning ionisation of target mol., for $He(2^3S)$ 79−41228
N_2+He, rot. inelastic scatt., appl. of sudden approx. 80−95705
N_2+He differential scatt. 0 to 5×10^{-2} rad. detector angle, 800 eV He *(Russian)* 77−79674
N_2+He^+, 0.7-2 MeV, charge-changing collisions, electron capture 80−58372
N_2+He^+, K-shell ionisation, total cross-sections calcs. 79−31663
N_2+He^+, up to 70 keV, symmetric (antisymmetric) reson. charge transfer cross sections *(Korean)* 78−50636
$N_2+He^+(Ar^+)$, small angle charge exchange, 0.5 to 1.0 keV, time of flight spectra 78−33604
$N_2+He^+(Ne^+)$, charge exchange, time-resolved emission probe 78−86946
N_2+He^+(2s), metastable ion electron capture, loss and de-excitation 77−6904
N_2+He^*, Penning ionisation, ejected electron spectra obs. 80−48074
$N_2+He(2^{1,3}S,2^{1,3}P)$, Penning ionis., N_2^+, $B^2\Sigma_u^+$ state effective cross sections 77−79688
N_2+heavy inert gas, small clusters, beam cluster intensity and collision cross section 77−38711
N_2+Hg, $6(^3P_0)\rightarrow6(^3P_1)$ excitation, double modulation obs. 79−27072
N_2+HgBr, vibr. relax., rate coeffs., fluoresc. obs. 80−63697
N_2+HgX_2 (X=halide), $A^3\Sigma_u^+$-state quenching obs. 80−108693
N_2+I_2, $(A^3\Sigma_u^+)$ state quenching 78−13580
$N_2+I_2^+\rightarrow I^++I+N_2$, 0.65-3.2 keV, dissoc. cross-section, internal excitation effects 78−64813
N_2+inert gas, state-to-state rates from press.-broadened linewidths, data reduction method 78−46430
N_2+K, rot. inelastic scatt., quantum effects, simple model surfaces 80−48064
N_2+K (Na), atom electronic excitation, vibr. to electronic energy transfer, seeded mol. beam studies 80−47919
N_2+K collision, electronic excitation and energy transfer, time of flight spectra 80−43151
N_2+K+Cd, optical excitation, rate consts., collisional energy transfer kinetics 80−32801
N_2+Kr^{2+}, charge transfer reactions, rate coeffs. and product-ion distributions meas. 80−104431
$N_2+Kr^{2+}(Xe^{2+})(C^{2+})$, charge transfer reaction rate consts. 80−7779
N_2+Li, vibr.-rot. relax., optical pot. method 78−62886
N_2+Li^+, comparison with classical small-ang. pot. scatt. theory 80−1043
N_2+Li^+, inelastic scatt., initial rot. and vibr. excitation effects 77−14543
N_2+Li^+, ion-molecule forces, generalised electron gas Drude model appl. 79−98183
N_2+Li^+, rot. and vibr. inelastic collisions, trajectory calcs. rel. to previous data 78−62878
N_2+Li^+, rot. polarisation, spectator model 77−30970
N_2+Li^+, rot.-vibr. energy transfer, 1-10 eV, calc. 79−45799
N_2+Li^+, vibr. excitation cross sections, 100-1200 eV 79−27077
N_2+Li(Na)(K), excited atom quenching, semi-empirical model 78−1065
N_2+Li(2p), Li(2p) excitation, alignment and orientation obs. 80−63794
N_2+methane, compressed-liquid dielectric const., derived excess vol. 79−11377
N_2+methane, liquid mixture, press. effect on excess thermodynamic functions 78−47494
N_2+methane, N_2 fixation, catalytic processes in non-equilibrium plasma chemical reactors *(French)* 80−89483
N_2+methyl cation, ternary assoc. reaction, rate coeffs., 100-300K 79−61845
N_2+methylmercury halides, $A^3\Sigma_u^+$-state quenching obs. 80−108693

nitrogen continued
N_2+N_2, dispersion forces calcs. 80−9675
N_2+N_2, interaction energy, multipole anal., change overlap, orientation and bulk props. 77−34715
N_2+N_2, isotopic variants, V-T and V-V exchanges 78−90270
$N_2+N_2^+$, first negative bands, excitation cross-section calcs. 77−68100
$N_2+N_2^++He\rightarrow N_4^++He$, transition state theory 78−27755
$N_2+N_2O_4\rightarrow N_2+2NO_2$, turbulent mixing in shear layer 77−75989
$N_2+N_2^*(A\Sigma)$, rot. energy transfer, power law scaling 79−98204
$N_2+N_2(Ar)(H_2)$, $(A^3\Sigma_u^+, \nu=0,1)$ metastable state quenching rate coeffs. 78−90206
$N_2+N_2(CO)$, in matrix, vibr. energy transfer and relax. 78−46426
$N_2+N_2(CO)(O_2)$, collinear collisions, anharmonicity effects, vibr. excitation 79−31656
$N_2+N_2(HF)(CO_2)(LiH)(H_2)$, intermol. forces, multipole results validity, charge overlap effects 79−89730
N_2+N^+, charge exchange, 1-3 keV, $N^+(^3P)$ and (^1D) states 79−36760
N_2+N^+, collision, isotope exchange, ion cyclotron reson. obs. 77−52618
N_2+N^+, molecular-orbital X-rays, recoil effects 78−66645
N_2+NH_3, collisional broadening of NH_3 inversion spectrum lines 80−99521
N_2+NO, $^2\Pi_{3/2}$, $^2\Pi_{1/2}$ states, line broadening, mag. moment effect 79−72391
N_2+NO, electronic energy transfer, spectroscopic obs. 78−82716
N_2+NO^+, reaction rate consts. meas. 80−7782
N_2+Na, collisional deactivation of Na excited states, time resolved fluoresc. 78−42197
$N_2+Na^*(3^2P)$, electronic to vibr.-rot. energy transfer, differential cross sections 77−38715
$N_2+Na(3p^2P_{3/2})$, electronic energy quenching dynamics, crossed beam expt. 80−9683
N_2+Ne, fluoresc. spectra, mol. bands, 0.1 to 6 atm., 3000-8200 Å 79−3394
N_2+Ne, K-X-ray spectrum, collisional configuration-rearrangement 78−82816
N_2+Ne^{2+}, charge transfer reactions, rate coeffs. and product-ion distributions meas. 80−104431
$N_2+Ne^{m+}(N^+)$, K-shell vacancy prod. cross-section, charge state depend. 78−17751
N_2+Ne^*, quenching rate const. for metastable $Ne(^3P_2)$, flowing afterglow 78−46295
N_2+Ne(Ar), rot. excitation, body-fixed approx. 77−19015
N_2+negative ion, electron-loss cross sections 80−37877
N_2+O, excitation and deactivation at above-thermal energies 80−43171
N_2+O, quenching of $O(^1D)$ state at 300K, semiclassical study 79−45823
N_2+O_2, binary diffusion coeff. pressure depend. meas. 80−43826
N_2+O_2, molecular fluid mixtures, equilibrium props. 80−64867
N_2+O_2, N_2 fixation, catalytic processes in non-equilibrium plasma chemical reactors *(French)* 80−89484
N_2+O_2 collinear collision, quantum-mech. model 77−30955
N_2+O_2 plasma jet, NO synthesis, chem. kinetics anal., model 80−38728
N_2+O_2 vibr. transitions, semiclassical theory 78−66633
N_2+O_2+NO, mixtures with nonthermal vibr. excitation of mol. N_2, formula for calc. equilib. const. 80−76545
$N_2(+O_2)$ electron beam irrad., rel. to exhaust gas treatment 78−80765
N_2+O^+, charge exchange collision, rate coeff. and ionosphere implications 80−87224
$N_2+O^+(^2D)$, charge exchange rate coefficient, effect of N_2^+ recomb. on aeronomic determ. 78−88954
$N_2+O^+(^2D)$, thermal rate coeff., products and branching ratios in ionosphere 80−82117
$N_2+O^+(^4S)(^2D)$, charge transfer reactions, cross-sections meas. 78−92462
$N_2+O^{n+}(Xe^{n+})(Pb^{n+})$, 50 keV, multiple scatt., target at.+energetic ion spatial correlation influence 79−27062
N_2+OCS, collisional line broadening of microwave spectra, semiclassical theory, calcs. 78−25516
N_2+OCS, gas, EPR of rot. transitions, T_1 press. depend. 80−9621
N_2+OH, mean collision cross sections from microwave spectroscopy 80−1046
N_2+OH, rot. inelastic collision, microwave spectra 79−45806
$N_2+OH^+(H_2O^+)$, reaction, ICR obs. 79−8429
$N_2+OH(A^2\Sigma^+)$, quenching rates and fluoresc. efficiency, rel. to atmosphere 80−14199
$N_2+O(^1D)$, energy transfer, classical trajectory model *(Spanish)* 79−89745
N_2+O(He), intermolecular pots. from Thomas-Fermi-Dirac functional 77−19009
$N_2+O(2^1D_2)$, collisional deactivation meas., 295K, rel. to atmospheric processes 80−16663
N_2+PH, collisional deactivation of $PH(b^1\Sigma^+)$, time resolved quenching 79−54948
N_2+propane, system, vapour-liq. equilib. data 78−83929
N_2+propene system, vapour-liq. equilib. data 78−83929
N_2+S, collision-induced emission of $S(^1S)$, 232 and 425K 79−81264
N_2+S_2, fluoresc. quenching and lifetimes of S_2 78−46386
N_2+SF_6, pulsed H^+ excitation, fluoresc. decay and press. depend. 77−14483
N_2+SO_2, collisional quenching of $^3B_1$ state, 8-1300 torr 78−86906
N_2+SO_2, rot. linewidths (intensities) of $^{32}S^{16}O_2(^{34}S^{16}O_2)$, 91.5 95.5 GHz 78−42044
N_2+Si^*, collisional quenching, reson. line absorpt. expt. 78−46297
N_2+Tl, Hg sensitised fluoresc., quenching 79−22643
N_2+X^{n+}, (X=Ar,Kr,Xe,U), Auger emission line shape after dissoc. 78−86838
N_2+Xe, ^{129}Xe chem. shielding, second virial coeff. 78−66563
N_2+Xe^{2+}, charge transfer from ground and metastable states 79−31677
$N_2^++2N_2\rightarrow2N_3^+$, reactions of electronically excited N_2^+ 77−1915
N_2^++first row transition metal surface reactions 79−96363
N_2^++Group IV elements and oxides, XPS and UPS prod. determ. 78−73084
N_2^++H, reaction, ion cyclotron reson. mass spectrometric obs. 79−64098
$N_2^++H_2$, collisional dissoc. cross-section, 2.4-24.3 keV 80−58373
$N_2^++H_2O$, 50 to 250 keV, OH radical form. 78−56890
$N_2^++H_2O$, reaction rate consts., product distrib., ICR obs. 79−8428
$N_2^++H^+$, fluoresc. efficiency, 3914 Å band of N_2^+ (1N), 100 eV-10 MeV 78−74697
N_2^++He, ion loss cross-section, 2.4-24.3 keV 80−58373
N_2^++He, low energy collisions, vibronic excitation model 77−83689

nitrogen continued
N_2^+ + He, N_2^+ selectively excited, collisional deactivation 80−83338
N_2^+ + He collisions, vibronic excitation, curve-crossing trajectories 80−23520
N_2^+ + Li(Na)(K), 50-1000 eV, crossed beams, electron transfer and excitation 80−14226
N_2^+ + N_2, three-body ion-neutral assoc. reactions, saturation 79−39134
N_2^+ + N_2 + He→N_4^+ + He, ternary assoc., selected ion flow tube obs. 79−39128
N_2^+ + N_2→N^+ + N + N_2, with reactant $X^2\Sigma_g^+$, $A^2\pi_u$ and excited metastable states 77−29001
N_2^+ + O reaction, in ionosphere, rate coeff. determ. 77−53288
N_2^+ + O_2, collisional dissoc. cross-section, 2.4-24.3 keV 80−58373
N_2^+ + O_2, electron capture and ion loss cross-section, 2.4-24.3 keV 80−58373
N_2^+ + $O_2(H_2)$(He), ($A^2\Pi_u$) Meinel band deactivation cross sections above thermal energies 78−66635
N_2^+ + O→NO^+ + N, aeronomical determ. of rate coeff. 79−75000
N_2^+ + Re(metal), reaction dynamics studied by XPS and thermal desorpt. spectrometry 80−93797
N_2^+ + SO_3, in mass spectroscopy of SO_3 mixtures 78−3415
N_2^+ + Th, charge transfer cross-section, 1-500 eV 78−82835
N_2^+ + U, charge transfer cross-section, 1-500 eV 78−82835
N_2^+ + fluoromethanes, thermal energy charge transfer reactions mechanism 77−63889
$^{14}N_2$ + CO, vibr.-vibr. energy transfer, long and short range pot. effect 80−99556
$^{15}N_2$ + CO, vibr.-vibr. energy transfer, long and short range pot. effect 80−99556
$(N_2)_2$, Van der Waals molecule, struct. and internal rot. barriers determ., interaction pot. from ab initio calcs. 80−91626
N_3 generation in NaN_3 thermal decomp. 79−100351
N_3, polarisability correl. with mol. dimens. 80−23288
N_3^- electronic struct., SCF Xα scatt.-wave calcs. 77−50364
N_3, high press. IR vibr. spectroscopy *(German)* 80−74170
N_3, low-lying excited states 79−31425
N_3^+, lateral diffusion in N_2, mass spectra meas. 78−91055
N_3 + NCl, reaction rate consts. calc. 79−74342
N_3^+ + O_2, drift tube mass spectra, rate coeffs. and prod. distrib. 77−77746
N_4^+, lateral diffusion in N_2, mass spectra meas. 78−91055
N_4^+ mobility in N_2 78−60985
N_4^+, photodissoc. cross sections meas., 3500-8600 Å 79−24763
N_4^+ + $O_2(CO_2)(H_2)(D_2)$ reactions, flow-drift tube obs. 78−60985
N_x^+, (x=1 to 4) stratospheric chemistry, reaction rate coeffs. and product distribs. 78−81305
N_2(-Ne), gas, 77K, positron annihilation lifetime spectra 79−10630
N_2(-methane), heat transfer in nucleate boiling of liquified gases and binary mixtures *(German)* 79−18687
N_2^+($A^2\Pi_u$-$X^2\Sigma_g^+$) system in aurora, vibr. development and quenching effects 78−88967
$N_2(A^3\Sigma_u^+, \nu_i)$ + $N(^4S)$→$N(^2P$ or $^2D)$ + $N_2(X^1\Sigma_g^+, \nu_f)$, energy partitioning 78−66636
$N_2(A^3\Sigma_u^+)$, auroral, quenching by O and O_2 from rocket meas. of emission 78−57380
N^+Ar, electron emission, double differential cross sections, Auger spectra 79−45684
$N_2(B^3\Pi_g$-$A^3\Sigma_u^+)$ system in aurora, vibr. development and quenching effects 78−88967
$N_2^+(B^2\Sigma_u^+)$, $N_2(C^3\Pi_u)$ and $N_2(C'^3\Pi_u)$ molecules, emissions obs. in yellow N_2 afterglow 80−63649
$N_2^+(B^2\Sigma_u^+)$, perturbation of ν=1 vibr. level, rot. lines freqs. and intensities *(French)* 77−79640
$N(^2D,^2P)$ metastable ats. prod. in N_2 DC glow discharge 80−38758
$N(^2D,^2P)$ metastable production by electron collisions in DC glow discharge 80−59274
$N(^2D)$ chemistry in ionospheric F-region 78−16241
$N(^2D)$ + O, associative ionisation 80−4161
$N(^2D)$ + O_2 as source of $O(^1D)$ atoms in aurorae 79−35028
NH_3-$N_2(H_2)$(Ne)(Ar)(Kr)(Xe), as R(1,1) vibr-rot. line parameters, ν_2 band, using CO_2 laser light 79−3444
NH_3 + NH_3(He)(Ar)(N_2)(O_2), ν_2 state vibr. relax., laser induced vibr. fluoresc. obs. 79−18269
NH_3Cl, ^{15}N zero point vibr. energy from nuclear photon scattering 80−59593
NII, NIII level lifetimes, beam-foil method meas. 78−94314
$^{14}N^{14}N$, Raman spectra, direct determ. of rotation-vibration coupling coeff. 77−38675
$^{14}N^{15}N$ + CO, vibr.-vibr. energy transfer, long and short range pot. effect 80−99556
$^{14}N^{15}N$ + O plasma reaction system, isotope fractionation under simulated space conditions 78−73623
$N_2(N_2^+)$, UV, visible spectra in Ar plasma, 230-620 nm 78−13456
$N_2(N_2$ + Ar) pulse excited microwave discharge diagnostics at moderate press. 78−9873
$N_3^+(N_4^+)$, ion transport in electrical discharge 78−87435
NO, core photoelectron line shape, localisation role 79−59512
NO^-, ($a^3\Sigma^+$), prod. from N^+ + O_2 reaction 80−7784
NO + N_2, NO γ(0,0) band, oscillator strength and line broadening 80−106356
NO + O_3*, laser excitation effects, fluoresc. meas. 77−21372
NO^+ + $2N_2$⇌$NO^+.N_2$ + N_2, rate const., enthalpy and bond strength 77−16809
NO^+ + N_2, vibrational radiation quenching in upper atmosphere 79−3543
NO_2 and NO_3, photodissociation solar radiation effects in atmosphere 79−58045
NO_3 in nighttime stratosphere, composition change following sunset 80−31097
$N_2O/N_2/H_2O$, CW gasdynamic laser, numerical anal. 78−29935
N_2O-N_2, CW gasdynamic laser, qualitative comparison with CO_2-N_2 laser 78−25856
N_2O-N_2, CW mixing gasdynamic laser, saturation parameter and small signal gain 79−45923
N_2O-N_2 mixture, thermalisation under reson. excitation by laser radiation *(Russian)* 78−26231
N_2O-N_2-He, gasdynamic laser, effect of weak flow perturbations on gain 80−14316
N_2O-N_2-He, population inversion of N_2O vibr. levels behind shock wave front 79−31886
nitrogen continued
N_2O-N_2-He mixture, radiation amplification factor in supersonic expanding stream of gas 77−10896
N_2O + N_2, vibr. population distrib. energy depend., ν_3, ν_2 and ν_1 mode exchanges *(French)* 79−10187
N_2O + N_2*, vibr. population studied by IR emission spectra *(French)* 77−14544
NO^+e = N + O, in hypersonic air wake, temp. depend. meas. 79−27834
NO^+(ν=1,2) + N_2, vibr. transfer, vibr. absorption coeff. 79−6994
$N^-(^3P)$, energy and width after form. by N_2 and NO dissoc. electron attachment 78−90308
$N^{2+}(^2P^0)$ + H, charge transfer, ab initio CI pot. curves and coupling-matrix elements 80−37878
$N(^4S)$ recombination rate in Lewis-Rayleigh afterglow 79−68968
$N^+(^5S)$ + inert gas, de-excitation cross section, 2-30 keV 78−25695
$N^{3+}(^1S)$ + H, charge transfer, ab initio CI pot. curves and coupling-matrix elements 80−37878
$N(^4S) + N^+(^3P) = N^+(^3P) + N(^4S)$, gerade-ungerade splitting of N_2^+ pots., cross sections 77−30987
$N(^4S) + O_2(^3\Sigma_g^-)$→$NO(^3\pi_u) + O(^3P)$ doublet surface minimum energy path calcs. 78−7194
$N(^4S) + O_3$, rate const. at 298K, upper limit determ. 79−74360
$N(^4S) + S(^3P) + M$→$NS(B^2\Pi) + M$ kinetics, chemilum. obs. 79−39151
$N_2(^1\Sigma_g^+)$, diatomic molecular form factors, vibr. average, study of convolution approx. 79−50926
$N_2^+(^2\Sigma_u^+)$, B and C states, unimolecular decay, nonadiabatic interactions, transition probability as function of Massey parameter 80−35503
$N_2(X^1\Sigma_g^+) + Ar(^3P_{2,0})$→$Ar(^1S) + N_2(C^3\Pi_u)$, sensitised fluoresc., vel. depend. 78−90204
$N_2(X^1\Sigma_g^+) + O^+(^4S)$→$NO^+(X^1\Sigma^+) + N(^4S)$, MCSCF potential energy surface for collinear $^4\Sigma$ pathway 80−63540
^{13}N, absorbed dose comparison rel. to γ-ray emitters 79−70647
^{13}N labelled NH_3 production for medical appl. 80−72327
^{13}N prod. by accelerators for nitrosourea-^{13}N prep. 79−53242
^{13}N production for nuclear medicine use 80−30889
^{13}N production in cyclotron by $^{16}O(p,\alpha)^{13}N$, water loop target 80−23201
^{13}N radioisotope preparation at variable energy cyclotron of Frederic Joliot Hospital Service *(French)* 77−65361
^{13}N species formed by proton irradiation of water 80−45532
^{13}N use for functional lung exploration *(French)* 77−70521
^{14}N, ^{15}N, laser isotope separation, by NH_3 photodissoc., book contrib. 78−9208
^{14}N, nuclear polarised ions, grazing incidence refl. from Cu surface 79−64077
^{14}N pulsed NQR-FFT radiofrequency spectrometer description and operation 80−17982
$^{14}N_2$ + CO, vibr. energy transfer, laser fluoresc. obs. 80−28050
$^{14}N^+$ implanted in Ta, target preparation 79−45501
$^{14}N^{14}N$ + $^{14}N^{15}N$, vibr. distrib., electron impact excitation, isotopic composition, interaction depend. 79−29332
$^{14}N^{15}N$ + CO, vibr. energy transfer, laser fluoresc. obs. 80−28050
^{15}N 6.5 MeV ions in solids, energy loss distrib. meas. 78−59845
^{15}N, anal. by proton scatt. 79−61926
^{15}N, beam foil and quantum beat spectra *(Chinese)* 80−32638
^{15}N, highly ionized, atomic transition polarisation by beam-foil interaction, 3-8 MeV 80−18908
^{15}N NMR heteronuclear spectroscopy, two dimensional Fourier transform technique 80−31818
^{15}N, NMR signal intensity enhancement by polarisation transfer 79−94013
^{15}N rel. to atmospheric nitrogenous trace gases 78−73470
^{15}N, spin-lattice relax. time, quantum effect of NH_4-ion rot. 80−75875
^{15}N, use in determ. denitrification rate seasonal var. in sediment 79−100883
$^{15}N/^{14}N$ ratio and solar nebula differentiation 80−36519
$^{15}N/^{14}N$ ratio in lunar microbreccias indicating ancient solar wind composition 80−62046
$^{15}N/^{14}N$ ratio in solar wind from lunar samples 77−87354
$^{15}N/^{14}N$ ratios in gaseous NH_3, NO_2 and NO_3^- in aerosols and precip. 78−44896
$^{15}N_2$, solid struct., and thermodynamic props. *(Russian)* 80−88083
^{15}N-^{13}C spin-spin coupling constants calc. using SCF and INDO method 80−32609
^{15}N-$^1H^+$ NMR, coupling consts., double reson., difference proton Fourier transform spectroscopy 79−3467
^{15}N-NH_4, absorpt. and transfer to amino-N, rat small intestinal sac 80−16909
$^{15}N^+$, implantation in Al, Ti, Ni, Cu, Zn, Mo, Ag, Ta, W, Au, ranges, conc. distrib. meas. 79−37749
^{15}N + CO, vibr. energy transfer, laser fluoresc. obs. 80−28050
N_2^* ($A^3\Sigma_u^+$), electron impact ionisation cross section 80−78718
N_2^*, metastable, collisional form., C-B emission spectrum 77−19019
N_2^* + CO, vibr. excitation and quenching, long contact time effect 79−86040
N_2^* + ClCN(BrCN), vibr. energy transfer, α_3 vibr.-rot. const., microwave meas. 77−83578
N_2^* + H_2O, vibr. deactivation rate, hard core calc. 79−31651
N_2^* + $H_2O(H_2S)$(methane), deactivation, from laser-induced CO_2 fluoresc. obs. 80−63776
N_2^* + H_2O→N_2 + H_2O^* 80−87212
N_2^* + $HgBr_2$, dissociative excitation, mol. fluoresc. obs. 80−91634
N_2^* + OCS 80−48063
N_2^* + SO_2, quenching of vibr. excited N_2, photoionis. detect. technique 78−46388
N2 + K, anisotropy of the repulsive intermolecular potential from rotationally inelastic scattering 79−41226
N6d2-Ne discharge lamp, meas. method for partial H_2 press., selective gettering action 77−87775
N_2⇌2N layer, hydrodynamic stability anal. 77−75993
Na-CO_2 mixing-type gasdynamic laser, experimental and theoretical studies *(Japanese)* 80−23666
Na-He-N_2 dense vapour system, optical pumping, RF spectrum analyser appl. 79−76393
Na + N_2, higher Na s and manifold states deactivation cross sections 79−10176
Na + N_2, Na excitation in non-equilib. conditions behind shock wave 77−23539
Na + N_2, rot. excitation and fine struct.-changing collisions 78−42176
Na + N_2, total elastic cross sections meas. 77−30954
$N_2(a'^1\Sigma_u^-)$ state radiative lifetime, VUV emission 79−18226

nitrogen continued
Na^*+N_2, differential quenching cross-section, polarisation effects 77−27019
N_2(active)+SO_2, excited neutral metastable SO_2 form. mass spectrometric study 80−83300
$Na(n^2D)+N_2(CO)$, collisional l-mixing, highly excited states, fluoresc. obs. 77−83686
Nb:N, deviations from Matthiessen's rule 78−39092
Nb:N, H, atomic tunnelling of interstitial pair, specific heat meas. 78−47600
Nb:N, H_{c2} anisotropy, impurity and temp. dependence 78−43533
Nb:N, neutron diffuse-scatt. intensities 80−59597
Nb:N,H(D), thermal cond., 0.07 to 1.5K, influence of N interstitials 79−65601
Nb-N, diffusion of H, incoherent neutron scatt., interstitial effects 79−60558
Nb-N system, ion-implanted, supercond. crit. temp., effect of implantation conditions 78−19176
Nb-Re-(Ru)-N system, N_2 solubility and solubility limit *(German)* 77−4205
Nb-Re(Ru)-N system, spectral emissivity, lattice parameter, initial rate of N_2 absorption *(German)* 77−4204
Nb_3Sn, vap. deposited supercond. film, effect of N_2 and tape heating 78−34939
Ne, electron impact, collision freq. in ionospheric F-region 79−53641
Ne:N_2, long wave UV luminesc. *(Russian)* 78−88347
Ne-N_2, atomic N nuclear pumped lasers, surface effects 80−63996
Ne-N_2, energy transfer, H^+ ion beam produced plasma, ion density and temp. 80−38539
Ne-N_2, N_2^+ ($B^2\Sigma_u^+$) state excitation kinetics 78−9239
Ne-N_2 AC discharge, pulse to continuous mode transition, Ne metastable effects *(German)* 80−84011
Ne-N_2 laser, energy pathways by proton excitation 78−5459
Ne-N_2 mixture, cataphoretic segregation in DC discharge, mass spectral anal. 77−32799
Ne-N_2 mixture, plasma created by electron beam, spectral composition *(Russian)* 78−30453
Ni:N, hyperfine interactions, recoil-implanted β-NMR method *(Japanese)* 79−51865
Ni(001) surface N adsorption due to ion beam irrad., surface struct. LEED study *(Chinese)* 80−84364
Ns+Ne, metastable state de-excitation, rate consts., radiolysis obs. 80−40709
$O+N_2^+(O^+)(O^{2+})$, rate coeffs. in thermosphere, AE satellite meas. 79−48594
$O^- + N_2 \rightarrow N_2O + e$, rate studies 78−40036
$O^- + N_2$, atom transfer, reaction rates and cross-section determ. 77−60052
$O^+ + N_2$, excited ion reactions, charge transfer coeffs. at thermal energy 80−95721
$O^- + N_2$, ion speed distribution effects in flow-drift tubes 77−56219
$O^- + N_2$, reaction rate coeff. in ionosphere 77−87167
$O^- + N_2(O_2)$, reaction rates, 300-900K 79−8434
$O^- + N_2(O)$, rate coeffs. in thermosphere, AE satellite meas. 79−48594
$O^- + N_2 \rightarrow N + NO^-$ react., mechanism, ab initio SCF calcs. 78−60996
O_2-He(N_2)(CO_2), O_2 electron attachment coeff. meas., O_2 partial press. depend. *(German)* 79−13821
O_2-N_2, gas mixture, mag. field effect on thermal conductivity 78−59533
O_2-N_2, gas mixtures, mass transfer, mag. field effects 78−63535
O_2-N_2 mixture, attachment cooling, press. depend. 80−91663
O_2-N_2 plasma mixture decay, effective recombination coeffs. *(Russian)* 77−47144
O_2+N_2, 118750 GHz transition, press. broadening 77−75136
O_2+N_2, collision induced UV absorpt., Herzberg continuum, dimer form. 78−9167
O_2+N_2, O_2 absorption in Herzberg region, N_2-induced, temp. effect 78−87429
$O_2+N^+(O^+)(C^+)$, rate coeffs. meas. at 300 and 100K in flowing afterglow 79−20346
OCS-N_2-SF_6 mixture laser, OCS photodissociation, electron dipole forbidden transition, absorpt. spectra 79−68389
$O^+(^2D)+N_2$ charge exchange, rate coeff. temp. depend. 80−77179
$O(^1D)+N_2$, electronic quenching resons., collinear collision, quantum mech. calcs. 77−60050
$O(^1D)+O_2(N_2)(CO_2)(O_3)(H_2O)$, 100-350K, reaction rate consts. 77−21355
OH ($A^2\Sigma^+$)+$H_2(N_2)$(Ar), collisionally induced population change rates, laser-induced fluoresc. obs. 78−5326
$OH^- + C(N_2)$, electron stripping and breakup, proton spectra 77−83685
$O^{+*}+N_2$, metastable ion reactions, rate consts. and ion mobility at 300K 80−95722
Rb+N_2, spin relax. rate 77−19027
reactant ion electronic states, effect on charge transfer cross sections 80−63809
S+inert gas (N_2)(H_2), rare gas sulphide $S(^1S)$ emissions 78−82828
S_2+N_2 *(Russian)* 80−99711
$S_2(B\ ^3\Sigma_u^-)$+inert gas (H_2)(N_2)(S_2), collision-induced energy transfer 79−3544
SF_6-N_2, dielec. props., ionisation and attachment coeffs. 80−33726
SF_6-N_2, horizontal cylindrical power cable, convective heat transfer, simulation *(Russian)* 77−58676
SF_6-N_2 mixture, discharge inception voltages, calc. 79−68966
SF_6-N_2 mixture, electron swarm development, Boltzman eqn. anal. 80−87841
SF_6-N_2 mixture in rod-plane gaps, static field breakdown 79−68965
SF_6-N_2 mixtures, attachment coeffs. and ionic mobilities, 1.2-4 eV 80−96338
SF_6-N_2-Ar mixture high-current multispark discharge switching characteristic 78−67444
SF_6+N_2, simultaneous vibr. transition, absorpt. band intensity 77−50474
SeO_2+N_2, radiative lifetime and quenching rates 80−95685
Si, commercial, nitridation, effect of BaF_2 80−81359
Si:B, N-implanted junction capacitance meas., appl. of dynamic lateral photovoltaic effect 77−85304
Si:N, amorphous, DC sputtered, enhanced, photocond. 78−56183
Si:N, amorphous, prep. by RF sputtering and props. 80−44229
Si:N, conc. profiles of ions and recoiled N after implantation through Si_3N_4 films 79−55764
Si:N, high energy ion implantation of buried insulating layers 80−88188

nitrogen continued
Si:N, implantation at high doses, annealing conditions for homogeneous buried insulating layer *(French)* 80−59498
Si:N, interstitial Si atom formation by light ion bombardment 78−47406
Si:N, ion implantation, refractive index, IR spectra, ion range and straggling meas. 80−34020
Si:N, ion implanted, IR transmission and rel. spectra study 80−108244
Si:N, ion implanted, nature of defect reverse annealing 80−88875
Si:N, ion implanted, oxidation characts. 80−89385
Si:N, laser-annealed, Jahn-Teller distorted donor, EPR meas. 80−84642
Si:N, struct. defects formed by 50 keV N^+ irrad., depth distrib. 78−18688
Si:N wafers, Si_3N_4 layer growth by high dose implantation and annealing, elec. props. 80−70227
p-Si:N_2^+ implanted, anneal behaviours of lateral photovoltaic method 79−14825
Si:P, N implantation through Si_3N_4 film, depth distrib. of knock-on N, SIMS meas. 78−10066
SiC, crysts., tetrahedral bond deformation variation with hexagonality and doping degree of N 79−94977
SiC, exam. of N solubility, in epitaxial layers 80−6520
SiC, N doping inhomogeneities due to growth conditions 78−22741
SiC:Al,N, blue cathodolum. spectra obs. 78−19574
SiC:Al,N (6H), ODMR for effective-mass-like acceptor 80−93213
SiC:N, conversion factor at high doping levels 78−22744
SiC:N, impurity effect on stress gradients and dislocation development 77−4116
n-SiC:N, O, cathodolum. spectra meas. 78−19573
α-SiC:N, paramag. N impurity levels, IR absorpt. and ESR expts. 77−59598
SiC:N (6H), photoluminesc., site-depend. donor and acceptor levels 79−61421
SiC-N_2 system, high temp.-processes, thermodynamics 77−85105
Si_3N_4-SiO_2:N,Zn ion-implanted multiple layers, ion range distribs., secondary ion microprobe meas. 79−42129
SiO_2 film, on GaP substrate, N ion implantation, optical refl. and EPR meas. 80−84197
T 79−45757
Ta film, determ. of thickness and O, N content 78−80824
Ta:N, H_{c2}-anisotropy obs. 78−80105
Ta:N, superconductive to normal transition anisotropy 80−25031
Ta:N film, triode sputtered, struct.-related cond. props. 79−78225
Ta-N film, reactively sputtered, N content determ. from Fourier anal. of X-ray diffr. profile 77−76693
Ta-Nb(Re)(W) (50,20,0 at.%), with N_2, spectral emissivity, N_2 absorption rate, N_2 solubility, thermodynamic data *(German)* 77−25026
Ti, nitriding kinetics at 1230 to 1500°C, diffusion and struct. investig. *(French)* 77−36683
$U^+ + N_2(D_2)(CD_4)$, endothermic reactions, heat of formation 77−73444
UF_6 admixture effect on N_2 and Ar excited state lifetimes 79−10281
V:N, ion bombard., void form. 80−34097
W, cast state, interaction nature between C, O_2 and N_2 *(Russian)* 79−70114
Zn single cryst. deform. in liquid N_2, gas bubble form. on growing twins *(Russian)* 79−60378
ZnSe:N, ion implanted cond. type conversion on annealing *(Korean)* 78−18668
p-ZnSe:N, LPE layers, photocapacitance and photocond. meas. 79−99572
Zr-O-N system, struct. and plastic deform. *(Russian)* 78−80588
ZrC:N, emissivity, integral hemispherical and monochromatic 78−91457
ZrN-Al_2O_3, effect of N on sintering 79−33991

nitrogen compounds
see also ammonia; ammonium compounds
acetylene-N_2O flame, chem. equilib. rel. to AAS 77−4957
adsorption and cryogenic refrigeration systems 79−58722
air pollution removal mechanisms and processes *(Dutch)* 77−70824
alkali halide:NO_x, EPR isotropic hyperfine triplets 80−2636
atmospheric NO_2 total content meas. by absorption spectroscopy *(Japanese)* 80−12469
bridged complexes, vibr. and electronic props., reson. Raman spectra appl. 80−52996
chloropentafluoroethane-NO, multiphoton dissoc., ^{13}C enrichment factor, CO_2 laser wavelength and fluence depend. 80−58331
dichlorodifluoromethane, rate const. for reaction with OH and tropospheric lifetime 77−64366
electroionisation synthesis 78−23937
ESCA shifts and effective charges 80−78648
fertilizers, nitrogenous and phosphate, pollution problems from manufacture 79−34450
gas mixture, thermal diffusion const. 78−67300
graphite nitrate, structural ordering in intercalation compounds 78−26539
graphite-Na-N-H intercalation compounds *(French)* 79−52633
HCl-NOCl gas mixture, vibr. relaxation, collisional de-excitation *(French)* 78−86934
hydrazinium hydrogen oxalate, electron and proton distrib. in the short O-H-O bond 79−14789
hydrazinium iron tri(hydrazoformate) monohydrate single cryst., effective EFG tensor, Mossbauer spectra obs. 79−56628
L(+) hydrazonium tartrate, soln. growth and cryst. morphology 79−33914
interstellar cloud gas phase chemistry 80−105319
metal surface hardening by plasma nitriding 79−8400
methoxy+NO, reaction rate upper limit, laser induced fluoresc. 80−85200
methyl radical+O_2 (NO), mass spectra, absence of reaction in combustion system 78−53195
modeling of elementary step of chemical transform. of crysts., appl. to decomp. 79−15985
molecule, ground state MNDO calcs. 78−911
muonic capture rates in elements of compounds, influence of chemical bond 78−58874
N_2H_4, electrochem. oxidation on Au, appl. to gas monitoring 79−39248
sym-N_2O_3, mol. vibr. in N_2 matrix, normal coord. anal. 79−59432
$^{14}N^{16}O$, 1-0 band at 1900 cm^{-1}, meas., interpret. 78−58651
nitrate, artifact, formation on filter media, interference effects 79−83668
nitrate and static stability in Peru coastal waters 79−74899
nitrate conc. in aerosols, SO_2 photochem. effects 77−49103
nitrate detection in aerosol particles using nitron 79−12280

nitrogen compounds continued
nitrate determ., improved hydrazine reduction method for freshwater samples 79−34467
nitrate determ. in atmosphere using HNO_3 collection on NaCl impregnated filters 80−81509
nitrate determ. in estuarine waters, UV absorption technique 79−16719
nitrate salts, Raman spectra, thermally disordered energy states '78 38122
nitrates, aq. solns., high resolution AC coupled Raman spectra 79−40619
nitrates, atmospheric sampling with glass fibre filters, errors 78−16169
nitrates, detection by chemiluminescence analyser 78−40094
nitrates, distrib. in Pacific ocean waters 80−31065
nitrates, gaseous, in atmosphere, investigations in urban and rural area 80−94123
nitrates in Bering Sea shelf sediments, denitrification estimates 80−12433
nitrides, structs. and cryst. growth 80−29865
nitrides, XPS *(Japanese)* 80−16154
nitrites and nitrates in wastewater, simultaneous automated determ. 77−29511
nitrogenous trace gases in atmosphere, preliminary ^{15}N studies 78−73470
nitroso and nitrosyl cpds., ^{14}N chem. shifts correl. with nuclear quadrupole coupling consts. 77−30888
nitroxide free radical spin label EPR spectra, determ. of rot. correl. time and HFS coupling 80−74260
nitroxide free radicals, neutral, EPR spectra, localised solvent-radical adducts 79−96290
nitroxide groups in crystals, H bonds and short intermolecular contacts 80−63855
ocean-atmosphere-continent system, N compounds exchange 78−3794
oxides, atmospheric pollution, ozone depletion *(Russian)* 78−16154
oxides, effect on stratospheric ozone calc. 77−53269
oxides, formation in simulated MHD combustion chamber working on natural gas and O^2 enriched air, investigation 80−106984
oxides, plasma chemistry *(Russian)* 78−92482
oxides, produced by thermonuclear explosions, effect on atmospheric ozone 79−84345
oxides, rain and snow acidity, release by burning of fossil fuels 80−26590
oxides, tropospheric photochemistry 78−44914
oxides+hydrocarbon mixtures in air, photochemistry 79−53427
oxides and ammonia, atmospheric cycles 79−48562
oxides in atmospheric samples, meas. using luminescence *(Dutch)* 80−3565
positronium nitrate, $[NO_3^-;e^+]$, existence, Hartree-Fock-Roothaan calcs. 80−83254
positronium nitrite, $[NO_2^-;e^+]$, existence, Hartree-Fock-Roothaan calcs. 80−83254
Purex process, concs. of U, Pu, HNO_3, fission products, in LMOM2 extractor, expt., graphical determ. 78−41843
rot. spectra, 714-1667 μm, Fourier interferometric spectrometer 77−83765
thionitrates, mol. struct., S-substitution effect *(French)* 80−23335
thunderstorm production of O_3 and N oxides 77−37300
$2NO_2 \rightleftharpoons N_2O_4$, multiple stationary states, hysteresis 77−9074
$2NO_2 \rightleftharpoons 2NO+O_2$, gas mixture turbulent concurrent double pipe heat exchanger equilib. and nonequilib. reaction 78−94856
$3NO \rightarrow N_2O+NO_2$, irreversible thermal decomposition, rate consts., 440 to 650°C *(Russian)* 79−70322
$Al+NO_3^-$, reactions between metal and aq. nitrate solns., XPS 77−12825
$Al+NO+Ar \rightarrow AlNO+Ar$, rate coeff., 600K, fluoresc. and absorption spectrum obs. 77−40521
$Ar:N_2O$, $O(^1S)$ photodissociative prod., photoluminesc. excitation spectra, exciton energy transfer 80−89508
Ar-Xe-NF_3, mixture in XeF laser, discharge stabilised by short-pulse electron beam 80−14358
Ar-Xe-NF_3 mixture, fluorescence from e-beam excitation at low temp. and high press. *(French)* 78−58727
$Ar+NO(X^2\pi)$, intermol. pot. surfaces, electron gas model calcs. 77−34721
$Ar^+ + NO$, charge transfer cross sections 77−34751
BH_3NH_3, microwave spectra, rot. consts., dipole moment, mol. struct. 79−85957
Ba-N_2O flame, candidate chem. laser reactions, intracavity dye laser absorpt. meas. 78−63108
$Ba+N_2O$, crossed mol. beams, BaO recoil vel. spectra 78−7184
$Ba+N_2O \rightarrow BaO+N_2$, chemiluminesc., ang. distrib. 78−44361
$Ba+N_2O \rightarrow BaO^*+N_2$, model electronically nonadiabatic reaction, large quantum effects 77−4897
$Ba+NO_3(N_2O)$, chemiluminesc., absolute photon yields determ. 77−86317
$Br+O_2(NO)$, quencher paramagnetism, deactivation rate const., spin-orbit relax. study 80−21263
C-O-H-N-Si-Ar, computer calculations of heterogeneous equilib. 79−66044
CN, free radical, anticrossing spectra for fine struct. consts. 79−68270
CN+NO, reaction rate constants 79−1935
CO-N_2O reacting gas mixture, gain due to CO_2 $00^01\text{-}10^00$ transition 80−74337
CO-NO mixtures, Ar matrix isolation, laser-included vibr. fluoresc. 80−9707
$CO+N_2O$ catalytic reaction on Sc_2O_3 and MgO, kinetic obs. 79−29389
$CO+NO(O_2)(D_2)$, (v=1) relax., temp. depend. 78−17760
$CO^+ + NO \rightarrow CO_2^+ + N$, crossed beam study 80−104436
CO_2-N_2O, laser optical pumping in 4.3 μ band 77−7060
CO_2-N_2O, mixed cryst., librational motion, Raman obs. 78−6661
$CO_2+C^+(N_2H^+)$, rate coeffs. meas. at 300 and 100K in flowing afterglow 79−20346
$CS_3+N_2O+O_2$ combustion, CO laser performance characts. *(Russian)* 78−55348
Ca-N_2O-CO flame, Ca catalyzed, gain meas., emission band assignment 78−66815
Ca-N_2O-CO flame, candidate chem. laser reactions, intracavity dye laser absorpt. meas. 78−63108
$Ca_{10}(PO_4)_6F_2:NO_2^-$ apatite, ESR, struct. of ions *(French)* 78−43640
$Cl+NO+N_2 \rightarrow NOCl+N_2$, rate const. temp. depend. 78−76828
$ClO+NO_2 \rightarrow ClONO_2$, fall-off curves, N inclusion effects 77−63910
$ClO+NO_2 \rightarrow ClONO_2$, reaction kinetics 77−86303

nitrogen compounds continued
$ClO + NO(NO_2)(SO_2)(CO_2)$, rate consts. at 300K 78−76829
$CsBr:NO_2^-$, luminesc. centre polarisation and reorientation *(Russian)* 78−76529
$CsCl(Br)(I):NO_2^-$, vibronic and reson. Raman spectra of BCC cryst. 79−87468
$CsI:NO_2^-$, luminesc. centre polarisation and reorientation *(Russian)* 78−76529
DBr-N_2O mixture, third harmonic generation obs. 79−23018
FCN, photoelectron spectrum 77−30920
FNNF, mol. struct., cis effect 80−91434
FNO, Stark spectroscopy of ν_1 band, rot. consts., dipole moment 79−13710
FNO_2, UV photoabsorption spectrum 79−10123
Ge-N_2O, rate coeff. meas. for $Ge+N_2O \rightarrow GeO+N_2$ reaction 78−63110
$Ge(^3P_0)+N_2O$, reaction rate const. meas., in flowing afterglow 77−77731
$H+NO_2 \rightarrow OH+NO$, energy disposal, information theory appl. 78−15658
$H+NO_2 \rightarrow OH+NO$, $H+NOCl \rightarrow HCl+NO$, rate meas. by Lyman-$\alpha$ fluoresc. 77−21353
$H+NO_2 \rightarrow OH+NO$, laser induced fluorescence for OH, $^2\pi$ to $^2\Sigma$ region, preferential population of Λ doublets 78−31620
$H+NO_2 \rightarrow OH+NO$, primary energy disposal, laser-induced fluoresc. 79−24726
$H^+ + NO$, ~10 eV, anomalous excitation of NO Rydberg states 77−14546
$HCO+NO(O_2)$, reaction rate consts. 78−31617
$HCl+O^-(O_2^-)(NO_2^-)(CO_3^-)(CO_4^-)$, rate consts. at 300K 78−76829
HN_3, ground $^1A'$ state, SCF and CI calcs., conform., geom., vibr. freqs. and dissoc. 80−18806
HNCO, 193 nm photolysis, photodissoc. products, $NH(a^1\Delta)$ internal energy distrib. reaction rate with 0_2 79−83489
H_2NNH_2, nuclear fuel processing solutions 78−78487
HNO, pot. energy functions for ground state surfaces 79−89620
HNO_3, aqueous soln., reflectance and complex refractive index, IR spectra, vibr. modes 80−66168
HNO_3, high resolution spectral meas. of 11.3 μm band, using tunable diode lasers 78−33504
HNO_3, nuclear fuel processing solutions 78−78487
HNO_3, overlapping Raman lines resolution by coherent ellipsometry 79−98110
HNO_3/NO_2 conc. ratio in daytime stratosphere 78−73460
HO_2+NO_2, UV irradiated, kinetics and mechanism, peroxynitric acid form., smog 77−63885
HONO+NO+NO_2+CO+air, UV irradiated, computer simulation, peroxynitric acid form., smog 77−63885
HO_2NO_2, thermal decay kinetics 79−5135
$HOONO_2$, FT IR spectral obs. of $HOO+NO_2 \rightarrow HOONO_2$ 77−28993
H_2S+NO_2, SO chemiluminesc. in Ar matrix 79−5146
$He^+ + N_2O$, rate coeffs. meas. at 300 and 100K in flowing afterglow 79−20346
$HeNO_2$ van der Waals complex, fluoresc. spectrum 77−46591
$HgH+NO \rightarrow HNO+Hg$, reaction rate temp. depend., chemiluminescence 78−68885
$KBr:NO_2$, X-irrad., paramag. and nonparamag. hole centres 77−16176
$KCl:NO_2^-$, Stokes' losses on cryst. vibrs. in luminesc. spectra of mol. centres *(Russian)* 77−55827
$KCl:NO_3^-$, colloid centre formation, absorpt. spectra, 300-1000 nm 79−78710
$KCl_{1-x}Br_x:NCO^-$, absorpt. band defect broadening *(Russian)* 78−72526
$KCl(I):NCO^-$, shift and broadening of local vibr. bands, temp. depend. 78−87755
$KCl_{1-x}I_x:NCO^-$, absorpt. band defect broadening *(Russian)* 78−72526
$Kr:N_2O$, cryodeposited film, exciton-enhanced KrO excimer luminescence 77−36288
$Kr:N_2O$, photoluminesc. from KrO (^1S) excimers 78−68544
Kr-NO, thermodynamics, monomer-dimer assoc. of NO, vap. press. meas. 79−90798
KrF+He(Ne)(Xe)(NF_3), quenching rate consts. meas. 79−24718
$Kr^*(Kr^+)+NF_3$, rate consts., electron attachment coeffs., flowing afterglow 78−13578
Mg-N_2O-CO flame, efficient chem. generation of $Mg(^3P)$ 78−63109
Mg-N_2O-CO flame, Mg catalyzed, gain meas., emission band assignment 78−66815
N_2O, remote conc. meas. using tunable IR laser 77−87118
N-Fe solid soln. in equilibrium with N_2 gas, partial molar enthalpy and excess entropy 80−60838
N_2 gasdynamic laser, active medium increased lifetime 79−68388
$N_2:N_2O$, liq., vibr. relax., Raman scatt. obs. 78−92061
N_2+HBr, rate consts. for vibr. energy transfer meas. using laser. induced fluorescence technique 80−87206
$N_2+N_2O_4 \rightarrow N_2+2NO_2$, turbulent mixing in shear layer 77−75989
N_2+N^+, charge exchange, 1-3 keV, $N^+(^3P)$ and (^1D) states 79−36760
N_2^++methane, charge transfer cross-section, low energy 78−58791
N_3^-, theoret. electron density distrib. cf. expt. density distribs. of NaN_3 and KN_3 77−46489
N_2BF_3, microwave spectrum and struct. 79−76420
NBr, in solid Ar, $b^1\Sigma^+ \rightleftarrows X^3\Sigma^-$ transitions 80−32702
NBr, mol. pot., r-centroids, $A^1\Sigma^+$-$X^3\Sigma^-$ band system 77−3373
NC+H, bimolecular exchange reactions, dynamical-statistical method calcs. 80−104435
$N(CH_3)_4GeCl$, cryst. and powder diffr. data 80−24422
NCNCO, geometrical struct., INDO calcs. 79−22602
$NCNO \rightleftharpoons NC+NO$, ground state pot. energy surface, ab initio calcs. 77−90593
NCO, $A^2\Sigma$ state, Fermi resonance and vibr. relax. in solid Ar 78−5212
NCO as possible interstellar species 79−17065
NCO^+, CI-SCF-MO basis function calc. 77−42246
NCS, force field in alkali halide lattices 79−51224
NCS^-, fluoresc. quenching of organic excited singlet states, rate meas., mechanism 77−38685
NCl, in solid Ar, $b^1\Sigma^+ \rightleftarrows X^3\Sigma^-$ transitions 80−32702
$NCl+N_3$, reaction kinetics calc. 79−74342
NCl_3, ab initio LCAO SCF calc. for ground state, inversion barrier 78−25426
NCl_3, bond polarisability and force constants 80−69260
$NCl_3.NH_3$, force const. calcs. 79−36603
ND, $b^1\Sigma^+$ state, collisional quenching, isotope effects, rate coeffs. 77−19018

nitrogen compounds continued
ND, $b^1\Sigma^+$ state, radiative lifetime, Einstein coeff. 78−90217
ND $c\,^1\Pi$-$a\,^1\Delta$ system, new bands, spectroscopic consts. 80−9612
ND, $d^1\Sigma^+$-$c^1\Pi$, spectra, equilib. consts., dissociation energy 78−33517
ND, dissoc. energy, calc. from $c^1\Pi$ state predissoc. *(German)* 78−90237
ND in solid Ar, role of rotational and translational modes, in vibr. relax. 78−10132
ND radical, metastable $b^1\Sigma^+$ state, tunable laser fluoresc. obs. 79−22744
ND, singlet-triplet transitions, high resolution spectrosc. with new emission source *(French)* 80−57383
ND_3, cryst. struct. between 2-180K, neutron powder profile refinement 79−73134
ND_3, vibr. levels inversion splitting, generalised WKB method 80−9585
$^{14}ND_3$, $^{15}ND_3$, ν_2 fundamentals and isotope shift 79−59456
ND_4^+ ions, rapidly reorienting deuteron NMR lineshape 79−19800
N_2D^+, dissociative recomb., interstellar mols. appl. 79−31704
N_2D^+, interstellar, radio detect. 78−16492
N_2D^+, interstellar strongly deuterated mol. obs. and implications for interstellar chemistry 79−5891
N_2D^+, lab. rest frequencies 78−1102
N_2D_2, near UV spectrum, vibr. assignment 78−78717
N_2D_4, ^{14}N quadrupole coupling consts., inversion barrier, microwave spectrum 77−54556
N_2D_4, microwave spectrum, barrier to inversion determ. 78−62793
ND_4Br, phase states and transition, from ESR of Cu^{2+} 79−99762
$ND_2(NH_2)$, ν_2 band, laser mag. reson., 9-10 micron 80−9601
ND_4NO_3, cubic, mol. orientation determ. by multipole anal. 79−73136
$ND^* + DN_3 \rightarrow ND_2^* + N_3$, chemiluminesc. reaction of electronically excited species, rate const. 78−80771
$ND(b^1\Sigma^+)$, quenching rate consts. *(German)* 79−41189
NF, $b^1\Sigma^+$ state, enhancement by I laser pumping, lasing potential 78−79012
NF, chem. pumped electronic transition laser system, chem. and scale-up 78−63103
NF, excited, lasing potential, prod. by $N+O_2F$ reaction 78−63106
NF, lasing due to electronic transitions, H_2+NF_2 chain reaction kinetics 79−89899
NF, pot. energy curves and dissoc. energy, Hulbert-Hirschfelder calc. 80−30210
NF produced by $H+NF_2$ in subsonic CW laser device $a^1\Delta$ state scale up 77−79815
NF+Bi, near-resonant electronic energy transfer, surface-hopping model 79−86030
NF+H(NF), electronically-excited free radical reactions 80−97707
NF_2, IR spectra, ν_1 and ν_2 bands, vibr. excitation and spin-rot. interaction, doublet splitting 80−28011
NF_2, ionis. pot., many-body diagrammatic RSPT calc. 79−31378
NF_2+H(O)(N), electronically-excited free radical reactions 80−97707
NF_3, bond charge parameters from integrated IR absorption intensities 77−6853
NF_3, bond order and Raman intensity, delta function eqn. 77−61693
NF_3, disappearance and appearance in excimer lasers, reaction kinetics 77−38860
NF_3, dissoc. electron attachment, rate consts. meas. 78−3326
NF_3, dissoc. electron attachment, negative ion prod. rates 80−18938
NF_3, electron dissociative attachment rate consts. at 300 and 500K, in discharge plasma 80−43849
NF_3, gas and liquid Ar soln., IR spectra, binary overtone and combination band intensities 77−79658
NF_3, IR intensity anal. 77−58081
NF_3, IR spectrum in liquid Ar, vibr. anal. 78−21927
NF_3, liq., plastic cryst., gas, Raman spectra, Coriolis coupling and transition dipole 78−39533
NF_3, mol. orbital calcs. core-valence approx. scheme 80−42927
NF_3, mol. vibr., G-intensity sum rule 78−74632
NF_3, NF_3^-, and NF_3^+, optimised struct. and bonding, ab initio SCF MO calc. 80−23334
NF_3, nuclear resonance, effects of intermolecular interactions and intramolecular dynamics 80−63658
NF_3, shock induced decomposition in Ar, IR emission, reply 77−63907
NF_3 shock-induced decomposition in Ar, IR emission, comment 77−63906
NF_3, thermal cond. in parallel const. and alternating elec., mag. fields, parametric reson. 78−83515
NF_3, thermal decomp. in shock waves, rate consts. meas. 77−16810
NF_3, thermal dissoc. behind shock waves, rate meas. 78−61002
NF_3-He hollow-cathode laser using F transitions 80−48289
NF_3-N_2(Ar)(He), electron attachment coeffs. using swarm techniques 80−53915
NF_3+Al chemiluminescent reactions 77−9086
NF_3+Cu, photon yields, chemi- and photo-luminesc. 79−5157
$NF_3+Kr(^3P_2)$, KrF* bound-free oscill. emission spectra calc. 80−7799
NF_3+WO_2, reaction product thermodynamic stability *(German)* 79−8449
NF_3+XeF*, quenching rates for XeF in (B) state 78−58730
N_2F_2, trans- and cis-isomers, photoelectron spectra, Green's function calc. 77−83650
N_2F_4, centrifugal distortion effect in microwave rot. spectrum 77−30859
N_2F_4, collisionless dissociation kinetics in highpower IR radiation field 80−66853
N_2F_4, mol. photodissoc. using CO_2-laserradiation, rate const. meas., mol. fluoresc. and time-resolved UV spectra obs. *(German)* 80−83434
N_2F_4, multiphoton excitation and vibr. energy flow, fluoresc. obs. 80−95673
N_2F_4, photodissoc. by ns CO_2 laser pulse 77−71840
N_2F_4+Ne*, quenching rate const. for metastable $Ne(^3P_2)$, flowing afterglow 78−46295
NF_2H, centrifugal distortion anal., microwave rot. spectrum 78−58650
NF*+HF*, microscopic vibrotational-electronic energy transfer, IR chemiluminesc. obs. 79−31662
$NF^*(a^1\Delta$ and $b^1\Sigma^+)$ production in $F+HN_3$ reaction 79−11770
$NF(a^1\Delta)$+Bi, near-reson. electronic energy transfer, rate const. and cross-section meas. 79−18273
$NF(a^1\Delta)+I(^2P_{1/2})$ system, electronic angular momentum transfer, chem. kinetic model 78−63104
$NF(b^1\Sigma^+)$ enhancement by I laser pumping 78−63105
NH, 3Π states, MC wavefunctions, rot.-vibr. anal. 79−13652
NH, atmospheric, IR emission studied using Fourier spectroscopy 80−95628
nitrogen compounds continued
NH, $b^1\Sigma^+$ and $d^1\Sigma^+$ states, multiconfig. wavefunctions, optimal config. selection 77−34566
NH, $b^1\Sigma^+$ state, radiative lifetime, Einstein coeff. 78−90217
NH, $c^1\Pi$ state anomalous populations following NH_3 photodissoc. 79−10133
NH, $d^1\Sigma^+ - c^1\Pi$, $d^1\Sigma^+$-$b^1\Sigma^+$, spectra, equilib. consts., dissociation energy 78−33517
NH, dissoc. energy, calc. from $c^1\Pi$ state predissoc. *(German)* 78−90237
NH, electron affinity and intercombination separation 77−18970
NH, fine struct. in $X^3\Sigma^-$ and $A^3\pi$ states, STO and GTO calcs. 77−6679
NH, heat of formation, review and new value 79−70362
NH in F- and G-type stars, bands oscillator strengths rel. to N abundances 77−91530
NH in solid Ar, crystal impurity librational relax., phonon assisted transitions, direct, Orbach and Raman processes 78−83887
NH in solid Ar, role of rotational and translational modes in vibrational relax. 78−10132
NH, interstellar, search for spectral lines below 3400 Å in ζ Persei 77−45509
NH, laser-excited A-X system fluoresc. 79−50060
NH, lower valence states, predissociations, Franck-Condon anal. 80−5590
NH, multipole expansion of diatomic overlap, MEDO calcs. 78−46264
NH, ND, $(b^1\Sigma^+)$ states quenching by deuterated cpds., kinetic isotope effects 77−63891
NH, ND, $d^1\Sigma^+$ state lifetimes, rot. struct., electron excited emission spectra 77−79654
NH, ND, $X^3\sigma^-$ state vibr. relax. Ar matrix, energy gap law breakdown 77−30963
NH, photofragment, energy distrib., chemiluminesc. reaction rates 77−90618
NH, pure rot. lasing after flash photolysis of HN_3 79−86175
NH, radiative lifetimes, electron-photon delayed coincidence meas. 78−50594
NH radical formed in NH_3 dissoc., fluoresc. spectrum, rotational relaxation 80−58310
NH radicals, metastable, production in discharge, spectra, rot., vibr. consts. determ. *(German)* 77−34642
NH reactions obs. using photolysis of HN_3 in C_2H_6 or C_3H_8 soln. 79−83471
NH, rot.-vibr. anal. by finite difference perturbation method 77−50420
NH, singlet-triplet transitions, high resolution spectrosc. with new emission source *(French)* 80−57383
NH, spectroscopic consts., FSGO calcs. 77−6758
NH^-, photoelectron spectra, NH electron affinity and intercombination separation 77−18970
NH^+, interstellar, Λ-doublet population inversion by collisions 80−22065
NH^+, PNO-CI and CEPA calcs. of electron correl. effects 77−34561
NH^+, pot. curves, ab initio CI calcs., equilib. distances 78−17579
NH^{3+}, pot. energy curves, model pot. method, orbiting and reson. effects 80−63815
NH+CO, vibrational energy transfer in solids, rot. mode participation 78−63815
$NH+HN_3$, intermediate reaction of laser photolysis of HN_3 78−61037
$NH+HN_3$ rate consts. from HN_3 UV photolysis data 80−101027
NH_2, (A^2A_1 state), rot. energy transfer, absolute rate coeffs. 79−50119
NH_2 (A^2A_1), excited state dynamics and bimol. quenching processes 80−9681
NH_2, ($\tilde{A}^2A_1$), fluoresc., form. by photolysis of $NH_3(\tilde{A}^1A_2'')$ 78−13547
NH_2, A^2A_1-X^2B_1 absorpt. spectrum, 6250-9500 Å, rot. and vibronic anal. 77−472
NH_2 fragments, multiple photon dissoc. of CH_3NH_2 and NH_3, laser-excited fluoresc. obs. 80−11938
NH_2, free radical, isotope effect on spectroscopic parameters *(Russian)* 77−54577
NH_2 free radical recombination meas. using intraresonator laser spectroscopy 77−86292
NH_2, geometry, SCF and CI calcs., basis set effects 78−62715
NH_2, ground state mol. consts., absorption spectra 80−28030
NH_2 group, hybrid lone pair problem in perturbational molecular orbital anal. 79−89608
NH_2 group, rate of dissociation at SiO_2 surface *(Russian)* 78−53233
NH_2, hyperfine level crossing spectroscopy of (0, 9, 0) and (0, 10, 0) vibr. states 78−17728
NH_2, hyperfine struct. of u-state, microwave optical double reson. 79−68246
NH_2, in Sagittarius B2 interstellar cloud, limit on peak line temp. 77−29900
NH_2, lab. obs. of 16 GHz rotational transition 77−3389
NH_2, microwave modulated saturation spectroscopy, hyperfine energy levels 79−68245
NH_2, microwave-optical double reson., collision-induced transitions, vibronic state obs. 77−34667
NH_2, ν_2 band, laser mag. reson. 80−83523
NH_2, optogalvanic spectroscopy in discharge, 570 to 620 nm 79−54862
NH_2, pot. energy curves of X^2B_1, A^2A_1, $^2B_2$ valence-shell and $\pi_u{}^2$3s-type Rydberg states calc. by CI 80−74138
NH_2, radical, laser mag. reson. spectra in 9 μm region, ν_2 band 79−45724
NH_2 radical, mag. hyperfine interactions, zero-point vibrs. effects 80−58167
NH_2, spin and rot. fine struct., orbital angular momentum 80−83247
NH_2, vibr. and rot. struct., intensity factors and orbital angular momentum 80−83246
NH_2, vibr.-rot. transitions, IR laser mag. resonance 77−27098
NH_2, vibronic levels, excited by blue CW dye laser 78−86907
NH_2, $X^-{}^2B_1$ rot. transition, MODR 78−66571
NH_2, X^1B_1 ground state, 010 level, mol. consts., emission spectra obs., 0.4-0.89 μ 78−74688
NH_2, X^2B_1, A^2A_1 and B^2B_2 states, ab initio SCF CI calcs. 78−29746
NH_2^-, dipole centre in alkali halide, paraelectric alignment 77−12413
NH_2^-, mol. geom., diffuse functions in SCF calcs. 79−10226
NH_2^-, photodetachment energy calcs. 77−27123
NH_2^-, photodetachment energy, eqn. of motion method 78−5301
NH_2^+, low lying states, ab initio MRD-CI pot. surface calcs. 79−89611
NH_2^+, quintet states, pot. energy surfaces, ab initio SCF MO calc. 78−25419
NH_2^+, triplet state ab inito CI pot. energy surfaces 78−74729

nitrogen compounds continued
NH_2 radical, heat of form., a diabatic electron affinity, from proton affinity meas. 79−91987
NH_2+H, spin exchange effects, rot. energy transfer, absolute rate coeff. 79−50119
NH_2+H rot. energy transfer in vibronic levels, absolute transfer rates 80−9701
NH_2+HN_3, rate consts. from HN_3 UV photolysis data 80−101027
NH_2+HO_2, rate const., in NH_3+O_2 flash photolysis 79−47943
NH_2+H→NH_3 react., force, density anal. 78−60997
NH_2+NO_2, reaction rate const. meas. 80−7772
NH_2+O_3, reaction mechanism, flash photolysis obs. 80−104425
NH_2+O_3, reaction rate const., rel. to atmospheric processes 80−85155
NH_2+propylene, reaction kinetics, laser reson. absorpt. obs. 77−9096
NH_2^-+H_2⇌NH_3+H^-, chem. equilib., ab initio calcs. 79−34282
NH_2^++H_2, reaction products translational energies 77−86298
NH_2^++H_2O, bimolecular reactions, product. distrib., rate consts. 78−11513
$(NH_2)_2$, ^{14}N quadrupole coupling consts., ab initio calcs. 80−58283
NH_3, detection by chemiluminescence analyser 78−40094
NH_3 photodissociation, appl. to solar energy conversion 80−30513
NH_3 small scale prod. for H storage 80−45782
NH_3^+ radical, mag. hyperfine interactions, zero-point vibrs. effects 80−58167
NH_3-NO mixtures, combustion emission spectra, identification of NH_2, NH, OH, NO by rapid scanning spectra *(French)* 79−52665
NH_4^+, dissoc. electron recombination cross-sections. 0.065-2 eV 78−66671
NH_n^++molecule (n=0 to 4), reactions, selected ion flow tube obs. 80−45489
N_2H^+, dissociative recomb., interstellar mols. appl. 79−31704
N_2H^+, electron impact rot. excitation, Glauber approx. with Coulomb effect 80−63840
N_2H^+, in Orion Nebula mol. cloud, distrib. obs. rel. to HCO^+ and SO_2 77−26034
N_2H^+, interstellar, relationship to HCO^+, HCN and CN 77−33587
N_2H^+, ion mobility in N_2, flow drift tube obs. 77−19663
N_2H+He, scattering cross-sections, factorisation and fitting, IOS approx. 78−33575
N_2H_2, CEPA-PNO calcs., band functions, correl. and polarisation roles 77−71758
N_2H_2, electron impact, N_2H^+ appearance pot., N_2 proton affinity 78−58869
cis-N_2H_2, ionisation and excitation energies depend. on bond angle, ab initio MO calc. 79−72236
N_2H_2, isomers, photoelectron spectra, vibr. struct., ionisation pots., Green's function calcs. 77−75213
N_2H_2, lone pair orbital explicit representation, augmented contracted Gaussian basis set 78−25423
N_2H_2, model rearrangement system, electron correlation and basis set effects 80−3317
N_2H_2, $N_2H_2^+$, ab initio calcs., electronic struct., geometries relative energies 77−46487
N_2H_2, near UV spectrum, vibr. assignment 78−78717
N_2H_2, nucl. spin-spin coupling, scanning MO HF LCAO calc. 79−50045
N_2H_2, variationally deorthogonalised localised molecular orbitals, electronic struct. 79−97968
cis-N_2H_2+ethylene, chem. reaction, intermediate geom. calcs. 78−35655
N_2H_2+ethylene reaction, H transfer, ab initio SCF GO calcs. 77−44469
N_2H_4 (gas)+TaS_2(2H) react., intercalation, X-ray diffr. investig. 77−12828
N_2H_4, adsorpt. on Cu, photoelectron spectra 78−6830
N_2H_4, dissociative adsorption on Fe(111) 79−46956
N_2H_4, heat of form. determ. by electron impact dissoc. 78−61040
N_2H_4, IR multiphoton dissoc., NH_2 prod. fluence depend. 79−68275
N_2H_4, intercalation of layer structures, charge density waves or artefacts 80−100221
N_2H_4 intercalation of TaS_2 polytypes, in situ expts. using TEM 79−8254
N_2H_4, nucl. spin-spin coupling, scanning MO HF LCAO calc. 79−50045
N_2H_4 production from NH_3 in atmospheric press. electron-beam controlled discharge 80−38799
$N_2H_4^+$ radical, mag. hyperfine interactions, zero-point vibrs. effects 80−58167
N_2H_4-F_2 flame, chemiluminesc., HNF A-X emission spectrum 79−50033
N_2H_4-H_2O, isolation of singular component for heat capacities of supercooled H_2O 80−107437
N_2H_4+H_2+H_2, mixtures with nonthermal vibr. excitation of mol. N_2, formula for calc. equilib. const. 80−76545
$N_2H_6^{2+}$ salts, NMR spin lattice relaxation study, ^{14}N-^1H dipole-dipole contrib. to relax. 80−75878
N_3H_3 radical, lowest two electronic states 80−925
$NH_2(A^2A_1,X^2B_1)$, obs. in UV laser photodissoc. of NH_3 80−11901
NH($A^3\Pi$, $b^1\Sigma$), two-photon generation in NH_3 UV laser photodissoc. 80−11901
NH($A^3\Pi$, $c^1\Pi$) radicals, electron impact of NH_3, H_2NNH_2 and organic mols., emission spectra 77−83752
$NHBr_2$, He(I) photoelectron spectra of NH_3+Br_2 gas phase reaction 79−31599
NH_2Br, He(I) photoelectron spectrum 78−25615
NH_4Br, dislocation influence on phase transition and light scatt. *(Russian)* 80−59648
N_2H_5Br, mol. ion motion and barriers to rot., PMR and neutron scatt. meas. 79−24226
NH_2Cl, $NHCl_2$, NCl_3, UV photoelectron spectra, assignments 78−86911
N_2H_5Cl, mol. ion motion and barriers to rot., PMR and neutron scatt. meas. 79−24226
NHD, electronic absorption spectrum, 5750-6450 Å, rot. assignments 79−64013
NH(D) radical, and isotopic species, laser mag. reson., hyperfine parameters 77−10694
NHD, rotational transitions, microwave optical double resonance obs. 80−58293
NH_xF_{3-x}, geometry changes during inversion, ab initio calcs. 78−5154
$NH_2(F_2)(Cl_2)$, SCF-MO-HF calc., struct. and one-electron props., population anal. indices 79−76338
$(N_2H_6)_2F_2[TiF_6]$, X-ray cryst. struct. determ. 80−54182

nitrogen compounds continued
$N_2H_6FeF_5$, Mossbauer spectra, 1D antiferromag. 80−15886
$N_2H_6FeF_5$, one-dimens. magnetism, mag. suscept. and Mossbauer reson. exam. 77−51893
$N_2H_6FeF_5$, one-dimens. antiferromagnetism 77−66444
$N_2H_6FeF_5$, one-dimensional antiferromagnetism, Mossbauer study 80−65872
$(NH_3)_nH^+$, n=1-9, detected in photoionisation of supersonic mol. beam mass spectra, H-bonding 79−74356
NH(ND), $b^1\Sigma^+$ state, collisional quenching, isotope effects, rate coeffs. 77−19018
NH(ND) $X^3\Sigma^-$, in inert gas solid, vibr. relax., matrix and isotope effects 80−95713
$N_2H_2(N_2D_2)$, ground and first excited state small vibr. coupling, ab initio CI calc. 78−62791
NH(NF)(NCl), effective spin-spin parameter and singlet-triplet transition intensities, ab initio calc. 78−9067
$NH(NH_2)$ obs. in laser photolysis of methylamine, fluoresc. obs. 80−97710
NH_2O_2, long-lived radical prod. by photolysis of ammoniacal KO_3 soln. 77−16838
NH_2OH, ionisation energies, He I photoelectron spectra, orbital calcs. 77−88497
$N_2H_6SO_4$, orthorhombic, low-temp. phase transition, Raman spectra meas. 77−24849
$NH_2(X^2B_1)$, laser mag. reson. spectra, Zeeman and hyperfine effects, rot. consts. 77−30892
$NH_2(X^2B_1)$, MODR, hyperfine coupling consts., spin rot. consts. 78−1010
$NH_2(X^2B_1)$ radical, and ND_2, ionisation pot., vibr. anal., ab initio calcs. and vacuum UPS obs. 80−53047
$NH(X^3\Delta^-)$ radical, form., detect. and reactions 79−64036
NH*+HCl(methane)(ethylene)(cyclopropane) (cyclohexane), rate const., time resolved chemiluminesc. 78−60982
NH*+HN_3→NH_2*+N_3*, rate const., time resolved chemiluminesc. 78−60982
NH_2HF, H-bonded complex, ab initio calcs. *(French)* 80−52866
NH($b^1\Sigma^+$), quenching rate consts. *(German)* 79−41189
NI, in solid Ar, $b^1\Sigma^+$⇌$X^1\Sigma^-$ transitions 80−32702
NNO, linear mol., Compton profile bond additivity, HF calc. 79−68268
NO, ^{129}Xe chem. shift, chem. shielding 77−6706
NO, $^2\Pi_{1/2}$ and $^2\Pi_{3/2}$ band centre freqs., opto-acoustic detection 77−58108
NO, 3sσ($A^2\Sigma^+$), in Ar Kr Xe matrices, Rydberg state 'bubbles', reson. fluoresc. obs. 77−83636
NO, 4-photon ionis. spectrum 2- and 3-photon resons., low temp. assignments 78−70887
NO, ($A^2\Sigma^+$) excitation using SHG from $KB_5O_8.4H_2O$ 77−3632
NO ($C\,^2\pi$), radiational transitions probability calc. 77−1924
NO ($a^4\Pi$), condensed phase vibr. relax., isotope effect, time resolved obs. 78−94233
NO (υ=1), vibr. fluoresc. detection of trifluoroformamide photodissoc. 78−74712
NO, $A^2\Sigma^+$ state, two-photon excitation and emission spectra 77−83666
NO, $A^2\Sigma^+$ two-photon excitation, radiation lifetime, quenching 77−3426
NO, $a^4\Pi$ and $b^4\Sigma^-$ states, electron impact spectra 78−58733
NO, absorpt. characts. of γ-O band, rel. to atm. meas. 78−57316
NO, absorpt. characts. of γ-0 band 79−39845
NO, absorpt. lines, spectral coincidences with CO laser lines 77−54559
NO, absorpt. lines spectral coincidences with CO laser lines 79−86162
NO abundance meas. in equatorial upper atm. 77−78547
NO admixture effect on electron beam controlled CO laser energy and spectral characts. 80−9867
NO, adsorbed layer, electron impact, electron impulsive ionisation spectroscopy obs. 80−60720
NO, adsorbed monolayer on graphite, melting and polymorphism 78−84063
NO, adsorbed on α-cyclodextrin, positron annihilation, effects of adsorbed gases 79−65952
NO, adsorbed on cleavage face of lamellar halides, polymorphic phase changes 77−31900
NO, adsorbed on Cu, species identification, struct., dissoc. chemisorption, desorption, UV photoelectron spectroscopy 78−52635
NO, adsorbed on Fe surface, anal. at low press., XPS, UPS 77−7970
NO, adsorbed on IR surface, oxidation of CO, XPS and UPS 78−15702
NO, adsorbed on Ir(111), flash desorption spectra, identification of recombined mols. 79−86996
NO, adsorbed on MgO, dimer form., heat of dissoc., EPR obs. 78−82755
NO, adsorbed on Pt(111), anal. of adsorption processes and surface reactions, vibration spectroscopy 78−87868
NO, adsorbed on Rh/Al_2O_3 catalyst, interaction with CO, IR study 79−70369
NO, adsorbed on Ru (001), inelastic electron scatt. dissoc. energies adsorbed state depend. 78−95956
NO, adsorbed on Si (111) surface, electron energy loss spectroscopy 78−2374
NO, adsorbed on SiO films, infrared spectra exam. 79−45725
NO, adsorpt. and decomp. on stepped Pt surface, LEED, AES and desorption expts. 78−38943
NO, adsorpt. and dissociative chemisorpt. on Cu, photoelectron spectra 78−6830
NO, adsorpt. on W (100), 300K and 100K, XPS, UPS and XAES, rel. to catalytic decomp. 79−28204
NO, adsorption, on Al, 80 to 290K, 10^{-6} to 10^{-2} Pa, XPS study 78−95657
NO adsorption, reactions, catalysis by ferroelectric $KNbO_3$ 80−30282
NO, adsorption and reactivity on Co (0001), LEED, AES, and thermal desorption study 80−80090
NO, adsorption of Pd (111), LEED, UPS, and thermal desorpt. expts. 77−69179
NO, adsorption on Fe (110), UPS and LEED/Auger meas. 77−72773
NO, adsorption on MgO powder, 77 to 150K, mol. motion anal. 78−84051
NO, adsorption on Ni, ground and core hole states, config. depend. HF LCAO SCF calc., relax. and binding energy 80−29453
NO, adsorption on Pd (111), LEED, photoelectron spectra and thermal desorpt. expts. 77−69180
NO, adsorption on Pt (100), 40-400°C LEED, AES, XPS and UPS obs. 77−35820

nitrogen compounds continued
NO, adsorption on Pt (111), EELS, thermal desorption, LEED, and AES study 80−80086
NO, adsorption on Re(0001), XPS, UPS and temp. programmed desorption 80−71574
NO, adsorption on Ru (001), KPS, UPS, and X-ray AES meas. 80−6655
NO, adsorption on Ru (001) surface, EELS obs. 80−20741
NO, adsorption on SiO_2-supported Pt or Pt-Pd, IR spectrosc. obs. 80−92780
NO adsorption on Ti, W evaporated films, mutual replacement of CH_4, CO and NO *(Japanese)* 78−22949
NO, adsorption on W, dissociative, FEM obs. 77−4258
NO, adsorption on W, FEM obs. 80−84390
NO, adsorption on W (110) surface, chemical changes detected by AES 80−10787
NO, adsorption on W(100) surface, adsorbate density determ. 77−1320
NO, adsorption on Zr, dissoc. and diffusion 80−80085
NO, air pollutant, collection method and conc. determ. *(French)* 77−81999
NO, air pollutant, deposition onto soil and cement surfaces, lab. meas. 79−70477
NO airglow, 2150 Å (1,0) γ-band intensity meas. with polarising NO photometer 78−45076
NO and CO, coadsorbed on Ru(001), adsite symmetry by electron energy loss 79−99412
NO, and isotopic forms, $X^2\Pi$ state, IR obs., mol. consts. 78−42045
NO, and isotopic forms, $\nu=0$ electronic states, spin-rot. doubling 80−5540
NO and NO_2 mixing ratio profiles of stratosphere from IR sunset spectra 80−94563
NO and O_3 meas., mixing ratio in stratosphere 78−44915
NO, ang. distrib. valance photoelectron spectra, vibr. depend., autoionisation and Franck-Condon factors 79−72356
NO, atm., form. in instantaneous linear discharges, variable energy input effect 79−20952
NO, atm. trace gases and pollutants, data compilation on mag. tape 78−44995
NO, atmospheric, high-altitude rocket meas. of density 78−45068
NO, atmospheric auroral concs. 77−2291
NO, Auger peak kinetic energy compared to $Cr(NO)_4$, complex bonding 80−58317
NO, autoionisation struct. at first ionisation limit, photoionis. data 78−58748
NO, $b^4\Sigma^- \rightarrow a^4\Pi$ band system, rot. consts. 79−72312
NO, boiling/condensation heat transfer props., cryogenic appls. 78−79192
NO $C^2\Pi(\nu'=0)$, lifetime meas., predissoc. and non-predissoc. rot. levels 78−62849
NO, calibration standards, generated by gas phase titration 78−69507
NO, catalytic decomp. over brownmillerite like compounds 79−43631
NO, catalytic reduction with CO by rare earth oxides 77−81422
NO, chemiexcitation in $N(^2D)+O_2$, 90-180K, IR obs. 78−90163
NO chemiluminescent emission at 2.9 μm wavelength, auroral enhancement 80−12586
NO, chemisorbed on transition metals at high pressures, XPS 77−20990
NO, chemisorbed on W (100) surface, UPS studies 79−23841
NO, chemisorpt. and decomp. on Ru 78−18903
NO, chemisorption and surface reactivity on clean and Na dosed (110) surface of Ag 77−31882
NO, chemisorption Ni, XPES meas. 79−77922
NO, chemisorption on Cu, cluster theory 80−29264
NO, chemisorption on goethite, IR spectra 80−7855
NO, chemisorption on Ir, chemisorptive bonding and reaction 77−51596
NO, chemisorption on Ni, Cu, Pd and Ag, semiempirical calcs. 78−14611
NO, chemisorption on Ni, angle-resolved UPS in modified LEED system 78−15293
NO, chemisorption on Ni, cluster theory 80−29264
NO, chemisorption on Ni (110), LEED, AES and thermal desorption meas. 77−15695
NO, chemisorption on Ni (100), LEED, AES, UPS, and thermal desorption study 80−39449
NO, chemisorption on Pt, effect of particle size of Pt supported on inorganic oxide carriers *(French)* 78−11552
NO, chemisorption on Pt(100), vibr. spectra, electron energy loss, LEED and Auger investig. 79−90866
NO, chemisorption on Rh, reactions with CO over Rh, flash desorption spectra, titration, reaction kinetic calcs. 78−61045
NO, chemisorption on Rh (755), (331), desorpt. temp. and decomp. characts. 79−65318
NO, chemisorption on Rh (110), LEED, AES, XPS, UPS, and desorption obs. 79−77899
NO, chemisorption on Ru(10$\bar{1}$0) surface 77−72783
NO, chemisorption on Ru(101) via mobile precursor state 78−43247
NO, chemisorption on W, 80K, FEM obs. 77−39733
NO, chemisorptive bonding and reaction on Ir (100) and (111) surfaces, UPS obs. 77−72786
NO, coadsorpt. and reactivity with Na on Ag (111) 78−38948
NO, combustion gas sampling system and valves for sampling during engine expansion process 78−24380
NO, conc. in auroral arc from ionic struct. meas. 77−2292
NO concentration in thermosphere, depend. on solar activity 80−77178
NO concentration meas. in gas mixtures, chemiluminescence method *(Russian)* 79−16094
NO concentrations in lower stratosphere, geographical vars. 78−73438
NO, daytime conc. in thermosphere 79−2408
NO decomp. in industrial exhaust gases by electron beam irradiation 79−29490
NO densities, horizontal winds effects in aurora 80−26656
NO density enhancement on winter anomalous day at S. Uist 80−82130
NO, density in lower E-region, diurnal and seasonal effects at low latits. 78−88976
NO, density profile from airglow obs., 72-120 km altitude 80−105094
NO density variations in E-region, theory, ion-neutral chem. constraints 79−75027
NO, desorption, associative, from Pt, Ni, Ru 80−54512
NO, desorption in Ni/SiO_2, 200 to 400K *(German)* 78−30835
NO detection using optoacoustic cell with improved performance 77−66987

nitrogen compounds continued
NO, diatomic mols., internal partition functions for O_2, N_2, NO and their ions, max. summation indices 80−27995
NO, diffusion in plastic solids, ELDOR 77−1618
NO dimer, asymmetric, characterisation, Raman, IR spectroscopy 79−41176
NO dimerisation, equilib. const. anal., trans-/cis-$(NO)_2$ zero pt. correlation energy difference 78−11509
NO, dipole moment derivatives, MINDO/3 semiempirical calcs. 77−75055
NO, dipole oscill. strength distribs., sums 78−21975
NO, dipole properties and dispersion energies additivity, using atoms and small mol. models 80−53091
NO, dispersion energy consts., dipole oscill. strength, refractivity 77−50492
NO, dissociation in AC field, kinetics and energetics *(French)* 78−64824
NO, dissociative adsorpt. on Ru (10$\bar{1}$0), LEED and AES expts. 77−90642
NO, dissociative and mol. adsorption on Re *(French)* 79−69344
NO dissociative chemisorption and mol. adsorption on Ni (100) 80−65373
NO, dissociative electron attachment 77−42431
NO, dissociative electron attachment, $N^-(^3P)$ form. 78−90308
NO, doublet-quartet transitions, 5-7.4 eV, electron-impact spectroscopy, 5-80° 78−37754
NO, doublet-quartet transitions, low energy variable-ang. electron scatt. obs. 78−62933
NO δ-bands in Venus UV nightglow, IUE obs. 79−62782
NO, EPR line shape in solvating mixtures 78−33532
NO, electrocatalytic decomp. on electrochem. reduced zirconia surface 80−61113
NO, electron impact, absolute emission cross-sections meas., calibration appls. 79−85996
NO, electron impact, energy loss spectra, electronic transitions obs. 78−17805
NO, electron impact dissoc. ionisation, N^- form., mass spectra 77−75320
NO, electron impact excitation, high vibr. levels of ground state, decay of reson. states 77−88581
NO, electron impact ionisation, metastable state mol. ion form. 77−14594
NO, electron radial diff. coeff. to mobility ratio 77−19666
NO, electronic quenching rates, two-photon spectrosc. meas. 79−50097
NO, electronic spectrum, press. induced config. demixing 78−42090
NO, electronic to vibr. energy transfer from excited halogen atoms, IR fluoresc. 78−63113
NO, electronic-vibr. energy transfer from $Br(4^2P_{1/2})$, 5.5 μm transition 77−31094
NO electronically excited photofragment of VUV photodissoc. methylnitrite, identification and quantum yield 80−99527
NO, emissivity calc. 78−90675
NO excited state vibrational energy transfer, for optoacoustic spectroscopy 78−37724
NO, far IR spectral lines and absorptance calcs. 77−46564
NO, Feshbach resonances, energy dependence of electronic coupling to ground state 79−89616
NO, Feshbach resonances, dynamic coupling to Rydberg states 79−89617
NO, first adsorbed layer on graphite, BN, and lamellar halides, critical and triple point temps. 78−91548
NO, first monolayer on MgBr cleavage face, triple point 78−6227
NO, fluoresc. spectra, $3s\sigma(A^2\Sigma^+)$ Rydberg state, vibr. relax. 79−13759
NO formation in constant volume combustion, prediction *(Japanese)* 79−16002
NO, Fourier transform spectra, intensity and self-broadening coeff. meas. 80−102503
NO, fundamental band spectrum, determ. of rotational, spin-orbit coupling and Λ type doubling consts. *(French)* 77−6768
NO, fundamental intensity and linewidth of IR absorpt. spectra, press. broadening 78−25530
NO, gamma band emission rate factor, rel. to upper atm. comp. determ. 77−54572
NO, gamma system in sunspots, equivalent widths calcs. 79−12457
NO gas, reduction of Pu(VI) to Pu(IV) 79−31108
NO, gas complex analysis method, resonance absorption with pulsed laser light *(Japanese)* 80−36421
NO, global morphology in lower E-region 78−88975
NO, γ (1,0) band auroral emission at 2150 Å probably N_2 feature 78−45083
NO, γ and β system, electronic transition probability 80−106332
NO, γ and δ bands auroral emission, from radiative recomb. of N and O 77−91343
NO, γ band lines, collisional broadening coeff. and optical collision diameter 80−63714
NO, γ-band collisional broadening parameters from resonance line absorpt. 77−10704
NO, γ-band excitation of fluoresc. in SO_2 in atm. 78−73121
NO γ-bands at 2259 Å, shock wave effective absorption coeffs., empirical determ. 79−64799
NO, γ(0,0) band, collisional broadening parameters 80−63713
NO, high frequency discharge 79−82105
NO, high mag. field spectroscopy 79−72445
NO, high resolution absorpt. spectrum in region of first ionization limit 77−461
NO, hyperfine splitting const., H-bond contrib. 78−74799
NO, $I^2\Sigma^+$ state, valence bands, absorpt. spectra 78−46361
NO, IR band absorpt. derivation from vibr.-rot. band spectroscopic variables 77−14434
NO, IR band nonrigid rot. absorption 78−91060
NO, IR emission Fourier transform spectroscopy, mol. rot.-vibr., RKR potential curve calc. 80−95618
NO, IR radiation spectral absorptance and transmittance, accurate modelling technique 78−91062
NO impurity in N plasma, effect on heating in RF discharge 80−59312
NO, in Ar and N_2 matrices, 6K, vac. UV photolysis, β and M band emissions 78−73069
NO in atmosphere, automatic meas., luminescence appls. *(Dutch)* 79−88041
NO, in atmosphere, meas. in equatorial Pacific region 79−100893

nitrogen compounds continued
NO in D-region, positive ion chemical scheme for electron density and comp. 79−40007
NO in disturbed thermosphere, conc. rel. to anharmonic N_2 mols. vibr. relaxation 79−12322
NO, in exhaust gas, direct optical detect., transverse sensitivity *(German)* 78−35751
NO, in high-latit. lower thermosphere 77−37467
NO in lower ionosphere, height profile during auroral absorpt. event 80−36443
NO in lower thermosphere, joint meas. by rocket borne UV photometer and mass spectrometer 78−40723
NO in mesopause region, density vars. rel. to ion-clustering during winter anomaly 79−21087
NO in mesosphere, conc. geomag. control from simultaneous D and F regions ionisation meas. 79−8651
NO in middle atmosphere, role of eddy diffusion in mesosphere and lower thermosphere 80−109198
NO in middle atmosphere, prod. by energetic particle precip. 80−109213
NO in rare gas matrix, radiationless processes in luminesc. spectra 79−36689
NO, in stratosphere, conc. vars. at twilight rel. to interpetation of solar occultation meas. 80−85756
NO, in stratosphere, obs. in N.hemisphere for three seasons 78−81288
NO in thermosphere, temperature-depend. model 78−16226
NO, in upper atmosphere, excitation of auroral 2150 Å emission 77−9594
NO, in upper atmosphere, prod. by meteoroids 79−2404
NO, internal partition function calc. 78−55159
NO, interstellar, ion-molecule reactions rel. to candidate mols. form. 78−28739
NO, interstellar microwave detection in Sagittarius B2 direction 78−93378
NO, intracavity Zeeman modulation detect., passive Q-switching, CO IR laser obs. 80−9597
NO, ionic ground state, photoelectron spectra vibr. intensity Franck-Condon factors 77−79650
NO, ionis. pot. and electron affinity, overlapping sphere MS $X\alpha$ calc. 78−41948
NO, ionisation by electron bombard., empirical and semi-empirical calcs. 79−36784
NO isotopes, spectrophone meas. at selected CO, CO_2 laser wavelengths 78−57310
NO, laser mag. reson. and IR-RF double-reson. near 5.3 μm 78−5258
NO, laser stimulation optimisation for intraresonator spectroscopy 80−77881
NO, latitudinal gradient in thermosphere 79−100991
NO, Lennard-Jones 12:6 parameters calc. from viscosity data 77−46612
NO, master eqn. theory, dissoc. rate consts. 77−77742
NO meas. in atmosphere, monitors, intercalibration 78−69529
NO, measured lifetimes of A $^2\Sigma^+$, D $^2\Sigma^+$ and C $^2\Pi$ states 78−90219
NO measurements in CH_4-O_2-N_2 flame by laser fluorescence 80−61178
NO, microwave absorpt. coeff. 77−64378
NO mixing ratios near stratopause, chemiluminescent meas. 79−34893
NO, mol. beam tunable diode laser sub-Doppler spectra, $^2\Pi_{1/2,3/2}$ Λ splittings 79−41180
NO, mol. parameters determ. 77−83571
NO molecular predissociation, quantum mechanics expt. test 79−17274
NO, multiphoton ionis. spectrum 79−10157
NO, N 1s photoelectron spectrum, correl. effects 77−10702
NO, NO_2, air pollutants three-dimens. distrib. in Los Angeles basin 78−61542
NO, NO_2, O_3, in atmosphere, photostationary state assumption 79−88391
NO, NO_2, pollutants conc. meas. at ground level at unpolluted maritime site 78−3951
NO, NO^+, in winter anomalous D-region over Sardinia (40°N), densities 80−21871
NO, nondispersive IR analyzer with compensation for optical bias 79−16103
NO nonlinear laser spectroscopy, VUV harmonic generation 80−74175
NO, nonlinear optical polarisability meas. 79−54991
NO, optical detection in air, gamma band fluoresc. *(German)* 77−60494
NO, oxidation by electron beam irrad., appl. to exhaust gas treatment 78−80765
NO, oxidation in O_2 matrix, IR spectra of products 78−23936
NO oxidation to NO_2 in power plant chimney plume 79−12178
NO, photoabsorpt. cross section, 10 to 50 nm 77−61797
NO, photoabsorpt. cross-section, 50-340 Å, as sum of empirical at. cross-sections 78−58718
NO, photoabsorption and photionisation, UV region meas. 78−42087
NO, photodissoc. at 184.9 nm, quantum yield, and quenching by N_2 78−80773
NO, photodissoc. in mesosphere and stratosphere, theory 80−41580
NO, photodissoc. ionis., 16-41 eV 77−18995
NO, photofragment of NO_2, Doppler spectroscopy 80−53124
NO, photoionis., vibr.-excited ions form. in Franck-Condon gaps, threshold photoelectron spectra obs. 79−68262
NO, photoionis. resonant processes, preionis. and predissoc. 77−65516
NO, photoionisation and ionisation pot., mol. beam meas. 77−10709
NO, photoionisation by vac. UV laser *(Russian)* 78−9205
NO photometric process analyser using resonance absorption method 80−57360
NO, positron energy levels, rel. to Rydberg levels of Na, NO 79−86089
NO, predissoc. rates and pertrubations in certain electronic states, time resolved spectra 77−27131
NO predissociation in mesosphere and stratosphere, photochemistry 80−21802
NO, press. broadening coeffs., spin-flip Raman laser spectrosc. 80−43147
NO, press.-broadened linewidths of $R(9.5)_{3/2}$ transition 78−70824
NO, prod. in D-region rel. to winds and electron densities time vars. correl. 79−25389
NO, prod. in Venus atmosphere by thunderstorms 80−98587
NO production by lightning in clouds, odd N chem. reactions on Venus 80−26768
NO, production by lightning, shock and channel heating methods 80−72581
NO profile in auroral E-region 77−41258
NO, pseudospectral dipole oscillator strength distribs. 78−50503
nitrogen compounds continued
NO, Q-branch spectra, external-resonator controlled Raman laser pumped by CW CO laser 80−9624
NO, quenching of pyrene dual fluoresc. 78−5266
NO $R_{1/2}(25/2)$ transition, extinction coeff. at 8-7 P(11) CO laser line 79 - 45711
NO radical, EPR (ST-EPR) spectra, fast computation, master supermatrix eqn. soln. 78−62213
NO, radical spin labels, appl. to solvent-solute interactions 78−17698
NO radicals, slow rot., modulated EPR spectra 79−38382
NO, reaction with CO on polycrystalline Pt surface at low press., reaction kinetics study *(German)* 79−15989
NO, reaction with CO on polycrystalline Pt at low press., reaction kinetics study *(German)* 79−15988
NO, reaction with O^+, nonthermal rate coeffs. in ionosphere 78−57375
NO, reactivity on Rb-dosed Ag 79−28207
NO, reduction with NH_3 and laterite catalyst 79−91993
NO, relative Raman scatt. cross section 80−100061
NO, reson. absorpt. meas. with CO laser, spectroscopic data for pollution monitoring 77−37350
NO, resonance-enhanced multiphoton ionis. and fragmentation of mol. beam 79−100411
NO, rot. line strengths in multiphoton transitions 80−48051
NO, rot.-vibr. fundamental obs., mol. consts. 77−57971
NO, Rydberg absorpt. bands 800-850 Å, isotope shift 79−13734
NO, Rydberg states quenching rate consts., two photon excitation method 80−5581
NO, Salyut 4 IR spectral obs. in upper atmosphere mid-latitudes 78−16223
NO, selectively excited rovibrational states, multiphoton ionisation spectra 80−69202
NO, self-N_2- and O_2-broadened linewidths 5.4 micron band, quadrupole moment 77−30930
NO, simultaneous one- and two-photon spectroscopy, Λ-doubling, spin-rot. splitting 78−66560
NO, spectroscopic consts., rot. const. of fundamental band 77−68027
NO, spectroscopic data calc., 2-0 and 3-0 overtone bands 79−36623
NO spin label, EPR (ST-EPR) spectra, fast computation perturbation approach 78−62212
NO, spin labels, EPR spectral simulation 78−78730
NO, spontaneous vibr.-rot. Raman scatt. from $X^2\Pi$ state 79−36646
NO, state selective step-wise photoionis. with mass spectroscopic ion detect. 80−43119
NO, stratospheric, balloon-borne chemiluminesc. meas. 77−29397
NO, stratospheric and mesospheric photodissoc. rate, calc. 80−51498
NO, stratospheric comp., IR meas. 79−8671
NO, stratospheric growth before sunrise by photolysis 77−29356
NO, sub-Doppler resolution IR spectra 78−86860
NO synthesis, reactions of vibr. excited N_2 in nonequilib. plasmachem. system 77−86310
NO synthesis in DC plasma jet 80−61099
NO synthesis in N_2+O_2 plasma jet, chem. kinetics anal., model 80−38728
NO, thermal cond. Senftleben effect meas. 79−18985
NO thermal desorption from Re single cryst. surface *(French)* 78−22959
NO, thermosphere composition and UV spectral absorpt. 80−85781
NO, thermosphere radiative cooling 80−72656
NO, thermospheric conc. diurnal variability 77−78549
NO, triple-dipole energy calcs. using pseudo spectral theory 78−46418
NO, troposphere content, 0-7 km altitude over clean and polluted areas 80−51478
NO, tropospheric production by lightning discharges 77−17189
NO, two-photon excitation to levels near and above the dissoc. limit 79−10161
NO, two-photon spectra by three-wave mixing 78−29826
NO, UV absorpt. spectra, 600-1000 Å, Rydberg series, ionisation energy 77−75180
NO, UV fluorescence, IR laser induced 80−53032
NO, UV irrad. photoionisation, NO^+ high vibr. excitation, photoelectron spectra 77−71830
NO, UV photoelectron spectrum, autoionisation from Rydberg state, vibr. progressions, Franck-Condon factors 78−50583
NO, upper atmosphere concs. rel. to temporal vars. of mid-latit. HF ionospheric absorpt. 77−53305
NO, v=0,1 states, spectroscopic data calc. 78−86851
NO, v=2←1 absorption band two-and multiphoton spectra, Λ-doubling const. vibr. depend. 77−30942
NO, vapour, four-wave sum mixing, 130 to 180 nm, third harmonic generation 77−10970
NO, var. in ionospheric E-region correl. with solar activity 78−49207
NO, vertical density profiles in midlatit. mesosphere 77−87012
NO, vibr. excited, form. in charge transfer reactions 77−3455
NO vibr. overtone band, mag. rot. spectrosc. obs. 80−86446
NO, vibr.-rot. bands in sunspots, equivalent widths 77−2395
NO, vibr.-rot. bands of Raman spectra 78−29173
NO, $X^2\Pi$ state, vibr. relax., IR-UV double reson. obs. 80−106338
NO $X^2\Pi(v''=0)$, ionis. energies to NO^+ $X^1\Sigma^+(v=0\text{-}34)$, NO^+ mol. consts., UPS obs. 80−14177
NO, Zeeman effect, relativistic corrections 77−83646
NO, Zeeman modulation IR spectroscopy using spin-flip Raman laser 79−18181
NO, Zeeman modulation spectroscopy, line shape analysis 80−74197
NO, Zeeman spectrum, mol. beam elec. reson. spectrosc. 80−91621
NO, Zeeman spectrum with magnetospectrophone 77−83647
NO^-, $^3\Sigma^-$ and $^1\Delta$ resonances, excitation in electron scatt. 77−31010
NO^- destruction in collisions with excited molecules 80−14189
NO^+ +molecule, reaction rate consts. meas. 80−7782
NO^+, $A^1\Pi$-$X^1\Sigma$ system, Franck-Condon factors, r-centroids calc., program 77−27121
NO^+ cluster ion formation in D-region, temp. control by ion obs. 80−61931
NO^+, dissoc. recombination, $N(^2D)$ atom quantum yield 77−63905
NO^+, electron impact, rate coeff. in thermosphere, AE satellite meas. 79−48594
NO^+, electron impact dissociative recombination, ion-beam expt. 79−54981
NO^+, fragmentation ang. distrib., energy disposal, branching, photoelectron-photoion coincidence spectra 79−68263
NO^+, in ionosphere, form. by $N(^2D)$+O associative ionisation 80−4161
NO^+ in ionosphere mid-latit. F_1-layer, mean diurnal var. 79−96856

nitrogen compounds continued
NO^+ in lower thermosphere, daytime chemistry from Atmosphere Explorer-C meas. 77−33230
NO^+, interstellar transitions in mm and IR wavelengths 80−56906
NO^+ meas. and water vapour concs. above mesopause 77−73898
NO^+, mobility in CO_2, obs. using injected-ion drift tube mass spectrometer 78−1784
NO^+, mobility in CO_2 80−43834
NO^+, multichannel dissociative electron recombination theory 77−83753
NO^+, N 1s photoelectron spectrum, correl. effects 77−10702
NO^+, pot. energy curves, dissoc. energy 79−22623
NO^+, pot. energy curves calcs. 80−5602
NO^+, protonation pot. energy surface, ab initio calcs., 4-31G basis set 77−83489
NO^+, R_e-function of A-X system, rel. to astrophysical meas. 78−13554
NO^+ recombination in mid-latitude trough and polar ionization hole 80−12575
NO^+, stratospheric chemistry, reaction rate coeffs. and product distribs. 78−81305
NO^+, symmetric charge transfer reaction cross section, selected kinetic energies, vibr. states 77−16813
NO^+, three-body reactions, rate coeffs. rel. to cluster ion form. in D-region 77−53308
NO^+, $X^1\Sigma^+$ state, UV irrad., high vibr. excitation, photoelectron spectra 77−71830
NO^+ $X^1\Sigma^+(v'=0\text{-}34)$←NO $X^2\Pi(v''=0)$ ionis. energies, NO^+ mol. consts., UPS obs. 80−14177
NO radical-paramagnetic transition metal interactions, EPR spectra rel. to dipolar interactions 79−95647
NO radicals, saturation transfer EPR effects anal. using hole-burning concept 79−94022
$^{14}N^{16}O$, overtone bands, determ. mol. consts. 78−58652
^{15}NO, vibr.-rot. transitions, Λ-doubling, optoacoustic spectroscopy meas. 78−42062
NO-Ar(He), thermal cond. Senftleben effect meas. 79−18985
NO-H_2 flame, OH form., collisional broadening parameter, curve of growth method 80−53052
NO-N_2, discharge ionisation growth, diffusion coeffs. 78−83636
NO-N_2-(H_2) mixtures, thermal cond., mag. field effect 79−94764
NO-O_2-acetylene, combustion products, 1400-2600K, minimisation of NO, computer model 78−85161
NO-SF_6, single-photon absorption reaction chemistry in solid state 77−73454
NO^+-N_2, temp.-dependent ion mobilities 79−86553
NO+Ar^+, reaction kinetics, mass spectrometer with selective introduction drift tube *(French)* 79−11839
NO+Ar^+, reaction product ratios, 300K 80−7783
NO+Ar^+(He^+)(Ne^+), charge transfer, thermal energy, product distrib. obs. 78−25656
NO+aromatic compounds mixture, charge transfer equilib. consts. adiabatic ionis. energies, entropy changes 78−37738
NO+BrO, temp. depend. kinetic study, stratospheric Br photochemistry implication 80−50866
NO+Br→Br+NO_2, reaction rate const., mass spectrometric determ. 79−34288
NO+bromomethyne radical, absolute reaction rate parameters 77−1909
NO+C_2, IR laser photolysis of polyat. mols. photochem. appls. 80−66835
NO+C_2, laser-induced chemilum. reaction 80−61101
NO+C_2H_4, HNO excitation by $O_2(^1\Delta_g)$ 79−52674
NO+C_2O, absolute reaction rate consts. meas. by laser induced fluoresc. 80−93738
NO+$C_2(a^3\Pi_u)$, laser-generated radical kinetics 79−100352
NO+C_3, reaction kinetics, laser induced fluoresc. obs. of allene photolysis 80−66820
NO+CCl_2FO_2, reaction, photolysis obs. 79−74931
NO+CH_3O_2, rate const., flash photolysis and kinetic spectroscopy 79−70305
NO+CO_2, Senftleben-Beenakker effect, saturation field, Kohler-Raum theory and obs. 80−28596
NO+CO_2 collisions in CO_2 gasdynamic laser, causing depopulationg of lower active level 80−74336
NO+CO+H_2 interaction over Pt, Rh, Ru and Os, NH_4OCN formation 78−73082
NO+CO(N_2), electronic energy transfer, spectroscopic obs. 78−82716
NO+Cd($5^3P_{0,1}$), absolute quenching cross section, phase-shift method 80−58340
NO+Cl^-, reactions at room temp. 80−93749
NO+ClO_2 reaction initiating HCl chemical laser 80−14333
NO+$ClONO_2$ react., gas phase, kinetics, mechanism, IR photometric investig. *(German)* 78−76834
NO+ClOO, reaction in stratosphere 79−34889
NO+ClO→NO_2+Cl, rate const. meas. 77−60059
NO+dimethylamino radical, reaction rate constants, FTIR obs. 80−16652
NO+ethylperoxy radicals reaction, flash photolysis and kinetic spectroscopy obs. of rate consts. 79−83470
NO+fluoromethylene, vibr. energy distrib., lasing action 78−48644
NO+formaldehyde(-d_2), laser beam-induced free radical reactions, quenching 78−44387
NO+Ge(Si), reaction rate consts. at 350K 78−53186
NO+H_2, vibr. relax. rate, stimulated Raman scatt. obs. 77−75269
NO+H^+, vibr. excitation, differential scatt., low energy meas. 79−89749
NO+H^+(He^+)(O^+), dissociative ionis. 79−10188
NO+HBr, rate consts. for vibr. energy transfer meas. using laser. induced fluorescence technique 80−87206
NO+HNO_3, rate consts. determ. with diode laser 79−70310
NO+HO_2, reaction kinetics meas. 78−31624
NO+HO_2 reaction rate constant effects on O_3 perturbations, model of stratosphere 78−73474
NO+HO_2(DO_2), reaction kinetics, near IR chemiluminesc. determ. 80−21261
NO+HO_2→OH+NO_2, kinetics temp. depend. 80−3313
NO+HO_2→OH+NO_2, rate constant determination in Arrhenius form 79−47904
NO+H+H_2→HNO+H_2, rate of reaction, temp. depend., third body efficiencies 78−23933
NO+H+M→HNO+M, NO+HgH→HNO+Hg, rate consts. of photosensitised reactions 77−36757
NO+He, anisotropic intermol. pots., crossed beam expts. 79−31639
nitrogen compounds continued
NO+He, multiphoton ionisation spectra in supersonic expansion, laser entranced collisional effects 80−83459
NO+He, Penning ionisation of target mol., for He(2^3S) 79−41228
NO+heavy inert gas, small clusters, beam cluster intensity and collision cross section 77−38711
NO+Hg, vibr. relax. of states v=2-10 79−89752
NO+Hg(6^3P_1)(6^3P_0), electronic-vibr. energy transfer collision, IR obs. 79−45716
NO+I, vibr. relax. rate const. determ. 77−19013
NO+I($5^2P_{1/2}$), electronic-vibrational energy transfer, fluoresc. obs. 78−66579
NO+inert gas, cross section meas. with state selected beams 78−62910
NO+Kr^+, charge-transfer reaction rel. to vibr. state of NO^+ 77−1916
NO+Li^+, vibr. excitation cross sections 79−54946
NO+methoxy radical, reaction rate meas. 80−76534
NO+N ^{4}(S) state reaction rate, discharge flow and photolysis reson. fluoresc. method 79−5142
NO+N_2, ionis. at low energy 78−58791
NO+N_2*, vibr. excited quenching temp. depdn., flowing afterglow 77−54595
NO+N_2(Ar), $^2\Pi_{3/2}$, $^2\Pi_{1/2}$ states, line broadening, mag. moment effect 79−72391
NO+N_2(CO_2)(CO)(CH_4)(Ar), NO γ(0,0) band, oscillator strength and line broadening 80−106356
NO+N^+, product distribs., rate consts., ion cyclotron reson. obs. 77−52618
NO+NO collisions, semi-empirical non-Lorentzien line shape determ. 77−34699
NO+NO_2+CCl_3O_3, photolysis, $CCl_3O_2NO_2$ thermal decomposition in stratosphere 79−57256
NO+Na($3p^2P_{3/2}$), electronic energy quenching dynamics, crossed beam expt. 80−9683
NO+Ne^+, thermal energy, reaction rate coeffs. and product distrib. 79−29333
NO+Ne(AR)(Kr)(Xe), angle depend. intermolecular pot., crossed beams study 80−9682
NO+Ne(Ar)(N_2)(H_2)(CO), $E^2\Sigma^+$ and $B'^2\Delta$ states fluoresc. collisional deactivation 79−6965
NO+Ni, complex form. in NiCa-Y zeolite, EPR, UV obs. 77−63949
NO+O, chemiluminesc., absolute rate consts., O_3 effect 80−45507
NO+O, chemiluminesc., rate const., optical comparison method meas. 77−90603
NO+O, in Ar matrix, chemiluminesc. 78−35688
NO+O, vibr. relaxation of NO, laser induced IR fluoresc. study 80−9626
NO+O_2+N_2, mixtures with nonthermal vibr. excitation of mol. N_2, formula for calc. equilib. const. 80−76545
NO+O_3, (001), laser enhanced reaction, temp. depend., reactive and non-reactive channels 78−48642
NO+O_3, chemilum. reaction, NO_2 light amplification *(Russian)* 77−88717
NO+O_3, fs-states and rot. states, effect on reactivity 80−89473
NO+O_3, IR laser enhanced reactions 79−66286
NO+O_3, laser enhanced reaction, fluoresc. obs. 79−66285
NO+O_3(001), laser-enhanced reaction, rates, temp. depend. 78−48675
NO+O_3(001)→NO_2($^2B_{1,2}$)+O_2, laser enhanced reaction, temp. depend. 77−81397
NO+O_3→NO_2^*+O_2, kinetic energy and internal state depend. 79−66287
NO+O_3→NO_2+O_2, rate const., 203-361K, fast flow method 77−33143
NO+O_3→NO_2*, mol. beam chemiluminesc., kinetic and internal energy depend. 78−31638
NO+O_3→NO_2*+O_2→NO_2+hν+O_2, chemiluminesc., translational and rot. energy effects 80−30218
NO+O_4, IR laser enhanced reaction rate. vibr. excitation 77−1911
NO+O^+(^4S)(^2D), charge transfer reactions, cross-sections meas. 78−92462
NO+OH, OH(v=1) relax., time resolved spectra 80−74240
NO+OH radical-molecule reactions, relax. and rate consts. 80−11918
NO+OH^+(H_2O^+), reaction, ICR obs. 79−8429
NO+O(^1S), product channels 78−46422
NO+PH, collisional deactivation of PH($b^1\Sigma^+$), time resolved quenching 79−54948
NO+peroxymethyl radical, reaction rate const. 79−61848
NO+S^+→NO^++S+1.1 eV, rate consts. kinetic energy depend., drift tube meas. 80−7778
NO+Sc(Y), nascent product state distribs., laser fluoresc. detect. 78−7187
NO+Si*, collisional quenching, reson. line absorpt. expt. 78−46297
NO^++2N_2⇌NO^+.N_2+N_2, rate const., enthalpy and bond strength 77−16809
NO^++Ar, reaction product ratios, 300K 80−7783
NO^++atmospheric gases, thermal energy reaction rates 78−92443
NO^++e^-→N+O, recombination rate const. determ. in flames 78−48632
NO^++metal atom reaction, obs. using magnetically confined afterglow 77−34750
NO^++N_2, vibrational radiation quenching in upper atmosphere 79−3543
NO^++NO_2^- neutralisation reaction, spectroscopic study 79−13819
NO^++X^-→NO+X (X=Cl, Br, I), rate const. determ. in flames 78−48633
NO_2, $^2B_1$ state fluoresc., bending vibr. progression 77−83638
NO_2, $^2B_2$ state, fluoresc. anomalous mag. depolaris. 78−21962
NO_2, $^2B_2$ state photodecomposition in 2nd predissoc. region 77−10712
NO_2, $^2B_2$-state excitation, fluoresc. lifetime 77−61780
NO_2, 6480 Å absorption, rot. anal. 79−45731
NO_2, 7390 Å band, vibronic transition within ground state manifold 78−21919
NO_2, 8170-8280Å absorption spectrum, rot. struct., assignments 79−6937
NO_2, 8920 Å band temp. depend., location of 000-000 band of A^2B_2-X^2A_1 transition 78−70826
NO_2, (101) band, line strengths, spin-splittings and forbidden transitions 80−47987
NO_2, A-X band system, visible absorption, fluoresc., vibronic coupling 77−58030
NO_2, absolute integrated intensity for 3.44 μm band 77−3418
NO_2, adsorbed gas, on glassy AsSe, surface cond., photocond. 78−80038
NO_2, adsorbed on SiO films, infrared spectra exam. 79−45725

nitrogen compounds continued
NO_2, adsorption on W, FEM obs. 80−84390
NO_2, air over N.Germany coast, obs. 80−26584
NO_2, air pollutant, deposition onto soil and cement surfaces, lab. meas. 79−70477
NO_2, air pollutant, spectroscopic analysis using scanning tunable dye laser 78−81362
NO_2 and isotopic forms, total quartic potential function 78−13486
NO_2, and N_2O_4, adsorption on W (110), 300K and 100K, XPS, UPS and XAES 79−28203
NO_2, atm. conc., from solar and lunar spectra in visible region obs. from ground *(French)* 79−53511
NO_2 atm. pollutant, effect of sunlight UV on photochem. reactions 77−21894
NO_2, atm. total content, var. during solar eclipse, diurnal var. in tropics *(French)* 77−2208
NO_2, atm. trace gases and pollutants, data compilation on mag. tape 78−44995
NO_2, atmospheric, dispersion correlation spectroscopy 77−73857
NO_2, atmospheric, gas chromatographic meas. using electron capture detect. 79−57549
NO_2, atmospheric, tangent ray meas. technique, effects of NO_2 conc. vars. at twilight 78−32141
NO_2, atmospheric abundance meas. using solar absorpt. method *(Japanese)* 80−94556
NO_2, atmospheric concentration determ. dye laser differential lidar system 78−32250
NO_2, atmospheric content optical determ. *(Russian)* 77−81962
NO_2, atmospheric content from aircraft-borne spectrophotometry *(Russian)* 79−34903
NO_2, atmospheric pollution monitoring by lidar systems 78−53765
NO_2, calibration standards, generated by gas phase titration 78−69507
NO_2, coherence time rel. to radiative lifetime, theory 79−18240
NO_2, complete quartic force field calc., algorithm 80−37736
NO_2 concentration in stratosphere, HNO_3 simultaneous meas. *(French)* 78−16107
NO_2 concentration in stratosphere, simultaneous inference using inversion algorithm 80−82000
NO_2 concs. in dwellings with gas or electric stoves 78−16086
NO_2, continuum emission in aurora 79−2422
NO_2, core-electron excitation, absorpt. spectrum and CI calcs. 77−75181
NO_2, coupling of vibronic states induced by messenger state 79−72226
NO_2, cyclic chemiluminescent monitoring device, NO conc. effects 77−49177
NO_2 decomposition by electron beam irradiation treatment of exhaust gases 79−79423
NO_2, detailed spectroscopic study, sub-Doppler spectroscopic techniques 80−52339
NO_2, direct CI calcs. 80−52889
NO_2, direct CI method generalised to HF interacting space 79−85908
NO_2, discrete reson. CARS emission, temporal and spectral props. 80−95630
NO_2, dissociation in AC field, kinetics and energetics *(French)* 78−64824
NO_2, dissociative limit, mol. beam characts. determ. by fluoresc. excitation spectra 80−53074
NO_2, EPR, mag. dipole transitions, Zeeman parameters 78−17697
NO_2, electron attachment, ECR obs. *(German)* 79−10201
NO_2, electronic states, pot. energy surface calcs. 77−6673
NO_2, electronic struct., $A^2B_2 \leftarrow X^2A_2$ and $B^2B_1 \leftarrow X^2A_1$ absorpt. bands 77−3257
NO_2 emission meas., Baden-Wurtemberg network *(German)* 79−52977
NO_2 evolution during HNO_3 intercalation of graphite 79−43564
NO_2 excited, fluoresc. spectrum, IR multiphoton vibr. pumping, photon absorpt. probability distrib. study 80−18854
NO_2, excited electronic states, time-resolved spectrosc. 79−45747
NO_2, excited state, ODMR obs. 79−36670
NO_2, excited-state rot. const., 5933 Å vibronic band reassignment 77−58196
NO_2, fluoresc. excited by laser, spin-orbit effects 79−64030
NO_2, fluoresc. lifetime and quenching mechanism 79−89701
NO_2, fluoresc. quenching mechanism 78−25599
NO_2, fluoresc. quenching mechanism in mag. field 78−74696
NO_2, fluoresc. spectra and collisional quenching 80−102538
NO_2, fluoresc. spectra from selectively excited HFS levels 78−21961
NO_2, fluoresc. spectra near 5000 Å, rotationally-forbidden bands 77−79639
NO_2 fluorescence monitor with flashlamp pumping atm. tests 77−64443
NO_2, force fields using Redington method 77−18899
NO_2, g-factors of electronic transitions determ., use of resonance optical rot. 79−54876
NO_2 gas, reduction of Pu(VI) to Pu(IV) 79−31108
NO_2, gas phase, chem. relax. times for dissoc. reactions *(Russian)* 77−70288
NO_2, ground state pot. surface, ab initio LCAO MO SCF calcs. 80−102461
NO_2 Hanle effect, nonstationary states in molecular spectroscopy, level splitting 80−23465
NO_2, Hanle effect, using Doppler reduced laser excitation 78−25627
$(NO)_2$, heat of form., UV spectrum temp. depend. 78−64872
NO_2, high-press. Raman matrix isolation spectra 78−45721
$(NO)_2$, IR spectra in O_2 matrix, vibr. freqs. 78−23936
NO_2, IR-optical double reson., fluoresc. obs., high-energy vibr. levels 78−55188
NO_2, in Ar matrix, Raman spectra, high press., low temp. effects 78−52479
NO_2 in atmosphere, remote sensing via computer assisted correl. spectrometer 78−4002
NO_2 in nonane, supersaturated gas, photoinduced nucleation 78−80760
NO_2 in stratosphere, conc. var. during total solar eclipse 80−105017
NO_2, in stratosphere, global behaviour 80−17334
NO_2, in stratosphere, meas. method and behaviour at mid-latit. 80−17414
NO_2, in stratosphere, obs. rel. to instantaneous global O_3 balance 80−109211
NO_2, in stratosphere at latitude 45°S at midsummer, ground based meas. 79−96784
NO_2 in stratosphere during Antarctic winter 79−34892
NO_2, inter and intramolecular radiationless transitions, relax., time resolved excitation and fluoresc. spectra 80−27966
NO_2, ionis. pot., many-body diagrammatic RSPT calc. 79−31378

nitrogen compounds continued
NO_2, laser and flash lamp fluoresc. monitors, comparison 80−17367
NO_2, laser excited fluoresc. lifetime 79−50076
NO_2, laser fluoresc., $^2B_1$ vibronic states 77−27109
NO_2 laser fluoresc. meas. in flames 78−56923
NO_2, laser spectroscopy by cascade photoionisation method in mass spectrometer 80−99496
NO_2, laser-induced fluoresc. spectrum near 6125 Å 77−58069
NO_2, laser-induced fluoresc. quenching rate const. and lifetimes 80−11930
NO_2, lowest quartet state theoretical excitation energy 79−68221
NO_2, mag. fluoresc. quenching mechanism, up to 18 kG, press. and λ depends. 77−65498
NO_2, mag. quenching of fluoresc. 79−31582
NO_2, magnetic quenching, enhancement of radiationless decay, direct and indirect mechanisms 77−42345
NO_2, matrix elements for multiplet spin-orbit interaction 77−57905
NO_2 meas. in ambient air, Dutch-German programme 77−29443
NO_2, meas. in atmosphere, monitors, intercalibration 78−69529
NO_2, microwave absorpt. coeff. 77−64378
NO_2, minor atm. components, visible absorpt. spectra, temp. depend. *(French)* 80−36355
NO_2 mixing ratio profiles from IR solar spectra obs., in stratosphere 80−105015
NO_2, mol., spin-rot. Hamiltonian in reduced form 79−63976
NO_2, molecular geometry, vibr. anharmonicity effects 79−50159
NO_2, NO_2^+, NO_2^-, SCF and MC SCF CI calcs. 78−46280
NO_2, NO_3^-, in atm. aerosols and precip., $^{15}N/^{14}N$ isotope ratios 78−44896
NO_2, $NO+O_3$, chemiluminescent reaction, theory of light amplification *(Russian)* 77−88717
NO_2, Ne matrix isolated, 6K, B←X band system 78−993
NO_2 nighttime concs., hydrocarbon reductions, potential effects, outdoor smog chamber expts. 77−70720
$(NO)_2$, normal coordinate anal. 78−90144
NO_2 on Cu, ultrahigh vacuum ESR studies 80−97729
NO_2, one-photon dissoc. to NO+O, Doppler spectroscopy 80−53124
NO_2 optical depths rel. to atmospheric turbidity studies 77−17216
NO_2, optical RF double reson. showing nonstationary state 79−59492
NO_2, optical RF double reson. for $^2B_2$ state g values 79−64022
NO_2, optimisation of diffuse Gaussian exponents 79−3364
NO_2, optoacoustic detect. using pulsed dye laser 78−27835
NO_2, optogalvanic spectroscopy in discharge, 570 to 620 nm 79−54862
NO_2, peroxy isomer, stability, ab initio SCF calcs., bond strength 77−14605
NO_2, perturbed $^2B_2$ state fluoresc. lifetime, excitation energy depend. 78−90202
NO_2, photodissoc. rate constant depend. on altitude 78−11949
NO_2, pollution meas. in ambient air, International Comparison Programme 77−87066
NO_2, quantitative detect. in N_2 using CO laser mag. resonance 77−12855
NO_2, quantitative intracavity laser detect. by optical multichannel anal. 77−77846
NO_2 radical, adsorption anisotropy on ionic cryst. surface, SCF MO LCAO calcs. 77−89643
NO_2, radical, ENDOR and ESR obs. ^{14}N hyperfine coupling tensor 77−50455
NO_2 radicals adsorbed on silica gel, averaging-out of ESR spectrum 77−60119
NO_2, real time method using tapered variable area flowmeter 78−71410
NO_2, reduction by electron beam irrad., appl. to exhaust gas treatment 78−80765
NO_2, relative Raman scatt. cross section 80−100061
NO_2, remote sensing of air pollution using optical multichannel analyser 79−79439
NO_2, reson. coherent antiStokes Raman and absorpt. spectra 79−54860
NO_2, reson. fluoresc. excited by visible laser, force consts. of ^{15}N mol. 79−72343
NO_2, reson. Raman spectra, vibr.-rot. scatt. Q branch enhancement 78−989
NO_2, rot. cooled, vibronic band lifetimes, time resolved fluoresc. excitation spectra obs. 79−94025
NO_2, rot. Q-branch effective line strength at 37.7 cm^{-1} 77−6859
NO_2, rot. spectra at 93 GHz, press. broadened hyperfine multiplet 78−90156
NO_2, rot. Zeeman spectroscopy, 8_{08} to 7_{17} rot. transition 78−25610
NO_2, shock heated, visible emission 80−58274
NO_2, single and double ionisation by electron impact, ionisation pot. determ. 80−95730
NO_2, solar radiation absorpt. causing stratospheric heating 77−17199
NO_2 source of artifact nitrate, formation on filter media, interference effects 79−83668
NO_2 spatial distribution, detectivity estimation of DAS lidar 78−92991
NO_2 species in an irrad. single crystal of uridine 5′-phosphate (Na salt), EPR obs. 80−40719
NO_2, stack plume obs. by laser radar *(Japanese)* 78−11990
NO_2, Stark spectroscopy using CW dye laser 77−38026
NO_2, stratosphere, spacecraft solar extinction data inversion 79−74961
NO_2, stratospheric, ground based obs. 80−85697
NO_2, stratospheric composition during major warming, 1979 obs. 80−51476
NO_2, stratospheric vertical distrib. at night, NO_3 layer effect *(French)* 77−66947
NO_2, sub-Doppler laser spectrosc., high resolution 80−52320
NO_2, sub-Doppler spectra, laser-beam system, HFS excitation, radiative, non-radiative decay 78−90210
NO_2 teledetection of gaseous atmos. pollutants, data acquisition and anal., pollution mapping *(French)* 80−7989
NO_2, thermal cond. in parallel const. and alternating elec., mag. fields, parametric reson. 78−83515
NO_2, thermal decomposition, kinetics in medium pressure region *(Russian)* 79−70321
NO_2, thermal decomposition kinetics *(Russian)* 80−3329
NO_2, transport into stratosphere, prod. in thunderstorms 80−8376
NO_2, two step photoionisation by vac. UV laser *(Russian)* 78−9205
NO_2, UV photodissoc. quantum yield, absolute absorption cross section 77−90616
NO_2, unimolecular reactions, rate theory 79−74348
NO_2, VUV absorption spectra, Rydberg states assignments 77−58040
NO_2, vacuum ultraviolet absorpt. spectra, absorpt. coeffs. 78−70846

nitrogen compounds continued
NO_2, valence shell ionis. spectra, theory and dipole (e-2e) spectra expts. 79−76522
NO_2, vertical column abundance in troposphere, optical absorpt. meas. 78−85632
NO_2, vertical electronic spectrum, SCF and CI calcs. 77−30878
NO_2, vertical electronic spectra, ab initio calcs. 78−66538
NO_2 vertical profile, balloon obs. in stratosphere *(Japanese)* 80−31086
NO_2, visible fluoresc., rotational structure of vibronic bands 79−98146
NO_2, visible spectrum simplification, rot.-vibr. levels, excitation, polarisation labelling spectroscopy 80−32730
NO_2^-, ab initio VB wave functions, π-electrons 78−70748
NO_2^- centres in CsBr and CsI, polarisation of luminesc. and reorientation processes 79−95823
NO_2^-, direct CI calcs. 80−52889
NO_2^-, direct CI method generalised to HF interacting space 79−85908
NO_2^-, electron detachment energy, equations of motion method calcs. 77−50478
NO_2^-, electronic struct., X-ray spectra obs. 78−55185
NO_2^-, heavy cation effect on singlet-triplet intercombination 79−85946
NO_2^-, high press. IR vibr. spectroscopy *(German)* 80−74170
NO_2^- hydrate clusters, ground-state HF pot., Monte Carlo simulation, energy surfaces and rot. barriers 80−106412
NO_2^- impurity, in alkali halide, effect on lattice vibrs. 77−35654
NO_2^- impurity anion in aqueous soln. of LiCl(Br), temp. quenching of luminesc. *(Russian)* 77−1714
NO_2^- impurity in alkali halides, reorientation, linear dichroism *(Russian)* 80−45127
NO_2^-, impurity induced Raman scatt. in alkali halides 77−52085
NO_2^-, in KI matrix, Raman spectra, high press., low temp. effects 78−52479
NO_2^- ion in nitrite salt cryst., $^{1,3}B_1 \rightarrow {}^1A_1$ transition spectra, reasons for diffuseness 80−97276
NO_2^-, microwave transition probability in zero field, spin-orbit interaction 78−25518
NO_2^- molecular ion in alkali halide crysts., peculiarities of luminesc. spectra 77−52174
NO_2^-, $NO_2^-.H_2O$, and peroxy isomers, photodissoc. and photodetachment 3500-8250 Å, rel. to ionosphere 80−35554
NO_2^-, optimisation of diffuse Gaussian exponents 79−3364
NO_2^-, photolysis as source of free radicals in productive surface seawater 79−62522
NO_2^-, solvated, in H_2O, ethanol, cyanomethane, and DMF lowest n-π^* transition 79−85960
NO_2^- triplet state lifetimes and fine structs., CNDO-CI calcs. 77−57897
NO_2^-, vertical electronic spectra, ab initio calcs. 78−66538
NO^-_2, molecular vibrational constants in KBr crystal, impurity effects 77−20035
$(NO)_2^-$, binding energy from photoionis. data 77−61811
NO_2^+, gas phase equilib. geometry, force consts., vibr. freq., dipole moment function MCSCF/CI calcs. 80−78520
NO_2^+, vertical electronic spectra, ab initio calcs. 78−66538
$^{14}NO_2$, and $^{18}NO_2$, inertia defects and dipole moments by kinetic consts. method 80−928
$^{14}N^{16}O_2$, IR spectra, $2\nu_2+\nu_3$ and $\nu_1+\nu_2+\nu_3$ bands, vibr. and vibr.-rot. consts. 78−983
$^{14}N^{16}O_2$, ν_1 band, high resolution IR spectra 78−55173
$^{14}N^{16}O_2$, $\nu_1+\nu_3$ band, IR absorpt. spectra 78−78693
$^{15,14}NO_2$, predissoc. rot. struct. in 2490 Å band 80−87192
NO_2-cyclohexane-air mixtures, photochem. particulate form. 78−11529
NO_2-N loss from microcosms as soil pollution indicator 78−16019
NO_2-N_2O_4 gaseous system, self-association theory 79−29347
NO_2-NaCl, atmospheric reaction, in situ TEM studies 80−104544
NO_2^--IO_4^- aqueous redox mixtures, γ-radiolysis 79−20392
NO_2+acetylperoxy radicals, absorpt. spectrum and reaction kinetics 80−91571
NO_2+$Ar(CO_2)(NH_3)$, continuum quenching in upper atmosphere 79−88520
NO_2+B, chemiluminesc. metal oxide formation 80−35509
NO_2+CCl_2FO_2, reaction, photolysis obs. 79−74931
NO_2+CO, E-V energy transfer reactions, electronically excited NO_2 78−64814
NO_2+Cl, (ClO)+M, reaction rate constants 79−100350
NO_2+Cl, ClONO prod., FT IR obs. 79−8427
NO_2+Cl, matrix reactions, IR absorpt. obs. 78−15667
NO_2+dimethylamino radical, reaction rate constants, FTIR obs. 80−16652
NO_2+ethylperoxy radical, reaction rate const. meas. 80−21262
NO_2+H, population inversion of Λ doublets in microwave spectrum of $OH(^2\Pi_{3/2}, v=1)$ 80−974
NO_2+H_2, vibr. relax. rate, stimulated Raman scatt. obs. 77−75269
NO_2+HO_2, form. and react. in aq. soln., pulse radiolysis 79−24805
NO_2+HO_2, reaction rate consts. by laser mag. reson. 78−27748
NO_2+H→NO+OH, hydroxyl group internal state distrib., laser-induced fluoresc., crossed mol. beams 77−4905
NO_2+H→OH+NO, vel. and angular distrib., Fourier transform Doppler spectrosc. obs. 79−80692
NO_2+He(Ne)(Ar), Penning ionis., electron spectra, vibr. transfer 77−14555
NO_2+K, charge transfer reactions, energy and ang. differential cross-sections meas. 80−53125
NO_2+K, ion pair form. reaction, energy loss spectra obs. 79−91921
NO_2+Li($4^2S_{1/2}$), crossed beam, search for collisional ionisation 79−64087
NO_2+NH_2, reaction rate const. meas. 80−7772
NO_2+N→N_2O+O, crossed beam study, produce ang. distrib. 79−34311
NO_2+O^- (O_2^-), charge exchange excited NO_2^- formation 77−75236
NO_2+OH, colisional relax., laser mag. reson. study of press. broadening 79−94020
NO_2+OH, mean collision cross sections from microwave spectroscopy 80−1046
NO_2+OH, OH(v=1) relax., time resolved spectra 80−74240
NO_2+OH, rot. inelastic collision, microwave spectra 79−45806
NO_2+OH+M→HNO_3+M, reaction kinetics, temp. and press. depend. 79−66284
NO_2+OH+M→HNO_3+M, rate constant under simulated atmospheric conditions 80−50846
NO_2+ROO→$ROONO_2$, (R=C_nH_{2n+1}), Fourier transform IR spectroscopic meas. 78−53194
nitrogen compounds continued
NO_2+SO_2 aerosol, form. kinetics, irrad. by 488 nm light 78−40067
NO_2+Sc(Y), oxidation, single collision chemiluminesc. 77−25267
NO_2^-+$O_2(CO_2)(NO_2)$, photodetachment and de-excitation rates 77−75236
NO_2^++O→NO^++O_2, rate constant rel. to atm. ion chem. 77−41245
$(NO_2)_2$, struct. and force fields of isomers, ab initio calcs. 77−18783
NO_3, atmospheric, obs. 78−88880
NO_3, atmospheric particles, size distrib. and chem. comp., Nagoya area, Japan 78−11980
NO_3, detect. in polluted troposphere by differential optical absorpt. 80−77036
NO_3 in troposphere, obs. of content in mountain air 80−72582
NO_3, mag. hyperfine interactions, MO LCAO UHF calcs. 77−14369
NO_3^-, aq. soln., vibr. width and dephasing, conc. depend. 80−43029
NO_3^-, contrib. to acidity of rain 79−2327
NO_3^-, detect. in subway air 78−36273
NO_3^-, determ. in surface and effluent water, potentiometric and colorimetric methods 79−100476
NO_3^-, determ. in waste and treated waters by laser Raman spectroscopy 79−92113
NO_3^- effect on spectral distribution and intensity of sonoluminescence of Ar saturated solutions 80−76091
NO_3^- electron scavenger, positronium form. inhibition in H_2O and D_2O 79−66325
NO_3^-, electronic struct., X-ray spectra obs. 78−55185
NO_3^-, geometry in crystals *(French)* 79−65045
NO_3^-, in ambient aerosols, assay via ion chromatography anal. 78−68974
NO_3^- in Antarctic ice, γ- and X-irrad. due to supernovae 80−31314
NO_3^-, in aq. nitrate solns., vibr. dephasing process, Raman obs. 79−51936
NO_3^- in aqueous electrolyte solution, vibr. relax. theory 79−94862
NO_3^- in E United States precip., concs. behaviour 78−92962
NO_3^-, in $MClO_3$ and $MClO_4$ matrix, vibr. spectra, anion site asymmetry 77−27062
NO_3^-, in molten monovalent metal nitrates, ion struct., pulsed neutron diffr. obs. 78−22631
NO_3^-, in rain water collected at Julich, Germany, N isotope comp. 78−57284
NO_3^- ions, inhibition of Ps form. in H_2O-ethylenediamine mixtures 78−95988
NO_3^-, level in reacting atmospheric aerosol, calcs. 80−26056
NO_3^-, $NO_3^-.H_2O$, and peroxy isomers, photodissoc. and photodetachment 3500-8250 Å, rel. to ionosphere 80−35554
NO_3^-, PO_4^{3-}, $Si(OH)_4$, ratios in Moroccan upwelling region 80−4045
NO_3^-, particulate, air pollution, lab. and field studies of major sampling interferences 79−92105
NO_3^-, particulate, global tropospheric meas. 78−88904
NO_3^-, positronium formation, Doppler broadened positron annihilation line shapes 80−45164
NO_3^-, Raman spectrum of ν_1 mode in soln., reorientation 78−92067
NO_3^-, triplet state lifetimes and fine structs., CNDO-CI calcs. 77−57897
NO_3^-, X-ray fluorescence, electronic struct. determ. 78−86887
NO_3^{2-}, coupling consts., geometry, LCAO UHF and ENDOR data calcs. 77−14369
NO_3^{2-}, ENDOR and ESR obs., ^{14}N hyperfine coupling and g-tensors 77−50455
NO_3^{2-}, in γ-irrad. Y-type zeolite, EPR triplet assignment, instead of H_2O^- 78−11534
NO_3^--N export from drainage basins, Toronto, Ontario 79−66729
NO_x, air pollution in Sheffield, conc. var. 80−16863
NO_x, atmospheric, interaction with airborne particles 78−81342
NO_x atmospheric chemistry, significance of HO_2NO_2 78−11971
NO_x, atmospheric monitoring, chemiluminesc. method 79−16062
NO_x biradicals, conform., spin probe appls. 78−86895
NO_x chemiluminescent analysis using diffusion interface module 78−40095
NO_x chemiluminescent monitor for air pollution investigations 80−72118
NO_x control in MHD coal-fired process 79−52947
NO_x, detection by chemiluminescence analyser 78−40094
NO_x emission from thermal power plants, review of preventive measures *(Croatian)* 78−3935
NO_x emissions from coal-fired MHD power plants, simplified correlations for prediction 80−97842
NO_x, emissions from domestic kerosene-fired and gas-fired appliances 79−88023
NO_x emissions from European cars, control 79−48198
NO_x, form. in combustion, oxidising agent excess depend., thermodynamic anal. 78−15677
NO_x, formation by heated corona wires of electrostatic precipitator 80−47081
NO_x formation steam boiler convective heating surface fouling with ash, dependence 79−83678
NO_x formation steam generator TP-87 with bottom burners *(Russian)* 77−83072
NO_x from SST and subsonic aircraft emission, potential O_3 column increase 78−11979
NO_x in flue gases, determination various methods, comparative evaluation 79−53014
NO_x in flue gases, measuring instruments, calibration and checking 79−53015
NO_x production in atm. due to lightning 77−56677
NO_x reduction on Fe-based catalysts containing V 79−12285
NO_x removal from air, chemical reagents based on $NaClO_2$ and K_2CO_3 (MARTZCLEAN) *(Japanese)* 79−52976
NO_x removal from atmosphere, using MARTZCLEAN reagents based on $NaClO_2$ and K_2CO_3 *(Japanese)* 80−61147
NO_x removal rate in urban atmosphere 80−56524
NO_x, Stark effect investig., using two-way EPR cavity system 80−90872
NO_x, surface reaction on Cu, relative humidity depend. 79−5176
NO_x, urban air pollution in Genoa, Italy 78−11981
NO_x^--HNO_x-H_2O clusters, gas phase, thermodynamic quantities, mass spectra obs. 80−50875
NO_y in stratosphere, effects of NO photolysis on mixing ratios 77−29399
N_2O, ^{14}N quadrupole coupling consts., ab initio calcs. 80−58283
N_2O, ^{15}N NMR, chem. shift., determ. of virial coeffs., rovibr. motion 78−58720

nitrogen compounds continued
N_2O, 12°1 band lines, precise meas. with compact vacuum IR spectrometer 80−95157
N_2O, 40°00-00°0 band, IR high press. absorpt. spectra profiles 80−52988
N_2O, absorption spectrum anal. press., temp. quantity and spectral resolution retrieval 79−100462
N_2O, abundance in air, IR spectrochem. anal. 78−15738
N_2O, adsorbed on α-cyclodextrin, positron annihilation, effects of adsorbed gases 79−65952
N_2O, adsorbed on SiO films, infrared spectra exam. 79−45725
N_2O adsorption on Cu (100) surface, reaction with CO 80−103583
N_2O, adsorption on W (110), 300K and 100K, XPS, UPS and XAES 79−28203
N_2O, air pollutant, remote meas. using chem. laser lidar system 77−21910
N_2O, and isotopic forms, pot. energy function determ. from vibr. data 77−18812
N_2O, and mixtures with CO_2 viscosity and thermal cond. coeffs. predictions, 180-900K, ≤23 MPa 77−84383
N_2O and NO in atmosphere, biomass burning as source 80−26586
N_2O, anomalous Zeeman effect, nonlinear optical techniques, book contrib. 78−9279
N_2O, as mol. probe in MBBA, solute solvent interaction, IR spectra vibr.-rot. fundamental 80−29155
N_2O, atm. absorption line parameters, AFGL, compilation update 79−21013
N_2O, atm. conc., rel. to tropospheric OH conc. 77−45069
N_2O, atm. distrib., mixing ratio 78−32175
N_2O, atm. life cycle, ground surface sink mechanism 77−66971
N_2O, atmos. warming due to N_2O release from fertiliser 80−94579
N_2O, atmospheric, greenhouse effect and climatic implications 77−9460
N_2O, atmospheric, instantaneous global photochemical reaction rates 80−17335
N_2O, atmospheric, potential of soil as natural sink 77−21772
N_2O, atmospheric, prod. by coal and fuel oil combustion 77−21890
N_2O, atmospheric, sources and sinks, O_3 reduction due to industrial fixed N fertilizers 77−78383
N_2O, atmospheric, sources, sinks and vars. meas. 78−85631
N_2O, atmospheric, three-dimens. distrib. and variability, numerical simulation 79−58006
N_2O, atmospheric abundance determ. by analysing solar spectra 78−85643
N_2O, atmospheric abundance meas. over USSR *(Russian)* 78−96265
N_2O, atmospheric anal. using electron capture-gas chromatography technique 77−9531
N_2O, atmospheric cycle, sources and sinks 79−70871
N_2O, atmospheric life cycle rel. to O_3 reductions 78−16140
N_2O CW gasdynamic mixing lasers, pumped by N_2 or air, low stagnation temp. characts. 78−63053
N_2O, chemisorbed on transition metals at high pressures, XPS 77−20990
N_2O, combination and difference bands, IR intensities 77−466
N_2O, conc. diurnal variability in surface air 79−84369
N_2O, conc. meas. in stratosphere 78−32171
N_2O, concs. in Michigan waters and USA municipal waters 78−57223
N_2O, continuous meas. in troposphere 78−81318
N_2O crystal, vibrational exciton bands, impurity modes 77−28560
N_2O, decomposition on titanate catalyst, energy reson. hypothesis 78−95947
N_2O, decomposition over particulate matter 79−16014
N_2O, destruction by siliceous land surfaces, possible tropospheric sink 79−12168
N_2O, determ. in blood or gas by polarographic sensor 79−62412
N_2O, determ. in water using electron capture detection gas chromatography, multiple equilib. 80−76566
N_2O, diffraction-limited IR spectroscopy, normalised slit width appls. 77−71388
N_2O, dipole moment functions 80−87094
N_2O, dipole oscill. strength distribs., sums 78−21975
N_2O, dipole properties and dispersion energies additivity, using atoms and small mol. models 80−53091
N_2O, dispersion energy consts., dipole oscill. strength, refractivity 77−50492
N_2O, dissoc. electron attachment, O^- ang. distrib. 77−75315
N_2O, dissoc. in alternating elec. field, kinetic and energetic data *(French)* 78−13620
N_2O, dissolved, consumption in anoxic basin, Saanich Inlet, British Columbia 78−40594
N_2O dissolved in liq. cryst., NMR, relax. times 80−25233
N_2O dissolved in SF_6, IR and Raman rot. correl. functions, expt. and theory 79−46541
N_2O, electron energy loss spectrum, optically forbidden transitions 77−31015
N_2O, electron impact, dissoc. patterns 79−7021
N_2O, electron impact, energy loss spectra, electronic transitions obs. 78−17805
N_2O, electron impact excitation, ionisation, emission spectrum 77−50469
N_2O, electron impact ionisation and dissociation, radiation emission 78−90304
N_2O, electron scavenging on irradiated silica gel surface 79−24762
N_2O, electronic autoionisation branching 80−91614
N_2O, electronic-vibr. energy transfer from $Br(4^2P_{1/2})$, 10.9 μm transition 77−31094
N_2O emission from soils, effects of acetylene and soil water content 79−83672
N_2O emission from soils during nitrification of fertiliser 78−57313
N_2O from soil treated with nitrogenous fertilisers, atmospheric source 78−61419
N_2O, fundamental vibr. bands in liq. phase 79−54856
N_2O, gas, up to 50 atm, refr. index, 328, 3103 MHz *(French)* 78−14129
N_2O, gas 80−95664
N_2O, gas phase electron attachment, temp. depend., pure, and in ethane and neopentane mixtures 79−36757
N_2O, gasdynamic laser, flow inhomogeneity effect on gain distrib. 78−1205
N_2O, gasdynamic laser, population inversion mechanism, kinetics 77−7074
N_2O, gaseous impurity, role in H_2 embrittlement of steel 77−59904
N_2O, global and regional meas. 78−73471
nitrogen compounds continued
N_2O, global atmos. and Pacific Ocean composition 80−51519
N_2O, ground level abundance, simultaneous determ. of CO_2, CO and H_2O 78−11969
N_2O, high-power tunable laser for 9 to 12.5 μm range 77−83884
N_2O, IR absorpt. spectra, N_2-broadened lines of ν_3 band 78−5228
N_2O, IR band nonrigid rot. absorption 78−91060
N_2O, IR bands, parametric deconvolution method 78−78697
N_2O, IR combination band spectral emissivity, 1200, 1700, 1900K, shock tube obs. 78−5287
N_2O, IR emissivity and band-model parameters, 200-500K 77−83591
N_2O, IR intensities by electron impact spectroscopy 77−6851
N_2O IR laser, transients obs. by modulation of intracavity absorber 78−74933
N_2O, IR spectrum in liquid Ar, vibr. anal. 78−21927
N_2O, impurity lines in He resonance source for photoelectron spectroscopy 77−14787
N_2O in agricultural soil, losses in solution in drainage water 79−43797
N_2O in Ar matrix, fluoresc. and thermoluminesc. after photolysis 79−89700
N_2O, in atm., sources and sinks 77−37374
N_2O, in atmosphere, from N fertilisers, effects on stratospheric O_3 78−73505
N_2O, in atmosphere, interhemispheric gradients meas. 78−81289
N_2O in atmosphere, laboratory intercalibration of meas. 78−81277
N_2O in atmosphere at mid-latitude of S. hemisphere 79−100908
N_2O, in liq. inert gas, electron attachment, elec. field effects 77−31009
N_2O in lower stratosphere, latitudinal profiles 78−44989
N_2O in N.American troposphere and stratosphere 79−79430
N_2O, in O_2 min. of tropical north Pacific Ocean, consumption during denitrification 79−5501
N_2O, in soln., IR and Raman band shapes, mol. dynamics, ν_3 band 77−36238
N_2O, in soln., Raman and IR ν_1 and ν_2 band shapes, mol. motion dynamics 78−64352
N_2O in stratosphere, altitude profiles at five latitudes 77−78318
N_2O in stratosphere, height profile meas. at several latits. 80−72601
N_2O in tropical E.Pacific Ocean, meas. in sea water and marine air 80−94542
N_2O in troposphere, absence of photolysis 79−53493
N_2O, interaction with Cu (111), kinetics using AES, LED and ellipsometry 79−65317
N_2O interaction with Cu (110) surface, ellipsometry, AES, LEED study 80−6635
N_2O, interactions with Ru ($10\bar{1}0$) surface 80−55713
N_2O, ionis. by low-energy electrons and near thermal inert gas ions, emission obs. 79−31707
N_2O isotopes, laser transitions near 4.6 μm, HF laser optical pump 78−58995
N_2O, K-shell photoabsorpt. spectra using synchrotron radiation 78−74711
N_2O, K-shell photoabsorption coeffs., 500-600 eV 80−9617
N_2O, laser, CW, thermally excited and selectively-pumped mixing comparison with CO_2 laser 77−42521
N_2O laser, mass spectra of positive ions in discharge plasma 77−89315
N_2O laser, new lines in 10 μm region, rot.-vibr. transitions in $(00^02\text{-}10^01)$ band 77−27281
N_2O laser as IR pump for obtaining far IR emissions in NH_3 80−74345
N_2O, liq., transient stimulated vibr. Raman scatt. 78−71144
N_2O, liq. phase vibr. spectra, anharmonicity effects 79−50022
N_2O, mech. of thermal electron attachment, microwave cond. meas. 78−59536
N_2O, microwave absorpt. coeff. 77−64378
N_2O mixing ratio meas. and residence time 78−49088
N_2O, multiple reflection cell, laser spectroscopic meas. 78−86359
N_2O, N $1s^{-1}$, π^*-state decay, fragment ion relative abundance by electron-ion coincidence technique 80−9743
N_2O, negative Van der Waals polymer mols., formed by nozzle expansion 78−90307
N_2O, non-Franck-Condon transitions in resonant autoionization 79−50092
N_2O, ν_2 band as freq. standard in 17 μm spectral region 79−63991
N_2O, ν_3 and $2\nu_3$ IR bandshape and dipole correl. functions 80−91560
N_2O ν_3-fundamental at 4.52 μ, shock wave effective absorption coeffs., empirical determ. 79−64799
N_2O, partial photoionisation cross-sections meas. 20 to 60 eV 79−31624
N_2O, photoabsorpt. cross section, 10 to 50 nm 77−61797
N_2O, photoabsorpt. cross-section, 50-340 Å, as sum of empirical at. cross-sections 78−58718
N_2O, photoabsorption and photionisation, UV region meas. 78−42087
N_2O photodissociation, CC $O(^1S)$, prod. and props. in liq. Ar and N_2 80−43063
N_2O, photoelectron spectrum, vibronic interaction and autoionis. effects 80−95680
N_2O, photoionisation, partial oscill. strengths 79−6973
N_2O, photoionisation and ion dissoc., isotope effects, mass spectra 78−9203
N_2O, photolysis, $O(^1S)$ absolute quantum yield spectral depend. meas. using XeO luminesc. 80−35561
N_2O, photolysis, relative rate consts. of $O(^1D_2)$+olefin reactions 79−83472
N_2O, polar gas thermomagnetic torque meas. 77−42960
N_2O, preionis. and predissoc., rel. to spectral line shape 80−63724
N_2O, prod. in ocean, Atlantic and Pacific meas. 79−48518
N_2O production in electric discharge 79−96786
N_2O, pseudospectral dipole oscillator strength distribs. 78−50503
N_2O, pulsed photoacoustic Raman spectrosc., gaseous trace anal. 80−40769
N_2O, pure and in mixtures, electron attachment near 1 atm., microeave cond. meas. 80−1063
N_2O, pure liq., mol. motion, anisotropic interaction 80−24345
N_2O, pure rotational stimulated Raman photoacoustic spectroscopy 80−32724
N_2O quadrupole hyperfine struct., vibr. depend. obs. using twin-laser spectrometer 80−43097
N_2O, rates of evolution from N fertilised soil 79−16656
N_2O, rot. Raman spectra, 01^10 state effects on intensity distrib. *(German)* 77−10679
N_2O, rot. Raman spectrum, meas. using Fabry-Perot interferometers with 20 cm^{-1} free spectral range *(Japanese)* 77−87847
N_2O, rot. transitions, self-broadening and self-shifting meas. 79−59426

nitrogen compounds continued
N_2O, satellite struct. and momentum distrib., binary (e,2e) spectroscopy 80−69125
N_2O, simple high-power TEA laser operating in IR 79−94251
N_2O, soil gas fluxes determ. by chamber methods, numerical evaluation 79−16700
N_2O solutions and aq. thymine, radiolysis products anal. 80−30257
N_2O, spin polarised photoelectrons, synchrotron excited 80−43101
N_2O, stratospheric conc. 77−78304
N_2O, stratospheric conc. meas., mixing ratio 78−81281
N_2O, submillimetre rot. lines, press. shifts 80−23463
N_2O submillimetric high-resolution Fourier transform spectra 79−31509
N_2O, submm wave spectra, 375-565 GHz, isotopic species, mol. consts. 77−3346
N_2O, synthetic absorption spectra rel. to quantitative anal. 79−100461
N_2O, thermal decomp., unimol. reaction theory 79−15954
N_2O, triboelectric discharge of Hg rolling on glass, chem. effect *(French)* 79−77438
N_2O, triple-dipole energy calcs. using pseudo spectral theory 78−46418
N_2O, vac. UV photodissoc., kinetic energy and ang. distribs. of fragments 77−30938
N_2O, valence and core photoionisation, spectral lines, many body effects 80−47853
N_2O, valence excitation energy and UV spectra, HAM/3 calc. 78−25454
N_2O, valence shell ionic photofragmentation, oscill. strengths, EELS and electron-ion coincidence meas. 80−37879
N_2O, vertical profile meas. in seawater *(German)* 78−3814
N_2O, weak nonlinear waves, struct. and propag., effect of vibr. relaxation 79−64683
N_2O, $X_2\Pi$ state, Ne I photoelectron spectra 77−30924
N_2O, X-ray fluoresc. obs., ionis. pot., fine struct., LCAO SCF calc. 77−68055
N_2O^-, N_2O, ground state potential energy surfaces 77−27175
$N_2O^- \rightarrow N_2 + O^-$, nanosec. pulse radiolysis, rate consts. meas., N_2O^- lifetime 77−16843
N_2O^+, dissoc., threshold photoelectron-photoion coincidence obs. 80−87189
N_2O^+, electronic ground state, INDO SCF MO calcs. 78−82644
N_2O^+, emission in $Ne^+ + N_2O$ charge transfer excitation; down to 1 eV 79−45835
N_2O^+, fluoresc. and dissociation lifetimes of vibr. excited states 78−42108
N_2O^+, fluoresc. and production cross-sections by photoionis. of N_2O 78−9204
N_2O^+, fluoresc. quantum yields and lifetimes, meas. method, ion form. 77−6815
N_2O^+, force fields and force const. of electronically excited states 80−69116
N_2O^+, mobility in Ne gas 78−14125
N_2O^+, photodissoc. cross section, time of flight anal. of reaction products 77−83664
N_2O^+, photodissociation 77−34705
N_2O^+, pot. energy hypersurface characts. calc. in $O^+ + N_2 \rightarrow N + NO^+$ react. 78−60996
N_2O^+, thin foil impact, dissoc. struct. effects in ionic fragment energy spectra 78−50631
$^{14}N_2{}^{16}O$, elec. and mag. props., hyperfine struct., mol. beam elec. reson. obs. 78−62792
$^{15}N_2O$, $^{14}N^{15}NO$, $^{15}N^{14}NO$, optically pumped by pulsed HF laser, emission obs. at 4.6 μm 79−50283
$N_2O/N_2/H_2O$, CW gasdynamic laser, numerical anal. 78−29935
N_2O-acetylene flame, background compensation in differential atomic emission spectrometry *(French)* 78−7296
N_2O-acetylene flame, spectral source using Reticon photodiode array 77−63999
N_2O-CO, flame, alkaline earth atom catalysed combustion 77−9081
N_2O-CO, gasdynamic laser, CO_2 vibr. level superequilib. chem. pumping 79−76666
N_2O-CO flame, alkaline earth catalyzed chain reaction chemiluminesc. 77−40548
N_2O-CO flame, Mg catalyzed chain reaction chemiluminesc. 77−36758
N_2O-CO_2, optically pumped transfer lasers, continuously tunable 78−13678
N_2O-CO_2(-ethane), gas phase thermal electron N_2O attachment mechanism, 5-120 torr 79−27085
N_2O-CO-He mixture, radiation amplification factor in supersonic expanding stream of gas 77−10896
N_2O-H_2 flame, appls. to Mn determ. in gasoline by AAS 78−15729
N_2O-He, species concentrations in glow discharge and afterglow, mass spectra, laser conditions 78−14241
N_2O-He(Kr), thermal diffusion factors meas. 80−10344
N_2O-hydrocarbon mixtures, mech. of thermal electron attachment, microwave cond. meas. 78−59536
N_2O-KOH-O_2-t-butane, pulse radiolysis, kinetics of transient O compound form. meas. from Cherenkov emission 77−70321
N_2O-N_2, CW gasdynamic laser, qualitative comparison with CO_2-N_2 laser 78−25856
N_2O-N_2, CW mixing gasdynamic laser, saturation parameter and small signal gain 79−45923
N_2O-N_2 mixture, conc. depend. of thermodiffusion const. 77−7503
N_2O-N_2 mixture, thermalisation under reson. excitation by laser radiation *(Russian)* 78−26231
N_2O-N_2-He, gasdynamic laser, effect of weak flow perturbations on gain 80−14316
N_2O-N_2-He, population inversion of N_2O vibr. levels behind shock wave front 79−31886
N_2O-N_2-He mixture, radiation amplification factor in supersonic expanding stream of gas 77−10896
N_2O-SF_6, single-photon absorption reaction chemistry in solid state 77−73454
N_2O+Al, AlO chemilum., perturbations and vibr. population anomalies obs., mechanism 77−63917
$N_2O + Al^+$, reaction cross sections 77−29000
$N_2O + Ar^+(He^+)(Ne^+)$, charge transfer, thermal energy, product distrib. obs. 78−25656
N_2O+B, chemiluminesc. metal oxide formation 80−35509
N_2O+B, chemiluminesc. reaction, vibr. state distrib. 79−20354
N_2O+B, gas phase rate consts., 300K, at. absorption obs. 79−83445
N_2O+Ba, chemiluminescent flame, BaO states population 79−39153
nitrogen compounds continued
N_2O+Ba, reaction, electronic branching, statistical and dynamical influences 78−92451
N_2O+Ba(Sm), chemiluminesc., absolute photon yields determ. 77−86317
N_2O+Br*, electronic-vibr. energy transfer, time-resolved fluoresc. obs. 79−89753
N_2O+CO, adsorption on NiO, catalysed reaction in Neel transition region 78−53258
N_2O+CO, CO_2 vibr. temps. under gasdynamic laser conditions 80−21276
N_2O+CO, Na catalysed, Na chemiluminesc., excitation mechanism, appl. chem. laser 77−63916
N_2O+CO, nonequilibrium reaction in shock waves *(Russian)* 78−76845
N_2O+CO, use of steady state chemical reaction for vibr. excitation of CO_2 and N_2 80−50851
$N_2O + CO_2$, vibr. energy transfer, relax. times 79−72401
N_2O+CO+Ba(Ca)(Sr) reaction, intracavity dye laser spectroscopy 77−86293
$N_2O + C \rightarrow CN + NO$, chemiluminesc., CN ($A^2\Pi_i$) vibr. distrib. 79−39152
N_2O+Ca, reaction, electronic branching, statistical and dynamical influences 78−92451
N_2O+Ca($4s4p^3P$), absolute chemiluminesc. cross-section and photon yield 78−53208
$N_2O + Cl^+$, reactions at room temp. 80−93749
N_2O+CsF, rot. inelastic collisions, mol. beam meas. 80−1049
N_2O+deuteromethane, time resolved fluoresc. for vibr. relax 79−31659
N_2O+formaldehyde, mol. isolated Voigt line, off-peak spectral absorpt. coeff. 80−106355
N_2O+Ge, chemiluminesc. reaction, HTFFR kinetics study 80−76496
N_2O+Ge(Si), reaction rate consts. at 350K 78−53186
$N_2O + H_2$, (oriented), total collision cross-sections, anisotropic pot. parameters calcs. 78−13568
$N_2O + H_2$, HO radical form. on Pt surface, laser-induced fluoresc. obs. 80−108738
$N_2O + H^+$, electron capture into n=3 states, 2.2-8.2 keV 79−50129
N_2O+HBr, rate consts. for vibr. energy transfer meas. using laser. induced fluorescence technique 80−87206
N_2O+HBr, V-V energy transfer, 300-900K 79−59539
N_2O+HCl, vibr. relax., 300-900K, by laser fluoresc. 79−31658
N_2O+HF, HF(v=3) relax. and rate consts. 80−61069
$N_2O + H \rightarrow N_2 + OH$, rate const., 2000-2850K, combustion of $H_2/N_2O/CO/Ar$ 78−85162
N_2O+He, binary gas mixture, mutual diffusion press. depend. 77−24047
N_2O+He, collisionally excited neutral and ionic emission, flowing afterglow 77−51248
N_2O+He, Penning ionisation of target mol., for He(2^3S) 79−41228
N_2O+He(He^+), in afterglow, $N_2{}^+$ (N_2O^+) optical emission obs. 79−68251
N_2O+He(Ne)(Ar), Penning ionis., electron spectra, vibr. transfer 77−14555
$N_2O + Ho \rightarrow HoO^* + N_2$, chemiluminesc. reaction, cross-section 78−76847
N_2O+inert gas, reactant decomp., rot.-vibr. energy transfer, relax. analytic soln. 80−55650
$N_2O + Li^+$, vibr. excitation, time of flight meas. 77−79682
N_2O+Mg($^3P_1$) metastable atom, afterglow quenching rate consts. 77−6720
$N_2O + N_2$, vibr. population distrib. energy depend., ν_3, ν_2 and ν_1 mode exchanges *(French)* 79−10187
$N_2O + N_2$, vibr. transfer from N_2O ν_3 to ν_1 and ν_2 modes, rate const. 79−22796
$N_2O + N_2$, vibroluminesc., V-V transfer consts., quadrupolar transition moment, IR spectra 79−10112
$N_2O + N_2$*, vibr. population studied by IR emission spectra *(French)* 77−14544
$N_2O + N(^2D)$, $NO(B^2\Pi_r)$ form., quenching 79−64038
N_2O+Na*(3^2P), electronic to vibr.-rot. energy transfer, differential cross sections 77−38715
$N_2O + Ne^+$, charge transfer excitation, down to 1 eV 79−45835
$N_2O + Ne^+$, thermal energy, reaction rate coeffs. and product distrib. 79−29333
N_2O+Ne*, quenching rate const. for metastable Ne($^3P_2$), flowing afterglow 78−46295
$N_2O + O_2(D_2)(H_2)$, Wassiljewa coeffs., thermal conds., 50 and 100°C 79−37437
N_2O+OH, rate consts. 77−16781
N_2O+OH, reaction, rate const. meas., N_2O atmospheric residence time appl. 77−21352
$N_2O + O(^1D_2)$, chemical-ionisation mass spectrometry, branching ratio measurements in N_2O/He mixtures 79−47905
$N_2O + O(^1D)$, rate consts., temp. depend. 78−27747
$N_2O + O(^1S)$, product channels 78−46422
$N_2O + O(2^1D_2)$, collisional deactivation meas., 295K, rel. to atmospheric processes 80−16663
N_2O+Pb→PbO+N_2, chemiluminesc. reaction, vel. depend. 78−27762
$N_2O + SF_6$, vibr.-vibr. energy transfer, fluoresc. 80−78688
N_2O+Sc(Y), oxidation, single collision chemiluminesc. 77−25267
N_2O+Si($3p^2(^1S_0)$), attenuation of reson. radiation, time-resolved kinetic obs. 78−5329
N_2O+Sm, mol. beam chemiluminescence, cross section energy depend. 77−32792
N_2O+Sn, chemiluminesc., high temp. fast flow reactor kinetics obs. 78−88636
$N_2O + Sn \rightarrow SnO(a^3\Sigma) + N_2$, chemiluminesc. high temp. fast flow reactor obs. 80−45493
$N_2O + X^+$, charge transfer excitation channels, emission cross-sections meas. 77−61851
$(N_2O)_2$, IR continuum spectrum at low temps. 80−980
N_2O_2, IR spectra of solid, Raman spectra of solid and liq., vibr. anal. 77−81093
N_2O_2, localised mol. orbitals from semiempirical CNDO calcs. 78−62726
$(N_2O)_2$, photo-induced vibr. predissoc. of van der Waals mol. 78−90242
N_2O_3 gas as possible photorecomb. laser medium 77−71981
N_2O_3, localised mol. orbitals from semiempirical CNDO calcs. 78−62726
N_2O_4, as working medium, thermodynamic cycle, approx. model *(Russian)* 77−73464

nitrogen compounds continued
N_2O_4 atmosphere, oxidation of stainless steel, 200 to 700°C, anal. *(Russian)* 77−73377
N_2O_4 atmosphere and γ radiation effects on polyethylene sorption props. *(Russian)* 77−72796
N_2O_4, chemically reactive working fluid for solar gas turbine plant 79−39316
N_2O_4 circular channel hydraulic resistance and heat transfer expts. *(Russian)* 79−14213
N_2O_4 coolant action on stainless steel, TEM study of intergranular corrosion *(Russian)* 78−58357
N_2O_4 corroded annular channels, heat transfer and pressure drop 80−1569
N_2O_4, dissoc. flow in tube, heat transfer and drag 78−71402
N_2O_4, dissoc. laminar gas flow, heat exchange with triangular bundle of rods 77−42930
N_2O_4, dissociated, enthalpy, 310-782K 78−73073
N_2O_4, dissociating, nonsteady flow in steam-generating channel 79−37422
N_2O_4, dissociating, turbulent pipe flow, heat transfer, resistance 78−91026
N_2O_4 dissociating coolant, chemical reaction kinetics in transient regimes *(Russian)* 78−58344
N_2O_4 dissociating coolant, O_2 generation time constant, enthalpy change *(Russian)* 78−58345
N_2O_4 dissociating gas flow in channel, turbulent boundary layer *(Russian)* 79−60067
N_2O_4, dissociating in vertical tube, boiling heat transfer 80−1568
N_2O_4, dissociating system, dynamic sorption of ^{131}I from gas phase *(Russian)* 78−58356
N_2O_4, dissociating turbulent convection on horizontal plate *(Russian)* 80−1587
N_2O_4, dissociation, reaction with H_2O, HNO_3, N_2O_3 *(Russian)* 77−86313
N_2O_4, effect on mech. props. of Cr and Cr-Ni steels and alloys after long-time exposure *(Russian)* 78−48573
N_2O_4 enthalpy measurement calorimeter, other corrosive gases and liquids 77−79097
N_2O_4, evaporation in enclosed containers, N_2 medium, 1.12-4.96 gauge atm. 77−47564
N_2O_4, fission reactor coolant, heat transfer on condensation *(Russian)* 80−57860
N_2O_4 flow in axisymmetric channels, heat transfer calc. *(Russian)* 79−14214
N_2O_4 flowing in axisymmetric channels, mass and heat transfer calcs. 80−1570
N_2O_4, gas phase, chem. relax. times for dissoc. reactions *(Russian)* 77−70288
N_2O_4, He I photoelectron spectrum 77−6845
N_2O_4, He I photoelectron spectrum, new interpretation 78−17713
N_2O_4, heat and mass transfer in turbulent stream in axisymmetric channel *(Russian)* 79−18960
N_2O_4, IR spectra in O_2 matrix, vibr. freqs. 78−23936
N_2O_4, ionis. by mol. orbital method, many-body calc. 79−36512
N_2O_4 liquid *(Russian)* 79−59863
N_2O_4, localised mol. orbitals from semiempirical CNDO calcs. 78−62726
N_2O_4, mol. force consts. and vibr. amplitude, force field study 79−31730
N_2O_4, paramag. shift effects on PMR spectra of electron donating organic compounds *(Russian)* 78−21946
N_2O_4, photoelectron spectrum interpretation 79−22761
N_2O_4, photoelectron spectra, 304 Å 79−59510
N_2O_4, reactive turbulent flow, heat and mass transfer anal. *(Russian)* 77−42932
N_2O_4, reactor coolant, stability in two-phase flow *(Russian)* 80−609
N_2O_4, second ionis. pot. by CI wavefunction 79−31732
N_2O_4, solid, solubility in liquid N_2 at 77.4K 77−32827
N_2O_4, sound dispersion and velocity mol. dissoc. effects *(Russian)* 80−1730
N_2O_4, turbulent dissoc. flow, along heated tubes, heat transfer 80−63225
N_2O_4, UV photodissoc., NO_2* form. and emission, quantum yield 79−66298
N_2O_4, UV photoelectron spectrum, variable temp./fast pumping technique, ionis. pots. 77−30926
N_2O_4, vibr. assignment 79−6940
N_2O_4, viscosity and thermal cond., approx. polynomials *(Russian)* 80−59739
N_2O_4-HNO_3-H_2O dissociating system, surface tension at liquid-vapour boundary *(Russian)* 78−47643
N_2O_4-NO mixtures, attainable superheating temp., depend. on NO conc. *(Russian)* 77−72140
N_2O_4-NO-H_2O, distrib. coeff. for N_2O_4 on liquid-vapour equilib. *(Russian)* 80−55699
N_2O_5, from smouldering discharge at O_3 liq. surface in N_2, thin solid pellicle formation 80−38827
N_2O_5 gaseous, integrated band intensity data, stratospheric detection implications 80−58250
N_2O_5, IR spectra in O_2 matrix, vibr. freqs. 78−23936
N_2O_5, stratospheric abundance upper limit 77−5299
N_2O_5, thermal dissoc. in N_2 79−96294
$N_2O_5+CO_3^-(NO_2^-)(F^-)(Cl^-)(Br^-)(I^-)=NO_3^-+XNO_2$, rate consts. 78−56879
$N_2O_5+H_3O^+$, rate consts. 78−56879
$N_2O_5+NO^+=3NO_2^+$, $N_2O_5+NO_2^+$, rate consts. 78−56879
$N_2O_5+O_2^+=NO_2^++NO_3+O_2$, rate const. 78−56879
$(^{14}NO)_2$ and $(^{15}NO)_2$ solids, Raman spectra at 20K 77−73139
$NO(A^2\Sigma^+, v'=0,1,2)$ lifetimes, $A^2\Sigma^+$-$X^2\Pi$ transition moment, oscill. strengths, internucl. separation depend. 78−82787
$NO(A^2\Sigma^+)$, prod. by near reson. electronic energy transfer, initial rot. state population 79−68304
$NO(B^2\Pi_r)$, form., quenching 79−64038
NOBr, photoabsorption and photodissociation, 190-300 nm 79−50038
NOBr+Br, primary and secondary photochemistry, vibrationally excited NO, IR fluoresc. obs. 80−48030
NO_2Br, formation and IR spectrum 79−98097
NOCN, struct., dipole moment, quadrupole coupling, microwave spectra 78−94238
NOCl laser, for 16 μm range, review *(Rumanian)* 80−87408
NOCl, molecular laser operating in 16 μm region 77−50656

nitrogen compounds continued
NOCl, optically pumped laser, 11-17 μm 78−46581
NOCl, vibr. energy transfer, (001) level activation/deactivation rate consts. meas. 77−79677
NOCl+Cl, primary and secondary photochemistry, vibrationally excited NO, IR fluoresc. obs. 80−48030
NO_2Cl, force fields calc. 78−42241
NO_2Cl, rot. distortion parameters for force consts. determ. in parametric method 79−76401
NO_2Cl, transformation and compliance matrices determ. 77−18898
$NOClBCl_3$, solid, Raman spectroscopy study *(French)* 79−69834
NOF and ONF, ab initio calcs. of geometry and electronic struct. 79−76342
NO_2F, force fields calc. 78−42241
NO_2F, rot. distortion parameters for force consts. determ. in parametric method 79−76401
NO_2F, transformation and compliance matrices determ. 77−18898
NOH, groundstate electronic struct., MRD CI calc., dissoc. energy, isomerisation energy 80−14088
NOH isomerism, low lying electronic states, ab initio MRD-CI calcs. 80−83291
NOH polycryst. radicals, low temp. PMR 80−25220
NOH^+, ab initio pot. surface, and isomerisation barrier of lowest states 79−22622
NOH^+, ab initio SCF and CI comparison of struct. and spectra with HNO^+ 77−26972
NOH^+, vertical spectra, heat of form., ab initio MRD-CI calcs. 79−49934
$NOHSO_4$ identification in stratospheric aerosols, rel. to N oxides pollutants removal 79−39795
$NOHS_2O_7$, identification in stratospheric aerosols, rel. to N oxides pollutants removal 79−39795
NOI, IR matrix isolated spectra, force consts. 79−10111
NO_2I, formation and IR spectrum 79−98097
$NONO^+$, photodissoc. cross sections meas., 3500-8600 Å 79−24763
$NO^+(NO)+SO_2$, cluster form., equilib. const. and rate coeffs., UV irrad. effects 77−60060
$NO(NO_2)+O_3$ reactions in power plant plumes 78−3923
$NO(N_2O)$-SF_6, single-photon absorption reaction chemistry in solid state 77−73454
$NO(N_2O_3)$-SF_6, single-photon absorption reaction chemistry in solid state 77−73454
$NO_2(NO_2^-)$, ionis. pot. and electron affinity, overlapping sphere MS Xα calc. 78−41948
$NO_2(N_2O_4)$ surface decomposition, resonance and spontaneous Raman spectra 80−61144
$NO_3(NO_3^-)$, ionis. pot. and electron affinity, overlapping sphere MS Xα calc. 78−41948
$N_2O(NO_2)$, Penning ionisation and photoelectron spectra 77−83653
$NO(^2\Pi_{3/2}, J=3/2)$ at X-band, high resolution EPR spectra 78−37661
$NO_2(SO_2)^-$, photodestruction 80−63722
$NO_3(SO_2)^-$, photodestruction 80−63722
$NO(X^2\Pi)+Ar(NO)$, lower vibr. states relax. rates meas. 77−65527
$NO(X^2\Pi)+Cd(^1P_1)\rightarrow NO(A^2\Sigma^+, v=0)$ electronic energy transfer react., collisional fluoresc. quenching 77−14548
$NO(X^2\Pi)+Zn(^1P_1)\rightarrow Zn(^1S_0)+NO(A^2\Pi^+, v=0,1)$, near-resonant electronic energy transfer, fluoresc. quenching 77−14549
$NO(X^2\Pi)+Zn(^1P_1)\rightarrow Zn(^1S_0)+NO(A^2\Sigma^+)$, near reson. electronic energy transfer, initial rot. state population 79−68304
$N_2O(X^1\Sigma^+)\rightarrow N_2(^1\Sigma_g^+)+O(^1S)$, photodissoc., exact collinear calcs. 77−30937
NO*+NO, van der Waals mols. in mol. fluoresc., vibr. predissoc. model 78−42120
NO_2*, multiple IR photon fluoresc. excitation and dissoc., electronically excited 80−48050
NO_2* visible emission, formed in N_2O_4 UV-irrad., quantum yield 79−66298
NO_2*+CO→CO_2+NO, laser-stimulated reaction 77−9075
NO_2*+CO→NO+CO_2, laser stimulated reaction, rate const. 78−40044
$(NO_2)_2\rightleftarrows 2NO+O_2$, chemically unstable mixture laminar flow in channel, heat and mass transfer *(Russian)* 77−68707
$(NO_2)_2\rightleftarrows 2NO_2+O_2$, nonequilibrium mixture laminar flow in channel, zone method anal. of heat and mass transfer *(Russian)* 77−72370
$N_2O_4\rightleftarrows 2NO_2$ equilib. system, condensation heat transfer on horizontal tube bundle *(Russian)* 78−46970
$N_2O_4\rightleftarrows 2NO_2$, heat transfer meas. *(Russian)* 77−84128
$N_2O_3\rightleftarrows 2NO_2\rightleftarrows 2NO+O_2$, heat exchange calc. *(Russian)* 77−84127
$N_2O_4\rightleftarrows 2NO_2\rightleftarrows 2NO+O_2$, precipitation of corrosion products in a fractionating column *(Russian)* 80−25707
$N_2O_4\rightleftharpoons 2NO_2$, chem. equilib., struct., statistical mech. calcs. 77−9111
$N_2O_4\rightleftharpoons 2NO_2$, gas mixture turbulent concurrent double pipe heat exchanger equilib. and nonequilib. reaction 78−94856
$N_2O_4\rightleftharpoons 2NO_2\rightleftharpoons 2NO+O_2$ dissociating system with NO added, phase equilibria *(Russian)* 79−19363
$N_2O_4\rightleftharpoons 2NO_2\rightleftharpoons 2NO+O_2$ dissociating system, behaviour with BaO *(Russian)* 79−20363
$N_2O_4\rightleftharpoons 2NO_2\rightleftharpoons 2NO+O_2$, quasi-equilib. and quasi-frozen flows, criteria and calc. formulae *(Russian)* 79−68824
$N_2O_4\rightleftharpoons 2NO_2\rightleftharpoons 2NO+O_2$, working fluid for power-producing thermodynamic cycles 80−13536
$NO_3^-.(HNO_3)_n$ clusters, form. studied by mass spectrometer, thermodynamic functions, sol. struct., 80−95754
$NO^+.H_2O$, photodissoc. cross sections, mass spectrometric determ. 78−1038
$NO^+.H_2O+O\rightarrow NO_2^++H_2O$, rate constant rel. to atm. ion chem. 77−41245
$(NO^+.H_2O)/(NO^+)$ ratio at mesopause, rel. to temp. 79−96849
$NO^+.N_2$ formation rate consts. at low temps. in lower ionosphere 77−60538
$NO^+.N_2$, rate const., enthalpy and bond strength 77−16809
$NO^+.NO$, photodissoc. cross sections, mass spectrometric determ. 78−1038
$NO(a^4\Pi)$ dipole moment, meas. by mol. beam electron impact vibr. excitation 79−72440
$NO(a^4\Pi)$, in Ar(Kr)(ArKr), matrices, multiphonon vibr. relax., time-resolved emission obs. 80−18861
$NO(b^4\Sigma^-)$, electron impact excitation energy, radiative lifetime, quenching in NO 77−79642
$NO^+(v=1,2)+N_2$, vibr. transfer, vibr. absorption coeff. 79−6994
$N_3P_3Br_6$, ^{81}Br NQR, conformation investig. 80−63665
$N_4P_4Br_8$, Br NQR expts. 79−76446

nitrogen compounds continued
$(NPCL_2)_3$, trimer and polymer, polycrystn., resistivity 77−51735
$N_3P_3Cl_6$, ionisation energy and electronic struct., UV photoelectron spectra and Xα calcs. 78−94281
$N_3P_3F_6$, ionis. energies, Xα scatt. wave calcs. 77−42242
$N_4P_4F_8$, ionis. energies, Xα scatt. wave calcs. 77−42242
α-NPO, two-photon fluoresc. 77−30896
$N_3P_3Pr_6$, Br NQR expts. 79−76446
NS, ground ionic state, photoelectron spectra determ. 77−46596
NS, interstellar radio emission theory 78−54031
NS, presence or absence in solar atm., theory 78−69765
NS radical chemiluminescence produced by active $N+S(S_2Cl_2)$, kinetics study 79−39151
NS, spectrum, perturbations in $A^2\Pi_{1/2}$-$X^2\Pi_{1/2}$ transitions, constants of $B'^2\Sigma^+$ state 78−70845
NS, Zeeman effect, relativistic corrections 77−83646
NSCl, force consts. and mean amplitudes of vibr. *(German)* 79−50005
NSF, forbidden transitions, laser optoacoustic spectroscopic obs. 77−61756
NSF, geometry and stability, LCAO-MO SCF calcs. 79−31391
NSF, NSCl, NSBr, force field determ., Redington's method applicability 79−81168
NSF_3, IR spectra, matrix isolated, force const. calc. 78−62802
NSF_3, microwave spectra in vibr. excited states, mol. consts. 79−50009
NSF_3, RF-mm wave double reson. of vibr. excited state 79−50054
N_2SO_3, weakly bound complex, dipole moments, MBER obs. 80−95701
NSi+H, bimolecular exchange reactions, dynamical-statistical method calcs. 80−104435
N_2O, viscosity meas. at low temps. 80−6193
^{14}N, isotropic hyperfine coupling consts. in small radicals 80−52894
$^{14}N^{16}O$, $^{15}N^{16}O$ isotopic species determ. using Zeeman scanning of atomic line, vibr.-rot. line profiles 79−49983
$^{14}N^{16}O$, overtone region IR emission spectra, vibr.-rot. Dunham coeffs. 79−41164
$^{14}N^{16}O$, v=2←0 overtone band IR spectra, Λ doubling, hyperfine struct. 79−41165
$^{14}NH^+(^{15}NH^+)(^{14}ND^+)$, ab initio CI calc. Λ type doubling in $X^2\Pi$ states 78−82714
$Na+N_2O$, Na chemiluminesc., excitation mechanism, appl. chem. laser 77−63916
Na+NO, energy transfer collisions via collision complex 77−83695
Na+NO, total cross sections 79−27064
$NaOH:NO_2^-$, electron tunnelling, pulse radiolysis 80−108722
Ne-NF_3, long pulse UV laser emission in electron beam excited supersonic flow 78−66801
Ne-Xe-NF_3, excited states quenching 79−18406
$NiSi_2$ epitaxial film on (111) Si substrate, interfacial order, backscatter, channelling study 80−65390
No, $C^2\Pi(v=0)$ state, two-photon absorpt. spectra, predissociation 77−79664
No_2 concentrations in stratospheric, experimental investigation *(Russian)* 77−49109
No_2 oxidation of C fibres, modification of struct., props. 78−44237
No_3^--Cl^- soln., inhibition of o-Ps formation 80−1089
O+NO binary reaction, crossed beams, NO_2 chemiluminesc. 78−64843
O+NO+M, rate const., 217-500K 79−52626
O+NO+M→NO_2+M, (M=He, Ne, Ar, Kr), 217-500K, absolute rate consts. 77−16787
O^++NO, charge transfer, reaction rates and cross-section determ. 77−60052
O^++NO, ion speed distrib. effects in flow-drift tubes 77−56219
$O_2+NO(NO_2)$, rate constants determ. as function of relative kinetic energy 80−81292
O_2^++NO→NO_2^++O, photoionis. mass spectra, photoionis. efficiency 77−40537
O_3+NO reaction in turbulent jet 77−62310
$ON^{81}Br$, anharmonic force field from IR and microwave data 78−82809
ONCN, far IR spectra, pure rot. and vibr.-rot. bands 78−82731
ONCN, IR spectra isotope shifts and ab initio calc. for harmonic force field 79−13715
$ON^{35}Cl$, anharmonic force field from IR and microwave data 78−82809
ONF, J transitions, rot. Zeeman effect 80−63707
ONF, vertical electronic spectrum, CI and SCF calcs. 77−75123
ONF_3, vibr. anal. using Green function 77−57962
$O(^3P)$+n-butane(NO(M=Ar)), reaction rate constants using flash photolysis-NO_2 chemiluminesc. method 77−44458
$O(^1S)+N_2O$, quenching rate const. determ. 77−10626
Pb+N_2O, pBo chemiluminescence spectra 77−9087
S-N system, inorganic, electronic struct. obs. by photoemission XPS and UPS, CNDO calcs. 80−78653
SF_6+NO+O_3, laser sensitised reaction, time-resolved NO_2* emission obs. 78−20017
SNF, geometry and stability, LCAO-MO SCF calcs. 79−31391
$SOCl_2$, photoabsorotion and photodissociation, 190-300 nm 79−50038
$Sb(5^4S_{3/2})+NO(O_2)$, rate consts., time-resolved reson. fluoresc. meas. 78−27732
Sc+NO_2, chemiluminesc., nonequilib. product distrib. 80−101014
Si+N_2O, flame chemiluminesc., SiO emission, $A^1\Pi$, $b^3\Pi$ and $a^3\Sigma$ states 77−77767
Si_5-Al-O-N_7, hot pressed, exam. of fracture mechanisms 78−72879
Sn+N_2O, oxidation chemiluminesc., quenching kinetics 79−52672
$Sn+O_2(NO_2)$, chemiluminescence and photon yields 77−29012
Sr-N_2O-CO flame, candidate chem. laser reactions, intracavity dye laser absorpt. meas. 78−63108
Sr-N_2O-CO flame, Sr catalyzed, gain meas., emission band assignment 78−66815
$SrFeO_{3-x}$, NO absorpt., IR spectroscopic study 79−78675
Sr*+N_2O→SrO*+N_2, visible chemiluminescence, absolute cross section and photon yields 78−92463
T_2+NF_3, chem. laser, TF spontaneous emission, Einstein coeffs. determ. 77−58073
Ti-V-C-N, solid solns., quasibinary cross sections 78−23676
$Ti(^5F)+N_2O(O_2)(NO_2)$, chemiluminesc., TiO dissoc. mechanisms, confirmation of $D^0_0(TiO)$ 77−40534
U+NO_2, UN reaction product identification in Ar matrix, vibr. energy distrib. 77−9066
V+$O_2(NO_2)$, oxidation, VO chemiluminesc. 77−9077
Xe:N_2O, photoluminesc. from XeO (^1D) excimers 78−68544
Xe^++NF_3 reaction, XeF^+ form., $Xe^+(^2P_{1/2})$ radiative deactivation 78−27737

NMR line breadth
A-phase, order parameter collective modes, effect on NMR and US attenuation 79−46866
acetic acid-methanol-tetrahydrofuran-d_8, superimposed intermolecular spin exchange reactions, NMR lineshape theory 80−32740
acetone, ^{17}O chemical shift and NMR linewidth meas., self-association equilib. const. determ., mol. reorientations obs. 80−87148
acetonitrile, dissolved in liq. cryst., NMR, ^{13}C, ^{14}N relax. times, temp. depend. 79−94016
adamantane, heteronuclear spin coupling and decoupling dynamics 77−48066
L-alanine, ^{17}O NMR chemical shifts and linewidths, pH dependence 80−80625
alkali chloride aqueous solutions, ^{35}Cl relax. rates of chloride ions 77−88471
amide C-N bond character, metal ion bonding effects 77−6801
aminobenzonitrile, para- and meta-, NQR linewidth, Zeeman effect, mol. config., H bonding, cryst. struct. 77−51986
ammonium hydrogen oxalate hemihydrate, single cryst., DNMR obs., elec. field gradients, reorientation 77−85618
arsonium salts, aq. soln., ^{75}As NMR spectra, mol. correl. time and symm. species 77−69714
asymmetric top molecules, complex polarisabilities, NMR line dipolar broadening 79−54058
AX_3 type spin coupled system, two-position exchange, NMR line shape function 77−90600
benzene, partially ordered solid, NMR line shape, orientational distrib. 78−35048
biased spectral decomposition in glass, ^{11}B, NMR spectroscopy 78−88198
bispenol-A epoxy resin, glass transition temp., effect of absorbed water, PMR line width 79−90766
borate glass, biased spectral decomposition 78−88198
borate glass, of ^{11}B, fast stable analysis technique 78−6585
broadening effects associated with cryst. imperfections, theory 78−35021
9-bromo-meta-carborane, mol. reorientation, ^1H and ^{11}B NMR 77−16185
n-butane, solid, mol. reorientation, PMR 77−8431
d-camphor, high resolution ^{13}C NMR spectra, 275 to 343K 79−56621
carbon tetrabromide, ^{13}C NMR in liq., FCC plastic cryst. and monoclinic cryst. 79−78549
chemical kinetics, line-shape anal. of peaks broadened by hidden exchange partner 79−43554
chemical shift between two sites in rapid exchange limit; Fourier transform method 79−24743
chlorophyll radical cations, NMR, hyperfine coupling 79−8482
cholesteryl decanoate, NMR spectroscopy of blue phase 79−4236
cholesteryl m-fluorobenzoate, NMR spectroscopy of blue phase 79−4236
cholesteryl myristate, cholesterogenic, blue phase, D NMR obs. 80−97151
cholesteryl nonanoate, cholesterogenic, blue phase, D NMR obs. 80−97151
clathrate deuterohydrates, ^1H NMR lineshape of tunnelling methyl group, <5K 78−46370
clathrate hydrates, identification from NMR line shapes 78−27861
computer analysis, iterative, of complex exchange-broadened bandshapes 79−35805
copper formate tetradeuterate, paramag., induced staggered magnetisation 77−12212
coupled multispin systems, simple line approx. anal. 79−75561
coupled systems, A-line intensity, phase, oscill. with time, heteronuclear double reson. spectra 80−34823
cytochrome c, PMR, eight-ring current model heme ring, conformation depend. shifts 80−74185
di-tert-butyl radical, ^1H NMR in organic solvents, press. depend. 79−31546
diamagnetic metal, crit. point of diamag. transition of first kind, and NMR linewidth 77−59469
p-dichlorobenzene, ^{35}Cl NQR line narrowing by nonreson. RF photon dressing 80−63662
1,2-dichloroethane, enclathrated, conform., reorientation, PMR line shape anal. 79−91300
p-dihalobenzenes, apparent NQR spin-spin relax. times obs. 80−54991
diheptyloxyazoxybenzene, smectic-C phase, proton NMR 77−11474
2,5-dihydroxy-p-benzoquinone, proton tautomerism dynamics, ^{13}C NMR obs., CNDO calc. 79−52632
dilute paramagnet, mag. reson. linewidth due to two-particle interaction 77−90012
dimethylacetylene, solid-solid phase transition, NMR meas. 78−6583
dimethylammonium copper chloride bromide, mag. props., pulsed NMR expts. 80−11292
2,6-dimethylbenzoic acid, ^1H chem. shift recovery from combined multiple pulse NMR and sample spinning 80−32738
N,N-dimethylcarbomoylchloride, chem. exchange rate by NMR method, temp. depend. 79−79243
dipolar interaction, reduction by off-resonance phonon avalanche 77−63260
dipolar linewidth in asymmetrically broadened NQR spectra 80−71230
dipole NMR line width red. under magic angle conditions 80−60435
dispersion vs. absorption curve method for distinguishing peak position distrib. from linewidth distrib. 80−4775
double NMR, dipolar broadening in solids 79−61265
dynamic NMR spectroscopy, mechanistic obs. df rearrangements and exchange reactions, review, book contrib. 79−30521
entangled polymer chain solutions, dipolar spin coupling modulation effect obs. on NMR spectra 78−56381
ethane, solid, PMR line shape, band width and second moment, phase transition 77−85584
ethanol, polymorphic forms, mol. motion, NMR obs. 80−88885
exchange broadening in two-site system with unequal populations, limiting eqns. 79−76448
exchange narrowed absorption lineshapes for Heisenberg paramag. 77−69717
exchange-broadened NMR bandshape, improved algorithm 78−91963
fatty carboxylic acids, C_{15} to C_{19}, solid phase, ^1H and ^{13}C NMR spectra 79−95653
ferromagnet, 1- and 2-dimens. Heisenberg systems 77−48064
ferromagnet, microscopic theory of NMR for low conc. case, lineshapes 77−59467
first order spin-spin multiplets, AX⇄BY system, T_1 spin decoupling and chem. exchange 77−71818

NMR line breadth continued
free induction decay, initial behaviour 78−80227
FTNMR, effect of inhomogeneous mag. field on line shape and resolution enhancement 79−63289
gas, effect of static and alternating field inhomogeneities 78−50491
gas, low density, non-Lorentzian NMR spectra, spin rotation 78−94259
Gaussian second derivative lines, modulation broadening calcs. 77−16147
glycine, ^{17}O NMR chemical shifts and linewidths, pH dependence 80−80625
graphite intercalation compound, LiC_6, ^{7}Li NMR *(French)* 78−35050
graphite-DNO_3, intercalation cpd., mol. dynamics 79−28631
graphite-SbF_5 intercalation cpd., carrier density from ^{19}F NMR line shapes 80−25224
haemoglobin, hyperfine-shifted PMR, mag. field and temp. induced line broadening 77−60184
heteroatomic cpds., paramag. reagents for ligand mol. struct. determ. from NMR 79−13741
heteronuclear spin coupling and decoupling dynamics 77−48066
heteronuclear system, line narrowing in many-pulse NMR expts. 80−71200
hexamethylenetetramine, ultraslow tetrahedral jumps, deuteron NMR spin alignment obs. 80−66046
high-resolution multipulse NMR spectrometer 78−58000
high-resolution NMR by double Fourier transform, chem. shift and spin echoes 77−57375
insulator, exchange-coupled, interference effects at finite temp., with anisotropic hyperfine interactions 77−81022
insulators, mag., interference effects due to electronic reson. 77−8435
intermolecular mechanics, T_1 and T_2, by microwave meas., zero- and non-zero field 79−45738
lattice nuclear mag. system simulation by classical mag. moments 77−69713
lecithin-deoxycholate mixed micelles, surface curvature and mobility, PMR study 80−21452
line broadening in nonuniform RF field, interpretation 78−60343
line narrowing, selective population transfer induced 80−31827
line narrowing with large reson. offset, appls. to solids *(German)* 80−7176
lineshape fitting, iterative least-squares method, symm. and mag. equiv. factorisation 77−69715
liquid, undergoing inhomogeneous Poiseuille flow, spin echo signal shape *(Russian)* 80−50225
liquid crystal, lyotropic, free induction decay, Jeener echoes 77−63291
lithium perfluoro-octanoate-water, liquid crystal, ^{19}F multipulse NMR obs. 80−34795
Lorentzian second derivative lines, modulation broadening calcs. 77−16147
lysine, aq. solns., $H^+(D^+)$ exchange rates, ^{17}O NMR linewidths, pH depend. 80−91661
macromolecule, NMR estimation of equilib. consts., intermediate exchange processes effect 80−1094
MBBA-d_8, mol. order and conformation, ^{2}D NMR line shape obs. 77−61771
methacryloyloxyethyleneoxycarbonyloxypropylene, NMR relaxation mechanism *(German)* 78−33527
methanol:chromium acetylacetonate, NMR, degenerate transitions, selective excitation transfer and separated relax. meas. 78−80235
methyl iodide, ^{13}C NMR with coherent proton decoupling, peak-height distortions within spin multiplets 79−31547
methyl piperidines, PMR spin-lattice relax. times and lineshapes, 100-300K 77−81027
methyl-containing mol. solids, proton NMR line shape, methyl group tunnelling 78−6588
molecule, homonuclear dipolar broadening removal using multiple pulse-magic angle spinning probe 78−12735
molecules, indistinguishability of permutations in same NMR mode 78−33524
monovalent ions in aq. metal ion solns., ^{14}N NMR relax. 80−20481
motion of spin between two positions and magnetic relaxation 79−69742
motionally narrowed NMR line shapes in solids 78−76325
multiple pulse NMR of solids, accurate phase adjustment 80−22404
multipulse NMR, nuclear magnetisation relax. *(Russian)* 79−19799
multipulse NMR, relax. processes anal. 80−34798
multipulse NMR line narrowing, appl. to solids and liq. crysts. 78−72424
multipulse NMR line narrowing in solids, thermodynamic theory *(Russian)* 79−19789
myoglobin, hyperfine-shifted PMR, mag. field and temp. induced line broadening 77−60184
naphthalene-d_{8}, in diethylether soln., ^{2}H NMR, mag. field induced alignment effects 79−13740
nematic liq. cryst., PMR line breadth temp. depend. 77−8419
NH_4Cl, PMR free induction decay shape and moments 78−68394
noise reduction filter in resolution enhancement 80−73403
nonequidistant NMR spectrum, spin-spin width suppression by RF pulses *(Russian)* 78−23357
NQR, inhomogeneous line narrowing by RF pulse sequence 80−93206
Nylon 6 and 12 films, drawn, NMR, mol. orientation, motions *(Japanese)* 77−32268
oxide glasses, charact. by magnetic resonance and optical absorption of metallic probe ions *(Japanese)* 79−95640
PAA-d_8, mol. order and conformation, ^{2}D NMR line shape obs. 77−61771
paramagnet, low-dimens., model 78−23356
paramagnetic contribs. calcs. 80−58286
paramagnetic ion nuclei in magnetically conc. solid, theory 80−25238
paramagnetic material effect on chem. shift and relax. times, mol. struct. effect 78−46373
paramagnetic metal ions as structural probes for NMR investigation of inorganic and bioinorganic compounds 78−62828
PEBAP, nematic liq. cryst., PMR line breadth temp. depend. 77−8419
peptides, effect of internal librational motion on ^{13}C NMR relax. times 78−85293
phospholipids, ^{31}p NMR, slow-motional lineshapes for very anisotropic rot. diffusion 80−5644
piperazines, PMR spin-lattice relax. times and lineshapes, 100-300K 77−81027
plastic crystal, anomalous high resoln. of NMR linewidths 77−12218
PMR, delayed Fourier transformation technique for resolution enhancement 80−74181
poly-β-benzyl-L-aspartate, soln., ^{13}C and ^{1}H NMR dynamic study 79−69737
poly-γ-benzyl-L-glutamate, soln., ^{13}C and ^{1}H NMR dynamic study 79−69737
poly-L-alanine, soln., ^{13}C NMR dynamical study 79−69737
polybutadiene, NMR line narrowing *(German)* 78−76341
polycarbonate, amorphous morphology, from NMR obs. of swelling penetrant mol. motion 79−27929
polydimethylsiloxane-bisphenol-A polycarbonate block copolymer, PMR spin diffusion effects 77−66431
polydimethylsiloxane-solvent system, NMR spectrum narrowing, dipolar spin coupling modulation 78−39413
polyethylene, chain end fixing, NMR line shape calcs. *(German)* 78−76322
polyethylene, fibre, phase structure and molecular mobility, broad-line NMR spectroscopy 78−14290
polyethylene, molecular motions, exam. by PMR line shape anal. 79−41982
polyethylene, NMR with rotation through magic angle *(German)* 78−76341
polyethylene terephthalate, mech. props., influence of cryst. arrangement and noncryst. region struct. 78−76707
polyisobutylene, ^{13}C spin-relaxation parameters rel. to effect, mol. wt., temp. 77−40146
polymer, cryst., broadline PMR spectra, math. separation procedure 80−2647
polymer, glassy state, ^{13}C NMR *(German)* 80−93188
polymer-solvent system, NMR spectrum narrowing, dipolar spin coupling modulation 78−39413
polymers, magic angle rotation ^{1}H NMR, appls. 78−43649
polymethacrylic acid aq. solns., PMR spectra 78−27099
polypyromellitimide, low temperature relax., NMR, dielec. and mech. losses 78−71686
polystyrene, plasma produced, struct., NMR 77−25264
polyvinylidene fluoride foil, piezoelectric effect, 100 Hz acoustic and NMR meas. 78−60396
powders, rot. spin-echoes and high resolution NMR 77−43901
powders with spin 1/2 nuclei arranged in isosceles triangular mag. config., shape function 80−2648
proteins, effect of internal librational motion on ^{13}C NMR relax. times 78−85293
proteins, line narrowing, convolution and pulse methods 78−78729
protocatechualdehyde, PMR, 77-427K, OH group rot., struct. 77−30886
proton chemical shifts, combined pulse NMR and magic-angle spinning 80−44934
PVC foil, piezoelectric effect, 100 Hz acoustic and NMR meas. 78−60396
pyrene-d_{10}, in diethylether soln., ^{2}H NMR, mag. field induced alignment effects 79−13740
pyridinium molten salts, $^{1}HNMR$ rel. to transport props. 77−73087
pyrrole, liq. and nonaq. solns., ^{14}N NQR, ^{1}H line shape anal. 78−6598
rare earth rhodium borides, RRh_4B_4, NMR and sp. ht. in supercond. and mag. ordered phases 80−7037
rare-earth vanadates, transferred hyperfine effects, ^{51}V NMR studies 79−82893
relaxation measurements, Markov theory, systems with multiple degrees of freedom 78−46368
RF field effect in system with nonequidistant spectrum 78−10788
ruby, ^{27}Al NMR line width, charact. features of behaviour 79−69734
ruby, ESR and NMR correl. line broadening effect assoc. with external mag. field inhomogeneities 80−50227
slow motional NMR lineshapes for very anisotropic diffusion I=1 nuclei 79−78533
solid, partially ordered, orientational distrib. from NMR and EPR line shapes 78−35048
solid state ^{2}H NMR, magic angle sample spinning to remove quadrupole broadening 79−97410
solid-state NMR, deuteron spin decoupling from protons 79−61266
solid-state NMR lineshapes, method for separating homonuclear and heteronuclear broadening 80−77828
solids, selective spin imaging 80−29629
solution, ^{89}Y spin-spin relax. times, no pH depend. 80−2657
sphingomyelin bilayer systems, monolayer coupling, choline methyl proton line width 78−35807
spin echo, phase-modulated, derivation of pure absorpt. spectra 80−22410
spin echo, rot., in solids, anisotropic interaction recovery 78−68410
spin systems under multiple pulse NMR conditions, chem. shift relax. 80−34808
spin-lattice relax., periodically-irrad. system, master eqn. predictions 78−43664
succinonitrile, plastic and liq., NMR, ^{13}C spin-lattice relax. and ^{14}N linewidth 79−24227
surfaces line broadening, quantum mechanical calc. 80−29639
TCNQ salt, $Qn(TCNQ)_2$, phase transition, paramag. shifts and PMR line width *(Russian)* 77−43892
terephthalic acid polyester in solution, ^{13}C spin relaxation study 79−87327
tetrafluoromethane, bond length and chemical shielding, NMR lineshape anal. of multispin system 80−32741
TGS, proton and deutron NMR anal. of temp. depend. 80−33919
transition metal hydrides, proton diffusion mechanisms, NMR determ. 77−90060
trichlorofluoromethane, ^{19}F spin-rot. tensors, appl. to liq.-phase rot. diffusion 80−43068
trichlorophosphazoperfluoro-1,1-dimethylethane, cryst., ^{19}F NMR and mol. mobility, fluorination influence 80−34809
trigonometric functions, for line broadening and narrowing 78−91925
two spin system in molecular medium, time correl. functions 77−32275
two-dimensional NMR spectra, elimination of dispersion-mode contribs. 80−20508
two-dimensional NMR spectra in phase-sensitive mode 80−20470
two-dimensional resolved spectroscopy, phase separation techniques, rare nuclei 78−19341
Van Vleck compounds, LF dynamics, NMR linewidth, RKKY exchange mechanism role 80−103812
vanadyl triisopropylate, chem. shifts, NMR line widths, temp. and solvent depend. 78−70853
Varytemp NMR for pulse spectrometers, applic. to lineshape determ. 77−2674

NMR line breadth continued
Voigt profile, revised tabulation for solids 77−36139
weakly coupled nuclear systems, theory of NMR line profiles *(Russian)* 77−46577
zeolite inclusion complexes, LiA.$LiNO_3$ and LiX.$LiNO_3$, ^{7}Li NMR motional line narrowing 79−56618
zeolites, type Y, Sc-, Zr-, catalytic activity, NMR, mechanism 79−29405
AgBr:$Na^+(Li^+)$, correlated diffusion of impurities, nuclear spin relax. meas. 80−108094
AgF, heteronuclear spin coupling and decoupling dynamics 77−48066
$(AgI)_x(Ag_2O\ B_2O_3)_{1-x}$, amorphous superionic compound, ^{11}B lineshape and relaxation 80−108107
$AgNa(NO_2)_2$, ^{23}Na elec. field gradient tensor from NMR satellite lines near phase transition 80−71191
Al, acoustic NMR saturation studies 79−73835
Al wires, eddy current effects on NMR 80−2645
Al-Ni system, Knight shift, NMR line widths determ. *(French)* 77−77113
β-AlO_3-(Na,Li)$_2$O, NMR, Raman and IR spectra, and X-ray diffr., heat treatment induced changes 80−107508
Al_2O_3:Fe^{3+}, dynamic nuclear polarisation, correl. ESR and NMR strain-broadening effects 77−48090
β-Al_2O_3-(Na,Li)$_2$O solid electrolyte, Li motion and activation obs. using ^{7}Li NMR 80−108100
β-Al_2O_3-NH_4^+ and β''-Al_2O_3-NH_4^+-H_3O, single cryst. PMR and proton motion 80−108101
β-Al_2O_3-Na_2O, ^{23}Na NQR and two-dimens. diffusion, model analysis 80−108111
β-Al_2O_3-Na_2O, ^{27}Al NMR obs., Na motion and cond. characts. 80−108096
β''-Al_2O_3-Na_2O, absorbed water effect on NMR lineshape and spin-lattice relax. time 80−108098
β-Al_2O_3-Na_2O, anomalous Na behaviour obs. using pulsed and CW NMR 80−108095
As, amorphous and cryst., NQR for tunnelling modes and local struct. order 79−61261
Au-V, dil., ^{51}V CW NMR line width anal., RKKY broadening 78−15033
B hydrides, relaxation time meas., ^{11}B NMR spectroscopy 77−32276
B_4H_{10}, ^{11}B NMR line broadening, B-B coupling 78−62826
B_5H_9, ^{11}B NMR line broadening, B-B coupling 78−62826
B_2O_3, vitreous, struct. and bonding determ., NMR obs. 77−39545
B_2O_3 vitreous and liq., ^{11}B NMR line shape and spin-lattice relax. meas. 77−4575
$Ba(ClO_3)_2.H_2O$, Γ-irrad. defects, ^{35}Cl NQR, 77 and 300K 78−91981
2,4-$C_2B_5H_7$, polyhedral, spin coupled ^{11}B-^{1}H systems, 2-dimens. correl. NMR 80−69166
CO, solid, anisotropy of chem. shift tensor, ^{13}C NMR obs. 77−90054
CS_2, in alkane soln., ^{33}S NMR linewidth for mol. correl. times 79−95661
CS_2, liq., ^{33}S NQR, quadrupole coupling const. from linewidth data 78−91985
CaF_2, ^{19}F NMR, free induction decay, initial behaviour 78−80227
CdSe(Te), chemical shift and linewidth determ. 79−19792
$CeAl_2$, antiferromag. ordering and Kondo behaviour, ^{27}Al NQR study 80−71231
$CePt_3$, ^{195}Pt NMR and susceptibility meas. 77−63299
ClO_3F, ^{19}F NMR line shape temp. depend. and spin-lattice relax. 78−91969
ClO_3F, ^{19}F spin-rot. tensors, appl. to liq.-phase rot. diffusion 80−43068
ClO_xF_y, ^{17}O NMR, chem. shifts, indirect coupling consts. 77−14453
Co complex, Co(III) diamine, ^{13}C NMR, spin-spin coupling const. *(Japanese)* 79−6952
Co, HCP, ferromag., anisotropic hyperfine interactions, NMR expt. 78−43658
$CoSe_2$, bulk mag. susceptibility, anomalous temp. depend., NMR and X-ray diffr. meas 79−87229
^{59}Co NMR line breadth and chemical shift data compilation *(Japanese)* 78−15045
CsAu, semicond. and metallic, NMR line shape, Knight shift, X-ray diffr. study 78−68402
Cu complexes, Cu(I)-P tetrahedral, ^{63}Cu FT-NMR 80−53021
Cu, NMR study on nuclear ordering below 1 μK 80−93187
Cu-Mn, dil. alloy, spin glass, host NMR, spin freezing 77−40138
Cu-Mn, dil. alloy, spin glass, host NMR, spin freezing 77−40139
Cu-Mn, spin glass, ^{63}Cu NMR linewidth and relax. meas. 77−69583
Cu-V, dilute, Knight shift of ^{51}V reson., and host satellite resonances 77−85594
$Cu_x(As_{0.4}Se_{0.6})_{1-x}$, amorphous, ^{77}Se NMR, comp. depend. 78−76329
$CuBr_2$, ^{63}Cu and ^{81}Br NQR line width obs. 80−50219
CuF_2, ^{63}Cu NQR meas. 80−50219
$CuM_2X_4.2D_2O$, MX=alkali or ammonium halide, quadrupolar interaction, 4-300K, reorientation 79−73848
D_2, solid, quadrupolar glass ordering NMR adsorption line shapes 80−7178
D_2O, $H^+(D^+)$ exchange rates, ^{17}O NMR linewidths, pH depend. 80−91661
$Dy_{1-x}Gd_xAl_2$, ordered alloys, hyperfine field, anomalous con. depend. NMR 80−75868
Fe:^{95}Nb NMR 77−59482
$FeBr_2$:Mn^{2+}, layered antiferromag., infinity mode NMR study 79−38390
Gd_2Co, amorphous ferromag. obtained by splat cooling, local and bulk mag. props. 79−1685
H_2, solid, enhanced quantum diffusion, below 0.3K 79−90845
H_2, solid, NMR, pulsed, linewidth transition, T_1, low ortho conc. 78−43667
p-H_2, solid, NMR lineshape due to unpaired o-H_2 mols. 79−47341
HCl and $(HCl)_2$, matrix isolated, pulsed NMR 79−22730
HIO_3, cryst., ^{1}H NMR, −165 to 25°C 79−73828
HIO_3, PMR spectra, homonuclear and heteronuclear broadening separation 80−77828
$H_{0.36}MoO_3$ and $H_{1.71}MoO_3$ bronzes, NMR relax. obs. at 77<T<450K, H diffusion 80−108089
$H_{1.6}MoO_3$ bronze, proton shift tensors PMR meas. 80−71202
HN_4^+, in crystalline cpds., tunnelling, PMR, generalised line shape, theory 79−73827
H_2O, $H^+(D^+)$ exchange rates, ^{17}O NMR linewidths, pH depend. 80−91661

NMR line breadth continued
$HTaWO_6$, and $HTaWO_6.H_2O$ defect pyrochlores, NMR study of proton motion 79−82889
^{3}He, adsorbed film on Grafoil, NMR, intermediate and near-monolayer coverages 79−46878
^{3}He, B-phase, superfluid, orientational electric field effect 79−46868
^{3}He monolayer, quantum tunnelling 77−39720
^{3}He, optically oriented nuclei, in two-chamber cell, NMR linewidth obs. 78−17591
^{3}He, superfluid, hydrodynamic parameters and correlation functions 79−82406
^{3}He, superfluid A-phase, effect of order-parameter collective modes on NMR and US attenuation 79−51344
^{3}He, superfluid A-phase, have persistent currents been obs.? 80−10731
^{3}He, superfluid A-phase, slab in mag. field, deformed textures 77−39718
^{3}He, superfluid A-phase, spin relax. and zero sound attenuation at low temp. 80−107595
^{3}He, superfluid B phase, textural singularities, NMR analysis 77−89608
^{3}He, superfluid B-phase, microscopic evaluation of transport parameters 79−51354
^{4}He:^{3}He, solid spin diffusion coeff. and T_2, impuritons, temp. depend. 78−34675
Hg, liq., nucl. spin relax. and quadrupolar relax. mech. 78−64292
HgSe(Te), chemical shift and linewidth determ. 79−19792
^{201}Hg, NMR line shape, effect of static and alternating field inhomogeneities 78−50491
$HoVO_4$, NMR, parameters in nuclear Hamiltonian 78−72422
IF_6, NMR and NQR of ^{127}I and ^{19}F, solid-solid transitions and mol. motions 79−99784
KB_3H_8, NMR study of proton and boron dynamics 80−71210
$KClO_3$, Γ-irrad. defects, ^{35}Cl NQR, 77 and 300K 78−91981
$KCoF_3$, Co^{2+} spin-lattice relax. narrowing of ^{19}F NMR 77−85611
KH_2PO_4, paraelectric, dynamic central peak depend. on deuterium content 79−65752
$KH_3(SeO_3)_2$, ferroelastic, central peak in local proton fluctuation spectrum 78−23363
$KMnF_3$, temp. depend. of NMR linewidth of ^{19}F in paramag. region 78−60346
$K_2Pt(CN)_4Br_{0.3}3.2H_2O$, linear cond., ^{195}Pt NMR evidence of low lying non-linear excitation 80−44933
$K_2Pt(CN)_4Br_{0.30}.3H_2O$, dynamic ^{195}Pt NMR meas. below metal-insulator transition 80−34810
K_2SiO_3 aqueous soln., ^{29}Si NMR expts. 78−15051
$KniF_3$, antiferromagnetic, field-induced domain reorientation, NMR obs. 79−82816
^{138,139}La, Fourier transform NMR 80−57354
$La_{1-x}Gd_xAg$, antiferromagnet, spin echo NMR anal. 80−15821
$LaNi_5$, Pauli paramagnet, adsorption of H, proton and ^{139}La NMR 79−78535
$LaNi_5$-H, with small Cr additions, NMR parameters *(Russian)* 80−29637
$LaNi_5H_{6.6}$, $LaNi_5H_{6.2}$, H diffusion NMR spectra *(Russian)* 78−2287
$LaPt_3$, ^{195}Pt NMR and susceptibility meas. 77−63299
$LaVO_4$, dimorphic, NMR of ^{51}V and ^{139}La 77−63310
Li wire, NMR line shape, eddy current effect in presence of self-diffusion 80−54955
Li_5AlO_4, NMR relaxation by paramag. impurities 79−42866
β-LiAlSiO$_4$, superionic cond., ionic cond. and NMR line narrowing 79−42306
LiCd intermetallic cpd., temp. depend. 80−75537
$LiCuCl_3$-$2H_2O$, ^{7}Li NMR lineshape 77−48061
LiH, solid, anion and cation diffusion, NMR relax. and linewidth obs., Schottky disorder 80−15815
$LiIO_3$, cross relax. in two-spin system, inhomog. broadened line 78−88218
Li_3N, diffusion processes and struct. NMR study 80−108090
Li_3N layer structure with fast ion cond., ^{6}Li NMR obs. of diffusion 80−108102
Li_2O-B_2O_3 glasses, low Li_2O content, ^{7}Li NMR study 80−84657
LiOH, NMR study, motional narrowing 79−42863
$Li_2S(O)$, cation diffusion NMR investigation up to 800°C 80−108092
$Li_2Ti_3O_7$, superionic cond., ionic cond. and NMR line narrowing 79−42306
$LiTmF_4$, strongly isotropic Van Vleck paramag., nucl. spin interaction *(Russian)* 80−34792
$^7Li_2O$, β-radiation detected NMR of ^{8}Li obs., double freq. irradiation, ^{7,8}Li hyperfine struct. anomaly 78−91994
$^7Li_2S$, β-radiation detected NMR of ^{8}Li obs. double freq. irradiation, ^{7,8}Li hyperfine struct. anomaly 78−91994
$LuCrO_3$:Er^{3+}, doping effect on ^{53}Cr NMR in domain walls 80−71219
Mn II complex with amino acids and peptides in D_2O, NMR line widening 77−56328
Mn^{2+} compounds, strongly exchange coupled, solid and liq. states, 300-1450K 77−73077
Mo, nuclear indirect interaction, NMR line shape anal. 78−52360
$MoO_{4-n}Sn^{2-}$, (n=0-4), ^{17}O(^{33}S)(^{95}Mo)(^{97}Mo) NMR investig. 80−53022
N_2, solid, anisotropy of chem. shift tnesor, ^{15}N NMR obs. 77−90053
ND_4^+ ion, tunnelling, deuteron NMR lineshape computations, first order quadrupolar interactions 79−15362
ND_4^+ ions, rapidly reorienting deuteron NMR lineshape 79−19800
NH_4 Br single cryst., low temp. PMR lineshapes of tunnelling NH_4^+ ions 80−25223
NH_4^+ ions undergoing slow tunnelling rotations, proton NMR line shapes 79−90576
NH_4^+, NMR absorpt. lineshape rel. to ion reorientation 77−48074
NH_4^+, NMR line shapes at low temp., composite tunnelling, reorientation 78−48054
$NH_4Cl(Br)(I)$, NMR under high press. 78−84485
$NH_4H_2AsO_4$, paraelec. phase, ^{75}As NMR linewidth, near transition temp. 77−36184
NH_4HF_2, powder, proton and fluorine 2nd moments meas., 77-395K 80−34803
$(NH_4)_2HPO_4$, NH_4^+ motions, PMR relax. times obs., 77-430K, struct. transition 77−85599
NH_4LiSO_4, ferroelec., PMR line shape and spin-lattice relax. 78−88205
NH_4ReO_4, PMR, NH_4^+ tunnelling, ground torsional level struct. 78−27097
$(NH_4)_2TiF_6$, ^{1}H-^{19}F coupled NMR, line shapes, spin-lattice relax. 79−73839

NMR line breadth continued
$NaAsO_2$ aq. solns., O exchange between $AsO_3(OH_2)^-$ and water 78−92459
NaCl, electric field gradients near dislocations, resulting NMR lineshapes 80−75225
$NaClO_3$, Γ-irrad. defects, ^{35}Cl NQR, 77 and 300K 78−91981
$NaNO_2$, ^{23}Na elec. field gradient tensor from NMR satellite lines near phase transition 80−71191
$NaNO_3$, double quantum nuclear magnetic resonance of ^{23}Na by double resonance, line shape 80−75886
$Na_2S(O)$, cation diffusion NMR investigation up to 800°C 80−108092
Na_2SiO_3 aqueous soln., ^{29}Si NMR expts. 78−15051
Nb-Pt, A15- and δ-phases, Knight shift of ^{195}Pt meas. 78−19350
NbD, orthorhombic β phase, ^{93}Nb Knight shift and quadrupole coupling parameters 78−19352
NbH, orthorhombic β phase, ^{93}Nb Knight shift and quadrupole coupling parameters 78−19352
$NbSe_2$ (2H), CDW amplitudes determ. by ^{77}Se NMR 77−77116
$Nb_{1-x}V_xH_x$, interaction between interstitial H and V, NMR meas. 77−59471
Ni-P alloy, amorphous, NMR expts. and interpretation 79−8060
Ni-Pd-P, Ni-Pt-P, amorphous and electronic structs., NMR Knight shifts and linewidths meas. 78−68400
$Ni(CN)_2$-dodecylamine, lamellar paraffinic system, phase transitions, wide-line NMR obs. *(French)* 80−44929
NiPB amorphous alloys, ^{31}P and ^{11}B NMR near paramag.-ferromag. transition 79−33558
O, metastable ^5S-state, optical pumping 80−32678
^{17}O NMR, proton decoupling 78−2752
^{17}O nuclear quadrupole double resonance spectroscopy, line shapes and examples 80−31820
P, amorphous, NMR studies 79−69740
P+Nb, dil. alloy, NMR obs. of ^{93}Nb 80−71203
PF_3Br_2, spin systems under multiple pulse NMR conditions, chem. shift relax. 80−34808
PbF_2, ^{19}F NMR, free induction decay, initial behaviour 78−80227
PbF_2:Mn, mag. tagging of ion diffusion, ^{19}F NMR meas. 80−108106
PbF_2:Mn, NMR relaxation by paramag. impurities 79−42866
PbF_2:Mn^{2+}, NMR linewidth with mag. tagging for superionic cond. parameters determ. 77−81021
$Pb(NO_3)_2$, ^{207}Pb NMR linewidth, angular depend. due to ^{14}N-^{207}Pb direct dipole-dipole interaction 80−11280
$Pb(NO_3)_2$, nucl. mag. shielding tensors of $^{207}Pb^{2+}$, NMR obs. 80−44939
PbSe(Te), chemical shift and linewidth determ. 79−19792
PdF_2, motionally narrowed NMR line shapes, free-induction decay meas. 78−68406
PdNb, dilute, NMR obs. of ^{93}Nb 80−71203
$PrCu_4$ and $PrCu_5$, Knight shift, mag. susceptibilities 79−95570
$PrNi_5$, LF dynamics and ^{141}Pr thermal relax., coupling parameter and RKKY exchange mechanism 80−103812
$PrNi_5$, metallic Van Vleck paramag., nucl. interactions, NMR meas. 80−44953
$PrNi_5$, nucl. cooling agent, relax. and exchange, EPR and NMR study 80−25237
$PrPt_3$, ^{195}Pt NMR and susceptibility meas. 77−63299
PtV, dil. alloys, NMR obs. of ^{51}V 80−71203
RbAu, NMR line shape, Knight shift, X-ray diffr. study, struct. props. 78−68402
$Rb_2CuCl_4.2H_2O$, and isomorphs fine struct. on NMR lines due to indirect nuclear spin-spin coupling 79−61244
$RbMnF_3$, antiferromag., temp. depend. of NMR linewidth 77−63292
$RbMnF_3$, Heisenberg antiferromagnet, paramag. region, NMR, spin pair correl. 78−15032
Rb_2ZnBr_4, incommensurate phase, ^{87}Rb NMR lineshape 80−93191
Rb_2ZnCl_4, spin-lattice relax. in incommensurable phase, phason and amplitudon excitations 80−50213
SF_6, solid, NMR line shape and relax. 77−51978
Si:P, electronic states, NMR of metallic and intermediate samples 79−4511
SiH_4, NMR linewidths and relax. times at 6.7 to 124K 77−85602
SiO_2:Co(II), adsorption of H_2O, coord. lifetime, surface effect, NMR obs. 80−34299
SmB_6, intermediate valence, ^{11}B NMR study 80−93193
$SnBr_2$, ^{81}Br NQR line width obs. 80−50219
SnF_2, second order $\beta \rightleftarrows \gamma$ transition, neutron diffr. and NMR obs. 80−107095
^{119}Sn NMR by pulse Fourier transform, T_1, T_2 and chem. shifts 77−55715
$Sr(NH_3)_6$, PMR linewidth, proton tunnelling and NH_3 rot., rapid NH_3 diffusion 78−35045
$SrO-B_2O_3$, ^{11}B NMR lineshape, BO_3^{-3} triangle, perfect trigonal symm. *(Korean)* 78−19367
Ta_6SH_x, H locations and motions, PMR linewidth meas. 77−77115
$TaSe_2$ (2H), CDW amplitudes determ. by ^{77}Se NMR 77−77116
$TaSe_2$ (2H), CDW and discommensurations, ^{77}Se NMR study 80−88883
^{181}Ta nuclear acoustic reson. line shapes, quadrupole exchange contrib. 79−61242
Th_4H_{15}, NMR investig. of proton environment and motion 77−48077
$TiH_{1.45}$, PMR study of spin correl. and saturation effects 77−59477
Tl complex of lasalocid (X-537A), ^{205}Tl NMR study 80−58288
U complex, tetrakis(dipivaloylmethanato)uranium IV, in CS_2 soln., ^1H NMR, intramol. rearrangement 79−19784
$UNi_{5-5x}Cu_{5x}$, NMR and press. effects 80−25230
V_2O_5, quadrupole broadening in ^{51}V NMR spectrum 80−20469
W, acoustic NMR line shape, effect of demagnetisation 79−95654
W, with H adatoms, PMR meas. of adsorption state, surface migration 78−10275
WF_6, effect of high hydrostatic press. in reorientation and internal motion, ^{19}F NMR spectra 79−15364
^{89}Y spin-spin relaxation times, pH depend. 80−66059
$ZnBr_2$, ^{81}Br NQR line width obs. 80−50219
ZnO, accumulation layer, ESR and NMR studies of adsorbed H_2 *(Japanese)* 80−50186
ZnS, ^{67}Zn and ^{33}S nuclear magnetic shielding, chemical shifts and linewidths 80−60434
ZnSe, ^{67}Zn nuclear magnetic shielding, chemical shifts and linewidths 80−60434
ZnSe(Te), chemical shift and linewidth determ. 79−19792
ZnTe, ^{67}Zn nuclear magnetic shielding, chemical shifts and linewidths 80−60434

nobelium
No entries

nobelium compounds
NoH^+, YbH_2, relativistic (non-relativistic) HF one-centre expansion calcs. 80−52908

noble gases *see inert gases*

noctilucent clouds *see clouds*

noise
see also acoustic noise; atmospherics; electron device noise; interference; random noise; roundoff errors; white noise
AC voltmeter, ambiguity in equivalence noise bandwidth approximation 78−4662
aerodynamic noise, generation by jets and boundary layers *(French)* 79−81867
aerodynamic noise prediction, acoustic dipole model, effect of motion 77−80148
aerodynamically generated *(French)* 79−77090
angiography visual perception limits 78−73231
arc discharge, low pressure, electrical noise in longitudinal mag. field *(Russian)* 79−10730
at-power reactor noise, second-order coherent functions 78−94070
atmospheric radio noise field strengths prediction for Indian subcontinent 79−84578
atmospheric radio noise vars. at Ping-Cheng, Taiwan 77−45246
atomic absorpt. flame spectrometry, noise level meas., single and double beam instrum. comparison 80−76584
automated measurement of noisy voltages with preset confidence level 77−37906
avalanche noise theory 79−24043
bidirectional laser amplifiers, amplified spontaneous emission intensity fluctuations 80−37988
bilinearly distorted image linear restoration using Wiener filters 80−83557
binary image in noise, detection 79−36848
biochemical model, phase transition induced by external noise 79−17377
biological evoked potentials, single trial, S/N ratio and response variability 78−61159
biomagnetic measurement facility installation in hospital environment, design criteria and procedure 80−104707
biomedical metal microelectrodes, noise characts. *(Japanese)* 80−3846
biomembrane flexural fluctuations and non-equilib. noise 80−76712
biomembranes, low noise amplification of voltage and current fluctuations 78−44741
birefringence modulator devices for sensitive polarisation determ. 78−8437
black-body radiation field interaction with photoconductor, noise, Langevin method 78−30950
BWR, neutron noise field, two-group diffusion theory 80−18461
BWR, noise anal. model 78−50237
BWR, noise sources of neutron flux, coherence anal. 77−88199
BWR power fluctuations, noise source estimation by autoregression 78−78476
C-CD imagers, evaluation techniques 77−83990
cardiac ejection fraction determ. from left ventricular time-activity curves 77−40741
cavitating orifice under reattached flow conditions, noise and vibration characteristics 80−83829
cavity flow, broadband noise generation, vortex model 77−75900
chemisorption kinetics, determ. from substrate current fluctuations 80−84383
chromatography, correlation type, noise sources eval. and practical considerations 80−40771
coded aperture γ-ray imaging, multiplex noise *(French)* 77−90887
coded aperture imaging, predicted performance of uniformly redundant arrays 79−18351
coded aperture imaging, signal to quantum noise ratio 78−37122
coherent line-frequency noise in evoked pot. recordings, cancellation 80−98161
colorimetric system chromaticity fluctuations anal. *(Russian)* 80−42249
colour film archival storage, white light processing technique 80−99637
coloured noise induced transitions, results for external dichotomous Markovian noise 79−58638
complex system characteristic derivative meas. by input deep modulation *(Russian)* 78−45588
computed tomographic reconstruction, detective quantum efficiency in detection of small objects 80−46046
computed tomography image second-order statistics, information and artifacts 80−46040
computerised tomography, detectability in CT images 80−3806
computerised tomography, dual energy scanning, noise considerations 80−3804
computerised tomography, noise and dose comparison, conventional and energy selective systems 79−66540
computerised tomography, reconstruction noise rel. to detectability 78−69213
computerised tomography scanners, image noise and smoothing 78−85368
computerised tomography scanners, smoothing and image noise 78−69190
computerised tomography scanners, survey of noise, dose and contrast detectability and resolution 80−104750
computerised X-ray tomography, noise power spectrum 78−53492
cone ionic channel closure, turtle 78−15830
cosmic radio noise absorpt. events meas. on riometers, due to backscatt. by E-region irregularities 77−25831
cross-modulation of radio cosmic noise in ionospheric propag. 77−70936
current noise parameters in embryonic heart cell aggregates 80−21459
data processing by coherent light, photographic noise *(Italian)* 78−22088
DC flux flow voltage and flux flow noise power spectrum local primary interactions 77−72953
deconvolution of high energy edge of noise distorted backscatt. spectra 79−56903
diagnostic method based on distorted signal 77−41540
discontinuous metal films, electrical noise, high temp. behaviour 80−54807
display design, visual psychophysics appl. 78−65017
displays, speckle noise min. detectable contrast 77−19411
dissipative steady state, stability 79−9187
distribution function peaks generated by noise 78−93611

noise continued
dominant noise process slope intersections, time/frequency-domain conversion 79−54107
dye laser, mode-locked, synchronously pumped, pulse-width stabilization 80−83622
dye laser, superluminescent source of optical noise for nonlinear optics *(Russian)* 78−79033
ECG, QRS detection accuracy rel. to anal. of HF components 80−17158
ECG, surface potential distributions, equiv. dipole recovery in presence of noise 79−70671
ECG telephone transmission, analogue and digital, errors and noise 80−94398
electrical noise thermometer, novel circuit 78−54364
electro-optical system image evaluation, subjective effects of electronic and turbulent noise 78−65023
electrocardiogram baseline noise estimation and removal using cubic splines and state space computation techniques 78−11755
electrocrystallisation noise, phenomenological model 78−51845
electron micrograph, 500 kV, atomic resolution, computer image processing 80−100149
electron micrograph image reconstruction, 3-dimens., electron noise effects 77−13829
electron micrographs, noisy, phase retrieval algorithms for semi-weak objects 78−78047
electron microscopy, correlation analysis of radiation damage 80−100282
electronic speckle pattern interferometry, optimal signal processing 78−16837
electrophotographic images, electrophoretically developed, applicability of Siedentopf's law 79−45881
electrophotography, noise perception and level of graininess 80−62753
electrostatic noise at solar wind plasma freq. beyond Earth's bow shock, mag. field-shock connection 79−70939
EM particle simulation codes, initial noise, quiet start 78−1883
EM propagation in multilayered struct., noise calculations by flow graph anal. 78−22069
emission CT system, expt. meas. of impulse response and noise 80−56182
exhaust jet, swirling, noise and flow characts. obs. 77−75950
exposure effect on human body *(Japanese)* 77−40709
external noise effect on transition to turbulent convection 80−96263
eye, human, detective quantum efficiency 78−56976
field scatt. by large cylinder of finite length *(Russian)* 78−55284
film grain multiplicative noise anal. 78−58932
film-grain noise degraded image estimation 78−54479
flaw detection system, noise immunity 80−104385
flaw-detection apparatus, noise immunity, sounding signal freq. modulation 80−89441
flicker, nerve membrane model 77−29125
fluctuation dissipation theorem for excess noise 78−70059
Fourier spectroscopy, S/N ratio 78−32885
Fourier transform spectrometer, SNR enhancement by elec. filter compensation of slide velocity errors 80−95151
Fourier transform spectrometry, broad band absorpt., noise levels 77−45901
fringe mode fluorescence velocimetry, organic dye appl. 77−39380
gallbladder images obtained by radiographic magnification technique 78−69186
gamma-Lorentzian intensity fluctuations, integrated, statistics 80−102685
gas lasers, low frequency noise 80−69364
gravitational wave noise, from spontaneous prod. of gravitons, energy density distrib. *(Russian)* 79−12551
ground thermal radio emission, effects on meas. of galactic radio background linear polarisation 77−2500
hair cells of organ of Corti, thermal noise 78−15845
heat conduction eqn., Crank-Nicolson noise control 77−75769
Helmholtz resonator as optoacoustic detector 80−31896
heterodyne optical radar S/N ratio in atmospheric turbulence 80−106558
HF range, noise intensity distrib., empirical laws approx. 77−9603
high-speed optical systems at 0.85 μm, modal noise and optical feedback 80−87323
hollow cathode tubes noise levels for at. absorpt. spectroscopy, pulsed *(Russian)* 77−71385
hologram, volume phase, signal, distortion noise 77−79782
hologram memory, DATA pattern construct., SNR 77−79771
holograms recorded using time-dependent reference wave, S/N ratio, energy characts. 80−32935
holographic correlator, noise sources, accuracy improvement 77−23636
holographic reversal of path of ray through nonuniform phase medium, S/N ratio 77−31075
image local segmentation, statistical segmentation algorithm construction 79−55074
image restoration by Wiener filtering, signal dependent noise 77−88645
image restoration degraded by multiplicative noise, optimum spatial filter 77−10857
imagery, 2-D sampled, aliasing and blurring effects 80−99635
immunity of optical signal reception with unstable modulator characts. 78−46690
inertial seismographs, sensitivity and dynamic range 79−39910
instrumental, of radiation flaw detector, optimal relative sensitivity 77−90554
intensity correlations in presence of additive background noise 79−27167
interferometry, noise reduction by averaging over optical path 77−18080
ion-cyclotron noise in topside ionosphere 80−101470
ion-selective membrane, flicker noise and turbulent convection in depleted layer 78−48692
i.r. imaging, NETD calc., radiation slide rule 77−124
IR noise caused by turbulent flows, IR detector obs. 79−31799
IR spectroscopy, computerised, noise props. 80−86466
ISR, longitudinal bunch dilution due to RF noise 77−83260
Josephson junction, pumped, noise down-conversion 79−56432
Josephson junctions, series-connected, noise characts. 77−66229
Josephson parametric amplifiers, gain-dependent noise temp. 80−84552
kinetic systems, differentiation between equilib. and nonequilib. systems 78−44439
Korteweg de Vries soliton, collapse into weak noise shelf 78−57792
laser, multimode, containing saturable absorbers, bistable operation 80−91862

noise continued
laser Doppler anemometry, S/N, detector influence *(German)* 77−19651
laser Doppler velocimeter, output data anal., noise rejection 77−39378
laser light scattering technique for turbulent mixing meas. 77−11285
laser single transverse mode radiation, spatial coherence 77−14733
laser tracker, target induced pointing noise 78−5519
laser with saturable absorber, correlation function, near threshold 79−27266
level crossing time interval fluctuations 79−21534
LF fluctuation, dissipation and relaxation properties, universality 80−84687
LF noise induced in dipole antenna in ionospheric plasma 79−80072
lidar for atmospheric multiple backscatt. and depolarisation obs. 78−36292
light flash envelope isolation from fluctuating background 77−37993
lipid bilayer, hydrophobic ion current noise, autocorrel. anal. 80−30676
LMFBR PHENIX vibration-induced neutron noise obs. 79−13453
low temperature NMR and SQUIDs, low-noise circuitry 78−4672
magnetic brush xerographic development, image noise 79−17526
magnetic modulator operating near Curie point temp., equivalent input noise study 77−74462
magnetometer, induction type, for biomag. fields *(German)* 79−88207
magnetosphere noise spectrum, influence of CW whistler injection 77−82087
magnetotelluric data, signal/noise ratio enhancement 77−53227
mammographic screen-film systems, comparison of laboratory and clinical evaluations 78−69187
mammography, detective quantum efficiency anal. of electrostatic imaging and screen-film imaging 80−41232
mammography, utility of modelling 78−69188
marginal oscillator optimised for RF size effect meas., noise anal. 77−26377
measurement system noise spectra determ., simultaneous eqns. soln. method 78−57354
mechanical light modulator, harmonic anal. of noise spectrum 78−1362
medical imaging systems, information capacity considerations 80−98090
metal film, discontinuous, elec. cond. and current noise mechanism, theory 78−56244
metals, resistance fluctuation spectroscopy, power spectrum of density fluctuations 79−65428
Michelson interferometer, active noise compensation *(Russian)* 78−12751
Michelson laser interferometers, noise limitations 80−82808
microbalance system, detection of minimum weight difference *(Japanese)* 79−26032
microcalorimeters, conductive, limiting potentialities, anal. 80−17942
modal, in fibre optic systems, suppression by dithering laser's operating point 79−94357
modal noise in multimode optical fibre systems 79−46083
modulation radiometer, limiting pulse noise *(Russian)* 77−67497
multilayer semiconductor structure, current noise 80−20302
muscle cells in tissue culture, acetylcholine-induced current fluctuations 77−29119
near-space radio noise environment characteristics and sources 78−89034
nerve membrane permeability changes, fluctuation anal. 78−11636
neuron, stochastic electronic model 77−48775
neutron counter, scintillation, photomultiplier noise characteristics 80−74077
neutron noise, space-depend., induced by vibr. absorber 77−74900
neutron noise as information carrier for early detection of fuel rod malfunction 77−14242
neutronic noise, relations with coolant temp. fluctuation and control rod vibr. at KUR 78−58327
NMR, Fourier transform, small signals meas. in presence of intense peaks 79−93196
NMR meas. at ultra-low tapes, S/N ratio, appl. to thermometry 80−73400
NMR spectroscopy, Fourier, S/N ratio optimisation, influence of receiver circuit and digital processing *(Czech)* 79−17461
NMR wideband detectors, R-LC and autodyne types, performance comparison 77−74473
nonlinear holography, multiple-reference-beam, intermodulation background noise suppression appl. 80−99674
nonlinear network noise anal., algorithm *(German)* 77−88997
in nonlinear optics 79−23015
nonlinear systems, white and coloured external noise and transition phenomena 78−45569
nuclear medicine images, controllable parameters affecting number of false positives and negatives 78−69191
nuclear reactor, HFIR, dimensionality reduction of noise signatures, improved automated noise anal. 77−6499
nuclear reactor, noise experiments with delayed neutrons, general theory 77−54316
nuclear reactor anal. using noise techiques, polarity correlations 77−14219
nuclear reactor behaviour unattended surveillance system 78−29621
nuclear reactor core, VVEH type, neutron noise, diagnostic method of mech. vibrs. *(Czech)* 77−3120
nuclear reactor core reactivity and space-domain noise effects of randomly dispersed materials 78−94071
nuclear reactor noise, nonMarkovian formulation, hidden state-variables 77−54281
nuclear reactor noise analysis, irreversible circulation parameter 78−94069
nuclear reactor noise analysis, time series modelling methods, comparative eval. *(Japanese)* 80−13552
nuclear reactor noise theory, adjoint space applic. 78−13202
nuclear reactor noise theory, fluctuation coarse-graining and normality preservation 78−94068
nuclear reactors, coupled-core, irreversible circulation of fluctuation 80−27700
nuclear spectrometry, detector signal and noise parallel meas. 77−61667
nucleic acids, discontinuous mag. field effects, room temp. superconductivity 79−62195
optical bistable memory switching in presence of external noise 79−59747
optical bistable system, noise transform. 79−59746
optical communication systems, nonlinear distortions and noise due to fibre connectors 80−96001

noise continued
optical communication using two-photon laser, optimum control of quantum noise 78−71049
optical correlation detection, optimization by prewhitening 80−95802
optical fibre attenuation meas. by backscattering method, effect of noise 80−102824
optical fibres, multimode, freq. depend. of modal noise, speckle theory 80−102817
optical fibres, step-index, modal-noise probability distrib. meas. and anal. 80−99859
optical films communication systems, low noise regeneration using optical repeaters 78−66920
optical goniometer accuracy effect of atm. turbulence 78−55461
optical heterodyne line-scan imagery, speckle noise model 79−50337
optical image processing, noise fluctuations and coherence 78−66771
optical image processing by spatial filtering, noise problems 78−37817
optical imager, linearly degraded, iterative restoration 80−95807
optical images, linearly degraded, iterative restoration, reblurring procedure 80−99640
optical noise and temporal coherence 80−102611
optical noise filter with two aperture stops, numerical analysis *(Japanese)* 77−14812
optical noise reduction, space appls. 78−59153
optical pulsed signals, time position accuracy determ. for correlated noise types 78−12761
optical radar, S/N ratio statistics 78−17866
optical receiver noise analysis, time-domain impulse response technique 77−68280
optical resolution, S/N ratio and meas. precision, revised numerical results 80−95806
optical resolution, S/N ratio and meas. precision 79−59643
optical signal processor, 2-dimens., high accuracy 78−46532
optical systems, noisy image restoration 78−63020
optical velocimeters, S/N ratio and scatt. power, detection angle effect 77−42936
optical waveguides, multichannel, cross-talk noise anal. 80−91922
optimal estimation in signal-dependent noise 79−41344
optomechanical scanner, noise analysis 80−47090
OTF synthesis, pupil function replication 79−27182
parametric generation from quantum noise, depend. on intermodal correlations 79−36958
particle flux, due to reduction and multiplication processes 79−21672
pattern selection in non-equilib. processes, marginal stability theory, eutectic solidification model 80−60852
periodic grating oscillator performance 77−39190
peripheral auditory system, anal., noise appls. 78−80888
Permalloy, oxidised film, magnetic noise, low temp. depression *(Russian)* 79−99734
Permalloy film magnetometer, mag. props. and LF noise 78−48005
phase measurement, synchronous marker for meas. in noise 78−12725
phase transition, noise induced, in parametric oscillator 79−58665
phase transition induced by external noise 78−16764
photoconductors, noise theory and measurements for modelling electronic processes and transport phenomena 79−56264
photoelectron statistics, joint moment method, phase radiation 80−23647
photographic emulsion, photon noise rel. to granularity 77−2708
photographic film, noise diffraction spectra 80−27368
photographic image optical power spectra anal., S/N concepts 78−63028
photographic image threshold luminance detail value, effect of target and photographic parameters 78−56989
photophoretic spectroscopy, broadband 80−86469
photoreceiver number of signal levels in presence of additive noise 77−58458
photoreceptor noise suppression, rel. to incremental intensity thresholds 79−43895
physical theory, fluctuations and noise 77−87
piezoelectric semiconductors, nonlinear noise amplification 78−60167
plasma, broadband noise effect on plasma instability 77−68778
polarimetry, noise suppression by polarization-plane rotation-angle amplification 80−68241
positron camera, 3-D imaging, noise anal. 78−85445
positron camera, 3-dimens. imaging using Fourier techniques 77−32951
power reactor, neutron density fluctuations, stochastic nonlinear model, Fokker-Planck eqn. 78−58316
premixed gaseous flame noise, influence of combustion substrate parameters 79−74384
pseudocolour density encoding, white-light, using contrast reversal 80−83560
pulsar timing noise anal. 80−77431
pulse discriminator, timing distrib., effect of randomizing time 78−58555
pupil noise amplitude control, interaction of sensory and motor mechanisms 78−64998
PWR internal vibrations, neutron noise monitoring 79−13445
PWR internal vibrs., multiple noise source model 77−26831
PWR neutron noise sources 78−94108
quantised dissipative systems, noise operator approach 77−30099
quantum noise source for Brownian oscillator, whiteness 78−75
quantum statistics of photocurrent in optimal light detector, atm. 'seeing' conditions 80−53244
radiographic granularity, of screen-film systems, assessment by entropy method 80−98070
radiographic screen-film systems, quantum fluctuations 79−58857
radiography, detection of bars and discs in quantum noise [radiography] 80−41042
radiography, fan beam computerised tomography, scatter effects 77−5097
radiography, medical diagnosis, information storage requirements 80−98086
radiography, threshold detection in visible noise 77−86624
radiological imaging systems, unified view using Schade aperture theory, noisy images 77−73563
radiometry, second order, radiant noise coherence 78−287
radionuclide angiocardiography determ. of ventricular ejection fraction, correction of noisy data 77−48868
radionuclide imaging, fundamental limitations 80−30882
random signal detection in noise, accounting for polarisation 77−61672
random walk timing noise anal. for pulsar timing 80−77432
rating of noise nuisance 79−86292
reactor noise anal., system size expansion method 77−26830
reactor noise theory as a Markov process 78−74420
noise continued
regularized object restoration, resolution beyond the diffr. limit 80−87324
renogram, comparison of techniques for filtering of noise 77−32952
resonant optoacoustic cells for trace gas analysis 79−11840
retinal bipolar cell dark noise and stability of rod rhodopsin 78−11644
RF SQUID, hysteretic, input noise 80−70905
RF SQUID magnetometer, effect of noise on performance 79−54159
RF SQUIDs, extension to noise theory rel. to gravit. radiation detectors 77−87685
ring laser, two-mode, intensity fluctuations 80−33038
satellite imagery, cloud cover noise and filtering theory 77−56744
SAW 300 MHz resonator oscillator close-in phase noise rel. to vibration 79−55289
scalar diffraction, inverse theory, eigenvalue formulation 80−102613
scanning background-limited IR sensor with adaptive threshold signal processing logic, performance 80−37082
scanning electron microscope, noise in deflection channel, effect on resolution *(Russian)* 78−86391
secondary ion images observation, using channel plate *(French)* 79−58840
seismic noise level meas. at NORSAR 77−73657
seismic signal, additive noise effect on digital processing steady solns. *(Russian)* 79−53317
seismic wide-band recorders specification 79−39908
seismographs, noises and generating mechanisms in long-period equipment 78−12017
seismology, signals resolution from coherent and incoherent noise, operators efficiency *(Russian)* 79−39963
SEM, note on signal-to-noise ratio when recording magnetic contrast 79−12910
semiconductor, anisotropic conductivity and ambipolar drift noise 77−20375
semiconductor, hot carriers, spreading and noise diffusion coeffs., identity 78−64047
semiconductor, n-type, quasisteady noise effect on thermionic emission 78−2974
semiconductor detector with alternating bias, energy resolution 77−10553
semiconductor junction noisy transient meas. 78−62205
semiconductor laser, quantum noise 78−1228
semiconductor-liquid electrolyte interface, conduction noise *(French)* 80−20306
semiconductors, anisotropic, voltage fluctuations associated with carrier drift 79−51644
signal detection, optical vs digital Fourier transform computers 79−27181
single-threshold detection of random signal in noise, appl. to optical communications 79−18353
sky fluctuating emission in airborne IR astronomy, meas. and interpretation 78−81552
solar fine structure radio bursts at meter wavelengths, review *(Russian)* 78−16386
solar radiation scatt. from gradient particulate atm., background noise in optical communication 79−62576
space-time signal processing, optimal versus conventional detectors 79−27467
speckle, dynamic props., zero-crossing study 80−63923
speckle interferometry S/N ratio, photon counting autocorrelation mode at low light levels 79−76613
spectrometer, double beam, with pulsed dye laser excitation, instrumental noise sources 78−88662
spectrometer, Fabry-Perot, signal noise limitations in data retrieval, winds, temp. and emission rate 78−93763
spectrometer efficiency, S/N ratio formula 80−31881
spectroscopy, noise reduction by low pass filter for DC signal, appl. chlorophyll-a fluoresc. 80−87249
SQUID, rel. to brain mag. response monitoring 77−29231
SQUID, single contact RF bias, low freq. external interference 79−67361
SQUID gradiometer, thin film DC device 77−30187
stellar interferometry, long baseline, S/N ratio 80−26749
stellar speckle interferometry, S/N ratio 78−12102
STEM examination of Bacillus subtilis cell wall struct., S/N enhancement by interactive computation 79−5427
sudden cosmic noise absorpt., solar Zenith angle depend. 78−12047
superconducting magnetic gradiometer, LF noise spectra 77−33203
target discrimination methodology in remote sensing 80−58470
teaching, Campbell's theorem, use in elec. noise formulae derivation 78−24602
temporal frequency dependence of modal noise in fibres [optical] 80−58687
theory, linear and nonlinear, use of general equation for Markov processes 79−21533
thermal electrostatic noise in solar wind, LF obs. from ISEE 3 80−101519
thermocouples, voltage spikes and temp. error due to time varying mag. fields 78−4617
thermometry, appl. to meas. of W specific heat *(Russian)* 77−76573
thermoplastic recording media, dynamic range, noise effect *(Russian)* 77−88675
time variant filter performance in 1/f noise, Si(Li) detector-opto feedback FET system 77−57830
time-varying, rel. to articulation of speech *(Japanese)* 79−81654
transaxial X-ray tomography reconstruction using convolution methods, digital simulation *(Japanese)* 78−35931
transducer noise in locust photoreceptor, intracellular responses 79−34560
transverse section picture reconstruction, correction functions and statistical noise 77−12989
transverse section reconstruction, statistical errors, effects of projection angle number and projection sampling 77−52869
turbulence, subgrid-scale modelling, eddy diffusivity, eddy noise 77−72292
turbulence structure and mechanisms, conference, Berlin, Germany (Aug. 1977) 78−94647
turbulent jet noise and diffusors *(Chinese)* 79−55367
two coupled systems, reduction of effective noise temp. *(Russian)* 77−75790
type II superconductor, flux-flow noise in rectangular sample 77−63043
US material inspection, signal-to-noise ratio improvement 77−16767

noise continued
Vibroseis deconvolution method, noise effects 80−90232
visible imaging CCD and charge injection device arrays 77−19446
vision, conditions for motion flow in dynamical visual noise 80−72174
vision, contrast thresholds of random patterns 78−65020
vision, influence of bandwidth and temporal props. of spatial noise on binocular masking-level differences 77−44681
vision, pursuit movements in absence of target, perceptual effect 78−73162
vision, temporal noise, detectability of power fluctuations 78−48811
vision, temporal stereopsis and dynamic noise 78−7368
visual dynamic noise, coherent motion and stereopsis 77−86503
visual evoked response, digital inverse filtering 79−53098
visual perception, complementary images, time-course of induction 79−2070
visual task subjective performance, noise and quality influence 78−53416
volume conductor electrical source information from elec. and mag. surface data 79−83727
wavefront reversal in stimulated light scatt., focused spatially inhomogeneous pump beam 79−27331
white light processing using diffr. grating method 80−106470
X-ray, film-screen characteristics effects on threshold detectability of small low-contrast objects 78−53487
X-ray backscattering, interface co-ordinate determ., signal-noise ratio 80−77925
X-ray microchannel plate image intensifier, noise charact. 78−53483
xeroradiography, physical theory and photon noise obs. 77−5072
ZPR, noise analyses, determination of kinetic parameters *(Rumanian)* 78−46139
Al films, plastic deformation, appl. of current noise technique for dislocation processes 80−35442
Al shielded room for biomag. meas. 80−104846
Au discontinuous film, elec. cond. and current noise, temp. depend. meas. 78−56245
Au discontinuous films, on sapphire substrates, electrical noise, high temp. behaviour 80−54807
n-$Cd_{0.21}Hg_{0.79}Te$, excess generation-recombination noise 80−107880
n-$Cd_xHg_{1-x}Te$, in strong mag. field, 10 to 1000 Hz noise oscillations 78−87980
CdS crystal, SAW amplification, bulk and acoustic noise 80−39637
CdS film, anomalous noise rel. to photomemory effect 77−20374
CdS, localised level anal. from generation-recomb. noise spectra 78−14777
CdS, optical quenching of noise photooscillations, connection with photoconduction *(Russian)* 77−20363
CdS sintered film, photolum. and recomb. photocurrent noise spectra 78−6743
Cs beam frequency standard drift and noise performance rel. to velocity distributions 78−57912
Fe-Ni-Co-Mo-Ge alloy 40NKM, excess mag. noise after various thermomag. treatments *(Russian)* 80−29575
GaAlAs CW DH diode lasers, optical emission and current noise obs. in LF range 77−3585
(GaAl)As CW DH lasers with stripe geometry, LF intensity noise obs. 77−38887
GaAlAs, diode laser, CW radiation, intensity noise spectra of axial mode groups 77−34890
GaAs DH laser, self-induced modulation, noise, instability 80−48250
GaAs p-n junctions, direct biased, temp. depend. of low freq. voltage fluctuations 79−56298
GaP Schottky barriers, voltage fluctuations, meas. 80−15604
p-Ge, diffusion coeff. for hot holes in mag. field 80−39614
Ge, magnetic field effects on hot-hole noise 77−4415
p-Ge, noise, energy relax. time and diffusion of hot holes 77−76839
p-Ge, noise calc. in strong elec. field using Monte Carlo method 80−15578
n-Ge, noise spectra of hot carriers 78−76083
Ge position sensitive γ-ray detectors using resistive charge division readout 77−54420
p-Ge, temp. depend. of noise and diffusion of hot holes 78−39174
GeTe film, amorphous, specific current noise power 77−66190
He-Cd, metal ion laser *(Japanese)* 79−64209
He-Cd extended-life laser charact. 78−46586
He-Ne laser, 0.63 μm emission intensity fluctuations, spectral correl. 78−1212
He-Ne laser, low noise manufacturing 78−79038
He-Ne laser, manufacturing problems with low noise specification 78−59047
He-Se, metal ion laser *(Japanese)* 79−64209
He-Se laser, noise props. 77−83857
n-$Hg_{1-x}Cd_xTe$, photoconductor, contact noise at 77K 78−88028
InP, diffusion and power spectral density of velocity fluctuations for electrons, Monte Carlo calc. 79−51572
InSb MIS structure, effect of room background on noise props. 80−103755
n-InSb, noise, round trip acousto-electronic amplification, anodic piezoelectric transducer *(Russian)* 78−23139
InSb-NiSb, 8 mm band noise generation *(Russian)* 78−39175
La-Gd (8 at.%), FCC, under hydrostatic pressure, resistivity meas., comparison with positive-J spin glasses 80−59958
$LiIO_3$, freq. up-conversion, spontaneous parametric noise 77−75622
$LiNbO_3$, freq. up-conversion, spontaneous parametric noise 77−75622
$LiNbO_3$, holographic storage and retrieval 80−99669
MBBA, nematic, anomalous spectra of current induced noise under high DC field 78−38617
Nd^{3+}:YAG multimode laser radiation noise 80−74366
Ni, electrodeposit structure, rel. to electrochem. noise 78−67916
β-PbF_2, anion mobility from noise meas. 79−46836
Se, amorphous, monostable switching, current noise 80−44682
Se, amorphous thin film, elec. noise, monostable switching 80−44684
Se-Ag_2Se, thin film polycrystalline heterostructure, exhibiting memory switching, noise level 78−84288
n-Si and FETs at high elec. fields 77−8163
n-Si, anisotropy of differential conductivity and transverse diffusion coefficient 78−76078
Si bars, generation-recombination noise at 77K 79−60883
Si, hole diffusivity, time-of-flight and noise meas. 79−56233
n-Si, hot carrier noise and generation-recomb. noise 79−38140
Si, hot hole diffusion and white noise, microscopic Monte Carlo model 78−30937
noise continued
n-Si, hot-electron diffusion noise, meas. using radiometric method in X-band region 77−39905
n-Si, low noise ohmic contact prep., transport props. 77−43723
Si, n-type, noise meas. on ohmic point contact 77−4443
n-Si, noise, small signal conductivity and diffusion in strong elec. fields 79−11192
n-Si, noise and hot carrier diffusion in mag. fields 79−11193
Si photodiode, avalanche, $n^+p\pi p^+$-type, primary photocurrent anal. by noise measurements *(French)* 80−88624
Si photodiode imaging array design factors 77−39085
Si, with dislocations, noise spectrum 80−107881
p-Si:B, reduction of vibration noise, suitable orientation of element, rel. to crystallographic axes 79−11123
VO_2 film, sensitivity to heat perturbation and current noise, effect of temp. 77−66215
VO_2 single cryst., noise in presence of current filament 80−92952
W_2O_{5-x} film, current, excess noise 78−6421
Zn, electrodeposit structure, rel. to electrochem. noise 78−67916
ZnS, metal-semiconductor LED, injection electroluminescence 77−62992

noise abatement
see also acoustic wave absorption
A/D convertor immunity noise, methods *(Russian)* 77−54838
absorber/barrier materials for noise control enclosures 77−23810
absorbers, dimensioning of facings for acoustically effective structural elements *(German)* 80−74600
absorption in rooms, meas. 77−39161
absorption mechanism of porous material of sound pulse 80−38170
absorptive barrier noise control, theory *(Japanese)* 77−3700
AC power line radio and TV interference control 77−75745
acoustic barrier performance, scale model studies of effects of wind 77−23806
acoustic enclosures, construction materials acoustic properties determination 77−23808
acoustic enclosures for noisy machines, user's guide 79−68481
acoustic insulating material complex elastic modulus meas. and transfer function theory *(Hungarian)* 80−106765
acoustic insulation by double wall technique *(Spanish)* 78−66985
acoustic insulation techniques for horizontal walls *(Spanish)* 78−87207
acoustic intensity measurement during noise abatement exercises *(German)* 80−1389
acoustic paths between two rooms connected by ventilation duct, anal. 80−10074
acoustic planning of plants, technical and economic advantages 80−3561
acoustic requirements and testing, standard light rail vehicle for mass transportation 78−87191
acoustic switch, employing monostable multivibrator, with 600 μW power consumption *(German)* 77−65649
acoustic wave diffr. by absorbing semi-infinite plane in moving fluid 77−50830
acoustic waveguide, active noise suppression 78−5613
acoustically absorptive room boundaries, industrial plant appl. 77−75741
active compensation, of vibrs. of inhomogeneous elastic structs. 78−18103
active noise control expt. for transformers 79−37085
active noise suppression, nonsteady problem 77−27426
active noise-suppression, influence of random errors on acoustic fields compensation 77−14852
active sound absorption, duct carrying uniformly flowing fluid 80−74556
active sound absorption theory, appl. of Huygens principle *(French)* 77−14840
active suppression systems, effectiveness of criteria for placement of compensating sources 78−18099
active suppression systems with finite number of couplings, approximation and stability aspects 78−18111
agricultural tractor operator noise, investigations on cab 80−43529
air compressor used in system for treatment of decubitus ulcers 80−48513
air conditioning plants, sound attenuators, attenuation charact. 78−30123
air conditioning systems 77−11083
air ejectors in punch pressing operations 78−90600
air transport noise reduction measures 78−1505
airborne noise level criteria for buildings 80−10075
aircraft, noise shielding 77−54840
aircraft, Siements airport noise monitoring systems 80−99895
aircraft, the Netherlands, legal and economic factors 80−72112
aircraft and missiles, effect of intense noise on equipment 79−3853
aircraft jet noise reduction test facility 77−845
aircraft jet noise reduction test facility 77−11096
aircraft landing trajectories of minimum noise *(Spanish)* 80−53546
aircraft noise, insulation of buildings 78−55508
aircraft noise identification system by correlation technique 79−23131
aircraft noise pollution, numerical representation, control methods 79−3846
aircraft power plants, mixer nozzle appl. 77−42662
aircraft takeoff procedures, effectiveness 80−16880
airports, control agency and Noise Bureau Factor proposals 77−23802
airports, general aviation, noise policies 79−18587
ambient noise indices, control instruments and systems *(French)* 79−76913
American National Standard S1.21-1972 qualification procedures 77−62120
antiphase signal for sound attenuation in ducts, expt. 77−31168
apartment blocks, noise transmission through wood joist floors, sound insulation methods 80−38178
arbitrary random noise and vibration waves, statistical consideration of peak distribution 80−23836
architectural acoustics, sound transmission between absorbing parallel planes 80−33344
attenuation by absorptive barriers *(Japanese)* 78−59198
auditoria, receiver sound control 77−68328
automobile exhaust system design, finite element acoustic analysis 78−51003
automotive noise legislation 79−34465
autonomous active sound suppression systems, efficiency and stability 79−64375
autonomous active systems for sound field suppression in single mode waveguides 77−50831
axial flow fan, control of tip-vortex noise 78−90593

noise abatement continued
axial flow fans with nonuniformly distrib. stator rows, interaction tones reduction 77−14847
background noise levels in buildings, design targets 77−54835
background noise levels in United Kingdom, prediction model 77−14843
baffles in closed spaces, dependence of effectiveness on nature of closed space, economic and annoyance factors 80−67019
barriers, sound attenuation estimation via calculating charts *(Japanese)* 78−30126
barriers, tree-lined earth, effects on sound propag. 79−18588
barriers and absorbing surfaces, mirror image anal. method 79−23135
barriers on finite impedance ground for noise reduction 80−33301
bearings, means 79−64398
British Government transport policy criticised 78−55512
building acoustics in America (1920-1940) 77−45663
building barriers for traffic noise protection 77−68324
building design, selection of mechanical services equipment 79−18598
building services design, roles of noise control and environmental engineering 79−23144
building sound insulation against aircraft noise, German federal regulation 79−90083
bulldozers, use of retrofit noise control treatments 80−43532
car cavity, simplified finite element method of analysis 79−81627
cavities, suppression of aerodynamically induced pressure oscillations 79−98523
centrifugal blower noise, exptl. studies 80−14518
centrifugal fan noise reduction by acoustically lined casing 78−1494
circular saws in S.Australia's woodworking and metal industries 80−48517
closed building, forecasting program for determ. of noise abatement measures efficacy *(French)* 78−13856
club noise control by electronic power reduction 78−51004
cold heading equipment noise and control 80−43538
combustion noise, flow induced, suppression using appl. of DC elec. field 80−38176
commercial environment with modern equipment 79−76912
community, estimation of L_{eq} using Weibull distribution *(Japanese)* 80−55964
community, industrial noise control conf., Inter-Noise 78, San Francisco, USA, 1978, May 79−18594
community noise, scaling of loudness, noisiness and annoyance 77−11086
community noise surveys, stratification to improve design efficiency 79−81623
community sound level prediction, convolution method 77−11084
complex dynamic system statistical energy analysis 77−75740
compound metal sheet, means *(German)* 77−19481
compressible fluid flow in pipes and valves, acoustic noise, damping *(French)* 77−19477
computer simulation of traffic flows, car following theory, intersections having traffic lights 80−72109
computerised noise environment modelling at General Motors Corporation 80−43542
construction machinery, project for noise control materials in RS4000 machine cabs 79−68484
control, engineering approach 80−16879
control factors, decision processes for public policy making 79−18595
control systems, probabilistic evaluation and appl. to single-wall *(Japanese)* 79−18582
control technique fundamentals *(Japanese)* 78−18107
cooling towers, water noise, meas. and reduction techniques 79−52997
covered panels, sound insulation characteristics of panels having porous material coverings *(Japanese)* 80−33334
critical tendencies in subjective assessment of environmental noise 80−72111
cylindrical duct with impedance walls, attenuation calc. 78−83146
dairy packaging industry, survey procedures 80−53551
Demey metro station, noise level increase due to echoes from passing vehicles *(French)* 80−69600
dieing machine, 300 ton, acoustic and vibratory characts. 80−43541
diesel, engine exhaust noise, single monopole very low freq. noise source in air duct 80−64282
diesel engine, freq. content of surface vib. rel. to noise reduction 77−80011
diesel engine noise, Lucas CAV research 79−50507
diesel engine noise generation, diagnosis and control 80−58857
diesel engine noise radiation mechanisms 79−32135
diesel engine powered installations, noise reduction programme 80−96106
diesel generator noise control 79−43800
diesel-engined ships, noise in cabins and engine room, reduction by abatement at source *(Japanese)* 80−79052
diesel-powered underground mining equipment 80−53557
diffracted field formed by rigid scatterers in field of harmonic point sound source, compensation 78−18112
diffraction by acoustically penetrable or electromagneticlly dielectric half plane, noise barrier model 78−5595
digital telemetry signal wire transmission using IC pulse regenerator *(Russian)* 77−58503
dissipative mufflers with locally reactive lining, modelling 78−13849
domestic acoustic noise control and measurement *(Spanish)* 80−1380
domestic roofing sound insulation, expt. facilities of meas. laboratory, test details 80−79058
domestic sound insulation deficiencies and remedies 78−83175
domestic water supply system, energy absorption technique appl. 77−19487
double walls, influence of cavity-volume damping on air layers stiffness *(German)* 77−80016
droplets in gas, heat and mass transfer rel. to high-intensity sound attenuation 77−62082
duct noise active attenuation meas. 78−90592
ducts, attenuation of lined plenum chambers, meas. and theory 79−81625
dumper, modifications to reduce noise levels 77−68325
ear, airborne sound destructive interference applicability for personal sound protection *(German)* 77−66817
ear protectors, use of sound levels for assessing adequacy 80−104771
elastic floor coverings, effect of thickness and hardness on impact sound insulation props. *(Japanese)* 80−79053
electric machines, acoustic noise meas. errors *(Hungarian)* 80−96102
electric power plant, noise emission controls 77−23811
electric utilities, impact of noise control regulations 78−33958

noise abatement continued
ELMO-G quiet running vacuum pumps and compressors for plant noise reduction 80−5872
EM in induction machines, method *(Hungarian)* 77−14841
engine components and vibration isolation 80−53552
engine muffler design, scaling rules using Buckingham's pi principle 79−14152
engine noise control 77−31171
engine structure vibrations, transmission path and dynamic behavior, background and static tests 80−43520
engine structure vibrations, transmission path and dynamic behavior, motoring tests 80−48487
engines, small two-cycle, low-pass filter muffler 79−18585
England and Wales, noise abatement zones 80−16881
environmental, urban, computer aided evaluation and control *(Japanese)* 79−88033
environmental noise, absorption by walls, statistical evaluation of noise control mechanisms *(Japanese)* 80−33336
environmental noise, annoyance due to different sources 80−48504
environmental noise, study re. nuclear power plant construction 78−87194
environmental railway noise impact assessment, high speed trains in AMTRAK Northeast corridor 80−48507
epoxy resin use in noise and vibration control 77−50829
exhaust noise and its control for construction equipment 80−43531
exhaust system, procedures for evaluation of acoustical performance 79−18645
exhaust systems, appl. of transmission matrices 80−53554
factories appl., computer simulation technique 80−64285
factory noise, materials and methods for reduction 77−39149
factory spaces, performance of absorptive treatments 80−48514
fan drives on construction equipment 80−43530
fan noise reduction by single- and double-wall barriers 80−87648
fanjet engines, discrete freq. noise reduction modelling 80−106652
felt sound absorption rel. to airflow resistance, obs. 77−58506
fibrous glass and mineral fibre acoustical materials, development 80−33341
finite sound absorbing panels, edge phenomena 77−27425
flexural mode vibration damping by reinforcing beams 78−18097
foliage as low-pass filter, expts. with model forests in anechoic chamber 80−33303
food plants, conflict of noise exposure control with sanitation requirements 79−18593
food processing industry, noise reduction materials 78−38132
forge hammers, control of impact noise 80−43539
foundry industry, investigation of acoustical barriers 80−48515
foundry operations 77−72115
freeway noise barrier, expt. eval. 79−34463
Gaussian white noise in telex-communication system, reduction *(Rumanian)* 77−27427
general aviation airport, practical noise abatement 77−65653
glass isolating panes, influence of gas filling on sound isolation *(German)* 77−80017
hearing protector attenuation: a perspective view 79−81619
hearing protector attenuation of random noise, testing 77−46866
hearing protectors, determination of effectiveness 79−14156
hearing protectors, meas. of real-ear attenuation by standardised test methods 78−1508
hearing protectors, performance estimation 78−40192
heavy commercial vehicle cab noise reduction techniques 79−37087
helicopter environmental noise impact obs. and evaluation 80−104539
high speed trains, aerodynamic noise study 80−48512
highway noise barriers, optimum weight with respect to effectiveness and cost 80−67021
highway noise shielding methods 78−9492
highway traffic noise, noise screening elements in highway design *(Hungarian)* 80−106662
housing, classes of acoustical comfort, measurement and control methods 79−23143
hydraulic, source and reduction method *(German)* 79−98545
hydraulic equipment 80−53561
impact noise from industrial machinery, effect on hearing loss 79−18599
impact noise level criteria for buildings 80−10075
impact noise reduction by floor coverings *(Japanese)* 80−33331
impact sound insulation, new rating system 77−11082
impact sound loudness meas. *(Japanese)* 79−98546
impulse method of measuring acoustic normal impedance at oblique incidence 80−53582
indoor machinery, sound transmission loss for various ventilation louvre geometries 80−45839
induced draft cooling towers, noise prediction and control 80−16878
induction motors in air/air heat-exchangers for ventilation *(Hungarian)* 80−102923
industrial, control services including acoustic enclosure with calculation of ventilation requirements 79−23138
industrial, protecting workers on an individual basis, Occupational Safety and Health Act 80−45841
industrial, sound attenuation by multiple barriers 80−43524
industrial building, system effectiveness study *(German)* 78−5612
industrial cost-effective noise control 78−55515
industrial ear protectors, standardisation of testing, current developments 78−22225
industrial hearing protection, types and limitations 78−55509
industrial machine design engineering, noise reduction techniques appl. 79−18596
industrial machinery, acoustic environment improvement for in situ meas. 77−39155
industrial machinery, sound power determ., environmental corrections 77−39153
industrial machinery, surface acoustical intensity method for in situ meas. 77−39156
industrial noise and hearing conservation 78−22223
industrial noise control, costs and legal requirements 78−33957
industrial noise control, systematic approach 79−68483
industrial noise hazard control programme 78−9490
industrial noise induced deafness and protective measures 78−22224
industrial noise regulation, acoustic press. level limits *(French)* 77−19480
industrial plants, heavy, reduction of occupational noise exposure 79−14153
industrial process burners, suppression methods 80−74597

noise abatement continued
industry, choice of engineering or administrative controls or personal protection 78−33956
inexpensive community noise assessments in small cities 77−54841
infinite plate with losses, flexural vibrs. in fluid 78−83319
infra-sound reduction from auxiliary compressors of large wind tunnels 79−81628
infrasound, problems on environmental pollution *(Japanese)* 80−35805
insulating material losses and performance factors *(Spanich)* 78−55516
interoffice speech privacy criteria and suspended ceiling acoustic insulation 78−83173
intracochlear interference effect applicability for personal sound protection *(German)* 77−66816
jet, free, silencing, operational engineering principle *(French)* 79−32494
jet noise suppressors, lab. comparison 78−59193
job shop environment, analysis for noise regulations 80−45840
lagging configurations, effective selection 77−84078
lathes, stock feed tubes silencing with ultrahigh molecular weight polyolefin 80−10085
legal considerations, statutory law, construction and demolition sites 78−87197
legal remedies for noise and vibration problems 80−10084
legislation and the noise consultant 80−10083
LF acoustic reduction of rectangular panel 79−32142
LF industrial noise problem 80−33339
lining design, finite length tuning concept expt. verification 77−31170
long-hole drilling machine 80−53559
low frequency noise breakout from air conditioning ducts 80−74594
machine noise, conf., St. Louis, USA (Nov. 1974) 77−39151
machine noise, solid and air borne sound and vibration, causes and remedies *(German)* 79−3847
machine panels, insertion loss, meas. and evaluation 78−87193
machine sound power meas. indoors by two-surface method 77−39152
machine tools, methods 79−50506
machine tools, vibration-damping plug 80−43525
machine vibration control, active vibr.-mounting techniques 78−18102
machinery, activities of EPA Office of Noise Abatement and Control 80−43527
machinery, conf., W.Lafayette, IN, USA (Apr/May 1979) 80−43526
machines employing circular saw blades 80−43533
marine structures, noise exposure and control 77−84079
materials for environmental noise control, review 77−42664
materials for noise and vibr. control, review 78−13854
materials for noise and vibration control 77−11089
mathematical model of sound transmission into orthotropic shell 79−81626
maximum acceptable noise levels in quiet rooms *(German)* 77−68307
mechanical input power meas. method for wall structures 80−19176
mechanical ventilation systems noise control, design approach 78−42489
metal cutting methods and machinery 80−53548
microjet noise and micropore diffuser-muffler design 78−30335
military occupational hearing conservation and noise control 79−14154
mining industry 80−53556
mobile equipment noise control in surface mining 80−53558
monetary charges, for road traffic and airport noise abatement 79−23133
muffler chambers, flow-reversing, anal., testing and design 77−11085
muffler characts., acoustic impulse technique 78−59217
mufflers, reactive, performance evaluation 77−14844
muffling dissipative device description 77−19482
multi-screen flow expanders for noise reduction 78−63236
multimode waveguide sound fields, active suppression system 78−18113
multiple acoustic screens, influence of physical factors on noise reduction *(French)* 78−13844
municipal noise control program development 79−74577
Murphy's laws appl. in noise control engineering 77−65650
N-fold walls, unified theory for sound shielding charact. determ. *(Japanese)* 79−90082
New York City, environmental noise codes 78−59202
newspaper pressroom, noise level reduction by screens and insulation 80−14517
noise characteristics of information systems with digital laser radiation scanning *(Russian)* 79−68478
noise control in industry, costs 80−16877
noise control system design, panel systems 80−87649
noise excluding audiometric headsets, perform. characts. 79−32157
noise generation by railroad coaches 80−48498
noise path diagnostics in dispersive structural systems, crosscorrelation anal. 77−23807
noise source contribution to observed noise estimation, digital signal processing techniques appl. 79−18617
noise source location in industry, microphone arrays appl. 79−18601
noise transmission through stiffened panels 80−102922
nonrectangular reverberation chamber design and construction 78−83196
nuclear power stations, environmental acoustic protection *(French)* 80−19155
occupational noise standard, 29 CFR 1910.95, problems in enforcement 80−43528
oil-fired boilers, noise reduction by casing *(Hungarian)* 80−106663
open plan offices, noise abatement via sound absorbing partial partitions 78−18116
open-plan offices, acoustical parameters 78−55520
opencast coalmining, principal noise sources 80−81505
optimised multisectioned acoustic liners 80−19145
outdoor noise control barriers, practical appls. and attenuation estimation procedures 80−33340
outdoor noise of coal-fired power plants, possible controls 80−76683
paging systems, noise reduction using selective methods 80−40944
paper mills equipment, means 77−7256
partitions, statistical energy anal. for sound insulation 79−23129
party wall and floor transmitted noise nuisance survey 78−42491
perforated facings with porous backing material as sound absorbers 77−62115
perforated tube muffler components, modelling method, theory 79−98543
perforated tube muffler components, modelling method appls. 79−98544
petro-chemical industrial plants, piping networks, noise abatement 80−28381
petrochemical process plant expansions, noise levels control 79−68480
physical and technical acoustics, conference, Zvenigorodskii, USSR (Sep. 1977) 78−18081
noise abatement continued
piezoelectric transducer systems, noise suppression and prevention for shock and vibration meas. 80−22353
pile driving devices 80−23832
pipe with turbulent air-flow, acceleration response and acoustic power spectral meas. 77−19484
pipeline under hydraulic impact 80−102927
plasterboard sound reduction indices and meas. 78−87196
plate radiation compensation at subcritical freqs., coupling of sound and vibr. fields 78−18110
plates with irregular shock response, sound power level and noise reduction parameters *(German)* 79−81616
pneumatic motors, noise reduction 77−19488
pneumatic silencers for exhaust valves and parts ejectors 77−84080
polyurethane foam on circular plate for noise reduction 77−62102
power hacksaw machines, study of noise emission 79−68482
power plant effects on environment, protection measures *(German)* 80−26574
power plants, design objectives 77−75739
power plants, procedures and equipment 77−35002
power plants steam venting noise characts. 79−7257
power transformer prediction and control 79−18648
power transformers, recent techniques, Fuji product appl. 77−72113
Poznan district post and telecommunication premises, reduction problems *(Polish)* 79−37088
prediction of emission from air conditioning and ventilation systems 77−7252
pressure reducing valves, causes and elimination 79−46108
pressure reducing valves, generated noise reduction methods 79−27463
propeller fans, noise reduction measures *(Japanese)* 80−64284
property line noise control limits statistical representation 77−54842
punch presses, noise reduction by means of shock absorbers 80−43540
quarrying, use of electronic transient recorders for meas. explosion noise and vibration 80−67023
radio studio acoustics planning for SDR's Stuttgart Broadcasting House *(German)* 78−71243
rail traffic, noise reduction *(German)* 77−821
rail traffic noise, attenuation by tree belts, pilot study 80−48501
railway, effect of train noise on sleeping subjects 80−48509
railway, environmental controls for new housing sites 80−48505
railway, environmental impact in Britain 80−48508
railway floating track slab resolution for noise and vibration reduction 77−68321
railway noise and estimation, for newly established line in Japan *(Japanese)* 79−10428
railway traffic, Dutch study 80−48511
railway vehicle internal design and wayside noise abatement 78−55514
railway wayside noise, high-speed trains 80−48497
railways, meas. on noise protection screens *(German)* 80−102916
reactive acoustic attenuator for air conditioning 78−38140
rectangular cavity with rigid incomplete partition, acoustic modes 77−84031
rectangular multielement acoustically lined ducts, sound attenuation 77−84030
rectangular wide barriers for sound reduction, approx. formula for calculation 80−38175
reduction by absorptive barrier, diffr. theory 77−84061
refining factory, cost-effective noise control 79−23139
regulation rel. to noise emission meas. 77−62108
research index, for UK (1975/1976) 77−7257
residences, energy conservation and noise control measures comparison 80−35807
resonators, concentric tube, with unpartitioned cavities, anal. 78−90587
reverberation control, room acoustics determination 78−75016
rigid planar screens, diffr. of arbitrarily oriented directional sources 78−83137
road traffic, control of noise level of moving vehicles 80−99894
road traffic, highway noise barrier perceived benefit 80−102920
road traffic, improvements to the equally-spaced vehicles model, grouping effect *(Japanese)* 80−55963
road traffic, noise control procedures 79−34464
road traffic, noise propag. characts. identification under different conditions, Kalman filter theory appl. *(German)* 80−99896
road traffic, noise with interrupted flow 77−62106
road traffic, prediction of time pattern of fluctuating sound levels *(Japanese)* 80−55965
road traffic, prediction problem for various types of vehicles and multilanes *(Japanese)* 77−3699
road traffic, reduction by correct building placement, noise emitted by single source in open space 80−87647
road traffic, use of sloped barriers for noise abatement 80−102925
road traffic noise, analysis of sequence of sound level readings *(Japanese)* 80−35806
road traffic noise, effect of structure-borne tunnel vibrations on buildings 80−48492
road traffic noise, human response in residential areas, possibility of reduction for the future 80−55962
road traffic noise, its relation to traffic volume *(Japanese)* 80−33335
road traffic noise, meas. radiating height of cars and lorries, effectiveness of sound barriers 80−64325
road traffic noise, new theoretical model *(Japanese)* 80−35804
road traffic noise, prediction using a scale model 80−45838
road traffic noise attenuation by masonry subdivision perimeter fence 79−74578
road traffic noise effect on hearing levels, academic achievement of children, exp. study 79−20553
road traffic noise level definitions and building design criteria 78−83174
road traffic noise levels on high rise building balconies 79−50504
road traffic noise prediction, use of theoretical and empirical models *(French)* 80−67020
road vehicle vibration analysis, digital modal analysis system 80−38173
rockwool and glasswool isolating materials for floating floors *(Japanese)* 78−59200
rolling-contact noise generation in wire stranding machines, use of elastomers 80−43534
room noise reduction, use of window cills and reveals 80−33343
rotary lawn mower noise control methods 77−34995
rotary scrap chopper noise 80−53549
saws, control of vibrations through thermal tensioning 80−48516
schoolroom acoustic insulation check allowing for boundary absorption *(Hungarian)* 80−106664

noise abatement continued
self excitation of active noise suppression in a waveguide 78−18109
self-protecting buildings, acoustical performance 80−23839
service evaluation tests on locomotives, AMTRAK Northeast corridor 80−48506
service system noise faults survey at Liverpool University 77−7251
sheet-steel manufacturing plant, partial enclosures for noise control 79−29495
shielding, mathematical theory 77−54839
shielding effect of noise barriers in open-plan offices, industrial halls 79−18610
ship, using viscoelastic materials 78−22226
ships, noise control problems 79−32134
ships, reduction of structure-borne sound, model tests 79−32133
silencers, optimisation of silencing characteristics and positioning of expansion chamber mufflers *(Japanese)* 80−33333
silencing systems, acoustic charact. anal., 4-terminal matrices of tube system *(Japanese)* 80−10082
silencing systems, acoustic charact. anal., attenuation const. of plane wave in tube *(Japanese)* 80−10081
single screen noise barrier 79−23136
single vehicle noise, stationary test method 77−34998
small elec. appliances, time-average holography appls. *(German)* 79−37086
sonic boom, pressures inside room with open window 80−69602
sound absorption, perforated facings on porous backings, calculation of specific normal impedance 80−64281
sound absorption materials, effects of outdoor exposure 77−88985
sound and vibration fields suppression, synthesis of systems 78−9494
sound attenuation by wide barriers, acoustical scale model study 78−1499
sound barriers acoustic diffraction, Z-lines method for far field anal. 77−50822
sound distrib. control in tubes by auxiliary driving sources, air conditioning duct appls. 79−14133
sound insulation design and transmission field meas. 78−87206
sound insulation meas. for light struct. *(Chinese)* 79−10427
sound isolation tests of residential buildings, correlation with subjective privacy opinions, standard sound source requirements 80−64323
sound power estimation in free field above refl. plane 77−39154
sound propagation in urban and forest areas, prediction of noise appl. *(German)* 80−38142
sound reduction by barriers *(Japanese)* 79−68479
sound rooms for measurements on domestic appliances 79−18604
sound transmission meas. 77−19486
sound-absorbing wedge design, reflection charact., materials and dimens. *(Japanese)* 80−64322
speech noise suppression using spectral subtraction 79−46124
splitter type silencers, acoustic attenuation in lined ducts, theory 77−23801
standard, OSHA regulation, effectiveness 79−14158
standard, OSHA regulation at 29 CFR 1910.95 (b) (1), review 79−14157
standardisation, activities of ISO *(Japanese)* 80−19154
standards, criteria for environmental noise control 79−18597
statistically stationary traffic noise shielding by simple obstacles 78−90590
steam turbines, 200 MW, with accessories, noise reduction research and development 80−91958
steel wheel/steel rail vehicles using steerable steel wheel system for noise reduction 78−26005
STOL aircraft and helicopters, interior noise control 80−14519
stoper drills for coal mines 80−53560
structure borne sound insulation on pipelines, insulation 79−50501
structure damping, evaluation of viscoelastic props. 80−43632
structure vibrations, reduction by increase in damping factor *(French)* 77−19472
structure-borne and air-borne sound levels rel. to insulation of appliances in buildings *(German)* 79−94404
structure-borne sound levels, effects of walls and floors in multistorey buildings *(German)* 78−94483
structures under impact loading, finite element modelling as tool for noise analysis and control 80−43535
subjective annoyance by low level sound, sound character as a physical attribute 80−35902
sugar mills, noise reduction of cane locomotives, shredders, and steam systems 79−18586
supersonic jet noise suppression by coaxial cold/heated jet flows 78−63468
supersonic transport planes, reduction of local ground noise 80−38174
surface effect vehicles, design problems 80−74598
telephone exchanges, PTT premises *(French)* 80−10079
telephone operator's office 80−10086
test facilities Boeing Commercial Airplane Co. 79−18603
thermal power stations, design concepts 77−75738
thick barrier, excess attenuation of noise band 77−62103
thin screen, study of shielding efficiency *(French)* 78−87188
thnadners, shaped noise barriers for control of diffracted sound 79−50502
timber frame constructions, sound insulation of wood joist floors 78−87203
traffic noise, attenuation around buildings 78−1498
traffic noise, cost and safety aspects of quiet tyres use 77−65652
traffic noise, model investigation on acoustical performance of courtyard houses 80−10077
traffic noise reduction by closed balcony shielding on buildings 78−33951
traffic noise reduction by multiple finite barriers, prediction method 80−38171
traffic noise screening effect by buildings *(German)* 80−10076
traffic noise spectra, simulation model 77−46865
training courses for non-specialists 79−23140
trains, annoyance in residential areas from noise and vibration 80−48503
transformer noise reduction by acoustic compensation 78−38134
transformer substations, means 77−23812
transport systems, natural rubber for vibration insulation 80−96099
transportation noise, LF, effects on human performance, tests 77−19483
transportation systems, importance in France 80−48510
trucks and portable compressors, enforcement of EPA regulations 80−53550
TV and motion picture stages, noise and insulation 78−79169
noise abatement continued
tyre/road noise mechanism study 77−19485
underground transit systems, noise control for fan and vent shafts in subways 79−18589
unsealed window sound insulation rel. to frame construction 79−68485
urban, noise mapping using grid method with Rohde and Schwarz integrating sound level meter ELDO 4 80−48533
urban noise level variation and attenuation with height 80−10078
urban noise survey, behaviour of exposure variables 78−87192
urban railway vehicles with sound absorbing wheel systems, noise emission reductions *(German)* 79−50508
urethane foams for acoustic absorber, physical and acoustical props. 79−18592
USA, 1977 state noise restrictions 78−59203
USA, environmental noise control programs 78−59201
USA Quiet Communities Act (1978), implementation by Environmental Protection Agency 80−72113
valves, methods 78−50999
vehicle cab noise control 78−55511
ventilation and air conditioning plants, ideal charact. of sound attenuators 77−54836
ventilation plant, noise and vibr. control 77−54834
vents and blowdown value orifice above 15 lb/in^2 gauge pressure 77−11088
vibration and noise control systems, review 77−11090
vibration and noise control systems, review 78−30127
vibration control, energy propag. in absorbing structs. 78−9596
vibration isolation, survey of use and characterization 80−19144
vibration sources, special treatments for reduction of plant noise 77−54833
vibration-absorbing coatings, constrained, optimality 77−823
vibration-absorbing coatings, detachable, investigation of energy losses 79−90078
vibration-stimulated material handling equipment 80−43537
Viennese Subway stations, noise control problems 77−68314
wall insulation, prediction of output probability distribution of noise level, road traffic noise 80−69593
wall systems, design for desired STC ratings 79−18608
wide cylindrical tubes with wall-mounted resonators, sound attenuation 77−11063
window-glasses, most effective window configurations 80−87655
wood joist floor-ceiling systems, sound-insulating efficiency upgrading 78−1515
wooden house, noise insulation against transportation noise *(Japanese)* 77−54832
work places, industrial installations, noise levels, limits *(French)* 77−19479
workplace noise exposure control, costs and benefits 77−23809
Fe, cast, noise reduction by electrolytic coating 78−80681
Mn-Cu alloy, high-damping, acoustic shock pulse propag., rel. to noise control appl. 77−15503

noise control (acoustic) *see noise abatement*

noise control (interference) *see interference suppression*

noise elimination *see interference suppression*

noise generators
600 MHz to 1 GHz coaxial thermal noise standard 80−98875
analytical method to predict noise radiation from vibrating machine systems 80−43521
comb-filtered noise, for auditory neurophysiological and psychophysical experiments 79−29676
fission reactor noise analysis, simulation using nucleate boiling noise generator 78−54840
high-level, for calibration of Johnson noise power thermometers 78−82005
microwave noise standards, Japanese, 10 GHz system *(Japanese)* 78−57985
pseudo-random sound absorption and buildings, insulation testing *(Spanish)* 78−13861
pseudorandom binary noise US correlation system for nondestructive evaluation 79−52612
self-diffusion NMR pulsed-gradient meas. noise pulse generator 77−53965
sonic anaesthesia during tooth hard tissue operations, BN-1 apparatus 78−85350
Ar microwave noise sources, new similarity rules 77−55177
He gas jet noise source, absolute calibr. 78−59228

noise levels, acoustic *see acoustic noise*

noise measurement
see also acoustic noise measurement; electric noise measurement; optical noise measurement
aircraft voice communications, expt. study 79−81662
antenna in plasma, detect. of natural noises 80−24181
BWR boiling noise, local and global component obs. and calc. 78−94066
BWR core flow fluctuation and neutron noise obs. 78−94060
BWR in-core instrument tube vibration obs. by reactor noise techniques 78−94064
BWR neutron noise local component meas., two phase flow study 78−94059
BWR neutron noise source identification, stochastic model data anal. 78−94106
BWR neutron noise source identification from existing instrumentation 79−13483
BWR power plant, neutron noise meas. and analysis 78−94105
BWR simulation diagnosis by noise analysis 78−94062
BWR stochastic neutron flux fluctuation obs. and modelling, thermohydraulic parameters 78−94065
BWR-4 neutron noise analysis spectra, instrument tube flow-induced vibr. 78−94063
BWR-4 neutron noise analysis spectra characterisation 79−13482
combustion products, noise temp. meas. using contactless capacitive convertor 78−9830
conference, Bad Nauheim, West Germany (Mar. 1978) 79−24031
Dounreay Fast Reactor surveillance, noise analysis development 79−3215
far IR lasers, optically pumped, frequency modulated noise measurements 78−55392
fast reactor boiling detection by noise analysis 79−13449
fast reactor neutron noise analysis, energy-dependent formalism 79−13489

noise measurement continued
ferromagnetic materials, noise charact., applicability of physical similitude 79−4705
fission reactor noise analysis, simulation using nucleate boiling noise generator 78−54840
Fourier transform as perturbation criterion, appl. to NMR intensity 78−65948
jet noise, appl. of cepstral techniques to ground refl. effects in acoustic spectra 77−31165
KEMA Suspension Test Reactor neutron flux and Dodewaard BWR temp. noise 79−3193
liquid, piezoelectric transducer appl. *(Russian)* 78−49799
liquid Na, thermocouple transfer function and flow velocity meas. by temp. noise 79−13394
LMFBR coolant flow monitoring by balanced outlet temp. signals 79−13393
LMFBR subchannel coolant flow behind blockage, temp. noise obs. 79−13389
magnetic, meas. method based on periodicity of Barkhausen jumps 79−17452
magnetoinductive pick-up for Barkhausen noise spectra meas. *(Russian)* 78−65945
mechanical Nyquist noise in cryogenic gravitational wave antenna 77−30078
microprocessor for optical processing system noise analogue signals 78−81955
neutron noise in coupled swimming pool reactor *(French)* 77−10462
nonstationary signal, with modulation radiometer 77−61048
nuclear power plants, diagnostic system using noise anal. 78−50279
nuclear reactor, two-phase flow characterisation by neutron noise techniques 78−94058
nuclear reactor noise, specialists' meeting, Gatlinburg, USA, Sept. 1977 78−94057
online Reactor Noise, Vibration and Loose Parts Monitor 79−3212
Permalloy ferromagnetic noise eval. 79−2799
pool-type reactor noise analysis and expt. 79−3195
power reactor noise anal. *(Bulgarian)* 78−82488
power reactor noise analysis, nonlinear kinetics effects and new techniques 79−13454
PWR, 450 MWe, noise obs., analysis and interpretation 78−94072
PWR neutron noise increase with operating time 79−13447
PWR neutron noise interpretation by vibration analysis 78−94073
PWR neutron noise meas. and modelling 79−13443
PWR pressure vessel vibration excitation, noise correlation and modelling 79−13442
reactor noise analysis, Polish developments 79−3216
sinusoidal signal, in presence of noise via synchronous marker 78−12725
two-dimensional analysis, applic. to Hall generator 78−6420
VHF noise field strength at 95 MHz over India, meas. techniques and obs. 80−109294
VLF vertical seismic noise 79−20763
West German LWR primary system online surveillance 79−3217
X-ray image intensifier noise evaluation, digital method 80−98097
X-ray image intensifiers, quantum noise meas. 80−46033
Na cooled power reactor noise analysis for malfunction diagnosis 79−13450

nomenclature and symbols
see also units (measurement)
amphiboles 79−66677
Arctic geophysical review, sea floor features, nomenclature *(French, English)* 79−48452
asteroid satellites, new nomenclature for announcing discoveries 78−69734
asteroids, Minor planet circulars 5017-5066, new names for seven objects 80−17533
asteroids, new names for 26 objects 80−77325
asteroids, new names for 35 objects 80−46459
asteroids, new names on Minor Planet Circulars 5249-5286 for 48 objects 80−67632
asteroids, new names on Minor Planet Circulars 5423-5454 for 26 objects 80−98599
aurora borealis, origin of metaphor 79−58512
axicon measn axial image 79−81499
carbohydrate nomenclature, digital representation, chemistry education 80−62435
chemical analysis, nomenclature for scales 79−66387
chemical rotation evolution, changing role of symbol 77−87621
climatology, confusions terminology *(German)* 78−65380
colloids, rheological props., terminology and symbols 80−26065
comets, 1976 perihelion passage designations 78−36523
comets, perihelion passage designations for 1978 period 80−31241
comets in 1977, perihelion passage designations on Minor Planet Circulars 4583-4622 79−16871
crystal-chemical formulae, for simple inorganic cryst. structs. 80−33910
crystallography and mineralogy, report of joint committee 77−65927
Earth spheroidal modes, classification and nomenclature 79−44129
electrical quantities, units, symbols and definitions *(German)* 80−86248
electroanalytical chemistry, terms, symbols and definitions 80−21348
elements of atomic numbers >100, nomenclature 80−3295
graphic symbols denoting types and methods of NDT 80−86042
graphite intercalation compounds, nomenclature 80−1948
heliotechnics, basic values, symbols, units and definitions *(Rumanian)* 80−57243
International Union of Pure and Applied Physics recommendations 78−93645
ion selective electrodes, review 78−85165
light measurement, units and terminology for photometry and displays 79−21691
line spread function, notation 77−620
linear and angular dimensions, classification and symbols for means of meas. 79−6081
magnetic structure, neutron determ., book contrib. 79−61064
magnetism teaching w.r.t. chemistry, guide to units 80−12871
Mars surface features nomenclature, Latin and Russian versions 79−8870
mean solar time on Greenwich meridian, definitions and terminology 79−21155
measurement technical term translation problems *(German)* 80−36965
measurement units, historical review and current systems in use *(German)* 80−68166

nomenclature and symbols continued
Mercury albedo features, IAU nomenclature 78−53848
Mercury albedo features, longits. and nomenclature 78−53849
microcomputer-based multiboard communication system for nonverbal handicapped children 78−57126
modulated non-commensurate layer structures, nomenclature and classification 79−94931
Moon surface features nomenclature, reason for name Aristarchus for brightest crater 79−49004
Mossbauer spectroscopy, nomenclature and conventions for reporting of data, IUPAC recommendations 77−68066
Munsell renotations for samples of OSA uniform colour scales 79−12833
nearby stars, priority list for nomenclature 77−78660
NMR spectroscopy, nomenclature and data presentation for publication in chemical journals, IUPAC recommendations 77−68065
open clusters, transit tables for star numbering, magnetic tape 79−44573
organic chemistry, isotopically modified compounds, nomenclature 80−3294
OTF testing, USA standards 78−50725
p-n junction photodiode terminology 80−70800
photoelectron spectroscopy, nomenclature and spectral presentation IUPAC recommendations 77−68075
photometric and radiometric equipment designations *(German)* 79−75570
photometric terminology for refl., transmission, scatt. and emission 77−74477
physicochemical quantities and units, symbols and terminology 79−63187
physiochemical quantities, symbols and terminology 80−3296
planetary satellites, new nomenclature for announcing discoveries 78−69744
planetary satellites, unconfirmed, suggested nomenclature 79−16877
Pleistocene period stages, terminology reconsidered in light of Plio-Pleistocene glaciation in N.America 79−62470
polarised light definitions and nomenclature 78−29897
polymers, stereochemical definitions, IUPAC nomenclature 80−23593
PVC, suggested morphology-characterisation terminology 79−7555
reflectance, geometrical considerations and nomenclature 78−29146
reflection, transmission, scatt. and emission terminology 78−37044
retroreflector and corner reflector terminology 77−11043
scintars−new class of compact galactic radiosources 79−44579
SI units, conventions and practices, physics teacher's viewpoint 80−36968
SI units, rationalisation and need for approximation to SI 80−36969
SI units development and implementation in Portugal *(Portuguese)* 77−37839
six-membered rings, conformation, nomenclature 80−78721
solar energy, units and symbols 79−12756
star names register *(Swedish)* 78−4188
steel ball bearing, fatigued, phase changes, nomenclature 80−89198
stellar data, conf. (Strasbourg, France, 19-21 Aug. 1976) 77−78828
stellar designation ambiguities, improvement proposals, IAU list 77−78661
stellar designation organization using bibliography-type data base 77−78658
supernova remnants, naming of Crab-type objects 79−35338
surface chemistry, rheological props., terminology and symbols 80−26065
terminology, gravis as synonym for the phrase, force of gravity 78−69936
testing equipment, uniform nomenclature 79−6109
thin layer chromatography, high performance, efficiency parameter terminology 78−20098
USSR-East German joint optical glass catalogue 79−76775
weather and climate, definitions 80−41540

nomograms
see also graphs
acoustic resonator parameters calc., for pneumatic-acoustic automation appl. 77−11098
air humidity meas. above 100°C 78−226
antireflection coating, three-layer, refractive index optimum combination 80−28306
black body monochomatic emissive power, fast calc. by nomograph 78−22257
bladder pressure noninvasive determ. from micturition cinecystourethrogram 79−92370
deconvolution nomogram for single exponential fluoresc. decays 80−67290
dew point temp. change with pressure, calc. 80−77607
distant light visibility calc., colour and flash time corrections 79−83781
electric machine air cooling using evaporative thermosiphon design 77−71194
electromagnetic inspection, parameter calc. using nomographs 79−79215
electron brightness meas. by 2-limiter method, accuracy calc. 79−6234
ellipsometry of dielectric films on GaAs 79−69894
ellipsometry of elec. conducting films on transparent ceramic 79−67376
fatigue with programmed loading of steel, nomogram construction 79−38964
fibre, self-focusing, matching elements calc. 80−28339
filters, basic theory and utilisation 77−17791
flash lamp load conditions, nomogram for calc. 77−58411
flow of air calc., dry, through pipe kinetic tenacity calc., with aid of nomogram *(German)* 77−35244
geomagnetic field total intensity anomalies, charts for quick determ. using horizontal plates *(Spanish)* 79−100982
gratings, ruled, lamellar and holographic, equivalence in const. deviation mountings 80−87474
gravitational parameter inaccuracy consequences computation, for orbits in Earth's gravitational field 78−40460
gravity vertical gradients, charts for quick determ. using horizontal plates *(Spanish)* 79−100982
heat transfer coefficient determ., water flowing in pipes or tubes 78−9641
HF heated cylindrical component temperature field computation for quench control 78−90632
hollow cylinder, internal one sided heating, nomogram construction, for computing temp. state 78−63271
impurity distribution coeffs., in crystals obtained by directed crystallisation 79−51133

nomograms continued
invertors, design and development *(Russian)* 77−53761
laser beams, construction of nomograms 79−98421
MV overhead line conductor cross-section optimum choice *(Bulgarian)* 77−60917
MV transformer optimum rating *(Bulgarian)* 77−60916
nuclear power reactor accidental release, isopleth method for population reaction 79−13533
optical fibre system design charts 79−7200
paraxial optical systems, nomographic diagrams for design and anal. 80−48377
physics undergraduate courses, role of nomograms 77−49519
pore size in thin dielec. films 78−6632
pressure inside hollow organs, recording through tubes, nomograms for calc. of system parameters 80−3836
radiation therapy, practical nomogram for correcting nominal standard dose *(Italian)* 77−81581
rainfall frequency relationships study for Karnataka region, India 80−31094
Schottky barrier IR detector, nomographs for parameter evaluation, 77K 80−31870
solar power satellite design appl. 79−70433
sound attenuation by barriers, estimation via calculating charts *(Japanese)* 78−30126
spent nuclear fuel decay heat production, prediction by nomogram 77−38358
stars photoelectric positions, chromatic refr. correction tables *(Russian)* 79−96889
steel, pearlitic structural, austenite grains, growth rate during heating 80−100860
stellar azimuth determ. method *(Russian)* 77−60579
US propag. calcs., multiple nomogram 80−28371
US tissue characterisation model selection nomogram 79−62321
US tool, radial mode, with statically loaded inner surface, reson. condition nomogram 78−183
vacuum pumpdown, nomogram for required time or pumping capacity 77−10035
visual pigment spectra nomograms, wavelength depend. 77−25430
Voigt contour of spectral line, nomogram for parameters determ. 80−52321
NH_3 continuous absorption cooling flat plate collector design and optimisation 79−62081

nomographs *see nomograms*

non-Newtonian flow
see also non-Newtonian fluids
a boundary layer theory for non-Newtonian fluids 80−83818
accelerating thin falling film, on inclined surface, gas absorption 78−93632
anisotropic liquid, axially symmetric flow 80−103050
in annular conduits *(Japanese)* 78−9660
annular flow between parallel but offset axis cylinders 79−60008
annular liq.-air flow, film thickness rel. to rate 77−3860
annular two-phase flow of non-Newtonian liqs. and gases, press. drop and gas vol. fraction 80−10286
annulus with negligible diffusion, laminar non-Newtonian flow, residence time distrib. 80−79357
annulus with non-Newtonian fluids, mass transfer to inner wall, Leveque soln. adaptation 80−10267
asymmetrical fluid, thermoconvection wave propagation, microinertial and couple stress effect 80−19446
axially symmetric squeeze-film flows, viscoelastic props. 79−98764
balance rheometer, inertia effects in rheometrical flow systems 77−68722
between rotating porous cylinders, flow stability in wide gap case 79−68761
between two rotating cylinders, nonconcentric 79−68759
Bingham fluid, entrance flow through noncircular ducts, finite difference anal. 80−1684
Bingham fluid, flow in entry region of circular pipe 77−42876
Bingham plastic flow between parallel plates, effect of asymmetric vel. profile 78−75175
blood, sickle cell rheology, press.-flow curves 77−25503
blood flow in artery, pulsatile flow 80−106845
boundary layer, in convergent channel, eqn. derivation by perturbation method 78−30322
boundary-layer theory in non-Newtonian nonlinearly viscous media 79−90289
bubble formation in nozzle flow 79−23356
bubble motion and deformation, drag coeffs. 77−89184
bubble rupture between two solid walls, effect of drag-reducing polymers on cavitation 80−106822
bubble swarm behaviour and gas absorption in non-Newtonian fluids in sparged columns 79−4061
bubble translational motion in a viscoelastic liquid, retarded motion approx. 80−83777
bubbles, fluid flow in Newtonian and non-Newtonian fluids *(French)* 79−46374
bubbles and drops coalescence rate, ambient liq. viscoelasticity effect 78−67248
bubbles in viscoelastic fluid, dynamics and dissolution 78−90970
buoyancy-thermocapillary convection layers with free surface, energy stability theory 80−87768
capillary and slit methods of normal stress measurements 80−43807
capillary rheometer, viscous heating from power law fluid, perturbation expansion anal. 78−63519
carboxy methyl cellulose solns., mass transfer from cylinders to power law fluids 80−83826
carboxy methyl cellulose solns., mass transfer from spheres to power law fluids 80−83825
carboxymethylcellulose, aq. soln., hydrodynamics of falling liquid film *(Russian)* 79−64715
carboxymethylcellulose, aq. soln., real flow curve determ., with wall effects, in rotation viscosimeters *(Russian)* 79−64714
carboxymethylcellulose soln., flow in profile channel of extrusion head 79−98780
Casson fluid flow between approaching discs, plug flow region 78−67230
Casson fluids flow in non-circular ducts, appl. to haemodialyser 79−20563
cavitation onset on cylinder, effect of dil. aqueous polymer solns. 77−68645

non-Newtonian flow continued
CBOOA, smectic, anisotropic shear viscosity meas. 77−15310
circular cylinder, non-Newtonian fluid flow boundary layer eqn. approx. soln. 80−14752
circular tube, non-Newtonian fluid linear flow, heat transfer 79−98810
classification criteria for rigid motions, viscometric flow and elongational flow 80−69881
clay aqueous suspension turbulent flow, average velocity profile and functional loss in pipe 80−48778
clay-water suspension turbulent flow in tube, velocity profile and frictional losses *(Russian)* 77−31364
co-rotational and other rate type constitutive equations 78−90942
coagulated suspensions, flow equation 78−63487
cochlear fluid mechanics, kinetic theory 78−53440
colloidal suspensions, coagulated, expt. props. of flow curve parameters 77−938
colloidal suspensions, coagulated, flow props., elastic floc model 77−939
colloidal suspensions, coagulated, flow props., energy dissipation in flow units 77−3862
conducting non-Newtonian liq., shear disturbance propag., mag. field effect *(Russian)* 77−65809
conference, Louvain-la-Neuve, Belgium, Sept. (1978) 79−60007
conference, stretching flow, Edinburgh, Scotland, (Sept. 1977) 78−71373
conical flow of non-Newtonian elastic power law fluid with injection/suction, similarity solns. 79−14439
constitutive equations, alternative approaches 79−60011
constitutive equations, deformation and convected derivatives 79−60013
constitutive models, with kinematic slip hypothesis 79−60009
convection, free, heat and mass transfer 79−68765
convection, past hot porous circ. cylinders, of 2nd-order liq. 79−14476
convection, stationary, vibr. instability 79−94683
convective heat and mass exchange, $Pe \leq 1000$, in power-law liq. 78−55683
convective stability, energy method 80−38455
converging and stretching flow 78−71374
cooperative phenomenon, theory 80−69878
Cosserat fluid, flow stability 78−51203
Cosserat fluid flow in curved pipe. 78−14048
Cosserat fluids, radial flow in convergent channels 80−74988
Couette flow, viscoelastic fluid *(French)* 77−65767
Couette flow with moving boundaries 79−23343
creeping flow, variational principles, entropy prod. 77−75946
creeping flow around rotating spheroidal spindle, torque calcs. 77−15073
creeping flow round sphere, fluid elasticity effect on drag coefficient 80−43742
creeping motion of fluid past sphere 80−24057
critical fluids, non-Newtonian effect and normal stress effect 80−49396
critical point region, theory 78−22377
curly-viscous fluids, free convection under boundary conditions of second kind 77−75942
curly-viscous fluids, three-dimens. free convection about slender bodies of revolution 77−75943
current carrying non-Newtonian fluid past a nonconducting sphere at low Reynolds number 79−64784
cylinder oscillating in viscoelastic fluid, secondary flow 79−60037
dental composite paste, rapid setting non-Newtonian viscosity eval. with parallel-plate plastometer 79−27610
die entry flow, kinematics and stability 79−60026
die swell from capillary, for Maxwell fluid 78−90939
die swell from capillary amendment of Tanner's theory 79−60020
die swell problem, free surface separation 79−90295
die swell problems, viscoelastic fluid flow, collocation and Galerkin finite element anal. 80−14751
diffusion coeffs., measurement by flow method 77−55045
diffusion flow on interacting surfaces, laminar and turbulent, in Newtonian or nonNewtonian fluids *(French)* 77−27516
dilatant liquid, plane laminar boundary layer 79−64712
dilute polymer soln. heterogeneity, ageing and non-Newtonian characts. 79−60030
dilute polymer solns., flow activation energy *(German)* 79−77191
dilute polymer solns., rheology, role of rigidity constraints 79−81928
dissipation effects on viscosity, critical eqns. *(German)* 79−27611
drag reducing polymer solns., dynamical behaviour, mol. conformation and optical props., expt. and rheological model 79−60034
drag-reducing flows, calc. of velocity profiles 77−35185
drop, deformable, motion in second-order fluid 79−64754
droplet deformation in extensional flow 80−19449
duct, rectangular, laminar non-Newtonian flow, vel. profiles 80−92217
duct entrance region flow, loss coeffs. calcs. 77−89166
duct flow, wall heat transfer in entrance region 79−4049
dumbbell shaped particles in power-law liq., struct.-phenomenological theory 78−1730
dusty gas, unsteady flow in channel with annular sector cross section 79−77247
dusty viscous flow through a cylinder of elliptic section under time-dependent pressure gradient 79−77248
Earth mantle, non-Newtonian corner flows press. rel. to plate subduction angle 79−39695
Earth mantle antiplane flow, appl. to tectonic plate deform. 77−73704
Earth mantle convection theory *(German)* 77−70631
eccentric rotating discs, torque and energy balances for flow 77−68641
EHD flows, one-dimens. steady-state 77−7464
elastic flow between eccentric co-rot. cylinders, material lines 77−23966
elastic liquid, long range memory effects in flows involving abrupt changes in geometry 77−35182
elastic liquid flow past porous plate 77−15078
elastic liquids, stability of plane Poiseuille flow 78−9662
elastic polymer solution, shear flow, rel. to rheologic theory 77−55051
elastic viscous fluid, unsteady flow past infinite porous plate 79−68794
elastic-viscous fluid, steady flow through annulus of porous rotating coaxial cylinders 77−72349
elastico-viscous flow, due to oscillating plate 79−4043
elastico-viscous flow around oscillating cylinder 77−35177
elastico-viscous flow reversal, stationary and torsionally oscill. disc 78−1698
elastico-viscous fluid rot. in mag. field, unsteady flow induced by oscill. plate 78−67273
elastico-viscous liquid, atomisation, drop size rel. to elasticity 77−35220
elastico-viscous liquid flow in axisymmetric pipe of slowly varying cross-section 80−83774

non-Newtonian flow continued
elastico-viscous MHD fluctuating flow past porous plate, heat transfer 79−90342
elasticoviscous capillary jet stability 79−90303
elasticoviscous flow along plane wall with periodic suction 79−10594
elastohydrodynamic lubrication, non-Newtonian effects of volume relaxation 80−103009
elastohydrodynamic lubrication at high press., non-Newtonian behaviour 79−46350
elastohydrodynamic oil film, shear behaviour 77−68635
elastohydrodynamic point contact, mathematical model for lubricating film thickness *(German)* 78−63464
elastoplastic flow, stability 79−14442
electrohydrodynamic instability 80−14832
elliptic variational equality, of Bingham type, approximation *(French)* 77−47048
emulsion, concentrated unstable, turbulent flow in pipes 80−28537
emulsions, unstable water-oil type, rheological props. obs. non-Newtonian obs. 77−75866
entangled monodisperse polymers kinetic network model for nonlinear viscoelastic flow props. 80−28538
entrance region of tubes, non-Newtonian flow, press. drop 77−27563
erythrocyte filtration through polycarbonate filter determ. method *(German)* 79−79708
exit flow through capillaries, effect of vibrations 80−79358
extruded polymer soln. through capillary, flow instability and electrostatic effects 79−60035
extrusion and forming of solids, plastic deform., nonNewtonian flow, numerical solns. 78−19824
Eyring falling film, Taylor diffusion of solute 77−39317
Eyring model fluid, dispersion in laminar falling film 77−89167
falling films, nonisothermal flow *(German)* 78−83439
fibre lightguide form., from tubular blank, optimisation 77−75719
fibre suspension, dil., mechanistic aspects of drag reduction in turbulent pipe flow 80−6102
fibre suspension flow in pipes, transition regime analysis, drag reduction 77−89186
film entrained by moving surface, thickness calc. 79−72916
filtration equation for non-Newtonian liq. 78−55690
filtration motion of non-Newtonian fluids *(Italian)* 77−55044
finite element method, mixed, for plane and axisymmetric flow 79−60017
finite element method for memory effect fluids 79−60016
finite element routine using mixed method 80−103045
flat plate, MHD unsteady flow of Maxwell fluid, relaxation parameter 80−24101
flow curves determ. by method of representative viscosity *(German)* 77−68642
flow model, for anisotropic viscosity tensor, shear and pipe flow 78−90938
flow of generalized Newtonian and Bingham liquids in an annular capillary 79−41758
flow past sphere, finite difference numerical solns 78−9661
flow regulating system operating with Newtonian and non-Newtonian fluids *(German)* 80−1535
flow structure in immediate vicinity of wall 79−1215
fluid flow past sphere, anomalous separation, wake formation 77−51091
fluid motion stability, book, part II 77−3811
fluid properties for control value operation *(German)* 79−7390
fluid spheres in viscoelastic fluid, drag coeff., low Reynolds number *(Japanese)* 78−9694
fluid-film flows, of differential fluids of complexity n dimensional approach, lubrication theory appl. 80−16492
fluid-particle dynamic interactions *(Portuguese)* 80−19452
force multipole moments for a spherically symmetric particle in solution 80−92185
forced convection, on circular cylinder, suction and slip velocity effects 78−34169
forced convection with rheological systems, review 79−1222
forced heat convection of linear flow of non-Newtonian fluids through rectangular channels 80−92141
free convection from vertical plate, variable gravity force effect 77−42878
frictional force and torque in anisotropic spatially inhomogeneous viscosity fluid, variational principle 79−37367
gas bubble formation at single submerged orifice, model 79−32640
gas bubble motion in power-law fluid, heat and mass transfer with chemical reaction 79−77227
gas bubble suspensions, incompressible nonNewtonian and Newtonian fluids, dilatational props. 78−30343
generalised measures in fluid mechanics 77−42877
glass-forming liquids, viscous flow and valence config. theory 80−14756
Glen body, steady flow of viscous nonlinear fluid around perfectly smooth sphere *(French)* 79−7387
granular cohesionless material, gravity flow in chutes and channels 79−64753
haemolytic secondary effects in cone-plate viscometers 79−62281
harmonically oscillating visco-elastic boundary layer flow 79−55401
heat flux from nonisothermal surfaces to gradient flows *(Russian)* 79−68767
heat transfer by fluctuating flow past porous plate 78−38309
heat transfer from cylinder submerged in non-Newtonian fluid 79−1221
heat transfer in duct flow 79−1219
heat transfer in non-Newtonian flow through pipes 79−32592
heat transfer in polymeric and disperse Bingham fluids during forced convection in ultradeep boreholes 79−68762
Hele-Shaw unsteady flow 80−14754
helical coil flow studies 78−51204
high viscosity fluids in circular tubes *(German)* 77−15124
hydraulic behaviour research, rheology *(Italian)* 78−38376
hydraulic resistance of channels calc. *(Russian)* 80−38451
hydrodynamic calculations for container pipeline systems with non-Newtonian liquids 80−106817
hydrodynamic resistance reduction by surfactant, rel. to micelle form. 77−7438
hydrodynamic stability of free convection in vertical layer 78−59430
hydrodynamic thermal explosion in power-law fluid flow 79−77158
hydroxylpropylmethyl cellulose, aq. solns., turbulent flow characts., friction-reducing props. 78−94649
hydroxypropyl cellulose-water, bubble elongation dynamics, modelling with viscoelastic constitutive relations 79−37388

non-Newtonian flow continued
ideal plastic material, film flow along oscillating wall 79−81927
impurity, effective diffusion in laminar liq. flow 78−67228
incompressible fluid, variational principle for flow 78−51207
incompressible fluid with pressure gradient and fluid injection, MHD flow 80−33686
incompressible isotropic simple fluids, universal motions 79−68758
incompressible liquid film, surface waves 80−43748
incompressible simple fluid with fading memory, stability 80−43741
inelastic power-law fluid, unsteady flow in circular tube; implicit finite difference anal. 80−83821
inertial effects of liquid flow with an anisotropic viscosity tensor 80−83820
infinite oscillating plate in viscoelast. fluid 79−27670
infinite vertical porous plate, unsteady free convective elastica-viscous flow, viscous dissipation heat 80−24012
inhomogeneous flows of non-Newtonian fluids: generation of spatial concentration gradients, stress and diffusion effects 79−60032
injection effects of viscoelastic liquid flowing into channel 80−53823
integral type incompressible simple fluids, uniqueness of some flows 77−19629
irregular viscous fluid between rot. cylinders, temp. and press. distribs. 77−65769
isochoric simple extensional flows, steady and unsteady 77−75944
isothermal circular cylinder, unsteady combined convection in viscous incompressible flow 79−55391
isothermal Couette flow in slowly converging channel with complex shear 77−15069
jet, flat submerged, in non-Newtonian liq. with power-law behaviour 80−59078
jets, micropolar fluid, impinging normally on flat plate, thermal boundary layer 80−28536
kinematical tensors, rheological eqns. of state 78−30326
laminar and turbulent flow in noncircular pipes 78−18315
laminar boundary layer, elongational viscosity and secondary instability 77−23997
laminar boundary layer flow, mass transfer 77−27562
laminar boundary-layer flow of non-Newtonian fluid, surface heat transfer rate 80−24055
laminar falling film with smooth wave free gas-liq. interface, heat transfer 79−7389
laminar far wake flow of non-Newtonian power law fluid 80−53824
laminar flow in porous annulus 77−72333
laminar flow in thin layer, two-dimensional problem 79−86474
laminar flow through parallel plates, kinetic energy correction factor 77−31271
laminar jet flow 80−1662
laminar natural convection heat transfer to a viscoelastic fluid 78−83436
laminar non-Newtonian falling liquid films, dynamics 79−7393
laminar non-Newtonian fluid jet, swirling, impinging on normal plane 77−42889
laminar pipe flow, nonisothermal, heat transfer, with internal heat sources 79−68763
laminar tube flow, dispersion 77−27561
laminar two-dimens. wake of incompressible pseudoplastic fluid 77−51089
laminar viscoelastic boundary layers, role of fluid relaxation time 79−81829
laminary flow through curved pipe, asymptotic theory *(German)* 77−24000
liquid crystal, dissipative structures in turbulent movement *(Russian)* 78−55808
liquid drop motion in non-Newtonian media 78−75184
liquid film, falling, hydrodynamic entrance length 77−58743
longitudinal vibration effects on Poiseuille non-Newtonian flow in non-circular pipe 79−86514
low Reynolds-number flow in the vicinity of axisymmetric constrictions 80−6147
lower critical Reynolds number, pipes and annuli, Newtonian and non-Newtonian flow, stability parameter anal. 78−87363
macromolecular liquids, flow alignment, non-Newtonian viscosity and normal press. 77−35183
macromolecular solutions, kinetic theory and rheology 77−7424
mass transfer from cylinders to power law fluids 80−83826
mass transfer from spheres to power law fluids 80−83825
mass transfer to power law fluids in fluidised beds 80−100032
Maxwell fluid, diffusion of vortex line in stagnation point flow 80−74892
Maxwell fluid, time depend. flow, between parallel inclined plates 79−37358
Maxwell fluid, unsteady flow past flat plate, transform technique 78−59428
Maxwell fluids, immiscible, hydrodynamic flow through non-conducting rectangular channel 80−100038
Maxwell viscoelastic liquid, drag on circular cylinder with transient vel. 78−18270
Maxwellian fluid, line vortex diffusion *(French)* 77−65765
MBBA, homeotropic nematic layer, torsional shear flow in normal elec. field 79−82155
MHD convective instability in rot. viscoelastic fluid layer heated from below 77−58800
MHD flow of a viscoelastic conducting fluid 80−92229
MHD viscoelastic free convection boundary layer flow past porous plate 80−10317
micropolar fluid, heat transfer in stagnation point flow 80−79356
micropolar fluid, laminar boundary layer, longitudinal surface curvature effects 80−48669
micropolar fluid, laminar flow through slot 80−10313
micropolar fluid, nonsimilar incompressible laminar boundary-layer flow 77−35184
micropolar fluid, second order, fund. and constitutive eqns., thermodynamics and flow 78−20970
micropolar fluid, steady incompressible flow, linear steady-state system of eqns. 80−83819
micropolar fluid, thermal boundary layer at stagnation point 80−53820
micropolar fluid drop in viscous fluid, flow, stream functions, velocities, spins, drag 80−53821
micropolar fluid flow, circular cylinder asymptotic boundary layer 79−18916
micropolar fluid flow between concentric cylinders 78−5767

non-Newtonian flow continued
micropolar fluid flow due to an oscillating plane subject to rotation 79−98763
micropolar fluid flow in channels, convective heat transfer *(Russian)* 79−18920
micropolar fluid flow on arbitrary surface, three-dimens. boundary layer eqns. 77−68633
micropolar fluid flows, kinematic props., Bernoulli surfaces 79−23341
micropolar fluid movement in presence of orientable particles, numerical study *(French)* 80−74924
micropolar fluid on circular cylinder, thermal boundary layer 78−75174
micropolar fluid theory, Stokes flow existence and uniqueness 80−69877
micropolar fluid with stretch, convection, appl. to Earth mantle 78−51202
micropolar fluids, potentials and Green's functions 80−96286
micropolar laminar radial channel flow, heat transfer 78−30328
micropolar liquid between two infinite slowly rotating discs 80−53796
micropolar liquids, laminar plane channel flow, stability *(German)* 78−94773
mixing, axial force on agitators 79−37356
nearly extensional flow, consistency relations 80−53822
nearly extensional flow, theory 79−60018
nearly extensional flows, derivation of constitutive eqns. 78−90944
needle, thin, external laminar flow, skin friction, vel. profile 78−67229
nematic liquid crystals, Couette flow, orientation instability for finite anchoring energies 80−74923
non-Newtonian pulsatile laminar flow in tube 78−79346
nonisothermal, through structures, heat dissipation and expansion effects *(German)* 77−15082
nonisothermal flow, in slowly converging channel 77−89168
nonisothermal flow of anomalous systems in pipes, rheological aspects *(Russian)* 80−43775
nonisothermal flow of anomalously viscous liquids in channels of screw extruders 80−19305
nonisothermal laminar flow in pipes 77−58741
nonlinear rheological fluids, functional description method for turbulence 79−72913
nonlinear viscoelastic fluid, kinematical flow anal. *(Polish)* 77−55049
nonlinear viscoelastic fluid, steady shearing flow instability 79−32461
nonlinear viscous flow, in two and three dimens., kinetic theory 78−71372
nonlinearly viscoplastic fluid, Couette flow 79−18918
nonstationary viscous flow of thermally conductive gas around semi-infinite plate, numerical anal. 80−6104
oil transport as oil-in-water emulsions 79−77192
Oldroyd B-fluid flow between porous plates with fluctuating vel. 78−26168
Oldroyd liquid, unsteady flow between two porous walls 78−63452
orientable polymer fluid, Ericksen's anisotropic fluids theory extension 80−79359
orthogonal stagnation flow, a framework for steady extensional flow experiments 80−1653
oscillatory tube flows of viscoelastic fluids 79−77252
parallel plates, torsional oscill. of one plate, radial-axial flow 78−38375
parallel walls, unsteady flow, velocity and temp. fields 77−39314
particle distribution in Poiseuille flow of suspension in micropolar fluid model 80−10314
particles in non-Newtonian fluid, constitutive models 79−60049
paste-like composite with polymer binding, rheological props., wall effect 77−47072
peristaltic non-Newtonian flow in oscillating pipe, peristaltic and Poiseuille flow phenomena 78−63463
petroleum, model validity 77−89170
phase-equilibria of rod-like molecules in extensional flow field 78−26158
physical constants of a flowing continuum, theory 79−60012
pipe, containing anomalously viscous liq., convection intensification by spiral swirlers 79−94461
pipe flow, heat and mass transfer 79−46309
pipe flow, parallelogram section, time variable press. grad. 79−68760
pipe flow, second order fluid, finite difference methods 78−94770
pipe flow, viscosity-shear rate depend., computer method 77−15066
pipe flow 79−7388
pipe flow turbulent entrance region, drag reducing fluid, expt. and anal. 78−63458
pipeline systems, problems in fluid mechanics for hydraulic transport of solid materials 80−106836
plane flow of second grade fluid through contraction 77−3870
plane jet, stability to infinitely small perturbations 78−51211
plane non-Newtonian Couette flow, heat transfer 79−86471
plane shear waves in viscoelastic fluids as motions with proportional stretch history 79−64613
plane squeeze-film flows, in convected coords. 78−90940
plastic disperse systems, generalised flow theory with account of wall effect 78−87320
plate suddenly accelerated in non-Newtonian fluid 78−90935
Poiseuille flow, applicability of the theory of directed jets 79−60019
Poiseuille flow, influence of vibrs. 79−7391
Poiseuille flow in cooled channel, hydrodynamic stability 79−14441
Poiseuille flow of viscoelastic fluid between eccentric cylinders 80−1652
Poiseuille pipe flow of incompressible second order fluid *(German)* 78−87395
polar fluid, two-dimensional internal flows 79−59988
poly-1-olefin melts, viscous flow activation energy, melt struct. 77−7654
polyacrylamide Separan MG200, aq. soln., rheological props. 80−64507
polyacrylamide soln., films, hydrodynamics *(Russian)* 77−31338
polyacrylamide solution, tube flow, friction and convective heat transfer, rheological changes effect 79−1220
polyacrylamides-water-glycerol, streaming birefringence in extensional flow 80−6013
polyethylene, high-density, mixed with gypsum, flow props. *(Japanese)* 77−7357
polyethylene, high-density, mixed with gypsum, flow props. *(Japanese)* 77−7358
polyethylene, low density, melt flow, mech. degradation *(Russian)* 79−50691
polyethylene high density melts, anomalous flow behaviour *(German)* 79−77048
polyethylene melt, flow in profile channel of extrusion head 79−98780
polyethylene oxide aqueous solns., spectroscopic obs. of structural variability WRT turbulent resistance reduction 77−7356

non-Newtonian flow continued
polyethyleneoxide dilute solns., flow birefringence at high rates 79−81834
polyisobutylene-oil, laminar plane stagnation flow kinematics, laser Doppler anemometry 78−38374
polymer, frost deform. 77−50624
polymer additives diffusion in turbulent boundary layer 77−35176
polymer dilute solution, elongational flow, meas. using tubeless siphon apparatus 77−7486
polymer extrusion flow and heat transfer relationships, numerical anal. 79−77188
polymer flow, birefringence meas. of normal and tangential stresses 77−58625
polymer flow on inclined plane, edge effects 80−19451
polymer fluids, complex modulus, freq. depend. var. during extensional flow 79−55351
polymer liq. flow, hydrodynamic eqns., centre of mass model, friction approx. 78−55664
polymer melt, viscosity under hydrostatic pressure, falling cylinder viscometer *(German)* 77−55115
polymer melt flows, propag. of large amplitude low frequency vibration 77−65770
polymer melts, blended resins, flow charact. *(Japanese)* 80−24059
polymer melts, elongational behaviour in const. elongation rate, tensile stress and tensile force expts. 80−38372
polymer melts, flow analysis of the non-isothermal two-dimensional filling process in injection molding 79−77038
polymer melts, flow in cooled channels, dimensional anal. *(German)* 79−81833
polymer melts, shear flow, network theory in nonlinear region *(German)* 79−77050
polymer melts and solutions, rheological equations, review 79−86391
polymer solns., dilute, extensional and sink flow in channel 80−74925
polymer solns., hydraulic resistance of channels calc. *(Russian)* 80−38451
polymer solns., turbulent flow through smooth and rough tubes, viscoelastic flow models *(German)* 77−11224
polymer solns., unstable flow, reservoir to capillary, jet instability onset and flow patterns, obs. 78−87364
polymer solns., weak, turbulence near walls *(German)* 77−15109
polymer solns. and suspensions, hydrodynamic interactions, Navier-Stokes eqn. calc. *(Russian)* 79−32652
polymer solution, admixtures influence on origin of vortices in wake behind cylinder 77−58744
polymer solution, bubble elongation dynamics, modelling with viscoelastic constitutive relations 79−37388
polymer solution, conc., constitutive eqn. applic. to shear and elongational flow 79−90292
polymer solution, dil., rotating Couette flow, elongational viscosity and stability 79−27669
polymer solution, dil., turbulent flow behaviour in annulus 80−33633
polymer solution, flow in exit region of tube, jet swell problem 80−38452
polymer solution, flow visualization near rot. disc 79−72914
polymer solution, free precipitation of spherical particles in centrifugal force field 77−11247
polymer solution, laminar wake behind cylindrical body 79−37355
polymer solution, power laws of reduced turbulent friction for pipe flow 77−15068
polymer solution, turbulent flow investig. using laser Doppler velocimeter 77−58822
polymer solution, viscoelastic, in annular die entry, upstream flow charcts., instability onset 79−60036
polymer solution, viscoelastic, radial flow, expt. 77−15072
polymer solution, vortex inhibition, velocity profile meas. 77−19628
polymer solution laminar capillary flow, excess press. drop 79−60038
polymer solutions, concentrated, rheological relationships 77−75867
polymer solutions, diffusion of ionic species, meas. by diffusion controlled electrolysys 80−74920
polymer solutions, liquid cryst., rheo-optics of shear and elongational flow, quiescent and flow birefringent charcts. 80−83773
polymer solutions, weak, flow anomalies *(Russian)* 80−19454
polymer thickened motor oil, flow in convergent jet thrust nozzles 77−75959
polymer-thickened oil, flow in convergent jet-thrust nozzles at 84°C 79−23348
polymeric, liq., spike-strain test relevance for network connectivity destruction by deformation 80−60013
polymeric liquid, steady shear flow, parallel superposition of oscillatory motion 79−18919
polymeric liquid pulsatile flow in circular tubes, flow enhancement, Goddard-Miller model 78−30324
polymeric liquids, rheology, fluid mechanics, book 77−65772
polymeric liquids in pipes, non-steady two-phase stratified laminar flow 79−81832
polymeric systems, fluid, rheology, characterised by mol. int. distrib., review 80−1504
polymers, flow in channels of noncircular cross-section 77−7451
polymers flow through a noncircular channel *(Rumanian)* 79−50795
polymethylphenylsiloxane liquid, pumped, improved heat transfer near crit. press. 77−7421
Polyox dilute soln., elongational flow obs. 79−60029
polyoxyethylene, dil. solns., laminar flow in tubes, scale effect 79−86472
polyoxymethylene-copolyamide melts, flow, fibrillation, mechanism 77−4765
polypropylene, melt and glass bead filled melt, velocity field rearrangement in stagnation flow leading to diverging radial flow between parallel plates 79−37360
polypropylene melt, flow in profile channel of extrusion head 79−98780
polystyrene, ordered monodisperse latexes, viscoelasticity and flow props. 80−58992
polystyrene, solns., nonlinear viscoelasticity, stress development at start of shear flow 77−3800
polystyrene melts, flame-retardant high-impact, shear viscosity-temp.-shear rate relationships 80−59691
polystyrene solution, internal viscosity, model for Lamb-Matheson-Philippoff increment 77−62284
polystyrene-Aroclor 1254, streaming birefringence in extensional flow 80−6013
polytropic plastic gas, nonstationary shock wave propag., closed form soln., thermonuclear microfusion 80−28534

non-Newtonian flow continued
pore geometry effects on pressure loss, model channels with varying diameter *(German)* 80−1677
porous channel inlet region, second order fluid flow, injection effects 79−68804
power law fluid, approx. soln. of two-dimens. laminar boundary layer flow *(Japanese)* 77−72337
power law fluid Couette flow, entrance region heat transfer 79−32587
power law fluid flow in pipes, entrance region heat transfer 79−1218
power law fluids, laminar flow through granular beds 80−38488
power law fluids, mass transfer into boundary layers 79−32588
power law fluids laminar pipe flow, heat transfer 78−59425
power law liquid, flow between eccentric rotating cylinders 77−65766
power law liquid flow around rigid sphere, asymptotic analysis *(Russian)* 77−31337
power law non-Newtonian liquid, stability of laminar boundary layer 77−55048
power law pseudoplastic laminar tube flow, heat transfer 77−80184
power-law fluid, fluctuating flow past porous flat plate 77−68639
power-law fluid, free convection around thin bodies of revolution under second kind boundary conditions 77−7422
power-law fluid, nonsteady heat exchange during steady flow in initial thermal section of tube 77−47046
power-law fluid, two-stream mixing along flat plate, variational solns. 80−53817
power-law fluid laminar jet flow 79−32619
power-law fluids, laminar flow in concentric annuli, vol. flow, press loss. calcs. 79−94681
power-law fluids flowing between two rot. coaxial circular cylinders, heat transfer rates 77−58742
power-law liquid, dil. suspensions of dipole dumbbells, rheological eqns. of state and shear flow in elec. field 79−86473
power-law non-Newtonian conducting fluid, laminar boundary layer in transverse mag. field 80−33694
Prandtl-Eyring fluid, flow between parallel plates, and in plain bearings *(German)* 78−94771
Prandtl-Eyring law appl., jetstream pump parameters *(German)* 78−30331
pseudoplastic fluid, flowing upward in vert. heated tube, variable physical props. 78−90945
pseudoplastic fluid, nonlinear singular boundary value problem 80−79362
pseudoplastic fluid crossflow around circular cylinder, heat and mass transfer 80−19370
pseudoplastic fluid flow in pipes, press. loss 79−98765
pseudoplastic fluids, heating in laminar flow 78−34128
pseudoplastic liquid film, wave motion 79−32583
pseudoplastic liquid flow in planar laminar boundary layer 79−86470
pulsatile flow, in circular pipes, Maxwell model 78−90937
pulsatile laminar pipe flows, multiviscous approx. 77−3871
pump with fixed and moving wall, steady shear flow *(German)* 78−87367
PVA soln., flow in profile channel of extrusion head 79−98780
PVC, emulsion, melts, slip, visual observations 79−4047
PVC, flow behaviour, particulate and melting flow, rheology 79−3981
PVC, rheology, viscoelasticity 79−3982
PVC, suspensions, melts, rheological props. rel. to struct. 79−3983
PVC cpds., rigid, plasticised, capillary flow 79−4046
PVC plastisol, flow behaviour at high shear rate *(German)* 80−92186
PVC suspension rheological props. *(German)* 79−94579
quadratic shear flow, rigid sphere and drop migration 77−84309
Rayleigh problem for purely viscous fluid, pseudosimilarity soln. *(German)* 79−37364
rectilinear flow, pressure error upper and lower bounds with pressure gradient 80−6010
rectilinear pipes, triangular and elliptical cross section, stress distrib. and thrust on walls 79−32585
recuperative heat exchanger, convective heat transfer, nonNewtonian carrier, conjugated problem 79−1086
Reiner effect, hydrodynamics of viscous fluid in A.S. Predvoditelev's form 77−55046
Reiner-Rivlin fluid, circular cylinder longitudinal motion in coaxial cylinder 79−10597
reinforced fluid rheology 77−51017
review 79−60010
rheological electrokinetic phenomena in rectangular capillary, numerical simulation 80−26023
rheological models, choice of expt. plan and model 77−7420
rheometry, flow curve evaluation 78−83352
Rivlin-Ericksen fluid, flow about rot. sphere 78−30323
Rivlin-Ericksen fluids, steady universal motion 79−68757
Rivlin-Ericksen viscoelastic fluid, unsteady flow through confocal elliptic cylinders 79−37354
rolling, Newtonian or non-Newtonian liqs., two-roll mill problem 78−42616
rotating cylinders, roll separating forces and specific power consumption 77−80186
rotating disc induced flow, mass transfer 79−41717
rotating liquid film, of 2nd order fluid, free surface instability 79−37294
rotational flow between 2 parallel plates, unsteady flow of Rivlin-Ericksen liq. 78−30320
rotational quasi-viscometric flows around a rotating sphere 79−60023
rotational viscometric flow around rotating sphere *(German)* 77−80187
rotatory oscillatory flow, rheological consts. determ. 78−30251
round tubes, non-Newtonian fluid transition and turbulent flow regions *(Russian)* 80−59077
rubber toughened plastics, ABS- and AAS-resin, flow props., effect of heating and shearing hysteresis *(Japanese)* 79−94685
sand, fluidised, determ. of flow parameters by simple model and new distributor design 78−83493
second order fluid, oscillatory convection flow from vertical plate 77−7423
second order fluid, unsteady motion between parallel plates 78−30321
second order fluid in curved annulus 79−72915
second order liquid porous parallel walled channel flow with free and forced convection 78−42635
second-order fluid, flow separation at straight edge 77−15079
second-order fluid, migration of spheres in two-dimens. unidirectional shear flow 77−940
second-order fluid, plane flow past submerged boundaries 77−75945
non-Newtonian flow continued
second-order fluid, rectilinear flow, pressure error, boundary integral approach 80−59081
second-order fluid between infinite rot. discs with injection 77−11223
second-order fluid creeping flow, stick-slip and die swell 78−30325
second-order fluid flow in curved pipe 78−59427
second-order fluid forced flow against rot. disc with uniform high suction 77−27564
second-order fluids, oscillatory free convection from infinite horizontal cylinder 77−72332
second-order viscoelastic fluids, superposition theorems 77−35181
secondary flow in cylindrical tubes 78−30327
shear flow, eqns. of state 79−23344
shear flow, non-Newtonian effect and long-range correlation 79−46349
shear-thinned fluid, laminar heat transfer and drag 79−68764
sheared coagulated sols, energy dissipation during sheared flow 78−63461
shock wave reflection from concave surface, numerical simulation 79−18913
simple fluids, small strain oscillatory squeeze film flow, polymeric liquids 80−92765
slip phenomena, thermodynamic approach 80−59083
slotted extrusion head channels, flow mechanism in *(Russian)* 77−55933
solid-fluid interaction in flow through porous media, fluidised beds *(Portuguese)* 80−38454
solid-liquid mixtures, rheological charact., shear stress/strain rate relationships 80−10287
solute dispersion in non-Newtonian fluids, chemical reaction effects 80−38503
sphere behaviour in non-homogeneous flow of viscoelastic fluid 77−68640
sphere surface viscoelastic Prandtl boundary layer flow, separation point 78−63460
spherical gas bubble in unsteady viscous flow, unsteady boundary layer 79−55357
spherically symmetric polymer, time depend. compressible flow, Faxen theorems 79−23345
spinning, isothermal, of Newtonian and viscoelastic liq., draw reson. instability 79−60027
spreading of film between two colliding surfaces produced by shock wave 77−7419
square duct entrance region, Laminar flow and heat transfer to non-Newtonian fluid 80−10243
squeeze-films, elastico viscous, torsional balance rheometer meas. 77−3851
squeeze-films, elastico-viscous, superimposed rotation 77−3850
steady Ekman flow of micropolar fluid, geometrical aspects 77−89169
stiff polymer dilute solutions, non-Newtonian viscosity 77−35103
Stokes flow due to body rot. in micropolar fluid 78−38372
stream falling under gravity, horizontal displacement causing curved stream 79−72917
stress field of slender particles oriented in extensional flow 77−19632
stress power and boundedness of flow 79−27668
stretching jet, convected Maxwell model 78−71379
stretching jet profiles, simple rheological models 77−75955
structural relaxing fluids, hydrodynamics theory *(Russian)* 80−19453
structured hydrocarbon systems, flow, rheological behaviour 78−59429
styrene-acrylonitrile copolymer, of azeotropic composition, Mark-Kuhn-Houwink relations *(Russian)* 79−50176
surface diffusion flux in Newtonian or nonNewtonian fluid, laminar flow, double pulse meas. *(French)* 78−40055
surfactant solns., rheological props., hydraulic loss reduction in tube flow 77−65768
suspension, dil., of spherical particles in non-Newtonian liq., rheological behaviour 80−24058
suspension, dilute, arbitrary-shape particles, time-depend. flow, Brownian rot. effect 78−26188
suspension, effective viscosity, statistical theory 79−90290
suspension in polymer melt, plastic-viscoelastic constitutive eqn. 79−60014
between symmetric rotating bodies of revolution, natural coord. system 77−15081
thermal boundary layers, in suddenly started viscoelastic fluid in circular pipe entrance region 78−9658
thermorheological secondary flow in cylindrical tube 79−60015
thermoviscous fluid, steady flow through straight tubes 80−33636
third grade fluids, viscometric flows 80−69883
thixotropic fluid, shear flow, oscillatory Couette flow, apparent viscoelasticity 79−90288
thixotropic fluid, shear flow *(Russian)* 78−87365
thixotropic fluids, rheological characterisation 80−38373
torsional oscillations of a non-Newtonian fluid with a free surface 79−94682
transient viscosity determination method 80−43746
tube during steady flow, small internal press. meas. 78−51260
tubular reactor with non-Newtonian laminar flow, diffusion and raction analysis 77−68703
turbulence, book 78−90839
turbulence, book contrib. 77−58775
turbulent boundary layer flow of power law fluid, mass transfer 77−31339
turbulent flow, in coiled tubes, anal. and exptl. verification 77−55052
turbulent flow with polymeric additives, convective heat transfer 79−77098
turbulent heat transfer in dilute surfactant or polymer solutions 79−77101
turbulent jets, influence of drag reducing polymers on cavitation inception 80−106823
turbulent pipe flow, use of eddy viscosity expressions for vel. profiles in Newtonian, non-Newtonian and drag-reducing flows 80−83789
turbulent shear flow without solid boundaries, effect of polymeric additives 79−77084
turbulent transport in circular tube 77−39313
two infinite parallel plates, non-Newtonian fluid linear flow, heat transfer 79−98810
two-phase flow through rectangular duct, interfacial instability 77−31359
tyre treads, scrap, rheological behaviour of rubber and crumb mixtures 78−55619

non-Newtonian flow continued
ultimate shear stress meas. by modified impact viscometer at high pressures 79−18980
uniqueness and drag for fluids of second grade in steady motion 79−32584
unsteady compressible flow in ducts, modified governing eqns. 79−46392
unsteady laminar flow of elastic viscous fluid through porous channel, applied mag. field effects 80−38499
unsteady laminar incompressible boundary layer eqns., flow, heat and mass transfer, similarity solns. 79−32590
unsteady pipe flow of viscoelastic fluids−possibilities of volume discharge increase *(German)* 79−50797
viscoelastic, test particle approach to flow classification 77−23996
viscoelastic (viscoplastic) fluid, free coating of vert. surface 78−42576
viscoelastic and inelastic fluid flow past sphere, creeping and boundary layer flows, drag coeff. 77−51090
viscoelastic boundary layer flow, second order, at stagnation point, heat transfer 80−103025
viscoelastic boundary-layer flow past a parabola and a paraboloid 80−83817
viscoelastic capillary jets, stability 79−46352
viscoelastic conducting fluid on oscill. plate in mag. field 77−72365
viscoelastic converging pipe flow, vel. vectors and radial stresses, rheological model and laser anemometry 79−60028
viscoelastic droplet break-up, in nonuniform shear flow 80−64588
viscoelastic Ekman layer on porous plate 77−72336
viscoelastic flow, continuum thermodynamic theory, configurational entropy effects 78−1621
viscoelastic flow, finite element simulation 80−43745
viscoelastic flow at stagnation point over moving wall 78−18319
viscoelastic flow in tube, eddy diffusion reduction for heat and momentum transfer 78−22382
viscoelastic flow past stationary and rotating cylinders 80−43744
viscoelastic flows involving abrupt geometry changes, long-range memory effects 77−15077
viscoelastic fluid, axial laminar flow, force exerted on wall *(German)* 77−68643
viscoelastic fluid, bubble and solid particle separation through apertures *(German)* 79−37389
viscoelastic fluid, creeping flow through tapered contraction 77−55050
viscoelastic fluid, deformed sphere motion 79−81831
viscoelastic fluid, effect of small polymer additions *(Russian)* 77−39316
viscoelastic fluid, elongational flow, elongational viscosity 78−14061
viscoelastic fluid, elongational flow, gas bubble collapse 78−14060
viscoelastic fluid, flow induced by elliptic harmonic oscills. of disc 79−4044
viscoelastic fluid, flow stability in converging channel against perturbations *(German)* 80−1654
viscoelastic fluid, fluctuating flow in a porous channel 79−64774
viscoelastic fluid, free convection flow past a vertical wall 80−10239
viscoelastic fluid, free surface between cylinders rotating at different speeds 80−59082
viscoelastic fluid, homogeneous shear flow, rigid particle slow motion 77−84308
viscoelastic fluid, MHD flow past porous plate in slip flow 79−4084
viscoelastic fluid, motion of rigid particles 80−103044
viscoelastic fluid, nonlinear stress relax. after steady shear flow 77−51015
viscoelastic fluid, oscillatory flow past infinite porous plate with variable suction 78−38373
viscoelastic fluid, Poiseuille flow and temp. distrib. 79−60039
viscoelastic fluid, stability of laminar boundary layers *(German)* 77−72335
viscoelastic fluid, stability of steady shearing flows, energy method and parabolic maximum principle 80−74926
viscoelastic fluid, steady flow and heat transfer between two coaxial rot. discs 80−14755
viscoelastic fluid, suspension of two identical spheres, interaction anal., general homogeneous flow 78−63455
viscoelastic fluid, thermal boundary layer on porous plate 77−84283
viscoelastic fluid, turbulent flow, frictional drag reduction 78−1696
viscoelastic fluid, turbulent wall motion 77−55047
viscoelastic fluid, unsteady flow through long circular ducts 79−77249
viscoelastic fluid, unsteady motion due to sphere rotation 78−59426
viscoelastic fluid film, flow along conical rotor 78−1697
viscoelastic fluid flow, eqns. of state and motion, direct numerical soln. 79−60021
viscoelastic fluid flow, mixed finite element anal. 77−39315
viscoelastic fluid flow between parallel plates, inertia elasticity and shear thinning props. *(German)* 78−55665
viscoelastic fluid flow in annulus entrance region, boundary layer anal. 78−63459
viscoelastic fluid flow in fixed geometry, collocation and Galerkin finite element methods 80−14750
viscoelastic fluid flow in nozzles, entrance press. losses 78−59442
viscoelastic fluid fluctuating flow past infinite porous wall in slip flow regime 79−18917
viscoelastic fluid in annulus, entry flow anal. 78−1699
viscoelastic fluid in channel entrance, hydrodynamic and thermal boundary layers 79−18915
viscoelastic fluid layer, convective instability, boundary thermal cond. independence 78−9659
viscoelastic fluid layer heated from below, vertical periodic oscillations, convection, overstability 80−48755
viscoelastic fluid lubrication, slider-bearing config., non-Newtonian normal stresses 80−69753
viscoelastic fluid tubular entry flow, velocity field in stable flow 79−50757
viscoelastic fluid unsteady flow through pipes under different press. gradient conditions 78−75172
viscoelastic fluids, dumbbell shaped particles, orientation in shear flow *(German)* 79−27673
viscoelastic fluids, heat transfer at low Deborah numbers, rheological effects 80−19445
viscoelastic fluids, material parameter meas. system 79−32722
viscoelastic fluids, secondary flows 77−68644
viscoelastic free convection boundary layer flow past infinite plate with constant suction 78−90936
viscoelastic laminar flow, combined generalised measure approach, pseudoplasticity 80−64586
non-Newtonian flow continued
viscoelastic laminar flow round spherical obstacle, finite boundaries effect 77−15076
viscoelastic layer, flow down inclined plane, finite amplitude long wave stability 79−37365
viscoelastic linear fluid, viscous dissipation of flow between eccentric rotating discs 77−58745
viscoelastic liq., motion of slender rod falling near vertical wall 80−43743
viscoelastic liq. film in rot. mixer 79−90291
viscoelastic liquid, boundary layer anal. of oscillating cylinder flows 77−65771
viscoelastic liquid, boundary-layer flow past symmetric wedge or right circular cone 80−64513
viscoelastic liquid, flow through porous channel, free and forced convection effects 80−53861
viscoelastic liquid, pulsatile flow in elliptic cross-section channel 79−7392
viscoelastic liquid, radial flow, expt. 77−15072
viscoelastic liquid, radial flow, theory 77−15071
viscoelastic liquid, with allowance for yield stress 77−84280
viscoelastic liquid channel flow, boundary-initial value problem 79−4045
viscoelastic liquid in corner, flow under pressure *(German)* 78−94772
viscoelastic liquid injected into Newtonian turbulent pipe flow, diffusion and drag reduction *(German)* 79−77251
viscoelastic liquid steady flow about porous rotating disc 79−32586
viscoelastic liquids, Poiseuille flow, hole-press. meas., computer model 80−59080
viscoelastic liquids, steady non-viscometric flow, review, book contrib. 77−47049
viscoelastic materials, time-depend. non-linear stresses, constitutive eqn. 77−35178
viscoelastic materials, time-depend. nonlinear stresses, memory function nonlinearity 77−35180
viscoelastic materials, time-depend. nonlinear stresses, shear and uniaxial elongation 77−35179
viscoelastic Maxwell fluid, unsteady flow between parallel planes, in transverse mag. field 78−38411
viscoelastic Maxwell liquid, torsional transient motion between concentric spheres 77−62283
viscoelastic medium, transitional flow, lag time eval. 80−38371
viscoelastic non-Newtonian fluid flow between eccentric rotating cylinders 77−84282
viscoelastic polymers, surface wave calcs. 79−32593
viscoelastic radial flow between parallel discs 78−67223
viscoelastic reacting fluids flowing over flat plate, boundary layer anal. of surface deposition 78−42675
viscoelastic Rivlin-Ericksen fluids, unsteady flow through circular and coaxial ducts in radial mag. fields 78−42632
viscoelastic solutions, first and second normal stress differences in steady laminar shearing flows 79−46348
viscoelastic squeeze films, effect of normal oscill. and fluid inertia 78−67224
viscoelastic tube, pulsatile flow, non-Newtonian effects *(French)* 80−59113
viscoelastic tube filled with viscoplastic media, unsteady motion 78−87366
viscoelastic unsteady flow through tubes 80−14753
viscoelastoplastic laminar tube flow, heat transfer 80−10269
viscolastic fluid velocity profiles at annulus inlet 80−64583
viscoplastic conducting liq., finite perturbations, Hartman flow instability *(Russian)* 78−47049
viscoplastic fluid Couette flow, heat transfer 80−10270
viscoplastic liq. in slot channel, peristaltic flow 78−5770
viscoplastic liquid, steady free convection 77−35175
viscoplastic liquid film on vertical vibr. wall, with slip, shaking loose 78−59371
viscoplastic media, flow in channels with varying cross section 79−94680
viscosity measurement, error correction in Couette viscometer *(German)* 78−94868
viscous drag reduction by polymer injection at high Reynolds number *(Chinese)* 79−32582
viscous flow in porous solid, relaxation phenomena *(French)* 78−87385
viscous fluid, flow and heat transfer due to disc small torsional oscills. 79−68691
viscous fluid under cyclic deform., self-heating, hydrodynamic thermal explosion 80−58993
viscous fluids, infinitesimal inviscid like motions 79−50761
viscous incompressible, finite element method, Bingham fluid 80−92184
viscous liquid in cylindrical nozzles, entrance press. losses 78−47012
wall region heat and mass transfer in turbulent Newtonian and viscoelastic flow 80−14680
wavy rod rotated, induced secondary flow, method of domain perturbations 78−63456
Weissenberg effect, review of expts. 79−60025
NaBr in hexantriol-1.2.6, structural relaxation shear and compressional viscous processes, electrolyte effects 79−94686
NaBr in hexantriol-1.2.6, shear relaxation 79−94687
Si_3N_4, aqueous suspension rheological and processing props. 77−23928
TiO_2 suspension in glycerine, Bingham plastic flow through annuli 80−64521

non-Newtonian fluids
see also colloids; polymer melts; polymer solutions; rheology
amorphous plastic injection moulding, frozen-in orientation, pressure loss during filling 79−77047
annular film, collapse under axial impact 77−84281
annulus with non-Newtonian fluids, mass transfer to inner wall, Leveque soln. adaptation 80−10267
basaltic lava flows, degassing effects on rheology 79−12115
Bingham fluids, single bubble motion and mass transfer 79−50758
bituminous pitch oils, flow curves, mag. field effect 80−33553
BKZ fluid tubular membrane, simultaneous elongation and inflation 79−90294
book, liquids and their props., mol. and macroscopic treatise 78−87604
butadiene-styrene three-block copolymer, rheological props., 60-110°C *(Russian)* 79−23292
carboxymethylcellulose, aq. soln., hydrodynamics of falling liquid film *(Russian)* 79−64715
carboxymethylcellulose, aq. soln., real flow curve determ., with wall effects, in rotation viscosimeters *(Russian)* 79−64714

non-Newtonian fluids continued
Casson fluid, gas bubble motion, behaviour, appl. to bubble in blood stream 79−10605
channel, cylindrical, arbitrary cross section, nonlinearly viscous medium motion 80−69928
concentrated disperse systems, non-Newtonian shear viscosity in steady flows 79−81957
concentrated disperse systems, non-Newtonian viscosity model 79−77231
constitutive equation 79−7388
constitutive equation derived from Lodges network theory 79−90207
convection, steady-state 78−22376
convective heat transfer theory in mixing 79−77094
Cosserat continuum, kinetic energy, linear and angular momentum densities, invariance 80−74829
Couette flow, vel. profile determ. 77−15074
Couette flow, with uniform suction at stationary plate 79−32637
couple stress theory, integral representation 80−33639
crosslinked polymer systems, probabilistic theory 80−19314
in cylindrical annulus, axial flow iterative calcs. *(German)* 77−11225
die-swell theory, analytical results 77−58624
diffusion coeffs., measurement by flow method 77−55045
dilatant liquids, propag. of shear perturbations 80−6103
disc rotating in non-Newtonian liquid, rheodynamics 77−15067
drag for fluids of grade three 80−33635
draw resonance theory, power-law and Maxwell fluids 78−83351
dumbbell kinetic problem, rheology, Langevin approach 78−42633
Earth upper mantle, viscosity, non-Newtonian fluid 79−79770
elastico-viscous fluid, compressible, nonperiodic wave propag. 80−43724
elastohydrodynamic problems for rough bodies with non-Newtonian lubrications *(Ukrainian)* 80−24054
elastohydrodynamic traction, non-Newtonian thermo-viscoelastic, from combined slip and spin 80−103043
elongational flow, effects on product rheology 77−23998
extensional flow capillary rheometer for extensional viscosity meas. 78−55704
extrudate swell, inelastic theory 80−43684
film flow along vertical oscillating plate *(German)* 78−59431
film flow over soluble wall, solvent layer form 78−42634
fluid mechanics, non-Newtonian, scope, critical examination 77−3849
fluid-film flows, of differential fluids of complexity n dimensional approach, lubrication theory appl. 80−16492
free convection effect on Stokes problem for vertical plate in elasto-viscous fluid 78−67226
gas and non-Newtonian liquid, stratified flow in horizontal pipes 80−48787
gas bubble oscills. in viscoelastic liq. 77−80202
hard-sphere liquid, shear viscosity, from nonequilib. mol. dynamics 79−19132
Hartmann flow, hydrodynamic stability, viscous core effects *(Russian)* 77−27611
heat transfer in jacketed agitated vessel, viscosity correl. 78−75143
heat transfer to pseudoplastic fluids in agitated vessel 77−35174
heating of viscous and non-Newtonian fluids on a rotating disk 79−77095
highly viscous fluids, nonisothermal flow in tubes and ducts *(German)* 79−32594
hydrodynamic calculations for container pipeline systems with non-Newtonian liquids 80−106817
ideal plastic material, film flow along oscillating wall 79−81927
incompressible viscoelastic fluid, Rayleigh-Taylor instability 80−79363
inelastic power-law, characterisation using falling sphere data 77−42875
interpenetrating EM structural continua, constitutive eqns. *(Russian)* 77−65805
kaolin suspensions, aq., flocculated and dispersed, rheological behaviour in pipe flow 80−64510
laminar flow in thin layer, two-dimensional problem 79−86474
laminar forced convection heat transfer in square duct, numerical solns. 78−18318
laminar heat transfer, in tubes 78−9624
laminar source flow between parallel disks 79−37363
Langevin analysis of dumbbells with hydrodynamic interaction 79−77042
liquid mixture separation by thermal diffusion in parasitic convection 80−64587
lubricant, frictional behaviour 79−87736
lubricant hydrodynamic theory *(German)* 78−79341
lubrication, elastohydrodynamic, between two rot. cylinders 78−83435
macromolecular solutions, laminar filtration under low polarization conditions 80−24056
mass and heat transfer, literature review 77−23999
Maxwell fluid, die swell, finite element anal. 80−83822
Maxwell fluid, Rayleigh-Taylor instability 80−33631
melt spinning for model viscoelastic liquids 78−71377
micropolar fluid, second order, fund. and constitutive eqns., thermodynamics and flow 78−20970
micropolar fluid layer subject to magnetic field, thermal instability 80−64585
micropolar fluids, thermodynamical aspects, non-linear approach 80−105598
momentum transfer in curved pipes 79−68814
multiphase non-Newtonian systems, rheological props. variation in barotreatment 80−19304
nearly viscometric glide bearing fluid *(German)* 79−81830
negative wake behind bubbles 79−64716
non-similar laminar boundary layers, rapid calc. procedure 78−90943
nonisothermal flow of viscous or non-Newtonian fluids over rotors of centrifugal heat exchangers 79−77097
nonlinear convection in elasticoviscous layer heated from below 77−68634
nonlinear viscoplastic media, dispersion in circular tubes for laminar motion case 77−58626
oscillating pipe flow, shear dependent viscosity effects 79−77190
pathological synovial fluids, viscoelastic props. at different shear rates 79−32430
peristaltic transport, long wavelength, stream function and pressure field solns. 80−74922
plastic non-Newtonian fluids in circular pipes, laminar flow stability loss 78−79342
Poiseuille flow, influence of vibr. 79−81930
polymer melt in intermittent shear flow, transient birefringence 78−63457
polymer processing, applications of rheology 77−23925
polymer solution, bubble collapse calcs. 77−933
polymer solution, dilute, aq., appl. of Hildebrand's fluidity model, apparent viscosity temp. depend. *(German)* 79−37366
polymer solution, viscoelastic properties, direct meas. method using channel flow 79−37265
polymer solution rheology based on a finitely extensible bead-spring chain model 80−83775
polymer solutions, dilute, normal stress difference and shear rate 80−83776
polymer solutions, flow behaviour in porous media *(German)* 78−55666
polymeric liquid, entropic elasticity and time temp. superposition principle, thermodynamic eqn. of state 78−63406
polymeric systems, rheology, review 78−87317
polymers, linear, viscoelastic props. under flow conditions, transition to highly elastic state *(Russian)* 79−50690
polypropylene melt, zero-shear-rate viscosity, press. depend. meas. 78−43164
polystyrene melt, normal and shear stress relax., Rheometrics mech. spectrometer transient response 78−42577
power law, heat transfer in plane Couette flow with additional pressure gradient including entrance effects 79−50760
power law fluid, rheology 77−3893
power law fluid, swarm of bubbles motion, mass transfer 79−50759
power law fluids, single bubble motion and mass transfer 79−50758
power law fluids containing oriented slender fibres, tensile behavior 79−37362
power-law liquid, dil. suspensions of dipole dumbbells, rheological eqns. of state and shear flow in elec. field 79−86473
power-law liquid, shear flow, general soln. for mag. rheology *(Russian)* 78−47003
Prandtl-Eyring fluid, flow between parallel plates, and in plain bearings *(German)* 78−94771
primary macromolecules, mol. wt. distrib. influence on crosslinked polymer systems 80−19313
pseudoplastic fluid, upper and lower Newtonian fluid behaviour 77−15080
pseudoplastic non-Newtonian liquid, laminar natural convection heat transfer 79−64713
Rayleigh classical equation generalisation to several non-Newtonian liquids 80−19444
Reiner-Rivlin fluids, rheological props. 80−14646
review, description and behaviour 80−33637
rheological props., pressure induced change of yield stress 80−53736
Rivlin-Ericksen fluid, dispersion medium on rheological behaviour of dilute suspension of dipolar dumbbells, viscoelastic props. 80−99983
Rivlin-Ericksen fluids, unsteady flow through circular and coaxial ducts in radial mag. fields 78−42632
roll clearance, control 79−41718
rotating disc induced flow, mass transfer 79−41717
rotationally symmetric flow *(German)* 78−55667
scale-up problems, review 79−23342
second order fluids, model, anomalous features 80−33632
secondary flow in noncircular pipe 77−15075
secondary flows, review 77−68644
Separan AP 30 aqueous soln., origin of hole press. in slit die apparatus 78−63462
shear rate calc. in coaxial viscometer, method comparison 79−4048
simple fluid shear depend. viscosity, central force interactions 80−79970
solid-filled systems, transfer phenomena, interface-adjoining phase struct. effects 79−77099
spheres falling in viscoelastic fluid, interactions along line of centres 77−15106
spherical gas bubble, in nonNewtonian liquids, growth by solute diffusion 78−34677
steady flow of non-Newtonian fluid through contraction 78−51205
stress relation to deformation, theory 79−59958
suspension, particle movement, appl. to dyeing and haematology *(German)* 78−87369
suspension of spheres in non-Newtonian fluid, viscosity 78−90807
thermomechanics, introduction, book 78−54187
thermoviscous fluid, steady slow motion through a circular tube 80−74921
third grade fluids, thermodynamics and stability 80−33638
thixotropic fluids, coagulation kinetics, diffusion effects and rheological models 80−43740
thixotropic fluids, rheological characterisation 80−38373
thixotropic liquid mixing, power requirement 77−15070
turbulent flow in absence of anomalous wall effects 80−69880
turbulent free convection heat transfer from flat vertical plate to power law fluid 78−67225
viscoelastic, resist. to tensile stress 80−1505
viscoelastic flow, heat transfer at low Deborah numbers, rheological effects 80−19445
viscoelastic fluid, flow anal. between 2-D surfaces subject to normal high freq. oscillations 80−16493
viscoelastic fluid, work estimate, convergence to equilib. 79−64718
viscoelastic fluid theory, entropy effects 77−14971
viscoelastic fluids, unstable tubular entry flow 79−90218
viscoelastic theories based on left Cauchy-Green tensor history 80−4534
viscosity measurement in rotational viscometer 80−19529
viscosity using capillary rheometer, end correction for power-law fluids 78−91037
Weissenberg effect, higher order theory 79−68766
C black conc. suspensions in low mol. wt. vehicles, rheology anal. 80−19312

noncrystalline state structure
see also amorphous state; vitreous state
Agave cantala natural fibre, small-angle X-ray scatt. of densely packed colloidal system, scatt. inhomogeneities 80−76565
aliphatic polymer fibres, supermol. struct., X-ray diffr. and acoustic methods 78−75570
alkali borate glass, IR absorption spectra and structure 79−8148
alkali borate glass, Mossbauer expts., 85-500K 78−80260
alkali borate glasses, Mossbauer effect 78−39476
alkali borates, vitreous and cryst., vibr. spectra and struct. comparison 78−23470
alkali germanate crystals and glasses, struct. and stability, IR spectra meas. 80−64911

noncrystalline state structure continued
alkali germanate glasses, struct., Raman scatt. obs. 80−1936
alkali metal oxide glass, composition dependence of activated processes, mixed alkali effect 79−77525
alkali silicate glass, suitability of small angle neutron scatt. for struct. determ. 78−22663
alkali silicate glasses, high temp. relax. mechanisms 80−70134
alkali silicate glasses, struct. and thermal props. 80−84075
alkali-silicate glasses and melts, partial molar vols. 79−94915
alkaline earth phosphate (MO-Al_2O_3-P_2O_5) irradiated electret glasses, relax. of external field intensity on heating 80−25282
alkaline earth silicate glasses, morphology effects on props. 80−49118
allophane, synthetic, amorphous mineral struct. obs. using ^{57}Fe Mossbauer effect 80−34836
alloys, amorphous, exhibiting Mossbauer spectra, elec. props. *(French)* 80−80244
alloys, amorphous, struct. disorder rel. to mag. moment, Curie temp. review *(Japanese)* 78−52259
alumina deposition by activated reactive evaporation, struct. obs. 77−44176
amgnetic thin films, amorphous, struct. and mag. props., review 80−93148
amino acid block copolymers, morphology and mech. props. 78−91264
amorphous alloys, struct. determ. by energy dispersive X-ray diffraction 80−84063
amorphous alloys, struct. phase transition *(Chinese)* 79−82336
amorphous and liquid semiconductors, conference, Cambridge, MA, USA (Aug. 1979) 80−41933
amorphous and ordered films, adsorbed on metal surface, electron state of adsorbed atoms *(Russian)* 79−51425
amorphous ferrimagnet, molecular field theory, struct. fluctuations 77−40018
amorphous ferromagnet, spin wave spectrum rel. to struct. 77−66290
amorphous materials, small area struct. studies 80−44087
amorphous metal, struct., simple computer modelling 79−19154
amorphous metals, elec. resist. temp. depend., phonon characterisation 79−60782
amorphous metals, low-temp. annealing, geometrical relaxation model on struct. charge and kinetics *(Japanese)* 79−94908
amorphous metals, struct., harmonic approx. model 77−47331
amorphous metals, struct. imperfections, review of expt. evidence 79−37630
amorphous metals and alloys, struct. modelling 77−31596
amorphous metals and ion implantation, review 79−14686
amorphous polymer, Rayleigh-Brillouin spectroscopy 79−38556
amorphous sample, struct. from inelastic and elastic electron scatt. *(French)* 79−90554
amorphous semiconductor, defect chemistry and states in gap, models 79−38030
amorphous semiconductor, local order as determined by electronic and vibrational spectroscopy 79−37627
amorphous semiconductor, tetrahedrally bonded, random stacking model, X-ray scatt. intensity 78−9953
amorphous semiconductor, tetrahedrally co-ordinated, random stacking model 77−62479
amorphous semiconductor alloy, bonding and transport properties 79−90950
amorphous semiconductors, fluctuations and non-randomness in continuous network models 80−49112
amorphous semiconductors, props., principles, appls. review 77−4287
amorphous solid, structural defects, computer simulation study 80−88040
amorphous solid, supercooled liquid-glass transition region, short-range order, simulation 80−44127
amorphous solids, low-energy excitations of phonons, magnons, electrons rel. to struct. factor 80−44488
amorphous solids, structure and low temp. props. 79−37631
amorphous structure, computer simulation 78−30541
amorphous tetrahedrally coord. solids, bond charge model 80−49108
amorphous thin films, crack networks of voids 78−2399
aromatic polymer fibres, supermol. struct., X-ray diffr. and acoustic methods 78−75570
asymmetric skinned synthetic polymeric membranes struct. 79−29417
atomic scale struct. determ., direct methods, review 79−37623
atomic-scale structure of amorphous solids, conf., Yorktown Heights, USA (Apr. 1978) 79−37622
B_2O_3-Li_2O-LiCl, ionic conductor, IR refl. Raman study 80−66173
BBB polybisbenzimidazobenzophenanthroline-dione, films, dynamic mechanical investig. at high temps. 77−4800
Bernal holes, size statistics 80−33892
bis-(p-toluene-sulphonate) of 2,4 hexadiyne 1,6 diol, X-ray scattering obs. of polymerisation mechanism and phase transition *(French)* 80−70399
bisphenol A polycarbonate, end-cap ratio and mech. props. of block copolymer 78−91266
bisphenol-A-diglycidyl ether epoxies, amine-cured, microscopic failure 77−90441
block copolymers, as ideal model system for a pseudo two phase solid texture, small-angle X-ray scatt. 79−14693
block copolymers, IR spectroscopy for struct.-props. relations 78−91268
block copolymers, morphology rel. to stress/strain props., deform. hardening effect, birefringence meas. 77−48501
borate glass: Ni, absorption spectra, mag. props., coordination behaviour *(German)* 80−40147
borate glass, ESR study of effect of glass composition on symmetry of Cr complexes 80−88052
borate glasses, mechanical relax. in transition range 78−80575
borate laser glasses, Cl^-coordinated, Tl^+, Mn^{2+} and Nd^{3+} impurities, absorpt. and X-ray obs. 79−38575
borophosphate glasses, effect of F on props. 78−67657
borosilicate glass, IR refl. spectra resulting from phase separation *(Japanese)* 78−39542
borosilicate glass film, vapour-deposited, structural model, IR spectra meas. 77−1084
borosilicate glass sputtered film, phys. and chem. props., B diffusion into Si, SiO_2 80−29040
borosilicate glasses, porous, IR spectroscopic obs. of coordination state of B atoms 77−24268
borosilicate microporous glasses, structural anisotropy and birefringence 79−8114
borozirconia glazes, low-melting, struct. and liq.-phase separation 79−60282

noncrystalline state structure continued
Bragg bubble glass, struct. and plastic flow 80−84091
butadiene, styrene, 4-vinylpyridine terpolymer, cross-linked by coordination with Fe (III) chloride, ion clustering 78−83748
butadiene-acrylonitrile elastomer, supramol. formations *(French)* 80−1941
butadiene-isoprene copolymers, monomer unit distrib., ^{13}C NMR determ. 78−26456
butadiene-styrene block copolymer, oriented, isotropic, struct. changes during deformation *(Russian)* 78−88512
butanediol terephthalate-polytetramethylene oxide terephthalate copolymers, dielec. props. 78−95546
cabal glass:SiO_2(TiO_2), microheterogeneity, and elec. cond. 78−83997
caprolactam oligomers, low-mol. wt., crystallisation kinetics from melt, solid structs. *(Russian)* 79−69034
carboxyl terminated butadiene nitride-diglycidyl ether of bisphenol A epoxy resin, struct. and mech. props. 78−52901
carnauba wax, thermoelectret orientation parameters, solidification with different cooling rates 79−38444
cellulose, mol. motions, role of water, temp. and morphology 77−89386
cellulose fibres, from jute, crystallinity percentage, estimation by X-ray methods 79−7553
cellulose hydrate, pulsed laser irrad., struct. changes *(Russian)* 77−66560
cellulose hydrated film, orientational heterogeneity, IR spectra and dichroism obs. *(Russian)* 78−38990
cellulose II, paracrystalline lattice disorder, X-ray diffractograms 78−83751
cellulose II, unit cell parameters, neutron diffr. 77−1086
cellulose triacetate, pulsed laser irrad., struct. changes *(Russian)* 77−66560
ceramics, glassy, struct. and electron beam sensitivity 80−79841
chalcogenide amorphous semiconductors, ESR studies of doped Mn, review *(Japanese)* 77−90019
chalcogenide glass, partial values and structure features 79−41969
chalcogenide glass films, photostructural changes, photodarkening 80−49121
chalcogenide glass structure modelling by Monte Carlo method *(Russian)* 79−55672
chalcogenide glasses, heteropolar, coordinations of ground state and of negative U defects 80−54137
chalcogenide glasses, struct. and growth kinetics, topological principles 80−49123
chemical bond stiffness, rel. to thermodynamic and kinetic props. *(French)* 77−72561
cholesteryl methyl carbonate, liq. cryst., low-ang. X-ray diffr. obs., solid and liq. 80−49093
Cl ThO_2 glasses, thermal anal. *(French)* 78−14282
conference on noncrystalline solids, Clausthal, Germany (Sept. 1976) 78−22654
copolyimide glass based on benzophenone tetracarboxylic acid dianhydride 77−63720
copolymers with interchanging struct. units, quasi-equilib. states 79−41975
covalent alloys, amorphous, dimensionality of subnetworks 80−28916
covalent amorphous semiconductors, local struct., bonding and electronic props. 78−51882
covalent elements, cohesion in condensed phases, corrections to simple Huckel approx. 78−59779
covalent elements, cohesion of σ and π bonds in condensed phases, simple Huckel approx. 78−59778
crystallography of amorphous solids, tentative description 80−6360
cyclohexanol, glassy cryst., diffuse X-ray scatt. study 80−100171
defects, EPR characterisation 79−38379
diepoxide-polyepoxide, relax. props. of cross-linked system *(Russian)* 78−51450
dispersion relation of phonon-like excitations 78−18727
elastic amorphous medium, relax. by defect diffusion 80−58925
elastometric glasses and porous network polymers, review of future developments 78−22657
electropolymerisation, on electrodes, book contribs. 80−50854
element, polymorphic bonding and thermal stability 77−31597
EM scattering techniques, phase retrieval methods 78−22656
epoxides, dielectric relax. and deform props., cross-link density effect *(Russian)* 80−60942
epoxy resin, low temp. thermal props., phonon states and crosslinked struct. *(German)* 78−75846
epoxy resin, nitroxide spin label doped, EPR study 79−78523
epoxy resin, thermosetting, crosslinking kinetics and structure *(German)* 78−76624
epoxy resin cross linked with aliphatic polyamines, struct. and dynamic mech. props. *(Japanese)* 80−38956
epoxy resins, struct. changes under mag. field action 80−40516
epoxy-anhydride-polycaprolactone, cross-linked block copolymer, morphology and impact strength 78−91265
ethanol-water system, metastable states, hydrates existence and props., low temp. 78−71835
ethylene copolymers, partially cryst. pseudoeutectoid, swelling, thermodynamics 80−39311
ethylene copolymers with acrylic monomers, NMR investig *(Russian)* 80−54959
ethylene-vinyl acetate copolymers, extrusion and heavy duty films, radiation crosslinking, struct. effect 80−66844
ethylene-vinyl alcohol copolymer, drawn samples, annealing effect around T_g temps. on shrinkage and mol. orientation 80−79712
EXAFS, for disordered solid struct. determ. 79−37624
extended X-ray absorption fine structure using real space transform, struct. determ. technique 78−23553
ferrimagnetic alloy, dipolar mechanisms for mag. anisotropy 78−64233
ferrocene, Willis disorder model *(French)* 78−83732
ferromagnetic amorphous system, directional order and induced anisotropy energy, theory 78−95431
film, high resolution STEM 79−37597
film, microporosity induced by nucleation and growth processes, TEM expt. 78−10303
fluoride systems, fundamental condition for glass formation 80−44135
fluorophosphate system glasses alkali free and crystn. products, struct. and IR spectra 79−94913
GdCo films, deposited on glass substrates *(Russian)* 80−24747
general theory development 79−41971

noncrystalline state structure continued
glass: ^{57}Fe, 2-parameter distrib. analysis using general inversion method 80−66079
glass, coloured, toughening process, spectral characts. 80−43416
glass, disclination lines, topological stability 80−33902
glass, elementary defect creation during glassmaking, model 78−22668
glass, glass surface, inhomogeneities and defects, detection using micro-bubbles, implantation technique *(German)* 78−47647
glass, heat treated, thin foil prep. for TEM obs. 78−7154
glass, homogeneity by Christiansen filter method 80−84066
glass, insulating, thermal, acoustic props., low temp. anomaly microscopic model 80−28921
glass, isobaric thermal behaviour during heating and cooling, rate of recovery, one-parameter model 80−75165
glass, low freq. Raman scattering by defects 77−8580
glass, microstructure, origin and meaning 78−88442
glass, molecular water, IR spectra 77−43992
glass, NMR investig. techniques 78−23358
glass, nonuniformities and basic principles of struct. 79−41970
glass, phase separated, EPR rel. to struct., elec. and opt. props. 78−23333
glass, phase separation and glass structure concept changes, review 77−65955
glass, relaxation memory effects, exactly soluble one-dimensional model 79−1398
glass, relaxation phenomena, review 78−2014
glass, relaxation phenomena and Raman spectroscopy, review of developments 78−22665
glass, review 78−2013
glass, rupture behaviour, long-term strength, thermofluctuation theory *(Russian)* 80−40536
glass, silicate, ultimate strength, and max. breaking rate 80−25863
glass, single-component, structure, crystallite and disordered-network hypotheses, review 79−41964
glass, struct. determ. using EXAFS 80−45169
glass, struct. formation during crystallisation, Mossbauer obs. 77−48106
glass, struct. relax., order parameter model 78−83740
glass, structure, influence of thermal history *(German)* 80−38930
glass, surface layer, model *(German)* 78−30817
glass, X-ray, neutron and electron diffr. studies, review 77−65954
glass fibre, elastic moduli, thermal history depend. *(Japanese)* 80−45333
glass fibre reinforced polyester resin composites, microstructure 79−37625
glass film, SiO_2 rich, prepared by modified CVD, refr. index behaviour 78−60526
glass local structure exam. by EXAFS 80−108301
glass porous, struct. and texture rel. to heat treatment effects *(German)* 78−44140
glass state, microscopic theory 80−44137
glass struct. study using small-angle X-ray scatt. 80−84071
glass structure, isobaric variation, phenomenological theory *(French)* 80−59393
glass transition temperature, determ from expansion and elec. cond. temp. depend. 80−19967
glass workability rel. to melting history, microstruct., apparent liquidus temp., mechanical props. 80−11633
glass-ceramics and photosensitive glass, microstructure rel. to properties *(German)* 80−38926
glass-forming systems, struct. transforms, temp. effect on chem. equilib. 79−94912
glass-forming systems, structure *(Russian)* 80−38925
glass-forming systems, structure and thermodynamics *(German)* 80−38924
glasses, inorganic, struct. by X-ray scatt. diffr. obs. 80−84069
glasses and ceramics, characterisation with analytical electron microscope 80−84068
glaze, effect of CaO and MgO content on microstructure 77−21083
hard sphere model of noncrystalline solids, homogeneous and isotropic appl. to metallic glasses 78−83731
hexamethyldisiloxane, polymer film, struct. determ., IR spectra, elemental anal. *(German)* 77−59224
high polymer physics, conf., Washington, USA (March 1978) 79−11633
hole structure of computer models 80−49109
ice orientational correlation parameter, water mol. dipole moment 80−59407
inorganic amorphous solids, struct., review 80−15004
inorganic glass, viscosity and free vol. 79−94916
inorganic glasses, thermal expansion coeff. rel. to phys. props. 80−49389
interpenetrating polymer networks, and related materials, review 78−42923
intertransition metal alloys, short-range struct. 79−50995
ion distribution function for complex solid, appl. to cond. of glasses 78−47585
kaolinite-mullite thermal sequence, structural analysis and transition phases 77−36484
Kevlar 29 and 49, aramid fibres, microvoid obs. 80−38960
Kevlar 49 fibre, macromol. struct., electron diffr. and dark-field electron microscope obs. 78−34446
lamellar structures, effects of distortions, small angle scattering, finite cluster model 79−10814
lead borate glasses, struct. 77−35485
Lennard-Jones amorphous solid, edge and screw dislocation, stability, elasticity, simulation 80−15099
lithium polyisoprene, struct. regularity and crystn. 80−103269
macromolecular aggregates, estimation of locations of subunits from neutron interference data 79−86716
macromolecular chains, coordinated motion simulation 79−86721
magnetic amorphous alloys, atomic struct., energy dispersive X-ray diffr. meas. 79−73100
materials props. microstruct. depend., book 78−88470
metal, amorphous, icosahedral microclusters as possible structural unit 78−34439
metal, amorphous, struct. model and SRO characts. *(Japanese)* 77−84654
metal film, amorphous, structural and amorphous props. 78−84323
metallic glass, atomic position correlations, nearly free electron approx. 77−39529
metallic glass, bulk and surface properties, review 80−44147
metallic glass, composition, mech. props., simulation 80−49117

noncrystalline state structure continued
metallic glass, density and Young's modulus, struct. relax. effects 78−72804
metallic glass, packing models and structural specificity 79−37629
metallic glass, prep. and phys. props. development 80−81003
metallic glass, review of current exptl. data 80−88058
metallic glass struct., one- and two-component hard sphere models 77−76312
metallic glasses, aged, atomic clustering exam. using positron annihilation methods 77−84655
metallic glasses, atomic struct., mech. and mag. props., prod. methods, uses 77−1081
metallic glasses, electronic structure, neutron scatt., elec. resist., Hall coeff., mag. susceptibility and XPS 78−23013
metallic glasses, electronic structure rel. to elec. cond., supercond. and mag. props. 80−65429
metallic glasses, free vol. theories of glass transition 78−14284
metallic glasses, glass transition temp. 79−99081
metallic glasses, mag. props., struct., and prep., book contrib. 79−65665
metallic glasses, mag. props. exam. *(German)* 77−89977
metallic glasses, mats. props. review 77−4043
metallic glasses, physical principles, manufacture, mech. and mag. props. *(French)* 78−83744
metallic glasses, Polk model and struct. 78−42916
metallic glasses, prep., characterization, review struct., formation, electronic, mag. and mechanical props., review 78−3074
metallic glasses, review *(German)* 79−41962
metallic glasses, review 80−88051
metallic glasses, stability, microscopic calcs. 79−32914
metallic glasses, struct. characts., preparation techniques, potential appls. *(Croatian)* 79−10800
metallic glasses, structure and crystallisation, review 78−2008
metallic glasses, structure direct obs. by bright field TEM 80−10502
metallic glasses and amorphous magnetism, review 79−82818
metallic glasses manufacture, struct. and stability *(Norwegian)* 79−14687
metallic glasses props., developments and appl. 80−19710
metallic layer, vapour deposited, struct., resist. component manufacture appl. *(German)* 77−55467
metalloid-transition metal amorphous surface alloys formed by ion implantation, TEM study 78−67730
metallomacrocytes, mixed valent, cofacial assembly, cond. polymeric material 80−70143
metals, amorphous, structure model, structural changes 80−92462
metals, glassy, structure, transport props., magnetic behaviour, review 80−70138
metals, rapidly quenched, conf., Brighton, England (July 1978) 80−67934
metals, struct. determ. by X-ray diffr. method *(Chinese)* 79−82126
metglas type system, structural and amorphous props. 78−84323
methacrylic acid-N,N'-ethylenedimethacrylamide crosslinked copolymer soln., 3-dimens. struct. peculiarities *(Russian)* 79−55678
methane-O_2, solid mixture, electron diffraction study *(Russian)* 78−83953
methanol-H_2O matrix, 77K, electron solvation and presolvation, electron spin-lattice relax. 79−57260
α,ω-methoxy-poly(ethylene oxide) effect of swelling on longitudinal acoustic mode 80−29739
microfibils of oriented polymers, struct. of amorphous sections 78−18559
microparacrystals, struct., theory *(German)* 80−59545
migration in Na_2O-Al_2O_3-SiO_2 glass 77−7902
mixed alkali glasses, Raman and far IR spectra, vib. at cation site, struct. 78−60435
models and exptl. methods, review 78−22655
multiphase polymer systems, conf., Ohio, USA (May 1976) 78−91262
multiphase polymers, morphology using electron microscopy 78−91271
multipolymers, glass transition rel. to phase separation 78−91270
Nafion, densities and expansion coeffs. as function of various parameters 80−79711
naphthalene derivatives, film struct., electron microscope and diffr. obs. 79−11029
network polymers, heterogeneous, from partially hydrolysed poly(methyl D-glutamate) and poly(oxyethylene glycol) *(Japanese)* 78−95002
neutron diffraction spectrometer, resolution and luminosity study for liquid on amorphous samples anal. 78−87591
nitrate glass: Eu^{3+} struct. reorganisation in glass transition interval, polarised luminesc. obs. 80−45141
nonvinyl polymers, diffusion of simple penetrants, statistical mechanical model 80−6556
nylon 66, doubly oriented, annealing of drawn and rolled samples, struct. 78−52859
nylon 6, α-form, crystal struct. and molecular packing 80−33905
Nylon 6, fibre, crystallite dimensions, effect on struct., mech. and diffusive props. 78−11273
nylon 6, relationship between morphology and dynamic mech. props. 79−4992
Nylon 6, small-angle X-ray scatt. struct. changes w.r.t. thermal and mech. history 79−41976
Nylon 6, solution crystallization 79−86719
nylon 6 fibres, highly oriented, fatigue process, struct. changes 77−90447
nylon 6 fibres, struct. changes due to strain annealing 79−15692
Nylon 6 film, prior high-press. treatment effects, weight swelling, density, IR crystallinity, X-ray and viscosity obs. 80−81025
Nylon 6 gut yarn, fine struct. change in twisting, annealing and untwisting, microbeam X-ray obs. 80−81026
Nylon 6 gut yarn, fine struct. change in twisting, annealing and untwisting, X-ray and electron microscopy obs. 80−84904
Nylon 6 yarns, NMR, fibre struct. rel. to annealing, drawing *(Japanese)* 77−32269
nylon 6-LiCl mixtures, DC cond. and struct., Lill effects 80−44149
Nylon-12, hydrostatic extrusion, struct. change *(Japanese)* 79−15693
Nylon-6, injection moulded, struct. and morphology 80−38949
nylon-6 dilute soln., gelation and crystallisation, struct. determ. 79−37635
Nylon-6 fibre, crystal struct., WAXS obs. 80−15015
nylons, glass transition temp., thermal, mech. meas. 77−31758
one-dimensional disordered system withshort-range order, struct. and model and config. entropy 77−80422
opal glasses, phosphate opacified, phase comp. and struct. 80−64919

noncrystalline state structure continued
optical fibres, UV radiation-induced losses rel. to colour centre form. 80−87517
optical spectroscopic methods of anal. *(French)* 77−77284
organic liquids, glasses and glassy crystals, entropy of struct. disorder, rel. to mol. struct. 79−65219
organosilicon ladder polymers, struct. and phys. props., book contrib. 79−65012
oxide glasses, γ-irrad., CuO effects on EPR 80−84645
oxide glasses with Bi or Se granules, elec. props. and microstructure 78−2490
PA-6, polymer fibre, orientation changes during stretching, IR spectra 78−75568
pair distribution functions, non-cryst. material, neutron diffr. data parameter calc. program 79−14652
pair distribution functions, non-cryst. materials, neutron diffr. data calc. program 79−14653
paracrystal theory, thermodynamic stability, statistical mechanics 78−75592
paracrystal theory appl. to real systems *(German)* 78−75591
perfluorocarbocyclic ethers, NMR, microstruct. 79−51863
PET, fibre, crystallite dimensions, effect on struct., mech. and diffusive props. 78−11273
PET, glassy polymer, local struct. determ. 80−33904
PET, uniaxially drawn, comparison of polarised fluorescence, polarised Raman and IR dichroism measurements 79−99084
PET fibre, molecular orientation determ. by US propag. velocity 77−58961
PET fibre, rel. to anisotropy of dielec. relax. 80−25297
PET fibres, amorphous, exam. of birefringence 80−11360
phosphate glass: Ni, absorption spectra, mag. props., coordination behaviour *(German)* 80−40147
phosphate glasses, non-alkaline, transition states, phys. effects of fluors, phase diagrams and optical effects *(German)* 80−88045
phosphate glasses, optical breakdown rel. to microscopic inhomogeneous struct. 80−102784
phosphosilicate glass film, vapour-deposited, structural model, IR spectra meas. 77−1084
photoemulsions, gels, coloured component addition, struct. form., dynamic shear modulus, viscosity meas. *(Russian)* 80−7871
pivalolactone-α-methyl-α-propyl-β-propiolactone copolymers, struct., thermal and mech. props. 79−43582
PMMA, amorphous, structural cause of orientation modification, exam. 78−67664
PMMA, amorphous, thermophysical props. depend. on hydrostatic press. 78−47612
PMMA, multicomponent network, pulsed NMR study of mol. motions 77−55724
PMMA, oriented, hypersound propag., elastic props. 78−75737
PMMA, struct.-prop. relationship between mol. wt. and fracture surface energy 78−80633
poly(1-butene), melting and annealing behaviour, X-ray diffr. and DTA 79−28083
poly(γ-n-amyl L-glutamate), crystal transition, X-ray diffr. exam. of structure 80−24374
poly(γ-n-butyl L-glutamate), crystal transition, X-ray diffr. exam. of structure 80−24374
poly(γ-n-ethyl L-glutamata), crystal transition, X-ray diffr. exam. of structure 80−24374
poly(γ-n-propyl L-glutamate), crystal transition, X-ray diffr. exam. of structure 80−24374
poly(alkyl methacrylate), vitreous state, thermal cond., hole theory of liqs., press. 78−84013
poly(m-methylene terephthalate) polymers, IR and Raman spectra 77−52088
poly(N-vinylcarbazole) layers, supermol. struct. effect on elec. props. 80−44606
poly(p-phenylene), AsF_5 doped, highly cond. charge transfer complexes, elec. and optical props. 80−70778
poly(p-phenylene terephthalamide) fibres, chain orientation distrib., and elastic props. 78−75566
poly(S)-2-methylbutyl vinyl ether, conformation, IR spectra 78−1116
poly(S)-5-methyl-1-heptene, conformation, IR spectra 78−1116
poly(tetramethylene terephthalate), IR obs. of reversible stress induced crystal-crystal phase transition 80−20627
poly(tetramethylene terephthalate), struct., X-ray obs. 80−19725
poly(tetramethylene tetraphthalate), IR studies of α crystal phase 77−62486
poly 2,3-dichlorobutadiene, struct., morphology, polymorphism 79−65008
poly (N,N-dipropylacrylamide), 'feathered' polymer resin, prep. from suspension 80−35533
poly-ε-caprolactone-PVC blends, morphology 79−69019
poly-arylate-dimethyl siloxane, polyblock copolymers, struct., thermodynamic stability *(Russian)* 80−64931
poly-m-phenylene, isophthalamide-b-dimethyl siloxane, morphology and tensile deform. 78−91263
poly-m-phenylene isophthalamide, precipitated from soln., morphology *(Japanese)* 79−14706
poly-m-phenylene isophthalamide-b-ethylene oxide, morphology and tensile deform. 78−91263
poly-m-toluenylsilsesquioxane mesomorphic struct., form. during polymerisation *(Russian)* 80−61095
poly-N-vinylcarbazole, polymerisation, struct., props., elec. characts., review 79−41972
poly-N-vinylcarbazole, struct. model, using NMR and diffr. data 78−83750
poly-p-benzamide fibre, supermol. struct., X-ray diffr. and acoustic methods 78−75570
poly-p-phenylene terephthalate, high modulus fibre, struct. obs. 78−75564
poly-tetramethyl-p-silphenylene-dimethylsiloxane block copolymers, crystn., morphology, kinetics 79−14695
polyacetylene:I charge transfer complex, struct. 79−74052
polyacetylene, AsF_5 doped, X-ray absorpt. meas., 5K to room temp. 80−71516
cis-polyacetylene, cryst. struct. determ. 78−75556
polyacetylene, nascent morphology obs. 80−24379
polyacetylene film, $(CH)_x$, synthesis, struct. and elec. props., doped materials, review 80−15623
polyacetylene-iodine derivatives, cryst. struct. determ. 78−75556
noncrystalline state structure continued
polyacrylamide gel structure inhomogeneity from permeability and viscoelasticity 77−89384
polyacrylic acid film, structurisation and mech. props., EM obs. *(Russian)* 80−59406
polyacrylonitrile, new model for structure, small-angle X-ray scattering and TEM study 79−77531
polyacrylonitrile, struct. of heat treated fibres, X-ray diffr. 78−83752
polyalkane imides, crystallisability, supermol. and crystalline structures 80−84100
polyalkenamers, longitudinal accordion mode, low frequency Raman spectroscopy 80−25369
polyamide, aromatic, fibre, high modulus, mol. and supramol. struct. 80−79710
polyamide blends, formation by injection moulding, structs. *(Russian)* 80−44155
polyamide-6, fibrillar struct. and annealing, small-angle X-ray diffr. 78−75565
polyamide-polyoxirane copolymers, mechanical properties evaluated 80−11700
polyamides, preoriented, method for increasing elastic moduli 77−80425
polyarylate organosiloxane polyblock copolymer, struct., props., phase conversion *(Russian)* 79−65010
polyarylbutadiene, microstructure, NMR and IR obs. *(Japanese)* 79−24488
polybiphenylacrylate, atactic, crystalline character effect on dynamic mech. response 78−56686
polybut-1-ene, cryst. forms I and II, far IR spectra 79−33708
1,2-polybutadiene, crosslinked in states of strain, entanglement networks, swelling anisotropy obs. 80−79666
high cis-,1,4-polybutadiene, orientation effects induced by shear rate in capillary extrusion 77−48389
polybutadiene-poly-α-methylstyrene copolymers, struct. obs., prep. *(French)* 80−59401
polybutene-1, microstructure determ. by ^{13}C-^{1}H NMR 78−26455
polybutene-1 film, tubular-extended, anal. of orientational and form birefringence 80−29712
polybutene-1 film, tubular-extruded, light scatt. from crystn. superstruct. 77−55796
polybutylene terephthalate, melt crystallised, solvent crystallised films and moulded bars, morpholigical obs. 80−84101
polybutyleneterephthalate, drawn annealed, struct. and props., X-ray scattering 79−7552
polycaprolactam, fibre, struct. change when used as resin reinforcement *(German)* 77−21091
polycaprolactam film, subjected to 9 kV elec. discharge, X-ray obs. *(Russian)* 79−23536
polycarbonate, amorphous, thermophysical props. depend. on hydrostatic press. 78−47612
polycarbonate, amorphous morphology, from NMR obs. of swelling penetrant mol. motion 79−27929
polycarbonate, bisphenol A, WAXS pattern, temp. effect and thermal history 80−93583
polycarbonate, electron microscopy 79−55675
polycarbonate, highly hot-drawn, mechanical prop. and phys. struct. changes 78−14293
polycarbonate, struct. ordering changes after annealing 79−94921
polycarbonate fibre, highly-oriented, drawing behaviour and mech. props. 78−76708
polycarbonate film, struct. and mech. props. 79−19160
polycarbonates unstretched and stretched, orientation relationships, ^{13}C NMR meas. *(German)* 80−20474
polychloroprene, microstruct. determ. by ^{13}C NMR 79−33546
polychloroprenes, microstruct., IR digital subtraction method, struct. irregularities effect on copolymer IR bands 79−38543
polychloroprenes, microstruct., IR digital subtraction method, struct. irregularities 79−42965
trans-1,4-polychloroprenes, prep. and struct., Raman spectra 77−66496
polycyclohexylphenyl acrylate, crystalline character effect on dynamic mech. response 78−56686
polydimethylsiloxane, end-cap ratio and mech. props. of block copolymer 78−91266
polydimethylsiloxane chains, with known radiative side chain amounts, model elastomeric networks prep. by sel. crosslinking 79−73106
polydioxolan, crystn. kinetics, dilatometric analysis and microscopy obs. 80−79706
polyelectrolyte, plasticised, effect of ion placement and struct. on props. 79−7679
polyester-polyurethane semi-interpenetrating networks, mech. props., morphology 80−45362
polyesteramide 6NT6 crystals, lamellar thickness invariance with crystallisation temp. 80−24380
polyesterimide polymers, quasicrystalline struct. 78−75571
polyesters, linear aliphatic, chem. struct. rel. to viscoelastic props. 79−41977
polyesters from bridged bicyclic lactones, struct. characterisation by NMR 80−20476
polyether sulphone, evidence for crystallinity 80−28928
polyethers, NMR, microstruct. 79−51863
polyethylend, high molecular weight film, fibril structure induced by oriented crystallisation *(Japanese)* 79−90575
polyethylene, amorphised by γ-irrad., interchain ordering, X-ray obs. 78−30545
polyethylene, amorphised by γ-irradiation, radial distribution function anal. for degree of interchain ordering 79−23530
polyethylene, amorphous, struct. from NMR line shape analysis and MAR-NMR 80−28931
polyethylene, amorphous fraction determ., multiple pulse NMR 77−77107
polyethylene, branched, annealing effect on lattice consts. 79−14698
polyethylene, bulk-crystallised, linear, PMR, phase struct. 77−84665
polyethylene, chain conform. in solid and melt, low angle neutron scatt. 77−76329
polyethylene, chain end fixing, NMR line shape calcs. *(German)* 78−76322
polyethylene, chain end fixing, spin-lattice relax. time *(German)* 78−76340
polyethylene, chain-extended, oriented, microindentation hardness 78−76728
polyethylene, chlorinated, microstructure, use of ethylene vinyl chloride and copolymers as macromolecular models *(German)* 77−27838

noncrystalline state structure continued
polyethylene, chlorinated, partial struct. anal. of methane component by ^{13}C nuclear magnetic resonance *(German)* 79−73110
polyethylene, cross-linked and low-density, pseudo spherulite structures and elec. discharges 78−42920
polyethylene, crystalline linear produced by rapid cooling from melt 77−19879
polyethylene, crystallinity, Raman spectral investig. 79−14696
polyethylene, crystallised from oriented melt, mech. and thermomech. props., framework struct. 77−63756
polyethylene, crystn. at high press., small-angle neutron scatt. 77−55248
polyethylene, dynamic mech. behaviour, longitudinal cryst. thickness 78−76691
polyethylene, effect of morphology on viscoelastic props. *(Polish)* 79−51008
polyethylene, extended chain crystal, fine structure and nucleation mechanism 78−14287
polyethylene, far IR absorption rel. to crystallinity 77−40242
polyethylene, fibre, phase structure and molecular mobility, broad-line NMR spectroscopy 78−14290
polyethylene, fibrous samples, struct. obs. by low-angle X-ray diffr. 78−34445
polyethylene, fine struct., prep., O_3 selective degradation, chromatographic obs. 78−92475
polyethylene, flow-induced fibril form. from soln. 80−59402
polyethylene, high density, hydrostatic extrusion conditions effect 77−63722
polyethylene, high density, oriented extended chain crystals, transparency *(Japanese)* 80−38955
polyethylene, high press. phase, US, DTA, and X-ray diffr. study 80−75188
polyethylene, high- and low-density, crystallinity degree, comparative obs. *(Polish)* 80−1943
polyethylene, high-density, lamellar sep. during deform. 78−23775
polyethylene, high-density, semicryst., fold-surface morphology effect on deform. processes 78−34447
polyethylene, high-density fibres, extrusion conditions influence on thermal props. and morphology 79−61617
polyethylene, high-density oriented, lamellar struct. obs. 77−55244
polyethylene, lamellar structs. nucleated onto fibrous substrates for high modulus 78−75578
polyethylene, lamellar two-phase systems, interface distrib. function determ. small-angle scatt. 79−10812
polyethylene, laser irrad. chem. and struct. modifications *(Russian)* 79−27931
polyethylene, lightly crosslinked, processed under mol. orient., struct., props., review 80−38957
polyethylene, linear, ^{13}C spin-lattice relaxation 80−25235
polyethylene, linear, γ-irradiated, crystallite size distrib. and lattice distortions 79−69157
polyethylene, linear, bulk-crystallised, morphology study 79−32918
polyethylene, linear, injection moulded at high press. struct. 79−11640
polyethylene, linear, melt-crystallised sharp fraction, lamellar morphology, electron microscopy obs. 80−84099
polyethylene, linear, quenching of thin films to amorphous state 80−28929
polyethylene, linear, single cryst., surface melting, X-ray diffr. 77−31755
polyethylene, linear, solution-crystallized, NMR anal. of phase struct. 78−71684
polyethylene, linear, struct. and relax. transitions, pulsed NMR and X-ray diffr. *(Russian)* 77−47357
polyethylene, low density, deformed in tension, lamellar reorientations 78−84914
polyethylene, low density, morphology and props. 80−64926
polyethylene, low-temp. relax., effects of chem.- and electron irrad.-crosslinking 79−4990
polyethylene, melt crystallized, amorphous phase, IR spectrum 78−76463
polyethylene, melting, equilib. temp., confomational modifications *(Russian)* 79−51240
polyethylene, mixed morphology and linear fractions, light scatt. obs. 78−2023
polyethylene, molecular motions, exam. by PMR line shape anal. 79−41982
polyethylene, NMR with rotation through magic angle *(German)* 78−76341
polyethylene, obtained with heterogeneous Ziegler-Natta catalysts, nascent struct. and morphology 79−96307
polyethylene, one dimens. synthesis of SAXS pattern 78−75589
polyethylene, oriented, partially crystalline, amorphous component obs., X-ray diffr. *(Russian)* 79−23534
polyethylene, polarised Raman studies of crystalline and amorphous orientation 78−67660
polyethylene, protonated and deuterated, neutron scatt. at intermediate Q-values 79−10807
polyethylene, pulsed NMR obs., crystallinity effects 78−76342
polyethylene, rapid crystn. from melt rel. to struct. 80−44152
polyethylene, SEM meas. of fine lamellar struct. 79−51007
polyethylene, short chain branching, ^{13}C NMR 79−33557
polyethylene, single cryst. and spherulites, microstruct., deform. micromechanisms 78−83758
polyethylene, single crystal, estimation of fold surface densities using space filling models 80−10507
polyethylene, single crystal, fold domain boundaries, TEM 80−107065
polyethylene, single crystal, structural changes due to electron irrad. 80−29053
polyethylene, solid, heterogeneity investigation by small angle neutron scattering 78−14298
polyethylene, straight chain segment length distrib., from Raman LAM-1 band 79−41981
polyethylene, stresses at spherulite boundaries causing black lines 77−72568
polyethylene, stretched, birefringence rel. to struct. changes 80−84714
polyethylene, supermolecular structure study, IR spectroscopy *(Spanish)* 79−77532
polyethylene, ultra-high modulus, micromorphology 77−63621
polyethylene, ultrahigh modulus linear, annealing effects on mech. stiffness and struct. 79−91717
polyethylene, ultrahigh-modulus, thermal cond. in region 2 to 100K 77−62690
polyethylene, ultraoriented, fibrillar struct. 77−89389

noncrystalline state structure continued
polyethylene, ultraquenched, electron diffr., morphology and thermal anal. 79−15640
polyethylene, uncrosslinked amorphous matrix embedded cryst. orientation distrib., strain energy and hydrodynamic pot. effects 78−9968
polyethylene, uniaxially stretched, density fluctuations 78−75587
polyethylene, vinyl group reactions during γ-irrad., crystallinity effect, absorbance obs. 80−81346
polyethylene, X-ray scatt., models for stacks of lamellae 79−37638
polyethylene crystal, longitudinal growth in flowing soln., melting of continuous fibrillar crystal 80−19917
polyethylene fibres, electron microscope investig. of internal struct. 80−28926
polyethylene fibril, high mol. wt., high melting point crystal *(Japanese)* 80−38954
polyethylene film, gauche-trans transition, activation energy meas. by IR spectra 79−57220
polyethylene films, uniaxially and doubly oriented, crystallite size determ., microparacrystallite lamellar surface identification 78−48431
polyethylene films modified by polyacrylonitrile grafting before, after orientating elongation, struct. *(Russian)* 77−32554
polyethylene high press. phase, struct., phase diagram and compressibility 78−9961
polyethylene lattice, inclusion of chain defects, stat. approach 80−75190
polyethylene melt, rheology and molecular struct., melt identification from mech. props. 77−11490
polyethylene oxide, low mol. wt., effect of end-group on crystallinity and fusion 77−84897
polyethylene oxide, nascent and annealed, X-ray study of crystal structure 80−64922
polyethylene oxide, peculiarities of struct. form. near below the melting point 80−54150
polyethylene oxide 2000-200 mixtures, Raman scatt., small-angle X-ray scatt. 77−52089
β-polyethylene oxybenzoate, cryst. struct. and mol. conformation 79−55674
polyethylene single cryst., FT IR spectra, CH_2 rocking mode 78−2843
polyethylene single cryst., FT IR spectra, CH_2 wagging mode 78−2842
polyethylene spherulites, lamellar struct. obs. 78−30547
polyethylene spherulites, STEM and microdiffr. obs. of micromorphology 78−34444
polyethylene sulphide, thermal stability and stability against solvents *(Russian)* 78−51449
polyethylene terephthalate, amorphous material orientation determ. *(Polish)* 79−73111
polyethylene terephthalate, conformation rel. to orientation, pot. energy surfaces study 79−68338
polyethylene terephthalate, effect of excess thermodynamic props. versus struct. form. on dynamic moduli 77−86053
polyethylene terephthalate, electron microscopy 79−55675
polyethylene terephthalate, far IR absorption rel. to crystallinity 77−40242
polyethylene terephthalate, fibre, melting in crystn., intermediate and amorphous phases 77−84898
polyethylene terephthalate, glassy and partially cryst., X-ray scatt., differential radial distrib. function 79−14704
polyethylene terephthalate, mech. props., influence of cryst. arrangement and noncryst. region struct. 78−76707
polyethylene terephthalate, NMR relax. and mol. mobility *(Russian)* 78−88219
polyethylene terephthalate, oriented amorphous phase 78−95003
polyethylene terephthalate, stretching, heat effects, struct. transforms. 79−15735
polyethylene terephthalate fibres, high freq. US effects on physical and chem. structs. *(Polish)* 78−51446
polyethylene terephthalate fibres, interdependence between struct. and thermal contraction *(Rumanian)* 78−91259
polyethylene terephthalate film, gauche-trans transition, activation energy meas. by IR spectra 79−57220
polyethylene terephthalate film, X-ray diffr. exam. of morphology 78−18558
polyethylene terephthalate yarns, NMR, fibre struct. rel. to annealing, drawing *(Japanese)* 77−32269
polyethylene total joint replacement, props. improvement by C fibre reinforcement, SEM obs. 78−24183
polyethylene-polyoxymethylene mixtures connection of melt thermodynamic props. with solid state struct. *(Russian)* 80−54152
polyethylene-propylene copolymers, branching effect on struct. and mech. props. *(Russian)* 79−52333
polyethylenes, extrusion and heavy duty films struct. parameters influence on cross-linking by radiation 80−66844
polyethyleneterephthalate, crystallised from thin layer melts, temp. depend. of morphology 80−54149
polyethyleneterephthallate, sorption of low MW solvents on struct. and mech. props. *(Russian)* 78−11358
polyhexamethylene sebacate-poly 2-methyl-2-ethyl-1,3-propylene sebacate, cryst. multiblock copolymers, crystallisation 78−91269
polyhexamethylene terephthalate/polyoxytetramethylene block copolymers, supramolecular texture 78−91261
polyimide PMF1, macrochains packing in atom-atom approx. 79−41973
polyimide polymers, quasicrystalline struct. 78−75571
cis-polyisoprene, ^1H NMR, T_1 and T_2 meas., −50-170°C 79−69738
cis-polyisoprene, ^1H NMR of γ-induced cross-linked polymer 79−69739
polymer, amorphous, bulk, structure models and exptl. methods, review 78−22671
polymer, amorphous, chain conform., small-angle neutron scatt. obs. *(Polish)* 80−10511
polymer, amorphous, light scatt. and local struct. 77−81111
polymer, amorphous, molecular origin of relaxations 78−26058
polymer, amorphous, stress-optical investig. of short-range order 78−22672
polymer, amorphous state struct., conf., Atlantic City, USA (Sept. 1974) 77−76327
polymer, brittle, in vitreous state, resistance to brittleness and fracture kinetics *(German)* 77−32688
polymer, creep tests for determining degree of cross-linking *(German)* 78−76822
polymer, crosslinked *(German)* 78−75584
polymer, crystalline, dynamic mech. props., influence of struct. 79−4991
polymer, dielec. breakdown theories, mol. and morphological features rel. to elec. strength, review *(Japanese)* 80−60501

noncrystalline state structure continued
polymer, diffusion of simple penetrants, statistical mechanical model 80−10704
polymer, drawing properties, role of interfibrillar tie mols. 78−76706
polymer, ESCA investigations on selected systems, struct. and bonding obs. 78−14302
polymer, fibrillation during cold drawing *(Russian)* 77−63691
polymer, filled, thermosetting, anisotropic structure on injection moulding *(German)* 78−76625
Polymer, free vol. theory 79−94919
polymer, glass-like, DSC obs. of mol. interaction variations *(Russian)* 79−32924
polymer, isotropic, oriented, thermal cond., 2-100K, crystallinity effect 77−20137
polymer, melt-crystallised, one-dimensional characterisation of microstruct. 78−75588
polymer, microinhomogeneous, elastic props. description rel. to crystallinity 79−19307
polymer, molecular dynamics simulation of struct. 80−28923
polymer, molten or amorphous, chain conform. determ. by diffr. 77−80429
polymer, multicomponent, homopolymer blends, macroscopic phase separation 80−45289
polymer, noncrystalline solid, preferred orientation from scatt. ang. distribs. 78−75560
polymer, oriented, amorphous-crystalline low ang. X-ray diagrams, supermol. struct. models, schematic representation *(Russian)* 78−87630
polymer, oriented, thermostable, relax. transitions, thermomech. and isometric heating obs. *(Russian)* 79−23538
polymer, oriented crystalline, anisotropic thermal expansion 80−39324
polymer, packing coefficient determ. from acoustical meas. data 80−38959
polymer, plastoelasticity theory 78−75712
polymer, recrystallisation during drawing 78−76658
polymer, rigid-chain, unity of deform. and spontaneous elongation mechanism 79−20138
polymer, semicrystalline, model for thermal cond., orientation effects 77−85004
polymer, semicrystalline, mol. morphology 78−38631
polymer, semicrystalline, small-angle neutron scatt. function computation 79−10811
polymer, short range order, radial distrib. functions from X-ray diffr. 77−76330
polymer, solid, orientation meas. and characterisation methods uing X-rays 78−75559
polymer, stressed, config. free energy change due to partial crystn. of chains, distrib. of cryst. orientations 79−94923
polymer, yield behaviour, interpret. w.r.t. correlated motion 78−6973
polymer blends, morphology and compatibility, X-ray and optical obs. 79−69026
polymer blends, selective staining method for TEM obs. of morphology 80−84103
polymer chain, amorphous state, configs. 77−80427
polymer chain, Pade approximant method, appl. to excluded vol. effect 79−94918
polymer chain conformation, determ. by neutron scatt. in amorphous polymers 77−76328
polymer chain conformations in liq. and cryst. slates *(French)* 78−18552
polymer chain in bulk and soln., elastic, coherent small-angle neutron scattering 77−80428
polymer chain subjected to elongation, conformational microstruct. variation *(Russian)* 79−31756
polymer crystal, hydrostatic compressibility, H_2 bonding effect on anisotropy 80−25782
polymer crystalline structure stability *(Russian)* 77−19880
polymer fibre, highly oriented, struct. and mech. props. 78−75563
polymer fibrils, formation by flow-induced crystallisation 80−33908
polymer film, semicrystalline, tear resist. 77−52488
polymer film, stretched, mol. distrib. determ. by polarised spectra 78−27298
polymer films, rod-like superstruct., small-angle light scatt., vol. fraction, orient. effects 79−1795
polymer films, vertical development, from gas phase, computer simulation *(German)* 77−27839
polymer glasses, review of expt. results 79−37636
polymer lamella structure, crystallisation under high supercooling 79−69028
polymer mech. or elec. props., struct. recovery *(French)* 80−59393
polymer microstructure morphogenesis, book contrib. 78−83757
polymer network, crosslinks and trapped entanglements, two-network model 80−38962
polymer network, crystn. and form. through crystn., crystallinity influence on radiation induced form. 80−38964
polymer network, permanently crosslinked, topological struct. and macroscopic behaviour 80−37919
polymer network, Riemann's metric degeneration to graph metric demonstration, chain entanglement problems 80−38963
polymer network, small ang. neutron scatt. 79−90569
polymer network, small-angle neutron scatt. obs. of mol. behaviour 80−37918
polymer network formation, pre-gel intramol. reaction and gelation, shear moduli and glass transition 80−45501
polymer network formation, relaxational props. variation 80−38961
polymer network formation, struct. and mech. props., computer simulation 80−38965
polymer networks and semi-crystalline polymers, diffusion mechanism and model, local conform. change 80−15288
polymer orientation measurement, in solid, by spectroscopic techniques, mech. anisotropy 78−75558
polymer relaxation in glassy state, free vol. fluctuation effects 79−69022
polymer structure and mech. props., book 78−83756
polymer structure and optical behaviour 80−106583
polymer surfaces, appl. of ESCA to struct. and bonding 79−57344
polymeric chain orientation evaluation, with polarised fluorescence method *(Japanese)* 80−6368
polymeric compositions containing elec. cond. filler, struct. effect on elec. props., review *(Russian)* 79−33317
polymers, aliphatic and aromatic, mean mol. orientation factors, from IR spectra and acoustic method 80−70142
noncrystalline state structure continued
polymers, amorphous, segmental distrib., crystallisation and viscoelastic relax. meas. 78−51443
polymers, amorphous, semi-cryst., mech. motions, review 77−32616
polymers, amorphous, struct. rel. to mech. props. 80−79713
polymers, cluster model from acoustical props. 77−51446
polymers, conference, Shrivenham, England (Sept. 1977) 78−75576
polymers, crystallinity, kinetic and morphological aspects *(French)* 80−1942
polymers, crystallinity determ. by thermal method *(Russian)* 80−38966
polymers, defocus transmission electron microscopy 80−28927
polymers, elec. props. and morphology, correl. review 78−43786
polymers, Fourier anal. of X-ray diffr. patterns 80−15016
polymers, glassy, improvement of alignment in diffuse fibre diffr. patterns 77−55243
polymers, morphological study, using C replicas, wide angle electron scatt. *(Russian)* 79−32923
polymers, multicomponent, props. and struct., review 78−44076
polymers, multicomponent-multiphase, bulk struct. by rheo-optical techniques 78−91267
polymers, oriented, partly cryst., macromols. in amorphous regions, length, mobility 80−49132
polymers, processing of small-angle X-ray patterns *(Russian)* 78−71642
polymers, short range order, amorphous and liquid, ideal peak method calcs. 80−28900
polymers, small angle neutron scattering studies, deuteration effects 79−50956
polymers, solid, orientation effects, conf., Budapest, Hungary (April 1976) 78−75557
polymers, struct. determ. from elastoosmometric parameters 80−64923
polymers, structure and molecular dynamics, neutron scatt. meas. 79−51009
polymetallomethacrylates, Mossbauer spectra, long-range ordering 79−65776
polymethineimine, all-trans, ab initio cryst. orbital calcs. 79−77530
polymethyl acrylate, head-to-head, high-resolution PMR spectra 79−73834
polymethyl acrylate, multicomponent network, pulsed NMR study of mol. motions 77−55724
polymethyl cinnamate, head-to-head, high-resolution PMR spectra 79−73834
polymethyl crotonate, head-to-head, high-resolution PMR spectra 79−73834
polymethylene sulphide, thermal stability and stability against solvents *(Russian)* 78−51449
polyolefins, isotropic semicryst., neutron scatt. obs. of struct., radius of gyration 79−94922
polyoxymethylene, drawn, extra meridional reflections 80−24376
polyoxymethylene, low-strain deform., transmission electron microscope exam. 79−5013
polyoxymethylene, mol. struct., least squares refinement 79−86720
polyoxymethylene, rapid crystn. from melt rel. to struct. 80−44153
polyoxymethylene copolymers, solid, mol. motions, 4-315K, dynamic-mech. study 79−4258
polyoxymethylene-copolyamide mixtures, melt rheological props., extrudate microstruct. *(Russian)* 80−7530
polypentamethylene terephthalate, oriented fibres, struct. anal. of two cryst. phases 79−73108
polypeptides, poly-L-lysine based, comb-like, struct., physicochem. props. *(Russian)* 79−55644
polyphenylacetylene films, phys. struct., AC and DC cond. 80−44750
polypropylene, change of crystn. forms during purification 77−55934
polypropylene, isothermal crystn., effect of contact with fibrous substrates 80−79708
polypropylene, isotropic, molten and cryst., small-angle neutron scatt., chain-folding 78−63680
polypropylene, molten and cryst., mol. conformation, small angle neutron scatt. study 79−51012
polypropylene, oriented, thermooxidative degradation kinetics, durability, influence of mech. initiated processes *(Russian)* 79−24591
polypropylene, preoriented isotactic sheet, mol. behaviour in uniaxial drawing *(Japanese)* 77−68928
polypropylene, quenched form, struct., X-ray obs. 78−67661
polypropylene, shear effect on crystallisation *(German)* 78−75586
polypropylene, thermoplastic, supramolecular struct. and frictional props. of surface layers 77−70188
polypropylene fibers, and films, and their hard elastic precursor small-angle X-ray diffr. studies 79−10815
polypropylene fibre, melt-spun with twist, helical orientation and mech. props. 78−75569
polypropylene fibres, γ-irrad., microstruct. changes in glassy-high elastic state transition *(Rumanian)* 80−49347
polypropylene fibres, helically twisted, small-angle light scatt. 79−1765
polypropylene fibres, high strength, elastic 80−20992
polypropylene fibres, homologue mixtures, props. 78−76709
polypropylene film, effect of crystallinity on deformation mechanism of biaxial stretching 77−80426
polypropylene film and fibre, plasma etching 78−95871
polypropylene spherulites, refl. acoustic microscopy obs. 80−28922
polypropylene systems, elastomeric impact modifiers rel. to morphology 79−66154
polypropylene-nylon 11 fibres, bimodal cryst. texture, X-ray diffr. and electron microscopy 78−75567
polypropylene-PMMA graft copolymer, X-ray meas. of crystallinity of component polymer *(Japanese)* 77−58962
polysiloxane dizwitterionomers, mech. props., microstruct. 80−49131
polysiloxane dizwitterionomers, morphology, ionic aggregation 80−49130
polysiloxane dizwitterionomers, sorption of H_2O, mechanism 80−49506
polystyrene, (-Kraton G blend), rubber toughened, charact. by SEM 79−14697
polystyrene, amorphous, structural cause of orientation modification, exam. 78−67664
polystyrene, amorphous, thermophysical props. depend. on hydrostatic press. 78−47612
polystyrene, atactic, effect of excess thermodynamic props. versus struct. form. on dynamic moduli 77−86053
polystyrene, chain conform. in solid and melt, low-angle neutron scatt. 77−76329
polystyrene, conform. and near all-trans extended-chain model relevant in gels, X-ray diffr. patterns interpret. 80−79707
polystyrene, electron microscopy 79−55675

noncrystalline state structure continued
polystyrene, end group modified, chain dynamics studied by fluorescence depolarization 80−19724
polystyrene, glassy atactic, struct. anal. from small-angle X-ray scattering 79−73109
polystyrene, head-to-head, high-resolution PMR spectra 79−73833
polystyrene, isotactic, morphology and growth of chain struct. *(German)* 78−75597
polystyrene, isotactic and static cold-crystallised blends, thermal transitions 80−24381
polystyrene, laser irrad. chem. and struct. modifications *(Russian)* 79−27931
polystyrene, Millar interpenetrating network, viscoelasticity and phase domain form. 78−83749
polystyrene, mol. conform., craze fracture 79−15835
polystyrene, oriented amorphous, supermol. structures rel. to mech. behaviour 78−22673
polystyrene, oriented high-molecular, physicocomech. props. *(Russian)* 79−33028
polystyrene, shrinkability, orient. 79−11660
polystyrene, soln. grown isotactic crystals, degree and distrib. of crystallinity, thermal stability 78−9964
polystyrene, solution grown isotactic crystal, thermal change kinetics study by X-ray diffr. 78−9965
polystyrene, stereostruct. of samples obtained by extraction of isotactic polystyrene with butanone 79−73112
polystyrene, X-ray scatt. and conformational analysis 78−26449
polystyrene amorphous film, cyclically fatigued, molecular behaviour 80−35310
polystyrene films, amorphous, X-ray small angle scatt. near glass transition, struct. *(Russian)* 77−31606
polystyrene model-networks, structure 77−89385
polystyrene sphere crystals, in aqueous suspensions, solid-like phase transiton 80−50893
polystyrene-b-isoprene-b-styrene, struct. regularity and crystn. 80−103269
polystyrene-poly(styrene-b-butadiene-b-styrene) polyblends, electron micrographs for struct. 78−51442
polystyrene-polybutadiene block copolymer, oriented microlattice obs. 78−2025
polystyrene-polydivinylbenzene, interpenetrating network, IR, NMR and chromatographic anal. of intermediate regions 77−55711
polystyrene-polyethylene(ethylene-propylene) blends, copolymer modified, mech. props., morphology 79−57088
polystyrene-polyethylene oxide, cryst. multiblock copolymers, crystallisation 78−91269
polystyrene-polyisoprene copolymers, macromol. chain conform. in lamellar phase *(French)* 80−2720
polysulphone-polydimethylsiloxane, linear block copolymer, morphology and impact strength 78−91265
polytetrahydrofuran, line-broadness in X-ray diffr. 77−19878
polytetramethyl-p-silphenylenesiloxane, degree of crystallinity 78−26453
polytetramethylene glycol, short range order, amorphous and liquid, ideal peak method calcs. 80−28900
polytetramethylene terephthalate, monofilaments, chain conform. rel. to strain 77−4055
polytrimethylene terephthalate, struct. determ. 80−19727
polytrioxane, γ-irrad., layer-like void formation 78−22760
polyurethane, interpenetrating network, IR, NMR and chromatographic anal. of intermediate regions 77−55711
polyurethane, segmented, domain struct., deform. effect 80−93623
polyurethane, segmented, time depend. struct. changes on annealing, X-ray meas. 77−4052
polyurethane, stress relax. meas., effect of cure temp. on network struct. 77−84674
polyurethane foam, X-ray exam. *(German)* 78−75596
polyurethane-polyurethane acrylate network, microinhomogeneities and props. *(Russian)* 78−51452
polyurethanes, crosslinked, effect of oligoglycol mol. wt. and SiO_2 filling on viscoelasticity and supermol. struct. *(Russian)* 79−34092
polyurethanes, domain struct. obs. by NMR 77−47355
polyurethaneurylenes, segmented, structural features *(Russian)* 77−47356
polyvinyl acetate, struct. relax., enthalpy and elec. polarisation obs. 79−41978
polyvinyl alcohol, laser irrad. chem. and struct. modifications *(Russian)* 79−27931
polyvinyl chloride, electron microscopy 79−55675
polyvinyl cyclohexane, head-to-head, prep., characterisation 79−70036
polyvinyl cyclohexane, head-to-head high-resolution PMR spectra 79−73833
polyvinylacetate films, amorphous, X-ray small angle scatt. near glass transition, struct. *(Russian)* 77−31606
polyvinylidene chloride, crystalline, preferred chain conform., mol. models 80−79709
polyvinylidene chloride, vibr. spectra, amorphous and cryst. state conforms. 79−27930
polyvinylidene fluoride, cryst., struct. phase transition theory, free energy, uniaxial stress 80−64924
polyvinylidene fluoride, dielec. props. and phase transitions *(French)* 80−55008
polyvinylidene fluoride, piezoelec. and pyroelec. props., struct. model 79−11386
polyvinylidene fluoride, relax., influence of monomeric unit conform. and supermol. struct. *(Russian)* 79−23537
polyvinylidene fluoride, struct. study, piezoelec. and pyroelec. props. 80−7300
polyvinylidene fluoride, TSC and thermoluminescence, reln. to molecular motion *(Japanese)* 80−55200
polyvinylidene fluoride, X-ray high press. study 80−6369
polyvinylidene fluoride film, stretched, struct. and elec. props. 79−90572
polyvinylidene fluoride film, uniaxially stretched and corona poled, piezoelec. meas. 80−25311
polyvinylidene fluoride films, stretched and rolled, electrostriction and piezoelectric effects *(Japanese)* 80−55041
polyvinylidene fluoride X-ray diffr. pattern changes due to corona charging 78−14285
polyvinylidene fluoride-PTFE, thermoelectret, IR spectra, struct. modifications and dielec. props. 77−55785
propylene, isotactic, crack propag. rel. to morphology *(German)* 78−76749

noncrystalline state structure continued
propylene-butadiene, alternating copolymer, struct., fractional composition obs. *(Russian)* 79−65011
propylene-butene-1 copolymers, thermal and mech. props. 79−34091
prosthesis block copolymers, non-thrombogenic, struct. and mech. props. 77−52925
PTE, polymer fibre, orientation changes during stretching, IR spectra 78−75568
PTFE, processing parameter effect on thermal props. and crystal struct. *(German)* 78−63679
PTFE copolymer, melting point, cryst. struct., modification *(Russian)* 77−31607
PVA, swollen crystallinity determ. by laser Raman spectroscopy 80−38953
PVC, amorphous, orientation study by creep thermomechanical method, computer anal. 78−75561
PVC, chlorinated, microstructure, use of ethylene vinyl chloride and copolymers as macromolecular models *(German)* 77−27838
PVC, crystalline syndiotactic, exam. of chain folding, lattice energy 80−24373
PVC, enthalpy determ. of order 79−7556
PVC, exam. of microstructure, using X-ray and light scattering 79−41983
PVC, film, uniaxially stretched, effect of mol. orientation on anisotropy of Young's modulus 77−86076
PVC, plasticised, processing-morphology-mech. props. relation 79−8264
PVC, plasticised film, defect form. study, turbidity and shrinkage meas. *(Russian)* 77−62490
PVC, Raman spectrum, C-Cl stretching region 78−84583
PVC, rheology, viscoelasticity, panel discussion 79−3984
PVC, rigid, microdomains, small angle X-ray scattering study 80−28930
PVC, rigid, tensile fracture morphology, rel. to mol. props. 77−59883
PVC, rigid resin, TEM studies of morphology, processing effects 80−108385
PVC, suggested morphology-characterisation terminology 79−7555
PVC chlorinated, mol. parameters determ. 79−41974
PVC particles, Raman spectra, conform. during polymerisation 79−33709
PVC physics symposium, Lyon-Villeurbanne, France (July 1976) 79−7554
PVC plastisols, thermally hardened, rheological props. *(German)* 79−29154
PVC products, quality control on basis of particle structure 79−8265
PVC-chlorinated polyethylene blend, optical characterisation methods 79−8408
Pyrex, ion bombardment, form. of cpds., IR spectrosc. exam. *(German)* 80−88173
quartz, amorphous layer on mech. treated single crysts. electron microscope and RHEED obs. 80−24721
quartz, fused, rel. to hyper-Raman scatt. and longit.-transverse splitting of vibrs. 79−73953
α-quartz and quartz glass, neutron irradiated struct., neutron diffr. meas. 78−22769
quartz fibre, ESR and IR obs. of microinhomogeneities 77−8401
quartz glasses, viscosity rel. to crystallisation 77−24386
radial distribution function peaks and coord. numbers 77−76271
random close packed, examination of cavities for applicability as model for O in silicate melt 78−55802
rare earth alloys, amorphous, mag. props. rel. to struct., review 79−15298
rare earth sulphides-1.8 Ga_2S_3 glasses, vibr. spectra, electronic transitions, short range order 77−69820
rare earth-transition metal alloys, amorphous, struct. and mag. props., book contrib. 80−39818
rare earth-transition metal alloys amorphous thin films, anisotropic mag. and microstruct. props. 78−95487
rare earth-transition metal amorphous film, microstruct. 77−51619
rare earth-transition metal film, amorphous, microstruct., TEM obs. 78−72018
rare earth-transition metal film, amorphous, microstruct. and magnetism 78−64230
review of properties, current and potential applications 78−30539
rheology of glassy state and highly viscous liq. 80−70130
rubber, Mooney-Rivlin constants correl. with polymer chain cross-section 77−11624
rubber, network, highly swollen, long time dynamics 80−38291
rubber, network entanglement contrib. to elasticity 80−39203
rubber, nitrite, heat ageing, light scatt. method study *(Russian)* 80−40407
rubber, X-ray scatt., differential radial distrib. function 79−14703
rubber elasticity, molecular aspects book contrib. 78−84886
rubber network elasticity, mol. theory 80−38290
rubber-epoxy resins, heterogeneity analysis, light scatt. and statistical methods 78−2024
selenide systems, binary, glass transition behaviour, model, comp. depend. 78−26673
semiconductor, amorphous, electronic props. and struct. *(Japanese)* 79−47179
semiconductor, amorphous or disordered, cond. mechanisms, model of medium-range comp. disorder 78−79994
semiconductor glass, tetrahedral, disorder 78−51423
semiconductors, amorphous, elementary excitations, struct. 80−49577
semiconductors, amorphous, short-range order, theory and probes 80−79698
semiconductors, chem. bonding, struct., pseudopot. theory *(German)* 78−30581
semiconductors, glassy, diamag., photostructural changes, mechanism 80−92557
semiconductors and insulators, struct. models 79−37628
semiconductors in noncrystalline states, diffr. investigations review 77−72559
silica gel, infrared absorpt. spectra *(Russian)* 77−55794
silicate glass, hydrated, proton and ^{23}Na wide-line NMR study 80−84659
silicate glass, IR refl. spectra resulting from phase separation *(Japanese)* 78−39542
silicate glass, neutron diffr. determ. of struct. 78−79533
silicate glass, thermodynamic theory of structural relaxation *(German)* 80−38929
silicate glass containing subcolloidal Ag, full-colour photosensitive glass, processing and struct. 79−10369

noncrystalline state structure continued
silicate glasses, local order around Fe, exam. using X-ray absorpt. spectrometry 80−79701
silicate glasses, longit. and transverse elastic wave vels., temp. and comp. variations 80−88258
silicate glasses, model of struct. element, calc. of physicochem. props. 79−69016
silicate glasses, struct. and phase transform. 78−64538
silk fibroin films, conformational changes induced by water immersion 80−10498
siloxane, temp. transitions, linear dilatometry and X-ray diffr. obs. *(Russian)* 80−59404
sodium iron fluorophosphate glasses, EPR and Mossbauer resonance study 80−39968
sodium tetraborate glass, melt, temp. depend. of high viscosity property *(Russian)* 80−39336
spherulite, two-phase, ht. cond. anisotropy 78−2316
splat quenched metal, electron transparent area prod. 77−4754
splat quenched metal, electron transparent prod., comment 77−4755
static structure factor, non-cryst. material, neutron diffr. data, normalisation, instrument correction program 79−14651
steel, stainless, alloyed with C, magnetron-sputtered, microstruct., and cryst.-amorphous transition 80−19719
steel, stainless, amorphous film, sputtered, prep. and characterisation 78−43266
structural relaxation, order parameter model *(German)* 80−44146
structure, stability, phys. charcts., prod. principles *(Hungarian)* 77−84656
styrene-butadiene block polymers, multiphase systems, struct., props. 77−31600
styrene-butadiene copolymers, struct. study by pyrolytic capillary gas chromatography *(German)* 78−18557
styrene-butadiene triblock copolymer film, rel. to effect of casting solvent on mech. props. 79−11651
styrene-butadiene-styrene triblock copolymers, dielec. props. 78−95545
styrene-diene triblock copolymer, hexagonal struct., flow props. of melt and fracture 78−76729
styrene-divinylbenzene grafted copolymer, structure investigation by IR spectroscopy *(Russian)* 77−62487
succinonitrile, plastic and liq., NMR, ^{13}C spin-lattice relax. and ^{14}N linewidth 79−24227
superconducting metastable alloys, review of current work 80−81002
supercooled amorphous state, Gaussian core model 79−73101
tellurite glasses, binary, struct. and props. *(Japanese)* 79−32917
tetrahedrally bonded solids, struct. theory 78−59757
tetramethyl-p-silphenylenesiloxane-dimethyl siloxane copolymers, degree of crystallinity 78−26453
thermoplastic elastomers, crosslinked by secondary valence interactions, elasticity and processing, crosslinking behaviour 80−40320
tie chain content of oriented partially crystalline polymer *(Russian)* 77−47358
transition metal, amorphous and liq. state, simulated model 79−14733
transition metal alloys, amorphous, mag. props., structure and preparation 80−75737
transition metal metalloid glasses, computer simulation of atomic struct. 77−31598
transition metal-metalloid glass, struct. simulation 78−38624
transition metal-metalloid glasses, short range order of dense-random-packing models 80−64907
transition metal-metalloid glasses, struct., compositional effects *(Japanese)* 80−84086
transition metal-metalloid glasses, struct. and plastic flow, review 80−84090
transition metal-metalloid glasses, struct. model 79−64997
transition metal-metalloid glasses, structural model 79−14690
transition metal-nonmetal glasses, with defined local coordination, struct. model 80−84092
transition metals, amorphous, prep. and struct., rel. to liq. struct. 77−51323
vibrational spectra and glass structure 80−84732
vinyl and related polymers, diffusion of simple penetrants, statistical mechanical model 80−10705
vinylidene fluoride-trifluoroethylene film, cryst. phase transition 80−66120
vinylidenechloride-vinylchloride latex copolymers grafted on to elastomers, film struct. and props. *(Russian)* 77−21090
vitrification and crystallisation conf. Lyon, France (Dec. 1976) *(French)* 77−72560
Voronoi polyhedra, construction procedure 79−71236
Vycor glass, manufacture, struct., physical and chem. props. 80−7527
water, low-density amorphous solid, OH stretching spectrum 79−11413
window glass, knots and cords, EPMA characterisation 80−84085
X-ray diffraction, frequency modulated, for multi-element disordered system struct. 77−72525
X-ray Raman edge extended modulation for struct. study of low atomic number materials 80−49111
Zachariasen's rules, Madelung constant, and network topology 79−27926
Ag-Ge-S glasses, X-ray determ. of struct. *(Japanese)* 80−10501
AgI-Ag oxysalt high cond. glasses, struct. obs. 79−32908
$AgI-Ag_2O-MoO_3$, superionic conducting glass, IR spectra and struct. 79−10804
$AgI-Ag_2O-MoO_3$ glass glass superionic cond., struct. and transport props. 80−88602
$AgI-Ag_2O.B_2O_3$ system, ionic cond., struct., electrochem. prop. in galvanic cell 78−95181
$(AgI)_x(Ag_2O.B_2O_3)_{1-x}$ glass, ionic cond. and disorder modes 80−39344
$AgPO_3-HgI_2(CdI_2)(PbI_2)$ glass, elec. cond. and Raman. spectra rel. to struct. *(French)* 79−10979
Al, and Al-Cu(Pb) dil. alloys, pulsed ruby laser irrad., noncryst. phase form 80−35012
Al-Cu, splat quenched, amorphous regions 77−4047
Al-Cu, splat quenched, amorphous regions, comment 77−4048
$Al_{20}As_{40}Te_{40}$, amorphous alloy, radial distribution function anal., X-ray diffr. *(Spanish)* 80−28915
AlF_3 based glasses, chem., thermal and optical props. *(French)* 80−70139
AlF_3-M_2F glasses, M=alkaline earth, density-of-states and structural forms, Raman spectra study 80−97255
Al_2O_3, amorphous anodic film, struct. anal. 79−51452
Al_2O_3 amorphous films, struct., electron diffr. investigation 80−20046

noncrystalline state structure continued
$Al_2O_3-Ln_2O_3$, Ln=La,Ce,Pr,Nd,Sm,Gd,Tb, struct. and thermal charcts. of amorphous phases *(French)* 77−72558
$Al_2O_3-SiO_2$, struct., localised radiation centres, spectroscopic investig. *(Russian)* 77−69844
$Al(PO_3)_3$, vitreous struct. 78−26443
$Al(PO_3)_3$-NaF-LiF glasses, mixed-alkali effect 80−19715
$AlPO_4$, amorphous, struct. determ. by radial distrib. functions derived from X-ray diffr. 77−43151
$Al_{0.23}Te_{0.77}$, amorphous semicond., radial distrib. anal. by X-ray diffr. 78−71678
amorphous, Raman scatt. investig. of irreversible thermostruct. transform. 77−48163
As, amorphous, intermediate range order from polarised features of Raman spectrum 80−49113
As, amorphous, low-temp., elementary excitations, struct. 80−49577
As, amorphous, neutron diffr. investig. of local order 77−35480
As, amorphous, optical, vibr., transport and defect-related props., review 79−51935
As, amorphous, vibr. excitations at defect sites, IR and Raman spectra calc. 80−49329
As, amorphous and cryst., NQR for tunnelling modes and local struct. order 79−61261
As amorphous films, interference enhanced Raman scatt. 80−50326
As, pulsed NQR, bonding, bond angle distrib. obs. in different phases 80−54984
As-S, amorphous, glass transition and specific heat, intermolecular bond saturation 80−15011
As-S amorphous film, photo-induced optical changes, annealing effect 78−27345
As-S glasses, acousto-induced structural changes, optical props. 80−49122
As-S glasses, resonance Raman scatt. 80−50325
As-S-I system, glasses, Raman spectra, struct. 79−65857
As-S-I system glasses, IR transmission spectra, structure-chem. comp. 79−42974
As-S-Tl, glass, viscosity and elastic props. 80−100180
As-Se, amorphous, glass transition and specific heat, intermolecular bond saturation 80−15011
As-Se amorphous films, photo-induced changes in IR vibr. spectra 79−91514
As-Se amorphous system, Raman scatt. 80−88984
As-Se glass film, rel. to photoinduced absorpt. changes 79−87519
As-Se-Sb, crystallised glasses, struct. from Mossbauer spectra 80−64917
As-Se-Te glasses, glass form., charact. temp., density, thermal expansion and dynamical viscosity, struct. model 78−26672
$AsO_{3/2}-BO_{3/2}$, glass, props. and struct. *(Japanese)* 77−27836
As_2O_3 crystalline and amorphous, EXAFS study of struct. 80−19776
As_2O_3 cubic and glassy, phase shift calc. for EXAFS 77−48275
As_2O_3, glassy, intermediate range order from polarised features of Raman spectrum 80−49113
$As_x(S,Se)_{1-x}$, chalcogenide, covalent non crystalline topology, short range order 80−15009
$As_{1-x}S_x$ glasses, building blocks and bonds 80−54141
As_2S_3 (Se_3), electron irradiated, effects on elec., photoelec. and optical props. 80−49806
As_2S_3, amorphous, luminesc. and optically detected ESR, photoinduced struct. change 80−50399
As_2S_3, amorphous semicond., photo-induced optical and structural changes *(Japanese)* 78−47244
As_2S_3, crystalline and amorphous, inelastic neutron scatt. spectra 77−24276
As_2S_3 glass, at. struct. changes due to irrad., comp. variations and annealing 77−76323
As_2S_3 glasses, quasi-eutectic structure, X-ray and IR investig. 77−15320
As_2S_3, glassy, photoinduced defects, EPR and absorpt. spectra 80−59398
As_2S_3 structure simulation of some tellurite and chalcogenide glasses quasi-crystalline structural diffusion method *(Russian)* 80−54147
As_2S_3:Ga system chalcogenide glasses, thermophysical and struct. props. 80−15007
As_2S_3-PbS glasses, structural props. 79−27925
As_2S_5, amorphous, struct., vibr. and electronic spectra 80−64908
As_2S_x glass, Raman and IR spectra, struct. model 78−80330
$As_{40}S_{60}$ glass, structure modelling by Monte Carlo method *(Russian)* 79−55672
As_xS_{1-x} glass, Raman spectra, chem. struct. *(Russian)* 78−76469
As_xS_{100-x} amorphous films, optical props. and photoinduced changes 80−60700
As_xS_{100-x} glasses, band gap and neighbouring order *(Russian)* 79−60694
As_xS_{100-x} glasses, Raman spectrum and structure 80−60593
As_xS_{100-x}, structural changes *(Russian)* 78−51427
As_xS_y, bulk and vapour deposited films, comparison of struct., X-ray diffr. meas. 77−69195
$(As_2S_3)_{1-x}(AsBr_3)_x$ glass, struct. interpretation of Raman spectra 79−65856
$(As_2S_3)_x(AsI_3)_{1-x}$, glass, Raman spectra, chem. struct. *(Russian)* 78−76469
$(As_{0.4}S_{0.6})_{100-x}Cu_x$, glassy, struct. and elec. cond. study 80−59399
$As_2S_3Ge_x$ glasses, vibr. props. and struct., IR refl. and Raman scatt. 79−78682
$(As_2S_3)_{1-x}(GeS_2)_x$ and $As_2S_3Ge_x$ glasses, struct. and vibr. spectra 79−91440
$(AsSI)_x(GeS_2)_{1-x}$ glasses, Raman and long-wave IR spectra obs. of struct. 79−51964
$As_2S_3(Se_3)$ evaporated films, optical absorpt. and thermally induced effects 79−42989
$As_2S_3(Se_3)$ evaporated films, struct. and thermally induced effects 79−41963
$As_4Sb_2Se_9$ glassy semiconductors, electronic props. 80−103712
AsSe-GeSe$_2$-PbSe, glass form., struct. defects, elec. cond., assoc. *(Russian)* 80−54144
$AsSe_{10}$, stable thermoelectret, effects of anisotropic external perturbation *(Russian)* 77−63361
As_2Se_3, amorphous, laser radiation induced struct. changes, electron microdiffr. obs. 79−10874
As_2Se_3, and As_4Se_5Ge glasses, struct. changes, Mn^{2+} EPR expts. 78−79534
As_2Se_3, crystalline and amorphous, inelastic neutron scatt. spectra 77−24276
As_2Se_3 glass, microwave elec. cond. and struct. 80−49793

noncrystalline state structure continued
As_2Se_3 glass, mol. struct. model 80−100179
As_2Se_3, glassy, rel. to photostimulated changes in contact props. 78−19162
As_3Se_2, electron irradiated, effects on elec., photoelec. and optical props. 80−49806
$As_2Se_3Hg_x$, semicond. glassy system, struct. 77−35489
$AsSeI_{0.1}$, glassy, rel. to photostimulated changes in contact props. 78−19162
$As_2Se_3(S_3)$, glassy film, photostructural effects, NQR study 80−49549
As_2Te_3, $As_4Te_5I_2$, $TlAsTe_2$, local struct. changes on crystal-glass transition, Mossbauer spectra 77−36157
$As_xTe_{90-x}Ge_{10}$, $As_{35}Te_{55}Ge_{10-x}Si_x$ glasses, elec. and optical props., comp. depend. 77−24555
$As_4Te_5Ge(Si)$ glass, struct. changes, Mn^{2+} EPR expts. 78−79534
$As_xTe_xSe_{100-2x}$, x=2.5 and 5.0, chalcogenide glasses, IR absorpt. spectra 77−24842
Au film, discontinuous, centre-to-centre particle distrib. determ. 80−96761
Au solar black, optical props., microstruct. influence 79−42937
Au-Ge-Si, influence of struct. on elec. resist. of glass forming alloys 80−65518
$Au_{35}Si_{65}$, amorphous vacuum-deposited and liquid-quenched films, diffusion and crystn. 80−84094
B, amorphous, X-ray Raman edge extended modulation for struct. study 80−49111
B amorphous film, interference enhanced Raman scatt. 80−50326
B dispersed fractionated powder, struct. obs. 80−19703
B films, amorphous, prep., struct., props., review, book contrib. 78−48321
B, struct. changes on Zn incorporation 78−79596
B_2O_3 and alkali borate glasses, Raman study at high temps. 80−93306
B_2O_3 glass, nonlinear structural relaxation model for glassy state 78−26448
B_2O_3 glass, struct. and phonon spectra 80−50324
B_2O_3, vitreous, BO_3 triangles in boroxyl rings and random networks, Raman intensity investig. 80−45058
B_2O_3, vitreous, struct. and bonding determ., NMR obs. 77−39545
B_2O_3, vitreous, struct. obs. using small-angle X-ray scatt. 79−41966
B_2O_3, vitreous, struct. study using ^{10}B NMR 80−84658
B_2O_3-K_2O-Na_2O-Rb_2O-Cs_2O glass, small angle X-ray scatt. exam. of struct. 80−38922
B_2O_3-SiO_2 glass film, CVD, differential IR studies 80−55213
BaB_2O_4-RF_2, R=Mg, Ca, Sr, Ba, glass form., struct. and props. 80−84077
$BaCl_2$, film, very-low-freq. inelastic light scatt. 80−25367
BaFCl film, very-low-freq. inelastic light scatt. 80−25367
BaO-Al_2O_3-SiO_2-Ta_2O_5-Mo glass ceramic metal composites, cermet prep. 80−11618
BaO-Al_2O_3-TiO_2-SiO_2, glass formation, structure of cations *(Russian)* 80−38933
BaO-B_2O_3-SiO_2:Ti^{3+}, elec. cond., struct. 78−72148
BaO-Fe_2O_3, splat quenching struct. and crystn. mechanism *(French)* 78−51426
BaO-Fe_2O_3 system, splat cooled phases struct., magnetisation and susceptibility 300-1100K *(French)* 77−48017
BaO-Fe_2O_3-B_2O_3 glass, Mossbauer study of struct. and mag. props. 79−47369
BaO-Fe_2O_3-B_2O_3 glass, struct. and mag. props., Mossbauer spectra 80−7226
BaO-WO_3-P_2O_5 glass, struct. and IR spectra 80−64914
$Ba(PO_3)_2$-fluoride glass, elec. cond., struct. 80−88056
$Ba_3(PO_4)_2$ glass, phase equilibrium data 79−27922
$Ba_3(PO_4)_2$ glass, phase equilibrium data 79−27923
$BaPO_3F$-Al_2O_3-B_2O_3 glasses, phys. props. 78−63676
Be-Nb-Zr alloys, glassy and partially crystalline, supercond. T_c and struct. props. 78−60239
Be-Zr alloy, glassy, rel. to supercond. props. 78−26983
BeF_2 glass transition, Monte Carlo study 80−75343
BeF_2:Eu^{3+} glass, struct. and optical props. 80−84067
BeF_2:Eu^{3+} glass, struct., Monte Carlo simulations 80−96448
BeF_2-KF-CaF_2-AlF_3-EuF_3 fluoroberyllate glass, Eu^{3+} fluoresc. linewidth 80−66285
C, activated, interaction with H_2, alteration of paramag. props., structural defects 77−63957
C, amorphous, diamond-like 3-fold coord. 80−50323
C, amorphous, X-ray and electron diffr. intensities, model struct. 78−26441
C, amorphous film, struct. props., Raman scatt. study 80−11417
C amorphous film struct., TEM obs. using bright field hollow cone illum. 78−22609
C, anthracene char, density fluctuations effect on physical properties 78−51420
C characterisation, using dark-field electron microscopy 79−77464
C fibre, prep. from benzene, struct. changes with stepwise heat treatment up to 3000°C 77−12649
C fibres with large breaking strain, prep., mech. props., struct., appl. 78−44077
C film, amorphous, struct. and semicond. props. and heterojunction form. with single cryst. Si 80−25002
C film, sputtered glassy, prep., mech. and struct. props. 77−66588
C, glassy, struct. evolution due to thermal treatment at 1000 to 2700°C, layers evolution 77−68923
C, glassy, struct. evolution due to thermal treatment at 1000 to 2700°C, tridimens. config. 77−68924
C, glassy, struct. parameter var. with heat treatment temp. 77−11488
C materials, fine structure characteristics by integral method 77−43153
C, structure change, during thermal ordering, radiation disordering 80−54283
$Ca_{1-x}La_xMgAl_xSi_{2-x}O_6$, crystalline and vitreous phase comp. and props. 77−44221
CaO-Al_2O_3-SiO_2 glasses, density-of-states and structural forms, Raman spectra study 80−97255
CaO-Al_2O_3-TiO_2-SiO_2, glass formation, structure of cations *(Russian)* 80−38933
CaO-B_2O_3-Fe_2O_3 glasses, effect of heat treatment on electronic props. 78−2480
CaO-Fe_2O_3-B_2O_3 glasses, phys. props. rel. to struct. and comp. 78−23331
CaO-Fe_2O_3-SiO_2 glass, struct. behaviour at melting, Mossbauer exam. 79−10802

noncrystalline state structure continued
CaO-Na_2O-B_2O_3, Raman scatt. studies of glass struct. 77−90147
CaO-SiO_2 glass, solid reactions, study by hot stage electron microscope *(Japanese)* 78−12798
CaO-SiO_2 system glasses, IR absorpt. struct. obs. of phases and struct. 80−34918
$Ca_3(PO_4)_2$, amorphous, reduced intensity functions, thermal vibr. coupling 78−42910
$CdGeAs_2$, glassy, structural model 77−35490
$CdGeAs_2$, short-range order, Mossbauer expts. 78−22648
$CdGe_{1-x}M_xAs_2$ (M=Si,Sn,Pb), (x=0.0,0.1,0.2), amorphous struct. 78−22651
$CdGe_{1-x}Sb_xAs_2$ system, amorphous and cryst. phases, DTA and microhardness obs. 78−22835
$CdGe_{1-x}Sn_xAs_2$, amorphous, radial distrib. anal. and mag. susceptibility meas. 77−43152
CdO-Bi_2O_3-Al_2O_3, glass formation and IR transmission *(Japanese)* 80−54146
Co based amorphous alloys, struct. and thermomag. meas. 77−16055
Co-B glass, X-ray obs. of struct. 79−1399
Co-B-Si amorphous alloy, liq. quenched, rel. to elec. resist. and cyclic deform. 80−59949
Co-Fe-Si-B, decomp. of amorphous state during annealing below recryst. temp., electron microscope study *(Russian)* 80−75164
Co-Gd amorphous film, struct., mag. anisotropy consts., saturation magnetisation *(Russian)* 79−99735
Co-Gd film, amorphous, prep. conditions influence on supernetwork struct. 77−76709
Co-P, amorphous electrodeposited foils, struct. characterisation by X-ray scatt. 79−77932
Co-P alloys, geometric struct. models and diffraction exam. techniques 80−79700
Co-Zr, amorphous phase form. in Zr-poor region, hardness and fracture strength *(Japanese)* 80−84914
$Co_{67}Er_{33}$ amorphous alloy, sputtered, local order and amorphous struct. 80−88061
$(Co_{0.93}Fe_{0.07})_{75-x}Cr_xSi_{15}B_{10}$ amorphous alloy, thermal stability, Cr conc. effects, DTA expts. 80−59395
CoP amorphous alloy, heat treatments influence on opt. props., struct. and DC resist. obs. 80−80892
$Co_{0.9}P_{0.1}$ noncrystalline ferromagnet, electroless deposited, struct. and microscopic mag. props. 80−88063
Cr-Ge amorphous films, annealing effect on elec. resistance and struct. 80−54667
$Cr_{11}Ge_8$, CrGe, and $Cr_{11}Ge_{19}$ amorphous films, short-range order, electron diffr. obs. *(Russian)* 78−56050
Cr_3Ge amorphous films, short range order struct. *(Russian)* 78−30841
Cr_5Ge_3, amorphous film, short-range-order struct., electron diffr. meas. 79−15047
$Cs_{1-x}O_x$, metallic glass, prep., elec. props. and struct. 78−67652
Cs_2O-MgO-SiO_2 system, glasses, crystn. prods., composition, props. 79−41961
$Cs_2O.4SiO_2$, glass, behaviour of VO^{2+} as spectroscopic probe 79−78510
Cu-Ag-Ge, Hume-Rothery glass form. 80−96449
Cu-Ag-P(6-14, 11-14 wt.%) amorphous, crystn. and elec. props., X-ray diffr., elec. resist. and DTA meas. *(Japanese)* 80−84088
Cu-Cd-Cl stretched photochromic glass, polorisation effects 79−95729
Cu-Sb-I system, glass form., struct. and IR spectra 80−64915
Cu-Zr alloys, amorphous, struct. X-ray scatt., rel. to Ni-P alloys 77−51324
Cu-Zr amorphous alloy, splat cooled, local order and amorphous struct. 80−88061
$CuInSe_2$ amorphous thin film, flash evaporation, struct., stoichiometry 80−89150
$Cu(NO_3)_2$, frozen aq. soln., phase transitions, struct., ESR 77−16154
$Cu_{0.57}Zr_{0.43}$, amorphous, partial struct. factor, TOF pulsed neutron 79−14684
$Cu_{0.57}Zr_{0.43}$ amorphous alloy, neutron diffr. obs. of struct. 80−88060
$Cu_{46}Zr_{54}$, metallic glass, dynamical struct. factor and freq. distrib. meas. 80−54136
$Cu_{57}Zr_{43}$, amorphous alloy, computer simulation of atomic structure 80−70125
$Cu_{60}Zr_{40}$, metallic glass, composition, mech. props., simulation 80−49117
$Cu_{66}Zr_{34}$, amorphous metallic glass, differences caused by preparation technique *(French)* 80−103247
$DyFe_2$, amorphous, struct. determ. EXAFS exam. 78−51421
DyIG, non-cryst., Mossbauer and magnetisation studies 80−44979
Eu-As-S, glass forming region, Raman and IR obs. *(French)* 79−99080
EuIG, non-cryst., Mossbauer and magnetisation studies 80−44979
EuS-Ga_2S_3-GeS_2, chalcogenide glasses, conditions of form. of glassy prod. *(French)* 80−100325
Fe, amorphous, relaxed Bernal structure, model 78−2007
Fe, amorphous chain of Bernal holes, dislocation model 79−4249
Fe, amorphous structure obtained by liq. state quenching 79−46573
Fe based alloy, amorphous, liq. quenched, struct., thermal stability and mech. props. 80−88059
Fe based amorphous alloys, struct. and thermomag. meas. 77−16055
Fe based metallic glasses, Curie temp., struct. relax. effects 77−8313
Fe, glassy, heat of crystn., and bulk modulus, calc. using struct. model 78−51428
Fe, realistic relaxed struct. model pair distrib. function 78−30544
Fe, struct. relax. of dense random packing model 78−30540
Fe-B, amorphous, short-range order, Mossbauer meas. 80−44986
Fe-B, amorphous alloys, compositional study on short-range struct. 80−84095
Fe-B, metallic glass, theoretical studies on structural models 79−37633
Fe-B (15-25 at.%) glass, quasicryst. struct. Mossbauer expts. 79−4255
Fe-B amorphous alloy, annealed, microstruct. and mag. domain changes 80−75790
Fe-B glass, X-ray obs. of struct. 79−1399
Fe-B metallic glass, struct. and crystallisation, Mossbauer spectra, calorimetry and magnetisation meas. 79−23528
Fe-B metallic glass, X-ray diffr. meas., semi-empirical struct. model 80−107059
Fe-B metallic glasses, short range order 79−77528
Fe-B metallic glasses, struct., stability and crystn. 80−75173
Fe-B-C amorphous alloys, atomic struct., energy dispersive X-ray diffr. meas. 79−73100
Fe-B-Si amorphous alloy, liq. quenched, rel. to elec. resist. and cyclic deform. 80−59949

noncrystalline state structure continued
Fe-B(-Si) alloy filaments produced by glass-coated melt spinning 80−76213
Fe-B(Si) amorphous alloys, Mossbauer spectra, struct. 80−15840
Fe-Cu alloy, vapour-deposited, struct. and thermal stability 78−43265
Fe-Ge, amorphous, atomic struct., neutron diffr. study 80−59392
Fe-Ge amorphous alloys, radial distrib. funct., electron diffr. exam. 77−68922
Fe-Ni-B metallic glass, X-ray diffr. meas., semi-empirical struct. model 80−107059
Fe-Ni-P-B, amorphous, crystn. and struct. 80−75175
Fe-O noncrystalline RF sputtered film, vapour species control 78−60575
Fe-P, metallic glass, theoretical studies on structural models 79−37633
Fe-P alloys, X-ray exam. of amorphous structure *(Japanese)* 77−84661
Fe-P film, amorphous, ion implanted, struct. and domain struct. obs. 79−91272
Fe-P-C, amorphous, crystn. and struct. 80−75175
Fe-P-C, amorphous, struct. and mag. props., Mossbauer, X-ray diffr. and elec. resist. meas. 78−2009
Fe-P-C amorphous alloys, Mossbauer spectra, struct. 80−15840
Fe-Zr, amorphous phase form. in Zr-poor region, hardness and fracture strength *(Japanese)* 80−84914
$Fe_{1-x}B_x$ metallic glasses, struct. and cryst., Mossbauer spectra, DSC, and magnetisation meas. 79−94906
$Fe_{100-x}B_x$, mag. and struct. props., comp. depend. 78−60314
$Fe_{80}B_{20}$, amorphous, cold neutron scatt., local and extended defects 80−84089
$Fe_{80}B_{20}$, amorphous struct., Mossbauer spectroscopy investigation 80−84677
$Fe_{80}B_{20}$, metallic glass, Mossbauer spectroscopy 78−60365
$Fe_{80}B_{20}$, metallic glass, triplet correlation, field-ion microscopy study 80−38921
$Fe_{80}B_{20}$ metallic glass, crystn. and struct. relax., Mossbauer effect study 80−75182
$Fe_{83}B_{17}$ metallic glass, struct. from neutron diffr. study 80−6363
$Fe_{83.4}B_{16.6}$, amorphous, mag. props. and microstruct., cooling rate and melt overheating effects 80−65965
$Fe_{83.4}B_{16.6}$ amorphous, mag. props., melt overheating and cooling rate effects 80−89371
Fe_xB_{100-x}, rel. to stress relax. after annealing 80−55447
$(Fe_{0.06}Co_{0.94})$-B, amorphous, ferromag., mag. instability rel. to struct. 79−99729
FeF_3, amorphous, struct. and mag. props., computer model 80−96446
Fe_xGe_{1-x}, amorphous alloy, short range order anal. 77−80423
$(Fe_{1-x}Mn_x)_{75}P_{15}C_{10}$, amorphous pair radial distrib. functions, neutron scatt. study 80−49128
$Fe_{78}Mo_2B_{20}$, metallic glass, triplet correlation, field-ion microscopy study 80−38921
Fe_xNi_{1-x} amorphous film, growth stress and structure factor, stabilisation by conduction electrons 80−38920
$(Fe_{0.6}Ni_{0.4})_{100-x}B_x$ and $(Fe_{100-x}Ni_x)_{80}B_{20}$ amorphous alloys, X-ray diffr. struct. determ. 80−64906
$Fe_{40}Ni_{40}B_{20-x}P_x$ metallic glasses, local struct. and dynamic disorder of Fe and Ni, EXAFS obs. 80−89088
$Fe_{40}Ni_{40}P_{14}B_6$, amorphous ribbon, cold rolling, annealing mag. props. 77−8958
$Fe_{40}Ni_{40}P_{14}B_6$, amorphous, energy dispersive X-ray diffr. study of structural relaxation 79−14689
$Fe_{40}Ni_{40}P_{14}B_6$, amorphous, resistometric study of short-range ordering rel. to heat treatment 80−70140
$Fe_{40}Ni_{40}P_{14}B_6$ glass, struct. relax., ferromag. reson. and X-ray scatt. 79−90566
$Fe_{40}Ni_{40}P_{14}B_6$, Metglas 2826, hot forming 80−84980
$Fe_{40}Ni_{40}P_{14}B_6$, quenched amorphous, high field susceptibility and microstructure 77−69506
$(Fe_{0.5}Ni_{0.5})_{75}P_{16}B_6Al_3$ glass, struct. relax. as origin of Curie temp. ageing 78−84418
Fe_2O_3, powder, preparation conditions rel. to morphology 77−8777
Fe_2O_3-P_2O_5 system, vitreous, struct. obs. using neutron scatt. 78−22667
Fe_2O_3-PbO-B_2O_3 glass, X-ray and electron microscope studies, mag. and Mossbauer effect meas. 80−28919
$Fe(OH)_3$ thin films, elec. cond. var. with temp., amorphous struct. 80−75566
FeOOH, ferric hydroxide gel, struct. determ. 79−11832
$(Fe_2O_3)_x(3B_2O_3.PbO)_{1-x}$ glass, X-ray diffr. struct. obs. 79−32915
$Fe_{100-x}P_x$, structural analysis of models for amorphous metallic alloys 80−103249
$Fe_{75}P_{25}$ amorphous alloy, atomic struct., computer simulation 80−88043
FePC molten and amorphous alloys, struct. factors 80−79674
Fe_2S_3, existence and thermal stability, Mossbauer study 78−83733
FeSb alloy films, vapour-deposited, formation of metastable phase 80−44437
Fe_xSi_{1-x}, amorphous, struct. and mag. props., giant moment form. at mag. ordering 78−68192
Ga, amorphous film, X-ray diffr. 79−51451
Ga_2O_3-R_2O_3:Nd^{3+} glass, prep., characts., X-ray diffr., absorpt. and thermal anal. obs. *(French)* 78−19704
$Ga_{20}Te_{80}$, amorphous, splat cooled, thermoelectric props. 78−43426
Gd-Ag, vap. quenched alloys, struct. and mag. props. 78−84461
Gd-Ag (0-16 at.%), vapour-quenched, struct. and mag. props. 78−38980
Gd-Ag(Cu) alloy film, amorphous, struct. and mag. props. 78−52318
Gd-Co, film, evaporated and sputtered, struct. and mag. anistoropy, electron microscopy 79−56578
Gd-Co amorphous films, correlation between struct. and mag. props. *(Chinese)* 80−54532
Gd-Co based amorphous sputtered films, microstruct. variability and mag. anisotropy, implanted ion effects 80−88459
Gd-Co film, amorphous, Ar sputtered, struct. 78−63946
Gd-Co film, amorphous, phase separation as source of perpendicular anisotropy 78−64244
Gd-Co film, bias-sputtered, dipolar mechanisms for mag. anisotropy 78−64233
Gd-Co film, vapour quenched, amorphous, struct., electron diffr. meas. 77−28086
Gd-Co-Mo film, amorphous, Ar sputtered, struct. 78−63946
Gd-Fe film, amorphous, in-situ ion beam sputtered, microstruct. and Lorentz mag. struct. 78−63947
GdFe films, deposited on glass substrates *(Russian)* 80−24747
$(Ge,Si)_{1-x}Y_x$, Y=H,F,B,P,..., amorphous struct., kinetically determined topological model 79−55666
Ge, amorphous, dislocation model 80−1929
noncrystalline state structure continued
Ge, amorphous, dislocation model 80−1930
Ge, amorphous, growth rate of crystallisation, Raman spectroscopy study 80−44227
Ge, amorphous, IR absorpt., first-order effective charges due to at. displacements 77−48164
Ge, amorphous, molecular liquid model and electronic structure 80−54133
Ge, amorphous, struct., dislocation model 78−42911
Ge, amorphous, struct. and growth kinetics, topological principles 80−49123
Ge, amorphous, vibrational spectra, struct. model calcs. 78−22806
Ge amorphous film, bright-field hollow cone images 80−75136
Ge amorphous films, structural relaxation and crystallisation 80−100170
Ge, amorphous whisker growth 78−2400
Ge, electrodeposited, X-ray, electrochem., and electrorefl. characterisation 78−14624
Ge film, amorphous, ^{74}Ge ion implanted, defect struct. obs. 78−51848
Ge film, amorphous, high resolution electron microscopy, digital processing use 78−37116
Ge film, amorphous, prep. conditions influence on supernetwork struct. 77−76709
Ge film, amorphous, thermoelec. power and structural investigs. using in-situ electron microscopy 77−76983
Ge, nearest-neighbour atom mean-square relative displacements, EXAFS spectra 79−91532
Ge:O, Cu, amorphous thin film, impurity effects on struct. 80−107054
Ge-As-Se, amorphous film, condensation formation and struct. props. *(Russian)* 78−38629
Ge-As-Se films, light irrad., heat treatment rel. to optical props. *(Russian)* 79−4858
Ge-Ga amorphous alloy, co-evaporated elec. and optical props. 80−70860
Ge-Ni, amorphous, struct., EXAFS study 80−49110
Ge-P-S glass system, EPR of intrinsic and Mn^{2+} impurity centres 80−88870
Ge-S, Ge-S-Ag, amorphous prop. and origin of paramagnetic defects 79−10801
Ge-S-Ga(In) system glasses, photoinduced changes 80−24365
Ge-S-Se system, glass-forming, struct. and props. 80−19713
Ge-Se glass, rel. to elastic props. under press., US interferometry 78−79658
Ge-Se glass film, rel. to photoinduced absorpt. changes 79−87519
Ge-Se glass system, effect of changes in local surrounding of atoms on optical props. *(Russian)* 78−80414
Ge-Se-Ga(In) system glasses, vitreous phase struct. 77−76320
Ge-Te alloy films, amorphous, semicond. props., refr. index, struct. study 78−26978
Ge-Te and Ge-Te-As system glasses, local struct., ^{119}Sn Mossbauer obs. 79−41968
$Ge_{33}As_{27}S_{15}Te_{25}$ glass, switching, microstructural changes 79−65523
$Ge_xAs_xSe_{100-2x}$, x=2.5 and 5.0, chalcogenide glasses, IR absorpt. spectra 77−24842
$Ge_xAs_xTe_xSe_{100-3x}$, glassy, rel. to IR absorpt. spectra 78−23448
$Ge_{1-x}H_x$, amorphous, atomic struct., X-ray study 80−49106
GeO_2, amorphous, obtained by hydrolysis of $GeCl_4$, exam. of props. 79−95956
GeO_2 particles used for optical fibre fabrication, struct. props. 80−89167
GeO_2, vitreous, neutron diffr. obs. using Harwell linac 78−22666
GeO_2, vitreous, struct., contrasted with EXAFS obs. of $ZnCl_2$ liq. and glass struct. 80−70133
GeO_2:Mn^{2+}, EPR, struct. of vitreous and crystn. states 77−48039
GeO_2-K_2O, glass composition effect on solubility in H_2O 80−39303
GeO_2-$K_2O(Na_2O)(Li_2O)$, glass, Raman spectra, struct. and crystn. 80−92463
GeO_2-Na_2O, glass composition effect on solubility in H_2O 80−39303
GeO_2-$PO_{5/2}$ glass, struct. and props. *(Japanese)* 77−27837
GeP, thin films, vacuum-deposited, struct. characterisation 77−47691
$Ge(S,Se)_2$ glasses, comparison A_1 Raman line, microscopic origin 80−29740
$Ge_x(S,Se)_{1-x}$ chalcogenide covalent non crystalline topology, short range order 80−15009
GeS_{11} glass, neutron irrad., thermal and elec. props. 79−19286
GeS_2, amorphous film, reversible and irreversible photostructural changes 79−74061
GeS_2, chalcogenide glass, hollow cluster model of atomic structure 80−6366
$Ge_{1-x}S_x$ glasses, building blocks and bonds 80−54141
Ge_2S_3, electron irradiated, effects on elec., photoelec. and optical props. 80−49806
Ge_2S_3, glass form. and characterisation *(German)* 80−64913
$Ge_{25}S_{75}$:Mn, bond struct. and character in Ge-S system, EPR obs. 80−66014
$Ge_{40}S_{60}$:Mn (Ag)(Cu), bond struct. and character in Ge-S system, EPR obs. 80−66014
$GeS(S_2)$ amorphous films, photostructural changes, UPS study 80−49550
GeSe, amorphous, pair distrib. function, anomalous X-ray scatt. 80−49126
$GeSe_2$, chalcogenide glass, hollow cluster model of atomic structure 80−6366
$GeSe_2$ evaporated films, struct. and thermally induced effects 79−41963
$GeSe_2$ evaporated films, optical absorpt. and thermally induced effects 79−42989
Ge_2Se_3, glass form. and characterisation *(German)* 80−64913
Ge_xSe_{1-x}, amorphous, exponential absorpt. edge rel. to struct. 79−99902
Ge_xSe_{1-x}, amorphous, X-ray diffr. and local order modelling 80−49125
Ge_xSe_{1-x} glass, $1/3 \leq x \leq 1/2$, Raman scatt., local order 78−23442
Ge_ySe_{1-y}, glass, bulk and film, IR transmission and reflectivity meas., struct. mode assignments 78−79537
$GeSe(Se_2)$ amorphous films, photostructural changes, UPS study 80−49550
GeTe film, amorphous and crystalline, electron diffr. meas. 77−39748
GeTe, film, local order, electron diffraction study 79−77485
GeTe, X-ray emission spectra, amorphous and cryst. struct. *(Russian)* 78−88385
$Ge_{15}Te_{85}$, splat-cooled, rel. to thermoelec. props. 78−43426
Ge_xTe_{1-x}, amorphous, struct., quadrupole splitting of $^3/_2$ spin state of ^{125}Te calc. 77−65950
$Ge_xTe_xSe_{100-2x}$, x=2.5 and 5.0, chalcogenide glasses, IR absorpt. spectra 77−24842

noncrystalline state structure continued
H-bonded solid, bond failure theory 79−73246
$H_{5n-2}UO_2(IO_6)_n.4H_2O$, n=0.5 to 2.0, high proton cond. 80−107562
Hg-As-S modulating glasses, optical parameters and struct. *(Russian)* 78−63159
Ho-Co film, evaporated, struct. and mag. anistoropy, electron microscopy 79−56578
Ho-Co film, vapour quenched, amorphous, struct., electron diffr. meas. 77−28086
$HoFe_2$, amorphous, struct. determ., EXAFS exam. 78−51421
In-S system, vac. deposited films, form., reacts. 78−43259
In_2O_3:Sn, sputtered film, optical and elec. props. 78−76177
$In_{20}Te_{80}$, splat-cooled, rel. to thermoelec. props. 78−43426
K_3AsO_4-$KAsO_3$, glass and cryst., Raman and IR spectra 79−99862
$K_2(F,O)$-B_2O_3-SiO_2, effect of replacing B_2O_3 by Al_2O_3 or Ga_2O_3 78−63677
K_2O-Al_2O_3-P_2O_5-Nb_2O_5 glasses, struct. singularities, IR spectra *(Russian)* 78−2861
K_2O-Al_2O_3-P_2O_5-Nb_2O_5 glasses, struct. role of Nb 78−67653
K_2O-Al_2O_3-P_2O_5-TiO_2, structural role of Ti, kinetic study of chem. destruction 80−88055
K_2O-Al_2O_3-SiO_2 system, crystallisation of glasses in primary phase field of leucite 78−67658
K_2O-B_2O_3-Fe_2O_3, γ-irrad., Mossbauer spectroscopic study 80−108132
K_2O-B_2O_3-P_2O_5 glass struct. studies using NMR 79−24221
K_2O-B_2O_3-SiO_2, glass, crystallisation range *(German)* 80−38934
K_2O-CaO-B_2O_3:CuII, immiscibility, ESR detect. 78−80200
K_2O-CaO-BaO-SiO_2 (B_2O_3) (GeO_2), calc. of network refraction and exam. of glass structure 79−4783
K_2O-MgO-B_2O_3:Cu^{2+}, micro-inhomogeneities, EPR and Raman study 80−84080
K_2O-PbO-SiO_2, structural units, Raman spectroscopy 77−20847
K_2O-SiO_2-GeO_2 digermanosilicate glass, Raman study of structure 79−77524
K_2O-SiO_2-GeO_2 metagermanosilicate glass, Raman study of structure 79−77523
K_2O-TiO_2-SiO_2 system, vitreous, struct. obs. using neutron scatt. 78−22667
$K_2O.SiO_2$ glass, X-ray diffr. *(Japanese)* 80−19720
$K_2O.2WO_3$ glasses, X-ray diffr. study of struct. *(Japanese)* 77−11489
$K_2O.3CaO.BaO.xSiO_2$, property-comp. relns. 78−67655
$K_2O.4SiO_2$, glass, behaviour of VO^{2+} as spectroscopic probe 79−78510
La-Au, splat-quenched, Mossbauer effect and elec. resist., amorphous struct. 80−84676
La-Au liq.-quenched alloys, Mossbauer spectra, struct. 80−15841
LiF-$NaPO_3$-MeF_x (Me=Mg, Ca, Al) glasses, IR spectroscopy study 80−16042
$(Li_{0.63}Na_{0.37})_2O.2SiO_2$, short range struct. by pulsed neutron scatt. 80−59396
LiO_2-Al_2O_3-SiO_2, glass containing ZrO_2, cryst. process 80−103253
Li_2O-Al_2O_3-P_2O_5:V^{4+}, glass exam. of ESR spectrum of V^{4+}, optical spectra, and structure 78−88180
Li_2O-Al_2O_3-SiO_2, phase separation of initial stages of sitallisation 80−88053
Li_2O-Al_2O_3-SiO_2 glass, He migration, struct. effects 77−55389
Li_2O-B_2O_3 glass struct. study using ^{10}B NMR 80−84658
Li_2O-B_2O_3-SiO_2 glass systems, phase separation effect on the diffusion processes 78−26734
Li_2O-Fe_2O_3-SiO_2 glass, struct. and crystallisation behaviour 78−83738
Li_2O-GeO_2 glass, synthesis, Ge coordination state 77−24271
Li_2O-LiF-B_2O_3-Li_2SO_4 glasses, DC cond. and secondary struct. relax. 80−107469
Li_2O-SiO_2-GeO_2 digermanosilicate glass, Raman study of structure 79−77524
Li_2O-TeO_2 glasses, struct., IR reflection spectra 78−68516
Li_2O-TiO_2-Al_2O_3-SiO_2 glass, γ-irrad., struct. position of Ti, EPR study 80−84644
$Li_2O.2SiO_2$, short range struct. by pulsed neutron scatt. 80−59396
Li_2S-GeS_2, glass forming region, struct. and ionic cond. 80−88358
$Li_2Si_2O_5$-Li_2SO_4 glasses, electrical cond. and Raman study of struct. *(French)* 79−65482
$Li_2Si_2O_5$-TiO_2 glasses, struct. and crystn. investigation using Raman spectra 80−38918
M_2O-MnO-B_2O_3 glasses, M=Li, Na, K, glass-forming region and physicochem. props. 78−63678
$M_2O(MF_y)$-BeO-P_2O_5 glasses, M=alkali metal, alkaline earth, Cd or Zn, glass-formation 78−67656
Mg-Ga, metastable cryst. and glassy phases, X-ray struct. anal. and electron microscopy *(German)* 79−46601
MgO-Al_2O_3-SiO_2 system glasses and glass ceramics, EPR obs. of transition elements, crystn. effects 78−23332
MgO-Al_2O_3-TiO_2-SiO_2, glass formation, structure of cations *(Russian)* 80−38933
MgO-BaO-Al_2O_3-SiO_2, glass, IR absorpt. spectra and solid struct. exam. 78−88314
MgO-Na_2O-B_2O_3, Raman scatt. studies of glass struct. 77−90147
MgO-TiO_2-Al_2O_3-SiO_2 glass, γ-irrad., struct. position of Ti, EPR study 80−84644
$Mg_{70}Zn_{30}$ metallic glass, struct. and dynamics 79−37632
Mn-Ge amorphous films, short-range order, electron diffr. obs. 80−39473
y$(Mn_xFe_{3-x}O_4)$-(1-y)B_2O_3 glasses, elec. and struct. props., 400-1000K 79−51575
Mn_3Ge_2, $Mn_{11}Ge_8$, amorphous thin films, quasieutectic model, electron diffr. investigation of short range order 79−69013
MnO-CdO(ZnO), solid solns. prep., struct. 78−95157
MnSi, amorphous, sputtered, mag., elec., struct. and thermal props., spin glass behaviour 80−50124
Mo-Si(Ge)(Al), amorphous supercond. alloy, produced by coevaporation, struct. and supercond. 79−91179
MoF_5, mol. and electronic struct., vitreous, liq., and tetrameric states, ^{19}F NMR obs., mol. mobility 80−34787
$(Mo_{1-x}Ru_x)_{80}P_{20}$ alloys, liq. quenched superconductor 78−88057
MoS_3, amorphous struct., X-ray radial distrib. anal. and XPS 80−49115
N_2, liq. and glassy state, spin density and current correl. functions, computer simulation 79−14661
Na-Fe fluorophosphate glass, EPR and Mossbauer resonance study 80−15838
Na_2S-GeS_2 system, glass formation, struct. and ionic conduction 80−54138

noncrystalline state structure continued
$NaAlSi_2O_6$ melts quenched at high press., struct. from IR and Al K-radiation data 79−32907
NaBr-H_2O, quick-frozen aq. soln., XPS 79−38713
NaCl-H_2O, quick-frozen aq. soln., XPS 79−38713
NaF-H_2O, quick-frozen aq. soln., XPS 79−38713
NaI-H_2O, quick-frozen aq. soln., XPS 79−38713
$NaNO_3$-H_2O, quick-frozen aq. soln., XPS 79−38713
Na_2O-Ag_2O-B_2O_3 glass, Ag^+ ion distrib., X-ray diffr. study 80−84076
Na_2O-B_2O_3 glass, struct. interpretation of ^{10}B and ^{11}B NMR spectra 78−80241
Na_2O-B_2O_3 glass struct. study using ^{10}B NMR 80−84658
Na_2O-B_2O_3-Bi_2O_3, glass with metallic Bi granules, elec. cond. 80−84493
Na_2O-B_2O_3-SiO_2 glass, ^{11}B NMR obs. of struct. 78−38625
Na_2O-B_2O_3-SiO_2 glass, NMR, struct. 79−87325
Na_2O-B_2O_3-SiO_2:Yb(Tb), luminesc. cooperative processes, glass struct. and comp. effect 80−16101
Na_2O-CaO-MgO-Al_2O_3-SiO_2 glasses, ternary and quaternary, struct., Raman spectra obs. 77−36229
Na_2O-CaO-SiO_2, glass, light scatt. rel. to heat treatment *(German)* 78−84598
Na_2O-CaO-SiO_2 glass, surface viscous flattening kinetics, sinusoidal profile decay method 79−79139
Na_2O-CaO-SiO_2 glass, effect of phase on liquids and gas diffusion *(German)* 80−38931
Na_2O-GeO_2 glass, X-ray diffr. study of Ge coordination number 80−10503
Na_2O-GeO_2 glasses, neutronographic study of Ge^{4+} struct. state 80−19711
Na_2O-GeO_2 glasses, rel. to low temp. viscosity, as function of composition 78−38865
Na_2O-GeO_2 glasses, struct. changes, X-ray diffr. study *(Japanese)* 78−91254
Na_2O-GeO_2-Yb_2O_3, glass struct., Yb^{3+} ion segregation 78−87620
Na_2O-MgO-B_2O_3:Cu^{2+}, micro-inhomogeneities, EPR and Raman study 80−84080
Na_2O-P_2O_5 glass, XPS quantitative struct. anal. 80−2917
Na_2O-P_2O_5-SiO_2 glass, metastable liquid immiscibility 80−100331
Na_2O-SiO_2, ion bombardment, form. of cpds., IR spectrosc. exam. *(German)* 80−88173
Na_2O-SiO_2 glass, bridging to non-bridging ratio and correl. to glass density and refr. index, ESCA study 80−84832
Na_2O-SiO_2 glass, internal and surface struct. by X-ray scatt. 80−84074
Na_2O-SiO_2 glass, OH^- content effect on mech. and other props. 80−89337
Na_2O-SiO_2 glasses, Si-O bonds, effect of Na_2O *(Japanese)* 78−42918
Na_2O-SiO_2 glasses, struct., mol. dynamic calcs. 80−24366
Na_2O-SiO_2:Cu^{2+} glass ESR and optical absorption 79−77526
Na_2O-SiO_2-GeO_2 digermanosilicate glass, Raman study of structure 79−77524
Na_2O-SiO_2-GeO_2 metagermanosilicate glass, Raman study of structure 79−77523
Na_2O-SiO_2-NaF, elec. cond. of melt, and IR absorpt. spectra of glassy phase *(Japanese)* 77−62657
Na_2O-TiO_2-Al_2O_3-SiO_2 glass, γ-irrad., struct. position of Ti, EPR study 80−84644
Na_2O-TiO_2-SiO_2 glass, IR refl., Raman and EPR spectra, struct. *(Russian)* 78−2860
Na_2O-TiO_2-SiO_2 glass, co-ordination of Ti, X-ray emission spectra study 80−84072
NaOH water solution, struct. props. of disordered systems, Raman spectral study 77−4631
$Na_2O.2SiO_2$, short range struct. by pulsed neutron scatt. 80−59396
$Na_2O.4SiO_2$, glass, behaviour of VO^{2+} as spectroscopic probe 79−78510
Na_2S-P_2S_5, glass forming region, struct. and ionic cond. 80−88358
Na_2S-$SiS_2(GeS_2)(P_2S_5)$, synthesis, structure and ionic conduction *(French)* 80−65291
Na_2S-XS_2, X=Si, Ge, glass forming region, struct. and ionic cond. 80−88358
Na_2SO_4-H_2O, quick-frozen aq. soln., XPS 79−38713
$Na_2Si_3O_7.xH_2O$, amorphous, pulsed NMR study 79−78555
Nb films electron beam evaporated, struct. defects *(German)* 77−76684
Nb-Ge(Si), amorphous supercond. alloy, produced by coevaporation, struct. and supercond. 79−91179
Nb-Ni, amorphous, synthesis by vapour quenching, and struct. 78−11111
Nb-Ni, glassy alloy, struct. anal. using X-ray diffr. 79−51004
Nb-Ni glasses, struct. factor temp. depend. 80−28920
Nb-Si liquid quenched alloy, metastable A-15 and amorphous phases, interstitials 80−54394
Nb_3Ge amorphous films, X-ray diffr. analysis of microstruct. 78−72035
$Nb_3Ge(Si)$, amorphous films, thermally-activated internal friction peaks, structural obs. 80−80147
$Nb_3Ge(Si)$, RF sputtered films, amorphous atomic scale struct. 80−84064
$Nb_{0.4}Ni_{0.6}$, amorphous, pair distrib. function, temp. depend., rel. to glass transition 80−24368
$Nb_{60}Ni_{40}$, metallic glass, obs. of temp. depend. of struct. factor 78−87624
Nb_2O_5-V_2O_5-P_2O_5, glasses and glass ceramics, elec. cond., struct. 80−84466
$NdFe_2$, amorphous, magnetization and neutron scatt. meas. 79−78314
Ni based alloy, amorphous, liq. quenched, struct., thermal stability and mech. props. 80−88059
Ni, splat quenched, gaseous impurities effect on struct. 77−4042
Ni-B glass, X-ray obs. of struct. 79−1399
Ni-Co-P, ferromag. film, amorphous to cryst. transition, diffr. and resistivity meas. 78−60587
Ni-Cr-P, amorphous, corrosion behaviour, immersion tests and electrochem. meas. *(Japanese)* 80−85085
Ni-Fe (20%) film, condensed, struct. from electron diffr. 77−59222
Ni-Ge, amorphous, atomic struct., neutron diffr. study 80−59392
Ni-P, amorphous, low P, struct. study using high-angle X-ray diffr. 80−107055
Ni-P, amorphous, reversible effects of temp. on struct. 78−34442
Ni-P, amorphous, struct., X-ray scatt., rel. to Cu-Zr alloys 77−51324
Ni-P alloy, amorphous, NMR expts. and interpretation 79−8060
Ni-P amorphous alloys, electrodeposited and melt-quenched atomic and electronic structures 80−88062
Ni-P film, amorphous, ion implanted, struct. and domain struct. obs. 79−91272

noncrystalline state structure continued
Ni-P metal metalloid glass forming alloys, gram atomic volumes 78−38628
Ni-Pd-P, Ni-Pt-P, amorphous and electronic structs., NMR Knight shifts and linewidths meas. 78−68400
Ni-Ta (70, 30 wt.%) metallic glass, struct. and crystn. *(Russian)* 80−70136
Ni-Ti-P, amorphous, corrosion behaviour, immersion tests and electrochem. meas. *(Japanese)* 80−85085
Ni-Zr, amorphous phase form. in Zr-poor region, hardness and fracture strength *(Japanese)* 80−84914
NiGe, and Ni_2Ge, amorphous film, electron diffr. exam. of struct. 77−35828
Ni_3Ge, amorphous film, electron diffr. exam. of struct. 77−35827
$Ni_{35}Nb_{38}$, metallic glass, struct., neutron diffr. study 80−54148
NiP amorphous alloy, heat treatments influence on opt. props., struct. and DC resist. obs. 80−80892
$Ni_{77}P_{23}$ metallic glass, struct. relax., X-ray expts. 79−1400
$Ni_{80}P_{20}$, amorphous, struct. factor temp. depend., X-ray diffr. study *(Japanese)* 79−51005
$Ni_{80}P_{20}$ amorphous alloy, liquid-quenched structure 77−1082
$Ni_{78}Si_{10}B_{12}$, amorphous, struct. factor temp. depend., X-ray diffr. study *(Japanese)* 79−51005
$Ni_{40}Ti_{60}$, amorphous, chem. short-range-order, X-ray and neutron scatt. obs. 80−96447
P, amorphous, prepared by chem. transport in low-press. H_2 plasma, radial distrib. function 80−64899
P, amorphous, struct. by electron microscopy 80−84065
P-As-Se glasses, mag. susceptibility, dielec. const., opt. props. 78−64184
P-S, amorphous, glass transition and specific heat, intermolecular bond saturation 80−15011
P-Se, amorphous, glass transition and specific heat, intermolecular bond saturation 80−15011
P-Se system glasses, magnetochem. investig. 77−51325
P-Se-Tl glasses, NMR of ^{31}P and ^{205}Tl 80−15812
P_2O_5, pure vitreous, Raman spectra and struct. 79−69838
$P_2Se_xS_y$ glass, thermophysical props., 303-413K, struct. interpretation 78−47615
Pb-Ge-S semiconducting glasses, far IR transmission and struct. 79−65855
Pb-Si-Sb amorphous alloys, electrical resistometric detection of relaxation 79−60278
PbO, stoichiometric deviations on heating in vacuum 77−25035
$PbO-2B_2O_3-Fe_2O_3$ glass, Mossbauer study, struct., crystallite formation, broadened quadrupole doublet 78−59761
$PbO-B_2O_3$ glass-forming melt, specific volume and viscosity, temp. depend. 80−84073
$PbO-B_2O_3-Bi_2O_3$, glass with metallic Bi granules, elec. cond. 80−84493
$PbO-Bi_2O_3-Al_2O_3$, glass formation and IR transmission *(Japanese)* 80−54146
$PbO-GeO_2$, glass, structure of anionic network, IR spectra 80−103256
$PbO-GeO_2$ glass, synthesis, Ge coordination state 77−24271
$PbO-SiO_2$ and $PbO-SO_3-SiO_2$ system glasses, struct. and IR absorpt. spectra 79−41967
$PbO-SiO_2$ glass, IR and Raman spectra interpreted in terms of struct. 78−27213
$PbO-SiO_2$ glass, rel. to EPR of Cu^{2+}, V^{4+}, and Mn^{2+} 78−39392
$PbO-SiO_2$ glasses, density-of-states and structural forms, Raman spectra study 80−97255
$PbO.2B_2O_3$, vitreous, structural aspects studied by Raman scattering 77−8575
PbSe-GeSe-AsSe, glass form., elec. cond., struct. defects, assoc. *(Russian)* 80−54145
Pd-Au-Si, influence of struct. on elec. resist. of glass forming alloys 80−65518
Pd-Cu-Si, glass form., crit. cooling rate 80−75169
Pd-Ge, metallic glass, theoretical studies on structural models 79−37633
Pd-Ge glass, short range order obs. for $Pd_{80}Ge_{20}$ and $Pd_{78}Ge_{22}$, EXAFS expts. 78−55815
Pd-Ge metallic glass, appl. of EXAFS methods for struct. determ. 79−37624
Pd-Si, amorphous, compositional study on short-range struct. 80−84095
Pd-Si, amorphous, struct., crystn. and Hall effect meas. 80−75178
Pd-Si, amorphous metallic glass, with defined local coordination, struct. model 80−84092
Pd-Si, amorphous $Pd_{0.8}Si_{0.2}$, struct. anal. by dense random packing model 79−51003
Pd-Si, metallic glass, theoretical studies on structural models 79−37633
Pd-Si alloys, metallic glass, structural model 79−14690
Pd-Si amorphous alloy, neutron irradiation effects *(Japanese)* 77−84806
Pd-Si metallic glass, high-resolution electron microscopy 80−84097
Pd-Si-Fe amorphous alloy, Mossbauer spectra, struct. and bonding 80−7224
Pd-Si-Sb, amorphous, phase separation and crystallisation 79−51002
$(Pd_{80}Au_7Si_{13})/Fe_{30}$, compositionally modulated amorphous film, diffusion, struct. relax. 80−103518
$Pd_{68.5}Cu_{15}Si_{16.5}$ glass, elec. resist., struct. and mag. props. 79−65423
a-$Pd_{0.8}Si_{0.2}$ alloy, struct. factor determ. rel. to short-range correlations 77−1060
$Pd_{0.8}Si_{0.2}$, amorphous, He^{2+} ion irradiation effect on structure 79−42120
$Pd_{0.8}Si_{0.2}$, amorphous ribbon, struct. factor anisotropy, pulsed neutron diffr. study 78−87619
$Pd_{80}Si_{20}$, amorphous, structural changes by neutron irradiation, X-ray scatt. meas. 78−6104
$Pd_{80}Si_{20}$, amorphous, struct. factor temp. depend., X-ray diffr. study *(Japanese)* 79−51005
$Pd_{80}Si_{20}$, amorphous, structural changes with neutron irrad., X-ray scatt. obs. 80−33898
$Pd_{80}Si_{20}$, amorphous alloy, partial struct. functions, X-ray, electron and neutron diff. studies *(Japanese)* 80−88050
$Pd_{80}Si_{20}$ glass, struct. simulation 78−38624
$Pd_{80}Si_{20}$ metallic glass, struct. relax., X-ray expts. 79−1400
$Pd_{80}Si_{20}$, metallic glass, composition, mech. props., simulation 80−49117
$Pd_{82.5}Si_{17.5}$, amorphous compared with liq. X-ray diffr. 77−24275
$(Pd_{85}Si_{15})_{61}/(Fe_{85}B_{15})_{39}$, compositionally modulated amorphous film, diffusion, struct. relax. 80−103518
$Pd_{100-x-y}Si_xFe_y$, amorphous, ^{57}Fe Mossbauer spectra, X-ray diffr., ageing behaviour 79−28651
$Pd_{82-x}V_xSi_{18}$, amorphous, effect of structural relax. on elec. resist. 79−56186

noncrystalline state structure continued
$R_{1-x}Co_x$, rare earth amorphous alloys, thermal stability, elec. cond. enthalpy 80−100172
$RbO_2-Na_2O-P_2O_5$ glasses, Raman and far IR spectra, vib. at cation site, struct. 78−60435
$Rb_{1-x}O_x$, metallic glass, prep., elec. props. and struct. 78−67652
$Rb_2O-Li_2O-P_2O_5$ glasses, Raman and far IR spectra, vib. at cation site, struct. 78−60435
S, random chain assembly model 78−6015
$(SN)_x$, brominated, X-ray absorpt. meas., 5K to room temp. 80−71516
$(SN)_x$, halogenated, struct. behaviour, TEM obs. 80−70126
SSe_9, stable thermoelectret, effects of anisotropic external perturbation *(Russian)* 77−63361
Sb-O-Cl(Br)(I), glass-forming regions 80−88057
$SbO_{3/2}-BO_{3/2}$, glass, struct. and props. *(Japanese)* 77−27836
Sb_2O_3 glass, X-ray diffr. anal. of struct. 78−87621
$Sb_2S_3(Se_3)$, IR spectra rel. to bonding, amorphous film and cryst. 77−16410
Se, amorphous, elec. cond., activation energy, density, cryst. Se effect 80−65548
Se, amorphous, far IR investigation of structure, ring and polymeric chain components *(Japanese)* 77−76311
Se, amorphous, random chain assembly model 78−6015
Se, amorphous and liquid state, Raman spectra, crystn. processes 80−60608
Se, amorphous evaporated layers, struct. inhomogeneities due to prep. technology fluctuations 77−76710
Se, amorphous film, highly disordered, UPS study 80−76148
Se amorphous film, interference enhanced Raman scatt. 80−50326
Se, amorphous film, photocond., dark cond., rel. to crystn. 80−88596
Se amorphous layer structure, influence of vacuum deposition conditions *(German)* 78−63957
Se, correl. between mol. struct. and props. 77−11484
Se, crystallisation kinetics correlation with molecular structure 78−94998
Se, DSC and X-ray diffr. expts. 78−22662
Se film, amorphous, struct. and crystn., far IR transmission spectrum and DSC obs. 77−85106
Se film, noncryst., ageing and crystn. obs., tentative struct. model 80−2295
Se, glassy, structural excitation energies of defects, pseudopot. approach 80−107061
Se, liq. and amorphous, struct. by pulsed neutron diffr. using an electron LINAC 77−51307
Se, liquid and amorphous, struct. modelling using Monte Carlo method 80−59391
Se, mol. structure, local atomic arrangement at intrinsic bonding defects 80−59374
Se, relax of sound velocity, struct. determ. 78−38786
Se, trigonal and amorphous, electronic struct. and nonempirical calc. of struct. props. 80−59866
$Se-As_2Se_3$ system glasses, vibr. spectra and partial vols. of components 79−42973
Se-Ge, amorphous, Raman spectra and average band gap 80−50327
Se-Ge glass, lattice vibr. spectra, photostruct. change, far IR absorpt. 78−72494
Se-Si system glasses, vibr. IR spectra 80−20643
Se-Te crystallised glasses, struct. transforms. and IR spectra 80−19712
Se-Te solid solutions, ordering, diffuse X-ray scatt. 77−65965
$Se_{0.95}Te_{0.05}$, glass crystallisation, effect of an alternating electric field 80−88054
$Se_{1-x}Te_x$, amorphous film, photo-crystallisation 80−59839
$Se_{1-x}Te_x$ systems, amorphous and liq. states, short range order, neutron scatt. study 80−49124
Se_xTe_{1-x}, amorphous, structural relaxation and crystallisation kinetics study by DTA 80−59394
Si, amorphous, hydrogenated, recent advances 79−28103
Si, amorphous, hydrogenated and deuterated, struct. 80−103245
Si, amorphous, IR absorpt., first-order effective charges due to at. displacements 77−48164
Si, amorphous, molecular liquid model and electronic struct. 80−54133
Si, amorphous, photostructural changes, photodarkening 80−49121
Si, amorphous, reduced intensity functions, thermal vibr. coupling 78−42910
Si, amorphous, scatt. intensity and radial distrib. function, random stacking model 79−27919
Si, amorphous, struct. and growth kinetics, topological principles 80−49123
Si, amorphous, structural disorder rel. to electronic props. 78−34756
Si amorphous film, vacuum deposited, microscopic voids, gas absorpt., crystn. study 80−49534
Si, amorphous film prepared by CVD, optical props. and struct., solar absorber appl. 79−52035
Si, amorphous layers, recrystallisation, pulsed laser annealing 80−65404
Si, effect of disorder on H content 80−75258
Si film, amorphous, high resolution electron microscopy, digital processing use 78−37116
Si, film, amorphous, prep. conditions influence on supernetwork struct. 77−76709
Si noncrystalline film, struct., interatomic distances, SRO 80−107053
Si plasma deposited amorphous hydrogenated film, optical props., annealing effect 79−56874
Si:As, amorphous, appl. of EXAFS methods for struct. determ. 79−37624
Si:F, amorphous, pure and doped, vibr. excitations at defect sites, IR and Raman spectra calc. 80−49329
Si:H, amorphous, defect creation and H evolution 80−50392
Si:H, amorphous, glow discharge deposited, laser annealing 80−49104
Si:H, amorphous, structural model 80−49105
a-Si:H, electronic states and bonding config. 80−64900
Si:H amorphous film, plasma-deposited, growth morphology and defects 80−44128
Si:H amorphous films, IR spectrum and struct. 80−97277
Si:H amorphous films, interference enhanced Raman scatt. 80−50326
Si:P, heavily doped, glow-discharge-produced, elec. and optical props 80−2497
Si-H, amorphous, H three-dimens. distrib., ion-induced AES and Rutherford backscattering 80−44132
Si-H, amorphous, random network model 80−1932
Si-H, amorphous, struct. anomalies, theoretical interpretation 79−90556
Si-H, amorphous, struct. and press. induced transition 80−44131

noncrystalline state structure continued
Si-H, amorphous, thermal stability and decomp. kinetics 80−24758
Si-Te system glasses, local struct., ^{119}Sn Mossbauer obs. 79−41968
Si(-H), amorphous, H atom effect on Si-Si atomic short-range order, X-ray diffr. obs. 79−64996
Si_xAs_{1-x}:H, amorphous system, struct. and defects, Raman and EPR meas. 80−49103
SiC, on Si and metal silicides, formation characteristics and mechanism, by ion backscattering techniques 79−60653
Si_xC_{1-x}:H reactive sputtering deposition, compositional and structural props. 79−99077
SiH_x polymer film, struct. rel. to amorphous solid 78−72048
$Si_{1-x}H_x$, amorphous, atomic struct., X-ray study 80−49106
$Si_{1-x}H_x$, noncrystalline film, struct., interatomic distances, SRO 80−107053
Si_3N_4, amorphous, CVD prep., struct. characts. by pulsed neutron diffr. 80−33891
Si_3N_4, CVD, chem. bond nature, Compton scatt. expts. 80−49539
Si_3N_4, CVD, effect of deposition parameters 77−55272
Si_3N_4, CVD amorphous film, X-ray diffr. 79−87013
Si_3N_4 film, amorphous, AES and EELS characterisation 79−90905
Si_3N_4, films, ion-beam synthesis, IR spectra, struct., crystallisation on annealing 77−16705
Si_3N_4 films, struct. 80−54545
Si_3N_4, non-stoichiometric films, struct. 79−42412
Si_3N_4-Al_2O_3-SiO_2 systems, glass forming regions 80−84070
SiO_2, amorphous, intrinsic defects, photoluminesc. 79−78740
SiO_2, amorphous, local at. struct., XPS obs. 80−20042
SiO_2, amorphous, optical and elec. props., comparison with chalcogenide semiconds. 78−6721
SiO_2, amorphous, struct. and chem. bonding 78−51422
SiO_2, amorphous, struct. model, surface struct. *(German)* 79−90859
SiO_2, amorphous, very small angle X-ray scatt. before and after thermal neutron irrad. 80−75270
SiO_2, amorphous and cryst., neutron irrad. and unirrad., intrinsic defect photolum. 80−50401
SiO_2, amorphous film, form. by thermal oxidation of Si, struct., mechanism 77−12725
SiO_2 and SiO_2-B_2O_3 glasses, struct. and phonon spectra 80−50324
SiO_2, cryst. and vitreous, struct. sensitive expansivity 78−22873
SiO_2 films, Si-rich, amorphous Si region obs. 80−84400
SiO_2, fused, broken bond defect generation mechanisms 80−88044
SiO_2 gel, internal and surface struct. by X-ray scatt. 80−84074
SiO_2 glass, crystallinity positron annihilation study 78−72629
SiO_2 glass, electron microscopic determ. of struct. 79−90561
SiO_2 glass, formation by hydrolysis of $Si(OC_2H_5)_4$ with NH_4OH and HCl soln., and characterisation 80−71622
SiO_2 glass, heat treatment study by positron annihilation 78−55812
SiO_2, glassy-amorphous, light scatt. exam. 78−14281
SiO_2 glassy-amorphous system, struct. *(German)* 78−38626
SiO_2, ion bombardment, form. of cpds., IR spectrosc. exam. *(German)* 80−88173
SiO_2 layers, crystallisation, structural props. rel. to annealing 78−34724
SiO_2, noncryst., radiation-induced defect centres, ESR spectra and struct. 78−23343
SiO_2, small amorphous particles, high resolution TEM 79−82157
SiO_2, stoichiometric condensate form. during electron beam evaporation of quartz, electrophysical props. 77−16496
SiO_2, vitreous, fast neutron irrad. effect on struct., interstitials role 78−26599
SiO_2, vitreous, Fe^{2+} absorpt. spectra in polarised light and struct. position 79−43007
SiO_2, vitreous, heat treatment effect on viscosity and struct. 80−19714
SiO_2, vitreous, intrinsic radiation defects, nonbridging O 80−19837
SiO_2, vitreous, paramag. centres associated with bonding defects 80−80609
SiO_2 vitreous film on Si, defect struct. comparison with crystalline SiO_2 and Si-O bond nature 80−54557
SiO_2:Fe, vitreous and cryst., with or without Al_2O_3, Na_2O additions, exam. of Fe^{2+} coordination, IR spectroscopy 78−88344
SiO_2:Fe^{2+}, vitreous silica, absorpt. spectra and structural state 80−16071
SiO_2:TiO_2, prep., amorphous struct., effect of roasting, bonds 78−44061
SiO_2-Al_2O_3-Fe_2O_3-Na_2O-K_2O-CaO-MgO glasses, Mossbauer spectra study 80−39967
SiO_2-B_2O_3 glass system, gel hot pressing synthesis and characterisation *(French)* 80−66468
SiO_2-B_2O_3 glasses, Brillouin scattering meas. of attenuation and vel. of hypersounds 80−100309
SiO_2-based glass, with thin metal films, exam. using emission electron microscope 77−1285
SiO_2-GeO_2, synthetic, struct, IR spectra 79−42993
SiO_2-glass fibres, struct. anal. using X-ray diffr. and optical microscopy 77−65952
SiO_2-glasses, radial distrib. functions 80−44136
SiO_2-Li_2O-Li_2SO_4, glass-forming region, struct. and ionic cond. 80−84320
SiO_2-Na_2CO_3, sodium Erevanit-25, sintering, struct. 79−43284
SiO_2-Na_2O-CaO-MgO glasses, surface and near surface struct. 78−87850
SiO_2-$PO_{5/2}$ glass, props. and struct. *(Japanese)* 77−27837
SiO_2-TiO_2-Al_2O_3-SrO(BaO), glasses, ceramic form. rel. to Al_2O_3 content 77−25005
SiO_2-ZrO_2 adsorbents, coprecipitated, porous struct. rel. to form. conditions 78−53263
SiO_2-ZrO_2-Li_2O-Na_2O based crystallisable glasses composition and properties 80−50731
SiO_x amorphous films, high energy electron diffr. study 80−38911
SiO_x film, amorphous, AES and EELS characterisation 79−90905
SiO_x, powder and vac. deposited, amorphous struct., X-ray diffr. meas. 80−1931
$Si_xO_yN_z$, non-stoichiometric films, struct. 79−42412
Sn-O system, amorphous, characterisation by appl. of Mossbauer effect 79−61283
SnO-GeO_2 system, glass form., compound anal. 77−35486
SnO-SiO_2 glass, struct., X-ray density, IR obs. 79−46574
$SrCl_2$ film, very-low-freq. inelastic light scatt. 80−25367
SrO-Al_2O_3-TiO_2-SiO_2, glass formation, structure of cations *(Russian)* 80−38933
SrO-Fe_2O_3, splat quenching struct. and crystn. mechanism *(French)* 78−51426

noncrystalline state structure continued
Ta, film, CVD on silica, struct. and mech. props. 77−24965
Ta-Co(Ni)(N)(Ar), amorphous metal films, struct. and elec. characterisation 79−87017
Ta_2O_5, defective anodic film on Ta, elec. characts. 77−12039
Tb-Fe film, undoped and O-doped, amorphous, microstruct. and mag. props. 79−91273
$TbFe_2$, amorphous, struct. determ., EXAFS exam. 78−51421
Te, amorphous, random chain assembly model 78−6015
Te, Raman spectra, crystn. processes 80−60608
Te, trigonal and amorphous, electronic struct. and nonempirical calc. of struct. props. 80−59866
Te-Si glassy alloys, IR transmission and sp. ht. changes in glass interval, vibr. modes, struct. models 78−23474
$Te_{80}Ge_{20-x}Sb_x(Bi_x)$, DSC studies of struct. phase transformation 80−66505
TeO-V_2O_5 glass system, X-ray diffr. study 79−10805
TeO_2, structure simulation of some tellurite and chalcogenide glasses quasi-crystalline structural diffusion method *(Russian)* 80−54147
TeO_2-Fe_2O_3 system, glass structure 79−90562
TeO_2-Li_2O glassy system, struct. recomb. model 80−19707
TeO_2-MoO_3-V_2C_5, phase comp. determ. using X-ray diffr., electron microscopy and DTA *(German)* 80−88046
TeO_2-P_2O_5 system, glass struct., neutron diffr. study 80−70128
Te_xSi_y, (x=78,87, y=22,13), amorphous, struct., X-ray diffr. study 80−6362
TiO_2, amorphous film, vac. deposited, struct. and crystn., TEM obs. 80−2291
TiO_2-Ti_2O_3-P_2O_5, glass form., struct. and elec. props. 80−44592
$TlAsS_2$, glass, crystallisation, effect of an alternating electric field 80−88054
$TlAsTe_2$, local struct. changes on crystal-glass transition, Mossbauer spectra 77−36157
TlS_2, amorphous, struct. and origin of crystn. process 77−76322
TlS_x, struct. from radial electron density distrib. curves 79−23527
$TlSe_x$ amorphous phase struct., rapid electron density distrib. curves 80−33896
$Tl_{1-x}Se_x$, amorhpous, IR spectra, structure 77−77194
Tl_xSe_{1-x}, amorphous and cryst., IR transmission spectra and struct. interpret. 78−23471
V_2O_5, amorphous, electronic cond., effect of random glass struct. 79−23972
V_2O_5, amorphous, hydration and fibrous texture, EPR study *(French)* 79−24826
V_2O_5 amorphous films, CVD prep., structural characts. 80−49114
V_2O_5, water in noncryst. solid, quenching of molten V_2O_5 *(French)* 78−42912
V_2O_5-BaO-K_2O-ZnO glasses, elect. props. and struct. 80−15547
V_2O_5-P_2O_5 glass, density and O molar volume 78−59759
V_2O_5-P_2O_5 glasses, Raman spectra 79−78667
V_2O_5-P_2O_5-MO system glasses, (M=Ba,Ca,Cu and Mg), phase separation, crystn. and EPR spectra 77−76321
V_2O_5-TeO_2 system, vitreous, struct. obs. using neutron scatt. 78−22667
$V_{1+x}P_{1-x}O_{5-c/2}$, density and struct. from X-ray scatt. meas. 77−89380
$V_{1+x}P_{1-x}O_{5-c/2}$ glasses, structure, adiabatic hopping conduction model 77−43588
W-Cu(N) amorphous metal films, struct. and elec. characterisation 79−87017
W-Ru based refractory transition metal-metalloid glass, X-ray determ. 80−1938
WO_3, amorphous film, vac. deposited, struct. and crystn., TEM obs. 80−2291
WS_3, amorphous struct., X-ray radial distrib. anal. and XPS 80−49115
Y-Si-Al-O-N glass, prep. and props. 80−25647
YIG, amorphous, ionic glass, hard-sphere random-packing model 80−24369
YNi_2 amorphous alloy, at. struct. 80−19704
ZnB_2O_4-RF_2, R=Mg, Ca, Sr, Ba, glass form., struct. and props. 80−84077
$ZnCl_2$, glassy and liq, EXAFS obs. of struct., comparison with vitreous GeO_2 80−70133
Zr-Co(Ni) amorphous alloy, thermal stability and electronic props. 79−73487
Zr-Cu, glassy alloy, struct. anal. using X-ray diffr. 79−51004
Zr-Ti-Be metallic glass, phase separation 80−97464
$Zr_{70}Co_{30}$, $Zr_{70}Fe_{30}$, $Zr_{70}Ni_{30}$ and $Zr_{70}Pd_{30}$ amorphous alloys, struct. factors and radial distrib. functions 80−84096
ZrF_4-BaF_2-NdF_3 glass, vitreous domain, prep. and optical props. 78−27304
$Zr_{0.7}Pd_{0.3}$, supercond., rel. to sp. ht. and thermal cond., 0.1-10K 78−26991

nondestructive readout
charge injection devices for astronomy 77−41317
MWPC, nondestructive readout system 79−3315
MWPC of focusing spectrometer 79−3280
superconducting film, memory device storage of Abrikosov vortices 79−28487
Si array/$LiNbO_3$ gap-coupled imaging devices 79−46057

nondestructive testing
see also crack detection; ultrasonic materials testing; X-ray fluorescence analysis
accelerated electrons, use in NDT, review 80−35480
accelerated testing and Arrhenius eqn. 78−53182
accountability, nondestructive assay using neutron counting, calorimetry and gamma spectrometry 80−63266
acoustic emission, cast iron, Cu alloy, and Al alloy 77−25221
acoustic emission, principles of technique and measuring instrums. 80−28375
acoustic emission, random signal parameters, computer calc. 77−44454
acoustic emission analysis for vibration and shock testing of industrially produced substances *(German)* 80−3279
acoustic emission NDT appls., review 78−11489
acoustic emission optical interfereometer and auxiliary direct viewing system 79−79217
acoustic emission technique, twinning characts. in In 77−4873
acoustic emission transducers and systems, spectral calibration by He gas jet 77−835
acoustic microscopy for NDT of electronic devices 79−37094
acoustic waves generation, by pulsed electron flux, for nondestructive inspection 80−5905

nondestructive testing continued
acoustic-emission pulse distrib., statistical investigation 80−87638
acoustical imaging, US visualization and characterization, conf., vol.8, Key Biscayne, FL, USA (May-June 1978) 80−83720
active thermal NDT, review 79−70282
adhesive bondline interrogation, using Stoneley wave methods 80−49530
adhesive joints, thin films, thick films and bulk coatings, conf. Philadelphia, USA (Nov. 1976) 80−46729
aerospace components, holographic interferometry 77−7039
aerospace test meas. symposium, San Diego (1976) 77−41284
AES of surfaces 78−85277
airframe material defectometry, quantitative test specifications *(German)* 80−89427
alloys, machining damage, depth of surface layers determ. 80−85094
alloys, metalloceramic, hard, homogeneity and wear resistance estimation, by magnetic method 77−90558
amorphous layer thickness meas. by electron back scattering method 80−100721
amorphous materials, high resolution imaging by electron microscopy 79−99039
amphibole fibre conc. in water, interlaboratory meas. by TEM 78−88590
amplitude and time analyzer for flaw detect. 79−70288
amplitude phase methods of testing, design relationship for eddy current transducers 78−53152
anisotropic body, nondestructive thermophysical checking methods 78−79196
anistropic specimen, dielectric const., NDT 80−35475
asbestos-cement pipes, nondestructive neutron-radiation testing of moisture content 79−75539
astigmatic X-rays, diaphragm for investigating materials by this method 80−25935
attachable electromagnets of ferroprobe coercimeters, use of pole shoes 78−45662
automated, vehicle reliability improvement on structural and motor parts 79−91859
automatic defect signaller for the ASNK-U assembly system for nondestructive testing 79−39101
automatic digital circuit for selecting information bearing components of output voltage of electromagnetic transducer 79−2760
automatic inspection of materials using lasers 80−66734
automatic magnetic inspection system for oil country tubular goods 77−81361
automatic test equipment for material props. determ. and quality control 77−86236
automatic visual inspection of moving steel surface 77−81349
autoradiographic inventory methods for nondestructive assay of reactor fuels and fuel assemblies 80−71875
autoradiography of thin laminars, resolution improvement *(French)* 80−35438
axisymmetric bodies, integrated photoelasticity, nondestructive anal. 79−18842
axisymmetric transducers, with various boundary conditions, single integral computer method for Green's function 80−87591
bar insulation in stator winding of large turbogenerator, inspection using microwave defectoscope 80−35474
Barkhausen noise anal. appl. 79−70261
base for inspection *(German)* 77−32741
beam-wave reflectometer for complex permittivity meas. at microwave freqs. 78−74030
bending wave propag. in transversely struck plate, birefringence obs. *(German)* 78−48582
bi-layer struct., radiation attenuation technique for simultaneous layer thickness determ. 77−12758
biomedical scattered radiation grids, method for testing 80−81717
blind hole drilling technique for residual stress measurement: application in NDT 80−40660
bonded interface defect testing by differential interferometric Stoneley wave meas. 80−76444
book 78−44340
brass, nondestructive determ. of in-depth profile 80−93836
brittle coating analysis of orthotropic materials 79−27606
brittle coatings 80−11851
brittle fracture growth dynamics, crack vel. meas. using evaporated thin conducting film 78−83347
brittle lacquer technique for strain measurements, book contrib. 79−20332
brush-type self-propelled ferrets for equipment in pipelines 79−34249
calibration and standards 79−11738
calorimetric nondestructive assay for in-field meas. of Pu-bearing materials 80−71874
CANDU fuel, post-irradiation test facilities at Chalk River 80−30206
CANDU fuels, nondestructive determ. of burnup by gamma scanning, fission monitor appl. 78−94076
CANDU nuclear reactors, in-situ inspection of press. tubes, nonrotating device 78−25259
cantilever fastened plate, structural sensitivity of magnetoelastic effect 79−39095
cast turbine blade microporosity, X-radiographic method appl. 77−86276
castings, defect classification 78−27690
cellulose hydrate, nondestructive control of mech. props. anisotropy, appl. of capacitance method 77−86277
ceramic components scanning laser acoustic microscopy, appl., comparison with SEM and optical microscopy results 80−58875
characterisation by precision gamma scanning 79−49688
charcoal filters, NDT of residual adsorption capacity 80−89523
cholesteric liquid crystals 77−73395
chrome plating, thickness meas., model PINT-3 electromagnetic instrument 78−70162
chromorheology, exptl. verification of numerical solns. of elastic-plastic problems 80−48659
chromorheology, new exptl. method 80−48658
chrysotile fibre conc. in water, interlaboratory meas. by TEM 78−88590
circular ring, inner boundary shapes, optimised, diametral compression 80−38369
clad optical fibres, nondestructive interferometric meas. of α and Δ 77−84013
coating thickness measurement using bremsstrahlung radiation from monoenergetic fast electrons 77−77609
coating thickness measurement using nuclear resonance methods 77−81334
nondestructive testing continued
coatings, brittle, strain sensitive, for stress, strain testing of surfaces of loaded structs. 79−29311
coatings, methods and instruments for measuring the thickness, review 78−73000
coatings on plates. determ. of residual stresses using curvature gauging method *(Russian)* 79−98674
coercimeter, electromagnetic, magnetising current amplitude and turn off speed effect 78−39997
coercimeter, with cylindrical attachable electromagnet, exam. of design 78−76809
coercimeter KIFM-1 with automatic measurement of the demagnetizing current 80−68229
coercive force, differential meas., appl. to ELA steel 77−71351
coercivity meter magnetic heads 78−57996
coercivity meter with portable display system 78−53135
coherent optical defectoscopy, signal processing *(German)* 78−7110
coherent optical materials testing procedure, filtered vibration patterns *(German)* 79−15882
cold rolling rolls, magnetic inspection at heat treatment quality 78−88613
colorimeters, used for corrosion meas. production control, quality monitoring *(German)* 77−48603
column buckling criteria determ. using vibr. data 78−34098
complete inspection principle 78−88598
complex mass production parts, choice of testing methods 79−5105
complex shape product inspection, local eddy current transducer 80−108671
composite materials, damage studying by NDT 80−66735
composite materials, thermographic technique, for examining damage extent 79−43540
composite materials damageability, NDT methods 80−11867
composite pressure vessel, holographic exam. 77−28957
composites, appl. of exptl. methods to fracture 80−11869
computer-based information system description and advantages 77−81366
concrete, density meas. by back-scattered gamma radiation 77−36699
concrete, strength, NDT standardization 79−91902
concrete *(Japanese)* 80−30188
concrete structures, reinforcement position measurement 77−90534
controlled regenerated inhibited solvent process, CRISP 77−12762
conveyor belts with steel reinforcing cables, computer-aided magnetic defectoscopy 77−73417
corrosion damage in nonmagnetic parts electromagnetic determ. of degree, apparatus *(Russian)* 77−70207
corrosion monitoring by eddy current 78−88584
corrosion monitoring by magnetic susceptibility variation meas. 79−29292
cotton fibre fineness and maturity comparison on air flow instruments 78−88591
creativity and imagination *(German)* 79−20316
CRISP-E, use in a phase-in mode 80−40654
critical evaluation of test results, representation, processing *(German)* 78−7145
current limitations of non-destructive testing in engineering 79−74326
cutting tools, stress anal., Moire technique 78−64799
cyclically loaded structures, effects of periodic proof and nondestructive testing 79−15946
cylindrical part edge quality determ., acoustic method and equipment 80−35491
cylindrically layered conductors, electromagnetic NDT 79−74318
cylindrically loaded structures NDT effect on reliability, assessment 77−81362
data processing and acquisition 80−11862
defect, thermal inspection 79−79208
defect detection by holographic interferometry 79−15935
defect-marking system, position-delay, pulse signals of scanning defectoscope conversion 77−90566
deformation state determ. by holographic interferometry *(German)* 77−77653
destructive materials testing anal. by nondestructive electromagnetic methods *(German)* 77−86267
device for checking airtightness by parameter changes in object and medium 80−104404
dielectric constant calculation by measuring porosity change using radio wave phase method 79−39096
dielectric material, NDT using Kirlian effect, high freq. technique 80−66749
dielectrics, potential distrib. determ., non-destructive method *(French)* 80−40060
diesel nozzle sprayer castings, heat treatment quality inspection 80−35471
diffusional homogenisation in compacted powder blends, X-ray diffr. line profile analysis 78−80491
digital filtering of speckle-photography data 80−27338
discontinuity detectio n 77−81360
discontinuous variations of stress, detection by magneto-inductive method *(German)* 79−52547
dye penetrant method using sorption developer, developer indications/single void diameter relation 79−70287
echo pulse thickness gauge, type UT-31MTs, portable 78−70108
economic signficance, of non-destructive testing *(German)* 80−7735
eddy current, primary eddy current transducers, response approx. 77−73419
eddy current defectoscope performance analysis with series tank circuit in input stage 78−53106
eddy current electromag. convertor, forming part of unbalanced bridge circuit, exam. of charact s. 78−85100
eddy current fastener hole tester, improved design 80−30194
eddy current flaw detector, feedback phase effects on response to displacements 77−73418
eddy current inspection, possibilities of phase generator circuits 78−88614
eddy current inspection of fastener holes, computer automation, exam. 78−53040
eddy current inspection system with simulated signal, calibration 78−3285
eddy current meter standards 78−27709
eddy current method, pulse-excited systems frequency spectrum analysis *(Czech)* 79−39071

nondestructive testing continued
eddy current method appl., distribution in plate of finite thickness calc., due to coil of arbitrary shape *(German)* 79−27129
eddy current modulation defectoscopy, defect parameter determination 78−60937
eddy current modulation inspection unit, for examining surface defects in petroleum pipes 78−76814
eddy current nondestructive evaluation, finite element analysis appl. 80−35439
eddy current probe, high saturation with internal reference, design and specifications 80−40658
Eddy current pulsed method theoretical and expt. foundations *(German)* 79−15920
eddy current spatial harmonics, spectra density meas. 78−53141
eddy current testing, numerical and expt. investigation *(German)* 77−12763
eddy current testing, signal to noise ratios and sensitivity increase 77−73393
eddy current testing devices, operation, appl., set up and evaulation, Verimet method *(German)* 79−70263
eddy current testing of tubes, rods and wires *(German)* 80−25971
eddy current testing of wire and bar 80−71819
eddy current thickness gauge, total factor experiment exam., metrological characteristics determ. 78−39999
eddy current transducer, electrical conductivity meas. of coatings, tuning out of gap instability 78−36994
eddy current transducer, impedance introduced by nonmagnetic plate 78−60939
eddy current transducer parameters, effect of moving inspected plate 78−60938
eddy current transducer part geometry effect on inspection 78−53078
eddy current transducer with electrical commutation of excitation field, NDT 80−105633
eddy current transducers, for meas. thickness of lacquer coloured coating on mag. base 78−85101
eddy currents in non-magnetic tubular conductors, NDT appl. *(French)* 80−83541
eddy-current feed-through transducer, approx. calc. of mag. field, nonferromag. media 80−78746
eddy-current probes, rotary, for defects scanning and detection 77−90557
elastic waves, attenuation and propag. speed in materials under uniaxial static compression, installation for determ. 80−21233
electrical circuit, hidden partial fault detection method 79−39097
electrical contact tip for magnetic inspection 79−66248
electrical Fe sheet, single sheet tester for 20 Hz to 20 kHz range *(Japanese)* 77−70251
electrically conducting spherical specimens, electromagnetic control 78−53138
electrographic porosity test, reclassification as nondestructive method *(German)* 80−97652
electroinductive, using nonsinusoidal EM fields *(Czech)* 79−20311
electromagnetic, nonharmonic development of multifrequency and harmonic methods 78−88607
electromagnetic inspection, parameter calc. using nomographs 79−79215
electromagnetic inspection of railway rails, high speed, objective rating 79−47858
electromagnetic inspection review 80−35468
electromagnetic inspection units, type MD-3 and 77PMD-3M, improvements 79−100318
electromagnetic instruments, interference factors on readings 78−48601
electromagnetic method, used for destructive materials testing anal. *(German)* 78−23909
electromagnetic methods, use in anal. of destructive materials testing *(German)* 77−73396
electromagnets used in NDT equipment, geometrical design expressions 78−85102
electron beam, surface thickness monitoring, object accessible from one side 78−60944
electron diffraction pattern analysis, design and development of projection system, for a negative viewer 80−22476
electron microscopy, solid surface characterisation, combined SEM-XPS-micro AES methods 79−30625
electron probe determ. of pn-junction depth in Si *(German)* 78−2552
electronic speckle pattern interferometry 77−74491
electrostatic application of red dye penetrants and dry powder developers to massive nuclear components 79−91872
elongated part of noncircular cross section, straight through eddy current transducer inspection 79−47860
EM, field components calc. radiated by rectangular waveguides *(Russian)* 78−82884
EM coating thickness meter, standardisation in Soviet Union 77−90561
EM field induction in vacuum by US wave in magnetostrictive conductive half space, anal. 77−73415
EM field of eddy current transducer, calc. for conducting bodies of complex shape 78−72964
EM NDT phenomena, fissile element modelling 80−40633
EM response of anisotropic cylindrical shell within solenoid 79−13867
EM transient response of solenoid driven conducting cylinder 80−23599
equipment, calibration using reference materials for fissile material assay 80−71880
equipment, circuit for selecting signals in specified phase range 78−56863
equipment for production line inspection 79−29320
ESCA, of ion beam effects on surfaces 78−52612
exoelectron emission defectoscopy, metal fatigue strength prediction 78−76807
exoemission defectoscopy in initial stages of fatigue fracture 78−53126
experimental mechanics compatibility 78−53181
failure anal. by SEM 78−27710
failure prevention, test methods and equipment *(German, English)* 79−52560
fast reactor burnup, correlation of $^{134}Cs/^{137}Cs$ 80−677
fatigue life prediction, acoustic emission signals distrib. anal. 80−25852
feed through eddy current transducer, numerical anal. or operating mode during ferromagnetic rod inspection 80−108670
ferrite probe, even-harmonic, with axial rectangular pulse excitation 77−77704
ferritometer testing, using DC magnetic field 77−16766
Ferrography, use of temper colours 78−3302
Ferrography, use to predict wear, for maintenance 78−3303
nondestructive testing continued
ferrography application to human joint wear 79−34694
ferrography of polymer form. under lubricated nibbing contact 77−21292
ferromagnet, Rayleigh const. determ. method 78−12732
ferromagnetic article, surface monitoring by defect field harmonics 79−39093
ferromagnetic half space, density of eddy currents induced by a transient magnetic field 78−71002
ferromagnetic material, inspection by method of two harmonics 78−88608
ferromagnetic material, NDT stress determ. by portable magnetic equipment 78−53172
ferromagnetic material, residual and active leakage field round artificial flaw 78−88595
ferromagnetic material thickness determ. 79−79187
ferromagnetic materials, demagnetisation level determination, after NDT 79−49261
ferromagnetic materials, higher harmonic signal analysis for eddy current transducer 78−70109
ferromagnetic materials, magnetoelastic effect/stress and strain in plane stressed state 77−77718
ferromagnetic materials, transducer for electromag. inspection 79−87771
ferromagnetic metals, thermal oxidation rate determ. using nanowebermeters 80−61045
ferromagnetic object inspection, investigation of the through-transducer signal spectrum 80−35487
ferromagnetic object inspection, method of higher harmonics, difference schemes 80−89444
ferromagnetic probe, core prep. method 78−44334
ferromagnetic probe coercimeter for inspecting the quality of parts with variable geometric dimensions 80−35488
ferromagnetic probe unit, MD-10F, automatic 78−56861
ferromagnetic product sorting by long coil system 79−29297
ferromagnetic round bar, high energy alternating field stray flux testing technique 80−100972
ferromagnets, cyclically remagnetised, discrete spectra of induction calcs., demagnetising factor 80−103859
ferromagnets, nondestructive inspection by magnetic noise method 78−72997
ferroprobe monitoring of rolled steel products with local transverse alternating magnetisation 77−73420
ferroprobe performance under neutron irradiation 78−60960
ferroprobe tube testers, automatic checking system 79−79211
ferroprobes appl., use of composite cores 77−87796
ferrous materials surface defect detection by portable EM inductors *(French)* 78−35616
ferrous metallurgy, nondestructive inspection and quality control review 80−21201
FFTF fuel and other core components 77−12757
FFTF Fuels & Materials Examination Facility equipment design and development 79−9747
fibre composite structure, thermal field techniques for NDT 80−66737
fibre optic CRT recorder appl. 79−27389
fibre reinforced composite, fatigue damage, early detection by NDT 77−28951
fibre reinforced struct., vibration technique for NDT 79−57183
fibre texture, quantitative determ. of volume fraction, analytical method by pole figures 80−11863
fibreglass laminates, thermal NDT using liq. crysts. 80−93709
fibrous materials, NDT determ. of mech. strength anisotropy using radiowave method 80−25969
film adhesion testing, simple real-time holographic interferometry method 78−92411
film coatings, use of steady heating, in thermal defectoscopy 78−85108
film roughness evaluation from interference extremum amplitudes 79−78766
films and powders, using electron spectroscopy 78−3430
finite elastic cylinder longitudinal collinear impact acoustodynamics 77−75743
fissile and fertile material, non-destructive testing 77−74917
fission materials analysis development, for EURATOM (CEC) Safeguards Directorate 79−85693
fission reactor fuel, irradiated, nondestructive assay methods *(Slovenian)* 80−27744
fission reactor pressure vessel, safeguarding containment *(German)* 79−13433
fission reactor US testing to ensure safety, trends *(German)* 77−26847
fission reactors, detection of flaws in metal during operation, review 78−17343
flash radiography, high energy, for dynamic NDT 78−15624
flaw detection in thin walled tubes with flaw depth in μm-range *(German)* 77−56195
flaw detection using proton radiography, exam. for Al foil 79−15939
flaw detector for revealing fatigue cracks 79−66244
flaw dimensions in direction of irradiation determ. from radiographs with aid of defectometer 80−71863
flexible scanning industrial X-ray fluoroscopic inspection 80−100971
flexible scanning industrial X-ray/fluoroscopic inspection 80−89459
fluid film lubrication, velocity profile meas., using ZnS phosphorescent tracer method 78−94866
fluorescent penetrant inspection, heat assisted 80−45466
focusing beams, incident angles on covered area of tube wall outer surface *(Chinese)* 78−80686
fractography, applications *(Japanese)* 80−16446
fracture analysis, use of microfractography 77−32750
fracture mech., conf., Washington, USA (Sept. 78) 79−43422
fracture mechanics anal. and NDT/destructive test correlations 77−90526
fragile materials, mech. props. meas. using disc-shaped specimens *(French)* 80−104367
fuel elements, quality inspection by eddy currents, unit 79−100315
fusion reactor JT-60 toroidal field coil, brazed connection, nondestructive test methods 80−13930
gamma-ray angular correlation measurement 77−74563
gamma-ray backscattering coefficients, Monte Carlo calcs. 77−61171
gamma-ray radiography, use of Se electroradiographic plates 78−72978
gamma-ray spectrometry method for fuel burn-up control *(Slovak)* 78−21672
glass, medieval, simulated, durability anal. using IR reflection spectroscopy 80−40777

nondestructive testing continued
glass, raster technique for automatic checking in sheets 78−23883
glass fibre reinforced epoxy, multilayer circuit board, holographic interferometry appl. to real-time studies of heat effects 79−91873
glass fibre reinforced epoxy pipe, radiometric inspection by image analysing system 77−90532
glass fibre reinforced plastic, failure due to deform., optical investigation method *(Russian)* 80−35437
glass fibre reinforced plastic, thermal inspection, one sided for separation of parts 79−79206
glass fibre reinforced plastics, exposed to liq. media, dynamic high-speed Young's modulus determ. *(German)* 80−85123
glass reinforced plastic, microwave determ. of mech. strains, anisotropic props. in millimeter range 77−9023
glass-plastic, engineering, nondestructive structural identification 78−92422
glass-textolite shells, NDT 78−11471
grain size meas., deep-drawing steel sheet and band, method and instrum. *(German)* 78−85059
granular material, simultaneous moisture content/thermal cond. meas. apparatus 78−53064
graphic symbols denoting types and methods of NDT 80−86042
graphite, artificial, residual macrostresses 77−16642
graphite, bending strength testing, quality improvement 79−52581
graphite fibre reinforced epoxy resin, radiographic technique for resin content meas. 78−3286
hardened components, residual stress, elastic characts. after surface plastic stress 78−60901
hardness measurement, colorimetric method for high frequency treated bandsaw blades 79−74325
hardness test, determ. of elastically homogeneous struct. elastic limit 77−66719
harmonic thermal flux monitoring quasistationary temp. distrib. 78−51040
Harwell nondestructive testing centre, UKAEA experience 79−34212
heat exchange tube thickness meas. by eddy current for corrosion testing, computer study 78−68852
heat treatment, coercivity meter attachment, with automatic current setting and recording 77−87795
heat treatment, electromagnetic quality inspection with specified intensity of internal field 80−108677
hermetic sealing of film products, use of $_{86}Rn^{220}$ 78−48595
high-resolution photoacoustic spectroscopy for dopant depth profiling 80−77883
hologram interferometry using double exposure/double direction illumination 79−27206
holographic, method for fringe control 80−31851
holographic, nondestructive testing of brazed, and epoxy bonded honeycomb panels 78−40017
holographic 79−43497
holographic instrumentation and materials developments *(German)* 78−39975
holographic interferograms, computer anal. for nondestructive testing 80−9836
holographic interferometry, appl. to materials and components *(German)* 78−48576
holographic interferometry, double exposure, appl. 79−6175
holographic interferometry and speckle photography for stress anal. 78−70095
holographic interferometry appl. *(French)* 78−42305
holographic interferometry appl. 78−53164
holographic interferometry appl. to study of structures and materials 79−8420
holographic interferometry applic. 78−35628
holographic NDT fringe control techniques 80−45450
holographic NDT system application of laser speckles 77−75457
holographic nondestructive testing at Fourier plane 78−46536
holographic techniques used in non-destructive testing, book contrib. 79−18380
holographic techniques using photothermoplastic film *(German)* 78−22097
holographic test system, quantitative fringe interpretation 77−75454
holography, significance in measuring techniques *(German)* 78−90395
holomoire interferometry applied to NDT 79−20294
homogeneous conducting cylinder, dynamic EM response for symmetric excitation 79−94125
honeycomb panels, holographic interferometry appl. 77−34843
IAEA safeguards, instruments and techniques, for nondestructive assay 78−33302
IC nondestructive evaluation by improved reflective scanning acoustic microscope 79−50551
ICs, ellipsometry appl. 79−85161
identification of materials, review of available methods 78−95876
image converters, thermoluminescent metal sulphate types, contrast functions conversion efficiency, NDT uses 79−9271
impedance inspection unit for inspecting joints in multilayer parts 78−44335
impedance type ferromagnetic probe sensors for magnetic inspection 78−48599
impurity determination, neutron activation analysis program for multielement analysis with abs. counting 77−21439
inaccessible pipes, optimised procedure for leak detect. using radioactive tracers 79−34217
Inconel, steam generator tubing, mag. probe inspection 80−85119
induction inspection unit with spaced windings, increasing sensitivity over magnetising and measuring length 78−56864
industrial optical microscopy, qualitative and quantitative surface testing 80−9033
industrial plant and machines, radioactive tracer techniques *(German)* 77−70522
industrial X-ray defectoscopy, devices to improve X-raying conditions 77−73405
industrial X-ray film information processing methods *(German)* 78−15637
industrial X-ray installation, spectroscopic anal. *(German)* 80−97668
inelastic critical strength prediction by vibration testing 78−35611
inhomogeneous material structural characts., automatic test system 78−48586
inspection methods, review 79−43535
insulators, nondestructive acoustic elec. field probe 80−47076
interactive graphics system developed for NDT 80−66729
nondestructive testing continued
interface waves for inspection of engineering materials 77−40481
interferometry, double-exposure, with instant Polaroid film 79−221
interferometry, electronic speckle pattern, for NDT 79−24702
internal cavities in objects, exam. by scanning with ionising radiation beams, from radioactive sources 78−40003
internal friction technique, computer-assisted digital processing system 79−43537
International Advances, (1977) 78−53162
inverse signal filtering, method in nondestructive testing 80−7749
IR ellipsometry of polySi-SiO_2-monoSi structure thickness 79−56287
IR interferometer appl. 79−8419
IR laser and defectograph, semicond. flow detection 78−3299
IR non-destructive testing of bonded materials, theory and practice 80−93708
IR scanning, three-component method of data analysis 77−48613
IR techniques for evaluation of SiC heat-exchanger tubing 80−76435
irradiated fissile materials in extended configurations, nondestructive assay 80−71872
irradiated fuel rod NDT using encircling and probe eddy-current systems 79−9751
kevlar-epoxy composites pressure vessels, holographic nondestructive eval. 80−81275
laboratory and field equipment in India 80−108650
laminated structure, thermal monitoring by near surface thermoelectric receivers 78−53107
laminates, exposed to liq. media, dynamic high-speed Young's modulus determ. *(German)* 80−85123
lapped paper and plastic insulated cables, butt gap distribution and spliced joints study using X-ray method 77−77726
laser beam 77−21345
laser energy deposition method for determination of elastic moduli, stress waves 79−20309
laser fusion, glass microballoon selection, wall thickness and uniformity meas. 78−87469
laser holographic and speckle detection of defects and strain in pressure vessels 77−81365
laser microprobe mass analyser (LAMMA) appl. 80−18041
laser speckle interferometry for nondestructive evaluation 78−60976
laser speckle photography, for nondestructive testing 77−67515
laser speckle photography, strain and movement meas. of steel structures 78−76797
LASL Van de Graaff accelerator, nondestructive assay of fissile nuclear material 77−83182
layered orthogonally reinforced plastics, strength and stiffness prediction in interlaminar shear 77−9025
layered reinforced plastic, light propagation for NDT 77−9024
leak test, automatic, nondestructive, design, evaluation and implementation for IC assemblies 78−53180
leak testing with dyed liquid tracers 78−23907
light and sound wave imaging at liquid surface 78−53175
linear accelerator for nondestructive inspection appl. 79−41046
linear electron accelerator appl. to NDT 78−40009
linear wave motions study using FFT, NDT appl. 80−92038
LMFBR, inservice inspection methods 77−38357
LMFBR, US testing, of austenitic steel welds 77−1903
local field image recording on magnetic tape without bias 78−53130
low thermal cond. materials, anal. of optimum method of inspecting by active thermal method 78−72996
luster quality, meas. method, texture and microreflection characteristics *(Japanese)* 80−35466
LWR irradiated fuel assemblies, nondestructive exam. using γ-ray and neutron techniques 80−66760
LWR spent fuel, nondestructive meas. and verification for materials safeguards 80−78420
machine fault diagnosis, vibr. anal., bispectrum method 79−8404
magnetic, using automatically compensated Burrows permeameter 77−10067
magnetic defectoscopes, nonsinusoidal periodic currents meas. 80−104386
magnetic field intensity meter, detection of magnetic oxide in stainless steel boiler tubes 78−76794
magnetic induction defectoscope with adjustment 78−53105
magnetic inductive method appl. *(German)* 78−48581
magnetic leakage fields, methods 78−3296
magnetic loss during polarity reversal, stress determ., mech. props. determ. 77−59879
magnetic methods, elongation of mag. field at defects 79−15932
magnetic particle inspection, arc strikes and counter meas. *(German)* 77−4880
magnetic particle inspection, nature of magnetic inks and powders 80−100974
magnetic particle inspection fundamentals 78−44285
magnetic powder inspection of thin parts using electromagnet 77−73424
magnetic powder testing, particle coagulation, effect on sensitivity 78−60942
magnetic sheets, NDT by external induction and field selective display 78−15618
magnetic sound determ. of H_2 absorpt. in metals *(Russian)* 77−60009
magnetic stray fields, optical detection 78−31602
magnetic stray flux technique 79−83401
magnetizing device for inspection of products of ferromagnetic materials according to parameters of Barkhausen discontinuity 80−89457
magnetodynamic method of part inspection 79−96272
magnetoelastic probe with controlled magnetic reluctance under poles 78−40011
magnetoferroprobe rail defectoscope, MRD-72, electronic circuit 78−53128
magnetographic fault location, local field representation using biased magnetic tape 78−72965
magnetographic fault location, local field representation using biased magnetic tape 78−72966
magnetographic inspection, determ. of magnetisation regimes 80−108665
magnetostatic field of defect in plane parallel plate, calc. 78−72986
magnetostrictive hysteresis determ. by inductive method *(Russian)* 77−56171
magnified dark-field image holographic recording 77−19214
material and structure evaluation by laser methods 77−21345
material with fluctuating parameters, by radiometric method, smoothing filter synthesis 77−90553
materials and structures testing 78−3298

nondestructive testing continued
materials failure and corrosion, microstructural aspects, obs. 79−52610
materials testing, radionuclide methods, in West Germany, industrial use impetus *(German)* 79−96231
medical implant device evaluation by holographic interferometry and optical correl. 80−40659
medical X-ray diagnostics, NDT impetus, novel techniques *(German)* 78−7146
medium with large no. of cracks, direct elec. current calcs. 80−96233
metal, internal friction determ. using sound emission during vibration 77−77715
metal, plastic deform. effects from X-ray diffr. data, moment method *(Czech)* 78−31593
metal, polycryst., electron or proton irrad., coherent acoustic emission *(Russian)* 77−81355
metal, surface contamination detection by nondestructive test, surface potential difference meas. method 79−83424
metal fatigue, eddy current sensors, tuning method 80−21231
metal machined surface, defect detection by laser scanning 78−40018
metal object in media, depth measurement instrument, eddy current transducer 79−39091
metal parts, large, without taking specimens, portable grinding and polishing machine 80−61042
metal pipe, thermal strain recording at elevated temp., photographic technique 77−66731
metal plate transient temperature field in active thermal test methods, calc. 77−75775
metal substructure exam. by astigmatic X-ray microbeam method 78−85076
metal surface, AES anal. in adhesion, friction and wear 78−53179
metal surface replica production, nondestructive mech. and electrolytic grinding and polishing *(German, English)* 77−48607
metal using positron annihilation technique 78−3293
metal using positron annihilation technique 78−3294
metal wire and bar NDT, electrical and EM methods 80−11865
metallic coatings, holographic interferometry appl. *(German)* 79−79186
metallic cylinder in electromagnetic field of noncoaxial coil, AC current, field calc. 78−53153
metallic objects with complex shape, eddy-current inspection 80−89446
metallic structures, magnetostriction method of measuring elastic stresses 78−72985
metallic substrate surface charact. prior to adhesive bonding 78−53166
metals, acoustic emission *(French)* 77−56207
metals, autoradiographic study of H distrib., exptl. difficulties 77−52586
metals, magnetostriction effects appl. *(German)* 78−23311
metals, NDT of hardness using applied EM transducer 77−56178
metals, positron annihilation, localised probe of lattice defects 80−55224
metals, strength and corrosion tests, NDT, electromagnetic methods, use in anal. of destructive materials testing *(German)* 77−73396
method comparison and optimum combination determ. 78−44308
methods review, including ultrasonic, X-ray and magnetic *(German)* 77−77724
metla, magnetic, and SEM exam. of fatigue, dynamic strength problems *(German)* 77−86272
metrological provisions for nondestructive testing equipment 79−74322
metrological provisions for thermal methods of inspection 79−100314
microelectronics and microprocessor impact on metals prod. and NDT 79−74320
micropipette electrode tips, beveled, non-destructive electron microscopic exam. 80−89915
microprocessor and microcomputer appl. 79−91891
microtrons, appl. in nondestructive inspection of industrial products 80−81267
microwave detection of third-order nonlinearities 80−55594
microwave testing of nonmetals *(German)* 77−44435
mining equipment, critical parts, exam. of rejection standards 78−73002
mobile nondestructive assay system for nuclear materials safeguarding 80−71876
Mossbauer ferritometer 79−17453
Mossbauer spectroscopy appl. 78−3295
moving material fault test rig *(German)* 80−11855
multicomponent assemblies, moire inspection 80−35434
multifrequency eddy current inspection with continuous wave methods 80−71844
multilayer cylindrical parts, thermal inspection unit for NDT 79−52606
multilayer object, layer separation detection by thermal method using thermal visualizer 78−53127
multilayer part, discontinuity type defect revealability, comparison of thermal inspection methods, computer simulation 79−79207
multilayer parts, thermal quality inspection two dimensional problem soln. 79−70283
multilayer product, theory of laid-on shielded transducers for inspection 78−88610
multiparameter methods, linear, nonlinear and transcendental transformations 78−35600
multiparameter methods *(German)* 77−44434
multivariant inspection methods, theory 78−88609
NBS reactor, summary of activities, (July 1976 to June 1977) 78−82435
NDT instrument for grain size and anisotropy meas. 79−11753
neutron, tomography investigation using research reactor 78−23915
neutron absorption radiometric testing of materials, review 80−71860
neutron activation analysis, sample posture convertor 80−35497
neutron activation analysis of air pollutants 77−25772
neutron appl. in industry and technology 77−25244
neutron conversion efficiency enhancement in neutron radiography 78−7444
neutron dosimetry characterization of spent thermal reactor fuel assemblies 80−23164
neutron generator appls., activation analysis, material investigation, radiotherapy *(Czech)* 79−31279
neutron radiography, 14.5 MeV, image improvement 77−52594
neutron radiography, contrast enhancement using gaseous ^{3}He penetrant 80−93707
neutron radiography, high-speed system, modulation transfer function 78−7158
neutron radiography, nuclear engineering appl. *(Slovak)* 80−76430
neutron radiography, trends *(German)* 77−32745
neutron radiography image quality 77−81347
neutron radiography of electronic piece parts reliability evaluation 78−31610
nondestructive testing continued
neutron radiography of mixed oxide reactor fuel, possible Pu particle detection 77−71637
neutron radiography with electron linear accelerator *(German)* 78−7150
NIIEFA linear accelerator−flaw detectors for nondestructive inspection of atomic power plant equipment 79−47856
nitriding process, monitoring systems 79−52556
NMR imaging, appl. to unsaturated water flow obs. within porous materials 79−98840
noncontact material testing using laser energy deposition and interferometry 80−71846
nondestructive, dye penetrant and magnetic particle methods 77−9022
nonmagnetic electrically conducting rod, section shape effect on eddy current transducer parameters with uniform field 78−53132
nonmetallic plates, sensitivity of thermal inspection, mathematical model 78−72995
nonsinusoidal periodic current meas. using standard DC shunt with magnetic powder monitoring, frequency errors 80−104398
nonsteady electromagnetic field outside a solid conducting cylinder surrounded by a coil with current 79−96273
nonuniformity of dielec. props., at mm wavelengths, method of determining 78−40001
nuclear, using 14 MeV neutron generator, density distribution variation effects *(German)* 77−25349
nuclear analytical techniques, applics. 77−16884
nuclear fuel and materials, nondestructive surface exam. 80−21246
nuclear fuel assay, highly enriched, using Ge(Li) detector and ^{235}U fission chambers 79−89522
nuclear fuel cycle materials, neutron and photon assay techniques and instrumentation 80−18426
nuclear fuel nondestructive assay techniques and instruments *(Japanese)* 77−57716
nuclear fuel shell inspection, mag. method for detecting ferromag. particles 80−66746
nuclear fuels, elemental and isotopic conc. anal. using nondestructive assay 79−49691
nuclear fuels, nondestructive measurement of U and Th conc. and quantities using XFA and gamma spectrometry 80−71877
nuclear material safeguarding, nondestructive meas. 80−76457
nuclear materials, NDT 78−82443
nuclear materials, neutron assay for accountability and criticality control 80−66759
nuclear materials, nondestructive element and isotope assay of Pu and U 80−71870
nuclear materials, results of international collaboration in the ESARDA working group 80−71879
nuclear materials accountability, U and P NDA of crated waste by gamma-ray and neutron coincidence counting 80−83166
nuclear materials safeguarding, nondestructive measurements of irradiated fuel assemblies at a reprocessing facility 80−95392
nuclear materials safeguards, assay of dissolver solns. by totally sampled wavelength dispersive X-ray fluorescence 80−83160
nuclear materials safeguards, collection and analysis of measured fission product data 80−95354
nuclear materials safeguards, mathematical simulation of calorimeters used for rapid nuclear fuel assay 80−95355
nuclear materials safeguards, nondestructive, energy-dispersive, X-ray fluorescence analysis of product-stream concentrations from reprocessed nuclear fuels 80−83163
nuclear materials safeguards, prototype, reference materials for nondestructive assay 80−78372
nuclear materials safeguards reference measurement system utilizing resonance neutron radiography for nondestructive assay meas. 80−78377
nuclear methods, sensitivites and detection limits 77−32756
nuclear power industry, nondestructive testing standards, role of NBS 79−54612
nuclear power plant at Obrigheim, inservice inspection of primary components *(German)* 77−34406
nuclear power plant components, acceptance tests, using X- and gamma ray images *(German)* 78−44297
nuclear power plant piping weld, by in-process acoustic-emission monitoring 77−14823
nuclear power plant system, optimisation with regard to design, materials and testing *(German)* 80−42739
nuclear power plants, in-service inspection requirements, impact of changes 79−54589
nuclear power plants, utility requirements for in-service inspection 79−54588
nuclear power station heat exchangers, eddy current probe for nondestructive testing of transfer tubes *(Japanese)* 80−81246
nuclear reactor components, NDT using acoustic emission *(Spanish)* 80−57871
nuclear reactor components, weld seam inspection, steam supply system, quality assurance *(German, English)* 77−83052
nuclear reactor fuel burnup, nondestructive verification, γ-ray spectrometry 77−3137
nuclear reactor material control or verification non-destructive techniques 79−87813
nuclear steam generators, inservice inspection, book contrib. 79−100322
NVM-5 nanowebermeter and its use for obtaining defect records 79−52602
object geometries comparison, speckle pattern interferometry, holographic illum. elements 78−66785
optical fibre characterisation techniques compared 80−64202
optical fibre endoscope type OD-20Eh, internal surface inspection 79−79216
optical fibre preform, simultaneous determ. of refractive-index profile and cross-sectional geometry 80−1312
optical fibre preform core diameter and Ge doping profile meas., X-ray nondestructive method 80−64231
optical fibre preform rod, refractive index profile meas. by transverse differential interferogram 80−64141
optical fibre refractive index profile meas., nondestructive transverse interference method 78−38024
optical fibres, measurement of refractive-index profiles in optical-fibre preforms by spatial-filtering technique 80−48403
optical methods for determining strain and displacement, book 79−20331
optical reflectance method, for anal. of anodic films on Al 80−37073
optical spatial filtering, of visualised results of flaw detection monitoring, rational regions of appl. 80−7751

nondestructive testing continued
optically isotropic mats., stress intensity factor determ. by dynamic method of caustics 80−33546
optimisation of inspection technique, as operations research problem 77−90548
optimum parameter determ., for critical parts inspection 78−44307
p-n junction, planar, nondestructive determ. of depth by SEM 78−19132
p-n junction thermal second breakdown prediction test 79−82668
pacemakers and batteries, microcalorimetric study 78−57130
paint, non-magnetic, thickness measuring instrums. 79−52557
passive neutron assay of Pu contaminated solid waste streams 79−36373
peeling detection in three layer objects by high-speed thermal scanning 78−44324
penetrant, new, for composite and adhesively bonded struct. 77−32739
penetrant inspection, high temp. 77−12756
penetrant inspection, modern techniques *(French)* 77−9028
penetrants, high temp., precautions in use 80−30192
penetration technique, S and halogen traces dosage methods *(French)* 78−15625
phase defect inspection for determ. of moment of origin of fatigue cracks 79−52578
photoelasticity, 3-d, matrix method for determination 79−41636
photogrammetry, close range X-ray and cold neutron techniques at Rolls-Royce 79−75637
photographic pulp quality control using He-Ne laser scanning system *(German)* 80−3272
photometric calibrator appl., inverse fourth power, NBS development 80−73412
photometry of interference patterns, noise elimination 79−97414
piezoceramic articles, nonuniform polaris. investig. using microwave Kerr effect 78−72969
piezoceramic materials, industrial using radiodefectoscopy 77−90555
piezoelectric transducers, acoustically loaded, expt. method for equivalent circuit parameter determination 78−51036
piezoelectric transducers, bandwidth enlargement 78−71257
piezoelectric transducers, input electrical impedance expression, internal loss correction 78−53101
pipeline girth welds, NDT of defects 78−27704
pipes, hot-rolled, automatic mag. quality control on prod. line 80−108661
plastic foam layer beneath sheets, NDT *(German)* 77−1896
plastic parts, holographic interferometry method 77−7037
polychromatic X-ray technique *(Japanese)* 77−48600
polycrystals, deformed, particle sizes and mean square strains *(German)* 78−3284
polymer, thermal inspection by one side method 79−52604
polymer materials, rigidity and hardness from acoustic, thermal, optical and dielectric props. *(Russian)* 77−48601
polymer objects, IR inspection 78−72971
polymers, stress-state meas. using chemiluminesc. system 80−40628
polyurethane, void detection by neutron gauging 78−23910
portable comprehensive irradiated-fuel inspection stand 79−9836
portable temperature measurement instrument for thermal monitoring 78−49837
portable X-ray analyser for residual stresses, design, operation and testing 78−53058
positron measurements, for NDT of metals and alloys 80−55222
potential developments for metal inspection appls. 77−12752
pressure vessel, C-fibre reinforced plastic immersion technique for acoustic emission detection 77−1902
pressure vessels, acoustic emission inspection during water pressure testing 77−1901
pressure vessels, heat treated, fracture modelling, acoustic emission 80−35303
pressure vessels, water pressure testing, test method and anal. *(German)* 78−25260
production methods, impact of electronics on control *(French)* 77−44425
professional qualifications, for flaw-detection workers, redefinition 79−9048
prosthesis wear, holographic studies using optical contouring 80−67288
protective coating thickness meas. using radioisotope method 77−90520
pulse eddy current methods *(German)* 77−90533
pulsed eddy current testing, for smooth and ribbed tubing 78−23906
pulsed interferometric holography, for nondestructive evaluation and anal. of structs. 78−60977
pulsed magnetic analyser, IMA-5 80−104399
punched artificial defects for calibration of NDT equipment 79−34228
PVF_2 transducers for NDT 80−76476
PWR, primary circuits in-service inspection 80−5268
quality control, NDT inspection reliability 79−66229
quality control, physical methods 79−79202
quality control in castings 79−29321
quartz-LZT wide-range instrument transducer, practical feasibility 78−51035
radial clearance determ. for engine crankshafts by γ-ray method 78−53147
radiation detectors, effects of averaging within field of view on recording equipment 78−53098
radiation-optical converter of single crystal, diameter calc. 79−68445
radio detection of local defects, strongly absorbing dielec. medium 80−35481
radio wave inspection with one sided access to object, conditions of coating and compensation 80−108679
radiographic image enhancement and anal. system, digital computer eval. 78−27708
radiographic inspection, spectra and angular distrib. meas. of scattered X-radiation *(German)* 78−7148
radiographic inspection method, productivity 80−71861
radiographic monitoring of thick walled parts via stereomicrotron 77−65064
radiographic testing equipment, device charact.: *(German)* 80−76438
radiographic weld testing between tubes and tube-plates in heat exchangers *(German)* 78−7151
radiographs optical and digital image processing 77−70241
radiography, Industrex Instant 600 paper system evaluation 77−52592
radiography, planar defect depth determ. 77−81350
radiography, possibilities of low temp. 77−81348
radiography gamma ray source, choice for welded joint monitoring 80−104396
nondestructive testing continued
radiography method of internal corrosion and wall thickness meas. 77−32737
radiography while maintaining temp. of 300°F 77−66723
radioisotope instrumentation, industrial appl. *(German)* 77−70245
radioisotopic wall thickness gauge, description 78−44310
radiometric flaw detector, relay-type with time delay signal smoothing, prob. anal. 77−81377
radiometric monitoring, smoothing filter synthesis 77−90553
radiometry methods, automatic data processing, development of models and algorithms 78−72991
railway rail steel, residual stresses meas. using magnetoelastic effect 77−81379
railways by X-ray 77−11436
reactor fuel cladding, diametral meas. by precision laser extensometer 78−57896
reactor vessels, thin-walled, radiographic testing, sensitivity using 10 MeV microtron 78−70603
recent developments, book 78−56873
reflector shape and size determ. by US spectroscopy, use of radiation field theory 77−25227
refractory products, apparent density determination, using surface γ densimeter 80−35464
refractory slabs, radio wave phase method for quality control 80−40667
reinforced concrete structural integrity assessment 78−56847
reinforced plastic, fatigue mech., charact. and defect detection 79−24687
reliability and nondestructive evaluation in materials and structs. 77−9004
reliability indices, methods of increasing them 78−40010
reliability rel. to human factors 79−24703
repair machining and inspection of cracked Al alloy components 78−80689
replication, NDT anal. and inspection technique 78−11467
research and development, book 79−100321
residual stress determ. 79−96267
residual stress meas., using elastic punching method 79−34264
residual stresses in thin specimens, layer-by-layer X-ray diffr. analysis, additional strains and corrections 78−39964
residual stresses measurement using X-rays 79−97484
resonance neutron radiography using a position-sensitive proportional counter, appl. to meas. of nuclear fuel 80−13597
review, nondestructive evaluation 80−71855
review 77−36700
rising purification method from penetrant liquid method *(German)* 77−90540
road construction, principles, instruments and methods *(German)* 79−11742
rocks, internal cracks, nondestructive obs. in stressed state 77−73726
roentgenographic method of crankshaft bush checking 78−53149
rolled sheet thickness effect in magnetic inspection of mech. props. 79−91894
rubber, nondestructive testing during production, portable instrument 78−23892
rubber-metal facings, vulcanisation degree determ., γ-ray method 80−61043
sapphire and Si surfaces, using IR and UV specular reflectance meas. 80−108684
SAW edge bonded transducer design and application 79−55304
SAW generation using CW laser, NDT appl. 80−87683
scanner development, for surface inspection of cold rolled sheets *(German)* 79−43533
scanning radiography beam-absorption system, param. selection for extended sources 77−81376
science base, coupling to technology 79−100323
scientific film for science and engineering students 79−80395
semiautomatic digital coercimeter, exam. of design 78−76817
semiautomatic portable coercimeter 79−34250
semiconductor, high resoln. SEM 78−64794
semiconductor dislocation Burgers vector exam., birefringence method 78−30626
semiconductor materials and devices, SEM characterisation methods 80−49064
semiconductor power devices, stacked, thermal device for inspection of contact joints 78−76819
semiconductor resistivity and Hall effect meas., nondestructive four-electrode characterization 80−49743
semiconductor resistivity profile meas. using two-probe spreading resistance techniques 80−49742
semiconductor surface characterisation using SAW 80−11069
sheet material surface density nonuniformity using beta radiation, effect on energy spectrum 77−77717
shells, determ. of critical loads by nondestructive methods 77−62181
shift registers, reliability assessment by scanning electron microscope 78−29215
signal processing in ultrasonics, conf., London, England, Jan. 1980 80−33351
simulated neutron tomography for nondestructive assays 80−99218
single electron field emission non-destructive SEM method 78−88410
sintered metalloceramic materials microstructure and porosity using mag. props. 77−73416
site training for radiography 78−25329
skull, holographic interferometric NDT 80−41162
slag-metal interface determination using electrochem. conc. element 78−7114
solar cell welds, mechanical strength evaluation 78−35630
solar cell welds, system selection 78−35629
soldered materials, US method for compatibility evaluation 77−40486
special nuclear materials, assay and accountability using neutron correlation meas. tech. 80−69015
special nuclear materials, nondestructive assay techniques for control and accountability 80−81270
speckle interferometry, pulsed lasers, appl. to NDT 78−65961
speckle pattern interferometer for measurement of displacements and surface tilt, book contrib. 79−20334
speckle technique for 3D nondestructive photoelasticimetry 77−58623
spectral nuclear materials, control and accountability, reliability of nondestructive assay techniques 80−76456
spent fuel subassemblies, nondestructive assay, comparison of calcs. and meas. 80−78421
spent fuel waste products, delayed neutron nondestructive assay instrumentation, Monte Carlo calculational design 80−81271

nondestructive testing continued
spent reactor fuel, nondestructive burnup determ. calibration using destructive radiochem. anal. 79−89372
spontaneously fissioning material, assay using neutron correl. counting 79−85605
spray coatings, NDT methods and measurable properties 79−83431
stamped disc surface inspection by automated eddy current unit 78−92430
steel, 11YuA, cold worked, heat treated, electromagnetomech. props. NDT 79−4980
steel, 38KhS, heat treatment quality inspection by magnetic method 79−52574
steel, 45, case hardening quality control by ferromagnetic coercive force transducer probes 78−53151
steel, austenitic, heat resistant, mag. permeability increase, measurement method 78−53039
steel, austenitic, Mn-Al-V-F2, EM characts. after nitriding, aging, austenitizing, NDT of nitrided layer depth 79−11750
steel, austenitic, thermonuclear reactor walls, ferromagnetic layer form. magneto-optical testing method 80−35465
steel, austenitic stainless, magnetic phase content determ. via permeability meas. using MF-10F probe 77−77648
steel, austenitic stainless, weld metal, delta ferrite content measurement 78−31600
steel, C, cold rolled St3Kp, annealed, mag. nondestructive inspection of strip and ribbon 78−60913
steel, C, ferromagnetic parts, mech. property meas., method and instrument 80−35469
steel, C, residual stress induced by uniaxial deform., mag. meas. 77−73390
steel, C, texture effect on mech. props./magnetic props. relationship, NDT appl. 79−96274
steel, case hardened gas carbonitrided, holographic interferometry study of plastic flow *(German)* 77−77723
steel, cast, heat treated, exam. of surface defects using fluorescent liquids 79−5101
steel, cast, heat treated, exam. of surface defects using fluorescent liquids 79−15933
steel, circular hot rolled stock, magnetic inspection of external surface, zond automated installation 79−79210
steel, coercive force measurement method of quality inspection of heat and thermomechanically treated parts 79−5113
steel, cold rolled strip, surface defects, online automatic system, design study 79−34231
steel, cold-formed, NDT of mech. props., coercimeter results 79−34240
steel, cutting high-speed, hardened by quenching 77−90559
steel, detector designed to meas. retained austenite 78−35602
steel, electric generator, anisotropic mag. props. obs. using NDT 80−21212
steel, electrical, crystal orientation and dimension determ. by magnetic method 79−70278
steel, electrical, sheet, systematic and random errors, in wattmeter apparatus for measuring unit losses 80−71858
steel, electrical sheet, wattmeter unit for measuring specific losses, system errors 79−91893
steel, ferritic, magnetomechanical acoustic emission for residual stress NDT 80−71149
steel, hardened, stress determ. from X-ray meas. by fixed time method 78−90801
steel, heat treated, electromagnetic device for quality inspection 78−53104
steel, heavy gauge rolled, mechanical props. using a type KIFM-1 coercimeter 78−72973
steel, high speed, anode potential determ. of tempering quality 78−53139
steel, high strength low-alloy, AE appl. to nondestructive testing 79−83419
steel, internal cavities exam. by scanning with ionising radiation beams, from radioactive sources 78−40003
steel, KhVG, annealed, mag. inspection of hardness and struct. 80−7750
steel, low alloy and C, hardened and tempered parts, nondestructive magnetic inspection 78−95889
steel, low alloy and C, hardened and tempered parts, nondestructive magnetic inspection 79−1929
steel, low C, mech. props. determ., NDT methods 79−29176
steel, low C and low alloy, rolled, nondestructive impact strength testing by coercive force meas. 79−52601
steel, magnetis. in LF mag. field, oscillations in envelope of harmonic levels, struct.-mech. characts. determ. 78−60940
steel, mild, plastic deform. during fatigue, detection by Barkhausen noise meas. 79−43524
steel, Mn-Si, mag. method of NDT of mech. props. 80−21211
steel, monitoring with pulsed magnetic analyser, IMA-5 80−104399
steel, neutron quasialbedo thickness meas. of single layer product, optimization 80−105611
steel, nitrided layer depth, electroinduction meas. method 80−104379
steel, positron meas., for trapping mechanism detection 80−84798
steel, residual stress determ. by X-ray integration *(German)* 79−52551
steel, rimming, continuously cast ingot, honeycomb blowhole depth, absorption-scattering method 78−53148
steel, rolled sheet, mag. testing of mech. props. 78−72972
steel, rolled sheet, mech. props. study with KF-1 coercimeter 79−87769
steel, Si, highly-oriented domain and grain obs. methods, using ferromagnetic colloid technique 80−11856
steel, square parts, surface inspection, defect depth meas., eddy current method 79−29307
steel, stainless, IR electro-thermal exam. 77−44428
steel, stainless, pipes, electro-thermal method for NDT of welds 80−35447
steel, stainless type SUS 304, diffusion welded joints, sound emission during tensile testing *(German)* 80−61062
steel, strength determ. from dynamic hysteresis loop EMF spectral content of coil, expt. 77−73414
steel, structural, nondestructive method of struct. damage investig. using cyclic loading effects and mag. characts. 78−3275
steel, structural heterogeneities, detection by mag. aerosol method 78−44314
steel, structural ties, NDT by eddy current transducer, optimum parameters and capabilities 80−108669
steel, thread rolled, Moire fringe method for examining local deform. zones 80−21220
nondestructive testing continued
steel, tube, mech. prop. testing by harmonic method using instrument type KAP with feedthrough transducer 78−53154
steel, tubing, NDT method comparison, optimum combination determ. 78−44308
steel, weldable C and alloy, brittle fracture, metallurgical factor effects, NDT data, impact tests *(French)* 79−5128
steel 17G1S, magnetic method of mech. prop. determ. of thick sheet 78−48600
steel articles thickness and continuity monitoring by neutron radiometry 79−93100
steel bar, Hall probe meas. of residual and active leakage fields round artificial flaw 78−88595
steel bearing balls, exoelectron emission for surface fatigue wear testing 78−39960
steel bearing parts, magnetic inspection of heat treatment quality 78−73007
steel billets, bars, tubes 77−12759
steel case depth after quench hardening, inspection using coercimeters 80−104377
steel fibre reinforced Al alloy, stressed state nondestructive testing method *(Russian)* 80−40631
steel mild, acoustic emission during magnetisation, stress effects 79−82854
steel parts, cylindrical, hardness inspection by EM method with higher harmonics 78−23891
steel spring wire, two frequency defectoscope 78−72963
steel struct. testing from anal. of Barkhausen noise statistics 77−77647
steel tubes, ferromag., complex of devices for automatic nondestructive testing 78−53092
steel tubing, cold rolled, nondestructive mag. method for determ. of mech. props. 78−23903
steel weld fatigue life estimation, multichannel NDT monitor 78−56846
steels, constructional and tool, heat treatment effects on elec., mag. and mech. props. expt. 77−77719
steels, heat treatment of 30KhN2MFA and 40Kh, nondestructive mag. quality control method 80−108662
stoneware sewer pipes, resonant frequency and acoustic emission meas. *(German)* 77−9010
strain and damage electrical measurement method *(French)* 80−71854
strain gauge for recording deformation of rotating parts, exam. of design 78−76820
strain meas. by X-ray diffraction *(French)* 78−15626
stress meas., nondestructive X-ray diffr. method 78−68853
stress measurement, ferromag. sample, by internal induction 77−62222
stress measurement by sandwich speckle photography *(German)* 80−10216
stress pattern analysis by thermal emission 80−33552
structural material analysis by computerized tomography 80−101001
structural stress distrib. determ. by remote IR thermometry 80−87749
superconductors, high field, large internally cooled, development, production and testing 79−54144
superficial temperature testing, thermographic method *(Polish)* 79−67299
surface coating technology, conference, London (1978) 79−83358
surface defect parameter determ. of a thin wire, capacitance method 80−35489
surface defects appearance, effects of roughness and method of surface preparation of rods 77−63860
surface layer thickness-composition monitoring by high energy electron backscattering 78−53146
surface layers and thin films, thermal diffusivity of microsections, IR and X-ray electron-probe microanal. 78−2314
surface potential pattern measurement by potential probes, crevice depth determination in metallic testpieces *(German)* 78−35597
surface stress meas. by optical waveguide effect 80−43681
surface topography quantitative determ. by Nomarski differential interference contrast microscopy 80−73318
survey assay meter developments at BNL for nuclear materials safeguarding appls. 80−69038
Symphonie communications satellite components, NDT *(German)* 77−1899
technological strength and nondestructive methods of testing during heat treatment 78−85090
television projector for optical materials inspection 78−73006
texture, evaluation by X-ray and neutron diffr. anal., comparison *(French)* 79−91882
texture, nondestructive investigation by neutron diffr. 79−87795
texture determination by magnetic texture gauge 79−66238
thermal, comparison of contact and contact free methods 79−70284
thermal, vortex tube appl. 80−89453
thermal detection of cracks in fatigue testing of parts 78−92423
thermal flow method, algorithm for calc. temp. field of object containing a defect 78−72970
thermal imaging in temp. and strain field meas. 77−70240
thermal inspection of plates with internal defects, one and two sided, heat transfer intensity effect 78−88616
thermal method of investigating hidden nonuniformities in flat dielectric materials 78−56868
thermal methods, review of theoretical and experimental problems 78−44325
thermal methods and apparatus for NDT of weld joints 78−88615
thermal monitoring, emissivity effects on temp. data 78−60946
thermal monitoring with maximal temperature differences over flaws 78−60945
thermal NDT of large shells under prod. conditions CCTV system with combined scanning 79−11751
thermal testing, scanning and printing head 78−44329
thermal testing with heat source and detector on same side, optimisation 77−77703
thermal vision systems, theoretical basis of use to monitor boundary stratification in hot metals 80−7748
thermography, NDI method for damage detection 80−35445
thermography, temp. and temp. pattern monitoring 78−68851
thermoplastic moulding quality assurance using holography and speckle photography 78−27720
thick film, adhesion to ceramic, destructive and nondestructive meas. 80−50809
thickness gauge, to meas. Ni coating thickness on mag. steel 78−76821
thickness gauge meas. of polymer protective coatings, on pipes 78−76818

nondestructive testing continued
thin coatings thickness monitoring using slow-neutrons 77−71297
thin crystals and films, nondestructive microhardness testing of near-surface layers 80−71829
thin rolled sheet, IMA-4 impulse magnetic analyser 80−35470
thin walled bearing races eddy current inspection of hardening and tempering quality 78−95892
thin walled cylinders, flaw detection, using inductive transducer 78−72962
THTR fuel reprocessing, destructive and nondestructive physical testing appls. 79−13512
tightness control by IR gas method 79−66236
tightness of mating parts 79−66234
tissue analysis by IR microinterferometer 79−79714
TLD, aluminophosphate glass, improvement of fast neutron response 80−13932
tomography, computerized, NDT appls. *(German)* 80−76439
transducer, force measuring, EM, design and appl. *(Russian)* 78−16784
transducer, matrix eddy-current, with magnetic circuit, design and construction 80−68228
transducer, straight-through screened circular primary, between multilayer cylinder and tube, EM field 80−71856
transducer orientation system in screen methods of NDT 80−66745
transient skin effect in laminated cores with sectionally different material props. *(German)* 79−41280
transition elements, 3d, ESR for valency assessment, appl. to ceramics and glass industries *(German)* 80−34757
transmission X-radiographic development trends *(German)* 78−15636
transparent microtarget, for laser fusion, interference method 77−9012
tube, magnetization with transverse field, approx. soln. 80−69321
tube inspection, magnetic leakage flux method 78−95891
tube to tubesheet welds, X-ray and isotropic techniques for boroside radiography 77−86261
tubing, ferromagnetic probe coercive force meter, different heads 78−60943
turbine blades, crack detect., holographic interferometric method 78−35625
turbine blades, fatigue crack detect., strobed hologram method 78−35624
TV analyzer for material structure studies 78−27696
ultracentrifuge with magnetic suspension, contactless meas. of adhesivity and cond. appl. 77−16776
ultrasonic concrete analyser, pulse velocity method 80−45472
ultrasonic testing techniques review 77−74899
ultrasonics symposium, Annapolis (1976) 77−19469
uniaxial tension, effect of material strain rate sensitivity and specimen heterogeneity *(Polish)* 78−84887
US, spectrum anal. for NDT of layered composite materials 77−81357
US applications, conference, Brighton (1977) 78−59223
US imaging using Bragg diffraction *(French)* 79−81664
US probe array using 4 transducers 80−35499
US visualisation for NDT of solids 80−22424
vibrational spectroscopy, use in NDT 78−76800
vibratory magnetometer, for high temp. anal. of low stability carbon steel 77−28946
visual inspection, human eye props. and defects *(German)* 77−86488
wear, debris anal. and condition monitoring review 78−68854
wear, laboratory measurement method using Ferrography, study of diesel engine wear 78−3304
wear debris analysis for machinery health monitoring 79−61807
wear measurement of cloth materials, nucleonic NDT instrument 78−53171
weld flaws, acoustic emission monitoring, with aid of microcomputer 80−11866
weld inspection system for Space Shuttle external fuel tank, automatic, interim report 80−76463
weld joint, use of flux sensitive magnetic heat for magnetographic inspection 78−44328
weld joint in stainless steel tubing of OK18T1 steel, ferromag. probe inspection unit 77−77721
weld seam defect parameters, measurement using TV-computer unit 79−67451
welded joint non-metallic inclusions, metallography method, and X-ray spectrum microanalysis appl. 77−76245
welded pipe joint, efficency of various methods of NDT 79−39103
welds, residual stresses, evaluation by Barkhausen noise meas. 80−76436
welds and castings, differential method of balancing out thickness-variation effects in radiography 80−66748
wire bonds on Si chips, IR microscopy 78−95867
wire rope, homogeneous, conducting, EM scattering by a slender void 78−74813
wire rope, NDT appl. of EM interaction between conducting cylinder and solenoid in relative motion 79−98261
wire rope NDT, EM field perturbation by internal void in conducting cylinder 79−34213
wire ropes using EM methods, review wire ropes using EM methods 79−83423
wood, impulse method of determining moduli of elasticity, shear moduli 77−77661
X-radiography, microfocus projection, scattering effect on contrast 80−100973
X-ray apparatus, portable, half-weight using ceramic tube 79−57193
X-ray beam, half-value layer determ., analytic method 80−66747
X-ray defectoscopy, evaluation of electroluminescent memory screen parameters 78−72992
X-ray defectoscopy, films sensitivity increase 77−90552
X-ray diffraction stress analyser, for large structures *(Japanese)* 77−48599
X-ray effective coeff. determ. 78−49950
X-ray emission analyser, data evaluation on Intel 8080A *(Hungarian)* 79−43522
X-ray film processing 78−27707
X-ray flash methods and equipment *(German)* 80−97669
X-ray flaw detection, electroluminescent storage screens, expt. results 77−77722
X-ray images, CALTIX systems, description *(French)* 77−4872
X-ray inspection of welded seams in heavy engineering using Philips MG 420 and MG 300 systems 79−93269
X-ray integration method, extension of $\sin^2\psi$ method *(German)* 80−92420
nondestructive testing continued
X-ray line profile test method, for plastic deform. *(Hungarian)* 80−97663
X-ray microfocus equipment 77−9008
X-ray NDT using 420 kV equipment incl. metal-ceramic tube *(German)* 78−4747
X-ray photographs, determ. of structral and quantum granularity 80−35477
X-ray portable stress analyser using position-sensitive scintillation detector 80−13190
X-ray portable unit, RAPS-1, for quality control, defectoscopy 79−44998
X-ray quality control, automatic exposure relay 78−95893
X-ray residual stress anal. theory 77−84200
X-ray screens consisting of scintillating crystal fibers, for nondestructive testing 79−6244
X-ray spectra of industrial radiographic units *(German)* 78−7149
X-ray stress anal., recent German activities 77−81359
X-ray stress analyser, field type, applicability *(Japanese)* 77−52591
X-ray stress meas., computer-aided system *(Japanese)* 80−104366
X-ray stress measurement method, appl. to practical materials *(Japanese)* 80−52379
X-ray structural anal., high temp. system, for examining liquid metals 80−25950
X-ray technique for nuclear fuel element assembly 78−72940
X-ray television system, based on vidicons, used for defectoscopy 78−72977
X-ray tube with variable focus, aerospace industry appls. 79−80734
x-rays and vidicon TV combine for instant inspection of precision components 79−74321
Zircaloy, claddings for irradiated UO_2 fuel, stability during long-term storage 79−26588
Zircaloy-UO_2 fuel rods, eddy-current testing of claddings using encircling and probe coils 80−21245
Ag-Cu-Pb coin chem. anal. by low energy γ-rays and neutron transmission meas. 80−35591
Ag_3Mg, ordered alloy, projected pot. image of defect obs. 79−99176
Al alloys, contamination, automated nondestructive inspection 80−16629
Al alloys, crack opening stress level in fatigue, determ. by eddy current technique 80−16617
Al, appl. of current noise technique for dislocation processes during plastic deform. 80−35442
Al coated steel, porosity evaluation, micro X-ray spectral anal. *(Russian)* 80−35389
Al foil, deformation, laser optical scanning obs. 80−100995
Al parts, radiographic testing *(German)* 77−1900
Al-Cu, high strength, type 2024-T3, crack growth, fatigue induced surface deform., holographic detect. 80−85120
Al-reinforced plastic honeycomb structures, active thermal inspection 78−72994
Al-Zn-Mg, acoustic emission meas. during tensile testing, reproducibility of results 80−50782
$Al_xGa_{1-x}As$-GaAs heterostruct., varizonal, parameter determ. by photoluminescence method *(Russian)* 80−108291
Al_2O_3 moisture sensor for sealed hybrid packages 77−87754
Au plated layer thickness meas., ^{195}Au nondestructive method 79−96244
B fibre reinforced Al, stressed state nondestructive testing method *(Russian)* 80−40631
B_4C absorber rods, nondestructive exam. with dual-energy gamma gauge and multigauge scanners 79−93721
Be bronze, BrB2 grade, heat treatment quality evaluation, using eddy current device 77−90562
Be coatings, thickness meas. using α-particles 78−82600
Be lightweight optical substrate fabrication 79−23107
C fibre reinforced epoxy resin, eddy current methods of exam. 77−12760
C fibre reinforced epoxy resin, diamag. susceptibility as fibre alignment characterisation method 78−84381
Ca, determination, image vol. samples 78−53308
CdS thin films on brass substrates, nondestructive resistivity meas. tech. 80−93898
Cr-Mn-Si steel, heat-treatment quality, higher harmonics of EMF obs. 78−60941
Cr-Y coatings, spectral determ. of Y content 77−90681
Fe, cast, grey, eddy current test for hardness certification 80−7733
Fe, coercive force measurement method of quality inspection of heat and thermomechanically treated parts 79−5113
Fe, high dispersion ferromagnet, magnetic powder defectoscopy material 80−35137
Fe, magnetomechanical acoustic emission for residual stress NDT 80−71149
Fe polycrystalline, two ferromag. methods for eval. of fatigue limit 80−89438
Fe, residual stress induced by uniaxial deform., magnetic meas. 77−73390
Fe-Cr, nondestructive in-depth surface anal. by XPS with different excitation X-ray energies 79−20328
Fe-graphite, porous sintered, determ. of impregnation depth with polycaprolactam-finely divided Cu metallic polymer 79−70272
Fe-Ni alloys, cold rolled, exam. of phase composition using Mossbauer spectroscopy 80−21204
Fe-Si (3.5 wt.%), microstructure inhomogeneity testing using Barkhausen noise strain depend. 77−12155
Fe-Si sheets, grain oriented, with insulating coating, nondestructive grain identification methods *(Slovak)* 79−5090
FeTi ferrite, H trapping study by high resolution autoradiography and degassing *(French)* 77−81368
GaP:N LED, acoustic emission, NDT of dislocation motion 78−91759
Gd, neutron radiography uses 77−66722
Ge amorphous film, evaporated, non-destructive density meas. 80−6680
H content of thin surface layers, nondestructive anal. by alpha-particle scatt. 77−56297
He-Ne lasers, sealed, using spectral emission methods 80−1210
Li nuclear microprobe method, appl. to in situ anal. of H-related materials problems 78−7299
Li-I_2 pacemaker battery electrolyte exam. by neutron radiography 80−30940
Mn determ. in Fe-, Ni-alloys by neutron activation anal., nondestructive, destructive methods 77−63987
Ni, acoustic emission during magnetisation, stress effects 79−82854

nondestructive testing continued
Ni base alloys, oxidation reaction investigation by X-ray diffr. and fluorescence *(German)* 79−57345
Ni, residual stress determ. by X-ray integration *(German)* 79−52551
Ni-Cd battery, state-of-charge determ., using impedance parameters 79−57423
Pb, parts, albedo thickness meas., neutron technique 79−29309
Pb, plastically deformed, annealed, positron trapping rate, 4-100K 78−31275
Pb, SO type, commercial purity, local deform. meas., using Moire method 80−21219
Pb-Sn (20wt.%), eddy current study of solidification 80−104141
Pu, accountability and control, field nondestructive assay measurements as applied to process inventories 80−63265
Pu, assay of large samples using portable neutron coincidence counter 80−69041
Pu nondestructive analysis, calibration by calorimetric assay 80−71878
Pu, nondestructive assay of large samples using passive neutron coincidence counting and gamma spectrometry 80−71871
Pu passive assay using Euratom variable dead-time neutron counter 80−69042
Pu safeguards, nondestructive assay using automated in-line instrumentation 80−95353
Pu safeguards, product soln. gamma-ray NDA using K-absorption edge densitometer 80−83162
Pu safeguards accountability, gamma-ray meas. of Pu and Am in molten salt residues 80−83165
Pu safeguards assay, isotopic meas. by gamma ray spectrometry using two-detector method 80−83161
Pu-U anal., in-line evaluation of nondestructive assay instruments 79−85589
Si crystal inclusions, microscopic, using X-ray diffraction and IR microscopy methods 79−55749
Si monocrystal peripheral fusion channelling under HF heating *(Russian)* 80−59627
Si, optical reflectance rel. to surface damage 79−14985
Si, polycrystalline Czochralski-grown, MIS solar cell characterisation using scanned laser response exam. 80−93884
Si polycrystalline film, effect of defects/grain boundaries on photovoltaic mech. 80−93883
Si:B, inhomogeneous surface layer, diffusion and implanted, X-ray rocking curves 80−6603
SiC-ceramic, nondestructive evaluation, scanning photoacoustic microscopy 80−85115
Si_3N_4-ceramic, nondestructive evaluation, scanning photoacoustic microscopy 80−85115
SiO_2 glass, stressed state investigation by NDT using UHF waves 78−11460
SiO_2 glasses surface textures and defects, exam. using liq. crysts. 80−6364
Sn-Pb composition anal. of PCBs using beta-backscatter gauge 80−16631
steel, C, magnetomechanical acoustic emission for residual stress NDT 80−71149
Ta capacitor, stress wave emission anal. in resistance welding 79−11739
thin film and surfaces, quantitative anal., He^{2+} induced X-ray emission technique 79−43548
Ti, pure (0.9998), positron annihilation study of defects 80−3281
Ti-Al-Mo-Sn alloy, elastically and plastically deformed, positron annihilation meas. of deformation 80−21038
Ti-Ti joints, soldered, exam. of active thermal method of inspecting 78−72993
TiC coating thickness meas. using X-ray diffr. 80−21243
$(U,Pu)O_2$, nondestructive active assay of ^{235}U and ^{239}Pu 80−71873
U assay, experimental comparison of the active well coincidence counter with the random driver 80−78503
U, nondestructive assay of mixed samples using neutron activation anal. 80−18423
U, nuclear fuel conversion plant, nondestructive assay 80−66761
U/Pu fuel reprocessing solutions, NDA using X-ray L-edge densitometer for materials safeguards 80−83167
UO_2 fuel elements cores, electrically conducting inclusions detection, using eddy current flaw detector 77−90560
UO_2-PuO_2 fuel pellets, porosity meas. methods *(German)* 80−73915
^{233}U safeguards, expt. nondestructive assay using a random driver 80−83164
^{235}U isotopic content determ. of nuclear materials using gamma spectrometry 79−85756
^{235}U, nondestructive assay, appl. to decommissioning of fuel reprocessing facility 80−81269
^{235}U, nondestructive determ. of content in fuel elements using passive gamma ray spectrometry 80−18418
W alloy, determ. of mean grain size by acoustic method 78−72961
W-Mo-Co high-speed cutting steels, Co determ. 78−3416
WC-TiC(TaC, NiC)-Co, hard, homogeneity and wear resistance estimation, by magnetic method 77−90558

nondeterministic systems
thermal deformation of structures with temp.-dependent material props. 77−65679

nonelectric final control devices
see also brakes; clutches; fluidic amplifiers; variable speed gear
water bath level control device 79−67283

nonelectric sensing devices
acousto-optic sensor development 80−14542
airflowmeter using wire-mesh element 77−39388
angle synchronous contact sensing for noise investigations, anal. of gear wheels machining errors appl. *(German)* 79−68477
capillary temperature sensor, using laminar fluidic amplifier 78−24793
chromatography, liquid, detector characts. and use, book 78−15751
combustible gas detector, operational tests 79−16105
extensometers, description, and appl. to buildings and public works *(French)* 77−5828
fibre optic rotation sensor, signal detection and processing 79−37034
fibre optics sensors for measurement and control appls. 80−58780
fluidic, principles and appls. *(German)* 77−53886
fluidic temperature sensors 80−73342
fusion thermal tracers, thermophys. characts. investig. 77−5837
gyrostabiliser, single-axis with pneumatic stabilising circuit, description and appl. *(Russian)* 77−26283
level gauge checking methods and facilities 77−22526

nonelectric sensing devices continued
linear meas. extension-nozzle ejector-transducer design 77−57313
liquid level sensor for process-control appls., utilizing pneumatic capacitor 79−71438
magnetic suspension densimeter, differential capacitance sensor as position detector 80−196
membranes appl., silicone rubber, physical props. *(Slovak)* 80−61141
microhole axis perpendicularity deviation meas. device 77−13739
optical fibre hydrophone, high-linearity multimode optical fibre sensor 79−68429
optical sensor using optical fibres *(Japanese)* 80−78997
optical-sensing systems, with automatic light-intensity control, stabilisation 77−54784
passive optical rotation sensors using guided waves, developments 80−58781
Permalloy magnetoresistive mag. field sensor, performance calc. 80−57342
photoacoustic detector, for laser beam energy monitoring, construction and calib. *(Czech)* 78−29156
photoelastic sensor for stress meas. *(Russian)* 77−11150
quartz cryst., piezoelec., coated, detection of HCl gas in ambient air 78−92532
rotary encoder for optical angle meas. *(Japanese)* 77−22523
seismic sensors, frequency charact., influencing factors *(Japanese)* 78−85722
slit die rheometer for polymer melt pressure meas. 77−27501
velocity measurement for moving surface using sensing arrays 79−58677
velocity sensor, optical, for liquid flow *(Russian)* 78−1759
viscosimeter solar radiation tracking sensor 80−86295
water-sensitive detector, emergency switch design 78−81962

nonleptonic decays
see also baryon hadronic decay; meson hadronic decay
$\Delta I=1/2$ enhancement, $SU(2)\otimes(1)\otimes U(1)'$ gauge model 77−6073
baryon pair production with large decay Q-value. Brasil-Japan emulsion chamber collaboration 79−58992
bottom mesons, weak decays, strong correction meas. 80−82970
charm decay and u-s symmetry 79−13078
charmed particle decays, semileptonic, nonleptonic, isospin restriction on charge distibs., branching ratios 77−54099
charmonium state decay, nonrelativistic and relativistic theory 78−58221
constituent rearrangement model and hadron reactions review 79−26294
enhancement and suppression factors for left handed current, K decay 79−385
flavour changing self energies, contrib. to $\Delta S=1$ hadronic weak decays 79−71713
gauge model of weak and electromag. interactions, $\Delta T=1/2$ rule *(Russian)* 78−45838
hyperon decay, implications for right handed current 77−67651
hyperon decays, CP violation, deviations from $\Delta I={}^1/_2$ rule 78−70367
hyperon nonleptonic decays, $\Delta I={}^1/_2$ rule violation 79−45087
hyperon nonleptonic decays in SU(3) 79−97624
parity violating non-leptonic hyperon and charmed baryons in SU(8) 77−26523
pseudosymmetry, weak decays and gauge group $U(1)\times SU(2)\times SU(2)\times U(1)$ 77−18214
QCD, six-quark model, $\Delta S=1$ weak nonleptonic decays 80−22582
quark density model, SU(3) symmetry breaking and nonleptonic decays 79−13079
reduction formula and non-leptonic decays in light-front formalism 78−12911
right handed currents, $\Delta I=1/2$ rules, nonleptonic decays, heavy-quark expansion, Zweig's rule 77−61217
strange particle nonleptonic decay, asymptotic freedom, light quarks and $\Delta T=1/2$ rule 77−38164
$SU_3\times U_1$ calibrating theory, weak and EM interactions appl. *(Russian)* 79−35964
SU(2) gauge invariance, spontaneously broken, $\Delta I=1/2$ rule, nonleptonic weak interactions model 77−41786
$SU(3)\times SU(3)$ chiral renormalisable gauge model, nonleptonic decays 78−24938
top mesons, weak decays, strong correction meas. 80−82970
weak, $\Delta I=1/2$ rule and strong interactions 77−46046
weak nonleptonic decays in SU(4) and SU(8), adjoint representation admixture 78−21426
η^0-π^0 mixing effects and $\Delta S=1$ nonleptonic weak decays 80−4991
Ω^- nonleptonic decay branching ratios from Weinberg-Salam and MIT bag models 80−37261
$\phi\phi$ decay as a parity and signature test 79−17722
$\Sigma^\pm$ lifetimes, decay asymmetry and nonleptonic decay branching ratio, $|\Delta I|=1/2$ rule 80−78061
$\tau\rightarrow 3\pi$ or 5π, decay rate using current algebra and PCAC 79−3062
$\tau\rightarrow$charged hadron+neutrals, branching ratio from e^+e^- annihilation 78−78200
X° pair production and decay in 400 GeV/c proton interactions 79−17768
$\Xi^-\rightarrow\Lambda\pi^-$, asymmetry parameter 80−42457

nonlinear acoustics
2D finite amplitude acoustic waves radiating from flat plate in arbitrary periodic vibrations 80−33283
absorbent materials, models for propag. 80−53524
absorbing solid, laser irradicted, relationships in formation of shock waves 79−55825
acoustic discontinuities, interfaces 78−46857
acoustic emission systems, amplitude-response variations 78−48605
acoustic focusing systems, nonlinear effects 79−32126
acoustic generation of harmonics 77−27417
acoustic interactions in media with weak periodic inhomogeneities 79−32124
acoustic streaming in Hg 79−64380
acoustic wave evolution in incompressible flow with density as function of time *(French)* 80−53517
acoustic waveguide, nonlinear interaction of elastic waves with resonance *(Russian)* 78−6206
acoustic-gravity waves in plane waveguide, interaction and self action *(Russian)* 78−36221
acoustic-vortical turbulence struct. 78−83373
acoustoelasticity of isotropic elastic materials, thermal effect 80−33276
aeroacoustic fluid dynamic equations, acoustic energy conservation, vibrational relaxation effects 78−90566
aeroacoustics and aircraft 80−53532

nonlinear acoustics continued
alkanes, fourth order nonlinearity acoustic parameter 78−51612
amplification of an acoustic signal by a laminar, pre-mixed, gaseous flame 79−29357
amplitude density of a finite amplitude wave 79−68462
amplitude shading of irregular acoustic arrays 78−83178
analytical description of wave propagation and interaction in confined beams 78−1470
anisotropic piezoactive wavegyide, normal waves 77−88975
antiferromagnet, acoustic SHG near first oder onentational phase transition 78−27067
antiferromagnet, effective anharmonicity of elastic subsystem *(Russian)* 77−90010
antiferromagnet, with easy plane anisotropy, nonlinear self-interaction of acoustic waves *(Russian)* 78−80187
artificial control of the laminar-turbulent transition of a two-dimensional wake by external sound 78−34139
astrophysical gravitating gas, nonlinear waves 78−28512
asymmetric double exponential waveform, weak-shock soln. for nonlinear propag. 80−10061
asymptotic analysis of the possibilities of making use of non-linear effects in acoustic-diagnostics of layered media 77−84090
asymptotic approximations of the solutions of a system of two non-linearly coupled harmonic oscillators 77−23792
asymptotic solutions of model equations in nonlinear acoustics 79−76905
atmosphere, generation of LF component of intense modulated acoustic wave *(Russian)* 79−98522
atmosphere, sound interaction with gravity waves *(Russian)* 77−3693
atmosphere acoustic and radio acoustic exploration, effects of sound nonlinear absorpt. *(Russian)* 80−94567
atmospheric acoustics 78−73493
atmospheric attenuation of explosion waves 77−31155
attenuation in superconductors 77−43780
attenuation of slightly nonlinear waves 77−50801
axial field of parametric acoustic radiator 80−33290
axisymmetric parametric radiation, weak interaction model 79−90053
backward waves and acoustic scanning, nonlinear interaction of vol. and surface waves 80−79040
boundary layers, acoustic streaming 79−86544
bounded heat evolving medium, nonlinear stabilization of unstable acoustic vibrations 80−6028
α-brass, acoustic harmonic generation by long-range dislocation motion 79−42150
broadband parametric array with Gaussian primary directivity patterns 80−96066
bromobenzene+m-xylene, US vel. and adiabatic compressibility 78−51614
bubble dynamics in the vicinity of a spherical radiator 77−68679
Burgers eqn., finite-amplitude propagation through gas droplet mixture 80−33282
Burgers equation, exact solutions 79−32125
cancellation of the distortion of finite-amplitude sound wave *(Japanese)* 77−14832
caster oil, calculation of nonlinearity parameters thermodynamic method 80−79880
cavitating water, matching optimisation for magnetostrictive transducers 78−94503
cavitation gas bubble, inhomogeneous sound field effect 80−6131
cavitation threshold meas. for polyalkylene glycol and castor oil 80−107374
cepstral technique appls. to ground reflection effects in acoustic spectra 77−31165
characteristic functional of the sound field in randomly inhomoge; neous media 79−64383
circular crystal plates, accel. effects on resonance freqs. 78−59189
circular lined ducts, nonlinear attenuation 79−23118
circular pipe, simulation of finite amplitude sound wave 78−13834
circumferential waves for a cyclindrical shell supported by a continuum 78−90564
closed tube, nonlinear resonant acoustic oscillators, finite rate theory 80−92171
coarse grained eqns. of propagation in two-phase random media 79−86280
collinear interaction of noise with finite amplitude tone 78−55490
combination normal mode-ray technique for the calculation of sound fields in waveguides 77−50800
combustion zones, nonlinear feature of coherent acoustic amplification 80−38156
comparison with nonlinear optics *(French)* 80−33293
compensation by the diffracted field formed by rigit scatterers in the field of a harmonic point sound source 78−18112
composite, fibre-reinforced, layered, harmonic elastic waves, dispersion 78−63223
compressible heavy fluid, variational principle 78−83426
compressible liquid, sound and hydrodynamic turbulence *(Russian)* 78−55633
conference on acoustic propag., Marseille, France, 1978, May *(French)* 79−41484
conformal array beam patterns and directivity indices 78−55523
constructive methods for solving the exterior neumann problem for the reduced wave equation in a spherically symmetric medium 77−50799
contactless semiconductor surface charact. using nonlinear SAW interaction 80−11069
convergent sound beam in a nonlinear medium 78−1468
correlation of nonlinear orifice impedance 77−23837
coupled system for subharmonics of any order 80−43504
coupled-mode-vector analysis of reflective arrays 79−7241
crystal nonlinear electroacoustics, dynamical eqns. and constitutive relations 79−56734
cubic crystals, acoustic non-linearity parameter 77−51444
cumulative nonlinear distortion of an acoustic wave propagating through non-uniform flow 78−22367
curved face parametric projector for marine sediment penetration 78−51032
cutting-out techniques *(French)* 79−41476
cylindrical cavity, excitation of nonlinear acoustic resonances by unsteady heat input 79−41483
deep water propagation, shadow and convergence zones *(French)* 79−41504
degenerate parametric amplification of sound 77−27414

nonlinear acoustics continued
detecting signals with random phase modulation in a nonlinear, nondispersive medium *(Russian)* 77−75606
diagnosis using nonlinear effects, asymptotic feasibility anal., props. of layer on halfspace object 78−63248
dielectric, piezoelectric and pyroelectric crystal, theory of nonlinear electroacoustics 78−79155
dielectric crystals, nonlinear electroacoustic, fundamentals and appl. 80−34489
dielectrics, electric, optic and acoustic interactions 80−2715
diffraction effects in finite-amplitude sound beams 78−1471
diffraction of sound beams in inhomogeneous media 79−64377
diffusivity of nonlinear wave propagation in pipes 80−33286
discontinuous noise waves, spectra 79−94389
discontinuous waves in nonlinear media 78−5601
dispersive acoustic systems, nonlinear and parametric phenomena 78−55489
dispersive waves, characterization using freq. approach 80−87606
dual nonlinear interactions of the tolmin-schlichting waves in shear flows *(Russian)* 77−58708
duct propagation, initial values for integration scheme to compute eigenvalues 77−46839
eccentric spheres, internal and extornal waves 77−75384
Eckart flow in conducting liq. or gas, acoustoelectric current prod. 79−27707
elastic interactions between acoustic bulk and surface waves 77−50797
elastic materials, isotropic, nonlinear acoustoelasticity 79−72740
elastic solids, homogeneous and heterogeneous, nonlinear waves 80−34134
elastic waves, nonlinear mode coupling, numerical investigation 79−7240
electroacoustic echo in powders, formation by freq. modulation mech. 78−19421
electron gas, nonlinear theory of sound wave propag. *(Russian)* 79−76904
electronic signal processing devices, photoelastic materials, nonlinear elastic interactions *(French)* 79−41525
end-fire arrays, exponentially schaded, nearfield axial levels 77−39127
end-fire line arrays with arbitrary shading, near field beam patterns 77−46857
energy eqns. for acoustic fields in stationary and moving fluids 80−53525
enhancement of the absorption coefficient of acoustic waves due to acoustic streaming in fluids 78−9471
evaporation rates of drops in forced convection with superposed transverse sound field 78−51224
evolution of nonlinear standing waves in bounded media 77−49607
explosive wave profile transformation, time constant derivation 80−48485
fibrous networks in viscous media, acoustic theory of wave motion 78−59177
film, dimensionally quantised, nonlinear US absorption in EM wave field 78−87745
finite amplitude distortion of intense sinusoidal pressure waves in air 80−33273
finite amplitude sound beam propag. in dissipative medium 79−32122
finite amplitude sound wave propag. in inhomogeneous medium with caustics 77−68295
finite-amplitude saturation of plane sound waves in air 78−1465
finite-amplitude wave propag. in media of various degrees of nonlinearity 80−53528
first passage time for oscillators with non-linear restoring forces 78−42562
fixed intensity approximation in the theory of nonlinear waves *(Russian)* 78−9410
flint glass, dense, nonlinear elastic props. *(French)* 80−34132
fluid and flat plate with harmonic excitation, nonlinear interaction 79−23250
fluid-loaded cylindrical shell, resonant component isolation in acoustic scatt. 80−5864
focused acoustic beam in nonlinear medium 80−33287
focused high-amplitude sound beams 78−94465
focusing transducers, study of parametric radiation *(French)* 79−41486
fourth-order acoustic torque in intense sound fields 78−63220
frozen oceans, wave propag. in random media 77−50814
gas bubbles, effect of backscattered acoustic wave on bubble oscillation 79−1021
gas bubbles in liquid, multiple resonances in sound scatt. 79−81606
gas bubbles in liquid, propag. of disturbances 80−59104
gas cavitation nuclei, stabilization mechanism 79−81611
gas column response to destabilising boundary condition, nonlinear self excited acoustic oscillations 79−41492
gas in open tube, nonlinear oscillations 78−18091
gas in rectangular cavities, nonlinear acoustic resonances 78−71240
gas-liquid medium, standing waves 78−9474
gas-liquid mixture, propag. of arbitary amplitude waves 78−38122
gas-liquid mixture, propag. of disturbances 78−9473
gas-liquid mixture, self action mechanisms 78−38118
gases, weak nonlinear waves, struct. and propag., effect of vibr. relaxation 79−64683
gases with weak relaxation influence 77−55100
Gaussian beam propag. 80−87609
Gaussian noise and its transformation by moving boundary condition effect 80−33281
generalised harmonic balance method for combination resonance in parametric dynamic systems 78−90753
generator, axial dynamic, model of theoretical acoustic system 79−14181
glass, US props. at ultra low temps. 77−39635
granular solid, one-dimens., small amplitude wave behaviour 78−59339
gravitational and acoustic waves in an elastic medium 78−24712
growth and decay of sonic discontinuities in non-equilibrium gasdynamics 78−34209
harmonic generation in piezoelectric crystals under the action of homogeneous external fields 79−32121
harmonic generation in sound beams 80−5862
harmonic generation of longitudinal elastic waves 77−79991
harmonic oscillator, perturbation theory 80−19272
harmonically vibrating flat plate, 2D acoustic wave radiation 79−81597
harmonics of the difference frequency in saturation-limited parametric sources 78−30110
heat transfer in acoustic wave 78−5599
HF sound propagation, non-linear effects in tubes 80−87614

nonlinear acoustics continued
HF sound propagation in metals and semiconduction 80−88279
high thermal conductivity mecia, model equations for the nonlinear acoustics 78−90565
high-permittivity crystals, modulation oscills. of travelling EM wave 80−24962
highly electrostrictive ceramic capacitor 79−47390
hyperbolic waves, comparison of perturbation methods 77−7236
impact testing of floors *(German)* 77−825
impulsive discharge noise, balloon burst problem and engine exhaust pulses 78−90588
inbonded interfaces and fatigue cracks, acoustic harmonic generation 78−90562
indirect interaction frequency shift of radiation 77−38983
inharmonic musical oscillators, nonlinearly excited, mode locking 79−14165
inhomogeneity of medium, determination by means of sound signals 80−87610
inhomogeneous absorbing layer, refractive index distributions 78−38117
inhomogeneous medium with slightly varying sound vel., beam propag. 78−1467
integral equation methods in duct acoustics for nonuniform ducts with variable impedance 77−58498
intense perturbations, nonlinear waves and appls. *(Russian)* 79−37073
interaction of acoustic radiators moving at supersonic velocity 77−815
interaction of acoustic waves and microwave radiation fields: depletion and mixing effects 79−90056
interaction of determinate packet with random noise, in Burgers' equation 80−106650
interaction of diffracting sound beams and the theory of highly directional ultrasonic radiators 78−38121
interaction of fields with plates under harmonic excitations 79−23246
interaction of plane acoustic wave and plane shock, wavenumber jump condition 78−1466
interaction of pulses with discontinuous edges 77−50802
interaction of two collinear, spherically spreading beams, appl. to parametric acoustic arrays 80−48484
interaction of weakly modulated sound and surface waves *(Russian)* 80−12402
interferometer nonlinear transducer motion 79−50540
ionic crystal, nonlinear elastic behaviour 78−59851
Isom's thickness noise formula, extension to near field 80−53520
Korteweg-de Vries solitary waves, cylindrical and spherical 79−77371
Korteweg-de Vries waves and solitons, three dimensional stability 78−83540
Lagrangian and Eulerian representations *(French)* 80−33285
Lagrangian-mean flow, exact theory of nonlinear waves 79−37331
Lamb wave propag. on isotropic plates, second harmonic acousto-optic interaction 80−34886
laminated composite, nonlinear transient pulse propag., interface reflection effect 78−63222
laminated material, geometrical acoustics 77−42774
Landau damping in regular wave interaction with noise 80−33284
large amplitude vibration of plates and membranes 77−50959
large amplitude vibrations of circular plates with varying thickness 77−50960
large-scale spatial oscillations of a cavity in a sound field 78−94775
laser interference microphone for ultrasonics and nonlinear acoustics 77−46874
LF harmonics generation in field of high power AM wave 78−50976
line acoustic waves, unusual parametric effects 80−5854
liquid, pot. energy effects on sound speed 79−81595
liquid, weakly assoc., US wave reson. absorpt. 80−34141
liquid containing gas bubbler, effect of polymer additives on acoustic props. 78−38779
liquid crystal, nematic, orientational acoustic nonlinearity 80−34143
liquid filled tubes, weak shock propag. 78−26004
liquid with gas bubbles, acoustic wave self-transparency effect *(Russian)* 80−14509
liquid-gas system near crit. point, sound alternations and dispersion 79−42149
liquid-solid interface, plane sound wave reflection and refraction in mag. field 80−38150
longitudinal wave propagation 78−25998
low-frequency parametric radiation of sound 77−39128
Mach number expansion of Navier-Stokes eqns. 78−90567
magnetically ordered media, self-induced transparency in nucl. acoustic reson. 79−69733
magnetoelastic crystal, cubic, acoustic SHG, static magnetisation effects *(Russian)* 78−56362
magnetoelastic media, nonlinear effects 77−36109
magnetoelastic media, nonlinear effects associated with social propag. 77−27413
magnetoelectric media, generation of second magnetoacoustic harmonics *(Russian)* 79−42816
many-valley semiconductor, US propag. 77−59305
marine sediments, saturated, nonlinear parameter 80−19132
melts, acoustic streaming 80−5861
metal, nonlinear effects on strong and weak sound wave propag. *(Russian)* 78−60168
metal, nonlinear interaction of strong and weak sound waves 78−59865
metal, Raman scatt. of sound in quantising mag. field 78−60171
metals and semimetals, higher sound harmonics generation, momentum nonlinearity regime *(Russian)* 78−38783
minerals, acoustic non-linearity parameter 78−20392
mode coupling of elastic waves 77−79990
model equations, book contrib., review 80−19126
monochromatic US signal interaction with AF noise underwater 79−14147
monochromatic wave modulation in underwater acoustics 79−41503
Mossbauer spectroscopic study of ultrasonic anharmonicity 78−52411
moving fluids, transport eqns. and acoustic motion 80−53523
moving sources in flow, acoustic radiation, appl. to aircraft noise 80−53526
multi-mode cylindrical surface wave excitation 78−26000
multicomponent chemically active gas mixtures, acoustic vels. 77−35261
mutual focusing of an intensive longitudinal sound wave in a non-linear medium 78−26001
mutual interaction of nearest neighbours in compact planar array 78−50979
mutual radiation impedances between circular pistons 79−1016

nonlinear acoustics continued
N-wave propagating in circular tube, nonlinear attenuation and wall effects 78−50972
near field parametric emission study by Fourier anal., appl. to focal emitter *(French)* 80−33291
nematic liquid crystal, US propag. 77−59069
neutrino detection in ocean by nonlinear sound generation by hadron showers 80−36465
noise spectrum evolution, Gaussian, intensive, plane wave in lossless fluids 80−69581
non-homogeneous marine media, numerical approx. of hyperbolic evolution problem 79−41489
nonadiabatic weakly ionized gases with applied magnetic fields, acoustic instabilities 78−9719
noncollinear three-phonon interaction in an isotropic plate 78−66970
nondissipative medium, nonlinear propag. of sound beam 77−34979
nonequilibrium effects on breakdown of weak solutions 78−94890
nonlinear acoustics 8th symposium, conf., Paris, France, July 1978 80−33277
nonlinear media containing chaotic inhomogeneities, equation closure for average field 79−81601
nonlocal diffusion theory of wave propagation in highly viscous liquids 80−102897
nonpolar liquids, cavitation threshold under ionising acoustic radiation 79−37074
nonreflecting boundary conditions for nonlinear hyperbolic systems 79−50748
nonstationary ultrasonic self-focusing in a nonlinear medium 77−27412
nonuniform gas with droplets, acoustic attenuation 78−83154
numerical simulation of shock-wave reflection from a concave surface 79−18913
numerical solution of wave scattering problems in the parabolic approximation 79−50491
ocean, approx. eqns. for powerful acoustic signal propag. *(Russian)* 79−98526
ocean acoustic transfer function 79−59861
oceans, propag. in fluctuating media 77−53073
one dimensional waves in near sonic flows 79−41701
optoacoustic exciter, nonlinear limit on efficiency 80−28406
orifice impedance meas. under turbulent boundary layer 77−23838
orthotropic plate vibration, finite element anal. 77−7237
parametric acoustic array, effect of finite aperture 80−106648
parametric acoustic array max. conversion efficiency anal. 78−71242
parametric acoustic arrays, nonlinear interaction of finite-amplitude sound waves 80−53529
parametric acoustic arrays, theory 80−33289
parametric acoustic arrays with intermediate directivity in water, expt. study 80−74569
parametric acoustic radiators, high-power, operating characts. 78−94469
parametric acoustic receiving array response to transducer vibration 80−74570
parametric acoustic receiving array vibration sensitivity anal. 78−66971
parametric acoustic source, numerical method for nearfield calc. 78−63221
parametric acoustic source model 77−46836
parametric acoustic sources of rectangular aperture, source level and beam pattern prediction 78−63219
parametric array, finite amplitude wave reflection 77−84036
parametric array, selected mode excitation in shallow-water sound propagation 78−59182
parametric array theory 78−38119
parametric arrays, beam pattern and propag. curve for air *(Japanese)* 80−83693
parametric excitation of low-frequency noise waves in a nonlinear medium 78−9472
parametric excitation of sound in an acousto-optical deflection of luminous radiation *(Russian)* 78−33850
parametric excitation of ultrasonic beams in a dissipative medium 79−18570
parametric hydrophone, compact, using nonlinear interaction within cylindrical rubber waveguide 79−98535
parametric interaction of two HF collinear beams 80−43507
parametric radiator, influence of dispersive medium on characts. 78−94470
parametric sound generation, liquid containing gas bubbles 80−87615
parametric sound generator theory 77−50849
parametric sound reception in freq. range 10 to 20000 cps, expt. research 80−33391
parametric transmitting arrays, weak interaction model for axial difference freq. field 79−81599
parametric US radiator, saturation-limited operation 78−94467
passive range estimation from array of sensors 80−53583
Pekeris operator, resolvent in dispersive media *(French)* 79−41488
perforated plate, nonlinear acoustic resistance *(Chinese)* 79−23119
periodic structures on solids, shear surface acoustic waves 79−90055
perturbation solution of a highly non-linear oscillation equation 78−33938
physical and technical acoustics and ultrasonics 78−1451
piezoceramic material, non-collinear SAW's, non-synchronous interaction *(Russian)* 78−26002
piezoelectric crystal, acoustic transverse wave polarisation and energy flow in external static fields 80−19123
piezoelectric crystal, excitation of acoustic harmonic and its energy flux 79−15404
piezoelectric crystals, acoustic wave mixing 78−83155
piezoelectric crystals, variation of phase vel. and wave struct. of finite amplitude SAW 78−95219
piezoelectric devices, variational principle for soln. of nonlinear acoustoelectronic problems 78−90621
piezoelectric effect, nonlinear, in crystals, transform. of acoustic waves into microwaves 78−10521
piezoelectric film, third-order piezoelec. and dielec. consts. meas. using surface acoustic waves *(Japanese)* 80−55042
piezoelectric problem parameters, variational limits 79−81594
piezoelectric semiconductor, nonlinear acoustical noise amplification, theory 78−47837
piezoelectric semiconductor, nonlinear interaction of acoustic waves with microwave elec. fields 79−42593
piezoelectric semiconductor, nonlinear interaction of quasicollinear acoustic waves 77−59306

nonlinear acoustics continued
piezoelectric semiconductor, US parametric amplification effects, contributions to nonlinear material coefficients 80−34144
piezoelectric semiconductor combinatorial scatt. of acoustic waves by electron beam *(Russian)* 77−11963
piezoelectric semiconductors, soln. by perturbation techniques 78−57796
piezoelectric surface waves, influence of uniaxial biasing stresses 77−27416
piezoelectric-semiconductor interface, acoustic wave amplification by reflection from uneven boundary *(Russian)* 78−30819
piezosemiconductors, second harmonics of acoustoelectric current 80−80329
pipes and ducts, standing waves near resonance 79−3823
piston source, circular, meas. of fundamental and second harmonic pressures in acoustic field 79−46101
plane wave diffraction by variable density cylinder 78−50977
plasmas, nonlinear acoustic waves *(Russian)* 79−55491
Poincare-Lighthill-Kuo method and non-dinear hyperbolic waves 78−41166
polarisation effects in crystal acoustics, linear and nonlinear 80−5855
polyvinylidene fluoride films, SH and Lamb waves propag. 80−75948
propag. of sound beams with uniform amplitude distrib. 80−102896
propagation and damping within fluids *(French)* 77−19467
propagation eqn. with energy loss *(French)* 80−8808
propagation in absorbant fluid, Fourier propag. theory *(French)* 80−33288
propagation loss enhancement in noise 77−35000
propagation of a strong sound wave in a plane layered medium 77−34980
propagation of plane harmonic waves, infinite isotropic medium having embedded doubly periodic array of cylindrical fibres 80−87607
propagation of waves induced by vibr. cylinder, 2-dimens. case 79−23120
propagation of waves induced by vibr. cylinder, 3-dimens. case 79−23121
propagation speeds for perturbations in a flow of a two-phase mixture 78−42642
pulsation noise damping from small air bubbles in water 80−64253
pulse propag. in nonlinear media, linear approx. 79−94390
pulse propagation in inhomogeneous atm., flow struct. near intersection between shock and caustic 79−14139
pulsed radiolysis, nonlinear radiation-acoustic phenomena 80−79029
quadrupole resonance of drops driven by modulated acoustic radiation pressure, experimental props. 80−33275
quartz, fast neutron irradiated, saturation of 9.4 GHz hypersonic attenuation 79−23682
radiating gas, attenuation of plane acoustic pulses 77−35259
radiation due to a fluctuating acoustic ring source in motion 77−50796
radiation force on sphere in quasistationary wave field, expt. 79−41482
radiation force on sphere in quasistationary wave field, theory 79−41481
radiation from a source near a jet 77−31169
radiation of plane circular source, nonlinear solutions *(French)* 80−33280
radiation patterns of acoustical arrays with quantized time delays 80−74566
radiation press. on an absorbing sphere 78−79154
radiation pressure, historical review 78−59178
radiation pressure on a sphere 77−84035
radiation pressure on rigid sphere in spherical wave field 80−64251
radiation pressure on sphere in standing wave field, meas. 77−79989
random, methods of analysis 80−53527
random quasimonochromatic waves, statistical props. 78−38116
Rayleigh and Langevin radiation pressure 78−25999
Rayleigh wave interaction in $LiNbO_3$-CdS system, expt. investigation 80−102946
Rayleigh wave scatt. by normal discontinuities, influence of elastic props. 77−46835
Rayleigh waves, normally incident, scatt. by thin strips 77−11773
real gas effects in non-equilibrium gas dynamics 78−47086
rectangular cavity in viscous gas flow, numerical anal. of acoustic resonance 79−64378
rectangular duct, finite amplitude two dimensional waves 79−72739
rectangular ducts, complex sound fields, self-excitation 77−46838
rectangular plates, averaging technique for nonlinear vibrations 78−63362
reflection from curvilinear boundary, field amplitude calc. 77−33874
reflection from obstacle in one-dimens. medium with random inhomogeneities 80−58839
relativistic cosmology, nonlinear HF waves 79−48968
relativistic shock damping 77−75994
resonance interaction of sound waves with a plane-parallel flow 77−814
resonance standing wave meas. anal. 79−10436
resonator, nonlinear thermoelastic couplings *(French)* 80−34118
resonator cavity, influence of depth on acoustical props. 80−58838
resonator in a field of finite-amplitude sound waves 78−1469
resonators, theory of nonlinear oscillations 78−50974
SAW, parametric mixing, approx. theory 79−86279
SAW, parametric mixing and harmonic generation anal. 79−50489
SAW and anomalous sound absorpt. for fluid-fluid interface 80−74562
SAW elastic convolver, degenerate, nonlinear interactions 80−64254
SAW generation, linear and nonlinear growth 79−56057
SAW generation by nonlinear mixing of bulk waves in isotropic fused samples 79−50490
SAW harmonic generation, overlap-integral anal. 79−55259
SAW power densities, simple method of approx. 77−79987
SAW propag., photographs on TV images of travelling waves using strobed electron beam 80−102894
SAW scatt. by post spacers 79−27456
SAWs of finite amplitude excited by monochromatic line source, propag. characts. 80−96091
scale invariance and asymtotic solutions of the Zabolotskaya-Khokhlov equation 77−11065
scanning acoustic microscopy, nonlinear imaging of an edge 78−38158
scattering of an acoustic line-source radiation from a rotating cylinder 77−50795
scattering of sound by sound, relation to the parametric receiving array 78−90563
scattering of sound by sound 77−27942
scattering of sound by sound *(Chinese)* 77−34978
scattering of sound by sound 79−10424
seawater and distilled water nonlinearity parameter meas. 78−75727

nonlinear acoustics continued
second acoustic harmonics generation, effect of crystal misalignment *(Russian)* 78−75009
second harmonic generation in an electric field 77−11962
second harmonic generation in finite amplitude SAW, anisotropic media *(French)* 80−34285
second harmonic SAW generation in devices involving semiconductor coupling 79−46148
second-harmonic generation in resonator of multilayered interference filter type 80−58840
second-harmonic generation in the field of a piston radiator 79−32123
self focusing of acoustic waves during cavitation 79−3821
self-defocusing of a sound beam in the presence of acoustic streaming 77−14833
self-detection of finite amplitude sound waves with large Reynolds numbers 78−5600
self-excitation frequencies of an annular jet 78−94782
self-focusing of an intense ultra- and hypersonic beam in an inhomogeneous and absorbing solid 77−84038
self-focusing of beams, simulation 77−75628
self-focusing of nonaxisymmetric beams 77−75627
semiconductor, SHG by hot-electron and electron transfer effects, optimum conditions 79−41491
semiconductor US absorption intermediate frequency 79−28380
semiconductor-piezoelectric structure, vol. acoustic wave excitation in nonlinear interaction with surface waves 80−69582
semimetal, Raman scatt. of sound in quantising mag. field 78−60171
semimetal, US propag. 77−59305
shape oscillation and static deformation of drops and bubbles driven by modulated acoustic radiation stresses 80−33274
shock pulses in Al rods, amplitude-dependent attenuation 78−55503
shock spectrum of a two-degree-of-freedom nonlinear vibratory system 77−27421
shock tubes of varying area, acoustic resonances 77−50803
shock wave generation in solids *(Japanese)* 79−68475
shock wave-acoustic wave interactions in elastic solids 79−98521
silicate glasses, phonon echoes at low temp., coherent acoustic echo generation 79−65163
simulation of impacting oscillations of a piezoelectric resonator with a vibrating wall *(Japanese)* 78−9483
solid, interaction of first and second sound *(Russian)* 79−86841
solid-solid interface, anomalous reflection of acoustic shock pulse 77−19466
sonic discontinuities nonuniform propag. in thermally conducting gases 79−3822
sonic wave, excitation by quasi-monochromatic Alfven pumping 80−106649
sound absorbing turbulent jet, scattered signal spectrum 79−94695
sound amplification in nonuniform flow 78−83158
sound field of plane radiator with arbitrary contour shape 80−79028
sound wave interaction with shock waves 79−27457
sources, nonlinear and thermal, due to thermoviscous heating of fluid by modulated sound wave 79−23122
spectral method appl. to nonlinear propag. 77−5672
spherical wave reflection from a boundary of reactive impedance using a modification of Cagniard's method 77−11064
stable arrays of resonant bubbles in a 1-MHz standing-wave acoustic field 77−79988
stationary self-focusing of ultrasound and hypersound in nonlinear media 77−813
steered planar nearfield transducer calibration array 78−59214
stellar winds, radiative amplification of sound waves 79−96999
stepped pressure concentrator, anal. of reson. freq., gain, and press. distribs. under reson. and nonreson. conditions 78−90619
stochastic instability of rays in inhomogeneous media 79−64379
stochastic ray theory relations, expt. agreement 77−84051
stratified media investig. using algorithms from inverse scatt. problem in quantum mechanics *(French)* 79−41490
streaming, dynamic characts. in field of acoustic dipole 78−50973
streaming in vicinity of plate possessing propagating longitudinal strain wave 80−87758
strength of nonlinear interaction between collinear surface acoustic waves 80−33295
strong nonlinear and dissipative effects in the acoustic diagnostics of layered media 78−1472
strong shock wave diffraction near the angle *(Russian)* 78−75171
structure of sound field in arbitrary smoothly inhomogeneous medium 80−38155
sub-bottom profiling sonar with nonlinear sound source 77−45198
subharmonic nonlinear acoustic reson. in open tubes, open-end boundary conditions 79−14137
superconducting and normal metal, non-linear acoustic props. of cond. electrons 79−60975
superconductor, nonlinear effects on threshold absorption *(Russian)* 79−19691
superconductor, sound velocity *(Russian)* 77−4468
superfluid, sound field due to moving source 79−90054
supersonic heat source, sound radiation 78−1688
suppression of finite-amplitude primary wave attenuation, parametric acoustic arrays, use of bubbles 80−74563
surface charge on unapodized periodic IDI 80−91947
surface wave attenuation due to elec. cond. of films, perturbation anal. 77−31154
surface wave formation rel. to resonance in acoustic scattering *(French)* 80−8809
surface wave in RF electric field noncollinear reaction 79−69566
surface wave memory correlator using nonlinear interactions *(French)* 80−33294
surface waves on anisotropic substrates, transverse amplitude depend. 79−7242
surface-wave harmonic generation on $LiNbO_3$ 77−31153
synthesis of cylindrical arrays with directivity patterns uniformly approximating a predetermined function 78−38123
ternary liquid mixtures, nonlinear effects with high amplitude US prop. 78−51613
TGS, ferroelec. single crystal, low freq. nonlinear effects 80−84490
TGS crystal, generation of second acoustic harmonics 78−18711
thermal generation of acoustic pulses by laser radiation, temp. nonlinearity 79−99271
thermal self-action of sound waves 77−3692
third and fourth order elastic consts. *(French)* 80−34116

nonlinear acoustics continued
transient parametric acoustic sources 80−10060
transonic flow, excitation on nonlinear plane waves by volume sources 80−38154
transonic gas flow, optical excitation of intense acoustic waves 80−74564
turbulent jet, sound radiation due to nonlinear interaction of instability waves 79−50720
turbulent media, scatt. and interaction of sound with sound *(Russian)* 79−18571
turbulent shear layer, sound and aircraft noise, spectral broadening 79−37076
turbulent shear layer, sound transmission 79−37075
two-phase medium, sound wave absorpt. and dispersion 78−94466
ultrasensitive US system for NDT, medical diagnosis and nonlinear US 78−59224
ultrasonic transducers, study of nonlinear parametric radiation using Fourier anal. *(French)* 79−41485
underwater absorption of sound by sound 78−59180
underwater explosion generation of sound pulse, nonlinear region 80−56493
underwater explosive shock waves, weak shock soln. 78−26003
underwater noise, determ. of spatial coherence using model *(French)* 79−41487
underwater parametric acoustic source beamwidth control 78−75011
underwater sound propagation in presence of randomly perturbed parabolic profile 78−94477
US absorption in liquid with gas bubbles, acoustic streaming appl. 80−5863
US and hypersonic waves, theory of self-action 78−75010
US beams in single crystals, diffr. and propag. 78−94468
US fields in air, numerical representation, microphone signal example *(French)* 80−53521
US imaging using arrays 79−64460
US nonlinearity parameter for solids, relationship with Gruneisen parameter 80−74561
US SAW, nonlinear interaction in 2-6 MHz range *(French)* 80−33296
US transmission in nonlinear layer in linear medium 79−47867
US wave in cavitating liquids, optical visualisation 80−106651
vapour-gas bubbles, heat transfer and phase transition effects 80−6133
variable area duct, effect of flow on quasi-on-dimensional wave propag. 77−84037
vibrationally relaxing gas, wavefronts of nonlinear waves 78−83431
viscous gas, in cylindrical channel of finite length, nonlinear acoustic effects 79−18958
viscous medium, sound field near boundery of confined beam, charcts. 78−18092
volume and surface wave interactions, functional signal transformations *(Russian)* 77−3703
vortex sound generators 78−50975
wall absorption coeff *(French)* 77−54823
water saturated marine sediments, finite amplitude wave propag. 78−1476
water-ethanol(methanol) mixtures, nonlinear acoustic coeff. meas., 0-50°C *(French)* 80−34142
wave propagation, fundamental principles *(French)* 77−42647
wave propagation as guided modes, parabolic approx. 80−43506
wave propagation on turbulent jets using organ pipe flue 80−91946
wave-front method for determining the dynamic properties of high damping materials 77−23895
waveguides with moving medium, energy transport 77−46837
weak acoustic signal enhancement using parametric mode interaction 79−94391
weak interaction of two beams in absorbing fluid, parametric emission, Fourier anal. *(French)* 79−94388
weak-shock transmission coefficient via harmonic generation 77−68294
weakly dispersive media, nonlinear sound interaction 77−807
weakly forced third order wekaly non-linear system 78−30119
weakly nonlinear dispersive wave propag. comments and reply 78−83156
wide band array synthesis 78−38120
Zabolotskaya-Kokhlov eqn. use of symmetries to find exact soln. 77−805
Al alloys, fatigue, microcrack development, acoustic SHG study 80−35440
Al cylindrical rod, stress wave propag. from electrical discharge 78−59866
$Bi_{12}GeO_{20}$, finite amplitude SAW distorted rippling profiles, optical probing obs. 80−34287
CdS, acoustic phonon intensity fluctuations after strong nonlinear amplification 78−59909
CdS, amplification of high intensity ultrasound *(Russian)* 77−28222
CdS film, on $LiNbO_3$, acoustic harmonic generation 77−89812
CdS, high intensity sound self-defocusing obs. 80−24972
CdS, self-defocussing of large intensity sounds obs. *(Russian)* 78−26916
Cds, nonlinear electronic absorption of sound 79−15196
Cu, nonlinear acoustics, third-order elastic const. meas. 80−33292
$CuCl_2$, aqueous soln., nonlinear conversion of acoustic pulses with thermooptic excitation 80−14510
$Cu_{2-x}O$, nonlinear elastic props., nonstoichiometry effects *(French)* 80−34133
Fe_2O_3, haematite, doubling freq. of sound and acoustic detection *(Russian)* 78−43623
Ge, nonlinear acoustics, third-order elastic const. meas. 80−33292
^3He-^4He, superfluid solns., nonlinear sound interaction 80−34267
KH_2PO_4 electro-optic modulator crysts., piezoelec. induced acoustic transients 80−70316
$LiNbO_3$, and $LiTaO_3$, finite amplitude SAW distorted rippling profiles, optical probing obs. 80−34287
$LiNbO_3$, fundamental and second harmonic SAW's, phase and amplitude relations 77−69157
$LiNbO_3$, opposed interaction of elastic waves 77−24360
$LiNbO_3$, parametric mixing of SAW in 20 to 100 MHz range 79−86279
$LiNbO_3$, parametric phonon echo obs. 80−59588
$LiNbO_3$, piezoelectric plate resonator, acoustic correl. 79−76929
$LiNbO_3$-p-Si, frequency doubling of the two-pulse and three-pulse echoes in surface acoustic waves 79−69335
Nb third-order elastic consts. using nonlinearity parameter 78−75733
Sb_2S_3 crystals, dielec. and acoustic nonlinarity 78−15107
SbSI, nonlinear sound propagation in case of polarisation switching 79−27458

nonlinear acoustics continued
SiO_2, finite amplitude SAW distorted rippling profiles, optical probing obs. 80−34287
SiO_2, fundamental and second harmonic SAW's, phase and amplitude relations 77−69157
SiO_2, vitreous, Suprasil-I, spectral diffusion at 0.5K, acoustic hole burning expts. 79−60439
TeO_2 crystal, parametric excitation in an acoustic interferometer 79−64381
TeO_2 paratellurite crystals, parametric excitation of sound, calc. 80−24537
Ti, acoustic harmonic generation by long-range dislocation motion 79−42150
$TlCdF_3$, third and fourth order elastic consts., press. depend. near phase transition *(French)* 80−34116
Xe, liq., nonlinearity and related parameters *(German)* 79−77685
$(YGd)(GaFe)_5O_{12}$ epitaxial film, nonlinear magnetoelastic effects *(French)* 80−34745
ZnO, acoustic phonon intensity fluctuations after strong nonlinear amplification 78−59909
ZnO thin-film transducer, bulk wave generation due to nonlinear interaction of SAW 79−42359

nonlinear control systems
see also control nonlinearities
active adaptive vibr. suppressing system, stabilisation of cylindrical panel motion *(Russian)* 77−68498
arm prosthesis, hydraulically actuated, performance criterion 77−48951
articulation development, possible nonlinear time varying control in feedback path 78−35870
dynamic, limit cycles, Hamiltonian systems and Lie's theory connections 77−78957
nuclear power reactor, model control 77−14252
proportionate Coulomb and viscously damped isolation system 78−42561
reactor nonlinear control system, relative stability anal. 77−3116
sounding rocket attitude stabilisation H_2O_2 jet system *(Japanese)* 78−28482
sounding rocket three-axis attitude control system *(Japanese)* 78−24422

nonlinear differential equations
$\epsilon XY(dY/dX)=X-Y(Y+1)$, exact perturbation soln., stellar struct. theory 78−32439
Alfven waves, circularly polarised, spiky soliton soln. to nonlinear evolution eqn. 80−38590
anthropomorphic mechanism compensating synergy *(Slovenian)* 77−64920
artificial compression method for shocks and contact discontinuities 78−70298
asymptotic analysis of nonlinear systems by method of averaging 77−82382
asymptotic solution of a nonlinear singular perturbation problem 79−12576
auto-immunity, math. model of cell dynamics 77−16900
autonomous dynamic systems, limit cycles and one parameter transformation groups 78−49641
axisymmetric gravitational fields, nonlinear differential eqn. giving exact eigenfunction solns. 78−77779
Backlund transformations and solns. for nonlinear field eqns. in 4-dimens. spacetime 80−338
Backlund transformations as canonical transformations 78−81855
Backlund transformations as nonlinear Dirac eqns. or Cauchy Riemann eqns. 78−49965
beam, buckled, eqns. for nonplanar, nonlinear motions 78−83316
beam, rotating, nonlinear flap-lag-axial eqns. derivation 77−84134
beams, frames, arches, axisymmetric shells, finite element anal., Newton Raphson method, nonlinear equilib. eqns. 78−22282
beams, nonlinear bending, finite element anal. 78−26068
Benjamin-Ono eqn., props. 79−63050
Benjamin-Ono equation, internal wave solitons, linear stability 80−53802
Benjamin-Ono equation, meromorphic solns. 79−62998
Benjamin-Ono equation, meromorphic solutions 80−31980
bifurcation and nonequilibrium phase transitions of limit cycles and multiperiodic flows in continuous media 78−81937
bifurcation into invariant tori at points of reson., use of Poincare maps 79−44707
bifurcation problems, left branching soln., appl. to nonlinear buckling 77−67222
bifurcations, singular perturbations 78−16626
biochemical pathway enzymes kinetics simulation appl. *(German)* 77−5102
biological systems, nonlinear diffusion 79−74589
Blasius eqn., generalised, boundary value problem 79−35567
blast waves, spherical, time-depend. energy deposition 78−9655
Boltzmann equation, nonlinear, for internal state and Maxwell models 80−77733
Boltzmann equation, nonlinear, solns. of Krook-Tjon-Wu model, Laguerre expansion of distrib. function 80−68157
Boltzmann equation, nonlinear, with soft potential, spatially periodic problems 80−77731
Boltzmann equations for internal state and Maxwell models, similarity solutions 80−86231
Bose gas, impenetrable, one particle reduced density matrix, Painleve-type eqn. 80−62576
Bossinesq equation, similarity solutions and Backlund transformation 80−68056
bound state energy levels, quantum mechanical formalism, convergent perturbation theory *(Russian)* 80−4573
boundary layer flow singular nonlinear differential eqns. 78−63413
boundary value problems, second order, iterative method 78−32660
boundary-value problem, incremental var. formulation, rel. to elasticity *(German)* 77−33866
Boussinesq equation, group theoretical approach 80−82914
bubbles motion dynamics in oscillating fluids 80−38483
buckling, tall vertical column, optical load, optimal shape, nonlinear differential-integral equation 80−53663
Burgers, finite difference solution, computational accuracy 79−3997
Burgers' equation for nonlinear shallow water waves, Galerkin method soln., expansion of B-splines 78−87352
Burgers eqn., equivalence transformations 77−74196
cantilever columns, spring hinged, post-buckling anal. 79−46235
cantilever minimum weight design with plural torsional frequency constraints 79−68629

nonlinear differential equations continued
capillary-porous body, nonlinear heat/mass transfer problem, soln. using invariant groups 78−55688
catalyst deactivation, nonlinear partial differential eqns. 79−39123
catastrophe theory, bifurcation properties of solutions of nonlindear operator equations 80−8789
Cauchy problem, existence and uniqueness of smooth global soln. *(French)* 78−93513
Cauchy problem, general case, class of nonlinear Schrodinger equations 79−84994
cerebral blood flow control in hypercapnia, model 79−100641
chaos in simple nonlinear differential eqns. 77−13584
circular plates subjected to transient loads, nonlinear dynamic response 78−16648
classical gravitational collapse problem, solns. 78−93099
classical nonconservative systems, appl. of time depend. canonical transforms 80−17792
cochlear hydrodynamics model, digital simulation 78−31821
completely integrable operator evolutionary eqns., Schrodinger Korteweg-de Vries, KdV eqns. 79−97248
completely integrable systems for Schrodinger and KdV equations *(French)* 79−25879
complex potential eqns., all solns. to nonlinear system 80−46795
complex variables method for soln. of large nonlinear differential eqns. systems 78−62062
composite layered slab, solute diffusion, conc. depend., with/without chem. reactions 80−54427
compressible plane subsonic flow, integration *(German)* 77−11218
concentric shock waves in inhomogeneous medium, self-similarity exponent 78−75168
conference, nonlinear problems in theoretical physics, Jaca, Gain 1978 80−4478
conference on solitons and condensed matter physics, Oxford, England (June 1978) 79−75364
conference proceedings, nonlinear dynamics, tribute to Sir Edward Bullard 78−93603
constants of motion of nonlinear equations in an extended Poisson formalism 79−49061
continuous system, sufficient condition for stability in first approximation 77−50883
continuum Heisenberg spin system, stationary spherically and axially symm. spin waves 80−34615
convection along plate, MHD boundary layer eqns. soln. 77−11276
convection flow, free, between heated vertical parallel plates, quasi-linearization 80−92148
counterflow processes, nonlinear modelling using weighted residual methods 80−69754
coupled bilinear eqns., exact one- and two-periodic wave soln. 80−68050
coupled nonlinear evolution eqns., infinite sequence of conservation laws 77−57156
curvilinearly aeolotropic thin rubber tubes, forced oscillations soln. 78−9589
cylindrical KdV equations, soln. asymptotic behaviour (in t), Cauchy problem 80−98803
damped, forced, continuation and boundedness of solutions 77−9855
deep water gravity waves, two-dimens. nonlinear wave eqn., exact envelope soliton solns. 80−43725
deflagration waves, heterogeneous, flame model for gas phase, nonlinear differential eqn. 80−81326
delay inequalities, n^{th} order, nonlinear oscillations 78−89300
diatomic lattice, solitary wave solns., ϕ^4 kink, struct. phase transition, phonon dispersion curves 79−80544
difference analogues to nonlinear partial differential eqns., reducible to linear eqns. 79−25831
difference eqns. with N-depend. coeff. 79−71274
difference eqns. with N-depend. coeff. 79−71275
diffusion, approach of solns. to travelling front solns. 78−24743
diffusion, asymptotic behaviour of solns. 78−24744
diffusion, finite element method appl. *(French)* 77−78965
diffusion eqn., evolution of stable profile 79−17363
diffusion equation, general class of similar solns., laser interactions, thermal cond. 77−37827
diffusion equation, nonlinear, invariance props., Lie-Backlund groups 80−62596
diffusion equation, similarity solutions 80−27239
diffusion equation, stable profile evolution 80−82731
diffusion problem, dual extremum principles 77−67218
diffusion process, nonlinear, path integral evaluation by Fourier series 78−70075
diffusion reaction nonlinear eqns., secondary bifurcation 77−9860
Dirac eqn. in four dimens., asymptotic solns. 77−6016
dispersive equation, weak solns. 77−74194
dispersive nonlinear wave eqn., soliton like solns. 78−93538
dispersive nonlinear waves, conservation laws group theoretic aspects 77−30016
dispersive systems, 2-D lumps 79−92955
dispersive wave eqns., modulational instability and envelope solns. 78−54199
dispersive waves, nonlinear model eqn., parametric growth rate 79−12615
double sine-Gordon equation, perturbation theory 79−75403
Duffing's equation, steady and chaotic motions 80−77616
Duffing's equation, strange attractors, explosion, chaotic behaviour 80−77617
Duffing eqn., large nonlinearity, subharmonic solns. 79−65
Duffing oscillator, statistical linearisation approx. method for nonlinear stochastic processes 77−17790
dynamic nonlinear systems containing limit cycles 78−77666
E×B effects on nonlinear mode-converted lower-hybrid waves 80−1785
education, soliton solns. to nonlinear wave eqns. 80−17737
Einstein-Maxwell equations, coupled, general soln., Ernst-Maxwell eqn. depend. on arbitrary harmonic function 77−74
elastic porous media, transient compressible liq. flow, linearisation of nonlinear partial differential eqn. 78−63490
elastic stability of Beck's column, harmonic nonlinear response to lateral excitation 79−10517
elastic-plastic torsion, nonlinear boundary value problem 77−89043
elastoplastic thin vertical columns, postbuckled, deflections 80−87728
electrochemical machining, approx. method for solving problems 78−44241
electron beam focusing theory *(Chinese)* 79−31783

nonlinear differential equations continued
electron optics aberrations, algorithm computation using Chebyshev polynomials 79−27156
electron plasma waves, nonlinear evolution equation including collision effects 79−82056
electron propagator, Dyson-Schwinger eqn. solns. 78−24984
elliptic, constructive methods based on analytic characterisations 79−71225
elliptic operators, Cauchy problem uniqueness *(French)* 77−17773
elliptic partial differential equations, nonlinear, approx. soln. by mesh refinement and local inversion 77−26160
elliptic problems involving a free boundary 80−24130
elliptic sine-cosine eqn., solitonlike solns. using harmonic functions 78−57741
elliptic type equations, num. soln. of mixed boundary-value problem *(Russian)* 77−67243
elliptic-hyperbolic sine eqn. in 2+1 dimens. space-time 77−49567
Emden-Fowler eqns., nonlinear boundary and eigenvalue problems by group methods 79−71224
envelope solitons and holes for sine-Gordon, nonlinear Klein-Gordon eqns. 77−2553
Ermakov systems generalized, nonlinear superposition law 80−86074
estimation of parameters for a beam on an elastic foundation with large deflections and built in at both ends 79−27520
evaluation equations, nonlinear, canonical transforms. 77−87643
evolution eqn., Cauchy problem 79−75353
evolution eqn., family of H-theorems 80−31685
evolution eqns., conservation laws, group theoretical derivation 80−57520
evolution eqns., conserved densities 79−71256
evolution eqns., equivalence transformations 77−74196
evolution eqns., multi-soliton solns. 79−58556
evolution eqns., prolongation structs. 78−24637
evolution eqns., prolongation structs. in two-dimens. 77−36
evolution eqns. generated from Boussinesq eqn. Backlund transform. 77−53748
evolution equation class solvable by spectral transform technique 79−75370
evolution equation soln., spectral transform method, cylindrical KdV eqn. 79−2657
evolution equation soln. by spectral transform, conservation laws, cylindrical KdV eqn. 79−2658
evolution equation with linearly x-depend. coeffs., spectral transform, single soliton soln. 78−57746
evolution equations, completely integrable, natural generalisation *(French)* 80−27152
evolution equations, connection to P-type differential eqns. 80−57078
evolution equations, integrable, inverse scatt. method 80−12913
evolution equations, inverse scattering method 80−12919
evolution equations, nonlinear, connection with Painleve type ordinary differential eqns., inverse scatt. transform 80−62486
evolution equations, nonlinear, inverse spectral transform, generalisation of Klein-Gordon problem 80−68055
evolution equations, reverse scattering method, Hamilton's structure and Beklund's transformations *(Russian)* 80−86090
evolution equations, symplectic operators and hereditary symmetries 80−82650
evolution equations and conservation laws, spectral transform method 80−62488
evolution equations in fluid dynamics, soln. by second order backward difference method 79−92950
evolution equations soln. using spectral transform method 78−57745
excitable fibre, steady speeds of spread of stable and unstable impulses, depend. on membrane ionic currents 78−53382
extension of nonlinear evolution equations of the K-dV (mK-dV) type to higher orders 80−105508
factorization theorems, stability and repeated bifurcation 78−65751
fast local convergence using single and multistep methods 77−53733
Fermi-Pasta-Ulam lattice, continuum approx. using Korteweg-de Vries eqn. 79−71375
fermion system of self-interacting particles, field patterns 78−16909
film boiling destabilisation in liq.-liq. systems 78−94588
filtering, nonlinear, conditional laws, smoothness, stochastic calculus of variations *(French)* 80−68128
fingero-imbibition phenomena with varying phase density, two parameter singular perturb. soln. 79−29789
finite element anal. of nonlinear partial differential eqns., appl. to estuarine flow *(Japanese)* 78−8233
fins, nonlinear problems, 1-D conduction, initial value problem 80−83726
flagella bend propagation, derivation of eqns. of motion and simulation 78−77074
flow between coaxial discs, multiple solutions 77−55002
flow between porous walls of different permeability, quasilinearisation soln. 79−55415
flow between rotating discs, finite element anal. using exponentially weighted basis functions 78−16655
flow-induced oscillations, bifurcation to divergence and flutter, infinite dimensional anal. 78−89336
fluctuations, random, moment behaviour of soln. processes for nonlinear stochastic differential eqns. *(Japanese)* 80−95039
fluid and isotropic solid acoustic harmonic generation 77−27417
fluid dynamics, small-disturbance transonic flow, nonlinear mixed elliptic hyperbolic eqn., finite element anal. 80−83814
fluids of finite depth, exact one- and two-periodic wave solns. 80−53797
fluids of finite depth, N-soliton soln. of higher order wave eqn. 80−48724
flutter eqn., continuation and direct soln. 78−34047
Fokker Planck eqn., non-linear, with nonconstant diffusion, non-Gaussian time dependent 80−31686
forced van der Pol oscillator, frequency entrainment 78−57794
forced van der Pol oscillator, variational eqn. bifurcations 78−77681
forced vibrs. of nonlinear systems, Duffing eqn. 77−33842
formal series solutions, rational solns., soliton eqns. 78−57747
free boundary eigenvalue problem in plasma confinement *(French)* 77−67200
friction, stochastic quantisation, nonlinear Schrodinger equation 80−27164
friction, stochastic quantisation, nonlinear wave eqn. 80−98825
functional differential equation, compactness of bounded trajectories of dynamical systems 80−82636
gas flow in catalytic convertor, numerical soln. 78−67281

nonlinear differential equations continued
gas flows in inclined mag. field, simple stationary waves *(Russian)* 77−27603
gas nonisothermal stationary motion in pipe anal., solution by iterative method 77−89086
gauge generators, Cawley's counter example to Dirac conjecture 80−13225
general nonlinear differential difference eqns., solvable by inverse method, complete integrability 79−62999
generalised Feller eqn., initial condition solns. 79−12579
generalized symmetries of nonlinear partial differential equations, Lie derivatives 80−4886
geomagnetism, tipping over of terrestrial mag. field *(Hungarian)* 79−16368
glass cylinder refractive index variation by field-assisted ion exchange 80−14500
global aspects of bifurcation and stability 78−69964
gradually varying channel, solitary wave evolution, KdV eqn. soln. 80−24040
gravitating disc, rotating, nonlinear stability theory 80−17488
gyroscopic systems, appl. of theory of singularly perturbed eqns. 77−57183
Hamiltonian formalism for higher order eqns. 77−74278
Hartree equations, time-dependent, global solutions, and nonlinear Schrodinger eqn. 80−73193
heat and electrical transfer differential eqns. 78−67004
heat and mass transfer, finite element soln., for chemically reacting system 80−68153
heat cond., cylindrical inverse transient, numerical soln. 77−6501
heat cond. eqn. soln. *(Russian)* 79−32187
heat cond. eqn. soln. *(Russian)* 79−37125
heat conduction, combination of Lagrange and Euler methods 79−76941
heat conduction, nonsteady, various boundary conditions 79−37116
heat conduction, quasilinear equations, approx. Galerkin method 80−33416
heat conduction eqn., nonlinear boundary control problems, maximum principle *(German)* 78−9528
heat conduction eqns., analytic solns. 78−63264
heat conduction in solids, nonlinear, direct and inverse problems, approx. soln. method 78−94510
heat conduction problems, soln. construction procedure, Kantorovich method 78−59264
heat eqn. soln. by Picar's method *(Russian)* 78−51041
heat exchanger true vibrations numerical soln. 78−75094
heat transfer, nonlinear, iterative-variational method 78−94511
heat transfer and evaporation from cooled surfaces, nonlinear eqns. numerical soln. *(German)* 80−58893
heat-pulse experiments, nonlinear effects, theory 80−96182
Heisenberg chain, classical, solitons and magnons 80−60161
Heisenberg spin chain, operator equation, nonlinear differential form, auxiliary constraint 80−65762
helical electron beam in resonator of gyro device with uniform EM field, nonlinear eqns. soln. 79−81348
higher order Korteweg de Vries eqn., Backlund transform 80−105510
higher order modified KdV eqns., bilinearisation 80−105509
Hilbert spaces, stability of solns. *(Russian)* 77−22377
hydrodynamic numerical modelling of tidal basins, Lagoon of Venice appl. 79−34832
hyperbolic, governing nonlinear vibr. systems in resonance 77−39242
hyperbolic balance laws in continuum physics 80−4525
hyperbolic conservation laws; initial and initial-boundary value problems, large-time behaviour 77−74233
hyperbolic eqn., special classes of solns. *(German)* 79−21526
hyperbolic system soln. decay, conservation laws with convex extension 77−49599
hyperbolic wave eqn., approx. periodic solns. 77−17778
hyperbolic waves, Poincare-Lighthill-Kuo method secular term elimination 78−41166
hypergeometric functions, partial differential matrix eqns. 77−37730
inhomogeneous overdense plasma, nonlinear penetration of strong EM waves 78−75355
integrability of general nonlinear differential-difference equations by inverse scattering method 79−12575
integrable nonlinear evolution eqns. with saturation effects, inverse scatt. 79−92995
integrable nonlinear evolution equation, soliton soln. from inverse scatt. method 80−73186
integral solutions, linearised non-linear evolution eqns. 78−93512
integro-differential mixed systems with polyvibrating operators, possible soln. determ. *(French)* 77−37726
invariant group of KdV, MKdV or Burgers eqn., commutative Lie algebra 80−365
inverse method for solving differential-difference and difference-difference eqns. 80−105513
inverse scatt., generalised problem prolongation structs., soliton solns. 77−3833
inverse scatt. method for general evolution eqn. 77−87629
inverse scattering formalism, self induced transparency, physical interpretation 79−85005
inverse scattering method, massive Dirac system soln. using connection with matrix Schrodinger eqn. 79−2655
inverse scattering transform eqns., survey of developments 78−57795
inverse scattering transform solvable nonlinear evolution eqns., existence, Lax's method extension 78−32711
inverse spectral transform solns. of nonlinear evolution eqns. 77−57228
inversion equation method generalised to matrix NLPDE 78−8223
Jaulent-Miodek family of nonlinear evolution eqns., Hamiltonian formulation 80−31511
Josephson junction, in inhomogeneous field *(Russian)* 78−84350
Josephson junction, solns. of nonlinear eqn. of resistively shunted model 78−2628
Kadomstev-Petviashvile eqn., reduction to Painleve transcendents 79−92954
Kadomtsev-Pyatviashvili eqn., asymptotic behaviour of solns. (two-dimensional Korteweg-de Vries eqn.) 80−52036
KdV, recurrence of initial state, numerical soln. using Fourier expansion 79−92924
KdV eqn. with damping, rational solns., appl. to plasma physics 79−27743
KdV equation, perturbative expansion and initial value problem 80−62487
nonlinear differential equations continued
KdV equation for collisionless multi-ion plasmas 79−77351
KdV equations, general similarity soln. in terms of second Painleve transcendents 79−63051
kidney model, numerical soln. by multiple shooting 80−104609
Klein Gordon, nonlinear generalisations, exact solns. 79−35569
Klein Gordon eqns., localised nondissipative stationary solns., quantum droplets 78−12819
Klein-Gordan equations with logarithmic nonlinearities, classical theory 79−5996
Klein-Gordon eqn., nonlinear interactions of counter-travelling waves 80−77627
Klein-Gordon eqns., non-dissipative character, confinement principle 78−62361
Klein-Gordon equation, inverse spectral transform 80−68055
Klein-Gordon equation, stringlike solns. 78−82114
Klein-Gordon nonlinear eqn., generalised susceptibility of solitary wave 79−75357
Klein-Gordon nonlinear eqn., solitary wave exist. in higher dimens. 77−74232
Klein-Gordon nonlinear equation, numerical soln. 78−89352
Kolmogorov direct equation, solution, Galerkin measures *(Russian)* 80−46981
Korteweg de Vries eqn., second modified, exact multi-soliton soln. 80−73180
Korteweg de Vries eqn. equivalence transformations 77−74196
Korteweg de Vries equation, Pade approximants, soliton solns. 80−42071
Korteweg de Vries equation, second order non-linear dispersive wave eqn. as alternative 78−57791
Korteweg de Vries equations, higher order, soliton solns., inverse scatt. problems 77−45741
Korteweg de Vries integrals and Poisson's theorem 79−69
Korteweg-de Vries, and conservative evolution eqns., generalization of potential operators and variational principles 79−75352
Korteweg-de Vries, complex modified eqn., dispersion, self-propagation in anisotropic medium 79−75371
Korteweg-de Vries, cylindrical eqn., soln. asymptotic behaviour 80−31526
Korteweg-de Vries, generalised Hamiltonian dynamics, appl. to nonlinear field theory 79−75678
Korteweg-de Vries eqn., bilinearization of nonlinear evolution equations 80−90654
Korteweg-de Vries eqn., exact soln. 77−26138
Korteweg-de Vries eqn., explicit solns. without scattering data 79−67167
Korteweg-de Vries eqn., generalised, conserved quantities 80−68054
Korteweg-de Vries eqn., higher order, prolongation struct., Lie algebra, soliton solns. 78−8249
Korteweg-de Vries eqn., Lie-Backlund transformation group study 80−9114
Korteweg-de Vries eqn., rational solns., spectral representation 78−69991
Korteweg-de Vries eqn., slowly varying solitary wave solns. 80−72
Korteweg-de Vries eqn. and 2nd Painleve transcendent, boundary value problem in plasma theory 80−69971
Korteweg-de Vries eqn. solns , existence and regularity 79−71265
Korteweg-de Vries eqn. with coord. stretchings, soliton plasma waves 77−58859
Korteweg-de Vries eqns., perturbed solns. and soliton production 80−42074
Korteweg-de Vries equation, algebraic soliton 77−9858
Korteweg-de Vries equation, discrete version with x-dependent coefficients 79−17239
Korteweg-de Vries equation, numerical methods of solution, difference and transform schemes, accuracy 80−46833
Korteweg-de Vries equation, perturbation theory 77−33852
Korteweg-de Vries equation, solns. for slowly decreasing boundary conditions 80−36872
Korteweg-de Vries equation, statistical theory of nonlinear, dispersive system with small dissipation 78−70058
Korteweg-de Vries equation, two-dimens. distrib. soliton soln., asymptotic anal. 79−49376
Korteweg-de Vries equation and nonlinear waves 79−92956
Korteweg-de Vries equation solns. 79−84964
Korteweg-de Vries equations, N-soliton soln., functional integral representation 80−4542
Korteweg-de Vries generalised eqn., pseudopotentials and inverse scatt. problems 77−87627
Korteweg-de Vries solitary waves for cylindrical and spherical symmetric ion acoustic waves 79−77371
Korteweg-de Vries soliton solutions, perturbations 80−105511
Korteweg-de Vries type eqns., group-theoretical interp. 80−77624
Korteweg-de Vries-Burgers eqn., invariant solns. 79−63052
Korteweg-de Vries-Burgers equation, time evolution, stability, of shock soln. 77−37743
Korteweg-de-Vries eqn., exact soln. via a generalisation spectral transform 78−65786
Kortweg-de Vries equation, perturbations conserving solitons 78−49642
laminar boundary layer, solution of the Falkner-Skan equation by quasi-linearization 79−1156
laminar flows of viscoelastic fluids in concentric annuli with axially moving boundaries 78−79295
Langmuir multidimensional nonlinear waves 78−63555
Langmuir waves, modulated, nonlinear Landau damping effect 78−81849
Laplace operator on spherical domain, fundamental eigenvalue numerical determ. 77−87628
laser, free electron type, nonlinear theory, efficiency enhancement 80−43317
Lienard type, exactly solvable 78−57740
light ray tracing through deformed glass rods with radially graded RI 79−64338
limit cycles and conservative Hamiltonian systems 77−78957
limit cycles and multiperiodic flow bifurcation and nonequilibrium phase transitions 78−24759
linear correspondents of nonlinear eqns. 78−20949
liquid-liquid extraction column online control by modal control techniques 78−54865
liquid-solid phase transition, dynamic Ginzburg-Landau theory 80−44292
local fluctuations in chemical reactions, nonlinear master eqn., dimensionality expansions, augmented mean field theory 78−73019
Lorenz system, 14-D generalization, appl. to atm. convection 78−75131

nonlinear differential equations continued
Love waves, hypoelastic stratified solid with material boundary 78−30225
magnetic domain boundary, interacting with localised defects, unidimensional flow of configs. *(Russian)* 80−65954
magnetic gap, soliton bound states in Ising model, quantum double sine Gordon eqn. solns. 79−78288
magnetic quark confinement, flux tube in gauge field model 77−6084
magnetoionic plasma, hyperbolic eqn. system, inverse problem 78−75354
Magnus method appl. to nonlinear eqns. near stability boundaries *(Russian)* 78−87331
massive Dirac system, nonlinear evolution eqns., inverse scatt. method soln. 79−2654
Mathieu equation with damping, variational anal. 80−57079
mathieu stability analysis of non-linear third-order weakly forced systems 79−30261
matrix Riccati eqn., quasi-linearisation, iterative approx. 78−57871
matrix Riccati equation, numerical soln. method *(Russian)* 79−25822
mechanical equations with slowly varying coefficients, approx. integration *(Italian)* 77−5627
mechanical system, periodic vibr. 80−33513
mechanical systems with time optimal condition 80−31492
membrane dynamic equation solving, practical algorithm 78−77038
meromorphic solutions of nonlinear partial differential equations and many-particle completely integrable systems 80−31523
MHD convective viscous flow past porous plate with suction, mass transfer effects 78−87398
MHD flow over infinite rotating disc with suction, existence of soln. 78−30366
Michaelis Menten mechanism, modified, global asymptotic stability of soln. 79−79456
Mielnik's generalised quantum mechanics, nonlinear model, simplex for mixed states set 78−57852
Miura's transform. of modified Korteweg deVries eqn. 79−75356
modified dissipativity for a non-linear evolution equation arising in turbulence 79−94594
modified Korteweg-de Vries eqn., N-soliton solns. 80−36876
modified Korteweg-de Vries solitary wave in a slowly varying medium 80−36873
modulated electron beam in inhomogeneous isotropic plasma, nonlinear wave generation 78−1852
molecules, linear, forced rot. diffusion, nonlinear aspects 79−90503
moment equation methods for nonlinear stochastic systems 79−21666
monodromy- and spectrum-preserving deformations. I, soln. of nonlinear differential eqns. 80−98802
multi-soliton soln. construction, direct method for sine-Gordon and Zakharov-Shabat eqns. 79−75360
multi-soliton solutions of a derivative nonlinear Schrodinger equation 80−105528
multibody system equations of motion, computer-aided formulation *(German)* 78−39
multidimensional partial, integration by inverse scatt. problem method 77−60905
multiphase wave interactions, instabilities and solitary envelope soln. 77−9888
muscle, striated, analytical soln. to isometric mechanogram of Hill's model 78−73168
N-soliton solns. of nonlinear evolution eqns., Wronskian representation 79−25867
Nernst-Planck analog equations and stationary state membrane electric potentials 79−92196
nerve, temporal stability of solitary impulse solns. of nerve eqn. 78−35830
nerve conduction eqn. periodic travelling wave solns. stability 79−16194
nerve fields, topographic organisation 80−89742
non-Newtonian pulsatile laminar pipe flows, multiviscous approx. 77−3871
nonautonomous eqns., periodic solns. 78−55583
nonlinear differential-difference and difference-difference eqn. generation, exactly soluble 77−49564
nonlinear elastic stability problems using a finite difference perturbation method 78−83273
nonlinear estuarine response to tidal action for potential hydroelectric power generation 77−70692
nonlinear evolution eqns. in one space dimens., inverse scatt. soln. 79−97222
nonlinear excitations by numerical determination 79−71372
nonlinear field eqn. and differential Schrodinger eqn. correction *(French)* 80−77637
nonlinear hydrodynamical eqn. of Kaup, periodic and N-soliton solns. *(French)* 80−31521
nonlinear Klein-Gordon equation, solitary wave collisions 79−80761
nonlinear mechanical system with time optimal condition, synthesis 78−54176
nonlinear mechanical systems, constraint simulation 80−62461
nonlinear network noise anal., algorithm *(German)* 77−88997
nonlinear Schrodinger equation, spectral transform soln., charact. behaviour of solitons 78−70005
nonlinear Schrodinger equation solns., recurrent motion in continuum dynamical systems 80−22235
nonlinear string dynamics, rigid body motions, space curves, prolongation structures, fiber bundles, and solitons 79−97213
nonlinear third order systems, pulse response 78−83313
nonrelativistic limits for Klein-Gordon and Dirac eqn. 80−330
nuclear reactor dynamics, numerical integration using real integrating factors 80−68730
nuclear reactor kinetics, quasistatic solutions, nonlinear system, iterative procedure 80−52711
nuclear reactor optimal shutdown control, quasilinearisation and numerical soln. *(Korean)* 79−89395
olfactory bulb model, spatial and temporal charact. freqs. of interactive neural masses 77−25476
open dynamic subsystem, nonlinear eqn. with fluctuating parameters derivation 80−94991
oscillating control system theory 77−25360
oscillation equation, single particle analogue of field equations of chiral Lagrangian theories of pion interactions, soln. 80−62470
oscillations in nearly conservative systems *(Russian)* 78−62069
oscillations of round plate, difference eqn. approx., Lyapunov methods *(Russian)* 77−39259
oscillator, nonlinear, stochastic instability 79−67150
nonlinear differential equations continued
oscillator eqn., Poincare-Lindstedt solns. 78−30
oscillators, coupled, with slow, nonexplicitly time-depend. evolution 80−52009
oscillators, necessary-sufficient condition for synchronisation 77−39
oscillators, nonlinear stochastic, triangular wave, optimally controlled, Weiner process and Poisson process, numerical studies 80−52128
oscillatory systems, u-procedure applic. for asymptotic soln. *(Ukrainian)* 77−49561
oscillatory systems with delay, stability props. of differential eqn. solns. *(Russian)* 77−41475
otolith membrane, finite element model, computer soln. of differential eqns. 77−40636
Painleve nonlinear ordinary differential eqns. and nonlinear partial differential eqns., corrections 79−5966
Painleve transcendents, linearisation 77−49568
parabolic, constructive methods based on analytic characterisations 79−71225
parabolic, optimal control processes *(German)* 77−22416
parabolic differential eqns., max. principles 77−29996
parabolic eqn. in noncylindrical domain, existence of weak solns. 77−67208
parabolic eqns., control to meet finitely many terminal conditions 77−5647
parabolic Feller diffusion eqn., Maxwell and Wien processes 77−26251
parabolic nonlinear partial differential equation, numerical soln. using asymm. finite difference eqns. 77−33845
parametric excitation of combined resonant systems 77−2539
partial. differential eqn. soln. by discrete least squares 78−45474
partial, elastic stability theory *(Russian)* 79−9128
partial, Galerkin method error analysis 77−78986
partial, interactions between short and long waves 77−67299
partial, Runge-Kutta method appl. to fluid flow problem 77−42796
partial, special multi-soliton solns. 80−105763
partial appls. 80−4510
partial differential eqns., partial spectral expansions 79−32193
partial differential equations, time depend., Method of Lines compared to finite difference scheme 78−79291
partial differential equations soln., using inversionlike integral eqns. generalisation 78−86117
partial nonlinear evolution eqns., solitons on moving space curves 77−74254
particle diffusion across mag. fields, stable profile for nonlinear diffusion eqns. 78−22456
pendulum motion, computer simulation, undergraduate teaching aid *(German)* 77−67166
periodic solutions of semilinear elliptic equations in a strip 79−17196
permeability of saturated steel calc., Stefan's equation with small parameter solution *(French)* 77−28409
perturbed solitons, interaction, and struct. of oscillatory shocks 79−64868
piezoelectric SAW velocity rel. to uniaxial biasing stresses 77−27416
piezoelectric semiconductors, growth of wave discontinuities 80−34488
pipe, of variable thermal and elec. conds., elec.-heated, flow-cooled, temp. distrib. 78−90626
plane entry flows and energy estimates for Navier-Stokes eqns. 79−37278
plane wedge under large deform., eqn. of compatibility *(German)* 77−23889
plasma, ion-acoustic waves, Korteweg-de Vries soliton, higher order terms in reductive perturbation theory 78−1824
plasma, Korteweg de Vries waves and solitons, three-dimens. stability 78−83540
plasma nonlinear wave interactions, symbolic computation code MCCSYMA 77−27660
plasma sheath, integro-differential eqns., nonlinear, nonlocal, soln. formalism 80−43936
plasma three-wave damped interaction 77−979
plasma wave propagation, nonlinear Schrodinger equation, modified Zakharov-Shabat inverse scatt. problem 80−59200
point charge as electrically invisible object, nonlinear Poisson-Boltzmann theory Coulomb singularity 80−43228
Poisson's equation, linear and nonlinear numerical solution including spatially variable dielectric const. 80−6825
Poisson brackets and related evolution equations 79−30263
Poisson-Boltzmann eqn., spherical, Debye-Huckel linearisation 80−35538
pole expansions of nonlinear partial differential eqns., corresponding many body problems 77−82372
prolongation structure for a nonlinear equation with explicit space dependence 80−82664
prolongation structure of AKNS eqns. system, generalisation, multicomponent nonlinear Schrodinger eqn. 77−45730
pulse response of nonlinear system, Krylov and Bogoliubov approx. 79−84962
QED, invariant charge from asymptotic soln. of non-linear eqn. 79−35974
quantal Coulomb excitation scattering matrix, asymptotic approxs., error estimates, using nonlinear Riccati matrix differential eqn. 77−49866
quantised frictional forces, nonlinear wave equation solutions 79−85
quantum dissipative systems, finite-difference retarded equation 80−12935
quantum electrodynamics, nonlinear problems 80−4901
quantum eqn. of motion for nonlinear oscillator in harmonic force field 78−54232
quasilinear partial differential equations, separability 78−65784
radiation defect production, exact solns. of models for continuous and pulsed irrad., implications for stability and fluctuations 80−65041
random behaviour 80−77706
random choice soln. of nonlinear hyperbolic systems of conservation laws 77−7362
rarefied binary gas mixture, two-dimens. channel flow, separation phenomena, num. soln. 77−58740
rate equations, soln. by matrix inversion 78−93520
reaction kinetics of solid pellet, nonlinear partial differential eqns. 79−39123
reaction-diffusion eqns., integral bounds for solns. 77−64928
reaction-diffusion eqns., large time behaviour of solns. 79−12741
reaction-diffusion models for interacting populations 78−65886
reaction-diffusion problem, nth order, asymptotic anal. 79−11764
rectangular orthotropic plates with nonlinear stress-strain relns., large deflections 78−26040

nonlinear differential equations continued
renal countercurrent model eqns., numerical soln. 77−40698
renal counterflow systems differential equation, soln. by numerical method 78−24082
renal network flow eqns. anal. 79−11961
respiration rhythmogenesis model, Lotka-Volterra equations *(German)* 77−48772
respiratory control, human, input stimulus design for model discrimination 79−53183
Reynolds equation, asymptotic soln. 79−14369
Riccati equations, numerical algorithm for reducing order *(Russian)* 77−49583
rigid wall-hot gas stream interaction, heat cond. eqns. soln. 78−79194
rotating machinery subharmonic vibration diagnosis 79−3971
round buoyant jets in stratified flows, integral eqns. 79−27680
Saint Venants eqns., three point weighted scheme for numerical soln. 78−30356
scalar field, complex, one-dimens., with fourfold phase anisotropy, solitary-wave solns. 79−58553
scattering theory, general case, class of nonlinear Schrodinger equations 79−84995
Schrodinger, perturbed equation with cubic linearity, soliton-like soln. 79−7765
Schrodinger eqn., slowly varying solitary wave solns. 80−73
Schrodinger eqn., soliton solns. 80−27173
Schrodinger eqn. inverse scatt. problem, prolongation structs. 77−33890
Schrodinger equation, Benjamin-Feir instability and recurrence 78−81874
Schrodinger equation, classical systems with infinite set of conservation laws 80−86102
Schrodinger equation, damped, appl. to high-freq. electrostatic plasma oscills. 77−7530
Schrodinger equation, existence, uniqueness and regularity *(French)* 77−67202
Schrodinger equation, nonlinear, constrained harmonic motion 80−77625
Schrodinger equation, relativistic wave equations, scattering theory 80−4882
Schrodinger equation, soliton soln. *(Chinese)* 79−92987
Schrodinger equation, strongly nonlinear, variational approach 79−58583
Schrodinger equation with periodic pot., existence of solns. 78−57820
Schrodinger equation with variable coefficients, differential-difference analogue, single-soliton solution behaviour 80−8819
Schrodinger invariant generalised heat eqns., similarity methods and trivial solns. 78−62164
Schrodinger nonlinear eqns., Cauchy problem soln. blowing up 78−8220
Schrodinger-Hartree nonlinear eqns., soln. asymptotic behaviour 77−37728
second order, series truncation method solution 79−4019
self-dual network eqn., shock wave and hole type soliton 78−27
semiconductor-on-piezoelectric SAW convolver saturation phenomena 78−2358
semigroup generation by second-order hypoelliptic differential operators 78−65755
shells, cylindrical homogeneous, nonlinear partial differential eqn. system, soln. existence and uniqueness 79−71249
sine Gordon, Josephson junction dynamics anal. 79−28481
sine Gordon equations, complex solitons and poles 79−30264
sine wave generator giving two signals in quadrature, mathematical model *(French)* 78−86114
sine-Gordon, two-dimens. eqn., reduction to Painleve transcendents 79−92954
sine-Gordon chain, effect of external field 78−62145
sine-Gordon chain, evidence for breather excitations 79−63054
sine-Gordon chains, role of breather solns. in statistical mechanics 79−85212
sine-Gordon eqn., Goursat and Cauchy problems 78−77682
sine-Gordon eqn., inverse method for solving differential-difference and difference-difference eqns. 80−105513
sine-Gordon eqn., separability 78−65784
sine-Gordon eqn. in 2+0 dimens., solns. 79−71258
Sine-Gordon eqn. in 3-D, diffusion theory *(French)* 77−61174
sine-Gordon eqn. with perturbative term, synchronised solitons 77−57204
sine-Gordon equation, 3 and 4 dimens., exact solns. 80−86091
sine-Gordon equation, approx. rotationally symmetric solns. 80−8807
sine-Gordon equation, Backlund transform., physical space-time solitons 80−77629
sine-Gordon equation, Backlund transformations and Dirac factorisation 80−73185
sine-Gordon equation, classical solns. of field eqns., moving t'Hooft-Polyakov monopole *(Russian)* 78−16935
sine-Gordon equation, difference analogue 78−20976
sine-Gordon equation, discretisation 79−21931
sine-Gordon equation, double, multidimensional multisoliton kink solutions 80−73184
sine-Gordon equation, exact mass spectrum, WKB approx. 77−33896
sine-Gordon equation, in one and more dimensions, break-up of quasi-soliton solns. 80−8806
sine-Gordon equation, intrinsic geometry 80−86553
sine-Gordon equation, nonlinear, constrained harmonic motion 80−77625
sine-Gordon equation, one dimens., group of invariance, dimens. anal. method 78−54528
Sine-Gordon equation, soliton solns., boson transformation 79−17611
sine-Gordon equation, two soliton solutions, breather solution 80−12945
sine-Gordon equation, two-dimensional, separable solns. 78−89614
sine-Gordon equation and nonlinear σ model on a lattice 79−21932
sine-Gordon equation in 2+1 dimensions, particular solns. 79−85211
sine-Gordon equations with multisoliton solutions, polynomial conserved densities 77−9887
sine-Gordon interaction solitons and classical particles 77−74589
sine-Gordon pendulum eqn. and $\lambda\phi^4$ model, generalisation 77−49610
sine-Gordon perturbed equation, soliton mass formulae 80−22200
sine-Gordon theory, soliton mass 77−13848
sine-Gordon with boundary conditions, soln. applicable to oscill. superfluorescence 79−27221
singular diffusion eqn., perturbation soln. 79−71387
singular perturb. problems, asymptotic equiv. 77−9875
singular perturbations for initial value problems, hyperbolic nonlinear partial differential eqns. 78−58111
smooth vector fields, geometrical generalization of relation between limit cycles and symms. 78−54163
solid propellent burning in three coord. systems, anal. 78−1558

nonlinear differential equations continued
solitary wave solns. of classical nonlinear field eqns., for teaching 80−17756
soliton collisions, structural stability 80−10382
soliton eqns., Lie group framework 78−24635
soliton equation, geometrization 79−75358
soliton equations, perturbed, variational approach 78−89366
soliton evolution of modified Korteweg-de Vries eqn. under action of perturbations 79−84970
soliton generation, nonlinear differential evolution eqns., 3+1 dimens. 80−46828
soliton history in mathematics of solns. to nonlinear evolution eqns. 79−75365
soliton instability in one-dimensional nonlinear systems *(Russian)* 80−52039
soliton perturbations and nonlinear focusing, anal. method for fluid dynamics 79−75369
soliton resonant production in regularised long wave eqn. 79−97216
soliton solns. of nonlinear partial differential eqns. 77−82368
soliton solution to Korteweg-de Vries equation using matrix trace 80−36870
soliton solution to modified Korteweg-de Vries equation, matrix trace method 80−36871
soliton solutions and dispersion relation 78−45467
soliton solutions and their applications 80−8813
soliton studies in mathematical physics 79−75366
solitons, geometrical interpretation, rigid body motion along helical space curves 78−24684
solitons, lecture 78−24690
solitons, nonlinear self dual network, with saturable property Korteweg-de Vries eqns. 79−21560
solitons, nonlinear wave equations solns., classical, quantal, appls. 78−57793
solitons, numerical studies, historical review 79−75367
solitons, weakly damped, mechanical model, anharmonic oscillator in pot. well 78−86192
solitons and SL(2,R) 78−57748
spectral transform, nonlinear discrete evolution equations 80−4553
spectral transform and nonlinear evolution equations 80−4551
spectral transform method extension for solving nonlinear differential difference eqns. 78−81804
spectral transform method for nonlinear evolution eqns. from Zakharov Shabat linear problem 78−65785
spectral transforms, nonlinear evolution equations 80−4552
spherical shells, nonlinear state and dynamic response 79−32236
spiral vibration of rotating shaft rubbing against interference element *(German)* 78−87252
stability anal. of nonlinear systems 79−84947
stability criterion, of third order non-linear differential eqns. 78−81801
stable limit cycles of vector fields, new negative criteria 78−57756
stagnation point flow, least square finite element soln. 77−14981
Stefan problems with nonlinear boundary conditions, polygonal method soln. 79−26010
stochastic, comparison of statistical linearisation, diagrammatic expansion, and projection operator methods 78−54306
stochastic, integral representation soln. 77−13730
stochastic 78−93516
stochastic differential eqn., perturbation theory, projection operator method, statistical linearisation 78−41229
stochastic differential eqns. excited by Gaussian noise and harmonic disturbances 77−87631
stochastic differential equations, approx. soln. by statistical linearization method, variational procedure 77−17789
straight elliptical jet motion, influence of twist using nonlinear differential equations 79−46354
strange attractors in 3-variable reaction systems 79−1939
stratified atmosphere, nonadiabatic heat dynamics with mass exchange and water phase transitions 79−58004
string, nonlinear stretched, randomly excited, anal. 78−83312
SU(2) gauge field theory, nonlinear scalar field eqn., spherical symmetric exact solns. *(Chinese)* 80−62886
subharmonic and superharmonic synchronisation in weakly nonlinear systems 77−2534
sublinear Hill's equation, nonoscillatory solns. 78−77675
superposition of solitons from same nonlinear differential eqns. 80−67
surface gravity wave packet development when moving over an uneven bottom 79−41700
symmetry approach to exactly solvable evolution equations 80−82648
temporally inhomogeneous nonlinear scatt. theory 77−37788
thermal reistance minimisation, solid with heat-exchanging surfaces, variational method 78−94512
third order, multiple time scaling, comments and reply 79−30262
third order equations analysis, multiple time scaling 77−82369
third order nonlinear differential eqns., stability criterion, comments and reply 79−94540
three-wave eqns. in 3 spatial dimensions, solns. 79−97212
time periodic solutions of a semilinear wave equation 79−17246
Toda equation, difference analogue 78−20975
Toda lattice, generalised eqn., solitons 80−95040
Toda lattice, poles, soliton solns. 79−75368
Toda lattice eqns. of motion, multi-soliton soln. construction, direct method 79−75360
Toda lattice equation, nonlinear, constrained harmonic motion 80−77625
toroidal shells, branching solns. to nonlinear eqns. *(Russian)* 79−27557
torsional creep problem, appl. of maximum principle 78−71284
transformation group and limit cycle containing nonlinear differential eqns., connection with perturbation techniques 78−20941
transformations for partial differential eqns. 80−42043
transient creep analysis, finite-element and analytical soln. superposition 77−75820
transient field initial-boundary value problems, hybrid simulation 77−41469
transient vibration problems, solution bounds 77−67226
transport equations, use of transformation groups to deduce properties 80−4680
two dimensional, nonlinear partial difference eqns., two point function 80−101762
two-dimensional infiltration in unsaturated soils, nonlinear diffusion eqn. numerical soln. 80−69918
two-dimensional space isothermal and nonisothermal turbulent flow *(German)* 80−28505

nonlinear differential equations continued
unified wave propagation theory, tenuous random medium 78−4491
variational principle, applied to nonlinear Schrodinger eqn. 79−63065
vascular bed modelling, optimal dialysis appl. 80−30758
vibrating symmetric system under nonlinear forces, group representation theory 77−2536
vibrating system defined by characteristic quantities bounded by nonlinear equation *(French)* 80−33278
vibrating systems, fourth order parametric resonance, influence of frictions 77−58620
viscoelastic circular membrane, nonlinear, large axisymmetric deform. under its own weight 80−64380
viscous liquid emerging from slot, nonlinear differential equation, Runge-Kutta numerical integration 80−52030
Volterra and nonlinear self-dual network eqns., conservation laws generation 77−53749
Volterra competition eqn., inverse scatt. soln., N-soliton solns. 77−49565
Volterra integro-differential equation, heat flow appl. 79−18668
Volterra series soln. 79−58527
water wave caustic region, nonlinear theory 77−11211
water waves, in nonhomogeneous incompressible fluid, nonlinear differential eqns. 78−55657
water-cooled water-moderated reactor cooling system faults, hybrid simulation *(Russian)* 78−5008
wave and spinor eqns., causal solns. by regularisation 77−33872
wave eqns. in n-dimensional space, periodic solns. 78−93540
wave equation, periodic solutions 80−73188
wave equations, asymptotic solns. using methods of averaging and two-timing 78−59
wave equations, symm. of solitons and general solns. 79−85210
wave evolution, nonlinear, in free shear layers, effects of critical layer structure 80−83809
wave phenomena, numerical and theoretical study 78−81851
wave propagation, nonlinear lattice 77−13707
wave propagation hyperbolic partial differential eqns. and mathematical models 78−77729
Zabolotskaya-Khokhlov eqn., exact solns. determ. via symmetries 77−805
He, superfluid B phase, spin wave breathers, double sine-Gordon equations 80−15329

nonlinear equations
see also nonlinear differential equations
aerosol coagulation, simplified model 77−56254
analytical approximate solutions of the nonlinear basic equations in classical physics 80−52001
applied inverse problems, book 79−49017
approximation method for solution of nonlinear integral equation with error estimation for problems in heat or mass transfer *(Russian)* 78−57879
atmosphere, squall line formation, nonlinear process 78−81323
axisymmetric surfaces of revolution, numerical soln. *(Russian)* 78−81838
background ensembles, nonlinear modeling 80−95037
Backlund transformation, simple structure of superposition formula, 79−12616
Backlund transformations, canonical struct. 80−86141
Ball-Zachariasen model of diffractive scattering, numerical soln. near singularity of Frechet derivative 80−9158
beam torsional vibration frequency optimisation 78−83288
Benjamin-Ono equation, periodic wave and soliton solns. 79−35570
Bessel functions, infinite systems of nonlinear equations containing zeros 80−46786
Bessel functions, squares of positive zeros, infinite nonlinear algebraic eqns. 78−20942
Bessel functions, squares of positive zeros, nonlinear eqns. and sum rules 78−49639
boomeron equation, asymptotic behaviour (in t) of solutions 79−9082
Born-Infeld equation, two-dimensional system of conservation laws *(Russian)* 80−42365
bound state, two charged media interaction, self-consistent field theory 78−16667
buckling of reticulated shells, nonlinear strain displacement relationship 77−54908
butadiene-styrene gum elastomers, compounds, viscoelastic props., stress relaxation meas. 77−7321
canonical transformations theory for nonlinear evolution eqns. 77−29993
catastrophe theory solution, application to n^{th} order chem. reactions 79−70296
Chandrasekhar nonlinear H-eqn., iteration 79−58652
chemical reaction diffusion equation, nearly degenerate bifurcations, mode interactions 80−85149
chemically reacting system with physical interactions, nonlinear eqns. 80−81288
Choquard nonlinear eqn. minimising soln. existence and uniqueness 78−67315
classical hard sphere system, statistical theory of freezing 80−33868
classical Q solitons, two space dimens. interaction 79−45015
CO_2-laser, numerical soln. to nonlinear rate eqns. of population level density *(Bulgarian)* 78−33720
Cole-Hopf transformation for nonlinear parabolic and hyperbolic equations, diffusion and turbulence 79−41680
Compton effect, multiple scatt., operator formalism, nonstationary electrons 78−12846
concentric shock wave self-similarity exponent approximation 78−75169
confluent hypergeometric functions, high order nonlinear eqns., sum rules, zeros 79−92923
confluent hypergeometric functions, nonlinear eqn. infinite system, zeros 79−92922
convex analysis and variational inequalities *(Japanese)* 80−77606
convex nonlinear boundary value problems, iterative bounds for stable solns. 78−54167
cosmology, Friedmann model, expanding Universe, nonlinear acoustic effects *(French)* 80−67921
creep buckling theory, nonexistence of global solns. for nonlinear eqn. 79−30251
creep problems in symm. press. vessels, uniqueness of integral eqns. positive solns. 77−65694
cubic eqn. root finding, symmetrical component method *(Russian)* 79−62993
derivative nonlinear Schrodinger eqn, soliton solns. 79−44773

nonlinear equations continued
difference eqn. and soln. by inverse scatt. 77−9861
diffusion eqn., with nonlinear terms, Fourier transform 80−103514
diffusion-reaction systems, effect of gravity on pattern formation 79−70302
Dirac equation with SU(3) colour symmetry, vanishing soliton solns. 79−71693
discrete exactly soluble evolution eqns. generation by Wronskian technique 77−49564
dispersive waves, nonlinear interaction between strong and weak waves 79−17242
double soliton solutions for multidimensonal eqn., quasiclassical quantisation 78−54569
Eells-Sampson heat eqn., lifetime *(French)* 78−86227
elastic bar structures, exact anal. with nonlinear eqn. system, stresses 79−81731
elastic nonlinear media, antiplane deform. soln. representation *(Russian)* 77−84145
elastic shells, stable solutions, finite element and Newton-Raphson methods 80−14593
electrodynamics, three-dimensional soliton solution *(Russian)* 79−22884
electron cyclotron maser in overmoded cavity, nonlinear multimode formulation 80−58495
elementary particle theory, mathematical method, conf., Liblice, Czechoslovakia (June 1978) 79−21891
EM wave propagation in ferromag. material, nonlinear waves and strong discontinuities *(Russian)* 78−74819
EMF in ferromag. material under torsion *(Rumanian)* 78−86986
evolution equation, exact two-periodic wave soln. 80−12914
evolution equation, explicit two-soliton solution 79−84965
evolution equations, conservation laws by spectral transform 79−5985
evolution equations, exact solns. 79−25873
evolution equations simulating pair production and annihilation, solitary wave solns. 78−86167
evolution equations solvable by inverse spectral transform of rank 4 matrix Schrodinger eqn. 78−41187
explosion, thermal, crit. parameters analysis 80−11891
FBR safety analysis, multicomponent hydrodynamics, implicit Eulerian technique 79−634
field eqns., time discretisation and mixed finite element methods 79−40384
finite element analysis, solution techniques, review 79−3914
fluid dynamics, free boundary flow, surface tension effects, finite element fluid flow simulators 80−82647
fluid dynamics, pseudoplastic non-Newtonian fluid, nonlinear singular boundary value problem 80−79362
frame nonlinear postbuckling behaviour, finite element analysis 77−62183
gas, two dimensional, initial value problem for model Boltzmann eqn. 79−44885
group representation theory and branch points of nonlinear function eqns. 77−67195
hard-sphere fluid, modified nonlinear Enskog eqn., entropy function 78−63526
Hartree eqn., quasiclassical soliton soln., Newtonian interaction with screening 80−68569
heat conduction with absorpt., similarity of nets method *(Russian)* 80−53603
heat generation eigenfunctions 77−49553
Hermite polynomials, systems of nonlinear eqns. for zeros 78−69961
Hermite polynomials, zeros of combinations, n-body problems 78−45466
higher order Benjamin-Ono equation, N-soliton and N-periodic wave solns. 80−12915
infinite systems, proof of Calogero's real and unique solutions 78−24636
instanton applications in statistical mechanics 79−75450
inverse problems, nonlinear eqn. soln., Tikhonov algorithm 77−41200
inverse scatt. method generalisation, generalised nonlinear Schrodinger eqn. eigenfunction 79−92994
inverse scatt. transform method, relativistic invariant formulation, sine-Gordon/massive Thirring model appl. 79−71598
inverse scattering method for nonlinear evolution eqns. under nonvanishing conditions 78−57808
inverse scattering method for solving nonlinear evolution equations 79−49096
3×3 inverse scattering transform, soliton perturb. scheme 80−27151
Ising model correlation quadratic identities, discrete-time Toda eqn. 80−105582
KdV, Backlung transform. for pole movement *(French)* 79−12711
kidney modelling, numerical continuation method 79−43944
Kirkwood-Salsburg equation, derivation and low-density soln. 79−9177
Klein Gordon equation, propag. of solns. with arbitrary complex mass 79−21924
Klein-Gordon eqn., two dimensional model anomalously slow stochastisation *(Russian)* 79−89068
Klein-Gordon equations, three dimens. multiple soliton-like solns. 78−49955
Korteweg de Vries eqn., soliton soln., Hugoniot conditions for gas dynamics 80−42069
Korteweg-de Vries eqn. difference analogue 78−55
Laguerre polynomials, nonlinear eqns. systems and sum rules for zeros 78−69962
Laguerre polynomials, zeros satisfying nonlinear eqn. 79−97182
Landau-Lifshitz nonlinear equation, N-soliton solutions *(Russian)* 79−24184
Lorenz equation in high Rayleigh number limit, periodic soln. using perturbation theory of nonlinear oscills. 79−68681
macromolecules, interacting, spherical, light scatt., conc. fluctuations, transport eqn. 79−1775
Mathieu eqn., chaos and successive subharmonic bifurcations 79−63153
metal creep, nonlinear integral eqn., existence and approx. solns. 78−13931
modified conservation laws for nonlinear waves *(Russian)* 77−45706
multi-spiral electron current, interaction with EM wave, nonlinear anal. *(Russian)* 79−22886
multidimensional solution based on inverse scatt. problem *(Russian)* 77−74600
multisoliton breakdown criteria and implications 77−29994
Nambu-Goldstone realisations of dynamical groups and nonlinear eqns. *(Russian)* 78−89632
Newton's method for solving nonlinear inequation systems, convergence 77−30001

nonlinear equations continued
Newton Raphson algorithm, standard and damped least squares methods, convergence 77−9878
nondissipative medium, boundary problem soln. with surface discontinuity *(Russian)* 80−101716
nonlinear Dirichlet problems, exponential decay estimates, elasticity and heat conduction 79−92939
nonlinear quantum mechanics, Gauss transform. appl., Schrodinger eqn., nonlinear integro-differential eqn. 79−6013
nonlinear reaction-diffusion equations, pattern selection at the bifurcation point 80−50827
nonlinear wave envelope equations for plasma physics, Fourier's method convergence 79−55463
nuclear physics nonlinear integral eqn. solution *(Chinese)* 78−74324
numerical study of solitons *(Chinese)* 79−35529
orthogonal polynomials, nonlinear eqns. for zeros 80−12888
Percus-Yevick eqn., existence and local uniqueness of solutions 80−36936
perturbed wave eqn., Pettis integration initial-value problem 79−71285
petroleum, two phase flow in underground reservoirs, soln. of nonlinear eqn. by random choice method 79−50773
plasma, collisionless drift modes, graphical method for finding complex roots of nonlinear eqn. 80−33762
plasma, ion acoustic soliton, Boussinesq eqn. description 79−46449
plasma low-hybrid wave nonlinear eqns. and solitons 78−75323
plasma nonlinear theory of unstable plane waves and solitons 80−87888
plasma transverse Cherenkov mode nonlinear stabilisation by external mag. field 80−38642
plasma wave self-modulation by ponderomotive force, nonlinear analysis 78−75326
plates, circular, variable thickness, numerical solution for flexure 80−99951
progressively changing equilib. eqns. soln. for nonlinear struct. 78−1581
pseudo nonlinear regression 77−64933
pumpdown time eqn. and system selection 80−82785
quantum dissipative system, nonlinear von Neumann equations 79−25976
reaction-diffusion systems, bifurcation theory, classification 80−108713
rectangular plates, non-linear vibration, theoretical anal. 78−90750
regularised long wave equation, anelastic collision of solitary waves, numerical anal. 78−77724
relativistic QFT, inverse scatt. problem and 5th Painleve transcendent 79−54260
retina of Limulus, spatially synchronised oscillatory response theory 78−73158
sandwich shells and Cosserat surfaces, nonlinear compatibility equations 79−53976
Schrodinger equation, appl. to deep water waves, $O(\varepsilon^4)$ perturb. anal. 80−4569
Schrodinger equation, explicit formulae for solns. *(Ukrainian)* 77−30031
semiconductor, nonlinear equation, asymptotics of spectral boundary-value problem 80−6851
$(\sin\phi)_2$ interaction in box, soliton soln. fermionisation 79−88840
sine-Gordon system, solitons and bion dissoc. 79−63048
solenoid windings, nonlinear eqn. for equal loading 79−55028
soliton, dimensioned profile for propagation *(French)* 77−35155
soliton and appls. *(Japanese)* 79−80418
soliton equations and pseudospherical surfaces, conservation laws, Backlund and scale transformations 79−75688
soliton solns., importance in low temp. physics 79−63057
soliton trajectories from nonlinear field eqns. of Dirac field, Lorentz and gauge invariant 78−4791
solitons, in dispersive media, nonlinear evolution eqns. soln., review 78−60
solitons, review of concepts and methods in theory *(Polish)* 80−68057
solitons, theory and applications 78−36811
spectral transform method for solving nonlinear evolution equations 79−49019
spinor theory, nonlinear, two-point function 79−63366
stochastic integral equations, nonlinear, mixed type, existence, uniqueness and stability of solutions 80−68131
tachyon solitons and their interactions, Backlund transformations in nonlinear systems 78−54181
thin elastic pivots theory, nonlinear balance equations, constructive method *(Russian)* 79−49050
thin elastic plate, dynamic buckling, nonlinear theory 79−37160
three wave interactions, space-time evolution in homogeneous medium 79−84966
three wave interactions, space-time evolution in inhomogeneous medium 79−84967
toroidal pinch equil. config., nonlinear operator eqn., optimisation soln. 78−59649
transcendental equations, for Fraunhofer diffraction, numerical soln. method 77−33750
transport processes, nonlinear, hydrodynamics 80−22310
transport theory, nonlinear integral equations 79−30393
two-bar frame, eccentrically loaded, nonlinear stability anal. 78−63343
two-dimensional nonlinear magnetostatic fields, isoparametric Hermite finite element program 79−41275
uniaxial crystals, refl. ellipsometry nonlinear eqn. inversion 80−95120
variational principle in nonequilibrium nonlinear statistical thermodynamics *(Russian)* 79−85058
viscoelastic media constitutive eqn. 78−81839
viscous fluid unsteady periodic flow, Galerkin finite element method 77−75872
visual impedance, nonlinear integral equation 79−100599
Volterra nonlinear integral eqn., Mellin transform for asymptotic soln. 77−5636
Volterra nonlinear integral eqns. solns., existence, continuous depend. *(Chinese)* 77−67213
Volterra stochastic nonlinear integral eqns., interconnected systems stability 79−71368
wave propagation, spectral and pseudospectral methods, turbulent sound wave appl. 77−5672
waves in nonlinear media, Poincare normal form method 80−36875
weakly dissipative system, higher order approx. in reductive perturbation method, shock wave appl. 80−14743

nonlinear equations continued
XY one dimensional model, transverse correlations, eqns. of motion of finite temp. 80−105581
$^{12}C+^{6}Li(^{16}O)$ scatt., anomalous backscatt. from nonlinear Schrodinger eqn. for nuclear matter 79−6465

nonlinear field theory
(1+1) dimensional field theoretic models with soliton behaviour, exact S-matrices and form factors 79−26240
(1+1) dimensional model field, fermion-boson correspondence, Klein transformation 80−42379
1/N expansion, classical dynamics in large N limit 80−101923
1/N expansion and the theory of composite particles 80−73604
$\lambda\phi_6^3$ field theory, renormalisation group and ladder approx. 79−97524
$\lambda\phi_6^4$, extended objects in quantum systems and soliton solns. 79−35945
$\lambda\phi^4$ theory, dynamical mass generation in $S^1\times R^3$ 80−99046
$\lambda\phi^4$ theory, trial wave function renormalisation using effective pot. 80−105791
$\lambda(\phi^6-\phi^4)$ bound state in weak coupling, Bethe Salpeter eqn. 77−5992
ν-dimensional Yang-Mills and (ν-1)-dimens. nonlinear σ-model connection, quark confinement, dual strings 80−90978
σ model, appl. of pure gauge fields on coset space 79−40673
σ model, instantons and 1/N expansion 80−42339
σ model, nonlinear, quantum fluctuations of pseudoparticles 77−87897
σ model, $SU_2\times SU_2$, modified Goldberger-Treiman relation, pseudoscalar form factor 80−27421
σ model, supersymmetric chiral field, 1/N perturbation theory and quantum conservation laws 80−68373
σ model, supersymmetric nonlocal conservation laws 80−46938
σ model, two and four-dimens., classical solns., instantons and merons 80−86548
σ model, two dimens., nonlinear, three loop calc., minimal subtraction method 78−62289
σ model, two-dimens., nonlinear, anal., nonlocal charges determ. 78−54532
σ model in $2+\varepsilon$ dimens., renormalisation 77−13866
σ model in symmetric spaces 80−42341
σ model representation of Yang-Mills theory as a spontaneous violation *(Russian)* 80−13220
σ models, nonlinear, perturbative approach to symmetry restoration 80−37163
σ models, nonlinear, soft mass renormalisation of 1/N expansion 80−47164
σ models of nonlinear evolution equations 80−57487
σ models with instantons, 1/n expandable series 79−21909
σ SU(N) model, spontaneous symmetry breaking, renormalisation 80−42340
σ-model, classical solns., stability props. 80−77954
σ-model, finite action solns. 79−80739
σ-model, finite energy solution 79−17618
σ-model, generally covariant 4-dimens., dimensionless coupling upper bound 80−86584
σ-model, Hamiltonian lattice formulation 77−10183
σ-model, nonlinear, curved space, spontaneous compactification, Grassmann manifold 80−57467
σ-model, nonlinear, local conservation law existence in various generalisations 79−71621
σ-model, nonlinear, n-component, on lattice of arbitrary dimensions, 1/n expansion 80−73576
σ-model, nonlinear, order-parameter relaxation from renormalisation group 80−57504
σ-model, nonlinear, superconformal invariance in 4-dimens. space-time 80−37154
σ-model, nonlinear, sypersymmetric, Ricci-flat Kahler manifolds and supersymmetry 80−90994
σ-model, nonlinear two dimens., finite action solns. of Euclidean eqns. of motion 78−37133
σ-model, O(2k+1), Euclidean, nonlinear, local theory of solutions, Euler-Lagrange eqns. 80−52387
σ-model, similar to anti-self-dual field in 4-D Euclidean space 80−52386
σ-model, U(N,r), supersymmetric, and O(2) extended supersymmetry 80−82878
σ-model, UV infinity suppression in gravity modified field theories 80−105787
σ-model and classical solns. of instanton and meron type 79−21905
σ-model appl. to nuclear physics in one dimension, fission, Hartree approx. 79−80890
σ-model instanton, interpretation as tunelling process through pot. barrier between two vacuums 79−49399
σ-model supersymmetric dynamics on pre-QCD level with elementary quarks and composite gluons 80−82886
σ-model supersymmetric extensions, dynamical conservation laws, symmetric space valued fields 80−95227
σ-model with quadratically broken symmetry, cross-over behaviour 79−17601
σ-model with quarks of π decays and π electromag. form factor 79−22100
σ-models, conservation laws, infinite series, differential geometric content 80−62841
σ-models, non-linear, and universality in 3-D, scaling limit, and critical behaviour, chirality 80−62824
σ-models, nonlinear, classical two dimens., dual symmetry 79−80750
σ-models, nonlinear, generalisation with gauge invariance 80−57469
σ-models, nonlinear, supersymmetric, nonlocal conserved currents and instanton-like solutions 80−86544
σ-models, nonlinear, with N=Z extended supersymmetry in 4-dimens. 80−47174
σ-models, supersymmetric, Kahler geometry and renormalisation 80−105789
σ-models, two-dimens., nonlocal invariance and hidden symmetry 80−86596
σ-models, two-dimens. nonlinear, on Riemannian and Hermitian symmetric spaces 80−52404
σ-models with dynamical charges, two-dimensional, renormalisation 79−85223
$\sigma SU(2)\otimes SU(2)$ model, asymptotic chiral invariance 77−71431
τ-vacuum for ϕ^4 and sine-Gordan theories, stationary solitons *(Chinese)* 80−101932
ϕ_1^4 theory, eigenvalues, Schwinger functions, critical behaviour 77−45931

nonlinear field theory continued
$\phi^{3,4}$ theory, conformal anomalies for interacting scalar fields in curved spacetime 79−49396
ϕ^3, conformally invariant amplitudes and field theory in a spacetime of constant curvature 79−49395
$(\phi^3)_6$, asymptotic freedom, zero charge and internal symmetry *(Russian)* 77−49864
$(\phi^3)_6$ theory, composite particle form factor, asymptotic behaviour 80−86595
ϕ^3 and ϕf^2 scalar nonrenormalisable field theories, scale-invariant solns. *(Russian)* 77−34097
ϕ^3 field theory, vacuum instability in scalar field theories 79−58872
ϕ^3 theory in 6-ϵ dimens., SU(3)×SU(3) strong interaction model 77−82726
ϕ^4, mass divergences of wide angle scatt. amplitudes 79−49402
ϕ^4, massive and massless, elliptic function methods 80−4829
ϕ^4 asymptotic free theory, renormalisation-group method 77−22652
ϕ^4 kink behaviour in presence of inhomogeneous perturbation 79−75692
ϕ^4 model, Altman's contractor techniques, appl. to nonlinear integral eqns. for Green's functions 79−45005
ϕ^4 model, strong coupling and infrared struct., renormalisation 80−101921
ϕ^4 quantum field theory, crit. point existence 77−10170
ϕ^4 soliton behaviour in presence of an impurity potential, collective coordinate method 80−31528
ϕ^4 theory, renormalisation groups transformation explicit construction 80−4832
ϕ^4 theory, spontaneous symmetry breakdown in finite systems 79−45011
ϕ^4 theory with spontaneous symmetry breaking, kink state 77−30235
ϕ^4 two-dimens. model, kink-antikink collisions 79−85218
ϕ^4-model, dimensional regularisation and instantons, scalar field theory model 80−4830
ϕ^4-theory, soliton soln., fluctuation renormalisation and extended particles 77−5996
$\Phi^4/4!$ scalar theories, perturbation theory divergence, pseudoparticles *(Russian)* 77−30273
$(\bar{\psi}\psi)^2$ model, spontaneous symmetry breaking, renormalisation 80−42340
Abelian Higgs model, lattice version, phase transitions and confinement 79−49398
AKNS-ZS inverse method, canonical struct. and generalised Marchenko eqn. calcs. 80−47192
anisotropic nonlinear σ-model, two dimens., instanton quantum fluctuations *(Russian)* 80−86600
anomalies of quantum conserved currents in exactly solvable models 78−387
antisoliton-soliton reflection in sine-Gordon model, single-loop approx. 79−21960
axially symmetric multi-instanton solutions generated by conformal mappings in SU(2) Yang-Mills field 80−42337
Backlund transform. derivation in inverse scatt. formalism 80−8810
Backlund transformation, dynamical systems, field theories calcs. 80−27386
Backlund transformation in the classical massive Thirring model 80−57456
Backlund transformations, group struct. 80−13219
Backlund transformations and solns. for nonlinear field eqns. in 4-dimens. spacetime 80−338
Backlund transformations in four-dimensional space-time 80−105768
Backlund transforms and symmetries of Yang eqns. 80−52393
bagged complex scalar field, EM interaction, fine struct. const., possible dynamic origin 80−86635
bell's inequalities from the field concept in general relativity 80−105771
Bethe-Salpeter eqn., quantised solitons 78−32985
Bethe-Salpeter model, scaling reconstruction using renormalisation group, Callan-Symanzik eqn., ϕ_6^3 theory *(Russian)* 80−42351
bilocal Lie groups and solitons 77−67194
binding energy in model classical field theories 80−4927
Bogomolny-Prasad-Sommerfield one-monopole soln. by Backlund transformation 80−99059
boson-fermion system, semiclassical anal. approach 80−27401
boson-soliton scatt., sine-Gordon model 80−9109
bound states of nonlinear scalar field in general relativity 78−77778
Cabibbo angle, gauge invariant rearrangement and theory, SU(2) symmetry breakdown 79−22027
charged particles, classical field model 78−12807
charged soliton long range interactions 79−63373
chiral dynamics, kink solns. of extended nonlinear model and particle interpretation 78−89612
chiral field model diagram techniques for low temp. phase 79−58882
chiral field theories with sophisticated topology 79−30650
chiral fields, two-dimens., hidden symm. 78−29243
chiral Gross-Neveu model, antiparticle as bound states of particles, factorised S-matrix framework 79−49411
chiral Gross-Neveu model embedded in U(1) gauge theory, fractional winding 80−86569
chiral invariant Gross-Neveu model, Hamiltonian diagonalization 80−22516
chiral model analog 80−52415
chiral nonlinear field eqns., exact solns. 78−54527
chiral $SU_4 \times SU_4$ breaking in nonlinear Lagrangian, pseudoscalar meson mass 77−57513
chiral SU(2)×SU(2) theory, localised solns. 77−26451
chiral SU(3)×SU(3) models, soliton solns. 78−4761
chiral SU(N) Thirring model, S-matrix bound state poles fixing 80−360
chiral theory, renormalisations 77−65112
chirality invariance and 'chiral' fields, book contrib. 79−58892
classical, relativistic, new solutions, charge barrier mechanism 78−54211
classical, spherically symm. solns. 77−45941
classical electrodynamics, nonlinear gauge approach, charged particle solns. 78−32695
classical Euclidean 2-D nonlinear σ-models, continuity eqns. 78−54210
classical Euclidean solns., pseudoparticle 77−67577
classical field eqns., mathematical aspects 80−4882
classical field theory, nonlinear one-dimensional model with internal degrees of freedom 78−49684
classical fields, stationary localised solns. 77−74572
classical nonlinear σ-model, two dimens., scatt. of massless lumps, nonlocal charges 78−62300
classical nonlinear scalar field, solns. with props. of shock waves 78−81865
classical scalar field theory, localised solns. 78−32976
nonlinear field theory continued
classical sine Gordon equation, exact time depend. solns. in 2+1 and 3+1 dimens. 78−78074
classical solns. 78−21327
classical solutions by inverse scatt. method 79−9272
classical solutions of a nonlinear field equation 80−4841
classical theory with positive mass square, static finite energy solns. 80−31984
closed vortices and Hopf index in Abelian and non-Abelian Higgs model, and nonlinear σ model 79−12960
collapsons, new form of nonlinear excitations 80−4876
collective phenomena and renormalisation of non-linear spinor theories 77−71441
collective state renormalisation, improper initial or final states in nonlinear field theory 79−439
colour geometrodynamics, eightfold way, review 80−95243
complex scalar field with nontrivial asymptotic behaviour of soliton solns. 80−4867
condensation of the vortex solitons in a 2+1 dimensional Abelian Higgs model 80−99048
conference, nonlinear problems in theoretical physics, Jaca, Gain 1978 80−4478
conformal and chiral anomalies, anomalous Ward-Takahashi identities 80−86612
conformal and superconformal gravity and non-linear representations 79−17308
conformal invariant nonlinear field equations, geometric soln. 79−93273
conformal supergravity, superconformal group, nonlinear representation 79−12695
conformally invariant σ-model in four dimens., instantons 80−95215
constrained systems, absence of classical lumps 79−2904
continuous spectrum decay, sine-Gordon eqn., nonlinear optics appl. 78−71143
cosmological constant, broken gauge theories and 3K black-body radiation 78−28870
coupled non-linear field eqns., soliton solns. 80−68338
coupled scalar field theories in 2-dimens., exact soliton solns. 79−21920
covariant σ models, first order system of differential eqns. 80−31978
covariant CP^2 non-linear σ-model, classical solns. 79−54020
covariant derivatives without gauge fields 80−73584
covariant quantisation of solitons in gauge theories 78−16916
CP_{n-1} models and non-Abelian HP_{n-1}, quantum props., σ relation, renormalisation 80−13210
CP^1 model, instanton interaction with fermion field 79−97514
CP^2 model, classical real configuration quantisation 80−73606
CP^2 vierbien singularities in half integral spin fields with EM background 80−73572
CP^{N-1} σ-model, N-component scalar QED model, renormalisation group functions 79−97500
CP^{n-1} σ-models, vacuum struct., statistical fluctuation effects 79−89101
CP^{N-1} model, (2+1) dimens. supersymmetric, supersymmetry algebra and central charge 80−86568
CP^{n-1} model, embeddings of classical solns. of O(2p+1) nonlinear σ-models, instantons 80−86562
CP^{N-1} model, instanton and large-N methods, QCD similarity 80−77963
CP^{n-1} model, pair prod. absence up to 3rd order perturbation theory 80−90990
CP^{N-1} model, QCD toy model, instantons θ vacua and confinement 80−9138
CP^{n-1} model, quantum fluctuations in the one-instanton sector 79−85209
CP^{N-1} model (D=2,3), UV renormalisation and phase transition 80−31989
CP^{n-1} model with non-Abelian gauge symmetry, generalisation in 2+ϵ dimensions 80−77953
CP^{n-1} model with quarks, confinement and chiral symmetry breaking 79−54302
CP^{N-1} model with unconstrained variables, Lagrangian and Hamiltonian formulations 80−105780
CP^{n-1} models, effective lagrangian with no U(1) current problem 79−89066
CP^{n-1} multi-instanton fields, quantum fluctuation 80−329
CP^{n-1} nonlinear σ-model, lattice formulation 79−58870
CP^{n-1} supersymmetric model, central charge, superalgebra and Dirac brackets 80−99044
CP^{N-1} two-dimens. model, infinitely many conserved local charges 80−47179
CP^{n-2} models in more than 2-dimens., confinement props. 80−86570
CP^N σ-models, 2-dimens., local conserved currents, conservation laws 80−86579
CP^N model, generalisation with gauge invariance 80−57469
CP(N) (N≥2) chiral theory, 2-dimens., non-selfdual instantons 80−86585
critical exponents, three dimensional system with short-range interaction, calc. 80−42348
current conservation in perturbative sine-Gordon and massive Thirring models 79−9273
currents and continuous symmetry restoration in two dimens., perturbation theory 79−21910
damped nonlinear Schrodinger equation, exact soln. for parabolic profile 79−17278
dense and dilute instanton-anti-instanton pair configurations 80−52424
dilute gas approximation, higher order corrections, appl. to gluon propagator and static quark pot. 79−49400
Dirac's monopole and the Hopf map 80−27402
Dirac field, kinks and the Heisenberg uncertainty principle 79−35943
Dirac field, self-interacting, Coulomb-like potential, localised solns. 80−68351
Dirac field eqn., Lorentz and gauge invariant 78−4791
Dirac field free soln., classical electrodynamics 79−80752
Dirac nonlinear eqn., soliton solns. 79−71591
Dirac nonlinear spinor eqns. with localised solns. 78−49964
double quadratic chain, statistical mech., nonreflectionless solitary wave 80−22518
driven sine-Gordon chain, periodic and solitary states 80−82881
dynamic charges in field theories 79−54251
dynamical and kinematical charges in classical nonlinear scalar field 78−54208
dynamical groups of completely integrable eqns., nonlinear realisations 80−4885

nonlinear field theory continued
Dyon solutions, existence, rigorous results 80−73595
education, topological solitons in physics, vortices and mag. monopoles as examples 79−25793
effective-potential approach to the quantization of the sine-Gordon theory in 1+1 dimensions 80−73608
Eguchi-Hanson instanton, TP inversion in quantum gravity, appl. to scatt. theory 79−58613
Einstein-Klein-Gordon eqn. solns. in stationary axially symmetric space-time *(French)* 79−25921
Einstein-Klein-Gordon equations, Killing field vectors, theorem *(French)* 79−30340
electrodynamics, photon-gravitation coupling 79−97276
electrons and gravitational instantons 79−25961
elementary length in nonlinear classical scalar field 77−45942
elementary particle theory, mathematical method, conf., Liblice, Czechoslovakia (June 1978) 79−21891
EM field, charged particle config., stability 80−57109
EM model for charge confinement 78−78078
equivalence theorem, path integral formulation 79−12933
Euclidean approach in curved spacetime, functional anal. 80−27181
Euclidean field theory, nonlinear elliptic eqn., classical solns. 79−21569
Euclidean manifolds, N-dimensional instantons and monopoles 80−42321
euclidean nonlinear classical field equations with unique vacuum 79−5989
Euclidean $P(0)_2$ model, quasiclassical expansions 80−47200
Euclidean space, spherically symmetric self-dual eqns., representation theory and integration 80−77936
Euclidean SU(2) Yang-Mills theory, pseudoparticle solns. 79−35931
exact from factors in field theoretic models with soliton behaviour 78−82211
exotic meson ($Q^2\bar{Q}^2$) spectroscopy, instanton effects 79−89140
extended structures described by Z(N) spin and gauge models, applications 79−67479
exterior calculus and two-dimensional supersymmetric models, super sine-Gordon model 80−47214
factorised completely X symmetric S-matrix characterisation, multicomponent field theories 80−105800
factorised gauge solitons for compact gauge groups in n dimens. 79−21944
factorised S-matrices in 2-dimens., relativistic QFT model exact solns. 79−93274
factorized U(n) symmetric S-matrices, two dimens., scatt. of solitons 78−45802
Fermion contribution to instantons 78−78079
fermion fields with $(\sin\phi)_2$ interaction, quantum solitons 77−41780
fermion number nonconservation in the presence of instantons *(Russian)* 79−49408
fermion-instanton coupling in two dimens., using perturbation theory for fermion sector 79−67475
fermionic solitons in gauge theories and their quantum corrections 80−101927
fermions, quantum field theory, large order perturb. theory, more than one coupling constant 80−77940
fermions and vortex solutions in Abelian and non-Abelian gauge theories 79−12959
Feynman path integrals on nonlinear phase space 78−37147
finite element method, with variable basis functions *(Russian)* 80−37160
flux line collapse, invisible string 77−57451
four dimensional nonlinear σ-model in Euclidean space 78−93801
four fermion interaction, Heisenberg spinor theory, counterterms 77−26455
four-dimensional σ-model on quaternionic projective space 80−9092
four-fermion Lagrangian interaction, fermion number conservation spontaneous breakdown 77−67584
free Klein Gordon fields, conservation laws 80−340
free relativistic spin-1/2 particle energy-momentum invariants and kinetic moment *(French)* 78−62287
frequency decompositions in curved space-time 80−31973
fully symmetric nonlinear theories, Green's function methods, SCF theory 77−61180
$g\phi^4$ model perturbation theory, anal. continuation to $g\geq 1$ region 79−97525
$g\phi^4$ static ultralocal field, path integral anal. of spontaneous breakdown of symmetry 79−54249
$g\bar{\psi}\psi\phi$ theory, trial wave function renormalisation using effective pot. 80−105791
gauge ambiguities and nonlinear σ-model relations in Yang-Mills vacuum sector 80−105767
gauge equivalent fields, existence near instantons *(Russian)* 80−27414
gauge field in stability subgroup of vacuum in nonlinear realization 78−390
gauge formalism, sine Gordon eqn. derivation 77−57437
gauge theories and strong gravity 79−58869
gauge theory formulation 79−71627
Gel'fand-Levitan method as a generalized Jordan-Wigner transformation 80−77962
general covariant group, nonlinear realisation, invariant theoretical consideration 79−35612
general relationship between linear and nonlinear realisations of supersymmetry 79−9297
general relativistic kink soln. props. for nonlinear scalar field 79−85226
general relativistic nonlinear field, kink soln. in generalised geometry 79−21922
generalised Parseval eqn. 78−54204
generalised sine-Gordon eqn., Backlund transformation, nonlinear σ model 80−4844
generalized Hamiltonian dynamics, appl. to nonlinear field theory 79−75678
geometrodynamical model of extended baryons 77−79251
$GL_{4,R}$, nonlinear two valued realizations, Dirac eqn. nonlinear form 79−80748
gluons *(Chinese)* 79−58923
grand partition function in field theory, appl. to sine-Gordon theory 79−6276
gravitation, in plane space, equivalence, massive bodies of electromag. struct. *(Russian)* 79−21610
gravitation, Newton constant's role 80−90761
gravitational duality and Backlund transformations 80−12971
gravitational fields, stationary, axi-symmetric, soliton solutions 80−73253
nonlinear field theory continued
gravitational instanton symmetries, classification 79−63110
gravitational instantons and their interactions 80−90766
gravitational solitons with axial symmetry *(Russian)* 79−93030
Green's exponential functions, chiral and gravitational 79−97490
Gribov's ambiguities and horizons 79−71639
Gross-Neveu and nonlinear σ-model, scatt. amplitudes in $1/N^2$ perturbation theory 78−70261
Gross-Neveu chiral model, scatt. theory, 1/N expansion 80−348
Gross-Neveu model, chiral invariant, S-matrix direct calc. 80−68362
Gross-Neveu model, irrelevant operators and equivalent field theories 79−21912
Gross-Neveu model, mass generation, renormalisation 80−27393
Gross-Neveu model, spontaneous mass generation 79−21907
gross-Neveu model as $Z_3=0$ limit of the two-dimensional SU(N) σ model 79−35949
Gross-Neveu model in $2+\epsilon$ dimens., composite operator anomalous dimens. 77−67660
Gross-Neveu type models, quantisation of a nonlinear phase space classical mechanics 79−6255
group theoretical construction of two-dimensional models with infinite sets of conservation laws 80−99056
H-spaces, gravitational instantons, spin coeff. method 80−31654
hadron nonlinear string model 77−87901
hadronic structure theory, derivation of static bag and bag constant estimation 79−58932
harmonic maps as models for describing broken symmetries 79−26222
Heisenberg Klein Gordon eqn., soln. in space time of const. curvature 80−62829
Heisenberg-Klein-Gordon equation, localised solns. in flat Schwarzschild space-time 80−4620
Higgs model, 1+1 dimensional, charge confinement and vacuum struct., instantons 80−341
Hilbert space sectors for solns., of relativistic eqns. 77−38080
holistic physics in the theory of magnetic monopoles 79−49369
homotopy theory for soliton solns. classification *(German)* 78−78062
Hopf fibrations of the sphere-constraints in the non-linear σ models 80−86573
hydrodynamic model, nonlinear pion+pion chiral Lagrangian, $e^+ + e^-$ and p+p collisions 78−32966
hydrodynamics, quantum relativistic, nonlinear generalised equations 80−68380
identical motion in relativistic quantum and classical mechanics 77−61177
index symmetry of classical Yang-Mills fields, symmetry effect on instantons 79−71631
infinite constituent bound states, quantum correction soliton states 79−2903
instanton calculations using dimensional regularisation 79−2908
instanton classical solution of a conformally invariant field theory 79−93285
instanton correction to vac. energy densities and bag const. 80−37211
instanton density in a theory with massless quarks 80−37210
instanton distribution, external field effects in SU(2) gauge field 80−4849
instanton effects on static $\bar{Q}Q$ potential 79−9333
instanton Green functions and tensor products 79−54252
instanton quantum fluctuations, in 2-D nonlinear theories *(Russian)* 80−4868
instanton singularities, Borel summing, method introduction 79−71624
instanton solns. for coupled nonlinear scalar and fermion fields 77−79220
instanton statistical mechanics in QCD 80−57567
instantons, θ-vacua, confinement in 1+1 Abelian Higgs model 80−77979
instantons, differential geometry and global anal., appl. to Yang-Mills equations 79−30641
instantons, geometrical description of parameter space 79−30653
instantons, high-dimens., topological charges in SU(3) group 79−30638
instantons, variational anal. 78−24934
instantons, virial theorems, variational arguments 77−49857
instantons and antiinstanton forces in sigma model and Yang-Mills theory 77−26462
instantons and characters in non-Abelian Yang-Mills theory 79−63345
instantons and embeddings in gauge field configurations, group theoretic study 80−4878
instantons and fermions in the field of instanton 79−26217
instantons and Kahler manifolds 79−12925
instantons and monopoles in Yang-Mills gauge field theories 80−91003
instantons and the 1/N expansion 80−400
instantons and vacuum tunnelling, canonical formalism in (1+1)-dimens. Higgs model 79−63348
instantons as link between weak and strong coupling in QCD 80−42403
instantons in a quark plasma, superheavy hadrons and neutron stars *(Russian)* 79−36039
instantons in field theory 79−71642
instantons in the presence of a fixed density of massless fermions in two dimensions 80−62853
interacting EM waves in general relativity exact solns. of Einstein-Maxwell eqns. 77−60985
intersoliton forces in weak-coupled quantum field theories 77−71430
invariant renormalization for theories with nonlinear symmetry 78−70290
inverse scattering method for equation $\sigma_{xt}=e^{\sigma}$, soliton soln. 78−389
inverse scattering method for the classical massive Thirring model with anticommuting variables 79−12626
inverse scattering problem and instanton construction by algebraic geometry, review 80−47203
inverse scattering transformation, correl. with exact quantum eigenstates 79−58873
Ising two-dimens. model and quantum field theory 77−69471
k-instantons in Sp(1) Yang-Mills theory, calculation method 80−13223
Kadomtsev-Petviashvili eqn., appl of variation of action method of one field solitons 80−331
kerr-Schild geometry, spinors, and instantons 79−35601
kink solution in ϕ^4 lattice field theory 77−22651
kink theories, approximately straight 80−82871
kinks and cobordism in field theories, general relativity fermions 80−98835
Klein-Gordon eqn., two dimensional model anomalously slow stochastisation *(Russian)* 79−89068

nonlinear field theory continued
Klein-Gordon eqn. in stationary space times, positive and negative frequency solns. 78−29002
Klein-Gordon eqns., nonlinear, with localised solns. 78−89620
Klein-Gordon equation, stringlike solns. 78−82114
Klein-Gordon equation and scattering theory 77−5986
Klein-Gordon equations, nonlinear model, particle-like piecewise analytical soln. *(Russian)* 77−30228
Klein-Gordon kinks with fourth order derivative self coupling 78−32970
Klein-Gordon nonlinear eqn., solitary wave exist. in higher dimens. 77−74232
Klein-Gordon nonlinear problems, existence of standing waves *(French)* 79−63339
Klein-Gordon-Schrodinger coupled eqns. 79−35955
Korteweg-de Vries equation, invariances and conservation laws 79−26244
Korteweg-de Vries equation, two-dimens. distrib. soliton soln., asymptotic anal. 79−49376
Korteweg-de Vries system, Lax representation, conservation laws 80−82893
Korteweg-de Vries theory, Hamiltonian structures and Miura like transformation 80−95216
Lagrangian, exact solutions in field thory 79−75677
lattice gauge theories, chiral symmetry dynamical breaking 80−99061
lattice nonlinear $O(2)_3$ model, phase transition between broken/unbroken symmetries 79−9147
lattice quantisation of Sine-Gordon system, single-site approx. 79−17603
Lie-Backlund operators props. from variational derivatives 80−37159
linearisation program for nonlinear field eqns., Lie groups 80−105784
linearization of relativistic nonlinear wave equations 80−62837
local field theory of solitons 79−12953
localised solns. of nonlinear spinor field 77−71223
Lund-Regge system, prolongation structures and connection forms 78−93805
magnetic fields, flux string and monopole, geometric configuration, compared to O(3) nonlinear σ-model 80−57527
mass generation for fermion field in absence of chiral symmetry breaking 80−347
massive CP^n sigma models, topological struct., finite action configurations 80−57476
massive gauge theories, with instantons, wave functions, energies, vacuum and heavy quarks, WKB Schrodinger eqn. 79−35951
massive Thirring model, inverse scatt. transform method, relativistic invariant formulation 79−71598
massive Thirring model, multisoliton solns. in Pohlmeyer-Lund-Regge system 80−47195
massive Thirring model, S-matrix calcs., required number of conserved currents 80−42329
massive Thirring model, sine-Gordon eqn., soliton struct., Coleman correspondence 78−8509
massive Thirring model, struct. and soln. 79−85230
massless boson, unified nonlinear theory 80−376
massless Euclidean Thirring field, four point Schwinger function, Lorentz group invariant forms *(German)* 80−90980
massless scalar and EM field equations interacting with gravit. field, particle-like solns. 79−54290
massless Thirring model, saturating field configurations for two point Green's function 79−35923
massless Wess-Zumino model in 4-dimens., asymptotic estimates 80−82877
massless $[g\phi^4]_4$ theory, functional integrals, complex instantons and asymptotic perturbation series 80−86571
membrane models and generalized Z_2 gauge theories, renormalisation props. 80−86587
meron pair, introduction, motivation and formalism 80−82861
meron pairs, bare activity 80−82862
meson interactions, LSZ reduction formulae, soliton asymptotic theory 78−4774
meson spectroscopy based on nonlinear field proper oscills., equivalence theorem 78−89689
mesonic octet decays, chiral QFT description using one loop approx. *(Russian)* 79−63471
microscopic causality for quantised solitary wave theories 78−82095
microscopic system mechanics, solitons and 1-dimens. Schrodinger eqn. 79−12934
Minkowski-space formulation of two-pseudoparticle processes 80−95220
multi-soliton solutions of nonlinear partial differential eqns. 80−105763
multicomponent chiral and gauge models, stationary solns. 79−85213
multidimensional nonlinear eqns., N-soliton solns. by Hirota's method 80−105797
multidimensional stable relativistic solitons *(Russian)* 80−13224
multisoliton solutions of nonlinear Klein-Gordon eqns. 79−12617
multisolitons, kinklike, in polynomial field theories 78−21014
multivacuum field theory models; cascade evolution of spherically symmetric pulsons 77−61192
multivortex solutions of the Ginzburg-Landau equations 79−71634
N-soliton states in polynomial field theories 77−18174
non-Abelian plane EM wave analogues 77−87904
non-linear wave equations in a curved background space 78−65827
non-one-dimensional soliton-like solutions for some field theories 77−67560
nonAbelian, nonlinear Yang-Mills field eqns., self-duality, helicity, coherent states 80−31988
nonlinear 3-dimens. chiral field, phase transition, 1/N renormalised expansion 79−49365
nonlinear σ model, 2-D, topology and higher symmetries 79−26241
nonlinear Bose systems, Dyson-Wick expansions 78−73921
nonlinear gauge fields and the structure of gravity and supergravity theories 78−77791
nonlinear Klein-Gordon eqn. related to Riemannian geometry, localised solns. 79−26223
nonlinear scalar field theory, space-time metric *(Russian)* 78−74127
nonlinear spinor field quantum theory, unitarisation 79−45021
nonlinear SU(n) a lattice field theory, phase transition 79−252
nonlinear super-Poincare fermion, quantisation in bag like formulation 80−4923
nonlinear superfields and quark confinement *(Chinese)* 80−42346
nonliner Schrodinger eqn., appl of variation of action method of one field solitons Kadomtsev-Petviashvili eqn., appl of variation of action method of one field solitons 80−331
nonlocal currents for supersymmetric nonlinear models 80−52414
nonlinear field theory continued
nonperturbative methods stability of soliton-like solns. 77−2750
nonpolynomial scalar interactions in four dimens., bounded interactions 80−82895
nonpolynomial scalar interactions in four dimens., quartic interaction 80−82894
nonrelativistic effective πN vertex, PCAC and σ-model 80−52591
nontopological solitons, hadron appl. 80−47191
null-plane quantisation in nonlinear Lagrangian theories 77−61194
O(2N) Gross-Neveu model, O(8) Dynkin diagram P_3 symmetry 80−77968
O(3) σ model, struct. of instanton plasma anal. 78−16912
O(3) σ-model, confinement in two dimens. models with factorisation 79−36011
O(3) σ-model, nonlinear, quantum fluctuations of instanton solns. *(Russian)* 78−74161
O(3) invariant theory, quantisation in neighbourhood of classical soln. 79−97522
O(3) nonlinear δ-model, instanton-anti-instanton interactions, fermion theory *(Russian)* 80−47193
O(3) nonlinear σ model, quantisation ambiguity and nontrivial vacuum struct. 79−40662
O(3) nonlinear σ model, quantum fluctuations of instantons 79−71610
O(3) nonlinear σ-model, mass generation in dense instanton gas approx. 80−82880
O(5) nonlinear σ-model as a SU(2) gauge theory 79−35937
O(n+1) symmetric, classical solns., symm. breaking, finite energy solns. 77−10172
O(n) σ model, nonlocal charges in two dimensions 80−18075
O(N) σ-model, two-dimens., mag. susceptibility, phase transitions and high temp. expansion 80−47177
O(N) σ-model with gauge interactions, two-dimens., phase transitions 77−6029
O(N) invariant $(\phi^2)_3{}^2$ model, chiral field model and universality in 3-dimens space 80−105796
O(N) model, dynamical mass generation in $S^1 \times R^3$ 80−99046
O(N) nonlinear σ-model, analyticity of solns. 80−52384
O(n) nonlinear σ-model, field eqn. reduction 80−31979
O(N) nonlinear σ-model, particle prod. and factorising S-matrix 79−71613
O(N) nonlinear σ-model, two-dimens., fifth Painleve transcendent 80−32002
on-shell counterterms and nonlinear invariances 80−22522
one-dimensional ϕ^4 and double quadratic systems, kinks, quantum statistical mechanics 80−47197
one-dimensional backward-scattering model with generalised coupling const., variational soln. 78−66036
one-dimensional complex scalar fields with phase anisotropy, statistical mech. 80−22517
one-dimensional field theories with odd-power self-interactions 79−254
one-dimensional solitary-wave-bearing scalar fields, statistical mechanics, ideal-gas phenomenology 80−105792
one-dimensional systems, variational soln. of sine-Gordon theory and Luther-Emery backward scatt. model for one-dimens. systems 79−40447
one-soliton sector, covariant functional approach 78−78092
order, disorder and generalized statistics 80−99055
ordered physical line structures, nonlinear local field theory, appl. to high polymers, supercond. flux line lattices 78−81859
$P(\phi)_2$ models, soliton solns. 80−42333
particle model based on stringlike solitons 78−62294
particle stability in nonlinear scalar field theory 80−91004
partition function for two-dimensional solitons 79−6039
path integrals definition, rules for nonlinear transform. of variables 78−78072
path-integral quantisation using zero-mode Feynman rule 78−70276
Penrose theory in particle physics 78−29321
percolation problem, high order behaviour in 0^3 field theories 78−65883
periodic vacuums, functional integrals, classical sine-Gordon solns., Coulomb gas props. 79−26226
phase transition in 2D Coulomb gas, sine-Gordon theory and XY model, renormalisation group anal. 80−36950
phase transitions, structural, first order, anharmonic oscillator model in (1+1) dimensions 80−86239
pion-nucleon field interactions, covariant perturbative expansion in SU(2)×SU(2) model 77−5983
planar diagrams, SU(N) asymmetric model, semiclassical approach 80−77957
Poincare self-stresses, model and field Lagrangian densities 80−52438
point transformations and non-linear system quantisation, S-matrix from perturbation theory 79−109
polynomial conservation laws in (1+1) dimens. classical and quantum field theory, nonlinear Schrodinger eqn. 78−54224
polynomial field, extended hadron bag model based on exact soln. 77−5997
polynomial field theories, nonlinear Klein Gordon eqn., exact multiple solution solns. 78−45773
Prasad-Sommerfield soliton, excited states, SU(3) generalisation 80−4877
Prasad-Sommerfield soliton mag. monopole, excited states and SU(3) generalisation 79−40665
pulsons, spherical symm., large amplitude, dynamics *(Russian)* 77−30274
QCD, effective Lagrangian, possible σ-model 80−86679
QCD vacuum struct. in chiral U(N)⊗U(N) symmetry 79−93347
QED, nonlinear approach, charged fermion fields 79−97545
QED in nonlinear gauge, for processes involving soft photons 77−79236
quantum action method in quantum field theory 79−40659
quantum aspects of classical and statistical fields 79−58585
quantum chiral model, local polynomial current conservation in renormalised 1/N perturbation theory 80−13232
quantum corrections to soliton mass in QFT, Feynman rules 78−78069
quantum field theory, nonperturbative, resonance states, solitons 78−380
quantum gravity, positive action conjecture and asymptotically Euclidean metrics 79−58611
quantum mass corrections to supersymmetric soliton theories in two dimensions 79−54254
quantum soliton and classical soliton 80−12986
quantum soliton operators for monopoles and Fermionization mechanism of dyons 79−35940
quantum theory of solitons, review 78−70288

nonlinear field theory continued
quantum vortex soliton operators in canonical formalism, gauge theory superselection rules 79−49386
quark field quantum fluctuation computation in arbitrary Yang-Mills instanton background 80−13268
quarks, fermion field, nonlinear, origin of four quark flavours, quantum numbers, isosymmetry breaking 80−62920
quartz resonator, large mag. field effect on rate of time 80−27195
quasilinear partial differential equations, separability 78−65784
quaternionic multi $S^4 \approx HP(1)$ gravitational and chiral instantons 80−31656
radiation damping force, 1-D, new mechanics 80−82632
relativistic classical nonlinear field eqns., virial theorem, solns. and nonlinear scatt. 79−97218
relativistic field eqns., geometric and algebraic foundation of spinor formalism 78−37128
relativistic field eqns., two-soliton solns. 78−74124
relativistic models of nonlinear quantum mechanics 79−12927
relativistic nonlinear spinor eqns. *(Russian)* 77−45751
relativistic strings, exceptional waves and characteristic shocks 78−89618
relativistic vortices interacting through scalar field, solns. for nonlinear coupled equations 79−22039
renormalisability of superconductivity models, nonlinear spinor models, fermions, collective bosonic states 77−18179
renormalisable theories from nonrenormalisable interactions 78−383
renormalised perturbation theory, model of 3-D nonlinear field, free of UV divergences 78−54567
review, classical soliton solns. and semi-classical quantisation techniques 78−8255
scalar complex field, Lorentz invariant system, exact many soliton solns. *(Russian)* 77−30275
scalar field with scalar pot., localised solns. 77−71419
scalar fields in 1+1 dimensions with spontaneously broken U(1) symmetry 78−54554
scalar interactions, 1/N expansion 78−16903
scalar relativistic fields, symmetry groups, with self-interaction 79−30664
scalar theory in isotropic homogeneous space-time 79−2676
scale-invariant gauge theories, instanton role in QCD, QED and $CP^{(N-1)}$ 80−27400
scattering operator, analyticity in nonlinear relativistic classical and prequantised field theories 80−73611
Schrodinger eqn., nonlinear variants, proposed neutron interferometer expt. 79−92984
Schrodinger equation, nonlinear field equations, quantum inverse scattering transform method, 2-D ice and ferroelectric lattices 80−68348
Schrodinger theory, scatt. of quantised solitons 77−49842
Schwarzschild geometry, nonlinear scalar field dynamics 79−275
self-interacting theory of nonlinear quantum field 78−70251
semiclassical fields in soliton sectors 78−29232
semiclassical soliton solns. in quantised field theories 80−4874
semiclassical spectrum of two dimens. nonlinear σ models 78−378
shock wave solutions, massless self-interacting theories 77−2727
sigma model, nonlinear, soliton stability in S^2 80−37165
$(\sin \phi)_2$ interaction in box, soliton soln. fermionisation 79−88840
sine Gordon field, thermodynamics 77−87913
sine Gordon model, quantum inverse problem method 80−68377
sine Gordon theory, derivation based on infinite set of coupled pendula 79−92962
sine Gordon theory, equivalence to z-dimens. ferromag. classical X-Y model low temp. behaviour 77−13873
sine-Gordan theory, Hamiltonian structures and Miura like transformation 80−95216
sine-Gordon chain, displacement fluctuations, long-time behaviour and dynamic scaling props. 80−101764
sine-Gordon eqn., geom. prop. of Backlund transform. 79−12620
sine-Gordon eqn., separability 78−65784
sine-Gordon eqn. as nonlinear scalar field model in Duffin-Kemmer formalism *(Russian)* 80−86599
sine-Gordon eqn. generalisation for any symmetric space, eqns. of motion 80−32001
sine-Gordon eqn. in 2+0 dimens., solns. 79−71258
Sine-Gordon eqn. in 2+1 dimens., special solns. 79−12932
Sine-Gordon eqns., differential geometry appls., soluble relativistic field theories *(Russian)* 78−74162
sine-Gordon eqns., Lax pairs for certain generalisations 80−31997
sine-Gordon equation, Backlund transform., physical space-time solitons 80−77629
sine-Gordon equation, classical solns. of field eqns., moving t'Hooft-Polyakov monopole *(Russian)* 78−16935
sine-Gordon equation, discrete, on SU(2) lattice, group theory aspects 80−57486
sine-Gordon equation, discretisation 79−21931
sine-Gordon equation, intrinsic geometry 80−86553
sine-Gordon equation, multidimensional soliton solns. 79−49383
sine-Gordon equation, nonlinear field equations, quantum inverse scattering transform method, 2-D ice and ferroelectric lattices 80−68348
sine-Gordon equation, one dimens., group of invariance, dimens. anal. method 78−54528
sine-Gordon equation, polynomial field theories, solitary wave solns. 77−2726
sine-Gordon equation, regular solns. using surfaces of const. negative curvature *(Russian)* 78−20980
sine-Gordon equation, rotationally symmetric breather-like solns. 80−77955
sine-Gordon equation, supersymmetric, prolongation struct. inverse scatt. formalism 80−99032
sine-Gordon equation and nonlinear σ model on a lattice 79−21932
sine-Gordon equations for 3-D solitons, classical $\lambda\phi^4$, double and single eqns. 78−45785
sine-Gordon field, topology and static-soliton solns. 77−49850
Sine-Gordon field theory, ferromag. model, existence and renormalisation in all dimensions 79−26248
sine-Gordon field theory, two dimens., second order phase transition, lattice model 78−78095
sine-Gordon field theory Coulomb gas equivalence, classical gas with logarithmic pot. 80−4850
sine-Gordon finite-energy two-dimens. solns. and Yang-Mills pseudoparticles, transformation 77−65100
sine-Gordon model, inverse scatt. transform method, relativistic invariant formulation 79−71598
sine-Gordon model, supersymmetric solitons and monopoles 80−31991
sine-Gordon model for large coupling consts., soliton scatt. matrix *(Russian)* 80−13221
sine-Gordon N-soliton quantum scatt. 77−34084
sine-Gordon pendulum eqn. and $\lambda\phi^4$ model, generalisation 77−49610
sine-Gordon soliton mass, higher order correction 77−61188
sine-Gordon solitons, exact two-particle S-matrix 77−74608
sine-Gordon supersymmetric model, higher local quantum conserved currents 80−52435
sine-Gordon supersymmetric model, quantisation of conservation laws and superrenormalisation 79−89058
sine-Gordon supersymmetric theory, infinite set of bosonic conserved currents 78−62313
sine-Gordon system, bion dissoc. 80−13201
sine-Gordon system, breathers, extended object QSM 80−42347
sine-Gordon system, Lax representation, conservation laws 80−82893
sine-Gordon theory, bound state of massive Thirring model 78−74141
sine-Gordon type field eqn., two-dimens., solitons, quark confinement 78−74160
singular gauge instanton field, gauge zero modes, instanton determinants, and quantum-chromodynamic calculations 79−71635
singular perturbations for initial value problems, hyperbolic nonlinear partial differential eqns. 78−58111
singular potentials in non-relativistic quantum theory, review *(Russian)* 80−68345
Skyrme gauge model, topological solitons 80−9086
solitary solutions collision in nonlinear field theory, variational anal., ϕ^4 appl. 79−35922
solitary wave exchange in NN pots. 78−70457
solitary wave exchange potential in pseudoscalar and scalar meson fields 79−71617
solitary wave transport, nontrivial example soln., numerical method 80−77971
soliton, extended particle, quantisation, degeneracy of eigenstates 80−73594
soliton, massive elementary particle, maintenance of size and shape 79−71643
soliton, non-topological, non-Abelian internal symmetry in 3+1 dimensional space-time, quantisation, collective coord. and Lorentz covariant methods 80−47199
soliton dynamics in nonintegrable systems, classical solns. 78−28996
soliton equations and pseudospherical surfaces, conservation laws, Backlund and scale transformations 79−75688
soliton field theory, construction of Green's functions from an exact S matrix 79−71629
soliton free energies calcs., WKB approx. failure 80−42073
soliton local field theory construction, extension to (non)Abelian (2+1) and (3+1) dimens. 79−71622
soliton mass, surface tension, in $(\lambda|\phi|^4)_2$ quantum field theory 77−30240
soliton mass two-loop quantum correction in scalar field theories 77−10175
soliton models of hadrons, semiclassical approach to quantum field theory 77−5981
soliton quantisation using Bogolyubov transformation 78−16695
soliton quantised states in non-perturbative field theory 77−67564
soliton quantum mechanical mass in supersymmetric theories 80−22536
soliton scattering in non-linear Schrodinger theory 78−8256
soliton solutions, nontopological, conservation laws 79−45022
soliton solutions, radiative corrections in infinite volume 77−13865
soliton solutions, renormalisation and quantum corrections 80−82884
soliton theory, review 80−47204
solitonlike fields, gauge phase factor operators, extended Higgs models and 't Hooft algebra 80−42324
solitons, charged, stability, relativistic complex scalar field, direct Lyapunov method 80−62827
solitons, effective Lagrangian, soliton form-factor and intersoliton asymptotic force 79−45010
solitons, geom. interpretation 79−54266
solitons, multidimens., additive topological laws of conservation *(Russian)* 77−74601
solitons, nontopological, and appls. to hadrons 78−32968
solitons, pulsating, energy of n-particle bound state *(Russian)* 77−74267
solitons, scale invariance 79−58866
solitons, solution of nonlinear Liouville equation 80−68374
solitons, static form factor, quantum correction in 2-D field theory with classical lump, asymptotic behaviour 80−52395
solitons and instantons in field theory 78−8495
solitons and nonlinear waves, stability in three dimens. 79−97211
solitons in some geometrical field theories 80−27390
solitons in Yukawa and Georgi-Glashow models with dynamical spontaneous symmetry breaking 79−6264
solitons with particle properties, real scalar fields anal. 77−45936
solitons with quantised charge, mass formula 79−93282
solvable models, common features 77−67573
spherical symmetric solution stability, influence of weak perturbations *(French)* 78−16904
spherically symmetric solitons for nonlinear or scalar field-gauge field interactions 79−97521
spin glasses and other glasses, symmetry and topology concepts 79−28541
spin in kink-type classical field theories 78−81861
spin-orbit terms of the heavy-quark potential in the presence of instantons 79−71710
spinless particle interaction with electromag. field, path integrals, Klein-Gordon eqn. 78−58144
spinor models, integrability in two-dimens. space-time 80−77935
spinor soliton as elementary particle, wave packet-soliton equivalence 78−12814
spinor soliton stability 79−97532
spinor theories in curved space-time, nonlinear invariances 79−54029
spinor theory, gravit. interaction *(Russian)* 77−79023
spinor theory, nonlinear, two-point function 79−63366
spontaneous symm. breaking and nonlinear Lagrangian 78−70303
static radially symmetric exact multinodal solns. to nonlinear coupled field eqns. 78−74131
stationary multisolitons, existence 80−13218
statistical mechanics, classical, universal features for continuum-field nonlinear Hamiltonians 78−93543

nonlinear field theory continued
Stiefel manifolds, 2-dimens. nonlinear σ-model, S-matrix regularities 80−86576
string representations and hidden symmetries for gauge fields 79−49378
strongly interacting Higgs bosons, gauged nonlinear σ-model, $SU(2)_L \times U(1)$ extension 80−86656
SU_∞ nonlocal conserved currents for two-dimensional chiral theories 80−52413
SU_N/Z_N gauge invariant theory, phase factor operators and soliton fields 80−77947
SU(2,1;1) nonlinear invariant σ model, superconformal group and curved fermionic twistor space 80 62831
$SU(2)_L \times U(1)$, nonlinear realisation of Weinberg-Salem model for chiral $SU(4) \times SU(4)$ meson theory *(Russian)* 79−30693
$SU(2) \times SU(2)$ and $SU(2) \times SU(1,1)$ chiral theories, exact finite energy solns. 79−54253
SU(2) gauge field theory, nonlinear scalar field eqn., spherical symmetric exact solns. *(Chinese)* 80−62886
SU(2) multi-instanton solutions, conformal transformation props. of one-loop tunnelling amplitudes 78−12822
SU(2) nonlinear σ model, kink solns., form factor interpretation 78−24964
SU(2) theory with four fermion interaction and asymptotic freedom, exact soln. 80−4858
SU(2) Yang-Mills gauge theory, two meron configurations in transverse gauge 79−71637
SU(2)/U(1) nonlinear theory, solitons with nonvanishing Hopf index 78−86410
SU(2n) principle models for integrable nonlinear systems, current constraints, conservation laws 80−86619
SU(3) quark-meson σ-model, quark masses 80−47178
SU(3) Yang-Mills theory, study of O(3) symmetric merons 79−30651
$SU(N+1)$ σ model (or CP^N model) as nonlinear realisation of $SU(N+1)$ symmetry 79−58871
$SU(N)_L \times SU(N)_R$ nonlinear σ-model, renormalisability and struct. 79−6279
$SU(N) \times SU(N)$ chiral symmetry, spontaneous breaking, instanton role 80−47219
SU(N) chiral Gross-Neveu spectrum derivation 80−47176
SU(N) gauge groups, N=2,3,4, meron and meronlike configurations 79−71636
SU(N) Higgs theory, two-dimens., instanton approach 80−99053
SU(N) invariant non-linear σ models 79−17613
super $(\phi^3)_2$ model, large order perturbation theory 80−82876
super sine-Gordon eqn., supergroup geometrical interpretation, supersymmetric extension 80−57475
(super-ϕ^3)$_4$, Euclidean model, normalisation of Schwinger functions 79−89060
(super-ϕ^3)$_4$, regularisation of Euclidean model, supersymmetry Ward identity derivation 79−89059
superconformal group and quark-like fermionic coordinates 80−9145
supercurrent, existence and deduction from an arbitrary superfield Lagrangian *(Russian)* 78−89633
supersymmetric σ model, nonlocal charges from zero curvature 80−31995
supersymmetric chiral models, instanton type solns. *(Russian)* 79−58901
supersymmetric extension, Kahler manifolds, Grassmann manifolds and CP^{n-1} models 80−9113
supersymmetric form of nonlinear σ model in two dimens. 78−24957
supersymmetric nonlinear σ model, nonlocal charges and currents 80−27410
supersymmetric nonlinear σ model, S-matrix determ. 78−66052
supersymmetric nonlinear σ model, spontaneous breakdown of chiral symmetry 78−54549
supersymmetric quantum theory construction around supertranslated soliton soln., Dirac's method 78−45783
supersymmetric sine-Gordon eqn., polongation struct. and inverse scatt. formalism 80−47173
supersymmetric sine-Gordon kink struct., and 'doubled' supersymmetric Ising model 79−71614
supersymmetric sine-Gordon model, exact soliton like solns. 79−30643
supersymmetric theories with solitons, algebra including topological quantum numbers as central charges 78−89630
supersymmetric theory, canonical quantisation 79−97283
supersymmetric theory, quantisation 77−65088
supersymmetry Volkov-Akulov model, constrained linear realisation 78−78107
tachyons, monopoles and related topics, book 79−44718
Thirring model, 2-D, complete integrability 78−49685
Thirring model, chiral, CP^{n-1} and SU_n, exact S-matrix 80−90985
Thirring model, massive, existence and relation to Sine-Gordon theory 77−57433
Thirring model coupled to gravity, classical solns. in generally covariant model with fermions 80−9091
Thirring model Lagrangian, generalised, interacting fermions, interacting solitons 77−45937
Thirring model massive phase, dynamic mass generation 80−4851
Thirring model SU(1,1) group representation theory algebraic struct. *(German)* 79−89055
Thirring-Weiss model, massless, saturating field configurations 79−35953
three body forces, nonlinear field theories equivalence to action-at-a-distance 77−26181
topological currents for chiral groups in three space dimens. 77−71451
topological solitons and duality *(German)* 80−91010
transverse pure gauge fields and nonlinear chiral solitons, Coulomb condition 78−78068
twisted scalar field, vacuum solns. 78−93804
two dimensional field theories with infinite number of conservation laws and Backlund transformations 80−9095
two dimensional models, nonlocal charges, existence 79−49385
two soliton sectors of two dimens. canonical quantum fields, semiclassical approx. 79−12939
two-dimens. Thirring and Schwinger models, solitons and confinement *(German)* 77−82665
two-loop divergences 78−54529
two-point function 77−65078
two-soliton soln. of coupled nonlinear evolution eqn. 77−79210
U(N,r) σ models, generalisations of σ and Cp^N models, and instantons 79−49377
nonlinear field theory continued
unified interactions, nonlinear realisation, spontaneous symmetry breaking 79−13010
unitary invariant generalisations *(Russian)* 78−66024
unitary quantum mechanics, nonlinear and relativistic invariant fields 80−4567
unstable solitons, semiclassical calc. of half-life 77−45953
vacuum decay, effective pot., vacuum tunnelling and 1/N expansion 79−93289
vector fields, classical theory, nonlinear generalisation, internal symms., conservation laws *(Russian)* 78−62328
vortex solitons, nonlocal field theories 79−49384
wave functionals, soliton sector and asymptotic vacuum states, Creutz quantisation method 80−68340
weak interactions, CP violation and instantons 80−354
Weiss-Zumino model, three loop β-function for superfield techniques 80−99043
WKB wave function, systems with many degrees of freedom, solitons and pseudoparticles 78−29255
Yang-Mills, dyon solns. and symmetry, elec. and mag. charge conservation 77−26183
Yang-Mills, nonstatic solns. of sourceless equation for SO(4) and SO(3,1) 77−65101
Yang-Mills eqns., new multipseudoparticle solns. 78−74152
Yang-Mills equations, SL(3,C) self dual instanton solns. 79−63369
Yang-Mills field, isodoublet-scalar field coupled, large order estimates for perturbation theory 79−71632
Yang-Mills multi-instantons, quantum fluctuations, Seeley coeffs. 80−77934
Yang-Mills pseudoparticle solns., quantisation, conformal group contraction 79−67464
Z(2) and Z(3) cyclic symmetric vector field theories, 1-dimens. solitons 80−77950
zero frequency mode contributions in soliton quantisation general scatt. amplitude 78−29234
zero frequency modes in perturbation expansion about classical field theory configs. 77−18169
zero-component field theories, high order behaviour without $n \to 0$ limit 79−75438
$K \to \pi e(\mu)\nu$, form factors, SU(3) σ-model one loop calc., chiral symmetry breaking 80−52506
ϕ^4 3-D field theory, IR behaviour and connection with critical phenomena 79−71601
ϕ^4 model, free energy, spontaneous symmetry breaking 80−101925
ϕ^4 theory, radiative corrections and dynamical symmetry breaking 77−18196
ϕ^4-field model with image mass, spontaneous coherent state transition 80−99057
π condensed phase, σ-model, alternating-layer-spin struct. 80−83057
$\pi \to e\nu_e\gamma$, isospin-breaking, chiral limit, conserved-vector-current violation, σ model 80−62988
π field, nonlinear chiral models, many dimensional solitons 78−4792
$(\bar{\psi}\psi)^2$ two dimensional model, equivalence to sine Gordon systems, conservation laws 79−2917
σ-model, classical solns. of nonlinear 4-dimens. model 79−63347
H atom, relativistic quantum mech. as weak-field limit of nonlinear theory 79−6878
^{3}He, superfluid, chiral fields, in Ginzburg-Landau region 79−55991
$\lambda\phi^4_2$, quantum field as limit of sine Gordon field 78−82094

nonlinear network analysis
basilar membrane, nonlinear electric circuit model, distortion 77−25459
coupled dynamic physiological systems, network thermodynamic simulation 79−96504
exploding wire discharge in RCL circuit with greatly nonlinear resistance *(Russian)* 79−41854
JET, synchronous-generator/bridge-convertor/ohmic heating circuit anal. 80−13893
modulational instability expt. using nonlinear transmission line 77−82397
noise anal. using computer *(German)* 77−88997
nongradient systems, nonlinear instability behaviour 79−75331
quartz crystal resonator nonlinear analysis 79−55299
Schottky-barrier solar cell sensitivity computation 79−62004
solar cell string disturbances, large-signal analysis 79−96461
TWT nonlinear theoretical problems *(Chinese)* 78−74824
Wien bridge oscillator, critical phenomena simulation, threshold instabilities 77−1211

nonlinear network synthesis
adaptive spatial filter for image classification *(Russian)* 78−42292
logarithmic frequency-voltage convertor design 77−13775
SAW filter design for nonlinear phase response, building-block method 77−27433

nonlinear optical susceptibility
aerosol of glass spheres, broadband degenerate four-wave mixing medium 80−43390
air, nonlinear susceptibility and self-focusing *(Russian)* 79−86224
akali metal vapour, seventh and ninth order nonlinear susceptibility meas. 79−55186
m-aminophenol, nonlinear optical susceptibility, second order, calc. from mol. spectra *(Russian)* 79−27318
ammonium malate, SHG, 492-640 nm, phase matching, refr. index and nonlinear susceptibility 77−72031
ammonium malate, single cryst., optical SHG, refr. index, susceptibility 78−63152
antisymmetric components interrel. with symmetric components, in Kleinman symmetry relation 78−33770
atomic resonant lines, ang. momentum depend. of laser-induced birefr. and dichroism 79−10367
atomic systems, nonlinear magnetoelec. susceptibility, Faraday effect, laser intensity depend. 78−59076
atomic vapours, effects of magnetic fields on four-wave mixing processes 79−23024
barium formate, nonlinear optical susceptibility tensor, Maker fringes 78−13751
benz-1,2, anthracene, nonlinear third-order electric susceptibility 78−74944
benzene, liq., third order optical susceptibility *(German)* 79−50358
benzene, Raman nonlinearity characterisation by two-beam interferometry 77−38986

nonlinear optical susceptibility continued
benzene, third-order nonlinear electric susceptibility, from CNDO wavefunction 78−37558
benzene-cyclohexane mixture, interference between Raman resonances in four-wave difference mixing 77−23712
benzenes, m-disubstituted, nonlinear optical props. 77−58373
benzenes, substituted, liq., optical nonlinearities and hyperpolarisabilities meas. 77−88857
benzoquino-dimethanes, nonlinear third-order electric susceptibility 78−74944
2-bromo-4-nitroaniline, nonlinear optical susceptibility, second order, calc. from mol. spectra *(Russian)* 79−27318
bromobenzene, liq. third order optical susceptibility *(German)* 79−50358
carbon tetrachloride, neat and cyclohexane mixture, nonlinear susceptibility, $\chi^{(3)}$, reson. and non-reson. contribs. 79−987
CARS in condensed phases, perturbation theory of third-order nonlinear susceptibility 80−14393
2-chloro-4-nitroaniline, nonlinear optical susceptibility, second order, calc. from mol. spectra *(Russian)* 79−27318
chloroform. liq., reson. nonlinear susceptibilities using IR optical parametric oscillator 79−10347
cholesteric liquid crystal, third harmonic generation, third order susceptibility 78−30021
chrysene, nonlinear third-order electric susceptibility 78−74944
coherent anti-Stokes Raman spectroscopy, polarisation sensitive, resonant susceptibility meas. 79−75605
conjugated hydrocarbon chains, linear and nonlinear elec. susceptibilities calcs. 78−19437
crystals, nonlinear susceptibility determ. using 4th and 5th harmonic generation 77−50717
cyclohexane, neat and CCl_4-C_6H_{12} mixture, nonlinear susceptibility, $\chi^{(3)}$, reson. and non-reson. contribs. 79−987
degenerate 4-wave mixing in plasmas 80−24179
dense optically transparent media, third-order optical susceptibilities 77−38981
density operator, diagrammatic evaluation 78−5523
diamond, nonlinear optical susceptibility, tight binding bonding orbital model 80−5784
dibenz-1,2,3,4-anthracene, nonlinear third-order electric susceptibility 78−74944
m-dinitrobenzene, nonlinear optical susceptibility, second order, calc. from mol. spectra *(Russian)* 79−27318
m-dinitrobenzene, nonlinear optical susceptibility tensor, calc. 79−23011
discrete multilevel system, nonlinear polarisations and excitations, time depend. 77−27313
Doppler-free two-photon dispersion problem 80−106562
fifth order atomic optical nonlinearities in multiphoton resonances 80−28275
four-photon spectroscopy of condensed media, nonlinear spectroscopy developments 80−91860
four-wave mixing spectroscopy, coherent cancellation of background 80−91842
four-wave mixing spectroscopy in crysts., nonlinear spectroscopy developments 80−91861
gas, third harmonic generation near two-photon reson. 79−59760
hexafluoroisopropanol, third order optical susceptibility obs. 77−34906
higher-order nonlinearities, theory 77−50717
hydrazonium tartrate enantiomers, and deuterates, struct. and opt. props. 77−68954
interference between SHG signals, accurate determ. of nonlinear optical coeffs. 77−31115
m-iodobenzene, nonlinear optical susceptibility, second order, calc. from mol. spectra *(Russian)* 79−27318
ionic crystal, nonlinear third-order susceptibility near Raman, two-photon resonances 79−94282
ionic crystals, centrosymmetric, stimulated excitation of second harmonic, microscopic theory 80−91849
ionic crystals, dispersion calcs. of cubic nonlinear susceptibility near Raman resonance 79−94292
isotropic liquid, polarisation props. of CARS 78−80334
isotropic media with fifth-order nonlinear susceptibility, focusing effects on six-photon processes *(Russian)* 78−25917
isotropic medium, three-photon light scatt. phenomenological theory *(Russian)* 78−83024
layered compounds, SHG at 0.6943 and 1.06 μm, energy gap depend. 78−30019
liquid, optical Kerr const., electronic and orientational contribs., obs. by coherent Raman techniques 77−88874
liquid, third-order nonlinear susceptibility ratio meas. by CARS Maker fringe technique 79−989
liquid crystal, isotropic phase, self-focusing stability of laser beam 80−99812
liquid crystals, pretransitional behaviour, nonlinear optical obs. 77−51483
magneto-optic Raman scattering of Raman-inactive phonon polaritons 80−91843
MBBA, nematic liq. cryst., nonlinear optical suscept. using light combination scatt. *(Russian)* 80−38064
MBBA liquid crystals, meas. in isotropic and nematic phases *(Russian)* 78−74945
measurement by interferometric and polarimetric methods *(Russian)* 77−61112
methanes, halogenated, nonlinear optical polarisability, bond-bond interaction role 78−18010
methylene blue in methanol, Nd laser radiation *(Russian)* 77−54753
molecular crystals, nonlinear optical susceptibility, second order, calc. from mol. spectra *(Russian)* 79−27318
molecular nonlinear vibrations, selective laser excitation 77−23522
multiparticle correlation function and nonlinear suscept. *(Russian)* 77−61999
naphthacene, nonlinear third-order electric susceptibility 78−74944
naphthalene, nonlinear third-order electric susceptibility 78−74944
naphthoquino-dimethanes, nonlinear third-order electric susceptibility 78−74944
β, β,-naphthyl ethylene, nonlinear third-order electric susceptibility 78−74944
nematic liquid crystal, SHG, mol. symmetry and macroscopic nonlinearity *(Russian)* 78−90457
m-nitroaniline, cryst., nonlinear optical susceptibility and spontaneous polarisation 77−58372
m-nitroaniline, nonlinear optical susceptibility, second order, calc. from mol. spectra *(Russian)* 79−27318
m-nitroaniline, nonlinear optical susceptibility tensor, calc. 79−23011
NMBA, monoclinic, cryst. struct. and nonlinear optical props. 78−26560
one-dimensional semiconductor, delocalisation and superalternation effects in nonlinear susceptibilities 77−11840
organic molecules, conjugated, nonlinear props. of new class of cpds. 79−41413
organic system, nonlinear second-order optical susceptibility 80−9947
parathymol, negative uniaxial cryst., linear and nonlinear optical and dielec. props. 77−75602
phase conjugation in nonlinear molecular gases 79−31618
phenanthrene, nonlinear third-order electric susceptibility 78−74944
1-phenyl butadiene, nonlinear third-order electric susceptibility 78−74944
picene, nonlinear third-order electric susceptibility 78−74944
plasma, fluctuation-dissipative relation in nonlinear electrodynamics *(Russian)* 78−79410
polarisation state evolution near self-focusing or stimulated Raman threshold 78−50867
polydiacetylene solutions, third-order nonlinear mixing (CARS) 79−10354
polymer, one dimensional, nonlinear optical props. 78−46708
propagator approach for calculation, appl. to atomic reson. fluoresc. in gas 79−98436
properties, dispersion, band theory 77−50716
pyrene, nonlinear third-order electric susceptibility 78−74944
pyroelectric, uniaxial, spontaneous polarisation, calc. from results of optical meas. 78−27162
quantum electrodynamics, CPT invariance, permutation symmetry and crossing symmetry 79−55176
Raman scattering, reson., coherent, lineshape, 3rd order nonlinear optical susceptibility 78−42378
rectification effect and meas. appls. 80−91835
reflection-transmission hybrid regime, plane wave soln. *(Russian)* 77−72025
resonant and non-resonant contribs. to $\chi^{(3)}$, time resolved obs. 79−987
resonant Rayleigh-type mixing spectroscopy using ps light pulses, ultrafast relax. study 80−91834
resonator, containing medium with quadratic susceptibility, props. 80−33074
resorcinol, cryst., nonlinear optical susceptibility and spontaneous polarisation 77−58372
α-resorcinol, nonlinear optical susceptibility, second order, calc. from mol. spectra *(Russian)* 79−27318
α-resorcinol, nonlinear optical susceptibility tensor, calc. 79−23011
rhodamine 6G, resonant interference of nonlinear optical suscept. *(Russian)* 77−7160
rhodamine dye, coherent ellipsometry determ. of third order polarisability 79−71511
semiconductor, degenerate four-wave mixing near band gap 80−5782
semiconductor, one-dimensional nonlinear optical props. 78−46708
semiconductor with forbidden band, quadratic nonlinearity 79−10345
semiconductor with zero band gap, freq. tripling and self-interaction of strong EM wave 79−10355
semiconductors, mixed and binary, nonlinear polarisability, self-action effects 80−99786
semiconductors, nonlinear effects, induced by lasers 79−94300
semiconductors, nonlinear optical props., book contrib. 80−78899
semiconductors with superlattice, third harmonic generation *(Russian)* 77−27315
SHG determ. of ferroelec. and antiferroelec. props. 78−74947
spectral representation, asymptotic relns. 77−50715
stimulated Raman scattering frequency shifts, nonreson. contribs. to nonlinear susceptibility 80−53373
styrolene, nonlinear third-order electric susceptibility 78−74944
succinonitrile, plastic crystal, HF electro-optical Kerr effect, orientation depend. 77−24822
tendon, rat-tail, coherent optical SHG 80−89796
tensorial properties 77−24661
three-level system, narrow nonlinear resonances *(Russian)* 80−78898
m-toluylenediamine, dispersion of quadratic susceptibility 79−18477
triphenylbenzene, cryst., nonlinear optical susceptibility and spontaneous polarisation 77−58372
two-photon resonant four-wave mixing with non-monochromatic waves 80−38066
two-photon resonant Rayleigh-type optical mixing and relax. 78−42380
uniaxial pyroelectric, phenomenological approach 77−23705
urea, single cryst., optical SHG, refr. index, susceptibility 78−63152
vapour, radiatively cooled resonant, 3rd order nonlinear optics processes 79−81477
AlN film, SHG expt. 78−30012
AlN, nonlinear susceptibilities 79−27312
$Ba_2NaNb_5O_{15}$, dispersion of quadratic optical susceptibility *(Russian)* 77−3635
$Ba_{0.25}Sr_{0.75}Nb_2O_6$, quadratic susceptibility dispersion meas., oscillator model including structure 78−59078
$BaTiO_3$, ferroelec., nonlinear optical susceptibility calc. 78−9409
$Ba_2TiSi_2O_8$, fresnoite, unsuitability for phase matched SHG 78−46721
CO, gas, phase matched, IR third harmonic generation 77−38985
CO, liq., IR four-wave mixing 78−18006
CS_2 filled waveguide, time-reversed wave generation by nonlinear refraction 78−90447
CS_2 in benzene, third-order nonlinear susceptibility ratio by CARS 78−46713
$CaCO_3$, third order nonlinear optical difference frequency generation 78−22176
$CaCO_3$, with and without inversion centres, nonlinear susceptibilities *(Russian)* 78−13750
$CdGeAs_2$, phase matched fourth harmonic generation, cascade process contrib. 79−76761
CdS, biexciton, low intensity nonlinear coherent mixing study 80−49619
CdS, resonant excitonic contrib. 77−3633
CdS, third order nonlinear optical difference frequency generation 78−22176
CdS(Se), optical detection near absorption band edge 77−749
CdSe 16 μm parametric amplification with HF laser pumping 80−78910
CdTe, backward degenerate four-wave mixing obs. 80−53361
$Cr_3B_7O_{13}Cl$, cubic, approx. nonlinear optical susceptibility 80−78904
$Cu_3B_7O_{13}Cl$, cubic, approx. nonlinear optical susceptibility 80−78904

nonlinear optical susceptibility continued
$Dy_2(MoO_4)_3$, cryst. growth and props. 79−55727
$Fe_3B_7O_{13}I$, cubic, approx. nonlinear optical susceptibility 80−78904
GaAs, electro-optic meas. 77−23707
GaAs, nonlinear electro-optical susceptibility, coupled anharmonic oscill. model 80−2723
GaN, nonlinear susceptibility and coherence length, SHG meas. 78−25924
GaP, electro-optic meas. 77−23707
$Gd_2(MoO_4)_3$, ferroic, linear and nonlinear optical susceptibility 78−22164
Ge, four-wave mixing at room temp. for tunable IR generation 80−9940
Ge, nonlinear optical susceptibility, tight binding bonding orbital model 80−5784
Ge, nonlinear susceptibility, 10 μm, determ. by time resolved ellipse rotation 80−83633
Ge optical switch, picosecond pulse generation at 10.6 μm 79−7159
Ge, phase conjugation of 4 μm for single line and multiline radiation 80−83641
n-Ge:P(As) strong impurity-induced reson. in third order susceptibility 77−46759
H, third-order optical harmonic coeffs., R-matrix calc. 77−57955
H_2, two-photon enhanced third harmonic generation and Raman scatt. 77−88843
He, third-order optical harmonic coeffs., R-matrix calc. 77−57955
$Hg_{1-x}Cd_xTe$, degenerate four-wave mixing of 10.6 μm radiation 80−95943
n-$Hg_{1-x}Cd_xTe$, optical phase conjugation 80−83644
$Ho_{2x}Gd_{2(1-x)}(MoO_4)_3$, ferroic, linear and nonlinear optical susceptibility 78−22164
I_2, molecular vapour, saturable absorpt., self-focusing and nonlinear susceptibility 80−83647
n-InSB, spin resonant four-wave mixing, CW meas. and transient effects 80−48344
n-InSb, cond. electron spectra in quantised mag. field, impurity resonance scatt. *(Russian)* 80−93178
InSb, low intensity nonlinearities, induced by lasers 79−94300
n-InSb, nonlinear optical susceptibility, cyclotron reson. meas. *(Russian)* 79−50341
n-InSb, nonlinear optical susceptibility spin reson. *(Russian)* 79−59749
InSe, SHG 79−81489
$KB_5O_8.4H_2O$, tunable UV generation at 1966 Å 77−68238
KH_2PO_4, third order nonlinear optical difference frequency generation 78−22176
KH_2PO_4, with and without inversion centres, nonlinear susceptibilities *(Russian)* 78−13750
KH_2PPO_4, KD_2PO_4, nonlinear electrooptic effects 80−29721
$KNbO_3$, ferroelec., nonlinear optical susceptibility calc. 78−9409
Kr gas, nonlinear susceptibility meas. via third harmonic generation, Lyman-α 1216 Å source 80−95947
$La_2Ti_2O_7$, ferroelecs., nonlinear optical props. 80−33086
$LiIO_3$, active spectroscopy of polaritons, interf. of direct and cascade processes *(Russian)* 77−38982
$LiIO_3$, dispersion of cubic nonlinear susceptibility meas. 79−76747
$LiNbO_3$, dispersion of quadratic optical susceptibility *(Russian)* 77−3635
$LiNbO_3$, non-centrosymm. crystal, hyper-Raman scatt. obs. 78−94409
$LiNbO_3$, spontaneous parametric light scatt. charcts. meas., 1000-4000 cm^{-1} 77−8640
$LiNbO_3$, third order nonlinear optical difference frequency generation 78−22176
$LiTaO_3$, dispersion of quadratic susceptibility crystal struct. 79−18478
$MgBaF_4$, nonlinear optical susceptibility tensor, Maker fringes 78−13751
NH_3, phase conjugation via degenerate four-wave mixing 80−106566
$(NH_4)_2BcF_4$, incommensurate phase superstructure, linear and nonlinear cryst. optics *(Russian)* 80−14387
$(NH_4)_2BeF_4$, unmatched phase, second optical harmonic generation *(Russian)* 78−79073
NH_4Cl, order-disorder phase transition, type of multicritical point, nonlinear quadratic susceptibility 78−83947
NO nonlinear laser spectroscopy, VUV harmonic generation 80−74175
Na, radiatively cooled vapour, 3rd order nonlinear optics processes 79−81477
Na, two and three photon resonances in strong nonmonochromatic field 77−34908
Na, vap., effective fifth order nonlinear susceptibility 77−65606
Na vapour, effective freq. conversion of radiation 80−28278
Na-Ar, nonlinear optical 5th order susceptibility meas., VUV harmonic generation 78−42381
Na-Ar(Xe) phase-matched mixtures, seventh and ninth order nonlinear susceptibility meas. 79−55186
$Nd_{2x}Gd_{2(1-x)}(MoO_4)_3$, ferroic, linear and nonlinear optical susceptibility 78−22164
$Nd(NO_3)_3$, aqueous soln., single photon absorpt. band struct., electronic resons. coherent ellipsometry 80−90881
$Ni_3B_7O_{13}Br$, cubic, approx. nonlinear optical susceptibility 80−78904
$Pb_3(Ge_{1-x}Si_x)_2O_7$, optical SHG and pyroelectric effect 77−10982
$PbTiO_3$, ferroelec., nonlinear optical susceptibility calc. 78−9409
Rb, vap., 1.06 micron conversion to 420 nm range 79−14040
Rb vapour, Doppler-free two-photon dispersion and optical bistability 80−95940
Rb-Xe mixture, third harmonic generation with Nd:glass mode-locked laser 77−27318
SF_6 multiphoton absorpt. meas. by third harmonic generation 80−1036
SF_6, third harmonic generation at 10.6μ 77−14775
Si, nonlinear optical susceptibility, tight binding bonding orbital model 80−5784
n-Si:P, Sb, reson. four wave mixing, valley orbit splitting 79−89960
$Sm_{2x}Gd_{2(-x)}(MoO_4)_3$, ferroic, linear and nonlinear optical susceptibility 78−22164
Sr, vapour, effects of magnetic fields on four-wave mixing processes 79−23024
$Sr_2Nb_2O_7$, ferroelecs., nonlinear optical props. 80−33086
$Tb_{2x}Gd_{2(1-x)}(MoO_4)_3$, ferroic, linear and nonlinear optical susceptibility 78−22164
Te, SHG under two-photon reson. conditions, third-order nonlinear susceptibility 80−99803
TeO_2, antisymm. components 78−13755
TeO_2, paratellurite cryst., polariton Raman scatt., nonlinear susceptibility 78−25928

nonlinear optical susceptibility continued
TiO_2, third order nonlinear optical difference frequency generation 78−22176
$Yb_{2x}Gd_{2(1-x)}(MoO_4)_3$, ferroic, linear and nonlinear optical susceptibility 78−22164
ZnO, third order nonlinear optical difference frequency generation 78−22176
ZnSe crystal, difference freq. generation of 2 CO_2 lasers 79−10362
ZnSe single crystal, nonlinear optical coeff. and SHG coherence length 77−79893
ZnTe, electro-optic suscept. dispersion curve 77−3620

nonlinear optics
see also nonlinear optical susceptibility; optical coherent transients; optical frequency conversion; optical parametric devices; optical phase conjugation; optical saturation; optical self-focusing; self-induced transparency; stimulated scattering
absorbing inhomogeneity molten zone, laser beam nonlinear scatt. 79−89969
absorbing liquid, coherent light transient self-diffr., simulated thermal scatt. laser expt. 80−48361
absorption of EM waves by band charge carriers in laser field 77−14767
absorptive optical bistability, transmitted light spectrum and dynamic response function 80−99789
absorptive optical bistability, two-level atom system, photon antibunching 80−58486
absorptive optical bistability transient, local relax., quantum statistical treatment 80−91838
active medium in Gaussian random optical field, stimulated emission statistics 80−58488
active periodic structure with quadratic nonlinearity, wave spatial harmonic spectra transformation 79−72630
adaptive focusing of light in inhomogeneous nonlinear medium, interf. criteria 80−99633
adaptive optics, book 79−31921
adaptive optics in high energy laser systems, book contrib. 79−31971
adaptive optics technology overview, book contrib. 79−32030
adaptive system, characteristic purposes 80−28273
aerosol, aqueous, thermal clearing by laser radiation *(Russian)* 78−28312
aerosol of glass spheres, broadband degenerate four-wave mixing medium 80−43390
algebraic model for CW thermal-blooming effects 79−94303
alkali halides, pulsed-laser-induced damage, role of avalanche multiplication and multiphoton absorpt. 80−48316
alkali halides, two-photon absorpt. 80−50292
alkaline earth fluorides, UV window and coating materials, two-photon absorpt. coeffs. 79−59734
alkoxyazoxybenzenes, isotropic-nematic transitions, RI, orientational relax. times 77−24390
alternating electric field generation in nonlinear cryst. on light irradiation *(Russian)* 77−83920
amplification of strong light-pulse in multicomponent media 78−30006
amplifying region, exponential, enhanced internal refl. 78−37939
angle tuned nonlinear optical crystals, exam. of performance for new cell with new index matching fluid 78−55401
anharmonic oscillator model for dispersive optical bistability 80−58623
anthracene vapour, optically induced dynamic gratings 80−28289
antiferromagnets, magnon parametric generation with impulses at Brillouin zone boundary *(Russian)* 80−29540
applied solid state physics, book 80−94936
aqueous aerosol cloud containing medium, light beam propag., thermal self-interaction 80−91750
atmosphere radiative t0ansfer, nonlinear propag. effects, conference, San Diego, California (1979 August 29 to 30) 80−62376
atmospheric propagation enhancement of CO_2 laser line, thermal blooming reduction 79−84472
atom, nonlinear resonance fluoresc., negative time pair correlation of photons *(Russian)* 79−59750
atom-atom collisions in strong light field, reson. broadening *(Russian)* 77−27149
atomic, two-level system, absorption spectrum, intense two-photon excitation obs. *(Russian)* 78−33465
atomic close collisions, optical processes 79−13790
atomic collisions, nonlinear optical phenomena 80−99788
atomic degenerate system, Doppler-free laser-induced dichroism and birefringence, linearly polarised laser 78−82711
atomic gas with resonant levels, mag. rot. of ellipse of polarisation of propagating rad. 79−50340
atomic intermediate states, far off-reson., temporal coherence in multiphoton absorpt. 78−50458
atomic resonant media, nonlinear Faraday effect 79−32001
atomic RF spectroscopy, nonlinear and parametric effects, review 80−18816
atomic system, nonlinear reson. induction in continuum 79−64273
atomic system, transient four-wave mixing and real time holography 79−55171
autoionising resonances, vac. UV nonlinear optical props. 77−50565
autorotation of polarisation ellipse in nonlinear medium *(Russian)* 77−58374
background ensembles, nonlinear modeling 80−95037
bandpass filter, narrow, via nearly degenerate four-wave mixing 79−23013
benzene, crysts., Raman and two-photon reson. in three wave mixing 79−38538
benzene, liquid, polarised light two photon thermal blooming near UV spectra 80−66216
biexcitons, nonlinear laser spectrosc., multiphoton transitions 80−84433
bilevel absorber, partial differential rate eqns. 78−37950
biphenyl, crysts., Raman and two-photon reson. in three wave mixing 79−38538
bistability, absorptive and dispersive, in Fabry-Perot and ring-cavity geometries 80−95942
bistability, critical slowing down 79−55174
bistability, exact semiclassical treatment of ring cavity 80−58627
bistability, space and time depend. effects 79−94279
bistability, space and time-depend. effects 79−55173
bistability and anomalies in absorption and resonance scattering of intense light 79−95803
bistability and photon antibunching in sub-SHG 79−31991
bistability and spectrum of fluctuations, quantum anal. 78−71067

nonlinear optics continued
bistability equations for standing wave cavity, analytic solns. 80−48328
bistability in bad cavity limit, Fokker Planck eqn. approach 80−64116
bistability in nonlinear distributed feedback structs. 80−5780
bistability in optical cavity filled with Kerr dielectric, nonlinear effect of powerful laser radiation field 80−99787
bistability in resonant two photon absorber 78−90448
bistable absorption, self-pulsing 79−86204
bistable memory switching in presence of external noise 79−59747
bistable nonlinear Fabry-Perot resonator switching speed and energy calc. 80−64095
bistable optical device, transient response and applications 80−33214
bistable optical device development from integrated two-arm interferometer, appls. *(French)* 80−69555
bistable optical devices: an overview 80−58625
bistable optical devices, overshoot and alternate switching, subharmonic generation 80−99790
bistable optical devices, overshoot switching 80−58776
bistable optical devices for integrated optics and fibre optics appls. 79−55175
bistable steady states in optical subharmonic generation, Wigner distrib. 80−53370
bistable system, noise transform. 79−59746
bistable TV-optical feedback system using optical flip-flops 80−53354
book 77−62000
bounded medium, nonlinear parametric reson., limit cycle solns. 80−19071
carrier scattering by lattice defects, nonlinear optical props. 80−29399
cavity, optical bistability, long-time behaviour 80−78892
chalcopyrite crystals, refractive index, temp. depend., appl. to nonlinear devices 80−60555
chemical spectroscopy and dynamics, higher-order susceptibility effects, laser appls. 79−40625
chirp reversal, optical integration in degenerate four-wave mixing 78−46730
chirped steady π-pulses of arbitrary duration in lossy, exactly resonant inverted medium 79−89947
chlorophyll-a, nonlinear absorpt. spectra 78−25522
coherence oscillations in nonlinear media, coherent state lifetime 78−66862
coherent and nonlinear optics, conf., Leningrad, USSR (Jun. 1978) 80−98753
coherent and nonlinear optics, Conf., Leningrad, USSR (June 1978) 80−27027
coherent ellipsometry of Raman light scatt., four-photon spectroscopy *(Russian)* 77−58387
coherent excitations interacting in dispersive medium, envelope-soliton propagation 79−2639
coherent multiphoton intense interactions, convergent perturbation anal. 80−1037
coherent optical spectroscopy of molecules and molecular beams 78−82054
coherent propagation, two-photon quasi-reson. pulses, multi-level atom medium 77−68196
coherent pulse propagation, 0π pulse generation from zero-area pulse 80−48352
coherent pulse propagation, complete solution and McCall-Hahn theory calcs. 77−88836
coherent Raman spectroscopy using powerful tunable lasers 77−53985
coherent waves in nonlinear medium, nonresonant interaction, eqns. system development and examples *(Czech)* 80−24149
collision effects on nonreson. interactions, nonlinear spectrosc. obs. 80−23496
collision induced resonant four photon parametric generation for spectroscopy 77−3627
combustion, coherent Raman spectrosc. obs. 80−16691
comparison with nonlinear acoustics *(French)* 80−33293
complex diamond like crystals, optical nonlinearity and average refractive index 78−30011
condensed matter, review lecture 78−25918
cone-type light beam structure in nonlinear medium 79−98437
conference, basic optical props. of materials, Gaithersburg, MD, USA (May 1980) 80−101668
conference, Novosibirsk, USSR (June 1977) 79−36953
conjugate wavefront generation and image reconstruction by four-wave mixing 78−13746
conjugated one-dimensional system optical nonlinearities 77−50714
continuous spectrum decay, sine-Gordon eqn., nonlinear optics appl. 78−71143
continuum self-phase modulation and stimulated Raman scatt., combined effects 80−69460
contrast magnification of spectral distrib. by freq. spatial filter *(Russian)* 77−747
convolution of ps optical signals 80−58629
cooperative multiphoton ionisation, bistability effects, Bonifacio-Lugiato model 80−19010
corundum particle aerosol, nonlinear propag. of laser radiation 79−23033
crossed Gaussian volume grating, Bragg diffr. of Gaussian beam 77−65569
cryogenic liquids, vibr. kinetics, nonlinear optics appls. 80−13082
cryptocyanine-methanol, soln., nonlinear optical absorpt., 310-815 nm 79−85973
crystal accelerator, radiative energy loss 80−23611
crystal lattice, interaction of mode-locked pulse train, helium temps. 79−23012
crystals, nonlinear refractive index coefficient at 1064 nm, meas. methods 79−3737
crystals, water-soluble, characts. of laser pulse damage 79−45987
cubic media, four photon interaction, collective self-focusing, integrals of motion 77−83935
CW backward-wave generation, degenerate four-wave mixing in CS_2 filled optical fibres 79−27327
cyanine dyes, substituted symmetric, optical nonlinearities, free-electron like model 79−41407
cytochrome c, fast Raman spectroscopy using dye laser intracavity reson. Raman amplification 77−66794
degenerate four-wave mixing, amplified refl., phase conjugation and oscill. 77−83927
degenerate four-wave mixing, hysteresis and optical bistability 80−69446
nonlinear optics continued
degenerate four-wave mixing for Doppler-free two-photon spectroscopy 79−31490
degenerate four-wave mixing in absorbing media 78−71138
degenerate parametric generation from quantum noise, photon statistics 79−81398
degenerate states, magnetoelec. susceptibilities, numerical calcs. 78−55143
density matrix, time evolution, graphical representation 80−64097
density operator, diagrammatic evaluation 78−5523
density operator, for pulsed and CW responses, diagrammatic anal. 79−14027
dielectric, circ. polaris. waves refl. and transmission 79−72616
dielectric liquid nonlinear third-order polarisation, transient effects elucidating molecular props. 80−15955
dielectric medium, steady propag. of coherent light pulse, dynamic behaviour of long pulse 79−98433
dielectric molecular fluid, optical props., internal forces effects, theory 77−28534
dielectrics, nonlinear phonon-photon interactions, physical basis 77−61998
1,1′-diethyl-4,4′-quinocyanine iodide, S_0-S_1 transition, relax. time meas. by reson. Rayleigh technique 78−42374
diffraction and freq. conversion, similitude theory 78−46710
digital data acquisition and on-line processing at Moscow State University 78−46709
dihydroxyanthraquinone, light-induced proton transfer, photochem. hole-burning obs. 80−76535
trans-4-dimethylamino-4′-nitrostilbene, mol. hyperpolarisability in soln., UV dispersion of charge transfer contrib. 79−31986
β-dinaphthylene oxide vapour, optically induced dynamic gratings 80−28289
discrete multilevel system, nonlinear polarisations and excitations, time depend. 77−27313
disorienting collisions, nonlinear resonance induction 80−37900
dispersion of opt. characts. in amplification range, freq. spectrum of stimulated emission, calcs. *(Russian)* 77−54757
dispersive media, interaction between weak pulses and high intensity low freq. wave *(Russian)* 80−48332
dispersive optical bistability, anomalous switching 80−23740
dispersive optical bistability with inhomogeneous broadening, exact soln. 80−53360
dispersive waves interaction, equal group vel. 77−75607
distortion induced in laser beam amplifier, removal by dynamic holographic correction *(Russian)* 78−55326
distortions, nonlinear, of scanning light beams 80−14407
DNA light induced diffusion in solutions due to laser cutting *(Russian)* 80−81646
DODCI dye dissolved in glycerine, time delayed picosecond pulse transmission obs. 80−48355
Doppler less spectroscopy, wave front convolution in parametric nonmonochromatic wave interaction *(Russian)* 79−94280
Doppler-free many-photon spectroscopy, obs. of transient optical processes 79−35845
dye, two-photon fluoresc. quenching, phase fluctuations and phase modulation effect 78−50570
dye laser, narrow band CW oscillator/pulsed amplifier system for precision nonlinear spectrosc. 80−53318
dye laser, superluminescent source of optical noise for nonlinear optics *(Russian)* 78−79033
dye molecules, dissolved, influence of environment on luminesc., intense laser excitation 78−84622
dye soln. tensor susceptance, reson. linearly polarised radiation, optical dye maser polarisation rot. *(Russian)* 77−58325
dye two-photon absorption, for picosecond laser pulse stabilisation, attenuation and shaping 79−55165
dynamic behaviour of optical bistability, time depend. Fokker-Planck eqn. soln. 80−37980
dynamic self-diffraction of coherent light beams, review 80−102777
electro-optical fourth-order effect, calc. of sixth-rank tensor 79−24291
electro-optical nonlinear Fabry-Perot resonator, for optical signal processing 78−42460
electrooptic crystals, holographic recording, photogalvanic effect mechanism of nonlinear wave interaction 80−102672
elliptically polarized Gaussian beams, nonlinear precession 80−28269
EM field, eigensolutions of field strength operator *(German)* 78−83028
EM wave propag., nonlinear media, integral eqns. 77−58375
EM wave reflection coeff. of nonlinear medium, discontinuity 80−28151
empirical relationship for a nonlinear index coefficient 80−74445
excimer lasers applied to nonlinear optical processes in atoms and mols. 79−59745
exciton-coherent light nonlinear interaction theory 77−54754
exponential transformation using film nonlinearity for optical homomorphic filtering 80−58467
extinction theorem, integral eqns. 77−14770
Fabry-Perot cavity, absorptive bistability, mean-field approx., truncated Bloch hierarchy 80−83631
Fabry-Perot cavity, dispersive optical bistability 80−78889
Fabry-Perot cavity, instabilities for coherently driven absorber 80−53387
Fabry-Perot cavity, optical bistability, spatial effects 80−83632
Fabry-Perot cavity, optical bistability, standing wave effects 80−91837
Fabry-Perot cavity, optical pulse tailoring and termination by self-sweeping 80−23760
Fabry-Perot cavity containing ruby, optical bistability and differential gain, 85 to 296K 77−39025
Fabry-Perot interferometer, lossless nonlinear 78−42375
Fabry-Perot interferometer, optical bistability, inhomogeneous broadening, mean field approx. 80−90885
Fabry-Perot interferometer, transient behaviour 78−33787
Fabry-Perot non-linear optic media devices, instability and regenerative pulsation phenomena 78−46685
Fabry-Perot nonlinear interferometer, beam profile hysteresis variations 80−86393
famatinite crystals, optical nonlinearity 77−61996
Faraday rotation, intensity depend., nonlinear refr. index effect 77−77181
fast transform calcs., appl. to SHG with depletion and diffraction 80−53376
ferroelectric oxide crystals for electrooptics and nonlinear optics, optical inhomogeneities, review *(Japanese)* 77−65613

nonlinear optics continued
ferroelectric theory and dynamics, optical, acoustic electro-optical props., Brillouin zone struct. 80−11347
ferromagnetic semiconductor, nonlinear magnetoelec. effect 77−20676
ferromagnetic semiconductor, refr. index variation in strong alternating mag. field 80−23741
fixed intensity approximation *(Russian)* 78−9410
flame diagnosis, CARS appls. 80−16689
fluid, molecular, multiphoton Raman scatt. spectra 77−63404
fluoride crystals, nonlinear refr. index, 1064 nm 78−30005
FM light pulse shape change on amplification 77−3564
fog, laser light nonlinear transmission 80−1256
Fokker-Planck equation for optical bistability 79−75456
1-formyl 2(4-nitrophenyl) hydrazine, preparation, optical and electro-optical props. 77−36201
four counterpropagating wave interaction in medium with cubic nonlinearity, dynamic holography concepts 80−91839
four photon parametric freq. adjustable picosecond lightwave packet mixing *(Russian)* 78−1296
four wave interaction, light induced crit. behaviour in nonlinear system 80−95941
four wave mixing, Raman spectroscopy background suppression 77−5924
four-photon processes stimulated by fluctuating pump in dispersive medium 79−23017
four-wave mixing, nearly degenerate, resonantly enhanced medium, narrow bandwidth optical filter appl. 79−31976
four-wave mixing spectroscopy, recent developments 80−53383
free atoms and molecules, nonlinear optics, book 80−73111
frequency shift by indirect parametric interaction with acoustic radiation 77−38983
g-factor difference between atomic transition levels, nonlinear spectroscopic determ. 80−23346
gas, anisotropy in strong EM field 79−98434
gas, nonlinearly absorbing medium, light-induced optical activity 79−72615
gas, reson. four-photon parametric processes, influence of collisions 77−79899
gas, Stark tunable, mirrorless optical bistability and optical limiting, obs. 80−38056
gas, two-photon absorpt. of ultrashort pulses, reson. intensities 78−59077
gas flow through optical train, thermal blooming control, optical degradation 80−33045
gating, subps, by optical wavefront conjugation 79−46004
gaussian beam formalism applied to nonlinear propag. problem 79−14046
Gaussian-averaged nonlinear function, exact decomposition 79−27319
glass:Nd^{3+}, resonantly enhanced four-wave mixing in absorbing media *(Chinese)* 80−102764
glass fibre signal propagation, nonlinear effects *(German)* 79−89996
glasses, nonlinear refractive index coefficient at 1064 nm, meas. methods 79−3737
grating echoes, in Na gas, the temporally recurrent spatial ordering of at. population 79−98447
grating phenomena, laser-induced review 77−46752
high power laser pulses, localisation in plasmas 79−14554
high resolution spectroscopy of atoms and mols., without Doppler broadening, laser techniques 77−54631
high-resolution laser spectroscopy, techniques and applications 77−57403
highly directional light beams by wave front convolution *(Russian)* 80−14385
hole burning into molecular velocity distribution due to monochromatic radiation and molecular elastic collision 80−43116
holographic interferometry, nonlinear recording, fringe location errors 79−76633
holography, image contrast changes during recording in nonlinear media with local response 80−69346
homogeneously broadened medium, absorption spectra of optical bistability with dispersion 80−102757
homogeneously broadened medium, dispersive bistability 79−50355
homogeneously broadened medium with dispersion, optical bistability 80−83630
hyper-Raman effect, scatt. intensity enhancement, light source statistical props. 77−42572
hysteresis reflection and refraction of light at boundary of nonlinear medium *(Russian)* 77−62001
II-VI semiconductor, laser beam spontaneous action, nonlinear props. *(Russian)* 77−88820
II-VI semiconductor, self-interaction dynamics of Nd laser radiation 79−27342
image and signal processing, United States Air Force programmes 78−74854
image processing, analogue and digital, feedback, review 80−102639
incoherent holographic record 77−38828
incoherent two photon amplification of laser pulse 78−63150
inelastic light scattering conference, Santa Monica, CA, USA (Jan. 1979) 79−95762
inhomogeneity influence on nonlinear cryst. effective length 80−106568
inhomogeneous nonlinear medium and time-varying medium, decay interaction of wave packets 80−14386
inhomogeneous waveguide, nonlinear pulse (soliton) propag. theory 79−72617
inhomogeneously amplifying medium, light beam deflection 77−88689
inhomogeneously broadened resonant medium, steady pulse propagation 79−59748
initial-value problem for zero-area pulses, anal. props. 80−23756
intense radiation in a liquid, propag. instability 79−10346
interference filters, nonlinear, spectral characts. in strong fields *(Russian)* 77−54718
intramolecular longit. relax. in mol. system with Rabi oscills., transient regime theory 78−46404
intramolecular memory effects in second-order optical processes 78−94270
invariant molecular tensors, definition in origin change, refraction and Faraday, effect 80−53363
invariant molecular tensors, definition in origin change 80−53362
inverse Raman scattering, highly fluorescent substances 78−4702
IR and FIR tunable coherent sources utilising modulational instability 80−95967
IR and UV nonlinear processes 79−3738
isotropic medium, three-photon light scatt. phenomenological theory *(Russian)* 78−83024
nonlinear optics continued
isotropic medium with two-photon absorpt., propag. of polarised radiation 80−28290
kinetic cooling of CO_2 laser beam 77−62018
laser, damage of laser components, threshold meas. 78−13740
laser, nonlinear stratified system, plane wave propagation 80−43343
laser, pulse width, meas. by two-photon absorpt. fluoresc., contrast ratio variation 79−76737
laser amplification of incoherent radiation 78−55334
laser amplifier with spatial filters, graphoanalytic determ. of energy parameters 80−48322
laser beam, high power, focusing props., influence of nonlinear refractive index medium *(French)* 78−46696
laser beam, thermal self-action over path in medium moving at variable vel., expt. and numerical simulation 79−32003
laser beam path design for reduced thermal blooming in axial pipe flow 79−94268
laser beam propagating in liquid, polarization, DC elec. field influence 80−91828
laser beam self-channeling, Schrodinger nonlinear eqn., exact soln. *(Ukrainian)* 79−94278
laser beam spatial coherence in a randomly inhomogeneous medium, effect of thermal nonlinearity 80−9926
laser beam transient self-diffraction in absorbing liquid 80−9927
laser beams, long-range photon spin interactions in at. vapour 77−27324
laser dyes, ultrafast gating and amplification of broadband signals 77−38987
laser engineering advances, conf., San Diego, CA, USA (Aug. 1977) 78−59017
laser engineering and appls., conf., Washington, USA (May-June 1979) 80−1216
laser focus movement, nonlinear optical technique 80−74446
laser frequency switching, subnanosec. expts. 78−42391
laser interaction with matter, nature of light, nonlinear spectroscopy 77−50712
laser light pulse parameter meas., integral method 77−72018
laser light sources, appl. in atomic and mol. optics *(Polish)* 79−36951
laser light with time-varying intensity in optical medium, temp. field kinetics 78−59098
laser material nonlinear refractive index meas. by time-resolved interferometry 77−18088
laser pulse amplification in medium with single photon stimulated emission and two photon absorpt. 79−45922
laser pulse propag. in absorbing medium *(Russian)* 79−59752
laser radiation wavefront instability and optical inhomogeneity evolution dynamics 80−9876
laser spectroscopy, density matrix methods, review 78−74071
laser spectroscopy, review 77−5927
laser spectroscopy, theoretical foundations 79−35846
laser spectroscopy inside Doppler line *(Russian)* 78−21231
laser wave propagation in piezoelectric crystal, lax's estimates appl. to critical crystal thickness 79−98440
laser waveguide mode propag. in nonlinear amplifying medium 77−58308
laser-induced gratings, book 79−42428
laser-induced gratings, method for study of optically excited solids, forced light scatt. 79−41408
lasers and applications, conf., Dresden, Germany (Mar.-Apr. 1977) 77−83881
lasers and applications, conference Erice, Italy (May-Jun. 1970) 77−38906
lasers and their applications, conf., Dresden, East Germany (Mar.-Apr. 1977) 79−7137
lasers for industrial chemistry, thermal lensing effect 80−87427
lattice vibration nonlinear interaction with powerful light beam 78−46711
lattice vibrations, nonlinear interaction with light beam 78−30034
lectures on interaction of radiation with condensed matter, Trieste, Italy (Jan.-March 1976) 78−27172
light beam quantum fluctuations meas. using nonlinear interferometer 79−80672
light beam refl. from active medium, lateral wave struct. 79−27315
light wave diffr. by complex spectral composition US 80−95939
light-induced grating, possible energy transfer control by acoustic vibrs. 80−28267
limited light beam, nonlinear reflections and transmission 80−58624
linear dynamic mol. system, correlated radiation impulse sequence interaction 80−38058
liquid, thermal lens effect meas. by photomixing method, laser system 77−42577
liquid crystals, four wave mixing and relaxation effects *(Chinese)* 80−53351
long-range interaction between CW laser beams in at. vap. 78−87110
longitudinally inhomogeneous running waves and their role in the nonlinear reflection and refraction of light 80−38059
longitudinally inhomogeneous travelling waves in nonlinear electrodynamics 79−10348
lower hybrid waves, quasi-optical beam self-action in magnetoplasma 80−38657
luminescence quenching at high pumping levels, microscopic theory 80−89040
magnetoplasma, hot collisionless, upper hybrid wave resonant excitation, nonlinear dielectric const. 79−77384
magnon coherent generation by optical technique using mag. Raman nonlinearity 78−68201
many-photon ionization, resonance scattering on a nonstationary potential, and complex poles of the S-matrix 79−22677
many-photon resonant absorpt., multimode radiation struct. effects 77−23708
materials, principles of nonlinear optics *(French)* 78−71140
materials for nonlinear optical appls., review 80−74450
Maxwell-Bloch equations, breakdown of soliton behaviour 77−72024
MBBA, nematic liq. cryst., nonlinear optical amplification above Frederiks transition 80−95937
MBBA, nematic liq. cryst., nonlinear optical processes near Freedericks transitions 79−69011
mean field theory of optical bistability 78−79068
metal, light refl., nonlinear thermo-optic effect at high intensity 80−93289
methane, continuous coherent radiation in spatially separated fields 78−30007

nonlinear optics continued
methane, nonlinear optical reson. shift in mag. field, vibr.-rot. transition 78−13549
methyl iodide mol. nonlinear resonant interaction with pulsed subMM radiation *(Russian)* 80−99523
methyl-(2,4-dinitrophenyl)-aminopropanoate, efficient cryst. 77−79890
microemulsions, heat transfer meas. by laser-induced thermal blooming 80−91833
mirror, nonlinear interf., reflection of light 80−102761
mirror coatings, selective reflectors, and antireflection coatings for nonlinear optics, chemical method 80−28300
mode-locked binary laser oscillator, bistability induced by optical nutation 79−31958
model equation in dispersive medium, wave interactions, self-precession and freq. shift 80−78900
molecular crystals, self-induced nonlinear optical rotation 78−1308
molecular electric polarisabilities, hyperpolarisabilities, nonlinear optical coeffs., MNDO calc. 79−13641
molecular intermediate states, far off-reson., temporal coherence in multiphoton absorpt. 78−50458
molecular mixed crystals, electronic transition props., Redfield theory 79−46008
molecular systems, identification by spectroscopic methods 78−29168
monochromatic radiation in gas media, near resonance nonlinear propagation 79−76748
moving medium, light beam instability and its decomposition with thermal self-stress 79−94305
multi-level atom with Raman reson., time-delayed laser scatt. 80−48343
multifrequency laser radiation, nonlinear power type interaction with matter 80−53356
multilevel atomic system, thermally relaxing, coherent radiation reson. scatt. and absorpt. 79−81401
multimode laser radiation field, multiphoton ionisation probabilities *(Russian)* 77−42560
multiphoton absorption, Kerr nonlinearity, cone-type light beam struct. 78−33790
multiphoton cross-section determination by means of luminescence experiments 80−93377
multiphoton detectors of laser radiation, statistical characts. 80−86408
multiphoton processes, equilibrium between radiation and matter 77−50713
multiple pulse thermal blooming, phase compensation 77−50732
multiquantum resonant interactions, canonical description *(Russian)* 77−10714
N two-level atoms, quantum theory of nonlinear optical phenomena 80−5790
n-order nonlinear phenomena, dispersion rels. 79−41410
naphthalene, crysts., Raman and two-photon reson. in three wave mixing 79−38538
narrow nonlinear resonance for transitions to continuum 77−750
narrow resonances, ultrahigh resolution laser spectroscopy *(Russian)* 78−70974
nematic liq. crystal, EM wave nonlinear interaction 80−19698
nitroanilines, hyperpolarisability, second harmonic generation and four wave mixing, excited dipole moment 77−54624
nitrobenzene, DC elec. field induced optical rectification 77−38980
noise in nonlinear optics 79−23015
non-classical effects in the statistical properties of light, review 80−99686
nondegenerated wave interaction with amplification, stochasticity occurrence *(Russian)* 78−83027
nonequilibrium quantum statistics of lasers and nonlinear optics 79−31848
nonlinear coherent coupler, new optical logic device 80−58630
nonlinear crystals, interference of optical harmonics 80−64102
nonlinear Fabry-Perot filled with Kerr liquids CS_2 and nitrobenzene 79−27316
nonlinear Schrodinger equation, exact solution, localised wavefield evolution 80−53191
nonresonant chirp compensation with counterpropagating optical pulses 77−58371
nonstationary interaction of opposite waves in quadratically nonlinear medium−numerical experiment *(Russian)* 78−83026
nuclear matter as optical medium, nonlinear phenomena, possible investigation methods 77−2924
opacity wave in optical breakdown of condensed transparent media, steady-state motion 77−14768
optical bistability, nonlinear polarisability model 80−37976
optical bistability in dispersive and absorptive media 79−14025
optical bistability with dispersion 80−78893
optical communication systems, nonlinear distortions and noise due to fibre connectors 80−96001
optical echo spectroscopy 80−48357
optical fibre, high power narrow band laser radiation transmission, nonlinear optical processes 80−53443
optical fibre, Raman oscillators and nonlinear effects 77−88854
optical fibre, soliton pulse propag. 80−58759
optical fibres, nonlinear pulse propagation 79−18536
optical glass, Raman scatt. and nonlinear refr. index 80−2749
optical irradiance determ. to stimulate nonlinear processes 79−18467
optical multistability, light self-modulation in double resonance *(Russian)* 80−106560
optical resonators, radiation excitation, review 80−69462
optical solids, nonlinear refr. index, empirical relationships 78−83025
organic compounds usable as solvents in laser saturable absorber, nonlinear refr. index meas. 80−102758
organic crystals for SHG, selection and characterisation 77−3626
organic laser dyes, nonlinear transmission including stimulated emission influence 80−99720
oscillators, two-mode self-excited, synchronisation and stochastisation by external field 79−80524
over-pumping energy effect, two interfering beams in nonlinear medium *(Russian)* 77−7161
paramagnetic centre crystals, nonlinear optical Faraday effect 80−99811
paramagnetic ion spectra perturbation by high-intensity nonreson. EM radiation 78−71137
parametric generation, from quantum noise effect of photon statistics 78−25921
parametric image convertor with freq. rise, phase aberrations *(Russian)* 78−9455
parametric instabilities, theory 78−14151

nonlinear optics continued
parametric interaction increment of modulated light beams *(Bulgarian)* 79−10351
parametric interaction of random waves in nonlinear nondispersive media *(Russian)* 77−31117
parametric interaction of two waves, scatt. radiation ang. struct., amplification *(Russian)* 77−58381
parametric resonance in transverse disturbing RF fields *(Russian)* 77−3624
parametric wave excitation in bounded systems 80−6252
partial spatial coherence blur correction by postdetection image processing 80−78792
particle acceleration in nonlinear crystal by 'rectified' light 80−23610
perovskite and tungsten bronze cryst. struct. types, ionic grouping theory, electrooptical, nonlinear optical effects *(Chinese)* 78−52472
perovskite-type crystals, microscopic origin, expt. *(Japanese)* 77−38990
phase adaptation by nonlinear techniques, optical propag. distortion compensation, book contrib. 79−31973
phase compensation of thermal defocusing of light beams 80−64121
phase-switching of a dispersive non-linear interferometer 80−82810
photoelectric current in case of nonlinear interference of EM fields 80−80324
photon antibunching enhancement by interf., polarisation effects 79−31990
photon antibunching enhancement by interf., Young's interf. expt. 79−27313
photon antibunching simulation 79−72543
photon fluctuations and interaction with solids 77−748
photon stationary distribution in optical bistability 80−48197
photon statistics after destructive interf. of two-photon absorbed light 80−48199
picosecond light continua generation depending on various nonlinear processes 80−33095
picosecond light pulse, meas. techniques *(Japanese)* 80−52291
picosecond light pulse techniques and applications, book 77−61137
picosecond nonlinear optics, book contrib. 77−65609
picosecond pulse duration, determ. from luminesc. intensity 78−71134
picosecond pulse measurement techniques, book contrib. 77−61139
picosecond resonant spectroscopy, using nonlinear cryst. parametric excitation, stroboscopic method *(Russian)* 77−83930
Planck constant, upper limit determ. to freq. dispersion by nonlinear spectroscopy 77−79050
plane wave reflection from nonlinear absorbing medium 79−81478
plane waves self-action in cubic medium, statistical phenomenon 77−68237
plane-parallel absorbing layer, in strong laser light field 80−58631
plant leaves, spectra of nonlinear optical effects *(Russian)* 78−48829
plant leaves, spectral transmission coeff. changes, nonlinear optical effect 79−57707
polarisation effects in nonlinear scatt., hyper-Rayleigh (Raman) scatt. 77−88858
polarisation ellipse rotation in one- and two-photon resonances 77−3621
polarisation resonance in a continuum, optical activity, spin-orbit interactions *(Russian)* 80−53391
polarisation-sensitive nonlinear spectroscopy, improved geometry 80−1285
polarised waves interaction in reson. medium in mag. field 79−64278
polaritons, bulk and surface, nonlinear spectroscopy 77−50730
polaritons, two-photon absorption and stimulated Raman effect 77−50729
polydiacetylene polymer crystals, optical nonlinearities, chain pairing effects, one dimens. band model 77−69851
polydiacetylenes, cryst., picosec. pulse, nonlinear optics appls. 79−46017
POPOP vapour, optically induced dynamic gratings 80−28289
power breakthrough in nonlinear process, stabilisation by electro-, piezo-optical tuning 77−88856
probe frequency gain in optically bistable system, quantum theory 79−98435
processing with Fabry-Perot interferometers containing phase recording media 80−48158
properties, dispersion, band theory 77−50716
ps light pulse length determ. by parametric amplification in nonlinear crysts. 78−1306
pulse propagation in inhomogeneous media 78−94408
pulsed laser spectroscopy, review 79−26140
Q-switched pulse stretching by intracavity nonlinear ellipse rot. 78−17991
quadratic nonlinear process, depend. on intermodal correlations 79−36958
quadratic optical processes, intermodal correls. efficiency effect 79−31978
quantum electronics, conf., New York, USA (Jun. 1980) 80−90614
quantum optics, introductory lecture 78−25843
quantum systems, wave packet behaviour in pseudo-coherent state method *(Russian)* 80−1175
quartz, nonlinear polarisation plane rotation due to ruby laser irrad. *(Russian)* 80−53390
quartz slab, ruby laser interaction, SHG 77−7159
quartz slab between linear media, laser wave propag. 77−14769
quasiequilibrium sample, light scatt. and thermal radiation, phenomenological approach 80−91840
radiation propagation in nonlinear media problems, decomposition method 79−84971
radiation self-synchronisation during stimulated Raman scatt. in external resonator *(Russian)* 80−102772
Raman amplification, high-efficiency narrow-linewidth, spectral compression 80−102770
Ramsey fringes in saturation spectroscopy 78−82868
rare earth titanates, pseudoperovskite struct., nonlinear spectral and luminesc. characts. 80−29771
rarefied absorbing gas, coherent rad., in time separated fields 78−37938
ray propagation and self-focusing, variational principle derived theories 79−27339
ray tracing in nonlinear moving media 77−14644
real time processing 80−87338
recent advances, review 80−33075
recoil effects in nonlinear spectroscopy, quantum representation of mol. motion 77−39000
rectification effect and meas. appls. 80−91835
rectification in nonlinear cryst. in external resonator 78−13748

nonlinear optics continued
reflection and refraction and boundary, between transmission and total internal refl. cases 79−18470
reflection by nonlinear absorbing medium, plane wave *(Russian)* 79−984
refraction into a nonlinear medium: wave profiles and hysteresis 80−43395
refractive index changes on degenerate four-wave mixing 80−9936
relaxation characteristics determ. by polarisation technique *(Russian)* 77−75603
resonance light scattering, spectral props. and photon correls. 80−91510
resonance medium, high power radiation polarisation ellipse, mag. rot *(Russian)* 78−70794
resonance medium, induced dichroism and gyrotropy 80−9971
resonance two-photon absorption, theory 80−28268
resonant amplification, total absorption in thin film *(Russian)* 77−7153
resonant e.m. pulse freq. modulation 77−734
resonant interaction of light pulses with matter, lattice vibr. enhancement, relax. role 79−23009
resonant media, pulse counterpropagation and nonlinear interaction, transverse effect computation 80−106563
resonant media, pulse steady propag. 79−72633
resonant media, transverse relax. effect and spatial optical parametric coupling of picosecond light pulses 80−19070
resonant media, two-photon coherent interaction of light pulses, phase modulation 77−79905
resonant medium, transient energy transfer between coherent light beams 79−27317
resonant nonlinear optics, randomly modulated light field excitation, statistical effects 77−50718
resonant optical phenomena in fluctuating laser fields, quantum statistical theory 79−14042
resonant orientation of tunnelling centres, self-induced anisotropy 78−79075
resonant propagation of two concomitant optical pulses interacting with three-level atomic system, num. modelling 80−9942
resonant Raman scattering in laser fields of arbitrary strength, antibunching effects 80−23653
resonant Rayleigh type optical mixing, appl. to ultrafast relax. process obs. 78−42373
resonant Rayleigh type optical mixing, appl. to ultrafast relax. in dye solns. 78−42374
resonant scanning optical microscope, nonlinear interaction enhancement 78−93758
resonant three level spin system, two-photon spectra 78−30017
resonant two-level medium, ultrashort light pulse propag. 78−50849
resonantly absorbing media, instability of coherent pulse propag. *(Russian)* 77−62017
resonantly excited laser media, possible use in wavefront reversal 79−94281
review, new results and problems *(Russian)* 79−36952
review of work at Ukrainian SSR Acad. of Sci. *(Russian)* 79−45950
rhodamine 6G alcohol soln., two-photon absorpt. efficiency 78−13749
ring cavity, chaotic behaviour of transmitted light, optical turbulence 80−102760
ring cavity, dressed mode dynamics of optical bistability 80−19013
ring dye laser, optical bistability and first order phase transition 80−95918
ring laser, nonlinear polarisability of two-isotope active medium 80−14369
ring laser, nonreciprocal effects on appl. of transverse mag. field to active medium 80−53341
ruby:Cr, lifetimes of laser-induced population density gratings, comparison with fluoresc. lifetimes 79−64276
ruby, forced Rayleigh scatt., 50 to 300K 77−42564
ruby, induced lattice formed by interference of atomic states *(Russian)* 78−66861
ruby, multiple optical hole burning obs. using Stark field sweeping 77−46768
ruby, phonons, at 29 cm^{-1}, stimulated emission 80−45114
ruby far IR quantum counter, optically pumped 77−38001
scattering of atoms by stimulated light freqs. appl. to isotope separation 78−66526
scattering of light in limit of ultra-strong fields 78−79067
scattering of two light beams, ultrastrong fields, differential scatt. power 80−43388
second and third order nonlinear optical polarisations, general effects of cryst. symmetry and orientation 77−19358
selective interactions, conf. Tsakhkadzor, USSR (Jan, 1976) 77−23706
self diffraction of laser beam by liquid crystal struct. 80−5803
self pulsing in absorptive optical bistability, analytical description 80−78891
self pulsing in dispersive optical bistability in ring cavity 80−78890
self-action problems, finite element method appl. 80−9941
self-diffraction of light by excitons 80−53389
self-diffraction of polarised light waves in two photon absorpt. in isotropic media 80−38077
self-imaging, light-optical experiments *(German)* 80−63938
self-induced thermal effects on SHG 77−736
semiconductor, ambipolar diffusion meas. using nonlinear transient gratings 78−80000
semiconductor, degenerate four-wave mixing near band gap 80−5782
semiconductor, energy transfer due to dynamical self diffraction of light beams of same freq. *(Russian)* 77−58397
semiconductor, heavily doped film, laser irradiation, spontaneously broken gauge symmetry 79−47531
semiconductor, high-power light pulse propag. under interband interaction conditions 79−10366
semiconductor, highly excited states, ps spectroscopy 77−48245
semiconductor, ionic, nonlinear intraband absorpt. and harmonic generation 78−33779
semiconductor, IR switching, ultrafast optically controlled 80−58626
semiconductor, layered, direct and indirect two photon processes 77−40261
semiconductor, luminescence in presence of intense laser field 79−38621
semiconductor, many-photon absorption by intraband transitions in mag. field 78−27261
semiconductor, noncoherent interaction of a light pulse 80−106561
semiconductor, nonequilibrium processes exam. by method of transient holograms 78−23105

nonlinear optics continued
semiconductor, nonlinear light absorption in presence of laser wave field 78−13747
semiconductor, nonlinear optical props., non-stationary density matrix of electron-phonon system 78−71818
semiconductor, nonlinear optical props. 80−25333
semiconductor, nonlinear refractive index under many-photon resonance conditions 78−90449
semiconductor, optical parameters in strong EM field, effects of finite wavelength of light 77−44050
semiconductor, picosecond spectroscopy, nonlinear optical interactions 79−93230
semiconductor, two-photon absorpt., free carrier storage by deep centres *(Russian)* 78−23131
semiconductor, two-photon resonance absorption *(Russian)* 77−61997
semiconductor etalon, optical bistability and ns modulation 80−64096
semiconductor film, size-quantised with tilted valleys, two-photon absorpt. 79−95869
semiconductor film, two-photon absorpt., optically induced diffr. 77−7154
semiconductor photostimulated light absorption in Burnstein-Moss effect *(Russian)* 79−28706
semiconductor physics, conf., Edinburgh, Scotland (Sept. 1978) 79−95303
semiconductor thin-film nonlinear Fabry-Perot interferometer for optical pulse shaping 79−89945
semiconductor with impurities, laser beam induced synergetic-phenomena 79−74021
semiconductor with superlattice, nonlinear EM wave amplification 77−88835
semiconductors, direct-gap, two-photon absorpt. 80−50292
semiconductors, free carrier optical props., book contrib. 80−80738
semiconductors, II-VI and III-VI types, competition between two-photon absorption and two-stage absorption via deep traps 80−29764
semiconductors, mixed and binary, nonlinear polarisability, self-action effects 80−99786
semiconductors, nonlinear effects, induced by lasers 79−94300
semiconductors and insulators, nonequilib. electron Coulomb collisions during optical pulse interband interaction 80−76049
short duration Gaussian pulses calc. *(Russian)* 78−55402
signal measurement with nonlinear conversion of multimode laser radiation 77−23715
signals with random phase modulation in nonlinear dispersive medium, statistical charact. *(Russian)* 77−75606
single mode laser, photon statistics, intracavity two-photon absorption effect *(German)* 77−10933
single-beam two-photon absorbed light, off diagonal density matrix 78−30009
solid in equilibrium with radiation field, reconciliation of photon noise statistics with electron statistics 79−23014
solid laser, undamped spiking, dynamical theory 77−14724
solid transparent dielectrics, pre-breakdown optical phenomena induced by coherent radiation *(Russian)* 79−86207
solid under excitonic state reson. conditions, laser pulse propag. theory 80−87430
soliton solutions, light beam self-action in nonlinear media 80−14404
sooty diffusion flame, CARS obs. 80−16690
spatial convolution and correlation of optical fields via degenerate four-wave mixing 78−71044
spatial filtering, nonlinear medium, loss formation 80−53357
spatial frequency resonances in nonlinear absorbing cell 79−31977
spatial frequency response of a nonlinear absorbing medium 79−27314
spectroscopy, atomic and molecular, high resolution, review 77−50564
spectroscopy, conf., Varenna, Italy (July 1975) 77−49778
spectroscopy, development and theory 77−49779
spectroscopy, dye laser design 77−79852
spectroscopy, nonlinear laser, gravitational effects 79−67391
spectroscopy, resolvent formalism appl. *(Japanese)* 80−82833
spin oscillators, optically pumped, orientation depend. of oscill. freq. 80−78896
spontaneous anti-Stokes scattering as high-resolution and ps-time-scale vacuum UV light source 78−9411
stannite crystals, optical nonlinearity 77−61996
state of art in 1978, fundamentals and appl. *(Czech)* 79−18468
stationary optical wave mixing, relax.-time determ., inhomogeneously broadened resonant transition *(German)* 78−1297
statistical properties of light, change by multiphoton absorbers with intermediate reson. 79−86208
stimulated Raman scattering, review of appls. 77−735
stochastic multiphoton resonance interaction with matter 80−33073
stratified media for IR image visualisation 79−32071
superlattices, nonlinear optical props. 77−50728
surface polaritons, linear photon and two photon absorpt. 80−49863
surface polaritons, Raman scatt., active spectroscopy theory 77−59576
surface waves at absorbing/amplifying media interface 80−43239
synchronous nonlinear interaction between waves on Bragg diffr. in media with periodic struct. *(Russian)* 80−14399
ternary semiconductor crystals for nonlinear optical applics., review 78−33782
ternary semiconductors, pot. practical appl., review 79−10344
ternary semiconductors, review of developments 78−34737
tetracene in alcoholic glasses, laser-induced hole burning mechanisms, zero-phonon fluoresc. 78−43912
thermal blooming: round beam vs square beam, computer study 80−38076
thermal blooming, continuum-lens model 80−78918
thermal blooming cell design for adaptive optics evaluation 80−33096
thermal blooming cell design for use in evaluating adaptive optics 80−102780
thermal blooming compensation, equivalent thin lens model 78−87108
thermal blooming compensation with multidither COAT system 78−33789
thermal blooming effect on laser beam propag. with on-axis null 77−27323
thermal blooming in a diagonal wind 80−95965
thermal blooming in atmosphere, book contrib. 79−34961
thermal blooming in axial pipe flow: comment [and reply] 80−95966
thermal blooming in laboratory expts., index of refr. turbulence effects 79−50357
thermal blooming in multiphoton absorption, applic. to benzene spectroscopy 77−30940

nonlinear optics continued
thermal blooming in multiphoton absorption, theory 77−30939
thermal blooming of slewed laser beam, stagnation and transonic effects 77−34903
thermal blooming of slewed laser beam with stagnant absorber region 77−38966
thermal blooming reduction vice phase correction, experimental demonstration 79−98449
thermal blooming spectroscopy for enzymatic anal. 80−86441
thermal defocusing of light beams, phase conjugation compensation method 80−64123
thermal halo effect, nonlinear scatt. by moving particles, symm. distortions 78−66875
thermal lens, pulsed source 80−95968
thermal lens in laser cavity, focal length 77−61977
thermal self-action problems and their compensation 80−106579
thermal self-interaction of annular laser beams in moving medium 78−71159
thermal-blooming compensation, using closed-loop adaptive single parameter system 78−94407
three boson field modes with trilinear interaction, statistical behaviour 78−87093
three level atoms, coherent nonlinear mechanism for optical bistability 80−102756
three level molecular system interaction with two laser fields 77−54685
three mode process, crit. comparison between quantum mechanical and classical approach 78−59079
three-level atom system, distortionless optical pulse propag. 78−22179
three-level system, narrow nonlinear resonances *(Russian)* 80−78898
three-level system, reson. interaction of opposite waves, relax. consts. of common level 78−50511
three-photon absorbers, effect on stabilisation and smoothing for signal intensity correl. charact. *(German)* 77−23709
three-wave interaction, review 79−86209
three-wave interactions in randomly inhomogeneous dispersive media *(Russian)* 80−53364
time evolution operators and Feynman diagrams appl. 78−18004
transient response in optical bistability 79−3666
transient scattering, stochastic theory of intermediate state interaction 78−13756
transparent layer, nonlinear, light reflection 79−55172
transparent materials, laser light refl. and transmission, high power densities 79−27305
transparent nonlinear layer, light refl. and transmission *(Russian)* 78−71142
transport equation for electrons in nonmonochromatic EM field 80−10937
turbulent absorbing liq. medium, laser radiation thermal self-interaction 80−91868
turbulent medium, pulsed laser radiation intensity fluctuations during thermal selfinteraction 80−102781
two interacting intensities, evolution in space and time 78−18005
two level atom, coherent and Raman scatt. spectra, secondary emissions 80−69449
two level atoms, method of separated optical fields 78−30008
two level atoms, nonlinear Ramsey reson. 77−3622
two level system, relax. consts. meas., two travelling waves reson. interaction 77−38644
two photon coherent states in degenerate four wave mixing 80−5717
two-level atom gas, optically induced optical activity 79−18490
two-level Doppler-broadened medium in Fabry-Perot, optical bistability 80−102759
two-level molecular gas, nonlinear absorption near gas-medium reson. 79−41409
two-level system, nonmonochromatic radiation excitation, nonlinear optical phenomena *(Russian)* 78−87101
two-photon absorbents for multicomponent laser systems 79−94240
two-photon absorption, coherent, near reson. media 79−14026
two-photon absorption in liquids, optical system 79−17500
two-photon absorption of randomly phase modulated laser beam 78−55400
two-photon double-beam optical bistability 80−64113
two-photon field nonlinear optical efficiency 80−9949
two-photon resonance, coherence effects on summation of optical frequencies *(Russian)* 77−62012
two-photon spectroscopy, ultra-high-resolution, Doppler-free 78−49909
ultra-short light pulse generation, review *(Japanese)* 79−45973
ultrashort consecutive light pulse four-wave interaction in media *(Russian)* 80−78897
ultrashort light pulses, shaping and shortening in excited level by optical controlled absorber *(German)* 78−87106
ultrashort pulse attenuation in active medium, calc. *(Russian)* 78−1295
uniaxial crystals, nonlinear optical props., review and summary of data 77−75615
urea, electro-optical coeffs. meas., rel. to nonlinear optics calcs. 80−34889
urea, second and third order hyperpolarisabilities, SHG and four-wave mixing meas. 79−59759
UV nonlinear optical processes using excimer lasers 80−38060
UV single freq. tunable source using dye laser 77−42547
UV transparent materials, 355 and 266 nm absolute two-photon absorption coeff. obs. 79−18493
vapour, radiatively cooled resonant, 3rd order nonlinear optics processes 79−81477
vector matching ang. width, for optical harmonics 80−9946
volume phase holography, crystal two light wave interaction, photoexcited, photogalvanic effects 79−27214
wave beam distortion by thermal self-interaction in droplet medium 80−19082
wave front reversal accompanying VRMB of depolarised pumping *(Russian)* 78−90458
wave rectification, quantum limit 80−83634
wavefront registration and volume object image reconstruction by stimulated Raman scatt. *(German)* 80−53367
wavefront rotation for light beam nonlinear deformation compensation *(Russian)* 80−64094
waveguides, optical, nonlinear pulse propag. theory 80−83669
wurtzite-type crystals, optical second-order nonlinear polarisability 78−25919
Zeeman laser or amplifer, bistability and intensity fluctuations 80−53254

nonlinear optics continued
$AgGaSe_2$, two-photon absorpt. and short pulse stimulated recombination 80−89054
$Al_{0.42}Ga_{0.58}As$-GaAs-$Al_{0.42}Ga_{0.58}As$, etalon, optical bistability and modulation 80−58628
AlN, epitaxial film growth by MBE, physical and optical props. 80−2293
As_2S_3, cryst. and vitreous, nonlinear light absorpt. 77−75605
As_2S_3, crystalline and vitreous, nonlinear absorption of ruby laser radiation *(Russian)* 78−22165
$As_2S_{3-x}Se_x$, amorphous, ps. relax., optically induced absorpt. 80−48325
As_2Se_3, cryst. and amorphous, optically induced absorption in band gap, picosec. dynamics 79−87439
Au, multiphoton photoeffect, induced by single selected ultrashort laser pulses, anomalies 77−28692
Ba atomic beam, light-shift induced zero-field level crossing, optical Hanle effect 80−52947
Ba, vapour, laser excited, anomalous conical emission and self focusing 80−43411
$Ba(NO_2)_2.H_2O$, nonlinear optical props. and polariton scatt. spectra 77−75616
$Ba_2TiSi_2O_8$, fresnoite, Czochralski growth and phys. props. 78−3026
BeF_2 glass, nonlinear refr. index, meas. of electronic and nucl. contribs. 78−50866
$Bi_{12}SiO_{20}$, photorefractive medium, real-time image processing via four-wave mixing 80−95944
$Bi_{1-x}Te_xO_{3/2+x/2}$ ($0.33 \lesssim x \lesssim 0.50$) solid solutions, low temp. phase stable at 20 degrees C, properties *(French)* 79−55886
CO, hole burning in single quantum power spectrum due to Autler-Townes splitting 80−9671
CO_2 laser pulse, nonlinear propag. charact., computer simulation 80−106575
CO_2 laser radiation, single pulse, thermal blooming 80−19080
CO_2 laser self-modulation by means of nonlinear absorbing filters, anal. 78−37925
CS_2, intensity dependent total refl., ps pulses 77−14781
CS_2-glass boundary, optical bistability at nonlinear interface 80−33094
Ca, weak intercombination line, Lamb-dips obs. by resonance fluorescence monitoring 79−3392
$Ca_3(VO_4)_2$, linear and nonlinear optical props. 79−23010
$CdCr_2Se_4$, refr. index variation in strong alternating mag. field 80−23741
$CdGeP_2$ synthesis and cryst. growth 79−87577
$CdGeP_2$ thermo-optic coefficient, dispersion 80−71396
CdP_2, 442 class gyrotropic crysts., self-induced rot. of light polarisation plane 80−99810
CdP_2, self-induced optical rotation of polarisation direction 79−19860
CdS nonlinear lens, with variable focal length 79−81511
CdS, nonlinear refr. index coeffs. meas. by nonlinear refraction method *(Russian)* 78−79066
CdS, nonlinear refr. index meas. by nonlinear lens method *(Russian)* 79−26111
CdS, nonlinear self-action effect and absolute two-photon absorption coeff. 80−83649
n-CdS, spin-flip Raman echo obs. 77−19370
CdS thermo-optic coefficient, dispersion 80−71396
CdS, three-photon absorpt. coeff. determ. by nonlinear luminesc. expt. 80−14384
CdS, two-photon absorption coefficient rel. to inverse Raman cross section 78−6678
CdS_xSe_{1-x}, photosemiconductor, optically controlled deflector based on thin-film waveguide 80−33206
CdSe, self-diffraction at induced phase lattice 77−3638
CdSe thermo-optic coefficient, dispersion 80−71396
CdTe, nonlinear optical effects in rotationally twinned crysts., phase matching 77−42570
^{113}Cd, two-level system, absorption spectrum, intense two-photon excitation obs. *(Russian)* 78−33465
$CoCl_2.6H_2O$ solution in ethanol, thin absorbing film, nonlinear optical props., Q-switch appl. 80−91836
Cs, vap., dispersive delay line, pulse squaring effects 77−72035
Cs vapour, self-phase modulation complete compensation at 1.06 μm 77−58395
CsD_2AsO_4 Fourier transform plane superposition multiplier, for optical processing 79−7084
CuCl, reson. coherent nonlinear scatt., biexciton autoionising states 79−51978
$CuGaS_2$ thermo-optic coefficient, dispersion 80−71396
D_2O, single 1.06 μm picosecond pulse superbroadening, concurrence with dielec. breakdown 79−86223
D_2O, superbroadening, by self-focused picosec. laser pulses 77−75612
GaAlAs-GaAs-GaAlAs etalon, optical bistability 80−5781
GaAs, amorphous sputtered films, hydrogenated, photoinduced optical absorpt. 80−50362
GaAs, DC biased, filamentation of laser radiation 80−74428
GaAs, nonlinear refractive index dispersion at helium temp. 78−2820
$Ga_xIn_{1-x}P$, refractive index comp. depend., nonlinearity parameter *(German)* 77−32344
n-GaP, optical rectification due to free carriers, detector appl. 77−10967
GaP single cryst., Raman scatt. cross section, nonlinear optical coeffs. 79−56784
GaP, surface polariton linear photon and two photon absorpt. 80−49863
GaP, two-photon absorption coefficient rel. to inverse Raman cross section 78−6678
GaP:Te, photon drag, optical rectification response meas., anomalous polarisation depend. 78−33769
GaP_xAs_{1-x}, refractive index comp. depend., nonlinearity parameter *(German)* 77−32344
GaS, anti-Stokes photon replica emission under two photon excitation 77−52175
GaS(Se), optical and nonlinear optical props. *(Russian)* 79−51943
Ge, amorphous sputtered films, hydrogenated, photoinduced optical absorpt. 80−50362
p-Ge modulation of 3.39 μm abs. by CO_2 laser irrad. *(Japanese)* 80−74410
n-Ge, nonlinear absorption of CO_2 laser radiation by nonequilib. carriers 79−32000
p-Ge, nonlinear IR absorpt., theory 79−65868
Ge, nonlinear reflection props. rel. to thermal effects 78−42371
Ge, picosecond Nd laser pulse reflectivity 79−18469

nonlinear optics continued
Ge, picosecond optical response, effects of parametric scatt., energy-gap narrowing and state filling 80−11424
Ge, plasma excitation, ultrafast optical props. 78−31248
Ge, reflectivity, picosec. laser pulses and electron-hole plasma 79−47463
Ge, refr. index and refl. changes due to intense laser irrad., surface heating effect 78−42372
Ge, Sellmeier coeffs. temp. depend., nonlinear optics average power limit 79−50349
Ge, ultrashort optical pulse transmission, pulse-width depend. 78−55403
α-HIO_3, nonlinear conical refraction, second-harmonic cone 79−27329
H_2O, single 1.06 μm picosecond pulse superbroadening, concurrence with dielec. breakdown 79−86223
H_2O, superbroadening, by self-focused picosec. laser pulses 77−75612
He, 2^3S and 2^1S states, two-photon ionization 80−37791
He-Ne, single mode laser, emission zone nonlinear active lens effect 80−32960
^3He-$^{20,22}Ne/^{127}I_2$, 0.63 micron laser generated contrasting power resons. *(Russian)* 77−23651
$Hg_{1-x}Cd_xTe$, avalanche formation, high intensity IR transmission limit 79−78684
$Hg_{1-x}Cd_xTe$, high intensity IR transmission limit 78−79074
I_2, reson.-enhanced three-photon absorption, CW intracavity absorption 79−10160
$^{127}I_2$, Doppler-free optoacoustic spectroscopy 80−57396
n-InAs, avalanche formation, high intensity IR transmission limit 79−78684
InS(Se), optical and nonlinear optical props. *(Russian)* 79−51943
InSb, absorpt. processes near bandgap, laser-induced hot electron and photocond. meas. 79−42584
InSb, avalanche formation, high intensity IR transmission limit 79−78684
InSb, degenerate four-wave mixing obs. at 5K 80−53355
InSb, low intensity nonlinearities, induced by lasers 79−94300
InSb, nonlinear absorption and pulse shaping for 10.6, 9.6 μm laser radiation 78−79077
InSb, nonlinear optical properties, hot electron effects 78−71139
InSb, nonlinear optical effects obs. using CW CO laser 79−3752
InSb, nonlinear refraction and absorpt. 80−9939
InSb, nonlinear transmission of picosecond 10.6 μm pulses 80−106559
InSb, optical bistability, signal amplification, low power nonlinear effect applications 80−19066
InSb optical signal amplification and bistability 80−9937
KBr, transient infrared absorption of bound polarons 78−92071
KD_2PO_4, nonlinear electrooptic coeffs. near Curie temp. 80−11366
KD_2PO_4, SHG efficiency, 532 to 266 nm 77−23710
KD_2PO_4, two photon absorption at 266.1 nm 77−88844
KH_2PO_4,(KD_2PO_4), photoelectric phenomena, nonlinear optical rectification *(Russian)* 79−19628
KH_2PO_4, KD_2PO_4 crystals, photoresponse under laser irrad., nonlinear optical rectification 80−100479
$K_xRb_{1-x}TiOPO_4$, new nonlinear optical material 77−14784
Kr-Xe, absorpt. spectra line-narrowing, with reson. excitation transfer 79−89973
LaF_3:Pr^{3+}, ultraslow optical dephasing for $^3H_2$-$^1D_2$ transition 79−64290
LaF_3:Pr^{3+}, pseudo-Stark effect meas. using population hole burning and optical free-induction decay 79−24292
LiH_2PO_3, nonlinear and linear optical props. 80−48330
LiH_2PO_3, P-H bond dipole direction, nonlinear optical coeffs. meas. 80−69253
α-$LiIO_3$, energy band struct., nonlinear optical absorpt. obs. 79−64277
$LiIO_3$, nonlinear light scatt. on cryst. defects 78−5527
$LiIO_3$, nonlinear optical activity *(Russian)* 79−45994
α-$LiIO_3$, two-photon absorption spectra, energy struct. anal. 80−99785
$LiNbO_3$, energy band struct., nonlinear optical absorpt. obs. 79−64277
$LiNbO_3$, two-photon absorption spectra, energy struct. anal. 80−99785
$LiNbO_3$, wave front convolution in 4-wave interaction with nonlocal nonlinear media *(Russian)* 79−86205
$LiNbO_3$:Fe, nonlinear image processing in 3-dimens. hologram 80−14303
$LiNbO_3$:Fe(Cu)(Co), pure and doped, nonlinear excitation, multiphoton photorefractive process 79−36950
$LiNbO_3$:Ti, nondegenerate four-wave mixing in integrated optics 79−46088
$LiNbO_3$:Ti waveguide, ps signal processing with planar, nonlinear integrated optics 80−64208
LiO_3, up-conversion of signal from thermal source 80−9938
$LiTaO_3$, wave front convolution in 4-wave interaction with nonlocal nonlinear media *(Russian)* 79−86205
$LiYF_4$, UV window and coating materials, two-photon absorpt. coeffs. 79−59734
$lInBO_3$:Ti crystals and waveguides, absorption loss and photorefractive index changes 80−58787
N_2, vibration stimulated Raman scatt., four photon parametric effects 80−33087
$NH_4H_2PO_4$, SHG efficiency, 532 to 266 nm 77−23710
$NH_4H_2PO_4$, two photon absorption at 266.1 nm 77−88844
Na atomic vapour, Doppler-broadened system, degenerate four-wave mixing, line shape and strength angular depend. 80−43391
Na, mag. perturbed gas, distortionless optical pulse propag. 78−22179
Na, radiatively cooled vapour, 3rd order nonlinear optics processes 79−81477
Na_2SbF_5, linear and nonlinear optical props., hyperpolarisability 78−30010
$Na_5W_3O_9F_5$, single cryst., prep., optical and dielec. studies *(French)* 80−15994
Nd^{3+}:glass, nonlinear refractive index, two-photon resonant absorption by Nd^{3+} *(Chinese)* 80−43387
Ne gas, laser induced birefr., polarised light interf. obs. 77−19368
Ne, reson. interaction of opposite waves, relax. consts. of common level 78−50511
Ne, reson.-absorpt. plasma of glow discharge positive column, Ne superradiation pulse variation 78−71489
Ne, two and three level systems, laser induced dichroism and birefr. 78−79065
Ni complex, BDN, saturable absorber, degenerate four-wave mixing, amplification and phase conjugation 80−43394
OsO_4, tunable diode laser spectrosc. obs. 78−82061
PbI_2, three-photon absorpt. coeff. determ. by nonlinear luminesc. expt. 80−14384

nonlinear optics continued
$PbMg_{1/3}Nb_{2/3}O_3$, electro-opt., elasto-opt., opt. and photo-induced props. 78−95560
$PbZn_{1/3}Nb_{2/3}O_3$, electro-opt., elasto-opt., opt. and photo-induced props. 78−95560
Rb, $5^2D_{3/2,5/2}$ and $7^2S_{1/2}$ two-photon excitation stimulated and parametric emission 77−10651
Rb vapour, Doppler-free two-photon dispersion and optical bistability 80−95940
Rb vapour, Gaussian pulse propag. under two-photon near reson. conditions 80−87441
SF_6, polarization-rotation and thermal-motion studies via resonant degenerate four-wave mixing 80−5779
SF_6 rarefied gas, coherent emission in time-separated fields 79−36954
SF_6 saturable absorber for CO_2 laser prepulse elimination 77−19337
SF_6, saturation absorpt. characts. at 10.53 μm CO_2 P(14) line 77−38999
SF_6, soln., cryosystem, vibr. relax. times, pulsed IR absorpt. spectral obs. 80−66188
SF_6, tunable diode laser spectrosc. obs. 78−82061
SbSI, cryst. and vitreous, nonlinear light absorpt., effect of temp. and phase transitions 77−75604
SbSI, photoelectric current, modulated due to light intensity 79−19626
Si, amorphous sputtered films, hydrogenated, photoinduced optical absorpt. 80−50362
Si, and Si:H, amorphous, ps. relax., optically induced absorpt. 80−48325
Si, degenerate four wave mixing of 1.06 μm laser radiation 80−5794
Si, excited by ultrashort laser pulses, self-diffr. effects 78−18022
Si:H amorphous films, photoinduced optical absorpt. and photocond. 80−50361
SiC nonlinear lens, with variable focal length 79−81511
SiC, nonlinear refr. index meas. by nonlinear lens method *(Russian)* 79−26111
α-SiC(6H), two stage transitions, nonlinear absorpt., thermoluminesc. method 80−7425
SiO_2, fibre waveguide, backward Raman amplification and pulse steepening 77−23740
SiO_2 optical fibres, self-phase modulation 78−66874
$SrTiO_3$ 78−6678
TiO_2, two-photon absorption coefficient rel. to inverse Raman cross section 78−6678
Tl $GaS_2(Se_2)$, optical and nonlinear optical props. *(Russian)* 79−51943
$TlInS_2(Se_2)$, optical and nonlinear optical props. *(Russian)* 79−51943
$ZnGeP_2$ thermo-optic coefficient, dispersion 80−71396
ZnO, surface exciton polariton, nonlinear optical excitation 77−59259
ZnO, surface exciton polaritons, nonlinear optical excitation and dispersion relation 79−82657
ZnP_2, 442 class gyrotropic crysts., self-induced rot. of light polarisation plane 80−99810
ZnP_2, self-induced optical rotation of polarisation direction 79−19860
ZnSe, nonlinear optical effects in rotationally twinned crysts., phase matching 77−42570
$(ZnSe)_{1-x}(GaP)_x$, two-photon absorpt. at ruby laser freq., clarification *(Russian)* 79−15505
ZnTe, nonlinear absorpt., temp. depend. *(Russian)* 77−20899
ZnTe, nonlinear optical effects in rotationally twinned crysts., phase matching 77−42570
ZnTe, two-photon absorpt. line shape near direct band gap and critical point 79−65898

nonlinear programming
see also convex programming; quadratic programming
Calvin photosynthesis cycle parameter identification 79−92186
data inversion via nonlinear programming, appl. to aerosols size distrib. meas. by impactors 77−2258
diagonal-wall MHD generator design optimisation by nonlinear programming *(Polish)* 78−79477
fast power reactor, material distrib. optimisation by nonlinear programming method 77−14210
FBR, optimisation of burnup characteristics, nonlinear programming method 77−14239
gas dynamic variational problems, nonlinear programming methods *(Russian)* 77−51074
heat exchanger optimisation 79−3895
limit analysis in continuum mechanics, nonlinear optimisation problems, numerical methods 79−2628
loudspeaker system, phase inverter, design using nonlinear optimization method *(Japanese)* 79−18659
marine boundary layer microwave sensing, estimation techniques 79−74993
neuronal response in rat hippocampus, dynamic model 79−34547
nuclear power stations, optimal size and location in energy parks 80−95489
optimal nodal point distribution for improved accuracy in computational fluid dynamics 80−48670
optimum laminate design, natural frequency restraints 80−53688
orbit transfer, three burn, optimal, nonlinear programming trajectory simulation 77−84133
PHWR-1000, uniformity factor maximisation, nonlinear programming 80−739
respiratory ventilator model and design optimisation 79−20713
SAW filter design using optimisation technique 80−74671
soil mechanics, optimal lower bounds 77−72262
strength of axisymmetric body, optimum shape calc., finite element technique 78−51060
structural reliability, using chance-constrained programming, appl. to reinforced silo 78−63338
tidal sea level extremes calc. 77−78479
viscoplastic flow, finite element method with added boundary terms 78−42543
water pollution dynamic models synthesis, finite-difference method 77−81950
water utilisation system, area wide multimodal system, nonlinear goal programming model 79−57518
system reliability appl., NATO Advanced Study Institute, Liverpool, England (Jul. 1973) 77−38396
P control in estuaries, parallel shooting models, Corpus Christi Bay (Texas) and Jamaica Bay (New York) appls. 79−57521

nonlinear symmetries
σ-models, nonlinear, classical two dimens., dual symmetry 79−80750

nonlinear symmetries continued
affine gravity and strong interactions in SL(4,R) nonlinear representations 80−18108
chiral dynamics, kink solns. of extended nonlinear model and particle interpretation 78−89612
chiral symmetry, nonlinear realisations and local invariance 80−361
de Sitter symmetry and restricted space-time regions for gravity and supergravity 79−85043
dissipative classical systems, time-depend. canonical transforms. 80−62885
extended hadrons and quark confinement, description using nonlinear De Sitter symmetry 78−58140
gauge field in stability subgroup of vacuum in nonlinear realization 78−390
Higgs like mechanism, nonlinear group realisations 79−45031
O(3) nonlinear σ model, quantum fluctuations of instantons 79−71610
O(N) nonlinear σ-model, particle prod. and factorising S-matrix 79−71613

nonlinear systems
see also bang-bang control; nonlinear control systems
acoustic nonlinear orifice impedance correlation curves 77−23837
acoustic orifice under turbulent boundary layer 77−23838
active, self-consistent soln. method for calc. of power spectrum of fluctuations 78−16735
arterial system nonlinear model validation 79−96600
asymptotic stability, geom. props. of Lyapunov functions *(German)* 78−87286
basilar membrane, nonlinear model rel. to two-tone suppression 77−48811
beam, buckled, eqns. for nonplanar, nonlinear motions 78−83316
beam, nonlinear elastic foundation, comment on fundamental freq. of vib. 78−90756
beams, tapered clamped, large amplitude vibr. 78−83311
bilinear system Volterra-kernel estimation 79−26512
biological, analysis by Wiener kernel estimation in freq. domain 77−1973
biological membrane, electrically excited, nonlinear dynamic models for simulation 80−94178
chemical system, open, information, critical fluctuations and phase-transition-like phenomena 79−24720
coupled dynamic physiological systems, network thermodynamic simulation 79−96504
crayfish stretch receptor repetitive firing behaviour nonlinear systems anal. 78−80853
crystallographic structures, non-linear physics anal. 80−10631
diffusion in nonuniform multicomponent system with multidimensional regions *(Russian)* 79−12743
dry-friction periodic relay system analysis *(Russian)* 79−10455
dual input nonlinear system characterisation using impulse trains 78−31761
dynamic system, piecewise-linear non-linear, several degrees of freedom, forced oscillations 78−54173
dynamical system, limit cycles and symmetries 80−62462
forced vibrations of systems with retardation and damping 78−83290
forced vibrs. of nonlinear systems, Duffing eqn. 77−33842
Hamiltonian systems of Vaslov and Hartree type, uniformisation method 79−21588
hydrological system, state space modelling and identification 79−79908
liver disease computer-aided diagnosis using nonlinear stochastic modelling technique 78−36024
lumped system in conflict with environment, Liapunov type design 79−57498
lung, nonlinear mathematical model, parameter tracking adaptive algorithm 77−60227
magnetic field calc., saturable, by finite element method, using scalar magnetic potential 77−38773
mathieu stability analysis of non-linear third-order weakly forced systems 79−30261
mechanical struct., Duffing asymmetric model dynamic prop. 77−19556
mode-locking in nonlinear systems, computer simulation 77−12872
moment equation methods for nonlinear stochastic systems 79−21666
multi-input nonlinear system statistical anal. by optimal linearisation *(German)* 78−64918
neural system Wiener anal. using Poisson-Charlier crosscorrelation 78−24055
neural transformations of random signals, Wiener and of functionals of Markov chain 80−76727
nonhamiltonian systems with one degree of freedom, forced periodic motion *(Russian)* 78−20959
nonholonomic Chetaev systems, Lagrange eqns. derivation from modified Pontryagin maximum principle 78−12557
nonlinear experimental design, information measures 80−62616
nonlinear third order systems, pulse response 78−83313
nuclear industry, nonlinear systems, nonparametric system identification 80−32325
nuclear reactor, modal control based on nonlinear model 77−38339
oscillating, delay effects *(German)* 77−53773
oscillator systems, nonlinear stochastic models 79−80525
oscillators, planar, nonlinear, stability of modes 80−74790
oscillators, weakly nonlinear, system with slowly varying parameters, resonance 80−62463
oscillators with nonlinear restoring forces, first passage failure probability calc. 78−42562
parametric dynamic systems, combination reson. determ., generalised harmonic balance method 78−90753
parametric excitation of combined resonant systems 77−2539
parametric vibration of systems with one degree of freedom 77−53770
perturbed motions, estimates *(Russian)* 77−54871
physiological, Volterra kernels representation determ. 79−2034
physiology, martingale model for estimation in nonlinear stochastic systems 77−77865
plasma nonlinear problem variational soln. *(French)* 78−63539
power reactor, neutron density fluctuations, stochastic nonlinear model, Fokker-Planck eqn. 78−58316
prosthetic arm decentralised control hierarchical approach 77−40924
pulse response, Krylov and Bogoliubov approx. 79−84962
PWR core, Xe oscillation model, neutron diffusion eqn., nonlinear system 78−58322
PWR system nonlinear model comparison with test results 78−29571
repetitive firing computer models nonlinear systems anal. 78−80854

nonlinear systems continued
resonant vibrations, modified single mode method 79−86371
response under combined forcing and parametric excitation 77−68517
second order system, eigenfunction expansion solutions of Fokker Planck eqn. 80−73172
shock spectrum of two degree of freedom nonlinear vibratory system 77−27421
Sobolev equations for nonlinear dispersive systems 79−21528
somatosensory system afferent signals, modulatory effect of prior input 77−90758
stability anal. method 79−84947
stability of periodic motion and nonlinear oscillation theory *(Russian)* 78−86147
stochastic stability of dynamic multi-nonlinearity systems, action of white noise 80−68135
stretched strings, occurrence of subharmonic resonances of order 1/3 78−90580
string, nonlinear stretched, randomly excited, anal. 78−83312
third order, forced periodic response stability 78−90763
third-order nonlinear systems with aperiodic excitations, Laplace transform technique 78−81830
time varying systems, stability anal. 78−37
variable-thickness elastic orthotropic annular plate nonlinear oscillations 79−68630
vibrating curved elements, asymptotic solutions to nonlinear vibrs. 78−90757
vibrating systems, nonlinear, multi-degree-of-freedom, harmonic excitation, instability 80−73162
Volterra kernel estimation of bilinear systems, cross correlation algorithm 79−80919

nonlinearities of control systems *see control nonlinearities*

nonparametric statistics
EEG automatic classification, decision rules comparison 80−109054
Kuwait hourly stochastic insolation model 79−58068
leucocyte classification by parametric and nonparametric analysis 77−78016
methods, probabilistic models and test problems *(French)* 78−12538
nuclear reactor normal and abnormal behaviour nonparametric recognition 79−81044
speech quality parametric objective measures correlated with subjective results 80−91980
van der Waerden's nonparametric X test in data processing 77−71304

nonradiative transitions
acceptor centres, radiationless transitions probabilities *(Russian)* 79−87507
acetaldehyde+CO_2, vibr. relax., search for unquenchable species, room temp., 5-2200 torr 78−9229
acetone, photochem. and photophysics, 330-250 nm, 0-1000 torr 78−17706
acetones, fluorinated, absorpt., fluoresc. spectra, quantum yields, decay times meas., mechanism 77−3410
acetophenone, T_1-S_0 intersystem crossing, nonradiative decay rate, excitation energy depend. 80−63609
acridine, electronic relax., internal conversion, intersystem crossing, psec. spectra 77−65499
acridine, nonradiative electronic relax., picosecond absorption spectrosc. obs. 78−82053
acridine, solvent depend. of radiationless relax., singlet lifetime, picosecond spectroscopy 78−66582
acrolein, vap., visible luminesc. excited by pulsed CO_2 laser 79−54894
activated crystal, electron excitation energy transfer, collective coherent phenomena 77−90189
activated crystal, electronic excitation energy migration efficiency, inverse transfer influence 78−19546
adiabatic potential crossing system, non-radiative transition 79−28817
adiabatic separation, theory, book contrib. 77−34687
alkali halides, luminescence quenching of F-centres 80−50417
alkyl aryl ketones, in homogeneous n-heptane solns., quasi-isoenergetic triplet energy migration, photolysis obs. 79−61878
8-anilino-1-naphthalenesulfonic acid, fluoresc. probe mol. in mixed solvent 79−45746
1,8-anilinonaphthalene sulphonate, aq. and ethanolic solns., excited singlet state decay pathway 78−17703
anthracene, carbonyl derivatives, triplet state population, picosec. laser obs. 78−13544
anthracene, chemisorbed on Al_2O_3, radiative and nonradiative processes 79−36686
anthracene, diacetyl-sensitised delayed fluoresc. 79−54888
anthracene, pure and d_n, PMMA soln., triplet lifetimes, 77-300K 78−25594
anthracene, theory of fission of singlet Frenkel exciton into two localised triplet excitons 79−23901
anthracene-N,N-diethylaniline exciplex, intersystem crossing 77−30905
anthracenes, in soln., triplet-triplet fluoresc. 79−59501
anthracenes, meso-substituted, thermally assisted and heavy atom assisted intersystem crossing 79−31573
anthracenes, nonradiative relax. of higher excited triplet states, double excitation obs. 78−29805
anthrone, 533 nm excited state absorpt. kinetic, triplet quenching solvent, internal conversion, vibr. relax. 78−21935
anthrone, intersystem crossing rates, ps time-resolved spectra 77−6821
antiresonance line shapes and radiationless decay, compatibility restrictions 80−48040
aromatic amides, intersystem crossing, mol. geom. effects 77−6828
aromatic compounds, intersystem crossing theory, El-Sayed rule extension, anomalous rate consts. 77−30911
aromatic compounds, with nonbonding electrons, proximity effect and radiationless transitions 78−58736
aromatic hydrocarbon, centrosymmetric, two photon excited upper state fluoresc. spectra, reson. fluoresc. and vibr. mode selectivity 80−18878
aromatic hydrocarbon, quenched with Ag^+ in ethanol, triplet state form. 79−11801
aromatic hydrocarbon derivatives, low-temp. singlet-triplet conversion probability rel. to optical parameters 79−54898
aromatic hydrocarbons, ethanol-KI solns., fluoresc. affected by I^- 79−13749
aromatic hydrocarbons, excimer decay dynamics, rate const. rel. to solvent 78−58729
aromatic hydrocarbons, intersystem crossing mechanism, rate consts. 77−65497

nonradiative transitions continued
aromatic hydrocarbons, sequential coupling 80−58297
aromatic hydrocarbons, singlet-triplet conversion at low temp. 80−43094
aromatic impurity molecule, internal conversion processes 78−82776
aromatic isolated mol. nonradiative conversion, internal and S-T conversion, vibr. excitation and fluoresc. quantum yield 80−43095
aromatic molecule with nonbonding electrons, $T_1(\pi\pi^*)\rightarrow S_0$ radiationless transition, vibr. coupling 77−18957
atom, exchange and relax. effects in low-energy transitions, appl. to Zn 3p vacancy deexcitation 79−3396
atom, L-subshell Auger and Coster-Kronig rates and fluorescence yields, relativistic calcs. 79−81180
atomic radiative and radiationless yields, K and L shell 79−76376
atoms, autoionising and inner shell vacancy states, decay, time independent multichannel scatt. theory 80−47854
atoms, excited, located near absorptive medium surface, energy dissipation 77−61692
atoms, relativistic transitions, Dirac-Fock formalism 78−37574
Auger kinetic and relax. energies in atoms and solids 78−15297
aza-aromatic molecules, intersystem crossing, quantum interference effects 80−53037
azulene, nonradiative relax. lifetime of first excited singlet state, subpicosecond optical technique 78−78741
azulene, picosecond dynamics 77−30896
azulene($-d_8$), ultrafast $S_2\rightarrow S_0$ internal conversion 79−3474
azulenes, substituted, internal conversion, energy gap correl. 79−54901
azuleno[5,6,7-cd]phenalene, slow internal conversion between close lying singlet state 77−30907
basis set choice criterion, for closely coupled electronic states 78−33546
basis set for describing transitions, method for determ. 77−6831
benzaldehyde gas, nonradiative electronic transition 80−83413
benzene, $^1B_{2u}$ and $^3B_{1u}$ states nonradiative decay, collisional deactivation 77−6819
benzene, $-d_0-d_8$ vapour at low press., intersytem crossing and internal conversion, press. depend. of triplet form. 77−30918
benzene, intramol. nonradiative transitions, Franck-Condon principle at high energies 77−14478
benzene, intramolecular vibr.-electronic conversion, relative rate calcs. method 77−65496
benzene, lowest triplet state, pulse radiolysis obs. 79−39168
benzene, phosphoresc., radiative and non-radiative decay routes, spin sublevel origin 77−58064
benzene, single vibronic level decay rate, analytical representation 77−79645
benzene, T_1-S_0 intersystem crossing vibronic interactions IR absorpt. spectrum obs. 80−28042
benzene, third channel decay mechanism, radiationless transitions 77−50463
benzene, vapour-phase, absolute fluoresc. quantum yields, nonradiative processes 77−6829
benzene ($^1B_{2u}(S_1)$)+Ar(benzene), rot. relax. to Boltzmann distrib. 78−86936
benzene-d_0,-d_6, phosphoresc., Boltzmann population and spin-lattice relax., decay processes 78−31230
benzene-d_0($-d_6$), radiationless triplet decay, non-Condon effects 80−83405
benzophenone, fluoresc. quenching and intermol. intersystem crossing, nonlinear press. depend. 78−25603
benzophenone vapour, fluoresc. and phosphoresc., nonradiative transitions between triplet and singlet state obs. 80−99516
benzophenones, in host crysts., triplet state PMDR, phosphoresc. spectra, transitions mechanisms 77−46585
p-benzoquinone($-d_4$), n-π^* excited states, distant intramol. interaction between identical chromophores 78−90203
benzo[α]pyrene-DNA complex, triplet state props., optically detected zero-field mag. reson. obs. 77−79636
1,12-benzperylene exciplexes, radiative and radiationless decay 77−6817
biacetyl in supersonic jet, emission spectra, energy-resolved decay times 79−81224
9,9′-bianthryl, excited, proton-induced radiationless processes 77−88486
biphenyl, carbonyl derivatives, absorpt. and luminesc. spectra, solvent effects and triplet lifetimes 77−24889
biphenyl, in propylene glycol, mol. fluoresc., effect of mol. conformation 78−78736
biphenylene, fluoresc. from higher singlet levels 79−83473
Bixon-Jortner approx. limitation, coupling strength incoherence 77−57960
borate glass: $UO_2^{2+}\rightarrow Ho^{3+}$, energy transfer processes 78−10969
Born-Oppenheimer and true eigenstate prep. by coherent light, large mol. nonradiative relax. 77−88490
calibo glass:Eu^{3+}, Ho^{3+}, energy transfer 78−76510
calibo glass, quantum efficiency of non-radiative energy transfer 79−33832
camphorquinone, cryst., PMDR and fluoresc., S_2 state, intersystem crossing 77−32296
camphorquinone, vapour, nonradiative electronic relax. rate, excess energy depend. 77−38687
carbazole, triplet state of X-traps, ODMR 79−24231
carbocyanine dye solns., photoisomerisation and internal conversion rates, time-resolved spectra 77−75201
carbocyanine dyes, triplet state quenching by nitroxyl radical, charge transfer complexing 78−25585
carbonyl fluoride, IR laser driven reverse internal conversion 79−81230
chalcogenide glass, mech. for electron-hole recomb. 78−72196
chalcogenide glasses, Luminescence, temp. depend. rel. to nonradiative transitions 80−71485
chalcogenide glasses, non-radiative recombination of electron-hole pairs 78−6759
chalcogenide semiconductors, optical and elec. props., comparison with SiO_2 78−6721
chemiluminescence in soln., energy transfer 79−11479
chloroacetylene dissoc. and predissoc., state selected unimolecular reaction dynamics 77−36744
chlorophyll, a and b, lowest singlet-singlet transition, solvent effects 79−24952
chlorophyll b derivatives, metal substitution effect on triplet state, intersystem crossing 77−88476
chlorophyll solutions, triplet state props., ODMR meas. 79−20517
chloroquinolines, photophys. behaviour, substituent and solvent effects 80−106342
CIDEP, examples of S-$T_{\pm 1}$ polarisation 78−86891

nonradiative transitions continued
collision free triplets, spectrum, temporal evolution 78−33441
collision-induced state-changes, intermol. pot. well depth role 79−81257
complex Franck-Condon overlap integral in nonradiative decays 79−50066
complex molecules, fluoresc. quenching by strong radiation due to linear Stark effect 77−58074
complex potential energy surface systems, nonradiative processes, WKB calcs. 80−45133
conference, luminescence, Paris (July 1978) 79−33755
coronene, sub psec radiationless relax. in soln. 77−18955
coumarin laser dyes, solvent effects on photophysical parameters 80−91598
coupled molecular normal vibr. system, radiationless energy relax. *(German)* 78−35184
diacetyl vapour, fluoresc. and phosphoresc., nonradiative transitions between triplet and singlet state obs. 80−99516
dialkylaniline derivatives, twisted intramol. charge transfer states, dual fluoresc. obs. and form., dipole moments 80−18881
3,6-diaminophthalimide vapour, mol. electronic excitation energy degradation path depend. on pentane 80−74195
diatomic molecule, neutron scatt. induced electronic transitions, tunnelling 80−63844
diatomic molecule in crystal, rate of radiationless electronic transitions 80−93373
diatomic molecule in solid lattice, nonradiative relax. of intramolecular vibr. 77−52178
diatomic molecules, matrix isolated, vibr. relax., rot.-translational coupling 80−53102
diazanaphthalenes, excited state absorpt. spectra and intersystem crossing kinetics 80−74176
p-diazines, polycyclic, $T_1(\pi\pi^*)\rightarrow S_0$ intersystem crossing, isotope effects, ODMR and phosphoresc. obs. 80−91586
dibenzofuran, triplet state of X-traps, ODMR 79−24231
dibenzothiophene, triplet state of X-traps, ODMR 79−24231
1,4-dibromonaphthalene, phosphorescence microwave photoexcitation spectrum (PMPS) 77−32294
9,10-dichlorophenanthrene, intramol. heavy atom effect, PMDR obs. 79−13745
3,3′-diethyl-2,2′-thiatricarbocyanine iodide, solns., photoisomerisation and internal conversion rates, time-resolved spectra 77−75201
3,3′-diethyloxadicarbocyanine iodide, lasing and photoisomerisation, conc. and temp. effects 77−7081
diethynylbenzene, radiative and nonradiative processes, triple bond effects 79−3481
p-difluorobenzene, $^1B_{2u}$, fluoresc. quantum yield, radiative and nonradiative lifetimes, vibronic level depend. 77−75204
dihydrophenazine derivatives, in 3-methylpentane (ethanol) (PMMA), radiationless processes, temp. depend. 80−43087
9,10-dimethyl anthracene, excited singlet state quenching by nitroxyl radical, triplet form. 77−88487
6,6′-dimethyloxyindigo, picosec. kinetics, and photostability, spectrosc. obs. 79−45748
2,6,dimethylpyrazine, PMMA soln., fluoresc. and phosphoresc. quantum yield and lifetime, 20-120 kbar 79−54902
dimethylsulphoxide, $Eu^{3+}\rightarrow Pr^{3+}$ and $Eu^{3+}\rightarrow Er^{3+}$ non-radiative energy transfer 79−47510
dinaphtho-(2′.3′:1.2);(2″3″:6.7)-pyrene, triplet state, phosphoresc. and ODMR obs. 79−27013
9,10-dioxa-anti-bimanes, fast intersystem crossing, picosecond spectrosc. obs. 79−85998
1,8(6′,7′-dioxododecamethylene) phenanthrene, intramol. electronic energy transfer, emission obs. 79−31571
9,10-diphenyl anthracene, excited singlet state quenching by nitroxyl radical, triplet form. 77−88487
1,8diphenyl-1,3,5,7-octatetraene, high press. fluoresc. studies of radiative and nonradiative processes 80−1011
1,6-diphenyl-1,3,5-hexatriene, high press. fluoresc. studies of radiative and nonradiative processes 80−1011
1,6-diphenylhexatriene, radiationless transitions and natural lifetimes, solvent effects 80−63622
2,5-diphenyloxazole, phosphoresc., 77K, solvent effect 78−42118
dissociating molecule, vibr. spectra *(Russian)* 78−21864
DNA, proton radiationless transitions for hydrogen bonds *(Russian)* 80−97857
duraldehyde, S_1-T_1 nonradiative transition mechanism, double reson. obs. 77−30893
dye solution, fluoresc. yield, photoacoustic determ. method 78−42117
dye solutions, mixed, fluoresc. conc. quenching, sensibilisation 79−24347
dyes, rot. diffusion of prolate, oblate mols. from absorpt. relax. 80−1008
dyes for tunable lasers, intersystem crossing rates and saturation parameters in triplet state 77−36280
dynamic multiphoton processes as criteria for luminesc. of electronically excited centres 80−11463
dynamic theory, selective mol. excitation by laser pulses 77−54570
electric field induced radiationless transitions, theory 78−74690
electro-optic laser technique for probing coherent and incoherent decay processes 77−75338
electron-hole drops, non-radiative recombination by phonon-assisted Auger recomb. 79−60716
electron-phonon system strongly coupled localised potential curve crossing problem, Landau-Zener formula *(Japanese)* 79−87049
electronic processes and energy transfer, conf., Tallahassee, Fla., USA (Jan. 1976) 77−27042
energy transfer, between ions in solutions under conditions of n-pair formation 79−4843
energy transfer, unified model, arbitrary Franck-Condon offset and temp. 79−1781
energy transfer between ions in solutions 79−10140
enhanced Raman scattering by adsorbates on metals, including nonlocal metal response, nonradiative modes excitation 80−88994
ethynylbenzene, radiative and nonradiative processes, triple bond effects 79−3481
excitation energy transfer and migration, spectral line broadening 80−2841
excited atoms ejected in ion-surface bombard., effect on optical emission intensity of radiationless transitions 78−39652
excited mol. states, preparation and decay, dephasing relax. and pulse fall time effects 78−94200
excited single state kinetics on a subnanosecond time-scale 79−36677
excited state electronic rearrangement, rate const. calcs. 77−3411

nonradiative transitions continued
fluorene, triplet state of X-traps, ODMR 79−24231
fluorenone, intersystem crossing rates, ps time-resolved spectra 77−6821
fluorescein dye(-Yb^{3+}), triplet state energy transfer, fluoresc. quenching obs. 79−54897
fluorescence, depolarisation, orientation factors, excitation energy transfer between isolated donor-acceptor fluorophore pairs 79−22740
fluorescence quenching and intermol. intersystem crossing, nonlinear press. depend. 78−25603
fluorescence quenching measurements, inner filter effects for different illumination geometries 78−92548
fluoride, Mn^{4+} activated, configurational co-ordinate model, predictive use 79−19918
fluorobenzene cations, fluoresc. quantum yields and lifetimes, electronic state relax. processes 80−48027
fluorophosphate glasses, rare-earth activated, luminesc., bonding 78−64415
formadelhyde(-d_2), S_1 rot. levels, collisionless nonradiative decay rates 79−72346
formaldehyde, $^1A_2$-state, radiative and nonradiative decay calcs., rel. to photochem. decomp. 78−37669
formaldehyde, intramol. energy transfer, photodecomp., radiationless decay 77−29027
formaldehyde, nonradiative transition rates and predissociation process 77−54574
formaldehyde, sequential coupling 80−58297
formaldehyde, vibronic and spin-orbit coupling, radiative and non-radiative transitions 77−3414
formaldehyde-d_0, -d_1, -d_2, single vibronic level photochem., radiative and nonradiative processes 78−66583
formaldehyde-d_0, -d_2, $^1(n\pi^*)$ radiationless transition, ab initio CI calc. 79−767
formaldehyde-d_2, inert gas and N_2 matrix fluoresc. spectra, radiationless transitions and lifetimes 79−3469
formaldehydes, (deuterated), A^1A_2 state, photoluminesc. in low temp. matrices, vibr. relaxation 79−50070
Forster migration of electronic excitation, randomly oriented system 78−48211
germanate glass:Bi^{3+}, time-resolved spectra, radiative and nonradiative processes 79−47501
germanate glass:Bi^{3+},Eu^{3+}, time resolved spectra for Bi-Eu energy transfer 79−33748
glass:Nd^{3+}, ED-2 laser glass, transition probabilities and quantum efficiency 77−58330
glass, trapped electrons, electron-phonon interaction 79−78697
glasses, non-radiative recombination at valence-alternation pairs 80−89048
glyoxal, ^1A_u state energy transfer, D effects 77−58066
glyoxal, internal conversion, energy redistrib. 80−53036
glyoxal, intersystem crossing in weak mag. field 78−78743
glyoxal, radiationless transitions in weak mag. field, fluoresc. quenching 77−58062
glyoxal, singlet-triplet radiationless processes in mag. field 80−106347
glyoxal, vibr. energy redistrib. following internal conversion 80−23452
glyoxal (^1A_u), fluoresc. quantum yields, radiative and nonradiative lifetimes 80−32759
glyoxal in supersonic jet, fluoresc. excitation, collision-induced intersystem crossing, van der Waals complex 79−81223
haemoproteins, fluoresc., reson. Raman and radiationless decay 77−30916
halides, aryl and aryl-alkyl 193 nm photodissoc., fragment translational energy distrib. 80−48048
haloazulenes, S_2-state deactivation, intersystem crossing and heavy atom effects 78−13545
halobenzenes, singlet excited states decay, substituent effects 77−75175
halofluorescein dyes, fluoresc. internal conversion, intersystem crossing 77−3405
halonaphthalenes, heavy atom effect on radiative and nonradiative decays 79−31584
halonaphthalenes, intersystem crossing-singlet excited state to triplet state spin sublevel 80−53035
1-halonaphthalenes, lowest triplet state, spin sublevels decay, internal heavy atom effects 79−95819
halotoluenes, singlet excited states decay, substituent effects 77−75175
helicenes, fluoresc., intersystem crossing, rate parameters 77−3392
N-heteroarenium cations B, resonant, nonradiative energy transfer *(German)* 78−25659
heteroaromatic mol. radiationless transition decay rate freq. shift depend., quantum statistical mechanics anal. 78−74691
heterocyclic aromatic molecules, nonradiative transitions activated by external fields 77−65501
heterocyclic N compounds, radiationless transitions, isotope effects 80−48033
N-heterocyclics, radiationless transitions, vibronic coupling effect 78−33543
hexamethyl-2,2′-indotricarbocyanine iodide, solns., photoisomerisation and internal conversion rate, time-resolved spectra 77−75201
high Rydberg atom+neutron atom (molecule), collisional quenching, theory 79−86051
high-overtone spectra, reson. struct. and background absorption 79−54833
higher order cross type mechanisms in radiationless transition theory 79−6960
hot luminescence in F centres, nonradiative quenching 80−11467
ortho-hydroxybenzophenone, soln., intramol. proton transfer and energy relax. photostability, transient absorption obs. 80−28032
hydroxypyridines, phosphoresc. emission, polarisation and lifetimes 78−31232
impurity centre, nonradiative transitions, with participation of short-wavelength phonons 80−16099
impurity ions and molecules in solids, non-radiative decay, book 80−2858
impurity molecule in crystal 80−103645
1-indanone, T_1-S_0 intersystem crossing, nonradiative decay rate, excitation energy depend. 80−63609
indigo, picosec. kinetics, and photostability, spectrosc. obs. 79−45748
indigo dye, excited state lifetime, influence of inter- and intramol. H bonding 77−79659
indigo dyes, triplet state config., laser flash absorpt. spectrosc. obs. 80−5557
nonradiative transitions continued
indole, and derivatives, temp. fluoresc. quenching, rel. to H_2O solvent struct. 78−5265
intermolecular energy transfer and high energy excitations, in condensed phase 80−66269
internal conversion, matrix elements 78−86903
intersystem crossing, collision-induced, reduced eqn. of motion 79−18227
intersystem crossing rates, triplet sublevel decay, vibronic coupling 78−5271
intramolecular dynamics, random coupling model, math. approach 80−58308
intramolecular dynamics, random coupling model, multiphoton excitation, kinetic eqns. 80−63700
intramolecular energy transfer, quantum effects 80−42964
intramolecular energy transfer, stochastic, crit. point anal. of Hamiltonian system instabilities 79−98005
intramolecular memory effects in second-order optical processes 78−94270
intramolecular nonradiative transitions of gaseous small molecules, rovibronic level, lineshapes 80−95667
intramolecular radiationless transitions, Franck-Condon factors of polyatomic mols. 77−14478
intramolecular radiationless transitions, theory, line broadening effects 78−90201
intramolecular vibr.-electronic conversion, relative rate calcs. method 77−65496
intrastate scrambling in large mol. bound level struct., appl. to tetracene 80−63696
9-iodoanthracene, picosecond fluoresc. lifetimes, thermally activated $S_1 \rightarrow T_n$ intersystem crossing 80−28045
ion fragmentation mechanisms and photoelectron spectroscopy, book contrib. 80−14179
ionic crystal, exciton mechanism model for defect form. 80−80187
ionic crystals, nonradiative multiphonon transitions in impurity centres with extremely weak electron-phonon coupling 80−25436
isomerisation, thermal, rate theory 79−34291
isoquinoline, radiationless transition branching ratio, temp. effects 79−54900
isoquinoline, radiationless transitions, internal conversion, energy depend. 78−94272
ketone chemiluminescence during disproportionation, nonradiative transition processes 79−87846
lanthanides complexes with L-histidine, intermolecular energy transfer, influence of metal-to-ligand ratio 80−32763
large molecules, excited state radiationless processes, time-resolved optoacoustic spectroscopy 78−89550
large molecules, nonradiative transitions activated by external fields 77−65501
laser excitation of stationary molecular states, coupling of real eigenstates to phonons and photons 77−68084
lattice relaxation and time resolved polarization of emission from localized electron with level crossing 79−4840
liquid, low-viscosity, Forster kinetics breakdown, time-depend. rate const. 79−86033
luminescence conference, Szeged, Hungary (Aug. 1976) 78−27279
luminescence decay, exchange mechanism, parameters 80−28051
luminescent solid, photoacoustic spectroscopy obs. 77−90185
2,6-lutidine, fluoresc. of vap. phase, nonradiative electronic relax. 79−86000
M-shell radiationless transitions, subshell fluoresc., Coster Kronig yields and X-ray linewidths, relativistic Dirac Hartree Slater calcs. 80−52959
macromolecular interactions, effects of intervening medium and polar mode energy feeding 79−13857
magnesium porphin, lowest triplet state, zero-field ODMR 79−31562
magnesium tetraphenylchlorin, lowest triplet state, zero-field ODMR 79−31562
magnetic quenching, enhancement of radiationless decay, direct and indirect mechanisms 77−42345
magnetic-field-induced radiationless transitions, quantum mech. theory 79−36676
metal complex, internal ligand modes 79−22750
metal-ion point defects in solids, non-radiative relax. 78−6753
methyl halide ions, unimol. dissoc. and internal conversions, coincidence meas. 77−6869
methylated benzene+tetracyanobenzene, fluorescent exciplex form., electronic relax. 80−5573
N-methylphthalimide in ethanol soln., gain and induced absorpt., struct. props. 77−24890
5-methylpyrimidine, singlet-triplet intersystem crossing, ODMR and MIDP in matrix at 1.6K 79−50055
micellar solutions, fluoresc. quenching rel. to aggregation numbers 79−34364
microemulsions, aerosol OT, inhomogeneous interior, fluoresc. and polarisation decay probes 80−50891
Migration of the excitation energy in luminescent media 78−27280
model, time development *(German)* 77−38686
molecular $\pi\pi^*$ and $n\pi^*$ states, rel. positions, single-triplet conversion probability, low temp. 79−816
molecular $\pi\pi^*$ and $n\pi^*$ states relative position, optical props., singlet-triplet conversion processes 79−3484
molecular beam, collisionless, high-resolution time-resolved laser spectroscopy 79−3501
molecular chemical tunnelling, facts and hypotheses 79−59520
molecular collision induced intersystem crossing, dynamics 78−90276
molecular crystal, multicomponent, energy migration master eqn. 80−16075
molecular crystal, sensitised fluoresc., energy transfer rate 79−38586
molecular dimers, intersystem crossing, struct. 78−33537
molecular electron-vibration system, nonequilib. first-order type phase transition 80−9633
molecular excited state relaxation processes, oscillatory versus dissipative limits, education appl. 80−31468
molecular gas, radiationless transitions in mag. field 78−66580
molecular multiphoton ionisation dynamics, rate eqn. modelling 80−48046
molecular optical spectroscopy, by 90° photon echo, during reson. scatt. and radiationless transitions 78−86978
molecular relax. phenomena, quantum statistical mechanical approach, irreversible thermodynamic theory 80−48028
molecular solids, electronic energy transport, picosec. transient grating technique obs. 79−47028

nonradiative transitions continued
molecular system, picosecond relax. processes, book contrib. 77−61788
molecular vibrational promoting modes, geometry, effect on radiationless transition rate consts. 80−5569
molecule, nonstationary state time evolution, vibr. redistrib., nonradiative mechanism 77−83575
molecule, optically prepared state undergoing radiationless decay, three-state model 78−5260
molecule located in condensed medium, vibr. relax. effect 80−80848
molecules, and condensed phases, book 77−34686
molecules, isolated, intersystem crossing, rot. motion effect 80−95669
molecules, transition probability studies, review of recent advances 78−17655
molecules, vibronic interactions, out-of-plane vibrs. 78−17705
molecules, with single and double minima pot. energy surfaces 79−50067
multicomponent luminescent system, nonradiative transfer of electronic excitation energy 79−28804
multiphonon nonradiative transition rate for electrons in semicond. and insulators 78−60503
multiphonon nonradiative transition rates, quadratic impurity-phonon coupling 78−23506
multiphonon tunnel processes in homogeneous elec. field *(Russian)* 78−39607
myosin-auramine O system, conform. changes and excitation energy transfer 79−96512
naphthalene:azulene, reson. fluoresc., Raman spectra, single vibronic level relax. 79−38588
naphthalene, $^1B_{3u}$-state lifetime, temp. depend. under Boltzmann conditions 79−86008
naphthalene, chemisorbed on Al_2O_3, radiative and nonradiative processes 79−36686
naphthalene, fluoresc. lifetimes of single vibronic levels 79−27016
naphthalene, internal conversion rate, effect of benzene triplet state self-quenching 78−25586
naphthalene, nonradiative transition rates, rot. struct. 78−42119
naphthalene, radiationless transitions, sharp Doppler-free resons. *(German)* 77−58076
naphthalene, theory of fission of singlet Frenkel exciton into two localised triplet excitons 79−23901
naphthalene, triplet state time evolution after radiationless transition, initial vibronic distrib. effects 80−23450
naphthalene, vapour-phase, absolute fluoresc. quantum yields, nonradiative processes 77−6829
naphthalene molecule in durene and xylene crystals, vibronic interactions 80−84755
naphthalene-d_0(-d_8), radiationless triplet decay, non-Condon effects 80−83405
1,2-naphthalocyanine-rare earth ion complexes, electronic excitation deactivation mechanism 79−85988
β-naphthylmethyl amine, solvent-induced intramol. exciplex fluoresc. 78−25592
non-Condon approximation calcs. of theory of radiationless processes *(Russian)* 78−72599
non-Condon scheme for nonradiative decays 77−34674
non-equilibrium phonon distrib., in cryst., spectral line shape theory 80−60530
nonrandom sequential coupling influence on radiationless relax. processes 78−90205
octaethylporphin, radiationless transitions, fluoresc. and phosphoresc., isotope effects 77−65502
ODMR, spin-lattice relax. and triplet-triplet. absorpt. effects 79−19807
optical dephasing in condensed phases, coherent spectrosc. obs., theory 79−36693
optical free induction decay, of mols. undergoing radiative and radiationless relax 78−83040
optical probing of excited mols. that have undergone radiationless transitions 77−27106
orbital correspondence anal. in max. symm., appl. to spin-forbidden processes 78−78631
organic dye, excited mol. decay near metal surface, energy transfer to plasmon surface polaritons 80−50440
orientation factor in conc. effects due to nonradiative energy transfer in luminescent system 80−25425
oxalyl fluoride, radiative and nonradiative transitions, self-quenching, unimol. dissoc. 78−17708
pentacene, intersystem crossing and internal conversion rates, fluoresc. transient and optical FID spectrosc. 79−81229
pentacene, laser fluoresc. of mol., excitation bandwidth and optical dephasing 79−36679
pentacene, mol. dephasing, radiationless decay meas. by laser-acoustic diffr. spectroscopy 78−37667
pentacene in naphthalene, intersystem crossing rates following single-mode laser excitation 80−43085
perylene, excimer form. process, ps laser fluoresc. obs. 79−11448
perylene, excited singlet state quenching by nitroxyl radical, triplet form. 77−88487
phase relaxation of excited molecule vibrations in dense medium *(German)* 77−40275
phenanthrene, and dideuteroisomers, vapour phase fluoresc. lifetimes, position dependent D effects 77−30901
phenanthrene, chemisorbed on Al_2O_3, radiative and nonradiative processes 79−36686
phenanthrene-PMDA, spin polarization of charge-transfer excitons, EPR meas. 79−19766
phenazine, triplet state intersystem crossing, picosec. singlet excitation 77−6824
phenol biradical prod. from O+benzene(-d), crossed mol. beam investig. 80−71902
2-phenylcycloalkane, photolysis products studied by ^{13}C CIDNP and intersystem crossing 79−79275
bis-(phenylethinyl)-mercury, spin-orbit coupling, heavy atom and D isotope effects 79−59372
photoacoustic spectroscopy, freq. and time-domain, relax. time meas. condensed phases 80−82826
photoacoustic spectroscopy, time-domain, nonradiative lifetime meas. of condensed phases 80−55232
photoacoustic spectroscopy in solids, phase measurement, appl. to nonradiative transitions, optical absorpt. 80−31885
photochemical processes, internal conversion, intersystem crossing 78−13548
nonradiative transitions continued
photochemical reactions, isomerisation, complexing, proton transfer, initiation of internal conversion processes 80−40713
photogeneration and fluoresc. quenching theory, appl. to x-metal-free phthalocyanine 79−65513
photoluminescence of solutions, decay and self-depolarisation 79−24351
photosynthesis, fluoresc. and energy transfer, time resolved obs. 79−48216
photosynthetic membrane, in vivo, light collection and exciton dynamics 79−48215
photosynthetic pigment, intersystem crossing 77−58057
photosynthetic systems, reaction centre struct., triplet state ODMR 77−29093
β-picoline, fluoresc. of vap. phase, nonradiative electronic relax. 79−86000
pigment associations, conc. effects, luminesc., absorpt. spectra and dichroism obs. 80−1007
pinacyanol, picosecond photobleaching and absorpt. recovery, solvent effects 77−44493
pinacyanol in ethanol, electronic relax., analysing light ps spectroscopy 80−99517
poly-2-vinylnaphthalene, soln., lowest triplet props., flash photolysis and radiolysis obs. 80−32861
polyacenes, alternant, internal conversion, energy gap correl. 79−54901
polyacenes, S_1-T_1 interconversion, excitaiton indices calcs. 79−54830
polyatomic molecule, electronic relax. process, energy depend., book contrib. 77−34688
polyatomic molecule, luminesc. parameters, intramol. vibr.-energy redistrib. effect 79−54890
polyatomic molecules, collision induced crossing, model 79−50059
polyatomic molecules, intramolecular dephasing processes 78−74695
polyatomic molecules, multiphoton absorpt., inverse radiationless transitions detect. *(Russian)* 79−22753
polyatomic molecules, nonradiative transitions, theory, anharmonicity effects 77−58072
polyatomic molecules, picosecond fluoresc. gating, intra- and intermol. transfer processes 78−78745
polyatomic molecules, primary photochem. processes *(French)* 77−90620
polyatomic molecules, radiationless conversion processes, regularities 80−14171
polyatomic molecules, radiationless transitions, Fermi resons. and quasidiscrete spectrum 80−95665
polyatomic mols., isolated, theory including vibronic level width 77−79646
polyatomic mols., quantum beats 80−37826
polycyclic monoazines, temperature dependence, triplet formation, radiationless transitions 79−54900
polyene derivatives, horizontal radiationless transitions, singlet-pot. and rot. angle, semi-empirical model 78−42109
polymethine dye nonequilib. protolytic forms, lasing, fluoresc. and nonradiative transitions 80−102722
polyphenyls, S_1-T_1 interconversion, excitaiton indices calcs. 79−54830
porphin (-d_2,d_4,d_6,d_8,d_{10},d_{12},d_{14}), nonradiative transition probabilities, deuteration effects 79−3485
porphyrin free base, spin-dependent D isotope effect in triplet state decay, N-H vibrs. 77−30909
porphyrin free lasers, radiationless decay of triplet state, position dependent D effect 77−30902
porphyrin solns., quenching of excited states by nitro-cpds., donor-acceptor interactions 78−2899
porphyrins, non-radiative deactivation of lower excited states, effect of mol. struct. 78−68987
porphyrins, solid solns., phosphoresc. rel. to solvent heavy ats. *(Russian)* 77−40286
probe by electro-opt. single laser mode switching 77−10698
proximity effect, vibrational tuning, vibronic interaction probe, QSM approach 78−94274
pseudoazulenes, anomalous fluoresc., radiationless transitions 80−91593
pyrazine, excited and N_{1s} ionised states, ab initio calcs. broken orbital symm. 80−27931
pyrazine, lowest triplet state, phosphoresc., intersystem crossing 78−5269
pyrazine, PMMA soln., fluoresc. and phosphoresc. quantum yield and lifetime, 20-120 kbar 79−54902
pyrazine, single vibronic level fluoresc., non-exponential decay 77−27108
pyrene+N,N-dimethylaniline (deuterate)(3,5 dimethoxy-N,N-dimethylaniline), geminate recomb., solvent, isotope, mag. field effects 78−56888
pyrene-diethyl aniline in acetonitrile-toluene, triplet exciplex state in pulsed laser photolysis 77−16836
pyridine, fluoresc. of vap. phase, nonradiative electronic relax. 79−86000
pyridine and methyl derivatives, fluoresc. and nonradiative processes 79−36684
pyrimidine, and derivatives, intersystem crossing rates, triplet sublevel decay, vibronic coupling 78−5271
pyrimidine, bi-exponential decay, methylation and vibr. excitation, proximity effects 80−78641
pyrimidine, singlet-triplet intersystem crossing, ODMR and MIDP in matrix at 1.6K 79−50055
pyromellitic dianhydride-phenanthrene, single cryst., charge-transfer triplet excitons, spin polaris. 79−11069
quinoline, radiationless transition branching ratio, temp. effects 79−54900
quinoline, radiationless transitions, internal conversion, energy depend. 78−94272
quinoxaline$^+$, (singly protonated), struct. and kinetics of fluoresc. and phosphoresc. states 77−30906
quinoxaline, fluoresc. quenching and intermol. intersystem crossing, nonlinear press. depend. 78−25603
radiative and nonradiative recomb. at metal ions, core struct. effects, review 79−4834
radical radiation formation in solid organic compounds 80−85201
rapid intramolecular radiationless transitions, decay rate by time resolved reson. Raman spectra 79−76434
rare earth activated phosphors, chemistry and physics, book contrib. 80−55187
rare earth doped cystals, intra- and inter-ionic multiphonon transitions 80−34973
rare earth ions in crystals, nonradiative processes, book contrib. 80−55188

nonradiative transitions continued
rare earth tetracyanoplatinates, energy transfer from linear stacks of donors 78−68546
rare-earth ions in soln., radiationless energy transfer and complexation processes 79−10144
rate calculations, integral eqn. method 78−76827
rate constant, electronic rearrangement effect 79−54907
rate constant of radiationless electron transition, diatomic molecule in crystal at zero temperature 79−43011
rate process theory, role of coherent mechanical vibr. 77−509
rate processes in condensed media, anharmonicity effects 79−19349
redox enzyme, Fe-, Cu-, or Mo-containing, electron transfer peculiarities 80−16896
retinal, isomers, intersystem crossing quantum efficiencies, solvent effects 79−22751
trans-retinal, picosecond photophysics 77−9169
retinyl acetate, high press. fluoresc. studies of radiative and nonradiative processes 80−1011
rhodamine 6G soln., cyclooctatetraene effects on laser props. *(Russian)* 78−25875
rhodamine 6G-ketocyanine mixed solns., wideband lasing 79−957
rhodamine dye, intercombination conversion rate consts. from triple quenching by 1,4-diphenylbutadiene 79−956
rhodamine dye solutions, additional heavy atom effects on triplet state transitions *(Russian)* 77−85800
rhodamine-B and -6G, sub psec radiationless relax. in soln. 77−18955
rhodamines in ethanol soln., gain and induced absorpt., struct. props. 77−24890
rotational selection rules for nonradiative processes 78−62838
rubrene-in-benzene, excited state migration and charge transfer 77−55559
ruby, energy transfer between different emitters and spatial diffusion 80−103978
ruby, nonequilibrium luminesc. of hot electrons, nonradiative transition probability 77−32436
ruby, nonradiative spectral and spatial energy transfer 77−44037
ruby, optical energy storage and retrieval 77−73165
ruby, optical pumping, bottlenecked 29 cm^{-1} phonon spectral width 77−12425
ruby, photoacoustic spectroscopy obs. 77−90185
ruby laser, cryst., excited state absorpt. and energy output 77−65595
semiconductor, acoustic studies progress *(Japanese)* 80−49310
semiconductor, Auger transition probability, phonon-assisted 79−15120
semiconductor, deep centres, nonradiative de-excitation 79−38644
semiconductor, indirect band gap, Auger recomb. of electron-hole drops 78−39600
semiconductor, multiphonon electron-hole recomb. processes 78−6750
semiconductor, multiphonon recombination processes 79−38643
semiconductor, non-radiative multiphonon carrier-capture cross-sections of deep traps, high-temp. limit 77−90191
semiconductor, nonradiative multiphonon carrier capture and ejection props. of deep traps 78−35190
semiconductor, recomb.-enhanced defect reactions 77−51377
semiconductor, recombination enhanced defect reactions 79−38094
semiconductor, strong electron-lattice interaction, review *(Japanese)* 80−49664
semiconductor laser, atom displacement as result of nonradiative recomb., defect form. mechanism 79−10308
semiconductors, Auger and radiative recombination of acceptor bound excitons 79−47023
semiconductors, multiphonon electron-hole recomb. processes 78−6751
semiconductors and insulators, non-radiative processes multiphonon recomb. 78−6752
Shpolskii system, 77K, sensitised phosphoresc. spectra 79−815
solid, phonon dispersion effects on nonradiative transitions 78−43926
solid, photoacoustic measurement of absolute quantum efficiencies 79−19924
solid, radiationless relax. meas. by heat-pulse method 77−36277
solid low temp., radiationless relax. dynamics, absorpt. spectra, thermal detection 77−74522
solute-solvent system, radiationless transitions, solvent effect, electronic relax. 77−6842
solution, assoc., ion pair radiationless energy transport 79−56835
solution, electronic excited state transport, Green function soln. 79−68994
solution, multicomponent, excitation energy transfer 78−84621
solution, nonlinear luminesc. quenching kinetics, high excitation power 79−56834
solution, rigid, luminesc. exchange promotion kinetics 80−50387
solutions, photoluminesc. decay time, donor conc. effect 80−66299
solvent effects, dynamic coupling model, quantum mechanical theory 80−29787
spectroscopic channel basis for radiative and radiationless processes, absorpt. spectra 77−14411
stilbene, direct photoisomerisation theory, from fluoresc. and absorption spectra 79−79262
trans-stilbene, fluoresc. decay, picosecond anal. 79−31569
stilbene, horizontal radiationless transitions, singlet-pot. and rot. angle, semi-empirical model 78−42109
stilbene aza-analogues, lowest excited states, INDO/S calcs. 80−95545
styrene (-d_3, d_5, d_8), fluoresc. quantum yields and lifetimes, 298 and 77K 79−59500
supernonradiative phase transition, appl. to paramag. impurities in strong mag. field 79−14898
symmetric top molecule, radiationless processes, angular momentum constraints 80−28052
synchrotron radiation obs. 80−63706
synchrotron radiation techniques for studying atomic physics 80−63583
tellurite glasses: Ho^{3+}, nonradiative relax. 77−24881
temperature effects on decay constants 77−46592
tetraalkylammonium tetrahalometalates, opt. lifetimes rel. to thermal transitions 77−28608
tetracene, theory of fission of singlet Frenkel exciton into two localised triplet excitons 79−23901
tetracene-Kr(Xe), intramol. intersystem crossing in supersonic beam, external heavy atom effect 80−14167
tetrachlorobenzene, in durene, 1.6K, $S_1 \sim\!\!\rightarrow T_1$ relax. mechanism, Zeeman phosphoresc. and PMDR obs. 77−30912
1,2,3,4-tetrachloronaphthalene, intramol. heavy atom effect, PMDR obs. 79−13745

nonradiative transitions continued
tetracyanoethylene(d), charge-transfer complex, fluoresc. quantum field and decay time 78−42107
tetracyanoethylene charge transfer complex, nonradiative decay of excited states, D isotope effect 79−31580
tetracyanoethylene-benzene(-toluene), and isotopic forms, excited charge-transfer state nonrad. decay, vibrs. role 78−82765
tetramethylpyrazine, PMMA soln., fluoresc. and phosphoresc. quantum yield and lifetime, 20-120 kbar 79−54902
tetramethylpyrazine-d_{12}, in durene matrix, intersystem crossing of 859.5 MHz transition 79−27015
tetraphenylchlorin-d_0, -d_1, lowest triplet state, intersystem crossing rates, temp. and isotope effects 80−48026
s-tetrazine, vapour, reson. CARS spectrosc., radiationless relax. rate 80−78614
thioindigo dyes, triplet state config., laser flash absorpt. spectrosc. obs. 80−5557
thionine-monohaloaniline triplet exciplex, quenching position dependent heavy atom effect, intersystem crossing 78−53197
thiophosgene vapour, fluoresc. from S_2 single vibronic states, quantum yields and quenching 77−34675
thioxanthone, fluoresc. and internal conversion, rel. to proximity effects 80−91592
three component system, energy transfer parameters 78−27292
three-electron atomic systems, autoionising states decay calcs. 78−78670
time resolved spectroscopy using new laser techniques 77−79162
time-resolved, opto-acoustic spectroscopy, nonradiative yields and rate consts. 78−58052
toluene+O_2, fluoresc. quenching kinetics 77−18964
toluene-d_8, soln., fluoresc. quantum yields, temp. and deuteration effects 77−3396
TP-C-DMP, new bifluorophoric laser dye with intramolecular energy transfer, lasing characts. 78−74899
TP-CSC-DMP, bifluorophoric mol. ultrafast intramolecular energy transfer 78−74900
trans-stilbene, fluoresc. lifetimes, 77-295K 78−1029
transition metal ion, in inert medium, electronic relax., coupling mechanism 79−76466
transition metal ion, in inert medium, electronic relax., theory 79−76465
transition probabilities, mol. cryst. model 78−10973
1,1,1-trifluoroacetone, photochem. and photophysics, 330-250 nm, 0-1000 torr 78−17706
trifluoroformamide, radiationless pathways, time-resolved fluoresc. obs. 78−66577
triphenylmethane dye soln., electronic relax., viscosity-depend., using picosec. flash photolysis 80−66258
triplet exciplexes, rapid rot., spin-selective depopulation of sublevels, heavy atom-induced mag. field effect 80−95552
triplet state, intersystem crossing rates from ODMR 78−78735
tropolone, in water and cyclohexane, electronic relax., absorption, excitation and fluoresc. spectra 78−66588
two-k-shell-vacancy systems, excited states, radiationless decay probability calcs. 78−41993
two-level atoms, Dicke model, nonradiative relax. *(Russian)* 79−50273
uniform interactions mixing assumption in radiationless transitions theory 79−86001
unimolecular radiationless decay, coupling strength incoherence 78−70865
unlike molecules, in soln., electronic excitation energy transitions *(German)* 77−34749
unstable molecular states, with memory effects, prep., decay, EM pulse excitation 78−46384
uranine, intercombination conversion rate consts. from triplet quenching by 1,4-diphenylbutadiene 79−956
vibrational relaxation of molecules in condensed media, survey, book contrib. 77−36295
vibronic level, single, analytical representation of decay rate 77−79645
vibronically coupled electronic states, radiationless decay, non-Condon effects 80−52966
vibronically coupled electronic states 79−22747
xanthene dye, solute-solvent hydrogen bonding and temp. effects on internal conversion 77−3402
xanthene dyes, internal heavy atom effect on radiative and non-radiative rate consts. 80−32765
xanthione, solns., triplet state quenching by ground state xanthione 78−42180
xanthone in host crysts., triplet state PMDR, phosphoresc. spectra, transition mechanisms 77−46585
p-xylene-d_{10}, soln., fluoresc. quantum yields, temp. and deuteration effects 77−3396
xylenes, singlet excited states decay, substituent effects 77−75175
Z=11 to 103, theoretical, L-shell Coster-Kronig energies 77−83524
zinc octaethylporphin, radiationless transitions, fluoresc. and phosphoresc., isotope effects 77−65502
zinc porphin in n-octane, population hole-burning using triplet reservoir 79−87491
$0s0_4$, multiphoton absorpt., inverse radiationless transitions detect. *(Russian)* 79−22753
Al, sputtered excited Al particles, effect of O during ion bombardment on spectra 79−38703
AlAs-GaAs:Ge double heterojunctions, efficiency of radiative recombination 77−77286
AlGaAs heterojunctions, nonradiative recomb. vel. estimate from edge luminesc. props. 80−65668
AlGaAs-GaAs heterostructures, luminescent characts., efficiency and radiative lifetime conc. depend. 80−55151
$Al_xGa_{1-x}As$-GaAs heterostructure, nonradiative large dark spots rel. to minority carrier transport 78−9378
$Al_{2x}Ga_{2(1-x)}O_3:Cr^{3+}$, luminesc., lifetime, 77 and 4K, struct., energy transfer 79−28798
$Al_2O_3:Cr^{3+}$, Jahn-Teller system, zero-phonon line broadening due to nonradiative transitions 80−108258
$Al_2O_3:V^{4+}$, dil. solution, stimulated phonon emission 78−63817
Al_2O_3-Cr (III), radiationless relax., heat-pulse meas. technique 77−36277
Ar, ($3s^{-1}4p^1P$) autoionising state decay, triple differential cross section 78−86831
$Ar^+ + H_2$, collinear reactions, electronic nonadiabatic transitions 78−7180
Ar^{z+}+inert gas atom (z=1-8), radiative and non-radiative deexcitation after electron capture 79−7008

nonradiative transitions continued
As_2S_3:Fe glass, photolum. and ESR, Fe impurities as non-radiative recomb. centres 80−29788
As_2Se_3, amorphous, nonradiative recombination of photocarriers 80−11046
B_2O_3-Na_2O-BaO glass, rare earth doped, nonradiative decay and multiphonon relax. 77−85802
$BaBr_2:Sm^{2+}$, radiationless coupling, $4f^55d$ band effects, spectra 77−8627
$BaCl_2:Sm^{2+}$, radiationless coupling, $4f^55d$ band effects, spectra 77−8627
BaCl($C^2\Pi$)+He(Ar)(N_2), collisional quenching, laser induced fluoresc. decay meas. 79−27075
BaClF:Sm^{2+}, radiative and radiationless transition rate meas. using tunable pulsed dye laser 77−24891
BaClF:Sm^{2+}, radiationless processes 79−33792
$BaF_2:Er^{3+}$, fluoresc. spectra of charge compensated cryst., multiphonon and energy transfer relax. 79−87496
BaO-B_2O_3 glass, $Mn^{2+}\rightarrow Nd^{3+}$ energy transfer, fluoresc. obs. 77−8621
BaO-B_2O_3:UO_2^{2+}, Nd^{3+} glass, radiative and nonradiative energy transfer 78−60508
BaO-B_2O_3:$UO_2^{2+}\rightarrow Er^{3+}$ glass, energy transfer 78−2895
BaO*, quenching of excited species formed by Ba+NO_2 chemiluminesc. reaction 77−58140
BrCN, photodissoc. energy disposal, electronic branching, vibr. and rot. transfer, CN(B→X) fluoresc. 77−42364
C in molecule, K-shell fluoresc. yield, statistical scaling 80−78644
C_2, Swan transitions, relax. dynamics and two-photon excitation, in inert gas matrix 77−505
C_2^-, matrix isolated, vibr. relax., absorpt. spectra 77−75172
C_2+O_2, $C_2(X^1\Sigma_g^+)$ and $C_2(a^3\Pi_u)$ intersystem crossing and free radical kinetics 80−95668
C_3, matrix isolated, vibr. relax. 78−66637
CN, fluoresc. spectra, time resolved, radiative decay and radiationless deactivation in Ar 79−98142
CN, matrix isolated, interstate cascading radiationless transitions 77−46594
CN, radical, nonradiative transition rates, matrix isolated molecule 78−78740
CN in solid Ne, internal conversions and relax. dynamics 77−34678
CO, $A^1\Pi(v'=1)$, vibr. relax. by reversible intersystem crossing, fluoresc. obs. 80−14170
CO^+, vibr.-excited $A^2\Pi$ state, radiative and radiationless vibronic deactivation rates with He 79−10134
CO+inert gas, collision-induced intersystem crossing, reversibility 77−50465
CO+inert gas, collision-induced intersystem crossing mechanism 78−74689
CO_2+inert gas, intramol. energy transfer, 153-393K, photoacoustic obs. 79−54943
CS_2, laser fluoresc., discrete and continuum, time and freq. resolved obs. 79−41195
$CaF_2:Er^{3+}$, fluoresc. spectra of charge compensated cryst., multiphonon and energy transfer relax. 79−87496
$CaF_2:Eu^{2+}$, energy transfer to luminesc. centres, pulsed excitation obs. 77−85781
$CaF_2:Eu^{2+}$, Sm^{2+}, relaxed resonance acoustic phonons in vibronic anti-Stokes luminescence *(Russian)* 80−93404
$CaF_2:Eu^{2+}$, X-ray induced luminesc. kinetics, energy transfer processes 79−8181
CaO-Li_2O-B_2O_3, calibo glass, $Dy^{3+}\rightarrow Ho^{3+}$ non-radiative energy transfer, diffusion limited relaxation 79−65925
CaO-Li_2O-B_2O_3:Er, Tb, calibo glass, nonradiative energy transfer 78−19541
$CdIn_2S_4$, photoluminesc., thermal quenching and recomb. centres 79−24362
Cd($^1P_1$) excited state quenching by mols., cross sections, chem., phys. exit channels 79−779
CdS, photoconductivity, luminescence, radiative and radiationless transition mechanisms 78−10948
CdS:In(Cl) concentration quenching mechanism of luminescence 80−97336
CdSe, low resist., mech. for nonradiative recombination of carriers, photoluminesc. and photocurrent charcts. 78−19092
ClFCS, second excited singlet state fluoresc., spectra 79−6957
ClFCS, second excited singlet state photophysics, laser excitation obs. 80−32758
Co complex, [^{57}Co(1,10-phenanthroline)$_3$]$(ClO_4)_2.2H_2O$, time differential Mossbauer spectra, aftereffects 78−27131
Cr^{3+} in crystals, radiationless relax., photoacoustic spectra 78−27264
CrO_2Cl_2, electronically induced IR multiphoton absorpt., quasicontinuum states, excited singlet radiationless decay 80−48049
CrO_2Cl_2, inert gas matrices, IR spectra, emission spectra, photoselection 77−14443
$CsMnBr_3:Nd^{3+}$, nearly 1-dimens. cryst., emission spectrum, extensive energy transfer 79−15516
$Cs_2NaYCl_6:Bi^{3+}$, luminescence props., emission and excitation spectra 80−108262
Dy^{3+}, in soln., non-radiative transitions as Forster's energy transfer to solvent vibrations 80−1014
Er^{3+} implanted crystals, laser active media, nonradiative losses due to $^4I_{11/2}$-$^4I_{13/2}$ transition 79−31911
ErP_5O_{14}, single cryst., radiative and non-radiative transitions 79−19920
Eu^{3+}, in soln., non-radiative transitions as Forster's energy transfer to solvent vibrations 80−1014
Eu^{3+}, nonradiative $^5D_1$-$^5D_0$ transition in various solvents 79−3479
$EuNa_2Mg_2(VO_4)_3$, disordered, thermal quenching of luminesc. 80−71472
$Eu_2[Pt(CN)_4]_3.18H_2O$, nonradiative energy transfer from tunable donor states to Eu^{3+} 79−43018
Fe XXIII and XXIV, reson. and intersystem transitions, oscill. strength, lifetime, beam-foil spectra 78−82685
Fe-Al, X-ray emission spectra 80−25489
FeVIII-XXVI energy level tables and Grotrian diagrams 80−74142
(GaAl)As, DH lasers, degradation mechanisms, temp. depend. 78−66825
n-GaAs, Auger transitions, nonlinear extrinsic luminesc. study sublinear emission 79−95833
GaAs, deep radiation centres from heat treatment, γ-irrad., deform., probability of nonradiative electronic transitions 80−50408
GaAs, γ- and electron irradiation, influence on recomb. charcts. near surface 80−71478
GaAs, nonradiative capture and recomb. by multiphonon emission 77−43533
GaAs, nonradiative capture, direct obs. of phonons 78−30976
nonradiative transitions continued
GaAs-Al,$Ga_{1-x}As$, DH laser, effect of bulk nonradiative recombination 78−82967
GaP epitaxial layer, crystal defects influence on luminesc. obs. 79−87511
n-GaP, LPE, non-radiative recombination 78−19565
GaP, non-radiative recombination and structural defects 78−19566
GaP, nonradiative capture and recomb. by multiphonon emission 77−43533
GaP:Cu, deep levels, photoluminesc. and optical cross sections 79−38653
GaP:Zn,O, Auger coeff. from luminesc. decay and Hall effect 77−48226
GaP:Zn,O, Auger coeff. from luminesc. efficiency and Hall effect 77−48227
Ga_2S_3-La_2S_3-Nd_2S_3:Nd^{3+} chalcogenide glass, Nd^{3+} emission and absorption spectra, nonradiative relax. 77−40268
Ge, nonradiative transitions at impurity centre with participation of short-wavelength phonons 80−16099
GeO_2-Na_2O-BaO glass, rare earth doped, nonradiative decay and multiphonon relax. 77−85802
He, electron impact ionisation, decay modes investig. 79−72422
I, $^2P_{1/2}$ state, relax. between hyperfine levels 80−18880
I_2, mol. dephasing, radiationless decay meas. by laser-acoustic diffr. spectroscopy 78−37667
$I_2Ne_aHe_b$ van der Waals complexes photodissoc. 80−50864
$KAlSi_3O_8$:rare earth ion, glass, nonradiative energy transfer and fluoresc. quenching 77−20905
KBr:Tl, nonradiative transitions in colour centres, WKB approximation 77−85803
KCl, F-centre first excited state radiationless decay, cluster model 77−52158
KCl, F-centre formation at highly excited triplet states of self-trapped excitons 80−76066
KCl, perturbed M-centre triplet state, M-F centre exchange mechanisms 79−69884
KCl:Eu^{2+}, radiationless transitions, photoacoustic spectra 77−32405
KCl:Eu^{2+}, spectroscopic anal. 78−80391
KI:Tl^+, A_T emission, mag. circular polarisation, WKB approx. for nonradiative transition rate 80−55180
KI:Tl, A_T emission, linear polarisation, appl. of semi-classical WKB formalism 80−45134
KI:Tl, decay of fast component of impurity luminesc. excitation in A-absorption band *(Russian)* 80−84767
KI:Tl, nonradiative transitions in colour centres, WKB approximation 77−85803
KI:Tl, triple decay-time in low-energy emission 78−43929
KY_3F_{10}:Eu^{3+}, fluoresc. decay, radiative and nonradiative transition probabilities 78−72581
Kr:N_2O_3 photoluminesc. from KrO (^1S) excimers 78−68544
$LaF_3:Pr^{3+}$, anomalous luminesc. decay, phonon reson. trapping and bottlenecking 79−43023
$La_{1-x}Nd_xP_5O_{14}$, Nd^{3+} luminesc. anomalously weak quenching 77−75533
Li, autoionisation states, config. decays and excitation energies 78−13475
Li-La phosphate glass, Nd, Cr activated, Nd luminesc. quantum efficiency meas., Nd-Cr nonradiative transfer 80−66296
Li-Nd-La phosphate glass, nonradiative losses, pulse periodic stimulated emission and luminesc. 77−83878
^{7}LiH, $A^1\Sigma^+$ state, vibr. levels, radiative and nonradiative lifetimes 78−66604
$LiTaO_3$:Cr (III), radiationless relax., heat-pulse meas. technique 77−36277
Lu porphyrin complexes, luminesc. 77−18958
Mg XI-S XV ions, 2131-1s31 and 2121-1s21 radiative transitions and nonradiative decay probabilities 78−70781
MgO:Cr(III), radiationless relax., heat-pulse meas. technique 77−36277
MgO:V^{2+}, Jahn-Teller system, zero-phonon line broadening due to nonradiative transitions 80−108258
Mn^{2+}, in soln., non-radiative transitions as Forster's energy transfer to solvent vibrations 80−1014
MnX_2 solns., (X=Cl, Br, I), heavy at. effect on rate consts. of radiative and non-radiative transitions 79−78736
N_2 film, on metal or sapphire substrates, luminescence and nonradiative energy transfer to surfaces 80−97350
NO in rare gas matrix, radiationless processes in luminesc. spectra 79−36689
NO_2, inter and intramolecular radiationless transitions, relax., time resolved excitation and fluoresc. spectra 80−27966
NO_2, sub-Doppler spectra, laser-beam system, HFS excitation, radiative, non-radiative decay 78−90210
N_2O^+, fluoresc. and dissociation lifetimes of vibr. excited states 78−42108
N_2*+CO, vibr. excitation and quenching, long contact time effect 79−86040
Na borate glass, nonradiative energy transfer from $Sm^{3+}\rightarrow Nd^{3+}$ 78−80394
Na-fluorescein, glycerol-alcohol soln., luminesc. decay time, conc. depend. 80−34960
$Na_3La_{1-x}Gd_x(PO_4)_2$, UV excitation, nonradiative transfer 79−38595
Na_2O-B_2O_3 glass, $Eu^{3+}\rightarrow Nd^{3+}$ diffusion-limited energy transfer, quantum efficiency 78−31238
Nd^{3+} ions, in solids, radiationless decay processes, laser photoacoustic spectroscopy meas. 80−84766
Nd^{3+}:inorganic glass, energy transfer processes, nonradiative transitions *(Chinese)* 79−64232
$NdCl_3$-$AlCl_3$ vap. complexes, Nd^{3+}, $^4F_{3/2}$ level deactivation 77−61786
$Nd_xY_{1-x}P_5O_{14}$, fluoresc. energy transfer and radiationless relax. 79−38625
Ne, solid, doped with Xe and benzene, energy transfer 77−32416
Ne-Xe-F_2(NF_3), excited states quenching 79−18406
O in molecule, K-shell fluoresc. yield, statistical scaling 80−78644
O_2 singlet-state luminesc. in energy transfer from dissolved pigments 79−54886
O_3+p-H_2(n-H_2), vibr. relax. quenching rate consts. meas. 79−13792
$O(2^1D_2)$, prod. by O_3 photolysis, collisional deactivation 79−20384
$O_2(c^1\Sigma_u^-)$, in Ar(Kr)(Ar-Kr) matrices, multiphonon vibr. relax. time-resolved emission obs. 80−18861
P_2, intersystem transition obs. in absorpt. spectrum 80−48008
P_2O_5-Na_2O-BaO glass, rare earth doped, nonradiative decay and multiphonon relax. 77−85802
$POCl_3:Pr^{3+}$, fluoresc. and lifetimes of excited states 80−71466

nonradiative transitions continued
Pb_2, in Ar matrix, excitation and emission spectra, vibr. freq. 78−13507
$Pb_{1-x}Sn_xSe$ epitaxial layers, radiative and nonradiative recomb. processes 80−60670
$Pb_{0.78}Sn_{0.22}Te$, $Pb_{0.91}Sn_{0.09}Se$, radiative and nonradiative recombination 80−80849
PbTe epitaxial film, stimulated emission, absorption spectra and recombination 78−80409
$RbMg_xMn_{1-x}F_3$, impurity induced fluorescence, thermal depend. 77−85776
$RbMnF_3:Er^{3+}$, absorption, emission, excitation and lifetime meas. 80−71460
Rb_2^*, optically excited, cascade predissoc. *(Russian)* 79−10159
$Re(C0)_5Br$-$Mn(C0)_5Br$, polycryst., ν(C0) vibr. intermol. Raman intensity transfer 80−60564
rhodamine 6Zh, quantum efficiency of intercombination conversion to triplet state by sensitised phosphoresc. *(Russian)* 77−85798
Ru complexes, luminescent, non-radiative pathways in solvents 77−3393
Ru complexes, $Ru(bipy)_3Cl_2.6H_2O$ and $Ru(bipy\text{-}d_8)_3\ Cl_2.6H_2O$, soln. electronic excitation energy, deactivation determ. 80−55173
S_2, in Ar matrix, fluoresc. and excitation spectra 78−94271
SF_6, nonradiative collisionless dephasing rate, two-photon coherent transient meas. 80−14176
SF_6, partial saturation of ν_3 ladder in IR absorpt., rate process model 80−58645
SO_2, fluoresc. and photosensitised phosphoresc. of biacetyl, quenching and triplet theory transfer 78−25608
SO_2, nonradiative transitions and intersystem crossing rates in gas phase, theory 80−23451
Se_2, laser induced fluoresc. in inert gas matrix 80−87161
Si, amorphous, electron-hole recombination, mech. 78−72196
Si, amorphous, mag. field depend. of luminesc. 79−43034
Si, amorphous, radiative and non-radiative tunnelling, photoluminesc. decay meas. 79−83026
Si, amorphous, spin depend. recomb., luminesc. and light induced ESR 80−50393
Si, nonradiative deexcitation in O_2 atmos., using differential meas. of excited state lifetime 78−2920
Si, nonradiative recombination and luminesc. 79−33770
Si, phonon-assisted Auger recomb., direct calc. of overlap integrals 80−107808
Si:H sputtered amorphous film, luminesc. and non-radiative decay 80−50395
α-SiC:Al diodes, ion implanted, transient characts. of electrolum. 79−24369
SiO_2, amorphous, optical and elec. props., comparison with chalcogenide semiconds. 78−6721
SiO_2-Na_2O-BaO glass, rare earth doped, nonradiative decay and multiphonon relax. 77−85802
$SrF_2:Er^{3+}$, fluoresc. spectra of charge compensated cryst., multiphonon and energy transfer relax. 79−87496
SrO, neutron- or proton-irrad., F^+ centre fluoresc. yield and lifetime, 5 to 140K 80−55181
TR^{3+} ion excited state population depend. on lattice on IR excitation. *(Russian)* 80−50425
Te_2, laser induced fluoresc. in inert gas matrix 80−87161
TeO_2-Al_2O_3-WO_3 glass, rare earth doped, nonradiative decay and multiphonon relax. 77−85802
Th porphyrin complexes, luminescence 77−18958
Ti atoms sputtered from Ti, Ti oxides, photon emission, nonradiative transition effects 80−58208
Tl+N_2, Hg sensitised fluoresc., quenching 79−22643
Tm^{3+}, in oxide glasses, multiphonon relax. rates and fluoresc. lifetimes 77−77266
UO_2^{2+}, excited, in liq. and glassy media, luminesc. decay processes, temp. activation 79−91978
Xe:N_2O, photoluminesc. from XeO (^1D) excimers 78−68544
Y porphyrin complexes, luminesc. 77−18958
YAG:Nd^{3+}, many-phonon nonradiative transition probabilities 79−95842
$Y_3(Al_{1-x}Ga_x)_5O_{12}$:Nd, fluoresc. energy transfer and radiationless relax. 79−38625
$Y_3Al_5O_{12}:Nd^{3+}$, transition probability $^4I_{11/2}$ to $^4I_{9/2}$ of Nd^{3+} states calcs. 79−56853
YE+AG:Er^{3+}, laser material, radiative and nonradiative transitions, conc. quenching 77−16391
Yb^{3+}, in soln., non-radiative transitions as Forster's energy transfer to solvent vibrations 80−1014
Yb^{3+}:phosphate glass, relation between absorption and equilib. luminesc. spectra 77−85754
Zn-porphin($-d_4,d_8,d_{12}$), nonradiative transition probabilities, deuteration effects 79−3485
ZnS:Cu, Er, Na, phosphor, mechanism of sensitisation effect of Cu and Na ions 77−16369
ZnS:Cu, trap parameters, thermostimulated luminesc. and cond. meas. *(Russian)* 77−72868
ZnS:Mn films, photoluminesc. and electroluminesc., excitation mechanism of luminesc. centres 79−11459
ZrO, in Ne matrix, laser photoluminesc. 77−14481

NOR gates *see logic gates*

normalising
heat treatment apparatus 79−79005
hydrologic data set distribution functions, extremes and confidence intervals 78−24313
products for nuclear power stations, research and development *(Russian)* 79−34080
stainless steel, laser surface melting for corrosion protection 80−93698
steel, alloy, U20Kh6T2D, structural transformations during heat treatment, and wear resistance 78−88484
steel, austenitic, low-C, transform. kinetics rel. to temp., deform., struct., mech. props. 79−24519
steel, austenitic stainless, struct. and mech. props. under low temp. deform. under linear and plane stress conditions 79−1902
steel, C, normalising device, for decarburisation determ. 79−87663
steel, C, type 1792AF 79−38966
steel, cast, high tensile strength, heat treatment 80−16358
steel, comp. and processing effects on microstruct. and props. rel. to low temp. applic. 77−52365
steel, Cr-Mo-V, normalised and tempered, size and geometry effect on creep cracking behaviour 78−64630
normalising continued
steel, electric sheet, hot-rolled, recrystallization and texture formation during ht. treatment 77−44271
steel, fatigue strength with stress concentrator, mean compressive stress effect 77−21264
steel, impact and tensile props., Si effects 79−24614
steel, low alloy effect of grain size, and amount of pearlite on fracture resistance 79−100255
steel, low C, bainitic, optimal struct., heat treatment effects 77−16624
steel, low C, Mn, strain hardening parameters, electron microscope obs. 77−63690
steel, low C, strain ageing, effect of prestrain *(Korean)* 77−8865
steel, low pearlite, low alloy, low temp. strength props., heat treatment 77−12658
steel, low-alloy, transform. of austenite, cooling rate effect 79−38821
steel, maraging, Cr-Ni-Ti, effect of Ti addition on hardness and energy scatt. 79−15687
steel, medium C, static and dynamic stress effect on hardenability and grain growth *(Korean)* 78−35404
steel, medium C, tempered, normalised or quenched, statistical property of fatigue limit, press-fitted axles *(Japanese)* 77−12693
steel, Mn-Cr, normalised, shot peening effect on bending fatigue strength *(German)* 78−35401
steel, Ni (9 wt.%), mech. props., effect of alloying 77−48462
steel, plate, alloying, normalising, controlled rolling 77−48459
steel, Si-Mn, 27SG, heat treated sheets, underwater explosive forming *(Polish)* 79−34052
steel, structural, brittleness susceptibility rel. to heat treatment 79−24620
steel, wear resistance of 30KhGSA and 40 kHNMA after thermal and thermomech. treatment 77−70087
steel, work-hardenable, N26T low magnetic phase, fatigue strength effect of surface treatment 77−48546
steel *(German)* 80−100869
steel nitride phase hardening, precipitation and solution kinetics after heat treatment 78−95756
steel-cast Fe cam-roller pair, wear resistance after strengthening treatment *(Russian)* 78−31542
steels, martensitic-ferritic, microdefect accumulation during creep, effects of heat treatment, hardening 79−24550
Fe, cast, high Cr, phase composition, mech. props. rel. to heat treatment 79−29108
Fe, cast, spheroidal graphite, degree of normalization effect on mech. props. *(Korean)* 79−87664
Fe, cast, steel cam-roller pair, wear resistance strengthening treatment *(Russian)* 78−31542
Mg cast iron, effect of heating temp. on microstruct. and mech. props. 77−56005

NOT gates *see logic gates*

notch brittleness
angled elliptic notch problem in compression and tension 79−18824
composites, single fibre-brittle zone model, fracture behaviour 80−97570
crack extension criterion of maximum shear or principal stress 78−79278
edge notch, semicircular, in semi-infinite plate, stress anal. 78−38258
fracture, notch angle effects obs. *(Japanese)* 80−6459
PMMA, ductile glassy, notch brittleness under plane strain 80−100900
polycarbonate, ductile glassy, notch brittleness under plane strain 80−100900
PVC, ductile glassy, notch brittleness under plane strain 80−100900
semielliptic notch with crack, micro- and macro-stress concentration correlation *(German)* 78−83330
steel, C, type 1792AF 79−38966
steel, heat-treatment furnace trays, in service embrittlement, microstruct. and props. changes 77−63784
steel, low alloy, blunt-notched, fracture mechanism and failure assessment 80−16450
steel, low C, specimens with notch and fatigue crack, fracture surface features 79−43417
steel, mild, microbehaviour of notch tip during increasing load in brittle fracture beyond general yield 78−35487
steel, tempered, notched, impact bending tests, cold brittleness curves 80−71758
steel for nuclear reactor press. vessels, criteria for brittle fracture, neutron effects *(German)* 77−34389
Al alloys, cryogenic, AMg5 and AMg6, mech. props. at −196°C 77−63748
Fe, cast, grey, fracture kinetics, surface hardening effect 80−76354
Fe, cast, grey pipe, resist. to fracture under hydraulic pressure 79−96124

notch ductility
cylindrical shell under internal pressure, ductile growth of longitudinal flow 79−10530
geometry of notch-tip, influence on stress and strain distrib. 80−33535
glass fibre reinforced plastic, load-time history anal. in instrumented Charpy test *(Japanese)* 80−55511
heat resistance testing, massive sample for mech. prop. changes obs. 78−7124
metal ductile fracture, void growth stress/strain relations *(French)* 80−19280
polycarbonate, brittle fracture of notched ductile polymers *(Japanese)* 80−16448
polyethylene, brittle fracture of notched ductile polymers *(Japanese)* 80−16448
PVC, brittle fracture of notched ductile polymers *(Japanese)* 80−16448
steel, C, inclusions, influence on toughness and fatigue props. 80−40533
steel, Cr-Mo-V, stress rupture, notch influence, temp. depend. *(German)* 80−60945
steel, low C, crack initiation at root of circumferential notch of round bar specimens *(Japanese)* 80−60947
steel, nil ductility transition temp., and Charpy V-notch fracture appear transition temp. relationship between them, determ. *(Czech)* 79−91783
steel, nonmetallic inclusions effect on ductility 80−30042
steel, tempered, notched, impact bending tests, cold brittleness curves 80−71758
steel PWR pressure components, mechanical factors affecting reliability *(French)* 79−20198
Al notched bars, deform. behaviour and strength having biaxial state of stress at notch root *(Japanese)* 80−81116

notch ductility continued
Al-Cu-Si-Mn, type 2017S-T4, crack initiation at root of circumferential notch of round bar specimens *(Japanese)* 80−60947
Cr-Mo-V steel, creep rupture tests on notched cylindrical specimens at 600°C 77−32670
Fe, cast flake and nodular, rupture strength, circumferential notch *(Japanese)* 80−93649
Fe-Ni-Mo alloy, high-strength ferritic, for cryogenic service, mech. characteris. 77−70143
Zr_3Al, ordered, notch sensitivity, neutron suppression 78−23779

notch sensitivity *see notch strength*

notch strength
see also fracture toughness
acetal copolymer, notches effect on fatigue strength 80−25857
Al alloy 7075-T6, fatigue crack propag. rate rel. to accumulated plastic strain rate, cold work effect *(Japanese)* 79−96115
alloy, superplastic, anomalous response to notch under superplastic conditions 78−52930
analysis using conformal mapping, book contrib. 78−94620
austenitic stainless steel, for cryogenic appl., tensile testing, room temp. and 4K 77−25119
bars, elastic plastic stress and strain conc. factor *(Japanese)* 78−26052
body force method of soln., book contrib. 78−94619
bone, impact loading, anisotropy of compact bone tissue 77−25491
borate glass, crit. stress intensity factor and fracture surface energy *(French)* 77−76487
borsic fibre reinforced Ti, unidirectional, K-calibration and compliance curves 78−88518
α-brass, plane stress ductile fracture, prestrain effects 80−108532
circumferentially notched tensile specimen, finite element anal. 78−67150
composite laminate, notch strength 79−57095
crack extension, fracture toughness and fatigue crack propagation threshold 77−35086
creep rupture of circumferentially notched circular tension bars 78−39901
creep rupture strength at nonstationary loading, stress conc. influence 78−31514
creep rupture strength under longit. shear and torsion 78−5689
deep circular notches, plane strain general yielding under loads and bending 79−18809
ductile crack extension, evaluation of resistance in single notch edge specimens 78−68807
edge notch stress anal., book contrib. 78−94621
fatigue behaviour, multiaxial stress-strain approx. 77−40446
fatigue crack growth in notched components 78−83329
fatigue crack growth model, notch analysis of fracture approach 78−52984
fatigue cracks, nonpropagating, analytical explanation, strain intensity factor criterion, in notches 79−68655
fatigue cracks, notch contribution to length 77−65715
fatigue damage detection, using optical correlation technique 78−35511
fatigue life of notched components, generalised design procedure for estimating 78−63388
fatigue life predictions, using smooth bar fatigue data 78−63387
fatigue limit of notched bodies, exam. 78−71291
fatigue limit of notched bodies *(Czech)* 79−70166
fibre reinforced plastic, props., implications for structural design 80−81174
fracture strength, fatigue crack emanates from notch root 78−72866
GFRP, unidirectional, compressive fracture mode 77−21251
glass fibre reinforced epoxy, fracture mechanics 80−35294
glass fibre reinforced resins, fatigue damage in notched samples 78−15496
glass-ceramic composite, internal stress effects on mech. props. 77−21250
glass/C fibre reinforced plastic, hybrid effects between interlaminar and translaminar config., mech. props. 79−52351
graphite, notch sensitivity, 20 to 2800°C 80−76353
graphite fibre reinforced epoxy, fracture mechanics 80−35294
graphite fibre reinforced epoxy, notched, fatigue initiation 77−52471
graphite reinforced epoxy laminate, fracture behaviour 79−83294
graphite reinforced epoxy laminate plates with cracks, strain and failure anal. 79−29170
graphite ring, eccentric, under radial thermal load, stress state 80−76351
gust loading test results, appl. of relative Miner rule for notched specimen 79−83308
heat shrinkage tubing, crack resistance *(Japanese)* 79−61709
impacted pretensioned plate, dynamic finite element and photoelastic analyses 78−67111
Inconel 718, creep fracture characts. 79−52339
Long-life notch strength reduction due to local biaxial state of stress 78−9612
low-alloy cast steel, high-strength, fracture toughness 77−56109
metal, notched, cyclic stress/strain behaviour, random fatigue life *(German)* 80−100907
metal, notched, fatigue under alternately over- and under-stresses *(Japanese)* 80−35307
metal, notched sheet, thickness effect on deform. and fracture under tension 79−70113
notched flat tensile specimens, deform. zone *(German, English)* 78−64603
notched specimen, brittle fracture characts. under impact bending 78−23810
nylon, partially crystn., temp. effects on fracture 77−63771
plant fibre, fracture energy 79−52355
plastics, mechanical strength and brittleness, effect of moisture and notches *(German)* 77−48543
plastics and reinforced plastics, tabulated data as design guide 77−21087
PMMA, defect build up in service, effect on notch sensitivity 77−66694
PMMA, effect of surface finish on strength, and craze reistance 78−76724
PMMA, fatigue crack growth under biaxial stress 79−70144
PMMA, fracture morphology in notched tension, mol. wt. effects 77−52487
PMMA notched beam, fracture due to central impact 80−16426
polycarbonate, notched specimens, impact fracture behaviour 77−28888
polycarbonate, notched specimens deform. and fracture 78−11293
polycarbonate notched beam, fracture due to central impact 80−16426

notch strength continued
polyisocyanurate foams, strength, cellular struct. effect 80−40518
polymer, crack tip failure mechanism modelling 80−108565
polymer concrete, fracture toughness meas. 79−70168
polypropylene partially crystn., temp. effects on fracture 77−63771
polyurethane foams, strength, cellular struct. effect 80−40518
polyurethane rigid foam, fracture props. over range of densities 79−79106
powder metallurgy, fatigue strength significance *(German)* 80−60946
PVC, rigid, fatigue crack growth, under biaxial stress 79−70144
PVC, rigid plate, notching method effect on Charpy impact values, fractographic considerations *(Japanese)* 80−108541
PVC sheet, notched, yielding 78−56708
reactor vessel, neutron irrad. effect on brittle fracture characts. *(Slovak)* 78−50254
rectangular bars , stresses at plastic deflection *(German)* 78−34025
rim of semi infinite plate, crack originating from triangular notch under transverse bending 79−77009
rods, round and flat, stress conc. coeff. in sharp circular notch zone, design feature effects 79−14350
specimen configuration effect on crack initiation in delayed fracture, apparent stress intensity factor anal. *(Japanese)* 79−77676
stainless cast high-strength steel, fracture toughness 77−56109
steel, 17G2SF, large diameter pipe, load carrying ability, failure charact. 79−5055
steel, 40Kh, effect of deform. ageing *(Russian)* 78−31427
steel, alloy, Cr-Mo, alloy SCM3, hydrogen embrittlement, delayed fracture, exam. *(Japanese)* 78−64620
steel, alloy, toughness evaluation inconsistency of AISI 4340 austenitised at increasing temp. 78−52982
steel, austenite decomposition, controlled rolling rel. to substruct., props. 79−29014
steel, austenitic, 30KhGSA, heat treatment, preliminary, cold deform., elec. heating rel. to mech. props. 79−24554
steel, austenitic stainless, type SUS 304, low cycle fatigue strength reduction factor *(Japanese)* 80−104259
steel, austenitic stainless type SUS 316, low cycle fatigue tests, freq. effect on notch sensitivity at elevated temps. *(Japanese)* 80−104260
steel, C, crack initiation and propagation life under repeated impact tensile loads *(Japanese)* 80−104264
steel, C, fatigue, residual stress and crack growth expts., notch and surface treatment effects 79−8356
steel, C, pressure vessel and piping, factors affecting notch toughness 79−61730
steel, C, spheroidised, fracture toughness, cementite particle effects, optic and electron obs. 78−60785
steel, C, type 1792AF 79−38966
steel, C, type SFVV1, low cycle fatigue strength reduction factor *(Japanese)* 80−104259
steel, C and alloy, notched beam, fatigue crack emanates from notch root, fracture strength 78−72866
steel, C and low alloy, structural, ductile and brittle fracture resist. in stable crack growth stage 79−52369
steel, C-Mo-P, intergranular fracture and grain boundary segregation, P, H, Mo effects *(Japanese)* 79−15775
steel, cast, fatigue from cast-to-shape notches 77−16679
steel, cast, plain C, C-Mn and low-alloy fatigue from notches 77−16678
steel, CC Cr-Ni, soaking at forging temp., effect on struct. and mech. props. *(Czech)* 78−64628
steel, Charpy V-notch toughness test, computer simulation 79−70138
steel, comp. and processing effects on microstruct. and props. rel. to low temp. applic. 77−52365
steel, complex alloy, exam. of temper brittleness 78−44209
steel, Cr, hypereutectic, structural, critical rates of impact, kinetics of failure 80−35325
steel, Cr (12wt.%), mech. props, carbide phase struct. 79−15702
steel, Cr-Mo, Mn-V, V, fracture toughness, pressure vessel appl. *(Czech)* 79−79094
steel, Cr-Mo, notched specimens, statistical eval. of fatigue life and fatigue limit and life distrib. *(Japanese)* 79−61702
steel, Cr-Mo-V, medium strength, correlation between crack initiation, propag. and microstruct. 78−60787
steel, Cr-Mo-V, normalised and tempered, size and geometry effect on creep cracking behaviour 78−64630
steel, Cr-Mo-V, notch geometry influence on creep rupture props. *(German)* 80−30055
steel, Cr-Mo-V, stress rupture, notch influence, temp. depend. *(German)* 80−60945
steel, Cr-Mo-V, stress rupture strength at high temps. *(German)* 80−40474
steel, crack opening displacement in deeply notched specimens 78−27617
steel, CrMo and CrMoV, creep resistant, ductile-brittle transition temp., precipitation effects *(German)* 78−19856
steel, decarburised layer effects on fracture toughness of 60S2 77−59930
steel, dual-phase, notched, fatigue 79−100253
steel, eutectoid notch toughness, tempering at moderate temps., effect of quenching temp. 77−21193
steel, ferritic, impurity defect interaction influence on radiation hardening and embrittlement 80−35199
steel, ferritic-pearlitic, low C, low alloy, low temp. effects on fatigue strength 79−5057
steel, finite life characteristics, notch effects *(German)* 77−90434
steel, hardened and casecarburized, fatigue crack initiation, propag. and termination, notch depth effects *(Japanese)* 78−7022
steel, heat resist., crack growth resist. on long-term loading 79−29178
steel, high purity, low S content, for tough semi-finished products in nuclear power plant *(German)* 80−45393
steel, high strength, low alloy, fatigue crack growth from a surface flaw 78−68803
steel, high strength, state of stress effects on ductile failure initiation 77−56070
steel, high-speed, quenched and tempered notch toughness, ultimate and yield strength in tension and compression 78−95782
steel, hot forging die type, fractography *(Japanese)* 80−108547
steel, hot rolled strip formability, mech. testing and mech. props. *(German)* 79−66089
steel, inclusion effect on cold formability 80−29975
steel, low alloy, metallurgical factors and toughness in structural steel welds *(Japanese)* 79−52377
steel, low alloy, naval, stretch zone width meas., COD for ductile crack initiation 78−68813

notch strength continued
steel, low alloy, pressure vessel and piping, factors affecting notch toughness 79−61730
steel, low alloy, tempered martensite embrittlement and crack initiation *(Japanese)* 79−66149
steel, low alloy, tempered martensite embrittlement mechanisms 79−8351
steel, low alloy, thermally fatigued, fracture toughness 78−72872
steel, low alloy effect of grain size, and amount of pearlite on fracture resistance 79−100255
steel, low and medium C, fatigue strength, small defect effect 80−104255
steel, low C, brittle fracture of notched specimens, ferrite grain size and notch geometry effects 78−19860
steel, low C, dual phase, impact props., microstruct. element influence 80−40525
steel, low C, effect of grain size on transition behaviour and bending speed correl. *(Japanese)* 79−8345
steel, low C, notched sheet under tensile loading, notch tip opening/contraction, J-integral relationship *(Japanese)* 77−4840
steel, low C, notched specimens, brittle fracture stress, effect of ferrite grain size, notch acuity and notch length 79−20187
steel, low C, S 35 C, annealed, crack initiation life, anal. of smooth and notched specimens *(Japanese)* 79−8347
steel, low pearlite, low alloy, low temp. strength props., heat treatment 77−12658
steel, low S, ESR and electric arc, notch toughness, interaction between overheating and tempering temp. effects 78−52970
steel, low strength notched specimens, preloading effects on brittle fracture 78−27642
steel, martensitic, Cr-Co-Ni-Mo, notch toughness, rel. to sensitivity to stress conc. 78−31532
steel, medium C type JIS S45C, multiple notched specimens, fatigue props. 79−61729
steel, mild, fatigue crack growth from a surface flaw 78−68803
steel, mild, fatigue crack growth in compression, notch effect 80−30065
steel, mild, notch effect on impact fatigue strength *(Japanese)* 79−43400
steel, mild, subject to three point bending and tensile load, acoustic emission 80−3154
steel, mild, transgranular stress corrosion cracking in H_2So_4-KI soln. 80−71797
steel, Ni (9 wt.%), effect of repeated tempering on notch strength *(Japanese)* 79−43280
steel, Ni-Cr, temper embrittlement by Sb, Ni, Cr effects 77−36628
steel, Ni-Cr-Mo, Ni effect on fracture toughness, heat treatment effect *(Korean)* 79−91781
steel, Ni-Cr-Mo, quenched and tempered, nothced bar tensile tests *(German)* 80−35247
steel, Ni-Cr-Mo and Cr-Cu-Mo and sintered, ductile fracture, microvoid effects *(Japanese)* 80−108542
steel, Ni-Si-Nb (1.5,0.02,0.03 wt.%), fatigue crack growth under bending *(French)* 80−21089
steel, notch sensitivity in fatigue 78−60757
steel, notched 1018, air fatigue in endurance limit range 77−36631
steel, pearlitic, heat treatment effects on mech. props. and microstruct. *(German)* 77−8857
steel, prestrained pressure vessel, dynamic toughness characts., expt. correlations 79−15783
steel, quenched, notch sensitivity, effect of tempering temp. 77−1846
steel, reinforcement, low, high temp. static strength testing 79−15902
steel, SHE 4340, tempered martensite embrittlement 80−30084
steel, sintered, mech. props. 77−40439
steel, spheroidised AISI 1095, U-notched bend specimens, hydrogen effect on fracture 79−52363
steel, spheroidized AISI 1095, ductile fracture of U-notched bend specimens 79−24616
steel, stainless, Kh18N10T, ionised gas effects 79−70252
steel, stainless, maraging, high strength, exam. of ageing embrittlement *(Japanese)* 78−84972
steel, stainless and low alloy, PWR primary circuit constituent materials, design features verification *(French)* 79−17976
steel, structural, brittleness susceptibility rel. to heat treatment 79−24620
steel, structural, crack growth under cyclic load, stress intensity factor 79−87709
steel, structural, effect of rare earth metals on cold temper brittleness 79−29202
steel, structural, influence of deform. heat on the mech. props. *(German)* 78−84904
steel, structural, lateral notches rel. to ductile fracture characts. 79−43392
steel, structural, notched, cathodic polarisation effect on fatigue in seawater 79−47805
steel, structural, unalloyed, brittle fracture, grain size and precipitate thickness effect 78−60786
steel, V and V-N , high strength, mech. props. and strain ageing, processing variables effects 77−59819
steel *(French)* 80−66670
steel 12Kh18N10T, struct. and mech. props. after prolonged working at −183°C 77−55988
steel 15Kh1M1F, temperature-time dependence of long-time structural strength 79−100232
steel 18Kh2N4MA, phase transformations and props. 77−12614
steel 40Kh, notch sensitivity under cyclic impact loads 78−3220
steel creep resistant, rare earth metal effect on inclusion charact. *(Czech)* 77−86134
steel low alloy, high strength, ductile failure criteria for blunting crack 78−64657
steel low C, fatigue strength of notched specimen, low-temp. quenching and quench ageing effects 79−100173
steel low C, notched, fatigue strength, crack propagation, plastic torsional prework depend. *(Japanese)* 79−15744
steel notched rods in tension, 20-700°C, yield conditions *(Polish)* 78−80604
steel plates, C and alloy steels, comparison of dynamic tear and Charpy V notch impact props. 78−92357
steels, cleavage fracture model at low temperatures *(German)* 80−35293
steels, S 45 C, SK 5 SCM 3, SNCM 8 and SUS 403, heat treated JIS, statistical fatigue props. 78−44222

notch strength continued
strain energy density and surface layer energy for blunt cracks or notches, book contrib. 78−94618
strain velocity effects on critical crack opening displacement 79−18818
stress anal., book 78−94617
stress intensity factor crack opening displacement relationship for compact tension specimen 78−90778
stress intensity factor formula for side notches with cracks 78−79264
stress intensity factors, mixed mode, photoelastic determ., notch effects 80−14632
three dimensional notch problems, elastic medium, book contrib. 78−94622
tip of blunt notch, plastic yielding during static and fatigue loading 79−77010
tip stress distrib. in strain hardening material 79−3927
tube with hexagonal bore, crack formation during rolling *(Russian)* 78−80622
wedge shaped notches with large flank angles, plane strain general yielding under loads and bending 79−18808
weld defects, toughness, crack growth anal. 79−43429
Al alloy, 2024-T3, notched sample fatigue damage detection via optical correlation technique 78−35511
Al alloy, accumulation of damages in stress concentration zones in alternating creep and fatigue 79−100261
Al alloy, high strength, fatigue crack propag. and fatigue life, shallow notch effect *(Japanese)* 79−29199
Al alloy 01205, mech. props. at cryogenic temps. 79−29206
Al alloy 2024-T4, ductile fracture, microvoid effects *(Japanese)* 80−108542
Al alloy 7075, modified, fatigue and failure mechanisms 79−100252
Al alloy 7075-T6, notched sheet under tensile loaded, notch tip opening/contraction, J-integral relationship *(Japanese)* 77−4840
Al alloy JIS A5083-O, notch sensitivity in fatigue 78−60757
Al alloy JIS A5083-0, multiple notched specimens, fatigue props. 79−61729
Al alloy V93, high strength, notch sensitivity in static and repeated loading 78−27639
Al alloys, critical stress intensity factor determ., fatigue tests on notched specimens *(French)* 78−35502
Al alloys AMg6M, AMg6, 5083, weld at cryogenic temps., mech. props. 79−66136
Al alloys A5083 and A7075, statistical fatigue props. 79−5060
Al, high purity 6061, thermomechanical treatment 77−44277
Al notched bars, deform. behaviour and strength having biaxial state of stress at notch root *(Japanese)* 80−81116
Al-Cu (4 wt.%), aged to contain Guinier Preston zones, crystallographic fatigue crack growth 78−60832
Al-Cu-Mg-Mn-Fe-Si, alloy D16, effect of mechanisothermal treatment on mech. props. 78−56674
Al-Mg (2.4 wt.%) alloy, solution-treated, grain size effects on fatigue strength 77−4839
Al-Mg sheet, artificial stress raiser effect on strength and local plasticity of weld joint 80−81130
Al-Mn sheet, artificial stress raiser effect on strength and local plasticity of weld joint 80−81130
Al-Zn-Mg-Cu (6.76, 2.37, 1.80 wt.%), cyclic SCC in salt water *(Japanese)* 80−45435
Al_2O_3, fracture toughness determ. using four-point-bend specimens 80−108536
Al_2O_3-Ca (0.6 to 1.6 at.%), fracture behaviour, Ca segregation effect 80−40504
B fibre reinforced Al, fracture mechanical study, unidirectional composites 78−88520
B fibre reinforced Al, unidirectional, K-calibration and compliance curves 78−88518
B fibre reinforced Al alloy 6061, cross plied laminate, tension-compression fatigue 79−38940
B fibre reinforced epoxy, fracture mechanical study, unidirectional composites 78−88520
B fibre reinforced epoxy, fracture mechanics 80−35294
B fibre reinforced epoxy composites, notched, tensile strength and failure modes 80−81205
C steel, impact-fatigue strength , notch strength, rel. to comp. and ductility of core 77−56093
Cu-Be alloy, notched specimen, static and dynamic behaviour 78−27634
Fe, Armco, texture role in prestrain embrittlement 78−60796
Fe, cast, notch strength, non-uniform stress distrib. effect *(Japanese)* 79−79090
Fe, cast, pearlitic, residual compressivel stress distrib. effect on resultant stress conc. in notched samples 78−92336
Fe, cast, spheroidal graphite pipe, fatigue strength 80−16419
Fe, cast flake and nodular, rupture strength, circumferential notch *(Japanese)* 80−93649
Fe, high-purity, notch toughness 77−44353
Fe, nitrogen, impurity defect interaction influence on radiation hardening and embrittlement 80−35199
Fe-C-Fe_xO_y, cleavage initiation by ductile tearing 78−64656
Fe-Ni-C (9, 0.1 wt.%), effect of intercritical tempering on impact energy, exam. of mech. props. 78−52861
Fe-Ni-Mn, martensite, aged, grain boundary embrittlement 79−96144
Fe-Ni-Mo alloy, high-strength ferritic, for cryogenic service, mech. characteris. 77−70143
Fe-Si (3.12 wt.%), brittle fracture, work hardening effect at notch tip 78−44220
Fe-Si (3wt.%), notched sheet under tensile loading, notch tip opening/contraction, J-integral relationship *(Japanese)* 77−4840
Na_2O-CaO-SiO_2 glass rods, prediction of thermal fatigue resist. 78−84955
Pb, model material, specimen size effect on plastic deform. around deep notches 79−70142
Si, monocrystalline, effect of notch root radius on fracture behaviour 78−76751
Si_3N_4, hot-pressed, fracture toughness determ. using specimens with chevron and straight through notches 80−108538
α-β Ti alloy, fatigue crack initiation from notches 77−21259
Ti, notched sample, fatigue damage detection via optical correlation technique 78−35511
Ti-Al-Cr-Mo-Fe(V)(Zr), effect of structure and heat treatment on tensile strength, ductility, fatigue limit and notch sensitivity 78−56711
αTi-Al-(Zr), embrittlement due to ageing 78−56673
UO_2, strength recovery and crack healing 77−8918

notch strength continued
V, oxygen impurity defect interaction influence on radiation hardening and embrittlement 80−35199
WC-Co alloys, single edge notched beams, exam. of fracture toughness 78−52975
Zn, pure, polycrystalline, cleavage fracture, hydrostatic tension effect 78−52990
Zr-Nb, pressure tube alloy, initiation COD as fracture criterion 78−72862

notch testing
see also fracture toughness testing
ABS polymer, transparent, fracture of notched tensile specimens 77−63772
alumina, polycrystalline, subcritical crack extension and crack resist. 77−8911
brittle materials, crack size and effective specific work for failure determ. 80−85108
Charpy tests, instrumented, evaluation of reliability 77−25243
chevron notched short bar specimens, compliance and stress intensity coefficients 80−96232
companion-specimen method verification of Neuber-based notch analysis 77−50985
crack opening displacement testing 77−36722
cylindrical notched specimen, four-point bending, crack resist. tests 80−53735
device for producing fatigue cracks in specimens 80−61051
epoxy resin microcircuitry elements, thermoelastic phenomena testing *(Polish)* 80−93724
fatigue life estimates 80−100999
fibrous cracking, COD and initiation, replication technique 77−56069
fracture evaluation at high loading rate by extrapolation method 77−36723
fracture toughness reference curve development 80−97588
fracture toughness screening using sharp notch tension 77−56169
glass fibre reinforced plastic, load-time history anal. in instrumented Charpy test *(Japanese)* 80−55511
glass microcircuitry element thermoelastic phenomena testing *(Polish)* 80−93724
graphite, effective specific work of fracture, evaluation method 79−57170
heat resistance testing, massive sample for mech. prop. changes obs. 78−7124
impact fatigue testing machine 78−56838
impact three point bend testing for notched and precracked specimens, testing and data analysis procedures 78−53053
impression method for plastic deforms. determ. at apex of stress concentrator, bare choice considerations 77−52571
notch like defects, echo signal depend. on sound field and frequency *(German)* 77−90537
notched and bend specimens with equivalent geometries, cyclic deform. *(German)* 77−86271
notched bar design for creep-rupture testing under tri-axial stresses 77−62165
notched bars, creep stress redistrib., finite element anal. 77−62164
nuclear power engineering materials certification testing for safety and reliability 80−78360
plates, V-notched elastic, symm. loaded, stress intensity factors, caustic method 80−83770
PMMA, crack size and effective specific work for failure determ. 80−85108
precompression cracking method, for fracture toughness testing *(Japanese)* 78−15612
rectangular bar, notched, strain meas. *(German)* 78−11451
round notch tension test, computer simulation 79−24705
rubber, instrument for controlled notching 79−70258
silicone rubber, crack tip replica, for determ. of J-integral values 79−52475
static bend testing by unit with energy accumulator 77−86251
statistical analysis of data 79−61818
steel, 35, fracture characteristics, notch sharpness effect in impact tests 79−52536
steel, C, fatigue crack propagation in sheet, influence of struct. of ferrite-pearlite bands *(French)* 80−76338
steel, Charpy type bars of AISI 4340, varying notch root radii, fracture initiation and propag. at notch root 80−85050
steel, Cr-Mn, low-cycle fatigue at 20 and −196°C 80−81196
steel, Cr-Mo-V (0.5, 0.5, 0.25 wt.%), creep crack growth in notched bend test, microstruct. effect 77−21261
steel, dynamic fracture toughness meas. by instrumented impact bend and compact K testing 77−36718
steel, EI643 and 30KhGSNA, notch sensitivity, in mains water *(Russian)* 77−77624
steel, heat treated, test specifications changes *(German)* 77−9019
steel, high temp. props. determ. with grooved tensile specimens 78−23902
steel, low C, impact strength and crit. brittleness temp., sample thickness and notch radius influence 80−85018
steel, maraging, notch strength 77−56056
steel, mild, dynamic flat fracture resistance, shear lip effects 77−44451
steel, notched bar impact test specimens, strain hardening distrib. *(German)* 77−60004
steel, pearlitic constructional, K_{IIIc} expt. determ. 80−100985
steel, S45C notched specimens, Charpy impact tests, notch angle effects *(Japanese)* 80−85124
steel, stainless, IR electro-thermal exam. 77−44428
steel, stainless SUS 316, creep fracture at elevated temps. vacuum environment effect *(Japanese)* 77−8942
steel, structural, susceptibility to brittle fracture criteria, comparison of notch impact and fracture toughness testing *(German)* 77−70237
steel, weldable C and alloy, brittle fracture, metallurgical factor effects, NDT data, impact tests *(French)* 79−5128
steel 15G2AFDps, fatigue to brittle fracture transition at low temp., stress raiser effect 77−12696
steel components, safety anal. for loading conditions 78−39979
steel plate, rolling direction determ. with notched bend test specimen *(German)* 77−60003
steel sheet, hot and cold rolled, cold formability, notched tensile test and stretch bend test *(German)* 80−61031
steels, structural St 37-2, cleavage fracture, report 80−25868

notch testing continued
steels, wide plate and V-notch bending tests evaluation on basis of materials mechanics *(German)* 80−66571
steels 30 KhGSNA and VNS-2, fatigue life diagrams plotting 79−70246
strain distribution near notch tip under mixed plane stress-plane strain condition *(Japanese)* 77−8891
strip with semicircular notches, tensile load conditions at end, interf. effects obs. 80−64455
structural steel, microstruct. and brittleness, rel. to austenizing and heat treatments 77−56091
tension tests, short term, review 79−61829
three point bend tests, notched or precracked specimens, load displacement measurement and work determ. 78−53054
Al alloy, 7175 T 651, crack tip opening under cyclic loading, effect of environmental and R-ratio 80−45377
Al alloy, stress corrosion cracking, active path form., electrolytically notched specimens 77−16713
Al alloy AK4-1, crack growth rate prediction under creep conditions 80−85107
Al alloy V95T1, endurance determ. method over wide range of load asymmetry 78−56836
Al, superplastic deformation depend. on subgrain struct. electron microscope study *(Russian)* 79−83257
Al_2O_3 brittle ceramic fracture toughness meas. notch requirements *(German)* 77−59937
B fibre reinforced epoxy, tensile anal. of edge notch 77−70159
Be, high-strength, fracture toughness determ. 77−73336
Cr-Mo-V steel, creep rupture tests on notched cylindrical specimens at 600°C 77−32670
Fe, slip-initiation phenomenon by fatigue, appl. to stress meas. 80−45342
Ni-Nb-Al-(Cr), eutectic, mech. props., high press. H_2 effects 77−63779
Ni-W (45.5 wt.%), eutectic, mech. props., high press. H_2 effects 77−63779
Ti alloy VT-20, fatigue life diagrams plotting 79−70246
α-U, mech. props. at very high strain rates, double-notch shear test use 80−85131

novae
see also supernovae
A0620−00, transient X-ray source, spectrophotometry 78−4400
A0620−00, X-ray nova, Ariel V crystal spectrometer/polarimeter obs. 77−2494
A0620−00, X-ray nova, distance determ. from reddening 77−2495
A0620−00, X-ray nova, spectroscopic obs. 77−87417
2A 0526−328 optical counterpart, X-ray emitting cataclysmic variable, spectrum and photometry 79−97103
accretion belts on white dwarfs, rel. to nova phenomenon 78−36582
accretion disc models and cataclysmic variables, H line blocking of UBV colours 79−101155
accretion discs theoretical photometric and spectroscopic props., cataclysmic variables appl. 79−80312
accretion disk stability 77−82244
Z Andromedae, UV spectra, 1979 Feb. 17, quiescent phase 79−40202
anomalous nova-like object in M31 79−80316
AE Aquarii, cataclysmic variable, IUE satellite UV obs. 80−72985
AE Aquarii, rapid light oscills. rel. to white dwarf oblique rotator model 80−36634
AE Aquarii, spectroscopic binary variable, X-ray source, orbital element determ. 80−105288
V603 Aquilae, accretion disc radiation of cataclysmic binary 77−91537
Aquilae 1891 (T Aurigae), spectrophotometry of shell 80−72955
Aquilae 1918 (V603 Aquilae), IUE obs. of periodic light vars. 80−105251
Aquilae 1918 (V603 Aquilae), old nova, eclipses obs. 80−90476
Aquilae 1918 (V603 Aquilae), periodic light vars. detect. 80−82391
Aquilae 1975 (V1301 Aquilae), dust grain IR emission model 80−105254
Aquilae 1975 (V1301 Aquilae), IR development 77−17570
V603 Aquilae (Nova 1918) 77−82247
V1301 Aquilae (Nova 1975), VBLUW photometry, absolute magnitude, distance and reddening 79−58342
Ariel 0620−00 (V616 Monocerotis), transient X-ray source, spherical model 78−12415
Ariel 1524-61 optical counterpart, identification and light curve 77−45611
astrometric posns. and identifications 79−21315
T Aurigae, eclipsing binary nova, times of minima 77−22267
Aurigae 1891 (T Aurigae), old nova, photometric and spectroscopic obs. 80−90446
BD−7°3007, nova-like variable, simultaneous spectroscopy and photometry 78−12250
bloated dwarf model of nova light curves 77−82251
UZ Bootis, cataclysmic variable similar to WZ Sagittae, outburst characts. 80−17596
Z Camelopardalis, dwarf nova, photometric obs. and light curve (1973-77) 80−56853
Z Camelopardalis, dwarf nova, spectrophotometry at standstill and in eruption 80−82366
TX Canum Venaticorum, cataclysmic variable, P Cygni type, visible spectral obs. 80−105249
AM Canum Venaticorum, orbital period increase 80−12765
η Carinae, earliest spectroscopic obs. and interaction of star with Carina Nebula 77−45433
OY Carinae, eclipsing ultrashort periodic dwarf nova discovery 79−53823
OY Carinae, white dwarf cataclysmic, eclipsing binary, parameter determ. 80−82385
HT Cassiopeiae, spectroscopic obs. of dwarf nova 79−88668
cataclysmic binaries, circumstellar material geometrical and photometric parameters 80−109492
cataclysmic binaries, connection as source of accretion disc viscosity 78−93307
cataclysmic binaries, evolution and origin 80−56885
cataclysmic binaries, gas flow hydrodynamic calc. 77−57037
cataclysmic binaries, masses and evolution 77−57031
cataclysmic binaries, role of white dwarf component 80−82356
cataclysmic binaries evolution, ang. momentum loss 77−57032
cataclysmic variable stars, multiple periodicities 77−87434
cataclysmic variables, period change due to mass transfer 80−82425

novae continued
cataclysmic variables, pulse timing meas., accretion disc models 79−62831
cataclysmic variables, role of accretion disks *(Polish)* 80−26739
cataclysmic variables, theoretical UBV colours of accretion discs 78−61865
cataclysmic variables, visual continuum flux distribs. 80−36636
cataclysmic variables, XUV emission *(German)* 80−109372
cataclysmic variables and nova explosions 77−82242
cataclysmic variables in globular clusters, preliminary report 80−109505
CD−42°14462, peculiar white dwarf, noneruptive close binary 77−53630
CD−42°14462 (V3885 Sagittarii), dwarf nova in permanent outburst 78−53966
CD−42° 14462, binary nature of nova-like variable 77−87435
BV Centauri, dwarf nova, identification as spectroscopic binary 80−51775
V436 Centauri, dwarf nova, no periodic modulation in quiescent state light curve 79−88677
V436 Centauri, dwarf nova, photometry during superoutburst (May 1978) 80−46570
Centauri 1979, optical novalike object discovery and identification with X-ray transient 79−62842
Centauri 1979, radio detect. of novalike object 79−67026
Centaurus X-4, magnitude of optical counterpart 1979 June 14 79−75220
Centaurus X-4, X-ray burst from novalike object 79−62935
Cephei 1971, chemical comp. of ejecta 78−12244
Cephei 1971 (IV Cephei), ejecta He abundance 79−40203
WX Ceti, cataclysmic variable similar to WZ Sagittae, outburst charcts. 80−17596
Z Chamaeleontis, cataclysmic binary, possible gravit. radiation emission 80−4386
Z Chamaeleontis, eruptive binary, model from photoelectric data anal. 80−72961
Z Chamaeleontis, gravitational waves from eclipsing cataclysmic binary 80−90439
Z Chamaeleontis, monitoring of southern dwarf nova, 1954-76 period 78−93272
Z Chamaeleontis, photometry of dwarf nova 79−67028
classical and dwarf novae, energy sources and systematics 79−67041
classical and dwarf novae explosions, review 79−67042
classical novae, minimum number of outbursts determ. 78−28692
classical novae, photospheric props. of optically thick winds 78−24516
CNO abundances and hydrodynamics, 1 M⊙ models with small mass envelopes 79−12475
coronal line emission origin 79−16965
SS Cygni, 1896-1975 study of dwarf nova 79−16986
SS Cygni, accretion disc radiation during dwarf nova outburst 77−91537
V1500 Cygni, accurate position and praenova search 77−2440
EM Cygni, cataclysmic variable, red and white dwarf binary, period change, B photometry 80−90434
SS Cygni, colour variations during dwarf nova outbursts 80−46576
SS Cygni, dwarf nova, ANS detection of both soft and hard X-ray emission 78−36579
SS Cygni, dwarf nova, identification as hard X-ray source by HEAO 1 scanning modulation collimator 79−2548
EM Cygni, dwarf nova, photographic study 77−33529
SS Cygni, dwarf nova, rapid optical oscills. phase variability 80−85947
SS Cygni, dwarf nova, soft X-ray pulsation obs. 80−46563
SS Cygni, dwarf nova, spectrophotometry rel. to accretion disc models in erruption and at min. light 80−36635
SS Cygni, dwarf nova, UV spectrum obs. by International Ultraviolet Explorer (IUE) 78−96474
SS Cygni, dwarf nova, X-ray polarisations discovery 78−65628
SS Cygni, dwarf nova during outburst, accretion disk model 77−82247
V1500 Cygni, expansion rate and distance 77−2439
ss Cygni, hard X-ray source, obs., accretion onto white dwarf 79−30078
SS Cygni, light curve periodicity 79−21300
V1500 Cygni, post-nova light curve development, UBV and Hβ obs. 77−71115
SS Cygni, radial vel. of dwarf nova 79−62833
V1500 Cygni, search for gamma ray lines 78−8013
V1500 Cygni, spectral development, visible and near IR obs. 78−4231
1500 Cygni, spectrophotometry of early phase with objective prism plates 77−17576
SS Cygni, spectroscopic binary variable, X-ray source, orbital element determ. 80−105288
V1500 Cygni, UBV obs. and two-colour method appls. 79−71042
V1500 Cygni, visual magnitude estimates 1976, Nov. and Dec. 77−9758
Cygni 1975, continuum periodic variability 77−13365
Cygni 1975, Copernicus near UV spectral obs. 77−29844
Cygni 1975, diminishing of emission line widths in postmax. spectrum *(Russian)* 77−74075
Cygni 1975, Hα, Hβ emission lines equivalent widths, scanner obs. 77−2430
Cygni 1975, light fluctuations period var. 79−97012
Cygni 1975, low resolution spectrophotometry 77−49403
Cygni 1975, photographic obs. 77−5535
Cygni 1975, polarisation obs. *(Chinese)* 77−67097
Cygni 1975, rapid vars. of emission line profiles 77−45434
Cygni 1975, shell phase obs. 77−49392
Cygni 1975, speckle interferometry with linear digicon detector 77−78648
Cygni 1975, spectrophotometric exam. *(French)* 77−22240
Cygni 1975, spectrophotometric obs. 77−49402
Cygni 1975, spectroscopic obs., detect. of diffuse enhanced spectrum 77−29850
Cygni 1975, spectrum around max. light 77−87411
Cygni 1975, spectrum obtained with small image-intensifier spectrograph 78−73647
Cygni 1975, stellar wind and light vars. 77−82237
Cygni 1975, synchrosignal for extraterrestrial civilizations 78−28546
Cygni 1975 (V1500 Cygni), 3 hour photometric period stabilisation 79−92776
Cygni 1975 (V1500 Cygni), 3 hour var. 79−16966
Cygni 1975 (V1500 Cygni), Balmer line emission profiles evolution in early decline phase 80−82371
Cygni 1975 (V1500 Cygni), binary nature, spectral meas. 77−87446
Cygni 1975 (V1500 Cygni), brightness meas., (1917 to 1976) 78−36618
Cygni 1975 (V1500 Cygni), BV photometric obs. 78−36613

novae continued
Cygni 1975 (V1500 Cygni), BV photometry 78−36619
Cygni 1975 (V1500 Cygni), continuous energy distrib., IR obs., thermal bremsstrahlung 79−80315
Cygni 1975 (V1500 Cygni), distance and temp., visible spectral obs. *(Chinese)* 80−85955
Cygni 1975 (V1500 Cygni), emission line profiles during early nebular stage 79−53826
Cygni 1975 (V1500 Cygni), emission line vars. rel. to struct. of central object 80−82367
Cygni 1975 (V1500 Cygni), fine-struct. lines rel. to 10 micron excess 78−93269
Cygni 1975 (V1500 Cygni), Hα and Hβ emission line vars. 80−4389
Cygni 1975 (V1500 Cygni), H I emission line profiles vars., envelope ejection vels. determ. 79−35281
Cygni 1975 (V1500 Cygni), He abundance of ejecta 78−28691
Cygni 1975 (V1500 Cygni), heavy element abundances 79−21295
Cygni 1975 (V1500 Cygni), high-energy gamma-ray flux upper limit 78−36603
Cygni 1975 (V1500 Cygni), interstellar reddening and distance 78−4230
Cygni 1975 (V1500 Cygni), light curve 77−2437
Cygni 1975 (V1500 Cygni), light curve for 1975 Aug.-1977 July period 80−4372
Cygni 1975 (V1500 Cygni), line spectrum evolution 78−32493
Cygni 1975 (V1500 Cygni), linear polarization obs. 78−36601
Cygni 1975 (V1500 Cygni), luminosity and distance, light curve obs. 80−72981
Cygni 1975 (V1500 Cygni), meas. and nova outburst model 77−87448
Cygni 1975 (V1500 Cygni), mechanism of quasieclipses after outburst *(Russian)* 78−93280
Cygni 1975 (V1500 Cygni), minute time scale flickering and 6.6 hour light period 77−17582
Cygni 1975 (V1500 Cygni), model for spectrographic obs. 77−87444
Cygni 1975 (V1500 Cygni), multiband photometry 77−87445
Cygni 1975 (V1500 Cygni), near IR spectroscopy 78−36599
Cygni 1975 (V1500 Cygni), near IR spectrum 78−36606
Cygni 1975 (V1500 Cygni), obs. of magnitude and spectrum charges *(French)* 77−82258
Cygni 1975 (V1500 Cygni), optical polarisation obs. 78−36622
Cygni 1975 (V1500 Cygni), periodicity investigation at 21 cm 80−82529
Cygni 1975 (V1500 Cygni), photoelec. obs., period decrease, visual magnitude estimates 77−22252
Cygni 1975 (V1500 Cygni), photoelectric obs. 78−36620
Cygni 1975 (V1500 Cygni), photometric and spectroscopic obs. 78−36604
Cygni 1975 (V1500 Cygni), photometric obs. 78−36616
Cygni 1975 (V1500 Cygni), photometric obs. at Skalnate Pleso Observatory 78−36617
Cygni 1975 (V1500 Cygni), photometry, light curves, magnitude estimates 78−85960
Cygni 1975 (V1500 Cygni), photometry rel. to 3.3 hour var. and flickering 78−36591
Cygni 1975 (V1500 Cygni), polarimetric and photometric obs. 78−36612
Cygni 1975 (V1500 Cygni), pre-maximum spectra 77−87449
Cygni 1975 (V1500 Cygni), radio emission from expanding shell 80−26868
Cygni 1975 (V1500 Cygni), radio obs. and analysis 80−67726
Cygni 1975 (V1500 Cygni), review of development *(French)* 80−17598
Cygni 1975 (V1500 Cygni), shell electron temps., densities and other props. 79−30068
Cygni 1975 (V1500 Cygni), short-term light vars. 78−36609
Cygni 1975 (V1500 Cygni), small amplitude light var. 78−36608
Cygni 1975 (V1500 Cygni), spatial and kinematic envelope model 78−36600
Cygni 1975 (V1500 Cygni), spectral energy distrib. 78−36605
Cygni 1975 (V1500 Cygni), spectral evolution 77−87447
Cygni 1975 (V1500 Cygni), spectral features during early decline phase 77−22245
Cygni 1975 (V1500 Cygni), spectrographic obs. *(Chinese)* 79−16982
Cygni 1975 (V1500 Cygni), spectrophotometric study *(French)* 77−82259
Cygni 1975 (V1500 Cygni), spectroscopic data 79−16988
Cygni 1975 (V1500 Cygni), spectroscopic developments and kinematics 77−45446
Cygni 1975 (V1500 Cygni), spectroscopic obs., three hour periodicity, nebula model 78−12235
Cygni 1975 (V1500 Cygni), spectroscopic studies, models for 3 hour profile vars. 79−8920
Cygni 1975 (V1500 Cygni), spectroscopic studies, nebular and central binary system 79−62830
Cygni 1975 (V1500 Cygni), spectrum variations 78−36607
Cygni 1975 (V1500 Cygni), thirteen-colour photometry and anal. of short period variability 79−92788
Cygni 1975 (V1500 Cygni), three hour light var. 79−80314
Cygni 1975 (V1500 Cygni), TV photometry 78−36602
Cygni 1975 (V1500 Cygni), UBV photometry, short period variability 78−61862
Cygni 1975 (V1500 Cygni), UBVR Hα photometry and polarimetry 78−36611
Cygni 1975 (V1500 Cygni), UBVRI photometry and polarimetry 78−36614
Cygni 1975 (V1500 Cygni), UV photometry 77−64766
Cygni 1975 (V1500 Cygni), UV photometry after visual max. 77−82260
Cygni 1975 (V1500 Cygni), visible and near UV photoelec. photometry 78−36610
Cygni 1975 (V1500 Cygni), visible and near UV spectrophotometric obs. 78−32492
Cygni 1975 (V1500 Cygni), visible and near UV spectrophotometry 78−32494
Cygni 1975 (V1500 Cygni), visible and UV spectra and light curve 80−12771
Cygni 1975 (V1500 Cygni), visible spectroscopy 78−36598
Cygni 1975 (V1500 Cygni), visible-band linear polarimetry 78−36621
Cygni 1975 (V1500 Cygni), visual magnitude estimate (1977, February 10) 77−29853
Cygni 1975 (V1500 Cygni), visual magnitude estimates (1977 Aug.-1978 Jan.) 78−32474
Cygni 1975 (V1500 Cygni), wide-band IR photometry 78−36615
Cygni 1975 (V1500 Cygni) as thermonuclear runaway event 77−82261

novae continued
Cygni 1975 (V1600 Cygni), 3.35 hour 1978 light curve, rel. to possible double period 79−67039
Cygni 1978, discovery report and precise position 78−85962
Cygni 1978, distance and interstellar reddening 79−21310
Cygni 1978, photoelectric obs. and visual magnitude estimates 78−89214
Cygni 1978, photometric obs., light vars., IR obs. showing dust form. phase 78−96494
Cygni 1978, prediscovery mags. and 1978 September spectral features 78−93282
Cygni 1978, rapid flickering and UBV photometry (1978 Sept.) 79−16985
Cygni 1978, spectra, polarisation, photometry and visual magnitude estimates 78−93283
Cygni 1978, spectrum, distance and absolute magnitude 78−89212
Cygni 1978, spectrum, polarisation and visual magnitude estimates 78−89213
Cygni 1978, spectrum, precise position and photometry 78−89211
Cygni 1978, spectrum and visual magnitude estimates 78−89210
Cygni 1978, UBV photometry, brightnesses and distance 78−93284
Cygni 1978, UBV photometry and short-period vars. 79−5835
Cygni 1978, V photoelectric and visual magnitudes (1978 Sept.-Nov.) 79−5837
Cygni 1978, visual magnitude estimates (1978 September 10 to 12) 78−85963
Cygni 1978, visual magnitude estimates for 1978 Oct. 78−93286
Cygni 1978 (V1668 Cygni), BV photometry 79−67035
Cygni 1978 (V1668 Cygni), JHKLM photometry 79−53828
Cygni 1978 (V1668 Cygni), linear polarisation obs. 80−26875
Cygni 1978 (V1668 Cygni), multifilter photometry and polarimetry 80−90454
Cygni 1978 (V1668 Cygni), optical light curve, uvby photometry 80−62154
Cygni 1978 (V1668 Cygni), photoelec. photometry, rapid flickering 80−36640
Cygni 1978 (V1668 Cygni), post-max. short period oscills., photoelectric photometry 80−82380
Cygni 1978 (V1668 Cygni), spectrographic obs. around max. brightness *(French)* 79−58343
Cygni 1978 (V1668 Cygni), spectroscopic and photometric obs., (1978 to 1979) *(Russian)* 80−109444
Cygni 1978 (V1668 Cygni), UBV light curve 80−46565
Cygni 1978 (V1668 Cygni), UV spectrum, emission lines 79−62837
Cygni 1978 (V1668 Cygni), visual mag. estimate (1979 April 25) 79−53824
Cygni 1978 (V1668 Cygni), visual magnitude estimates, 1978 Nov.-1979 Apr. 79−48819
Cygni 1978 (V1668 Cygni), visual magnitude estimates, 1979 June 79−80324
Cygni 1978 (V 1668 Cygni), spectral development 80−51789
V1500 Cygni (Nova 1975), visual magnitude estimates (1977 May-Aug.) 77−82230
V1500 Cygni (Nova Cygni 1974), periodicities and rapid line variability 77−33524
V1500 Cygni (Nova Cygni 1975), IR photometry and spectroscopy 77−53599
V1500 Cygni (Nova Cygni 1975), spectroscopic obs. of coronal line phase 77−33504
V1500 Cygni (Nova Cygni 1975), UBV photometry 77−33525
V1500 Cygni (Nova Cygni 1975), UBVRI photometry 77−33509
V1500 Cygni (Nova Cygni 1975), visual magnitude estimates (1977, April-May) 77−53610
HR Delphini, determ. of mass of ejected nebula 77−74068
HR Delphini, two-colour diagram 79−71042
Delphini 1967, central star props. and envelope ionisation conditions *(French)* 77−53603
Delphini 1967, emission line spectrum *(Russian)* 78−16440
Delphini 1967, He I triplet lines *(French)* 77−56939
Delphini 1967, spectrophotometry in 3400 to 6500 A range 78−16430
Delphini 1967 (HR Delphini), cataclysmic binary spectrum 80−4359
Delphini 1967 (HR Delphini), emission line spectrum peculiarities 79−35280
Delphini 1967 (HR Delphini), emission lines at nebular stage *(Russian)* 80−17597
Delphini 1967 (HR Delphini), envelope, photoionization models in nebula stage, 1969 June-July 79−62835
Delphini 1967 (HR Delphini), He I radial vel. var. 77−82249
Delphini 1967 (HR Delphini), models of envelope ionization 77−87439
Delphini 1967 (HR Delphini), photoionisation models, binary system evolution 80−17590
Delphini 1967 (HR Delphini), photoionisation models of envelope in nebular stage, obs. data 78−61864
Delphini 1967 (HR Delphini), physical conditions in envelope at max. light 78−24519
Delphini 1967 (HR Delphini), physical conditions of different regions of envelope 80−4369
Delphini 1967 (HR Delphini), physical props. and element abundances in nebular state 78−36573
Delphini 1967 (HR Delphini), premax. and principal absorpt. line systems in spectrum 79−35279
Delphini 1967 (HR Delphini), premax. outflow 80−82378
Delphini 1967 (HR Delphini), radio emission from expanding shell 80−26868
Delphini 1967 (HR Delphini), short period light vars. from UBV photometry 80−67744
Delphini 1967 (HR Delphini), short period photometric vars. obs. 79−44503
Delphini 1967 (HR Delphini), simultaneous X-ray, UV and optical obs. 80−109440
Delphini 1967 (HR Delphini), spectra, line ident., radial vels. 80−17594
Delphini 1967 (HR Delphini), spectral evolution during decline 77−87440
Delphini 1967 (HR delphini), spectral evolution during decline period 78−40957
Delphini 1967 (HR Delphini), spectroscopic orbit 79−44510
Delphini 1967 (HR Delphini), UV spectrum, stellar wind 80−26880
Delphini 1967 (HR Delphini) circumstellar envelope props. *(Russian)* 78−77564
Delphini 1967 (HR Delphini) premax. envelope conditions 78−24518
Delphini (1967), photoelectric and spectrographic obs. 78−20844
dust formation and ionisation in nova envelopes, theory 80−98678
novae continued
dust formation time scale 77−67093
dust grains, IR spectra and props 80−26943
dust grains surrounding source, effect on nova model 80−105324
dusty circumstellar envelopes *(French)* 77−56940
dwarf nova brightening, magnetic fields and outburst phenomena *(Afrikaans)* 78−32481
dwarf nova outbursts, colour vars. 80−46576
dwarf novae, cataclysmic variables, review of spectroscopic and photometric obs. 77−56959
dwarf novae, eruption types and superhumps, obs. 79−75212
dwarf novae, EUV obs. from Apollo-Soyuz Test Project 78−93252
dwarf novae, hard X-ray emission from 47 objects 78−93275
dwarf novae, HEAO-A2 soft X-ray survey during optical outburst 80−46574
dwarf novae, mass transfer instabilities and accretion disk structure 77−82243
dwarf novae, mass transfer instability in semidetached binary systems 78−8047
dwarf novae, nature, H accretion, mag. field, radiation mechanisms *(Russian)* 78−93277
dwarf novae, outbursts, accretion model 79−88680
dwarf novae, photometry of rise to max. and decline 77−9753
dwarf novae, quasi-periodic oscills. and nonradial pulsations of accretion disks 80−46568
dwarf novae, quasiperiodic luminosity vars. 79−80311
dwarf novae, rapid brightness oscills. obs. 78−40968
dwarf novae, review 77−78799
dwarf novae, satellite UV obs., temp. calc. 77−57033
dwarf novae, search for light oscills. during outbursts 78−40966
dwarf novae, soft X-ray emission 77−45457
dwarf novae, spectra *(Russian)* 80−8638
dwarf novae, spectrophotometry, 1250-7500 Å region 80−46577
dwarf novae, X-ray emission 79−67031
dwarf novae and possibly related objects, IR photometry 78−8015
dwarf novae binaries, theory 77−56962
ejecta, dust grains sudden nucleation and growth 80−26941
emission line asymmetry 79−101214
envelope, grain formation 77−82254
envelope collisions model, dynamics of transition from premax. to principal spectrum 78−8025
envelope model and total energy considerations 77−82250
envelopes, CNO composition 77−87453
evolution from white dwarf binary system 80−109465
expanding dust shells, IR obs. 77−41404
expanding shells, matter-bound or radiation-bound 77−64780
expansion before light max. and principal envelope formation 77−87436
explosions, Rayleigh-Taylor instability 78−36551
extragalactic distance indicators 78−93396
fast nova model evolution from pre-explosion to decline 79−35273
fast nova occurrence, mechanism for envelope C enhancement 80−85936
flare-ups theory, exact analytic self-similar solns. for shock waves 79−35269
galactic nova, discovery in Curtis Schmidt thin prism survey of extragalactic emission-line objects 78−28538
U Geminorum, 1978 February magnitude estimates 78−36589
U Geminorum, dwarf nova, M-type dwarf companion spectral type 79−62851
U Geminorum, dwarf nova, radial vels. from emission line obs. 77−57029
U Geminorum, dwarf nova, spectrophotometric parallax 79−67012
U Geminorum, dwarf nova, visual magnitude estimates, (1979, March 23 to 24) 79−44501
U Geminorum, dwarf nova, visual magnitudes during outburst, (1980 May 6 to 9) 80−72978
U Geminorum, eclipsing binary dwarf nova, times of minima 77−22267
U Geminorum, HEAO 1 obs. of hard X-rays 79−21299
U Geminorum, HEAO obs. of low-energy X-ray emission 79−21298
U Geminorum, magnitude estimates for 1978 Oct. 78−96493
U Geminorum, model of disk and accreting stream 77−82246
U Geminorum, period-amplitude relationship for dwarf nova 77−91545
U Geminorum, radial vel. meas., rot. accretion disc and hot spot model 77−33561
U Geminorum, soft X-ray emission and visual magnitude estimates 77−91544
U Geminorum, V mag., primary eclipse and visual mag. estimates 79−44505
U Geminorum, visual magnitude estimates during outburst (1980 Oct.) 80−109439
U Geminorum, visual magnitudes for 1978 Jun. 78−65627
in globular clusters, intracluster gas heating and nova driven winds 78−57596
grain formation in ejected envelopes 77−91548
Harvard Photographic Collection, recent novae and variable star research 78−32486
HD 245770 (BD+26°883=A0535+26), spectroscopic obs. 77−87577
HDE 245770, spectroscopic obs. of X-ray nova Ariel 0535+26 optical counterpart 77−45450
AH Herculis, dwarf nova, changes in rapid oscills. during outburst 79−88686
AH Herculis, dwarf nova outburst, rapid oscills. evolution 80−94805
DQ Herculis, emission lines phase depend. in accretion disc 77−74095
AM Herculis, highly magnetised, accreting white dwarf 77−49396
DQ Herculis, photometric study of light curve 71 s oscill. 78−93259
DQ Herculis, X-ray obs. from Ariel 5 satellite 77−37671
Herculis 1934 (DQ Herculis), eclipsing binary, emission line eclipse phenomena 80−94800
Herculis 1934 (DQ Herculis), extended nova shell spectra 78−93253
Herculis 1934 (DQ Herculis), high time resolution spectrophotometry 80−22017
Herculis 1934 (DQ Herculis), light curve and double maxima 77−82255
Herculis 1934 (DQ Herculis), short-period oscills. modulation and pulsed emission lines asymmetry interpretation 80−22044
Herculis 1934 (DQ Herculis), UBV photometry of visual binary 80−8661
Herculis 1934 (DQ Herculis), white dwarf rot. period rel. to nova remnant shape 80−105244
Herculis 1960 (V446 Herculis), ejecta He abundance 79−92775
Herculis 1963 (V533 Herculis), 63 sec. oscill., UBV photometry 80−17592
Herculis 1963 (V533 Herculis), periodic light oscills. obs. 78−93285

novae continued
DQ Herculis (Nova 1934), masses of interactive binary 79−97029
DQ Herculis (Nova 1934) He II 4686 Å line phase shift from spectrophotometry 79−21296
historical novae, Latin terminology 80−62437
historical records, possible supernovae amongst comet and nova descriptions 77−2448
hot CNO nucleosynthesis, $^{18}O/^{17}O$ abundance ratio 77−78767
EX Hydrae, 2:3 period ratio in light curve 80−46580
EX Hydrae, dwarf nova, identification with high galactic latit. X-ray source (4U 1249−28) 80−22118
EX Hydrae, dwarf nova, IR and optical light curves 80−67747
EX Hydrae, dwarf nova lightcurve, periodic and secular vars. 80−77413
EX Hydrae, eclipsing binary dwarf nova, times of minima 77−22267
EX Hydrae, soft X-ray emission during optical quiescence, HEAO-A2 obs. 79−71054
EX Hydrae, spectra of dwarf nova 80−98670
EX Hydrae, U Geminorum type star, possible counterpart of (4U 1249-28) 78−36729
VW Hydri, colour variations during dwarf nova outbursts 80−46576
VW Hydri, dwarf nova, IR light curves 80−67747
VW Hydri, dwarf nova, light curve superhumps model 80−4381
VW Hydri, dwarf nova, model 79−16977
WX Hydri, dwarf nova, obs. of superhumps during supermaximum 79−88677
VW Hydri, dwarf nova, short period light oscills. 78−20837
VW Hydri, light curves of dwarf nova 78−12245
VW Hydri, outbursts of dwarf nova, long and short eruptions comparison 79−88669
IR emission by dust grains near variable primary sources 79−44358
KUV09313+4052, variable UV excess object and possible dwarf nova, discovery 80−62159
Lacertae 1936 (CP Lacertae), ejecta He abundance 79−92775
X Leonis, period-amplitude relationship for dwarf nova 77−91545
light curves, as manifestation of nonuniform stellar wind 80−62160
light echoes, obs. of seven galactic novae 78−12246
line transfer, Monte Carlo calcs. 79−48902
in LMC, discovery and spectrum 79−8931
in LMC, discovery confirmation, magnitude, photometric obs., premax. spectra 78−49456
in LMC, discovery obs. 77−33513
LMC, discovery of nova near HV 12080 (1977, February 26) 77−37605
in LMC, IR obs. with HJKL filters 77−33518
in LMC, photometric obs. 77−60769
LMC, probable nova discovered 1978 March, position and magnitude 78−45341
LMC 1977b, photometry, light curves, distance modulus 78−8019
LMC 1977b, VBLUW photometry, absolute magnitude, distance and reddening 79−58342
LMC nova, UBV photometric meas. (1977, March-April) 77−53608
LS55° −8, high-speed photometric obs. of new nova-like variable 78−57565
AY Lyrae, soft X-ray emission detect. from dwarf nova, H1839+37 79−75227
Magellanic Cloud (LMC) nova, premaximum spectrum 79−62853
magnetic field generation by close binary interaction 80−26903
magnetic white dwarf in binary system, collapse, mass ejection, nova mechanism 78−32485
maximum of outburst as opportunity for mutual CETI search strategy 80−56723
model evolution with Z=0.03 envelope 77−82265
V616 Monocerotis, spectroscopic obs. of X-ray nova, Ariel 0620−00 optical counterpart 77−45450
Monocerotis 1975 (Ariel 0620−00), linear polarisation obs. 77−13351
Monocerotis 1975 (V616 Monocerotis=A0620−00), 8-day modulation 77−87442
Monocerotis 1975 (V616 Monocerotis=A0620−00), spectral characts. 77−87443
Monocerotis 1975 (V616 Monocerotis=A0620−00), spectroscopic obs. 77−82257
Monocerotis 1975 (V616 Monocerotis=A0620−00), X-ray and visible light curves 77−82331
Monocerotis 1975 (V616 Monocerotis=A 0620−00), UBV photometry *(Russian)* 79−58360
Monocerotis 1975 (V616 Monocerotis=A 0620-00), UBV photometry 80−56846
Monocerotis 1975 (V616 Monocerotis), photographic photometeric obs. 78−36587
Monocerotis 1976 (Ariel 0620−00), Ariel 5 obs. of decay 77−29950
V616 Monocerotis (A0620-00), light curve 77−64777
V616 Monocerotis (Ariel 0620-00), distance from interstellar colour excess 77−64744
V616 Monocerotis (Nova 1975=A0620−00), spectroscopic obs. 77−87577
MXB 1730−335, comparison with dwarf novae rel. to neutron star model 78−12410
nebular stage, abundance determ. methods 77−87279
nebular stage, collisional spectrum development 77−87441
in NGC 5272, photometry and identification as W Virginis variable 79−75224
in NGC 5272 (=M3), discovery, V mags. and spectrum 79−71050
nonejecting novae as EUV sources 78−12238
IM Normae (Nova 1920), recovery, spectral obs. of faint candidate stars 79−71058
novae, spectrophotometric estimate of electron density in rapidly rot. accretion discs 79−16968
novae and related stars, conf. (Paris, 7-9 Sept. 1976) 77−82240
nucleosynthesis, by n-process of neutron capture 77−2336
nucleosynthesis induced during outburst 77−82263
old novae, search for rapid photometric oscills. 78−4251
RS Ophiuchi, recurrent nova, spectrum obs. 79−62848
Ophiuchi 1976, precise position 77−2444
Ophiuchi 1977, identification with X-ray transient 77−91540
Ophiuchi 1977, X-ray intensity on 1978 Mar. 9 78−40961
Ophiuchi 1977, X-ray transient, positions and independent discoveries 77−82234
Ophiuchi 1977 (H1705−25), X-ray light curve 78−49453
Ophiuchi 1977 (H1705−25), X-ray nova, HEAO 1 obs. 78−49452
optical and Z-ray novae, comparison 79−58350
optically thick time-dependent wind model for postmax. phase 79−12476
optically thick winds in classical novae 77−87450

novae continued
optically thin winds struct. in classical novae 80−36643
outburst, equatorial belt formation, plasma current rings model, double adiabatic MHD 80−67757
outburst models 77−82248
outbursts, effect of binary companion 80−82394
p-nuclei, low-temp. photonuclear nucleosynthesis in degenerate H burning zones 78−57540
RU Pegasi, dwarf nova, rapid and ultrarapid light vars. 77−53596
RU Pegasi, radial vel. of dwarf nova 79−62833
AG Pegasi, symbiotic binary system, UV and optical spectrum rel. to nature of components 80−109449
AG Pegasi, symbiotic nova, radio emission obs. 77−22232
KT Persei, dwarf nova, brightness oscills. during two outbursts 77−2438
UV Persei, dwarf nova, characts. of outbursts 79−71052
Gk Persei, visual magnitude estimates (1978 July) 78−69809
GK Persei, X-ray outburst detect. from old nova 79−67033
Persei 1901 (GK Persei), nearly new X-ray source (Ariel 0327+43) discovery 78−69910
Persei 1901 (GK Persei), visual magnitude estimates for 1978 Jul. 78−73718
Persei 1974 (V400 Persei), spectral evolution 78−73715
GK Persei (Nova 1901), visual magnitude estimate for 1978 July 78−69807
V400 Persei (Nova Persei 1974), photoelectric obs. 78−4252
PG 2337+12, high latitude blue variable, possible old nova 77−22241
photometry of nova-like variables 77−82245
RR Pictoris, accretion disc radiation of cataclysmic binary 77−91537
Pictoris 1925 (RR Pictoris), spectrophotometry of surrounding filaments, abundances, ionization 79−40194
RR Pictoris (Nova 1925) 77−82247
piston problem, one-dimensional, in non-ideal gas, time-dependent soln. 80−82185
polytropic envelopes, thermal wave propag. *(Russian)* 77−82213
Population II stars in M31 and Galaxy 79−30074
potential novae and kinds of objects 77−82241
prenova model with shell in thermal imbalance, pulsational stabilities 78−45316
prenovae and outburst amplitudes, physical parameters 77−87437
BX Puppis, cataclysmic variable, possible member of Hyades-like cluster (NGC 2482) 80−31289
VV Puppis, dwarf nova, spectroscopic obs., broad absorpt. features discovery 79−44502
VV Puppis, dwarf nova, spectroscopic obs. during active phase 79−80322
Puppis 1942 (CP Puppis), soft X-ray emission detect. 79−80325
T Pyxidis, recurrent nova, photoelectric obs. 78−4252
radio emission from nova shells, review of obs. 80−26868
recurrent, magnitude-frequency relation 78−28699
recurrent novae and symbiotic stars, survey at 1612 MHz 80−12774
relativistic particle generation 77−74062
remnants shapes, effects of white dwarf rotation 80−105244
review of 50 years research 78−4239
WZ Sagittae, 1978-9 outburst of dwarf nova, spectra 80−94801
WZ Sagittae, B mags. and total visual magnitude estimates 79−21308
WZ Sagittae, BV photometry and magnitudes (1978 Nov.-Dec. outburst) 79−12484
WZ Sagittae, eclipsing binary, outburst of December 1978, UV obs. 80−72982
WZ Sagittae, eruptive binary, model from hot spot eclipses anal. 80−72962
WZ Sagittae, image-tube spectroscopic obs. of 1978 Dec. outburst 80−72958
V Sagittae, light curve coherent oscills. 78−8022
WZ Sagittae, orbital parameter determ. for recurrent nova 78−93317
WZ Sagittae, period change and magnitudes (1978 Dec.-1979 Jan.) 79−21309
V Sagittae, periodicity disclaimed due to telescope periodic drive error 79−92763
WZ Sagittae, physical parameters from eclipse anal. 79−80336
WZ Sagittae, recurrent nova, IUE obs. in outburst 80−109448
WZ Sagittae, recurrent nova, light curve superhumps model 80−4381
WZ Sagittae, recurrent nova, photometric study at minimum light 78−24513
WZ Sagittae, recurrent nova, physical parameters, present state, past and future evolution 78−85948
WZ Sagittae, recurrent nova, spectroscopic obs. and model for superhump phenomena 80−82368
WZ Sagittae, recurrent nova, spectroscopic obs. during 1978 outburst 80−26862
WZ Sagittae, recurrent nova, spectroscopic study during 1978 outburst 80−56849
WZ Sagittae, spectroscopic obs. (1978 December 1 and 2) 79−16983
WZ Sagittae, spectroscopic obs. and photoelectric V-magnitudes 79−16984
WZ Sagittae, time of minimum light, period, magnitudes 79−21353
WZ Sagittae, time-resolved broadband obs., optical pulsations, period 79−92781
WZ Sagittae, UBV photometry and spectroscopy of 1978 Dec. outburst 79−12483
WZ Sagittae, visual magnitude 1979 April 8 79−44508
WZ Sagittae, visual magnitude estimate 1979 June 20 for recurrent nova 79−84800
WZ Sagittae, visual magnitude estimates, 1978 Nov., 1979 Jan.-Feb. 79−30075
WZ Sagittae, visual magnitude estimates, (1978, November 28 to December 11) 79−12481
V1500 Sagittae, visual magnitude estimates 1977, Feb. and Mar. 77−37607
Sagittae 1977, discovery obs. 77−9759
Sagittae 1977, precise position, photographic and visual magnitudes 77−17602
Sagittae 1977, spectral obs., visual magnitude estimators 77−22253
Sagittae 1977, visual magnitude estimate 77−17601
Sagittae 1977, visual magnitude estimates 77−60768
Sagittae 1977, visual magnitude estimates 1977, FEb. and Mar. 77−37607
Sagittae 1977, visual magnitude estimates (1977, April-May) 77−53610
Sagittae 1977, visual magnitude estimates (1977 Aug.-Oct.) 78−8021
Sagittae 1977, visual magnitude estimates (1977 January-February) 77−29853

novae continued
Sagittae 1977, visual magnitude estimates (1977 June 26-July 27) 77−74064
Sagittae 1977, visual magnitude estimates (1977 November 6 to 1978 January 7) 78−36593
Sagittae 1977 (HS Sagittae), visual magnitude estimates, (1978, August 5 to September 3) 78−89209
Sagittae 1977 (HS Sagittae), visual magnitude estimates 78−61872
Sagittae 1977 (HS Sagittae), visual magnitude estimates 1978 June 78−85961
V1017 Sagittarii, recurrent nova, decline obs. 77−82233
Sagittarii 1974 (V3888 Sagittarii), line identifications and radial vels. 77−22246
Sagittarii 1977, discovery report 77−33516
Sagittarii 1977, early spectrum 78−32496
Sagittarii 1977, image-tube spectra (April 1977) 77−41384
Sagittarii 1977, IR obs., high temp. dust shell form., visual magnitudes 77−60766
Sagittarii 1977, photometry, spectrum, absolute magnitude and distance 78−53955
Sagittarii 1977, position and visual magnitude estimates 77−33519
Sagittarii 1977, UBV photoelec. obs. (1977, March-April) 77−53607
Sagittarii 1977, visual magnitude, UBV and Hα obs. (1977, March) 77−33517
Sagittarii 1977, visual magnitude estimates (1977, April-May) 77−53610
Sagittarii 1977, visual magnitude estimates (1977, Aug.-Oct.) 78−4246
Sagittarii 1977, visual magnitude estimates (1977 June 12-Aug. 2) 77−74064
Sagittarii 1977 (V4021 Sagittarii), visual magnitude estimates for 1978 May and July 78−69806
Sagittarii 1978, discovery on 1978 April 7, position, Balmer emission lines 78−45342
Sagittarii 1978, identified with IRC −20494=V3876 Sagittarii, IR obs. 78−49459
Sagittarii 1978, precise position, visual magnitude estimates 1978 Apr. 78−49458
Sagittarii 1978, probable nova magnitudes (1978 June 30 to October 3) 79−101164
Sagittarius, discovery of probable declining nova (1978 March) 80−4376
U Scorpii, 1979 March outburst, visual magnitude estimates 79−44504
U Scorpii, magnitudes and UBVRI photoelectric obs. of 1979 June outburst 79−71049
U Scorpii, probable identification at minimum 78−45343
U Scorpii, recurrent nova, 1979 March outburst unconfirmed 79−44506
U Scorpii, recurrent nova, spectroscopic obs. during outburst 79−75225
Scorpius X-1, extended X-ray obs. with Bragg crystal spectrometer 79−12543
VY Sculptoris, novalike variable, precise position 80−101597
Scuti 1975, spectrum, line identifications 78−45335
Scuti 1975, UBVRI photometry 77−33520
Scuti 1975 (V373 Scuti), spectral evolution 78−73715
V373 Scuti (Nova 1975), VBLUW photometry, absolute magnitude, distance and reddening 79−58342
searching, projection blink comparison method 79−12407
RT Serpentis, symbiotic star/nova, possible H_2O maser obs. 79−8932
FH Serpentis, two-colour diagram 79−71042
Serpentis 1909 (RT Serpentis), spectrum in 1964, 1975 and (1978) 80−46566
Serpentis 1970, search for gamma ray lines 78−8013
Serpentis 1970, thick inhomogeneous shell model for radio emission 78−12236
Serpentis 1970 (FH Serpentis), dust grain IR emission model 80−105254
Serpentis 1970 (FH Serpentis), outburst model test 77−82253
Serpentis 1970 (FH Serpentis), radio emission from expanding shell 80−26868
Serpentis 1978, discovery obs. 78−36594
Serpentis 1978, evolution of dust shell 80−90430
Serpentis 1978, image tube spectrograms, emission lines 78−40964
Serpentis 1978, IR magnitudes and BVR photometry 78−65629
Serpentis 1978, IR photometry 80−4365
Serpentis 1978, precise position, spectra, visual magnitude estimates 78−36596
Serpentis 1978, UBV photoemtry, visual magnitude estimates, spectrographic obs. 78−40963
Serpentis 1978, UBV photometry and magnitude estimates 78−40959
Serpentis 1978, VBLUW photometry, absolute magnitude, distance and reddening 79−58342
Serpentis 1978, visual magnitude estimates 1978 Mar.-Apr. 78−49457
Serpentis 1978, visual magnitude estimates (1978 April) 78−53959
Serpentis 1978, visual magnitude estimates (1978 April-June) 78−61873
shell ejection in nova outbursts, time before max. 77−2441
shell ejection timing in nova outbursts 77−82252
shell expansion and IR brightening, model 79−97007
shell ionisation, time-depend. model 79−53816
shells, structural development theory 77−64746
slow deflagration front stability at degenerate star surface 80−67729
slow nova, evolution of model with Z=0.03 envelope from pre-explosion to extinction 78−32468
slow nova, hydrodynamic study of outburst 78−40954
slow nova with 1.25 M⊙ white dwarf model 77−82264
slow novae and symbiotic stars, late-type components spectral classifications 80−94813
slow recurrent novae, relationship to type II symbiotic stars 80−62144
southern dwarf novae, image tube spectra 77−56960
space density, recurrence rate and classification 78−53964
Star of Bethlehem, Far East record searches 80−17507
Star of Bethlehem, possible nova in 5 BC 78−32365
Star of Bethlehem, role of comets/novae in 5 and 4 BC 79−67136
supercritical accretion discs winds struct. and appearance, numerical models 80−21984
surface nucl. reactions and origin of mag. fields 80−101616
symbiotic stars, obs. of unidentified bands at 6830 and 7088 Å 80−46573
symbiotic stars and recurrent novae, high speed photometry 77−60799
Tauri 396 AD (V471 Tauri), identification of possible outburst *(Russian)* 79−101162
RR Telescopii, C III spectral lines, IUE obs. 79−71089
RR Telescopii, cm wavelength radio emission detect. 77−17573
RR Telescopii, slow nova, evolution of nebular spectrum 77−60771

novae continued
RR Telescopii, slow nova and symbiotic stars 77−82256
thermonuclear runaway model of nova outburst, review 77−82262
thermonuclear runaways in white dwarf envelopes 77−56961
transient thermal X-ray emission from shocked circumstellar gas 77−45437
transition zone oscillations, inception 77−87402
RW Trianguli, nova-like binary star, eclipse timings 79−21357
RW Trianguli, nova-like eclipsing binary radial vels., dimens. from visible spectra 80−82418
EK Trianguli Australis, peaks in lightcurve during 1979 June outburst 79−75222
EK Trianguli Australis, SU Ursae Majoris dwarf nova, superhumps, light curve UBV obs. 80−105255
UBV obs. and two-colour method appls. 79−71042
UX Ursae Majoris, anomalous 1977 period change for nova-like eclipsing binary 78−85956
SU Ursae Majoris, period-amplitude relationship for dwarf nova 77−91545
AN Ursae Majoris, polarisation of AM Herculis-type nova-like binary 78−85958
SU Ursae Majoris, probable 1980 March super outburst 80−51785
SU Ursae Majoris, soft X-ray halo around dwarf nova 80−98677
SU Ursae Majoris stars, important sub-group of dwarf novae, photometric props. 80−101596
V3888 Sagittarii (1974), photometry during decline stage 78−20836
Vulpecula, novalike object, 1980 May-June spectra and magnitudes 80−82392
Vulpecula, novalike object, UV decline and expanding cooling photosphere 80−67741
Vulpecula, novalike object visual magnitude estimates (1980 February 2 to May 9) 80−72980
Vulpecula 1976 (NQ Vulpeculae), isothermal dust condensation phase, broad-band photometry 78−36586
Vulpecula novalike object, photometry, June 1980, and spectral classification 80−94807
LV and NQ Vulpeculae, two-colour diagram 79−71042
NQ Vulpeculae, visual magnitude estimates 1977, Feb. and Mar. 77−37607
NQ Vulpeculae, visual magnitude estimates (1977 January-February) 77−29853
Vulpeculae 1968 No.1 (LV Vulpeculae), spectroscopy 77−87438
Vulpeculae 1976, Hα emission line profile variations *(Russian)* 77−74074
Vulpeculae 1976, IR energy distrib. 1976, Nov./Dec. 77−9757
Vulpeculae 1976, IR spectrum *(Russian)* 78−16441
Vulpeculae 1976, magnitudes and photoelectric obs. (1976 October-November) 77−5538
Vulpeculae 1976, photoelec. obs., visual magnitude estimates 77−33533
Vulpeculae 1976, photoelectric V measures and visual magnitude estimates 1976, Dec. 77−17600
Vulpeculae 1976, polarisation meas., reddening and distance 77−29855
Vulpeculae 1976, polarization and magnitude obs. 1976, Nov. 77−2442
Vulpeculae 1976, spectra and light curve 77−33510
Vulpeculae 1976, spectra in range .38 to 1.12 microns *(French)* 77−53606
Vulpeculae 1976, spectrograms and photoelectric V obs. 1976, Oct. and Nov. 77−2443
Vulpeculae 1976, visual magnitude estimates 1976 Nov.-Dec. 77−17598
Vulpeculae 1976, X-ray emission upper limits, Ariel V data 77−64781
Vulpeculae 1976 (NQ Vulpeculae), CO emission and η Carinae stage 79−25609
Vulpeculae 1976 (NQ Vulpeculae), Hα emission line profiles in 1976 November to December *(Russian)* 78−40971
Vulpeculae 1976 (NQ Vulpeculae), Hα var. 79−58352
Vulpeculae 1976 (NQ Vulpeculae), IR photometry, dust form. in exploded shell 79−48832
Vulpeculae 1976 (NQ Vulpeculae), light, colour and vel. curves 78−28708
Vulpeculae 1976 (NQ Vulpeculae), photometric obs., visual magnitudes 77−60767
Vulpeculae 1976 (NQ Vulpeculae), spectral evolution 78−89205
Vulpeculae 1976 (NQ Vulpeculae), spectroscopic 79−21316
Vulpeculae 1976 (NQ Vulpeculae), spectroscopic obs. of slow nova 78−85955
Vulpeculae 1976 (NQ Vulpeculae), UV and visible spectra anal. *(Chinese)* 80−12770
Vulpeculae 1976 (NQ Vulpeculae), visual magnitude estimates 77−22254
Vulpeculae 1976 (NQ Vulpeculae), visual magnitude estimates for 1978 Aug.-Oct. 79−5839
Vulpeculae 1976 (NQ Vulpeculae), visual magnitudes, 1977 Nov.-1978 Jun. 78−65626
Vulpeculae 1976 (NQ Vulpeculae), visual magnitudes (1977 Aug.-Nov.) 78−16434
Vulpeculae 1976 (NQ Vulpeculae), visual magnitudes (1978 June 29 to July 13) 78−85959
Vulpeculae 1979, discovery on 1979 April 5, position, visual magnitude 79−44507
Vulpeculae 1979, photoelectric obs., (1979 April 21 and 25) 79−53822
Vulpeculae 1979, photometric history (1898 to 1978) 79−53819
Vulpeculae 1979, posn., magnitudes, spectrum and photometry 79−48818
Vulpeculae 1979, prediscovery obs. and visual magnitude estimates 79−48817
Vulpeculae 1979, slow nova, pre-maximum light curve 80−4364
Vulpeculae 1979, spectroscopic and photometric obs., (1958 and 1968) 79−58344
Vulpeculae 1979, spectroscopic and photometric obs., possibly exceptionally slow nova 79−48820
Vulpeculae 1979, visual magnitude estimate, (1979, May 2) 79−58348
Vulpeculae 1979, visual magnitude estimates, 1979 Jun. 79−75221
NQ Vulpeculae (Nova 1976), visual magnitude estimates (1977 June 20-July 27) 77−74064
NQ Vulpeculae (Nova Vulpeculae 1976), photoelectric obs. 78−4252
NQ Vulpeculae (Nova Vulpeculae 1976), visual magnitude estimates (1977, April-May) 77−53610
white dwarf surface accretion, thermal runaway, nova phenomenon 77−82222
white dwarfs, accreting, thermonuclear runaways 78−40937
white dwarfs, He flash and nova evolution 80−72938

novae continued
X-ray binary sources rel. to old novae 77−87576
X-ray nova at $\alpha=1^h14^m$, $\delta=+64.4^\circ$, discovery obs. 78−24515
X-ray novae, spectroscopic obs. of optical counterparts 77−45450
X-ray source in Norma, novalike increase, SAS-3 obs. 77−67142
X-ray transient sources, discoveries and obs., review *(Polish)* 77−17720
^{26}Al, synthesis in explosive H burning 80−85929
CNO nuclei enhancement in nova progenitors 77−33484
CNO nucleosynthesis 77−87452
SS Cygni, soft X-ray emission detect. during optical outburst 80−46574
Fe II, Fe III line emission in optical and UV, theory and anal. technique 77−13364
U Geminorum, soft X-ray emission detect. during optical outburst 80−46574
H-rich envelope mass 77−87451
Li/Na ratio upper limit 79−101156
^7Li, prod. in nova explosions 78−57555
^{15}N production, effects on $^{15}N/^{14}N$ ratio evolution 78−93201
^{22}Ne and ^{26}Al nucleosynthesis in novae and supernovae outbursts 80−62143

novoids *see novae*

nozzles
accelerating two-phase nozzle/diffuser flows, virtual mass effects on numerical stability 80−92204
acoustic disturbance from gas nonuniformities convected through a nozzle 78−34179
air bubbles, production, pulsation and damping, in dil. polymer solns. 80−69879
air ejectors in punch pressing operations, noise abatement methods 78−90600
air in supersonic nozzle, shock activation with overexpansion, jet form. 78−18330
air jet, heat transfer coeff. for quenching of hot plate 77−47053
air suction noise, separation flow theory 77−50832
airdroplet flight in air, drift loss from spray cooling pond, numerical estimation 80−19471
annular, design for supersonic flow generation *(French)* 77−7433
annular, swirled jet form., stream parameters at exit cross section 77−15090
anomalous glow discharge transition to nozzle hollow cathode discharge 78−67531
aortic stenosis, turbulent wall press. meas. in exptl. model 78−3538
arc nozzle clogging theory 80−38791
aspirating choked-nozzle probe for gas density meas., time response 77−84351
asymmetric nozzle, off-design regimes with supersonic inlet vel. 77−24009
atomic beam, produced from He nozzle flow, high speed ratio 80−5636
atomic beam production, He skimmed from freejet zone of silence 80−5635
atomisation of high-viscosity liqs. by parallel flow air-liq. nozzle *(Japanese)* 78−38385
axisymmetric afterbodies, separated turbulent flows, wakes, exhaust plume effects 80−74885
axisymmetric choked, transonic swirling flow analysis 77−58761
axisymmetric hypersonic nozzle. viscous gas flow calc. with departure from vibr. equilib. 80−33649
axisymmetric impinging jet, transfer characteristics at conical surfaces 77−3889
axisymmetric Laval nozzles, numerical flow study including overexpansion and breakaway 79−90304
beam expansion, Monte Carlo simulation 79−94675
boiling, expt. study of outflow from accelerating two-phase nozzle 78−1721
boundary layer equations for laser heated flow, similarity soln. 77−31355
bubble formation in flowing liq. 79−64741
bubbly liquid, choking phenomena in nozzle flows 77−62300
bubbly liquid, nozzle flow based on Wijngaarden's model 78−26182
buoyancy-induced flow stratification in cylindrical plenum 77−46366
cavitation pressure meas. to determ. mechanism of cavitation erosion in nozzle-type venturi 79−90298
cavitation regimes of a hot-water flow in a Laval nozzle 78−75181
centrifugal nozzle, similarity criterion and flow swirl ratio 77−24010
chamber-orifice interaction in bubble formation 77−89185
chemical and vibrational nonequilibrium flow, general formulation 79−7416
chemical laser, low pressure, line-shape flattening resulting from hypersonic nozzle wedge flow 80−91783
chemical laser nozzle, effect of geometry and boundary layers on flowfield 77−27622
chemical laser nozzle, gas flow 77−42529
chemical laser nozzle, TRW CL XV, fluid mechanical and optical analysis, LAMP and BLAZER code calcs. 79−98350
chemical laser resonator modelling, LAMP and BLAZER code calcs. comparison with CL XV meas. 79−36890
choked foam flow in convergent-divergent nozzle 80−74940
circuit breaking arcs, current zero arc model based on forced convection 80−33831
circular impinging jet, heat transfer characts., stagnation point, boundary layers 80−79303
circular semi-infinite liquid jet, harmonically forced at nozzle, instability and wave propagation 79−32618
cluster beam, nozzle flow formation and detection, high energy beam 80−5638
cluster formation, in rarefied nozzle flowfield 80−5639
coaxial air stream, self-oscillatory liquid film flow regime 79−86498
compressible and incompressible flows, recent theoretical and expt. developments, book 80−1620
compressible flow, variational principle and finite element method 79−46336
compressible gas flow through exhaust valve, analytical calc. using flux analysis method *(Japanese)* 80−69896
condensation, heterogeneous, in Lavale nozzle *(Russian)* 77−89007
condensing injector, optimal diffusor throat cross section dimensions 77−31356
condensing steam, method for calculating expansion 77−27573
conical, flow characts., obs. *(Russian)* 80−33650
conical annulus, turbulent exit vel. calc. method 77−55069

nozzles continued
conical nozzle and diffuser, laminar compressible boundary layer swirling flow 80−48768
constriction meter orifice, swirling flow component effect on discharge coeffs. 78−63514
control jets, gasdynamic features, 3-D subsonic and supersonic flows 80−6112
convective heat transfer, turbulent boundary layer regime 78−9670
convergent nozzles, swirl effects on mass flux and thrust 80−74936
convergent nozzles incorporated into gas flowmeter, comparison with standard 80−6126
convergent-divergent, flashing flow of initially subcooled water 77−80195
critical air flow, heat transfer, numerical study 79−98778
critical flow through axisymmetric nozzle, discharge coeffs. 78−38381
critical flow venturi nozzle, calibration in high pressure gas 79−68844
critical flow venturi nozzles, primary calibration in high pressure gas 80−53832
critical two-phase flow, multidimens. effects 79−14461
crystal resonator electrode deposition from nozzle beam type metal vapour source 77−40376
CW supersonic chemical laser, porous nozzle, chemically reacting boundary layer 80−100022
cylindrical nozzles with sharp upstream edges, critical flowmetering appl. 80−28546
DC arc in blocked nozzle, boundary layer integral method anal. 80−6295
DC arc in supersonic nozzle flow, appl. to gas blast circuit breaker 79−23469
degeneration of supersonic flow due to interaction of centered compression and rarefaction waves 80−69864
diatomic homonuclear molecules, vibr. relax. in nozzle expansions *(French)* 78−62877
die entry flow, kinematics and stability 79−60026
die swell problem, free surface separation 79−90295
different jet regimes, internal and external flows, separation and wakes 80−100023
diffuser, conical, swirl effect on press. recovery coeffs. 78−63474
discharge coefficients, boundary layer soln. 79−32626
dispersed supersonic two-phase flow, shock characts., droplet size depend. at nozzle 80−106815
dispersive compressible fluid, transonic nozzle flows 80−69895
drop formation hydrodynamics, macorencapsulation 80−64603
drop size in nozzle flow of moist water vapour 77−42904
dry vapour discharge theory, rel. to heat pipe performance 78−75033
duct, supersonic flow downstream oscillations from abrupt cross section increase, nozzles 80−74976
ducted and exhaust plume flow fields, computer anal. 79−7397
ejector nozzle starting parameters, press., calc. technique 79−37375
electric arcs in nozzle flow, high current, scaling characts. 78−59707
electrohydrodynamic convertor or nozzle for jet printer, output parameter exact solns. *(Russian)* 78−75230
ferroliquid, deviation of free flow by inhomogeneous mag. field 77−65800
flame, atm. press., ion sampling aerodynamic disturbance by sampling system 77−60142
flame, atm. press., supersonic sampling, boundary layer cooling 77−60143
flange tap orifice flowmeters, Stolz and ASME-AGA orifice eqns., lab. data comparison 80−64604
flat and axisymmetric, supersonic flow calc. method for arbitrary inlet gas props. 77−68657
flow visualization using two-phase flow 80−33714
flowmeter calibration method using sonic nozzles *(Japanese)* 77−65821
flows with vibrational relaxation, sudden-freezing analysis 77−58806
foam flow, choked, in convergent-divergent nozzle 79−64750
free jet development, turbulence effects *(German)* 77−84291
free surface flows from nozzle at low Reynolds number 80−43758
friction area and nozzle area as flow parameters 77−42895
gas binary mixtures, flowing, probe for conc. meas. 79−4098
gas blast circuit breakers, three nozzle arc models, review 79−27862
gas blast flow with arc heating 79−46502
gas curtain thermal protection, supersonic nozzle, vel. gradient 78−51215
gas ejector, energy separation mechanism *(Russian)* 78−34178
gas ejector, inverse energy separation 78−47013
gas ejector, with slotted nozzle, effect of viscosity on limiting performance 77−27572
gas flow in duct, self-excited oscillations 78−55670
gas flow into duct, self-excited oscillations 80−33647
gas flow parameters in Laval nozzles and curvilinear channels, 1-D theory 80−6124
gas flow rate standard appl., characts. *(Japanese)* 77−39375
gas flow with particles, nonsymmetric 2D nozzle, nonuniform wear 77−47075
gas injection technique, rapid response, design 78−94865
gas jet blowing into supersonic flow without 3-dimens. boundary layer separation, nozzle shape 80−100009
gas jet expsn. into vacuum, rot. relax. 79−32625
gas jet-liquid bath interaction for different degrees of assimilation during blowing 80−43754
gas mixture in quasi-one-dimens. flow, vel. slip and temp. difference 79−64735
gas mixtures with vibr. relax., nozzle flow 79−64727
gas of variable density, channel flow, discontinuity evolution 77−58734
gas turbine, noise, acoustic disturbance propagation in gas stream anal. *(Russian)* 79−32131
gas-film cooling efficiency in supersonic axisymmetric nozzles 79−98715
gas-liquid bubble flow accelerating in nozzle, slipping of phases *(Russian)* 77−35202
gas-liquid nozzle design, inverse problem formulation 78−47015
gas-liquid swirl nozzle, gas dispersion, discharge coeff. 77−89187
gas-liquid system discharging from nozzle, phase slip *(Russian)* 77−55067
gasdynamic laser flow, vibr. wall accomm. for CO_2-N_2-H_2O 79−98340
gasdynamic laser nozzle wake, flowfield props. boundary layers 80−24027
gasdynamic laser resonator cavity, flow fields and amplification coeffs., 2-D calc. 80−5722
gases, thermal shock prod. with conc. solar energy *(French)* 78−91056
halogens, supersonic atomic and mol. nozzle beam source 77−31028

nozzles continued
Hartmann-Sprenger tube, air jet from convergent nozzle, air column oscillations generative mech. 80−14828
heat exchange between two-phase flow and nozzle wall with condensate film 79−46357
heat flux determ. using computer 77−42894
heat fluxes, nonstationary meas. method using probe 77−42942
heat transfer in aerodynamic-tube nozzles 80−24068
heat transfer in turbulent boundary layer, subsonic and supersonic 79−1229
heat transfer of transonic air flow 79−1230
heavy isotope separation using nozzles, jets and channels, investig. 79−94097
helical gas stream from nozzle, quasi-one dimens. theory 79−64734
high pressure flow, importance in gas turbines and circuit breakers *(Spanish)* 79−98781
high subsonic nozzle flows, pressure waves from convection of temp. disturbances 80−6125
high-velocity gas jets, interaction, photographic study 78−42695
highly viscous chemical laser nozzles flow, two dimens. Navier Stokes eqns., implicit marching method 78−63506
holographic shearing interferometer for recording of pulsed gasdynamic processes 77−47117
holographic shearing interferometer with narrow ref. beam for flow investig. in reflecting nozzle of shock wave 77−47118
hydraulic characts., measurement precision 79−82004
hydrocarbon vapour, spontaneous condensation in submerged turbulent jet 79−64721
hyperbolic Laval nozzles, transonic flow in throat region *(Chinese)* 80−6122
hypermixing nozzle in thrust augmentor, three dimens. turbulent mixing 78−51214
hypersonic, tunable dye laser meas. 77−68719
hypersonic, viscous flow 79−64733
hypersonic conical nozzle, boundary layer separation from compression shock 80−48766
hypersonic flow, vibr. relax. in air 79−68781
hypersonic flow from high enthalpy supersonic flow 80−74937
hypersonic nozzle boundary layer, static press. variation and Reynolds stress 77−84294
hypersonic wind tunnel, flow core relative area, nozzle similitude ratios 80−48747
ideal gas flow, choked and supercritical, through orifices and convergent conical nozzles, numerical soln. 80−38474
ideal gas flow in tapering nozzles 79−81944
ideal gas in ejector nozzles, theory of combined flow of high/low pressure streams 80−6123
ideal radial free jet, nozzle length effects 80−14768
immersed nozzle, liq. gas discharge processes 78−83451
impactor performance, effect of boundary layers 77−60133
injector with distrib. multijet liquid supply, efficiency and performance 80−74939
ink jet nozzle flow, 100:1 scaled-up model 77−75957
internal gas flow anal. by large particles method *(Russian)* 78−79355
internal profiling of the nozzles of model systems 80−92198
isotope separation by laser photochemistry in nozzle flows with heterogeneous condensation 80−50862
jet, meas. of plane-wave noise radiation 77−58758
jet, turbulent, radial, flow at and after attaching point 79−37369
jet-generating nozzle system, hydraulic characts. 77−84295
jets, two-dimensional water, sensitive to sound, behaviour *(Japanese)* 80−79376
laminar boundary layer effect on jet turbulence 77−55065
laminar boundary layer swirling flow with heat and mass transfer in conical nozzles and diffusers 79−81842
laminar compressible boundary layer swirling flow in nozzle, flow and heat tranfer 78−94795
laminar compressible boundary layers for laser heated swirling nozzle and diffuser flow 80−53831
Langley expansion tube, flow characts. from vel. meas., He, CO_2, air 78−14057
laser, chemical, pressure recovery, 1D flow model, comparison with DF laser results 77−71979
laser evaporation of target, nozzle for impulse augmentation 79−23439
laser heated nozzle flow with swirl, axisymmetric comp. boundary layer 80−14775
laser-heated H_2 rocket, analysis of nozzle flow 80−10283
Laval, boiling water discharge and dynamic characteristics 80−19470
Laval, self-similar nonsteady gas flow from finite vol. 79−81942
Laval, vortical helical ideal gas flow, asymptotic series soln. 79−81943
Laval nozzle, reflection of acoustic waves from subcritical inner parts 77−27574
Laval nozzle, supercritical steam supersonic discharge 80−48765
Laval nozzle, surface burning in two-phase flow, boundary layer interaction, Rakhmatulin model 78−83452
Laval nozzle, two-dimens. two-phase flows with nonequil. phase transition 77−51101
Laval nozzle, two-dimensionality of flow 79−90305
Laval nozzle flow of gas-foreign particle mixture, direct problem soln. 77−35218
Laval nozzle with gasdynamic regulation, characts. 80−33651
Laval nozzles, adiabatic expansion of water vapour from the saturation line 78−79356
Laval nozzles, flows with heat addition, book contrib. 80−1671
Laval nozzles, subsonic, transonic, supersonic flow characts. calc. *(Chinese)* 79−32623
Laval nozzles with heat input, flow lines 78−90961
Laval plane nozzles, approx. for special flows *(Russian)* 78−87374
Laval two-dimensional supersonic nozzles, numerical construction method 80−92197
linear meas. extension-nozzle ejector-transducer design 77−57313
liquid, pulse bombardment of liq. interface, gas transfer rate 77−7434
liquid ejector with perforated nozzle 80−24069
liquid jet breakup, second perturbation soln. for one-dimensional Cosserat theory 79−86478
liquid metal jet, borehole casing perforation feasibility, nozzle design, theory *(Russian)* 78−51216
loss characteristics of orifices and nozzles 79−32627
low-density flows through tubes and nozzles 79−94658
Ludwieg tube, steady flow duration extension, reservoir orifice method, variable opening area effect 80−64579

nozzles continued
Mach wave radiation of hot supersonic jets 80−69894
mass gas flow stabiliser, expt. 77−75960
medium speed turbulent, two dimens. meas. near nozzle outlet using laser Doppler anemometer 80−28582
metallic particles, two-phase nozzle flow into vacuum, laser scatt. 77−35194
MHD, gas boundary layer swirling nozzle and diffuser flows with mag. field 80−1693
MHD convertor, acceleration nozzle, with supersonic flow deformation 78−26181
MHD flow, secondary flow, axisymmetric elec. current 78−79381
microjet noise and micropore diffuser-muffler design 78−30335
microwave discharge, supersonic flow in waveguide, electron densities, possible laser 80−38842
mixed 2-D flows of supersaturated and two-phase medium with nonequilib. phase transitions 79−77224
mixer for aircraft power plant noise control 77−42662
mixing nozzle reattachment of two-dimensional turbulent jet 79−23347
molecular beam mass spectroscopy, sampling nozzle gas dynamics 79−49330
molecular beams, intense condensed, for injector for heating and fuelling of toroidal plasma expt. 77−24179
monatomic gas, rarefied flows in axisymmetric expansion nozzle 80−92182
monatomic gas, rarefied flows in two-dimens. expansion nozzle 80−28547
multiphase mixture, two-dimens. nozzle and jet supersonic flows 80−48780
multiple jets in crossflow, characts. obs. 79−14444
multitube, investig. of noise reduction in two parallel flow jets 79−41723
Navier-Stokes solutions using Stetter's method 79−32551
non-Newtonian liquid flow from nozzle, bubble form. 79−23356
nonequilibrium gas relaxation in supersonic nozzle, analysis method 80−74941
nonequilibrium nozzle flow, similarity considerations 78−90959
nonequilibrium two-phase flow in Laval nozzles 79−68820
nonsteady flow with spontaneous condensation 78−47011
nonuniform flow through propulsion nozzle 78−94796
nozzle, convergent-divergent, compressible turbulent boundary-layer heat transfer *(German)* 78−22399
nozzle expansion in turbulent flow, downstream heat and mass transfer 80−1669
nozzle fluid concentrations, probability density functions in free-diffusion flames, laser-light technique 80−10235
nozzle-to-cylinder structures subjected to internal pressure, finite plate method 78−34007
nuclear reactor, control rod drive hydraulic return nozzle repair 80−23043
nucleation homogeneous, gasdynamics of supersonic flow with condensation 77−62292
optical fibre coating concentricity improvement by tapered nozzles *(German)* 78−38095
orifice plate calibrations, extrapolation to high Reynolds no. 80−53833
orifice plate discharge coeffs. at low Reynolds no. 77−84296
orifices in decreasing flows, unsteady characteristics *(Japanese)* 79−10600
pipe, swirled flow, friction law and form parameters, exit nozzle effect 79−37329
pipes and bends, structure-borne sound behind a jet nozzle *(German)* 80−87804
planar sonic nozzle, three dimens. wave struct. of nonstationary gas outflow 77−55068
plane asymmetric, flow calculations in overexpanded flow regimes 79−41730
plasma flame, with rectangular cross section, prod. by nozzle *(Japanese)* 78−47108
polydisperse gaseous suspension, heat transfer between subsonic nozzle walls, rel. to particle motion parameters 77−24019
polymer thickened motor oil, flow in convergent jet thrust nozzles 77−75959
polymer-thickened oil, flow in convergent jet-thrust nozzles at 84°C 79−23348
Prandtl supersonic jet problem, linear aerodynamic theory formulae, validity, book contrib. 80−6090
Prandtl-Meyer expansion with access of heat *(German)* 79−86484
pressure losses across fluid metering nozzle, anal. and reduction method 77−51144
primary coolant inlet of PWR vessel, fracture mech. exam. of integrity *(German)* 78−17327
profile for free molecules flow simulation of air-intakes and cascades 79−94652
pulsed nozzle jet struct., direct shadow method and streak photography 80−10323
PWR components subject to thermal shock, heat transfer coeffs. 80−32332
PWR pressure vessel nozzle, comparison of 3-D and axisymm. finite element anal. 79−13423
quarter circle and combined, investigation *(Russian)* 78−42689
quasi-one-dimensional fluid, boundary conditions on time depend. computations 77−84324
reactor pressure vessel, stress intensities for nozzle cracks 78−70583
reattachment flow issuing from finite width nozzle, bubble press. parameter 80−10275
resonance tube, jet flow and heating, unsteady complex shock struct. 80−6115
ring slit nozzle, coaxial flow with post expansion and heat input *(German)* 78−90960
ring type supersonic nozzle for pulsed gasdynamic device 77−75998
rocket nozzle, compressible turbulent boundary layers, heat transfer and skin-friction 79−14451
rotating, thin film flow of quasiviscous fluid over surface 77−54965
rotating hollow gas jets, nozzle exit flow angle and pressure forces effects *(German)* 80−69887
rotating propulsive nozzle flowfields for nonequilibrium chemically reacting supersonic flow 80−48764
rotational transonic flow and inviscid potential computation by quasi-natural numerical methods 79−64666
round jet of inviscid liquid from nozzle of slowly varying profile 78−14055

nozzles continued
sampling probe, molecular beam mass spectrometry, in situ anal. in crystal growth ambients 80−52357
separation nozzle, for ^{235}U enrichment, double deflection type *(German)* 77−46383
sharp-lip capillary nozzle production and meas. precision 77−80246
shear layer instability noise produced by various jet nozzle configurations 80−69791
shuttered nozzle, for atmospheric press. species stroboscopic extraction into high vacuum regions 77−77858
slit nozzle, for cluster beam generation with strong flux intensity *(Japanese)* 80−52361
sonic nozzle expansions, rot. relax. theory 80−43827
sonic nozzles, expt. study using gas flow dimensionless characts. 79−81945
sonic venturi nozzle, for volume or mass flow, differential interferometric meas. 79−68872
sound attenuation in low Mach no. nozzle flow 79−50721
sound pulsation noise damping from small air bubbles in water 80−64253
sound spectra radiated by gas jets, influence of closely located solid surfaces 80−69800
spherical nozzles of high-temperature heaters, heat transfer calcs. 80−103022
spray, air atomised, dispersion characts., orifice shape depend. 78−34182
spray mixing, effect of sharp-edged orifice type and cavitation 77−51107
spray nozzle, transfer processes in droplet plume during counterdirectional atomisation in gas flow 77−24014
spray nozzles, stability of thin, radially moving liquid sheets 78−71381
spray production, drop size distrib. 79−32633
spray pyrolysis, aerodynamics of nozzles 79−68782
square, transonic flow, 3-dimens. density field meas., holographic technique 78−47080
steady state arcs, nozzle flow 78−32664
steady state Navier-Stokes equation, numerical method and appl. *(Japanese)* 77−68564
steady transonic Euler eqns., Newton's method soln., nozzle appl. 80−38437
steam, 2-D two-phase flow, nucleating and wet steam, time-marching method 80−69906
steam condenser, supersonic nozzle discharge, heat transfer and gasdynamics 78−55671
steam droplets growth in Laval nozzle 79−32648
steam turbine nozzle cascades, local heat transfer, approach flow turbulence effects 80−38381
steam turbine turbulent flat jet condenser, nozzle hydraulic and heat transfer characts. 78−94793
steel, stainless, cylinder, in thermal aerodynamic tube, nonsteady heat transfer method 79−37147
stress intensity factors for reactor vessel nozzle cracks 79−15796
submerged jets in water with slit nozzles, interaction between two opposed jets 80−6113
submerged jets issuing from conical radially slit nozzles 77−35195
subsonic flow, entropy noise, model 79−60046
subsonic nozzle flow, response to acoustic and entropy disturbances 77−75958
suction nozzle, resuspension of spheres from a surface 79−37386
superheated liquid discharge from nozzle, pressure calc. 80−92199
supersonic, influence of transonic flow throat region for maximum thrust 79−41729
supersonic, jet flow from nozzle, coords. of acoustic cross-section 78−5778
supersonic, nonequilibrium heterogeneous-homogeneous condensation of gas *(Russian)* 77−51096
supersonic, pulsed jet wave struct. in nonstationary flow stage 80−59094
supersonic, radiative recombination of shock heated Cl under nonequilib. expansion *(Ukrainian)* 79−37421
supersonic, start-up shock wave struct. 79−7398
supersonic, use in CO_2 gasdynamic laser, two-stage expansion of N_2 78−71076
supersonic air ejector, constant-area-mixing type, design theory 79−86482
supersonic and sonic annular jets, 80−100019
supersonic axisymmetric, film cooling efficiency 80−48710
supersonic conical nozzle, flowfield induced by secondary gas injection 77−62290
supersonic flow, amplification coefficient, effect of mixing conditions in a laval nozzle 80−6085
supersonic flow, finite difference method calcs. *(French)* 78−34157
supersonic flow, sonic injection, auxiliary blowing effect on conc. profiles downstream *(French)* 77−65778
supersonic jet from nozzle with inclined rim 79−64724
supersonic molecular beam nozzle, use of pulse valve 80−100045
supersonic nozzle, chem. nonequilib. flow, specific momentum losses 78−59505
supersonic nozzle beam, high temp. and press. device 80−37907
supersonic nozzle design, nonlinear programming method *(Russian)* 77−51074
supersonic nozzle flowfields, fully viscous and Navier-Stokes solns., comparison, book contrib. 80−1641
supersonic nozzle flows of condensible vapour, near-equil. heterogeneous nucleation and similarity rules 77−58759
supersonic space flows, irrotational, characteristics method *(Russian)* 79−18908
swirl nozzle with annular exit section, anal. of outlet flow rate *(Chinese)* 79−32624
swirl spray atomising nozzle, coefficient of discharge and spray cone angle 80−64602
swirled flow characts. in swirl-nozzle type injector 79−86444
tall-form spray chamber, residence-time distribution of air 78−9679
thermally nonequilibrated flow through supersonic nozzle, cooling, population inversion *(Russian)* 77−7412
throttling liquids, temp. field near boundary 80−43757
transonic channel flow, unsteady, with shock waves 77−23991
transonic flow, gases with rate process 78−14058
transonic flow, rotational, relaxation solution 78−30312
transonic flow, upstream-downstream speed transition 79−98779
transonic flow fields, quasi-one-dimens., time depend. calc. *(Japanese)* 77−58760
transonic nozzle flow of gases with rate and nonuniform props. 77−62289
nozzles continued
transonic nozzle flow of vibr. relax. or chem. reacting gases 78−59506
transonic potential flows past cascades, in nozzles and channels, pseudo-unsteady method 80−14727
transonic unsteady-state flow of supersaturated vapour, in presence of condensation 77−35162
turbine blade and nozzle guide vane, transient cascade, heat transfer meas., wind tunnel 78−94768
turbojet nozzle model used for investigating internal noise of turbojet engine 80−87644
turbulence of free coaxial jets with independent air supply to nozzles *(Bulgarian)* 78−59436
turbulent jet mixing, effect of nozzle wall boundary-layer state 77−27568
turbulent jets, two-dimens., vel. and press. distribs. at confluence 77−24004
turbulent mixing noise, aircraft, in-flight simulation expt. 78−1501
turbulent shear layers on plug nozzles, mixing 77−89182
two dimensional Laval micronozzles, laminar boundary layer approx. calcs. 80−24070
two phase, efficiency at high rates of heat and mass transfer 80−48767
two phase flow heat transfer in convergent part of nozzle, correl. of expt. data 79−81958
two-dimensional long slots, rarefied gas transition flow 80−43738
two-dimensional supersonic flows of mixture, vapour and drops in nozzle and submerged jet, determ. 79−23357
two-phase flow, critical, nonequilibrium vapour production model 80−52719
two-phase flow in a nozzle, max. mass flow rate determ. 78−71384
two-phase flow in Laval nozzle, direct problem, numerical soln. 78−63475
two-phase flow in nozzles, subsonic and transonic 79−81950
two-phase flow through sharp-edged orifices, pressure-drop study 78−1726
two-phase flow through variable cross section channels, critical flow rate 79−55410
two-phase flows, specific impulse estimation 77−47065
two-phase nozzle flow, liq. film size at mouth, holographic meas. 79−86537
two-phase nozzle flows from separate phase model 80−74938
underexpanded jet, first roll geometrical struct., cone angle and degree of contraction effects 77−11229
valve connected to pipe, acoustic oscills. from flow 78−59491
variable pressure drop flowmeters, drainage coefficient reliability 77−58824
vibration relaxation time in nozzle and shocktube expansion flows, physical model 80−24067
vibrational nonequilibrium flow, computational methods comparison 79−60073
viscoelastic fluid flow in nozzles, entrance press. losses 78−59442
viscous flow, time-dependent two-dimensional, moving boundary walls 78−14059
viscous liquid in cylindrical nozzles, entrance press. losses 78−47012
vortex ring formation at a circular nozzle, rolling-up and circulation prod. 79−50738
vortex stretching, due to shear layer instability 77−65776
wall jet on flat smooth plate, mean vel., turbulence and press. distribs. 77−62288
water, subcooled, choked expansion and the isentropic homogeneous equilib. model for 2-phase flow 78−91034
water flow through orifice, polymer additives effect on cavitation and noise 79−98768
water jet appearance, nozzle shape and polymer additive effects, boundary layers 80−53828
water vapour expansion with condensation, nozzle flow at high pressure 80−106828
wet steam flow in nozzles, choking conditions 79−72926
wetting of a vertical plate by a liquid, model 78−22319
whistler, formula for acoustic resonance freqs. 79−72741
wind tunnel contraction section, smoothly varying nozzle construction method 78−47081
wind tunnel nozzles, low-speed, effect of inflow nonuniformity *(German)* 78−71382
Ar, cluster formation and homogeneous nucleation, comparison of expt. and theory, for supersonic nozzle flow 80−79925
Ar, gas in planar nozzle, shock-wave propag., effect of transverse mag. field 80−6094
Ar nucleation, Ar in He carrier gas, supersonic nozzle flow 78−94871
Ar plasma, hypersonic nozzle, radiation field characts. 77−84340
Ar, supersonic pulsed flow from conical nozzle 80−103056
Ar-He rarefied mixture in supersonic nozzle and jet, longit. translational nonequilib. 79−27678
Br_2, dissociating flow in supersonic nozzles, atomic recomb. and vibr. relax. effects 78−42677
Br_2 recombination in supersonic expansion in nozzle *(Russian)* 78−1757
CO, vibr. population distrib. in supersonic expansion 78−71364
CO_2 aerosol/hypersonic air stream interaction, gasdynamic CO_2 laser energy characts. 80−48211
CO_2 gasdynamic laser, gain supersonic flow heating effect, condition optimisation 78−82947
CO_2, gasdynamic laser, optimisation of gain coeff. in nozzle stream *(Russian)* 77−27272
CO_2 gasdynamic laser power, free-piston shock tube expts. *(Japanese)* 79−76661
CO_2-He-N_2, gas dynamic laser, gain coeff. numerical estimates, book contrib. 80−1183
CO_2-N_2, gasdynamic laser mixture, vibr.-nonequilib. nozzle flows, numerical and approx. solns. 78−74881
CO_2-N_2-H_2O gas mixture, oscillatory nonequilib. in planar supersonic nozzle flow 78−1758
CO_2-N_2-He mixture in gas-dynamic system with independent thermal excitation, population inversion in two-step mixing 79−89888
CO_2-N_2-He nozzle flows with boundary layer, gain coefficients 80−14312
Cl_2 partially dissociated, recomb. reaction freezing in supersonic nozzle, chemiluminescence *(Russian)* 77−52644
D_2-HCl electric discharge gasdynamic laser, turbulent mixing characts. 78−9366
Ga, liq. particles-He(N_2)(CO_2)(air), nonequilib. Laval nozzle flow calib., numerical soln. 77−75967
H_2, cluster beam formed from nozzle flow, isotope effect 80−6127

nozzles continued
He-N_2-CO_2 mixture in supersonic nozzle, shock activation with overexpansion, jet form. 78−18330
Li/Li_5 supersonic nozzle beam characts. by spectroscopic techniques 78−55255
N_2 gas jet injection into Hg, interaction at submerged orifice 80−59102
N_2, hypersonic nozzle flow, supercooling and spontaneous condensation 78−1549
N_2 in supersonic nozzle, shock activation with overexpansion, jet form. 78−18330
N_2-CO_2, expanding stream of CO_2 laser, effect of H_2 addition on gain coeff. *(Russian)* 77−27271
NH_3, condensation by homogeneous nucleation in supersonic nozzles 77−11230
SF_6, condensation in supersonic nozzle flow 78−34611
SF_6 condensation in supersonic nozzle expansions, trimerscritical model derivation 79−77211
SF_6-Ar, condensing flow, gasdynamic and IR meas. 80−6501
^{235}U enrichment, separation nozzle process 79−31106
^{235}U, large scale enrichment using separation nozzle 79−94654
NTC thermistors *see thermistors*
ν (neutrino) *see neutrinos*
nuclear acoustic resonance *see acoustic nuclear magnetic resonance*
nuclear alignment *see nuclear polarisation*
nuclear binding energy
see also nuclear forces
^{145}Sm neutron separation and level exciton (n,γ) and (d,p) correlations 80−22756
$^{298}114$, high spin pot. energy surfaces, fission barrier, α-, γ-decay half lives, yrast spectrum 80−73764
A=10-58, neutron separation energies, self consistent set from (n,γ) reaction 80−52563
A=18 shell model spectra and 3 nucleon force 78−25124
A=32 to 140, nuclear struct., binding energies, dipole moments *(French)* 77−46098
A=3,4, finite nuclei, binding energy in Jastrow-Factor-Cluster method 79−49575
A=3 nuclei, charge asymm. from EM contribution to ^3He-^3H binding energy difference 78−29378
A=3-4 hypernuclei, binding energy anal., Λ-N pot., scatt. length and effective range 80−9256
abnormally large density and binding energy states, book contrib. 80−489
alpha cluster role in natural α-decay 79−6519
atomic mass evaluation 1977: mass table, mass excesses, total BEs, β-decay energies 78−4894
BCS techniques applied to self-consistent shell model 79−89249
Bethe homework problem, variational calcs. for neutron and nuclear matter 78−37292
Bethe-Goldstone eqn., nucl. matter, nucleon optical pot. anal. 78−12981
Bloch density for nonlocal pots., ħ-expansion partial resummation, average binding energies 80−86797
bound state problems, scatt. theory methods, binding energies 79−17823
Brueckner and Jastrow methods comparison 77−290
Brueckner expansion, embedding in Green's function theory for nuclear matter binding energy 79−22220
Brueckner theory for finite nuclei, effective particle potentials 77−6248
central-tensor coupled effective interaction pot., binding energy shape, electric moment 77−14036
charge symmetry breaking nuclear forces, two-body, many-body nuclear systems 78−17109
charge-dependent three-body force with N* (1236) in the intermediate states 79−67677
classical many-body model for heavy ion collisions nuclear binding energy and density 78−66302
closed shell nuclei, binding energies, Sussex interaction and delta force 79−22182
compressibility of nuclear matter, density depend. of binding energy, hyperspherical functions method *(Russian)* 78−17093
compressible nuclei, surface energy 80−83031
conference, 11th Masurian school in nuclear physics, Mikolajki, Poland (Aug.-Sept. 1978) 79−63605
conference on many-body theories, Trieste, Italy (Oct. 1978) 80−22135
continuum effects in thermodynamical calcs. of binding energy shell corrections 77−71555
deformed nuclei, energy density formalism 79−9451
deformed nuclei, fragmentation of single-particle states, neutron strength functions 77−6233
deformed nuclei calc. by HF method with Skyrme's interaction *(Russian)* 79−456
deformed nuclei energy density mass formula, approx. method, binding energy, quadrupole moments 79−13195
density isomers, schematic model of mass distrib. 77−6219
density-dependent HF description, of nuclei in rare earth and Ni regions 77−54170
deuterons, D-state probability, review of spin, binding energy, magnetic and quadrupole moment 78−62488
dipole interaction between nucleons, steps in binding energy and mag. moment energy *(German)* 78−74306
doubly magic nuclei, Skyrme force calc. for nuclear struct. 78−49721
effective interaction calcs., symmetry coeff., isospin-spin depend. of single particle pot. compressibility, rearrangement energy 77−46126
effective interactions, folded diagram expansion, self consistent and oscillator sd shell model spaces 78−21502
electronuclear sum rules, linear energy weighted, nuclear struct. determ. method 79−75897
energy density formalism, charge distrib. fine structure, spherical nuclei 77−6251
energy density formalism calcs. with Fermi type distrib. of nucleons 77−46121
Eotvos expts. and weak interactions, anal. 78−78129
even-even nuclei, phenomenological calcs. in n-p interacting boson approx. 80−27597
even-even nuclei, semi-empirical correlation energy 78−17092
even-even nuclei in 2p1f shell, HF calcs. using velocity depend. effective interaction 79−71792
even-even nuclei in 2p-1f shell, binding energy, quadrupole moment, by HF calc. 79−17843
even-even spherical nuclei far from stability, Hartree-Fock calc. *(Russian)* 77−41908
nuclear binding energy continued
even-odd mass difference ratio, mass and binding energy formula 80−47361
exotic nuclei, stability calcs. using Hartree-Fock approx. with Skyrme interaction 78−82273
$f_{7/2}$ shell nuclei, two-body spin-orbit coupling interaction, energy spectra *(Chinese)* 79−93531
Fermi systems, semi-infinite, surface props., thickness and energy 80−52600
few-body systems, photon and lepton probes 77−26591
few-nucleon systems, analytical continuation of the core constants 79−71803
g-shell nuclei, charge distrib., self consistent calc. *(Russian)* 77−38234
generalised vibrational rule 80−105971
giant dipole resonance energy calcs., pair correlations 78−93924
hadronic colour induced Van der Waals force consequences 78−45863
heavy atom nuclei, presence of π^- from binding energy calcs. 78−82275
heavy nuclei, charge asymmetry of nuclear forces and binding energies 79−75866
heavy nuclei, charge symmetry breaking nuclear forces 77−88047
heavy nuclei, contrib. of charge-symmetry-breaking nuclear forces 79−75826
heavy nuclei, Z=68-72, nucleon separation, pairing and decay energies and mass defect 77−79301
HF calculations of masses and BE 77−22862
high order partial wave contrib. to nuclear matter binding energy for model interactions 79−45144
hypernuclei, ΔN effective force, binding energy, excitation spectra, self consistent calcs. 77−6283
hypernuclei, Friedel sum rule, hadron phys. meaning, nuclear matter density, binding energy 78−82305
hypernuclei, produced by strangeness exchange reactions, ground state binding energy 78−17130
hypernuclei, recoilless Λ prod., Λ binding energy 78−50116
hypernuclei studies in nuclear emulsions 77−22923
impure nuclear matter with Λ, binding energy, functional variational approach 80−22744
infinite nuclear matter, response function, quantum field theory of fermion systems 78−70480
infinite system of nucleons and Δ resonances, pot. energy, neutron stars 80−86836
isobar degrees of freedom, binding energy from BHF approx. 80−22734
isobar degrees of freedom in nuclear matter, binding, NN interactions and 2π exchange 80−22735
level density, analytic formula, shell and pairing effects 78−50092
light nuclei, alpha cluster model, 3-body problem 80−32217
light nuclei, hyperspherical functions for size, excited states, compressibility, binding energy 80−22679
liquid drop energy, shell correction determ. 78−12992
many body problem in Lee model, NN scatt. and matter binding energy 80−63116
many-body forces in nuclear physics, review, book contrib. 79−97670
many-body interactions from quark exchanges, nuclear tetrahedral struct. and props. 79−6459
many-body theory, comparison of Brueckner and λ_{00} approx. 77−2929
matrix element for binding energy, integral form 78−70435
matter distribution in nuclei far from β stability valley, charact. features 77−64635
medium and heavy nuclei, binding energy shell effects, universal behaviour 79−447
microscopic binding energy calcs., modified Strutinsky correction 79−67638
multiparticle cores in nuclei, matter fluctuations, binding energy, repulsion correlations 79−75864
N=28 isotones, effective interactions, Coulomb displacements and separation energies 78−50077
N=50 isotones, effective interactions, Coulomb displacements and separation energies 78−50077
N=Z even-even nuclei, 2s-1d shell Hartree-Fock calcs. s-wave interaction 79−26385
neutron binding energy in compound nucleus formed from $^{124}Sn+^{86}Kr$ 78−54797
neutron matter, energy per particle and effective mass 77−30499
neutron-rich nuclear potential energy surfaces 80−18183
non-self-consistent energy calculations with a density-dependent effective interaction 79−36170
nuclear, matter, V^8 models, variational calcs. for binding energy and density 80−42571
nuclear bound states of k−, p̄ and Σ 80−13399
nuclear matter, Λ^0 binding energy, many-body cluster contribs., Jastrow calc. 79−93545
nuclear matter, hard core pots., crystalline struct. binding energy, HF calcs. 79−93543
nuclear matter, hypernetted chain approx., impurity ground state energy 80−83055
nuclear matter, symm. and asymm., simple effective interaction for props. 78−25141
nuclear matter, variational approach, hyper-netted-chain calcs. 77−2926
nuclear matter, variational approach with realistic potentials 77−18463
nuclear matter, variational theory 79−40867
nuclear matter BBG theory, auxiliary single particle field for binding energy 80−22723
nuclear matter binding energy, Δ(1236) effect, lowest order reaction matrix calc. 77−6278
nuclear matter binding energy, charge dependent N-N potential, HF calcs. 78−50115
nuclear matter binding energy, corelated basis functions method appl. 78−45998
nuclear matter binding energy expansion convergence in Brueckner-Bethe-Goldstone theory 80−488
nuclear matter binding energy from low density expansions, Brueckner-Hartree-Fock approx. 80−22720
nuclear matter binding energy variational calcs. in two- and three-body cluster approx. 77−26603
nuclear matter nonstatic OBEP, vel. depend. tensor pot., BE calc. 77−88065
nuclear matter properties, velocity dependent effective potential of s-wave interaction 78−58247
nuclear matter with n excess spin-up p and n, binding energy 79−13232
nuclei in fp shell, statistical spectroscopy 77−6255

nuclear binding energy continued
nucleon, bound in harmonic oscill. pot., coupled to pion field, EM struct. 78−8732
nucleon binding in nuclei at high ang. momentum 78−25104
nucleon fluid, excitation to N*(1234) state, lowest order constrained variational calcs. 79−40864
nucleon motion in nuclei, determ. using high energy electron induced knock-out reactions *(French)* 79−445
nucleon pairing and quadrupoling effects, appl. of 5D quasi-spin group 79−9494
nucleon-nucleon potential, tensor contrib. for total ang. momentum depend. pots. 77−2915
optical nucleon-nucleus potential *(Russian)* 78−37321
orbital excitation of the hyperon in hypernuclei 80−106001
p-f shell nuclei, HF calcs., vel. depend. effective pot., binding energy, quadrupole moment 80−461
p-shell hypernuclei, shell model anal. of Λ binding energies 78−78300
p-shell hypernuclei with effective Λ-nucleon potentials, binding energy and well depth 79−36184
pairing correlation treatment, single particle levels, binding energy, spectra, branching ratios *(Chinese)* 80−102107
pairing with a delta interaction in the energy density nuclear mass formula 79−36143
Paris NN pot. parametrisation, phase shifts, nuclear matter binding energy 80−47405
Pauli principle effect in nuclear matter, exchange of interacting two pions 78−12983
pionic condensation, superdense nuclei *(Russian)* 77−46129
polarised nuclear matter, binding energy, spin energies, relativistic calc. 80−102134
pure hard core interaction in neutron excess matter, third order binding energy calc. 78−89784
quark exchange, nuclear force model 78−41648
quark exchange model, for nuclear binding energies 79−93533
radiative strength functions in spherical nuclei, giant dipole resonance influence, ^{124}Te, ^{140,142}Ce appls. 78−89774
relativistic effects on the two-nucleon and nuclear matter systems 79−89261
relativistic sum rule for total binding energy 77−14023
repulsive core regularisation, two-body binding energy 77−82814
ring diagrams, Landau parameters, pion condensation, binding energy, of nuclear matter 78−74321
s-d shell nuclei, HF calcs., vel. depend. effective pot., binding energy, quadrupole moment 80−461
s-shell nuclei, binding energy scheme with soft core nucleon-nucleon potential *(Russian)* 79−3077
saturation in finite nuclei, nuclear matter density and binding energy 80−83029
sd-shell nuclei heavy-ion reaction resonances, low level density regions, shell model 80−57757
sd-shell nuclei with realistic effective Hamiltonian, binding energies using Brueckner shell model 77−57594
self-consistent field calcs., HF calcs., NN interactions, and results of appl., book contrib. 79−75880
separation and alpha- and beta-decay energies, 1977 at. mass evaluation tables 78−4895
separation and nuclear-reaction energies, 1977 at. mass evaluation tables 78−497
shell correction, account of continuum in thermodynamic calc. *(Russian)* 78−29409
shell correction method for finite well potentials, appl. to ^{240}Pu nucleus 78−37298
shell corrections to semi-empirical formulae for binding energy and radius *(Russian)* 78−78283
shell effects in nuclear radii and binding energies, prediction of relative radii 79−45149
shell model, globally self-consistent, magic nuclei and spherical nuclei calculations 79−59020
shell model calculations, strong two body correls. 77−6259
short-range forces and surface tension, surface isomers 77−57596
single particle nuclear density struct., Hartree-Fock and model independent anal. *(Russian)* 79−80941
single particle states, systematics in a Woods-Saxon potential *(Rumanian)* 79−59003
single-particle motion in nucleus, forces between constituent nucleons, shell model 80−47408
single-particle potential, symmetry coefficient and effective mass in nuclear matter 79−13234
single-particle response and ground-state properties, Hartree-Fock theories 80−105997
spherical nuclei, Hartree-Fock-Bogolyubov calcs., D1 effective interaction, nuclear matter, binding energies 80−63105
spherical nuclei, masses determ. by energy-density method 77−6215
spherical nuclei, nuclear mass formula, energy density functional, self-consistent calc. 78−78244
spherical nuclei, self-consistent Thomas Fermi method 77−57607
spherical nuclei, total binding energy, many body field theory, ^{16}O, ^{40}Ca, ^{58}Ni appls. 77−30482
spin orbit interaction of nucleons, relative motion dependent, universal coeffs. of hyperspherical function method 77−61354
spin unsaturated systems, finite range two- and three-body interactions 78−66220
stable charmed hyperfragments containing charmed baryon+nucleons, binding energies, lifetimes 78−89815
strongly bound π^- nuclear states, vel. depend. pot. binding, pionic atoms 80−37331
structure of nuclear energy surface, binding energy eqn., corrections 77−61344
subcoulomb fusion, effective barrier at low energies, total reaction cross section 78−37385
subshell closure effects of nuclear binding energies, neutron rich nuclei 78−58230
subshells, exact eqn. for binding energy *(Russian)* 77−71575
super-dense nuclei, stability and pion condensation 77−18375
superdense nuclei, search for neutrons with binding energy >40 MeV *(Russian)* 79−89515
superdense nuclei, search in reactor active zone 79−75824
superdense nuclei stability region, pion condensation *(Russian)* 77−46128
superheavy nuclei and multineutron systems, possibility of existence *(Russian)* 80−462

nuclear binding energy continued
surface energy of very neutron rich nuclei, Thomas-Fermi model 77−22870
surface tension coefficient, surface energies, and scalar meson mass *(Chinese)* 79−49574
symmetry effects on nuclear binding energy and rest mass of constituents *(French)* 80−63068
T matrix, $^1S_0$ two-nucleon, interior wave function 77−14038
tensor contrib. to nuclear matter in first order perturbation theory, binding energy 77−18410
Thomas-Fermi, extended model, binding energies and liq. drop parameters 77−67699
three body forces from cluster terms, binding energy and tensor forces 79−45176
three body problem with three body forces, special solns. to integral eqns. 79−75869
three neutron resonance, enhancement factors, forces, and binding energy 79−45230
three nucleon bound states, Δ (1236) effects, on binding energy and form factors 79−75858
three nucleon clusters in nuclear matter, energy per particle density dependence 78−17112
three particles, binding energy and scatt. state calcs. using boundary condition model *(Russian)* 79−40837
three particles with Coulomb interaction, binding energy and scatt. states *(Russian)* 80−5051
three-body cluster energy, lowest order constrained variational calc. 79−13233
three-body forces in 3- and 4-nucleon systems 78−29400
three-body nuclear forcesin σ-model, nuclear matter and triton BE 77−71568
three-body problem with Bargmann potentials 78−82274
three-nucleon forces, nuclear matter and BE 77−74773
three-nucleon potentials due to π, S and ω, binding energy in nuclear matter 78−62486
three-nucleon system, Faddeev eqns. perturbation, nucleon-nucleon interaction with tensor force 78−70463
trinucleon bound state using Paris pot., binding energy and form factors 78−89803
trinucleon ground state observables, new harmonic oscill. basis calc. 77−74776
trinucleon properties, one-boson-exchange potentials 77−18433
trinucleon props. with one-boson exchange potls. 77−18421
triton, momentum space calculations, Faddeev bound-state eqns., binding energy 78−25122
triton *(Russian)* 78−29376
Woods-Saxon potential spectrum, pairing force strength, Nilsson model comparison 80−57704
Z=N nuclei, pot. calc. from α-α interaction 79−6661
(α,^{2}He) reaction in 1p- and 2s1d-shell nuclei, A-depend. of neutron binding energy 78−74379
α-nucleus separation energies, Woods-Saxon pot., A depend., closed shell effects 78−25107
d propagation in nuclear matter, spin depend. of d optical pot. and binding energy 78−70545
Δ resonance inclusion in one-boson-exchange potential, Brueckner-Hartree-Fock calcs. for ^{16}O 77−54155
(K̄,K̄), isobar doorway model, optical pot., Λ-nuclear matter binding energy 80−106079
Λ, binding energy in nuclear matter, reaction-matrix calculation 79−36185
Λ binding energy in nuclear matter with Nijmegen baryon-baryon interaction 80−13400
Λ binding to nuclear matter in Fermi hypernetted chain approx. 79−85396
Λ s-shell hypernuclei, general props. and developments in experimental methods, review 79−22224
ΛN distrib. function, Λ-binding to nuclear matter, Fermi hypernetted chain approx. 80−78131
ΛNN correlations and Λ binding in nuclear matter 80−106000
N-nucleus optical potential from realistic Hamada-Johnston internucleon pot., binding energy 78−54730
^{3}n binding energy, calc. from ^{3}H, ^{3}He, ^{4}H, ^{4}He and ^{4}Li ground-state properties 80−83044
^{3}n system, bound state, Faddeev eqn. calc. 80−105989
^{4}n binding energy, calc. from ^{3}H, ^{3}He, ^{4}H, ^{4}He and ^{4}Li ground-state properties 80−83044
NΔ conversion, two-channel formalism and three-body forces approaches 78−8733
NNN bound state problems, hyperspherical harmonic expansion, review 80−91136
np effective interaction in mirror nuclei, charge exchange part, linear binding energy relation 77−22901
(π,π), Weinberg chiral Lagrangian nonlinear terms, nuclear binding, optical pot. 80−78329
π bound states in finite nuclei, π-nuclear optical pot. 78−46013
π-nucleus scattering, binding effects in optical pot. of pion in nucleus 78−41685
^{27}Al(π,^{2}Xγ), 190, 220 MeV, multinucleon removal cross sections and γ-ray spectra, binding energy effects 79−3183
^{28}Al, neutron binding energy precision meas. 80−18182
Ba, charge radii and binding energy per nucleon, linear relationship evidence 80−68520
^{8}Be, cluster formation, multicentre variational model *(Chinese)* 78−25128
^{8}Be, ground state props., modified Brueckner-Bethe-Goldstone method 78−50076
^{9}Be, α-cluster struct., binding energy determ., Faddeev eqn. soln. 78−41640
^{9}Be, binding energies, three body calcs., Faddeev formalism, alpha cluster model 79−75876
^{9}Be, three body calc. with separable pots. for binding energy 79−45145
^{9}Be, three body molecular calc. of low-lying spectrum 79−93534
^{9}Be, three-body model of bound state struct. 79−6374
^{9}Be, binding energy calcs., clustering 79−9501
$^{\Lambda}$C, A=13,14, neutron binding energy from ^{1}H(n,γ) 80−52564
$^{\Lambda}$C, A=13,14 neutron binding energy 80−47362
^{12}C, α-cluster model, binding energy, RMS radii, and form factors 79−75825
^{12}C, α-cluster struct., binding energy determ., Faddeev eqn. soln. 78−41640

nuclear binding energy continued
C, binding energies, three body calcs., Faddeev formalism, alpha cluster model 79−75876
C, constrained variational calcs. for binding energy and RMS radii, N*(1234) allowance 79−3074
C, ground state props., modified Brueckner-Bethe-Goldstone method 78−50076
C, saturating effect of N*(1234) on binding 78−58231
^{9}C struct., determ. of Brink's model parameters, calc. of binding energy, 2^{+} level lifetime 79−85358
^{12}C structure, energy levels, binding energy, cluster model with varying hinge angle 78−4907
^{12}C, three body calc. with separable pots. for binding energy 79−45145
^{40}Ca, magic nucleus, nonlocal pots., binding energies 77−41877
^{40}Ca structure, supersoft-core pot., HF approx., ground state props. 78−533
^{114}Cd, neutron binding energy precision meas. 80−18182
^{12}C hypernucleus detection in p+emulsion nucleus, 250 GeV, Λ binding energy *(Russian)* 78−89816
Co isotopes, shell model 78−62479
Cu, isotopes, shell model calcs. of BE, spectroscopic factors and excit. energies 77−22860
^{165}Dy, neutron binding energy precision meas. 80−18182
^{166}Er, Skyrme-HF calcs., deformation, electric moments, spin-orbit potentials 78−62480
^{68}Er, neutron binding energy precision meas. 80−18182
Fe, single neutron separation energies determ. from doublets 77−26566
^{252}Fm, pot. energy surface, liquid model, deformation energy formulae *(Chinese)* 80−102106
^{2}H, binding energy meas. *(Russian)* 79−9453
^{2}H D-state probability lower bound, binding energy, quadrupole moment 80−91137
^{2}H deformation effects in nuclear interaction, DWBA anal. *(Japanese)* 78−21575
^{2}H γ-energy and binding energy from ^{1}H(n,γ) 80−52564
^{2}H neutron binding energy and n mass excess from ^{1}H(n,γ) 80−47362
^{2}H-^{3}H binding energy correlation, ^{4}He theory and Tjon line 79−89227
^{2}H(d,n)^{3}He, struct. and form factor models in mass-3 system 79−45274
^{2}H(d,p)^{3}H, struct. and form factor models in mass-3 system 79−45274
^{3}H, binding energies, three body calcs., Faddeev formalism, alpha cluster model 79−75876
^{3}H binding energy, 3N bound state with separable interactions, Faddeev theory corrections 80−13388
^{3}H binding energy, D-state percentage of deuteron, wave function shape 77−2902
^{3}H binding energy, energy depend. boundary condition model 79−13194
^{3}H, binding energy, local soft core NN pots., quasiparticle formalism 79−6529
^{3}H binding energy, quantum theory evolution law approach appl. *(Russian)* 79−80866
^{3}H binding energy, relativistic calc., Bethe Salpeter eqn. 80−68519
^{3}H, binding energy, truncated t-matrix approx., trinucleon bound state problem 79−448
^{3}H, binding energy, unitary pole and Adhikari-Sloan expansions 78−499
^{3}H, binding energy and charge form factor, internucleon force 77−18438
^{3}H binding energy from 1-boson exchange, n-d and n-(pn)* momentum distribs. 79−67639
^{3}H binding energy in $J=1/2^{+}$ three-N state calc. with super-soft core 77−71570
^{3}H bound state for Reid soft-core pot. perturbational exact calc., binding energy 79−63602
^{3}H, ground-state calc., harmonic oscillator basis 79−71807
^{3}H hypernucleus, binding energy, role of spin forces in Λ-N interactions *(Russian)* 78−54718
^{3}H model, appl. of three particle bound state eqns., binding energy 78−78276
^{3}H, NN realistic nonlocal pots. from inverse scatt. theory for $^{3}S_1$-$^{3}D_1$ interaction 78−41651
^{3}H neutron binding energy 80−47362
^{3}H neutron binding energy from ^{1}H(n,γ) 80−52564
^{3}H, partly non-local pots. model 77−54157
^{3}H, props. calc. by interpolation approach *(Russian)* 77−22903
^{3}H realistic wave function, energy and density distribs. 80−86794
^{3}H, relativistic bound state calcs., off shell depend., binding energy 78−82295
^{3}H, relativistic correction to binding energy 77−79302
^{3}H, relativistic corrections to two-body pot., binding energy 78−74301
^{3}H, soft core potentials 77−18378
^{3}H, three body calc. with separable pots. for binding energy 79−45145
^{3}H, three nucleon observables with meson theoretical interactions, binding energy, form factors 79−67676
^{3}H, three-particle bound states for partly nonlocal interactions with continuum bound states 80−32206
^{3}H, unitary scheme model anal. with Gogny, Pires and de Tourreil interaction 79−59016
$^{3}H_{\Lambda}$, and contrib. of spin forces to Λ-N interaction *(Russian)* 77−79319
$^{3}H_{\Lambda}$, binding energy, Fadeev equation in coord. space, Lambda-nucleon potential 80−63120
^{3}H→n+d, s-wave asymptotic normalisation consts. in one-boson exchange model 80−37334
^{A}H, A=2,3, binding energy from Brillouin-Wigner perturbation method, strong short ranged interactions 80−86796
$_{\Lambda}{}^{3}$H binding energy using phenomenological ΛN pots. 80−9254
He, A=3, 5, BE, level calcs. using new boson expansion to n-fermion problem 78−511
He, A=3,4, relativistic corrections to two-body pot., binding energy 78−74301
^{2}He, ground state level determ. 80−99136
^{3}He, BE, 4 boson approx. and ^{4}He BE 77−61351
^{3}He, binding energies, three body calcs., Faddeev formalism, alpha cluster model 79−75876
^{3}He, Coulomb energy, charge symmetry breaking 80−27564
^{3}He Coulomb energy, quasiparticle method 77−18416
^{3}He Coulomb energy from configuration space Faddeev calcs. 80−102131
^{3}He, one-boson exchange pot. 78−41652
^{3}He, three body calc. with separable pots. for binding energy 79−45145
^{3}He, trinucleon bound state problem, binding energy, form factors and mag. moment 80−22710
^{3}He-^{3}H binding energy difference, Coulomb energy contribution 79−491
^{3}He-^{3}H binding energy difference, charge asymmetry 79−71808
nuclear binding energy continued
^{3}He-^{3}H Coulomb energy difference and charge dependent three-body force 79−45181
^{4}He BE calc. in 4 boson approx. 77−61351
^{4}He binding energy, 4-nucleon problem, integral eqn. approach 80−91183
^{4}He binding energy, Δ(3-3) effects, reaction matrix calc., Δ degrees of freedom 80−9218
^{4}He binding energy, nonrelativistic theory of four nucleon systems *(Russian)* 79−80881
^{4}He, binding energy, truncated t-matrix approx., trinucleon bound state problem 79−448
^{4}He binding energy, unitary pole approx. 78−25103
^{4}He, binding energy and form factor calcs., Reid interaction 78−54678
^{4}He, constrained variational calcs. for binding energy and RMS radii, N*(1234) allowance 79−3074
^{4}He, four-body problem unitary pole approx. calc. 78−516
^{4}He, from Alt-Grassberger-Sandhas eqns. 78−41650
^{4}He, ground state props., modified Brueckner-Bethe-Goldstone method 78−50076
^{4}He, magic nucleus, nonlocal pots., binding energies 77−41877
^{4}He, nucl. binding energy, radius and charge form factor, Brueckner calcs. 79−71787
^{4}He, reaction matrix calc. with three and four particle correls. 77−34218
^{4}He, saturating effect of N*(1234) on binding 78−58231
^{4}He, shell model calcs. 80−13393
^{4}He, structure in the translation-invariant oscillator basis *(Russian)* 78−25123
$^{4}He_{\Lambda}$-$^{4}H_{\Lambda}$ binding energy difference, exact 4-body calc. 79−63622
^{4}He(π,π), single scatt. optical pot., Pauli principle and binding effects on cross section 80−86933
^{5}He, effective 3- and 4-body forces in 5 nucleon system 79−477
$^{5}He_{\Lambda}$, Λ-N pot. Majorana component on B_{Λ} value, overbinding 80−99144
$^{6}He_{\Lambda\Lambda}$, ΛΛα binding Feddeev's method 77−38238
$_{\Lambda}{}^{4}$He-$_{\Lambda}{}^{4}$H binding energy difference, particle mixing and charge asymmetric ΛN forces 79−75891
$_{\Lambda}{}^{4}$He-$_{\Lambda}{}^{4}$H binding energy difference, bound states, exact four body calc. 80−9255
^{200}Hg, neutron binding energy precision meas. 80−18182
^{5}Li, effective 3- and 4-body forces in 5 nucleon system 79−477
^{6}Li, α+p+n model, numerical soln. of coupled Faddeev eqns. 79−17831
^{6}Li, binding energies, three body calcs., Faddeev formalism, alpha cluster model 79−75876
^{6}Li, cluster formation, multicentre variational model *(Chinese)* 78−25128
^{6}Li ground state, separable pot. three body model 78−50090
^{6}Li, hyperspherical L_m approx., even parity states binding energy 78−74311
^{6}Li, RMS radii, binding energy, electric quadrupole transitions using generalised hyperspherical functions *(Russian)* 78−86469
^{6}Li, three body calc. with separable pots. for binding energy 79−45145
^{6}Li, three-body model using hyperspherical harmonics 78−29411
^{10}Li neutron binding energy from ^{7}Li(t, ^{9}Li)^{1}H *(Russian)* 80−105961
^{24}Mg, Brink α-cluster model 77−6195
^{15}N, neutron binding energy 80−47362
^{15}N, neutron binding energy from ^{1}H(n,γ) 80−52564
^{151}Nd, rot. states populated through neutron capture 77−6196
^{20}Ne, Brink α-cluster model 77−6195
Ni isotopes, shell model calcs. of BE, spectroscopic factors and excit. energies 77−22860
^{A}O, A=16, 17, valence-core self-consistency, wave functions, binding energy, levels, spectra 80−63123
^{16}O, 0^{+} level pot. harmonics and matrix elements, BE contrib. *(Russian)* 77−82835
^{16}O and Sd shell nuclei, binding energy from realistic Hamiltonians and spectral distrib. theory 80−22678
^{16}O, binding energy, wave function of ground state, orthogonal schema model 79−63582
^{16}O, charge distribution, orthogonal scheme model *(Russian)* 78−29382
^{16}O, constrained variational calcs. for binding energy and RMS radii, N*(1234) allowance 79−3074
^{16}O, energy calcs., Jastrow variational method extension, FAHT cluster expansion 80−22677
^{16}O ground state and binding energy, microscopic calc. with realistic NW interaction *(Russian)* 80−5052
^{16}O, ground state props., modified Brueckner-Bethe-Goldstone method 78−50076
^{16}O ground-state energy, nonunitary model operator approach 80−83030
^{16}O, magic nucleus, nonlocal pots., binding energies 77−41877
^{16}O, mesonic and isobar degrees of freedom, Brueckner Hartree Fock calc., binding energy 79−63600
^{16}O, oscillator matrix elements from NN phase shifts and short range correl. 77−271
^{16}O, relativistic self-consistent nuclear model, separation energy, mean square radius *(Russian)* 79−97654
^{16}O, saturating effect of N*(1234) on binding 78−58231
^{16}O structure, energy levels, binding energy, cluster model with varying hinge angle 78−4907
^{16}O, third order contributions to binding energy 77−30481
^{17}O valence energies, extended multiple scatt. approach to 2p1h system 78−29396
^{208}Pb, charge and proton distribs., single particle model 78−50074
Ru, even isotopes, potential energy surfaces and ground state equilib. deformation 80−73789
^{32}S α-cluster struct., ground and first excited states, energies, radii and moments 80−102122
^{32}S, Brink α-cluster model 77−6195
^{32}S, nucl. saturation props. 79−6395
^{132}Sb, doubly closed shell nuclide, β-spectra, total binding energy determ. 77−50046
^{41}Sc-^{41}Ca Coulomb displacement energy, HF calcs. 80−42527
^{28}Si ($\pi^{\pm}$,Xγ), 190, 220 MeV, multinucleon removal cross sections and γ-ray spectra, binding energy effects 79−3183
^{28}Si, Brink α-cluster model 77−6195
^{145}Sm primary γ-rays, direct capture and neutron separation energy, (d,p),(n,γ) correlation 80−57738
^{154}Sm, Skyrme-HF calcs., deformation, electric moments, spin-orbit potentials 78−62480

nuclear binding energy continued
Sn from ^{122,124}Sn(n,γ) up to 20 keV, level schemes, spin-parity assignments, neutron separation energies 77−54215
^{A}Sn, A=113,115,117,118,119,120, rms neutron orbit sizes, DWBA anal. of Sn(t,d) data 79−36145
^{132}Sn, doubly closed shell nuclide, β-spectra, total binding energy determ. 77−50046
Sn(d,t)Sn, even A=112 to 124, deeply bound hole states of odd A Sn 78−8725
Sr, even isotopes, potential energy surfaces and ground state equilib. deformation 80−73789
^{93}Sr neutron binding energy from transitions and β-delayd neutron defined level correspondences 80−63070
^{A}Tb, A=149, 151, 153, 155, 157, prop. anal. on function of nuclear shape 79−75828
^{100}Tc level scheme, transitions and J^{π} values, n binding energy from ^{99}Tc(n,γ) 79−63590
Ti, single neutron separation energies determ. from doublets 77−26566
^{235}U, pot. energy surface, liquid model, deformation energy formulae *(Chinese)* 80−102106
^{237}U levels, bands and J^{π} assignments, n binding energy from ^{236}U(n,γ) 80−5041
^{239}U, neutron binding energy precision meas. 80−18182
Xe, charge radii and binding energy per nucleon, linear relationship evidence 80−68520
^{137}Xe neutron binding energy, determ. from ^{136}Xe(n,γ) 77−41879
^{91}Ze primary γ-rays and binding energies from ^{90}Zr(n,γ) 80−52566
Zn isotopes, A=62-68, shell model calc. 77−270
Zn, single neutron separation energies determ. from doublets 77−26566
Zr, even isotopes, potential energy surfaces and ground state equilib. deformation 80−73789
Zr, isotopes, neutron separation energies, (d,t) reactions *(German)* 77−57592
Zr neutron separation energies from (d,t) and (d,p) reactions 80−47489
^{A}Zr, A=90, 92 and 94, charge densities and single-particle structure 80−9224
^{A}Zr, A=91, 92, 94, binding energy and primary γ-ray intensities from Zr(n,γ) 80−52565
^{92}Zr, neutron binding energy precision meas. 80−18182

nuclear bombardment targets
see also nuclear reactions and scattering
2.6 T supercond. magnet design and manufacture for polarised target 79−31293
actinide target prep. for synthesis of transactinide elements 80−23206
actinide target preparation by focused ion beam sputtering 80−23219
amorphous targets, energetic in transport, Monte Carlo program 80−102411
axially polarised proton target, for A and R parameter meas. in $\pi^- p \rightarrow K^0 \Lambda^0$ 79−63834
biomedical target, water-cooled pion-production, remote exam. and disassembly 80−25975
2,3-butanediol doped with Cr(V)-complex, materials with adjacent hydroxyl groups, dynamic proton polarisation 77−79492
Butanol recycling from irradiated proton target material 79−63852
CERN polarised d target, apparatus for two-body scatt. expts. 79−31287
composition determ. from α-scatt. and (p,γ) meas. 77−75019
conference on high energy phys. with polarised beam and target, Argonne, USA (Oct. 1978) 79−63526
cryogenic target containing liquid He, H_2 and D_2 79−68111
cryogenic targets for streamer chambers and cryofluid target supply *(Russian)* 78−13381
cryogenically pumped gas target for γ-ray ang. distrib. meas. 78−55076
curved plunger for TDPAC meas. on recoil into gas 79−76313
deuterated polarised target, calibration of deuteron polarisation 77−3200
deuterated polystyrene targets, solid, preparation method 78−82554
diamond target preparation for tandem expts. 80−23222
dispersion aerosols for transport of deuteron and ^{84}Kr induced reaction products 77−34502
dynamic polarization in radiation resistant materials 79−31283
electron spectroscopy, target sources, centrifuge method of prep. 80−74060
EM isotope separation and in-beam electron spectroscopy, Pt target preparation 80−52812
enriched gaseous isotopes, recovery systems 78−58525
enriched isotope target preparation, design of quasi-hyperbolic electrostatic fields 80−23597
Erlangen windowless high density gas target for nuclear scattering experiments 79−54735
explosively clad uranium targets 80−18737
frozen polarised proton target 79−26795
frozen spin polarised targets 77−38526
frozen spin target, horizontal dilution refrigerator with high cooling power 80−73372
gas, high pressure, liquid N cooled, intense fast-neutron prod. by ^{2}H(d,n) reaction 77−3201
gas, small medium press. target cell for polarised and unpolarised ion beams 78−17460
gas cell target for studying fusion and damped collisions of light nuclei 79−76250
gas jet recoil transport system, aerosol formation using pure gas as carrier 79−97921
gas target, differentially pumped and recirculating 79−13570
gas target neutron generator, Canadian research 77−83427
gaseous windowless high density target for scatt. expts. 80−23210
goniometer, precision three axis UHV bakeable system 78−70673
goniometer for nuclear reaction cross section and channelling expts. 78−21801
graphite targets for use in LAMPF high intensity beams 79−68107
Havar foil, stopping power and multiple scatt. for low energy protons 79−31339
heating by ion beam, thermal charact. *(Japanese)* 80−99374
heavy ion beam targets, damage, lifetime, uniformity, book contrib. 79−31291
heavy ion facility, target production 80−23213
heavy ions, experimental methods, targets and detectors, book 79−31242
heavy-ion recoil target system, high intensity, gas cooling 77−10508
high density windowless gas jet target 79−22512
high pressure gas target system for the determination of absolute electron scattering cross sections 79−26798

nuclear bombardment targets continued
high pressure sample container for thermal neutron inelastic scattering on fluids 80−37681
intense sources of fast neutrons 79−22522
isomeric state g-factor meas., target preparation 80−23217
isotope, quartz crystal thickness sensor 80−17923
isotope compounds, conversion to metals by reduction-distallation methods 80−23223
isotope induction at LAMPF, fabrication, cladding, handling of irrad. targets 80−23231
isotope target preparation by laser beam evaporation techniques 80−18735
isotopic target preparation by ion beam sputtering 80−23220
Kapton foil, stopping power and multiple scatt. for low energy protons 79−31339
LAMPF high power pion prod. target mechanism 77−83387
laser fusion cryogenic target characterisation by wavefront shearing interferometer 80−74008
Linac, inexpensive positron converter of high reliability and high yield 79−68108
liquid target mounting 78−46197
mass separators, on-line, progress in targets and ion sources 77−14300
membranes in pulsed electron beam, temp. and ultimate load calcs. 79−45484
metal target preparation for stopping power meas. of channelled ions in low energy region 80−63431
metal vapour targets for HIXE anal. 78−80822
multiple rabbit, pneumatic multi-target transfer system, design, operation 77−54385
multitarget assembly for high energy irrad., simultaneous prod. of ^{123}I, ^{62}Zn and $^{13}NH_3$ 77−90896
muon transfer in gas targets 77−42445
neutrino target complex at Fermilab, operating experience 80−23230
neutron generator facility with alternative 30° target 80−9444
neutron production, by electron accelerator 3 to 10 MeV *(Rumanian)* 79−63855
NIM-controlled rabbit system 80−18731
nuclear polarization, recent advances in technique 79−30822
optically pumped electron spin polarised targets, polarised ion beam prod. 80−27851
ORNL EM isotope separation program 80−18673
pion conversion target for Saclay electron linear accelerator 77−54384
polarised, ^{3}He cooled cryostat development 77−13760
polarised, cryostat with large cooling power, for electron synchrotron 77−34496
polarised, frozen spin and deuterated targets at CERN 77−38523
polarised, proton and deuteron, for precise polarisation meas. at KEK 80−37670
polarised ^{3}He continous flow cryostat 80−52240
polarised materials, proton beam effects 78−29723
polarised nucleon targets, meson photoprod. amplitudes 77−34162
polarised proton, using high homogeneous field supercond. magnet 77−26911
polarised proton production in Yb, spin refrigeration of $(Yb,Y)(C_2H_5SO_4)_3.9H_2O$ cryst. in nonuniform mag. field 77−83435
polarised proton target, 50 kG 1K, construction, performance 77−38524
polarised proton target using split pair superconducting magnet system 77−14291
polarised target 'R and A' magnet, ANL 77−38525
polarised target materials, radiation damage, clean materials and dynamic polarisation 79−63832
polarised targets, discussion 79−68065
polarised targets, materials research, recent developments at CERN 79−63835
polarised targets, meas. using Q-meter with automatic phase control and tuning 79−228
polarised targets and cryogenics at Laboratori Nazionali di Legnaro 80−106219
polarized target, horizontal dilution refrigerator construction 78−86708
polarized target experiments at CERN 79−63850
polyethylene, precise low-energy ^{2}H(n,n) cross sections 78−82342
polyethylene foils, deuterated, prep. technique 77−88313
polyimide substrate foils for nuclear targets 80−18739
powdered, thickness determ. using α-ray and β-ray gauges 79−22519
powdered isotopic material prod. by centrifugal method 80−18738
powdered target prod. by centrifugal precipitation method 78−841
preparation techniques 79−85201
preparation with isotope separator using retardation collector system 77−14284
projected inertial confinement fusion reactor target evaluation by buoyancy analysis 80−78442
proton cyclotron targets for prod. of e^{+}-emitting radionuclides for medical appl. 79−53241
rabbit fast transport system for fragile targets in high vac. 77−83417
rabbit system with 8-targets, appl. to ^{53}Ti and ^{59}Mn decays 77−26635
radioactive, for study of nuclei far from stability by particle transfer spectroscopy 77−22990
radioactive target preparation and characterisation 80−18734
radioactive target production for use in charged particle reaction spectroscopy 78−70670
radioactive targets, preparation by on-line isotope separation 77−23328
recoil products of high-energy nuclear reactions ang. distrib. meas., geometry calcs. 77−6596
reference fission foils preparation by fluoride deposition, characterisation 80−23218
refractory matrices, fast release of reaction products from 600 MeV irradiation 78−29652
remotely controlled target transport system for cyclotron irradiations 80−69005
rotating accelerator targets, method for increasing lifetime 79−89513
rotating target wheel with thin targets for heavy ion beams of high current densities 79−76241
scattering chamber, rotatable lid, vacuum sealed, with semicond. detector arrays, INS cyclotron accessory 77−6599
solid target preparation by reactions with gases 80−18733
solid targets from gaseous elements, prod. and use 80−23212
SOLIS, surface ionisation integrated target-ion source 77−14303
superconducting magnet system, polarised proton target, for pion photoproduction 79−22508
surface ionisation integrated target-ion source for Sr, Ba 77−88314
thickness determination method using series integration 80−18748

nuclear bombardment targets continued
thickness meas. by photon induced X-ray fluorescence 77−18728
thickness uniformity gauge using ^{147}Pm beta source 77−10512
thin film target preparation using glow discharge ion source 78−55067
thin target manufacture methods for studying heavy particle reactions 79−68112
track sensitive target expts., automatic film meas. 78−55105
transuranic production for medical use, chemical treatment of targets *(French)* 77−42203
transuranics production by irradiation in expt. reactors, medical *(French)* 77−42202
TRISTAN facility, target developments 77−23353
ultra-high vac. harmonic drive as rotary motion feedthrough 77−2661
ultra-high-temperature, for on-line isotope separators 77−23337
UNILAC, He-jet transport system for short-lived nuclei 79−13569
vacuum evaporation, substrate temp. meas. by laser beam 80−20794
water-cooled target for the 14 MeV neutron source, design and experiment 80−47795
Weapons Neutron Research Facility initial target/moderator configuration 79−9933
X-ray fluorescence thin film calibration standards 80−22496
ZGS, polarised targets 80−91309
13 self supporting film production 80−18747
Al foils, thickness uniformity determ. from proton backscatt. yield 77−10510
^{241}Am, target prep. for synthesis of transactinide elements 80−23206
Ar isotopically enriched solid target prod. and use 80−23212
^{75}As(α,2n)^{77}Br production excitation curves 79−85468
^{10}B self supporting target preparation up to 500 μg/cm^2 80−18745
^{11}B self supporting target preparation up to 500 μg/cm^2 80−18745
Be, absolute neutron yield meas. for protons from threshold to 3 MeV 77−79498
Be, chemical procedure for preparation 79−63854
Be compact target, fast neutron prod. by 30 MeV deuteron irradiation 77−83424
Be foil, rolling procedures 80−23225
^{9}Be(d,n)^{10}Be, neutron distrib. from bombardment of thick Be target 77−83408
^{249}Bk, target prep. for synthesis of transactinide elements 80−23206
^{79}Br(p,3n)^{77}Kr→^{77}Br, production excitation curves 79−85468
Br(p,xn)^{77}Kr, prep. of carrier free ^{77}Kr using natural Br 78−29678
C accumulation on accel. target surfaces irradiated by protons 77−83380
C deposition on targets during beam bombardment 80−18741
C evaporated thin films, yield tensile strength meas. 80−23214
C foil, ion irradiation, correlation of energy loss and crystallographic transform. 80−23215
C foils, impurity anal. by PIXE 80−18740
C stripper foil, lifetime meas. 80−23216
C stripper foil preparation, under heavy ion bombardment 80−18717
C stripper foils, ethylene cracking in glow discharge, irradiation lifetimes 80−23207
C stripper foils, lifetime enhancement by slackening technique 80−23186
^{11}C isotopes, production and transport system 78−46200
Ca, evaporation preparation 80−23224
CaO, isotopically enriched target preparation using electron gun 80−23226
Cd, isotopic enrichment during zone melting process *(Russian)* 77−10522
^{249}Cf, target prep. for synthesis of transactinide elements 80−23206
Cl target prod. 80−9441
^{248}Cm, target prep. for synthesis of transactinide elements 80−23206
Co, absolute neutron yield meas. for protons from threshold to 3 MeV 77−79498
Cr complex, Cr^{V}, doping agent for polarised targets 78−46198
Cr(V) complex, paramagnetic, dynamic polarisation of protons and deuterons 79−36453
Cu, absolute neutron yield meas. for protons from threshold to 3 MeV 77−79498
Cu+Fe+Cd, nuclear target preparation by evaporation and rolling 80−23224
Cu+Fe+Sn, nuclear target preparation by evaporation and rolling 80−23224
D gas target with compact medical cyclotron, dosimetry of neutron field 77−73592
D, solid, construction and operation 77−6590
DT miniature target assembly, neutron yield calib. with associated particle monitoring 79−45505
^{166}Er preparation by retardation and direct deposition technique in mass separator 77−14285
Eu_2O_3 suitability, Gd impurity determ. by activation anal. and cation-exchange 77−16874
Fe complex $Fe(NO)[S_2CN(C_2H_5)_2]_2$ in frozen toluene, for dynamically proton polarised target 78−52378
Fe, proton bombardment, stable nuclide form. and separation 78−20045
Gd_2O_3, isotopically enriched target preparation using electron gun 80−23226
H atomic polarised beam target 77−34495
H gas jet target for p polarisation meas. in high energy elastic scatt. 77−30439
H, liq. target for neutron scatt., H vap. cooled 79−706
H scintillating gaseous drift chamber for use as positron sensitive target 80−9457
H, solid, construction and operation 77−6589
H_2, liq., prep. of Lawsonite end plates for working spaces 77−67926
H_2, liquid, fabrication of mylar caps for working cavities 77−46441
H_2 target, liquid, microprocessor-based cryogenic refrigerator controller 79−45491
H_2, thin liquid target for low energy nuclear physics expts. 80−78471
^{2}H cryogenic gas target design for neutron therapy 77−75020
He jet system for radioactivity studies 79−93855
He jet transport system, benzene and diethyl sulphide additives 79−76245
He jet transport system, operation with solid monodisperse aerosols 79−22507
He thin-window gas cell, calibration of magnetic quadrupole spectrometer 79−93859
He-jet transport system for nuclear reaction prods. using heavy ion accelerator ALICE *(French)* 77−3202
^{3}He liquid target for scatt. expts. 78−70663
^{3}He optically pumped target, polarisation enhancement and measurement 77−34531
^{4}He liquid target with remote handling for TRIUMF cyclotron 78−25364
Hf, preparation from HfO_2 reduction by Ca 80−18746
Hg, thick target preparation 79−63851
HgS target preparation for high resolution particle spectroscopy 77−30690
^{127}I(p,5n)^{123}Xe, in-beam collection of ^{123}Xe for carrier-free ^{123}I prod. 78−44610
^{82}Kr(d,3n)^{81}Rb, non-linear behaviour of gas targets for isotope prod. 78−25361
LaC_2, high-temperature carbide targets for fast on-line mass separation of alkali and noble gas elements 79−22515
Li, absolute neutron yield meas. for protons from threshold to 3 MeV 77−79498
Li, evaporation preparation 80−23224
^{6}LiD, new material for polarised targets for pol. neutron prod. *(French)* 80−68987
^{6}LiD, polarised target material, DNP 80−87007
Me, isotopically enriched target preparation using electron gun 80−23226
MgO target elements for Pu production *(French)* 77−42199
$^{14}N^{+}$ implanted in Ta, target preparation 79−45501
^{14}N(d,n)^{15}O, non-linear behaviour of gas targets for isotope prod. 78−25361
Na-vapour jet charge-exchange continuous-action target 80−23205
Nd_2O_3, isotopically enriched target preparation using electron gun 80−23226
Ni foil, crystal struct. as function of substrate temp. during deposition 80−18742
NpO_2 target elements for Pu production *(French)* 77−42199
^{16}O(p,α)^{13}N, in-cyclotron ^{13}N prod., water loop target 80−23201
P, thin red target preparation 78−46196
Pb isotopically enriched rotating sandwich targets for high intensity heavy ion beams 80−18743
Pb, self supporting O_2 free targets 78−13365
Pb targets for superheavy element synthesis 77−82960
Pt foil, crystal struct. as function of substrate temp. during deposition 80−18742
Pt target preparation using EM isotope separators 78−70676
^{238}Pu production, chemical treatment of Np targets *(French)* 77−42201
^{238}Pu production from targets in Celestin reactors, medical use *(French)* 77−42200
^{84}Rb, preparation by on-line isotope separation 77−23328
S isotopic targets prod. by evaporation technique 77−34500
Se+p→^{77}Br production excitation curves 79−85468
Si live targets, transversal filter approach of trapezoidal pulse shaping 79−36487
SiO_2, isotopically enriched target preparation using electron gun 80−23226
Sm_2O_3, isotopically enriched target preparation using electron gun 80−23226
^{144}Sm, enriched isotope target preparation, design of quasi-hyperbolic electrostatic field 80−23597
sputter, isotopically enriched targets for ^{148}Ca and ^{14}C prod. 80−23221
T gas target as intense 14 MeV neutron source 77−83429
T gas targets, pressure monitoring system 80−99370
T, low-temp. gas target fast neutron prod. facility 77−30691
TaC, Ta_2C, prod. of $^{14}C^{-}$ beam for tandem accelerator *(French)* 79−76243
^{122}Te on Au target fabrication for cyclotron isotope prod. 77−83406
^{124}Te, prod. of ^{123}I for radiopharmaceuticals 77−60252
^{124}Te(p,2n)^{123}I, improved targetry and radiochem. for ^{123}I prod. 78−28064
^{124}Te(p,2n)^{123}I, new approach to target chem. for ^{123}I prod. 77−60250
^{124}Te(p,n)^{124}I, improved targetry and radiochem. for ^{124}I prod. 78−28064
Ti high pressure gas target 78−70671
Ti rolled foil preparation 80−18744
Ti, tritiated self supported target prep. 80−23211
Ti-T target system for production of 14 MeV neutrons, improvements 80−63433
TiT targets, prod. of DT neutrons by d^{+} beam irradiation analysed 77−18727
Tl+p, ^{201}Tl and ^{203}Pb radioisotope preparation 79−88184
U deposit spray painting on metallic backing 80−18736
U films, production techniques 77−389
UC, high-temperature carbide targets for fast on-line mass separation of alkali and noble gas elements 79−22515
$^{235}UO_2$ single crystals, electrochemical prep. 78−37478
^{235}U, muonic, fission studies, target preparation 80−23217
^{238}U, muonic, fission studies, target preparation 80−23217
^{238}U target for pulsed spallation neutron source, design 77−67930
^{238}U thin self supporting foils 80−9440
V foil, rolling procedures 80−23225
VC, high-temperature carbide targets for fast on-line mass separation of alkali and noble gas elements 79−22515
W foil, rolling procedures 80−23225
W, isotopically enriched target preparation using electron gun 80−23226
W+p, 25 GeV, antiproton prod., flux optimisation using hadron cascade calcs. 77−83411
Zn, isotopic enrichment during zone melting process *(Russian)* 77−10522

nuclear branching and mixing ratios
^{24}Mg radiative decays of unbound high spin states from ^{20}Ne(α,γ), ^{20}Ne(α,α′γ) 79−6484
A=134-144, fission yields from spectroscopic meas., γ-branching and half-lives 80−78213
A=149, data sheets to August 1974 77−10305
A=163, nuclear data sheets to April 1979 80−98762
A=16, (π^{-}, γ) and (μ^{-}, ν_μ) capture reactions on ^{16}O, branching ratios 78−17105
A=190 to 220 even-even nuclei, 2_2^{+} level deexcitation *(Russian)* 77−2939
A=21-44, energy levels, excitation energies, branching and mixing ratios, lifetimes, J^{π}, resonances 79−13208
A=24-28 nuclei, reliability of calculated decay props. 78−93970

nuclear branching and mixing ratios continued
A=4N nuclei, lowest T=2 state isospin forbidden decays, branching ratios 79−67703
A=60 to 150 even-even nuclei, 2_1^+ level deexcitation *(Russian)* 77−2939
A≤57 nuclei, E2, M1 multipole mixing ratios 80−22751
computer program for meas. gamma-gamma directional correlations and anal. of ang. distrib. data 78−86503
delayed neutron spectra, gross props. 78−78327
E2:M1 multipole mixing ratio, sign change in A=150 region 80−493
E2, M1 multipole mixing ratios in odd-mass nuclei, A>150 77−30503
E2 α_k conversion coeffs. for $2^+ \rightarrow 0^+$ transition, review 78−17143
E2/M1 mixing ratio, in vibr. yrast band, sign rule 79−17855
eikonal approx., electron-oriented nucleus scatt., polarisation of e^-, nuclei and emitted γ rays 78−37331
even-even nuclei, 58≤A≤150, E2, M1 multipole mixing ratio, data survey 78−50118
light nuclei, schematic model for isospin mixing 78−66198
linear polarisation mixing coeffs. for mixed dipole and quadrupole γ-radiations, Compton polarimeter 80−73110
nanosecond isomers, in-beam gamma spectroscopic investigation, Ge(Li) detector 78−86506
odd mass nuclei, 59≤A≤149, E2, M1 multipole mixing ratios 78−4911
odd-odd deformed nuclei, mag. props. 77−82822
pair rotational (vibrational) spectra formulae, branching ratio, selection rules, two particle transfer reaction *(Chinese)* 79−9448
pairing correlation treatment, single particle levels, binding energy, spectra, branching ratios *(Chinese)* 80−102107
particle rotor model study of transitional N=89 and N=91-95 nuclei 80−42529
positronium production in nucl. monopole transitions 77−54635
shape isomers, spontaneous fission, static and decay props. and excitations, review, book contrib. 78−82402
T=1/2 mirror nuclei, half-lives and branching ratios meas. 77−74805
XX ^{126}Xe, $2_2^+ \rightarrow 2_1^+$ transition multipole mixing ratio 80−78198
$(n,\gamma\gamma)/(n,\gamma)$ branching ratios for ^{2}H, ^{3}He, ^{16}O, and ^{208}Pb 77−14131
ν-nucleus reactions, multimuon events, QCD predictions for associated prod. of charm 78−25034
(π^-,π^0) absorpt. by complex nuclei 77−88174
π^-, radiative capture, branching ratio with respect to stopped π^- absorpt. 78−89914
^{134}Ba level scheme obs. from ^{134}La decay 77−10360
^{A}Ag, A=105,107, positive parity band, mixing and branching ratios lifetimes from $(^{16}O,2np)(^{14}N,3n)$ 80−9197
^{109}Ag levels from ^{109}Pd decay, spins, γ cascades, mixing ratios 77−22930
^{110}Ag^m, oriented, T-reversal test and struct. study 78−86505
^{111}Ag, 376.7 keV level lifetime, shape coexistence, γ-branching 78−551
^{122}Ag decay, struct. of neutron rich even-even Cd nuclei 78−66249
^{A}Al, A=25,26,27 levels, resonances, γ-ray branching ratios from Mg(p,γ) 80−86875
^{26}Al, isoscalar and isovector E2 transition matrix elements 78−25148
^{26}Al low energy resonances, decay and J^π assignments, branching ratios from ^{25}Mg(p,γ) 80−42624
^{26}Al T=1 states, resonances, J^π and transitions from ^{25}Mg(p,γ) 80−99131
^{27}Al bound state parity and spin assignments, level struct. from ^{26}Mg (p,γ) resonances 78−66206
^{27}Al isobaric analogue resonances, spectroscopic factors and γ-rays from (p,p), (p,γ) 80−86873
^{27}Al levels, resonances, J^π, branching and mixing ratios from ^{26}Mg(p,γ) 80−99132
^{28}Al levels, spins and γ-rays, multipole mixing from ^{27}Al(n,γ), pol. thermal 80−47398
^{31}Al, radioactive half-life and branching ratios 79−22240
^{35}Ar→^{35}Cl superallowed decay, branching ratio meas., Cabibbo angle anomaly 79−26399
^{36}Ar, obs. of decay of T=2 state in ^{35}Cl(p,γ) 77−6294
^{38}Ar yrast levels, J^π assignments, transitions, branching and mixing ratios from ^{35}Cl(α, pγ), ^{24}Mg(^{16}O, 2pγ) 79−67625
^{39}Ar, energy level spin and parity assignments, level spectroscopy from (α,nγ), (d,pγ) 78−93943
^{40}Ar, yrast levels, J^π, branching and mixing, via (^{16}O, 2pγ) 34 MeV 77−74759
^{74}As decay, branching ratios and $T_{1/2}$ meas., K-fluorescence yield of Ge 77−3300
^{75}As, transitions populating and depopulating 279 keV level, δ(E3/M2) 77−82852
^{75}As(n,n'γ)^{75}As, deexcitation gammas, energy levels, branching ratios, spins, parities, excitation function meas. 78−89869
^{85}As, β-decay delayed n emission, simple statistical model description 79−67714
Au, A=189, 191, 193, γ-ray ang. distrib. meas., particle-hole symm. 77−88074
^{A}Au, A=181, 182, alpha decay, half lives, decay energies and branching ratios 79−45215
^{9}B, isospin forbidden nucleon decays of T=3/2 levels 77−6320
^{10}B T=1 states, γ-transition strengths, lifetimes, branching and mixing ratios from ^{6}Li(α,α) 80−27594
^{10}B(n,α_1), 2 and 24 keV, ang. distribs., branching ratio 79−54440
^{11}B(d,p)^{12}B reactions, 1.3 to 3.0 MeV, DWBA analysis of magnetic substate populations of residual nucleus 78−29480
^{12}B, β-ray branching and $T_{1/2}$ 78−41674
^{A}Ba, A=142,144,146, transition γ-γ ang. correlations, levels, J^π, mixing ratios 80−73823
^{138}Ba, E(1) and E(2) transitions via (γ, γ) at E<5 MeV 77−74797
^{142}Ba, $\gamma\gamma$ ang. correlations, levels, spins and mixing ratios from ^{142}Cs decay 80−57734
^{143}Ba decay to ^{143}La, β-branching and log ft values 78−50129
^{8}Be isovector radiative decay, E2-M1 mixing ratio, conserved vector currents from ^{4}He(α,γ) 79−6488
^{9}Be, first T=3/2 states, γ-decay, branching ratios and total widths from ^{7}Li(^{3}He, pγ) 79−6489
^{9}Be, isospin forbidden nucleon decays of T=3/2 levels 77−6320
^{9}Be(d,p), 12 MeV polarised deuterons, analysing powers, j-mixing ratio 77−82937
^{9}Be(d,t), 12 MeV polarised deuterons, analysing powers, j-mixing ratio 77−82937
^{206}Bi, decay investig. from nuclear orientation of ^{206}Bi in Ni 77−41911
^{206}Bi, nucl. orientation in ferromag. BiMn 78−13010
^{207}Bi, nucl. orientation in ferromag. BiMn 78−13010

nuclear branching and mixing ratios continued
^{209}Bi EM props. of particle vibration coupling states from ^{208}Pb(^{7}Li, ^{4}He 2nγ) 78−70485
^{242}Bk electron capture half life and α-branching ratio from ^{238}U+^{10}B, ^{235}U+^{11}B, ^{232}Th+N 79−67716
^{248}Bk, 23.7 h, spectroscopic studies 78−78314
^{76}Br(n,p)^{76}Se, thermal energy, ^{77}Br proton branches 78−89878
^{87}Br, β-decay delayed n emission, simple statistical model description 79−67714
C+K at rest, absorpt. branching fractions determ. 77−67771
^{12}C, 15.1 MeV level decay branching ratios, meas. with NBS positron annihilation in flight facility 79−31306
^{12}C, branching ratio of 7.654 MeV state meas., rate of stellar He burning 77−2941
^{12}C, radiative transitions and isospin mixing 77−38242
^{12}C(^{12}C,n)^{23}Mg, 3.54-4.94 MeV, cross section, neutron branching ratio, stellar processes estimates 77−34336
^{12}C(γ,γ), 15.11 MeV energy level excitation, branching ratio 77−30548
^{12}C($\mu^-,\nu_\mu\gamma$)^{12}B, impulse approx. calc., photon branching ratios 78−37315
^{12}C(π, 2γ), limit on 2γ/1γ branching ratio 77−10447
^{12}C($\pi^-\gamma\gamma$), branching ratio, ang. correlation 79−85526
^{12}C(π^-, 2γ), doubly radiative capture theory, branching ratio and ang. correlations 80−9314
^{14}C first excited 0^+ state, lifetime and E^0 decay from (d,p), (^{13}C,p) 80−102145
^{40}Ca, branching ratio and electric, monopole strength excited in ^{40}Ca(p,p') at 7-10 MeV 77−30505
^{40}Ca($\mu,\nu\gamma$), ^{40}K,*, 85 MeV/c, radiative capture branching ratio, photon asymm. 77−79365
^{42}Ca, high spin states from ^{39}K(α,p), lifetimes, multipole mixing ratios 78−50186
^{A}Cd(n,nγ) A=114,116, energy levels, spins, and gamma-ray multipole mixing ratios investig. 80−52580
^{114}Cd(e,e'), 40-110 MeV, vibr. nuclei, branching ratios 77−6356
^{141}Ce, γ-decay, levels, J^π, branching via ^{140}Ce(d,pγ) 8 MeV 77−14064
^{34}Cl, high spin negative parity states, lifetimes meas. 78−74327
^{34}Cl, J^π, levels, mixing ratios, $T_{1/2}$ via ^{33}S(p,γ) and ^{33}S(p,p) 1.0, 2.0 MeV 77−26613
^{34}Cl, levels Γ, γ-branching, $T_{1/2}$ via ^{33}S(p,γ) 1.0, 2.0 MeV *(French)* 77−26612
^{37}Cl, in-beam γ-ray spectroscopy via ^{3}H(^{35}Cl,pγ) 78−13013
^{55}Co, resonance decays, branching ratios and analogue resonances from ^{54}Fe(p,γ) 80−52643
^{56}Co, γ-ray transitions, branching ratios, spin assignments, energy level lifetimes from ^{54}Fe(^{3}He, pγ) 79−497
^{57}Co, $g_{9/2}$ IAR in ^{56}Fe(p,γ) 78−70504
^{57}Co, $g_{9/2}$ isobaric analogue resonances, obs. in ^{56}De(p,γ)^{57}Co 78−82332
^{59}Co (n, n'γ), 1.3-3.9 MeV, energy level structure and decay scheme 79−45164
^{59}Co level energies, branching ratios lifetimes and spins from (p,p'),(α,pγ) 80−63093
^{59}Co(n,n'γ), 1.1-3.3 MeV, level inelastic scatt. cross section, decay γ-rays, spins, branching ratio 79−6605
^{60}Co low lying states from ^{57}Fe(α,pγ), spin constraints, γ mixing ratios 78−29487
^{49}Cr low lying states, deformed configuration mixing shell model calcs. 77−6302
^{51}Cr, bands, levels, EM transitions, J^π, branching and mixing ratios from ^{48}Ti (γ,nγ)^{51}Cr and ^{51}V(p,nγ)^{51}Cr 80−52606
^{51}Cr, strongly deformed $K^\pi=1/2^-$ bands from γ meas., level transition parameters 79−3113
^{52}Cr, γ-decay of analogue states obs. in ^{51}V(p,γ) 78−70503
^{52}Cr(e,e'), 40-110 MeV, vibr. nuclei, branching ratios 77−6356
^{A}Cs, A=142, 144, 146, low lying levels, J^π, mixing ratios and γ-γ ang. correlations 80−102119
^{114}Cs β-decay, half life and branching ratio, ^{114}Xe excited states and γ-rays 80−47436
^{114}Cs, neutron deficient isotopes from ^{58}Ni(^{58}Ni,xpyn), alpha decay studies 79−93567
^{133}Cs, 161 keV transition M1-E2 mixing ratio and nucl. struct. parameter 78−74332
^{133}Cs(α,α'), 161 keV state magnetic moment and B(E2) values, Coulomb excitation 79−45159
^{62}Cu, yrast states obs. in ^{60}Ni(α,pnγ) and ^{63}Cu(p,pnγ) 78−12945
^{63}Cu(p,p') negative parity level excitation, gamma ray obs., test for core excitation model 80−68534
^{64}Cu, γ-spectra, J^π assignments via ^{64}Ni(p,nγ) 2.75-3.75 MeV 77−18470
^{65}Cu(p,p'γ), 5.25, 6.0 MeV, levels, transition energies, lifetimes, branching ratios determ. 77−41960
^{162,164}Dy, γ-mixing, J^π values, levels via (n,n'γ) reaction 77−74768
^{160}Dy, meas. of 1178-87 keV cascade ang. correl. function 77−14061
^{162}Dy, level scheme, γ-branchings following ^{162}Tb decay 77−34246
^{164}Dy multipole mixing in γ to ground bands from ^{163}Dy(n,γ) 80−52615
Er, A=162, 164, 166, (α,2nγ) studies of vibr. and other side bands 77−2893
^{19}F, 3907 keV state, lifetime meas. by Doppler shift attenuation method 77−88079
^{19}F levels, studied via ^{19}F(p,p'γ), 5 to 9 MeV 77−297
^{19}F reson. levels from ^{15}N(α,γ)^{19}F reaction 77−65211
^{19}F(p,p'γ), 1459→110 keV transition, E2/M1 mixing ratio 80−106013
^{A}Fe, A=57, 59, levels, J^π and transition branching ratio from Fe(n,γ) 80−105976
^{53}Fe, strongly deformed $K^\pi=1/2^-$ bands from γ meas., level transition parameters 79−3113
^{56}Fe, level struct. via (^{12}C,α2p), (α,2p) and (α,α) reactions 77−67702
^{56}Fe low lying levels, J^π, γ-γ coincidences, internal conversion from ^{56}Co β^+-decay 80−86815
^{58}Fe high spin states from ^{55}Mn(d,pγ), decay props., γ-γ coincidence 78−21515
^{67}Ga, levels, branching, mixing, $T_{1/2}$, via ^{67}Zn(p,nγ) 3.6-4.3 MeV 77−34247
^{67}Ga levels below 2.5 MeV populated in ^{64}Zn(α,pγ) 77−88042
^{69}Ga(n,n'γ), fast n, levels, J^π, transitions and mixing ratios, statistical anal. *(Russian)* 80−13382
^{71}Ga ang. correlations, level spin assignments and multipole mixing ratios from ^{71}Zn^m decay 78−78305
^{72}Ga→^{72}Ge, gamma and beta-ray spectra, intensities, branching ratios, spin and parity assignments *(Korean)* 78−50128
^{154,156}Gd, pairing-plus-quadrupole calcs. 77−82807

nuclear branching and mixing ratios continued
$^{\vee}$Gd, A=150-156, E2:M1 multipole mixing ratio, sign change in A=150 region 80−493
^{67}Gd, γ-spectroscopy of high-spin levels via ^{64}Zn(α,pγ), ^{53}Cr(^{16}O,pnγ) 78−93960
^{145}Gd EC/β^+-decay branching ratio anomalies, ^{145}Eu level and transition effects 80−32244
^{150}Gd levels and transitions, J$^{\pi}$ assignments mixing ratio, nuclear orientation from ^{150}Tb decay 79−13205
^{154}Gd, elec. monopole and quadrupole matrix elements for the K$^{\pi}$=0$^+$ bands 77−57626
^{154}Gd, γ-γ directional correls., coincidence meas. 77−65212
^{156}Gd, elec. monopole transitions from excited 0$^+$ states, ^{156}Eu decay obs. 77−18478
^{156}Gd transitions from second K$^{\pi}$=0$^+$ band following ^{156}Eu decay, branching, mixing ratios 78−25150
^{66}Ge levels, lifetimes and mixing ratio, in-beam γ-spectroscopy from ^{54}Fe(^{14}N,npγ) 80−42541
^{69}Ge excited states, lifetimes and J$^{\pi}$ assignments, mixing ratios from ^{66}Zn(α,nγ) 79−63629
^{69}Ge high spin states, EM props., Branching and mixing ratios from ^{55}Mn(^{16}O,pn) 80−13347
^{71}Ge, levels, studied via ^{68}Zn(α,nγ), 8 to 10 MeV, comparison with coupling model calcs. 78−8742
^{2}H+π$^-$→π^{0}nn, rest capture branching ratio, impulse approx. 78−62957
^{3}H$_{\Lambda}$→π$^-$^{3}He branching ratio calc. 79−63620
^{3}H(π$^-$, γ)3n, rest π, resonance branching ratio, bound state upper limit 80−99162
^{3}He(n,γγ), thermal neutrons, cross section and branching ratio 79−45263
Hf, alpha decay studies of the isotope 79−63636
^{180}Hf, internal conversion coeff., penetration effect 79−6500
^{A}Hg, A=177-183, 188, alpha decay, half lives, decay energies and branching ratios 79−45215
^{201}Hg γ-γ directional correlations, level transitions, spin assignments, mixing ratios from ^{201}Tl decay 79−496
^{201}Hg missing f$_{5/2}$ state Coulomb excitation, level scheme, J$^{\pi}$, transitions using (α,α), (^{18}O, ^{16}O) 80−47386
^{152}Ho α-decay and branching ratio 79−89241
^{A}I, A=110-113, neutron deficient isotopes from ^{58}Ni(^{58}Ni,xpyn), alpha decay studies 79−93567
^{137}I, β-decay delayed n emission, simple statistical model description 79−67714
^{A}In, A=119, 121, unified model description, vibr. multiplet yrast struct., branching ratios 80−105953
^{111}In band structure and hole-core coupling, ^{109}Ag(α,2nγ), branching and mixing ratios 78−58249
^{112}In low lying levels, transitions, T$_{1/2}$, multipolarities and mixing ratios from ^{112}Cd(p,nγ) 80−68545
^{A}Ir, A=189, 191, levels, J$^{\pi}$, transitions and mixing ratios from Pt decay 80−68602
^{38}K, lifetime and E2/M1 branching ratio of second excited state 77−34254
^{40}K, spin and mixing ratio determ. from ang. distrib. meas. 79−93551
^{40}K, yrast levels, J$^{\pi}$, branching and mixing, via (^{16}O,pnγ) 34 MeV 77−74759
^{41}K, l-forbidden M1 decay from 1st excited state 78−13024
^{41}K, populated by ^{38}Ar(α,pγ), levels props., shell model calc. 78−62588
^{42}K, yrast state J$^{\pi}$ assignments via ^{26}Mg(^{18}O, pnγ) anal. at 25,34 MeV 77−57618
^{84}Kr levels, γ-cascades, J$^{\Pi}$, mixing ratios and correlations from ^{84}Br decay 80−63134
^{139}La, nuclear structure effect on internal conversion of l-forbidden transitions 79−63632
^{7}Li(π$^-$, t)^{4}H, study of particle-unstable state ^{4}H, branching ratio 79−93528
^{11}Li beta decay, γ activity 80−106018
^{7}Li(γ,n), photo neutron cross sections, branching ratios 77−41943
^{157}Lu, short lived α emitter, α energy, T$_{1/2}$ and branching ratio 80−501
^{177}Lu, 150 keV state, mag. dipole moment, TDPAC 77−41886
^{176m}Lu, electron capture meas. *(German)* 78−33153
^{A}Mg, A=29-32, radioactive half-life and branching ratios 79−22240
^{24}Mg 6$_3^+$ level, α and γ decays, branching ratios from ^{12}C(^{16}O,α) 79−75901
^{24}Mg continuum states, branching ratios from ^{12}C(^{16}O, αα) 80−22661
^{24}Mg, multipole mixing ratios from polarised beam γ-ray singles meas. 77−46132
^{24}Mg, T=2 state props., obs. in ^{23}Na(p,γ)^{24}Mg reaction 78−8767
^{24}Mg(d,pγ)^{25}Mg, particle-gamma and gamma-gamma coincidence, energies and branching ratios 77−22892
^{26}Mg, isoscalar and isovector E2 transition matrix elements 78−25148
^{26}Mg, multipole mixing ratios from polarised beam γ-ray singles meas. 77−46132
^{27}Mg, excited states up to E$_x$=7976 keV, studied via ^{26}Mg(d,pγ) reaction 77−41981
^{28}Mg ΔT=1 0$^+$→0$^+$ β-decay, isospin forbidden branching ratio to ^{28}Al 79−93560
^{28}Mg, isospin forbidden β-decay 78−78315
^{51}Mn, EM transitions, J$^{\pi}$, half-lives, branching and mixing ratios 77−18471
^{52}Mn, high spin state spectroscopy via ^{39}K(^{16}O,2pnγ) 37-52 MeV 77−10321
^{52}Mn, low-lying states J, γ-branching and mixing via ^{52}Cr(p,nγ) 77−14028
^{53}Mn high spin states, decay scheme, J$^{\pi}$ assignments, mixing ratios from ^{40}Ca(^{16}O, 3pγ) *(French)* 79−67627
^{53}Mn lifetimes meas. from ^{50}Cr(α,pγ)^{53}Mn *(French)* 79−67711
^{55}Mn, levels, J$^{\pi}$, γ-branching via (n,n′γ) 1.0-3.6 MeV 77−79310
^{55}Mn(n,n′γ), 2.2-3.2 MeV energy level J$^{\pi}$ assignments, transition branching and mixing ratios 79−40881
^{59}Mn, β-decay scheme, mass, branching ratios 77−82873
^{94}Mo high spin state transitions, mixing ratios, spins, shell model calcs. from ^{94}Tc decay 79−97678
^{94}Mo, level spins and multiple mixing ratios from γ-γ correlation meas. 78−21517
^{95}Mo, levels, B(E2), B(M1), branching ratios populated in ^{95}Tc^{m,g} decay 77−82856
^{104}Mo, first excited 0$^+$ state, E0^2/E2$^+$ ratio 79−17819
^{12}N, β-ray branching and T$_{1/2}$ 78−41674
^{14}N 9.13 MeV state, obs. in ^{13}C(p,γ) 78−41641
nuclear branching and mixing ratios continued
^{14}N unbound 4$_1^+$, 5$_1^+$, 3$_2^+$ states from ^{13}C(p,γ), lifetimes, branching ratios 78−25184
^{17}N, excited states obs. in ^{18}O(t,αγ) at 3.5 MeV *(French)* 77−14031
^{A}Na, A=27-32, radioactive half-life and branching ratios 79−22240
^{22}Na bound and analogue state lifetimes, branching ratios, DSA method from ^{21}Ne(p,γ) 0.5-6.0 MeV 78−93967
^{22}Na, ground state band struct., J$^{\pi}$, E2 transitions, T$_{1/2}$ *(French)* 77−34210
^{22}Na, isoscalar M2 transition, γ-ray spectra obs. 77−10363
^{23}Na, spectroscopy of high-spin states in ^{12}C(^{12}C,pγ) 77−46131
^{25}Na, τ, J, π, branching and mixing ratios for lowest 5 levels 77−57624
^{91}Nb, struct. anal. from ^{91}Zr(p,nγ) at 3.5-4.8 MeV 78−13011
^{94}Nb, spin parity determ., excitation energy 979 keV 79−9551
^{146}Nd(γ,γ′), reson. fluoresc., J$^{\pi}$, M2/E1 and Γ meas. 77−26663
^{20}Ne, alpha-cluster states, spin, parity and branching ratios 78−50066
^{20}Ne, α decay from 8p-4h O$^+$ state, branching ratios 78−50132
^{20}Ne continuum states, J$^{\pi}$ and branching from ^{12}C(^{12}C, αα) 80−22660
^{20}Ne, from ^{16}O(α,γ), 10.27 MeV, first T=1,2$^+$ state radiative width meas. rel. to analogue β-decays 78−549
^{20}Ne, gamma decays of some T=0, 1 and 2 states above 9.5 MeV 77−34244
^{20}Ne high spin states, J$^{\pi}$ and α-decay branching ratios from ^{16}O(^{12}C,^{8}Be) 80−18166
^{20}Ne levels, J$^{\pi}$, branching ratio and EM transition rates from ^{16}O+α 80−42540
^{20}Ne levels and branching ratio from ^{12}C(^{16}O, αα) 80−22661
^{20}Ne resonances, J$^{\pi}$, excitation functions and branching ratio from ^{19}F(p,γ) 80−22787
^{21}Ne(p,γ)^{22}Na, γ-ray ang. distrib. and mixing ratios, analogue resons. 78−62504
^{22}Ne(α,nγ)^{25}Mg, particle-gamma and gamma-gamma coincidence, energies and branching ratios 77−22892
^{A}Ni(A=58, 59, 61), thermal neutron induced charged particle spectroscopy 77−71611
^{58}Ni, isoscalar giant quadrupole reson., decay modes 79−63649
^{60}Ni, 1173 keV transition M3/M2 mixing ratio meas. 80−52608
^{61}Ni, γ-spectroscopy above 2.2 MeV excit., J$^{\pi}$,T, branchings 77−54172
^{61}Ni, low-lying levels, J, B(E2), B(M1) from Coulomb excit. 77−26610
^{61}Ni, spectroscopy of levels below 2.2 MeV obs. in ^{58}F(α,nγ) 77−6289
^{252}No spontaneous fission, fragment mass and kinetic energy distribs. 77−46194
^{239}Np, absolute meas. of branching ratio for the 277.6 keV line 80−86854
^{237m}Np fission isomer from ^{238}U(p,2n), statistical model anal., fission to γ branching ratio 78−25256
^{15}O, reson. widths and branching ratios meas. from ^{14}N(p,γ)^{15}O 77−38244
^{16}O, alpha-cluster states, spin, parity and branching ratios 78−50066
^{16}O high spin states, J$^{\pi}$ and α-decay branching ratios from ^{12}C(^{12}C,^{8}Be) 80−18166
^{16}O, search for 0$^-$→0$^+$ pair transition 78−86508
^{19}O β-decay, Fermi to Gamow Teller mixing ratio meas., ^{19}F isospin mixing 79−9520
^{19}O, p-γ correl. meas., form. from ^{18}O(d,p) reaction 77−10353
^{A}Os, A=169, 170, α-branching ratios 79−503
^{A}Os, A=188, 189, levels, J$^{\pi}$, transitions and mixing ratios from Ir decay 80−68602
^{171}Os, alpha decay, half lives, decay energies and branching ratios 79−45215
^{186}Os, levels deduced from ^{186}Ir decay and ^{186}W,(α,4n)^{186}Os 78−86481
^{194}Os beta decay, X-ray/gamma relative intensities, L$_1$ subshell yields 78−4919
^{30}P T=1 state decay, lifetimes and branching ratios, analogue E2 transitions from ^{29}Si(p,γ) 80−68598
^{31}P(p,γ)^{32}S resonances below E$_p$=1.5 MeV 77−50141
^{A}Pb, A=190,192, level scheme, γ-branching, ^{192m}Pb half life from Gd+^{40}Ar and ^{182}W+^{16}O 79−75854
^{204}Pb(n,n′γ), 1.5-3.1 MeV, levels, J$^{\pi}$, excitation functions and mixing ratios 80−102123
^{206}Pb γγ directional correlations, multipole mixing ratios, transition strength limits from ^{206}Bi decay 80−86849
^{208}Pb region, finite Fermi systems, review 78−537
^{101}Pd nonyrast rotational states, transitions, T$_{1/2}$, branching and mixing ratios from ^{92}Zr(^{12}C,3n) 80−105950
^{105}Pd E2/M1 mixing ratios from decay of polarised ^{105}Rh 77−6315
^{105}Pd, high-spin particle-core multiplets via ^{96}Zr(^{12}C,3nγ)^{105}Pd, rot. model 77−54140
^{106}Pd, gamma-gamma ang. correlation meas. from decay of ^{106}Rh^{g} 77−79325
^{106}Pd, γ-γ directional correlations, mixing ratios 77−82853
^{110}Pd(e,e′), 40-110 MeV, vibr. nuclei, branching ratios 77−6356
^{147}Pm, β-decay, branching ratio and K-shell autoionisation 80−42598
^{147}Pm energy levels and γ-ray transitions E2/M1 mixing ratio from ^{147}Nd β-decay 79−67655
^{147}Pm, low-lying levels, spin-parity and multipole mixing ratios 77−88043
^{151}Pm level scheme in low excitation region <1 MeV 77−54173
^{141}Pr, nuclear structure effect on internal conversion of l-forbidden transitions 79−63632
^{A}Pt, A=173-179, 188, alpha decay, half lives, decay energies and branching ratios, rot. struct. 79−45215
^{188}Pt α-decay energy and branching ratio 79−22237
^{196}Pt (^{20}Ne, ^{20}Ne′), excited states, lifetime meas. using recoil-distance method 80−13413
^{196}Pt (^{58}Ni, ^{58}Ni′), excited states, lifetime meas. using recoil-distance method 80−13413
^{239}Pu, spectroscopy in second minimum of pot. energy surface 79−30805
^{80}Rb, level struct., quasi-rot. bands, via ^{79}Br(α,3n) 30-55 MeV reaction 77−88028
^{85}Rb, single-particle estimate of γ-γ transition probability 78−13023
Re, alpha decay studies of the isotope 79−63636
^{A}Re, A=166, 167, 168, α-branching ratios, decay characterics 79−503
^{187}Re, 36.23 keV transition, penetration coeff. and mixing ratio determ. 77−50080
^{187}Re low lying level struct. and transitions, E2/E1 mixing ratios from ^{187}W decay 80−27557
^{103}Rh E2/M1 mixing ratios from decay of polarised ^{103}Ru 77−6315
^{103}Rh level scheme from fast n scatt., γ transitions, spins, parities, cross sections 78−78374
^{105}Rh E2/M1 mixing ratios from decay of polarised ^{105}Ru 77−6315

nuclear branching and mixing ratios continued
^{103}Rh gamma transitions, directional correl., multiple mixing ratios 79−80897
^{105}Rh, in Fe, oriented nuclear decay, mag. moments 77−46111
Ru, A=102, 104, collective states, J, B(E2), B(E3) via (d,d′) scatt. 77−26557
^{A}Ru(p,p′γ), A=96, 98, 5-8 MeV, level schemes, transitions, vibr. state, mixing ratios 80−18199
^{97}Ru populated in ^{88}Sr(^{13}C, 3nγ), band-like structures 80−32146
^{100}Ru, negative parity bands obs. in ^{100}Mo(α,4n)^{100}Ru 77−6291
^{104}Ru level energies, B(E2) ratio, mixing ratios, γ-ang. correlations, from ^{104}Tc β-decay 79−493
^{105}Ru, γ-γ ang. correl. meas., spin and γ-ray mixing ratios 78−21516
^{33}S, excited states, ang. correl. meas. 77−38239
^{33}S, state spectroscopy via ^{30}Si(α,nγ), E1,E2, J$^{\pi}$ assignments <5 MeV 77−34227
Sb isotopes, fission product conc., sensitivity anal. of branching ratio effects 78−82428
^{A}Sb, A=121,123, levels below 2 MeV, spins, transitions and mixing ratio from (p,γ), (n,n′γ) 80−32191
^{119}Sb, γ-γ and γ-e directional correls. following ^{119m}Te decay, branching ratios 78−546
^{135}Sb, β-decay delayed n emission, simple statistical model description 79−67714
^{42}Sc, β^{+} decay, isospin symm. hindered, branching fraction 78−21526
^{42}Sc, ground state β-decay, weak non-analogue Fermi branch, branching ratio upper limit 78−70495
^{45}Sc, fragmented analogue state, ^{44}Ca(p,p′γ) amplitudes 79−17882
^{51}Sc β-decay to ^{51}Ti, γ-ray spectra, β branching ratios, ^{51}Ti levels 77−6318
^{76}Se high spin states, bands, J$^{\pi}$, transitions and $T_{1/2}$ from ^{71}Ga(^{7}Li,2n) 80−105951
^{26}Si, isoscalar and isovector E2 transition matrix elements 78−25148
^{27}Si, γ-branchings and mixing ratios determ. from ^{24}Mg(α,nγ) 78−17224
^{28}Si, 12917 and 12924 keV level gamma-gamma directional correl. 79−536
^{28}Si levels, obs. in (α,γ) and (p,γ) reacts. 78−66205
^{28}Si, prolate and oblate intrinsic states *(French)* 78−70482
^{28}Si, T=1 positive parity analogue states, lifetimes and branching ratios 77−34249
^{28}Si(α,γ)^{32}S resonances below E_{α}=3.83 MeV anal. 77−50141
^{A}Sm, A=147, 149, levels, J, γ-transitions and multipole mixing ratios, γγ correlations from Eu EC decay 80−106012
^{A}Sm, A=148,9, structural connections, levels, bands, J$^{\pi}$, transitions and mixing ratios from Nd+^{3}He(α) 79−63576
^{A}Sm, A=150, 152, E2:M1 multipole mixing ratio, sign change in A=150 region 80−493
^{143}Sm, T$_{>}$ hole analogue states, p decay, deduced states and p branching ratio 78−70451
^{149}Sm, γ-γ ang. correl. meas., transition multipolarities, multipole mixing ratios 77−41910
^{150}Sm, nucl. struct. from ^{150}Pm decay *(Japanese)* 77−41889
^{150}Sm, yrast bands anal. from ^{150}Nd(α,4n), interacting boson approx. 78−13124
^{151}Sm, β-decay, branching ratio and K-shell autoionisation 80−42598
^{154}Sm(γ,γ′), reson. fluoresc., J$^{\pi}$, M2/E1 and Γ meas. 77−26663
Sn isotopes, fission product conc. sensitivity anal. of branching ratio effects 78−82428
Sn, odd isotopes, number-projected three-quasiparticle description 78−93953
^{116}Sn(^{16}O,^{16}O) 48 MeV, collective states, E2, E0 transition probabilities, halflife, branching ratios 80−18172
^{116}Sn(e,e′), 40-110 MeV, vibr. nuclei, branching ratios 77−6356
^{117}Sn^{m}, E5 transition, branching ratio from ^{120}Sn(p,3np) 79−45200
^{121}Sn$^{m}\rightarrow{}^{121}$Sn$^{g}\rightarrow{}^{121}$Sb, branching fraction, K-shell IC coeff. 78−82319
^{A}Sr, A=94,96 direct and skip cascades, γγ ang. correlations, levels, mixing ratios from Rb decay 80−86851
^{87}Sr excited levels from ^{87}Rb(p,nγ), spin, parity, branching ratios, lifetimes 77−50076
^{92}Sr γγ ang. correlations, levels, J$^{\pi}$, mixing ratios from ^{92}Rb decay 80−57725
Ta, alpha decay studies of the isotope 79−63636
^{166}Ta, isotope identification in ^{159}Tb(^{16}O,9n) reaction, half-life and decay scheme 77−79331
^{173}Ta, levels, rot. parameters, γ-mixing 77−34248
^{177}Ta, γ-transition 55/22$^{+}\rightarrow$77/22^{+}, E2/M1 mixing, μ determ., $T_{1/2}$ 77−10355
^{180}Ta^{m}, β^{-} and EC branching ratios, K-internal conversion coeff., γ-intensities, T 1/2 80−68601
^{181}Ta, anomalous M1-conversion, 482-keV transition, penetration parameter meas. 77−61382
^{149}Tb compound nucleus, statistical model de-excitation calcs. 78−50146
^{155}Tb, oriented in Gd, γ-decay ang. distrib., hyperfine splitting, moment and mixing ratios 79−45242
^{156}Tb, orientation in Gd matrix, γ-ray ang. distrib. anisotropy meas. 79−59031
^{160}Tb β-decay, oriented nuclei, γ transitions multipole mixing parameters 80−18240
^{95}Tc, energy levels from ^{95}Mo(p, nγ)^{95}Tc 80−37372
^{95}Tc in Fe, oriented nuclear decay, mag. moments 77−46111
^{97}Tc E2/M1 mixing from 785 keV ^{97}Tc γ-γ correl. 77−54178
^{97}Tc E2/M1 mixing ratios from decay of polarised ^{97}Ru 77−6315
^{97}Tc, γ-γ ang. correl. study, E2/M1 mixing ratios, transition strengths 77−71584
^{97}Tc levels, decay props., mixing ratios and J$^{\pi}$, from directional correlations in ^{97}Mo(p,nγ) 79−89240
^{99}Tc, β-decay, branching ratio and K-shell autoionisation 80−42598
^{99}Tc^{m} β-decay, β-branching, ^{99}Ru decay scheme 80−42596
^{95m}Tc$\rightarrow{}^{95g}$Mo, K capture branching ratio 77−6308
Te isotopes, fission product conc., sensitivity anal. of branching ratio effects 78−82428
^{A}Te, A=107-110, neutron deficient isotopes from ^{58}Ni(^{58}Ni,xpyn), alpha decay studies 79−93567
^{123}Te levels, spin assignments and E2/M1 multipole mixing ratio from ^{123}I decay 79−75836
^{126}Te(p,n), $2_2^{+}\rightarrow 2_1^{+}$ transition multipole mixing ratio 80−78198
^{228}Th decay, γ-ray and internal conversion intensities 78−41669
^{230}Th α-decay, search for the K$^{\pi}$=0^{+} excited states in ^{226}Ra 78−86504
^{44}Ti, lowest T=2 state decay, branching ratios from ^{46}Ti(p,t) 42 MeV 78−78304

nuclear branching and mixing ratios continued
^{46}Ti(α,nγ)^{49}Cr, gamma-ray ang. distrib., ang. correlation, linear polarisation and Doppler-shift attenuation meas. 77−82941
^{203}Tl, nuclear structure effect on internal conversion of l-forbidden transitions 79−63632
^{204}Tl, β-decay, branching ratio and K-shell autoionisation 80−42598
Tl(n,n′γ), 1.03-2.26 MeV, ang. distribs. meas., intermediate coupling model 77−38276
^{153}Tm, short lived α emitter, α energy, $T_{1/2}$ and branching ratio 80−501
^{163}Tm, high spin rot. levels, studied via ^{165}Ho(^{3}He,5n) and ^{165}Ho(α,6n) reactions 78−8722
^{167}Tm rotational bands, J$^{\pi}$, γ-transitions and branching ratios from ^{165}Ho(α,2nγ) 80−86781
^{169}Tm, studied via ^{169}Tm(^{32}S,^{32}S′γ), EM props. of ground state rot. band 78−8726
^{233}U levels, bandheads, total α-branching and transitions from ^{237}Pu α-decay 79−93516
^{236}U, odd-parity level at 687.59 keV, mixing ratios, half-life 77−50079
^{236}U shape isomer, γ branch upper limit, γ-yields from ^{235}U(d,p) 80−99145
^{237}U shape isomer, γ-decay search, branching ratio from ^{238}U(Γ,2nγ′) 45 MeV 78−93961
^{238}U, multipolarities involved in electrodisintegration 78−590
W, alpha decay studies of the isotope 79−63636
^{134}W, E1+M2+E3 multipolarity mixtures 536.7 and 920.9 γ-transition 79−6474
^{182}W high spin states, J assignments and mixing ratios from ^{182}Re isomer decay 80−42593
^{A}Xe, A=111-113, neutron deficient isotopes from ^{58}Ni(^{58}Ni,xpyn), alpha decay studies 79−93567
^{A}Xe, A=129, 131, populated in (α,nγ), props. of low-lying levels 80−464
^{127}Xe decay, absolute gamma-ray intensities 78−548
^{128}Xe, collective excitations obs. following decay of ^{128}Cs and ^{128}I 79−45143
^{131}Xe, ang. correl. meas. of γ-γ cascades from ^{131}I decay 77−6292
^{132}Xe level struct., J$^{\pi}$, transitions and multipole mixing ratio from ^{132}I decay 80−91134
^{167}Yb→^{167}Tm mass difference, from positron spectrum, level transition branching ratio 79−6376
^{171}Yb, EM transitions, mixing of states having different quantum numbers 79−6493
^{64}Zn, γ-ray spectroscopy from ^{61}Ni(α,nγ)^{64}Zn 78−21514
^{64}Zn, struct. of quasi-bands from (α,nγ) and (^{11}B,p2nγ) 78−70424
^{67}Zn, populated in ^{64}Ni(α,n), level struct. below 2.0 MeV, γ-ray studies 78−62483
^{90}Zr, γγ directional correl. meas. 78−33144
^{97}Zr, T$_{>}$ hole analogue states, p decay, deduced states and p branching ratio 78−70451
^{100}Zr, lifetime meas. of 331.3 keV 0_2^{+} state 78−21523

nuclear charge
see also form factors (nuclear)
1p shell isotensor charge depend. contrib. to isobaric mass multiplets, shell model anal. 79−67632
1p-shell nuclei, HF charge distribs. 77−14024
A=16-58, charge, proton and neutron density distribs. calc. 80−22680
A=3 nuclei, charge asymm. from EM contribution to ^{3}He-^{3}H binding energy difference 78−29378
A=3 nuclei, charge asymmetry 79−71808
A=40-100, charge distrib. from (e,e) and muonic X-ray meas. 78−54679
A=42 isotopic spin triplet, Coulomb energies and shifts, microscopic calcs. 80−9200
A=42 nuclei, T=1, J=0 states, Coulomb displacement energies, Hartree-Fock wave functions, charge depend. 78−89773
A=76-79 charge dispersion curve from ^{232}Th(p, f) 80−18349
abnormal nuclei, critical charge *(Russian)* 77−273
actinide fission, statistical anal. of gamma emission 78−17255
anomalous nuclei, crit. charge *(Russian)* 78−8736
asymmetry of forces, effects for np→dπ^{0} reaction 77−10332
charge distribution in heavy ion-reactions 78−74304
charge symmetry breaking forces, heavy nuclei binding energies 77−88047
collective props. of nuclei deduced from electron scatt., deformed nuclei, review 78−50064
compound-nucleus cross sections from nuclear charge-density distributions 79−9605
core polarisation effects in inelastic scatt. and charge exchange 77−22983
Coulomb and charge dependent effects in nuclei 77−54131
Coulomb displacement energies and n-p density distribs. 78−17084
Coulomb displacement energies of A=4n+3, T=1/2 mirror nuclei in $1f_{7/2}$ shell 77−57590
Coulomb energy differences, Cottingham formula appl. 78−37256
Coulomb energy of circular torus, application to crit. fissility *(French)* 79−6373
Coulomb Green function for extended, uniformly charged nucleus 79−13199
deep inelastic heavy ion collisions, charge and mass distrib. variances, time depend. 79−97651
deep inelastic heavy ion collisions, mass and charge distribs., statistical model 80−18332
deep inelastic heavy ion reactions, high multipole isovector modes and charge fluctuations 80−57793
deep lying level props. in strong electrostatic field *(Russian)* 77−2910
deep reconstruction of Coulomb field, shake-up of vacuum *(Russian)* 78−4910
deeply inelastic heavy ion collisions, charge transfer ang. momentum depend., fragment kinetic energies 80−47505
deformation energies for nuclei with different charge-to-mass ratio for fusion or binary fragmentation 79−80869
density distrib., Glauber-Sitenko approx. fast hadron scatt. anal. *(Russian)* 78−25161
deuteron, EM form factor, data anal. and asymptotic behaviour 79−89155
double magic nuclei, self consistent description of low lying collective states *(Russian)* 78−89783
E2 core-polarisation charge, nuclei near ^{16}O and ^{40}Ca 77−22888
effective charge evaluation using perturbation theory 78−78250

nuclear charge continued
effective interaction constraints imposed by antisymm. and charge independ. 78−86500
electric charge density of atomic nuclei *(French)* 78−86470
electron+nucleus scattering, three body correlations, influence on charge form factor of closed shell nuclei 79−6571
electron charge and velocity, independence limit, atomic neutrality 79−97549
electron scattering, inelastic, charge distribs. expansions for model independent anals. 77−50114
even-even deformed nuclei, coupled rot. bands, charge and density distribs. 78−89776
exotic atoms, E2 and E4 nucl. moments from HFS, review 78−37265
fermion charge accumulation in nucl. matter rel. to existence and props. *(Russian)* 77−57597
fission, droplet model of charge division 78−17173
fission, isobaric widths, frozen quantal fluctuations, charge equilibration 80−37365
fission, most probable charge, shell and deform. effects 78−29440
fission, spontaneous, mass and charge division, asymmetry, order-disorder model 80−22866
folded diagram calculation of effective charges, valence nucleon in 1s0d shell 78−4905
form factors, dispersion relation approach, pole and quark-counting model 77−26568
form factors, pion exchange currents effects 77−18379
fractional electric charges and mag. monopoles, existence in matter, model 79−13238
g-shell nuclei, charge distrib., self consistent calc. *(Russian)* 77−38234
Hartree-Fock expectation value variation, asymptotically linear functions 79−44776
heavy ion collisions, charge equilibrium and mass transfer, liquid drop model 79−97722
heavy ion collisions, charge equilibrium model using collective high freq. mode and quantal master eqn. 80−27667
heavy ion collisions, statistical model for mass and charge distrib. 79−17929
heavy ion deep inelastic reactions, charge equilibration 79−49635
heavy ion fusion reactions, charge density asymmetry liquid drop model 80−63220
heavy nuclei, charge asymmetry of nuclear forces and binding energies 79−75866
heavy particle track grain counting for nucl. charge determ. 78−17528
heavy-ion reactions, time for charge equilibration, microscopic hydrodynamical model 78−8857
heavy-ion sub-Coulomb collisions, e^+-e^- pair creation as probe for strong Coulomb fields 78−12962
isoscalar effective charge in large A limit Tamm-Dancoff and RPA calcs. 80−42534
light natural elements, muonic X-ray transitions, nuclear charge radii 80−99589
light ternary fission product charge distributions and fission probabilities 79−9643
linearised Hartree Fock model, effective charge, isoscalar nuclear shifts, rms radius ^{208}Pb, ^{90}Zr 78−25138
low energy fission, charge distrib., quantum mechanical phenomenon of GDR 80−86945
many-body charge density operators, breakdown of Siegert theorem 78−29379
multiquantum excitation calculation of density distrib. and charge form factors 77−41885
neutron rich nuclei; β^--emitters, deformation and spectroscopy 80−78223
nuclear forces, charge dependence and nuclear struct. effects, nuclear charge distribs. 80−32197
nuclear forces, charge symm. breaking, test by np elastic scatt. 78−89798
nuclear forces, charge symm. breaking, two-body, many-body nuclear systems 78−17109
nuclei stopping in nuclear emulsion, charge determ. 79−85363
nucleonic mass distrib. using mag. spectrometer *(French)* 79−449
odd-A deformed nuclei, EM and electron scatt. form factors, selection rules 79−9458
pion exchange contrib. to nuclear charge, current and Hamiltonian operators 77−41881
proton RMS charge radius from ^{1}H Lamb shift meas. 77−50047
quadrupole moments and rms charge radii, shell model calcs. 80−47369
relativistic electron scattering, expt. techniques for excited nuclei studies 77−30701
relativistic heavy ion reactions, target residue mass and charge distribs., calcs. 79−3172
RMS radii mass number depend., fine struct. 78−501
shape and charge polarisation of fission fragments, fusioning nuclei, and heavy ion scatt. 79−9543
shell effects in the RMS radii of the nuclear charge distributions determined by electron scattering 79−13200
spherical nuclei, energy density formalism, charge distrib. fine structure 77−6251
spherical nuclei, nuclear mass formula, energy density functional, self-consistent calc. 78−78244
supercharged nuclei, vacuum charge distrib., relativistic Thomas-Fermi approx. *(Russian)* 77−41876
transitional nuclei, particle-rotor recoil term and pairing interaction, Fermi surface 80−32174
trinucleon system, evidence of three body force, effect on charge density *(French)* 79−75857
two pion exchange charge density in static approx. ^{3}He, ^{3}H form factors 78−66222
two-body $1f_{7/2}$ nuclei, B(E2) transition probabilities, effective charge concept 77−18477
two-electron atoms, nucl. charge correl. with $(r_{12}^n)^{-1/n}$ function 79−68178
uncorrelated cluster model, generating functional formulation, charge transfer 79−49590
(e,e), virtual photon intensity and finite nuclear size effects, PWBA calcs. 79−26424
μ^- K-shell X-ray transitions in F, Na, Al, Si, P, S, K, nuclear charge radii 78−66195
n-p residual interaction effect on elastic electron scatt. by dipole giant resonance positioning 77−82914

nuclear charge continued
(p,t), deformed nuclei, quadrupole vibr. excitation in two nucleon transfer reactions *(Russian)* 79−30780
π^- condensation in electric field of supercharged nucleus *(Russian)* 78−54717
ρ-ω mixing charge symmetry breaking force, nonlocal contribs., ^{3}He-^{3}H mass difference 78−70458
^{27}Al, inelastic electron scatt., charge distrib., Coriolis band mixing calc., C2 form factors 79−529
Ar isotopes, meas. of 280 MeV/nucleon particles with plastic detector 77−38561
^{36}Ar, charge distrib. via ^{36}Ar(e,e′) 65-115 MeV 77−18527
^{40}Ar, charge distrib. via ^{40}Ar(e,e′) 65-115 MeV 77−18527
^{197}Au+^{129,132,136}Xe, near interaction barrier, charge asymm. equilibrium 78−8843
^{197}Au(^{A}Xe,X), A=129, 132, 136, <787 MeV, light and heavy fragment N/Z ratios 80−32292
^{197}Au(^{132}Xe,X), damped collisions, charge distrib. second moments and giant E1 quantal fluctuations 80−27547
Ba, charge radii and binding energy per nucleon, linear relationship evidence 80−68520
Ba, neutron deficient, charge radii, moments, transitions and isomers, atomic beam laser spectroscopy 80−102141
^{A}Ba,(A=134-138), quadrupole moments and change in mean square radii of charge distrib. 79−50154
^{A}Ba, A=126 to 135, charge radii, mag. dipole and elec. quadrupole moment 79−72436
^{A}Ba A=128, 131, 133, charge radii and nuclear moments 79−9460
^{128}Ba, charge radius determ. using Doppler free laser spectroscopy 77−71558
^{131}Ba, magnetic mom. and charge determ. using Doppler free laser spectroscopy 77−71558
^{9}Be, molecular model, charge form factors for electron scatt. 78−46015
^{209}Bi, charge distrib. from elastic electron scatt. and muonic X-ray data anal. 78−54681
^{209}Bi+^{12}C reaction, fission product charge distrib., 40 to 66 MeV 77−79406
^{209}Bi(^{56}Fe,X), damped collisions, fast A/Z equilibration and correlated nucleon exchange 80−86798
^{12}C, charge transition density, sum rules, oscillation form factors *(Russian)* 79−22186
^{12}C, isospin mixing of 1^+ states 78−4898
^{12}C, pion-exchange contribs. to charge densities, HF calcs. 78−46001
^{12}C, pot. and charge deform. of rot. states 77−46106
^{12}C(e,e), 25-115 MeV, ground state charge distrib. and RMS charge radius 80−57672
^{13}C(^{14}N, ^{14}C)^{13}N, sub-Coulomb charge exchange *(Russian)* 78−46106
Ca, isotopic sequence charge distrib. calc. 79−85361
Ca, radial charge distrib. moments, ground state correlations, generator coordinate model 79−30785
Ca stable isotopes, nucl. charge distrib. from isotope shift in Ca I resonance line 79−9461
^{A}Ca A=40, 48, charge density and single particle state struct. 79−36144
^{A}Ca, A=40 to 46,48, nuclear charge distrib., from isotope shift of 6573 angstrom line 80−57674
^{40}Ca, charge density calcs. K_{mm} approx. 79−9456
^{40}Ca, ground state energy and RMS charge radius 78−58242
^{40}Ca, pion exchange currents and charge form factors, shell model anal. 77−10338
^{40}Ca, pion-exchange contribs. to charge densities, HF calcs. 78−46001
^{40}Ca(e,e), cross sections, model independ. charge density 80−27548
^{41}Ca, E2 core polarisation charge, Woods-Saxon shell model compared to harmonic oscillator model 80−63072
^{41}Ca, mean square nuclear charge radius, correl. with doubly magic ^{40}Ca 79−54385
^{45}Ca, nuclear charge radius, spin, moments, by laserspectroscopy 80−18187
^{48}Ca, neutron radius determ., charge symm. 78−29380
^{48}Ca, pion-exchange contribs. to charge densities, HF calcs. 78−46001
Cd, A=110, 116, difference in nuclear charge radius, X-ray isotopic shift meas. 77−18382
^{A}Cd, A=110, 112, 114, 116 nuclear charge radius differences 79−26365
^{249}Cf(n,f), thermal., yields of isotopes of Nb, I and Cs, charge distrib. 78−41789
^{252}Cf, SF, charge distrib., determ. of fractional cumulative yields of ^{134}Te and ^{135}I 78−41791
^{252}Cf, spontaneous fission product charge distrib. 78−13176
^{A}Cl(e, e′), 116, 194 MeV, A=35, 37, charge distrib. and RMS charge radius 80−102109
^{245}Cm (n,f), thermal, charge distrib., ^{135}I and ^{190}Ba fractional cumulative yields 80−63074
^{59}Co, electron elast. scatt. cross sections, phase shift anal. and HF calcs. *(Russian)* 78−41707
Cr, A=48-52, effective charges and E2 transitions in 1f-2p shell nuclei 78−544
^{A}Cr(e,e), A=50,52,53,54, 226.7 MeV, charge density distrib. *(Russian)* 78−86473
^{50}Cr(e,e), 227 MeV, differential cross sections, Fermi charge density distribs. *(Russian)* 78−89785
Cs, ground state spins, moments, charge radii by laser spectroscopy 80−78147
Cu, A=63, 65, electron elast. scatt. cross sections, phase shift anal. and HF calcs. *(Russian)* 78−41707
^{147}Dy charge states and charge distrib. from ^{113}Cd(^{40}Ar,6n) *(Russian)* 79−40840
^{148}Dy$_{82}$ 10^+ isomer, $\pi h_{11/2}$ effective E2 charge 78−93964
^{161}Dy, E0, E2 and E4 charge moment determ., using muonic atoms 78−21490
^{166}Er(^{86}K,X), deep inelastic collision, charge drift and dispersion calc., thermal eqn. model based on shell model 80−57798
^{166}Er(α,α'), 11.25 to 12 MeV, elec. moment, charge deform. parameters 77−54233
^{166}Er(e,e′), 35-350 MeV, coupled channels anal., rot. band excited states, charge densities 79−3139
^{17}F, effective charges and radial integrals calc. 78−4897
Fe, A=52, 4, effective charges and E2 transitions in 1f-2p shell nuclei 78−544
Fe, radial charge distrib. moments, ground state correlations, generator coordinate model 79−30785

nuclear charge continued
^{A}Fe(e,e), 100-275 MeV, A=54,56,57, cross sections and muonic X-ray meas., charge distrib. systematics 80−86801
^{A}Fe(e,e), A=54,56, 226.7 MeV, charge density distrib. *(Russian)* 78−86473
^{54}Fe(p,d)^{53}Fe, 40 MeV spectroscopic factors, ang. distrib., DWBA anal. 79−22287
^{154}Gd(α,α'), 11.8 MeV, charge deform. parameter determ. 78−33201
^{156}Gd(α,α'), 11.25 to 12 MeV, elec. moments, charge deform. parameters 77−54233
Gd(α,α'), 11.8 MeV, A=154, 156, electric quadrupole and hexadecapole moments, charge deform. parameters 77−30489
^{1}H(n,π^{0})^{2}H, nuclear forces charge symmetry test 80−5071
^{2}H charge operator, retardation, quasipot. eqns. and rel. corrections 80−99122
^{2}H(d,n)^{3}He, 1.5-15.5 MeV, tensor anal. power, charge symmetry violation in mirror reaction 80−13368
^{2}H(d,p)^{3}H, 1.5-15.5 MeV, tensor anal. power, charge symmetry violation in mirror reaction 80−13368
^{2}H(e,e), charge and structure radius, form factor and structure function *(Russian)* 79−40841
^{3}H, binding energy and charge form factor, internucleon force 77−18438
^{3}H charge form factors, harmonic oscillator basis 79−71807
^{3}H, EM form factors, 3-nucleon wave function calc. 80−95302
^{3}H$_{\Lambda}$, charge symm. breaking, Λ separation energy in hypertriton 78−17132
^{3}H$_{\Lambda}$ charge symm. breaking considerations for hypertriton 78−17133
^{3}H-^{3}He charge asymm., neutron-proton mass difference 78−70464
^{3}He change form factor, relativistic corrections for three nucleon observables 79−85383
^{3}He charge form factor, internucleon force 77−18438
^{3}He, charge form factor, n+d collision anal. 77−18439
^{3}He charge form factor 79−71806
^{3}He, charge form factor one-boson exchange pot. 78−41652
^{3}He charge form factors, harmonic oscillator basis 79−71807
^{3}He, EM form factors, 3-nucleon wave function calc. 80−95302
^{3}He, elastic electron scatt. data, comparison with charge form factor calcs. 79−71848
^{3}He, nuclear charge form factor, two-boson exchange charge density π, ρ, ω exchanges 80−63073
^{3}He, rigorous bounds for charge densities from form factor data 80−5055
^{3}He(e,e), 29-95 MeV, RMS charge radius and charge form factor 77−57653
^{3}He(e,e), charge density distrib., charge form factor, of ^{3}He 78−29453
^{3}He(e,e), model depend. of charge densities 78−78248
^{3}He(e,e) 170 to 750 MeV, EM structure, form factors and distribs. 77−54208
^{4}He, ground state energy and RMS charge radius 78−58242
^{4}He, nucl. binding energy, radius and charge form factor, Brueckner calcs. 79−71787
^{4}He nuclear charge density determ. using form factor analyticity 80−63077
^{4}He, pion exchange currents and charge form factors, shell model anal. 77−10338
^{4}He, soft-core radial wave function, photo-disintegration calculation 80−18209
^{4}He, structure in the translation-invariant oscillator basis *(Russian)* 78−25123
^{4}He(e,e), cross section anal., nuclear charge form factor, short range correl. 78−8746
^{4}He(e,e) 170 to 750 MeV, EM structure, form factors and distribs. 77−54208
^{A}He, A=3, 4, charge structure, effect of neutron charge 80−105963
^{178}Hf, 2^{+}-0^{+} transitions, mean square nuclear charge radius change, Mossbauer expt. 78−25109
^{A}Hg, A=198-202,204, muonic X-ray transitions, nuclear state quadrupole moments and charge distrib. 79−41253
^{39}K, charge density and single particle state struct. 79−36144
^{6}Li, charge form factor, short range Jastrow correls. in harmonic oscillator shell model 78−70467
^{6}Li, Coulomb energy determ. from electron scatt. spectrum *(Russian)* 77−30479
^{6}Li, EM form factors and vertex consts. 78−12958
^{7}Li charge form factor with resonating group wave function, quad. moment, charge radius 80−102110
^{24}Mg, pot. and charge deform. of rot. states 77−46106
^{24}Mg(e,e), 4_{1}^{+} 4.12 MeV and 2_{2}^{+} 4.24 MeV level resolution, E2 and E4 form factor meas. 79−17811
^{A}Mo, A=92, 94-98, 100, muonic atom X-ray transitions, nuclear charge radii 80−27545
^{14}N(e,e) in storage ring, elastic form factor, charge distributions 80−22819
^{23}Na α-transfer spectroscopic factors from shell model wave functions of ^{19}F(^{6}Li,d) 79−36149
^{150}Nd(α,α'), 11.5 MeV, electric quadrupole and hexadecapole moments, charge deform. parameters 77−30489
Ne isotopes, meas. of 280 MeV/nucleon particles with plastic detector 77−38561
^{20}Ne hexadecapole moments, quadrupole deformation effects, E4 effective charge, valence polarisation 80−78142
^{20}Ne, pot. and charge deform. of rot. states 77−46106
Ni mean square charge radii from isotope shifts 80−99484
Ni, radial charge distrib. moments, ground state correlations, generator coordinate model 79−30785
^{A}Ni(e,e), 100-275 MeV, A=58,60,62,64, cross sections and muonic X-ray meas., charge distrib. systematics 80−86801
^{58}Ni, charge density, HF calcs. from (e,e) data 79−89260
^{58}Ni, charge density, single particle struct., using proton wave functions 78−45995
^{60}Ni, electron elast. scatt. cross sections, phase shift anal. and HF calcs. *(Russian)* 78−41707
O, isotopic sequence charge distrib. calc. 79−85361
^{16}O, 0^{+} states, appl. of K-harmonics method 78−54685
^{16}O, charge distribution, orthogonal scheme model *(Russian)* 78−29382
^{16}O, contrib. of meson exchange currents to charge density and RMS radius 77−10313
^{16}O, ground state energy and RMS charge radius 78−58242
^{16}O, pion exchange currents and charge form factors, shell model anal. 77−10338
^{16}O, pion-exchange contribs. to charge densities, HF calcs. 78−46001
nuclear charge continued
^{17}O, charge distrib. differences between A=16, 17, and 18 isotopes 79−63583
^{17}O, effective charges and radial integrals calc. 78−4897
^{17}O(e,e), elastic and inelastic, cross sections, excited states, charge radii 78−46049
^{18}O($\pi^{\pm}$,$\pi^{\pm\prime}$) ^{18}O(2^{+}), DWIA anal. with microscopic form factors, effective charges 79−85549
^{192}Os, muonic, dynamic hyperfine effect, model independ. anal. 78−22057
Pb, A=204-208, charge distrib. from elastic electron scatt. and muonic X-ray data anal. 78−54681
^{198}Pb, E2 transition probability and effective charge for neutron $i_{13/2}$ subshell 78−78309
^{208}Pb, charge and proton distribs., single particle model 78−50074
^{208}Pb, partly self-consistent potl., charge distrib. and Fermi surface *(Russian)* 77−272
^{208}Pb, pion-exchange contribs. to charge densities, HF calcs. 78−46001
^{208}Pb(e,e), 502 MeV, charge density distrib. variations 79−75830
^{105}Pd muonic X-rays, nuclear charge parameters, quadrupole moments 78−29377
^{110}Pd(^{208}Pb, X), 1.18-1.28 GeV, charge equilib. time scale, relaxation time 80−18188
^{110}Pd(^{208}Pb, X), equilibrium process time evolution, mass and charge distribs., energy loss 79−97725
^{199}Po charge states and charge distrib. from ^{164}Dy(^{40}Ar,5n) *(Russian)* 79−40840
^{192}Pt(α,α'), 24 MeV, coupled channels anal. of ground state band, negative β_{4} deformation 78−70550
^{239}Pu, highly deformed, muonic X-rays, nuclear charge distrib., elec. quadrupole moment 78−70440
Rb, ground state spins, moments, charge radii by laser spectroscopy 80−78147
^{A}Sb, A=121, 123, elec. and mag. hfs. 79−10224
Si, A=28, 29, 30, charge distrib. in ground, excited states via (e,e') 18.5-117.1 MeV 77−54142
^{28}Si, pot. and charge deform. of rot. states 77−46106
Sm, A=152, 154, electric quadrupole and hexadecapole moments, charge deform. parameters, Coulomb excitation expts. 77−30489
Sm, stable even isotopes, mean-square charge radii 79−67647
^{A}Sm, A=144-154, mean square nuclear charge radius, laser atomic beam spectroscopy 80−102468
^{A}Sm, A=144-154, nuclear charge density and quadrupole moments from muonic X-rays 79−40838
^{A}Sm, A=150, 152, muonic, X-ray spectra meas. and anal., charge radii, multipole moments 79−3600
^{152}Sm(e,e'), 35-350 MeV, coupled channels anal., rot. band excited states, charge densities 79−3139
Sm(α,α'), 11.25 to 12 MeV, a=152,156, elec. moments, charge deform. parameters 77−54233
^{88}Sr(e,e), 400 MeV, charge density distrib. variations 79−75830
^{181}Ta, radial charge parameters, quadrupole moment, from muonic atom transitions 77−34226
^{181}Ta+^{20}Ne, 8.0 GeV, target residue mass, charge distrib. determ. 79−17930
^{232}Th, highly deformed, muonic X-rays, nuclear charge distrib., elec. quadrupole moment 78−70440
^{232}Th(p,f), 28 GeV, charge dispersion, mass yields 77−3062
^{232}Th(p,f), 29-97 MeV, Rb, In and Cs relative independ. yields, charge division 80−102218
Ti, A=44-50, effective charges and E2 transitions in 1f-2p shell nuclei 78−544
Ti, A=46,50, neutron radius determ., charge symm. 78−29380
^{48}Ti(e,e), 227 MeV, differential cross sections, Fermi charge density distribs. *(Russian)* 78−89785
Tl, A=205,203, charge distrib. from elastic electron scatt. and muonic X-ray data anal. 78−54681
U, A=235, 238, highly deformed, muonic X-rays, nuclear charge distrib., elec. quadrupole moment 78−70440
U+^{12}C, 25.2 GeV, large collision residues and fission 77−71618
^{235}U(n,f), thermal, charge and mass yields of light fission products 77−23122
^{235}U(n,f), thermal, charge distrib. of fission products 77−23123
^{235}U(n,f), thermal, fragment ionisation, charge distribs., stat. and instant perturbation theory *(Russian)* 80−63219
^{235}U(n,f), thermal n, fission product isobaric charge distrib., parity effects 79−17791
^{235}U(n_{th},f), charge distrib. of products in mass chains 79 to 100 77−10456
^{236}U* fission fragment charge distrib. in statistical model *(Russian)* 79−59102
^{238}U, proton-induced fission, asymm. region, nucl. charge distrib. 78−4967
^{238}U(γ,f), 20 MeV, fission product yields, charge distrib. 80−42533
^{238}U(p,f), 11-29 GeV, three dimens. charge dispersion curves, isobaric yields 80−102111
^{238}U(p,f), 35-85 MeV, nuclear charge dispersion in light mass region 78−8864
U(γ,f) A=235,238, 25 MeV bremsstrahlung, prod. yields, mass chains, charge distribs. 77−6470
V, A=47-51, effective charges and E2 transitions in 1f-2p shell nuclei 78−544
^{51}V(e,e'), shell model calcs., effective charges 77−26674
Xe, charge radii and binding energy per nucleon, linear relationship evidence 80−68520
Zn, radial charge distrib. moments, ground state correlations, generator coordinate model 79−30785
^{A}Zn(e,e), 100-275 MeV, A=64,66,68,70, cross sections and muonic X-ray meas., charge distrib. systematics 80−86801
^{A}Zr, A=90, 92 and 94, charge densities and single-particle structure 80−9224
^{90}Zr, pion-exchange contribs. to charge densities, HF calcs. 78−46001

nuclear chemistry
see also chemical effects of nuclear reactions and scattering; radiation chemistry; radiochemistry
acetic acid-formic acid, 'dimer', tritium β^{-}-decay causing H^{+} transfer, ab initio MO calc. 80−3391
chemonuclear synthesis, product purification, cost anal. 79−61889
Coulomb capture ratios of negative mesons in chemical compounds 79−20453

nuclear chemistry continued
ethanol-t, charge spectrometer studies of chem. effects of nucl. transforms. *(Japanese)* 77−57420
formamide dimer, tritium β^--decay causing H^+ transfer, ab initio MO calc. 80−3391
formic acid dimer, tritium β^--decay causing H^+ transfer, ab initio MO calc. 80−3391
hot-atom reactions, Boltzmann eqn. for hot-atom relax. 79−100423
interfaces of nuclear and chemical physics, elementary particles and biochemistry 77−6284
neutron capture recoil reactions in mixed crystals, effects on chem. processes 77−90632
rapid automated nuclear chemistry facility for the study of short lived fission products 79−71978
B_2H_6 compounds, doubly-isotopic, laser driven nuclear fusion, energy release 78−78499
^{57}Co, disintigrating nucleus, energy absorpt. by mol. environment 78−80775
^{18}F+hexafluoropropylene nonequilibrium effects in moderated nuclear recoil experiments 80−89509
^{18}F+methane, nonequilibrium effects in moderated nuclear recoil experiments 80−89509
Fe, proton bombardment, stable nuclide form. and separation 78−20045
^{16}O ions, mag. hyperfine interactions, PAC meas. 80−95734
T, release behaviour and chem. forms on heating neutron irradiated UO_2(Li) pellets 78−40071
T+chloroethane(cyclobutane), recoil reaction, 5×10^{-2} torr 78−44389
T_2O, charge spectrometer studies of chem. effects of nucl. transforms. *(Japanese)* 77−57420

nuclear cluster model
3-cluster systems, orthogonality condition model, appl. to 3-α model 78−530
3-cluster systems, resonating group method, appl. to 3α system 78−50108
^{12}C-α-^{12}C nuclear molecular states, quantum mechanical three-body approach 79−97692
^{4}He(d,t)^{3}He, charge asymmetry effects 77−14136
α-clustering in heavy nuclei, pre-equil. model, nuclear matter NN, Nα interactions 80−63111
A=12 to 24, nuclear cluster norm determ. using integral transform and SU(3) recoupling techniques 79−22214
A=15-18, effective interaction from coupled cluster many-body method extension 80−22701
A=16 to 28, α-structure amplitudes and shell model wavefunctions for nuclear states 79−45192
A=16-40, α-spectroscopic factors between ground states, shell model prediction 79−13204
A=18, α-clustering on odd-parity levels 78−74318
A=3,4, finite nuclei, binding energy in Jastrow-Factor-Cluster method 79−49575
A=3, d+n clustering, D-state effects in (d,t) and (d,^{3}He) 79−22302
A=50 to 150, even-even, odd-even, odd-odd, cluster vibr. model 80−68567
A$\leq$44, fp-shell nuclei struct., effect of core-excitation and α-clustering correl. 80−9245
A(p,d)X, A(p,t)X, inclusive reaction clustering phenomena, scaling behaviour, knockout mechanism, review 79−6441
advances in nuclear physics, clustering and self-consistent field theory, book 79−75879
alpha cluster reactions, effective single particle operator 80−32218
alpha cluster role in natural α-decay 79−6519
alpha clustering, vacuum ground state, nuclear matter theory calc. 79−40876
alpha matter, abnormal boson occupation 79−26387
alpha Q values, first excited 2^+ states, even-even nuclei 79−6458
alpha-alpha interaction for coupled channels 77−18489
alpha-deuteron cluster anal. of ^{6}Li(e,d)e'^{4}He 77−6355
angular correlation anal. 78−634
angular correlation anal. 79−6547
antisymmetrisation effects in Jastrow cluster expansion for nucl. matter 77−10352
antisymmetrisation effects in nuclear collisions, projection operator techniques 78−46036
antisymmetrisation in α-decay and α-transfer based on cluster representation 78−86514
antisymmetrized four-body wave function and coexistence of single particle and cluster structures 79−54399
antisymmetrized n-nucleon problems, refined resonating group calcs., reduction to cluster modes 78−17123
BBG theory developments, hole and particle lines, dispersion effects and healings 80−22719
Bose fluids, two-body density matrix 79−40875
bound state poles, effect on N-body scatt. amplitudes *(Chinese)* 80−5111
break up process as three body problem, Faddeev eqns. 78−89842
Brink model, α-cluster sd shell nuclei, binding energies, rotational band energies 77−6195
Brueckner theory, unification with HFB theory 80−105995
cluster states in reaction theory, breakup into composite fragments 79−36207
cluster systems, normalisation kernels, SU(3) prop., generator coordinate theory 80−73814
clustering aspects of nuclear struct. and nuclear forces, review 79−80887
clustering aspects of nuclear structure and nuclear reactions, review 79−3100
clustering in heavy and light nuclei, fresh look at concept 77−22827
collective clustering effects in nuclei information from heavy-ion transfer reaction 77−14171
complex nuclei, α-clusters, preequilibrium model approach 79−6457
composite particle scatt., integral eqns. taking Pauli principle into account 78−86496
composite particles, N-cluster dynamics and effective interaction, dynamical eqn. 80−42560
composite-particle interactions, computational procedures 79−13225
conference on few body systems and nuclear forces, Graz, Austria (Aug. 1978) 79−80880
conference on many-body theories, Trieste, Italy (Oct. 1978) 80−22135
conference on nuclear structure and reactions, clustering aspects, Winnipeg, Canada (June 1978) 79−3099

nuclear cluster model continued
correlated cluster model for energetic proton inclusive spectra is p-nucleus collisions 77−71600
correlated-basis-functions approach to realistic nuclear matter 79−40872
correlation expansions for light nuclei, higher order term effects 79−75877
cosmic ray clusters, size and mass determ. NN interactions 77−71548
coupled channel variational method for microscopic study of reactions between complex nuclei 79−13263
coupling effects of two-particle and alpha two-hole states in A=18 nuclei 80−5081
deuteron form factors and spectroscopic factors in heavy spherical nuclei, shell model *(Russian)* 80−63078
distortion correction of N-cluster wave functions 79−6448
double core model for fission 77−30546
double folding pot. for inelastic scatt. between nuclei 80−13425
double nuclear cluster system in heavy ion deep inelastic collisions 79−6438
double well cluster shell model folding potential *(Chinese)* 80−52596
(e,e), elastic and inelastic A=12-40, 22 79−63571
effective internuclear potential, odd-even l-depend. 79−6450
exchange kernels, analytical derivation methods 79−13228
Faddeev equations, generalised, for many-cluster problems 77−88058
few-body systems, bound states, bridge concept 77−22927
fission fragment formation as clustering effect, many-nucleon correl. 79−6561
fission of actinides, fragment shell effects determ. from ^{32}S many nucleon correlations 78−41690
four cluster problem, appl. of hyperspherical harmonics 79−6447
four particle systems, reaction dynamics 79−80905
four-body system, energy dependent pole approx. 79−71801
fragmentation, clustering and absorption mechanisms in p and π induced reactions 79−6546
hadron+nucleus, high energy, cluster cascade model 80−18300
hadron-nucleus interaction, cluster prod., at cosmic ray energies 80−13467
hadron-nucleus interactions, secondary particle multiplicity, one-cluster model *(Russian)* 78−17165
hadron-nucleus reactions, quasi-elastic cluster knock-out, multiplicities 78−46042
heavy ion clustering aspects and nuclear quasimolecular resonances 79−6439
heavy ion reactions, cluster correlation, review, book contrib. 80−27670
heavy ion resonance reactions as orbiting cluster phenomena 80−47446
heavy-ion reaction, cluster transfer, shell model investig. 77−14172
integral transformations, generator coordinates and the evaluation of resonating group kernels 79−6446
interaction matrix elements, canonical transformations and Gaussian integral kernels 77−18453
Ising struct. in shell-cluster model 77−26601
K-harmonics method for cluster spectroscopic factors 78−62512
kernels of GCM, RGM and OCM and their calculational methods 79−13227
kinetic energy of nucleus centre-of-mass motion, single particle functions with realistic behaviour *(Russian)* 77−74785
light nuclear systems, microscopic approx. for sequential decay processes in 3-body breakup 77−18500
light nuclei, α transfer and knockout reactions, α clustering 78−41687
light nuclei, α-particle and trinucleon clusters 78−54706
light nuclei, alpha cluster model, 3-body problem 80−32217
light nuclei, cluster struct., review 78−50107
light nuclei, high spin dinuclear states 79−3103
light nuclei, hyperspherical functions for size, excited states, compressibility, binding energy 80−22679
light nuclei, microscopic theory of three cluster problem 78−54707
light nuclei, props. from double well cluster shell model 80−27572
light nuclei coupling constants from dispersion anal. of N and d scatt. amplitudes 78−29399
light nuclei structure, multicluster model, review 79−3102
low density α clustering effects of Skyrme N+N interactions in nuclear matter 78−29398
low density nuclear matter, calc. of energy expectation value 79−6451
many-body interactions from quark exchanges, nuclear tetrahedral struct. and props. 79−6459
many-particle correls. of nuclear sub-structs., ^{16}O, ^{18}O particle and hole clusters *(Chinese)* 77−57614
microscopic cluster model, light nuclei as proving ground, reviews 79−3101
microscopic description, review 80−487
multi-cluster problems, interaction kernels using SU(3) recoupling techniques 79−45193
multichannel nuclear reactions, connected kernel formalism 78−46038
multicluster allowed states, spectroscopic amplitude of cluster transfer 77−88059
multicluster problem based on microscopic theory, 3α system 77−18455
neutron matter, spin and tensor correlations, cluster expansion hypernetted chain eqns. 80−22728
neutron or nuclear matter, spin depend. correlations, variational method 80−22726
neutron resonances, nuclei from ^{64}Zn to ^{177}Hf, total α-widths 77−26708
nuclear matter, Λ^0 binding energy, many-body cluster contribs., Jastrow calc. 79−93545
nuclear matter, Brueckner Bethe and variational calcs. review, nuclear saturation problem 80−22745
nuclear matter, constrained variational calcs., three body and N* (1234) contribs., cluster energy 80−22743
nuclear matter, three nucleon clusters with intermediate Δ-states exchange diagrams calc. 78−17112
nuclear matter BBG theory, auxiliary single particle field for binding energy 80−22723
nuclear matter binding energy variational calcs. in two- and three-body cluster approx. 77−26603
nuclear molecules, clusters of protons and neutrons 79−54400
nuclear structure, conf. 78−50059
nuclear surface phenomena, Yakubovski eqn. appl. to N-body systems 79−75931
nucleon-alpha particle, two-channel potl., exact method for calc. 77−18488
nucleosynthesis, clustering in charged particle reactions 79−5744
orthogonality condition model, appl. to 2α+t system 78−50110

nuclear cluster model continued
(p,α) direct reactions on light nuclei, alpha cluster breakup effects 79−6550
Pauli principle in multiple scatt. theory, exact eqns., cluster exchange 80−106024
Pauli-principle effects, simulation 78−8756
polarisation and correlation probes of nuclear clustering, (^{6}Li,^{6}Li) scatt. 79−6437
pre-compound decay into complex particle channels 79−6456
preformation coeffs. and level densities from (p,α) and α-decay 77−71579
proton-nucleus inclusive collisions, very large momentum transfer, cluster representation 79−93615
PWIA cross section for quasifree reactions, nuclear cluster struct. investigation 78−82324
quasi-free cluster knockout calcs. in DWIA 77−34273
quasi-free scatt. model in (α,α′) 77−14139
quasielastic cluster knockout theory, review, book contrib. 79−75874
quasifree cluster knockout reactions, cluster spectroscopic factors, medium and high energies, review 79−6440
rare earth nuclei, cluster-rotor-coupling approach to backbending 79−45129
reaction matrix approach to the cluster state, Brueckner generator coordinate method, appl. to α-α scatt. 80−9250
reduced α-amplitude in exactly solvable model, one-body transition matrix 79−85387
resonating group method, simplified calc. of analytical kernals 79−6449
resonating group method alternative, comments, many body Lippmann-Schwinger eqns., cluster approx. 80−83052
resonating-group method for nuclear many-body problems, review 79−9497
rotational state energies, α-cluster nuclei, Brink's model, functions with exponential asymptotics *(Russian)* 77−6212
scattering reactions, cluster effects, spectroscopic information on cluster structure 77−67711
sd-shell nuclei, ground state alpha cluster correl. calcs. 78−74314
sd-shell nuclei, ground-state alpha-cluster correl. 79−6402
self consistent long range order in nuclear matter Hartree Fock Overhauser orbitals 78−17127
separable interaction of composite particles with inclusion of the Pauli principle 79−85389
six-nucleon system, cluster model, resonating group, and integral eqns. approach, appl. to ^{6}Li 79−80888
Sp(6,R) symmetry, α-breakup amplitudes, of giant E2 excitations in light nuclei 78−29435
spectroscopic factors for p-shell nuclei, cluster transfer reactions 77−30486
spectroscopic information from nuclear reactions 79−6455
spherical nuclei, probabilities of α-transitions, effect of higher configs. of α-particle internal waves functions 78−17155
spin and isospin stability of dense neutron and nuclear matter with hard core interaction 79−26386
stable nuclei, charting based on number of alpha-particles *(French)* 77−88057
static density waves of nuclear matter, cluster-variational investigation 79−40868
Su(3) symmetry and integral kernals in cluster problems 80−9251
sU(3) techniques for angular momentum projected matrix elements in multi-cluster problems 79−6445
SU(4) theory, role in nuclear struct. theory 79−3097
theory of resonating group method and generator coordinate method, and orthogonality condition model 79−13226
three body forces from cluster terms, binding energy and tensor forces 79−45176
three cluster resonating group method, cluster struct. in light nuclei and cluster rearrangement collisions 78−54705
three neutron resonance, enhancement factors, forces, and binding energy 79−45230
three nucleon, finite range microscopic form factors, zero range DWBA calcs. 79−6525
three particle nuclear molecular states, Schrodinger eqn., wave functions and energy spectrum *(Russian)* 78−86497
three-body cluster energy, lowest order constrained variational calc. 79−13233
three-body scatt. problem, cluster expansions, effective intercluster pots. 80−5082
three-cluster distorted-wave methods 79−6524
three-nucleon wavefunctions, appl. to (^{2}H,^{3}H) and (^{2}H,^{3}He) 77−54168
time dependent coupled cluster approx., general formulation 79−67695
time dependent coupled cluster approx. to nuclear dynamics, solvable model appl. 79−9496
trineutron confirmed nonexistence, Faddeev-UPE method 79−63612
two charged clusters collision, scatt. amplitudes and integral eqns. 80−68614
two-centre generator coordinate model functions, ang. momentum eigenstates projection 78−12994
two-centre molecule-like states, generator coordinate wave function projection 78−12995
uncorrelated cluster model, generating functional formulation, charge transfer 79−49590
wave functions from shell and cluster model 78−29412
wavefunctions, correlation operators, variational techniques, review 80−22748
Z=N nuclei, pot. calc. from α-α interaction 79−6661
(α, 2α) 700 MeV, cross section, effective cluster number from PWIA, momentum distrib. 79−40940
(α,^{12}C), 90.3 MeV, cross sections and systematics multi-α-cluster transfer implications 80−42675
(α,^{12}C), 90.3 MeV, multi-α-cluster transfer and direct pickup cross sections 80−57760
α cluster amplitudes and core excitations in s-d shell nuclei 77−57615
α particle nuclei, cluster struct., ground state energy lower bounds 78−46017
α strength factors for (α,p) and heavy-ion α-transfer reactions on medium nuclei 77−18454
α surface clustering, effect of pairing and four-body interactions in 41≤A≤45 nuclei 77−10344
α-cluster deformation inside light nuclei 79−17829
α-clustering and spectroscopic factors, shell effects and deformation correlations in (^{6}Li,d), (d,^{6}Li) 79−6436

nuclear cluster model continued
α-clustering in nuclei, phenomenological pot. and folding model results relation 78−78289
α-decay width calc. in meth. not involving arbitrary channel radii 77−54192
α-nucleus separation energies, Woods-Saxon pot., A depend., closed shell effects 78−25107
α-particle effective surface pot. and OCM justification 79−97715
α-preequilibrium decay, emission rate, α-preformation factor 78−41676
α-spectroscopic factors, pseudo SU(3) approx. 78−70471
α-transfer, spurious C.M. effects separation in shell nucleon configuration framework 79−45194
α-transfer to α-decaying nuclei 77−79396
α-vibrations, proton and neutron pairing vibrs. 77−289
αα and NN scatt. analogies, quark struct. and clustering connections 79−6442
(d, ^{6}Li), 54.25 MeV, α-cluster spectroscopic factors, DWBA anal. 80−52571
(d,^{6}Li), A=144-238, alpha-cluster transfer from alpha-decaying nuclei 80−91166
(γ,d), odd-Z light nuclei, from (e,e′d), cross section, E2 transistors giant resonance and clusters 80−63169
^{6}Li, d+α clusters, break up in nuclear field, ^{118}Sn+^{6}Li study 78−46092
^{6}Li(α,α), resonant-group kernel function, analytical computation 79−40941
(n, α) with resonance neutrons, properties of highly-excited states of nuclei *(Russian)* 80−106053
(p, α) microscopic form factors, DWBA cluster form factor replacement 80−47478
(p,χ), inclusive backward collision, intermediate energies, correlated nucleon clusters 79−40914
(p,d) reaction, nuclear cluster effects 79−6576
(P,X), 400 GeV, correlation strength, dependence on target size, multiplicity and cluster size 80−78287
(p,X), emulsion, particle production by clusters at 200 GeV/c 79−89302
(p,X), inclusive pion prod., forward and backward π spectra 79−85484
(p,X) in emulsion 24 GeV, clusters in rapidity interval method, multiperipheral model 80−5135
p-N reaction, high energy, as probe of cluster structure *(Hungarian)* 77−50124
p+nucleus, 200 GeV/c, clusterisation and secondary particle correl. *(Russian)* 78−33133
(π^-, γ), pion absorption by two nucleon cluster, high spin state excitation probability 79−49570
π pairs, dynamical and Bose-Einstein inclusive correlations, from cluster decay 78−62463
π+nucleus, 200 GeV/c, clusterisation and secondary particle correl. *(Russian)* 78−33133
^{20}Ne cluster struct., rot. bands from (^{16}O-α)+(^{12}C-^{8}Be) coupled channel orthogonality condition model 79−97647
^{16}(γ,X), bremsstrahlung weighted cross section, two-body correlations effects, linked cluster expansion 80−106047
A=12-15, heavy ion induced α-transfer α-clusters, DWBA anal. 79−26454
^{A}Ag, A=105-109, negative parity states, vibr. versus rot. descriptions 80−73781
^{27}Al+^{14}N, 100 MeV, α preequilibrium decay 79−6666
^{27}Al(^{6}Li,d)^{31}P, 36 MeV, absolute cross sections, ang. distribs. 79−89321
^{27}Al(p,α)^{24}Mg, finite-range cluster-model description, DWBA approach 80−52667
^{27}Al(p,pα), 600 MeV, α-cluster quasielastic knockout, expt. methods, separation energy spectra 79−13275
^{27}Al(π,xγ), gamma ray coincidence spectra, nuclear surface clustering evidence 79−6707
^{27}Al($\pi^\pm$,$\pi^\pm$X), 190 MeV, multiparticle removal occurring as separate particles, cluster removal 79−85498
^{27}Al($\pi^\pm$,xγ), 300 MeV, gamma-ray coincidence spectra, clustering evidence 79−6706
^{36}Ar(^{6}Li,d)^{40}Ca, 0$^+$ levels of ^{40}Ca, cluster-transfer model 78−62571
^{193}Au levels, three holes cluster vibr. and particle asymmetric rotor descriptions 80−57668
^{10}B, cluster effects, low-lying states determ. 77−6228
^{11}B, struct. study of 2α+t system in orthogonality condition model, level energies and parity 80−5080
^{7}Be, ^{4}He^{3}He coupling from ^{3}He+^{4}He scattering, dispersion anal. 78−89889
^{8}Be, α-cluster excitation via α-α-scatt., coupled channel calcs. 78−529
^{8}Be, α-particle and Sp(2,R) model connection 77−65207
^{8}Be, αα$^+$ rotational band existence 79−13192
^{8}Be cluster amplitudes and core excitations in s-d shell nuclei 77−57615
^{8}Be, cluster formation, multicentre variational model *(Chinese)* 78−25128
^{8}Be high spatial symmetry excited states, resonances, rot. band from (d,αt), (p,αt) 80−86780
^{8}Be high-lying reson. below α-α* threshold, cluster model calc. 77−82840
^{8}Be, highly excited αα* states from ^{7}Li+p and ^{6}Li+d 78−78262
^{8}Be lowest negative parity state, shell and cluster model calcs. from ^{7}Li(p,p), ^{8}Be lowest negative parity state, shell and cluster model calcs. 80−18205
^{8}Be, microscopic wave function, α-α scatt. phase shift calc. 78−62503
^{8}Be, quasi-mol. struct. model observed from α-α scatt. 79−6397
^{8}Be resonant state, αα* cluster and sympletic model anal. from ^{7}Li(p,α), ^{6}Li(d,α) 79−9537
^{8}Be rot. levels using α-α cluster model with effective pot. interaction 77−22915
^{8}Be, scattering system, microscopic nucl. cluster model 78−54703
^{8}Be spontaneous fission pot. energy curve, cluster shell model *(Chinese)* 80−22867
^{9}Be, 1/2$^+$ resonance state at 1.68 MeV 79−6398
^{9}Be, α-cluster behaviour via ^{9}Be(α,α) anomalous 40 MeV effects 78−615
^{9}Be, α-cluster struct., binding energy determ., Faddeev eqn. soln. 78−41640
^{9}Be, binding energies, three body calcs., Faddeev formalism, alpha cluster model 79−75876
^{9}Be, HF and GCM calc. in α-cluster molecular model, ground state props. 77−54137
^{9}Be low lying spectrum, 3-body molecular description, adiabatic one level approx. 80−78150
^{9}Be, n+α+α cluster model 79−6452

nuclear cluster model continued
^{9}Be, positive parity excited energy levels, three well cluster shell model study *(Chinese)* 79−93518
^{9}Be, three body molecular calc. of low-lying spectrum 79−93534
^{9}Be(^{3}He, αα)^{4}He, 2.8 MeV, quasi-free and sequential processes 79−67789
^{9}Be, binding energy calcs., clustering 79−9501
^{12}C, 3 alpha force and 3α model 79−30798
^{12}C, 3-α struct. in boson model 78−17124
^{12}C, 3α model, props., stochastic variational method 77−41891
^{12}C, 3α system, resonating group method for nuclear props. 78−50108
^{12}C, alpha cluster in Hartree Fock calcs. 80−63110
^{12}C, α-cluster model, binding energy, RMS radii, and form factors 79−75825
^{12}C, α-cluster struct., binding energy determ., Faddeev eqn. soln. 78−41640
^{12}C, α-particle model, amalgamation of two nucleon correl. into multiple scatt. process 77−54169
^{12}C, α-particle model 77−82839
^{12}C, α-particle model of ground and 0^{+} excited states, hyperspherical method 77−6272
^{12}C, binding energies, three body calcs., Faddeev formalism, alpha cluster model 79−75876
^{12}C, boson 3α model and effective inter-α forces 78−66232
^{12}C, Efimov state search using Ali-Bodmer α-α force and Faddeev technique 79−6420
^{12}C, excited state struct., anomalous α-decay props. 3-cluster GCM model 79−6399
^{12}C, excited state struct., α-particle model 80−47385
^{12}C $J^{\pi}=0^{+}$ isoscalar levels, α-particle model with group theoretical methods 77−74766
^{12}C, positive-parity states, anomalous α-decay props. 78−62511
^{12}C, proton total cross section, 0.15 to 1 GeV, α-particle model and Glauber multiple scatt. theory 77−18538
^{12}C relativistic ions, Coulomb disintegration into 3 α-particles, total cross section 79−40943
^{12}C struct. calcs. via 3α system resonating group method 78−531
^{12}C, struct. of excited states in 3-α model 77−65201
^{12}C structure, energy levels, binding energy, cluster model with varying hinge angle 78−4907
^{12}C, three alpha struct. in Faddeev formalism 77−14048
^{12}C, three α model calcs. and O_2^{+} state 79−75856
^{12}C, three α-particle model calcs., Faddeev formalism, low lying states 77−18399
$^{12}C_1$ 3α model, composite particle interactions, Pauli principle *(Russian)* 80−18214
^{12}C-^{12}C resonances, speculation of nature, excited α-particles 79−13339
^{12}C+^{12}C system, nuclear molecule microscopic description, HF and coupled channel calcs. 80−13493
^{12}C+γ→3α, photodisintegration theory using 3α model and hyperspherical functions *(Russian)* 78−78365
^{12}C+π, Glauber theory in microscopic α-cluster model 79−13346
^{12}C(^{12}C,xα), 12-31.5 MeV, inclusive α-particle yield, resonant like structs. 80−42691
^{12}C(^{6}Li,d), ^{16}O level configuration mixing anal., α-spectroscopic strengths 79−6683
^{12}C(^{6}Li,d)^{16}O(α)^{12}C, 35 MeV, d-α coincidence spectra meas. after ^{16}O break-up, α-cluster state energies 79−63688
^{12}C(^{9}Be, ^{9}Be)^{12}C(g.s.), 39.68, 43.75 MeV, back angle cross section enhancement, Hauser Feshbach anal. 79−89324
^{12}C(^{9}Be,^{8}Be)^{13}C, 20 MeV, α-cluster transfer process contrib. 79−6668
^{12}C(^{9}Be,^{9}Be), cluster effects *(German)* 79−76015
^{12}C(^{9}Be,^{9}Be), possibility of ^{3}He exchange 79−6669
^{12}C(^{9}Be,^{9}Be)$^{12}C_{gs}$, cluster effects *(German)* 79−76015
^{12}C(^{9}Be,α)^{17}O, ang. distrib. from pick-up model anal. of cluster transfer *(Russian)* 80−37396
^{12}C(^{9}Be,α)^{17}O, cluster effects *(German)* 79−76015
^{12}C(α,α), α-particle elastic scatt. excitation functions, α-cluster state energies 79−63688
^{12}C(α,α), spectra and widths of quasistationary α-cluster states *(Russian)* 77−46180
^{12}C(p,^{6}Li)^{7}Be, 51.9 MeV, cluster coupling shell model 78−46058
^{12}C(p,α), 45.2 MeV, cross sections, finite range DWBA anal., cluster form factors 80−68666
^{12}C(p,p), 3-61.4 MeV, α-cluster contribs., semi-classical model 79−36233
^{12}C(p,p), 3.0 MeV, elastic scattering, discrepancies from optical model, possible α-cluster struct. 78−62528
^{12}C(p,p)^{12}C, elastic and inelastic, 1 GeV, α-particle model in Glauber multiple scatt. theory 77−30577
^{12}C(p,pα), 600 MeV, α-cluster quasielastic knockout, expt. methods, separation energy spectra 79−13275
^{12}C(p,pd), (p,pt), (p,pα), spectroscopic data on quasielastic ejection on nucleon clusters from 1p shell nuclei 79−80931
^{12}C(p,px), x=d,t, ^{3}He, 75 MeV, spectroscopic factors, cluster model, DWIA 77−54214
^{12}C(π^{+},2p), cluster effects in in-flight π^{+} capture 78−89916
^{12}C(π^{+},p^{3}He), cluster effects in in-flight π^{+} capture 78−89916
^{12}C(π^{+},pd), cluster effects in in-flight π^{+} capture 78−89916
^{40}Ca, ^{36}Ar+α model, energy levels, spin and parity 77−57602
^{40}Ca composite system, heavy ion resonances from ^{24}Mg+^{16}O, ^{28}Si+^{13}C 80−86874
^{40}Ca+$\pi^{\pm}$, multinucleon removal, prompt de-excitation γ-spectra obs. 79−6708
^{40}Ca(^{12}C,^{8}Be)^{44}Ti, 45 MeV, semiclassical analysis of α-transfer reactions, partial wave amplitudes 79−45283
^{40}Ca(α, α), generator coordinate method for arbitrary cluster widths 77−18581
^{40}Ca(p,pα), 600 MeV, α-cluster quasielastic knockout, expt. methods, separation energy spectra 79−13275
Ca(α,α), large angle scatt., cluster exchange and one-nucleon exchange 77−88152
^{110}Cd, O^{+} bands from cluster-vibration coupling, semimicroscopic mechanism for band mixing 79−36121
^{143}Ce quasi-$f_{7/2}$ low lying states spectroscopic factors, cluster-vibr. model from ^{142}Ce(d,p) 80−47391
^{15}F alpha particle cluster states, rot. bands in ^{14}N+α model 78−8757
^{18}F, semi-microscopic calc. of α-cluster states, shell model approx. 80−465
^{18}F, shell and cluster admixtures, T=0 positive parity levels, E2 rates 77−18396
nuclear cluster model continued
^{18}F, trinucleon cluster states, low lying negative parity states 78−29387
^{19}F, alpha-particle and triton cluster states anal. 77−41907
^{19}F, coupled channel orthogonality condition model 80−47384
^{19}F, energy levels from α-^{15}N and t-^{16}O coupled channel orthogonality condition model 80−37326
^{19}F final state selective population, triton clustering from band anal. from (^{7}Li,t), (^{6}Li,^{3}He) 80−9306
^{19}F levels, resonances and phase shifts, resonating group calcs. from ^{15}N(α,α) 80−32189
^{19}F positive parity alpha clusters, Woods-Saxon well calcs. 79−26383
^{19}F+^{28}Si spin orbit pot., single folding model and cluster model 80−9196
^{19}F(d,X), X=^{7}Li, ^{7}Be, 13.6 MeV, diff. cross sections, ^{5}He cluster direct transfer *(Russian)* 80−52650
^{A}Fe(^{16}O, ^{12}C), 50 MeV, a=54, 56, 58, α-spectroscopic factors, DWBA anal., (^{6}Li, d) comparison 79−63585
^{56}Fe(e,e′α), 60 and 120 MeV, evidence for α-clusters 79−6569
Ga, odd, single particle and collective degrees of feedom, clustering, shell model anal. 80−68510
Ge, odd, single particle and collective degrees of feedom, clustering, shell model anal. 80−68510
(HI,X), inclusive pion prod., forward and backward π spectra 79−85484
^{3}H, binding energies, three body calcs., Faddeev formalism, alpha cluster model 79−75876
^{4}H, cluster model, energy levels by interaction set anal. 78−25136
^{3}He, binding energies, three body calcs., Faddeev formalism, alpha cluster model 79−75876
^{3}He(t,d)^{4}He, symmetry breakdown as cluster spatial effect 79−6619
^{3}He(t,d)^{4}He asymmetry, cluster model anal., isobaric analogue states 78−78389
^{4}He, (3+1) cluster model of the T=0 0_2^{+} state by GCM 79−6396
^{4}He binding energy, Δ(3-3) effects, reaction matrix calc., Δ degrees of freedom 80−9218
^{4}He, nucl. binding energy, radius and charge form factor, Brueckner calcs. 79−71787
^{4}He photodisintegration, clustering effects 79−6562
^{4}He scatt. system, multichannel cluster model description 77−82902
^{4}He-cluster pickup anal. of (α,^{8}Be) reactions for A=9-16 65-72.5 MeV 77−6418
^{4}He(α,α), natural boundary condition methods for the microscopic treatment of composite-particle scattering 79−63680
^{4}He(α,α), nuclear separable plus Coulomb interaction 80−83106
^{4}He(α,α), size change of α effect on phase shift, generator coordinate and variational methods *(Chinese)* 80−68683
^{4}He(d,d), low energy, resonating group method anal. with distortion effect 80−73851
^{4}He(p,pn)^{3}He, ^{3}He momentum spectra determ. by cluster model interpretation 79−6577
^{4}He(π,π), 75-260 MeV, dibaryon contrib. to πNN cluster 79−89328
^{4}He(π^{+},π^{+}p)^{3}He, 105 to 135 MeV, cluster effects 79−85513
^{4}He(π^{+},π^{+}n)^{3}He, cluster effects 79−85513
^{4}He(π^{+},π^{+}p)^{3}H, 135 to 155 MeV, cluster effects 79−85513
^{5}He, 16.7 MeV states energy calc. using mixed cluster representation 80−27555
^{6}He β-decay from three body model of A=6 system, α-N, N-N interactions 78−46032
^{121}I, excited by (α,t), (^{3}He,d), three particle cluster-phonon coupling model calcs. 79−63572
^{16}L(α,d)^{18}F, 29.8 MeV, cluster form factors, DWBA calcs. 79−6643
^{4}Li, cluster model study using generator coord. method on ^{3}He+p scatt. 80−27581
(^{6}Li,d) on odd A, sd shell nuclei, α-cluster spectroscopic strengths, DWBA anal. 79−3104
^{6}Li, α+p+n cluster model with local interactions, Faddeev eqns., energy and charge radius calc. 79−22215
^{6}Li, α+p+n model, numerical soln. of coupled Faddeev eqns. 79−17831
^{6}Li, αnp elastic scatt., 0.2-5.0 keV, three body model, phase shift, total cross section 79−75875
^{6}Li, binding energies, three body calcs., Faddeev formalism, alpha cluster model 79−75876
^{6}Li, cluster formation, multicentre variational model *(Chinese)* 78−25128
^{6}Li, cluster struct., multivalley character of isoenergetic surfaces *(Russian)* 79−26384
^{6}Li, Coulomb disintegration in field of heavy target nucleus, perturbation theory 78−66319
^{6}Li, EM form factors and spectroscopic factors in phenomenological cluster models 80−496
^{6}Li, EM form factors and vertex consts. 78−12958
^{6}Li ground state, cluster struct. obs. in ^{6}Li(p,pα)np 77−88129
^{6}Li ground state, double well-cluster shell model, d-cluster contraction and deform. *(Chinese)* 78−78290
^{6}Li, Pauli distortion effects in folded optical pot. 79−6454
^{6}Li, self-consistent desorption using four and two body substructures 79−63611
^{6}Li, three-body model of bound state struct. 79−6374
^{6}Li, three-body model using hyperspherical harmonics 78−29411
^{6}Li, transition probabilities between cluster structure states and r.m.s. radius, double well-cluster model *(Chinese)* 80−63128
^{6}Li+n, effective internuclear potential, of cluster blocking effect 78−50159
^{6}Li(^{3}He,^{3}H)^{6}Be, 27 MeV, comparison of experimental data and cluster and distorted wave calcs. 79−76010
^{6}Li(^{3}He,^{3}He)^{6}Li*, 27 MeV, comparison of experimental data and cluster and distorted wave calcs. 79−76010
^{6}Li(^{3}He,αα p), 2.5 MeV, ^{5}Li or ^{8}Be formation, direct or compound nucleus mechanism 77−57678
^{6}Li(^{3}He,pα), 2.9 MeV, quasifree reaction, ^{2}H(^{3}He,pα) contrib., cluster motion 80−13485
^{6}Li(α,π^{+})^{6}He, threshold prod. in α-d cluster model 77−79356
^{6}Li(d,X) system, resonating group method, single channel approx., cluster states 80−57782
^{6}Li(e,e′), 102, 123 MeV, excitation form factor, ^{3}H-^{3}He cluster model 80−78190
^{6}Li(e,e′d)^{4}He, ^{6}Li(e,e′τ)^{3}H, d-α cluster model anal. 77−26673
^{6}Li(γ,d)^{4}He, cross section calc. by cluster model *(Japanese)* 77−67733
^{6}Li(p,p) 0.6, 1.04 GeV, α-d cluster model and Glauber multiple scatt. theory 79−85476
^{6}Li(p,pd), 590 MeV, α-d motion, impulse distrib., cluster momentum distrib. 80−52679

nuclear cluster model continued
^{6}Li(p,pd), 670 MeV, large angle quasifree scatt., spectroscopic factor, momentum distrib., cluster model 80−63184
^{6}Li(p,pd)α, 156 MeV, relative wave function of d and α clusters, PWIA, DWIA anal. *(Chinese)* 79−59068
^{6}Li(τ,τ)^{6}Li, 27 MeV cross-section calc. by Amado 3-body model 79−6617
^{6}Li(τ,τ)^{6}Li*, 45 MeV, cross-section calc. by Amado 3-body model 79−6616
^{6}Li→^{3}He+^{2}H+n (^{3}H+^{2}H+p), zero degree fragmentation of relativistic ^{6}Li 79−85438
^{6}Liμ^{-}→^{3}H^{3}Hν in ^{6}Li loaded photoemulsion, secondary particles ang. distrib. and energy *(Russian)* 78−89855
^{7}Li, cluster model wave function and r.m.s. radius 78−70442
^{7}Li, cluster struct. interplay model and appl., energy levels and shell clusters 79−17842
^{7}Li clustering, ^{7}Li+^{3}He three-body final states and impulse approx. calcs. 77−3023
^{7}Li, dσ(p,p'd)/dσ(p, nd), 670 MeV, cross section ratio, cluster model estimate 80−22829
^{7}Li, model for coupling two cluster structs., influence on shape and states 78−78288
^{7}Li, photodisintegration, cluster model wave function, bremsstrahlung weighted cross section 80−63163
^{7}Li two centre model, Brinks α-cluster model generalisation for odd nuclei *(Russian)* 79−30797
^{7}Li(α,α), low energy elastic and inelastic scatt., Pauli principle effect 78−4953
^{7}Li(d,$\alpha\alpha$)n, 2 MeV, quasi free reaction, ^{7}Li struct. 78−41727
^{7}Li(γ,t), <50 MeV, total and differential cross sections, levels, cluster model calcs. 80−32265
^{7}Li(π^{+},2p), cluster effects in in-flight π^{+} capture 78−89916
^{7}Li(π^{+},p^{3}He), cluster effects in in-flight π^{+} capture 78−89916
^{7}Li(π^{+},pd), cluster effects in in-flight π^{+} capture 78−89916
^{8}Li scattering system, microscopic multichannel cluster model calc., resonating group calc. 78−4906
^{A}Li(p,pα), A=6,7, 600 MeV, α-cluster quasielastic knockout, expt. methods, separation energy spectra 79−13275
Λ^{9}Be multiparameter variational calc., clustering in hypernuclei *(Russian)* 77−74791
Mg, α- and ^{8}Be-spectroscopic factors determ. 78−62494
^{24}Mg, ^{16}O+α+α cluster model, energy level structure 80−18215
^{24}Mg K=2 band and alpha cluster model state point symmetry 80−105946
^{24}Mg, novel cluster model descript., ^{16}O+^{8}Be, energy levels 78−62495
^{24}Mg, struct. determ. from ^{16}O+α+α model 79−6401
^{24}Mg(p,pα), 600 MeV, α-cluster quasielastic knockout, expt. methods, separation energy spectra 79−13275
^{95}Mo, neutron cluster-quadrupole vibr. coupling model for levels via ^{95}Tc^{m,g} decay 77−82856
^{14}N+^{12}C, 112 MeV, alpha clustering, multiple shape vibrs., TDHFC calcs. 79−3164
^{14}N(d, α), pol.d, 1.5-3 MeV, vector anal. capacity for two α-particle groups 80−78266
^{15}N(p,pα), (p,pt), (p,pα), spectroscopic data on quasielastic ejection on nucleon clusters from 1p shell nuclei 79−80931
^{15}N 9.155 MeV state, lifetime, cluster nature and parity from ^{12}C(^{7}Li,$\alpha\gamma$), ^{12}C(^{6}Li,^{3}Heγ) 79−6424
^{23}Na level α-spectroscopic strengths assuming direct cluster transfer from ^{19}F(^{6}Li,d) 80−27552
Nb, high spin negative parity states from cluster vibration coupling model 79−75823
^{93}Nb, 1 quasiparticle 2 phonon multiplet, microscopic quasiparticle cluster phonon coupling model 77−2908
^{20}Nd, low lying positive parity states by (^{16}O-α)+(^{12}C-^{8}Be) orthogonality condition model 79−6400
^{19}Ne alpha-particle and triton cluster states anal. 77−41907
^{19}Ne, final state selective population, triton clustering from band anal. from ^{16}L(^{6}Li,t) 80−9306
^{20}Ne, alpha-cluster states, spin, parity and branching ratios 78−50066
^{20}Ne, α-and ^{8}Be-spectroscopic factors determ. 78−62494
^{20}Ne α-cluster levels, props., hard-core potential calcs. 77−30614
^{20}Ne α-cluster states and backward angle anomaly in ^{16}O(α,α)^{16}O 77−38287
^{20}Ne, α-cluster struct. at excit. energy >30 MeV *(Russian)* 77−74784
^{20}Ne cluster struct., coupled channel orthogonality condition model, α-decay, excited states, transitions 79−97681
^{20}Ne, cluster struct. study in ^{16}O-α+^{12}C-^{8}Be coupled channel orthogonality condition model 79−89258
^{20}Ne, coexistence of shell struct. and cluster struct. 78−78279
^{20}Ne, positive parity alpha clusters, Woods-Saxon well calcs. 79−26383
^{20}Ne+^{58}Ni, 164 MeV, alpha clustering, multiple shape vibrs., TDHFC calcs. 79−3164
(^{20}Ne+α) system, effect of nuclear deform. on folded pot. 79−6453
^{A}Ni(p,α), A=58, 60, 30 MeV, α-particle angular distrib. 79−6588
^{16}O, 3 α forces, ground state energy and form factor 80−86817
^{16}O (α, 2α), DWIA calc., cross section and spectroscopic factors 79−63681
^{16}O, alpha-cluster states, spin, parity and branching ratios 78−50066
^{16}O α-cluster levels, props., hard-core potential calcs. 77−30614
^{16}O, α-cluster model, clustering and nuclear forces in terms of quark struct. 79−6443
^{16}O, α-cluster model comparison with giant E2 excitations 78−50109
^{16}O α-cluster states, widths and resonances, optical model, direct transfer in ^{12}C(^{6}Li,d) 80−105975
^{16}O, α-spectroscopic amplitudes in shell model 77−71564
^{16}O, cluster expansions for normalisation integral calc. 80−86831
^{16}O, configuration mixing and α-cluster transfer 78−46004
^{16}O, energy calcs., Jastrow variational method extension, FAHT cluster expansion 80−22677
^{16}O, π^{-} capture reactions, neutron spectra determ. by 2 and 4 nucleon cluster expansions 79−6703
^{16}O structure, energy levels, binding energy, cluster model with varying hinge angle 78−4907
^{16}O, tetrahedral rotor behaviour, charge form factors, deformed α clusters 79−45141
^{16}O+^{16}O, 384 MeV, alpha clustering, multiple shape vibrs., TDHFC calcs. 79−3164
^{16}O+^{20}Ne, elastic and inelastic 50 MeV, contribution of α-cluster exchange 77−10429
^{16}O+^{4}He, group theory appl. to reaction studies 80−9276

nuclear cluster model continued
^{16}O(^{9}Be,^{5}He)^{20}Ne*, sub-Coulomb alpha transfer cross sections 80−37394
^{16}O(α,α), α-particle elastic scatt. excitation functions, α-cluster state energies 79−63688
^{16}O(α,α), spectra and widths of quasistationary α-cluster states *(Russian)* 77−46180
^{16}O(d,d), treatment as three-body problem 79−6618
^{16}O(p,p), 49.48 MeV, elastic scattering, discrepancies from optical model, possible α-cluster struct. 78−62528
^{16}O(p,pd), (p,pt), (p,pα), spectroscopic data on quasielastic ejection on nucleon clusters from 1p shell nuclei 79−80931
^{16}O(p,px), x=d,t, ^{3}He, 75 MeV, spectroscopic factors, cluster model, DWIA 77−54214
^{16}O→^{12}C+α, alpha spectroscopic factors, K-harmonics method 78−62512
^{17}O α-cluster states, α-decay orbital momenta and parities from ^{13}C(^{6}Li,d) and α-decay *(Russian)* 78−86486
^{18}O alpha particle cluster states, rot. bands in ^{14}C+α model 78−8757
^{18}O, dineutron cluster states, single-channel resonating group calc., levels, J^{π} 77−82841
^{18}O, trinucleon cluster states, low lying negative parity states 78−29387
^{18}O, two-body surface correls. in extended basis shell model 78−532
^{18}O$_{2}$ shell-cluster admixtures, spectra, α-widths and electric transitions 77−54136
^{31}P(^{6}Li,d)^{35}Cl, 36 MeV, absolute cross sections, ang. distribs. 79−89321
^{205}Pb, ^{206}Pb, cluster vibrational field coupling model description 77−57604
^{208}Pb, energy of two-phonon α-vibration 77−14019
^{208}Pb(^{16}O,^{12}C)^{212}Po and α-decay, comparison for α-transfer reaction mechanism 79−6652
^{208}Pb(^{16}O,^{12}C)^{212}Po, 93 MeV, semiclassical analysis of α-transfer reactions, partial wave amplitudes 79−45283
^{208}Pb(^{6}Li,d), 90 MeV, alpha-cluster transfer from alpha-decaying nuclei 80−91166
^{208}Pb(d,^{6}Li) ^{204}Mg, SS MeV, levels and spectroscopic factors, α clustering, DWBA anal. 79−67694
^{208}Pb(π^{-},^{4}n), 120 MeV, tetraneutron possible existence, cross section and lifetime bounds 79−40958
^{212}Po, surface α-clustering and α-decays 79−75926
^{85}Rb levels, J^{π} and transitions from Kr^{m,g}, Sr^{m,g} decay, cluster-vibr. model 80−78162
^{32}S α-cluster struct., ground and first excited states, energies, radii and moments 80−102122
^{32}S, comparison of cluster and two-centre shell models 79−6444
^{32}S deformed states, comparison of cluster and shell model wave functions 79−22187
^{32}S, nuclear saturation props. 79−6395
^{44}Sc, $(f_{7/2})^{4}$ states populated in ^{41}Ca(α,p) 25 MeV reaction, relative transition strengths, semi-microscopic model calcs. 79−6645
^{28}Si, highly excited ^{12}C-α-^{12}C molecular state, symmetrical decay *(Russian)* 80−86861
^{28}Si, three body nuclear molecular resonances for ^{12}C-α-^{12}C 79−75949
^{28}Si, three particle (^{12}C-α-^{12}C) struct., highly excited state calcs. *(Russian)* 79−3073
^{28}Si, tri-nuclear cluster state of ^{12}C-^{12}C-α 78−50189
^{28}Si(α,d)^{30}P, spectroscopic factor calcs. 79−6384
^{28}Si(e,f), alpha cluster model approach, intermediate state to ^{12}C+^{16}O 79−40972
^{29}Si(^{6}Li,d)^{33}S, 36 MeV, absolute cross sections, ang. distribs. 79−89321
^{A}Sm, A=146,147, excited states, energy levels, spin, parity, shell and cluster-vibration models, from (α,xn) and (^{3}He,xn) 80−57683
Sr, high spin negative parity states from cluster vibration coupling model 79−75823
^{85}Sr, lifetime DSA meas. in ^{85}Rb(p,nγ) 79−36196
Tc, high spin negative parity states from cluster vibration coupling model 79−75823
^{95}Tc, 1 quasiparticle 2 phonon multiplet, microscopic quasiparticle cluster phonon coupling model 77−2908
^{44}Ti, yrast states as α-particle cluster states 78−33114
^{205}Tl, level excitation energies and ang. distribs. cluster model DWBA calcs. from ^{208}Pb(p,α) 79−17814
Zn even isotopes in cluster-vibr. model, energy spectra, EM props. 78−54708
^{64}Zn(d,^{6}Li), 55 MeV, cluster model DWBA anal. 78−21573
^{67}Zn, role of cluster-vibr., coupling in struct. of negative parity states 77−34206
Zr, high spin negative parity states from cluster vibration coupling model 79−75823
^{92}Zr(p_{pol}, A)^{89}Y, finite-range cluster-model description, DWBA approach 80−52667

nuclear collective model
see also nuclear cranking model; nuclear liquid drop model
2_{γ}^{+} level depopulation, reduced quadrupole transition probabilities, neutron-proton mass deformation difference 77−34203
2p1h multiple scatt. formalism, effective interactions, energy spectra 77−67709
^{24}Mg states, Nilsson model spectroscopic factors, collective model rot. bands 79−6421
γ vibrations in permanently deformed nuclei 78−86465
A=12-240, even-even, dynamic deformation theory, B(E2) values, quadrupole and mag. moments 80−68591
A=158-176, 'extension of variable moment of inertia model to high spins', comments 80−86791
A=228 to 240 even nuclei, anharmonicity of vibr. states superfluid model 77−61340
A=50 to 150, even-even, odd-even, odd-odd, truncated quadrupole phonon model 80−68567
A=50 to 150, shell, dynamical deformation and interacting boson models, limitations 80−68563
A=88-96, collective treatment of pairing Hamiltonian, transfer data anal. 79−13220
A~150, yrast states, deformed oscillator Hamiltonian calcs. 80−78126
A~150 transitional region, collective props., interacting boson model 80−27538
actinides, level energies and B(E2) ratios of deformed even nuclei 79−13221
adiabatic approx., time evolution of state vectors 77−88056
adiabatic collective motion, quantum Hamiltonian microscopic derivation 80−47345

nuclear collective model continued
adiabatic time dependent Hartree Fock theory of collective paths 78−525
adiabatic time-depend. theory, classical Hamiltonian quantisation for collective phenomena 78−526
algebraic formulation, collective and intrinsic submanifolds 80−73811
anharmonic collective motion, adiabatic TDHF as consistent theory 78−78291
anharmonic vibrator model, appl. of relation between 6-j and 9-j symbols 77−17838
axially symmetric nuclei, soln. of HF eqns. in coord. space 77−88060
backbending, effect of protons 77−82816
backbending phenomena, two fluid model of nuclear rots. ^{164,166}Er, ^{166,168,170}Yb 77−50049
band crossing in interacting boson model, E2 transition probabilities and g-factors 80−102101
basis states for rotational and vibrational limits 80−86775
Bohr's collective Hamiltonian soln. for transitional odd-mass nuclei 77−6221
Bohr collective Hamiltonian and interacting boson model relationship 80−86825
book, collective and single-particle models 77−41904
boson description, coupled system of quadrupole and octupole vibr. 79−484
boson expansions, convergence of various methods 79−93037
bound proton-neutron system, basis functions and collective states 79−67688
bound proton-neutron system, operator averaging technique, recurrent construction of collective variables 79−67689
canonical conjugate momenta to collective coords. 78−17119
classification of states in the unitary scheme for complex nuclei and commutation properties of SU_3-irreducible ε-tensors 79−63598
closed shell nuclei, elementary excitations unified model 77−67712
clustering effects in nuclei information from heavy-ion transfer reaction 77−14171
cold nuclear matter, hydrodynamical approximations 79−22219
collective 0^+ state, sum rules and breathing mode 80−86778
collective excitation of three particles, outside closed shell, propagator method 79−17830
collective mass parameter, super-normal phase transition effect 80−5046
collective motion, consistent microscopic theory in an ATDHF approach framework 78−70472
collective motion, self-consistent treatment, appl. giant dipole resons. 77−61362
collective path curvature as collectivity meas., quasi-boson approx. validity 80−22658
collective potentials and dipole and quadrupole giant resonances 78−78286
collective quasiparticle pairs, many phonon norm matrix orthogonality 79−71810
collective regularity, shell model appl. to microscopic description 78−50069
conference on interacting bosons in nuclear physics, Erice, Italy (June '78) 80−27042
constant temperature model, decay widths of highly excited nuclei *(Russian)* 77−74783
core-quasiparticle model, odd transitional nuclei 78−12988
Coriolis attenuation factors in particle plus rotor model 79−40862
Coriolis decoupling model, two quasiparticle plus rotor bandmixing calcs. 77−6205
cranked Hartree-Fock-Bogoliubov theory extension 80−105996
decoupled bands of odd-A nuclei in core-particle coupling model 77−10340
deformation of neutron-density in inelastic scatt. 78−46000
deformed even nuclei, level energies, γ transitions, moment of inertia, collective Hamiltonian 78−25133
deformed even-even nuclei, angular mom. coeff. distrib. for ground state band 79−13182
deformed even-even nuclei, real and complex boson expansions for vibr. anharmonicities 78−527
deformed nucl., shape anal. by collective rot. and SU(3) models 77−41880
deformed nuclear states in yrast-band, microscopic model 79−6365
deformed nuclei, new isovector collective modes 79−9443
deformed nuclei, nuclear collective rot., microscopic description 79−26357
deformed nuclei, positive parity isovector collective states 79−93483
deformed translationally invariant model, ^{12}C rotational band 79−58996
depairing probability for high spin states, rotational energy spectrum, rotor model anal. *(Chinese)* 79−80864
dissipation effects in presence of nuclear collective motion, nuclear friction 79−75810
dynamic polarisability and macroscopic eqns. of motion 77−41903
E1 giant resonances, features 77−79350
effective Coriolis coupling and nuclear Kondo effect 79−36174
effective interaction energy dependence, collective state partitioning model 77−22911
eigenvalue distribution in scalar space for noninteracting and interacting bosons 80−78177
electric quadrupole moments, quasi-rotational states in even-even nuclei 78−82281
elementary excitations 79−17836
energy dissipation, into internal energy superfluid wall formula 80−63108
energy-weighted moments, relations between nucl. collective theories 78−33130
even-even deformed nuclei, nonadiabatic effects 78−528
even-even nuclei, decoupled bands, Hamiltonian in body fixed frame 79−36176
even-even nuclei, low lying collective states from p-n interacting boson model 80−32158
even-even nuclei, microscopic anal. of low-lying collective states 78−12941
even-even nuclei, phenomenological calcs. in n-p interacting boson approx. 80−27597
even-even nuclei, resonance model of backbending and downbending 77−67694
even-even nuclei, semi-empirical correlation energy 78−17092
even-even nuclei, spectra calcs., interacting boson model 80−68590
even-even nuclei, yrast band energies, coherent states model, three parameter formula 78−17091
nuclear collective model continued
even-even nuclei with A≈150, excited states calculation, phenomenological models: band-mixing, vibrational-rotational and interacting-boson model 80−22653
even-even nuclei with collective oscillations, surface probabilities of α-particle formation *(Russian)* 78−41677
exact canonically conjugate momentum to the quadrupole tensor and a microscopic derivation of the nuclear collective hamiltonian 78−78251
exact fermion model with monopole and quadrupole low lying collective states 79−9495
excitation, elementary modes, conference, Varenna, Italy, July-Aug. (1976) 79−17834
extended generator coordinate method with HFB states excitation energies, B(E2) values of ^{72,74}Ge, ^{70}Zn 77−6203
Fermi liquid model anharmonic effects in collective excitations *(Russian)* 77−2922
Fermi liquid theory and giant resonances in nuclei 79−3095
finite nuclei, pairing and seniority 79−17840
fission, relaxation phenomena, collective deformation, and internal excitation energy *(Russian)* 79−80920
fluid dynamic approach to nuclear collective motion 78−17121
fluid dynamic relativistic model appl. to $^{20}Ne^{+}$ ^{238}U reaction 77−74877
fluid dynamical model, single-particle Schrodinger fluid 77−54165
fluid dynamical model, spin-, isospin-, spin-isospin-, and normal sound 77−54167
frictional effects in nuclear reactions with large scale collective motion, review 78−78336
generalised collective model, surface tension, energy spectra, and E2 γ-transitions 79−6432
generalised Schwinger representation, time depend. Hartree Bogoliubov theory quantisation, anharmonic vibr. 78−54673
generator coordinate method with conjugate parameters 80−47413
generator coordinate Peierls-Yoccoz method, applicability 77−67708
generator coordinate treatment of scatt., appl. of variational principle with natural boundary condition 77−54196
generator-coordinate method, props. of Griffin-Hill-Wheeler spaces 77−54166
generator-coordinate method extension to two quasi-particle excited states, appl. to fp-shell nuclei 77−54153
giant monopole resonance, self-consistent generator coord. method 77−2891
giant monopole states in the Suzuki model 79−45189
giant monopole vibrs., RPA and collective field description, surface compressibility 80−102100
giant multiple resonances, excitation strength functions 80−5037
giant multipole resonances, Regge poles and collective model 80−13436
giant multipole resonances, spin-isospin vibrs., spin waves, Regge poles in collective model 78−89777
giant resonances, damping theory, correlation function method *(Russian)* 77−10309
giant resonances in nuclear reactions, microscopic theory of intermediate struct. 80−99161
governor model for asymmetric deformed nuclei, band anal. 80−86776
gradient formula for the group U(2l+1) in nuclear collective model theory 78−37300
gradient formula for the O(5)⊃O(3) chain of groups 78−78285
Griffin-Hill-Wheeler eqn., solvable model 78−50105
group theoretical advances in collective motion anal. 80−9201
hadron-nucleus collisions at high energies, simple collective effects model *(Russian)* 78−89809
Hamiltonian decompositions, restricted dynamics, microscopic nuclear theory *(Russian)* 80−52594
harmonic quadrupole collective Hamiltonian, exact soln. 78−37301
Hartree model, decoupling of collective monopole and quadrupole oscills. 77−10343
heated fast rotating nuclei, equilib. props. 78−70439
heavy deformed nuclei, flow patterns for collective rotations 79−75816
heavy ion reactions, deflection function, effect of nuclear vibr. mode and orientation 79−59080
heavy ion scatt., nucleon transfer in dynamical two centre shell model, mol. single particle effects 79−89325
heavy-ion collisions, Thomas Fermi static and dynamic theory for collective motions 77−18599
heavy-ion reactions, time for charge equilibration, microscopic hydrodynamical model 78−8857
HF, adiabatic time-depend. description of nucl. collective motion 77−74786
HF, adiabatic time-depend. theory of collective motion in finite systems 79−486
high energy heavy ion collisions, hydrodynamic and classical microscopic descriptions 78−54791
high energy nuclear collisions, isobaric-gas model, shock waves, temp., density, pionisation 78−94022
high spin rotational states of Sm, Gd, Dy, Er, Yb doubly even isotopes, lifetimes meas. 77−30511
Hill-Wheeler integral for rotational energies, polynomial expansion 79−95
hole-line expansion convergence in nuclear matter 78−8762
hydrodynamic model predictions for p-nucleus collisions 77−50070
hydrodynamical model of nuclear fluid, spin and isospin props. 78−70479
i13/2 shell, particle-rotor model exact soln., cranking model connection 79−93485
$i_{13/2}$ shell, particle-rotor model soln., backbending, transition rates, ang. momentum spread 80−47344
interacting boron model of collective state, O(6) limit 80−32214
interacting boson and triaxial rotor models, O(6) limit 80−27579
interacting boson approx. and Frankfurt model, collective model confrontation 80−57706
interacting boson approx. s.bosons, exact calcs. and fermion pair description 80−57707
interacting boson model, collective motion descript., shell model test 80−27542
interacting boson model, collective state description, shell model connection 80−37341
interacting boson model, collective states of even-even nuclei, shell model descript. 78−62493
interacting boson model, electron scatt. data anal., Sm-Nd region 78−62522
interacting boson model, monopole and quadrupole pairing 80−73812

nuclear collective model continued
interacting boson model, relation to expanding boson and truncated quadrupole phonon models 80−27580
interacting boson model, rot. limit 78−46016
interacting boson model, shell model and microscopic nuclear struct. 80−27575
interacting boson model, shell model description 80−27574
interacting boson model, shell model fermion Hamiltonians with monopole and quadrupole pairing 80−27576
interacting boson model, shell model foundation 80−37340
interacting boson model, sphericity 77−41902
interacting boson model, transition from SU(5) to SU(3) limits 79−13218
interacting boson model 80−52595
interacting boson model classical limits 80−86826
interacting boson model for collective states, present status 80−27573
internal dynamics and collective rot., double variational method 77−50071
isobaric distributions in deep inelastic reactions 80−18270
isoscalar giatn resonances, sum-rule approacH 77−82898
isospin forbidden beta decays, collective model, Fermi matrix elements, appl. to ^{8}Li, ^{134}Cs 77−67722
isovector pairing vibrations, in two nucleon transfer ion-nucleus reactions 78−21487
kinetic energy, geometric derivation 79−49589
kinetic energy in the mass quadrupole oscillation collective model 78−66231
Kostant-Souriau geometric quantization of nuclear collective models 80−9247
l-azimuthal spherical harmonics in collective models 80−91139
large amplitude collective motion, adiabatic time-depend. HF method 77−88061
large amplitude collective motion, collective subspaces and generator coordinate method 80−9199
large amplitude collective motion coupling to RPA excitations 77−74787
large amplitude collective motion in a nontrivial schematic model 80−73816
large amplitude motion, microscopic theory 77−38231
level crossing effect on collective dynamics 77−50042
level density of interacting bosons 80−105974
level density of nuclei, role of collective effects and neutron resonances *(Russian)* 79−49586
light nuclei, shape in translationally invariant shell model 79−26367
local harmonic approach and ATDHF theory 77−71578
low lying states in collective nuclei, boson expansion theory 80−78118
macroscopic nuclear dynamics 78−12993
macroscopic rotation of cold nuclei 79−17785
many phonon systems, projection operator method 78−25130
many-body problem, classical hydrodynamics and collective motion approx. 80−83027
many-phonon monopole pairing vibrs. interaction in nuclear field theory, IBM 80−27578
mass quadrupole model, algebraic formulation 80−18211
microscopic collective Hamiltonian, spin-isospin part of the matrix element 79−63609
microscopic description of direct processes in (N,N′), effective interaction 78−12979
microscopic description of nuclei collisions, GCM and RGM framework, appl. to ^{4}He+^{4}He 77−34272
microscopic inertial functions for barium region nuclei 77−18448
microscopic model, wobbling motion in fast rotating nuclei 78−21505
microscopic theory, coeffs. for SU_3-irreducible decomposition of operators and props. of basic interactions 79−63608
microscopic theory, definition and eval. of collective energy 79−63607
microscopic theory for large amplitude collective motion in soft nuclei 80−86824
microscopic theory of collisions between complex nuclei based on generator coord. method 78−13145
modified one body nuclear dissipation 78−50071
modified oscillator potential description of high spin rotational states 77−67696
moment map and collective motion, Hamiltonian action of Lie group 80−91138
moment of inertia, connection with collective variables 79−75820
negative collective masses, nonlocal effective Hamiltonian 77−6191
neutron pickup reactions to $(i_{13/2})^2$ bands, theoretical rot. signatures, backbending 80−52558
nonadiabatic rotational model, mag. dipole moments j≥9/2 rot. bands 79−6388
nuclear collective rot. microscopic theory, general description of rots. 79−26356
nuclear field theory of Fermi systems in an external field, path integrals 78−93954
nuclear field theory treatment of the interacting boson model 80−27577
nuclear matter collective excitation stability with Skyrme interaction *(Russian)* 79−13239
nuclear shape meas. and collective model validity for N≠Z nuclei 78−45999
nuclei far from stability, spectroscopy 77−22910
nucleon-nucleus reactions, particle production, Fermi motion versus collective tube model 79−93659
nucleus-nucleus reactions, particle production, Fermi motion versus collective tube model 79−93659
O(5)×SU(1,1) symmetric irreducible representations, orthonormal basis, interacting boson model appl. 80−78178
octupole vibration, collective, wave functions, spherical harmonics 80−68532
odd mass nuclei, Hamiltonian in body fixed frame 79−36176
odd nuclei, soft and deformed, rotor plus quasiparticle approach, moments, transition probabilities 80−78214
odd-A $1f_{7/2}$ nuclei, high spin states, shell model analysis 78−62560
odd-A nuclei, O(6) spectra, interacting boson-fermion model, new coupling scheme 80−57727
odd-A nuclei collective states, interacting boson-fermion model 80−95296
odd-odd man nuclei, decoupled and strongly coupled particles system 78−8727
one body nuclear dynamics, classical theory for collective motion 78−8755
one-body dissipation, general classical theory, quantal corrections 78−86494
nuclear collective model continued
one-body dissipation formula derivation from Boltzmann eqn. 79−67686
one-body dissipation of nuclear deformation collective energy, semiclassical approx. *(Russian)* 78−86502
oscillator basis for octupole collective motion in nuclei 78−70470
p-shell nuclei, generator coordinate anal. of molecular like states 78−54664
pairing collective degrees of freedom, Dyson-like representation of fermion space 78−25134
pairing vibration in closed-shell nuclei, RPA calc. 77−67710
pairing with a delta interaction in the energy density nuclear mass formula 79−36143
particle rotor model for doubly odd transitional nuclei in Tl region 79−13223
particle rotor model study of transitional N=89 and N=91-95 nuclei 80−42529
particle-phonon coupling, unified theory, appl. to Sb and In isotopes 77−61360
particle-rotor model, band crossing 79−17833
particle-rotor model, characteristic features of backbending curves, B(E2) values *(German)* 77−71554
particle-rotor model, pairing interaction treatment, yrast and yrare bands 80−83028
particle-rotor model, two-body nature of recoil term 80−22713
particle-rotor model Hamiltonian, Coriolis interaction and recoil term attenuations, possible connection 80−32215
particle-vibration coupling, radial transition density of shape oscills., ^{208}Pb example 77−50048
particle-vibration coupling model, octupole mode 79−17839
particle-vibrator model, microscopic foundation 80−78179
path-integral approach to time-dependent self-consistent field theories 79−59023
perturbative treatment of nuclear rots., two-dimens. rotor, bands, moments of inertia 80−78111
potential energy surface and collective spectra 78−86464
projection of ang. mom. eigenstates from two-centre generator coord. model functions 77−22912
propagation and damping of collective modes in nuclear matter 78−25132
pseudomagic nuclei, yrast bands, variable moment of inertia model 80−449
quadrupole collective model with γ-independ. pot. energy surface 77−61363
quadrupole collective operators, matrix element closed form, spherical phonon operators 79−17832
quadrupole phonon states, fifth label values, exact derivation 80−31664
quadrupole transition densities and electron scatt. in the interacting boson model 80−27598
quadrupole vibration theory, potential oscillations and collective motion *(Russian)* 79−13222
quadrupole vibrs., group theory and nuclear collective model 77−57610
quantised rotator, classical correspondence of Schwinger boson representation 79−9492
quasiparticle excitations in rot. deformed nucleus *(Russian)* 79−26364
quasiparticle-phonon nuclear model, basic assumptions *(Russian)* 79−13219
rapidly rotating nuclei, semiclassical HF description, smooth quantal corrections, density and total energy 80−32171
rare earth even nuclei, Woods Saxon pot., very high spin Strutinsky calcs. 77−88055
rare earth nuclei, cluster-rotor-coupling approach to backbending 79−45129
relativistic hadron+nucleus reactions, degree of collectivisation 79−40956
relativistic heavy-ion collisions, π^- multiplicity distribs., collective tube model 78−89902
resonating group calcs., odd-even dependence of the optical optical potential 79−97687
rotating fermion systems, quantum mech. treatment 79−17337
rotating nuclei, two-phase model 78−33113
rotating toroidal nuclei, ang. mom. thresholds 78−41629
rotation aligned coupling, ang. momentum projection method, odd-A La isotopes 77−2921
rotation effects on collective props. review *(Russian)* 78−37299
rotation of light nuclei, quantum mechanical probability current 78−29410
rotation-alignment model and high-spin states in ^{189,191,193}Au 77−14016
rotation-vibrational motion with nonvanishing vortex-spin 77−18447
rotational and intrinsic motions, semimicroscopic derivation of coupling 77−38232
rotational and intrinsic nuclear motions, semimicroscopic derivation of coupling 77−30498
rotational band approach, pure zero-rank operators 80−47341
rotational collective microscopic theory in Sp(3,R) model 77−26600
rotational model, current operator 79−3096
rotational motion, in many paritcle systems, description using collective variables 79−40830
rotational motion, particle-rotation coupling 79−17838
rotational motion, selected topics 79−17835
rotational states in HF calc. with Skyrme interactions 77−34212
rotor plus particle model, odd neutron deficient Cd isotopes 79−36127
RPA derivation using generalised Schwinger representation of fermion pairs 77−38233
Schwinger boson representation, quantised rotator 80−18164
Schwinger representation of fermion pairs, anharmonicity 78−74316
semimicroscopic description of nucl. states at low, intermediate and high excitation energies 78−54666
shape anal., HF calcs. for light nuclei 77−41882
shell model description of the optical model potential 79−93580
Sp(n,R) discrete series, harmonic oscill. eigenstates, nuclear collective model 78−71
spherical even-even nuclei, anharmonicity effect in many phonon states 77−61361
spherical nuclei, fragmentation of hole states in quasiparticle-phonon model 80−83020
spherical nuclei, quasi-particle theory, modification of BCS basis 80−63109
spherical nuclei, quasiparticle-phonon model, iterative method 80−68566
spherical nuclei, self consistent theory of finite Fermi systems and low lying collective states 79−45130

nuclear collective model continued
spherical nuclei, small amplitude vibrs., giant resonances, TDHF, fluid dynamics comparison 78−66233
spherical shell model, renormalisation for collective model within truncated space 78−54697
spin rotation, high angular velocity, collective aspects of heavy ion collisions 80−78309
Stephens rotation alignment model, limits of application *(French)* 78−8754
superfluid deformed rare earth nuclei, quasiparticle-phonon coupling, self-consistent calcs. 77−54138
superfluid model, n-quasiparticle states of nuclei, statistical characts. *(Russian)* 79−3072
superfluid model, paired matrix elements for a spherical nucleus with variable pairing 79−6433
superfluid model, quasiparticle number conservation 77−6269
superfluid nuclei, pairing correls. in excited states, low seniority shell model approx. improvement 77−54163
superfluid nuclei, quasiparticle-phonon self-consistent coupling 77−54164
superfluidity and field theory of elementary excitations 79−17837
symplectic collective model, irreducible U(3) tensor interactions 80−83048
Tamm-Dancoff method based on SO(2N+1) regular representation of fermion many body systems 79−35629
Thomas-Fermi approach to rotating nuclei 78−41657
extended Thomas-Fermi density matrix 78−41658
Thomas-Fermi model of finite nuclei 78−8747
thomas-Fermi study of nuclei at high angular momenta 78−66197
three-particle system outside closed-shell nuclei, nucl. field treatment 78−25129
time dependent Hartree-Fock theory for nuclear collective motion *(German)* 77−67714
time dependent HF polarisability and RPA sum rules, collective model restoring force 79−6461
time dependent HF theory, collective path concept, validity range 79−17844
transitional nuclei, doubly even, validity of collective phonon truncation 79−36134
transitional nuclei, dynamical interplay between pairing and quadrupole modes, shell model anal. 79−89252
transitional nuclei, particle-rotor recoil term and pairing interaction, Fermi surface 80−32174
transitional odd mass nuclei, asymmetric rotor model for decoupled bands 77−22913
transitional odd-mass nuclei, beta decay log ft values from asymmetric rotor model 79−67715
transitional odd-odd mass nuclei, gamma deformed rotor model 79−93498
triaxial quantum rotor in high spin limit, matrix mechanics appl., yrast states 79−67687
triaxial rotor+hole for ^{191,193}Pt high-spin levels 77−34213
triaxial rotor at high ang. momentum near yrast line, microscopic theory 79−30795
two-dimensional, for even-even nuclei 77−61358
two-fluid model of nuclear rotations and surface vibrations, appl. to rare-earth nuclei 78−62474
two-phonon states, effect of Pauli principle 80−68565
variable moment of inertia model, theories of collective motion 77−57611
velocity fields and transition densities in nuclear collective modes 79−89255
vibrational collective motion, shell model anal. using algebraic approach 78−50072
vibrational nuclei, variable moment of inertia model, relation to interacting boson model 80−83051
viscosity, single-particle Schrodinger fluid 77−71577
vorticity in nuclear fluid dynamics 78−33131
Weizsacker mass formula based on consistency conditions, parameters calc. *(Russian)* 77−38220
wobbling motion at high spin, microscopic model in small oscillation approx. 80−22666
yrast level spacing discontinuity, rotation alignment mechanism 78−17085
yrast levels, ang.-momentum-projection from coherent phonon state 77−82808
yrast wave function, variational principle used to solve Hartree Fock problem 79−93537
yrast-band of odd nuclei 80−22651
Z=50 region odd-A nuclei, band structures and particle vibration coupling 77−54132
α-vibrations, proton and neutron pairing vibrs. 77−289
(n,γ), interacting boson and Nilsson model tests, Pt-Os transition region 80−37380
(n,p) excitation functions for Z≥48 nuclei, 10 to 20 MeV *(Russian)* 77−34305
π condensation in nuclear matter, Hartree-Fock and generator coord. methods 78−17129
π-nucleus, barionic cumulative effect in nuclei collective nature *(Russian)* 79−22339
^{232}Th(α, α'), coupled channel Born anal. of deformation correl 80−5149
^{A}Ag, A=105,107, positive parity band, mixing and branching ratios lifetimes from (^{16}O,2np)(^{14}N,3n) 80−9197
^{A}Ag, A=105-109, negative parity states, vibr. versus rot. descriptions 80−73781
^{A}Ag, A=105-109, negative parity states, EM props. from particle-asymmetric rotor model 80−102097
^{103}Ag collective excitation and J^{π} following ^{94}Mo(^{12}C,p2nγ), rotor-plus-particle model 80−86782
Au odd mass isotopes, particle rotor descriptions 77−22914
^{A}Au, A=189, 193, 195, particle-asymmetric rotor description of $h_{11/2}$ levels system 78−70425
^{A}Au, A=193-199, positive parity states, particle-asymmetric rotor description 78−46005
^{193}Au, intermediate coupling vibr. models 77−22845
^{193}Au levels, three holes cluster vibr. and particle asymmetric rotor descriptions 80−57668
^{195}Au, intermediate coupling vibr. models 77−22845
^{197}Au(p,X)^{149}Tb, target fragmentation momentum transfer, collective tube model, collectivity effects 80−37359
^{120}Ba, low lying struct., collective model discussion 79−22244
nuclear collective model continued
^{8}Be collective excitation spectra from generalised hyperspherical functions method *(Russian)* 80−91133
^{9}Be, HF and GCM calc. in α-cluster molecular model, ground state props. 77−54137
^{76}Br, Coriolis distorted bands, common $g_{9/2}$ parentage in N=41 nuclei 80−13349
CC ^{158}Dy high spin states B(E2) values, IBA model test from ^{26}Ng(^{136}Xe, 4n) CC ^{158}Dy high spin states B(E2) values, IBA model test 80−27541
^{12}C (^{12}C, ^{12}C), molecular collective excitation theory in two centre model 79−89256
^{12}C, monopole excitations, transition densities from simple collective model 79−40834
^{12}C, multipole elec. giant resons., anomalous parity isovector states, Coulomb excitation cross sections 79−9439
^{12}C+^{12}C, mol. resonance props. by GCM 79−13321
^{12}C(K^{+},$K^{+\prime}$), form factors, cross sections, interior probing capability 80−73866
^{12}C(e,e'p)^{11}B, energy spectra calc. in terms of dynamic collective model *(Russian)* 78−8804
^{12}C(p,p'), 20-40 MeV, pol. p, anal. powers, imaginary spin-orbit pot., coupled channels anal. 80−102179
^{12}C(p,p), below 8 MeV, iterative R-matrix in collective rot. model, phase shifts, inelasticity 79−3141
Ca, radial charge distrib. moments, ground state correlations, generator coordinate model 79−30785
^{A}Ca(α,α) and (α,α'), (A=40,42,44,48), single pole dominance 77−41985
^{42}Ca, collective states, quasi-degenerate intrinsic Hamiltonian, variational methods 80−68505
Cd 2_1^+ excitation, α-spectroscopic factors in IBA model from Sn(d,^{6}Li) 80−105967
^{1}Cd, A=113, 115 from ^{113,115}Ag β-decay 80−47432
^{103}Cd levels, J^{π} and positive parity decoupled band, rotor anal. of ^{94}Mo(^{12}C, 3nγ) 80−102096
^{104}Cd quasirot. ground state band and γ-transition from ^{102}Pd(α,2nγ) 80−105955
^{106}Cd collective and yrast levels, γ-transitions, 2 quasiparticle+rotor model from (heavy ion, xnγ) 79−22169
^{110}Cd, collective excitations in the interacting boson model *(Russian)* 80−5044
^{112}Cd(p,p'), 30 MeV polarised proton inelastic scatt., phonon states 77−2982
Ce, A=137, 139, high spin levels, γ spectra, hole-core coupling 77−50063
Ce, A=138,140, levels from (p,p'), (p,t) reactions, spin, parity, deform. parameters, enhancement factors 77−54217
^{132}Ce. pairing correlation for fast rot. nuclei 78−78284
^{37}Cl(ν_e,e^-)^{37}Ar, rot. model for mass-37 system, cross section calcs. 77−88114
^{A}Cs, A=119 , 121, 123, 125, collective props. and level schemes from (^{10}B,p2n), (^{14}N,3n) (^{10}B,3n) 79−22171
^{A}Cs A=127, 129, 131, 133, high spin states and collective properties from (^{10}B, 3n), (α, 2n) (^{6}Li, 3n) 79−22170
^{127}Cs collective quadrupole dynamics, band struct., transitions, collective model anal. from ^{127}I(α,4n) 80−78112
^{155}Dy, weakly deformed, isomeric $^{9+}/_{2}$ and lowest $^{7-}/_{2}$ states decay 79−89231
^{156}Dy, superband in backbending, band-mixing model 77−34209
^{156}Er, non axial deformability of rotating nuclei in two-phase model *(Russian)* 78−46002
^{158}Er, anomalous rotational bands−a model of a soft rotor coupled with $i_{13/2}$ particles 79−85356
^{164}Er, two-fluid model of nuclear rotations and surface vibrations, energy levels 78−62474
^{166}Er, non axial deformability of rotating nuclei in two-phase model *(Russian)* 78−46002
^{166}Er(γ,γ'), 14.4-16.6 MeV, γ-vibr. band head transitions, dynamic collective model 80−57662
^{A}Eu, A=151, 152, 153, 154, 155, excited states of transitional region nuclei, rot. bands *(Russian)* 80−52556
^{151}Eu level scheme from excitation functions, rotor and interacting boson anals. from ^{152}Sm(p,2nγ) 79−45163
^{19}F, even parity excited states, collective props., EM moments, generator coordinate method 78−78259
Fe, radial charge distrib. moments, ground state correlations, generator coordinate model 79−30785
^{57}Fe, rot. band mixing microscopic theory using modified Kuo-Brown interaction 80−68513
^{154,156}Gd, pairing-plus-quadrupole calcs. 77−82807
^{A}Gd, A=152, 154, 156, 158, excited states of transitional region nuclei, rot. bands *(Russian)* 80−52556
^{152}Gd, vibrational states, B(E2) branding rates and interband transitions, pairing plus quadrupole calcs. 80−78127
^{153}Gd, weakly deformed, isomeric $^{9+}/_{2}$ and lowest $^{7-}/_{2}$ states decay 79−89231
^{154}Gd, two-fluid model of nuclear rotations and surface vibrations, energy levels 78−62474
Ge, A=70, 72 and 74, dynamic deformation theory, energy levels 78−58235
Ge, doubly even nuclei, quasiparticle+phonon model calcs. 78−41626
^{A}Ge, A=71-74, electric quadrupole moments, nonadiabatic rot. model calcs. 79−6389
^{4}He, monopole excitations, transition densities from simple collective model 79−40834
$^{5}_{\Lambda}$He, Λ-particle induced excitation probability, ang. pot. functions method *(Russian)* 79−26389
^{175}Hf, three- and five-quasiparticle isomers, rotational bands and residual interactions from ^{170}Er(^{9}Be, 4n) 80−83022
Hg, even-A, possible triaxial shape and phase transition, triaxial rotor model 79−93503
Hg, positive-parity states, Coriolis antipairing effect, deformed-rotor model 78−12950
^{A}Hg, A=198, 200, rigid asymmetric rotor model descript., E2 and E4 props. 80−13403
I, 123≤A≤133, coupled quadrupole model, spectra, B(E2), B(M1), moments calcs. 77−82837
I, A=117-127, odd, collective props. determ. 77−46124
Ir odd mass isotopes, particle rotor descriptions 77−22914
^{A}Ir, A=187, 189, 191, 193, positive parity states, particle asymmetric rotor descriptions 79−49572

nuclear collective model continued
Kr even isotopes, collective levels and B(E2) values, IBA calcs. 80−27539
Kr even-even isotopes, collective states and transitions, interacting boson approx. 80−73773
^{A}Kr, A=74-82, even-even isotopes, B(E2) values and collectivity, interacting boson approx. 80−27537
^{78}Kr bands, lifetimes and E2 transitions from interacting boson model and (^{16}O,p2n), (^{19}Fe,α2n) 80−73771
^{A}Mg, A=24,26, second order nonspherical quadrupole phonon effects 80−86790
^{23}Mg even parity excited states, collective props., EM moments, generator coordinate method 78−78259
^{24}Mg, highly-excited rot. band obs. from ^{10}B(^{14}N,α)^{20}Ne 78−33218
^{24}Mg isoscalar quadrupole excitations in 2 centre shell model, collective approach, particle-hole excitations 79−45139
^{24}Mg, low spin rotational states, energy props., extended deformation model 80−86785
^{24}Mg, monopole excitations, transition densities from simple collective model 79−40834
^{24}Mg, rotational band fragmentation and rotation-vibr. model, ^{12}C+^{12}C appl. 78−25096
^{24}Mg, rotational band fragmentation, rotation-vibr. model 78−54665
^{24}Mg, triaxial nuclei rots., extended cranked shape consistent oscillator model 80−102133
^{24}Mg(α,α'), 120 MeV, ground and gamma band excitation, coupled channel calcs. in rotational model 79−89315
^{24}Mg(p,p'), polarised p, 20.3 MeV, low lying states, collective and microscopic model 78−82287
^{24}Mg(p,p), 40 MeV, natural parity transitions 78−66277
^{26}Mg(^{3}He,^{3}He'), 4^{+} states, B(E2) values, and band mixing, rot.-vibr. model 80−83019
^{95}Mo, neutron cluster-quadrupole vibr. coupling model for levels via ^{95}Tc^{m,g} decay 77−82856
^{96}Mo vibration-rotation struct. and yrast levels from variable moment of inertia model 80−73778
^{A}Na, A=21, 23, even parity excited states, collective props., EM moments, generator coordinate method 78−78259
^{23}Na, particle-rotor model with s-d shell pairing, BCS approx. 80−57705
Nd, A=139, 141, high spin levels, γ spectra, hole-core coupling 77−50063
Nd, even-even, E2 transition probabilities from multiple Coulomb excitation, IBA comparison 80−78212
^{147}Nd low spin states ns lifetimes, particle rotor model interpretation 80−78207
^{148}Nd, vibrational states, B(E2) branding rates and interband transitions, pairing plus quadrupole calcs. 80−78127
^{149}Nd, weakly deformed, isomeric $^{9+}/_{2}$ and lowest $^{7-}/_{2}$ states decay 79−89231
^{A}Ne, A=19, 21, even parity excited states, collective props., EM moments, generator coordinate method 78−78259
^{20}Ne collective motion, B(E2) rates, algebraic formulation in symplectic shell model 80−83015
Ni, radial charge distrib. moments, ground state correlations, generator coordinate model 79−30785
^{16}O, giant dipole resonance fine struct., 5p-5h excitation model *(Chinese)* 78−82271
^{16}O, tetrahedral rotor behaviour, charge form factors, deformed α clusters 79−45141
^{16}O+^{16}O elastic scattering, GCM calcs., phase shifts, ang. distribs. 77−30625
^{16}O(^{16}O,^{16}O), 10-41 MeV, molecular resonances γ-yield, band crossing model 80−106032
^{16}O(p,p'), 150 MeV, spin-orbit interaction within collective model and DWBA 79−45128
^{16}O(p,p'), 20-40 MeV, pol. p, anal. powers, imaginary spin-orbit pot., coupled channels anal. 80−102179
^{18}O struct. calcs., collective Hamiltonian approach 79−22212
Os even-even isotopes, excitation energies and EM props. from interacting boson model 80−106005
^{A}Os, A=186, 188, 190, 192, rigid asymmetric rotor model descript., E2 and E4 props. 80−13403
^{A}Os, A=186,188, levels and transitions from Re decay, triaxial rotor model 80−91155
^{A}Os, A=186-194, collective levels, transitions, mag. and quadrupole moments, boson expansion theory 80−105954
^{190}Os, collective states and static quadrupole moment, boson expansion theory 80−47346
Os(t,p), 17 MeV, two neutron transfer strength, O(6) limiting symmetry in IBA, Pt comparison 80−32287
Pb, odd-A isotopes, weak coupling calc. for high spin neutron hole excitations 78−62475
Pb pairing vibr. band, microscopic struct. and wave functions from (p,t), (t,p) 80−91126
Pb region, forbidden charge exchange collective modes, β- and γ-decay processes 80−86784
^{205}Pb, ^{206}Pb, cluster vibrational field coupling model description 77−57604
^{207}Pb(p,p'), excitation of neutron-hole states, 61.2 MeV protons 78−8724
^{208}Pb monopole vibr. vel. field, asymptotic form 80−78115
^{208}Pb, Thomas-Fermi model 78−8747
^{208}Pb($\pi^{\pm}$,$\pi^{\pm}$), 80, 116 MeV, elastic and inelastic, optical and collective model anal. 79−22329
Pd, even isotopes, low lying collective states, IBA 80−27540
Pd, even-even, collective states, B(E2), branching ratios and moments, boson expansion method 80−102099
Pd, even-mass isotopes, collective model with deform., vibr., rot. energy levels, B(E2) ratios 78−17120
^{A}Pd, A=106, 108, collective excitations in the interacting boson model *(Russian)* 80−5044
^{105}Pd, high-spin particle-core multiplets via ^{96}Zr(^{12}C,3nγ)^{105}Pd, rot. model 77−54140
^{109}Pd low spin odd parity levels, γ-rays, particle-rotor comparison from ^{108}Pd(n,γ) 80−73805
^{109}Pd unique parity states, particle rotor model low spin test 79−93515
^{145}Pm level struct., J$^{\pi}$ and lifetimes, cluster-vibr. model anal. of ^{146}Nd(p,2n) 80−91125
^{149}Pm high spin states and bands, rot. description and in-beam study from ^{150}Nd(p,2nγ) 80−32153
^{149}Pm levels, bands, transitions, in-beam spectroscopy, particle-rotor anal. from ^{150}Nd(p,2nγ) 80−78125

nuclear collective model continued
Pt, even mass, ground and gamma band EM transition rates, asymmetric rotor model 80−32231
Pt even-even isotopes, excitation energies and EM props. from interacting boson model 80−106005
Pt, positive-parity states, Coriolis antipairing effect, deformed-rotor model 78−12950
^{A}Pt, A=188-198 collective levels, transitions, mag. and quadrupole moments, boson expansion theory 80−105954
^{A}Pt, A=190,192,194, state struct. in interacting boson model 80−83047
^{A}Pt, A=192, 194, 196, rigid asymmetric rotor model descript., E2 and E4 props. 80−13403
^{A}Pt, A=192, 194, β_4 deformations, anomalous interference terms, rigid asymmetric rotor model 79−75832
^{190}Pt, collective excitations in the interacting boson model *(Russian)* 80−5044
^{194}Pt(^{12}C,^{12}C), 78 MeV, elastic and inelastic differential cross section, triaxial rotor anal. 79−63689
^{196}Pt, collective states and static quadrupole moment, boson expansion theory 80−47346
^{196}Pt, O(6) symmetry of interacting boson approx. model in shape transition 80−27550
Pt(t,p), 17 MeV, two neutron transfer strength, O(6) limiting symmetry in IBA, Os comparison 80−32287
^{240}Pu fission, dynamic excitation and collective energy, quasiparticles 79−67792
Rb odd-even isotopes, collective states and transitions, interacting boson approx. 80−73773
^{A}Re, A=181, 182, 187, spin polarisation, state struct. and mag. moments in rot. model 80−18194
^{A}Re, A=186,188, β-decay, weak magnetism effects, triaxial rotor model 80−91155
Ru, even isotopes, low lying collective states, IBA 80−27540
Ru, even-even, collective states, B(E2), branching ratios and moments, boson expansion method 80−102099
^{A}Ru, A=104,106,108, level scheme and transitions, collective model anal. of Tc decay 80−78166
Sb, neutron rich nuclei, IBM and shell model approaches, collective modes 80−78129
^{74}Se, collective excitations in the interacting boson model *(Russian)* 80−5044
^{A}Si(e,e'), 126-293 MeV, A=28,29, levels and form factors, particle-phonon coupling anal. 80−105977
^{30}Si nuclear structure model in coupled channels calc. for ^{30}Si+^{12}C scatt. 79−97721
Sm isotopes, shape transition, s-d IBA model Hamiltonian struct. 80−32173
^{A}Sm, A=148, 150, 152, 154, 156, excited states of transitional region nuclei, rot. bands *(Russian)* 80−52556
^{147}Sm, deformed 1h$_{11/2}$ neutron hole states 78−86466
^{150}Sm deformation, collective spectra and moments of inertia starting from nuclear force 79−17790
^{150}Sm, vibrational states, B(E2) branding rates and interband transitions, pairing plus quadrupole calcs. 80−78127
^{151}Sm, struct. determ. from gamma ray spectra in (n,γ) 77−22853
^{153}Sm, spin, parity, deduced levels, using ^{150}Nd(α,n), comparison with particle-rotor model 79−58999
Sm(n,n), (n,n'), (n,n'γ), A+148,150,2, E=2.47 MeV collective excitations obs. 78−33187
Sn 2$_1^{+}$ excitation, α-spectroscopic factors in IBA model from Te(d,^{6}Li) 80−105967
Sn, even isotopes, collective states and transitions from simple phenomenological model 80−73787
Sn isotopes, relation between interacting boson approx. and quasiparticle formalism 80−32216
^{177}Ta spin polarisation, state struct. and mag. moments in rot. model 80−18194
^{48}Ti(γ,n), 15-27.5 MeV, giant dipole resonance splitting, dynamic collective model 80−57755
Tl odd mass isotopes, particle rotor descriptions 77−22914
^{A}U(α, α'), A=234, 236, 238, coupled channel Born anal. of deformation correl 80−5149
^{236}U, induced fission dynamics 78−66261
^{238}U collective and deformation props., general collective model 80−86827
^{238}U, Xe-induced Coulomb fission, rotation-vibration model for target nucleus 79−13367
^{48}V, low-lying positive parity states, deformed config. mixing model 77−6198
W even nuclei, pairing phonons or SU(3) bosons 79−93532
^{A}W, A=184, 186, rigid asymmetric rotor model descript., E2 and E4 props. 80−13403
^{133}Xe, semi-microscopic anal. by generalised vibrational intensity and selection rules and diagonalisation 77−2901
^{166}Yb multiple band crossing, (gSS'S''S'') system gamma correlation patterns 80−106008
^{167}Yb i$_{13/2}$ band, spin alignment in the particle-rotor and cranking models 80−42536
^{168}Yb, two-fluid model of nuclear rotations and surface vibrations, energy levels 78−62474
Zn, doubly even nuclei, quasiparticle+phonon model calcs. 78−41626
Zn, radial charge distrib. moments, ground state correlations, generator coordinate model 79−30785

nuclear collective motion *see nuclear collective model*

nuclear collective states and giant resonances
see also isobaric analogue resonances
1f$_{7/2}$-shell nuclei, selective population of high-spin states in heavy ion reactions 77−18374
1p nuclei, M2 giant resonance calcs. from (e,e'),(π^{-},γ)$_{g}$,(μ^{-},ν) 80−22784
^{116}Xe quasi-rotational bands, levels J$^{\pi}$ and T$_{1/2}$ from ^{116}Cs decay 80−83021
^{154}Er, high-spin states 78−29373
^{239}U vibr. states, obs. in ^{238}U(n,γ) 78−41627
^{298}114, high spin pot. energy surfaces, fission barrier, α-, γ-decay half lives, yrast spectrum 80−73764
^{A}Er, A=156, 160, yrast level population, decay, and lifetimes from Sn(^{40}Ar, 4n), ^{A}Er, A=156, 160, yrast level population, decay, and lifetimes *(Russian)* 79−97648
^{A}S, A=32,34, E1 and E2 strength, E1 giant resonance decay, isospin 79−89266

nuclear collective states and giant resonances continued
β band influence on structure of decoupled bands 78−93921
γ vibrations in permanently deformed nuclei 78−86465
γ-ray yield functions from high spin states, comparison with 79−93492
γ-vibrational levels, Coriolis effects and microscopic structure 77−82809
A=12-208, adiabatic TDHF approx. isoscalar quadrupole collective motion, cranking mass 80−68507
A=158-176, 'extension of variable moment of inertia model to high spins', comments 80−86791
A=187-199 odd-A nuclei, structure and formation of rot. bands based on intruder orbitals 77−22829
A=19-31 odd nuclei, $K^{\pi}=1/2^{-}$ bands, spectroscopic factors and transitions 80−32151
A=228 to 240 even nuclei, anharmonicity of vibr. states superfluid model 77−61340
A=24-60, yrast lines using Strutinsky method, empirical fusion bands 80−42514
A=36-39, energy levels and effective interactions from large scale shell model calcs. 79−59011
A=40-56, spectroscopy props. using pure configuration shell model *(Chinese)* 80−42584
A=40-80, yrast props. and high spin isomers, cranking plus Strutinsky formalism 80−32152
A=4-16, monopole giant resonances, state density radii and compressibility using hyperspherical functions *(Russian)* 80−27615
A=4n nuclei, energy levels, BE(2) transition rates, HF calcs. with Skyrme force 78−82315
A=60-80 even-even nuclei, collective motions and band structs. 80−9202
A=70, heavy-ion induced fission-evaporation reactions, magnetic substrate distribs., nuclear alignment 80−73857
A=72 region, evidence for coexistence of spherical and deformed states 77−6192
A=88-96, collective treatment of pairing Hamiltonian, transfer data anal. 79−13220
A=90 region, core pol. effects and giant quadrupole resonances, HF and macroscopic calcs. 80−57756
A≤28, giant quadrupole resonance, E2 intensity distrib., from (α, α′), DWBA anal. *(Hungarian)* 80−52642
A∼150, yrast states, deformed oscillator Hamiltonian calcs. 80−78126
A∼150 transitional region, collective props., interacting boson model 80−27538
A∼90 nuclei, isomeric states, spin polarisation, M4 transitions and giant resonances 80−63157
a giant resonance theory in the 1p1h+2p2h+continuum approximation 79−67628
actinide nuclei, cranking model, collective inertia parameters 80−57665
actinide nuclei, modified oscillator potential, dynamical moment of inertia, single particle levels 79−67637
actinide nuclei, photo- and electro-fission cross sections and yields, giant resonances 80−5187
adiabatic collective motion, quantum Hamiltonian microscopic derivation 80−47345
adiabatic TDHF approx., mass parameters, single collective variable, theoretical aspects 80−73765
angular momentum depend. cranked HFB inertia parameter, high spin states 80−42524
asymmetric nuclear matter, isospin waves, IAS and giant Gamow-Teller resonance 80−91142
asymmetric rotator, yrast states, wobbling freq., boson representation 80−32167
atomic negative meson capture, nuclear giant resonance excitation *(Russian)* 80−42623
back bending, Hartree-Fock Bogolyubov approach, cranking method 78−58228
back bending effect, Hartree-Fock-Bogolyubov treatment of cranking method, yrast states 78−82264
backbenders, rot. energy expressions and least squares fitting 80−27531
backbending, core-particle coupling model appl. band construction 79−97645
backbending, effect of protons 77−82816
backbending, ground state band and aligned two quasiparticle band crossing interpretation 79−22167
backbending associated with alignment of quasiparticle momenta 78−33112
backbending curves, characteristic features, B(E2) values, particle-rotor model *(German)* 77−71554
backbending nuclei, HFB cranking wave functions 80−83049
backbending phenomena in even-even nuclei, mechanism *(Chinese)* 79−22177
band crossing anomalies in cranking model 78−25127
band crossing in interacting boson model, E2 transition probabilities and g-factors 80−102101
band crossing region, self consistent cranking model discontinuities and ang. momentum fluctuations 79−482
band head splittings, residual n-p interaction in doubly odd deformed nuclei 77−14012
band level staggering in doubly-odd nuclei, evidence for predicted phase change 80−32144
band mixing with several valence nucleons, E2 and M1 matrix elements *(French)* 78−45994
band structures, generalised HFB approach in intrinsic frame of reference, equilib. deformation 80−22664
band structures, generalised HFB approach in SU(3) framework 80−22663
boson expansion technique description of collective motion 77−279
bound proton-neutron system, basis functions and collective states 79−67688
bound proton-neutron system, operator averaging technique, recurrent construction of collective variables 79−67689
Cl ^{208}Pb(α,α′), 120 MeV, new giant resonance at 80 $A^{-1/3}$ MeV 77−41939
coherent rot. states, quantum flow pattern and vortex struct. 80−22656
coherent rotational states, alpha decay, α-emission probability 80−102155
coherent rotational states formed in heavy ion collisions, γ-decay 80−27657
coincidence method for Coulomb excitation studies of weakly populated vibr. like levels 78−70716
collective 0^{+} state, sum rules and breathing mode 80−86778
collective angular momentum in classical mechanics 80−4516

nuclear collective states and giant resonances continued
collective coordinates in RPA, systematics of giant multipole resonances *(Russian)* 77−74751
collective excitation, interplay of pairing and intrinsic modes 79−36132
collective excitations from high-q electron scatt., RPA AND ATDMF calcs. 80−22673
collective excitations in nuclear matter with Skirm type effective interaction *(Russian)* 78−54716
collective excitations of nuclei in a relativistic mean-field theory 80−95300
collective excited states, pairing degrees of freedom influence, shell model anal. 79−89250
collective mass parameter, super-normal phase transition effect 80−5046
collective model of giant multipole resonances, spin-isospin vibrs., spin waves, Regge poles 78−89777
collective modes in fission and deep inelastic scatt., ang. momenta equilib. statistical treatment 80−42688
collective motion, basis states for rotational and vibrational limits 80−86775
collective motion, gauge invariant periodic TDHF eigenstates 80−27532
collective motion, self-consistent treatment, appl. giant dipole resons. 77−61362
collective motion frictional and conservative forces, frictional Schrodinger eqn. 79−85357
collective parameter dynamics, monopole vibrs., variational principles 80−95298
collective path curvature as collectivity meas., quasi-boson approx. validity 80−22658
collective potentials and dipole and quadrupole giant resonances 78−78286
collective props. of nuclei deduced from electron scatt., deformed nuclei, review 78−50064
collective regularity, shell model appl. to microscopic description 78−50069
collective rotation, quantisation, Schwinger boson representation 80−18164
collective spectra, two dimens. interacting boson and variable moment-of-inertia models 79−67633
collective state renormalisation, improper initial or final states in nonlinear field theory 79−439
collective states and crossing symmetry 79−93497
collective states description in terms of SU(6) group 77−54134
collective structure inferred from heavy ion Coulomb excitation 80−5167
collective transition average lifetimes, spin (30-50) region in heavy ion-nucleus reactions 78−89822
complex cascade processes decay law, high spin state mean lifetime corrections *(Chinese)* 80−22761
complex deformed and spherical nuclei, giant resonances within quasiparticle phonon model 79−63648
compound deformed state g-factors and moments of inertia *(Russian)* 77−74757
compound neutron absorption processes, optical pots., one particle vibr. state effects *(Russian)* 80−105956
compound nucleus, giant resonances, force functions for partial E1-transitions 78−12985
compound nucleus radiative decay, population of aligned rotational bands *(Russian)* 78−86467
conference, 11th Masurian school in nuclear physics, Mikolajki, Poland (Aug.-Sept. 1978) 79−63605
conference, Les Houches, France (July-August 1977) 79−71864
conference on interacting bosons in nuclear physics, Erice, Italy (June '78) 80−27042
conference on medium heavy nuclei structure, Rhodes, Greece (May 1979) 80−67935
Conference on meson-nuclear physics, Houston, USA (Mar. 1979) 79−85489
conference on neutron capture gamma ray spectroscopy, Upton, USA. (Sep. '78) 80−36780
conference on nuclear interactions, Canberra, Australia (Aug.-Sep. 1978) 80−4476
conference on nuclear physics with EM interactions, Mainz, Germany (June 1979) 80−22145
conservation laws and collective excitations in nuclei, microscopic model of giant dipole resonance 77−54135
continuum transitions in nuclei at high ang. momenta, are multipolarity 79−17849
core polarisation in inelastic scatt., extension to include charge-exchange reactions 78−78359
Coriolis decoupling model, two quasiparticle plus rotor bandmixing calcs. 77−6205
Coriolis effect in odd-A nuclei, computer program 77−61341
Coulomb effect in rotating nuclei in the Thomas-Fermi approach 80−47355
Coulomb fission prompt component, model including rot. states and vibr. motion 79−67783
Coulomb-nuclear interference for high spin states 78−46097
coupled rotational bands in even-even nuclei, model 80−27529
cranked Hartree-Fock-Bogoliubov wave functions, ang. momentum distribs. at band crossings 78−93956
cranked HFB treatment of pairing force, back-bending model 77−278
cranking, microscopic derivation for nuclear systems with large angular momentum 79−40829
cranking calculations with self-consistent symmetries in a triaxial basis 79−54374
cross sections, energy-averaged, for resonant elastic scattering *(Russian)* 77−46153
damping of collective motion, time depend. Hartree model study 78−54711
decoupled bands and antialigned states 78−78236
deep inelastic heavy ion collisions, quantal theory of Brownian motion, collective vibrs. 79−67774
deep inelastic processes, large scale collective motion in nuclear matter 80−5087
deformation changes rel. to α-decay rotation signatures 79−13258
deformed even-even nuclei, ^{152}Sm to ^{238}U, semimicroscopic calcs. of giant dipole resonances 77−50096
deformed even-even nuclei, angular mom. coeff. distrib. for ground state band 79−13182
deformed even-even nuclei, E2 transitions within ground state band 78−13012

nuclear collective states and giant resonances continued
deformed even-even nuclei, real and complex boson expansions for vibr. anharmonicities 78−527
deformed nuclear states in yrast-band, microscopic model 79−6365
deformed nuclei, bandcrossing in K≠0 bands, odd-A rare earths 80−5045
deformed nuclei, coupled rot. bands, RPA type approach 78−89775
deformed nuclei, level densities, K-band positions 77−22855
deformed nuclei, low and high energy collective states and giant resonances, RPA calc. 79−17779
deformed nuclei, new isovector collective modes 79−9443
deformed nuclei, nuclear collective rot., microscopic description 79−26357
deformed nuclei, positive parity isovector collective states 79−93483
deformed nuclei, splitting of giant multipole states, vibr. pot. model 78−4893
deformed nuclei, state microscopical structure in neighbourhood of yrast line 79−45137
deformed nuclei, yrast level ground state correlations, RPA anal. 80−86777
deformed nuclei fusion reactions, γ-multiplicities, collective and statistical γ-rays Monte Carlo calcs. 79−578
deformed nuclei with isoscalar and isovector interactions, one-phonon states 79−3071
deformed rare earth nuclei, bandcrossing in K≠0 bands, backbending 80−9204
depairing probability for high spin states, rotational energy spectrum, rotor model anal. *(Chinese)* 79−80864
dipole giant reson., energy splitting connection with deform. 77−2975
dipole giant resonance in fissioning nuclei, microscopic calcs., excitation energies, dipole strengths, transition densities 78−29442
dipole reson. excited by free-bound muon atomic transition 77−26630
dipole resonance, even-even deformed nuclei, quasiparticle-phonon nuclear model *(Russian)* 80−52641
dipole sum rule schematical eval., collective isovector quadrupole strength 80−47428
dissipation effects in presence of nuclear collective motion, nuclear friction 79−75810
doorway mechanism in deep inelastic heavy ion reactions 78−632
doorway states, energy dependence of inelastic cross-section, shell model, coupled channel anal. 80−73854
doorway states reln. to optical model *(Russian)* 77−6213
double crossing of ground rotational band and super band 78−45996
double magic nuclei, self consistent description of low lying collective states *(Russian)* 78−89783
doubly closed shell nuclei, isovector giant monopole resonances, sum rule approach 80−78244
doubly even deformed nuclei, excited states, Pauli principle effects, quasiparticle-phonon model 80−63094
doubly even nuclei, yrast band B(E2) values, hydrodynamical model and CAP effect 80−86793
doubly magic nuclei, giant monopole resonances calcs. using adiabatic HF theory 79−22260
E1 giant resonance of deformed nuclei in the region 150<A≤186 *(Russian)* 78−78348
E1 giant resonances, features 77−79350
E1 transitions from octupole vibrational states 79−93548
E1-giant dipole resonance, strength function pygmy anomaly, nonstatistical background coupling 80−37358
E2-giant resonances, results obtained with Darmstadt electron Linac 77−83183
E2-transition rates of the ground state rotational member 78−89821
E2/M1 mixing ratio, in vibr. yrast band, sign rule 79−17855
effective Coriolis coupling and nuclear Kondo effect 79−36174
effective moment of inertia, effective freq. depend. in deformed oscillator basis model 79−75811
electric multipole modes in the fluid-dynamical approximation 80−106029
electronuclear sum rules, linear energy weighted, nuclear struct. determ. method 79−75897
electroproduction and decay of giant resonances 79−26413
elementary excitations 79−17836
EM sum rules for (γ,γ), (e,e), transitions and giant resonances 80−5090
ensemble of random particle-hole matrices with collective eigenstates 77−61388
even actinides, lowest 0^+ state excitation, collective phonon state, spectroscopic factors from (p,t), (t,p) 80−13410
even actinides, two-nucleon transfer, first 0^+ collective state excitation, spectroscopic factor *(Russian)* 80−42530
even-even deformed nuclei, aligned rot. of octupole vibrational states 78−12955
even-even deformed nuclei, ang. momentum depend. of collective parameters *(Russian)* 77−6210
even-even deformed nuclei, backbending from band crossing 77−14022
even-even deformed nuclei, collective $K^\pi=0^+$ states, realistic boson expansion comparison 80−5043
even-even deformed nuclei, coupled rot. bands, charge and density distribs. 78−89776
even-even deformed nuclei, giant E_λ resonances of high multipolarity, force functions 79−75944
even-even deformed nuclei, multiphonon $K^\pi=0^+$ states, matrix elements of general Hamiltonian 78−41621
even-even deformed nuclei, multiphonon $K^\pi=0^+$ states, norms 78−17089
even-even deformed nuclei, nonadiabatic effects 78−528
even-even nuclei, decoupled bands, Hamiltonian in body fixed frame 79−36176
even-even nuclei, low lying collective states from p-n interacting boson model 80−32158
even-even nuclei, microscopic anal. of low-lying collective states 78−12941
even-even nuclei, resonance model of backbending and downbending 77−67694
even-even nuclei, yrast band backbending mechanism criteria 80−91128
even-even nuclei, yrast band energies, coherent states model, three parameter formula 78−17091
even-even nuclei, z=6 to 100, probable members of quasi-bands in spherical and deformed regions 80−13357
even-even nuclei with A≈150, excited states calculation, phenomenological models: band-mixing, vibrational-rotational and interacting-boson model 80−22653

nuclear collective states and giant resonances continued
even-even rare earth nuclei, rotational energies, microscopic calcs. 77−54133
exact fermion model with monopole and quadrupole low lying collective states 79−9495
excitation during collective deformation, time depend. Hartree Fock Bogolyubov method, fission process 78−58229
excited nuclei, self-consistent theory of giant dipole resonance, thermodynamic RPA *(Russian)* 80−5106
excited simple and yrast states, mag. moments, transient mag. fields 80−5064
$f_{7/2}$ shell nuclei, odd-A, collective bands of positive parity states 78−54677
fast nonadiabatic nuclear rotation theory *(Russian)* 77−88036
fast rotating heated nuclei, collective excitation microscopic description, statistical characts. *(Russian)* 79−97649
fast rotating nuclei, harmonic oscillator approx., moments of inertia and yrast lines 79−30765
fast rotating nuclei, yrast traps 79−71786
Fermi liquid model anharmonic effects in collective excitations *(Russian)* 77−2922
Fermi liquid theory and giant resonances in nuclei 79−3095
fission, isobaric widths, frozen quantal fluctuations, charge equilibration 80−37365
fission lifetime distribution and probability estimates 78−659
fluid-dynamical approximation for finite Fermi systems 79−89259
fp-shell nuclei, high-spin states 78−12946
fragmentation of nucleus caused by decay of bound muon *(Russian)* 79−68333
functional approach to nuclear field theory, schematic model, monopole pairing, particle-hole forces 78−50095
Gamow Teller giant resonance struct., consequences for delayed neutron spectra and nucleosynthesis 77−2950
Gamow-Teller giant resonance struct., anal. of beta-delayed neutron spectra 77−22974
GDR in droplet model 77−74781
generalised Schwinger representation, time depend. Hartree Bogoliubov theory quantisation, anharmonic vibr. 78−54673
giant dipole reson., 3 isospin modes in mass 24 isobars 77−6338
giant dipole resonance, γ-emission spectrum 79−59065
giant dipole resonance, Galilei invariance of pairing interactions, effects of breaking *(Russian)* 77−74750
giant dipole resonance, isospin structure 77−79352
giant dipole resonance, particle-hole calcs., M1 strength 80−22785
giant dipole resonance, role of compound nucleus levels *(Russian)* 78−25164
giant dipole resonance decay, photonucleon emission in shell model 79−45233
giant dipole resonance decoupling and threshold states in schematic and shell models 80−78245
giant dipole resonance energy calcs., pair correlations 78−93924
giant dipole resonance intermediate struct. using (n,γ) and (γ, n), Brink hypothesis test 80−63150
giant dipole resonances, translationally invariant model for spherical nuclei 79−9431
giant E0 resonances, effect on lifetime of excited 0^+ states 79−17878
giant E1 mode, energy broadening in heavy ion reactions 79−30815
giant E1 resonance, Galilean invariant pairing 77−88094
giant isobaric resonances, A* resonances appl. to pion-induced reactions 79−67776
giant isobaric resonances, isobar doorway model 79−85428
giant isoscalar and isovector resonances, TDHF calc. 79−85433
giant isovector monopole states, isospin splitting and mixing 80−27609
giant magnetic resonances and effective Mλg-factors, RPA anal. 77−2897
giant monopole electro-excitation, energy-weighted isoscalar sum rules 80−63174
giant monopole resonance, self-consistent generator coord. method 77−2891
giant monopole states in the Suzuki model 79−45189
giant monopole vibrs., RPA and collective field description, surface compressibility 80−102100
giant multiple resonances, excitation strength functions 80−5037
giant multipole reson. fragmentation over two-phonon states in spherical nuclei 78−575
giant multipole resonance excitation through inelastic scatt. 77−57593
giant multipole resonances, isotopic splitting 79−6378
giant multipole resonances, light deformed nuclei via radiative capture, microscopic study 77−54139
giant multipole resonances, Regge poles and collective model 80−13436
giant multipole resonances, review 78−13044
giant multipole resonances, survey 77−79351
giant multipole resonances and inelastic pion scattering 79−85426
giant multipole resonances in excited core model 77−30539
giant octupole reson. in deformed nuclei 77−280
giant quadrupole capture of energetic nucleons by nuclei 77−10398
giant quadrupole reson. splitting in light deformed nuclei 78−4924
giant quadrupole resonance in deformed nuclei 78−86519
giant quadrupole resonances in even-even deformed nuclei, RPA calcs. *(Russian)* 77−50045
giant reson. and quasielastic excit. in electron scatt. and muon capture 77−57651
giant resonance electroexcitation 77−82897
giant resonance production mechanisms *(French)* 80−78243
giant resonance simple microscopic model *(Russian)* 78−578
giant resonances, electric monopole and dipole vibrations, TDHF equations, fluid dynamical Lagrangian 80−47447
giant resonances, self-consistent microscopic anal. including particle continuum 77−2896
giant resonances in many particle systems, microscopic derivation of classical eqns. of motion 80−102199
giant resonances in nuclear reactions, microscopic theory of intermediate struct. 80−99161
governor model for asymmetric deformed nuclei, band anal. 80−86776
Griffin-Hill-Wheeler spaces, 1- and 2-conjugate parameter generator states, giant resonances and scatt. 80−42618
ground state deformation energy, rot. band inertial parameter depend. 80−18185
ground state rot. band transitions and delayed feeding via (d,3n) for A=158-180 77−34211
groundstate bands in coherent states, vibr. and rot. limits 77−82811

nuclear collective states and giant resonances continued
group theoretical advances in collective motion anal. 80−9201
growth points in nuclear physics, book 80−94928
harmonic quadrupole collective Hamiltonian, exact soln. 78−37301
Hartree Fock Bologiubov theory, appl. to light/heavy nuclei, book contrib. 79−75881
Hartree-Fock-Bogolyubov approach to nuclear band description *(Russian)* 79−3107
heated fast rotating nuclei, equilib. props. 78−70439
heavy deformed nuclei, flow patterns for collective rotations 79−75816
heavy ion collisions, charge equilibrium model using collective high freq. mode and quantal master eqn. 80−27667
heavy ion collisions, collective effects rel. to pion prod. 80−37392
heavy ion collisions on UNILAC, review of the spectroscopy of high spin states 78−50194
heavy ion deep inelastic collision, high lying vibrational and incoherent excitations, simultaneous treatment 79−36256
heavy ion deep inelastic reactions, particle transfer, excitation of collective surface vibrs., in damping processes 78−70555
heavy ion fusion reactions, statistical yrast line 80−86948
heavy ion inclusive cross sections, collective and statistical effects, fluctuations for complex collisions 79−36258
heavy ion induced fusion, yrast lines versus entrance channel limitation 78−89929
heavy ion inelastic scattering, form factors 79−26458
heavy ion large-angle scatt., inelastic cross-section and collective state excitation 80−52690
heavy ion optical pot. contrib. from coupling to vibrational states 79−67726
heavy ion reaction, high energy nuclear collective states; existence 77−82804
heavy ion reactions, deflection function, effect of nuclear vibr. mode and orientation 79−59080
heavy ion scattering, angle depend. phase shifts, coupled channel formalism 80−18253
heavy nuclei, photoproton reaction, isospin effect 79−80926
heavy nuclei tensor forces, unnatural parity excitations, high momentum collectivity 80−63065
HF pot., particle vibration coupling effects 79−93578
(HI,xn), cranking model for E1 polarization charge in rotating nuclei 79−85405
high amplitude oscillatory states and external fields, in heavy ion interaction and fission *(Russian)* 79−97650
high angular momenta nuclei, backbending, yrast states, large moment of inertia band 77−14027
high angular momenta nuclei, shell effects on moment of inertia and level density *(Russian)* 79−67635
high angular momentum behaviour, transitional nuclei and backbending 79−17789
high angular momentum fusion compound nucleus deexcitation, high spin states, rare earths 80−9259
high lying intermediate excitations in effective interaction with super soft core pot. 79−36173
high spin effects in nuclei with proton no. 40-60, shape, deforms. 78−503
high spin rot. motion, TDHF cranking model and RPA descript. 80−102091
high spin rotational states description with modified oscillator potential 77−67696
high spin state studies, (n,γ) and heavy ion reaction complementarity 80−37381
high spin states, identification method at high excitation energies 79−17788
high spin states 79−71785
high spin states and band coupling, theory and heavy ion expts. *(Russian)* 80−18160
high-spin nuclear rotations, single particle Nilsson model 78−12943
high-spin selectivity of heavy-ion compound reactions 80−5048
high-spin states, means and methods of investig. 78−86722
high-spin states, spectroscopy with heavy-ion compound reactions 77−14176
high-spin states and shell struct. in N=Z nuclei, ^{20}Ne appl. 80−47342
high-spin states of transitional and spherical nuclei, decoupled and strongly coupled bands 78−12939
highly excited nearly spherical nuclei, ang. momentum effects, backbending, yrast states 79−49566
hot nuclei with high angular momenta, γ-ray emission in heavy ion reactions, rot. bands 78−13133
hydrodynamical model, plasma oscills. appl. to collective states and giant resonance energies 78−70479
i13/2 shell, particle-rotor model exact soln., cranking model connection 79−93485
$i_{13/2}$ shell, particle-rotor model soln., backbending, transition rates, ang. momentum spread 80−47344
inelastic form factors properties from energy weighted sum rules 78−37319
inelastic scattering, evidence for giant resonances 79−17883
inertia ellipsoid axes from hyperspheric functions method, nuclear struct. and shape *(Russian)* 79−30767
inertia parameter approximations 78−50073
interacting boron model of collective state, O(6) limit 80−32214
interacting boson model, collective motion descript., shell model test 80−27542
interacting boson model, collective state description, shell model connection 80−37341
interacting boson model for collective states, present status 80−27573
interacting boson model for collective states in even even nuclei 80−22715
intermediate structure of giant analogue reson. in medium and heavy nuclei 78−62517
isobar propagation and collective effects, pion-nucleus and photonuclear investigation 80−22676
isobaric distributions in deep inelastic reactions, collective model and independent particle model 80−18270
isoscalar dipole strength excitation in GQR region by inelastic electron and hadron scatt. 80−47448
isoscalar giant electric resonances, excitation and decay 80−5108
isoscalar giant monopole and quadrupole resonances, new formulae 78−93925
isoscalar giant monopole resonance systematics from 60 MeV (p,p′) 79−17879

nuclear collective states and giant resonances continued
isoscalar giant quadrupole reson., Skyrme interaction and effective mass 77−14088
isoscalar giant resonances and pair correlations, variational calcs. 79−75945
isoscalar giatn resonances, sum-rule approacH 77−82898
isovector M6 excitations, open shell RPA calcs., appl. to electron scatt. form factors 78−50112
isovector pairing collective motions and transition rates, projected BCS solns., generator coordinate simplification 80−22654
isovector pairing vibrations, in two nucleon transfer ion-nucleus reactions 78−21487
large amplitude collective motion, collective subspaces and generator coordinate method 80−9199
large amplitude collective motion, semiclassical approach, degenerate shell model appl. 80−27535
large amplitude collective motion coupling to RPA excitations 77−74787
large deformations and dissipation in a random-matrix model approach for fission or colliding nuclei 80−18162
large maplitude collective motion, field theory, excitation energies 80−22665
large scale collective motion in very heavy ion reactions, macroscopic description 80−5049
large-amplitude collective nuclear motion in fission and heavy ion reactions 80−22675
level density just above yrast line *(Chinese)* 78−86485
light heavy ion induced fusion, cross sections and yrast line limitations 80−5192
light nuclei, giant quadrupole resonances excited by α or p inelastic scatt. 78−624
light nuclei, m-particle n-hole struct. from few nucleon transfer reactions, review 78−50062
light nuclei, multipole giant resonances 78−86462
light nuclei, role of complicated configs. in giant resonances, continuum shell model 78−86463
light nuclei rotational bands, independent-particle description 77−14021
liquid drop model description *(French)* 80−22669
low energy fission, charge distrib., quantum mechanical phenomenon of GDR 80−86945
low lying states in collective nuclei, boson expansion theory 80−78118
low-lying collective states, Fermi liquid approach *(Russian)* 78−89772
low-spin low-energy phase transitions 77−22834
macroscopic rotation of cold nuclei 79−17785
magnetic dipole and quadrupole state excitation, inelastic electron scatt., various nuclei 78−50154
many body effective interaction theory problem, comparison with atoms 80−47406
many-body interactions from quark exchanges, nuclear tetrahedral struct. and props. 79−6459
many-body problem, classical hydrodynamics and collective motion approx. 80−83027
medium nuclei, photoproton spectra and preequilib. decay, microscopic theory 80−47464
meson capture, giant dipole resonance properties *(Slovak)* 77−61395
microscopic damping model for giant resonances *(Russian)* 77−10309
microscopic derivation of quantum fluctuations in nuclear reactions, collective and intrinsic state coupling 79−45138
microscopic description of direct processes in (N,N′), effective interaction 78−12979
microscopic description of giant electric and magnetic multipole resonances in ^{12}C, ^{16}O, ^{90}Zr, ^{208}Pb 78−538
microscopic nuclear Hamiltonian matrix elements in space of collective fermion states 77−88022
microscopic theory of one-body dissipation, collective motion, independ. particle model 78−54700
moderately deformed nuclei, high-spin states studied in (heavy ion, xnγ) reaction 77−14180
modified one body nuclear dissipation 78−50071
moment of inertia, connection with collective variables 79−75820
monopole excitations and K-harmonic model 77−6194
monopole excitations in heavy nuclei, hadron induced 78−86471
monopole vibrations and effective interactions, hyperspherical model 78−58223
multi-quasi-particle excitation bands, moments of inertia and blocking effect *(Chinese)* 79−49568
multipion production, π^- multiplicity distrib. and $\pi^-\pi^-$ correlation function, collective phenomena search 79−85485
multipole giant resonances, characteristic features *(Dutch)* 79−17875
multipole phonon states, G_2 group shift operator properties 80−99139
multipole phonon states, R(7) group shift operators 80−99140
multipole residual interaction strength, radial depend. in RPA 80−83026
multipole reson., review 77−14087
N=5 shell, deformed odd-neutron nuclei, band ordering and spectrum 80−83018
N=82 region, high spin isomers, cranked HF calcs., deformation shapes, excitation energies 80−99121
N=82 region, high spin isomers, deformation energy surface, shape constrained cranked HF theory 80−57666
N=82-86, high spin isomers, gamma spectroscopy 80−47358
n-deficient even-mass isotopes near Pb, yrast states, shape transitions 77−61345
N-quadrupole and N-octupole state construction, practical method 79−75817
negative collective masses, nonlocal effective Hamiltonian 77−6191
neutron collectivities from α-particle scatt., implications for giant-resonance excitations 77−26558
neutron induced yrast isomer prod., pulsed beam meas. using plastic scintillation spectrum 80−27871
neutron pickup reactions to $(i_{13/2})^2$ bands, theoretical rot. signatures, backbending 80−52558
neutron rich transitional fission fragments, spectroscopy, 0^+ states and octupole vibrs. 80−78204
new giant resonances, unfolded spectra, decomposition into multipole resonances 78−54670
nonadiabatic rotational model, mag. dipole moments j≥9/2 rot. bands 79−6388
nuclear collective rot., microscopic theory, SDHFB and HFBP methods test 79−67619
nuclear collective rot. microscopic theory, general description of rots. 79−26356

nuclear collective states and giant resonances continued
nuclear dynamics, TDHF and ATDHF, nuclear vibrs., heavy ion collisions and Fermi hydrodynamics 79−67696
nuclear field theory, phonon renormalisation, eigeneqns. and sum rules *(Chinese)* 80−102127
nuclear field theory treatment of the interacting boson model 80−27577
nuclear inertia for excited states, adiabatic cranking model calcs. 80−9216
nuclear rotational motion, particle-rotation coupling 79−17838
nuclear structure, conf. 78−50059
nuclear structure at high angular momenta, review *(German)* 79−40832
nuclei far from stability, spectroscopy 77−22910
nucleon radiative capture model, through collective M1 excitation, photon angular distrib. 78−58276
octupole excit. in deformed nuclei, translational invariance *(Russian)* 77−61343
octupole low-energy resonances in deformed nuclei, RPA calc. 77−82892
octupole resonance, even-even deformed nuclei, quasiparticle-phonon nuclear model *(Russian)* 80−52641
odd A shell nuclei, positive parity states, collective bands, Hartree-Fock calcs. 79−30778
odd mass nuclei, Hamiltonian in body fixed frame 79−36176
odd-A nuclei collective states, interacting boson-fermion model 80−95296
odd-odd fission products, level schemes, rot. bands, shell model states 80−78167
odd-odd man nuclei, decoupled and strongly coupled particles system 78−8727
one particle density distrib., nucleon density, from nuclear ellipsoid of inertia *(Russian)* 79−30784
oscillator basis for octupole collective motion in nuclei 78−70470
p-shell nuclei, generator coordinate anal. of molecular like states 78−54664
pair field of yrast state with quadrupole pairing 77−22832
pair rotational (vibrational) spectra formulae, branching ratio, selection rules, two particle transfer reaction *(Chinese)* 79−9448
pairing correlation for fast rot. nuclei 78−78284
pairing resonances at high levels 77−71552
pairing vibrational and isospin rot. states in particle number and isospin projected GCM 78−54696
particle rotor model study of transitional N=89 and N=91-95 nuclei 80−42529
particle-phonon coupling, unified theory, appl. to Sb and In isotopes 77−61360
particle-rotor model, band crossing 79−17833
particle-rotor model, pairing interaction treatment, yrast and yrare bands 80−83028
particle-vibration coupling form factor from simple model 80−57663
particle-vibration coupling model, octupole mode 79−17839
particle-vibrational doorway states 78−70421
Pauli principle and quasirotational structure of excited nuclei spectra 77−6193
perturbative treatment of nuclear rots., two-dimens. rotor, bands, moments of inertia 80−78111
phase transition in rotational band of excited state *(Russian)* 77−6211
photo-nucleon spectra, shell and pre-equilibrium decay model of giant reson. decay *(Russian)* 78−579
photon scatt., exchange effects, scatt. amplitude and integrated photoabsorpt. cross section 77−82910
photonuclear giant dipole resonance, isospin shift of energy 77−50111
photonuclear reactions, Saclay linac, photon beam prod., 10-100 MeV, giant dipole resonance *(French)* 79−523
photonuclear reactions review, giant dipole resonances and cross sections 80−5125
photonuclear reacts., conf., International school, Erice, Italy, 1976 77−88111
photonuclear reacts., coupled channels method *(Russian)* 78−50153
photoscattering by giant resonances in deformed nuclei, cross section determ. by semimicroscopic approach 79−9545
pigmy resonance, EM transitions, threshold states effects *(Hungarian)* 78−89818
polarised nucleus fission, parity nonconservation mechanism, rot. state mixing *(Russian)* 80−37408
potential model, energy dissipation heavy ions reactions 80−22849
pre-actinide nuclei, fission barriers, level density collective effects *(Russian)* 80−106092
pre-actinide nuclei, level density and fission probability collective effects *(Russian)* 80−13455
prolate symmetry axis, rotation of nuclei at high spin states, yrast states 78−70431
proton scattering at 1 GeV, reviews 79−26428
pseudomagic nuclei, yrast bands, variable moment of inertia model 80−449
quadrupole excitations, microscopic approach to description *(Russian)* 77−50041
quadrupole isoscalar and isovector capture of 5-50 MeV nucleons 77−2994
quadrupole oscillation wave functions, multiplicity factor *(Chinese)* 80−102103
quadrupole resonance, even-even deformed nuclei, quasiparticle-phonon nuclear model *(Russian)* 80−52641
quadrupole strength, giant quadrupole resonance 80−52575
quadrupole vibration theory, potential oscillations and collective motion *(Russian)* 79−13222
quadrupole vibrations, excitations in two nucleon transfer reacts. 79−17786
quasiparticle spectra near the yrast line 80−453
quasirotational bands, non-adiabatic effects 78−54663
radiative strength distrib. with energy, E1, M1 giant resonances, particle-hole calcs. 80−37349
radiative strength functions in spherical nuclei, giant dipole resonance influence, ^{124}Te, ^{140,142}Ce appls. 78−89774
rapidly rotating nuclei, high spin rot. including shell fluctuations, semiclassical description 80−47348
rapidly rotating nuclei, semiclassical HF description, smooth quantal corrections, density and total energy 80−32171
rapidly rotating nuclei, shell struct., collective motion and elastic deformation 79−71782
rare earth deformed nuclei, high spin region excited rot. bands, RPA calcs. 80−78108

nuclear collective states and giant resonances continued
rare earth nuclei, cluster-rotor-coupling approach to backbending 79−45129
rare earth nuclei, cranking model, collective inertia parameters 80−57665
rare earth nuclei, high spin isomer α-decay search 80−102158
rare earth nuclei, high spin states from (HI, xn) reactions, discrete γ-transitions 80−5050
rare earth nuclei (d,t) reactions, band heads, two-step process 78−62551
rare earths, yrast band energy calcs., exponential model with pairing attenuation, backbending 79−9446
rare-earth nuclei, back-bending phenomena, high spin states 78−74300
rare-earth nuclei transition density, ang. momentum projection corrections to rot. model 78−500
relaxation effects in collective transitions 79−9437
rotating deformed nucleus, quasiparticle excitations *(Russian)* 79−26364
rotating nuclei, critical ang. momentum and equilibrium figures from ellipsoid, liquid drop model *(Russian)* 80−37339
rotating nuclei, current distribs., cranked HF model 80−63059
rotating nuclei, M1 and E1 transitions within and between bands, cranking model 80−494
rotating nuclei, two-phase model 78−33113
rotating nuclei of high and v.high nucl. spin *(German)* 78−25102
rotating toroidal nuclei, ang. mom. thresholds 78−41629
rotation, inertial parameters in microscopic theory 80−91132
rotation, zero point energy 78−25101
rotation excitation, Coulomb-nuclear interf. in heavy-ion collisions 77−14151
rotation for large deformation using spherical basis 77−18371
rotation for low and high spin values, appl. of Peierls Yoccoz ang. mom. projection method 77−2899
rotational and vibr. states, interacting boson model, sphericity 77−41902
rotational band approach, pure zero-rank operators 80−47341
rotational band termination, shell model calcs. in sd shell 80−32145
rotational bands, probabilities of α-, β- and γ-transitions accompanied by changes in nuclear shape *(Russian)* 78−89820
rotational excitation ang. momentum transfer in inelastic scatt., coupled channel and adiabatic method 77−50094
rotational motion, in many paritcle systems, description using collective variables 79−40830
rotational motion, nuclear, microscopic description via SU(3) 79−36133
rotational motion, selected topics 79−17835
rotational nuclear struct., moment of inertia, ang. momentum sel. using total γ-energies 79−89221
rotational nuclei, high-spin, variable moment of inertia model, microscopic-macroscopic approach 80−63058
rotational spectra calc. using ang. momentum constraint, HF method 79−85403
rotational state energies, α-cluster nuclei, Brink's model, functions with exponential asymptotics *(Russian)* 77−6212
rotational states, coherent, γ-decay, random quantum meas. 80−73855
rotational states, Coulomb excitation by spherical nucleus, distortion, semiclassical model 79−67620
rotational states, transverse electroexcitation, cranking model velocity fields 77−10342
rotational states in heavy deformed nuclei, high-spin anomaly 78−93934
rotational states in HF calc. with Skyrme interactions 77−34212
RPA, for open shell nuclei by seniority and reduced isospin projections 80−47415
RPA, GCM, and semiclassical theories unification for giant resonances descript. 78−54671
RPA anal. of strongly disturbed bands in the high spin region described by rotating bosons 78−78239
RPA equations, sum rules for giant multipole resonances, energies, transition densities 77−61365
S and ground band interaction in cranked HFB model 80−95299
s-d shell nuclei, isoscalar, quadrupole, and monopole giant resonances, recent developments 79−26415
Schwinger boson representation for the quantized rotator 78−93602
self consistent cranking model, anomalies 79−26382
self-consistent field calcs., NN interactions, and results of appl., book contrib. 79−75880
self-consistent mean-field theory, progenitor sum rules, giant dipole reson. 77−67729
semi-infinite nuclear medium, kinetic energy density, simple approx., giant monopole resonance 80−32222
semiempirical rotational formulae for energy of rot. levels 78−17070
semimicroscopic description of nucl. states at low, intermediate and high excitation energies 78−54666
semimicroscopic method for level density calcs. *(Russian)* 77−34202
shadowing measurements in low $|Q^2|$ inelastic electron scatt. expts. 79−59053
shape changes at high excitation energies *(German)* 79−54384
shape isomer prod. in nuclear reactions and β-decay 79−6377
shell model, SU_6(s,d) boson model, collective states struct., Ba, Sm appls. 78−54672
shell model tests of interacting boson model descript. of nuclear collective motion 78−78280
single particle Schrodinger fluid, nuclear fluid dynamics, shell model basis, shape distortions 79−93484
single unperturbed level, large energy shift due to residual interaction 79−444
Sp(6,R) symmetry, α-breakup amplitudes, of giant E2 excitations in light nuclei 78−29435
special shell structure for nuclei at high angular momenta 79−17825
spherical even-even nuclei, phonon picture, n-quasi-particle collective states 77−10307
spherical nuclei, collective rot. state 77−10300
spherical nuclei, dipole states, transition densities and electroexcitation, GDR form factors *(Russian)* 80−52611
spherical nuclei, excitation of collective states in high-energy proton interactions 78−17073
spherical nuclei, giant monopole resonance transition densities, dynamical Thomas-Fermi theory 80−9278
spherical nuclei, self consistent theory of finite Fermi systems and low lying collective states 79−45130
spherical nuclei, small amplitude vibrs., giant resonances, TDHF, fluid dynamics comparison 78−66233
spherical nuclei with pairing, M1-reson. calc. 79−6390
spherical shell model, collective features, review 78−50098

nuclear collective states and giant resonances continued
spin giant resonance and core polarization effects, coupling term effects *(Chinese)* 80−47450
spin rotation, high angular velocity, collective aspects of heavy ion collisions 80−78309
statistical model calcs. of α-emission from excited nuclei 78−17157
statistical model radiation widths for $75<A<130$ 78−33161
strongly deformed nuclei, shortlived states, g-factor meas. method 80−52577
SU_6, dynamical symmetries, in nuclei, energy levels, transitions and collective states 78−74317
subCoulomb elastic heavy ion scatt., influence of low lying collective states 78−78414
sudden shape transitions, pair correlation association, E2 transition rate and backbending *(Chinese)* 79−59007
sum rules electron scatt., giant reson. 77−14114
sum rules for collective excitations 79−59002
superband and ground band ang. momentum difference *(Chinese)* 80−102102
superheavy elements, collective motion, stability and prod. in heavy ion collisions 80−18169
symmetric couplings of proton and neutron pairs, SU(6)×SU(2) group 77−26561
Thomas-Fermi approach to rotating nuclei 78−41657
three parameter rotational formula, physical meaning, rot. and vibr. limits 80−18157
three particle excitation, outside closed shell, propagator method 79−17830
threshold states in different schematic models 78−82272
time dependent HF polarisability and RPA sum rules, isovector giant resonances 79−6462
total γ-decay energy meas., selection of high spin nuclear states 79−26391
transient nuclei, spherical states, energies, degeneracy multiplicities *(Russian)* 77−34217
transitional nuclei, doubly even, validity of collective phonon truncation 79−36134
transitional nuclei, dynamical interplay between pairing and quadrupole modes, shell model anal. 79−89252
transitional nuclei, pairing rotations and quadrupole modes, dynamical interplay 80−18165
transitional nuclei, rotation along axis of symmetry 80−448
transitional nuclei, single particle and collective degrees of freedom coupling *(Russian)* 80−13345
transitional odd mass nuclei, asymmetric rotor model for decoupled bands 77−22913
transitional odd-man nuclei, diagonalisation of collective quadrupole Hamiltonian 77−6221
transitional odd-odd mass nuclei, gamma deformed rotor model 79−93498
transitional odd-odd mass nuclei, strong and decoupling struct. 77−30476
transplutonium elements, excited quasiparticle states of odd mass deformed nuclei 77−26565
triaxial quantum rotor in high spin limit, matrix mechanics appl., yrast states 79−67687
triaxial rotor at high ang. momentum near yrast line, microscopic theory 79−30795
two rotation regimes, cranked harmonic oscillator soln. 80−22657
two-fluid model of nuclear rotations and surface vibrations, appl. to rare-earth nuclei 78−62474
two-particle high spin states, crude shell model location, max. spin coupling 79−22172
two-quasi particle excitations, high-spin rot. state, ang. momentum projection 78−41615
velocity fields and transition densities in nuclear collective modes 79−89255
very high spin states from liquid drop model 80−5047
vibration coupling in fast neutron capture, refined direct-semidirect model 77−18541
vibrational collective motion, shell model anal. using algebraic approach 78−50072
vibrational nuclei, quasiparticle RPA nonlinear generalisation for anharmonic effects 79−63579
vibrational nuclei, variable moment of inertia model, relation to interacting boson model 80−83051
vibrational transitional nuclei, quasirotational states 78−12942
vibrations, review 79−89219
volume and surface vibr. relations, quantum hydrodynamics 80−9227
vorticity in nuclear fluid dynamics 78−33131
VV ^{173}Yb, e.m. consts. of lower rot. bands determ. 77−82802
wobbling motion at high spin, microscopic model in small oscillation approx. 80−22666
yrast and statistical cascades, M1 radiation after (MI, XN) reactions 80−42583
yrast band, backbending, canonical formalism *(French)* 80−52555
yrast bands of negative parity, gapless superconductivity, exactly solvable R(8) model 77−14015
yrast decay schemes from ^{48}Ca+heavy ion fusion evaporation reacts., appl. to Fe, Cr and Mn 78−66308
yrast level spacing discontinuity, rotation alignment mechanism 78−17085
yrast levels, ang.-momentum-projection from coherent phonon state 77−82808
yrast region of rapidly rotating nuclei, instability toward nucleon emission 77−88027
yrast spectroscopy, nuclei with high angular momentum, review 78−50063
yrast traps, island of high spin isomers near N=82 78−8844
yrast traps, obs. in heavy ion collisions 80−37319
yrast traps, single particle calcs. for rare earth nuclei 77−88031
yrast traps, struct., nuclear deform. 78−21486
yrast traps at very high angular momenta, microscopic description 78−70426
yrast-band of odd nuclei 80−22651
yrast-yrare interaction in $i_{13/2}$ shell, oscillating behaviour 79−93481
Z=34-94, high spin yrast isomers and nuclear deformation 79−6369
Z=50 region odd-A nuclei, band structures and particle vibration coupling 77−54132
(α,α'), A=40-208, low energy octupole resonances, 96 and 115 MeV 79−511

nuclear collective states and giant resonances continued
$(\alpha,\alpha'X)$, isoscalar giant quadrupole resonance decay props. 80−22792
(α,γ), direct and resonance capture, giant dipole and quadrupole resonances 80−37385
(d,d'), A=40 to 208, 108 MeV, giant monopole resonance excitation and ang. distribs. 80−102164
(e,e), low-q, A=14 nuclei, isospin T=2, 1 and 0 collective resonances, shell model 80−510
(e,e'), 70 MeV, 1p shell nuclei, shell model cross sections, giant M2, transversal E1 resonances 80−63143
(e,e') in giant resonance region, review 79−93585
(γ,d), odd-Z light nuclei, from (e,e'd), cross section, E2 transistors giant resonance and clusters 80−63169
(γ,n), preequilibrium exciton model with evaporative component, photoneutron spectra, giant resonances 80−57762
(γ,X), A=14 nuclei, isospin T=2, 1 and 0 collective resonances, shell model 80−510
(^{3}He,n), 25.4 MeV, N=82 nuclei, n ang. distrib., transitions, vibr. band search 79−63574
(K^-,π^-), strange giant resonance, DWIA calc. 77−14187
μ capture, subsequent excitations and particle emission cascade, hydrodynamical model 78−89825
(n,2n), 14.7 eV, isomeric cross-section ratios, statistical theory, moment of inertia 79−97701
(n,f), themal, parity violation from opposite parity rot. states 80−95303
(n,γ), direct and resonance capture, giant dipole and quadrupole resonances 80−37385
(n,γ), E1 and M1 strength functions, A- and energy-depend., giant dipole resonances 80−37348
(n,γ), Fast n, gamma rays in giant dipole region, review 80−37351
(n,γ), polarized space parity nonconservation, optical pot. and GDR parameters *(Russian)* 80−86803
(n,γ), valence model, mass range $40<A<70$ 79−45256
(N,γ) reactions in giant dipole resonance region, role of exchange forces 77−88126
(n,p) reactions on ^{6,7}Li, ^{12}C, ^{14}N, ^{16}O, ^{20}Ne, ^{27}Al, ^{209}Bi, isovector analogue giant resonances study 77−26726
n-p residual interaction effect on elastic electron scatt. by dipole giant resonance positioning 77−82914
^{20}Ne, rotational bands 78−45993
(p,d), 52 MeV, deeply bound hole state transition strength giant resonance, DWBA anal. 80−47426
(p,γ), direct and resonance capture, giant dipole and quadrupole resonances 80−37385
(p,γ_0), polarised p in giant dipole resonance region on ^{14}C, ^{30}Si, ^{54,56,58}Fe, ^{59}Co, ^{88}Sr 78−82346
(p,n), anomalous optical potential for sub-Coulomb barrier protons, 2 particle 1 hole states 80−105948
(p,n) scattering, charge exchange, isobaric analogue state, giant resonance effect, semimicroscopic model 78−89868
(p,p'), deformed nuclei, ground state rot. band, shape meas. and exchange contrib. 79−451
(p,p'), hadronic transition operator for collective state transition rates 79−45262
(p,p') to collective states, medium energies, spin-orbit deformation from DWBA calcs. 79−9565
(p,t), deformed nuclei, quadrupole vibr. excitation in two nucleon transfer reactions *(Russian)* 79−30780
pp scattering, dibaryon resonance behaviour, nonadiabatic rotational bands in light nuclei 80−13353
(π,γ), A=14 nuclei, isospin T=2, 1 and 0 collective resonances, shell model 80−510
(π^-,γ), high spin isomer state excitation, review 79−49569
(π^-,γ), pion absorption by two nucleon cluster, high spin state excitation probability 79−49570
(π,π), intermediate energies, collective isobaric resonance 80−63208
(π,π) scatt. in 3,3 resonance region, Δ-isobar dynamics, optical potential and RPA calcs. 77−34347
(π,π'), collective transitions, giant resonances, isospin content and spin transfer 80−42580
(π^-,X) slow pion capture in deformed nuclei, effects on high spin state excitation 80−18345
π^- absorption at rest, high spin state excitation, π-condensation and Δ^{++} *(Russian)* 80−86927
^{20}Ne cluster struct., rot. bands from (^{16}O-α)+(^{12}C-^{8}Be) coupled channel orthogonality condition model 79−97647
^{208}(N,γ), pol. N, anal. power and giant multipole resonances, direct-semidirect model 80−18265
^{238}(e,e'), scatt. from octupole band, model for nuclear surface vibrations 78−37333
Ac, A=229, 231, levels via (t,α) 15 MeV 77−74749
^{227}Ac, 7 to 16 MeV photofission, giant resonance and nuclear deformation *(Russian)* 78−41795
^{227}Ac levels and bands from ^{231}Pa α-decay 79−45217
^{A}Ag, A=105,107, positive parity band, mixing and branching ratios lifetimes from (^{16}O,2np)(^{14}N,3n) 80−9197
^{A}Ag, A=105-109, negative parity states, vibr. versus rot. descriptions 80−73781
^{A}Ag, A=105-109, negative parity states, EM props. from particle-asymmetric rotor model 80−102097
^{103}Ag collective excitation and J^π following ^{94}Mo(^{12}C,p2nγ), rotor-plus-particle model 80−86782
^{103}Ag high spin states, bands transitions, intermediate deformation Coriolis coupling from (^{3,4}He, xnγ) 80−105944
^{104}Ag levels, J^π, $T_{1/2}$, bands and transitions from ^{103}Rh(α, 3nγ) 80−102093
^{105}Ag high spin states and bands, g-factor and isomeric state from ^{103}Rh(α, 2nγ) 79−36125
^{107}Ag high spin states, J^π assignments, polarisations and transitions from (^{7}Li,4nγ), (^{6}Li,3nγ) 80−27536
^{A}Al, A=24,25,26, giant M1 strength, comparison with cross sections from Mg(p,n) 80−86878
^{26}Al, coherence widths, level density param. and effective moment of inertia 78−37360
^{27}Al, levels, GDR isospin mixing via (γ,p) 28 MeV 77−74832
^{27}Al, low lying states, band mixing effects, quadrupole moment 78−490
^{27}Al+^{12}C, 83 MeV, giant resonance excitation 78−17235
^{27}Al+^{16}O fusion, 30-70 MeV, statistical model calcs., yrast states and continuum feeding times 79−579
^{27}Al(α,α'), 106, 120, 145, 172.5 MeV, giant quadrupole reson. obs. 77−6415

nuclear collective states and giant resonances continued
^{27}Al(γ,X), 3-30 MeV, photoabsorption cross section, giant dipole resonances 80−78254
^{27}Al(p,γ)^{28}Si, radiative capture of intermediate-energy protons to high-lying states 79−36243
^{36}Ar, resonances populated in ^{24}Mg(^{12}C,α) 79−67629
^{38}Ar high spin state density, γ-decay mode, deformed states from ^{35}Cl(α,pγ) 80−32168
^{38}Ar yrast levels, J^{π} assignments, transitions, branching and mixing ratios from ^{35}Cl(α, pγ), ^{24}Mg(^{16}O, 2pγ) 79−67625
^{40}Ar(α,α′), 172.5 MeV, isoscalar giant quadrupole resonance 79−45231
^{40}Ar(γ, xp yn), 9-29 MeV, cross sections in giant resonance region, particle decay modes 80−13462
As isotopes, A=69, 71, 73, level scheme, cf. with Alaga model 77−22835
^{69}As 1306 keV state mag. moment, g-factor, rot. aligned band 80−86807
^{73}As core-coupled states, studied via (p,t) reaction 77−54212
^{212}At high spin states, decay, g factor, J^{π} assignments, level energies from ^{208}Pb(^{7}Li,3n) 80−5042
^{189,191,193}Au, high-spin states, blocking effect in rot.-alignment model 77−14016
^{193,195}Au, decoupled bands and rot. alligned coupling to triaxial shape 77−65191
Au, A=189, 191, 193, level schemes, gamma spectroscopy of high-spin states 77−22848
Au isotopes, A=184-197, β^{+}-decay, single particle and collective degrees of freedom 77−22956
Au, odd isotopes, $9/2^{-}$ level excitation energy, semi-empiricle method 77−22844
Au odd mass isotopes, odd proton effects on potl. energy surfaces 77−22877
Au odd mass isotopes, particle rotor descriptions 77−22914
Au odd mass isotopes, statistical anal. of levels 77−22842
Au, photonuclear cross-sections in giant reson. region 78−17178
^{A}Au, A=189, 191, 193, high spin states and transitions, isomeric states from Ir(α,xnγ) 80−5038
^{A}Au, A=189, 193, 195, particle-asymmetric rotor description of $h_{11/2}$ levels system 78−70425
^{A}Au A=190, 192, 194, levels, J^{π}, isomers and rot, aligned bands from Ir(α,xn) 80−9215
^{A}Au A=190, 192, 194, quasi-rotation aligned bands 79−40833
^{185}Au, collective band structure from ^{175}Lu+^{16}O, ^{170}Yb+^{19}F, ^{165}Ho+^{24}Mg reactions 79−22166
^{190}Au, obs. of rotation aligned bands 79−17783
^{192}Au, obs. of rotation aligned bands 79−17783
^{193}Au levels, three holes cluster vibr. and particle asymmetric rotor descriptions 80−57668
^{194}Au, obs. of rotation aligned bands 79−17783
^{197}Au natural line shape of giant dipole resonance 77−88096
^{197}Au+^{14}N, 161 MeV, giant resonances in inelastic scatt. 78−62564
^{197}Au(^{132}Xe,X), damped collisions, charge distrib. second moments and giant E1 quantal fluctuations 80−27547
^{197}Au(α,α′), 120 MeV, new giant resonance at 80 $A^{-1/3}$ MeV 77−41939
^{197}Au(e,xn), 37 to 147 MeV, cross sections, giant dipole reson. 79−89296
^{11}B non-normal parity state electroexcit. calcs., E1, M2 giant reson. 77−57643
^{11}B(^{3}He,^{3}He) 17.5 and 40.0 MeV, elast. and inelast. scatt. from ground state and low excited levels 77−65229
^{11}B(α,γ$_0$)^{15}N, giant dipole reson. region 77−26777
^{11}B(γ,nγ′) 30 MeV giant dipole resonance decay, ^{10}B transitions *(Russian)* 80−13433
^{11}B(p,γ)^{12}C, radiative capture of intermediate-energy protons to high-lying states 79−36243
^{12}B analogue states at 4.5 MeV giant resonance region, strong spin-isospin mode, from ^{12}C(e,e′π^{+}) 80−78250
Ba isotopes, collective states, soln. of Schrodinger eqn. with Bohr Hamiltonian 77−67695
Ba isotopes, microscopic dynamic calc. of collective states 78−17075
Ba odd neutron isotopes, microscopic struct. of low lying collective excited states *(Japanese)* 79−3065
Ba odd-mass isotopes, A=125-133, high spin level systematics and triaxial shapes 77−22838
^{A}Ba, A=126 to 135, charge radii, mag. dipole and elec. quadrupole moment 79−72436
^{A}Ba, A=135,137, Coulomb excitation, transition probabilities, γ-rays and level collectivity from (^{16}O,^{16}O′), (α,α′) 80−78201
^{123}Ba, high spin levels and bands from ^{114}Sn(^{12}C, 3n)^{123} Ba 79−45127
^{125}Ba, $7/2^{\pm}$ states, populated in ^{116}Sn(^{12}C, 3n), explained by triaxial core model 78−37258
^{126}Ba backbending, shell model calc., pair realignment and Coriolis antipairing 80−32164
^{126}Ba, backbending and E2 transition strengths of yrast states 79−26363
^{128}Ba, level scheme, near instability against γ-deformation via ^{128}La decay 77−82806
^{129}Ba, triaxial shape and high-spin bands obs. in ^{124}Sn(^{12}C,3n) 77−34219
^{8}Be, 1^{+} reson. parameters via ^{4}He(d,d)^{4}He, 6-7 MeV 77−88095
^{8}Be, 3^{+} doublet at 19 MeV, level-parameters, isospin mixing model 78−89789
^{8}Be, $\alpha\alpha^{+}$ rotational band existence 79−13192
^{8}Be $\alpha\alpha$* rot. levels search in ^{2}H(^{6}Li,α) 79−22175
^{8}Be collective excitation spectra from generalised hyperspherical functions method *(Russian)* 80−91133
^{8}Be, effective nucleus eccentricity depend. on total momentum *(Russian)* 79−3078
^{8}Be fission mode, large amplitude collective motion, adiabatic TDHF calcs. 80−86786
^{8}Be high spatial symmetry excited states, resonances, rot. band from (d,αt), (p,αt) 80−86780
^{8}Be, reson. level, J^{π}, via ^{7}Li (p,γ)^{8}Be 380 to 960 keV 77−88131
^{8}Be rot. levels using α-α cluster model with effective pot. interaction 77−22915
^{9}Be deformed nucleus, continuum states in strong coupling model 80−22682
^{9}Be, level structs. in terms of rot. bands, molecular α-cluster model 77−54137
^{10}Be, form. in ^{7}Li(t,γ) reaction, excitation functions and resonant struct. for 17.79 MeV state 78−13110

nuclear collective states and giant resonances continued
^{207}Bi high spin states, level decays, three particle interactions from ^{205}Tl(α,2n), ^{208}Pb(d,3n) 79−49567
^{208}Bi M1 isobaric analogue resonances and giant spinflip resonances from ^{208}Pb(p,n) 80−106030
^{209}Bi, effect of pairing modes in multiplet struct. 78−12973
^{209}Bi+^{14}N, 161 MeV, giant resonances in inelastic scatt. 78−62564
^{209}Bi(α,α′), 120 MeV, new giant resonance at 80 $A^{-1/3}$ MeV 77−41939
^{209}Bi(γ,X), 3-30 MeV, photoabsorption cross section, giant dipole resonances 80−78254
^{76}Br, Coriolis distorted bands, common $g_{9/2}$ parentage in N=41 nuclei 80−13349
^{76}Br long-lived positive parity isomer from ^{75}As(α,3n) 79−54375
^{77}Br collective bands, lifetimes, spins and E2 transition probabilities from ^{64}Ni(^{16}O, 2nP) 80−13415
C, photonuclear cross sections in giant reson. region 78−17178
CC ^{158}Dy high spin states B(E2) values, IBA model test from ^{26}Ng(^{136}Xe, 4n) CC ^{158}Dy high spin states B(E2) values, IBA model test 80−27541
CC ^{20}Ne 8^{+} level radiative width, resonance strength from ^{16}O(α,γ) 80−83065
(^{12}C,X) on A=144-164, search for high spin isomeric states, shell effects 79−71784
^{12}C, collective nuclear wave function, deformed translationally invariant model 79−58996
^{12}C, isoscalar giant quadrupole resonance obs. 77−307
^{12}C, isoscalar giant quadrupole resonance 78−78238
^{12}C, isoscalar giant quadrupole resonances, RPA calcs., E2 strength fragmentation, spectroscopic factors 80−13437
^{12}C, isoscalar giant reson. in ^{11}B(p,α)^{8}Be 6.0-18.0 MeV 77−46152
^{12}C, isoscalar giant reson. *(French)* 78−78341
^{12}C isoscalar giant resonance from ^{10}B(d,α)^{8}Be(g.s.) excitation functions struct. 78−46073
^{12}C, isovector GQR splitting 77−22988
^{12}C, monopole excitations, transition densities from simple collective model 79−40834
^{12}C, multipole elec. giant resons., anomalous parity isovector states, Coulomb excitation cross sections 79−9439
^{12}C p_0 channel E2 strength from ^{11}B(p,γ) pol p. 80−22790
^{12}C spin-orbit force and deformation, self-consistent HF calc. 79−455
^{12}C, spreading widths of giant reson. calc., core-coupling RPA approx. 77−74827
^{12}C+^{12}C in elastic scatt., high energy, resonances obs., evidence for band crossing model 78−66305
^{12}C+^{12}C scatt., intermediate molecular resonances, band crossing model anal. 79−6655
^{12}C(^{12}C,^{8}Be)^{16}O(GS), excitation functions and Legendre anal. for resonance J^{π} assignments 78−78347
^{12}C(^{16}O, n)^{27}Si, 12.8 MeV resonance investig. by time-of-flight spectra and n-γ coincidence 79−9627
^{12}C(^{16}O,^{16}O′), 315 MeV, giant multipole resonance excitation 79−30812
^{12}C(^{3}He,^{3}He), E2 strength distrib., giant quadrupole reson. 77−30612
^{12}C(^{3}He,γ$_0$)^{15}O, differential cross section in giant dipole reson. region 78−78395
^{12}C(^{6}Li,^{6}Li′), 153 MeV, isoscalar giant quadrupole resonances 80−13440
^{12}C(α,p)^{15}N, 50 MeV, proton spectra, excitation of high-spin states *(Russian)* 77−6209
^{12}C(α,p)^{15}N ($3/2^{-}$, 6.328 MeV) transition, giant resonance effects 79−9601
^{12}C(e,e), 180° scatt., transverse inelastic form factors and spectra, collective 2^{+} state 80−9261
^{12}C(γ,γ), 23.5-39 MeV, cross sections and giant resonances, E2 strength 80−63122
^{12}C(γ,nα)^{7}Be, electric quadrupole transition cross-sections, behind giant resonance *(Russian)* 80−78281
^{12}C(γ,p)^{11}B, 40-120 MeV, reaction mechanism *(Russian)* 77−65221
^{12}C(γ,p)^{11}B, electric quadrupole transition cross-sections, behind giant resonance *(Russian)* 80−78281
^{12}C(γ,pα)^{7}Li, electric quadrupole transition cross-sections, behind giant resonance *(Russian)* 80−78281
^{12}C(p,2p), asymmetric energy-sharing mode, half distorted-wave formalism, intermediate giant resonance 80−68656
^{12}C(p,p′)^{12}C*, pol. p., 19-23 MeV, giant resonances as doorway states, virtual excitation 80−5102
^{12}C(p,p), 14-45 MeV, differential cross section and spin-flip probabilities, giant resonances 80−73850
^{12}C(p,p) dispersive effects in ground state rot. band excitation, coupled channel calcs. 79−40828
^{12}C(π,π′) collective resonances 78−78415
^{12}C(π,π′)^{12}C*, giant dipole resonance, Glauber theory 77−6467
^{12}C(π^{-}, γ)^{12}B*, excitation of collective states, shell model 80−22652
^{12}C(π^{+},π^{+}′), 180 MeV, 1^{+} T=0,1 collective states anal. 79−85540
^{13}C, decay props. of giant dipole reson. photoreactions anal. in continuum shell model 77−26665
^{13}C, giant quadrupole resonance blocking mechanism 80−13437
^{13}C, giant reson. isospin splitting, photonuclear and e-scatt. cross-sections 78−577
^{13}C, photoexcited giant dipole resonace, continuum shell model anal. 80−18266
^{13}C(γ,n) 7.6 to 41.8 MeV, photoneutron cross section meas., giant resonance isospin splitting 79−63657
^{13}C(π$^{\pm}$,π$^{\pm}$), near πN (3,3) resonance, 180 MeV, collective states and cross sections 80−13507
^{14}C(πγ), collective resonances, A=14 isobaric states, shell model predictions 79−85386
^{22}C, electroexcitation of collective M1 resonances, RPA calcs. 77−46104
Ca isotopes vibrational states, single pole dominance in (α,α) and (α,α′) reactions 77−41985
^{A}Ca, A=40,48, static and transition densities, self consistent RPA theory test in fast particle (p,p), (e,e) scatt. *(Russian)* 79−49604
^{A}Ca, A=40 to 48, giant multipole resonances, mass dependence of energy weighted sums 80−63144
^{A}Ca(^{6}Li,^{6}Li′), A=40, 44, 48, 153 MeV, isoscalar giant quadrupole resonances 80−13440
^{A}Ca(α,α), 40-62 MeV, A=40,44, elastic and inelastic, ang. distribs. and collective state excitation 79−6650
^{A}Ca(p,p′), pol. p, A=40,48, 800 MeV, diff. cross sections, anal. powers, DWIA anals., high spin levels 80−83067
^{A}Ca(π$^{\pm}$,π$^{\pm}$), A=40,42,44,48, 180 MeV (in)elastic scatt. differential cross-sections, Pauling blocking 79−85539
^{40}Ca (α,α′), 104 MeV, giant resonance ang. distribs., L-transfer contribs. 80−27610

nuclear collective states and giant resonances continued
^{40}Ca, α-and p-spectra from giant reson. region via ^{40}Ca(α,2α) and ^{40}Ca(α,αp) 77−30523
^{40}Ca, excitation of low lying collective states by (n,n′) scatt. 78−17205
^{40}Ca, GQR, J^{π}, via (^{3}He,^{3}Heα) and (^{3}He,^{3}He′p) 70 MeV ang. distribs. 77−50097
^{40}Ca, giant isoscalar monopole state energies in generator coordinate method 80−37317
^{40}Ca, giant monopole resonance widths, RPA calcs. based on Skyrme interaction 78−93984
^{40}Ca giant resonances prod. from ^{40}Ca(^{3}He,^{3}He′)^{40}Ca*→^{36}Ar+^{4}He 79−93479
^{40}Ca, high-spin members of 4p-4h triaxial band 77−74742
^{40}Ca, isoscalar giant resonances and Landau parameters with density-dependent effective interactions 79−71827
^{40}Ca, magic nuclei at collective excitations, energy spectrum and shape *(Russian)* 80−106015
^{40}Ca, monopole vibration damping, TDHF calcs. 80−22667
^{40}Ca, vibrating nucleus, adiabatic anal. of time-dependent HF solns. 79−40863
^{40}Ca+^{14}N, 161 MeV, giant resonances in inelastic scatt. 78−62564
^{40}Ca+^{3}He inelastic scatt., isoscalar multipole reson. 78−66190
^{40}Ca+^{40}Ca, 284 MeV, energy spectra struct. obs. 78−4958
^{40}Ca+^{40}Ca, collective modes excitation 79−54448
^{40}Ca(^{16}O,^{16}O), rot. band of molecular resonances, generator coordinate model 80−13428
^{40}Ca(^{40}Ca, ^{40}Ca), generator coordinate study, rot. band of molecular resonances 79−75948
^{40}Ca(^{40}Ca,X), 400 MeV, fragment energy spectra struct., giant resonances, direct process 80−47452
^{40}Ca(^{9}Be, ^{9}Be′), 45, 60 MeV, low lying collective states, ang. distribs., DWBA double folding pot. anal. 80−78113
^{40}Ca(K^{-}, π^{-}) $^{40}_{\Lambda}$Ca, possible strange giant reson. 77−82969
^{40}Ca(α,α), 20-50 MeV anomalous elast. and inelast. scatt. optical model anal. 77−88161
^{40}Ca(α,α), 6-18 MeV, resonances, anomalous large angle scatt. and quasi-molecular states 80−27613
^{40}Ca(α,α), giant isoscalar quadrupole resonance, α-over p-decay ratio, SU(3) and shell model 80−27608
^{40}Ca(e,e′), microscopic model of isovector multipole giant resonances *(Russian)* 78−54747
^{40}Ca(n,γ_0)^{41}Ca, 6 to 13 MeV quadrupole radiation, direct-semidirect model calcs. 79−545
^{40}Ca(p, p′), isovector dipole strength excitation in giant resonance region 80−83066
^{40}Ca(p,p′), 800 MeV, high energy octupole giant resonance, ang. distribs. 80−86879
^{40}Ca(p,p′), giant resonances from antisymmetrised DWBA anal. 79−85432
^{40}Ca(π^{+},π^{+}′), 241 and 163 MeV, giant resonance studies 79−85512
^{41}Ca E2 resonance, cross sections and γ-spectrum from ^{40}Ca(n,γ) 80−57759
^{41}Ca, giant dipole resonance determ. in ^{40}Ca(p,γ) 79−93620
^{41}Ca giant dipole resonance, isospin struct., direct-semidirect anal. from ^{40}K(p,γ) 80−47449
^{41}Ca, spin and parity from ^{38}Ar(α,nγ) angular distrib. and linear polarisation of γ 80−63079
^{41}Ca yrast states from ^{26}Mg(^{18}O, 3nγ), γ meas., spin, parity, branching and mixing 78−58250
^{42}Ca, collective states, quasi-degenerate intrinsic Hamiltonian, variational methods 80−68505
^{42}Ca high spin state density, γ-decay mode, deformed states from ^{39}K(α,pγ) 80−32168
^{44}Ca(e,e′p), (γ,p) cross-sections determ., giant dipole reson. anal. 77−26666
Ca(π^{+},π^{+}′), 163,241 MeV, giant quadrupole resonances 79−40893
Cd even-even nuclei, low lying collective states, two-photon character 80−57667
Cd, even-mass, shape coexistence, quasi-rot. band 78−496
Cd even-mass isotopes, vibr. excitations 77−54129
Cd, isotopes A=109, 106, 105, 104, high spin states excited by (α,xnγ) *(French)* 78−29394
^{A}Cd, (A=106, 108, 110, 112, 114, 116, 118), so-called two phonon states, quasiparticle shell model calcs. 79−89251
^{A}Cd, A=105,107,109,111, odd neutron deficient, rotor+particle model anal. 79−36127
^{A}Cd, A=107, 109, 111, from Pd(α,3nγ)Cd, high spin states obs. 80−450
^{A}Cd, A=111-115, electric quadrupole moments, nonadiabatic rot. model calcs. 79−6389
^{A}Cd, A=112, 114, 0_2^{+} and 0_3^{+} states, E0, E2 transitions and collectivity 80−102144
^{A}Cd(^{16}O,^{16}O′), 44 MeV, A=112, 114, 0_2^{+}, 0_3^{+} state collectivity, E0 and E2 decay, $T_{1/2}$ 80−73784
^{103}Cd levels, J^{π} and positive parity decoupled band, rotor anal. of ^{94}Mo(^{12}C, 3nγ) 80−102096
^{104}Cd quasirot. ground state band and γ-transition from ^{102}Pd(α,2nγ) 80−105955
^{106}Cd collective and yrast levels, γ-transitions, 2 quasiparticle+rotor model from (heavy ion, xnγ) 79−22169
^{110}Cd, collective excitations in the interacting boson model *(Russian)* 80−5044
^{110}Cd, O^{+} bands from cluster-vibration coupling, semimicroscopic mechanism for band mixing 79−36121
^{112}Cd, negative parity yrast band, E1 transitions polarisability, quadrupole-octupole coupled vibr. system 79−484
^{114}Cd(e,e′), 40-110 MeV, vibr. nuclei, branching ratios 77−6356
^{116}Cd(p,p′γ), 5-20 MeV, lowest 3^{-} collective level identification from decay excitation function 79−9444
^{135}Ce, yrast cascade dipole component from ^{122}Sn(^{16}O,4n) 80−9266
^{140}Ce, hexadecapole motion obs. from α-scatt., EM transitions and conversion electron spectra 78−25097
^{140}Ce(N,γ_0), 2-10 MeV, giant M1 resonance in direct-semidirect model 79−17898
^{140}Ce(e,e′), 50-92 MeV, E0, E1, E2, E3 and E4 giant resonances, cross section, shell model anal. 79−54423
^{140}Ce(e,e′), giant dipole resonance, E1 form factor and breathing mode existence 79−3125
^{141}Ce collective M1 excitation effects on γ-ang. distribs., direct semidirect model of ^{140}Ce(n,γ) 80−57733
nuclear collective states and giant resonances continued
^{250}Cf energy levels, bands and transitions from ^{250}Bk, β^{-} decay 79−22205
^{250}Cf low spin states, bandheads, J^{π} and transitions from ^{250} Es EC decay 80−105952
^{250}Cf(d,d′), 15 MeV, vibr. states, J^{π} and reduced transition probabilities 80−47351
^{34}Cl high spin states 78−82289
^{37}Cl high spin state decay, spin assignments, yrast level lifetime from ^{27}Al(^{19}F,2αp), ^{27}Al(^{12}C,2p), ^{34}S(α,p) 79−6490
^{A}Cm, A=246,248, fission isomer rot. spectra $I^2(I+1)^2$ correction 80−18229
^{55}Co, GDR, (p,γ) cross section determ. in shell model 78−78345
^{59}Co, isospin effects in GDR region 78−78344
^{59}Co(γ,xn), 10-36.5 MeV, photoneutron cross sections, integrated cross sections, giant dipole resonance 79−89289
^{48}Cr high spin states, yrast levels and 6^{-} isomeric state from ^{40}Ca(^{10}B,np) 80−454
^{48}Cr, spectroscopy of high spin states 79−59032
^{51}Cr, bands, levels, EM transitions, J^{π}, branching and mixing ratios from ^{48}Ti (γ,nγ)^{51}Cr and ^{51}V(p,nγ)^{51}Cr 80−52606
^{51}Cr, strongly deformed $K^{\pi}=1/2^{-}$ bands from γ meas., level transition parameters 79−3113
^{52}Cr high spin states, transitions and J^{π} values from ^{50}Ti(α,Znγ) 80−455
^{52}Cr, high-spin states, populated by ^{50}Ti(α,2nγ) spectroscopic meas. 77−65190
^{52}Cr, total photoneutron cross section, high resolution meas., isospin effects 78−8792
^{52}Cr(α,α′), 8-18 MeV, cross sections, search for giant dipole resonance 80−9281
^{52}Cr(α,$p_0(p_1)$) differential cross section in giant dipole resonance region from (e,$p_0(p_1)$) 79−63655
^{52}Cr(e,e′), 40-110 MeV, vibr. nuclei, branching ratios 77−6356
^{52}Cr(e,$p_0(p_1)$), differential cross section in giant dipole resonance region 79−63655
^{53}Cr, possible deformed $7/2^{-}$ states with $\Delta J=1$ band 79−45170
^{53}Cr, yrast level lifetimes and J^{π} assignments from ^{48}Ca+^{9}Be 79−9445
Cs, low-lying collective states anal. 77−88030
^{A}Cs, A=119 , 121, 123, 125, collective props. and level schemes from (^{10}B,p2n), (^{14}N,3n) (^{10}B,3n) 79−22171
^{A}Cs, A=119-133 odd isotopes, collective props., bands and transitions from heavy ion reactions 80−68512
^{A}Cs, A=121, 123, 125, $g_{9/2}$ and $h_{11/2}$ bands 78−50067
^{A}Cs A=127, 129, 131, 133, high spin states and collective properties from (^{10}B, 3n), (α, 2n) (^{6}Li, 3n) 79−22170
^{124}Cs, β-decay props. of collective 1^{+} states 78−13028
^{126}Cs, β-decay props. of collective 1^{+} states 78−13028
^{127}Cs collective quadrupole dynamics, band struct., transitions, collective model anal. from ^{127}I(α,4n) 80−78112
^{62}Cu, yrast states obs. in ^{60}Ni(α,pγ) and ^{63}Cu(p,pγ) 78−12945
^{63}Cu, paradoxical octupole-multiplet pattern 78−41617
^{63}Cu+^{63}Cu, 450 MeV, energy spectra struct. obs. 78−4958
^{63}Cu(p,p′), 40 MeV, octupole states, weak coupling model 79−93495
^{158}Cy, double crossing of ground rotational band and super band 78−45996
Dy (A=154, 156), negative parity band crossing in even-even nuclei 78−21488
Dy deformed nuclei, particle ang. momentum alignment effects 80−68522
Dy even isotopes, aligned Stockholm band intrinsic spin I_0^{eff} 80−13363
Dy, N=85 isotones, bands and transitions from α and HI excitation, in-beam study 80−78123
Dy, odd mass isotopes, rot. excitations anal. 77−82813
^{A}Dy, (A=151,152), high spin yrast states, γ-ray polarisation in (^{32}S,sn) reactions 80−497
^{A}Dy, A=152, 153, isomeric states and complex band structs. from Nd(^{12}C, xnγ), Gd(α, xnγ) 79−67624
^{A}Dy, A=158, 160, high spin rot. state pairing correlation, self-consistent treatment 79−3070
^{A}Dy, A=161, 163, Nilsson state $\Delta N=2$ mixing, rot. bands from (d,t), (d,p) 80−95295
^{A}Dy, A=161, 163, rotational bands, coupled-channels Born approx. anal. of ^{162,164}Dy(d,t) 80−83104
^{A}Dy A=162, 164, gamma to ground band transitions, γ-γ directional correlations from (n,γ) 80−68579
^{148}Dy, p single particle states and pairing force calcs., high spin states 80−42522
^{149}Dy, collective and noncollective excitations, Hamiltonian calc. for level density 79−36139
^{150}Dy, high-spin isomers produced by ^{144,146}Nd(^{12}C,xn), gamma-ray spectra 78−50075
^{151}Dy high spin states, isomers, α-decays and yrast sequence from (^{32}S,3n), (^{18}N,4n) 79−93493
^{151}Dy high spin yrast isomers, shell model configs. from ^{152}Gd(α,5n) and ^{136}Ce(^{18}O,3n) 79−49573
^{151}Dy levels, bands and transitions, in-beam γ-rays from ^{142}Nd(^{12}C,3nγ) 80−458
^{152}Dy, collective bands and absence of yrast traps 80−9207
^{152}Dy high spin isomeric states, g-factors from ^{140}Ce(^{16}O, 4n) 80−13377
^{152}Dy high spin isomers, yrast traps, oblate shape at high ang. momenta 79−97646
^{152}Dy high spin isomers, yrast states and level lifetimes from (^{15}N, 4n), (^{16}O, 4n) 80−13361
^{152}Dy, high spin state populations from ^{124}Sn(^{32}S,4n) 80−57660
^{152}Dy high spin struct., in beam γ meas. from (^{15}N, 4n), (^{16}O, 4n) 80−18179
^{152}Dy, high-spin isomer at high excitation energy obs. in ^{154}Gd(α,6n) 77−22841
^{152}Dy, rotation along axis of symmetry 80−448
^{152}Dy yrast continuum γ-ray multipolarity via polarisation meas. from ^{140}Ce(^{16}O,4n) 80−9264
^{152}Dy yrast isomers, γ-rays from compound nuclei 80−86789
^{152}Dy, yrast isomers, oblate shape, excitation energies, spin and parity 79−17795
^{152}Dy yrast line single particle nature at high ang. momentum from Sn(^{32,34}S, 4n) 79−71783
^{152}Dy, yrast states of isomers at high angular momenta, particle-hole struct. 79−36124
^{152}Dy, yrast traps, and very high spin states, populated in (^{32}S,4nγ) 78−89778

nuclear collective states and giant resonances continued
^{152}Dy yrast traps, isomers and oblate deformations from ^{124}Te(^{32}S, 4n) 80−13362
^{153}Dy, collective bands anal. using (α,3nγ) at 35-45 MeV 77−61342
^{153}Dy, populated in ^{153}Ho β-decay, lower excited states 80−22765
^{154}Dy N=88 nuclei quasirot. bands and J^{π} from beta-decay 80−83025
^{156}Dy, $\beta\gamma$ two phonon vibr. via (p,t) 29.9 MeV reaction 77−14018
^{156}Dy, collective struct., J^{π}, via (p,t) reaction below 2.3 MeV excit. 77−74747
^{156}Dy, gamma-band anomalous behaviour 77−82812
^{156}Dy high spin states, γ-ang. distribs., lifetimes and feeding times from ^{148}Nd(^{13}C, 5n) 80−13364
^{156}Dy high spin states lifetimes and feeding times, quadrupole moments from ^{24}Mg(^{136}Xe,4n) 80−32239
^{156}Dy rotational levels obs. in ^{159}Tb(p,4nγ) at 27-51 MeV 77−6199
^{156}Dy, superband 78−29374
^{156}Dy, superband in backbending, band-mixing model 77−34209
^{158}Dy band side feeding pattern and γ-multiplicities, statistical model from ^{26}Mg(^{136}Xe, 4n) 79−75821
^{158}Dy collective excitations as populated in ^{158}He^{g,m} decay 78−82270
^{158}Dy, Yrast states from heavy ion collisions, lifetimes 78−54793
^{161}Dy, Nilsson bands, J^{π} via (d,p), (d,t) and (n,γ) 77−34215
^{162}Dy, intraband transition rates in gamma vibr. bands 78−45992
^{162}Dy, level scheme, γ-branchings following ^{162}Tb decay 77−34246
^{162}Dy rotational states lifetime meas. using ^{162}Dy(^{40}Ar,^{40}Ar'γ) 78−50123
^{162}Dy+^{16}O, Coulomb-nuclear interference for high spin states 78−46097
^{162}Dy(^{136}Xe,^{136}Xe'), 547, 612 MeV, high spin state energies and reduced transition probabilities 80−18232
^{163}Dy(α,α'), E2 and E4 transition moments, rotational states 78−41740
^{164}Dy, low lying spectra and EM transitions, level struct. in quasirotational bands 79−36141
^{164}Dy multipole mixing in γ to ground bands from ^{163}Dy(n,γ) 80−52615
^{164}Dy, recoil distance meas. of lifetimes of rotational states 78−66242
^{165}Dy, collective contributions to E1, $\Delta K=1$ matrix elements in odd-odd deformed nuclei 79−17857
Dy(α, xn γ) equilib. and pre-equilib. reactions, ang. momentum transfer, ground state bands 79−45277
(e,e'), giant multipole resonance width, momentum transfer dependence 79−54420
Er, A=162, 164, 166, (α,2nγ) studies of vibr. and other side bands 77−2893
Er, deformed nuclei, particle ang. momentum alignment effects 80−68522
Er even isotopes, aligned Stockholm band intrinsic spin I_0^{eff} 80−13363
Er rotational nuclei, transition energy correlations, very high ang. momentum 80−86787
Er yrast levels, spin alignment, populated by preequilibrium (α,xnγ) reactions 80−52557
^{A}Er, (A=154,155), rotational struct. at high spins 80−457
^{A}Er (A=156,157,158), high spin yrast states, γ-ray polarisation in (^{32}S,xn) reactions 80−497
^{A}Er, A=154, 155, γ-ray spectra, ang. distrib., high spin states 79−9503
^{A}Er, A=156, 164, aligned positive parity bands from rot. aligned model 80−9209
^{A}Er, A=158,160,162, high spin states and deformation, number conservation effects 79−89225
^{A}Er, A=159,160, energy levels, deexcitation γ-rays, g-factors and hyperfine interaction from ^{28}Si(^{136}Xe, xn) 80−102114
^{A}Er, A=165, 167, rotational bands, coupled-channels Born approx. anal. of ^{166,168}Er(d,t) 80−83104
^{A}Er, A=166-170, α-particle Coulomb excitation of octupole vibr. states 78−41618
^{153}Er 360 ns yrast trap, γ transitions and lifetimes from ^{144}Sm(^{12}C,3n) 80−9205
^{154}Er, collective bands and absence of yrast traps 80−9207
^{154}Er, high-spin yrast states, lifetime meas. using recoil-distance method 79−40884
^{154}Er yrast cascade to spin 36, side feeding, energy, multipolarity irregularities from (^{16}O, 4n), (^{64}Ni, 4n) 79−36191
^{154}Er yrast trap and transitions, decay scheme from (^{64}Ni,4n), (^{16}O,4n) 80−9206
^{155}Er, backbending effects via (^{12}C, xn) excit. 77−71556
^{156}Er, level struct. determ. in ^{156}Tm (β^++EC) decay 77−22957
^{156}Er N=88 nuclei quasirot. bands and J^{π} from EC decay 80−83025
^{156}Er, negative parity band crossing in even-even nuclei 78−21488
^{156}Er, negative parity yrast states, microscopic calc. 78−495
^{156}Er, non axial deformability of rotating nuclei in two-phase model *(Russian)* 78−46002
^{156}Er, rotating nuclei, two-phase model 78−33113
^{157}Er low-lying scheme determ. from ^{157}Tm decay 77−22958
^{158}Er, anomalous rotational bands−a model of a soft rotor coupled with $i_{13/2}$ particles 79−85356
^{158}Er, double crossing of ground rotational band and super band 78−45996
^{158}Er, high spin state anomaly, backbending 79−22173
^{158}Er, high-spin yrast levels, second discontinuity obs. 77−61373
^{158}Er, level struct. determ. in ^{158}Tm (β^++EC) decay 77−22957
^{158}Er moment of inertia curve behaviour in recrossing ground state band and superband 79−59001
^{158}Er, number conservation, effect on energy spectra, deform. and B(E2) values 79−36122
^{158}Er, second backbending using cranked Hartree-Fock-Bogoliubov method 79−13188
^{158}Er, var. calc. and HFB calc. of back-bending 77−57584
^{160}Er continuum γ-ray multipolarity by linear polarisation meas. from ^{148}Nd(^{16}O,4n), yrast levels 79−85408
^{160}Er high spin yrast states and transitions from ^{152}Sm(^{13}C,5n) 80−9208
^{160}Er, number conservation, effect on energy spectra, deform. and B(E2) values 79−36122
^{160}Er, produced in ^{124}Sn+^{40}Ar, γ-ray multiplicity spectra, nuclear shape at high angular momentum 78−37260
^{162}Er 0^- band, angular momentum projection method for even-even nuclei excited states 79−3069
^{162}Er, ang. momentum projection for rot. nuclei, numerical aspects 79−63575
^{162}Er energy spectrum anomalies, rot. bands, cranking model with Hartree-Fock-Bogolubov theory 79−3064
^{162}Er, microscopic calc. of high-spin rot. states 78−8730
^{162}Er, negative parity excited bands, exact ang. momentum and particle number projection 79−45135
^{163}Er, excited states populated in ^{163}Tm decay 78−17146
nuclear collective states and giant resonances continued
^{164}Er deformed nucleus, excited rot. bands, selfconsistent HFB treatment 80−42515
^{164}Er high spin props. in multiple band crossing region from (^{18}O,4nγ), (α,4nγ), (^{136}Xe,^{136}Xeγ) 80−83023
^{164}Er multiple high spin band struct. from ^{160}Gd(^{9}Be,5n), backbending 78−70429
^{164}Er, populated via ^{150}Nd(^{18}O,4n)^{164}Er, multiple band crossings 78−37257
^{164}Er rot. states, HF and HFB self consistent calc. with Skyrme interaction 80−22662
^{164}Er, two-fluid model of nuclear rotations and surface vibrations, energy levels 78−62474
^{166}Er, low lying spectra and EM transitions, level struct. in quasirotational bands 79−36141
^{166}Er, non axial deformability of rotating nuclei in two-phase model *(Russian)* 78−46002
^{166}Er, rotating nuclei, two-phase model 78−33113
^{166}Er(e,e'), 35-350 MeV, coupled channels anal., rot. band excited states, charge densities 79−3139
^{166}Er(γ,γ'), 14.4-16.6 MeV, γ-vibr. band head transitions, dynamic collective model 80−57662
^{167}Er(α,α), E2 and E4 transition moments, rotational states 78−41740
^{168}Er γ-vibr. band, M1 admixtures in intra-band transitions 80−99149
^{168}Er, intraband transition rates in gamma vibr. bands 78−45992
^{168}Er(d,t)^{167}Er, 17 MeV, band heads, two-step process 78−62551
^{172}Er levels, bands, J^{π} and transitions from ^{170}Er(t,p) 80−83038
^{A}Eu, A=151, 152, 153, 154, 155, excited states of transitional region nuclei, rot. bands *(Russian)* 80−52556
^{A}Eu, A=157, 159, single proton states, rot. bands, J^{π} assignments and mass from Gd(t,α) 79−45132
^{A}Eu(p,p'), A=151-3, 12 MeV, rot. states, deformation parameters, DWBA and coupled channel anal. 79−9459
^{145}Eu high spin and isomeric states, transitions, weak coupling from ^{144}Sm(α,2npγ) 80−13348
^{145}Eu high spin core coupled states and transitions from ^{142}Nd(^{6}Li, 3nγ) 80−42520
^{145}Eu high spin levels, isomers and in-beam γ-spectroscopy from ^{144}Sm(α,2np) 80−78124
^{145}Eu high spin states, J^{π} and transitions from (^{7}Li,4nγ) and (^{6}Li,3nγ) 80−47350
^{146}Eu 9^+ isomer, γ-decay, high spin particle-hole multiplet population from ^{147}Sm(p,2n) 80−63066
^{151}Eu narrow band and pickup strength, shape coexistence from (d,t) 80−86799
^{152}Eu, transitional nucleus, ground state rotational struct. stability 78−93929
^{153}Eu $5/2^+$ ground state rot. band, J^{π}, shape coexistence from (d,p) 80−86799
^{153}Eu(n,X), gamma transitions and band levels *(Russian)* 79−67700
^{154}Eu low lying levels, bands, transitions from ^{153}Eu(n,γ) 80−57694
^{154}Eu(p,p'), 12 MeV, ground band rot. states, deformation parameters, coupled channels anal. 80−9195
^{155}Eu, single proton states, spins and parity, rot. bands from ^{156}Gd(t,α), ^{154}Sm(α,t) 79−30766
^{18}F, 4p-2H, 1^+ rot. band anal. from ^{14}N(^{7}Li,t)^{18}F 77−79299
^{18}F compound nucleus rot. band structure, ^{16}O(d,d) study with resonating group method 77−10415
^{18}F, negative parity states, dynamic interaction propagator approach 79−13191
^{19}F, decoupled bands and antialigned states 78−78236
^{19}F, electroexcitation of ground state rotational band 78−66191
^{19}F, even parity state, EM props., collective struct., generator coord. method, HF method anal. 79−89220
^{19}F final state selective population, triton clustering from band anal. from (^{7}Li,t), (^{6}Li,^{3}He) 80−9306
^{19}F isospin mixing in yrast $I=5/2^+$ level 79−93508
^{19}F, level struct. J^{π}, spectroscopic factors via (^{13}C, ^{9}Be) reaction 77−14033
^{19}F low lying band state lifetimes, stopping power, transition strengths from ^{15}N(α,γ) 80−42585
Fe, A=54, 56, intermediate struct. via (γ,n) 5-26.3 MeV 77−74824
Fe isotopes A=53-58, spectroscopic calcs. using mass independ. effective interaction, yrast levels 78−41638
Fe, photonuclear cross sections in giant reson. region 78−17178
^{A}Fe, A=54-56, high spin states, energy levels, spectroscopic factors, EM props., shell model 80−47359
^{A}Fe, A=56-60, shell struct. of collective states, level spectra 79−93494
^{A}Fe(α,α'), A=54,58, 8-18 MeV, cross sections, search for giant dipole resonance 80−9281
^{A}Fe(p,γ_0)Co, A=54,56, giant dipole resonance splitting, direct-semidirect capture model anal. 80−106055
^{52}Fe yrast state properties, transitions and decays from ^{40}Ca(^{14}N,np) 79−67631
^{53}Fe, strongly deformed $K^{\pi}=1/2^-$ bands from γ meas., level transition parameters 79−3113
^{54}Fe 8^+ and 10^+ level spin assignments and lifetimes from (^{16}O,2p), (^{6}Li, pn) 80−68531
^{54}Fe high spin states, transitions and J^{π} values from ^{52}Cr(α,Znγ) 80−455
^{54}Fe(α,α'), coupled channels calc., capture cross section, GQR decay modes 80−27654
^{54}Fe(γ,n), cross section meas., E1 giant dipole isospin splitting 79−17892
^{54}Fe(p,p'), 39, 62 MeV, DWBA anal., collective spectra, direct process contrib. *(Russian)* 80−13408
^{55}Fe, possible deformed $7/2^-$ states with $\Delta J=1$ band 79−45170
^{56}Fe yrast band, coexistence of prolate and oblate shapes 78−12947
^{56}Fe+n, 0-2.2 MeV, doorway state struct. 77−88143
^{56}Fe(e,e'), Coulomb form factor for $0^+\rightarrow 4^+$ transition, collective 4^+ states, shell model 80−57664
^{56}Fe(p,p), elastic scatt. in giant reson. region of ^{57}Co 77−18542
^{56}Fe(p,p), elastic scatt. in giant reson. region of ^{57}Co 77−18543
^{57}Fe, Mossbauer effect in Ge, appl. of in-beam implantation method 78−25372
^{57}Fe, rot. band mixing microscopic theory using modified Kuo-Brown interaction 80−68513
^{213}Fr, high spin yrast states in N=126 isotones 79−45131
Ga, odd, single particle and collective degrees of feedom, clustering, shell model anal. 80−68510
^{A}Ga, A=65,67, high spin states and transitions from Fe+^{12}C(^{14}N) 80−68516

nuclear collective states and giant resonances continued
^{67}Ga high spin states, J^{π} and transitions, triaxial struct. from ^{54}Fe(^{16}O,αp),(^{6}Li,Zn) 80−63062
^{67}Ga, high spin states, using ^{57}Fe(^{12}C,pnγ) at 40 MeV 79−36128
^{148}Gd, pairing-plus-quadrupole calcs. 77−82807
Gd (A=154-156), collective properties 77−6192
Gd, N=85 isotones, bands and transitions from α and HI excitation, in-beam study 80−78123
$^{154-160}$Gd, vibrational state B(E2), B(E3) via (α,α′)Coulomb excit. 77−74803
^{A}Gd A=144,146,147,148, high spin isomer g-factors yrast traps from (^{28}Si,^{28}Si′), (α,α′) 80−78146
^{A}Gd, A=146-7, high spin yrast traps, g-factors 79−63578
^{A}Gd, A=146.7, particle hole yrast states and Z=64 shell closure from Sm (α, xn) 79−49571
^{A}Gd, A=152, 154, 156, 158, excited states of transitional region nuclei, rot. bands *(Russian)* 80−52556
^{A}Gd, A=154, 156, energy levels and E2 transition rates from three-band mixing model, backbending 79−67623
^{146}Gd, high multiplicity yrast isomers prod. in (α,xn) reactions 78−41666
^{146}Gd, p single particle states and pairing force calcs., high spin states 80−42522
^{147}Gd, collective and noncollective excitations, Hamiltonian calc. for level density 79−36139
^{147}Gd, high multiplicity yrast isomers prod. in (α,xn) reactions 78−41666
^{147}Gd^{m} high spin yrast trap, oblate deformation and quadrupole moment 80−32157
^{150}Gd, collective bands and absence of yrast traps 80−9207
^{150}Gd, high spin states, pairing correlations and nuclear shape, HFB approach 80−42517
^{150}Gd negative parity yrast states, obs. in (α,xn) and ^{150}Tb decay 77−88033
^{150}Gd, negative parity yrast band, E1 transitions polarisability, quadrupole-octupole coupled vibr. system 79−484
^{151}Gd, collective bands anal. using (α,3nγ) at 35-45 MeV 77−61342
^{151}Gd, high spin states, gamma ray and conversion electron obs., level struct. 77−46130
^{152}Gd β- and octupole bands, downbending moments of inertia from ^{150}Sm(α, 2n) 80−91131
^{152}Gd N=88 nuclei quasirot. bands and J^{π} from EC decay and (α,xnγ) 80−83025
^{152}Gd, negative parity band crossing in even-even nuclei 78−21488
^{152}Gd, negative parity bands, coherent state model 78−89782
^{152}Gd, vibrational states, B(E2) branding rates and interband transitions, pairing plus quadrupole calcs. 80−78127
^{154}Gd levels, bands, J^{π}, DWBA anal. of ^{152}Gd(t,p) 80−78110
^{154}Gd levels from γ ang. distribs., populated by ^{152}Sm(α,2nγ) and ^{154}Tb decay 79−442
^{154}Gd multiphonon vibr. bands, dynamic deformation theory 80−5035
^{154}Gd, two-fluid model of nuclear rotations and surface vibrations, energy levels 78−62474
^{155}Gd, vibr. state, level scheme, γ and conversion electron spectra from ^{154}Gd(n,γ) 80−57696
^{158}Gd excited states from ^{157}Gd(n,γ), level struct., rot. bands, transition probabilities 78−89819
^{158}Gd, rotational bands, coupled-channels Born approx. anal. of ^{166}Gd(d,t) 80−83104
Ge, doubly even nuclei, quasiparticle+phonon model calcs. 78−41626
Ge isotopes A=68 to 78, potential energy surface and collective spectra 78−86464
Ge, odd, single particle and collective degrees of feedom, clustering, shell model anal. 80−68510
^{A}Ge, A=66,69,70, negative parity high spin states, spin and lifetimes from HI reactions 80−73768
^{A}Ge, A=68,70,72, discovery of multiple collective band struct. *(Chinese)* 79−80865
^{A}Ge A=68,70,72,74, deformations and collective spectra, reaction mechanisms from Ge(p,t) 79−22168
^{19}Ge excited state, J, mean lifetimes and transitions from ^{64}Za(^{7}Li,ph)
^{19}Ge excited state, J, mean lifetimes and transitions 80−68517
^{68}Ge, ground and both neutron and proton rotational aligned bands, model calcs 79−54377
^{68}Ge multiple band struct., $g_{9/2}$ orbital, level lifetimes from ^{58}Ni(^{12}C, 2p) 80−13358
^{69}Ge high spin states, EM props., Branching and mixing ratios from ^{55}Mn(^{16}O,pn) 80−13347
^{69}Ge high spin states, J assignment, decay scheme from ^{55}Mn(^{16}O,pn) 80−68518
^{69}Ge level structure and lifetimes, decay through negative parity band from ^{55}Mn(^{16}O,pnγ) 79−45172
^{72}Ge excitation energies, B(E2) values, extended generator coordinate method 77−6203
^{72}Ge high spin levels obs. in ^{70}Zn(α,2nγ) *(French)* 79−22304
^{72}Ge levels pop. in ^{8}Zn(^{6}Li,pn), in beam gamma-ray spectroscopy 80−47343
^{74}Ge excitation energies, B(E2) values, extended generator coordinate method 77−6203
^{2}H(^{3}He,^{4}He)^{1}H, 27 and 33 MeV, polarised ^{3}He beam analysing power and cross sections 79−89316
^{4}He, giant dipole reson., shell model calcs. including noncentral forces and target recoil corrections 79−17824
^{4}He, monopole excitations, transition densities from simple collective model 79−40834
^{4}He, one particle density distrib., nucleon density, from nuclear ellipsoid of inertia *(Russian)* 79−30784
^{4}He(α,α), large amplitude collective motion, adiabatic TDHF calcs. 80−86786
Hf (A=176-180), collective properties 77−6192
Hf, A=166, 168, 170, yrast feeding and lifetimes via Sn(Ti,4n) 195, 198 MeV 77−50078
$^{176-180}$Hf, vibrational state B(E2), B(E3) via (α,α′)Coulomb excit. 77−74803
^{A}Hf, A=166, 168, 170, 172, yrast states, quadrupole moments and B(E2) values, microscopic calcs. 80−32147
^{A}Hf, A=171, 173, three quasiparticle isomers and rot. bands 79−26354
^{A}Hf, A=172-180, prolate isotopes, Yrast traps using cranked modified oscillator pot. 78−93923
^{A}Hf(HI,xn), A=170-173, two and three quasiparticle isomers, rot. bands, decays and lifetimes 80−9211

nuclear collective states and giant resonances continued
^{171}Hf one- and three-quasiparticle states, high spin rot. bands from (^{16}O,5n), (^{13}C,4n) 80−18163
^{172}Hf, decoupled two-quasiparticle bands, backbending 78−4890
^{172}Hf, negative parity excited bands, exact ang. momentum and particle number projection 79−45135
^{172}Hf rotation bands from ^{160}Gd(^{16}O,4n), high spin states, halflives 78−25217
^{172}Hf yrast band and high spin states, $22^{+}\rightarrow 20^{+}$ transition, band crossing from ^{160}Gd(^{16}O,4n) 80−42523
^{174}Hf, angular momentum fluctuation energy in the cranking model 79−89254
^{174}Hf, approximate ang. momentum projection from cranked HFB wave functions, yrast energies 79−30776
^{174}Hf, double crossing of ground rotational band and super band 78−45996
^{174}Hf, microscopic calc. of high-spin rot. states 78−8730
^{175}Hf multi-quasiparticle states and bands, isomeric states, lifetimes from ^{170}Er(^{9}Be,4n) 80−9213
^{175}Hf, three- and five-quasiparticle isomers, rotational bands and residual interactions from ^{170}Er(^{9}Be, 4n) 80−83022
^{176}Hf, ground rotational band level energies calc. 78−45996
^{176}Hf yrast traps, cranking Hartree Fock Bogoliubov calcs. 78−25100
^{178}Hf, energy levels, K-forbidden decays, M4 decay of yrast state 80−68506
^{178}Hf, yrast states struct. changes via ^{176}Yb(α,2n)^{178}Hf 77−50044
^{180}Hf band crossing and giant backbending 80−32156
^{180}Hf, nonrotational interpretation of E_4 matrix element 78−33111
Hf(γ,xn), x=1, 2; A=176, 178, 180, 8-21 MeV, GDR, neutron yields and multiplicities *(Russian)* 77−82894
Hf(n,n′γ), 2.75 MeV, direct excitation of some collective levels 77−26720
Hg, even-A, possible triaxial shape and phase transition, triaxial rotor model 79−93503
Hg high spin states and rotation alignment in ^{198}Hg 77−57591
Hg isotopes, A=184-197, β^{+}-decay, single particle and collective degrees of freedom 77−22956
^{A}Hg, A=198-204, reorientation effect meas. on 2^{+} states 78−37282
^{A}Hg(α,α′), A=198, 200, 204, 16-27 MeV backward scatt., collective states 80−13365
^{188}Hg, HF calc., shape and lowest band struct., B(E2) values 80−32148
^{190}Hg, 21 ns isomer $(\nu i_{13/2})^{2}$ interpretation from g-factor meas. 80−105945
^{195}Hg level scheme and transitions, band population from ^{195}Tl (1.13 h) decay 79−17807
^{196}Hg, band crossing, level scheme, J^{π} 77−65192
^{197}Hg, non-axial deform. anal., $i_{13/2}$ neutron coupling to triaxial rotor and to anharmonic vibrator 77−22847
Ho, A=163,165, collective state form factor effects in Dy(^{3}He,d) at 46.5 MeV 77−14138
^{149}Ho low lying yrast states from ^{122}Te(^{32}S,X), ^{121}Sb(^{32}S,X) 80−91151
^{155}Ho high spin states, lifetimes, J^{π} and rot. parameters from ^{145}Nd(^{14}N,4n) 79−85354
^{155}Ho, negative-parity bands 78−93937
^{159}Ho, level scheme determ. from (^{3}He,3nγ) 77−22840
^{159}Ho, rotational states determination from ^{159}Tb(α,4nγ)^{159}Ho and ^{159}Tb(^{3}He,3nγ)^{159}Ho 77−26556
^{165}Ho natural line shape of giant dipole resonance 77−88096
^{165}Ho(γ,γ′) 8.5-11.4 MeV, elastic and Raman scatt., giant reson. struct. 77−34284
^{166}Ho, energies of low-lying high spin levels *(Russian)* 78−89793
I energy levels, collective excitations, spin,parity, populated in ^{121,125}Sb(α,2n), γ spectra 78−4891
I isotopes 121, 123, 125, rotational bands meas. 77−22837
I, low-lying collective states anal. 77−88030
I odd-A nuclei, deformed $9/2^{+}$ proton-hole states, Nilsson calc. 77−74746
^{A}I, A=115-127 odd isotopes, collective props., bands and transitions from heavy ion reactions 80−68512
^{121}I single particle strength distrib., determ. from ^{120}Te(^{3}He,d) 78−70423
^{123}I, bands and decay props., core-particle coupling and polarisation effects 80−13354
In, photonuclear cross sections in giant reson. region 78−17178
^{A}In, A=119, 121, unified model description, vibr. multiplet yrast struct., branching ratios 80−105953
^{108}In high spin struct., in-beam spectroscopy, conversion electrons from ^{98}Mo(^{14}N,4nγ) 80−73782
^{109}In high spin states, γ-transitions, ang. distribs. from ^{108}Cd(α,2np) 80−73783
^{109}In high spin states, transitions, isomeric state, negative parity bands from ^{107}Ag(α, 2nγ) 80−451
^{109}In, levels and transitions obs. in ^{107}Ag(α,2n) 77−22836
^{111}In $21/2^{+}$ isomeric state g-factor and relaxation time from ^{109}Ag(α,2nγ) 80−73794
^{111}In band structure and hole-core coupling, ^{109}Ag(α,2nγ), branching and mixing ratios 78−58249
^{111}In, rotational band detect., internal conversion electron spectra from ^{111}Cd(p,nγ)^{111}In 79−6362
Ir, A=191, 193, shape of stable transition nuclei, photoabsorpt. cross-sections *(Russian)* 77−79307
Ir, odd isotopes, $9/2^{-}$ level excitation energy, semi-empiricle method 77−22844
Ir odd mass isotopes, odd proton effects on potl. energy surfaces 77−22877
Ir odd mass isotopes, particle rotor descriptions 77−22914
Ir odd mass isotopes, statistical anal. of levels 77−22842
^{A}Ir, A=187, 189, 191, 193, positive parity states, particle asymmetric rotor descriptions 79−49572
^{A}Ir, A=191,193 photoneutron yield curves, nuclear shape and giant dipole resonances, 8-21 MeV *(Russian)* 79−13268
^{183}Ir, high spin states of rotation aligned bands, backbending 77−30485
^{185}Ir, high spin states of rotation aligned bands, backbending 77−30485
^{185}Ir level scheme determ. from ^{185}Pt decay 77−22843
^{185}Ir levels excited in (α,xn) reactions, positive parity band 80−9231
^{185}Ir levels populated in ^{185}Pt^{m+g} decay 80−9269
^{187}Ir, diagonalisation of collective quadrupole Hamiltonian 77−6221
^{191}Ir, levels excited in (p,2n) and (d,3n) 79−22164
^{41}K yrast states from ^{26}Mg(^{18}O, p2nγ), γ meas., spin, parity, branching and mixing 78−58250
^{43}K high spin states, J^{π} and lifetimes from ^{40}Ar(α,pγ) 79−67621

nuclear collective states and giant resonances continued
Kr even isotopes, collective levels and B(E2) values, IBA calcs. 80−27539
Kr even-even isotopes, collective states and transitions, interacting boson approx. 80−73773
^{A}Kr, A=74,76, rot. bands, band crossing and backbending 80−18176
^{A}Kr, A=74,76,78,80, discovery of multiple collective band struct. *(Chinese)* 79−80865
^{A}Kr, A=74-82, even-even isotopes, B(E2) values and collectivity, interacting boson approx. 80−27537
^{A}Kr, A=76,78,80, yrast states and band struct., backbending from Zn(^{12}C, 2n) 80−13359
^{A}Kr, A=78, 80, quasi-γ bands and negative parity levels from Br(p,2nγ) 80−456
^{A}Kr, A=79, 81, high spin E2 bands, J^{π}, transitions from Ge(^{10,11}B, xγ) 80−63061
^{78}Kr band struct., level scheme, from γγ-coincidence from ^{65}Cu(^{16}O, 2np) 80−18177
^{78}Kr band struct., lifetimes and E2 transitions n-p boson model anal. from ^{65}Cu (^{16}O, 2np) 79−80863
^{78}Kr band structs., in-beam γ-rays from ^{68}Zn(^{12}C, 2n) 80−22672
^{78}Kr bands, lifetimes and E2 transitions from interacting boson model and (^{16}O,p2n), (^{19}Fe,α2n) 80−73771
^{78}Kr high spin levels, bands and transitions, level lifetimes from ^{68}Zn(^{12}C,Zn) 80−42525
^{78}Kr high spin states, transitions and lifetimes from (^{16}O,2np), (^{19}F,2nα), (^{16}O,2n), (^{12}C,2n) 80−27534
^{78}Kr high spin states from ^{65}Cu(^{16}O,p2n), band struct. 78−74387
La, low-lying collective states anal. 77−88030
^{A}La, A=125, 127, collective props., bands and transitions from heavy ion reactions 80−68512
^{133}La level struct., parity levels, decoupled band struct. from ^{133}Ce β-decay 79−9476
^{139}La(e,p), 15-25 MeV, T_0+1 giant dipole resonance and characteristic decay mode 80−78247
^{167}Lu intrinsic and rotational levels, obs. in (^{3}He,5n), (α,6n) and (p,4n) 77−88026
^{174}Lu, populated by ^{176}Lu (p,t)^{174}Lu, energy levels and rotational bands 78−37346
^{175}Lu, nuclear rot. band energies *(Russian)* 78−54720
^{175}Lu(γ,γ′), elastic and Raman scatt. at 8.5-11.4 MeV, GDR parameters 78−587
^{176}Lu deformed odd-odd nucleus, γ transition probabilities, rot. band mixing 77−61375
Mg, giant quadrupole resonance strength, p- and α-inelastic scatt. and α capture 78−37323
^{A}Mg, A=24,26, second order nonspherical quadrupole phonon effects 80−86790
^{A}Mg(p, p′), A=24, 26, isovector dipole strength excitation in giant resonance region 80−83066
^{23}Mg, even parity state, EM props., collective struct., generator coord. method, HF method anal. 79−89220
^{24}Mg, ^{16}O+α+α cluster model, energy level structure 80−18215
^{24}Mg (γ,p), 17-30 MeV, giant dipole resonances and transitions, shell effects *(Russian)* 80−13434
^{24}Mg continuum states, branching ratios from ^{12}C(^{16}O, αα) 80−22661
^{24}Mg Coulomb matrix elements, isospin mixing in giant dipole resonance from ^{20}Ne(α,γ) 79−93507
^{24}Mg, evidence for rotational band and its fragmentation in ^{12}C(^{12}C, α)^{20}Ne reaction 79−9449
^{24}Mg, form. in ^{12}C+^{12}C reaction at 10.5 to 15 MeV, possible rot. band 78−13134
^{24}Mg giant isoscalar quadrupole fission/fusion doorway states from ^{12}C(^{12}C, ^{12}C) 80−37410
^{24}Mg ground and γ-bands, direct and multistep processes from (α,^{6}He), (p,t), (^{16}O, ^{16}O) 80−102094
^{24}Mg ground state band from ^{12}C(^{12}C,X) 80−42727
^{24}Mg, ground state rot. bands from shell-model Hamiltonians 77−79298
^{24}Mg high spin selectivity, critical ang. momentum effects from ^{10}B(^{16}O,d) 80−13366
^{24}Mg high spin states, high spin particle spectroscopy upper limits for compound reactions from ^{10}B(^{16}O,d) 79−36126
^{24}Mg high spin states from selective compound reactions, stat. anal. from ^{10}B(^{16}O,d) 80−18180
^{24}Mg, intermediate structure resonances in ^{10}B+^{14}N and ^{12}C+^{12}C near Coulomb barrier 79−9450
^{24}Mg, $K^{\pi}=0^{-}$, $K^{\pi}=3^{-}$ bands, radiative and α-widths from (α,γ), (^{16}O,αγ) 80−18173
^{24}Mg K=2 band and alpha cluster model state point symmetry 80−105946
^{24}Mg, levels, GDR isospin mixing via (γ,α) 28 MeV 77−74832
^{24}Mg low lying K-band from ^{28}Si α-decay 80−47438
^{24}Mg, low lying rot. bands from extended deformation model, parity violating deformations 79−6360
^{24}Mg, low spin rotational states, energy props., extended deformation model 80−86785
^{24}Mg, lowest lying rotational band energies, Brink α-cluster model 77−6195
^{24}Mg, microscopic model of 2_1^{+} and 3_1^{+} states, inelastic p scatt. test 79−26358
^{24}Mg, molecular configuration 79−13193
^{24}Mg, monopole excitations, transition densities from simple collective model 79−40834
^{24}Mg nucleus, ^{12}C+^{12}C quasimolecular rotational band resonances *(Russian)* 79−13269
^{24}Mg, populated via ^{12}C(^{12}C,γ), resonance in γ yields, $J^{\pi}=2^{+}$ resonance 78−54799
^{24}Mg radiative decays of unbound high spin states, resonance J^{π} assignment from ^{20}Ne(α,γ) 79−67701
^{24}Mg, rot. band, reson. states, J^{π} via ^{12}C+^{12}C 78−491
^{24}Mg, rot. band obs. with ^{12}C(^{12}C,α)^{20}Ne 78−12951
^{24}Mg rot. band termination, level lifetimes from ^{12}C(^{16}O, α) 80−18174
^{24}Mg rotational band collectivity, shell model excitation in Sp(4, R) symmetry 80−102095
^{24}Mg, rotational band fragmentation and rotation-vibr. model, ^{12}C+^{12}C appl. 78−25096
^{24}Mg, rotational band fragmentation, rotation-vibr. model 78−54665
^{24}Mg, rotational band struct., obs. in (^{3}He,^{3}He′) 78−41616
^{24}Mg states, Nilsson model spectroscopic factors, collective model rot. bands from ^{23}Na(^{3}He,d) 79−6421
nuclear collective states and giant resonances continued
^{24}Mg, triaxial nuclei rots., extended cranked shape consistent oscillator model 80−102133
^{24}Mg yrast and high spin states up to 24 MeV, ang. distribs. from ^{10}B(^{16}O, d) 80−18175
^{24}Mg yrast line, Strutinsky type cranking calc., pairing correlation inclusion 80−13355
^{24}Mg yrast states up to 24 MeV excitation energy from ^{10}B(^{16}O,d), 60 MeV 78−89781
^{24}Mg+e, 21 to 32 MeV, E0 and E2 excitations, fission into two ^{12}Cg.s. nuclei 78−54744
^{24}Mg(^{3}He,^{3}He), 130 MeV, giant reson. excitation, DWBA anal. 79−89319
^{24}Mg(p,p′), 0.8 GeV, rot., γ and β bands, ground state deformation, DWBA, coupled channels anal. 80−9198
^{24}Mg(p,p′), 20, 40, 800 MeV, γ-vibr. band, coupled channels anal. 80−9194
^{24}Mg(p,p′), 22.5 to 28.5 MeV, giant reson. effects 78−4923
^{24}Mg(p,p′) 15-35 MeV, low lying state differential cross sections, two step effects 79−89304
^{24}Mg(p,p′), 40 MeV, DWBA anal., positive parity states, transitions and giant resonance 79−6419
^{24}Mg(p,p), 14-45 MeV, differential cross section and spin-flip probabilities, giant resonances 80−73850
^{24}Mg(p,p), 15 Mev, excitation functions 80−22825
^{24}Mg(p,p), 40 MeV, natural parity transitions 78−66277
^{25}Mg coherence moment-of-inertia from ^{12}C(^{13}C,α) 79−75815
^{26}Mg, GDR proton channel decay, isospin effects *(Russian)* 77−14020
^{26}Mg(^{3}He,^{3}He′), 4^{+} states, B(E2) values, and band mixing, rot.-vibr. model 80−83019
^{26}Mg(γ,n)^{25}Na, 19.5 to 27.0 MeV, giant dipole resonance decay channel determ., isospin component 79−26423
^{26}Mg(p,p′), 24 MeV, rot. description of low lying states, coupled channels anal. 79−54376
^{27}Mg, excited states up to E_x=7976 keV, studied via ^{26}Mg(d,pγ) reaction 77−41981
Mg(α,α′), A=24,5,6, 106, 120, 145, 172.5 MeV, giant quadrupole reson. obs. 77−6415
Mn photonuclear cross sections in giant reson. region 78−17178
^{52}Mn yrast state properties, transitions and decays from ^{52}Fe $^{M}\beta^{+}$-decay 79−67631
^{53}Mn high spin states, decay scheme, J^{π} assignments, mixing ratios from ^{40}Ca(^{16}O, 3pγ) *(French)* 79−67627
^{53}Mn high spin states, lifetimes, shell model calcs., yrast levels from ^{48}Ca(^{10}B, 5n) 79−6425
^{54}Mn, populated in ^{52}Cr(α,pnγ), low lying intruder states 79−58998
^{55}Mn(γ,xn), 10-36.5 MeV, photoneutron cross sections, integrated cross sections, giant dipole resonance 79−89289
^{A}Mo+^{86}Kr, A=92, 98, deep inelastic reactions, fast collective mode, quantal fluctations 79−67636
^{A}Mo(^{3}He,^{3}He′), A=92,94,96,98,100, 110 MeV, giant quadrupole resonance isotopic depend. 80−9282
^{92}Mo(π^{+},π^{+}), 180 MeV, octupole transitions 79−85542
^{94}Mo high spin state transitions, mixing ratios, spins, shell model calcs. from ^{94}Tc decay 79−97678
^{96}Mo vibration-rotation struct. and yrast levels from variable moment of inertia model 80−73778
^{100}Mo resonances, search for valence neutron capture in 3p neutron giant resonance 77−30587
^{A}N, A=16,18, E1 and M2 giant resonance excitation from O(π^{-},γ) 79−89280
^{13}N, giant dipole reson. excited in ^{12}C(p,γ) and ^{12}C(p,p′), doorway-states 77−6336
^{13}N giant dipole resonance population amplitude and phase, E1 reaction amps. from ^{12}C(p,γ_0), pol. p 80−63145
^{14}N+^{12}C, 112 MeV, alpha clustering, multiple shape vibrs., TDHFC calcs. 79−3164
^{14}N(^{6}Li,^{6}Li′), 153 MeV, isoscalar giant quadrupole resonances 80−13440
^{14}N(γ,n_0)^{13}N, 17 to 26 MeV, angular distrib., giant dipole resonance, single-particle nuclear model 80−52659
^{15}N, giant reson. excitation around 17 MeV, J^{π},Γ assignments 77−34277
^{15}N giant resonance and cross sections from (γ,d) and (d,γ) pol. d 79−93587
^{15}N, photoabsorption, shell-model anal. of giant dipole state 78−29447
^{15}N, spin assignments for giant resonances from ^{11}B(α,γ_0), 15.5-19.5 MeV 78−94019
^{15}N(e,e′), 52-195.3 MeV, giant resonance electroexcitation, C1, C2 strength distribs. 79−510
^{A}Na, (A=21, 23), even parity state, EM props., collective struct., generator coord. method, HF method anal. 79−89220
^{22}Na, ground state band struct., J^{π}, E2 transitions, $T_{1/2}$ *(French)* 77−34210
^{22}Na, band mixing, E2 and M1 matrix elements *(French)* 78−45994
^{23}Na, decoupled bands and antialigned states 78−78236
^{23}Na high spin positive parity state, approx. microscopic methods, shell model comparison 79−85352
^{23}Na high spin states, excitation functions, nonstatistical effects, Hauser-Feshbach anal. of ^{12}C(^{15}N,α) 80−106041
^{23}Na levels and spectroscopic amplitudes, J^{π} assignments, high spin states from ^{20}Ne(α,p) 79−75848
^{23}Na, levels populated by ^{12}C(^{15}N,α) 78−50070
Nb, high spin negative parity states from cluster vibration coupling model 79−75823
^{89}Nb, level scheme determ. from (^{3}He,3nγ) 77−22840
^{90}Nb giant particle hole resonances, Gamow-Teller strength from ^{90}Zr(p,n) 80−86877
^{93}Nb high-spin three-quasiparticle states obs. in ^{93m} Mo decay 77−34262
Nd, N=85 isotones, bands and transitions from α and HI excitation, in-beam study 80−78123
^{A}Nd, A=138,139, high spin states, isomers and γ-cascade from ^{140}Cd(α, xzn) 80−78120
^{A}Nd, A=138,139, high spin states, J^{π}, γ-cascades and shape transition from ^{140}Ce(α, xn) 80−102090
^{A}Nd(^{32}S,^{33}S^{1}), 56 MeV, A=144,146,148, first excited 2^{+} state mag. moment meas. 79−17798
^{133}Nd, high spin states, negative parity level band based $h_{11/2}$ state from ^{116}Sn(^{20}Ne, 3n) 79−75813
^{140}Nd ns isomers and yrast isomers, γ-transitions from ^{128}Te(^{16}O,4n) 80−78121

nuclear collective states and giant resonances continued
^{142}Nd(^{16}O, ^{14}C), 104 MeV, two proton transfer between pairing rot. states 77−10430
^{144}Nd, collective and noncollective excitations, Hamiltonian calc. for level density 79−36139
^{148}Nd from ^{148}Pr β-decay, low lying energy levels, quasi band description 80−5096
^{148}Nd, vibrational states, B(E2) branding rates and interband transitions, pairing plus quadrupole calcs. 80−78127
^{150}Nd, Doppler shift meas. of ground state bands using ^{150}Nd(^{40}Ar, ^{40}Ar γ) 78−50124
^{150}Nd, vibr. bands, population by ^{150}Pr decay 78−89817
^{150}Nd(^{20}Ne, x$n\gamma$), multipolarities of yrast and statistical cascades, total γ conversion coeff. 78−70484
^{150}Nd(^{20}Ne,X), 115, 130 MeV, γ-continuum multiplicity distrib., yrast bump 80−9265
^{150}Nd(e,e′), possible $K^{\pi}=0^{-}$ octupole band, e scatt. form factors 79−9447
^{151}Nd, rot. states populated through neutron capture 77−6196
Ne, A=20, 22, isoscalar giant quadrupole resonance obs. 77−307
^{A}Ne, (A=19,21) , even parity state, EM props., collective struct., generator coord. method, HF method anal. 79−89220
^{19}Ne, final state selective population, triton clustering from band anal. from ^{16}L(^{6}Li,t) 80−9306
^{20}Ne, alpha-cluster states, spin, parity and branching ratios 78−50066
^{20}Ne cluster struct., coupled channel orthogonality condition model, α-decay, excited states, transitions 79−97681
^{20}Ne, cluster struct. study in ^{16}O-α+^{12}C-^{8}Be coupled channel orthogonality condition model 79−89258
^{20}Ne collective motion, B(E2) rates, algebraic formulation in symplectic shell model 80−83015
^{20}Ne continuum states, J^{π} and branching from ^{12}C(^{12}C, $\alpha\alpha$) 80−22660
^{20}Ne cranking model rot. behaviour from Strutinsky method 77−2894
^{20}Ne, deformed nuclei, giant multipole resonances, and transitions, microscopic theory from ^{19}F(p,γ) 79−513
^{20}Ne E1 resonance from ^{19}F(p,γ) pol. p 80−22790
^{20}Ne, effective nucleus eccentricity depend. on total momentum *(Russian)* 79−3078
^{20}Ne giant E1 resonance intermediate struct. from ^{19}F(p,γ), pol. and unpol. 80−78251
^{20}Ne, giant multipole reson. via ^{19}F(p,γ)^{20}Ne, microscopic calc. 77−22987
^{20}Ne, giant multipole resonances in excited core model 77−30539
^{20}Ne, ground state rot. bands from shell-model Hamiltonians 77−79298
^{20}Ne high spin states, J^{π} and α-decay branching ratios from ^{16}O(^{12}C,^{8}Be) 80−18166
^{20}Ne high spin states, J^{π} assignments from ^{16}O(^{6}Li,d) 80−18167
^{20}Ne high-spin states studied via α-transfer reaction ^{16}O(^{14}N,^{10}B)^{20}Ne, 155 MeV 77−14164
^{20}Ne, level struct., J^{π}, spectroscopic factors via (^{13}C,^{9}Be) reaction 77−14033
^{20}Ne, lowest lying rotational band energies, Brink α-cluster model 77−6195
^{20}Ne, possible rot. band spectrum 77−79297
^{20}Ne, rotational moment of inertia, cranked HF formalism with Skyrme force 77−30477
^{20}Ne with backbending, first excited 4^{+} state g-factor 80−78144
^{20}Ne+^{58}Ni, 164 MeV, alpha clustering, multiple shape vibrs., TDHFC calcs. 79−3164
^{20}Ne(e,e′), E1 and E2 giant resonances excitation at 60-120 MeV 78−50144
^{20}Ne(γ,n) cross sections and giant resonance struct. 80−13441
^{21}Ne states, spins and rotational bands from ^{12}C(^{13}C,α) 79−75815
^{22}Ne backbending, yrast line and rotational motion, Strutinsky method from ^{11}B+^{13}C 79−36135
^{22}Ne, giant multipole resonances in excited core model 77−30539
Ni even isotopes, quasiparticle RPA nonlinear generalisation for anharmonic vibr. spectra 79−63580
Ni giant resonances using virtual and real photons 80−22791
^{A}Ni, A=60,61, giant resonance decay modes in (e,p), (e,α) cross section study 79−17877
^{A}Ni(e,e′), 102 MeV, A=58,60, E1-E4 giant multipole resonance comparison, shell model anal. 80−42614
^{57}Ni high spin yrast cascade, decay modes J assignment from ^{54}Fe(α,nγ) 80−68514
^{58}Ni, GDR proton channel decay isospin effects *(Russian)* 77−14020
^{58}Ni, giant electric resonances, study of ^{54}Fe(α,γ)^{58}Ni 78−41739
^{58}Ni, giant resonance αecay modes in (e,p) and (e,d) cross section study 79−17877
^{58}Ni, HFB and dynamic anal., collective motion, zero point energy correction 80−18161
^{58}Ni, isoscalar giant quadrupole reson., decay modes 79−63649
^{58}Ni, mag. quadrupole resonance, M2 strength distrib., quasiparticle-phonon model 79−75947
^{58}Ni, T_0+1 giant M1 resonance, electroexcitation 77−14118
^{58}Ni+^{16}O fusion, 30-70 MeV, statistical model calcs., yrast states and continuum feeding times 79−579
^{58}Ni(^{16}O,^{16}O′), 315 MeV, giant multipole resonance excitation 79−30812
^{58}Ni(α,α'c), 150 MeV, c=charged particle, particle decay from isoscalar giant resonance region 80−13439
^{58}Ni(e,e′α), electric quadrupole giant resonance α-decay *(Russian)* 79−85434
^{58}Ni(e,e′p), electric quadrupole giant reson. decay *(Russian)* 79−85434
^{59}Ni, and N=29 nuclei isobaric analogue resonances in unified model description 78−78343
^{60}Ni, GDR proton channel decay, isospin effects *(Russian)* 77−14020
^{60}Ni, hexadecapole motion obs. from α-scatt., EM transitions and conversion electron spectra 78−25097
^{60}Ni high spin states, J^{π}, $T_{1/2}$, ang. distribs. and polarisations from ^{56}Fe(^{7}Li, p2nγ) 80−99116
^{60}Ni, photon scatt., direct obs. by giant dipole reson. 78−93988
^{60}Ni, T_0+1 giant M1 resonance, electroexcitation 77−14118
^{60}Ni yrast state lifetimes and parities from ^{51}V(^{12}C,2np) 79−45134
^{60}Ni(α,α'), 8-18 MeV, cross sections, search for giant dipole resonance 80−9281
^{62}Ni low lying collective states populated in ^{61}N(d,p), spectroscopic factors 77−61433
^{62}Ni(γ,X), 19.2-26.2 MeV, photoneutron and photoproton spectra, giant dipole resonance-decay, isospin conservation 80−13443

nuclear collective states and giant resonances continued
Ni(e,e′) A=58, 60, 64, isospin splitting of giant dipole resonance *(Russian)* 77−50116
^{235}Np deduced levels and Nilsson band configurations from ^{234}U(^{3}He,d) and ^{234}U(α,t) 79−468
^{237}Np(e,f), 10-34 MeV, electrofission cross section, E2 transition mode and giant resonances 80−106084
^{237}Np(γ,γ') 8.5-11.4 MeV, elastic and Raman scatt., giant reson. struct. 77−34284
^{16}O, giant dipole and quadrupole resonances 77−2965
^{16}O, alpha-cluster states, spin, parity and branching ratios 78−50066
^{16}O, α-cluster model comparison with giant E2 excitations 78−50109
^{16}O, breathing mode, K-harmonics calc. 77−6200
^{16}O collective and giant multipole states, Brueckner RPA particle-hole state description 80−32169
^{16}O E1 and p_0 channel E2 strength from ^{15}N(p,γ) 80−22790
^{16}O excited state GDR from ^{15}N(p,γ), coupled channels version of continuum shell model 79−542
^{16}O excited state giant resonance populated in ^{15}N(p,$\gamma_{0,1,2}$), ang. distrib., γ correl. 77−82926
^{16}O, giant dipole reson. struct. anal. from ^{15}N(p,γ)^{16}O 78−4942
^{16}O, giant dipole resonance fine struct., 5p-5h excitation model *(Chinese)* 78−82271
^{16}O, giant E1 resonance obs. in ^{15}N(p,γ_0) at 8.6-18 MeV 78−66256
^{16}O, giant isoscalar monopole state energies in generator coordinate method 80−37317
^{16}O, giant monopole resonance widths, RPA calcs. based on Skyrme interaction 78−93984
^{16}O high spin states, J^{π} and α-decay branching ratios from ^{12}C(^{12}C,^{8}Be) 80−18166
^{16}O, isoscalar giant monopole vibrs., time-depend. HF calc. 77−22986
^{16}O isoscalar giant quadrupole resonance, α-decay dominance from ^{16}O(α,α'+charged particle) 78−46035
^{16}O, isoscalar giant quadrupole resonances, RPA calcs., E2 strength fragmentation, spectroscopic factors 80−13437
^{16}O, isoscalar giant resonances and Landau parameters with density-dependent effective interactions 79−71827
^{16}O, isovector GQR splitting 77−22988
^{16}O, magic nuclei at collective excitations, energy spectrum and shape *(Russian)* 80−106015
^{16}O, monopole vibration damping, TDHF calcs. 80−22667
^{16}O, octupole GR strength via ^{16}O(p,p′)^{16}O, 42.5-49.3 MeV, polarised protons 77−57644
^{16}O, positive parity giant multipole resons., particle hole shell model 79−30811
^{16}O, rotational band collectivity, shell model excitation in Sp(4, R) symmetry 80−102095
^{16}O, spreading of giant quadrupole resonance, calcs. using 2p-2h admixtures 78−21485
^{16}O, spreading widths of giant reson. calc., core-coupling RPA approx. 77−74827
^{16}O, struct. in giant resonance region obs. in ^{13}C(^{3}He,γ), 25 to 30 MeV 79−63650
^{16}O, T=0 pairing vibr. determ. from ^{14}N(^{3}He,p) 78−70422
^{16}O, vibrating nucleus, adiabatic anal. of time-dependent HF solns. 79−40863
^{16}O+^{12}C, isobar total prod. cross-sections, target giant reson. excitation 79−85429
^{16}O+^{16}O, 384 MeV, alpha clustering, multiple shape vibrs., TDHFC calcs. 79−3164
^{16}O(^{16}O,^{16}O), 10-41 MeV, molecular resonances γ-yield, band crossing model 80−106032
^{16}O(^{16}O,^{16}O), quasimolecule dynamical study, L=0 to 30 phase shifts 77−26784
^{16}O(^{28}Si,X), 55-96 MeV, γ-ray yield functions from high spin states, comparison with ^{12}C+^{24}Mg 79−93492
^{16}O(^{3}He,^{3}He), E2 strength distrib., giant quadrupole reson. 77−30612
^{16}O(^{3}He,γ)^{19}Ne, E_x=11 to 25 MeV, g.s. giant dipole resonance 79−6539
^{16}O(^{6}Li,^{6}Li′), 153 MeV, isoscalar giant quadrupole resonances 80−13440
^{16}O(K,K′), low lying collective state selective excitation, ang. distribs. and cross sections 79−6368
^{16}O(α,α), giant isoscalar quadrupole resonance, α-over p-decay ratio, SU(3) and shell model 80−27608
^{16}O(γ,n), 25-45 MeV, isovector giant quadrupole resonance evidence, E2 cross section 80−18268
^{16}O(γ,n)^{15}O, ang. distrib. asymmetry anal. 78−25172
^{16}O(γ,p)^{15}N, electric quadrupole transition cross-sections, behind giant resonance *(Russian)* 80−78281
^{16}O(μ^{-},e^{-})^{16}O*, shell model anal. of μe conversion rate *(Russian)* 79−89300
^{16}O(p,p′), 135 MeV, high spin particle-hole states, 4^{-} states 80−9217
^{16}O(p,p′), giant resonances from antisymmetrised DWBA anal. 79−85432
^{16}O(p,p′), microscopic anal. of doorway states in giant resonance region 77−2966
^{16}O(π,π)^{16}O, microscopic isobar-hole calc. doorway states 78−4965
^{16}O(π^{+},π^{+}), 50-340 MeV, isobar hole doorway states, collective Δ-hole states 79−85350
^{17}O compound nucleus rot. band structure, ^{16}O (N,N) study with resonating-group method 77−10415
^{17}O, giant reson. isospin splitting, photonuclear cross-sections 78−577
^{17}O(γ,n), 8.5-39.7 MeV, cross section, giant dipole and pygmy resonance decays 80−42619
^{18}O, modified HF calcs. for low-lying collective states 77−22916
^{18}O, negative parity states, dynamic interaction propagator approach 79−13191
^{18}O struct. calcs., collective Hamiltonian approach 79−22212
^{18}O(e,e′), 80-165.7 MeV, giant dipole and quadrupole resonances, form factors 80−102168
^{18}O(γ,n) 8.0 to 41.8 MeV, photonuclear cross section meas., resonance decay branching 79−63656
^{18}O(π,π'), 164 MeV, yrast state and level excitation, DWIA calcs., shell model context 80−42526
Os, A=190, 192, possible hexadecapole vibrs. via Ir(t,α)Os 15 MeV reactions 77−26560
^{A}Os, A=182, 184, 186, high spin yrast states, back-bending 80−86802
^{A}Os, A=186-194, collective levels, transitions, mag. and quadrupole moments, boson expansion theory 80−105954
^{A}Os(α,α') A=188,190,192, 4_3^{+} level population, hexadecapole vibrs. 78−89780

nuclear collective states and giant resonances continued
^{A}Os(γ,xn), 7-30 MeV, A=186,188-190,192, photoneutron cross section and giant resonances 79−54422
^{182}Os, K-isomer populations, (p,xnγ), (He,xnγ) reaction study 78−93927
^{186}Os, K=0 rot. band collective states, populated in ^{186}Ir decay 77−82803
^{188}Os, ground and γ-band level energies, B(E2) values and EM moments, triaxial description 79−36140
^{190}Os, collective states and static quadrupole moment, boson expansion theory 80−47346
^{191}Os, Nilsson model strength fragmentation obs. in ^{190}Os(n,γ) 77−74844
^{192}Os level scheme and rot. bands, from ^{191}Os(n,γ), interacting boson approx. anal. 79−6413
^{30}P high spin two nucleon states decay props. from ^{28}Si(α, dγ) 80−13402
Pa, A=233, 235, 237, levels via (t,α) 15 MeV 77−74749
Pb cored nuclei, high spin stater energies, quadrupole interaction, yrast traps 77−34223
Pb even isotopes, two quasiparticle 2^{+} state coupling to T=0 giant quadrupole resonance 80−68618
Pb isotopes, occupation number calc., pair correlations 79−30783
Pb, odd-A isotopes, weak coupling calc. for high spin neutron hole excitations 78−62475
Pb pairing vibr. band, microscopic struct. and wave functions from (p,t), (t,p) 80−91126
Pb region, forbidden charge exchange collective modes, β- and γ-decay processes 80−86784
Pb region, particle-vibration multiplet spectra, self-consistent framework 80−102089
^{A}Pb(α,α′), A=204, 206, 208, 16-27 MeV backward scatt., collective states 80−13365
^{200}Pb, obs. of levels in ^{198}Hg(α,2n) 78−66192
^{203}Pb in-beam electron conversion from high spin states from ^{204}Hg(α,5n) 79−93554
^{203}Pb multiplet struct., DWBA anal. from ^{205}Pb(p,t) 79−17784
^{204}Pb yrast levels populated in ^{204}Hg (α,4n), spin, parity, γ spectra 78−12954
^{205}Pb multipole resonance E1-E2 and E1-M1 interference from ^{206}Pb(γ,n) 80−32251
^{205}Pb(d,d′), 14, 17 MeV, direct population of collective states, multiplets, deform. parameters 78−74376
^{206}Pb proton pairing vibr. obs., using (^{3}He,n) reaction at 33.3 MeV 78−13128
^{206}Pb(α,α′), 120 MeV, new giant resonance at 80 $A^{-1/3}$ MeV 77−41939
^{207}Pb, muonic, octupole doublet isomer shifts, octupole vibrs. 80−95750
^{207}Pb neutron hole states, core vibration effects, shell model energies 79−36142
^{208}Pb, alpha-particle vibr. states, obs. in ^{204}Hg(^{16}O,^{12}C) 77−38218
^{208}Pb (α,α^{1}), 100-172 MeV, giant monopole resonance evidence from strong energy depend. 80−13432
^{208}Pb (e,e′), 2^{-} giant resonance twist mode excitation, B(M2) values, form factors 80−78246
^{208}Pb breathing model transition density, single particle and collective state dynamical coupling 80−106007
^{208}Pb core with valence nucleon or hole, mag. props., exchange currents, electron scatt. 80−22689
^{208}Pb, core-coupling RPA calcs. of NGR, electric multipole strength fragmentation 78−50142
^{208}Pb, damping of single particle states and giant resonances 79−17782
^{208}Pb, energy of two-phonon α-vibration 77−14019
^{208}Pb, excitation of low lying collective states by (n,n′) scatt. 78−17205
^{208}Pb, fine struct. of M1 giant resonance obs. in ^{207}Pb(n,γ) 77−79347
^{208}Pb, from ^{207}Pb(n, γ), primary E2 transitions to ground state 78−58284
^{208}Pb, giant dipole resonance struct. 77−88023
^{208}Pb, giant M1 resonance near 8 MeV 79−6541
^{208}Pb giant magnetic dipoles states obs. in ^{207}Pb+n, spin parity assignments 77−57666
^{208}Pb giant monopole and quadrupole resonances, multipole excitations from (α,α′)(d,d′) 80−106031
^{208}Pb, giant monopole reson struct. 78−82331
^{208}Pb, giant multipole reson. electroexcitation 77−34279
^{208}Pb, high-spin states, form factors for electroexcitation 77−14116
^{208}Pb, isoscalar breathing mode state obs. in (α,α′) scatt. at 96 MeV 78−17086
^{208}Pb, isoscalar electric giant dipole resonance, from RPA calc., nuclear compressibility 78−86520
^{208}Pb, isoscalar giant multipole resonances, simple macroscopic model, damping mechanisms 80−42617
^{208}Pb isoscalar giant reson., decay scheme 80−9277
^{208}Pb, M1 collective strength, evidence from ^{208}Pb(γ,n$_{pol}$) 77−38255
^{208}Pb, mag. quadrupole resonance, M2 strength distrib., quasiparticle-phonon model 79−75947
^{208}Pb, magnetic high spin states, microscopic struct. 80−95297
^{208}Pb, mode coupling theory for two particle-two hole states 77−6214
^{208}Pb, monopole giant resonances, position and width 77−82896
^{208}Pb monopole vibr. vel. field, asymptotic form 80−78115
^{208}Pb, photonuclear induced high multipole giant reson., Australian nuclear physics review 77−88021
^{208}Pb region, finite Fermi systems, review 78−537
^{208}Pb, search for collective M1 resonance in ^{208}Pb(γ,n$_{0}$) 77−46103
^{208}Pb, static and transition densities, self consistent RPA theory test in fast (p,p), (e,e) scatt. *(Russian)* 79−49604
^{208}Pb, twist mode 77−88037
^{208}Pb+^{12}C(^{14}N), giant resonances, ang. distrib., inelastic scatt. 78−62564
^{208}Pb+^{208}Pb deep inelastic processes, TDHF and elementary modes of excitation 79−63695
^{208}Pb(^{12}C, ^{12}C′), 200 MeV, evidence for giant quadrupole excitation 79−49637
^{208}Pb(^{14}N,^{14}N′), 266 MeV, giant resonance excitation 80−78253
^{208}Pb(^{16}O,^{16}O′), 315 MeV, giant multipole resonance excitation 79−30812
^{208}Pb(^{16}O,^{16}O′), 315 MeV, continuous spectrum and giant resonance excitation, coherent state model test 80−32252
^{208}Pb(^{208}Pb, X), giant resonance polarisation pots. from nucleus-nucleus effective pot. 80−78248
^{208}Pb(^{3}He,^{3}He′), 108.5 MeV, giant monopole resonance, DWBA anal. 79−71828
nuclear collective states and giant resonances continued
^{208}Pb(^{3}He,^{3}Ne), 130 MeV, giant reson. excitation, DWBA anal. 79 89319
^{208}Pb(^{3}He,t)^{208}Bi, 80 MeV, Gamow-Teller M1 state excitation 78−50184
^{208}Pb(^{6}Li,^{6}Li′)^{208}Pb, 156 MeV, giant quadrupole reson. excitation 77−67767
^{208}Pb(N, γ$_{0}$), γ-ray ang. distribs., giant E3 resonances, direct-semidirect model 79−67727
^{208}Pb(N,γ$_{0}$), 2-10 MeV, giant M1 resonance in direct-semidirect model 79−17898
^{208}Pb(α, α′), neutron collectivities, E2 giant resonance excitation 77−26558
^{208}Pb(α,α′), 65 MeV, inclusive reaction, giant resonance background, heavy ion model anal. 80−5150
^{208}Pb(α,α′), 96 MeV, ang. distribs., breathing mode states, DWBA calcs. 78−50183
^{208}Pb(α,α′), RPA calcs., existence of breathing mode 78−25163
^{208}Pb(α,α), 172 MeV, giant resonance structures 80−91163
^{208}Pb(α,α), 172 MeV, strongly excited giant monopole resonance 80−18273
^{208}Pb(d,d′), RPA calcs., existence of breathing mode 78−25163
^{208}Pb(e,e^{1}), E2 transitions of fragmented isoscalar quadrupole giant resonance 80−22758
^{208}Pb(e,e′), 50-335 MeV, J^{π}=12^{-}, 14^{-} high spin states, DWBA anal. 79−93490
^{208}Pb(e,e′), 70-335 MeV, natural parity high spin state excitation 80−63060
^{208}Pb(e,e′), giant multipole resonance excitation, particle-hole interaction 80−22789
^{208}Pb(e,e′), M2 giant resonance excitation, spin-magnetism mass depend. quenching, M1 strength reduction 78−86521
^{208}Pb(e,e′), RPA calcs., existence of breathing mode 78−25163
^{208}Pb(γ,n), 7.4-8.4 MeV, cross section, E1 and M1 transitions, collective and giant M1 resonance 79−89267
^{208}Pb(n,n′γ), 5.2-8.5 MeV, E1 excitations, collective states and spin assignments, statistical model anal. 79−54405
^{208}Pb(p, γ), γ ang. distrib., isovector giant quadrupole resonance, direct-semidirect model 79−63647
^{208}Pb(p,γ) fast capture, direct-semidirect model excitation function calcs. 78−94004
^{208}Pb(p,p′), 135 MeV, normal parity level excitation, J^{π}, differential cross sections 80−57690
^{208}Pb(p,p′), 135 MeV, normal parity excitations, microscopic description, NN interaction shape 80−57691
^{208}Pb(p,p′), 39, 62 MeV, DWBA anal., collective spectra, direct process contrib. *(Russian)* 80−13408
^{208}Pb(p,p′), 40, 45 MeV, fine struct. in giant resonance region, collective dipole spin flip excitation 78−46056
^{208}Pb(p,p′), 800 MeV, high energy octupole giant resonance, ang. distribs. 80−86879
^{208}Pb(p,p′), giant resonances from antisymmetrised DWBA anal. 79−85432
Pd, A=102,4,6, collective and two-quasiparticle excitation for Zr (^{13}C, 3nγ) 77−18601
Pd, even isotopes, low lying collective states, IBA 80−27540
Pd, even-even, collective states, B(E2), branching ratios and moments, boson expansion method 80−102099
Pd, even-mass isotopes, collective model with deform., vibr., rot. energy levels, B(E2) ratios 78−17120
^{A}Pd, A=106, 108, collective excitations in the interacting boson model *(Russian)* 80−5044
^{14}Pd, A=101, 103, 105, decoupled rotational band struct., in spherical quasiparticle theory 78−66193
^{101}Pd nonyrast rotational states, transitions, T$_{1/2}$, branching and mixing ratios from ^{92}Zr(^{12}C,3n) 80−105950
^{105}Pd, high-spin particle-core multiplets via ^{96}Zr(^{12}C,3nγ)^{105}Pd, rot. model 77−54140
^{108}Pd, vibr. states study, elastic and inelastic electron scatt., anharmonic vibrator model 78−62520
^{110}Pd(e,e′), 40-110 MeV, vibr. nuclei, branching ratios 77−6356
Pd(n,n′), near threshold energy for first 2^{+} collective levels excitation, statistical model test 77−61408
^{141}Pm medium spin states, J^{π}, transitions and shape from (p,2n), (^{3}He,3n), (α,4n) 80−86779
^{143}Pm high spin states, J^{π}, transitions, isomer g-factors from (d,2N), (α,2N) 80−32154
^{145}Pm level struct., J^{π} and lifetimes, cluster-vibr. model anal. of ^{146}Nd(p,2n) 80−91125
^{149}Pm high spin states and bands, rot. description and in-beam study from ^{150}Nd(p,2nγ) 80−32153
^{149}Pm levels, bands, transitions, in-beam spectroscopy, particle-rotor anal. from ^{150}Nd(p,2nγ) 80−78125
^{151}Pm single proton states, rot. bands, level J^{π} assignments, spectroscopic strengths from ^{150}Nd(^{3}He,d), and ^{152}Sm(t,α) 79−67626
^{153}Pm 5/2^{-} h$_{11/2}$ dominated band, anomalous ang. distribs., CCBA calcs. for ^{154}Sm(t,α) 80−86788
Pr, low-lying collective states anal. 77−88030
^{139}Pr medium spin states, J^{π}, transitions and shape from (p,2n), (^{3}He,3n), (α,4n) 80−86779
^{141}Pr, natural line shape of giant dipole resonance 77−88096
^{141}Pr(e,p), 15-25 MeV, T$_{0}$+1 giant dipole resonance and characteristic decay mode 80−78247
^{143}Pr, 57 keV state, from ^{143}Ce 1404 keV beta transition spectrum shape 78−74339
^{191,193}Pt high-spin levels via ^{190,192}Os(α,3nα), triaxial rotor model 77−34213
Pt, A=194, 195, 196, 198, shape of stable transition nuclei, photoabsorpt. cross-sections *(Russian)* 77−79307
Pt, even mass, ground and gamma band EM transition rates, asymmetric rotor model 80−32231
Pt rot. states and moments of inertia staggering from ^{A}Hg, A=181-185 α-decay 78−89779
^{A}Pt, A=173-179, 188, alpha decay, half lives, decay energies and branching ratios, rot. struct. 79−45215
^{A}Pt, A=186,188,190, subnanosecond high spin isomers, decay chains and lifetimes from Yb(^{16,18}O, xn) 79−45140
^{A}Pt, A=188-198 collective levels, transitions, mag. and quadrupole moments, boson expansion theory 80−105954
^{A}Pt, A=190-193, lifetimes of rotation-aligned states 78−93969

nuclear collective states and giant resonances continued
$^{\wedge}$Pt, A=194-8 photoneutron yield curves, nuclear shape and giant dipole resonances, 8-21 MeV *(Russian)* 79−13268
^{182}Pt, low-energy collective states 77−22846
^{187}Pt→^{185}Pt, oblate to prolate transition meas. 77−22878
^{188}Pt, ground and γ-band level energies, B(E2) values and EM moments, triaxial description 79−36140
^{188}Pt side band, low lying and high spin states populated in ^{191}Ir(p,4nγ) 78−4936
^{190}Pt, collective excitations in the interacting boson model *(Russian)* 80−5044
^{191}Pt, non-axial deform. anal., $i_{13/2}$ neutron coupling to triaxial rotor and to anharmonic vibrator 77−22847
^{194}Pt, determ. of sign of $P_3=M(0_1^+2_1^+)M(2_1^+2_2^+)M(2_2^+0_1^+)$ 79−63588
^{194}Pt, populated in ^{194}Ir decay, level scheme determ. 77−2900
^{194}Pt(^{16}O,^{16}O′), 7-17.5 MeV, Coulomb excitation, low lying collective state reduced matrix elements, triaxiality 78−82269
^{194}Pt(α,α′), 7-17.5 MeV, Coulomb excitation, low lying collective state reduced matrix elements, triaxiality 78−82269
^{195}Pt(n,γ)^{196}Pt, low spin positive-parity states struct., O(6) limit of IBA model 78−33110
^{196}Pt, collective states and static quadrupole moment, boson expansion theory 80−47346
^{196}Pt negative parity states in partially decoupled bands, γ-transitions from ^{195}Pt(n,γ) 80−47360
^{196}Pt rotation-vibration struct., O(6) interacting boson description alternative 79−59019
Pu, even isotopes, $K=0^+$, 0^- bands, energies, inverse moments of inertia 80−63063
$^{\wedge}$Pu, A=238,240, fission isomer rot. spectra $I^2(I+1)^2$ correction 80−18229
^{239}Pu, giant resonance in total photoabsorpt. cross-section 77−6347
^{239}Pu, spectroscopy in second minimum of pot. energy surface 79−30805
^{243}Pu, J^{π}, Nilsson and rot. bands via (n,γ), (d,p) and (d,t) 77−6202
Ra, even isotopes, $K=0^+$, 0^- bands, energies, inverse moments of inertia 80−63063
^{214}Ra, high spin yrast states in N=126 isotones 79−45131
^{225}Ra rotational band level diagram from α-decay and conversion electrons 80−18156
Rb odd-even isotopes, collective states and transitions, interacting boson approx. 80−73773
$^{\wedge}$Rb, A=79, 81, decoupled $g_{9/2}$ bands, level lifetimes and E2 transitons from (^{16}O, 2n)(^{19}F, p2n) 80−73772
^{78}Rb band struct. and level scheme from ^{64}Zn(^{16}O,np) 79−54380
^{79}Rb positive parity decoupled band, levels and J^{π} from (^{9}Be,Xγ), (^{10}B,Xγ), (^{12}C,Xγ), (^{28}Si,3pγ) 79−89223
^{83}Rb band struct., spin assignments and transitions from (^{6}Li,3n), (^{16}O,p2n), (α,2n) 80−73774
^{83}Rb high spin states, Jπ and transitions from HI and α reactions 80−105949
^{83}Rb high spin states, positive and negative parity bands from (^{6}Li, 3n), (α, 2n) 80−18178
^{85}Rb high spin states, yrast cascade, J^{π}, γ-transitions from ^{82}Se(Li,xnγ) 80−73775
Re odd mass isotopes, odd proton effects on potl. energy surfaces 77−22877
$^{\wedge}$Re, A=181,182,187, rotational struct., spin polarization 80−83016
^{181}Re states and transitions, rot. bands and Nilsson states from ^{181}Ta(^{3}He,3nγ) 79−36152
Rn, even isotopes, $K=0^+$, 0^- bands, energies, inverse moments of inertia 80−63063
^{210}Rn high spin states, decay and lifetimes, spin assignments from ^{204}Pb(^{9}Be,3n) 80−18168
^{212}Rn high spin isomers, excited core states coupled to valence protons 77−74745
^{212}Rn, high spin yrast states in N=126 isotones 79−45131
Ru, A=102, 104, collective states, J, B(E2), B(E3) via (d,d′) scatt. 77−26557
Ru, even isotopes, low lying collective states, IBA 80−27540
Ru, even-even, collective states, B(E2), branching ratios and moments, boson expansion method 80−102099
$^{\wedge}$Ru(p,p′γ), A=96, 98, 5-8 MeV, level schemes, transitions, vibr. state, mixing ratios 80−18199
^{97}Ru high spin states, band like structs., transitions from ^{88}Sr(^{12}C,3nγ) 80−73779
^{97}Ru populated in ^{88}Sr(^{13}C, 3nγ), band-like structures 80−32146
^{100}Ru, negative parity yrast band, E1 transitions polarisability, quadrupole-octupole coupled vibr. system 79−484
Ru(n,n′), near threshold energy for first 2^+ collective levels excitation, statistical model test 77−61408
^{32}S, giant dipole reson., doorway structs. in radiative capture of neutrons 79−532
^{32}S(γ,p_0), giant dipole resonance decay model, cross section and p spectrum 79−6563
^{32}S(γ,p), 17-30 MeV, giant resonance p decay channel, state transition distrib. *(Russian)* 78−89840
^{32}S(p,p), 14-45 MeV, differential cross section and spin-flip probabilities, giant resonances 80−73850
Sb isomer ratio, high spin trapping from (α,xn)(α, pn) 80−22655
Sb, neutron rich nuclei, IBM and shell model approaches, collective modes 80−78129
$^{\wedge}$Sb, A=113,115,117,119, high spin states, J^{π} assignments, decay schemes and lifetimes from Cd(^{6}Li,3n) 79−54381
$^{\wedge}$Sb, A=113-175, odd isotopes, collective props., bands and transitions from heavy ion reactions 80−68512
^{119}Sb intrinsic high spin state population, cluster DWBA anal. of ^{116}Sn(α,p) 79−67630
^{125}Sb high spin levels, gamma transition energies and intensities from ^{125}Sn, decay 80−73819
^{127}Sb states, collective neutron excitation role, spectroscopic factors and form factors from ^{30}Te(p,α) 79−67622
$^{\wedge}$Sc A=44,46,48, HF projection formalism, energy levels, static moments, EM transition probabilities 79−3083
^{43}Sc, analogue resonances and struct. props. from ^{42}Ca(p,p) at 1.2-3.0 MeV 77−6374
^{43}Sc, $J^{\pi}=19/2^-$ isomer, high-spin precursors, from ^{29}Si(^{16}O,pn) 80−57656
^{45}Sc(e,e′p), (γ,p) cross-sections determ., giant dipole reson. anal. 77−26666
nuclear collective states and giant resonances continued
^{48}Sc spin-flip isovector giant resonance, $T_>$ Gamov-Teller strength from ^{48}Ca(p,n) 80−106019
$^{\wedge}$Se, A=70,72,74, discovery of multiple collective band struct. *(Chinese)* 79 80865
$^{\wedge}$Se, A=74, 76, vibr. states and transition from dynamic deformation theory 80−73770
^{72}Se side band struct., negative parity states and transitions from ^{58}Ni(^{16}O,2p) 80−73769
^{72}Se yrast states from ^{58}Ni(^{16}O,2pγ), γ spectra, lifetimes, nuclear model predictions 77−54176
^{73}Se high-spin states via ^{70}Ge(α, nγ) at 10-18 MeV 77−10324
^{74}Se, collective excitations in the interacting boson model *(Russian)* 80−5044
^{74}Se level scheme, J^{π} assignments, bands and transitions from ^{60}Ni(^{16}O,2p), ^{64}Ni(^{12}C,2n) and ^{65}Cu(^{11}B,2n) 79−54393
^{74}Se quasi-γ bands and negative parity levels from ^{75}As(p,2nγ) 80−456
^{76}Se high spin states, bands, J^{π}, transitions and $T_{1/2}$ from ^{71}Ga(^{7}Li,2n) 80−105951
^{79}Se high spin levels, transitions, J^{π} assignments from ^{76}Ge(α,nγ) 80−459
^{25}Si(p,p), 14-45 MeV, differential cross section and spin-flip probabilities, giant resonances 80−73850
^{27}Si, levels, GDR isospin mixing via (γ,n) 28 MeV 77−74832
^{28}Si 8^+ state, level systematics and energy spectra from ^{25}Mg(^{12}C,^{9}Be) 80−42528
^{28}Si (p,p′), 14-40 MeV, low lying states, optical and statistical model anals., giant resonances 79−40894
^{28}Si dipole reson., effect of 2^+ core excitation 78−17166
^{28}Si, giant dipole reson., doorway structs. in radiative capture of neutrons 79−532
^{28}Si, giant reson. multipolarities via (α,α′), 120 MeV reactions 77−54201
^{28}Si, isoscalar giant quadrupole resonance obs. 77−307
^{28}Si, isoscalar giant quadrupole resonances, RPA calcs., E2 strength fragmentation, spectroscopic factors 80−13437
^{28}Si, microscopic model of 2_1^+ and 3_1^+ states, inelastic p scatt. test 79−26358
^{28}Si, prolate and oblate intrinsic states *(French)* 78−70482
^{28}Si, shell model and statistical spectroscopic anal. 78−29390
^{28}Si, three particle (^{12}C-α-^{12}C) struct., highly excited state calcs. *(Russian)* 79−3073
^{28}Si(^{9}Be, ^{9}Be′), 45, 60 MeV, low lying collective states, ang. distribs., DWBA double folding pot. anal. 80−78113
^{28}Si(α,α′c), c=charged particle, 150 MeV, isoscalar giant quadrupole resonance struct. 80−13438
^{28}Si(e,e′), 92 MeV, E2 strength distrib., giant quadrupole 79−36192
^{28}Si(e,e′), M2 giant resonance excitation, spin-magnetism mass depend. quenching, M1 strength reduction 78−86521
^{28}Si(γ, p), 18.1-29 MeV, giant dipole resonance, contrib. from various configs. 80−18264
^{28}Si(γ,p), 18.1-29 MeV, photoproton energy spectra, contribs. to giant dipole resonance 80−78242
^{28}Si(p, p′), isovector dipole strength excitation in giant resonance region 80−83066
^{28}Si(π^+,$\pi^{+\prime}$), 162 MeV, high spin particle-hole state excitation 79−85541
^{29}Si rot.-vibr. coupling effects, excitation spectrum and ang. distribs. from ^{28}Si(d, p) 80−57661
^{32}Si Coulomb matrix elements isospin mixing in giant dipole resonance from ^{28}Si(α,γ) 79−93507
Si(p_{pol},p_{pol}), giant multipole resonance region, optical model anal. 80−57779
Sm, even isotopes, n ang. distrib., transitions, vibr. band search from Nd(^{3}He,n) 79−63574
Sm(^{16}O, ^{18}C) A=144, 148, 152, 104 MeV, two proton transfer between pairing rot. states 77−10430
$^{\wedge}$Sm, A=148, 150, 152, 154, 156, excited states of transitional region nuclei, rot. bands *(Russian)* 80−52556
$^{\wedge}$Sm, A=148,9, structural connections, levels, bands, J^{π}, transitions and mixing ratios from Nd+^{3}He(α) 79−63576
$^{\wedge}$Sm, A=152, 154, energy levels and E2 transition rates from three-band mixing model, backbending 79−67623
$^{\wedge}$Sm(p,p′), A=144,154, 67 MeV, giant isoscalar monopole resonance excitation 79−22259
$^{\wedge}$Sm(p,p), 1 GeV, A=152, 154, dispersive effects in ground state rot. band excitation, coupled channel calcs. 79−40828
^{145}Sm ns isomers and yrast isomers, γ-transitions from (^{24}Mg,4n), (^{19}F,4n) 80−78121
^{144}Sm, isoscalar breathing mode state obs. in (α,α′) scatt. at 96 MeV 78−17086
^{144}Sm, p single particle states and pairing force calcs., high spin states 80−42522
^{144}Sm, produced in ^{100}Mo+^{48}Ca 78−37260
^{144}Sm(α,α′), 96 MeV, ang. distribs., breathing mode states, DWBA calcs. 78−50183
^{145}Sm, collective and noncollective excitations, Hamiltonian calc. for level density 79−36139
^{147}Sm, deformed $1h_{11/2}$ neutron hole states 78−86466
^{149}Sm, collective bands anal. using (α,3nγ) at 35-45 MeV 77−61342
^{150}Sm deformation, collective spectra and moments of inertia starting from nuclear force 79−17790
^{150}Sm, negative parity band crossing in even-even nuclei 78−21488
^{150}Sm, negative parity bands, coherent state model 78−89782
^{150}Sm, negative parity yrast band, E1 transitions polarisability, quadrupole-octupole coupled vibr. system 79−484
^{150}Sm, vibrational states, B(E2) branding rates and interband transitions, pairing plus quadrupole calcs. 80−78127
^{151}Sm, populated in ^{151}Pm decay, level scheme, γ-ray spectra 77−74792
^{151}Sm, struct. determ. from gamma ray spectra in (n,γ) 77−22853
^{152}Sm, giant resonance excitation by (e,e′) at 60-105 MeV, DWBA analysis *(Russian)* 78−41686
^{152}Sm ground and γ-bands, direct and multistep processes from (α,^{6}He), (p,t), (^{16}O,^{18}O) 80−102094
^{152}Sm, ground-state rot. band via electron scatt., charge distrib. 77−30475
^{152}Sm, level population by (t,α) reaction 77−67755
^{152}Sm(e,e′), 35-350 MeV, coupled channels anal., rot. band excited states, charge densities 79−3139
^{152}Sm(n,n′γ), 2.5 MeV, direct excitation of rotational levels 77−30594

nuclear collective states and giant resonances continued
^{152}Sm(n,n'γ), 2.75 MeV, direct excitation of some collective levels 77−26720
^{152}Sm(n,n'γ), 2.5 MeV, rot. level direct excit. 77−14127
^{153}Sm, spin, parity, deduced levels, using ^{150}Nd(α,n), comparison with particle-rotor model 79−58999
^{154}Sm (p,p')^{154}Sm, 1 GeV, giant reson. excit., Glauber calc. 77−82891
^{154}Sm, giant multipole reson. fragmentation among two-phonon states 80−78238
^{154}Sm giant multipole resonance fragmentation among two-phonon states 80−18260
^{154}Sm(p,p'), 35 MeV, ground state rot. band and multipole moment 80−32178
^{154}Sm(p,p'), 1 GeV, possibility of observing giant resonances with high multipolarities *(Russian)* 78−78350
Sn, deep h-le state fragmentation, strength functions, giant resonances, quasiparticle phonon model 80−37320
Sn, even isotopes, collective states and transitions from simple phenomenological model 80−73787
Sn, single closed shell even mass nuclei, collective bands, spin, parity, from Cd(α,2nγ), γ meas. 78−54719
^{A}Sn, (A=112, 114, 116, 118, 120, 122), so-called two phonon states, quasiparticle shell model calcs. 79−89251
^{A}Sn, A=106-108, yrast levels and transitions from ^{54}Fe(^{58}Ni, X) 80−105957
^{A}Sn, A=108 to 126, quasi-particle coupling to pairing and quadrupole vibrs. 79−54373
^{A}Sn, A=112, 114, 116, 118, positive parity band heads, excitation energies and transitions from Cd(α, 2nγ) 79−45136
^{A}Sn, A=112-124 even isotopes, 0^+ state collectivity, E0 and E2 transition rates 80−73785
^{A}Sn(n,n'), A=116, 118, 120, 122, 11 MeV, octupole vibr. states, diff. cross section, deformation length, DWBA anal. 80−102092
^{A}Sn(p,p'), A=115, 117, 119, 18 MeV, state spin assignment, particle-vibr. coupling 80−32160
^{112}Sn 6^+ isomeric state g-factor and relaxation time from Cd(α,2nγ) 80−73794
^{116}Sn, collective states and E0, E2 transition rates 79−17787
^{116}Sn particle-hole states, strength decoupling form giant dipole resonance, Gaussian force, δ-force diagonalisation 78−25125
^{116}Sn(^{16}O,^{16}O) 48 MeV, collective states, E2, E0 transition probabilities, halflife, branching ratios 80−18172
^{116}Sn(α,α'), 96, 129 MeV, giant resonance excitation, isoscalar breathing mode state, nuclear incompressibility 80−68620
^{116}Sn(e,e'), 40-110 MeV, vibr. nuclei, branching ratios 77−6356
^{116}Sn(p,p'), 800 MeV, high energy octupole giant resonance, ang. distribs. 80−86879
^{117}Sn, substructure in radiative strength function using quasiparticle-phonon nucl. model 79−40901
^{118}Sn(^{6}Li,^{6}Li'), 153 MeV, isoscalar giant quadrupole resonances 80−13440
^{119}Sn, substructure in radiative strength function using quasiparticle-phonon nucl. model 79−40901
^{120}Sn(γ,n), giant mag. dipole resonance location, photoneutron polarisation method 80−37357
^{120}Sn, giant multipole reson. fragmentation over two-phonon states 78−575
^{120}Sn(^{3}He,^{3}He), 130 MeV, giant reson. excitation, DWBA anal. 79−89319
^{124}Sn, electron excitation of giant multipolar resonances *(Russian)* 78−8802
^{124}Sn(e,e) ^{150,225}MeV giant multipole resonances, positions and half widths *(Russian)* 78−78349
^{132}Sn, doubly magic nucleus, level scheme 78−54668
Sn(α,3n), 16-38 MeV, Te isomer ratio, high spin trapping 80−22655
Sr, high spin negative parity states from cluster vibration coupling model 79−75823
^{A}Sr, A=81, 83, yrast and high spin states of neutron deficient isotopes from Kr(α,xn) 80−73776
^{A}Sr, A=98, 100 rot. struct. sudden onset, gamma transitions from Rb decay 80−73777
^{83}Sr high spin states, J^π and de-excitation from Kr(α,xn) 80−42516
^{84}Sr quasi-γ bands and negative parity levels from ^{85}Rb(p,2nγ) 80−456
^{88}Sr(γ,γ), 14 MeV, highly excited spin-1 resonances, spin and radiative widths 80−86876
^{88}Sr(n,n'), 11 MeV, octupole vibr. states, diff. cross section, deformation length, DWBA anal. 80−102092
^{98}Sr very low lying 0^+ state, shape coexistence bands, $T_{1/2}$, transitions from ^{98}Rb decay 80−78148
^{100}Sr ground state rot. band transitions, deformations and lifetimes from ^{100}Rb β-decay 79−93550
^{166}Ta, isotope identification in ^{159}Tb(^{16}O,9n) reaction, half-life and decay scheme 77−79331
^{173}Ta, levels, rot. parameters, γ-mixing 77−34248
^{176}Ta, decay of four-particle isomer 78−70481
^{177}Ta, rotational struct., spin polarization 80−83016
^{178}Ta level properties, rot. bands, transitions and level lifetimes from ^{176}Lu(α, 2n), ^{178}Hf(d, 2n), ^{178}Hf(p, n) 79−36158
^{181}Ta, 136 keV level, g-factor meas. 79−6387
^{181}Ta, ground state rotational band, electroexcitation 78−33168
^{181}Ta(^{84}Kr,^{84}Kr'γ), 348 MeV, ground-state rotational band obs. 77−6197
^{181}Ta(e,e'), 79-119 MeV, DWBA anal., giant multipole resonance parameters 77−30558
^{181}Ta(e,e'), giant monopole and quadrupole resonances excitation 78−17184
^{181}Ta(γ,X), 3-30 MeV, photoabsorption cross section, giant dipole resonances 80−78254
^{181}Ta(γ,γ')^{181}Ta, elastic and Raman scatt. at 8.5-11.4 MeV, GDR parameters 78−587
^{182}Ta, configuration mixing in positive parity states 77−22854
^{182}Ta deformed odd-odd nucleus, γ transition probabilities, rot. band mixing 77−61375
^{182}Ta rot. bands, bandheads and decay data from ^{181}Ta(n,γ) 79−93491
^{185}Ta single proton states and rot. bands, J^π from ^{186}W(t,α),pol.t 80−91130
^{A}Tb, A=147, 148, high spin particle-hole states, octupole M2/E3 isomers from ^{151}Eu(α,xn) 80−18171
^{A}Tb, A=149, 151, 153, 155, 157, prop. anal. on function of nuclear shape 79−75828
^{149}Tb, high spin states obs. 80−18158
nuclear collective states and giant resonances continued
^{153}Tb excited states from Eu(α, xn), rot. bands, spin, parity, γ spectra 78−62552
^{153}Tb, negative-parity bands 78−93937
^{155}Tb, excited state lifetimes 79−6494
^{156}Tb, orientation in Gd matrix, γ-ray ang. distrib. anisotropy meas. 79−59031
^{159}Tb(γ,γ') 8.5-11.4 MeV, elastic and Raman scatt., giant reson. struct. 77−34284
Tc, high spin negative parity states from cluster vibration coupling model 79−75823
^{93}Tc, J=17/2 doublet, parity mixing, weak NN interaction 80−73791
^{95}Tc, energy levels from ^{95}Mo(p, nγ)^{95}Tc 80−37372
^{95}Tc, high momentum states band structs. obs. in (α,2nγ) 78−33109
^{96}Tc, high spin states, γ-energy, intensity, coincidence, ang. distrib. and electron conversion from ^{93}Nb(α,n) 80−52554
^{97}Tc high spin states, spins and transitions from ^{94}Zr(^{6}Li,3nγ) 80−73780
Te evaporation residues from (^{12}C,xnγ), and (^{40}Ar,xnγ), shell effects at high spin 79−22165
Te isomer ratio, high spin trapping from Sn(α,3n) 80−22655
Te, multipole-multipole interaction in particle-particle channel 79−6364
Te odd neutron isotopes, microscopic struct. of low lying collective excited states *(Japanese)* 79−3065
^{A}Te, A=117, 119, 121, collective excitations, high spin states and transitions from (α, Zn)(d, Zn)(^{3}He, 3n) 80−13346
^{A}Te, A=117,119,121, ΔJ=1 band structures on ns isomeric states 79−54382
^{A}Te, A=122,124,126 yrast band double backbending, possible mechanisms *(Chinese)* 80−99120
^{118}Te, produced in ^{82}Se+^{40}Ar, γ-ray multiplicity spectra, nuclear shape at high angular momentum 78−37260
^{120}Te quasi-rot. band based on proton 4p-2h state, level scheme, transitions from ^{118}Sn(α,2nγ) 80−78119
^{124}Te, giant multipole reson. fragmentation over two-phonon states in spherical nuclei 78−575
^{125}Te low lying negative parity high spin states multistep induced population from (d,t)(^{3}He,α) 80−57657
^{126}Te, M1, giant resonance and radiative strength functions 80−57731
^{132}Te from fission, 10^+ isomeric state, J^π from deexcitation pattern, half life 80−460
Th, even isotopes, $K=0^+$, 0^- bands, energies, inverse moments of inertia 80−63063
^{A}Th, A=231, 233, vibr. band systematics, excitation energies and rot. parameters 79−36137
^{231}Th, asymmetrically deformed, rot. bands from ^{230}Th (n,γ) 79−3068
^{231}Th excited states and bands, spins, γ-transitions from ^{230}Th(n,γ) 80−57699
^{231}Th, rotational band level diagram from α-decay and γ-transitions 80−18156
^{232}Th, giant resonance in total photoabsorpt. cross-section 77−6347
^{232}Th, vibr. states, Coulomb excitation 79−9432
^{232}Th(α,α'), 120 MeV, isoscalar giant resonances, DWBA anal. 80−42621
^{232}Th(γ,X) 5-18.3 MeV, photoneutron and photofission cross sections, giant resonance and deformations 80−68712
^{232}Th(n,f), 1.35-5.3 MeV, yields and kinetic energies, vibrational states 79−45307
^{232}Th(n,f), cross section up to 6 MeV, rotational states obs. 77−23161
^{232}Th(n,f) cross-section meas., rotational bands 77−26803
^{232}Th(p,p'), 35 MeV, ground state rot. band and multipole moment 80−32178
^{233}Th, excited levels, using thermal and average reson. neutron capture in ^{232}Th 79−45166
^{233}Th, vibrational states determ. following (n,e$^-$) 77−30514
^{233}Th(α,α') 120 MeV, isoscalar giant quadrupole resonance fission decay channel inhibition 79−54419
Ti, A=45-51 odd isotopes, spectra and EM transitions, spin assignments, rot. bands 77−74793
Ti, A=51, 52, mean lifetimes of yrast states populated in ^{48}Ca+Li 77−2942
Ti(^{12,13}C,X) 45, 46 MeV, particle-gamma coincidences, isotope assignment for yrast spectroscopy 80−68593
^{43}Ti positive parity states, mean lifetimes, quasirotational band from ^{40}Ca(α,n) 20 MeV 79−6415
^{44}Ti, yrast states as α-particle cluster states 78−33114
^{44}Ti* band crossing search, Hauser-Feshbach calcs. for ^{28}Si(^{16}O,α) 79−22174
^{46}Ti (γ,N), 12-25 MeV, isospin splitting in giant dipole resonance 79−45152
^{46}Ti(e,e'p), (γ,p) cross-sections determ., giant dipole reson. anal. 77−26666
^{48}Ti, (A+2)particles-2 holes excitations, interaction renormalisation 78−29375
^{48}Ti high spin states, γ-decay, J^π assignments, lifetimes from ^{45}Sc(α,pγ) 80−13356
^{48}Ti+^{16}O, anisotropy of yrast γ-transmissions 79−93650
^{48}Ti(γ,n), 15-27.5 MeV, giant dipole resonance splitting, dynamic collective model 80−57755
^{50}Ti high spin states, transitions and J^π values from ^{48}Ca(α,Znγ) 80−455
^{50}Ti(γ,X), photoneutron and photoproton cross sections, giant dipole resonance isospin splitting 80−13442
^{50}Ti(γ,n_0), cross sections in giant dipole reson. energy range 79−89286
^{50}Ti(γ,n), cross sections in giant dipole reson. energy range 79−89286
Tl, A=195, 197, rot. bands, high spin states 78−62476
Tl isotopes, A=184-197, β^+-decay, single particle and collective degrees of freedom 77−22956
Tl, odd isotopes, $9/2^-$ level excitation energy, semi-empiricle method 77−22844
Tl odd mass isotopes, odd proton effects on potl. energy surfaces 77−22877
Tl odd mass isotopes, particle rotor descriptions 77−22914
Tl odd mass isotopes, statistical anal. of levels 77−22842
Tl region, particle rotor model for doubly odd transitional nuclei 79−13223
^{192}Tl high spin band struct. and transitions, isomeric state from ^{181}Ta(^{16,18}O,xnγ) 80−47353
^{194}Tl high spin states, excitation functions, $I^\pi=8^-$ isomeric state from ^{181}Ta(^{18}O,5n) 80−32163
^{196}Tl high spin states, γ-decay and rot. structs. from ^{197}Au(α,5n), ^{194}Pt(^{6}Li,4n) 79−440

nuclear collective states and giant resonances continued
^{197}Tl, diagonalisation of collective quadrupole Hamiltonian 77−6221
^{197}Tl, level scheme determ. from (^{3}He,3nγ) 77−22840
^{198}Tl rotational structure, studied via ^{197}Au(α,3n) using in beam γ-ray spectroscopy 77−54130
^{201}Tl core-coupled states, studied via (p,t) reaction 77−54212
^{203}Tl core-coupled states, studied via (p,t) reaction 77−54212
^{167}Tm, energy level scheme from ^{165}Ho(α,2nγ) *(German)* 80−68576
^{167}Tm, levels and transitions from ^{165}Ho(α,2n) 80−73766
^{167}Tm rotational bands, J^{π}, γ-transitions and branching ratios from ^{165}Ho(α,2nγ) 80−86781
^{169}Tm, studied via ^{169}Tm(^{32}S,^{32}S′γ), EM props. of ground state rot. band 78−8726
^{173}Tm level and band struct., spin assignments, ang. distribs. from ^{176}Yb(p,α), 16 MeV, ^{173}Tm level and band struct., spin assignments, ang. distribs. 79−474
^{175}Tm single proton states, rot. bands, J^{π} assignments from ^{176}Yb(t,α), pol. t 80−452
U, even isotopes, $K=0^{+}$, 0^{-} bands, energies, inverse moments of inertia 80−63063
^U A=235, 239, vibr. band systematics, excitation energies and rot. parameters 79−36137
^U, A=236, 238, strength function of β-transitions, probability of delayed fission 80−22764
^U, A=236,238, fission isomer rot. spectra $I^{2}(I+1)^{2}$ correction 80−18229
^U(γ,X), A=235, 236, 238, 5-18.3 MeV, photoneutron and photofission cross sections, giant resonance and deformations 80−68712
^{230}U decay chain, γ-ray single and coincidence meas., internal conversion spectra obs. 77−6319
^{232}U high spin states and ground state rot. band from ^{232}Th(α,4nγ) 80−47349
^{232}U→^{212}Pb decay chain, obs. of collective states fed by weak α-transitions 78−8786
^{233}U, excited octupole states in odd U isotopes, vibr. states, deuteron scatt., 13.1 MeV 77−46099
^{233}U levels, bandheads, total α-branching and transitions from ^{237}Pu α-decay 79−93516
^{233}U(d,d′), multipolarities and reduced transition probabilities 78−17215
^{235}U, excited octupole states in odd U isotopes, vibr. states, deuteron scatt., 13.1 MeV 77−46099
^{235}U, giant resonance in total photoabsorpt. cross-section 77−6347
^{235}U vibrational and single particle states from ^{234}U(n,γ) 79−36123
^{235}U(d,d′), 13.1 MeV multipolarities and reduced transition probabilities 78−17215
^{236}U, giant E2 isoscalar resonance determ. 80−27607
^{236}U, pairing energy gap determ. from ^{235}U(n,f) 79−80962
^{236}U shape isomer, rot. band and const. via ^{235}U(d,p) 12 MeV 77−34208
^{237}U levels, bands and J^{π} assignments, n binding energy from ^{236}U(n,γ) 80−5041
^{238}U (^{6}Li, ^{6}Li′f), 150 MeV, isoscalar giant resonance struct. 79−89275
^{238}U collective and deformation props., general collective model 80−86827
^{238}U deformed even-even nucleus, rot. vibr. band excitation, classical limit S-matrix 79−3067
^{238}U, giant resonance in total photoabsorpt. cross section 77−6347
^{238}U, ground rotational band level energies calc. 78−45996
^{238}U, microscopic calc. of high-spin rot. states 78−8730
^{238}U, negative parity band crossing in even-even nuclei 78−21488
^{238}U, negative parity bands, coherent state model 78−89782
^{238}U, neutron elastic and inelastic ang. distribs., 1.1 to 3.1 MeV, to ground state rot. band 77−26717
^{238}U, struct. in sequence of s-wave levels 77−22857
^{238}U(e,α), 40 MeV, isoscalar E2 giant resonance α particle search 79−9549
^{238}U(e,α)e′^{234}Th cross section, giant quadrupole resonance 78−58262
^{238}U(e,e′), 87.5 MeV, deformed fissionable nucleus, giant multipole resonances and isovector states 80−42612
^{238}U(e,e′α), 13.1 MeV, cross section in giant quadrupole resonance region 79−6573
^{238}U(e,e′f), 5.5-28.3 MeV, E2 isoscalar giant resonance in photofission cross section 79−512
^{238}U(n,n′), 0.3 to 3.0 MeV, ground state rot. band excitation 77−23085
^{238}U(p,p′), 22 MeV, rot. band, multipole deformation parameters from coupled channel anal. 80−13369
^{238}U(p,p′), 35 MeV, ground state rot. band and multipole moment 80−32178
^{239}U, population in direct and collective neutron capture by ellipsoidally deformed nucleus 78−94001
uncorrelated target, optical pot. unitary content, DWIA and Glauber theory from (α,α)(α,γ) 80−105947
^{48}V, $K^{\pi}=4^{-}$ rotational band 78−12944
^{48}V, low-lying positive parity states, deformed config. mixing model 77−6198
^{48}V, odd-parity rotational band structure 77−46102
^{51}V, isospin effects in GDR region 78−78344
^{51}V(α,p_0), differential cross section in giant dipole resonance region from (e,p_0) 79−63655
^{51}V(e,p_0), 15-26 MeV, differential cross section in giant dipole resonance region 79−63655
^{52}V, mean lifetimes of yrast states populated in ^{48}Ca+Li 77−2942
W, A=174, 175, from (^{16}O, xn), γ continuum spectra, yrast cascades, dipole component 78−54794
W, A=178, 180, 182, high spin states, microscopic-macroscopic model 79−438
W, A=182, 180, 178, pair excitations via (p,t) 21 MeV reaction 77−88032
W high spin states, A=172, 174, 176, from Dy(^{16}O, xn), decoupled quasiparticle bands, backbending 78−50199
W isotopes, A=172-176, high spin states and backbending 77−34204
W, produced in (^{16}O,xn) 78−37371
^W (^{84}Kr,^{84}Kr′γ) A=183, 184, 186, 340 MeV, Coulomb excitation, energy levels and bands 79−63577
^W, A=170-182, even isotopes, yrast states, spectra and quad. moments, variation formulation 80−99119
^W, A=172-175, bands and backbending, $i_{13/2}$ neutron decoupling from Dy(^{16}O,xn) 80−9212
^W, A=173, 175, high-spin states, single-particle structure 78−93922
^W, A=174, 175 quasicontinuum γ-rays yrast cascade dipole component, moment of inertia from Dy(^{16}O, xnγ) 80−47424

nuclear collective states and giant resonances continued
^{170}W, nonspherical nucleus after backbending, crit. spin rel. to angular vel., bands *(Russian)* 79−75822
^{174}W, decoupled two-quasiparticle bands, backbending 78−4890
^{178}W high spin rot. levels and bands from ^{177}Hf(α,3nγ) 79−26359
^{178}W high spin states, yrast bands and backbending from ^{170}Er(^{12}C,4n) 80−13352
^{179}W, backbending, high spin isomer decay 78−45997
^{180}W ground and $K=2^{-}$ octupole band ang. momenta coupling, lifetimes from ^{181}Ta(p,2nγ) 80−9214
^{180}W, $K=2^{-}$ octupole alignment, ground-band angular momenta 78−78237
^{180}W octupole vibr. states, J^{π} and transitions from ^{180}Re decay 80−83024
^{180}W, rot. and vibr. bands, γ-vibr. band, metastable state half life from ^{181}Ta(p,2nγ) 79−54378
^{181}W levels (neutron and collective) and J^{π}, ang. distribs. from ^{183}W(p,t) 80−78160
^{182}W high spin states, J assignments and mixing ratios from ^{182}Re isomer decay 80−42593
^{183}W(α,α′), 15 MeV, level and band Coulomb excitation, B(E2) values 80−32233
^{184}W, quadrupole mom. of second 2^{+} state 77−30490
W(n,n′γ), 2.75 MeV, direct excitation of some collective levels 77−26720
Xe isotopes, A=118, 120, 122, level schemes and quasi-rotational bands 77−22839
Xe isotopes, collective states, soln. of Schrodinger eqn. with Bohr Hamiltonian 77−67695
Xe isotopes, microscopic dynamic calc. of collective states 78−17075
Xe, odd neutron isotopes, microscopic struct. of low lying collective excited states *(Japanese)* 79−3065
Xe-Nd region, microscopic anal. of core deform. 78−74303
^{116}Xe level scheme and yrast band, in-beam γ-study from ^{106}Cd(^{12}C, 2n) 80−13360
^{124}Xe, energy level scheme, ^{124}Cs decay 78−13033
^{125}Xe $11/2^{-}\rightarrow 9/2^{-}$ transition in odd parity band from ^{124}Te(α, 3n) 80−9203
^{125}Xe odd and even parity band structs., level lifetimes from ^{125}Te(^{3}He,3nγ) 80−27533
^{128}Xe, collective excitations obs. following decay of ^{128}Cs and ^{128}I 79−45143
^{133}Xe, semi-microscopic anal. by generalised vibrational intensity and selection rules and diagonalisation 77−2901
^{89}Y, giant reson. pionic excitation 80−73834
^{89}Y high spin states and decay scheme from ^{87}Rb(α,2nγ) 80−32166
^{89}Y(e,e′), 92.5 MeV, giant reson. and bound collective states 78−13070
^{89}Y(p,γ_0)^{90}Zr, 14-27 MeV, E_2 and E_3 radiation anal. in direct-semidirect model 77−38266
^{89}Y(π, π^{1}), 163, 240 MeV, giant resonance pionic excitation 80−52561
Yb, A=163, 165, 167, backbending of rotational bands 78−8728
Yb, A=172,174,176, Mossbauer effect in Yb cpds., appl. of in-beam implantation method 78−25372
^Yb, (A=168, 170), angular momentum fluctuation energy in the cranking model 79−89254
^Yb, A=160, 161, backbending, multiple band crossing freq. and alignment from Sm(^{16}O,3n) 80−47347
^Yb, A=161, 162, 166, yrast cascade dipole component from Sm(^{16}O,4n) 80−9266
^Yb, A=163, 165 level schemes and backbending behaviour of neutron deficient isotopes 79−40836
^Yb, A=164, 166, high spin yrast states and transitions from Gd(^{13}C,5n) 80−9208
^Yb, A=166, 168, 170, backbending and moment of inertia in HFB cranking method 80−42521
^Yb, A=166,168,170, Yrast band investigation, self consistent cranking model anal. 79−6367
^Yb, A=168, 170, approximate ang. momentum projection from cranked HFB wave functions, yrast energies 79−30776
^Yb(^{16}O,^{16}O′γ), A=168-176, even nuclei, 58-62 MeV, Coulomb excitation, vibr. and rot. states 80−32162
^Yb(^{40}Ca,^{40}Ca′), A=170,172,174, 168 MeV, rotational g-factor meas. using transient field interactions 80−18193
^{160}Yb double backbending and rot. states, HFB cranking model anal. 80−32155
^{160}Yb yrast levels, 2nd and 3rd backbending, cranked HFB calcs. 80−63064
^{160}Yb, yrast line irregularity, backbending effect 79−30777
^{161}Yb from (^{16}O, xn), γ continuum spectra, yrast cascades, dipole component 78−54794
^{161}Yb, produced in (^{16}O, xn), γ-ray spectra, dipole moment in yrast cascade 78−37371
^{161}Yb quasicontinuum γ-rays yrast cascade dipole component, moment of inertia from Sm (^{16}O, xnγ) 80−47424
^{162}Yb high spin states, HF self consistent calc. with Skyrme interaction, cranking approach 80−9210
^{162}Yb high spin states with Skyrme interaction, cranked Hartree-Fock calcs. 79−13189
^{162}Yb rot. states, HF and HFB self consistent calc. with Skyrme interaction 80−22662
^{164}Yb, levels populated in ^{164}Lu decay, band struct. 77−82805
^{166}Yb, high spin state anomaly, backbending 79−22173
^{166}Yb multiple band crossing, (gSS′S″S‴) system gamma correlation patterns 80−106008
^{167}Yb $i_{13/2}$ band, spin alignment in the particle-rotor and cranking models 80−42536
^{168}Yb low lying collective excitation energies calcs. at high angular momenta 79−13190
^{168}Yb, low lying spectra and EM transitions, level struct. in quasirotational bands 79−36141
^{168}Yb, microscopic calc. of high-spin rot. states 78−8730
^{168}Yb, two-fluid model of nuclear rotations and surface vibrations, energy levels 78−62474
^{169}Yb, E2 transitions in rot. bands, partial probability calcs. 79−75835
^{170}Yb negative parity yrast band, rot. aligned n, deformation coupled bandhead from Er(α,xn) 79−93489
^{171}Yb, EM transitions, mixing of states having different quantum numbers 79−6493
^{172}Yb levels, bands, J^{π} and $T_{1/2}$ from ^{170}Er(α,2n) 80−91127
^{172}Yb octupole band, particle vibrational alignment from ^{170}Er (α,2n) 80−13351

nuclear collective states and giant resonances continued
^{174}Yb, pairing vibr. character of 1494 keV 0^+ state via ^{172}Yb(t,p), 15 MeV 77−18572
^{175}Yb level structure, band structure and J^π assignments from ^{176}Yb(d,t) and ^{174}Yb(d,p) 79−40850
^{176}Yb(p,p′), 35 MeV, ground state rot. band and multipole moment 80−32178
^{177}Yb level structure, band structure and J^π assignments from ^{176}Yb(d,p) 79−40850
Zn, A=64, 66, 68 transition charge density, and radius to collective states via (e,e′) 77−50077
Zn, doubly even nuclei, quasiparticle+phonon model calcs. 78−41626
Zn, even isotopes, effect of particle-vibr. coupling in nucl. struct. 78−12940
^{A}Zn(α, α'), A=64, 66, 129 MeV, isoscalar giant monopole resonances, nuclear incompressibility 80−83083
^{62}Zn, band mixing HF model, struct. and electromag. transitions 78−54676
^{62}Zn yrast states, possible decay scheme from ^{40}Ca(^{28}Si,α2pγ) 79−54379
^{64}Zn, electroexcitation of giant multipole reson. *(Russian)* 78−58264
^{64}Zn, electron excitation of giant multipolar resonances *(Russian)* 78−8802
^{64}Zn, γ-ray spectroscopy and role of $g_{9/2}$ orbital 78−33142
^{64}Zn high spin states, J^π, $T_{1/2}$, γ-decays from (α,nγ), (^{11}B,p2nγ) 80−73767
^{64}Zn, quasi-rotational states populated in ^{51}V(^{16}O,p2nγ), lifetimes and effective population times 78−17140
^{64}Zn, struct. of quasi-bands from (α,nγ) and (^{11}B,p2nγ) 78−70424
^{64}Zn(γ, n)^{63}Zn, giant dipole reson. isospin splitting, reaction cross section *(Russian)* 78−46040
^{64}Zn(γ,n), photoneutron energy spectra and intermediate struct. of the giant dipole reson. *(Russian)* 79−22270
^{65}Zn, γ-ray spectroscopy and role of $g_{9/2}$ orbital 78−33142
^{66}Zn negative parity high spin states, spin and lifetimes from HI reactions 80−73768
^{67}Zn, role of cluster-vibr., coupling in struct. of negative parity states 77−34206
^{68}Zn low lying collective states populated in ^{67}Zn(d,p), spectroscopic factors 77−61433
^{70}Zn excitation energies, B(E2) values, extended generator coordinate method 77−6203
Zr, high spin negative parity states from cluster vibration coupling model 79−75823
^{85}Zr yrast and high spin states of neutron deficient isotopes from Sr(α,xn) 80−73776
^{89}Zr high spin states, J values, γ ang. distrib. from (α, 2nγ) and (α, nγ) 79−89217
^{90}Zr (p, p′), 57.5 MeV, polarised p, low lying level and giant resonance excitation 79−36157
^{90}Zr (p,p′), 0.8 GeV, low energy giant octupole resonance excitation, deformation length 79−93593
^{90}Zr, giant multipole reson. fragmentation over two-phonon states 78−575
^{90}Zr, giant resonance levels, study by proton and electron scatt. *(Russian)* 79−3127
^{90}Zr, mag. quadrupole resonance, M2 strength distrib., quasiparticle-phonon model 79−75947
^{90}Zr, neutron absorpt. cross section, optical pot. imag. part 79−9536
^{90}Zr neutron absorption, multipole giant resonance contrib. to optical pot. imaginary part 80−18263
^{90}Zr, static and transition densities, self consistent RPA theory test in fast (p,p), (e,e) scatt. *(Russian)* 79−49604
^{90}Zr+^{12}C(^{14}N), giant resonances in inelastic scatt. 78−62564
^{90}Zr(^{3}He,^{3}He′), 108.5 MeV, giant monopole resonance, DWBA anal. 79−71828
^{90}Zr(^{3}He,^{3}He), 130 MeV, giant reson. excitation, DWBA anal. 79−89319
^{90}Zr(^{3}He,t)^{90}Nb, 130 MeV, giant Gamow-Teller resonance, T=4, T=5 components 78−46081
^{90}Zr(^{3}He,t)^{90}Nb, 80 MeV, Gamow-Teller M1 state excitation 78−50184
^{90}Zr(^{6}Li,^{6}Li′), 153 MeV, isoscalar giant quadrupole resonances 80−13440
^{90}Zr(^{6}Li,^{6}Li′), 74 MeV, excitation of giant quadrupole reson. 78−8854
^{90}Zr(α,α'), 96, 129 MeV, giant resonance excitation, isoscalar breathing mode state, nuclear incompressibility 80−68620
^{90}Zr(e,e′), 2^- giant resonance twist mode excitation, B(M2) values, form factors 80−78246
^{90}Zr(e,e′), M2 giant resonance excitation, spin-magnetism mass depend. quenching, M1 strength reduction 78−86521
^{90}Zr(γ,α) statistical and pre-equilibrium cross sections and multipolarities from (e,α) 80−68646
^{90}Zr(n,X), 10-20 MeV, multipole giant resonance contrib. to optical pot. imaginary part 80−78241
^{90}Zr(n,n′), 11 MeV, octupole vibr. states, diff. cross section, deformation length, DWBA anal. 80−102092
^{90}Zr(π,π'), 226 MeV, giant reson. examination 80−73871
^{90}Zr(π^+,$\pi^{+\prime}$), 241 and 163 MeV, giant resonance studies 79−85512
^{96}Zr, shape transition microscopic study using shell model 79−40835
^{98}Zr, shape transition microscopic study using shell model 79−40835

nuclear coupling, molecular *see molecular nuclear coupling*

nuclear cranking model
^{298}114, high spin pot. energy surfaces, fission barrier, α-, γ-decay half lives, yrast spectrum 80−73764
A=12-208, adiabatic TDHF approx. isoscalar quadrupole collective motion, cranking mass 80−68507
A=40-80, yrast props. and high spin isomers, cranking plus Strutinsky formalism 80−32152
actinide nuclei, cranking model, collective inertia parameters 80−57665
adiabatic, validity for appl. to fission 77−18517
adiabatic TDHF approx., mass parameters, single collective variable, theoretical aspects 80−73765
angular momentum depend. cranked HFB inertia parameter, high spin states 80−42524
back bending, Hartree-Fock Bogolyubov approach, cranking method 78−58228
back bending effect, Hartree-Fock-Bogolyubov treatment of cranking method, yrast states 78−82264
backbending associated with alignment of quasiparticle momenta 78−33112
backbending nuclei, HFB cranking wave functions 80−83049
nuclear cranking model continued
band crossing, of particle-rotor model 79−17833
band crossing anal. 77−6270
band crossing anomalies, large angular momentum fluctuation 80−73815
band crossing anomalies in cranking model 78−25127
band crossing region, self consistent cranking model discontinuities and ang. momentum fluctuations 79−482
collective motion at large amplitudes and finite velocities 77−18449
coupled bands in even-even nuclei in RPA approach 80−32143
cranked harmonic oscillator, complete soln. 79−67690
cranked harmonic oscillator pot., self-consistent condition 78−17122
cranked Hartree-Fock-Bogoliubov wave functions, ang. momentum distribs. at band crossings 78−93956
cranked HFB treatment of pairing force, back-bending model 77−278
cranking, microscopic derivation for nuclear systems with large angular momentum 79−40829
cranking calculations with self-consistent symmetries in a triaxial basis 79−54374
cranking model, perturbation theory and Dalgarno Lewis method 77−45640
EM properties of deformed nuclei, approximate projection technique 79−93510
giant resonance description, RPA, GCM, and semiclassical theories unification 78−54671
harmonic oscillators, cranked, in coordinate space 78−25135
Hartree Fock Bogoliubov method, high nuclear spins, quadrupole pairing, moment of inertia, yrast traps 78−54712
Hartree-Fock-Bogolyubov approach to nuclear band description *(Russian)* 79−3107
HF calcs. of gyromagnetic ratio and moment of inertia 79−93482
(HI,xn), cranking model for E1 polarization charge in rotating nuclei 79−85405
high spin rot. motion, TDHF cranking model and RPA descript. 80−102091
high spin states and band coupling, theory and heavy ion expts. *(Russian)* 80−18160
i13/2 shell, particle-rotor model exact soln., cranking model connection 79−93485
Inglis cranking formula, temp. dependent mass parameter behaviour 80−22714
lagrange multipliers in the cranked harmonic oscillator model 79−45190
moment of inertia, particle-number-projected BCS wavefunctions 77−22830
N=82 region, high spin isomers, cranked HF calcs., deformation shapes, excitation energies 80−99121
N=82 region, high spin isomers, deformation energy surface, shape constrained cranked HF theory 80−57666
nuclear inertia for excited states, adiabatic cranking model calcs. 80−9216
nuclear inertia in fission and heavy ion reacts. 78−41656
nuclear struct. calcs. *(Rumanian)* 77−26602
odd-A 1-p shell nuclei, projected HF method 77−6207
pairing interactions at high spin 77−54162
quadrupole pairing forces influence on backbending, cranked Hartree Fock Bogoliubov approach 78−29401
rare earth nuclei, cranking model, collective inertia parameters 80−57665
rare-earth nuclei, inertial functions of Bohr's collective Hamiltonian 77−61359
rotating nuclei, current distribs., cranked HF model 80−63059
rotating nuclei, M1 and E1 transitions within and between bands, cranking model 80−494
rotating nuclei, selfconsistency conditions in cranked harmonic oscillator model, HF calcs. 78−58239
rotational current and velocity fields, transverse electroexcitation of rot. states 77−10342
rotational nuclei, high-spin, variable moment of inertia model, microscopic-macroscopic approach 80−63058
S and ground band interaction in cranked HFB model 80−95299
Schrodinger eqn., all orders solution 77−82838
self consistent cranking model, anomalies 79−26382
self consistent cranking model with RPA corrections, high spin states, conservation laws 77−14047
spontaneous fission mass parameters, cranking and hydrodynamic models, deformation depend. *(Russian)* 80−13511
two rotation regimes, cranked harmonic oscillator soln. 80−22657
wave function, investigation w.r.t. angular momentum 79−483
wave functions, matrix elements, cranked deformed harmonic oscillator, high spin nucleus appl. 78−25131
Woods-Saxon potential spectrum, pairing force strength, Nilsson model comparison 80−57704
yrast bands of negative parity, gapless superconductivity, exactly solvable R(8) model 77−14015
yrast region of rapidly rotating nuclei, instability toward nucleon emission 77−88027
yrast spectroscopy, nuclei with high angular momentum, review 78−50063
yrast-yrare interaction in $i_{13/2}$ shell, oscillating behaviour 79−93481
^{158}Er, moment of inertia anomaly at ang. momentum of 26 to 30 78−62496
^{162}Er energy spectrum anomalies, rot. bands, cranking model with Hartree-Fock-Bogolubov theory 79−3064
^{A}Hf, A=172-180, prolate isotopes, Yrast traps using cranked modified oscillator pot. 78−93923
^{174}Hf, angular momentum fluctuation energy in the cranking model 79−89254
^{174}Hf, approximate ang. momentum projection from cranked HFB wave functions, yrast energies 79−30776
^{176}Hf yrast traps, cranking Hartree Fock Bogoliubov calcs. 78−25100
^{24}Mg, molecular configuration 79−13193
^{24}Mg, triaxial nuclei rots., extended cranked shape consistent oscillator model 80−102133
^{24}Mg yrast line, Strutinsky type cranking calc., pairing correlation inclusion 80−13355
^{20}Ne, moment of inertia from cranked HF method 80−102098
^{20}Ne rotational behaviour from Strutinsky method 77−2894
^{20}Ne, rotational moment of inertia, cranked HF formalism with Skyrme force 77−30477
^{240}Pu, moments of inertia of fissioning isomers 78−74299
^{32}S, cranked Hartree-Fock-Bogolyubov calcs., p,n pairing correlations 79−6460

nuclear cranking model continued
^{236}U, moments of inertia of fissioning isomers 78−74299
^{A}Yb, (A=168, 170), angular momentum fluctuation energy in the cranking model 79−89254
^{A}Yb, A=166, 168, 170, backbending and moment of inertia in HFB cranking method 80−42521
^{A}Yb, A=166,168,170, self-consistent cranking model anal. of Yrast bands 79−6367
^{A}Yb, A=168, 170, approximate ang. momentum projection from cranked HFB wave functions, yrast energies 79−30776
^{160}Yb double backbending and rot. states, HFB cranking model anal. 80−32155
^{162}Yb high spin states, HF self consistent calc. with Skyrme interaction, cranking approach 80−9210
^{167}Yb $i_{13/2}$ band, spin alignment in the particle-rotor and cranking models 80−42536

nuclear decay schemes *see radioactive decay schemes*

nuclear decay theory
see also alpha decay theory; beta decay theory
Bateman equations solution using transition matrix approach 77−57632
beta-delayed particle emission A>70 77−22972
composite exponential decay curve anal. 78−46241
compound nuclei, Z=98, 100, 102, statistical description of decay widths *(Russian)* 78−86549
delayed neutron emission, struct. of Gamow-Teller giant resonance 77−22974
delayed neutrons, single-particle approach, β-strengths to configs. in emitter nuclides 77−22975
delayed-neutron spectra characterisation 77−79345
disintegration into two and three fragments 77−71596
exchange effects in radioactive decay 77−10372
exotic light nuclei, with unequal numbers of protons and neutrons 78−89831
exponential decay law, corrections 77−67639
Fermi model for high multiplicity compound nucleus decay 80−22799
gamma transitions and coincidences, construction of decay schemes, SMUDLA code 80−83063
Gamow state vectors as functionals over subspaces of the nuclear space 80−32227
gravitational baryon annihilation *(Russian)* 77−26470
highly excited nuclei, decay widths in constant temperature model *(Russian)* 77−74783
highly excited nuclei, lifetime *(Russian)* 78−29430
K-harmonics method for cluster spectroscopic factors 78−62512
light nuclei, schematic model for isospin mixing 78−66198
low-energy nucl. physics, test of elementary particle theory 78−21361
nucleon emission stability, shell model anal. 77−22969
parity nonconserving nuclear interactions and weak neutral currents, review 77−41936
preequilibrium decay, exciton model formulation, reply to comments 78−78354
preequilibrium decay, microscopic exciton model 77−41935
preequilibrium decay models *(Rumanian)* 80−47457
prequilibrium decay, differences of alternate formulations, possible exciton formulation errors 78−70507
proton decay, β-delayed proton radioactivity, book contrib. 78−82322
quantum states and systems, decay law 78−62112
rate variations produced by physical or chem. means 77−41931
regeneration rate of decay processes and continuous quantum observations 77−17834
rotational states, coherent, γ-decay, random quantum meas. 80−73855
statistical model for delayed proton emission, appl. to Ba and rare-earth neutron deficient isotopes 77−22953
strengh distributions and statistical spectroscopy, general theory 77−79322
strength distributions and statistical spectroscopy, shell model comparisons 77−79323
SU(3) model of EM transitions, selection rules, transition probabilities *(German)* 77−2943
supernuclei containing bound states of charmed baryons, existence, decay, phys. significance 77−79320
three-particle nucleus, virtual decay, vertex form factors *(Russian)* 77−26607
transformations of physical systems, decay, molecular rearrangements, causality 77−2551
two peaked pot. barrier, quasi-stationary state decay, semiclassical approx. *(Russian)* 80−37366
two photon decay, time correlation 80−27506
unstable particles in elec. field 78−562
vertex constants *(Russian)* 78−33155
yrast region of rapidly rotating nuclei, instability toward nucleon emission 77−88027
α-decay lifetimes and resonance widths, comparison of calc. methods 78−78325
β-delayed neutron decay, statistical model, Monte Carlo techniques, fictional pandemonium nucleus calcs. 78−89830
μ capture, subsequent excitations and particle emission cascade, hydrodynamical model 78−89825
t→dn vertex constant from Faddeev eqn. *(Russian)* 80−83079
Ba, A=117, 119, 121, delayed proton emitters, positron-proton coincidence meas. 78−78326
^{8}Be, γ-decay strength of isovector M1 transition, microscopic wave function 78−62503
^{9}Be, molecular model, n and α-particle decay widths, charge form factors 78−46015
^{12}C, excited state decay, axion emission search 80−32235
^{3}H, props. calc. by interpolation approach *(Russian)* 77−22903
^{4}He, vertex consts. calc. by method of integral equations 77−14076
^{176m}Lu, electron capture meas. *(German)* 78−33153
Na neutron rich isotopes, β-delayed emission of n, 2n, α, t 78−74343
^{16}O, two nucleon emission following bound pion absorption 78−82395
^{33}S levels, excited by α-capture reactions 78−33124
^{28}Si, highly excited ^{12}C-α-^{12}C molecular state, symmetrical decay *(Russian)* 80−86861

nuclear deformation *see nuclear shape*

nuclear density
^{16}O(p,p), spin orbital interaction and nucl. matter density distrib. *(Russian)* 79−22176
β-active superdense nuclei search in (p,X), (d,X) reactions *(Russian)* 80−42535

nuclear density continued
A=16-58, charge, proton and neutron density distribs. calc. 80−22680
A=4n, densities, form factors, transitions, multipole moments in s-d shell, HFC 80−37321
abnormal density, possible existence, from study of π^0 prod. in Xe+π 77−54143
abnormal nuclei, critical charge *(Russian)* 77−273
abnormally large density and binding energy states, book contrib. 80−489
asymmetric nuclear matter, isospin and density waves, Landau theory 78−66235
bubble and string nuclei, shell and cluster concepts, role of mesons, fresh look at concepts 77−22827
charge- and mass-density waves in finite nuclei, possible expt. test 77−54144
classical many-body model for heavy ion collisions nuclear binding energy and density 78−66302
collective props. of nuclei deduced from electron scatt., deformed nuclei, review 78−50064
colliding nuclear slabs, density compression 78−642
compressibility of nuclear matter, density depend. of binding energy, hyperspherical functions method *(Russian)* 78−17093
compression wave propagation direction in nuclear matter 79−75882
Coulomb barriers, thermal Hartree-Fock approx. excitation-energy depend. 77−10346
Coulomb displacement energies and n-p density distribs. 78−17084
critical opalescence, percursor to pion condensation 78−62498
deformed nuclei calc. by HF method with Skyrme's interaction *(Russian)* 79−456
density isomer formation in high energy heavy ion collisions, 3-dimens. fluid dynamical calcs. 79−49578
density isomers, schematic model of mass distrib. 77−6219
density matrix approx. 78−33128
density-dependent HF description, of nuclei in rare earth and Ni regions 77−54170
diffuse-surface density distrib., moments, potentials, energies calc. 77−10311
direct energy minimisation methods in self-consistent nuclear fields, ground state props. 80−22702
doubly magic nuclei, Skyrme force calc. for nuclear struct. 78−49721
droplet of nucl. matter under rapid rot., anal. using Thomas-Fermi method 79−36179
eikonal anal. of high energy proton and electron scatt. *(Russian)* 77−22908
even-even deformed nuclei, coupled rot. bands, charge and density distribs. 78−89776
even-even spherical nuclei far from stability, Hartree-Fock calc. *(Russian)* 77−41908
exact density matrix expansion in solvable model, local density approx., local Fermi momentum approx. 78−50099
FCC lattice model of nuclear struct. 77−14042
flucton model of coherent fluctuations of nuclear density 79−75959
fluctuation of nucleon density, application to scattering 79−517
fluctuations, large momentum pion prod. in proton-nucleus reactions 77−38267
folding model calcs. of optical potls., nuclear density distribs. 77−30535
Glauber approx. corrections, nucleon-nucleus scatt., nuclear density distrib. 78−50166
hadron-nucleus total cross-sections, moments of nucl. densities 78−78252
Hamiltonians, semiclassical approx., spin-independ. pots. 80−32208
heavy ion collisions, fluid dynamical and TDHF models, abnormal nuclear matter, density isomers 80−47502
heavy ion deep inelastic collisions, kinetic energy dissipation, nuclear matter density oscillations *(Russian)* 80−37397
heavy ion fusion cross section, energy depend., nuclear matter density distrib., depend. 80−47519
heavy-ion interactions, magic nuclei, real part of nucl.-nucl. interaction anal. 77−6426
high energy nuclear collisions, isobaric-gas model, shock waves, temp., density, pionisation 78−94022
hypernuclei, Friedel sum rule, hadron phys. meaning, nuclear matter density, binding energy 78−82305
kaon-nucleus reactions, low energy, nuclear density shape optical pot. kaonic atom level shifts 80−63213
large momentum transfer reactions, density fluctuations, quark-parton mechanism *(Russian)* 79−80868
matter distribution in nuclei far from β stability valley, charact. features 77−64635
multiquantum excitation calculation of density distrib. and charge form factors 77−41885
neutron density distrib., probing with hadrons 78−66196
neutron distribution in nuclei, elastic and inelastic proton scattering, review 80−22649
neutron skin, compared with droplet model theory 80−52599
nuclear, matter, V^8 models, variational calcs. for binding energy and density 80−42571
nuclear density distrib., Glauber-Sitenko approx., fast hadron scatt. anal. *(Russian)* 78−25161
nuclear fireballs, break-up densities 78−8790
nuclear matter, pion condensation and density isomerism 80−5085
nuclear matter density determ., HF versus droplet model 80−68574
nucleon fluid, excitation to N*(1234) state, lowest order constrained variational calcs. 79−40864
nucleonic mass distrib. using mag. spectrometer *(French)* 79−449
nucleus-π^+ total cross-section, nuclear density and π-N off-shell amplitude effect 77−3050
nucleus-nucleus interaction pot. using energy dependent delta interaction, Skyrme interaction folding 79−36269
one-body density matrix determ. by iterative steepest descent approach, appl. to ^{20}Ne 78−17125
oscillations, from semi-infinite nuclear matter calc., Regge type oscillation comparison 80−57671
particle-hole type matrix elements for density-dependent interactions 79−40856
pion condensation in nucl. matter, role of effective nucleon mass 78−74323
rapidly rotating nuclei, density distrib. 78−8734
rapidly rotating nuclei, semiclassical HF description, smooth quantal corrections, density and total energy 80−32171
saturation in finite nuclei, nuclear matter density and binding energy 80−83029

nuclear density continued
scattering of electrons and protons, calcs. from nucleon density distrib. 78−54738
self-consistent field calcs., HF calcs., NN interactions, and results of appl., book contrib. 79−75880
semi-infinite nuclear matter calc., nuclear density oscillations 80−22681
sensitivity of real part of nucleus-nucleus potential to nuclear densities 78−82291
single particle nuclear density struct., Hartree-Fock and model independent anal. *(Russian)* 79−80941
single-particle potential, symmetry coefficient and effective mass in nuclear matter 79−13234
spherical nuclei, self-consistent Thomas Fermi method 77−57607
statistical description of nuclear compound states, temp. Green's functions method *(Russian)* 78−17115
superdense nuclei, possible existence *(Russian)* 79−13198
superdense nuclei, search for and synthesis, review of expts. and π-condensation theory 79−6463
superdense nuclei, search for neutrons with binding energy >40 MeV *(Russian)* 79−89515
superdense nuclei, search in reactor active zone 79−75824
superdense nuclei stability region, pion condensation *(Russian)* 77−46128
superheavy elements, variations in nuclear skin thickness 77−14025
surface energy of very neutron rich nuclei, Thomas-Fermi model 77−22870
surface thickness of nuclear densities and single particle pots., self consistent study 79−85360
Thomas-Fermi approx. extensions, finite nuclei 77−6256
extended Thomas-Fermi density matrix 78−41658
Thomas-Fermi model of finite nuclei 78−8747
three nucleon clusters in nuclear matter, energy per particle density dependence 78−17112
two-body correlations 77−14037
two-particle density matrix, for U(3(n−1)) states with $E_{min}+1$ in nuclei with $n \leq 16$ 78−41624
Wigner transform props., and nonlocality expansions of one body density matrix using Wigner function moments, review 79−67641
(e,e), 25-302 MeV, nucleon density distribution in nucleus 79−75831
(e,e), proton and neutron densities 80−22684
(K,X) optical pot. from KN scatt. and kaonic atom pot. models 79−97731
(p,p), polarised p, 0.8 GeV, neutron isotopic density differences and RMS radii 79−67643
(p,p) 800 MeV, polarised p, n density uncertainties from optical model anal. 79−22185
(p,X), total reaction cross sections and the matter density of finite nuclei 79−45150
π condensation in neutron matter, N-N interaction, critical density 80−57711
π condensation induced density oscillations, infinite nuclear matter and pions atoms calcs. 78−70476
π-condensate structure *(Russian)* 78−58236
πN scattering amplitude in nuclear matter, quantum field theory approach 80−42570
^{8}Be, ground state props., modified Brueckner-Bethe-Goldstone method 78−50076
^{209}Bi(p,n) pre-compound process, 18 to 64 MeV, cross sections, hybrid models anal. 79−3140
^{12}C, ground state props., modified Brueckner-Bethe-Goldstone method 78−50076
^{12}C, monopole excitations, transition densities from simple collective model 79−40834
^{12}C(^{17}O,^{16}O), single-n sub-Coulomb transfer reactions, single particle wave function RMS radius, n-excess 79−85355
^{12}C(π,π), total cross section, density distribs. and ray bending effects 80−47509
^{A}Ca, A=40, 48, neutron densities and single particle struct. 80−32165
^{A}Ca, A=40, 48, nuclear matter density distrib., saturation effect, optical potential from (α,α) 80−63115
^{A}Ca(α,α), A=40, 42, 44, 48, 104 MeV nuclear size and density distrib. from folding model anal. 80−68525
^{A}Ca(e,e), A=40, 48, (in)elastic scatt., self-consistent calcs. of nuclear density *(Russian)* 79−80928
^{A}Ca(p,p), 0.6, 1 GeV, A=40,42,44,48, matter density, Glauber model anal. 79−93500
^{A}Ca(p,p), A=40, 48, (in)elastic scatt., self-consistent calcs. of nuclear density *(Russian)* 79−80928
^{14}Ca(p,p), A=40, 42, 44, 48, 1 GeV, cross sections using nuclear densities from self-consistent methods *(Russian)* 78−41724
^{40}Ca, finite nuclear props. in relativistic quantum field theory, mass and p densities 80−9219
^{40}Ca, two-parameter nucleon density distrib., form factors calc. 77−65193
^{252}Cf fission, search for abnormal energy release reln. to superdense nuclei *(Russian)* 79−89340
^{54}Fe(p,p), 800 MeV, polarised differential cross sections and anal. powers, n density 79−13297
^{2}H(e,e), elastic and deep inelastic, nuclear matter density at large momentum transfers *(Russian)* 78−86529
^{3}H realistic wave function, energy and density distribs. 80−86794
^{4}He, ground state props., modified Brueckner-Bethe-Goldstone method 78−50076
^{4}He, monopole excitations, transition densities from simple collective model 79−40834
^{4}He, one particle density distrib., nucleon density, from nuclear ellipsoid of inertia *(Russian)* 79−30784
^{4}He(α,α) microscopic optical pot. for elastic scatt. in terms of nuclear density 79−54444
^{6}He, density distribution function of nucleons 80−22650
^{24}Mg, monopole excitations, transition densities from simple collective model 79−40834
^{A}Ni, A=58, 64, neutron densities and single particle struct. 80−32165
^{58}Ni(p,p), 800 MeV, polarised differential cross sections and anal. powers, n density 79−13297
^{64}Ni(p,p) 800 MeV, polarised differential cross sections and anal. powers, n density 79−13297
^{16}O, ground state props., modified Brueckner-Bethe-Goldstone method 78−50076
^{16}O, one particle density distrib., nucleon density, from nuclear ellipsoid of inertia *(Russian)* 79−30784

nuclear density continued
^{16}O, two-parameter nucleon density distrib., form factors calc. 77−65193
^{16}O(p,p), 1 GeV, cross sections using nuclear densities from self-consistent methods *(Russian)* 78−41724
Pb, A=204,206,208, neutron density RMS radii determ. from (α,α) scatt. 78−17088
^{208}Pb (e,e), 502 MeV, high-momentum-transfer, charge-density distrib. anal. 77−38258
^{208}Pb, charge and proton distribs., single particle model 78−50074
^{208}Pb, eikonal anal. of high energy proton and electron scatt. *(Russian)* 77−22908
^{208}Pb, finite nuclear props. in relativistic quantum field theory, mass and p densities 80−9219
^{208}Pb, isoscalar electric giant dipole resonance, from RPA calc., nuclear compressibility 78−86520
^{208}Pb, neutron and proton surface thickness, HF calcs. 77−71557
^{208}Pb, neutron densities and single particle struct. 80−32165
^{208}Pb, Thomas-Fermi model 78−8747
^{208}Pb+^{12,13}C, single-n sub-Coulomb transfer reactions, single particle wave function RMS radius, n-excess 79−85355
^{208}Pb+^{16,17,18}O, single-n sub-Coulomb transfer reactions, single particle wave function RMS radius, n-excess 79−85355
^{208}Pb(^{16}O,X), 80-313 MeV, optical model anal., dynamic shape or density changes 80−18186
^{208}Pb(α,α'), 96 MeV, ang. distribs., nuclear compressibility 78−50183
^{208}Pb(e,e), (in)elastic scatt., self-consistent calcs. of nuclear density *(Russian)* 79−80928
^{208}Pb(p,p), 1 GeV, cross sections using nuclear densities from self-consistent methods *(Russian)* 78−41724
^{208}Pb(p,p), (in)elastic scatt., self-consistent calcs. of nuclear density *(Russian)* 79−80928
^{208}Pb(π,π), total cross section, density distribs. and ray bending effects 80−47509
^{210}Po, excited, deformed, fission or neutron emission, shell-correction approach to nuclear densities 77−30483
^{32}S(π,π), total cross section, density distribs. and ray bending effects 80−47509
^{144}Sm(α,α'), 96 MeV, ang. distribs., nuclear compressibility 78−50183
^{A}Sn, A=116, 124, neutron densities and single particle struct. 80−32165
^{120}Sn(π,π), total cross section, density distribs. and ray bending effects 80−47509
^{48}Ti(p,p), 1 GeV, cross sections using nuclear densities from self-consistent methods *(Russian)* 78−41724
U+U high energy nuclear collisions, large baryon densities prod. 78−86540
^{236}U, nuclear matter density distrib., in asymmetric two centre shell model 80−32209
^{238}U, nuclear excitation rate in high-temp. environment 78−66244
^{238}U(e,e'), scatt. from octupole band, HF calc. of intrinsic equilib. density 78−37333
^{90}Zr(e,e), (in)elastic scatt., self-consistent calcs. of nuclear density *(Russian)* 79−80928
^{90}Zr(p,p), (in)elastic scatt., self-consistent calcs. of nuclear density *(Russian)* 79−80928
^{90}Zr(p,p), spin orbital interaction and nucl. matter density distrib. *(Russian)* 79−22176

nuclear electric moment
see also molecular nuclear coupling
A=12-240, even-even, dynamic deformation theory, B(E2) values, quadrupole and mag. moments 80−68591
A=17, 18 and 20, multipole matrix elements, HF calcs. 78−50098
actinide ions, tetrapositive, nucl. hexadecapole antishielding factors 79−26909
actinides, effect of simple consistency condition on multipole moments 78−86475
central-tensor coupled effective interaction pot., binding energy, shape, electric moment 77−14036
collective contributions to E1, $\Delta K=1$ matrix elements in odd-odd deformed nuclei 79−17857
collective props. of nuclei deduced from electron scatt., deformed nuclei, review 78−50064
core polarisation, multiple scatt. eqn. for two particle one hole system and generalised vertex 77−65204
deformed nuclei, approximate projection technique for EM properties calc. 79−93510
deuteron, EM quadrupole form factor peak value, determination of percentage D-state 78−93950
deuterons, D-state probability, review of spin, binding energy, magnetic and quadrupole moment 78−62488
E0 conversion, reduced probability, quadrupole moment effects 80−18235
E0-conversion, reduced probability, quadrupole moment effect 80−78138
E1-E2 direct-semidirect model for fast nucleon radiative capture, γ ang.-distribs. 78−62536
E2 core-polarisation charge, nuclei near ^{16}O and ^{40}Ca 77−22888
E2 matrix calc., band mixing with several valence nucleons *(French)* 78−45994
E2 strength distribution in 1s nuclei, isospin sum rules 77−30550
E2 transition selection rule, pñ signature, shell model 78−50069
E2/M1 mixing ratio, in vibr. yrast band, sign rule 79−17855
electric quadrupole moments, quasi-rotational states in even-even nuclei 78−82281
electronuclear energy weighted sum rules and excited state quadrupole moments 79−36150
electronuclear sum rules, linear energy weighted, nuclear struct. determ. method 79−75897
even nuclei, 2^{+} excited states quadrupole moments, energy weighted sum rule appl. 80−9229
even-even nuclei, electric and dynamic quadrupole moments 78−66203
even-even nuclei, static quadrupole moments of arbitrary excited states, sum rule approach 80−91135
even-even nuclei in 2p-1f shell, binding energy, quadrupole moment, by HF calc. 79−17843
even-even rare earths, microscopic quadrupole and hexadecapole moments 80−13376
excited state quadrupole moments meas. using Coulomb excitation 80−5065
exotic atom X-ray meas., review 78−50061
exotic atoms, E2 and E4 nucl. moments from HFS, review 78−37265
fast nonadiabatic nuclear rotation theory *(Russian)* 77−88036

nuclear electric moment continued
fission isomers, meas. of extreme nucl. deform. *(German)* 79−40971
fission isomers, spectrosc. props. 80−105966
generalised collective model, surface tension, energy spectra, and E2 γ-transitions 79−6432
heated spherical nuclei, quantal model of fluctuation E2 radiation *(Russian)* 78−78306
heavy nuclei, quadrupole moment effect on internal conversion coeff. *(Russian)* 77−82867
internal conversion coefficients, $30 \leq Z \leq 104$, Hartree-Fock-Slater model calcs. 79−36199
intrinsic multipole moments in deformed nuclei, correls. effects 78−29385
isoscalar E1/broad resonances (T=0) 79−13250
lanthanide ions, tripositive nucl. hexadecapole antishielding factors 79−26909
laser-RF double reson. spectroscopy of nucl. quadrupole moments, ^{55}Mn and ^{50}V appls. 80−57682
Mossbauer isomer shifts and nuclear models, book contrib. 79−85385
Muonic atoms, X-ray vacuum corrections, nuclear moments, transitions and deformation parameters 80−37912
N=28 region, $1f_{7/2}$ nuclei, low lying and high spin states 78−54667
N=50 isotones, effects of $1p_{3/2}$ core excitations 79−466
nuclei, transitional, pairing rotations and quadrupole modes 80−18165
octupole vibration, collective, wave functions, spherical harmonics 80−68532
odd-neutron spherical nuclei, isomeric state lifetimes, inhibited electric quadrupole transitions 78−78310
orientation with combined elec. and mag interactions 78−41633
p-f shell nuclei, HF calcs., vel. depend. effective pot., binding energy, quadrupole moment 80−461
quadrupole moment of heavy deformed nuclei in pseudo-SU(3) model 77−71565
quadrupole moments and rms charge radii, shell model calcs. 80−47369
quadrupole pairing forces influence on backbending, cranked Hartree Fock Bogoliubov approach 78−29401
quadrupole strength, giant quadrupole resonance 80−52575
quadrupole transfer strength, deformed rare-earth nuclei, heavy ion reactions 77−336
relativistic many-body bound systems, quantum field theory calc. 77−74765
review, spin and moment data tables 77−22881
review of meas. 78−37266
s-d shell nuclei, HF calcs., vel. depend. effective pot., binding energy, quadrupole moment 80−461
s-d shell nuclei, isomorphic model 77−50069
shape isomers, spontaneous fission, static and decay props. and excitations, review, book contrib. 78−82402
short living nuclear states, optical orientation, γ-spectrum anisotropy, lifetime, moments *(Russian)* 80−63090
short-range correlations and pseudopotentials, even-even isotopes, Hartree Fock Bogoliubov method 78−535
spectroscopic quadrupole moment extraction from muonic atom hyperfine structure, polarisability correction 77−18391
spherical nuclei, static quadrupole moments of vibr. states 78−62481
stable odd-mass sd nuclei, EM multipole moments of ground states 80−102116
thermonuclear fusion plasmas, effect of nucl. elec. quadrupole moments 78−83524
transitional nuclei, ang. momentum projected quasiboson states 78−41637
valence nucleons in $i_{13/2}$ orbit about strongly deformed core, model calc. 77−18371
(e,e) on nuclei with quadrupole moment, differential cross section static correction 79−6570
in (p,n) reactions quadrupole moment, isovector component, nuclear spin re-orientation effect 80−52573
^{27}Al, low lying states, band mixing effects, quadrupole moment 78−490
^{27}Al(α,α′), 145 MeV, excitation energy anal., octupole strength conc. 78−21584
^{29}Al, mag. moment quadrupole coupling const. β-ray detected NMR in Al_2O_3 cryst. 78−37267
^{10}B, energy level struct., admixed wave functions, ground state quadrupole moment, deformability 77−50054
^{11}B, determ. of hexadecapole mom. and quadrupole deform. from ^{11}Be(^{3}He, ^{3}He) 77−65229
^{11}B, quadrupole transitions from ^{12}C(γ,p) *(Russian)* 80−78281
Ba isotopes, ang. momentum projected quasiboson states 78−41637
Ba, neutron deficient, charge radii, moments, transitions and isomers, atomic beam laser spectroscopy 80−102141
^{A}Ba,(A=134-138), quadrupole moments and change in mean square radii of charge distrib. 79−50154
^{A}Ba, A=126 to 135, charge radii, mag. dipole and elec. quadrupole moment 79−72436
^{A}Ba, A=130, 132, 134, 136, levels and EM props., ang. momentum projected quasiboson model 80−5067
^{126}Ba, backbending and E2 transition strengths of yrast states 79−26363
^{134}Ba, reorientation effect and multiple Coulomb excitation meas. 77−61450
^{135}Ba, nucl. quadrupole moment, calc. using NQR, HFS and fine struct. data 78−50081
^{137}Ba, nucl. quadrupole moment, calc. using NQR, HFS and fine struct. data 78−50081
^{9}Be, struct., size, quadrupole moment, generator coord. method calc. 79−71788
^{209}Bi, Q value via ^{210}Po E2 transitions 77−14068
^{209}Bi/^{208}Pb isotone pair, charge distrib. polarisation from e^- scatt. and muonic X-ray data consistency 77−22873
^{80}Br, 37 keV level quadrupole moment, shell model anal. *(French)* 79−85366
^{12}C, isoscalar giant quadrupole resonance 78−78238
^{12}C, pot. and charge deform. of rot. states 77−46106
^{A}Ca, A=41,43,45, quadrupole moments, from hyperfine struct. splitting of $4s4p\,^3P_1$ 80−57674
^{A}Ca, A=47, 49, single particle states lifetimes calcs. 80−105943
^{43}Ca, nucl. quadrupole moment, HFS in at. beam mag. reson. 79−63940
^{45}Ca, nuclear charge radius, spin, moments, by laserspectroscopy 80−18187
Cd, A=106-116, Q_{2+} mass depend. via Cd(α,α′) and Cd(^{16}O,^{16}O′) 77−18390
nuclear electric moment continued
Cd, even-mass, B(E2) and $Q(2_1{}^+)$ via (e,e′) 68, 112 MeV scatt. 77−71585
Cd, multipole-multipole interaction in particle-particle channel 79−6364
Cd, quadrupole moments of first excited states of even isotopes 78−17099
^{A}Cd, static quadrupole moments determ. for A=111, 113, 115 78−37281
^{111}Cd $5/2^+$ quadrupole moments, evaluation using antishielded field gradients 78−51951
^{111}Cd, elec. quadrupole moment from elec. field gradients of trans-dimethyl organometallic moieties 80−29371
^{111}Cd^m, nuclear orientation in Zn and Be, 245 keV state quadrupole moment, half-life 80−37324
^{116}Cd(^{16}O,^{16}O′γ), 33 MeV, ^{116}Cd(α,α′γ), 8.5 MeV, quadrupole moments determ. 77−41887
^{140}Ce, hexadecapole motion obs. from α-scatt., EM transitions and conversion electron spectra 78−25097
^{131}Cs, 133.5 keV state, electric quadrupole interaction 80−32228
^{133}Cs, quadrupole interaction of 81 keV state in Te 78−48088
(d,d), A=24-54, pol.d, 20 MeV, quadrupole transition amplitudes 80−99148
Dy, deformed nuclei, quasicontinuum γ-spectrum, M1, E1, E2 components 80−498
Dy, quadrupole moment calc. using HF method *(Russian)* 80−13375
^{A}Dy, A=156-164, deformation hexadecapole moments, Hartree-Fock calcs. *(Russian)* 80−63081
^{148}Dy$_{82}$ 10^+ isomer, $\pi h_{11/2}$ effective E2 charge 78−93964
^{156}Dy high spin states lifetimes and feeding times, quadrupole moments from ^{24}Mg(^{136}Xe,4n) 80−32239
^{161}Dy, E0, E2 and E4 charge moment determ., using muonic atoms 78−21490
^{163}Dy(α,α′), E2 and E4 transition moments, rotational states 78−41740
^{164}Dy, recoil distance meas. of lifetimes of rotational states 78−66242
Er *(Russian)* 80−13375
^{A}Er, A=158,160,162, high spin states and deformation, number conservation effects 79−89225
^{A}Er, A=162-170, deformation hexadecapole moments, Hartree-Fock calcs. *(Russian)* 80−63081
^{166}Er, Coulomb excitation with ^{4}He and ^{16}O ions 78−8839
^{166}Er, Skyrme-HF calcs., deformation, electric moments, spin-orbit potentials 78−62480
^{166}Er(α,α′), 11.25 to 12 MeV, elec. moment, charge deform. parameters 77−54233
^{167}Er(α,α), E2 and E4 transition moments, rotational states 78−41740
^{19}F low lying positive parity states from rot. model, moments and deformation 79−6410
^{19}F, transition probabilities and multipole moments between states calc. by generator coordinate method 78−13022
^{54}Fe^m, static moments, perturbed ang. distribs. with combined dipole and quadrupole interactions 78−62482
Gd, isotope shifts and deform. obs. 77−65433
Gd, quadrupole moment calc. using HF method *(Russian)* 80−13375
^{A}Gd, A=152-160, deformation hexadecapole moments, Hartree-Fock calcs. *(Russian)* 80−63081
^{147}Gd^m high spin yrast trap, oblate deformation and quadrupole moment 80−32157
^{155}Gd, 86.54 keV state, Mossbauer meas. 77−85635
^{156}Gd(α,α′), 11.25 to 12 MeV, elec. moments, charge deform. parameters 77−54233
^{157}Gd quadrupole electric moment determ. 79−31723
Gd(α,α′), 11.8 MeV, A=154, 156, electric quadrupole and hexadecapole moments, charge deform. parameters 77−30489
Ge, doubly even nuclei, quasiparticle+phonon model calcs. 78−41626
^{69}Ge, transitions, spin and parity, and mag. moments determ. from β-decay of ^{69}As 79−22245
H^+, upper limit from P- and T-violating interactions in hyperfine struct., mol. beam reson. expt. on TlF 80−53019
H^+, value from electric dipole hyperfine struct. calc. of TlF 80−53162
^{2}H D-state probability lower bound, binding energy, quadrupole moment 80−91137
^{2}H D-state probability measurability in meson exchange current theory, moments and RMS radius 79−89246
^{2}H, quadrupole form factor and D-state probability 77−71571
^{2}H, quadrupole moment, calc. from D_2 elec. field gradient 79−93511
^{2}H quadrupole moment, energy depend. of NN interaction anal. 77−74775
^{2}H, quadrupole moment and percentage D state lower bounds 78−37286
^{2}H, quadrupole moment operator *(French)* 79−461
^{2}H quadrupole moments, $^3S_1$-$^3D_1$ and $^3D_2$ states simple pot. model 78−78271
^{2}H, repulsive nonlocal potl. models 77−88050
^{2}H, two-nucleon bound state description 77−38221
^{3}H, enhancement factor calc. in photonuclear electric dipole sum rule 78−37288
^{3}H photoeffect, electric dipole sum rules 79−36231
^{3}H photoeffect, hyperspherical harmonics and elec. dipole sum rules 77−57650
^{A}H, A=1, 2, nuclear electric dipole moments from P nonconserving atomic transitions 80−57681
^{3}He, enhancement factor calc. in photonuclear electric dipole sum rule 78−37288
^{4}He harmonic oscillator sum rules for photonuclear reactions, dipole moments, E1 transitions 78−41692
Hf, quadrupole moment calc. using HF method *(Russian)* 80−13375
Hf-Ir, isotopes, deformation, level assignments, static moments, modified oscill. model 77−22872
^{A}Hf, A=166, 168, 170, 172, yrast states, quadrupole moments and B(E2) values, microscopic calcs. 80−32147
^{A}Hf, A=176-180, deformation hexadecapole moments, Hartree-Fock calcs. *(Russian)* 80−63081
^{177}Hf, nucl. quadrupole moments and hyperfine struct. in ground multiplet ^{3}F of ^{179}Hf 77−83520
^{179}Hf, nucl. quadrupole moments and hyperfine struct. in ground multiplet ^{3}F 77−83520
^{180}Hf(α,α′), 21, 24 MeV, ang. distrib. meas., sensitivity to excited-state quadrupole moments 77−88158
^{A}Hg, A=193, 195-198, electric quadrupole moments, nonadiabatic rot. model calcs. 79−6389
^{A}Hg, A=198,200,202,204, reorientation effect, Coulomb excitation, oblate shapes 79−71790

nuclear electric moment continued
^{A}Hg, A=200,202,204, oblate shape determ. 79−17792
^{A}Hg, quadrupole moment, change between first $5/2^-$ states for A=197,199, shell model anal. 80−52576
^{197}Hg, quadrupole moment of $5/2^-$ 134 keV state 77−34225
^{198}Hg, static quadrupole moment of 1st excited state 78−17095
^{166}Ho, internal hyperfine field obs. using β-γ directional correl. 80−32229
^{129}I time depend. quadrupole interactions, γ-γ correlations from ^{129}Te^{m+g} decay 80−78145
^{132}I 3^+ and 1^+ state electric and mag. moments 79−63587
^{132}I isotope, doubly odd, quadrupole moments, PAC meas. 78−37280
^{115}In, elec. quadrupole moment from elec. field gradients of trans-dimethyl organometallic moieties 80−29371
^{186,188,190}Ir in Re crystal, electric quadrupole orientation, elec. field gradient 80−78140
Ir, A=191, 193, hyperfine struct. of low lying fine struct. levels, hyperfine anomaly, electronic g-factor 78−66214
^{186}Ir anomalous I$^{\pi}$K=5^+1 ground state config. confirmation, spectroscopic quadrupole moment 79−93506
^{192}Ir ground state spectroscopic quadrupole moment, g-factor, hyperfine quadrupole splitting 79−89235
^{47}K, single particle states lifetimes calcs. 80−105943
^{138,139}La, Fourier transform NMR 80−57354
La odd-A isotopes, rot. aligned coupling, ang. momentum projection 77−2921
^{138}La/^{139}La nuclear electric quadrupole moment ratio, laser RF double reson. obs. 80−23447
^{6}Li, RMS radii, binding energy, electric quadrupole transitions using generalised hyperspherical functions *(Russian)* 78−86469
^{7}Li charge form factor with resonating group wave function, quad. moment, charge radius 80−102110
^{7}Li, proton scatt., $3/2^-\rightarrow 1/2^-$ transition, LS coupling shell model, isoscalar quadrupole renormalisation 77−14046
^{7}Li, quadrupole moment from HFS 78−66678
^{175}Lu, muonic, nuclear spectroscopic ground state quadrupole moments from X-rays 79−98252
^{24}Mg 2_1^+ state quadrupole moment from ^{208}Pb(^{24}Mg,^{24}Mg) 80−9230
^{24}Mg first excited state static quadrupole moment, B(E2) value from ^{208}Pb(^{24}Mg,^{24}Mg) 79−45161
^{24}Mg, pot. and charge deform. of rot. states 77−46106
^{24}Mg+e, 21 to 32 MeV, E0 and E2 excitations, fission into two ^{12}Cg.s. nuclei 78−54744
^{26}Mg, 2_1^+ state quadrupole moment in band mixed HF model 80−52578
^{26}Mg, quadrupole moments meas. in (^{12}C,^{12}C′) excitation at 41.3 MeV 77−65231
Mo, A=94-100 static quadrupole moment determ. from α- and ^{16}O-scatt. 77−6226
Mo complex, ^{97}Mo and ^{95}Mo nuclear elec. quadrupole moment, nuclear quadrupole double reson. spectra 78−10802
^{A}Mo, A=94, 96, 98, multiparticle states, method of generalised seniority 80−22759
^{A}Mo, A=95, 97, nucl. quadrupole moments from laser-RF double reson. spectroscopy 80−57682
^{98}Mo static quadrupole moment of first 2^+ state from (α,α′), (^{16}O,^{16}O′) 80−5061
^{100}Mo(α,α′γ), 8.5 MeV, ^{100}Mo(^{16}O,^{16}O′γ), 33 MeV, quadrupole moments determ. 77−41887
^{104}Mo, first excited 0^+ state, E0^2/E2$^+$ ratio 79−17819
^{12}N ground state electric quadrupole moment from ^{12}C(γ, π), ^{12}N ground state electric quadrupole moment *(Russian)* 80−42538
^{13}N, quadrupole strength, from ^{12}C(p,γ)^{13}N, semi-direct capture model calcs. 80−47370
^{15}N, quadrupole transitions from ^{16}O(γ,p) *(Russian)* 80−78281
^{23}Na, band mixing, E2 and M1 matrix elements *(French)* 78−45994
^{23}Na, transition probabilities and multipole moments between states calc. by generator coordinate method 78−13022
Nd(^{16}O,^{16}O), 40-48 MeV, even nuclei, 2^+ state E2 transition probabilities and quadrupole moments 80−18234
^{150}Nd, Doppler shift meas. of ground state bands using ^{150}Nd(^{40}Ar,^{40}Ar′γ) 78−50124
^{150}Nd(α,α′), 11.5 MeV, electric quadrupole and hexadecapole moments, charge deform. parameters 77−30489
^{20}Ne hexadecapole moments, quadrupole deformation effects, E4 effective charge, valence polarisation 80−78142
^{20}Ne, pot. and charge deform. of rot. states 77−46106
^{20}Ne, transition, intrinsic hexadecapole and static quadrupole moments from ^{208}Pb(^{20}Ne,^{20}Ne′) 131 MeV 78−66204
^{20}Ne(e,e′), E1 and E2 giant resonances excitation at 60-120 MeV 78−50144
^{21}Ne, transition probabilities and multipole moments between states calc. by generator coordinate method 78−13022
^{22}Ne lifetime of 6^+ member of ground state band by DSAM, B(E2) values 79−26395
^{58}Ni, giant electric resonances, study of ^{54}Fe(α,γ)^{58}Ni 78−41739
^{60}Ni, hexadecapole motion obs. from α-scatt., EM transitions and conversion electron spectra 78−25097
^{16}O, α-cluster model comparison with giant E2 excitations 78−50109
^{16}O(^{10,11}B, ^{10,11}B), 33.7-49.5 MeV, mag. distribs., ground state quadrupole moment contrib. 80−42689
^{18}O 1.98 MeV 2^+ state static quadrupole moment, from nuclear sum rules 80−13374
^{18}O 1.982 MeV state, static electric quadrupole moment determ. 77−74763
^{18}O, quadrupole moment of first excited state 77−22886
^{18}O, quadrupole moment of first 2^+ state, SU(3) representation 77−46113
^{18}O, static quadrupole moment of first excited state, reorientation effect in Coulomb scatt. 77−82823
^{19}O first excited state electric moment, B(E2) transition from ^{208}Pb(^{18}O,^{18}O′) 79−67651
Os even nuclei, spin expsn. Hamiltonian, quadrupole moments 80−5058
^{A}Os, A=182, 184, 186, high spin yrast states, back-bending 80−86802
^{A}Os, A=186, 188, 190, 192, electromagnetic moments from muonic X-rays 78−12972
^{A}Os, A=186-194, collective levels, transitions, mag. and quadrupole moments, boson expansion theory 80−105954
^{A}Os, A=191,193, ground state spectroscopic quadrupole moment meas. 80−27553
nuclear electric moment continued
^{188}Os, muonic resonance spectra, deduced isomer shifts and electric moments 80−18948
^{190}Os, collective states and static quadrupole moment, boson expansion theory 80−47346
^{192}Os, muonic, dynamic hyperfine effect, model independ. anal. 78−22057
^{192}Os, Wilets-Jean Hamiltonian for energy levels, transitions, moment, etc. 79−9457
^{192}Os(^{12}C,^{14}C)^{190}Os, 70 MeV, shape transition effect on quadrupole transfer strength 78−644
Pb, A=204,6, quadrupole moments of first excited state meas. 78−21491
Pb cored nuclei, high spin stater energies, quadrupole interaction, yrast traps 77−34223
Pb region, even-odd nuclei, EM moments and transitions 77−88040
Pb(^{12}C,^{12}C′), A=204,206,208, 60 MeV, quadrupole moment and B(E3) values 79−17797
Pb(^{16}O,^{16}O′), A=204,206,208, 52 MeV, quadrupole moment and B(E3) values 79−17797
^{A}Pb, A=200,206, 12^+ isomer states, quadrupole moments 80−27554
^{208}Pb, charge distrib. polarisation from e$^-$ scatt. and muonic X-ray data consistency 77−22873
^{208}Pb, core-coupling RPA calcs. of NGR, electric multipole strength fragmentation 78−50142
^{208}Pb, from ^{207}Pb(n,γ), primary E2 transitions to ground state 78−58284
^{208}Pb, quadrupole moment of 3^- excited state 77−38222
Pb(α,α′), A=204,206,208, 13.8 MeV, quadrupole moment and B(E3) values 79−17797
Pd, even-even, collective states, B(E2), branching ratios and moments, boson expansion method 80−102099
Pd, quadrupole moments of first excited states of even isotopes 78−17099
^{102}Pd, meas. of Q(2_1^+) by reorientation precession technique 78−12971
^{104}Pd, meas. of Q(2_1^+) by reorientation precession technique 78−12971
^{105}Pd muonic X-rays, nuclear charge parameters, quadrupole moments 78−29377
^{108}Pd, vibr. states study, elastic and inelastic electron scatt., anharmonic vibrator model 78−62520
^{A}Pt, A=188-198 collective levels, transitions, mag. and quadrupole moments, boson expansion theory 80−105954
^{194}Pt, determ. of sign of P_3=M($0_1^+2_1^+$)M($2_1^+2_2^+$)M($2_2^+0_1^+$) 79−63588
^{196}Pt, collective states and static quadrupole moment, boson expansion theory 80−47346
^{236}Pu, 40 ps fission isomer quadrupole moment 77−50053
^{239}Pu, highly deformed, muonic X-rays, nuclear charge distrib., elec. quadrupole moment 78−70440
^{A}Rb, A=90-93, nucl. moment and charge radius using fast-beam laser spectroscopy 79−40839
^{87}Rb, low-lying level struct. in quasiparticle-core model 77−82825
^{89}Rb, nucl. moment and charge radius using fast-beam laser spectroscopy 79−40839
Re, A=183, 184, 186, 188, nuclear quadrupole alignment in Re single cryst. at low temp. 78−48091
^{183}Re, elec. quadrupole moment of 514 Nilsson state, TDPAC meas. 78−37276
^{103}Rh, quadrupole moments of $3/2^-$ and $5/2^-$ states, reorientation precession meas. 77−2905
Ru, A=99, 101, hyperfine struct. and nucl. moments determ. 77−26575
Ru, even-even, collective states, B(E2), branching ratios and moments, boson expansion method 80−102099
Ru, quadrupole moments of first excited states of even isotopes 78−17099
^{A}Ru, A=96, 98, 100, multiparticle states, method of generalised seniority 80−22759
^{A}Ru, first excited 2^+ states, quadrupole moments meas. for A=96, 100 and 104 78−78260
^{A}Ru(^{16}O,^{16}O′), 36-45 MeV, A=96, 98, 100, 102, 104, first 2^+ excited state quadrupole moment 80−47374
^{A}Ru(α,α′), 8.5-9.5 MeV, A=96, 98, 100, 102, 104, first 2^+ excited state quadrupole moment 80−47374
^{102}Ru 2^+ state quadrupole moment, reorientation effects and multiple Coulomb excitation from (α,α), (^{16}O,^{16}O) 80−5063
^{102}Ru(^{16}O,^{16}O), 38-42 MeV, Coulomb excitation, 2^+ state electric quadrupole moment 80−73793
^{102}Ru(α,α), 8.5, 9.0 MeV, Coulomb excitation, 2^+ state electric quadrupole moment 80−73793
^{32}S α-cluster struct., ground and first excited states, energies, radii and moments 80−102122
S6, A=120, 122, 3^+ isomeric states quadrupole moments, (p,n) excited, TDPAD method 78−41635
^{121}Sb, elec. quadrupole moment from elec. field gradients of trans-dimethyl organometallic moieties 80−29371
^{49}Sc, single particle states lifetimes calcs. 80−105943
Se, A=76, 78, 80, 82, static quadrupole moments of first 2^+ excited states 77−65197
Se isotopes, excited states struct., energy systematics 78−54687
^{74}Se(^{16}O,^{16}O′), 33, 34 MeV, first excited state, static quadrupole moment, deformation evidence 79−17802
^{74}Se(α,α′), 7.3 MeV, first excited state, static quadrupole moment, deformation evidence 79−17802
^{28}Si, giant reson. multipolarities via (α,α′), 120 MeV reactions 77−54201
^{28}Si, pot. and charge deform. of rot. states 77−46106
^{28}Si, quadrupole moments meas. in (^{12}C,^{12}C′) excitation at 41.4 MeV 77−65231
^{30}Si, 2_1^+ state quadrupole moment in band mixed HF model 80−52578
^{30}Si first excited state, static quadrupole moment from ^{208}Pb(^{30}Si,^{30}Si) 80−13373
Sm, A=152, 154, electric quadrupole and hexadecapole moments, charge deform. parameters, Coulomb excitation expts. 77−30489
^{A}Sm, A=148, 150, 152, 154, levels, moments, isomer shifts, spectroscopic amplitudes, sixth order boson expansion 79−89242
^{A}Sm, A=150, 152, muonic, X-ray spectra meas. and anal., charge radii, multipole moments 79−3600
^{154}Sm, Skyrme-HF calcs., deformation, electric moments, spin-orbit potentials 78−62480
^{154}Sm(p,p′), 35 MeV, ground state rot. band and multipole moment 80−32178

nuclear electric moment continued
Sm(α,α'), 11.25 to 12 MeV, a=152,156, elec. moments, charge deform parameters 77−54233
Sn, odd isotopes, number-projected three-quasiparticle description 78−93953
^{A}Sn(e,e') A=116, 120, 124, electric moment distrib., lowest lying quadrupole states excitation 79−6392
^{117}Sn, collective states and E0, E2 transition rates 79−17787
^{119}Sn elec. quadrupole moment from elec. field gradients of trans-dimethyl organometallic moieties 80−29371
^{11x}Sn, (x=3-6,8) quad. moment, γ-ray spectra of Cd:Sn 77−26571
^{A}Sr, A=89-94, mag. and electric quadrupole moments 79−6408
TaS_3(1T), inequivalent lattice sites in charge density distorted phases 80−15835
^{181}Ta, elec. quadrupole interactions in 482-keV level, meas. using Ge detector 79−40842
^{181}Ta, pionic X-rays, effective quadrupole moment determ. 78−66200
^{181}Ta, radial charge parameters, quadrupole moment, from muonic atom transitions 77−34226
^{A}Tb, A=149, 151, 153, 155, 157, prop. anal. on function of nuclear shape 79−75828
^{160}Tb, orientation in Gd matrix, γ-ray ang. distrib. anisotropy meas. 79−59031
Tc, A=93-101 odd isotopes, levels, EM moments in unified model 77−82826
^{99}Tc, 740 keV gamma transition quadrupole content, ^{99}Mo beta-decay obs. 77−54145
^{122}Te, backscatt. of ^{4}He, ^{14}N, ^{16}O, and ^{18}O, reorientation effect meas. 78−50209
^{125}Te, 9/2$^-$ 321 keV level, quad. moment from PAC of implanted Te metal 77−28488
^{128}Te backscatt. of ^{4}He, ^{14}N, ^{16}O, and ^{18}O, reorientation effect meas. 78−50209
^{232}Th, highly deformed, muonic X-rays, nuclear charge distrib., elec. quadrupole moment 78−70440
^{232}Th(p,p'), 35 MeV, ground state rot. band and multipole moment 80−32178
^{205}Tl, electric dipole interaction energy from electric dipole hyperfine struct. calc. of TlF 80−53162
^{169}Tm, studied via ^{169}Tm(^{32}S,^{32}S'γ), EM props. of ground state rot. band 78−8726
U, A=235, 238, highly deformed, muonic X-rays, nuclear charge distrib., elec. quadrupole moment 78−70440
^{233}U, monopole conversion, magnetic dipole transitions, latent penetration effect 79−9464
^{238}U, quadrupole moment meas., using ^{238}U(d,pn) 79−71856
^{238}U(^{136}Xe,^{136}Xe), multiple Coulomb and nucl. excitation 78−21603
^{238}U(^{238}U,^{238}U), multiple Coulomb and nucl. excitation 78−21603
^{238}U(p,p'), 35 MeV, ground state rot. band and multipole moment 80−32178
V isotopes, A=47-51 78−25114
^{48}V, low-lying positive parity states, deformed config. mixing model 77−6198
^{50}V quadrupole moment and atomic ground state hyperfine intervals, laser spectroscopic determ. 79−89234
W isotopes, A=182, 184, 186, Coulomb excitation with ^{4}He and ^{16}O ions 78−8839
W, quadrupole moment calc. using HF method *(Russian)* 80−13375
W, reorientation meas. quadrupole moment determ. 78−12968
^{A}W, A=170-182, even isotopes, yrast states, spectra and quad. moments, variation formulation 80−99119
^{A}W, A=182-186, deformation hexadecapole moments, Hartree-Fock calcs. *(Russian)* 80−63081
^{184}W, quadrupole mom. of second 2$^+$ state 77−30490
^{186}W quadrupole mom. of second 2$^+$ state 77−30490
^{129}Xe, low-lying levels determ. from Coulomb excitation and (α,n) reacts. 78−70450
^{131}Xe, low-lying levels determ. from Coulomb excitation and (α,n) reacts. 78−70450
Yb, quadrupole moment calc. using HF method *(Russian)* 80−13375
^{A}Yb, A=168-176, deformation hexadecapole moments, Hartree-Fock calcs. *(Russian)* 80−63081
^{169}Yb, E2 transitions in rot. bands, partial probability calcs. 79−75835
^{172}Yb, muonic resonance spectra, deduced isomer shifts and electric moments 80−18948
^{176}Yb(p,p'), 35 MeV, ground state rot. band and multipole moment 80−32178
Zn, doubly even nuclei, quasiparticle+phonon model calcs. 78−41626
^{62}Zn, band mixing HF model, struct. and electromag. transitions 78−54676
^{67}Zn 9/2$^+$ quadrupole moments, evaluation using antishielded field gradients 78−51951
Zr even isotopes, quadrupole moments and E2 transition rates, broken pair approx. 80−52579
^{A}Zr, A=92, 94, 96, multiparticle states, method of generalised seniority 80−22759

nuclear electric shielding *see nuclear screening*

nuclear electromagnetic transitions *see nuclear energy level transitions*

nuclear electron capture
see also beta-decay
atomic electron excitation probabilities during orbital electron capture by the nucleus 79−45211
atomic inner shell ionisation phenomena, conf., Freiburg, West Germany (March.-Apr. '76) 77−27040
atomic shell rearrangement during electron capture 79−75921
crystal field effects on probability of K-capture 77−18480
decay rate 77−57804
double K-shell vacancy creation per internal conversion 79−45212
energy loss rate due to electron capture in highly evolved stars 77−64752
inner shell electron rearrangements in radioactive decay 77−18881
inner shell ionisation in electron capture decay 77−18882
inner-shell vacancy filling detector, scintillation counter 77−18749
internal bremsstrahlung in s-electron capture 80−63133
Kβ/Kα ratio anomalies, K-capture rel. to bremsstrahlung excitation 77−18825
K-capture probability, strong mag. field effect *(Russian)* 77−34266
laser spectroscopic techniques involving atom, mol. excited states, book contrib. 78−9212
odd nuclei, second forbiddeness order, matrix element determ. 79−6508

nuclear electron capture continued
radioactive decay constant, effect of chem. surroundings, electron capture 80−42601
radioactive decay constants, constancy limits 80−78217
radioactive decay constants constancy limits 80−18245
recoil effects, elementary particle treatment 77−79339
relative orbital electron capture probabilities, experimental techniques, review 77−18893
review of theoretical status and exptl. methods 77−26629
screening effect on electron capture rates at high densities, stellar interiors 77−33478
screening effects in radiative orbital electron capture by an atomic nucleus 79−67717
semi-leptonic weak interactions 78−555
weak interaction treatment, modifications to $Re/R_{\beta+}$ ratio from finite size and Coulomb corrections 77−46143
^{106}Ag^{m}, L/K ratios, Q-value 78−29426
^{106}Ag^{m} decay, IC and γ-rays, ^{106}Pd energy states and J$^{\pi}$ 80−18197
^{108}Ag^{m} (127 yr.), K-electron capture probability, ^{108}Ag-^{108}Pd ground state mass difference 79−59038
^{26}Al, in interstellar medium, galactic source of γ-ray line emission 77−33692
^{244}Am decay, relative probability of electron capture 78−17153
^{37}Ar atomic electron correlation in M electron capture 79−63634
^{37}Ar, double internal bremsstrahlung in electron capture, ang. correl. meas. 78−25157
^{37}Ar, M/L capture ratio, multiconfig. Hartree-Fock calc. atomic electron correlations 78−62510
^{74}As decay, branching ratios and $T_{1/2}$ meas., K-fluorescence yield of Ge 77−3300
^{206}At→^{206}Po, EC-β$^+$ decay, Po excited levels 77−79340
^{211}At half life, branching ratio of electron capture and α decay modes 78−58253
^{187}Au decay, ^{187}Pt, levels, J$^{\pi}$, $T_{1/2}$, possible E0 transitions *(French)* 80−32230
^{195}Au decay, K-shell capture fractions, internal conversion electrons, coincidence techniques 80−57743
^{196}Au, L/K, M/L electron-capture ratio determ., derivation of exchange and overlap corrections 79−22233
^{131}Ba decay, ^{131}Cs level struct. obs. 77−10359
^{131}Ba decay, gamma-ray spectra of ^{131}Cs 79−85400
^{131}Ba, L/K and M/L capture ratios 78−29425
^{133}Ba decay data and standardisation 77−88081
^{7}Be decay, radiative capture of orbital electrons, inner bremsstrahlung spectrum, decay energy 79−500
^{7}Be, electron capture decay, internal ionisation 77−18892
^{7}Be, electron capture radioactive decay probabilities in atoms and ions 79−59556
^{7}Be, inner bremsstrahlung spectrum, partial decay energy 79−6512
^{7}Be, L/K capture ratio, multiconfig. Hartree-Fock calc. atomic electron correlations 78−62510
^{7}Be→^{7}Li, inner bremsstrahlung spectra, disintegration energies 77−54191
^{7}Be→^{7}Li, total electron capture decay energy from inner bremsstrahlung spectrum, student experiment 78−24611
^{206}Bi decay, ^{206}Pb γγ directional correlations, multipole mixing ratios, transition strength limits 80−86849
^{207}Bi EC decay, ^{207}Pb, 569.65-1063.63 keV cascade γ-γ ang. correl. meas. 80−86847
^{207}Bi, gamma-ray transitions following electron capture, 1.44 and 1.46 MeV γ-rays 79−85399
^{209}Bi→Pb, electron capture decay, LL-vacancy production by KLl Auger transitions 77−18832
^{A}Bk, A=240, 242, electron capture, delayed fission prob. and fission barrier height *(Russian)* 80−42722
^{242}Bk electron capture half life and α-branching ratio from ^{238}U+^{10}B, ^{235}U+^{11}B, ^{232}Th+N 79−67716
^{248}Bk, 23.7 h, spectroscopic studies 78−78314
Cd decay and half life, ^{A}Ag A=99, 101, 103, levels, transitions and J$^{\pi}$ 80−47383
^{104}Cd, β$^+$/(EC+β$^+$) probability ratio, EC decay energies, mass excesses 80−27543
^{105}Cd decay, ^{105}Ag, excited level struct. and transitions 79−97655
^{109}Cd decay, double K-shell vacancy creation per internal conversion 79−45212
^{109}Cd, double K-shell vacancy creation probability 77−54182
^{109}Cd EC decay data revision 80−5095
^{109}Cd, LX-, LX-coincidences during decay 78−17149
^{109}Cd nuclear transformation rate meas. using 4π proportional counter 78−21826
^{139}Ce, half-life determ. 77−34498
^{139}Ce→^{139}La, internat. comparison of activity meas. March 1976 79−13613
^{247}Cf decay, ^{247}Bk proton states, transitions and spectroscopic factors 79−89224
Co complex, bis-(β-diketonato) Co(II) dihydrate, Fe chem. states, Mossbauer emission 80−15917
Co complex, Werner complexes, ^{57}Fe partial quadrupole splitting, emission Mossbauer spectra 80−15919
$CoSO_4.7H_2O$, electron capture aftereffects, time differential Mossbauer coincidence technique 80−39927
^{57}Co in cosmic rays, abundance rel. to pre-accel. radioactive decay 79−40044
^{57}Co, Mossbauer gamma-X-ray coincidence meas. 80−14041
^{58}Co, student expt. 80−12875
$Co^{2+}[Fe^{III}(CN)_6]^{3-}$, time depend. linewidth of Mossbauer spectrum 80−15911
Cr, K_β/K_α following K-electron capture and X-ray excitation 78−13031
^{51}Cr→^{51}V, inner bremsstrahlung spectra, disintegration energies 77−54191
^{128}Cs decay, ^{128}Xe, collective excitations obs. 79−45143
^{129}Cs decay, ^{129}Xe excited state lifetimes, γ-transitions 80−78205
Cu, K_β/K_α following K-electron capture and X-ray excitation 78−13031
^{64}Cu, autoionisation of K-shell following β-decay 78−13029
^{64}Cu decay in Cu-Ag, electron density change 79−99519
^{151}Dy decay, ^{151}Tb lower excited state lifetimes, ^{151m}Tb isomer 79−75919
^{159}Dy evaluation for transmission imaging and bone mineral anal. 77−48861
^{A}Es, A=244, 246, 248, electron capture, delayed fission prob. and fission barrier height *(Russian)* 80−42722

nuclear electron capture continued
^{250}Es decay, ^{250}Cf E0 transitions and excited 0^+ states 79−45173
^{250}Es EC decay, ^{250}Cf low spin states, bandheads, J^π and transitions 80−105952
^{250}Es^m EC decay, ^{250}Cf two-quasiparticle states 77−46140
^{252}Es, half-life, γ-ray decay obs. 78−4914
^{A}Eu EC decay, A=147, 149, ^{147,149}Sm levels, J, γ-transitions and multipole mixing ratios, γγ correlations 80−106012
^{152}Eu decay, ^{152}Sm γ-transition energy and intensity meas. 80−73818
^{152}Eu, X-ray emission probabilities per decay 80−14027
^{155}Eu decay, Gd $L_{2,3}$ subshell X-ray fluorescence and Coster-Kronig yields 80−69102
^{150m}Eu, 35.8 y, decay coincidence study, ^{150}Sm levels 77−82858
Fe, K_β/K_α following K-electron capture and X-ray excitation 78−13031
^{55}Fe β-decay surface contamination monitoring probes, comparison of response between detectors 78−25398
^{55}Fe electron-capture decay double internal bremsstrahlung 79−63633
^{251}Fm, e′ capture decay, ^{251}Es level struct. and p states, level transitions 78−78268
^{67}Ga γ- and X-ray emission probabilities and half-life obs. 80−32242
^{70}Ga, β-decay to excited states, β- and γ-ray meas. 77−41933
^{143}Gd^{m+g}, β^+ and EC decay 78−50130
^{145}Gd EC/β^+-decay branching ratio anomalies, ^{145}Eu level and transition effects 80−32244
^{145}Gd, ε/β^+ anomalous values, reinvestigation 77−79332
^{145}Gd→^{145}Eu, weak interaction treatment, modifications to $Re/R_{\beta+}$ ratio from finite size and Coulomb corrections 77−46143
^{146}Gd decay, γ- and internal conversion electron spectra 79−75916
^{147}Gd→^{147}Eu decay, γ-ray spectra obs. at small-source detector distance *(Russian)* 79−93520
^{71}Ge, energy release accompanying electron capture 78−17148
^{71}Ge, LX-, LX-coincidences during decay 78−17149
^{71}Ge, radioactive decay rate in GeS and GeS_2 79−97683
^{1}H, capture probabilities for 4.25 and 61.8 MeV protons in a neutron beam facility 80−78222
^{158}He^{g,m} decay, obs. of ^{158}Dy collective excitations 78−82270
^{172}Hf EC decay, ^{172}Lu levels, transitions and J^π values 80−18249
^{197}Hg (64 h) decay γ intensities, obs. 79−75922
^{A}Ho, A=150, 151, 152, high spin isomer EC, ^{150,151,152}Dy levels, J^π and transitions 79−89241
I, A=124, 6, nucl. reson. fluoresc. in ^{124}Te and ^{126}Te 77−2953
^{123}I decay, ^{123}Te levels, spin assignments and E2/M1 multipole mixing ratio 79−75836
^{123}I, isomer shift calibration of ^{29}I and ^{127}I, lifetime variations in electron capture decay 80−39925
^{123}I production from ^{123}Xe formed in spallation reactions by 660 MeV protons, medical appls. 80−85494
^{125}I, electron capture decay lifetime, calibration of Mossbauer isomer shift of ^{127}I and ^{129}I 80−39922
Ir decay, oriented nuclei, ^{188,189}Os levels, J^π, transitions and mixing ratios 80−68602
^{40}K, pressure-induced changes in electron-capture decay const., theory 80−22771
^{A}La A=131,133, decay, ^{131,133}Ba l-forbidden M1 transitions, energy level lifetime meas. *(Russian)* 79−49603
^{138}La, radioactive decay meas., half life, γ energies 80−13418
Lu, A=162,4,5, prod. Yb 78−62509
^{169}Lu decay, ^{169}Yb γγ ang. correlations, levels and spins *(Russian)* 80−83069
^{171}Lu decay, ^{171}Yb level scheme, γ-transitions, spin-parity assignments 77−46133
^{172}Lu decay, identification of γ-spectra unplaced energies by delayed coincidence meas. 80−78221
^{A}Md, A=248, 250, electron capture, delayed fission prob. and fission barrier height *(Russian)* 80−42722
^{258}Md isomer, EC decay, ^{258}Fm spontaneous fission, mass and kinetic energy distribs. 80−47518
^{54}Mn, electron-capture decay, K X-ray emission rate determ. 78−21530
^{22}Na, anomalous electron capture/β^+ decay ratio, second forbidden corrections 79−22238
^{22}Na, EM corrections for electron capture to β^+ decay ratio 79−89269
^{22}Na, electron capture/positron emission ratio 77−30522
^{92}Nb, half life determ. by gamma spectroscopy, comparison of ^{92}Nb, ^{94}Nb activities and abundances 78−29423
^{59}Ni, nuclear electron capture theory 77−82869
^{59}Ni, radiative capture of K-electrons, γ spectra anal. 77−61384
Pb, 0.43-1.71 MeV electrons 79−6513
^{201}Pb decay, ^{201}Tl levels, transitions and J^π assignments 80−5099
^{201}Pb→^{201}Tl following ^{203}Tl(p,3n) or ^{205}Tl(p,5n), E_p=15 to 60 MeV, yields and excitation functions 79−5369
^{205}Pb, decay, orbital electron capture ratios 77−18894
^{205}Pb decay, orbital electron capture ratios, half-life 78−74340
^{103}Pd decay, 357 keV γ:K X-ray abundance ratio obs. 79−498
^{103}Pd, K-electron capture decay, double K-shell vacancy creation 80−22773
^{109}Pd decay, double K-shell vacancy creation per internal conversion 79−45212
^{204}Po, EC, ^{204}Bi excited states, γ rays, conversion electrons and γγ coincidences 80−18241
^{207}Po half life, charact. γ meas. 78−58253
^{140}Pr, $P_K/P_{\beta+}$ ratio for allowed decay 77−61386
Pt decay, oriented nuclei, ^{189,191}Ir levels, J^π, transitions and mixing ratios 80−68602
^{188}Pt decay, ^{188}Ir level scheme and transitions 79−22237
^{237}Pu , half-life determ. by gamma counting in NaI(Tl) 78−8775
^{81}Rb, β^+-EC decay, $T_{1/2}$, ^{81}Kr levels 77−79309
^{180}Re decay, ^{180}W octupole vibr. states, J^π and transitions 80−83024
^{94}Rh decay, $T_{1/2}$, ^{94}Ru levels and γ-transitions 80−18244
^{208}Rn decay, ^{206}At energy levels and transitions, IC electrons 80−18242
^{210}Rn decay, ^{210}At excited states, spins, parities and rate of population 79−75917
^{97}Ru 2.9 day decay, γ-γ correls. from ^{97}Tc 785 keV 77−54178
^{97}Ru→^{97}Tc, polarised nuclei ^{97}Ru mag. moment, E2/M1 mixing ratios 77−6315
^{44}Sc, electron capture to positron emission ratio, $4\pi\beta$-γ coincidence meas. 77−18479
^{145}Sm, electron capture decay to ^{145}Pm, γ-transition decay rate and intensities 78−13030
^{145}Sm, electron capture decay, internal bremsstrahlung 78−13035
^{A}Sn, A=106,108, $\beta^+/(EC+\beta^-)$ probability ratio, EC decay energies, mass excesses 80−27543
nuclear electron capture continued
^{106}Sn β^+/EC decay, ^{106}In level scheme determ. 78−93971
^{108}Sn, electron capture decay to ^{108}In, level scheme 77−71589
^{113}Sn, chem. effect on electron capture probability and decay const. 79−54412
^{113}Sn, decay, electron capture probability 77−67720
^{85}Sr, decay to ^{85}Rb, two-quantum γ-γ decay of 514 keV excited state 78−13009
^{85}Sr, electron capture decay, K X-ray emission probability, half-life, decay scheme 79−17862
^{85}Sr^{m,g} decay, ^{85}Rb levels, J^π and transitions 80−78162
^{178}Ta 2.45 h decay, J^π assignment, ^{178}Hf 9^- to 8^- transition 79−45201
^{180}Ta^m, β and EC branching ratios, K-internal conversion coeff., γ-intensities, T 1/2 80−68601
^{146}Tb decay and T1/2, ^{146}Gd lowest 2^+ state, J^π and transitions 80−105979
^{149}Tb^g, 4.15 h, decay γ-spectrum, ^{149}Gd level scheme and transitions 79−9477
^{150}Tb decay, ^{150}Gd levels and transitions, J^π assignments mixing ratio, nuclear orientation 79−13205
^{151}Tb decay, ^{151}Gd excited state spin assignments γ-γ ang. correlations *(Russian)* 79−49597
^{152}Tb decay, ^{152}Gd N=88 nuclei quasirot. bands and J^π 80−83025
^{153}Tb decay, ^{153}Gd γ-directional distrib., levels, spin assignments 79−13241
^{154}Tb decay, ^{154}Gd levels from γ ang. distribs. 79−442
^{155}Tb, oriented in Gd, γ-decay ang. distrib., hyperfine splitting, moment and mixing ratios 79−45242
^{160}Tb→^{160}Dy, γ-transitions and angular distributions 80−83060
^{94}Tc decay, ^{94}Mo high spin state transitions, mixing ratios, spins, shell model calcs. 79−97678
^{95m}Tc→^{95g}Mo, K capture branching ratio 77−6308
^{119m}Te, electron capture decay, γ-ray spectra, ^{119}Sb level scheme determ. 77−50088
Ti, K_β/K_α following K-electron capture and X-ray excitation 78−13031
^{195}Tl (1.13 h) decay, ^{195}Hg level scheme and transitions, band population 79−17807
^{197}Tl decay, half life and decay scheme, ^{197}Hg level scheme and transitions 79−67719
^{201}Tl decay, ^{201}Hg γ-γ directional correlations, level transitions, spin assignments, mixing ratios 79−496
^{201}Tl γ- and X-ray emission probabilities and half-life obs. 80−32242
^{204}Tl first forbidden K-capture decay, internal bremsstrahlung spectra 79−45213
^{156}Tm decay, ^{156}Er N=88 nuclei quasirot. bands and J^π 80−83025
^{169}Tm, high resolution meas. of anisotropic directional correl. between γ-rays and KX rays 80−32243
V, K_β/K_α following K-electron capture and X-ray excitation 78−13031
^{50}V, half lives of β-decay and e^--capture in ΔJ=4 transitions 79−22246
^{50}V, half-life limits for β-decay and electron capture 77−79334
^{181}W electron capture decay, ^{181}Ta L X-ray spectrum, L_1 subshell yield 79−49608
$^{260}X_{105}$, prod., L X-ray spectra, decay 78−8780
Xe isotope shifts of 1s electron in K-X-rays following electron capture 77−23454
Xe, K X-ray energy shifts following electron capture beta decay, role of nucl. hyperfine struct. 78−5166
^{123}Xe→^{123}I, generator prod. for radiopharmaceutical appls., high energy alpha reactions 77−37053
^{127}Xe decay, absolute gamma-ray intensities 78−548
^{88}Y solution, standardisation using efficiency extrapolation method, β-γ coincidence meas. 78−21832
^{169}Yb, double K-shell vacancy creation by internal conversion 77−57627
Zn, K_β/K_α following K-electron capture and X-ray excitation 78−13031
^{65}Zn, EC decay rate determ. using X-ray gamma-ray summing 77−57804
^{65}Zn, electron capture/positron emission ratio 77−30522
^{89}Zr allowed β-decay, K-electron capture/e^- emission ratios 79−93557
^{89}Zr, electron capture decay lifetime in $BaTiO_3$, $PbZrO_3$ and ZrO_2 77−28523

nuclear emulsions *see nuclear track emulsions*

nuclear energy *see nuclear power*

nuclear energy level lifetimes
^{116}Xe quasi-rotational bands, levels J^π and $T_{1/2}$ from ^{116}Cs decay 80−83021
^{154}Er, high-spin states 78−29373
^{298}114, high spin pot. energy surfaces, fission barrier, α-, γ-decay half lives, yrast spectrum 80−73764
^{54}Fe, mean lifetime of 6.38 MeV 8^+ state *(French)* 79−45204
^{A}Er, A=156, 160, yrast level population, decay, and lifetimes from Sn(^{40}Ar, 4n), ^{A}Er, A=156, 160, yrast level population, decay, and lifetimes *(Russian)* 79−97648
A=134-144, fission yields from spectroscopic meas., γ-branching and half-lives 80−78213
A=21-44, energy levels, excitation energies, branching and mixing ratios, lifetimes, J^π, resonances 79−13208
A=24-28 nuclei, reliability of calculated decay props. 78−93970
A=4n nuclei, energy levels, BE(2) transition rates, HF calcs. with Skyrme force 78−82315
charge plunger technique, nuclear lifetime meas. 78−29698
collective transition average lifetimes, spin (30-50) region in heavy ion-nucleus reactions 78−89822
complex cascade processes decay law, high spin state mean lifetime corrections *(Chinese)* 80−22761
conference on nuclear interactions, Canberra, Australia (Aug.-Sep. 1978) 80−4476
conference on nuclear spectroscopy and structure, Alma Ata, USSR, (Mar. 78) 79−75809
conference on nuclear struct. spectroscopy and atomic nucleus struct., Tashkent (Mar. 77) 79−6470
curved plunger for TDPAC meas. on recoil into gas 79−76313
determination by reson. fluoresc. under bremsstrahlung bombardment *(French)* 77−54179
Doppler shift attenuation method, environment slowing down effect 77−38245
Doppler shift attenuation method, ion stopping cross sections 78−70725
Doppler shift lifetime meas., attenuation factor, recoiling nuclei velocity calcs. *(Rumanian)* 77−46134
Doppler-shift attenuation meas., light ion ranges meas. by (p,γ) reson. broadening 77−69023

nuclear energy level lifetimes continued
DSA meas., ion-atom interaction 79−749
DSA meas. of heavy-ion stopping in matter 77−10569
DSA meas. of nuclear excited state lifetimes, centroid shift and line shape anal. *(Rumanian)* 77−46135
DSA recoil distance lifetimes, comprehensive anal. formalism, computer code 77−6653
DSAM, nuclear spectroscopy techniques *(Hungarian)* 80−14036
electronic lifetime meas. with Ge(Li) detector using centroid-shift method 79−6790
excited nuclear states, 10^{-18} to 10^{-6} s, lifetimes, direct meas. 79−30804
excited nuclear states, lifetime meas. 80−5093
fission isomers, meas. of extreme nucl. deform. *(German)* 79−40971
fission lifetime distribution and probability estimates 78−659
fp-shell nuclei, high-spin states 78−12946
gamma ray ang. distrib., Doppler effect appl. in nucl. spectroscopy *(Hungarian)* 80−14036
gamma-ray delayed coincidence summing 78−55088
giant E0 resonances, effect on lifetime of excited 0^+ states 79−17878
ground state rot. band transitions and delayed feeding via (d,3n) for A=158-180 77−34211
high spin rotational states of Sm, Gd, Dy, Er, Yb doubly even isotopes, lifetimes meas. 77−30511
in-beam gamma-ray spectroscopy, book 77−83449
interacting boron model of collective state, O(6) limit 80−32214
isomer shifts, total conversion coefficients, nuclear electron and gamma transitions importance 79−85411
laser radiation effects on nuclear transition lifetime 80−22760
measurement, plunger device piezoelec. fine adjustment and PLL distance regulation 79−6806
measurement using on-line computer and registration time shift compensation 80−68577
measurement using recoil distance method expts. 80−73825
moderately deformed nuclei, high-spin states studied in (heavy ion, xnγ) reaction 77−14180
N=82-86, high spin isomers, gamma spectroscopy 80−47358
nanosecond isomers, in-beam gamma spectroscopic investigation, Ge(Li) detector 78−86506
nuclear excited states, 10^{-10} to 10^{-6} s, lifetime meas. by time spectrometer system 79−31313
odd-neutron spherical nuclei, isomeric state lifetimes, inhibited electric quadrupole transitions 78−78310
plunger device for in-beam meas. of nuclear lifetimes, tested on ^{22}Na and ^{153}Dy 78−13375
Poisson and Brockwell-Moyal freq. distribs., χ-square test 80−5430
preequilibrium decay, microscopic exciton model 77−41935
recoil distance meas. in coincidence mode, corrections calc. 77−10565
recoil distance method, Doppler effect appl. in nucl. spectroscopy *(Hungarian)* 80−14036
recoil distance method for excited state lifetimes, zero order description corrections *(Rumanian)* 79−36198
short living nuclear states, optical orientation, γ-spectrum anisotropy, lifetime, moments *(Russian)* 80−63090
spontaneous fission of transuranium nucl. isomers, exptl. work review 77−79405
SU_6, dynamical symmetries, in nuclei, energy levels, transitions and collective states 78−74317
superheavy region, neutron drip line, energy density mass formula extrapolation 78−93932
time-dependence of reson. scatt. radiation 77−14060
walk-free centroid method for lifetime meas. with pulsed beams 78−70715
yrast decay schemes from ^{48}Ca+heavy ion fusion evaporation reacts., appl. to Fe, Cr and Mn 78−66308
yrast isomer prod., pulsed beam meas. using plastic scintillation spectrum 80−27871
γ-γ coincidence techniques, lifetime meas. following fusion evaporation reaction 79−59318
^{99}Tc^m compounds, chemically induced decay constant variation 78−93968
^{161}Dy, in Gd_2O_4, and Gd, TDPAC meas. 78−10809
Ag, odd-mass isotopes, $9/2^+ \rightarrow 7/2^+$ transitions, transition probabilities, half-lives 77−18475
^{A}Ag, A=105,107, positive parity band, mixing and branching ratios lifetimes from (^{16}O,2np)(^{14}N,3n) 80−9197
^{104}Ag levels, J^π, $T_{1/2}$, bands and transitions from ^{103}Rh(α, 3nγ) 80−102093
^{105}Ag absolute transition probabilities from 53.2 keV level, half-life 79−49605
^{108}Ag, populated in ^{108}Pd(p,nγ), level struct., spin and parity, isomeric state lifetimes and g-factors 77−18392
^{110}Ag low lying states, decay scheme and $T_{1/2}$ from ^{109}Ag(n,γ) 80−47393
^{110}Ag, populated in ^{110}Pd(p,nγ), level struct., spin and parity, isomeric state lifetimes and g-factors 77−18392
^{111}Ag, 376.7 keV level lifetime, shape coexistence, γ-branching 78−551
^{111}Ag, excited state lifetimes, γγ ang. correls. 77−6298
^{27}Al bound state parity and spin assignments, level struct. from ^{26}Mg (p,γ) resonances 78−66206
^{27}Al excited states, recoil-distance method 77−30510
^{27}Al(p,α)^{24}Mg resonance, nuclear lifetime meas. problems in single cryst. blocking expt. 77−47500
^{28}Al, $T_{1/2}$, J^π, levels below 5.45 MeV via ^{27}Al(d,pγ) 77−57623
^{39}Ar, energy level spin and parity assignments, level spectroscopy from (α,nγ), (d,pγ) 78−93943
^{39}Ar, lifetimes of high-spin levels meas. Doppler shift technique 77−61380
^{40}Ar, lifetime determ. using Doppler shift attenuation 79−93551
^{40}Ar(α,pγ)^{43}K, 10.4 MeV, lifetime of 738 keV level of ^{43}K, M2 transition strength meas. 77−65226
^{41}Ar states from ^{40}Ar(d,p), lifetimes meas. by DSA method 78−78308
^{A}As, A=70, 72, level scheme, transitions, J^π and lifetimes from Ge(p,nγ) 80−22695
^{A}As, A=71, 73, levels, J^π, transitions, T1/2 from Se decay, Ge(^{3}He,d), (p,xnγ) 80−57684
^{69}As, recoil distance level lifetime meas. from ^{16,18}O collisions 78−78311
^{70}As states, excitation functions, spin and halflifes from ^{69}Ga(α,3n), ^{60}Ni(^{13}C,np), ^{63}Cu(^{10}B,2np) 79−6414
^{72}As, new 87 ns isomer, g-factor via ^{59}Co(^{16}O,2pn) 53-56 MeV 77−54149
^{75}As, level lifetimes, bremsstrahlung, reson. fluoresc. *(French)* 79−13248
^{75}As, nucl. reson. fluoresc. meas., spins and level widths determ. 77−61379
^{213}At levels, J^π, transitions and lifetimes from ^{208}Pb(^{7}Li,X) 80−68542
^{197}Au(^{20}Ne,^{20}Ne), 90 MeV, state lifetimes, weak coupling core excitation model, translation rates 79−63630
^{197}Au(^{35}Cl,^{35}Cl), 120 MeV, state lifetimes, weak coupling core excitation model, translation rates 79−63630
^{10}B, 3590 keV excited state lifetime from ^{9}Be(p,γ) 79−9510
^{10}B T=1 states, γ-transition strengths, lifetimes, branching and mixing ratios from ^{6}Li(α,α) 80−27594
^{11}B analogue of ^{11}C 6478 keV state, lifetime from ^{7}Li(α,γ) 80−5092
^{A}Ba, A=131,133, l-forbidden M1 transitions, energy level lifetime meas. from La decay *(Russian)* 79−49603
^{A}Ba, A=135,137, Coulomb excitation, transition probabilities, γ-rays and level collectivity from (^{16}O,^{16}O′), (α,α′) 80−78201
^{126}Ba, backbending and E2 transition strengths of yrast states 79−26363
^{7}Be, lifetimes of first excited levels meas. 77−22943
^{203}Bi high spin states from ^{203}Tl(α,4n), lifetimes meas. 78−29485
^{73}Br, excited state lifetimes by particle X-ray coincidence technique 78−86507
^{76}Br, new isomeric state with half-life 1.49 sec 79−17858
^{76}Br^M decay props., half life and γ-transitions, level scheme 80−83071
^{77}Br collective bands, lifetimes, spins and E2 transition probabilities from ^{64}Ni(^{16}O, 2nP) 80−13415
^{77}Br E2 transition probabilities and mean lives from ^{64}Ni(^{16}O,2npγ) 80−13414
^{11}C negative parity states lifetime limits and transition strengths from ^{10}B(p,γ) 80−5092
^{12}C struct., determ. of Brink's model parameters, calc. of binding energy, 2^+ level lifetime 79−85358
^{13}C, 1-20 ps region mean lifetime meas., high-vel. DSA method 77−65200
^{14}C first excited 0^+ state, lifetime and E^0 decay from (d,p), (^{13}C,p) 80−102145
^{A}Ca, A=47, 49, single particle states lifetimes calcs. 80−105943
^{41}Ca, lifetimes of excited $3/2^-$ states from ^{2}H(^{40}Ca, p) 60 MeV 78−70487
^{41}Ca parity doublet gamma lifetimes, 3/2 levels, parity mixing from ^{40}Ca(d,pγ) 80−78209
^{42}Ca, high spin states from ^{39}K(α,p), lifetimes, multipole mixing ratios 78−50186
^{48}Ca, lifetime of 5147 keV, 4504 keV, levels determ. by (p,p′γ) at 28 MeV 77−79381
cc ^{160}Tm doubly odd deformed nucleus, excited states and state lifetimes from ^{160}Yb decay 79−13209
^{1}Cd, A=113, 115 from ^{113,115}Ag β-decay 80−47432
^{A}Cd(^{16}O,^{16}O′), 44 MeV, A=112, 114, 0_2^+, 0_3^+ state collectivity, E0 and E2 decay, $T_{1/2}$ 80−73784
^{106}Cd, 4659.8 keV isomeric level 77−30508
^{111}Cd^m, nuclear orientation in Zn and Be, 245 keV state quadrupole moment, half-life 80−37324
^{119g,m}Cd, decay schemes, half-lives, excited levels 77−296
^{138}Ce, ^{139}Ce, high-spin states, lifetime meas. using (α,xn) reactions 77−18476
^{34}Cl, high spin negative parity states, lifetimes meas. 78−74327
^{34}Cl high spin states 78−82289
^{34}Cl, J^π, levels, mixing ratios, $T_{1/2}$ via ^{33}S(p,γ) and ^{33}S(p,p) 1.0, 2.0 MeV 77−26613
^{34}Cl, levels Γ, γ-branching, $T_{1/2}$ via ^{33}S(p,γ) 1.0, 2.0 MeV *(French)* 77−26612
^{34}Cl negative parity high spin states, ang. distribs. and lifetimes from ^{31}P(α,n) 79−17812
^{36}Cl, 1-20 ps region mean lifetime meas., high-vel. DSA method 77−65200
^{37}Cl high spin state decay, spin assignments, yrast level lifetime from ^{27}Al(^{19}F,2αp), ^{27}Al(^{12}C,2p), ^{34}S(α,p) 79−6490
^{55}Co excited levels and IAS meas. with ^{54}Fe(p,γ) 77−18509
^{56}Co, γ-ray transitions, branching ratios, spin assignments, energy level lifetimes from ^{54}Fe(^{3}He, pγ) 79−497
^{56}Co levels populated in ^{58}Ni(d,αγ), 7 MeV, mean lifetimes 78−4950
^{56}Co, populated in ^{54}Fe(α,pn), transition rates of high spin states 77−6301
^{59}Co, energy levels, lifetimes, deexcitation following (n,n′γ) studies 80−83059
^{59}Co level energies, branching ratios lifetimes and spins from (p,p′),(α,pγ) 80−63093
^{59}Co, mean lifetime meas., 1400 to 1650 keV range, by reson. scatt. of bremsstrahlung *(French)* 79−75905
^{59}Co(n,n′γ), level transitions, deexcitations and lifetimes 80−18222
^{60}Co, 2505 keV gamma ray intensity in β-decay 79−13249
^{48}Cr, spectroscopy of high spin states 79−59032
^{49}Cr low lying states, deformed configuration mixing shell model calcs. 77−6302
^{51}Cr, EM properties, lifetimes of 749 and 777 keV levels, E2/M1 mixing ratio 80−63127
^{51}Cr, strongly deformed $K^\pi=1/2^-$ bands from γ meas., level transition parameters 79−3113
^{53}Cr excited state lifetimes from ^{50}Ti(α,n) 79−26392
^{53}Cr, yrast level lifetimes and J^π assignments from ^{48}Ca+^{9}Be 79−9445
^{54}Cr levels, transitions, $T_{1/2}$, J^π, shell model anal. from ^{51}V(α,pγ) 80−47381
^{127}Cs, 66-keV decay, $T_{1/2}$, K conversion coeff. 77−54184
^{129}Cs $11/2^-$ isomer, g-factor and lifetime in CsI cubic environment from ^{127}I(α,2n) 79−6394
^{133}Cs, excited levels lifetime meas. using retarded coincidence method *(French)* 78−62507
^{A}Cu A=29,63, Doppler shift attenuation factors, level lifetimes, resonances from Ni(p,γ) 80−57741
^{A}Cu, A=63,65, mean lifetime meas., 1400 to 1650 keV range, by reson. scatt. of bremsstrahlung *(French)* 79−75905
^{59}Cu, reson. lifetime, J, via ^{58}Ni(p,γ) 1833 and 3547 keV 77−26621
^{63}Cu EM decay transitions, level J^π assignments, level lifetimes from (α,pγ), (^{11}B, 2pγ) 79−85402
^{63}Cu low excitation states, level struct. and lifetimes from ^{60}Ni(α,pγ) 80−86813
^{65}Cu(p,p′γ), 5.25, 6.0 MeV, levels, transition energies, lifetimes, branching ratios determ. 77−41960

nuclear energy level lifetimes continued
Dy, studied via $^{164}Dy(^{32}S,^{32}S'\gamma)$, recoil distance lifetimes of ground state bands 78−8774
^{A}Dy, A=159,161, lifetimes of low excited states, delayed e-γ and γγ coincidences *(Russian)* 80−68596
^{152}Dy 60 ns isomer deexcitation E2 x- (orΔ) transition, half life, γγ-coincidence from $^{152}Gd(\alpha,4n)$ 80−86859
^{152}Dy high spin isomers, yrast states and level lifetimes from (^{15}N, 4n), (^{16}O, 4n) 80−13361
^{156}Dy high spin states, γ-ang. distribs., lifetimes and feeding times from $^{148}Nd(^{13}C,5n)$ 80−13364
^{156}Dy high spin states lifetimes and feeding times, quadrupole moments from $^{24}Mg(^{136}Xe,4n)$ 80−32239
^{158}Dy, Yrast states from heavy ion collisions, lifetimes 78−54793
^{162}Dy rotational states lifetime meas. using $^{162}Dy(^{40}Ar,^{40}Ar'\gamma)$ 78−50123
$^{162}Dy(^{136}Xe,^{136}Xe')$, 547, 612 MeV, high spin state energies and reduced transition probabilities 80−18232
^{164}Dy, recoil distance meas. of lifetimes of rotational states 78−66242
^{165}Dy, collective contributions to E1, ΔK=1 matrix elements in odd-odd deformed nuclei 79−17857
^{153}Er 360 ns yrast trap, γ transitions and lifetimes from $^{144}Sm(^{12}C,3n)$ 80−9205
^{154}Er, high-spin yrast states, lifetime meas. using recoil-distance method 79−40884
^{157}Er, lifetimes of excited states, delayed e-γ coincidences *(Russian)* 80−68597
^{170}Er, studied via $^{170}Er(^{32}S,^{32}S'\gamma)$, recoil distance lifetimes of ground state bands 78−8774
^{144}Eu, multiplet splitting and isomerism, J, π, T1/2 via (d,2n) and (p,n) 77−14014
^{152}Eu doubly odd nucleus, transition probabilities and deformations, obs. in (n,γ) 79−97680
^{18}F 1.04 MeV state lifetime and γ-transition polarisation from $^{18}O(p,n)$ 80−106016
^{19}F, 3907 keV state, lifetime meas. by Doppler shift attenuation method 77−88079
^{19}F levels, studied via $^{19}F(p,p'\gamma)$, 5 to 9 MeV 77−297
^{19}F low lying band state lifetimes, stopping power, transition strengths from $^{15}N(\alpha,\gamma)$ 80−42585
^{52}Fe, low-lying excited states, $^{50}Cr(^{3}He,n\gamma)^{52}Fe$ reaction 78−4952
^{53}Fe, strongly deformed $K^{\pi}=1/2^{-}$ bands from γ meas., level transition parameters 79−3113
^{54}Fe 8^{+} and 10^{+} level spin assignments and lifetimes from (^{16}O,2p), (^{6}Li, pn) 80−68531
^{56}Fe, level struct. via (^{12}C,α2p), (α,2p) and (α,α) reactions 77−67702
^{56}Fe, populated in $^{54}Fe(\alpha,pp)$, transition rates of high spin states 77−6301
^{58}Fe energy level lifetimes up to 4213 keV from $^{55}Mn(\alpha,p\gamma)$ 79−17853
^{58}Fe high spin states from ^{55}Mn(d,pγ), decay props., γ-γ coincidence 78−21515
^{68}Fe low lying state mean lifetimes and transitions from $^{64}Zn(^{7}Li,p2n)$ 80−68599
Ga, A=66, 68 isomeric state from $^{56}Fe+^{13}C$ and $^{56}Fe+^{15}N$ reactions, lifetimes, g-factors 78−33147
^{67}Ga, levels, branching, mixing, $T_{1/2}$, via $^{67}Zn(p,n\gamma)$ 3.6-4.3 MeV 77−34247
^{67}Ga levels below 2.5 MeV populated in $^{64}Zn(\alpha,p\gamma)$ 77−88042
$^{69}Ga(p,p'\gamma)$, 3.0-5.1 MeV, low lying state struct., lifetimes, spin and parity 79−467
^{74}Ga, half-life of 56.5 keV level by delayed coincident summing 77−34255
$Gd(^{35}Cl,^{35}Cl'\gamma)$, A=154, 6, 132-43 MeV, lifetime meas. of high spin states 78−13140
^{67}Gd, γ-spectroscopy of high-spin levels via $^{64}Zn(\alpha,p\gamma)$, $^{53}Cr(^{16}O,pn\gamma)$ 78−93960
^{142}Gd, populated in (α,6n), ground state bands obs. 77−2938
^{146}Gd, 3^{-} 1579 keV first excited state 78−41670
^{146}Gd, O_2^{+} state EM decay, $T_{1/2}$ and monopole strength 80−95310
^{147}Gd, high-spin states and particle-core coupling 77−26614
^{151}Gd, 108 and 395 keV levels, mag. moments and half-lives, PAC 77−22883
Ge, A=68, 70, lifetime meas. by DSAM, using (α, 2nγ) reaction at E_{α}=30 MeV 78−8773
^{A}Ge, A=66,69,70, negative parity high spin states, spin and lifetimes from HI reactions 80−73768
^{A}Ge, A=70, 72, 74, appl. of crystal blocking technique to study highly excited nuclear continuum using (p,p') 79−45261
^{19}Ge excited state, J, mean lifetimes and transitions from $^{64}Za(^{7}Li,ph)$
^{19}Ge excited state, J, mean lifetimes and transitions 80−68517
^{66}Ge levels, lifetimes, J^{π} and transitions from $^{58}Ni(^{10}B,pn\gamma)$ 80−73799
^{66}Ge levels, lifetimes and mixing ratio, in-beam γ-spectroscopy from $^{54}Fe(^{14}N,np\gamma)$ 80−42541
^{66}Ge states and decay scheme, polarisations J^{π} and ang. distribs. from $^{58}Ni(^{10}B,pn\gamma)$ 80−22692
^{67}Ge excited state decay scheme, mean lifetimes from $^{64}Zn(\alpha,n\gamma)$ 79−26393
^{67}Ge, M2 transition half-life 78−89823
^{67}Ge, mass excess and low lying states, comparison with ^{63,65}Ni, ^{65,67}Zn and ^{69}Ge, from $^{65}Zn(\alpha,n\gamma)$ 78−66213
^{68}Ge, excited states populated in $^{58}Ni(^{12}C,2p)$, spins and parities of levels 78−13020
^{68}Ge multiple band struct., $g_{9/2}$ orbital, level lifetimes from $^{58}Ni(^{12}C,2p)$ 80−13358
^{69}Ge excited states, lifetimes and J^{π} assignments, mixing ratios from $^{66}Zn(\alpha,n\gamma)$ 79−63629
^{69}Ge level structure and lifetimes, decay through negative parity band from $^{55}Mn(^{16}O,pn\gamma)$ 79−45172
^{72}Ge high spin levels obs. in $^{70}Zn(\alpha,2n\gamma)$ *(French)* 79−22304
^{A}Hf(HI,xn), A=170-173, two and three quasiparticle isomers, rot. bands, decays and lifetimes 80−9211
^{171}Hf, hindered electric dipole transitions and lifetimes from (HI,xn) reactions 80−9263
^{171}Hf one- and three-quasiparticle states, high spin rot. bands from (^{16}O,5n), (^{13}C,4n) 80−18163
^{172}Hf rotation bands from $^{160}Gd(^{16}O,4n)$, high spin states, halflives 78−25217
^{175}Hf multi-quasiparticle states and bands, isomeric states, lifetimes from $^{170}Er(^{9}Be,4n)$ 80−9213
^{175}Hf, three- and five-quasiparticle isomers, rotational bands and residual interactions from $^{170}Er(^{9}Be,4n)$ 80−83022
Hg, A=199, 197, 5/2^{-} state halflife and mag. moments 78−506

nuclear energy level lifetimes continued
Hg high spin states and rotation alignment in ^{198}Hg 77−57591
$^{184}Hg\rightarrow^{184}Au$ decay, energy levels and lifetimes *(French)* 78−41661
^{155}Ho high spin states, lifetimes, J^{π} and rot. parameters from $^{145}Nd(^{14}N,4n)$ 79−85354
^{157}Ho, lifetimes of excited states, delayed e-γ coincidences *(Russian)* 80−68597
^{158}Ho, isomeric state and rotational band meas. in $^{159}Tb(\alpha,5n)$ and $^{160}Dy(p,3n)$ 77−2890
^{165}Ho, excited state lifetimes, delayed coincidences method 77−6298
^{127}I 57.6 keV level half-life meas., β-γ delayed coincidences 77−6300
^{128}I, on-line data acquisition system for monitoring high resolution multi-dimensional spectra 78−58567
^{A}In, A=113,115, mean lifetime meas., 1400 to 1650 keV range, by reson. scatt. of bremsstrahlung *(French)* 79−75905
^{107}In nucleus and K shell excitation, lifetime meas. from $^{106}Cd(p,p')^{106}Cd$ 80−63130
^{111}In $21/2^{+}$ isomeric state g-factor and relaxation time from $^{109}Ag(\alpha,2n\gamma)$ 80−73794
^{112}In, 8^{-}, 6^{+} isomeric states, $T_{1/2}$, g-factors via $^{112}Cd(p,n)$, $^{109}Ag(\alpha,n)$ 77−10318
^{112}In, half-lives and mag. moments of two high spin states, γ-ray spectra 77−22940
^{112}In low lying levels, transitions, $T_{1/2}$, multipolarities and mixing ratios from $^{112}Cd(p,n\gamma)$ 80−68545
^{119g,m}In, decay schemes, half-lives, excited levels 77−296
^{191}Ir, excited nuclei mean precession time depend. on γ-spectral width, g-factors *(Russian)* 80−78211
^{A}K, A=45,46, levels, lifetimes and transitions from Ar β-decay 80−42597
^{38}K, lifetime and E2/M1 branching ratio of second excited state 77−34254
^{40}K, lifetime determ. using Doppler shift attenuation 79−93551
^{41}K, l-forbidden M1 decay from 1st excited state 78−13024
^{41}K states from $^{40}Ar(d,n)$, lifetimes meas. by DSA method 78−78308
$^{41}K(p,p\gamma)$, 1.58 MeV, parity doublet gamma lifetimes, 3/2 levels, parity mixing 80−78209
^{43}K, $(7/2)^{-}$ 738 keV state g-factor and lifetime 77−10367
^{43}K high spin states, J^{π} and lifetimes from $^{40}Ar(\alpha,p\gamma)$ 79−67621
^{44}K excited levels, J^{π}, transitions and lifetimes from $^{48}Ca(p,\alpha n)$ 80−68544
^{47}K, single particle states lifetimes calcs. 80−105943
^{78}Kr band struct., lifetimes and E2 transitions n-p boson model anal. from ^{65}Cu (^{16}O, 2np) 79−80863
^{78}Kr bands, lifetimes and E2 transitions from interacting boson model and (^{16}O,p2n), (^{19}Fe,α2n) 80−73771
^{78}Kr high spin levels, bands and transitions, level lifetimes from $^{68}Zn(^{12}C,Zn)$ 80−42525
^{78}Kr high spin states, transitions and lifetimes from (^{16}O,2np), (^{19}F,2nα), (^{16}O,2n), (^{12}C,2n) 80−27534
^{79}Kr excited states, J^{π} assignment, transitions, level lifetimes from ^{79}Rb β^{+} decay 79−17810
^{81}Kr levels, transitions and J^{π} assignments, first excited state lifetime from $^{81}Br(p,n\gamma)$ 79−75849
^{7}Li, lifetimes of first excited levels meas. 77−22943
Lu, A=162,4,5, from Eu(^{16}O, xn), gamma transitions, half-lives anal. 78−62509
^{174}Lu isomeric levels, γ-spectra, T 1/2 and decay modes from $^{176}Yb(p,3n)$ 80−99151
^{177}Lu, excited state lifetimes by delayed coincidence method 80−18231
^{177}Lu excited state lifetimes, γ-transitions from β-decay transitions 80−78205
^{24}Mg rot. band termination, level lifetimes from $^{12}C(^{16}O,\alpha)$ 80−18174
^{27}Mg, excited states up to E_x=7976 keV, studied via $^{26}Mg(d,p\gamma)$ reaction 77−41981
^{51}Mn, EM transitions, J^{π}, half-lives, branching and mixing ratios 77−18471
^{51}Mn, lifetimes of some low-lying l=1 states 77−79393
^{52}Mn, high spin state spectroscopy via $^{39}K(^{16}O,2pn\gamma)$ 37-52 MeV 77−10321
^{53}Mn high spin states, lifetimes, shell model calcs., yrast levels from $^{48}Ca(^{10}B,5n)$ 79−6425
^{53}Mn lifetimes meas. from $^{50}Cr(\alpha,p\gamma)^{53}$Mn *(French)* 79−67711
^{54}Mn excited state lifetimes from $^{51}V(\alpha,n)$ 79−26392
^{54}Mn, excited states populated in $^{51}V(\alpha,n\gamma)$, Doppler shift attenuation mesa. of lifetimes 78−17141
^{55}Mn, energy levels, bound state mean lifetimes and spins from $^{54}Cr(p,\gamma)$ 80−42586
Mo neutron rich isotopes, excited 0 states 77−22937
Mo(A=94, 95, 96), nuclear reson. fluoresc., line profiles, level lifetimes 77−71586
$^{89}Mo^{m}$ levels, transitions and half life from $^{93}Mo(p,p'3n)$ 80−86858
^{92}Mo in beam γ-spectroscopy, level, lifetimes and excitation functions from $^{90}Zr(\alpha,Zn)$ 79−13240
^{93}Mo excited state lifetimes, delayed coincidences method 77−6298
^{93}Mo, excited state lifetimes and widths populated in $^{92}Mo(\gamma,\gamma)$ to 5.1 MeV 77−30512
^{99}Mo, short lived isomers from photonuclear reactions, internal conversion coeffs. 78−37308
^{14}N, DSA lifetimes determ. from exptl. stopping powers 78−17142
^{14}N, g-factor, lifetime meas. of 5.106 MeV 2^{-} state of ^{14}N 78−93965
^{14}N unbound 4_1^{+}, 5_1^{+}, 3_2^{+} states from $^{13}C(p,\gamma)$, lifetimes, branching ratios 78−25184
^{15}N 9.155 MeV state, lifetime, cluster nature and parity from $^{12}C(^{7}Li,\alpha\gamma)$, $^{12}C(^{6}Li,^{3}He\gamma)$ 79−6424
^{15}N states, cross sections and lifetimes, EM decay strengths from 3 and 4 particle transfers 80−9237
^{16}N, 1-20 ps region mean lifetime meas., high-vel. DSA method 77−65200
^{21}Na DSA lifetime of 2425 keV state via $^{20}Ne(p,\gamma)^{21}$Na 1.7 MeV 77−82860
^{21}Na, mag. moment and lifetime of first excited state determ. 78−550
^{21}Na, produced in $^{2}H(^{20}Ne,n\gamma)^{21}$Na energy level lifetime 78−41631
^{22}Na 0^{+} level mean life, isovector mag. dipole transition from $^{19}F(\alpha,n)$ 80−68595
^{22}Na, 4.52 MeV state, J^{π}, lifetime, via $^{12}C(^{12}C,d\gamma)^{22}$Na 77−54147
^{22}Na bound and analogue state lifetimes, branching ratios, DSA method from $^{21}Ne(p,\gamma)$ 0.5-6.0 MeV 78−93967
^{22}Na excited states, recoil-distance method 77−30510
^{22}Na, ground state band struct., J^{π}, E2 transitions, $T_{1/2}$ *(French)* 77−34210

nuclear energy level lifetimes continued
^{22}Na, recoil-distance lifetime meas. 77−34252
^{23}Na levels, resonance strengths, γ-decays and level lifetimes from ^{22}Na(p,γ) 79−45229
^{23}Na, spectroscopy of high-spin states in ^{12}C(^{12}C,pγ) 77−46131
^{24}Na, τ, J, π, branching and mixing ratios for lowest 5 levels 77−57624
Nb, A=90, 92, short lived isomers from photonuclear reactions, internal conversion coeffs. 78−37308
^{91}Nb 21/2$^+$ state, lifetime, g-factor meas. 77−30487
^{91}Nb, struct. anal. from ^{91}Zr(p,nγ) at 3.5-4.8 MeV 78−13011
^{92}Nb, high-spin states, EM props. via ^{88}Sr(^{7}Li, 3n)^{92}Nb 34 MeV 77−74770
^{90m}Nb, decay rate perturbation by implantation in metals 78−21524
^{141}Nd, ^{142}Nd, high-spin states, lifetime meas. using (α,xn) reactions 77−18476
^{143}Nd, high-spin states and particle-core coupling 77−26614
^{147}Nd low spin states ns lifetimes, particle rotor model interpretation from ^{146}Nd(d,pγ) 80−78207
^{150}Nd, Doppler shift meas. of ground state bands using ^{150}Nd(^{40}Ar,^{40}Ar′γ) 78−50124
^{19}Ne, mean lifetimes via ^{19}F(p,nγ)^{19}Ne at 12 MeV 77−54180
^{21}Ne 2796, 1747, 2867 keV level mean lifetimes from ^{4}He(^{18}O,n) 79−93553
^{21}Ne, Doppler shift attenuation lifetime meas. at high recoil velocity 77−30513
^{21}Ne, mag. moment and lifetime of first excited state determ. 78−550
^{21}Ne, TDPAC obs. on ions recoiling in vacuum 77−22942
^{21}Ne*, produced in ^{2}H(^{20}Ne,p)^{21}Ne*, 351 keV 5/2$^+$ state lifetime and mag. moment 78−41631
^{22}Ne 3.34 MeV level lifetime meas. by Doppler-shift method, slowing down environment effect 77−38245
^{22}Ne excited states, recoil-distance method 77−30510
^{22}Ne, interpretation of Z_2 variation in low velocity DSAM results 79−26394
^{22}Ne lifetime of 6$^+$ member of ground state band by DSAM, B(E2) values 79−26395
^{22}Ne, lowest 4$^+$ state lifetime meas. via Doppler shift technique 78−37307
^{22}Ne, recoil-distance lifteime meas. 77−34252
^{22}Ne(2$^+$), g-factor and τm via ^{4}He(^{19}F,pγ) 38.5 MeV 77−34224
^{22}Ne(4$_1^+$) from ^{4}He (^{19}F,pγ), lifetime meas. by high vel. coincidence DSA method 78−33148
^{22}Ne(γ,γ), up to 18 MeV, nuclear resonance fluorescence, states, transitions and lifetimes 79−45234
^{58}Ni, mean lifetime meas., 1400 to 1650 keV range, by reson. scatt. of bremsstrahlung *(French)* 79−75905
^{60}Ni high spin states, J^π, T$_{1/2}$, ang. distribs. and polarisations from ^{56}Fe(^{7}Li, p2nγ) 80−99116
^{60}Ni yrast state lifetimes and parities from ^{51}V(^{12}C,2np) 79−45134
^{61}Ni, γ-spectroscopy above 2.2 MeV excit., J^π,T, branchings 77−54172
^{61}Ni low lying states, lifetime meas. using ^{58}Fe(α,nγ) 77−88078
^{61}Ni, spectroscopy of levels below 2.2 MeV obs. in ^{58}F(α,nγ) 77−6289
^{62}Ni excited states from ^{59}Co(α,pγ), B(E2) values 79−3115
^{62}Ni level struct. and decay scheme, shell model calcs. from ^{59}Co(α,pγ), 10 MeV 79−3085
^{237}Np, lifetime of 60 keV state, undergraduate expt. 79−20
^{15}O, lifetimes of bound states populated in ^{14}N(p,γ) 77−82928
^{15}O, nucl. g-factor and lifetime of 5.24 MeV 5/2$^+$ level 78−37269
^{18}O, 2$^+$ 1.98 MeV level lifetime and g-factor determ. from high velocity recoil in vacuum 77−18474
^{20}O, 1-20 ps region mean lifetime meas., high-vel. DSA method 77−65200
^{20}O first excited state, g-factor and lifetime from ^{3}H(^{18}O, pγ) 80−102115
^{A}Os, A=186, 188, 7$^-$ isomeric state lifetime from W(α,2nγ) 79−17854
^{28}P, T=1 positive parity analogue states 77−34249
^{30}P, recoil-distance lifetime meas. 77−34252
^{30}P T=1 state decay, lifetimes and branching ratios, analogue E2 transitions from ^{29}Si(p,γ) 80−68598
^{31}P, interpretation of Z_2 variation in low velocity DSAM results 79−26394
^{31}P, precision Doppler-shift attenuation lifetime meas. from γ-ray lineshapes 79−36195
Pb, A=194, 196, 198, 12$^+$ isomeric states, T$_{1/2}$, g-factor 77−74762
^{A}Pb, A=190,192, level scheme, γ-branching, ^{192m}Pb half life from Gd+^{40}Ar and ^{182}W+^{16}O 79−75854
^{A}Pb, A=197, 198, low energy γ-transitions and level lifetimes from ^{186}W(^{16}O, xn) 80−18221
^{197}Pb isomers, half lives and decay 79−36197
^{203}Pb, 480 ms isomeric 29/2$^-$ state, decay scheme 77−22893
^{204}Pb, populated by ^{204}Bi decay, isomeric transitions 78−50122
^{206}Pb, half-lives of two-neutron-hole 0$_2^+$ state 77−10323
^{207}Pb, 569.6 keV level, half-life meas. 78−55090
^{210}Pb levels, J^π, transitions and lifetimes from ^{208}Pb(^{7}Li,X) 80−68542
^{101}Pd, level struct. obs. in ^{101}Ag β-decay 78−37311
^{101}Pd nonyrast rotational states, transitions, T$_{1/2}$, branching and mixing ratios from ^{92}Zr(^{12}C,3n) 80−105950
^{102}Pd, 1592 keV E0 transition T$_{1/2}$ meas. using e-γ coincidence 80−22762
^{106}Pd, reson. scatt. of annihilation quanta, excited state lifetime meas. *(Russian)* 77−26651
^{109}Pd, level structure and half life 77−82827
^{142}Pm, multiplet splitting and isomerism, J, π, T1/2 via (d,2n) and (p,n) 77−14014
^{145}Pm level struct., J^π and lifetimes, cluster-vibr. model anal. of ^{146}Nd(p,2n) 80−91125
^{147}Pm, level struct. via ^{148}Nd(p,2nγ) 12.1-20.2 MeV 78−510
^{151}Pm, excited state lifetimes, delayed coincidences method 77−6298
^{208}Po, half-lives of two-neutron-hole 0$_2^+$ state 77−10323
^{212}Po, levels, J^π, transitions and lifetimes from ^{208}Pb+^{7}Li 80−68542
^{214}Po, half life of α-emitting excited 0$^+$ state 79−45205
^{139}Pr isomeric 11/2$^-$ state, half-life, g-factor, and nuclear orientation relaxation from ^{140}Ce(p,2nγ) 79−75837
^{A}Pt, A=186,188,190, subnanosecond high spin isomers, decay chains and lifetimes from Yb(^{16,18}O, xn) 79−45140
^{A}Pt, A=190-193, lifetimes of rotation-aligned states 78−93969
^{187}Pt, levels, J^π, T$_{1/2}$, possible E0 transitions from ^{187}Au decay *(French)* 80−32230
^{192}Pt 3$^+$ and 4$_1^+$ states from ^{192}Ir β decay, lifetime meas. by β-γ coincidence 78−25153
^{192}Pt, lifetimes of first four excited states 77−294
nuclear energy level lifetimes continued
^{192}Pt, lifetimes of ground-band states, B(E2) values, (Ar,Ar′γ) reaction 77−54181
^{194}Pt, lifetimes of ground-band states, B(E2) values, (Ar,Ar′γ) reaction 77−54181
^{196}Pt (^{20}Ne, ^{20}Ne′), excited states, lifetime meas. using recoil-distance method 80−13413
^{196}Pt (^{58}Ni, ^{58}Ni′), excited states, lifetime meas. using recoil-distance method 80−13413
^{237}Pu fission isomers, half lives and yield ratio, statistical model anal. from ^{239}Pu(γ,Zn) 79−40885
^{237}Pu fission single particle isomers, half lives and isomeric ratio from ^{239}Pu(γ,2n) 80−18181
^{A}Rb, A=79, 81, decoupled g$_{9/2}$ bands, level lifetimes and E2 transitons from (^{16}O, 2n)(^{19}F, p2n) 80−73772
^{82}Rb, level structure, gamma angular and time distribs. from ^{81}Br(α,3n) 80−52583
^{94}Rh, γ-spectrum and half-lives 80−83062
^{100}Rh, lifetime measurements in excited states 79−63631
^{108}Rh, level structure and half life 77−82827
^{210}Rn high spin states, decay and lifetimes, spin assignments from ^{204}Pb(^{9}Be,3n) 80−18168
^{212}Rn, shell model states, semiempirical calcs. half lives, mag. moments, excitation functions 80−63083
^{101}Ru, short lived isomers from photonuclear reactions, internal conversion coeffs. 78−37308
^{34}S(γ,γ), E<18 MeV, state lifetimes, excitation energies and level cross sections 78−93966
Sb, A=108,109,110, gamma-ray meas., decay scheme calc. 77−18473
Sb, A=115, 117, 11/2$^-$ isomeric states, half-life, and g-factor 78−33122
^{A}Sb, A=113,115,117,119, high spin states, J^π assignments, decay schemes and lifetimes from Cd(^{6}Li,3n) 79−54381
^{112}Sb, ^{114}Sb, 8$^-$ states, half-life and mag. moment, γ-ray spectra 77−22941
^{113}Sb, 15 MeV excitation, average nucl. lifetime determ. 80−43164
^{113}Sb mean nuclear lifetime from X-ray spectrum in ^{112}Sn(p,p′) 80−9267
^{115}Sb, high-spin states anal., ^{113}In(α,2nγ) at 20-30 MeV 77−41982
^{121}Sb, bremsstrahlung reson. fluoresc. obs. in natural isotopic mixture *(French)* 79−13247
^{122}Sb, low-lying state props., coupled neutron quasiparticle-proton model 77−61378
^{123}Sb, bremsstrahlung reson. fluoresc. obs. in natural isotopic mixture *(French)* 79−13247
^{43}Sc, g-factor of 3/2$^+$ hole state meas. in (α,p) react. 78−21492
^{43}Sc, J^π=19/2$^-$ isomer, high-spin precursors, from ^{29}Si(^{16}O,pn) 80−57656
^{44}Sc, mean lifetimes of 1648-1768 keV levels via ^{41}K(α,n) 5-11 MeV, DSA method 77−6299
^{45}Sc levels, J^π, transitions and lifetimes from (p,p′)(^{3}He,^{3}He′)(α,α′) 80−63091
^{49}Sc, single particle states lifetimes calcs. 80−105943
^{72}Se recoil distance level lifetime meas. from ^{58}Ni(^{16}O,2p) 78−78311
^{72}Se yrast states from ^{58}Ni(^{16}O,2pγ), γ spectra, lifetimes, nuclear model predictions 77−54176
^{76}Se high spin states, bands, J^π, transitions and T$_{1/2}$ from ^{71}Ga(^{7}Li,2n) 80−105951
^{27}Si, γ-branchings and mixing ratios determ. from ^{24}Mg(α,nγ) 78−17224
^{28}Si, 12.44 MeV 2$^+$ level lifetime meas. by crystal blocking 77−34253
^{28}Si 4$^+$ state lifetime by blocking effect method from ^{27}Al(p,α) *(Russian)* 80−91152
^{28}Si compound states populated in ^{27}Al(p,α), 937 and 885 keV resonance lifetime meas. using crystal blocking technique 79−63671
^{28}Si, interpretation of Z_2 variation in low velocity DSAM results 79−26394
^{28}Si lifetimes in selected materials, DSA study, theoretical stopping power predictions 78−74329
^{28}Si, precision Doppler-shift attenuation lifetime meas. from γ-ray lineshapes 79−36195
^{28}Si, prolate and oblate intrinsic states *(French)* 78−70482
^{28}Si, T=1 positive parity analogue states, lifetimes and branching ratios 77−34249
^{30}Si, recoil-distance lifetime meas. 77−34252
Sm, ion recoiling into gas and vac., hyperfine field and correl. time meas. 78−66240
^{140}Sm, populated in (α,n), ground state bands obs. 77−2938
^{142}Sm isomers, lifetimes and transitions from ^{142}Nd(α,4n) 80−78122
^{145}Sm, excited state lifetimes γγ ang. correls. 77−6298
^{145}Sm, high-spin states and particle-core coupling 77−26614
^{152}Sm(^{35}Cl,^{35}Cl′γ), 132-43 MeV, lifetime meas. of high spin states 78−13140
Sn, odd isotopes, number-projected three-quasiparticle description 78−93953
Sn(^{16}O, 4nγ), 76 MeV, lifetimes of yrast states of even Ce nuclei 78−21589
^{A}Sn, A=120,122,124,126,128, levels, transitions and J^π values from In isomeric decays 79−75851
^{112}Sn 6$^+$ isomeric state g-factor and relaxation time from Cd(α,2nγ) 80−73794
^{115}Sn, Coulomb excit. via (^{4}He,^{4}He) and (^{16}O,^{16}O) reactions 77−67719
^{116}Sn(^{16}O,^{16}O) 48 MeV, collective states, E2, E0 transition probabilities, halflife, branching ratios 80−18172
^{119}Sn, 23.87 keV level half-life 80−47433
^{132}Sn, doubly magic, RPA calc. of level scheme 78−50087
^{132}Sn level struct., lifetimes, γ-γ coincidences, internal conversion from ^{235}U fission 80−52584
^{132}Sn levels, isomers, lifetimes and transition probabilities from fission 80−78163
^{119m}Sn, by X- and γ-ray intensity meas. 77−26620
Sn(p,2nγ)Sb, A=111, 3, 5, excited states of Sb anal. 77−2911
^{85}Sr, lifetime DSA meas. in ^{82}Rb(p,nγ) 79−36196
^{87}Sr excited levels from ^{87}Rb(p,nγ), spin, parity, branching ratios, lifetimes 77−50076
^{98}Sr very low lying 0$^+$ state, shape coexistence bands, T$_{1/2}$, transitions from ^{98}Rb decay 80−78148
^{100}Sr ground state rot. band transitions, deformations and lifetimes from ^{100}Rb β-decay 79−93550
^{176}Ta, decay of four-particle isomer 78−70481

nuclear energy level lifetimes continued
^{176}Ta, isomeric states and rot. struct. anal., in-beam γ-ray spectroscopy 78−78312
^{177}Ta, γ-transition $55/22^+ \rightarrow 77/22^+$, E2/M1 mixing, μ determ., $T_{1/2}$ 77−10355
^{178}Ta level properties, rot. bands, transitions and level lifetimes from ^{176}Lu(α, 2n), ^{178}Hf(d, 2n), ^{178}Hf(p, n) 79−36158
^{149}Tb, lifetimes of low-lying levels *(Russian)* 78−46027
^{151}Tb lower excited state lifetimes, ^{151m}Tb isomer from ^{151}Dy decay 79−75919
^{153}Tb, low excited states, lifetime meas. 79−6492
^{155}Tb, excited state lifetimes 79−6494
Tc, A=98, 100, 101, short lived isomers from photonuclear reactions, internal conversion coeffs. 78−37308
^{96}Tc, low-lying levels, γ-transitions via ^{93}Nb(α,n)^{96}Tc 10.8, 14.0 MeV 77−2931
^{97}Tc excited state lifetimes, delayed coincidences method 77−6298
^{98}Tc, lifetimes of isomeric states from ^{98}Mo(p,n), 4-5 MeV 78−82314
^{100}Tc internal conversion, isomeric level half life from ^{100}Mo(p,n), 3.7 MeV 78−78313
^{100}Tc low lying and isomeric levels, transitions and mean lines from ^{100}Mo(p,nγ) 80−42548
^{100}Tc μs isomers, isomeric transitions and mean lives from ^{100}Mo(p,n) 80−73803
^{120}Te quasi-rot. band based on proton 4p-2h state, level scheme, transitions from ^{116}Sn(α,2nγ) 80−78119
^{121}Te isomeric state, spin, lifetime and mag. moment from (α,n),(d,Zn) 80−47387
^{125}Te, levels and transitions following decay of ^{125}Sb 79−71816
^{132}Te from fission, 10^+ isomeric state, J^π from deexcitation pattern, half life 80−460
Ti, A=51, 52, mean lifetimes of yrast states populated in ^{48}Ca+Li 77−2942
^{43}Ti, lifetime and γ decay of isomeric $19/2^-$ state from ^{40}Ca(α,nγ) 20 MeV 78−70486
^{43}Ti positive parity states, mean lifetimes, quasirotational band from ^{40}Ca(α,n) 20 MeV 79−6415
^{44}Ti levels, lifetimes and spins meas. from ^{40}Ca(α,γ)^{44}Ti 77−79328
^{46}Ti, lifetime meas. by γ-γ coincidence technique following ^{40}Ar(^{9}Be,3n) 79−59318
^{48}Ti high spin states, γ-decay, J^π assignments, lifetimes from ^{45}Sc(α,pγ) 80−13356
Tl, A=201,203, levels via (d,3nγ), J^π,$T_{1/2}$, $9/2^-$ band discovery 77−34207
^{198}Tl rotational structure 77−54130
^{206}Tl, excitation of 12^- isomeric state in Bi(n,α) at 14 MeV, half life 78−70453
^{169}Tm, studied via ^{169}Tm(^{32}S,^{32}S′γ), EM props. of ground state rot. band 78−8726
^{1}u2C mean life, Pauli exclusion principle validity for nucleons 80−18233
^{A}U, A=237,238, nuclear excitation rate for low lying states, e and γ induced transitions 79−17856
^{236}U, odd-parity level at 687.59 keV, mixing ratios, half-life 77−50079
^{238}U shape isomeric γ-decay, in μ^- atoms, isomer lifetime 77−34245
^{238}U(p,nf), multiple scatt. effect due to filling in of blocking patterns 78−21617
^{45}V level scheme, γ-rays, level lifetimes, internal conversion from ^{40}Ca(Li,xn) 80−63085
^{50}V excited states populated in ^{42}Ti(α,pγ), lifetimes 78−21583
^{A}W, A=173, 175, hindered electric dipole transitions and lifetimes from (HI,xn) reactions 80−9263
^{180}W ground and K=2^- octupole band ang. momenta coupling, lifetimes from ^{181}Ta(p,2nγ) 80−9214
^{180}W, rot. and vibr. bands, γ-vibr. band, metastable state half life from ^{181}Ta(p,2nγ) 79−54378
^{118}Xe, decay investig. using mass separator on-line with synchrocyclotron 78−17139
^{119}Xe, decay investig. using mass separator on-line with synchrocyclotron 78−17139
^{125}Xe odd and even parity band structs., level lifetimes from ^{125}Te(^{3}He,3nγ) 80−27533
^{129}Xe, excited state lifetimes by delayed coincidence method 80−18231
^{129}Xe excited state lifetimes, γ-transitions from ^{129}Cs decay 80−78205
^{A}Yb, A=163, 165 level schemes and backbending behaviour of neutron deficient isotopes 79−40836
^{172}Yb levels, bands, J^π and $T_{1/2}$ from ^{170}Er(α,2n) 80−91127
^{174}Yb, studied via ^{174}Yb(^{32}S,^{32}S′γ), recoil distance lifetimes of ground state bands 78−8774
^{63}Zn, $5/2^-$ 193 keV level, γ-ray ang. distrib. integral rot. 77−41912
^{63}Zn EM decay transitions, level J^π assignments, level lifetimes from (α, nγ), (^{11}B, npγ), (^{7}Li, pnγ) 79−85402
^{64}Zn, γ-ray studies of levels above 3.1 MeV 80−32238
^{64}Zn high spin states, J^π, $T_{1/2}$, γ-decays from (α,nγ), (^{11}B,p2nγ) 80−73767
^{64}Zn, populated in ^{51}V(^{16}O, p2nγ) 78−13019
^{64}Zn, quasi-rotational states populated in ^{51}V(^{16}O,p2nγ), lifetimes and effective population times 78−17140
^{64}Zn, struct. of quasi-bands from (α,nγ) and (^{11}B,p2nγ) 78−70424
^{65}Zn, EM transition probabilities, lifetimes, weak coupling model 77−74804
^{65}Zn, high spin states obs. in (α,nγ), and (^{16}O,np) 78−13016
^{66}Zn negative parity high spin states, spin and lifetimes from HI reactions 80−73768
^{67}Zn, excited state lifetime, DSA meas. *(Russian)* 78−41668
^{67}Zn, γ spectroscopy of low spin states from ^{64}N(α,nγ), 8.2 MeV 78−78303
^{67}Zn, high spin states obs. in (α,nγ) 78−13016
^{67}Zn, populated in ^{64}Ni(α,n), level struct. below 2.0 MeV, γ-ray studies 78−62483
^{70}Zn, lifetime meas. by DSAM, using (α, 2nγ) reaction at E_α=30 MeV 78−8773
Zr neutron rich isotopes, excited 0 states 77−22937
^{86}Zr, populated in ^{73}Ge(^{16}O,3n), lifetime meas. by Doppler shift method 78−25152
^{100}Zr, lifetime meas. of 331.3 keV 0_2^+ state 78−21523

nuclear energy level transitions
see also internal conversion; Mossbauer effect; nuclear branching and mixing ratios; nuclear energy level lifetimes
2_γ^+ level depopulation, reduced quadrupole transition probabilities, neutron-proton mass deformation difference 77−34203

nuclear energy level transitions continued
150<A<190 odd-mass deformed nuclei, absolute EM transition probabilities *(Russian)* 77−34251
^{145}Sm neutron separation and level exciton (n,γ) and (d,p) correlations 80−22756
^{208}Pb (N,N^1) unnatural parity state excitation, π− condensate instability proximity, DWBA 79−97660
^{24}Mg radiative decays of unbound high spin states from ^{20}Ne(α,γ), ^{20}Ne(α,α′γ) 79−6484
^{298}114, high spin pot. energy surfaces, fission barrier, α-, γ-decay half lives, yrast spectrum 80−73764
^{A}S, A=32,34, E1 and E2 strength, E1 giant resonance decay, isospin from Si(α,γ) 79−89266
β band influence on structure of decoupled bands 78−93921
A=105, nuclear data sheets, levels, decays and J^π assignments 79−93486
A=119, nuclear data sheets, level and decay props. 79−71780
A=11, 12, energy levels, transitions and resonances, compilation 80−46743
A=120-150, levels and EM props., recent results 80−68592
A=121 nuclear data sheets, level schemes and decay properties 79−75818
A=12 to 40, (α,^{2}He) reaction, high spin state transition cross sections in 1p and 2s1d shell 79−6644
A=12-240, even-even, dynamic deformation theory, B(E2) values, quadrupole and mag. moments 80−68591
A=134-144, fission yields from spectroscopic meas., γ-branching and half-lives 80−78213
A=135-143, odd A fission products, delayed n, decay studies and Q_β meas. 80−78227
A=136 nuclear data sheets, level schemes and decay props. 79−75819
A=140, nuclear data sheets, levels and transitions 80−31435
A=144 nuclear data sheets, levels, decays and J^π assignments 79−93487
A=154, nuclear data sheets, levels, decay props., isomeric states, Nilsson orbitals 79−71781
A=159, nuclear data sheets, levels, decays, and J^π assignments 79−93488
A=160-180 nuclei, manifestations of oblate shapes at high spin, transition energies in yrast region 78−78249
A=184, 194, 200, 208, pygmy resonance, E1 transition probabilities, BCS wave functions, spin-isospin oscillation *(Chinese)* 80−63087
A=18-38, inelastic scatt. E4 transition probabilities in the 0d, 1s shell 80−78210
A=190 to 220 even-even nuclei, 2_2^+ level deexcitation *(Russian)* 77−2939
A=199, nuclear level scheme data sheets, decay scheme 79−13186
A=19-31 odd nuclei, $K^\pi = 1/2^-$ bands, spectroscopic factors and transitions 80−32151
A=1-257, nuclear excitation by atomic electron transitions, nuclear levels 80−78191
A=203, nuclear data sheets, level struct., decay schemes 79−13187
A=204, nuclear data sheets, levels, J^π and transitions 80−31429
A=212, nuclear data sheets, levels, J^π, transitions 80−31430
A=221, nuclear data sheets, levels, J^π, transitions 80−31431
A=225, nuclear data sheets, levels, J^π, transitions 80−31432
A=40-56, spectroscopy props. using pure configuration shell model *(Chinese)* 80−42584
A=46, nuclear data sheets, level struct. and decay props. 79−13185
A=4n, densities, form factors, transitions, multipole moments in s-d shell, HFC 80−37321
A=4N nuclei, lowest T=2 state isospin forbidden decays, branching ratios 79−67703
A=54-82, ground state transition strengths from (p,t) reactions 80−95305
A=58 nuclear data sheet to June 1976 77−18372
A=60, nuclear data sheets, levels and transitions 80−31433
A=60 to 150 even-even nuclei, 2_1^+ level deexcitation *(Russian)* 77−2939
A=64, nuclear data sheets, levels and transitions 80−31434
A=6-44, gamma-ray transition strengths, data tables 80−37345
A=71 nuclear data sheets, levels, J^π and transitions 80−31428
A=73, nuclear data sheets, levels, J^π and transitions 80−101673
A=76 nuclear data sheet to June 1976 77−18373
A=77, nuclear data sheets, levels, J^π and transitions 80−105439
A=7-40, EM transition strength distribs. *(Russian)* 80−86855
A<100, average E1/M1 strength ratio 80−52621
A<45 nuclei, EM transition strengths 77−46109
A≤28, giant quadrupole resonance, E2 intensity distrib., from (α, α′), DWBA anal. *(Hungarian)* 80−52642
A∼90 nuclei, isomeric states, spin polarisation, M4 transitions and giant resonances 80−63157
A = 202 nuclear data sheets, levels and transitions 79−40831
A = 86, nuclear data sheets, level and decay schemes 79−30774
actinide fission, statistical anal. of gamma emission 78−17255
actinide nuclei, even-even, E_2 transitions from 2^+ state of gamma-vibrational band 80−91150
actinides, level energies and B(E2) ratios of deformed even nuclei 79−13221
aligned states with high spins 77−82845
analog-antianalog gamma transition strength 80−13429
analogue states, dipole radiative decay 78−17135
atomic negative meson capture, nuclear giant resonance excitation *(Russian)* 80−42623
average resonance neutron capture, completeness in nuclear spectroscopy 80−106006
axion emission in decay of excited nucl. states 78−49975
B(E_2) values of gamma-ray cascades and empirical relation 80−91145
band crossing in interacting boson model, E2 transition probabilities and g-factors 80−102101
biparametric γ-γ coinc. method, γ-transition intensity meas. *(French)* 78−29697
Chung-Wildenthal hamiltonians in sd shell, possible unifaction, few particle spectra 79−85406
coherent rotational states formed in heavy ion collisions, γ-decay 80−27657
coincidence method for Coulomb excitation studies of weakly populated vibr. like levels 78−70716
collective state excitation in high-energy proton interactions with spherical nuclei 78−17073
collective structure inferred from heavy ion Coulomb excitation 80−5167

nuclear energy level transitions continued
common doorway resonance, decay amplitude phase relation from (n,γ) reactions 80−57758
complex cascade processes decay law, high spin state mean lifetime corrections *(Chinese)* 80−22761
compound highly excited states populated in (n,α) *(Russian)* 78−29472
compound nucleus, giant resonances, force functions for partial E1-transitions 78−12985
compound nucleus radiative decay, population of aligned rotational bands *(Russian)* 78−86467
compound state statistical description, single particle states, radius and excitation energy *(Russian)* 79−22180
Compton excitation of nuclear levels, cross section estimation *(Russian)* 79−49620
conference on medium heavy nuclei structure, Rhodes, Greece (May 1979) 80−67935
conference on neutron capture gamma ray spectroscopy, Upton, USA. (Sep. '78) 80−36780
conference on nuclear spectroscopy and structure, Alma Ata, USSR, (Mar. 78) 79−75809
conference on nuclear spectroscopy of fission products, Grenoble, France (May 1979) 80−77546
conference on nuclear struct. spectroscopy and atomic nucleus struct., Tashkent (Mar. 77) 79−6470
continuum γ rays, multipolarity, enhanced ang. correlation meas., heavy ion-compound nucleus reactions 78−93963
continuum transitions in nuclei at high ang. momenta, are multipolarity 79−17849
Coriolis decoupling model, two quasiparticle plus rotor bandmixing calcs. 77−6205
Coulomb and charge dependent effects in nuclei 77−54131
Coulomb excitation of sd shell nuclei, B(E2) values, lifetime meas. 78−25216
data sheets for A=184 nuclei 78−12948
data sheets for A=231, 235, 239 nuclei 78−12949
decay scheme construction from gamma transitions and coincidences, SMUDLA code 80−83063
deep inelastic heavy ion reactions, high multipole isovector modes and charge fluctuations 80−57793
deformed even nuclei, level energies, γ transitions, moment of inertia, collective Hamiltonian 78−25133
deformed even-even nuclei, E2 transitions within ground state band 78−13012
deformed even-even nuclei, SU_3 description of energy levels and reduced E2 transition probabilities *(Russian)* 79−13251
deformed nuclei, approximate projection technique for EM properties calc. 79−93510
deformed nuclei, magnetic dipole γ-transitions, one particle matrix element tables 79−6472
deformed nuclei, single particle matrix elements of electric quadrupole γ-transitions 77−88072
deformed nuclei, single particle matrix elements of radiative M2-transitions, Nilsson model 80−22753
deformed nuclei, surface thickness effects and multipole excitation splitting, sum rule approach 79−453
deformed nuclei fusion reactions, γ-multiplicities, collective and statistical γ-rays Monte Carlo calcs. 79−578
degenerate single-particle oscillator shells, particle-vibr. coupling, exact selection rule for l-forbidden M1 transitions 78−78278
delayed fission product γ spectra following short neutron irrad. 79−9645
dipole sum rule schematical eval., collective isovector quadrupole strength 80−47428
double magic nuclei, self consistent description of low lying collective states *(Russian)* 78−89783
doubly even nuclei, yrast band B(E2) values, hydrodynamical model and CAP effect 80−86793
doubly odd deformed nuclei, EM transitions, nanosec. lifetimes 78−62505
dynamic electron screening in mesonic atom and nuclear E1 transitions 78−55260
E0 transition probabilities, and 0^+ states of even-even nuclei 79−6406
E1, E0 and M1 transitions, results obtained with Darmstadt electron Linac 77−83183
E1, following l=1 neutron capture near 24 keV, width correlations 77−26765
E1 sum rule, photoabsorption and beta decay, exchange current effects 77−41950
E1 transition selection rule, light nuclei transition strengths 80−106014
E1 transitions from octupole vibrational states 79−93548
E1-radiative force function is half magic nuclei *(Russian)* 77−57620
E2 α_k conversion coeffs. for $2^+ \rightarrow 0^+$ transition, review 78−17143
E2 core-polarisation charge, nuclei near ^{16}O and ^{40}Ca 77−22888
E2-transition rates of the ground state rotational member 78−89821
E2/M1 mixing ratio, in vibr. yrast band, sign rule 79−17855
E_2-transition probabilities and Davydov-Rostovsky model 78−74330
eikonal approx., electron-oriented nucleus scatt., polarisation of e^-, nuclei and emitted γ rays 78−37331
electric dipole sum rule in correlated nuclear matter 80−83056
electron scatt. theory, EM struct. from DWBA and other models 80−5133
electron-positron internal pair formation following heavy ion collisions, conversion coeff. calcs. 78−50135
EM multipole transitions, nuclear force contrib., model independ. of energy weighted sum rules 78−66241
EM sum rules for (γ,γ), (e,e), transitions and giant resonances 80−5090
empirical $(1f_{7/2})^n$ model, review 79−17826
energy standard value and accurate determ. *(Czech)* 80−22755
energy weighted electronuclear sum rules, centre-of-mass corrections 80−5091
ensemble of random particle-hole matrices with collective eigenstates 77−61388
even actinides, lowest 0^+ state excitation, collective phonon state, spectroscopic factors from (p,t), (t,p) 80−13410
even actinides, two-nucleon transfer, first 0^+ collective state excitation, spectroscopic factor *(Russian)* 80−42530
even-even neutron-rich fission products, de-excitation spectra, β-decay, deformation 80−78203
even-even nuclei, 1^- excitations, self consistent shell model description *(Russian)* 80−13407
even-even nuclei, heavy, deformed, B(E2; $2^+ \rightarrow 0^+$) values calc. 78−74325
even-even nuclei, microscopic anal. of low-lying collective states 78−12941
even-even nuclei, phenomenological calcs. in n-p interacting boson approx. 80−27597
even-even nuclei, spectra calcs., interacting boson model 80−68590
even-even nuclei with N=66, spectra, quadrupole transition probabilities 77−26577
even-even spherical nuclei, 2_1^+ state deformation parameter from (p,p) and EM excitation 80−27549
exchange current contribs. to parity violating elec. transitions 78−29383
excitation energies, calc. by energy density method 80−47425
excitation energies in hot matter, limits 80−56703
excitation of nucleus from bound μ^- decay *(Russian)* 79−22869
excited nuclear levels, polarisation induced by at. orientation 80−91144
exciton model of γ-emission in (N,γ) reactions 78−62539
few-body problem, deuteron, EM effects, three body bound state, break-up reactions 79−85384
fission fragment deexcitation, statistical model anal. of spin influence 79−17941
fission products, short-lived, rapid paper electrophoretic separation, γ-rays and half-lives determ. 77−44498
fluctuating hyperfine field I-depend. 77−22880
form factors of 0^+-0^- transition in A=16 system, nuclear struct. effects 80−18246
fragmentation of nucleus caused by decay of bound muon *(Russian)* 79−68333
gamma ray decay scheme computation on basis of γ-γ coincidence meas. 79−59295
generalised Schwinger representation of fermion pairs to anharmonicity 78−89807
generalised vibrational rule 80−105971
giant dipole resonance, particle-hole calcs., M1 strength 80−22785
giant dipole resonance decay, photonucleon emission in shell model 79−45233
giant dipole resonance intermediate struct. using (n,γ) and (γ, n), Brink hypothesis test 80−63150
giant E0 resonances, effect on lifetime of excited 0^+ states 79−17878
giant multiple resonances, excitation strength functions 80−5037
groundstate and β-band simultaneous description, new model 77−2898
half life measurements for 35 radioisotopes 80−83070
heated spherical nuclei, quantal model of fluctuation E2 radiation *(Russian)* 78−78306
(heavy ion, xn) reactions, higher moments of γ-ray multiplicity 77−18604
heavy ion deep inelastic reactions, γ-ray multiplicity, partial ang. momenta *(Russian)* 80−37346
heavy ion induced reactions, γ multiplicity, compound nucleus deexcitation *(Rumanian)* 78−89906
heavy ion inner shell excitations, multistep processes, quasimolecular model, coupled channels calc. 80−9303
heavy ion large-angle scatt., elastic cross-section, excitation functions 80−52689
heavy ion large-angle scatt., inelastic cross-section and collective state excitation 80−52690
heavy ion reactions, 10-200 MeV/N, Markovian and non-Markovian effects in transition probabilities 80−102175
heavy ion reactions, phenomenological nuclear friction mechanism, particle-hole excitation, nucleon exchange *(Chinese)* 80−42694
heavy nuclei, β and γ transitions, effective coupling consts. 78−46026
heavy nuclei, fission process gamma ray analysis *(Rumanian)* 79−40973
heavy-ion excitation functions in (HI,xn) reaction, Fermi gas model 77−18602
(HI,xn), cranking model for E1 polarization charge in rotating nuclei 79−85405
high angular momentum fusion compound nucleus deexcitation, high spin states, rare earths 80−9259
high-spin states, means and methods of investig. 78−86722
hole excitation spectrum in finite Fermi system, many body field theory 80−102105
hot nuclei with high angular momenta, γ-ray emission in heavy ion reactions, rot. bands 78−13133
$i_{13/2}$ shell, particle-rotor model soln., backbending, transition rates, ang. momentum spread 80−47344
internal conversion coefficients, higher approx. and near-threshold behaviour 79−6501
internal conversion coeffs. for E5, M5 transitions, $30 \leq Z \leq 104$ 79−26396
ion, free, aligned, static hyperfine interaction, gamma-ray ang. distrib. 79−9508
ion induced γ-rays, thick sample reaction yields, energies, appl. in prompt nuclear anal. 78−62502
irreducible spin precession theory applied to atomic and nuclear RF spectroscopy 80−27969
isolated doorway resonances, spreading width and branching ratios 77−57645
isomer shifts, total conversion coefficients, nuclear electron and gamma transitions importance 79−85411
isoscalar dipole strength excitation in GQR region by inelastic electron and hadron scatt. 80−47448
isoscalar E1/broad resonances (T=0) 79−13250
isoscalar giant electric resonances, excitation and decay 80−5108
isovector M6 excitations, open shell RPA calcs., appl. to electron scatt. form factors 78−50112
isovector pairing collective motions and transition rates, projected BCS solns., generator coordinate simplification 80−22654
K-shell internal conversion coeffs. for pure E2 transitions compilation anal. 79−75910
l-forbidden M1 transitions, shell effects, reduced transition probabilities 80−68594
l-forbidden M1 transitions, single pion exchange effects 77−6286
large maplitude collective motion, field theory, excitation energies 80−22665
laser radiation effects on nuclear transition lifetime 80−22760
laser spectroscopic technique involving atom, mol. excited states, book contrib. 78−9212
laser-induced resonant absorption of γ radiation 80−18290
level density, shell. struct. effect excit. energy depend. 77−79311
level density in large spectroscopic spaces, statistical spectroscopic methods 80−86814

nuclear energy level transitions continued
light deformed nuclei, Skyrme interaction spin components, spectra, projected HF theory 80−73820
light nuclei, E1 transitions from reson. states, probability distribs. 78−13021
light nuclei, multipole giant resonances 78−86462
linear polarisation mixing coeffs. for mixed dipole and quadrupole γ-radiations, Compton polarimeter 80−73110
linearly transformed energy spectra perturbation by configuration mixing 79−59034
Lipkin Meshkov Glick model multilevel extensions, ground state energy phase transitions 79−85404
low energy positive parity spectra, $2\hbar\omega$ excitations, ang. momentum projected deformed particle-hole model calcs. 78−25119
M1 transitions in spherical nuclei, finite Fermi systems theory *(Russian)* 77−6296
macroscopic rotation of cold nuclei 79−17785
magic and doubly magic nuclei, A=129, 131, 133 chains, 0^+ states, spectroscopy 80−78165
magic Z (N) isotopes (isotones), calc. of first 2^+ and 3^- excited levels and transition prob. 79−80874
magnetic dipole transitions near ^{208}Pb 79−6393
magnetic multipole transitions, energy weighted sum rule 79−9505
mathematical modelling for radionuclide gamma emission 80−32236
medium nuclei, β and γ transitions, effective coupling consts. 78−46026
mesoatoms, prompt fission internal γ-ray conversion, fragment radiative transitions *(Russian)* 80−86944
mirror state EM decay rates, multipole matrix element isospin decomposition 79−36190
mixed parity radiation, polarised nucleus, higher order approxs. in ang. distrib. 77−6288
mono-energy pair conversion of nuclear multipoles, form factors, Hartree-Fock-Slater wave functions *(Russian)* 79−93555
monopole excitations in heavy nuclei, hadron induced 78−86471
Mossbauer isomer shifts, book 79−87346
Mossbauer transition characts. tabulation book contrib. 79−87364
multiple angular correlation between many quanta in coincidence, populated by heavy ion reactions 79−36193
multipole matrix elements from classical field with sources 79−9504
multipole radiation theory, in senior undergraduate physics course 78−54120
muonic atoms, energy shifts and polarisability of deformed nuclei 80−86893
muonic atoms, isomer shifts, book contrib. 79−86093
Muonic atoms, X-ray vacuum corrections, nuclear moments, transitions and deformation parameters 80−37912
N=28, 50, 82 isotones, effective interactions and low lying state energy spectra 79−22208
N=50 isotones, transition probabilities, $1p_{3/2}$ and $0f_{5/2}$ hole excitation effects 80−47431
N=5 shell, deformed odd-neutron nuclei, band ordering and spectrum 80−83018
N=82 region, high spin isomers, cranked HF calcs., deformation shapes, excitation energies 80−99121
N=82-86, high spin isomers, gamma spectroscopy 80−47358
neutral current, P-violation in nuclear transitions 79−13243
neutron capture, total radiative width and degree of freedom, statistical model calcs. 80−57732
neutron excess nuclei, near equality of isoscalar and EM transition rates 78−8770
neutron resonance capture anal. 77−26693
neutron rich nuclei; β^--emitters, deformation and spectroscopy 80−78223
neutron rich transitional fission fragments, spectroscopy, 0^+ states and octupole vibrs. 80−78204
neutron-rich nuclei in A∼100 region, decay props. 77−22961
nuclear continuum spectrum from disintegration by high energy particles, direct and resonant mechanisms *(Russian)* 79−30803
nuclear excitation by electron transition (NEET) 77−34256
nuclei far from stability, β-decay energies, γ-rays, Q_β values and masses 80−78225
nuclei in intense laser fields, spontaneous-stimulated γ-ray emission 77−83843
nuclides for Interlaboratory LMFBR reaction rate program, γ-ray intensities 77−22928
odd deformed nuclei, E2-transition probabilities with ΔK=1 79−6495
odd deformed nuclei, M1 transitions, one particle intranuclear conversion matrix elements 79−6473
odd mass nuclei with 51 neutrons or 51 protons, radioactivity, expt. theory *(French)* 77−293
odd nuclei, soft and deformed, rotor plus quasiparticle approach, moments, transition probabilities 80−78214
odd-A nuclei, E2 transition probabilities between Nilsson states, odd-A nuclei 77−57622
odd-A nuclei, O(6) spectra, interacting boson-fermion model, new coupling scheme 80−57727
oriented radioactive nuclei, JINR investigs. using SPIN equipment *(Czech)* 77−42220
P-shell hypernuclei, formation, γ-radiation, and spin values, shell model 79−22223
pairing correlation treatment, single particle levels, binding energy, spectra, branching ratios *(Chinese)* 80−102107
pairing rotations and quadrupole modes, dynamical interplay 80−18165
parity nonconserving nuclear interactions and weak neutral currents, review 77−41936
parity violating one-body potl. effects 77−18383
parity violating terms in nuclear EM operators and struct. effects 79−6482
parity violation in nuclear forces, neutron capture γ-ray expts. 80−37322
parity violation in nuclear processes with polarised neutrons 79−59008
particle spectra line shapes after γ emission in flight 78−41665
pf-shell nuclei, Hermitian operator method calcs., energy levels, transitions 78−54702
pigmy resonance, EM transitions, threshold states effects *(Hungarian)* 78−89818
positron annihilation in heavy at. shells, nuclear orientation *(Russian)* 79−49602
positronium production in nucl. monopole transitions 77−54635
preactinide nuclei, fission excitation functions and fission barrier height, liquid drop model 80−47513

nuclear energy level transitions continued
probabilities of α-, β- and γ-transitions accompanied by changes in nuclear shape *(Russian)* 78−89820
quadrupole transition densities and electron scatt. in the interacting boson model 80−27598
quasiparticle spectra near the yrast line 80−453
qunatum beats in atomic and nuclear physics 78−70772
radiative strength distrib. with energy, E1, M1 giant resonances, particle-hole calcs. 80−37349
radiative strength functions in spherical nuclei, giant dipole resonance influence, ^{124}Te, ^{140,142}Ce appls. 78−89774
radioactive decay constant, effect of chem. surroundings, electron capture 80−42601
radionuclide decay, computer simulation, levels, transitions, internal conversion 80−63136
rare earth nuclei, even-even, E_2 transitions from 2^+ state of gamma-vibrational band 80−91150
rare earth nuclei, high spin states from (HI, xn) reactions, discrete γ-transitions 80−5050
rare-earth nuclei transition density, ang. momentum projection corrections to rot. model 78−500
ratio of $\Delta\langle r^2\rangle$ for pairs of elements with analogous electronic structure, tabulation, book contrib. 79−85410
ratios of $\Delta\langle r^2\rangle$ for two transitions in the same element or nuclide, tabulation, book contrib. 79−85409
recoil corrections in electric gamma transitions 79−89263
resonance gamma-ray absorpt. method 78−55089
rotating nuclei, M1 and E1 transitions within and between bands, cranking model 80−494
rotational nuclear struct., moment of inertia, ang. momentum sel. using total γ-energies 79−89221
rotational spectra calc. using ang. momentum constraint, HF method 79−85403
rotational states, coherent, γ-decay, random quantum meas. 80−73855
screening effects in radiative orbital electron capture by an atomic nucleus 79−67717
semimicroscopic description of nucl. states at low, intermediate and high excitation energies 78−54666
semiphenomenological model, unified description of reactions, states and transitions 79−75844
short living nuclear states, optical orientation, γ-spectrum anisotropy, lifetime, moments *(Russian)* 80−63090
Sn Z=50 region isotopes, system struct calcs. 80−18192
spectroscopic information from nuclear reactions: applications 79−459
spectroscopic information from nuclear reactions: theory 79−458
spectroscopy using (γ,γ′) and (n,γ) scatt. 80−18287
spherical even nuclei, role of doorway states in gamma decay of highly-excited states 77−30581
spherical nuclei, compound state γ-transitions, reduced γ-widths, Wigner stat. matrix method *(Russian)* 80−68587
spherical nuclei, dipole states, transition densities and electroexcitation, GDR form factors *(Russian)* 80−52611
spherical nuclei, giant monopole resonance transition densities, dynamical Thomas-Fermi theory 80−9278
spherical nuclei, M1 transition strength distrib. at high excitation energies 79−75895
spin-alignment attenuation factors in mass 61-67 nuclei populated by (α, n) and (α, p) reactions 79−26390
strengh distributions and statistical spectroscopy, general theory 77−79322
strength distributions and statistical spectroscopy, shell model comparisons 77−79323
SU(3) model of EM transitions, selection rules, transition probabilities *(German)* 77−2943
sudden shape transitions, pair correlation association, E2 transition rate and backbending *(Chinese)* 79−59007
sum rules for spin-dependent excitations of nuclei 79−59018
total γ-decay energy meas., selection of high spin nuclear states 79−26391
transitional odd-odd mass nuclei, gamma deformed rotor model 79−93498
two-body $1f_{7/2}$ nuclei, B(E2) transition probabilities, effective charge concept 77−18477
U(3(n-1)) scheme, translationally invariant wave function, proton-neutron states, electromag. transition operators 77−41906
weak γ-ray transitions observed in coincidence with summed cascades 79−76264
weak interaction between nuclear particles, parity violation, review 77−6295
weak neutral currents, internal conversion probe from M1 decay, nuclear matrix elements 79−67712
XX ^{126}Xe, $2_2^+ \rightarrow 2_1^+$ transition multipole mixing ratio 80−78198
yrast and statistical cascades, M1 radiation after (MI, XN) reactions 80−42583
yrast decay schemes from ^{48}Ca+heavy ion fusion evaporation reacts., appl. to Fe, Cr and Mn 78−66308
(α,α′X), isoscalar giant quadrupole resonance decay props. 80−22792
(α,xnγ), rare earth nuclei, complete fusion process n and γ multiplicity 80−18363
β^+-decay, e^+ annihilation in atomic K-shell, nuclear excitations *(Russian)* 80−42602
(d,d′), A=40 to 208, 108 MeV, giant monopole resonance excitation and ang. distribs. 80−102164
(d,^{6}Li), A∼60,116, L=0 transitions, cross sections, microscopic anal. 80−78189
(dx) breakup on nucleus, adiabatic treatment stripping and forbidden transition cross section 80−9299
(e,e) elastic scatt., spectroscopic information and form factors 80−9260
(e,e′), light and medium nuclei, high energy approx. anal., transition densities and probabilities *(Russian)* 80−63129
(e,e′), transition strengths, unnatural parity state excitation of stretched configs., NN forces 79−63626
(γ,d), odd-Z light nuclei, from (e,e′d), cross section, E2 transistors giant resonance and clusters 80−63169
(γ,γ), 2.5-3.5 MeV, level photoexcitation 80−78193
γ spectra of millisecond isomers, 38 MeV α-induced reactions, abs. cross-section determ. 79−9502
γ-ray absorption, enhancement using radiation field of high-power laser, cross section determ. 79−59033
(^{3}He,n), 25.4 MeV, N=82 nuclei, n ang. distrib., transitions, vibr. band search 79−63574

nuclear energy level transitions continued
(K⁻,π⁻), hypernuclei generation, γ-spectroscopy and lifetimes 79−75890
Λ s-shell hypernuclei, general props. and developments in experimental methods, review 79−22224
Λ- and Σ-hypernuclei, γ-transitions, spin-orbit components of single particle pots. 80−42574
(n,γ), A=20 to 240, E1 and M1 strength functions 80−52625
(n,γ), A=75 to 103, γ-strength functions and stat. model cross section calcs. 80−52612
(n,γ), A=94-190, resonance capture, low lying level population fluctuations, γ-rays 80−52619
(n,γ), E1 and M1 strength functions, A- and energy-depend., giant dipole resonances 80−37348
(n,γ), Fast n, gamma rays in giant dipole region, review 80−37351
(n,γ), γ-rays, QED test review 80−37199
(n,γ), mechanism in 3s size resonance, s-wave radiative width partition 80−37387
(n,γ), mechanism in 3s size resonance, radiative width statistical and valence effects 80−37388
(n,γ), non-spherical even-even nuclei, energy gap from γ-transitions 80−47395
(n,γ), on-line gamma anal. using Ge detector 80−52624
(n,γ), spin assignments using polarised beams and gamma spectroscopy 80−37323
(n,γ) gamma ray spectra calc. 80−52620
(n,γ) gamma ray study at Tehran nuclear research centre 80−57735
(n,γ) spectroscopy, nuclear struct. investigation, review 80−37379
(n,γα), (n,γf), low energy γ-transitions between compound states, statistical theory 80−57737
(n,γα), thermal n, systematic search, γ-spectra and selective state population 80−37390
(n,γp), thermal n, systematic search, γ-spectra and selective state population 80−37390
(n,n′), odd mass nuclei, 2-4.5 MeV, level excitation functions, Hauser-Feshbach-Moldauer model test 79−36238
(n,n′γ), A=28-152, spherically doubly even nuclei, level excitation cross sections, statistical anal. *(Russian)* 79−67707
(n,n′γ) cross section, effect of intensive EM wave on γ decay *(Russian)* 79−59070
(n,nγ), A=19-207, neutron scattering resonance radiative widths 80−99146
(n,xγ) reactions, ENDF/B prompt γ-ray evaluations, models and data 77−26753
NN amplitude recovery from high energy nucleon-nucleus scatt., γ-transition data *(Russian)* 77−74855
np doubly radiative capture, M1-M1 transitions and cross section calcs. 79−13292
^{194}Os, populated in ^{192}Os(2n,γ), level transitions, prolate-oblate transition 78−62540
(p,d), 51.9 MeV, forbidden transition ang. distribs., CCBA and DWBA anals. 80−86848
(p,d), 52 MeV, deeply bound hole state transition strength giant resonance, DWBA anal. 80−47426
(p,γ), isobaric analogue doorway states, excitation functions 80−47388
(p,p′), hadronic transition operator for collective state transition rates 79−45262
(p,p′), transition strengths, unnatural parity state excitation of stretched configs., NN forces 79−63626
(p,p′) and (e,e′) scattering, core polarisation, microscopic models, transitions, cross sections, form factors 78−604
(p,xnγ), rare earth nuclei, complete fusion process n and γ multiplicity 80−18363
p̄p atom and NN̄ nucl. interaction, radiative transitions 78−25065
(π,γ), γ-transitions on and off line 80−37912
(π⁻,γ), high spin isomer state excitation, review 79−49569
(π⁻,γ), pion absorption by two nucleon cluster, high spin state excitation probability 79−49570
(π,π′), 1p shell targets, DWIA calcs., strong transitions, isospin effects 80−42708
(π,π′), collective transitions, giant resonances, isospin content and spin transfer 80−42580
(π,π′), particle-hole state excitation, field theory calcs. *(Russian)* 80−37318
(π⁻,X) slow pion capture in deformed nuclei, effects on high spin state excitation 80−18345
π- and ρ-exchange pots., influence on mag. resonances, mag. moments, and transition probabs. 80−99133
π⁻ absorption at rest, high spin state excitation, π-condensation and Δ⁺⁺ *(Russian)* 80−86927
^{134}Ba level scheme obs. from ^{134}La decay 77−10360
^{18}O(γ,σ$_0$), 19-32 MeV, E1 and E2 cross section, E1-E2 phase difference 80−63172
^{208}(N,γ), pol. N, anal. power and giant multipole resonances, direct-semidirect model 80−18265
A=12, nuclear axial dipole transition moment in the sigma model for 1⁺, T=0→0⁺, T=0 transition 79−45184
^{227}Ac, high pressure meas. of gamma transitions 80−18225
^{230}Ac levels, Jᵠ and transitions, Nilsson assignments from ^{230}Ra decay 80−68543
Ag, odd-mass isotopes, 9/2⁺→7/2⁺ transitions, transition probabilities, half-lives 77−18475
^{A}Ag, A=104, 106, levels, Jᵠ, and isobaric analogue resonances from Pd(p,n) 80−32180
^{A}Ag, A=105, 107, 109, 111, isomeric transition internal conversion, γ-transition energies and e intensities 79−6503
^{A}Ag, A=105-109, negative parity states, EM props. from particle-asymmetric rotor model 80−102097
^{A}Ag A=99, 101, 103, levels, transitions and Jᵠ from Cd decay, Pd(p,2nγ) 80−47383
^{A}Ag(^{86}Kr,X), A=107,109, 620 Mev, deep inelastic scatt., ang. momentum transfer, γ-ray multiplicities 80−27665
^{A}Ag(^{86}Kr,X) A=107,109, γ-ray multiplicities from diffusion model with one body dissipation 79−6487
^{103}Ag collective excitation and Jᵠ following ^{94}Mo(^{12}C,p2nγ), rotor-plus-particle model 80−86782
^{103}Ag high spin states, bands transitions, intermediate deformation Coriolis coupling from (^{3,4}He, xnγ) 80−105944
^{103}Ag levels and spectra from ^{103}Cd decay 79−22235
^{104}Ag levels, Jᵠ, T$_{1/2}$, bands and transitions from ^{103}Rh(α, 3nγ) 80−102093
^{105}Ag decay, γ-ray spectra, γ-γ coincidence and ang. correl. meas. 78−13007
^{105}Ag, excited level struct. and transitions populated by decay of ^{105}Cd 79−97655
^{105}Ag, γ-transitions, level scheme via (p,nγ) reaction *(Russian)* 77−74801
^{106}Ag low-lying excited states from ^{103}Rh(α,nγ) and ^{104}Pd(α,pnγ) 80−57693
^{107}Ag high spin states, Jᵠ assignments, polarisations and transitions from (^{7}Li,4nγ), (^{6}Li,3nγ) 80−27536
^{108}Ag levels and γ-transitions, population-spin correlation from ^{107}Ag(n,γ) 80−63097
^{108}Ag transition multipolarity and conversion electrons from ^{107}Ag(n,e⁻) 80−52627
^{109}Ag levels from ^{109}Pd decay, spins, γ cascades, mixing ratios 77−22930
^{110}Ag 118.718 keV isomer, low lying states and transitions, coincidence study from ^{109}Ag(n,γ) 80−73806
^{110}Ag low lying states, decay scheme and T$_{1/2}$ from ^{109}Ag(n,γ) 80−47393
^{110}Ag^{m} cascade decay, γ-γ linear polarisation direction correls., Ge detectors *(Japanese)* 78−41903
^{110}Ag^{m} decay, precise γ-ray spectroscopy 78−58251
^{111}Ag, obs. in ^{111}Pd^{g,m} β-decay 78−541
^{110m}Ag, gamma transitions to ^{110}Cd 79−85401
Al, A=25, 27, M1, E2, transition probabilities between differently deformed states, Nilsson model 77−61376
^{A}Al, A=24,25,26, giant M1 strength, comparison with cross sections from Mg(p,n) 80−86878
^{A}Al, A=25,26,27 levels, resonances, γ-ray branching ratios from Mg(p,γ) 80−86875
^{24}Al, ^{24}Al^{m}, decay to γ-ray and α-particle emitting ^{24}Mg states 79−49607
^{24}Al, effective M3 matrix elements and transitions from shell model 80−102143
^{25}Al, T=3/2 states γ-decay, ^{24}Mg(p,γ)^{25}Al 77−26608
^{26}Al, isoscalar and isovector E2 transition matrix elements 78−25148
^{26}Al low energy resonances, decay and Jᵠ assignments, branching ratios from ^{25}Mg(p,γ) 80−42624
^{26}Al T=1 states, resonances, Jᵠ and transitions from ^{25}Mg(p,γ) 80−99131
^{27}Al, analogue-antianalogue M1 transitions, nucl. shape change influence 78−13006
^{27}Al isobaric analogue resonances, spectroscopic factors and γ-rays from (p,p), (p,γ) 80−86873
^{27}Al levels, resonances, Jᵠ, branching and mixing ratios from ^{26}Mg(p,γ) 80−99132
^{27}Al+^{20}Ne, 120 MeV, prompt γ emission, reaction products deexcitation 78−74396
^{27}Al(^{12}C,^{12}C), 14-25 MeV, 180° scatt. excitation function and ang. distrib. struct. 80−32253
^{27}Al(e,e′), 62 to 112 MeV, form factors, ^{27}Al energy spectrum, transition probabilities 77−34288
^{27}Al(e,e′), 70-340 MeV, odd parity state electroexcitation, form factors, transition probabs. 80−78208
^{27}Al(e,e′), transition widths, multipolarity assignment DWBA calc. 78−13068
^{27}Al(n,α), 4.5-18.3 MeV, cross sections and excitation curves *(Chinese)* 79−49601
^{27}Al(p,γ)^{28}Si, 2046 keV, gamma-ray intensity calibration standard 77−30698
^{27}Al(p,γ)^{28}Si, standard resonance strength 77−30565
^{28}Al E1 transitions and partial radiative widths from ^{27}Al(n,γ) 80−52618
^{28}Al levels, spins and γ-rays, multipole mixing from ^{27}Al(n,γ), pol. thermal 80−47398
^{28}Al levels, transitions and spin from ^{27}Al(n,γ), pol. Al and n 80−78153
^{243}Am, absolute yields of 43.5, 74.7 and 117.8 keV photons 80−32568
^{245}Am, high pressure meas. of gamma transitions 80−18225
^{32}Ar, high spin states from heavy-ion fusion evaporation reactions, decay schemes 77−2932
^{35}Ar levels, transitions and β-delayed protons from ^{35}K decay 80−91156
^{35}Ar lowest T=3/2 state excitation energy from ^{35}K decay, ^{35}Ar lowest T=3/2 state excitation energy 79−85407
^{36}Ar deduced levels from ^{36}K beta-delayed particle emission 80−83074
^{36}Ar, delayed proton and alpha emission, transition energies, levels, Jᵠ, from ^{36}K decay 80−52629
^{36}Ar, obs. of decay of T=2 state in ^{35}Cl(p,γ) 77−6294
^{38}Ar high spin state density, γ-decay mode, deformed states from ^{35}Cl(α,pγ) 80−32168
^{38}Ar levels, Jᵠ and transition strengths, DWBA anal. of ^{40}Ar(p,t) 80−47378
^{38}Ar yrast levels, Jᵠ assignments, transitions, branching and mixing ratios from ^{35}Cl(α, pγ), ^{24}Mg(^{16}O, 2pγ) 79−67625
^{40}Ar, lifetime determ. using Doppler shift attenuation 79−93551
^{46}Ar decay, gamma-ray spectra meas., half-life determ. 78−21513
Ar(e,e′), A=36, 40, 65 to 115 MeV, low lying level struct., lifetimes 78−8798
As isotopes, levels and spectra from broken pair model 80−73801
^{A}As, A=70, 72, level scheme, transitions, Jᵠ and lifetimes from Ge(p,nγ) 80−22695
^{A}As, A=71,73,75, E1 γ-ray strength function from Ge(p,γ) 79−75902
^{A}As, A=73,75,77, probabilities for analogue-antianalogue transitions 79−6496
^{70}As, hyperfine struct. investig. using at. beam mag. reson. 77−22933
^{71}As intermediate struct., resonance spin from ang. correlations of ^{70}Ge(p,p′γ) 79−67729
^{74}As level structure, studied via ^{72}Ge(α,npγ), 30 to 50 MeV 77−10357
^{75}As populated in ^{75}Se decay, E0 transitions 80−22752
^{75}As, stopped π⁻ absorption, in beam and activation γ-ray spectroscopy 79−40960
^{75}As, transitions populating and depopulating 279 keV level, δ(E3/M2) 77−82852
^{76}As excited states, excitation functions and decays ang. distribs., cross sections from ^{76}Ge(p,nγ) *(Russian)* 80−63089
^{76}As, level structure, transitions and Jᵠ, from ^{76}Ge(p,nγ) 80−47379
^{208}At energy levels and transitions, IC electrons from ^{208}Rn decay 80−18242
^{209}At, gamma-ray spectra, produced by ^{209}Bi(^{3}He, 3nγ)^{209}At, 28 and 26 MeV 78−74377

nuclear energy level transitions continued
^{209}At, γ-transition, multipolaritis, level scheme following ^{208}Rn decay 80−83072
^{209}At high spin states from ^{206}Pb(^{6}Li, 3nγ), γ meas., neutron hole influence 77−2934
^{212}At high spin states, decay, g factor, J^{π} assignments, level energies from ^{208}Pb(^{7}Li,3n) 80−5042
^{213}At levels, J^{π}, transitions and lifetimes from ^{208}Pb(^{7}Li,X) 80−68542
Au, A=189, 191, 193, level schemes, gamma spectroscopy of high-spin states 77−22848
^{A}Au, A=189, 191, 193, high spin states and transitions, isomeric states from Ir(α,xnγ) 80−5038
^{A}Au, A=193-199, positive parity states, particle-asymmetric rotor description 78−46005
^{187}Au energy states from ^{187}Hg decay, parities γ-spectra, triaxial nuclear deform. *(French)* 78−33143
^{193}Au, intermediate coupling vibr. models 77−22845
^{194}Au decay scheme, γ-spectrum, low-intensity transitions and level energies of ^{194}Pt 78−13003
^{195}Au, intermediate coupling vibr. models 77−22845
^{196}Au, studied via ^{197}Au(n,2n), isomeric cross-section ratio and spin-cut-off factor 78−13096
^{197}Au, stopped π⁻ absorption, in beam and activation γ-ray spectroscopy 79−40960
^{197}Au+^{136}Xe, 1064 MeV, fragment spin orientation from continuum γ-ray anisotropy meas. 80−22853
^{197}Au(^{86}Kr,X), 620 Mev, deep inelastic scatt., ang. momentum transfer, γ-ray multiplicities 80−27665
^{197}Au(^{86}Kr,X) 612 MeV, γ-ray circular polarisation 80−13453
^{197}Au(α,α′), 120 MeV, isoscalar resonance excitation, low lying transitions, DWBA calc. 80−512
^{198}Au, 411 keV transition energy, absolute meas. rel. to He-Ne laser freq. *(Czech)* 80−22755
^{198}Au, energy level spin from ^{197}Au(n,γ) with polarised n and Au 79−457
^{198}Au gamma-ray strength functions from spectrum fitting method from ^{197}Au(n,γ) 80−52616
^{198}Au level spin assignments from γ ang. distrib. and circular polarisation from ^{197}Au(n,γ) 80−52570
^{198}Au, populated in ^{198}Au(n,γ), high energy transitions 80−22878
^{198}Au(n,γ), 0.5-3.0 MeV, γ-spectra strength functions 80−32240
^{199}Au, populated in ^{198}Au(n,γ), high energy transitions 80−22878
(α,γ), excitation function competition cusps, Mauser-Feshbach calcs. 80−13404
^{9}B complex system, excitation functions for 17.19 and 17.64 MeV levels from ^{6}Li+^{3}He 80−78188
^{10}B, EM transitions, model anal. based on [42] representation dominance 79−40880
^{10}B T=1 states, γ-transition strengths, lifetimes, branching and mixing ratios from ^{6}Li(α,α) 80−27594
^{10}B transitions and levels from ^{11}B(γ,nγ′) *(Russian)* 80−13433
^{10}B(^{9}Be, X), total reaction cross sections for sub-Coulomb energies, neutron transfer reaction 79−80950
^{10}B(e,e′), 67-194 MeV, form factors, transitions and ground state radiative width 79−75898
^{10}B(e,e′)^{10}B, 40-61 MeV, multipolarities, transition widths 77−10356
^{11}B, +ve parity states in weak coupling model, E1 and β strengths 77−34228
^{11}B intermediate resonance and electric quadrupole transition contribution to ^{12}C(γ,pα)^{7}Li *(Russian)* 79−40896
^{11}B, radiative widths meas., 2.125 to 8.92 MeV levels, intensity calibration of photon spectrum 79−13242
^{11}B(e,e′), E1 transitions to unnatural parity states 80−22758
^{11}B(γ,nγ′) 30 MeV giant dipole resonance decay, ^{10}B transitions *(Russian)* 80−13433
^{12}B(1^{+},g.s.), induced pseudo-scalar coupling constant in ^{12}C(μ,ν_{μ}) 79−49606
Ba, neutron deficient, charge radii, moments, transitions and isomers, atomic beam laser spectroscopy 80−102141
^{A}Ba, A=130, 132, 134, 136, levels and EM props., ang. momentum projected quasiboson model 80−5067
^{A}Ba, A=132, 134, 136, negative parity states, J^{π}, transitions, DWBA anal. of Ba(p, t) 80−86810
^{A}Ba, A=135,137, Coulomb excitation, transition probabilities, γ-rays and level collectivity from (^{16}O,^{16}O′), (α,α′) 80−78201
^{A}Ba, A=142,144,146, transition γ-γ ang. correlations, levels, J^{π}, mixing ratios 80−73823
^{A}Ba(γ,γ) A=136-8, 1.68-5.0 MeV, nuclear resonance fluorescence, levels transitions and spins 79−6543
^{123}Ba, high spin levels and bands from ^{114}Sn(^{12}C, 3n)^{123} Ba 79−45127
^{126}Ba, backbending and E2 transition strengths of yrast states 79−26363
^{129}Ba, excitation and props. of high-spin levels using ^{120}Sn(^{12}C,3nγ) 78−17104
^{129}Ba, γ-ray linear polarisation meas. from ^{120}Sn(^{12}C,3n) 78−50121
^{129}Ba, struct. determ. from ^{129}La β-decay 79−22244
^{133}Ba, 12.34 keV M1 transition 80−106004
^{133}Ba decay data and standardisation 77−88081
^{134}Ba, inversion of 0^{+} phonon states and γ softness 77−10364
^{135}Ba(α,α′), 8-10 MeV Coulomb excitation, reduced E2 transition probabilities 78−13127
^{138}Ba+α, closed shell 82 neutron nucleus, B(E2)-values 78−66296
^{139}Ba β⁻ decay into ^{139}La, γ-rays, energy levels 78−70492
^{139}Ba level scheme, J^{π} and γ-transitions from ^{139}Cs β-decay 80−42590
^{142}Ba, γγ ang. correlations, levels, spins and mixing ratios from ^{142}Cs decay 80−57734
^{143}Ba, nuclear spectroscopy of neutron rich A=143 nuclei 79−59039
^{144}Ba beta and gamma spectroscopy 77−22962
^{7}Be effective for charge exchange analogues of Gamow-Teller transitions from ^{7}Li(p,n) 80−57726
^{7}Be excitation functions from ^{6}Li(^{3}He, d) 80−18223
^{8}Be, 0^{+}, T=2→I^{+}, T=1 width via ^{6}Li(d,γ)^{8}Be 77−14130
^{8}Be collective excitation spectra from generalised hyperspherical functions method *(Russian)* 80−91133
^{8}Be, ΔT=1 γ-decay from 16.6-16.9 MeV states 78−8771
^{8}Be, γ-decay strength of isovector M1 transition, microscopic wave function 78−62503
^{8}Be isovector radiative decay, E2-M1 mixing ratio, conserved vector currents from ^{4}He(α,γ) 79−6488
^{8}Be, level feeding via β and γ transitions, role of spatial quantum numbers 77−67723

nuclear energy level transitions continued
^{9}Be, first T=3/2 states, γ-decay, branching ratios and total widths from ^{7}Li(^{3}He, pγ) 79−6489
^{9}Be low lying spectrum, 3-body molecular description, adiabatic one level approx. 80−78150
^{10}Be, form. in ^{11}B(γ,p) reaction, 18 to 31 MeV, photoproton spectra and ang. distrib., excited state transitions 78−13056
^{9}Be, excited states and spectra, continuum effects calcs. 80−57720
^{204}Bi excited states, γ rays, conversion electrons and γγ coincidences from ^{204}Po, EC 80−18241
^{205}Bi high spin states populated in Tl(α,xn), yrast states, isomers 77−30616
^{207}Bi, decay, time differential perturbed ang. γ-γ correl. meas. 78−17134
^{207}Bi, gamma-ray transitions following electron capture, 1.44 and 1.46 MeV γ-rays 79−85399
^{207}Bi high spin states, level decays, three particle interactions from ^{205}Tl(α,2n), ^{208}Pb(d,3n) 79−49567
^{208}Bi, 0^{+} IAS, spreading width and isospin impurity, isovector monopole state influence 80−78155
^{208}Bi isobaric analogue resonances, spin assignments, decay amplitudes from ^{207}Pb(p,p) 79−75946
^{208}Bi two-particle, two-hole configuration, levels, J^{π} and excitation energies from ^{210}Bi^{m}(p,t) 80−32190
^{209}Bi EM props. of particle vibration coupling states from ^{208}Pb(^{7}Li, ^{4}He 2nγ) 78−70485
^{209}Bi, effect of pairing modes in multiplet struct. 78−12973
^{209}Bi energy and transition probability convergence in Dyson's boson expansion 80−78206
^{209}Bi from ^{208}Bd(d,nγ), half life of 2442.8 keV lowest 2p 1h state 78−74331
^{209}Bi, stopped π⁻ absorption, in beam and activation γ-ray spectroscopy 79−40960
^{209}Bi(α,α′), 120 MeV, isoscalar resonance excitation, low lying transitions, DWBA calc. 80−512
^{247}Bk proton states, transitions and spectroscopic factors from (α,t), α-decay, electron capture 79−89224
^{251}Bk level structure from ^{251}Cm beta decay 79−36200
^{75}Br, first 9/2^{+} state and prolate deform. from ^{75}As(α,4nγ) 78−50088
^{76}Br level structure studied via the ^{75}AS(α, 3nγ) reaction, 30 to 55 MeV 77−54174
^{76}Br^{M} decay props., half life and γ-transitions, level scheme 80−83071
^{78}Br, high-spin states, from ^{77}Se(α,2np), decay into isomers 80−52569
^{78}Br level struct. determ. from (α,nγ), (^{3}He,d) and (p,d) reacts. 79−59010
^{80}Br level struct. and transitions, DWBA anal. spectroscopic factors from ^{81}Br(p,d), 22.8 MeV 79−3084
^{80}Br, study of excited states from ^{79}Br(n,γ) and ^{80}Se(p,nγ) *(French)* 78−29393
^{82}Br, study of excited states from ^{82}Se(p,nγ) and ^{81}Br(n,γ) *(French)* 78−29393
^{88}Br→^{88}Kr, γ-ray spectrum, transitions 77−295
CC ^{158}Dy high spin states B(E2) values, IBA model test from ^{26}Ng(^{136}Xe, 4n) CC ^{158}Dy high spin states B(E2) values, IBA model test 80−27541
CC ^{168}Er high intrinsic excitation levels, γ-decay props. from ^{167}Er(n,γ) 80−52588
CC ^{20}Ne 8^{+} level radiative width, resonance strength from ^{16}O(α,γ) 80−83065
CC Rb cross sections and decay props. from ^{85}Rb(γ,n), ^{85}Rb(n,2n) 79−49600
^{A}C(π,π′), A=12, 13, ~180 MeV, isospin mixing, levels, excitation functions and ang. distribs. 80−42543
^{11}C intermediate resonance and electric quadrupole transition contribution to ^{12}C(γ,nα) *(Russian)* 79−40896
^{11}C levels and resonance, γ-ray excitation curves from (p,αγ), (p,pγ) 80−9280
^{12}C 1^{+}(T=1, 15.1 MeV) state excitational pionic modes, M1 form factor for (p,p′), (e,e′) 80−78195
^{12}C, 15.1 MeV level decay branching ratios, meas. with NBS positron annihilation in flight facility 79−31306
^{12}C 2^{+} (4.43 MeV) state, transition DWA anal. from (p,p') and (e,e') 79−67704
^{12}C, α-transfer spectroscopic factors for O^{+}, 2^{+} and 4^{+} states, transitions from (d, ^{6}Li) 80−13370
^{12}C, EM and allowed weak transitions, improved impulse approx. treatment 78−41662
^{12}C, excited state decay, axion emission search 80−32235
^{12}C, excited state struct., α-particle model 80−47385
^{12}C gamma line Doppler broadening in ^{12}C(n,n'γ)^{12}C and ^{9}Be(α,nγ)^{12}C, 4438 keV 80−91147
^{12}C isovector M1 excitations, current and spin contribs. from (e,e′), (p,n) 80−68582
^{12}C M1 (15.11 MeV) form factor, evidence for nuclear pion field critical opalescence 80−32232
^{12}C mag. transition form factors, core polarisation and exchange current effects 79−75899
^{12}C, transition densities, form factors and transient radii 79−6481
^{12}C$_{2+}$ spin alignment using γ-decay in flight in ^{16}O(^{12}C,^{12}C$_{2+}$)^{16}O and ^{12}C(^{16}O,^{12}C$_{2+}$)^{16}O interactions 78−41767
^{12}C+^{12}C gross struct. resonances in excitation functions from ^{12}C(^{12}C, ^{10,11}B) 80−102167
^{12}C+^{16}O, 11 to 27 MeV, structure in gamma-ray yields 77−34250
^{12}C(^{12}C, ^{12}C)^{12}C*, 0$_2^{+}$, 3$_1^{-}$, 4$_1^{+}$ state excitation functions, resonance structures 80−42616
^{12}C(^{12}C,^{12}C′), 14.5-32 MeV, gross structure peaks, particle-γ coincidences 79−97693
^{12}C(^{12}C,α), 7-15 MeV, excitation function statistical anal., nonstatistical features 80−99167
^{12}C(^{14}N,^{13}N)^{13}C at high energies, simplified DWBA anal. 79−93643
^{12}C(^{14}N,α), 10.1-15.9 MeV, forward angle excitation function structure, nonstatistical struct. 80−86885
^{12}C(^{16}O, ^{12}C*), 45-53 MeV, ^{12}C* m-substate population, spin alignment and excitation functions 80−42615
^{12}C(^{16}O, ^{16}O), 35 to 50 MeV, backscatt., dynamic deformation and excitation functions, optical anal. 80−18227
^{12}C(^{16}O,^{16}O), elastic and inelastic, 23-32 MeV, strong absorption region resonances, excitation functions 80−86884
^{12}C(^{16}O, α), ^{24}Mg low spin resonances, excitation functions and ang. distribs. 80−63151
^{12}C(^{20}Ne,^{20}Ne), back angle scatt. systematics, structured excitation functions and oscillatory ang. distribs. 80−32295

nuclear energy level transitions continued
^{12}C(^{24}Mg,^{24}Mg), back angle scatt. systematics, structured excitation functions and oscillatory ang. distribs. 80−32295
^{12}C(^{28}Si,αX), 87-91.5 MeV, α-HI angular correlations, excitation functions, statistical anal. 80−86915
^{12}C(^{40}Ca,^{40}Ca), 90° and 180° excitation functions energy depend., DWBA anal. 80−42582
^{12}C(K^+,$K^{+\prime}$), form factors, cross sections, interior probing capability 80−73866
^{12}C(α, α′γ),γ angular correlation function obs. *(Russian)* 79−13246
^{12}C(α,α′γ)^{12}C, 17.6 to 21.8 MeV 'rotation' of ang. correl. function 77−6406
^{12}C(e,e′), 12.71 MeV 0^+ to 1^+ transition, axial isoscalar neutral current, polarisation asymmetry 79−26425
^{12}C(e,e′), E2 transitions, convection currents and spin magnetisation 79−13244
^{12}C(e,e), 180° scatt., transverse inelastic form factors and spectra, collective 2^+ state 80−9261
^{12}C(γ,γ), 23.5-39 MeV, cross sections and giant resonances, E2 strength 80−63122
^{12}C(γ,γ), total photoabsorption and elastic cross sections, spectroscopic information *(Russian)* 80−83095
^{12}C(n, X), compound resonance decay based on bound and metastable single nucleon states *(Russian)* 80−5107
^{12}C(ν,ν′), ($\bar{\nu}$,$\bar{\nu}$′), 15.11 MeV state excitation, cross sections, level decay 80−9258
^{12}C(p,d)^{11}C, 700 MeV, transitions confirm multistep processes 78−46110
^{12}C(p,p′), 1 GeV, proton polarisation in natural parity level excitation *(Russian)* 80−42634
^{12}C(p,p′), 122 MeV, level excitation, cross sections, effective NN interaction, DWIA anal. 80−78197
^{12}C(p,p′), 22-27 MeV, 1^+ state de-excitation γ-ray ang. distrib., tensor force effects, DWBA anal. 80−68580
^{12}C(p,p′), pol. p, 800 MeV, unnatural parity states excitation, anal. powers and isospin 80−68538
^{12}C(π,π′), A* excitation, A* model unified description 80−102205
^{12}C(π,π′γ), 30-150 MeV, calc. π-γ ang. correls. 77−10452
^{12}C(π^-, 2γ), doubly radiative capture theory, branching ratio and ang. correlations 80−9314
^{12}C(π^+,d)^{10}C, transitions to low lying states in ^{10}C 78−46110
^{12}C(π^+,p)^{11}C, 49.3 MeV, transitions confirm multistep processes 78−46110
^{12}C($\pi^\pm$,πN), 40-600 MeV, excitation functions and absolute cross sections 80−18226
^{13}C, ΔT=0,1 E1 or M2 population of isospin splitting of giant reson. 78−577
^{13}C, state transition ang. distrib., optical parameters from ^{12}C(^{7}Li, ^{6}Li) 79−75904
^{13}C, T=3/2 resonance parameters, ground state γ-decay width from ^{9}Be(α,n) and ^{9}Be(α,α′) 79−3123
^{13}C, transitions from lowest T=3/2 states 77−88075
^{13}C(^{12}C,^{12}C), molecular neutron orbit formation, $1/2^+$ state excitation, coupled channels calcs. 80−78156
^{13}C(α,α′), 22, 36 MeV, resonant state line shapes 80−91148
^{13}C(γ,n), 6.5-9.3 MeV, ang. distribs., E1, M1 and E2 excitations, resonance radiative widths 80−68581
^{13}C(p,γ), pol. p, 6.25-17.0 MeV, anal. power and cross section ang. distribs., E1, E2 amplitudes 80−47461
^{14}C first excited 0^+ state, lifetime and E^0 decay from (d,p), (^{13}C,p) 80−102145
^{14}C(^{12}C,X), 40-57 MeV, strong resonant behaviour in inelastic and transfer channels, γ-yields 80−52644
^{17}C populated in ^{48}Ca(^{18}O, ^{17}C), mass excess, low lying level struct. 78−8744
Ca(^{12}C,X), 3, 4.8 GeV, in-beam transition γ-rays 79−6483
^{A}Ca, A=40,42,44, E0 matrix elements 79−45203
^{A}Ca, A=40,48, static and transition densities, self consistent RPA theory test in fast particle (p,p), (e,e) scatt. *(Russian)* 79−49604
^{A}Ca, A=44,46 excited states and transition ang. distribs. from Ti(^{14}C,^{16}O) 80−95308
^{A}Ca(e,e′), backward scatt., A=40, 42, 44, 48, mag. dipole ground state transition search 80−106009
^{A}Ca(p,p′), pol. p, A=40,48, 800 MeV, diff. cross sections, anal. powers, DWIA anals., high spin levels 80−83067
^{44}Ca, A=40,42,44,48, E0 matrix elements determ. from (e,e′) scatt. 78−33141
^{40}Ca, core polarisation charge for E6 transition, Bohr Mottelson model calc. 79−36194
^{40}Ca, effective convection current in shell model 79−63606
^{40}Ca ions recoiling in vacuum, decoupling of hyperfine interactions 77−22931
^{40}Ca, magic nuclei at collective excitations, energy spectrum and shape *(Russian)* 80−106015
^{40}Ca, weak s resonance γ-ray decay in negative parity low lying levels 80−27591
^{40}Ca(^{9}Be,^{9}Be′), 45, 60 MeV, 1^- state excitation Frahn scaling formula for cross section 80−102136
^{40}Ca(d,d), 4.5-5.4 MeV, excited states, excitation functions and ang. distribs., statistical anal. 80−57686
^{40}Ca(e,e′), strong mag. dipole transition, coherent spin flip transitions, ground state correlations 79−71817
^{40}Ca(γ,γ), 6.95, 7.12 MeV, strengths of isospin forbidden E1 transitions 78−13059
^{40}Ca(p, p′), isovector dipole strength excitation in giant resonance region 80−83066
^{40}Ca(p,p′γ), 6.25 MeV, triple ang. correlation, 3^- exit channel, resonances, single particle states 80−68626
^{40}Ca(p,p′), DWIA test in Glauber theory, transition density 80−99173
^{41}Ca, E2 core polarisation charge, Woods-Saxon shell model compared to harmonic oscillator model 80−63072
^{41}Ca E2 resonance, cross sections and γ-spectrum from ^{40}Ca(n,γ) 80−57759
^{41}Ca excited states, excitation functions and ang. distribs., statistical anal. from ^{40}Ca(d,p) 80−57686
^{41}Ca, giant dipole resonance determ. in ^{40}Ca(p,γ) 79−93620
^{41}Ca, highly stripped ions, recoiling in vacuo, γ-decays of isomeric states obs. 78−50119
^{41}Ca, spin and parity from ^{38}Ar(α,nγ) angular distrib. and linear polarisation of γ 80−63079
^{41}Ca, transverse decoupling of hyperfine interactions in free atoms 77−18468
^{41}Ca, two particle-one hole states, EM transition probabilities 77−88035
^{42}Ca high spin state density, γ-decay mode, deformed states from ^{39}K(α,pγ) 80−32168
^{43}Ca γ-ray spectroscopy, levels and decay scheme deform. 79−80896
^{43}Ca high spin positive parity states, struct., from ^{40}Ar(α,nγ) 78−46025
^{44}Ca, γ-ray spectra from ^{43}Ca(n,γ) 77−38278
^{45}Ca levels, excitation functions and J^π from ^{45}K β-decay 80−105978
^{140}Ca, level density from ^{143}Nd(n,α) reaction 79−9558
Cd 2_1^+ excitation, α-spectroscopic factors in IBA model from Sn(d,^{6}Li) 80−105967
Cd, A=104 and 105, populated in α+Pd reactions, high spin states 78−62484
Cd, even-mass, B(E2) and Q(2_1^+) via (e,e′) 68, 112 MeV scatt. 77−71585
Cd, isotopes A=109, 106, 105, 104, high spin states excited by (α,xnγ) *(French)* 78−29394
^{A}Cd, A=112, 114, 0_2^+ and 0_3^+ states, E0, E2 transitions and collectivity 80−102144
^{A}Cd(^{16}O,^{16}O′), 44 MeV, A=112, 114, 0_2^+, 0_3^+ state collectivity, E0 and E2 decay, $T_{1/2}$ 80−73784
^{A}Cd(n,nγ) A=114,116, energy levels, spins, and gamma-ray multipole mixing ratios investig. 80−52580
^{103}Cd levels, J^π and positive parity decoupled band, rotor anal. of ^{94}Mo(^{12}C, 3nγ) 80−102096
^{103}Cd levels and spectra from ^{103}In decay 79−22235
^{104}Cd quasirot. ground state band and γ-transition from ^{102}Pd(α,2nγ) 80−105955
^{106}Cd collective and yrast levels, γ-transitions, 2 quasiparticle+rotor model from (heavy ion, xnγ) 79−22169
^{107}Cd, g-factor of 845.6 keV state, differential PAC 77−6225
^{107}Cd, heavy ion nucl. alignment, recoil in vac., time-differential meas. 78−37304
^{108}Cd levels from ^{96}Zr(^{16}O, 4nγ), γ meas., decay scheme, band struct. 78−66301
^{109}Cd, gamma-ray precision energy meas. 78−58533
^{110}Cd, γ-ray spectra using coincidence and sum method *(French)* 78−62675
^{110}Cd, O^+ bands from cluster-vibration coupling, semimicroscopic mechanism for band mixing 79−36121
^{110}Cd, transition determ. in ^{110}Ag^m spectroscopy 78−58251
^{111}Cd, 1330 keV level excitation cross section from positron annihilation 80−68583
^{111}Cd, excitation by photon less positron annhilation, isomeric γ-transitions *(Russian)* 80−5089
^{111}Cd, pionic, E2 nuclear resonance effects 78−29868
^{112}Cd, $0_1^+ \rightarrow 0^+$ elec. monopole transition in low-lying ^{112}Cd levels prod. in ^{112}I decay 79−54406
^{112}Cd, E0 transition from o_1^+ state following ^{112}In beta decay 80−68578
^{112}Cd, kaonic, E2 nuclear resonance effects 78−29868
^{112}Cd, negative parity yrast band, E1 transitions polarisability, quadrupole-octupole coupled vibr. system 79−484
^{176}Cd(p,p′γ), 5-20 MeV, lowest 3^- collective level identification from decay excitation function 79−9444
Cd(n,nγ), γ spectra and ang. distrib., ^{114,116}Cd energy levels, spins, particles 77−88070
Ce, A=136,137,138, high spin states and isomers obs. using in-beam γ-spectroscopy 78−82309
Ce, A=137, 139, high spin levels, γ spectra, hole-core coupling 77−50063
Ce band structures populated in ^{116,118}Sn(^{16}O,3n), high spin levels, yrast cascade 78−8842
Ce isotopes, neutron rich, decay properties 78−13032
^{135}Ce, yrast cascade dipole component from ^{122}Sn(^{16}O,4n) 80−9266
^{140}Ce γ-spectra, E1 and M1 hindrance factors from ^{143}Nd(n,γα) 80−37386
^{140}Ce, hexadecapole motion obs. from α-scatt., EM transitions and conversion electron spectra 78−25097
^{140}Ce, M1 transition enhancement from neutron resonances quasiparticle-phonon model 79−9506
^{140}Ce+α, closed shell 82 neutron nucleus, B(E2)-values 78−66296
^{141}Ce collective M1 excitation effects on γ-ang. distribs., direct semidirect model of ^{140}Ce(n,γ) 80−57733
^{144}Ce, $0^- \rightarrow 0^+$ beta transition spectral shape anal. 77−38246
^{144}Ce, e-γ and e-e coincidences, improved detection system 80−52605
^{144}Ce, gamma-ray precision energy meas. 78−58533
^{250}Cf E0 transitions and excited 0^+ states from ^{250}Es decay 79−45173
^{250}Cf energy levels, bands and transitions from ^{250}Bk, β^- decay 79−22205
^{250}Cf low spin states, bandheads, J^π and transitions from ^{250} Es EC decay 80−105952
^{250}Cf(d,d′), 15 MeV, vibr. states, J^π and reduced transition probabilities 80−47351
Cl, A=35,36,37 high spin states from heavy-ion fusion evaporation reactions, decay schemes 77−2932
^{A}Cl, A=34, 38, effective M3 matrix elements and transitions from shell model 80−102143
^{34}Cl high spin states 78−82289
^{35}Cl(n,γ)^{36}Cl, E1 and M1 radiative strength functions 78−4940
^{36}Cl anomalous M1/E1 strength ratio and doorway states from ^{35}Cl(n,γ) 80−57730
^{37}Cl, in-beam γ-ray spectroscopy via ^{3}H(^{35}Cl,pγ) 78−13013
^{39}Cl excited states and transitions from ^{39}S decay 80−42595
^{A}Cm, A=246,248, fission isomer rot. spectra $I^2(I+1)^2$ correction 80−18229
^{249}Cm excited and single particle states, γ-transitions from ^{248}Cm(n,γ) 80−47399
^{A}Co, A=55, 59, energy levels from Ni(p_{pol},α) 80−68663
^{A}Co, A=55,57,59,61, deduced levels, proton-hole states, semimicroscopic model from Ni(p,α) 79−45171
^{55}Co, γ decay and splitting of analogue states from ^{54}Fe(^{3}He,dγ) at 18 MeV 78−70505
^{55}Co isobaric analogue resonances, J^π, partial widths and spectroscopic factors from ^{54}Fe(p,γ), (p,p′) 79−85431
^{55}Co, resonance decays, branching ratios and analogue resonances from ^{54}Fe(p,γ) 80−52643
^{56}Co, relative intensities of γ-transitions meas. 79−97930
^{57}Co, $g_{9/2}$ IAR in ^{56}Fe(p,γ) 78−70504
^{57}Co, $g_{9/2}$ isobaric analogue resonances, obs. in ^{56}De(p,γ)^{57}Co 78−82332
^{57}Co, gamma decay of $g_{9/2}$ isobaric analog resonance 79−63674

nuclear energy level transitions continued
^{57}Co, level props. study from ^{57}Fe(τ,d) reaction, DWBA calcs. 78−93946
^{57}Co state alignment, γ-transitions and ang. distribs. from ^{56}Fe(p,γ) 80−73797
^{59}Co (n, n′γ), 1.3-3.9 MeV, energy level structure and decay scheme 79−45164
^{59}Co, energy levels, lifetimes, deexcitation following (n,n′γ) studies 80−83059
^{59}Co level struct., from ^{59}Fe decay γ-spectrum 77−14063
^{59}Co, radiative transitions from unbound states obs. in neutron inelastic scatt. *(Russian)* 78−41664
^{59}Co, stopped π^- absorption, in beam and activation γ-ray spectroscopy 79−40960
^{59}Co+n, 16-22 MeV, cross sections for prompt γ, compound statistical model calcs. 79−543
^{59}Co(α,xnyp), 20-172.5 MeV, cross sections excitation functions, hybrid model, preequilib. effects 80−57784
^{59}Co(n,2n), isomeric cross-section ratio and excitation function, mixed-powder method and gamma-ray spect. 80−47472
^{59}Co(n,α), excitation function, mixed-powder method and gamma-ray spect. 80−47472
^{59}Co(n,n′γ), 1.1-3.3 MeV, level inelastic scatt. cross section, decay γ-rays, spins, branching ratio 79−6605
^{59}Co(n,n′γ), level transitions, deexcitations and lifetimes 80−18222
^{60}Co, 2505 keV gamma ray intensity in β-decay 79−13249
Cr, A=48-52, effective charges and E2 transitions in 1f-2p shell nuclei 78−544
Cr isotopes populated in (n,n′γ) scatt., γ-ray assignments to transitions 77−26767
^{49}Cr levels, transitions, and Gamow-Teller matrix elements from ^{49}Mn, β^+-decay 80−57746
^{49}Cr low lying states, deformed configuration mixing shell model calcs. 77−6302
^{51}Cr, bands, levels, EM transitions, J^π, branching and mixing ratios from ^{48}Ti (γ,nγ)^{51}Cr and ^{51}V(p,nγ)^{51}Cr 80−52606
^{51}Cr, gamma-ray precision energy meas. 78−58533
^{52}Cr, 1p5h config., high-spin neutron-hole states, EM transition rates 78−70430
^{52}Cr, decay of highly excited nuclei following ^{48}Ti(^{16}O,^{12}C) at 120 MeV 79−45289
^{52}Cr, EM decay of isobaric analogue states to low lying states 78−86492
^{52}Cr, γ-decay of analogue states obs. in ^{51}V(p,γ) 78−70503
^{52}Cr high spin states, transitions and J^π values from ^{50}Ti(α,Znγ) 80−455
^{52}Cr, high-spin states populated by ^{50}Ti(α,2nγ), assignment from spectroscopic states 77−65190
^{52}Cr(γ,γ′), 35 MeV, 2^+ state deexcitation γ-rays, differential cross sections, deformation *(Russian)* 80−13406
^{52}Cr(γ,γ), up to 12 MeV, highly excited spin-1 resonances, γ-transitions 80−13427
^{53}Cr, excited negative parity states to 2322 keV via (p,p′γ) and (α,α′γ) 77−82851
^{53}Cr levels, J^π, γ-transitions and 1626 eV resonance from ^{52}Cr(n,γ) 80−42610
^{54}Cr levels, transitions, $T_{1/2}$, J^π, shell model anal. from ^{51}V(α,pγ) 80−47381
^{56}Cr, γ-ray spectroscopy of low-lying states studied via ^{54}Cr(t,pγ) 77−10358
^{56}Cr, yrast decay schemes for heavy-ion fusion evaporation reactions 77−82854
Cs, fission fragment, delayed neutron branches from γ-spectroscopy 80−78230
Cs→Xe, neutron deficient isotopes, Xe low lying levels 77−22947
^{A}Cs, A=119-133 odd isotopes, collective props., bands and transitions from heavy ion reactions 80−68512
^{A}Cs, A=121, 123, 125, $g_{9/2}$ and $h_{11/2}$ bands 78−50067
^{A}Cs, A=142, 144, 146, low lying levels, J^π, mixing ratios and γ-γ ang. correlations 80−102119
^{123}Cs, decoupled band obs. by in-beam γ-ray spectra of ^{115}In(^{12}C,4n) 78−21520
^{123}Cs(^{123m}Cs), gamma and conversion electron radiation 80−106017
^{127}Cs, 66-keV decay, $T_{1/2}$, K conversion coeff. 77−54184
^{127}Cs collective quadrupole dynamics, band struct., transitions, collective model anal. from ^{121}I(α,4n) 80−78112
^{131}Cs, 133.5 keV state, electric quadrupole interaction 80−32228
^{131}Cs, gamma ray spectra from ^{131}Ba decay 79−85400
^{131}Cs, level struct. obs. from ^{131}Ba decay 77−10359
^{131}Cs populated in ^{131}Ba decay, E0 transitions 80−22752
^{133}Cs, populated in (n,n′γ) reaction, level scheme and deexcitation 78−13004
^{133}Cs(N,γ)^{134}Cs, exciton model, γ spectra calc. 78−62539
^{133}Cs(α,α′), 161 keV state magnetic moment and B(E2) values, Coulomb excitation 79−45159
^{134}Cs 176.403 keV isomer, populating γ-rays, low lying levels from ^{133}Cs(n,γ), ^{134}Cs 176.403 keV isomer, populating γ-rays, low lying levels 80−78200
^{137}Cs excited levels from ^{137}Xe β decay, γ spectra, coincidences, branching, logft values 77−54186
^{139}Cs level scheme, J^π and γ-transitions from ^{139}Xe β-decay 80−42590
^{143}Cs, nuclear spectroscopy of neutron rich A=143 nuclei 79−59039
^{144}Cs, beta and gamma spectroscopy 77−22962
Cu, A=61,63, analogue state decay modes from Ni (^{3}He,dp) 79−67702
Cu odd isotopes populated in ^{58,61}Ni(p,γ), analogue to antianalogue M1 transitions 77−67718
^{A}Cu A=29,63, Doppler shift attenuation factors, level lifetimes, resonances from Ni(p,γ) 80−57741
^{A}Cu, A=59, 61, 63, 65, f and p shell analogue resonances, γ-decay *(Russian)* 79−30800
^{59}Cu, analogue resons. excited in ^{58}Ni(p,γ), γ-decay 78−13005
^{59}Cu, determ. of total and partial widths of unbound states 77−74802
^{59}Cu, γ decay and splitting of analogue states, from ^{58}Ni(^{3}He,dγ) at 18 MeV 78−70505
^{60}Cu levels from ^{60}Ni(^{3}He,t) 78−46079
^{61}Cu γ-cascade multiplicities, entry state depend. on excitation energy from ^{58}Ni (α,pγ), 17 and 19.5 MeV 78−82311
^{61}Cu, J^π assignments, E1 photon strength functions, partial radiative widths 79−59063
^{62}Cu, γ-ray transitions from ^{59}Co(α,n)^{62}Cu, ^{60}Ni(^{3}He,p)^{62}Cu,^{62}Ni(p,n)^{62}Cu *(French)* 77−26615
^{62}Cu, yrast states obs. in ^{60}Ni(α,pnγ) and ^{63}Cu(p,pnγ) 78−12945

nuclear energy level transitions continued
^{63}Cu, decay of analogues, γ-ray ang. distribs. and spins of resons. 78−13002
^{63}Cu EM decay transitions, level J^π assignments, level lifetimes from (α,pγ), (^{11}B, 2pγ) 79−85402
^{63}Cu, EM props., J^π, via (p,p′γ) 5.0 MeV 77−74800
^{63}Cu $g_{9/2}$ analogue state fragmentation from γ-transitions in ^{62}Ni(p,γ) 79−22202
^{63}Cu, level struct. from ^{63}Cu(p,p′γ) react. 78−78378
^{63}Cu levels, transitions and ang. distribs. from α-transfer in ^{59}Co(^{6}Li,d) 80−73798
^{63}Cu levels and transition j-depend., DWBA anal. of ^{60}Ni(^{19}F, ^{16}O) 80−42542
^{63}Cu low excitation states, level struct. and lifetimes from ^{60}Ni(α,pγ) 80−86813
^{63}Cu state alignment, γ-transitions and ang. distribs. from ^{62}Ni(p,γ) 80−73797
^{63}Cu(p,p′) negative parity level excitation, gamma ray obs., test for core excitation model 80−68534
^{64}Cu, γ-spectra, J^π assignments via ^{64}Ni(p,nγ) 2.75-3.75 MeV 77−18470
^{64}Cu levels and transitions, stat. anal. of ^{64}Ni(p, nγ) *(Russian)* 80−5104
^{65}Cu analogue $P_{1/2}$ resonance, γ-decay and energy levels from ^{64}Ni (p, γ) 79−80907
^{65}Cu levels and transitions, γ-strength function using average resonance capture from ^{64}Ni(p,γ) 80−13411
(d,d), A=24-54, pol.d, 20 MeV, quadrupole transition amplitudes 80−99148
(d,p), A=88-106, pol. d, excitation curve isospin anomaly, neutron single particle resonances 80−27595
Dy equilibrium and pre-equilibrium decay, α-multiplicities, energies and entry lines from ^{160}Gd(α,xn) 79−93549
Dy K-shell internal conversion yields, gamma transition multipolarities from (α,xn), (^{12}C,xn) 80−78215
Dy, N=85 isotones, bands and transitions from α and HI excitation, in-beam study 80−78123
^{A}Dy, A=150, 151, 152, levels, J^π and transitions from Ho EC decay 79−89241
^{A}Dy, A=152, 153, isomeric states and complex band structs. from Nd(^{12}C, xnγ), Gd(α, xnγ) 79−67624
^{A}Dy A=158,160, quasi-continuum γ-ray cascades, neutron drip line from ^{160}Gd(α, xn) 79−75903
^{A}Dy A=162, 164, gamma to ground band transitions, γ-γ directional correlations from (n,γ) 80−68579
^{A}Dy(α,α), A=161,163, 9.0-13.5 MeV, B(E2) values, rigid rotor model validity 79−494
^{148}Dy$_{82}$ 10^+ isomer, $\pi h_{11/2}$ effective E2 charge 78−93964
^{150}Dy, gamma-decay, produced by ^{144,146}Nd(^{12}C,xn)^{150}Dy, high-spin isomers of ^{150}Dy 78−50075
^{151}Dy high spin states, isomers, α-decays and yrast sequence from (^{32}S,3n), (^{14}N,4n) 79−93493
^{151}Dy levels, bands and transitions, in-beam γ-rays from ^{142}Nd(^{12}C,3nγ) 80−458
^{152}Dy 60 ns isomer deexcitation E2 x- (or Δ) transition, half life, γγ-coincidence from ^{152}Gd(α,4n) 80−86859
^{152}Dy continuum γ-ray multipolarity by linear polarisation meas. from ^{140}Ce(^{16}O,4n) 79−85408
^{152}Dy high spin struct., in beam γ meas. from (^{15}N, 4n), (^{16}O, 4n) 80−18179
^{152}Dy yrast continuum γ-ray multipolarity via polarisation meas. from ^{140}Ce(^{16}O,4n) 80−9264
^{152}Dy yrast isomers, γ-rays from compound nuclei 80−86789
^{152}Dy yrast line single particle nature at high ang. momentum from Sn(^{32,34}S, 4n) 79−71783
^{155}Dy, weakly deformed, isomeric $9^+/_2$ and lowest $7^-/_2$ states decay 79−89231
^{156}Dy high spin states lifetimes and feeding times, quadrupole moments from ^{24}Mg(^{136}Xe,4n) 80−32239
^{158}Dy band side feeding pattern and γ-multiplicities, statistical model from ^{26}Mg(^{136}Xe, 4n) 79−75821
^{158}Dy collective excitations as populated in ^{158}He^{g,m} decay 78−82270
^{158}Dy γ-spectrum from ^{158}Gd(α,4n), 40 MeV, fusion and neutron evaporation, ^{158}Dy γ-spectrum 79−36291
^{160}Dy anomalous γ-L X-ray directional correlations from ^{160}Tb decay 80−52610
^{160}Dy, γ transitions following ^{160}Tb decay 80−83060
^{160}Dy, γ-ray intensity and ang. correl. meas. 77−10354
^{160}Dy γ-spectrum from ^{160}Gd(α,4n) 40, 49 MeV, fusion and neutron evaporation 79−36291
^{160}Dy, meas. of 1178-87 keV cascade ang. correl. function 77−14061
^{160}Dy, quasi-continuum transitions multipolarities from ICC via ^{160}Gd(α,4n)^{160}Dy 77−82945
^{162}Dy, intraband transition rates in gamma vibr. bands 78−45992
^{162}Dy(n,n′γ), study of ^{162}Dy levels up to 2 MeV 77−6285
^{164}Dy, low lying spectra and EM transitions, level struct. in quasirotational bands 79−36141
^{164}Dy multipole mixing in γ to ground bands from ^{163}Dy(n,γ) 80−52615
^{164}Dy(α,α′), 11.5-12 MeV, E_2 and E_3 transition strengths meas. 77−26618
^{164}Dy(n,n′γ), γ spectrum, level populations 77−61406
^{165}Dy, collective contributions to E1, ΔK=1 matrix elements in odd-odd deformed nuclei 79−17857
Dy(α,α′), A=156,8, E=12-13 MeV, E2, E4 transition matrix elements determ. 78−33202
Er, A=161,162, high ang. momentum states from Nd+^{16,18}O, γ decay modes from multiplicity meas. 78−29419
Er γ-multiplicities and cross sections, neutron evaporation from ^{130}Te(^{32}S,X), (^{16,18}O,X) 80−73824
Er rotational nuclei, transition energy correlations, very high ang. momentum 80−86787
^{A}Er, A=156-162, transitions from ^{158}Gd+^{12}C fusion 79−580
^{A}Er, A=158,160,162, high spin states and deformation, number conservation effects 79−89225
^{A}Er, A=159,160, energy levels, deexcitation γ-rays, g-factors and hyperfine interaction from ^{28}Si(^{136}Xe, xn) 80−102114
^{153}Er 360 ns yrast trap, γ transitions and lifetimes from ^{144}Sm(^{12}C,3n) 80−9205
^{154}Er, high-spin yrast states, lifetime meas. using recoil-distance method 79−40884
^{154}Er yrast cascade to spin 36, side feeding, energy, multipolarity irregularities from (^{16}O, 4n), (^{64}Ni, 4n) 79−36191

nuclear energy level transitions continued
^{1}Er yrast trap and transitions, decay scheme from (^{64}Ni,4n), (^{16}O,4n) 80−9206
^{58}Er, anomalous rotational bands−a model of a soft rotor coupled with $i_{13/2}$ particles 79−85356
^{58}Er continuum γ-ray multipolarity by linear polarisation meas. from ^{148}Nd(^{16}O,4n), yrast levels 79−85408
^{60}Er high spin yrast states and transitions from ^{152}Sm(^{13}C,5n) 80−9208
^{61}Er, excited states populated in ^{163}Tm decay 78−17146
^{64}Er high spin props. in multiple band crossing region from (^{18}O,4nγ), (α,4nγ), (^{136}Xe,^{138}Xeγ) 80−83023
^{166}Er (α,α′), 11.5-12 MeV, E_2 and E_3 transition strength meas. 77−26618
^{166}Er, Coulomb excitation with ^{4}He and ^{16}O ions 78−8839
^{166}Er, low lying spectra and EM transitions, level struct. in quasirotational bands 79−36141
^{166}Er, spin dependence of E2/M1 admixtures 77−6192
^{166}Er(^{86}Kr, X), 600 MeV, deeply inelastic, alignment of transferred ang. momentum, discrete γ-ray ang. correlations 80−47498
^{166}Er(γ,γ′), 14.4-16.6 MeV, γ-vibr. band head transitions, dynamic collective model 80−57662
^{167}Er levels and transitions, spectroscopic factor bombarding energy depend. from ^{168}Er(d,t), 9-15 MeV 79−495
^{167}Er(α,α), 9.0-13.5 MeV, B(E2) values, rigid rotor model validity 79−494
^{168}Er, $2_\gamma \rightarrow 2_g$ transition, band mixing, electric monopole contrib. 77−2940
^{168}Er, 80 and 1094 keV states, g-factors from ang. correlation methods 80−83035
^{168}Er γ-vibr. band, M1 admixtures in intra-band transitions 80−99149
^{168}Er, intraband transition rates in gamma vibr. bands 78−45992
^{172}Er levels, bands, J^π and transitions from ^{170}Er(t,p) 80−83038
Er(α,α′), A=162, 4, E=12-13 MeV, E2, E4 transition matrix elements determ. 78−33202
^{251}Es level struct. and p states, level transitions from ^{250}Cf(α,t) and ^{251}Fm decay 78−78268
^{A}Eu, A=145, 147, 149, mag. moments of $11/2^-$ states 79−40846
^{147}Eu, transitions in ^{147}Gd decay 79−6475
^{143}Eu^{m}, decay obs., struct. determ. 78−50130
^{145}Eu high spin and isomeric states, transitions, weak coupling from ^{144}Sm(α,2npγ) 80−13348
^{145}Eu high spin core coupled states and transitions from ^{142}Nd(^{6}Li, 3nγ) 80−42520
^{145}Eu high spin levels, isomers and in-beam γ-spectroscopy from ^{144}Sm(α,2np) 80−78124
^{145}Eu high spin states, J^π and transitions from (^{7}Li,4nγ) and (^{6}Li,3nγ) 80−47350
^{145}Eu level and transition effects on ^{145}Gd decay anomalies 80−32244
^{146}Eu 9^+ isomer, γ-decay, high spin particle-hole multiplet population from ^{147}Sm(p,2n) 80−63066
^{147}Eu populated in ^{147}Gd decay, γ-ray spectra obs. at small-source detector distance *(Russian)* 79−93520
^{149}Eu, proton states and transitions shell model anal. of ^{148}Sm(α,t) 79−30781
^{151}Eu level scheme from excitation functions, rotor and interacting boson anals. from ^{152}Sm(p,2nγ) 79−45163
^{152}Eu 89.8488 keV isomeric state feeding, delayed coincidence meas., level scheme from ^{151}Eu(n,γ) 80−63126
^{152}Eu ($T_{1/2}$=12.4 yr) neutron resonances 0 to 14 eV, radiation width, level spacings 77−26583
^{152}Eu, isomeric levels and transitions, Nilsson model 80−18195
^{152}Eu, level scheme, low energy transitions, reaction data, Nilsson model interpretation 78−66215
^{153}Eu, EM transitions, multipole, internal conversion coeffs. *(Russian)* 80−63121
^{153}Eu(n,X), gamma transitions and band levels *(Russian)* 79−67700
^{154}Eu low lying levels, bands, transitions from ^{153}Eu(n,γ) 80−57694
^{150m}Eu, 35.8 y, decay coincidence study, ^{150}Sm levels 77−82858
^{9}F+n, 16-22 MeV, cross sections for prompt γ, compound statistical model calcs. 79−543
^{A}F, A=18, 19, E2 transition rates calc., shell model with effective interaction and charges 80−47423
^{18}F 1.04 MeV state lifetime and γ-transition polarisation from ^{18}O(p,n) 80−106016
^{18}F, 1.08 MeV γ transition, circular polarisation affected by neutral weak currents 78−41663
^{18}F, 1.08 MeV γ transition, circular polarisation affected by neutral weak currents 79−13243
^{18}F, 5603 keV level, isospin mixing via (α,γ) and (p,γ) reactions 78−543
^{18}F, effective interaction, nonlocal pot. reaction matrix free scatt., spectra 77−46122
^{18}F resonances, α-widths, isospin and parity mixing, R-matrix anal. of ^{14}N(α,α) 80−91162
^{19}F, coupled channel orthogonality condition model 80−47384
^{19}F, decoupled bands and antialigned states 78−78236
^{19}F, hyperfine interactions of fast ions recoiling in noble gases 77−18469
^{19}F low lying band state lifetimes, stopping power, transition strengths from ^{15}N(α,γ) 80−42585
^{19}F, parity mixing and weak parity nonconserving NN interaction 77−6223
^{19}F reson. levels from ^{15}N(α,γ)^{19}F reaction 77−65211
^{19}F, spectra and E1 transitions, ang. momentum projected HF and Tamm-Dancoff methods 77−54139
^{19}F $T=^3/_2$ states resonance energy, γ-decay and J^π, capture strength from ^{16}O(p,γ) 79−67728
^{19}F, transition probabilities and multipole moments between states calc. by generator coordinate method 78−13022
^{19}F(p,p′γ), 1459→110 keV transition, E2/M1 mixing ratio 80−106013
^{20}F 2.97 MeV doublet γ-decay, J^π assignment from ^{11}B(^{13}C,αγ) 79−6491
^{20}F cross sections and anal. power, compound nucleus contrib. Ericson fluctuations from ^{18}O(d,p), pol. d 80−22803
Fe, A=52, 4, effective charges and E2 transitions in 1f-2p shell nuclei 78−544
^{A}Fe, A=54-56, high spin states, energy levels, spectroscopic factors, EM props., shell model 80−47359
^{A}Fe, A=56-58, shell model calcs., static moments and EM transition rates 79−17853
^{A}Fe, A=56-60, shell struct. of collective states, level spectra 79−93494
^{A}Fe, A=57, 59, levels, J^π and transition branching ratio from Fe(n,γ) 80−105976

nuclear energy level transitions continued
^{52}Fe yrast state properties, transitions and decays from ^{40}Ca(^{14}N,np) 79−67631
^{54}Fe high spin states, transitions and J^π values from ^{52}Cr(α,Znγ) 80−455
^{54}Fe(α,α′), coupled channels calc., capture cross section, GQR decay modes 80−27654
^{54}Fe(p,p′), 39, 62 MeV, DWBA anal., collective spectra, direct process contrib. *(Russian)* 80−13408
^{54}Fe(p,p′), pol. p, 800 MeV, diff. cross sections, anal. powers, DWIA anals. 80−83067
^{54}Fe(ρ,α)^{51}Mn, 35 MeV, nuclear struct. study 79−75980
^{55}Fe resonances, levels, J^π, valence capture γ-ray spectrum from ^{54}Fe(n,γ) 80−86852
^{56}Fe, 6^+ doublets populated in heavy-ion compound reactions, side feeding 78−13014
^{56}Fe, fp shell model calcs., spectra and spectroscopic factors 80−68588
^{56}Fe isobaric analogue resonances, γ ang. distribs., spin assignments, decay characts. 78−78342
^{56}Fe isobaric analogue resonance levels, branching ratios, from ^{55}Mn(p,γ) 80−68617
^{56}Fe low lying levels, J^π, γ-γ coincidences, internal conversion from ^{56}Co β^+-decay 80−86815
^{56}Fe, partial radiation widths from neutron capture resonances, valency model calcs. 77−26707
^{56}Fe, radiative transitions from unbound states obs. in neutron inelastic scatt. *(Russian)* 78−41664
^{56}Fe+n, 16-22 MeV, cross sections for prompt γ, compound statistical model calcs. 79−543
^{56}Fe(^{16}O,^{16}O′)^{56}Fe, magnetic substate population, closed formalism based on DWBA 77−6424
^{56}Fe(e,e′), Coulomb form factor for $0^+ \rightarrow 4^+$ transition, collective 4^+ states, shell model 80−57664
^{56}Fe(γ,γ), up to 12 MeV, highly excited spin-1 resonances, γ-transitions 80−13427
^{56}Fe(n,γ)^{57}Fe, high energy γ-ray transitions of ^{56}Fe resonances, E_n=7 to 70 keV 77−23081
^{56}Fe(n,n′γ), 14.6 MeV, maximum excitation state γ-decay, cross section *(Russian)* 80−68586
^{56}Fe(n,n), 14.6 MeV, radiation widths and particle widths of highly excited states, γ-transitions 79−6409
^{56}Fe(ρ,α)^{53}Mn, 35 MeV, nuclear struct. study 79−75980
^{57}Fe anomalous M1/E1 strength ratio and doorway states from ^{56}Fe(n,γ) 80−57730
^{57}Fe, gamma decay of 1.167 keV $p_{1/2}$ resonance obs. in ^{56}Fe(n,γ) 77−30585
^{57}Fe, Mossbauer absorption line function for a polycrystalline quadrupole-split absorber situated in a large applied magnetic field 79−87340
^{58}Fe levels, J^π, anal. powers and cross sections from ^{56}Fe(t,p) pol.t 80−68539
^{59}Fe resonances, primary γ-intensities, E1-M1 correlation from ^{58}Fe(n,γ) 80−57740
^{68}Fe low lying state mean lifetimes and transitions from ^{64}Zn(^{7}Li,p2n) 80−68599
Fe(n,n′γ), 8.5 to 14.2 MeV, differential cross section for prod. of 0.847 MeV γ-ray 77−23080
Ga from ^{66,68}Zn(p,γ), γ-ray ang. distrib. 78−74353
^{A}Ga, A=65,67, high spin states and transitions from Fe+^{12}C(^{14}N) 80−68516
^{65}Ga, 1.286 MeV state spin 9/2 determ. from ^{64,66}Zn(p,γ) obs. 79−63663
^{65}Ga high spin states, J^π and transitions, triaxial struct. from (^{12}C,αp),(^{7}Li,Zn) 80−63062
^{67}Ga γ- and X-ray emission probabilities and half-life obs. 80−32242
^{67}Ga, high spin states, using ^{57}Fe(^{12}C,pnγ) at 40 MeV 79−36128
^{69}Ga state alignment, γ-transitions and ang. distribs. from ^{68}Zn(p,γ) 80−73797
^{69}Ga(n,n′γ), fast n, levels, J^π, transitions and mixing ratios, statistical anal. *(Russian)* 80−13382
^{72}Ga, 3^--2^+ first forbidden beta transitions, β-γ ang. correlation, nuclear matrix elements 80−42599
^{154,156}Gd, pairing-plus-quadrupole calcs. 77−82807
Gd (A=154-156), collective properties 77−6192
Gd even nuclei, A=152-160, dynamic deform. theory, level energies B(E2) values 78−89795
Gd, N=85 isotones, bands and transitions from α and HI excitation, in-beam study 80−78123
$^{154-160}$Gd, vibrational state B(E2), B(E3) via (α,α′)Coulomb excit. 77−74803
^{A}Gd A=144,146,147,148, high spin isomer g-factors yrast traps from (^{28}Si,^{28}Si′), (α,α′) 80−78146
^{A}Gd, A=152, 154, γ-transition energy and intensity meas. from Eu decay 80−73818
^{A}Gd A=152, 154, negative parity states and β-γ-γ correlations from Eu β-decay 79−97676
^{A}Gd, A=154, 156, energy levels and E2 transition rates from three-band mixing model, backbending 79−67623
^{A}Gd(n,γ), A=154,156-8, 2, 24 keV, resonance averaged γ-spectra, level and J^π appls. 80−37347
^{67}Gd, γ-spectroscopy of high-spin levels via ^{64}Zn(α,pγ), ^{53}Cr(^{16}O,pnγ) 78−93960
^{144}Gd level scheme, delayed transitions, in-beam study from ^{144}Sm(α,4nγ) 79−17809
^{145}Gd levels, J^π and transitions, neutron hole coupling to ^{146}Gd core from ^{144}Sm(α,3n) 80−78164
^{146}Gd decay, γ- and internal conversion electron spectra 79−75916
^{146}Gd, high multiplicity yrast isomers prod. in (α,xn) reactions 78−41666
^{146}Gd lowest 2^+ state, J^π and transitions from ^{146}Tb decay 80−105979
^{146}Gd, O_2^+ state EM decay, $T_{1/2}$ and monopole strength 80−95310
^{146}Gd region, proton subshell effects from α-decay and spectroscopy, self-consistent study 80−57748
^{147}Gd, high multiplicity yrast isomers prod. in (α,xn) reactions 78−41666
^{147}Gd, high-spin states and particle-core coupling 77−26614
^{149}Gd level scheme and transitions from ^{149}Tb^{g} electron capture 79−9477
^{150}Gd levels and transitions, J^π assignments mixing ratio, nuclear orientation from ^{150}Tb decay 79−13205
^{150}Gd negative parity yrast states obs. in (α,xn) and ^{150}Tb decay 77−88033

nuclear energy level transitions continued
^{150}Gd, negative parity yrast band, E1 transitions polarisability, quadrupole-octupole coupled vibr. system 79−484
^{151}Gd excited state spin assignments γ-γ ang. correlations from ^{151}Tb decay *(Russian)* 79−49597
^{151}Gd, high spin states, gamma ray and conversion electron obs., level struct. 77−46130
^{152}Gd, populated in ^{152}Eu decay 80−22768
^{152}Gd, vibrational states, B(E2) branding rates and interband transitions, pairing plus quadrupole calcs. 80−78127
^{153}Gd γ-directional distrib., levels, spin assignments from ^{153}Tb decay 79−13241
^{153}Gd levels and γ-ray spectra from ^{152}Gd(n, γ) 80−57736
^{153}Gd, weakly deformed, isomeric $^{9+}/_{2}$ and lowest $^{7-}/_{2}$ states decay 79−89231
^{154}Gd multiphonon vibr. bands, dynamic deformation theory 80−5035
^{155}Gd, vibr. state, level scheme, γ and conversion electron spectra from ^{154}Gd(n,γ) 80−57696
^{155}Gd(α,α), 9.0-13.5 MeV, B(E2) values, rigid rotor model validity 79−494
^{156}Gd, elec. monopole transitions from excited 0^+ states, ^{156}Eu decay obs. 77−18478
^{156}Gd(n,γ), up to 2.24 keV, n resonances, spectra fluctuation, statistical theory test 79−36188
Gd(α,α′), 11.5-12 MeV, E_2 and E_3 transition strengths meas. 77−26618
Gd(α,α′), A=154,156,158,160, E2 and E4 reduced matrix elements 78−29490
Ge, even-even nuclei, γ-spectroscopy, exptl. results and models 80−68589
^{A}Ge, A=68, 70,72,74, level excitation, n-p interaction role from α-transfer in Zn(^{6}Li,d) 80−73821
^{A}Ge A=68,70,72,74, deformations and collective spectra, reaction mechanisms from Ge(p,t) 79−22168
^{A}Ge(t,p), pol.t, A=70,72, octupole oscillations modes from anal. powers, 3^-_1 octupole transition 80−102142
^{19}Ge excited state, J, mean lifetimes and transitions from ^{64}Za(^{7}Li,ph) 80−68517
^{19}Ge excited state, J, mean lifetimes and transitions 80−68517
^{66}Ge levels, lifetimes, J^π and transitions from ^{58}Ni(^{10}B,pnγ) 80−73799
^{66}Ge levels, lifetimes and mixing ratio, in-beam γ-spectroscopy from ^{54}Fe(^{14}N,npγ) 80−42541
^{66}Ge states and decay scheme, polarisations J^π and ang. distribs. from ^{58}Ni(^{10}B,pnγ) 80−22692
^{69}Ge excited states, spin and γ-decay, parity state struct. from ^{69}Ga(p,nγ) 3-5.6 MeV, ^{69}Ge excited states, spin and γ-decay, parity state struct. 79−464
^{69}Ge high spin states, EM props., Branching and mixing ratios from ^{55}Mn(^{16}O,pn) 80−13347
^{69}Ge high spin states, J assignment, decay scheme from ^{55}Mn(^{16}O,pn) 80−68518
^{69}Ge, transitions, spin and parity, and mag. moments determ. from β-decay of ^{69}As 79−22245
^{71}Ge, levels, studied via ^{68}Zn(α,nγ), 8 to 10 MeV, comparison with coupling model calcs. 78−8742
^{71}Ge negative parity states, J^π, energy spectra and spectroscopic factors 79−59013
^{72}Ge excitation energies, B(E2) values, extended generator coordinate method 77−6203
^{74}Ge excitation energies, B(E2) values, extended generator coordinate method 77−6203
^{75}Ge, beta decay of 83 min ground state, decay characts. and scheme 79−67713
^{76}Ge(n,n′γ), 2.0 to 4.1 MeV, level and decay schemes 77−23092
^{2}H γ-energy and binding energy from ^{1}H(n,γ) 80−52564
^{2}H(γ,pπ) photoexcitation in Δ(1236) region 80−22813
^{2}H(p,γ), 7-15 MeV, polarised and unpolarised p, cross section and anal. power 79−40921
^{3}H photoeffect, electric dipole sum rules 79−36231
^{3}H, total photodisintegration cross-section calc. using coupled hyperspherical harmonics 77−18525
^{A}H, A=2, 3, EM sum rules, total absorption cross sections 79−71818
^{A}H(π^+, π^+), A=1,2, 130-280 MeV, 180° excitation function, dibaryon resonance signals 80−68619
^{3}He trinucleon photoeffect, electric dipole transitions to isospin 1/2 trinucleon states 79−45246
^{3}He(^{3}He,d^{3}He), three body break up reaction energy spectra, computer program 80−27593
^{3}He(^{3}He,p^{3}He), three body break up reaction energy spectra, computer program 80−27593
^{4}He deduced monopole excitation to O^+ state DWBA anal. from (α,α′) 79−22226
^{4}He harmonic oscillator sum rules for photonuclear reactions, dipole moments, E1 transitions 78−41692
^{4}He, parity mixing below 30 MeV excitation energy for ΔT=0,1 transitions 80−52604
^{4}He photodisintegration, electric dipole transitions, photoeffect cross section 79−67742
^{4}He, second O^+ state, excitation energy 79−67658
^{4}He(α,αd), 119 MeV, excited states, J^π and γ-ang. correlations 80−86809
^{A}He, A=3, 4, EM sum rules, total absorption cross sections 79−71818
^{A}He, prod. cross section calc., γ decay spectrum, shell model theory 78−62501
He(γ,pπ), photoexcitation in Δ(1236) region 80−22813
Hf (A=176-180), collective properties 77−6192
$^{176-180}$Hf, vibrational state B(E2), B(E3) via (α,α′)Coulomb excit. 77−74803
^{A}Hf, A=166, 168, 170, 172, yrast states, quadrupole moments and B(E2) values, microscopic calcs. 80−32147
^{A}Hf(n,nγ), 2.75 MeV, A=180,178,176, levels and excitation cross sections 79−75839
^{171}Hf, hindered electric dipole transitions and lifetimes from (HI,xn) reactions 80−9263
^{172}Hf, decoupled two-quasiparticle bands, backbending 78−4890
^{172}Hf yrast band and high spin states, $22^+ \rightarrow 20^+$ transition, band crossing from ^{160}Gd(^{16}O,4n) 80−42523
^{177}Hf neutron resonances, high energy γ-rays 77−22938
^{178}Hf 9^- to 8^- transition from ^{178}Ta 2.45 h decay 79−45201
^{178}Hf, energy levels, K-forbidden decays, M4 decay of yrast state 80−68506
Hf(α,α′), A=176,8,180, E2 and E4 reduced matrix elements 78−29490
nuclear energy level transitions continued
Hg, A=191,2,3,5,7,9, rot. aligned bands, high spin states, energy levels B(E2) values 78−70483
Hg, even-A, possible triaxial shape and phase transition, triaxial rotor model 79−93503
^{A}Hg, A=196 to 204, E2 values for excitation of 2^+, $2^{+\prime}$ and 4^+ states 79−17792
^{A}Hg, A=198, 200, rigid asymmetric rotor model descript., E2 and E4 props. 80−13403
^{180}Hg, $T_{1/2}$=3s decay chain, on-line γ-ray spectroscopy 78−13034
^{184}Hg, excited deformed band, shape isomerism anal. 77−6234
^{184}Hg→^{184}Au decay, energy levels and lifetimes *(French)* 78−41661
^{188}Hg, HF calc., shape and lowest band struct., B(E2) values 80−32148
^{195}Hg level scheme and transitions, band population from ^{195}Tl (1.13 h) decay 79−17807
^{197}Hg (64 h) decay γ intensities, obs. 79−75922
^{197}Hg energy levels from ^{195}Pt(α,2n), γ and conversion electron spectra, spins, parities 78−25149
^{197}Hg level scheme and transitions from ^{197}Tl electron capture 79−67719
^{201}Hg γ-γ directional correlations, level transitions, spin assignments, mixing ratios from ^{201}Tl decay 79−496
^{201}Hg missing $f_{5/2}$ state Coulomb excitation, level scheme, J^π, transitions using (α,α), (^{16}O, ^{16}O) 80−47386
^{203}Hg, gamma-ray precision energy meas. 78−58533
Ho, A=161,163,165, E1 transitions, hexadecapole deforms., Nilsson model calc. 77−82861
^{A}Ho, A=153, 160, isomeric levels and transitions, Nilsson model 80−18195
^{A}Ho, A=167,169, energy levels from Er(t,α), polarised t 79−36155
^{149}Ho low lying yrast states from ^{122}Te(^{32}S,X), ^{121}Sb(^{32}S,X) 80−91151
^{159}Ho, rotational states determination from ^{159}Tb(α,4nγ)^{159}Ho and ^{159}Tb(^{3}He,3nγ)^{159}Ho 77−26556
^{165}Ho, electron-oriented nucleus scatt., eikonal approx. calc. 78−37331
^{165}Ho(^{86}Kr,X), 620 Mev, deep inelastic scatt., ang. momentum transfer, γ-ray multiplicities 80−27665
^{166}Ho, energies of low-lying high spin levels *(Russian)* 78−89793
^{166}Ho, internal hyperfine field obs. using β-γ directional correl. 80−32229
^{166}Ho low lying levels and transitions, 54.24 keV level mag. moment from ^{166}Dy decay 80−13380
^{166}Ho, spin assignments to levels, using ^{165}Ho(n,γ) polarised target and projectile 79−59062
I energy levels, collective excitations, spin,parity, populated in ^{121,123}Sb(α,2n), γ spectra 78−4891
^{A}I, A=115-127 odd isotopes, collective props., bands and transitions from heavy ion reactions 80−68512
^{123}I, bands and decay props., core-particle coupling and polarisation effects 80−13354
^{123}I decay, gamma-ray spectra, ^{123}Te level scheme obs. 77−10361
^{127}I γ cascade following ^{127}Te decay, 360.3-57.6 keV γ-γ directional correl. 78−25151
^{127}I(n,2n), 4.5-18.3 MeV, cross sections and excitation curves *(Chinese)* 79−49601
^{127}I(n,n′γ), 3, 14 MeV, 57 and 202 keV γ-ray prod. cross section 79−67706
^{127}I(n,n′γ), fast n, γ-ang. distribs., level ang. momenta 80−18224
^{129}I energy levels populated in ^{129}Te decay, γ spectra, coincidence spectra 77−2935
^{129}I time depend. quadrupole interactions, γ-γ correlations from ^{129}Te^{m+g} decay 80−78145
^{132}I decay, weak transition energies and intensities, γ-spectrum, ^{132}Xe levels 79−9521
^{132}I isomer and gamma-ray spectrum from ^{133}Cs(π^-,p) 80−78199
^{133}I yield and γ-ray spectra from ^{133}Cs(π^-,p) 80−86857
^{136}I, isomeric ratio, γ-spectra thermal neutron and 3 MeV fission of ^{235}U *(French)* 80−68709
In light isotopes, decay study with LISOL on-line mass separator 77−23361
In populated in ^{111,113}Cd(p,nγ), energy levels, spins, lifetimes, shape 77−320
^{A}In, A=104, 106, β-decay half lives and decay schemes 78−74333
^{A}In, A=113, 115, excitation by photon less positron annhilation, isomeric γ-transitions *(Russian)* 80−5089
^{A}In, A=119, 121, unified model description, vibr. multiplet yrast struct., branching ratios 80−105953
^{108}In high spin struct., in-beam spectroscopy, conversion electrons from ^{98}Mo(^{14}N,4nγ) 80−73782
^{108}In, level scheme determ. from ^{108}Sn decay and ^{108}Cd(p,n) 78−41636
^{109}In high spin states, γ-transitions, ang. distribs. from ^{108}Cd(α,2np) 80−73783
^{109}In high spin states, transitions, isomeric state, negative parity bands from ^{107}Ag(α, 2nγ) 80−451
^{109}In, levels and transitions obs. in ^{107}Ag(α,2n) 77−22836
^{111}In, populated in ^{111}Cd(p,nγ), γ-ray spectra, level scheme 78−13083
^{112}In low lying levels, transitions, $T_{1/2}$, multipolarities and mixing ratios from ^{112}Cd(p,nγ) 80−68545
^{113}In levels, from decay of ^{113}Sn 77−38247
^{114}In, internal conversion on outer electron shells, 191 keV E4 transition 80−42587
^{115}In 597 keV level J^π assignment from ^{115}Cd^{g} β-decay 79−80900
^{115}In, K-shell positron annihilation, excitation of nucleus *(Russian)* 78−33171
^{115}In^{m}, nuclear excitation by e^+ annihilation with K-shell electrons 79−22230
^{117}In level scheme, J^π and transitions from ^{117}Cd isomer decay, unified model anal. 80−32193
Ir, A=187, 189, triaxial rotor model and γ-vibr. model comparison, γ decay, level schemes 78−54695
^{A}Ir, A=189, 191, levels, J^π, transitions and mixing ratios from Pt decay 80−68602
^{181}Ir, γ-ray spectra, half-life, decay scheme 78−41672
^{188}Ir level scheme and transitions from ^{188}Pt electron capture 79−22237
^{191}Ir 129 keV transition, atomic screening, time reversal violation 80−106011
^{191}Ir, excited nuclei mean precession time depend. on γ-spectral width, g-factors *(Russian)* 80−78211
^{191}Ir γ transition, time reversal like phase shift between competing multipoles 79−30801
^{192}Ir levels, resonances and low energy γ-rays from ^{191}Ir(n,γ) 80−47397
^{193}Ir, muonic, mag. hyperfine anomaly 77−83768
K, A=48, 49, 50, half lives, γ meas. 78−74341

nuclear energy level transitions continued

$^{\wedge}$K, A=37,39, levels, excitation and microscopic form factors, DWBA calcs. from Ca(p,α) 80−32185
$^{\wedge}$K, A=40,42, EM transitions and transition probabilities for low lying states 79−75896
$^{\wedge}$K, A=43,44, levels, spin and parity assignments, decay scheme from ^{43,44}Ar β-decay 79−13210
$^{\wedge}$K, A=45,46, levels, lifetimes and transitions from Ar β-decay 80 42597
^{18}K, effective M3 matrix elements and transitions from shell model 80−102143
^{18}K level spectrum and (^{3}He,t) reaction mechanism from ^{38}Ar(^{3}He,t) 79−22229
^{39}K 9/2^{+} forbidden transition, cross section CCBA anal., L=1 transitions from ^{40}Ca(^{15}N,^{16}O) 79−9507
^{39}K, evaporation residue from ^{27}Al+^{12}C, prompt γ deexcitation 78−74395
^{40}K excitation energy, γ decay, of lowest T=2 state populated in ^{40}Ar(p,n) 78−8769
^{40}K, lifetime determ. using Doppler shift attenuation 79−93551
^{41}K, highly stripped ions, recoiling in vacuo, γ-decays of isomeric states obs. 78−50119
^{41}K, l-forbidden M1 decay from 1st excited state 78−13024
^{44}K excited levels, J$^{\pi}$, transitions and lifetimes from ^{48}Ca(p,αn) 80−68544
^{44}K excited states from ^{44}Kr β decay, weak coupling predictions, γ-ray meas. 78−74336
Kr even isotopes, collective levels and B(E2) values, IBA calcs. 80−27539
Kr even-even isotopes, collective states and transitions, interacting boson approx. 80−73773
$^{\wedge}$Kr, A=74-82, even-even isotopes, B(E2) values and collectivity, interacting boson approx. 80−27537
$^{\wedge}$Kr, A=79, 81, high spin E2 bands, J$^{\pi}$, transitions from Ge(^{10,11}B, xγ) 80−63061
$^{\wedge}$Kr(p,p'), 51.9 MeV, A=78, 80, 82, 84, 86, 2_2^+ and 4_1^+ state excitation 79−54389
^{78}Kr band struct., level scheme, from $\gamma\gamma$-coincidence from ^{65}Cu(^{16}O, 2np) 80−18177
^{78}Kr band structs., in-beam γ-rays from ^{68}Zn(^{12}C, 2n) 80−22672
^{78}Kr bands, lifetimes and E2 transitions from interacting boson model and (^{16}O,p2n), (^{19}Fe,α2n) 80−73771
^{78}Kr high spin levels, bands and transitions, level lifetimes from ^{68}Zn(^{12}C,Zn) 80−42525
^{78}Kr high spin states, transitions and lifetimes from (^{16}O,2np), (^{19}F,2nα), (^{16}O,2n), (^{12}C,2n) 80−27534
^{78}Kr high spin states from ^{65}Cu(^{16}O,p2n), band struct. 78−74387
^{79}Kr, low lying levels from ^{79}Br(p,nγ) 80−105972
^{81}Kr low lying states populated in ^{81}Br(p,nγ), γ spectra, γ-γ coincidences 78−25195
^{84}Kr levels, γ-cascades, J$^{\Pi}$, mixing ratios and correlations from ^{84}Br decay 80−63134
^{88}Kr level scheme and transitions, delayed neutrons from ^{88}Br β-decay 80−42600
^{16}L(d,^{6}Li)^{12}C, 50 to 80 MeV, spectroscopic factors energy depend. 79−6622
$^{\wedge}$La, A=123-125, half lives, low energy γ-data, β decay probabilities 79−499
$^{\wedge}$La, A=125, 127, collective props., bands and transitions from heavy ion reactions 80−68512
^{131}La→^{131} decay scheme, γ, X-ray and conversion electron spectra *(Russian)* 80−32241
^{138}La, radioactive decay meas., half life, γ energies 80−13418
^{139}La from ^{139}Ba β^- decay, γ-rays, energy levels 78−70492
^{139}La(n,γ), non-statistical capture, radiative widths, γ-ray doorway state model 80−37389
^{140}La γ-ray intensities, meas. with coaxial Ge(Li) detector *(French)* 78−58534
^{140}La, s- and p-wave resonances, obs. in La(n, γ) 78−17186
^{140}La, spectra from ^{139}La(n, γ) 78−17185
^{141}La, γ-γ coincidence and elec. conversion meas. 79−13252
^{143}La, gamma-ray spectra, half-life 77−82859
^{143}La, level scheme obs. in ^{143}Ba decay 78−50129
^{144}La beta and gamma spectroscopy 77−22962
(^{6}Li,d), A$\sim$60,116, L=0 transitions, cross sections, microscopic anal. 80−78189
^{6}Li, 5.36 MeV level electroexcitation form factor via ^{6}Li(e,e')^{6}Li at 40.5 and 50.5 MeV 77−54177
^{6}Li, even parity levels, anal. using P-model *(Russian)* 79−49585
^{6}Li, transition probabilities between cluster structure states and r.m.s. radius, double well-cluster model *(Chinese)* 80−63128
$^{6}_{\Lambda}$Li, supermultiplet struct. and decay props. of hypernuclear 1^{+} resonances from (K^-,π^-) 80−78186
^{6}Li(^{3}He, ^{3}He), excitation functions 80−18223
^{6}Li(e,e'), 102, 123 MeV, excitation form factor, ^{3}H-^{3}He cluster model 80−78190
^{6}Li(e,e'), 76-141 MeV, form factors, appl. to (π^-,γ), phenomenological model 80−83068
^{7}Li, proton scatt., 3/2^{-}→1/2^{-} transition, LS coupling shell model, isoscalar quadrupole renormalisation 77−14046
$^{7}_{\Lambda}$Li($K^-,\pi^-\gamma$), hypernuclear γ-ray line 78−37377
^{8}Li, form. in ^{11}B(n,α) reaction, 14.4 MeV, spectra and ang. distribs., recoil nucl. transitions 78−17193
$^{8}_{\Lambda}$Li possible γ-transition from ^{9}Be(K^-,π^-p) 80−106002
$^{9}_{\Lambda}$Li, prod. cross section calc., γ decay spectrum, shell model theory 78−62501
$^{\wedge}_{\Lambda}$Li, A=6,7, excited states and spectra, continuum effects calcs. 80−57720
$^{\wedge}$Lu, A=158, 159, alpha decay and gamma transitions 80−73827
$^{\wedge}$Lu A=171, 173, Nilsson state transitions from 1/2 life, Coriolis coupling matrix from Yb(p,n), 13 MeV 79−6485
^{170}Lu→^{170}Hf, beta decay, reduced transition probabilities 77−22945
^{172}Lu, decay scheme, γ-ray, conversion electron spectra 79−75913
^{172}Lu levels, transitions and J$^{\pi}$ values from ^{172}Hf EC decay 80−18249
^{174}Lu isomeric levels, γ-spectra, T 1/2 and decay modes from ^{176}Yb(p,3n) 80−99151
^{175}Lu delayed transitions from ^{176}Yb(p,3n) 80−99151
^{175}Lu(α,α), 9.0-13.5 MeV, B(E2) values, rigid rotor model validity 79−494
^{176}Lu deformed odd-odd nucleus, γ transition probabilities, rot. band mixing 77−61375

nuclear energy level transitions continued

^{176}Lu, reson. spins, secondary γ-transition intensity, from ^{175}Lu(n,γ) 78−21512
^{177}Lu, reson. spins secondary γ-transition intensity meas. in ^{176}Lu(n,γ) 78−21512
^{177}Lu excited state lifetimes, γ-transitions from β-decay transitions 80−78205
^{178}Lu isomeric states and spins, transition probability from ^{181}Ta(n,α) 80−52582
$^{\wedge}$Mg(p, p'), A=24, 26, isovector dipole strength excitation in giant resonance region 80−83066
^{23}Mg hole states, transitions and spectroscopic factors, DWBA anal. of ^{24}Mg(p,d) 80−32161
^{23}Mg j-forbidden $^{7}/_{2}^{+}$ state excitation, CCBA calculations, two step processes from ^{24}Mg(p,d), 49.5 MeV 79−26369
^{23}Mg, produced in 32-14.4 MeV ^{16}O+^{9}Be, gamma transitions 79−49599
^{23}Mg resonances through γ-decay excitation functions from ^{12}C(^{12}C,n) 80−63148
^{24}Mg, ^{16}O+α+α cluster model, energy level structure 80−18215
^{24}Mg 6_3^+ level, α and γ decays, branching ratios from ^{12}C(^{16}O,α) 79−75901
^{24}Mg ($\alpha,\alpha'\gamma$) 104 MeV, nuclear deformation from ang. correlations, coupled channel anal. 78−78301
^{24}Mg (γ,p), 17-30 MeV, giant dipole resonances and transitions, shell effects *(Russian)* 80−13434
^{24}Mg continuum states, branching ratios from ^{12}C(^{16}O, $\alpha\alpha$) 80−22661
^{24}Mg first excited state static quadrupole moment, B(E2) value from ^{208}Pb(^{24}Mg,^{24}Mg) 79−45161
^{24}Mg ground and γ-bands, direct and multistep processes from (α,^{6}He), (p,t), (^{16}O, ^{16}O) 80−102094
^{24}Mg intermediate struct. correlations, elastic and reaction channel excitation functions from ^{12}C(^{12}C,X) 80−68625
^{24}Mg isovector M1 excitations, current and spin contribs. from (e,e'), (p,n) 80−68582
^{24}Mg, K$^{\pi}$=0^{-}, K$^{\pi}$=3^{-} bands, radiative and α-widths from (α,γ), (^{16}O,$\alpha\gamma$) 80−18173
^{24}Mg, multipole mixing ratios from polarised beam γ-ray singles meas. 77−46132
^{24}Mg, O_1^+, 2_1^+, 4_1^+ states, EM props. from large basis shell model 79−75900
^{24}Mg, produced in 3.2-14.4 MeV ^{16}O+^{9}Be, gamma transitions 79−49599
^{24}Mg radiative decays of unbound high spin states, resonance J$^{\pi}$ assignment from ^{20}Ne(α,γ) 79−67701
^{24}Mg rotational band collectivity, shell model excitation in Sp(4, R) symmetry 80−102095
^{24}Mg, T=2 state props., obs. in ^{23}Na(p,γ)^{24}Mg reaction 78−8767
^{24}Mg, triaxial nuclei rots., extended cranked shape consistent oscillator model 80−102133
^{24}Mg yrast and high spin states up to 24 MeV, ang. distribs. from ^{10}B(^{16}O, d) 80−18175
^{24}Mg(^{13}C,^{13}C'), 35 MeV, γ-rays and spin flip 80−18189
^{24}Mg(^{13}C,^{13}C'), 35 MeV, 2^{+} population probab., spin-flip and spin orbit pots., coupled channel anal. 80−99125
^{24}Mg(^{16}O,^{16}O), 24-40 MeV, backward angles, excitation functions, ang. distribs. and resonant behaviour 80−68622
^{24}Mg(α,α'), 120 MeV, ground and gamma band excitation, coupled channel calcs. in rotational model 79−89315
^{24}Mg(p,p'), 49.5 MeV, consistent folding model, HF calc. for E2, E4 transitions 79−22288
^{24}Mg(p,p') 17.5 MeV 79−22288
^{25}Mg (e,e) 80-215 MeV, magnetic moment form factors, M1, M3, M5 transitions 79−40844
^{26}Mg ($\alpha,\alpha'\gamma$) 104 MeV, nuclear deformation from ang. correlations, coupled channel anal. 78−78301
^{26}Mg, isoscalar and isovector E2 transition matrix elements 78−25148
^{26}Mg, multipole mixing ratios from polarised beam γ-ray singles meas. 77−46132
^{26}Mg transition strength n and p components, $\pi^{\pm}$ inelastic scatt. comparison, shell model 80−68585
^{26}Mg(^{3}He,^{3}He'), 4^{+} states, B(E2) values, and band mixing, rot.-vibr. model 80−83019
Mn, A=54-6, yrast decay schemes from heavy-ion fusion evaporation reactions 77−82854
^{52}Mn yrast state properties, transitions and decays from ^{52}Fe ^{M} β^+-decay 79−67631
^{53}Mn fragmented $g_{9/2}$ isobaric analogue resonance, transitions, J$^{\pi}$ assignments from ^{52}Cr(p,γ) 79−45240
^{53}Mn fragmented $g_{9/2}$ isobaric analogue resonances, γ-transitions from ^{52}Cr(p,γ) 79−85430
^{53}Mn fragmented $g_{9/2}$ isobaric analogue resonance, γ-spectra and excitation functions from ^{52}Cr(p,γ) 80−68627
^{53}Mn, γ decay and splitting of analogue states from ^{52}Cr(^{3}He,dγ) at 18 MeV 78−70505
^{53}Mn high spin states, decay scheme, J$^{\pi}$ assignments, mixing ratios from ^{40}Ca(^{16}O, 3pγ) *(French)* 79−67627
^{53}Mn(ρ,α)^{52}Cr, 35 MeV, nuclear struct. study 79−75980
^{54}Mn, populated in ^{52}Cr(α,pnγ), low lying intruder states 79−58998
^{55}Mn energy level excitation curve, bound state and resonance γ-decay from ^{54}Cr(p,γ) 79−476
^{55}Mn transitions to low lying levels, α spectroscopic strengths, DWBA anal. of ^{51}V(^{6}Li,d) 79−45156
^{55}Mn(α,α), 4.5 to 7 MeV, Coulomb excitation, search for 1.29 MeV 1/2^{-} level 78−82360
^{55}Mn(n,n'γ), 2.2-3.2 MeV energy level J$^{\pi}$ assignments, transition branching and mixing ratios 79−40881
^{56}Mn, gamma intensity, from ^{55}Mn(n, γ) cross-section meas., k_0 factors calcs. 79−26433
^{56}Mn levels, transitions and spins from ^{55}Mn(n,γ), pol. Mn and n 80−78154
Mn(n,γ), primary transitions using focused 24 keV filtered neutron beam 80−63436
Mo, A=103-5, half-lives and γ-ray energies of short-lived isotopes following ^{235}U fission 78−17137
Mo, A=94-100, B(E2; 0^{+}→2^{+}) via ^{4}He and ^{16}O scatt. 77−6226
Mo, even-even isotopes, first excited 0^{+}' states, energy systematics 78−54683
Mo isotopes struct., spectroscopy weak coupling approx. in shell model 79−22194
Mo neutron rich isotopes, excited 0 states 77−22937

nuclear energy level transitions continued
A Mo, A=94, 96, 98, multiparticle states, method of generalised seniority 80−22759
A Mo, A=98,102, anal. powers, transitions, shape coexistence states, DWBA anal. of Mo(t,p), pol.t 80−86895
A Mo(n,γ) A=98, 100 resonance parameters, capture Γ-rays and reaction mechanism 80−18272
^{89}Mo^{m} levels, transitions and half life from ^{93}Mo(p,p'3n) 80−86858
^{92}Mo(p,p'), time development function at isobaric analogue resonances, compound nuclear level decays 79−3124
^{93}Mo, shell model calcs., energy levels, transitions and spectroscopic factors 79−63593
^{94}Mo high spin state transitions, mixing ratios, spins, shell model calcs. from ^{94}Tc decay 79−97678
^{98}Mo neutron resonances, spin-parity determ. using low energy γ-rays 77−26570
^{98}Mo static quadrupole moment of first 2^+ state from (α,α'), (^{16}O,^{16}O') 80−5061
^{98}Mo(,α,α'), 8 MeV, multiple Coulomb excitation, fast $2^+ \rightarrow 0^+$ transition 79−17846
^{99}Mo, levels and gamma decay scheme obs. in ^{98}Mo(n,γ) 77−30580
^{100}Mo(n,n'γ), fast n, gamma transitions, level energies and scheme 80−73822
^{100}Mo(p,p'), 6.975 MeV, E0 transition probability for 0_1^+-0^+ transition 77−41963
^{101}Mo levels, γ-rays and p-wave resonance partial radiative widths from ^{100}Mo(n,γ) 80−57739
^{101}Mo, levels and gamma decay scheme obs. in ^{100}Mo(n,γ) 77−30580
^{93m}Mo→^{93}Nb, high-spin three-quasiparticle states of ^{93}Nb 77−34262
Mo(p,p'γ), odd isotopes, excited d-states from analogue resonances and p-γ correlations 80−68546
NN potential from baryonium data, spin forces and radiative decay widths 79−45175
A N, A=16,18, E1 and M2 giant resonance excitation from O(π$^-$,γ) 79−89280
^{13}N giant dipole resonance population amplitude and phase, E1 reaction amps. from ^{12}C(p,γ$_0$), pol. p 80−63145
^{13}N state transition ang. distrib., optical parameters from ^{12}C(^{7}Li, ^{6}He) 79−75904
^{13}N, transitions from lowest T=3/2 states 77−88075
(^{14}N,xnγ), rare earth nuclei, complete fusion process n and γ multiplicity 80−18363
^{14}N (e,e'), 40-60 MeV, at 180°, M1 transitions and transition widths 79−49598
^{14}N, energy levels up to 11.05 MeV, transitions and resonance decay from ^{13}C(p,γ) 80−47376
^{14}N levels and excitation energies, kinematically complete investigation from ^{16}O(π$^-$, 2n) 80−99128
^{14}N(γ,π$^-$)^{14}O, 145-325 MeV, Gamow-Teller suppression and M1 radiative widths 80−52609
^{14}N(n,γ), γ-ray energies, calibration standards 80−52613
^{14}N(p,p'), 122 MeV, level excitation, cross sections, effective NN interaction, DWIA anal. 80−78197
^{15}N excited states and transitions from ^{15}C beta decay 80−18248
^{15}N low lying states, cross sections and anal. power, transitions, spectroscopic factors from ^{14}N(d,p), pol. d 80−32183
^{15}N, obs. of high spin states in ^{12}C(^{6}Li,t) and ^{12}C(^{6}Li, ^{3}He) 78−13015
^{15}N polarisation, spin alignment and excited state ang. distrib. from ^{88}Sr(^{16}O, ^{15}N) 79−67709
^{15}N three particle states at high excitation energies, J^π, selective population from ^{12}C(^{7}Li, α) 80−99129
^{15}N(e,e'), excitation of energy levels 9.7 to 14.7 MeV, 60-194 MeV, EM form factor meas. 78−25175
Na, A=21, 2, 3, absolute reson. strengths meas. in Ne(p,γ), Ne(p,pγ) 77−38272
Na, A=21, 23, M1, E2, transition probabilities between differently deformed states, Nilsson model 77−61376
^{22}Na 0^+ level mean life, isovector mag. dipole transition from ^{19}F(α,n) 80−68595
^{22}Na, isoscalar M2 transition, γ-ray spectra obs. 77−10363
^{22}Na levels, resonances in ^{21}Ne+p reactions, 0.4 to 1.6 MeV 77−18540
^{23}Na, decoupled bands and antialigned states 78−78236
^{23}Na, E1 decays, high spin state identification 77−26617
^{23}Na high spin positive parity state, approx. microscopic methods, shell model comparison 79−85352
^{23}Na high spin states, excitation functions, nonstatistical effects, Hauser-Feshbach anal. of ^{12}C(^{15}N,α) 80−106041
^{23}Na, produced in 32-14.4 MeV ^{16}O+^{9}Be, gamma transitions 79−49599
^{23}Na resonances through γ-decay excitation functions from ^{12}C(^{12}C,p) 80−63148
^{23}Na, transition probabilities and multipole moments between states calc. by generator coordinate method 78−13022
^{24}Na, effective M3 matrix elements and transitions from shell model 80−102143
^{24}Na, produced in 32-14.4 MeV ^{16}O+^{9}Be, gamma transitions 79−49599
A Nb, A=92, 94, γ-ray multipolarities, internal conversion coeffs., energy levels 79−63625
A Nb, A=93,95,97, quasiparticle-phonon coupling model calcs. levels, transitions and spectroscopic factors 79−472
^{90}Nb isovector resonance analogues, Gamow-Teller transition from ^{90}Zr(^{3}He,t) 79−9539
^{91}Nb analogue state decay modes from ^{90}Zr (^{3}He,dp) 79−67702
^{91}Nb, energy spectra and EM props. using broken pair model 80−499
^{92}Nb, γ-spectra, level and decay scheme for states to 1.6 MeV excit. 77−30504
^{92}Nb, shell model calcs., energy levels, transitions and spectroscopic factors 79−63593
^{93}Nb (e,e), 80-215 MeV, magnetic moment form factors, M1, M3, M5 transitions 79−40844
^{93}Nb B(Eλ) transitions, quasiparticle-phonon multiplet, nuclear field theory for superfluid nuclei 80−47427
^{93}Nb neutron resonances, spin and parity assignments from (n,γ) meas. 77−26569
^{93}Nb^{m}, γ-ray transitions of isomeric level, K-conversion coeff., exchange effects 77−6304
^{93}Nb(α, X), 15-72 MeV, excitation functions and spallation cross-sections 80−18274
^{93}Nb(n,γ)^{94}Nb, exciton model, γ spectra calc. 78−62539
^{93}Nb(n,n'γ), 1.3-2.7 MeV, energy levels, decay scheme, de-excitation gammas 78−41710
^{94}Nb excited states from ^{94}Zr(p,nγ), spin, parity, γ-spectra 77−88125

nuclear energy level transitions continued
^{97}Nb level structure from ^{97}Zr decay, spins, parities γ ang. correls. 78−29418
^{133}Nb, high-spin levels, in-beam γ-ray spectra meas. *(French)* 77−61372
^{93m}Nb, gamma-emission from 30 keV level *(French)* 77−57617
^{93m}Nb, radioactive decay period meas. *(French)* 77−79341
Nd, A=139, 141, high spin levels, γ spectra, hole-core coupling 77−50063
Nd, even-even, E2 transition probabilities from multiple Coulomb excitation, IBA comparison 80−78212
Nd, N=85 isotones, bands and transitions from α and HI excitation, in-beam study 80−78123
Nd(^{16}O,^{16}O), 40-48 MeV, even nuclei, 2^+ state E2 transition probabilities and quadrupole moments 80−18234
A Nd, A=138,139, high spin states, isomers and γ-cascade from ^{140}Cd(α, xzn) 80−78120
A Nd, A=138,139, high spin states, J^π, γ-cascades and shape transition from ^{140}Ce(α, xn) 80−102090
^{140}Nd ns isomers and yrast isomers, γ-transitions from ^{128}Te(^{16}O,4n) 80−78121
^{142}Nd+α, closed shell 82 neutron nucleus, B(E2)-value 78−66296
^{143}Nd, high-spin states and particle-core coupling 77−26614
^{144}Nd excited state charact., level scheme extension 77−6231
^{144}Nd levels and transitions, γ-ray spectra from ^{144}Pr^{m}β-decay *(French)* 80−18250
^{144}Nd, neg. parity states, γ-transition multipolarity 79−40882
^{146}Nd, from ^{146}Pr decay, level props., 104 γ-ray transitions 78−86476
^{147}Nd, beta spectrum, hard component 80−22769
^{148}Nd, vibrational states, B(E2) branding rates and interband transitions, pairing plus quadrupole calcs. 80−78127
^{149}Nd, weakly deformed, isomeric $^{9+}/_2$ and lowest $^{7-}/_2$ states decay 79−89231
^{150}Nd+^{20}Ne, 128 to 172 MeV, γ-ray multiplicities in evaporation residues 77−14065
^{150}Nd(^{20}Ne,X), 115, 130 MeV, γ-continuum multiplicity distrib., yrast bump 80−9265
^{150}Nd(α,α'), 11.5-12 MEV, e$_2$ and E$_3$ transition strengths meas. 77−26618
^{151}Nd, rot. states populated through neutron capture 77−6196
^{18}Ne cross section, excitation function and double isobaric analogue state from ^{18}O(π$^+$,π$^-$) 80−27596
^{19}Ne, spectra and E1 transitions, ang. momentum projected HF and Tamm-Dancoff methods 77−54139
^{20}Ne 13482 keV level, parity violating effects in two resonance interference from ^{19}F(p,α) pol. p 80−83033
^{20}Ne $2^+ \rightarrow 0^+$ transition from ^{12}C(^{16}O,^{16}O) 80−63125
^{20}Ne cluster struct., coupled channel orthogonality condition model, α-decay, excited states, transitions 79−97681
^{20}Ne, coexistence of shell struct. and cluster struct. 78−78279
^{20}Ne collective motion, B(E2) rates, algebraic formulation in symplectic shell model 80−83015
^{20}Ne continuum states, J^π and branching from ^{12}C(^{12}C, αα) 80−22660
^{20}Ne, deformed nuclei, giant multipole resonances, and transitions, microscopic theory from ^{19}F(p,γ) 79−513
^{20}Ne excitation functions, resonance search from ^{10}B(^{14}N,α) 80−27614
^{20}Ne, form. in ^{19}F(p,γ) reaction, 668 keV, γ-ray transitions to ground state, rel. to stellar nucleosynthesis 78−17191
^{20}Ne, from ^{16}O(α,γ), 10.27 MeV, first T=1,2^+ state radiative width meas. rel. to analogue β-decays 78−549
^{20}Ne, gamma decays of some T=0, 1 and 2 states above 9.5 MeV 77−34244
^{20}Ne high spin states, J^π and α-decay branching ratios from ^{16}O(^{12}C,^{8}Be) 80−18166
^{20}Ne levels, J^π, branching ratio and EM transition rates from ^{16}O+α 80−42540
^{20}Ne non-isolated resonances, excitation functions and ang. distribs. from ^{20}Na(p,α) *(Chinese)* 80−22788
^{20}Ne, 0_1^+, 2_1^+, 4_1^+ states, EM props. from large basis shell model 79−75900
^{20}Ne, produced in 3.2-14.4 MeV ^{16}O+^{9}Be, gamma transitions 79−49599
^{20}Ne quadrupole transitions, electron scatt. form factors, shell model calcs. 78−62523
^{20}Ne resonances, J^π, excitation functions and branching ratio from ^{19}F(p,γ) 80−22787
^{20}Ne resonances through γ-decay excitation functions from ^{12}C(^{12}C,α) 80−63148
^{20}Ne, spectra and E1 transitions, ang. momentum projected HF and Tamm-Dancoff methods 77−54139
^{20}Ne, unnatural parity levels at high excitation, γ spectra from ^{12}C(^{12}C, αγ) 77−2933
^{20}Ne+^{12}C, 6.3-13.8 MeV, total fusion cross section, S-factor, γ-yields 80−22877
^{20}Ne(^{12}C,X), 24-42 MeV, complete fusion, total cross section, excitation function 80−68717
^{20}Ne(p,p') 24.5 MeV, consistent folding model, HF calc. for E2, E4 transitions 79−22288
^{21}Ne, E1 decays, high spin state identification 77−26617
^{21}Ne, γ-ray circular polarisation, parity mixing 78−70443
^{21}Ne low lying levels, EM transitions, 2.80 MeV $1/2^±$ doublet parity mixing 79−9462
^{21}Ne, produced in 3.2-14.4 MeV ^{16}O+^{9}Be, gamma transitions 79−49599
^{21}Ne, transition probabilities and multipole moments between states calc. by generator coordinate method 78−13022
^{22}Ne 2^+ state excitation in ^{126}Te(^{22}Ne, ^{22}Ne') 79−54404
^{22}Ne compound states from ^{18}O(α,γ), transitions, spins, parities, astrophys. reaction rate 78−57545
^{22}Ne(e,e'), 60 to 110 MeV, spin, parity, form factor, reduced transition prob. determ. 79−63661
Ni, fp shell model calcs., spectra and spectroscopic factors 80−68588
Ni isotopes, from thermal neutron capture study, M1 and E2 strength functions 77−57674
Ni isotopes populated in (n,n'γ) scatt., γ-ray assignments to transitions 77−26767
Ni+^{16}O, 100 MeV, deep inelastic, γ-circular polarisation and spin orientation 79−17848
A Ni, A=57, 59, 61, 63, variation of spectra, isospin mixing 80−13401
A Ni, A=60, 62, 66, levels, J^π, anal. powers and cross sections from Ni(t,p)pol.t 80−68539
A Ni(^{40}Ca, fusion), A=58, 60, 62, 113-170 MeV, fusion cross sections and excitation functions 80−32315

nuclear energy level transitions continued
^{57}Ni(π^+,xγ), 100-200 MeV, prompt and delayed γ spectra, nuclide yields 79−22332
^{56}Ni excitation functions from ^{40}Ca(^{16}O,X) fusion 80−18362
^{57}Ni high spin yrast cascade, decay modes J assignment from ^{54}Fe(α,nγ) 80−68514
^{58}Ni, isovector M8 strength fragmentation, inelastic electron scatt. meas. 78−37305
^{58}Ni, mag. quadrupole resonance, M2 strength distrib., quasiparticle-phonon model 79−75947
^{58}Ni, partial radiation widths from neutron capture resonances, valency model calcs. 77−26707
^{58}Ni(^{16}O,X), 100 MeV, deep inelastic, fragment spin polarisation and alignment, γ-rays 80−18284
^{58}Ni(d,d′), 10 MeV, diff. cross sections and d-γ ang. correlations, multi-shell coupled channel calcs. 80−83064
^{58}Ni(e,e′), 120-264 MeV, $J^\pi=6^+$, 5.125 MeV state isoscalar character, form factors, transition strengths 80−9262
^{58}Ni(e,e′) 5.125 MeV $J^\pi=6^+$ state excitation, isoscalar character 79−22227
^{58}Ni(γ,γ), M1 strength isospin splitting for dipole ang. distrib. states 80−13412
^{59}Ni, levels and new γ-transitions following ^{59}Cu(β^+)^{59}Ni 77−22935
^{60}Ni, 1173 keV transition M3/M2 mixing ratio meas. 80−52608
^{60}Ni, aero-phonon, $4_1^+\rightarrow 2_2^+$ γ-ray transition 78−17136
^{60}Ni, Coulomb contributions to nuclear radii and energies 80−68515
^{60}Ni, hexadecapole motion obs. from α-scatt., EM transitions and conversion electron spectra 78−25097
^{60}Ni high spin states, J^π, $T_{1/2}$, ang. distribs. and polarisations from ^{56}Fe(^{7}Li, p2nγ) 80−99116
^{60}Ni level scheme and γ-rays from ^{59}Ni(n,γ) 80−63099
^{60}Ni, partial radiation widths from neutron capture resonances, valency model calcs. 77−26707
^{60}Ni populated in ^{60}Co beta decay, 2506 to 2159 keV γ transition 77−22929
^{60}Ni, spin of 1.33 MeV level, anisotropy coefficients in $4^+\rightarrow 2^+\rightarrow 0^+$ cascade *(Spanish)* 79−89525
^{61}Ni, spectroscopy of levels below 2.2 MeV obs. in ^{58}F(α,nγ) 77−6289
^{62}Ni excited levels from ^{62}Cu decay, transition energies and intensities *(Spanish)* 77−67716
^{62}Ni(γ,X), 19.2-26.2 MeV, photoneutron and photoproton spectra, giant dipole resonance-decay, isospin conservation 80−13443
Ni(e,α), E2 strength in resonance regions statistical decay 80−91146
Ni(n,γ), primary transitions using focused 24 keV filtered neutron beam 80−63436
^{237}Np electron transition excitation following K-shell photoionisation, deexcitation γ-rays 80−78196
^{237}Np, energy levels from ^{241}Am α-decay, γ transitions 79−6480
^{237}Np, gamma-ray spectra following ^{231}Am α-decay *(French)* 79−492
^{237}Np(e,f), 10-34 MeV, electrofission cross section, E2 transition mode and giant resonances 80−106084
^{238}Np levels, resonances and transitions from ^{237}Np(n,γ) 80−52589
^{239}Np, high pressure meas. of gamma transitions 80−18225
^{242}Np levels, J^π and transitions from ^{242}U decay 79−67664
^{A}O, A=16, 17, valence-core self-consistency, wave functions, binding energy, levels, spectra 80−63123
^{A}O, A=18, 19, E2 transition rates calc., shell model with effective interaction and charges 80−47423
^{15}O, obs. of high spin states in ^{12}C(^{6}Li,t) and ^{12}C(^{6}Li, ^{3}He) 78−13015
^{16}O $3^-\rightarrow 0^+$ gamma transition from ^{12}C(^{16}O,^{16}O) 80−63125
^{16}O 4^+ state nonstatistical population in compound nucleus calcs. of ^{12}C(^{6}Li,d) 80−102137
^{16}O α-cluster states, widths and resonances, optical model, direct transfer in ^{12}C(^{6}Li,d) 80−105975
^{16}O, calc. of spectrum of O^+ levels 79−63627
^{16}O high spin states, J^π and α-decay branching ratios from ^{12}C(^{12}C,^{8}Be) 80−18166
^{16}O, hyperfine interactions of highly stripped ions recoiling into H and He 77−22932
^{16}O, isospin forbidden 7.12 MeV E1 transition, continuum shell-model calc. 77−18472
^{16}O, isospin mixing in 7.12 MeV 1^- state 77−283
^{16}O level excitation functions, resonances from ^{12}C(^{16}O,^{12}C) 80−63146
^{16}O mag. dipole strength, M1 resonances from ^{15}N(p,γ), polarised p 79−80898
^{16}O, magic nuclei at collective excitations, energy spectrum and shape *(Russian)* 80−106015
^{16}O magnetic dipole strength 80−37385
^{16}O, rotational band collectivity, shell model excitation in Sp(4, R) symmetry 80−102095
^{16}O, search for $0^-\rightarrow 0^+$ pair transition 78−86508
^{16}O+^{16}O, fusion cross section gross struct., excitation functions, coupled channel method 80−52705
^{16}O(^{16}O, X), 9.3 MeV, fusion reaction residue partial prod. cross sections from γ-detection 79−67804
^{16}O(^{16}O,^{16}O), 10-41 MeV, molecular resonances γ-yield, band crossing model 80−106032
^{16}O(α,α) 17 to 27 MeV, backscatt., dynamic deformation and excitation functions, optical anal. 80−18227
^{16}O(e,e), T=1 level form factors, Helm model, pion photoprod. and muon capture appls. 80−52553
^{16}O(γ,γ), 6.95, 7.12 MeV, strengths of isospin forbidden E1 transitions 78−13059
^{16}O(γ,γ), total photoabsorption and elastic cross sections, spectroscopic information *(Russian)* 80−83095
^{16}O(γ,n), 25-45 MeV, isovector giant quadrupole resonance evidence, E2 cross section 80−18268
^{16}O(p,p′), 1 GeV, proton polarisation in natural parity level excitation *(Russian)* 80−42634
^{16}O(p,p′), 40 MeV, retarded isoscalar M2 strength obs. 78−93962
^{16}O(π,π'), ~180 MeV, isospin mixing, levels, excitation functions and ang. distribs. 80−42543
^{16}O(π^-,γ), one and two neutron emission, decay channels 79−45300
^{17}O, ΔT=0,1 E1 or M2 population of giant reson. isospin splitting 78−577
^{17}O levels, resonances, J^π and radiative width from ^{14}N(t,γ) 80−47389
^{17}O, produced in 3.2-14.4 MeV ^{16}O+^{9}Be, gamma transitions 79−49599
^{17}O(γ,n), 8.5-39.7 MeV, cross section, giant dipole and pygmy resonance decays 80−42619
^{18}O 6p-4h states and composite spectra from ^{12}C(^{18}O,^{12}C) 80−63096
nuclear energy level transitions continued
^{18}O E2 transition probabilities, coexistence of spherical and deformed states 77−18394
^{18}O, effective interaction, nonlocal pot. reaction matrix free scatt., spectra 77−46122
^{18}O level gamma decay from ^{17}O(n,γ) 80−52623
^{18}O, transition strength n and p components, $\pi^\pm$ inelastic scatt. comparison, shell model 80−68585
$^{18}O_2$ shell-cluster admixtures, spectra, α-widths and electric transitions 77−54136
^{18}O(e,e′), isovector mag. dipole and quadrupole transitions, analogues, ($\pi^-\gamma$) relation 80−106010
^{18}O(π,π′), 164 MeV, yrast state and level excitation, DWIA calcs., shell model context 80−42526
^{19}O first excited state electric moment, B(E2) transition from ^{208}Pb(^{18}O,^{18}O′) 79−67651
(^{17,18}O,^{17,18}O′), 54-69 MeV, on A=48-92, excited states and ang. distribs., DWBA anal. 79−67705
Os even-even isotopes, excitation energies and EM props. from interacting boson model 80−106005
Os, O(6)→rotor transition, interacting boson approx. model, levels and transitions 79−13224
^{A}Os, A=186, 188, 190, 192, rigid asymmetric rotor model descript., E2 and E4 props. 80−13403
^{A}Os, A=186,188, levels and transitions from Re decay, triaxial rotor model 80−91155
^{A}Os, A=186-194, collective levels, transitions, mag. and quadrupole moments, boson expansion theory 80−105954
^{A}Os, A=188, 189, levels, J^π, transitions and mixing ratios from Ir decay 80−68602
^{186}Os, K=0 rot. band collective states, populated in ^{186}Ir decay 77−82803
^{188}Os, ground and γ-band level energies, B(E2) values and EM moments, triaxial description 79−36140
^{189}Os, level scheme from ^{189}Re beta-decay 79−54388
^{189}Os, nuclear excitation by electron transition, (NEET) 77−34256
^{190}Os levels and γ-ray transitions, (n,γ) and (n,e$^-$) reactions 79−36189
^{192}Os level scheme and rot. bands, from ^{191}Os(n,γ), interacting boson approx. anal. 79−6413
^{192}Os, Wilets-Jean Hamiltonian for energy levels, transitions, moment, etc. 79−9457
^{193}Os level scheme and transitions, Coriolis coupled Nilsson states from ^{192}Os(n,γ) 80−57698
^{196}Os, $T_{1/2}$ and partial decay scheme 78−21527
P, A=30, 32, high spin states from ^{16}O+^{16,18}O reactions and ^{27}Al(α,n), γ-ray meas. 78−74386
^{A}P, A=31, 33, levels and transition j-depend., DWBA anal. for Si(^{19}F, ^{16}O) 80−42542
^{29}P, determ. of total and partial widths of unbound states 77−74802
^{29}P excitation functions and spectroscopic factors from ^{28}Si(p,γ) resonant and direct capture 79−80912
^{30}P high spin two nucleon states decay props. from ^{28}Si(α, dγ) 80−13402
^{30}P level width isospin depend., excitation functions, statistical anal. of ^{29}Si(p,α) 80−78152
^{30}P positive parity states, transitions and spectroscopic strengths, DWBA anal. of ^{29}Si(^{3}He,d) 80−102138
^{30}P T=1 state decay, lifetimes and branching ratios, analogue E2 transitions from ^{29}Si(p,γ) 80−68598
^{31}P, analogue-antianalogue M1 transitions, nucl. shape change influence 78−13006
^{31}P transition cross sections from ^{33}S(p,^{3}He) 79−67660
^{32}P spectroscopic factors and level transition excitation function anal. from ^{31}P(d,p), 1.5-2.5 MeV 78−74371
^{141}P(n,γ), resonance parameters, s-wave radiative and reduced neutron widths 80−47471
^{231}Pa α-decay, γ-rays and internal conversion spectrum, ^{227}Ac levels and bands 79−45217
^{231}Pa, high pressure meas. of gamma transitions 80−18225
^{233}Pa decay emission probability of 312 keV gamma-ray 79−59035
^{233}Pa excited level scheme and γ-transitions from ^{237}Np α-decay 79−80876
^{233}Pa, high pressure meas. of gamma transitions 80−18225
^{234}Pa isomers from ^{234}Th β^- decay, low energy γ-spectrum 78−70493
Pb, 1^+ state and effective g-factor anal. 77−74764
Pb, A=204,6, quadrupole moments of first excited state meas. 78−21491
Pb region, even-odd nuclei, EM moments and transitions 77−88040
Pb region, forbidden charge exchange collective modes, β- and γ-decay processes 80−86784
Pb region, mag. moments and M1, M2 and M4 values, self consistent calcs. 80−47371
Pb region, particle-vibration multiplet spectra, self-consistent framework 80−102089
Pb, strongly forbidden T1-transition, parity nonconservation *(Russian)* 77−10366
^{A}Pb, A=197, 198, low energy γ-transitions and level lifetimes from ^{186}W(^{16}O, xn) 80−18221
^{A}Pb, A=197,198, low energy γ-transitions 80−83058
^{A}Pb, A=202, 204, spectra from multistep shell model method 80−78194
^{A}Pb(α,α), A=206, 208, 120 MeV, isoscalar resonance excitation, low lying transitions, DWBA calc. 80−512
^{198}Pb, E2 transition probability and effective charge for neutron $i_{13/2}$ subshell 78−78309
^{204}Pb, muonic, first excited 2^+ state, isomer shift of E2 transition 80−99150
^{204}Pb populated by ^{204}Bi decay, isomeric transitions, J^π assignments 78−50122
^{204}Pb(n,n′γ), 1.5-3.1 MeV, levels, J^π, excitation functions and mixing ratios 80−102123
^{205}Pb, ^{206}Pb, cluster vibrational field coupling model description 77−57604
^{206}Pb γγ directional correlations, multipole mixing ratios, transition strength limits from ^{206}Bi decay 80−86849
^{206}Pb, population of 0^+, alpha-decay of ^{210}Po 80−22775
^{206}Pb+n, 3-50 KeV, neutron resonances, J^π assignments, decay scheme 79−36217
^{207}Pb 569.65-1063.63 keV cascade, γ-γ ang. correl. meas. from ^{207}Bi decay 80−86847
^{207}Pb doorway resonances, M1 ground state radiative strength, level density from ^{208}Pb(n,n), (n,γ) 79−93589

nuclear energy level transitions continued
^{207}Pb, γ-γ directional correls. in ^{207}Bi decay, mag. perturbation obs. 77−74796
^{207}Pb, muonic, octupole doublet isomer shifts, octupole vibrs. 80−95750
^{207}Pb muonic isomer shifts, neutron hole anomalous moment contribs. 80−78728
^{207}Pb neutron separation energy and resonances, decay transitions from ^{206}Pb(n,γ) 79−36217
^{207}Pb p-wave resonances, enhanced primary M1 transitions from ^{206}Pb(n,γ) 80−57728
^{207}Pb parity assignments and M1 radiative strength from ^{206}Pb(n,n) 80−52614
^{207}Pb(n,p) reaction, isobar analogue state excitation *(Russian)* 80−102124
^{208}Pb 1^+ states, fine struct., energy levels, transition probabilities, matrix diagonalised method *(Chinese)* 78−78269
^{208}Pb 7064 keV level negative parity, EM deexcitation pattern from ^{207}Pb(d,p) 79−36148
^{208}Pb (e,e′), 2^- giant resonance twist mode excitation, B(M2) values, form factors 80−78246
^{208}Pb breathing model transition density, single particle and collective state dynamical coupling 80−106007
^{208}Pb compound nucleus, γ-decay spectral function depend. on ang. momentum *(Russian)* 78−86467
^{208}Pb, excitations, EM transitions in renormalised RPA 77−82857
^{208}Pb, fine struct. of M1 giant resonance obs. in ^{207}Pb(n,γ) 77−79347
^{208}Pb giant monopole and quadrupole resonances, multipole excitations from (α,α′)(d,d′) 80−106031
^{208}Pb M1,E1,M2,E2 localised γ-ray strengths from ^{207}Pb(n,γ) 80−37350
^{208}Pb, mag. quadrupole resonance, M2 strength distrib., quasiparticle-phonon model 79−75947
^{208}Pb magnetic susceptibility and M1 transitions, nuclear interaction role 79−45160
^{208}Pb, muonic, isomer shift of 2.61 MeV gamma transition 77−38753
^{208}Pb region, mag. transition strength, core polarisation effects, form factor shape 80−86850
^{208}Pb, static and transition densities, self consistent RPA theory test in fast (p,p), (e,e) scatt. *(Russian)* 79−49604
^{208}Pb(^{12}C,^{11}B), 77 MeV, bound and continuum state excitation, direct and two step processes 80−63205
^{208}Pb(^{14}N,^{14}N′), 266 MeV, giant resonance excitation 80−78253
^{208}Pb(^{16}O,^{16}O′), 315 MeV, continuous spectrum and giant resonance excitation, coherent state model test 80−32252
^{208}Pb(^{49}Ca,Xn), excitation functions for compound-nucleus and transfer reactions of magic nuclei 79−22310
^{208}Pb(N, γ_0), γ-ray ang. distribs., giant E3 resonances, direct-semidirect model 79−67727
^{208}Pb(α,α′), levels, B(E3), transition density and nuclear pot., folding model anal. 80−86812
^{208}Pb(d,d′), 24 MeV, mag. dipole states, spin, parity, transition strengths 77−14129
^{208}Pb(e,e′), E2 transitions of fragmented isoscalar quadrupole giant resonance 80−22758
^{208}Pb(e,e′), 60 MeV, backward scatt., $2\hbar\omega$ M1 excitation search 80−32234
^{208}Pb(e,e′), 70-335 MeV, natural parity high spin state excitation 80−63060
^{208}Pb(γ,n), 7.4-8.4 MeV, cross section, E1 and M1 transitions, collective and giant M1 resonance 79−89267
^{208}Pb(n,n′γ), 5.2-8.5 MeV, E1 excitations, collective states and spin assignments, statistical model anal. 79−54405
^{208}Pb(p, γ), γ ang. distrib., isovector giant quadrupole resonance, direct-semidirect model 79−63647
^{208}Pb(p,p′), 135 MeV, normal parity level excitation, J^π, differential cross sections 80−57690
^{208}Pb(p,p′), 135 MeV, normal parity excitations, microscopic description, NN interaction shape 80−57691
^{208}Pb(p,p′), 24 MeV, mag. dipole states, spin, parity, transition strengths 77−14129
^{208}Pb(p,p′), 39, 62 MeV, DWBA anal., collective spectra, direct process contrib. *(Russian)* 80−13408
^{208}Pb(p,p′), 40, 45 MeV, fine struct. in giant resonance region, collective dipole spin flip excitation 78−46056
^{210}Pb ground state decay 80−47429
^{210}Pb levels, J^π, transitions and lifetimes from ^{208}Pb(^{7}Li,X) 80−68542
Pb(α,α), 104 MeV, nucl. matter sizes and isoscalar octupole transition rate 77−6422
Pd, A=101-5, particle-core coupling, Nilsson model rot. model at intermediate deform. 77−10362
Pd, even-even, collective states, B(E2), branching ratios and moments, boson expansion method 80−102099
Pd, even-mass isotopes, collective model with deform., vibr., rot. energy levels, B(E2) ratios 78−17120
^{99}Pd level scheme, γ-ray cascade, studied via heavy-ion reactions 77−30506
^{100}Pd levels and γ-transitions from ^{100}Ag^{g,m} decay 80−83077
^{101}Pd nonyrast rotational states, transitions, $T_{1/2}$, branching and mixing ratios from ^{92}Zr(^{12}C,3n) 80−105950
^{102}Pd(p,p′:γ,γ), population of low spin levels, level scheme 79−36153
^{102}Pd(p,p′γ), long lived O^+ state, E0 transitions 80−73804
^{103}Pd decay, 357 keV γ:K X-ray abundance ratio obs. 79−498
^{104}Pd, characts. of the levels excited in ^{104,104m}Ag decay 79−9515
^{105}Pd, from decay of ^{105m,g}Ag 78−37306
^{106}Pd, E0 transition from 0_1^+ state following ^{106}Rh beta decay 80−68578
^{106}Pd levels and E0 transitions from ^{106}Ru β-decay 79−75894
^{108}Pd, vibr. states study, elastic and inelastic electron scatt., anharmonic vibrator model 78−62520
^{109}Pd levels, J^π, transitions, unique parity states, and spectroscopic factors from ^{108}Pd(n,γ) 80−42547
^{109}Pd low spin odd parity levels, γ-rays, particle-rotor comparison from ^{108}Pd(n,γ) 80−73805
^{109}Pd low spin odd parity states, rot. aligned model, Coriolis calc. of ^{108}Pd(n, γ) 80−57695
Pm, A=143, 144, 145, ICC, γ-spectra, multipolarities for low-lying levels 77−50081
^{A}Pm, A=143, 145, proton states and transitions, stripping strength, shell model anal. from Nd(^{3}He,d) 80−68508
^{141}Pm medium spin states, J^π, transitions and shape from (p,2n), (^{3}He,3n), (α,4n) 80−86779
nuclear energy level transitions continued
^{143}Pm high spin states, J^π, transitions, isomer g-factors from (d,2N), (α,2N) 80−32154
^{145}Pm, form. in electron capture decay of ^{145}Sm, γ-transition decay rate and intensities 78−13030
^{147}Pm energy levels and γ-ray transitions E2/M1 mixing ratio from ^{147}Nd β-decay 79−67655
^{147}Pm, γ-γ cascades angular correlations in ^{147}Nd beta decay 79−63624
^{147}Pm, level scheme and transitions following ^{147}Nd 80−83073
^{147}Pm levels, transitions, $\gamma\gamma$-coincidences and IC electrons from ^{147}Nd decay 80−18243
^{147}Pm proton states and transitions shell model anal. of ^{148}Sm(t,α), ^{146}Nd(^{3}He,d) 79−30781
^{149}Pm, β^- decay, ^{149}Sm level scheme 80−22750
^{149}Pm, β-decay, nucl. matrix elements, calc., γ-transitions 80−52628
^{149}Pm high spin states and bands, rot. description and in-beam study from ^{150}Nd(p,2nγ) 80−32153
^{149}Pm levels, bands, transitions, in-beam spectroscopy, particle-rotor anal. from ^{150}Nd(p,2nγ) 80−78125
^{149}Pm, populated in ^{149}Nd β decay 79−63628
^{149}Pm, shape factor anal. of β-transitions 78−21532
^{151}Pm level scheme in low excitation region <1 MeV 77−54173
^{152}Pm decay, β and γ rays, spins, half lives, ^{152}Sm levels 78−542
^{204}Po, γ-rays, conversion electron spectra, $\gamma\gamma$ coincidences 80−83061
^{206}Po, excited levels, populated by ^{206}At EC-β^+ decay 77−79340
^{210}Po, alpha-decay, population of 0^+ of ^{206}Pb 80−22775
^{212}Po, isomer with spin and parity 8^+, α- and γ-decay 78−82283
^{212}Po, levels, J^π, transitions and lifetimes from ^{208}Pb+^{7}Li 80−68542
^{215}Po, excited states, half-life meas. *(French)* 79−97679
p$\bar{p}$ atom, nucl. level shift and radiative transitions *(Russian)* 80−28121
^{139}Pr medium spin states, J^π, transitions and shape from (p,2n), (^{3}He,3n), (α,4n) 80−86779
^{140}Pr isobaric analogue resonances, de-excitation cascade, K-shell ionisation, spin depend. from ^{140}Ce(p,n) 80−78202
^{141}Pr, ICC, γ-spectra, multipolarities for low-lying levels 77−50081
^{141}Pr, positive parity levels, gamma-ray yields and ang. distribs. 80−105962
^{141}Pr(n,γ), non-statistical capture, radiative widths, γ-ray doorway state model 80−37389
^{142}Pr, $2^-\rightarrow 2^+$ β spectrum, shape meas. 77−50083
^{144}Pr levels and transitions, studied via ^{144}Ce decay 77−14070
^{146}Pr→^{146}Nd, decay scheme and energy levels, log ft values 78−4912
^{150}Pr decay into ^{150}Nd vibr. levels 78−89817
^{191,193}Pt γ-spectra, high-spin levels and triaxial rotor model 77−34213
Pt, even mass, ground and gamma band EM transition rates, asymmetric rotor model 80−32231
Pt even-even isotopes, excitation energies and EM props. from interacting boson model 80−106005
Pt, O(6)→rotor transition, interacting boson approx. model, levels and transitions 79−13224
Pt+^{136}Xe, A=192, 194, 196, Coulomb excitation, γ softness from E2 transition strengths 77−82951
^{A}Pt, A=188-198 collective levels, transitions, mag. and quadrupole moments, boson expansion theory 80−105954
^{A}Pt, A=190, 192, 194, levels and γ-transition reduced probab., interacting boson model 80−18196
^{A}Pt, A=190,192,194, state struct. in interacting boson model 80−83047
^{A}Pt, A=192, 194, 196, rigid asymmetric rotor model descript., E2 and E4 props. 80−13403
^{A}Pt, A=192, 194, 196, states, J^π, ang. distribs. and transitions, DWBA anal. of Pt(p,t) 80−468
^{187}Pt, levels, J^π, $T_{1/2}$, possible E0 transitions from ^{187}Au decay *(French)* 80−32230
^{188}Pt, ground and γ-band level energies, B(E2) values and EM moments, triaxial description 79−36140
^{191}Pt energy levels, γ and conversion electron spectra, spins, parities 78−25149
^{192}Pt, Coulomb excited, transition probabilities 78−62506
^{192}Pt, lifetimes of ground-band states, B(E2) values, (Ar,Ar′γ) reaction 77−54181
^{194}Pt, determ. of sign of $P_3=M(0_1^+2_1^+)M(2_1^+2_2^+)M(2_2^+0_1^+)$ 79−63588
^{194}Pt, lifetimes of ground-band states, B(E2) values, (Ar,Ar′γ) reaction 77−54181
^{194}Pt, populated in ^{194}Ir decay, level scheme determ. 77−2900
^{194}Pt+^{136}Xe, multiple Coulomb excitation, E2 transition probabilities of ^{194}Pt 78−4961
^{196}Pt (^{20}Ne, ^{20}Ne′), excited states, lifetime meas. using recoil-distance method 80−13413
^{196}Pt (^{58}Ni, ^{58}Ni′), excited states, lifetime meas. using recoil-distance method 80−13413
^{196}Pt negative parity states in partially decoupled bands, γ-transitions from ^{195}Pt(n,γ) 80−47360
^{193m}Pt decay, K-shell conversion coeff. of 135.5 keV, M4 transition 77−2944
^{A}Pu, A=238,240, fission isomer rot. spectra $I^2(I+1)^2$ correction 80−18229
^{239}Pu, high pressure meas. of gamma transitions 80−18225
^{239}Pu(n,X), thermal n, gamma spectra from capture, fission and fission products 80−37352
^{240}Pu, 42.9 keV γ transition, Mossbauer reson. obs. 79−36229
^{241}Pu level structure and γ-transitions from ^{245}Cm decay 80−105980
^{244}Pu(n,γ) resonance integral meas. 80−73846
^{246}Pu excited states, mass excess and shell gap, L=0 transition from ^{244}Pu(t,p) 80−9236
^{223}Ra decay chain, precise γ-ray spectroscopy 77−54175
^{223}Ra, excited states, half-life meas. *(French)* 79−97679
^{226}Ra levels from ^{230}Th α decay, search for $K^\pi=0^+$ excited states 78−86504
^{228}Ra-^{228}Ac decay and ^{228}Th decay chain, gamma ray energies 79−85857
^{230}Ra levels, J^π and transitions, Nilsson assignments from ^{230}Ac decay 80−68543
Rb, fission fragment, delayed neutron branches from γ-spectroscopy 80−78230
Rb odd-even isotopes, collective states and transitions, interacting boson approx. 80−73773
^{A}Rb, A=79, 81, decoupled $g_{9/2}$ bands, level lifetimes and E2 transitons from (^{16}O, 2n)(^{19}F, p2n) 80−73772
^{A}Rb, A=96,98, β-decay schemes and total energies, mass excess and separation energies 80−27601

nuclear energy level transitions continued
^{A}Rb(n,n′γ), 550-2100 keV, A=85,87, levels, excitation functions, J$^{\pi}$, Hauser-Feshbach anal. 80−105982
^{81}Rb band struct., spin assignments and transitions from (^{6}Li,3n), (^{16}O,p2n), (α,2n) 80−73774
^{83}Rb high spin states, Jπ and transitions from HI and α reactions 80−105949
^{81}Rb high spin states, positive and negative parity bands from (^{6}Li, 3n), (α, 2n) 80−18178
^{85}Rb high spin states, yrast cascade, J$^{\pi}$, γ-transitions from ^{82}Se(Li,xnγ) 80−73775
^{A}Rb levels, J$^{\pi}$ and transitions from Kr^{m,g}, Sr^{m,g} decay, cluster-vibr. model 80−78162
^{85}Rb, single-particle estimate of γ-γ transition probability 78−13023
^{85}Rb, two-quantum γ-γ decay of 514 keV excited state 78−13009
^{88}Rb decay, γ-ray energy meas. 79−22530
^{90}Rb, β,γ, conversion electron spectra obs. 77−71583
^{90}Rb level scheme, transitions, J$^{\pi}$ assignments and internal conversion coeffs. from ^{90}Kr β-decay 79−67663
^{A}Re, A=181, 182, 187, magnetic moments meas. by PAC 80−22688
^{A}Re, A=183,184, nuclear K-X-ray satellites, Z=50-83, decay scheme 80−42984
^{177}Re, isomeric states, γ-ray transition 79−9433
^{177}Re, populated in decay of Os isotopes, lower excited state obs. 78−17145
^{179}Re, populated in decay of Os isotopes, lower excited state obs. 78−17145
^{181}Re states and transitions, rot. bands and Nilsson states from ^{181}Ta(^{3}He,3nγ) 79−36152
^{187}Re, 36.23 keV transition, penetration coeff. and mixing ratio determ. 77−50080
^{187}Re low lying level struct. and transitions, E2/E1 mixing ratios from ^{187}W decay 80−27557
^{94}Rh, γ-spectrum and half-lives 80−83062
^{97}Rh levels and γ-transitions, 3QP model anal. of ^{97}Pd β^{+}-decay 80−102120
^{99}Rh γ-ray cascade, obs. in ^{90}Zr+^{12}C, and ^{91}Zr+^{11}B 78−41762
^{99}Rh isomer, ($T_{1/2}$=4.5 hr.), decay, anticoincidence and integral coincidence spectra meas. 79−6479
^{99}Rh, possible high-spin cascade obs. in heavy ion reactions 77−30506
^{100}Rh, γ-ray spectrum and ang. γγ correlations, ^{100}Ru level struct. study 79−6510
^{100}Rh short lived isomer, decay scheme from (α,pn), (p,n) and (p,3n) 79−75920
^{103}Rh level scheme from fast n scatt., γ transitions, spins, parities, cross sections 78−78374
^{103}Rh, neutron elastic and inelastic cross sections up to 1500 keV, γ-ray transitions, 40 keV isomeric state 77−23089
^{104}Rh(n,γ), 0.5-3.0 MeV, γ-spectra strength functions 80−32240
^{105}Rh gamma transitions, directional correl., multiple mixing ratios 79−80897
^{208}Rn→^{208}At, γ-ray, conversion electron spectra 80−83072
^{210}Rn decay, ^{210}At excited states, spins, parities and rate of population 79−75917
^{212}Rn, shell model states, semiempirical calcs. half lives, mag. moments, excitation functions 80−63083
^{224}Rn→^{224}Fr→^{224}Ra decay, γ-rays IC electrons and eγ coincidences 80−18239
Ru, even-even, collective states, B(E2), branching ratios and moments, boson expansion method 80−102099
^{A}Ru, A=101, 103, 105, quasiparticle-phonon coupling model, spectra, moments and transitions 79−22231
^{A}Ru, A=104,106,108, level scheme and transitions, collective model anal. of Tc decay 80−78166
^{A}Ru, A=106, 108, levels, transitions, J$^{\pi}$ and shape from Tc decay 80−57744
^{A}Ru, A=96, 98, 100, multiparticle states, method of generalised seniority 80−22759
^{A}Ru(p,p′γ), A=96, 98, 5-8 MeV, level schemes, transitions, vibr. state, mixing ratios 80−18199
^{94}Ru levels and γ-transitions from ^{94}Rh decay 80−18244
^{95}Ru level scheme, low lying states, g-factor spin, parity 77−88071
^{97}Ru high spin states, band like structs., transitions from ^{88}Sr(^{12}C,3nγ) 80−73779
^{97}Ru populated in ^{88}Sr(^{13}C, 3nγ), band-like structures 80−32146
^{99}Ru decay scheme from ^{99}Tc^{m} β-decay 80−42596
^{100}Ru, negative parity yrast band, E1 transitions polarisability, quadrupole-octupole coupled vibr. system 79−484
^{102}Ru 2^{+} state quadrupole moment, reorientation effects and multiple Coulomb excitation from (α,α), (^{16}O,^{16}O) 80−5063
^{103}Ru, gamma-ray precision energy meas. 78−58533
^{103}Ru, level struct. from ^{103}Tc decay 79−9470
^{103}Ru, levels and gamma decay scheme obs. in ^{102}Ru(n,γ) 77−30580
^{104}Ru level energies, B(E2) ratio, mixing ratios, γ-ang. correlations, from ^{104}Tc β-decay 79−493
^{105}Ru, γ-γ ang. correl. meas., spin and γ-ray mixing ratios 78−21516
^{105}Ru, levels and gamma decay scheme obs. in ^{104}Ru(n,γ) 77−30580
^{106}Ru 512 keV γ-ray, precise meas., Ge(Li) detector, comparison with positron annihilation radiation standard 77−6610
^{31}S level J$^{\pi}$ assignments, transition cross section from ^{33}S(p,t) 79−67660
^{32}S, decay of reson. states populated in ^{31}P(p,γ) 78−13085
^{32}S levels and J$^{\pi}$ from ^{32}Cl β^{+} decay 80−22772
^{32}S, O_1^+, 2_1^+, 4_1^+ states, EM props. from large basis shell model 79−75900
^{32}S resonances and excitation functions, Hauser Feshbach anal. of ^{20}Ne(^{12}C,X), X=p,d,α 80−78249
^{32}S(γ,p), 17-30 MeV, giant resonance p decay channel, state transition distrib. *(Russian)* 78−89840
^{32}S(n,n′γ), 13.9 MeV, 2^{+} (2.23 MeV) excitation, spin flip probab., deexcitation γ-rays 80−86853
^{34}S(α,Γ)^{38}Ar, 2-3.5 MeV, reson. levels, mixing ratio 79−71859
Sb, A=108,109,110, gamma-ray meas., decay scheme calc. 77−18473
^{A}Sb, A=113-175, odd isotopes, collective props., bands and transitions from heavy ion reactions 80−68512
^{A}Sb, A=115, 117, M2, E3 transition reduced matrix elements, EM core polarisation 79−17847
^{A}Sb, A=121,123, levels below 2 MeV, spins, transitions and mixing ratio from (p,γ), (n,n′γ) 80−32191
^{113}Sb, 15 MeV excitation, average nucl. lifetime determ. 80−43164
^{119}Sb intrinsic high spin state population, cluster DWBA anal. of ^{116}Sn(α,p) 79−67630
nuclear energy level transitions continued
^{119}Sb, transitions to low lying states from ^{118}Sn(^{7}Li,^{6}He) 79−6688
^{122}Sb energy levels populated in ^{121}Sb(n,γ), spin, parity, γ and conversion electron spectra 78−54721
^{123}Sb populated in ^{123}Sn^{m} decay, γ-ray, X-ray and electron spectra 77−88073
^{123}Sb(γ,γ′), energy levels, spin and parity, strong M1 transitions 78−93940
^{124}Sb, first forbidden β-transitions, β-γ circular polarisation correlations 79−9517
^{125}Sb decay, gamma-ray spectra, ^{125}Te level scheme obs. 77−10361
^{125}Sb high spin levels, gamma transition energies and intensities from ^{125}Sn^{9}, decay 80−73819
^{131}Sb partial level scheme from ^{131}Sn beta decaying isomer, γ spectra 77−50091
^{A}Sc A=44,46,48, HF projection formalism, energy levels, static moments, EM transition probabilities 79−3083
^{A}Sc, A=45, 47, HF projection formalism, energy levels, EM moments, transition probabilities 79−22199
^{41}Sc, decay and partial widths of 2883 and 5037 keV levels 77−88077
^{41}Sc, determ. of total and partial widths of unbound states 77−74802
^{41}Sc, two particle-one hole states, EM transition probabilities 77−88035
^{43}Sc, J$^{\pi}$=19/2^{-} isomer, high-spin precursors, from ^{29}Si(^{16}O,pn) 80−57656
^{43}Sc, resonance struct obs. in ^{42}Ca(p,γ)^{43}Sc below 2.75 MeV 78−13072
^{44}Sc, $(f_{7/2})^4$ states populated in ^{41}Ca(α,p) 25 MeV reaction, relative transition strengths, semi-microscopic model calcs. 79−6645
^{44}Sc, population of $f_{7/2}{}^4$ states in ^{41}Ca(α,p) reaction 79−59077
^{45}Sc levels, J$^{\pi}$, transitions and lifetimes from (p,p′)(^{3}He,^{3}He′)(α,α′) 80−63091
^{45}Sc, low-lying negative parity levels, Coulomb excitation 79−93552
^{45}Sc resonance decays, energy levels and J_{π} values from ^{44}Ca (p,γ) 79−80908
^{45}Sc(π^{-},X), stopped π^{-}, yields and γ-rays 80−86857
^{46}Sc energy levels, resonances, spin and parity from ^{45}Sc(n,γ) 80−52673
^{46}Sc level deexcitation, E1 and M1 absolute radiative widths from ^{45}Sc(n,γ) 80−52622
^{46}Sc, s- and p-wave radiative widths obs. in ^{45}Sc(n, γ) 78−17187
^{46}Sc transition polarisation, levels and spin assignments from ^{45}Sc(n,γ), pol. n 80−52656
^{49}Sc proton single particle states, spectroscopic factors, DWBA anal. of ^{48}Ca(d,n) 80−99118
Se, evaporation residue from Ni+^{12}C, prompt γ deexcitation 78−74395
Se, even-even isotopes, first excited 0^{+} states, energy systematics 78−54683
Se, even-even nuclei, γ-spectroscopy, exptl. results and models 80−68589
Se isotopes, excited states struct., energy systematics 78−54687
^{A}Se, A=74, 76, vibr. states and transition from dynamic deformation theory 80−73770
^{72}Se from ^{58}Ni(^{16}O, 2pγ), high spin and excitation energy regions, γ cascade 78−54795
^{72}Se side band struct., negative parity states and transitions from ^{58}Ni(^{16}O,2p) 80−73769
^{74}Se level scheme, J$^{\pi}$ assignments, bands and transitions from ^{60}Ni(^{16}O,2p), ^{64}Ni(^{12}C,2n) and ^{65}Cu(^{11}B,2n) 79−54393
^{74}Se transition energy correlations in γ-continuum from ^{64}Ni(^{16}O,α2n) 80−95309
^{75}Se decay, gamma transitions 78−13008
^{76}Se high spin states, bands, J$^{\pi}$, transitions and $T_{1/2}$ from ^{71}Ga(^{7}Li,2n) 80−105951
^{76}Se, level scheme from γγ coincidence meas. of ^{76}As decay 80−22754
^{79}Se, 96 keV transition, conversion coeff., γ-spectrum 80−63131
^{79}Se high spin levels, transitions, J$^{\pi}$ assignments from ^{76}Ge(α,nγ) 80−459
^{83m}Se, decay scheme refinement, ^{83}Br levels 78−17147
Se(n,n′γ), even-A isotopes, 2.0 to 4.1 MeV, level and decay schemes 77−23092
^{2}Si(π$^{\pm}$, π$^{\pm 1}$) 130, 180, 226 MeV, πN(3), region, inelastic transitions, optical and DWIA anal. 79−97677
^{26}Si, isoscalar and isovector E2 transition matrix elements 78−25148
^{28}Si 8^{+} state, level systematics and energy spectra from ^{25}Mg(^{12}C,^{9}Be) 80−42528
^{28}Si (α,α′γ) 104 MeV, nuclear deformation from ang. correlations, coupled channel anal. 78−78301
^{28}Si excitation functions, ang. distribs. and resonant behaviour from ^{24}Mg(^{16}O,^{12}C) 80−68622
^{28}Si excitation functions, ang. distribs., resonance spin assignments from ^{24}Mg(^{16}O,^{12}C) 80−68623
^{28}Si, excitation functions for O^{+} and 2^{+} states, meas. from ^{24}Mg(^{16}O,^{12}C) 78−54800
^{28}Si isovector M1 excitations, current and spin contribs. from (e,e′), (p,n) 80−68582
^{28}Si levels and J$^{\pi}$ from ^{28}P β^{+} decay 80−22772
^{28}Si, O_1^+, 2_1^+, 4_1^+ states, EM props. from large basis shell model 79−75900
^{28}Si p3/2 neutron resonance γ-decay, partial rad. widths from Si(n,γ) 80−52617
^{28}Si, shell model and statistical spectroscopic anal. 78−29390
^{28}Si(^{12}C,^{12}C), 27.8-31.5 MeV, elastic and inelastic excitation functions, fine struct., statistical anal. 80−18269
^{28}Si(^{16}O, ^{12}C)^{32}S, transitions to g.s., meas. of excitation functions 79−17920
^{28}Si(^{16}O,^{16}O), 30-32.7 MeV, elastic and inelastic excitation functions, fine struct., statistical anal. 80−18269
^{28}Si(e,e′), 38.7-57.5 MeV, energy levels, isovector M1 strength, DWBA anal. 79−75847
^{28}Si(e,e′), 92 MeV, E2 strength distrib., giant quadrupole 79−36192
^{28}Si(n,γ), 565, 813 keV, resonance γ, spectra, valence model test 80−63124
^{28}Si(n,n′γ), 13.9 MeV, spin flip probability from 1.78 MeV state, direct theory 80−9234
^{28}Si(n,n′γ), 1.96-4.15 MeV, prod. cross section for 1780 keV transition 79−59058
^{28}Si(p, p′), isovector dipole strength excitation in giant resonance region 80−83066
^{29}Si 3/2^{+} and 5/2^{+} states population, (d,p) and (p,π^{+}) comparison 80−95307
^{29}Si doorway state neutron capture, levels and γ-spectra from ^{28}Si(n,γ) 80−57729
^{29}Si excitation functions from ^{27}Al(^{3}He,p) 80−47493

nuclear energy level transitions continued
^{29}Si, low lying energy level structure, from ^{28}Si(d_{pol},pγ) and multi-step reaction calcs. 80−68537
^{29}Si neutron resonance, γ-spectra, partial and total radiative widths from ^{28}Si(n,γ) 80−42578
^{29}Si rot.-vibr. coupling effects, excitation spectrum and ang. distribs. from ^{28}Si(d, p) 80−57661
^{29}Si(d,p), 1.1-2.1 MeV, excitation functions, statistical fluctuations anal. 80−95322
^{29}Si(e,e′), 63-112 MeV, ground state transitions props. and transition radii of excited levels 77−50115
^{30}Si(^{16}O,^{16}O), elastic and inelastic, 60 MeV, to 1st excited 2^+ state, coupled channels anal. 78−82377
^{30}Si(p,γ), pol.p, 6.4-15.0 MeV, cross section and anal. power ang. distribs. 80−99168
Sm equilibrium and pre-equilibrium decay, α-multiplicities, energies and entry lines from ^{150}Nd(α,xn) 79−93549
Sm, even isotopes, n ang. distrib., transitions, vibr. band search from Nd(^{3}He,n) 79−63574
Sm, ion recoiling into gas and vac., hyperfine field and correl. time meas. 78−66240
^{A}Sm, A=147, 149, levels, J, γ-transitions and multipole mixing ratios, γγ correlations from Eu EC decay 80−106012
^{A}Sm, A=148,9, structural connections, levels, bands, J^π, transitions and mixing ratios from Nd+^{3}He(α) 79−63576
^{A}Sm, A=150, 152, muonic, X-ray spectra meas. and anal., charge radii, multipole moments 79−3600
^{A}Sm, A=152, 154, energy levels and E2 transition rates from three-band mixing model, backbending 79−67623
^{A}Sm(^{3}He, ^{3}He′), A=144, 148, 152, 154, 150, 40.9 MeV, transition cross sections, deformation parameters, coupled channels anal. 79−67640
^{A}Sm(^{86}Kr,X), A=144, 154, 490 MeV, transfer reactions and associated γ-multiplicity moments 80−18342
^{A}Sm(n,nγ), 2.75 MeV, A=150,152,154, levels and excitation cross sections 79−75839
^{141}Sm, M4 $11/2^- \rightarrow 3/2^+$ transition, level energy 77−10365
^{142}Sm isomers, lifetimes and transitions from ^{142}Nd(α,4n) 80−78122
^{142}Sm ns isomers and yrast isomers, γ-transitions from (^{24}Mg,4n), (^{19}F,4n) 80−78121
^{144}Sm+α, closed shell 82 neutron nucleus, B(E2)-value 78−66296
^{144}Sm(n,γ), resonance and thermal n, γ-spectra, recent expt. review, non-statistical effects 80−37383
^{145}Sm, high-spin states and particle-core coupling 77−26614
^{145}Sm primary γ-rays, direct capture and neutron separation energy, (d,p),(n,γ) correlation 80−57738
^{146}Sm, high spin states and transitions from ^{146}Nd(α,4n) 79−6423
^{147}Sm(n,α)^{144}Nd, 2 keV, statistical model anal. 80−102186
^{150}Sm, calc. of ^{149}Sm(n,γ) spectra 78−94006
^{150}Sm, γ-spectra, levels in ^{150m}Eu, 35.8 y decay 77−82858
^{150}Sm γ-spectra from ^{150}Nd(α,4n), 45 MeV, fusion and neutron evaporation 79−36291
^{150}Sm, negative parity yrast band, E1 transitions polarisability, quadrupole-octupole coupled vibr. system 79−484
^{150}Sm, nucl. struct. from ^{150}Eu decay *(Japanese)* 77−41888
^{150}Sm, vibrational states, B(E2) branding rates and interband transitions, pairing plus quadrupole calcs. 80−78127
^{151}Sm, gamma spectra, energy levels *(Dutch)* 80−47430
^{151}Sm low energy levels from expt. and Coriolis mixing calcs. of ^{150}Sm(n,γ) 80−57697
^{151}Sm, transition probabilities determ. 77−79329
^{151}Sm transitional nucleus, neg. parity states, spectroscopic factors, B(E2) values, particle-rotor model 78−50080
^{152}Sm ground and γ-bands, direct and multistep processes from (α,^{6}He), (p,t), (^{16}O,^{18}O) 80−102094
^{152}Sm, γ-transition energy and intensity meas. from ^{152}Eu decay 80−73818
^{152}Sm, level population by (t,α) reaction 77−67755
^{152}Sm levels populated in ^{152}Pm decay, γ spectra 78−542
^{152}Sm, populated in ^{152}Eu decay 80−22768
^{152}Sm(n,n′γ) spectra and ang. distribs. anomalous excitation *(Russian)* 77−54224
^{153}Sm, spin, parity, deduced levels, using ^{150}Nd(α,n), comparison with particle-rotor model 79−58999
^{154}Sm, strength functions for transitions to $I^\pi=2^+$ states 78−86519
Sm(α,α′), 11.5-12 MeV, E_2 and E_3 transition strengths meas. 77−26618
Sn 2_1^+ excitation, α-spectroscopic factors in IBA model from Te(d,^{6}Li) 80−105967
Sn, deep h-le state fragmentation, strength functions, giant resonances, quasiparticle phonon model 80−37320
Sn from ^{122,124}Sn(n,γ) up to 20 keV, level schemes, spin-parity assignments, neutron separation energies 77−54215
Sn isotopes, levels and spectra from broken pair model 80−73801
Sn odd isotopes, A=109-117, high spin states, level schemes 78−54684
Sn odd-mass isotopes, hole-state analogues, line broadening and Coulomb displacement energies 80−52560
Sn, photoactivation by 42 MeV bremsstrahlung, gamma transition energies and line intensities 78−13057
Sn, simple configurations in capture states 77−22939
Sn, single closed shell even mass nuclei, collective bands, spin, parity, from Cd(α,2nγ), γ meas. 78−54719
^{A}Sn, A=106-108, yrast levels and transitions from ^{54}Fe(^{58}Ni, X) 80−105957
^{A}Sn, A=112, 114, 116, 118, positive parity band heads, excitation energies and transitions from Cd(α, 2nγ) 79−45136
^{A}Sn, A=112-124 even isotopes, 0^+ state collectivity, E0 and E2 transition rates 80−73785
^{A}Sn, A=115,117, transition strengths from Sn(p,t) 79−89307
^{A}Sn, A=118,120,122, deep hole states, excitation energies and ang. distribs. from Sn(p,t) 80−86792
^{A}Sn, even A=116, to 124, $2_2^+ \rightarrow 2_1^+$ energy level transitions in (n,n′γ) reaction, pair interaction effects *(Russian)* 79−3114
^{106}Sn excited states from ^{106}Co (^{3}He,3n), coincidence experiments 80−52607
^{112}Sn, determ. of multipole mixture values in $2_2^+ \rightarrow 2_1^+$ transitions *(Russian)* 79−89268
^{112}Sn(p,p′), 20.51, 25.0 MeV, energy levels, excitation functions and ang. distribs. 80−32184
^{114}Sn, determ. of multipole mixture values in $2_2^+ \rightarrow 2_1^+$ transitions *(Russian)* 79−89268
^{116}Sn, collective states and E0, E2 transition rates 79−17787
^{116}Sn levels, J^π and transitions from ^{115}Sn(n,γ) 80−52587

nuclear energy level transitions continued
^{116}Sn(α,α′), 96, 129 MeV, giant resonance excitation, isoscalar breathing mode state, nuclear incompressibility 80−68620
^{117}Sn 6517 keV level, effective cross section, transition widths, from γ resonant scatt. 79−3135
^{117}Sn, substructure in radiative strength function using quasiparticle-phonon nucl. model 79−40901
^{117}Sn^m, E5 transition, branching ratio from ^{120}Sn(p,3np) 79−45200
^{119}Sn, substructure in radiative strength function using quasiparticle-phonon nucl. model 79−40901
^{119}Sn(p,n′)^{119}Sb, 17-19 MeV, analogue state excitation and decay 79−6542
^{120}Sn 6730 keV level, spin, absorpt. cross section, from nuclear resonant scatt. 79−3134
^{120}Sn 7310 keV level, effective cross section, transition widths, from γ resonant scatt. 79−3135
^{120}Sn γ-spectra, E1 and M1 hindrance factors from ^{123}Te(n,γα) 80−37386
^{122}Sn excitation of 6^+, 8^+, 10^+ and 9^- states, DWBA anal. from ^{122}Sn(p,p′) and ^{124}Sn(p,t) 79−89264
^{122}Sn, kaonic, E2 nuclear resonance effects 78−29868
^{123}Sn^m decay scheme, γ-ray, X-ray and electron spectra, ^{123}Sb transitions 77−88073
^{132}Sn, energy levels, gamma transitions, spin and parity 80−9239
^{132}Sn level struct., lifetimes, γ-γ coincidences, internal conversion from ^{235}U fission 80−52584
^{132}Sn levels, isomers, lifetimes and transition probabilities from fission 80−78163
^{A}Sr, A=80,82,84-86, levels and transitions from Kr(^{3}He,n) 80−18201
^{A}Sr, A=89 to 94, struct. of states in the generalised seniority shell model 79−6408
^{A}Sr, A=94,96 direct and skip cascades, γγ ang. correlations, levels, mixing ratios from Rb decay 80−86851
^{A}Sr, A=96,98, β-decay schemes and total energies, mass excess and separation energies 80−27601
^{A}Sr, A=98, 100 rot. struct. sudden onset, gamma transitions from Rb decay 80−73777
^{83}Sr high spin states, J^π and de-excitation from Kr(α,xn) 80−42516
^{85}Sr, β-decay, γ-ray weak transitions, intensities 77−79326
^{87}Sr(p,p′), 20.5 MeV, level scheme, ang. distribs., transitions and deformation parameter 79−22195
^{88}Sr(γ,γ), 14 MeV, highly excited spin-1 resonances, spin and radiative widths 80−86876
^{89}Sr level transitions and spin assignments from ^{88}Sr(d,p)^{89}Sr, polarised d 78−66286
^{90}Sr, energy spectra from nuclear shell model 79−22225
^{92}Sr γγ ang. correlations, levels, J^π, mixing ratios from ^{92}Rb decay 80−57725
^{93}Sr excited state depopulation γ-rays, n coincidence from ^{94}Rb β-delayed n decay 80−52631
^{93}Sr neutron binding energy from transitions and β-delayd neutron defined level correspondences 80−63070
^{98}Sr very low lying 0^+ state, shape coexistence bands, $T_{1/2}$, transitions from ^{98}Rb decay 80−78148
^{48}T excited states from ^{45}Sc(A,pγ), level struct., lifetimes, from DSA and pγ coincidence meas. 78−74326
^{177}Ta, magnetic moments meas. by PAC 80−22688
^{180}Ta^m, β$^-$ and EC branching ratios, K-internal conversion coeff., γ-intensities, T 1/2 80−68601
^{181}Ta, freq. modulation of 6.2 keV Mossbauer states 79−13202
^{182}Ta, decay scheme, conversion electron spectra, K-line transitions 78−13025
^{182}Ta deformed odd-odd nucleus, γ transition probabilities, rot. band mixing 77−61375
^{182}Ta rot. bands, bandheads and decay data from ^{181}Ta(n,γ) 79−93491
^{A}Tb, A=147, 148, high spin particle-hole states, octupole M2/E3 isomers from ^{151}Eu(α,xn) 80−18171
^{A}Tb, A=149, 151, 153, 155, 157, prop. anal. on function of nuclear shape 79−75828
^{148}Tb, high spin states, transitions J^π assignments from (Li,xn) and (^{10}B,xn) 79−49582
^{151}Tb 11/2 isomer, high spin few-particle states, in beam study from (^{3}He,3n) and (α,4n) 79−17805
^{153}Tb excited states from Eu(α, xn), rot. bands, spin, parity, γ spectra 78−62552
^{153}Tb low excited states, γ-ray angular distrib. in ^{153}Dy decay 79−6471
^{156}Tb, orientation in Gd matrix, γ-ray ang. distrib. anisotropy meas. 79−59031
^{159}Tb 58 keV transition, obs. of one phonon transitions in Tb 79−38416
^{160}Tb β-decay, oriented nuclei, γ transitions multipole mixing parameters 80−18240
^{160}Tb→^{160}Dy, γ-transitions and angular distributions 80−83060
^{A}Tc, A=93-96, excitation functions and isomer ratios from ^{93}Nb(α,xn) (x=1 to 4) 80−492
^{A}Tc, A=94 to 98, γ-ray multipolarities, internal conversion coeffs., energy levels 79−63625
^{93}Tc $^{17}/_2$ isomer, parity mixing search, partial γ-decay widths from ^{65}Cu(^{32}S,2n2p), 120 MeV 78−93936
^{95}Tc, energy levels from ^{95}Mo(p, nγ)^{95}Tc 80−37372
^{95}Tc, transition rates of even-parity states calc. 77−74806
^{96}Tc energy level diagram, γ transitions and parities from ^{96}Mo(p,nγ) 79−9479
^{96}Tc, high spin states, γ-energy, intensity, coincidence, ang. distrib. and electron conversion from ^{93}Nb(α,n) 80−52554
^{96}Tc low lying states, level scheme, parities, from conversion electron, γ spectra 78−46024
^{97}Tc, energy levels, low-lying, decay properties 80−63084
^{97}Tc, γ-γ ang. correl. study, E2/M1 mixing ratios, transition strengths 77−71584
^{97}Tc high spin states, spins and transitions from ^{94}Zr(^{6}Li,3nγ) 80−73780
^{97}Tc, K-capture probability for β-transition to 216 and 324 keV levels 79−6511
^{97}Tc levels, decay props., mixing ratios and J^π, from directional correlations in ^{97}Mo(p,nγ) 79−89240
^{98}Tc 14 μs isomer, low lying levels and transitions from ^{98}Mo(p,n) 80−73802
^{98}Tc, low-lying levels obs. in ^{98}Mo(p,n) 77−88076
^{100}Tc level scheme, transitions and J^π values, n binding energy from ^{99}Tc(n,γ) 79−63590
^{100}Tc low lying and isomeric levels, transitions and mean lines from ^{100}Mo(p,nγ) 80−42548

nuclear energy level transitions continued
^{100}Tc μs isomers, isomeric transitions and mean lives from ^{100}Mo(p,n) 80−73803
^{102}Tc decay scheme and γ-intensities from ^{102}Mo fission product decay 80−78229
^{102}Tc deduced levels, tentative J^{π} and transitions from ^{102}Mo decay 80−52630
^{A}Te, A=117, 119, 121, collective excitations, high spin states and transitions from (α, Zn)(d, Zn)(^{3}He, 3n) 80−13346
^{m}Te, A=125,127,129, internal conversion of M4 transitions at 109.27, 88.26, 105.50 keV 77−65214
^{120}Te quasi-rot. band based on proton 4p-2h state, level scheme, transitions from ^{118}Sn(α,2nγ) 80−78119
^{124}Te, energy levels spectroscopy by ^{123}Te(d,p)^{124}Te 77−41973
^{124}Te, level struct. determ. from ^{124}Sb beta-decay 79−54387
^{125}Te, levels and transitions following decay of ^{125}Sb 79−71816
^{125}Te low lying negative parity high spin states multistep induced population from (d,t)(^{3}He,α) 80−57657
^{126}Te, M1, giant resonance and radiative strength functions 80−57731
^{126}Te(^{22}Ne, ^{22}Ne′), 93.5 MeV, 2^{+} state mutual excitation and transitions 79−54404
^{126}Te(p,n), $2_2{}^{+}\rightarrow 2_1{}^{+}$ transition multipole mixing ratio 80−78198
^{127}Te, energy levels spectroscopy by ^{120}Te(d,p)^{121}Te 77−41973
^{130}Te(n,γ), resonance and thermal n, γ-spectra, recent expt. review, non-statistical effects 80−37383
^{131}Te γ-transitions, spectroscopic factors and reduced transition intensities from ^{130}Te(n,γ) 80−91143
^{132}Te low lying levels and EM props., shell model description 80−42549
^{A}Th, A=231, 233, vibr. band systematics, excitation energies and rot. parameters 79−36137
^{228}Th decay, γ-ray and internal conversion intensities 78−41669
^{228}Th, high pressure meas. of gamma transitions 80−18225
^{228}Th, precise γ-ray energy meas. with Ge(Li) detectors 78−13376
^{230}Th, precise γ-ray energy meas. with Ge(Li) detectors 78−13376
^{231}Th excited states and bands, spins, γ-transitions from ^{230}Th(n,γ) 80−57699
^{231}Th, rotational band level diagram from α-decay and γ-transitions 80−18156
^{232}Th level structure and decay parameters from (n,n′) and (n,n′γ) meas. 77−30494
^{232}Th, vibr. states, Coulomb excitation 79−9432
^{232}Th(^{16}O,γ), transfer induced fission, excitation functions and cross sections 80−13515
^{232}Th(^{19}F,γ), transfer induced fission, excitation functions and cross sections 80−13515
^{232}Th(p,X), 10-100 MeV, spallation residue excitation functions, fissionability 80−18353
Ti, A=44-50, effective charges and E2 transitions in 1f-2p shell nuclei 78−544
Ti, A=45-51 odd isotopes, spectra and EM transitions, spin assignments, rot. bands 77−74793
Ti(^{12,13}C,X) 45, 46 MeV, particle-gamma coincidences, isotope assignment for yrast spectroscopy 80−68593
^{A}Ti, A=44, 46, 48, 52, energy levels and EM props. using classical semimicroscopic model 79−59012
^{A}Ti, A=44, 48, ang. distribs. for transitions, DWBA anal., spectroscopic strengths from Ca(^{7}Li,t) 80−68584
^{A}Ti, A=48,50, excited states and transition ang. distribs. from Cr(^{14}C,^{16}O) 80−95308
^{42}Ti, $6_1{}^{+}$ state lifetime, B(E2) value 77−82863
^{44}Ti, lowest T=2 state decay, branching ratios from ^{46}Ti(p,t) 42 MeV 78−78304
^{44}Ti lowest T=2 state isospin forbidden γ-decay from resonances in ^{40}Ca(α,γ) 79−22228
^{45}Ti, weak E1 transitions examined using γ-ray, γ-γ coincidence and n-γ coincidence techniques 80−57724
^{46}Ti deduced levels, spin assignments and γ-decay, band struct. from ^{43}Ca(α,nγ), 8-15 MeV 78−78302
^{46}Ti(n,p), 4.5-18.3 MeV, cross sections and excitation curves *(Chinese)* 79−49601
^{48}Ti levels and transition ang. distribs., form factors, DWBA anal. of ^{45}Sc(α,p) 79−45202
^{48}Ti+^{16}O, anisotropy of yrast γ-transmissions 79−93650
^{48}Ti(n,p), 4.5-18.3 MeV, cross sections and excitation curves *(Chinese)* 79−49601
^{49}Ti, $3/2^{-}\rightarrow 7/2^{-}$ 1381 keV transition, B(E2) value 78−74328
^{49}Ti(α,α′) 5.2-5.8 MeV, B(E2) value meas. for $3/2^{-}$ to $7/2^{-}$ transition 78−82308
^{50}Ti, 1p7h config., high-spin neutron-hole states, EM transition rates 78−70430
^{50}Ti high spin states, transitions and J^{π} values from ^{48}Ca(α,Znγ) 80−455
Tl, A=185,187 isomeric decays, half-life, $h_{9/2}$ intruder state 77−26616
Tl, strongly forbidden T1-transition, parity nonconservation *(Russian)* 77−10366
^{A}Tl, A=199, 200 cross section and excitation function statistical anal. from ^{197}Au(α,xn) *(Rumanian)* 80−22846
^{192}Tl high spin band struct. and transitions, isomeric state from ^{181}Ta(^{16,18}O,xnγ) 80−47353
^{193}Tl, studied via decay ^{193}Pb$\rightarrow$^{193}Tl 77−6587
^{194}Tl high spin states, excitation functions, $I^{\pi}=8^{-}$ isomeric state from ^{181}Ta(^{18}O,5n) 80−32163
^{196}Tl high spin states, γ-decay and rot. structs. from ^{197}Au(α,5n), ^{194}Pt(^{6}Li,4n) 79−440
^{201}Tl γ- and X-ray emission probabilities and half-life obs. 80−32242
^{201}Tl levels, transitions and J^{π} assignments from ^{201}Pb decay 80−5099
^{203}Tl, ^{205}Tl, core excitations to low-lying states, e.m. props., hyperfine splittings, isomer shifts 78−89794
^{205}Tl transition strengths from ^{208}Pb(p,α) 79−13271
^{206}Tl resonances, neutron strength functions and radiative widths 77−22898
Tm, A=163-171, E1 transitions, hexadecapole deforms., Nilsson model calc. 77−82861
^{163}Tm, high spin rot. levels, studied via ^{165}Ho(^{3}He,5n) and ^{165}Ho(α,6n) reactions 78−8722
^{165}Tm, levels excited by β-decay of ^{165}Yb 78−74334
^{166}Tm decay, ^{166}Er level population 79−93556
^{167}Tm, energy level scheme from ^{165}Ho(α,2nγ) *(German)* 80−68576
^{167}Tm, levels and transitions from ^{165}Ho(α,2n) 80−73766
^{167}Tm rotational bands, J^{π}, γ-transitions and branching ratios from ^{165}Ho(α,2nγ) 80−86781
nuclear energy level transitions continued
^{167}Tm(HI,xnγ), ang. distrib., multipolarities *(French)* 80−68575
^{169}Tm, excited state lifetime meas. 80−32237
^{169}Tm, γ-ray transitions for level struct., obs. in ^{169}Yb electron capture decay 78−82307
^{169}Tm, studied via ^{169}Tm(^{32}S,^{32}S′γ), EM props. of ground state rot. band 78−8726
^{170}Tm gamma-ray strength functions from spectrum fitting method from ^{169}Tm(n,γ) 80−52616
^{170}Tm(n,γ), 0.5-3.0 MeV, γ-spectra strength functions 80−32240
U (M,f), muon excitation probabilities, muonic atoms, Schrodinger eqn. 80−47515
U gamma abundances 77−65270
U spontaneously fissionable isomers, excitation by K shell e^{+} annihilation, shape isomery model *(Russian)* 79−30802
U(Xe,f), Coulomb fission problem, uniform semi-classical approach to forbidden transitions 79−36287
^{A}U A=235, 239, vibr. band systematics, excitation energies and rot. parameters 79−36137
^{A}U, A=236,238, fission isomer rot. spectra $I^{2}(I+1)^{2}$ correction 80−18229
^{A}U(n,X), A=233, 235, thermal n, gamma spectra from capture, fission and fission products 80−37352
^{232}U, high pressure meas. of gamma transitions 80−18225
^{232}U$\rightarrow$^{212}Pb decay chain, obs. of collective states fed by weak α-transitions 78−8786
^{233}U levels, bandheads, total α-branching and transitions from ^{237}Pu α-decay 79−93516
^{233}U, monopole conversion, magnetic dipole transitions, latent penetration effect 79−9464
^{233}U(d,d′), multipolarities and reduced transition probabilities 78−17215
^{235}U, K-shell positron annihilation, excitation of nucleus *(Russian)* 78−33171
^{235}U vibrational and single particle states from ^{234}U(n,γ) 79−36123
^{235}U^{M} prod. by nuclear excitation by electron transition in plasma 80−22668
^{235}U^{m}, highly converted nuclear transitions, electronic bridge theory appl. 79−67708
^{235}U($1/2^{+}$; 73 eV) isomer *(Russian)* 79−9511
^{235}U(d,d′), 13.1 MeV multipolarities and reduced transition probabilities 78−17215
^{235}U(n,γ) resonance capture, primary γ-transitions, parity assignments 77−26619
^{236}U fission shape isomer, γ-decay from ^{238}U(γ,2n) 80−18230
^{236}U γ-transitions from ^{235}U(n,γf) 80−106085
^{236}U low lying levels from 4^{-} isomer decay in (n,e), (n,γ) 80−47396
^{236}U shape isomer, γ branch upper limit, γ-yields from ^{235}U(d,p) 80−99145
^{237}U shape isomer, γ-decay search, branching ratio from ^{238}U(Γ,2nγ′) 45 MeV 78−93961
^{237}U virtual photon excited state decay and total cross section of ^{238}U(e,n) 80−22757
^{238}U, multipolarities involved in electrodisintegration 78−590
^{238}U, strength functions for transitions to $I^{\pi}K=2^{+}0$, $2^{+}1$, $2^{+}2$ and $I^{\pi}=2^{+}$ states 78−86519
^{238}U(n,γ), 2, 24 keV, resonance averaged γ-spectra, level and J^{π} appls. 80−37347
^{238}U(n,n′γ), 1.06 MeV, cross sections and γ spectra for various energy levels *(Russian)* 79−40883
^{238}U(n,n′γ) technique for study of levels near 1 MeV 77−26719
uncorrelated target, optical pot. unitary content, DWIA and Glauber theory from (α,α)(α,γ) 80−105947
V, A=47-51, effective charges and E2 transitions in 1f-2p shell nuclei 78−544
V, A=52, 3, yrast decay schemes from heavy-ion fusion evaporation reactions 77−82854
V isotopes, A=47-51 78−25114
^{45}V level scheme, γ-rays, level lifetimes, internal conversion from ^{40}Ca(Li,xn) 80−63085
^{47}V $3/2^{-}$ analogue state decay amplitudes, common doorway state phase relation from ^{46}Ti(p,p′γ) 79−89276
^{51}V, γ-strength function, γ-ray spectra, average resonance method from ^{50}Ti(p,γ) 80−9257
^{51}V, levels populated in 200 MeV (π,π′γ) 78−21611
^{51}V, shell model, pairing-plus-surface-tensor interaction, energy levels, B(E2) values 78−78282
^{51}V(n,α), 4.5-18.3 MeV, cross sections and excitation curves *(Chinese)* 79−49601
^{51}V(p,p′), 6 MeV, levels, spins and EM props., shell model anal. 80−63092
^{52}V, mean lifetimes of yrast states populated in ^{48}Ca+Li 77−2942
W high spin states, A=172, 174, 176, from Dy(^{16}O, xn), decoupled quasiparticle bands, backbending 78−50199
W isotopes, A=182, 184, 186, Coulomb excitation with ^{4}He and ^{16}O ions 78−8839
^{A}W (^{84}Kr,^{84}Kr′γ) A=183, 184, 186, 340 MeV, Coulomb excitation, energy levels and bands 79−63577
^{A}W, A=170-182, even isotopes, yrast states, spectra and quad. moments, variation formulation 80−99119
^{A}W, A=173, 175, high-spin states, single-particle structure 78−93922
^{A}W, A=173, 175, hindered electric dipole transitions and lifetimes from (HI,xn) reactions 80−9263
^{A}W, A=174, 175 quasicontinuum γ-rays yrast cascade dipole component, moment of inertia from Dy(^{16}O, xnγ) 80−47424
^{A}W, A=184, 186, rigid asymmetric rotor model descript., E2 and E4 props. 80−13403
^{A}W(n,nγ), 2.75 MeV, A=182,184,186, levels and excitation cross sections 79−75839
^{174}W, decoupled two-quasiparticle bands, backbending 78−4890
^{180}W octupole vibr. states, J^{π} and transitions from ^{180}Re decay 80−83024
^{182}W 100 keV E2-transition, L-subshell internal conversion coeff. from ^{182}Ta decay 79−75909
^{183}W(α,α′), 15 MeV, level and band Coulomb excitation, B(E2) values 80−32233
^{184}W, 1285 keV 5^{-} state struct. anal. 79−9467
^{184}W (n,n′γ), fast n, level struct. and populations, γ-transitions 79−75841
^{184}W, T-invariance violation, test in 922 keV γ-ray 77−71581
^{184}W(^{12}C,^{12}C′), 70 MeV, 4^{+} state excitation ang. distrib., hexadecapole deformation length effects 80−68521

nuclear energy level transitions continued
^{186}W(n,n'γ), fast n, level struct. and populations, γ-transitions 79−75842
Xe levels populated in ^{129}Cs, ^{133}I β decay energy level scheme, γ spectra meas. 77−2936
^{A}Xe, A=122,124,126,128, 0^+ excited state spin assignments and transitions from Cs β-decay 79−67649
^{A}Xe, A=124,126-8,130,132, levels, transitions and J^π values, DWBA anal. from Te(^{3}He, n) 79−75852
^{114}Xe excited states and γ-rays from ^{114}Cs β-decay 80−47436
^{116}Xe level scheme and yrast band, in-beam γ-study from ^{106}Cd(^{12}C, 2n) 80−13360
^{118}Xe, decay investig. using mass separator on-line with synchrocyclotron 78−17139
^{119}Xe, decay investig. using mass separator on-line with synchrocyclotron 78−17139
^{125}Xe $11/2^- \rightarrow 9/2^-$ transition in odd parity band from ^{124}Te(α, 3n) 80−9203
^{129}Xe excited state lifetimes, γ-transitions from ^{129}Cs decay 80−78205
^{132}Xe level struct., J^π, transitions and multipole mixing ratio from ^{132}I decay 80−91134
^{136}Xe(n,γ), resonance and thermal n, γ-spectra, recent expt. review, non-statistical effects 80−37383
^{137}Xe neutron unbound states, high energy X-rays from ^{137}I decay 80−86856
^{A}Y, A=85,87,89, E1 γ-ray strength function from Sr(p,γ) 79−75902
^{A}Y^{m,g}, A=86, 87, isomeric yield ratios and γ-spectra from ^{93}Nb(π^-,X) 80−86857
^{85}Y, from ^{85}Zr decay 77−34258
^{87}Y level struct., γ-spectroscopy and J^π from (p,2nγ), (α,2nγ) 80−83040
^{89}Y, energy spectra and EM props. using broken pair model 80−499
^{89}Y excited state ang. distrib. from ^{88}Sr(^{16}O, ^{15}N) 79−67709
^{89}Y gamma transitions, microscopic finite-range anal. of ^{92}Zr(p,α) 80−63181
^{89}Y high spin states and decay scheme from ^{87}Rb(α,2nγ) 80−32166
^{89}Y(π,π'), 163, 240 MeV, giant resonance pionic excitation 80−52561
^{90}Y, 7^+ to 2^- E5 transition probability 78−66243
^{90}Y, energy spectra from nuclear shell model 79−22225
^{90}Y, shell model calcs., energy levels, transitions and spectroscopic factors 79−63593
^{98}Y^{g}, β-decay schemes and total energies, mass excess and separation energies 80−27601
^{171}Y populated in ^{171}Lu decay, level scheme, γ-transitions, spin-parity assignments 77−46133
^{90m}Y, ^{90g}Y decays, weak β transitions, γ-ray emission 77−34265
^{A}Yb, A=158, 159, alpha decay and gamma transitions 80−73827
^{A}Yb A=160-163, γ-transitions from Lu decay 80−102146
^{A}Yb, A=160-166, transitions from ^{158}Gd+^{12}C fusion 79−580
^{A}Yb, A=161, 162, 166, yrast cascade dipole component from Sm(^{16}O,4n) 80−9266
^{A}Yb, A=164, 166, high spin yrast states and transitions from Gd(^{13}C,5n) 80−9208
^{A}Yb, A=169-x, γ de-excitation and ang. momentum distribs. after fast α-emission from ^{159}Tb(^{14}N,αxn) 80−18228
^{A}Yb A=172, 174, electric monopole transitions from excited $K^\pi=0^+$ levels from Yb(n,γ) 79−6486
^{A}Yb(^{16}O,^{16}O'γ), A=168-176, even nuclei, 58-62 MeV, Coulomb excitation, vibr. and rot. states 80−32162
^{159}Yb, identification 77−50075
^{161}Yb quasicontinuum γ-rays yrast cascade dipole component, moment of inertia from Sm (^{16}O, xnγ) 80−47424
^{166}Yb multiple band crossing, (gSS'S''S'') system gamma correlation patterns 80−106008
^{167}Yb, spin and parity determ. from ^{167}Lu→^{167}Yb data, e/β^+ anomaly 79−6380
^{167}Yb→^{167}Tm mass difference, from positron spectrum, level transition branching ratio 79−6376
^{168}Yb, low lying spectra and EM transitions, level struct. in quasirotational bands 79−36141
^{168}Yb(α,α'), 12-13 MeV, E2, E4 transition matrix elements determ. 78−33202
^{169}Yb $^7/_2^+$[404]→$^7/_2^+$[633] transition ft value from ^{169}Lu allowed hindered β^+ decay 80−102148
^{169}Yb, EM transitions, mixing of states having different quantum numbers 79−6493
^{169}Yb, E2 transitions in rot. bands, partial probability calcs. 79−75835
^{169}Yb γγ ang. correlations, levels and spins from ^{169}Lu decay *(Russian)* 80−83069
^{169}Yb, populated in ^{169}Lu decay, meas. of γ-ray and conversion electron spectra 80−22766
^{169}Yb populated in ^{169}Lu decay, γ-ray and conversion electron spectra 80−22767
^{172}Yb, gamma ray spectra, β-decay of ^{172}Hf and ^{172}Lu 78−33140
^{173}Yb, γ-transitions from 7/2, $7/2^-$ [514] 636 keV level 80−78187
^{173}Yb M1 transitions from 636 keV level, multipole mixture parameters, penetration effect 80−18220
^{174}Yb, width correlation in ^{173}Yb(n,γ) 77−79370
^{91}Ze primary γ-rays and binding energies from ^{90}Zr(n,γ) 80−52566
Zn, A=64, 66, 68 transition charge density, and radius to collective states via (e,e') 77−50077
Zn, even isotopes, effect of particle-vibr. coupling in nucl. struct. 78−12940
Zn, even isotopes, weak-coupling model, level struct., E2 transition rates 77−54159
^{A}Zn, A=64, 66 levels and primary E1 transition strength functions from Cu(p,γ) 80−91149
^{A}Zn(p,γ), A=64, 66, $g_{9/2}$ isobaric analogue resonances 79−63663
^{62}Zn ang. distribs. for transitions, DWBA anal., spectroscopic strengths from ^{58}Ni(^{7}Li,t) 80−68584
^{62}Zn, band mixing HF model, struct. and electromag. transitions 78−54676
^{62}Zn yrast states, possible decay scheme from ^{40}Ca(^{28}Si,α2pγ) 79−54379
^{63}Zn EM decay transitions, level J^π assignments, level lifetimes from (α, nγ), (^{11}B, npγ), (^{7}Li, pnγ) 79−85402
^{63}Zn, low-lying negative parity states anal. by ^{60}Ni(α,nγ) ^{63}Zn 78−21521
^{64}Zn, electroexcitation of giant multipole reson. *(Russian)* 78−58264
^{64}Zn, γ-ray spectroscopy and role of $g_{9/2}$ orbital 78−33142
^{64}Zn, γ-ray studies of levels above 3.1 MeV 80−32238
^{64}Zn high spin states, J^π, $T_{1/2}$, γ-decays from (α,nγ), (^{11}B,p2nγ) 80−73767

nuclear energy level transitions continued
^{64}Zn, J^π assignments from γ-ray linear polarisation meas. from ^{59}Co(^{7}Li,2n) 79−6383
^{65}Zn gamma intensity, from ^{64}Zn(n, γ) cross-section meas., k_0 factors calcs. 79−26433
^{65}Zn, γ-ray spectroscopy and role of $g_{9/2}$ orbital 78−33142
^{65}Zn, high spin states obs. in (α,nγ), and (^{16}O,np) 78−13016
^{65}Zn odd-parity states from ^{62}Ni(α,nγ), γ study, energies, branching and mixing ratios, lifetimes 78−50120
^{67}Zn, Coulomb excitation, gamma-ray spectra 79−9434
^{67}Zn, high spin states obs. in (α,nγ) 78−13016
^{70}Zn excitation energies, B(E2) values, extended generator coordinate method 77−6203
^{70}Zn(p,p'), 3.825 MeV, E0 transition probability for 0_1^+-0^+ transition 77−41963
Zr, A=86, 87, 88, high spin states 78−74383
Zr even isotopes, quadrupole moments and E2 transition rates, broken pair approx. 80−52579
Zr isotopes populated in (n,n'γ) scatt., γ-ray assignments to transitions 77−26767
Zr neutron deficient isotopes, studied via heavy ion induced compound reactions 77−57621
Zr neutron rich isotopes, excited 0 states 77−22937
^{A}Zr, A=91, 92, 94, binding energy and primary γ-ray intensities from Zr(n,γ) 80−52565
^{A}Zr, A=92, 94, 96, multiparticle states, method of generalised seniority 80−22759
^{A}Zr, A=92, 96, first excited 0^+ state transition strength from (^{6}Li,^{8}B), (d,^{6}Li) correlation 80−78260
^{A}Zr(n,n'γ) 2.2-3.7 MeV, A=92, 94, level and decay scheme, J^π assignments 79−17850
^{A}Zr(p,p'), A=94,96, 11.2-13.4 MeV, anal. power and excitation function $T_<$ fluctuations 80−42626
^{87}Zr, in-beam γ-ray spectroscopy of excited states 79−17852
^{88}Zr transitions and high spin states above 8^+ isomer, ^{86}Sr(α, 2nγ)^{88}Zr 79−40848
^{90}Zr (p, p'), 57.5 MeV, polarised p, low lying level and giant resonance excitation 79−36157
^{90}Zr, anal. of spectrum of transitions to low-lying 2^+ states 78−17138
^{90}Zr, E1 γ-ray strength function from ^{89}Y(p,γ) 79−75902
^{90}Zr, energy spectra from nuclear shell model 79−22225
^{90}Zr, mag. quadrupole resonance, M2 strength distrib., quasiparticle-phonon model 79−75947
^{90}Zr, proton orbit sizes and E0 matrix element for 2 lowest 0^+ states 80−27546
^{90}Zr, static and transition densities, self consistent RPA theory test in fast (p,p), (e,e) scatt. *(Russian)* 79−49604
^{90}Zr(^{3}He,t)^{90}Nb, 18.5 MeV resonance, isovector dipole and Gamow-Teller transitions 80−86881
^{90}Zr(α,α'), 96, 129 MeV, giant resonance excitation, isoscalar breathing mode state, nuclear incompressibility 80−68620
^{90}Zr(e,e'), 2^- giant resonance twist mode excitation, B(M2) values, form factors 80−78246
^{91}Zr, populated in thermal neutron radiative capture reactions, γ-ray line obs. 78−17190
^{91}Zr, shell model calcs., energy levels, transitions and spectroscopic factors 79−63593
^{92}Zr, gamma-gamma directional correl. study 78−29422
^{93}Zr, populated in thermal neutron radiative capture reactions, γ-ray line obs. 78−17190
^{95}Zr, gamma intensity, from ^{94}Zr(n, γ) cross-section meas., k_0 factors calcs. 79−26433
^{95}Zr, populated in thermal neutron radiative capture reactions, γ-ray line obs. 78−17190
^{96}Zr, obs. of levels populated in β-decay *(German)* 77−67726
^{97}Zr, gamma intensity, from ^{96}Zr(n, γ) cross-section meas., k_0 factors calcs. 79−26433
^{97}Zr, populated in thermal neutron radiative capture reactions, γ-ray line obs. 78−17190
^{98}Zr, obs. of levels populated in β-decay *(German)* 77−67726
Zr(p,p'γ), odd isotopes, excited d-states from analogue resonances and p-γ correlations 80−68546

nuclear energy levels
see also isobaric analogue states; nuclear collective states and giant resonances; nuclear resonances; nuclear spectroscopic factors
0^- level positions, effects of one pion exchange 77−6232
$1f_{7/2}$ neutron single particle energy systematics 77−30480
2s-1d shell nuclei, cluster struct. and inelastic scatt. of polarised protons 79−6557
^{18}F levels, J^π and ang. distribs. DWBA anal. of ^{19}F(p,d) 80−42545
^{208}Pb (N,N^1) unnatural parity state excitation, π− condensate instability proximity, DWBA 79−97660
^{24}Mg radiative decays of unbound high spin states from ^{20}Ne(α,γ), ^{20}Ne(α,α'γ) 79−6484
^{54}Fe, mean lifetime of 6.38 MeV 8^+ state *(French)* 79−45204
^{5}Li states, phase shift anal. of ^{3}He(d,d) 80−47382
^{90}Y, 1^+ and 0^+ states populated in ^{88}Sr(^{3}He,p) 78−25116
A=105, nuclear data sheets, levels, decays and J^π assignments 79−93486
A=119, nuclear data sheets, level and decay props. 79−71780
A=11, 12, energy levels, transitions and resonances, compilation 80−46743
A=120-150, levels and EM props., recent results 80−68592
A=121 nuclear data sheets, level schemes and decay properties 79−75818
A=136 nuclear data sheets, level schemes and decay props. 79−75819
A=140, nuclear data sheets, levels and transitions 80−31435
A=144 nuclear data sheets, levels, decays and J^π assignments 79−93487
A=149, data sheets to August 1974 77−10305
A=154, nuclear data sheets, levels, decay props., isomeric states, Nilsson orbitals 79−71781
A=159, nuclear data sheets, levels, decays, and J^π assignments 79−93488
A=16, 17 nuclei, energy levels, struct., review 77−46116
A=16 to 28, α-structure amplitudes and shell model wavefunctions for nuclear states 79−45192
A=176, data sheets to April 1976 77−10306
A=18, 2p1h multiple scatt. formalism, effective interactions, energy spectra 77−67709

nuclear energy levels continued
A=18 nuclei, importance of high lying intermediate excitations on nuclear effective interactions 78−70460
A=18 shell model spectra and 3 nucleon force 78−25124
A=18 to 38 nuclei, anal. of nuclear spectroscopic data 79−26381
A=190, Nilsson strength fragmentation, quadrupole and hexadecapole deformations 80−47394
A=199, nuclear level scheme data sheets, decay scheme 79−13186
A=1-257, nuclear excitation by atomic electron transitions, nuclear levels 80−78191
A=203, nuclear data sheets, level struct., decay schemes 79−13187
A=204, nuclear data sheets, levels, J^{π} and transitions 80−31429
A=212, nuclear data sheets, levels, J^{π}, transitions 80−31430
A=215, nuclear data sheets, decay characteristics and level struct. 78−58224
A=219, nuclear data sheets, decay characts. and level struct. 78−58225
A=21-44, energy levels, excitation energies, branching and mixing ratios, lifetimes, J^{π}, resonances 79−13208
A=221, nuclear data sheets, levels, J^{π}, transitions 80−31431
A=223, nuclear data sheets, decay characts. and level struct. 78−58226
A=225, nuclear data sheets, levels, J^{π}, transitions 80−31432
A=227, nuclear data sheets, decay characts. and level struct. 78−58227
A=230 to 254 nuclei semi-microscopic calcs. of level density *(Russian)* 77−277
A=237, nuclear data sheets to November 1977 78−82267
A=241, nuclear data sheets to November 1977 78−82268
A=24-108, level widths in charged particle induced reactions, stat. anal. 80−68535
A=36-39, energy levels and effective interactions from large scale shell model calcs. 79−59011
A=40-56, spectroscopy props. using pure configuration shell model *(Chinese)* 80−42584
A=46, nuclear data sheets, level struct. and decay props. 79−13185
A=48, nuclear data sheets, to September 1977 78−82266
A=4-16, monopole giant resonances, state density radii and compressibility using hyperspherical functions *(Russian)* 80−27615
A=4N nuclei, lowest T=2 state isospin forbidden decays, branching ratios 79−67703
A=50, nuclear data sheets 77−10304
A=50-57, N=28-30, effective interactions and energy spectra from shell model calc. 78−82299
A=58 nuclear data sheet to June 1976 77−18372
A=5 to 10 nuclei, energy levels 79−49583
A=60, nuclear data sheets, levels and transitions 80−31433
A=64, nuclear data sheets, levels and transitions 80−31434
A=6 extended shell-model calcs. 77−14017
A=71 nuclear data sheets, levels, J^{π} and transitions 80−31428
A=73, nuclear data sheets, levels, J^{π} and transitions 80−101673
A=76 nuclear data sheet to June 1976 77−18373
A=77, nuclear data sheets, levels, J^{π} and transitions 80−105439
A>228 odd mass nuclei, single particle states, nuclear deform. 78−12952
A≈90 nuclei, studied by transfer reactions induced by ^{1}H, ^{2}H, ^{3}He 77−46118
A = 143, nuclear data sheets, level energies, J^{π} assignments 79−30775
A = 202 nuclear data sheets, levels and transitions 79−40831
A = 86, nuclear data sheets, level and decay schemes 79−30774
actinide nuclei, modified oscillator potential, dynamical moment of inertia, single particle levels 79−67637
actinides, level energies and B(E2) ratios of deformed even nuclei 79−13221
asymptotic nucleus-nucleus states using momentum projection methods 78−78403
average resonance neutron capture, completeness in nuclear spectroscopy 80−106006
average resonance parameter eval. and calcs., statistical model for capture process 80−18271
backbending even-even nuclei, particle-rotor model with VMI core *(German)* 77−6258
baryon-antibaryon nuclei, energy spectra and properties 80−22709
BCS techniques applied to self-consistent shell model 79−89249
boson model, interacting, shell-model basis, correspondence between fermion and boson states and operators 80−52593
bound states, systematics, simple physically realistic pot. 79−13181
classification of states, unitary scheme 80−42550
classification of states in the unitary scheme for complex nuclei and commutation properties of SU_3-irreducible ϵ-tensors 79−63598
clustering of levels in regular spectrum 77−71237
compound state statistical description, single particle states, radius and excitation energy *(Russian)* 79−22180
Compton excitation of nuclear levels, cross section estimation *(Russian)* 79−49620
conference on medium heavy nuclei structure, Rhodes, Greece (May 1979) 80−67935
conference on neutron capture gamma ray spectroscopy, Upton, USA. (Sep. '78) 80−36780
conference on nuclear physics with EM interactions, Mainz, Germany (June 1979) 80−22145
conference on nuclear spectroscopy and structure, Alma Ata, USSR, (Mar. 78) 79−75809
continuum effects in thermodynamical calcs. of binding energy shell corrections 77−71555
correlation expansions for light nuclei, cluster model higher order term effects 79−75877
Coulomb and charge dependent effects in nuclei 77−54131
Coulomb displacement energies, charge and mass number depend. in isotope shifts 78−8729
Coulomb displacement energies and n-p density distribs. 78−17084
Coulomb displacement energies of A=4n+3, T=1/2 mirror nuclei in $1f_{7/2}$ shell 77−57590
Coulomb displacement energy, T=1/2 mirror nuclei 77−282
Coulomb energy differences, Cottingham formula appl. 78−37256
Coulomb energy differences, dispersion theory using Cottingham formula 77−2895
coupled bands in even-even nuclei in RPA approach 80−32143
data sheets for A=184 nuclei 78−12948
data sheets for A=231, 235, 239 nuclei 78−12949
decoupled bands, perturbative anal. level energies 78−41623
deep hole states observed in particle transfer reactions 80−68511
deep lying level props. in strong electrostatic field *(Russian)* 77−2910
deep nuclear levels, practicability of kaon probe 78−25237

nuclear energy levels continued
deformed even nuclei, level energies, γ transitions, moment of inertia, collective Hamiltonian 78−25133
deformed even-even nuclei, SU_3 description of energy levels and reduced E2 transition probabilities *(Russian)* 79−13251
deformed nuclei, effect on Coriolis interaction, Nilsson model and Woods-Saxon pot. calcs. 80−63071
deformed nuclei, first monopole excitation energies in systems with pairing forces 77−61364
deformed nuclei, fragmentation of single-particle states, neutron strength functions 77−6233
deformed nuclei, gaps in single-particle level scheme and backbending 78−17072
deformed nuclei, one-particle state fragmentation, general regularities *(Russian)* 78−494
deformed nuclei, single particle level blocking in BCS approx. 80−99117
deformed single-particle basis for pot. energy surfaces and spectra 78−8735
dense Fermi systems, generalised perturbation theory, ground and low excited states 80−22741
densities, SCF approximation 77−2909
densities, shell effects and pairing effects, SCF theory of statistical thermodynamics *(Chinese)* 80−63088
density of states of spherical nuclei calc. 78−513
diffuse-surface density distrib., moments, potentials, energies calc. 77−10311
direct nucleon transfer reactions, model-independent spectroscopic information, use of spectroscopic factor and vertex constants 78−17168
doorway states mixing via fine-structure states, appl. to fission isomers 77−34231
doubly even deformed nuclei, excited states, Pauli principle effects, quasi-particle-phonon model 80−63094
electropion prod., deep inelastic scatt. and struct. from electron coincidence expts. at Stanford 80−22821
empirical $(1f_{7/2})^{n}$ model, review 79−17826
emulsion, K^{-} capture, neutron to proton ratio on surface 79−76024
even actinides, lowest 0^{+} state excitation, collective phonon state, spectroscopic factors from (p,t), (t,p) 80−13410
even nuclei, 2^{+} excited states quadrupole moments, energy weighted sum rule appl. 80−9229
even-even neutron-rich fission products, de-excitation spectra, β-decay, deformation 80−78203
even-even nuclei, backbending mechanism anal. *(Chinese)* 78−78247
even-even nuclei, props. of 0^{+} states and E0 transitions 79−6406
even-even nuclei with N=66, spectra, quadrupole transition probabilities 77−26577
even-even spherical nuclei, $2_1{}^{+}$ state deformation parameter from (p,p) and EM excitation 80−27549
even-even transitional nuclei, bunching of spin states in γ-band, asymm. rotor model 78−62485
excited nuclear states, lifetime meas. 80−5093
excited simple and yrast states, mag. moments, transient mag. fields 80−5064
excited state quadrupole moments meas. using Coulomb excitation 80−5065
excited states, β-decay and electron capture rates, gross theory, astrophysics implications 77−41927
excited states, Young's diagram 80−42566
exotic light nuclei , masses and energy levels 77−22866
$f_{7/2}$ shell nuclei, odd-A, collective bands of positive parity states 78−54677
$f_{7/2}$ shell nuclei, shell model study in pure $f_{7/2}{}^{n}$ config. 79−36162
$f_{7/2}$ shell single particle state systematics, centroid energies, Saxon-Woods pot. 79−3066
Fermi surface in double magic nuclei, self consistent description *(Russian)* 78−33120
fermion system, classification of states, spin 1/2, using chain of subgroups of unitary scheme 79−63597
few nucleon systems, description via analytical continuation in copuling constant 77−18420
few quasi-particle components of nuclear states in quasi-particle-phonon model 79−75843
field theory, renormalisation of single particle states 78−24926
finite nuclei and inhomogeneous infinite systems, ground states, FHNC method extension 80−22736
finite temperature shape transitions, stability conditions, level density, HF and HFB calcs. 79−67644
fission lifetime distribution and probability estimates 78−659
fixed angular momentum moments and level densities, statistical spectroscopic methods 80−467
folded diagrams and s-d shell effective interactions, excit. spectra and ground state binding 77−79315
generalised collective model, surface tension, energy spectra, and E2 γ-transitions 79−6432
generalised vibrational rule 80−105971
generator-coordinate method extension to two quasi-particle excited states, appl. to fp-shell nuclei 77−54153
giant quadrupole capture of energetic nucleons by nuclei 77−10398
gross-shell effects in the single-particle level distribution with fixed angular momentum projection *(Russian)* 79−22179
gross-shell structure in deformed oscillator pot., semiclassical anal. *(Russian)* 79−22178
ground state deformation energy, rot. band inertial parameter depend. 80−18185
ground-state proton-neutron occupancies in the f-p shell 80−13381
groundstate and β-band simultaneous description, new model 77−2898
growth points in nuclear physics, book 80−94928
heavy even-even nuclei, spectra from shell model and interacting bosons 79−6411
heavy ion collisions, complete fusion cross sections, compound nucleus props. *(French)* 79−577
heavy ion collisions, nuclear level shifts, generalised relativistic Coulomb problem *(Russian)* 80−52586
heavy ion induced few nucleon transfer reactions, proton pairing and four nucleon correl., reaction kinetics *(French)* 79−557
heavy ion induced reactions, information from γ-spectroscopy *(Rumanian)* 78−58300
heavy ion stripping and pickup reactions on closed shell nuclei, level shifts, DWBA 80−91168
high angular momenta nuclei, shell effects on moment of inertia and level density *(Russian)* 79−67635

nuclear energy levels continued
high-spin selectivity in heavy-ion compound reactions, critical ang. momenta determ., spectroscopy 77−54238
high-spin states, light particle emission, deformation effects 79−22198
high-spin states in N=28 nuclei 78−29407
hole excitation spectrum in finite Fermi system, many body field theory 80−102105
hole states, continuum shell model approach for (p,2p) and (e,e'p) reactions 79−22162
hypernuclei, ΛN effective force, binding energy, excitation spectra, self consistent calcs. 77−6283
hypernuclei, produced by strangeness exchange reactions, level structure 78−17130
hypernuclei, symmetry classification for excited states, appl. to Be isotopes *(Chinese)* 78−25144
interacting boson model, band struct. of heavy even/even nuclei *(Dutch)* 79−17841
internal conversion due to hyperfine interaction, shift effect in generated X-ray lines *(Russian)* 78−58234
isobar propagation and collective effects, pion-nucleus and photonuclear investigation 80−22676
isospin dependence of level density 77−61349
isospin mixing in nuclei, matrix elements explained by Coulomb interaction 78−37264
large deformations, single particle levels, self-consistent field rearrangement, HF method 80−78107
level densities, thermodynamic temps., spin cutoff factors, nuclei with $23 \leq A \leq 40$, expt. calcs. 77−30492
level density, analytic formula, shell and pairing effects 78−50092
level density, shell. struct. effect excit. energy depend. 77−79311
level density in large spectroscopic spaces, statistical spectroscopic methods 80−86814
level density of interacting bosons 80−105974
level density of nuclei, role of collective effects and neutron resonances *(Russian)* 79−49586
level density of nuclei and the superconductive-type pair interaction *(Russian)* 80−13383
level density with schematic forces, appl. to ^{116,117}Sn 78−41639
level shift non-measurability due to pion diamagnetism in Mossbauer effect 80−73808
light muonic atoms, nuclear size effects, energy levels, Lamb shift 80−14254
light nuclei, hyperspherical functions for size, excited states, compressibility, binding energy 80−22679
light nuclei, m-particle n-hole struct. from few nucleon transfer reactions, review 78−50062
low level excitation, inelastic electron scatt. *(Russian)* 78−58265
magic and doubly magic nuclei, A=129, 131, 133 chains, 0^+ states, spectroscopy 80−78165
magic Z (N) isotopes (isotones), calc. of first 2^+ and 3^- excited levels and transition prob. 79−80874
maximum overlap and shape instabilities 79−40401
mean field theory of nuclear dynamics, time depend. 78−12986
microscopic model, wobbling motion in fast rotating nuclei 78−21505
mirror nuclei, A=13-33, transverse photon effect 77−6229
mirror state EM decay rates, multipole matrix element isospin decomposition 79−36190
multipole excitation of doubly-open shell spherical nuclei 78−21507
N=27 nuclei levels and analogue states, DWBA anal., from (^{3}He,α) reaction 79−17808
N=28 isotones, effective interactions, Coulomb displacements and separation energies 78−50077
N=28 nuclei, energy spectra calc. in shell model 79−13206
N=28 region, $1f_{7/2}$ nuclei, low lying and high spin states 78−54667
N=29 nuclei, effective 2-body interactions and level spectra 78−41647
N=50 isotones, effective interactions, Coulomb displacements and separation energies 78−50077
N=50 isotones, effects of $1p_{3/2}$ core excitations 79−466
N=50 isotones, transition probabilities, $1p_{3/2}$ and $0f_{5/2}$ hole excitation effects 80−47431
N∼28 nuclei, shell model study of high-spin states 79−3087
neutron, alpha and nuclear matter, ground vacuum states 80−22738
neutron capture, total radiative width and degree of freedom, statistical model calcs. 80−57732
neutron excess deformation, coupled channel anal. of (p,n) elastic and inelastic scatt. 79−93480
neutron level spacing distrib., nonstatistical effects *(Russian)* 78−41625
neutron rich fission fragments, excited state spin assignment, various methods 80−78506
neutron rich transitional fission fragments, spectroscopy, 0^+ states and octupole vibrs. 80−78204
neutron s-wave strength functions, odd-even fluctuations 77−22856
neutron strength function, spin depend. *(Russian)* 78−17069
neutron strength functions in deformed nuclei, semi-microscopic approach 77−22851
non-normal parity states, 1p shell nuclei, $1\hbar\omega$ spectra 78−12977
nuclear matter momentum distribs., single particle orbitals, Fermi hypernetted chain theory 80−86841
nuclear matter with neutron excess, thermal props. and level density parameter 80−91141
nucleon, bound in harmonic oscill. pot., EM struct. and binding energy 78−8732
nucleon excitation of levels with anomalous parity, rel. to models of nucleon-nucleon amplitudes *(Russian)* 77−79383
odd mass nuclei, $1g_{9/2}^+$ shell region, low lying states, anharmonic effects 80−57687
odd mass nuclei, 2s-1d shell, nuclear forces, energy levels 77−2917
odd mass nuclei in $1f_{7/2}$, level density and spacings from resonance data anal. 80−18206
odd nuclei states, Coriolis mixing, phonon admixture and non-adiabatic effects in even-even core 78−74310
odd p-shell nuclei, lowest positive parity state from projected HF theory 79−463
odd-odd fission products, level schemes, rot. bands, shell model states 80−78167
odd-odd nuclei, pn multiplets x=I(I+1) energy depend., parabolic rule, nuclear states 80−13379
odd-odd nuclei near A=50 statistical props. of low-lying 1^+ levels 77−6243
one-hole states, in double magic nuclei, form factors, spectroscopic factors, centroid energies 78−17090
nuclear energy levels continued
pairing correlation treatment, single particle levels, binding energy, spectra, branching ratios *(Chinese)* 80−102107
pairing properties and superconductivity, semiclassical treatment, local density approx. of nuclear gap 80−32188
particle-hole conjugation and protection theorems *(Chinese)* 80−73796
particle-hole states, microscopic self-consistent calc., ^{16}O levels 77−67713
pear-shaped nuclei, 3-D representation of pot. energy *(French)* 79−67645
perturbative approximations to Bloch-Horowitz effective Hamiltonian, energies, bounds, ^{18}O calcs. 78−70466
pf-shell nuclei, Hermitian operator method calcs., energy levels, transitions 78−54702
pole expansions for resonance functions, scatt. amplitudes and continuum states *(Russian)* 80−86871
p$\bar{p}$ atom, ground state energy displacement *(Russian)* 79−89813
pre-actinide nuclei, level density and fission probability collective effects *(Russian)* 80−13455
projection of wave functions on states with definite ang. momentum 78−12590
propagation by pairing and surface excitations, nuclear states description 78−46007
proton-neutron basis, decomposition matrix rel. to basis of specified isospin T 80−37337
quasi-elastic direct transfer reaction to continuum states, DWBA and diffraction model 80−18277
quasi-particle factorisation scheme, appl. to $1f_{7/2-}$ shell 79−80875
quasiparticle-phonon nuclear model, few quasiparticle components of nuclear states 79−13216
radiative strength distrib. with energy, E1, M1 giant resonances, particle-hole calcs. 80−37349
radionuclide decay, computer simulation, levels, transitions, internal conversion 80−63136
rare earth nuclei, modified oscillator pot. parameters, single particle levels 80−68509
rare earths, pairing energy, single particle levels and interaction matrix elements 78−8721
relativistic electron scattering, expt. techniques for excited nuclei studies 77−30701
rotating deformed nucleus, quasiparticle excitations *(Russian)* 79−26364
rotational, projected HF method appl. to 1-p shell odd-A nuclei 77−6207
rotational levels from α-nucl. folded pot. 77−67703
s-d shell nuclei, Coulomb energies, isomorphic model 77−50069
s-wave neutron reduced widths 77−22850
Sb, A=111, 3, 5, excited states anal. with Sn(p,2nγ)Sb 77−2911
sd shell nuclei, effective interaction between nucleons 78−17117
sd-shell levels, fixed-JT averaging method rel. to projected HF method 77−10345
sd-shell nuclei, ground-state alpha-cluster correl. 79−6402
sd-shell nuclei heavy-ion reaction resonances, low level density regions, shell model 80−57757
self-consistent field rearrangement in large nuclear deformations, HF calcs. 80−18184
self-consistent wave functions, oscillatory parameters *(Russian)* 78−21506
semiempirical nuclear level density formula with shell effects 78−82290
semileptonic weak and EM interactions, (e,e) P-vibrations and state abnormal P admixtures 79−75977
semimicroscopic description of nucl. states at low, intermediate and high excitation energies 78−54666
semiphenomenological model, unified description of reactions, states and transitions 79−75844
shape isomers, spontaneous fission, static and decay props. and excitations, review, book contrib. 78−82402
shell depend. level density formula 77−22849
shell model, globally self-consistent, magic nuclei and spherical nuclei calculations 79−59020
shell model calcs. A=24, mass, spectra and β decay 78−4903
shell model calculation techniques *(French)* 79−45188
shell model calculations, strong two body correls. 77−6259
shell model level densities in evaporation calculations 79−45241
shell structure, trend towards certain shapes 77−14026
short living nuclear states, optical orientation, γ-spectrum anisotropy, lifetime, moments *(Russian)* 80−63090
short-lived isotopes, laser spectroscopy in fast atomic beams and resonance cells 80−57700
single particle energies, by nonhermitian potential *(Chinese)* 79−93496
single particle energies of neutrons and protons, semiempirical formulas 78−78235
single particle levels, one boson exchange potentials, spin orbit splittings 79−9436
single particle levels, spin orbit splitting, 1 boson exchange pot. contribs. *(Russian)* 78−78243
single particle nuclear density struct., Hartree-Fock and model independent anal. *(Russian)* 79−80941
single particle orbitals, Coriolis attenuation problem, pairing plus recoil model 80−32159
single particle potentials, theorem *(Chinese)* 77−34201
single particle pots., Lehmann representation discrete and continuous energy spectra *(Chinese)* 80−102104
single particle realistic level schemes, nuclear shell correction energies, temp. smearing method 78−17118
single particle states, discrete expansions of continuum wave functions, convergence props. 80−57659
single particle states in 1f 2p shell, energy calcs. 78−25098
single particle width in nuclei, deviations of mass operator from HF values 78−62477
single-particle density, decomposition in time-even and time-odd parts 78−17074
single-particle energies from momentum-depend. pot. approximated by Morse function 77−6190
single-particle energy levels, shell-model anal. 78−17071
single-particle level density, excitation dependence of nuclear level density parameter 80−32149
single-particle states, eigenvalues near zero energy 77−67693
single-particle states in nuclear matter and in finite nuclei 80−78117
single-particle strengths of states, Green's function calc. 77−41875

nuclear energy levels continued
Skyrme-type interactions, spectroscopy of light nuclei, density dependent Hartree-Fock 80−22717
Sn Z=50 region isotopes, system struct calcs. 80−18192
spectral distrib. method for approximated level densities, validity in boson space 79−462
spectroscopic factors for single-nucleon transfer in A=21-44 region 77−46109
spectroscopy by continuation of polarisation observables into nonphysical region, nuclear struct. 78−78356
spherical even-even N or Z≈40, 0^+ anomalous state struct. 77−18397
spherical near magic nuclei, blocking effects on j=1/2 level 79−6363
spherical nuclei, fragmentation of hole states in quasiparticle-phonon model 80−83020
spherical nuclei, level density rel. to eqn. of state at subnuclear densities 80−77278
spherical nuclei, low lying states, effects of particle-particle channel residual interaction 78−12978
spherical nuclei, M1 transition strength distrib. at high excitation energies 79−75895
spherical nuclei, total binding energy, many body field theory, ^{16}O, ^{40}Ca, ^{58}Ni appls. 77−30482
spheroidal asymmetric oscillator pot., shell model calcs. 77−74779
spin, parity and spectroscopic factors of excited states populated in ^{24}Mg(d,p) 78−8826
spin orbit interaction of nucleons, relative motion dependent, universal coeffs. of hyperspherical function method 77−61354
stable odd-mass sd nuclei, EM multipole moments of ground states 80−102116
statically deformed nuclei, level spacing by statistical methods 79−45165
strength functions, shell model calc. 80−32187
SU_3 representation 80−42552
SU_6, dynamical symmetries, in nuclei, energy levels, transitions and collective states 78−74317
subshells, exact eqn. for binding energy *(Russian)* 77−71575
superfluid model, isotopic invariance and pairing energies 80−22687
superheavy nuclei, HF calcs. using Skyrme and finite range forces 77−46101
superheavy region, neutron drip line, energy density mass formula extrapolation 78−93932
superheavy region, spin-orbit pot. effect on single particle levels 79−59000
superheavy shell struct. in 250≤A≤500 mass region 77−22833
surface thickness of nuclear densities and single particle pots., self consistent study 79−85360
three particle level spectrum, Thomas theorem and Efimov effect, N/D eqns. 80−42562
total single particle energies, energy and N-averagings in shell correction method 80−22671
transition radiation in nucl. dispersive medium, nucl. levels and permittivity meas. *(Russian)* 77−59635
translational nuclei, ang. momentum projected quasiboson states 78−41637
translationally invariant effective interactions, factorisation 77−82833
transplutonium elements, excited quasiparticle states of odd mass deformed nuclei 77−26565
two-particle fractional parentage coeffs. in unitary scheme 77−41905
U(3(n-1)) scheme, translationally invariant wave function, proton-neutron states, electromag. transition operators 77−41906
unbound levels, reson. nucleon-nucleus scatt. 77−23005
UPEAK spectral decomposition routine 78−32798
warm nuclei, Thomas-Fermi model rel. to stellar collapse 80−51648
yrast traps, single particle calcs. for rare earth nuclei 77−88031
Z=114-126, nuclear stability reexamination using deformed Woods-Saxon pot. lifetimes level density 79−3094
Z=55-63, odd proton nuclei, low lying even parity states 80−27551
(d,p), reduced normalisations 78−86522
Δ(1236), virtual isobar admixtures in complex nuclei, OBE approx. 78−17107
(e,e′), transition strengths, unnatural parity state excitation of stretched configs., NN forces 79−63626
(γ,γ), 2.5-3.5 MeV, level photoexcitation 80−78193
(γ,p), >100 MeV, using monochromatic photons, leading to final nuclear states 80−22814
(n,2n) reactions at 14.8 MeV, isomeric ratios in 107<A<143 mass range 78−13073
(n,e$^-$) high precision spectroscopy, internal conversion coeffs. for nuclear struct. 80−37353
(n,γ), A=94-190, resonance capture, low lying level population fluctuations, γ-rays 80−52619
(n,γ), non-spherical even-even nuclei, energy gap from γ-transitions 80−47395
(n,γ) spectroscopy, nuclear struct. investigation, review 80−37379
(n,n), single particle bound state, energy independ. optical model, asymmetry term 80−37316
(n,n′γ), A=28-152, spherically doubly even nuclei, level excitation cross sections, statistical anal. *(Russian)* 79−67707
(N̄,X), complex shell model, narrow resonances and bound states *(Chinese)* 80−42622
NN̄ quasinuclear systems, review 78−25065
(p,2p), 1p shell nuclei, high lying one hole states *(Russian)* 79−59004
(p,d), 52 MeV, deeply bound hole state transition strength giant resonance, DWBA anal. 80−47426
(p,n), anomalous optical potential for sub-Coulomb barrier protons, 2 particle 1 hole states 80−105948
(p,p), single particle bound state, energy independ. optical model, asymmetry term 80−37316
(p,p) quasifree scatt., polarised p, nuclear state information 79−75846
(p,p′), ground state correlation, continuum spectra 78−94007
(p,p′), light and intermediate nuclei, analysing capacity, 2^+ state excitation 79−6558
(p,p′), single neutron states, two step process and effective interaction 80−78290
(p,p′), transition strengths, unnatural parity state excitation of stretched configs., NN forces 79−63626
(p,p′), unnatural parity states excitation, π-condensate instability effects, DWBA anal. 80−78168
pp̄ atom, nuclear energy level shift *(Russian)* 78−37295
(π^-,2n) struct. and reaction information, two hole states, direct mechanism 79−85496
(π,γ), inverse pion photoprod., level struct. determ. 80−22863
nuclear energy levels continued
(π,π′), particle-hole state excitation, field theory calcs. *(Russian)* 80−37318
($\pi^\pm$,$\pi^\pm$′), π^- nuclear response enhancement, continuum effects, stretched state isospin mixing 80−86929
(t,p) ground state cross section systematics in 2s-1d shell 80−5148
Tl(γ,γ), 4.5 MeV to neutron emission threshold, strengths in energy levels 79−36164
^{51}Mn levels studied via high resolution proton scatt. from ^{50}Cr 77−54151
^{134}Ba level scheme obs. from ^{134}La decay 77−10360
^{159}Tb, 58 keV level, nuclear reson. fluorescence 78−33121
^{207}(e,e′), transverse scatt. amplitude suppression, form factors, neutron hole states 80−91129
^{227}Ac levels and bands from ^{231}Pa α-decay 79−45217
^{230}Ac levels, J^π and transitions, Nilsson assignments from ^{230}Ra decay 80−68543
^{109,111}Ag, particle-vibr. multiplet excit. by two-neutron stripping 77−34214
Ag, A=109,111, proton hole states via ^{110,112}Cd(d,^{3}He) 50 MeV 77−18369
^{A}Ag, A=104, 106, levels, J^π, and isobaric analogue resonances from Pd(p,n) 80−32180
^{A}Ag, A=105-109, negative parity states, EM props. from particle-asymmetric rotor model 80−102097
^{A}Ag A=99, 101, 103, levels, transitions and J^π from Cd decay, Pd(p,2nγ) 80−47383
^{103}Ag levels and spectra from ^{103}Cd decay 79−22235
^{105}Ag, excited level struct. and transitions populated by decay of ^{105}Cd 79−97655
^{105}Ag, γ-transitions, level scheme via (p,nγ) reaction *(Russian)* 77−74801
^{105}Ag, high spin states γ-single spectra, γγ coincidence, excitation functions, ang. distrib., polarisation meas. 78−21519
^{105}Ag, high spin states populated in ^{103}Rh(α,2n) 77−22936
^{106}Ag low-lying excited states from ^{103}Rh(α,nγ) and ^{104}Pd(α,pnγ) 80−57693
^{108}Ag, form. in ^{107}Ag(n,γ) reaction, isomeric level scheme at 215.38 keV 78−12975
^{108}Ag levels and γ-transitions, population-spin correlation from ^{107}Ag(n,γ) 80−63097
^{108}Ag, low-lying states and state distrib. following ^{107}Ag(n,γ) 78−50084
^{108}Ag, populated in ^{108}Pd(p,nγ), level struct., spin and parity, isomeric state lifetimes and g-factors 77−18392
^{109}Ag levels from ^{109}Pd decay, spins, γ cascades, mixing ratios 77−22930
^{110}Ag 118.718 keV isomer, low lying states and transitions, coincidence study from ^{109}Ag(n,γ) 80−73806
^{110}Ag low lying states, decay scheme and $T_{1/2}$ from ^{109}Ag(n,γ) 80−47393
^{110}Ag low-lying levels from ^{109}Ag(n,γ) obs. 80−47422
^{110}Ag, populated in ^{110}Pd(p,nγ), level struct., spin and parity, isomeric state lifetimes and g-factors 77−18392
^{111}Ag, level struct. via ^{110}Pd(^{3}He,d)^{111}Ag 33.2 MeV 77−88045
Ag(p,f), 600 MeV, fragment energies, cross sections level density and barrier heights 80−42723
^{A}Al, A=25,26,27 levels, resonances, γ-ray branching ratios from Mg(p,γ) 80−86875
^{24}Al, 1^+ states anal. in ^{24}Mg(^{3}He,t)^{24}Al at 44 MeV 77−79390
^{24}Al, low-lying 1^+ state anal. in ^{24}Mg(^{3}He,t) 78−29484
^{26}Al 1^+T=0 states, isobaric analogue state, spin-isospin effective interaction from ^{26}Mg(p,n) 80−68553
^{26}Al, coherence widths, level density param. and effective moment of inertia 78−37360
^{26}Al excited states, isobaric analogues, spins, DWBA anal. of ^{27}Al(^{3}He,α) 80−105981
^{26}Al level anal. from ^{25}Mg(^{3}He,d)^{26}Al at 18 MeV 78−62554
^{26}Al long lived nucl. isomeric states, thermalization in stars 80−85846
^{26}Al T=1 states, resonances, J^π and transitions from ^{25}Mg(p,γ) 80−99131
^{26}Al^m, relative yield from ^{25}Mg(p,γ) reaction 79−101058
^{27}Al, absolute excitation energy meas. using electrostatic analyser 77−30741
^{27}Al bound state parity and spin assignments, level struct. from ^{26}Mg (p,γ) resonances 78−66206
^{27}Al, J^π=5/2 state, cross section and analysing power ang. distribs. 80−18296
^{27}Al, levels, GDR isospin mixing via (γ,p) 28 MeV 77−74832
^{27}Al levels, resonances, J^π, branching and mixing ratios from ^{26}Mg(p,γ) 80−99132
^{27}Al, proton hole states obs. via (e,e′p) 77−10389
^{27}Al, shape mixing using ang. momentum projection from Hartree-Fock intrinsic states 78−86472
^{27}Al(e,e′), 62 to 112 MeV, form factors, ^{27}Al energy spectrum, transition probabilities 77−34288
^{27}Al(e,e′), 70-340 MeV, odd parity state electroexcitation, form factors, transition probabs. 80−78208
^{28}Al, ang. correls. and branching ratios meas. using (^{3}He,pγ) at 11-15 MeV 78−13129
^{28}Al ground state doublet ang. distrib., direct charge exchange model anal. from ^{28}Si(^{18}O,^{18}F) 80−9307
^{28}Al, high spin states anal. in ^{27}Al(d,p) at 3.1 MeV 77−74856
^{28}Al levels, spins and γ-rays, multipole mixing from ^{27}Al(n,γ), pol. thermal 80−47398
^{28}Al levels, transitions and spin from ^{27}Al(n,γ), pol. Al and n 80−78153
^{28}Al, spectroscopic meas. in ^{30}Si(d,α) react. with polarised deuterons 78−41728
^{28}Al, spin-parity assignment, from ^{30}Si(d,α)^{28}Al at 8.12 MeV 77−6222
^{A}Am, A=240, 242, 244, energy levels from deuteron-induced neutron transfer 77−26578
^{32}Ar, high spin states from heavy-ion fusion evaporation reactions, decay schemes 77−2932
^{35}Ar levels, transitions and β-delayed protons from ^{35}K decay 80−91156
^{35}Ar lowest T=3/2 state excitation energy from ^{35}K decay, ^{35}Ar lowest T=3/2 state excitation energy 79−85407
^{36}Ar deduced levels from ^{36}K beta-delayed particle emission 80−83074
^{36}Ar, delayed proton and alpha emission, transition energies, levels, J^π, from ^{36}K decay 80−52629
^{36}Ar, mode-mode coupling model for four-body correl. 77−10322
^{36}Ar(^{6}Li,d)^{40}Ca, 0^+ levels of ^{40}Ca, DWBA calcs. with optical model parameters 78−62571

nuclear energy levels continued
^{38}Ar high spin states from ^{27}Al(^{14}N,2pn), decay scheme 78−25232
^{38}Ar levels, J$^{\pi}$ and transition strengths, DWBA anal. of ^{40}Ar(p,t) 80−47378
^{38}Ar, model independ. J$^{\pi}$ assignments from ^{24}Mg(^{16}O,2pγ) 77−18384
^{39}Ar, energy level spin and parity assignments, level spectroscopy from (α,nγ), (d,pγ) 78−93943
^{39}Ar low lying states from ^{37}Cl(α,d), spectra, ang. distribs., spins 78−25212
^{40}Ar, yrast levels, J$^{\pi}$, branching and mixing, via (^{16}O, 2pγ) 34 MeV 77−74759
^{40}Ar(α,α$_1$), 12-15 MeV, J$^{\pi}$ assignments for deduced levels 79−89232
Ar(e,e′), A=36, 40, 65 to 115 MeV, low lying level struct., lifetimes 78−8798
As isotopes, A=69, 71, 73, level scheme, cf. with Alaga model 77−22835
As isotopes, levels and spectra from broken pair model 80−73801
^{A}As, A=70, 72, level scheme, transitions, J$^{\pi}$ and lifetimes from Ge(p,nγ) 80−22695
^{A}As, A=71, 73, levels, J$^{\pi}$, transitions, T1/2 from Se decay, Ge(^{3}He,d), (p,xnγ) 80−57684
^{A}As, A=78,80,82, ground state mass meas. and excited state energies 79−63595
^{68}As β-decay, γ coincidence and singles spectra, spin, parity assignments, half-life meas. 77−79333
^{70}As, hyperfine struct. investig. using at. beam mag. reson. 77−22933
^{70}As states, excitation functions, spin and halflifes from ^{69}Ga(α,3n), ^{60}Ni(^{12}C,np), ^{63}Cu(^{10}B,2np) 79−6414
^{72}As, populated in ^{72}Ge(p,nγ), level scheme determ. 77−14032
^{73}As bound and isobaric analogue states, spectroscopic factors, DWBA anal. of ^{72}Ge(^{3}He,d) 79−54391
^{73}As, energy levels, meas. from ^{72}Ge(p,γ) 2213 keV 78−93939
^{74}As level structure, studied via ^{72}Ge(α,npγ), 30 to 50 MeV 77−10357
^{75}As, obs. of levels from (n,nγ) at 1.3-2.8 MeV 77−26611
^{75}As populated in ^{75}Se decay, E0 transitions 80−22752
^{75}As(n,n′γ)^{75}As, deexcitation gammas, energy levels, branching ratios, spins, parities, excitation function meas. 78−89869
^{76}As excited states, excitation functions and decays ang. distribs., cross sections from ^{76}Ge(p,nγ) *(Russian)* 80−63089
^{76}As, level structure, transitions and J$^{\pi}$, from ^{76}Ge(p,nγ) 80−47379
^{76}As, low-lying states via ^{75}As(d,p) at 11 MeV, spectroscopic factors, DWBA anal. 77−10319
^{78}As, level struct. determ. in ^{80}Se(d,α) at 16 MeV 78−8827
^{79}As levels, J$^{\pi}$ and ang. distribs. from ^{76}Ge(α,p) 80−78161
^{71,73}As, γ-spectroscopy of high-spin states via heavy-ion reactions 77−74795
^{207}At, g-factor of 25/2^{+} isomeric state, evidence for neutron excitation 78−70447
^{208}At energy levels and transitions, IC electrons from ^{208}Rn decay 80−18242
^{209}At, gamma-ray spectra, produced by ^{209}Bi(^{3}He, 3nγ)^{209}At, 28 and 26 MeV 78−74377
^{209}At, γ-transition, multipolaritis, level scheme following ^{208}Rn decay 80−83072
^{209}At high spin states from ^{206}Pb(^{6}Li, 3nγ), γ meas., neutron hole influence 77−2934
^{210}At excited states, spins, parities and rate of population from ^{210} Rn decay 79−75917
^{212}At excitation functions and isomer ratios from ^{209}Bi(α,n) 80−83039
^{212}At, relative α-decay width and excited levels, nuclear field theory 80−47437
^{213}At levels, J$^{\pi}$, transitions and lifetimes from ^{208}Pb(^{7}Li,X) 80−68542
Au isotopes, A=184-197, β^{+}-decay, single particle and collective degrees of freedom 77−22956
Au isotopes, statistical anal. of level schemes 77−6230
Au levels from p stripping reactions on ^{194,196,198}Pt, high spin states 78−78398
Au, odd isotopes, pot. energy surfaces and quadrupole deformation parameters, deformed basis model 79−80867
Au, odd mass isotopes, h$_{9/2}$ intruder state 77−88024
Au odd-mass isotopes, 9/2^{-} level excitation energies, estimates 77−275
^{187}Au, high-spin states anal, h$_{9/2}$ and i$_{13/2}$ bands 78−25117
^{187}Au energy states from ^{187}Hg decay, parities γ-spectra, triaxial nuclear deform. *(French)* 78−33143
^{194}Au, isomeric states anal. conversion electron and γ-ray spectra from ^{194}Pt(p,n) and ^{195}Pt(p,2n) 77−71582
^{196}Au energy levels and Q-value from ^{197}Au(γ,n) 80−37329
^{198}Au level spin assignments from γ ang. distrib. and circular polarisation from ^{197}Au(n,γ) 80−52570
^{9}B, 17.11 MeV energy level of T=3/2 quadruplet from ^{6}Li(^{3}He,γ), ^{6}Li(^{3}He,p) 79−22193
^{9}B 17.637 MeV state form., α-α coincidence meas. from ^{6}Li(^{3}He,α)^{3}Li(GS), ^{9}B 17.637 MeV state form., α-α coincidence meas. 79−475
^{9}B complex system, excitation functions for 17.19 and 17.64 MeV levels from ^{6}Li+^{3}He 80−78188
^{9}B, energy levels anal. in ^{9}Be(p,pn)^{8}Be 78−21550
^{9}B, isospin forbidden nucleon decays of T=3/2 levels 77−6320
^{10}B, cluster effects, low-lying states determ. 77−6228
^{10}B, energy level struct., admixed wave functions, ground state quadrupole moment, deformability 77−50054
^{10}B, first four levels from ^{12}C(p,pd)^{10}B data at 58 MeV 79−6578
^{10}B levels, J$^{\pi}$, ^{12}C(p,^{3}He) at 51.9 MeV 77−30566
^{10}B levels, J$^{\pi}$ and ang. distribs. from ^{9}Be(^{3}He,d) 80−42546
^{10}B levels and differential cross sections PWBA and coupled channel anal. of (α, t) 80−102121
^{10}B spectroscopic factors, ^{9}Be(^{3}He,d) with 33 MeV polarised beam 77−328
^{10}B T=1 states, γ-transition strengths, lifetimes, branching and mixing ratios from ^{6}Li(α,α) 80−27594
^{10}B transitions and levels from ^{11}B(γ,nγ^{1}) *(Russian)* 80−13433
^{11}B, 5/2^{-} level from ^{10}B(n,αγ)^{7}Li, 5 to 700 keV 78−89866
^{11}B, 2α+t model, parity states, shell and cluster structs. 78−50110
^{11}B (e,e′) 120-250 MeV, excited state form factors, shell and diagram model anal. *(Russian)* 79−40852
^{11}B, absolute excitation energy meas. using electrostatic analyser 77−30741
^{11}B, energy levels, using ^{10}B(p,π^{+}) 163 to 186 MeV 79−59061
^{11}B, excited states parameters from ^{7}Li(α,α)^{7}Li expt. *(French)* 79−93637
^{11}B, projected HF calc. in intermediate coupling 77−18460
nuclear energy levels continued
^{11}B, radiative widths meas., 2.125 to 8.92 MeV levels, intensity calibration of photon spectrum 79−13242
^{11}B states, spectroscopic factors from DWBA anal. of ^{12}C(p,2p) 80−5057
^{11}B, struct. study of 2α+t system in orthogonality condition model, level energies and parity 80−5080
^{11}B, studied via ^{10}B(d,p)^{11}B, 1 to 2 MeV, ang. distribs., reduction factor, spectroscopic factors 77−41977
^{11}B(e,e′), E1 transitions to unnatural parity states 80−22758
^{12}B, hyperfine interactions in Mg, decoupling by external mag. field 77−24756
^{12}B levels, J$^{\pi}$ and diff. cross sections, R-matrix anal. of ^{11}B(n,n) 80−78151
^{12}B state excitation energies and widths, DWBA ang. distribs. from ^{10}B(t,p) 23 MeV 78−70544
^{13}B state excitation energies and widths, DWBA ang. distribs. from ^{11}B(t,p), 23 MeV 78−70544
^{14}B, mass excess and excited states from ^{14}C(^{14}C,^{14}B) 80−42676
Ba isotopes, ang. momentum projected quasiboson states 78−41637
Ba, neutron rich nuclei from N=82, energy level systematics 77−22896
^{A}Ba, A=130, 132, 134, 136, levels and EM props., ang. momentum projected quasiboson model 80−5067
^{A}Ba, A=132, 134, 136, negative parity states, J$^{\pi}$, transitions, DWBA anal. of Ba(p, t) 80−86810
^{A}Ba, A=142,144,146, transition γ-γ ang. correlations, levels, J$^{\pi}$, mixing ratios 80−73823
^{A}Ba(^{32}S,^{32}S′), A=130, 132, 134, 136, 72-80 MeV, 2$_1^{+}$ state mag. moments 80−47373
^{127}Ba high spin level structure studied via ^{118}Sn(^{12}C,3n)^{127}Ba 77−38226
^{128}Ba, level scheme, near instability against γ-deformation via ^{128}La decay 77−82806
^{129}Ba, excitation and props. of high-spin levels using ^{120}Sn(^{12}C,3nγ) 78−17104
^{130}Ba, Wilets-Jean Hamiltonian for energy levels, transitions, moment, etc. 79−9457
^{139}Ba level scheme, J$^{\pi}$ and γ-transitions from ^{139}Cs β-decay 80−42590
^{142}Ba, γγ ang. correlations, levels, spins and mixing ratios from ^{142}Cs decay 80−57734
^{143}Ba, nuclear spectroscopy of neutron rich A=143 nuclei 79−59039
^{6}Be, levels and parentage via (p,pn) 47 MeV reactions 77−50132
^{7}Be effective for charge exchange analogues of Gamow-Teller transitions from ^{7}Li(p,n) 80−57726
^{7}Be excited state from ^{4}He(^{3}He,^{3}He) polarised scatt. study 78−46078
^{8}Be 1^{+} and 1^{-} levels, expt. and shell model calcs. from ^{7}Li(p,γ$_0$) 80−63095
^{8}Be, 2^{-} threshold states 77−54150
^{8}Be, α-particle and Sp(2,R) model connection 77−65207
^{8}Be, energy levels deduced from ^{6}Li(^{6}Li,αα)α reaction mechanism 80−83113
^{8}Be, highly excited αα* states from ^{7}Li+p and ^{6}Li+d 78−78262
^{8}Be isospin mixed 2^{+} doublet, level parameters from ^{4}He(α,α) 80−27556
^{8}Be, isospin mixing of states near 17 MeV, from ^{9}Be(d,t)^{8}Be and ^{9}Be(d,^{3}He)^{8}Li 77−65198
^{8}Be level energies, Brink's model with single-particle functions with realistic behaviour *(Russian)* 77−74785
^{8}Be, level feeding via β and γ transitions, role of spatial quantum numbers 77−67723
^{8}Be low lying states, Sp(2, R) model with generator coordinate method 79−45169
^{8}Be lowest negative parity state, shell and cluster model calcs. from ^{7}Li(p,p), ^{8}Be lowest negative parity state, shell and cluster model calcs. 80−18205
^{8}Be, mixed T=0 and 1 states, isospin mixing matrix elements 78−37289
^{8}Be, obs. of 2^{+} state from ^{8}Li(β)^{8}Be(α)α 78−93938
^{8}Be, quasi-mol. struct. model observed from α-α scatt. 79−6397
^{8}Be, reson. level, J$^{\pi}$, via ^{7}Li (p,γ)^{8}Be 380 to 960 keV 77−88131
^{8}Be spectroscopic factors, ^{9}Be(^{3}He,α) with 33 MeV polarised beam 77−328
^{9}Be, 2s$_{1/2}$ state obs. in ^{10}B(t, α) 80−22691
^{9}Be, HF and GCM calc. in α-cluster molecular model, ground state props. 77−54137
^{9}Be, isospin forbidden nucleon decays of T=3/2 levels 77−6320
^{9}Be low lying spectrum, 3-body molecular description, adiabatic one level approx. 80−78150
^{9}Be, n+α+α cluster model 79−6452
^{9}Be, positive parity excited energy levels, three well cluster shell model study *(Chinese)* 79−93518
^{9}Be quasibound states, refined resonating group calc. 77−2907
^{9}Be, three body molecular calc. of low-lying spectrum 79−93534
^{9}Be$_{\Lambda}$, hypernuclear excited states in 1p shell *(Chinese)* 78−82306
^{9}Be(α, α′), 65 MeV, levels and differential cross sections, optical anal. 80−102121
^{9}Be(e,e′p), single hole state momentum and energy distribs. 80−22674
^{9}Be(γ,π), photoabsorption and sum rules, structure, RMS radius, polarisability and exchange parameters 80−22686
^{9}Be(n,2n) pseudolevel eval. validation 80−22697
^{9}Be(p,pn)^{8}Be, 10-24 MeV, cross section, reaction mechanism, ^{9}Be level excitation 79−22284
^{9}Be(p,pn)^{8}Be, kinematically complete exam. of ^{9}B and ^{9}Be levels 78−21550
^{10}Be levels and differential cross sections DWBA and coupled channel anal. of (α, ^{3}He) 80−102121
^{10}Be near threshold state from ^{7}Li(t,^{9}Li) *(Russian)* 80−13484
^{11}Be single neutron strength, levels, spin assignments, spectroscopic factors from ^{10}Be(d,p) 79−36156
^{11}Be state excitation energies and widths, DWBA ang. distribs. from ^{9}Be(t,p) 23 MeV 78−70544
^{12}Be core excited T=2 levels, spin, half life from ^{10}Be(t,p), 12 MeV 78−66210
^{12}Be mass excess and excited states from ^{10}Be(t,p) 79−22183
$^{}_{\Lambda}$^{9}Be, excited states and spectra, continuum effects calcs. 80−57720
Bi, A=206, 208, 211, two-particle states anal. 77−38289
^{203}Bi high spin states from ^{203}Tl(α,4n), lifetimes meas. 78−29485
^{204}Bi excited states, γ rays, conversion electrons and γγ coincidences from ^{204}Po, EC 80−18241
^{205}Bi high spin states populated in Tl(α,xn), yrast states, isomers 77−30616
^{206}Bi, high-spin states anal. from ^{205}Tl(α,3n) 78−82368
^{208}Bi, influence of nucl. polarisation on level props. 78−54686

nuclear energy levels continued
^{208}Bi two-particle, two-hole configuration, levels, J^{π} and excitation energies from $^{210}Bi^{m}$(p,t) 80−32190
^{209}Bi, effect of pairing modes in multiplet struct. 78−12973
^{209}Bi energy and transition probability convergence in Dyson's boson expansion 80−78206
^{209}Bi from ^{208}Bd(d,nγ), half life of 2442.8 keV lowest 2p 1h state 78−74331
^{209}Bi, levels, ground state widths via reson. fluoresc. 77−74799
^{209}Bi levels and spectroscopic factors, ^{210}Bi(9$^-$) parentage from $^{210}Bi^{m}$(d,t) 80−78158
^{209}Bi low lying levels and spectroscopic factors, EFR-DWBA anal. of ^{208}Pb(^{7}Li, ^{6}He) 80−32182
^{209}Bi single particle levels, ang. distribs., spectroscopic factors, DWBA anal. of ^{208}Pb(^{7}Li,^{6}Me) 80−63067
^{209}Bi, single particle state mag. moment in large shell model space 79−45162
^{209}Bi(γ,γ'), 7.28, 7.63 MeV, energy levels anal. 78−13058
^{209}Bi(γ,γ), 4.5 MeV to neutron emission threshold, strengths in energy levels 79−36164
^{210}Bi, influence of nucl. polarisation on level props. 78−54686
^{211}Bi, 410 keV state single particle component determ. from DWBA anal. of (α,p) reacts. 77−88034
^{211}Bi levels, spin assignments and spectroscopic strengths from $^{210}Bi^{m}$(d,p), 20 MeV 79−6418
^{212}Bi, isomeric states from α-activities 78−82282
^{247}Bk, proton orbital 1/2$^-$[521] obs., stability of superheavy elements 77−67698
^{247}Bk proton states, transitions and spectroscopic factors from (α,t), α-decay, electron capture 79−89224
^{251}Bk level structure from ^{251}Cm beta decay 79−36200
Br, A=80,2, energy levels anal. from Se(p,nγ) 77−71609
^{75}Br, first 9/2$^+$ state and prolate deform. from ^{75}As(α,4nγ) 78−50088
^{76}Br level structure studied via the ^{75}AS(α, 3nγ) reaction, 30 to 55 MeV 77−54174
^{76}Br populated by ^{76}Se(p,nγ), level scheme 78−50091
$^{76}Br^{M}$ decay props., half life and γ-transitions, level scheme 80−83071
^{77}Br, level struct., l-transfers, spectroscopic factors, DWBA anal. from ^{76}Se(^{3}He,d), 41 MeV 78−86479
^{77}Br, low energy states from ^{77}Se(p,nγ)^{77}Br reaction 79−6407
^{78}Br level struct. determ. from (α,nγ), (^{3}He,d) and (p,d) reacts. 79−59010
^{79}Br, level struct., l-transfers, spectroscopic factors, DWBA anal. from ^{78}Se(^{3}He,d), 41 MeV 78−86479
^{80}Br level struct. and transitions, DWBA anal. spectroscopic factors from ^{81}Br(p,d), 22.8 MeV 79−3084
^{80}Br, level struct. determ. from thermal (n,γ) meas. 78−41667
^{80}Br, study of excited states from ^{79}Br(n,γ) and ^{80}Se(p,nγ) *(French)* 78−29393
^{82}Br, level struct. determ. from thermal (n,γ) meas. 78−41667
^{82}Br, study of excited states from ^{81}Br(n,γ) and ^{82}Se(p,nγ) *(French)* 78−29393
^{83}Br, levels assignment, ^{83m}Se decay scheme obs. 78−17147
C_{Λ}, A=12,13, hypernuclear excited states in 1p shell *(Chinese)* 78−82306
CC ^{168}Er high intrinsic excitation levels, γ-decay props. from ^{167}Er(n,γ) 80−52588
CC Rb cross sections and decay props. from ^{85}Rb(γ,n), ^{85}Rb(n,2n) 79−49600
C(^{16,17}O,^{16,17}O), two centre shell model, molecular single particle states at level crossings 80−47354
^{A}C(p,p), A=12, 13, 0.8 GeV, elastic and inelastic, ang. distribs., states, optical and DWBA anal. 79−3154
^{A}C(p,π$^{\pm}$), A=12,13, 200 MeV, analogue and nonanalogue state cross sections 80−99130
^{A}C(π,π'), A=12, 13, ~180 MeV, isospin mixing, levels, excitation functions and ang. distribs. 80−42543
^{10}C levels, spin and parity, ^{12}C(p,t) and ^{12}C(p,^{3}He) comparative study 77−30566
^{10}C low lying level ang. distribs., zero range DWBA anal. from ^{12}C(p,t) 79−67656
^{10}C, T=2 state total width and first excited state excitation energy 78−66211
^{11}C levels and resonance, γ-ray excitation curves from (p,αγ), (p,pγ) 80−9280
^{11}C negative parity states lifetime limits and transition strengths from ^{10}B(p,γ) 80−5092
^{11}C spectroscopic factors, ^{12}C(^{3}He,α) with 33 MeV polarised beam 77−328
^{11}C/^{11}B, mirror level pair cross sections from ^{12}C(π$^{\pm}$,πN) 79−67665
^{12}C, 17.77 and 18.36 MeV state struct., from ^{11}B(p,p) 1.9 to 3.0 MeV R-matrix study 79−9435
^{12}C, 19.25 MeV level spin assignment from ^{11}B(p,n)^{11}C, 3-49 MeV 78−93996
^{12}C 2$^+$ level, transverse EM form factor, convection current contrib. 80−63076
^{12}C, 3-α struct. in boson model 78−17124
^{12}C, absolute excitation energy meas. using electrostatic analyser 77−30741
^{12}C, α-particle model of ground and 0$^+$ excited states, hyperspherical method 77−6272
^{12}C deduced levels and spectroscopic factors, ang. distribs., DWBA anal. from ^{16}O(d,^{6}Li) 80 MeV 78−94013
^{12}C, Efimov state search using Ali-Bodmer α-α force and Faddeev technique 79−6420
^{12}C energy levels from (p,d) 80−42667
^{12}C, excited state struct., anomalous α-decay props. 3-cluster GCM model 79−6399
^{12}C, excited state struct., α-particle model 80−47385
^{12}C excited states, obs. in ^{10}B(d,3α) and ^{9}Be(^{3}He,3α) 77−18576
^{12}C, excited states ang. distrib. in ^{16}O(d,^{6}Li) 79−6624
^{12}C excited states between 29 and 34 MeV, obs. in ^{10}B(d,αα)α, and ^{9}Be(^{3}He,αα)α 78−21494
^{12}C ground state, dispersion anal. of ^{12}C+p forward scatt. 77−34297
^{12}C high lying continuum states populated by inelastic p and α scatt. 77−82925
^{12}C, isospin mixing of 1$^+$ states 78−4898
^{12}C J^{π}=0$^+$ isoscalar levels, α-particle model with group theoretical methods 77−74766
^{12}C, lowest T=2 state excitation energy from ^{14}C(p,t), 27.6 MeV 78−66211
nuclear energy levels continued
^{12}C, mixed T=0 and 1 states, isospin mixing matrix elements 78−37289
^{12}C, multipole elec. giant resons., anomalous parity isovector states, Coulomb excitation cross sections 79−9439
^{12}C negative parity states from ^{13}N isospin forbidden p decays in ^{11}B(^{3}He,np) 79−26372
^{12}C, positive-parity states, anomalous α-decay props. 78−62511
^{12}C, shell model proton transition densities from (e,e') data 79−93517
^{12}C, spin flip excitation of 1$^+$ T=0 state in (p,p') 78−8817
^{12}C struct. calcs. via 3α system resonating group method 78−531
^{12}C, struct. of excited states in 3-α model 77−65201
^{12}C structure, energy levels, binding energy, cluster model with varying hinge angle 78−4907
^{12}C, study of isospin mixing 77−18385
^{12}C, three alpha struct. in Faddeev formalism 77−14048
^{12}C, three α model calcs. and O_2^+ state 79−75856
^{12}C, three α-particle model calcs., Faddeev formalism, low lying states 77−18399
$^{12}C_{2+}$ m-state population in ^{64}Zn (^{12}C, $^{12}C_{2+}$*) 79−93521
^{12}C(^{12}C, ^{12}C)^{12}C*, 0_2^+, 3_1^-, 4_1^+ state excitation functions, resonance structures 80−42616
^{12}C(^{6}Li,d), ^{16}O level configuration mixing anal., α-spectroscopic strengths 79−6683
^{12}C(α,α'), generator coordinate multichannel calc., levels and resonances 80−78149
^{12}C(e,e') excitation of 2$^+$ T=1 state at 16.11 MeV, radiative width, magnetisation density 78−25176
^{12}C(e,e) , 12.71 and 15.11 MeV level struct. and isospin mixing from form factors 80−32186
^{12}C(n, X), compound resonance decay based on bound and metastable single nucleon states *(Russian)* 80−5107
^{12}C(ν,ν'), ($\bar{\nu}$,$\bar{\nu}$'), 15.11 MeV state excitation, cross sections, level decay 80−9258
^{12}C(p,p'), 1 GeV, proton polarisation in natural parity level excitation *(Russian)* 80−42634
^{12}C(p,p'), 122 MeV, level excitation, cross sections, effective NN interaction, DWIA anal. 80−78197
^{12}C(p,p'), 22-27 MeV, 1$^+$ state de-excitation γ-ray ang. distrib., tensor force effects, DWBA anal. 80−68580
^{12}C(p,p'), 800 MeV, 15.11 MeV state diff. cross section, nuclear critical opalescence search 80−105984
^{12}C(p,p'), pair decay of 7.65 MeV level meas. 78−29469
^{12}C(p,p'), pol. p, 800 MeV, unnatural parity states excitation, anal. powers and isospin 80−68538
^{12}C(p,p'γ), 23.5-27 MeV, 1$^+$ state spin flip meas. DWBA anal., cross sections 80−68529
^{12}C(π$^+$,π$^+$), 148 MeV, inelastic scatt., 15.1 MeV (1$^+$) state, differential cross section 78−89792
^{12}C(π$^{\pm}$,π$^{\pm}$'), 162 MeV, strongly isospin-mixed 79−93505
^{13}C, 1-20 ps region mean lifetime meas., high-vel. DSA method 77−65200
^{13}C, reson. struct. anal. from ^{13}C(γ,n$_0$)^{12}C 78−586
^{13}C(^{12}C,^{12}C), molecular neutron orbit formation, 1/2$^+$ state excitation, coupled channels calcs. 80−78156
^{13}C(γ,n), 7.6-24 MeV, photoneutron ang. distribs., level scheme and J^{π} assignments 80−466
^{13}C(π,π'), 162 MeV, pure n and p transitions, differential cross sections 80−5040
^{14}C, (sd)^2 positive-parity states, shell model calcs. 78−54674
^{14}C energy levels from ^{12}C(t,p), spins, parities 78−70542
^{14}C, energy states from ^{12}C(t,p) 23 MeV 78−78392
^{14}C first excited 0$^+$ state, lifetime and E^0 decay from (d,p), (^{13}C,p) 80−102145
^{14}C, populated by ^{12}C(t,p)^{14}C, spin and parity of states near 10 MeV excitation in ^{14}C 78−37263
^{14}C state excitation energies and widths, DWBA ang. distribs. from ^{12}C(t,p) 23 MeV 78−70544
^{14}C(e,e'), 37, 50.5, 60.5 MeV, 180° scatt. cross sections, excited states, spin parity 77−30557
^{15}C 0.74 MeV 5/2$^+$ state g-factor, shell model interpretation from ^{3}H(^{13}C,p) 80−32176
^{16}C, (sd)^2 positive-parity states, shell model calcs. 78−54674
^{16}C mass excess and final states, DWBA anal. of ^{14}C(t,p) 23 MeV 78−78392
^{16}C, spectroscopy with ^{14}C(t,p)^{16}C at 3.02-6.1 MeV 78−613
^{17}C populated in ^{48}Ca(^{18}O, ^{17}C), mass excess, low lying level struct. 78−8744
^{18}C mass excess and discrete nuclear states from ^{18}O(π$^-$,π$^+$) 79−13196
Ca, A=38, 40, 42, level props. from Ar(^{3}He,n) reacts. 77−65227
Ca isotopes, $f_{7/2}$ neutron occupancies 78−78240
Ca isotopes, neutron RMS radii from pion total cross-sections 77−57589
Ca, neutron densities from 1 GeV proton scatt. 78−17087
^{A}Ca (α,α') A=40, 44, nuclear level mag. moments, ^{40}Ca 2$_1^+$ level, ^{44}Ca 3$_1^-$ level 79−85368
^{A}Ca A=40, 48, charge density and single particle state struct. 79−36144
^{A}Ca, A=40, 48, neutron densities and single particle struct. 80−32165
^{A}Ca, A=40, 48, single particle levels, rms charge radius, Wood-Saxon pot. 80−63106
^{A}Ca, A=44,46 excited states and transition ang. distribs. from Ti(^{14}C,^{16}O) 80−95308
^{A}Ca, A=47, 49, single particle states lifetimes calcs. 80−105943
^{A}Ca(α,α'), A=40, 42, 44, 1.37 GeV, low lying state ang. distribs., Glauber rigid body approx. 79−54394
^{38}Ca, J^{π} and configuration mixing via ^{40}Ca(p,t)^{38}Ca 51.9 MeV 77−26684
^{39}Ca/^{39}K mirror level pair cross sections from ^{40}Ca(π$^{\pm}$,πN) 79−67665
^{40}Ca, ^{36}Ar+α model, energy levels, spin and parity 77−57602
^{40}Ca, ^{48}Ca RMS radii, RPA ground state correls., isotope effect 77−6238
^{40}Ca, 1$^-$, T=0 state at 6.95 MeV, isospin forbidden electroexcitation 78−25177
^{40}Ca, alpha transfer to 4p-4h states obs. in ^{36}Ar(^{6}Li,d) 78−21590
^{40}Ca α-spectroscopic factors, direct α-stripping, zero range DWBA anal. of ^{36}Ar(^{6}Li,d) 79−45157
^{40}Ca, energy levels, using ^{40}Ca(p,π$^+$) 163 to 186 MeV 79−59061
^{40}Ca, ground state energy and RMS charge radius 78−58242
^{40}Ca, proton hole states obs. via (e,e'p) 77−10389
^{40}Ca, shell model anal. of ground state energy 78−29389
^{40}Ca(^{9}Be,^{9}Be'), 45, 60 MeV, 1$^-$ state excitation Frahn scaling formula for cross section 80−102136

nuclear energy levels continued
^{40}Ca(d,d), 4.5-5.4 MeV, excited states, excitation functions and ang. distribs., statistical anal. 80−57686
^{40}Ca(e,e'), strong mag. dipole transition, coherent spin flip transitions, ground state correlations 79−71817
^{40}Ca(p,p')^{40}Ca, 185 MeV, scatt. from 3$^-$ and 5$^-$ states, DWIA anal. 77−18537
^{40}Ca(p,p'γ), 6.25 MeV, triple ang. correlation, 3$^-$ exit channel, resonances, single particle states 80−68626
^{41}Ca 1f$_{7/2}$ neutron radial distrib., single particle, orbits, RMS radii from ^{40}Ca(^{13}C,^{12}C) 80−42532
^{41}Ca, DWBA anal. of ^{9}Be elastic scatt. on various nuclei *(German)* 78−70552
^{41}Ca excited states, excitation functions and ang. distribs., statistical anal. from ^{40}Ca(d,p) 80−57686
^{41}Ca, high-spin positive parity states anal. with ^{38}Ar(α,nγ)^{41}Ca 77−38224
^{41}Ca parity doublet gamma lifetimes, 3/2 levels, parity mixing from ^{40}Ca(d,pγ) 80−78209
^{41}Ca, positive parity levels via ^{40}Ca(d,p)^{41}Ca with polarised deuterons 77−6402
^{41}Ca, two particle-one hole states, EM transition probabilities 77−88035
^{42}Ca 0$^+$ 4p-2h and 6p-4h configs. populated in ^{38}Ar(^{6}Li,d) 78−25220
^{42}Ca, extended Skyrme force versus realistic interactions, effective interactions 79−54395
^{42}Ca from ^{41}Ca(d,p), 11 MeV, cross section, vector analysing power, spectroscopic strengths 78−74374
^{42}Ca, high spin states from ^{39}K(α,p), lifetimes, multipole mixing ratios 78−50186
^{42}Ca high spin states from ^{28}Si(^{16}O,2pγ), γ meas. 78−89787
^{42}Ca, state calc. by shell model including 1g$_{9/2}$ orbit 79−80873
^{42}Ca, wavefunctions of O$^+$ states 78−74308
^{43}Ca, four-particle one-hole states anal. by ^{41}K(α,d) 78−21580
^{43}Ca high spin positive parity states, struct., from ^{40}Ar(α,nγ) 78−46025
^{44}Ca 3.59 MeV 0$^+$ state config. from ^{48}Ti(d,^{6}Li) 79−9472
^{44}Ca, mode-mode coupling model for four-body correl. 77−10322
^{45}Ca levels, excitation functions and J^π from ^{45}K β-decay 80−105978
^{45}Ca(f$_{7/2}$)$^{-3}$ configuration states via ^{48}Ca(^{3}He,^{6}He)^{45}Ca, 70 MeV 77−14034
^{47}Ca high spin states through double step processes, CCBA calcs. from ^{48}Ca(^{3}He,α) 78−89797
^{47}Ca, low-lying levels anal. in ^{48}Ca(d,t) reactions 78−13114
^{48}Ca(^{12,13}C,X), elastic, inelastic and single nucleon transfer excitation functions, ^{49}Ca levels 80−13492
^{49}Ca levels from ^{48}Ca(d,p), analysing power, cross section, spins, parities, spectroscopic factors 78−78391
Ca(p,p'), 19 MeV, nuclear struct. anal. 78−17197
cc ^{160}Tm doubly odd deformed nucleus, excited states and state lifetimes from ^{160}Yb decay 79−13209
cc ^{42}K levels and ang. distribs., spectroscopic factors, DWBA anal. from ^{41}K(d,p) 79−17806
Cd, A=104 and 105, populated in α+Pd reactions, high spin states 78−62484
Cd, A=105 to 109, parity assignments from (^{16}O,xnγ) obs. 78−41630
Cd, A=106-112, L,J,π via (^{3}He,n) 25.4 MeV reaction to 0$^+$ states 77−50050
Cd, even isotopes, effect of residual interaction in particle-particle channel on low-lying states 78−21503
^{1}Cd, A=113, 115 from $^{113, 115}$Ag β-decay 80−47432
^{A}Cd, A=104-116, low lying level scheme, mass excess from Cd(p,t) 80−73807
^{A}Cd(^{32}S,^{32}S'), A=106, 108, 110, 112, 114, 116, 72-80 MeV, 2$_1^+$ state mag. moments 80−47373
^{A}Cd(n,nγ) A=114,116, energy levels, spins, and gamma-ray multipole mixing ratios investig. 80−52580
^{103}Cd levels and spectra from ^{103}In decay 79−22235
^{106}Cd, high-spin states via γ-spectra populated in ^{104}Pd(α,2nγ) 77−30508
^{108}Cd levels from ^{96}Zr(^{16}O, 4nγ), γ meas., decay scheme, band struct. 78−66301
^{109}Cd, low lying level struct. via γ-γ correls. following ^{109}In decay 77−30509
^{110}Cd level scheme from ^{110}Ag^m *(French)* 78−58248
^{111}Cd, 1330 keV level excitation cross section from positron annihilation 80−68583
^{111}Cd^m, nuclear orientation in Zn and Be, 245 keV state quadrupole moment, half-life 80−37324
^{113}Cd, level scheme from ^{113}Ag 5.3 h β-decay 78−46028
^{114}Cd proton hole states populated in ^{115}In(d,^{3}He), DWBA anal. 78−8829
^{115}Cd, level scheme from ^{115}Ag 20 min decay 78−46029
^{122}Cd, struct. determ. from ^{122}Ag β-decay 78−66249
^{119g,m}Cd, decay schemes, half-lives, excited levels 77−296
Cd(n,n'γ), A=114,6, E=2.67 MeV, ang. distribs. meas., 3$^-$ octupole states anal. 77−38275
Cd(n,nγ), γ spectra and ang. distrib., ^{114,116}Cd energy levels, spins, particles 77−88070
Ce, A=136,137,138, high spin states and isomers obs. using in-beam γ-spectroscopy 78−82309
Ce, A=137, 139, high spin levels, γ spectra, hole-core coupling 77−50063
Ce, A=138,140, levels from (p,p'), (p,t) reactions, spin, parity, deform. parameters, enhancement factors 77−54217
Ce band structures populated in ^{116,118}Sn(^{16}O,3n), high spin levels, yrast cascade 78−8842
^{136}Ce, 10$^+$ isomeric states, systematic behaviour 79−30791
^{140}Ce+n, 20-240 keV total cross section, resonance multilevel shape anal., level spacings 79−3148
^{140}Ce(e,e'), giant dipole resonance, E1 form factor and breathing mode existence 79−3125
^{141}Ce levels, single neutron holes, spectroscopic factors, DWBA anal. of ^{142}Ce(d,t), (^{3}He,α) 79−85353
^{141}Ce, spin-parity assignments from ^{140}Ce(d,p)^{141}Ce 77−38283
^{143}Ce quasi-f$_{7/2}$ low lying states spectroscopic factors, cluster-vibr. model from ^{142}Ce(d,p) 80−47391
^{144}Ce level scheme determ. 77−22962
^{144}Ce levels from ^{144}La decay 80−13417
^{145}Ce, level schemes determ. from β-decay of A=145 nuclei 78−78323
Ce(d,^{6}Li), (A=140, 142), 35 MeV, ang. distrib. meas., deduced α-particle spectroscopic factors, reduced widths, decay lifetimes 77−18571
^{250}Cf E0 transitions and excited 0$^+$ states from ^{250}Es decay 79−45173
nuclear energy levels continued
^{250}Cf energy levels, bands and transitions from ^{250}Bk, β$^-$ decay 79−22205
^{250}Cf two-quasiparticle states populated by ^{250}Es^m EC decay 77−46140
Cl, A=35,36,37 high spin states from heavy-ion fusion evaporation reactions, decay schemes 77−2932
^{34}Cl high spin states 78−82289
^{34}Cl, J^π, levels, mixing ratios, T$_{1/2}$ via ^{33}S(p,γ) and ^{31}S(p,p) 1.0, 2.0 MeV 77−26613
^{34}Cl, levels Γ, γ-branching, T$_{1/2}$ via ^{33}S(p,γ) 1.0, 2.0 MeV *(French)* 77−26612
^{34}Cl negative parity high spin states, ang. distribs. and lifetimes from ^{31}P(α,n) 79−17812
^{34}Cl states populated in ^{32}S(^{3}He,p) at 18 MeV 77−88046
^{35}Cl, model independ. J^π assignments from ^{24}Mg(^{16}O,pαγ) 77−18384
^{36}Cl, 1-20 ps region mean lifetime meas., high-vel. DSA method 77−65200
^{36}Cl, spin and parity of 3723, 4294 and 5313 keV levels 77−88038
^{37}Cl high spin state decay, spin assignments, yrast level lifetime from ^{27}Al(^{19}F,2αp), ^{27}Al(^{12}C,2p), ^{34}S(α,p) 79−6490
^{39}Cl excited states and transitions from ^{39}S decay 80−42595
^{12}C low lying excited states, ang. distribs. from ^{12}C(K$^-$,π$^-$) 80−32226
^{242}Cm levels via ^{246}Cf α-decay *(Russian)* 77−82882
^{245}Cm, from ^{249}Cf α-decay, γ-spectra and internal conversion spectra 79−6477
^{249}Cm excited and single particle states, γ-transitions from ^{248}Cm(n,γ) 80−47399
Co, A=59,60, yrast decay scheme from ^{48}Ca+^{15}N(^{18}O) fusion-evaporation reactions 78−13154
Co isotopes, shell model 78−62479
^{A}Co, A=55,57,59,61, deduced levels, proton-hole states, semimicroscopic model from Ni(p,α) 79−45171
^{A}Co A=55,57,59,61, level direct and compound cross sections from ^{A}Ni(p,α), A=58,60,62,64 79−9474
^{54}Co deduced levels, J-depend., two-step processes from ^{54}Fe(^{3}He,t) 37.7 MeV 79−6412
^{55}Co, spectroscopic study via ^{54}Fe(^{3}He,d)^{55}Co and ^{54}Fe(τ,dp)^{54}Fe reactions 77−88029
^{56}Co, ang. correls. and branching ratios meas. using (^{3}He,pγ) at 11-15 MeV 78−13129
^{57}Co, levels anal. with ^{54}Fe(α,p) and ^{48}Ti(^{12}C,p2n) 77−46115
^{57}Co levels and analogue states, J^π from DWBA anal. of ^{58}Ni(^{3}He, α) 79−63592
^{57}Co state alignment, γ-transitions and ang. distribs. from ^{56}Fe(p,γ) 80−73797
^{58}Co 1$^+$ level population, shell model calcs., (t,^{3}He) and (e,e') comparison from ^{58}Fe(p,n) 79−9481
^{59}Co (n, n'γ), 1.3-3.9 MeV, energy level structure and decay scheme 79−45164
^{59}Co, energy levels, lifetimes, deexcitation following (n,n'γ) studies 80−83059
^{59}Co level energies, branching ratios lifetimes and spins from (p,p'),(α,pγ) 80−63093
^{59}Co, nucl. level densities, using single particle states for Woods-Saxon and Nilsson potentials 78−50086
^{59}Co(e,e), mag. elastic scatt., radial distrib. of 1f$_{7/2}$ proton orbit using cross sections 78−13067
^{59}Co(n,n'γ), 1.1-3.3 MeV, level inelastic scatt. cross section, decay γ-rays, spins, branching ratio 79−6605
^{60}Co, level struct., spectroscopic factors, DWBA anal. from ^{59}Co(d,p), 14 MeV 78−86478
^{60}Co low lying states from ^{57}Fe(α,pγ), spin constraints, γ mixing ratios 78−29487
^{60}Co low lying states struct., orbital ang. momentum, spectroscopic factors 78−29478
^{49}Cr energy levels, spins, parities, spectroscopic factors, from ^{50}Cr(τ,α) 78−33199
^{49}Cr ground analogue state fine struct., l=3 states differential cross section from ^{50}Cr(p,d) 80−63152
^{49}Cr levels, transitions, and Gamow-Teller matrix elements from ^{49}Mn, β$^+$-decay 80−57746
^{51}Cr, bands, levels, EM transitions, J^π, branching and mixing ratios from ^{48}Ti (γ,nγ)^{51}Cr and ^{51}V(p,nγ)^{51}Cr 80−52606
^{51}Cr level scheme, DWBA and optical model anal. from ^{52}Cr+^{13}C 79−36159
^{51}Cr, level struct. to E$_x$=8.1 MeV via ^{50}Cr(d,p) 77−50059
^{51}Cr levels, spectroscopic function and analogue states, PWBA anal. of ^{52}Cr(^{3}He,α) 80−68547
^{52}Cr, 1p5h config., high-spin neutron-hole states, EM transition rates 78−70430
^{52}Cr 4.75 MeV excited state from ^{50}V(α,d), 8$^+$ assignment 78−74380
^{52}Cr, γ-spectra, levels, J^π via α+^{50}Cr reaction 77−74794
^{52}Cr, level scheme determ. from ^{52}V γ-ray spectrum *(French)* 77−14066
^{52}Cr levels populated in decay of ^{52}V, ^{52}Mu^g and ^{52}Fe→^{52}Mn→^{52}Cr 78−21529
^{52}Cr studied via (α,2nγ), high spin states, shell model calcs. 78−54675
^{52}Cr(^{12,13}C,X), elastic, inelastic and single nucleon transfer excitation functions, ^{53}Cr levels 80−13492
^{52}Cr(γ,γ'), 35 MeV, 2$^+$ state deexcitation γ-rays, differential cross sections, deformation *(Russian)* 80−13406
^{53}Cr, excited negative parity states to 2322 keV via (p,p'γ) and (α,α'γ) 77−82851
^{53}Cr levels, J^π, γ-transitions and 1626 eV resonance from ^{52}Cr(n,γ) 80−42610
^{53}Cr low-lying level structure via ^{52}Cr(d,p) with 10 MeV polarised beam 77−18395
^{53}Cr, possible deformed 7/2$^-$ states with ΔJ=1 band 79−45170
^{54}Cr levels, transitions, T$_{1/2}$, J^π, shell model anal. from ^{51}V(α,pγ) 80−47381
^{54}Cr, proton-neutron correl., shell model for collective motion 77−79312
^{55}Cr deduced levels and spins, from ^{54}Cr(d$_{pol}$,p), cross section and vector analysing power 80−52684
^{56}Cr, γ-ray spectroscopy of low-lying states studied via ^{54}Cr(t,pγ) 77−10358
Cs, A=119, 121, 123, 125, deformed 9/2$^+$ proton hole states 78−41620
Cs, deformed nuclei, low-lying positive parity states 77−6240
^{A}Cs, A=119, 121, 123, 125, collective props. and level schemes from (^{10}B,p2n), (^{14}N,3n) (^{10}B,3n) 79−22171
^{A}Cs A=127, 129, 131, 133, high spin states and collective properties from (^{10}B, 3n), (α, 2n) (^{6}Li, 3n) 79−22170

nuclear energy levels continued
$^{\wedge}$Cs, A=142, 144, 146, low lying levels, J^{π}, mixing ratios and γ-γ ang. correlations 80−102119
^{129}Cs 11/2 isomer, g-factor and lifetime in CsI cubic environment from ^{127}I(α,2n) 79−6394
^{129}Cs, band struct., in-beam γ-ray spectroscopy after (γ,2n) reaction 78−4951
^{131}Cs, level struct. obs. from ^{131}Ba decay 77−10359
^{131}Cs populated in ^{131}Ba decay, E0 transitions 80−22752
^{133}Cs, populated in (n,n'γ) reaction, level scheme and deexcitation 78−13004
^{134}Cs 176.403 keV isomer, populating γ-rays, low lying levels from ^{133}Cs(n,γ), ^{134}Cs 176.403 keV isomer, populating γ-rays, low lying levels 80−78200
^{137}Cs excited levels from ^{137}Xe β decay, γ spectra, coincidences, branching, logft values 77−54186
^{139}Cs level scheme, J^{π} and γ-transitions from ^{139}Xe β-decay 80−42590
^{143}Cs, nuclear spectroscopy of neutron rich A=143 nuclei 79−59039
Cu, A=59,61,63,65, levels and spectroscopic strengths via Ni(τ,d)Cu 18 MeV, centroid energies 77−10303
Cu, A=64, 66, 68, 70, level schemes, mass excesses via (t,^{3}He) reactions 77−46117
$^{\wedge}$Cu A=29,63, Doppler shift attenuation factors, level lifetimes, resonances from Ni(p,γ) 80−57741
$^{\wedge}$Cu, A=61, 63, 65, nucl. level densities, using single particle states for Woods-Saxon and Nilsson potentials 78−50086
$^{\wedge}$Cu, A=65,67,68, energy levels, core coupling model calcs. 80−9238
^{58}Cu, ^{60}Cu, populated in Ni(π^+, π^0), deexcitation γ spectra 78−89912
^{59}Cu, reson. lifetime, J, via ^{58}Ni(p,γ) 1833 and 3547 keV 77−26621
^{60}Cu, ang. correls. and branching ratios meas. using (^{3}He,pγ) at 11-15 MeV 78−13129
^{60}Cu levels from ^{60}Ni(^{3}He,t) 78−46079
^{60}Cu spin states, shell model, 6^- and 9^+ states in odd odd Cu isotopes 78−74313
^{61}Cu γ-cascade multiplicities, entry state depend. on excitation energy from ^{58}Ni (α,pγ), 17 and 19.5 MeV 78−82311
^{62}Cu high spin states populated in ^{60}N+α, ^{63}Cu+p, ^{52}Cr+^{14}N, level scheme *(French)* 78−21496
^{63}Cu EM decay transitions, level J^{π} assignments, level lifetimes from (α,pγ), (^{11}B, 2pγ) 79−85402
^{63}Cu, level struct. from ^{63}Cu(p,p'γ) react. 78−78378
^{63}Cu, levels, J^{π} via ^{64}Zn(d,^{3}He) polarised d, 13 MeV 77−88100
^{63}Cu levels, transitions and ang. distribs. from α-transfer in ^{59}Co(^{6}Li,d) 80−73798
^{63}Cu levels and transition j-depend., DWBA anal. of ^{60}Ni(^{19}F, ^{16}O) 80−42542
^{63}Cu low excitation states, level struct. and lifetimes from ^{60}Ni(α,pγ) 80−86813
^{63}Cu, paradoxical octupole-multiplet pattern 78−41617
^{63}Cu state alignment, γ-transitions and ang. distribs. from ^{62}Ni(p,γ) 80−73797
^{63}Cu(p,p') negative parity level excitation, gamma ray obs., test for core excitation model 80−68534
^{64}Cu, γ-spectra, J^{π} assignments via ^{64}Ni(p,nγ) 2.75-3.75 MeV 77−18470
^{64}Cu levels and transitions, stat. anal. of ^{64}Ni(p, nγ) *(Russian)* 80−5104
^{65}Cu analogue $P_{1/2}$ resonance, γ-decay and energy levels from ^{64}Ni (p, γ) 79−80907
^{65}Cu levels and transitions, γ-strength function using average resonance capture from ^{64}Ni(p,γ) 80−13411
^{65}Cu, low-lying level struct. via (e,e') 120 MeV *(Russian)* 77−74838
^{65}Cu(p,p'γ), 5.25, 6.0 MeV, levels, transition energies, lifetimes, branching ratios determ. 77−41960
^{69}Cu mass excess and low lying states, DWBA anal. from ^{70}Zn(d,^{3}He) 79−6422
^{162,164}Dy, γ-mixing, J^{π} values, levels via (n,n'γ) reaction 77−74768
$^{\wedge}$Dy A=148, 149, deduced levels from ^{148,149}Ho β-decay 79−36166
$^{\wedge}$Dy, A=150, 151, 152, levels, J^{π} and transitions from Ho EC decay 79−89241
$^{\wedge}$Dy, A=152, 153, isomeric states and complex band structs. from Nd(^{12}C, xnγ), Gd(α, xnγ) 79−67624
$^{\wedge}$Dy, A=159,161, lifetimes of low excited states, delayed e-γ and $\gamma\gamma$ coincidences *(Russian)* 80−68596
^{148}Dy, p single particle states and pairing force calcs., high spin states 80−42522
^{148}Dy$_{82}$ 10^+ isomer, $\pi h_{11/2}$ effective E2 charge 78−93964
^{149}Dy, $27/2^-$ three-particle isomer on ^{146}Gd doubly closed shell nucleus 77−22895
^{151}Dy levels, bands and transitions, in-beam γ-rays from ^{142}Nd(^{12}C,3nγ) 80−458
^{152}Dy, yrast isomers, oblate shape, excitation energies, spin and parity 79−17795
^{153}Dy, populated in ^{153}Ho β-decay, lower excited states 80−22765
^{156}Dy, prompt transitions multipolarities, γ and conversion electron spectra, energy level bands, spin, parity 78−8768
^{157}Dy, decoupled bands, perturbative anal. level energies 78−41623
^{161}Dy, Nilsson bands, J^{π} via (d,p), (d,t) and (η,γ) 77−34215
^{162}Dy, level scheme, γ-branchings following ^{162}Tb decay 77−34246
^{162}Dy(n,n'γ), study of ^{162}Dy levels up to 2 MeV 77−6285
^{157}Er, ^{155}Er nucl. energy levels from obs. of ^{157}Tm, ^{155}Tm decay *(French)* 77−57630
^{157}Er, lifetimes of excited states, delayed e-γ coincidences *(Russian)* 80−68597
^{158}Er, high-spin yrast levels, second discontinuity obs. 77−61373
^{159}Er, decoupled bands, perturbative anal. level energies 78−41623
^{162}Er, energy levels determ. from ^{165}Ho(p,4nγ) obs. 77−61348
^{162}Er, microscopic calc. of high-spin rot. states 78−8730
^{163}Er, excited states populated in ^{163}Tm decay 78−17146
^{163}Er level struct., DWBA anal. of ang. distribs. from ^{166}Er(d,t) 79−30788
^{166}Er, 2-quasiparticle states obs. 80−18198
^{166}Er, level population by radioactive decay of ^{166}Ho *(French)* 78−545
^{166}Er, level population from ^{166}Tm decay 79−93556
^{166}Er(d,^{6}Li), 35 MeV, ang. distrib. meas., deduced α-particle spectroscopic factors, reduced widths, decay lifetimes 77−18571
^{167}Er level struct., DWBA anal. of ang. distribs. from ^{166}Er(d,p) 79−30788
^{167}Er levels and transitions, spectroscopic factor bombarding energy depend. from ^{168}Er(d,t), 9-15 MeV 79−495
^{168}Er, 80 and 1094 keV states, g-factors from ang. correlation methods 80−83035
nuclear energy levels continued
^{170}Er level struct. obs. in ^{170}Ho β^--decay 78−41675
^{172}Er levels, bands, J^{π} and transitions from ^{170}Er(t,p) 80−83038
^{251}Es level struct. and p states, level transitions from ^{250}Cf(α,t) and ^{251}Fm decay 78−78268
^{251}Es, proton orbital $1/2^-$[521] obs., stability of superheavy elements 77−67698
Eu, A=147, 149, 151, band struct. obs. via heavy-ion reactions 77−82855
Eu, A=149, 151, band struct. anal. with Sm(d,3nγ) at 18-25 MeV 77−41913
$^{\wedge}$Eu, A=145, 147, 149, mag. moments of $11/2^-$ states 79−40846
$^{\wedge}$Eu, A=153,155, single proton hole states in pickup reactions from (p,α) 80−78128
$^{\wedge}$Eu, A=157, 159, single proton states, rot. bands, J^{π} assignments and mass from Gd(t,α) 79−45132
^{144}Eu, multiplet splitting and isomerism, J, π, T1/2 via (d,2n) and (p,n) 77−14014
^{145}Eu level and transition effects on ^{145}Gd decay anomalies 80−32244
^{147}Eu populated in ^{147}Gd decay, γ-ray spectra obs. at small-source detector distance *(Russian)* 79−93520
^{149}Eu level structure populated in ^{150}Sm(p,2nγ), spin, parity 78−21561
^{149}Eu, proton states and transitions shell model anal. of ^{148}Sm(α,t) 79−30781
^{151}Eu, energy levels and coexistence of three shapes 77−79304
^{151}Eu level scheme from excitation functions, rotor and interacting boson anals. from ^{152}Sm(p,2nγ) 79−45163
^{151}Eu(^{16}O,^{16}O'γ), 25-42 MeV, energy levels, transitions, spin assignments determ. 77−38294
^{152}Eu 89.8488 keV isomeric state feeding, delayed coincidence meas., level scheme from ^{151}Eu(n,γ) 80−63126
^{152}Eu, level scheme, low energy transitions, reaction data, Nilsson model interpretation 78−66215
^{154}Eu, level scheme, populated by thermal neutron capture, conversion electron spectra 77−61374
^{154}Eu low lying levels, bands, transitions from ^{153}Eu(n,γ) 80−57694
^{155}Eu, single proton states, spins and parity, rot. bands from ^{156}Gd(t,α), ^{154}Sm(α,t) 79−30766
$^{\wedge}$F, A=18, 19, deduced levels and spectroscopic factors from ^{14,15}N(^{11}B,^{7}Li) 79−26454
^{15}F mass excess and T=3/2 levels from ^{20}Ne(^{3}He,^{8}Li) 78−78264
^{16}F levels populated in ^{19}F(^{3}He,^{6}He) and ^{16}O(^{3}He,t) 78−17231
^{17}F 14.174 MeV T=3/2 level, spin assignment from ^{16}O(p,p'), polarised p 79−67648
^{18}F 1.04 MeV state lifetime and γ-transition polarisation from ^{18}O(p,n) 80−106016
^{18}F, 5603 keV level, isospin mixing via (α,γ) and (p,γ) reactions 78−543
^{18}F compound nucleus in ^{16}O+d reactions, level characts. from vector analysing power 77−61434
^{18}F integrated cross sections to excited residual states from ^{19}F(γ,n) 80−18200
^{18}F isospin mixed states seen via ^{14}N(α,α_1)^{14}N, 7.6 to 16.9 MeV 77−14029
^{18}F, $J^{\pi}=5^+$ excited state, populated by ^{16}O(α,d)^{18}F, 28 to 33.6 MeV 78−58291
^{18}F level spin, isospin and parity assignments, from ^{20}Ne(d,α) tensor analysing power meas. 78−74305
^{18}F levels and resonances, cross sections in R-matrix formalism from ^{17}O(p,α) 80−18267
^{18}F, levels from ^{16}O(^{3}He,p) at 18 MeV 77−34325
^{18}F, semi-microscopic calc. of α-cluster states, shell model approx. 80−465
^{18}F, shell and cluster admixtures, T=0 positive parity levels, E2 rates 77−18396
^{18}F, trinucleon cluster states, low lying negative parity states 78−29387
^{19}F 5.10 MeV level parity from ^{17}O(^{3}He,p) 79−45155
^{19}F, energy levels from α-^{15}N and t-^{16}O coupled channel orthogonality condition model 80−37326
^{19}F, even parity excited states, collective props., EM moments, generator coordinate method 78−78259
^{19}F even-parity states, generator coord. method, projected Hartree-Fock, and complete diagonalisation calcs. comparison 78−89796
^{19}F final state selective population, triton clustering from band anal. from (^{7}Li,t), (^{6}Li,^{3}He) 80−9306
^{19}F level scheme, anal. using parity mixing 77−18387
^{19}F level struct., ang. distribs. anal. using DWBA of ^{17}O(^{3}He,p) 80−9232
^{19}F, level struct. J^{π}, spectroscopic factors via (^{13}C, ^{9}Be) reaction 77−14033
^{19}F level structure populated in ^{16}O(α,p), spin, parity *(Spanish)* 77−67756
^{19}F levels, resonances and phase shifts, resonating group calcs. from ^{15}N(α,α) 80−32189
^{19}F, levels, spectroscopic factors via ^{16}O(α,p)^{19}F 77−14140
^{19}F low lying positive parity states from rot. model, moments and deformation 79−6410
^{19}F, low-lying excited states calc. by generator coordinate method 78−12974
^{19}F, produced in ^{15}N(α,γ)^{19}F, 5.2 to 8.4 MeV, resonances and gamma decay schemes 78−37358
^{19}F, reson. levels from ^{15}N(α,γ)^{19}F, 2.8 to 4.0 MeV 77−65211
^{19}F, spectra and E1 transitions, ang. momentum projected HF and Tamm-Dancoff methods 77−54139
^{19}F, studied via ^{19}F(p,p'γ), 5 to 9 MeV 77−297
^{19}F, transition probabilities and multipole moments between states calc. by generator coordinate method 78−13022
^{19}F(p,p), 17.5 and 30 MeV, low lying level cross-sections, coupled-channel method 80−42649
^{20}F 2.97 MeV doublet γ-decay, J^{π} assignment from ^{11}B(^{13}C,$\alpha\gamma$) 79−6491
^{20}F, 4 to 6 MeV levels populated in ^{19}F(d,p) 78−25118
^{20}F, ang. correls. and branching ratios meas. using (^{3}He,pγ) at 11-15 MeV 78−13129
^{20}F energy levels populated in ^{14}N(^{7}Li,p), spin, parity 78−21596
^{20}F excited states from ^{16}O(^{7}Li,^{3}He), energies, spins 78−82369
^{20}F states up to 7 MeV excitation, studied via ^{22}Ne(d,α)^{20}F 77−10414
Fe, A=59,60, yrast decay scheme from ^{48}Ca+^{15}N(^{18}O) fusion-evaporation reaction 78−13154
Fe isotopes A=53-58, spectroscopic calcs. using mass independ. effective interaction, yrast levels 78−41638

nuclear energy levels continued
A Fe, A=54-56, high spin states, energy levels, spectroscopic factors, EM props., shell model 80−47359
A Fe, A=57, 59, levels, J^π and transition branching ratio from Fe(n,γ) 80−105976
A Fe(n,γ), A=54,56,58, resonance capture, ^{55,57,59}Fe level schemes 79−547
^{52}Fe, γ-spectra, levels, J^π via α+^{50}Cr reaction 77−74794
^{52}Fe levels, J^π, via ^{54}Fe(p,t)^{52}Fe 52 MeV reaction 77−50058
^{52}Fe levels from ^{54}Fe(p,t), ang. distrib., spin, parity, $f_{7/2}$ shell model 78−74362
^{52}Fe low lying level ang. distribs., zero range DWBA anal. from ^{54}Fe(p,t) 79−67656
^{52}Fe, low-lying excited states, ^{50}Cr(^{3}He,nγ)^{52}Fe reaction 78−4952
^{53}Fe, levels, J^π, populated via (τ,α) 18 MeV 77−74767
^{54}Fe, studied via (α,2nγ), high spin states, shell model calcs. 78−54675
^{54}Fe(^{12,13}C,X), elastic, inelastic and single nucleon transfer excitation functions, ^{53}Fe levels 80−13492
^{54}Fe(p,d)^{53}Fe, 40 MeV spectroscopic factors, ang. distrib., DWBA anal. 79−22287
^{54}Fe(p,p′), testing self consistent models of collective and single particle struct. 78−82300
^{55}Fe deduced levels, from ^{54}Fe(d_{pol},p), cross section and vector analysing power 80−52684
^{55}Fe levels, J^π, spectroscopic factors, DWBA anal. of ^{56}Fe(^{3}He,α) 80−99127
^{55}Fe, possible deformed $7/2^-$ states with ΔJ=1 band 79−45170
^{55}Fe resonances, levels, J^π, valence capture γ-ray spectrum from ^{54}Fe(n,γ) 80−86852
^{56}Fe, absolute excitation energy meas. using electrostatic analyser 77−30741
^{56}Fe, level struct. via (^{12}C,α2p), (α,2p) and (α,α) reactions 77−67702
^{56}Fe low lying levels, J^π, γ-γ coincidences, internal conversion from ^{56}Co β^+-decay 80−86815
^{56}Fe, nucl. level densities, using single particle states for Woods-Saxon and Nilsson potentials 78−50086
^{56}Fe, proton-neutron correl., shell model for collective motions 77−79312
^{56}Fe, semi-microscopic calc. of levels, spectroscopic factors and EM props. 77−2912
^{56}Fe(n, n), up to 1 MeV, cross section by coupled channels method, simple vibrational model 78−70535
^{56}Fe(n,n′γ), 1.57-2.8 MeV, low levels excitation *(Russian)* 78−41722
^{56}Fe(n,n′γ), up to 14.6 MeV, radiation and neutron widths for highly excited levels *(Russian)* 78−605
^{56}Fe(n,n), 14.6 MeV, radiation widths and particle widths of highly excited states, γ-transitions 79−6409
^{57}Fe, semi-microscopic calc. of levels, spectroscopic factors and EM props. 77−2912
^{57}Fe(p,p′)^{57}Fe*, excited $5/2^-$ state mag. moment 79−93512
^{58}Fe levels, J^π, anal. powers and cross sections from ^{56}Fe(t,p) pol.t 80−68539
^{58}Fe(n,n), 0.03-500 keV, total cross section, resonance parameters and level spacings 79−6603
^{59}Fe deduced levels and spins, from ^{58}Fe(d_{pol},p), cross section and vector analysing power 80−52684
^{59}Fe, spin assignments to p-wave neutron states 77−22852
^{60}Fe, level struct., spin and parity assignments, mass excess from ^{58}Fe(t,p) 17 MeV 78−82288
^{60}Fe struct. and new level from ^{60}Mn decay, mass excess 78−78317
^{68}Fe low lying state mean lifetimes and transitions from ^{64}Zn(^{7}Li,p2n) 80−68599
from ^{16}O(d,α_3), J^π assignments 79−3160
Ga, odd, single particle and collective degrees of feedom, clustering, shell model anal. 80−68510
A Ga, A=67 to 69, energy spectra, shell model calc. 79−17818
A Ga, A=69, 71, spectroscopic factors, occupation number anomalies from Ge(d,He) 26 MeV 78−82279
A Ga, A=71,73, levels, ang. distribs., spin assignments and deformation transition from Ga(t,p) 79−54392
A Ga, A=73, 75, deduced levels, occupation number anomalies, spectroscopic factors from Ge(d,^{3}He) 26 MeV 78−82279
^{65}Ga, 1.286 MeV state spin 9/2 determ. from ^{64,66}Zn(p,γ) obs. 79−63663
^{65}Ga, spin assignments of levels by forward-angle j dependence 78−93935
^{66}Ga high spin states, shell model interpretation from ^{64}Zn(α,pnγ) and ^{63}Cu(α,nγ) *(French)* 79−3086
^{67}Ga, high spin states, using ^{57}Fe(^{12}C,pnγ) at 40 MeV 79−36128
^{67}Ga, levels, branching, mixing, $T_{1/2}$, via ^{67}Zn(p,nγ) 3.6-4.3 MeV 77−34247
^{67}Ga levels below 2.5 MeV populated in ^{64}Zn(α,pγ) 77−88042
^{68}Ga, spectroscopy with ^{69}Ga(d,t) and ^{70}Ge(d,α), DWBA 77−57603
^{69}Ga state alignment, γ-transitions and ang. distribs. from ^{68}Zn(p,γ) 80−73797
^{69}Ga(n,n′γ), fast n, levels, J^π, transitions and mixing ratios, statistical anal. *(Russian)* 80−13382
^{69}Ga(p,p′γ), 3.0-5.1 MeV, low lying state struct., lifetimes, spin and parity 79−467
^{70}Ga, high spin levels via ^{68}Zn(α,pnγ)^{70}Ga 77−30611
^{71}Ga ang. correlations, level spin assignments and multipole mixing ratios from ^{71}Zn^m decay 78−78305
^{73}Ga, levels, J^π and ang. distribs. from ^{70}Zn(α,p) 80−78161
Gd even nuclei, A=152-160, dynamic deform. theory, level energies B(E2) values 78−89795
A Gd, A=146.7, particle hole yrast states and Z=64 shell closure from Sm (α, xn) 79−49571
A Gd A=152, 154, negative parity states and β-γ-γ correlations from Eu β-decay 79−97676
A Gd(n,γ), A=154,156-8, 2, 24 keV, resonance averaged γ-spectra, level and J^π appls. 80−37347
^{142}Gd, populated in (α,6n), ground state bands obs. 77−2938
^{144}Gd level scheme, delayed transitions, in-beam study from ^{144}Sm(α,4nγ) 79−17809
^{145}Gd levels, J^π and transitions, neutron hole coupling to ^{146}Gd core from ^{144}Sm(α,3n) 80−78164
^{146}Gd, 1579 keV state, assignment of isospin and parity, using γ-ray ang. distrib. 78−21489
^{146}Gd, 3^- 1579 keV first excited state 78−41670
^{146}Gd, excitation energy of lowest 2^+, 3^- levels, energy density method 79−3088
^{146}Gd lowest 2^+ state, J^π and transitions from ^{146}Tb decay 80−105979
nuclear energy levels continued
^{146}Gd, mag. moments of isomeric states 79−40847
^{146}Gd, O_2^+ state EM decay, $T_{1/2}$ and monopole strength 80−95310
^{146}Gd, p single particle states and pairing force calcs., high spin states 80−42522
^{149}Gd level scheme and transitions from ^{149}Tb^g electron capture 79−9477
^{150}Gd levels and transitions, J^π assignments mixing ratio, nuclear orientation from ^{150}Tb decay 79−13205
^{150}Gd, vibr. levels anal. from ^{150}Tb decay 78−8772
^{151}Gd excited state spin assignments γ-γ ang. correlations from ^{151}Tb decay *(Russian)* 79−49597
^{153}Gd γ-directional distrib., levels, spin assignments from ^{153}Tb decay 79−13241
^{153}Gd levels and γ-ray spectra from ^{152}Gd(n, γ) 80−57736
^{154}Gd levels, bands, J^π, DWBA anal. of ^{152}Gd(t,p) 80−78110
^{155}Gd, vibr. state, level scheme, γ and conversion electron spectra from ^{154}Gd(n,γ) 80−57696
^{156}Gd transitions from second $K^\pi=0^+$ band following ^{156}Eu decay, branching, mixing ratios 78−25150
Ge, even-even nuclei, γ-spectroscopy, exptl. results and models 80−68589
Ge excited states from ^{72,74,76}Ge(p,t), spins, parities 78−25194
Ge, odd, single particle and collective degrees of feedom, clustering, shell model anal. 80−68510
A Ge, A=68, 70,72,74, level excitation, n-p interaction role from α-transfer in Zn(^{6}Li,d) 80−73821
A Ge, A=68 to 70, energy spectra, shell model calc. 79−17818
A Ge, A=70, 72, 74, appl. of crystal blocking technique to study highly excited nuclear continuum using (p,p′) 79−45261
A Ge, A=72, 74, 0_2^+ levels, struct. transition between N=40 and 42 from Ga(α,p) 80−73800
A Ge, A=72,74,76,78, ang. distribs., levels and spin assignments, deformation transition from Ge(t,p) 79−54390
A Ge(d,d) 16 MeV, A=70-74, polarised d, elastic and inelastic, levels and deformation 79−554
^{66}Ge levels, lifetimes, J^π and transitions from ^{58}Ni(^{10}B,pnγ) 80−73799
^{66}Ge levels, lifetimes and mixing ratio, in-beam γ-spectroscopy from ^{54}Fe(^{14}N,npγ) 80−42541
^{66}Ge states and decay scheme, polarisations J^π and ang. distribs. from ^{58}Ni(^{10}B,pnγ) 80−22692
^{67}Ge, mass excess and low lying states, comparison with ^{63,65}Ni, ^{65,67}Zn and ^{69}Ge, from ^{65}Zn(α,nγ) 78−66213
^{68}Ge, energy levels populated in ^{70}Ge(p,t), 26 MeV, spin-parity assignments 77−54216
^{69}Ge excited states, lifetimes and J^π assignments, mixing ratios from ^{66}Zn(α,nγ) 79−63629
^{69}Ge excited states, spin and γ-decay, parity state struct. from ^{69}Ga(p,nγ) 3-5.6 MeV, ^{69}Ge excited states, spin and γ-decay, parity state struct. 79−464
^{69}Ge level structure and lifetimes, decay through negative parity band from ^{55}Mn(^{16}O,pnγ) 79−45172
^{70}Ge, high-spin states anal. from γ-ray spectra of heavy-ion reactions 78−33146
^{70}Ge level spin and parity assignments from ^{56}Fe(^{16}O,2pγ), ^{67}Zn(α,nγ), ^{68}Zn(α,2nγ) 79−3081
^{71}Ge, levels, studied via ^{68}Zn(α,nγ), 8 to 10 MeV, comparison with coupling model calcs. 78−8742
^{71}Ge negative parity states, J^π, energy spectra and spectroscopic factors 79−59013
^{72}Ge, gamma-ray spectra, energy levels, spin and parity assignments, from ^{72}Ga beta-decay *(Korean)* 78−50128
^{72}Ge spin, parity assignments, new O^+ states 79−63594
^{74}Ge, 26 MeV levels from ^{75}As(d,^{3}He) 78−25112
^{74}Ge, energy levels, shape transition from 15 MeV ^{72}Ge(t,p) study 78−93945
^{76}Ge levels, J^π assignments, shape transition DWBA anal. from ^{74}Ge(t,p) 79−17815
^{76}Ge(n,n′γ), 2.0 to 4.1 MeV, level and decay schemes 77−23092
^{78}Ge level struct., J^π values from DWBA anal. of ^{76}Ge(t,p), 17 MeV 79−6417
^{78}Ge level struct., proposed nuclear shape transition, DWBA anal. from ^{77}Ge(t,p), 15 MeV 78−78266
Ge(n,n′), 2^+ level excitation cross sections, intermediate resonances, optical model with coupled channels *(Russian)* 79−40897
H, A=4,5, levels determ. from Li(^{6}Li,^{8}B) 77−46183
^{2}H D-state, asymptotic normalisation 78−41653
^{2}H quadrupole moments, $^3S_1$-$^3D_1$ and $^3D_2$ states simple pot. model 78−78271
^{2}H(^{3}He,2pt), 2.2-6 MeV, A=5 levels coupled to nucl.-^{4}He*(0^+) channel 77−2906
^{2}H(e,e′p), single hole state momentum distrib. 80−22674
^{3}H, energy levels using ATMS method and realistic nuclear forces 80−22707
^{3}H, ground state energy, second order Brueckner-Baranger approx. 80−63082
^{3}H, three-particle system for nonlocal interactions with continuum bound states 79−75870
^{4}H, cluster model, energy levels by interaction set anal. 78−25136
He, A=157, 159, 161, 163, single proton states, Dy(^{3}He,d) and Dy(α,t) reactions 78−489
He, A=3, 5, BE, level calcs. using new boson expansion to n-fermion problem 78−511
^{2}He, ground state level determ. 80−99136
(^{3}He,^{6}He), 70 MeV, mass excess and excited states for proton-rich medium nuclei 79−6375
^{3}He(e,e), elastic and inelastic cross sections 40-60 Mev, possible 10 MeV state 79−40908
^{3}He(p,p), polarised p, below 6 MeV, anal. power meas. for four nucleon system levels 79−71837
^{4}He, (3+1) cluster model of the T=0 0_2^+ state by GCM 79−6396
^{4}He (e,e′pp) reaction cross-section and ground state shell model calcs. *(Russian)* 80−78283
^{4}He broad level search from ^{2}H(d,n) 80−102117
^{4}He continuum, microscopic calcs., dynamical R-matrix, model for struct. and reactions 77−14043
^{4}He continuum microscopic calcs. cross sections and levels from ^{3}He+n, ^{3}H+p channels 80−57702
^{4}He, effects of three body force on energy levels 78−54692
^{4}He, energy levels using ATMS method and realistic nuclear forces 80−22707

nuclear energy levels continued
^{4}He excited states obs. in ^{1}H(p,γ) induced by 6 to 16 MeV polarised protons 77−18559
^{3}He, ground state energies, four order high lying contribs. 79−75850
^{4}He, ground state energy, second order Brueckner-Baranger approx. 80−63082
^{4}He, ground state energy and RMS charge radius 78−58242
^{4}He ground state wave function in translationally invariant oscillator basis 77−6262
^{4}He isospin splitting of 1p-1h excitation, obs. in ^{3}H(p,p) 78−41622
^{4}He level density and J^π calcs. 79−63596
^{4}He level energies, Brink's model with single-particle functions with realistic behaviour *(Russian)* 77−74785
^{4}He, particle hole calculations, centre of mass subtracted kinetic energy 78−62491
^{4}He, shell model calcs. 80−13393
^{4}He, struct. of 2nd 0^+ state 78−93947
^{4}He system, high spin states 78−86484
^{4}He system, O^+ states, microscopic wave function 80−463
^{4}He, T=1 excited negative parity state struct. 80−57688
^{4}He(α,αd), 119 MeV, excited states, J^π and γ-ang. correlations 80−86809
^{4}He(γ,2d), 30-35 MeV, 2^+ state search *(Russian)* 80−42553
^{4}He(γ,n), 30-35 MeV, 2^+ state search *(Russian)* 80−42553
^{5}He, 16.7 MeV states energy calc. using mixed cluster representation 80−27555
^{5}He energy levels deduced from d(t,t)d 80−47488
^{5}He first excited state characts. from ^{7}Li(d,αα)n 77−276
^{6}He state excitation energies and widths, DWBA ang. distribs. from ^{4}He(t,p), 23 MeV 78−70544
^{7}He, levels determ. from ^{9}Be(^{6}Li,^{8}B) 77−46183
$^{\Lambda}_{\Lambda}$He-$^{\Lambda}_{\Lambda}$H binding energy difference, bound states, exact four body calc. 80−9255
Hf-Ir, isotopes, deformation, level assignments, static moments, modified oscill. model 77−22872
Hf-Os region, high lying states, Nilsson strength fragmentation 80−42539
$^{\Lambda}$Hf(n,nγ), 2.75 MeV, A=180,178,176, levels and excitation cross sections 79−75839
^{174}Hf, microscopic calc. of high-spin rot. states 78−8730
^{177}Hf(n,γ), 1-165 eV, γ-ray spectra obs., level scheme determ. 77−50130
^{179}Hf energy levels from decay of ^{179}Lu 77−54185
Hg, A=191,2,3,5,7,9, rot. aligned bands, high spin states, energy levels B(E2) values 78−70483
Hg even isotopes, nonaxial deforms., odd parity states, semidecoupled model 77−34220
Hg isotopes, A=184-197, β^+-decay, single particle and collective degrees of freedom 77−22956
Hg, positive-parity states, Coriolis antipairing effect, deformed-rotor model 78−12950
$^{\Lambda}$Hg, A=184, 186, 188, shape coexistence and energy level schemes 79−97652
$^{\Lambda}$Hg, A=190-200, even, phase transition and possible triaxial shape, energy levels 80−63098
$^{\Lambda}$Hg, A=198-202,204, muonic X-ray transitions, nuclear state quadrupole moments and charge distrib. 79−41253
^{184}Hg, excited deformed band, shape isomerism anal. 77−6234
^{194}Hg, level density calc., shell and pairing effects, deformation, excitation energy dependence 79−67662
^{195}Hg level scheme and transitions, band population from ^{195}Tl (1.13 h) decay 79−17807
^{196}Hg, band crossing, level scheme, J^π 77−65192
^{197}Hg energy levels from ^{195}Pt(α,2n), γ and conversion electron spectra, spins, parities 78−25149
^{197}Hg level scheme and transitions from ^{197}Tl electron capture 79−67719
^{197}Hg, quadrupole moment of $5/2^-$ 134 keV state 77−34225
^{201}Hg missing $f_{5/2}$ state Coulomb excitation, level scheme, J^π, transitions using (α,α), (^{16}O, ^{16}O) 80−47386
^{202}Hg, transfer strengths from 17.5 MeV ^{204}Hg(p,t) reaction 78−94005
^{206}Hg, energy level spectra, random-phase method calcs. 79−9469
^{206}Hg excited states from ^{204}Hg (t,p), neutron pairing vibr. 78−62549
^{206}Hg, obs. of excited states in (^{18}O,^{16}O) and (^{17}O,^{16}O) reactions 77−6242
Hg(γ,γ), 4.5 MeV to neutron emission threshold, strengths in energy levels 79−36164
$^{\Lambda}$Ho, A=167,169, energy levels from Er(t,α), polarised t 79−36155
^{157}Ho, lifetimes of excited states, delayed e-γ coincidences *(Russian)* 80−68597
^{159}Ho, level scheme, γ-singles, conversion electron spectra via ^{159}Er decay 78−547
^{165}Ho level scheme determ. *(French)* 77−274
^{165}Ho levels from ^{166}Er(t,α), 17 MeV polarised tritons, analysing powers, spins 78−78390
^{165}Ho(π^-,X), 175 MeV/c, monopole and quadrupole strong interaction effects in pionic atoms 78−41777
^{166}Ho, energies of low-lying high spin levels *(Russian)* 78−89793
^{166}Ho low lying levels and transitions, 54.24 keV level mag. moment from ^{166}Dy decay 80−13380
^{167}Ho, level scheme determ. from β^- decay of ^{167}Dy 77−26580
^{170}Ho, 43 s and 2.76 min states, energies and intrinsic structs. 78−78321
^{123,125}I, levels, J^π, spectroscopic factors 77−34230
I, 123≤A≤133, coupled quadrupole model, spectra, B(E2), B(M1), moments calcs. 77−82837
I, A=123,125, level struct. from Te(^{3}He,d) 24 MeV reactions 77−50057
I β^+ decay force function resonance struct., level populations *(Russian)* 80−102154
I energy levels, collective excitations, spin,parity, populated in ^{121,123}Sb(α,2n), γ spectra 78−4891
I, odd-mass nuclei, $9/2^+$ bands, deformed states 78−17106
$^{\Lambda}$I, A=121 to 131, comparative study of proton states excited by (α,t), (^{3}He,d) 79−63572
^{121}I energy levels from ^{120}Te(^{3}He,d) and ^{120}Te(α,t) 78−78246
^{121}I mass excess, energy levels and single particle strength distrib. from ^{120}Te (^{3}He,d) 80−5053
^{121}I single particle strength distrib., determ. from ^{120}Te(^{3}He,d) 78−70423
^{127}I(n,n'γ), fast n, γ-ang. distribs., level ang. momenta 80−18224
^{129}I energy levels populated in ^{129}Te decay, γ spectra, coincidence spectra 77−2935
^{136}I level scheme via ^{135}Te (20.9 s) β decay 77−82877
In isotopes, A=110, 112, 114, np coupling const. determ. 77−34205
nuclear energy levels continued
In, odd-mass isotopes, positive parity bands in deformed and spherical representation 78−21495
In populated in ^{111,113}Cd(p,nγ), energy levels, spins, lifetimes, shape 77−320
^{108}In, level scheme determ. from ^{108}Sn decay and ^{108}Cd(p,n) 78−41636
^{108}In, levels, J^π from ^{108}Sn decay γ- and conversion electron-spectra 77−71589
^{111}In band structure and hole-core coupling, ^{109}Ag(α,2nγ), branching and mixing ratios 78−58249
^{111}In, isospin mixing obs. in ^{110}Cd(p,p'), ^{110}Cd(p,α), ^{107}Ag(α,α') and ^{107}Ag(α,p) 77−57598
^{111}In, populated in ^{111}Cd(p,nγ), γ-ray spectra, level scheme 78−13083
^{112}In low lying levels, transitions, $T_{1/2}$, multipolarities and mixing ratios from ^{112}Cd(p,nγ) 80−68545
^{113}In, unified model description of odd mass In nuclei 78−66251
^{115}In 597 keV level J^π assignment from ^{115}Cd^g β-decay 79−80900
^{115}In unified model description of odd mass In nuclei 78−66251
^{117}In level scheme, J^π and transitions from ^{117}Cd isomer decay, unified model anal. 80−32193
^{122}In, states and masses determ. from (t,^{3}He) 78−66290
^{124}In, states and masses determ. from (t,^{3}He) 78−66290
^{126}In levels from ^{126}Cd β-decay 79−3117
^{119g,m}In, decay schemes, half-lives, excited levels 77−296
Ir, A=187, 189, triaxial rotor model and γ-vibr. model comparison, γ decay, level schemes 78−54695
Ir, A=191, 193, hyperfine struct. of low lying fine struct. levels, hyperfine anomaly, electronic g-factor 78−66214
Ir, A=193, 195, proton states, populated via Pt(t,α), A=194, 196 78−33123
Ir, odd isotopes, pot. energy surfaces and quadrupole deformation parameters, deformed basis model 79−80867
Ir odd-mass isotopes, $9/2^-$ level excitation energies, estimates 77−275
$^{\Lambda}$Ir, A=189, 191, levels, J^π, transitions and mixing ratios from Pt decay 80−68602
^{183}Ir levels, J^π assignments, Nilsson states for N=105 isotones from ^{183}Pt fast β-transition 79−22206
^{185}Ir levels excited in (α,xn) reactions 80−9231
^{185}Ir levels populated in ^{185}Pt^{m+g} decay 80−9269
^{186}Ir anomalous $I^\pi K=5^+1$ ground state config. confirmation, spectroscopic quadrupole moment 79−93506
^{188}Ir level scheme and transitions from ^{188}Pt electron capture 79−22237
^{189}Ir low lying positive parity bands, state anomalous angular distribs. from ^{191}Ir(p,t), 34.7 MeV 78−66212
^{191}Ir low lying positive parity bands, state anomalous angular distrib. from ^{193}Ir(p,t) 34.7 MeV 78−66212
^{192}Ir levels, resonances and low energy γ-rays from ^{191}Ir(n,γ) 80−47397
Ir(p,t)^{189,191}I, 18 MeV, ground state rot. band, 7/2 gamma vibr. levels 78−74360
K odd isotopes, $2s_{1/2}{}^{-1}$ and $1d_{3/2}{}^{-1}$ hole state separation energies 79−67634
$^{\Lambda}$K, A=37,39, levels, excitation and microscopic form factors, DWBA calcs. from Ca(p,α) 80−32185
$^{\Lambda}$K, A=43,44, levels, spin and parity assignments, decay scheme from ^{43,44}Ar β-decay 79−13210
$^{\Lambda}$K, A=45,46, levels, lifetimes and transitions from Ar β-decay 80−42597
^{37}K (sd)$^{-3}$ g.s band investigation in ^{40}Ca(p,α)^{37}K study 79−6587
^{38}K excitation spectrum and distrib. from ^{40}Ca(π^-, 2n), absorpt. at rest 78−66322
^{38}K level spectrum and (^{3}He,t) reaction mechanism from ^{38}Ar(^{3}He,t) 79−22229
^{38}K low lying 1^+, T=0 states, DWBA anal. of ^{40}Ca(p,^{3}He) 80−470
^{39}K, charge density and single particle state struct. 79−36144
^{39}K high spin states, J^π assignments, DWBA anal. of ^{41}Ca(d,α), 22 MeV, ^{39}K high spin states, J^π assignments, DWBA anal. 79−40851
^{39}K high spin states from ^{24}Mg(^{18}O, p2nγ), decay scheme 78−25232
^{39}K high spin states from ^{28}Si(^{16}O,αpγ), γ meas. 78−89787
^{39}K, J^π, hole-core wave functions via ^{39}K(α,α') 31 MeV 77−50056
^{39}K, produced in ^{40}Ca(p, 2p), ground and excited states, DWIA calcs. 78−62535
^{39}K $s_{5/2}$ and $d_{3/2}$ states from ^{40}Ca heavy ion L=1 pickup reactions 79−67734
^{39}K states and spectroscopic strengths DWBA anal. of ^{40}Ca(^{7}Li,^{8}Be) 80−5069
^{40}K energy levels and spectroscopic strengths from ^{41}Ca(d,^{3}He) 79−89238
^{40}K excitation energy, γ decay, of lowest T=2 state populated in ^{40}Ar(p,n) 78−8769
^{40}K, yrast levels, J^π, branching and mixing, via (^{16}O,pnγ) 34 MeV 77−74759
^{41}K, populated by ^{38}Ar(α,pγ), levels props., shell model calc. 78−62588
^{41}K(p,pγ), 1.58 MeV, parity doublet gamma lifetimes, 3/2 levels, parity mixing 80−78209
^{42}K, levels, studied by ^{44}Ca(d,α)^{42}K reactions, 11 MeV, DWBA analysis 78−8723
^{42}K, yrast state J^π assignments via ^{26}Mg(^{18}O, pnγ) anal. at 25,34 MeV 77−57618
^{43}K 738 keV state g-factor, PAC technique 77−6227
^{44}K excited levels, J^π, transitions and lifetimes from ^{48}Ca(p,αn) 80−68544
^{45}K deduced energy levels from ^{45}Ar decay 78−78319
^{46}K deduced energy levels from ^{46}Ar decay 78−78319
^{46}K levels, J^π and tensor anal. powers from ^{48}Ca(d,α), pol.d 80−102113
^{47}K, single particle states lifetimes calcs. 80−105943
^{48}K mass excess and 0.58 MeV excited state from ^{48}Ca(^{7}Li,^{7}Be), 52 MeV 79−446
^{48}K mass excess and states from ^{48}Cu(^{7}Li,^{7}Be) 80−9221
$^{\Lambda}$Kr, A=78, 80, quasi-γ bands and negative parity levels from Br(p,2nγ) 80−456
$^{\Lambda}$Kr(p,p'), 51.9 MeV, A=78, 80, 82, 84, 86, $2_2{}^+$ and $4_1{}^+$ state excitation 79−54389
^{77}Kr, low lying state J^π assignments, anal. powers from ^{78}Kr(d,t) 79−45153
^{79}Kr excited states, J^π assignment, transitions, level lifetimes from ^{79}Rb β^+ decay 79−17810
^{81}Kr levels, J^π, ICC via ^{81}Rb 77−79309
^{81}Kr levels, transitions and J^π assignments, first excited state lifetime from ^{81}Br(p,nγ) 79−75849
^{81}Kr low lying states populated in ^{81}Br(p,nγ), γ spectra, γ-γ coincidences 78−25195

nuclear energy levels continued
^{84}Kr levels, γ-cascades, J^{Π}, mixing ratios and correlations from ^{84}Br decay 80−63134
^{85}Kr level struct. and spectroscopic factors from ^{84}Kr(d,p), polarised and unpolarised d 79−471
^{85}Kr positive-parity states calc. by quasiparticle phonon coupling 79−75845
^{87}Kr energy levels from ^{87}Br β-decay, delayed neutrons, high energy γ spectra 78−25155
^{87}Kr ground state spin assignment from ^{86}Kr(d,p), polarised and unpolarised d 79−471
^{87}Kr levels in ^{86}Kr(n_{th},γ) 77−74798
^{88}Kr level scheme and transitions, delayed neutrons from ^{88}Br β-decay 80−42600
^{93}Kr, γ-ray decay scheme, levels, J^{π}, logft values 77−54152
Kr(p,p′), 51.9 MeV, low-lying octupole states anal. 78−21497
La, A=144-6, β-decay, γ-ray singles and coincidence meas. 78−4913
La odd-A isotopes, rot. aligned coupling, ang. momentum projection 77−2921
^{133}La, band struct., in-beam γ-ray spectroscopy after (^{3}He,3n) reaction 78−4951
^{133}La level struct., parity levels, decoupled band struct. from ^{133}Ce β-decay 79−9476
^{134}La levels anal. using decay of ^{134}Ce 77−6290
^{135}La, band struct., in-beam γ-ray spectroscopy after (α,2n) reaction 78−4951
^{139}La, level props., Coulomb excitation obs. 80−13378
^{139}La(γ,γ′), 7.28, 7.63 MeV, energy levels anal. 78−13058
^{139}La(p,f), 600 MeV, fragment energies, cross sections level density and barrier heights 80−42723
^{143}La, nuclear spectroscopy of neutron rich A=143 nuclei 79−59039
^{145}La, level schemes determ. from β-decay of A=145 nuclei 78−78323
Li, A=10, 11, ground-state config. anal. 77−22859
(^{6}Li,d), ground state transitions in 1f-2p shell, 34 MeV, spectroscopic factors 79−6670
^{6}Li, (αnp) 3 body model using hyperspherical harmonics, bound states 78−70469
^{6}Li, absolute excitation energy meas. using electrostatic analyser 77−30741
^{6}Li, α+p+n cluster model with local interactions, Faddeev eqns., energy and charge radius calc. 79−22215
^{6}Li, α+p+n model, numerical soln. of coupled Faddeev eqns. 79−17831
^{6}Li, electron excitation cross sections, short-range correlations *(Russian)* 79−36169
^{6}Li energy levels, d-α elastic scatt., three body calcs. 77−54158
^{6}Li energy levels from (p,d) 80−42667
^{6}Li, even parity levels, anal. using P-model *(Russian)* 79−49585
^{6}Li, excitation energy of second excited state meas. in (p,p′) and (p,α) 77−57619
^{6}Li excited states, D(α,α)D cross-sections, α-d systems 80−47491
^{6}Li excited states, final state interactions, three-body force effects from ^{2}H(α,αp) 80−57692
^{6}Li, highly excited states obs. in ^{9}Be(p,α) 77−6244
^{6}Li, levels anal. from ^{3}H(^{3}He,^{3}He), 20-33 MeV 78−17227
^{6}Li low lying positive parity energy levels, effects of weak compression *(Russian)* 78−78270
^{6}Li, nucleon spectral function, K-harmonics calc. 79−75834
^{6}Li structure, three-body NNα model with separable interactions *(French)* 77−71598
^{6}Li(e,p), 16 MeV, nonexistence of 16.1 MeV state in (γ,p) cross section 79−45174
^{7}Li 3/2^{-} state from ^{6}Li(n,−a) 80−18297
^{7}Li, ang. momentum eigenstates projection from two-centre generator coordinate model functions 78−12994
^{7}Li, cluster struct. interplay model and appl., energy levels and shell clusters 79−17842
^{7}Li, electron excitation cross sections, short-range correlations *(Russian)* 79−36169
^{7}Li, energy of first 3/2^{-} excited state from S-matrix anal. from ^{6}Li(n,t)^{4}He, 0-3.9 MeV, ^{7}Li, energy of first 3/2^{-} excited state from S-matrix anal. 79−473
^{7}Li, model for coupling two cluster structs., influence on shape and states 78−78288
^{7}Li, non-central forces and spectrum *(Russian)* 79−89243
^{7}Li, two-centre molecule-like states, generator coordinate wave function projection 78−12995
^{7}Li(γ,t), <50 MeV, total and differential cross sections, levels, cluster model calcs. 80−32265
^{8}Li state excitation energies and widths, DWBA ang. distribs. from ^{6}Li (t,p), 23 MeV 78−70544
^{9}Li, levels determ. from ^{11}B(^{6}Li,^{8}B) 77−46183
^{9}Li state excitation energies and widths, DWBA ang. distribs. from ^{7}Li(t,p), 23 MeV 78−70544
^{A}Li(γ,π), A=6, 7 80−22686
$^{A}_{\Lambda}$Li, A=6,7, excited states and spectra, continuum effects calcs. 80−57720
Lu β^{+} decay force function resonance struct., level populations *(Russian)* 80−102154
^{172}Lu levels, transitions and J^{π} values from ^{172}Hf EC decay 80−18249
^{174}Lu, populated by ^{176}Lu (p,t)^{174}Lu, energy levels and rotational bands 78−37346
^{175}Lu, level schemes from ^{176}Yb(p,xnγ) and ^{176}Yb(d,xnγ) reaction 79−75838
^{175}Lu(π^{-},X), 230 MeV/c, monopole and quadrupole strong interaction effects in pionic atoms 78−41777
^{176}Lu, level schemes from ^{176}Yb(p,xnγ) and ^{176}Yb(d,xnγ) reactions 79−75838
^{177}Lu excited state lifetimes, γ-transitions from β-decay transitions 80−78205
^{148}m, struct. anal. from decay of ^{148}Pm, ^{148m}Pm gamma-ray spectra 77−67717
^{23}Mg even parity excited states, collective props., EM moments, generator coordinate method 78−78259
^{23}Mg, high spin states anal., ^{12}C+^{12}C reson. at $E_{c.m.}$=19.3 MeV 77−26579
^{23}Mg hole states, transitions and spectroscopic factors, DWBA anal. of ^{24}Mg(p,d) 80−32161
^{23}Mg j-forbidden $^{7}/_{2}^{+}$ state excitation, CCBA calculations, two step processes from ^{24}Mg(p,d), 49.5 MeV 79−26369
^{23}Mg/^{23}Na, mirror level pair cross sections from ^{24}Mg($\pi^{\pm}$,πN) 79−67665

nuclear energy levels continued
^{24}Mg, 11.86 MeV level, confirmation of $J^{\pi}=8^{+}$ assignment from ^{12}C(^{16}O,αγ) 42 MeV 78−70445
^{24}Mg 2_1^{+} state quadrupole moment from ^{208}Pb(^{24}Mg,^{24}Mg) 80−9230
^{24}Mg 2_1^{+} substate parameters near Coulomb barrier from ^{12}C(^{16}O, α) 79−67657
^{24}Mg, 2^{+} level, 8^{+} member, radiative width meas. 77−71613
^{24}Mg, 6 MeV 4^{+} state, configuration anal., electron scatt. form factors 78−25115
^{24}Mg 6_3^{+} level, α and γ decays, branching ratios from ^{12}C(^{16}O,α) 79−75901
^{24}Mg coherence width, intermediate structure effects from ^{23}Na(p,α)^{20}Ne 79−45133
^{24}Mg, form. in ^{12}C+^{12}C reaction at 10.5 to 15 MeV, possible rot. band 78−13134
^{24}Mg, γ-ray and α-particle emitting states form., from ^{24}Al and ^{24}Al^{m} decay 79−49607
^{24}Mg, identification of 10^{+} levels using ^{12}C(^{16}O,α) at 26.7 MeV 78−33119
^{24}Mg isoscalar quadrupole excitations in 2 centre shell model, collective approach, particle-hole excitations 79−45139
^{24}Mg, levels, GDR isospin mixing via (γ,α) 28 MeV 77−74832
^{24}Mg, low spin rotational states, energy props., extended deformation model 80−86785
^{24}Mg lowest $J^{\pi}=0^{+}$, T=Z level from ^{23}Na+p reactions, narrow resonance, isospin forbidden particle decays 78−89871
^{24}Mg lowest T=2 state from ^{23}Na(p,γ), total width 78−89870
^{24}Mg, novel cluster model descript., ^{16}O+^{8}Be, energy levels 78−62495
^{24}Mg, population of resonant ^{12}C+^{12}C states in ^{12}C(^{16}O, α) 78−62563
^{24}Mg states, Nilsson model spectroscopic factors, collective model rot. bands from ^{23}Na(^{3}He,d) 79−6421
^{24}Mg, struct. determ. from ^{16}O+α+α model 79−6401
^{24}Mg(^{16}O^{16}O), entrance, exit and reaction channel data at backward angles 79−36254
^{24}Mg(α,α′), 1.37 GeV, low lying state ang. distribs., Glauber rigid body approx. 79−54394
^{24}Mg(e,e), 4_1^{+} 4.12 MeV and 2_2^{+} 4.24 MeV level resolution, E2 and E4 form factor meas. 79−17811
^{24}Mg(p,p′), 135 MeV, large momentum transfer, excitation of high-spin particle-hole states in ^{24}Mg 77−61420
^{24}Mg(p,p′), 40 MeV, two step pickup-stripping process, negative parity states 80−32256
^{24}Mg(p,p′), polarised p, 20.3 MeV, low lying states, collective and microscopic model 78−82287
^{24}Mg(p,p′)^{24}Mg, 20 MeV, excitation energies up to E_x=13.2 MeV 77−317
^{24}Mg(p,p'), 40 MeV, DWBA anal., positive parity states, transitions and giant resonance 79−6419
^{25}Mg, energies and branching ratios, α and d reactions 77−22892
^{25}Mg highly excited states from ^{24}Mg(d,p), fluctuation anal. 78−46071
^{25}Mg, low-lying excited states calc. by generator coordinate method 78−12974
^{26}Mg, energy levels anal. with ^{12}C(4u^{16}O,2p)^{26}Mg 77−38293
^{26}Mg, spectroscopic factors, via ^{27}Al(n,d) 56.3 MeV 78−4935
^{26}Mg(p,p′)^{26}Mg, 20 MeV, excitation energies up to E_x=11.2 MeV 77−317
^{27}Mg energy levels, spectroscopic factors, DWBA, Hauser-Feshbach anals. from ^{26}Mg(d,p) 80−52581
^{28}Mg, differential cross sections for lowest four states from ^{26}Mg(^{18}O,^{16}O) 79−67661
^{32}Mg, excitation energy of lowest 2^{+}, 3^{-} levels, energy density method 79−3088
Mn levels from ^{50,52,54}Cr(α, p), 18, 26 MeV, J-depend., spins, parities 78−78397
^{A}Mn, A=51, 53 small angle cross sections for levels, DWBA anal. from Cr(^{3}He,d) 79−22203
^{51}Mn, 21 MeV analogue state, excitation 80−13471
^{51}Mn, EM transitions, J^{π}, half-lives, branching and mixing ratios 77−18471
^{52}Mn, γ-spectra, levels, J^{π} via α+^{50}Cr reaction 77−74794
^{52}Mn, high spin state spectroscopy via ^{39}K(^{16}O,2pnγ) 37-52 MeV 77−10321
^{52}Mn, low-lying states J, γ-branching and mixing via ^{52}Cr(p,nγ) 77−14028
^{52}Mn populated in Cr(π^{+}, π^{-}), deexcitation γ spectra 78−89912
^{53}Mn level scheme, DWBA and optical model anal. from ^{52}Cr+^{13}C 79−36159
^{53}Mn low lying states, DWBA anal., shell model wave functions from ^{56}Fe(p,α) 80−32211
^{54}Mn, intruder states and configuration purity 77−38223
^{54}Mn low lying 2p-4h states, J^{π} from tensor anal. powers of ^{56}Fe(d,α), pol.d 80−99124
^{55}Mn energy level excitation curve, bound state and resonance γ-decay from ^{54}Cr(p,γ) 79−476
^{55}Mn, energy levels, bound state mean lifetimes and spins from ^{54}Cr(p,γ) 80−42586
^{55}Mn, levels, J^{π}, γ-branching via (n,n′γ) 1.0-3.6 MeV 77−79310
^{55}Mn, proton-neutron correl. shell model for collective motion 77−79312
^{55}Mn(α,α), 4.5 to 7 MeV, Coulomb excitation, search for 1.29 MeV 1/2^{-} level 78−82360
^{55}Mn(n,n′γ), 2.2-3.2 MeV energy level J^{π} assignments, transition branching and mixing ratios 79−40881
^{56}Mn levels, transitions and spins from ^{55}Mn(n,γ), pol. Mn and n 80−78154
^{57}Mn levels and J^{π} restrictions, from ^{57}Cr β-decay 78−70436
^{57}Mn, low lying level struct. via ^{55}Mn(t,p)^{57}Mn, shell model comparison 77−74769
^{58}Mn energy levels populated in ^{58}Fe(t,^{3}He), mass excess, spin-parity assignments 77−54230
Mo, even-even isotopes, first excited 0^{+}′ states, energy systematics 78−54683
Mo isotopes struct., spectroscopy weak coupling approx. in shell model 79−22194
^{A}Mo, A=98,102, anal. powers, transitions, shape coexistence states, DWBA anal. of Mo(t,p), pol.t 80−86895
^{89}Mo mass excess and excited states from ^{92}Mo(^{3}He,^{6}He) 80−42531
^{89}Mo^{m} levels, transitions and half life from ^{93}Mo(p,p′3n) 80−86858
^{92}Mo energy levels calc. from two-body effective parameters 77−57608
^{92}Mo high spin states from ^{90}Zr(α,2nγ), negative parity states 78−89786
^{92}Mo in beam γ-spectroscopy, level, lifetimes and excitation functions from ^{90}Zr(α,Zn) 79−13240

nuclear energy levels continued
^{91}Mo, shell model calcs., energy levels, transitions and spectroscopic factors 79−63593
^{92}Mo even parity states, shell model calc. 77−50061
^{95}Mo, first excited 3/2$^+$ state, g-factor determ. 77−26574
^{95}Mo, levels, B(E2), B(M1), branching ratios populated in ^{95}Tc^{m,g} decay 77−82856
^{98}Mo static quadrupole moment of first 2$^+$ state from (α,α′), (^{16}O,^{16}O′) 80−5061
^{100}Mo(n,n′γ), fast n, gamma transitions, level energies and scheme 80−73822
^{101}Mo levels, γ-rays and p-wave resonance partial radiative widths from ^{100}Mo(n,γ) 80−57739
^{101}Mo resonances, levels, J^π, level spacings, cross section from ^{100}Mo(n,γ) 79−89278
^{93,95}Mo, transfer $\mathcal{L}$ values, spectroscopic factors, J^π via (p,d) and (d,t) 40 MeV 77−74748
Mo(p,p′γ), odd isotopes, excited d-states from analogue resonances and p-γ correlations 80−68546
^{12}N ground state electric quadrupole moment from ^{12}C(γ, π), ^{12}N ground state electric quadrupole moment *(Russian)* 80−42538
^{13}N ground state, dispersion anal. of ^{12}C+p forward scatt. 77−34297
^{13}N, level parameters determ. from ^{12}C(p,p) at 0.3-2.0 MeV 77−3007
^{13}N level structure via ^{12}C(p,p) scatt. with 11.5 to 18 MeV polarised beam 77−315
^{13}N spectroscopic factors, ^{13}C(^{3}He,d) with 33 MeV polarised beam 77−328
^{14}N 1$^+$ state cross sections, effective two nucleon interaction, isovector tensor component from ^{14}C(p,n) 80−18208
^{14}N 9.13 MeV state, obs. in ^{13}C(p,γ) 78−41641
^{14}N, energy levels up to 11.05 MeV, transitions and resonance decay from ^{13}C(p,γ) 80−47376
^{14}N levels and excitation energies, kinematically complete investigation from ^{16}O(π^-, 2n) 80−99128
^{14}N, meas. of nucl. g-factor of 5.11 MeV 2$^-$ state by recoil distance technique 78−37268
^{14}N residual states, vector anal. power. optical pot. from ^{12}C(^{6}Li,α), pol. ^{6}Li 79−97697
^{14}N unbound 4$_1^+$, 5$_1^+$, 3$_2^+$ states from ^{13}C(p,γ), lifetimes, branching ratios 78−25184
^{14}N(p,p′), 122 MeV, level excitation, cross sections, effective NN interaction, DWIA anal. 80−78197
^{14}N(p,p′), 25-40 MeV, level cross sections, optical parameters, DWBA anal., tensor effective interaction 80−68555
^{15}N 3/2$^-$ state spin alignment and polarisation, 1/2-spin orbit interaction from ^{27}Al, ^{88}Sr(^{16}O,^{15}N) 80−27622
^{15}N 9.155 MeV state, lifetime, cluster nature and parity from ^{12}C(^{7}Li,αγ), ^{12}C(^{6}Li,^{3}Heγ) 79−6424
^{15}N, direct evidence for 3p-4h excitations 79−67659
^{15}N energy levels populated in ^{13}C(^{3}He,p), p ang. distrib. 78−21581
^{15}N excited states and transitions from ^{15}C beta decay 80−18248
^{15}N integrated cross sections to excited residual states from ^{19}F(γ,α) 80−18200
^{15}N level excitation functions, resonance, p ang. distribs. from ^{13}C(^{3}He,p), 3.6-6.6 MeV 78−93942
^{15}N low lying states, cross sections and anal. power, transitions, spectroscopic factors from ^{14}N(d,p), pol. d 80−32183
^{15}N low-lying positive parity states, Nilsson scheme from ^{14}C(^{3}He,d) 79−80871
^{15}N low-lying states, obs. in (e,e′) scatt. 78−12976
^{15}N, spins of p-h states from analysing powers of (d,τ) reacts. 78−25111
^{15}N states, cross sections and lifetimes, EM decay strengths from 3 and 4 particle transfers 80−9237
^{15}N three particle states at high excitation energies, J^π, selective population from ^{12}C(^{7}Li, α) 80−99129
^{15}N$_{3/2}$ (6.33 MeV) state, spin alignment meas. from (^{16}O,^{15}N) using γ-recoil 79−17796
^{15}N+X, X=^{11}B,^{12}C,^{18}O,^{13}C, deduced excited states, shell model wave functions, DWBA anal. 79−45284
^{16}N, 1-20 ps region mean lifetime meas., high-vel. DSA method 77−65200
^{16}N ground state quadruplet, DWBA anal. of ^{14}N(t,p) 79−22200
^{16}N, J^π=1$^-$ assignment from ^{15}N(d,p) 79−30786
^{16}N, levels at 5.5-8.5 MeV from ^{14}N(t,p) 78−66207
^{16}N levels from ^{18}O(d,α) using polarised deuterons, spin parity assignments 78−89886
^{16}N particle hole spectra, spectroscopic strengths, from ^{17}O(d,τ) tan studies 78−58288
^{16}N structure of 1$^+$ states populated in two nucleon transfer and ^{14}C beta decay 78−50085
^{17}N, 1p spin-orbit splitting anal. with ^{18}O(d,τ) at 52 MeV 77−41980
^{17}N 2p-1h states from ^{15}N(t,p), spins, parities. cross sections 78−62548
^{17}N, excited states obs. in ^{18}O(t,αγ) at 3.5 MeV *(French)* 77−14031
^{17}N levels and ang. distribs. meas., shell model calcs. from ^{15}N(t,p) 80−9233
^{18}N, mass excess and excited states from ^{14}C(^{18}O,^{18}N) 80−42676
^{A}Na, A=21, 23, even parity excited states, collective props., EM moments, generator coordinate method 78−78259
^{A}Na, A=22,23 J^π assignments from ^{12}C(^{12}C,Xγ), X=p or d 79−45154
^{21}Na deduced levels and cross sections from ^{12}C(^{12}C,t) 80−469
^{21}Na levels obs. in ^{20}Ne(p,p) with polarised protons 77−2913
^{21}Na, produced in ^{2}H(^{20}Ne,nγ)^{21}Na energy level lifetime 78−41631
^{22}Na 0$^+$ level mean life, isovector mag. dipole transition from ^{19}F(α,n) 80−68595
^{22}Na deduced levels from ^{12}C(^{14}N,α) and ^{14}N(^{12}C,α) 78−93944
^{22}Na excitation functions determ. in ^{12}C(^{12}C,d)^{22}Na at 14.3 MeV 77−82956
^{22}Na levels, resonances in ^{21}Ne+p reactions, 0.4 to 1.6 MeV 77−18540
^{22}Na, resonance levels obs. in ^{20}Ne(d,p$_0$) 78−46072
^{23}Na, DWBA anal. of α-spectroscopic factors in ^{19}F(^{6}Li,d) 78−82383
^{23}Na energy levels from ^{25}Mg(d,α), spin, parity, angle-integrated cross section 78−50179
^{23}Na even parity states, generator coord. method, projected Hartree-Fock, and complete diagonalisation calcs. comparison 78−89796
^{23}Na, high spin states anal., ^{12}C+^{12}C reson. at E$_{c.m.}$=19.3 MeV 77−26579
^{23}Na, high-spin states, shell-model calc. in sd shell 77−65213
^{23}Na levels, resonance strengths, γ-decays and level lifetimes from ^{22}Na(p,γ) 79−45229
^{23}Na levels and spectroscopic amplitudes, J^π assignments, high spin states from ^{20}Ne(α,p) 79−75848
^{23}Na, low-lying excited states calc. by generator coordinate method 78−12974
^{23}Na, populations of half integer spin mag. substates, determ. from (n,n′γ) distribs. 77−30493
^{23}Na positive parity states ang. distrib., DWBA anal. from ^{21}Ne(^{3}He,p), 18 MeV 78−82284
^{23}Na, reson. levels via ^{19}F(α,n)^{22}Na at 2.3-4.7 MeV 77−65199
^{23}Na, spectroscopy of high-spin states in ^{12}C(^{12}C,pγ) 77−46131
^{23}Na, transition probabilities and multipole moments between states calc. by generator coordinate method 78−13022
^{23}Na(p,p′)^{23}Na, 20 MeV, excitation energies up to 11.2 MeV 77−317
^{24}Na, J^π assignments via ^{22}Ne(^{3}He,p)^{24}Na 18 MeV reaction 77−74760
^{24}Na, level struct. and spin assignments, DWBA anal. from ^{22}Ne(^{3}He,p), 18 MeV 78−86477
^{24}Na, reported 2.46 MeV state not seen ^{24}Mg(t,^{3}He)^{24}Na 77−34229
^{27}Na excited states and mass excess from ^{26}Mg(^{18}O,^{17}F) 79−3075
^{A}Nb, A=90,91,94 neutron spectra, level density, direct processes from Zr(p,n) *(Russian)* 79−67666
^{A}Nb, A=93,95,97, quasiparticle-phonon coupling model calcs. levels, transitions and spectroscopic factors 79−472
^{89}Nb, excited states studied by (^{3}He, 3nγ) in-beam γ-ray spectroscopy 77−41983
^{91}Nb, 17$^-$/2 state, g-factor meas. 80−32179
^{91}Nb 21/2$^+$ state, lifetime, g-factor meas. 77−30487
^{91}Nb from ^{89}Y(α,2nγ)^{91}Nb, high spin states, shell model structure 79−93514
^{91}Nb, level struct., p$_{3/2}$ core excitations 77−50060
^{91}Nb, two-body effective parameters calc., energy levels 77−57608
^{92}Nb energy levels populated in ^{92}Zr (p, n), spins, parities 77−14125
^{92}Nb, high-spin states, EM props. via ^{88}Sr(^{7}Li, 3n)^{92}Nb 34 MeV 77−74770
^{92}Nb low lying multiplets, DWBA anal. for spectroscopic factors from ^{91}Zr(α,t) 80−57685
^{92}Nb, shell model calcs., energy levels, transitions and spectroscopic factors 79−63593
^{92}Nb, spectroscopic factors and levels obs.in ^{93}Nb(^{3}He,α) 77−88154
^{93}Nb, 1 quasiparticle 2 phonon multiplet, microscopic quasiparticle cluster phonon coupling model 77−2908
^{93}Nb(γ,γ′), energy levels, spin and parity, 6465 KeV resonance total width 78−93940
^{93}Nb(n,n′γ), 1.3-2.7 MeV, energy levels, decay scheme, de-excitation gammas 78−41710
^{93}Nb(n,n′γ), up to 14.6 MeV, radiation and neutron widths for highly excited levels *(Russian)* 78−605
^{94}Nb excited states from ^{94}Zr(p,nγ), spin, parity, γ-spectra 77−88125
^{94}Nb level density, neutron spectra and ang. distribs. nonequilib. processes from ^{94}Zr(p,n) *(Russian)* 80−37376
^{97}Nb, 1251 keV level spin-parity characteristics, ^{97}Zr β-decay meas. 77−22879
^{99}Nb, level schemes, from ^{99}Zr β-decay obs. 79−17863
^{100}Nb mass and excited states from ^{100}Mo(t,^{3}He) 79−63581
^{133}Nb, high-spin levels, in-beam γ-ray spectra meas. *(French)* 77−61372
Nd, A=139, 141, high spin levels, γ spectra, hole-core coupling 77−50063
Nd isotopes, prolate-oblate transition from ^{128}Te(^{16}O,5nγ) 78−70438
Nd odd isotopes, 1h$_{11/2}^{-1}$ neutron state strength distrib. 77−46100
Nd(^{16}O,^{16}O), 40-48 MeV, even nuclei, 2$^+$ state E2 transition probabilities and quadrupole moments 80−18234
^{A}Nd, A=145, 147, 149, single neutron hole states spectroscopic factors, DWBA anal. of (d,t), (^{3}He,α) 80−78109
^{20}Nd, low lying positive parity states by (^{16}O-α)+(^{12}C-^{8}Be) orthogonality condition model 79−6400
^{138}Nd, 10$^+$ isomeric states, systematic behaviour 79−30791
^{139}Nd, N=79, states populated in ^{139}Pm decay 77−41929
^{141}Nd, level struct. determ. from (d,t) at 17 MeV and (^{3}He,α) at 24 MeV 77−41979
^{142}Nd(γ,γ), 1.85-5.0 MeV, resonance fluorescence, level radiative widths, spin assignments 79−9538
^{143}Nd, from ^{144}Nd(d,t)^{143}Nd, nuclear levels, intermediate coupling unified model calcs. 78−89791
^{143}Nd, levels, J, π, via ^{142}Nd(n,γ) with E=thermal 77−10320
^{144}Nd capture states partial α-decay widths from ^{143}Nd(n,γα) 80−37328
^{144}Nd excited state charact., level scheme extension 77−6231
^{144}Nd, high-spin states anal. from ^{142}Ce (α,2n)^{144}Nd 77−82940
^{144}Nd, level props. from ^{143}Nd(d,p) and ^{146}Nd(p,t) 77−6241
^{144}Nd levels and transitions, γ-ray spectra from ^{144}Pr^{m}β-decay *(French)* 80−18250
^{145}Nd energy levels from ^{144}Nd(d,p) and ^{146}Nd(d,t), DWBA calcs. 80−68533
^{145}Nd level scheme from ^{144}Nd(n,γ) 78−8823
^{146}Nd, from ^{146}Pr decay, level props., 104 γ-ray transitions 78−86476
^{147}Nd, energy levels anal. from ^{148}Nd(d,t)^{147}Nd 78−507
^{147}Nd, level scheme from (n,γ) meas. 77−34232
^{147}Nd low spin states ns lifetimes, particle rotor model interpretation from ^{146}Nd(d,pγ) 80−78207
^{148}Nd from ^{148}Pr β-decay, low lying energy levels, quasi band description 80−5096
^{149}Nd, level scheme from (n,γ) meas. 77−34232
^{149}Nd, level struct. determ. from decay of ^{149}Pr 77−71591
^{151}Nd, level scheme from (n,γ) meas. 77−34232
Nd(d,^{6}Li) (A=142, 144, 146), 35 MeV, ang. distrib. meas., deduced α-particle spectroscopic factors, reduced widths, decay lifetimes 77−18571
Ne, low spin states populated in ^{16,18}O(^{3}He,n) 77−14141
^{A}Ne, A=19, 21, even parity excited states, collective props., EM moments, generator coordinate method 78−78259
^{18}Ne analogue and nonanalogue states, π double charge exchange form factors from ^{18}O(π^+,π^-) 80−13405
^{18}Ne ground state obs. in ^{18}O(π^+,π^-)^{18}Ne at 148, 187 MeV 77−74883
^{19}Ne 3/2$^+$ state config. from ang. distribs. and cross section of ^{21}Ne(p,t) 79−9473
^{19}Ne 5.09 MeV level parity from ^{21}Ne(p,t) 79−45155
^{19}Ne, final state selective population, triton clustering from band anal. from ^{16}L(^{6}Li,t) 80−9306
^{19}Ne, spectra and E1 transitions, ang. momentum projected HF and Tamm-Dancoff methods 77−54139
^{20}Ne, 0g orbit mixing via (e,e′), one-step forbidden transition anal. 78−493
^{20}Ne 13482 keV level, parity violating effects in two resonance interference from ^{19}F(p,α) pol. p 80−83033

nuclear energy levels continued
^{20}Ne, [211] quartet state, by study of ^{19}F(p,α)^{16}O, 1.5 to 2 MeV 78−46006
^{20}Ne, appl. of cluster expansion theory *(Spanish)* 79−88868
^{20}Ne, α decay from 8p-4h O^+ state, branching ratios 78−50132
^{20}Ne α-cluster levels, props., hard-core potential calcs. 77−30614
^{20}Ne, coexistence of shell struct. and cluster struct. 78−78279
^{20}Ne, configuration mixing and α-cluster transfer on ^{16}O 78−46004
^{20}Ne ground state level calc., maximum method 80−73795
^{20}Ne, highly excited α-unbound states, cluster model 78−634
^{20}Ne level density from Hauser-Feshbach anal. of ^{19}F(p,α_0)^{16}O, 1.5 to 3.8 MeV *(Spanish)* 77−30562
^{20}Ne, level struct., J^π, spectroscopic factors via (^{13}C,^{9}Be) reaction 77−14033
^{20}Ne levels, J^π, branching ratio and EM transition rates from ^{16}O+α 80−42540
^{20}Ne, levels, J^π and ang. distribs. from ^{18}O(t,p) 80−18204
^{20}Ne levels and branching ratio from ^{12}C(^{18}O, $\alpha\alpha$) 80−22661
^{20}Ne low lying levels and intermediate structure J^π from ^{16}O(^{12}C, ^{8}Be) 80−102166
^{20}Ne low lying states, configuration mixing calcs. with basis states from variational method 80−22693
^{20}Ne narrow $J^\pi=10^+$ resonance in strong absorption region, excited states from ^{12}C(^{16}O,^{8}Be) 79−30814
^{20}Ne, quartet states from ^{19}F(p,α)^{16}O 80−105973
^{20}Ne, rot. levels from α-^{16}O folded pot. model 77−67703
^{20}Ne, spectra and E1 transitions, ang. momentum projected HF and Tamm-Dancoff methods 77−54139
^{20}Ne states, J^π, differential cross sections and ang. distribs. from ^{16}O(α,α') 80−18203
^{20}Ne, suitability of lowest T=1 states for parity nonconservation experiments from ^{16}O(α,γ) 79−22189
^{20}Ne, unnatural parity levels at high excitation, γ spectra from ^{12}C(^{12}C, $\alpha\gamma$) 77−2933
^{20}Ne* low lying states and resonances, J^π assignments and energies from ^{12}C(^{16}O,^{8}Be) 79−93592
^{20}Ne(^{12}C,^{12}C), symmetry and shell struct. effects on absorption, precompound states 80−27666
^{21}Ne α-spectroscopic strengths and level J^π assignments from ^{17}O(^{6}Li,d) α-stripping 79−516
^{21}Ne configuration level density calcs. using spectral distrib. expansion, operator traces 79−71791
^{21}Ne, decay widths of lowest T=3/2 level, obs. as isospin forbidden resonance in ^{17}O(α,n) 77−6322
^{21}Ne deduced spectroscopic factors, levels and anal. powers from ^{20}Ne(d_{pol},p) 80−83087
^{21}Ne even parity states, generator coord. method, projected Hartree-Fock, and complete diagonalisation calcs. comparison 78−89796
^{21}Ne low lying states from ^{17}O(^{6}Li,d), weak coupling behaviour, ^{20}Ne+n 78−46100
^{21}Ne, low-lying excited states calc. by generator coordinate method 78−12974
^{21}Ne states, spins and rotational bands from ^{12}C(^{13}C,α) 79−75815
^{21}Ne states cross section, coupled channel and fluctuations anal. from ^{20}Ne(d,p) 80−27617
^{21}Ne, transition probabilities and multipole moments between states calc. by generator coordinate method 78−13022
^{21}Ne*, produced in ^{2}H(^{20}Ne,p)^{21}Ne*, 351 keV $^{5}/_{2}^{+}$ state lifetime and mag. moment 78−41631
^{22}Ne 2^+ state excitation in ^{126}Te(^{22}Ne, ^{22}Ne′) 79−54404
^{22}Ne levels, J^π, α-particle spectroscopic strengths studied via ^{18}O(^{6}Li,d) at 32 MeV 77−18594
^{23}Ne structure, differential cross sections from ^{27}Al (α, ^{8}B) 80−5153
Ni doubly even nuclei, eqns. of motion method, pairing correlations, ground state energies 80−52585
Ni even isotopes, negative parity levels, Tam-Dancoff approx., single particle energies 79−3080
Ni isotopes, from thermal neutron capture study 77−57674
^{A}Ni A=57-59, $f_{7/2}$ hole configuration effects, shell model calcs. 80−22670
^{A}Ni, A=58, 64, neutron densities and single particle struct. 80−32165
^{A}Ni, A=60, 62, 66, levels, J^π, anal. powers and cross sections from Ni(t,p)pol.t 80−68539
^{A}Ni, A=60, 62, nucl. level densities, using single particle states for Woods-Saxon and Nilsson potentials 78−50086
^{A}Ni, A=64, 58, level ang. momentum and spin values, DWBA anal. from (t,d) polarised t 79−36163
^{57}Ni energy levels, spin and parity assignments from ^{59}Ni(p,t) 79−9475
^{57}Ni levels and analogue states, J^π from DWBA anal. of ^{58}Ni(^{3}He, α) 79−63592
^{57}Ni, studied via ^{54}Fe(^{6}Li,t)^{57}Ni, t-energy spectra and reaction mechanism 78−41756
^{58}Ni, charge density, single particle struct., using proton wave functions 78−45995
^{58}Ni compound nucleus decay, fusion products from ^{46}Ti+^{12}C 79−40979
^{58}Ni, neutron densities from 1 GeV proton scatt. 78−17087
^{58}Ni(^{6}Li,^{6}Li′), 71 MeV, excited states deformation lengths, DWBA and coupled channels anals. 80−68541
^{58}Ni(^{7}Li,^{7}Li′), 19 MeV, first 2^+ states Coulomb-nuclear interference, optical and DWBA anal. 80−22852
^{58}Ni(α,α') 1.37 GeV, low lying state ang. distribs., Glauber rigid body approx. 79−54394
^{58}Ni(e,e′), 120-264 MeV, $J^\pi=6^+$, 5.125 MeV state isoscalar character, form factors, transition strengths 80−9262
^{58}Ni(e,e′) 5.125 MeV $J^\pi=6^+$ state excitation, isoscalar character 79−22227
^{58}Ni(γ,γ), M1 strength isospin splitting for dipole ang. distrib. states 80−13412
^{59}Ni deduced levels, from ^{58}Ni(d_{pol},p), cross section and vector analysing power 80−52684
^{59}Ni levels, cross section and vector anal. power, ang. distribs. from ^{58}Ni(^{7}Li,^{6}Li), pol.^{7}Li 80−106044
^{59}Ni, levels and new γ-transitions following ^{59}Cu(β^+)^{59}Ni 77−22935
^{59}Ni, semi-microscopic calc. of levels, spectroscopic factors and EM props. 77−2912
^{59}Ni, studied via ^{56}Fe(^{6}Li,t)^{59}Ni, t-energy spectra and reaction mechanism 78−41756
^{60}Ni deduced levels from ^{58}Fe(^{16}O,^{14}C)^{60}Ni, DWBA anal., spectroscopic strengths 80−47380
^{60}Ni level scheme and γ-rays from ^{59}Ni(n,γ) 80−63099
nuclear energy levels continued
^{60}Ni, spin of 1.33 MeV level, anisotropy coefficients in $4^+\rightarrow2^+\rightarrow0^+$ cascade *(Spanish)* 79−89525
^{61}Ni level ang. distribs., DWBA anal. from ^{59}Ni(t,p) 79−17816
^{61}Ni, low-lying levels, J, B(E2), B(M1) from Coulomb excit. 77−26610
^{61}Ni, multiparticle configurations, obs. in ^{61}Cu decay 78−70496
^{62}Ni, 6-11 MeV, levels determ. from ^{59}Co(α,p)^{62}Ni *(French)* 77−26615
^{62}Ni excitation level calcs., critical comparison of several methods *(Spanish)* 79−67654
^{62}Ni level struct. and decay scheme, shell model calcs. from ^{59}Co(α,pγ), 10 MeV 79−3085
^{65}Ni, spin assignments to p-wave neutron states 77−22852
^{235}Np deduced levels and Nilsson band configurations from ^{234}U(^{3}He,d) and ^{234}U(α,t) 79−468
^{237}Np electron transition excitation following K-shell photoionisation, deexcitation γ-rays 80−78196
^{237}Np, energy levels from ^{241}Am α-decay, γ transitions 79−6480
^{237}Np level scheme, α-decay of ^{241}Am *(French)* 78−74342
^{237}Np, quasi-stationary state decay through two bump barrier *(Russian)* 80−13420
^{238}Np energy level scheme determ. by Nilsson model 79−26370
^{238}Np levels, resonances and transitions from ^{237}Np(n,γ) 80−52589
^{242}Np levels, J^π and transitions from ^{242}U decay 79−67664
^{243}Np energy level spin assignments and anal. power from ^{244}Pu(t,α), polarised t 79−36165
^{A}O A=16, 17, deduced levels, spectroscopic factors from ^{12,13}C(^{13}C,^{9}Be) 79−26454
^{A}O, A=16, 17, valence-core self-consistency, wave functions, binding energy, levels, spectra 80−63123
^{A}O, A=17, 19, level scheme, two-step transfer contribs., coupled channel anal. from O(^{13}C,X) 80−32181
^{14}O low lying states, exact finite and zero range DWBA anal. from ^{12}C(^{3}He,n), 12-24 MeV 78−82286
^{15}O, level scheme determ. from ^{14}N(p,γ) 77−38243
^{15}O, normal parity levels from P-model calcs. with realistic NN interaction *(Russian)* 80−32194
^{15}O T=3/2 levels from ^{17}O(p,t) 78−78264
^{16}O, 0^- levels, energy shift, two channel anal. 79−75840
^{16}O, 0^+ states, appl. of K-harmonics method 78−54685
^{16}O, 3 α forces, ground state energy and form factor 80−86817
^{16}O 4^+ state nonstatistical population in compound nucleus calcs. of ^{12}C(^{6}Li,d) 80−102137
^{16}O α-cluster levels, props., hard-core potential calcs. 77−30614
^{16}O α-cluster states, widths and resonances, optical model, direct transfer in ^{12}C(^{6}Li,d) 80−105975
^{16}O, binding energy, wave function of ground state, orthogonal schema model 79−63582
^{16}O, bound isobars Δ(1236), single particle energies, wave functions *(Chinese)* 80−52562
^{16}O, Brueckner-Hartree-Fock approach, variational definition of single particle pot. 80−32170
^{16}O, calc. of spectrum of O^+ levels 79−63627
^{16}O collective and giant multipole states, Brueckner RPA particle-hole state description 80−32169
^{16}O, configuration mixing and α-cluster transfer 78−46004
^{16}O determ. of widths of 14.32 and 14.40 MeV levels from ^{14}N(α,d) 79−93513
^{16}O, energy levels, ^{13}C(^{3}He,$\alpha\gamma$)^{12}C radiative capture reaction, particle-hole picture 79−9471
^{16}O excited 0^+ levels 80−42551
^{16}O excited states from ^{14}N(^{3}He,p), ang. distrib. meas. 78−89891
^{16}O excited states near 15 MeV, R-matrix anal. of ^{15}N+p reactions 78−29460
^{16}O ground state and binding energy, microscopic calc. with realistic NW interaction *(Russian)* 80−5052
^{16}O, ground state energies, four order high lying contribs. 79−75850
^{16}O, ground state energy and RMS charge radius 78−58242
^{16}O ground state energy and low odd parity states, correlated basis function method 80−57689
^{16}O, isospin mixing anal. 78−8832
^{16}O level excitation functions, resonances from ^{12}C(^{16}O,^{12}C) 80−63146
^{16}O levels, Hauser Feshbach and DWBA anal. α-spectroscopic strengths from ^{12}C(^{6}Li,d), 20-34 MeV 79−569
^{16}O levels and ang. distribs., ^{3}He spectroscopic strengths, Hauser-Feshbach/DWBA anals. of ^{13}C(^{6}Li,t) 80−47390
^{16}O, levels near 13 MeV via ^{15}N+p 0.9-1.25 MeV 78−509
^{16}O, mixed T=0 and 1 states, isospin mixing matrix elements 78−37289
^{16}O, odd parity levels, correlated basis functions method 80−22721
^{16}O, particle hole calculations, centre of mass subtracted kinetic energy 78−62491
^{16}O particle-hole spectra, spectroscopic strengths, from ^{17}O(d,t) triton studies 78−58288
^{16}O residual states, vector anal. power. optical pot. from ^{12}C(^{6}Li,d), polarised ^{6}Li 79−97697
^{16}O, search for 0^+ level near 8.87 MeV 2^- level using ^{4}He(^{12}C,^{4}He) 77−88044
^{16}O, search for quartet excited states via ^{14}N(d,α)^{12}C and ^{14}N(d,p)^{15}N 77−57600
^{16}O, spin-orbit coupling in relativistic Hartree model 78−8731
^{16}O states, J^π from ^{12}C(^{12}C, $\alpha\alpha$) 80−22660
^{16}O states obs. in ^{12}C(^{7}Li,t), ^{12}C+4 particles vertex 77−14030
^{16}O structure, energy levels, binding energy, cluster model with varying hinge angle 78−4907
^{16}O two boson approach test, interacting boson approx., 0^+ and 2^+ levels 79−9489
^{16}O+X, X=^{11}B,^{12}C,^{13}C,^{18}O, deduced excited states, shell model wave functions, DWBA anal. 79−45284
^{16}O(^{16}O,^{16}O), symmetry and shell struct. effects on absorption, precompound states 80−27666
^{16}O(e,e′p), single hole state momentum and energy distribs. 80−22674
^{16}O(e,e), T=1 level form factors, Helm model, pion photoprod. and muon capture appls. 80−52553
^{16}O(γ,p)^{15}N up to 120 MeV, cross-sections, energy levels *(Russian)* 80−47465
^{16}O(γ,π), total cross section, Δ-hole states damping, π^0,ρ exchange, Δ isobar hole model 80−91174
^{16}O(p,p′), 1 GeV, proton polarisation in natural parity level excitation *(Russian)* 80−42634
^{16}O(p,p'), 135 MeV, 4^- particle-hole states, J^π ambiguity removal 80−5036

nuclear energy levels continued
$^{16}O(\pi,\pi')$, ~180 MeV, isospin mixing, levels, excitation functions and ang. distribs. 80−42543
^{17}O, 1p spin-orbit splitting anal. with $^{18}O(d,t)$ at 52 MeV 77−41980
^{17}O α-cluster states, α-decay orbital momenta and parities from $^{13}C(^6Li,d)$ and α-decay *(Russian)* 78−86486
^{17}O, cross sections to ground, 0.87 and 5.09 MeV states, neutron strength from $^{16}O(d,p)$ 80−5066
^{17}O, delayed neutron emission following ^{17}N β-decay 77−18481
^{17}O, energy multiple-scatt. contrib. using energy-depend. reaction matrix 77−14013
^{17}O high spin 4p-3h strength location from excited peaks of $^{13}C(^6Li,d),(^7Li,t)$ 79−3082
^{17}O levels, resonances, J^π and radiative width from $^{14}N(t,\gamma)$ 80−47389
^{17}O valence energies, extended multiple scatt. approach to 2p1h system 78−29396
^{17}O, widths of isospin forbidden neutron decays of T=3/2 levels, obs. in $^{13}C(\alpha,n)$ 77−6321
$^{17}O(e,e)$, elastic and inelastic, cross sections, excited states, charge radii 78−46049
^{17}O(g.s.), $((sd))_{5/2^+1/2}(1p^{-2})_{01}$ component determ. from $^{17}O(^3He,p)^{19}F$ data 78−78263
^{18}O 6p-4h states and composite spectra from $^{12}C(^{18}O,^{12}C)$ 80−63096
^{18}O, coexistence of spherical and deformed states 77−18394
^{18}O deduced levels and ang. distribs., cross sections from $^{12}C(^7Li,p)$, 16, 18 MeV 79−6686
^{18}O, dineutron cluster states, single-channel resonating group calc., levels, J^π 77−82841
^{18}O integrated cross sections to excited residual states from $^{19}F(\gamma,p)$ 80−18200
^{18}O level gamma decay from $^{17}O(n,\gamma)$ 80−52623
^{18}O low excitation struct., model calcs. 78−70452
^{18}O, low-lying positive-parity states, wave functions 77−6239
^{18}O, neutron deform. param. determ. from (π,π') scatt. 78−29502
^{18}O probable 6p-4h states from weak coupling calcs. 79−443
^{18}O, struct. of negative parity states, consistency and ghost elimination 77−26595
^{18}O, trinucleon cluster states, low lying negative parity states 78−29387
$^{18}O_2$ shell-cluster admixtures, spectra, α-widths and electric transitions 77−54136
$^{18}O+^{18}O$, scatt. and neutron transfer reactions, excitation levels, recoil DWBA analysis 78−8837
$^{18}O+\pi^\pm$, inelastic and elastic scatt., neutron-proton radius differences and isovector deform. 79−40963
$^{18}O(^{18}O,^{18}O)$, symmetry and shell struct. effects on absorption, precompound states 80−27666
$^{18}O(p,t)$, polarised p, 24.4 MeV, two-step reaction to unnatural parity state, anal. power 79−67739
^{19}O first excited state electric moment, B(E2) transition from $^{208}Pb(^{18}O,^{18}O')$ 79−67651
^{19}O high spin states populated in $^{13}C(^7Li,p)$ 78−21595
$^{19}O_\Lambda$, pairing correlation effects *(Chinese)* 80−47420
^{20}O, 1-20 ps region mean lifetime meas., high-vel. DSA method 77−65200
^{20}O, 4p and 6p-2h states obs. in $^{18}O(t,p)$ 79−40849
^{20}O, determ. by $^{18}O(^{18}O,\ ^{16}O)^{20}O$ reaction at 52 MeV 79−26450
^{20}O first excited state, g-factor and lifetime from $^3H(^{18}O,p\gamma)$ 80−102115
^{20}O states below 6 MeV, J^π assingments, DWBA anal. of $^{18}O(t,p)$ 79−22201
$(^{17,18}O,^{17,18}O')$, 54-69 MeV, on A=48-92, excited states and ang. distribs., DWBA anal. 79−67705
Os, O(6)→rotor transition, interacting boson approx. model, levels and transitions 79−13224
^{A}Os, A=186, 188, 190, 192, electromagnetic moments from muonic X-rays 78−12972
^{A}Os, A=186,188, levels and transitions from Re decay, triaxial rotor model 80−91155
^{A}Os, A=188, 189, levels, J^π, transitions and mixing ratios from Ir decay 80−68602
^{A}Os, A=190,192, two-quasiproton states, level struct., DWBA anal. of Ir(t,α) 79−89237
^{A}Os(α,α') A=188,190,192, 4_3^+ level population, hexadecapole vibrs. 78−89780
^{186}Os, levels deduced from ^{186}Ir decay and $^{186}W,(\alpha,4n)^{186}Os$ 78−86481
^{189}Os, level scheme from ^{189}Re beta-decay 79−54388
^{189}Os spectroscopy, Nilsson model description, triaxiality 77−14035
^{190}Os levels and γ-ray transitions, (n,γ) and (n,e^-) reactions 79−36189
^{191}Os, energy levels and spectra from $^{190}Os(d,p)$, $^{192}Os(d,t)$, $^{190}Os(n,\gamma)$ reactions 77−41917
^{192}Os level scheme and rot. bands, from $^{191}Os(n,\gamma)$, interacting boson approx. anal. 79−6413
$^{192}Os(p,p')$ and (d,d'), γ-ray spectra, energy level scheme 77−34243
^{193}Os, energy levels and spin assignments using $^{192}Os(n,\gamma)$ 79−36161
^{193}Os, energy levels investig. using $^{192}Os(d,p)^{193}Os$ and $^{192}Os(n,\gamma)^{193}Os$ reactions 78−41642
^{193}Os level scheme and transitions, Coriolis coupled Nilsson states from $^{192}Os(n,\gamma)$ 80−57698
^{194}Os, obs. of levels populated in $^{192}Os(t,p)$ 78−50181
^{A}P, A=31, 33, levels and transition j-depend., DWBA anal. for $Si(^{19}F,\ ^{16}O)$ 80−42542
^{28}P, energy levels and spectroscopic assignments using $^{28}Si(^3H,t)$ *(French)* 79−45167
^{28}P, nucleon unbound states, spin, parity, partial width, from $^{28}Si(d,pn)$ 80−102118
^{29}P deduced levels from ^{29}S β^+-delayed proton decay, half life 79−22241
^{29}P, unbound states via $^{28}Si(d,pn)$ 10-11.8 MeV ang. distribs., DWBA anal. 77−6236
^{30}P, 1st excited state, α-isospin forbidden transition probability in $^{32}S(d,\alpha)$ 78−89882
^{30}P level width isospin depend., excitation functions, statistical anal. of $^{29}Si(p,\alpha)$ 80−78152
^{30}P positive parity states, transitions and spectroscopic strengths, DWBA anal. of $^{29}Si(^3He,d)$ 80−102138
^{30}P T=1 state decay, lifetimes and branching ratios, analogue E2 transitions from $^{29}Si(p,\gamma)$ 80−68598
^{31}P high E_x states, J^π, DWBA anal. $^{29}Si(^3He,p)$ 80−68536
^{31}P states from $^{29}Si(^3He,p)$, energy levels, ang. distribs., L-values 78−82361
^{31}P transition cross sections from $^{33}S(p,^3He)$ 79−67660
nuclear energy levels continued
^{32}P, ang. correls. and branching ratios meas. using $(^3He,p\gamma)$ at 11-15 MeV 78−13129
^{32}P, spin-parity assignments from $^{34}S(d,\alpha)^{32}P$ 78−17219
^{34}P, excited states and mass excess via $^{34}S(t,^3He)^{34}P$ 23.0 MeV reaction 77−34229
^{34}P mass and energy levels from $^{36}S(d,\alpha)$ 79−6632
^{141}PM struct. determ. from $^{141}Sm^g$ decay 77−46142
^{233}Pa anal. power for spin states from $^{234}U(t,\alpha)$, polarised t 79−36165
^{233}Pa excited level scheme and γ-transitions from ^{237}Np α-decay 79−80876
^{234}Pa isomers from ^{234}Th β^- decay, low energy γ-spectrum 78−70493
^{206,207,208}Pb levels, ground state widths via reson. fluoresc. 77−74799
Pb, 195-203, high-spin neutron hole excitations, hole-core weak coupling 77−50062
Pb, A=193, 5, 7, 9, high-spin states anal. by heavy ion reactions 78−21500
Pb, A=200, 202, 204, seniority four admixtures in low lying 0^+ states 78−8741
Pb even isotopes, two quasiparticle 2^+ state coupling to T=0 giant quadrupole resonance 80−68618
$Pb(^{12}C,^{12}C')$, A=204,206,208, 60 MeV, quadrupole moment and B(E3) values 79−17797
$Pb(^{16}O,^{16}O')$, A=204,206,208, 52 MeV, quadrupole moment and B(E3) values 79−17797
^{A}Pb, A=202, 203, 204, transfer strengths from 17.5 MeV $^{204,205,206}Pb(p,t)$ reaction 78−94005
^{A}Pb, A=190,192, level scheme, γ-branching, ^{192m}Pb half life from Gd+^{40}Ar and $^{182}W+^{16}O$ 79−75854
^{A}Pb, A=200,206, 12^+ isomer states, quadrupole moments 80−27554
^{A}Pb, A=205-207, neutron hole states, spectroscopic factors, DWBA anal. of $Pb(^3He,\alpha)$ 80−47352
^{A}Pb, A=207,209, single particle state mag. moment in large shell model space 79−45162
^{A}Pb(e,e'), A=204, 206-208, levels and inelastic cross sections 80−22698
^{A}Pb(γ,γ), A=206-8, 4.5 MeV to neutron emission threshold, strengths in energy levels 79−36164
^{A}Pb(γ,n), A=206, 208, levels using tagged photons 80−23245
^{105}Pb, level scheme, from nuclear reactions and ^{105}Ag β decay 77−82849
^{194}Pb, excited level scheme from ^{194}Bi decay 77−6306
^{196}Pb, excited level schemes from ^{196}Bi decay 77−6306
^{199}Pb, level scheme from ^{199}Bi decay 78−78316
^{201}Pb, level scheme from ^{201}Bi decay 78−78316
^{203}Pb, 480 ms isomeric $29/2^-$ state, decay scheme 77−22893
^{203}Pb, high-spin level struct. determ. from $^{202}Hg(\alpha,3n\gamma)$ at 38.2 MeV 78−29489
^{204}Pb, muonic, first excited 2^+ state, isomer shift of E2 transition 80−99150
$^{204}Pb(n,n'\gamma)$, 1.5-3.1 MeV, levels, J^π, excitation functions and mixing ratios 80−102123
^{205}Pb, ^{206}Pb, cluster vibrational field coupling model description 77−57604
^{205}Pb, hole states below 2.56 MeV, spectroscopic strengths via $^{204}Pb(d,p)$ 77−30478
^{205}Pb, particle states via $^{204}Pb(d,p)$, spectroscopic factors 77−34216
^{206}Pb $\gamma\gamma$ directional correlations, multipole mixing ratios, transition strength limits from ^{206}Bi decay 80−86849
^{206}Pb, level scheme including conversion electrons $\lesssim$40 eV 78−21518
^{206}Pb low lying level ang. distribs., zero range DWBA anal. from $^{208}Pb(p,t)$ 79−67656
^{207}Pb doorway resonances, M1 ground state radiative strength, level density from $^{206}Pb(n,n)$, (n,γ) 79−93589
^{207}Pb inner hole states, spectroscopic strengths DWBA anal. from $^{208}Pb(^3He,\alpha)$ 79−17813
^{207}Pb muonic isomer shifts, neutron hole anomalous moment contribs. 80−78728
^{207}Pb neutron hole states, core vibration effects, shell model energies 79−36142
^{207}Pb parity assignments and M1 radiative strength from $^{206}Pb(n,n)$ 80−52614
$^{207}Pb(\gamma,n)$, 7632 keV level photoexcitation, cross section and J^π 80−37330
$^{207}Pb(p,p')$, excitation of neutron-hole states, 61.2 MeV protons 78−8724
^{208}Pb 1^+ states, fine struct., energy levels, transition probabilities, matrix diagonalised method *(Chinese)* 78−78269
^{208}Pb 7064 keV level negative parity, EM deexcitation pattern from $^{207}Pb(d,p)$ 79−36148
^{208}Pb breathing model transition density, single particle and collective state dynamical coupling 80−106007
^{208}Pb core with valence nucleon or hole, mag. props., exchange currents, electron scatt. 80−22689
^{208}Pb, damping of single particle states and giant resonances 79−17782
^{208}Pb, excitations, EM transitions in renormalised RPA 77−82857
^{208}Pb, magnetic high spin states, microscopic struct. 80−95297
^{208}Pb, neutron densities and single particle struct. 80−32165
^{208}Pb region, finite Fermi systems, review 78−537
^{208}Pb single particle and hole states, renormalisation, core polarisation, spectroscopic factors 80−57658
$^{208}Pb(^{12}C,^{11}B)$, 77 MeV, bound and continuum state excitation, direct and two step processes 80−63205
$^{208}Pb(\alpha,\alpha')$, levels, B(E3), transition density and nuclear pot., folding model anal. 80−86812
$^{208}Pb(d,^6Li)$ ^{204}Mg, SS MeV, levels and spectroscopic factors, α clustering, DWBA anal. 79−67694
$^{208}Pb(e,e')$, 50 to 335 MeV, 12^- mag. spin state excitations 78−50155
$^{208}Pb(\gamma,\gamma)$, parity of bound J=1 levels 79−22188
$^{208}Pb(p,p')$, 135 MeV, normal parity level excitation, J^π, differential cross sections 80−57690
$^{208}Pb(p,p')$, 135 MeV, normal parity excitations, microscopic description, NN interaction shape 80−57691
$^{208}Pb(p,p')$, precritical behaviour in pionlike excited states in nuclear matter 79−49593
$^{208}Pb(p,p)$, 0.8 GeV, elastic and inelastic, ang. distribs., states, optical and DWBA anal. 79−3154
$^{208}Pb(p,\pi^+)$, 180 MeV, ang. distribs., discrete states, differential cross section 79−13298
^{209}Pb excited states, $3/2^-$ resonances from shell model of $^{208}Pb(n,n)$ 80−78240
^{209}Pb excited states and $3/2^-$ resonances, shell model, calcs. from $^{208}Pb(n,n)$ 80−18262
^{209}Pb levels obs. in $^{210m}Bi(t,\alpha)$ 77−34320

nuclear energy levels continued
^{209}Pb unbound high spin shell model states, single nucleon states 78−25126
^{210}Pb levels, J^{π}, transitions and lifetimes from ^{208}Pb(^{7}Li,X) 80−68542
^{211}Pb, Pauli principle effects on level spectrum, ^{210}Pb(t,d) spectroscopic factors 78−17108
Pb(α,α'), A=204,206,208, 13.8 MeV, quadrupole moment and B(E3) values 79−17797
^{108,110}Pd, particle-vibr. multiplet excit. by two-neutron stripping 77−34214
Pd, A=102,4,6, collective and two-quasiparticle excitation for Zr (^{13}C, 3nγ) 77−18601
^{A}Pd(^{32}S,^{32}S'), A=102, 104, 106, 108, 110, 72-80 MeV, 2_1^+ state mag. moments 80−47373
^{99}Pd level scheme, γ-ray cascade, studied via heavy-ion reactions 77−30506
^{100}Pd levels and γ-transitions from ^{100}Ag^{g,m} decay 80−83077
^{101}Pd, level struct. obs. in ^{101}Ag β-decay 78−37311
^{102}Pd(p,p':γ,γ), population of low spin levels, level scheme 79−36153
^{102}Pd(p,p'γ), 8 MeV, ang. correl. meas. to determ. level scheme 78−21559
^{102}Pd(p,p'γ), long lived O^+ state, E0 transitions 80−73804
^{104}Pd, characts. of the levels excited in ^{104,104m}Ag decay 79−9515
^{104}Pd levels populated in ^{104m,g}Ag β^+ decay , spins, parities 78−13018
^{105}Pd, from decay of ^{105m,g}Ag 78−37306
^{105}Pd levels with large spin, γ spectra 79−6478
^{106}Pd energy states and J^{π} from ^{106}Ag^{m} decay 80−18197
^{106}Pd, excited states and transitions from decay of ^{106}Rh^{g} 77−79324
^{106}Pd, gamma-gamma ang. correlation meas. from decay of ^{106}Rh^{g} 77−79325
^{106}Pd levels and E0 transitions from ^{106}Ru β-decay 79−75894
^{109}Pd, energy levels determ. from decay of ^{109}Rh 78−25154
^{109}Pd, level structure and half life 77−82827
^{109}Pd levels, J^{π}, transitions, unique parity states, and spectroscopic factors from ^{108}Pd(n,γ) 80−42547
^{109}Pd low spin odd parity levels, γ-rays, particle-rotor comparison from ^{108}Pd(n,γ) 80−73805
^{109}Pd low spin odd parity states, rot. aligned model, Coriolis calc. of ^{108}Pd(n, γ) 80−57695
^{109}Pd unique parity levels, interacting boson approx. model test for odd-A nuclei 79−85369
^{109}Pd unique parity states, particle rotor model low spin test 79−93515
^{A}Pm, A=143, 145, proton states and transitions, stripping strength, shell model anal. from Nd(^{3}He,d) 80−68508
^{A}Pm, A=144,148,152, strong exhaustion of deeply-bound proton hole states 79−45142
^{A}Pm, A=147,149,151 single proton hole states in pickup reactions from Sm(p,α) 80−78128
^{A}Pm, A=149,151, shape coexistence, deformed states from Nd decay 80−78135
^{142}Pm, multiplet splitting and isomerism, J, π, T1/2 via (d,2n) and (p,n) 77−14014
^{143}Pm, p single particle states and pairing force calcs., low lying levels 80−42522
^{145}Pm, low-lying levels anal. using ^{145}Sm decay 78−29420
^{147}Pm energy levels and γ-ray transitions E2/M1 mixing ratio from ^{147}Nd β-decay 79−67655
^{147}Pm, level scheme and transitions following ^{147}Nd 80−83073
^{147}Pm, level struct. via ^{148}Nd(p,2nγ) 12.1-20.2 MeV 78−510
^{147}Pm levels, transitions, $\gamma\gamma$-coincidences and IC electrons from ^{147}Nd decay 80−18243
^{147}Pm, low-lying levels, spin-parity and multipole mixing ratios 77−88043
^{147}Pm proton states and transitions shell model anal. of ^{148}Sm(t,α), ^{146}Nd(^{3}He,d) 79−30781
^{149}Pm, energy levels from ^{149}Nd beta decay 80−27592
^{149}Pm levels, bands, transitions, in-beam spectroscopy, particle-rotor anal. from ^{150}Nd(p,2nγ) 80−78125
^{149}Pm single proton states, spin assignments, spectroscopic factors from ^{150}Sm(t,α), pol.t 80−18170
^{151}Pm single proton states, rot. bands, level J^{π} assignments, spectroscopic strengths from ^{150}Nd(^{3}He,d), and ^{152}Sm(t,α) 79−67626
^{153}Pm struct., spin and parity assignments, Nilsson model interpretation from ^{154}Sm(t,α) polarised t 79−469
Po, A=202-210, isomeric levels, g, $T_{1/2}$ 77−14068
^{A}Po, A=209, 211 deduced levels, J^{π} assignments, spectroscopic factors from stripping and pickup reactions 79−22197
^{208}Po, yrast two proton-two neutron hole states 78−78307
^{209}Po, 31/2$^-$ isomeric state, g-factor meas. 77−10317
^{210}Po, level density calc., shell and pairing effects, deformation, excitation energy dependence 79−67662
^{211}Po excitation functions and isomer ratios from ^{208}Pb(α,n) and ^{209}Bi(α,np) 80−83039
^{212}Po excitation functions and isomer ratios from ^{209}Bi(α,p) 80−83039
^{212}Po, isomer with spin and parity 8$^+$, α- and γ-decay 78−82283
^{212}Po, levels, J^{π}, transitions and lifetimes from ^{208}Pb+^{7}Li 80−68542
^{212}Po levels and J^{π}, weak coupling calc. using realistic matrix elements 80−5068
^{143}Pr, 57 keV state, from ^{143}Ce 1404 keV beta transition spectrum shape 78−74339
^{144}Pr levels and transitions, studied via ^{144}Ce decay 77−14070
^{145}Pr, level schemes determ. from β-decay of A=145 nuclei 78−78323
^{146}Pr→^{146}Nd, decay scheme and energy levels, log ft values 78−4912
Pt, A=192, 194, 2^+, 3^+ states via (α,α') Coulomb excit. 78−622
Pt even isotopes, nonaxial deforms., odd parity states, semidecoupled model 77−34220
Pt isotopes, use of (p,t) reaction to study low lying states 77−54212
Pt, O(6)→rotor transition, interacting boson approx. model, levels and transitions 79−13224
Pt, positive-parity states, Coriolis antipairing effect, deformed-rotor model 78−12950
^{A}Pt, A=190, 192, 194, levels and γ-transition reduced probab., interacting boson model 80−18196
^{A}Pt, A=190,192,194, state struct. in interacting boson model 80−83047
^{A}Pt, A=191 to 197, odd, levels excited via (p,d) and (d,t) 78−50089
^{A}Pt, A=192, 194, 196, states, J^{π}, ang. distribs. and transitions, DWBA anal. of Pt(p,t) 80−468
^{185}Pt from ^{190}Pt(p,t), 0^+ and ground state population 78−86532
^{186}Pt, level scheme 79−97652
^{187}Pt, levels, J^{π}, $T_{1/2}$, possible E0 transitions from ^{187}Au decay *(French)* 80−32230
nuclear energy levels continued
^{188}Pt, level scheme 79−97652
^{191}Pt energy levels, γ and conversion electron spectra, spins, parities 78−25149
^{192}Pt 4^+ and 3^+ levels populated in ^{192}Ir β decay, spectral shapes, quadrupole vibr. levels 77−50086
^{192}Pt(α,α'), 24 MeV, α-angular distrib. for 0^+, 2^+, $2^{+\prime}$, 4^+, $4^{+\prime}$ and 3^- state excitation 78−70550
^{193}Pt low lying negative parity states and shape from ^{195}Pt(p,t) 80−68540
^{194}Pt, determ. of sign of $P_3=M(0_1^+2_1^+)M(2_1^+2_2^+)M(2_2^+0_1^+)$ 79−63588
^{196}Pt (^{20}Ne, ^{20}Ne'), excited states, lifetime meas. using recoil-distance method 80−13413
^{196}Pt (^{58}Ni, ^{58}Ni'), excited states, lifetime meas. using recoil-distance method 80−13413
^{196}Pt level struct. and J^{π} assignments, interacting boson approx. O(6) limit from ^{195}Pt(n,γ) 79−75853
^{197}Pt states populated by (d,p), (d,t) and (n,γ) reactions 78−78267
^{239}Pu(n,f), 0.1-1 Mev, light charged particle emission, saddle point states 79−22343
^{240}Pu, level density calc., shell and pairing effects, deformation, excitation energy dependence 79−67662
^{240}Pu levels via ^{236}U α-decay *(Russian)* 77−82882
^{241}Pu level structure and γ-transitions from ^{245}Cm decay 80−105980
^{242}Pu level scheme from ^{242}Np β-decay 79−67664
^{244}Pu levels via ^{248}Cm α-decay *(Russian)* 77−82882
^{246}Pu excited states, mass excess and shell gap, L=0 transition from ^{244}Pu(t,p) 80−9236
^{226}Ra levels from ^{230}Th α decay, search for $K^{\pi}=0^+$ excited states 78−86504
^{226}Ra, total enutron cross-section up to 1 keV 77−26745
^{230}Ra levels, J^{π} and transitions, Nilsson assignments from ^{230}Ac decay 80−68543
^{A}Rb(n,n'γ), 550-2100 keV, A=85,87, levels, excitation functions, J^{π}, Hauser-Feshbach anal. 80−105982
^{74}Rb, N=Z nucleus with T=1, $I^{\pi}=0^+$, half life 77−26627
^{80}Rb, level struct., quasi-rot. bands, via ^{79}Br(α,3n) 30-55 MeV reaction 77−88028
^{82}Rb, level structure, gamma angular and time distribs. from ^{81}Br(α,3n) 80−52583
^{84}Rb levels from ^{85}Rb(p,d), spin and parity determ. 78−82338
^{85}Rb levels, J^{π} and transitions from Kr^{m,g}, Sr^{m,g} decay, cluster-vibr. model 80−78162
^{87}Rb, low-lying level struct. in quasiparticle-core model 77−82825
^{90}Rb level scheme, transitions, J^{π} assignments and internal conversion coeffs. from ^{90}Kr β-decay 79−67663
^{93}Rb, γ-ray decay scheme, levels, J^{π}, logft values 77−54152
Re, A=187, 189, 191, obs. of proton hole states via (t,α) 77−88025
Re, odd isotopes, pot. energy surfaces and quadrupole deformation parameters, deformed basis model 79−80867
^{A}Re, A=181, 182, 187, magnetic moments meas. by PAC 80−22688
^{A}Re, A=181, 182, 187, spin polarisation, state struct. and mag. moments in rot. model 80−18194
^{177}Re, populated in decay of Os isotopes, lower excited state obs. 78−17145
^{179}Re, populated in decay of Os isotopes, lower excited state obs. 78−17145
^{187}Re, 206 keV state, g-factor, time differential PAC meas. 78−505
^{187}Re low lying level struct. and transitions, E2/E1 mixing ratios from ^{187}W decay 80−27557
^{188}Re, energy levels obs., form. by ^{189}Os(t, α)^{188}Re 80−47487
^{97}Rh levels and γ-transitions, 3QP model anal. of ^{97}Pd β^+-decay 80−102120
^{103}Rh level scheme from fast n scatt., γ transitions, spins, parities, cross sections 78−78374
^{103}Rh, quadrupole moments of 3/2$^-$ and 5/2$^-$ states, reorientation precession meas. 77−2905
^{105}Rh, particle-vibr. multiplet excit. by two-neutron stripping 77−34214
^{108}Rh, level structure and half life 77−82827
^{212}Rn, shell model states, semiempirical calcs. half lives, mag. moments, excitation functions 80−63083
^{A}Ru, A=104,106,108, level scheme and transitions, collective model anal. of Tc decay 80−78166
^{A}Ru, A=106, 108, levels, transitions, J^{π} and shape from Tc decay 80−57744
^{A}Ru(^{16}O,^{16}O'), 36-45 MeV, A=96, 98, 100, 102, 104, first 2^+ excited state quadrupole moment 80−47374
^{A}Ru(α,α'), 8.5-9.5 MeV, A=96, 98, 100, 102, 104, first 2^+ excited state quadrupole moment 80−47374
^{A}Ru(p,p'γ), A=96, 98, 5-8 MeV, level schemes, transitions, vibr. state, mixing ratios 80−18199
^{94}Ru level structure, spin and parity, from beta decay of ^{94}Rh isomers 80−57747
^{94}Ru levels and γ-transitions from ^{94}Rh decay 80−18244
^{95}Ru level scheme, low lying states, g-factor spin, parity 77−88071
^{97}Ru, ^{101}Ru, studied via ^{96,100}Ru(d,p) reactions at 11.5 MeV 77−18570
^{97}Ru levels anal. with ^{96}Ru(d,p) at 16 MeV 77−38284
^{100}Ru, energy levels from ^{100}Rh decay 79−6510
^{100}Ru, negative parity bands obs. in ^{100}Mo(α,4n)^{100}Ru 77−6291
^{102}Ru levels populated in ^{102}Tc^{g} β^--decay 78−86513
^{102}Ru(^{16}O,^{16}O), 38-42 MeV, Coulomb excitation, 2^+ state electric quadrupole moment 80−73793
^{102}Ru(α,α), 8.5, 9.0 MeV, Coulomb excitation, 2^+ state electric quadrupole moment 80−73793
^{103}Ru, level scheme determ. from ^{103}Tc β-decay 79−85413
^{103}Ru, level struct. from ^{103}Tc decay 79−9470
^{104}Ru level energies, B(E2) ratio, mixing ratios, γ-ang. correlations, from ^{104}Tc β-decay 79−493
^{104}Ru, level scheme determ., β^- and γ-activities of ^{104}Tc 78−82313
^{105}Ru, level and γ-decay scheme determ. 78−82312
^{31}S level J^{π} assignments, transition cross section from ^{33}S(p,t) 79−67660
^{31}S, studied via ^{28}Si(^{6}Li,t)^{31}S, t-energy spectra and reaction mechanism 78−41756
^{32}S α-cluster struct., ground and first excited states, energies, radii and moments 80−102122
^{32}S energy levels and ang. distribs., DWBA anal. from ^{31}P(^{3}He,d), 25 MeV 78−78265
^{32}S levels and J^{π} from ^{32}Cl β^+ decay 80−22772
^{32}S levels and spectroscopic factors, DWBA anal from ^{28}Si(^{16}O,^{12}C) 79−22204

nuclear energy levels continued
S levels and spectroscopic factors from pickup DWBA anal. of ^{3}S(^{3}He,α) 80−9235
^{3}S(d,p), DWBA anal. converging overlap integrals, stripping to decaying states 79−6530
^{32}S(n,γ), single particle resonances and doorway states, K matrix formalism 80−37384
^{33}S(n,n′γ), 13.9 MeV, 2^{+} (2.23 MeV) excitation, spin flip probab., deexcitation γ-rays 80−86853
^{33}S compound nculeus from ^{31}P(d,p)^{32}P ang. distrib. DWBA anal. and level widths 78−74371
^{34}S levels, excited by α-capture reactions 78−33124
^{34}S, state spectroscopy via ^{30}Si(α,nγ), E1,E2, J$^{\pi}$ assignments <5 MeV 77−34227
^{34}S, populated in ^{32}S(t,p) at 10 MeV 78−50180
^{34}S(γ,γ), E<18 MeV, state lifetimes, excitation energies and level cross sections 78−93966
^{35}S, total ang. mom. of levels up to 5.058 MeV, obs. in ^{34}S(d,p) 77−88149
^{36}S, mode-mode coupling model for four-body correls. 77−10322
^{37}S energy level scheme from (d,p) study, proton spectra *(Russian)* 78−41733
^{37}S level scheme and excitation energies from ^{36}S(d,p) *(Russian)* 79−30790
Sb, A=127-33, fission fragments, partial level schemes determ. 78−29392
Sb, odd-mass nuclei, 9/2^{+} bands, deformed states 78−17106
^Sb, A=119,122, level density, neutron spectra and ang. distribs. nonequilib. processes from Sn(p,n) *(Russian)* 80−37376
^Sb, A=121,123, levels below 2 MeV, spins, transitions and mixing ratio from (p,γ), (n,n′γ) 80−32191
^Sb, A=123,125,127,129, cross-sections, ang. distribs., spectroscopic factors, DWBA anal. of Te(t,α) 80−52572
^{115}Sb, high-spin states anal., ^{113}In(α,2nγ) at 20-30 MeV 77−41982
^{117}Sb, levels studied via ^{116}Sn(^{16}O,^{15}N)^{117}Sb, ang. distrib. anal. of 64 MeV reacts. 78−8836
^{119}Sb, low-lying states obs. in decay of ^{119m}Te 77−50088
^{120}Sb low lying level scheme, J$^{\pi}$ assignments from ^{120}Sn(p,nγ) 79−22196
^{121}Sb, positive parity levels, Coulomb excitation obs. 78−21522
^{122}Sb energy levels populated in ^{121}Sb(n,γ), spin, parity, γ and conversion electron spectra 78−54721
^{123}Sb, positive parity levels, Coulomb excitation obs. 78−21522
^{123}Sb(γ,γ′), energy levels, spin and parity, strong M1 transitions 78−93940
^{130}Sb levels, spin-parity assignments, from ^{130}Sn β decay 77−34264
^{133}Sb, level scheme of one proton and doubly closed shell core 78−37291
Sc, A=43, 47, $d_{3/2}$ hole states, wave functions mag. moment, M2 transitions, shell model 78−17116
^Sc A=44,46,48, HF projection formalism, energy levels, static moments, EM transition probabilities 79−3083
^Sc, A=45, 47, HF projection formalism, energy levels, EM moments, transition probabilities 79−22199
^{41}Sc, two particle-one hole states, EM transition probabilities 77−88035
^{42}Sc, energy levels anal. by ^{40}Ca(α,d) at 40 MeV 78−21579
^{42}Sc two particle states, spectroscopic strengths and J$^{\pi}$ values from ^{41}Ca(^{3}He,d) 79−63591
^{43}Sc, state calc. by shell model including $1g_{9/2}$ orbit 79−80873
^{44}Sc, 68 keV state, g-factor, time differential PAC meas. 78−505
^{44}Sc, $(f_{7/2})^{4}$ states populated in ^{41}Ca(α,p) 25 MeV reaction, relative transition strengths, semi-microscopic model calcs. 79−6645
^{45}Sc levels, J$^{\pi}$, transitions and lifetimes from (p,p′)(^{3}He,^{3}He′)(α,α′) 80−63091
^{45}Sc, neutron stripping and pick-up, reanalysed data, sum rule anal. and spectroscopic factors 78−8828
^{45}Sc resonance decays, energy levels and J$_{\pi}$ values from ^{44}Ca (p,γ) 79−80908
^{46}Sc energy levels, resonances, spin and parity from ^{45}Sc(n,γ) 80−52673
^{46}Sc level deexcitation, E1 and M1 absolute radiative widths from ^{45}Sc(n,γ) 80−52622
^{46}Sc transition polarisation, levels and spin assignments from ^{45}Sc(n,γ), pol. n 80−52656
^{49}Sc, levels via ^{48}Ca(τ,d)^{49}Sc 18 MeV 77−10303
^{49}Sc, location of major $2p_{1/2}$ strength using (^{7}Li,^{6}He) react. 78−25095
^{49}Sc proton single particle states, spectroscopic factors, DWBA anal. of ^{48}Ca(d,n) 80−99118
^{49}Sc, single particle states lifetimes calcs. 80−105943
Se, A=76, 78, 80, 82, static quadrupole moments of first 2^{+} excited states 77−65197
Se even isotopes, A=76-82 level struct. from (n,n′γ) 77−34233
Se, even-even isotopes, first excited 0^{+}′ states, energy systematics 78−54683
Se, even-even nuclei, γ-spectroscopy, exptl. results and models 80−68589
Se isotopes, excited states struct., energy systematics 78−54687
Se isotopes level structures from ^{76,78,80,82}Se(d,p) spins, parities, spectroscopic factors, l-values 78−89885
^Se, A=75, 77, 79, 81, levels and ang. distribs., spectroscopic factors from Se(p, d) 80−22696
^Se(p,p), A=76-82, doubly even nuclei, deformation parameters 79−97705
^{72}Se, high spin and excitation regions anal., ^{58}Ni(^{16}O,2pγ) 78−25226
^{74}Se level scheme, J$^{\pi}$ assignments, bands and transitions from ^{60}Ni(^{16}O,2p), ^{64}Ni(^{12}C,2n) and ^{65}Cu(^{11}B,2n) 79−54393
^{74}Se quasi-γ bands and negative parity levels from ^{75}As(p,2nγ) 80−456
^{75}Se energy levels from ^{74}Se(d,p), DWBA, sum rule anals., spectroscopic factors 78−66285
^{76}Se, level scheme from γγ coincidence meas. of ^{76}As decay 80−22754
^{79}Se, level structure study via ^{80}Se(p,d)^{79}Se 78−93993
^{83}Se, IAS, J$^{\pi}$ via ^{82}Se(p,pγ) 4.5-7.7 MeV 78−573
^{76,74}Se, 33 MeV levels, J$^{\pi}$ via Se(p,t)Se 77−67700
Se(n,n′) 2^{+} level excitation cross sections, intermediate resonances, optical model with coupled channels *(Russian)* 79−40897
Se(n,n′γ), even-A isotopes, 2.0 to 4.1 MeV, level and decay schemes 77−23092
^Si(e,e'), 126-293 MeV, A=28,29, levels and form factors, particle-phonon coupling anal. 80−105977
^{27}Si, levels, GDR isospin mixing via (γ,n) 28 MeV 77−74832
^{27}Si, shape mixing using ang. momentum projection from Hartree-Fock intrinsic states 78−86472
^{27}Si, studied via ^{24}Mg(^{6}Li,t)^{27}Si, t-energy spectra and reaction mechanism 78−41756

nuclear energy levels continued
^{28}Si 12.291 MeV level width, axial blocking meas. from ^{27}Al(p,α) 80−63086
^{28}Si, 17.62 and 17.71 MeV level struct. 79−9468
^{28}Si, 2^{+} 1.78 MeV state, reduced matrix element and deformation length from (^{16}O,^{16}O) 79−13317
^{28}Si 4^{+} state lifetime by blocking effect method from ^{27}Al(p,α) *(Russian)* 80−91152
^{28}Si (e,f), K=2 symmetry intermediate state 80−47514
^{28}Si, appl. of theory of bi-determinantal intrinsic states 79−9484
^{28}Si α-doorway states in α-decay to ^{24}Mg low lying K-band 80−47438
^{28}Si, energy levels populated in ^{24}Mg(α,n)^{27}Si, threshold to 13.1 MeV 78−618
^{28}Si, excited levels populated in ^{27}Al(p,α)^{24}Mg at E$_{p}$=1540-2220 keV 78−17189
^{28}Si, investigation of levels and resonances in ^{27}Al(p,γ) and ^{24}Mg(α,γ) 78−66205
^{28}Si levels and J$^{\pi}$ from ^{28}P β^{+} decay 80−22772
^{28}Si, sd-shell calcs. for O^{+} states, particle-hole conjugation 77−67704
^{28}Si, shell model and statistical spectroscopic anal. 78−29390
^{28}Si spectrum, central and noncentral components of effective sd-shell interaction 77−54160
^{28}Si(^{12}C,^{16}O)^{24}Mg, entrance, exit and reaction channel data at backward angles 79−36254
^{28}Si(e,e′), 38.7-57.5 MeV, energy levels, isovector M1 strength, DWBA anal. 79−75847
^{28}Si(n,γ), single particle resonances and doorway states, K matrix formalism 80−37384
^{28}Si(n,n′γ), 13.9 MeV, spin flip probability from 1.78 MeV state, direct theory 80−9234
^{28}Si(p,p′), 135 MeV, large momentum transfer, excitation of high-spin particle-hole states in ^{28}Si 77−61420
^{28}Si(p,p), pol. p, 12-18 MeV, cross section, anal. power and states, ^{29}P resonance coherence widths 80−32258
^{28}Si(π$^{\pm}$,π$^{\pm}$′), 162 MeV, excitation of high-spin particle-hole states 79−93667
^{29}Si 3/2^{+} and 5/2^{+} states population, (d,p) and (p,π^{+}) comparison 80−95307
^{29}Si, DWBA anal. of ^{9}Be elastic scatt. on various nuclei *(German)* 78−70552
^{29}Si doorway state neutron capture, levels and γ-spectra from ^{28}Si(n,γ) 80−57729
^{29}Si levels, J$^{\pi}$, spectroscopic factor, DWBA anal. of ^{28}Si(^{3}He, ^{2}He) 80−86811
^{29}Si levels and ang. distribs., DWBA anal. of ^{27}Al(α,d) 80−78157
^{29}Si, low lying energy level structure, from ^{28}Si(d_{pol},pγ) and multi-step reaction calcs. 80−68537
^{29}Si, nucleon unbound states, spin, parity, partial width, from ^{28}Si(d,pn) 80−102118
^{29}Si, unbound states via ^{28}Si(d,pn) 10-11.8 MeV ang. distribs., DWBA anal. 77−6236
^{30}Si first excited state, static quadrupole moment from ^{208}Pb(^{30}Si,^{30}Si) 80−13373
Sm odd isotopes, $1h_{11/2}{}^{-1}$ neutron state strength distrib. 77−46100
^Sm, A=146,147, excited states, energy levels, spin, parity, shell and cluster-vibration models, from (α,xn) and (^{3}He,xn) 80−57683
^Sm, A=147, 149, levels, J, γ-transitions and multipole mixing ratios, γγ correlations from Eu EC decay 80−106012
^Sm, A=148, 150, 152, 154, levels, moments, isomer shifts, spectroscopic amplitudes, sixth order boson expansion 79−89242
^Sm, A=148,9, structural connections, levels, bands, J$^{\pi}$, transitions and mixing ratios from Nd+^{3}He(α) 79−63576
^Sm(n,nγ), 2.75 MeV, A=150,152,154, levels and excitation cross sections 79−75839
^{140}Sm, 10^{+} isomeric states, systematic behaviour 79−30791
^{140}Sm, populated in (α,α4n), ground state bands obs. 77−2938
^{141}Sm, M4 11/2^{-}→3/2^{+} transition, level energy 77−10365
^{144}Sm, p single particle states and pairing force calcs., high spin states 80−42522
^{146}Sm, high spin states and transitions from ^{146}Nd(α,4n) 79−6423
^{146}Sm levels excited by ^{146}Eu decay, spin-parity assignment *(Russian)* 77−14062
^{148}Sm compound states partial α-widths, α-spectra of ^{147}Sm(n,α) 80−47392
^{148}Sm levels from ^{148}Eu decay, struct. interpretation from boson expansion model *(Russian)* 78−78261
^{149}Sm 286 keV level J$^{\pi}$ character from ^{149}Pm first forbidden β-decay, β-γ ang. correlation 79−49609
^{149}Sm, level scheme following ^{149}Pm β^{-} decay 80−22750
^{150}Sm, γ-spectra, levels in ^{150m}Eu, 35.8 y decay 77−82858
^{150}Sm, nucl. struct. from ^{150}Eu decay *(Japanese)* 77−41888
^{150}Sm, nucl. struct. from ^{150}Pm decay *(Japanese)* 77−41889
^{150}Sm, nucl. struct. from Coulomb excitation *(Japanese)* 77−41890
^{150}Sm, yrast bands anal. from ^{150}Nd(α,4n), interacting boson approx. 78−13124
^{151}Sm, gamma spectra, energy levels *(Dutch)* 80−47430
^{151}Sm, low energy levels, spin values, ga gamma-gamma ang. correl. meas. 77−18398
^{151}Sm low energy levels from expt. and Coriolis mixing calcs. of ^{150}Sm(n,γ) 80−57697
^{151}Sm transitional nucleus, neg. parity states, spectroscopic factors, B(E2) values, particle-rotor model 78−50080
^{153}Sm level struct., DWBA anal. of ang. distribs. from ^{154}Sm(d,t) 79−30788
^{155}Sm, level struct., DWBA anal. of ang. distribs. from ^{154}Sm(d,p) 79−30788
Sm(d,^{6}Li) (A=144, 148, 150, 154), 35 MeV, ang. distrib. meas., deduced α-particle spectroscopic factors, reduced widths, decay lifetimes 77−18571
Sm(p,t), even isotopes, high energy neutron pairing strength, two neutron holes, resonances 80−78116
Sn, A=104, 106, 108, seniority four admixtures in low lying 0^{+} states 78−8741
Sn, A=108-118, L,J,π via (^{3}He,n) 25.4 MeV reaction to 0^{+} states 77−50050
Sn, A=114, 6, 8, struct. of quintet states of negative parity 77−288
Sn, deep h-le state fragmentation, strength functions, giant resonances, quasiparticle phonon model 80−37320
Sn deeply bound hole states and isobaric analogue states populated in ^{116,118,120,124}Sn neutron pick-up reactions 77−30570

nuclear energy levels continued
Sn from ^{122,124}Sn(n,γ) up to 20 keV, level schemes, spin-parity assignments, neutron separation energies 77−54215
Sn isotopes, levels and spectra from broken pair model 80−73801
Sn odd isotopes, A=109-117, high spin states, level schemes 78−54684
Sn, odd isotopes, number-projected three-quasiparticle description 78−93953
Sn odd isotopes, spreading widths of deep lying hole states 78−29388
Sn, odd mass isotopes, low lying negative parity states, energy levels, shell model calc. 80−5076
^{A}Sn (t,α), 4.75-5.25 MeV, A=112, 116, 118, 120, 124, single proton states RMS radius 80−13350
^{A}Sn, A=109,111,113,115,117, level scheme, J^{π} assignments, high spin states from Cd(α,xn) 79−45168
^{A}Sn, A=111,115,119, neutron hole distribs., IAS and spectroscopic factors from Sn(^{3}He,γ) 80−42519
^{A}Sn, A=113, 115, 117, 119, deeply bound hole state struct. from (^{3}He,α) 78−93930
^{A}Sn, A=113,115,117,118,119,120, rms neutron orbit sizes, DWBA anal. of Sn(t,d) data 79−36145
^{A}Sn, A=116, 118, 120, 122, 124, 0^{+}, 2^{+} and 4^{+} states 1 number conserving approach 80−22694
^{A}Sn, A=116, 124, neutron densities and single particle struct. 80−32165
^{A}Sn, A=118,120,122, deep hole states, excitation energies and ang. distribs. from Sn(p,t) 80−86792
^{A}Sn, A=120,122,124,126,128, levels, transitions and J^{π} values from In isomeric decays 79−75851
^{A}Sn(e,e′) A=116, 120, 124, electric moment distrib., lowest lying quadrupole states excitation 79−6392
^{A}Sn(n,γ) A=114,116,118, ^{115,117,119}Sn resonance meas., weak coupling model calc. for levels, J^{π} assignments 79−6416
^{A}Sn(n,n′), A=116, 118, 120, 122, 124, 11 MeV, levels, deformation parameters, isospin effects, optical parameters 80−57679
^{A}Sn(p,p′), A=115, 117, 119, 18 MeV, state spin assignment, particle-vibr. coupling 80−32160
^{110}Sn, level struct. determ. from decay of ^{110}Sb 77−18473
^{112}Sn(p,p′), 20.51, 25.0 MeV, energy levels, excitation functions and ang. distribs. 80−32184
^{113}Sn, decay to levels of ^{113}In 77−38247
^{115}Sn, Coulomb excit. via (^{4}He,^{4}He) and (^{16}O,^{16}O) reactions 77−67719
^{115}Sn, fine struct. in deeply bound hole states 77−41874
^{115}Sn, levels, J^{π} via ^{116}Sn(d,t)^{115}Sn 23 MeV 78−612
^{115}Sn weak coupling neutron hole states from ^{116}Sn(^{3}He,α) 80−73786
^{116}Sn, level density with schematic forces 78−41639
^{116}Sn levels, J^{π} and transitions from ^{115}Sn(n,γ) 80−52587
^{116}Sn, levels studied via ^{116}Sn(^{16}O,^{16}O) and ^{116}Sn(^{16}O,^{16}O′), ang. distrib. anal. of 64 MeV reacts. 78−8836
^{116}Sn, π content of ground and low-lying states 77−38225
^{116}Sn, state excitation energies and partial half lives from ^{115}Sn(^{3}He,d), 28.4 MeV 78−66295
^{117}Sn 6517 keV level, effective cross section, transition widths, from γ resonant scatt. 79−3135
^{117}Sn, level density with schematic forces 78−41639
^{118}Sn excited states, studied via β-decay of ^{118g}In and ^{118}Sb 77−54187
^{119}Sn, 23.87 keV level half-life 80−47433
^{119}Sn, magnetic moment, of $I=+^{3}/_{2}$ level *(Russian)* 78−50083
^{120}Sn 6730 keV level, spin, absorpt. cross section, from nuclear resonant scatt. 79−3134
^{120}Sn 7310 keV level, effective cross section, transition widths, from γ resonant scatt. 79−3135
^{120}Sn, level struct. from ^{120}In β-decay 78−86510
^{121}Sn level props. determ. from ^{120}Sn+n transmission and capture gamma-ray meas. 77−3004
^{122}Sn excitation of 6^{+}, 8^{+}, 10^{+} and 9^{-} states, DWBA anal. from ^{122}Sn(p,p′) and ^{124}Sn(p,t) 79−89264
^{132}Sn, doubly magic, RPA calc. of level scheme 78−50087
^{132}Sn, exact and statistical results for multi-proton cases 78−86483
^{132}Sn level struct., lifetimes, γ-γ coincidences, internal conversion from ^{235}U fission 80−52584
^{132}Sn levels, isomers, lifetimes and transition probabilities from fission 80−78163
^{132}Sn region, level spectra, shell model anal. 78−86482
Sn(d,t)Sn, even A=112 to 124, deeply bound hole states of odd A Sn 78−8725
^{A}Sr, A=80,82,84-86, levels and transitions from Kr(^{3}He,n) 80−18201
^{A}Sr, A=89 to 94, struct. of states in the generalised seniority shell model 79−6408
^{A}Sr, A=94,96 direct and skip cascades, γγ ang. correlations, levels, mixing ratios from Rb decay 80−86851
^{83}Sr, excited states struct. ^{83}Y β^{+} decay, γ-ray coincidence meas. 77−6309
^{83}Sr levels from ^{84}Sr(^{3}He,α), 18 MeV, DWBA calcs. using optical model 78−41738
^{84}Sr quasi-γ bands and negative parity levels from ^{85}Rb(p,2nγ) 80−456
^{85}Sr, high-spin states obs. from ^{82}Kr(α,n) and ^{84}Kr(α,3n) 77−41915
^{86}Sr, populated in ^{89}Y(p,α), DWBA microscopic anal. 78−70449
^{87}Sr 1 $g_{9/2}$ neutron distrib. radial size, states, differential cross sections from ^{86}Sr(^{18}O,^{17}O) 80−95301
^{87}Sr excited levels from ^{87}Rb(p,nγ), spin, parity, branching ratios, lifetimes 77−50076
^{87}Sr produced in ^{88}Sr(p,d), two step processes, excitation of core coupled states 77−88150
^{87}Sr(p,p′), 20.5 MeV, level scheme, ang. distribs., transitions and deformation parameter 79−22195
^{88}Sr populated in ^{86}Kr(^{3}He,n), subshell closure, 0^{+} states 78−21582
^{88}Sr, populated in ^{87}Sr(n,γ) 77−30584
^{88}Sr(γ,γ), reson. fluoresc. yield meas. width of 1.836 MeV level determ. 77−79357
^{89}Sr, populated in ^{88}Sr(n,γ) 77−30584
^{89}Sr produced in ^{88}Sr(d,p), two step processes, excitation of core coupled states 77−88150
^{90}Sr, level struct. determ. from decay of ^{90}Rb 77−71583
^{92}Sr γγ ang. correlations, levels, J^{π}, mixing ratios from ^{92}Rb decay 80−57725
^{93}Sr excited state depopulation γ-rays, n coincidence from ^{94}Rb β-delayed n decay 80−52631
^{93}Sr, γ-ray decay scheme, levels, J^{π}, logft values 77−54152
^{98}Sr very low lying 0^{+} state, shape coexistence bands, $T_{1/2}$, transitions from ^{98}Rb decay 80−78148
^{48}T excited states from ^{45}Sc(A,pγ), level struct., lifetimes, from DSA and pγ coincidence meas. 78−74326

nuclear energy levels continued
^{166}Ta, isotope identification in ^{159}Tb(^{16}O,9n) reaction, half-life and decay scheme 77−79331
^{173}Ta, levels, rot. parameters, γ-mixing 77−34248
^{177}Ta, magnetic moments meas. by PAC 80−22688
^{177}Ta spin polarisation, state struct. and mag. moments in rot. model 80−18194
^{178}Ta level properties, rot. bands, transitions and level lifetimes from ^{176}Lu(α, 2n), ^{178}Hf(d, 2n), ^{178}Hf(p, n) 79−36158
^{180}Ta, evidence for Gallagher-Moszkowski doublets from ^{181}Ta(p,d) reaction 78−58233
^{182}Ta, levels, J^{π}, via 2-3 eV neutron capture γ-spectra 78−602
^{185}Ta single proton states and rot. bands, J^{π} from ^{186}W(t,α),pol.t 80−91130
^{147}Tb, p single particle states and pairing force calcs., low lying levels 80−42522
^{148}Tb, high spin states, transitions J^{π} assignments from (Li,xn) and (^{10}B,xn) 79−49582
^{149}Tb compound nucleus, statistical model de-excitation calcs. 78−50146
^{151}Tb 11/2 isomer, high spin few-particle states, in beam study from (^{3}He,3n) and (α,4n) 79−17805
^{151}Tb lower excited state lifetimes, ^{151m}Tb isomer from ^{151}Dy decay 79−75919
^{159}Tb(p,f), 600 MeV, fragment energies, cross sections level density and barrier heights 80−42723
Tc, A=93-101 odd isotopes, levels, EM moments in unified model 77−82826
Tc, A=94,8, levels determ. from Mo(^{3}He,t)Tc at 24 MeV 77−26778
^{93}Tc $^{17}/_{2}$ isomer, parity mixing search, partial γ-decay widths from ^{65}Cu(^{32}S,2n2p), 120 MeV 78−93936
^{93}Tc $17/2^{-}$ isomer, internal conversion coeffs., parity mixing search from ^{92}Mo(α,2np) 43 MeV 78−78255
^{93}Tc, level struct., $p_{3/2}$ core excitations 77−50060
^{94}Tc levels and J^{π}, coupled channel and DWBA anal. of ^{92}Mo(^{3}He,p) 79−89239
^{95}Tc, 1 quasiparticle 2 phonon multiplet, microscopic quasiparticle cluster phonon coupling model 77−2908
^{95}Tc, energy levels from ^{95}Mo(p, nγ)^{95}Tc 80−37372
^{95}Tc, high spin states, coupled proton-neutron excitations 78−17225
^{96}Tc energy level diagram, γ transitions and parities from ^{96}Mo(p,nγ) 79−9479
^{96}Tc even mass odd nucleus, proton spectroscopy, from ^{95}Mo(^{3}He,d), shell model anal. 79−63573
^{96}Tc low lying states, level scheme, parities, from conversion electron, γ spectra 78−46024
^{96}Tc, low-lying levels, γ-transitions via ^{93}Nb(α,n)^{96}Tc 10.8, 14.0 MeV 77−2931
^{97}Tc, energy levels, low-lying, decay properties 80−63084
^{97}Tc levels, decay props., mixing ratios and J^{π}, from directional correlations in ^{97}Mo(p,nγ) 79−89240
^{97}Tc, spin of 785.0 keV level from γ-γ ang. correl. study 77−71584
^{98}Tc 14 μs isomer, low lying levels and transitions from ^{98}Mo(p,n) 80−73802
^{98}Tc energy levels from ^{99}Tc(p,d), l-values, spectrocopic factors, parities 78−25183
^{98}Tc, excited by (d,t) and (p,d)$_{g}$ l,J,π determ. 77−18370
^{99}Tc, 920 keV level spin, from ^{99}Mo beta decay gamma-ray obs., 0.1-1 MeV 77−54145
^{99}Tc level structure, spin-parity, from inelastic scatt. and proton stripping studies 78−8743
^{99}Tc, low-lying states via ^{98}Mo(^{3}He,d)^{99}Tc, proton config. 77−22894
^{100}Tc level scheme, transitions and J^{π} values, n binding energy from ^{99}Tc(n,γ) 79−63590
^{100}Tc low lying and isomeric levels, transitions and mean lines from ^{100}Mo(p,nγ) 80−42548
^{100}Tc μs isomers, isomeric transitions and mean lives from ^{100}Mo(p,n) 80−73803
^{102}Tc deduced levels, tentative J^{π} and transitions from ^{102}Mo decay 80−52630
Te, even isotopes, effect of residual interaction in particle-particle channel on low-lying states 78−21503
Te levels from ^{112,116,118,120,124}Sn(^{3}He, n) reactions, ang. distribs. 78−89890
^{118}Te, levels studied via ^{116}Sn(^{16}O,^{14}C)^{118}Te, ang. distrib. anal. of 64 MeV reacts. 78−8836
^{121}Te isomeric state, spin, lifetime and mag. moment from (α,n),(d,Zn) 80−47387
^{123}Te level scheme obs., ^{123}I decay, gamma-ray spectra meas. 77−10361
^{123}Te levels, spin assignments and E2/M1 multipole mixing ratio from ^{123}I decay 79−75836
^{124}Te capture states partial α-decay widths from ^{123}Te(n,γα) 80−37328
^{124}Te, energy levels spectroscopy by ^{123}Te(d,p)^{124}Te 77−41973
^{124}Te, level struct. determ. from ^{124}Sb beta-decay 79−54387
^{125}Te, level scheme, from radioactive decay of ^{125}Sb *(French)* 77−65202
^{125}Te level scheme obs., ^{125}Sb decay, gamma-ray spectra meas. 77−10361
^{125}Te, levels and transitions following decay of ^{125}Sb 79−71816
^{126}Te, 0^{+} states populated by β-decay of ^{126}I 77−74810
^{126}Te, level struct. obs. in ^{125}Te(n,γ) 77−34308
^{126}Te(^{22}Ne, ^{22}Ne′), 93.5 MeV, 2^{+} state mutual excitation and transitions 79−54404
^{127}Te, energy levels spectroscopy by ^{120}Te(d,p)^{121}Te 77−41973
^{132}Te 2^{+} level, shell model calc., Lanczos and Householder method comparison 80−22711
^{132}Te low lying levels and EM props., shell model description 80−42549
^{134}Te, levels, J^{π}, 6^{+} isomer level mag. moment 77−82824
^{229}Th levels from γ-spectra following ^{233}U decay 77−26636
^{231}Th β decay and ^{235}U α decay, γ-radiation study, energy level scheme *(Russian)* 78−17160
^{231}Th excited states and bands, spins, γ-transitions from ^{230}Th(n,γ) 80−57699
^{231}Th, levels via ^{230}Th(d,p) 17 MeV 77−79388
^{232}Th level structure and decay parameters from (n,n′) and (n,n′γ) meas. 77−30494
^{233}Th, excited levels, using thermal and average reson. neutron capture in ^{232}Th 79−45166
Ti, A=42, 44, level props. from Ca(^{3}He,n) reacts. 77−65227
^{A}Ti, A=44, 46, 48, 52, energy levels and EM props. using classical semimicroscopic model 79−59012
^{A}Ti, A=48,50, excited states and transition ang. distribs. from Cr(^{14}C,^{16}O) 80−95308

nuclear energy levels continued
^{43}Ti(Li, Li'), A=46,48, 17 MeV, first 2^+ states Coulomb-nuclear interference, optical and DWBA anal. 80−22852
^{44}Ti positive parity states, mean lifetimes, quasirotational band from ^{40}Ca(α,n) 20 MeV 79−6415
^{44}Ti, mode-mode coupling model for four-body correl. 77−10322
^{45}Ti $d_{3/2}$ hole states, wave functions, mag. moment, M2 transitions, shell model 78−17116
^{47}Ti, integral rot., hyperfine field and g-factor of $3/2^+$ state 77−50052
^{46}Ti deduced levels, spin assignments and γ-decay, band struct. from ^{43}Ca(α,nγ), 8-15 MeV 78−78302
^{47}Ti, integral rot., hyperfine-field and g-factor of $7/2^-$ state 77−50052
^{47}Ti levels, DWBA and Hauser Feshbach anal., compound nucleus cross sections from ^{46}Ti(d,p) 80−47377
^{48}Ti high spin states from ^{45}Sc(α,pγ) 78−74378
^{48}Ti levels and transition ang. distribs., form factors, DWBA anal. of ^{45}Sc(α,p) 79−45202
^{48}Ti(n,n'γ), 1.57-2.8 MeV, low levels excitation *(Russian)* 78−41722
^{49}Ti nuclear levels from n-capture γ-rays in ^{50}Ti(γ,n) 80−37327
^{49}Ti(γ,γ'), nuclear levels from n-capture γ-rays 80−37327
^{50}Ti, 1p7h config., high-spin neutron-hole states, EM transition rates 78−70430
^{50}Ti, shell model calcs. using surface delta interaction 78−37290
^{50}Ti, studied via (α,2nγ), high spin states, shell model calcs. 78−54675
^{50}Ti(^{12,13}C,X), elastic, inelastic and single nucleon transfer excitation functions, ^{49}Ti levels 80−13492
^{51}Ti, populated in ^{51}Sc β-decay spin-parity values 77−6318
Tl, A=201,203, levels via (d,3nγ), J^π,$T_{1/2}$, $9/2^-$ band discovery 77−34207
Tl, A=203,5,7, proton hole states obs. with Pb(t,α) 77−41978
Tl, A=208,206,204, high-spin states, α-spectra via (d,α) 80 MeV 78−504
Tl isotopes, A=184-197, β^+-decay, single particle and collective degrees of freedom 77−22956
Tl, odd isotopes, negative-parity level props. 78−17103
Tl, odd isotopes, pot. energy surfaces and quadrupole deformation parameters, deformed basis model 79−80867
Tl, odd mass isotopes, $h_{9/2}$ intruder state 77−88024
Tl odd-mass isotopes, $9/2^-$ level excitation energies, estimates 77−275
^Tl, A=196, 198, staggering of even and odd spin states 78−70446
^Tl, A=203, 205, excited state g-factor from Tl(^{40}Ca, ^{40}Ca'γ) 79−22191
^{196}Tl high spin states, γ-decay and rot. structs. from ^{197}Au(α,5n), ^{194}Pt(^{6}Li,4n) 79−440
^{197}Tl, levels determ. from ^{197}Au(^{3}He, 3nγ) at 24-28 MeV 77−46177
^{201}Tl levels, transitions and J^π assignments from ^{201}Pb decay 80−5099
^{203}Tl, ^{205}Tl, core excitations to low-lying states, e.m. props., hyperfine splittings, isomer shifts 78−89794
^{204}Tl neutron hole states, J^π and spectroscopic factors from ^{205}Tl(p,d) 80−86783
^{205}Tl, level excitation energies and ang. distribs. cluster model DWBA calcs. from ^{208}Pb(p,α) 79−17814
^{205}Tl(α,3n), 35-51 MeV, ^{206}Bi high-spin states anal. 78−82368
^{206}Tl, excitation of 12^- isomeric state in Bi(n,α) at 14 MeV, half life 78−70453
^{206}Tl, influence of nucl. polarisation on level props. 78−54686
^{206}Tl, isomeric yrast states obs. 77−281
^{207}Tl, single particle state mag. moment in large shell model space 79−45162
^{208}Tl, influence of nucl. polarisation on level props. 78−54686
^{165}Tm, levels excited by β-decay of ^{165}Yb 78−74334
^{167}Tm, energy level scheme from ^{165}Ho(α,2nγ) *(German)* 80−68576
^{171}Tm, g factor of 635.4 keV level meas. 77−10316
^{173}Tm level and band struct., spin assignments, ang. distribs. from ^{176}Yb(p,α), 16 MeV, ^{173}Tm level and band struct., spin assignments, ang. distribs. 79−474
^{175}Tm single proton states, rot. bands, J^π assignments from ^{176}Yb(t,α), pol. t 80−452
^U, A=232, 234, 236, octupole-octupole residual interactions and low lying 0^+ excited states 79−36136
^{233}U, high-energy spin state obs. using Coulomb excitation 78−17102
^{233}U, states excited by ^{234}U(d,t) and ^{234}U(^{3}He,α) 78−66208
^{235}U, levels, J^π, multipolarities via (n,γ) 5-49 MeV 78−512
^{235}U vibrational and single particle states from ^{234}U(n,γ) 79−36123
^{236}U low lying levels from 4^- isomer decay in (n,e), (n,γ) 80−47396
^{236}U nuclear instability and fission in strong mag. field energy level deformation *(Russian)* 79−13360
^{237}U levels, bands and J^π assignments, n binding energy from ^{236}U(n,γ) 80−5041
^{237}U virtual photon excited state decay and total cross section of ^{238}U(e,n) 80−22757
^{238}U, 0.9-2.7 MeV neutron elastic and inelastic diff. cross sections for scatt. from ground, 45, 148 keV states 77−26770
^{238}U, microscopic calc. of high-spin rot. states 78−8730
^{238}U, shell corrections for finite depth single particle potentials 79−30782
^{238}U, struct. in sequence of s-wave levels 77−22857
^{238}U(e,e'), 87.5 MeV, deformed fissionable nucleus, giant multipole resonances and isovector states 80−42612
^{238}U(e,e'f), 5.5-9 MeV, fission fragment ang. distribs. DWBA anal., low lying fissioning levels 80−42713
^{238}U(n,γ), 2, 24 keV, resonance averaged γ-spectra, level and J^π appls. 80−37347
^{238}U(n,n'γ), 1.06 MeV, cross sections and γ spectra for various energy levels *(Russian)* 79−40883
^{238}U(n,n'γ) technique for study of levels near 1 MeV 77−26719
^{239}U, energy level assignments from ^{238}U(d,p) at 12 MeV 78−66209
U(p,f), 600 MeV, fragment energies, cross sections level density and barrier heights 80−42723
V, A=47,59,51, spectra, e.m. moments, B(E2) and B(M1) values calc. 78−8745
^{31}V level scheme, DWBA and optical model anal. from ^{52}Cr+^{13}C 79−36159
^{45}V level scheme, γ-rays, level lifetimes, internal conversion from ^{40}Ca(Li,xn) 80−63085
^{47}V spin values and level scheme recalc. 78−78256
^{49}V proton hole, analogue and high spin states, distorted wave anal. from ^{52}Cr(p,α) 79−9482
^{50}V excited states populated in ^{42}Ti(α,pγ), lifetimes 78−21583
^{50}V, γ-ray spectrum from thermal neutron capture 78−21568
^{50}V, high-spin levels anal. in ^{48}Ti(α,pnγ) reaction *(French)* 78−21572
nuclear energy levels continued
^{51}V high spin states, lifetimes, shell model calcs., yrast levels from ^{48}Ca(^{10}B, α3n) 79−6425
^{51}V, proton hole states obs. via (e,e'p) 77−10389
^{51}V, shell model, pairing-plus-surface-tensor interaction, energy levels, B(E2) values 78−78282
^{51}V, shell model calcs. using surface delta interaction 78−37290
^{51}V struct., pairing plus surface tensor interaction 77−18411
^{51}V(e,e), mag. elastic scatt., radial distrib. of $1f_{7/2}$ proton orbit using cross sections 78−13067
^{51}V(p,p'), 6 MeV, levels, spins and EM props., shell model anal. 80−63092
^{52}V capture area, resonance parameters and mean level spacings from ^{51}V(n,γ) 79−6608
^{52}V, spin assignments to p-wave neutron states 77−22852
^{54}V energy levels populated in ^{54}Cr(t,^{3}He), mass excess 77−54230
^W (^{84}Kr,^{84}Kr'γ) A=183, 184, 186, 340 MeV, Coulomb excitation, energy levels and bands 79−63577
^W, A=178, 180, 182, 184, levels and J^π, ang. distribs. from W(p,t) 80−78159
^W(n,nγ), 2.75 MeV, A=182,184,186, levels and excitation cross sections 79−75839
^{181}W, level absolute density from n spectra, statistical anal. of ^{181}Ta (p, n) *(Russian)* 79−97657
^{181}W level density, n spectra and ang. correls., direct and nonequilib. processes from ^{181}Ta(p,n) *(Russian)* 80−68631
^{181}W levels (neutron and collective) and J^π, ang. distribs. from ^{183}W(p,t) 80−78160
^{182}W, level struct. determ. from (α,2nγ) and ^{182m}Re decay 77−41914
^{184}W, 1285 keV 5^- state struct. anal. 79−9467
^{184}W (n,n'γ), fast n, level struct. and populations, γ-transitions 79−75841
^{184}W(^{12}C,^{12}C'), 70 MeV, 4^+ state excitation ang. distrib., hexadecapole deformation length effects 80−68521
^{186}W levels, spin-parity assignments, via ^{184}W(t,p) at 15 MeV 77−18572
^{186}W(n,n'γ), fast n, level struct. and populations, γ-transitions 79−75842
^{188}W levels, spin-parity assignments, via ^{186}W(t,p) at 15 MeV 77−18572
Xe, A=118,120,122, level struct., J, π, following Cs β-decay 77−57601
Xe, beta decay of neutron deficient Cs isotopes 77−22947
Xe levels populated in ^{129}Cs, ^{133}I β decay energy level scheme, γ spectra meas. 77−2936
Xe, neutron rich nuclei from N=82, energy level systematics 77−22896
^Xe, A=122,124,126,128, 0^+ excited state spin assignments and transitions from Cs β-decay 79−67649
^Xe, A=124,126-8,130,132, levels, transitions and J^π values, DWBA anal. from Te(^{3}He, n) 79−75852
^Xe, A=129, 131, populated in (α,nγ), props. of low-lying levels 80−464
^{114}Xe excited states and γ-rays from ^{114}Cs β-decay 80−47436
^{116}Xe level scheme and yrast band, in-beam γ-study from ^{106}Cd(^{12}C, 2n) 80−13360
^{124}Xe, energy level scheme, ^{124}Cs decay 78−13033
^{124}Xe, level struct. exam. using β^+-decay of Cs 78−21498
^{125}Xe, negative parity levels in odd-A neutron deficient isomers 79−17817
^{126}Xe, level struct. exam. using β^+-decay of Cs 78−21498
^{127}Xe level scheme from decay of ^{127}Cs 77−299
^{128}Xe levels, J^π, log ft values, deduced from ^{128}Cs decay 77−54189
^{129}Xe excited state lifetimes, γ-transitions from ^{129}Cs decay 80−78205
^{129}Xe, low-lying levels determ. from Coulomb excitation and (α,n) reacts. 78−70450
^{131}Xe, low-lying levels determ. from Coulomb excitation and (α,n) reacts. 78−70450
^{131}Xe, negative parity states, nucl. orientation, γ-ray spectra of Fe:^{131}Xe 77−28487
^{132}Xe level struct., J^π, transitions and multipole mixing ratio from ^{132}I decay 80−91134
^{132}Xe levels, from ^{132}I β-decay 79−9521
^{136}Xe, neutron particle-hole states determ. from ^{136}I β-decay 77−74811
^{137}Xe level and decay scheme from ^{136}Xe(n_{th},γ) 78−13102
^{137}Xe low lying state parentage coeffs., anal. of ^{136}Xe(p,p_1) 78−66282
^{137}Xe neutron unbound states, high energy X-rays from ^{137}I decay 80−86856
^{137}Xe, populated in ^{138}I β-decay, delayed neutrons feeding excited states obs. 80−27600
^{139}Xe, populated in ^{138}I β-decay, level scheme 80−27600
Y level scheme from Sr β-decay 77−26632
^{85}Y, from ^{85}Zr decay 77−34258
^{87}Y level struct., γ-spectroscopy and J^π from (p,2nγ), (α,2nγ) 80−83040
^{87}Y, low-lying states anal. in ^{84}Sr(α,p) at 18 MeV 78−17228
^{89}Y, first four energy levels, from ^{92}Zr($\tilde{p}$,α)^{89}Y reaction *(French)* 79−75981
^{89}Y high spin states from γ-ang. distribs. in ^{87}Rb(α,2nγ), 30-55 MeV 78−93941
^{89}Y, level struct., $p_{3/2}$ core excitation 77−50060
^{90}Y low lying multiplets, DWBA anal. for spectroscopic factors from ^{91}Zr(d,^{3}He) 80−57685
^{90}Y, shell model calcs., energy levels, transitions and spectroscopic factors 79−63593
^{94}Y deduced levels spectroscopic factors, spin and parity from ^{96}Zr(^{3}He,αp) 39 MeV 78−70451
^{171}Y populated in ^{171}Lu decay, level scheme, γ-transitions, spin-parity assignments 77−46133
Yb, A=164,5, from Lu decay, level schemes determ. 78−62509
Yb isotopes, A=160-165, decay spectra meas. 77−22959
^{168}Yb, microscopic calc. of high-spin rot. states 78−8730
^{169}Yb $\gamma\gamma$ ang. correlations, levels and spins from ^{169}Lu decay *(Russian)* 80−83069
^{169}Yb populated in ^{169}Lu decay, γ-ray and conversion electron spectra 80−22767
^{171}Yb level struct., DWBA anal. of ang. distribs. from ^{170}Yb(d,p) 79−30788
^{173}Yb, γ-transitions from 7/2, $7/2^-$ [514] 636 keV level 80−78187
^{173}Yb, level struct. determ. from (d,p) and (d,t) reactions 78−29482
^{173}Yb M1 transitions from 636 keV level, multipole mixture parameters, penetration effect 80−18220
^{175}Yb level structure, band structure and J^π assignments from ^{176}Yb(d,t) and ^{174}Yb(d,p) 79−40850
^{177}Yb level struct., DWBA anal. of ang. distribs. from ^{176}Yb(d,p) 79−30788

nuclear energy levels continued
^{177}Yb level structure, band structure and J^{π} assignments from ^{176}Yb(d,p) 79−40850
Zn, A=65,7, particle-vibr. coupling among positive parity states 77−38241
Zn, A=66,67, level struct. determ. from ^{64}Ni(α,n), (α,2n), spin-parity assignments 77−46178
Zn, even isotopes, effect of particle-vibr. coupling in nucl. struct. 78−12940
Zn, even isotopes, weak-coupling model, level struct., E2 transition rates 77−54159
^{A}Zn, A=64, 66 levels and primary E1 transition strength functions from Cu(p,γ) 80−91149
^{A}Zn, A=65 to 68, energy spectra, shell model calc. 79−17818
^{60}Zn level determ. from ^{58}Ni(^{12}C,^{10}Be) of 77 MeV 79−26371
^{61}Zn level determ. from ^{58}Ni(^{12}C,^{9}Be) at 77 MeV 79−26371
^{61}Zn states, pseudo LS coupling model 80−68548
^{61}Zn, studied via ^{58}Ni(^{6}Li,t)^{61}Zn, mass, t-energy spectra and reaction mechanism 78−41756
^{62}Zn, band mixing HF model, struct. and electromag. transitions 78−54676
^{62}Zn, in beam gamma spectroscopy using ^{63}Cu(p,2nγ), ^{60}Ni(α,2nγ) 77−6297
^{62}Zn levels from ^{58}Ni(^{16}O,^{12}C) 79−6694
^{63}Zn EM decay transitions, level J^{π} assignments, level lifetimes from (α, nγ), (^{11}B, npγ), (^{7}Li, pnγ) 79−85402
^{63}Zn level scheme, spin and parity assignments from (p,d), (p,nγ), (α,nγ), (^{12}C,pnγ) 79−465
^{63}Zn, levels, J^{π} via ^{64}Zn(d,t) 13 MeV, polarised d 77−88100
^{64}Zn, γ-ray spectroscopy from ^{61}Ni(α,nγ)^{64}Zn 78−21514
^{64}Zn, high-spin states anal. from heavy-ion reactions 78−33145
^{64}Zn, J^{π} assignments from γ-ray linear polarisation meas. from ^{59}Co(^{7}Li,2n) 79−6383
^{65}Zn odd-parity states from ^{62}Ni(α,nγ), γ study, energies, branching and mixing ratios, lifetimes 78−50120
^{66}Zn(d,p)^{67}Zn, 12 MeV, levels, ang. distribs., spectroscopic factors meas. 77−22891
^{67}Zn, Coulomb excitation, gamma-ray spectra 79−9434
^{67}Zn, γ spectroscopy of low spin states from ^{64}N(α,nγ), 8.2 MeV 78−78303
^{67}Zn, multiparticle configuration obs. in ^{67}Cu and ^{67}Ga decay 78−70496
^{68}Zn, 26 MeV levels from ^{69,71}Ga(d,^{3}He) 78−25112
^{68}Zn low lying states, S-values from DWBA anal. of ^{64}Ni(^{6}Li, d) 79−36160
^{69}Zn, energy levels, core coupling model calcs. 80−9238
^{70}Zn, 26 MeV levels from ^{69,71}Ge(d,^{3}He) 78−25112
Zr, A=86, 87, 88, high spin states 78−74383
Zr level scheme from Y β-decay 77−26632
Zr neutron deficient isotopes, studied via heavy ion induced compound reactions 77−57621
^{A}Zr, A=92, 96, first excited 0^{+} state transition strength from (^{6}Li,^{8}B), (d,^{6}Li) correlation 80−78260
^{A}Zr, A=93, 95, $1h_{11/2}$ neutron single particle strength, quasiparticle-phonon coupling 79−89226
^{A}Zr(^{35}Cl,^{35}Cl′), 90 MeV, A=92, 94, 2_1^{+} levels mag. moments 80−105968
^{A}Zr(n,n′γ) 2.2-3.7 MeV, A=92, 94, level and decay scheme, J^{π} assignments 79−17850
^{88}Zr transitions and high spin states above 8^{+} isomer, ^{86}Sr(α, 2nγ)^{88}Zr 79−40848
^{90}Zr (p, p′), 57.5 MeV, polarised p, low lying level and giant resonance excitation 79−36157
^{90}Zr (p,π^{+}), 180 MeV, ang. distribs., discrete states, differential cross section 79−13298
^{90}Zr, proton orbit sizes and E0 matrix element for 2 lowest 0^{+} states 80−27546
^{90}Zr, two-body effective parameters calcs., energy levels 77−57608
^{91}Zr, level struct. via (d,p), (p,p′) and (p,d) reactions, DWBA, CCBA anal. 77−18393
^{91}Zr, shell model calcs., energy levels, transitions and spectroscopic factors 79−63593
^{92}Zr level struct. and reduced spectroscopic factors from ^{91}Zr(d,p) 80−32192
^{92}Zr levels, J^{π}, cross sections, vector anal. power, optical parameters from ^{91}Zr+pol. d 80−78268
^{92}Zr(n,n′γ), 1.57-2.8 MeV, low levels excitation *(Russian)* 78−41722
^{94}Zr(n,n′γ), 1.57-2.8 MeV, low levels excitation *(Russian)* 78−41722
^{96}Zr, unusually strong excitation of 1.59 MeV 0^{+} state in ^{100}Mo(d, ^{6}Li) 79−49584
^{98}Zr, level scheme determ. from β-decay of ^{98}Y 77−41934
^{99}Zr→^{99}Nb, half life, level schemes and β-decay investigation 79−17863
^{100}Zr, confirmation of 331 keV 0^{+} state 78−41643
^{100}Zr, levels, J^{π} via ^{100}Y β-decay 77−82878
Zr(p,p′γ), odd isotopes, excited d-states from analogue resonances and p-γ correlations 80−68546

nuclear engineering
see also fission reactors
air sampling system at HFEF/N 79−45441
air-core Tokamak, optimisation of ohmic heating coil configurations 80−14914
American Nucl. Soc. winter meeting 1977 78−58315
American Nucl. Soc. Winter Meeting 1977 78−82408
American Nuclear Society Transactions, Washington, USA (November 1978) 79−85570
Argentinian industrial development 77−65352
atomic power engineering development in CMEA countries *(Polish)* 77−65344
atomic science and engineering, measuring informational basis, nuclear instrument making 79−684
Bangladesh, development policies 77−61627
basic nuclear engineering, book 78−54810
breeder reactor development, survey *(German)* 78−5007
BWR, technology transfer experience 77−65349
Canadian industry, technology transfer 77−57760
CANDU, nuclear quality high pressure valve bellows, development, report 78−82490
centrifugal separators, two-phase flow distribs., nuclear power appl. *(German)* 77−6574
CIRENE reactor, technological aspects, materials *(Italian)* 77−14214

nuclear engineering continued
Colgate fission plasma reactor, high temp., gaseous fissionable material, design, technical problems *(Dutch)* 78−50249
components and vessels, underwater plasma arc and explosive cutting 79−9922
computer assisted learning in nuclear engineering 77−13557
concrete structs., steady-state stresses under sustained and cyclic temp. 77−83024
conference, San Diego, Calif., USA (June 1978) 79−17972
conference, San Diego, Calif., USA (June 1978) 79−49650
conference, world nuclear energy, Washington, D.C., USA (Nov. 1976) 77−34361
conference on nuclear engineering remote systems technology, San Francisco, USA (Nov.-Dec. 1977) 79−45438
control rod drive system penetration assemblies for Caorso Mark 2 primary containment 78−58368
cooperative education programs in Omaha Public Power District 78−4429
cooperative utility programs at North Carolina State University 78−4430
CRBR carbide reload design, comparison with reference oxide design during TUC 79−85658
CRBR piping, structural reliability uncertainties 77−46350
CRBR primary piping reliability, stress-strength overlap method 77−46349
criticality safety of large facility, neutron interaction anal. 79−63822
criticality safety workshop for graduate students 77−37699
democratic control 79−75316
desalination by very low temp. nuclear waste heat 78−41850
design, one term vs. one year projects 77−45632
design at Idaho State Univ. 77−45631
design course at Ohio State Univ. 77−45630
design curriculum at Univ. of Illinois 77−45628
design education at Mississippi State Univ. 77−45629
dynamic isotope power system, PuO_2 fuelled, organic Rankine cycle turbine power system for space appls. 80−18692
dynamic measurements of a nuclear reactor using low-peak-factor excitation signals 79−36349
EBR-II, dynamic response of ducts to press. pulse, finite element calcs. using STRAW 77−3124
EBR-II steam generator tube bore side inspection probe and drive 79−9850
education, energy from nuclear sources, outline for secondary school students 79−80975
education, energy option for undergraduates 80−31447
education facilities and problems in India 77−37680
education in Japan *(Japanese)* 80−27067
educational programme, eval. for accreditation, design component role 77−41430
Egypt's technological experience in radioisotope production 77−65358
energy conversion engineering, alternative energy sources *(Japanese)* 80−26105
energy production, research review *(Hungarian)* 78−74414
Exxon nuclear fuel recovery centre, maintenance philosophy 79−45459
FBR accident, TRANSIT computer code for mechanistic analysis of transition phase 77−46328
FFTF core component measuring system 79−45446
FFTF fuel element measuring system 79−45447
FFTF interim examination and maintenance cell, equipment testing program 79−45451
French nuclear industry competitiveness *(French, English)* 79−89489
fuel and waste management schemes for nuclear power implementation 77−57773
fuel cycle management, interdisciplinary approach in education and research activities 77−38433
fuel defect test loop, remote handling system design 79−45395
fuel element postirradiation test facilities, Chalk River 79−45460
fuel pin profilometry adaptation, cutoff saw 79−45452
fuel reprocessing, remote handling experience, Windscale 79−45456
fuel reprocessing hot cell facilities and techniques, Karlsruhe 79−45458
fuel services, analysis, costing and economics of cooperative facilities 77−57772
Fuels and Materials Examination Facility, design features and objectives 79−45448
fusion design team, undergraduate education 78−58469
fusion engineering developments review 79−3240
fusion experiments, microprocessor applications in data acquisition and control 80−13918
fusion power plants, engineering limitations 78−74473
fusion power status and prospects 77−67878
fusion reactor, MFTF, sustaining neutral beam power supply, shunt preconditioner, IBM-ASTAP anal. 80−102332
fusion reactor, PHIBEX, poloidal field power supply for ignition, computer based cct. anal. 80−102329
fusion reactor maintenance considerations 79−45417
fusion-fission concepts, nuclear energy systems synthesis 80−13838
globe main steam isolation valve unbalanced forces and novel actuator design 78−50288
graduate cooperative program with industry, experience over 3 years 78−4434
heavy water dielectric constant meas. over temp. range 473K to 643K 80−103912
HFEF, irradiated fuel examination by eddy currents 79−45461
HFEF/N, equipment repair room modifications 79−45439
HFEF/N, handling equipment for neutron radiography facility 79−45443
HFEF/S air cell, decontamination and refurbishment 79−45445
high level waste, retrieval system design, Hanford 79−45380
high-speed slitter for irradiated stainless-steel tubing 79−45450
hockey stick heat exchanger, elbow centroid 80−9329
HTR, coal gasification appl. 80−11996
HTR, inelastic structural anal. for component design 79−6734
ignition test reactor, remote maintenance system requirements 79−45420
industrial internship programme in nuclear engineering education 78−4432
inertial confinement from reactors, remote system needs 79−45421
irradiated fuel rods, examination by eddy currents 79−45464
irradiated fuel rods, storage options, comparisons 79−45383
irradiated fuel sipping, inspection, and repair at Point Beach Nuclear Plant 79−45384

nuclear engineering continued
JAERI program, probabilistic risk assessment techniques in Japan 80−18515
JASON low power reactor, nuclear engineering education and training 77−41431
laboratory course at Purdue University 78−4443
laser driven fusion reactors, assessment of engineering problems 79−36413
liquid to vapour transformations, mechanics of two phase flows 77−89532
LMFBR, 1000 MW(e) pool plant, fabrication and construction 80−5213
LMFBR, fuel handling and storage system 79−45394
LMFBR, pool-type, engineering design and construction 80−5212
LMFBR, spent fuel shipping system 79−45385
LMFBR, squeeze flow between two adjacent subassemblies, discrete model 78−86634
LMFBR concrete containment struct., exptl. anal. of dynamic loading 78−41867
marine reactor systems, Monte Carlo reliability anal. of power and heat removal systems *(Japanese)* 78−58396
master slave manipulator SM-229, compact servo system 79−45454
medical radiological physics education based on nucl. engineering 80−31448
Na loop safety facility expts., disassembly at HFEF/N 79−45444
nondestructive analysis applications in the nuclear industry 80−13706
NRC standardisation in licensing, B and W viewpoint 80−23023
nuclear engineering, teaching project management as part of international technology transfer 78−4428
nuclear power in Czechoslovakia, review *(Czech)* 79−31157
nuclear power stations, applications of multi-directional seismic inputs in the design of components 79−31238
nuclear reaction flow boiling nucleate region, dynamics 77−88205
nuclear reactor redundancy systems, common mode failures 80−13641
O-ring compounds, resistance to heat and ionizing radiation 78−29584
Philippine experience in technology transfer 77−65355
portable glove box system, HFEF/N 79−45440
power implementation in Argentina 77−57771
power plant implementation in developing countries, particularly Egypt 77−57768
power station development in Soviet Union, problems and solution 80−102290
pressure vessel surveillance capsules, remote disassembly and examination 79−45463
probabilistic systems reliability analysis for students 77−37698
process heat as energy supply in developing countries 77−57735
process instrumentation lab. 78−17447
pulsed neutron physics facility, remote operation and maintenance 79−45465
PWR, control of fission products activity in primary coolant, computer code 80−32537
PWR, implementation in Iran 77−57769
PWR coolant water pumps, cavitation detection, brief review *(German)* 77−74906
PWR cooling and heat recovery, circulating pump development 77−82993
PWR fuel dissolution, Idaho processing plant remote systems 79−45455
PWR pressure vessel safety, term paper from course at Georgia Tech 78−58379
quality control and safety, West German practice *(German)* 77−75004
radiation damage test facility, LAMPF 79−45466
radiation protection optimisation in nuclear engineering, cost, risk *(Czech)* 78−33295
radioactive waste, underground repository, design and operation 79−26589
radioactive waste calcining facility, process filters, remote handling system 79−45382
radioactive waste disposal in geological formation, general considerations *(German)* 79−9757
radioactive waste management, regional cooperation in India 77−57730
radioisotope production technology transfer to developing countries 77−65357
reactor fuel, selected enrichments for minimisation of blending losses, optimal set 78−17402
reactor heat, limiting conditions for use in thermoelectrochemical cycle for water decomposition *(Russian)* 78−46183
reactor safety, nucl. engineering programme at UCLA 78−58377
reactor safety education at Northwestern Univ. 78−58376
reactor safety educational programme at Purdue 78−58380
reactor safety teaching, MIT nucl. engineering dept. courses, USA 78−58378
remote decontamination facility and repair station for hot-cell manipulators, Whiteshell, Canada 79−45453
remote inspection system, for nuclear power stations 79−45386
remote systems and maintenance, Japanese reprocessing plant 79−45457
research programs in nuclear centres of developing countries 77−57767
risk estimates, communication techniques 80−18514
safeguards technology, present status *(Japanese)* 79−26783
safety, instructional programs at RPI, LWR and FBR appl. 78−58375
seismic safety of power plants, review 77−374
SGHWR fuel pins, fuel cladding ratchetting study 78−54855
site radiography training 78−25329
spent fuel storage expansion, planning, site preparation, installation considerations 79−45381
standards development, current status and long term objectives 77−67908
standby diesel units behaviour on load takeover 77−46341
Stirling isotope power system for space appls., development and test results 80−18693
structural mechanics in reactor technology, conf. 78−41874
structural reliability of mech. components and subassemblies of nuclear power plants, conf. 79−594
teaching laboratory, development at Ecole Polytechnique 78−4444
teaching laboratory for expansion of student knowledge horizons 78−4445
technology transfer, collaboration of R&D centre in Sweden with small countries 77−57766
technology transfer, experience of Argentina 77−57763
technology transfer, experience of Federal Republic of Germany 77−57762
technology transfer, French/Iranian nuclear research centre 77−57764
technology transfer, IAEA experience 77−57758
nuclear engineering continued
technology transfer, India 77−57759
technology transfer, Iran conf. 77−57757
technology transfer, Japanese power plants 77−57770
technology transfer, Pakistan experience 77−57765
technology transfer, US experience 77−57761
technology transfer to developing countries, IAEA's contribution 80−13952
thermal reactor, homogeneous, critical size calc. 77−23171
Tokamak experimental power reactor, remote maintenance considerations 79−45418
Tokamak fusion test reactor remote maintenance 79−45419
Tokamak next generation reactors, remote servicing considerations 79−45422
Tokamak power reactors, remote system requirements 79−45423
training of existing staff for new nuclear units at university 78−4431
transient fluid and structural dynamics problems, flow singularity methods 78−86633
TREAT, neutron radiography equipment improvements 79−45462
undergraduate cooperative industrial program at Cincinnati University 78−4433
undergraduate reactor laboratory course 77−37697
USA nuclear standards index 78−29662
VHTR in Japan, energy problems and development 77−57736
world nuclear energy, conf. (Washington, 1976) 77−67779
^{10}B neutron capture method appl. *(German)* 77−42006
Na, liquid, heat transfer in crossflow around circular cylinder *(Japanese)* 77−57706
^{238}Pu fuel form facility, Savannah River 79−45396
U isotope separation appl. to nucl. fuel cycle, teaching module 80−36805

nuclear engineering computing
see also computerised control; computerised instrumentation
accident risk calcs., models and data, CRAC 80−47613
accidents due to loss of coolant, multiple-element model, program in ALGOL-60 and FORTRAN IV 78−66358
activation analysis and γ-ray spectroscopy, conference, Mayaguez, Puerto Rico (May 1978) 79−1983
ADDJA computer code, statistical reson. parameters for ^{238}U 77−26650
advanced continuous fluid Eulerian comput. scheme for flows with large density gradients 77−46236
advanced reactor cycles, total core analysis 79−9782
AGR, helical monotube vapour generator, density wave instability, experimental-stochastic and theoretical anal. 80−47539
AGR fuel pins, pellet-clad interactions, comparison of expts. and SLEUTH-SEER code results 80−42755
air cool transformers for fusion reactors, computer aided design 80−18662
ALMOS, BWR plant model, appl. to turbine trip transient analysis *(German)* 80−83177
AMPX code, operating experience 80−68743
AMPX code for coupled multigroup n-γ cross section sets 80−68741
AMPX code implementation problems at KFA Julich 80−68742
analogue simulation for continuous gas flow control, nuclear fuel production *(German)* 80−78416
analytical modeling of fuel rod ramp experiment 78−86590
ANS annual meeting, 1977 78−663
Arkansas Nuclear One, refueling shuffle movement sequencing program 80−9357
artificial earthquake generation for dynamic anal. of nuclear power stations 79−97850
atmospheric dispersion calcs. for nuclear plants, EFFAIR code 79−18007
automatic stochastic data processing system for reactor monitoring 79−97962
BABEL, multigroup neutron library for fast reactor, shielding design studies 80−68745
BACO code, simulation of fuel rod performance 80−37450
Baseball II-T experiment, microcomputer-based pellet trajectory guidance system 78−62623
BEHAVE-SST interpretation of TREAT experiments HUT 5-5A and HUT 5-5B 79−85659
benchmark γ-spectrometry, unfolding codes 79−26802
benchmark computation 77−79417
benchmark rod-bundle thermal-hydraulic analysis using boundary-fitted coordinates 80−47548
BERTA, laser-driven fission-fusion microexplosions, nuclear and thermohydrodynamic calcs. 80−47696
BNL-TWIGL, anal. of BWR rod drop accident, effect of thermal-hydraulic feedback 80−42815
BNL-TWIGL anal. of BWR turbine trip without bypass transient 80−42814
book, advances in nuclear science and technology (vol.9) 77−14202
breached element location from mixture of Xe tags, MIXTAG code 78−33274
BRINE, cross-section self shielding factors, analytic bounds 80−37426
bubble and spark chamber photographs analysis with PA-BESM-4 system, exchange apparatus 78−9045
building walls, differential press. during tornadoes, computer program 77−38349
burnup calculation code for cluster-type fuel lattices, BUNDLE 78−33246
burnup codes for calc. of fuel depletion and fission product poisoning 77−67800
BWR, benchmarking ARMP system against Quad Cities Unit 1 Cycle 1 meas. 80−27712
BWR, block-monitoring index for diagnosis of power station operating characts. 79−59185
BWR, bypass flow distrib. 77−42017
BWR, condensate feedwater system dynamics anal. 80−23025
BWR, control rod programming using heuristic and mathematical methods 80−52766
BWR, control rod sequence exchanges utilizing an off-line predictive code 78−21725
BWR, coupled problems in transient fluid and structural dynamics 77−71646
BWR, emergency core cooling system, unreliability estimates, comp. programs 77−54280
BWR, expt. reactor, design of control systems using Horowitz method 79−45338

nuclear engineering computing continued
BWR, fast moderator feedback effects during severe press. transients 78−4990
BWR, feasibility study of core management system by data communication 78−13254
BWR, fuel element positioning and control patterns, optimisation system 80−733
BWR, Hatch-1, core management data magnetic tape transfer to central office 78−21719
BWR, HDR reactor, design of blowdown loading expts., dynamic response of PWR-vessel internals 77−88204
BWR, improved fuel utilisation 80−732
BWR, KKM turbine trip simulation with a one-dimensional transient model 80−18510
BWR, min. critical power ratio thermal limit 80−18398
BWR, on-line core performance evaluation and operating guidance system 79−97859
BWR, ONDA-3 system for in-reactor fuel management 80−735
BWR, operating reactivity and power distrib. data base for nuclear methods qualification 79−89404
BWR, optimal fuel pin enrichment distribs. 77−83008
BWR, optimal in-core fuel management using OPTLWR computer code 78−17363
BWR, optimum fuel loading and operation planning, FAPMAN model 80−47606
BWR, prediction model for shutdown margin reactivity 79−26476
BWR, process monitoring and parameter estimation, multivariate signal analysis algorithms 80−47585
BWR, safety evaluation, experiments and analytical analysis, NRC codes 80−13703
BWR, startup control rod programming code system 80−13688
BWR, TRAB transient analysis program for pressure vessel and subsystems 80−73978
BWR, transactinide buildup in nuclear fields, sensitivity anal. rel. to neutron flux and spectra *(Italian)* 79−45356
BWR, vent clearing transients calc., press. suppression system, digital computer simulation 77−3132
BWR, void reactivity feedback, space-time anal. 79−22414
BWR control rod programming, heuristic and mathematical approaches 79−9779
BWR core, moderator temp. coeff. and neutron leakage, DIFFUSION-ACE calc. 78−54844
BWR core simulation, few group coarse mesh diffusion scheme, expt. verification 77−23223
BWR dynamics, imbedded flux calc. 80−714
BWR fuel assembly, radiant heat transfer 78−17287
BWR fuel management anal., consistent modelling procedure 80−23052
BWR licensing basis transients, computer anal. of turbine trip without bypass transient 80−42814
BWR LOCA, computer prediction of loading conditions on pressure suppression system 80−764
BWR LOCA, RELAP4 (MOD7/Version 1) core spray cooling calcs. compared with data 79−49730
BWR LOCA analysis, jet pump modelling using RELAP4 80−68850
BWR LOCA analysis, RELAP4/MOD7 calc. of level swell test data 80−23003
BWR neutron noise source identification, stochastic model data anal. 78−94106
BWR of Hamaoka nuclear power station, operating experience *(Japanese)* 78−17333
BWR power distrib. prediction system, on-line performance test 80−13689
BWR power distribution analysis, three-dimensional calc. program 79−9674
BWR power distribution changes, online prediction evaluation 79−9780
BWR power plant, computerised core component accounting system shortens shuffling time 80−699
BWR pressurisation effects of bypass streamline transient modelling 79−89408
BWR pressurisation transient anal. using MEKIN neutronics/thermal-hydraulic code 80−47626
BWR reactivity feedback modelling effects 80−22927
BWR rod drop accident, effect of thermal-hydraulic feedback, BNL-TWIGL code anal. 80−42815
bWR servicing and refueling improvement program 80−9390
BWR shutdown dose rate prediction, calc. code 80−23061
BWR subchannel code with drift flux and vapor diffusion transport 79−59149
BWR suppression pool temperature transients following LOCA, computer anal. 80−762
BWR transient anal., iterative procedure for predicting critical power ratio 80−42816
BWR transient anal. model for pressurisation transients 80−18509
BWR turbine, simulation 78−737
BWR turbine trip, RELAP/RETRAN steam line models, accuracy considerations 79−59197
BWR turbine trip test, computer anal. 80−692
BWR turbine trip transients, additional separator modelling considerations 80−18511
BWR turbine valve closure, pressure transients 79−89441
BWR vent clearing hydrodynamics, numerical simulation using SOLA-VOF code 79−49659
BWR vent clearing hydrodynamics, SOLA VOF simulation 80−32356
BWR with fracture live steam line, isolating valve loading *(German)* 77−38340
BWR WNS, a new core design with improved performance 79−59151
BWR-6 computer anal. of fission product release to containment via press. suppression pool 79−59223
BWR-II containment vessel, soil-struct. interaction for transient loads 78−29604
BWR/6 axial reflectors, Monte Carlo modelling 80−22939
CACECO, FFTF containment response to postulated core meltdown accidents 80−32381
CACTUS, a characteristics solution to the neutron transport equations in complicated geometries 80−95336
CAMAC-controlled calibration system for nucl. reactor systems 78−37532
CANDU, feedback coeff. anal. 80−27716
CANDU, LOCA, space-time neutronic anal. 80−13663
CANDU advanced BLWR with enriched fuel, controllability studies 77−71683
CANDU distributed computer control systems 79−76105
CANDU fuel channels, power rundown, computer programs for fuel and struct. element decay heat 77−57711
CANDU fuel pellet stacking, mathematical model of automatic assembler 80−37464
CANDU PHWR heat transport network, SOPHT computer model 77−83025
CANDU reactor, integral transport code PEAKAN for flux peaking anal. 79−59135
CANDU reactor, shutdown system design, performance during commissioning 78−25319
CANDU reactor kinetics benchmark activity 77−79416
Candu reactor moderator effectiveness as LOCA heat sink 79−81021
CANDU secondary coolant circuit chemistry control, automated system development 78−66359
CANDU simulated core in ZED-2, transient meas. anal., CERKIN code exam. 78−58386
CANDU simulated cores, transient expts., validation of computer codes 78−54825
CANDU-PHW 600 MWe reactors, channel power mapping and calibration routing 80−57892
CANDU-PHW thorium convertor, study of running-in period 78−25313
capacitor fed fusion expts., computer based control system 80−13912
carbide fuel elements, response to fast thermal transients, UNCLE-T-BUBE code 79−93715
carbide fuel-coolant interactions, PLUTO code 79−85613
CATFISH for LMFBR core flow distrib. anal. 80−23018
cause analysis algorithm using cause consequence method 79−97823
CEGB nuclear power station emergency monitoring procedures 78−55053
CERN 400 GeV proton synchrotron control consoles 77−38518
CIRENE, heavy water moderated BWR, LOCA simulation of recirculation circuit rupture 79−30949
CIRENE LWCHW reactor, two-phase flow rods for neutron flux control, computer anal. 79−59217
CIRENE reactor control, two phase flow rods, BUANA and TICO codes 79−17994
clad failure prediction during FBR overpower transiency, JANE 80−78363
coarse mesh methods for benchmark and realistic reactor problems 77−88191
coated fuel particles, automatic size anal. 77−79460
COBRA, fuel bundles, thermal-hydraulic anal., comparison of computational techniques in COBRA-IIIC and COBRA-IIIP *(Japanese)* 80−95374
COBRA code for LMFBR fuel assemblies, thermal-hydraulic anal. wire-wrap modelling 80−47549
COBRA III/MELT code, anal. of FFTF transient overpower accidents 80−32373
COBRA subchannel anal. code, LMFBR whole core transient anal. 80−18388
COBRA-IV comparison with the W-ARD 11:1 LMFBR air flow tests 80−27734
CODA 1-D coolant dynamics code for PWR flow transients, critical heat flux predictions 80−42817
collective dose distribution anal. using census data, graphical method 77−6567
collision probability program for uniform slab lattices 79−89350
COMETHE code, benchmarking results 80−37452
COMETHE code with transient capability 80−42761
COMETHE III-J code, fuel behaviour models 80−42752
COMETHE III-J code improvements for fuel rod modelling 80−42754
COMETHE III-J programme, anal. of integral fuel rods 80−37448
commercial reactor code incorporation into nuclear engineering course 78−4448
complex particle transport problem soln., general-purpose Monte Carlo codes 79−583
complex repairable systems, Karlsruhe computer program for availability and reliability evaluation 77−88249
computer assisted learning in nuclear engineering 77−13557
computerised reactor safety systems, design, specification and implementation 79−63783
concrete reactor pressure vessels, finite element creep anal. 78−41813
conduction controlled surface rewetting, general 1-D model 77−83011
conference, Berlin, Germany (Aug. 1979) 80−77539
conference, San Diego, Calif., USA (June 1978) 79−17972
conference, San Diego, Calif., USA (June 1978) 79−49650
containment accident analysis using CONTEMPT4/MOD2 compared with experimental data 79−49738
containment analysis by ALICE code after HCDA 79−49736
containment blowdown following LOCA, press. and temp. transients and COPDA results 78−13303
containment leakage from Na fire anal., response surface method, SPOOL-FIRE code 79−18004
containment response to accidents, comparison of CONTEMPT-LT calculations with Marviken experiments 79−49737
containment structures pressure tightness verification, pressurisation plant, data acquisition and processing *(Spanish)* 80−13775
Controlled Fusion Atomic Data Center 78−17432
cooling medium pressure calc. using ZOCO VI program *(German)* 78−21668
CORA transient anal. code for cluster of reactor core assemblies 80−18389
core disassembly calculations, vapour press. eqn. of state, VENUS-II code studies 78−8908
core operating limit supervisory system stochastic simulation 79−630
core pin power distribution det. based on nodal coarse mesh calcs. 77−88195
core power distribution calc., FLAME3 nodal code accuracy 79−9703
core transient thermal-hydraulic anal., computer code 77−83022
core-wide fuel performance assessment 79−93766
COROPT code, anal. of LMFBR design 80−27714
CORTAC 3-D thermal hydraulic model of LMFBR core restraint transient responses 80−18390
CORTRAN code, LMFBR whole core transient thermal hydraulic anal. with CORTRAN code 80−18392
cost comparison of PWR and PHWR nuclear power plants in Korea using ORCOST and POWERCO-50 80−57821
coupled hydrodynamic and struct. response, splitting method 77−74958
coupled problems in transient fluid and structural dynamics 77−71646

nuclear engineering computing continued
CRAC, accident risk calcs., models and data 80−47613
CRATER code calc. of LWR fuel rod under power transients *(French)* 80−42789
CRBR, primary pipe rupture accident anal. with DEMO code 78−70621
CRBR mild transient overpower accidents with advanced fuels 80−18539
CRISIS code for LWR critical heat flux calc., anal. of empiric relations *(Bulgarian)* 80−68766
criticality control of intermediate U enrichments, computer calcs. 80−37435
criticality safety anal., quality assurance for computer programs 79−63766
criticality safety anal. at Oak Ridge 80−37431
criticality safety broadgroup library validation using uranium systems 79−26564
criticality safety program, role of computers in quality assurance 79−63765
criticality search techniques for low and high switched systems 80−37494
CRNL NOS/BE 1.3 system, dynamic core allocation 80−78425
CRONOS code development, PWR fast transients anal. 80−23055
cross-section self shielding factors, analytic bounds 80−37426
Culham fusion expts., distributed control systems using microcomputers 80−13909
Culham fusion expts., integrated data network for microcomputer based diagnostics 80−13910
Culham fusion studies, appl. of microcomputer to data acquisition and control 80−13908
CUPIDON code anal. of PWR fuel rod during depressurisation accident *(French)* 80−42791
data acquisition/analysis, modular-programmed systems 77−18766
data centres of NSRDS, role in technical information transfer 78−13402
data covariance estimation methods for sensitivity-based data assessment 78−13400
data evaluation at Nuclear Safety Information Center, products and available services 78−17545
data evaluation using lognormal distribs. in least squares algorithm 79−93902
data processing system of Dungeness 'B' power station 77−67831
deep-penetration radiation transport, event and point value in Monte Carlo importance sampling 78−8869
defense waste processing facility, anal. of radionuclides 80−37518
depletion chain eqns., FORTRAN program for solns. using analytical methods 78−74423
development of maneuvering strategies using optimal control theory 79−30959
diffusion problems, two dimens., nuclear reactor structs., singularities in finite element approx. 77−6496
digital computer applications in reactor instrumentation and control 80−106134
digital computer control in Canadian nuclear plants, past performance and future outlook 78−58383
DIGRAS, dynamic intragranular fission gas release and swelling 80−32345
directional integration method for 2-D fluid transients 78−683
DISCAL, HCDA, neutronics and hydrodynamics equations, energy release 80−68842
discrete angle finite element formulation of radiation transport 78−13197
discrete cross-section expansion for discrete ordinate codes, TDA computer code 79−69162
DNB open core algorithm for on-line thermal margin evaluation 80−27782
dosimetry, thermoluminescence, automatic, for personnel monitoring *(German)* 77−10493
DOT 3.5, use in fast power reactor shield configuration calcs. 80−68749
DOT-IV neutron transport theory code, use on vector processing computer 80−47836
dynamic analysis facility at Chalk River National Laboratory 80−58106
dynamic materials accounting for LWR fuel cycle 79−36325
dynamic safeguards accounting and material control via modern estimation methods 77−34417
EBR II, transient testing and simulation for LMFBR plant dynamic modelling 79−54558
EBR II gas-tagging anal., isotopic weighting factors 79−59221
EBR-II cover gas, second Xe tag identification, code MIXTAG 77−42145
EBR-II cover gas clean-up system, transient anal. 77−46357
EBR-II delayed neutron concentrations, computer modelling 80−27717
EBR-II primary system piping evaluation for safety research modification 79−9785
ECC reflood characts., effect of bottom injection location, SUNYAB/EPRI program 79−49726
ECC system, treatment of water packing effects [in fission reactors] 79−89401
educational module, in-core fuel management computer system 80−36826
ELESIM computer code for fuel element performance prediction 79−81007
emergency monitoring procedures at CEGB stations, UK 77−54322
ENDF/B-IV, absorption effects on decay heat and spectral pulse kernels 80−22931
ENDF/B-V, prompt fission neutron spectra 80−22869
ENDF/B-V cross section data for shielding appls., Monte Carlo MCNP integral calcs. 80−47744
ENDF/B-V cross-section covariance data for neutronics anal. of fusion reactor materials 80−47710
ENDF/B-V nuclear data for shielding appls., energy balance anal. 80−47745
ENDF/B-V uncertainty data processing into multigroup covariance matrices 80−68752
enrichment facility, at Savannah River Plant, diversion path analysis 79−85739
enrichment zoning and control rod programming for reactivity and power shape control 79−18003
epithermal 1/V self-shielding of reactor poisons using Nordheim integral method 78−17306
ESSOR heterogeneous reactor, calc. of reactivity, flux distrib. and power by CART loop 79−30891
ETA-BETA fusion expt., data acquisition and anal. programs 80−13914
nuclear engineering computing continued
EULFCI code for numerical anal. of LMFBR HCDA fuel-coolant interaction 80−68733
Euratom Data Acquisition Co-ordinating Committee activities 80−13904
EURDYN, nonlinear transient dynamics programs for fast reactor safety 80−91234
EURDYN-1M, containment and fuel subassembly analyses for fast reactor safety studies 80−52772
EURDYN-1M, safety studies on LMFBR, computer program 80−99267
Evaluated Nuclear Data File, ENDF/B-V, at Brookhaven Nat. Lab. 78−13398
Evaluated Nuclear Structure Data File for basic and applied research 78−17544
expanding nuclear power systems, initial fissile U requirements for fuel cycle, computer simulation 78−17320
explicit iterative technique for FX2 reactor analysis computer code 78−17302
FACSIMILE VSI code for void swelling calcs. 80−42782
failure analysis and failure prevention in nuclear elec. power plants 77−79450
failure location algorithm for complex networks 80−99228
FAPMAN8, LWR, operation planning, optimum fuel loading and generation planning 80−47673
FAPMAN-5, a computer code for optimum operation of LWR power stations 79−22450
FAPMAN-IC program module for LWR power stations, incremental fuel cost calcs. 80−95356
Farley Nuclear Plant Data Link System 79−9797
fast breeder test reactor operator training simulator model development 80−91219
fast high-power reactor calcs. using ZELVA program *(Czech)* 77−6493
fast reactor containment, COVA program for computer code validation 78−41833
fast reactor containment safety, study using computer code SEURB-NUK-2 78−33260
fast reactor design data adjustments 79−9695
fast reactor finite difference diffusion theory codes, optimised iteration strategies and data management 77−83005
fast reactor models, iterative methods comparison 79−97752
fast reactor parameters, influence of fission spectra uncertainties 80−22928
fast reactor physics, assessment of JAERI fast group constants set version 2 80−602
fast reactor SDX cell homogenization code, validation results for pin geometry 79−80997
fast reactor three-dimensional hexagonal-Z systems anal. using THREET-RAN (hex,z) 79−80994
fast reactors, error anal. of computational models 79−97750
FASTA, fuel performance modelling, pellet-cladding interaction 80−63264
FASTA, fuel preconditioning, power shock anal. and sipping 80−63358
FATRAP, PWR accident anal. code, logic construction *(Czech)* 79−30957
fault tree anal. code SUPKIT *(Japanese)* 78−54847
fault tree analysis, development of DICOMICS-TWIN self-adaptive algorithm for minimal cut sets determ. 78−17380
fault tree and reliability analysis, modular decomp., PL/1 program 78−17381
fault trees, methodology for computer-aided construction, nuclear system appl. 78−37412
FAXMOD anal. of creep and sheath ballooning 80−42759
FBR, 2-D power distrib. calc. by appl. of Askew coarse mesh method 79−22372
FBR, above-core structural response to molten core disassembly 79−30992
FBR, comparison of computer code predictions with COVA expts. under postulated accident conditions 79−30995
FBR, energy increase from bubble collapse following recriticality in large molten pools 79−31023
FBR, experimental, math. model for control system design in FBR plants 79−17990
FBR, modelling molten fuel-coolant interaction, INTER and CEFRA *(Czech)* 78−66352
FBR, Monte Carlo benchamrk program for anal. of critical assemblies 79−89405
FBR, optimisation of burnup characteristics, nonlinear programming method 77−14239
FBR, rigorous and efficient struct. Doppler effect calcs. 78−33256
FBR, SAS3D prediction of intrasubassembly boiling incoherence, multipin boiling model 79−49662
FBR, space dependent simulation of transient behaviour using KINTIC-2 code *(German)* 80−83182
FBR, void reactivity effects on hypothetical core disruptive accident excursion energy 79−31024
FBR carbide fuel, Sphere-Pac form, performance evaluation using computer code SPECKLE-I 80−637
FBR containment code, structural deform., SEURBNUK-2 80−78404
FBR containment code validation program, SEURBNUK 80−78405
FBR containment response to HCDA, effect of struct. components, Eulerian hydrodynamic anal. 80−23014
FBR core disruptive accident, response of upper internal structures, finite element computer anal. 80−47645
FBR excursion model, ICECO predictions 77−42028
FBR fuel, accuracy and computational time of hierarchy of growth rate definitions 79−80979
FBR HCDA, fluid-struct. interaction anal., evaluation of computer code 80−23015
FBR HCDA, structural response of the upper internals, finite element anal. 80−18537
FBR probabilistic accident anal. 77−83054
FBR safety anal. modelling of fission gas behaviour 80−748
FEMAXI-II, fuel rod deform. code, appl. 80−37446
FFTF, containment response to postulated core meltdown accidents 80−32381
FFTF, HCDA, NASTRAN nonlinear dynamic transient accident anal. 77−42133
FFTF, interassembly flow redistribution at natural circulation conditions 79−85654
FFTF, transient overpower accidents, effect of intrasubassembly incoherencies 80−32373
FFTF control rod anal. with SCRAM program 77−46355

nuclear engineering computing continued
FFTF fuel, neutron source strength as function of irradiation 80−22929
FFTF loss-of-electric-power transient response, natural circulation tests, pre-test simulation using SSC-L code 80−42836
FFTF reactor shielding anal., spatial channel theory 77−6569
finite element code, neutron flux computation 78−50449
finite element heat cond. in reactor solids, review and TEMPEL computer program 78−62593
FIPMIGR program, fission product migration, anal. 80−37453
FISPIN, nuclide inventory calculation code 80−42781
fissile material inventory and criticality control system, on-line, INMACS 79−89486
fission gas, steady state behaviour in carbide fuels, modelling 78−78469
fission gas release and swelling in irradiated UO_2, model 77−6488
fission gas release from high burn-up oxide fuel, predictions in ELESIM code 80−57864
fission product migration in fuel pin, FIPMIGR program 80−37453
fission reactor, automatic diagnosis of abnormal phenomena 78−17330
fission reactor, functional anal. of multigroup neutron diffusion problem 78−58317
fission reactor, utility use of NSSS supplier reactor analysis code for operational support 78−21724
fission reactor, VVR-S, Bucharest, IRT-M expt. bundle power distrib., obs. and computer anal. 77−18655
fission reactor, zero-power control rod group reactivity worth, computerized determ. method 78−21702
fission reactor fuel, U enrichment, optimal blending 78−13309
fission reactor pressure vessels for high temp., computer appl. *(Japanese)* 78−673
fission-fusion systems, laser-driven, nuclear and thermohydrodynamic calcs. 80−47696
fission-gas-induced swelling in UC, porosity effects study by UCSWELL code 78−8959
fixed bed reactor radial flow, Runge-Kutta method soln. 79−10546
FLAIR-CENSOR, PWR core power manoeuvres, fuel duties and fuel preconditioning 80−63337
flow boiling anal., numerical standards 77−79448
flow-induced vibration anal. of nuclear reactor components 79−22380
fluence limit analysis of nuclear reactor component, damage function methods, computer simulation 77−18668
fluid dynamics, coarse mesh methods appl. *(German)* 77−88197
fluid dynamics, prospects for accurate computer simulation 77−79422
fluid dynamics eqns., asymmetric weighted residual method 77−79421
fluid flows with large density gradients, Eulerian finite difference technique 77−79424
fluid piping systems, transient cavitation effects 78−29554
flux synthesis program KASY, consideration and appl. to reactor design problems 77−88184
Fourier-transformed neutron slowing-down kernel moments, MAGGIE code 78−29540
fracture mechanics of reactor primary system under operating and accident conditions 78−66342
FRAP-S3, steady state fuel rod anal. program, calc. of stored energy for PWR-type fuels 80−9349
FTR, criticality expts. of fuel pins in water, computer calcs. 79−59162
FTR TOP accident, effect of power skew, computer code development 79−54481
fuel accountability and control, use of novel data collection and processing techniques 79−85749
fuel accounting system, nuclear inventory and management system program 78−13245
fuel assemblies in vertical flow channels, computer dynamic model 79−22379
fuel assembly spectrum code verification based on integral transport theory 79−80996
fuel behaviour models incorporated in COMETHE III-J 80−42752
fuel bundles, thermal-hydraulic anal., comparison of computational techniques in COBRA-IIIC and COBRA-IIIP *(Japanese)* 80−95374
fuel burnup calcs. in LASER code 79−59119
fuel cladding, slightly oval cylindrical shells, creep anal. 78−78468
fuel cycle, GASP IV simulation model 78−41847
fuel cycle cost sensitivity to data uncertainties, interactive graphic computation 79−9837
fuel cycle management, w.r.t. economics 77−14241
fuel cycle material shipment, transportation model 79−85743
fuel cycle strategies, simulation using FISS computer program 80−5317
fuel element codes, structural anal. 80−78362
fuel element modelling, LMFBR, LWR 78−86617
fuel element modelling at CNEA 80−37449
fuel element performance modelling, IAEA specialists meeting, 1978 80−36769
fuel element performance modelling using LIFE-III, UNCLE-I and LIFE-LWR codes 77−46229
fuel fabrication control system for remote operation 80−18571
fuel failure, relating uncertainty allowance in operating limits 80−13721
fuel failure prediction using POSHO model 77−46226
fuel management analysis core, computer code for teaching assistance 78−4449
fuel pellet storage facility, large dry, criticality eval. 79−26668
fuel performance anal. by finite element method, MIPAC code 80−42750
fuel performance data base EPRI 79−93731
fuel performance modelling, pellet-cladding interaction, FASTA 80−63264
fuel pin claddings, fission gas driven creep calcs. 79−26531
fuel pin gaps, probabilistic distrib. within wire-spaced fuel subassembly 78−78448
fuel pin heat transfer, digital transfer matrix 78−29548
fuel pin imagery, computer enhancement and mensuration 78−37395
fuel pin inelastic modelling and stress analysis using FULMOD code 77−46233
fuel pin modelling principles and developments 77−46232
fuel pin performance modelling codes for overpower performance analysis 77−46230
fuel pin-cell burnup code BETTY 78−89946
fuel pins, computer controlled meas. 80−5300
fuel pins, eccentrically placed pellets, finite difference method for heat transfer 78−82419
fuel preconditioning, power shock anal. and sipping, POSHA and FASTA 80−63358

nuclear engineering computing continued
fuel restructuring and relocation under irrad., COMETHE code calcs. 77−46235
fuel rod, heat transfer code for calc. effect of asymmetric geometries 79−49743
fuel rod, simulation of performance with BACO computer code 80−37450
fuel rod anal., statistical version of URANUS programme 80−42749
fuel rod anal. program, CYGRO-4 78−41805
fuel rod behaviour modelling using LIFE-III code 77−46234
fuel rod bowing, finite element computer model 77−46260
fuel rod deformation code FEMAXI-II and its application 80−37446
fuel rod mechanical design, DIMCO system 80−37418
fuel rod modelling complexities 77−46231
fuel rod modelling techniques, best-estimate calc. 79−17984
fuel rod ramp tests analysis using SAFE-2D program 77−46228
fuel rod simulation in COMETHE III-J code improvements 80−42754
fuel rod thermal characteristics, on-line simulation by elec. heated rod 77−46209
fuel rod thermal stored energy, calculational uncertainty anal. 80−47609
fuel rods, thermal and mechanical anal. with URANUS code 78−41803
fuel sheath deform. following fuel power transients, simulation 78−33258
fuel storage pool criticality calc., transport-consistent diffusion algorithm 79−9721
fusion experimental facilities, computerised control and data acquisition 80−13890
fusion experiments, 10 bit transient data recorded 80−13917
fusion experiments, fibre optic signalling in control 80−13919
fusion mirror reactors, finite orbit treatment of plasma buildup 80−37631
fusion plant, inertial confinement, commercialisation anal. 78−58410
fusion plasma, MHD behaviour computation *(Japanese)* 79−31178
fusion reactor, compact toroidal ignition experiment, support struct. anal. by numerical code 80−106167
fusion reactor, low power Tokamak experimental fusion power plant, scoping studies with empirical scaling, SISYFUS code 80−102309
fusion reactor, magnetic confinement, structural anal., combined interactive/batch computer environment 80−91255
fusion reactor, PDX Tokamak, finite element anal. using computer graphics 80−95424
fusion reactor, pulsed expts., computer-based control systems 78−62624
fusion reactor, SLPX TF coil, stress anal. using COSMIC-NASTRAN 80−106168
fusion reactor, stainless steel first wall, swelling and irradiation creep, FWLTB computer code 80−32446
fusion reactor, Tokamak constant tension D-shaped coils, lateral support struct. 78−55013
fusion reactor cavity gas response to particle beam target explosions 80−37602
fusion reactor coil design codes in FORTRAN IV 78−66367
fusion reactor design and performance requirements, cost and systems anal. 78−50357
fusion reactor first wall, lifetime calc. in FWLTB program 80−18646
fusion reactor first wall structural materials, prediction of life limiting props. 78−62605
fusion reactor inertial confinement pellets, neutronics modelling 80−37593
fusion reactor Ingra injector, control and data acquisition system 80−13913
fusion reactor insulators, radiation damage calcs. using MORSE code 80−34061
fusion reactor materials, neutronics analysis using ENDF/B-V cross-section covariance data 80−47710
fusion reactor materials, nuclear response functions library, MACKLIB-IV 79−67950
fusion reactor quantitative cross-section data assessment 78−9047
fusion reactor shielding, radiation attenuation meas., macroscopic cross-section sensitivity calc. 79−67951
fusion reactor superconducting magnet magentoelastic energy calcs., finite element anal. 78−55002
fusion reactor TESPE coil, finite element method calc., winding package modelling 78−50376
fusion reactor vacuum vessel, magnetic stress induced by plasma motion, 3-dimens. anal. 78−66370
fusion reactor vacuum vessel, stress anal. 78−66371
fusion reactors, air detritiation operation, computer model and scale expt. 78−66413
fusion reactors, interferometric phase detection system, using high speed digital techniques 78−62629
fusion reactors, sputtering erosion in inertial confinement reactors 79−22462
FWLTB computer code, stainless steel first wall, swelling and irradiation creep 80−32446
GAM library data formation in energy groups, PWR appl. 80−68746
gamma photons penetration, 6 MeV, through Al, concrete and graphite, expt. and computed results comparison 80−5256
gamma spectra of fission products, estimation using nucl. systematics 78−70587
gas cloud explosion pressure loading for reactor secondary containment 79−49789
GCFR, 1000 MW, calc. of depressurisation and flow coast down accidents 78−50274
GCFR, 1000 MW(e), reliability anal. of decay heat removal system 77−14223
GCFR, Argonne, calc. of void streaming in critical expts. 77−83007
GCFR, Pu fuelled, fission products and secondary gamma-ray spectra 78−676
GCFR, transient anal., systems simulation methods, development and validation 79−54486
GCFR, transient analysis of closed gas turbine cycles, TUGSIM-10 computer code 77−18675
GCFR fuel assembly thermal-hydraulic anal., modification of COBRA code 80−588
GCFR proliferation-resistant heterogeneous fuel cycles, computer neutronic anal. 80−18435
GCR implementation strategy anal. using MCFLOW program 77−57733
GETRANS, two-dimens. integral neutron transport code 79−22366
GRASS-SST code, LWR fuel, mechanistic prediction of transient fission gas release 80−47571

nuclear engineering computing continued
guard line circuits dual microprocessor system, decision-making and self-testing 80−57901
HCDA, first-generation model for UO_2 particle size distribs. 78−13295
HCDA, neutronics and hydrodynamics equations, energy release, DISCAL code 80−68842
HCDA, REXCO code, comparison with flexible vessel expts. 78−70618
HCDA due to transient overpower, model for prediction of press. in core and upper plenum 78−8926
HDR, numerical investigation of radial mixing capabilities in strongly buoyancy-influenced vertical, turbulent channel flows 79−93751
heat exchanger tube, vibratory contact with support plate, forces produced 77−88211
heat transfer finite difference computer programs 79−14221
heat transfer simulation using analogue computer elements *(Russian)* 80−52733
heating, nuclear, approx. method, direct energy balance calc., γ transport, accuracy 77−6495
HEATUP-R/AEP analysis of PWR LOCA reflood, effect of low containment press. on peak cladding temp. 80−57897
helical wire subassemblies, mechanical behaviour anal. with SWAMB code 77−46259
heterogeneous computer program for square fuel rod lattices in cylindrical tank 78−58346
heterogeneous fuel pin cells, nodal method in 2-D calcs. 78−21631
heterogeneous lattices, unified theory 80−37428
HEXAB-II-30E code for few group 2-D diffusion eqns. in hexagonal geometry, LWR core calcs. *(Bulgarian)* 80−68765
HFIR, dimensionality reduction of reactor noise signatures, improved automated noise anal. 77−6499
HFR test reactor, HIP-TEDDI code for neutron flux calcs. 79−3223
high flux test reactor, MARIA, nuclear power research programs *(Polish)* 79−93693
high-level radioactive waste storage, distribution calc. *(German)* 79−81014
HOTRAN-3, LWR core, thermal and hydraulic behaviour code *(Hungarian)* 80−32401
HOTROD code, fuel performance during LOCA 80−42790
HTGR, control rod ejection accident, comparison of one- and two-dimens. models 78−13279
HTGR, pebble-bed, computational procedure for xenon stability 77−61501
HTGR core, 2-D vibr. test for vertical slice model, COLLAN 2-V simulation code *(Japanese)* 78−58328
HTGR core during transient temp. excursion, fission product release analysis *(Japanese)* 78−82467
HTGR cores, graphite oxidisation analysis *(Japanese)* 79−81018
HTGR cores, transient thermal hydraulic anal., RETSAC code 77−46246
HTGR fuel and graphite structure stress analysis methods and programs *(Japanese)* 78−74434
HTGR fuel element graphite, determ. of ^{90}Sr diffusion coeffs. 79−67869
HTGR fuel particle, computer code for anal. of transient behaviour 78−8964
HTGR PCRV depressurisation accident, anal. of gas circulation using HAZARD code 79−54561
HTGR primary coolant system depressurisation accident, expt. and numerical anal. 80−775
HTGR steam power plant, nonlinear dynamic model 78−78437
HTR spent fuel reprocessing facility, real-time data acquisition and processing system *(German)* 80−106148
HWR, fuel cycle cost anal. using computer code HWRCOST on-power refuelling 77−83051
HWR, multidimens. space time kinetics studies 78−29547
HWR, multidimensional space time kinetics, TRIMHX code 80−47538
HWR reboiler hybrid computer dynamic simulation 78−8949
hydraulic pressure pulses with structural flexibility 77−50266
hydraulic pressure wave propagation in plastically deforming pipe, rel. to reactor HCDA 78−8876
hydrid reactor, reaction rate calcs. in ^{238}U and ^{232}Th blankets around D-T neutron source 80−52782
hydrodynamic oscillations in Gentilly-1 reactor steam mains, GISMO program 78−54824
ICECO code, anal. of LMFBR Na spillage 80−32364
ICEPEL code comparisons for flexible pipe elbow loop 79−49772
ICF, parametric studies 80−32507
imbedded neutron flux calc., reconstruction of original material struct. of fuel bundle 77−88196
in-core meas. of energy release *(Czech)* 78−86637
in-reactor fuel temperature, transient response of centreline thermocouples, appl. to fuel modelling 80−95372
inertial confinement fusion pellets, neutron moderation, effects on damage and radioactive inventory 80−47704
influence function method, fracture mechs. and residual fatigue life anal. of power station cracked components 77−80109
INSITE system for nuclear site data storage and retrieval 78−5109
integral rods, anal. with COMETHE III-J programme 80−37448
integrated PWR, anticipated transients without scram, calc. of dynamical behaviour 80−5250
interactive fuel management using a CRT 79−85594
IRAN-1,2, plants, calc. of radioactive releases 79−18056
irradiated fuel rods, computer-controlled gamma scanning 79−9753
IRT code for PWR non-LOCA transient anal. 80−42819
isolation and relief valve/piping transient force anal. program 78−50287
isotope composition tables for isotopes produced in CANDU reactors 78−29564
ISUNE-4 code for transient pellet-cladding interaction, in LWR 80−91228
JANE, clad failure prediction during FBR overpower transiency 80−78363
Japanese reactor noise pattern library 79−3338
JET, control and data acquisition system 80−13905
JET, control system, communications, diagnostics, data storage and anal., NORD computers 80−68943
JET, synchronous generator, bridge convertor and ohmic heating systems, digital simulation 78−54960
JT-60, control system 80−13906
kinetics eqns., piecewise polynomial approx. 78−4981
KINTIC-2, space dependent simulation of transient behaviour of FBR *(German)* 80−83182

nuclear engineering computing continued
laboratory computer system for routine, plant and environmental radiation monitoring appl. 79−9912
laboratory instructional programs in computer instrumentation at RPI 80−31472
Large Coil Test Facility, instrumentation system design 80−95446
large pools for spent fuel, LUSH code cf with design methods for struct. load calc. 78−17337
large-water reactor, TRAC-P1 post-test anal. of US standard problem 7 79−89433
laser fusion driven actinide waste burner, neutronics anal. 78−58459
laser fusion power plant, capital cost data base 80−32504
laser fusion system studies model, TROFAN 80−32505
laser plasma compression, computer simulation of implosion struct. *(Japanese)* 79−14587
laser-fission-fusion systems, coupled nuclear-thermohydrodynamic anal. 79−13520
leakage neutron spectrum in light water, ENDF/GASKET model in DTF-IV code 78−62592
LEVITATE code anal. of steel ablation and fuel-steel mixing phenomena following LMFBR accident 80−47649
Levitron experiment, Culham, plasma fluctuation and by microcomputer system 80−13911
light ion sputtering in fusion reactors, discrete ordinates method calcs., ANISN code 78−92158
LIMITS−a fast Monte Carlo code for system reliability 79−49783
linear acceleration reactors, anal. of neutron yield produced by high-energy protons 80−22895
liquid cooled fast reactor HCDA, fluid filled vessel response to internal explosions 79−49771
LMBFBR overpower accidents, mechanistic model of fuel flow regimes and fuel plateout 79−85615
LMFBR, accident conditions, theoretical anal. of Na fire using SPOOL-FIRE code 77−14248
LMFBR, accident progression within secondary containment boundary 80−32368
LMFBR, advanced, core design methods 78−8885
LMFBR, appl. of BWR simulator to neutronics calc. tool 79−40987
LMFBR, benchmark calc., neutronics codes validation 77−79415
LMFBR, benchmark calcs. by diffusion methods 77−79414
LMFBR, breeding ratio and fissile inventory for homogeneous and heterogeneous cover 80−32374
LMFBR, bubble collapse reactivity increases in boiling fuel/steel pools 79−31025
LMFBR, Clinch River, assessment of containment response to hypothetical core melt-through accident 78−8928
LMFBR, Clinch River, consequences of boiling in radial blanket due to hypothetical major pipe leak 78−8922
LMFBR, Clinch River, LOCA in one heat transport loop without reactor trip 78−8924
LMFBR, Clinch River Plant, pipe rupture simulation using DEMO code 78−8927
LMFBR, Clinch River Plant, sensitivity for radiological consequences to var. in aerosol parameters 78−13294
LMFBR, comparison of neutron diffusion computer codes 77−88188
LMFBR, comparison of REXCO and ICEPEL code calcs. with tests of plastically deformable pipes filled with compressible fluids 79−30994
LMFBR, computation studies of cladding relocation dynamics after transient undercooling accident 78−13255
LMFBR, computer control system for Na test loops 79−26550
LMFBR, computer model for ^{3}H transport and release 79−36371
LMFBR, computer modelling of piping components for transient hydrodynamic structural response 78−74449
LMFBR, containment, safety anal., conf., San Francisco (Aug. 1977) 77−71664
LMFBR, containment building response to HCDA, risk assessment, computer anal. 77−71678
LMFBR, containment codes appl., response predictions in HCDA conditions 77−71670
LMFBR, containment pressurisation by Na spray fires 80−32365
LMFBR, coolant cavitation in dynamic containment loading 80−32326
LMFBR, core design optimisation, simplified reactor physics model 78−8886
LMFBR, core designs, loss of flow transient anal. for 1200 MWe reactor 79−22415
LMFBR, core flow distrib., analytical prediction, using CATFISH hydraulic code 80−23018
LMFBR, core restraint systems, interassembly heat transfer model 80−567
LMFBR, development and Pu allocation, optimal policies 80−725
LMFBR, dynamic core deform. during local failure propag., subassembly expts., CORE-1 code 77−88244
LMFBR, dynamic response of containment vessel and coolant wave propag., REXCO-EUR code manual 78−58349
LMFBR, effective conduction mixing lengths for subchannel anal. of finite hexagonal bundles 78−13210
LMFBR, enrichment and control optimization for reactivity losses during burnup 78−21692
LMFBR, establishment of buoyancy induced natural circulation, CURL-L code anal. 79−49663
LMFBR, fast integral model for the transient analysis of a melting fuel pin 79−54552
LMFBR, fast integral modelling of HCDA 79−26555
LMFBR, finite element formulation for thin reactor struct. thermal stress anal. 78−70613
LMFBR, fuel and coolant motion following pin failure, EPIC code 77−83055
LMFBR, fuel pin coolability in low power voiding, SAS3A computer code anal. 79−49661
LMFBR, fuel pin deform. within wire-wrap fuel assembly, computer code anal. 79−71915
LMFBR, HCDA, Eulerian computer code anal., primary system response 77−3127
LMFBR, HCDA, structural response calcs., methods, codes development 77−3126
LMFBR, HCDA, two-phase momentum exchange experiment and analysis, using SIMMER code 79−49751
LMFBR, high power, optimisation by nonconvex programming mathematical model 78−41810
LMFBR, hypothetical loss of flow accident, computer simulation 79−3222

nuclear engineering computing continued
LMFBR, local boiling calculations in subchannel geometry, feasibility study using CLAYMORE code 78−25280
LMFBR, LOFA, fuel assembly boiling and voiding, THARC-S code 80−13646
LMFBR, LOFT for loss-of-piping-integrity transient, expt. data and COBRA-3M comparison 78−17370
LMFBR, loop-type, effect of pumped stored kinetic energy on natural circulation decay heat removal 80−23010
LMFBR, loop-type, transition to natural convection from low temp., low flow conditions 80−18533
LMFBR, modeling ejection of fresh fuel into sodium under prompt-burst conditions 79−85668
LMFBR, modelling in prompt burst HCDA calcs. 78−74454
LMFBR, molten cladding film relocation following HCDA, large wave dynamics 78−17365
LMFBR, Na incipient boiling under forced convection in seven pin bundle 79−22401
LMFBR, Na pump, multimode heat transfer, computer codes 79−610
LMFBR, Na spillage due to slug impact on reactor cover 80−32364
LMFBR, nonlinear structural dynamics of fuel elements, press. pulses, struct. models, expt. verification 77−3125
LMFBR, parametric safety analyses for reduced energetics in PLBR-sized core 78−13298
LMFBR, performance characts. in US nucl. energy system. rel. to breeding ratio, sp. power, discharge exposure 78−17404
LMFBR, pool-type, design effect on natural circulation establishment 77−6487
LMFBR, pool-type, PLOOP code for primary loop coolant flow and heat transfer anal. 79−31012
LMFBR, post HCDA aerosols, gravitational collision efficiency 80−32375
LMFBR, post-test anal. of transient overpower TREAT test R9 for BOL FFTF-type fuel 79−30985
LMFBR, primary containment response with upper internal struct. 80−32361
LMFBR, probabilistic accident anal. with deterministic codes 78−37420
LMFBR, SAS3A simulations for a 19-pin dryout experiment 79−54547
LMFBR, SNR-300, fuel rod performance and modelling at high burnup 78−58336
LMFBR, SNR-300, HCDA anal. by failure incoherence modelling, HOPE computer code 77−88237
LMFBR, struct. response to HCDA, appl. of coupled Euler Lagrange computer program 77−71671
LMFBR, subchannel deformation analysis code for wire wrap assemblies (SHADOW) 78−54829
LMFBR, temp. distrib. of subassembly including intersubassembly heat transfer 77−83014
LMFBR, thermal-hydraulic core anal., interassembly heat transfer, TRITON computer code 79−59153
LMFBR, thermohydraulic transients, numerical simulation using SSC-L code 79−54485
LMFBR, transient simulation code CURL 79−31011
LMFBR, U-Pu-Zr fuelled, study of core disruptive accidents 80−18540
LMFBR, W-ARD air flow tests, COBRA-IV comparison 80−27734
LMFBR, whole core thermal hydraulic transient code 80−18387
LMFBR accidents, steel ablation and fuel-steel mixing phenomena, LEVITATE code anal. 80−47649
LMFBR benchmark calcs. by 2 and 3 dimens. diffusion methods 78−74432
LMFBR containment, anal. of nonlinear fluid-struct. interaction, improved ICECO code 78−70615
LMFBR containment performance studies with simple computer code 79−93788
LMFBR containment response anal., Eulerian computer code MICE for multifield fluids 78−70616
LMFBR containment response to postulated Na spills and fires, computer anal. 79−54480
LMFBR control rod bowing, CRPBOW program 77−46262
LMFBR core and fuel design in Halian fast reactor programme 79−97795
LMFBR core assemblies, interassembly heat transfer, using CORTEMP code 79−59154
LMFBR core design optimisation, COROPT code 77−42041
LMFBR core disassemblies, damage potential sensitivity in prompt critical excursion 79−49766
LMFBR core disruptive accident, SIMMER-VENUS II comparison for mechanical disassembly 79−31018
LMFBR core orificing computer code 79−9681
LMFBR core structural analysis codes verification/qualification 79−89407
LMFBR coupled fluid-struct. problems, advanced Eulerian method 78−682
LMFBR design codes, multigroup diffusion, current weighted total cross section determ. in unresolved energy region 80−18365
LMFBR finite hexagonal bundles, three-dimensional coupled coolant cell heat transfer anal. 80−586
LMFBR fuel assembly, 19 pin, simulation of flow blockage 80−582
LMFBR fuel assembly, 3-D numerical simulation, thermal-hydraulic behaviour anal. 79−59143
LMFBR fuel assembly, anal. of loss of piping integrity accident 80−27783
LMFBR fuel assembly, thermal consequences of plenum fission gas release, TRUMP thermal anal. 80−47646
LMFBR fuel pin behaviour, computer code FRUMP, stress, strain, temp. distribs., displacements 77−14235
LMFBR fuel pin bundle, wire-spaced, three-dimens. deflection modes 78−13301
LMFBR fuel pins, computer anal. and control for nondestructive gamma scanning 79−9754
LMFBR fuel pins, reactor illuminated, coded aperture imaging 79−30989
LMFBR fuel subassembly, pin bundle deflection anal. 78−78449
LMFBR HCDA, containment response anal. to PAHR failure 79−49672
LMFBR HCDA, Na_2O aerosol gravitational fallout rate, validation of computer code 80−18535
LMFBR HCDA, simulation of fuel-speed pool during transition to transition phase 78−8937
LMFBR HCDA, wave propagation ICECO code predictions in rigid 2-dimens. vessel 79−49770

nuclear engineering computing continued
LMFBR HCDA anal. with FUTURE and FRUMP codes 79−85661
LMFBR HCDA analysis, uncertainty in accident consequences calculated by large codes due to uncertainties in input 80−78413
LMFBR HCDA containment response productions, validation of computer code 80−18538
LMFBR hypothetical core disruptive accident anal., hydrodynamic/neutronic coupled code FX2-POOL 77−23219
LMFBR hypothetical overpower accident, intersubassembly incoherencies and grouping techniques 79−31008
LMFBR intersubassembly transient heat transfer code, TCLUST1 80−63231
LMFBR LOF transient, integral model for voiding phase conditions 77−42032
LMFBR LOF-TOP, axial propagation of fuel failure, SAS3D-EPIC anal. 80−47650
LMFBR outlet plenum mixing, 3-D numerical simulation 78−8880
LMFBR outlet plenum transients, expt. and anal. using PLENUM-2 code 79−49664
LMFBR outlet plenums, transient anal. with PLENUM-2A program 80−32378
LMFBR oxide fuel analysis system 77−46227
LMFBR plant, modelling thermal hydraulic transients 77−88207
LMFBR plant, thermohydraulic transient simulation 77−83001
LMFBR power reactor, objective function optimisation *(Russian)* 78−70590
LMFBR prestressed concrete reactor vessels, analytical model and code applications 78−74448
LMFBR probabilistic accident anal., stochastically variable parameters 79−31021
LMFBR prompt burst calcs., FX2-TWOPOOL code for hydrodynamics, thermodynamics and neutronics 79−49767
LMFBR refuelling scheme optimisation by man machine interactive method 77−67826
LMFBR safety, collocation method soln. of radiation-conduction problems 80−13720
LMFBR safety, comparison of ICECO code with flexible vessel expts. 78−70619
LMFBR safety, comparison of ICEPEL code with straight flexible pipe expts. 78−70620
LMFBR safety, review of computer code packages 77−83053
LMFBR safety anal., theoretical interpretation of SCARABEE single pin in-pile boiling expts. 77−88239
LMFBR safety analysis, computational techniques 78−66355
LMFBR safety analysis, computer code for determ. of aerosol attenuation in leakage paths 78−13293
LMFBR shell structures, finite element elastic-plastic anal. 78−41804
LMFBR shielding calculations, accuracy of ENDF/B-IV cross sections 78−13401
LMFBR slow overpower transient, simplified computing method for cladding and fuel strain 79−31005
LMFBR soln. of COBRA energy equations during natural circulation conditions 79−89354
LMFBR spent fuel shipping cask designs, subcriticality guidelines, Monte Carlo calcs. 78−82470
LMFBR subassemblies, coolant boiling calc., using Claymore code 78−82473
LMFBR subassembly, central blockage wake anal. 78−29556
LMFBR subassembly, fuel coolant interaction anal.model and computer code SAMI 80−106136
LMFBR subassembly, multichannel model for fuel coolant interaction 80−13653
LMFBR subassembly, thermal hydraulics anal. 79−89396
LMFBR subassembly ducts dynamic response, comparison of finite element code with expts. 78−70614
LMFBR subassembly fault detection, microprocessor-based distributed system appl. *(Japanese)* 79−41002
LMFBR subassembly response to simulated local press. loadings, accident conditions, finite element anal. 77−3123
LMFBR subassembly simulation, finite element computer model, safety anal. 78−70612
LMFBR thermohydraulic transient simulation, appl. of multiple time-step integration in Super System Code 80−47552
LMFBR TOP accident, effect of transient power histories on intrasubassembly failure incoherencies 80−47647
LMFBR TOP accident, fuel pin failure, anal. 79−49699
LMFBR transient fission gas behaviour modelling, bubble equilibration effects FRAS 2 code 79−59168
LMFBR transient overpower accident anal. using PLUTO2 code 79−31004
LMFBR wire wrapped rods, 3-D thermal-hydraulic anal. 77−79425
LOCA, computer simulation of reflood heat transfer and hydrodynamics 79−67891
LOCA, condensing heat transfer 78−21684
LOCA, data analysis using computer-aided models *(Czech)* 80−73949
LOCA, effect of drop evaporation rate on containment pressure transients 79−22413
LOCA, experimental and theoretical study of the blowdown of the secondary side of a steam generator 80−761
LOCA, fuel element behaviour during high-temp. transients, ELOCA code 79−81043
LOCA, gravity-driven reflood hydrodynamics, EFLOD code 79−89426
LOCA, straight pipe blowdown tests and code verification [of reactor LOCA] 80−759
LOCA, thermal shock in nuclear containment wall, computer code for safety anal. 77−3135
LOCA anal. in Federal Republic of Germany, computer models 79−26642
LOCA anal. program TECAR 77−88250
LOCA analysis in small compact reactors uisng RELAP4/MOD5 thermal hydraulic code 80−68852
LOCA capability code for utility appl. 78−21690
LOCA codes, characteristics of two-phase one component flow with slip 77−83019
LOCA mathematical models for PWR safety analysis *(Russian)* 79−30963
LOCA quench front model for Transient Analysis Reactor Code 80−47550
LOCA reflood phase, thermo-hydrodynamic behaviour, REFLA-1D code 80−47592

nuclear engineering computing continued
local and general coincidence schemes assuming two failure modes 79−49787
LOFT, zero power physics testing, meas. vs. calcs. 80−27713
LOFT core fluid conditions during blowdown and refill 79−89440
LOFT L2-4 test and FLOOD4 code, PWR reflood behaviour anal. *(Japanese)* 79−97824
LOFT LOCE fuel module structural response, computer code prediction 79−89439
LOFT non nucl. test L1-4, TRAC anal. 80−13655
loss of coolant effect on resonance escape probability, COCAP and WIMS codes 80−22963
LWR, 3D flux distrib. calc., axial continuous synthesis model with finite element trial functions 80−713
LWR, actinide decay power 80−22930
LWR, anal. of BNL exponential expts. with ENDF/B-IV data 78−13218
LWR, analysis of operating reactors with the SIMULATE nodal program 79−59150
LWR, automated procedure for selection of optimal refueling policies 79−67892
LWR, B and W cross-flow anal. by LYNX codes 80−22906
LWR, calc. of optimum power profiles using pattern search techniques, PROFILE code 80−47557
LWR, ENDF/B-IV eigenvalue calcs. for UO_2 and mixed oxide critical lattice expts. 78−25272
LWR, first order perturbation methods in sensitivity anal. 80−37425
LWR, interpretation of in-core measurements by semianalytical approach 80−712
LWR, LOCA conditions, fuel rod behaviour, code system SSYST-Mod 1 calcs. 77−88248
LWR, NEPTUNE reactor calc. system, development and assessment 80−600
LWR, neutronic thermohydrodynamic interaction model *(French)* 79−89349
LWR, NRC safety research programs, fuel behaviour, operational safety, metallurgy and materials 80−13705
LWR, operation planning, optimum fuel loading and generation planning, comp. code FAPMAN8 80−47673
LWR, optimum fuel loading and operation planning, FAPMAN model 80−47607
LWR, outgoing neutron spectrum from H_2O in H_2OV interface 80−27697
LWR, pellet-clad interaction modelling 80−37445
LWR, PROFIP 3, fission product activities, fuel survey 80−736
LWR, Pu recycling, CEA-EdF studies 80−722
LWR, Pu recycling, technical and economic study 80−720
LWR, reactor cavity neutron flux calc. 79−89362
LWR, Scale system cross-section validation with shipping-cask critical experiments 80−37559
LWR, sensitivity of fuel cycle cost to uncertainties in nucl. data 80−680
LWR, spray droplet heat transfer in LOCA 80−32380
LWR, thermal-margin methodology improvements 80−23022
LWR, water props. modelling using splines 77−42033
LWR anal., CASMO fast transport theory assembly depletion code 78−25278
LWR anal., pressure-crossflow soln. method, COBRA-III codes 78−82417
LWR anal., verification of the RETRAN computer code with measured reactor coolant pump coastdown data 79−89406
LWR and HWR, anal. of UO_2-ThO_3 fueled exponential expts. with WIMS-D code and data 79−81000
LWR blow down accident, French studies, assessment codes *(French)* 79−26641
LWR cell depletion code EPRI-CELL 77−50225
LWR code analysis, qualification of SIMULATE against the Hatch-1 end-of-cycle 1 gamma scan 80−57921
LWR cones, computation of cell group consts. 80−566
LWR containment vessel, I removal by spray after LOCA, MIRA-PB code 80−47593
LWR core, few group 2-D diffusion eqns. in hexagonal geometry, HEXAB-II-30E code *(Bulgarian)* 80−68765
LWR core, thermal and hydraulic behaviour, modelling in HOTRAN-3 *(Hungarian)* 80−32401
LWR core barrel model, circular cylindrical shell, dynamic response to nonaxisymm. loading 77−88247
LWR core blowdown, dynamic behavior of valves, computer simulation 80−5288
LWR core flux distrib. using CETRA core simulator 80−716
LWR core following and in-core fuel management code package, benchmarking and operating experience 80−704
LWR core meltdown, accident anal. using computer system KESS 80−752
LWR core meltdown and containment anal., computer code solns. 80−753
LWR core performance studies in the UK, review of computer codes for static reactor physics anal. and kinetic anal. 80−703
LWR core transient anal. using coupled neutronics and thermal hydraulic models 80−715
LWR cores, single-fluid thermal hydraulic anal. 80−18410
LWR critical heat flux calc., anal. of empiric relations using CRISIS code *(Bulgarian)* 80−68766
LWR design codes EPRI-CELL and CPM, implementation 80−68751
LWR fuel, mechanistic prediction of transient fission gas release 80−47571
LWR fuel cycle effluent model for ENFORM system 78−94111
LWR fuel cycle resource requirements, implications of data uncertainties 80−18437
LWR fuel management, power distrib. calcs. by nodal one-group simulators 80−706
LWR fuel performance anal., WAFER-2 code 80−37447
LWR fuel rod, transient pellet-cladding interaction, ISUNE-4 computer anal. 80−91228
LWR fuel rod failure probability, comparison of FRAP T4 and meas. 80−13644
LWR fuel rod mechanical performance predictor, SPEAR code 79−93730
LWR fuel rod under power transients, CRATER code calc. *(French)* 80−42789
LWR fuel safety, failure thresholds, NSRR programme 79−26595
LWR LOCA, analysis, role of LOFT program 80−18531

nuclear engineering computing continued
LWR LOCA, assessment of the RELAP4/MOD6 reactor transient thermal-hydraulic code 80−42826
LWR LOCA, two-dimensional temperature distributions in fuel rods under blowdown conditions 80−774
LWR LOCA, utilisation of LOFT information for licensing 80−18532
LWR LOCA analysis, TRAC-1D code for Standard Problem 2 78−13288
LWR LOCA safety analysis, thermohydraulic phenomena, review *(German)* 79−13430
LWR neutron flux distrib. in hexagonal geom., appl. of transmission probability method 79−93680
LWR NRC safety research programs, thermo-hydraulics and computer code development 80−13704
LWR power stations, incremental fuel cost calcs. using FAPMAN-IC program module 80−95356
LWR ruptured fuel rods in LOCA, fission product release, computer modelling 79−49780
LWR spectral effects, corrected one-group coarse-mesh representation 79−59132
LWR utility, development of non-LOCA safety anal. methods 78−21691
LWR version of URANUS integral code for fuel rod mechanical calculations *(Spanish)* 79−36315
LWR version of URANUS integral fuel rod code 78−17278
MAC code, fuel rod behaviour in PWR assemblies *(French)* 80−37451
magnetic field and force eqns., solns. using programmable calculator 80−91721
MAKOKOT code, equilibrium of plasma without shell, impurities outside coronal equilibrium and hollow profiles 80−28774
MARC finite element program, PWR piping, circumferential cracks, opening and extension 80−78364
MARIA research reactor, dynamics model for fast transients anal., code TOTEM 80−37419
MASURCA LMFBR heterogeneous core design, performance characts. and computer calcs. 79−59124
material control system simulator 79−85685
material inventory, computer assisted accountancy and control system *(German)* 79−13415
material safeguarding, management information system at BWR fuel fabrication plant 79−85750
materials accounting and control system 79−13507
materials control and accountability system (DYMCAS), prototype terminal 79−89485
materials control system, real-time, generalised concept 79−89449
materials management, Conf., Cincinnati, OH., USA, (June 1978) 79−85672
materials monitoring VACOSS electronic sealing system appl. 79−85687
MEKIN, BWR benchmark calcs. 80−18385
MEKIN code, experience in LWR core anal. 80−23054
MEKIN neutronics/thermal-hydraulic code for BWR pressurisation transient anal. 80−47626
MELSIM-1 code, LWR core meltdown accident simulation 80−18507
mesh-packed cold traps, impurity interaction anal. 78−25262
MHSS, material handling system simulator 77−38337
microprocessor controlled multipoint recorder with graphical video output for reactor core temperatures 80−57873
microprocessor for nuclear reactor instrumentation 80−83147
microprocessor-based flux wire evaluation and anal. system 80−63353
microscopic depletion in UO_2 and mixed oxide fuel rods, MICBURN code 78−25276
MIPAC, fuel performance anal. by finite element method 80−42750
Mirror Fusion Test Facility, neutral beam injection, optimisation by computer graphics 78−66376
mixed oxide fuel cycles, cost sensitivity anal. 79−89369
MO200 model for evaluating safeguards in mixed-oxide fuel-rod fabrication plant 77−38372
Monte Carlo infinite cell calculations for TRX-1 and TRX-2 benchmarks 80−27711
MORSE continuous weights code 80−68748
MORSE transport code, fusion reactor insulator, radiation damage calcs. 80−34061
Muehleberg BWR, core simulation by fuel Management System, expt. verification 80−705
multidimensional neutron transport equation, spherical harmonics soln. by finite Fourier transform. 78−17269
multidimensional reactor calcs., interface current techniques 77−88193
multidimensional reactor dynamics equation, fast factorization and exponential transform. procedures 78−17303
MULTIFLEX, fluid-structural interactions, one-dimensional networks 80−13535
multigroup collision prob. method, applied to overlapping neutron spectra theory, THERMAL 80−52718
multigroup integral transport theory code, thermal reactor lattice studies 78−50225
multigroup libraries from radiation shielding information centre 78−13399
multigroup neutron flux calcs. with MURLAB program 78−29541
multigroup time-dependent delayed γ-spectra from fission and activation of U and Pu 78−13184
multigroup transfer coeffs., efficient eval. for shielding appls. 80−47747
multilayer radiation shielding optimisation, conversational procedure 77−14273
multiple volume blowdown expt. and prediction comparison 79−93814
multiple-support excitation piping problems, automated anal. 79−9773
multizone reactor, reactivity and power shape control, optimisation method 77−6529
multizone reactor neutron flux profile optimisation program *(Russian)* 79−13412
MWPC, cylindrical, event triggers, correlation of wire addresses 80−58092
MWR feedwater and recirculation flow, minicomputer-based digital control 80−23027
Netherlands fusion expts., data acquisition and anal. systems 80−13915
network computations using a transient two-phase velocity difference model 79−26477
neutral beam test stand, 120 keV, computer based diagnostic and control system 78−66389
neutral injection beam line, parameter studies, computer programme 78−66390
neutron, homogenized-cell diffusion parameters from transport codes 78−17300

nuclear engineering computing continued
neutron, p-cell homogenization, transient flux effects, incorporation into 2-D iteration scheme 78−17301
neutron diffusion, mixed-lattice multidimensional reactor calcs., coarse mesh finite difference method 77−34375
neutron diffusion, multigroup equation, synthesis-finite element method 80−27699
neutron diffusion and transport, GGTC-ENEL computer code for multi-group cross sections 78−58323
neutron diffusion code comparison for LMFBRs 80−95337
neutron diffusion eqns., param. adjustment with DELILAH correlation code 79−13413
neutron diffusion equation, multigroup theory 80−27695
neutron diffusion multigroup three dimensional calcs. with finite element method *(German)* 77−88189
neutron diffusion scheme, new brief three-dimens. calcs., BWR core 77−42014
neutron evaluated nuclear data files in unresolved resonance region, data representation 78−29459
neutron flux distributions in nuclear reactors, improved response matrix method calcs. 77−34363
neutron flux regulation, dynamic simulation of two-phase control absorber 80−13731
neutron information at National Neutron Cross-Section Center 78−13403
neutron radiography, high-speed system, modulation transfer function 78−7158
neutron reflection, plane-parallel concrete interfaces, Monte Carlo calc. 80−27686
neutron self-powered detectors with burn-up, sensitivity anal. 77−75024
neutron spectra evaluation, using multisphere response meas., iterative method appl. *(Slovak)* 77−83444
neutron spectrum calculating module of pin-cell burnup code BETTY 77−71634
neutron transient space-time simulation, computer code 77−18644
neutron transport, anisotropic scattering treatment using improved comput. code *(Japanese)* 80−13526
neutron transport, probability table method extension 79−584
neutron transport, state-space splitting in Monte Carlo calcs. 77−65264
neutron transport, transverse buckling effects in 2-D calcs. 80−32318
neutron transport, ZEPHYR code for general two-dimensional geoms. 77−65249
neutron transport eqn., response matrix finite element soln. 80−13527
neutron transport theory, buckling approximation inclusion in finite element calcs. 78−17276
neutron transport theory, S_N calcs. using ANL DIF3D diffusion code 80−47526
neutron two-group diffusion calc. by spatial synthesis algorithm 78−13200
neutronic analysis of the NBS intermediate-energy standard neutron field (ISNF) 80−27692
neutronic data base generation for transient reactor calcs. 77−83004
neutronics code, CONIFERS for reactors with channels 78−25281
NIRVANA high temp. creep model for Zircaloy fuel sheathing 79−87704
nodal expansion method and depletion program MEDIUM-2, validation by benchmark calcs. and comparison with expts. for PWR design appls. 77−88194
nonlinear coupled core reactor, computer simulation of decoupling theory appl. to power control 78−54845
nonlinear finite element anal. ADINA program for stress anal. 78−41148
Nordheim integral treatment for resonance processing, proper use 80−37427
NORMA-CLARA, laser-driven fission-fusion microexplosions, nuclear and thermohydrodynamic calcs. 80−47696
NORMA-LIBERTAS, laser-driven fission-fusion microexplosions, nuclear and thermohydrodynamic calcs. 80−47696
NOTUNG, anal. of ECCS dynamic procedures in SNR-300 LMFBR *(German)* 80−83185
NSSS, computerised simulator 80−22914
Nuclear Code Centre, Japan, history, activities *(Japanese)* 79−13618
nuclear containment vessel, dynamic response to fluid pressure pulses 78−26077
nuclear criticality data, computerised bibiliographic data base 80−13568
nuclear data files of UK Chemical Committee, summary of data, available in ENDF/B format 78−82425
nuclear facility safeguards effectiveness evaluation 78−82486
nuclear laboratory instruction with multichannel analyser/microcomputer system 80−31471
nuclear materials management, design of minicomputer system 79−22395
nuclear materials transportation, SABRE II combat simulation model 80−37542
nuclear pumped laser fusion blanket optimisation in space and time 80−37616
nuclear reactor constrained feedback control system design 77−88257
nuclear reactor optimal control using Walsh function variational synthesis technique 77−38347
nuclear reactor pressure vessels, stress analysis program, STANSAS *(Japanese)* 80−22969
nuclear safety inform. retrieval system, development 79−26551
nuclide inventory calculation code, FISPIN 80−42781
on-line nuclear materials accounting and control 78−29629
on-line surveillance of nuclear reactors based on decision theory 79−9775
online digital core protection calculator, thermal margin routine 79−9777
operating reactor data retrieval and evaluation system RECORDS 80−13690
optimum trip level of m-out-of-n reactor temperature trip-amplifier systems 79−93741
ORNL interface and logistics studies 80−37540
ORNL Nuclear Legislative Data Base program 80−37539
particle detectors, high speed data processing, histogram and tape writing 80−58101
PBHTR, closed Th cycles, computational reactor lifetime simulation 79−85643
PBHTR, depressurisation in primary circuit after failure of main coolant duct, analysis 78−25316
PBHTR, steady state coolant gas activity, STADIF-II code 78−29569

nuclear engineering computing continued
PBR, LOCA, evaluation code NAKOGAS-1 79−13492
PBR core, coolant flow predictions using PEBBLE computer code 79−54474
PDQ program, diffusion theory calcs., fuel swelling and cladding shrinkage effects 80−22926
PDQ-8 neutron diffusion-depletion program 79−71876
PECITIS-II program, anal. of UO_2 collapsible clad elements 80−42751
personnel monitoring for radiological protection, current status and developments, review 79−22490
PEST code, MHD stability limits of high-β Tokamaks 80−28643
Phenix fuel assembly and core performance anal., CAPHE code system *(French)* 79−97878
PHWR-1000, uniformity factor maximisation, nonlinear programming 80−739
Pickering reactor, simulation of wire activation expts. with SORGHUM code 78−25310
pipe whip restraints, conceptual design using interactive computer anal. 77−6513
pipework analysis using code PACE 2 79−93707
piping system anal. to nuclear standard regulations 77−6504
piping systems, pipe rupture and steam/water, hammer design loads for dynamic anal. 78−41868
PIRK 2 program, inverse reactor kinetic eqn. solns. 79−76095
PL-MODT: a modular fault tree analysis and transient evaluation code 79−49784
plasma simulation, heat transport 80−28817
PLENUM-2A, transient anal. of LMFBR outlet plenums 80−32378
point model nuclear reactor heuristic approach to reinforcement learning control 78−46144
POSHA, fuel preconditioning, power shock anal. and sipping 80−63358
power burst facility loop modification, appl. of RELAP4 code 79−89432
power economy, computer simulation 77−79486
power plant pathology 78−17345
power reactor, computational method of approximating discrete power distrib. meas. 78−17340
power reactor in-core fuel management, computer programs 79−71914
power reactor operational control algorithms 79−67896
power shape control, reactor fuel reliability constraints 77−83057
power station installation policies analysis using TOTEM-3 code 77−65323
power station performance evaluation by thermal hydraulic anal. 79−67831
power stations, computer control systems for data acquisition and process control 79−22426
PREP-KITT, HTGR core auxiliary cooling system, failure analysis 80−22964
pressure tube type reactors, SENHOR-IV computer code for small pipe break anal. 79−89397
pressure tube type reactors, small scale pipe rupture anal. 77−42034
pressure vessel and nozzle junction, optimum shape design 78−89941
pressure vessels, shearing stress minimisation by automated design optimisation 78−17289
prestressed concrete pressure vessels design, finite element anal., computer programs 77−23183
probabilistic fracture mechanics anal., nuclear power station structural components 77−81317
PROFILE, calc. of optimum power profiles using pattern search techniques for LWR 80−47557
PROFIP 3, PWR fuel clad failure characterisation based on fission product activity 80−95365
protection system software validation, quality assurance experience 80−57886
Purex process, first extraction, Pu accumulation, computer simulation, SEPHIS code 80−68907
PWR, bidimensional transport coeff. N_H, influence of transverse flow *(Spanish)* 78−8873
PWR, computer code for the study of migration and deposition of corrosion products 80−13700
PWR, computer program for accident anal. *(German)* 79−85623
PWR, core control optimisation for scheduled load changes 79−71911
PWR, core flux meas. by microprocessor based automatic flux mapping system 79−45359
PWR, critical B concs. and cycle lifetime predictions 80−9365
PWR, data acquisition system for high press. water loop *(Hungarian)* 78−82432
PWR, depressurisation accident, CUPIDON anal. of fuel rod behaviour *(French)* 80−42791
PWR, development and Pu allocation, optimal policies 80−725
PWR, effects of early core flow predictions and CHF correl. characts. in RELAP4/MOD5 best estimate blowdown calcs. 79−31059
PWR, HERMITE coupled neutronic thermal hydraulic code 80−23051
PWR, high-speed in-core fuel management system 79−30971
PWR, improved instrumentation and computer control systems 78−29601
PWR, JAERI, test of LOCA/ECCS anal., code verification, by participation in LOFT program *(Japanese)* 77−50256
PWR, KWU 1300 MWe facility, neutron flux computer calcs., radiation damage 77−34370
PWR, LOCA, anal. of LOFT semiscale test *(Japanese)* 79−17998
PWR, LOCA, steam-water mixing 80−13651
PWR, LOCA test, effect of LOFT pressurizer on RELAP4/MOD5 modelling 78−13286
PWR, loss of coolant accident, solving hydrodynamic conditions in reactor core and primary system *(Czech)* 77−3072
PWR, Markov model for quantitative systems interactions anal. of system unavailability 80−22898
PWR, modification of subcooled boiling calc. in COBRA-3/KFKI program *(Russian)* 78−82434
PWR, MULTIFLEX code, anal. of hydraulic force with hydro-structural interactions during LOCA 78−58373
PWR, operational dynamics, digital simulation model 80−27751
PWR, oxide fuel rods, computer program for mechanical and thermal anal. *(Korean)* 78−86571
PWR, physics design of reload with nodal code system 80−723
PWR, process monitoring and parameter estimation, multivariate signal analysis algorithms 80−47585
PWR, Pu isotope calcs. for steady-state core anal. 79−59126
PWR, Pu recycling, CEA-EdF studies 80−722
PWR, rod ejection accident anal. by reactivity weighting method 79−22419

nuclear engineering computing continued
PWR, sensitivity of LOCA heat transfer anal. 78−50246
PWR, shielding against neutron and gamma streaming, computational methods 78−21783
PWR, subcompartment pressure-temp. response comparison between anal. and exptl. results 79−31050
PWR, three loop, simulation in advanced recycle methodology program 80−68856
PWR, Tihange-type, Pu recycling, physics and safety anal. 80−724
PWR, two-phase critical flow in long nozzles 80−13550
PWR, velocity and press. distrib. at core inlet 77−83018
PWR accident consequences, with loss of coolant *(Slovak)* 78−29594
PWR and rod bundle cores, thermal-hydraulic THINC-IV computer program 77−46216
PWR assembly, MAC code model of fuel rod behaviour *(French)* 80−37451
PWR automated optimal multiple cycle fuel management code 79−85641
PWR blowdown, pressure field and core barrel loadings, computer codes 80−13665
PWR core, large, appl. of coarse-mesh finite difference eqns. for k_{eff} and peak power factors 78−17305
PWR core, steady-state single stage thermal anal. of hot assembly subchannels 78−13212
PWR core anal. using 3-D spatial neutronics codes 79−89360
PWR core analysis, methods and data validation 80−57924
PWR core analysis, steady-state core physics and thermal-hydraulic reload design calcs. 80−57923
PWR core analysis using EPRI ARMP program, calc. and meas. reactor physics parameters 80−57925
PWR core analysis verification, reactivity rundown and power distrib. accuracy 80−57922
PWR core meltdown accident, computer simulation of second phase 80−754
PWR core power manoeuvres, fuel duties and fuel preconditioning, FLAIR-CENSOR 80−63337
PWR core thermal-hydraulic response during steam line break accident 80−18384
PWR cores, thermohydrodynamic computer programs *(Polish)* 79−81031
PWR design, higher order nodal depletion program MEDIUM-2, exptl. verification 79−26492
PWR differential rod worth and feedback coeff. online estimation system 79−9798
PWR dynamical behaviour modelling in FORTRAN 80−91217
PWR dynamics, lumped parameter model, eval. of assumptions 80−585
PWR engineered safety features actuation system follow-up system logic 80−57879
PWR flow transients, critical heat flux predictions using CODA 1-D coolant dynamics code 80−42817
PWR fuel clad failure characterisation based on fission product activity, PROFIP 3 code 80−95365
PWR fuel mangement program 80−18434
PWR fuel pin transient heat conduction and open hot channel DNBR evaluation 79−9679
PWR hypothetical LOCA sensitivity to fuel rod material props. 79−89436
PWR in-core fuel management, nonequilib. fuel cycle for reload optimisation 79−30942
PWR internals, flow induced random vibr. anal. 77−83016
PWR internals, vibration mode shape computation and expts. 79−13444
PWR LOCA, determ. of 3-D props. of pressure wave propagation by method of characts. 79−89402
PWR LOCA, effect of steam generator tube rupture, computer simulation 80−23006
PWR LOCA, licensing evaluation calcs. at LOFT 80−23008
PWR LOCA, LOFT post-test anal. using RELAP4/MOD5 blowdown model 80−42825
PWR LOCA, LOFT tests, TRAC-P1A pre-test calculations 80−42824
PWR LOCA, subcooled decompression, multidimensional wave prop. with FLASH-genre codes 79−59194
PWR LOCA reflood, effect of low containment press. on peak cladding temp., HEATUP-R/AEP anal. 80−57897
PWR LOCA Standard Problem 5, TRAC-P1A anal. 80−42823
PWR natural circulation U-tube steam generator, digital code UTSG 78−50242
PWR neutronic calcs., subcooled boiling and open channel effects 80−23053
PWR non-LOCA transient anal. using IRT code 80−42819
PWR piping, circumferential cracks, opening and extension, MARC finite element program 80−78364
PWR plant, dynamics, digital simulation 78−8882
PWR plant simulator, load-follow methods computer design anal. 79−67917
PWR power plant, safeguard system, diagnosis of fault conditions using fault trees 77−6549
PWR pressure vessel failure probability from pressure transients, OCTAVIA computer code 79−18011
PWR pressure vessel vibration excitation, noise correlation and modelling 79−13442
PWR reflood, analytical treatment, computer code 79−89425
PWR reflood simulation of FLECHT-SET system using RELAP4/MOD6 78−13285
PWR steady state thermal anal., single-pass procedure using simplified nodal layout 78−50244
PWR steam generator force anal. during LOCA 80−13666
PWR thermodynamic design calcs., using iteration system based on secondary circuit system model *(German)* 80−13571
PWR transient anal. methods, qualification with plant startup meas. 80−18508
PWRs, fault analysis and calcs., FORTRAN program *(German)* 79−41018
quality control program in design planning for reliability, availability and maintainability 79−97774
quench front in 2-D, difference method 77−79419
radiation exposure near nuclear power plants, remote monitoring system 79−18055
radiation instrumentation, computer-based data acquisition system for multi-station teaching laboratory 78−4446
radiation safety monitoring instrumentation complex at the USSR nuclear power plants *(Russian)* 79−76108
nuclear engineering computing continued
radiation safety system 77−25562
radiation shielding, effects of thickness and geometry var. on neutron spectra 78−33300
radiation shielding, in 3-D direct-coupled-ray method 78−21785
radiation shielding, Monte Carlo calcs., event-value path-length biasing 77−38421
Radiation Shielding Information Center, international technology resource 78−17543
radiation transport, appl. finite element methods 78−13196
radiation transport calc., Monte Carlo approach for engineers 79−585
radioactive high-level waste disposal in salt formations, far-field temp. calcs. 80−5277
radioactive nuclide decay data for reactor calcs., activation products and related isotopes 78−82426
radioactive pollution from nuclear power stations, accident anal. 79−63782
radioactive waste management system, risk assessment for potential accidental releases 78−17353
radioactive waste source terms, calc. using computer code 79−54569
radioactive waste surveillance, using real-time unfolding algorithm 79−85679
radiograph feature extraction via least squares fit to model 77−14229
radioisotopes in reactor cooling system, prod., transfer, life cycle, radiation calcs. using program system TIBSO 78−54821
RAGRAF: temp. distrib. calc. code, multi-pin fuel assemblies in stagnant gas atmos. 79−85604
RCP01 Monte Carlo program, neutron capture and photon heating rates 79−71912
REACT/THERMIX, eval. of graphite *(German)* 80−83181
reactant distribution functions in fusion reactors, fast computing method using Legendre polynomials expansion 78−78491
reactimeter, microprocessor based, nucl. engineering lab. class enhancement 80−36825
reactivity calcs., correlated sampling Monte Carlo methods 79−22368
reactivity determination, real time program 79−45379
reactivity effect of cross-section processing for moist bulk-oxide criticals 80−37493
reactor, core power and flux distribs., BITNOD large-mesh code appl. 78−17304
reactor computational benchmark problems, review 77−79413
reactor containment, nonlinear dynamic response, seismic analysis 77−3180
reactor containment response to HCDA anal. with MICE code 77−42029
reactor control, digital load-follow concept, simulation in FRG-2 reactor *(German)* 77−50249
reactor coolant accidents, appl. of self-initialized RELAP4 momentum eqn. 78−13287
reactor coolant activity monitoring, automatic on-line system 80−684
reactor core and shield calc., radiation transport program benchmark tests 78−78440
reactor core bowing history computer program 79−9688
reactor core energy distribution, algorithm for extremal control 80−83209
reactor core system, bowed, NUBOW-3D program for static anal. including irrad. creep and swelling 80−5215
reactor criticality calculations, Monte Carlo MONK code 77−14226
reactor dynamics, finite element analysis for two dimensional eqn. *(German)* 77−88190
reactor dynamics, numerical integration using real integrating factors 80−68730
reactor fuel, rod modelling, utility requirements 78−21747
reactor fuel reprocessing, in-process inventory dynamic measurement simulation 77−38371
reactor kinetics, smoothing and extrapolation techniques 77−83002
reactor kinetics digital simulation 77−88216
reactor neutron field analogue simulation using one-group diffusion approximation and finite difference methods *(Russian)* 78−74416
reactor neutron flux regulation dynamic simulation algorithm 80−27738
reactor noise analysis, time series modelling methods, comparative eval. *(Japanese)* 80−13552
reactor operation and control simulation code 77−83006
reactor optimal shutdown problem algorithm by branch and bound method *(Japanese)* 79−36341
reactor physics codes, utility use and requirements 78−17299
reactor protection system performance, impact of ageing mechanism 79−18000
reactor risk analysis, computer role 77−38373
reactor safety, event tree construction by AUTOET 1 computer code 78−17379
reactor safety, fault tree anal., modular representation, PL-MOD code 78−78480
reactor scram system, digital computer module *(German)* 78−86635
reactor shielding computation methods and programs in Poland *(Russian)* 79−26767
reactor shielding materials, Pb and steel, γ leakage spectra computer calcs. 78−58350
reactor small pin bundles, thermal-hydraulic anal. using COBRA-3M computer code 79−76067
reactor space time kinetics, quasi-static synthesis method 79−26479
reactor spatial dynamics, hybrid computer simulation 78−29567
reactor spatial kinetics approx. techniques 77−38334
reactor structural analysis using CEASEMT computer codes 79−97911
reactor systems reliability, computer programs *(Slovak)* 78−82416
reactor technology structural mechanics, conf. 78−41874
reactor vessel design-basis-accident presure-pulse prediction using SPIRT code 79−89361
reflecting boundary conditions for diffusion coefficient calculations in Wigner-Seitz cells 80−27710
reinforced concrete structs., missile impact loading, nuclear power plant appl. 79−31237
RELAP4, jet pump modelling in BWR LOCA anal. 80−68850
RELAP4 BWR jet pump model, improved version 80−18380
RELAP4/MOD5 blowdown model of PWR LOCA LOFT experiment 80−42825
RELAP4/MOD6 LWR LOCA thermal-hydraulic anal. code 80−42826
RELAP4/MOD6 program, test prediction for German PKL test K5A 80−13642
RELAP 4/REPIPE, subcooled blowdown thrust force calc. 80−18382

nuclear engineering computing continued
RELAP-3B anal. of BWR turbine trip without bypass transient 80−42814
RELAP-4 code, self initialisation of momentum eqn. 79−36307
research reactor, core and console, long term service and reliability investig. 80−9359
research reactor, DIDO, three-dimensional SNAP diffusion theory calc., including up-scattering 80−5208
research reactor, IRT-2000, algorithms for direct digital control of neutron field 78−86643
response matrix eqns., properties 77−67795
RETRAN, LOFT test L2-2 pre-test calc. 80−18518
RETRAN, macroscopic balance equations for two-phase flow models 80−9332
RETRAN code, non-LOCA transient safety anal. 80−18506
RETRAN model analysis of TMI-2 accident 80−102263
RETRAN simulation of the Three Mile Island Unit 1 turbine trip test 80−18512
RETRAN two-phase flow model, comparison with expt. 80−32330
reversed field pinch, burn stability 78−58467
RFIT, data evaluation program, theoretical background 78−29562
risk studies, data specialisation, Bayes' theorem 80−47601
risks statistical assessment, of accidents and normal operation 78−50281
rocket propulsion using nuclear reactor, optimisation problem, calculus of variation 80−27694
rod bundle thermal-hydraulic anal., commix-1 program 80−13645
rod bundles with flow sweeping, SIMPLE-2 code for single phase thermal-hydraulic calcs. 77−46215
rod swap test results, VEPCO analytical methods for Surry 1, cycle 5 80−9338
SABRE II, nucl. materials transportation model 80−37542
safeguards effectiveness evaluation, SAFE methodology 79−85674
safety, Integrated Safeguards Information System requirements 79−85681
safety analysis, fluid-struct. system dynamics, computational algorithms 77−71669
safety problems analysis by fluid-struct. finite element method 77−3128
safety systems, time dependent unavailability anal., FRANTIC computer code 78−29588
SAND-II, neutron spectrum unfolding, ^{252}Cf 80−13514
SAREF test fuel motion reactivity feedback, experimentally based limits 79−49775
SAS3D-EPIC, anal. of axial propagation of fuel failure in LMFBR LOF-TOP 80−47650
Scale system cross-section validation with shipping-cask critical experiments 80−37559
scanning microprobe, digitally controlled for p and heavy ions 79−13571
SCAP-BR, multilegged duct γ streaming computer program 79−9906
Scylla IV-P, computer-based control and data acquisition system for CTR 78−62621
SDX cell homogenisation code validation for ZPPR pin geometry 80−86962
seed-blanket calcs., 2-D, one-channel synthesis method, transport and diffusion 80−73876
seismic design, automated generation of spectrum compatible artificial time histories 78−29661
self-shielding factors, discrepancies between ETOX and TIMS codes 80−68744
sensitivity-based cross-section data assessment for reactor core and shield anal. 78−9048
SEPHIS, Pu accumulation in Purex process, first extraction 80−68907
SETS, shutdown heat removal system failure, fault tree, common-cause anal. 80−63334
SEURBNUK, FBR containment code validation program 80−78405
SEURBNUK-2, FBR containment code, structural deform. 80−78404
SGHWR fuel pins, pellet-cladding interactions and length changes 80−42763
SHIELD system, nucl. fuel cycle appl. 80−37517
shielding benchmark calcs. by Discrete Ordinates and Monte Carlo methods 80−73886
shipping cask criticality safety, SCALE system, correl. with expt. 79−63775
shutdown heat removal system failure, fault tree, common-cause anal., SETS 80−63334
SIMMER II results, statistical anal. for postdisassembly in vessel dynamics 79−49786
SIMON cavitation model, anal. of LMFBR coolant cavitation in dynamic containment loading 80−32326
Simtron program for Zircaloy sheath tube oxidation calc. *(German)* 77−346
SIMULATE code for startup test predictions 80−18558
SIMULATE models, BWR split void assembly benchmark verification 80−22938
SIMULATE qualification against the Hatch-1 end of cycle gamma scan 80−57921
simulation, modular data based codes appl. *(German)* 78−17445
SLEUTH-SEER code predictions of pellet-clad interactions in AGR fuel pins 80−42755
SLIM, SGHWR fuel pins, pellet-cladding interactions and length changes 80−42763
SNR-300 LMFBR, ECCS, decay heat removal during heat sink failure, accident anal. using NOTUNG code *(German)* 80−83185
SNR-300 LMFBR steam generator transients, computer simulation 80−23012
software coding for reliable data communication in reactor safety system 79−13496
SOMIX-1 Na spray fire code, containment pressurisation 80−32365
special nuclear materials, computer-based in-plant nondestructive assay instrumentation 79−9752
spent fuel storage racks, design, safety calcs. and benchmarking 79−22416
spent reactor fuel, risk analysis of alternatives from reactor pool until final disposal 78−17355
spin lattice relaxation time meas. simulation, systematic and random error effects 80−37062
SSC-L simulation, FFTF loss-of-electric-power transient response, natural circulation tests 80−42836
statistical fuel model, FRP 80−42748
steam drum dynamics, analogue simulation 77−71645
steam generator, flow distribution anal., computer code 79−49653
steam generators, linearised transient anal. 80−18378
nuclear engineering computing continued
steel, austenitic stainless type 316, corrosion mechanism in hot flowing Na, computer simulation 80−3251
structural anal. of reactor fuel elements 78−41814
structure loading and response studies, testing philosophies, simulation techniques 77−71672
structure-fluid mesh partitions of explicit-implicit integration appl. to reactor safety 77−46238
subcritical reactor, neutron joint factorial moments and count bivariate distribs. 79−59120
suboptimal control of reactors with distributed parameters, computer model, singular perturbation theory 77−6530
Super System Code for LMFBR thermohydraulic transient simulation, appl. of multiple time-step integration 80−47552
Super-Phenix FBR, data processing and collection *(French)* 79−76107
Super-Phenix FBR control system evaluation *(French)* 79−76106
symbiotic system economic evaluation using SYMECON 80−106177
symmetric SOR and SIP methods, numerical soln. of multigroup diffusion eqn. 78−74431
synthesis finite element method for three-dimensional reactor calculations 80−13566
systems reliability analysis, cost effective quality control program 79−97775
tandem mirror fusion-fission system studies 80−37607
tandem mirror hybrid reactor, nucl. performance sensitivity of Be/molten salt blanket 80−37606
TCLUST1, LMFBR intersubassembly transient heat transfer code 80−63231
TCLUST1 transient code, anal. of LMFBR subassemblies 80−18391
teaching laboratory, computer modules for calculation of prompt-neutron generation time 78−4447
temperature-dependent resonance integral evaluation by HAMMER code 79−9708
TESHOM computer code, data format input data for lattice codes 79−22381
TEXTOR, computerised control system design 80−13907
TFR 600 Tokamak, plasma equilib., numerical simulation of multitransformer eqns. 78−55760
TFR Tokamak, microcomputer data acquisition system 80−13916
TFTR, isodose contour map construction using DOT 3.5 computer code 79−67949
TFTR breeding modules, neutronics 80−37611
TFTR vacuum system transient simulator 78−74496
THERMAL, multigroup collision prob. method, applied to overlapping neutron spectra theory 80−52718
thermal channel heat transfer gap calc. by numerical methods 78−21630
thermal hydraulic anal., of rod bundle fuel elements, COBRA-3C/KFKI digital computer program 78−54822
thermal hydraulic analysis of a wire-wrapped 19-rod bundle with edge blockage 79−59142
thermal hydraulic analysis of a wire-wrapped 19-rod bundle with edge blockage 79−71887
thermal hydraulics, sensitivity theory development 79−17963
thermal hydraulics anal., teaching appl. of computer graphics 80−36824
thermal lattice leakage calcs. using modified B_1 method 80−47545
thermal-hydraulic anal., COBRA IIIP/MIT code 77−79423
thermal-hydraulic conservation eqns., analytic integration 77−83012
thermal-hydraulic margin analysis, appl. response surface methodology 78−17378
thermal-hydraulic numerical calculations for VVER reactor cores *(Russian)* 79−26481
thermally expandable fluid transients, finite difference method 77−79418
thermohydraulic code verification by rod bundle expts. 79−97769
thermonuclear fusion research, user-engineered command language 80−27819
TIPSY program, thermal information processing system 79−67883
TLD, safety and reliability of decentralised reading in Sweden 77−40780
TMI-2 accident analysis using two-loop RETRAN model 80−102263
TNS Tokamaks, costing and sizing, computer code 78−50361
Tokamak, physics of burn control 80−37599
Tokamak fusion, Impurity Study Experiment, mag. field calcs. using GFUN-3D programme 78−66368
Tokamak ohmic heating pulsed power supply digital simulation 78−8991
Tokamak plant, superconducting toroidal field magnet model 78−17425
Tokamak reactor modelling, time-depend. computer codes 77−34468
tokamak reactor superconducting toroidal field magnet computational model, technical and economic 78−50375
Tokamak-hybrid reactor, comparative anal. 79−18043
Tokamaks, large, impurity effects and control, neutral beam injection, computational models 80−28773
Tokamaks, transport losses, computer modelling and scaling 80−28612
tomography for neutron radiography of nucl. fuel 78−82529
toroidal geometry effects in neutron transport eqn., discrete ordinate S_N method 78−13327
TRAC anal. of LOCA in PWR with combined ECC injection 80−18522
TRAC anal. of PWR LOCA 80−18521
TRAC calculations of ECC bypass phenomena in a 1/15-scale experimental facility 79−49725
TRAC code on RSR Standard Problem 5 79−49724
TRAC pre-test and post test calcs. of LOFT nucl. test L2-2 80−18519
TRAC-P1A anal. of PWR LOCA Standard Problem 5 80−42823
TRAC-P1a calcs. of blowdown expt. 80−18383
TRAC-P1A pre-test calculations of LOFT PWR LOCA tests 80−42824
TRANSENERGY, transient thermal hydraulic anal. in forced convection regime 80−18393
Transient Analysis Reactor Code LOCA quench front model 80−47550
transient fission gas behaviour, exptl. and analytical results 79−59190
transient heat conduction, soln. by hybrid method 78−681
transient heat transfer, COMETHE code 80−42761
transient overpower, comparison of EPIC and PLUTO fuel-coolant interaction codes 78−8920
transient process dynamics in reactor with dissociating coolant *(Russian)* 77−42050
transient thermal hydraulic analysis, RELAP4 transform. into fully implicit iterative code 77−65257
transient two-phase flow system, three-dimensional numerical simulation 80−687
transport codes DOT and TWOTRAN as standards for diffusion in pebble bed reactors 80−68750

nuclear engineering computing continued
transport package design, criticality evaluation, appl. of SCALE system 79−63774
transverse momentum eqn. for COBRA-IV-I, improved version 80−578
TREAT, fission gas non-equilib. behaviour during fast thermal transients, simulation 78−41831
TREAT fast-neutron hodoscope, time and mass resolution of fuel motion, data acquisition system 79−41003
TROFAN, laser fusion system studies model 80−32505
TRUMP thermal anal. of plenum fission gas release in LMFBR fuel assembly 80−47646
tubular joints stress anal., finite element anal., computer programs 78−41808
turbulent diffusion, connected flow passages, computer prediction using k-ε turbulence model 80−9331
two-dimensional fast reactor model, space-time synthesis 78−89935
two-phase flow instability, programme for heat removal expt. at low power 78−54814
two-phase nonstationary velocity tracking by adaptive cross-correl. algorithm 78−14074
TWOTRAN-DA, diffusion synthetic acceleration module, grid-coupling methods for the multigrid solution of the neutron diffusion equation 80−47555
UCFLOOD code for bottom reflooding heat transfer in LWR 79−49728
uncertainty anal. methods, comparison 77−79426
UNCLE finite element scheme, input specification 80−95512
unfolded neutron spectrum and foil reaction rate computation and meas. 79−9904
URANUS and EPRI code evaluation 80−42756
URANUS programme, statistical version 80−42749
validated computer codes for nuclear electric utility 78−17403
variable direction method, choice of optimal variant for 2-D reactor models 79−97751
vent clearing analysis of a mark III pressure suppression containment 80−32371
ventilation systems I trapping, user guide to codes ITRAP-A(B)(S)(L) 79−93843
vibration analysis of heat exchanger and steam generator designs 78−66333
video detection/tracking of tracer particles in model packed-bed reactor 77−42012
void swelling calculations using FACSIMILE VSI 80−42782
VVER reactors, neutron physics calcs. programs *(Russian)* 79−30884
WAFER-2, simulation fission gas release in UO_2-Zr BWR type fuel rods 80−42758
WAFER-2 code, LWR fuel performance anal. 80−37447
water radiolysis, mathematical modelling for kinetics in operating reactors 78−61036
water-cooled reactor core coolant flow calcs., computer code 77−74914
water-cooled water-moderated reactor cooling system faults, hybrid simulation *(Russian)* 78−5008
water-moderated water-cooled reactor operational mode anal. *(Russian)* 78−21760
Westinghouse nuclear training reactor fuel inventory reduction plan 80−23115
Westinghouse plant, hardware considerations for new DNB design procedure 80−18396
Westinghouse plant availability anal. with operating data base 80−23050
WIMS-D performance in cell parameters calculation for UO_2-D_2O systems 80−68747
Wolsung-1 CANDU-PHW generating station, nuclear computer design anal. 79−76060
WRAP-EM system, complete BWR-EM LOCA anal. 80−18523
WWER-440 reactors, neutron-physical charact. calc. by BIPR 5K programme *(Bulgarian)* 79−85601
Yankee reactor physics method verification 80−63323
ZED II reactor lattice parameter calcs. using LATREP CYCLE 4 80−27787
Zircaloy cladding, stresses due to pellet cladding interaction 80−42762
Zircaloy LWR cladding, modeling of deform. and fracture in SPEAR code system 79−93729
^{137}Cs, 10 GeV proton spallation for transmutation of radioactive waste, calc. of transmutation number 80−13470
D-D fusion-fission hybrid reactor, energy multiplication and fissile prod. 79−36409
D-T Tokamak reactor, costing and sizing using COAST code 79−76142
Ge on-line, hyperpure detector, radiation monitoring system 78−37493
^{16}N activity in water from $^{16}O(n,p)^{16}N$, computer code and expt., nuclear powered ship 78−13192
O_2 deposition in a mesh-packed cold trap 80−22905
Pt self-powered detector, neutron sensitivity calc. 78−37449
$(Pu,U)O_2$, criticality data generation using SU-HAMMER code 78−29581
Pu computerised inventory control system 79−36386
Pu fuel cycle back end services, utility optimisation model 78−41845
Pu-island element, B304, gamma scanning of power and burnup distrib. 80−721
^{239}Pu, criticality of thin flat foils versus spherical shells, two-group diffusion anal. 79−26530
^{239}Pu direct enrichment of LWR assemblies in a fusion hybrid 80−37604
^{90}Sr fission reactor waste management, by fusion reactor transmutation 78−70642
ThF_4, spallation cross section and recoils, range calcs. computer code MARLOWE 79−93736
ThO_2-UO_2 in PWR fuel rod, LIFE-THERMAL computer code anal. 78−86623
$(U,Pu)O_2$ fuels, O distrib. during irradiation, calc. using CODIF program 78−70604
U enrichment plant criticality analysis *(Japanese)* 78−46156
UC_x, computer simulation of C activity and transport 78−86618
UO_2 collapsible clad elements, PECITIS-II program 80−42751
UO_2-Zr BWR type fuel rods, fission gas release 80−42758
$UO_2(NO_3)_2$ highly enriched solns., benchmark critical expt. calc. study, KENO-IV code 79−18026
^{235}U, ^{235}U systems, criticality anal. using KENO and SU-HAMMER codes 78−89949
^{235}U-Al castings in water, pulsed reactivity meas., Monte Carlo anal. 79−26522
Xe oscillations, program for optimal control in 1-D slab reactor *(German)* 77−61529
nuclear engineering computing continued
Xe spatial oscillations, time optimal control 80−32320
Xe-I induced spatial power oscillations, integration method 80−13567

nuclear explosions
see also weapons
acoustic gravity waves in ionosphere, propag. *(French)* 78−12042
air-over-ground transport calcs. for various cross sections, weapon effect studies 77−23164
Alberta, Canada, 1966, high explosive analogue of Tunguska event 77−64287
atmospheric, low-altitude, Wilson Cloud form., model 78−53704
atmospheric, rel. to stratospheric O_3 depletion 79−70848
atmospheric chain reactions nuclear proliferation mobility 77−53731
atmospheric radiation environment, mass integral scaling 77−46406
atmospheric radioactivity, maximum credible concentrations and dose rates 79−83948
atmospheric thermonuclear, N oxide production, effect on ozone layer 79−84345
axially symmetric explosion in magnetogasdynamics 80−62007
Baneberry event, numerical simulation 80−841
biosphere, radioactive contamination, influencing factors, 1962-76, Hungary *(Hungarian)* 78−92711
body waves, short-period, conventional and spectral magnitudes 79−48417
bomb survivors' carcinogenesis and mortality (1950-74) 79−88136
cavity radius estimation for contained peaceful explosions 79−16712
China, influence on radioactive fallout in air and rain to end of (1978) 79−79997
Chinese, 19th, 1976, γ-ray spectra anal. of fallout particles using Ge(Li) detector *(Japanese)* 79−31219
Chinese, anal. of fission product mixtures by Ge(Li) gamma-ray spectrometry 77−26884
Chinese 19th nuclear test explosion, fractionation effect of hot particles 79−45424
Chinese atmospheric tests in 1976, fallout in air and rain over United Kingdom 77−73847
Chinese atmospheric thermonuclear explosions, ^{95}Zr data appl. to stratospheric transport parametrisation 79−2342
Chinese atmospheric weapons tests, 1976, USA population dose estimates for ^{131}I in thyroid 78−77116
Chinese explosion 1977 Sept. 18, time distrib. and anal. fallout particles 79−25796
Chinese nuclear test explosion, September 1976, hot particle anal. from γ-spectra *(Japanese)* 78−82519
Chinese nuclear weapon tests, fresh fallout anal. using beta counting technique 79−92106
civil defence aspects of US power stations as targets in nuclear war in year 2000 77−3188
civilisations possible self-annihilation through thermonuclear war 78−81562
detonation waves, initiation and propagation conditions 79−93834
discrimination between explosions and earthquakes 78−11809
education, nuclear fallout radioactivity γ-ray detection and anal., Chinese fission bomb anal. 78−49596
EM pulse, induced currents and charges on aircraft 78−42258
EM pulse, surface currents and charges on aircraft 78−42257
EM pulse measurement both inside and away from nuclear source regions 78−21773
EM pulse produced, anal. 78−21771
EMP, system generated by photoelectron emission current, anal. 78−21772
EMP radiation, electronic systems, protection 77−54366
Eurasian earthquakes and explosions, discrimination using P codes spectral charact. 78−7576
fallout, artificial radionuclides depositional history in Ross Ice Shelf, Antarctica 79−88027
fallout from atmospheric test as possible explanation of Ural contamination disaster 80−76666
fallout nuclide determination for 19th Chinese nuclear test 79−54601
fallout nuclides determ., 19th Chinese test 78−82520
fallout observation, Chinese A-tests 80−27820
fallout of highly radioactive particles originating from the Chinese nuclear explosions *(Japanese)* 79−63813
fallout on Taiwan, 1971 to 1975 period 77−90918
fission products, removal rate seasonal vars. in lower stratosphere 80−55957
gamma radiation EM effects in atmosphere, Compton electron currents 78−93020
geoelectric field, disturbed by gamma-ray pulse 79−70852
ground motion duration after nuclear explosions 79−48413
India, scientists' view of first Indian nuclear explosion 77−82362
industrial accident involving radiation exposure in Washington State, worldwide impact 77−3122
Japan atomic bombs, radiation doses received by survivors residing in USA 77−9260
late stage equivalence of near-surface explosions 78−61353
microexplosion ignition, magnetically insulated foil accel. to ultrahigh vel. 77−65327
microprocessor multiple arrays, operating systems for nuclear diagnostic system 79−49918
miniexplosion, critical masses in fission-fusion hybrid systems 77−3158
mining and construction uses, role in national economy of USSR 77−23314
multiburst cloud rise after nuclear explosion 78−94142
neutral particle transport in 2-D, appl. of space angle synthesis 77−83107
neutron air transport sensitivity to nitrogen cross section uncertainties 77−23165
neutron bomb radiation protection, calc. of rad. penetration in air and shielded human tissue dose equiv. 80−47743
neutron bombs, effects *(German)* 78−814
neutron stars, thermonuclear flahses model for X-ray bursts 78−12417
neutron weapons, physical and military problems *(Norwegian)* 79−81091
Nevada Test Site, geology effect on absolute travel-time residuals 79−16391
Nevada test site, nuclear testing fallout possible association with childhood leukaemia 80−12186
Nevada Test Site, site transfer functions, preliminary evaluation 79−88301

nuclear explosions continued
Nevada Test Site (NTS) explosions, Earth crustal structs. inferred from Rayleigh-wave signatures 79−66632
Nevada Test Site explosion, seismic waves group vel. anal. rel. to crustal struct. 78−81111
Novaya Zemlya, inversions of high freq. Q_γ^{-1}(f) from seismic Rayleigh waves 77−33000
Novaya Zemlya, phase-matched filtering of Love waves 79−92602
Novaya Zemlya events, P-wave travel time residuals vars. in central California 77−25658
ore mining uses, continuous underground operations 77−23302
P-wave codas, spectral composition of earthquakes and explosions 80−21640
P-wave signals, multivariate autoregressive model, short-period discrimination appl. 79−16385
P-wave travel times from Nevada explosions to Oroville dam, 1970-76 period 77−56581
P-waves records complexity appl. for discrimination of artificial and natural seismic sources 80−12340
pollution, radioactive dust captured by wind from Earth's surface *(Russian)* 80−16869
radiation transport in Earth for neutron and gamma-ray point sources above an air-ground interface 80−32526
radioactive contamination of biosphere, explosion and power plant influence *(Hungarian)* 80−21548
radioactive fallout on Milan 1976-7, influence of Chinese nuclear expts. *(Italian)* 78−58501
radioactive waste, comparison of USA military and civilian inventories 78−4995
radionuclide composition and activity over Bulgaria in 1976, including Sept. 26th nuclear test 79−88018
radionuclide migration at US ERDA Nevada test site 77−57752
rocket propulsion using staged thermonuclear microexplosions 77−91405
SALMON, short-period P-wave attenuation in USA from P-wave spectra 77−25650
seismic discrimination, via dynamic spectral ratios with variable freq. bands 77−81834
seismic discrimination improvement using pattern recognition 78−40694
seismic pattern, automatic recognition 77−81831
seismic pattern recognition, fundamental problems 78−81428
seismic source models for underground explosion 77−33004
seismic wave traces, multivariate autoregressive feature extraction and the recognition of multichannel waveforms 79−39878
seismological data collection and anal., detect. of possible violations of Nuclear Test Ban Treaty 79−39919
seismology, computer-aided anal. and discrimination, bibliography 77−81832
seismology, extraction and use of broad-band P-wave pulse for event classification 77−81830
S. Sinkiang, inversions of high freq. Q_γ^{-1}(f), from seismic Rayleigh waves 77−33000
Soviet disaster 1957-8, explosion of stored nucl. waste, causes 80−22974
space vehicle nuclear propulsion, historical review of advanced consent 80−36475
STARFISH, inner radiation belt energetic electron spectra before and after explosion 77−2305
STARFISH in inner radiation belt, max. radiation dose in 1962-71 period 78−69612
statistics for nucl. detonations, 1945 to 1975 77−71698
stratosphere, O_3 response to nuclear bomb tests 77−81966
structural integrity in postulated accidents, scaling laws for contained explosions 80−47604
surface waves anomalous propagation in Barents Sea, from NORSAR data 79−25202
teleseismic body wave radiation from seismic source in layered medium 77−9363
test explosions 1975-1978, review 79−67958
thermal neutron transport in moving media 79−63713
thermonuclear microexplosion, use of black-body radiation as inertial confinement fusion driver 80−91241
tissue neutron and gamma-ray response function, mid-head, military appl. 80−8185
Tunguska event, 1908, egregious theory involving Li meteorite nuclear explosion 79−21229
turbulent radiowave propagation, ionospheric phase and frequency spectra 78−24405
ultrahigh press. (TPa) shockwave from underground nuclear explosion for solid Hugoniot data 80−59580
underground, at Novaya Zemlya, P-waves travel time anal. 79−84115
underground, elastic seismic source model for 1 Mton explosion in tuff 77−44927
underground, far-field waveforms calc. 77−60356
underground, monitoring using Gauribidanur seismic array 79−39913
underground, P-signal complexity and upper mantle struct. 77−56596
underground, preprocessing of signals prior to input to pattern recognition scheme 79−62631
underground, seismic source functions and magnitude determ. 77−56584
underground, T-phase recordings at Rarotonga, S.Pacific Ocean 79−84138
underground, tectonic stress release effect on P-wave signature 77−25642
underground detonations, monitoring, book 79−681
underground explosions, hydrophone recordings of mantle-refracted P-waves 80−98257
underground fusion explosion, use as geothermal energy source 78−46176
underground nuclear explosion, gas flow in permeable Earth formation with crack 78−61372
underground nuclear explosions, complex P-wave signal coda power and modulation characteristics 79−79757
underground nuclear explosions, distinction from natural earthquakes *(French)* 78−20364
war, global consequences 77−57148
weapons testing, radionuclide distributions in oceans and marine sediments 78−13344
^{14}C contamination of Atlantic from weapons tests 80−89683
^{14}C production in reactors and explosions, population dose, health impact 77−14274
D-T layer implosion through nonhomogeneous transition layer 78−74465
DT near critical explosion compression, neutron output 77−67867
nuclear explosions continued
DT thermonuclear miniexplosion produced by explosion compression, energy output minimisation 77−67896
PuO_2 assemblies, fission and explosive energy releases 77−83108
PuO_2-UO_2 assemblies, fission and explosive energy releases 77−83108
^{239}Pu and ^{233}U droplets burning in air, aerosol generation investig. rel. to inhalation hazards 79−67959
^{239}Pu, use in weapons and energy prod., radiological hazards, security 77−10492
^{240}Pu content of commercial Pu, criticality of fast assemblies *(German)* 77−6564
^{240}Pu, effect of spontaneous fission on energy release in a nuclear explosive 80−95464
^{240}Pu, effect on neutron lifetime in nuclear explosives 79−13531
$UO_{2,3}$ assemblies, fission and explosive energy releases 77−83108
nuclear fission *see fission*
nuclear fission of plutonium *see fission of plutonium*
nuclear fission of uranium *see fission of uranium*
nuclear fission piles *see fission reactors*
nuclear fission products *see fission products*
nuclear forces
see also binding energy; meson field theory; nuclear binding energy
$0f_{7/2}$ and $0g_{9/2}$ nuclei, mag. form factors, core polarisation and exchange current effects 80−13409
0p shell nuclei, effective interaction spin-tensor decomposition 80−32198
1p shell isotensor charge depend. contrib. to isobaric mass multiplets, shell model anal. 79−67632
1p-shell, isospin mixing between T=0 and 1 states 79−6430
3N, 4N, 3α model systems, props., stochastic variational method 77−41891
3N bound state as probe of internucleon force 77−18438
^{208}Pb (N,N^1) unnatural parity state excitation, π− condensate instability proximity, DWBA 79−97660
α-clustering in heavy nuclei, pre-equil. model, nuclear matter NN, Nα interactions 80−63111
(π,π'), inelastic scatt. in Fermi liquid, nucleon-nucleon interaction effects 80−22862
πN interaction, resonance damping, (3,3) resonance width 77−10350
ρ-exchange isovector parity-violating potential 79−93525
σ-propagator, summation of two-pion inserts 77−10186
A=15-18, effective interaction from coupled cluster many-body method extension 80−22701
A=16 to 40, mag. moments, shell model calcs, mesonic exchange current effects, book contrib. 80−479
A=18, 3p1h multiple scatt. formalism for 2 valence nucleons, microscopic effective interaction 79−6428
A=18, effective interaction, 2nd order core polarisation diagrams with intermediate particle states 79−45180
A=18, multiple scattering, three-particle one-hole nuclear effective interaction 80−13384
A=18, shell-model spectra, one-boson-exchange potential 80−68550
A=18 nuclei, importance of high lying intermediate excitations on nuclear effective interactions 78−70460
A=18 shell model spectra and 3 nucleon force 78−25124
A=18 to 22, influence of non-central interactions on 1s-0d nuclei 78−93949
A=36-39, energy levels and effective interactions from large scale shell model calcs. 79−59011
A=3 systems, charge form factor and bound nucleon polarisation 80−22708
A=3-4 hypernuclei, binding energy anal., Λ-N pot., scatt. length and effective range 80−9256
A=40 to 60, neutron force function, role of input states 79−9486
A=41-55, charge dependent two body interactions from $1s_{7/2}$ shell displacement energies 79−67668
A=42, multiple scattering formalism for the effective interaction 80−102126
A=50-57, N=28-30, effective interactions and energy spectra from shell model calc. 78−82299
A=6-14, one π exchange currents effect on partial muon capture rates 79−22239
A=6-14 nuclei, OPE current effect on allowed β-decays in the 1p shell nuclei 79−54413
A≤44, fp-shell nuclei struct., effect of core-excitation and α-clustering correl. 80−9245
abnormal nuclear matter, many body forces, σ-model Lagrangian field theory 77−6277
abnormally large density and binding energy states, book contrib. 80−489
advances in nuclear physics, clustering and self-consistent field theory, book 79−75879
alpha cluster reactions, effective single particle operator 80−32218
alternating layer spin structure, one-dimensional, localised, in nuclear system, and π^0 condensation 78−4902
average effective-interaction calcs. in HF and harmonic oscill. basis 77−57605
axial currents in nuclei, one-pion exchange diagram 78−46008
axial meson exchange currents and hard pions in nuclear physics 79−40854
bag-model, interquark interaction effects 77−30315
baryon+antibaryon bound states, NN̄, quasinuclear levels, annihilation, influence of decay channels, multichannel model 79−2912
baryon-antibaryon nuclei, energy spectra and properties 80−22709
baryonium, review of QCD, duality, string models and bag models 78−78135
BBG theory developments, hole and particle lines, dispersion effects and healings 80−22719
Bethe Goldstone equation soln., rapidly convergent polynomial expansion 78−54689
Bethe homework problem, variational calcs. for neutron and nuclear matter 78−37292
Bethe Salpeter equation for I=1 NN scatt. with one boson exchange 77−57455
Bethe-Goldstone eqn., nucl. matter, nucleon optical pot. anal. 78−12981
binding energy of heavy nuclei, contrib. of charge-symmetry-breaking nuclear forces 79−75826
binding energy of nuclear matter, corelated basis functions method appl. 78−45998
boson model, interacting, shell-model basis, correspondence between fermion and boson states and operators 80−52593

nuclear forces continued
bound states in baryon-antibaryon systems, NN, NN̄, dispersion method *(Russian)* 78−16933
bound states of 2N, 3N and 4N systems, nuclear forces 79−71800
bound trinucleon soln. including Δ(1236) isobar effects 79−67674
Brueckner and Green's function theories, ground state props., nuclear matter calcs. 78−8750
Brueckner theory for finite nuclei, effective particle potentials 77−6248
Brueckner-generator-coord. method, α-α scatt. 78−62487
[CC] $^{12}C(\gamma,\pi^+)^{12}B$, nuclear critical opalescence study 80−105988
central p-wave parameter meas., p+polystyrene 5.9-9.9 MeV, nucleon-nucleon force 77−67748
central-tensor coupled effective NN interaction pot. 77−14036
charge asymmetry and charge dependence of two nucleon scattering 78−4899
charge asymmetry of forces, effects for np→dπ^0 reaction 77−10332
charge dependence and nuclear struct. effects, nuclear charge distribs. 80−32197
charge dependent nuclear forces, meson theory, book contrib. 79−97671
charge independent pairing Hamiltonian, variational approach 78−86488
charge symmetry breaking forces, heavy nuclei binding energies 77−88047
charge symmetry breaking in nuclear forces, test by np elastic scatt. 78−89798
charge symmetry breaking nuclear forces, two-body, many-body nuclear systems 78−17109
charge-dependent three-body force with N* (1236) in the intermediate states 79−67677
chiral symmetry and pion condensation, review book contrib. 80−437
chiral symmetry and the NN interaction, book contrib. 79−97669
cluster model, coupling effects of two-particle and alpha two-hole states in A=18 nuclei 80−5081
clustering aspects of nuclear struct. and nuclear forces, review 79−80887
coherent residual interactions, pairing, particle-hole 78−78272
collective mode of nucleon system with π^0 condensate 78−41660
collective modes in nuclear matter, propag., damping 78−25132
collective motion frictional and conservative forces, frictional Schrodinger eqn. 79−85357
composite particles, N-cluster dynamics and effective interaction, dynamical eqn. 80−42560
condensates and Bose-Einstein correlations, quantum optics formalism 79−59028
conference, 11th Masurian school in nuclear physics, Mikolajki, Poland (Aug.-Sept. 1978) 79−63605
conference on few body systems and nuclear forces, Graz, Austria (Aug. 1978) 79−67567
conference on few body systems and nuclear forces, Graz, Austria (Aug. 1978) 79−80880
conference on high energy physics and nuclear struct. Vancouver, Canada (Aug. 1979) 80−41936
conference on many-body theories, Trieste, Italy (Oct. 1978) 80−22135
Conference on meson-nuclear physics, Houston, USA (Mar. 1979) 79−85489
conference on mesonic interface in nuclear struct. Erice, Italy (Sept. 1976) 79−26374
configuration mixing, Coulomb energy anomaly, inmirror nuclei 78−25099
constrained Hartree-Fock calcs. 78−8758
continuum shell model, 3-particle system, limitations in reaction theory 79−75932
continuum shell model, recoil corrections for nucleon-nucleus scattering 78−8751
core polarisation, multiple scatt. eqn. for two particle one hole system and generalised vertex 77−65204
core polarisation contributions to two body effective interaction, centre of mass effects 78−66219
correlation expansions for light nuclei, cluster model higher order term effects 79−75877
Coulomb and charge dependent effects in nuclei 77−54131
Coulomb corrections in $^2H(p,p)^2H$ 77−10400
Coulomb displacement energies of analogue states in mirror nuclei, review 78−78242
Coulomb distortion effects on phase shifts and effective range parameter 79−85322
Coulomb energy anomaly and charge-dependent nuclear forces 79−58997
Coulomb problem, separation of EM effects in few-nucleon systems 77−23014
Coulomb-nuclear interference polarisation in high energy large momentum transfer hadron reactions 77−79282
Coulombian asymptotic states, appl. in partial wave space 77−18426
coupled channels method, applicability to nuclear physics with Ns and Δ's, book contrib. 79−97667
coupled equations for NN, NΔ, πd, NN scatt. above π prod. threshold 79−89244
coupling constants of dN and d*N three-body vertices, spectator functions 78−46011
deformation, unified microscopic description 77−79305
deformations of rare earth nuclei, Skyrme-HF calcs. 78−62480
deformed nuclei, first monopole excitation energies in systems with pairing forces 77−61364
deformed nuclei, pairing self-consistent description *(Russian)* 79−67646
degenerate many fermion system in exp. S form, linked valence expansions 78−41654
dense nuclear matter, construction in lab., book contrib. 80−490
density-depend. folding interactions, effect on nucl. shape 77−22871
density-dependent delta interaction, actinide pairing matrix elements 77−10334
density-dependent Hartree-Fock and Brueckner-Hartree-Fock theories, nuclear forces, nuclear struct. *(German)* 77−82842
deuteron photodisintegration, cross section calcs., local static pots. 77−22997
deuteron scattering from N-body scatt. theory, approx. three body model 79−75934
deuteron wave functions, relativistic, π-NN coupling 80−22595
deuterons, current conservation and off-shell effects with arbitrary interaction 79−45183
dibaryon resonances in πNN and ππNN dynamics 79−13177
dibaryon resonances in πNN and ππNN dynamics 79−75862
diffuse-surface density distrib., moments, potentials, energies calc. 77−10311
nuclear forces continued
dipole interaction between nucleons, steps in binding energy and mag. moment energy *(German)* 78−74306
direct energy minimisation methods in self-consistent nuclear fields, ground state props. 80−22702
discontinuous nuclear potential calcs., global element method appl. 79−3089
dispersion theoretical approach to NN interaction 79−85380
double folding pot. for inelastic scatt. between nuclei 80−13425
double stripping core independ. 2-nucleon transfer, Tang-Herndon effective interactions, (α,d), (t,p) 80−73836
doubly magic nuclei, Skyrme force calc. for nuclear struct. 78−49721
droplet-model theory of the neutron skin 80−47416
education, Schrodinger eqn. solns. using approximate nucleon-nucleon and Λ-nucleon pots. 80−62429
effective Coriolis coupling and nuclear Kondo effect 79−36174
effective fields on nucleus allowing 2p2h config., Green's function method eqns. 79−6361
effective form factor pot. due to unbound core after direct process, asymptotic behaviour 80−27560
effective interaction calcs., symmetry coeff., isospin-spin depend. of single particle pot. compressibility, rearrangement energy 77−46126
effective interaction energy dependence, collective state partitioning model 77−22911
effective interaction with three-body effects 80−27562
effective interactions, appl. to structure problems 77−46120
effective interactions, folded diagram expansion, self consistent and oscillator sd shell model spaces 78−21502
effective interactions, HF self-consistent potl. and linked valence expansions 77−6273
effective interactions in sd shell, two body matrix elements, spin tensors 79−9487
effective mass and exchange current effects in finite nuclei 80−78171
effective NN interaction, long range components, configuration mixing 78−41646
effective NN interaction and exchange current vel. depend., dipole sum rule enhancement 80−63100
effective potentials for heavy-ion scattering derived from channel coupling 80−57794
effective pots., energy depend. pole expansions in 4-body integral equations 79−45178
effective radius outside energy surface, approx. *(Russian)* 77−14039
effective sd-shell interaction, central and non-central components, appl. to ^{28}Si 77−54160
effective three-body interactions in $f_{7/2}$ shell 77−2920
effective two-body interaction near doubly closed shells 77−65206
electron+nucleus scattering, three body correlations, influence on charge form factor of closed shell nuclei 79−6571
electron-positron internal pair formation following heavy ion collisions, conversion coeff. calcs. 78−50135
elementarity of baryon resonances in nuclear matter 79−97666
elementary particle method for nuclei in weak and EM processes, book contrib. 79−97663
EM effects in precision anal. of low-energy np interaction data 78−93896
EM multipole transitions, nuclear force contrib., model independ. of energy weighted sum rules 78−66241
EM pot. between nucleons, anomalous mag. moments and orbit-orbit interaction 79−93524
energy depend. of NN interaction anal. 77−74775
even-even nuclei in 2p1f shell, HF calcs. using velocity depend. effective interaction 79−71792
even-even spherical nuclei, neutron strength function, spin depend., quasi-particle-phonon model *(Russian)* 80−42561
exchange and renormalisation phenomena due to pion-nucleon couplings 77−41893
exchange current affairs in electron scatt. off nuclei 79−71846
exchange current effects on orbital g-factor and E1 sum rule, photoabsorption and beta decay 77−41950
exchange effects, trace of energy-momentum tensor, in weakly bound states 78−37293
exchange effects in nuclei, introduction 79−26375
exchange mag. moments, meson exchange currents, field theoretical approach 80−52574
exotic nuclei, stability calcs. using Hartree-Fock approx. with Skyrme interaction 78−82273
Fadeev integral eqns. for 3 particles in boundary condition model, wave function determ. 78−54248
Fermi hypernetted chain calcs. for model nuclear matter 78−8759
Fermi liquid theory, tensor forces role 79−63616
few body dynamics, conf. 77−18368
few body systems and EM interactions, conference, Frascati, Italy (March 1978) 79−71804
few nucleon correlations from high energy scatt., review *(Russian)* 80−68549
few nucleon systems, 3N and 4N calcs., review 78−50094
few nucleon systems, realistic nucleon-nucleon interactions 78−62526
few-body methods, stat. mechanics, atomic and molecular physics, nuclear N-body problem 79−85379
few-nucleon systems, analytical continuation of the core constants 79−71803
few-nucleon systems, energy-weighted longit. sum rule for electron-nucleus scatt. and nuclear forces 78−58238
finite nuclei, Δ-resonance self energy, Fermi broadening, π-nucleus optical pot. 80−68707
five-body equation, wave function treatment for binary partitions 78−16686
folded diagrams and s-d shell effective interactions, excit. spectra and ground state binding 77−79315
force on nucleus in non-stationary state, definition and anal. 80−105526
four-body model of four-nucleon system, spin and isospin effects 79−71802
four-body model with separable NN interaction, neutron-trinucleon scattering lengths *(Ukrainian)* 77−30495
four-body system, Efimov effect and three-body effective pot. 80−86865
four-body system, energy dependent pole approx. 79−71801
four-nucleon integral eqn. solns. using effective UPA 79−71794
four-nucleon problem, integral eqn. approach, pair-wise interactions *(Russian)* 77−88052
four-nucleon systems, unitary pole approx. 78−516

nuclear forces continued
frictional effects in nuclear reactions with large scale collective motion, review 78−78336
Gamow Teller matrix elements and nuclear mag. moments, configuration mixing v. mesonic effects 79−26400
ghost-pole subtraction and the σ-exchange NN potential 80−86819
giant E1 resonance, Galilean invariant pairing 77−88094
Glauber approx. corrections, nucleon-nucleus scatt., nuclear density distrib. 78−50166
Glauber theory, relativistic correction, high-energy behaviour of scatt. amplitude *(Chinese)* 78−86427
grand unified model, Yukawa coupling radiative corrections, lepton and quark masses 79−97555
gravitational, electromagnetic, and nuclear theory 79−71677
Green's function method for many-body problem for relativistic meson field theory, book contrib. 80−357
growth points in nuclear physics, book 80−94929
hadron-nucleus interactions, existence of slowly moving sources, vel. depend. frictional sources 79−6690
half shell t-matrix parametrisation for delineated two-body bound state 77−18407
Hamada-Johnston interaction, nucleon optical pot. 78−12982
Hamiltonian field theory for systems of nucleons and mesons 79−75860
hamiltonian formulation in generalized linear electrodynamics 79−97543
Hamiltonian formulation of N-body theories, effective interactions and many-body corrections 79−75938
Hamiltonians, semiclassical approx., spin-independ. pots. 80−32208
hard core exponential pots., unitary pole approx. validity at positive energies 79−3093
hard-core spin-polarised neutron matter, ground state energy calc. 78−12999
Hartree eqn., quasiclassical soliton soln., Newtonian interaction with screening 80−68569
Hartree-Fock and linear response, coordinate space representation and gradient iteration 80−18216
Hartree-Fock calcs., fast iterative procedure 80−47414
Hartree-Fock calcs. of semi-infinite nuclear matter with complete forces (finite range and spin-orbit term) 78−86499
heavy atom, parity nonconservation, weak interaction *(Russian)* 79−45182
heavy ion collisions, collective effects rel. to pion prod. 80−37392
heavy ion deep inelastic reactions, Coulomb and nuclear forces effects on double differential cross section pattern 78−70560
heavy ion fusion, internuclear potential determ. 78−41800
heavy ion optical potential, real part, folding technique 80−73830
heavy ion reactions, phenomenological nuclear friction mechanism, particle-hole excitation, nucleon exchange *(Chinese)* 80−42694
heavy ion-nucleus reactions, Pauli blocking on exchange and dissipation mechanism 80−42684
heavy nuclei, charge asymmetry of nuclear forces and binding energies 79−75866
heavy nuclei tensor forces, unnatural parity excitations, high momentum collectivity 80−63065
heavy spherical nuclei, choice of density depend. interaction and α-decay *(Russian)* 78−46010
heavy-ion interactions, magic nuclei, real part of nucl.-nucl. interaction anal. 77−6426
HF calculations of masses and BE 77−22862
high density matter, relativisitc quantum many-body problem 78−4909
high lying intermediate excitations in effective interaction with super soft core pot. 79−36173
hypernuclei, ΛN effective force, binding energy, excitation spectra, self consistent calcs. 77−6283
hypernuclei, ΛN interaction and spin-orbit coupling 77−71580
hypernuclei, NN tensor force effect on Λ separation energy 80−86845
impulse approx. with nuclear current conservation, off-shell form factors 80−52632
inelastic nucleon scatt. anal., comparison of effective two-nucleon interactions 79−93608
inelastic scatt. interactions from realistic pots. 77−67727
infinite nuclear matter, saturation props. using HF calcs. on finite nuclei 79−45198
infinite system of nucleons and Δ resonances, pot. energy, neutron stars 80−86836
integral equations for three- and four-nucleon problem, resonating group approx. 77−18432
interaction potential between magic nuclei, Skyrme interaction energy functional, microscopic and proximity pots. 78−62556
interaction-time effects of quasifree processes 79−75863
inverse scatt. problem, off-shell transition amplitude generation, real symmetric function 79−6431
ion-ion pot., energy depend. from simplified energy density method, folding model combination 79−6429
isobar components of nuclei, experimental tests, review, book contrib. 79−97668
isobar configurations, transition potentials 79−71799
isobar degrees of freedom, binding energy from BHF approx. 80−22734
isobar degrees of freedom in nuclear matter, binding, NN interactions and 2π exchange 80−22735
isobar doorway model, pion absorpt. optical potential 79−85420
isobaric spin dependence of effective nuclear forces 77−79352
isoscalar effective charge in large A limit Tamm-Dancoff and RPA calcs. 80−42534
Jastrow correlations and nuclear photoeffect 78−4927
K-harmonics method for nuclear many body problem with two-body interaction 78−33125
Kerr-Newman background space, nonstatic nuclear forces, meson field at black hole event horizon 78−61880
in Kerr-Newman background space 77−60999
lepton-hadron relation and the nucleon-nucleon potential 79−22207
level density with schematic forces, appl. to ^{116,117}Sn 78−41639
light nuclei, alpha cluster model, 3-body problem 80−32217
light nuclei, isospin mixing, charge depend. nuclear forces and Coulomb interactions 80−5056
liquid neutron matter, pion condensation and the linear σ-model 79−59027
local pots. with Coulomb interactions, separable expansions 77−6247
local two-body interactions, general off-shell phase eqns. 78−36880
long range NN interaction, axial polarisability, two pion exchange 78−29397

nuclear forces continued
low density α clustering effects of Skyrme N+N interactions in nuclear matter 78−29398
low density expansion of nuclear matter optical pot., self consistency requirement 78−8760
many body effective interaction theory problem, comparison with atoms 80−47406
many body problem in Lee model, NN scatt. and matter binding energy 80−63116
many-body forces in nuclear physics, review, book contrib. 79−97670
many-body interactions from quark exchanges, nuclear tetrahedral struct. and props. 79−6459
mass depend. of spin-orbit splitting in A=176-208 region 78−29405
matter distribution in nuclei far from β stability valley, charact. features 77−64635
mean field theory of nuclear dynamics, time depend. 78−12986
meson dynamics in many-body problem, HF approx. 77−22917
meson exchange, relativistic corrections, book contrib. 80−475
meson exchange 80−32195
meson exchange current effects in hadron-nucleus scatt. 79−26380
meson exchange current theories 79−71798
meson exchange currents, configuration mixing, role in nucl. mag. moment, beta decay, review, book contrib. 80−478
meson exchange currents, conservation principles, symmetries, book contrib. 80−473
meson exchange currents, effect in electron inelastic scatt., book contrib. 80−480
meson exchange currents in nuclei 78−12980
meson exchange potential and isobar configs. in nuclei, review 78−50093
meson exchanges and finite Fermi system theory 77−74774
meson field theory, generalised one-boson-exchange pot. 78−66096
meson presence in nuclei, nuclear g-factor exchange current controls., EM interaction role 80−22706
meson theory of nuclear vector and axial vecotr exchange currents, review, book contrib. 80−474
meson-meson interactions, nuclear saturation, nuclear matter compressibility 79−22221
meson-nuclear phys. in 1979, current status and new development 79−85490
mesonic and relativistic effects in the nuclear electromagnetic interaction 80−22818
mesonic degrees of freedom, retardation effects in π, ρ, ω-exchange currents 77−34234
mesonic degrees of freedom, role in hadron-nucleus scatt. 79−26412
mesonic effects in photonuclear sum rules, book contrib. 80−476
mesonic exchange effect on nuclear mag. moment, expt. study, book contrib. 80−477
mesons in nuclei, and introduction, book contrib. 79−97662
mesons in nuclei, exchange current effects on nuclear mag. moments, book 80−471
mesons in nuclei, field theoretical aspects, book 80−481
mesons in nuclei, nuclear forces, baryon reson. effects, book 79−97661
micrononcausal Euclidean wave functions for hadrons, virtual mesons in deuterons 78−41408
microscopic cluster model, light nuclei as proving ground, reviews 79−3101
microscopic effective interactions in correlated model space, eqn. of motion method 80−86818
microscopic versus empirical effective interactions in a single j shell 80−18210
Migdal and surface δ interactions, strength consts. 78−8749
minimal relativistic dynamics of the 3π and ππN systems 79−75702
minimal three body scatt. effective interaction, Yukawa pot. 79−17820
modified Lipkin model, orthogonal polynomial expansion for effective interactions 79−26373
modified oscillator potential description of high spin rotational states 77−67696
momentum dependent δ interactions for nuclear struct. calcs., ground state props. 78−74309
momentum-depend. pot. approximated by Morse function 77−6190
momentum-dependent nuclear potential, group-theoretical derivation of matrix elements 77−26588
monopole vibrations and effective interactions, hyperspherical model 78−58223
multiparticle cores in nuclei, matter fluctuations, binding energy, repulsion correlations 79−75864
multiple pion exchange in nonstatic theory of NN→NN, NΔ 77−34236
multipole residual interaction strength, radial depend. in RPA 80−83026
N=28, 50, 82 isotones, effective interactions and low lying state energy spectra 79−22208
N=28 isotones, effective interactions, Coulomb displacements and separation energies 78−50077
N=29 nuclei, effective 2-body interactions and level spectra 78−41647
N=50 isotones, effective interactions, Coulomb displacements and separation energies 78−50077
N resonances in NN interaction 78−25066
N-body scatt., filter operators in linked-cluster formalism 79−45040
N-body systems, current research in N-particle scatt. 79−80906
neutral current effects in nuclei, review 79−40859
neutral meson condensation, one boson exchange model 79−13235
neutral pion condensation and ALS model including isobar Δ(1236) 79−71814
neutron distribution in nuclei, elastic and inelastic proton scattering, review 80−22649
neutron gas: temperature dependence of the effective interaction 79−36172
neutron gas ground state energy in theory with soft-core pot. 77−82843
neutron rich nuclei stability, HF calcs. *(Russian)* 80−78181
neutron star, relativistic quantum mechanical model for solid core 77−33546
neutron system, localised, tensor force effects, alternating layer spin config. 77−2925
neutron-proton asymmetry and Coulomb field in complex optical pot. 77−30529
NN potential and ^{2}H wave function 77−18418
non-self-consistent energy calculations with a density-dependent effective interaction 79−36170
nonlocal $^1S_0$ p-p pot., nuclear matter calcs. 77−38227
nonlocal continuous potentials, theory of integral operators and eigenvalue anal. 78−8274

nuclear forces continued
nonlocal separable interaction, πN and NN systems appl., odd-mass nuclei studies 77−2917
nonlocal separable interactions in the study of nucl. props. *(French)* 78−33115
nonrelativistic effective πN vertex, PCAC and σ-model 80−52591
nonrelativistic quark model study, resonating group method 80−47403
nuclear charge form factors, effect of N* (1688) resonance 79−93501
nuclear critical opalescence, pion field and condensation 80−42559
nuclear currents, elementary particle description, microscopic anal., book contrib. 79−97664
nuclear Dirac phenomenology, consistency with meson-nucleon interactions 80−9272
nuclear energy level shift non-measurability due to pion diamagnetism in Mossbauer effect 80−73808
nuclear field theory, Dyson boson expansion and Faddeev-Watson resummation technique 80−13385
nuclear field theory, phonon renormalisation, eigeneqns. and sum rules *(Chinese)* 80−102127
nuclear field theory, schematic model functional approach, diagram rules 80−102128
nuclear field theory foundation, schematic model, many-body problem 79−85378
nuclear matter, central spin- and isospin-dependent potentials 78−46023
nuclear matter, Hugenholtz Van Hove theorem and density depend. effective interactions 80−32219
nuclear matter, iterative isobar process role, effective NN interaction 80−99143
nuclear matter, Landau parameters sum rules, tensor force effects 79−80892
nuclear matter, N-N separable non-local interaction, single particle potential 78−58245
nuclear matter, S-wave πN interactions and PCAC 80−78185
nuclear matter, spin-isospin and pion condensation phase transistions, eqn. of state 80−86843
nuclear matter, symm. and asymm., simple effective interaction for props. 78−25141
nuclear matter Δ(1236) inobar probability is nuclear many-body system ground state 79−75859
nuclear matter binding energy, variational approach with realistic potentials 77−18463
nuclear matter charge symmetry breaking nuclear forces 77−26589
nuclear matter energy calc. with state depend. correls. and semirealistic N-N pot. 77−88066
nuclear matter nonstatic OBEP, vel. depend. tensor pot., BE calc. 77−88065
nuclear matter props., charge dependent N-N potential, HF calcs. 78−50115
nuclear matter transparency to fast particles, rel. to high-energy strong interactions range *(Russian)* 78−4901
nuclear pion field struct., book contrib. 80−482
nuclear proximity interaction from HF functional with Skyrme interactions 80−83043
nuclear scatt. from nuclei with nuclear matter t-matrices 79−93577
nuclear structure, conf. 78−50059
nuclei, description in relativistic field theory, book contrib. 80−358
nucleon, bound in harmonic oscill. pot., coupled to pion field, EM struct. 78−8732
nucleon binding in nuclei at high ang. momentum 78−25104
nucleon isobars in nuclear struct., Δ (1236) role in exchange currents 79−26378
nucleon potl. models from pp scatt. 77−6246
nucleon-nucleon interaction as derived from the De Rujula, Georgi, Glashow phenomenological quark-quark potential 80−78172
nucleon-nucleon potential, nuclear form factor behaviour at high transferred momenta 79−9485
nucleon-nucleon potential, tensor contrib. for total ang. momentum depend. pots. 77−2915
nucleon-nucleon repulsive core, quark model forbidden states explanation 78−12984
nucleon-nucleus optical pot. from nuclear matter t-matrix, effective force. 80−22783
nucleon-nucleus optical potential, exchange term and effect of odd forces 78−70500
nucleon-nucleus potential at low and intermediate energy in a Dirac-Hartree model 80−5070
nucleonic form factor, pion exchange, model 80−22608
nucleus-nucleus interaction pot. using energy dependent delta interaction, Skyrme interaction folding 79−36269
odd proton nuclei, parity nonconserving effects, phenomenological proton-nucleus weak interaction 79−40853
odd-odd nuclei, role of tensor force as an effective interaction 80−37332
off shell form factor model, NN scatt. appl. 80−86800
off-shell effects in (p,2p) reacts. 77−6376
one boson exchange potentials and low energy nuclear physics *(Russian)* 77−82834
one meson exchange potential, N-Δ equivalent potential *(Chinese)* 79−22209
one nucleon absorption of slow pions, pion condensate effect *(Russian)* 78−8765
one pion exchange currents, relativistic corrections 77−18400
one-boson-exchange model including N-Δ interaction 77−18422
one-boson-exchange pot. in relativistic config. space for two-fermion system *(Russian)* 77−88051
one-hole states, in double magic nuclei, form factors, spectroscopic factors, centroid energies 78−17090
optical anal. of resonances in velocity depend. square well pot. 78−62098
oscillator matrix elements from NN phase shifts with short range correl. 77−271
Overhauser's model, Skyrme force, Hartree-Fock test 78−12997
p-p bremsstrahlung, forbidden asymmetries and choices of geometry 79−58972
Pade approximants using effective interaction props., series convergence 78−86487
pair correlations, isotopically invariant, generalisation of Mottelson function 79−6366
pairing correlations in finite nuclei including virtual mesons 77−41899
pairing plus surface tensor interaction, appl. to ^{51}V 77−18411
pairing residual interaction in simple dynamical models 77−14040
pairing-force interaction many-fermion system, energy calc. 78−8339

nuclear forces continued
Paris NN pot. parametrisation, phase shifts, nuclear matter binding energy 80−47405
Paris NN potential, superposition of Yukawa terms, G-matrix, nuclear matter 78−70455
Paris nucleon-nucleon potential, book contrib. 79−97665
parity non-conserving processes, weak interaction theory, review 78−50002
parity nonconserving nuclear interactions and weak neutral currents, review 77−41936
parity violating, neutral current effects 77−30497
parity violating effects in vector-like quark models 77−61249
parity violating internucleon potential due to vector meson exchange, asymptotically free theories 77−10210
parity violating nucl. force, unified treatment 80−47400
parity violating nuclear effects, low energy anal., NN scatt. parametrisation 78−66218
parity violating observables in low energy pp scatt. 78−50045
parity violation in neutron-proton capture 77−46165
parity violation in nuclear forces, neutron capture γ-ray expts. 80−37322
parity-non-conserving nuclear forces, theoretical and phenomenological approach review 80−42556
parity-nonconserving nucl. force in np→dγ 77−10333
parity-violating potentials, coherent neutron scatt. 77−71599
partially conserved axial-vector current and model chiral field theories in nuclear physics 79−67698
particle hole effective interaction, empirical, enhanced isospin depend. 78−78274
particle-hole type matrix elements for density-dependent interactions 79−40856
particle-particle collision probability, vol. integral using preequilibrium exciton model 78−70477
Pauli principle effect in nuclear matter, exchange of interacting two pions 78−12983
Pauli-principle effects, simulation 78−8756
perturbative anal. of two-body effective interactions from large matrix diagonalisations 78−41644
PETRA results for fluons, nuclear forces, t-quarks and quark-lepton symmetry 80−86731
phase shift behaviour in Bakamjian-Thomas theory, relation nuclear force at high energy *(Chinese)* 79−80878
phenomenological nuclear force, strength and range in Bakamjian-Thomas theory *(Chinese)* 79−63603
photonuclear sum rules from continuum calcs., dependence on residual interactions 80−22807
pion Bose-Einstein condensation in energetic heavy ion collisions 80−22705
pion condensate, superconductivity in mag. field, critical field *(Russian)* 80−13387
pion condensates, supercond. props., σ model anal. with nucleons 79−59029
pion condensates existence in neutron stars, implications of cooling calcs. 79−101170
pion condensation, field theoretic many-body system 80−22703
pion condensation and the pion-nuclear interaction, book contrib. 80−485
pion condensation in dense nuclear and neutron matter 80−37333
pion condensation in finite nuclei, precritical phenomena, (p,p′) study 79−85377
pion condensation in isospin symmetric nuclear matter 79−80894
pion condensation in nucl. matter, role of effective nucleon mass 78−74323
pion condensation in nuclear matter, book contrib. 80−484
pion condensation precursor, quasi-elastic peak softening 80−78170
pion condensation threshold in finite nuclei 80−18218
pion exchange contrib. to nuclear charge, current and Hamiltonian operators 77−41881
pion exchange current operators, their construction and effect on nuclear props. and reactions 78−86490
pion exchange currents effects on charge form factors 77−18379
pion excitations and phase transitions in nuclear matter, review, book contrib. 80−483
pion field and weak interactions in nuclei 79−26376
pion non-radiative absorption by single nucleon in nuclei, pion condensation 77−42000
pion propagation and production in nuclear matter 79−80893
pion propagator in nuclear matter, optical pot. Pauli blocking corrections 77−22919
pion scattering by nuclear pion cloud 79−85372
pion spectrum and polariz. operator in nuclear medium in heavy nuclei collisions *(Russian)* 80−68558
pion-condensate instability of nuclear medium, temp. depend. *(Russian)* 79−80879
pion-few nucleon problems, Hamiltonian approach 77−6448
pion-nucleus coupling constants, deduction using PCAC 79−40855
pionic atom broadened X-ray lines, appl. of absorpt. edge technique 78−70976
pionic atoms and strongly bound states 79−86084
pionic condensation, superdense nuclei *(Russian)* 77−46129
pionic field, isobaric excitation effects as weak axial coupling consts. 77−10328
pions and isobars in nuclei−an overview, (π,π) and nuclear forces 79−85373
polar emission in fission, nuclear orbiting, three-body trajectory classical calc. 79−3131
potential energy surfaces, folded Yukawa-plus-exponential model 80−86816
potential scattering, boundary condition model, two and three nucleon problems *(Russian)* 78−86491
product represenation in effective range theory 78−78273
progenitor sum rules, nuclear theory appl., meson+nucleon interaction, inelastic form factors 78−54690
propagation by pairing and surface excitations, nuclear states description 78−46007
proton-neutron multiplets, odd-odd nuclei, parabolic Regge trajectories, exchange of quadrupole phonon 80−52590
proton-proton potential models obtained from the Virginia phase-shift analysis 80−47401
protonium annihilation widths from coupling channel boundary condition model 79−36803

nuclear forces continued
proximity friction, one body, calc. of key function using Thomas Fermi approx. 78−70454
pseudovector πN coupling and the relativistic model of pion condensation *(Russian)* 79−49596
pure hard core interaction in neutron excess matter, third order binding energy calc. 78−89784
QCD and superdense matter, quark and gluon plasma, hadronic structure, neutron stars, hadron collisions, review 80−73683
quark exchange, nuclear force model 78−41648
quark model, deep inelastic scatt., N and nucleus struct. *(Russian)* 77−61299
quasibound state wavefunctions for particles inside Coulomb barrier, computation 77−2914
quasiconfiguration approach to effective forces, appl. to $f_{7/2}$ problem 79−45187
radius perturbation theory, appl. to NN system and pionic atoms 78−21007
reaction matrices comparison for free scatt. and nucl. matter 79−59026
reaction matrix approach to the cluster state, Brueckner generator coordinate method, appl. to α-α scatt. 80−9250
realistic NN pot. construction for three body systems and nuclear matter 80−22699
Reid soft core pot., Talmi integral anal. for nuclear force separation 79−36171
Reid soft core potential, low-rank separable matrix formalism 80−22704
relativistic effects on the two-nucleon and nuclear matter systems 79−89261
relativistic mean field theories, correlation effects estimate 80−5073
relativistic N-N one-boson-exchange potentials with asymptotic power-law energy dependence 78−82293
relativistic nuclear field theory with π and ρ, cold nuclear matter calcs. 79−93527
relativistic nucleus-nucleus collisions, high density nuclear Mach shock waves 78−633
relativistic two-body forces in many-body systems, Weinberg and Yukawa interactions 80−32203
renormalised shell model matrix elements from nucleon-nucleon phase shifts 78−12991
repulsive core regularisation, two-body binding energy 77−82814
resonance degrees of freedom in the two-nucleon system 80−5072
ring diagrams in nuclear matter, many-body forces contrib., ρ and π exchange 80−22740
RPA coordinate space formalism derivation, interaction strength and transform. coeffs. for Skyrme interactions 78−70473
s-d shell, two nucleon effective interaction, intruder state, RPA correlation 80−57701
s-d shell effective interactions, effective single particle field sizes 79−89247
S-matrix pole trajectory in three neutron model 78−82296
S-wave πN interaction role in combined pion condensation 80−105998
S-wave nucleon-nucleon interaction, energy-dependent separable potential 80−68551
S-wave pion-nucleus dynamics in the $\sigma+\omega$ model 79−89245
Saito potential, off-energy-shell unitarity 80−18207
saturated nuclei, quantum chromodynamics of nucl. forces 79−13211
scalar meson field and many-body forces, book contrib. 80−359
scattering params. for separable potls. with Coulomb interaction 77−18425
sd shell nuclei; spin-tensor decomp. of effective interaction 79−93522
sd shell nuclei, effective interaction between nucleons 78−17117
second class current upper limit from β-decay data 80−47404
self-consistent calculations of nuclear properties with phenomenological effective forces, review 79−22218
self-consistent WKB calculation in a model nucleus with Skyrme interaction 79−45186
sensitivity of real part of nucleus-nucleus potential to nuclear densities 78−82291
shell model, Hartree-Fock self consistency and many body monopole forces 79−67685
shell model anal. of effect of geometry 78−4900
short range NN interaction from nonrelativistic QCD 80−32200
short range nucleon correl., high energy scatt. 77−71569
short-range central nucl. pot., two-nucleon problem 77−65203
short-range correlation effects, vel.-depend. pots. 77−30496
short-range forces and surface tension, surface isomers 77−57596
short-range repulsion, gauge theory of coloured quarks 78−12880
single particle levels, one boson exchange potentials, spin orbit splittings 79−9436
single particle levels, spin orbit splitting, 1 boson exchange pot. contribs. *(Russian)* 78−78243
single particle pots. and many body forces in NN interactions *(Chinese)* 79−59014
single-particle motion in nucleus, forces between constituent nucleons, shell model 80−47408
single-particle pot., nonhermitian *(Chinese)* 78−78241
single-particle response and ground-state properties, Hartree-Fock theories 80−105997
six-nucleon system, cluster model, resonating group, and integral eqns. approach, appl. to ^{6}Li 79−80888
Skyrme's interaction, correction to g-factors 77−65196
Skyrme's interaction, spin stability and mag. polarisability 77−2916
Skyrme force, use in HF calcs. of energy levels and transition rates 78−82315
Skyrme forces in nuclear matter, self consistent periodic quartet formation 77−14052
Skyrme forces used in self-consistent RPA calc. 77−50072
Skyrme interaction, mag. moments, polarisability, gyromag. factors 78−21501
Skyrme interaction and effective mass in isoscalar giant quadrupole reson. 77−14088
Skyrme interaction and spin stability of nuclear matter 77−54146
Skyrme interaction HF calc. for nuclear stability limits 77−18377
Skyrme interaction in HF calc. of rot. states 77−34212
Skyrme tensor interaction, HF spin-orbit effects in spherical nuclei 77−61350
Skyrme-type interactions, spectroscopy of light nuclei, density dependent Hartree-Fock 80−22717
small nuclear systems, deviation from saturation, mass formula correction 79−80891

nuclear forces continued
soft pion theorem, appl. to currents in nuclear forces and matter. 79−26377
soft-photon theorem for the electromagnetic interaction of the relativistic two-nucleon system 79−40858
solid like aspect with alternating layer spin and π condensation 80−22733
solitary wave exchange in NN pots. 78−70457
spectral distribution methods in effective interaction theory 78−86489
spherical nuclei, absolute α-decay widths, renormalised effective interaction contrib. in shell model 79−75925
spherical nuclei, Hartree-Fock-Bogolyubov calcs., D1 effective interaction, nuclear matter, binding energies 80−63105
spherical nuclei, isomer and isotope shifts, theory of finite Fermi systems 80−39929
spherical nuclei, low lying states, effects of particle-particle channel residual interaction 78−12978
spherical nuclei, total binding energy, many body field theory, ^{16}O, ^{40}Ca, ^{58}Ni appls. 77−30482
spin rotation, high angular velocity, collective aspects of heavy ion collisions 80−78309
spin unsaturated systems, finite range two- and three-body interactions 78−66220
spin-2 mesons exchange interaction in superdense neutron matter, relativistic theory 78−45349
spin-depend. N-N forces, ^{1}H(t,t) and ^{3}H(p,p) polarised scatt. 79−6634
spin-isospin density phase in finite nuclei, strongly oblate shape 80−22746
stable charmed hyperfragments containing charmed baryon + nucleons, binding energies, lifetimes 78−89815
static nuclear Laplacian force *(Bulgarian)* 78−54688
statistical description of nuclear compound states, temp. Green's functions method *(Russian)* 78−17115
stellar collapsing cores, effects of nuclear forces, partition function and dissoc. 79−48833
strong interactions in strange hadronic atoms 79−86083
strongly bound π^- nuclear states, vel. depend. pot. binding, pionic atoms 80−37331
strongly bound pion states in nuclei, optical model 80−68557
structure theory, nuclear reaction matrix and nuclear forces 80−9242
Sturm-Liouville equation, convergence, rel. to nucleon-nucleus pot. 79−6534
Sturm-Liouville equation, math. aspects rel. to nucleon-nucleus pot. 79−6533
sum rules for collective excitations 79−59002
super soft core model 78−66217
superfluid model, isotopic invariance and pairing energies 80−22687
superfluid model, paired matrix elements for a spherical nucleus with variable pairing 79−6433
superheavy nuclei and multineutron systems, possibility of existence *(Russian)* 80−462
superheavy nuclei stability, spin-orbit symmetry potential 78−50104
superposed Yukawa and inverse square potentials, eigenenergy expansion 79−30281
surface δ interaction for nuclear matter, effective interactions 79−67672
surface properties from Thomas-Fermi calc. 80−13394
surface tension coefficient, surface energies, and scalar meson mass *(Chinese)* 79−49574
T matrix, $^1S_0$ two-nucleon, interior wave function 77−14038
Tabakin rank-one potl. in orthogonality condition model, 3-body energy 77−18423
tensor contrib. to nuclear matter in first order perturbation theory, binding energy 77−18410
Thomas-Fermi kinetic-energy density with gradient corrections 80−91169
Thomas-Fermi model of finite nuclei 78−8747
three and four nucleon low energy scatt. expts., review 79−80945
three body forces from cluster terms, binding energy and tensor forces 79−45176
three body forces from meson exchange, status report 77−54154
three body problem with energy dependent potentials 77−18413
three body problem with three body forces, special solns. to integral eqns. 79−75869
three body systems in nuclear physics, review 78−517
three body unitary transformations, forces, bound state properties 77−18415
three fermion system with exchange potential, asymptotic soln. of Schrodinger eqn. 77−38229
three neutron resonance, enhancement factors, forces, and binding energy 79−45230
three nucleon bound states, Δ (1236) effects, on binding energy and form factors 79−75858
three nucleon clusters in nuclear matter, intermediate Δ-states, exchange diagrams calc. 78−17112
three- and four-body interaction props., hyperspherical expansion convergence *(Russian)* 78−518
three-body, two-pion exchange forces, ^{4}He calc. 77−41895
three-body Amado-Lovelace eqn. at positive energies, anal. soln. 78−16938
three-body cluster energy, lowest order constrained variational calc. 79−13233
three-body force from 2π, $\pi\rho$, and 2ρ exchanges 80−78169
three-body force from kinematical effects in the three-nucleon system 80−105986
three-body forces from triple Boson couplings 77−18409
three-body forces in 3- and 4-nucleon systems 78−29400
three-body forces in nuclear matter and nuclei 77−22900
three-body forces in the nuclear three-body problem 79−45177
three-body nuclear forcesin σ-model, nuclear matter and triton BE 77−71568
three-body problems with local potls. in coord. space 77−26594
three-body reactions with charged particles 79−75968
three-body scatt. problem, cluster expansions, effective intercluster pots. 80−5082
three-body vertices with two-body techniques 77−18435
three-nucleon bound state, perturbation approach to Faddeev eqn. 78−54691
three-nucleon bound state, soln., perturbational approach to Faddeev eqn. 79−30793
three-nucleon bound state computed with explicit Δ(1236) components 79−67673

nuclear forces continued
three-nucleon forces, nuclear matter and BE 77−74773
three-nucleon potentials due to π, S and ω, binding energy in nuclear matter 78−62486
three-nucleon system, Faddeev eqns. perturbation, nucleon-nucleon interaction with tensor force 78−70463
three-nucleon system, local strong and Coulomb potls. 77−18427
three-nucleon systems, props. and interactions 79−71805
three-nucleon two-pion exchange potl. for matter calcs. 77−26592
threshold states in different schematic models 78−82272
total single particle energy, asymptotic form of smooth part 78−4892
translationally invariant effective interactions, factorisation 77−82833
trinucleon bound state using Paris pot., binding energy and form factors 78−89803
trinucleon properties, one-boson-exchange potentials 77−18433
trinucleon system, evidence of three body force, effect on charge density *(French)* 79−75857
trinucleon system bound by one-boson-exchange force 77−18414
truncated space calcs. of exact bound state energies 79−3090
two and three-body problem, boundary condition model *(Russian)* 77−34237
two body problem solution, NN interaction with separable pots., models, computer calcs. *(German)* 77−54156
two pion exchange three nucleon pot. and nuclear matter, appl. of πN scatt. amplitude 79−40877
two pion exchange three-nucleon potential and nuclear matter 79−75865
two- and three-body scatt. amplitudes, separable expansion method 77−18431
two-body bound state and half off-shell t-matrix parametrisation 77−18424
two-body correlations 77−14037
two-body effective forces in light and medium nuclei via stripping reactions 77−88049
two-body effective residual interaction; universal relationship 77−18403
two-body force scatt. calculations, limitations 77−88089
two-body local potl., possible phenomenological form 77−18405
two-body transition matrix and UPA model, convergence props. of generalised separable expansion 78−16939
two-nucleon interaction isobar contributions from noncovariant perturbation theory 79−478
two-nucleon pot. and meson physics, nucleon-nucleon interactions, review 78−89802
two-nucleon soft-core potential with central, spin-orbital and tensor components *(Czech)* 77−41892
two-nucleon stripping reactions with Tabakin pot. 78−21570
two-nucleon system, Δ resonance, excitation spectrum 78−41649
two-nucleon system, isobar configs., relativistic model 77−41894
UCN, quasibound states in matter, reson. positions and widths 80−73833
unitarily equivalent multiparticle Hamiltonian systems yielding equal scattering for corresponding states 78−77756
unitary pole expansion, physical basis 77−18406
Universe and microcosm, gravitational-inertial field theory 80−8721
valence nucleon effective interactions 80−9244
van der Waals type model for pp elastic scattering at high energies 79−58977
variational techniques, wave functions correlation operators, review 80−22748
virtual mesons effect on hadron-nucleus reactions, book contrib. 80−472
virtual particle interactions *(Polish)* 79−40802
virtual pions, Yukawa field and effects on μ-capture, β-decay, mag. moment etc. 79−26379
weak, EM and strong interactions in the nucleus 80−4978
weak axial coupling constants in nuclei, polarizability, pionic field, PCAC 77−6055
weak interactions in nuclei, axial polarisability 77−22924
Woods-Saxon potential spectrum, pairing force strength, Nilsson model comparison 80−57704
Yukawa interaction among fermions, asymptotic estimates in perturbation theory 77−30092
Yukawa pot., superposition, off-shell Jost function 78−29415
Yukawa pot. problem, S-matrix exact evaluation from transformed Schrodinger eqn. 78−82120
Yukawa potential, scatt. amplitude, nonperturbative var. approx. calcs. 78−24981
Yukawa potential function, determ. of phase shifts 78−58237
Yukawa quantum field theory, Matthews-Salam integral representations 80−327
Yukawa quantum field theory in 2D space-time, linear N_r bound, locally Fock property 80−326
Yukawa spherical diffuse massless sources in relativity 77−87931
Z-boson and two-boson models, neutral current phenomena, μ-e universality 80−18109
(α,α), local density dependence of NN interaction, double-folding calcs. 80−83114
α particle nuclei, cluster struct., ground state energy lower bounds 78−46017
α surface clustering, effect of pairing and four-body interactions in 41≤A≤45 nuclei 77−10344
α-α effective interaction, energy density formalism *(Russian)* 77−46119
α-α interaction, consistent calc. by resonating group method 77−18491
αα and αN multichannel interactions, total cross sections, phase shifts determ. 77−38228
β-stable nuclear matter, electrically neutral, constrained variational calc. 78−58243
(d,x) deuteron break-up, dependence of differential cross section on n-p potential form *(Russian)* 80−78173
d, 6 quark system, wave function, elastic form factor, NN forces, spectroscopy *(Russian)* 78−50015
d photodisintegration, soft-core pots. calcs. 77−57648
d propagation in nuclear matter, spin depend. of d optical pot. and binding energy 78−70545
d stripping reactions, Tabakin pot. calcs., differential cross sections, ang. distribs. 78−611
Δ(1232) isobar in nuclei, one-boson-exchange and straton model anal. *(Chinese)* 78−78275
Δ(1236) resonance, effect on NN scatt., nuclear and neutron matter 77−41909
Δ(33) interaction with nucleus, effective shell model pot., pion scatt. test 80−32202
nuclear forces continued
Δ resonance inclusion in one-boson-exchange potential, Brueckner-Hartree-Fock calcs. for ^{16}O 77−54155
Δ resonance shifts, simple model 77−82829
Δ-N interaction and π photoproduction on few body systems 79−71842
(e,e) determination of valence nucleon radial distrib., exchange current role 79−40878
(e,e′), deep inelastic, meson exchange currents from Fermi gas model 78−66268
(e,e′), transition strengths, unnatural parity state excitation of stretched configs., NN forces 79−63626
ed→ed, nucleon forces, meson exchange current effects, impulse approx., review 80−57603
(γ,N), intermediate energies, nucleon current interactions, direct knock out mechanism 80−27624
^2H(p,p), theoretical anal. of nucleon-nucleon forces 79−9554
$^2H(\pi,\pi)$, relativistic three-body calc. 77−74715
$^2H(\pi^+,pp)$, pion absorpt., effect of ρπ exchange currents *(Korean)* 80−47402
Λ well depth with class of equiv. pots., nuclear matter appl. 77−26605
Λ-N two term separable pots., comparison 78−66239
ΛN distrib. function, Λ-binding to nuclear matter, Fermi hypernetted chain approx. 80−78131
ΛNN correlations and Λ binding in nuclear matter 80−106000
$\mu^+d\rightarrow\mu^+np$, ≤5 MeV, Coulomb break-up of deuteron and n-p off-shell effects 79−75777
(N,N′), microscopic description of direct processes, effective interaction 78−12979
N and Δ resonances in nuclei, coupled channel eqns. soln. for nuclear matter 79−17845
N-N interaction and nucleon struct. study by ep and ed elastic scatt. 79−71797
N-N interaction information from perturbative and variational nuclear matter calcs. 79−71796
N-N new interaction for heavy-ion optical pot. in folding model 77−18505
N-N potential, review 79−71795
N-N singlet even pot. from inverse scatt. problem algebraic method 77−18315
N-nucleus optical model potential, spin-orbit component from internucleon pot., $^{40}Ca+p$ appl. 78−46039
n-p final state interaction in ^2H(p,2p)n at high-energy 77−18533
n-p residual interaction effect on elastic electron scatt. by dipole giant resonance positioning 77−82914
^3n model with $^1S_0$ interaction in Faddeev eqn. framework, 3 neutron resonance 79−67680
^3n system, S-matrix pole trajectories 79−67679
N*(1688) resonance effects on nuclear reaction, NN scatt. phase parameters 80−105987
nd breakup reaction, Reid soft-core pot. calcs. at 22.7 and 46.3 MeV 77−74860
NΔ conversion, two-channel formalism and three-body forces approaches 78−8733
NΔ non-static interaction models, s-wave amplitudes and cross sections 79−67667
$\bar{N}N$ and $\pi\bar{N}N$, $\pi\pi\bar{N}N$ bound states from $\bar{N}N$ potentials 80−62951
$\bar{N}N\rightarrow B_i\pi$, B_i are $\bar{N}N$ quasinuclei 80−57624
NN correlations, anal. in elastic pion double charge exchange, reactions 77−10449
NN covariant dynamics and πD scatt. 77−6449
$N\bar{N}$ cross-sections and resonances in nonstatic OBEP 80−13386
NN dynamics at medium energies, elastic and inelastic scatt., unitary model 80−63101
NN dynamics at medium energies, phase parameters, one pion exchange model 80−63102
NN effective 2-body pot. in nuclear matter 78−54714
nn effective range, determ. in proposed ^2H(d,2n)2p expt. 77−18585
NN forces matrix elements in hyperspherical basis *(Russian)* 78−46009
NN forward scatt., two and three pion cut contribs., nucleon exchange model 80−63103
NN hard (soft) core pots., FPT and ACCBA anal. 77−18404
NN hard core as relativistic effect 77−87994
nn interaction, effective radius determ. using three nucleon motion for nuclear forces 79−6426
NN interaction, isobars, transition potentials, short-range repulsion 77−34235
NN interaction, meson field theory, one-boson-exchange model 78−66216
NN interaction, mesonic aspects, dynamical calcs. 77−10330
NN interaction, quark MIT bag model anal. 79−80806
NN interaction, time reversal noninvariant NN potential in two nucleon system 79−54352
NN interaction in pion exchange, nuclear matter and pion condensation, review 80−42557
$\bar{N}N$ interaction information from antiprotonic atoms strong interaction effects 77−18402
NN interaction matrix, irreducible basis of representations of group O(n-1) 77−6271
NN interactions, conf., Vancouver, Canada (July 1977) 78−62418
NN interactions, one-boson exchange, dispersion relation and multichannel approaches 77−22759
NN low-energy semi-phenomenological model, Nπ coupling const. *(French)* 77−18311
$NN\rightarrow NN\pi$, lowest order Feynman diagram calc. 79−63508
NN P-violating interaction in Bars-Halpern-Yoshimura gauge model 77−22758
NN parity nonconserving pot., evidence for enhanced ΔS=0, ΔT=2 weak interaction in nuclei 77−18419
NN potential, direct part, study through α+α scatt. 77−10420
NN potential, meson field theory two-pion exchange anal. 77−208
NN potential in multihadron systems, nonrelativistic covariant theory 78−70456
NN potential short range behaviour with the quark model 80−47409
NN potentials, based on meson exchange, discussion and appl. to nuclear matter 79−80815
NN potentials repulsive part, mesonic theory *(Russian)* 79−30792
$N\bar{N}$ quasinuclear states and the Bethe-Salpeter equation 79−13212
$N\bar{N}$ quasinuclear systems, review 78−25065
NN realistic nonlocal pots. from inverse scatt. theory for $^3S_1$-$^3D_1$ interaction 78−41651
NN resonances and total cross sections, expt. evidence review 80−42558

nuclear forces continued
NN scatt., 325 MeV, unique isospin-zero phase shift solution 78−50044
NN scatt., potential models, high-energy phase shifts and off-shell react. matrices 78−45936
NN scattering, role of noniterative π exchange in nuclear matter 79−40857
NN scattering dynamics, new approach 77−18412
NN̄ system, positions of resonances found by applying Faddeev's equations *(Russian)* 79−93529
NN system, ρ-meson exchange and reln. between pion-nucleus and NN interaction 77−10331
NN systems, resonances due to annihilation, baryonium states, many channel N/D method 78−66143
NN T-matrix, analyticity constraints 77−18408
NN tensor force and d(γ,p)n forward p prod. 77−57649
NN weak coupling constant magnitude, anal. of ^{41}K data, CVC hypothesis *(Russian)* 77−6144
NNN bound state problems, hyperspherical harmonic expansion, review 80−91136
NNN̄ system, bound and reson. states using Fadeev eqns. *(Russian)* 78−89804
NNπ system, effective 3-body with unusual disconnected struct. 79−75861
NNπ system, phenomenological relativistic quantum mechanics, scatt. theory 80−83082
np bremsstrahlung, effects of nonminimal currents and role of various couplings 78−70394
np bremsstrahlung, one-pion-exchange current 77−82828
np bremsstrahlung at 200 MeV 78−66144
np D-transfer effect on phase shift anal. near 325 MeV 78−82294
np effective interaction in mirror nuclei, charge exchange part, linear binding energy relation 77−22901
np interaction, definitive expts. at LAMPF 77−18557
np interaction and nucl. deformation 78−8748
ω meson contrib. to nucl. forces, field theory model 77−74772
(p,2p) DWIA calcs., N-N off shell t-matrix, optical model from N-N 77−88124
(p,p), pol. p, sd, fp shell nuclei, 65 MeV, effective two-body interaction range 80−32201
(p,p′), deformed nuclei, ground state rot. band, shape meas. and exchange contrib. 79−451
(p,p′), deformed nuclei, local approx. results for exchange effects 79−452
(p,p′), single neutron states, two step process and effective interaction 80−78290
(p,p′), transition strengths, unnatural parity state excitation of stretched configs., NN forces 79−63626
(p,p′), unnatural parity states excitation, π-condensate instability effects, DWBA anal. 80−78168
(p,π^+), π threshold prod. and absorption, pseudoscalar-pseudovector equivalence 79−80877
pp→^{2}He$^+\nu_e$, pionic exchange current contribs. 77−10329
p$\bar{\text{p}}$ atom, nuclear energy level shift *(Russian)* 78−37295
pp bremsstrahlung cross section, 11 and 13 MeV *(German)* 77−10275
pp reaction, exchange current corrections π and ρ exchange 80−26733
pp scatt., low energy, strong van der Waals interaction 78−41563
pp scattering up to 30 MeV, precision analyses 77−34172
(π,2π), possible probe for pion condensation precursor phenomena 80−78330
(π,$\gamma\gamma$), pion condensation studies status report 79−85524
(π^-, $\gamma\gamma$), existence test for pion condensation 79−85525
(π^-,n), π threshold prod. and absorption, pseudoscalar-pseudovector equivalence 79−80877
(π,π), Weinberg chiral Lagrangian nonlinear terms, nuclear binding, optical pot. 80−78329
(π,X), effective S-wave πNN interaction, effects in nuclear matter 80−105985
π bound states in finite nuclei, π-nuclear optical pot. 78−46013
π condensation, effects of short range nucleon repulsion 77−88064
π condensation effects in degenerate matter, appl. to theory of superdense celestial bodies *(Russian)* 79−96907
π condensation in isospin symm. nuclear matter, phenomenological approach 78−29414
π condensation in neutron matter, N-N interaction, critical density 80−57711
π condensed phase, σ-model, alternating-layer-spin struct. 80−83057
π electromag. processes, theoretical aspects 80−22822
Π field in nuclei, μ absorpt. and doubly radiative Π absorpt. as probes 77−88063
π(γ)+A→p+X, effect of short range pairing correl. in cumulative nucleon prod. *(Russian)* 79−30794
π propagator in nucl. matter, NN correls. 78−515
π- and ρ-exchange pots., influence on mag. resonances, mag. moments, and transition probabs. 80−99133
π^- absorption at rest, high spin state excitation, π-condensation and Δ^{++} *(Russian)* 80−86927
π^0 condensation in finite system, extended Thomas-Fermi model 78−41645
π^0 condensation in σ-model, chiral symmetry 79−80895
πd field theoretical model, effective semi-relativistic three-body problem 78−86454
πd→πd, 47 MeV, differential elastic cross section 79−85530
πd semi relativistic field theroretical model, extended Fadde'ev and Amado-Lovelace eqns. 78−89729
πd system, resonances near ΔN threshold, Argand diagrams 78−62582
π^-d→2n+γ, n-n scatt. length from γ spectrum 78−62576
π^3He^{3}He coupling, estimation methods 79−63599
π^3He^{3}He coupling constant determ. from ^{3}H(p,n)^{3}He differential cross section 78−89801
π^3He^{3}He coupling on basic of PCAC 80−32196
πN coupling in Δ(1231) isobar region, pion index of refraction, self-energy in low density limit 80−42554
πN effective interaction in nuclear matter, pion propagator modification 77−2927
πN elastic interactions, potential determination using Newton-Sabatier method, inverse scatt. problem 78−89731
πN elastic scatt., nonstatic model for nuclear reactions 80−102125
πN low energy partial wave anal., cross sections, Δ^0 and Δ^{++} 80−52531
πN off shell scatt. and πNN vertex function 79−85333
πN P11 ground state potential, meson probability density 80−27558

nuclear forces continued
πN scattering amplitude in nuclear medium at nuclear matter density 78−29500
πN scattering amplitude in nuclear matter, quantum field theory approach 80−42570
πNN form factor; relativistic calc. of Δ(1232) contribution to imaginary part *(Korean)* 80−47292
πNN(πNΔ)($\pi\Delta\Delta$) vertices, study of the finite range struct. 79−85370
πNN vertex, virtual nucleon propagator, and pionic vertex, form factor enhancement 80−22700
πNN vertex function, dispersion theory calc. 77−57509
πNN vertex function and low energy πN scatt. 79−85332
πNN-NN coupled problem, unitary model 80−99135
πNN-NN coupled system theory, practical eqns. and unitarity 79−97659
πNN-NN coupled systems theory, relativistic extensions 80−63104
πNN-NN system, coupled channel approach, coupled equations 79−85371
$\pi\omega$ meson exchange contribution to NN interaction 77−18401
ρ-meson intermediate states in πN scatt. Chew-Low theory modifications 79−479
ρ-ω mixing charge symmetry breaking force, nonlocal contribs., ^{3}He-^{3}H mass difference 78−70458
ρ^0-ω mixing, sign of single particle exchange nucleon force, charge asymm. pot. 77−88048
(t,p) stripping reactions, repulsive-core effects, Tabakin potential 77−30607
^{6}Li(p,n), 144 MeV, one pion exchange and PCAC expt. test 80−528
^{1}(π^-, γn) differential cross-sections in Δ(1232) region 79−93665
^{16}(0$^+$)(μ,ν)^{16}N(0$^-$), one pion exchange current problem for ^{16}O(0$^+$)⇄^{16}N(0$^-$) 79−85375
A=20,21, Preedom-Wildenthal interaction, influence of central and non-central components 79−45179
^{26}Al 1$^+$T=0 states, isobaric analogue state, spin-isospin effective interaction from ^{26}Mg(p,n) 80−68553
^{27}Al(^{3}He,p) 9-14 MeV, stat. multistep compound emission, residual two-body interaction 80−47493
^{10}B, triaxial deformation in shell model non-central forces, projected HF calc. 80−13367
^{11}B(p,γ), 30-100 MeV, meson exchange and nucleon correlation process calcs. 79−549
Be, neutron forces in relativistic electron radiation field in crystal, channelling *(Russian)* 80−70287
^{7}Be effective for charge exchange analogues of Gamow-Teller transitions from ^{7}Li(p,n) 80−57726
^{9}Be, binding energies, three body calcs., Faddeev formalism, alpha cluster model 79−75876
^{12}Be, Hartree-Fock calculations of nuclear bulk properties with density- and starting-energy dependent effective interaction 80−9246
Be(γ,p)X, 180-420 MeV, quasifree NN system photodisintegration, p spectrum 80−106049
^{207}Bi high spin states, level decays, three particle interactions from ^{205}Tl(α,2n), ^{208}Pb(d,3n) 79−49567
^{209}Bi(^{3}He,d), 30 MeV, effective residual interaction matrix elements, spectroscopic factors, cross sections 80−99134
^{209}Bi(α,t), 40 MeV, effective residual interaction matrix elements, spectroscopic factors, cross sections 80−99134
^{209}Bi(n,n), direct scatt., polarised thermal neutrons, empirical parity-violating potentials and neutron optical activity 79−59074
^{A}C, A=12, 13, nuclear critical opalescence, M1 form factor, pion field and condensation 80−73809
^{12}C 1$^+$(T=1, 15.1 MeV) state excitational pionic modes, M1 form factor for (p,p′), (e,e′) 80−78195
^{12}C, 3 alpha force and 3α model 79−30798
^{12}C, 3-α struct. in boson model 78−17124
^{12}C, boson 3α model and effective inter-α forces 78−66232
^{12}C, Efimov state search using Ali-Bodmer α-α force and Faddeev technique 79−6420
^{12}C M1 form factor, pion field critical opalescence, ρ role, polarisation phenomena 80−68552
^{12}C mag. transition form factors, core polarisation and exchange current effects 79−75899
^{12}C, saturating effect of N*(1234) on binding 78−58231
^{12}C, three α model calcs. and O$_2^+$ state 79−75856
^{12}C(^{12}C,p)X, 800 MeV/N, fireball and preequilibrium cross sections, π condensation proximity influence 80−27659
^{12}C(μ,γ), exclusive radiative capture, axial currents and induced pseudoscalar form factors 79−97699
^{12}C(μ,ν_μ)^{12}B, induced pseudo-scalar coupling constant 79−49606
^{12}C(μ^-,ν_μ)^{12}B, Hartree Fock wavefunction, correlations, pseudoscalar coupling constant, capture rates, recoil nuclear polarisation 80−22774
^{12}C(p,n), 144 MeV, one pion exchange and PCAC expt. test 80−528
^{12}C(p,p′), 122 MeV, level excitation, cross sections, effective NN interaction, DWIA anal. 80−78197
^{12}C(p,p′), 22-27 MeV, 1$^+$ state de-excitation γ-ray ang. distrib., tensor force effects, DWBA anal. 80−68580
^{12}C(p,p′), 800 MeV, 15.11 MeV state diff. cross section, nuclear critical opalescence search 80−105984
^{12}C(π $\gamma\gamma$), branching ratio, ang. correlation 79−85526
^{14}C$_{g.s}$ β-decay, mesonic exchange currents, weak process microscopic treatment 80−57742
Ca, extended Skyrme force calculation, spin instability 79−63601
^{A}Ca, (A=43-46), pairing force, seniority number 80−27563
^{A}Ca= A=40, 48, Hartree-Fock calculations of nuclear bulk properties with density- and starting-energy dependent effective interaction 80−9246
^{40}Ca, core polarisation J-averaged effects through 3rd order up to 10 $\hbar\omega$ excitations 79−67671
^{40}Ca, giant isoscalar monopole state energies in generator coordinate method 80−37317
^{40}Ca, magic nucleus, nonlocal pots., binding energies 77−41877
^{40}Ca, pion exchange currents and charge form factors, shell model anal. 77−10338
^{40}Ca, relativistic Hartree-Fock eqns., 1 boson exchange pot., spin orbit splitting 79−3106
^{40}Ca(^{16}O,X), ion-ion interaction pot., imaginary part, effective interaction 80−68692
^{40}Ca(^{6}Li,^{6}Li), 156 MeV, density depend. of N-N interaction 79−6660
^{40}Ca(n,n), 10 and 50 MeV, optical model real potential 78−58274
^{42}Ca, extended Skyrme force versus realistic interactions, effective interactions 79−54395

nuclear forces continued
Cd, even isotopes, effect of residual interaction in particle-particle channel on low-lying states 78−21503
Cd, multipole-multipole interaction in particle-particle channel 79−6364
^{40}Cd(d,p)^{41}Ca, 11 MeV, effect of Skyrme type density depend. effective pots. 78−46069
^{34}Cl, core polarisation J-averaged effects through 3rd order up to 10 $\hbar\omega$ excitations 79−67671
^{166}Er, Skyrme-HF calcs., deformation, electric moments, spin-orbit potentials 78−62480
^{17}F, axial vector decay, exchange corrections 79−36201
^{18}F, effective interaction, nonlocal pot. reaction matrix free scatt., spectra 77−46122
Fe isotopes A=53-58, spectroscopic calcs. using mass independ. effective interaction, yrast levels 78−41638
Ge, A=64, 66, 68, 70, Lipkin-Nogami method, ground state props. 78−50103
^{A}Ge, A=68, 70,72,74, level excitation, n-p interaction role from α-transfer in Zn(^{6}Li,d) 80−73821
H+H^{+}, nuclear repulsion, contrib. to charge transfer 80−18922
(HI,HI), local density dependence of NN interaction, double-folding calcs. 80−83114
^{1}H(γ,π^{+}), 3.4-18 GeV, πNN form factor and differential cross sections, one pion exchange 80−68526
^{1}H(n,γ)^{2}H, exchange current and interaction effects using unitary equivalent transforms. 79−9566
^{1}H(n,γ)^{2}H, repulse core effect 77−38259
^{1}H(n,$\gamma\gamma$), thermal, consistency between pion exchange currents and NN pot., cross sections 80−68556
^{1}H(n,π^{0})^{2}H, nuclear forces charge symmetry test 80−5071
^{1}H(p,π^{+})^{2}H, NN pot., isobar configurations and π prod., inelastic cross sections 79−63666
^{1}H(π^{-},γ), effective range theory parameters a_{nn} and r_{nn} 79−85381
^{1}H(π^{-},$\gamma\gamma$)n, off-mass shell πN amplitude, $\pi^{0}\rightarrow\gamma\gamma$ amplitude, chiral Lagrangian model 79−93669
^{2}H, $^{3}S_1$-$^{3}D_1$ n-p state, mixing parameter energy depend. pot. description 77−82830
^{2}H breakup induced by 12.5 MeV protons, Ebenhoh code anal. 77−18547
^{2}H charge operator, retardation, quasipot. eqns. and rel. corrections 80−99122
^{2}H D-state probability measurability in meson exchange current theory, moments and RMS radius 79−89246
^{2}H, Δ(1236) inobar probability is nuclear many-body system ground state 79−75859
^{2}H, EM props. in relativistic one boson exchange model 79−67678
^{2}H magnetic moment due to two boson exchange, pseudovector πN coupling model 79−40843
^{2}H photo- and electrodisintegration, meson exchange current and isobar config. effects 79−71840
^{2}H photodisintegration depend. on NN potential, 10 to 180 MeV *(Russian)* 77−6350
^{2}H, quadrupole form factor and D-state probability 77−71571
^{2}H, quadrupole moment and percentage D state lower bounds 78−37286
^{2}H quadrupole moments, $^{3}S_1$-$^{3}D_1$ and $^{3}D_2$ states simple pot. model 78−78271
^{2}H radial functions, pionic exchange current contribs. to pp$\rightarrow$^{2}He$^{+}\nu_e$ 77−10329
^{2}H, repulsive nonlocal potl. models 77−88050
^{2}H, weak and EM lepton reactions, exchange currents, isobaric excitations and form factors *(German)* 79−93523
^{2}H+n scattering, 14.4 MeV, parity nonconserving asymm. 78−21449
^{2}H(d,t)^{1}H, differential cross sections calc. using DWBA, distortions 78−54772
^{2}H(e,e'), 56.4 MeV, cross sections, form factors, meson exchange current contrib. 80−68649
^{2}H(e,e'p), consistent nonrelativistic treatment including meson exchange currents and isobar configurations 79−40905
^{2}H(e,e), electric and mag. scatt., tensor polarisation, mesonic exchange current effects 79−85374
^{2}H(e,e), form factors, tensor pol., and two-nucleon force calcs. 80−106045
^{2}H(e,e), tensor polarisation and d wave function short range behaviour 79−67564
^{2}H(e,n)p EM sum rules, exchange currents and isobar configurations 79−93526
^{2}H(μ^{-}, ν)2n, axial meson exchange currents, a_{nn} and g_p extraction 79−97658
^{2}H(μ^{-}, ν)2n, hard pions and axial meson exchange current effects 79−40906
^{2}H(n, nn)p, 25 MeV, neutron-neutron effective range 80−83041
^{2}H(n,n), 10 MeV, differential cross section, (p,p) comparison for Coulomb force 79−71793
^{2}H(n,n), (n,p), 24 MeV, quasifree scatt., n-n effective range, Monte Carlo anal. 80−68554
^{2}H(n,nn)p, 21.5 MeV, cross section, nn effective range parameter 79−67669
^{2}H(p,2p)n, 45 MeV, sensitivity to various separable S-wave NN potentials 77−313
^{2}H(p,p), 10 MeV, differential cross section, (n,n) comparison for Coulomb force 79−71793
^{2}H(p,p), rank-1 pots. using shielded Coulomb pot., separable nuclear forces 79−71854
^{2}H(p,π^{+})^{3}H, NN pot., isobar configurations and π prod., inelastic cross sections 79−63666
^{2}H(p_0,p_1p_2)n, 156 MeV, test on p_1-n-p_2 colliniarity reson. 79−75996
^{2}H(π,2nγ), final state interactions, n+n scatt. parameters 78−25245
^{2}H(π,π_{-}) low energy scatt., Afnan-Thomas anal. with exclusion principle 79−75792
^{2}H(π,π), 140-260 MeV, (3,3) region, tensor force, cross sections, pol. parameters 80−68641
^{2}H(π,π), 47 MeV, differential elastic cross section 79−85530
^{2}H(π,π), comparison of Faddeev eqn. approach with optical potential 79−76030
^{2}H(π,π), elastic differential cross section, Faddeev calc. and π-absorption 79−75793
^{2}H(π,π), pion absorption effect from threshold to resonance 80−99193
^{2}H(π,π), relativistic description, πN waves, NN rescatt., ρ-exchange, π absorption and emission 80−9310
^{2}H(π,π), scatt. length, exchange current contrib. 80−78328
nuclear forces continued
^{2}H(π,π)^{2}H, 142 MeV, elastic cross section and polarisation observables 79−75791
^{2}H(π^{-}, n)n, mechanism, cross-sections, EM form factors 79−89181
^{2}H(π^{-},γn)n, effective range theory parameters a_{nn} and r_{nn} 79−85381
^{2}H(π^{-},nγ)n, multiple scatt. corrections, off-shell rescatt. effects, effective range 80−83127
^{2}H(π^{+}, p)p, pπ exchange current effects on pion absorption, cross section enhancement 80−57803
^{3}H, binding energies, three body calcs., Faddeev formalism, alpha cluster model 79−75876
^{3}H, binding energy, truncated t-matrix approx., trinucleon bound state problem 79−448
^{3}H binding energy calcs., soft core potentials 77−18378
^{3}H binding energy from 1-boson exchange, n-d and n-(pn)* momentum distribs. 79−67639
^{3}H bound state for Reid soft-core pot. perturbational exact calc., binding energy 79−63602
^{3}H charge form factor calc. with pair and recoil exchange currents 77−34238
^{3}H, D-state asymptotic normalisation const., Faddeev eqn. with Reid soft core pot. 79−59017
^{3}H, energy levels using ATMS method and realistic nuclear forces 80−22707
^{3}H, meson exchange currents, effect on charge form factors 80−105990
^{3}H ν-decay, ρ exchange current, weak axial vector current low energy theorem 79−40886
^{3}H, relativistic corrections to two-body pot., binding energy 78−74301
^{3}H Sussex interaction, g-matrix and variational calcs. 79−3091
^{3}H, three nucleon observables with meson theoretical interactions, binding energy, form factors 79−67676
$^{3}H_{\Lambda}$, and contrib. of spin forces to Λ-N interaction *(Russian)* 77−79319
$^{3}H_{\Lambda}$, short range repulsion, separation energy, K-harmonics calcs. 80−86846
^{3}H(p,γ), 30-100 MeV, meson exchange and nucleon correlation process calcs. 79−549
^{3}H$\rightarrow$n+d, s-wave asymptotic normalisation consts. in one-boson exchange model 80−37334
^{A}H, A=2,3, binding energy from Brillouin-Wigner perturbation method, strong short ranged interactions 80−86796
$_{\Lambda}^{3}$H, binding energy via rank-2, two-body pots. 77−26604
He, A=3,4, relativistic corrections to two-body pot., binding energy 78−74301
He neutron rich isotopes, reaction matrix calcs., stability 78−66225
^{3}He, binding energies, three body calcs., Faddeev formalism, alpha cluster model 79−75876
^{3}He bound state, perturbation approach with Reid soft core pot. 79−67675
^{3}He breakup induced by 156 MeV protons, pd final state interactions 77−23013
^{3}He, charge form factor, n+d collision anal. 77−18439
^{3}He charge form factor calc. with pair and recoil exchange currents 77−34238
^{3}He, charge form factor one-boson exchange pot. 78−41652
^{3}He, Coulomb energy, charge symmetry breaking 80−27564
^{3}He Coulomb energy, quasiparticle method 77−18416
^{3}He, meson exchange currents, effect on charge form factors 80−105990
^{3}He, one-boson exchange pot. 78−41652
^{3}He, photonucl. sum rules 79−6427
^{3}He, trinucleon bound state problem, binding energy, form factors and mag. moment 80−22710
^{3}He-^{3}H binding energy difference, Coulomb energy contribution 79−491
^{3}He-^{3}H Coulomb energy difference and charge dependent three-body force 79−45181
^{3}He-^{3}H nuclei; charge asymmetric energy using different OBEP models 78−70372
^{3}He^{3}Hπ coupling constant, determ. from forward dispersion relations 78−58307
^{3}He(^{3}He,^{2}Hνe^{+})^{4}He, 11.5 MeV, search for high energy deuterons 79−76012
^{3}He(e,e'p), cross-section, Fadeev technique, nucleon-nucleon interaction *(Russian)* 80−73842
^{3}He(γ,π^{+})^{3}H, exchange current effects, two body processes 79−71839
^{3}He(p(polarised),p)^{3}He, nuclear force and T-violation effects 78−4797
^{3}He(π,π), 1 GeV, backward scatt., nonstable meson-nucleon interaction cross section, resonance *(Russian)* 80−68559
^{3}He(π,π), 145, 180, 195 MeV, differential cross section, mesonic exchange effects, form factors, optical pot. 79−85376
^{4}He, binding energy, truncated t-matrix approx., trinucleon bound state problem 79−448
^{4}He, effects of three body force on energy levels 78−54692
^{4}He, energy levels using ATMS method and realistic nuclear forces 80−22707
^{4}He, four-nucleon bound state with realistic NN interaction, hyperspherical harmonics *(Russian)* 80−83045
^{4}He, magic nucleus, nonlocal pots., binding energies 77−41877
^{4}He, N*-^{3}H configurations 79−17822
^{4}He, pion exchange currents and charge form factors, shell model anal. 77−10338
^{4}He, saturating effect of N*(1234) on binding 78−58231
^{4}He, soft-core radial wave function, photo-disintegration calculation 80−18209
^{4}He structure based on realistic two- and three-body interactions 77−18417
^{4}He, TRK dipole sum rule reevaluation including isobar effects 78−66221
^{4}He-^{4}He effective interaction, energy density formalism *(Russian)* 77−46119
^{4}He-$\bar{p}$, X-ray spectrum, energies and relative intensities for 3d and 2p levels 78−70979
^{4}He+α break-up reactions, 130 MeV, continuous energy spectra of emitted particles 79−76013
^{4}He(d,d), noncentral forces, Pauli principle effects on d polarisation, orthogonality condition model 79−6614
^{4}He(e,e), cross section anal., nuclear charge form factor, short range correl. 78−8746
^{4}He(p,d), intermediate energies, pion exchange currents in DWBA anal. 80−32199
^{4}He(p,d) pickup reaction, isobar configurations and short range correlations 80−22798

nuclear forces continued
^{4}He(π,π), low energy, first order optical pot., Pauli principle corrections, nuclear binding 80−27675
^{5}He, effective 3- and 4-body forces in 5 nucleon system 79−477
^{6}He$_{\Lambda\Lambda}$, short range repulsion, separation energy, K-harmonics calcs. 80−86846
^{6}He$_{\Lambda\Lambda}$ hyperfragment, $\alpha\Lambda\Lambda$ model, Faddeev formalism, two-body local potentials 77−18467
^{A}He, A=3,4, EM form factors and structure at large momentum transfer 79−67710
$_{\Lambda}{}^{4}$He-$_{\Lambda}{}^{4}$H binding energy difference, particle mixing and charge asymmetric ΛN forces 79−75891
$_{\Lambda}{}^{4}$He-$_{\Lambda}{}^{4}$H separation energy difference, Coulomb energy contribution 79−491
$_{\Lambda}{}^{5}$He, Λ-particle induced excitation probability, ang. pot. functions method *(Russian)* 79−26389
^{175}Hf, three- and five-quasiparticle isomers, rotational bands and residual interactions from ^{170}Er(^{9}Be, 4n) 80−83022
I, 123≤A≤133, coupled quadrupole model, spectra, B(E2), B(M1), moments calcs. 77−82837
^{123}I, bands and decay props., core-particle coupling and polarisation effects 80−13354
^{39}K(^{39}K,X), π^{0} condensation, spin-isospin instabilities, TDHF calcs. 80−83042
^{5}Li, effective 3- and 4-body forces in 5 nucleon system 79−477
^{6}Li, binding energies, three body calcs., Faddeev formalism, alpha cluster model 79−75876
^{6}Li excited states, final state interactions, three-body force effects from ^{2}H(α,αp) 80−57692
^{6}Li ground state, separable pot. three body model 78−50090
^{6}Li, hyperspherical L_{m} approx., interaction including Majorana exchange operator 78−74311
^{6}Li+α system, exchange effects, resonating-group study 80−9240
^{6}Li(^{3}He, ^{3}He^{3}He)^{3}H, 132 MeV, quasifree scatt., ^{3}He-^{3}He two body cross sections 79−76011
^{7}Li, non-central forces and spectrum *(Russian)* 79−89243
Mo even isotopes, HFB calc. of deform. due to isoscalar n-p interaction 78−74302
NN̄ potential from baryonium data, spin forces and radiative decay widths 79−45175
^{2}N breakup, nucleon induced, NN interaction parameters 77−18550
^{14}N 1^{+} state cross sections, effective two nucleon interaction, isovector tensor component from ^{14}C(p,n) 80−18208
^{14}N$_{g.s.}$ partial muon capture, mesonic exchange currents, weak process microscopic treatment 80−57742
^{14}N(p,n), 144 MeV, one pion exchange and PCAC expt. test 80−528
^{14}N(p,p′), 122 MeV, level excitation, cross sections, effective NN interaction, DWIA anal. 80−78197
^{14}N(p,p′), 25-40 MeV, level cross sections, optical parameters, DWBA anal., tensor effective interaction 80−68555
^{15}N(^{15}N,X), π^{0} condensation, spin-isospin instabilities, TDHF calcs. 80−83042
^{15}N(p,γ), 30-100 MeV, meson exchange and nucleon correlation process calcs. 79−549
^{15}N(π^{+}, π^{0})^{15}O, isobar hole model calc. of single charge exchange 79−85523
^{16}N(0^{-})→^{16}O(0^{+})+$\bar{\nu}$e+e^{-}, one pion exchange current problem for ^{16}O(0^{+})⇄^{16}N(0^{-}) 79−85375
N*(1236) propagator, momentum depend. in N*-excitation current 80−27559
^{22}Na, effective interactions for dominant shell-model configurations: ds-shell example 80−32204
^{20}Ne hexadecapole moments, quadrupole deformation effects, E4 effective charge, valence polarisation 80−78142
^{20}Ne, nuclear current from cranked HF solns. 80−9241
^{20}Ne, rotational moment of inertia, cranked HF formalism with Skyrme force 77−30477
^{21}Ne, energy moments, sd shell realistic effective interactions, shell model spectra 80−18190
^{21}Ne, parity-nonconserving nucleon-nucleon pot., large parity admixtures 78−82278
Ni, A=58, 60, 62, 64, 66, Lipkin-Nogami method, ground state props. 78−50103
Ni isotopes, pairing-plus-quadrupole interaction anal. 77−79313
O Hartree Fock pot., truncated space calcs. of exact bound state energies 79−3090
^{14}O$_{g.s.}$ β-decay, mesonic exchange currents, weak process microscopic treatment 80−57742
^{15}O, axial vector decay, exchange corrections 79−36201
^{16}O, 3 α forces, ground state energy and form factor 80−86817
^{16}O, α-cluster model, clustering and nuclear forces in terms of quark struct. 79−6443
^{16}O, bound isobars Δ(1236), single particle energies, wave functions *(Chinese)* 80−52562
^{16}O, Δ(1236) inobar probability is nuclear many-body system ground state 79−75859
^{16}O, Δ(3,3) excitations and effective 3-nucleon forces 80−27561
^{16}O, giant isoscalar monopole state energies in generator coordinate method 80−37317
^{16}O ground-state energy, nonunitary model operator approach 80−83030
^{16}O, Hartree-Fock calculations of nuclear bulk properties with density- and starting-energy dependent effective interaction 80−9246
^{16}O, magic nucleus, nonlocal pots., binding energies 77−41877
^{16}O, mesonic and isobar degrees of freedom, Brueckner Hartree Fock calc., binding energy 79−63600
^{16}O, pion condensation and short range correlation 77−6245
^{16}O, pion condensation effects, RPA calcs. *(Chinese)* 80−47407
^{16}O, pion exchange currents and charge form factors, shell model anal. 77−10338
^{16}O region, effect operators, number conserving set generalisation 80−42555
^{16}O, relativistic Hartree-Fock eqns., 1 boson exchange pot., spin orbit splitting 79−3106
^{16}O, saturating effect of N*(1234) on binding 78−58231
^{16}O+^{12}C, isobar total prod. cross-sections, target giant reson. excitation 79−85429
^{16}O+^{16}O, nucleon-nucleon forces and heavy-ion potentials 79−6657
^{16}O+^{16}O collisions, resonating group study, effective two-nucleon forces 79−59044
^{16}O+light ion scatt., exchange Coulomb kernel in resonating group formulation 79−6531

nuclear forces continued
^{16}O+μ, total muon capture rate, Skyrme forces, closure approx., sum rule technique 78−54742
^{16}O(0^{+})⇄^{16}N(0^{-}), beta decay and muon capture rate ratio, mesonic exchange currents 80−42594
^{16}O(0^{+})⇄^{16}N(0^{-}), nucl. wave functions and mesonic exchange currents 79−40887
^{16}O(γ, p), 300 to 900 MeV/c, p-shell momentum distrib. calc. 78−50151
^{16}O(γ,π), total cross section, Δ-hole states damping, π^{0},ρ exchange, Δ isobar hole model 80−91174
^{16}O(μ,γ), exclusive radiative capture, axial currents and induced pseudoscalar form factors 79−97699
^{16}O(π,2N), bound 2p pion absorpt., microscopic description, NN correls. 78−94030
^{17}O, third-order treatment of the one-body effective interaction 79−67670
^{17}O valence energies, extended multiple scatt. approach to 2p1h system 78−29396
^{18}O, effective interaction, nonlocal pot. reaction matrix free scatt., spectra 77−46122
^{18}O, effective interaction, Hartree-Fock effects 78−534
^{18}O, spurious centre of mass effects, effects on microscopic nuclear effective interactions 78−82292
^{18}O($\pi^{\pm}$,$\pi^{\pm}$′) ^{18}O(2^{+}), DWIA anal. with microscopic form factors, effective charges 79−85549
^{22}O, Hartree-Fock calculations of nuclear bulk properties with density- and starting-energy dependent effective interaction 80−9246
^{206}Pb, effect of renormalisation of effective interaction on ground state wave functions *(Russian)* 77−284
^{207}Pb(e,e), magnetisation distrib. from elastic mag. form factors, core polarisation, exchange currents 80−47372
^{208}Pb core with valence nucleon or hole, mag. props., exchange currents, electron scatt. 80−22689
^{208}Pb, mode coupling theory for two particle-two hole states 77−6214
^{208}Pb region, effective interaction and energy spectra 78−25121
^{208}Pb, shell-model interaction for neutron hole states 77−18446
^{208}Pb, Thomas-Fermi model 78−8747
^{208}Pb(^{208}Pb, X), giant resonance polarisation pots. from nucleus-nucleus effective pot. 80−78248
^{208}Pb(^{3}He,d), 30 MeV, effective residual interaction matrix elements, spectroscopic factors, cross sections 80−99134
^{208}Pb(α,t), 40 MeV, effective residual interaction matrix elements, spectroscopic factors, cross sections 80−99134
^{208}Pb(p,p′), precritical behaviour in pionlike excited states in nuclear matter 79−49593
^{210}Po, effect of renormalisation of effective interaction on ground state wave functions *(Russian)* 77−284
pp bremsstrahlung, intermediate nucleon isobars contrib., relativistic model, nuclear force significance 78−93899
^{32}S, nucl. saturation props. 79−6395
^{28}Si, spin cutoff factors, sd shell realistic effective interactions, shell model spectra 80−18190
^{28}Si(e,e′), 6^{-} T=1 resonance form factor, mag. strength quenching, meson exchange currents 80−86882
^{150}Sm deformation, collective spectra and moments of inertia starting from nuclear force 79−17790
^{154}Sm, Skyrme-HF calcs., deformation, electric moments, spin-orbit potentials 78−62480
Sn, extended Skyrme force calculation, spin instability 79−63601
^{93}Tc, J=17/2 doublet, parity mixing, weak NN interaction 80−73791
Te, even isotopes, effect of residual interaction in particle-particle channel on low-lying states 78−21503
Ti even isotopes, deformed nuclei in Lipkin-Nogami approach, Kuo Brown effective interaction 79−59006
^{48}Ti, (A+2)particles-2 holes excitations, interaction renormalisation 78−29375
^{49}Ti(e,e), cross section, $1f_{1/2}$ neutron orbit radial distrib. 79−93541
^{A}U, A=232, 234, 236, octupole-octupole residual interactions and low lying 0^{+} excited states 79−36136
^{238}U(d,d)^{238}U, 17 MeV elastic and inelastic scatt., nuclear-Coulomb interf., optical pot. 77−79389
Zn, A=60, 62, 64, 66, 68, Lipkin-Nogami method, ground state props. 78−50103

nuclear fusion
see also nuclear explosions; nuclear reactions involving few nucleon systems
1p and 2s1d shell nuclei, fusion cross sections, entrance channel versus compound nucleus limitations 80−78343
α-induced, γ-ray spectra calcs. 79−36291
A=70, heavy-ion induced fission-evaporation reactions, magnetic substrate distribs., nuclear alignment 80−73857
absorption effects in low energy heavy ion fusion reactions 78−8851
activation calc. and exptl. comparison for 14 MeV neutron source, fusion technique validation 79−9657
amorphous state analogy 79−54370
basic concepts involved in fusion processes 77−34451
chain reactions, kinetics, high electron temps., interactions with D-T plasma 80−68945
charge and slope polarisation of nuclei, liquid drop model anal. 79−9543
classical model, empirical nucleus-nucleus potl. 77−74870
cohesion of nuclear matter in heavy ion collisions 78−66314
complete fusion anal. for heavy ion reactions 79−49643
complete fusion excitation functions, systematic semiempirical anal. with modified proximity pot. 79−6720
complete fusion in heavy-ion collisions 80−37400
complete fusion systems, barrier penetration, enhanced fusion-fission yields 80−13520
composite nucleus scission, fusion and strongly damped collisions, rot. energy, boundary diffuseness 80−102224
compound nucleus, relatively cool, with high ang. momentum, production *(Russian)* 78−29519
compound nucleus formation cross section in heavy ion reactions, shell model calcs. 78−13132
compound nucleus reaction, superheavy element prod. method optimisation 78−46103
conference on heavy ion reaction dynamical props., Johannesburg, S.Africa (Aug. 78) 80−17715
conference on nuclear interactions, Canberra, Australia (Aug.-Sep. 1978) 80−4476

nuclear fusion continued
conference on nuclear physics, Mikolajki, Poland (2-14 Sept. 1979) 80−101662
controlled, present state and future prospects *(German)* 77−18692
controlled fusion research and the Joint European Torus project 80−18593
controlled thermonuclear fusion, contemporary state of research 79−680
cryogenic techniques development *(French)* 79−93677
deformation energies for nuclei with different charge-to-mass ratio for fusion or binary fragmentation 79−80869
deformed nuclei fusion reactions, γ-multiplicities, collective and statistical γ-rays Monte Carlo calcs. 79−578
electron beam heated solenoid reactors appl. 78−8992
electron screening effect, quantum theory for relativistic electron plasma *(Russian)* 77−17350
elementary reactions in plasma fusion, diffusion, contamination bremsstrahlung and electrostatic forces *(German)* 79−46429
energy generation appl., prospects 77−38399
energy option, recent developments 79−36416
exothermal nuclear reactions, quark catalysis 79−30873
focus plasma, CO_2 laser irradiated, neutron yield enhancement 77−62386
fragmentation theory, two body breakup channels in fission, fusion, heavy ion scatt. 78−46037
fusion power prospects in Soviet Union 77−67868
gas cell target for studying fusion and damped collisions of light nuclei 79−76250
heavy ion, critical angular momentum, phenomenological approach 78−33203
heavy ion, fusion barrier at sub-Coulomb energies 78−628
heavy ion, schematic classification of nuclear processes *(Rumanian)* 78−58313
heavy ion+nucleus, fusion cross section at sub-Coulomb energies, effective pot. barrier 78−58314
heavy ion collisions, classical microscopic description of particle cluster collisions 79−9533
heavy ion collisions, complete fusion cross sections, compound nucleus props. *(French)* 79−577
heavy ion collisions, resonance states in two-body breakup channels, theory of fragmentation 79−9619
heavy ion deep inelastic reactions, as probes of nuclear matter, review 78−46083
heavy ion dynamical props. from coupled channels calcs. total, direct and fusion cross sections 79−67772
heavy ion fusion, evaporation model breakdown, preequilibrium α emission 78−89927
heavy ion fusion, expt. data comparison with classical trajectory models, review 80−9324
heavy ion fusion, internuclear potential determ. 78−41800
heavy ion fusion, sensitivity to friction form factor, dissipative and conservative properties 79−67807
heavy ion fusion and damped reactions, rolling friction, nuclear pots., classical trajectories 80−78312
heavy ion fusion and deep inelastic scatt., shape degrees of freedom, classical dynamic model 80−22876
heavy ion fusion and transfer reactions, resonance effects 80−9283
heavy ion fusion barrier, penetrability calc. 78−41798
heavy ion fusion cross section, energy depend., nuclear matter density distrib., depend. 80−47519
heavy ion fusion reaction excitation function anal., nucleus-nucleus pots. 80−42728
heavy ion fusion reactions, charge density asymmetry liquid drop model 80−63220
heavy ion fusion reactions, statistical model calcs. 80−42726
heavy ion fusion reactions, statistical yrast line 80−86948
heavy ion fusion reactions in fragmentation theory 77−54239
heavy ion induced, fusion cross sections 80−86913
heavy ion induced fusion, yrast lines versus entrance channel limitation 78−89929
heavy ion induced reactions, information from γ-spectroscopy *(Rumanian)* 78−58300
heavy ion reactions, DWBA anal. 78−13143
heavy ion reactions, potential energy surface topography 77−330
heavy ion reactions, potential energy surfaces, binary fission, fusion, liquid drop model *(Rumanian)* 78−86547
heavy ion reacts., cross-sections for fusion, quasifission and deep inelastic collisions *(Russian)* 78−54801
heavy ion-nucleus collisions, friction model 78−86546
heavy-ion collision, fusion barriers calc. 78−25225
heavy-ion compound nucleus reaction 77−14173
heavy-ion deep inelastic collisions, classical model with friction and deformation 77−30633
heavy-ion fusion excitation functions, dynamical model, one-body friction 78−50224
heavy-ion induced fusion evaporation react., nucl. lifetime meas. by γ-γ coincidence techniques 79−59318
heavy-ion induced fusion reaction products, statistical and liquid drop model anal. 78−66312
heavy-ion induced fusion-evaporation, phenomenological restrictions for spin alignment attenuation factors 77−57686
heavy-ion reaction, fusion channel separation *(Russian)* 77−74880
heavy-ion reactions, collective pot. energy surfaces, appl. to Ar+Ag, Kr+Cu, and Xe+Bi 78−41748
heavy-ion static adiabatic cluster pots., K-matrix model 77−3033
high angular momentum fusion compound nucleus deexcitation, high spin states, rare earths 80−9259
idealized, one-body dissipation, general classical theory, quantal corrections 78−86494
inertia confinement, expt. *(Japanese)* 78−46121
inertial confinement fusion energy with particle beams 77−83074
inertial fusion, systems anal. of accelerator and storage ring systems 77−83474
influence of shell effect in nuclear level densities on compound nucleus decay 79−40979
ion+electron, energy transfer term in rate eqn., fusion targets 80−5331
ion-ion proximity pot. radial depend. test using fusion excitation functions 80−22859
laser, CO_2 laser systems development 79−49859
laser, for electrical power generation 77−26867
laser, Nova scientific feasibility experiment 79−49863
nuclear fusion continued
laser beam-plasma interaction, in mag. field, breakdown, heating, trapping, fusion, diagnostics, book contrib. 77−51196
laser fusion expt. using 4π illumination system 78−58312
laser fusion prod. of H by radiolytic-thermochem. cycles 80−45811
laser induced, X-ray diagnostics appl., review 77−55176
laser technique using H-B reaction, research in Australia 79−3234
laser thermonuclear fusion, review 77−34449
laser thermonuclear power plant, conceptual design study 80−78441
laser-fusion expts., calorimeters for meas. of ions, X-rays and scatt. radiation 78−16800
light heavy ion collision, resonant and non-resonant behaviour of complete fusion cross-sections 79−9625
light heavy ion induced fusion, cross sections and yrast line limitations 80−5192
light heavy-ion systems, fusion cross section variations, nuclear proximity pot. 80−57815
magnetic, 1978 status, expt. results survey 79−49864
magnetic containment testing for JET 78−54870
magnetic mirror experiments, measuring MeV ions from fusion reactions 80−6281
mass asymmetry due to valley fragmentation 77−71616
mean field theory of nuclear dynamics, time depend. 78−12986
micro-explosions, electron beams initiated, progress and future applicability *(French)* 78−746
microexplosion ignition, magnetically insulated foil accel. to ultrahigh vel. 77−65327
microfusion, reflection coefficients of stationary shock waves on rigid wall for profiled pressure 78−51303
microwaves appl., economic and safety aspects 80−3754
Migma IV high energy fusion apparatus 77−83075
miniexplosion, critical masses in fission-fusion hybrid systems 77−3158
muon catalysed fusion and hydrogenic mesomolecules 80−68719
muon catalysed fusion in cold H, new development *(German)* 79−67805
neo-Z-pinch, mag. fusion appls. 80−103180
neutron generation by implosion of D_2 gas target 78−54869
neutron stars, nuclear fusion and C flashes 78−93293
neutron weapons, physical and military problems *(Norwegian)* 79−81091
nuclear astrophysics, introduction to form. and evolution of matter in Universe, book 80−105447
nucleus-nucleus potential test using fusion excitation functions 78−50204
pellet fusion by high energy heavy ions 77−83354
plasma physics research, in USSR, superconducting magnet system appls. *(Slovak)* 78−87474
plasma simulation with parallel pipeline programming 79−68947
power, state-of-the-art and problems to be overcome *(Dutch)* 80−37574
power engineering developments review 79−3240
power generation by thermonuclear reactions 77−65330
power prod. in reactors, and astrophys. appl. *(Norwegian)* 79−30872
probability games, modelling stellar evolution and fusion 80−77590
promptly emitted particles in nuclear collisions, fusion nucleon spectra 80−42678
reaction rate enhancement due to strong screening 78−13186
relativistic heavy ion accelerator description and applications *(German)* 78−78522
research, appl. as future energy resource, review 79−49839
resonant thermonuclear reaction rate integrals, closed-form evaluation and approximation considerations 80−8535
review, worldwide variation of energy production, future Hungarian energy requirements *(Hungarian)* 78−70580
shell model level densities in evaporation calculations 79−45241
social aspects *(Dutch)* 80−106153
solar interior, ν-less fusion process, model based on composite neutron model n=p+φ meson 79−8898
static model of complete fission 78−86543
stellar evolved C cores, nuclear energy generation rates and energy dissipation 80−82339
stellar interiors, high energy particle excess, effect on secondary reaction rates *(Russian)* 80−77393
stellar interiors, thermonuclear reaction rate enhancement due to strong screening, ionic mixtures case 80−36613
subcoulomb fusion, effective barrier at low energies, total reaction cross section 78−37385
superconductor coils appls., based on Nb-Ti *(French)* 80−95399
superheavy element synthesis in fusion reactions, failure 79−45317
switch for mag. cct. supply *(German)* 78−37441
technology development in France and UK, review 77−18695
thermonuclear fusion plasmas, elem. processses and role of atomic, ionic and mol. data 80−14916
thermonuclear power plants, problems and perspectives *(Polish)* 78−54876
thermonuclear react. rates, computation with STEEP code 78−18375
thermonuclear reaction rate, parameter-depend. integral evaluation 79−29985
thermonuclear reaction rate data for intermediate mass nuclei 80−31427
thermonuclear reaction rates, thick target meas. 80−73108
thermonuclear reactions, laser compressed, thermalising and electrodynamic coupling 77−11374
thick target meas. technique for reaction rate determ. 77−23392
time-dependent variational approach to heavy ion reactions, appl. to fusion 78−50193
Tokamak, PLT, beam-heated, neutron emission profiles 78−63588
Tokamak devices, power supplies *(Dutch)* 78−741
two spherical nuclei system, pot. energy calcs. for fission and fusion 79−13326
underground fusion explosion, use as geothermal energy source 78−46176
unified nuclear pot. for heavy ion elastic scatt., fission, fusion, masses and deformations 80−5189
unified pot. from liquid drop model, description of nuclear props. 79−22213
p-xylene, plasma polymerised, as laser fusion target 78−88431
Z=103, 105, 107 element prod. from heavy ion fusion, cross sections from statistical model 80−32313
(α,X), complete fusion barrier and evaporation from ^{194}Hg 80−68715
(α,xnγ), rare earth nuclei, complete fusion process n and γ multiplicity 80−18363
d-d neutral beam facility neutron yield meas., shielding and diagnostics 79−9878
(p,X), complete fusion barrier and evaporation from ^{194}Hg 80−68715

nuclear fusion continued
(p,xnγ), rare earth nuclei, complete fusion process n and γ multiplicity 80−18363
pp→Dev, in Sun, exchange current contrib. *(Russian)* 78−93195
pp reaction, exchange current corrections π and ρ exchange 80−26733
ppe→Dν, in Sun, exchange current contrib. *(Russian)* 78−93195
Ag+^{20}Ne, 175 MeV, γ-ray multiplicities and energies, primary fragment angular momenta 78−46093
^{109}Ag+^{40}Ar, fusion excitation functions, dynamical model calc. 78−50224
^{109}Ag+^{86}Kr, 366-716 MeV, evaporation residue product cross sections 79−17947
^{27}Al+^{12}C, complete fusion cross sections, excitation functions *(Chinese)* 78−82406
^{27}Al+^{14}N or ^{16}O, high spin states prod in ^{35,36,37}Cl and ^{37}Ar, decay schemes 77−2932
^{27}Al+^{16,18}O, 34-81 MeV, total fusion-evaporation cross sections, fusion barrier 80−5190
^{27}Al+^{16}O, 60-80 MeV, fusion cross-sections 77−74898
^{27}Al+^{16}O, fusion cross section calc. in boundary condition model 79−9656
^{27}Al+^{16}O, fusion excitation functions, dynamical model calc. 78−50224
^{27}Al+^{16}O fusion, 30-70 MeV, statistical model calcs., yrast states and continuum feeding times 79−579
^{27}Al+^{20}Ne, 120 MeV, strongly damped collisions 77−34332
^{27}Al(^{15}N,X), 27-70 MeV, complete fusion, total fusion cross section, entrance channel effects 80−68716
^{27}Al(^{16}O,X), 88 MeV, inelastic scatt. and multinucleon transfer, Q-value depend. 80−42690
^{27}Al(^{28}Si,Xγ), 65-81 MeV, fusion evaporation products, reaction cross sections 79−17946
^{243}Am(^{49}Ca,xn), production of superheavy elements with A=114-116 78−29493
^{40}Ar+^{243}Am, 214-300 MeV, fusion-fission reaction, asymm. mass distrib. 77−82963
Au(Ar,X), 227 MeV, ang. momentum transfer in deep inelastic collisions 79−45281
Au(^{63}Cu,X), 365 and 443 MeV, ang. momentum transfer in deep inelastic collisions 79−45281
^{197}Au+^{40}Ar, 217 MeV, fusion and deep inelastic collision, charge and mass anal. 77−82959
^{197}Au+Ar, 183-248 MeV, fusion and deep inleastic collision, influence of bombarding energy 77−82958
^{197}Au(^{14}N, xn), in flight mass separation of Rn isotopes 78−25381
^{197}Au(^{16}O,X), colliding heavy ion interface, nucleon emission, fusion and strongly damped collisions 80−86922
^{197}Au(^{40}Ar,X), 222, 340 MeV, fusion cross sections, direct and evaporative p and α prod., evaporation, fission 80−13518
^{197}Au(HI,X), 60-120 MeV complete fusion cross sections from fission fragment ang. distrib. 80−13516
B_xH_y compounds, doubly-isotopic, laser driven nuclear fusion, energy release 78−78499
^{10}B+^{10}B, fusion below Coulomb barrier, quantum mechanical barrier penetration model anal. 80−18361
^{10}B(^{14}N,X), 2.9-7.5 MeV, evaporation residue and total fusion cross section 79−22348
^{11}B+^{10,11}B, fusion below Coulomb barrier, quantum mechanical barrier penetration model anal. 80−18361
^{11}B+p→^{4}He+^{8}Be→3(^{4}He) fusion power feasibility 77−38310
^{11}B+p→3 ^{4}He+6.8 MeV, calcs. of use in fusion reactor 77−83092
^{11}B(p,2α)α, reaction characts., potentiality for controlled thermonuclear fusion 77−30667
^{12}B+^{16}O→^{16}Al, fusion cross section comparison to ^{12}Cr^{14}N→^{26}Al 79−71873
^{134}Ba+^{16}O, compound nucleus, ^{150}Gd, deexcitation, evaporation calcs. comparison with exptl. decay data 77−61391
^{134}Ba+^{16}O, formation and decay of ^{150}Gd compound nucleus 77−61453
^{9}Be+^{12}C, 2.8-6.3 MeV, fusion and neutron transfer cross-sections 78−41746
^{9}Be+^{16}O, 2 to 5.1 MeV, sub barrier, cross sections and optical model calcs. 78−8838
^{9}Be(^{18}O,X), 1.8-6.7 MeV, total fusion and transfer cross sections ^{19}O, ^{21,22,23}Ne, ^{24,25}Na, ^{25}Mg prod. 80−91205
^{209}Bi+^{12}C, complete fusion cross sections, excitation functions *(Chinese)* 78−82406
^{209}Bi(^{48}Ca, X), fusion reactions from Cf and Fm integral yields, statistical model anal. *(Russian)* 79−97740
^{209}Bi(^{84}Kr, X), TDHF fusion calcs., fusion cross sections 80−37409
^{209}Bi(HI,X), 60-120 MeV complete fusion cross sections from fission fragment ang. distrib. 80−13516
C degenerate core thermonuclear reaction propag., neutrino mech. *(Russian)* 79−5812
(^{12}C,X), A=12-19, total fusion cross sections and fusion barrier parameters 80−9322
^{12}C-^{12}C scattering, fusion cross-section, folding model study, coupled channel effects 78−89893
^{12}C+^{10,11}B, fusion below Coulomb barrier, quantum mechanical barrier penetration model anal. 80−18361
^{12}C+^{10,11}B, sub Coulomb energy, fusion cross sections, elastic scatt., optical model anal. 77−34335
^{12}C+^{12}C, 2.5 to 6.2 MeV, γ-ray transitions and cross-section fluctuations 77−30628
^{12}C+^{12}C, 3.2-64 MeV/nucleon, time-depend. HF calcs. 77−3034
^{12}C+^{12}C, diffuse surface nuclear and Coulomb pot. energies 77−18593
^{12}C+^{12}C, fusion reactions, Woods Saxon, folding and proximity pot. anals. 79−45316
^{12}C+^{12}C, partial widths of molecular resonances 78−46094
^{12}C+^{12}C scatt. and fusion cross sections above Coulomb barrier, folding model, resonances 79−6687
^{12}C+^{12}C subCoulomb fusion cross-section, 6.5-12 MeV 77−50151
^{12}C+^{12}C system, inelastic scatt. and fusion cross section, folding model, resonances 79−13337
^{12}C+^{14}N fusion, 248 MeV, cross-section meas. liquid-drop limit for ^{26}Al 78−4959
^{12}C+^{16}O, 8.5-12.9 MeV, oscills. in excitation function for complete fusion 77−3037
^{12}C+^{16}O complete fusion, partial prod. cross section for nuclides, evaporation model calcs. 79−36294
^{12}C+^{18}O, excitation functions for dominant fusion channels 7 to 25 MeV, obs. of regular gross struct. 79−36293
^{12}C+^{9}Be, 11.4 MeV cm energy, p, d, t, α production 80−9302

nuclear fusion continued
^{12}C(^{12}C,X), 14-31 MeV, total and fusion cross sections, ^{24}Mg ground state band 80−42727
^{12}C(^{12}C,X), 27-60 MeV, evaporation residue cross sections from complete fusion, statistical anal. 79−13369
^{12}C(^{12}C,X) fusion cross section oscillations, overlapping compound states availability 80−9321
^{12}C(^{14}N,X), 27-60 MeV, evaporation residue cross sections from complete fusion, statistical anal. 79−13369
^{12}C(^{15}N,X), 27-60 MeV, evaporation residue cross sections from complete fusion, statistical anal. 79−13369
^{12}C(^{16}O,^{16}O)^{12}C, 15.4 to 30.9 MeV, correlation between fusion and inelastic scatt. 78−66310
^{12}C(^{16}O,X) 10.5-23.3 MeV, low energy fusion cross sections 77−14152
^{13}C+^{16}O, excitation functions for dominant fusion channels 7 to 25 MeV, obs. of regular gross struct. 79−36293
^{13}C(^{13}C,^{24}Mg), 3.05-6.88 MeV, fusion cross section energy depend., optical anal. 80−42724
^{A}Ca(α,X), 10-27 MeV, A=40,44, fusion cross sections, anomalous large angle scatt. 79−80966
^{40}Ca+^{16}O, 45-63 MeV, excitation function determ. 78−82404
^{40}Ca+^{40}Ca, 2- and 3-dimens. time depend. HF calc. comparison 79−17948
^{40}Ca+^{40}Ca, 278 MeV, comparison of 2-D and 3-D TDHF 78−82386
^{40}Ca+^{40}Ca, 3-dimens., time depend. HF calcs. for fusion cross sections 78−66318
^{40}Ca+^{40}Ca, evaporation-residue cross-sections meas. 78−33211
^{40}Ca+^{40}Ca, low impact parameters, energy dependence of fusion cross section 78−41751
^{40}Ca+^{40}Ca, total fusion cross section, time depend. HF calcs. 79−17945
^{40}Ca(^{16}O,X), 36-75 MeV, absolute and fusion total cross sections, ^{56}Ni excitation functions 80−18362
^{40}Ca(^{16}O,X), 40-214 MeV, fusion and elastic scatt. cross sections, optical anal. 80−32314
^{40}Ca(^{20}Ne,X), 44.1-70.4 MeV, fusion and elastic scatt. cross sections, evaporation residues 80−550
^{48}Ca+^{15}N(^{18}O) fusion-evaporation reaction, ^{59,60}Fe, ^{59,60}Co yrast decay scheme 78−13154
^{48}Ca+heavy ion fusion evaporation reacts., yrast decay schemes 78−66308
^{48}Ca(^{248}Cm, 2n)^{294}X$_{116}$, super-heavy elements prod. at barrier energies 79−13368
^{48}Ca(p, γ)^{49}Sc, 0.6-2.7 MeV, cross sections and thermonuclear reaction rates, Hauser-Feshbach calcs. 79−36239
^{48}Ca(p, n)^{48}Sc, 0.95-2.7 MeV, cross sections and thermonuclear reaction rates, Hauser-Feshbach calcs. 79−36239
^{35}Cl induced reactions, targets A=27-124, 70-170 MeV, fusion and interaction barrier parameters, critical angular momenta 77−10428
^{35}Cl+^{24,25,20}Mg(^{27}Al)(^{28}Si), 100-70 MeV, mass systematics of evaporation residues 77−38311
Cm(^{48}Ca,xn), production of superheavy elements with A=114-116 78−29493
^{248}Cm+^{48}Ca superheavy element prod., radiochem. separation 78−74390
^{12}Cr+^{14}N→^{26}Al, fusion cross section comparison to ^{10}B+^{16}O→^{26}Al 79−71873
^{52}Cr+^{12}C, 56 MeV, heavy ion fusion, evaporation model breakdown, preequilibrium α emission from ^{64}Zn 78−89927
^{65}Cu+^{86}Kr, 366-716 MeV, evaporation residue product cross sections mass-charge distrib. 79−17947
^{65}Cu(^{63}Cu, X) fusion, 55-105 Mev, evaporation residue excitation functions 79−63710
D-D fusion reactor, heliotron *(Japanese)* 78−54878
D-T, muon catalysed fusion for pellet ignition 77−3063
D-T compression, explosion-induced, cylindrical system with heavy inertial layer, neutron yield 80−68944
D-T fusion, energy deposition, damage and neutronics data 77−26880
D-T layer implosion through nonhomogeneous transition layer 78−74465
D-T thermonuclear plasma, neutron collision diagnostics *(Russian)* 77−34471
D+T→He^4+n+17.6 MeV, possibility of using U$^+$ accelerated ions *(Norwegian)* 79−30871
D(^{6}Li)-T, inertially-confined, high thermonucl. gain with low T inventory 78−58403
DT microspheres, laser fusion, 4 TW system, n and α meas. 78−74471
DT:^{239}Pu plasma, neutron induced fission, fusion enhancement 79−71946
D(d,n)^{3}He, fusion cross sections and thermonuclear reaction rates 80−533
D(d,p)T, fusion cross sections and thermonuclear reaction rates 80−533
^{147}Dy charge states and charge distrib. from ^{113}Cd(^{40}Ar,6n) *(Russian)* 79−40840
^{164}Dy(^{40}Ar,X) 222, 340 MeV, fusion cross sections, direct and evaporative p and α prod., evaporation, fission 80−13518
Er production in ^{A}Ge+^{86}Kr, A=70, 74, 76, and ^{A}Sn+^{40}Ar, A=122, 124, 50 to 120 MeV, angular momentum limits 78−25224
^{19}F+^{12}C, 92 MeV, fusion and direct reactions anal. 78−21591
^{19}F+^{12}C, fusion reactions, Woods Saxon, folding and proximity pot. anals. 79−45316
^{A}Fe(^{6}Li,X) A=54,56, 10-100 MeV, fusion and nonfusion processes, cross sections 79−45315
^{55}Fe(^{52}Cr, X), entrance channel mass asymmetry effects on reaction mechanism, fission and fusion 80−106077
^{56}Fe(^{16}O,X), 81 MeV, fragments in incomplete fission 77−14153
^{158}Gd+^{12}C, 112-164.7 MeV, fusion pre-equilibrium effects, $^{170-x}$Yb, $^{166-x}$Er, x=4-10, transitions 79−580
^{158}Gd+^{12}C, 152 MeV, pre-equilib. particle emission 79−581
^{160}Gd(^{12}C, αxn)$^{168-x}$Er, particle fragmentation accompanied by incomplete fusion, two step model 80−86947
^{160}Gd(^{12}C,xα), 120, 200 MeV, average α-multiplicities, incomplete fusion and breakup 80−27661
^{160}Gd(^{12}C,xαyn), 90-200 MeV, incomplete fusion, fast α prod. absolute cross sections 80−18359
^{70}Ge+^{32}S, 110, 132 MeV fusion evaporation residues, Monte Carlo simulation 78−41799
^{1}H+^{2}H burning star hypothesis for Jupiter 77−13282
^{2}H, superdense, cold, nuclear reaction energy output in mag. field *(Russian)* 77−29801
^{2}H^{3}Hμ→^{4}He+n+μ^-+17.6 MeV, muonic catalysis in synthesis reactions *(Russian)* 80−52706
^{2}H(^{2}H, n)^{3}H, fusion possibility in ^{2}H metallic state at low temp. 79−67806
^{2}H(^{2}H,n)^{3}He, fusion through metallic D 80−13517

nuclear fusion continued
$^{2}H(^{3}H,n)^{4}He$, muon catalysis kinetics *(Russian)* 80−91206
$^{2}H(t\mu,n\mu^{-})^{4}He$, fusion reaction, 2 GeV energy release 78−17250
$^{2}H(t\mu,n\mu)^{4}He$, muon catalysed fusion, neutron yield, muonic molecules 80−106095
^{3}H, production in fission and fusion reactors 79−71874
$^{3}H(^{2}H,n)^{4}He$, chain carriers in fusion reaction kinetics 80−86969
$^{3}H(d,n)^{4}He$, neutron fluence and energy transfer standard 80−102194
$^{3}He(d,p)^{4}He$, fusion cross sections and thermonuclear reaction rates 80−533
I prod. relative thresholds from fusion and transfer induced fission in $^{238}U(^{40}Ar,f)$ 79−9640
$^{139}La(^{86}Kr,X)$, TDHF fusion calcs., fusion cross sections 80−37409
$^{139}La(^{86}Kr,X)$, 505, 610, 710 MeV, TDHF calcs., fusion behaviour 80−9323
$^{6}Li+^{6}Li\rightarrow 3^{4}He$, 0.5-2.75 MeV, meas. of cross sections and fusion parameters 78−50223
$^{6}Li+p$ propagating fusion fuel cycle 80−37629
$^{6}Li(d,\alpha)$, cross sections, low energy extrapolation, 3 keV-1 MeV, thermonuclear reaction rate parameter 79−6635
$^{6}Li(p,^{3}He)^{4}He$, 100 to 700 keV, cross sections and angular distrib. meas., rel. to CTR 79−93618
$Mg+^{14}N$ or ^{16}O, high spin states prod. in $^{35,36,37}Cl$ and ^{37}Ar, decay schemes 77−2932
^{24}Mg giant isoscalar quadrupole fission/fusion doorway states from $^{12}C(^{12}C,^{12}C)$ 80−37410
$^{24}Mg+^{16}O$, 30-81 MeV, fusion cross section, elastic scatt. ang. distrib., optical model anal. 78−78412
$^{24}Mg+^{18}O$, 32-72 MeV, fusion cross section, elastic scatt. ang. distrib., optical model anal. 78−78412
$^{26}Mg+^{16}O$, 29-81 MeV 78−78412
$^{26}Mg(^{16}O,X)$, complete fusion, 25-70 MeV evaporation residue cross section, total fusion excitation functions 79−13370
$^{55}Mn\ (^{12}C,X)$, 77 MeV, fragments in incomplete fission 77−14153
$^{92}Mo(^{16}O,X)$, entrance channel mass asymmetry effects on reaction mechanism, fission and fusion 80−106077
$^{100}Mo+^{100}Mo\rightarrow{}^{200}Po$, two dimensional fusion barrier, penetrability calc. 78−41798
$(^{14}N,xn\gamma)$, rare earth nuclei, complete fusion process n and γ multiplicity 80−18363
^{14}N-induced reactions energy relax. during fusion determ. by preequilib. α emission 79−26446
$^{14}N+^{10}B$, sub Coulomb energy, fusion cross section, optical model anal. 77−34335
$^{14}N+^{12}C$, 34.1-178.1 MeV, fusion and peripheral reaction cross sections, direct yield 79−67771
$^{14}N+^{12}C$, fusion reactions, Woods Saxon, folding and proximity pot. anals. 79−45316
$^{14}N+^{16}O$, 20-60 MeV, compound nucl. form. 78−4954
$^{14}N(^{14}N,X)$ 9.4-22.0 MeV, low energy fusion cross sections 77−14152
$^{23}Na(^{19}F,X)$ complete fusion, 25-70 MeV evaporation residue cross section, total fusion excitation functions 79−13370
$Nd(^{16,18}O,4n)^{162}Er$, γ multiplicities, side feeding pattern, Monte Carlo calcs. 79−578
$^{146}Nd(^{16}O,X)$, 142 MeV, narrow window for incomplete fusion 80−95325
$^{150}Nd+^{20}Ne$, 174.8 MeV, pre-equilib. particle emission 79−581
$^{150}Nd+^{20}Ne$, 175 MeV, cross sections and energy spectra 78−41760
$^{20}Ne+^{12}C$, 6.3-13.8 MeV, total fusion cross section, S-factor, γ-yields 80−22877
$^{20}Ne(^{12}C,X)$, 24-42 MeV, complete fusion, total cross section, excitation function 80−68717
$^{20}Ne(^{20}Ne,X)$, 132 MeV, TDHFB calc. for total fusion cross section 80−13521
$^{A}Ni(^{40}Ca$, fusion), A=58, 60, 62, 113-170 MeV, fusion cross sections and excitation functions 80−32315
$^{58}Ni+^{16}O$ fusion, 30-70 MeV, statistical model calcs., yrast states and continuum feeding times 79−579
$^{58}Ni+^{23}Na$, deformed aligned projectile ions, elastic scatt., fusion, polarisation effects 78−58303
$^{58}Ni+^{32}S$, 110, 132 MeV, fusion evaporation residues, Monte Carlo simulation 78−41799
$^{60}Ni(^{12}C,X)$, 77 MeV, fragments in incomplete fission 77−14153
$^{62}Ni+^{35}Cl$, fusion excitation functions, dynamical model calc. 78−50224
^{252}No production, heavy ion complete fusion cross sections 79−67803
$^{A}O+^{12}C$, A=16,18,22 79−45316
$^{A}O(^{12}C,X)$, A=16,18, fusion cross sections by TDHF calcs. 79−89342
$^{16}O+^{12}C$, 17-28 MeV, total fusion cross section, γ-ray meas. 77−14162
$^{16}O+^{12}C$, 45-80 MeV, fusion cross sections using time-of-flight technique, TDMF calcs. 78−94043
$^{16}O+^{12}C$, fine struct. in fusion cross section 78−89928
$^{16}O+^{12}C$ system, exptl. survey of resonant structs. below and above Coulomb barrier 79−9616
$^{16}O+^{16}O$, 2- and 3-dimens. time depend. HF calc. comparison 79−17948
$^{16}O+^{16}O$, 3-dimens., time depend. HF calcs. for fusion cross sections 78−66318
$^{16}O+^{16}O$, 35-80 MeV, fusion cross sections using time-of-flight technique, TDMF calcs. 78−94043
$^{16}O+^{16}O$, 64, 80 MeV, fusion events, time dependent HF calcs. 79−36292
$^{16}O+^{16}O$, diffuse surface nuclear and Coulomb pot. energies 77−18593
$^{16}O+^{16}O$, fusion cross section gross struct., excitation functions, coupled channel method 80−52705
$^{16}O+^{16}O$, total fusion cross section and excitation function, statistical model anal. 79−13371
$^{16}O+^{16}O$, total fusion cross section, time depend. HF calcs. 79−17945
$^{16}O+^{16}O$ reaction cross sections, 12.5-30.5 MeV excitation functions 78−643
$^{16}O(^{12}C,X)$, sub-barrier energies, fusion cross section, static and dynamic deformation effects 80−42729
$^{16}O(^{16}O,X)$, 9.3 MeV, fusion reaction residue partial prod. cross sections from γ-detection 79−67804
$^{16}O(^{16}O,X)$, fusion limiting ang. momenta, from evaporation, mass distrib. stat. model fit 80−68714
$^{16}O(^{16}O,X)$, 30-40 MeV, complete fusion cross section, gross and intermediate width struct. 79−67808
$^{16}O(^{16}O,X)$, total fusion cross sections and fusion barrier parameters 80−9322
$^{16}O(^{40}Ca,X)$, ^{56}Ni formation cross section, TDMF calcs. for fusion 79−93676

nuclear fusion continued
$^{17}O+^{12}C$, 14-33 MeV, max. total fusion cross section 79−22349
$^{18}O+^{12,13}C$ fusion evaporation reactions, 100 MeV, comparison of residues with statistical calcs. 78−66311
Pb targets, possibilities for producing super-heavy elements Z>102, new projectiles *(Russian)* 78−86548
$Pb+^{14}N$, complete fusion cross sections, excitation functions *(Chinese)* 78−82406
$^{206}Pb(^{40}Ar,2n)^{244}Fm$, fusion reactions near Coulomb barrier, optical pot. parameter determ. 79−30874
$^{207}Pb(^{40}Ar,3n)^{244}Fm$ 79−30874
$^{208}Pb+^{40}Ca$, 255, 300 MeV, lowered fusion cross section 78−41797
$^{208}Pb+^{86}Kr$, 469 MeV, search for superheavy nuclei, Z>106, lifetimes >2 ps 78−46102
$^{208}Pb(^{16}O,X)$, 80-313 MeV, optical model anal., dynamic shape or density changes 80−18186
$^{208}Pb(^{48}Ca,X)$, fusion reactions from Cf and Fm integral yields, statistical model anal. *(Russian)* 79−97740
$^{110}Pd+^{40}Ar$, compound nucleus ^{150}Gd, deexcitation, evaporation calcs., comparison with exptl. decay data 77−61391
$^{110}Pd+^{40}Ar$, formation and decay of ^{150}Gd compound nucleus 77−61453
$^{118}Pd+^{118}Pd$, 637 MeV time depend. Hartree-Fock-Bogoliubov calc. for fusion and subsequent ^{236}U fission 79−36265
^{199}Po charge states and charge distrib. from $^{164}Dy(^{40}Ar,5n)$ *(Russian)* 79−40840
$^{141}Pr+^{35}Cl$, 135-170 MeV, evaporation residue excitation functions 77−88166
$^{242}Pu(^{48}Ca,xn)$, production of superheavy elements with A=114-116 78−29493
^{32}S compound nucleus formation and deexcitation entrance channel effects from $^{16}O+^{16}O$, $^{12}C+^{20}Ne$ 80−549
$^{32}S+^{24,25,26}Mg(^{27}Al)(^{28}Si)$ fusion reaction, 130 MeV, mass systematics of evaporation residues 77−38311
$^{32}S+Mg(^{27}Al)$, 160 MeV, evaporation residues, isotope and element distribs. meas. 78−13153
Si burning, during advanced evolution of massive stars 78−28652
$Si+^{16,18}O$, 34-81 MeV, total fusion-evaporation cross sections, fusion barrier 80−5190
$^{A}Si(^{12}C,X)$, 20-49 MeV, A=28-30, complete fusion cross sections, excitation function weak struct. 80−5188
$^{A}Si(^{16}O,X)$, 21-61 MeV, A=28-30, complete fusion cross sections, excitation function weak struct. 80−5188
$^{28}Si+^{16}O$, fusion oscillations, evaporation residue gamma yields, cross section 80−42725
$^{28}Si+^{28}Si$ fusion reaction, 117.5 MeV, mass systematics of evaporation residues 77−38311
$^{28}Si+^{6}Li(^{9}Be)(^{12}C)$, fusion and strong absorption from elastic scatt. optical pot. 80−102222
$^{28}Si+^{9}Be$, localisation of direct reaction processes, fusion and total cross sections 78−78353
$^{28}Si(^{28}Si,X)$, ^{56}Ni formation cross section, TDMF calcs. for fusion 79−93676
$^{28}Si(^{28}Si,X)$, 60 MeV, α-α correlations to probe fusion low ang. momentum window 80−106094
$^{28}Si(^{9}Be,^{9}Be)$, 121-201.6 MeV, strong absorption dominance, global optical model anal., fusion barrier 80−83116
$^{28}Si(^{9}Be,X)$, 30-60 MeV, total fusion cross section, evaporation residues, optical model 80−78344
$^{28}Si(^{9}Be,X)$, X=p,d,α, energy dependence, angular distrib. of spectra, optical and statistical model anal. 80−68710
$Sm+O^{16}$ fusion, cross sections for spherical and deformed Sm isotopes, shape effects 78−78407
$^{A}Sm(^{16}O,X)$, 60-75 MeV, A=148, 150, 152, 154 deformation effects on fusion 80−18360
$^{A}Sm(^{16}O,X)$, 60-75 MeV, A=148,150,152,154, fusion cross section, evaporation residues 80−83137
$^{A}Sm(^{40}Ar,X)$ A=144, 148, 154, 3.6-4.5 MeV/A, sub-barrier fusion, evaporation residue cross section, deformation 80−68718
$^{154}Sm(^{16}O,X)$, 153 MeV, angular momentum transfer in incomplete-fusion reactions 80−9320
$^{154}Sm(^{40}Ar,X)$, 222, 340 MeV, fusion cross sections, direct and evaporative p and α prod., evaporation, fission 80−13518
$^{112}Sn+^{32}S$, 160 MeV, mass, velocity, angular and charge state distribs. 78−82405
$^{112}Sn+^{35}Cl$, 135-170 MeV, evaporation residue excitation functions 77−88166
$^{116}Sn+^{35}Cl$, fusion excitation functions, dynamical model calc. 78−50224
$^{116}Sn(^{40}Ar,X)$ 187, 222, 340 MeV, fusion cross sections, direct and evaporative p and α prod., evaporation, fission 80−13518
$^{120}Sn+^{35}Cl$, 135-170 MeV, evaporation residue excitation functions 77−88166
T chemistry in nuclear fusion research, review *(Japanese)* 79−63806
$^{159}Tb(^{11}B,X)$, 51 MeV, fusion and deep inelastic, quantised frictional motion calcs. 80−102223
$^{159}Tb(^{14}N,X)$, 140 MeV, incomplete fusion reactions, sum rule model 80−95332
$^{159}Tb(^{40}Ar,X)$, 273 MeV, complete fusion and charge transfer reactions 79−45314
$T(d,n)^{4}He$, fusion cross sections and thermonuclear reaction rates 80−533
$Ti(^{16}O,X)$, 310 MeV, fusion, upper limit to compound nucleus formation 80−78315
$^{48}Ti+^{16}O$, 57.74 MeC, heavy ion fusion, evaporation model breakdown, preequilibrium α emission from ^{64}Zn 78−89927
$^{49}Ti(p,\gamma)$, 0.74-3.25 MeV, cross section and thermonuclear reaction rates, nucleosynthesis, IAR effects 80−102187
$^{49}Ti(p,n)$, 0.74-3.25 MeV, cross section and thermonuclear reaction rates, nucleosynthesis 80−102187
$^{A}Tl(^{48}Ca,X)$, A=203, 205, fusion reactions from Cf and Fm integral yields, statistical model anal. *(Russian)* 79−97740
$T(t,2n)^{4}He$, fusion cross sections and thermonuclear reaction rates 80−533
^{235}U fission fragment thermonuclear superheavy nuclei synthesis, prod. cross sections 80−95331
$^{238}U+^{40}Ar$, cross-sections for fusion, quasifission and deep inelastic collisions *(Russian)* 78−54801
$^{238}U+^{40}Ar(^{48}Ca)$, products from complete fusion and deep elastic processes 78−70565
$^{238}U(^{56}Fe,X)$, 538 MeV, binary coincident fragments, fragment mass and energy, fission following fusion 80−548

nuclear fusion continued
^{51}V (^{16}O,X), 81 MeV, fragments in incomplete fission 77−14153
^{182}W(^{12}C,X) 77-167 MeV, fusion cross sections, direct and evaporative p and α prod., evaporation, fission 80−13518
$^{186}W+^{86}Kr$, cross-sections for fusion, quasifission and deep inelastic collisions *(Russian)* 78−54801
$^{89}Y+^{40}Ar$, 237 meV, γ-ray multiplicities and energies, primary fragment angular momenta 78−46093
$^{90}Zr+^{86}Kr$, 366-716 MeV, evaporation residue product cross sections 79−17947

nuclear fusion reactors *see fusion reactors*

nuclear giant resonances *see nuclear collective states and giant resonances*

nuclear induction *see nuclear magnetic resonance*

nuclear instrumentation
see also angular correlation techniques; beam handling equipment; counters; counting circuits; nuclear reactor instrumentation; particle accelerators; particle detectors; particle track visualisation
accidents, use of mobile remote-handling equipment *(French)* 78−53525
activation meas. using Nairi-K multichannel installation 80−23271
amplifier, linear, solid-state, for photomultiplier pulses 80−5451
analog mean-timer circuit for use with large-volume scintillation counters 80−63477
atomic science and engineering, measuring informational basis, nuclear instrument making 79−684
AZ MS IV scanning measuring projector system, calibration methods 80−5449
BASIC overlay for CAMAC data and command handling 80−18772
CAMAC diagnostic module for on-line monitoring of CAMAC integrity 80−5459
CAMAC high rate data acquisition system 80−23281
CAMAC single crate controller, DMA-option for PDP-11 computers 77−10559
CAMAC-CAMAC linkage module 77−10557
CERN polarised d target, apparatus for two-body scatt. expts. 79−31287
colloqium on nucl. instrumentation, London, England 1979 80−4480
combustion system for liquid scintillation wastings *(Japanese)* 80−63503
communication network within hierarchical control system, appl. to Fermilab beam line 79−45610
compact tape transport station for on-line studies of short-lived nuclides 79−68116
computer network for on-line data processing 78−37529
computer-based data acquisition system for multi-station teaching laboratory 78−4446
computer-controlled pulser system 80−52841
conference, nuclear power systems, San Francisco, CA, USA (Oct. 1979) 80−56994
conference on nuclear power systems, Washington, USA (1978) 79−41045
conferences, nuclear science, nuclear power systems, San Francisco, USA, 19-21 Oct. 1977 78−33304
constant fraction differential discriminator for use in fast timing coincidence systems 79−45580
data acquisition and processing equipment, evolution 79−72219
data acquisition real time flexible processing software 79−36495
data acquisition system on-line, for particle physics expts. using PDP-11 computers 80−27913
data acquisition/analysis, modular-programmed systems 77−18766
data processing system for neutron expts. 79−81143
delay lines, multichannel remotely programmable 77−10560
dispersion aerosols for transport of deuteron and ^{84}Kr induced reaction products 77−34502
dual NIM standard 52 fold multiplicity unit 79−49914
dynamic analysis facility at Chalk River National Laboratory 80−58106
electrometer/ratiometer of high sensitivity and precision 78−70154
electronic systems based on the Harwell 6000 series 80−106242
electronic techniques for high energy expts. 79−59315
electronics in nuclear science and technology 80−9347
emergency conditions, monitoring and handling 78−57082
emitter-coupled integrated circuits, application to nanosecond nuclear electronics 78−5101
event handler, a fast, programmable, CAMAC-coupled data acquisition interface 79−45608
fast clustering processor for MWPC read out 79−63878
fast event recorder utilizing a CCD analog shift register 79−45578
FASTBUS, medium energy physics appls. 80−42912
FASTBUS, molecular data bus system for high energy physics 80−42911
FASTBUS project, development status of high speed standard data bus 79−45605
femtoamp current preamp for microprocessor controlled isotope calibrator 79−45586
Fermilab master slave servo-manipulator, control system 77−83309
fission materials nondestructive analysis development, for EURATOM (CEC) Safeguards Directorate 79−85693
fission multiplicity detectors, seldom exploited props. 77−46468
fluctuating analogue quantities averaging device 79−68170
fluid radioactive waste monitoring equipment, USSR standards *(Russian)* 78−89998
fuel reprocessing plant instrumentation for internat. safeguards 78−721
fusion reactor, MFTF, electrical systems, overview 80−91278
gas jet recoil transport system, aerosol formation using pure gas as carrier 79−97921
gas jet recoil transport system, continuous separation of Se and Te from fission products 78−70674
gas jet recoil transport system for fission products, appl. to chemical separation in gas phase 78−17459
gas jet transport system, steady state, radioactive distrib. in compressible stream tube *(German)* 78−90007
gas-jet transport system, aerosol size-depend. props. 77−79493
gas-jet transport system, optical investigation 77−14289
goniometer, precision three axis UHV bakeable system 78−70673
goniometer, ultra high vac., manipulator with six degrees of freedom 78−18509
HFR at Grenoble, neutron beam installations 77−26864
high energy physics program at BNL, equipment, experiments, future research 77−18716
high rate 4π β-γ coincidence counting system 79−45588

nuclear instrumentation continued
high rate liquid Ar calorimeter electronic systems, design and operating experience 80−58087
high speed top mounted bus, prototype crate and module system 79−45611
high-speed transfer system for short lived nuclides 77−30686
hot cell extension optical profilometer 80−68789
impurity monitor for liquid ionization chamber media 79−31331
Indian nuclear power station effluent monitoring system requirements and experience 79−13552
irradiation creep facility, materials testing for fast and fusion reactors 79−57192
irradiation facility of Stockholm 225 cm cyclotron 77−57781
isotopes appl. to contactless meas., of density and thickness *(Bulgarian)* 79−80578
Jupiter's radiation belt, nucl. meas. techniques 78−85895
KEKNET, a high speed on-line network for high energy physics 79−36493
laboratory course, computer based data acquisition and anal. 80−36820
least squares fitting procedure, errors of parameters 78−16768
level and density measurement using nuclear gauges 80−843
linear accelerator, magnetically insulated pulse power driven 78−5045
liquid sample holder for radioactive solutions, X-ray fluorescence anal. 79−24867
logarithmic converter stabilized by a baseline restorer employing gain switching 79−45582
magnetic spectrograph, multi-ang., for charged particles emitted in nucl. reactions 80−5429
magnetic tape interfaces for a dual-parameter coincidence experiment 80−14055
mechanical actuator, stepper motor, appl. to control of scientific apparatus 78−62683
microcomputer-based data acquisition system 80−63500
microprocessor multiple arrays, operating systems for nuclear diagnostic system 79−49918
minicomputer data acquisition system for Princeton cyclotron facility 78−90048
modular 125 ps resolution time interval digitizer for 10 MHz stop burst rates and 33 ms range 79−45591
modular instrumentation system for nuclear industry 77−67780
modular trigger processing system for high energy physics experiments 79−49919
multi-channel analyzer using a dedicated CAMAC memory 79−45592
multi-faceted data gathering and analysing system 78−37530
multi-parameter CAMAC compatible ADC scanner 79−31350
multi-parameter distributed processing data acquisition, display, and on-line analysis system 79−45612
multichannel radiometer automatic channel separating system *(Russian)* 80−58094
multiprocessor system for nucl. event picture anal. *(Italian)* 80−69047
NDT methods, sensitivities and detection limits 77−32756
neutron facility of Birmingham radiation centre based on Dynamitron accelerator 77−26887
neutron installations and facilities 77−23317
neutron physics, recent advances 77−26640
neutron physics at LAMPF 77−26951
neutron physics research trends 77−22825
neutron scatt. facility in 20-40 MeV range 77−26888
nuclear physics data acquisition with UNIX time-sharing system 79−41085
nuclei and particles, introductory text book 78−78234
nucleonic and other meas. methods compared 77−38594
nucleonics, review Nov. 1975 to Nov. 1977 78−82262
number oriented microprocessor appl. to real time data processing 79−49921
on-line separators, fast tape transport system 77−14328
online Reactor Noise, Vibration and Loose Parts Monitor 79−3212
op amp, type 108, radiation hardening by modified processing, failure anal. 77−18751
optical fibres, low-loss multimode, characterisation for nuclear diagnostics 80−78501
optical instrument for determining upper limit of neutron charge 80−63501
optimum filters, finite time width and area balance, for triangular or step current input waveforms 79−13610
particle-particle correlation experiment, on-line four parameter anal. system *(Chinese)* 80−42910
perimeter security system using ^{137}Cs γ-ray beams 77−18713
photomultiplier assemblies and associated electronics for high energy physics large counter expts. 77−83469
physical measurement and standardisation requirements *(Italian)* 79−93845
PIGMI, accelerator control system 79−45475
plunger device for in-beam meas. of nuclear lifetimes, tested on ^{22}Na and ^{153}Dy 78−13375
preamplifier, charge sensitive, loop phase shift and delays 80−58089
preamplifier, low noise 79−76307
programmable fast logic unit 80−52842
pulse height analyser, microprocessor based digital controller 79−3335
pulse height analysers, CAMAC data acquisition interface 79−3336
pulse height store for A/D conversion 80−14054
pulsed data A-D acquisition system 79−22572
pulsed feedback preamplifiers, energy depend. loss anal. 79−45581
PWR crosslinked polyethylene insulated low noise triaxial cable *(Japanese)* 78−670
rabbit fast transport system for fragile targets in high vac. 77−83417
radiation monitoring system, digital communication techniques 79−49866
radiation techniques and technology development in the Soviet Union 79−685
radioactive ion beams, for nucl. expts., review 79−97922
radiogauging, use of ionising radiation 79−41086
radionuclide conc. meas., portable three channel evaluation unit *(Czech)* 79−22538
remote solution meas., during cold checkout runs at nuclear fuel plant facility 79−85748
Rutherford Laboratory N5 expt. data acquisition system, program struct. and CAMAC hardware 78−90051
Saclay high-energy physics supercond. magnet programme 79−31352
signal interface element survey, low cost quantisers, fast ADC's, high energy physics appl. 79−45584

nuclear instrumentation continued
spectroscopy, in university science course for talented high-school students 78−89282
SPS control system, modifications since instalment 79−26866
SQUID appl. to nuclear gyros and magnetometers, high stability and sensitivity 80−98949
standard signal transmission over long cables, using ESL ICs 78−5102
surveillance of spent fuel 79−85679
target thickness uniformity gauge using ^{147}Pm beta source 77−10512
teaching, undergraduate, courses, facilities 80−27086
teaching laboratory, development at Ecole Polytechnique 78−4444
temperature controlled hybrid substrate for use as a building block in precision instrumentation design 79−45583
time coder with variable channel width for time-of-flight expts. 78−33403
time digitiser in CAMAC format 77−10558
time projection chamber multichannel ADC and readout system 79−45590
time to amplitude converters, precision 1 GHz time calibration 80−27903
time-to-amplitude convertors, spectral distortion *(Japanese)* 77−46469
TLD readers, safety and reliability of decentralised reading in Sweden 77−40780
transuranic waste assay instrumentation, Los Alamos Scientific Laboratory developments 79−85692
vacuum gauge design 78−17546
vaporisation apparatus for liquid scintillation wasting *(Japanese)* 80−63502
versatile data handling system for nuclear physics experiments based on PDP 11/03 micro-computers 79−76319
VICKSI beam line instrumentation and control system 77−83401
voltage dividers to stable photomultiplier running *(German)* 79−68172
wide-band measuring system for studying charge-coupled device characteristics 79−45585
C, stripper foil prepared by cracking hydrocarbon vapour in glow discharge 79−31286
Fe single crystal frames, use in transient field meas. 79−59324
Ge FET, fabrication on high purity substrate 79−45579
^{3}H concentration measurements in nuclear power plant atmosphere, instrumentation 79−26765
He jet, cryogenic, and recoil TOF apparatus 78−17458
He jet system for radioactivity studies 79−93855
He jet TOF mass spectrometer for nuclear spectroscopy of fission products 77−23355
He jet transport system, benzene and diethyl sulphide additives 79−76245
He-jet and skimmer system at Chalk River 77−14290
He-jet system, appl. for isotope separation 77−14287
^{125}I, counting device with automatic efficiency correction 80−42897
NaI detector system, front end electronic, pulse height anal. 79−45587
U exploration and assay, nuclear methods 77−41228

nuclear interactions *see nuclear reactions and scattering*

nuclear internal conversion *see internal conversion*

nuclear isobaric analogue resonances *see isobaric analogue resonances*

nuclear isobaric analogue states *see isobaric analogue states*

nuclear isomerism
see also nuclear energy levels
^{116}Xe quasi-rotational bands, levels J^{π} and $T_{1/2}$ from ^{116}Cs decay 80−83021
^{148}Pm^{m,g} isomeric pair prod., in (d,2n), (p,n) and (α,pn) reacts. 77−88144
^{154}Er, high-spin states 78−29373
A=154, nuclear data sheets, levels, decay props., isomeric states, Nilsson orbitals 79−71781
A=40-80, yrast props. and high spin isomers, cranking plus Strutinsky formalism 80−32152
A∼90 nuclei, isomeric states, spin polarisation, M4 transitions and giant resonances 80−63157
alkali metal radioisotopes, hyperfine spectroscopy, nucl. props. 80−57677
density isomer formation in high energy heavy ion collisions, 3-dimens. fluid dynamical calcs. 79−49578
density isomers, schematic model of mass distrib. 77−6219
density isomers in high energy heavy ion collisions, hydrodynamical model anal. 79−36138
fission isomeric states population via isobaric analogue resonances 77−34231
fission isomers, meas. of extreme nucl. deform. *(German)* 79−40971
fission isomers, spectrosc. props. 80−105966
heavy ion collisions, fluid dynamical and TDHF models, abnormal nuclear matter, density isomers 80−47502
high density isomeric state in nucleon matter relativistic heavy-ion collisions 79−85390
high-spin isomery, heavy ion experiments at UNILAC *(German)* 78−66435
high-spin states and shell struct. in N=Z nuclei, ^{20}Ne appl. 80−47342
independent fission-product yields to isomeric states, distrib. 77−50106
isomeric A=48-50 nuclei, mag. moments and core polarisation 78−37274
isomeric states prod. cross-sections at 14.8 MeV via (n,2n), (n,p), and (n,n'γ) 77−26744
laser induced nuclear orientation effects 77−30740
metastable isomer prod. via (γ, γ') at 6-8 MeV *(French)* 79−29433
N=82 region, high spin isomers, cranked HF calcs., deformation shapes, excitation energies 80−99121
N=82 region, high spin isomers, deformation energy surface, shape constrained cranked HF theory 80−57666
N=82-86, high spin isomers, gamma spectroscopy 80−47358
N≃50 nuclei, unsuccessful search with 42 MeV ^{16}O projectile 80−9223
nanosecond isomers, in-beam gamma spectroscopic investigation, Ge(Li) detector 78−86506
neutron induced yrast isomer prod., pulsed beam meas. using plastic scintillation spectrum 80−27871
nuclear matter, pion condensation and density isomerism 80−5085
oblate high spin isomers, pairing Hamiltonian anal. by RPA 78−12996
odd-neutron spherical nuclei, isomeric state lifetimes, inhibited electric quadrupole transitions 78−78310
photochemical separation of isomers 79−50153
photon induced spallation reactions, intermediate energies, isomeric cross-section ratios 77−41954
rare earth nuclei, high spin isomer α-decay search 80−102158

nuclear isomerism continued
reviews of isomers in the millisecond region, γ-ray and conversion electron spectra of decay 79−36167
s-process isotopes, nonthermal isomeric branching, importance of long-lived states 78−7983
shape isomer prod. in nuclear reactions and β-decay 79−6377
shape isomers, spontaneous fission, static and decay props. and excitations, review, book contrib. 78−82402
short-lived isotopes, laser spectroscopy in fast atomic beams and resonance cells 80−57700
spallation yield distribution calc. method, including isomeric state effects 79−93596
spherical nuclei, isomer and isotope shifts, theory of finite Fermi systems 80−39929
spin rotation, high angular velocity, collective aspects of heavy ion collisions 80−78309
spontaneous fission of transuranium nucl. isomers, exptl. work review 77−79405
unthermalised isomeric states, effect on red giant star s-branching ratios 80−90410
yrast traps, obs. in heavy ion collisions 80−37319
Z=34-94, high spin yrast isomers and nuclear deformation 79−6369
γ spectra of millisecond isomers, 38 MeV α-induced reactions, abs. cross-section determ. 79−9502
(n,2n), 14.7 eV, isomeric cross-section ratios, statistical theory, moment of inertia 79−97701
(n,2n) reactions at 14.8 MeV, isomeric ratios in 107<A<143 mass range 78−13073
(n,f), actinide nuclei, influence of isomeric states on independ. fission prod. yield 78−4968
(n,p) at 14.7 MeV, on 48 stable nuclides 77−61417
(π^-, γ), high spin isomer state excitation, review 79−49569
^{94}Rh isomers, beta decay, ^{94}Ru level structure, spin and parity 80−57747
^{A}Ag, A=105, 107, 109, 111, isomeric transition internal conversion, γ-transition energies and e intensities 79−6503
^{100}Ag^{g,m} decay, ^{100}Pd levels and γ-transitions 80−83077
^{105}Ag high spin states and bands, g-factor and isomeric state from ^{103}Rh(α, 2nγ) 79−36125
^{106}Ag low-lying excited states from ^{103}Rh(α,nγ) and ^{104}Pd(α,pnγ) 80−57693
^{108}Ag, form. in ^{107}Ag(n,γ) reaction, isomeric level scheme at 215.38 keV 78−12975
^{108}Ag, populated in ^{108}Pd(p,nγ), level struct., spin and parity, isomeric state lifetimes and g-factors 77−18392
^{108}Ag^{m}, neutron cross-section for production from ^{107}Ag 79−29625
^{110}Ag 118.718 keV isomer, low lying states and transitions, coincidence study from ^{109}Ag(n,γ) 80−73806
^{110}Ag low-lying levels, from ^{109}Ag(n,γ) obs. 80−47422
^{110}Ag, populated in ^{110}Pd(p,nγ), level struct., spin and parity, isomeric state lifetimes and g-factors 77−18392
^{110}Ag^{m}, oriented, T-reversal test and struct. study 78−86505
^{110}Ag^{m} decay, precise γ-ray spectroscopy 78−58251
^{110}Ag^{m} orientated, β-ray asymmetry, Fermi/Gamow-Teller matrix element ratio 79−93562
Al isomeric state formation cross section with 14.8 MeV neutrons, half-life, γ-ray spectra 77−30604
^{24}Al, ^{24}Al^{m}, decay to γ-ray and α-particle emitting ^{24}Mg states 79−49607
^{24}Al, 1^{+} isomer decay 79−85414
^{26}Al long lived nucl. isomeric states, thermalization in stars 80−85846
Am, 240-3, spontaneous fission, conversion electron spectra obs. 77−82864
^{A}Am(γ,n), 10-80 MeV, A=241, 243, delayed/prompt fission yield ratio, cross section, isomer prod. 79−80924
^{241}Am(n,f), 14.8 MeV, mass yield distrib., and absolute fission yield, isomer ratios 80−18352
^{241}Am(n,γ)^{242m}Am, γ-quanta in population of spontaneously fissile isomer *(Russian)* 79−30835
^{72}As, new 87 ns isomer, g-factor via ^{59}Co(^{16}O,2pn) 53-56 MeV 77−54149
At high spin isomers, deformed independent particle model, yrast lines, shape 79−480
^{A}At, A=198m,198g,199, alpha branching ratios 80−99154
^{207}At, g-factor of 25/2^{+} isomeric state, evidence for neutron excitation 78−70447
^{210}At, isomeric 19^{+} state, isospin depend. in two-particle core polarisation 78−21499
^{212}At excitation functions and isomer ratios from ^{209}Bi(α,n) 80−83039
^{A}Au, A=189, 191, 193, high spin states and transitions, isomeric states from Ir(α,xnγ) 80−5038
^{A}Au A=190, 192, 194, levels, J^{π}, isomers and rot, aligned bands from Ir(α,xn) 80−9215
^{194}Au, isomeric states anal. conversion electron and γ-ray spectra from ^{194}Pt(p,n) and ^{195}Pt(p,2n) 77−71582
^{196}Au, studied via ^{197}Au(n,2n), isomeric cross-section ratio and spin-cut-off factor 78−13096
^{197}Au(n,n')^{197m}Au, E$_n$=3 and 14.1 MeV, form. cross sections of short-lived isomer, cyclic activation technique 80−32283
Au(π^-,X), stopped π^- capture, product nuclei distribs., isomeric yield ratios, neutron multiplicity 77−18625
Ba, neutron deficient, charge radii, moments, transitions and isomers, atomic beam laser spectroscopy 80−102141
Ba, radioisotopes, at. beam laser spectroscopy, hyperfine struct., nucl. moments and radii 80−57678
^{136}Ba(n,2n)^{135}Ba^{m}, 14.2 MeV, neutron activation cross sections 80−91180
^{138}Ba(n,α)^{135}Xe^{m,g}, 14.2 MeV, neutron activation cross sections 80−91180
Bi, isomeric state formation cross section with 14.8 MeV neutrons, half-life γ-ray spectra 77−30604
^{207}Bi high spin states, level decays, three particle interactions from ^{205}Tl(α,2n), ^{208}Pb(d,3n) 79−49567
^{209}Bi EM props. of particle vibration coupling states from ^{208}Pb(^{7}Li, ^{4}He 2nγ) 78−70485
^{210}Bi^{m}(d,t), 17 MeV, ^{209}Bi levels and spectroscopic factors, ^{210}Bi(9^{-}) parentage 80−78158
^{212}Bi, isomeric states from α-activities 78−82282
Br, isomer ratios in fission fragments at high excitation 80−32261
^{76}Br, Coriolis distorted bands, common g$_{9/2}$ parentage in N=41 nuclei 80−13349

nuclear isomerism continued
^{76}Br long-lived positive parity isomer from ^{75}As(α,3n) 79−54375
^{76}Br, new isomeric state with half-life 1.49 sec 79−17858
^{76}Br^{M} decay props., half life and γ-transitions, level scheme 80−83071
^{78}Br, high-spin states, from ^{77}Se(α,2np), decay into isomers 80−52569
^{78}Br, in liq. metal target, in-beam γ-NMR-PAD 77−59465
(^{12}C,X) on A=144-164, search for high spin isomeric states, shell effects 79−71784
^{41}Ca, highly stripped ions, recoiling in vacuo, γ-decays of isomeric states obs. 78−50119
^{107}Ca 21/2^{+} 2679 keV three quasiparticle state, nuclear struct. of isomeric states using g-factor 77−88039
^{107}Cd, heavy ion nucl. alignment, recoil in vac., time-differential meas. 78−37304
^{109}Cd, 11 μs isomeric level, spin and parity determ. by ^{108}Pd(α,3n) *(French)* 78−8738
^{110}Cd(p,n)^{110m,g}In, anal. of isomer ratios in preequilibrium statistical model 77−6361
^{111}Cd, excitation by photon less positron annhilation, isomeric γ-transitions *(Russian)* 80−5089
^{111}Cd^{m}, nuclear orientation in Zn and Be, 245 keV state quadrupole moment, half-life 80−37324
^{111}Cd(γ,γ), isomeric states excitation, integral cross sections 80−27528
^{112}Cd(p,n)^{112m,g}In, anal. of isomer ratios in preequilibrium statistical model 77−6361
^{115}Cd^{m,g}, decay to ^{115}In, decay scheme, unified model description of odd mass In nuclei 78−66251
^{119g,m}Cd, decay schemes, half-lives, excited levels 77−296
^{133}Ce, 5-h isomer β-decay, ^{133}La level struct., parity levels, decoupled band struct. 79−9476
^{136}Ce, 10^{+} isomeric states, systematic behaviour 79−30791
^{138}Ce, ^{139}Ce, high-spin states, lifetime meas. using (α,xn) reactions 77−18476
^{252}Cf fission products, g-factors of isomeric states 77−22890
^{252}Cf, spontaneous fission, yields and isomer ratio in A=134 chain 78−41786
^{A}Cm, A=246,248, fission isomer rot. spectra $I^2(I+1)^2$ correction 80−18229
^{59}Co(n,α), thermal, isomer state excitation, relative probabilities 79−75814
^{48}Cr high spin states, yrast levels and 6^{-} isomeric state from ^{40}Ca(^{10}B,np) 80−454
^{129}Cs 11/2^{-} isomer, g-factor and lifetime in CsI cubic environment from ^{127}I(α,2n) 79−6394
^{129}Cs, band struct., in-beam γ-ray spectroscopy after (γ,2n) reaction 78−4951
^{134}Cs 176.403 keV isomer, populating γ-rays, low lying levels from ^{133}Cs(n,γ), ^{134}Cs 176.403 keV isomer, populating γ-rays, low lying levels 80−78200
^{62}Cu 390 keV state, ferromag. effect, spin assignment 77−2903
^{A}Dy, A=152, 153, isomeric states and complex band structs. from Nd(^{12}C, xnγ), Gd(α, xnγ) 79−67624
^{148}Dy$_{82}$ 10^{+} isomer, $\pi h_{11/2}$ effective E2 charge 78−93964
^{149}Dy, 27/2^{-} three-particle isomer on ^{146}Gd doubly closed shell nucleus 77−22895
^{150}Dy, high-spin isomers produced by ^{144,146}Nd(^{12}C,xn), gamma-ray spectra 78−50075
^{151}Dy high spin states, isomers, α-decays and yrast sequence from (^{32}S,3n), (^{14}N,4n) 79−93493
^{151}Dy high spin yrast isomers, shell model configs. from ^{152}Gd(α,5n) and ^{136}Ce(^{19}O,3n) 79−49573
^{152}Dy 60 ns isomer deexcitation E2 x- (orΔ) transition, half life, $\gamma\gamma$-coincidence from ^{152}Gd(α,4n) 80−86859
^{152}Dy, collective bands and absence of yrast traps 80−9207
^{152}Dy high spin isomeric states, g-factors from ^{140}Ce(^{16}O, 4n) 80−13377
^{152}Dy high spin isomers, yrast traps, oblate shape at high ang. momenta 79−97646
^{152}Dy high spin isomers, yrast states and level lifetimes from (^{15}N, 4n), (^{16}O, 4n) 80−13361
^{152}Dy, high spin state populations from ^{124}Sn(^{32}S,4n) 80−57660
^{152}Dy, high-spin isomer at high excitation energy obs. in ^{154}Gd(α,6n) 77−22841
^{152}Dy yrast isomers, γ-rays from compound nuclei 80−86789
^{152}Dy, yrast isomers, oblate shape, excitation energies, spin and parity 79−17795
^{152}Dy, yrast states of isomers at high angular momenta, particle-hole struct. 79−36124
^{152}Dy, yrast traps, and very high spin states, populated in (^{32}S,4nγ) 78−89778
^{152}Dy yrast traps, isomers and oblate deformations from ^{124}Te(^{32}S, 4n) 80−13362
^{153}Dy, weakly deformed, isomeric $^{9+}/_{2}$ and lowest $^{7-}/_{2}$ states decay 79−89231
^{164}Dy(n,γ), thermal, isomer state excitation, relative probabilities 79−75814
^{153}Er 360 ns yrast trap, γ transitions and lifetimes from ^{144}Sm(^{12}C,3n) 80−9205
^{154}Er, collective bands and absence of yrast traps 80−9207
^{154}Er yrast trap and transitions, decay scheme from (^{64}Ni,4n), (^{16}O,4n) 80−9206
^{256}Es 7.6 hr β-decaying high-spin isomer, discovery following ^{254}Es(t,p) 77−22964
^{143}Eu^{m}, decay obs., struct. determ. 78−50130
^{144}Eu, multiplet splitting and isomerism, J, π, T1/2 via (d,2n) and (p,n) 77−14014
^{145}Eu high spin and isomeric states, transitions, weak coupling from ^{144}Sm(α,2npγ) 80−13348
^{145}Eu high spin levels, isomers and in-beam γ-spectroscopy from ^{144}Sm(α,2np) 80−78124
^{146}Eu 9^{+} isomer, γ-decay, high spin particle-hole multiplet population from ^{147}Sm(p,2n) 80−63066
^{152}Eu 89.8488 keV isomeric state feeding, delayed coincidence meas., level scheme from ^{151}Eu(n,γ) 80−63126
^{152}Eu doubly odd nucleus, transition probabilities and deformations, obs. in (n,γ) 79−97680
^{152}Eu, isomeric levels and transitions, Nilsson model 80−18195
^{152}Eu, isomeric state struct. 80−83017
^{152}Eu^{m} (n,n'), thermal neutron acceleration by isomeric nuclei *(Russian)* 80−52680
^{141g}Eu, ^{141m}Eu β-decay props., J$^{\pi}$, decay energy, $T_{1/2}$ 77−82876
^{150m}Eu, 35.8 y, decay coincidence study, ^{150}Sm levels 77−82858

nuclear isomerism continued
^{57}Fe^{m}, Mossbauer level excitation using specific charact. of synchrotron radiation 78−66447
^{213}Fr, high spin yrast states in N=126 isotones 79−45131
Ga, A=66, 68 isomeric state from ^{56}Fe+^{13}C and ^{56}Fe+^{15}N reactions, lifetimes, g-factors 78−33147
^{A}Gd A=144,146,147,148, high spin isomer g-factors yrast traps from (^{28}Si,^{28}Si'), (α,α') 80−78146
^{A}Gd, A=146, 147, g-factors of yrast states 79−17800
^{143}Gd^{m+g}, β^{+} and EC decay 78−50130
^{146}Gd, high multiplicity yrast isomers prod. in (α,xn) reactions 78−41666
^{146}Gd, mag. moments of isomeric states 79−40847
^{147}Gd, high multiplicity yrast isomers prod. in (α,xn) reactions 78−41666
^{147}Gd^{m} high spin yrast trap, oblate deformation and quadrupole moment 80−32157
^{150}Gd, collective bands and absence of yrast traps 80−9207
^{153}Gd, weakly deformed, isomeric $^{9+}/_{2}$ and lowest $^{7-}/_{2}$ states decay 79−89231
^{67}Ge, mass excess and low lying states, comparison with ^{63,65}Ni, ^{65,67}Zn and ^{69}Ge, from ^{65}Zn(α,nγ) 78−66213
^{71}Ge, in liq. metal target, in-beam γ-NMR-PAD 77−59465
^{4}He, T=1 excited negative parity state struct. 80−57688
Hf, alpha decay studies of the isotope 79−63636
Hf, isomeric state formation cross section with 14.8 MeV neutrons, half-life, γ-ray spectra 77−30604
^{A}Hf, A=171, 173, three quasiparticle isomers and rot. bands 79−26354
^{A}Hf(HI,xn), A=170-173, two and three quasiparticle isomers, rot. bands, decays and lifetimes 80−9211
^{171}Hf one- and three-quasiparticle states, high spin rot. bands from (^{16}O,5n), (^{13}C,4n) 80−18163
^{175}Hf multi-quasiparticle states and bands, isomeric states, lifetimes from ^{170}Er(^{9}Be,4n) 80−9213
^{175}Hf, three- and five-quasiparticle isomers, rotational bands and residual interactions from ^{170}Er(^{9}Be, 4n) 80−83022
^{178}Hf, energy levels, K-forbidden decays, M4 decay of yrast state 80−68506
^{178}Hf, g-factor for K=6, J$^{\pi}$=6^{+} isomer, perturbed ang. distrib. meas. 78−37277
Hg isotope shifts, odd-even staggering, Coriolis effects in particle-core coupling 79−49580
^{184}Hg, excited deformed band, shape isomerism anal. 77−6234
^{185}Hg, nuclear shape isomerism detected by laser spectroscopy 79−49576
^{190}Hg, 21 ns isomer $(\nu i_{13/2})^2$ interpretation from g-factor meas. 80−105945
^{191}Hg^{m}, and $^{190m-185m}$Hg, nucl. spins, on-line quantum beat spectrosc. determ. 80−9562
^{197}Hg^{g,m}, prod. in ^{197}Au(γ,π^{-}) 79−9548
Hg(π^{-},X), stopped π^{-} capture, product nuclei distribs., isomeric yield ratios, neutron multiplicity 77−18625
^{A}Ho, A=150, 151, 152, high spin isomer EC, ^{150,151,152}Dy levels, J$^{\pi}$ and transitions 79−89241
^{A}Ho, A=152,160, isomeric state struct. 80−83017
^{A}Ho, A=153, 160, isomeric levels and transitions, Nilsson model 80−18195
^{157}Ho→^{157}Dy decay, internal conversion electron spectra and eγ coincidences *(Russian)* 80−68604
^{158}Ho, isomeric state and rotational band meas. in ^{159}Tb(α,5n) and ^{160}Dy(p,3n) 77−2890
^{166}Ho, energies of low-lying high spin levels *(Russian)* 78−89793
^{132}I isomer and gamma-ray spectrum from ^{133}Cs(π^{-}p) 80−78199
^{132m}I, ^{134m}I, isomer yield ratios in ^{235}U(n,f) 77−38306
In isomeric decays, ^{A}Sn, A=120,122,124,126,128, levels, transitions and J$^{\pi}$ values 79−75851
In, isomeric state formation cross section with 14.8 MeV neutrons, half-life, γ-ray spectra 77−30604
^{A}In, A=113, 115, excitation by photon less positron annhilation, isomeric γ-transitions *(Russian)* 80−5089
^{127}In, β-decay obs., decay scheme, half-lives 79−45207
^{109}In high spin states, transitions, isomeric state, negative parity bands from ^{107}Ag(α, 2nγ) 80−451
^{111}In 21/2^{+} isomeric state g-factor and relaxation time from ^{109}Ag(α,2nγ) 80−73794
^{112}In, 8^{-}, 6^{+} isomeric states, $T_{1/2}$, g-factors via ^{112}Cd(p,n), ^{109}Ag(α,n) 77−10318
^{114}In isomer decay, spin, excitation function, T_{112} γ-X-ray and γ-γ coinc. 77−6312
^{115}In^{m}, nuclear excitation by e^{+} annihilation with K-shell electrons 79−22230
^{115}In(γ,γ), isomeric states excitation, integral cross sections 80−27528
^{114m}In, prod. in Cd(d,xn) reactions, $E_d \leq 27.5$ MeV, cross sections 80−13482
^{116m}In, prod. in Cd(d,xn) reactions, $E_d \leq 27.5$ MeV, cross sections 80−13482
^{119g,m}In, decay schemes, half-lives, excited levels 77−296
^{191}Ir(n,γ), thermal, isomer state excitation, relative probabilities 79−75814
^{38}K^{m}, β and γ spectra meas., determ. of isomeric ratios *(Russian)* 77−74771
^{38}K^{m} superallowed Fermi β-decay half lives 78−82318
^{41}K, highly stripped ions, recoiling in vacuo, γ-decays of isomeric states obs. 78−50119
^{38m}K, end point energy of superallowed Fermi decay 78−46030
^{84}Kr, 1.84 μs isomeric state, g-factor meas. 78−17101
^{85}Kr^{m,g} decay, ^{85}Rb levels, J$^{\pi}$ and transitions 80−78162
^{125}La 27/2^{+} 2737 keV three quasiparticle state, nuclear struct. of isomeric states using g-factor 77−88039
^{174}Lu isomeric levels, γ-spectra, T 1/2 and decay modes from ^{176}Yb(p,3n) 80−99151
^{178}Lu isomeric states and spins, transition probability from ^{181}Ta(n,α) 80−52582
^{258}Md isomer, EC decay, ^{258}Fm spontaneous fission, mass and kinetic energy distribs. 80−47518
Mg, isomeric state formation cross section with 14.8 MeV neutrons, half-life, γ-ray spectra 77−30604
^{89}Mo^{m} levels, transitions and half life from ^{93}Mo(p,p'3n) 80−86858
^{99}Mo, short lived isomers from photonuclear reactions, internal conversion coeffs. 78−37308
^{100}Mo(n,γ)^{99}Mo^{m1,m2,g}, isomeric cross section ratios 78−29448
^{24}Na^{m}, 1^{+} isomer, mag. moment 80−32177

nuclear isomerism continued
^{24}Na^{m}, polarised, β-decay asymmetry and mag. moment from Na(n,γ) 80−91157
^{24m}Na, laser induced nuclear orientation 80−57680
Nb, A=90, 92, short lived isomers from photonuclear reactions, internal conversion coeffs. 78−37308
Nb isotopes, A=95, 97, 99, beta-decay schemes, level struct. 77−26631
^{91}Nb, 17^{-}/2 state, g-factor meas. 80−32179
^{91}Nb, 3.8 μs isomeric state, mag. moment, TDPAD meas. 78−41634
^{93}Nb^{m}, γ-ray transitions of isomeric level, K-conversion coeff., exchange effects 77−6304
^{94}Nb(n,γ)^{95m,g}Nb, isomeric cross section ratio 79−49623
^{93m}Nb, radioactive decay period meas. *(French)* 77−79341
^{A}Nd, A=138,139, high spin states, isomers and γ-cascade from ^{140}Cd(α,xzn) 80−78120
^{138}Nd, 10^{+} isomeric states, systematic behaviour 79−30791
^{140}Nd ns isomers and yrast isomers, γ-transitions from ^{128}Te(^{16}O,4n) 80−78121
^{141}Nd, ^{142}Nd, high-spin states, lifetime meas. using (α,xn) reactions 77−18476
^{149}Nd, weakly deformed, isomeric $^{9+}/_{2}$ and lowest $^{7-}/_{2}$ states decay 79−89231
^{237}Np, effect of isomer shelf in photofission cross sections *(Russian)* 79−9648
^{A}Os, A=186, 188, 7^{-} isomeric state lifetime from W(α,2nγ) 79−17854
^{182}Os, K-isomer populations, (p,xnγ), (He,xnγ) reaction study 78−93927
^{188}Os, muonic resonance spectra, deduced isomer shifts and electric moments 80−18948
Pb, A=194, 196, 198, 12^{+} isomeric states, $T_{1/2}$, g-factor 77−74762
Pb, isomeric state formation cross section with 14.8 MeV neutrons, half-life, γ-ray spectra 77−30604
^{A}Pb, A=200,206, 12^{+} isomer states, quadrupole moments 80−27554
^{197}Pb isomers, half lives and decay 79−36197
^{200}Pb, obs. of levels in ^{198}Hg(α,2n) 78−66192
^{203}Pb, 480 ms isomeric 29/2^{-} state, decay scheme 77−22893
^{204}Pb, muonic, first excited 2^{+} state, isomer shift of E2 transition 80−99150
^{204}Pb, populated by ^{204}Bi decay, isomeric transitions 78−50122
^{207}Pb, muonic, octupole doublet isomer shifts, octupole vibrs. 80−95750
^{109}Pd, level structure and half life 77−82827
^{111}Pd^{g,m}, γ-ray decay, ^{111g}Pd half-life, ^{111}Ag levels and decay 78−541
^{142}Pm, multiplet splitting and isomerism, J, π, T1/2 via (d,2n) and (p,n) 77−14014
^{143}Pm high spin states, J^{π}, transitions, isomer g-factors from (d,2N), (α,2N) 80−32154
Po, A=202-210, isomeric levels, g, $T_{1/2}$ 77−14068
Po high spin isomers, deformed independent particle model, yrast lines, shape 79−480
Po, neutron deficient isotope prod. in ^{182}W(^{20}Ne,xn) reactions 78−8835
^{207}Po^{m}(2.79 s), ^{207}Po^{g} decay, spin from conversion electrons meas. 78−58252
^{209}Po, 31/2^{-} isomeric state, g-factor meas. 77−10317
^{211}Po excitation functions and isomer ratios from ^{208}Pb(α,n) and ^{209}Bi(α,np) 80−83039
^{212}Po excitation functions and isomer ratios from ^{209}Bi(α,p) 80−83039
^{212}Po, isomer with spin and parity 8^{+}, α- and γ-decay 78−82283
^{139}Pr isomeric 11/2^{-} state, half-life, g-factor, and nuclear orientation relaxation from ^{140}Ce(p,2nγ) 79−75837
^{144}Pr^{m}β-decay, ^{144}Nd levels and transitions, γ-ray spectra *(French)* 80−18250
^{148}Pr isomerism study from β and γ decay meas. 80−5096
^{A}Pt, A=186,188,190, subnanosecond high spin isomers, decay chains and lifetimes from Yb(^{16,18}O, xn) 79−45140
^{185}Pt^{m+g} decay, population of ^{185}Ir levels 80−9269
Pt(π^{-},X), stopped π^{-} capture, product nuclei distribs., isomeric yield ratio, neutron multiplicity 77−18625
Pu, A=239, 241, spontaneous fission, conversion electron spectra obs. 77−82864
^{A}Pu, A=238,240, fission isomer rot. spectra $I^{2}(I+1)^{2}$ correction 80−18229
^{237}Pu fission isomers, half lives and yield ratio, statistical model anal. from ^{239}Pu(γ,Zn) 79−40885
^{237}Pu fission single particle isomers, half lives and isomeric ratio from ^{239}Pu(γ,2n) 80−18181
^{239}Pu, 8-μs fission isomer, quadrupole moment 77−30484
^{239}Pu, spectroscopy in second minimum of pot. energy surface 79−30805
^{239}Pu(n,n′), 3-5 MeV, fission isomer prod. 77−61462
^{240}Pu, hexadecapole shape isomeric state, shell correction method fission barrier calcs. 80−545
^{240}Pu, reson. in isomeric and prompt fission probabilities 78−78429
^{240}Pu^{m}, shape isomer, half-life and excitation function meas. *(Chinese)* 78−78253
^{241}Pu isomeric state non-existence 80−105983
^{244}Pu(n,2n)^{243}Pu, E_n=14 MeV, search for finite isomer 77−54222
^{214}Ra, high spin yrast states in N=126 isotones 79−45131
^{213m}Ra, 2.1 msec. isomer, gamma and alpha decay meas. 77−14067
^{78}Rb band struct. and level scheme from ^{64}Zn(^{16}O,np) 79−54380
^{78}Rb β-decay half lives of isomeric and ground state from (^{16}O,3n) 80−27534
^{81}Rb, β^{+}-EC decay, $T_{1/2}$, ^{81}Kr levels 77−79309
Re, alpha decay studies of the isotope 79−63636
^{172}Re, isomeric states, γ-ray transition 79−9433
^{182}Re isomer decay mag. moment, ^{182}W high spin states, J assignments and mixing ratios 80−42593
^{187}Re(n,γ), thermal, isomer state excitation, relative probabilities 79−75814
^{99}Rh isomer, ($T_{1/2}$=4.5 hr.), decay, anticoincidence and integral coincidence spectra meas. 79−6479
^{100}Rh short lived isomer, decay scheme from (α,pn), (p,n) and (p,3n) 79−75920
^{103}Rh, neutron elastic and inelastic cross sections up to 1500 keV, γ-ray transitions, 40 keV isomeric state 77−23089
^{103}Rh(e,e′), 350-800 keV, isomer Coulomb excitation cross sections 80−22659
^{108}Rh, level structure and half life 77−82827
Rn high spin isomers, deformed independent particle model, yrast lines, shape 79−480
^{199}Rn and ^{199}Rn^{m} alpha decay signatures from ^{169}Tm(^{35}Cl,5n) 80−68610
^{212}Rn high spin isomers with core excited neutron configs. from ^{204}Hg(^{12}C, 5n) 78−54792
^{212}Rn, high spin yrast states in N=126 isotones 79−45131
nuclear isomerism continued
^{101}Ru, short lived isomers from photonuclear reactions, internal conversion coeffs. 78−37308
^{102}Ru(γ,p)^{101}Tc^{m,g}, isomeric cross section ratios 78−29448
S, isomer ratios in fission fragments at high excitation 80−32261
^{32}S shape isomeric state from unconstrained variation 80−95306
S6, A=120, 122, 3^{+} isomeric states quadrupole moments, (p,n) excited, TDPAD method 78−41635
Sb, A=115, 117, 11/2^{-} isomeric states, half-life, and g-factor 78−33122
Sb isomer ratio, high spin trapping from (α,xn)(α, pn) 80−22655
^{115}Sb g-factor of 19/2^{-} and 11/2^{-} isomers from ^{115}In(α,4n) 79−40845
^{115}Sb, g-factor of 19/2^{-} isomeric state, time differential perturbed ang. distrib. method 79−22192
^{122}Sb, 5^{+} isomeric state, mag. moment determ. from ^{122}Sn(d,2n)^{122}Sb 78−21493
^{122}Sb, 5^{+} state, mag. moment, g-factor meas. 77−71567
^{A}Sc, A=44m,46,47,48, fragment emission, two-step model applicability from ^{238}U(p,X) 80−99177
^{42}Sc, weak neutral current props., search for 0^{-} isomer using ^{42}Ca(p,n) 79−45126
^{43}Sc, J^{π}=19/2^{-} isomer, high-spin precursors, from ^{29}Si(^{16}O,pn) 80−57656
^{45}Sc, low-lying isomeric level rel. to stellar ^{45}Sc(p,γ)^{46}Ti reaction rates 78−93090
^{A}Sm, A=148, 150, 152, 154, levels, moments, isomer shifts, spectroscopic amplitudes, sixth order boson expansion 79−89242
^{140}Sm, 10^{+} isomeric states, systematic behaviour 79−30791
^{142}Sm isomers, lifetimes and transitions from ^{142}Nd(α,4n) 80−78122
^{142}Sm ns isomers and yrast isomers, γ-transitions from (^{24}Mg,4n), (^{19}F,4n) 80−78121
Sn, photoactivation by 42 MeV bremsstrahlung, gamma transition energies and line intensities 78−13057
^{112}Sn 6^{+} isomeric state g-factor and relaxation time from Cd(α,2nγ) 80−73794
^{121}Sn^{m}→^{121}Sn^{g}→^{121}Sb, branching fraction, K-shell IC coeff. 78−82319
^{132}Sn, doubly magic nucleus, level scheme 78−54668
^{132}Sn, energy levels, gamma transitions, spin and parity 80−9239
^{132}Sn levels, isomers, lifetimes and transition probabilities from fission 80−78163
Sr isotopes, A=95, 97, 99, beta-decay schemes, level struct. 77−26631
^{85}Sr^{m,g} decay, ^{85}Rb levels, J^{π} and transitions 80−78162
Ta, alpha decay studies of the isotope 79−63636
^{176}Ta, decay of four-particle isomer 78−70481
^{176}Ta, isomeric states and rot. struct. anal., in-beam γ-ray spectroscopy 78−78312
^{180}Ta mass, 10^{13} y naturally occurring isomer state 80−57670
^{180}Ta^{m}, β^{-} and EC branching ratios, K-internal conversion coeff., γ-intensities, T 1/2 80−68601
^{181}Ta(n,2n)^{180}Ta^{m}, 14.68 MeV, cross section 80−68659
^{181}Ta(n,α), thermal, isomer state excitation, relative probabilities 79−75814
^{A}Tb, A=147, 148, high spin particle-hole states, octupole M2/E3 isomers from ^{151}Eu(α,xn) 80−18171
^{151}Tb 11/2 isomer, high spin few-particle states, in beam study from (^{3}He,3n) and (α,4n) 79−17805
^{151}Tb lower excited state lifetimes, ^{151m}Tb isomer from ^{151}Dy decay 79−75919
Tc, A=98, 100, 101, short lived isomers from photonuclear reactions, internal conversion coeffs. 78−37308
^{A}Tc, A=93-96, excitation functions and isomer ratios from ^{93}Nb(α,xn) (x=1 to 4) 80−492
^{93}Tc $^{17}/_{2}$ isomer, parity mixing search, partial γ-decay widths from ^{65}Cu(^{32}S,2n2p), 120 MeV 78−93936
^{93}Tc 17/2^{-} isomer, internal conversion coeffs., parity mixing search from ^{92}Mo(α,2np) 43 MeV 78−78255
^{93}Tc, g.m, γ-ray spectra 79−6476
^{98}Tc 14 μs isomer, low lying levels and transitions from ^{98}Mo(p,n) 80−73802
^{98}Tc, lifetimes of isomeric states from ^{98}Mo(p,n), 4-5 MeV 78−82314
^{98}Tc, low-lying levels obs. in ^{98}Mo(p,n) 77−88076
^{99}Tc^{m} β-decay, β-branching, ^{99}Ru decay scheme 80−42596
^{99}Tc^{m} decay constant, chemical state effect 80−42591
^{100}Tc internal conversion, isomeric level half life from ^{100}Mo(p,n), 3.7 MeV 78−78313
^{100}Tc low lying and isomeric levels, transitions and mean lines from ^{100}Mo(p,nγ) 80−42548
^{100}Tc μs isomers, isomeric transitions and mean lives from ^{100}Mo(p,n) 80−73803
^{99m}Tc, X_{α}-SW-calc. of chemically induced decay constant variation of Tc in TcO_4^- and hexahalides 79−54769
Te isomer ratio, high spin trapping from Sn(α,3n) 80−22655
^{A}Te, A=117,119,121, ΔJ=1 band structures on ns isomeric states 79−54382
^{A}Te^{m}, A=125, 127, 129, 11/2^{-} isomeric state magnetic moments 80−42537
^{m}Te, A=125,127,129, internal conversion of M4 transitions at 109.27, 88.26, 105.50 keV 77−65214
^{121}Te isomeric state, spin, lifetime and mag. moment from (α,n),(d,Zn) 80−47387
^{129}Te^{m+g} decay, ^{129}I time depend. quadrupole interactions, γ-γ correlations 80−78145
^{132}Te from fission, 10^{+} isomeric state, J^{π} from deexcitation pattern, half life 80−460
^{134}Te, levels, J^{π}, 6^{+} isomer level mag. moment 77−82824
^{232}Th(γ,f), deep subthreshold photofission, double humped fission barrier anal., shape isomer 80−5179
^{42}Ti, ^{6},$^{+}$ state lifetime, B(E2) value 77−82863
^{43}Ti, lifetime and γ decay of isomeric 19/2^{-} state from ^{40}Ca(α,nγ) 20 MeV 78−70486
Tl, A=185,187 isomeric decays, half-life, $h_{9/2}$ intruder state 77−26616
Tl, isomeric state formation cross section with 14.8 MeV neutrons, half-life, γ-ray spectra 77−30604
^{186}Tl, isomer and ground state half-lifes 79−97652
^{192}Tl high spin band struct. and transitions, isomeric state from ^{181}Ta(^{16,18}O,xnγ) 80−47353
^{194}Tl high spin states, excitation functions, I^{π}=8^{-} isomeric state from ^{181}Ta(^{18}O,5n) 80−32163
^{206}Tl, excitation of 12^{-} isomeric state in Bi(n,α) at 14 MeV, half life 78−70453
^{206}Tl, isomeric yrast states obs. 77−281

nuclear isomerism continued
U spontaneously fissionable isomers, excitation by K shell e^+ annihilation, shape isomery model *(Russian)* 79−30802
^{A}U, A=236,238, fission isomer rot. spectra $I^2(I+1)^2$ correction 80−18229
$^{A}U^{m}$, A=236,238, isomeric to prompt fission ratios; fission fragments from (d,pf), (d,pnf) 80−86940
^{A}U(γ,f), A=235, 236, 238, deep subthreshold photofission, double humped fission barrier anal., shape isomer 80−5179
^{235}U internal conversion from $1/2^+$ isomeric state, U^{4+} electron configuration 80−58146
$^{235}U^{M}$ prod. by nuclear excitation by electron transition in plasma 80−22668
^{235}U(1/2$^+$; 73 eV) isomer *(Russian)* 79−9511
^{236}U fission shape isomer, γ-decay from ^{238}U(γ,2n) 80−18230
^{236}U isomeric and prompt fission, nuclear superfluidity evidence from ^{235}U(d,pf) 80−68711
^{236}U low lying levels from 4^- isomer decay in (n,e), (n,γ) 80−47396
^{236}U shape isomer, γ branch upper limit, γ-yields from ^{235}U(d,p) 80−99145
^{236}U shape isomer, rot. band and const. via ^{235}U(d,p) 12 MeV 77−34208
^{236}U shape isomer populated in $^{235}U(n_{th},\gamma)$, isomeric/prompt fission ratio 77−323
^{237}U shape isomer, γ-decay search, branching ratio from $^{238}U(\Gamma,2n\gamma')$ 45 MeV 78−93961
^{238}U delayed fission cross-section for 14 MeV neutrons, shape isomer excitation 77−26808
^{238}U, quadrupole moment meas., using ^{238}U(d,pn) 79−71856
^{238}U shape isomeric γ-decay, in μ^- atoms, isomer lifetime 77−34245
^{238}U, spontaneous fission, conversion electron spectra obs. 77−82864
U(γ,f) A=235,238, 25 MeV bremsstrahlung, prod. yields, mass chains, charge distribs. 77−6470
^{46}V, weak neutral current props., search for 0^- isomer using ^{46}Ti(p,n) 79−45126
W, alpha decay studies of the isotope 79−63636
^{179}W, backbending, high spin isomer decay 78−45997
^{125}Xe, negative parity levels in odd-A neutron deficient isomers 79−17817
^{125}Xe odd and even parity band structs., level lifetimes from ^{125}Te(^{3}He,3nγ) 80−27533
Y isomeric state formation, cross section with 14.8 MeV neutrons, half-life, γ-ray spectra 77−30604
Y isotopes, A=95, 97, 99, beta-decay schemes, level struct. 77−26631
$^{A}Y^{m,g}$, A=86, 87, isomeric yield ratios and γ-spectra from ^{93}Nb(π^-,X) 80−86857
^{59}Y(n,γ), thermal, isomer state excitation, relative probabilities 79−75814
^{83}Y β^+-decay, ^{83}Sr nucl. energy levels, γ-ray coincidence meas. 77−6309
$^{87}Y^{m}$ orientation meas. in Al and Au hosts, mag. moment of $9/2^+$ isomeric state 78−41632
^{88}Y 14 ms 8^+ isomeric state, g-factor from ^{87}Rb(α,3n) 80−63080
^{99}Y→^{99}Zr, half life and beta decay investigation 79−17863
^{172}Yb, muonic resonance spectra, deduced isomer shifts and electric moments 80−18948
Zr isotopes, A=95, 97, 99, beta-decay schemes, level struct. 77−26631
^{88}Zr transitions and high spin states above 8^+ isomer, ^{86}Sr(α, 2nγ)^{88}Zr 79−40848

nuclear isospin
1p shell isotensor charge depend. contrib. to isobaric mass multiplets, shell model anal. 79−67632
1p-shell, isospin mixing between T=0 and 1 states 79−6430
$^{12}C(\pi^{\pm},\pi^{\pm\prime})$, isospin mixing doublet, possible isospin mixing matrix element extraction 79−85364
^{A}S, A=32,34, E1 and E2 strength, E1 giant resonance decay, isospin from Si(α,γ) 79−89266
A=200 region, macroscopic fission barriers, isospin depend., liquid drop model 80−57811
A=21 to 44, energy levels, energies, mixing rations, spin assignments 79−13208
A=24 isobars, excitation of three isospin modes of giant dipole resonance 77−6338
A=24 to 209, 7 to 26 MeV, neutron scattering and isospin dependence of the optical model potential 79−45250
A=26, isoscalar and isovector E2 transition matrix elements 78−25148
A=42 isotopic spin triplet, Coulomb energies and shifts, microscopic calcs. 80−9200
A=50-57, N=28-30, effective interactions and energy spectra from shell model calc. 78−82299
A-12, T=1 isospin triplet decay 78−78322
asymmetric nuclear matter, isospin waves, IAS and giant Gamow-Teller resonance 80−91142
charge independent pairing Hamiltonian, variational approach 78−86488
compound nuclear reactions, isospin mixing treatment 79−3119
compound nucleus mirror reactions, isospin mixing from Ericson fluctuations 79−22190
compound nucleus reactions, mirror channel and isospin mixing correlations 79−9488
core polarisation in inelastic scatt., extension to include charge-exchange reactions 78−78359
Coulomb isospin mixing, self consistent theory, isobaric states in RPA, isovector forces *(Russian)* 79−22181
dense neutron and nucl. matter, spin and isospin instability 78−86474
dense neutron and nuclear matter, spin and isospin stability 80−22737
double folding pot. for inelastic scatt. between nuclei 80−13425
four-body model of four-nucleon system, spin and isospin effects 79−71802
giant isovector monopole states, isospin splitting and mixing 80−27609
giant multipole resonances, isotopic splitting 79−6378
giant multipole resonances, spin-isospin vibrs., spin waves, Regge poles in collective model 78−89777
ground-state correlations observable in hard heavy-ion reactions 78−78406
heavy nuclei, photoproton reaction, isospin effect 79−80926
high energy hadron-nucleus scatt., correl. and isospin effects, multiple diffr. theory 78−94000
hydrodynamical model of nuclear fluid, spin and isospin props. 78−70479
intermediate and heavy nuclei, O^+ state, isospin purity violation 78−12964

nuclear isospin continued
isobaric quartets in nuclei, T=3/2 states, isobaric multiplet mass eqn. 79−93519
light nuclei, isospin mixing, charge depend. nuclear forces and Coulomb interactions 80−5056
light nuclei, isospin mixing matrix elements 78−37289
light nuclei, schematic model for isospin mixing 78−66198
medium nuclei, photoproton spectra and preequilib. decay, microscopic theory 80−47464
microscopic collective Hamiltonian, spin-isospin part of the matrix element 79−63609
mirror channel fluctuation reactions, isospin mixing 78−33157
mirror nuclei, spin and isospin distribs. in medium heavy nuclei 79−71789
mirror state EM decay rates, multipole matrix element isospin decomposition 79−36190
multipole giant resonances, characteristic features *(Dutch)* 79−17875
nonlocal optical pot., isospin depend. 79−93579
nuclear matter, polarised, thermal props., temp., spin isospin and spin-isospin pressure 80−102135
nuclear matter, spin-isospin and pion condensation phase transistions, eqn. of state 80−86843
open shell nuclei by seniority and reduced isospin projections 80−47415
pair correlations, isotopically invariant, generalisation of Mottelson function 79−6366
particle hole effective interaction, empirical, enhanced isospin depend. 78−78274
photonuclear reactions review, giant dipole resonances and cross sections 80−5125
proton-neutron basis, decomposition matrix rel. to basis of specified isospin T 80−37337
quadrupole moments and rms charge radii, shell model calcs. 80−47369
single-particle potential, symmetry coefficient and effective mass in nuclear matter 79−13234
spin and isospin stability of dense neutron and nuclear matter with hard core interaction 79−26386
spin-isospin density phase in finite nuclei, strongly oblate shape 80−22746
spin-isospin polarizability of nuclear matter and renormalization of weak currents 79−67697
strong isospin mixing in nuclei 78−37264
sum rules for spin-dependent excitations of nuclei 79−59018
superallowed Fermi β-decays, impurity correction 79−93563
superfluid model, isotopic invariance and pairing energies 80−22687
supermultiplet model, transformation matrices rel. to canonical basis of group SU_4 79−67693
T=2 states in T_z=1 nuclei, EN decays 78−13129
tensor quasiparticle interaction and spin-isospin sound in nuclear matter 79−63618
threshold states in different schematic models 78−82272
total neutron widths, isobaric analogue reson. 79−6540
trinucleon photoeffect to isospin 3/2, using coupled hyperspherical harmonics 78−41696
Z=73-85, preactinide nuclei, fission barriers in droplet model, isospin depend. *(Russian)* 80−5120
μ^- p→ν_μnγ, appl. to nuclear spin and isospin doublets 78−82320
(n,n), isospin depend. of nucleon-nucleus optical pots. 77−34311
NN interaction, isospin nonconservation using relativistic formalism 79−9500
(p,p), isospin depend. on analysing powers 78−82343
(π^+,π^-) A=9-32, 180 MeV 80−105960
(π,π'), 1p shell targets, DWIA calcs., strong transitions, isospin effects 80−42708
(π,π'), collective transitions, giant resonances, isospin content and spin transfer 80−42580
$(\pi^{\pm},\pi^{\pm\prime})$, π^- nuclear response enhancement, continuum effects, stretched state isospin mixing 80−86929
^{25}Al, isospin forbidden T=3/2 resonances, isospin mixing 77−18507
^{26}Al 1^+T=0 states, isobaric analogue state, spin-isospin effective interaction from ^{26}Mg(p,n) 80−68553
^{210}At, 19^1 isomeric state, g-factor 78−21499
^{8}B, isospin symmetry breaking in A=8 mirror decays 78−93973
^{9}B, 17.11 MeV level and second T=3/2 quadruplet 79−22193
^{10}B(d,d′), energy dependent isospin violation 77−14134
^{11}B+^{11}C, semi-leptonic weak and EM interactions, isoelastic processes 77−18528
^{12}B, polarised, higher order effects in determ. of asymmetry parameters in β-decay 79−22247
^{8}Be,(3^+,T=1 states) 78−89789
^{8}Be isospin mixed 2^+ doublet, level parameters from ^{4}He(α,α) 80−27556
^{8}Be, isospin states, spectroscopic factors 77−65198
^{8}Be, Z-state, threshold st at isospin mixing from ^{7}Be+n 77−54150
^{9}Be T-3/2 levels, isospin forbidden particle decays 77−6320
^{208}Bi, 0^+ IAS, spreading width and isospin impurity, isovector monopole state influence 80−78155
$^{A}C(\pi,\pi')$, A=12, 13, ∼180 MeV, isospin mixing, levels, excitation functions and ang. distribs. 80−42543
^{12}C, 1^+ states, isospin mixing 78−4898
^{12}C isospin mixing and violation from ^{11}C(d,d′) and ^{10}B(α,d) 77−18385
^{12}C isospin mixing from ^{10}B(^{3}He,pα) and ^{11}B(p,α) 77−38242
^{12}C J-transfer determ. and isospin mixing from ^{13}C(d,t) polarised d 79−49579
^{12}C, lowest T=2 state mass 78−66211
^{12}C negative parity states from ^{13}N isospin forbidden p decays in ^{11}B(^{3}He,np) 79−26372
$^{12}C(^6Li,\alpha)^{14}N$ (2.31 MeV), isospin violation 78−41763
^{12}C(d, d′), isospin violating direct reaction, Coulomb interaction role 80−102170
$^{12}C(d,\alpha)^{10}B$, (1.74MeV,T=1 state), isospin violation 78−70541
^{12}C(e,e) , 12.71 and 15.11 MeV level struct. and isospin mixing from form factors 80−32186
$^{12}C(\mu^-,\nu_\mu\gamma)^{12}B$, appl. of μ^- radiative capture to nucl. spin and isospin transitions 78−86511
^{12}C(p,p′), pol. p, 800 MeV, unnatural parity states excitation, anal. powers and isospin 80−68538
$^{12}C(\pi^+,\pi^{+\prime})$, 100-291 MeV, cross sections and ang. distribs., spin and isospin transfer 80−52697
$^{12}C(\pi^{\pm},\pi^{\pm}d)$, ^{10}B, 180 MeV, isospin effects in (3/2, 3/2) resonance region 79−85365
$^{12}C(\pi^{\pm},\pi^{\pm\prime})$, 162 MeV, strongly isospin-mixed 79−93505

nuclear isospin continued
$^{12}C(\pi^+,\pi^+p)^{11}B$, 180 MeV, isospin effects in (3/2, 3/2) resonance region 79−85365
^{13}C, giant resonance, isospin splitting 78−577
^{13}C, T=3/2 level from isospin forbidden resonance in Be(α, n) 79−3123
^{13}C-^{13}N mirror nuclei, 15.1 MeV resonance width, isospin forbidden transitions 79−13265
$^{13}C(d,{}^3He)$, isospin violating direct reaction, Coulomb interaction role 80−102170
$^{13}C(d,t)$, isospin violating direct reaction, Coulomb interaction role 80−102170
$^{14}C(\pi\gamma)$, collective resonances, A=14 isobaric states, shell model predictions 79−85386
^{A}Ca, A=40,48, states with definite isospin, RPA ground state correlations 77−6238
^{40}Ca, 1$^-$ T=0 state, isospin forbidden electroexcitation 78−25177
^{40}Ca, isospin forbidden E2 transition strengths 78−13059
$^{40}Ca(n,n')$ 1 isospin effects 77−34312
^{41}Ca giant dipole resonance, isospin struct., direct-semidirect anal. from $^{40}K(p,\gamma)$ 80−47449
$^{44}Ca(\gamma,p)$, isospin mixing estimates in giant dipole resonance region 77−26666
^{33}Cl, isospin forbidden T=3/2 resonances, isospin mixing 77−18507
^{55}Co, GDR, (p,γ) cross section determ. in shell model 78−78345
^{59}Co, isospin effects in GDR region 78−78344
$^{59}Co(p,\gamma_0)$ polarised p, 5.8 to 16.5 MeV, isospin splitting 78−70533
^{52}Cr, EM decay of isobaric analogue states to low lying states 78−86492
$^{53}Cr(\gamma,p)^{52}V$, cross-section, 14.4-27 MeV, isospin splitting 80−520
^{134}Cs isospin forbidden beta-decays 77−67722
(d,p), A=88-106, pol. d, excitation curve isospin anomaly, neutron single particle resonances 80−27595
^{18}F, 5605 and 5668 KeV states, isospin mixing 78−543
^{18}F isospin mixed states via $^{14}N(\alpha,\alpha')$ 77−14029
^{18}F $J^\pi=3^-$ doublet at 6241 keV, isospin mixing from (p,γ), (p,α), (α,γ) ($^{14}N,\alpha$) 80−511
^{18}F level spin, isospin and parity assignments, from $^{20}Ne(d,\alpha)$ tensor analysing power meas. 78−74305
^{18}F resonances, α-widths, isospin and parity mixing, R-matrix anal. of $^{14}N(\alpha,\alpha)$ 80−91162
^{19}F isospin mixing and ω_o value from ^{19}O β-decay 79−9520
^{19}F isospin mixing in yrast $I=5/2^+$ level 79−93508
$^{A}Fe(p,\gamma_0)Co$, A=54,56, giant dipole resonance splitting, direct-semidirect capture model anal. 80−106055
$^{54}Fe(\gamma,n)$, cross section meas., E1 giant dipole isospin splitting 79−17892
$^{2}H(d,n)^3He$, 15.5, 17 MeV, pol. d, anal. power direct reaction and isospin symmetries 80−515
$^{2}H(d,p)^3H$ and $^{2}H(d,n)^3He$, comparison of analysing powers 2.5 to 11.5 MeV 79−6628
$^{2}H(\pi,\pi)$, 142,180 MeV, isospin effects, three body calcs. 77−6450
$^{2}H(\pi^\pm,p\pi^\pm)$, 340 MeV/c, reaction mechanisms and isospin effects 80−32306
^{3}H, three particle photodisintegration, isospin transitions *(Russian)* 78−589
$^{3}H+^{3}He$, semi-leptonic weak and EM interactions, isoelastic processes 77−18528
$^{3}H(p,p)$, diffractional scatt., isospin depend. *(Russian)* 78−54763
$^{3}H(p,p)$,156 MeV, scatt. amplitude isospin depend. 77−61404
^{A}H, A-2,3, photodisintegration cross section quadrupole contrib. from isospin sum rules 77−30550
^{3}He, isospin 1/2 three body photodisintegration suppression 79−40902
^{3}He, three particle photodisintegration, isospin transitions *(Russian)* 78−589
$^{3}He+\mu^-\rightarrow\nu_\mu+^{3}H$, angular correlations and capture rates, spin and isospin transitions, hyperfine effects 78−70494
$^{3}He(\mu^-,\nu_\mu\gamma)^3H$, appl. to nuclear spin and isospin doublets 78−82320
$^{3}He(p,p)$, diffractional scatt., isopin depend. *(Russian)* 78−54763
$^{3}He(p,p)$,156 MeV, scatt. amplitude isospin depend. 77−61404
$^{3}He(\pi,\pi)$, role of spin isospin effects in Δ(1236) resonance domain *(Russian)* 78−78423
$^{3}He(t,d)^4He$, charge asymmetry effects 79−3159
^{4}He, low lying T=1 level ordering from p-^{3}He elastic scatt. 79−26438
^{A}He, A-3,8, photodisintegration cross section quadrupole contrib. from isospin sum rules 77−30550
^{111}In isospin mixing matrix element from (p,p′),(p,α) and (α,α′) 77−57598
^{6}Li, η meson photoprod. reaction amplitude, isospin character 77−14111
$^{6}Li+\mu^-\rightarrow\nu_\mu+^{6}He$, angular correlations and capture rates, spin and isospin transitions, hyperfine effects 78−70494
^{8}Li isospin forbidden beta-decays 77−67722
^{8}Li, isospin symmetry breaking in A=8 mirror decays 78−93973
^{20}Mg, β-delayed proton obs., mass excess of T=2 state in ^{20}Na 79−22234
^{24}Mg Coulomb matrix elements, isospin mixing in giant dipole resonance from $^{20}Ne(\alpha,\gamma)$ 79−93507
^{24}Mg lowest $J^\pi=0^+$, T=Z level from $^{23}Na+p$ reactions, narrow resonance, isospin forbidden particle decays 78−89871
^{26}Mg, giant dipole resonance formation, isospin effects *(Russian)* 77−14020
$^{26}Mg(\gamma,n)^{25}Na$, 19.5 to 27.0 MeV, giant dipole resonance decay channel determ., isospin component 79−26423
^{28}Mg $\Delta T=1$ $0^+\rightarrow0^+$ β-decay, isospin forbidden branching ratio to ^{28}Al 79−93560
^{28}Mg, isospin forbidden β-decay 78−78315
$^{A}Mo(n,n)$ A=92,96,98,100, E_n=7 to 26 MeV, determ. optical model pot. parameters 79−22286
$^{92}Mo(n,n')$, isospin effects 77−34312
$^{92}Mo(n,n')$ deformation parameter isospin depend. 77−82817
$^{92}Mo(n,n)$, elastic and inelastic, 11 MeV, isospin effects, optical and deformation parameters 79−17794
^{12}N, polarised, higher order effects in determ. of asymmetry parameters 79−22247
$^{14}N(\alpha,\gamma)^{18}F$, parity violation with isospin change 78−94018
$^{14}N(d,d')$, energy dependent isospin violation 77−14134
$^{14}N(d,d')$, 10-17 MeV, isospin non-conservation, direct DWBA and Hauser Feshbach anal. 79−67757
$^{14}N(\gamma,n_0)^{13}N$, 17 to 26 MeV, angular distrib., giant dipole resonance, single-particle nuclear model 80−52659
$^{146}Nd(n,n)$, 7 MeV, isospin effects 77−26768
^{21}Ne T=3/2 level decay width for isospin forbidden particle decays 77−6322

nuclear isospin continued
^{A}Ni, A-55,60, giant dipole resonance formation, isospin effects *(Russian)* 77−14020
^{A}Ni, A=57, 59, 61, 63, variation of spectra, isospin mixing 80−13401
$^{A}Ni(e,e')$, A=58,60,64, giant dipole resonance isospin splitting 77−50116
$^{A}Ni(\gamma,p)$, A=58,60, giant dipole resonance region, isospin effects 77−61398
^{58}Ni (p,p) 100 MeV, systematic optical model anal. 78−66274
^{58}Ni, $J^\pi=6^+$, 5.125 MeV state, isoscalar character 79−22227
$^{58}Ni(\gamma,\gamma)$, M1 strength isospin splitting for dipole ang. distrib. states 80−13412
$^{62}Ni(\gamma,X)$, 19.2-26.2 MeV, photoneutron and photoproton spectra, giant dipole resonance-decay, isospin conservation 80−13443
^{15}O T=3/2 levels from $^{17}O(p,t)$ 78−78264
^{16}O, 4$^-$ particle-hole states, isospin mixing 80−99123
^{16}O, 7.12 MeV 1$^-$ state, isospin mixing 77−283
^{16}O, α spectroscopic amplitudes using isotopic spin formation 77−14072
^{16}O, isospin forbidden 7.12 MeV transition, continuum shell model calc. 77−18472
^{16}O, isospin forbidden E1 transition strengths 78−13059
^{16}O isospin mixing matrix elements, three level model 80−78136
^{16}O, strong isospin mixing effect 78−8832
^{16}O, T=0 pairing vibr. determ. from $^{14}N(^3He,p)$ 78−70422
$^{16}O(\alpha,X)$, isospin mixing, shell model calcs. with and without continuous spectrum 77−2979
$^{16}O(\alpha,\alpha)^{16}O$, 6.9-10.2 MeV, level and isospin mixing parameters 78−66292
$^{16}O(\alpha,\gamma)^{20}Ne$, 6.9-10.2 MeV, level and isospin mixing parameters 78−66292
$^{16}O(p,{}^3He)^{14}N$, 27 to 30 MeV, isospin conservation 78−50170
$^{16}O(p,t)^{14}O$, 27 to 30 MeV, isospin conservation 78−50170
$^{16}O(\pi,\pi')$, ~180 MeV, isospin mixing, levels, excitation functions and ang. distribs. 80−42543
^{17}O, giant resonance, isospin splitting 78−577
$^{18}O+\pi^+(\pi^-)$, elastic and inelastic scatt., angular distrib., 180 MeV, comparison with ^{8}Si 78−94035
^{29}P, deduced levels from ^{29}S β^+-delayed proton decay 79−22241
^{29}P, isospin forbidden T=3/2 resonances, isospin micing 77−18507
^{30}P level width isospin depend., excitation functions, statistical anal. of $^{29}Si(p,\alpha)$ 80−78152
^{207}Pb, T=45/2 isobaric analogue state obs. in $^{208}Pb(^3He,\alpha)^{207}Pb$ 78−93928
^{208}Pb, fine structure between 8 and 12 MeV 78−13071
^{208}Pb, isobaric analogue states, effects of Coulomb isospin coupling, random-phase method *(Russian)* 80−86808
$^{208}Pb(^3He,\alpha)^{207}Pb$, 70 MeV, deephole states, $T_>=45/2$ components 78−82362
$^{208}Pb(n,n')$, isospin effects 77−34312
$^{208}Pb(p,p)$ 100 MeV, systematic optical model anal. 78−66274
^{32}S energy levels, spin, parity and isospin assignments from $^{31}P(^3He,d)$ 78−78265
^{42}Sc, beta decay, isospin symmetry hindered branch 78−21526
$^{45}Sc(\gamma,p)$, isospin mixing estimates in giant dipole resonance region 77−26666
$^{A}Se(n,n)$, 6-10 MeV, A=76,78,80,82, isospin effects in scatt. pots. 77−26757
$^{A}Se(n,n)$ 6-10 MeV, A=76,78,80,82, isospin effects 77−6383
^{24}Si, isobaric multiplet mass eqn., test from decay 79−40890
^{28}Si, $J^\pi=0^+$, T=2 level, isospin forbidden resonance 79−45236
$^{28}Si+\pi^+(\pi^-)$, elastic and inelastic scatt., angular distrib., 180 MeV, comparison with ^{18}O 78−94035
$^{28}Si(\gamma,X)$ giant dipole resonance isospin mixing 77−74832
^{32}Si Coulomb matrix elements isospin mixing in giant dipole resonance from $^{28}Si(\alpha,\gamma)$ 79−93507
$^{A}Sm(n,n)$, 7 MeV, A=148,150, isospin effects 77−26768
^{143}Sm, $T_>$ hole analogue states, p decay, deduced states and p branching ratio 78−70451
Sn (n,n′) deformation parameter isospin depend. 77−82817
$^{A}Sn(n,n')$, A=116, 118, 120, 122, 124, 11 MeV, levels, deformation parameters, isospin effects, optical parameters 80−57679
$^{120}Sn(p,p)$ 100 MeV, systematic optical model anal. 78−66274
$^{88}Sr(n,n)$, elastic and inelastic, 11 MeV, isospin effects, optical and deformation parameters 79−17794
^{A}Te, A=122,124,126 yrast band double backbending, possible mechanisms *(Chinese)* 80−99120
^{44}Ti, lowest T=2 state decay 78−78304
^{44}Ti lowest T=2 state isospin forbidden γ-decay from resonances in $^{40}Ca(\alpha,\gamma)$ 79−22228
^{46}Ti (γ,N), 12-25 MeV, isospin splitting in giant dipole resonance 79−45152
$^{46}Ti(\gamma,p)$, isospin mixing estimates in giant dipole resonance region 77−18528
$^{50}Ti(\gamma,X)$, photoneutron and photoproton cross sections, giant dipole resonance isospin splitting 80−13442
$^{64}Zn(\gamma,n)^{63}Zn$, giant dipole resonance, isospin splitting *(Russian)* 78−46040
$^{40}Zr(n,n')$, isospin effects 77−34312
^{90}Zr (p,p) 100 MeV, systematic optical model anal. 78−66274
$^{90}Zr(n,n')$ deformation parameter isospin depend. 77−82817
$^{90}Zr(n,n)$, elastic and inelastic, 11 MeV, isospin effects, optical and deformation parameters 79−17794
^{97}Zr, $T_>$ hole analogue states, p decay, deduced states and p branching ratio 78−70451

nuclear liquid drop model
A=200 region, macroscopic fission barriers, isospin depend., liquid drop model 80−57811
alpha decay as a fission-like process, Q-value and half-life calc. 79−93566
alpha-decay, decay periods in liq. drop model *(Russian)* 80−32246
arbitrary scalar functions, divergence relns. and multipole expansions 79−6434
binary fission saddle pints, shape parametrization for liquid-drop studies 80−106086
charge and slope polarisation of fission fragments, fusioning nuclei, and heavy ion scatt. 79−9543
CM(3) collective model, geometric quantisation 80−5078
compressible model and mass formula 77−74780
consistent two-centre model, appl. to ^{238}U asymmetrical fission *(Russian)* 77−2974

nuclear liquid drop model continued
Coulomb energy, of uniformly charged hollow circular cylinder *(French)* 77−42460
Coulomb energy of circular torus, application to crit. fissility *(French)* 79−6373
deep inelastic scattering, fragment nuclides distribs., neutron rich nuclei prod., diffusion model 78−58297
deformation energy calculation program 79−13197
deformation energy for axial symmetric nuclei 79−59022
deformed and superdeformed nuclei from heavy ion reactions, α-decay amplification 80−102156
deformed nuclei, surface thickness effects and multipole excitation splitting, sum rule approach 79−453
droplet of nucl. matter under rapid rot., anal. using Thomas-Fermi method 79−36179
ellipsoidal, liquid-drop model, irrotational incompressible hydrodynamic flow 80−83050
even-even nuclei, electric and dynamic quadrupole moments 78−66203
even-even rare earths, microscopic quadrupole and hexadecapole moments 80−13376
fission, charge division 78−17173
fission, most probable charge, shell and deform. effects 78−29440
fission barrier calculations, effect of simple consistency condition, drop model with shell corrections 77−67732
fission instability, high angular momentum, deformation energy surface calc. 79−93603
fission of heavy nuclei, calc. of Coulomb energy of distorted nuclei 79−63654
fission scission point model based on deformed shell effects 77−10455
fissionability, target mass depend. for π, γ, α, p, cascade-evaporation and liquid drop calcs. *(Russian)* 80−106089
fissioning nucleus, deformation process mass parameter, liquid drop model 80−102221
GDR in droplet model 77−74781
generalisation as theory for heavy ions collision *(Rumanian)* 78−58260
giant resonances, stability and polarisation *(French)* 80−22669
heavy ion collisions, charge equilibrium and mass transfer, liquid drop model 79−97722
heavy ion collisions, hot compressed zone stability and temp., liquid drop model 80−78316
heavy ion collisions, rarefaction of oblate shaped nuclear matter, hydrodynamics calcs. 78−89894
heavy ion deep inelastic reactions, charge equilibration 79−49635
heavy ion fusion reactions, charge density asymmetry liquid drop model 80−63220
heavy ion reactions, potential energy surface topography 77−330
heavy-ion diffuse surface nuclear and Coulomb pot. energies 77−18593
heavy-ion induced fusion reaction products, statistical and liquid drop model anal. 78−66312
identical nuclei, collisions, heavy ion real pots. *(German)* 77−57691
inert gas, electronic structure extension of nucl. model 79−94769
low-lying collective states, Fermi liquid approach *(Russian)* 78−89772
mass formula, higher-order vol. symm. terms, droplet model, Hartree-Fock effective interactions 78−89808
mass formulae considering spin and compressibility effects 77−22865
mass from inhomogeneous partial difference eqns. 77−6268
moment map and collective motion, Hamiltonian action of Lie group 80−91138
neutron skin, compared with droplet model theory 80−52599
neutron-rich nuclear potential energy surfaces 80−18183
nuclear matter density determ., HF versus droplet model 80−68574
nucleus-nucleus potential from liquid drop model 78−50204
one body dissipation and super viscidity of nuclei, nuclear fissior, collisions and deformation 78−86501
potential energy surfaces, binary fission, fusion, liquid drop model *(Rumanian)* 78−86547
potential energy surfaces, folded Yukawa-plus-exponential model 80−86816
preactinide nuclei, fission excitation functions and fission barrier height, liquid drop model 80−47513
rotating nuclei, critical ang. momentum and equilibrium figures from ellipsoid, liquid drop model *(Russian)* 80−37339
rotating nuclei, from heavy ion collision, high spin states instability against fission *(Rumanian)* 78−50150
rotational band struct. in deformed doubly even nuclei, two fluid model 77−10341
semiempirical droplet model, mass excess values reported 77−6266
semiempirical liquid drop model, shell correction formula 77−6267
semiempirical shell correction to droplet model, magic number effects 77−10339
shell correction for masses and radii 77−22863
shell correction to liquid drop energy 78−12992
shell corrections to semi-empirical formulae for binding energy and radius *(Russian)* 78−78283
statistical fission parameters, ang. momentum depend. in statistical/rotating liquid drop model 78−89846
superheavy nuclei, ^{300}120, effect of nuclear force finite range on fission and heavy-ion reactions 78−13180
superheavy nuclei, lifetime, theoretical prediction of nonoccurrence in nature 78−662
surface energy, spin-orbit interaction effects, Fermi liquid drop vibrs. *(Russian)* 78−86495
surface tension coefficient calc. in Fermi model *(Russian)* 77−74782
Thomas-Fermi, extended model, binding energies and liq. drop parameters 77−67699
unified nuclear pot. for heavy ion elastic scatt., fission, fusion, masses and deformations 80−5189
unified pot. from liquid drop model, description of nuclear props. 79−22213
very high spin states from liquid drop model 80−5047
Z=73-85, preactinide nuclei, fission barriers in droplet model, isospin depend. *(Russian)* 80−5120
μ capture, subsequent excitations and particle emission cascade, hydrodynamical model 78−89825
p induced reactions at intermediate energy, nuclear fissility anal. 78−70579
^{26}Al, liquid-drop limit, fusion of ^{12}C+^{14}N 78−4959
^{40}Ar+^{109}Ag, 170-340 MeV, fission barriers at high ang. momenta 77−26786
^{209}Bi+^{136}Xe, stochastic model for strongly damped collisions with liquid drop driving forces 78−89834

nuclear liquid drop model continued
Cf, splitting of cold and hot nuclei *(Russian)* 78−29516
^{244}Cm, nucl. shape of first saddle point 77−74756
^{A}Fm(n,f), A=253, 255, 257, 259, fission mass distrib. transition, liquid drop and shell model calcs. 80−32310
^{A}Fm(sf), A=254, 256, 258, 260, fission mass distrib. transition, liquid drop and shell model calcs. 80−32310
^{150}Nd+^{150}Nd→^{300}120, effect of nuclear force finite range on fission and heavy-ion reactions 78−13180
^{56}Ni from HI reactions, superdeformed nucleus decay, α-decay amplification 80−68608
^{62}Ni(^{32}Cl,f), statistical anal. of excitation functions, Bohr-Wheeler and liq. drop model 78−13181
Pb+heavy ion hard reaction, ground state correlations from liquid drop model 79−22308
^{141}Pr(^{35}Cl,f), statistical anal. of excitation functions, Bohr-Wheeler and liq. drop model 78−13181
^{240}Pu, hexadecapole shape isomeric state, shell correction method fission barrier calcs. 80−545
^{240}Pu, nucl. shape at first saddle point 77−74756
^{116}Sn(^{32}Cl,f), statistical anal. of excitation functions, Bohr-Wheeler and liq. drop model 78−13181
^{149}Tb from HI reactions, superdeformed nucleus decay, α-decay amplification 80−68608
^{236}U, effect of nuclear force finite range on fission and heavy-ion reactions 78−13180
^{236}U fission fragment kinetic energies, wall and window one body dissipation model 80−52703
^{236}U nuclear instability and fission in strong mag. field energy level deformation *(Russian)* 79−13360
^{238}U fission, pot.-energy surface calc. 77−61465

nuclear magnetic acoustic resonance *see acoustic nuclear magnetic resonance*

nuclear magnetic moment
see also gyromagnetic ratio; molecular nuclear coupling; nuclear magnetic resonance
β-emitting nuclei polarised by fast polarised beams 77−28502
A=12-240, even-even, dynamic deformation theory, B(E2) values, quadrupole and mag. moments 80−68591
A=15 mag. moments, nuclear Dirac wave function test 80−5060
A=16 to 40, mag. moments, shell model calcs, mesonic exchange current effects, book contrib. 80−479
A=6to 14, radiative pion capture, mag. dipole resonance excitation in 1p shell nuclei 78−74408
A≥208, accurate g-factor measurement using heavy-ion induced reactions 77−26572
axially symmetric rare earths, mag. moments, current densities in projected HF approach 79−89236
band crossing in interacting boson model, E2 transition probabilities and g-factors 80−102101
collective props. of nuclei deduced from electron scatt., deformed nuclei, review 78−50064
conference on mesonic interface in nuclear struct. Erice, Italy (Sept. 1976) 79−26374
conference on nuclear struct. spectroscopy and atomic nucleus struct., Tashkent (Mar. 77) 79−6470
cross conjugate nuclei, correl. between g-factors of cross-conjugate pairs of states 79−460
deformed nuclei, approximate projection technique for EM properties calc. 79−93510
deformed nuclei, HF approach to mag. moments 78−12967
deformed nuclei, magnetic dipole γ-transitions, one particle matrix element tables 79−6472
deuterons, D-state probability, review of spin, binding energy, magnetic and quadrupole moment 78−62488
dibenzoylperoxide, triplet sensitized photolysis, mag. isotope effect 77−60081
dipole interaction between nucleons, steps in binding energy and mag. moment energy *(German)* 78−74306
dipole mom. meas., use of Fe single crystal frames in transient field meas. 79−59324
E2/M1 mixing ratio, in vibr. yrast band, sign rule 79−17855
effective NN interaction and exchange current vel. depend., dipole sum rule enhancement 80−63100
EM pot. between nucleons, anomalous mag. moments and orbit-orbit interaction 79−93524
exchange corrections to dipole sum rule 78−17111
exchange mag. moments, meson exchange currents, field theoretical approach 80−52574
excitation of nucleus from bound μ^- decay *(Russian)* 79−22869
excited nuclei moving through ferromag. media, transient mag. field effect, mag. moment meas. 80−37325
excited simple and yrast states, mag. moments, transient mag. fields 80−5064
$f_{7/2}$ shell nuclei, shell model study in pure $f_{7/2}^n$ config. 79−36162
Gamow Teller matrix elements and nuclear mag. moments, configuration mixing v. mesonic effects 79−26400
hyperfine fields on fast ions in ferromagnetic media, review 78−37283
internal conversion coefficients, 30≤Z≤104, Hartree-Fock-Slater model calcs. 79−36199
internal conversion due to hyperfine interaction, shift effect in generated X-ray lines *(Russian)* 78−58234
inverse bremsstrahlung, high energy, nucl. mag. contribs. 78−74350
Isolde experiments, prod. of extreme neutron/proton ratio nuclei, nuclear props. study *(Danish)* 78−4972
isomeric A=48-50 nuclei, mag. moments and core polarisation 78−37274
isomeric state g-factor meas., target preparation 80−23217
isoscalar, deviations from Schmidt values 77−46112
isoscalar mag. moments, data tables 79−54407
light nuclei, mag. moments, configuration mixing and meson exchange contrib. 78−17100
light nuclei, short lived states, meas. techniques 77−46109
long lived high spin isomers, magnetic moments, nuclear struct. *(German)* 77−82820
M1 magnetic form factor and spin oscillations 79−67652
M1 matrix calc. band mixing with several valence nucleons *(French)* 78−45994
M1 transitions in spherical nuclei, finite Fermi systems theory *(Russian)* 77−6296

nuclear magnetic moment continued
magnetic dipole and quadrupole state excitation, inelastic electron scatt., various nuclei 78−50154
magnetic dipole excitation in (e,e′) scatt. 77−30560
magnetic dipole transitions in atomic and particle physics: ions and psions 79−9322
magnetic dipole transitions near ^{208}Pb 79−6393
magnetic multipole expansion, education 80−105456
magnetic order determ. using low-temperature techniques *(French)* 80−5062
meson exchange currents, configuration mixing, role in nucl. mag. moment, beta decay, review, book contrib. 80−478
meson presence in nuclei, nuclear g-factor exchange current controls., EM interaction role 80−22706
mesonic exchange effect on nuclear mag. moment, expt. study, book contrib. 80−477
mesons in nuclei, exchange current effects on nuclear mag. moments, book 80−471
^{13}C-methane-d_1:O, annealed, spin conversion and proton 2nd moment time-depends. 80−11283
mirror nuclei, iso-vector mag. moments in 1p-shell, β-decay ft values 77−88084
mirror nuclei, spin and isospin distribs. in medium heavy nuclei 79−71789
Mossbauer effect 77−85635
multipole interaction between two nonoverlapping charge distributions 79−89731
multipulse NMR, nuclear magnetisation relax. *(Russian)* 79−19799
N=126 isotones, mag. moments and core polarisation blocking 77−26573
N=50 isotones, effects of $1p_{3/2}$ core excitations 79−466
N=50 isotones populated in heavy-ion beam reactions, mag. moments, proton core polarisation 78−21598
nanosecond isomers, in-beam gamma spectroscopic investigation, Ge(Li) detector 78−86506
nonadiabatic rotational model, mag. dipole moments $j \geq 9/2$ rot. bands 79−6388
nuclear Dirac phenomenology and the Λ-nucleus potential, anomalous mag. moment 80−37344
odd deformed nuclei, M1 transitions, one particle intranuclear conversion matrix elements 79−6473
odd-A 1-p shell nuclei, projected HF method 77−6207
odd-A deformed nuclei, mag. dipole moment model, Coriolis coupling 77−30488
odd-odd deformed nuclei, mag. props. 77−82822
one pion exchange effects, l-forbidden M1 transitions 77−6286
orientation with combined elec. and mag interactions 78−41633
relativistic many-body bound systems, quantum field theory calc. 77−74765
review, spin and moment data tables 77−22881
review of meas. 78−37266
shell-model, mag. dipole moments 78−82280
short living nuclear states, optical orientation, γ-spectrum anisotropy, lifetime, moments *(Russian)* 80−63090
Skyrme's interaction, correction to g-factors 77−65196
Skyrme interaction, mag. moments, polarisability, gyromag. factors 78−21501
spherical nuclei with pairing, M1-reson. calc. 79−6390
stable odd-mass sd nuclei, EM multipole moments of ground states 80−102116
tensor M1 operator asymptotic cancellation, particle-vibration coupling 78−50082
three-nucleon systems, props. and interactions 79−71805
virtual pions, Yukawa field and effects on μ-capture, β-decay, mag. moment etc. 79−26379
Wigner scheme, Γ-decay of analogue states, β-decay 77−41930
(e,e), form factors, magnetisation density, mag. moments and valence nucleon orbits 80−22690
π- and ρ-exchange pots., influence on mag. resonances, mag. moments, and transition probabs. 80−99133
Ag, static mag. moments, spin, parity and excitation energy from nuclear orientation *(Dutch)* 79−80872
^{105}Ag high spin states and bands, g-factor and isomeric state from ^{103}Rh(α, 2nγ) 79−36125
^{106}Ag^{m}, mag. moment determ. from orientation meas. 77−10315
^{110}Ag^{m}, oriented, T-reversal test and struct. study 78−86505
^{24}Al, β-transitions, weak magnetism, nuclear struct., matrix elements 79−13253
^{29}Al, mag. moment quadrupole coupling const. β-ray detected NMR in Al_2O_3 cryst. 78−37267
^{242}Am, mag. dipole moment-atomic electron satellite states, influence on E0 conversion 80−18236
^{242}Am, reduced E0 conversion due to mag. moment effects 80−83034
Ar, A=37, 40, implantation in Fe, perturbed ang. distrib. 78−12969
^{69}As 1306 keV state mag. moment, g-factor, rot. aligned band 80−86807
^{70}As, hyperfine struct. investig. using at. beam mag. reson. 77−22933
^{71}As, ^{72}As, nucl. mag. moment by NMR/ON 77−12251
^{72}As, new 87 ns isomer, g-factor via ^{59}Co(^{16}O,2pn) 53-56 MeV 77−54149
^{207}At, g-factor of $25/2^+$ isomeric state, evidence for neutron excitation 78−70447
^{209}At high spin states from ^{206}Pb(^{6}Li, 3nγ), γ meas., neutron hole influence 77−2934
^{212}At high spin states, decay, g factor, J^π assignments, level energies from ^{208}Pb(^{7}Li,3n) 80−5042
Au, short-lived isotopes, spin and mag. moment meas. from atomic-beams 77−22882
Au, spin and mag. moment, trends in neutron deficient nuclei 78−37261
^{12}B, quadrupole coupling const. in ZrB_2 single cryst. 78−37279
Ba, neutron deficient, charge radii, moments, transitions and isomers, atomic beam laser spectroscopy 80−102141
^{A}Ba, A=126 to 135, charge radii, mag. dipole and elec. quadrupole moment 79−72436
^{A}Ba(^{32}S,^{32}S′), A=130, 132, 134, 136, 72-80 MeV, 2_1^+ state mag. moments 80−47373
^{131}Ba, magnetic mom. and charge determ. using Doppler free laser spectroscopy 77−71558
^{135}Ba, ^{137}Ba, nucl. mag. moments and ratios of quadrupole moments, NMR spectroscopy 77−73088
^{136}Ba, mag. moment of 2140.2 keV 5^- state 79−59009
^{138}Ba, 6^+ state, nucl. g-factor and nucl. spin relax. in Xe 77−22884

nuclear magnetic moment continued
^{209}Bi EM props. of particle vibration coupling states from ^{208}Pb(^{7}Li, ^{4}He 2nγ) 78−70485
^{209}Bi, mag. moments and core polarisation blocking 77−26573
^{209}Bi, single particle state mag. moment in large shell model space 79−45162
^{210}Bi, magnetic moment and beta-decay 77−41926
^{12}C, β-transitions, weak magnetism, nuclear struct., matrix elements 79−13253
^{12}C, M1 form factor, pion field, rho meson role 80−105970
^{12}C, magnetic dipole excitation in (e,e′) scatt. 77−30560
^{15}C 0.74 MeV $5/2^+$ state g-factor, shell model interpretation from ^{3}H(^{13}C,p) 80−32176
^{A}Ca (α,α′) A=40, 44, nuclear level mag. moments, ^{40}Ca 2_1^+ level, ^{44}Ca 3_1^- level 79−85368
^{40}Ca, hyperfine interaction of electron in L, M and N regimes 78−70448
^{40}Ca, mag. moment of 3^- level meas. 77−10314
^{45}Ca, nuclear charge radius, spin, moments, by laserspectroscopy 80−18187
Cd, even nuclei, systematic meas. of mag. moments of 2_1^+ states 78−54682
^{A}Cd, static quadrupole moments determ. for A=111, 113, 115 78−37281
^{A}Cd(^{32}S,^{32}S′), A=106, 108, 110, 112, 114, 116, 72-80 MeV, 2_1^+ state mag. moments 80−47373
^{110}Cd, recoiling in Fe, enhanced transient fields 78−37284
^{252}Cf fission products, g-factors of isomeric states 77−22890
^{36}Cl, g-factor determ. from perturbed ang. distribs. 78−12970
Cs isotopes, nucl. spins and mag. moments, atomic-beam mag. reson. expt. 78−17097
Cs isotopes, short-lived, determ. of nucl. spins by β radiation detected optical pumping 78−37262
Cs neutron rich isoptopes, nucl. spins and mag. moments 80−47367
Cs, short-lived isotopes, spin and mag. moment meas. from atomic-beams 77−22882
Cs, spin and mag. moment, trends in neutron deficient nuclei 78−37261
^{129}Cs $11/2^-$ isomer, g-factor and lifetime in CsI cubic environment from ^{127}I(α,2n) 79−6394
^{133}Cs(α,α′), 161 keV state magnetic moment and B(E2) values, Coulomb excitation 79−45159
Dy, deformed nuclei, quasicontinuum γ-spectrum, M1, E1, E2 components 80−498
^{152}Dy high spin isomeric states, g-factors from ^{140}Ce(^{16}O, 4n) 80−13377
^{152}Dy, yrast states of isomers at high angular momenta, particle-hole struct. 79−36124
^{A}Er, A=159,160, energy levels, deexcitation γ-rays, g-factors and hyperfine interaction from ^{28}Si(^{136}Xe, xn) 80−102114
^{168}Er, 80 and 1094 keV states, g-factors from ang. correlation methods 80−83035
^{A}Eu, A=145, 147, 149, mag. moments of $11/2^-$ states 79−40846
^{18}F ions recoiling in vacuum, mag. decoupling of hyperfine interaction 78−37270
^{19}F low lying positive parity states from rot. model, moments and deformation 79−6410
^{19}F, transition probabilities and multipole moments between states calc. by generator coordinate method 78−13022
^{20}F, β-transitions, weak magnetism, nuclear struct., matrix elements 79−13253
Fe, A=54,58, mag. moments of 2^+ first excited states, g-factors 77−88041
Fe, even nuclei, systematic meas. of mag. moments of 2_1^+ states 78−54682
Fe:^{106}Rh, nuclear orientation and mag. moment 77−85623
^{54}Fe^{m}, static moments, perturbed ang. distribs. with combined dipole and quadrupole interactions 78−62482
^{56}Fe, recoiling in Fe, enhanced transient fields 78−37284
^{57}Fe(p,p′)^{57}Fe*, excited $5/2^-$ state mag. moment 79−93512
^{59}Fe β-decay, nuclei polarised in iron foils cooled by dilution refrigeration 77−34263
Fr, spin and mag. moment, trends in neutron deficient nuclei 78−37261
^{212}Fr in liq. ^{203}Tl, $(h_{9/2})^n$ proton states, Knight shifts and absolute mag. moments 77−82821
^{A}Gd A=144,146,147,148, high spin isomer g-factors yrast traps from (^{28}Si,^{28}Si′), (α,α′) 80−78146
^{A}Gd, A=146, 147, g-factors of yrast states 79−17800
^{146}Gd, mag. moments of isomeric states 79−40847
^{151}Gd, 108 and 395 keV levels, mag. moments and half-lives, PAC 77−22883
^{153}Gd, mag. moment meas. of 129.2 keV 77−82850
Ge, A=70, 72 and 74, dynamic deformation theory, energy levels 78−58235
^{69}Ge, transitions, spin and parity, and mag. moments determ. from β-decay of ^{69}As 79−22245
HT, triton-proton mag. moment ratio determ. by NMR method with 10^{-6}% accuracy *(Russian)* 77−61773
^{2}H D-state probability measurability in meson exchange current theory, moments and RMS radius 79−89246
^{2}H, D-state wave function calc. 78−8740
^{2}H magnetic moment due to two boson exchange, pseudovector πN coupling model 79−40843
^{2}H, two-nucleon bound state description 77−38221
^{3}H, meson exchange contribs., and beta decay 77−6249
^{3}H, unitary scheme model anal. with Gogny, Pires and de Tourreil interaction 79−59016
^{3}He, nucl. mag. moment, ratio of precession freqs. of gas phase helions-proton mixture *(Russian)* 79−17803
^{3}He, meson exchange contribs. 77−6249
^{3}He, trinucleon bound state problem, binding energy, form factors and mag. moment 80−22710
Hf, static mag. moments, spin, parity and excitation energy from nuclear orientation *(Dutch)* 79−80872
Hf-Ir, isotopes, deformation, level assignments, static moments, modified oscill. model 77−22872
^{178}Hf, g-factor for K=6, $J^\pi=6^+$ isomer, perturbed ang. distrib. meas. 78−37277
Hg, A=199, 197, $5/2^-$ state halflife and mag. moments 78−506
Hg isotopes, nuclear ground state props. via atomic spectra 77−22874
Hg, nuclear magnetic moment ratio of odd isotopes *(French)* 77−75081
^{A}Hg, A=198-204, reorientation effect meas. on 2^+ states 78−37282

nuclear magnetic moment continued
^{190}Hg, 21 ns isomer $(\nu i_{13/2})^2$ interpretation from g-factor meas. 80−105945
Ho, magnetic moment of neutron resonances 77−26576
^{165}Ho in $HoVO_4$, NMR predictions of properties, dipolar interactions and antiferromagnetic exchange 80−50203
^{165}Ho, pseudomagnetic moment and spin-lattice relax. in holmium ethylsulphate 77−63306
^{166}Ho, internal hyperfine field obs. using β-γ directional correl. 80−32229
^{166}Ho low lying levels and transitions, 54.24 keV level mag. moment from ^{166}Dy decay 80−13380
^{166}Ho^{m} in $HoVO_4$, nuclear orientation study below 1K 80−88899
^{A}I, A=123, 125, mag. moments and polarisation NMR on oriented nuclei 79−75836
^{132}I 3^+ and 1^+ state electric and mag. moments 79−63587
^{132}I isotope, doubly odd, quadrupole moments, PAC meas. 78−37280
In, A=109, 110, 111, low temp. orientation, γ-ray spectra 77−79327
^{A}In, A=109,110, nucl. g-factor NMR-ON meas. on Fe-In alloys 78−37275
^{110}In, nucl. orientation, nucl. mag. moment, γ-ray spectra of Fe:^{110}In 77−28485
^{111}In $21/2^+$ isomeric state g-factor and relaxation time from ^{109}Ag(α,2nγ) 80−73794
^{111}In, nucl. orientation coeffs., nucl. mag. moment 80−97168
^{112}In, 8^-, 6^+ isomeric states, $T_{1/2}$, g-factors via ^{112}Cd(p,n), ^{109}Ag(α,n) 77−10318
^{112}In, half-lives and mag. moments of two high spin states, γ-ray spectra 77−22940
Ir, A=191, 193, hyperfine struct. of low lying fine struct. levels, hyperfine anomaly, electronic g-factor 78−66214
^{186}Ir decay, obs. of ^{186}Os levels 78−86481
K, A=40, 41, implantation in Fe, perturbed ang. distrib. 78−12969
^{40}K, g-factor determ. from perturbed ang. distribs. 78−12970
^{43}K 738 keV state g-factor, PAC technique 77−6227
^{84}Kr, 1.84 μs isomeric state, g-factor meas. 78−17101
^{138,139}La, Fourier transform NMR 80−57354
^{138}La, ^{139}La, nucl. mag. moments and ratios of quadrupole moments, NMR spectroscopy 77−73088
^{138}La, magnetic moment of the first excited state, meas. using TDPAD 79−63589
^{177}Lu, 150 keV state, mag. dipole moment, TDPAC 77−41886
^{24}Mg, velocity and Z-depend. of transient mag. field in Fe 77−71566
^{25}Mg (e,e) 80-215 MeV, magnetic moment form factors, M1, M3, M5 transitions 79−40844
^{25}Mg(e,e), 180° scatt., magnetisation distrib., mag. multipole moments 80−9228
^{25}Mg(e,e), 40-260 MeV, cross sections, Coulomb multipole moments and magnetic form factor 78−25178
^{A}Mo, A=94, 96, 98, multiparticle states, method of generalised seniority 80−22759
^{92}Mo, mag. moments of 8^+ and 11^- states anomalous orbital magnetism 79−6391
^{93}Mo^{m}, low temp. nucl. orientation, γ-ray spectra 77−79327
^{95}Mo, first excited $3/2^+$ state, g-factor determ. 77−26574
^{99}Mo first excited state g factor from ^{96}Zr(α,n) and ^{98}Mo(d,p) 79−17801
^{93m}Mo, nucl. g-factor NMR-ON meas. on Fe-Mo alloys 78−37275
^{12}N, β-transitions, weak magnetism, nuclear struct., matrix elements 79−13253
^{14}N, g-factor, lifetime meas. of 5.106 MeV 2^- state of ^{14}N 78−93965
^{14}N, meas. of nucl. g-factor of 5.11 MeV 2^- state by recoil distance technique 78−37268
Na neutron rich isotopes, nuclear ground state props. via laser spectroscopy 77−22875
^{A}Na, A=22, 24, β-transitions, weak magnetism, nuclear struct., matrix elements 79−13253
^{21}Na, mag. moment and lifetime of first excited state determ. 78−550
^{21}Na, mag. moment of first excited state, time differential plunger meas. 78−37271
^{23}Na, band mixing, E2 and M1 matrix elements *(French)* 78−45994
^{23}Na, transition probabilities and multipole moments between states calc. by generator coordinate method 78−13022
^{24}Na^{m}, 4^+ isomer, mag. moment 80−32177
^{24}Na^{m}, polarised, β-decay asymmetry and mag. moment from Na(n,γ) 80−91157
^{A}Nb, nucl. g-factor, A=90, 92 m, NMR-ON meas. on Fe-Nb alloys 78−37275
^{91}Nb, $17^-/2$ state, g-factor meas. 80−32179
^{91}Nb, 3.8 μs isomeric state, mag. moment, TDPAD meas. 78−41634
^{92}Nb, high-spin states, EM props. via ^{88}Sr(^{7}Li, 3n)^{92}Nb 34 MeV 77−74770
^{93}Nb (e,e), 80-215 MeV, magnetic moment form factors, M1, M3, M5 transitions 79−40844
^{93}Nb(e,e), 180° scatt., magnetisation distrib., mag. multipole moments 80−9228
^{A}Nd(^{32}S, ^{33}S^1), 56 MeV, A=144,146,148, first excited 2^+ state mag. moment meas. 79−17798
^{20}Ne, velocity and Z-depend. of transient mag. field in Fe 77−71566
^{20}Ne with backbending, first excited 4^+ state g-factor 80−78144
^{21}Ne, mag. moment and lifetime of first excited state determ. 78−550
^{21}Ne, recoil into vacuum g-factor meas. of $5/2^+$ state, 0.350 MeV 78−37272
^{21}Ne, transition probabilities and multipole moments between states calc. by generator coordinate method 78−13022
^{21}Ne*, produced in ^{2}H(^{20}Ne,p)^{21}Ne* mag. moment and g-factor of 351 keV $^3/_2^+$ state 78−41631
^{22}Ne, first excited 2^+ state, mag. moment determ. 77−18388
^{22}Ne(2^+), g-factor and τm via ^{4}He(^{19}F,pγ) 38.5 MeV 77−34224
Ni, even nuclei, systematic meas. of mag. moments of 2_1^+ states 78−54682
Ni isotopes, even determ. of g-factor of 2_1^+ states 78−43697
^{A}Ni, A=58-64 even, magnetic mom. of 2_1^+ states from (^{32}S, ^{32}S′) at 72 MeV 78−66202
^{57}Ni, various orbit contribs. to mag. moment 78−78254
^{15}O, nucl. g-factor and lifetime of 5.24 MeV $5/2^+$ level 78−37269
^{16}O, transient fields in magnetised Fe, g-factor meas. 77−22887
^{16}O(p,p′), 40 MeV, retarded isoscalar M2 strength obs. 78−93962
^{17}O, M3 suppression in HF theory 78−33134
^{17}O, mag. form factor, core polarisation and exchange current effects 78−46003

nuclear magnetic moment continued
^{18}O 2_1^+ states, coexistence of spherical and deformed states 77−18394
^{20}O first excited state, g-factor and lifetime from ^{3}H(^{18}O, pγ) 80−102115
^{A}Os, A=186, 188, 190, 192, electromagnetic moments from muonic X-rays 78−12972
^{A}Os, A=186-194, collective levels, transitions, mag. and quadrupole moments, boson expansion theory 80−105954
^{183}Os $9/2^+$ [624] ground state g-factor from NMR 80−83037
Pb, 1^+ state and effective g-factor anal. 77−74764
Pb, A=194, 196, 198, 12^+ isomeric states, $T_{1/2}$, g-factor 77−74762
Pb region, even-odd nuclei, EM moments and transitions 77−88040
Pb region, mag. moments and M1, M2 and M4 values, self consistent calcs. 80−47371
^{A}Pb, A=207,209, single particle state mag. moment in large shell model space 79−45162
^{202}Pb, 4_1^+ state g-factor 77−30491
^{207}Pb(e,e), magnetisation distrib. from elastic mag. form factors, core polarisation, exchange currents 80−47372
^{208}Pb core with valence nucleon or hole, mag. props., exchange currents, electron scatt. 80−22689
^{208}Pb, fine struct. of M1 giant resonance obs. in ^{207}Pb(n,γ) 77−79347
^{208}Pb, mag. moment, MI transition probabilities, one pion exchange calcs. 79−9463
^{208}Pb magnetic susceptibility and M1 transitions, nuclear interaction role 79−45160
^{208}Pb(e,e′), 50 and 63.5 MeV, mag. quadrupole strength fragmentation 78−41705
^{208}Pb(e,e′), M2 giant resonance excitation, spin-magnetism mass depend. quenching, M1 strength reduction 78−86521
Pd, even-even, collective states, B(E2), branching ratios and moments, boson expansion method 80−102099
^{A}Pd(^{32}S, ^{32}S′), A=102, 104, 106, 108, 110, 72-80 MeV, 2_1^+ state mag. moments 80−47373
Po, A=202-210, isomeric levels, g, $T_{1/2}$ 77−14068
$PrIn_3$:Gd, indirect nuclear exchange interactions, ESR-linewidth meas., sp. ht. determ. 80−103825
^{139}Pr isomeric $11/2^-$ state, half-life, g-factor, and nuclear orientation relaxation from ^{140}Ce(p,2nγ) 79−75837
^{143}Pr in Ce, $Ce(NO_3)_3$ soln., mag. dipole moment of 57 keV state, PAC meas. 77−46110
Pt, A=187, 189, 191, low-temp. orientation studies, mag. moment and E2/M1 ratios in daughters 77−22889
^{A}Pt, A=188-198 collective levels, transitions, mag. and quadrupole moments, boson expansion theory 80−105954
^{214}Ra in liq. ^{206}Rb, $(h_{9/2})^n$ proton states, Knight shifts and absolute mag. moments 77−82821
Rb isotopes, short-lived, determ. of nucl. spins by β radiation detected optical pumping 78−37262
Rb neutron rich isotopes, nucl. spins and mag. moments 80−47367
Rb, short-lived isotopes, spin and mag. moment meas. from atomic-beams 77−22882
Rb, spin and mag. moment, trends in neutron deficient nuclei 78−37261
^{A}Rb, A=77, 78, 78m, 79, 84m, nuclear spins and mag. moments, deformed shapes 79−17793
^{87}Rb, low-lying level struct. in quasiparticle-core model 77−82825
Re, A=183, 184, 186, 188, nuclear quadrupole alignment in Re single cryst. at low temp. 78−48091
^{A}Re, A=181, 182, 187, magnetic moments meas. by PAC 80−22688
^{A}Re, A=181, 182, 187, spin polarisation, state struct. and mag. moments in rot. model 80−18194
^{182}Re isomer decay mag. moment, ^{182}W high spin states, J assignments and mixing ratios 80−42593
Rh, static mag. moments, spin, parity and excitation energy from nuclear orientation *(Dutch)* 79−80872
^{105}Rh in Fe, oriented nuclear decay, mag. moments 77−46111
^{105}Rh, polarised, from γ-ray ang. distrib. following decay 77−6315
^{212}Rn, Knight shift and absolute mag. moment meas. in Hg 78−37278
^{212}Rn, shell model states, semiempirical calcs. half lives, mag. moments, excitation functions 80−63083
Ru, A=99, 101, hyperfine struct. and nucl. moments determ. 77−26575
Ru, even-even, collective states, B(E2), branching ratios and moments, boson expansion method 80−102099
^{A}Ru, A=96, 98, 100, multiparticle states, method of generalised seniority 80−22759
^{97}Ru ground state g-factor, relaxation time 80−83036
^{97}Ru, polarised, from γ-ray ang. distrib. following decay 77−6315
^{103}Ru, polarised, from γ-ray ang. distrib. following decay 77−6315
^{105}Ru, polarised, from γ-ray ang. distrib., following decay 77−6315
^{A}S(α,$\alpha'\gamma$), 8-9 MeV, A=32, 34, 2_1^+ state transient field g-factor meas. 79−36151
^{31}S, mag. dipole moment meas. using ^{31}P(p,n)^{31}S 77−18482
^{32}S, transient field g-factor meas. on 2_1^+ states 78−37273
^{34}S, transient field g-factor meas. on 2_1^+ states 78−37273
^{A}Sb, A=113,115,117,119, high spin states, J$^{\pi}$ assignments, decay schemes and lifetimes from Cd(^{6}Li,3n) 79−54381
^{112}Sb, ^{114}Sb, 8^-states, half-life and mag. moment, γ-ray spectra 77−22941
^{114}Sb, 8^-, 210 μs state, mag. moment, PAC of liq. Sn:^{114}Sb 77−26609
^{115}Sb g-factor of $19/2^-$ and $11/2^-$ isomers from ^{115}In(α,4n) 79−40845
^{115}Sb, g-factor of $19/2^-$ isomeric state, time differential perturbed ang. distrib. method 79−22192
^{122}Sb, 5^+ isomeric state, mag. moment determ. from ^{122}Sn(d,2n)^{122}Sb 78−21493
^{122}Sb, 5^+ state, mag. moment, g-factor meas. 77−71567
^{125}Sb, via nuclear orientation Mossbauer meas. 77−55713
Sc, A=43, 47, $d_{3/2}$ hole states, wave functions mag. moment, M2 transitions, shell model 78−17116
^{43}Sc, g-factor of $3/2^+$ hole state meas. in (α,p) react. 78−21492
^{43}Sc, mag. moments in $19/2^-$ state, time-differential perturbed ang. distrib. method 78−33117
^{28}Si(e,e′), M2 giant resonance excitation, spin-magnetism mass depend. quenching, M1 strength reduction 78−86521
Sn, odd isotopes, number-projected three-quasiparticle description 78−93953
^{A}Sn(^{35}Cl, ^{35}Cl′), 108 MeV, A=112-124 even isotopes, 2_1^+ mag. moments and shell model struct. 80−86805
^{112}Sn 6^+ isomeric state g-factor and relaxation time from Cd(α,2nγ) 80−73794
^{119}Sn, magnetic moment, of $I=+^3/_2$ level *(Russian)* 78−50083
^{A}Sr, A=89-94, mag. and electric quadrupole moments 79−6408

nuclear magnetic moment continued
^{86}Sr, 8$^+$ state, nucl. g-factor and nucl. spin relax. in Kr 77−22884
^{179}Ta, γ-transition 55/22$^+$→77/22$^+$, E2/M1 mixing, μ determ., $T_{1/2}$ 77−10355
^{177}Ta, magnetic moments meas. by PAC 80−22688
^{177}Ta spin polarisation, state struct. and mag. moments in rot. model 80−18194
^{178}Ta, nucl. orientation in Fe 78−39412
^{180}Ta nuclear spin and mag. dipole moment from laser resonance fluorescence 80−78143
^{181}Ta, 136 keV level, g-factor meas. 79−6387
^{181}Ta, freq. modulation of 6.2 keV Mossbauer states 79−13202
^{182}Ta, in Fe-Ta, nuclear mag. moment, NMR-ON study 80−78139
Tb, magnetic moment of neutron resonances 77−26576
^{A}Tb, A=149, 151, 153, 155, 157, prop. anal. on function of nuclear shape 79−75828
^{155}Tb, oriented in Gd, γ-decay ang. distrib., hyperfine splitting, moment and mixing ratios 79−45242
Tc, A=93, 94, 95, low temp. nucl. orientation, γ-ray spectra 77−79327
Tc, A=93-101 odd isotopes, levels, EM moments in unified model 77−82826
^{A}Tc, A=93-95, nucl. g-factor NMR-ON meas. on Fe-Tc alloys 78−37275
^{93}Tc, ^{94}Tc, mag. moment determ., γ-ray spectra of Fe:^{93,94}Tc 77−28484
^{95}Tc in Fe, oriented nuclear decay, mag. moments 77−46111
^{A}Te, A=127, 129, 131, ground state mag. moments 80−5059
^{A}Te^{m}, A=125, 127, 129, 11/2$^-$ isomeric state magnetic moments 80−42537
^{121}Te isomeric state, spin, lifetime and mag. moment from (α,n),(d,Zn) 80−47387
^{125}Te, via ^{125}Sb nuclear orientation Mossbauer meas. 77−55713
^{134}Te, levels, J^π, 6$^+$ isomer level mag. moment 77−82824
^{119m}Te, mag. moment, nucl. orientation, γ-ray spectra of Fe:^{119m}Te 77−28486
^{232}Th, thermal Westcott g-factor meas. 78−37287
^{43}Ti, mag. moments in 19/2$^-$ state, time-differential perturbed ang. distrib. method 78−33117
^{45}Ti, 5/2$^-$ 40 keV level, g-factor meas. 77−57599
^{45}Ti $d_{3/2}$ hole states, wave functions, mag. moment, M2 transitions, shell model 78−17116
^{45}Ti, integral rot., hyperfine field and g-factor of 3/2$^+$ state 77−50052
^{47}Ti, integral rot., hyperfine-field and g-factor of 7/2$^-$ state 77−50052
^{A}Tl, A=203, 205, excited state g-factor from Tl(^{40}Ca, ^{40}Ca′γ) 79−22191
^{203}Tl, ^{205}Tl, core excitations to low-lying states, e.m. props., hyperfine splittings, isomer shifts 78−89794
^{207}Tl, single particle state mag. moment in large shell model space 79−45162
^{163}Tm, high spin rot. levels, studied via ^{165}Ho(^{3}He,5n) and ^{165}Ho(α,6n) reactions 78−8722
^{169}Tm, studied via ^{169}Tm(^{32}S,^{32}S′γ), EM props. of ground state rot. band 78−8726
^{171}Tm, 635.4 keV level props., mag. moment from γ ang. correl. meas. 78−13017
^{233}U, monopole conversion, magnetic dipole transitions, latent penetration effect 79−9464
V isotopes, A=47-51 78−25114
^{51}V, ENDOR in $KMgF_3$ and $KZnF_3$, nucl. mag. moment 79−28638
Xe, A=126-132 even nuclei, gyromagnetic ratios of 1st 2$^+$ states 78−12966
^{126}Xe, first 2$^+$ excited state g-factor 77−18389
^{87}Y^{m} orientation meas. in Al and Au hosts, mag. moment of 9/2$^+$ isomeric state 78−41632
^{88}Y 14 ms 8$^+$ isomeric state, g-factor from ^{87}Rb(α,3n) 80−63080
^{A}Yb(^{40}Ca,^{40}Ca′), A=170,172,174, 168 MeV, rotational g-factor meas. using transient field interactions 80−18193
Zn, even nuclei, systematic meas. of mag. moments of 2_1^+ states 78−54682
^{A}Zn, A=64, 66, 68, 70, transient mag. field g-factor meas. 79−67653
^{A}Zr, A=92, 94, 96, multiparticle states, method of generalised seniority 80−22759
^{A}Zr(^{35}Cl,^{35}Cl′), 90 MeV, A=92, 94, 2_1^+ levels mag. moments 80−105968
^{90}Zr(e,e′), M2 giant resonance excitation, spin-magnetism mass depend. quenching, M1 strength reduction 78−86521
^{94}Zr, 2$^+$ state, recoiling in Fe, enhanced transient fields 78−37284

nuclear magnetic resonance
see also acoustic nuclear magnetic resonance; chemical shift; double nuclear magnetic resonance; ENDOR; Knight shift; molecular nuclear coupling; NMR line breadth; nuclear quadrupole resonance; nuclear spin-lattice relaxation; proton magnetic resonance; spin echo (NMR); spin-spin relaxation
^{31}P spectroscopic zeugmatography 80−76872
α,β-β-trifluoroacetonitrile, liq.-liq. transition rel. to mol. motion, NMR study 80−70383
A_3 spin system, NMR relax. kinetics 78−80238
absolute meas. of ampere 80−98941
absorption peak voltmeter cct. error analysis *(Russian)* 79−26079
acetic acid, methyl group dynamics, NMR 78−29802
acetic acid-$^{13}C_1$, in nematic phase soln., dipole-dipole couplings, selective spin population transfer investig. 80−60427
acetone, liq., rot. motion, nucl. mag. relax. obs. 78−88209
acetone-d_6, deuteron NMR spin echo, time domain spectrum 78−88223
acetonitride-d_1, ^{2}H NMR spectra, vibr. and asymmetry corrections to quadrupole coupling consts. 80−74184
acetonitrile, dissolved in nematic EBBA, oriented CH_3 group relax., multiple quantum NMR 80−66057
acetonitrile in liq. cryst., ^{13}C and ^{14}N relax. times 79−19793
N-acetyl-D-alloisoleucine, ^{13}C NMR, soln. struct., dynamics, proton relaxation mechanisms 80−76708
N-acetyl-l-phenylalanine methyl ester, model for amino acid side chains internal motions in peptides and proteins 80−48017
N-acetyl-valine, NMR of solid, ^{14}N-^{1}H dipolar spectra, NH bond length 78−48055
acoustic ringing effects in pulsed nuclear magnetic resonance probes 78−86313
acrylonitrile, NMR and relax. props., liq.-liq. transition rel. to mol. motion 80−70382
acrylonitrile-MMA copolymers, sequence distrib. determ. by NMR 77−14622
nuclear magnetic resonance continued
acrylonitrile-vinylidene chloride copolymerisation, sequence distrib. determ. by ^{13}C-NMR 79−79247
actinides, spin fluctuation theory, for mag. and elec. props. 78−91869
adamantane, ^{13}C NMR using high-speed magic angle spinner 78−89516
adamantane, derivatives in solution, mol. motion and methyl group rot. barriers from ^{13}C NMR relax. times 80−74179
adamantane, proton-enhanced NMR, magic-angle spinning, polarisation transfer 78−19349
adenosine 5′-diphosphate, interactions with myosin, intermolecular spin diffusion study 80−18951
adiabatic demagnetisation using near nπ RF pulse strings 77−90050
adsorbed molecules, NMR, effect of migration between physical and chem. adsorption sites 77−21422
aerobic Escherichia coli cells, metabolism, high resolution ^{31}P NMR studies 77−90741
agarose gels, $H_2{}^{17}O$ enriched, ^{17}O NMR, hydration anal. 77−81426
agriculture appls. of pulsed NMR 80−56297
albumin, human serum, AsF_3^- NMR probe for anion binding sites 78−48748
alcohol/water mixtures, NMR and IR obs., low temp., shifts, interpretation 77−52065
aliphatic alcohols in carbon tetrachloride, association processes, NMR spectroscopy 77−16792
alkali fluoroborates, ^{19}F chem. shift, multiple pulse zero crossing NMR obs. 79−9230
alkali halides, matter transport rel. to point defect parameters 80−107488
alkali iodates, chem. shift, NMR obs. 80−48015
alkali metal difluoride, MHF_2, ^{19}F free induction decay 78−2753
alkali metal salts, NMR spectra of alkali metal nuclei, shielding and quadrupole coupling consts. 78−84487
alkali metapenodates, chem. shift, NMR obs. 80−48015
alkali silicate and borate glasses, ionic motion, ^{7}Li NMR obs. 78−27107
alkali silicate glass, Li^+ motion, ^{7}Li NMR spectra, nucl. relax. 80−34804
alkenyl polysulphide, oligomeric, synthesis and characterisation by NMR 79−79248
p-alkoxybenzal-p′-ethoxyaniline, even-odd effect and chain config. 79−50989
p-alkoxybenzylidene-p-alkylaniline, liq. crysts., ^{2}H NMR, aliphatic and chain conformation 79−14670
alkyl chains, ^{13}C longitudinal relax. times and nuclear Overhauser enhancement anal. 80−83390
4-alkyl-3-phenyl-3 4-dihydrocoumarins cis- and trans-, ^{13}C NMR spectra 80−43067
alkylamines coordinated to Ni(II) acetylacetonate, ^{1}H and ^{13}C NMR, hyperfine coupling const. 79−41187
alternating copolymer of styrene and N-substituted maleimides, NMR relax. studies of mol. motion 77−85608
amino acid side chains, internal motions in peptides and proteins, N-acetyl-l-phenylalanine methyl ester model 80−48017
amino acid side chains, NMR relax. due to multiple internal rots. 78−94340
4-amino-2,2,6,6-tetramethylpiperidine-N-oxyl and deuterated derivatives, mag. resonance study 80−63686
amplification and dynamic shift of NMR freq., rel. to local mag. props. *(Russian)* 77−20722
ampoule for NMR meas. of self-diffusion coeffs. of liquid molecules under pressure 79−35773
analogue Fourier transforms, pulsed NMR spectroscopy methods 80−47085
analytical chemistry appls., conf., Denver, CO, USA (Aug. 1979) 80−90598
anisotropic media, simple spin systems, magnetisation modes and evolution matrices 79−4734
annular spinning sample, sideband structure 77−49761
anthracene, mag. susceptibility anisotropies, high field ^{2}H NMR quadrupolar effects obs. 80−25225
anthracene-tetracyanobenzene, charge transfer complex, phase transitions, deuteration effect, mag. reson., spectral and thermal meas. 79−4412
antiferromagnet, two-dimens., nucl. mag. relax. *(Japanese)* 78−19364
antiferromagnet, under magnon bottleneck conditions, eqns. of motion 77−66429
antiferromagnets, low anisotropy, nuclear spin waves spectra, relaxation, parametric excitation, NMR dynamic shift *(Russian)* 80−11180
antiferromagnets, nuclear magnetisation motion under parametric influence of longitudinal RF field *(Russian)* 79−82880
aqueous heterogeneous systems, NMR, substrate struct. and H_2O mol. relax. 78−7247
aromatic acids, mixtures, quantitative anal. by ^{13}C NMR 78−31716
aromatic hydrocarbons, in airborne particulates, gas chromatography/mass spectrometric, NMR analyses 77−13116
arsonium salts, aq. soln., ^{75}As NMR spectra depend. on alkyl chain 77−69714
aryl ammonium hydrogen difluorides, IR vibr. spectra and NMR reson. obs. 80−34788
2-aryl-3-benzylidenamino-4-thiazolidones, IR and NMR spectra, solvent effects and isomer conform. *(Italian)* 79−3596
atomic hyperfine coupling consts., calc. 77−39810
atomic systems, coherent transients theorem 80−99808
ATP, ^{31}P spectroscopic zeugmatography 80−76872
ATPase kinetics in E. coli cells, ^{31}P NMR meas. 78−77022
autodyne spin detector, broadband, for NMR signal detection 77−74471
automatic NMR gaussmeter *(Polish)* 77−79133
automatic system, for recording, processing and summation 80−27327
auxiliary system for broadband NMR on strongly magnetic systems 78−70172
averaging method in RF-atom system interaction calcs. *(Russian)* 79−26973
bacteria, yeast and leukaemic cells, dynamic struct. obs. by Overhauser enhanced ^{15}N NMR 77−90742
benzaldehydes in EBBA liq. cryst., NMR, mol. struct., reorientation and order matrix 78−5251
benzene, chem. shielding tensor obs. using proton-enhanced ^{13}C reson. in He-cooled probe 80−17978
benzene, cryst., press. depend. of nuclear spin-lattice relax. time 79−28635
benzene, frozen liquids, high-resolution ^{13}C NMR using magic angle spinning 79−33544

nuclear magnetic resonance continued
benzene, monohalogenated, orientation in lyotropic surfactant soln., NMR 77−28456
benzene adsorbed on graphite, melting and orientation, NMR study 80−100403
benzene submonolayer on silica gel, PMR and DMR dynamics and surface heterogeneity 79−69735
benzene-d_1, ^{2}H NMR spectra, vibr. and asymmetry corrections to quadrupole coupling consts. 80−74184
benzene-d_1, $(-d_2)(-d_3)$, oriented, order, D nucl. quadrupole coupling, mag. reson. spectra 78−74683
benzene-d_6, deuteron NMR spin echo, time domain spectrum 78−88223
benzene-hexa-n-alkanoates and benzene mixture, disc-like mesogens, thermotropic mesophases 79−86699
benzenes, monosubstituted, ^{13}C NMR chem. shifts 79−42850
benzenes, monosubstituted, high resolution, automated anal. by computer program DAVINS appl. 80−63669
benzenes, substituted, C-C coupling consts., coupled Hartree-Fock calcs. 77−27091
benzil, NMR of cryst., 77-367K 79−38387
benzonitrile, field depend. ^{13}C NMR spin-lattice relax. and anisotropic mag. shielding 79−76450
benzyl fluoride, mol. struct., NMR and gas electron diffraction obs., ab initio and mol. mechanics calcs. 80−23574
benzylidene anilines, nematic phase, dipole coupled ^{13}C NMR technique 79−99073
bilayer membrane head group, orientational order and rotational diffusion 80−21451
binary ^{13}C spectra, ^{1}H noise decoupled, classification 78−27832
binary mixtures, NMR longit. relax., mole fraction depend. 77−61767
biochemical applications, using supercond. magnets 79−74811
biological and medical imaging by NMR 78−69172
biological and medical imaging by NMR 80−26319
biological imaging, review *(Japanese)* 80−94312
biological information noninvasive meas., generation of mag. focus *(Japanese)* 78−85355
biological living tissue using ^{31}P 77−37117
biological NMR spectroscopy, instruments and techniques 78−28148
biological systems, entropy of fluctuations, time evolution, NMR obs. 79−53017
biological systems, simultaneous multinucl. NMR by alternate scan recording of ^{31}P and ^{13}C spectra 80−26426
biological technique, ^{31}P NMR of perfused working rat hearts, using ^{31}P 77−29236
biomedical whole-body imaging system design 80−98064
biomembrane, water transport determ. methods *(Rumanian)* 80−94435
biomolecules, Fe-containing, appl. of spectroscopy 79−24956
biotin, of ^{13}C, spectrum assignment 80−26204
bis-methyldigermyl chalcogenide, ^{1}H and ^{13}C NMR study, chemical shifts 80−71201
bis-methyldisilyl chalcogenide, ^{1}H and ^{13}C NMR study, chemical shifts 80−71201
bistrifluoromethylmercury, scalar coupling between rare spins 80−66047
Bitter magnet development, stabilisation and calibration 79−30501
Bloch equations solution in presence of varying B_1 field, selective pulse analysis 80−25222
blood flow evaluation in peripheral circulation, noninvasive techniques 80−56163
blood flow meas., cerebral 77−40730
blood flow measurement, flat crossed-coil detector 78−40284
blood flowmeter, noninvasive clinical diagnosis appls. 80−17178
BOBOA, deuteron mag. reson. of mol. order and dynamics 77−35469
body scanning appl. 79−53274
book, principles of magnetic reson. 78−80189
borate glass, Li^+ motion, ^{7}Li NMR spectra, nucl. relax. 80−34804
broad-line, reduction of spurious baseline effects 79−75562
broadband transmit/receive circuit for NMR spectrometer 78−89520
bromides, MAl_2Br_7, (M=Li, Na, K, Cs, NH_4, and $(CH_3)_4N$), ^{81}Br NQR and ^{27}Al NMR meas. 78−6597
9-bromo-meta-carborane, mol. reorientation, ^{1}H and ^{11}B NMR 77−16185
bromoform liquid, NMR spin-lattice relax. time 80−25232
brute-force nuclear orientation 77−28452
butadiene-isoprene copolymers, monomer unit distrib., ^{13}C NMR determ. 78−26456
butadiene-nitrile elastomers, high temp., and press. chem. transformations *(Russian)* 79−52659
n-,t-butanol in alkanes, molecular relaxation processes studied by ^{13}C NMR 80−63654
tert-butyl acetate, frozen liquids, high-resolution ^{13}C NMR using magic angle spinning 79−33544
caesium perfluoro-octanoate/D_2O system, ^{2}H NMR quantum orders, RF pulses 80−103892
caesium perfluorooctanate, thermodynamically independent nematic amphiphilic mesophase obs. 79−95126
calibration of large mag. field sweeps 78−261
camphene, plastic cryst., ^{13}C NMR obs. 79−95667
cancer, appls. of EPR and NMR, review 78−69173
cancer detection, behaviour of different nuclear probes 79−62326
cancer detection by NMR in living animal 77−44736
capsular polysaccharide antigen, structure investig. by ^{13}C NMR 80−35828
carbides, solid-state ^{13}C NMR spectra 79−24220
carborane anion, ^{11}B NMR 78−90190
Carr-Purcell-Meiboom Gill pulsed NMR sequence, errors in T_2 values 77−85604
Carr-Purcell-Meiboom-Gill pulsed NMR experiment, baseline drift 77−85603
CBOOA, deuteron mag. reson. of mol. order and dynamics 77−35469
CBOOA, with cholesterol decanoate, short range smectic A order in nematic phase, NMR meas. 77−28475
celenious acid, rel. determ. of protons coordinates using moments of NMR spectra 79−60239
cellular applications of ^{31}P and ^{13}C NMR 80−46110
cement, water adsorption, NMR relax. exam. 78−48354
CERN muon storage ring, calib. of NMR magnetometers and mag. field meas. system 77−57780
CERN muon storage ring, NMR mag. field meas./stabilisation system 77−57779
chemical applications, literature review July 1975-July 1977 78−85217

nuclear magnetic resonance continued
chemical exchanges, mechanisms, dynamic NMR spectrosc. obs. book contrib. 79−30521
chemical exchanges, rate parameters, NMR determ. method *(French)* 77−21383
chemical fast kinetics studied by NMR, review 80−55662
chemical reactions with electronic isotopic substitution in flow and stopped flow NMR 77−25265
chemical rearrangement mechanisms, dynamic NMR spectrosc. obs. book contrib. 79−30521
chemical shift, nucl. other than protons, semi-empirical calcs., review 77−75188
chemical shift data for ^{59}Co NMR *(Japanese)* 79−68242
4-chloro, 3-nitrotoluene, partially aligned in elec. field, ^{13}C NMR, dipole moment determ. 80−78633
chloroform-d_1, D NMR relax., in nematic liq. cryst., motion spectral densities determ. 77−63304
chlorophyll a-water interaction, NMR obs. in CCl_4 and trichloromethane 79−34501
cholesteric liquid crystal, proton NMR spectra, angular depend. of second moment *(Russian)* 77−62478
cholesterol, proton-coupled ^{13}C NMR spectrum, double Fourier transform 78−78725
cholesterol+water, interaction in organic media, dielec. and NMR spectroscopy 78−76979
cholesteryl myristate, cholesterogenic, blue phase, D NMR obs. 80−97151
cholesteryl nonanoate, cholesterogenic, blue phase, D NMR obs. 80−97151
cholesteryl-m-fluorobenzoate, cholesteric liq. cryst., NMR, orientational order parameter 77−8429
choline bromide, solid, mol. dynamics, NMR obs. 78−56390
choline chloride, solid, mol. dynamics, NMR obs. 78−56390
choline salts, hydration, NMR spin-lattice relax. obs. 79−87830
chromatin nucleosome core particle, ^{31}P mag. reson. of DNA 78−40112
chrysene, mag. susceptibility anisotropies, high field ^{2}H NMR quadrupolar effects obs. 80−25225
clay-water systems, NMR, substrate struct. and H_2O mol. relax. 78−7247
coal, chem. struct., NMR and IR obs. 77−40590
coherent averaging, and its appls. 78−73887
coherent averaging, modulation method 77−8424
coherent phenomena, in multilevel NMR system, review *(Japanese)* 79−73831
collagen, hydration and intramolecular fusion, NMR and calorimetry obs., dynamic model 79−79451
collagen fibril, ^{2}H NMR of mol. motion 80−67034
colour display technique for NMR imaging 77−57373
combined retrieval system for IR, ^{13}C NMR and mass spectral data 78−31717
computer applications to NMR 80−54958
condensed matter, Summer School, Pula, Yugoslavia (Sept., 1976) 78−76293
copolyesters, diol sequencing, NMR spectra 79−52657
copolymer, ^{13}C and ^{1}H NMR, monomer unit distrib. *(Russian)* 77−46664
copper chalcogen compounds, NMR chemical shifts 80−29636
coronene, mag. susceptibility anisotropies, high field ^{2}H NMR quadrupolar effects obs. 80−25225
correlation effects in solids, representative NMR expts. 78−76324
correlation NMR spectroscopy and appls. 79−49262
coupled spin systems, multiple quantum transitions, excitation, detection, Fourier transform multiple quantum NMR 80−31819
coupled spin systems, NMR correlation spectroscopy, interference effects 77−13789
coupled spin systems, review 78−48072
CP, ^{31}P spectroscopic zeugmatography 80−76872
cross-peptide bond ^{13}C-^{15}N coupling constant, NMR obs. 80−55980
cross-polarisation ^{13}C NMR with magic angle spinning, appl. to fossil fuels and polymers 80−77819
CRT display expansion, continuously variable knob-controlled 77−22578
cryogenic flow meas. using NMR double-tuned pickup 77−13756
crystal structure investigation, using NMR spectra moments, props. of orientation dependences 79−60239
Cu, complexes, ^{63}Cu and ^{65}Cu chemical shifts and coupling constants 78−94260
cyanoacetylene, liquid, N and ^{1}H relax. rates using pulsed NMR *(French)* 79−38394
cyanomethane, multiple quantum coherence in dipolar relaxation measurements 79−73845
cyanomethane-d_1, ^{13}C-D quadrupole coupling const., ^{2}H-NMR spectra 77−481
cyanomethane-d_3, deuteron NMR spin echo, time domain spectrum 78−88223
4-cyanphenylene-4'-n-alkoxybenzoates, pulsed NMR Fourier spectroscopy 77−24266
cyclic A_{2n}-systems, trans induction effect in NMR and ESR spectra 78−29799
cyclohexane, plastic cryst., NMR determ. of phase diagram 77−12210
cyclohexane, solid, NMR second moment calc. 77−8420
cyclopropane, liq., mol. dynamics, Raman and NMR studies of orientational motion 80−93296
data bank, ^{13}C, DARC PLURIDATA system 80−30298
DBS micelle solution, hydrophobe molecule solubility 79−83517
decylammonium chloride micelles, ^{13}C longitudinal relax. times and nuclear Overhauser enhancement anal. 80−83390
defect diffusion models in NMR and dielectric relaxation 79−15375
degenerate transitions, selective excitation transfer and separated relax. meas. 78−80235
detection, appl. of integrated cct. Robinson oscillator 77−74475
deuterated polarised target, calibration of deuteron polarisation 77−3200
deuteron quadrupole coupling constants, determ. from natural abundance ^{13}C satellites in ^{2}H NMR 79−31556
1,2-di(N-piperidyl)ethane-bis-N-oxide tetrahydrate, synthesis, cryst. and mol. struct. obs. 79−32985
di-(2-ethylhexyl)phthalate, ^{13}C and ^{1}H relax., reorientational correlation times 79−51869
dialkylammonium copper chloride, nearly 2-D ferromag., low temp. NMR 77−28455
dialkylammonium copper chlorides nearly two dimens. Heisenberg ferromagnet, NMR study of magnetisation 77−85586

nuclear magnetic resonance continued
diammonium oxalate monohydrate, NMR spectra, ^{13}C-^{13}C interaction, chemical shift effects 78−29800
diamond, ^{13}C NMR 79−51862
diastereotopic nuclei, magnetic nonequivalence, chiral shielding 77−3383
diatomic homonuclear mol., nuclear spin relax., intramol. quadrupole relax. 77−14450
diatomic molecules, NMR isotope shifts, theory 77−75186
dicarbaclosododecaboranes, icosahedral, electron transfer phenomena in isolated borane units 80−18871
o-dichlorobenzene, dil. soln. in CS_2, nucl. relax. and anisotropic mol. reorientation 79−95669
1,1-dichloroethane, tilt-effect and interference with rel. sign determination in weak irrad. expts. 80−32742
dicyanoacetylene, solns., NMR and mol. reorientation 79−73840
p-diethoxybenzene, ^{13}C shielding tensors determ., by NMR from powder patterns 78−25556
diethylammonium copper tetrabromide, mag. struct., NMR meas. 80−71192
diethylammonium copper tetrachloride, ^{63}Cu NMR, hyperfine interactions 80−54956
difference NMR spectroscopy, reference lineshape adjusted, expts. 78−17693
difference NMR spectroscopy, reference lineshape adjusted, theory 78−25561
diffusion and flow meas. by NMR system, spin phase graphing 78−47074
diffusion data obtained by NMR and Mossbauer expts., interpretation, mol. dynamics study 78−47567
difluoride ion, ^{19}F free induction decay in NH_4HF_2 and (substituted) phenylamine salts 78−2754
difluoride ion, ^{1}H and ^{19}F free induction decay in alkali metal difluorides, $TlHF_2$, $BaFHF_2$, $SrFHF_2$ 78−2753
1,1-difluorotetrachloroethane, in nematic liq-cryst., transient nutation, modulation effects 77−8424
digital lock-in amplifier simulation 77−151
digital NMR gaussmeter using hybrid IC 79−71501
digital phase-shifter for multiple quantum NMR 80−17974
p,p′-dihexyloxyazoxybenzene-fluorobenzene, solute orientational order, NMR obs. 77−84627
dihydromuconic acid, C=C bond, ^{13}C shielding tensor, NMR meas. 78−1005
dilute gases, nucl. mag. relax., theory 78−25559
dilute spin species in crystals, separated local field ^{13}C NMR 77−90044
dilution refrigerator for low temperature nuclear orientation experiments on line to an isotope separator 79−752
4-4′-dimethoxyazoxybenzene-d_{14}, orientational order and internal rot., D NMR obs. 79−50987
p-dimethoxybenzene, ^{13}C shielding tensors determ., by NMR from powder patterns 78−25556
dimethyl ammonium manganese trichloride, NMR for mag. ordered state at 3.6K 79−47340
dimethyl mercury, coupling consts., solvent depend., ^{1}H, ^{13}C and ^{199}NMR 78−76334
N,N-dimethylacetamide, amide band rot., ^{13}C NMR using modified DEFT pulse sequence 79−93191
dimethylformamide, intramolecular exchange rate determ. from ^{13}C spin-lattice relax. times 80−69169
dipalmitoyl lecithin bilayer, ^{2}H NMR in liq. cryst. and gel phases 79−92173
dipalmitoyl phosphatidylcholine, gel and liquid crystalline phases, deuterium mag. resonance obs. 79−91308
diplosporin derived from (1,2-^{13}C)acetate, ^{13}C-^{13}C coupling assignment using DANTE excitation 80−80617
dipolar energy relaxation time 77−24755
dipolar spin fluctuations in rot. frame 80−20465
dipolar system, spin correlation function for free induction decay appl. to CaF_2 77−8421
direct observation in rotating frame, method tested on chemical shifts in CaF_2 *(Russian)* 78−39422
DMSO-Tl^+, spin-lattice relax., chem. shift anisotropy 79−51870
DNA, double-stranded, ^{13}C NMR obs. 80−69281
DNA, molecular motions, investigated by ^{31}P and ^{13}C NMR relaxation 80−63657
DNA and polynucleotide hydration, γ-irrad effects, frozen H_2O and D_2O solns. 77−21484
DNA conformational fluctuations, internal motion correl. times, ^{31}P NMR obs. 80−72135
DNA internal motions, ^{31}P NMR and PMR 80−97855
dodecanate/decyltrimethylammonium micelles, type II mesophase, bilayer struct., NMR spectra study 80−75149
double γ-resonance, γ-ray scatt. 79−78593
double quantum transitions, heteronuclear excitation and detection in solids, cross polaris. appls. 80−97153
double sample cell NMR technique for mag. susceptibility meas. in solid ^{3}He 79−63225
doubly tuned oscillator configuration, nonlinear mode interactions, freq. jump effects 80−77824
dynamic ^{13}C NMR spectroscopy, review 77−51971
dynamic frequency shifts rel. to quadrupole interaction 79−81216
dynamic magnetoresonance effects in solids 80−20447
EABAC, smectic A, nematic, and isotropic phases, NMR and quasielastic neutron scatt. obs. 80−88022
EBBA, liq. cryst., isotropic phase, NMR pulsed field grad. study of self-diffusion 79−90814
EBBA, NMR and Raman scatt. studies in nematic phase 80−100619
EBBA-non-mesogenic binary liq. cryst. system, two-phase premelting, NMR obs. *(Russian)* 78−30743
electric quadrupole interactions measured by nuclear orientation and NMR on oriented nuclei, review 80−92868
electrolyte soln. struct. determ. 78−38605
electrolyte solutions, NMR relaxation of ^{1}H, ^{2}D, ^{23}Na *(Russian)* 78−15053
epoxy polymers, cured spin-spin and lattice relax., proton coupling, ^{13}C NMR obs. 80−34799
erythrocyte ghost membrane struct. effects of fusogenic agent, fusion mechanism 78−31782
erythrocyte membrane water permeability defect in human epilepsy 77−29122
ethane, ^{13}C NMR, density depend. mag. shielding in gas phase 77−75187
nuclear magnetic resonance continued
ethanes, diastereotopic nuclei, magnetic nonequivalence, chiral shielding 77−3383
ethyl-trimethyl phosphines, $(C_2H_5)_{3-n}P\{E^{IVB}(CH_3)_3\}_n$, ($E^{IVB}$=C;Si;Sn; n=0,1,2,3), ($^{1}H$, ^{13}C, ^{29}Si, ^{31}P, ^{119}Sn) NMR 80−32744
ethylene, ^{13}C NMR, density depend. mag. shielding in gas phase 77−75187
ethylene, matrix isolated, shielding tensor anisotropy, ^{13}C NMR meas. 79−59491
ethylene, solid, phase diagram and NMR at high press. 80−11279
ethylene copolymers with acrylic monomers, NMR investig *(Russian)* 80−54959
ethylene glycol, microprocessor-controlled target polarization monitor 79−88990
ethylene-β-chloroethylacrylate, ^{13}C-NMR microstruct. investigation, substitution increments, sequence distrib. *(German)* 78−13636
(ethylene-co-vinyl alcohol)-g-ethylene oxide graft copolymers, sol. behaviour 80−19682
ethylene-glycidylacrylate copolymer, ^{13}C-NMR microstruct. investigation, substitution increments sequence distrib. *(German)* 78−13636
exchange processes, two-dimensional NMR spectrosc. investig. 80−25218
excitonic insulators, study of coherence factors using NMR relaxation 78−76338
explosive device detection using NMR techniques 79−6158
eye cataractous lens, NMR study of state of water *(Hungarian)* 78−64986
eye lenses, crystalline, of humans, fish and birds, state of water, NMR meas. 79−48212
Fe-Cr-Co-Si-Mo, plastic deform. influence on structure and mag. props. *(Russian)* 79−70176
ferroelectric, H-bonded, soft and central modes, mag. reson., review 78−15108
ferroelectrics, order-disorder, pseudo-one-dimens. kinetic Ising model 80−71333
ferromagnet, microscopic theory of NMR for low conc. case, lineshapes 77−59467
ferromagnet, nuclear magnetisation motion, hyperfine field microscopic inhomogeneity, NMR freq. shift *(Russian)* 80−80623
ferromagnet, under magnon bottleneck conditions, eqns. of motion 77−66429
ferromagnetic alloys, dil., hyperfine field rel. to NMR meas. 77−24537
ferromagnetic film, electron-nuclear oscillations in conditions of strong coupling between electronic and nuclear subsystems *(Russian)* 79−19782
ferromagnetic film, magnon avalanche under NMR saturation 78−10783
ferromagnets, homogeneous, magnon effects in nucl. spin-lattice relax. 79−51877
FET Q-switch circuit for pulsed NMR 77−49760
field focusing NMR visualisation of tumour in live animal 77−32950
field-focusing NMR, formation of chemical scans in man 78−85354
Fischer-Tropsch wax, NMR investigation 80−7186
flow meas., CW NMR to determine volume fractions and flow rates of component mixtures 80−33710
flow-rate meas. for liquids, pulse-compensation method based on NMR 80−103088
flowing system meas. of transient species and effects, high resolution NMR set-up 77−150
flowmeter for automatic liquid dosage system 80−43815
fluid flow profiles, convective and press.-driven, meas. using pulsed NMR 78−14109
p-fluoranil, ^{19}F NMR and spin-lattice relax. meas., pot. profile calc., mole. reorientation 80−29634
fluoranil-macrocyclic polyether mol. complexes, configs., IR and NMR obs. 78−33529
fluorite lattices, $^{19}F^-$, self-diffusion, spin lattice relax., NMR techniques 80−34801
1-fluoro, 2,4-dinitrobenzene, partially aligned in elec. field, ^{13}C NMR, dipole moment determ. 80−78633
pfluorobenzaldehyde(-d_1), in smectic mesophase, mol. struct. and reorientation, NMR 77−27093
fluorobenzenes, partially oriented in lyotropic liq. cryst., NMR spectra 77−68059
fluorobenzenes, substituted, cryst., ^{19}F NMR, chem. shift tensor meas. 78−10789
fluoromethane, chem. shielding. mol. rot. and anharmonic vibr. 78−94258
fluoromethanes, ^{19}F shielding anisotropies, NMR of smectic mesophase solns. 77−34662
fluoromethanes, and perfluoroethane, NMR gas-to-liquid shifts, 2nd-virial coeff. of chem. shielding validity 79−85976
Fourier NMR spectrometer, TESLA BS 497 adaption *(Czech)* 79−6157
Fourier transform, digital quadrature detect. 78−24833
Fourier transform, line-broadening mechanisms, dispersion-absorption plots 78−89512
Fourier transform, NMR spectrometer, magic-angle rot. 80−105688
Fourier transform, pulse system, commercial waveform analyser use 80−17977
Fourier transform, resolution enhancement, digital filtering by sinusoidal window 79−93195
Fourier transform, resolution enhancement using double exponential function 79−35804
Fourier transform, small signals meas. in presence of intense peaks 79−93196
Fourier transform, water-eliminated, WEFT, modified pulse sequence technique 77−26373
Fourier transform interpolation of spectral segments 77−26374
Fourier transform NMR, selective excitation, theory and appls. 78−77953
Fourier transform NMR, two-dimens., sensitivity, comparison with one-dimens. FT NMR 78−78724
Fourier transform NMR spectroscopy, clipped free induction decay signal anal. 77−63976
Fourier transform NMR spectroscopy, review 80−104486
Fourier transform spectrometry, error estimates 80−37061
Fourier transform spectroscopy, flip angle depend., pulse cascade description 80−28036
Fourier transform spectroscopy, high-field, of biological systems 79−39457
Fourier transform spectroscopy, software wave correction 77−43891

nuclear magnetic resonance continued
free decay and side bands in Fourier transform of high resolution NMR in inhomogeneous field *(French)* 77−51965
free-precession signal, waveform 77−51972
frequency to magnetic field convertor, digital circuit 77−61097
from velocity measurement, repetitive pulse NMR technique 80−31829
FT NMR, digitisation and data processing 80−95115
FTNMR, effect of inhomogeneous mag. field on line shape and resolution enhancement 79−63289
gas chromatography peak identification by ^{13}C and ^{1}H Fourier transform NMR 77−77836
gas phase, spin-spin and spin-rot. relax., IOS calcs. 79−18209
gas phase NMR, kinetic theory, single relax. time approx. 77−14451
gelatin, water molecules state, NMR meas. *(Russian)* 79−52790
gelatin crosslinking by formaldehyde, ^{13}C NMR obs. 79−5187
geophsical NMR logging, probe polarization field *(Russian)* 77−87120
glass, B NMR spectra, singular-value decomposition 77−36141
glass, struct. investig. techniques 78−23358
glass dating by hydration layer thickness meas. by NMR 77−74567
glycerol, nucl. mag. spin relax. and high freq. motion 79−51874
glycerol-d_3(-d_4), compressed viscous liq., reorientational motion, NMR obs. 80−7183
1-glyceryl 1-octanoate-water-CsCl, Cs^+H_2O interaction in lamellar phase, NMR quadrupole splitting and chemical shift 80−50209
glycine, electron-irrad. polycrysts., stable products obs. by ^{13}C NMR 78−15775
gramicidin single-channel currents, rate theory calc. using NMR-derived rate consts. 80−94186
graphite, ^{13}C NMR 79−51862
graphite intercalation compounds, magnetic resonance determ. of oxidation state 78−35051
graphite intercalation compounds with Br, K, ^{13}C NMR spectra 80−66048
graphite intercalation cpds. with Li, nucl. relax. times 80−44947
graphite nitrate, $(C_{3.24})^+(NO_3)^-3HNO_3$, DTA, NMR and refl. meas., dynamical and electronic props. 77−59478
graphite-UF_6 intercalation compounds, NMR exam. 78−39416
group theory, independent-particle Hamiltonian 80−43074
gutta percha, partially hydrogenated, ^{13}C NMR 80−20472
gyromagnetic ratio of proton in strong mag. field, meas. 79−40527
haemoglobin, ^{15}N NMR determ. of residual struct. in backbone of unfolded mol. 77−90720
halides, NMR spectra of halogen nuclei, shielding and quadrupole coupling consts. 78−84487
halloysite, $Al_2O_3(SiO_2)_3(H_2O)_2$, study of adsorbed water 78−95226
haloalkanes, ^{19}F chem. shielding, temp. depend., FT NMR obs. 78−86888
halomethanes, ^{13}C chemical shifts, diamag. susceptibility, effect of non-bonded interactions 78−78726
heart physiology, ^{31}P NMR investigations of metabolism, pH and contractile performance 78−69018
Heisenberg paramagnet, electronic spin dynamics, NMR 78−76266
4-n-heptyl-d_{15}-oxybenzoic acid-d_1, nematic and smectic phases, mol. and relative segmental order 80−96439
heterogeneous systems, self-diffusion, NMR pulsed field gradient *(German)* 78−60341
heteronuclear spin coupling scaling by multipulse techniques 79−42843
heteronuclear spin system, second moments of NMR spectra, calc. 79−73836
hexadecapole spin resonance in cubic symm. cryst. by NQR, NMR, nuclear gamma reson. 80−20500
hexafluorobenzene, cryst., press. depend. of nuclear spin-lattice relax. time 79−28635
hexafluorobenzene-O_2, soln., NMR for translational O_2 diffusion 79−65749
hexafluorobutene, vibrational broadening, dense fluid region, Raman and NMR study 80−43056
hexamethyl benzene-d, NMR, 4π and 2π rot. symmetry in spin-1 system 78−62830
hexamethyldisilane, plastic cryst., NMR determ. of phase diagram 77−12210
hexamethylene tetramine, polycryst. ^{14}N NMR elec. field gradient effects 77−77112
n-hexatriacontane, cryst. struct., γ-ray effects obs. 78−43048
high frequency effects in NMR spectrometers 80−77829
high frequency NMR, use of slotted tube resonator as probe head 77−30192
high inductions, meas. using NMR device *(German)* 79−21789
high magnetic field behaviour of solids and plasmas, conference, Cambridge, MA, USA (Sept. 1978) 79−60667
high pressure solid state physics, review 79−90729
high resolution, automated anal., principles and computational strategy 80−58287
high resolution, automated anal. by computer program DAVINS appl. 80−63669
high resolution, high pressure, commercial NMR spectrometer modifications, vol. of activation meas. 78−45664
high resolution, in solids, pulse coherent averaging method *(Rumanian)* 79−78543
high resolution by susceptibility compensation of detection coil 78−12736
high resolution spectra, mag. field induced mol. alignment effects 79−18207
high-resolution, broadband decoupling and scaling of heteronucl. spin-spin interactions 80−17980
high-resolution NMR spectrometer field homogeneity rel. to pole tip edge saturation 79−30522
high-temperature minifurnace, homogeneous, 25 to 1600°C, for NMR measurements 79−49235
hippuric acid, solid, second moment meas. by wide-line NMR 80−108081
HOAB, liquid crystal, mol. orientational order in uniaxial and biaxial phases by NMR 77−84629
HOAB-d_{30}, biaxial liq. cryst., NMR of spinning sample 79−64987
homonuclear coupled NMR spectra, pulses applied to multiplets, mutual coupling determ. 80−18873
homonuclear selective population inversion in AB system 80−75865
hormonal steroids, ^{13}C NMR spectra 80−81543
human samples, elec. conducting, RF losses 80−21580
human samples, zeugmatographic expt. sensitivity 80−21579
human whole-body line-scan imaging 79−5334
nuclear magnetic resonance continued
hybrid relaxation and multiple pulse methods for studying chemical, physical and spin exchange 80−80629
hydrocarbon, ^{13}C NMR shielding constants and tensors, finite perturbation calcs. 77−27092
2-hydroxy-3-crotonyloxypropyl methacrylate, polymerisation photocross-linking *(Japanese)* 78−31376
hydroxyl protons, temp. depend. of chem. shift, in R-OH cpds. 78−35054
p-Hz:o-H_z, clustering rate and NMR obs., 25 mK-2K 78−47635
ice, melting, in porous solid, NMR and differential scanning calorimetry obs. 77−62621
III-V semiconductors, chemical shifts of NMR lines of Ga nuclei 78−88201
image recovery under nonuniform magnetic fields 78−40282
imaging, and biomedical appls. 80−46006
imaging, display of cross-sectional anatomy 78−44579
imaging, methods, medical applications 77−73552
imaging, selective irrad. line scan techniques 80−77822
imaging, selective pulses method 79−93190
imaging, thin-section 78−78728
imaging, three-dimens., using selective excitation 78−21190
imaging by multisensitive point method, appl. to ~10 cm biological systems 77−86581
imaging of biological objects, sensitivity, performance time 79−96718
imaging of living organisms *(Polish)* 78−77098
imidazoline nitroxide radical, H-bonding with H donors, NMR, DNP and spin lattice meas. 79−15971
indenyl-Li ion pair in dimethoxyethane, ^{13}C NMR, temp. and counterion depend. 78−48062
indenyl-Na ion pair in dimethoxyethane, ^{13}C NMR, temp. and counterion depend. 78−48062
inhomogeneous static field effect *(Russian)* 78−48053
insulators, neutron activated β-emitters, hyperfine interactions 78−39070
interaction between atoms and RF fields, averaging method 79−81172
intermolecular relaxation operator, dipole coupling 77−68057
intramolecular H-bonds, H, D and T NMR, isotope effects and pot. energy surfaces 79−76447
inversion-recovery NMR experiments, three-parameter-nonlinear fitting procedure 77−85605
iodomethane-d_1, ^{13}C enriched, NMR, oriented, symmetry related isotope effects 77−61772
ion, nuclear transition probability when Orbach-Aminov processes exist in electron system *(Russian)* 77−85597
ionic crystal defects, mag. reson. studies 80−108066
ionic solvation, spectroscopic data comparison for methanolic and aqueous solns. 80−26099
irreducible spin precession theory applied to atomic and nuclear RF spectroscopy 80−27969
isomeric states, in-beam γ-NMR-PAD 77−59465
J-resolved two-dimensional NMR, spin decoupling, appl. to 2,3,4-trichlorophenol 80−31823
KEL-F, ^{19}F, spectrum using multiple pulse decoupling-magic angle spinning NMR probe 78−12735
lactams, N-methylated, cis-trans isomerism, ^{1}H and ^{13}C NMR obs. 80−106335
lamellar intercalation compounds, NMR studies 80−39882
lanthanide complexes, paramag., and shift reagents, NMR, book contrib. 80−53023
lanthanide ion complexes, lanthanide-induced NMR shifts, temp. depend. 77−68061
lanthanide shift reagents, pseudocontact shift, temp. depend. 79−95659
LAOCOON3 analysis system, reliability efficiency and error estimates 78−258
lecithin bilayer, ion-induced changes in head group conform, ^{31}P and ^{2}H NMR 78−3452
lecithin translational diffusion, pulsed NMR 77−9176
librational motion effects on fluoresc. depolarisation and NMR relax. in macromols. and membranes 80−85324
line scanning method for NMR images, tumorous rat leg appl. 78−92683
linear field correction, optimum size of rectangular current shim off mag. pole face 78−86314
linear triatomic molecules, NMR isotope shifts, theory 77−75186
lineshape analysis of two-site exchange kinetics, student expt. 77−26118
lineshape fitting, iterative least-squares method, symm. and mag. equiv. factorisation 77−69715
lipid bilayer, of dipalmitoyl-lecithin, NMR dispersion of layers dispersed in D_2O 79−48223
lipid bilayer, paraffin chain dynamics, ang. correl. function decay by multiple rot. pot. diffusion 80−3569
lipid organisation in Acholeplasma laidlawii membranes, ^{2}H NMR 77−86456
liquid, J cross-polarisation, refocusing method 80−22406
liquid, resolution enhancement of spectra affected by mag. field inhomogeneity *(French)* 77−12208
liquid chromatography, high performance, direct-coupling to FT-NMR 79−34412
liquid crystal, lyotropic, phase diagrams and NMR, solubilised mols. effect on struct. 77−84628
liquid crystal, premelting, high resolution NMR 78−26671
liquid crystal, thermotropic mesophase, DMR chain segments assignment 80−24356
liquid crystal phase transforms. obs., state-of-the-art 78−75820
liquid crystalline solns. in p-Cresol-$CDCl_3$ mixed solvent system 79−91303
liquid crystals, biaxial and uniaxial, orientational order 78−75552
liquid crystals, deuterated, dueteron mag. resonance mol. odering, conformational changes 80−34789
liquid crystals, dipole coupled ^{13}C NMR technique 79−99073
liquid crystals, high-resolution ^{13}C NMR spectra 79−38388
liquid crystals, lyotropic, counterion binding, NMR, ion condensation model 80−1922
liquid crystals, mol. conformation and orientational order, NMR studies, review 80−75151
liquid crystals, nematic and smectic, EPR and NMR relax., first-rank tensor component effects 78−14275
liquid metal, nucl. quad. relax. rate temp. depend. calcs. 77−12273
liquid metal targets, ^{71}Ge, ^{78}Br nuclear states, in-beam γ-NMR-PAD 77−59465
liquid metals and alloys, review 78−2755

nuclear magnetic resonance continued
liquid system, Earth field range, review 80−50206
liquids, ^{15}N NMR using J cross-polarisation for signal enhancement 79−78537
lithium acetate, methyl group dynamics, NMR 78−29802
lithium acetate dihydrate, nearly free methyl rotors, rot. energy states, nucl. reson. props. 80−34784
lithium formate crystal, dehydration, influence of hydrostatic press., ^{7}Li NMR 78−2758
lithium perfluoro-octanoate-water, liquid crystal, ^{19}F multipulse NMR obs. 80−34795
lithium perfluoro-octanoate-water system, liq. cryst. struct., self-diffusion, NMR 78−15036
liver homogenate, rat, ^{23}Na intensity, effects of alkali cations 77−12893
lock-type cell for high pressures and low temps. 78−54416
low field magnet, computer controlled, for optical and magnetic resonance studies 80−95113
low gyromagnetic ratio nuclei, NMR recording by mag. coherent transfer technique 77−90068
low temperature NMR spectroscopy, low-noise circuitry 78−4672
low-noise broadband transmit/receive circuit for NMR 80−62706
low-temperature thermometer for ^{1}H, ^{19}F, and ^{13}C spectroscopy 78−65949
lyo-mesophases, induced chem. shift, NMR obs. 79−33548
lyotropic liquid crystals, orientation in mag. field, glass interface effects 79−1390
lyotropic nematic liquid crystals, mag. susceptibility, mol. aggregation meas. 80−19690
lyotropic systems, NMR of dissolved cations and D_2O molecules 79−22732
lysozyme, aq. solns., H_2O ordering, NMR relax. investig. 79−62171
lysozyme, spin echo and spin lock ^{13}C Fourier transform NMR 79−43824
macromolecular dynamics, high resolution NMR investig. 80−91708
macromolecule, microconformation by fast exchange NMR spectra 80−102593
macromolecules, internal motion, NMR spin-lattice relax. 79−41257
macromolecules, relaxation anal. of dynamic processes 79−8470
'magic angle' spinning apparatus in solid NMR spectroscopy 80−17983
magic-angle rotor, using forced air bearing for NMR of solids 80−47083
magnetic angle spinner, high-speed 78−89516
magnetic field distributions rapid meas. method 80−27322
magnetic field intensity meas. by NMR, meas. accuracy 78−249
magnetic field prod. and meas. 78−8425
magnetic focus generation for NMR biological meas. *(Japanese)* 79−12041
magnetic induction unit, 2 to 10 T, USSR special standard 77−30191
magnetic metals, hyperfine mag. fields at ^{119}Sn nuclei 80−60248
magnetic props. of materials, appl. of nucl. orientation, review 80−44928
magnetic relaxation depend. on internal motion in solid, correlations 80−25239
magnetic shielding constants calc. by GIAO method using Gaussian functions 80−1001
magnetically ordered cryst., indirect nuclear spin interactions 80−103847
magnetometer, type 9298, homogeneous mag. field meas. 78−32839
magnetometer display using freq. to magnetic field convertor 79−71490
magnetometer for solenoid calibration 78−21187
magnetometer large-scale automation 80−57343
magnetometer type 9298, for 1 to 68 kGr using NMR 78−77950
maleic acid, acid slats, melts, H_2 bonding, IR, NMR investigs. 79−65859
malignant cells, evidence for a condensed phonon state 79−62214
mangetically ordered crystal, dynamic shift of NMR freq. of nuclei located in domain walls 80−15823
many-spin system dynamics, group approach *(Russian)* 80−50221
MBBA:trichlorobenzene, solute orientation in nematic soln., temp. and conc. depends., NMR obs. 79−46556
MBBA, ^{13}C spin-lattice relax., Fourier-transform NMR, NOE 78−48064
MBBA, liq. cryst., isotropic phase, NMR pulsed field grad. study of self-diffusion 79−90814
MBBA, nematic liq. cryst., ^{2}H NMR, mol. order and reorientation 79−27906
MBBA, NMR and Raman scatt. studies in nematic phase 80−100619
MBBA, solid, metastable, wide-line NMR 77−51966
MBBA nematic liq. cryst. systems, orientational order rel. to solute size, shape 77−4565
measurement using SQUID magnetometer system 79−75560
measuring head for NMR expts. in supercond. mag., characts., appls. *(German)* 77−41661
medical imaging, conf., London, England (Nov. 1978) 79−83876
medical imaging, conference, San Diego, USA (Aug. 1979) 80−94919
medical imaging, physiological effect threshold for RF and mag. fields 79−66484
medical imaging by NMR, book 80−31426
medical imaging by NMR, book contrib. 80−36064
medical nuclear magnetography in weak field *(French)* 77−52858
medical technology, appl. *(Japanese)* 80−51202
membrane organisation using D-NMR and spin label EPR as probes 77−44600
mesophase, degree of order rel. to cholesterol additions, chain motions 77−24260
metabolite mapping by ^{31}P NMR in whole animals, diagnosis appl. 80−36211
metal, neutron activated β-emitters, hyperfine interactions 78−39070
metal, non-Arrhenius diffusion and NMR relax. relationship 78−47568
metal single crystal meas., sensitivity consideration 78−43659
metal tritides, ^{3}He NMR and distrib. 78−30661
metallic magnetic resonance meas. using limiting oscillator circuit with improved S/N ratio 79−26096
nido-metalloborane, high -resolution ^{11}B NMR obs. of $[(B_{10}H_{12})_2Ni]^{2-}$ 79−31553
metalloenzymes, ^{113}Cd as NMR active site probe 78−68999
metalloproteins, metal nuclei, biophysical appls. of NMR, review, book contrib. 80−109081
metals, BCC and FCC, H-diffusion and trapping 80−70447
metals, charge perturbations around impurities, NMR anal. 77−85582
metals, charge perturbations around impurities, quadrupole effects on NMR signal 77−85582
metals and alloys, NMR results, brief survey 79−73830
nuclear magnetic resonance continued
methacryloyloxyethyleneoxycarbonyloxypropylene, NMR relaxation mechanism *(German)* 78−33527
methane, ^{13}C and proton medium shifts in gas phase and in soln. 77−88467
methane, ^{13}C NMR, density depend. mag. shielding in gas phase 77−75187
methane, $^{13}CH_4$, spin conversion time constants, NMR meas. 78−64281
methane, adsorbed on graphite, NMR pulsed field gradient method, diffusion coeff. meas. 80−15362
methane, in alkane soln., ^{13}C nucl. spin-spin relax., for mol. correl. times 79−95661
methane, NMR chem. shift., temp. depend., virial coeffs. 78−58722
methane, solid, high press. NMR obs. 80−50214
methane+Kr(Xe), ^{13}C-mag. shielding density depend. 78−9173
methane-d_0,-d_1,-d_2,-d_3,-d_4, ^{13}C NMR chem. shifts, coupling consts. 78−37657
methane-d_1, solid, ^{23}C and ^{1}H NMR, spin conversion obs. 77−20731
methane-Kr mixtures, rot. self-diffusion and spin-lattice relax. *(Russian)* 79−69745
methanol, ^{13}C spin-lattice relax., cross correlation of rot. motion 79−42855
methanol, mol., nucl. spin-spin coupling const., Hartree-Fock calc. 80−9618
methanol-β-quinol clathrate, orientation and reorientation dynamics, dielec. and NMR obs. 79−99783
methanol-d_1, ^{13}C-D quadrupole coupling const., ^{2}H-NMR spectra 77−481
4-methyl 2,6 di-tertiary butyl phenol, gamma-irradiated, electron-methyl group dynamical interactions 77−43161
methyl bromide, liq., NMR relax., anisotropic mol. reorientation 78−2764
methyl chloroformate, struct., microwave, Raman, far IR and NMR spectra 77−34614
methyl compounds with hindered rot. ^{13}C spin-rot. relax. times 79−50049
N-methyl formamide, isotopically enriched, isotropic and nematic phases, NMR spectra 77−32270
methyl group, ^{2}H quadrupole coupling const. by high-resolution NMR spectroscopy 78−25563
methyl group, NMR relax., spin rot. and chem. shift anisotropy effects 78−31117
methyl group, NMR relax. due to dipolar interactions 77−14455
methyl group dynamics, NMR 78−29802
methyl iodide, ^{13}C NMR with coherent proton decoupling, peak-height distortions within spin multiplets 79−31547
methyl iodide, and -d_1, dissolved in nematic phase, C-H bond orientation, ^{13}C NMR 78−46371
methyl methacrylate-styrene copolymers, ^{13}C NMR 80−20473
methyl rotator in isotropic fluid, motional asymm. determ. from ^{13}C spin dynamics 77−69718
4-methyl-2,6-di-tert-butylphenol, methyl group rot. mechanisms, Raman effect 78−71691
methylammonium ion, deuterated, dissolved in lyotropic systems 79−22732
methylene bromide-d_0-d_2, liq., nucl. spin-lattice relax., rot. correl. times 77−59476
methylmercuric halides, partially oriented, ^{1}H and ^{13}C NMR obs. 80−23437
methylmercury nitrate, in nematic and lyotropic liq. crysts., r_α-struct. and anisotropy of Hg-C coupling const. 80−43071
micellar solutions, micellar aggregation number, ^{13}C NMR chemical shift conc. depend. 80−48016
microcomputer system, appl. *(Japanese)* 79−75564
microemulsions, stability, high field NMR investig. *(French)* 78−27827
microprocessor-controlled target polarization monitor 79−88990
moisture measurements, reference materials 79−34403
molecular crystals, chem. shielding, spin-lattice, quadrupole interactions, ^{2}D NMR spin echo spectroscopy 80−34817
molecular gas, low density, transverse nucl. mag. relax. 79−59490
molecular liquid, orientation dependent distrib. function from NMR relax. data 77−20737
molecular motion dynamics in crystal influence on spectral parameters of NQR, NMR and EPR 80−20486
molecular motion effect, averaging for quantum finite motion with large amplitude 77−58046
molecular relaxation, statistical treatment, review 77−51284
molecular reorientation of symmetric top molecules, in liquid state, book contrib. 78−22623
molecular solid, dynamic struct., NMR 79−73829
molecular solid, effect of rigid-body vibrs. on NMR, quadrupole, chemical shift and dipole-dipole interactions 78−15056
molecular spatial structure, spectra interpretation, computer method 79−49962
molecular spectroscopic laboratory strategies, queueing theory and digital simulation use 80−30299
molecule, diamagnetic, NMR shielding tensor and mag. susceptibility tensor, current density calc., appl. to H_2 *(German)* 79−76445
molecule adsorbed on solid, NMR, paramag. relax. times *(Russian)* 77−39737
molecules, C-N spin-spin coupling consts., NMR, MINDO/3 calcs. 78−17694
molecules, diamagnetic susceptibilties and NMR chemical shifts in terms of localised MO's 80−106256
molecules, NMR, ^{13}C chem. shifts, screening constant calcs., CNDO/S method *(French)* 79−94012
molecules, physisorbed on homogeneous surfaces, NMR study 80−97732
molten salts, IR, Raman, EPR and NMR spectroscopy, review *(French)* 79−69832
molybdates, ^{95}Mo and ^{97}Mo Fourier transform NMR, chem. shifts and Larmor freqs. *(German)* 77−59473
monochlorobenzene, partially oriented, r_α-struct., ^{13}C satellite PMR obs. 79−50048
motion induced NMR spin relax. times in low temp. HF limit 80−60443
trans,trans-mucodinitrile solid, NMR relax., mol. motions between unequal pot. wells 78−19353
multidimensional space and time signal processing in biology and medicine 80−85493
multiple pulse NMR cycle technique, appl. to homonuclear dipolar decoupling in solids 79−67365
multiple pulse NMR in solids, resolving power improvement 79−93183

nuclear magnetic resonance continued
multiple pulse technique for homonucl. dipolar modulation of chem. shift powder pattern 79−24224
multiple pulse zero crossing technique, appl. to ^{19}F chem. shift in solids 78−37041
multiple pulse-magic angle spinning combined technique for randomly oriented solids 77−32266
multiple quanta, in presence of nonreson. field, interpretation *(French)* 78−72421
multiple quantum effects, fictitious spin $^1/_2$ operator formalism 78−76319
multiple quantum transition in NMR, two-dimensional spectroscopy, selective detection 78−23353
multiple-pulse NMR, spin dynamics *(Russian)* 78−35057
multiple-pulse NMR examination relaxation processes *(Russian)* 78−35056
multiple-pulse sequence technique for NMR $T_{1\rho}$ measurements 77−85606
multiple-quantum coherence, selective excitation, appl. to benzene 80−23439
multiple-quantum transitions, separation of different orders using pulsed field gradients 80−50222
multipulse NMR, nuclear magnetisation relax. *(Russian)* 79−19799
multispin system, slow diffusion exam. by new NMR technique 77−51970
muonium-substituted transient radicals observed by muon spin rotation 78−74678
muscle, mouse, ^{13}C NMR and PMR 77−86463
muscle, skeletal, Na relaxation, spin echo study, evidence of Na ion binding inside a biological cell 78−88698
muscle, striated, of frog, pulsed NMR of ^{39}K 77−16920
muscle water transverse and longit. NMR relax. rates 78−35810
myosin, interaction with adenosine 5'-diphosphate, intermolecular spin diffusion study 80−18951
myosin, interactions with HDO, intermolecular spin diffusion study 80−18951
naphthalene-d_8, in diethylether soln., ^2H NMR, mag. field induced alignment effects 79−13740
naphthalene-tetracyanobenzene, charge transfer complex, phase transitions, deuteration effect, mag. reson., spectral and thermal meas. 79−4412
'nematic' amphiphilic liquid crystalline mesophases, thermodynamic stability 79−95126
nematic liq. crystal spin-relaxation, composite Markov process, rot. reorientation and director fluctuations 77−62471
nematic liquid crystal, ionic conduction-induced flow alignment angle, NMR evidence 80−44125
nematic liquid crystal, mol. reorientation, Fourier tranform NMR 77−35479
nematic liquid crystal, optical anisotropy, determ. from NMR and birefringence data *(German)* 77−40205
nematic liquid crystals, MHD effect, high resolution NMR *(Russian)* 78−15040
nematic liquid crystals, nucl. spin relax. and slow solute motion 79−95662
nematic-cholesteric liq. cryst. mixture, NMR, reordering, nucleation and growth model 77−72546
nematogenic substances in solid state, NMR spectra 77−16186
nematogens, molecular motion in solid phase 79−61239
neopentane, adsorbed on graphite (TiO_2), NMR pulsed field gradient method, diffusion coeff. meas. 80−15362
neopentane adsorbed on graphite, quasi two-dimens. fluid, NMR 80−102525
nitrobenzene, anisotropic mol. reorient., ^{13}C, ^{14}N and ^2H mag. relax. 77−48070
nitrobenzene, liq., ^{14}N and D NMR, ^{14}N quadrupole coupling const., environmental effects 78−48052
p-nitrofluorobenzene, nematic phase NMR, ^{19}F shielding anisotropy 78−62824
nitromethane, liq., NMR relax. obs. of internal mol. rot. 79−95668
NMR chem. shift., temp. depend., virial coeffs. 78−58722
NMR image resolution from sensitive line method, magnetisation vector 79−93182
NMR under optical pumping conditions 80−25253
NMR-ESR spectroscopy, miniature magnetic assembly, teaching 80−105467
noble metal complexes, hexafluoro, review of struct. obs., pseudorot., press. effects 78−6045
noise, Fourier transform as perturbation criterion, appl. to NMR intensity 78−65948
noise reduction filter in resolution enhancement 80−73403
noisy exponential decays, algebraic anal. for on-line computer anal. 77−67415
nomenclature and data presentation for publication in chemical journals, IUPAC recommendations 77−68065
non-secular spin-spin interactions, in nucl. relax. 78−91976
nonaqueous electrolyte solutions, ionic nuclei, quadrupolar interaction, mag. relax., infinite dilution limit 78−35692
nonequilibrium spin system *(Russian)* 78−64278
nonexponential nuclear relaxation data acquisition and processing system using Nairi-2 computer 78−32800
nonpolar molecule substituting polar mol. in mol. dipole lattice, dielectric alignment 77−89359
nonresonant RF excitation on mag. nuclei at low freq. 78−76326
nonrigid molecules, dipolar relax. and nuclear Overhauser effects, fluctuating internuclear distances effect 80−91578
norbornane, derivatives in solution, mol. motion and methyl group rot. barriers from ^{13}C NMR relax. times 80−74179
nuclear dipolar magnetic ordering, dipole-dipole interactions review 77−85475
nuclear echo formation in spin systems with dynamic freq. shift to NMR 80−93208
nuclear magnetic shielding constant, calc. by extended Huckel method with expansion by Gaussian functions 77−79634
nuclear magnetic shielding density 80−63559
nuclear magnetism and ultralow temperature, review *(Japanese)* 80−86806
nuclear spin relaxation spectroscopy, appls., review 77−83619
nuclear-spin subsystems, cross-relax., nonequilib. thermodynamics 79−58662
nucleic acid bases, ^{14}N relax. and N-proton spin coupling, NH-proton spin-lattice relax. 80−26202
nuclear magnetic resonance continued
nucleic acids studies, at. coords. of helices, by computer program 79−86095
nucleobases stacking interaction 79−62170
nucleoside conformations from NMR studies, review 78−76990
nucleotide conformations from NMR studies, review 78−76990
null line stabiliser of NMR spectrometer with time division 79−2800
4-n-octyl-d_{17}-oxybenzoic acid-d_1, nematic and smectic phases, mol. and relative segmental order 80−96439
off-resonance nuclear spin-lattice relaxation time, pulsed NMR method for mol. motion in condensed phases 79−78554
oil, lubricating, radn. effects and radn. dosimetry appl. 80−2069
oligoethylene glycol, crystallisation kinetics in presence of tetrachloromethane, NMR investig. *(Russian)* 80−54153
one-dimensional magnetic system, high-temp. dynamics 79−4716
one-dimensional planar magnets, low temp. NMR 80−44943
operator formation for double quantum NMR 78−2750
order parameter fluctuation spectrum, central peaks near ferroelectric phase transitions, review 79−19851
organic compounds, ^{13}C NMR, chem. shift, effective excitation energy calcs. 77−14457
organic molecular crystals, intermolecular interactions, spectroscopic studies, review 80−103958
organic molecules, NMR spectra, mag. field induced mol. alignment effects 79−18207
organic molecules, polycryst., NMR, selection of nonprotonated C resonances 80−50201
organic solids, frozen liquids, high-resolution ^{13}C NMR using magic angle spinning 79−33544
organoarsinoboranes, ^{11}B NMR 78−90190
organometallic, fluxional, solid state chem. exchange, ^{13}C NMR magic angle spinning 80−7775
organophosphorus compounds, liq., ^{31}P nucl. spin-lattice relax. and Overhauser effect 79−36666
organotin compounds, with remote substitutions, ^{119}Sn NMR constants 79−65748
oriented molecules, NMR spectra, vibr. correction study 80−18840
α-oxalic acid.$2H_2O$, proton mag. shielding, rel. to deuterium shielding 77−77106
oxalic acid dihydrate, NMR spectra, ^{13}C-^{13}C interaction, chemical shift effects 78−29800
β-oxy butyric acid ethyl ester, scaled spectra using three joined pulse sequences 80−73405
PAA, nematic, NMR study of ordering, intramol. mobility 80−100162
PAA, nematic and crystalline phases, NMR and relax. 79−4740
PAA, structural and optical anisotropy, NMR spectra 79−14675
PAA-di, nematic liquid crystal, NMR data, appl. of Landau-de Gennes theory 80−64893
pancreatic trypsin inhibitor, bovine, macromol. dynamics, high resolution NMR investig. 80−91708
PAP, structural and optical anisotropy, NMR spectra 79−14675
paramagnetic material effect on chem. shift and relax. times, mol. struct. effect 78−46373
paramagnetic metal ions as structural probes for NMR investigation of inorganic and bioinorganic compounds 78−62828
paramagnetic polycryst. mols., NMR 80−23436
paramagnetic systems, NMR shifts calc. using nonmultipole expansion method 80−2651
particles, quantum size effect obs. by CESR and NMR 77−20700
parvalbumins, Ca-binding, lanthamide-substituted, of muscle, ^{13}C NMR obs. 79−96516
pentachlorotoluenes, positional isomers, ^{13}C Fourier transform NMR spectrometry, struct. and compositional anal. 80−91576
pentacoordinated ferrous porphyrins, ^1H and ^{19}F NMR, hyperfine shift, π electron binding 78−78719
peptide, NMR spectroscopy study 78−88694
peptides, effect of internal librational motion on ^{13}C NMR relax. times 78−85293
perfluorocarbocyclic ethers, NMR, microstruct. 79−51863
phase and intensity anomalies reduction in FT NMR spectra of Varian XL-100 spectrometer 77−45873
phase device for low freq. NMR expts. 80−31837
phase diagrams, construction, use of NMR, Mossbauer effect, and gamma ray perturbed angular correlation 79−8417
phase transitions, high press., NQR and stationary NMR studies 80−19934
phenanthrenequinone, NMR of cryst., 77-480K 79−38387
phenyl alkyl ammonium copper chloride, quasi-two-dimens. Heisenberg ferromag., mag. props. 77−66273
phenylamine difluoride, and derivs., ^{19}F free induction decays 78−2754
phenylene sulphides, NMR relaxation for mol. motions *(German)* 80−11288
phenylphosphines, and derivatives, ^1H, ^{13}C and ^{31}P NMR studies 80−87152
phlogopites, mica, Fe^{2+}, F^-, and OH^- distrib. in octahedral sheet, NMR study 79−82183
phosphate glass, Li^+ motion, ^7Li NMR spectra, nucl. relax. 80−34804
phospholipid bilayer membrane, spin $^1/_2$-nuclei, in chain methylene groups 77−48767
phospholipid bilayers, carbonyl groups dynamics, ^{13}C chem. shift anisotropy obs. 80−85326
phospholipid membrane, polar head motion, NMR and EPR linewidth study using $TCNQ^-$ ion-radical *(French)* 80−45865
phospholipid transmembrane asymm. studied by NMR spectroscopy with displacing reagents 78−31984
phosphorous metabolites, ^{31}P spectroscopic zeugmatography 80−76872
phosphoryl transfer enzymes, biophysical appls. of NMR, review, book contrib. 80−109081
piperylene-acrylonitrile copolymers, polymerisation, monomer composition rel. to copolymer struct. *(Russian)* 80−5651
pivalic acid, liq. and plastic crysts., ^{13}C NMR chem. shift, temp. depend. 80−2652
plastic crystals, high-resolution ^{13}C NMR spectra 79−38388
plastic crystals, self-diffusion parameters from anal. of NMR relax data 79−42301
PMMA, mol. motions in benzene soln., ^{13}C NMR and EPR 79−78551
PMMA, multicomponent network, pulsed NMR study of mol. motions 77−55724
PMMA, syndiotactic, solns. in toluene, NMR obs. of struct. and dynamics of associates 80−75867

nuclear magnetic resonance continued
PMMA isotactic, syndiotactic stereocomplex formation in soln., composition, struct. 79−66292
pnictides, cubic Van Vleck compounds, paramag. fluctuations, ESR or NMR relax. 77−66420
polarised β-active nuclei, cross-relaxation processes 80−60431
polariser design, for magnetising liquid in NMR devices 80−57351
poly(γ-benyl-D-glutamate) liquid crystal, orientation in magnetic field, NMR study *(Japanese)* 77−72550
poly(γ-benzyl-L-glutamate), soln., rot. diffusion, ^{13}C NMR 77−75350
poly(diallyldimethylammonium) chloride, struct., ^{13}C NMR 77−565
poly(dimethyl siloxane) diffusion of dichlorodifluoromethane, conc. and pressure dependence 77−55392
poly(ethylene-but-1-ene) copolymer, gelation and precipitation from solutions, NMR exam. 79−43641
poly(L-histidine), molecular motions in solid state, NMR and dielec. meas. 80−11332
poly N,N-diallyldimethylammonium chloride, soln. props., struct. 79−94861
poly O-carbobenzoxyl-L-tyrosine, in soln., conformation, helix-coil transition, circular dichroism, NMR spectra 77−31037
poly-1,3-pentadiene, microstruct., IR, NMR, X-ray determs. 79−37637
poly-4-methyl-1-hexene, optically active, ^{13}C NMR obs. of conform. 77−10801
poly-β-benzyl-L-aspartate, soln., ^{13}C and ^{1}H NMR dynamic study 79−69737
poly-β-substituted vinyl ethers, cationic polymeris., stereochem. 80−21284
poly-γ-benzyl-L-glutamate, soln., ^{13}C and ^{1}H NMR dynamic study 79−69737
poly-L-alanine, soln., ^{13}C NMR dynamical study 79−69737
poly-L-ornithine solution, ^{15}N NMR, coil-helix transition, solvent effects and pH depend. 80−74275
poly-N-vinylcarbazole, struct. model, using NMR and diffr. data 78−83750
poly-p-chlorophenyl glycidyl ether, struct., tacticity and addition isomerism, ^{13}C NMR 80−58427
poly-p-phenylene sulphide, NMR relaxation for mol. motions *(German)* 80−11288
poly-thio-1-N,N-diethylaminomethylethylene, optically active samples, ^{13}C NMR spectra 80−28127
polyacetylene:AsF_5, mag. susceptibility, Fermi surface density of states, semicond.-metal transition 79−95566
polyacetylene:I, NMR investigation of struct. 80−39011
polyacetylene:I, NMR struct. investigation 80−108082
polyacetylene and polyacetylene: AsF_5, one-dimens. spin diffusion, NMR T_1 and dynamic nuclear polarisation meas. 80−44946
polyarylbutadiene, microstructure, NMR and IR obs. *(Japanese)* 79−24488
polyatomic fluid, local dynamics, spectroscopic studies, summer school lecture series 80−6343
polyatomic molecules, NMR isotope shifts, theory 77−75186
polyatomic molecules, structure recognition, from IR, UV, NMR and mass spectra, computer method 78−25737
1,4-polybutadiene, epoxidised, ^{13}C NMR, Overhauser effect 79−51872
polybutadiene, hexafluoro acetone substituted, H-NMR and ^{19}F-NMR spectroscopy *(German)* 80−103893
polybutadiene, low mol. wt., NMR study of terminal group struct. *(Russian)* 77−63912
polybutadiene, mol. motion in solid and soln., ^{13}C NMR relaxation meas. *(Japanese)* 80−2666
cis-1,4-polybutadiene, partially hydrogenated, ^{13}C NMR 80−20472
polybutadiene, transverse nuclear magnetisation decay rel. to slow mol. motions *(Russian)* 78−72423
polybutadiene-polystyrene, ^{13}C NMR assignments, rel. to mol. configurations 77−54640
polybutene-1, microstructure determ. by ^{13}C-^{1}H NMR 78−26455
polycarbonates unstretched and stretched, orientation relationships, ^{13}C NMR meas. *(German)* 80−20474
polychloroprene, microstruct. determ. by ^{13}C NMR 79−33546
polycrystal, struct. parameters determ. from NMR spectra anl. of two-spin system 77−89353
polycrystalline solids, spin-one NMR, ^{14}N shift, elec. field gradient effects 77−77112
polydimethylcarbosiloxane net-type, crystallisation, NMR obs. *(Russian)* 77−20744
polyesters, linear aliphatic, chem. struct. rel. to viscoelastic props. 79−41977
polyesters from bridged bicyclic lactones, struct. characterisation by NMR 80−20476
polyethers, NMR, microstruct. 79−51863
polyethylene, ^{13}C NMR rotating frame relaxation 80−7182
polyethylene, chlorinated, ^{1}H and ^{13}C NMR microstructural investigation *(German)* 77−55246
polyethylene, chlorinated, high resolution ^{1}H and ^{13}C NMR, group fractions *(German)* 77−65551
polyethylene, chlorinated, microstructure, use of ethylene vinyl chloride and copolymers as macromolecular models *(German)* 77−27838
polyethylene, chlorinated, partial struct. anal. of methane component by ^{13}C nuclear magnetic resonance *(German)* 79−73110
polyethylene, chlorination, rate const. determ. using NMR spectra of chain sequence *(German)* 79−100366
polyethylene, highly oriented fibres, 2-dimens. ^{13}C NMR 77−77114
polyethylene, homopolymers, copolymers and model systems, ^{13}C NMR chem. shifts and relax. times 79−72449
polyethylene, linear, cold-deformed, texture and molecular chain mobility 78−19805
polyethylene, linear, solution-crystallized, NMR anal. of phase struct. 78−71684
polyethylene, linear, struct. and relax. transitions, pulsed NMR and X-ray diffr. *(Russian)* 77−47357
polyethylene, mol. morphology determ. by NMR 78−94341
polyethylene, NMR, IR spectra and elemental anal. 80−29681
polyethylene, NMR relaxation times, computer-assisted meas. method 77−22586
polyethylene, pulsed NMR study of crystallization kinetics from melt and soln. 79−87624
polyethylene, short chain branching, ^{13}C NMR 79−33557
polyethylene, ultraoriented, ^{13}C-^{13}C dipolar satellites 77−28465
polyethylene glycol, transverse nuclear magnetisation decay rel. to slow mol. motions *(Russian)* 78−72423

nuclear magnetic resonance continued
polyethylene oxide, dilute solns., mol. motion, EPR and NMR investigations 79−94863
polyethylene oxide, NMR relaxation in melt, three component model 77−55723
polyethylene oxide soln., NMR meas. of dilute to semidilute regime crossover 79−11355
polyhedral A_{2n}-systems, trans induction effect in NMR and ESR spectra 78−29799
polyisobutylene, transverse nuclear magnetisation decay rel. to slow mol. motions *(Russian)* 78−72423
polyisobutylene soln., NMR, chain segment motions 80−20475
polyisocyanides, solns., struct. and acidification 80−19915
1,4-polyisoprene, epoxidised, ^{13}C NMR, Overhauser effect 79−51872
polymer, self-diffusion detection, NMR matrix technique 80−15806
polymer chain dynamics, ang. correl. function decay by multiple rot. pot. diffusion 80−3569
polymer glassy and crystalline, relax. process characterisation, ^{13}C NMR obs. 80−34802
polymer melt, NMR relaxation, mol. motion, local defect component theory 77−55722
polymer melts, defect fluctuations, reptation, Monte Carlo investig., NMR autocorrel. function 77−3499
polymer orientation measurement, in solid, by spectroscopic techniques, mech. anisotropy 78−75558
polymer solns., dynamical polymer coil overlap, NMR model 80−23583
polymers, oriented, partly cryst., macromols. in amorphous regions, length, mobility 80−49132
polymers, review 80−11277
polymers, synthetic, dil. solns., NMR relax., review 79−89693
polymers containing main chain heteroatoms, struct., ^{13}C NMR investigs., review 79−55013
polymetal phosphinates, linear chain magnet, ^{31}P NMR, spin density 77−77108
polymethacrylic acid: ^{23}Na, nuclear relax. correl. times and counterion behaviour 80−50212
polymethacrylic acid, stereoregular, synthesis, ^{13}C NMR obs. 80−58422
polymethacrylic acid, syndiotactic deuterated, aq. solns., methylene deuteron relax., freq. and temp. depend. 77−90062
polymethinecyanines, symm. solvent effects on electronic struct., ^{1}H, ^{13}C NMR 78−13516
polymethyl acrylate, multicomponent network, pulsed NMR study of mol. motions 77−55724
polynucleotides, double helix, high resolution NMR, review 77−86450
polypropylene, isomeric, microconformation from slow exchange ^{13}C-NMR spectra of low mol. wt. cmpds. 80−102592
polypropylene, stereochem. additions, sequence lengths, ^{13}C NMR 77−27212
polysiloxane oligomers, ^{29}Si NMR, chem. shift effects of end groups 79−33550
polystyrene, epimerised isotactic, methylene C mag. resonance spectra 80−63878
polystyrene, plasma produced, struct., NMR 77−25264
polystyrene, stereochem. additions, sequence lengths, ^{13}C NMR 77−27212
polystyrene-polydivinylbenzene, interpenetrating network, IR, NMR and chromatographic anal. of intermediate regions 77−55711
polyurethane, interpenetrating network, IR, NMR and chromatographic anal. of intermediate regions 77−55711
polyurethanes, cross-linked, mol. mobility and struct., thermomechanical and NMR obs. *(Russian)* 80−69285
polyurethanes, domain struct. obs. by NMR 77−47355
polyvinyl carbazole, and ring chlorinated derivatives, dielectric and NMR relaxation 79−73883
polyvinylidenefluoride, effect of structural factors on melting and freezing *(German)* 78−15389
population distribution to enhance NMR sensitivity and allow decoupling of low gyromagnetic ratio nuclei 80−73399
population inversion using composite sandwich 79−93197
positronium, ground state, fine struct. interval, NMR meas. 77−34787
potassium laurate-1-decanol-water mixtures, biaxial nematic phase obs. 80−107409
potassium palmitate-water bilayer, lamellar liq. cryst. polymorphism, NMR and birefringence 79−60270
potassium palmitate-water solution, deuterated, NMR asymmetry parameter 80−88882
powder patterns for integer spin nuclei in presence of asymmetric quadrupole effects 77−90046
powdered specimen, anisotropic mag. interactions, high resolution NMR *(Russian)* 78−39418
powders, high speed rot., spin diffusion, NMR spin lattice relax. obs. of D 80−66056
powders, rot. spin-echoes and high resolution NMR 77−43901
prepolymers, H-NMR and ^{19}F-NMR spectroscopy *(German)* 80−103893
principles, introduction to basics 80−77820
probe assembly, He-cooled, for proton-enhanced ^{13}C reson. 80−17978
probe for high-pressure and high-temp. expts. 80−22403
progressive-saturation selective population inversion technique, sensitivity gain 78−17692
propionitriles (-O, NH, S), conformational investig., NMR, IR and semiempirical MO methods 80−95650
n-propylammonium chloride, NMR, spin-lattice relax., cation dynamics 79−11353
propylene copolymers, ethylene incorporation meas. by ^{13}C NMR and IR spectrosc. 79−39225
propylene-alkyl acrylates alternating copolymers characterisation 79−51950
propylene-butadiene, alternating copolymer, struct., fractional composition obs. *(Russian)* 79−65011
propylene-butene copolymers, PB centred tetrad ^{13}C NMR spectra assignment 80−58428
propylene/butene-1 copolymers, coisotactic shift contribs. in ^{13}C NMR spectra 80−29635
protein, NMR spectroscopy study 78−88694
protein titrations by NMR, pH depend. of internal reference 77−86727
proteins, ^{13}C NMR, review 77−86449
proteins, effect of internal librational motion on ^{13}C NMR relax. times 78−85293
proteins, methine aromatic C sites, natural abundance ^{13}C NMR at high mag. field strength 77−86443

nuclear magnetic resonance continued
proteins, solid, NMR, detection of individual C resonances, appls. 80−51042
proton relaxation enhancement, biochem. appls., review 79−89692
PTFE, NMR and X-ray diffr. investig. of press. induced III-I transition and mol. motion 77−51969
pulse, spurious ringing 79−93187
pulse Fourier transform NMR, vomplex spin system nonequilib. state, Liouville space description 78−48057
pulse Fourier transform NMR, weakly coupled complex spin system 78−48058
pulse NMR, two channel analogue pulse generator design 78−45665
pulse NMR technique, chem., anal. appls. 77−29975
pulse programmer, microprocessor-based 80−52289
pulse programmer for high resolution multiple pulse NMR in solids *(German)* 77−41660
pulse programmer for single and double resonance expts. 80−57347
pulse radiolysis applic. 77−32814
pulse type, programmable pulse sequence generator 80−17979
pulsed, automatic trigger pulse logic for pulse programmer 80−47084
pulsed, flow velocity meas. in capillary 78−83506
pulsed, solid-state high-power RF amplifier for imaging expts., 1 to 22 MHz 79−54162
pulsed gradient diffusion meas. with microcomputer 80−17973
pulsed NMR, extremely fast recovery time receiver 77−26376
pulsed NMR data acquisition system, devel., appl. to polyisobutylene 80−34807
pulsed NMR experiments, microprocessor-controlled pulse sequencer 80−68231
pulsed NMR in solids, survey 80−34782
pulsed NMR relaxation, computer controlled, general programme 78−4669
pulsed NMR technique for meas. radiation effects in polymer 80−66051
pulsed NMR thermometry below 0.1K 77−5852
pulsed relaxation measurements, signal integration and S/N ratio 77−48030
pulsed spectrometer wideband preamplifier 79−71502
PVC, chlorinated, microstructure, use of ethylene vinyl chloride and copolymers as macromolecular models *(German)* 77−27838
PVC, reduced, NMR, IR spectra and elemental anal. 80−29681
PVC branching, origin, extent 79−7048
PVC-vinylchloride system, glass transition, nuclear mag. relax. obs. *(German)* 80−79917
pyrene-d_{10}, in diethylether soln., ^{2}H NMR, mag. field induced alignment effects 79−13740
pyrene-tetracyanobenzene, charge transfer complex, phase transitions, deuteration effect, mag. reson., spectral and thermal meas. 79−4412
pyridil-benzo-X-azoles, NMR spectra, chemical shift and coupling const. data *(Italian)* 77−54566
pyridine, ^{13}C-^{1}H spin-spin coupling consts. 78−25562
pyridine, proton-coupled ^{13}C J NMR, strong coupling 78−17691
pyridine, proton-coupled ^{13}C J spectra, strong coupling 77−68063
pyridine+HCl, proton transfer interactions, NMR obs. 78−20007
pyridine-3-aldehyde, partially oriented in nematic solvent, rot. isomerism and conformation, NMR obs. 77−71820
di-α-pyridyl hydroperchlorates, intramol. H bonds, steric conditions and polarisability obs. 80−53160
pyrochlore related structures, phases of type AM_2X_6, acentricity and phase transitions, X-ray diffr., DSC and NMR study 79−27943
pyromellitic acid dianhydride, cryst. struct., anisotropic proton mag. shielding 79−87326
Q-meter spectrometer modification, servomechanism for automatic tuning *(French)* 77−18061
qauche NMR effect in ^{13}C, ^{19}F and ^{31}P chem. shifts and directly bonded coupling consts., bond angle effects 77−68056
quadrupolar nuclei in solids, enhanced resolution NMR interferometric correl. of shifts 80−57355
quadrupole distorted NMR powder patterns, simulation, Fortran program 77−77105
quasi one-dimensional and two-dimensional crystals, NMR relaxation time mag. field depend. *(Russian)* 79−61254
quasilattice theory of solutions, use in mol. spectroscopy, thermodynamic parameters determ. 79−96350
quick sample change probe for magic-angle-spinning NMR in a superconducting magnet 80−31834
radiative detection, single-pulse and spin-echo NMR 78−8428
radiofrequency pulse sequences which compensate their own imperfections, appln. to population inversion 80−77827
radiospectrometer electromagnet field uniformity rel. to pole piece shape and material 78−86309
radiospectrometers, calc. of optimal configuration of shims 80−73398
rare earth alloys, RAl_2, RZn, ordered, NMR determ. of hyperfine fields 78−84180
rare earth cobaltides, R_2Co_{17}, ^{59}Co NMR obs. of hyperfine fields and mag. moments 77−20726
rare earth cobaltites, ^{59}Co NMR, quadrupolar and hyperfine interactions 79−15366
rare earth complexes, formation and props., book contrib. 80−43204
rare earth compounds, cryst. field effects on EPR and NMR *(Japanese)* 77−43879
rare earth compounds, cryst. field effects on EPR and NMR *(Japanese)* 77−43880
rare earth compounds, gyromagnetic resonance, study of magnetism *(Danish)* 79−15359
rare earth induced NMR shifts, temp. depend. 77−28464
rare earth intermetallic compounds, NMR anal. of indirect mag. interactions 80−71193
rare earth metal, alloy and cpd., static and dynamical aspects of hyperfine interaction, NMR investigation 79−91299
rare earth metals, heavy, NMR exam. of electric field gradient 78−52363
rare earth nuclei in cubic cpds., self polarisation field calc. 80−15487
rare earth orthoferrites, hyperfine interaction anisotropy, NMR study *(Russian)* 80−66052
rare earth phosphates, RPO_4, ^{13}P NMR exam. of transferred hyperfine effects 79−61241
rare earth systems, NMR, EPR, and Mossbauer effect, book contribs. 80−39883
rare earth-Al_2(Zn), mag. coupling mechanism 79−4655
rare earth-Co alloy, RCo_5, mag. anisotropy, individual Co site contribution 79−78366

nuclear magnetic resonance continued
rare earth-nonmagnetic metal intermetallic cpds., struct. and props., review 79−95377
rare earth-transition metal alloys, cryst. and amorphous, mag. props. 77−73008
rat liver isolated cells, ^{31}P NMR 78−61150
receiver, description and design 78−21193
relaxation, electron spectral densities calcs. 80−60436
relaxation data processing *(Japanese)* 77−34008
relaxation measurements, Markov theory, systems with multiple degrees of freedom 78−46368
relaxation parameters, use of superoperators *(Russian)* 77−14458
relaxation processes, macroscopic evolution eqns. and virtual spins importance *(French)* 80−32739
relaxation time relationship in rotating and laboratory coordinate systems 80−39887
relaxation times, computer-assisted meas. method 77−22586
relaxation times and magnetisation of slowly relaxing systems with weak NMR signals 77−49752
resolution enhancement of spectra by numerical treatment *(Spanish)* 77−67483
resonant NMR near mag. transition 78−76265
review of NMR and molecular biology research *(Chinese)* 79−39459
RF size effects meas., optimisation of marginal oscillator for 77−26377
rhodamine Zh, isomer separation, identification and emission efficiencies *(Russian)* 77−83871
ring current theory 80−87240
RNA, conformational fluctuations, internal motion correl. times, ^{31}P NMR obs. 80−72135
RNA, molecular motions investigated by ^{31}P and ^{13}C NMR relaxation 80−63657
rotating coordinate system, indirect NMR obs., suppression of nuclear dipole interactions *(Russian)* 77−40141
rotating frame, ^{13}C spin-lattice relax. using proton decoupled Fourier transform spectra, errors origin 80−18945
rotating frame, effect of nonresonant oscillating field, modification of Zeeman energy 77−28454
rotating frame demagnetisation, J-ordered magnetic states production 80−73404
rotating frame relax. time for spinning sample 79−47344
rotating frame selective pulses in NMR imaging 80−68232
rotating frame spin-lattice relax. in presence of off-reson. RF field 79−93193
rubber, natural, transverse nuclear magnetisation decay rel. to slow mol. motions *(Russian)* 78−72423
rubber, partially hydrogenated, ^{13}C NMR 80−20472
ruby, ^{27}Al NMR line acoustic saturation, appl. in quantum acoustic strain detector 77−51009
ruby laser, ^{27}Al nucl. spin system, collective ordering phenomena, instabilities 80−11278
ruby NMR laser, dynamic props. from point of view of synergetics 80−43341
sample tube self-positioning anti-vortex plug 77−21434
saturated bandshapes in high-resolution NMR relax., obs., three and four spin 1/2 systems 77−1611
saturation in rotating system of coordinates under magic angle conditions 78−19346
scaling of heteronuclear spin interactions by multipulse sequences 80−73405
screening constants of O and N in molecules, INDOS/S parameterisation scheme 79−76449
second moment, lattice vibrs. effect 80−20467
selective excitation with single-freq. off-reson. decoupling 80−17981
self-diffusion in cubic crystals, random motion of vacancies, correl. factor and NMR diffusion parameters 78−2284
self-diffusion measurement, restricted, with gradient modulation 77−4568
self-diffusion NMR pulsed-gradient meas. noise pulse generator 77−53965
semi-classical equations of motion, soln. by transform. to rot. co-ordinate frames 79−35586
semi-mean interaction regime *(Russian)* 78−80231
semiconductor solid solns., NMR of optically oriented nuclei, quadrupole effects *(Russian)* 77−85592
semiconductors, liq., NMR and metal-nonmetal transition 77−51973
semiconductors, optical orientation of electronic and nuclear spins 78−79928
semiempirical theory of NMR parameters, chem. shielding, ^{13}C chem. shifts 80−23435
shielding constant, cusp-type anomaly in fluid crit. region 78−39411
sigma phase alloys, NMR and electric-field gradients 80−108109
signal enhancement by rod-induced convection 80−77823
signal intensity enhancement by polarisation transfer 79−94013
signal to noise calculation for lines, direct vs. lock-in recording 77−65049
signal to noise ratio, reciprocity principle calcs. 77−13792
silicate glass, hydrated, proton and ^{23}Na wide-line NMR study 80−84659
simple cubic lattice, simple hopping, correlation functions, NMR relaxation rates 79−42864
single crystal NMR probe and circuitry *(Chinese)* 79−35807
single passage NMR on oriented nuclei experiencing small elec. quadrupole interactions, numerical solns. 78−15031
single- and double-pulse nuclear orientation NMR 79−42842
skin, rat, ^{1}H and ^{13}C NMR obs. 80−40965
smectic-C liquid crystals, biaxial mol. order, NMR meas. 80−25227
sodium dodecyl sulphate: Gd^{3+}, micellar system, chain folding, ^{13}C NMR obs. 80−61158
sodium oleate, frozen soln., NMR study of phase transitions 79−56617
solenoid, superconducting, homogeneous, for superconductor props. meas. by NMR *(Czech)* 78−29130
solid, double-cross-polarisation NMR 80−20468
solid, H-bonded, NMR chem. shift tensors *(German)* 78−84489
solid, pulsed NMR, adjusting conditions *(German)* 78−84486
solid electrolytes and solid soln. electrodes, review 80−60432
solid materials, high resolution ^{13}C NMR spectroscopy 80−97150
solid polymers, review 80−88888
solid state, simultaneous use of rotation and RF fields, selective investigation of interactions *(Russian)* 78−56385
solid state ^{2}H NMR, magic angle sample spinning to remove quadrupole broadening 79−97410

nuclear magnetic resonance continued
solid state physics applications *(Chinese)* 80−80622
solid with reorienting mol. groups, effective decay time for multipulse NMR 79−61238
solids, averaging method application to high resolution NMR, Magnus expansion *(Russian)* 80−34793
solids, calcs. of NMR spin echo responses 78−88221
solids, disorder of NMR and soft collective lattice modes, spins and pseudospins 78−88208
solids, high resolution multipulse techniques 78−60345
solids, high resolution NMR, review 78−6582
solids, high resolution pulsed NMR, adjusting conditions of pulse sequences 80−93184
solids, pulsed NMR, conf., London, England (Dec. 1978) 80−31404
solution film adsorbed on cryst. surface, NMR investig. 77−8426
solutions exhibiting chemical exchange, spin 5/2 and 7/2 nuclei 79−65750
spatial selection in NMR by spin locking 78−43656
spectra, computer-aided interpretation, minicomputer based file search system 80−62702
spectra, computer-aided interpretation using artificial intelligence system 80−62701
spectra calculation, general method, 2D spin-echo NMR spectroscopy appl. 78−86842
spectra recording processing and accumulation, using mag. tape system *(Russian)* 79−26097
spectrometer, commercial, modification for rot. frame spin-lattice relax. meas. 80−22407
spectrometer, CW, signal intensity, effect of coil design parameters 77−49756
spectrometer, pulse, controlled by programmable digital unit *(Czech)* 78−77952
spectrometer, widebore supercond. magnet systems, sideways-spinning 20 mm tube probe 79−30518
spectrometer for NMR in internal fields of ferromagnets for freq. range 10 to 230 MHz 80−27325
spectrometer pulse generator, programmable digital, for proton enhanced ^{13}C high-resolution NMR spectrometers 79−58762
spectrometer RF coil, CW operation, signal intensity 78−89515
spectrometer-computer interface, demonstration expt., signal averaging influences on S/N ratio 80−36813
spectrometers, SQUID-based, sensitivity limit 80−98961
spectrometers, time-sharing control by minicomputer 79−93192
spectrometry, electric furnace with RF coil for measurements up to 2000K 79−63214
spectroscopy, ^{1}H, automatic PMR spectra interpretation system 78−32840
spectroscopy, computer appl. *(Czech)* 80−17984
spectroscopy, frequency sweep nonlinearity, meas. and correction 78−24836
spectroscopy, high power pulsed, automation and control 80−86359
spectroscopy, high resolution, using nematic liq. crysts. with negative anisotropy 79−40596
spectroscopy, resolution enhancement, effective sample volume restriction effects 80−31836
spectroscopy, thermostatically controlled resonant cell 79−93181
spherical conductor, free induction decay and skin effect 80−2649
spin density imaging by NMR 77−43893
spin density imaging using line shaped mag. field 78−73190
spin glasses, spin dynamics, EPR, NMR, muon precession, Mossbauer, and neutron scatt. results 79−65689
spin imaging by mag. field modulation 80−90873
spin lattice relaxation time meas. simulation, systematic and random error effects 80−37062
spin relaxation and molecular rotation, review, book contrib. 79−31557
spin system, ABC type, matrix elements of tensor operators calc., transition probability matrix 80−25182
spin system orientation due to stimulated emission and absorpt. of radiation 77−52001
spin-density imaging technique 77−87799
spin-lattice relax., effect of correlated atomic diffusion 80−107495
spin-lattice relax. time meas. in FT NMR by variable nutation angle method 77−49757
spin-lattice relaxation times, measurement based on null method 80−22402
spin-one system, NMR response to three-pulse sequences in inhomogeneous B_0 field 79−42861
spin-one system, response to three-pulse sequence in homogeneous B_0 field 79−42860
spin-spin coupling consts., Fermi contact contrib., mol. orbital calcs. 77−68060
spinor interferometry, phase factor obs. by NMR spectroscopy 79−4731
squaric acid, antiferrodistortive phase transition, proton chemical shift tensor determ. 77−63300
squaric acid, H-bonded antiferroelec., cluster form., NMR obs. 79−28628
SQUID detection, low temp., NMR imaging improvement towards mol. kinetic meas. 80−104723
SQUID detection of NMR, appl. to liq. ^{3}He 79−67368
SQUID NMR meas. at low-temp., improved technique 78−54417
SQUID NMR techniques, appl. to liquid ^{3}He 79−26093
stationary NMR signals, theory, dynamic freq. shift effects *(Russian)* 79−22734
steroids, mixtures, quantitative anal. by ^{13}C NMR 78−31716
stochastic NMR spectroscopy, Ito and Stratonovich calculus calcs. 77−13787
strong magnetic field induction metrology 78−37040
strontium formate dihydrate, H bonds, deuteron mag. reson. meas. 77−85593
structure and conformation of dissolved mol. in liq. crystal, NMR 78−62829
styrene derivatives, ^{13}C NMR spectra, Hammett eqn. appl., undergraduate experiment 79−84913
styrenes, 4-substituted, NMR substituent parameters, pattern recognition interpretation 80−58284
substituent parameters, pattern recognition interpretation 80−58284
subsurface EM techniques for oil exploration 77−17263
Suhl-Nakamura interaction effects, nuclear spin motion in strong RF field 77−43905
superconducting fluctauations effect on relaxation of effective nuclear moment of van Vleck ions 79−7936
nuclear magnetic resonance continued
superconducting mag. field meas. using signal ave. 77−83231
superconducting solenoid, mag. parameters, NMR study of effect of constructional features 79−71488
superconducting solenoids fields meas., automatic 80−57344
superconducting spectrometer, efficient decoupler coil design to reduce heating in conductive samples 80−31828
superconductor with struct. transform., kinetic props. *(Russian)* 79−95544
superconductors, surface relax. time of conduction electron spins 78−91814
superconductors with paramag. impurities, NMR theory in singlet state 79−28445
superionic conducting materials, nucl. mag. relax. by paramag. impurities 79−42866
superionic conductor, paramag. impurity contrib. to NMR relax. in one-dimension 80−20477
superionic conductors, mag. reson., book contrib. 80−25240
superionic conductors, prefactor anomalies, effect of low dimensionality 78−48061
superionic conductors, transitions, structures, dynamics and spectra, review 79−60549
superspin, appl. to ABX system 80−60426
symmetric spin system, calc. of NMR spectra of SYMTRY computer program 77−85587
symmetry groups of nonrigid molecules as generalized wreath products and their representations 80−48013
TBBA, temp. depend. of deuteron NMR splittings in nematic and smectic phases 79−32898
TBBA liquid crystal, self diffusion coeffs., neutron diffr. and NMR study 80−19689
TBBA mesophases, mol. orientational order 79−37619
techniques *(Chinese)* 80−80621
techniques for determination of phys. and biological struct. *(Rumanian)* 78−49874
teflon, γ-irradiated, low dose range, rel. to positron lifetimes 78−76550
ternary superconductor, mag. interactions 79−73613
tetraalkylammonium halides, mol. reorientation, spin lattice relax. time study 80−18875
tetrafluoro-1,3-dithioethane, ^{19}F chem. shift tensor multiple pulse NMR 77−77111
tetrafluoromethane, ^{19}F NMR, chem. shielding, intermol. interactions and rovibr. motion effects 78−9171
tetrafluoromethane, compressed fluid ang. momentum relax., NMR 78−19354
tetrafluoromethane-inert gas, compressed fluids, ang. momentum relax., NMR 78−19355
tetrahydrofuran-propylene oxide copolymers, prep., ^{13}C NMR, end group anal. 79−66293
tetramethylaminoborane, $B_3H_8^-$ large-angle anisotropic motion, ^{11}B BMR, temp. depend. 77−90045
tetramethylammonium halides, libration amplitudes, NMR second moment determ. 77−1603
tetramethylammonium octahydrotriborate, NMR study of proton and B dynamics 80−93200
tetramethylammonium zinc tetrachloride, ^{13}C NMR and PMR study of incommensurate phase transition 80−34863
2,2,6,6-tetramethylpiperidine nitroxide radical.alcohol complex, NMR chem. shift 78−46366
1,1,3,5-tetramethylpiperidinium iodide, model cpd., struct., ^{13}NMR 77−565
1,1,3,4-tetramethylpyrrolidinium iodide, model cpd., struct., ^{13}C NMR 77−565
tetramethyltin, in liq. cryst., ^{1}H, ^{115}Sn, ^{117}Sn and ^{119}Sn NMR spin-spin relax. 78−91973
tetraoxane, NMR obs. of mol. motion, rel. to polymerisation temp. effects on polytetraoxane texture 77−84663
meso-tetraphenylporphine, NH H^+ tunnelling rate 80−97158
textures near $A \rightarrow A_1$ transition, NMR and current effects 78−59994
TGS, ferroelec. transition, struct. changes, ^{13}C NMR obs. 78−60344
TGS, temp. depend. of spontaneous polarisation, microscopic mechanism, NMR expts. 77−81070
TGS deuterised, radiospectroscopic studies, NMR of $^{2}D_1$ and $^{1}H_1$ nuclei 79−15341
theoretical chemistry, NMR, ESR and NQR, review 77−18943
thermodynamics of nuclear spins 80−54964
thermometer, for multinuclear Fourier transform NMR 80−57292
thermometry at ultra-low temperatures, technique 77−17985
thermotropic liquid crystals, NMR relax., review 78−39436
thiourea, polycryst., mol. dynamics under hydrostatic press., NMR study 80−80619
thiourea-d_4-ferrocene inclusion cpd. mol. motion, PMR spectrum 80−84656
three-level system, two-photon transient effects, NMR obs. 77−85588
thulium ethyl sulphate, Van Vleck paramag., mag. reson. on uniaxial and uniform compression *(Russian)* 79−61243
thylakoid membranes, pulsed NMR, photosynthesis appl. 78−80839
thymine+muonium, radical form. in aq. soln., spin reson. obs. 78−74679
time sharing method in high modulation NMR of fluids *(German)* 78−16822
tissue, living, biological and medical appls. 77−77959
tissue imaging, RF mag. field penetration, phase shift and power dissipation 78−73189
titanocene, alkyl-substituted ^{13}C and ^{1}H NMR, chemical shifts prediction 80−63671
TMNB, linear S=1 ferromag., easy plane anisotropy, low-temp. mag. props. 78−23250
TMNC, linear S=1 ferromag., easy plane anisotropy, low-temp. mag. props. 78−23250
TMNC, quasi one dimensional planar ferromag., low temp. NMR study im mag. field 80−97157
$(TMTSF)_2X$, ($X=PF_6^-$, AsF_6^-, SbF_6^-, BF_4^-, NO_3^-) highly conducting salts, props. 80−59969
transition metal 3d, spin-orbital interaction effect on NMR, g-factor anisotropy *(Russian)* 77−24752
transition metal complexes, $M(CN)_5X^{n-}$, ^{13}C NMR, chem. shifts 79−51866
transition metal complexes, vibronic coupling and spin relax. NMR decay rate study 80−18870
transition metal diborides, C32-type, phys., chem. props., appls., review, book contrib. 78−47308

nuclear magnetic resonance continued
transition metal hydrides, proton diffusion mechanisms, NMR determ. 77−90060
transition metal silicides, NMR and μSR, microscopic mag. props. *(Japanese)* 78−52368
transition metal tetrahedral complex ions, F NMR chem. shifts, outer sphere cation effects 80−102527
transition phenomena in region of equal NMR and ferromag. reson. frequencies *(Russian)* 77−32272
triated samples, hazard reduction using plastic tube insert 79−40546
trichloroacetic acid, proton chemical shift tensor 78−13520
triethylacetic acid, high resolution ^{1}H and ^{13}C NMR spectra at liquid-solid phase transition 80−11281
1,2,3-trifluorobenzene, ^{13}C, ^{19}F, and ^{1}H NMR spectral anal. 78−37659
trifluoromethyl systems, in smectic liq. cryst. soln., Fourier transform ^{19}F NMR 77−79631
2,4,6-trifluoronitrobenzene, ^{19}F shielding anisotropies, nematic phase NMR 77−27090
trimethylacetic acid, high resolution ^{1}H and ^{13}C NMR spectra at liquid-solid phase transition 80−11281
trimethylamino borane, ^{11}B NMR 78−90190
trimethylene oxide, ^{12}C NMR, coupling consts. 78−25570
trimethylene sulphide, ^{12}C NMR, coupling consts. 78−25570
trimethylphosphine, chem. shift anisotropy, struct., liq. cryst. NMR 77−61768
trimethylphosphonium oxide (sulphide) (selenide), chem. shift anisotropy, struct., liq. cryst. NMR 77−61768
triple NMR technique for N-containing molecules, ^{13}C-{^{1}H,^{14}N} triple reson. 79−81219
tris(dimethylamino)phosphorus, ^{15}N and ^{31}P NMR aligned in liq. cryst., geom. struct. 78−82751
triscyclopentadienyl uranium chloride, ^{13}C NMR shifts, 160-320K 77−16190
tristearin irreversible liq.-liq. phase transition, ^{13}C NMR meas. 78−26681
2-tromopropane, tilt-effect and interference with rel. sign determination in weak irrad. expts. 80−32742
TTF(MBDT) spin-Peierls transition, mag. exchange interactions, mag. props. 80−25138
tumour detection by NMR relax., spectrum anal. of multiple components data 78−48851
two dimensional ^{13}C NMR spectroscopy, high sensitivity 80−31826
two dimensional system, theory 77−51968
two-dimensional, state-of-the-art 78−74044
two-dimensional resolved spectroscopy, phase separation techniques, rare nuclei 78−19341
two-dimensional systems, order parameter from chemical shift anisotropy patterns 80−80624
two-phase fluid, void fraction, NMR meas. 77−15096
two-spin system, NMR relax. rate parameters, by nuclear Overhauser effect 77−69720
two-spin system, solid without spin-lattice relax., NMR theory *(German)* 78−88197
ultra-low temperature meas. of S/N ratio, appl. to thermometry 80−73400
undergraduate instruction, general purpose microcomputers use for hypothetical spectra synthesis 80−42009
unsaturated water flow within porous materials, obs. by NMR imaging 79−98840
urea-formaldehyde resins, ^{13}C Fourier transform NMR of chem. struct. 79−42849
urea-n-paraffin adducts, order-disorder transition, thermal anal., X-ray diffr., and NMR 79−33084
Varian EM-360 NMR spectrometer interface with Altair 8800B microcomputer 78−89519
Varytemp NMR for pulse spectrometers, applic. to lineshape determ. 77−2674
vinyl copolymers, containing fluorescent groups, optically active 80−102594
visual pigment unprotonated chromophore-protein bond, ^{13}C NMR spectra 78−11607
Voigt profile analysis, Fourier transform approach and least-squares curve fitting 77−20729
water, adsorbed on cellulose, NMR relaxation times 79−78552
water, lyotropic phase orientation, ^{17}O and ^{2}H NMR study 78−27905
water, NMR shielding constants of ^{1}H and ^{17}O, paramag. contrib., triple perturbation theory 79−10127
water, studies in biological systems 80−3886
water adsorbed on proteins, new programme for NMR study of diffusion 79−92139
water in biological cells *(French)* 77−90739
water-cetyltrimethylammonium bromide-haxanol system, ^{13}C NMR, catalysis in micellar and liq. cryst. phases 79−61909
weak signal recording by second-harmonic oscillogram 77−10080
wide-line, investigation of inorganic and organic solids, reference list 79−19786
p-xylene, ^{13}C chem. shielding tensors 78−60342
yeast cells, translational mobility of water, pulsed NMR obs. 79−57612
zeolite, hydrated Na-Y, ^{23}Na pulsed NMR free induction decay 80−84660
zeolite interface, ionic conduction bands 77−35745
zeugmatographic imaging, gradient control device using microprocessor 80−89822
zeugmatographic imaging 80−51203
zeugmatographic imaging of heart and lungs 80−17053
zeugmatography, criticism of selective pulse concept in presence of field gradient 77−74472
zeugmatography, medical imaging 79−66501
zeugmatography, rotating frame 79−93186
zeugmatography, state of the art 78−74043
zeugmatography by reconstruction from projections 80−77821
zirconocene dichlorides, alkyl-substituted, ^{13}C and ^{1}H NMR, chemical shifts prediction 80−63671
$LiTbF_4$, NMR shift tensors, temp. and field depend. 79−38391
- 78−18749
Ag complexes in organic solns., ^{109}Ag NMR, solvent effects 77−16191
Ag halides, matter transport rel. to point defect parameters 80−107488
$AgBF_4$, ionic radii and chem. shifts, correl. with electronegativity 80−66054
AgF(AgI,AgBr,AgCl), NMR chemical shifts 80−74180
$AgIO_4$, chem. shift, NMR obs. 80−48015

nuclear magnetic resonance continued
$Ag(NH_3)_2Ag(NO_2)_2$, and deuterate, proton and deuteron mag. reson., reorientation 79−11351
Al-Cr, neutron irrad., Cr atom distribution NMR study 80−54957
Al-Cu (4 wt.%), precipitation sequence of metastable phases, NMR meas. 78−23713
Al-Cu (4 wt.%) alloy, reversion process of Guinier-Preston zones, ^{63}Cu NMR obs. 80−60871
Al-Ga (10 wt.%), exam. of ^{27}Al diffusion by NMR technique 78−87813
Al-Mn, dilute, NMR investig. of spin density oscills. around Mn impurities 77−4570
Al_4C_3, solid-state ^{13}C NMR spectra 79−24220
β-Al_2O_3, additive modified charact. by NMR 78−10785
Al_2O_3-H_3O^+, β and β'' phases, protonic, conductance and spectroscopy 80−70450
β-Al_2O_3-Na_2O, ceramic and powder specimens, various Na_2O content, NMR study 79−61240
β-Al_2O_3-Na_2O, protonic, conductance and spectroscopy 80−70450
β-Al_2O_3-Na_2O ^{23}Na asymmetry parameter, temp. variations 80−6540
β-Al_2O_3-Na_2O-Li_2O, ^{7}Li NMR 79−15361
θ-$Al_{0.35}V_2O_5$, NMR of ^{51}V 80−71232
^{27}Al, NMR in MAl_2Br_2 crysts.(M=Li, Na, K, Cs, NH_4, $(CH_3)_4N$), quadrupole effect 78−6597
^{29}Al, mag. moment quadrupole coupling const. β-ray detected NMR in Al_2O_3 cryst. 78−37267
As-Se-Tl system, chalcogenide glasses, NMR spin-lattice relax. time meas. 79−95671
o-$As_2B_{10}H_{10}$, ^{1}H and ^{11}B CW NMR, mol. reorientation in cryst., phase transition 77−85583
AsF_5 intercalation with graphite and benzenoid systems, EPR, NMR and X-ray diffr. obs. 80−19775
As_2Se_3:X (X=Cu, Ag, Tl, I, Ge), effect of doping, NMR meas. 80−11282
As_2Se_3-$GeSe_x$-$SnSe_x$ (x=1,2), exam. of Sn valency and physical props. 79−4753
^{70}As, hyperfine struct. investig. using at. beam mag. reson. 77−22933
Au-Yb dilute, NMR investig. of anisotropic cond. electron exchange 77−63309
AuF_3, ^{19}F NMR chemical shift, crystal chemistry 78−87645
$AuIn_2$, pulsed NMR expts, rel. to performance as nuclear refrigerant 79−61259
Au_2MnAl, Heusler alloy, ferromag., NMR meas. 78−76320
Au_2MnIn, Heusler alloy, ferromag., NMR meas. 78−76320
B compounds, ^{13}C NMR spectroscopy 79−89691
B_4C, solid-state ^{13}C NMR spectra 79−24220
BF_3, ^{19}F NMR, chem. shielding, intermol. interactions and rovibr. motion effects 78−9171
$B_{10}H_{12}As^-$, ^{11}B NMR 78−90190
$B_{10}H_{12}S$, ^{11}B NMR 78−90190
$B_{10}H_{12}Se$, ^{11}B NMR 78−90190
$B_{10}H_{12}Te$, ^{11}B NMR 78−90190
B_2O_3, vitreous, struct. study using ^{10}B NMR 80−84658
B_2O_3-Li_2O-LiCl glasses, solid electrolyte, NMR meas. 80−29208
^{11}B, NMR, for senior level inorganic courses 78−4424
^{11}B, NMR in BF_3, chem. shift temp. depend. 78−58722
^{12}B, β decay, alignment prod. by NMR 78−50126
^{12}B, hyperfine fields in ferromag. Ni, NMR obs. 77−28476
^{12}B, NMR in Ni, hyperfine field determ. 77−8418
Ba hectorite, Ba ion position, water effect *(French)* 77−72593
Ba, nucl. mag. moments and ratios of quadrupole moments, NMR spectroscopy in aqueous soln. 77−73088
BaF_2:Y^{3+}, diffusion of bound and free $F_{(i)}^-$ interstitials, NMR meas. 79−78542
$BaFHF_2$, ^{19}F free induction decay 78−2753
^{135}Ba,^{137}Ba Fourier transform NMR, NQR studies 78−94261
$Ba[Fe(CN)_5NO]_2.2H_2O$, NMR, H_2O orient. *(French)* 78−52366
BeF_2 aqueous solns., mag. and quadrupole relax. 80−71226
^{9}Be, nuclear mag:spin-lattice relaxation times 78−86889
Bi-Mn, dil. liq. alloy, static and dynamic props. of localised Mn moments 79−82755
BrF_3 complexes with BF_3, PF_5 and AsF_5, F NMR, struct. and stability 78−37658
BrF_6, EPR spectra, 'NMR' transitions, mol. symmetry 77−46580
C black, IR-, UV- and NMK spectra, props. after extraction with organic solvents *(Polish)* 79−70010
C_8AsF_5 intercalation compound, NMR and static mag. susceptibility meas. 78−88214
2,4-$C_2B_5H_7$, polyhedral, spin coupled ^{11}B-^{1}H systems, 2-dimens. correl. NMR 80−69166
$(CF_x)_n$, fluorinated graphite, ^{13}C NMR and ^{19}F NMR spectra 80−15808
CO, ^{13}C NMR, density depend. mag. shielding in gas phase 77−75187
β-CO, ^{13}C NMR, self-diffusion activation parameter, press. depend. 77−69719
CO, adsorbed on Rh dispersed on Al_2O_3, ^{13}C NMR obs. of adsorbed states 80−96733
CO adsorbed on transition metal zeolite, ^{13}C NMR study 79−52751
CO chemisorbed on Rh dispersed on Al_2O_3, ^{13}C NMR obs. 80−1000
CO group, NMR chem. shift, solvent's dielectric const. effect, mag. anisotropy 79−42847
CO, in He bath, NMR spin-lattice relax., coupled states ang. momentum decoupling 77−77117
CO, liq., ^{13}C NMR for mol. diffusion and spin-rot. interaction, 0-1.73 kbar 79−99777
CO_2, ^{13}C NMR, chem. shift., determ. of virial coeffs., rovibr. motion 78−58720
CO_2, ^{13}C NMR, density depend. mag. shielding in gas phase 77−75187
CO_2+Kr(Xe), ^{13}C-mag. shielding density depend. 78−9173
^{13}C, 2D NMR spectra, off-resonance decoupling 80−74182
^{13}C, CIDNP, obs. in reactions of organic and inorganic radicals during pulse radiolysis 80−63660
^{13}C chem. shielding tensors in p-xylene 78−60342
^{13}C, chem. shift in CO_2 78−58720
^{13}C, chem. shifts, estimation by computer program based on additivity rules 78−13518
^{13}C, chem. shifts, natural abundance determ. in gas phase and extrapolation from liq. phase meas. 77−88470
^{13}C chemical shift calcs. for N-containing cpds., approx. SCF perturbation theory 77−18945
^{13}C, data analysis by pattern recognition 77−48059

nuclear magnetic resonance continued
^{13}C Fourier transform NMR, method for tailored detection of signals 79−40597
^{13}C NMR, ^{2}H label quantitative meas. 77−50456
^{13}C NMR, chem. shift, effective excitation energy calcs. 77−14457
^{13}C NMR, computer program chem. shift retrieval system 79−18206
^{13}C NMR, high-resoln. allowing spin coupling and mag. field inhomogeneity 77−20740
^{13}C NMR, low-temp. thermometer 78−65949
^{13}C NMR, poly(diallyldimethylammonium) chloride struct. 77−565
^{13}C NMR, RF amplitude effects in proton-spin decoupling 77−28463
^{13}C NMR in copolymers, monomer unit distrib. *(Russian)* 77−46664
^{13}C, NMR in methane, chem. shift temp. depend. 78−58722
^{13}C NMR in solids, high-resolution 80−34802
^{13}C NMR intensity meas. technique, chem. anal. appl. 77−51981
^{13}C NMR probe for high resolution Fourier spectroscopy, cw time sharing appl. *(German)* 78−16823
^{13}C NMR shielding constants and tensors in hydrocarbons, finite perturbation calcs. 77−27092
^{13}C NMR shifts in triscyclopentadienyl uranium chloride 77−16190
^{13}C, NMR spectra, transition intensities, off-resonance proton spin decoupling influence 80−74183
^{13}C, NMR spectra assignment, proton-C splitting scaling 78−46372
^{13}C NMR spectra of natural rubber latex 80−15816
^{13}C NMR spectroscopy, 270 and 90 MHz, ^{1}H noise decoupling field heating effects 79−38389
^{13}C NMR with off-reson. proton spin decoupling, proton chem. shift calc. methods 78−27101
^{13}C, obs. of adsorbed cyclopropane on Pt 77−51591
^{13}C, peptides and proteins, review 78−24023
^{13}C, phospholipid bilayer mol. motions 77−48767
^{13}C, relax. in nitrobenzene 77−48070
^{13}C, shielding consts. and anisotropy of NMR shielding tensor, modified CNDO/S calcs. *(French)* 80−32610
^{13}C, slow-spinning magic-angle, for amorphous solid 77−48068
^{13}C spectra, ^{13}C-X coupling consts., relative signs determ. using ^{13}C satellites 79−94018
^{13}C spectra, modified DEFT pulse sequence use 79−93191
^{13}C, spin conversion obs. in solid $^{13}CH_3D$ 77−20731
^{13}C-^{13}C dipolar satellites in ultraoriented polyethylene 77−28465
^{13}C-{^{1}H} off-resonance spin decoupling, variable decoupler field strength 77−67485
$^{13}C-^{13}C-^{1}H$ fragment, nucl. relax. and Overhauser effect 79−54868
C=C bond, ^{13}C shielding tensor, NMR meas. 78−1005
$CaB_3O_4(OH)_3.2H_2O$, NMR of ^{11}B in crit. region 77−16199
CaC_2, solid-state ^{13}C NMR spectra 79−24220
CaD_2, neutron diffr., NMR 77−15378
CaF_2, ^{19}F NMR chemical shift, press. depend. 0-4 kbar 77−20733
CaF_2, (n,γ) induced lattice defects, struct., polarised ^{20}F NMR 77−20724
CaF_2, (n,γ) induced lattice defect annealing, polarised ^{20}F NMR 77−20725
CaF_2, (n,γ) induced point defects, struct. and annealing 78−59842
CaF_2, heteronuclear mag. spin system relaxation in many pulse NMR expts. 80−93203
CaF_2:ErF_3, clustering, defect struct., NMR study 78−80229
CaF_2:Eu^{2+}, nuclear spin diffusion barrier, ^{19}F NMR Obs. 78−64282
CaF_2:Nd^{3+}(Eu^{3+})(Dy^{3+})(Ho^{3+})(Tm^{3+}), ^{19}F NMR studies 80−60429
CaF_2:Y^{3+}, diffusion of bound and free $F_{(i)}^-$ interstitials, NMR meas. 79−78542
CaF_2:YbF_3, clustering, defect struct., NMR study 78−80229
$CaF_{2-x}H_x$, ionic conductivity study *(French)* 80−29210
$Ca(OH)_2$, single cryst. NMR 77−48058
$(CaO)_3.SiO_2$, adsorption of H_2O, NMR exam. 78−48354
$Ca_5(PO_4)_3(F_{1-x}(OH)_x)$, apatites, lattice struct. NMR obs. 79−42845
$CdBr_2.4H_2O$, NMR, ^{113}Cd nucl. mag. shielding 78−68395
$CdCO_3$, NMR, ^{113}Cd nucl. mag. shielding 78−68395
$CdCl_2$, NMR, ^{113}Cd nucl. mag. shielding 78−68395
$CdCr_2S_4(Se_4)$, spontaneous magnetisation temp. depend., nuclear resonance freq. depend. *(French)* 80−80483
CdF_2, NMR, ^{113}Cd nucl. mag. shielding 78−68395
CdI_2, NMR, ^{113}Cd nucl. mag. shielding 78−68395
CdO, NMR, ^{113}Cd nucl. mag. shielding 78−68395
CdS, NMR, ^{113}Cd nucl. mag. shielding 78−68395
CdSe, NMR, ^{113}Cd nucl. mag. shielding 78−68395
CdSe(Te), chemical shift and linewidth determ. 79−19792
CdTe, NMR, ^{113}Cd nucl. mag. shielding 78−68395
CdTe, NMR, dipole-dipole coupling between ^{111}Cd, ^{113}Cd and ^{125}Te 79−91305
^{113}Cd probe for active sites of metalloenzymes 78−68999
Ce intermetallics, CeX_2Si_2 (X=Cu, Ag, Au), ^{29}Si NMR and mag. susceptibility 79−61246
$CeAl_2$, cryst. field effects and mag. order in low temp. phase 78−68391
ClF, gas, rot. frame NMR, reorientational and ang. correl. times 78−78721
ClO_xF_y, ^{17}O NMR, chem. shifts, indirect coupling consts. 77−14453
^{35}Cl NMR, medium effects 77−1612
Co complex, Co(III) diamine, ^{13}C NMR, spin-spin coupling const. *(Japanese)* 79−6952
Co complex, $Co(NH_3)_6I_3$, phase transition investig. by NMR 77−1608
Co complex, dipyridyl chloride, metamag., mag. struct., NMR 77−85418
Co complexes, Co(III) mixed complexes, orbital angular momentum reduction, ^{59}Co NMR chemical shift 80−58137
Co, FCC single-crystals, NMR freq. depend. on interatomic distances 79−69748
Co, NMR in paramagnetic and ferromagnetic states, crit. nucl. relax. 79−56622
Co, NMR spectra temp. depend. 78−52364
Co, NMR-ON meas., mag. hyperfine splitting const. of ^{60}Co, ^{52}Mn and ^{90}Nb 78−43651
Co-Fe, double hexagonal alloys, crystalline and mag. props. *(Japanese)* 79−73132
$CoCl_2$, antiferromag., elec. field effect in NMR 77−28459
Co_xGa_{1-x} alloys, cluster spin glass, host and impurity NMR and AC susceptibility 80−71194
$Co(NH_3)_5{}^{15}NH_3{}^{3+}$ complex prep. and Fourier transform NMR spectra *(Japanese)* 78−48060
$Co_{2-x}(Ni,Fe)_xTiSn$, Heusler alloy, positive contribs. to hyperfine fields, magnetisation and NMR meas. 78−43654
CoO, antiferromagnetic, ^{59}Co NMR and hyperfine field 77−77109

nuclear magnetic resonance continued
CoS_2, microscopic mag. props., NMR meas. 79−91306
$CoS_{2-x}Se$, magnetism and metamagnetic transition, neutron diffr. and NMR meas. 80−15717
$Co(S_xSe_{1-x})_2$, metamagnetic transition, ^{59}Co NMR 79−38322
$CoSe_{1.95}$, NMR and susceptibility meas., absence of antiferromag. 77−16060
$CoSe_2$, temp. induced local mag. moments, ^{59}Co NMR 79−65747
$CoSiF_6.6D_2O$, deuteron mag. reson. study 80−2646
$CoTi_{1-x}Al_x$, form. of mag. moment of Co atom, X-ray diffr., mag. meas. and NMR 77−43819
Co_2TiSn, Heusler alloy, positive contribs. to hyperfine fields, magnetisation and NMR meas. 78−43654
Cr complexes, NMR study ^{31}P chemical shift, substituents electronegativity steric hindrance and π-bonding effect 80−95651
CrB_2, itinerant antiferromag., sping fluctuations, NMR study 80−108119
CrB_2, NMR of ^{11}B meas. 78−56397
$CrPS_4$-Li intercalation cpd., phys. props. 79−19788
$Cr_{1-x}V_x$, nucl. spin relax., spin fluctuation effect 80−34811
$Cr_{1-x}V_xCo$, localised mag. moment of Co impurity 78−27014
^{53}Cr:$ErCrO_3$, anomalous freq. variation at 2-8K *(Russian)* 78−43650
Cs perfluoro-octanoate, amphiphilic liq. cryst., ^{19}F multipulse NMR study 78−76328
Cs^+, glycerol solns. quadrupole interactions, nucl. mag. relax., correl. time determ. 77−14449
$^{133}Cs^+$/Cs g-factor ratio, NMR and zeeman transition freqs. 78−17817
$Cs^+ + Cs$, reson. charge exchange cross section at thermal energies 79−854
Cs_2 molecules, magnetic shielding studies 77−42341
$CsBF_4$, ionic radii and chem. shifts, correl. with electronegativity 80−66054
$CsCoCl_3$, Ising like antiferromag., mag. phase transition, ^{133}Cs NMR 80−7184
$CsCuCl_3$, one-dimensional antiferromag., ^{63}Cu NMR mas. 78−2756
$Cs_2CuCl_4.2H_2O$, Bloch-wall NMR, anisotropic hyperfine interaction 79−51864
$Cs_2CuCl_4.2H_2O$, ferromag., hyperfine and exchange interactions, NMR study 80−50208
CsD_2AsO_4, ferroelect. phase transition, NMR study *(Chinese)* 79−33644
CsD_2PO_4, pseudo-one-dimens. ferroelec. transition, DMR and relax. study 80−71223
$CsFeCl_3$, linear chain cryst., quadrupole and mag. reson., rel. to $RbFeCl_3$ 79−38403
$Cs_2GeF_6.4HF$, cryst., H bond geometry, NMR obs. 79−42844
$Cs_2GeF_6.4HF$, molecular diffusion, spatial symmetry, HF molecule arrangement 79−42313
$CsHF_2$, struct. and phase transformation, NMR study 77−90047
CsH_2PO_4, NMR of ^{133}Cs, elec. field gradient 78−15034
$CsH_2PO_4(CsD_2PO_4)$, permittivity temp. depend., pseudo one-dimens. ferroelectric ordering and critical props., NMR 79−78635
$CsMnF_3$, mag. props. above T_n, NMR obs. of induced ferrimagnetism 79−99780
$CsMnF_3$, NMR saturation, nuclear spin wave excitation, large freq. shifts *(Russian)* 80−50207
Cs_2NaRCl_6 (R=Ce, Nd), tetragonal distortion from cubic symm., magnetisation and NMR meas. 80−34403
$CsNiBr_3$, double ordering in mag. linear chain system, sp. ht. and NMR data 79−28545
$CsNiBr_3$, nearly one-dimensional antiferromag., thermal and mag. props. meas. 77−77041
$CsNiCl_3$, double ordering in mag. linear chain system, sp. ht. and NMR data 79−28545
$CsNiF_3$, ^{19}F NMR, spin fluctuation suppression 78−91970
$CsNiF_3$, linear S=1 ferromag., easy plane anisotropy, low-temp. mag. props. 78−23250
$CsNiF_3$, quasi one dimensional planar ferromag., low temp. NMR study im mag. field 80−97157
$CsPbCl_3$, struct. phase transitions, NMR obs. 78−83943
$Cs_2SnF_6.4HF$, cryst., H bond geometry, NMR obs. 79−42844
$Cs_2SnF_6.4HF$, molecular diffusion, spatial symmetry, HF molecule arrangement 79−42313
$CsUOF_5$, struct. obs. using neutron diffr. and NMR 79−32962
$CsVO_3$, polycryst., quadrupole coupling const., asymmetry parameter, chem. shift, NMR computer calcs. 78−6584
^{133}Cs, nuclear mag:spin-lattice relaxation times 78−86889
^{133}Cs salts, powders, nucl. mag. shielding and quadrupole coupling 77−90056
Cu complex, $[C_6H_5(CH_2)_nNH_3]_2CuCl_4$, n=1,2,3, two-dimens. ferromagnet, NMR and mag. susceptibility 77−16058
Cu, from below 1 kHz to 100 kHz, use of transverse SQUID 80−37064
Cu, NMR at high polarisation and low field, nuclear spin exchange interaction 80−34790
Cu, nucl. demagnetisation expts. 77−45851
Cu, nuclear antiferromagnetism, NMR obs. 79−78538
Cu, nuclear antiferromagnetism, low temp. NMR study 80−66049
Cu, nuclear ordering below 1 μK, NMR study 80−93187
Cu^{2+} systems, magnetic, nuclear spin Hamiltonians *(Japanese)* 80−60430
Cu:Cr(Mn)(Fe), NMR satellite data rel. to impurity struct. 78−35052
Cu-Co(Fe)(Ni), dil. mag. alloy, NMR of ^{63}Cu around impurities 77−16187
Cu-Cr, Kondo alloy, NMR of Cu satellites, 1 to 4K 79−73837
Cu-Fe, dil., powder, transferred orbital hyperfine field on near neighbours, NMR meas. 78−27098
Cu-Fe group, dil., NMR satellite data calc., struct. of mag. impurities 80−103894
Cu-Ga, high dislocation density alloys and oxide precipitated struct., NMR, spin echo 80−39892
Cu-Mn, dil., Kondo deviations of Mn electron spin relax. and g-factor, NMR meas. 79−51747
Cu-Mn, dil., spin density magnetisation near magnetic atoms 79−33545
Cu-Mn alloy spin glass, macroscopic mag. anisotropy, transverse susceptibility and zero field NMR enhancement 80−80525
Cu-Mn(1%) spin glass, remanent mag., zero-field NMR obs. 79−33492
Cu-Si, high dislocation density alloys and oxide precipitated struct., NMR, spin echo 80−39892
Cu-Ti, solubility of Ti, exam. using NMR of ^{63}Cu *(French)* 80−7179
Cu-transition metal, alloys, satellite NMR study, lineshifts and splitting 80−34786

nuclear magnetic resonance continued
$Cu_x(As_{0.4}Se_{0.6})_{1-x}$, amorphous, ^{77}Se NMR, comp. depend. 78−76329
$CuBeF_4.5H_2O$, NMR, interactions between paramag. ion system and antiferromag. linear chains 77−63295
CuBr, NMR chemical shifts, temp. depend. 78−68401
CuCl, NMR chemical shifts, temp. depend. 78−68401
$CuCl_2.2H_2O$, antiferromag., range of existence of intermediate state 77−59410
$CuCl_2.2H_2O$, effect of press. on mag. phase transition, NMR meas. 78−19253
$CuCl_2.2H_2O$, flop of sublattice moments and Neel temp., press. effects, NMR obs. 77−40058
$CuCl_2.2H_2O$, influence of high hydrostatic press. on intermediate state associated with spin flopping 78−35020
$CuCl_2.2H_2O$, NMR, high press. effect on existence domain width of intermediate state 79−87255
CuCr(Fe)(Mn), dil., anisotropic hyperfine coupling, NMR study 80−65784
CuI, NMR chemical shifts, temp. depend. 78−68401
CuMn, spin glass, remanence, new approach from zero field NMR 80−34785
$Cu(NO_3)_2.2^1/_2H_2O$, high field phase transition, susceptibility and NMR meas. 77−69559
$CuSO_4.5H_2O$, $CuSeO_4.5H_2O$ and $CuBeF_4.5H_2O$, mag. ordering in external field 77−66350
$CuSeO_4.5H_2O$, $CuSO_4.5H_2O$ and $CuBeF_4.5H_2O$, linear-chain antiferromag., mag. phase transition investig. 77−55684
^{63}Cu,^{65}Cu, Fourier transform NMR studies 78−94262
D, in nitrobenzene, liq., ^{14}N quadrupole coupling const., environmental effects 78−48052
D NMR, appls. for physics, chemistry and biology 77−87801
p-D_2 adsorbed on graphite, NMR, orientational behaviour, weak crystal field 78−75935
D_2O, dissolved in lyotropic systems 79−22732
D_2O, nuclear mag. relax. of deuterons at identically oriented planar interfaces 77−36148
$DyAl_2$, conduction electron spin and orbital polarisation effects 78−80228
DyF_3, transferred hyperfine interaction, NMR study 78−68393
$DyFe_{0.998}Co_{0.002}O_3$, mag. transition, NMR meas. 78−27036
$Dy_{0.9}M_{0.1}Al_2$, (M=Sc, Y, La, Lu), hyperfine field, NMR spectra 80−15811
$ErAl_2$, conduction electron spin and orbital polarisation effects 78−80228
$ErCrO_3$, magnetisation, NMR freq. temps. depend. weak ferromagnetic-antiferromagnetic spin reorientation transition 80−29631
$ErCrO_3$:^{53}Cr, NMR frequencies, anomalous behaviour at low temps., 2-8K *(Russian)* 78−43650
$Er_{0.8}Dy_{0.2}FeO_3$, mixed orthoferrite crystals, ^{57}Fe NMR in spin reorientation range 78−15039
ErF_3, single cryst. ^{19}F NMR, ligand hyperfine field interactions 77−48067
$Er_{1-x}Gd_xAl_2$, effective mol. field at ^{167}Er, NMR meas. 80−71197
$Er_{0.3}Ho_{0.7}FeO_3$, mixed orthoferrite crystals, ^{57}Fe NMR in spin reorientation range 78−15039
$ErRh_4B_4$, mag. supercond., NMR study of ^{11}B 80−107957
$Er_{0.5}Tm_{0.5}FeO_3$, mixed orthoferrite crystals, ^{57}Fe NMR in spin reorientation range 78−15039
ethanol-water system, complex dielec. permitt. in UHF region and NMR spectra *(Japanese)* 80−100620
$EuLiH_3$, transferred hyperfine fields at Eu nuclei, NMR meas. 80−71195
EuO, dynamic dipolar cross over 78−76339
EuO(S)(Se)(Te), Heisenberg ferromag. semicond., hyperfine and exchange interactions 77−69530
EuS, hyperfine field and magnetisation temp. depend., NMR meas. 77−8422
$EuSe_{1-x}Te_x$, transferred hyperfine fields at Eu nuclei, NMR meas. 80−71195
$(Eu_xSr_{1-x})S$, transferred hyperfine fields, NMR 80−71196
F, spin-spin coupling constants, review 77−23511
FSO_2OF, wide-line NMR anal. of mol. struct., chem. shielding tensor 77−83622
^{19}F NMR, ligand hyperfine interaction, shift tensor determ., in TbF_3 and HoF_3 78−48056
^{19}F NMR, low-temp. thermometer 78−65949
^{19}F NMR, single cryst. ErF_3 determ. of ligand hyperfine field interactions 77−48067
^{19}F NMR chem. shifts in polar solvents, intermol. interactions 77−51975
^{19}F NMR imaging for biomedical application 78−20240
^{19}F, NMR in MHF_2 (M=alkali metal), $TlHF_2$, $SrFHF_2$, $BaFHF_2$ 78−2753
^{19}F, NMR in NH_4HF_2 and (substituted) phenylamine salts 78−2754
^{19}F NMR in one-dimensional ferromagnet $CsNiF_3$ 78−91970
^{19}F NMR solvent shifts, charge transfer contribs. 77−50454
^{19}F shielding anisotropies of fluoromethanes, NMR obs. of smectic mesophase solns. 77−34662
^{19}F-^{11}B spin-spin coupling in solns. of complex fluoroborates 77−23512
^{20}F NMR in CaF_2, rel. to (n,γ) damage annealing 77−20725
^{20}F NMR_2 in CaF_2, rel. to (n,γ) damage 77−20724
Fe, BCC, high field Knight shift and hyperfine anisotropy of ^{57}Fe 80−71205
Fe, implantation of ^{197m}Hg, NMR of oriented nuclei 77−81020
Fe, nuclear orientation-mag. reson. of ^{48}V 79−61288
Fe sheet, surface magnetisation, ferromag. nucl. reson. meas. 78−60348
Fe:^{103m}Rh, γ-detected NMR of 40 keV metastable state, 0.5 to 14 kG external fields 77−59499
Fe:^{129}Xe, implanted atom sites, NMR/ON 77−20723
Fe:^{129}Xe, implanted atom site populations, Mossbauer, NO and NMR/ON obs. 77−20755
Fe:^{199}Au, quad. interaction, orbital mag. hyperfine field by NMR/ON 77−12250
Fe:^{60} Co, nucl. orientation-pulsed NMR obs., γ-radiation anisotropy 77−59490
Fe:^{60}Co, elec. quad. interaction, single passage NMR/ON 77−16204
Fe:^{71}As(^{71}As), nucl. mag. moment by NMR/ON 77−12251
Fe:^{95}Nb NMR 77−59482
Fe:I, ^{131}I NMR, vacancy associated impurity sites 78−91964
Fe-^{48}V, nucl. orientation of ^{48}V, γ-ray anisotropy obs. and NMR meas. 80−97169

nuclear magnetic resonance continued
Fe-based alloys, volume interactions between substitutional sp and 3d solutes 79−78069
Fe-Co, dil., ensemble rotation concept in NMR on oriented nuclei 77−90061
Fe-Co, hyperfine field distrib., temp. and press. depend. 78−91651
Fe-Co based Laves phases, mag. saturation moment, Co conc. depend. 78−15037
Fe-Co-Cr-Si, structural transform. and mag. props. following heat treatment *(Russian)* 77−81274
Fe-In, NMR-ON meas. of nucl. g-factor for $^{109,110}In$ 78−37275
Fe-Mo, NMR-ON meas. of nucl. g-factor for ^{93m}Mo 78−37275
Fe-Nb, NMR-ON meas. of nucl. g-factor for ^{90}Nb and ^{92m}Nb 78−37275
Fe-Ni, hyperfine field distrib., temp. and press. depend. 78−91651
Fe-Ta, nuclear mag. moment of ^{182}Ta NMR-ON study 80−78139
Fe-Tc, NMR-ON meas. of nucl. g-factor for $^{93-95}Tc$ 78−37275
$FeBO_3$, dynamic NMR frequency shift for ^{57}Fe *(Russian)* 78−43677
$FeBr_2$:Mn^{2+}, layered antiferromag., infinity mode NMR study 79−38390
$Fe(CO)_2(PF_3)_3$, ^{31}P and ^{19}F NMR, 25 to −100°C axial and equatorial ligand interchange 77−73091
$Fe(CO)_3(PF_3)_2$, ^{31}F and ^{19}F NMR, 25 to −100°C, axial and equatorial ligand interchange 77−73091
$Fe_{3-x}Co_xAl$, site preference and local environment effects, Mossbauer and NMR meas. 80−71264
$Fe_{1-x}Co_xSi$, mag. props., sp. ht., n.m.r. and Mossbauer effect meas. 77−12129
$FeCr_2S_4$, normal ferrimag. spinel, NMR studies 2-77K *(Russian)* 79−19785
FeF_2:Mn, antiferromag., NMR relax., impurity bonding 80−66061
FeF_2:Mn, Heisenberg antiferromagnet, impurity thermodynamics, NMR meas. 79−61098
FeF_3, weak ferromag., NMR of ^{57}Fe nuclei 79−95676
$Fe_{3-x}Mn_xSi$, Mossbauer and NMR exam. of site substitution and mag. struct. 77−12092
$Fe_xNb_xV_{2-2x}O_4$, NMR analysis of semiconductor transitions 78−52367
Fe_3O_4, lattice parameters, NMR freqs., and magnetoelec. pots. near 12K 80−71146
Fe_3O_4, low temp. phase ionic ordering, NMR *(Russian)* 78−23354
Fe_3O_4, magnetite, electronic struct. at low temps., NMR anal. 78−67686
$Fe_{80}P_{13}C_7$, amorphous and crystalline, electrochemical and semicond. behaviour *(Russian)* 80−101021
$FePS_3$ and $FePSe_3$, antiferromag., mag. props., NMR meas. 79−24223
$Fe_3Si_{1-x}Al_x$, conc. depend. of NMR freq. 79−69732
β-$Fe_{0.35}V_2O_5$, NMR of ^{51}V 80−71232
^{57}Fe powder, NMR excitation function, drumhead model of Bloch walls 80−15810
$Ga+H_3PO_4$, interaction in aq. soln., ^{71}Ga and ^{31}P NMR obs. 79−22729
GaAs oxide growth kinetics and physical props. 79−77937
GaAs:Fe, ordering of Fe impurity, NMR anomalous line shift obs. 78−27102
$Ga_{1-x}Co_x$, cluster spin glass system, host and impurity NMR studies 79−65745
$GdAl_2$, hyperfine fields, ferromagnetic coupling between rare earth spins, NMR study 80−39880
$GdAl_2$, spin reorientation, NMR features rel. to preferred magnetisation direction change 77−63213
$GdCo_2$, ^{59}Co hyperfine field, temp. depend. splitting 77−8447
$Gd(Co_{1-x}Ni_x)_2$ compounds, NMR and thermal expansion 80−66070
$Gd_{1-x}La_xRh_2$, NMR, contribution of Gd neighbours to Gd hyperfine field 77−8423
$GdPt_x$, $Gd_{1-x}A_xPt_2$ (A=Sc, La), Laves phase alloy, NMR, nonstoichiometry 77−63298
$Gd_xY_{1-x}Co_2$, transferred hyperfine interactions, ^{155}Gd Mossbauer effect and ^{165}Ho NMR expts. 77−63339
$Gd_xY_{1-x}Fe_2$, s-d exchange interaction integral, change due to hydrostatic compression 78−88199
^{71}Ge, in liq. metal target, in-beam γ-NMR-PAD 77−59465
H high-temp. probe for proton magnetic resonance expts. 79−49234
H^+ chemical shifts, INDO calcs. 80−32743
o-H_2 adsorbed on graphite, NMR, orientational behaviour, weak crystal field 78−75935
H_2, adsorbed on Rh-TiO_2 catalyst, surface states, NMR spectrosc. investig. 80−103891
o-H_2 dilute impurity in rare gas solids and p-H_2, NMR study 80−25228
H_2, single crystals, NMR, dynamic effects 80−107608
p-H_2, solid, anisotropic NMR spectra and crystalline state 78−10786
p-H_2, solid, cryst. field energy for o-H_2 impurities, NMR studies 80−15331
H_2, solid, diluted ortho-para mixtures, NMR of ortho-H_2 79−60600
H_2, solid, glass phase, use of NMR *(French)* 80−93190
o-H_2, solid, NMR relax. and libron energy 78−88204
p-H_2, solid, NMR spectra, motional-narrowing model interpretation, order-disorder transition below 0.18K 78−79855
p-H_2, solid, NMR spectrum of isolated o-H_2 pairs 80−15332
H_2, solid, orientational order parameter at reduced ortho conc., NMR spectra meas. 77−4566
H_2, solid, orientational ordering effects at low ortho conc. 79−56018
H_2, solid, quadrupolar glass phases, evidence from NMR study 78−84027
p-H_2, solid, very low O-H_2 conc., order-disorder transition, NMR 78−56384
H_2, solid, with low ortho-fraction, ferrorotational transition *(Russian)* 79−60597
H_2, transverse NMR low density spectrum 78−74681
H_2-He, nucl. shielding, ab initio coupled HF calc. 79−89690
H_2-He(Ne), NMR longit. relax., mole fraction depend. 77−61767
o-H_2+Ar, relax. and kinetic cross sections, DWBA calc. 78−25655
o-H_2+He, relax. and kinetic cross sections, DWBA calc. 78−25655
H_3, transverse NMR of low-density gas 79−64017
HCl, del. gas, proton longit. relax. time 77−34720
HCl, in the bath, NMR spin-lattice relax., coupled states ang. momentum decoupling 77−77117
HD, liq., in He bath, NMR spin-lattice relax., coupled states ang. momentum decoupling 77−77117
HD, nucl. spin-spin coupling, diamag. contrib. 79−36665
HDO, interactions with myosin, intermolecular spin diffusion study 80−18951

nuclear magnetic resonance continued
$H_{3-n}D_nSe(n=0, 1 \text{ and } 2)$, ^{77}Se NMR on XL-100 spectrometer, isotope effects and spin-lattice relaxation 80−71211
HNO_3, H_2O, devitrification crystallisation, fast Raman and wide-line NMR obs. *(French)* 79−73915
H_2O, adsorbed, surface-induced NMR line splittings and augmented relax. rates 78−64288
H_2O, proton mag. moment in Bohr magnetons, g-factor ratio determ. 78−33526
$H_2O(D_2O)$ isotope effects, ^{17}O NMR 77−34663
H_2SeO_3, ^{77}Se Fourier transform NMR 78−95528
H_2SeO_4, NMR of ^{77}Se, chemical shift and screening tensors *(Russian)* 78−64285
HT, triton-proton mag. moment ratio determ. by NMR method with 10^{-6}% accuracy *(Russian)* 77−61773
$H(UO_2PO_4)4H_2O$, solid, fast hydrogen ion diffusion, NMR relax. time meas. 80−2205
^1H, hydrostatic liquids for obs. of NMR at high press. and low temp. 79−2801
^2H NMR, deuteron quadrupole coupling constants, determ. from natural abundance ^{13}C satellites 79−31556
^2H NMR of D_2O in lyotropic phase, T, calcs. 77−18944
^2H nuclei, spin-1 particle, eight-dimensional spin space determ. 80−60428
^2H, relax. in nitrobenzene 77−48070
^2H, spontaneous polarisation of TGS, temp. depend., microscopic mechanism determ. 77−81070
He beam, magnetic spectrom. meas. using automatic tracking NMR system 80−27869
He film, adsorbed, NMR measurements 80−107605
He, polarisation via collision with Tb atom 78−33453
He, solid, vacancy tunnelling freq. calc. 77−80678
^3He, liq., spin polarisation, rapid melting of polarised solid 79−46872
^3He, nucl. mag. moment, ratio of precession freqs. of gas phase helions-proton mixture *(Russian)* 79−17803
^3He, 1^1S_0 ground state, NMR obs. by transverse modulation of mag. field 78−82671
^3He, A-phase, superfluid, field-induced Ī textures and mag. resonance 79−46864
^3He, A-phase, superfluid, field-induced surface texture, in presence of superflow 79−46869
^3He admixed with C particles, surface induced ferromagnetism, pulsed NMR expts. 79−51362
^3He adsorbed layers, NMR studies 79−65286
^3He, adsorbed monolayers, nuclear magnetic relaxation for two dimensional systems 80−103534
^3He, adsorbed monolayers on Grafoil, NMR, low coverage 78−91503
^3He, adsorbed on graphite, NMR relax, times 79−51374
^3He, adsorbed on Vycor glass under press., nature of phases, entropy and magnetisation expts. 80−49458
^3He, anisotropic superfluid phases, book contrib. 79−99387
^3He film, adsorbed on graphite, nucl. mag. susceptibility below 4.2K 77−20155
^3He film, submonolayer and multilayer, adsorbed on Grafoil, pulsed NMR study 80−49456
^3He film, theory of motional inhibition of interlayer quantum tunnelling 80−54466
^3He, HCP solid, with ^4He impurities, ^3He nucl. mag. relax. behaviours 79−56027
^3He, in Grafoil, NMR obs. of magnetisation 79−51370
^3He in Grafoil, ultralow temp. NMR mag. susceptibility, surface magnetisation and transition 78−79843
^3He, liq. confined in Al_2O_3 and Pt powders and Grafoil, NMR expts. 79−51371
^3He, liquid, normal and superfluid phases, NMR and ion mobility experiments 78−91505
^3He, monolayer film, adsorbed on Grafoil, pulsed NMR meas. 79−33152
^3He, monolayer on grafoil, NMR relaxation time study 78−75902
^3He, optically oriented nuclei, maser excitation and characts., appls. 78−17891
^3He, optically oriented nuclei, in two-chamber cell, spin maser appls. 78−17892
^3He, solid, mag. ordering, NMR study 80−54470
^3He, solid, mag. susceptibility near ordering temp., pulsed NMR meas. 78−18869
^3He, solid, nuclear antiferromag. reson. 80−54471
^3He, solid, nuclear spin exchange interaction at high molar vol. 77−20160
^3He superfluid, A and B phases, pulsed NMR, nucl. susceptibility, spin-lattice relax., freq. shifts 78−47628
^3He, superfluid, A-phase, additional positive shift in Legget shift in transverse and longit. reson. freq. 79−7726
^3He, superfluid, A-phase, dissipation of flow, NMR study 80−92745
^3He, superfluid, A-phase, generation of textural defects 79−60588
^3He, superfluid, A-phase, hydrodynamics and macroscopic dynamics in high mag. field 77−72733
^3He, superfluid, A-phase, helical textures, NMR response 80−70496
^3He, superfluid, A-phase, mag. texture relax. 79−60581
^3He, superfluid, A-phase, order parameter singularities, confined to small cylinders, NMR 79−55994
^3He, superfluid, B-phase, low temp. spin relax. 80−15323
^3He, superfluid, B-phase, n-solitons, and NMR freq. calcs. 78−34670
^3He superfluid, B-phase, nonlinear NMR, instability analogous to ferromag. reson. predicted 78−43202
^3He, superfluid, distortion in elec. and mag. fields, NMR shifts 77−35780
^3He, superfluid, flowing, NMR 79−4448
^3He, superfluid, heat capacity, spin susceptibility, NMR and viscosity *(Danish)* 78−22921
^3He, superfluid, hydrodynamic parameters and correlation functions 79−82406
^3He, superfluid, longitudinal magnetisation, relax. meas. 79−51355
^3He, superfluid, low temp. orbital dynamics 77−66057
^3He, superfluid, mag. reson., electron cloud distortion, viscosity and density meas. 79−65277
^3He, superfluid, NMR, Ī-texture effects on satellite frequencies 79−60583
^3He, superfluid, order parameter relaxation and hydrodynamics near A-transition 77−66064

nuclear magnetic resonance continued
^3He, superfluid, surface energy assoc. with interface between A- and B-phases, NMR obs. 77−47641
^3He, superfluid, transport parameters, Kubo formulae and BCS-Green's functions 80−88382
^3He superfluid *(Russian)* 79−7727
^3He, superfluid A phase, effect of mag. dipole interaction on collective modes 77−89610
^3He, superfluid A phase, helical textures and NMR frequencies 79−95235
^3He, superfluid A phase, NMR on textural defects 78−38895
^3He, superfluid A-phase, composite solitons, mag. reson. 78−51779
^3He, superfluid A-phase, composite solitons in presence of superflow, satellite freq. 80−2233
^3He, superfluid A-phase, composite soliton in narrow circ. cylinder, satellite freq., thermal fluctuations 80−34266
^3He, superfluid A-phase, evidence for metastable mode, pulsed NMR meas. 77−85013
^3He superfluid A-phase, exptl. studies of solitons 80−88386
^3He, superfluid A-phase, longitudinal mag. relax. 80−59751
^3He, superfluid A-phase, NMR in presence of disgyration 79−19418
^3He, superfluid A-phase, phase diagram for helical texture 80−24704
^3He, superfluid A-phase, planar-twist soliton near A-A_1 transition, NMR props. 79−33145
^3He, superfluid A-phase, small cylinders, evidence for textural transition from NMR expts. 78−56015
^3He, superfluid A-phase, soliton lattice, flow induced 79−82407
^3He, superfluid A-phase, soliton lattice for NMR behaviour 80−2234
^3He, superfluid A-phase, textures in narrow cylinders 80−24703
^3He, superfluid A-phase, unusual NMR effects 77−66059
^3He, superfluid and normal, appl. of SQUID NMR techniques 79−26093
^3He, superfluid B phase, soliton-like spin waves 80−44385
^3He, superfluid B phase, surface textures and NMR 79−37895
^3He, superfluid B-phase, bound spin wave states associated with n-solitons 78−67884
^3He, superfluid B-phase, low-temp. spin relax. 79−55989
^3He, superfluid B-phase, textures and NMR, theory 77−39717
^3He, superfluid B-phase ferromagneticlike reson. behaviour obs. in NMR 78−10245
^3He, superfluid phases, NMR in restricted geometries 77−7933
^3He, two-dimens. solid, melting mechanism 80−10643
^3He with C particles, pulsed NMR, mag. susceptibility surface induced ferromagnetism, antiferromagnetic exchange interaction 78−79844
^3He-^4He film, adsorbed on graphite, nucl. mag. susceptibility below 4.2K 77−20155
^3He-^4He II, pulsed NMR investig. of ^3He flow vel. 77−59171
^3He-^4He liquid mixture, conc. ^3He spin diffusion expts. 78−34671
^3He-^4He solid mixture, dil. ^3He conc., diffusion coeff. obs. by NMR, impurity-phonon scatt. *(Russian)* 77−62701
^3He-A, superfluid, spin dynamics, spin-orbit configurations, spin waves *(Russian)* 80−54462
^3He-A superfluid, longit. and transverse NMR modes, satellite resons. 77−7936
^4He, diffusion of ^3He, pulsed NMR exam. *(Russian)* 78−71902
^4He, solid, diffusion coeff. of ^3He, detection and study of impuriton-phonon scatt. mech. 79−56029
Hg complexes, tertiary phosphines, NMR, ^{199}Hg-^{31}P spin-spin coupling, temp. depend. 78−62825
Hg, nuclear magnetic moment ratio of odd isotopes *(French)* 77−75081
$HgCr_2Se_4$, spontaneous magnetisation temp. depend., nuclear resonance freq. depend. *(French)* 80−80483
HgSe(Te), chemical shift and linewidth determ. 79−19792
^{199}Hg-^{31}P, NMR in Hg complexes (tertiary phosphines), temp. depend. 78−62825
^{203}Hg nuclei, optically pumped, anharmonic mag. resonance phenomena 79−94015
HoF_3, ^{19}F NMR, ligand hyperfine interaction, shift tensor determ. 78−48056
$HoVO_4$, NMR predictions of properties, dipolar interactions and antiferromagnetic exchange 80−50203
$HoVO_4$, parameters in nuclear Hamiltonian 78−72422
^{165}Ho, obs. of transferred hyperfine interactions in $Gd_xY_{1-x}Co_2$ 77−63339
IF_6, NMR and NQR of ^{127}I and ^{19}F, solid-solid transitions and mol. motions 79−99784
n-InAs, nucl. maser effect 78−19345
InAs:Mn, NMR, magnetoresist., Hall effect and mag. susceptibility meas. 78−26888
InSb:Mn, NMR, magnetoresist., Hall effect and mag. susceptibility meas. 78−26888
^{192}Ir orientated in Fe and Ni, nuclear mag. resonance 80−84661
$K_3Co(CN)_6$, NMR spin lattice relax. of ^{59}Co rel. to $Co(CN)_6$ octahedra vibr. modes 80−39885
$KCoF_3$, antiferromag., ^{59}Co NMR exam. 78−76332
$KCoF_3$, NMR, magnon-phonon interaction contribution to nuclear spin-lattice relax. 78−88207
$KCoF_3$, single crystal, mag. susceptibility, ^{19}F NMR and static measurements 79−11301
$K_2CuCl_4.2H_2O$, and isomorphous cpds., mag. interactions of H and D nuclei, NMR obs. 79−87251
$K_2CuCl_4.2H_2O$, Bloch-wall NMR, anisotropic hyperfine interaction 79−51864
$K_2CuCl_4.2H_2O$, ferromag., hyperfine and exchange interactions, NMR study 80−50208
$K_2CuCl_4.2H_2O$ structure compounds, 3-dimens. ferromag., exchange anisotropy by NMR 77−55714
$K_2CuCl_4.2H_2O$ structures, BCC Heisenberg ferromags., transferred hyperfine interactions of ^1H, ^2D and ^{17}O 77−69725
$KCuF_3$, hyperfine interactions of ^{19}F nuclei, n.m.r. meas. 77−12209
K_2CuF_4, hyperfine interactions of ^{19}F nuclei, n.m.r. meas. 77−12209
KD_2AsO_4, ferroelect. phase transition, NMR study *(Chinese)* 79−33644
KD_2PO_4, ferroelec. transition, ^{31}P chemical shift tensor meas. 77−28527
KD_2PO_4, ferroelec. transition, ^{31}P chem. shift obs. 78−76414
KD_2PO_4, ferroelect. phase transition, NMR study *(Chinese)* 79−33644
$KD_3(SeO_3)_2$, D NMR above and below ferroelec. transition, H-bond behaviour 78−52460
$KD_3(SeO_3)_2$, deuteron mag. reson. in ordered and disordered phase 78−39414
KH_2PO_4 (KDP) type crystals, discrepancy between ESR and NMR data 77−48035

nuclear magnetic resonance continued
KIO_3, temp. depend. Raman spectra and phase transitions *(Russian)* 78−15171
$K_2Mn_{1-x}Cu_xF_4$, dynamic Jahn-Teller effect, NMR *(Japanese)* 78−19347
$KMnF_3$:Rb, phase transition and atomic motions, NMR study 80−75872
K_2MnF_4, nucl. spin-magnon relax. time, temp. depend., NMR study 80−25117
K_2MnF_4, two-dimens. Heisenberg antiferromag., field and temp. depend. of magnetic 77−66272
K_2MnF_4, two-dimensional antiferromag., NMR, magnetisation field-depend., spin-wave theory 77−63294
K_2MnF_4:Zn(Mg)(Ni), local magnetisation, NMR and Green's function study 80−65870
$K_3Mn_2F_7$, quadratic double-layer antiferromag., NMR, spin-wave anal. of sublattice magnetisation 77−63293
$K_3Mn_2F_7$, quadratic double-layer Heisenberg antiferromagnet, sublattice magnetis. 77−66270
$KNbF_6$, NMR, quadrupole effects and struct. distortion 80−15809
K_2NiF_4, nucl. spin-magnon relax. time, temp. depend., NMR study 80−25117
K_2O-B_2O_3-P_2O_5 glass struct. studies using NMR 79−24221
$K_2Pt(CN)_4Br_{0.3}.3.2H_2O$, motion of Br^- ions 77−90051
K_2PtCl_6, K_2ReCl_6, K_2SnCl_6, solid state phase transitions, lattice vibr., NMR and NQR obs. 80−34814
$K_2SnF_6.4HF$, cryst., H bond geometry, NMR obs. 79−42844
$K_2SnF_6.4HF$, molecular diffusion, spatial symmetry, HF molecule arrangement 79−42313
$K_2Ta_4O_9F_4$, NMR meas. on ^{19}F, localisation of F^- ions *(French)* 79−77579
K_2TeO_3, D_2O soln., $^{123,125}Te$ Fourier transform NMR 78−15046
K_2TiF_6, anion motion and phase transition, NMR spectra 79−99788
^{39}K pulsed NMR obs. of whole body live and dead newborn mice 80−40964
Kr, polarisation via collision with Rb atom 78−33453
^{83}Kr, NMR gaseous study *(German)* 80−52917
^{83}Kr, nucl. mag. relax. meas. in gas 80−43072
$^{138,139}La$, Fourier transform NMR 80−57354
La intermetallics, LaX_2Si_2 (X=Cu, Ag, Cu), ^{29}Si NMR and mag. susceptibility 79−61246
La ions as probes of conform. of mols. in soln. 77−60324
La, nucl. mag. moments and ratios of quadrupole moments, NMR spectroscopy in aqueous soln. 77−73088
La-P-Ce, dilute, NMR investig. of anisotropic cond. electron exchange 77−63309
LaB_6, synthesis and props., review *(Japanese)* 80−40255
LaF_3, ^{19}F NMR study, relaxation times meas. 80−108093
LaF_3, ionic transport, NMR and cond. studies 80−107555
$La_{75}Ga_{25}$, amorphous, local symmetry around glass-former sites, elec. quadrupole effects, NMR 80−80618
$La_{1-x}Gd_x(Zn,Ag)$, resonance of ^{139}La 78−15038
$LaH_{2.69}$ ^{139}La NMR, Knight shift 79−91307
La_3In, mag. susceptibility and normal state NMR meas. 78−31118
β-$LaNi_{5-y}Al_y$ hydrides, H diffusion, NMR studies 80−15298
$LaNi_3H_x$ (x=4.7, 4.9), NMR line width, spin-lattice relaxation time temp. depend., H self-diffusion *(Russian)* 79−61248
β-$LaNi_5H_x$, H_2 diffusion, NMR meas. 79−82378
$La_2Ni_7H_x$ (x=9.9, 11.4), NMR line width, spin-lattice relaxation time temp. depend., H self-diffusion *(Russian)* 79−61248
La_2O_3-B_2O_3-P_2O_5 glasses, struct. changes during heat treatment 77−7672
La_3Tl, mag. susceptibility and normal state NMR meas. 78−31118
Li, Knight shift volume depend. 80−84663
Li, thermal mixing rate calc. 78−10795
Li^+-ligand complexes, ^7Li chemical shifts, expt. and ab initio studies 80−63670
LiAl, NMR relax. investig. of ^7Li self-diffusion 77−12217
Li_5B_4, cryst. struct., X-ray and neutron diffr., and NMR 79−23571
$Li_{4+x}B_7O_{12+x/2}Cl$, solid electrolyte, NMR meas. 80−29208
LiCl, frozen soln., NMR study of phase transitions 79−56617
LiCl glycerol solns. quadrupole interactions, nucl. mag. relax., correl. time determ. 77−14449
$LiCrS_2$, intercalation cpd., NMR 77−90048
$LiErF_4$ powder, ^{19}F NMR 77−48067
LiF, cross relaxation of β-active ^8Li nuclei *(Russian)* 80−103895
LiF, heteronuclear mag. spin system relaxation in many pulse NMR expts. 80−93203
LiF, NMR exam. of point defects generated in (n,γ)-reaction *(Russian)* 78−60347
LiF, thermodynamic effects of RF pulse pair on system with two spin species 77−66433
$Li_xFePS_3(Se_3)$, Li_xMnPSe_3 and $Li_xNiPS_3(Se_3)$, NMR and neutron diffr. obs., mag. props. 80−60433
LiH, nuclear antiferromagnetism, dynamic nuclear polaris., NMR 79−1724
$LiHoF_4$, NMR shift tensors, temp. and field depend. 79−38391
$Li_6In_2O_6$, ion mobility, NMR meas. *(French)* 79−65240
$Li_6In_2O_6$, pseudo-two-dimens. electrolytic solid, Li ion mobility, NMR study *(French)* 80−34235
Li_3N, superionic conductor, cryst. growth and struct., phys. props., book contrib. 79−42308
$LiNH_4SO_4$, ferroelect. and press. induced phase transitions 79−38473
$LiNH_4SO_4$, phase transitions and phys. props. 78−76399
$LiNH_4SO_4$, press.-temp. phase diagram, NMR and SHG meas. 78−23690
$LiNbO_3$, chemical, struct. and physical props., book contrib. 79−69783
Li_7NbO_6, ion mobility, NMR meas. *(French)* 79−65240
Li_7NbO_6, pseudo-two-dimens. electrolytic solid, Li ion mobility, NMR study *(French)* 80−34235
Li_xNiPS_3, antiferromag., mag. props. and ionic mobility, NMR meas. 79−24223
Li_xNiPS_3, microscopic diffusion studies by NMR technique 79−28138
Li_2O-B_2O_3 glass struct. study using ^{10}B NMR 80−84658
Li_2O-B_2O_3 glass system, 4-coordinated B atomic fraction determ. 78−94999
Li_2O-LiX-B_2O_3 glass, X=halogen, high anionic cond. of new solid electrolytes 80−107546
$LiRF_4$, R=Dy, Er, Ho, Tb, NMR rotation spectra, transferred hyperfine interaction 77−85590
Li_8SnO_6, ion mobility, NMR meas. *(French)* 79−65240
nuclear magnetic resonance continued
Li_8SnO_6, pseudo-two-dimens. electrolytic solid, Li ion mobility, NMR study *(French)* 80−34235
LiT, retention and distrib. of ^3He NMR studies 79−69153
$LiTmF_4$, ^{169}Tm NMR spectrum, hyperfine field parameters, and cryst. field calcs. 77−12213
$LiTmF_4$, local mag. field at ^{19}F rel. to paramag. susceptibility, NMR meas. *(Russian)* 77−81023
$LiTmF_4$, Van Vleck paramag., mag. reson. on uniaxial and uniform compression *(Russian)* 79−61243
$LiVS_2$, intercalation cpd., NMR 77−90048
^6Li, nuclear mag:spin-lattice relaxation times 78−86889
^8Li, in $LiTaO_3$, multiple quantum NMR transitions obs., quadrupole moment determ. 77−73090
Mg:^{12}B ions, decoupling of hyperfine interactions by external mag. field 77−24756
$MgCl_2$, aq. soln., ^{25}Mg NMR, longit. relax. rates 79−91309
$Mg(NO_3)_2$, aq. soln., ^{25}Mg NMR, longit. relax. rates 79−91309
Mn II-lecithin lipid-water system, NMR and EPR obs. 80−61168
Mn ternary carbides, Mn_3MC, M=metal, mag. props. 77−63116
Mn ternary nitrides, Mn_3MN, M=metal, mag. props. 77−63116
$Mn_{23}C_6$, solid-state ^{13}C NMR spectra 79−24220
$MnCO_3$, NMR saturation, nuclear spin wave excitation, large freq. shifts *(Russian)* 80−50207
$Mn(ClO_4)_2/NaClO_4$ in aq. soln., interaction between Mn^{2+} and ClO_4^-, NMR studies 80−71212
$Mn_{1-x}Cu_xSb$, ferromag., NMR exam. 77−12207
MnF_2, reson. NMR near phase transition 78−76265
$MnFeO_2$:^{55}Mn, NMR freq. dynamical shift for nuclei in domain walls *(Russian)* 77−40148
$MnFe_2O_4$, valence states, NMR investig. *(Czech)* 78−72420
$Mn_xFe_{3-x}O_4$ NMR of Mn^{3+} in B-sites 78−35061
MnII-ATP system, exchange mechanism, FT NMR and EPR obs. 79−22733
$Mn_4N_{0.8-1}$, NMR of ^{55}Mn, reson. curve fine splitting, spin echo meas. 78−2768
Mn_4N_x, non-stoichiometric, ^{14}N NMR 79−91302
MnO-B_2O_3, polycryst. cpds., mag. susceptibility and ^{11}B NMR 79−8056
MnO_4, aqueous soln., ^{55}Mn nuclear mag. shielding, NMR obs., O isotope exchange 77−10691
MnO_4^-, aq. soln., O isotope substitution, ^{55}Mn NMR 77−30890
$MnPS_3$ and $MnPSe_3$, antiferromag., mag. props., NMR meas. 79−24223
Mn_2Sb, domain and domain wall resons. in ^{55}Mn NMR spectrum 80−25219
$MnSb_{1-x}Sn_x$, zero-field NMR investig. of domains and domain walls 77−32271
MnSi, helically ordered state, ^{55}Mn and ^{28}Si NMR 78−43655
^{55}Mn, NMR in Mn_4N_x 78−2768
Mo complexes derived from electron-rich olefins, cryst. chem. 77−76372
$Mo_{70}B_{30}$, amorphous, local symmetry around glass-former sites, elec. quadrupole effects, NMR 80−80618
$Mo(CO)_6$, second-order quadrupole splittings of ^{95}Mo NMR signal 77−28461
MoF_5, mol. and electronic struct., vitreous, liq., and tetrameric states, ^{19}F NMR obs., mol. mobility 80−34787
MoO_4^-, aq. soln., O isotope substitution, ^{95}Mo NMR 77−30890
$MoO_{4-n}S_n^{2-}$ in aqueous soln., ^{95}Mo NMR identification 77−48069
$Mo_{48}Ru_{32}B_{20}$, amorphous, local symmetry around glass-former sites, elec. quadrupole effects, NMR 80−80618
MoS_4^{2-}, S isotope effect on ^{95}Mo nucl. mag. shielding 77−63301
^{95}Mo, ^{97}Mo, Fourier transform NMR, chem. shifts and Larmor freqs. *(German)* 77−59473
^{95}Mo NMR signal in $Mo(CO)_6$, second-order quadrupole splitting 77−28461
N containing molecules, N NMR, nuclear mag. shielding, X-ray photoelectron spectra 78−17695
N_2 complex, $NiC(C_6H_5NO)_6(NO_3)_2$, singlet ground-state systems, field induced mag. long range order 80−60266
$(N(CH_3)_3H)_2SnF_6$, phase transition and temp. effects, Mossbauer and NMR spectra 78−88236
ND_3, dissolved in poly-γ-benzyl-L-glutamate-chloroform, NMR study 80−34805
ND_4^+, dissolved in lyotropic systems 79−22732
$ND_4D_2AsO_4$, ND_4 role in antiferroelec. transitions, D NMR 77−52025
$(ND_4)_2PbCl_6$-ND_4Cl polycryst. mixture, D spin-lattice relax. times, ND_4^+ reorientation activation energies 78−6587
NF_3, nuclear resonance, effects of intermolecular interactions and intramolecular dynamics 80−63658
NH_3, adsorbed on graphite, NMR pulsed field gradient method, diffusion coeff. meas. 80−15362
$NH_3+He(H_2)$, rot. relax., double and triple reson. obs. 78−90196
NH_4 perfluoro-octanoate, amphiphilic liq. cryst., ^{19}F multipulse NMR study 78−76328
NH_4^+, ND_4^+, in lyotropic mesophase, ^{14}N NMR, and quadrupole splitting 78−17690
NH_4^+, proton-proton dipolar coupling in nematic soln. using high resolution NMR 77−3387
$N_2H_6^{2+}$ salts, NMR spin lattice relaxation study, ^{14}N-^1H dipole-dipole contrib. to relax. 80−75878
NH_4BF_4, ionic radii and chem. shifts, correl. with electronegativity 80−66054
NH_4Br, ^{14}N NMR obs., rel. to structural transforms. 79−15368
$(NH_4)_2CuBr_4.2H_2O$, ferromag., hyperfine and exchange interactions, NMR study 80−50208
$(NH_4)_2CuCl_4.2H_2O$, Bloch-wall NMR, anisotropic hyperfine interaction 79−51864
$(NH_4)_2CuCl_4.2H_2O$, ferromag., hyperfine and exchange interactions, NMR study 80−50208
$(NH_4)_4Fe(CN)_6.1.5H_2O$ cryst. struct. determ., and ionic conductivity using NMR technique 79−14758
$(NH_4)_2GeF_6$, NMR, nuclear dipolar energy relax. 79−42853
$NH_4HC_2O_4$, hemihydrate, ^{14}N NMR, high resolution spectra, elec. field gradient tensor 77−81018
NH_4HF_2, ^{19}F free induction decays 78−2754
$NH_4H_3(SeO_3)_2$, single crystal, ^{77}Se magnetic shielding, chemical shift tensors 80−71207
NH_4I, ^{14}N NMR obs., rel. to structural transformations 79−15368
NH_4IO_4, chem. shift, NMR obs. 80−48015
NH_4VO_3, polycryst., quadrupole coupling const., asymmetry parameter, chem. shift, NMR computer calcs. 78−6584

nuclear magnetic resonance continued
N_2O, ^{15}N NMR, chem. shift., determ. of virial coeffs., rovibr. motion 78−58720
N_2O dissolved in liq. cryst., NMR, relax. times 80−25233
^{12}N, β decay, alignment prod. by NMR 78−50126
^{12}N, NMR in Ni, hyperfine field determ. 77−8418
^{14}N, in nitrobenzene, liq., ^{14}N quadrupole coupling const., environmental effects 78−48052
^{14}N NMR, single cryst., separation of dipolar and quadrupolar splittings, new technique 80−25217
^{14}N NMR chemical shift, external neat nitromethane scale 78−24834
^{14}N, relax. in nitrobenzene 77−48070
^{14}N screening, absolute scale 78−2762
^{15}N, chem. shift in NNO 78−58720
^{15}N NMR chem. shift references evaluation 78−24835
^{15}N NMR heteronuclear spectroscopy, two dimensional Fourier transform technique 80−31818
^{15}N NMR of haemoglobin 77−90720
Na, self-diffusion mech., NMR meas. 80−44356
Na^+, dissolved in lyotropic systems 79−22732
Na^+-gramicidin D emulsion, NMR obs. 79−43805
Na_2, magnetic shielding studies 77−42341
Na_2, nuclear spin polarized, measurement of nuclear spin relaxation, comparison with ortho-para conversion rate 79−43568
Na_2+Na, spin polarisation exchange via opt. pumping, NMR 77−14452
$NaAlCl_4$, cryst. struct., charge distrib., X-ray, NMR and NQR meas. 77−11528
NaBr, ^{23}Na NMR chem. shift meas. 77−71817
$NaCN_x$ struct. domains, NMR determ. 80−50204
NaCl, ^{23}Na NMR chem. shift meas. 77−71817
NaCl, doubly rotating coordinate system, NMR multiple-quantum transitions 77−81019
NaCl, frozen soln., NMR study of phase transitions 79−56617
NaCl:Ca^{2+}, highly doped, aggregation of point defects, NMR and dielec. loss meas. 79−10847
NaCl:Sr, dimer and trimer aggregate formation by NMR, ionic cond. and dielectric losses 80−15094
$NaClO_4/Mn(ClO_4)_2$ in aq. soln., interaction between Mn^{2+} and ClO_4^-, NMR studies 80−71212
$NaClO_4.D_2O$, H bonding, D NMR 77−34664
$NaCrS_2$, intercalation cpd., NMR 77−90048
NaF, ^{23}Na NMR chem. shift meas. 77−71817
$NaHSeO_3$, ^{77}Se Fourier transform NMR 78−95528
$NaHSeO_3$, and $NaDSeO_3$, NMR of ^{23}Na and ^2D, hydrogen bonding 80−44190
$NaH_3(SeO_3)_2$, high-pressure phase transform., ^{23}Na NMR obs. 77−63380
NaI, ^{23}Na NMR chem. shift meas. 77−71817
$Na_xIn_xSn_{1-x}S_2$ ($1>x>0$), intercalation-substitution system, NMR study *(French)* 79−69095
NaK+Na, spin polarisation exchange via opt. pumping, NMR 77−14452
NaN_3, NMR, Na nuclear quadrupole moment, phase transition 77−73092
$NaNH_4SeO_4.2H_2O$, ferroelectric crystal, effect of hydrostatic pressure on phase transition 78−52453
$NaNO_2$, ferroelectric, NMR of ^{23}Na small particles 79−28629
$NaNO_3$, cryst., ^{23}Na transitions, two-photon transient effects, NMR obs. 77−85588
$NaNbF_6$, NMR, quadrupole effects and struct. distortion 80−15809
Na_2O-B_2O_3 glass, struct. interpretation of ^{10}B and ^{11}B NMR spectra 78−80241
Na_2O-B_2O_3 glass struct. study using ^{10}B NMR 80−84658
Na_2O-B_2O_3-SiO_2 glass, ^{11}B NMR obs. of struct. 78−38625
Na_2O-B_2O_3-SiO_2 glass, NMR, struct. 79−87325
β-$Na_2O.Al_2O_3$, high-field ^{23}Na NMR 78−64284
$NaReO_4$, ^{23}Na and ^{187}Re NMR and NQR temp. depend. 80−54973
$NaReO_4$, temp. depend. of nuclear quadrupole freq. of ^{23}Na, ^{187}Re, NMR and NQR meas. 78−95529
Na_2SeO_3, ^{77}Se Fourier transform NMR 78−95528
Na_2SeO_4, ^{77}Se Fourier transform NMR 78−95528
Na_2TeO_3, D_2O soln., $^{123,125}Te$ Fourier transform NMR 78−15046
$NaVO_2$, polycryst., quadrupole coupling const., asymmetry parameter, chem. shift, NMR computer calcs. 78−6584
β-$Na_{0.33}V_2O_5$, quasi-one-dimensional conductor, NMR studies 80−93204
$NaVS_2$, intercalation cpd., NMR 77−90048
Na_xWO_3, $0.22<x<0.84$, low temp. struct., press. effects, NMR study 80−59443
Na_xWO_3, Knight shift, spin-lattice and spin-spin relax., high press. NMR obs. 80−50211
^{23}Na in heterogeneous system, nuclear mag. relaxation time determ., rel. with dimensions of colloidal particles 80−75876
^{23}Na, relax. in polyelectrolyte solns. 79−20353
Nb-H system, NMR evidence for low temp. pseudo-cubic phase 78−80526
NbD_x, x=0.55 to 0.88, deuteron and ^{93}Nb mag. resonance, β-α transitions 77−20721
$Nb(OR)_2Cl_3.L$, halo-alkoxide complex, prep. and props. 78−18605
NbS_2-$(pyridine)_{1/2}$ intercalation complex, superlattice struct., NMR meas. 80−70180
$NbSe_2$, charge density wave state, NMR meas. 77−8430
$Nb_3Sn(Al)(Sb)$, NMR of ^{93}Nb and spin-lattice relax. time at low temp. 77−85388
Nd-Co alloys, NMR of ^{143}Nd and ^{145}Nd 78−19343
$NdAl_2$, conduction electron spin and orbital polarisation effects 78−80228
NdF_3, crystals, shift tensors and F-diffusion, ion interactions, F^- NMR study 80−20471
$NdFeO_3$, mag. transition, NMR meas. 78−27036
Ne, polarisation via collision with Rb atom 78−33453
Ni complex, hexamethylphosphorotriamide Ni (II), paramagnetic, pulsed NMR, substitution reaction *(French)* 78−10793
Ni, ferromag. hyperfine fields on ^{12}B, NMR obs., near T_c 77−28476
Ni, magnetisation temp. depend. exam. using ^{61}Ni NMR 77−73089
Ni, NMR study of metal precipitated onto a cathode *(Russian)* 80−93185
Ni:$^{12}B(^{12}N)$, hyperfine field determ. by NMR 77−8418
Ni:^{192}Ir, NMR/ON, resonant freq. shift with applied field 77−28462
Ni:B, impurity electronic struct. calc., ^{11}B NMR data anal., magnetisation decrease 79−47046

nuclear magnetic resonance continued
Ni:B(N), hyperfine interactions, recoil-implanted β-NMR method *(Japanese)* 79−51865
Ni-b, hyperfine interactions from 6 to 730K, ^{12}B NMR 80−29372
Ni-Cd, dil., ferromagnetic dynamic crit. exponent, hyperfine interaction vs. neutron scatt. expts. 78−84437
Ni-P, amorphous alloys, low temp. mag. props., comp. depend. 77−66387
Ni-P, amorphous magnetisation, NMR and coercive force meas. 77−32187
$Ni_{1-3x}{}^{2+}Fe_{2+2x}{}^{3+}$ $Vac_xO_4{}^{2-}$ (Vac=cation vacancy), solid solns., cryst. lattice imperfections 80−39069
$NiI_2.6H_2O$, disordered linear chain mag., ESR, mag. susceptibility and NMR meas. 77−20688
$Ni_{1-x}P_x$, electrodeposited, amorphous, mag. and transport props. 78−52106
$Ni_{78}P_{14}B_8$, amorphous, local symmetry around glass-former sites, elec. quadrupole effects, NMR 80−80618
$NiPS_3$, antiferromag., mag. props., NMR meas. 79−24223
$NiPS_3$-Li, chemical and electrochemical intercalation *(French)* 78−38679
$(Ni_xPt_{1-x})_{75}P_{25}$ metallic glass system, ^{31}P and ^{195}Pt NMR 77−12211
^{17}O NMR, proton decoupling 78−2752
^{17}O NMR in chlorine oxyfluorides 77−14453
^{18}O isotope shift in ^{13}C NMR, struct. depend. 80−69165
P compounds, solid, ^{31}P NMR and π bond 79−4732
^{31}P NMR analysis of intact tissue, review 80−26432
P-Se-Tl glasses, NMR of ^{31}P and ^{205}Tl 80−15812
P+Nb, dil. alloy, NMR obs. of ^{93}Nb 80−71203
$PBMoO_4$, ^{207}Pb mag. shielding anisotropy, Fourier transform NMR 77−90057
PBr_3, ^{31}P scalar relax. using off-reson. RF field 79−93193
PCl_5, ^{31}P NMR of three solid phases, ionis. of PCl_6^- at high-press. 79−82882
PCl_5, sublimed phase studied by ^{31}P NMR, Raman spectra and X-ray diffr. 80−100209
PF_3, cryst., mol. motion, ^{19}F NMR investig. 77−73093
PF_3, in smectic solvent, ^{31}P NMR, ^{19}F and ^{31}P mag. shielding 77−18942
PF_3, nuclear resonance, effects of intermolecular interactions and intramolecular dynamics 80−63658
PF_5, nuclear resonance, effects of intermolecular interactions and intramolecular dynamics 80−63658
PH_3, ^{31}P NMR chem. shift, virial coeff. determ. 78−58721
PH_3, and d_3, ^{31}P NMR of liq. and gas, isotope effect on coupling consts. 79−76451
$PH_3(D_3)$, ^{31}P NMR, chemical shielding, centrifugal distortion, anharmonic vibr., cubic force consts. 78−82752
$PO_4{}^{3-}$, O isotope effect in ^{31}P NMR spectra 78−42100
POF_3, nuclear resonance, effects of intermolecular interactions and intramolecular dynamics 80−63658
P_4S_3, ^{31}P NMR spectrum and spin-lattice relax. time, 77 to 500K and 7 to 25 MHz 79−8064
P_4S_9, P_4S_{10}, ^{31}P NMR spectra, cf. related cpds. 77−8427
PSF_3, in orienting smectic solvent, ^{19}F and ^{31}P mag. shielding anisotropies, F-P-F bond angle 77−18942
^{31}P, in inorganic solids, multiple pulse NMR 78−52369
^{31}P, NMR chem. shift in PH_3, virial coeffs. 78−58721
^{31}P NMR investigation of heart physiology 78−69018
^{31}P NMR of the perfused heart 80−77534
^{31}P NMR spectra of P_4S_9 and P_4S_{10}, cf. related cpds. 77−8427
^{31}P, shielding consts. and anisotropy of NMR shielding tensor, modified CNDO/S calcs. *(French)* 80−32610
^{31}P-NMR spectra of chicken erythrocyte nucleosomes, temp. dependence 80−94280
^{31}P-NMR study, crayfish perfused ventral nerve cords 79−79475
$PbCO_3$, ^{207}Pb mag. shielding anisotropy, Fourier transform NMR 77−90057
$PbCrO_4$, ^{207}Pb mag. shielding anisotropy, Fourier transform NMR 77−90057
PbFCl, ionic cond. mechanism, ^{19}F NMR meas. and struct. considerations 79−55927
Pb_2MnF_6, antiferromag. and superionic conductor, EPR and NMR meas. 79−99366
$Pb(NO_3)_2$, ^{207}Pb mag. shielding anisotropy, Fourier transform NMR 77−90057
PbSe(Te), chemical shift and linewidth determ. 79−19792
$PbSnF_4$, fast ionic cond. of F^- ions, NMR study *(French)* 80−39345
$Pb_{0.9}Sn_{0.1}F_2$, NMR study of F atom motion *(French)* 80−100622
$PbWO_4$, ^{207}Pb mag. shielding anisotropy, Fourier transform NMR 77−90057
$^{208}Pb(^3He,t)^{208}Bi$, 80 MeV, Gamow-Teller M1 state excitation 78−50184
Pr compounds, Van Vleck paramagnets, mag. props., anisotropy from NMR anal. 80−54862
Pr pnictides and chalcogenides, press. depend. of cryst. field splitting 78−68392
$PrAlO_3$, tetragonal, mag. props. 77−90052
$PrCl_3$, cooperative Jahn-Teller ordering of elec. dipoles in non-Kramers doublets 78−15115
PrF_3 crystals, shift tensors and F-diffusion, ion interactions, F^- NMR study 80−20471
$PrVO_4$, energy levels 78−80226
$PrVO_4$, of ^{141}Pr and ^{51}V 77−77110
n-propylboranes, ^{11}B NMR 78−90190
Pt, adsorption of cyclopropane, NMR and PMR obs. 77−51591
Pt cluster, conduction electron density oscills., NMR spin-echo meas., indirect exchange interaction 80−44954
Pt complex, chloro-bromo complexes of Pt (IV) and Pt (II), ^{195}NMR, cooperative shift effect 79−33547
Pt-Cr(Nb)(Re)(Rh)(V), dil. alloy, 0.5 at.%, ^{195}Pt NMR for local mag. susceptibility 78−84484
Pt-transition metal, dil., mag. susceptibility and NMR meas. 78−39290
^{195}Pt shifts, referencing convention 79−33547
$RbCaF_3$, ^{87}Rb NMR at cubic to tetragonal phase transition 79−82885
$RbCdCl_3$, struct. phase transitions, NMR obs. 78−83943
RbCl:Ag, dynamic behaviour of off-centre Ag^+ defects, NMR study 79−28634
$RbCoCl_3.2D_2O$, metamagnetic phase transition, crystallographic and mag. struct., neutron diffr. meas. 80−44174

nuclear magnetic resonance continued
$Rb_2CuBr_4.2H_2O$, ferromag., hyperfine and exchange interactions, NMR study 80−50208
$Rb_2CuCl_4.2H_2O$, BCC Heisenberg ferromag., transferred hyperfine interactions of ^1H, ^2D and ^{17}O 77−69725
$Rb_2CuCl_4.2H_2O$, Bloch-wall NMR, anisotropic hyperfine interaction 79−51864
$Rb_2CuCl_4.2H_2O$, ferromag., hyperfine and exchange interactions, NMR study 80−50208
$Rb_2CuCl_4.2H_2O$, NMR spectra, second-order effects of mag. hyperfine interaction, pseudoquadrupole interaction 79−78540
$Rb_2CuX_4.2H_2O$, (X=Cl, Br), fine struct. due to indirect coupling of nuclear spins 79−78541
$RbD_3(SeO_3)_2$, DMR, electric quadrupole coupling, ferroelec. transition 79−91312
$RbFeCl_3$, linear chain cryst., quadrupole and mag. reson., rel. to $CsFeCl_3$ 79−38403
$RbFeCl_3.2D_2O$, cryst. and mag. struct., neutron scatt. and NMR expts. 79−7969
$RbH_3(SeO_3)_2$, ^{87}Rb NMR, elec. field grad. temp. depend. 79−78536
$Rb_xK_{1-x}MnF_3$, struct. transitions, NMR and birefr. expts., 60-300K 77−47577
RbKr, magnetic resonance meas. of spin-rotational interaction 78−33528
$RbMnF_3$, antiferromag. domain struct. in fields exceeding spin-flop value 79−69693
$RbMnF_3$, modes interaction *(Russian)* 77−59468
$RbMnF_3$, nucl. spin waves *(Russian)* 78−34973
$RbMnF_3$, nuclear spin waves spectra, relaxation, parametric excitation, NMR dynamic shift *(Russian)* 80−11180
Rb_2NaHoF_6, NMR spectra of ^{165}Ho, 1.6 to 13K 80−80620
Rb_2NaTbF_6, NMR spectra of ^{159}Tb, 1.6 to 13K 80−80620
$RbNiCl_3$, cryst., ^{35}Cl and ^{87}Rb NMR down to 1.3K 79−42848
Rb_2ZnCl_4, incommensurate phase transition, ^{87}Rb NMR study 80−75967
Rh_2MnPb, hyperfine fields, ferromag., NMR and Mossbauer effect studies 80−71259
Rh_2MnSb, hyperfine fields, ferromag., NMR and Mossbauer effect studies 80−71259
Ru_2FeSn, ferromag. Heusler alloys, hyperfine fields at nonmagnetic atoms in various sites, Mossbauer effect and NMR meas. 80−66089
SF_6, ^{19}F NMR, chem. shielding, intermol. interactions and rovibr. motion effects 78−9171
SF_6, ^{19}F NMR vibr. anharmonicity effects 80−91580
$ScAl_2$ density of states, ^{45}Sc NMR 77−63276
ScOF, ordering and structure, NMR and crystallographic determ. *(French)* 79−90618
$ScVO_4$, ^{51}V NMR, nucl. quadrupole coupling const., chem. shift 77−90055
Se, trigonal tight-binding calc. of chem. shift 78−2759
^{77}Se, FT NMR in solns., chem. shift, I_1 relax. times, NOE enhancement 78−95528
Si, NMR of ^{29}Si in weak mag. fields 79−65746
SiC, solid-state ^{13}C NMR spectra 79−24220
$SiCl_4$ liquid, angular momentum relaxation, effective collision numbers 80−64873
$SiCl_4$ molecule, NMR relaxation expts. to study molecular reorientation 80−63673
SiF_4, ^{19}F NMR, chem. shielding, intermol. interactions and rovibr. motion effects 78−9171
SiO_2-B_2O_3-Al_2O_3-$Na_2O(K_2O)$ glasses, Ag interdiffusion, optical and NMR studies 80−24683
$SmAl_2$, hyperfine fields, ferromagnetic coupling between rare earth spins, NMR study 80−39880
$SmCo_5$, magnetic anisotropy, Co contrib., ^{59}Co NMR Obs. 78−43583
$Sm_3Fe_5O_{12}$, spin-reorientation phase transition, NMR spectra and anisotropy consts. meas. 77−28458
$Sm_{1-x}Gd_xAl_2$, hyperfine fields, ferromagnetic coupling between rare earth spins, NMR study 80−39880
SnTe, NMR of ^{119}Sn and ^{125}Te, low hole conc., 64-440K *(Russian)* 79−15365
SnTe:Mn, NMR study 4.2 to 300K *(French)* 80−54960
^{117}Sn, ^{119}Sn, low temp. NMR thermometry 80−82775
^{119}Sn NMR by pulse Fourier transform, T_1, T_2 and chem. shifts 77−55715
^{119}Sn-^{117}Sn primary isotope effect on mag. shielding, NMR of Sn cpds. 79−72338
SrF_2:Y^{3+}, diffusion of bound and free $F_{(i)}^-$ interstitials, NMR meas. 79−78542
$SrFHF_2$, ^{19}F free induction decay 78−2753
^{87}Sr, $^3P_2$ metastable state, hyperfine struct. at. beam mag. reson. obs. 78−17590
T_2, solid, radiation-catalyses ortho-para transition 79−73832
TGS, ferroelectric phase transition, high resolution NMR study 80−97214
TGSe, deuterated, NMR investig. of ferroelec. and press. induced transition mechanisms 77−16189
Ta_2D, atomic displacements determ. by deuteron magnetic resonance *(Japanese)* 78−15035
Ta_2D_{1+x}, atomic displacement of Ta determined by deuteron magnetic resonance 79−37701
$Ta(OR)_2Cl_3.L$, halo-alkoxide complex, prep. and props. 78−18605
$TaS_2(ND_3)$, intercalation system, wideline NMR, temp. effects 77−16184
$TaS_2(NH_3)$, intercalation complex, wideline NMR obs., translational and reorientational effects 77−1602
Tb, ferromagnetic, mag. dipole and elec. quadrupole hyperfine fields, NMR obs. 80−34791
$TbAl_2$, conduction electron spin and orbital polarisation effects 78−80228
TbF_3, ^{19}F NMR, ligand hyperfine interaction, shift tensor determ. 78−48056
TbF_3, transferred hyperfine interaction, NMR study 78−68393
$Tb_{1-x}Gd_xAl_2$, effective mol. field at ^{159}Tb, NMR meas. 80−71197
Te compounds, NMR orbital shift of ^{125}Te, depend. on ionicity and local struct. 77−32273
Te, trigonal, tight-binding calc. of chem. shift 78−2759
Th complex, tetramethylethyl-cyclopentadienyl thorium trichloride, prep., NMR and IR spectra 79−76425
β-$TiFeH_{1.03}$, H diffusion, NMR meas. 80−10707
$TiH_{1.8}$, tritiated, NMR of ^3He formed by β-decay, radiation damage, ageing 77−24751

nuclear magnetic resonance continued
γ-TiH_x, interstitial H diffusion mechanism, NMR spin-lattice relax. study 80−103515
TiO_2, rutile, superficial constitutive water, NMR study 80−88881
$TiS_2(ND_3)$, intercalation system, wideline NMR, temp. effects 77−16184
$TiS_2(NH_3)$, intercalation complex, wideline NMR obs., translational and reorientational effects 77−1602
Tl complex of lasalocid (X-537A), ^{205}Tl NMR study 80−58288
Tl+Cs, Tl $6^2P_{3/2}$-state relax., NMR obs. 80−95653
$TlCoCl_3$, paramag., spin density, NMR study 78−88200
$TlCoF_3$ paramagnetic, nonmagnetic atomic nuclei spin density, NMR study 80−29633
TlF, P- and T-violating interactions in hyperfine struct., mol. beam reson. expt. 80−53019
$TlHF_2$ ^{19}F free induction decay 78−2753
$TlHF_2$, struct. and phase change 77−51996
$TlMnCl_3$, paramag., spin density, NMR study 78−88200
$TlNiCl_3$, paramag., spin density, NMR study 78−88200
Tl_2O-B_2O_3, glass, ^{205}Tl NMR 77−59470
Tl_2O-GeO_2, glass, ^{205}Tl NMR 77−59470
Tl_2O-SiO_2, glass, ^{205}Tl NMR 77−59470
$TlPO_3$, vitreous and polycrystalline, NMR and IR exam. of cation motion 77−66041
^{205}Tl, solvated and adsorbed, chem. shift and nuclear relaxation *(Rumanian)* 79−82888
$^{205}Tl^+$, NMR in aq. soln., dissolved O_2 on nuclear spin relax. rate 78−19356
$TmVO_4$, Jahn-Teller distortion, RF susceptibility and NMR meas. 80−44930
U complex, tetramethylethyl-cyclopentadienyl uranium trichloride, prep., NMR and IR spectra 79−76428
UF_6, isotope enrichment, ^{19}F NMR in gas, liq. and solid 78−23364
$UNi_{5-5x}Cu_{5x}$, NMR and press. effects 80−25230
$UO_2(DMSO)_5^{2+}$ in DMSO soln. kinetics of DMSO exchange by NMR method 79−81214
$UO_2(NO_3)_2$, aq. soln., pulsed NMR relax. time, ^{235}U enrichment depend. 80−2658
UO_2(acac)DMSO, in DMSO soln. kinetics of DMSO exchange by NMR method 79−81214
UT_3, ^3He distribution from triton decay, NMR meas. 78−19360
V-Ni sigma phase alloys, NMR and electric-field gradients 80−108109
$V_{1-x}Al_xO_{2\pm y}$, mag. and struct. props. meas. 78−2658
VH_x, NMR, phase transition obs., activation energy for H diffusion meas. *(Russian)* 78−27506
V_2(Hf,Zr), NMR and mag. susceptibility, density of states determ. *(Russian)* 80−66053
V_2Hf, NMR meas., mag. susceptibility, Knight shift and elec. field gradient determ. *(Russian)* 78−23359
$VO_{1.25}$, ^{51}V NMR studies, microscopic mag. props. 80−108086
V_2O_{3+x}, $0 \le x \le 0.08$, mag. and elec. props. 80−49833
V_2O_5-Fe_2O_3-LiO_2 system, physical properties 78−84503
V_2O_5-MoO_3 system, X-ray diffr., IR absorption spectra, NMR and thermal analysis 77−24379
V_3O_7, microscopic mag. props., NMR 80−7177
V_4O_7, sublattice magnetisation temp. depend., ^{51}V NMR 79−91301
$V_{1+x}S_2$, local moment formation, X-ray, mag. susceptibility and NMR meas. 77−69511
V_3Se_4, itinerant antiferromag., spin fluctuations, NMR study 80−75874
V_5Se_8, itinerant antiferromag., spin fluctuations, NMR study 80−75874
V_2Ta, NMR meas., mag. susceptibility, Knight shift and elec. field gradient determ. *(Russian)* 78−23359
V_2Zr, NMR meas. mag. susceptibility, Knight shift and elec. field gradient determ. *(Russian)* 78−23359
$WSeF_4$, cryst. struct., and preparation 78−63730
Xe, liq.-vap. crit. exponents, NMR 78−18759
Xe, polarisation via collision with Rb atom 78−33453
^{129}Xe, NMR/ON in Fe, implanted atom sites 77−20723
^{129}Xe, NMR/ON in Fe, implanted atom site population 77−20755
(Y,Ho)VO_4: ^{165}Ho, enhanced NMR meas. 77−66428
Y_xCo_y, NMR meas. of ^{59}Co 77−85585
$YCrO_3$, antiferromag., mag. domain walls, ^{53}Cr NMR study 79−11327
$YCrO_3$, magnetisation, NMR freq. temps. depend. weak ferromagnetic-antiferromagnetic spin reorientation transition 80−29631
$Y_{1-x}Dy_xCo_5$, NMR meas. of ^{59}Co 77−85585
$YFeO_3$, influence of photomagnetic effects on ^{57}Fe NMR 78−52365
$YFeO_3$, mag. domain walls, photomagnetic effects, ^{57}Fe NMR obs. 78−95464
$Y_{1-x}Gd_xCo_2$, NMR meas. of ^{59}Co 77−85585
$(Y_{1-x}Gd_x)_2Co_{17}$, ^{59}Co NMR, hyperfine fields and contrib. of 4f electrons 77−20727
$Y_{1-x}Ho_xCo_5$, NMR meas. of ^{59}Co 77−85585
YIG, domain boundary nuclear spin echo excitation, NMR domain freq. capture effect *(Russian)* 80−44955
YOF, trigonal, NMR of F^{19} to detect paired formations 79−14788
YRh_4B_4, supercond., anomalous cond.-electron polaris. 80−25047
YVO_4, ^{51}V NMR, nucl. quadrupole coupling const., chem. shift 77−90055
^{89}Y in $Y(NO_3)_3$, YCl_3 and $Y(ClO_4)_3$ aqueous solns., NMR study 77−24754
^{89}Y spin-spin relaxation times, pH depend. 80−66059
Yb complexes, lanthanide-induced NMR shifts, temp. depend. 77−68061
YbCuAl, intermediate-valent, nucl. reson. and relax. 79−78550
$YbVO_4$, ^{51}V NMR, nucl. quadrupole coupling const., chem. shift 77−90055
Yfe_3, NMR investig. of Y hyperfine field temp. depend. 77−4567
Zn-nucleotide, triphosphate complexes, ^{35}Cl NMR obs. 80−63661
ZnSe(Te), chemical shift and linewidth determ. 79−19792
$ZnTiF_6.6H_2O$ and $ZnTiF_6.6D_2O$, ^{19}F NMR, phase transition 79−19790
Zr and its alloys, H diffusion, NMR study 80−108088
ZrF_4-BaF_2-$ThF_4(LaF_3)(NdF_3)(PrF_3)$, F^- ion cond. glasses, cond. process 80−107477
$Zr_{1-x}Nb_xZn_2$, microscopic mag. props., NMR investigation 80−15807
$Zr(V_{1-x}Co_x)_2$, pseudobinary intermetallic compound, relation between electronic struct. and H_2 storing props. 80−76662
$ZrZn_2$, itinerant electron ferromag., NMR exam. of effect of spin fluctuations 77−16192
$^{90}Zr(^3He,t)^{90}Nb$, 80 MeV, Gamow-Teller M1 state excitation 78−50184

nuclear magnetic shielding *see nuclear screening*

nuclear mass
see also atomic mass
^{67}Ge, mass excess and low lying states, comparison with ^{63,65}Ni, ^{65,67}Zn and ^{69}Ge 78−66213
A=12-208, adiabatic TDHF approx. isoscalar quadrupole collective motion, cranking mass 80- 68507
A=60-260 nuclei, violated Wigner SU(4) symmetry reconstruction from mass data *(Russian)* 80−37336
adiabatic TDHF approx., mass parameters, single collective variable, theoretical aspects 80−73765
alpha Q values, first excited 2^+ states, even-even nuclei 79−6458
charge RMS radii mass number depend., fine struct. 78−501
collective mass parameter, super-normal phase transition effect 80−5046
compressible liquid drop model 77−74780
conference on nuclear spectroscopy of fission products, Grenoble, France (May 1979) 80−77546
deep inelastic heavy ion collisions, charge and mass distrib. variances, time depend. 79−97651
deep inelastic heavy ion collisions, mass and charge distribs., statistical model 80−18332
deformation energies for nuclei with different charge-to-mass ratio for fusion or binary fragmentation 79−80869
deformed nuclei energy density mass formula, approx. method, binding energy, quadrupole moments 79−13195
density isomers, schematic model of mass distrib. 77−6219
difference operator decomposition, regional mass tables 77−22864
dilute Fermi gas, self energy, momentum distrib., and effective mass, nuclear matter 80−63119
droplet model, mass formula, higher-order vol. symm. terms, Hartree-Fock effective interactions 78−89808
droplet model with shell correction for masses and radii 77−22863
droplet of nucl. matter under rapid rot., anal. using Thomas-Fermi method 79−36179
effective mass and exchange current effects in finite nuclei 80−78171
ensemble averaging of mass values 77−6217
even-odd mass difference ratio, mass and binding energy formula 80−47361
exact canonically conjugate momentum to the quadrupole tensor and a microscopic derivation of the nuclear collective hamiltonian 78−78251
exotic light nuclei , masses and energy levels 77−22866
exotic light nuclei mass meas. via nucleon transfer reactions 77−22867
exotic nuclei, supermultiplet mass predictions 79−85359
experimental values of nucl. masses 77−6218
family of mass relations based on residual n-p interactions 77−54141
fission, asymmetric, nuclear mass parameter 78−13053
fission, spontaneous, mass and charge division, asymmetry, order-disorder model 80−22866
fission process, dynamic aspects, nuclear mass parameter, action integral minimisation, ^{252}Fm appl. 78−62586
fissioning nucleus, deformation process mass parameter, liquid drop model 80−102221
formulae considering spin and compressibility effects 77−22865
Franzini-Radicati mass relationship in isobars, Wigner SU(4) supermultiplet 80−105958
fundamental constants, self-consistent values *(German)* 79−12758
Garvey-Kelson generalised mass relations, review *(Rumanian)* 79−75827
Garvey-Kelson mass relations 77−6216
generalised mass relationships, prior to Garvey-Kelson type relationships *(Rumanian)* 78−58232
hadron-nucleus inelastic interactions, high energy, mean normalised multiplicity target depend. 80−47454
heavy ion collisions, charge equilibrium and mass transfer, liquid drop model 79−97722
heavy ion collisions, statistical model for mass and charge distrib. 79−17929
HF calculations of masses and BE 77−22862
Inglis cranking formula, temp. dependent mass parameter behaviour 80−22714
Isolde experiments, prod. of extreme neutron/proton ratio nuclei, nuclear props. study *(Danish)* 78−4972
light nuclides, proton rich, mass excesses 78−37259
liquid drop model, mass predictions 77−6268
mass fitting and averaging, correction due to one particle Hamiltonian symmetry *(Russian)* 80−83032
measurements on nuclei far from stability 77−22861
meson presence in nuclei, nuclear g-factor exchange current controls., EM interaction role 80−22706
momentum and mass distribs., form factors, short range correlation effects 80−105959
nuclear isotopes far off stability line, production, props., review *(Hungarian)* 79−9927
nuclear matter, finite temperature props., variational theory, effective mass 80−5084
nuclear matter properties, velocity dependent effective potential of s-wave interaction 78−58247
nuclei far from stability, β-decay energies, γ-rays, Q_β values and masses 80−78225
nucleon fluid, constrained variational calc. of symmetry coeff. 78−46022
one body mass radius operator of closed shell nuclei, convergence studies 79−45146
optimum atomic mass formula from nuclear mass shell and parity corrections *(Russian)* 80−37902
pairing with a delta interaction in the energy density nuclear mass formula 79−36143
particle transfer during nuclear deformation, Hartree-Fock calcs. *(Russian)* 79−3079
particle-number-projected mass tensor 80−9220
relations and eqns. 78−66194
relativistic heavy ion reactions, target residue mass and charge distribs., calcs. 79−3172
semiempirical droplet model, mass excess values reported 77−6266
semiempirical liquid drop model, shell correction formula 77−6267
semiempirical mass formulae, shell corrections, α-decay period estimates for heavy nuclei *(Russian)* 79−22184
semiempirical shell correction to droplet model, magic number effects 77−10339
semiempirical shell model, mass excess calc. 77−6260
shell model, anal. of mass formula and mass relationships 78−25108
shell model calcs. A=24, mass, spectra and β decay 78−4903
shell model mass formula 77−6261
single particle states, systematics in a Woods-Saxon potential *(Rumanian)* 79−59003
small nuclear systems, deviation from saturation, mass formula correction 79−80891
spherical nuclei, masses determ. by energy-density method 77−6215
spherical nuclei, nuclear mass formula, energy density functional, self-consistent calc. 78−78244
spin unsaturated systems, finite range two- and three-body interactions 78−66220
spontaneous fission mass parameters, cranking and hydrodynamic models, deformation depend. *(Russian)* 80−13511
stability against nucleon emission in shell model 77−22969
statistical theory of fission, nucleon tunnelling, mass distrib. widths *(Russian)* 80−5121
SU(4) theory, role in nuclear struct. theory 79−3097
superheavy region, neutron drip line, energy density mass formula extrapolation 78−93932
unified nuclear pot. for heavy ion elastic scatt., fission, fusion, masses and deformations 80−5189
unified pot. from liquid drop model, description of nuclear props. 79−22213
Weizsacker formula based on consistency conditions, parameters calc. *(Russian)* 77−38220
Z=37-43, neutron rich fission products, mass energy surface, decay props. 80−78228
(π^+,π^-) A=9-32, 180 MeV 80−105960
A=Rb, A=74-79, 90-99, direct meas. of masses, deformation onset at N=60 79−54383
^{A}Ac, A=209-214, 216, deduced mass from Fr direct mass meas. 80−78130
^{108}Ag^{m} (127 yr.), K-electron capture probability, ^{108}Ag-^{108}Pd ground state mass difference 79−59038
Ag(p,f), 1 GeV, binary fission, possible mass instability of correlated fragments 80−83133
^{22}Al, Coulomb matrix elements and energy shifts 77−10308
^{27}Al(e,e'), internuclear nucleon effective mass in quasielastic scatt. *(Russian)* 79−3076
Ar isotopes, meas. of 280 MeV/nucleon particles with plastic detector 77−38561
As, β-decay energies and masses, A=80, 81, 83 77−74808
As, stable isotopes, masses meas. 78−12956
^{A}As, A=78,80,82, ground state mass meas. and excited state energies 79−63595
^{A}As, A=79,81, Q-values and mass excess from Se(d,^{3}He) 80−9222
^{A}At, A=200-206, 208, deduced mass from Fr direct mass meas. 80−78130
^{197}Au+^{40}Ar, 217 MeV, fusion and deep inelastic collision, charge and mass anal. 77−82959
^{197}Au(p,X), 0.2-6.0 GeV, product cross sections, mass yields, spallation products 80−83088
^{A}B, mass excess and excited states from ^{14}C(^{14}C,^{14}B) 80−42676
^{15}B, mass excess from ^{48}Ca(^{18}O,^{15}B)^{51}V 78−70433
^{15}B mass meas. in ^{11}B(^{18}O,^{14}O)^{15}B at 96, 103 MeV 77−38219
^{9}Be(e,e'), internuclear nucleon effective mass in quasielastic scatt. *(Russian)* 79−3076
^{12}Be mass excess and excited states from ^{10}Be(t,p) 79−22183
^{A}Bi, A=196-202, 204, deduced mass from Fr direct mass meas. 80−78130
^{206}Bi, mass excess calc. from Pd(α,d)Bi 77−10312
^{209}Bi(^{56}Fe,X), damped collisions, fast A/Z equilibration and correlated nucleon exchange 80−86798
^{A}Br, A=79,81, mass using spectroscopic doublet method *(Russian)* 78−86468
^{12}C, adiabatic mass parameters, isoscalar quadrupole modes 77−14049
^{12}C(e,e'), internuclear nucleon effective mass in quasielastic scatt. *(Russian)* 79−3076
^{13}C, mass spectromatic calibration of mass and neutron separation energy 78−70434
^{16}C mass excess and final states, DWBA anal. of ^{14}C(t,p) 23 MeV 78−78392
^{17}C populated in ^{48}Ca(^{18}O, ^{17}C), mass excess, low lying level struct. 78−8744
^{18}C mass excess and discrete nuclear states from ^{18}O(π^-,π^+) 79−13196
Ca, A=40, 48, mass and neutron distribs., HF calcs. *(Russian)* 77−82815
^{36}Ca mass via ^{40}Ca(^{4}He,^{8}He), isobaric multiplet mass eqn. deviations 77−74754
^{40}Ca, adiabatic mass parameters, isoscalar quadrupole modes 77−14049
^{40}Ca, finite nuclear props. in relativistic quantum field theory, mass and p densities 80−9219
^{A}Cd, A=104-116, low lying level scheme, mass excess from Cd(p,t) 80−73807
^{104}Cd, $\beta^+/(EC+\beta^+)$ probability ratio, EC decay energies, mass excesses 80−27543
^{31}Cl, mass excess in ^{36}Ar(^{3}He,^{8}Li) 77−57595
^{43}Cl, observation and mass excess in ^{48}Ca(^{3}He,^{8}B)^{43}Cl at 74 MeV 77−10310
^{65}Co, mass excess meas. from ^{70}Zn(^{3}He,^{8}B)^{65}Co 78−93931
^{57}Cr mass excess, half life, ground state spin and parity, from ^{48}Ca(^{11}B, pn) 78−70436
Cs isotope, neutron deficient, supermultiplet mass predictions 79−85359
Cs neutron deficient isotopes, beta-decay energies and masses 77−22946
Cs, neutron rich isotopes, $Q_\beta$and direct mass meas. 80−78132
^{A}Cs, A=117-124, 126, 138, 140-147, direct meas. of masses, deformation onset at N=60 79−54383
Cu, A=64, 66, 68, 70, level schemes, mass excesses via (t,^{3}He) reactions 77−46117
Cu, effective mass determ. from (n,γ) line shapes 77−57660
^{69}Cu mass excess and low lying states, DWBA anal. from ^{70}Zn(d,^{3}He) 79−6422
^{69}Cu Q-values and mass excess from ^{70}Zn(d,^{3}He) 80−9222
^{153}Dy→^{153}Tb mass difference from β^+ spectrum *(Russian)* 79−13257
^{A}ER, A=167,168, absolute atomic masses 79−89228
^{A}Eu, A=157, 159, single proton states, rot. bands, J^π assignments and mass from Gd(t,α) 79−45132
^{15}F mass excess and T=3/2 levels from ^{20}Ne(^{3}He,^{8}Li) 78−78264
^{15}F mass excess from ^{20}Ne(^{3}He,^{8}Li), 88 and 75 MeV 78−78245
Fe, effective mass determ. from (n,γ) line shapes 77−57660

nuclear mass continued
^{50}Fe proton rich nucleus populated in ^{54}Fe(α,^{8}He), Q values, mass excesses 77−88162
^{60}Fe, level struct., spin and parity assignments, mass excess from ^{58}Fe(t,p) 17 MeV 78−82288
^{62}Fe mass excess from ^{64}Ni(^{18}O,^{20}Ne) at 63 MeV 77−335
^{62}Fe mass excess from ^{64}Ni(^{18}O,^{20}Ne)^{62}Fe reaction 77−41878
^{61,62}Fe, mass excess via ^{64}Ni(α,^{7}Be) and ^{64}Ni(^{11}B,^{13}N)^{62}Fe resp respectively 77−74752
^{A}Fr, A=201-203, alpha decay, branching ratios, mass excess and half life 80−99154
^{A}Fr, A=204-210, 212, 224-228, direct mass meas. 80−78130
Ga, β-decay energies and masses, A=76-79 77−74808
Ga, stable isotopes, masses meas. 78−12956
^{A}Ga, A=73,75, Q-values and mass excess from Ge(d,^{3}He) 80−9222
^{A}Gd, A=146,147, mass and Z=64 shell closure from ^{144}Sm(^{12}C,^{9,10}Be) 80−57669
Ge, β-decay energies and masses, A=79, 80 77−74808
Ge, stable isotopes, masses meas. 78−12956
^{67}Ge, mass excess and excited states from ^{70}Ge(^{3}He,^{6}He) 79−6375
H^- ion bound state, extensions to finite nuclear mass 78−29743
^{2}H, mass spectrometric redeterm. 78−70434
^{3}He-^{3}H mass difference, ρ-ω mixing charge symmetry breaking force, nonlocal contribs. 78−70458
^{6}He, mass meas. from ^{7}Li(d,^{3}He)^{6}He and ^{19}F(d,^{3}He)^{18}O* reactions 78−41628
^{8}He, mass determ. from spectra of ^{64}Ni(^{4}He,^{8}He)^{60}Ni, and ^{64}Ni(^{4}He,^{6}He)^{62}Ni 78−25106
^{A}Hf, A=179,180, absolute atomic masses 79−89228
^{A}I, A=121, 123, 125, mass excesses, ^{121}I energy levels from Te(^{3}He,d) and Te(α,t) 78−78246
^{121}I mass excess, energy levels and single particle strength distrib. from ^{120}Te (^{3}He,d) 80−5053
^{123}I, mass. meas., ground state Q-value of ^{123}Te (^{3}He,d) 78−4896
^{A}In, A=120-129, total β-decay energies and masses of strongly neutron rich isotopes 78−86512
^{111}In-^{109}In mass difference from Q values of Cd(^{3}He,d) 80−63069
^{122}In, states and masses determ. from (t,^{3}He) 78−66290
^{124}In, states and masses determ. from (t,^{3}He) 78−66290
^{48}K mass excess and 0.58 MeV excited state from ^{48}Ca(^{7}Li,^{7}Be), 52 MeV 79−446
^{48}K mass excess and states from ^{48}Cu(^{7}Li,^{7}Be) 80−9221
^{A}Kr, A=78,80,82,83,84,86, mass using spectroscopic doublet method *(Russian)* 78−86468
Li, A=10, 11, ground-state config. anal. 77−22859
^{20}Mg, β-delayed proton obs., mass excess of T=2 state in ^{20}Na 79−22234
^{29}Mg mass excess from ^{26}Mg(^{18}O,^{15}O) 79−3075
^{30}Mg mass excess from ^{26}Mg(^{18}O,^{14}O) 79−3075
^{58}Mn energy levels populated in ^{58}Fe(t,^{3}He), mass excess, spin-parity assignments 77−54230
^{59}Mn, β-decay scheme, mass, branching ratios 77−82873
^{59}Mn, observation and mass excess in ^{68}Ni(^{3}He,^{8}B)^{59}Mn at 74 MeV 77−10310
^{60}Mn, mass and β-decay half life, ^{60}Fe struct. and mass excess 78−78317
Mo, effective mass determ. from (n,γ) line shapes 77−57660
^{89}Mo mass excess and excited states from ^{92}Mo(^{3}He,^{6}He) 80−42531
^{14}N(e,e'), internuclear nucleon effective mass in quasielastic scatt. *(Russian)* 79−3076
^{18}N, mass excess and excited states from ^{14}C(^{18}O,^{18}N) 80−42676
^{19}N, mass excess via ^{18}O(^{18}O,^{19}N)^{17}F 91 MeV reaction 77−74753
^{19}N, mass meas. via ^{18}O(^{18}O,^{19}N)^{17}F 91 MeV 77−22868
Na neutron rich isotopes, mass meas. 77−22861
^{27}Na excited states and mass excess from ^{26}Mg(^{18}O,^{17}F) 79−3075
^{100}Nb mass and excited states from ^{100}Mo(t,^{3}He) 79−63581
Ne isotopes, meas. of 280 MeV/nucleon particles with plastic detector 77−38561
^{16}Ne mass excess and diproton decay width from ^{20}Ne(^{4}He,^{8}He) 117 MeV 78−78245
^{16}Ne, mass excess from π double charge exchange reactions 78−70573
^{54}Ni proton rich nucleus populated in ^{58}Ni(α,^{8}He) Q values, mass excesses 77−88162
^{57}Ni, mass excess determ. from ^{59}Ni(p,t)^{57}Ni and ^{58}Ni(^{3}He,α)^{57}Ni 77−18376
^{67}Ni mass excess from ^{70}Zn(^{4}He,^{7}Be) pick-up reaction 79−9452
^{68}Ni mass excess from ^{70}Zn(^{18}O,^{20}Ne)^{68}Ni reaction 77−41878
^{252}No, high mass asymmetry distribs. in fissioning nuclei, shell effects 79−3186
^{12}O mass excess and diproton decay width from ^{16}O(^{4}He,^{8}He) 117 MeV 78−78245
^{16}O, adiabatic mass parameters, isoscalar quadrupole modes 77−14049
$^{16}O_{\Lambda}$, Λ-N residual interactions, Λ spin-orbit splitting and effective mass 80−57722
^{16}O(e,e'), internuclear nucleon effective mass in quasielastic scatt. *(Russian)* 79−3076
^{21}O, mass determ. from ^{18}O(^{18}O,^{15}O) ^{21}O reaction at 91 MeV 78−50078
^{22}O, measured in ^{18}O(^{18}O,^{14}O)^{22}O 100 MeV reaction 77−22869
^{A}Os, A=189,190, absolute atomic masses 79−89228
^{27}P, mass excess in ^{12}S(^{3}He,^{8}Li) 77−57595
^{32}P mass from ^{34}S(d,α) 79−6632
^{A}Pa, A=215-218, deduced mass from Fr direct mass meas. 80−78130
^{208}Pb, finite nuclear props. in relativistic quantum field theory, mass and p densities 80−9219
Pd isotope cumulative yields, cumulative yields of Ru and Pd isotopes 79−576
^{110}Pd(^{208}Pb, X), equilibrium process time evolution, mass and charge distribs., energy loss 79−97725
^{188}Pt side band, low lying and high spin states populated in ^{191}Ir(p,4nγ) 78−4936
^{246}Pu excited states, mass excess and shell gap, L=0 transition from ^{244}Pu(t,p) 80−9236
Rb isotope, neutron deficient, supermultiplet mass predictions 79−85359
Rb neutron deficient isotopes, mass meas. 77−22861
Rb neutron deficient isotopes, beta-decay energies and masses 77−22946
Rb, neutron rich isotopes, $Q_{\beta}$and direct mass meas. 80−78132
^{A}Rb, A=85,87, mass using spectroscopic doublet method *(Russian)* 78−86468
^{A}Rb, A=96,98, β-decay schemes and total energies, mass excess and separation energies 80−27601
Ru isotope cumulative yields, cumulative yields of Ru and Pd isotopes 79−576
S, A=32, 34, mass and neutron distribs., HF calcs. *(Russian)* 77−82815
(^{32}S,X), 153-184 MeV, fission like processes around A_{CN}=100, mass distrib. strong change 80−9318
(^{32}S,X), A=59-89, double differential cross section, mass asymmetry, transport model 80−102203
^{34}S mass excess meas., comparison with theory 77−54188
Sb, A=128,130,131,134, total β decay energies, mass excesses, β-γ coincidence study 77−82870
Sb, effective mass determ. from (n,γ) line shapes 77−57660
Se, stable isotopes, masses meas. 78−12956
^{24}Si, isobaric multiplet mass eqn., test from decay 79−40890
^{24}Si, Q value and mass excess from ^{28}Si(α,^{8}He) 80−86795
^{27}Si, mass excess in ^{29}Si(p,t) 77−57595
^{28}Si, mass and neutron distribs., HF calcs. *(Russian)* 77−82815
Sn, A=127 to 131, total β decay energies, mass excesses, β-γ coincidence study 77−82870
^{A}Sn, A=106,108, β^+/(EC+β^+) probability ratio, EC decay energies, mass excesses 80−27543
^{A}Sr, A=96,98, β-decay schemes and total energies, mass excess and separation energies 80−27601
^{80}Sr ground state mass from Kr(^{3}He,n) 80−18201
^{180}Ta mass, 10^{13} y naturally occurring isomer state 80−57670
^{181}Ta+^{20}Ne, 8.0 GeV, target residue mass, charge distrib. determ. 79−17930
Te, A=134,135, total β decay energies, mass excesses, β-γ coincidence study 77−82870
^{232}Th(n,f), 2-8 MeV, fission product yields and mass distribs. 80−86939
^{232}Th(p,f), 28 GeV, charge dispersion, mass yields 77−3062
^{197}Tl, deduced mass from Fr direct mass meas. 80−78130
^{238}U, high mass asymmetry distribs. in fissioning nuclei, shell effects 79−3186
^{238}U(n,f), 14.5 MeV, neutron emission, mass distrib. and energetics 80−47512
^{238}U(p,f), 9.5-17 MeV, symmetric to asymmetric mass ratios for fragments 80−5178
U(γ,f) A=235,238, 25 MeV bremsstrahlung, prod. yields, mass chains, charge distribs. 77−6470
^{54}V energy levels populated in ^{54}Cr(t,^{3}He), mass excess 77−54230
^{55}V mass excess determ. and β-decay scheme 78−21528
^{98}Y^{g}, β-decay schemes and total energies, mass excess and separation energies 80−27601
^{167}Yb→^{167}Tm mass difference, from positron spectrum, level transition branching ratio 79−6376
Zn, β-decay energies and masses, A=75-78 77−74808
Zn, stable isotopes, masses meas. 78−12956
^{61}Zn ground state mass determ. from ^{64}Zn(^{3}He,^{6}He) 70 MeV, mass excess calc. 79−26371
^{61}Zn, studied via ^{58}Ni(^{6}Li,t)^{61}Zn, mass, t-energy spectra and reaction mechanism 78−41756

nuclear matter
α-clustering in heavy nuclei, pre-equil. model, nuclear matter NN, Nα interactions 80−63111
Δ(1232) isobar propagation 77−10349
Δ(1236) inobar probability is nuclear many-body system ground state 79−75859
ν_6 semirealistic model, variational theory accuracy and convergence 80−57712
A=16-58, charge, proton and neutron density distribs. calc. 80−22680
A=18 shell model spectra and 3 nucleon force 78−25124
A=4-16, monopole giant resonances, state density radii and compressibility using hyperspherical functions *(Russian)* 80−27615
abnormal neutron stars *(Chinese)* 78−85967
abnormal nuclear matter, many body forces, σ-model Lagrangian field theory 77−6277
abnormal nuclear states 77−22921
abnormal occupation, two body correlations and plane wave HF energy 80−86844
abnormal states, pion condensation *(Russian)* 78−37302
abnormally large density and binding energy states, book contrib. 80−489
absorption of leading particles, hadron compoiste model 77−88067
alpha matter, abnormal boson occupation 79−26387
alpha particle-nucleus scatt., critical radii, correl. with nuclear matter distribs. 79−45148
alternating layer spin phase, partial wave contrib. anal. 79−85391
analytic hydrodynamic model for expanding fireballs 78−41745
antinuclei and new long-lived particles, 10^{-8} to 10^{-14} s lifetimes, review of Serpukhov expts. *(Russian)* 79−63615
antisymmetrisation effects in Jastrow cluster expansion for nucl. matter 77−10352
asymmetric, coupling of isospin oscills. to density oscills. 78−21508
asymmetric, lowest order Brueckner theory, k-matrix calc. 77−2928
asymmetric nucl. matter, rearrangement effects 77−14050
asymmetric nuclear matter, compression modulus, neutron excess effects, neutron stars 79−36182
asymmetric nuclear matter, isospin and density waves, Landau theory 78−66235
asymmetric nuclear matter, isospin waves, IAS and giant Gamow-Teller resonance 80−91142
asymmetric semi-infinite nuclear matter, HF calcs., surface symmetry props., finite range forces 80−57713
axial current and pionic props. 77−88068
baryon matter struct. and pion condensation *(Russian)* 79−22222
baryon system, strong interacting, finite temp. many body theory, phase transition 77−65210
baryonic inclusive spectra in hadron-, photon- and HI-nucleus collisions, fireball model 80−86892
baryonic matter, transition to quark matter, appl. to neutron stars 77−5424
BBG theory, auxiliary single particle field for binding energy 80−22723
BBG theory developments, hole and particle lines, dispersion effects and healings 80−22719
Bethe homework problem, variational calcs. for neutron and nuclear matter 78−37292
Bethe-Faddeev wave function generalisation to N-body clusters 77−57639

nuclear matter continued
Bethe-Goldstone eqn., nucl. matter, nucleon optical pot. anal. 78−12981
binding energy, corelated basis functions method appl. 78−45998
binding energy, hypernetted chain approx., impurity ground state energy 80−83055
binding energy, variational approach, hyper-netted-chain calcs. 77−2926
binding energy, variational approach with realistic potentials 77−18463
binding energy, variational calcs. with state depend. correls. 77−26603
binding energy and rest mass of constituents, total symmetry effects *(French)* 80−63068
binding energy expansion convergence in Brueckner-Bethe-Goldstone theory 80−488
binding energy from low density expansions, Brueckner-Hartree-Fock approx. 80−22720
binding energy in nuclear matter, Δ(1236) effect, lowest order reaction matrix calc. 77−6278
Born-Green-Yvon eqns. for strongly interacting Fermi systems 79−71363
Bose fluids, two-body density matrix 79−40875
boson condensation, solvable quantum field theoretic model 77−57447
boson matter, Euler-Lagrange equations and hypernetted chain calcs. 79−40871
boson resonant state S-matrix pole residue relationship with wave function asymptote 79−9499
bound multineutron system, 8 and 20 neutrons, existence probability 80−68570
bound neutral polyneutron systems, existence anal. HFC 78−70475
Brueckner's theory of nuclear matter, external field 78−33137
Brueckner and Green's function theories, model nuclear matter calcs., ground state props. 78−8750
Brueckner and Jastrow methods comparison, binding energy 77−290
Brueckner Bethe and variational calcs. review, nuclear saturation problem 80−22745
Brueckner expansion, embedding in Green's function theory for nuclear matter binding energy 79−22220
Brueckner-Bethe calculations of nuclear matter 80−22718
cascade generation, 100-10000 GeV, anomalous effects *(Russian)* 78−70366
cell model, generalised, incorporating strong spatial correls. 77−55403
cell model, generalised for strong spatial correls. 77−57276
central spin- and isospin-dependent potentials 78−46023
Chakravarty-Woo eqn., extension and appl. to liq. ^{4}He, liq. ^{3}He, and nucl. matter 80−68124
charge constrained coherent pion states from transversing fast nucleon 80−27585
charge dependent N-N potential, nuclear matter props., HF calcs. 78−50115
charge symmetry breaking nuclear forces 77−26589
charged Bose condensates in supercritical external fields, relativistic field theory 78−8766
classical Yang-Mills solns., W meson condensation, superdense matter composition symmetry 79−93292
cluster variational calcs. for extended nuclear systems 77−6279
cohesion of nuclear matter in heavy ion collisions 78−66314
cold, stationary finite amplitude motions, quantum shock waves and solitons 80−42573
cold matter at super-nuclear densities including pion condensates 78−17128
cold matter in Einstein-Cartan gravitation theory, static spherical configurations 78−49308
cold nuclear matter, hydrodynamical approximations 79−22219
collapson concentration limit, neutron annihilation reaction *(Russian)* 77−38235
collective excitation stability with Skyrme interaction *(Russian)* 79−13239
collective excitations in nuclear matter with Skirm type effective interaction *(Russian)* 78−54716
collective mode of nucleon system with π^0 condensate 78−41660
collective modes in nuclear matter, propag., damping 78−25132
colliding ion system, projectile nucleon mean free path, nuclear matter approach, Pauli blocking 80−86920
collision integral in nuclear matter at zero temperature 79−17928
compressed nuclear matter, blast wave production in fireball explosions 79−49592
compressibility, asymmetric matter, one boson exchange model approach *(Russian)* 79−3112
compressibility effect on optical-pot. real part, n+^{40}Ca calc. 77−74823
compressibility of nuclear matter, density depend. of binding energy, hyperspherical functions method *(Russian)* 78−17093
compressible nuclei, surface energy 80−83031
compression and speed of sound, heavy-ion collisions 80−27584
compression wave front, width in nuclear matter *(Russian)* 77−34242
compression wave propagation direction in nuclear matter 79−75882
condensates and Bose-Einstein correlations, quantum optics formalism 79−59028
conference, 11th Masurian school in nuclear physics, Mikolajki, Poland (Aug.-Sept. 1978) 79−63605
conference, Les Houches, France (July-August 1977) 79−71864
conference on few body systems and nuclear forces, Graz, Austria (Aug. 1978) 79−67567
conference on many-body theories, Trieste, Italy (Oct. 1978) 80−22135
conference on nuclear spectroscopy and structure, Alma Ata, USSR, (Mar. 78) 79−75809
constrained variational calcs., three body and N* (1234) contribs., cluster energy 80−22743
correlated basis functions approach, comparison with Brueckner-HF approx. 79−40869
correlated nuclear matter, electric dipole sum rule 80−83056
correlated-basis-functions approach to realistic nuclear matter 79−40872
correlation function Euler eqn. when closed-form energy is used 77−49674
coupled channels method, applicability to nuclear physics with Ns and Δ's, book contrib. 79−97667
cranking model anal. of nuclear inertia in fission and heavy ion reacts. 78−41656
critical opalescence, a precursor to nuclear π condensation, local spin ordering 78−82303
critical opalescence, percursor to pion condensation 78−62498
deep inelastic processes, large scale collective motion in nuclear matter 80−5087
deep inelastic scatt. off nucl. matter, quark exclusion principle 77−38236
nuclear matter continued
deep reconstruction of Coulomb field, shake-up of vacuum *(Russian)* 78−4910
deformed nuclei, surface thickness effects and multipole excitation splitting, sum rule approach 79−453
degenerate electron-neutron plasma, energy release mechanism 77−74790
degenerate many fermion system in exp. S form, linked valence expansions 78−41654
dense Fermi systems, energy expectation values, numerical study of Fermi hypernetted chain method 79−40874
dense Fermi systems, generalised perturbation theory, ground and low excited states 80−22741
dense matter, transport props., neutron stars appl. 79−67236
dense matter, U(1) symm. gauge model, eqn. of state 78−62500
dense matter phase transitions, cusp catastrophe theory 77−22920
dense matter physics, conference, Paris, France (1979 September 17 to 21) 80−73094
dense neutron and nucl. matter, spin and isospin instability 78−86474
dense neutron and nuclear matter, spin and isospin stability 80−22737
dense neutron matter, ferromag. transition, pure hard core gas model 78−70478
dense neutron matter, zero sound propag., Landau theory 78−53977
dense neutron matter physics, implications for neutron star props. 80−77277
dense neutron star matter eqn. of state, QCD instanton effects 79−92796
dense nuclear matter, construction in lab., book contrib. 80−490
dense nucleon matter, density and isospin waves 79−93540
dense plasmas and nuclear reactions, astrophysical appls. 80−77281
dense stellar matter, diffusion approx. to neutrino transport 78−93096
dense stellar matter, nuclear reaction rate enhancement 79−21168
density calc. from ^{40}Ca(p,p)^{40}Ca at 1.04 GeV 77−34303
density compression in colliding nuclear slabs 78−642
density determ., HF versus droplet model 80−68574
density fluctuation in nuclear matter 80−86838
density isomer formation in high energy heavy ion collisions, 3-dimens. fluid dynamical calcs. 79−49578
density isomers, schematic model of mass distrib. 77−6219
density isomers in high energy heavy ion collisions, hydrodynamical model anal. 79−36138
density matrix, one-body, and momentum distrib. calc., Jastrow wave functions 77−85008
density oscillations, from semi-infinite nuclear matter calc., Regge type oscillation comparison 80−57671
density oscillations due to pion condensation, infinite nuclear matter and pionic atoms calcs. 78−70476
dilute Fermi gas, self energy, momentum distrib., and effective mass, nuclear matter 80−63119
dispersion energies and excitation parameters 77−74319
dispersion relations, HF method for hard core interactions *(German)* 78−54713
distribution of matter in nuclei far from β stability valley, charact. features 77−64635
droplet of nucl. matter under rapid rot., anal. using Thomas-Fermi method 79−36179
droplet-model theory of the neutron skin 80−47416
effective interaction calcs., symmetry coeff., isospin-spin depend. of single particle pot. compressibility, rearrangement energy 77−46126
effective interaction with three-body effects 80−27562
effective NN interaction and exchange current vel. depend., dipole sum rule enhancement 80−63100
effective nuclear matter interactions applied to finite nuclei 79−93546
elementarity of baryon resonances in nuclear matter, book contrib. 79−97666
ellipsoidal, liquid-drop model, irrotational incompressible hydrodynamic flow 80−83050
elongated soliton-type wave solutions, finite amplitude wave propagation *(Russian)* 80−13397
energy calc. with state depend. correls. and semirealistic N-N pot. 77−88066
energy calculations, comparison of Baker, Brueckner, and Jastrow methods 78−25143
equation of state, relativistic quantum field theory of neutron stars 80−5088
equation of state at subnuclear densities, theory 80−77278
equation of state at ultrahigh densities and the speed of sound 80−57716
equation of state for hot nuclear matter 79−93538
equilibrium process, hadronic momentum distribs. and relaxation process 79−40866
exp(S) formalism, n-body Schrodinger eqn. 77−22918
explosive quark matter, hypothesis for Centauro event 80−22648
extended Fermi system, optimum Jastrow function 78−8761
extended Fermi-hypernetted chain scheme, Landau parameters calc., transport coeffs., Jastrow theory 77−41529
extended Thomas-Fermi approx. to kinetic energy density 77−2919
Fermi hypernetted chain calcs. for model nuclear matter 78−8759
Fermi hypernetted chain equations, optimal correl. function 79−40870
Fermi liquid theory, one pion exchange processes, condensate effects 77−6276
Fermi liquid theory, tensor forces role 79−63616
Fermi liquid theory and giant resonances in nuclei 79−3095
Fermi model fluid eqn. of state via lowest order constrained method 77−18443
Fermi quantum crystals, melting curves low temp. anomalies rel. to neutron stars 78−24757
Fermi superfluid hydrodynamics, time-depend. BCS formalism, compared with He II, finite nuclear systems 78−22920
Fermi system particle distrib., nuclear matter, heavy ion collisions and fission 79−36183
Fermi systems, semi-infinite, surface props., thickness and energy 80−52600
Fermi-Bose similarity, parafermi and parabose algebras 77−30091
Fermi-hypernetted-chain method, upper bound on variational energy 77−291
Fermidynamics and time dependent Schrodinger-Hartree Fock theory 79−3105
fermion charge accumulation, rel. to superheavy nuclei *(Russian)* 77−57597
fermion hypernetted chain variational calc. 80−22725

nuclear matter continued
fermion matter with spin depend. correlations, variational theory 79−63614
fermion system, two-body propagations with dynamic effective interactions 77−41896
fermions, constrained variation in Jastrow method at high density, neutron system, liquid ^{3}He appls. 77−5753
finite Fermi system correlation energy, fast configuration interaction approach 80−22739
finite nuclei, low energy optical pot. from Reid hard core interaction 80−52640
finite nuclei and inhomogeneous infinite systems, ground states, FHNC method extension 80−22736
finite quark mass effects on superdense quarkion configurations 80−105852
finite temperature, neutron gas eqn. of state 77−67715
finite temperature props., variational theory, effective mass 80−5084
flow, Fermidynamics and commensurability; TDHF restructured into TD-$\mathcal{S}$-HF 79−93539
fluid dynamics of small finite systems, nuclear matter flow, time depend. Hartree Fock 78−46018
fluid theory, universality in short range struct. in simple classical fluids 80−75141
fractional electric charges and mag. monopoles, existence in matter, model 79−13238
free quark existence, theoretical possibilities 79−17744
Gamow-Teller β transition quenching in mirror nuclei A=3, 15, 17, 39, 41 79−17860
Gamow-Teller matrix element, axial currents in nuclei, quenching mechanism 79−17859
gasdynamic mechanisms of heavy nuclei inelastic collisions *(Russian)* 77−61452
gauge theory for superdense matter, symm. breaking 77−45955
generalised Fermi sea for plane wave HF theory, 3-dimens. semi-realistic interactions 80−105999
generalized Fermi sea for plane-wave Hartree-Fock theory: one dimensional model calculation 79−45196
Green's function method for many-body problem for relativistic meson field theory, book contrib. 80−357
ground state properties of Lipkin Meshkov Glick model using atomic coherent states, nuclear phase transitions 78−62489
ground-state energy, numerical calcs. 77−61367
hadron chemistry, heavy ion collisions 78−82389
hadron gas, non-ideal, eqn. of state appl. to universe Friedmann model *(Russian)* 79−44649
hadron matter, thermodynamic description, evolution, coupling const. depend., hot nucleon matter appl. *(Russian)* 79−3006
hadron matter phase transformation at high temps., cosmological consequences *(Russian)* 77−91674
hadron matter physics, determ. from pulsars and compact X-ray sources 80−77442
hadronic interiors, meas. and charge distrib., hadronic diffraction scatt. 80−73817
hadronic matter, phase transitions, eqn. of state 79−75889
hadronic matter, thermodynamic props. of class of solvable statistical models 79−63452
hadronic matter chemical equilibrium, statistical model for heavy ion collisions, nuclear fireball 79−40948
hadronic matter of finite no. of fireballs, phase transition struct. 79−36180
Hagedorn's bootstrap model of early Universe, dense matter eqn. of state, external mag. field 78−86044
Hamiltonian field theory for systems of nucleons and mesons 79−75860
hard core pots., crystalline struct. binding energy, HF calcs. 79−93543
hard sphere Fermi gas Jastrow correlations 79−40451
Hartree-Fock anal. of nucl. many-body problem 77−18457
Hartree-Fock calcs. of semi-infinite nuclear matter with complete forces (finite range and spin-orbit term) 78−86499
head on heavy ion collisions, compression and temp. extremes, nuclear matter phase changes *(Russian)* 80−83121
heavy ion collisions, critical scatt. and pionic instabilities 78−21586
heavy ion collisions, energy loss and ang. distribs., dissipation mechanism, hydrodynamic model 79−3175
heavy ion collisions, fluid dynamical and TDHF models, abnormal nuclear matter, density isomers 80−47502
heavy ion collisions, high energy, depend. of total pion prod. cross sections on eqn. of state 78−41772
heavy ion collisions, rarefaction of oblate shaped nuclear matter, hydrodynamics calcs. 78−89894
heavy ion collisions, relativistic hydrodynamical approach, shock compression effects *(Russian)* 79−30851
heavy ion deep inelastic collisions, kinetic energy dissipation, nuclear matter density oscillations *(Russian)* 80−37397
heavy ion deep inelastic reactions, as probes of nuclear matter, review 78−46083
heavy ion fusion cross section, energy depend., nuclear matter density distrib., depend. 80−47519
heavy ion relativistic collisions, pion bremsstrahlung and critical phenomena, nuclear matter phases 80−86919
heavy nuclei, charge asymmetry of nuclear forces and binding energies 79−75866
heavy nuclei, presence of π^- from binding energy calcs. 78−82275
heavy spherical nuclei, choice of density depend. interaction and α-decay *(Russian)* 78−46010
heavy-ion collisions, compressed nuclear matter classical microscopic calc. 77−10432
heavy-ion collisions, form. and disintegration of high-density nucl. matter 77−10423
heavy-ion collisions, prod. in tidal bore effect, 40-200 MeV/N 77−34331
heavy-ion interactions, magic nuclei, real part of nucl.-nucl. interaction anal. 77−6426
high densities, shock waves, pion condensation *(German)* 77−38237
high density and temp. effects from relativistic heavy ion collisions 77−26781
high density isomeric state in nucleon matter relativistic heavy-ion collisions 79−85390
high density matter, relativisitc quantum many-body problem 78−4909
high density nuclear Mach shock waves, central heavy ion collisions, compressed nuclear matter, meson condensation 78−46089
high excited nuclear matter, p-wave π absorption, high energy heavy ion appls. 79−93542
nuclear matter continued
high order partial wave contrib. to nuclear matter binding energy for model interactions 79−45144
high temperature thermally dissociated matter, comp. and adiabatic index 79−44354
high-temperature nuclear matter, neutral currents and neutrino Comptonisation 80−21905
highly dense nuclear matter, formation by relativistic nucleus-nucleus collisions 79−97675
hole states in nuclear matter, single-particle potential 80−32150
hole-line expansion convergence 78−8762
hot, equation of state 79−63619
hot hadronic matter in early universe, relativistic eqn. of state 78−45438
hot neutron star matter, neutrino transport, opacity 79−75238
Hugenholtz Van Hove theorem and density depend. effective interactions 80−32219
hydrodynamic and time-depend. HF calcs. comparison for nuclear matter slab collisions 77−18598
hydrodynamic model, nonlinear pion+pion chiral Lagrangian, $e^+ + e^-$ and p+p collisions 78−32966
hydrodynamic model predictions for arbitrary vel. of sound in nuclear matter 77−50070
hydrodynamical model of nuclear fluid, spin and isospin props. 78−70479
hypernetted chain integral eqns. 79−490
hyperspherical-expansion approach to bound state 77−79317
impure nuclear matter with Λ, binding energy, functional variational approach 80−22744
infinite, correlated basis functions method 80−22721
infinite finite temperature baryon matter, Green's function formalism, quantum correction 78−13000
infinite nuclear matter, PCAC relations, πN vertices, π condensate instability *(Russian)* 80−13398
infinite nuclear matter, response function, quantum field theory of fermion systems 78−70480
infinite nuclear matter, saturation props. using HF calcs. on finite nuclei 79−45198
infinite nuclear matter ambiguities, harmonic oscillator and infinite well solns. 80−22742
infinite system of nucleons and Δ resonances, pot. energy, neutron stars 80−86836
inhomogeneous many-body system integral equations 80−22732
intensification of pion beams by highly excited nuclear matter with inverse population *(Russian)* 79−49595
interacting neutron matter model at postsupernova temps. 77−45399
intranuclear cascade calcs., influence of mean free path parameter 78−93958
intranuclear cascade calcs. for $(\pi,\alpha X)$ reaction 79−575
ion beams, heavy, uses in nuclear physics *(French)* 80−78182
ion-ion pot., energy depend. from simplified energy density method, folding model combination 79−6429
isobar components of nuclei, experimental tests, review, book contrib. 79−97668
isobar degrees of freedom, binding energy from BHF approx. 80−22734
isobar degrees of freedom in nuclear matter, binding, NN interactions and 2π exchange 80−22735
isospin symmetric, pion condensation 79−80894
isospin symmetric nuclear matter, pion condensation, heavy ion collision appl. 80−9252
iterative isobar process role, effective NN interaction 80−99143
Jastrow trial wavefunction test 77−18465
Jastrow type calculation, normalisation condition, energy per particle, density 78−70474
Jastrow type calculations for nuclear matter with normalisation condition 78−66236
kinetic theory of nucl. fluids 78−8763
Landau parameters sum rules, tensor force effects 79−80892
large baryon densities, prod. by high energy nuclear collisions 78−86540
lattice density waves in nuclear matter 79−71815
leptoproduced high energy particles, nuclear attenuation, hadronisation time 80−102182
light nuclei, hyperspherical functions for size, excited states, compressibility, binding energy 80−22679
liquid neutron matter, pion condensation and the linear σ-model 79−59027
low density, α cluster model 79−6451
low density α clustering effects of Skyrme N+N interactions in nuclear matter 78−29398
low density expansion of nuclear matter optical pot., self consistency requirement 78−8760
many body problem in Lee model, NN scatt. and matter binding energy 80−63116
many body theory, appls. review of development 80−46968
many fermion energy calculations 78−66238
many-body correl. simulation by pair excit. amplitudes 77−2923
many-body theory, comparison of Brueckner and λ_{00} approx. 77−2929
massive neutron star, fermionic matter, coupled Dirac-Einstein eqns., self consistent soln. 78−73731
massive star core collapse, core processes 80−82335
mean field near Fermi surface, energy dependence, single-particle quantities, Brueckner-Hartree-Fock calcs. 80−68572
mean field theory, correlation corrections 79−6467
meson condensation, quasiclassical model *(Russian)* 80−5086
meson condensation and two photon emission in hadron capture by nuclei and heavy-ion collisions 79−3109
meson-meson interactions, nuclear saturation, nuclear matter compressibility 79−22221
mesonic wakes, appl. to meson prod. in nuclear collisions 77−6280
mesons in nuclei, field theoretical aspects, book 80−481
mesons in nuclei, nuclear forces, baryon reson. effects, book 79−97661
Migdal and surface δ interactions, strength consts. 78−8749
model calculation with fermion lowest order constrained variational method 77−14053
model energy calcs. in Jastrow variational approach 78−74322
model energy including δ-function contribs. Jastrow correlation factor 80−13396
momentum distrib., Fermi-hypernetted-chain theory 80−82716
momentum distribs., single particle orbitals, Fermi hypernetted chain theory 80−86841
monopole vibrations and effective interactions, hyperspherical model 78−58223

nuclear matter continued
Monte Carlo methods in quantum many-body problems 80−22727
Monte Carlo simulation of many-fermion system 78−12644
multihadron production in matter connection with hadron quark-glue model 79−356
multihadron production in nuclear matter and hadron struct., space-time description, review *(Russian)* 80−68571
multiparticle cores in nuclei, matter fluctuations, binding energy, repulsion correlations 79−75864
neutral meson condensation, one boson exchange model 79−13235
neutral pion condensation and ALS model including isobar Δ(1236) 79−71814
neutron, alpha and nuclear matter, ground vacuum states 80−22738
neutron $^3P_2$ superfluidity under π^0 condensation in neutron star matter 80−47417
neutron and nuclear matter, non-plane wave HF states, nuclear homework pot. 80−32224
neutron and nuclear matter, variational calc. models 80−22724
neutron and nuclear matter with isobars, transition pot. model, neutron stars 80−68573
neutron crystals, review rel. to pulsars *(Polish)* 77−61369
neutron distribution in nuclei, elastic and inelastic proton scattering, review 80−22649
neutron excess, thermal props. and level density parameter 80−91141
neutron gas: temperature dependence of the effective interaction 79−36172
neutron gas, crystallisation, zero-order, Bethe-Fermi homework potential 80−63117
neutron gas ground state energy in theory with soft-core pot. 77−82843
neutron gas interactions at high density and temp., supernova models appl. 77−33330
neutron matter, energy density in relativistic harmonic approx. 80−18217
neutron matter, energy expectation value, test of Wu-Feenberg and F_2 approximations 79−40873
neutron matter, energy per particle, effective mass and mag. susceptibility relations 79−75885
neutron matter, energy per particle and effective mass 77−30499
neutron matter, equilib. config. allowing for nuclear and gravit. interactions *(Russian)* 77−18462
neutron matter, hypernetted chain calcs. with the Paris pot. 80−57714
neutron matter, long range order, extended boson matter density matrices 80−22731
neutron matter, pair condensation, variational theory using correlated basis functions 80−32220
neutron matter, sigma model, pion condensation 77−88069
neutron matter, spin and tensor correlations, cluster expansion hypernetted chain eqns. 80−22728
neutron matter, spin zero sound and spin diffusion coeff. 77−57278
neutron matter, viscous, differential rot. 77−60788
neutron matter calcs. using Jastrow theory 77−34241
neutron matter densities in even Ni isotopes via (p,p) 1.047 GeV reactions 77−54171
neutron matter mag. susceptibility, lowest-order constrained variationsl calc. 79−75884
neutron matter props. 78−58242
neutron matter-quark matter phase transition, QCD and extended Higgs model, instantons 80−91062
neutron or nuclear matter, spin depend. correlations, variational method 80−22726
neutron skin, compared with droplet model theory 80−52599
neutron star, relativistic quantum mechanical model for solid core 77−33546
neutron star core, phase transition between nucl. and quark matter 80−67771
neutron star cores, AC Josephson effect rel. to pulsars emission 80−82404
neutron star crusts and white dwarf interiors, nuclear crystals form. *(Polish)* 77−17355
neutron star matter, $^3P_2$ pairing near transition temp. 78−57571
neutron star matter, π^- condensation 77−53420
neutron star matter, abnormal phase 78−20849
neutron star matter, decompression 77−33544
neutron star matter, eqn. of state rel. to max. mass 77−33545
neutron star matter, neutrino scatt. by phonons 79−12488
neutron star matter, physics rel. to mass constraints 77−5543
neutron star matter, superfluid phase transition 79−59025
neutron star matter at high temp. and density, bulk props. 78−89812
neutron star matter at ultrahigh densities, props. 77−91560
neutron star state equation and two nucleon nuclear interaction for nuclear matter *(Russian)* 79−40879
neutron stars, β-decay of π condensates as cooling mechanism 78−4271
neutron stars, eqn. of state for dense hadronic matter, asymptotic freedom 78−36627
neutron stars, hadronic matter components, leptons and baryons *(Polish)* 79−88587
neutron stars, inner crust nuclear compositions 80−31322
neutron stars, mass-radius relation, obs. constraints, dense matter eqn. of state 80−46597
neutron stars, maximum mass, Brans-Dicke theory 77−33543
neutron stars, microscopic interpretation of struct. 77−64790
neutron stars, neutrino cooling in pion-condensed phase 78−45351
neutron stars, neutrino-pair bremsstrahlung in collisions between neutrons and nuclei 77−74789
neutron stars, neutron-rich nuclei, energy density mass formula appl. 79−35290
neutron stars, Ni's theory of gravity 78−4273
neutron stars, review of nuclear physics 79−92797
neutron stars, structure and physics 79−67046
neutron stars, superdense quark core, spontaneous magnetisation possibilities 80−8646
neutron stars, superfluidity 80−77441
neutron stars, surface temp., density and mag. field determ. from thermal radiation 80−56869
neutron stars ν transport in π condensed matter 78−4270
neutron stars and physics of matter at high density 79−84815
neutron stars structure and evolution, relativistic eqns. 77−33471
neutron stars thermal properties and detectability, cooling and heating processes 80−31323
neutron stars with equation of state given by nuclear Thomas-Fermi model 79−48840

nuclear matter continued
neutron system, localised, tensor force effects, alternating layer spin config. 77−2925
neutron-proton electron mixture with zero charge density, eqn. of state, rel. to supernova explosions 77−53416
neutronization kinetics in superdense matter with frozen-in mag. field *(Russian)* 78−46019
neutrons, relativistic, ultra-degenerate, non-interacting gas, Fermi energy and eqn. of state in intense mag. field 78−89401
non-Abelian Cherenkov radiation of pions from a fast nucleon 79−40865
nonlocal $^1S_0$ p-p pot., nuclear matter calcs. 77−38227
nonlocal separable interactions in the study of nucl. props. *(French)* 78−33115
nonstrange baryonic matter, thermodynamic behaviour for rel. mean-field theory 79−75887
nonsymmetric, incompressibility anal. *(Russian)* 79−59030
nuclear currents, microscopic anal. of elementary particle description 78−82304
nuclear dynamics and renormalisation group relations, bulk props. 79−6469
nuclear free energy, variational description 79−45199
nuclear interaction investigation, use of theoretical techniques in nuclear matter theory 78−62497
nuclear radii from total neutron cross sections, optical model calcs. 79−9455
nuclear scatt. from nuclei with nuclear matter t-matrices 79−93577
nuclei excitation energies in hot matter, limits 80−56703
nucleon fluid, constrained variational calc. of symmetry coeff. 78−46022
nucleon fluid, excitation to N*(1234) state, lowest order constrained variational calcs. 79−40864
nucleon mean free path 77−10351
nucleon mean free path anal. exciton model 77−46127
nucleon resonances in nuclei, review 77−26563
nucleon-nucleon potential, tensor contrib. for total ang. momentum depend. pots. 77−2915
nucleon-nucleus optical model, nucl. matter approach 79−93574
nucleon-nucleus optical pot. from nuclear matter t-matrix, effective force. 80−22783
OBEP, nonstatic with retardation, vel. depend. tensor pot. 77−88065
one body dissipation and super viscidity of nuclei, nuclear fission, collisions and deformation 78−86501
one body nuclear dynamics, classical theory for collective motion 78−8755
one-body dissipation, linear response approach 77−57681
one-body dissipation of nuclear deformation collective energy, semiclassical approx. *(Russian)* 78−86502
one-boson-exchange model including N-Δ interaction 77−18422
optical medium, nonlinear phenomena, possible investigation methods 77−2924
optical model complex pots. determ. from Reid's hard core interaction 77−88092
optical model potential in Λ_{10} approx., complex mass operator 78−33138
correl. with optical nucleon-nucleus potential *(Russian)* 78−37321
optical potential, Coulomb components and symmetry, microscopic calc. 77−30529
optical potential of slow pions, P-wave screening, Lorentz-Lorenz factor *(Russian)* 77−6335
optimal plane-wave Hartree-Fock states for many-fermion systems 80−27587
optimised Jastrow correlations for Fermi liquids 80−32223
Overhauser's model, Skyrme force, Hartree-Fock test 78−12997
overlap integral calcs. in diffuse surface model 79−17821
Paris NN pot. parametrisation, phase shifts, nuclear matter binding energy 80−47405
Paris NN potential, superposition of Yukawa terms, G-matrix, nuclear matter 78−70455
partially conserved axial-vector current and model chiral field theories in nuclear physics 79−67698
particle-particle collision probability, vol. integral using preequilibrium exciton model 78−70477
partition functions, astrophysical implications 79−21167
partition functions at high temp. rel. to pre-supernova stellar collapse 79−101059
Pauli blocking effects in low-energy πN scatt. 77−6441
Pauli principle effect in nuclear matter, exchange of interacting two pions 78−12983
Pauli suppression of Born amplitude, effect on (3,3) resonance 77−6323
phase transition to abnormal nuclear matter at finite temperature and finite baryon density 80−86840
phase transitions and shock waves in nuclear matter 79−49594
phase transitions at finite temperatures 79−6468
phase transitions in nuclear matter described by pseudospin Hamiltonians 78−66237
photoneutrino reactions in superstrong magnetoactive plasma, neutron stars appl. 79−35105
pion condensate, structures for symmetric nuclear matter 80−86839
pion condensate existence determ. from π-nucleus total cross sections at ≈1.2 GeV 78−17249
pion condensates, supercond. props., σ model anal. with nucleons 79−59029
pion condensates existence in neutron stars, implications of cooling calcs. 79−101170
pion condensation, one nucleon absorption of slow pions *(Russian)* 78−8765
pion condensation and density isomerism 80−5085
pion condensation and dynamics of neutron stars 79−67047
pion condensation in dense nuclear and neutron matter 80−37333
pion condensation in neutron matter: effects of pion-nucleon scattering 79−26388
pion condensation in nucl. matter, role of effective nucleon mass 78−74323
pion condensation in nuclear matter, book contrib. 80−484
pion condensation precursor, quasi-elastic peak softening 80−78170
pion condensation threshold in finite nuclei 80−18218
pion condensation thresholds for nuclei with A=16 to 298 77−26606
pion condensed matter, solid-like struct. 79−71813
pion dispersion relation in nuclear matter 80−42572
pion excitations and phase transitions in nuclear matter, review, book contrib. 80−483
pion field and weak interactions in nuclei 79−26376
pion propagation and production 79−80893

nuclear matter continued
pion propagator in nuclear matter, optical pot. Pauli blocking corrections 77−22919
pion spectrum and polariz. operator in nuclear medium in heavy nuclei collisions *(Russian)* 80−68558
pion-condensate instability of nuclear medium, temp. depend. *(Russian)* 79−80879
pionic condensation, superdense nuclei *(Russian)* 77−46129
pionic degrees of freedom in nuclei 77−10326
pionic field, isobaric excitation effects as weak axial coupling consts. 77−10328
pionisation of degenerate matter *(Russian)* 77−91558
pionization in superdense degenerate matter *(Russian)* 78−46020
polarised, deform. of Fermi surface 78−12998
polarised, thermal props., temp., spin isospin and spin-isospin pressure 80−102135
polarised nuclear matter, binding energy, spin energies, relativistic calc. 80−102134
pomeron and critical temperature 79−3003
pre-equilibrium decay into complex particle channels−analysis of double differential cross sections 79−93599
preequilibrium phenomena and heat diffusion 77−79318
properties, and N=Z closed-shell nuclei 78−58242
pseudovector πN coupling and the relativistic model of pion condensation *(Russian)* 79−49596
pulsars outer crust, influence of mag. field on comp. 80−101610
QCD of quark matrer to nuclear matter transition at neutron star density 78−54608
QCD scale parameter from quark matter phase transition 79−89112
quark attenuation and recombination in nuclear matter, hadron-nucleus reactions 80−52601
quark confinement, phase transitions from nucleon to quark matter 79−63617
quark-nucleon phase diagram and quantum chromodynamics 80−105855
rapidly rotating nuclei, density distrib. 78−8734
Rayleigh and whispering gallery waves excited by heavy ion elastic and inelastic scatt. 80−91164
reaction matrices comparison for free scatt. and nucl. matter 79−59026
realistic NN pot. construction for three body systems and nuclear matter 80−22699
relativistic central heavy ion collisions, spherical and linear fluid dynamical models 80−86926
relativistic composite system, light-front wave functions 80−73592
relativistic condition of pion condensation 80−86837
relativistic dense matter, statistical mechanics using phenomenological quantum field model 78−89814
relativistic effects on the two-nucleon and nuclear matter systems 79−89261
relativistic heavy ion collisions, charged particle emission multiplicities and ang. correlations, firestreak models 80−18328
relativistic heavy-ion collisions, nuclear matter to hot quark matter phase transition 79−3170
relativistic non-ideal hadron gas universe, gravit. collapse *(Russian)* 79−44650
relativistic nuclear field theory with π and ρ, cold nuclear matter calcs. 79−93527
relativistic nuclear matter, shock waves, heavy ion collision hydrodynamics 80−52602
relativistic nucleus-nucleus collisions, high density nuclear Mach shock waves 78−633
relativistic quantum field theory of finite nuclei 79−6466
relativistic superdense matter 78−12091
relativistic Thomas-Fermi model, nuclear size correction, eqns. of state and mass of superdense matter 78−29413
review, comparison of perturbative to variational techniques 78−33136
ring diagrams, Landau parameters, pion condensation, binding energy, of nuclear matter 78−74321
ring diagrams in nuclear matter, many-body forces contrib., ρ and π exchange 80−22740
S-wave πN interaction role in combined pion condensation 80−105998
S-wave πN interactions and PCAC 80−78185
saturated nuclei, quantum chromodynamics of nucl. forces 79−13211
saturation in finite nuclei, nuclear matter density and binding energy 80−83029
Schrodinger fluid velocity field, fermion system moments of inertia 78−65868
self consistent long range order in nuclear matter Hartree Fock Overhauser orbitals 78−17127
self consistent periodic quartet formation in nuclear surface 77−14052
self-consistent pseudopots. in thermodynamic limit, correlation field, nuclear matter single particle orbitals 80−9253
semi-infinite nuclear matter calc., nuclear density oscillations 80−22681
semi-infinite nuclear medium, kinetic energy density, simple approx., giant monopole resonance 80−32222
semi-infinite nuclear slab dynamics of TDHF 79−75888
semiinfinite and infinite symmetric matter, relativistic Hartree and Thomas-Fermi calcs. 78−25142
sequential decay model for hadron-hadron multiparticle prod., appl. to nuclear matter 78−46021
shock wave dynamics, phase transition effects 78−21509
shock wave model for heavy ion high energy collisions 79−54402
shock waves in a hydrodynamic model of central heavy ion collisions 79−40946
shock waves in heavy ion-nucleus reactions 77−61447
shock waves in heavy-ion collisions, expt. search *(Russian)* 77−338
simple quantum liquids, Jastrow variational wave functions, for nuclear matter, liquid ^{3}He and ^{4}He 80−22729
single particle width in nuclei, deviations of mass operator from HF values 78−62477
single-particle response and ground-state properties, Hartree-Fock theories 80−105997
single-particle Schrodinger fluid dynamical eqns. 77−54165
single-particle states in nuclear matter and in finite nuclei 80−78117
small nuclear systems, deviation from saturation, mass formula correction 79−80891
soft nuclear matter eqn. of state, from heavy nuclei central collision fireballs 80−13395
soft pion theorem, appl. to currents in nuclear forces and matter. 79−26377
solid like aspect with alternating layer spin and π condensation 80−22733
nuclear matter continued
solidification of π^0 condensation in nucl. matter 78−89813
solidification of nucleon system, π^0 condensation, πN P-wave interaction 78−54715
spatial correlations and elementary excitations in many-body systems 80−22730
spherical nuclei, Hartree-Fock-Bogolyubov calcs., D1 effective interaction, nuclear matter, binding energies 80−63105
spin and isospin stability of dense neutron and nuclear matter with hard core interaction 79−26386
spin density wave and π^0 condensation 77−61368
spin stability and Skyrme interaction 77−54146
spin-dependent parameters in Landau-Migdal theory 77−82844
spin-isospin and pion condensation phase transistions, eqn. of state 80−86843
spin-isospin density phase in finite nuclei, strongly oblate shape 80−22746
spin-isospin polarizability of nuclear matter and renormalization of weak currents 79−67697
spin-orbit correlations in nuclear matter from correlated basis functions 80−37343
spin-polarised hard-core neutron matter, ground state energy calc. 78−12999
stable state of cold matter with super-strong magnetic field *(Russian)* 78−25140
static density waves, cluster-variational investigation 79−40868
stellar collapsing core, Thomas-Fermi model of warm nuclei 80−51648
stellar dense matter, nuclear size effect rel. to neutron stars limiting mass 80−101611
stellar hot dense matter, beta transition rates 78−73699
strong compression effects in high energy heavy ion reactions, nuclear fluid dynamics anal. 80−18341
structure, shell model, clustering concepts, role of mesons 77−22827
super-dense nuclei, stability and pion condensation 77−18375
superconducting props. of π condensates 78−32993
superconducting quark matter, asymptotically high density 78−12863
superdense celestial bodies, theory 80−67773
superdense magnetised astrophysical objects, interiors physical conditions 80−17603
superdense matter eqn. of state and relativistic nucleon-nucleus collisions *(Russian)* 78−606
superdense neutron matter, relativistic theory and eqn. of state 78−45349
superdense nonequilibrium cosmic objects, coherent boson graviton avalanche catastrophes 78−85844
superdense nuclei, possible existence *(Russian)* 79−13198
superdense nuclei, search for and synthesis, review of expts. and π-condensation theory 79−6463
superdense nuclei stability region, pion condensation *(Russian)* 77−46128
superdense radioactive nuclei, search in p-nucleus collisions, cross-section limit 77−26638
superdense stars, internal struct., effect of nucl. interactions *(Russian)* 77−13324
superdense stars, quantum theory of magnetism 79−92753
superdense stars, state of matter *(Japanese)* 77−29643
superdense stars in quantum limit of ultrastrong frozen-in mag. fields 77−53620
superdense states, parameter restrictions *(Russian)* 77−61370
superfluid model, quasiparticle number conservation 77−6269
superfluid neutron matter, $^3P_2$ pairing, mag. field effects, vortices 80−62174
superfluid quark matter 79−93340
superfluidity and field theory of elementary excitations 79−17837
supernovae, thermodynamic of nucleon, lepton, photon mixture, quantum mechanical calcs. 80−77273
supernuclear matter as quark bags or interacting neutrons, neutron star test 77−78812
surface δ interaction for nuclear matter, effective interactions 79−67672
surface properties from Thomas-Fermi calc. 80−13394
symmetric and asymmetric, simple effective interaction for props. 78−25141
temperature dependence of threshold for pion condensation in neutron matter 79−45197
tensor contrib. to nuclear matter in first order perturbation theory, binding energy 77−18410
tensor quasiparticle interaction and spin-isospin sound in nuclear matter 79−63618
thermal conductivity, volume and shift viscosities for neutron and nuclear matter *(Russian)* 79−93544
thermal conductivity calc. based on relativistic quantum field theory 79−75886
thermodynamic equilibrium for highly excited state *(Russian)* 78−21510
thermodynamic functions of nuclei *(Russian)* 78−539
thermodynamic model, shear viscosity temp. dependence 78−62499
thermonuclear explosions in stars 80−72766
third-order perturbation calcs. for realistic potentials 77−6281
Thomas-Fermi model of finite nuclei 78−8747
three nucleon clusters in nuclear matter, intermediate Δ-states, exchange diagrams calc. 78−17112
three-body cluster energy, lowest order constrained variational calc. 79−13233
three-body force from 2π, $\pi\rho$, and 2ρ exchanges 80−78169
three-body forces 77−22900
three-body forces from triple Boson couplings 77−18409
three-body problem, variational and Bethe-Faddeev methods 80−27586
three-nucleon forces, nuclear matter and BE 77−74773
three-nucleon potentials due to π, S and ω, binding energy in nuclear matter 78−62486
three-nucleon two-pion exchange potl. for matter calcs. 77−26592
threshold pion absorption in nuclei 78−82390
time dependent coupled cluster approx. to nuclear dynamics, solvable model appl. 79−9496
transparency to fast particles, rel. to range of high-energy strong interactions *(Russian)* 78−4901
transport coefficient temperature dependence 80−78184
two pion exchange three nucleon pot. and nuclear matter, appl. of πN scatt. amplitude 79−40877
two pion exchange three-nucleon potential and nuclear matter 79−75865

nuclear matter continued
two-nucleon interaction isobar contributions from noncovariant perturbation theory 79−478
UCN, quasibound states in matter, reson. positions and widths 80−73833
ultrarelativistic nuclear collisions, asymptotic hadron spectrum, hot hadronic matter 80−63118
uniform extended Fermi medium, correlated basis functions, graphical anal., integral eqn. methods 80−22722
Universe, high density matter, many body treatment, pulsars 80−26738
V^8 models, variational calcs. for binding energy and density 80−42571
vacuum ground state, nuclear matter theory calc. 79−40876
vacuum polarisation in strong fields, π condensation 79−314
valence nucleons, radial wave functions 80−73788
variational and Brueckner-Bethe calcs., review 78−93959
variational calculation for model nuclear matter using a new integral equation method 78−82301
variational techniques, wave functions correlation operators, review 80−22748
variational theory of nuclear matter, noncommuting pair correl. functions 78−58244
variational theory of nuclear matter, review 79−89262
variational theory of nuclear matter 79−40867
velocity dependent effective potential of s-wave interaction, props. calcs. 78−58247
warm neutron degenerate matter, eqn. of state 79−84810
Weizsacker mass formula based on consistency conditions, parameters calc. *(Russian)* 77−38220
(α,α) scatt. near Coulomb barrier and matter distribs. of medium and heavy nuclei 78−66291
β-stable nuclear matter, electrically neutral, constrained variational calc. 78−58243
d propagation in nuclear matter, spin depend. of d optical pot. and binding energy 78−70545
$\Delta(1226)$ resonance effects, one-boson exchange potentials 77−14051
$\Delta(1236)$ resonance, effect on NN scatt., nuclear and neutron matter 77−41909
$\Delta(1236)$-resonance effects 78−82302
Δ-Δ system, deeply bound, one boson exchange potl. model 77−30501
Δ-isobar, exclusion principle effects, Chew Low theory 77−6275
Δ-propagation in nuclear matter, Pauli principle effects 80−32221
(e,e) determination of valence nucleon radial distrib., exchange current role 79−40878
$(\bar{K},\bar{K})$, isobar doorway model, optical pot., Λ-nuclear matter binding energy 80−106079
K^1-nucleus optical pot. for kaonic atoms 79−98255
Λ, binding energy in nuclear matter, reaction-matrix calculation 79−36185
$\Lambda(1405)$ resonance behavior in nucl. matter 77−18466
Λ binding energy in nuclear matter with Nijmegen baryon-baryon interaction 80−13400
Λ binding to nuclear matter in Fermi hypernetted chain approx. 79−85396
Λ s-shell hypernuclei, general props. and developments in experimental methods, review 79−22224
Λ well depth with class of equiv. pots., nuclear matter appl. 77−26605
Λ^0 binding energy, many-body cluster contribs., Jastrow calc. 79−93545
ΛNN correlations and Λ binding in nuclear matter 80−106000
N and Δ resonances in nuclei, coupled channel eqns. soln. for nuclear matter 79−17845
n distribution from 1 GeV p scattering *(French)* 80−78183
n excess, spin-up n and p, effective NN pot., optical pot., binding energy 79−13232
N-N interaction information from perturbative and variational nuclear matter calcs. 79−71796
N-N separable non-local interaction, single particle potential 78−58245
^{3}n binding energy, calc. from ^{3}H, ^{3}He, ^{4}H, ^{4}He and ^{4}Li ground-state properties 80−83044
^{4}n binding energy, calc. from ^{3}H, ^{3}He, ^{4}H, ^{4}He and ^{4}Li ground-state properties 80−83044
NΔ conversion, two-channel formalism and three-body forces approaches 78−8733
NN effective 2-body pot. in nuclear matter 78−54714
NN interaction, isospin nonconservation using relativistic formalism 79−9500
NN interaction in pion exchange, nuclear matter and pion condensation, review 80−42557
NN potentials, based on meson exchange, discussion and appl. to nuclear matter 79−80815
NN scattering, role of noniterative π exchange in nuclear matter 79−40857
(p, p), 1 GeV, polarisation data, Glauber anal. spin-orbit parameters, matter distribs. 80−52655
(p,p), polarised p, 0.8 GeV, neutron isotopic density differences and RMS radii 79−67643
(p,p) 800 MeV, polarised p, n density uncertainties from optical model anal. 79−22185
(p,p) elastic and inelastic on s-d shell nuclei, polarised p, nuclear matter distrib. 78−78297
(p,p′), deformed nuclei, ground state rot. band, shape meas. and exchange contrib. 79−451
(p,p′), deformed nuclei, local approx. results for exchange effects 79−452
(p,X), total reaction cross sections and the matter density of finite nuclei 79−45150
$(\bar{p},X)$, $\bar{p}$ annihilation on heavy nuclei, nuclear matter props. 80−63185
p-nucleus interactions, 20 to 200 GeV/c, nuclear matter interaction model *(Russian)* 78−46065
(π,π) P-wave absorptive and dispersive effects, nuclear matter considerations 79−85558
(π,X), effective S-wave πNN interaction, effects in nuclear matter 80−105985
π condensate effect on one nucleon absorption of slow pions *(Russian)* 77−30639
π condensate instability and shell effects in nuclei from ^{16}O to ^{298}114 *(Russian)* 77−50074
π condensation, effect on π+nucleus scatt. total cross-section 77−61456
π condensation, effects of short range nucleon repulsion 77−88064
π condensation, finite two-level system *(Russian)* 77−6282
π condensation, relativistic Klein-Gordon-Fock treatment 77−65208
π condensation, statistical concepts in hadron physics 79−58945
nuclear matter continued
π condensation, vacuum instability in external fields 78−50114
π condensation and tensor binding, parity and isospin 78−33139
π condensation effects in degenerate matter, appl. to theory of superdense celestial bodies *(Russian)* 79−96907
π condensation in finite nuclei 78−78299
π condensation in isospin symm. nuclear matter, phenomenological approach 78−29414
π condensation in neutron matter, N-N interaction, critical density 80−57711
π condensation in nuclear matter, Hartree-Fock and generator coord. methods 78−17129
π condensation instability and inelastic nucleon scatt. *(Russian)* 77−61426
π condensed, eqn. of state of finite temp. 79−3110
π condensed phase, σ-model, alternating-layer-spin struct. 80−83057
π dispersion relation in nuclear matter using ν+nucleus reactions 79−488
π dispersion relns., $\gamma\rightarrow\pi^+\pi^-$ and $\bar{\nu}\rightarrow e^+\pi^-$ decays 77−65209
π double charge exchange in heavy nuclei, pion condensation 77−79402
Π field in nuclei, μ absorpt. and doubly radiative Π absorpt. as probes 77−88063
π field relaxation in nuclear materials *(Russian)* 78−8764
π fields in nucl. matter 78−58246
π propagator in nucl. matter, NN correls. 78−515
π-condensate phase transition at finite temp. *(Russian)* 79−3111
π-condensate structure *(Russian)* 78−58236
π-condensation in practical nuclei, effect of quasiparticle interaction amplitude 79−6464
π-nucleus scattering, binding effects in optical pot. of pion in nucleus 78−41685
π^- condensation, nonrelativisitc treatment, mean field method 77−30500
π^- condensation in electric field of supercharged nucleus *(Russian)* 78−54717
π^- in heavy atomic nuclei *(Russian)* 78−25139
$\pi^0\rightarrow 2\gamma$, decay width as signal for nuclear matter phase transition, Primakoff effect 80−86842
π^0 condensation in dense neutron matter resulting from alternate-layer-spin structure 77−18464
π^0 condensation in finite system, extended Thomas-Fermi model 78−41645
π^0 condensation in symmetric nuclear matter and pure neutron matter 79−3108
π^0 condensation in σ-model, chiral symmetry 79−80895
π^0-meson condensation, alternating layer-spin struct. of nucleon system 79−13236
$\pi^{\pm}(\pi^0)$ condensation in nuclear medium, possible coexistence 79−36181
π+nucleus scatt., hole-line expansion and Pauli principle 77−18627
πN coupling in $\Delta(1231)$ isobar region, pion index of refraction, self-energy in low density limit 80−42554
πN effective interaction in nuclear matter, pion propagator modification 77−2927
πN interaction, resonance damping, (3,3) resonance width 77−10350
πN interaction in nuclear matter 77−23115
πN P-wave interaction, effect of non-condensed pions in nuclear medium 79−13237
πN scattering amplitude in nuclear medium at nuclear matter density 78−29500
πN scattering amplitude in nuclear matter, quantum field theory approach 80−42570
$\pi\pi\pi$ absorpt. in nucl. matter 78−50049
σ model, pion condensation, use of chiral symmetries 79−296
Ag (α,x), 0.2-4.2 GeV/N, compression phenomena and Mach shock waves 80−22851
Ag+C(O), 0.2-4.2 GeV/N, compression phenomena and Mach shock waves 80−22851
(Ar,X), in emulsion, nuclear shock wave search 80−22747
Ar(HI,X) 0.2-4.2 GeV/N, nonperipheral collisions, forward-backward asymmetry, compression phenomena 80−18329
^{40}Ar+Au$\rightarrow{}^A$Z+X, 500 MeV/nucleon excited nuclear matter prod. 77−50154
Br+C(O), 0.2-4.2 GeV/N, compression phenomena and Mach shock waves 80−22851
Br(HI,X), 0.2-4.2 GeV/N, nonperipheral collisions, forward-backward asymmetry, compression phenomena 80−18329
Br(α,X) 80−22851
(^{12}C, X), in emulsion, 3.6 GeV/N, high energy multiply charged particle emission, nuclear shock waves *(Russian)* 80−86923
^{12}C+^{6}Li(^{16}O) scatt., anomalous backscatt. from nonlinear Schrodinger eqn. for nuclear matter 79−6465
^{12}C(^{12}C,X), optical potential, nuclear matter approach 80−57801
^{12}C(p,p′), 122 MeV, precritical phenomena 80−83089
^{12}C(p,p′), 800 MeV, 15.11 MeV state diff. cross section, nuclear critical opalescence search 80−105984
^{12}C(p,p), 0.8 GeV, polarised p, differential cross section, anal. power, nuclear matter densities 79−13299
Ca (p,p), 1 GeV, neutron and proton RMS radii differences in matter 79−54403
Ca, extended Skyrme force calculation, spin instability 79−63601
^{A}Ca, A=40, 48, nuclear matter density distrib., saturation effect, optical potential from (α,α) 80−63115
^{A}Ca(p,p), 0.6, 1 GeV, A=40,42,44,48, matter density, Glauber model anal. 79−93500
^{A}Ca(p,p), 800 MeV, polarised p, A=40, 42, 44, 48, differential cross sections and anal. powers 79−36244
^{40}Ca(^{16}O,^{16}O), optical pot., nuclear matter approach, energy density matter [-] 80−83112
^{40}Ca(^{40}Ca,^{40}Ca), optical pot., nuclear matter approach, energy density matter [-] 80−83112
^{40}Ca(^{40}Ca,x), relativistic, compression and pion distrib., Monte Carlo calc. 80−73853
^{40}Ca(p,p′), realistic complex nuclear matter t-matrix anal. Hamada-Johnston pot. 79−9564
^{40}Ca(π,π), nuclear matter distribs., density depend. HF anal. 79−487
^{48}Ca(π,π), nuclear matter distribs., density depend. HF anal. 79−487
^{48}Ca$(\pi^{\pm},\pi^{\pm})$, optical pot. ambiguities, neutron radius determ. 79−17872
(Fe,X), in emulsion, nuclear shock wave search 80−22747
^{2}H propagation in nucl. matter, spin depend. of optical pot. 79−93635
^{2}H, superdense, cold, nuclear reaction energy output in mag. field *(Russian)* 77−29801

nuclear matter continued
$^{3}He(\gamma,\pi^{+})^{3}H$, Fermi motion and off-shell effects, impulse approx. 80−27626
^{4}He elementary diagram calcs. with truncated sums 79−85382
^{4}He truncation influence, using recurrence relations for reaction matrices 79−489
^{A}He, A=3, 4, charge structure, effect of neutron charge 80−105963
$^{39}K(^{39}K,X)$, π^{0} condensation, spin-isospin instabilities, TDHF calcs. 80−83042
^{6}Li bound states, six body hyperspherical soln. to N-body Schrodinger eqn. 79−9490
$^{15}N(^{15}N,X)$, π^{0} condensation, spin-isospin instabilities, TDHF calcs. 80−83042
$^{20}Ne+U\rightarrow{}^{A}Z+X$, 400 MeV/nucleon, excited nuclear matter prod. 77−50154
$^{A}Ni(p,p)$, 1 GeV, A=58,60,62,64, elastic and inelastic, Glauber anal., matter distribs. 79−75883
$^{58}Ni(^{58}Ni,X)$, optical potential, nuclear matter approach 80−57801
$^{58}Ni(p,p)$, 0.8 GeV, polarised p, differential cross section, anal. power, nuclear matter densities 79−13299
$^{A}O(\pi^{\pm},\pi^{\pm})$, A=16, 18, resonance region, proton and neutron distribs. 80−91195
^{16}O and infinite nuclear matter, mesonic and isobar degrees of freedom 79−9491
^{16}O, pion condensation and short range correlation 77−6245
$^{16}O(^{16}O,^{16}O)$, optical pot., nuclear matter approach, energy density matter [-] 80−83112
$^{16}O(p,p)$, nucleon distrib. in nuclei, self-consistent anal. 79−9556
^{208}Pb, isoscalar electric giant dipole resonance, from RPA calc., nuclear compressibility 78−86520
$^{208}Pb(\alpha,\alpha')$, levels, B(E3), transition density and nuclear pot., folding model anal. 80−86812
$^{208}Pb(p,p')$, precritical behaviour in pionlike excited states in nuclear matter 79−49593
$^{208}Pb(p,p)$, 0.8 GeV, polarised p, differential cross section, anal. power, nuclear matter densities 79−13299
$^{110}Pd(^{208}Pb,X)$, 1.2 GeV, central collisions, neutron rich nucleon flow, mass, charge and energy 80−18337
Sn, extended Skyrme force calculation, spin instability 79−63601
^{A}Sn, A=116 and 124, neutron matter densities and RMS radii 78−70526
^{116}Sn, π content of ground and low-lying states 77−38225
Sn(p,n) (A=112,116,124), 22.8 MeV, ang. distribs. to isobaric analogue states, nuclear matter distrib. 77−10405
$^{49}Ti(e,e)$, cross section, $1f_{1/2}$ neutron orbit radial distrib. 79−93541
U(Ne,X), 250, 400, 800 MeV/N, nuclear matter collective sideward flow, nuclear fluid dynamics 80−57715
^{236}U, nuclear matter density distrib., in asymmetric two centre shell model 80−32209
$^{238}U+^{20}Ne$, expt. and relativistic two fluid model energy spectra 78−78298
$^{238}U+^{4}He$, expt. and relativistic two fluid model energy spectra 78−78298
$^{90}Zr(p,p)$, 0.8 GeV, polarised p, differential cross section, anal. power, nuclear matter densities 79−13299

nuclear models
see also nuclear cluster model; nuclear collective model; nuclear reaction and scattering models; nuclear shell model
asymmetric rotor model, bunching of spin states in γ-band of even-even transitional nuclei 78−62485
backbending even-even nuclei, particle-rotor model with VMI core *(German)* 77−6258
binding energy, relativistic sum rule 77−14023
boson approximation for deformed nuclei *(Russian)* 77−74778
boson model, two-dimens., spatially symmetric configurations for 4 particles 79−67691
boson sd model of nuclei, group O(6) 78−33132
bound states, systematics, simple physically realistic pot. 79−13181
classification of states, unitary scheme 80−42550
coherent state model, for negative parity bands 78−89782
collective spectra, two dimens. interacting boson and variable moment-of-inertia models 79−67633
core-particle coupling models, deform., ^{185}Re, $^{75,77}Se$ appls. 79−450
Coriolis mixing of odd nuclei states, phonon admixture and non-adiabatic effects in even-even core 78−74310
Coulomb form factors, effects of core polarisation 77−30474
coupled channels method, applicability to nuclear physics with Ns and Δ's, book contrib. 79−97667
elementary particle method for nuclei in weak and EM processes, book contrib. 79−97663
even-even deformed nuclei, aligned rot. of octupole vibrational states 78−12955
excited core model of giant multipole resonances 77−30539
exciton model, nucleon mean free path anal. 77−46127
fermion interaction theory of nuclear and atomic struct. models, singlet paired fermions 79−9180
form factors of 0^{+}-0^{-} transition in A=16 system, nuclear struct. effects 80−18246
hypernetted chain integral eqns. 79−490
hyperspherical harmonic expansion method, first order L_{m}-approx. 80−18212
interacting boson approx. model, Pt-Os transition region 79−6435
interacting boson model, band struct. of heavy even/even nuclei *(Dutch)* 79−17841
interacting boson model of nucleus in terms of Casimir operators of I(6) chains 79−45191
interaction Boson model, O(6) limit, reln. to triaxial nucl. models 79−71811
isobar components of nuclei, experimental tests, review, book contrib. 79−97668
K-harmonics in one dimension 79−2584
Lipkin model, quasi-spin pairing and struct. 79−485
low energy positive parity spectra, $2\hbar\omega$ excitations, ang. momentum projected deformed particle-hole model calcs. 78−25119
microscopic model with antisymmetrisation effects, target nucleon+α, target nucleon+^{6}Li, pots. calcs. 78−62516
microscopic models, core polarisation, transitions, cross sections, form factors 78−604
mode coupling method, a reformulation 80−37335
model density matrix, $U_{3(n-1)}$-irreducible decomposition 79−67692

nuclear models continued
modified Lipkin model, orthogonal polynomial expansion for effective interactions 79−26373
Mossbauer isomer shifts and nuclear models, book contrib. 79−85385
N-centre model, hole theory in nonorthogonal basis 77−57606
natural boundary condition methods for calc. of scatt. cross section 77−6327
neutron distribution in nuclei, elastic and inelastic proton scattering, review 80−22649
nuclear bag states containing quarks, detection 78−70465
nuclear currents, elementary particle description, microscopic anal., book contrib. 79−97664
nuclear field theory perturbation expansion for strongly anharmonic systems, convergence, phonons 78−62490
nuclear fission, excitation lifetimes model 79−521
nuclear matter, thermodynamic model, shear viscosity temp. dependence 78−62499
nucleon potl. models from pp scatt. 77−6246
odd-A deformed nuclei, mag. dipole moment model, Coriolis coupling 77−30488
order-disorder model of balance neutron distrib. in fission 79−13279
orthogonal schema model, ^{16}O binding energy, wave function of ground state 79−63582
pairing force model, perturbation theory for projected states 78−33126
pairing residual interaction in simple dynamical models 77−14040
proton-neutron model, translationally invariant wave function, U(3(n-1)) scheme appls. 77−41906
quadrupole surface vibr. model in body-fixed coords. 77−18450
quasiclassical model, meson condensation in nuclear matter *(Russian)* 80−5086
quasiparticle-phonon nuclear model, few quasiparticle components of nuclear states 79−13216
rare earths, yrast band energy calcs., exponential model with pairing attenuation, backbending 79−9446
schematic model for isospin mixing in light nuclei 78−66198
semidecoupled model of Pt and Hg even isotopes, nonaxial deforms., odd parity states 77−34220
semiphenomenological model, effective deformation and elasticity parameters 79−9454
semiphenomenological model, unified description of reactions, states and transitions 79−75844
single particle states, systematics in a Woods-Saxon potential *(Rumanian)* 79−59003
single particle width in nuclei, as resulting from two body collision 78−62477
single-particle models, relation between average kinetic energy and mean-square radius 80−52567
Sp(2,R) model, connection with α-particle model for ^{8}Be 77−65207
spherical nuclei, total binding energy, many body field theory, ^{16}O, ^{40}Ca, ^{58}Ni appls. 77−30482
static model of complete fission 78−86543
SU(5) interacting d-boson model, log. energy decreases 78−93955
superfluid model, isotopic invariance and pairing energies 80−22687
supermultiplet model, transformation matrices rel. to canonical basis of group SU_{4} 79−67693
Thomas-Fermi model calc. of surface energy of very neutron rich nuclei 77−22870
Thomas-Fermi model of warm nuclei 80−51648
unified model, semimicroscopic model, odd-mass nuclei with 51 neutrons or 51 protons *(French)* 77−293
unified model description of odd mass In nuclei 78−66251
α-clustering and spectroscopic factors, shell effects and deformation correlations, model comparisons 79−6436
^{209}Bi, particle-vibr. model 78−519
^{140}Ce, M1 transition enhancement from neutron resonances quasiparticle-phonon model 79−9506
$^{140}Ce(e,e')$, giant dipole resonance, E1 form factor and breathing mode existence 79−3125
$^{63}Cu(p,p')$ negative parity level excitation, gamma ray obs., test for core excitation model 80−68534
$^{A}Dy(\alpha,\alpha)$, A=161,163, 9.0-13.5 MeV, B(E2) values, rigid rotor model validity 79−494
$^{167}Er(\alpha,\alpha)$, 9.0-13.5 MeV, B(E2) values, rigid rotor model validity 79−494
^{19}F low lying positive parity states from rot. model, moments and deformation 79−6410
^{54}Fe, self consistent models, collective and single particle struct., test by inelastic p scatt. 78−82300
^{56}Fe, equilib. compound model invalidity for $E_{x}>13$ MeV *(Russian)* 78−605
$^{155}Gd(\alpha,\alpha)$, 9.0-13.5 MeV, B(E2) values, rigid rotor model validity 79−494
$^{2}H(d,n)^{3}He$, struct. and form factor models in mass-3 system 79−45274
$^{2}H(d,p)^{3}H$, struct. and form factor models in mass-3 system 79−45274
^{3}H binding energy, energy depend. boundary condition model 79−13194
^{3}H model, appl. of three particle bound state eqns., binding energy 78−78276
He, A=157, 159, 161, 163, single proton states, $Dy(^{3}He,d)$ and $Dy(\alpha,t)$ reactions 78−489
^{4}He continuum, microscopic calcs., dynamical R-matrix, model for struct. and reactions 77−14043
$^{191}Hg^{m}$, and $^{190m-185m}Hg$, nucl. spins, on-line quantum beat spectrosc. determ. 80−9562
Ir, A=187, 189, triaxial rotor model and γ-vibr. model comparison, γ decay, level schemes 78−54695
^{6}Li, (αnp) 3 body model using hyperspherical harmonics, bound states 78−70469
^{6}Li ground state, separable pot. three body model 78−50090
^{6}Li, nucleon spectral function, K-harmonics calc. 79−75834
$^{175}Lu(\alpha,\alpha)$, 9.0-13.5 MeV, B(E2) values, rigid rotor model validity 79−494
^{24}Mg, low lying rot. bands from extended deformation model, parity violating deformations 79−6360
^{24}Mg, microscopic model of 2_{1}^{+} and 3_{1}^{+} states, inelastic p scatt. test 79−26358
$^{14}N(\gamma,\pi_{0})^{13}N$, 17 to 26 MeV, angular distrib., giant dipole resonance, single-particle nuclear model 80−52659
^{A}Nb, A=93,95,97, quasiparticle-phonon coupling model calcs. levels, transitions and spectroscopic factors 79−472
^{93}Nb, equilib. compound model invalidity for $E_{x}>11$ MeV *(Russian)* 78−605

nuclear models continued
^{59}Ni, and N=29 nuclei isobaric analogue resonances in unified model description 78−78343
^{16}O, Hamiltonian matrix analysis, base model of orthogonal scheme for 0$^+$ state 79−63610
^{16}O, relativistic self-consistent nuclear model, separation energy, mean square radius *(Russian)* 79−97654
^{8}O low excitation struct., model calcs. 78−70452
Os, O(6)→rotor transition, interacting boson approx. model, levels and transitions 79−13224
^{192}Os level scheme and rot. bands, from ^{191}Os(n,γ), interacting boson approx. anal. 79−6413
^{53}Pm struct., spin and parity assignments, Nilsson model interpretation from ^{154}Sm(t,α) polarised t 79−469
Pt, O(6)→rotor transition, interacting boson approx. model, levels and transitions 79−13224
^{A}Ru, A=101, 103, 105, quasiparticle-phonon coupling model, spectra, moments and transitions 79−22231
^{72}Se yrast states from ^{58}Ni(^{16}O,2pγ), γ spectra, lifetimes, nuclear model predictions 77−54176
^{28}Si, microscopic model of 2_1^+ and 3_1^+ states, inelastic p scatt. test 79−26358
^{28}Si(μ^-, γν), γ−ν ang. correlation, pseudoscalar and tensor form factors, particle-hole model 79−13256
^{A}Sn(n,γ) A=114,116,118, ^{115,117,119}Sn resonance meas., weak coupling model calc. for levels, J$^\pi$ assignments 79−6416
U spontaneously fissionable isomers, excitation by K shell e$^+$ annihilation, shape isomery model *(Russian)* 79−30802

nuclear moment of inertia
^{148}Pm^{m,g} isomeric pair prod., in (d,2n), (p,n) and (α,pn) reacts. 77−88144
A=158-176, 'extension of variable moment of inertia model to high spins', comments 80−86791
A=170-212 nuclei, 20-60 MeV ^{3}He ion induced fission, effective momenta of inertia *(Russian)* 77−34360
actinide nuclei, cranking model, collective inertia parameters 80−57665
angular momentum depend. cranked HFB inertia parameter, high spin states 80−42524
back bending, Hartree-Fock Bogolyubov approach, cranking method 78−58228
backbending associated with alignment of quasiparticle momenta 78−33112
backbending curves, characteristic features, B(E2) values, particle-rotor model *(German)* 77−71554
backbending even-even nuclei, particle-rotor model with VMI core *(German)* 77−6258
backbending in $^{180-182}$Os and ^{181}Re Coriolis antipairing, rot. alignment, deform. jumps 78−70432
backbending nuclei, macroscopic foundation of model *(German)* 79−54386
backbending phenomena, two fluid model of nuclear rots., ^{164,166,}Er, ^{166,168,170}Yb 77−50049
backbending phenomena in even-even nuclei, mechanism *(Chinese)* 79−22177
compound deformed state g-factors and moments of inertia *(Russian)* 77−74757
coupled bands in even-even nuclei in RPA approach 80−32143
cranked HFB treatment of pairing force, back-bending model 77−278
cranking model, HF calcs. of gyromagnetic ratio and moment of inertia 79−93482
cranking model anal. of nuclear inertia in fission and heavy ion reacts. 78−41656
cranking moment of inertia, in a static potential 78−70437
deformation energy surfaces at very high spin states, microscopic determ. 77−71560
deformed even nuclei, level energies, γ transitions, moment of inertia, collective Hamiltonian 78−25133
dense matter phase transitions, cusp catastrophe theory 77−22920
depairing probability for high spin states, rotational energy spectrum, rotor model anal. *(Chinese)* 79−80864
double crossing of ground rotational band and super band 78−45996
even-even and odd A nuclei, nuclear shapes and motions, review 80−5054
even-even deformed nuclei, backbending from band crossing 77−14022
even-even nuclei, backbending mechanism anal. *(Chinese)* 78−78247
even-even nuclei, electric and dynamic quadrupole moments 78−66203
even-even nuclei, resonance model of backbending and downbending 77−67694
even-even nuclei, yrast band backbending mechanism criteria 80−91128
even-even nuclei, yrast band energies, coherent states model, three parameter formula 78−17091
even-even rare earth nuclei, microscopic calcs. 77−54133
fast nonadiabatic nuclear rotation theory *(Russian)* 77−88036
fission isomer properties investigation using Nilsson pot. 78−29403
fission isomers, spectrosc. props. 80−105966
generalised pairing calc. 77−10302
groundstate and β-band simultaneous description, new model 77−2898
Hartree Fock Bogoliubov method, high nuclear spins, quadrupole pairing, moment of inertia, yrast traps 78−54712
Hartree Fock Bologiubov theory, appl. to light/heavy nuclei, book contrib. 79−75881
heavy transition nuclei, self-consistent anisotropic oscill. model, shape parameters calc. 77−79306
high angular momenta nuclei, backbending, yrast states, large moment of inertia band 77−14027
high angular momentum behaviour, transitional nuclei and backbending 79−17789
high spin rotational states description with modified oscillator potential 77−67696
high spin states 79−71785
hot nuclei with high angular momenta, γ-ray emission in heavy ion reactions, rot. bands 78−13133
inertia parameter approximations 78−50073
odd-A 1-p shell nuclei, projected HF method 77−6207
particle number projection effects 77−22830
particle-rotor model, band crossing 79−17833
perturbative treatment of nuclear rots., two-dimens. rotor, bands, moments of inertia 80−78111
pseudomagic nuclei, yrast bands, variable moment of inertia model 80−449
quadrupole pairing forces influence on backbending, cranked Hartree Fock Bogoliubov approach 78−29401
quantum corrections to rigid body values 78−25105
quasirotational bands, non-adiabatic effects 78−54663
rare earth even nuclei, Woods Saxon pot., very high spin Strutinsky calcs. 77−88055
rare earth nuclei, cluster-rotor-coupling approach to backbending 79−45129
rare earth nuclei, cranking model, collective inertia parameters 80−57665
rare-earth nuclei, back-bending phenomena, high spin states 78−74300
rotating nuclei, current distribs., cranked HF model 80−63059
rotating nuclei deformation energy, Nilsson model dynamical moment of inertia, shell corrections *(German)* 78−82276
rotating nuclei of high and v.high nucl. spin *(German)* 78−25102
rotation, inertial parameters in microscopic theory 80−91132
rotational nuclei, high-spin, variable moment of inertia model, microscopic-macroscopic approach 80−63058
RPA anal. of strongly disturbed bands in the high spin region described by rotating bosons 78−78239
Schrodinger fluid velocity field, fermion system moments of inertia 78−65868
shape isomers, spontaneous fission, static and decay props. and excitations, review, book contrib. 78−82402
unified model with vibrating core of variable deform., appl. to ^{21}Ne, ^{21,22}Na 77−50068
variable moment of inertia model, theories of collective motion 77−57611
Woods-Saxon potential spectrum, pairing force strength, Nilsson model comparison 80−57704
yrast level spacing discontinuity, rotation alignment mechanism 78−17085
yrast spectroscopy, nuclei with high angular momentum, review 78−50063
Ag(α,f), fission fragments tracklength and ang. distribs., fission moment of inertia 77−50182
^{26}Al, coherence widths, level density param. and effective moment of inertia 78−37360
^{27}Al, coherence widths from ^{12}C(^{15}N,α) 78−41619
^{36}Ar, inverse inertia parameter calc. 78−50073
^{196}Au, studied via ^{197}Au(n,2n), isomeric cross-section ratio and nuclear moment of inertia 78−13096
Au(α,f), fission fragments tracklength and ang. distribs., fission moment of inertia 77−50182
^{126}Ba, backbending and E2 transition strengths of yrast states 79−26363
^{8}Be, αα$^+$ rotational band existence 79−13192
^{8}Be, effective nucleus eccentricity depend. on total momentum *(Russian)* 79−3078
^{12}C, inverse inertia parameter calc. 78−50073
Dy, odd mass isotopes, rot. excitations anal. 77−82813
Er rotational nuclei, transition energy correlations, very high ang. momentum 80−86787
^{155}Er, backbending effects via (^{12}C, xn) excit. 77−71556
^{158}Er, back-bending phenomenal, rotating potential *(Chinese)* 80−47357
^{158}Er, moment of inertia anomaly at ang. momentum of 26 to 30 78−62496
^{160}Er, produced in ^{124}Sn+^{40}Ar, γ-ray multiplicity spectra, nuclear shape at high angular momentum 78−37260
^{164}Er multiple high spin band struct. from ^{160}Gd(^{9}Be,5n), backbending 78−70429
^{152}Gd β- and octupole bands, downbending moments of inertia from ^{150}Sm(α, 2n) 80−91131
^{72}Ge levels pop. in ^{8}Zn(^{6}Li,pn), in beam gamma-ray spectroscopy 80−47343
^{6}He, density distribution function of nucleons 80−22650
^{171}Hf one- and three-quasiparticle states, high spin rot. bands from (^{16}O,5n), (^{13}C,4n) 80−18163
Hg, positive-parity states, Coriolis antipairing effect, deformed-rotor model 78−12950
^{18}Ir, high spin states of rotation aligned bands 77−30485
^{185}Ir, high spin states of rotation aligned bands, backbending 77−30485
^{23}Na, levels populated by ^{12}C(^{15}N,α) 78−50070
^{20}Ne, effective nucleus eccentricity depend. on total momentum *(Russian)* 79−3078
^{20}Ne, inverse inertia parameter calc. 78−50073
^{20}Ne, moment of inertia from cranked HF method 80−102098
^{20}Ne, rotational moment of inertia, cranked HF formalism with Skyrme force 77−30477
^{58}Ni(^{16}O, X), 70 MeV, compound nuclei charged particle evaporation, moment of inertia 80−57785
Pt, positive-parity states, Coriolis antipairing effect, deformed-rotor model 78−12950
Pu, even isotopes, K=0$^+$, 0$^-$ bands, energies, inverse moments of inertia 80−63063
^{240}Pu, moments of inertia of fissioning isomers, cranking model 78−74299
Ra, even isotopes, K=0$^+$, 0$^-$ bands, energies, inverse moments of inertia 80−63063
Rn, even isotopes, K=0$^+$, 0$^-$ bands, energies, inverse moments of inertia 80−63063
^{28}Si, inverse inertia parameter calc. 78−50073
^{28}Si, shell model and statistical spectroscopic anal. 78−29390
^{144}Sm, produced in ^{100}Mo+^{48}Ca 78−37260
^{A}Te, A=117,119,121, ΔJ=1 band structures on ns isomeric states 79−54382
^{118}Te, produced in ^{82}Se+^{40}Ar, γ-ray multiplicity spectra, nuclear shape at high angular momentum 78−37260
Te(α,f), fission fragments tracklength and ang. distribs., fission moment of inertia 77−50182
Th, even isotopes, K=0$^+$, 0$^-$ bands, energies, inverse moments of inertia 80−63063
^{230}Th(n,f), 0.68-1.10 MeV, fission fragment ang. distribs., resonance and moment of inertia 80−102219
^{233}Th, in shape isomeric deform., from ^{232}Th(n,f) 77−23161
^{163}Tm, high spin rot. levels, studied via ^{165}Ho(^{3}He,5n) and ^{165}Ho(α,6n) reactions 78−8722
U, even isotopes, K=0$^+$, 0$^-$ bands, energies, inverse moments of inertia 80−63063
^{236}U, moments of inertia of fissioning isomers, cranking model 78−74299

nuclear moment of inertia continued
^{48}V, low-lying positive parity states, deformed config. mixing model 77−6198
W isotopes, A=172-176, high spin states and backbending 77−34204
^{A}W, A=174, 175 quasicontinuum γ-rays yrast cascade dipole component, moment of inertia from Dy(^{16}O, xnγ) 80−47424
^{170}W, nonspherical nucleus after backbending, crit. spin rel. to angular vel., bands *(Russian)* 79−75822
^{178}W high spin states, yrast bands and backbending from ^{170}Er(^{12}C,4n) 80−13352
^{179}W, backbending, high spin isomer decay 78−45997
Yb, A=163, 165, 167, backbending of rotational bands 78−8728
Yb, A=169, 170, moments of inertia of excited bands, even-odd difference *(Chinese)* 78−498
Yb with high angular momentum from heavy ion reactions, moment of inertial using γ-spectra 78−13135
^{A}Yb, A=163, 165 level schemes and backbending behaviour of neutron deficient isotopes 79−40836
^{A}Yb, A=166, 168, 170, backbending and moment of inertia in HFB cranking method 80−42521
^{161}Yb quasicontinuum γ-rays yrast cascade dipole component, moment of inertia from Sm (^{16}O, xnγ) 80−47424
^{172}Yb levels, bands, J^{π} and $T_{1/2}$ from ^{170}Er(α,2n) 80−91127

nuclear moments
see also nuclear electric moment; nuclear magnetic moment; nuclear moment of inertia
A=32 to 140, nuclear struct., binding energies, dipole moments *(French)* 77−46098
A=4n, densities, form factors, transitions, multipole moments in s-d shell, HFC 80−37321
aligned states with high spins 77−82845
conference on nuclear interactions, Canberra, Australia (Aug.-Sep. 1978) 80−4476
deformed nuclei energy density mass formula, approx. method, binding energy, quadrupole moments 79−13195
density-dependent HF description, of nuclei in rare earth and Ni regions 77−54170
diffuse-surface density distrib., moments, potentials, energies calc. 77−10311
dipole moment of nuclear state using transient mag. field from ion passing through ferromag. *(Dutch)* 78−29386
electromagnetic multipoles and form factors 77−67701
even-even nuclei in 2p1f shell, HF calcs. using velocity depend. effective interaction 79−71792
fixed angular momentum moments and level densities, statistical spectroscopic methods 80−467
(heavy ion, xn) reactions, higher moments of γ-ray multiplicity 77−18604
in-beam gamma-ray spectroscopy, book 77−83449
ion implantation in samples colder than 0.5K, low temp. nuclear orientation studies 80−34033
mesoatoms in static electromagnetic fields, excited state lifetimes and population, nuclear moments *(Russian)* 80−53170
moderately deformed nuclei, high-spin states studied in (heavy ion, xnγ) reaction 77−14180
nuclear isotopes far off stability line, production, props., review *(Hungarian)* 79−9927
odd nuclei, soft and deformed, rotor plus quasiparticle approach, moments, transition probabilities 80−78214
odd-odd deformed nuclei, ground state static moments 78−66201
proper frequencies, weakly coupled moments in amplitude modulated mag. field *(French)* 77−10571
review, nuclear moments, and moment ratios determ. by Mossbauer spectroscopy 77−22885
^{A}As, A=69-72, $^{4}S_{3/2}$ ground state hyperfine struct. and nuclear moments 80−32853
Ba, radioisotopes, at. beam laser spectroscopy, hyperfine struct., nucl. moments and radii 80−57678
^{A}Ba A=128, 131, 133, charge radii and nuclear moments 79−9460
Ca, stable and radioisotopes, hfs, isotope shifts, dye laser saturation spectroscopy, beam expt. 80−58169
Cs, ground state spins, moments, charge radii by laser spectroscopy 80−78147
^{A}Cs, A=133, 137-139, hyperfine struct., isotope shifts, nuclear moments and radii, laser spectroscopy 79−10071
^{A}Cs, A=138 to 142, nucl. moments and charge radii changes from hyperfine struct. and isotope shifts 79−17804
^{62}Cu 390 keV state populated in ^{60}Ni(α,pnγ), ferromag. effect, spin assignment 77−2903
^{19}F, even parity excited states, collective props., EM moments, generator coordinate method 78−78259
^{19}F, even parity state, EM props., collective struct., generator coord. method, HF method anal. 79−89220
^{A}Fe, A=56-58, shell model calcs., static moments and EM transition rates 79−17853
^{154,156}Gd, pairing-plus-quadrupole calcs. 77−82807
^{154}Gd multiphonon vibr. bands, dynamic deformation theory 80−5035
^{2}H static moments, relativistic and exchange current corrections 79−17799
^{2}H(e,e), EM form factors, relativistic formulae, moment corrections 80−63075
^{A}Hg, A=198-202,204, muonic X-ray transitions, nuclear state quadrupole moments and charge distrib. 79−41253
I, 123≤A≤133, coupled quadrupole model, spectra, B(E2), B(M1), moments calcs. 77−82837
^{8}Li, in $LiTaO_3$, multiple quantum NMR transitions obs., quadrupole moment determ. 77−73090
^{23}Mg even parity excited states, collective props., EM moments, generator coordinate method 78−78259
^{23}Mg, even parity state, EM props., collective struct., generator coord. method, HF method anal. 79−89220
^{A}Na, (A=21, 23), even parity state, EM props., collective struct., generator coord. method, HF method anal. 79−89220
^{A}Na, A=21, 23, even parity excited states, collective props., EM moments, generator coordinate method 78−78259
^{23}Na high spin positive parity state, approx. microscopic methods, shell model comparison 79−85352
^{A}Ne, (A=19,21) , even parity state, EM props., collective struct., generator coord. method, HF method anal. 79−89220

nuclear moments continued
^{A}Ne, A=19, 21, even parity excited states, collective props., EM moments, generator coordinate method 78−78259
^{20}Ne, deformed nucleus, quadrupole moment, HF calc. exponential convergence and acceleration 79−85367
^{21}Ne, energy moments, sd shell realistic effective interactions, shell model spectra 80−18190
^{188}Os, ground and γ-band level energies, B(E2) values and EM moments, triaxial description 79−36140
^{208}Pb region, finite Fermi systems, review 78−537
^{188}Pt, ground and γ-band level energies, B(E2) values and EM moments, triaxial description 79−36140
Rb, ground state spins, moments, charge radii by laser spectroscopy 80−78147
^{185}Re/^{187}Re quadrupole moment ratio 79−9465
^{A}Ru, A=101, 103, 105, quasiparticle-phonon coupling model, spectra, moments and transitions 79−22231
^{A}Sc A=44,46,48, HF projection formalism, energy levels, static moments, EM transition probabilities 79−3083
^{A}Sc, A=45, 47, HF projection formalism, energy levels, EM moments, transition probabilities 79−22199
^{28}Si, deformed nucleus, quadrupole moment, HF calc. exponential convergence and acceleration 79−85367
^{A}Sm, A=144-154, nuclear charge density and quadrupole moments from muonic X-rays 79−40838
^{154}Sm(p,p′), 0.8 GeV, ang. distribs. and multipole moments, DWBA and coupled channel anals. 80−105969
V, A=47,59,51, spectra, e.m. moments, B(E2) and B(M1) values calc. 78−8745
W, produced in (^{16}O,xn) 78−37371
^{133}Xe, nuclear moments and optical isotope shift 78−33118
^{161}Yb, produced in (^{16}O, xn), γ-ray spectra, dipole moment in yrast cascade 78−37371
^{176}Yb(p,p′), 0.8 GeV, ang. distribs. and multipole moments, DWBA and coupled channel anals. 80−105969
Zn, even isotopes, effect of particle-vibr. coupling in nucl. struct. 78−12940

nuclear muon capture *see muon capture*

nuclear optical model
$1f_{7/2}$ neutron single particle energy systematics 77−30480
1f-shell nuclides, optical pot. imag. part, isotopic features 79−9535
1p shell nuclei, optical model anal. of elastic scatt. of 45 MeV ^{3}He 79−59078
^{12}C(^{16}O,^{16}O), anomaly at 13.7 MeV, optical model anal. 78−21587
^{16}O(π^{+},π^{+}), 50 MeV, Lorentz-Lorenz effect 78−17247
(^{6}Li,^{6}Li) 50.6 MeV elastic scatt. on A=12-208 nuclei, optical model parameters 77−18592
$^{A}Z(K^{-},\pi^{-})_{\Lambda}{}^{A}Z$, strangeness exchange reaction ang. distribs., Glauber theory 79−75892
Λ_{10} approximation, complex mass operator using nonlocal separable central pot. 78−33138
A=24 to 209, 7 to 26 MeV, neutron scattering and isospin dependence of the optical model potential 79−45250
A=40 to 56, two-nucleon transfer reactions, coupled channel formalism for isospin depend. optical pot. 80−42609
A=50 to 89, α-particle elastic scatt., neutron shell sensitivity, optical model parameters 79−6642
absorption and prod. of mesons, overview 79−85492
absorption effects in low energy heavy ion fusion reactions 78−8851
absorptive s-wave pion-nucleus optical pot., energy dependence 79−54418
alpha particle-nucleus scatt., antisymmetrisation effects 79−71826
alpha particle-nucleus scatt., critical radii, correl. with nuclear matter distribs. 79−45148
analogue resonances, finite Fermi systems, polarisation effects *(Russian)* 78−46041
annihilation nonlocality effects in the pion optical potential, dependence of (π,π) cross section 79−85550
atomic physics appl. 79−98223
Bethe-Goldstone eqn., nucl. matter, nucleon optical pot. anal. 78−12981
breakup reactions at intermediate energy 77−14086
charged particle scatt., optical pot. in approx. of strong absorption *(Russian)* 78−89839
Chew-Low model for p-wave pion absorpt. on z nucleons, low energy π-nucleus scatt. 78−70567
coherent nucleus approximation in kaonic atoms theory 79−86086
coherent parity-violation experiments with neutron beams 79−59073
common potential and peripheral processes for 1p shell nuclei 77−34276
compelx potl. theory, review 77−30538
complex particle elastic scattering, modified optical pot. reflecting coupled channel effects 78−70501
complex pot. barrier scatt. in semiclassical theory 77−9915
compound neutron absorption processes, optical pots., one particle vibr. state effects *(Russian)* 80−105956
compound nucleus, giant resonances, force functions for partial E1-transitions 78−12985
compressibility effect on real pot., n+^{40}Ca calc. 77−74823
Coulomb barriers, thermal Hartree-Fock approx. excitation-energy depend. 77−10346
Coulomb components and symmetry of complex optical pot., microscopic calc. 77−30529
coupled channel optical model calc. improvement *(Chinese)* 80−99159
deuteron folding model potentials, mass no. systematics 77−2964
deuteron-nucleus optical potential, imaginary L.S interaction 78−41729
deuteron-nucleus polarisation transfer in elastic scatt., tensor interaction 77−57647
diffraction scatt. of nucleons *(Russian)* 79−89285
diffractive semi-optical model for nucleus-nucleus collisions *(Russian)* 79−63646
direct reactions, semiclassical theory, complex paths and uniform approximations 77−71244
dispersion reln. anal. of potl. energy depend. 77−30537
doorway states, energy dependence of inelastic cross-section, shell model, coupled channel anal. 80−73854
doorway states reln. to optical model *(Russian)* 77−6213
double folding pot. for inelastic scatt. between nuclei 80−13425
education, multiple scattering theory, target nucleus wave function antisymmetry 77−49523
effective nuclear matter interactions applied to finite nuclei 79−93546

nuclear optical model continued
eikonal model description of Coulomb effects in inelastic pion-nucleus scattering 79−76025
eikonal model of hadronic matter distribution of particles and nuclei 79−26317
elastic projectile-nucleus scattering, optical pot. reactive content, DWIA justification 79−36211
elastic proton and neutron, cross sections, microscopic optical model pot. calcs. 78−593
elastic scatt. cross section ratio meas., appl. to Ca(p,p) 79−93634
elastic scatt. ion section, long range absorpt., and direct react. components 79−97689
elastic scatt. with optical potential, complex angular momentum methods, poles and zeros of S-matrix, REGGE 80−47445
elastic scattering, empirical optical model 80−509
elastic scattering between complex nuclei, barrier penetration effects, semiclassical theory 77−34339
elastic scattering cross sections with coupled channels, optical model fitting code 79−13264
elastic two fragment collisions, Pauli principle and optical pot. 80−63153
elastic two-fragment collisions, multiple scatt., optical pot. and N-body approaches 79−93573
elementary particle scattering, phenomenological approach to the inverse problem 79−49498
equations of motion with nuclear absorption in heavy ion collisions, optical model 79−6684
equivalent potls. for scatt. processes 77−30532
fast neutron capture and the microscopic isovector optical potential 79−63668
fast neutron scattering through small angles, U and Pb targets, test of optical model predictions 77−26769
Feshbach theory of nuclear reactions, α-decay width calcs., light Po isotopes appl. 78−89829
finite nuclei, Δ-resonance self energy, Fermi broadening, π-nucleus optical pot. 80−68707
finite nuclei, low energy optical pot. from Reid hard core interaction 80−52640
first order optical pot., knockout cross section approx. to total cross section 79−22254
fixed scatterer approx., corrections, correl. expansion 78−571
folded pot., effect of nucl. deform. 78−93983
folding calcs. and density depend. interactions 78−8852
folding description of elastic and inelastic scattering 79−93582
folding model, elastic scatt. of light heavy ions 80−13424
refined folding model, validity for complex projectile scatt. 79−509
folding model calcs. of optical potls., nuclear density distribs. 77−30535
folding model in momentum space, imaginary potential 77−57683
four body system, decoupled Yakubovski eqn. optical pot. and physical implications 78−78334
four-body problem, generalised optical potentials 80−22781
Fourier-Bessel-analysis of alpha-particle scattering optical potentials and nuclear matter densities 79−97716
fragment elastic scattering, unitarity and optical pot. 80−106028
Glauber high-energy approx. extension to composite particles 78−82328
Glauber model extension by means of optical potential, appl. to ^{4}He(p,p)^{4}He 77−50093
Glauber model relation to classical probability calculus 77−50095
Green function appraoch to single particle states 77−30533
hadron-nucleus collisions, two channel optical model 79−36210
hadron-nucleus reactions, optical pot. eqns. for low and moderate energies *(Russian)* 80−63214
hadron-nucleus scatt., cluster expansion of optical potential 77−10380
hadron-nucleus scatt., optical treatment in terms of scatt. amplitudes 78−89838
hadronic interiors, meas. and charge distrib., hadronic diffraction scatt. 80−73817
hadronic props. of photons, book contrib 78−82217
Hamada-Johnston interaction, nucleon optical pot. 78−12982
heavy ion+nuclear emulsion, 2.1 GeV/nucleon, projectile fragmentation optical model discussion 78−70561
heavy ion+nucleus scattering, Regge pole contrib., forward- and backward-angle, Coulomb and nuclear scatt. functions 80−57788
heavy ion collisions, deeply inelastic, random matrix model based transport theory, 1-dimens. model 79−49633
heavy ion deep inelastic collision processes, optical model description, statistical considerations 80−68687
heavy ion elastic and inelastic scatt., optical pots. and folding model 80−5169
heavy ion elastic and inelastic scatt., review, book contrib. 80−27668
heavy ion elastic scatt., diffr., refr., interf. effects 77−3031
heavy ion elastic scattering, folding model pots. from realistic NN interactions 80−5159
heavy ion elastic scattering, generalised Fresnel model rel. to optical model 78−74393
heavy ion elastic scattering, local optical potential determ., semiclassical derivation 79−59083
heavy ion elastic scattering 80−73858
heavy ion folding potentials 79−97728
heavy ion inelastic scatt., folding model, macroscopic formalism, form factors 78−25227
heavy ion inelastic scattering, optical pot. deformation 80−13505
heavy ion optical model, surface transparency and resonance phenomena 79−9617
heavy ion optical pot., imaginary part 79−97727
heavy ion optical pot., long range absorpt., from Coulomb distorted states and Green's functions 78−29494
heavy ion optical pot., real part energy depend. 79−63691
heavy ion optical pot. contrib. from coupling to vibrational states 79−67726
heavy ion optical potential, real part, effective pot. using folding models 78−70499
heavy ion optical potential, real part, folding technique 80−73830
heavy ion optical potential elastic scatt., energy depend., Regge pole and Coulomb amplitudes 78−25228
heavy ion optical potentials, energy and ang. momentum dependence 77−57692
heavy ion optical potentials, real part calc. by classical inversion procedure 78−89892
heavy ion pots., quasimolecular resonance phenomena 79−97730
heavy ion scatt., folding model in momentum space, formalism and real potential 77−57682

nuclear optical model continued
heavy ion scatt., optical potential resonances, semiclassical method, S-matrix amplitude 79−3120
heavy ion scattering, optical model code A-THREE 78−89837
heavy ion scattering cross-sections, WKB calcs., unphysical reflection phenomena 80−27656
heavy ion single nucleon transfer reactions, optical potential ambiguities, DWBA anal. 77−34341
heavy ion-light particle angular correlation, forward peaked, light particle emission from l-windows 80−63142
heavy-ion α-particle transfer calcs., rot. excitation 77−14168
heavy-ion elastic scatt., dynamic polarisation pot. 78−13136
heavy-ion elastic scatt. pots., spin-orbit terms, appl. to (^{6}Li,^{6}Li) 78−66313
heavy-ion high-energy scatt., optical phase shift function 78−639
heavy-ion optical pot. real part, new effective N-N interaction in folding model 77−18505
heavy-ion pot., density depend. interactions and folding model 78−17237
heavy-ion potential scattering, single reflection approx. 77−10422
heavy-ion pots., single-folding model 77−18597
heavy-ion scattering, dynamic polarisation pot. for Coulomb excitation effects 77−67765
heavy-ion transfer reactions optical model Coulomb terms in DWBA 77−10431
HF pot., particle vibration coupling effects 79−93578
Hilbert space theory of nonunitary scatt. and capture 80−52639
Hill-Wheeler eqns. direct solns., pot. scatt. and α-α calcs. 78−4956
imaginary inelastic transition form factor, microscopic theory 78−50175
imaginary part of the nuclear optical potential and inelastic form factor 79−93581
ion-ion pot., energy depend. from simplified energy density method, folding model combination 79−6429
ion-ion potls., and Coulomb barrier radius 77−3039
isobar doorway model, pion absorpt. optical potential 79−85420
kaon-nucleus reactions, low energy, nuclear density shape optical pot. kaonic atom level shifts 80−63213
kaonic atoms, quadrupole hyperfine structure 80−78726
L-depend. optical pots., local density models 79−93583
Levinson theorem, standard optical pots., nucleon+nucleus scatt. phases *(Russian)* 78−17214
light ion scatt., optical pot. and proximity pot. comparison 79−3121
Lorentz-Lorenz effect and ρ^2 terms in pion-nucleus scattering 78−82391
low density expansion of nuclear matter optical pot., self consistency requirement 78−8760
low energy one-neutron transfer reactions between heavy ions, optical model potential 79−45294
many-body scatt. theory, orthogonalised distorted waves and optical potentials 79−75940
many-body theory of complex potl. 77−30534
medium weight nuclei, polarised d elastic scatt., 10 to 15 MeV 79−36248
metallic reflection, absorpt. cross sections of potentials imaginary part 78−82329
microscopic calcs. of nucleon potls., review 77−26648
microscopic nucleus-nucleus optical potential 79−97688
microscopic optical model anal. of (n,n) and (p,p) cross sections 78−29434
microscopic optical pots., conference, Hamburg, Germany 1978 79−92904
microscopic pots., summary 79−97691
microscopic relativistic nucleon-nucleus model 79−67725
minimisation procedures for nuclear optical model parameter searches, use of derivatives 77−10379
model parameters for heavy-ion α-transfer reactions on targets with A=10-20 *(Japanese)* 78−4962
momentum projection methods in nucleus-nucleus scatt., optical pot. 1-channel problem 78−78403
multiple scatt. theory, spectator expansion of full Green's operator 78−17162
neutron coherent scatt., parity-violating pots., weak interaction probe 77−71599
neutron cross sections for ^{232}Th, ^{233}Th, ^{233}U and appl. to reactor design 77−54227
neutron elastic scattering, 11 MeV, isospin depend. of neutron-nucleus optical pot. 77−14126
neutron inelastic scatt., 14.2 MeV, optical model anal. 77−54225
neutron optical potl. from sub-Coulomb (p,n) data on ^{51}V, ^{54}Cr, ^{55}Mn, and ^{59}Co 77−26649
neutron resonances, partial E1 radiative strength functions, shell and optical model interpretation *(Russian)* 77−82895
neutron resonances, reaction mechanisms and nuclear struct. 77−26564
neutron s-wave strength functions, odd-even fluctuations 77−22856
neutron scattering cross sections for ^{48}Ti, ^{54}Fe, ^{56}Fe, ^{209}Bi *(Russian)* 77−26688
neutron strength function fluctuations 77−22858
neutron-nucleus in 4 to 100 MeV range, shell effects 77−54197
non-local potl., theoretical and phenomenological aspects 77−30536
nonlinear phenomena, nucl. matter and intense particle beams 77−2924
nonlocal optical pot., isospin depend. 79−93579
nonlocal pot. model, energy independent, bound and scattering states 77−18504
nuclean scatt. from nuclei with nuclear matter t-matrices 79−93577
nuclear bound states of k−, $\bar{p}$ and Σ 80−13399
nuclear fragmentation of ^{12}C, ^{16}O at high energies, phenomenological anal., diffractive excitation model 77−54247
nuclear matter, comparison of Brueckner and λ_{00} approx. 77−2929
nuclear matter, dispersion relations for generalised optical potential *(German)* 78−54713
nuclear matter, n excess, spin-up n and p, effective NN pot., optical pot. 79−13232
nuclear matter complex pots. determ. from Reid's hard core interaction 77−88092
nuclear optical pot., general theory 79−93576
nuclear radii from total neutron cross sections, optical model calcs. 79−9455
nucleon optical pot., spin-orbit term 80−27606
nucleon spin-orbit optical pot., energy depend. 80−68616
nucleon-nucleus, pot., three-body approach 77−18506
nucleon-nucleus elastic scatt., spin effects in framework of Glauber optical model 79−40909

nuclear optical model continued
nucleon-nucleus elastic scatt. at medium energies, microscopic optical pots. 79−97703
nucleon-nucleus multiple scatt., closure correction in optical potential 78−50141
nucleon-nucleus optical model, nucl. matter approach 79−93574
nucleon-nucleus optical model, nucl. struct. approach 79−93575
nucleon-nucleus optical pot. from nuclear matter t-matrix, effective force. 80−22783
nucleon-nucleus optical potential, exchange term and effect of odd forces 78−70500
nucleon-nucleus potential, correl. with nuclear matter characts. *(Russian)* 78−37321
nucleon-nucleus unstable hadron coherent prod., cross section errors from parton model 79−22253
nucleus+nucleus interaction potential, microscopic approach to real and imaginary parts calcs. 78−37372
nucleus-hadron total cross-section, 180-1600 MeV 79−6538
nucleus-nucleus interaction pot., transition from light to heavy ions, optical pots 80−63197
nucleus-nucleus interaction pot. using energy dependent delta interaction, Skyrme interaction folding 79−36269
nucleus-nucleus pot., folding model, single nucleon knock-out exchange contrib. 77−305
nucleus-nucleus potential from liquid drop model 78−50204
nucleus-nucleus scattering amplitude, using Glauber-Sitenko eikonal approx. *(Russian)* 79−80953
odd-even dependence of the optical optical potential 79−97687
off-shell ambiguities and phenomenological optical potentials 78−37379
optical anal. of resonances in velocity depend. square well pot. 78−62098
optical model potl., conf. 77−30530
optical potential, imaginary part, effect on total reaction cross sections 79−9534
OPTY, universal optical model code for elastic scatt. 80−73832
p-wave π absorpt. on two nucleons and low energy π-nucleus scatt. 79−76038
parabolic repulsion potential for scattering of ^{6}Li and ^{9}Be ions by light and medium nuclei 80−22782
parameters from pion low energy scattering, review 79−85529
particle-particle collision probability, vol. integral using preequilibrium exciton model 78−70477
phase-amplitude method for a separable non-local optical potential 80−78237
photon-nucleus interactions, optical model description, photon shadowing suppression 77−46158
photoneutron reactions near threshold, optical model, review *(Russian)* 77−82904
photonuclear reacts., coupled channels method *(Russian)* 78−50153
pion+nucleus total cross-sections in (3,3) resonance region 77−10437
pion propagator in nuclear matter, optical pot. Pauli blocking corrections 77−22919
pion s-wave absorpt., optical potl. calc. 77−10439
pion-nucleus, single charge exchange and inelastic scatt. cross sections relationship 80−102204
pion-nucleus elastic scatt. at low energies 77−6439
pion-nucleus interaction at low energy 77−6460
pion-nucleus low energy scatt., cross-section 79−3181
pion-nucleus low energy scatt., Lorentz-Lorenz effects 77−46151
pion-nucleus scatt. momentum space optical potl. code, PIPIT 77−6442
pionic atoms, quadrupole hyperfine structure 80−78726
potential based on folded Yukawa model 77−22985
potential for scatt. processes, survey 77−30531
potential in channel coupling array method 77−18496
potential with kinematic, absorption and correl. corrections for (π,π) scatt. at 50 MeV 77−50157
projectile fragmentation in nuclear emulsions at 2.1 GeV/nucleon 78−70561
proton absorbing optical pots., vol. integrals calc. 77−10403
proton scatt. parameters at subcoulomb energies 79−93584
proximity formulae for folding potentials 79−36209
proximity treatment of the interaction between deformed nuclei 78−78338
quantum corrections to optical potentials 79−97690
quasi elastic nucleus-nuclear scatt. differential cross section *(Russian)* 80−68696
radial moments of folding integrals, non-spherical distribs., inelastic scatt. off nuclei 77−2963
reflection effect in optical pot. absorption cross section *(Russian)* 79−22255
S(n,n) 20, 26 MeV, Coulomb correction term to optical model pot. 77−38280
S-matrix, energy depend. anal. using WKB 77−34275
S-wave π absorption, off shell effects, effect on π-nucleus optical pot. 78−70566
semi-classical analysis of optical model ambiguities 79−85419
sensitivity of alpha-decay to the real alpha-nucleus potential 79−97714
separable optical potential theory, Schwinger variational principle *(Russian)* 79−3122
shell model description of the optical model potential 79−93580
short range correlations in nucleus-nucleus scatt. amplitude, optical phase shift expansion 78−70502
Si (n,n), 20, 26 MeV, Coulomb correction term to optical model pot. 77−38280
single scattering optical model, three body approach, appl. to nucleon+nucleus scatt. 78−25162
single- or coupled-channel, calcs. for neutron scatt. from ^{208}Pb, ^{232}Th, ^{238}U 77−30595
slow π potential in nuclear matter, P-wave screening, Lorentz-Lorenz factor *(Russian)* 77−6335
spherical model calcs. of ^{94,96}Mo(n,n) ang. distrib. 77−26716
spherical pot. spin-orbit term anal. from neutron elast. scatt. ang. distrib. meas. 77−30599
spherical potl., spin-orbit term anal. from neutron elast. scatt. ang. distrib. meas. 77−30600
spin-orbit effects via (n,n) back angle elastic scatt., Fe,Co,In,Bi targets 77−67746
spin-orbit pot. for spin $^{1}/_{2}$ particles 79−97686
spin-unsaturated subshells and the nucleon-nucleus optical-model spin-orbit potential 80−18259
spline interpolation method appl. to optical potential 80−32272
stellar environment, nucl. struct. and reactions 80−72765

nuclear optical model continued
strongly bound pion states in nuclei, optical model 80−68557
strongly interacting particles, optical pot. theory 80−32250
sub Coulomb elastic scatt., adiabatic and dynamic polarisation effects 79−97698
theory of energy-dependent nuclear optical-model potentials 80−102163
three body problem with energy dependent potentials 77−18413
three-body Bethe-Faddeev equations and single-particle potentials in nuclei 79−97684
threshold pion absorption in nuclei 78−82390
total scattering cross sections for optical pots., quasiclassical calcs. 78−8270
two-channel Hamiltonians and the optical model of nuclear scattering 79−59043
ultracold neutrons in scatt. medium, optical potential *(Russian)* 77−34362
uncorrelated target, optical pot. unitary content, DWIA and Glauber theory 80−99160
variational principle based statistical theory of nuclear reactors, optical $\hat{S}$ matrix 79−36221
volume integrals of nucleon absorbing optical pot. 78−8789
volume integrals of real part of nucleon optical pot. for A=10-238 78−78339
West Yennie formula, assessment of validity for Bethe phase, using optical model framework 78−21608
(α,α), antisymmetrisation effects, α pot. form factor, optical model anal. 78−82366
(α,α), folding potentials, Woods-Saxon and squared Woods-Saxon parametrisations 80−102195
(α,α), local density dependence of NN interaction, double-folding calcs. 80−83114
(α,α) anomalous large angle scatt., optical model sensitivity 79−13309
(α, α) scatt., 120-172.5 MeV, optical pot, uniqueness and shape 79−97719
(α,α) scatt. near Coulomb barrier and matter distribs. of medium and heavy nuclei 78−66291
(α, α) scatt. on A=40 nuclei, accurate optical pots. 79−97718
α elastic scatt. at 100, 140 MeV, Fraunhofer diffr. oscills., refractive damping anal. 77−61445
α elastic scattering from ^{90,92}Zr, ^{124}Sn, ^{208}Pb, optical model parametrization 78−33196
α scattering from 2d-1s shell optical model and coupled-channel anal. 77−6407
α-decay width calc. in meth. not involving arbitrary channel radii 77−54192
α-nucleus elastic scatt., optical model analysis 78−41737
α-nucleus optical potential as three body problem, microscopic description 79−6536
α-nucleus pot., microscopic calc. 78−8788
α-particle effective surface pot. and OCM justification 79−97715
α-particle potential parameters, elimination of discrete multivaluedness 77−6333
(d,d), A=27-238, 12-90 MeV, global optical model pot. 80−78305
(d,d), folding model modification due to strong Pauli distortion 79−6620
(d,d), optical model analyses *(German)* 80−68676
(d,d), pol. d, 12 MeV, A=46-82, cross sections, anal. powers, global optical model anal. 80−47459
(d,d), pol. d, 56 MeV, A=16-208, cross sections, optical parameters, anal. powers 80−78270
(d,d), pol.d, 52 MeV, A=12-197, vector anal. power and optical parameters 80−57764
(d, d), uniqueness of optical pot. 79−97685
(d,d) 12 MeV, tensor polarised, differential cross section, vector and tensor analysing power 78−78357
(d,d) breakup channel contrib. to optical pot. in 3-particle approx. 79−6630
(d,d) medium heavy nuclei, optical model anal., cross sections, anal. powers 80−73839
d breakup effect on spin orbit and tensor pots. 80−32286
d propagation in nuclear matter, spin depend. of d optical pot. and binding energy 78−70545
d+nucleus optical model calcs., tensor spin-orbit interaction 78−13112
Δ spreading potential in pion-nucleus scatt., optical model approach 79−85422
(e,e′), cross section near quasielastic maximum, shell and optical models *(Russian)* 80−91179
(e,e′N) reaction, energy depend. optical potential calc. *(Russian)* 78−41706
(γ,n), valency mechanism near threshold, optical nuclear model *(Russian)* 77−6351
(γ,π), photopion reaction sensitivity to optical pot. 80−78278
(γ,Π) in nuclear matter, optical pot. and Fermi gas model, Li, Be appl. 79−36230
$(\bar{K},\bar{K})$, isobar doorway model, optical pot., Λ-nuclear matter binding energy 80−106079
(K,X) optical pot. from KN scatt. and kaonic atom pot. models 79−97731
$\bar{K}$-nucleus optical pot. at low energy 78−94032
K^- nucleus, optical model pots. 77−2962
K^--nucleus optical pot. for kaonic atoms 79−98255
K+nucleus, opt. pot., distorted waves, 100 to 200 MeV, difference between Schrodinger and Klein-Gordon wave functions 78−94033
(n,γ), polarized space parity nonconservation, optical pot. and GDR parameters *(Russian)* 80−86803
(n,n), A=90 region, elastic, inelastic and total cross section, statistical model calcs. 80−68674
(n,n), elastic and inelastic scatt. on various isotopes, cross sections meas. and calcs. 78−13081
(n,n), isospin depend. of N-nucleus optical pots. 77−34311
(n,n), pol. n, 16.1 MeV, differential cross section, optical model fit 80−32259
(n,n), single particle bound state, energy independ. optical model, asymmetry term 80−37316
(n,n) 2.9 MeV, elastic differential cross section and polarisation ang. depend., statistical anal. 79−45264
(n,n) compound scatt. and optical model polarisation 77−2971
N optical pot. for T=0 nuclei, Si, S, Ca 77−88137
N-nucleus optical model potential, spin-orbit component from internucleon pot., ^{40}Ca+p appl. 78−46039
$\bar{N}$-nucleus optical pot. strong interaction effects, implications for $\bar{N}N$ interaction 77−18402

nuclear optical model continued
N-nucleus optical potential from realistic Hamada-Johnston internucleon pot., binding energy 78−54730
(p,2p) DWIA calcs., N-N off shell t-matrix, optical model from N-N 77−88124
(p,2p) quasifree reactions, anal. of momentum distribs. distortion, complex optical pot. effects 78−54767
(p,2p) reaction for slightly deformed nuclei 77−57657
(p,n), 2.5-5.8 MeV, A=89-130, cross sections, sub-Coulomb proton anomalous optical pot. 80−32278
(p,n), A=89-130, anomalous optical pot. for sub-Coulomb protons 80−102190
(p,n), A=89-130, sub-Coulomb protons, anomalous optical pot. 80−102191
(p,n), A=90 region, reaction cross section, statistical model calcs. 80−68674
(p,n), anomalous optical potential for sub-Coulomb barrier protons, 2 particle 1 hole states 80−105948
(p,n) cross sections on nuclei with A=89 to 130, anomalous optical model pot. 78−25188
(p,n) excitation functions for A=45 to 80, proton optical pot. at sub-Coulomb energies 80−9292
(p,p), 0.1-1 GeV, optical pot., vol. integrals and root mean square radii 80−106054
(p,p), 10 to 50 MeV, scatt. data on nuclei of A≤70 79−93633
(p,p), 100-2200 MeV, total and reaction cross sections from optical pot. 80−18303
(p,p), 30 MeV, polarised protons 78−597
(p,p), A=9 to 70, differential cross sections, struct. effects, optical and coupled channel anal. 80−47482
(p,p), angular momentum depend. optical pots., physical interpretation 79−26431
(p,p), isobaric analogue resonances, microscopic and phenomenological parameters, S-matrix eval. methods 78−13045
(p,p), new type of parameter systematics 79−93630
(p,p), pol. p, sd, fp shell nuclei, 65 MeV, effective two-body interaction range 80−32201
(p,p), polarised p, 0.8 GeV, neutron isotopic density differences and RMS radii 79−67643
(p,p), semi-phenomenological anal. 79−93632
(p,p), single particle bound state, energy independ. optical model, asymmetry term 80−37316
(p,p) 800 MeV, polarised p, n density uncertainties from optical model anal. 79−22185
(p,p) scatt. on light nuclei, 6 MeV *(Russian)* 78−25200
(p,p′) to collective states, medium energies, spin-orbit deformation from DWBA calcs. 79−9565
(p, t) ang. distrib., zero-range DWBA calc., volume absorptive optical pot. singular prop. 80−523
p elastic and polarisation scatt., optical model pot. with l-depend. 77−61394
p+complex nuclei, 10 GeV, inelastic emulsion scatt., optical model anal. *(Korean)* 78−50165
(π^-, NN), low energy pion absorption, $\sigma+\omega$ model, optical pots., real $\rho^2(r)$ pot. 80−83125
(π^-,nn), S-wave and p-wave absorptive pion-nucleus optical pot. 80−27677
(π^+,p) near (3,3) resonance region, isobar doorway model 78−41778
(π, π), lowest order optical pot. containing π emission and absorption effects 80−73865
(π,π), phase shifts in (3,3) resonance region and diffractive nature 77−6462
(π,π), relativistic Schrodinger and Klein-Gordon optical models, off-shell sensitivity 80−5175
(π,π), Weinberg chiral Lagrangian nonlinear terms, nuclear binding, optical pot. 80−78329
(π,π) elastic scatt., covariant theory, first and second order optical pots. 79−85545
(π,π) elastic scatt. on light nuclei, optical pot. and scatt. amplitude model *(Russian)* 78−89918
(π,π) low energy, optical pot. 79−40965
(π,π) optical pot., possible local field correction from resonant scatt. cross section 79−85421
(π,π) scatt. in 3,3 resonance region, Δ-isobar dynamics, optical potential and RPA calcs. 77−34347
(π^+,π^0), isobar-doorway model optical pot. appl. to isospin nonzero nuclei 80−52699
(π,π') differential cross section calculation program modification 79−54457
(π,X), reaction mechanisms, at low energy and near 3.3 reson. region 79−80958
π bound states in finite nuclei, π-nuclear optical pot. 78−46013
π dispersion relns. in nuclear matter, $\gamma \rightarrow \pi^+\pi^-$ and $\bar{\nu} \rightarrow e^+\pi^-$ decays 77−65209
π s-wave absorption, sensitivity to off-shell props. of πN scatt. 77−50158
π-nucleus, calc. of strong interaction shifts and widths of pionic atom X-rays 77−23586
π-nucleus elastic scatt., momentum space optical pot. code PIPIT 77−38298
π-nucleus optical pot., first order, remarks on calculations 77−46150
π-nucleus optical potential, p-wave absorptive pot. and higher-order corrections 79−45303
π-nucleus scatt., nonrelativistic QFT formulation, Low eqn., optical pot. definition 79−6700
π-nucleus scatt., optical potl. for low and medium energies 77−6443
π-nucleus scattering, binding effects in optical pot. of pion in nucleus 78−41685
π-nucleus scattering, low energy, optical pot., quasideuteron model calcs. 78−74406
π^--mesonic atom, π^--nucleus optical pot. information 79−85559
$\pi^\pm$ 162 MeV elastic scatt., ang. distribs., diffraction patterns, optical model calcs. 78−58309
π+nucleus, opt. pot., distorted waves, 100 to 200 MeV, difference between Schrodinger and Klein-Gordon wave functions 78−94033
π+nucleus optical pot., off-shell sensitivity, repulsive correl. 77−71626
π+nucleus scatt., hole-line expansion and Pauli principle 77−18627
π+nucleus total cross section, A-depend. shift of peak 78−33226
πN low energy scatt., subtracted form of Low eqn. 78−66150
πnucleus scatt., nucleon Fermi motion, numerical approx. in momentum-space calc. 79−45302

nuclear optical model continued
(t,t), A=40-208, 17 MeV, pol. t, cross sections and anal. powers, optical anal. 80−47462
(t,t), elastic scatt., optical spin-orbit pot., spin-orbit strength 79−85480
^{208}Pb+p, 100-1050 MeV, optical pot. real part, nuclear matter approach 77−82890
^{12}(α, α), 1.37 GeV, microscopic anal. using modified Glauber model 78−617
^{A}Ag(p,p), A=107,109, 2.0-6.7 MeV, cross sections, Hauser-Feshbach optical calcs. for p absorption systematics 80−47483
^{107}Ag(n,n), 0.25-4.5 MeV, total, elastic and inelastic cross sections, optical-statistical anal. 80−27639
^{109}Ag(p,p′), pol.p, 6.06 MeV, anal. powers, large absorption pot., optical model 80−83092
^{27}Al, pionic, Lorentz-Lorenz quadrupote term, P-wave optical pot. 79−22252
^{27}Al, strongly bound π-nuclear states, criticality condition, optical pot. 78−90325
^{27}Al(^{3}He,^{3}He), 46 MeV, ang. distribs., optical and DWBA anal., scatt. pots. 79−556
^{27}Al(^{3}He,^{3}He) 39.7 MeV, optical pot. mass. depend. 77−34327
^{27}Al(^{6,7}Li, ^{6,7}Li), 90 MeV, real optical pot. continuous ambiguity 80−102200
^{27}Al(α,α), 41 MeV, elastic and inelastic, ang. distribs., optical and DWBA anal., scatt. pots. 79−556
^{27}Al(n,n), (in)elastic scatt. cross sections, duration of collision process *(Russian)* 79−80942
^{241}Am, neutron cross sections, 1 keV to 15 MeV, optical and stat. model calcs. 77−57655
^{A}Ar(α,α), A=36,40, 29 MeV, energy and mass depend. of extracted optical potentials 79−49632
^{36}Ar(^{6}Li,d)^{40}Ca, 0$^+$ levels of ^{40}Ca, DWBA calcs. with optical model parameters 78−62571
^{40}Ar(d,d), optical model parameter investigation using 9-12 MeV polarised d 78−94016
^{197}Au+p, 16 MeV, coherent optical model analysis 77−26750
^{197}Au(^{14}N,n), DWBA anal. above Coulomb barrier 80−86917
^{197}Au(^{3}He,^{3}He) 39.7 MeV, optical pot. mass depend. 77−34327
B, 20 to 50 MeV, total reaction cross sections compared to opaque-nucleus model 78−33174
B+^{27}Al, A=10,11, elastic scatt. quadrupole effects at 50 MeV, optical parameters 77−88169
^{10}B(^{9}Be, X), total reaction cross sections for sub-Coulomb energies, neutron transfer reaction 79−80950
^{10}B(α,α), 5-50 MeV, optical and Inopin-Ericson model anal. 77−3025
^{10}B(p,π^+), differential cross sections, DWBA calc. 79−85415
^{10}B(π^+,π^0), 1st order pion-nucleus pot. calc. 77−23113
^{11}B(^{3}He,^{3}He) 17.5 and 40.0 MeV, elast. and inelast. scatt. from ground state and low excited levels 77−65229
Ba, A=134-138, average neutron cross sections, statistical and optical model calcs. 78−29458
^{8}Be(α,α)^{8}Be elastic scatt. generalised optical potentials, three-body approximation *(Russian)* 79−13313
^{8}Be(n,n)^{8}Be elastic scatt. generalised optical potentials, three-body approximation *(Russian)* 79−13313
^{8}Be(t,t)^{8}Be elastic scatt. generalised optical potentials, three-body approximation *(Russian)* 79−13313
(^{9}Be,^{9}Be), optical pot. 79−59087
^{9}Be elastic scatt., 14-26 MeV, universal optical pot. determ. *(German)* 78−70552
^{9}Be elastic scattering on heavy target nuclei, 14-26 MeV, universal optical pot. 78−25219
^{9}Be+^{12}C, 2.8-6.3 MeV, fusion and neutron transfer cross-sections 78−41746
^{9}Be+^{12}C, 3.5 to 9.5 MeV, sub barrier, cross sections and optical model calcs. 78−8838
^{9}Be+^{16}O, 2 to 5.1 MeV, sub barrier, cross sections and optical model calcs. 78−8838
^{9}Be+^{19}F, 7 to 16 sub. barrier, cross sections and optical model calcs. 78−8838
^{9}Be(^{9}Be,^{9}Be) 14, 20 and 26 MeV, optical model parameters, 9 to 22 MeV excitation curves 79−26449
^{9}Be(α, α'), 65 MeV, levels and differential cross sections, optical anal. 80−102121
^{9}Be(d,d), 12.17 to 14.43 MeV, elastic and inelastic scatt., optical model anal. 78−89883
^{9}Be(π,π), ang. distribs., optical model calcs. 78−58308
^{9}Be($\pi^\pm$,$\pi^\pm$) elastic and inelastic quadrupole scatt., 162 MeV, rot. and optical model anal. 79−6714
^{9}Be(t,t)^{9}Be, 15, 17 MeV, polarised t, differential cross sections and optical model fits 78−41730
^{209}Bi(α,n), excitation functions and isomer ratios of ^{212}At 80−83039
^{209}Bi(α,np), excitation functions and isomer ratios of ^{211}Po 80−83039
^{209}Bi(α,p), excitation functions and isomer ratios of ^{212}Po 80−83039
^{209}Bi(n,n), 0.6 to 1.0 MeV, optical model params. 78−21557
^{209}Bi(n,n), direct scatt., polarised thermal neutrons, empirical parity-violating potentials and neutron optical activity 79−59074
C+π, 40 to 280 MeV, second order optical pot., effect of short range correls. 78−74407
^{A}C, A=12,13, large angle scatt. of ^{9}Be, optical model and DWBA anal. 79−36259
^{A}C(^{9}Be,^{9}Be) A=12, 13, 14, 20 and 26 MeV, optical model parameters 79−26449
^{A}C(p,p), A=12, 13, 0.8 GeV, elastic and inelastic, ang. distribs., states, optical and DWBA anal. 79−3154
^{12}C, vector polarised ^{6}Li elastic scatt., full optical model anal. 78−70553
^{12}C-^{12}C scattering, fusion cross-section, folding model study, coupled channel effects 78−89893
^{12}C+^{10,11}B, sub Coulomb energy, fusion cross sections, elastic scatt., optical model anal. 77−34335
^{12}C+^{12}C, optical pot. for nucleus-nucleus systems using double folding model 79−45225
^{12}C+^{12}C elastic scatt., optical model anal. 77−6429
^{12}C+^{12}C elastic scatt., induced rot., energy depend. of optical pot. real part 78−89903
^{12}C+^{12}C scatt., 10-20 MeV, optical model pot. 79−26456
^{12}C+^{12}C scatt. and fusion cross sections above Coulomb barrier, folding model, resonances 79−6687
^{12}C+^{16}O, elastic scatt., simple double folded optical pot. model for resonances 79−6535
^{12}C+^{16}O resonances, microscopic double folded model 78−41754

nuclear optical model continued
$^{12}C+^{20}Ne$ elastic scatt., strength of absorpt. 77−3028
$^{12}C+^{27}Al$, elastic scatt. quadrupole effects at 55 MeV, optical parameters 77−88169
^{12}C+p, 9.5 MeV, optical pot., inverse scatt. method *(Russian)* 79−552
$^{12}C+\pi$, P-wave pion absorption on two nucleons and low-energy pion-nucleus scattering 78−78416
$^{12}C+\pi$ optical potl. at 50 MeV 77−6440
$^{12}C+\pi$ optical potl. improved calcs. 77−6334
$^{12}C+\pi^-$, 40 GeV/c, multiplicity distribs. of secondary charged particles, Glauber model calcs. *(Russian)* 78−17252
$^{12}C(^{12}C,^{12}C)$, 35-63 MeV, elastic and inelastic, cross sections, DWBA and optical anal. 79−93656
$^{12}C(^{12}C,X)$, optical potential, nuclear matter approach 80−57801
$^{12}C(^{16}O,^{16}O')$, molecular resonances from coupling interactions derived by folding procedure 79−89279
$^{12}C(^{16}O,^{16}O)$, 35 to 50 MeV, backscatt., dynamic deformation and excitation functions, optical anal. 80−18227
$^{12}C(^{16}O,^{16}O^*)^{12}C^*$, 33-54 MeV, intermediate struct. resonances, ang. distrib. optical model fit, spin assignments 78−82330
$^{12}C(^{16}O,^{16}O)^{12}C$ scattering gross struct. features, optical model 77−88164
$^{12}C(^{16}O,X)$, transparency to l=9 partial wave in 14.7 MeV resonance region 80−78314
$^{12}C(^{16}O,\alpha)^{24}Mg$, anomaly at 13.7 MeV, optical model anal. 78−21587
$^{12}C(^3He,^3He)$. 20.5-33.0 MeV, energy depend. of analysing power optical model 78−17226
$^{12}C(^3He,^3He)$ 39.7 MeV, optical pot. mass. depend. 77−34327
$^{12}C(^3He,\alpha)^{11}C$, 11 MeV, multistep mechanism, CCBA calcs. 78−41734
$^{12}C(^6Li,^6Li)$ 5.8, 59.8 MeV, optical pot. inner part, elastic scatt. cross section 79−3173
$^{12}C(^6Li,^6Li)^{12}C$, 20 MeV and higher, diffraction model behaviour, anomalies caused by two step-processes 79−13344
$^{12}C(^9Be,^9Be)$ 14, 20 and 26 MeV, optical model parameters 79−26449
$^{12}C(K^-,K^+)$, 0.4-1.2 GeV/c, optical potl., cross-sections determ. 77−14184
$^{12}C(\alpha,\alpha)$, 20 to 24 MeV 77−65228
^{12}C(e, e'p), quasifree scatt., spin-orbit distortion of emerging nucleon 80−52664
^{12}C(e,e'p), cross sections from DWIA, optical, and shell model calcs. *(Russian)* 80−32270
$^{12}C(e,e'p)^{11}B$, recoil momentum distribs., optical potential variation effects, HF calcs. 77−41955
$^{12}C(\gamma,\pi^-)$, (γ,π^-p), knockout p interaction, optical model and quasifree π photoprod. mechanism *(Russian)* 80−42638
^{12}C(n,n), 14.2 MeV, elastic, inelastic, backscatt. meas., optical model test 78−58275
^{12}C(n,n), 15 to 18 MeV, resonance effects 77−30591
^{12}C(n,n), (in)elastic scatt. cross sections, duration of collision process *(Russian)* 79−80942
$^{12}C(p,^6Li)^7Be$, 51.9 MeV, spectroscopic factors and reaction mechanism 78−46058
^{12}C(p,X), reaction and scatt. dynamics, optical and coupled channel anal. 80−78297
^{12}C(p,p'), 185 MeV, elastic and inelastic scatt., proton polarisation and ang. distribs. 79−59060
^{12}C(p,p'), Glauber model, shell model wave functions, EM form factor, spin effects 77−46164
^{12}C(p,p'), 20-40 MeV, pol. p, anal. powers, imaginary spin-orbit pot., coupled channels anal. 80−102179
^{12}C(p,p), 1 GeV elast. and inelast. scatt. and nuclear deform., Glauber theroy 77−6377
^{12}C(p,p), 144 MeV, elastic scatt. cross sections, optical pot. 80−42660
^{12}C(p,p), 50-160 MeV, energy depend. optical pot. 80−22830
^{12}C(p,p), 60 to 183 MeV, folded potentials for d intermediate channels 79−17868
^{12}C(p,p), optical potential, spin-orbit term 80−52668
^{12}C(p,p), radial sensitivity of optical pot. 80−86869
$^{12}C(p,\pi^+)$, optical model orthogonality constraints for bound and continuum waves 79−89306
$^{12}C(p,\pi^+)^{13}C$, 185 MeV, DWBA with Kisslinger type optical pot. 78−4938
$^{12}C(\pi,X)$, deep inelastic, π and Δ optical pot. effects, semiclassical transport model 80−52698
$^{12}C(\pi,\pi')$, monopole scatt., opt. pot., coupled-channel formalism 78−94034
$^{12}C(\pi,\pi)$, 1.12 GeV, covariant optical model, nucl. struct. calc. 77−14197
$^{12}C(\pi,\pi)$, nonlinear meson dynamics and binding corrections, optical pots. 80−106080
$^{12}C(\pi,\pi)$ 28 to 260 MeV, corrections to optical potential, role of ρ^2 term 78−70574
$^{12}C(\pi,\pi)$ inelastic wavefunctions, optical model with Kisslinger pot. 77−18611
$^{12}C(\pi^+,\pi^+)$, 0-300 MeV, cross sections, pion-nucleus optical pot. including nuclear Hamiltonian 80−68706
$^{12}C(\pi^+,\pi^+)$, 40 MeV, differential cross sections and strength parameters, optical model fit 80−18347
$^{12}C(\pi^+,\pi^+)$, 49.9 MeV, differential cross sections, partial wave and optical model anal. 79−22333
$^{12}C(\pi^+,\pi^+)$, elast. and inelast. scatt., 50 MeV, ang. distrib. determ. optical model and DWBA 79−45304
$^{12}C(\pi^+,\pi^+)$, phase shift equivalent optical pots., π wave function constraint 79−9629
$^{12}C(\pi^\pm,\pi^\pm)$, resonance region, first order optical pot. calcs. 79−40957
$^{12}C(t,t)^{12}C$, 15, 17 MeV, polarised t, differential cross sections and optical model fits 78−41730
$^{13}C(\pi^+,\pi^0)$, angle integrated cross section, optical pot., n and p radius differences 80−32307
^{13}C spectroscopic factors, cross sections DWBA anal. optical model parameters from $^{12}C(^{16}O,X)$ 80−13371
^{13}C, state transition ang. distrib., optical parameters from $^{12}C(^7Li,^6Li)$ 79−75904
$^{13}C(^{13}C,^{24}Mg)$, 3.05-6.88 MeV, fusion cross section energy depend., optical anal. 80−42724
^{13}C(d,X), 13 MeV, cross section, vector and power, optical model parameters, DWBA anal. 79−22301
^{13}C(p,d) modified DWBA anal., optical model parameter influence on vertex consts. *(Russian)* 78−78340
$^{13}C(\pi^+,\pi^0)$, 0-300 MeV, cross sections, pion-nucleus optical pot. including nuclear Hamiltonian 80−68706
nuclear optical model continued
$^{13}C(\pi^+,\pi^0)$, 1st order pion-nucleus pot. calc. 77−23113
$^{13}C(\pi^+,\pi^0)$, total cross section energy depend., first order optical pots. 79−76028
$^{13}C(\pi^+,\pi^0)^{13}N$, charge-exchange transition vertex, optical pot. 77−6461
$^{13}C(\pi^+,\pi^0)^{13}N$ in (3,3) reson. region, optical model calc. 77−18610
^{14}C spectroscopic factors, cross sections DWBA anal. optical model parameters from $^{12}C(^{16}O,X)$ 80−13371
$(^{12,13}C,X)$ elastic, inelastic and single nucleon transfer excitation functions optical and DWBA anal. 80−13492
Ca isotopes, neutron RMS radii from pion total cross-sections 77−57589
^{A}Ca, A=40, 42-44, 48, pionic X-rays, strong interaction and isotope shifts, π-nuclear optical pot. 80−53169
^{A}Ca, A=40, 48, nuclear matter density distrib., saturation effect, optical potential from (α,α) 80−63115
$^A Ca(^{12}C,^{12}C)$, A=40,42,48, 47-51 MeV, ang. distribs. optical model anal., surface transparency 79−45291
$^A Ca(^7Li,^7Li)$, A=40, 48, 88 MeV, optical potentials, phenomenological and microscopic 80−52687
$^A Ca(\alpha,\alpha)$, 40-62 MeV, A=40,44, elastic and inelastic, ang. distribs. and collective state excitation 79−6650
$^A Ca(\alpha,\alpha)$, A=40, 42, 44, 48, 104 MeV, cross sections and optical pots., nuclear size 80−68524
$^A Ca(\alpha,\alpha)$, A=40, 42, 44, 48, 104 MeV nuclear size and density distrib. from folding model anal. 80−68525
$^A Ca(\alpha,\alpha)$, A=42,44,48, 29 MeV, energy and mass depend. of extracted optical potentials 79−49632
^{A}Ca(p,p), 30.3 MeV, A=40,44,48, cross section ratio, optical model anal. 79−54441
^{A}Ca(p,p), 800 MeV, polarised p, A=40, 42, 44, 48, differential cross sections and anal. powers 79−36244
$^A Ca(\pi,\pi)$, A=40,48, 40-241 MeV, first and second order optical pots., resonance behaviour 80−68624
^{14}Ca(p,p), A=40, 42, 44, 48, 1 GeV, cross sections using nuclear densities from self-consistent methods *(Russian)* 78−41724
^{40}Ca (α,α), α-nucleus pot., microscopic calc. 78−8788
^{40}Ca, anomalously small absorption of α-particles 79−93640
^{40}Ca, pionic, Lorentz-Lorenz quadrupote term, P-wave optical pot. 79−22252
^{40}Ca, radius difference to ^{48}Ca, from 104 MeV alpha scatt. optical model calcs. 79−454
$^{40}Ca+^{16}O$, inelastic scatt., exit channel distorting pot., DWBA calc. 78−94025
$^{40}Ca+^{20}Ne$, 36-95 MeV, Coulomb-nuclear interference 78−50210
$^{40}Ca+^{40}Ca$, elastic scatt. excitation functions, interf. effects 77−50155
^{40}Ca+P, 100-1050 MeV, optical pot. real part, nuclear matter approach 77−82890
$^{40}Ca(^AB,^AB)$, A=10,11, angular distrib., Woods-Saxon and double-folding optical models 80−52691
$^{40}Ca(^{11}B,^{10}B)$, 51.5 MeV, n stripping, DWBA anal. with Woods-Saxon and double folding optical pots. 80−102171
$^{40}Ca(^{11}B,^{12}C)$, 32, 68 MeV, single proton pickup, DWBA anal., optical pot. 80−106037
$^{40}Ca(^{11}B,^{12}C)$, 51.5 MeV, p pickup, DWBA anal. with Woods-Saxon and double folding optical pots. 80−102171
$^{40}Ca(^{13}C,^{14}N)$, 40, 68 MeV, single proton pickup, DWBA anal., optical pot. 80−106037
$^{40}Ca(^{16}O,^{16}O)$, 60 MeV, long range absorption and optical model effects from strong inelastic coupling 80−535
$^{40}Ca(^{16}O,^{16}O)$, complex heavy ion optical pot., microscopic BHF derivation 80−106067
$^{40}Ca(^{16}O,^{16}O)$, optical pot., nuclear matter approach, energy density matter [-] 80−83112
$^{40}Ca(^{16}O,X)$, 40-214 MeV, fusion and elastic scatt. cross sections, optical anal. 80−32314
$^{40}Ca(^{17}O,\ ^{17}O)$, 61 MeV, elastic and inelastic, microscopic single folding model anal. 80−52692
$^{40}Ca(^3He,^3He)$, 27-84 MeV, energy depend. of optical model param. 78−41736
$^{40}Ca(^3He,^3He)$, 90-120 MeV, cross sections, deduced unambiguous optical pot. 79−13311
$^{40}Ca(^3He,^3He)$, pol. ^{3}He, 33.3 MeV, differential cross section and anal. power, optical pots. 80−42627
$^{40}Ca(^{40}Ar,^{40}Ar)$, 191, 236, 272 MeV, cross sections, interaction radius, Fresnel and optical model anal. 79−59084
$^{40}Ca(^{40}Ar,^{40}Ar)$, 191, 236, 272 MeV, elastic cross sections, optical and Fresnel model anals. 80−22858
$^{40}Ca(^{40}Ca,^{40}Ca)$, 64-120 MeV, optical model and strong absorpt. model anal. 77−41994
$^{40}Ca(^{40}Ca,^{40}Ca)$, optical pot., nuclear matter approach, energy density matter [-] 80−83112
$^{40}Ca(^6Li,^6Li)^{40}Ca$, 30 MeV, ang. distribs. for elastic and inelastic scatt. at backward angles 79−13343
$^{40}Ca(^9Be,\ ^9Be')$, 45, 60 MeV, low lying collective states, ang. distribs., DWBA double folding pot. anal. 80−78113
$^{40}Ca(^9Be,\ ^9Be)$, 45, 60 MeV cross sections, ang. distribs., Wegner plot, optical and double folding anal. 80−47497
$^{40}Ca(K^+,K^+)$, 0.4-1.2 GeV/c, optical potl., cross-sections determ. 77−14184
$^{40}Ca(\alpha,\ \alpha)$, $(^6Li,\ ^6Li)$, velocity of refined folding model approaches 80−541
$^{40}Ca(\alpha,\alpha)$, 104 MeV, optical model analysis 78−41737
$^{40}Ca(\alpha,\alpha)$, 22 to 142 MeV, energy and mass depend. of extracted optical potentials 79−49632
$^{40}Ca(\alpha,\alpha)$, 27-9 MeV, anomalous large-angle scatt. 77−18583
$^{40}Ca(\alpha,\alpha)$, 29 MeV, optical pot., double folding model for anomalous large angle scatt. 78−70551
$^{40}Ca(\alpha,\alpha)$, 36-61 MeV, large angle struct. 78−41743
$^{40}Ca(\alpha,\alpha)$, back-angle anomaly, semi-microscopic absorpt. pot. 78−616
$^{40}Ca(\alpha,\alpha)$, optical pot., nuclear glory effect 78−21578
$^{40}Ca(\alpha,\alpha)$ 140 MeV, modified optical pot., folding pots. and energy depend. 78−70549
$^{40}Ca(\alpha,\alpha)^{40}Ca$, 166 MeV, matter density determ. from model-independ. anal. 77−38285
$^{40}Ca(\alpha,\alpha)$20-50 MeV anomalous elast. and inelast. scatt. 77−88161
$^{40}Ca(\alpha\alpha)$, 104 MeV, Fourier-Bessel anal. of optical pots. and nucl. matter densities 79−97716
$^{40}Ca(\alpha\alpha)$, <85.6 MeV, energy depend. of optical model params. 77−3024
^{40}Ca(d,p), 7 MeV, cross-sections calcs. from pseudopotentials, spectroscopic factors 78−572

nuclear optical model continued
^{40}Ca(e,e'p), multiparticle approach to expt. data anal. 77−88112
^{40}Ca(n,n')^{40}Ca, imaginary inelastic transition form factor, microscopic theory 78−50175
^{40}Ca(n,n), 10 and 50 MeV, optical model real potential 78−58274
^{40}Ca(n,n), 11-26 MeV, differential cross sections, global optical model anal. 80−18298
^{40}Ca(p,X), multiple scattering theory, validity of closure approx. 79−45269
^{40}Ca(p,p), 20-50 MeV differential cross section, polarisation ang. distrib., optical model exchange terms 80−27638
^{40}Ca(p,p), 30 MeV, optical pot. imaginary part calcs. 80−86868
^{40}Ca(p,p), 30.3 MeV, microscopic anal. 79−93631
^{40}Ca(p,p), absorbing optical pot., Coulomb correction term 80−73831
^{40}Ca(p,p), evidence for ang. mom. depend. optical model pots. 79−13290
^{40}Ca(p,p), imaginary spin-orbit term in proton optical potential, ang. distribs. 78 58273
^{40}Ca(p,p), spline interpolation method appl. to optical potential 80−32272
^{40}Ca(p,π^+), differential cross sections, DWBA calc. 79−85415
^{40}Ca(π^+,π^+), 40 MeV, differential cross sections and strength parameters, optical model fit 80−18347
^{40}Ca($\pi^\pm$,$\pi^\pm$), resonance region, first order optical pot. calcs. 79−40957
^{44}Ca(^{6}Li,^{6}Li)^{44}Ca, 30 MeV, ang. distribs. for elastic and inelastic scatt. at backward angles 79−13343
^{44}Ca(^{7}Li, ^{7}Li), 34 MeV, ang. distribs., cross sections, double folding model anal. 80−78313
^{46}Ca(α,α), 36-61 MeV, large angle struct. 78−41743
^{48}Ca (α, α), 104 MeV, Fourier-Bessel anal. of optical pots. and nucl. matter densities 79−97716
^{48}Ca, radius difference to ^{40}Ca, from 104 MeV alpha scatt. optical model calcs. 79−454
^{48}Ca, strongly bound π-nuclear states, criticality condition, optical pot. 78−90325
^{48}Ca+^{16}O 56 MeV, transitions to resolved levels, optical model parameter 78−41758
^{48}Ca(^{16}O, ^{15}N), ^{15}N excitation contrib. in optical pot., DWBA grazing peak shift 80−86921
^{48}Ca(^{6}Li, ^{6}Li), (α, α), velocity of refined folding model approaches 80−541
^{48}Ca(d,t)^{47}Ca, 13.5 MeV, polarised deuterons, low-lying levels in ^{47}Ca 78−13114
^{48}Ca(p,n), nucleon optical potential from Lane model 80−83097
^{48}Ca($\pi^\pm$,$\pi^\pm$), optical pot. ambiguities, neutron radius determ. 79−17872
Ca(n,n) 20, 26 MeV, Coulomb correction term to optical model pot. 77−38280
Ca(n,n)Ca, 11-26 MeV, optical model fit 77−79372
Ca(p,p), 30 MeV, A=40, 48, pick-up and inelastic scatt. contributions to p optical pot. 78−25182
^{114}Cd(p,p'), optical pot. deform. effect on analysing power and p-γ ang. correlations 79−17903
^{59}Co+n, 8-31 MeV, spin-spin depend. of total cross section 78−17172
^{59}Co(^{16}O,^{16}O), 142 MeV, optical model anal. of ang. distrib. meas. 78−58295
^{59}Co(^{16}O,^{16}O), 36-56 MeV, cross sections, optical and double-folding model anal. 79−6693
^{50}Cr(p,p) and (p,p'), E_p=6 MeV, cross sections, opt. pot. parameters 78−13086
^{52}Cr+^{13}C, 105 MeV, ^{51}V, ^{51}Cr, ^{53}Mn, level scheme, DWBA and optical model anal. 79−36159
^{52}Cr(^{16,18}O,^{16,18}O'), 30-42 MeV, excitation function differences, optical and DWBA anals. 79−63698
^{52}Cr(d,p)^{53}Cr, deuteron break-up model anal. of cross-section, vector analysing power and angular correlation 80−27648
^{52}Cr(p,p) and (p,p'), E_p=6 MeV, cross sections, opt. pot. parameters 78−13086
Cr(n,n), A=50, 52, 54, 1.5-3.0 MeV elast. and inelast. scatt., differential cross section *(Russian)* 78−25199
^{65}Cu(α,α), 27-9 MeV, anomalous large-angle scatt. 77−18583
Cu(α,α), A=63 and 65, 48 MeV, I.L. potential depth, optical model anal. 78−50187
Cu(n,n), 14.2 MeV, polarisation in forward angle scatt. 80−18282
Cu(n,n), 16.1 MeV, polarisation meas., optical model anal. 79−22264
Cu(n,n), fast neutrons, differential cross sections, optical model calcs. *(Chinese)* 79−9572
^{168}Er(d,t)^{167}Er, 17 MeV, band heads, two-step process 78−62551
^{19}F+^{28}Si spin orbit pot., single folding model and cluster model 80−9196
^{19}F(^{16}O,^{16}O)^{19}F, 32.0 MeV, parity-depend. optical model calc. 77−50152
^{19}F(d,d), elastic scatt., 1.2-2.5 MeV, excitation functions, ang. depend., optical model anal. 79−9594
^{54}Fe(^{16,18}O,^{16,18}O'), 30-42 MeV, excitation function differences, optical and DWBA anals. 79−63698
^{54}Fe(^{6}Li,^{6}Li), 38, 44, 50 MeV, elastic and inelastic scatt., optical model anal. and inelastic scatt. deformation lengths 79−59082
^{54}Fe(^{7}Li, ^{7}Li), 36, 42, 48, MeV, elastic and inelastic scatt., optical model anal. and inelastic scatt. deformation lengths 79−59082
^{54}Fe(p,p), 5.5-6.2 MeV, resonance effects, deformation, spectroscopic factors, statistical, optical and DWBA anal. 79−6593
^{56}Fe(^{3}He,^{3}He), 33-83 MeV, details of nuclear surface 77−34324
^{56}Fe(p,p), 6 MeV, elastic and inelastic, quadrupole deformation, IAR excitation, optical pots. *(Russian)* 80−63149
^{56}Fe(p,p), evidence for ang. mom. depend. optical model pots. 79−13290
^{58}Fe(^{7}Li, ^{7}Li), 34 MeV, ang. distribs., cross sections, double folding model anal. 80−78313
Fe(p,p'), A=54,6, E=17.2, 20.4, 24.6 MeV, polarised protons, optical model, DWBA anal. 78−13094
Fe(π^+,π^+) elast. and inelast. scatt., 50 MeV, ang. distrib. determ. optical model and DWBA 79−45304
Ge+^{12}C, 48 MeV, surface transparency of optical pots. 78−13146
Ge+^{16}O, 56 MeV, surface transparency of optical pots. 78−13146
Ge+^{18}O, 56 MeV, surface transparency of optical pots. 78−13146
^{74}Ge(^{18}O,^{16}O)^{76}Ge, coupled-channel Born approx. anal. 77−82954
^{76}Ge(^{16}O,^{18}O)^{74}Ge, coupled-channel Born approx. anal. 77−82954
Ge(n,n'), 2^+ level excitation cross sections, intermediate resonances, optical model with coupled channels *(Russian)* 79−40897
H(^{3}He,^{3}He), 33 MeV, ^{3}He polarisation anal. power meas. optical model anal. 77−38286
(HI,HI), local density dependence of NN interaction, double-folding calcs. 80−83114

nuclear optical model continued
^{1}H(p,X), elastic, inelastic and charge exchange cross sections in optical model 80−68665
^{2}H propagation in nucl. matter, spin depend. of optical pot. 79−93635
^{2}H scattering, deformed tensor interactions, folding model 80−57783
^{2}H(d,d), medium energy, total cross section, optical model calcs. 79−9593
^{2}H(π,p)p, absorptive P-wave pion-nucleus optical pot. 79−22327
^{2}H(π,p)p, reactive two body contrib. to pion-nucleus optical pot. 80−9313
^{2}H(π,π), comparison of Faddeev eqn. approach with optical potential 79−76030
^{2}H(π^+,p)p, pion absorption, absorptive P-wave pion-nucleus optical pot. 79−76031
^{2}H(π^+,p)p, pionic disintegration, absorptive π-nucleus optical pot., microscopic model 80−99191
(^{3}H,^{3}H), polarised scatt., optical model parameters 78−70540
^{4}H(p,p), microscopic optical pot. calc. 79−85423
He(^{3}He,^{3}He), 33 MeV, ^{3}He polarisation anal. power meas. optical model anal. 77−38286
(^{3}He,^{3}He), elastic scatt., optical spin-orbit pot., spin-orbit strength 79−85480
(^{3}He,^{4}He), microscopic optical pots. to overcome DWBA difficulties 77−54198
(^{3}He, ^{3}He), 119 MeV, optical pot. parameters energy and mass depend. 80−32289
(^{3}He, ^{3}He), uniqueness of optical pot. 79−97685
(^{3}He, ^{3}He) scatt., polarisation effects, phenomenological ^{3}He pots. 79−97112
^{3}He elastic scatt. angular distribs., optical potentials and volume integrals for targets with A=10 to 58 80−52686
^{3}He, optical pot., coupled reaction channel anal. 78−570
^{3}He(e,e), relationship to ^{3}He(π^-,π^-) 80−78323
^{3}He(n,n), 1-24 MeV optical model anal. 77−23027
^{3}He(p,p), 6.8 to 16.2 MeV, optical model pot. calcs. of cross section and polarisation data 79−63672
^{3}He(π,π), 145, 180, 195 MeV, differential cross section, mesonic exchange effects, form factors, optical pot. 79−85376
^{3}He(π,π), and charge exchange, calc. based on first order optical potl. 77−6454
^{3}He(π,π), optical potential in momentum representation 80−78324
^{3}He(π^-, π^0)^{3}H, 100 to 260 MeV optical-model calcs. 77−79403
^{3}He(π^-,π^-), 145, 180 and 195 MeV, relationship to ^{3}He(e,e) 80−78323
^{3}He(π^-,π^0)^{3}H, optical potential in momentum representation 80−78324
^{3}He($\pi^\pm$,$\pi^\pm$), 100-260 MeV, optical model calc. 77−79403
^{4}He (d,d), pol. d, 20 MeV, optical pot. strong tensor term, anal. powers 80−37364
^{4}He ($\pi^\pm$,$\pi^\pm$), 100-260 MeV, optical-model calc. 77−79403
^{4}He, π^0 coherent photoprod., screening corrections and rescatt. *(Russian)* 78−41697
^{4}He+N, potential calc. using microscopic model 77−88091
^{4}He+π^- second-order optical pot., multiple scatt. theory 77−82966
^{4}He(^{3}He,^{3}He), 60.2, 113.1 MeV, ang. distrib., optical and coupled channel anal., cross sections 80−47492
^{4}He(α,α), 158.2 MeV, differential cross sections, optical model anal. 79−22307
^{4}He(α,α), nonlocal and separable complex path *(Russian)* 77−306
^{4}He(α,α) microscopic optical pot. for elastic scatt. in terms of nuclear density 79−54444
^{4}He(p,X), multiple scattering theory, validity of closure approx. 79−45269
^{4}He(p,X)^{3}He, 6.85 GeV/c, Glauber multiple model 79−63664
^{4}He(p,p), 560-1730 MeV, Dirac eqn. optical model anal. 78−29467
^{4}He(p,p), 600, 1050 MeV, optical model partial-wave anal. 77−10406
^{4}He(p,p), 788 MeV, back angle diffraction struct., Dirac, eqn. optical model 80−68667
^{4}He(p,p), differential elastic scatt. cross-section, 1 GeV protons *(Russian)* 77−79382
^{4}He(p,p), intermediate energies, energy depend. of optical model 77−23006
^{4}He(p,p), intermediate energy, microscopic momentum space optical pot. calc. 79−71853
^{4}He(p,p), medium energy, anal. power, relativistic optical model anal. 79−40925
^{4}He(p,p)^{4}He, optical model anal. 78−78369
^{4}He(π,π), 1.12 GeV, covariant optical model, nucl. struct. calc. 77−14197
^{4}He(π,π), (3,3) region, multiple scatt. theory study by optical pot. method *(Russian)* 80−13509
^{4}He(π,π), calc. based on first order optical potl. 77−6454
^{4}He(π,π), low energy, first order optical pot., Pauli principle corrections, nuclear binding 80−27675
^{4}He(π,π), lowest order optical model 77−6456
^{4}He(π,π), single scatt. optical pot., Pauli principle and binding effects on cross section 80−86933
^{4}He(π,π) 28 to 260 MeV, corrections to optical potential, role of ρ^2 term 78−70574
^{4}He(π^-,π^-), 1.12 GeV, multiple scatt. theory 77−6466
^{4}He(π^-,π^-), total cross section, improved optical pot., second order correction 79−22330
^{4}He($\pi^\pm$, $\pi^\pm$), resonance region, first order optical pot. calcs. 79−40957
He(π^-,π^-), 1.12 GeV, multiple scatt. anal., optical model potl. 77−6453
^{165}Ho(π^-,X), 175 MeV/c, monopole and quadrupole strong interaction effects in pionic atoms 78−41777
H(p,x), direct and charge transfer scattering processes, second quantisation 80−78289
^{115}In(p,p), 2.0-6.7 MeV, cross sections, Hauser-Feshbach optical calcs. for p absorption systematics 80−47483
^{39}K(^{12}C,^{12}C), 54, 63 MeV, angular distrib., Woods-Saxon and double-folding optical models 80−52691
^{139}La(^{86}Kr,X), 505, 610 and 710 MeV, elastic and deeply inelastic reactions, optical model anal. 78−66316
(Li,Li) cross sections on 40≤A≤91 targets, 28 and 34 MeV, optical model parameters 77−54248
(^{6}Li,^{6}Li), 30, 88 MeV, M3Y folding model eval., model independ. anal. 80−78317
(^{6}Li, ^{6}Li), 22.8 MeV, optical model test from vector anal. power data 79−97729
(^{6}Li, ^{6}Li), 99 MeV, A=12-208, ang. distribs. from double folding model pots. 80−106074
(^{6}Li, ^{6}Li) elastic scatt., failure of double folded pot. model 78−62566

nuclear optical model continued
^{6}Li, Pauli distortion effects in folded optical pot. 79−6454
^{6}Li+n reactions, 4.4-7.3 MeV, DWBA and optical model anal. 77−18539
^{6}Li(^{3}He,^{3}He), 27 MeV, cross sections, three body and optical model calcs. 79−76009
^{6}Li(^{3}He,p)^{8}Be, 14 MeV, p-^{8}Be optical model parameters 78−25208
^{6}Li(p,p'), 185 MeV, optical model anal. of inelastic scatt. to 1st excited state, deformation parameters 79−22300
^{6}Li(p,p), 144 MeV, elastic scatt. cross sections, optical pot. 80−42660
^{7}Li(α,α)^{7}Li elastic scatt. generalised optical potentials, three-body approximation *(Russian)* 79−13313
^{7}Li(π,π), elastic and inelastic, nuclear struct. effects in optical model 77−23112
^{7}Li(π^{+},π^{-})^{7}Be, distorted wave impulse calc., optical pot., multiple scatt. 78−50138
^{7}Li(π^{+},π^{0}), 1st order pion-nucleus pot. calc. 77−23113
^{A}Li(π^{+},π^{+}), A=6, 7, 50 MeV, optical model anal., core+valence neutron model, isotopic effects 79−6715
Li(d,d), 3-10 MeV, A=6,7, differential cross section, optical model anal. 77−61435
^{175}Lu(π^{-},X), 230 MeV/c, monopole and quadrupole strong interaction effects in pionic atoms 78−41777
Mg isotopes, elastic proton scatt., 9.1 MeV, potential parameters 77−316
^{A}Mg(^{16}O,^{16}O), A=24, 26, 20-35 MeV cross sections and excitation functions, optical model anal. 79−93655
^{A}Mg(^{7}Li,^{7}Li), A=24, 26, 88 MeV, optical potentials, phenomenological and microscopic 80−52687
^{24}Mg+^{16}O, 30-81 MeV, fusion cross section, elastic scatt. ang. distrib., optical model anal. 78−78412
^{24}Mg+^{18}O, 32-72 MeV, fusion cross section, elastic scatt. ang. distrib., optical model anal. 78−78412
^{24}Mg+^{7}Li inelastic scatt., 34 MeV, microscopic interpretation, double folding model 77−14156
^{24}Mg(^{12}C,^{12}C), 20-36 MeV, ang. distribs., S-matrix elements, optical model parameters 79−93660
^{24}Mg(^{3}He,^{3}He), 130 MeV, elastic scatt. ang. distribs., optical model anal. 78−94020
^{24}Mg($\alpha,\alpha_{1}\gamma$), 104 MeV, alpha-gamma ang. correl., quadrupole deform. 77−88155
^{24}Mg(p,p') 15-35 MeV, low lying state differential cross sections, two step effects 79−89304
^{24}Mg(p,p'), 49.5 MeV, consistent folding model, HF calc. for E2, E4 transitions 79−22288
^{24}Mg(p,p') 17.5 MeV 79−22288
^{24}Mg(p,p), 22.5 to 28.0 MeV, differential cross sections, optical, coupled channel, core excitation anal. 79−6613
^{24}Mg($\pi^{\pm},\pi^{\pm}$) 180 MeV elastic and inelastic scatt., optical model and DWBA calcs. 78−89915
^{26}Mg+^{16}O, 29-81 MeV 78−78412
^{26}Mg(^{11}B,^{11}B), (^{11}B,^{10}B), (^{11}B,^{10}Be), 31 MeV, optical model and DWBA anal. 77−26785
microscopic optical model pot., (n,n) and (p,p) cross sections 78−54729
Mo stable isotope eval., 5 keV-5 meV neutrons, rel. to reactor structural steel 80−13620
^{A}Mo(d,d) A=92-100, 21.5 MeV, elastic and inelastic cross sections, RPA and folding model 79−553
^{A}Mo(n,n) A=92,96,98,100, E_{n}=7 to 26 MeV, determ. optical model pot. parameters 79−22286
^{A}Mo(p,n), A=94-96, 98, 1.7-6.7 MeV, total cross sections, p strength functions, optical model anal. 80−18301
^{92}Mo(N,N)^{92}Mo, optical model anal. 80−47473
^{92}Mo(n,n), 7-26 MeV, differential cross sections, global optical model anal. 80−18298
^{92}Mo(n,n), elastic and inelastic, 11 MeV, isospin effects, optical and deformation parameters 79−17794
Mo(d,d), A=92, 94, 96, 98, 100, elastic scatt., optical model anal., deformation parameters 78−94017
Mo(n,X), 2 keV-20 MeV cross sections, coherent optical and statistical model calcs. 80−18318
Mo(n,n), unified optical model anal., Lane model breakdowns 79−17873
Mo(p,p), unified optical model anal., Lane model breakdowns 79−17873
^{13}N state transition ang. distrib., optical parameters from ^{12}C(^{7}Li, ^{6}He) 79−75904
^{14}N residual states, vector anal. power. optical pot. from ^{12}C(^{6}Li,α), pol. ^{6}Li 79−97697
^{14}N spectroscopic factors, cross sections DWBA anal. optical model parameters from ^{12}C(^{16}O,X) 80−13371
^{14}N+^{10}B, sub Coulomb energy, fusion cross section, optical model anal. 77−34335
^{14}N(α,α), 20 to 24 MeV 77−65228
^{14}N(γ,π^{-}), DWIA anal., wave function and π optical pot. effects on cross section 80−63168
^{14}N(p,d) modified DWBA anal., optical model parameter influence on vertex consts. *(Russian)* 78−78340
^{14}N(p,p'), 25-40 MeV, level cross sections, optical parameters, DWBA anal., tensor effective interaction 80−68555
^{14}N(p,p), 144 MeV, elastic scatt. cross sections, optical pot. 80−42660
^{14}N(p,p), average geometry optical model potential, doorway state effects 77−79367
^{93}Nb(n,γ), cross-section below 3 MeV, coherent optical and statistical model calcs. 77−26713
Nd, A=148, 150, pionic X-rays in 4f→3d transition, neutron isotope shift 77−75347
^{A}Nd(n,n) A=142,144,146,148,150, 7 MeV, optical pot. and deformation, cross sections 79−89230
^{144}Nd(^{12}C,^{14}C)^{142}Nd, 78 MeV, Coulomb excitation effect 77−46186
^{20}Ne+^{12}C, 17 to 35 MeV, excitation functions, optical model anal. 78−41759
^{20}Ne(α,α), 20 to 24 MeV 77−65228
^{20}Ne(p,p') 24.5 MeV, consistent folding model, HF calc. for E2, E4 transitions 79−22288
^{21}Ne deduced spectroscopic factors, levels and anal. powers from ^{20}Ne(d_{pol},p) 80−83087
^{21}Ne(^{3}He,α)^{20}Ne, large angle excitation function fluctuations, DWBA and opt. model calcs. 79−89318
Ni+^{12}C, 48 MeV, surface transparency of optical pots. 78−13146
Ni+^{16}O, 56 MeV, surface transparency of optical pots. 78−13146
Ni+^{18}O, 56 MeV, surface transparency of optical pots. 78−13146

nuclear optical model continued
Ni(^{16}O,^{18}O), surface transparent pots., and CCBA anal. of diffractive behaviour 78−50206
^{A}Ni, A=58,60,62, elastic and inelastic neutron scatt., 1.5-3 MeV *(Russian)* 77−26689
^{A}Ni(^{7}Li, ^{7}Li), A=58, 60, 34 MeV, ang. distribs., cross sections, double folding model anal. 80−78313
^{A}Ni(n,n), A=58,60,62,64, 5 MeV, differential cross sections, optical, statistical and coupled channel anals. *(Russian)* 80−37377
^{A}Ni(p,p), 1 GeV, A=58,60,62,64, elastic and inelastic, Glauber anal., matter distribs. 79−75883
^{58}Ni (p,p) 100 MeV, systematic optical model anal. 78−66274
^{58}Ni vector polarised ^{6}Li elastic scatt., full optical model anal. 78−70553
^{58}Ni(^{16}O,^{16}O), 60 MeV, cross section ang. distribs., optical model parameters 79−6694
^{58}Ni(^{3}He,^{3}He), 27-84 MeV, energy depend. of optical model param. 78−41736
^{58}Ni(^{3}He,^{3}He), 90-120 MeV, cross sections, deduced unambiguous optical pot. 79−13311
^{58}Ni(^{58}Ni,X), optical potential, nuclear matter approach 80−57801
^{58}Ni(^{6}Li,^{6}Li), elastic and inelastic, 74 MeV, folding optical model parameters 80−102201
^{58}Ni(^{7}Li,^{7}Li'), 19 MeV, first 2^{+} states Coulomb-nuclear interference, optical and DWBA anal. 80−22852
^{58}Ni(α,α), 139 MeV, optical model analysis 78−41737
^{58}Ni(α,α), 27 to 49 MeV, cross sections, optical model anal. 79−85483
^{58}Ni(α,α), <85.6 MeV, energy depend. of optical model params. 77−3024
^{58}Ni(α,α), radial sensitivity of optical pot. 80−86869
^{58}Ni(α,α) 140 MeV, modified optical pot., folding pots. and energy depend. 78−70549
^{58}Ni(α-α), 50.2 MeV, composite particle optical pot. discrete ambiguities, partly Pauli-forbidden states 80−86870
^{58}Ni(d,d), 10 MeV, multishell form factors 79−93636
^{58}Ni(d,p)^{59}Ni, deuteron break-up model anal. of cross-section, vector analysing power and angular correlation 80−27648
^{58}Ni(p,p), 1 GeV, Fresnel and two-body correl. effects 78−82353
^{58}Ni(p,p), 800 MeV, elastic and inelastic, cross section, deformation lengths, optical and DWBA anals. 80−68664
^{58}Ni(p,p), evidence for ang. mom. depend. optical model pots. 79−13290
^{58}Ni(π,π), 162 MeV, elastic and inelastic ang. distribs., optical and PWIA anals. 80−42706
^{58}Ni(π,π), ang. distribs., optical model calcs. 78−58308
^{60}Ni+n, total and differential cross-sections, optical-statistical and coupled-channel models 80−13472
^{60}Ni(^{16}O,^{16}O), 142 MeV, optical model anal. of ang. distrib. meas. 78−58295
^{60}Ni(d, d), 9, 12 MeV, polarised d, excitation functions, optical model parameters and spin-orbit pot. 79−67756
^{60}Ni(t,d), sub-Coulomb region, neutron orbit radius determ. 77−38217
^{61}Ni(^{3}He,^{3}He) 39.7 MeV, optical pot. mass depend. 77−34327
^{64}Ni, elastic and inelastic scatt. of 1.5-3.0 MeV neutrons *(Russian)* 77−61428
Ni(α,α), A=62 and 64, 48 MeV, I.L. potential depth, optical model anal. 78−50187
Ni(p,p'), A=58,60,62, E=17.2, 20.4, 24.6 MeV, polarised protons, optical model, DWBA anal. 78−13094
^{A}O($\pi^{\pm},\pi^{\pm}$), A=16, 18, resonance region, proton and neutron distribs. 80−91195
(^{16}O,^{16}O), M3Y folding model eval., model independ. anal. 80−78317
^{16}O α-cluster states, widths and resonances, optical model, direct transfer in ^{12}C(^{6}Li,d) 80−105975
^{16}O residual states, vector anal. power. optical pot. from ^{12}C(^{6}Li,d), polarised ^{6}Li 79−97697
^{16}O, vector polarised ^{6}Li elastic scatt., full optical model anal. 78−70553
^{16}O+^{12}C, 15-72 MeV, gross struct. in γ-ray yields 78−78405
^{16}O+^{12}C elastic scatt. and total reaction cross sections near Coulomb barrier 77−54235
^{16}O+^{12}C scattering, l-depend. absorptive pot., long life pot. resonances 78−62570
^{16}O+^{16}O, elastic scatt. excitation functions, interf. effects 77−50155
^{16}O+^{16}O heavy ion folding potential, antisymmetrisation effects 78−94023
^{16}O+^{28}Si, 33-215 MeV, optical pots. anal. 77−41988
^{16}O+π, optical potential, p-wave absorptive pot. and higher-order corrections 79−45303
^{16}O(^{16}O,^{16}O), optical pot., nuclear matter approach, energy density matter [-] 80−83112
^{16}O(^{3}He, ^{3}He), pol. ^{3}He, 33.3 MeV, differential cross section and anal. power, optical pots. 80−42627
^{16}O(^{9}Be,^{9}Be) 14, 20 and 26 MeV, optical model parameters 79−26449
^{16}O(K^{+},K^{+}), 0.4-1.2 GeV/c, optical potl., cross-sections determ. 77−14184
^{16}O(α,α), 20 to 24 MeV 77−65228
^{16}O(α,α), 28 to 33.6 MeV, optical potential of incident channel 78−58291
^{16}O(α,α), effect of Pauli principle on optical potl. 77−6412
^{16}O(α,α) 17 to 27 MeV, backscatt., dynamic deformation and excitation functions, optical anal. 80−18227
^{16}O(α,d)^{18}F, 28 to 33.6 MeV, forward angle yield, optical potential of incident channel 78−58291
^{16}O(n,n), totally microscopic description, optical pot. and many-body theory 79−546
^{16}O(p,p'), 20-40 MeV, pol. p, anal. powers, imaginary spin-orbit pot., coupled channels anal. 80−102179
^{16}O(p,p), 1 GeV, cross sections using nuclear densities from self-consistent methods *(Russian)* 78−41724
^{16}O(p,p), 20-50 MeV differential cross section, polarisation ang. distrib., optical model exchange terms 80−27638
^{16}O(p,p), 50-160 MeV, energy depend. optical pot. 80−22830
^{16}O(p,p), average geometry optical model potential, doorway state effects 77−79367
^{16}O(p,p), evidence for ang. mom. depend. optical model pots. 79−13290
^{16}O(p,p), imaginary spin-orbit term in proton optical potential, ang. distribs. 78−58273
^{16}O(p,p), spline interpolation method appl. to optical potential 80−32272
^{16}O(p_{pol},2p), cross section, analysing power, energy sharing spectra, distorted wave impulse approx. 80−78291
^{16}O(π,π), 1.12 GeV, covariant optical model, nucl. struct. calc. 77−14197
^{16}O(π,π), 40-342 MeV, second order optical pot. parameters 79−22337

nuclear optical model continued
$^{16}O(\pi,\pi)$, binding effects in optical model with S-wave interaction 77−14196
$^{16}O(\pi,\pi)$, nonlinear meson dynamics and binding corrections, optical pots. 80−106080
$^{16}O(\pi,\pi)$, T-matrix from isobar-hole model, many-body corrections, optical pot. parameter 80−9312
$^{16}O(\pi,\pi)$ low energy p-wave optical pot., absorptive part from isobar-hole model 79−85556
$^{16}O(\pi,\pi)$ optical pot., local field correction 80−68705
$^{16}O(\pi^+,\pi^+)$, 40 MeV, differential cross sections and strength parameters, optical model fit 80−18347
$^{16}O(\pi^+,\pi^+)$ 40 and 49.7 MeV, differential cross sections, partial wave and optical model anal. 78−70570
$^{16}O(\pi^+,\pi^+)$ elast. and inelast. scatt., 50 MeV, ang. distrib. determ. optical model and DWBA 79−45304
$^{16}O(\pi^\pm,\pi^\pm)$, resonance region, first order optical pot. calcs. 79−40957
$^{17}O(n,n')^{17}O$, imaginary inelastic transition form factor, microscopic theory 78−50175
$^{18}O+^{18}O$, elastic scatt. excitation functions, interf. effects 77−50155
$^{18}O+\pi^+$, inelastic and elastic scatt., neutron-proton radius differences and isovector deform. 79−40963
$^{18}O(\pi^+,\pi^-)^{18}Ne(GS)$, optical model calc. including ^{18}F intermediate state coupling, cross section 79−13349
$^{207}Pb(p,p')$, excitation of neutron-hole states, 61.2 MeV protons 78−8724
^{208}Pb, fast neutron scatt. and capture, microscopic isovector optical pot. test 80−52682
$^{208}Pb+^{16}O$, elastic scatt., transfer reactions, fission, total cross sections, optical model parameters 77−54246
$^{208}Pb+^{6}Li$, Coulomb and nucl. excitation in ^{6}Li dissociation 78−41770
$^{208}Pb(^{16}O,^{16}O)$, elastic scatt., exponential optical pots. 80−42681
$^{208}Pb(^{16}O,^{15}N)$ 104, 138.5, 216.6 MeV, DWBA and optical model anal., energy dependence 78−82378
$^{208}Pb(^{16}O,^{15}N)$ 312.6 MeV, optical model and DWBA anal., energy depend., lower energy comparison 78−82379
$^{208}Pb(^{16}O,^{15}O)$, 312.6 MeV, optical model and DWBA anal., energy depend., lower energy comparison 78−82379
$^{208}Pb(^{16}O,^{16}O)$ 104, 138.5, 216.6 MeV, DWBA and optical model anal., energy dependence 78−82378
$^{208}Pb(^{16}O,^{16}O)$ 312.6 MeV, optical model and DWBA anal., energy depend., lower energy comparison 78−82379
$^{208}Pb(^{16}O,^{17}O)$ 104, 138.5, 216.6 MeV, DWBA and optical model anal., energy dependence 78−82378
$^{208}Pb(^{16}O,X)$, 80-313 MeV, optical model anal., dynamic shape or density changes 80−18186
$^{208}Pb(^{3}He,^{3}He)$, 130 MeV, elastic scatt. ang. distribs., optical model anal. 78−94020
$^{208}Pb(^{40,48}Ca,\ ^{40,48}Ca)$, optical model anal., strong absorption radius *(Russian)* 80−68697
$^{208}Pb(^{40}Ar,\ ^{40}Ar)$, optical model anal., strong absorption radius *(Russian)* 80−68697
$^{208}Pb(^{48}Ti,\ ^{48}Ti)$, optical model anal., strong absorption radius *(Russian)* 80−68697
$^{208}Pb(^{6}Li,^{6}Li)$, elastic and inelastic, 74 MeV, folding optical model parameters 80−102201
$^{208}Pb(N,N)$, <30 MeV, microscopic optical pot. in nuclear struct. approach, HF field 80−527
$^{208}Pb(\alpha,\alpha')$, levels, B(E3), transition density and nuclear pot., folding model anal. 80−86812
$^{208}Pb(\alpha,\alpha)$, 104 MeV, optical model analysis 78−41737
$^{208}Pb(\alpha,n)$, excitation functions and isomer ratios of ^{211}Po 80−83039
$^{208}Pb(n,n)$, 7-26 MeV, differential cross sections, global optical model anal. 80−18298
$^{208}Pb(n,n)$, (n,n'), 7-26 MeV, optical model anal. 78−37340
$^{208}Pb(p,P')$, pol. p, 9, 10 MeV, vol. integrals for optical pots., real symmetry pot. 80−42659
$^{208}Pb(p,\gamma)$ fast capture, direct-semidirect model excitation function calcs. 78−94004
$^{208}Pb(p,\bar{n})$, nucleon optical potential from Lane model 80−83097
$^{208}Pb(p,p)$, 0.8 GeV, cross sections, optical anal. np RMS radius difference, Δr_{np} 80−63187
$^{208}Pb(p,p)$, 0.8 GeV, elastic and inelastic, ang. distribs., states, optical and DWBA anal. 79−3154
$^{208}Pb(p,p)$, 1 GeV, cross sections using nuclear densities from self-consistent methods *(Russian)* 78−41724
$^{208}Pb(p,p)$, 1 GeV, Fresnel and two-body correl. effects 78−82353
$^{208}Pb(p,p)$, 20-50 MeV differential cross section, polarisation ang. distrib., optical model exchange terms 80−27638
$^{208}Pb(p,p)$, 30 MeV, optical pot. imaginary part calcs. 80−86868
$^{208}Pb(p,p)$, 30 MeV, pick-up and inelasti scatt. contribution to p optical pot. 78−25182
$^{208}Pb(p,p)$ 100 MeV, systematic optical model anal. 78−66274
$^{208}Pb(p,\pi^+)$, differential cross sections, DWBA calc. 79−85415
$^{208}Pb(\pi,\pi)$, 162 MeV, elastic and inelastic ang. distribs., optical and PWIA anals. 80−42706
$^{208}Pb(\pi,\pi)$, ang. distribs., optical model calcs. 78−58308
$^{208}Pb(\pi^+,\pi^+)$, 40 MeV, differential cross sections and strength parameters, optical model fit 80−18347
$^{208}Pb(\pi^\pm,\pi^\pm)$, 80, 116 MeV, elastic and inelastic, optical and collective model anal. 79−22329
$Pb(\alpha,\alpha)$, 104 MeV, A=204,206,208, neutron density RMS radii 78−17088
$Pb(\alpha,\alpha)$, 104 MeV, nucl. matter sizes and isoscalar octupole transition rate 77−6422
Pb(n,n), 13.7-15 MeV, differential cross section energy depend., meas. and optical model 80−18304
Pb(n,n), 14.2 MeV, polarisation in forward angle scatt. 80−18282
Pb(n,n), 16.1 MeV, polarisation meas., optical model anal. 79−22264
Pb(n,n), A=206,207,208, 0.6 to 1.0 MeV, optical model params. 78−21557
$^{A}Pd(p,X)$, 6 MeV, A=102,104,106,108,110, quadrupole deformation, cross sections, direct processes, optical parameters *(Russian)* 79−67753
$^{105}Pd(^{3}He,^{3}He)$ 39.7 MeV, optical pot. mass depend. 77−34327
$^{141}Pr+n$, spherical optical model anal., fast neutron differential elastic scatt. and total cross sections 78−46051
(π, X), theoretical approaches, in $\Delta(1232)$ energy regime 79−80960
^{32}S (n,n), 0.6 to 3.6 MeV, excitation functions meas., optical model anal. 78−58280
^{32}S, neutron scatt. obs., 1-3 MeV, ang. distrib., optical model anal. 77−50125
nuclear optical model continued
$^{32}S(^{3}He,^{3}He)^{32}S$, ambiguities in ^{3}He spin-orbit pot. radius, phenomenological optical-model anal. 79−36250
$^{32}S(n,n)$, 14.2 MeV, elastic, inelastic, backscatt. meas., optical model test 78−58275
$^{32}S(n,n)$, 21.5 MeV, optical model and coupled channel calcs. 77−26714
$^{32}S(n,n)$, 25-1100 keV, total cross section, multilevel anal., strength functions, optical parameters 80−78298
$^{34}S(d,d)$, elast. and inelast. scatt. of 11.8 MeV polarised deuterons 78−33191
$^{34}S(d,p)^{35}S$, 11.8 MeV vector polarised deuterons, optical pot. 77−88149
^{117}Sb, levels studied via $^{116}Sn(^{16}O,^{15}N)^{117}Sb$, ang. distrib. anal. of 64 MeV reacts. 78−8836
$^{45}Sc(\alpha,\alpha)$, 27-9 MeV, anomalous large-angle scatt. 77−18583
Se enriched even isotopes, neutron elastic and inelastic scatt., symmetry effects 77−26757
Se(d,d), polarised deuterons, vector analysing power, optical model calcs. 78−62550
$Se(n,n')\ 2^+$ level excitation cross sections, intermediate resonances, optical model with coupled channels *(Russian)* 79−40897
$^{2}Si(\pi^\pm,\pi^{\pm1})$ 130, 180, 226 MeV, $\pi N(3)$, region, inelastic transitions, optical and DWIA anal. 79−97677
$^{A}Si(^{16}O,^{16}O)$, A=28, 30, 20-35 MeV cross sections and excitation functions, optical model anal. 79−93655
$^{A}Si(^{3}He,^{3}He)$, 46 MeV, A=28-30, ang. distribs., optical and DWBA anal., scatt. pots. 79−556
$^{A}Si(\alpha,\alpha)$, 41 MeV, A=28-30, ang. distribs., optical and DWBA anal., scatt. pots. 79−556
$^{A}Si(p,p')$, A=28,29,30, 51.9 MeV, blocking effect and core-excitation DWBA and optical model 78−82336
$^{28}Si\ (p,p')$, 14-40 MeV, low lying states, optical and statistical model anals., giant resonances 79−40894
^{28}Si, vector polarised ^{6}Li elastic scatt., full optical model anal. 78−70553
$^{28}Si+^{12}C$ elastic scatt. ang. distribs., optical pot. 78−8855
$^{28}Si+^{6}Li(^{9}Be)(^{12}C)$, fusion and strong absorption from elastic scatt. optical pot. 80−102222
$^{28}Si+^{9}Be,\ ^{12}C,\ ^{14}N$ or $^{16,18}O$, low energy elastic scatt., global optical model anal. 78−25229
$^{28}Si(^{12}C,^{12}C)$, 19-48 MeV, ang. distribs., cross sections and optical parameters 80−5157
$^{28}Si(^{15}N,^{14}N)$, 44 MeV, modified optical pot. from backward elastic scatt. 80−32255
$^{28}Si(^{15}N,^{16}O)$, 44 MeV, modified optical pot. from backward elastic scatt. 80−32255
$^{28}Si(^{16}O,^{16}O)$, 55 MeV, Regge pole anal. using optical pots. 79−3174
$^{28}Si(^{16}O,^{16}O)$, 142 MeV, optical model anal. of ang. distrib. meas. 78−58295
$^{28}Si(^{16}O,^{16}O)$, 215 MeV, energy independent Woods-Saxon optical potential 77−14165
$^{28}Si(^{16}O,^{16}O)$, 45 to 63 MeV, energy depend. surface transparent optical pot. 78−46099
$^{28}Si(^{16}O,^{16}O)$, 50, 55 MeV, backward angle cross section, optical model calc. 79−9610
$^{28}Si(^{16}O,^{16}O)$, 65 MeV, elastic and inelastic, optical and coupled channels model anals. 79−45293
$^{28}Si(^{16}O,^{16}O)$, elastic and inelastic, coupled channels calcs., optical pot. energy depend. 79−571
$^{28}Si(^{16}O,^{16}O)$, parity depend. of heavy-ion optical pot. 78−74397
$^{28}Si(^{16}O,^{16}O)$, radial sensitivity of optical pot. 80−86869
$^{28}Si(^{16}O,^{16}O)$ optical pot. semiclassical anal. 79−17917
$^{28}Si(^{16}O,^{16}O)^{28}Si$, 45-64 MeV elastic scatt., quasi-molecular or barrier-top resonance 79−13341
$^{28}Si(^{18}O,^{18}O)$, 60 MeV, optical model parameters 79−22204
$^{28}Si(^{18}O,^{18}O)$, 65 MeV, elastic and inelastic, optical and coupled channels model anals. 79−45293
$^{28}Si(^{6}Li,^{6}Li)$, 154 MeV, differential cross section ang. distrib., optical anal. 80−63201
$^{28}Si(^{9}Be,\ ^{9}Be')$, 45, 60 MeV, low lying collective states, ang. distribs., DWBA double folding pot. anal. 80−78113
$^{28}Si(^{9}Be,\ ^{9}Be)$, 45, 60 MeV cross sections, ang. distribs., Wegner plot, optical and double folding anal. 80−47497
$^{28}Si(^{9}Be,^{9}Be)$, 121-201.6 MeV, strong absorption dominance, global optical model anal., fusion barrier 80−83116
$^{28}Si(^{9}Be,X)$, 30-60 MeV, total fusion cross section, evaporation residues, optical model 80−78344
$^{28}Si(^{9}Be,X)$, X=p,d,α, energy dependence, angular distrib. of spectra, optical and statistical model anal. 80−68710
$^{28}Si(\alpha,\alpha)$, elastic and inelastic scatt., compound nucleus contrib. anal. 78−37356
$^{28}Si(d,p)$, 18 MeV, cross-sections calcs. from pseudopotentials, spectroscopic factors 78−572
$^{28}Si(n,\gamma)$, n and γ width correlation, valence, optical and shell model comparison 79−6606
$^{28}Si(n,n)$, 0.6 to 3.6 MeV, excitation functions meas., optical model anal. 78−58280
$^{28}Si(p,p')$ 3.1-3.8 MeV, interference effects, β_2 and optical parameters 77−26685
$^{28}Si(\pi,\pi)$, 162 MeV, elastic and inelastic ang. distribs., optical and PWIA anals. 80−42706
$^{30}Si(^{12}C,^{12}C')$ 41.3 MeV, ^{30}Si angular distrib., coupled channels calc. 79−97721
$^{30}Si(p,\alpha)^{27}Al$, 17 MeV, polarised p, cross-section and analyzing power ang. distrib. 79−54427
$^{28,30}Si(^{19}F,^{16}O)^{31,33}P$ 60 MeV, j depend., spin-orbit effects, optical pot. 77−41993
Si(n,n)Si, 11-26 MeV, optical model fit 77−79372
$Si(p_{pol},p_{pol})$, giant multipole resonance region, optical model anal. 80−57779
$Si(\pi,\pi)$, ang. distribs., optical model calcs. 78−58308
$Si(\pi^+,\pi^+)$, elast. and inelast. scatt., 50 MeV, ang. distrib. determ. optical model and DWBA 79−45304
Sm isotopes, proton scatt., 16 MeV, coherent optical model analysis 77−26750
$^{A}Sm(^{3}He,^{3}He')$, A=144, 148, 152, 154, 150, 40.9 MeV, transition cross sections, deformation parameters, coupled channels anal. 79−67640
$^{A}Sm(N,N')$ A=152,154, deformed nuclei struct., rot. model with optical pot., coupled channel formalism 79−3146
^{152}Sm (n,n), 2.4-7.2 MeV, inelastic and elastic optical model and deformation parameter depend. *(Russian)* 80−13481
$^{154}Sm(\alpha,\alpha)$, 50 MeV, long range absorption and optical model effects from strong inelastic coupling 80−535

nuclear optical model continued
S(n,n)S, 11-26 MeV, optical model fit 77−79372
^{A}Sn(n,n′), A=116, 118, 120, 122, 124, 11 MeV, levels, deformation parameters, isospin effects, optical parameters 80−57679
^{A}Sn(n,n), 11-26 MeV, A=116, 118, 120, 122, 124, differential and total cross sections, optical pots. 80−78293
^{A}Sn(n,n) A=116, 124, 11, 24 KeV, differential cross sections, global optical model anal. 80−18298
^{A}Sn(p,p), A=116, 120, 4-9 MeV, proton optical pot. low energy behaviour 79−85469
^{116}Sn, levels studied via ^{116}Sn(^{16}O,^{16}O) and ^{116}Sn(^{16}O,^{16}O′), ang. distrib. anal. of 64 MeV reacts. 78−8836
^{116}Sn(^{3}He,^{3}He), 90-120 MeV, cross sections, deduced unambiguous optical pot. 79−13311
^{118}Sn(^{7}Li,^{7}Li), 48 MeV, optical model parameters for DWBA anal. 79−6688
^{120}Sn(^{3}He,^{3}He), 130 MeV, elastic scatt. ang. distribs., optical model anal. 78−94020
^{120}Sn(p,p) 100 MeV, systematic optical model anal. 78−66274
^{122}Sn(d,d), 15 MeV, optical model calc. 78−41729
^{124}Sn(^{6}Li,^{6}Li), elastic and inelastic, 74 MeV, folding optical model parameters 80−102201
Sn(p,n), 8.8 MeV polarised protons, optical model parameters 77−2972
Sn(p,n), even isotopes, 4-10 MeV, cross sections, optical parameters and nuclear radius A-depend. 80−57773
Sn(p,n) for A=117-124 at 2.6-7 MeV, p-wave size reson. optical model fit 77−30575
Sn(p,p), 8.8 MeV polarised protons, optical model parameters 77−2972
Sn(p,p$_0$), pol.p, 6.77-8.8 MeV, cross sections, optical parameters and nuclear radius A-depend. 80−57773
Sn(p,p)Sn, A=115-120, 14-18 MeV, optical model parameters, (p,n) analogue state reaction relevance 77−88132
Sr isotopes, $1g_{9/2}$ nucleon-transfer reactions, nucleon radical distrib. 78−50068
^{84}Sr(^{3}He,α)^{83}Sr, 18 MeV, ^{83}Sr levels, DWBA calcs. using optical model 78−41738
^{88}Sr(n,n), elastic and inelastic, 11 MeV, isospin effects, optical and deformation parameters 79−17794
^{181}Ta+^{16}O, elastic scatt. transfer reactions, fission, total cross sections, optical model parameters 77−54246
Te(^{3}He,^{3}He) A=122-128, 8-18 MeV, optical model and deform. parameters 77−34221
^{118}Te, levels studied in ^{116}Sn(^{16}O,^{14}C)^{118}Te, ang. distrib. anal. of 64 MeV reacts. 78−8836
Te(α,α) A=122-128, 8-18 MeV, optical model and deform. parameters 77−34221
Te(n,n′), A=124-130, scattering cross sections and optical model 78−4944
^{232}Th+α, 19.8 to 27.2 MeV, elastic scatt. or capture and fission, optical model pots. 77−88181
^{232}Th(n, γ), cross sections calc. optical model calcs. 79−30829
^{232}Th(n, N′), cross sections calc. optical model calcs. 79−30829
^{233}Th(N,N′), deformed nuclei struct., rot. model with optical pot., coupled channel formalism 79−3146
Ti, 20 to 50 MeV, total reaction cross sections, compared to optical model prediction 78−33174
^{A}Ti, A=46, 48, 50, pionic X-rays, strong interaction and isotope shifts, π-nuclear optical pot. 80−53169
^{A}Ti(^{7}Li,^{7}Li′), A=46,48, 17 MeV, first 2^+ states Coulomb-nuclear interference, optical and DWBA anal. 80−22852
^{A}Ti(α,α), A=46,48,50, 140 MeV, nuclear size comparison, optical model pot. 79−17913
^{46}Ti(d,d), 10 MeV, optical model calc. 78−41729
^{48}Ti(p,p), 1 GeV, cross sections using nuclear densities from self-consistent methods *(Russian)* 78−41724
^{50}Ti(α,α), 140 MeV, model independent description limits from local optical pots. 80−102196
Ti(n,n), 1-4.5 MeV, elastic inelastic, total cross sections, optical-statistical, coupled-channels models 79−539
^{169}Tm(n,γ), capture cross section from 10^{-5} eV to 2×10^{7} eV, statistical model 80−63189
^{238}U(N,N′), deformed nuclei struct., rot. model with optical pot., coupled channel formalism 79−3146
^{238}U(d,d)^{238}U, 17 MeV elastic and inelastic scatt., nuclear-Coulomb interf., optical pot. 77−79389
^{238}U(n,γ), 5-20 MeV, direct and collective capture, excitation curve, γ-spectra 78−94001
^{238}U(n,n′), cross section param. from optical model anal. 78−21557
^{51}V(^{3}He,d), (^{3}He,^{3}He), 15 MeV, ang. distribs. meas., optical model anal. 78−33192
^{51}V(p,n)^{51}Cr, 2.34 MeV, shell model anal. of analogue resonance 77−14122
^{89}Y(p,p), 0.8 GeV, elastic and inelastic, differential cross sections, relativistic optical model anal. 79−45270
^{89}Y(p,p), 185 MeV, ang. distribs., polarisation, cross section, optical pot. 78−89873
Zn even isotopes, fast neutron elastic and inelastic scatt. cross sections *(Russian)* 77−74853
^{A}Zn(p,p), A=66,68, 20-50 MeV differential cross section, polarisation ang. distrib., optical model exchange terms 80−27638
^{64}Zn(d,d), polarised d, 13 MeV, optical model parameters, vector analysing power 77−88100
^{68}Zn(α,α), 38 MeV, correls. of optical pot. parameters for elastic scatt. 78−13117
Zn(α,α), A=64 and 66, 48 MeV, I.L. potential depth, optical model anal. 78−50187
^{A}Zr (p,p), A=92, 94, 2-6.5 MeV, optical and Lane model anal. comparison 80−18302
^{A}Zr(p,n), A=92, 94, 1.7-6.7 MeV, total cross sections, p strength functions, optical model anal. 80−18301
^{40}Zr(α, α), energy depend. of phenomenological optical pot. 79−97717
^{90}Zr (α,α) 40 to 140 MeV, modified optical pot., folding pots. and energy depend. 78−70549
^{90}Zr (p,p) 100 MeV, systematic optical model anal. 78−66274
^{90}Zr, neutron absorpt. cross section, optical pot. imag. part 79−9536
^{90}Zr neutron absorption, multipole giant resonance contrib. to optical pot. imaginary part 80−18263
^{90}Zr(^{3}He,^{3}He), 130 MeV, elastic scatt. ang. distribs., optical model anal. 78−94020
^{90}Zr(^{3}He,^{3}He), 90-120 MeV, cross sections, deduced unambiguous optical pot. 79−13311

nuclear optical model continued
^{90}Zr(^{6}Li,^{6}Li), elastic and inelastic, 74 MeV, folding optical model parameters 80−102201
^{90}Zr(^{6}Li,^{6}Li) 34 MeV, optical model anal. 79−26448
^{90}Zr(^{7}Li,^{7}Li) 34 MeV, optical model anal. 79−26448
^{90}Zr(α,α), E=26.2-166 MeV, antisymmetrisation effects, α pot., form factor, optical model anal. 78−82366
^{90}Zr(α,α), form factor, coupling between real and imaginary optical potential 80−68680
^{90}Zr(d, d), 10, 11, 12 MeV, polarised d, excitation functions, optical model parameters and spin-orbit pot. 79−67756
^{90}Zr(d,d), 10 and 15 MeV, optical model calc. 78−41729
^{90}Zr(n,X), 10-20 MeV, multipole giant resonance contrib. to optical pot. imaginary part 80−78241
^{90}Zr(n,n), 11 MeV, differential cross sections, global optical model anal. 80−18298
^{90}Zr(n,n), elastic and inelastic, 11 MeV, isospin effects, optical and deformation parameters 79−17794
^{90}Zr(p,$\bar{n}$), nucleon optical potential from Lane model 80−83097
^{90}Zr(p,p), 0.8 GeV, elastic and inelastic, differential cross sections, relativistic optical model anal. 79−45270
^{90}Zr(p,π^+), differential cross sections, DWBA calc. 79−85415
^{90}Zr(π^+,π^+), 40 MeV, differential cross sections and strength parameters, optical model fit 80−18347
^{91}Zr(^{6}Li,^{6}Li) 34 MeV, optical model anal. 79−26448
^{92}Zr levels, J^{π}, cross sections, vector anal. power, optical parameters from ^{91}Zr+pol. d 80−78268
^{92}Zr(N,N)^{92}Zr, optical model anal. 80−47473
^{92}Zr(p,α), 35 MeV, polarised p, DWBA anal., anal. power, optical pot., J-depend. 79−3143
^{92}Zr($\bar{p}$,α)^{89}Y, 35 MeV, analysing power study *(French)* 79−75981
Zr(α,α), A=90,2, E=40-120 MeV, form factors, optical model anal. 78−13123

nuclear orientation *see nuclear polarisation*

nuclear Overhauser effect
acetonitrile, ^{13}C relaxation times anal. using J-diffusion model of mol. reorientation 80−87149
alkyl chains, ^{13}C longitudinal relax. times and nuclear Overhauser enhancement anal. 80−83390
bacteria, yeast and leukaemic cells, dynamic struct. obs. by Overhauser enhanced ^{15}N NMR 77−90742
benzene-2,5-dibromothiophene, self-association, proton mag. relax. 77−28471
benzonitrile, field depend. ^{13}C NMR spin-lattice relax. and anisotropic mag. shielding 79−76450
biological macromolecule, truncated driven nucl. Overhauser effect in presence of spin diffusion 80−1095
biological macromolecules, PMR, nuclear Overhauser enhancement difference spectroscopy 78−81091
bromobenzenes ^{13}CBr bond, spin-spin coupling consts., correl. with C hybridisation s-character 80−34806
camphene, plastic cryst., ^{13}C NMR obs. 79−95667
coupled spin systems, selective nucl. Overhauser effects calc., use in struct. chem. 80−23588
decylammonium chloride micelles, ^{13}C longitudinal relax. times and nuclear Overhauser enhancement anal. 80−83390
dinucleoside monophosphates, conformational anal. 79−20509
dioxane-D_2O mixture, nuclear Overhauser effect factors determ. using dynamic Overhauser enhancement with least square procedure 79−4746
dispiro compound I, pyrolysis, CIDNP, S-T mixing, nuclear Overhauser effect 77−6803
DNA, molecular motions, investigated by ^{31}P and ^{13}C NMR relaxation 80−63657
ferrocytochrome c, horse, transient proton-proton Overhauser effects 79−43822
formic acid, ^{13}C NMR spectra and relax. under intermediate decoupling power conditions 80−20515
Fourier transform double resonance NMR, two- and three-spin systems 78−80249
gramicidin-S, dissolved in deuterated ethylene glycol, interproton effects 79−16123
heteronuclear double resonance, individual Overhauser effects in coupled AX_2 and AX_3 spectra 79−31554
hydrocarbon chain, gauche-trans isomerisation, ^{13}C relax. times and nucl. Overhauser enhancement model 78−33520
III-V semiconductors, optical detect. of CESR, giant Overhauser shifts 78−80251
liquid, simultaneous meas. of NOE and T_1 79−42854
liquid binary mixtures, proton mag. relax. and mol. motion 77−28471
lysozyme, nuclear Overhauser effect in ^{1}H spectra 79−43823
lysozyme, tryptophan residues, H exchange for D, relax., proton NMR spectra 80−35846
MBBA, ^{13}C spin-lattice relax., Fourier-transform NMR, NOE 78−48064
methyl bromide, ^{13}C relaxation times anal. using J-diffusion model of mol. reorientation 80−87149
methyl iodide, ^{13}C relaxation times anal. using J-diffusion model of mol. reorientation 80−87149
methylene chloride, in EBBA-d_{23}, intermol. dipolar random field cross-relax. term obs. 80−60438
molecular multiple internal rot., ^{13}C-{^{1}H} nuclear Overhauser enhancement, ^{13}C spin lattice relax. 77−479
mononucleotides, conformation anal. 79−20509
multispin system, time development of nuclear Overhauser effects 80−34822
nonrigid molecules, dipolar relax. and nuclear Overhauser effects, fluctuating internuclear distances effect 80−91578
nonstationary nutations in heteronuclear double resonance 80−20516
nuclear spin polarisation intensities, exciting light polarisation plane depend. 79−89688
organophosphorus compounds, liq., ^{31}P nucl. spin-lattice relax. and Overhauser effect 79−36666
peptides, in soln., total conformational anal. 79−16136
peptides, soln. conformation by intramolecular effect 79−16135
poly-β-benzyl-L-aspartate, soln., ^{13}C and ^{1}H NMR dynamic study 79−69737
poly-γ-benzyl-L-glutamate, soln., ^{13}C and ^{1}H NMR dynamic study 79−69737
poly-L-alanine, soln., ^{13}C NMR dynamical study 79−69737
1,4-polybutadiene, epoxidised, ^{13}C NMR, Overhauser effect 79−51872

nuclear Overhauser effect continued
polybutadiene, mol. motion in solid and soln., ^{13}C NMR relaxation meas. *(Japanese)* 80−2666
polyethylene, linear, glass transition temp. upper limit, ^{13}C Fourier transform NMR 79−14918
polyfluorostyrene, para- and meta-, dil. soln., ^{19}F magnetic resonance 78−10792
polyisobutylene, ^{13}C spin-relaxation parameters rel. to effect, mol. wt., temp. 77−40146
polyisobutylene, linear, interpretation of spin relax. in terms of specific motion 79−42857
1,4-polyisoprene, epoxidised, ^{13}C NMR, Overhauser effect 79−51872
polystyrene, dilute soln., ^{1}H mag. relax., selective inversion technique appl. 80−44957
polystyrene soln., macromolecular chain dynamics, C^{13} and NMR 78−55267
protein, proton magnetic reson. and spin diffusion 77−28470
proteins, nuclear Overhauser effect in ^{1}H spectra 79−43823
pulsed NMR spectroscopy, pulse spacing selection for increased accuracy in meas. 77−28474
pyridazine, liq., nucl. relax. and mol. reorientation, nucl. Overhauser enhancement 78−60351
pyrimidine, liq., nucl. relax. and mol. reorientation, nucl. Overhauser enhancement 78−60351
randomly coiled polymer, in solution, models for spin relaxation 77−85607
$tRNA_{yeast}^{phe}$, Fourier transform PMR in aq. soln., ^{1}H exchange and relax. rates meas. method 78−15049
RNA, molecular motions investigated by ^{31}P and ^{13}C NMR relaxation 80−63657
RNA, nuclear Overhauser effect and solvent exchange rate, NMR expts. using supercond. magnet 79−74811
spin pair undergoing reorientations by jumping among inequivalent sites, nucl. mag. spin relax. 79−42862
terephthalic acid polyester in solution, ^{13}C spin relaxation study 79−87327
thermodynamics of nuclear spins 80−54964
tryptophan, Fourier transform PMR in aq. soln., ^{1}H exchange and relax. rates meas. method 78−15049
two-spin system, NMR relax. rate parameters 77−69720
vinyl bromide-d_3, ^{13}CBr bond, coupling consts., correl. with C hybridisation s-character 80−34806
vinyl polymer solutions, proton spin-lattice relax. and Overhauser enhancements 77−55721
^{9}Be, nuclear mag:spin-lattice relaxation times 78−86889
^{13}C, interacting with strongly irradiated proton system, longit. mag. relax., Overhauser enhancement 78−19377
^{13}C NMR, ^{2}H label quantitative meas. 77−50456
^{13}C NMR intensity meas. technique, chem. anal. appl. 77−51981
^{13}C, reduced value rel. to ^{1}H spin-lattice relax. 77−46581
^{13}C-^{1}H, spin-pair with time-dependent internuclear distance, nuclear Overhauser enhancement 79−42862
^{13}C-^{1}H long-range coupling assignment through selective ^{1}H decoupling 77−46582
^{13}C-enriched mols., proton relax. and nuclear Overhauser effect from NMR meas. 77−68058
$^{13}C-^{13}C-^{1}H$ fragment, nucl. relax. and Overhauser effect 79−54868
^{133}Cs, nuclear mag:spin-lattice relaxation times 78−86889
Fe:^{129}Xe, implanted atom site populations, Mossbauer, NO and NMR/ON obs. 77−20755
K_2SiO_3 aqueous soln., ^{29}Si NMR expts. 78−15051
$^{6}LiCl$, aq., temp.-depend. relax. 77−1613
^{6}Li, nuclear mag:spin-lattice relaxation times 78−86889
^{15}N, interacting with strongly irradiated proton system, longit. mag. relax., Overhauser enhancement 78−19377
Na_2SiO_3 aqueous soln., ^{29}Si NMR expts. 78−15051
^{77}Se, FT NMR in solns., chem. shift, I_1 relax. times, NOE enhancement 78−95528

nuclear particle track visualisation *see particle track visualisation*

nuclear photoeffect *see photon-nucleus reactions*

nuclear physics
see also fission; fission reactors; nuclear bombardment targets; nuclear decay theory; nuclear explosions; nuclear reactions and scattering; nuclear structure; radioactivity
activated metal foil experiments, teaching expts. 79−17165
American Nuclear Society Transactions, Washington, USA (November 1978) 79−85570
annual review book 80−67940
astrophysics, recent developments 78−4100
book, annual review of nuclear science (vol.26) 77−57583
CERN computing school, La Grande Motte, France (1976) 77−65414
computer in the nuclear science laboratory 79−72220
computer simulation techniques for an undergraduate nuclear physics course 80−36823
computer technology developments in relation to nuclear research 77−13566
conference, Mickolajki, Poland, 30 Aug.-11 Sep. 1976 78−21484
conference, Mikolajki, Poland, 1977 78−86461
conference, nuclei far from stability, Corgese, Corsica, France (May 1976) 77−22824
conference, Portoroz, Yugoslavia, 4-6 Nov 1976 78−12937
data file references to literature, Sept. to Dec. 1977 79−9430
display for data output in phys. expts. 78−9046
Duane, William (1872-1935), life and work 79−30183
Ernest Rutherford, biography 80−8768
fundamental nuclear constants, direct test of constancy 77−2889
international research, 1956 to 1976 activities of JINR 77−10299
laboratory course at Purdue University 78−4443
laser applications in nucleas physics, review, book contrib. 80−68504
libraries of nuclear data *(Spanish)* 79−36120
neutron physics research trends 77−22825
nonlinear integral eqn. solution *(Chinese)* 78−74324
nuclei and particles, introductory text book 78−78234
nucleonics, review Nov. 1975 to Nov. 1977 78−82262
recent references (May-August 1977) 79−441
reference data for space technology 78−82407
review of research programs at Saclay Nuclear Physics dept. *(French)* 79−437
Schwinger and nuclear physics 79−62987
Soddy, F., nuclear science, economics and social responsibility, holistic approach 80−90640
teaching, undergraduate, courses, facilities 80−27086
theoretical physics at Kharkov Inst., Ukrainian SSR *(Russian)* 79−12558

nuclear polarisation
see also dynamic nuclear polarisation; magnetic double resonance; nuclear polarisation in liquids and solids
$0f_{7/2}$ and $0g_{9/2}$ nuclei, mag. form factors, core polarisation and exchange current effects 80−13409
A=18, effective interaction, 2nd order core polarisation diagrams with intermediate particle states 79−45180
A=3 systems, charge form factor and bound nucleon polarisation 80−22708
A=70, heavy-ion induced fission-evaporation reactions, magnetic substrate distribs., nuclear alignment 80−73857
A=90 region, core pol. effects and giant quadrupole resonances, HF and macroscopic calcs. 80−57756
A≥208, accurate g-factor measurement using heavy-ion induced reactions 77−26572
A∼90 nuclei, isomeric states, spin polarisation, M4 transitions and giant resonances 80−63157
actinide fission, statistical anal. of gamma emission 78−17255
alpha-particle energy spectrum, fission-emitted, fission-fragment shape and orientation depends. 78−74346
angular correls. random perturbations, asymptotic attenuation coeffs. 77−30507
atom, resonant photoionisation, nuclear polaris. *(Russian)* 79−49997
atomic energy level isotopic shifts and nuclear polarisation *(Russian)* 78−13444
beam production by reson. at. ionis. 79−13576
charged particle polarisation, methods of meas. *(Rumanian)* 79−59321
collective excitations, macroscopic eqns. of motion and dynamic polarisability 77−41903
core polarisation, multiple scatt. eqn. for two particle one hole system and generalised vertex 77−65204
core polarisation contributions to two body effective interaction, centre of mass effects 78−66219
core polarisation effects in inelastic scatt. and charge exchange 77−22983
core polarisation in inelastic scatt., extension to include charge-exchange reactions 78−78359
Coulomb form factors, effects of core polarisation 77−30474
deformed nuclei, polarisation, and energy shifts in muonic atoms 80−86893
deformed nuclei, static isoscalar and isovector polarisability, isovector $K=\pm1^{+}$ modes 80−32260
dilution refrigerator for low temperature nuclear orientation experiments on line to an isotope separator 79−752
dipole polarisability sum rule, HF calc.,, ^{16}O, ^{40}Ca appl. 78−21504
dynamic polarisability, TDHF theory and RPA sum rules 78−78292
E2 core-polarisation charge, nuclei near ^{16}O and ^{40}Ca 77−22888
eikonal approx., electron-oriented nucleus scatt., polarisation of e^{-}, nuclei and emitted γ rays 78−37331
few body dynamics, conf. 77−18368
fission, order-disorder model of balance neutron distrib. 79−13279
heavy ion potentials, polarisation effects 77−18596
heavy ion reactions, deflection function, effect of nuclear vibr. mode and orientation 79−59080
(HI,xn), cranking model for E1 polarization charge in rotating nuclei 79−85405
high angular momenta nuclei, backbending, yrast states, large moment of inertia band 77−14027
hypernuclei, ΛN effective force, binding energy, excitation spectra, self consistent calcs. 77−6283
ion implantation in samples colder than 0.5K, low temp. nuclear orientation studies 80−34033
isomeric A=48-50 nuclei, mag. moments and core polarisation 78−37274
laser induced nucl. orientation, at. and nucl. applications, review 78−37310
laser induced nuclear orientation, ^{24m}Na appl. 80−57680
laser induced nuclear orientation effects 77−30740
matter current density and R parameter meas. 77−30544
muonic atoms, nuclear polarisation energy shifts, phenomenologically extended microscopic calcs. 78−94335
muonic atoms of deformed nuclei, nuclear polarisation correction 77−23584
neutron and nuclear polarisation expts., spin depend. of neutron cross-sections, mag. moments, radiation capture of neutrons *(Russian)* 80−52654
neutron excess nuclei, near equality of isoscalar and EM transition rates 78−8770
nuclear matter, polarised, thermal props., temp., spin isospin and spin-isospin pressure 80−102135
orbital angular momentum transfer to nucl. spin polarisation in external mag. fields 80−14217
orientation with combined elec. and mag interactions 78−41633
particle spectra line shapes after γ emission in flight 78−41665
polarised beams, review of appl. 79−45243
polarized source based on nuclear polarization by charge-exchange 79−22514
polarized target, horizontal dilution refrigerator construction 78−86708
positron annihilation in heavy at. shells, nuclear orientation *(Russian)* 79−49602
proper frequencies, weakly coupled moments in amplitude modulated mag. field *(French)* 77−10571
review of recent advances in technique 79−30822
short living nuclear states, optical orientation, γ-spectrum anisotropy, lifetime, moments *(Russian)* 80−63090
Skyrme's interaction, correction to g-factors 77−65196
Skyrme interaction, mag. moments, polarisability, gyromag. factors 78−21501
spectroscopic quadrupole moment extraction from muonic atom hyperfine structure, polarisability correction 77−18391
spherical tensor formalism, polaris. transfer *(Russian)* 79−59047
spin exchange and polarisation changes, RPA breakdown from HF connection 80−99142

nuclear polarisation continued
spin giant resonance and core polarization effects, coupling term effects *(Chinese)* 80−47450
spin-isospin polarizability of nuclear matter and renormalization of weak currents 79−67697
target ^{3}He continuous flow cryostat 80−52240
time dependent HF polarisability and RPA sum rules, collective model restoring force 79−6461
time dependent HF polarisability and RPA sum rules, isovector giant resonances 79−6462
valence nucleons, muonic atom analysis 80−27530
weak axial coupling constants in nuclei, polarizability, pionic field, PCAC 77−6055
weak interactions in nuclei, axial polarisability 77−22924
(e,e), A=60 region, nuclear radius, core polarisation and isotone shifts, muonic X-rays 80−22685
^{105}Ag, high spin states γ-single spectra, γγ coincidence, excitation functions, ang. distrib., polarisation meas. 78−21519
^{110}Ag^m, oriented, T-reversal test and struct. study 78−86505
^{240}Am^m, spontaneously fissioning isomer optical shift in pumped $^8S_{7/2}\rightarrow{}^{10}P_{7/2}$ transition, nuclear deformation 80−27971
^{76}As, dynamic orientation in n-Si crystals, ang. momentum, forbidden β transition 79−501
^{12}B, aligned, β ang. distribs., second class currents 78−50126
^{12}B, aligned, β-ang. distrib. asymmetry coeffs., pseudotensor interaction, T=1 isospin triplet decay 80−106021
^{12}B, hyperfine interactions in Mg, decoupling by external mag. field 77−24756
^{12}B, polarised, higher order effects in determ. of asymmetry parameters in β-decay 79−22247
^{12}B, produced in ^{12}C($\mu^-,\nu_\mu\gamma$)^{12}B, impulse approx. calc., nuclear polarisation 78−37315
^{12}B spin polarisation, obs. in ^{100}Mo(^{14}N,^{12}B) 79−3168
^{12}B, spin polarisation in ^{100}Mo(^{14}N,^{12}B), semiclassical anal. 78−33212
^{12}B spin polarisation in ^{100}Mo(^{14}N,^{12}B) 80−63160
^{12}B spin polarisation in ^{232}Th(^{14}N,^{12}B) 80−63161
^{12}B spin polarisation meas. from β-decay, product of ^{100}Mo(^{14}N,^{12}B)^{102}Ru 78−50196
^{12}B(1$^+$, g.s.), polarisation in ^{12}C(μ^-,ν_μ), effect of correlations 80−22774
^{12}B(1$^+$,g.s.), induced pseudo-scalar coupling constant in ^{12}C(μ,ν_μ) 79−49606
^{12}B→B$^-$+^{12}C, second-class current search, alignment correlation meas. by Zeeman technique 78−37313
^{12}B→β$^-$+^{12}C, alignment correlation meas. by Zeeman technique, vector currents and form factors 78−37312
^{138}Ba, 6$^+$ state, nucl. g-factor and nucl. spin relax. in Xe 77−22884
^{206}Bi, nucl. orientation in ferromag. BiMn 78−13010
^{207}Bi, nucl. orientation in ferromag. BiMn 78−13010
^{208}Bi, influence of nucl. polarisation on level props. 78−54686
^{210}Bi, influence of nucl. polarisation on level props. 78−54686
^{A}C, A=12, 13, nuclear critical opalescence, M1 form factor, pion field and condensation 80−73809
^{12}C, 2$_1^+$ state, rel. depend. of transient mag. field effect, recoil in Fe 78−37285
^{12}C M1 form factor, pion field critical opalescence, ρ role, polarisation phenomena 80−68552
^{12}C, M1 form factor, pion field, rho meson role 80−105970
^{12}C, weak hadronic form factor and recoil polarisation in muon capture 78−62508
^{12}C(π^-,π^-)^{12}C*, 4.5 GeV/c, gamma-ray decay obs., nucl. polarisation anal. 77−30636
^{40}Ca, core polarisation charge for E6 transition, Bohr Mottelson model calc. 79−36194
^{41}Ca, deorientation of highly stripped ions recoiling in vacuo 78−37325
^{41}Ca, transverse decoupling of hyperfine interactions in free atoms 77−18468
^{107}Cd, heavy ion nucl. alignment, recoil in vac., time-differential meas. 78−37304
^{111}Cd^m, nuclear orientation in Zn and Be, 245 keV state quadrupole moment, half-life 80−37324
^{34}Cl, core polarisation J-averaged effects through 3rd order up to 10 ħω excitations 79−67671
^{60}Co polarised nuclei, β-ray emission, directional distrib. and asymmetry factor 80−95315
^{152}Dy continuum γ-ray multipolarity by linear polarisation meas. from ^{140}Ce(^{16}O,4n) 79−85408
^{160}Er continuum γ-ray multipolarity by linear polarisation meas. from ^{148}Nd(^{16}O,4n), yrast levels 79−85408
^{19}F, 5/2$_1^-$ state, precession on recoil in Fe and Ni 78−37285
^{2}H, dynamic and static polarisability from Rayleigh scatt., two-photon disintegration 79−75867
^{3}He optically pumped target, polarisation enhancement and measurement 77−34531
^{3}He$^+$(2S) state ion beam with nuclear polarisation, RF source 79−59602
^{4}He muonic atom, nuclear polarisation corrections 78−22056
^{A}Hg, A=198-204, reorientation effect meas. on 2$^+$ states 78−37282
^{198}Hg rotation alignment and high spin states 77−57591
^{165}Ho, electron-oriented nucleus scatt., eikonal approx. calc. 78−37331
^{A}I, A=123, 125, mag. moments and polarisation NMR on oriented nuclei 79−75836
^{123}I, bands and decay props., core-particle coupling and polarisation effects 80−13354
^{112}In, half-lives and mag. moments of two high spin states, γ-ray spectra 77−22940
^{6}Li+n, spin depend. capture and scatt. of slow neutrons 78−46059
^{12}N, aligned, β ang. distribs., second class currents 78−50126
^{12}N, aligned, β-ang. distrib. asymmetry coeffs., pseudotensor interaction, T=1 isospin triplet decay 80−106021
^{12}N, polarised, higher order effects in determ. of asymmetry parameters in β-decay 79−22247
^{12}N→^{12}C(g.s.), second-class axial current, meas. alignment-positron-momentum correl. 78−82317
^{23}Na$^+$, production and detection of vector-polarised beam 79−13843
Nd ions recoiling in vac. or low press. He, nuclear deorientation, perturbation mech. model 77−50105
^{20}Ne from ^{16}O(^{16}O,^{12}C)^{20}Ne, polarisation measurements 80−9301
^{20}Ne hexadecapole moments, quadrupole deformation effects, E4 effective charge, valence polarisation 80−78142

nuclear polarisation continued
^{20}Ne, strong polarisation of levels obs. in ^{16}O(^{16}O,^{12}C) reaction 78−25213
^{61}Ni, spectroscopy of levels below 2.2 MeV obs. in ^{58}F(α,nγ) 77−6289
^{16}O, 31$^-$ state, precession in Fe foil, depend. on magnetisation 78−37285
^{16}O, weak hadronic form factor and recoil polarisation in muon capture 78−62508
^{17}O, mag. form factor, core polarisation and exchange current effects 78−46003
^{186}Os, levels deduced from ^{186}Ir decay and ^{186}W,(α,4n)^{186}Os 78−86481
Pb, muonic high-lying states transitions, electron screening effects 77−34786
Pb muonic isotopes, A=204, 206, 207, 208, nuclear polarisation energy shifts, RPA calcs. 78−94334
^{208}Pb core with valence nucleon or hole, mag. props., exchange currents, electron scatt. 80−22689
^{208}Pb, muonic atom, 2Z 79−64123
^{208}Pb region, mag. transition strength, core polarisation effects, form factor shape 80−86850
^{208}Pb single particle and hole states, renormalisation, core polarisation, spectroscopic factors 80−57658
^{A}Re, A=181, 182, 187, spin polarisation, state struct. and mag. moments in rot. model 80−18194
^{A}Sb, A=115, 117, M2, E3 transition reduced matrix elements, EM core polarisation 79−17847
^{112}Sb, ^{114}Sb, 8$^-$ states, half-life and mag. moment, γ-ray spectra 77−22941
^{114}Sb, 8$^-$, 210 μs state, mag. moment, PAC of liq. Sn:^{114}Sb 77−26609
^{86}Sr, 8$^+$ state, nucl. g-factor and nucl. spin relax. in Kr 77−22884
^{177}Ta spin polarisation, state struct. and mag. moments in rot. model 80−18194
^{155}Tb, oriented in Gd, γ-decay ang. distrib., hyperfine splitting, moment and mixing ratios 79−45242
^{156}Tb, orientation in Gd matrix, γ-ray ang. distrib. anisotropy meas. 79−59031
^{160}Tb β-decay, oriented nuclei, γ transitions multipole mixing parameters 80−18240
^{49}Ti, polarised, T violation test, γ-ray directional correlation 78−62330
^{206}Tl, influence of nucl. polarisation on level props. 78−54686
^{208}Tl, influence of nucl. polarisation on level props. 78−54686
^{180}W, K=2$^-$ octupole alignment, ground-band angular momenta 78−78237

nuclear polarisation in liquids and solids
see also dynamic nuclear polarisation
β-ray spectra of recoil nuclei polarised by fast polarised beams 77−28502
acridine in fluorene matrix, RF induced mag. reson. transitions, triplet state, optical nucl. polarisation 79−31561
adiabatic demagnetisation using near nπ RF pulse strings 77−90050
antiferromagnet, nucl. orientation 78−43652
aromatic molecular crystals, optical nuclear polarization by optically excited triplet states 79−19804
bromomethane, ^{79}Br, ^{81}Br quadrupole bond magnitude ratio *(Russian)* 79−76452
brute-force nuclear orientation, review of accomplishments and problems 77−59466
brute-force nuclear orientation 77−28452
cross polarisation in solids with flip-back of I-spin magnetisation 80−39894
cross-relaxation processes, polarised β-active nuclei 80−60431
p-dibromobenzene, crystal nucl. spin polarisation cross relax. study 80−29647
dilute alloy, appl. of low temp. nucl. orientation 80−15825
double-cross-polarisation NMR of solids 80−20468
electric quadrupole interactions measured by nuclear orientation and NMR on oriented nuclei, review 80−92868
fluorene: acridene, radical pair form. from excited states, optical nucl. polarisation obs. 80−14155
fluorene crystal, doped, photochemical hydrogen abstraction, proton hyperfine structure via optical nuclear polarisation 80−63659
gamma-ray laser, nuclear orientation techniques for directed emission 77−27268
generalised spin precession eqn., elec. quadrupole interaction sign 78−43744
graphite intercalation cpds. with Li, nucl. relax. times 80−44947
Haupt effect, coupled rotational and dipolar relaxation of methyl groups 77−32292
holmium ethylsulphate, pseudomagnetic moment of ^{165}Ho and spin-lattice relax. times 77−63306
insulators, neutron activated β-emitters, hyperfine interactions 78−39070
intermediate state perturbation in low temperature nuclear orientation 80−97168
Kondo system, comparison of nuclear orientation and magnetisation expt. 77−63297
magnetic props. of materials, appl. of nucl. orientation, review 80−44928
metal, neutron activated β-emitters, hyperfine interactions 78−39070
NMR J cross-polarisation in liquids, refocusing method 80−22406
NMR signal intensity enhancement by polarisation transfer 79−94013
nuclear elec. quadrupole coupling const. sign determ., appls. 77−12291
nuclear quadrupole alignment and low temp. systematics of elec. field gradients of ^{176}Lu^m and ^{177}Lu 79−78565
Nylon 66, stress-oriented NMR expt. using multiple impulses to achieve line narrowing *(German)* 77−28457
optical coherence storage in stimulated optically induced nucl. spin polaris. 80−58649
orientation with combined elec. and mag interactions 78−41633
polarised targets, meas. using Q-meter with automatic phase control and tuning 79−228
polyethylene, ultraoriented, ^{13}C-^{13}C dipolar satellites 77−28465
rare earth ferromagnet, polarisation in external mag. fields, TDPAC 77−8462
semiconductor, nuclear polarisation due to anisotropic size effect in weak elec. field 80−71199
solvent-paramagnetic solute system, nucl. spin-lattice relax. times, cross-correl. method 79−95679
spin polarisation torsional spectroscopy, four time domains 80−20510
spin system orientation due to stimulated emission and absorpt. of radiation 77−52001
Ag-Mn, dil., nuclear orientation expts. 78−43713

nuclear polarisation in liquids and solids continued
Al:^{12}B, relax. mechanism for polarised implant 78−87693
Al-Mn, dil., ^{54}Mn Knight shift meas. using nucl. orientation 78−68396
Al-Y, dil., hyperfine interactions, $^{87}Y^{m}$ nuclear orientation meas. 78−43715
$Al_xGa_{1-x}As$, optically magnetised, luminescence polarisation anisotropy, hysteresis effect symmetry props. 80−34982
Au-Ho nuclear orientation thermometer for use from 1-30 mK 79−17419
Au-Mn, dil., nuclear orientation of recoil implanted ^{52}Mn 78−43716
Au-Mn(Cr)(Fe), dil., spin glass state and Kondo effect, nucl. orientation of ^{54}Mn 78−6514
Au-Y, dil., hyperfine interactions, $^{87}Y^{m}$ nuclear orientation meas. 78−43715
BiMn, ferromag., nucl. orientation of Bi isotopes 78−13010
^{206}Bi, nuclear orientation in Ni for ^{206}Pb decay investig. 77−41911
CaF_2, (n,γ) induced lattice defects, struct., polarised ^{20}F NMR 77−20724
CaF_2, (n,γ) induced lattice defect annealing, polarised ^{20}F NMR 77−20725
^{111}Cd, nucl. orientation coeffs. with axially symm. elec. field gradient 80−97168
Co, nucl. orientation on implanted ^{114m}In 79−47345
Co-^{48}V, nucl. orientation of ^{48}V, γ-ray anisotropy obs. 80−97169
Co-Mn, dil., hexagonal hyperfine field at ^{54}Mn, nucl. orientation meas. 79−8057
$Co_{80}P_{20}$, amorphous, sign and magnitude of ^{60}Co hyperfine field, nucl. orientation 78−48100
Cu:^{69}Ge(^{67}Zn), nucl. alignment temp. depend. rel. to radiation damage during PAC obs. 77−27919
Cu-Cs diluted deuterated Tutton salts, electron non-Zeeman system, nuclear relaxation study 80−44951
Cu-Mn Kondo system, ^{54}Mn nucl. orientation 78−68421
Fe, implantation of ^{197m}Hg, NMR of oriented nuclei 77−81020
Fe, nuclear orientation and NMR/ON on implanted ^{114m}In 79−47345
Fe radiative detection of single- and multiple-pulse mag. reson. of oriented ^{60}Co radioactive nuclei 77−66437
Fe, triple pulse reson. studies of ^{60}Co nuclei 78−43675
Fe:^{105}Rh(^{95}Tc), nuclear orientation of nuclei, anisotropy of gamma-ray emission 77−46111
Fe:^{106}Rh, nuclear orientation and mag. moment 77−85623
Fe:^{110}In, nucl. orientation, nucl. mag. moment, γ-ray spectra 77−28485
Fe:^{119m}Te, mag. moment, nucl. orientation, γ-ray spectra 77−28486
Fe:^{129}Xe, implanted atom sites, NMR/ON 77−20723
Fe:^{129}Xe, implanted atom site populations, Mossbauer, NO and NMR/ON obs. 77−20755
Fe:^{131}Xe, negative parity states, nucl. orientation, γ-ray spectra 77−28487
Fe:^{199}Au, quad. interaction, orbital mag. hyperfine field by NMR/ON 77−12250
Fe:^{60}Co, nucl. orientation-pulsed NMR obs., γ-radiation anisotropy 77−59490
Fe:^{60}Co, elec. quad. interaction, single passage NMR/ON 77−16204
Fe:^{71}As(^{72}As), nucl. mag. moment by NMR/ON 77−12251
Fe:^{82}Br, nucl. orientation 77−59486
Fe:^{93,94}Tc, γ-ray spectra, nucl. mag. moment determ. 77−28484
Fe:^{95}Nb NMR 77−59482
Fe:Bi, impurity site distrib., channelling and nucl. orientation obs. 77−15447
Fe:I, ^{131}I NMR, vacancy associated impurity sites 78−91964
Fe-^{48}V, nucl. orientation of ^{48}V, γ-ray anisotropy obs. and NMR meas. 80−97169
Fe-In, dil., hyperfine field of In, clustering effect, nucl. orientation obs. 77−16188
Fe-Ta, nucl. orientation of ^{178}Ta 78−39412
Fe-Y, dil., hyperfine interactions, $^{87}Y^{m}$ nuclear orientation meas. 78−43715
p-GaSb, CESR, optically detected, giant Overhauser shift 79−4722
Gd:^{160}Tb, hyperfine interaction for ^{160}Tb *(Russian)* 77−63347
Gd-Sc, dil. alloy, ferromag. hyperfine field determ. 77−43919
Ge, polarisation of implanted ^{12}B 78−43653
^{3}He, liq., spin polarisation, rapid melting of polarised solid 79−46872
^{3}He, liq., spin polarised, quantum fluid *(French)* 79−46862
^{3}He, liq. and solid., spin polarised, thermodynamical nuclear orientation 79−46879
Ho-Au, dil., hyperfine interaction of Ho^{3+}, nuclear orientation expts. 78−43717
$HoAlO_3$, electronic and nucl. mag. ordering, mol. field approx. 80−60157
$HoVO_4$, below 1K, nuclear orientation study of Van Vleck enhanced nuclear antiferromagnet 80−88899
In_3Ce, nucl. orientation meas. 78−39415
^{111}In, nucl. orientation coeffs., nucl. mag. moment 80−97168
(La,Th)-Ce, dilute alloys, mag.-nonmag. transition of impurity moments, environment effects 77−40034
^{8}Li, in $LiTaO_3$, multiple quantum NMR transitions obs., quadrupole moment determ. 77−73090
Lu-Hf, elec. field gradient at ^{175}Hf nuclei aligned at low temps. 79−82884
Mg, elec. quadrupole interactions on ^{12}B and ^{12}N via depolarisation due to level mixing 77−55728
Mn-Tb, dil., hyperfine interactions, nuclear orientation 80−15929
$MnCl_2.4H_2O$, antiferromagn., nucl. orientation 78−43652
$MnCl_2.4H_2O$, single cryst., mag. phases, obs. by ^{54}Mn nucl. polarisation 77−81031
NaCl:Fe(Mn), nucleation of Au, surface imperfection effects 77−15699
Ni:^{192}Ir, NMR/ON, resonant freq. shift with applied field 77−28462
Ni:Bi, impurity site distrib., channelling and nucl. orientation obs. 77−15447
Pb_3Ce, nucl. orientation meas. 78−39415
Pd-Co alloy, dil., giant moment and Kondo-like coupling, nuclear orientation meas. 77−32160
Pd-Co(Mn), dilute, nuclear orientation expt., giant moments and Kondo coupling 77−63296
Pd-Mn, dil. alloy, giant moment at very low temp. 78−88094
Pd,H-^{54}Mn, dil., nucl. orientation of ^{54}Mn 77−12257
$PrIn_3$, nucl. orientation of ^{144}Pm in singlet ground state, exchange interaction and cryst. field splitting obs. 80−71275
Pt, A=187, 189, 191, low-temp. orientation studies, mag. moment and $E_2/M1$ ratios in daughters 77−22889
Pt-^{95}Nb, nuclear orientation meas. 79−65644

nuclear polarisation in liquids and solids continued
Pt-Mn dilute alloy, cubic foil, Mn spin behaviour, nuclear orientation technique 78−27044
Sb-Hg, quadrupole interaction, time differential perturbed ang. correl. and nucl. orientation 79−24250
^{120}Sb, nuclear alignment in Sn, temp. depend. 78−41720
^{125}Sb in Pd_2MnSb, orientation meas. with ^{125}Te Mossbauer effect 77−55713
Si:S, electron-nuclear interactions during pumping, influence of mag. field 79−95378
Sn:^{114}Sb, PAC, mag. moment of 8^-, 210 μs state of ^{114}Sn 77−26609
^{115}Te, nuclear alignment in Sn, temp. depend. 78−41720
$YLiF_4$:rare earth, spin-lattice relax. and nuclear polarisation *(Russian)* 79−8049
$^{87}Y^{m}$ orientation meas. in Al and Au hosts, mag. moment of $9/2^+$ isomeric state 78−41632
Yb, FCC, nucl. orientation of 3d impurities and magnetisation meas. 78−64280
Zn, EFG sign at ^{69m}Zn site 77−59492
Zn-^{54}Mn, nuclear orientation meas. 79−65644

nuclear power
25 years of nuclear power, UKAEA 25th anniversary 79−71901
abuses of nuclear power 77−67910
accident prevention and control *(French)* 80−52747
advanced nuclear energy systems, emerging concepts, conf., Graz, Austria (March 1978) 79−13381
AGR design for Heysham II and Torness 80−23108
AGR development and exploitation prospects 80−23109
AGR fuel element design improvement 80−23112
AGR line development status and performance *(German)* 78−86568
air-scooping nuclear-electric propulsion for advanced orbital transportation missions 78−45188
alternative versus conventional energy sources, advantaegs of controlled nuclear fusion *(German)* 80−72002
American Nuclear Society 25th Annual Meeting (Atlanta, GA, USA (June 1979)) 80−12847
American Nuclear Society proceedings (conf. Las Vegas, NV, June 1980) 80−94920
American Nuclear Society Transactions, Washington, USA (November 1978) 79−85570
American Power Conference, Chicago, Ill., USA, April 1976 77−46201
ANS annual meeting, 1977 78−663
Argentinian industrial development 77−65352
assessments of nuclear systems and use of nuclear power, review 79−45334
atomic energy and nonproliferation *(French)* 78−33303
balanced approach to excess fuel from breeder reactors 79−59248
Bangladesh, development policies 77−61627
benefit-cost analysis in nuclear fuel cycle 78−8957
book 80−46750
break-even rating of nuclear and conventional power. technico-economic parameters 79−79362
breeder reactor development, survey *(German)* 78−5007
breeder reactors introduction, essential conditions 80−829
Calvert Cliffs power manoeuvring control strategy 79−9863
Canada's effort, future routes 77−46388
Canadian nuclear controversy, educational responsibility 77−37711
Canadian power reactor programme, role of Chalk River research reactors 79−81073
CANDU-PHW program, status and prospects *(Czech)* 77−38387
centralised heat supply and central heating, reactor design and development 79−26730
centralised heat supply from nuclear boiler units, technoeconomic assessment 80−7899
chemical technology development in nuclear power generation fuel cycle factories 79−31096
China, R and D *(German)* 80−68971
civil AGR multistart helically ribbed fuel pin development 80−23111
coal gasification by nuclear steam reforming of methane 80−55775
coal gasification plant, high-temp. alloy evaluation for nucl. process heating 78−13237
coal gasification plant using nuclear process heat, material corrosion 78−13348
collective dose rate commitment in nuclear power industry, appl. to future dose rate eval. *(Spanish)* 79−63816
commercial nuclear capacity and spent-fuel accumulation, US projection 80−18574
comparability study of fission and fusion reactors w.r.t. safety, costs and development time 79−59114
conf., American Nuclear Society San Francisco, Calif., USA (Nov. 1979) 80−31414
conference, Berlin, Germany (Aug. 1979) 80−77539
conference, nuclear power plant construction, operation and development, Tokyo, Japan (Sept. 78) 78−86672
conference, San Diego, Calif., USA (June 1978) 79−17972
conference, San Diego, Calif., USA (June 1978) 79−49650
conference in Salzburg report *(German)* 78−8896
conference on nuclear power and its fuel cycle, Salzburg, Austria (May 1977) 79−26504
Conference on Nuclear Power and the Public, September 1977, Geneva, brief report 78−29520
controlled nuclear fusion, progress and problems review 79−36415
controlled thermonuclear fusion reactor problems and prospects 79−81075
Czechoslovakia, review *(Czech)* 79−31157
denatured Th cycle in symbiotic systems, potential role 79−26484
developing countries, regulatory capability transfer 80−13634
developing country, standards and standardisation in nuclear technology 77−65346
development, significance of failure of Harrisburg, PWR *(Swedish)* 79−92056
development and technology, surface science rel. problem areas 78−88553
development history *(Croatian)* 77−34479
development utilising FBRs, ACRs and alternative fuel cycles 80−47565
developments up to year 2000 demand and technology forecasting *(French)* 79−92048
disposal of radioactive waste by underground storage, geological aspects *(German)* 79−13431
district heating schemes, heat transport and storage 79−39321

nuclear power continued
district heating systems, nuclear power appl. 78−37454
dual purpose nuclear power station and integrated agro-industrial complex in E.India 80−7904
economic and sociological effects of development 77−33823
economic competitiveness, w.r.t. West German Government expenditure *(German)* 80−23180
economics, comparison with other energy sources 79−22499
economy planning, computer simulation 77−79486
education, nuclear nonproliferation, fuel cycle economics, numerical estimates 80−51982
education, undergraduate course evaluation on radiation and the environment 78−1
education in peaceful uses, high school curriculum in Japan 77−37682
educator involvement needs for nucl. controversy 77−37710
electric generating capacity for US by 2000 80−40846
electricity generation and use in energy conversion 79−9921
energy, environment and health, Failla Memorial Lecture, learning from nucl. experience 78−80982
energy conversion engineering, alternative energy sources *(Japanese)* 80−26105
energy production, research review *(Hungarian)* 78−74414
energy resources, fission and fusion processes *(Portuguese)* 77−3189
energy self-sufficiency by 1990, use of Nuclear forms - complex of reactors 80−18456
energy source in USSR, electricity generation *(Russian)* 79−26592
energy strategy, soft vs. hard energy technologies, review 79−24885
energy supply, future tasks for nuclear energy 80−61317
energy supply, transition from fossil fuel to nuclear and regenerative sources, technical, economic and ecological aspects 80−66955
engineering development in CMEA countries *(Polish)* 77−65344
environmental analysis, bi-Gaussian atmos. diffusion model, influence of turbulence typing scheme 80−3554
environmental effects, general radiation level and waste product disposal 79−18051
environmental effects, research at Chalk River Nucl. Laboratories 78−61222
environmental effects, some practical issues 80−94121
environmental effects from nuclear energy, effects of small radiation doses 79−2312
environmental impact, review 80−101143
environmental pollution, British Royal Commission Report evaluation 77−71705
environmental radiation dose assessment of a growing nuclear industry 80−3553
European Economic Community member states' nuclear achievements *(French)* 79−89490
European Nuclear Conf., Hamburg, Germany, May 1979 79−97841
European nuclear controversy, future educational plans 77−37712
European thermonuclear fusion programme, role of technology 80−86982
fast reactor design data adjustments 79−9695
fast reactors, programme and state of work in the Soviet Union 79−643
FBR, development, fuel cycle, hazards and alternatives, review 79−63715
FBR solution to world energy problem *(French, English)* 80−18591
FBR technology and strategies, role of nuclear power in world energy supply 80−50948
fission and fusion reactors, research and development in Japan 80−47701
fission electric cells, synergetics using catastrophe theory 80−45761
French nuclear fuel cycle activities and companies *(German)* 79−81054
French plan VII, energy forecasting 78−49628
French private nuclear fuel cycle industries *(German)* 79−81055
fuel cycle, national and international aspects *(German)* 78−86665
fuel cycle industry development, limiting factors *(French)* 78−66430
fuel cycles, reactor types, future role of nuclear energy *(German)* 78−29579
fusion, economic and environmental consequences 78−33285
from fusion, state-of-the-art and problems to be overcome *(Dutch)* 80−37574
fusion energy, appl. to thermochemical H_2 production 80−76658
fusion energy applications, anal. of nonelectric appl., 1977 79−18040
fusion energy heat source for N_2 fixation 80−32510
fusion energy prod. by plasma vortex struct. compression 79−9888
fusion engineering developments review 79−3240
fusion first-wall/blanket and associated structural mats., performance, safety and economics 80−32432
fusion power prospects in Soviet Union 77−67868
fusion power status and prospects 77−67878
fusion reactors, progress at Culham, descriptive survey 77−83073
fusion reactors for synthetic fuels 80−13793
fusion research, philosophy 80−42854
fusion technology development in France and UK, review 77−18695
fusion-supported decentralized nuclear energy system with 10 to 300 MW PWR 80−32515
future development, heat for dwellings and farming, industrial power 79−85759
future prospects, technical, economic and political review *(Spanish)* 79−59116
gas cooled reactor experience and programs in France, reviews 79−45332
gas cooled reactors, background and status in UK, review 79−45333
gas turbine waste heat utilisation for elec. energy generation and desalination *(German)* 79−87936
gaseous core reactor power production with minimal transuranic wastes 79−9806
German nuclear power development, review 79−63716
German public relations campaign 77−37709
global nuclear power is alternate source of energy, prospects and issues 80−7897
global problems and energy, nuclear power 78−45454
growth rates, influence on introduction dates for ACR and FBR 80−18379
H, thermochemical production by H_2O decomp., optimum temp. conditions utilizing HTGR nuclear heat 80−35781
hazards to human populations, from low-level radiation, review of current estimates 78−57043
health hazards from alternative electricity generation fuel cycles 78−11791
heat supply from nuclear reactors and coal combustion, appl. study 78−37455
heavy-ion beam inertial-confinement fusion, commercial power generation 79−6762
high-level radioactive waste storage, distribution calc. *(German)* 79−81014
high-level radioactive waste storage, temp. distribution simulation expts. *(German)* 79−81015
high-temperature power-technological industrial processes use of nuclear power, reviews 79−26729
Hinkley Point B AGR commissioning and three years' operational experience 80−23107
HTGR, nonelec. appl., prod. of H_2 and synthetic hydrocarbons, review 79−45329
HTGR and alternative nuclear strategies *(Chinese)* 80−78353
HTGR utilisation in technological processes and electric power generation, review 79−97886
HTR nuclear long distance energy system, heat transport by chemical circuit 80−7905
HTR plant with methane reformers for long distance energy system 80−7906
human health risk, comparison of conventional and nonconventional technologies 79−87956
HWR, option for technology transfer 77−46387
HWR dynamics modelling for digital control system design 79−9829
hydrogen power system, global energetic system, mathematical model *(Rumanian)* 80−35623
implementation on Argentina 77−57771
industry status, national and international recognition problems 79−93810
integrated nuclear power system, mathematical model *(Rumanian)* 79−41013
integrated reactor systems fuel strategy, review of future nuclear energy options 79−49696
International Nuclear Fuel Cycle Evaluation Association structure *(Dutch)* 80−7896
international symbiotic nuclear energy parks using breeders and advanced convertors, economic feasibility 80−57825
isotope fuelled Stirling cycle power system, 1 kWe 79−48176
isotope power system, Brayton cycle, dynamic power convertor for space appl. 79−48167
isotope-powered satellite design for Shuttle launches 78−61709
Italian nuclear power programme, fuel cycle industry development 79−31069
Italian power plant Caorso, technical parameters BWR 77−38388
laser fusion in power engineering, future prospects 77−38401
legislation changes in West Germany *(German)* 77−71703
light water hybrid breeding reactors, source driven 79−13518
LMFBR, energy investment 78−78512
LMFBR in Italian electric power program *(Italian)* 77−10483
LMFBR principles and potential advantages 79−81072
long-term nuclear energy strategies, role of fission and fusion 80−78354
low temperature nuclear heat utilisation 80−7903
low temperature nuclear heat utilization in Italy 80−7902
magnetic fusion reactor, current status 77−23290
mathematical modelling of nuclear power engineering development 80−7901
methane reforming by nuclear steam for coal hydrogasification 80−30325
methanisation plant ADAM I, nuclear long-dist. energy circuit *(German)* 78−25335
model of developing industry, estimation of Pu steady-state isotopic composition 79−59166
multicriterial optimization of the development of nuclear power in the framework of the perspectives of COMECON 80−7900
multistage flash distillation process using nuclear power, design aspects 77−38390
national energy and nuclear power system plans of the Federal Republic of Germany 79−26506
national energy programme of USA, nuclear power, fuel enrichment and waste disposal 79−26686
national programmes, survey 77−88267
net energy from nuclear power, energy accounts for realistic nuclear programmes 79−26594
neutronics rel. to energy problem 77−26827
nonconventional conversion systems *(Rumanian)* 78−86705
nondestructive testing standards, role of NBS 79−54612
nonelectrical energy production, review 79−26728
nonproliferation, nuclear fuel cycles and radiation damage 80−68934
nonproliferation and safeguards systems 79−81102
nonproliferation treaty safeguards implementation, nuclear facilities in USA 78−820
nuclear energy importance and developments in Great Britain *(German)* 80−99198
nuclear energy synergetics, characts. of integrated systems 79−13382
nuclear engineering, teaching project management as part of international technology transfer 78−4428
nuclear power stations, long term radioactivity values, meas. in marine life *(Spanish)* 80−7962
nuclear risks, energy source health effects 79−85696
nuclear symbiosis, development of FBR and thermal spectrum near breeder reactors, review 79−45335
optimal development strategies for a whole energy system based on hydrogen 80−45795
optimisation problems, system criterion appl. to problems 77−23313
optimum theory of nuclear plant mix with minimum natural fuel requirement 79−26469
option as long term investment 80−99351
PBHTR, design operation and applications, review 79−45328
peaceful use in Belorussia, historical review *(Russian)* 79−35517
pebble-bed high-temp. reactor as a source of nuclear process heat 77−10479
Philippine experience in technology transfer 77−65355
plant safety systems, common mode, failures, investigation *(German)* 78−694
PNP project, prototype HTR and coal gasification plant review 80−5393
process heat system, material screening studies 78−13236
progress review (1939-79) *(French, English)* 80−18590
proliferation and Pu recycling, effects of future nuclear power 79−18021
proton linear accelerator, high current, appl. 77−38450

nuclear power continued
public attitude formation 77−10496
public health aspects of radiation 78−35895
public opposition, international experience review 77−18642
public opposition, legislative aspects and effects *(German)* 80−23181
PWR, CANDU, operation, status and prospects of nuclear power in Canada 78−86664
PWR load factor statistical analysis 79−9789
quality assurance, international standardisation, FORATOM 80−58008
radiation protection programme in Iran, past, present, future trends 77−65337
radioactive contaminant unplanned release meas. and countermeasures 78−89994
radioactive impact of nuclear facilities, preoperational evaluation 80−3534
radioactive releases and waste disposal, CEGB Research Division report 78−46145
radioactive waste management 79−9763
radioisotope thermoelectric generator, high-temperature insulations testing 79−48145
radioisotope thermoelectric generator, selenide technology evaluation at JPL, for Galileo (NASA) spaceflight mission 79−48147
radioisotope thermoelectric generators, terrestrial and undersea appl. 79−48150
radiological impact of the Rhein-Maas region from nuclear facilities under normal operation 80−3535
reactor control, digital load-follow concept, simulation in FRG-2 reactor *(German)* 77−50249
reactor gaseous effluents reprocessing, radionuclide management 79−76078
reactor noise analysis, Polish developments 79−3216
reactor strategies in a global context 79−87937
reactors, factors affecting choice of type and power *(French)* 80−52712
research programmes of Swiss Federal Institute for Reactor Research 80−52722
review, worldwide variation of energy production, future Hungarian energy requirements *(Hungarian)* 78−70580
review of energy resources, reactor accidents, radioactive waste disposal 78−50413
risk assessment in European Community 80−106135
risk estimation methods and wider applications *(French)* 79−89492
rocket reactors, laminar flow, temp.-viscosity induced instabilities in gaseous heated channel 77−18689
Royal Commission Report, on Environmental Pollution, UK, overview 77−54267
safeguards in technology transfer to developing countries 77−65348
Salzburg conf., May 1977, overview *(German)* 77−88183
seawater desalination, evaluation of single purpose fission reactor 80−5319
security problems and solutions, technology transfer 77−61635
shale oil extraction using nucl. heat sources, feasibility 77−34422
ship propulsion, report on 1977 IAEA conference *(Dutch)* 77−83069
ship propulsion, technical and economic aspects of a nuclear-powered containership 80−5392
social and economic implications, United Kingdom view 77−33826
solar assisted LWR nuclear reactors, SOAR power system concept 80−55820
South Africa, industry development, book 80−73105
space appl., selenide isotope generator for Galileo mission 79−52951
space power systems using thermionic conversion, USSR activity and 1978 status, comparison with USA status 79−48158
space propulsion, NASA's thermionic technology program, 1978 status, objectives and plans 79−48159
space propulsion, nuclear-electric, Jupiter orbiter mission 78−45189
space propulsion, out-of-core thermionic power conversion system 79−48160
space vehicle appls., missions and planning, elect. and propulsion power requirements 80−30428
space vehicle nuclear propulsion, historical review of advanced consent 80−36475
space vehicle radioisotope power system, using Rankine conversion cycle, emergency cooling by multifoil insulation melting 79−48168
spacecraft, nuclear integrated multimission spacecraft, definition and evaluation 80−18715
spacecraft dynamic power system, thermally-integrated 79−48166
spacecraft radioisotope thermoelectric generator cooling, in Shuttle 79−48142
Spanish nuclear power program, technology transfer 77−65353
special applications, future outlook 77−42177
status and development trends, in late 1970s 79−57347
steam gasification of coal, test and development of heat-exchanger alloy 78−15589
steam generators, once-through, flow dynamics stability *(Czech)* 77−38386
Swedish energy policy up to the year 1990 *(Swedish)* 79−87982
Swiss energy program, overview *(French)* 77−88230
Swiss energy situation and nuclear development *(French)* 79−89491
synergetic aspects of solar energy and the fast breeder reactor 80−7907
synthetic fuel production application 77−34480
synthetic fuel production in a particle-beam driven fusion reactor 80−55780
technology and policies, book 77−6476
thermal power outputs of small high-temp. power plants 78−738
Turkey, nuclear power prod., utilisation and safety 80−3481
United States nuclear export policy 77−61634
United States nuclear industry, new energy policy, review 78−5061
United States policy towards nuclear power and nuclear weapon nonproliferation, overview 80−3484
urban district heating, review 80−26118
US breeder reactor programme 78−731
US energy policy 80−81426
US energy policymaking, suggested revision of production/consumption patterns 80−66954
US future development economic assessment, Pu recycle's influence 79−36394
USSR, nuclear power industry development and future plans *(Russian)* 79−26734
value of reliability analysis 78−29619
waste disposal problems, present and future trends 78−66350
waste management problem, reprocessing *(German)* 79−13499
world nuclear energy, conf. (Washington, 1976) 77−67779
nuclear power continued
worldwide energy prospects, synthesis of studies published in 1976 and 1977 *(French)* 79−29443
H production using fusion reactor heat and gas dynamic compression heating 80−35793
H production using nuclear process heat from HTRs 80−30595
H synfuel prod. by high temp. electrolysis using fusion energy 80−35792
H synfuel prod. from fusion power using hybrid thermochem. $Bi_2O_3.SO_3$ cycle 80−40931
H_2 production using high temp. reactors 80−97814
H_2 thermochemical production, plasmochemical H_2O decomposition using nuclear energy source 80−61436
Pu, toxicity, cancer risk. calc. 77−2025
^{232}Th utilisation in reactor fuel cycles, review 79−45390
U enrichment, market survey *(German)* 78−4999
U exploration in developing countries, facts and trends 80−16764
U, reactor fuel supply, exploration and production capacities, review 79−22388
U utilisation, improved fuel cycles 80−787
U-graphite channel reactor development in the USSR 79−602
UF_6-He circulating gas critical expts. 79−13488

nuclear power stations
see also power station control
250 MWe station, Phenix-250, with Na-cooled FBR, France *(Dutch)* 77−71686
440 MW water-moderated water-cooled reactors type VVER-440, description 77−18691
480 V and 125/250 V auxiliary elec. unit design, safety features 77−3143
840 MW Loviisa-1 Nuclear Power Station, in Finland, two years' operating experience *(Russian)* 80−106151
1200 MW, containment description *(German)* 77−42102
1980s world's trends and Czechoslovak nuclear power program *(Czech)* 80−47784
2000 MW by water-moderated water-cooled reactor, development possibility 77−67865
2056 MW nuclear reactor pressure tubes cracking 78−82463
4150 MW nuclear power station with PWRs, at Bugey, in France, commissioning report *(French)* 80−37571
abandonment at end of working life, problems *(French)* 80−18588
accident at Three Mile Island, lessons learned 80−57929
accident dispersion model, direction depend. probability limits consistent with NRC practice 78−17372
accident prevention, 1300 MW nuclear reactor steam isolating valve blowdown tests *(German)* 80−22967
accidents, coolant unsteady flow, with discharge from high-pressure vessel *(Russian)* 79−89448
accidents, Three Mile Island nuclear power station, viewpoint of member of Commission of Enquiry 80−83190
accidents due to loss of coolant, multiple-element model and computer solution 78−66358
accidents in power stations of Electricite de France, protection organisation *(French)* 78−55049
accumulation ponds cooling possibility analysis *(Slovenian)* 80−91208
acoustic monitoring equipment for nuclear power plants: research, development and industrial production 79−76076
advanced control concept, computer-based systems design 77−67909
advanced control room design 79−45362
advanced fuel fusion impact on electric power transmissions 77−83087
advanced power reactors, appl. in developing countries 77−57734
aerodynamic and thermodynamic effects on environment *(German)* 80−61469
AGR, commercial designs 77−71687
AGR, future energy generation prospects 78−729
AGR system for nuclear process heat, primary circuit component materials 78−13233
aircraft impact, simplified derivation of reaction-time history 78−89958
aircraft impact, structural response, reaction-time and impact area-time curves 80−78407
aircraft impact on reactor containment structures 78−29660
aircraft impact problem, review 78−41875
ambiental radiology, equipment and methods, review *(Spanish)* 79−45425
American Nucl. Soc. winter meeting 1977 78−58315
American Nucl. Soc. Winter Meeting 1977 78−82408
antiseismic supports of reinforced elastomer blocks *(French)* 79−54535
Arizona Nuclear Power Project waste water reclamation for cooling 79−9861
artificial earthquake generation for dynamic anal. of nuclear power stations 79−97850
aseismic bearing foundation system for power station earthquake protection 80−83206
aseismic design, using rubber mounts 77−79470
aseismic design and testing of equipment and components, Japan 80−52763
atmospheric pollution, nature and extent of unplanned releases, review 79−57530
atmospheric radioactivity, radiological impact from model coal-fired power plants and from nuclear systems 80−3557
availability improvement by acoustic emission surveillance 79−3213
availability improvement by surveillance techniques 79−9812
axisymmetric seismic response of thick circular plate supporting many rods, nuclear power plant appl. 80−1458
B&W integrated control system improvement 78−8946
Babcock & Wilcox steam supply system, operating experience 78−21752
battered piles for nuclear power plant support, dynamic stiffness and seismic input motion 80−13954
Beloyarskaya Atomic Electric Power Plant, channel reactors, permissible power operating calculations 79−80984
Biblis, radiation protection during first refuellling shutdown of unit A 77−65335
Biblis core protection and German safety regulations 77−88260
Biblis Nuclear Power Station, meas. and control system, fault statistics evaluation *(German)* 79−97819
Biblis nuclear power station, waste production, storage and disposal 80−68903
blast effects from accidental explosions, US regulatory requirements 78−41877
BN-350, design and experimental testing of intermediate heat exchangers *(Russian)* 79−97785

nuclear power stations continued
BN-350 fast reactor, operating experience (1972-77) *(Russian)* 79−97868
BN-600, design and experimental testing of intermediate heat exchangers *(Russian)* 79−97785
Bohunice A-1 power plant, nondestructive gamma-ray spectrometry method for fuel burn-up control *(Slovak)* 78−21672
boiler inlet temps. and corrosion product deposits, water chemistry effects 80−89528
boilers water conditions, chemical monitoring development in UK *(Russian)* 77−88217
BOPSSAR plant, radioactive waste management, influence on standardised plant design 77−46307
boric acid management in VVER reactor power plants *(Russian)* 79−30896
breakdown in Three Mile Island plant *(Hungarian)* 80−18454
breakdown in TMI-2 power plant, consequences *(Hungarian)* 80−18455
breeder nuclear power stations, introductory outline *(German)* 79−26731
breeder reactor, Super Phoenix, construction report *(French)* 79−63803
breeder reactor development, survey *(German)* 78−5007
breeder reactor liquid Na cooling pressure meas. using differential recorder *(German)* 77−88270
breeder reactors, current status in Europe 80−27796
Brunswick plant post-startup optimization 80−23048
BWR, ASEA-ATOM supplied, operating experience 80−9375
BWR, automatic protection system *(German)* 78−4989
BWR, Bilibino power station, internal power-distribution monitor system 78−17341
BWR, block-monitoring index for diagnosis of power station operating characts. 79−59185
BWR, design, construction and organisation of Caorso nuclear power station, Italy *(Italian)* 79−26471
BWR, Dresden 1 plant, prototype operation for decontamination of primary system 79−54538
BWR, dynamic loading of press. suppression containment blowdown, power station expt. data 77−3133
BWR, earthquake-proof component design, seismic analysis 78−21733
BWR, Fukushima Daiichi power station, preoperational test, start-up test, operating experience *(Japanese)* 78−29635
BWR, grid freq. and control capability 77−46396
BWR, Millstone Unit No. 1, augmented off gas system experience 80−22919
BWR, neutron flux monitoring instrum. 77−14240
BWR, off-gas recombiner operating experience at Chin-Shan 80−22920
BWR, radioactive corrosion products behaviour 78−21661
BWR, revised Inservice Inspection program, implementation at Millstone Unit 1 80−23020
BWR, sustaining improved plant operation 80−9374
BWR, Swiss 942 MWe project, Dutch (NUCON) development *(Dutch)* 79−3191
BWR, technology transfer experience 77−65349
BWR, TVO I, startup principles 80−9372
BWR, vent clearing transients calc., press. suppression system, digital computer simulation 77−3132
BWR, Wm. H. Zimmer station, startup and testing 80−9373
BWR and CANDU PHW, 2×200 and 2×220 MWe plants, operational experience in India *(Hungarian)* 77−3146
BWR building, soil-struct. interaction behaviour damping effects, expt. anal. 77−38434
BWR containment struct., appl. of frequency domain anal. 79−93753
BWR plant, heat drain deaeration under forward conditions 77−88212
BWR plant, LOCA capability code for utility appl. 78−21690
BWR plant diagnosis system, on line process computer appl. 78−46146
BWR plant in Japan, aseismic design 77−65267
BWR plants, I-131 airborne emission data for environmental impact evaluation 77−38391
BWR plants in Japan, seismic design and tests 78−86652
BWR power plant, computerised core component accounting system shortens shuffling time 80−699
BWR power plant, construction experience 78−86673
BWR power plant, routine checks and radiation protection 78−74462
BWR power plant appl. of computer based systems 77−88264
BWR power plant availability improvement by acoustic emission monitoring 79−9809
BWR power plant shielding concept 80−18712
BWR power plant stack effluent inert gas nuclide monitor 79−3255
BWR power plant turbine building, radiation protection, calc. and obs. 78−74461
BWR power stations, operating record and reliability, reviews 79−22403
BWR primary steam circuits, decontamination procedures *(German)* 79−89389
BWR reactor operation and management using minicomputer 79−81042
BWR refuelling schedule, minimisation of power peaking 77−61513
BWR steam turbine, blast cleaning to remove radioactive deposits 80−18554
BWR Vermont Yankee power station, external radiation field meas. 77−54368
cables, damage mechanisms in LOCA environment 80−13658
California underground siting study, anal. 80−18400
California underground siting study, effectiveness in mitigating health consequences 80−18402
California underground siting study, selection and analysis of accident sequences 80−18401
Canadian industry, technology transfer 77−57760
CANDU, 2000 MWe system, Canadian nuclear power programme 77−10481
CANDU, decommissioning 77−74973
CANDU, digital computer control 77−54324
CANDU, future developments 77−38381
CANDU, political and economic uncertainties 79−85758
CANDU, reliability of performance 79−18029
CANDU−Canadian experience and expectations with the heavy-water reactor 79−26593
CANDU 600 MW(e) station, man-rem expenditures 79−13493
CANDU design evolution 79−13417
CANDU nuclear power station safety, Atomic Energy Control Board guidelines 79−22425
CANDU operation for electricity prod. and district heating 78−41835
CANDU PHW commercial nucl. elec. stations, commissioning and operating experience 78−86656

nuclear power stations continued
CANDU PHWR heat transport network, SOPHT computer model 77−83025
CANDU plant construction, Bruce nuclear power development, Ontario Hydro 78−86676
CANDU plant DDC, dual redundant minicomputer system max. utilisation 79−36375
CANDU power plant deaerator dynamics 79−93708
CANDU power plants, automated anal. system for control of secondary coolant chemistry 80−18446
CANDU power stations, fuel safeguards scheme 80−63291
CANDU power stations, reduction, control and prediction of radioactivity transport 80−18448
CANDU reactors, present state and future development 77−74970
CANDU type reactor implementation in Pakistan 77−61596
CANDU-OCR power station options and costs 80−73989
CANDU-PHW, decommissioning cost, environmental impact hazards and size 77−61598
CANDU-PHW, waste management and its role in Canadian fuel cycle 79−89393
CANDU-PHW decommissioning, costs, environmental impact, radioactive waste management 80−13964
CANDU-PHW program, status and prospects *(Czech)* 77−38387
Caorso BWR power station, structural acceptance tests of primary containment *(Italian)* 79−30951
Caorso nuclear power station airborne and liquid radioactive release monitoring systems 79−13553
Caorso plant, dynamic tests and seismic records of RHR building 78−41872
Caorso station in Italy, Mark 2 primary containment structure, construction features 77−65322
capital cost considerations, optimum plant size 80−63416
CAS medium-size nuclear plants 79−31169
CDFR secondary cct. design from PFR operations 79−97788
CEGB nuclear power station emergency arrangements 78−55050
CEGB nuclear power station emergency monitoring procedures 78−55053
centralised heat supply and central heating 79−26730
channel type, graphite BWR, safety problems in USSR *(Russian)* 79−26637
chemical explosion induced, nuclear power plant protection 77−38351
civil defence aspects of US power stations as targets in nuclear war in year 2000 77−3188
class 1E auxiliary power systems, degraded or loss of voltage protection 79−45363
Clinch River Breeder Reactor Plant, role and progress in LMFBR development 80−13781
column section seismic design subjected to three components of earthquake 77−38355
combined heat and power, fusion reactor appls. *(German)* 79−67935
Commonwealth Edison's Zion Generating station, decontamination of radwaste evaporation 80−9376
component manufacture, quality control problems 79−22453
computational uncertainty anal. methods, comparison 77−79426
computer appl. to reactor scram system *(German)* 78−86635
computer control systems for data acquisition and process control 79−22426
computer modules, appl. to data handling, simulation, alarm anal., and safety *(German)* 79−49788
computerised monitoring fast analogue scanner for data acquisition 77−6656
concrete slab perforation by missiles, nuclear plant appl. 77−38352
concrete slab perforation by missiles, nuclear plant appl. 77−38353
concrete slab perforation by missiles, nuclear plant appl. 77−38354
condensate at BWR power stations, pulver resin on-floating method, construction and initial startup aspects *(Hungarian)* 79−76116
condenser coolant contamination control using atomic absorption spectrophotometer method 77−373
conference, nuclear power plant construction, operation and development, Tokyo, Japan (Sept. 78) 78−86672
conference, nuclear power quality assurance, Knoxville, USA (Oct. 1978) 79−97773
conference on nuclear power and fuel cycle, Salzburg, Austria, (May 77) 79−26503
conference on nuclear power and its fuel cycle, Salzburg, Austria (May 1977) 79−26504
conference on nuclear power systems, Washington, USA (1978) 79−41045
construction and engineering problems, layout aspects 78−86702
construction in the USSR 79−646
containment and surveillance techniques for the IAEA 79−85645
containment building, Mark III, advantages, Grand Gulf Nuclear Station project 80−106122
containment buildings, integrated leak rate testing *(Spanish)* 79−54518
containment integrated leak rate test *(Korean)* 78−54851
containment structures, integrity and safety aspects *(Spanish)* 79−93738
containment structures pressure tightness verification, pressurisation plant, data acquisition and processing *(Spanish)* 80−13775
contaminated live steam release into turbine hall at Brunsbuttel *(German)* 79−89388
contamination monitoring station of Zarnowiec plant *(Polish)* 80−74033
control and instrumentation designs beyond the 1980s 80−57872
control and instrumentation. [conf. Cannes, France (Apr. 1978)] 79−76096
control and protection system future trends justification 77−88263
control appls., problems and trends 78−70609
control guidelines 80−106119
control instrumentation, commissioning and maintenance experience at Rajasthan 79−89455
control problems survey 77−88258
control room and desk design, alarm system, information displays 79−89462
control room and desk design, alarm system, information displays 79−89464
control rooms, human factors design approaches, improvement of man-machine interface, error reduction 80−63327
coolant piping, relative rupture probabilities 78−21632
coolant pump, seismic anal. by response spectrum method 77−3183
cooling ponds, waste heat dissipation 79−48191

nuclear power stations continued
cooling system, flow around obstacles determ. *(Czech)* 78−66331
cooling system design, optimal system synthesis, tower, pond 77−14260
cooling water impact on water surface temps. and ice conditions *(Finnish)* 79−20868
corrosion damage, influence of water chemistry 79−54517
corrosion damage, overview of water chemistry 79−54553
corrosion product reduction program 78−21665
corrosion research in FBR and PWR nuclear power plants, review of problems *(Czech)* 78−62598
cost comparison of PWR and PHWR nuclear power plants in Korea 80−57821
cost reduction by containment elimination 79−13467
CRBRP, future design and construction of LMFBRs in USA 79−97804
Creys Malville station, Super Phenix project safety *(French)* 79−30948
Creys-Malville centre, siting, operation, safety, containment and waste *(French)* 79−30945
Creys-Malville plant, installation, design and construction planning *(French)* 80−47691
Creys-Malville plant worksite and progress *(French)* 80−47692
Creys-Malville station, nuclear boiler studies and construction, Super Phenix 1 *(French)* 79−36301
Creys-Malville station, safety arrangements *(French)* 79−30946
CRT man-machine communication system in nuclear power stations 79−45364
CTR, for power generation, design 77−3157
CTR central power station waste management 78−773
current nuclear power plant safety issues, 1980 conf. preview 80−95360
current status, USA, as of 31/12/1977 78−58398
Czechoslovak nuclear power station fluid radioactive release monitoring *(Russian)* 79−13555
Czechoslovak Research Institute activities, safety, waste disposal and personnel training *(Slovak)* 80−83188
Czechoslovakia, review *(Czech)* 79−31157
damaged fuel element detection and location at Atucha nuclear power station 79−89460
DC power failure following AC power failure 78−78483
decentralized instrumentation and control system with bus transmission in nuclear power plants 79−97847
decommissioning, alternative methods and regulations 79−54573
decommissioning, conf., Vienna, Austria (Nov. 1978) 80−12855
decommissioning, cost anal. for complete removal 79−67904
decommissioning, criteria for the management of redundant nuclear facilities 80−13975
decommissioning, deform. of acceptable residual radioactive contamination levels 80−13973
decommissioning, dismantling of French-type fast-neutron power reactors *(French)* 80−13968
decommissioning, disposition planning system for engineered approach 80−13963
decommissioning, establishment of activity limits for items to be released for unrestricted use 80−13972
decommissioning, experience gained with the decontamination of a shut-down reprocessing plant 80−13981
decommissioning, French experience rel. to safety *(French)* 80−13965
decommissioning, Halian experience 80−13967
decommissioning, IAEA defined options 79−81071
decommissioning, industrial experience gained in the decontamination and partial dismantling of a shut-down reprocessing plant 80−13985
decommissioning, legal aspects 80−13961
decommissioning, main problems 80−676
decommissioning, national policies and international aspects 80−13959
decommissioning, partial dismantling of the Avogadro RS-1 materials testing reactor *(French)* 80−13980
decommissioning, progress report on dismantling of the Sodium Reactor Experiment 80−13978
decommissioning, radioactive waste disposal *(French)* 80−13736
decommissioning, radioactivity limits for release of liquid radwaste, math. model 80−13737
decommissioning, residual activity levels allowing radioactive waste to be considered inactive 80−13735
decommissioning, state-of-the-art handbook 80−824
decommissioning, summary of US DOE handbook 80−13969
decommissioning, technical and economic aspects 79−26602
decommissioning, treatment of contaminated metallic wastes by smelting 80−13741
decommissioning, US policy and standards 80−13960
decommissioning and dismantling projects at Idaho National Engineering laboratory 80−13984
decommissioning and reconstruction of the fast reactor fuel reprocessing plant, Dounreay 80−13983
decommissioning and total dismantling of PWR power plant 80−13982
decommissioning aspects of a nuclear chemical plant 80−13986
decommissioning of a ^{239}Pu contaminated incinerator facility 80−13987
decommissioning of commercial power reactors, environmental, economic and sociological effects 79−67901
decommissioning of commercial power reactors, technical feasibility, cost, environmental effects 79−67902
decommissioning of LWR power plants by German utilities 80−13962
decommissioning of LWR power station, radioactive waste decay behaviour 80−13738
decommissioning of nuclear installations in the preliminary safety report *(French)* 80−13966
decommissioning of power reactor, NRC regulations 79−67905
decommissioning of PWR and fuel reprocessing plant 80−13970
decommissioning of PWR power station, safety, cost and occupational radiation exposure estimates 79−67903
decommissioning of the Lucens experimental nuclear power plant *(French)* 80−13979
decommissioning problem solutions and costs *(German)* 79−89487
decommissioning quantitative anal. of radioactive waste development 80−13974
decontamination, chelating agent appl. 78−50280
desalination by very low temp. nuclear waste heat 78−41850
desalination plant, steam-cycle and optimisation calc. 79−26724
design, appl. of multi-directional seismic inputs 79−31238
design, construction, operation and safeguard systems, book 79−30875
design basis R and D of power stations to cut costs and schedules 80−99204
design engineering for earthquake loads 78−66431
design for underground rock cavity location, safety aspects 79−13398
nuclear power stations continued
design management, plant replication for low-cost nuclear power, Philippines National Power Corp. 80−63242
design standardisation, scoping anal., and early site review for 1980's generation 80−22912
developing country, development of local engineering capability 77−65350
development in Soviet Union, problems and solution 80−102290
development of techniques for radwaste systems in CANDU power stations 80−37547
development trends, Soviet Union *(Russian)* 79−97885
diagnostic instrumentation experience 79−3218
digital computer control in Canadian nuclear plants, past performance and future outlook 78−58383
digital radiation monitoring 78−816
dissociating N_2O_4 power plants, safety and accident response *(Russian)* 79−31066
district heating, duplex chemical system for storage and transport of heat from LWR 78−37460
district heating, safety evaluation 78−37422
district heating and electricity prod., economy and safety, heat output optimum 78−37459
district heating from Kaiseraugst nuclear power station 78−37462
district heating in Stockholm, nuclear power and oil-fired plant comparison 78−37458
district heating plant, safety 80−767
district heating schemes, heat transport and storage 79−39321
district heating systems, combined generation by fossil fired and nuclear power plants 78−37457
double-wall piping welded joint residual stress study *(Russian)* 78−27541
Dresden Unit 1, chemical cleaning 79−54591
dual purpose nuclear power station and integrated agro-industrial complex in E.India 80−7904
dual-purpose nuclear-electric reverse osmosis seawater conversion plant design and cost study 80−47683
Dungeness A, radiation and contamination control 80−5386
dynamic response to earthquake, aircraft impact, soil structure interact. 79−3208
dynamic simulation, design anal. tool 77−88222
earthquake damage in UK, estimation of probability 79−93844
earthquake protection method design *(French)* 77−54332
earthquake response spectra 78−41871
earthquake response spectra determ. 79−97910
earthquake simulator operational principles 78−5681
earthquake site response anal., construction of smooth site dependent spectra 79−76086
earthquakes, records, optimal digitisation 77−91044
earthquakes, seismic faults, risk to power stations in New York and New Jersey 79−8611
EBR-II, wake and dispersion models rel. to released material 77−91186
economic analysis of nuclear electric power plants c.f. fossil fuel plants 79−92057
economic indices improvement for LWR power stations and fuel cycles *(Russian)* 79−26744
education, energy from nuclear sources, outline for secondary school students 79−80975
effluent analysis methods for environmental monitoring 79−13556
effluent discharge, atmospheric radioactivity inside buildings, absorbed dose estimation *(Spanish)* 78−8998
effluent environmental impact comparison 78−96290
effluent monitoring programme design and organisation principles 79−13548
electrical and mechanical equipment, improved seismic tests, research needs 78−94053
electrical power supply, safety requirements, emergency supplies 80−52762
electrical supply system performance, reliability of protection and control systems 80−52761
electricity supplies for safety system, German Regulation KTA 3701.1 *(German)* 80−37466
electrodialysis desalination plant, boundary layer thickness, effect on plant perform. and design 79−26725
electronic system of power-station control with modules and distributed software based on controbloc elements *(French)* 79−76110
elementary catastrophe theory modelling of Duffing's equation for seismic excitation of nuclear power facilities 79−31240
ELMO bumpy torus reactor reference design 78−803
emergency core cooling system motor operated valves, failure mode anal. 78−54866
emergency core cooling system motor operated valves, failure criteria 78−70592
emergency monitoring procedures at CEGB stations, UK 77−54322
energy analysis of nuclear power plants and their fuel cycle 79−26746
energy balance of nuclear power plant *(French)* 79−63729
energy self-sufficiency by 1990, use of Nuclear forms - complex of reactors 80−18456
energy storage for Tokamak reactor cycles 78−62661
engineering materials certification for safety and reliability testing 80−78360
environment protection problems during construction *(French)* 80−76663
environmental acoustic protection *(French)* 80−19155
environmental and safety aspects 78−766
environmental aspects *(Japanese)* 77−83112
environmental effects, nuclear and thermal power stations comparison 77−71706
environmental impact *(French)* 78−8994
environmental monitoring methods and techniques at nuclear facilities using thermoluminescence dosimeter 79−85819
environmental noise, study re. nuclear power plant construction 78−87194
environmental programmes for surveillance, implementation in Spain 77−65336
environmental protection, reactor safety and waste handling *(Hungarian)* 80−91224
environmental protection in Hungary *(Hungarian)* 80−91225
environmental radioactivity and dosage models *(Spanish)* 80−32518
environmental research data implementation *(French)* 80−74037
environmental studies organisation *(French)* 80−76664
equipment response to aircraft impact 78−50416

nuclear power stations continued
equipment response to airplane crash 77−3186
failure analysis and failure prevention in nuclear elec. power plants 77−79450
failure probability of battery system following loss of AC power 78−17376
FAPMAN-5, a computer code for optimum operation of LWR power stations 79−22450
Farley Nuclear Plant Data Link System 79−9797
fast alarm system to optimise protection of public 78−55048
fast breeder reactor, safety engineering technology aspects *(German)* 79−54567
fast breeder reactor boiler tubes, eddy current probe insertion for in service inspection, method development *(Japanese)* 80−822
fast reactor electricity generation, experience and future development 80−18587
fast reactor plant, future design and construction plans, review of national papers SM 225/81-87 79−97797
fast reactor projects, progress report 79−85757
fast-core experimental power station KNK II 79−81074
fault conditions diagnosis based on tree logic and probabilistic importance, appl. to nuclear power plant 77−6549
fault tree analysis, development of DICOMICS-TWIN self-adaptive algorithm for minimal cut sets determ. 78−17380
fault tree and reliability analysis, modular decomp., PL/1 program 78−17381
FBR, 1200 MWe Super Phenix, construction work in France 77−46391
FBR, 1200 MWe Super Phenix, steam generators design, France 77−46392
FBR, appl. in Spanish electricity supply system, review *(Spanish)* 79−59115
FBR, effect on world stockpile plutonium 78−86641
FBR, electric power generation, research, development and demonstration, risk and timing 80−57837
FBR power stations, development of modular steam generators 79−76058
Federal radiological emergency response planning and preparedness activities 78−46147
Fessenheim, France, PWR core physics meas. c.f. design values 80−718
FFTF, operator training simulator 78−5013
FFTF heat transport system, design construction and testing 79−97783
fire barriers, analytical hazards analysis 80−18534
fire frequency and core damage probability estimation 79−13461
fire hazard assessment 78−50269
fire occurrences, Bayesian prediction model 80−18527
fire protection policy 77−46356
fire protection research 78−21710
fire risk assessment 80−23002
fission reactor design, development and commercialisation of 17 types, review *(Japanese)* 79−80974
fission reactor fuel UF_6 advantages 78−8912
fission reactor neutron flux instrumentation commissioning, EM compatibility 79−89466
fission reactors testing using ultrasonic test apparatus *(German)* 80−13730
fission-fusion electric energy supply system modelling 78−740
fission-fusion hybrid energy storage system, economic feasability 78−796
fission-fusion hybrid power plant economics 78−789
flame resistant cable, develop. and qualification tests 79−687
flexible dual-containment approach design and licensing 79−13400
floating nuclear plant, shield design features 78−21777
floating plant, overview 78−21748
floating power plant, environmental and safety aspects 78−21750
floating power plant manufacture 78−21749
fluid radioactive waste monitoring equipment, USSR standards *(Russian)* 78−89998
fluid systems, program for initial cleaning 80−23047
Foratom member countries, nuclear power programme financial aspects 79−26697
forced outages, statistical data anal. 80−13776
Forsmark 3 plant, reactor safety study 80−18516
Fort Calhoun, operation with reduced complement of in-core detectors 78−21716
Fort St. Vrain HTGR power station, review of design and operation 79−45353
Fort St. Vrain HTGR rise-in-power test programme 79−9864
French nuclear power generation programme *(French)* 79−26732
French nuclear power plant gaseous and liquid effluent release monitoring *(French)* 79−13551
French nuclear power plant occupational radiation exposure meas. and prediction 79−9900
French safety reliability methods for power plants *(French)* 79−26644
fuel, rod modelling, utility requirements 78−21747
fuel accounting practices at Duke Power Company 78−13244
fuel and waste management schemes for nuclear power implementation 77−57773
fuel circuit review, radioactive conditioned waste final storage *(German)* 80−799
fuel cycle, industrial integration, Argentina *(Spanish)* 79−31154
fuel cycle alternatives for power reactors 77−42107
fuel cycle and nuclear power plant development in USSR, economic aspects 79−644
fuel cycle economics, tutorial paper 78−17446
fuel cycle length flexibility in C-E reactors 77−42116
fuel damage impact on plant operations 80−686
fuel element damage at Three Mile Island Nuclear Power Station, thermodynamic aspects *(German)* 79−93739
fuel handling system availability, minimum requirements 78−41820
fuel management, fuel cycle and in-core management 79−26702
fuel management reactor calcs., educational aspects 78−17298
fuel outage management and quality assurance 79−97862
fuel reprocessing, implementation 77−42162
fuel reprocessing at Windscale, possibilities and implications 77−79451
fuel reprocessing plants, economic anal. of alternate location strategies 79−59235
fuel reprocessing programme in W.Germany *(German)* 78−8954
fuel reprocessing technology status, large plants 78−21735
FUGEN project, Japan, construction and start-up 78−86675
full-scale reactor safety experiments performed in the Marviken power station, Sweden 79−26633
fusion, recirculating power, unit costs, thermal pollution 78−29643

nuclear power stations continued
fusion, UWMAK-III, non-circular, Tokamak, power reactor design 77−74979
fusion magnetic confinement near term designs, overview 78−58413
fusion mirror reactor studies 77−74980
fusion plant, inertial confinement, commercialisation anal. 78−58410
fusion plant design costs 78−791
fusion plant layout, CO_2 driven 80−32503
fusion plants, D-^{3}He field-reversed mirror concept appl. 80−23126
fusion plants with ^{3}He generator and D-^{3}He satellite design 79−76143
fusion power, parametric anal. of utility operations 78−58409
fusion power commercialisation 78−58405
fusion power plants, compact, magnetic mirror research 78−744
fusion power station economic anal. 78−788
fusion reactor, Culham Conceptual Tokamak Reactor Mk II, reactor costs and maintenance 77−74978
fusion reactor, inertial confinement, parametric studies 80−32507
fusion reactor, inertial confinement economics 80−32506
fusion reactor, laser systems, plant development problems in Yugoslavia *(Croatian)* 80−833
fusion reactor appl., present state and future prospects *(German)* 77−18692
fusion reactor costing methods 78−790
fusion reactor large magnet systems safety 78−770
fusion reactor second generation designs, safety anal. 78−771
fusion technology progress 78−62607
fusion Tokamak, development problems, Yugoslavia *(Croatian)* 80−832
fusion Tokamak, experimental fusion reactor preliminary design 77−74981
fusion-fission hybrid reactor system, energetics assessment 78−797
fusion-fission hybrid system using divertored Tokamak, optimisation 78−798
future advanced energy systems 77−57774
gas cooled fast neutron reactors, He and CO_2 coolant comparison 77−42046
gas phase cavity reactor design and operation with MHD generators and turbogenerators *(Russian)* 78−37435
gas turbine-HTGT system heat exchanger design 78−739
gaseous effluent standards comparison for nuclear and fossil fuel power prod. facilities 80−32536
gaseous reactor wastes, dispersal forecasting *(French)* 78−8995
GCFBR, research and development, current status *(Hungarian)* 79−6759
GCFBR symbiosis with thermal reactors 77−57738
GCFR, development of PCRV steam generator cavity closure 78−41849
GCFR, transient analysis of closed gas turbine cycles, TUGSIM-10 computer code 77−18675
GCFR core and core support struct., seismic model test 78−41869
GCFR power plants, 1200-1500 MW using dissociating coolant 79−31160
GCFR with N_2O_4 coolant, power plant nuclear and chemical safety 79−30969
GCHTR, steam gasification of coal using fluidised bed gasifier 77−83071
GCR implementation strategy anal. using MCFLOW program 77−57733
Genkai PWR plant operating experience 78−86655
German, assessment of accident risks 80−18517
German nuclear power development, review 79−63716
Glace Bay HWR, thermal effluent appl. to greenhouse heating 78−86678
Gosgen pressurized-water nuclear plant *(German)* 79−63763
Grand Gulf, BWR designed for improved operation 80−106121
Grand Gulf contributes to growth in the sunbelt 80−106150
gross operator error rates, evaluation of operator reliability 79−45371
Hamaoka BWR plant, operational experience 78−86654
Hamaoka nuclear power station, operating experience *(Japanese)* 78−17333
Harrisburg (TMI-2), fuel element defects quantitative calc. *(German)* 80−23105
Harrisburg nuclear power station failure, safety and control *(Norwegian)* 79−81017
heat appl. to space heating at Karlsruhe Nuclear Research Centre *(German)* 79−87943
heat discharge, agricultural uses *(French)* 78−5060
heat exchangers, eddy current probe for nondestructive testing of transfer tubes *(Japanese)* 80−81246
heat extraction from steam generators in nuclear plants 78−37465
heat rate improvement, design modifications to condenser air-removal system 79−67830
heat recovery from nuclear plants for agriculture and pisciculture 78−37464
heat supply, district heating, nuclear reactors, applicability *(Russian)* 79−31173
heating plants, big cities, industrial complexes, nuclear reactor applicability *(Russian)* 79−31174
hermetically sealed valve for the safety systems of a nuclear power station *(Russian)* 78−89952
high-temperature power-technological industrial processes use of nuclear power, reviews 79−26729
Hinkley Point B, AGR radiation protection, design criteria and operating experience 80−27832
Hinkley Point B AGR station computer control system, performance review 79−89457
HTGR, 330 MWe nuclear power station, start-up and operating experience since 1975 80−830
HTGR, He-cooled, status and prospects 77−79467
HTGR, Peach Bottom, decommissioning and component removal 78−21756
HTGR, performance assessment of Peach Bottom Unit 1 prototype 79−67906
HTGR, with direct cycle gas turbine, project development in Germany 77−46389
HTGR development and its process heat, steam-cycle and gas turbine appls. 80−63250
HTGR dual purpose plant for military installations 78−41855
HTGR plant, reoptimisation using nonproliferation fuel cycle 80−13576
HTGR plant seismic response, nonlinear soil-structure interaction from base slab uplift 77−3177
HTGR risk assessment, operator actions, event and fault tree anal. 80−63330

nuclear power stations continued
HTGR steam generator, construction and development *(German)* 77—369
HTGR steam power plant, nonlinear dynamic model, digital simulation 78—78437
HTGR steam supply, using once-through steam generator, modelling 77—88271
HTGR U reprocessing by graphite fuel element and C fluidised bed combustion 78—13314
HTGR with closed-cycle gas turbine, technological assessment 79—54490
HTR, control 77—14262
HTR, in West Germany 77—61594
with HTR and He turbine, dry closed circuit cooling, principles and advantages *(German)* 78—74426
HTR nuclear long distance energy system, heat transport by chemical circuit 80—7905
HTR plant with methane reformers for long distance energy system 80—7906
HTR plants components development and testing *(German)* 77—10482
HTR power station, design development, operation and appl., review *(German)* 79—76088
HTRs, current development and commercial advantages *(German)* 78—37433
human factors, normal operation and emergency procedures, errors, safety, maintenance, working conditions 80—63328
human factors engineering 78—21711
human factors in nuclear power plants, review 79—89463
human resources, quality assurance, reliability in nuclear power plant construction 79—97776
hydrobiological studies, conception and data obtained *(French)* 80—76665
IAEA's activities in safety codes and nuclear safeguards 77—65347
IAEA nuclear safety standards program for protection, electric, instrumentation systems 79—45365
IAEA safety codes and guides for thermal neutron power plants 79—26616
identification, plant responses 77—88213
Ikata Power Station Unit I, operating experience *(Japanese)* 79—36397
impact load for tornado generated missiles 78—51103
impact of new security regulations on nuclear plant design and operations 80—796
improved radiation shielding using packed mixed size Pb particles, nuclear plant maint. appls. *(Japanese)* 80—106207
in-service inspection methods and limitations 77—3169
in-service inspection requirements, impact of changes 79—54589
Indian nuclear power station effluent monitoring system requirements and experience 79—13552
Indian Point Unit No.2 reactor vessel, detection and identification of loose object 80—18553
induction motors, used in safety-related functions 77—3144
industrial activities nearby causing hazards, deterministic and probabilistic studies 80—78408
industrial process heat charact., potential for solar and nuclear power systems 78—822
inertial confinement fusion reactor and generating station concepts 78—753
inservice examinations, effective quality assurance 79—97861
inservice inspection, power plant design and fabrication 78—78451
inservice inspection of nuclear power plants in Japan, appl., problems *(Japanese)* 77—50255
INSITE system for nuclear site data storage and retrieval 78—5109
inspection practices and decisions for safety and availability 77—46304
installation policies analysis using TOTEM-3 code 77—65323
instrumentation and control, remote multiplexing appl. 80—52752
instrumentation system, practical implementation of regulatory guide 1.75, class 1E circuits 77—65345
integrated fusion-fission nuclear energy system with fuel self-sufficiency, thermal-electric conversion efficiency decrement 80—57907
integrated nuclear energy complex system of CMEA member countries *(Czech)* 80—52715
international symbiotic nuclear energy parks using breeders and advanced convertors, economic feasibility 80—57825
IRAN-1,2, plants, calc. of radioactive releases 79—18056
irradiated fuel, safe transport 77—79445
irradiated fuel visual inspection, design of compact, portable stand 79—67912
irradiated nuclear fuel transport and handling, French nuclear power plants *(French)* 79—31233
Isar BWR power station, transient expts. during startup and initial operation *(German)* 80—83187
isolation and relief valve/piping transient force anal. program 78—50287
Italian power plant Caorso, technical parameters BWR 77—38388
Italy, district emergency exercises 78—55052
Italy's electric power requirements, nuclear programme, pumped storage hydroelectric integration 79—26733
JOYO experimental fast reactor, test and operational experience 79—97867
KNK II fast breeder, construction and aseismic design 79—97778
Kori power plant unit I, startup and operating experience *(Korean)* 79—76080
Krsko, construction, architecture and reactor system cooling *(Croatian)* 80—37416
large-scale, safety considerations 78—8961
laser fusion deployment scenario 78—58411
laser fusion generating stations, safety, environmental effects 78—50337
laser fusion hybrid reactor, scoping studies for power generation 78—5026
laser fusion power plant, capital cost data base 80—32504
laser fusion power plants, final optics 78—50334
laser fusion power stations, potential accidents 78—776
laser fusion system studies model, TROFAN 80—32505
laser fusion-fission hybrid reactor design 78—802
laser thermonuclear power plant, conceptual design study 80—78441
laundry drain treatment system development 79—9788
leakage tests, Spanish safety policies *(Spanish)* 80—5247
licensing procedure, public participation under Atomic Energy Act *(German)* 80—102256
licensing procedures in the UK 80—27708
liquid and solid radioactive waste processing using fixation method *(Czech)* 77—74947
liquid discharge, radionuclide isotopic anal. *(Spanish)* 78—13250

nuclear power stations continued
LMFBR, 1200 MWe, Na-cooled, superphenix *(Norwegian)* 77—74913
LMFBR, components and fuel handling systems, Italian industry contrib. 79—97875
LMFBR, control rel. to operational safety aspects 77—14251
LMFBR, development areas 77—57737
LMFBR, equipment design, Na-NaK engineering handbook 79—97815
LMFBR, experience with Rapsodie and Phenix in France *(French)* 79—97892
LMFBR, future design and construction in USSR *(Russian)* 79—97803
LMFBR, future design and construction plans in Federal Republic of Germany 79—97799
LMFBR, future design and construction plans in Italy 79—97800
LMFBR, future design and construction plans in Japan 79—97801
LMFBR, future design and construction plans in UK 79—97802
LMFBR, HCDA, structural response calcs., methods, codes development 77—3126
LMFBR, insulations 77—83068
LMFBR, large EM induction pump for high-temp. appl. 78—17291
LMFBR, leak detection in steam generator, by acoustic spectra meas. *(Czech)* 78—54849
LMFBR, modular steam generators, breakdown protection 79—76059
LMFBR, past and present role in Federal Republic of Germany 79—97891
LMFBR, past and present role in Italy 79—97895
LMFBR, past and present role in UK 79—97894
LMFBR, past and present role in USSR *(Russian)* 79—97893
LMFBR, pool type, natural circulation cooling 80—102289
LMFBR, primary loop components, design and testing *(French)* 79—97782
LMFBR, safety c.f. thermal reactors 79—26562
LMFBR, selection of steam conditions 80—18404
LMFBR commercial plant design 78—8877
LMFBR critical technical issues 80—13779
LMFBR demonstration plant, design, construction and operating experience 79—97887
LMFBR design, reliability, risk assessment, power plant safety anal. 77—71665
LMFBR design, risk-based approach 77—88198
LMFBR fuel handling experience 79—97873
LMFBR plant, modelling thermal hydraulic transients 77—88207
LMFBR plant, thermohydraulic transient simulation 77—83001
LMFBR plant system design, review *(Japanese)* 79—80973
LMFBR power stations, electric power generation and fuel fabrication 80—57928
LMFBR steam cycle conditions, comparison 80—18406
LMFBR steam cycle selection 80—18403
LMFBR steam cycles comparison, PLBR design 80—18405
LMFBR steam generator tubes Cr-Mo low alloy steels suitability comparison 78—54834
LMFBR steam generators, mass transfer props. of steel, test *(Japanese)* 77—348
LMFBR steam generators, use of alloy 800 77—3108
LMFBRs in Japan, past and present role 79—97889
LMFBRs in USA, past and present role 79—97890
LMFISR, in France, Future design and construction plans *(French)* 79—97798
load factors and availability achieved with light water and heavy water reactors *(Slovenian)* 80—68843
LOCA, extreme loads and associated safety aspects, reviews 79—22405
LOCA, models for estimation of critical flow in two-phase systems 79—36361
LOCA, response of reactor containments 79—30958
locations around world, part in electrical energy production 80—18589
loose parts monitoring techniques and experience 79—3211
Loviisa Nuclear Power Station, in Finland, guarantee testing for output and efficiency *(Russian)* 80—102291
Loviisa-1 Nuclear Power Station, in Finland, safety during design, building, and operating stages *(Russian)* 80—106128
low temp. heat extraction from nuclear power plants for district heating 78—37456
low temperature nuclear heat utilization in Italy 80—7902
low-level radiation dose meas. 79—85820
LWR, 1000-2000 MVA range turboalternator design, problems *(French)* 77—3153
LWR, advanced reactor development 77—67861
LWR, commercial, evaluation of human errors and operator reliability 78—17373
LWR, condenser tube failures 78—21715
LWR, deterministic criteria vs. probabilistic analyses 80—32377
LWR, Dutch nuclear safety requirements 80—768
LWR, effect of district heat prod. on reactor operation and safety 79—85624
LWR, fuel cycle sensitivity anal. system 77—42119
LWR, heat supply for desalination, economics 78—41851
LWR, heavy water moderated, prototype, pressure tube monitoring with US devices 77—88268
LWR, human operator errors, analytical model 80—63329
LWR, liquid effluent treatment 80—18444
LWR, multigoal fuel cycle optimization including nonproliferation objectives 80—52764
LWR, optimum fuel loading and coastdown operation 79—30970
LWR, press. and temp. loads on containment after LOCA, scale model expts. 77—3134
LWR, Pu recycling experience 79—45391
LWR, radioactive discharges meas. *(German)* 77—42174
LWR, reliability demonstration test *(Japanese)* 79—26552
LWR and coal power stations, effects on ambient media from mining to waste disposal *(Spanish)* 77—75005
LWR at Genkai nuclear power plant, Japan, operating experience *(Japanese)* 77—79447
LWR circulator auxiliaries system modelling 77—88221
LWR diversion resistant processes and cycles 78—86677
LWR dynamics simulation, using hybrid computer system *(Czech)* 77—54309
LWR fossil fired superheater technical and economic assessments 78—8966
LWR nuclear power plant with passive containment system, surveillance system importance 80—795
LWR operation and maintenance 78—86653
LWR plant, decommisioning 78—29603

nuclear power stations continued
LWR plant, economic effect of increased seismic load on design and construction costs 78−66432
LWR plant, occupational radiation exposure, recommended limitations 79−59266
LWR plant availability rel. to refuelling cycle duration 79−22440
LWR plant control, linear quadratic theory appls. 77−88265
LWR plants in Japan, safety aspects and operating experience 79−26628
LWR power plant, general design philosophy *(Japanese)* 78−54816
LWR power plant, radioisotope activity meas. in secondary loop coolant 80−5345
LWR power plant human errors 79−13459
LWR power plants, inservice inspection 79−30944
LWR power plants, radioactivity release in LOCA uncertainties 79−26639
LWR power station construction in France, standardisation advantages *(French)* 78−58397
LWR power station radioactive unplanned dischage meas. 78−89995
LWR power stations, design features and instrumentation for materials safeguards *(Russian)* 80−63278
LWR power stations, R and D for improving seismic safety 80−99231
LWR primary circuit component production, metallurgical aspects 79−36330
LWR safety considerations in Sweden, reactor design for power plants 79−26631
LWR thermochemical energy cycle for management of reactor heat −15 to 180°C 79−22449
LWR utility, development of non-LOCA safety anal. methods 78−21691
LWR waste management, cf. fusion plant 78−773
LWRs, installation in small developing countries 79−31167
LWRs at Harrisburg and Mulheim-Karlich, safety systems comparison *(German)* 80−22966
LWRs in Japan, design improvement and standardisation 78−86579
machinery monitoring and online diagnostic systems 79−9810
machinery surveillance and diagnostics automation 79−641
Magnox power station, decommissioned, rad. levels, neutron activation, waste disposal 80−13976
main steam isolating valves, back pressure light, PWR appl. 78−29602
Maine Yankee power station uprate history 80−73967
maintainability, human factors engineering review of design, c.f. fossil plant 80−22913
maintenance optimization through trend monitoring 80−18552
management of low-level radwaste, book 79−54568
mathematical modelling and optimisation, methods 77−23315
metal structures, inelastic anal. 78−70586
metalwork fault monitoring, US flaw detection system *(Russian)* 78−25302
MHD pumps, cylindrical induction, research and development studies 79−77276
microprocessor control systems for nuclear power plants, program reliability *(Spanish)* 78−58369
Millstone power plant, Unit 3 design 80−22922
mirror fusion reactors, remote servicing features 78−58448
mirror hybrid reactor power plant, mechanical struct. 78−58449
mitigating community impacts of energy development 79−61938
modal control 77−14252
model validation and automatic control 77−88261
modification during plant startup and operation 78−21758
Monju heat transport system design and related R & D work 79−97791
MSR (Pu converters) and MSBR's in commercial nuclear power stations 79−26740
multi-site utilities, centralized in-house environmental laboratory services 79−85821
national nuclear power programmes, survey 77−88267
neutron flux optimum control during nuclear station load following 79−9761
NIIEFA linear accelerator−flaw detectors for nondestructive inspection of atomic power plant equipment 79−47856
noise analysis, time series modelling methods, comparative eval. *(Japanese)* 80−13552
noise measurements for plant surveillance and anomaly detection in nuclear power stations 79−97853
nonequilibrium fuel management policies at San Onofre unit 1 77−42117
NRC standardisation in licensing, B and W viewpoint 80−23023
nuclear chemical-bound energy system, short term market prospects *(German)* 78−82505
nuclear energy centres, power development, economic and ecological problems, USSR *(Russian)* 79−31149
nuclear energy complexes, economic and ecological problems of nuclear power development 79−645
nuclear fuel cycle facilities in USSR, nuclear material control and accounting *(Russian)* 79−26718
nuclear fuel movement monitoring, using dosimeter 77−67899
nuclear material and facilities, physical protection at plant, IAEA first training course, report 79−76077
nuclear materials, safeguarding experiences *(German)* 80−611
[nuclear plant] construction sequence scale model an aid to productivity and quality assurance 79−97777
nuclear power in Czechoslovakia, review *(Czech)* 79−31157
nuclear power nonelectrical energy production, review 79−26728
nuclear power plant emergencies, prevention of excessive irrad. of staff and population *(Russian)* 78−50286
nuclear power programme, Philippines, prospects, problems 79−31175
nuclear safety aspects at power and fuel cycle plants in USSR *(Russian)* 79−26709
occupational radiation exposure, evaluation and control, US research program 80−5370
occupational radiation exposure at nuclear power plants, meas. and prediction 79−59182
occupational radiation exposure minimisation, at Yankee Atomic, USA 77−18712
off-site emergency monitoring systems 78−46178
offshore environmental monitoring program for proposed nuclear power plant in Islote, Puerto Rico 78−11917
offshore floating plants, design and anal. methodologies 78−66336
on-power measurements of reactor parameters using dynamic meas. methods, computer system description 79−89467
one flow steam generator for PWR power plant, prototype research works *(Russian)* 79−26723
nuclear power stations continued
Ontario Hydro nuclear power plant stack effluent monitoring 79−3254
Ontario Hydro nuclear power program, occupational doses 77−88285
operating and startup experience, control, instrumentation and electrical systems, Trojan plant 77−65283
operating conditions in combined energy system *(Russian)* 77−38367
operating experience, conf., Arlington, Texas, USA (Aug. 1979) 80−8735
operating experience with control, instrumentation and electrical system, Three Mile Island 77−65285
operating margin optimisation 79−85592
operating plant experience utilisation in plant design 77−65325
operation, socio-economic effects on demography, finance and local activities of region *(French)* 80−74038
operation, with reduced utilisation of rated power, limit of fuel stay time in reactor type VVER-440 *(Russian)* 77−65274
operational diagnostics and control computerisation 79−3233
operational reliability of power stations with PWR, PHWR and BWR *(Czech)* 78−82500
operational safety, standardised international guide *(Czech)* 77−38383
operator performance and response time, stress degradation, Poisson model 80−63415
operator reliability modelling for nuclear power stations 79−85621
operator training, simulator 77−367
operator training simulator, design characteristics *(Spanish)* 80−58007
optimal cycle coastdown at San Onofre unit-1, reduced enrichment requirements 77−42118
optimal operating conditions 78−37427
optimal size and location in energy parks 80−95489
optimisation, with GCFR and N_2O_4 dissociating working substance *(Russian)* 79−59159
optimisation of the cyclical operating regime 79−71916
optimum fuel cycle strategy 78−54831
optimum theory of nuclear plant mix with minimum natural fuel requirement 79−26469
outages, turbine-generator reliability assurance through large scale test facilities 77−3151
Pakistan, transfer of control and instrumentation technology 77−65356
Palisades Plant steam generator operation rel. to water chemistry 79−9854
parameter identification methods 77−88219
PBHTR, design operation and applications, review 79−45328
PBHTR, source of nuclear process heat, development of power plant, overall time and cost estimates 77−3089
Peach Bottom 1, HTGR nuclear power station, review of design and operation 79−45327
Peach Bottom power station radwaste system backfit considerations 80−9351
performance analysis of power plants from operating experience data 78−21757
performance evaluation by thermal hydraulic anal. 79−67831
performance improvement by Reactor Power Cutback System 79−9795
personnel dosimetry and access monitoring by process computers *(German, English)* 78−17440
personnel monitoring concepts 79−85822
personnel radiation minimisation in nuclear power plants 78−21663
PFR, fuel and component handling, CDFR intentions 79−97872
Phenix and Super Phenix breeder reactor plants, status report 80−13780
Phenix and Super-Phenex, primary ccts. *(French)* 79−97780
Phenix LMFBR, radioactive effluent release, operating team irrad. results *(French)* 79−31163
Phenix plant operations and modifications *(French)* 80−47615
Philippsburg power station, personnel dosimetry monitoring, use of evaluation device for rod and process computer *(German, English)* 78−17441
photon radiation meas. in nuclear power stations 80−63403
PHWR, CANDU, fuel cost anal. 78−54832
PHWR, CANDU reactor system, appropriate technology 78−58338
PHWR, forced circulation steam generator selection criteria *(Rumanian)* 79−3232
PHWR design, integration into power stations, small plant role in developing countries 79−31170
pipeline system Cr-Ni alloyed austenitic steel, Ti stabilised, corrosion props. *(Hungarian)* 77−18658
piping system design, rationalisation of power plant pipe break criteria 80−99205
piping systems under seismic motion, method of residues 77−3182
piping weld inspection, by in-process acoustic-emission monitoring 77−14823
plan in Holland, critical review *(Dutch)* 78−13252
planning and construction of nuclear power plant *(Korean)* 78−54819
plant, contrib. of quality assurance to safety and reliability 79−22438
plant component design, dynamic analysis, nonlinear effects, research status and needs 79−593
plant diagnostic system using noise anal. 78−50279
plant efficiency, and heat rate improvement program 79−67829
plant efficiency at Beaver Valley power station number 1, anal. of generating capability deficiency 79−67828
plant safety systems, common mode, failures, investigation *(German)* 78−694
plant size, optimisation techniques appl. to energy planning 79−24886
plastics, applications in nuclear power industry 79−6744
PNP project, prototype HTR and coal gasification plant review 80−5393
Point Lepreau, radioactive waste management 78−29600
Point Lepreau, standard CANDU 600 MWe nuclear plant installation 78−29637
point model nuclear reactor heuristic approach to reinforcement learning control 78−46144
pollution resulting from release of Cu, impact and fate on aquatic environments 78−7665
polymer cable insulating materials radiation resistance, expt. 78−59835
portable radiation meters, accuracy checking facility at Berkeley Laboratories, UK 78−74507
power conf., Chicago, United States, July 1979 80−794
power conference, Lausanne, Switzerland (Oct. 1977) 79−36326
power control problems for PWR power plant *(Russian)* 79−31158
power plant implementation in developing countries, particularly Egypt 77−57768
power plant pathology 78−17345
power reactors, min. unit generation cost 80−734

nuclear power stations continued
preoperational tests, start up tests and operating experience of Japanese power station *(Japanese)* 79−67881
pressure component manufacture, new materials, technologies and equipment development 78−74436
pressure vessel components reliability, conf. Vienna, Austria, 1977 79−17986
pressure vessel surveillance capsule remote dismantling and testing 79−9817
pressure vessel testing, water pressure testing, test method and anal. *(German)* 78−25260
pressure vessels, exam. for compliance with safety regulations 78−89954
pressure vessels, remote controlled US pre-service and in-service inspections 78−89955
pressurised heavy water Candu nuclear power plants, cost and safety aspects *(French)* 80−18463
prestressed secondary containments, explosive characts. near ultimate load,, review 79−30968
primary and secondary water chemistry of PWR power stations, European experience 80−106110
principles underlying IAEA nuclear safety programme 80−95361
probabilistic fracture mechanics anal., nuclear power station structural components 77−81317
probabilistic methods for risk assessment and safety standard 78−21693
probabilistic siting analysis, atmospheric releases, health effects 80−106130
process heat as energy supply in developing countries 77−57735
process heat from nuclear steam supply systems, appl. to prod. and treatment of liquid and gaseous prime movers *(German)* 79−87944
processed fission product wastes as heat source 78−41838
projects status, USSR ninth five year plan 77−23316
prospects w.r.t. environmental problems *(Hungarian)* 80−13742
protection of nuclear power plant against seism-aseismic bearings 80−857
protection system, development of integrated numerical protection system *(French)* 79−76097
protection system equipment, class 1E, qualification requirement 77−67822
protection systems, treatment, analysis and presentation of information on component faults and [nuclear power] plant disturbances 79−76098
public attitudes in Switzerland 77−33824
public reaction to developments in Canada 77−33825
PWR, 836 MWe nuclear power station, operating experience since 1974 80−831
PWR, commissioning and start-up procedures *(Slovak)* 79−36346
PWR, comparison cost effectiveness of remote, centralised microprocessor based multiplexing control systems 78−89971
PWR, condensate treatment in secondary cct., optimisation *(Hungarian)* 77−30654
PWR, construction and operation experience in Japan 77−57732
PWR, dynamic testing for model validation 77−3087
PWR, fault tolerant multiplexed control rod position detection and system 77−65281
PWR, forced circulation steam generator selection criteria *(Rumanian)* 79−3232
PWR, German, U-tube steam generators, inspection findings 79−9849
PWR, heat transfer equations for boiler tubes *(Rumanian)* 79−3189
PWR, heating, ventilating and air conditioning systems *(Japanese)* 80−91213
PWR, ice condenser system *(Japanese)* 80−91214
PWR, implementation in Iran 77−57769
PWR, loss of coolant accident, mathematical model *(Czech)* 77−3072
PWR, occupational radiation exposure 78−21664
PWR, Oconee, occupational exposures, radiation levels and waste levels during operation 78−21726
PWR, Oconee station, steam generator availability 80−22921
PWR, optimal fuel loading and operation planning 78−50276
PWR, potential of Th cycle 77−42122
PWR, primary cct. leakage simulation, safety aspects *(German)* 78−33239
PWR, quality assurance during operation, France 77−61526
PWR, radiation safety of personnel and local population 77−71700
PWR, sensor response monitoring, time series modelling 79−26659
PWR, small, electricity and steam supply, technical and economic studies 79−31171
PWR, Three Mile Island, Pennsylvania, USA LOCA 79−89398
PWR, transient state studies 77−14263
PWR, two-unit, modification feasibility for radwaste volume reduction equipment 78−17395
PWR, vibrations due to cooling medium flow, meas. and evaluation *(Hungarian)* 80−63304
PWR accident prevention, extra instrumentation for Ringhals 2 station, Sweden 80−63369
PWR and LWR local corrosion causes and preventive methods *(French)* 78−8963
PWR appl. to multi-stage-flash desalination, small performance plants 78−37461
PWR automated optimal multiple cycle fuel management code 79−85641
PWR balance-of-plant design standardisation 80−22911
PWR boiler tubes, corrosion risk reduction methods 79−39045
PWR boiler tubes, denting type corrosion, control by use of neutralisers 80−106109
PWR containment building, design and anal. of cavity shield system 80−18713
PWR containment safety design margins *(German)* 78−717
PWR containment vessel wall electrical penetration tests *(Japanese)* 79−6747
PWR crosslinked polyethylene insulated low noise triaxial cable *(Japanese)* 78−670
PWR design and plant layout, safety criteria 80−102288
PWR development in France *(French)* 78−8962
PWR heat rate improvements, controllable loss system 79−67827
PWR instrumentation operating experience during start-up and operation 79−89456
PWR modular steam generator, application possibilities 79−76057
PWR natural circulation U-tube steam generator, digital code UTSG 78−50242
PWR nuclear steam supply system for district heating and elec. prod. 78−37466
PWR operation, statistical analysis *(French)* 78−58374
nuclear power stations continued
PWR plant, cut-and-cover construction, feasibility and safety *(German)* 78−82429
PWR plant, dynamics, digital simulation 78−8882
PWR plant, LOCA capability code for utility appl. 78−21690
PWR power plant, assessment of underground siting as engineered safety factor 78−13316
PWR power plant, dynamic model 77−46266
PWR power plant, radiation protection *(French)* 78−82521
PWR power plant dynamics, math. model *(Polish)* 79−63800
PWR power plant flow pressure fluctuations as vibration source, relationships *(Hungarian)* 80−47685
PWR power plant steam dump valve stability anal. 78−50289
PWR power plants, design concepts to facilitate dismantling 80−13577
PWR power plants, safety technical problems, core cooling *(Russian)* 79−31085
PWR power station operation in France, monitoring and control equipment eval. 79−89454
PWR power station secondary water chemistry study, progress report 80−106108
PWR power stations, operating record and reliability, reviews 79−22404
PWR power unit, automatic control and meas. system design lines *(Russian)* 79−30964
PWR pressure vessel design *(German)* 77−42180
PWR radiation shielding design 80−5372
PWR reactor dismantling, model scheme to meet West German regulations 80−825
PWR steam generator eddy-current inspection results 79−9855
PWR steam generator repair options 80−22923
PWR steam generator tubing, corrosion problems 79−24683
PWR three unit 1300 MW(e) plant, engineering and design 78−86578
PWR West German risk evaluation study, interim report 77−74960
PWR/BWR, waste-water treatment plants, engineering experience 77−6543
PWRs, 900 MW, in France, construction report *(French)* 79−63801
PWRs 1300 MW, in France, development report *(French)* 79−63802
quality and safety criteria, management aspects *(French)* 77−3154
quality assurance, cost effective programs 79−97863
quality assurance as management commitment and personnel indoctrination 77−61632
quality assurance as means of nuclear technology transfer in Iran 77−61630
quality assurance criteria, international standardisation 80−780
quality assurance in Japanese plants 77−61628
quality assurance principles by French Elec. Board *(French)* 77−3155
quality assurance program for nuclear plant operations 80−783
quality assurance requirements for reliability in developing countries 79−22452
quality assurance standards in USA, present status and appl. 80−781
quality control and maintenance of trained personnel in developing countries 77−61633
quality control and safety, West German practice *(German)* 77−75004
quality control in Iranian nuclear power station initiation 77−61629
quality systems standards comparison 79−22439
quantitative risk anal., limitations 77−46354
radiation dosage determination, monitoring and control for personnel safety *(German)* 80−842
radiation exposure ALARA concept 80−32388
radiation exposure and protection 78−25301
radiation exposure near nuclear power plants, remote monitoring system 79−18055
radiation hazards from emissions of thermal and nuclear power stations, comparative study 79−34460
radiation monitoring, decentralised system using microprocessors *(Spanish)* 80−47727
radiation monitoring, digital differential pulse rate meter 78−37451
radiation monitoring, on-line computer appl. 80−5391
radiation monitoring meter design 79−54604
radiation monitoring of deposited activity, use of CdTe γ spectrometer 77−42193
radiation monitoring programmes at Point Lepreau 78−29552
radiation monitoring system *(Russian)* 79−31230
radiation monitoring systems, review 78−33292
radiation protection, recommendations review *(Hungarian)* 78−74508
radiation protection, regulatory control, implications of ICRP publication 26 80−18706
radiation protection optimisation in nuclear engineering, cost, risk *(Czech)* 78−33295
radiation qualification of reactor components 77−88252
radiation safety in nuclear power stations, doses to personnel, local population 77−71701
radiation safety monitoring instrumentation complex at the USSR nuclear power plants *(Russian)* 79−76108
radiation safety prediction 79−45435
radiative waste water treatment methods *(Hungarian)* 80−18450
radioactive aerosol dispersiveness in main ventilation systems 78−70650
radioactive contamination of biosphere, explosion and power plant influence *(Hungarian)* 80−21548
radioactive contamination prevention methods *(Hungarian)* 79−88007
radioactive effluent discharge data intercomparability and EEC harmonisation 79−13546
radioactive effluent discharges, European Community, 1972-76, radiological aspects 79−41019
radioactive effluent monitoring, symposium, Portoroz (1977) 78−89985
radioactive emission meas. and control *(German)* 77−79484
radioactive emissions, heat emissions, other environmental effects, review 79−22491
radioactive emissions meas. and control, survey 79−85818
radioactive fission products formation and behaviour, Kr and Xe separation and processing *(Czech)* 79−49707
radioactive liquid direct meas. instrument design *(Russian)* 79−3250
radioactive material leakage, accident risk 77−67820
radioactive pollution, population dose in the Northern Hemisphere 80−104779
radioactive pollution from nuclear power stations, accident anal. 79−63782
radioactive sludge dehydration using Funda filter *(Japanese)* 77−88234
radioactive waste, high level, disposal in deep-sea bed, New Zealand 78−705
radioactive waste, low-level, from nuclear power plants, solidification 79−54540

nuclear power stations continued
radioactive waste, reprocessing, solidification vitrification of liquid waste, review 79−9762
radioactive waste disposal from nuclear power plants *(Russian)* 79−30966
radioactive waste disposal problem 77−363
radioactive waste management 77−74974
radioactive waste meas. and problems *(Hungarian)* 79−88008
radioactive waste treatment and disposal *(French)* 80−99221
radioactive waste water treatment by flocculation precipitation process 79−93797
radioactivity release, air monitoring, emergency procedures 78−70610
radiologcal environmental monitoring programs design 78−70647
radwaste disposal operations Peach Bottom power station system backfit considerations 80−5261
radwaste evaporator improvement 80−91232
radwaste management systems, engineering and operational principles 79−54576
Rancho Seco Generating Station, LIDAR obs. of plume diffusion 78−11991
Rancho Seco nuclear power plant dry site operation 79−9860
Rapsodie control plug replacement *(French)* 79−97871
with RBMK reactors, structural materials corrosion monitoring 79−9756
reactor, pressure recorder for liquid cooling pipe *(German)* 77−88218
reactor buildings safety, solid-structure interaction behaviour 79−97912
reactor containment, nonlinear dynamic response, seismic analysis 77−3180
reactor containment structures, design and construction, ACI-ASME code of practice impact 80−798
reactor control and safety, development of a reliable single-channel direct-digital reactor-control system 79−89458
reactor control data sheets for Stade Nuclear Power Station, West Germany *(German)* 78−58366
reactor cooling system, operational principles *(Slovenian)* 77−67858
reactor core anal. using digital simulation 77−67866
reactor diagnostic system tasks and installation *(Hungarian)* 80−18452
reactor fuel cycle costs 77−6575
reactor loose parts monitoring, USA technology status and recommendations 79−623
reactor monitoring system for energy liberation fields of Beloyarsk power station reactors 77−23232
reactor neutron kinetics digital simulation 77−88216
reactor noise analysis by multivariate statistical pattern recognition system 77−14228
reactor noise diagnostics and surveillance, experience of Babcock and Wilcox company 78−17346
reactor parameter monitoring system, microcomputer-based *(Hungarian)* 80−18451
reactor power control, dual 305 computer system at Stade nuclear power station 77−353
reactor primary containment vessel, design and fabrication 77−18659
reactor protection computer systems, statistical verification of reliability 80−32417
reactor protection system, development of integrated numerical protection system *(French)* 79−76097
reactor release, population risk, implication of WASH-1400 in FRG 77−46351
reactor safety, probable risk assessment 80−797
reactor safety, qualification of class 1E transmitters 77−65287
reactor safety, quantifying plant availability, ALARA, and occupational radiation exposure relationships 79−59183
reactor safety and protection, electrical isolation devices employing fiber optic cable 79−59218
reactor simulators and nuclear power plants, mutual dependency of numbers *(Czech)* 79−35499
reactor structural analysis using CEASEMT computer codes 79−97911
reactor trip system, design of internal architecture for Westinghouse microprocessor-based [nuclear reactor] integrated protection system 79−76100
reactors in use in West, important types *(German)* 78−74463
reference mirror hybrid fusion-fission reactor design 78−801
refueling, underwater fuel handling techniques 79−67911
regulatory activities and their research and developmental support in the CSSR 79−26625
reinforced concrete containment structures, improved design, research requirements 78−94049
reinforced concrete structs., missile impact loading, nuclear power plant appl. 79−31237
relativistic electron beam hybrid reactor, economic model 78−58412
reliability analysis, unavailability of systems under periodic test and maintenance 80−95368
reliability technology, role of ASTM in providing standards 79−22435
remote heat supply, technical and economical aspects *(German)* 77−352
remote inspection system 79−45386
remote inspection system for reduction of personnel radiation exposure 77−14275
remote maintenance to comply with new legislation limiting occupational radiation exposure, in United States 80−106210
remote multiplexing control and safety systems evaluation 79−76109
remote siting as risk-reduction method, cost effectiveness 77−67178
research criteria, economical nuclear power plant structs. and components 78−94045
research needs, standards improvement, nuclear power plant design 78−94046
risk anal. for Austrian nuclear power plant site *(German)* 77−65321
risk analysis of the fuel cycle in the Netherlands 79−26624
risk assessment, role in nuclear regulatory processes 79−71906
risk tree analysis in criticality control 79−85632
risks statistical assessment of accidents and normal operation 78−50281
rock cavity construction of a nuclear power plant−a case study 79−26485
safeguard application to Italian nuclear power plants and fuel cycle 79−26716
safeguarding of nuclear facilities, methodology to aid decision-making 80−18477
safeguards systems, directed graph and fault tree anal. of material theft detection 80−13728
safety, aircraft crash probabilities for selected parts of a nuclear plant 80−859
safety, availability of redundant safety systems with common-mode and undetected failures 80−91230
nuclear power stations continued
safety, Czechoslovak legislation and practices *(Slovak)* 80−13632
safety, merits of separation against multiple failures 79−26626
safety, regulatory control ot nuclear power stations in the United Kingdom 80−18707
safety, risk assessment of necessary functions for protection against external accidents 80−743
safety, seismotectonic map of France for appl. to antiseismic design of nuclear installations 80−860
safety, USSR basic approaches 79−627
safety, West German policy *(German)* 80−57865
safety analysis, human errors in high stress situations, data and assessment 78−17374
safety analysis, methodology and appls. of probabilistic risk assessment 80−63352
safety analysis and regulations in France, probabilistic methods 80−106123
safety analysis capability at nuclear utilities 80−23013
safety and influence upon environment *(Croatian)* 80−81492
safety and technology developments *(German)* 78−50282
safety aspects, Japanese regulations 80−47599
safety aspects *(Portuguese)* 80−68844
safety assessment in Germany probabilistic methods 80−106124
safety criteria for siting *(Spanish)* 79−59179
safety equipment qualification for dynamic loads 80−99233
safety estimation, using reliability analysis 77−10471
safety in nuclear power stations, statutory requirements 77−79485
safety in USSR *(Russian)* 79−26614
safety of nuclear plant and fissile material *(German)* 77−42158
safety of power plants with boiling-water graphite channel reactors 79−26561
safety problems in developing countries 77−67825
safety requirements implementing in rapidly industrialising countries 77−65304
safety research in Europe, role of Joint Research Centre 77−65299
safety standards and regulations in USA and Germany 77−65298
safety strategy and principles in nuclear power station practice *(German)* 78−37410
safety system, solid state trip system design 79−6753
safety system redundancy, cable routine inspection 78−735
safety systems, reliability criteria 79−18014
safety w.r.t. siting in densely populated areas, PWR protection *(Czech)* 77−50261
safety-economic assessment, w.r.t. siting, comparison with coal-fired power station *(Czech)* 78−50266
saturated steam parameters in reactor containments with escape of coolant, simplified calc. 80−68764
seawater desalting, reactors coupled to multieffect distillation plants, feasibility 79−31172
secondary system fission product transport study at the Oconee Nuclear Station 79−49781
secondary system radioactivity monitoring 80−18445
security, sabotage and terrorist attack, statistical anal. of threat reality and consequences 80−13727
seismic anal., Bell ring. vibr. of vessels with attached masses 77−3181
seismic anal., slab modelling 78−50414
seismic anal. for multicountry appl. 77−65306
seismic areas, nucl. power plant siting 78−82481
seismic category I building design, structural anal. 80−858
seismic design, automated generation of spectrum compatible artificial time histories 78−29661
seismic design of power plants 77−3179
seismic design requirements in Japan 79−26747
seismic effects in secondary containments: research needs 78−94050
seismic floor response spectra 78−819
seismic ground motions, vertical soil-structure interaction effects 79−92496
seismic input through rigid foundation filtering 78−29659
seismic load studies on nuclear power plants, research needs 78−94052
seismic qualification of Class 1E eqpt. 80−99234
seismic qualification of systems, structures, equipment and components 78−41878
seismic qualification tests of elect. eqpt., damage severity factor concept 80−99235
seismic response anal. of structures, new discrete models 78−67081
seismic response of flexible cylindrical liquid storage tanks 79−31241
seismic response spectrum normalisation 78−50415
seismic risk anal. of discrete system of sites in New England 77−86785
seismic safety, review 77−374
seismic safety margins research program of the US Nuclear Regulatory Commission 80−99229
seismic safety of mechanical eqpt., R and D program 80−99232
seismic testing for class 1E equipment 78−78475
seismic testing motions anal. with instantaneous response spectra 79−22498
seismic testing of structures and components using two axial shaking table 78−44300
seismic trip system, risk assessment 78−17377
SGHWR preliminary work at Winfrith, UK *(German)* 77−14261
Shimane BWR plant, generating experience 77−42178
Shimane nuclear power plant, Japan, operating experience *(Japanese)* 77−71659
Shimane power station operating experience 77−65351
short range system analysis method for nucl. utilities 77−50252
shutdown system reliability, effect of operator performance 78−29611
site comparison for United Kingdom including meteorological conditions and population distribs. 77−54376
site selection, pragmatic pairwise group-decision approach 80−102356
site selection, social aspects 78−5062
siting, appl. of remote sensor data 78−21744
siting, internalising social costs, United States experience 77−33827
siting, risk-benefit evaluation, practical calcs. for Helsinki 77−54375
siting, USA state laws for regulation 77−3187
siting criteria, population density limits proposed in NUREG-0625 80−102357
siting evaluation, environmental impact probabilistic assessment model 79−79412
siting of power plant, geological and seismology surveys of US midcontinent 78−85501
siting on rivers, ecological and environmental constraints *(Croatian)* 79−92092

nuclear power stations continued
siting policy in the USA 80−27835
Sizewell power station, radiation and contamination control 80−5387
skyshine dose due to gamma-rays from nucl. power plant *(Japanese)* 79−29917
small and medium power reactors, problems, prospects 79−31168
SNR 300, pumps, heat exchangers and manipulator systems 79−97784
SNR 300 LMFBR steam generators 79−97792
SNR-2, future design and construction plans in Federal Republic of Germany 79−97799
socioeconomic aspects during construction, minimisation of adverse effects 77−33828
soil warming, waste heat from nuclear power station 78−37463
soil-structure interaction, finite element and lumped parameter methods 77−3174
soil-structure interaction, impedance and finite element methods 77−3173
soil-structure interaction parameters, from finite element anal. 77−3175
soil-structure interaction with partial lifting of base slab 77−3178
soil-structure systems, probabilistic frequency variations 77−3176
Soviet building techniques, props., review *(Hungarian)* 79−45398
Spain, implementation 77−61597
spatial control during nuclear station load cycling, multivariable control algorithm 79−13490
spatial reactor control methods 77−83056
spent fuel element reprocessing, basic problems *(Russian)* 79−26692
spent fuel storage and disposal and plant building and operating legislature *(German)* 80−99223
spent fuel storage basins 78−725
spent LWR fuel, prospects for storage and reprocessing 78−5002
spray cooling, heat and mass atmospheric transfer 78−94078
spray ponds as large ultimate heat sink, thermal performance 78−13214
stack effluents, radiation monitoring 78−46179
standardisation, of plant design, General Electric standard safety anal. report for licensing 80−22908
standardisation, rel. to w.r.t. plant rating, plant engineering and system engineering 80−594
standardisation of balance-of-plant design and final design evolution 80−22909
standardisation of design, licensing experience at Palo Verde 80−22910
standards development, current status and long term objectives 77−67908
startup, benefits of standardisation 80−13686
startup, conduct of operations, organisation and personnel 80−63340
startup, staffing program, scope, tasks, resources, constraints, anal., implementation 80−63341
startup and operating experience including cable tray fire, Browns Ferry plant 77−65284
startup planning, comparison of domestic Westinghouse plant and PWR 80−9371
steam generator, flow distribution anal., computer code 79−49653
steam generator, inservice inspection, book contrib. 79−100322
steam generator, multiple tube rupture, radiological consequences 78−74452
steam generator design life, probabilistic approach 77−46395
steam generator inspection by photographic and visual methods 79−54557
steam generator leakage in the AVR nuclear power station 80−596
steam generator life evaluation, safety features in stress anal. for some accidents 79−54560
steam generator reliability, Canadian practice 79−22451
steam generator tube survey, causes of failures, repair procedure 78−54826
steam generators, Na-water type, design 77−50215
steam mains, Gentilly-I generating station, inertial analysis of hydrodynamic oscills. 78−89944
steam superheating in power stations, results and prospects *(Russian)* 79−26743
steam turbines for district heating in nucl. power plants 78−37437
steam turbines for power prod., district heating, desalination 78−37438
steel, AGR boilers, gas side corrosion, breakaway oxidisation treatment 78−48558
steel pressure vessel surveillance capsule exam., appl. of ASTM standards 79−22436
steel products for nuclear power stations, research and development *(Russian)* 79−34080
stress corrosion cracking prevention *(Japanese)* 77−26835
structural design and analysis, research survey, nuclear power plants 78−94048
structural design and analysis research programme for nuclear power stations 78−94047
structural protection measures, against disruptive accidents *(German)* 78−94118
structural reliability, conference, Berlin, Germany (Aug. 1979) 80−105422
structural system under multiple support excitation, seismic response anal. 78−53623
sulphonated cool, gamma radiation breakdown 78−693
Sundesert Nuclear Plant water supply 79−9862
Super Phenix fuel fabrication for Creys-Malville station, core controls *(French)* 79−31089
Super Phenix reactor vessel research and development *(French)* 79−30947
Super-Phenix fast reactor power station, in France *(French)* 80−86967
Super-Phenix FBR control system evaluation *(French)* 79−76106
Superphenix full-scale breeder reactor construction in France 77−65324
Superphenix internal shells, vibr. anal. *(French)* 78−50247
surface protection materials, tests on 900 commercial products *(German)* 80−35356
surface- and ground-water quality near power plants 78−7679
surveillance testing feedback to improve plant availability 80−9384
surveillance testing safety system unavailability 80−9385
Swedish agrothermal plant using BWR power station waste heat, heat cost 78−86704
Swedish State Power Board nuclear power stations, training of emergency organisation 78−50412
Swedish underground nuclear reactor containment studies, review 79−600
symbiotic reactor strategies, U demand 77−42120
Taipower, completion of first power plant, construction experience, testing and start-up 78−86674
nuclear power stations continued
Takahama power station, operation records *(Japanese)* 78−25304
tandem mirror fusion reactor, mechanical design 78−800
tandem mirror fusion reactor, parametric design 78−794
Tarapur Atomic Power Station radioactive waste discharge monitoring 78−89989
technical, economic and safety aspects *(Hungarian)* 78−82465
technology transfer, collaboration of R&D centre in Sweden with small countries 77−57766
technology transfer, experience of Argentina 77−57763
technology transfer, experience of Federal Republic of Germany 77−57762
technology transfer, India 77−57759
technology transfer, Iran conf. 77−57757
technology transfer, Japanese power plants 77−57770
technology transfer, Pakistan experience 77−57765
technology transfer, role of nuclear standards 77−65296
technology transfer, US experience 77−57761
technology transfer in nuclear power, quality assurance as training tool 77−61631
Texas nuclear power plant cooling water requirements 79−9859
TFTR, physics/engineering interface 78−750
TFTR electric power module, conceptual design 80−32508
Thailand's first nuclear power plant, radiation monitoring programme 80−57996
thermal efficiency, CO_2 fund. condensation cycles, performance characts. 80−63368
thermal plume monitoring by drogues 77−3192
thermal power stations, achievement of environmental harmony *(French)* 79−92094
thermal reactor stations in USSR, fuel reprocessing and waste disposal *(Russian)* 79−26592
thermonuclear, laser appl. as initiator 'Argus' system *(Czech)* 79−67943
thermonuclear microfusion using explosion-induced compression of D-T 78−82508
thermonuclear plants, international collaboration 77−79481
thermonuclear power plants, problems and perspectives *(Polish)* 78−54876
thermonuclear power station based on theta-pinch reactor with cumulating liner, engineering level and economic charact. *(Russian)* 80−68951
thermonuclear power stations and the environment *(Czech)* 78−86681
Three Mile Island, accident, malfunction development, prevention *(Hungarian)* 80−68846
Three Mile Island accident, ^{133}Xe in plume 80−89696
Three Mile Island accident, commission report 80−32372
three-loop, intermediate heat exchangers effectiveness determ. 80−608
THTR, core rod drive *(German)* 78−54837
TMI, the need for evacuation to protect public safety 80−99352
TMI-2 accident, cause, radiological consequences, NRC action 80−102262
TMI-2 accident analysis using two-loop RETRAN model 80−102263
Tokamak, fusion power plant economics, effect of major design parameters 79−76141
Tokamak advanced fuel power plant, capital cost anal. 79−18046
Tokamak fusion power plant, cost sensitivity anal. 78−17412
tokamak fusion power plants, major cost drivers 78−58443
Tokamak fusion power reactors 78−21764
Tokamak fusion reactors, commercial feasibility 78−58406
Tokamak fusion reactors, MAXAMAK and MULTIMAK approaches 78−804
Tokamak ignition test reactor, scoping studies 78−793
Tokamak power plants, impact of major design params. on economics 78−792
tokamak power reactors, design approaches for engineering feasibility 78−58442
Tokamak power systems, economics 78−54993
Tokamak reactors with elongated plasmas, parametric and economic anal. 78−795
tornado missile hazard, synthesized windfield model 79−31239
tornado vortex model, appl. to nuclear plant design 78−17444
transport process models for dissociative cooling *(Russian)* 79−13410
transuranium and other radionuclides, conc. and distribs. in nuclear power plant environs 79−93841
Trino power plant, in-service inspection and operating experience, main coolant circuit *(Italian)* 79−17992
tritium distribution in technological systems of Novovoronezh nuclear power station 80−32533
Tsuruga power station radioactive waste treatment system *(Japanese)* 78−74442
turbo-alternator driven by heat stored by NaOH fusion *(French)* 80−40915
turbogenerator overspeed protection, reliability study, design *(French)* 77−3156
Turkey Point nuclear power plant operation, steam generator tube denting effects 79−9852
Turkey Point steam generator repair and influence of water chemistry 79−54556
tVA pipe rupture evaluation and typical mitigation fixes 80−18549
UK nuclear power station radioactive effluent monitoring and public information 78−89992
UK standards and procedures 79−81032
underground containment, dynamic anal. for design criteria 77−3170
underground nuclear power plant, accidents, containment of fission products, finite element anal. 80−27768
underground nuclear power station design, safety and economic considerations 79−76068
underground siting, conceptual design and estimated cost of nuclear power plants in mined caverns 80−688
underground siting, cut-and-cover technique 77−3171
unsteady state processes for dissociative coolant *(Russian)* 79−13411
USA, reactors built, being constructed, or planned Dec. 1978 79−54491
USA background seismic risk and incremental risk due to nuclear power stations 79−70757
utilisation factors, economics, operating experience, Swedish nuclear power stations *(Swedish)* 77−79472
utility requirements for in-service inspection 79−54588
utility use of reactor physics core codes 78−17299
validated computer codes for nuclear electric utility 78−17403
vent-air monitoring by nuclide-specific detection system 79−3249
vertical steam generator tubes, forced convection heat transfer *(French)* 79−98729

nuclear power stations continued
VHTR in Japan, energy problems and development 77−57736
vibration analysis of heat exchanger and steam generator designs 78−66333
vibration monitor for rotating machines, ave. frequency technique 78−13299
vibration-acoustic diagnostics, random signal patterns recognition, with aid of computer *(Slovak)* 79−18612
vibrations caused by flow, indirect meas. methods *(Hungarian)* 80−18453
volume reduction and solidification of low level radioactive wastes 80−42794
VVER, for semi-peak load generation, mathematical model 80−68936
VVER, proposals for increasing power station efficiency 79−26491
VVER plant, gamma emitting radioactivity in heat transfer agent meas. *(Hungarian)* 77−26833
VVER safety 79−26560
VVER-400 reactor, primary circuit coolant pressure and quantity control *(Polish)* 80−91231
VVER-440 reactor power stations, design and operation 79−59127
WASH 1400 report, safety evaluation in France 77−46353
WASH-1400 study, implications 77−46352
waste disposal, discussion 79−39528
waste disposal, permanent home search discussion 77−42113
waste management, legal aspects 77−88229
waste management principles modifications *(German)* 80−102255
water cooled, steam generator tube failures, world experience in 1975 77−38394
water cooled and moderated reactors in Soviet Union nuclear power generation 79−642
water cooled channel reactor, electrical energy cost of change in fuel component 80−37480
water supply, B determ. by flame photometry 78−45672
water-cooled water-moderated reactor cooling system faults, hybrid simulation *(Russian)* 78−5008
water-graphite reactors, optimisation study for power stations 79−76089
water-moderated water-cooled reactor operational mode anal. by computer *(Russian)* 78−21760
water-moderated-water-cooled reactor VVER-1000, power plant technology 78−82501
water-water reactor parameters optimisation 77−74912
West German LWR power plant stack monitoring, legal and technical aspects 78−89988
West German nuclear power plant airborne radioactive release control 79−13549
West German nuclear power plant liquid radioactive effluent monitoring 79−13554
West German nuclear power plant liquid radioactive effluent control 79−13550
Westinghouse plant availability anal. with operating data base 80−23050
Westinghouse power plants, uprating capacity 80−68878
Westinghouse PWR, reduced temp. return-to-power 79−54559
Westinghouse steam generator experience with all volatile treatment 79−9853
Westinghouse steam generators, operations update 78−21683
Westinghouse steam generators, operations update 78−21751
Wolsung-1 CANDU-PHW generating station, nuclear computer design anal. 79−76060
workers' protection against radiation hazards 79−59267
world nuclear energy, conf. (Washington, 1976) 77−67779
worldwide ISO standards for nuclear technology safety 80−102266
WWER reactor safety problems, LOCA prevention *(Russian)* 79−26629
WWER reactors for district heating appl. 78−41854
Yugoslavia's first nuclear power plant construction 77−65354
zero liquid discharge considerations 79−9858
Zion Generating Station steam generator operating experience 79−9851
^{14}C production between now and year 2000 77−54367
CaF_2:Mn TLD, internal background build-up 77−54399
Cl ion concentration in nuclear power station loop waters, potentiometric method improvements 79−85599
Cl^- ions in nuclear reactor water coolant, determination by flow-type porous metallic Ag electrode 80−89577
^{60}Co long-lived γ-emitting aerosols, max. allowable emission rate from nuclear power station 80−32532
^{131}I in nuclear power plant gaseous discharge, cumulative meas. *(Russian)* 79−3224
N_2O_4 dissociating coolant reactors, power stations and radiation sterilization in Belorussia *(Russian)* 79−36398
N_2O_4 gas cooled fast reactor power stations, nuclear and chemical safety *(Russian)* 79−26655
Na heated steam generator, flow instability 77−46214
Na heated steam generators, tube degradation induced by dryout instability 77−46213
Na-cooled fast reactors, material corrosion problems 79−36328
SO_2, ground-level conc. calcs. near a nuclear facility 80−97823
T monitoring at Oconee 1 in-core sources and diffusion rates 80−18691
U supply study in Western world *(German)* 78−8960
Zr nuclear steam superheating channels, design testing 80−5211

nuclear pumped lasers
conference, Orsay, France (May 1978) 80−62393
deposition rates in fission fragment energy 77−23642
diatomic molecules, N_2 and CO nuclear pumped lasers, electron impact cross section meas. 80−63985
direct nuclear pumping, fission-induced, heavy particle energy distrib. function 77−23643
direct nuclear pumping, kinetic model of plasma generated by fission products 77−23644
fission fragment excitation of UF_6 and UF_6-Ar-N_2 mixture 77−23665
fission fragment volume source for direct nuclear pumping 79−36879
fission pumped gas lasers for H prod. by H_2O photolysis 80−45810
fusion blanket optimisation in space and time 80−37616
fusion feedback, self sustained 79−13516
gamma-ray laser pumping by neutron flux from thermonuclear microexplosion 80−28186
gamma-ray lasers, direct pumping by resonance capture of neutrons 80−14310
gas core reactor utilising UF_6 and CO_2 laser 80−23117
gas nuclear pumped laser simulation experiments 80−64042
gaseous core reactors 78−33725

nuclear pumped lasers continued
hybrid nuclear reactor appls. for fission neutron energy recirculation 80−95408
inert gas halide excimer lasers, electron beam, nuclear and discharge pumped, book contrib. 79−81418
inert gas IR lasers pumped by U fission fragments 80−28198
inert gas nuclear pumped lasers, electron impact cross section meas. 80−63985
inert gas nuclear pumped lasers, prod. efficiency of excited states 80−63998
inertial confinement fusion applications, 'next step' expt. 78−58997
inertial confinement fusion power system, nuclear pumped laser coupling 79−85775
ion kinetics in high-pressure laser plasmas 80−64002
large volume multiple pass nucl. pumped laser, output energy, laser media vol. effects 80−63982
laser fusion and laser heated solenoid reactors 78−5041
media 78−17916
neutrons from laser-fusion reactor 78−9364
optimisation expts. 78−9363
plasma, ^3He and $^{235}UF_6$ nucl. excitation, spectra obs. 80−83997
plasma science, conference, Monterey, CA, USA (May 1978) 79−37442
population processes, ion recombination 78−9361
power supply, gaseous and plasma U fueled fission reactors 80−63247
reactor-laser for disintegrating thermonuclear plasma 80−19598
research 78−33726
scale-up, potential appls. 78−9360
thermal neutron traps description 80−64041
trifluoroiodomethane nuclear pumped lasers, electron impact cross section meas. 80−63985
Ar, fission fragment energy deposition kinetics rel. to nucl. pumped laser 77−23652
Ar-Kr-F_2 nuclear pumped laser, high energy beam deposition 80−63999
Ar-N_2 mixture, fission fragment energy deposition kinetics, rel. to nucl. pumped laser 77−23652
Ar-Xe, low-threshold nuclear pumped laser, generation characts. 80−19018
C nuclear pumped lasers employing Ne(He)-CO(CO_2) mixtures, energy storage 80−63996
CO laser, cooled electroionisation type, in nucl. reactor active zone 80−64066
CO nuclear pumped laser, fission fragment excited with gas cooling, performance obs. 80−63997
CO room temperature nuclear pumped laser, parameter optimisation and spectral props. obs. 80−63995
CO-^3He nuclear pumped laser, optimisation with 2 MeV protons 80−64000
CO-He nuclear pumped laser, high energy beam deposition 80−63999
CO-N_2-^3He, laser mixture, excitation in externally maintained discharge in reactor core 80−28193
CO-N_2-^3He, nucl. reactor active zone, plasma and sustained discharge props. 80−5729
CO_2-N_2-^3He laser mixture, excitation in externally maintained discharge in reactor core 80−28193
$Eu^{3+}+UO_2^{3+}$ solution, nuclear pumped liq. lasers, LASL program 80−64011
HF/UF_6-H_2 nuclear pumped laser, characts. 80−78847
He, gain coeffs. for fission fragment generated plasma 77−31488
He-CO_2, nuclear pumped laser, use of fast burst Caliban reactor *(French)* 79−89889
He-CO_2 atomic C nuclear pumped laser collision processes, output delay 80−38002
He-Hg direct nuclear pumped laser, optimum conditions for lasing 77−50655
He-Hg nuclear pumped laser, charge exchange pumping 80−63996
He-Ne CW laser nuclear pumping demonstration 79−13949
He-Ne nuclear-pumped CW lasing 80−48216
He-Sr laser, possibility of nucl. pumping, 4305 Å Sr II transition 80−58518
He-Xe, low-threshold nuclear pumped laser, generation characts. 80−19018
He-Xe laser, nuclear pumping by vol. source of fission fragments 79−36879
^3He direct nucl. pumped laser, power density 78−58980
^3He-$^{20,22}Ne$/$^{127}I_2$, 0.63 micron laser generated contrasting power resons. *(Russian)* 77−23651
^3He-^{22}Ne laser, interaction of orthogonally polarised modes with various transverse distribs. *(Russian)* 77−27276
^3He-Ar (Xe)(Kr)(Cl), volume pumped nuclear laser, survey of lasing 80−63979
^3He-Ar laser, first order model, lasing action depend. on Ar conc. 79−76668
^3He-Ar volumetric nucl. pumped laser, dominating processes and reaction physics 80−63981
^3He-Ar(Xe)(Kr)(Cl), nucl. lasing, population inversion mechanism 80−63980
^3He-Ar(Xe)(Kr)(Cl) direct nuclear pumped lasers using $^3He(n,p)^3H$ reaction 79−31863
^3He-Kr, nucl. pumping by volumetric $^3He(n,p)^3H$ reaction 77−10886
^3He-Xe, direct nucl. pumping via $^3He(n,p)^3H$ 77−71972
^3He-Xe, nucl. pumped laser plasma, distrib. functions 79−36880
^3He-Xe, nucl. pumping by volumetric $^3He(n,p)^3H$ reaction 77−10886
^3He-Xe nuclear pumped laser, small signal gain coeff. and power output, theory comparison with expt. 80−63983
^3He-Xe nuclear pumped laser, electron distrib. function role 80−63984
$^3He(n,p)^3H$ direct nuclear pumped laser 77−83851
I, photodissociated by nucl. induced excimer fluoresc. 80−78846
KrF* nuclear pumped lasers, excited state prod. rate and fission power pulse shape matching 80−63998
N_2-He ion nuclear pumped lasers feasibility study and quenching 80−64001
$Nd^{3+}+UO_2^{3+}$, solution, nuclear pumped liq. lasers, LASL program 80−64011
Ne-N_2, atomic N nuclear pumped lasers, surface effects 80−63996
$Pm^{3+}+UO_2^{3+}$ solution, nuclear pumped liq. lasers, LASL program 80−64011
$Th^{3+}+UO_2^{3+}$ solution, nuclear pumped liq. lasers, LASL program 80−64011
Tl, UF_6-TlF-F_2 nuclear-reaction laser, possible steady-state operation 77−42527
UF_6 admixture effect on N_2 and Ar excited state lifetimes 79−10281

nuclear pumped lasers continued
UF_6, nucl. lasing, population inversion mechanism 80−63980
UF_6 nuclear pumped lasers, electron impact cross section meas. 80−63985
UF_6-He circulating gas critical expts. 79−13488
UF_6-He fission pumped nucl. laser, power deposition 78−58987
XeF laser excited by proton beam, stimulated emission at 351, 353 nm 79−98344
XeF(B), candidate laser fusion driver 79−86171
XeF* nuclear pumped laser obs. 80−63996
XeF*-UF_6, nuclear pumped excimer fusion lasers, kinetic model 79−18410
XeF*(B), buffer effects 80−37617

nuclear quadrupole moments *see nuclear electric moment*

nuclear quadrupole resonance
absorption at combination frequencies *(Russian)* 78−64295
3d-acetonitrile, cryst. struct., ^{14}N NQR free induction decay times meas. 80−54985
acoustic solid effect due to US stimulated transitions between NQR levels 77−12249
alkali halates, NQR freq. temp. depend., phonon spectra interpretation 77−12226
alkali metal bromates and chlorates, alkali and ^{17}O NQR, spin echo double reson. method, electronegativity 80−54970
amidinium salts, ^{14}N NQR spectra, H^+ relax. times 80−60448
2-amino-5-chloropyridine, rot. modes, ^{35}Cl NQR 78−74677
aminoarsines, NQR freq. of ^{14}N, ^{75}As, ^{35}Cl, N-As bonds 78−25566
aminobenzonitrile, para- and meta-, NQR linewidth, Zeeman effect, mol. config., H bonding, cryst. struct. 77−51986
aminoboranes, NQR freq. of ^{14}N, ^{75}As, ^{35}Cl, N-B bonds 78−25566
aminobromotoluenes, NQR freqs., temp. depend. 78−70850
aniline-chlorophenol complexes, ^{35}Cl NQR, inter- and intramol. interactions 80−63666
apparatus for study under high hydrostatic pressure 78−74038
apparent spin-spin relaxation time, super-regenerative NQR spectrometric obs. 80−54963
autotype detector, spin resonance detection 80−22397
aziridines, substituted, ^{14}N NQR, electron distribs. 77−3385
barbiturates, ^{14}N NQR freq. at 77K 77−43900
benzene-d_6, solubilization in hexadecyltrimethylammonium bromide aq. soln., D NMR 78−24015
biological and model systems, ion binding, from NMR quadrupole effects 79−39357
bisymmetric Zeeman modulator for NQR 80−98960
bridge RF spectrometer, high freq. preamplifier 80−22380
bromides, MAl_2Br_7, (M=Li, Na, K, Cs, NH_4, and $(CH_3)_4N$), ^{81}Br NQR and ^{27}Al NMR meas. 78−6597
1-bromo-2, 4-dinitrobenzene, cryst., ^{79}Br NQR Zeeman effect 78−2765
bromobenzene, in EBBA, ^1H NMR and NQR of D, geometric struct. 78−17689
bromocyclotriphosphazatrienes, ^{81}Br NQR, conformation investig. 80−63665
bromomethane, ^{79}Br, ^{81}Br quadrupole bond magnitude ratio *(Russian)* 79−76452
bromomethane derivatives, NQR frequency of Br, substituent group effects 80−95648
byotropic liquid crystals:Cs^+, ^{133}Cs NMR, chemical shift anisotropies 78−79525
caesium trichloroacetate, temp. depend. of ^{31}Cl NQR spectra 80−20495
charge ordered crystals, low lying collective electronic excitations, NQR study problems 79−78561
chloral hydrate, phase transform. rate, ^{35}Cl NQR rate 80−54983
chloranil, phase transition, Zeeman effect of ^{35}Cl NQR 78−59944
6-chloro 2,4-dimethoxypyrimidine, ^{35}Cl NQR, Zeeman effect 80−18874
2- chloro-1,3,2-dioxa-arsolane, temp. depend. of NQR spectra parameters of ^{75}As and ^{35}Cl 80−20494
2- chloro-1,3,2-X, Y-arsolanes, temp. depend. of NQR spectra parameters of ^{75}As and ^{35}Cl 80−20494
4-chloro-2-nitrobenzoic acid, ^{35}Cl NQR 79−50044
m-chloroacetanilide, cryst., ^{35}Cl NQR, Zeeman effect 77−8443
chloroacetanilides, NQR freqs., torsional vibr., temp. var. 78−2766
α-chloroacetic acid, ^{35}Cl and ^{37}Cl pure NQR, H bonding, isotope effects 78−27111
chloroacetic acid, acid salts, NQR obs. of H-bond pot. energy curves 77−18941
chloroacetoacetanilides, NQR freqs., torsional vibr., temp. var. 78−2766
chloroanisoles, ^{35}Cl NQR, inter- and intramol. interactions 80−63666
chlorobenzene in EBBA, ^1H, D NMR and NQR, geometric struct. 78−17689
chlorobenzenes, substituted, NQR freqs. 80−20504
chloromethoxyyaniline, NQR freqs., torsional vibr., temp. var. 78−2766
chloronitrotoluenes, ^{35}Cl NQR temp. depend. 80−106334
chlorophenols, ^{35}Cl NQR, inter- and intramol. interactions 80−63666
N-5-chlorosalicylideneaniline, H^+-^{14}N double reson. NQR spectra temp. depend. thermochromism and tautomeric mech. 78−70849
N-5′-chlorosalicylideneaniline, photochromism and thermochromism, NQR spectra, temp. and UV irrad. depend. 80−54968
coherent NQR relaxometer, two freq. processes by multichannel analyser 80−20498
coherent two-photon NMR, standard-basis operators, coherent averaging 80−82798
conference, 5th International Symposium on NQR spectroscopy, Toulouse, France (Sept. 79) 80−51947
conference, Moscow, USSR (Feb. 78) 79−78558
conference, Osaka, Japan (1977) 78−91980
copper acetate monohydrate, pure quadrupole reson., covalency 77−16205
coupling tensors and chemical shift, from single-cryst. data 78−91982
crystal, spectra of quadrupole nuclei, separation of chem. shift and quadrupole interaction *(Russian)* 78−39440
crystal symmetry determ. and elec. effects 77−11450
crystals, NMR quadrupolar effects, RF energy absorpt., relaxation times *(Russian)* 80−71235
3-cyanopyridine, NQR Zeeman obs., crystal packing 80−54978
cyclodiphosphazane, cryst., NQR study, intramol. interaction geom. and CCl_3 group dynamics 79−78564
cyclohexane-d_6, solubilization in hexadecyltrimethylammonium bromide aq. soln., D NMR 78−24015
n-decylammonium cadmium chloride, perovskite-type layer cmpd. n-decylammonium chain dynamics 79−99313

nuclear quadrupole resonance continued
deep struct. changes, NQR obs., high-press. and temp. effects 80−54139
detection-method 77−13786
deuterated compounds, molecular order and conformation changes in phase transitions 78−47237
diacetylhydrazine, ^{14}N NQR lines fine structure 80−63667
p-dibromobenzene crystal nucl. spin polarisation cross. relax. study 80−29647
2,6-dichloroacetanilide, NQR, cryst. struct., band character 78−6596
dichloroacetic acid-d_0, -d_1, ^{35}Cl, ^{37}Cl NQR, isotope effects 77−46578
p-dichlorobenzene, ^{35}Cl NQR line narrowing by nonreson. RF photon dressing 80−63662
p-dichlorobenzene, ^{35}Cl NQR spectrum using digital freq. modulation 78−21189
p-dichlorobenzene, ^{35}Cl powder Zeeman NQR, injection and phase locked NQR spectrometer 80−54979
p-dichlorobenzene, charge transfer complexes, NQR shifts 78−55186
p-dichlorobenzene, in p-dibromobenzene, optical detection of Cl NQR in mag. field 80−50228
p-dichlorobenzene, NQR study of zone melting purification 79−91583
p-dichlorobenzene, nuclear dipole absorpt. signal, under quadrupole reson. saturation conditions 78−48082
p-dichlorobenzene-naphthalene alloys, solid solns., NQR study 80−66063
4,4′-dichlorodiphenylsulphide, NQR line, Zeeman effect 77−59481
trans-1,2-dichloroethane, solid, NQR at high press., hindered rot. 79−95672
3,5-dichloronitrobenzene, NQR line, Zeeman effect 80−28034
3,5-dichlorophenol, torsional-vibr. freq., ^{35}Cl NQR 78−70851
2,4-dichlorophenoxyacetic acid, NQR of ^{35}Cl, 77-300K 78−50560
4,6-dichloropyrimidine, ^{35}Cl NQR, Zeeman effect 80−18874
diffusion in NaCl-type crystals, NQR caused by vacancy diffusion of impurities, spectral density 78−68408
diformylhydrazine, ^{14}N NQR lines fine structure 80−63667
p-dihalobenzenes, apparent NQR spin-spin relax. times obs. 80−54991
diphenyl halonium compounds, X-ray struct. anal. and NQR, chem. bonding 77−12232
diphenyl selenium halides, correlation between NQR spectra and cryst. struct. 77−12233
diphenyl tellurium halides, correlation between NQR spectra and cryst. struct. 77−12233
dipolar linewidth in asymmetrically broadened NQR spectra 80−71230
dipole width suppression by strong elec. field 80−20493
dipole-quadrupole nuclei interactions, quasi-rigid and tumbling lattice 77−66434
double quadrupole spin echo reson. 80−20513
double resonance, review 77−36153
double resonance detection, principles and appl. to D 78−76354
double resonance with spin mixing by continuous coupling for detection of ^2D NQR 77−77128
dynamic quadrupole spin relax., appl. to at. vacancy hopping 77−8436
echo in quadrupole spin-system, and energy levels in interaction representation 80−20492
electron density mapping in mols., cyrsts., conf., Rehovot, Israel, (Apr. 1977) 78−71622
electron ordered systems, orbital distrib. NQR spectra studies, review 79−78560
electron-nuclear quadrupole coupling induced by exchange interaction 79−73850
element-halogen bond, field consts. of NQR freqs. 78−25568
exchange clusters, hydbrid electronic-nuclear states, quadrupole moments *(Russian)* 80−34816
ferroelectric, H-bonded, soft and central modes, mag. reson., review 78−15108
formic acid(−d_1), dilute deuterated mixture, high-sensitivity NQR, double quadrupole reson. 78−68412
formic acid-d_1, NQR sensitive detection by double resonance with spin mixing by continuous coupling 77−77128
gas phase quadrupole coupling const. anomalous positive temp. coeff., vibr. depend. 80−53016
geophysical techniques, use of ^{27}Al as probe nucleus 80−67426
giant quadrupole reson. splitting in light deformed nuclei 78−4924
glasses, nuclear quadrupole spin-lattice relax., soliton-nucl. quadrupole moment interaction, temp. depend. 80−50220
graphite intercalation compound, LiC_6, ^7Li NMR *(French)* 78−35050
halogen derivatives of group IV elements, NQR correl. anal. 77−12239
halogen NQR spectra, struct. information for R_2MX_6 compounds 80−71228
Heisenberg ferromagnets, BCC, with $K_2CuCL_4.2H_2O$ struct., ^{17}O transferred hyperfine interactions 78−39439
heteroorganic group III compounds, NQR expts., review 78−25565
hexadecapole spin resonance in cubic symm. cryst. by NQR, NMR, nuclear gamma reson. 80−20500
hexamethylene tetramine, polycryst. ^{14}N NMR elec. field gradient effects 77−77112
hexomethylenetetramine complexes, ^{14}N NQR pulsed apparatus 77−10075
high-pressure chamber for pulsed NQR spectrometer 78−86308
Hirshfeld type deformation functions, and elec. field gradients calcs. by Fourier series 79−73479
hydrazide derivatives, symm., ^{14}N NQR echo envelope slow beats 80−29643
hydrazine monohydrate, ^{14}N NQR, echo envelope modulation obs. 80−50218
hydrocarbon chain ordering in model membrane, D quadrupole splitting 78−64947
hydroxypyrimidines, ^{14}N NQR, tautomerism 77−83620
I=1 NQR data fron single crystal ENDOR expts. 80−54994
ice, ^{17}O, NQR spectrum by double reson. with coupled multiplets, fine struct. 80−54969
ice, high-pressure forms, ^2D and ^{17}O NQR from double reson. obs., quad. coupling consts., 77−90069
ice Ih, NQR of ^{17}O, double NMR for ^1H tunnelling, 1.3 and 4.2K 79−47353
ice II, NQR of ^2D and ^{17}O 77−1617
imidazole, quadrupole coupling consts. interpretation, ab initio field gradient calcs. 80−58282
impulse thermometer 77−37887
impure crystal, nuclear quadrupole spin-phonon interaction mechanism 79−95674
inhomogeneous NQR line narrowing by RF pulse sequence 80−93206
interaction representation for spin=3/2 system 77−79633

nuclear quadrupole resonance continued
iodates, complex and simple, effects of bonding on NQR spectra of ^{127}I 77−12234
iodobenzoic acid, NQR of ^{127}I and Mossbauer spectra of ^{125}I, bonding 77−12241
iodohippuric acid, NQR of ^{127}I and Mossbauer spectra of ^{125}I, bonding 77−12241
iodomercuroates, complex, NQR spectra of ^{127}I and struct. 77−12230
iodomethane, IR-RF double reson., NQR of spin-rot. coupling consts. 78−66569
iodomethane-d_1, in nematic soln., D NQR coupling const., isotope effect 79−27009
ionic lattice $ABCL_3$ systems, covalency parameters estimation from nucl. quadrupole coupling 80−25246
isoscalar giant quadrupole reson., Skyrme interaction and effective mass 77−14088
isothiazole, ^{14}N NQR of mol., expt. and MO calc. 79−36667
isoxazole, ^{14}N NQR of mol., expt. and MO calc. 79−36667
layered compounds and intercalates, TDPAC studies 80−39890
line narrowing by intense RF irradiation 79−19801
liquid, nuclear quadrupole relaxation of non centre symm. mols. *(Russian)* 80−88889
liquid alloys, concentration fluctuations, nucl. quadrupole spin relax. 78−91975
liquid crystals, ^{14}N NQR in solid state 79−61260
liquid crystals, biaxial and uniaxial, orientational order 78−75552
liquid crystals, biaxial order parameters, NQR determ. 78−59750
liquid crystals, biaxial order parameters, NQR meas. 78−34432
liquid crystals, lyotropic, ^{23}Na NMR quadrupole splittings, elec. double layers 78−76345
liquid crystals in solid phase, nuclear quadrupole coupling consts. 77−8444
liquid metal, rel. to viscosity 77−1615
liquid metals, nucl. quadrupole relaxation, Sternheimer antishielding and fluctuating elec. field gradients 77−55726
liquid metals, quadrupolar relax. rate 78−48076
liquid metals and alloys, nuclear quadrupole relaxation 78−15050
liquids, nuclear spin quadrupole relaxation 79−78548
lyotropic liquid crystal, ^6Li, ^7Li, and ^{23}Na NMR, metal ion-polar head group interaction 79−4243
magnetic field sources, homogeneous, for studying NQR devices characts. 77−61102
malononitrile, ^{14}N PNQR obs. of phase transition press. depend., line splitting 77−77120
many-spin system dynamics, group approach *(Russian)* 80−50221
MBBA, nematic liq. cryst., ^2H NMR, mol. order and reorientation 79−27906
MBBA-d_{13}, nematic phase, mol. order and director fluctuations, ^2D NMR meas. 79−90529
membrane protein-lipid interactions, ^2H NMR investig. 78−80826
metal:D, dynamic quadrupole nuclear spin relax., α or α' phases 77−48085
metal complexes, NQR spectrosc. appls. 80−54986
methyl bromide, NQR and A_1-A_2 splitting, RF spectrosc. inside laser cavity 80−91579
methylammonium hexahalometallates (IV), halogen NQR obs. of struct. phase transition 79−95673
molecular crystal, p-$Cl_3P{=}NSO_2C_6H_4Cl$, quadrupole nature of spin-lattice relax. 77−59480
molecular crystals, NQR freq., intermol. force effect 80−66065
molecular crystals, nucl. quadrupole relax. of I=1 nuclei 77−12247
molecular crystals NQR freq. press. depend. 80−54971
molecular crystals of solid replacement solns., impurity distrib. 77−12222
molecular motion dynamics in crystal influence on spectral parameters of NQR, NMR and EPR 80−20486
molecular reorientation in crystal, nuclear quadrupole spin-lattice relax. 80−66062
molecular reorientations between unequal potential wells 80−54989
molecular solid, effect of rigid-body vibrs. on NMR, quadrupole, chemical shift and dipole-dipole interactions 78−15056
molecular torsional oscills., NQR freq. temp depend. electric field gradient asymmetry 80−18868
molecules, wavefunction shape, field gradient and density distrib. calcs. 80−53017
molten salt, nucl. quadrupolar spin-lattice relax., microscopic liq. dynamics 79−91313
monochloroacetic acid single crystal, Zeeman and ^{35}Cl NQR investig. 80−66066
multichannel synchronous detector for NQR signals 77−61098
multiple and combinational freq. NQR, dipole-dipole, spin-spin interactions 80−20499
multiple resonances, phase eqns. 77−16202
nitrile complexes, RCN...Cl-Cl' and RCN...$HCCl_3$, charge transfer and distrib., NQR 77−12244
nitrobenzenes, substituted ^{14}N-NQR, elec. field gradient of NO_2 78−21944
nitroso and nitrosyl cpds., ^{14}N chem. shifts correl. with nuclear quadrupole coupling consts. 77−30888
NMR-NQR double resonance, two-freq. methods, resonance spectrometers 80−20512
NQR-NMR double resonance line intensities, level crossing method, two freq. saturation 80−20514
nuclear quadrupole alignment and low temp. systematics of elec. field gradients of $^{176}Lu^m$ and ^{177}Lu 79−78565
OOAB, nematic thermotropic mesophases, end-chain ordering and even-odd effects, deuterium mag. reson. 79−82890
order parameter fluctuation spectrum, central peaks near ferroelectric phase transitions, review 79−19851
organic halides, NQR shift in external elec. field, rel. to bonding 77−12237
organic molecular crystals, intermolecular interactions, spectroscopic studies, review 80−103958
oxadiazoles, ^{14}N NQR of mol., expt. and MO calc. 79−36667
PAA, liq. crystal, ^{14}N NQR freqs., double-reson. level crossing method 78−6602
panoramic pulsed NQR spectrometer programmer, design, basic functions 77−61100
paradibromobenzene-paradichlorobenzene solid solutions, mol. cryst., NQR study 80−25242
nuclear quadrupole resonance continued
paradichlorobenzene, ^{35}Cl nucl. quadrupole spin-lattice relax. meas. 77−28469
paradichlorobenzene, NQR freq., intermol. force effect 80−66065
paradichlorobenzene, NQR study of the lattice dynamics *(Russian)* 80−97160
perchloro-3cyclopentenone, ^{35}Cl NQR Zeeman obs. 80−54981
phase transitions, high press., NQR and stationary NMR studies 80−19934
phase transitions, nuclear quadrupole splittings 80−20489
phenazine, first excited state ^{14}N quadrupole tensor by ODNQR 78−50561
phenazine, triplet state, ^{14}N quadrupole tensor, optical detection of NQR 79−18218
phosphamides, carcinostatic, ^{14}N NQR, electron distrib. and bonding configs. 80−48018
phospholipid bilayers, struct. dynamics from deuterium spin-lattice relax. time meas. 79−79485
phosphoranes, cryst., NQR study, intramol. interaction geom. and CCl_3 group dynamics 79−78564
poly-γ-benzyl-L-glutamate, sidechain order parameters, ^2H NMR meas. 80−1923
polycrystalline materials, effect of mag. field on quadrupole spin echo 77−12245
polycrystalline samples, ^{14}N NQR, Zeeman effect, second-order theory 80−20503
polycrystalline solids, spin-one NMR, ^{14}N shift, elec. field gradient effects 77−77112
polyelectrolyte solutions, counterion nucl. mag. relax., quadrupolar mechanism 80−2659
potassium palmitate-d_{31}, spin-lattice relax., chain position and temp. depends. 78−68405
PQR line shape, digital-analogue interface for data processing 79−45615
precision thermometry, freq. meas. improvement 80−22356
pressure sensitivity, vol. depend. of elec. field gradient and lattice vibrs. 77−12225
propyl-1,3-diamino manganese chloride, structural phase transitions at 336 and 305K, NQR meas., DTA 78−63855
pulse spectrometer modulator 80−17971
pulsed NQR-FFT radiofrequency spectrometer for ^{14}N, description and operation 80−17982
pulsed panoramic RF spectrometer for NQR 77−10074
pulsed spin locking technique, theory 80−98958
pyridine and salts, deuterium NQR, double reson. method, ring charge distrib. 80−53015
pyridine-H_2O, bonding, double quadrupole reson. obs. 80−32749
pyridinium salts, hydrogen-bonded systems, deuteron quadrupole coupling 79−78563
pyrrole, liq. and nonaq. solns., ^{14}N NQR, ^1H line shape anal. 78−6598
quadrupole spin echo envelope EFG tensor axisymmetry in mag. field 80−20497
quadrupole spin system, saturation by external elec. field 77−12246
quantum kinetic theory 80−52288
quartz glass surface, in vacuum, mechanism of appearance of elec. charges 79−69743
quinoxaline, in p-dibromobenzene, ^{81}Br, elec. field grad. distortion near defect sites, optically NQR 79−38409
quinoxaline, in p-dibromobenzene, triplet state NQR, nucl. spin polarisation effects 79−18208
rare earth Cu_2Si_2, interconfiguration fluctuation system, NMR meas. 80−15817
rare-earth vanadates, transferred hyperfine effects, ^{51}V NMR studies 79−82893
RF spectroscopy in laser cavity, pure nucl. quadrupole spectra 78−90320
rotating co-ordinate system, direct obs. of NQR 80−7188
rotating coordinate system with quadrupole splitting, paramag. susceptibility 80−11178
ruby, ^{27}Al NQR relax. times at very low temps. 79−65757
ruby, ESR and NMR correl. line broadening effect assoc. with external mag. field inhomogeneities 80−50227
salicylidene-2-chloroaniline, photochromism and thermochromism, NQR spectra, temp. and UV irrad. depend. 80−54968
N-salicylideneanilines, photo- and thermo-chromic, ^{14}N quadrupole resonance temp. depend. 78−48077
N-salicylideneanilines, thermochromic and photochromic, ^{14}N quadrupole coupling, NQR meas. 77−28480
saturation of NQR lines in presence of paramag. impurities 80−20491
scanning NQR spectrometer freq. marker system 78−21191
scanning NQR spectrometers, signal recovery system 78−74039
semiconductor solid solns., NMR of optically oriented nuclei, quadrupole effects *(Russian)* 77−85592
short range remote spectrometer for anal. 80−55742
signal detection using butterfly oscillators, 200 to 650 MHz 79−54163
signal register, IC, for pulsed two-freq. NQR spectrometer 77−61099
single channel two freq. ^{14}N NQR pulse spectrometer, multiplet spectra 80−17968
small sample enhanced coupling using ferrite coils 80−52287
solid, mol. and complex ion intramolecular configs., nucl. quadrupole double reson. obs. intramolecular configs., nucl. quadrupole double reson. obs. 80−34821
solids, NQR spectroscopy, elec. field gradient tensor parameters 78−72432
solids, nuclear electric hexadecapole interactions 79−1722
solutions exhibiting chemical exchange, spin 5/2 and 7/2 nuclei 79−65750
spectral parameters, accuracy monitoring method 77−13785
spectral parameters, baric dependences 79−78559
spectrometer, CW, signal intensity, effect of coil design parameters 77−49756
spectrometer, programming device for a spin-echo installation 80−17972
spectrometer, pulsed, for metre and decimetre range 77−10076
spectrometer, scanning, improved super-regenerative oscillator and quench generator 78−8429
spectrometer, super-regenerative, continuous freq. monitoring 79−63190
spectrometer, weak signal relax. meas. with Sigma type digital storage device, pulse-train program blocks 80−17970
spectrometer for Cl compounds, superregenerative oscillator scheme *(Slovak)* 77−18059
spectrometer for nuclear quadrupole double resonance with programmable calculator control 79−12830
spectrometer RF coil, CW operation, signal intensity 78−89515

nuclear quadrupole resonance continued
spectrometers for precision measurement of temp., optimisation *(Russian)* 80−22412
spectroscopy, electronics appls. 80−63668
spectroscopy, lock-in amplifier and bidirectional square wave modulator 78−256
spin 3/2 nuclei, Zeeman NQR powder spectra 80−20502
spin echo, two-frequency action, amplification and modulation 80−108116
spin generator appl. in NQR thermometry 77−10077
spin lattice relax. time meas., steady state pulse method, master eqn 80−54975
spin-lattice relax. due to mol. fragments reorientation *(Russian)* 80−7189
spin-lattice relaxation, quadrupole, in solids 78−39429
spin-lattice relaxation time in single crysts., orientation depend. 79−95666
steady-state NQR in solids, basic principles 78−76349
stroboscopic integrator for studying NQR relax. processes 80−17969
structural phase transitions, elec. field effects in NQR 80−20488
structural transitions, dynamic aspects, nuclear quadrupole relax. studies 78−76344
TBACA, chiral, smectic C* and H* phases, mol. orientational ordering, ^{14}N NQR study 80−75152
TBACA, liq. cryst., chiral, ^{14}N NQR of smectic phases 78−59749
TBBA, achiral liq. cryst., ^{14}N NQR of smectic phases 78−59749
TBBA, biaxial liq. cryst., orientational order, ^{14}N NQR meas. 77−32288
TBBA, biaxial smectic phases, orientational order, neutron scatt. and NQR results 78−91225
TBBA, smectic, freq. dispersion of proton Zeeman relax. time and quadrupole reson. of ^{14}N 77−62468
TBBA, smectic phases, orientational order, ^{14}N NQR and double NMR obs. 78−94974
TBBA, smectic VI and H phases, orientational order 77−84648
TBBA mesophases, mol. orientational order 79−37619
TCNQ, lattice vibrs., temp. depend., NQR obs. 79−38402
TCNQ salt, K-TCNQ, ^{14}N NQR temp. depend. rel. to Peierls transition 79−82892
TCNQ salt, Rb-TCNQ, ^{14}N NQR, Zeeman perturbation study, charge transfer 78−39438
temperature meas. methods *(Russian)* 80−223
temperature measurement and regulation, pulsed NQR system 77−10020
p-terephthal-bis-aminocinnamate, smectic phases, orientational order, ^{14}N NQR and double NMR obs. 78−94974
tetrachloroaurates and tetrachloroiodates, ^{35}Cl NQR freqs., correl. with crystallographic data 79−33559
tetrahalides of group IV elements, NQR spectra rel. to cryst. struct. 77−12231
tetramethylammonium chlorate, order-disorder transitions, DTA and NQR meas. 77−66022
tetramethylammonium hydrogen bis-trichloracetate ($-d_n$), ^{35}Cl NQR study 80−66064
theoretical chemistry, NMR, ESR and NQR, review 77−18943
thermometer, calibration in 203-398K range 80−42222
thermometer, NQR, capture effect 77−10018
thermometer, pulsed NQR, for temps. up to 870K 77−13749
thermometer circuit 77−10019
thermometer with 77 to 374K range, full automatic precision, appl. and operation 77−17979
thermometry, high-precision NQR 77−10017
thermometry appl. 77−65031
1,2,5-thiadiazole, NQR coupling const., dipole moment of mol. 79−27010
thiazole, ^{14}N NQR of mol., expt. and MO calc. 79−36667
three pulse echo detection and electroacoustic recording *(Russian)* 79−47129
three-level system, macroscopic reson. dynamics 78−76348
three-level system transition probabilities, molecular motion anisotropy 80−18867
transition metal alloys, A15 structure, nucl. quadrupole coupling const., at shear const., Born repulsion charge cloud 79−8070
transmitter for low-frequency pulsed NQR spectrometer 77−61101
s-triazene, second order phase transition, mol. reorientation, ^{14}N NQR 78−48074
s-triazine, low temp. phase, reconciliation with X-ray diffraction measurements 79−46798
s-triazine, mol. cryst., low temp. mol. reorientation, phase transition, ^{14}N NQR 77−36150
trichloroacetic acid-base H bonded complex, ^{35}Cl NQR meas. 78−25555
3,4,5-trichloroaniline, polymorphism, ^{35}Cl NQR 80−54163
1,3,5-trichlorobenzene, ^{35}Cl NQR, high press. behaviour 79−33560
trichloromethane glass:O_3, ^{17}O, NQR by proton double reson., broad reson. assignments 80−53014
trichlorophosphazenes, ^{35}Cl NQR spectra and reorientational motion of PCl_3 group 78−25567
trichlorophosphazo compound, $Cl_3P{:}NCCl(CF_3)_2$, nuclear quadrupole spin-lattice relax. 80−66062
tricritical point determ. by NQR 79−77746
trimethylene trinitroamine, ^{14}N NQR *(Chinese)* 79−91310
two frequency spin echo spectroscopy, review 80−20506
two-frequency NMR-NQR double reson. 79−95683
unmixed complexes with ligands, nuclear quadrupole relax. rate, temp. depend. 77−16203
vanadyl alkanoates, ^{51}V NMR, quadrupole splitting in nematic phases 79−28637
water, adsorbed on cellulose, NMR relaxation times 79−78552
Ag_3AsS_3, proustite, structural changes in low temp. phase transition, NQR study 80−19935
Ag_3AsS_3; NQR study of phase transitions, high press., tricrit. pt. determ. 79−77746
AgBr, diffusion of Na^+, NQR caused by vacancy diffusion of impurities, spectral density 78−68408
$AgClO_3$, ^{35}Cl NQR spectrum under press. at 311K 80−11291
$AgClO_3$, mol. torsional oscills., cooperative study by NQR 80−25244
$AgClO_3$, NQR and thermal expansion investig. of phase transform. 77−12229
$AgClO_3$, NQR freq. of ^{35}Cl, temp. depend., phase transition 77−12228
$AgClO_3$, NQR temp. depend., torsional mol. oscill. in solid 79−4743
$AgClO_3$, structural phase transition, ^{35}Cl NQR meas. 80−15819

nuclear quadrupole resonance continued
$AgNa(NO_2)_2$, ferroelec. transition, ^{23}Na elec. field gradient tensor, NMR meas. 79−4777
$AgReO_4$, NQR 77−20745
Ag_2SbS_3, order-disorder phase transition, NQR and spin-lattice relax. expts. 78−47523
Ag_3SbS_3, NQR elec. field effect, temp. depend. near ferroelec. transition 77−77121
Ag_3SbS_3, pyrargyrite, order-disorder phase transition and elec. polarisation 79−38468
Al alloys, dil., screening charge anisotropy around impurities, nucl. quadrupole couplings meas. 77−32286
Al, electron-irrad., NQR, EFG around vacancies and interstitials 78−88220
Al-V(Ti)(Fe), dil., screening charge around 3d impurities, NQR meas. 77−32287
$AlBr_3.SrBr_3$, $AlBr_3.BiBr_3$ complexes, NQR 77−20747
Al_2Cl_6 molten, nuclear mag. relax., mol. rot. 80−71209
Al_2O_3, ^{27}Al quadrupole splitting, strain effects, US modulation technique 79−28636
$Al_2O_3{:}Cr^{3+}$, corundum and ruby, ^{27}Al quadrupole, transitions, acoustic and elec. saturation 77−90071
β-Al_2O_3-$(Na,Li)_2O$, first-order quadrupole NMR obs. of cation distrib. and ion motion 80−108113
β-Al_2O_3-Na_2O, ^{23}Na NQR and two-dimens. diffusion, model analysis 80−108111
β-Al_2O_3-Na_2O, low-temp. ^{23}Na satellite spectra, Na ion motion 80−108112
β-Al_2O_3-Na_2O, nucl. double reson. interferometry, satellite spectrum 78−31123
β''-Al_2O_3-Na_2O, of ^{23}Na, elec. quad. interaction, 185 to 419K, ion motion obs. 80−108110
θ-$Al_{0.35}V_2O_5$, NMR of ^{51}V 80−71232
^{27}Al in aqueous soln., quadrupolar relax., motions of hydration water mols. 78−64291
As, amorphous and cryst., NQR for tunnelling modes and local struct. order 79−61261
As metal, electric field gradient, temp. and press. variation 80−93205
As, pulsed NQR, bonding, bond angle distrib. obs. in different phases 80−54984
As, rhombohedral, nucl. quadrupole spin-lattice relax. 79−15373
As_2I_4, ^{127}I, ^{75}As NQR freqs. meas. 80−58285
As_2S_3, glassy, deep struct. changes, NQR obs., high-press. and temp. effects 80−54139
As_2S_3, vitreous local struct., elec. field gradient tensor asymmetry obs. 79−73847
As_2Se_3, photodarkening and photostructural effects, Raman, IR and NQR studies 80−16036
$As_2Se_3(S_3)$, glassy film, photostructural effects, NQR study 80−49549
$As_{25}Te_{75}$, and $As_{45}Te_{55}$, vitreous, local struct., elec. field gradient tensor asymmetry obs. 79−73847
B hydrides, relaxation time meas., ^{11}B NMR spectroscopy 77−32276
$B(OH)_3$, $^1H/^2H$ quadrupole reson. freqs. detected by double reson. with level crossing 78−84497
$Ba(ClO_3)_2.H_2O$, ^{35}Cl NQR meas. 77−66435
$Ba(ClO_3)_2.H_2O$, Γ-irrad. defects, ^{35}Cl NQR, 77 and 300K 78−91981
$Ba(ClO_3)_2.2H_2{}^{17}O$, fine struct. in quad. reson. of ^{17}O, DNMR 77−8453
^{135}Ba,^{137}Ba Fourier transform NMR, NQR studies 78−94261
^{135}Ba, nucl. quadrupole moment, calc. using NQR, HFS and fine struct. data 78−50081
$^{135}Ba^{2+}$, $^{137}Ba^{2+}$, aq. ions, nucl. quadrupole relax. 78−64287
^{137}Ba, nucl. quadrupole moment, calc. using NQR, HFS and fine struct. data 78−50081
$^9Be^{2+}$, aq. ions, nucl. quadrupole relax. 78−64287
$BiCl_3$, nuclear electric hexadecapole interactions of ^{209}Bi 79−1722
$BiCl_3.GaCl_3$ complex, NQR of ^{209}Bi, $^{69,71}Ga$ and $^{35,37}Cl$ 78−25569
$BiCl_3$.nitrile complex, NQR spectra changes during complex form. 77−12242
BiOCl, nuclear electric hexadecapole interactions of ^{209}Bi 79−1722
$BiVO_4$, NQR spectra of ^{209}Bi 79−82891
BrF(Cl), rot. spectra in millimeter wave region, rot. transitions obs., equilib. const. determ. 80−78607
$BrF_3.SbF_5$, NQR anal. of complex ion struct. 77−12238
^{81}Br NQR in MAl_2Br_7 crysts. (M=Li, Na, K, Cs, NH_4, $(CH_3)_4N$), Zeeman effect 78−6597
CCl_3PCl_4, cryst., libration freqs., temp. depend., combination light scatt. and NQR obs. *(Russian)* 77−66436
$C(NH_2)_3Al(SO_4)_2.6H_2O$, temp. depend. quadrupole coupling const. for $^{27}Al^{3+}$ and $^{71}Ga^{3+}$ 78−19368
CS_2, liq., ^{33}S NQR, quadrupole coupling const. from linewidth data 78−91985
Ca dichlorophosphate complexes, cryst. struct. ^{35}Cl NQR obs. 80−108108
CaB_6, ^{11}B nucl. quadrupole interaction, NMR meas. 80−2660
$CaBr_2$-H_2O, ^{79}Br NQR, cryst. struct. 78−27110
$Ca(ClO_3)_2$, mol. torsional oscills., cooperative study by NQR 80−25244
$CaSnCl_6$, Cl NQR anomalous temp. depend., crystal struct. and phase transitions 80−54977
CaV_2O_6, elec. field gradient at ^{51}V, NMR meas. and ionic model calcs. 78−19370
$^{43}Ca^{2+}$, aq. ions, nucl. quadrupole relax. 78−64287
$CdBr_2$ and CdI_2(4H), electric field effect on NQR, elec. polarisation mechanism 77−20746
$CeAl_2$, antiferromag. ordering and Kondo behaviour, ^{27}Al NQR study 80−71231
$Ce_{1-x}Sc_xAl_2$, fluctuating valence system, quadrupole interaction temp. depend. 80−54972
Cl NQR spectrometer with exact reading of resonant freq. 80−42247
Cl NQR spectroscopy, parametric superrogenerator with phase quantisation application 80−22398
ClF, rot. spectra in millimeter wave region, rot. transitions obs., equilib. const. determ. 80−78607
$ClF_5.xSbF_5$ and $ClF_3.xSbF_5$, NQR anal. of complex ion struct. 77−12238
$Cl_3PNCCl(CF_3)_2$, cryst., ^{35}Cl NQR obs. of molecular reorientations between unequal potential wells 80−54989
$Cl_3PNPO(CCl_3)_2$, NQR spin-lattice relax. study of PCl_3 and CCl_3 group reorientation 78−2767
$Cl_nSi(CH_3)_{4-n}$, ^{35}Cl NQR, geminal and vicinal interactions on substituents electronic effect 80−63663

nuclear quadrupole resonance continued
$Cl_nSi(OCH_3)_{4-n}$, ^{35}Cl NQR, geminal and vicinal interactions on substituents electronic effect 80−63663
^{35}Cl, in organic compounds, crystal splitting, bonding effects 77−12221
Co complex, tris(ethylenediamine)cobalt(III) ion in complex anion solns., ^{59}Co NMR relax. obs. 80−25234
Co complex $[Co(NH_3)_4CO_3]Br$, ^{14}N quadrupole interaction, $^1H/^{14}N$ double reson. 79−51882
Co complexes, $Co(en)_2Cl_2.Cl.HCl.2H_2O$, temp. dependence of NQR frequencies 80−66068
$Co_{1-x}M_xSi$ (M=Fe, Ni), elec. field gradient, quadrupole splitting of ^{59}Co 80−29641
Cs_2CdBr_4, struct. phase transitions, NQR study 80−71343
$CsCdCl_3$ and $CsPbCl_3$, NQR investig. of press. induced phase transition 77−12224
$CsCdCl_3$, phase transition under pressure 78−51664
$CsCoCl_3$, covalency parameters estimation from nucl. quadrupole coupling 80−25246
$CsCuBr_3$, quasi-1-dimens., NQR obs. 80−54987
$CsCuCl_3$, phase transition, refr. index, electrooptic coeff., pyroelec. signal, and NQR meas. 80−70386
$CsCuCl_3$, quasi-1-dimens., NQR obs. 80−54987
$CsFeCl_3$, linear chain cryst., quadrupole and mag. reson., rel. to $RbFeCl_3$ 79−38403
Cs_2HgBr_4, phase transitions and singularities of cryst. struct., NQR study 80−19936
$CsIO_3$, hexagonal modification, temp. depend. of NQR freq., interpretation of long-wave spectra 80−25243
$CsPbCl_3$, n.q.r. spin-lattice relax. near cubic-tetragonal transition, soft modes 77−1616
$CsPbCl_3$, phase transition under pressure 78−51664
Cu complex, $(CH_3NH_3)_2Cu(Cl_{1-x}Br_x)_4$, ferromag., Br NMR mas. 80−29642
Cu complex, dichloro(N-nitrosopiperidine) Cu II, ^{14}N NQR obs. 80−54988
Cu complex, dichloro(dimethylnitrosamine)copper(II), magnetic phase transition, ^{14}N NQR obs. 80−11289
Cu complex, dichloro(dimethylnitrosamine) Cu II, mag. props., ^{14}N NQR obs. 80−54988
Cu compounds, NQR spectrum of $^{63,65}Cu$ 77−12235
Cu, electron-irradiated, monovacancy migration during stage III annealing, NQR study 80−107576
Cu, screening charge density round $\Delta Z=-1$ impurities, vacancies, NQR study 80−103897
Cu-Ni(Pd)(Pt), dil., screening charge density round $\Delta Z=-1$ impurities, vacancies, NQR study 80−103897
Cu_3BiS_3, wittichenite, NQR of $^{63,65}Cu$ and ^{209}Bi 80−20490
$CuBr_2$, ^{63}Cu and ^{81}Br NQR line width obs. 80−50219
$CuBr_2$, NQR freqs. temp. depend., paramag.-antiferromag. transition 79−42867
$CuBr_2$, quasi-1-dimens., NQR obs. 80−54987
$CuCl_2$, quasi-1-dimens., NQR obs. 80−54987
$Cu(ClO_3)_2$, mol. torsional oscills., cooperative study by NQR 80−25244
CuF_2, ^{65}Cu NQR meas. 80−50219
$CuFeS_2$, antiferromag., NQR local mag. field effects 80−71234
Cu(I) complexes, cuprous halide triphenylphosphines, NQR, Zeeman effect 80−54980
$CuM_2X_4.2D_2O$, MX=alkali or ammonium halide, quadrupolar interaction, 4-300K, reorientation 79−73848
Cu_2O, ^{63}Cu NQR spectrum using digital freq. modulation 78−21189
Cu_2O, NQR freq. of ^{63}Cu, temp. depend., mol. dynamics 77−12227
Cu_3SbS_3, skinnerite, polymorphism, X-ray diffr. and NQR meas. 80−49165
Cu_3VS_4, out of equil. mixed cond., chem. origin of mobile ions, spin-lattice relax. and NQR obs. 80−108104
DCl, orthorhombic, nucl. quadrupole double reson. obs. and interpret. 77−90070
DIO_3, cryst., NQR coupling const. and field gradient tensors 79−73828
^2D, NQR in ice II 77−1617
dimethylammonium cadmium chloride, proton-^{14}N double reson. exam. of struct. phase transitions 77−4583
$Dy_{1-x}Gd_xAl_2$, ferromag, easy axis rot., ^{163}Dy NMR obs. 79−78562
$Er_{1-x}Gd_xAl_2$, nuclear hyperfine field, quadrupolar splitting, NMR study 80−39888
$ErNbO_4$, ^{93}Nb NQR spectra, 77 to 450K 79−38401
EuB_6, ^{11}B nucl. quadrupole interaction, NMR meas. 80−2660
$EuCu_2Si_2$, fluctuating valence system, quadrupole interaction temp. depend. 80−54972
$EuCu_2Si_2$, interconfiguration fluctuation, NMR expts. 80−66069
$EuCu_2Si_2$, valence fluctuation and temp. depend. of Cu nuclear quadrupole interaction 80−15818
Fe complex, FE II cyclohexanone thiosemicarbazone, Mossbauer spectrum, quadrupole splitting 79−28641
Fe:^{199}Au, quad. interaction, orbital mag. hyperfine field by NMR/ON 77−12250
Fe:^{60}Co, elec. quad. interaction, single passage NMR/ON 77−16204
$FeBO_3$, suppression effect under hyperfine quadrupole splitting, Mossbauer study *(Russian)* 80−75906
θ-$Fe_{0.35}V_2O_5$, NMR of ^{51}V 80−71232
Ga, liq., nuclear quadrupole relax. rate for ^{69}Ga, 20-150°C, calc. 77−36151
Ga, NQR, press. depend. of elec. field gradient and Knight shift tensors 78−19366
GaAs, nucl. spin levels, elec. induced shifts 80−34408
GaAs:Al, optical detection of NQR 79−69752
GaAs:Te, powder, quadrupole interactions in NMR spectra 79−51880
$GaCl_3$, cryst. struct., Zeeman split fine struct. lines, FT NQR obs. 80−54982
GeI_2, ^{127}I NQR freqs. meas. 80−58285
H_2^+, floating orbital calc. of elec. field gradient, quadrupole coupling const. 77−12248
HCl and HCl-DCl, ferroelec. transition, ^{35}Cl NQR study 80−71233
HCl, solid, ferroelec. phase, spin-spin interactions, NQR meas. 77−85612
HI nuclear quadrupole HFS in IR spectrum, obs. using tunable diode laser 80−58412
HIO_3, $^1H/^2H$ quadrupole reson. freqs. detected by double reson. with level crossing 78−84497
α-HIO_3, HI_3O_8, I_2O_5 and deuterated cpds., crystalline, ^{127}I NQR, bonding and mol. dynamics 80−39889
HI_3O_8, NQR freqs. of ^{127}I 78−72433
nuclear quadrupole resonance continued
H_2O_2, ^{17}O pure NQR spectrum 80−9620
H_2SeO_3, $^1H/^2H$ quadrupole reson. freqs. detected by double reson. with level crossing 78−84497
^2H quadrupole resonance, double transitions, appls. 79−3465
Hg, liq., nuclear quadrupole relax. rate for ^{201}Hg, −35 to 80°C, calc. 77−36151
Hg, liq., relax. rate, temp. depend. 77−48084
Hg liquid, quadrupole relaxation rate temp. depend 80−88884
$HgCl_2$, ^{35}Cl powder Zeeman NQR, injection and phase locked NQR spectrometer 80−54979
$HgCl_2$, NQR freq., intermol. force effect 80−66065
$HgCl_2$, non-resonant impurity atom substitution effect on ^{35}Cl NQR reson. 78−5252
$HgCl_2$, Zeeman NQR spectra obs. asymmetry parameters 80−80634
I complexes, ICl.L (L=organic radical), charge transfer and quadrupole-interaction consts. calc. 77−10590
ICl(Br), rot. spectra in millimeter wave region, rot. transitions obs., equilib. const. determ. 80−78607
IF_6, NMR and NQR of ^{127}I and ^{19}F, solid-solid transitions and mol. motions 79−99784
I_2O_5, NQR freqs. of ^{127}I 78−72433
In, liq., nuclear quadrupole relax. rate for ^{115}In, 170-650°C, calc. 77−36151
In liquid alloys, ^{117m}Sb nucl. spin relax. 78−39437
In liquid alloys, $^{117}Sb^m$ nucl. quadrupole relax. rate, systematical trends 79−73849
InAs:Mn powder, quadrupole interactions in NMR spectra 79−51880
InBi, Knight shift and quadrupole interaction of ^{115}In 77−55717
$In_{1-x}I_x$, molten mixture, NMR, reson. shifts, relax. rates, quadrupole relax. 80−2654
InP:Te, powder, quadrupole interactions in NMR spectra 79−51880
InP:Te, quadrupole struct. of NMR line 80−20505
InSb:Mn, powder, quadrupole interactions in NMR spectra 79−51880
$In_{1-x}Sb_x$, liquid, nucl. quadrupole relax. of Sb, time depend. PAD meas. 77−43899
KAl_2Br_7, NQR double-reson., $Al_2Br_7^-$ ion in cryst. 78−91993
$K_2Al_2(SO_4)_4.24H_2O$, temp. depend. curves of quadrupole interaction parameter for $^{27}Al^{3+}$ 77−55727
$KBrO_3$, hexagonal modification, temp. depend. of NQR freq., interpretation of long-wave spectra 80−25243
$KClO_3$, ^{35}Cl NQR, Stark splitting *(French)* 79−47352
$KClO_3$, ^{35}Cl NQR appl. in thermometry below 77K 80−66067
$KClO_3$, Γ-irrad. defects, ^{35}Cl NQR, 77 and 300K 78−91981
$KClO_3$, NQR freq. of ^{35}Cl, temp. depend., mol. dynamics 77−12227
$KClO_3$, NQR temp. depend., torsional mol. oscill. in solid 79−4743
$K^{35}ClO_3$, NQR absorption precision thermometer 77−5841
$KClO_3$-$CsClO_3$, NQR, mag. susceptibility meas. 78−35059
$K_3Co(CN)_6$, ^{59}Co quadrupole coupling const., temp. depend. 80−44557
$K_3Co(CN)_6$, spin 7/2 system, quadrupolar relax. parameters 78−56392
$KCuF_3$, ^{63}Cu NQR meas. 80−50219
$K_{0.5}Eu_{0.5}Nb_2O_6$, ^{93}Nb NQR spectra, 77 to 450K 79−38401
KH_2AsO_4, ferroelec. phase transition under hydrostatic press., NQR spectra obs. 79−69785
KH_2AsO_4, ferroelec. phase, ^{75}As NQR, press. and temp. depend. 80−71227
KH_2AsO_4, ferroelectric phase transition under high hydrostatic press., mol. dynamics, NQR study 80−75880
$KHCO_3$, $^1H/^2H$ quadrupole reson. freqs. detected by double reson. with level crossing 78−84497
$KHSO_4$, $^1H/^2H$ quadrupole reson. freqs. detected by double reson. with level crossing 78−84497
α-$KIO_3.HIO_3$, ^{127}I NQR study of ferroelec. phase transition 79−38400
$KIO_3.HIO_3$, structural modifications, NQR study 80−20487
$KMnO_4$, ^{55}Mn NMR second-order quadrupole splitting, asymmetry parameter 77−63312
KNO_2, low temp. NQR spectrum of ^{14}N, poss. ferroelec. transition 77−12223
K_2OsCl_6, Cl NQR spectra by Fourier transform methods 80−75879
K_2OsCl_6, impurity H^+ ion motion, ^{35}Cl NQR obs., 77 and 298K 80−60451
K_2PtCl_6, K_2ReCl_6, K_2SnCl_6, solid state phase transitions, lattice vibr., NMR and NQR obs. 80−34814
$KReO_4$, NQR and thermal expansion 77−20745
$KReO_4$, nuclear electric hexadecapole interactions of ^{187}Re 79−1722
$KReO_4$, quadrupole coupling, cation electric field gradients 78−35060
$KSc(MoO_4)_2$, quadrupole interaction const., influence of phase transition, NMR meas. 77−16206
$K_{0.5}Tm_{0.5}Nb_2O_6$, ^{93}Nb NQR spectra, 77 to 450K 79−38401
K_2ZnCl_4, ^{35}Cl NQR study of incommensurate phase transition 80−60450
K_2ZnCl_4, incommensurate phase transitions, ^{35}Cl NQR study 80−75968
$KZnF_3$, cryst., ^{20}F elec. quadrupole interaction, NMR meas. 77−12253
La-D, phase transition, NMR meas. 80−66508
La-H, ordered struct. near $LaH_{2.65}$ at 250K, NMR 80−66508
LaB_6, ^{11}B nucl. quadrupole interaction, NMR meas. 80−2660
LaF_3:Pr^{3+}, nuclear quadrupole interaction, optical-RF double reson. meas. of ground electronic state 77−48092
$LaNbO_4$, ^{93}Nb and ^{139}La NQR spectra 79−38401
$LaVO_4$, dimorphic, NMR of ^{51}V and ^{139}La 77−63310
LiN_3, ionic nature, quadrupole splitting, mag. field depend., N^{3-} electron cloud deform., NMR 80−50210
$LiND_4SO_4$, ^7Li and ^2D NMR exam. of high-pressure phase 79−11396
$LiNH_4SO_4$, phase transitions, temp. depend. of NMR, spontaneous polarisation, birefringence and SHG 78−10191
$LiReO_4$, ^{187}Re HQR freq. temp. depend. 80−25245
$LiReO_4.2H_2O$, ^{187}Re HQR freq. temp. depend. 80−25245
$LiTaO_3$, ^{181}Ta NQR spectra, 77K to room temp. 79−38401
Mg dichlorophosphate complexes, cryst. struct. ^{35}Cl NQR obs. 80−108108
Mg, elec. quadrupole interactions on ^{12}B and ^{12}N via depolarisation due to level mixing 77−55728
$MgBr_2.2Et_2O$, NQR freqs. temp. depend., phase transition 79−42867
$MgO-B_2O_3$ system, glass and cryst. compd. struct. determ. by ^{11}B NMR 79−94905
$Mg_2V_2O_7$, quadrupole coupling tensor of ^{51}N nucleus 80−11290
$^{25}Mg^{2+}$, aq. ions, nucl. quadrupole relax. 78−64287
Mn dichlorophosphate complexes, cryst. struct. ^{35}Cl NQR obs. 80−108108
$Mn_{1-x}Co_xSb$, ferromagnetic, NMR exam. 79−24228
MnSi, NMR and susceptibility above T_c 78−43665

nuclear quadrupole resonance continued
Mo complex, ^{97}Mo and ^{95}Mo nuclear elec. quadrupole moment, nuclear quadrupole double reson. spectra 78−10802
N_2, in β-quinol clathrate, guest-host interaction, mag. reson. spectra 78−76346
α-N_2, solid, NQR echo envelope modulation due to intramol. dipole coupling 77−48083
α-N_2, solid, NQR meas. 77−12252
ND_3 dissolved in poly-γ-benzyl-L-glutamate-chloroform, NMR study 80−34805
ND_4^+ ions, rapidly reorienting deuteron NMR lineshape 79−19800
ND_4IO_4, NQR freq. in cryst. 79−65756
ND_4ReO_4, ^{187}Re NQR temp. and press. depend., deuteration shift 79−65756
NG_4HgCl_3, NQR freq. anomalous temp. depend., reorientation 80−54976
NH_4ReO_4, explanation of ^{187}Re NQR freq. anomalous behaviour 78−48075
$(NH_4)_2HAsO_4$, hydrogen bonded, ^{75}As NQR study 79−38399
$(NH_4)_2HAsO_4$, molecular motion, PMR meas. 77−85591
$(NH_4)_2HAsO_4$, Zeeman perturbed NQR spectra, EFG tensors and antiferroelectric ordering 77−43898
α-NH_4HgCl_3, NQR freqs., anomalous temp. depend. NH_4^+ ion reorientation 79−56624
NH_4I_3, NQR freq. anomalous temp. depend., reorientation 80−54976
NH_4IO_4, ^{127}I NQR rel. to thermal expansion 79−4742
NH_4IO_4, high order phase transition, quadrupole coupling temp. depend. 80−54371
$((NH_4)_xK_{1-x})_2SnCl_6$, mixed cryst., NQR relax. and reson. 80−54990
$(NH_4)_2PtBr_6$, cubic to tetragonal phase transition, data for Br nucleus 79−1500
$(NH_4)_2PtI_6$, crystal symm., struct. phase transition, ^{127}I NQR freq. 80−34815
NH_4ReO_4, ^{187}Re HQR freq. temp. depend. 80−25245
NH_4ReO_4, (ND_4ReO_4), nuclear electric hexadecapole interactions of ^{185}Re and ^{187}Re 79−1722
NH_4ReO_4, high order phase transition, quadrupole coupling temp. depend. 80−54371
NH_4ReO_4, NQR and thermal expansion investig. 77−12229
NH_4ReO_4, NQR and thermal expansion 77−20745
NH_4ReO_4, NQR freq. of ^{185,187}Re, temp. depend. 77−12228
NH_4ReO_4, NQR freqs., anomalous temp. depend. NH_4^+ ion reorientation 79−56624
NH_4ReO_4, NQR freq. anomalous temp. depend., reorientation 80−54976
NH_4ReO_4, nuclear quadrupole coupling, NQR temp., press. depend., continuous phase transition 78−27109
NH_4ReO_4, quadrupole coupling, cation electric field gradients 78−35060
$(NH_4)_2SO_4.Al_2(SO_4)_3.24H_2O$, temp. depend. curves of quadrupole interaction parameter for $^{27}Al^{3+}$ 77−55727
$(NH_4)_2SnCl_6$, ^{35,37}Cl NQR, Raman spectra and spin lattice relax., hindered rot. 80−54974
$(NH_4)_2ZnCl_4$, commensurate-incommensurate phase transition, ^{35}Cl NQR study 80−75966
$N_3P_3Br_6$, ^{81}Br NQR, conformation investig. 80−63665
$N_4P_4Br_8$, Br NQR expts. 79−76446
$N_3P_3Pr_6$, Br NQR expts. 79−76446
^{14}N, in organic compounds, correl. anal. 77−12240
^{14}N, NQR of TBBA and TBACA smectic liq. crysts., orientational ordering 78−59749
^{14}N, observation equipment and techniques 80−22399
$NaAlCl_4$, cryst. struct., charge distrib., X-ray, NMR and NQR meas. 77−11528
$NaAuCl_4.2H_2O$, ^{17}O and ^{23}Na pure quadrupole double reson., fine struct. 77−63323
NaCl, pure and doped, nucl. acoustic reson. 79−69746
$NaClO_3$, ^{35}Cl NQR meas. 77−66435
$NaClO_3$, ^{35}Cl NQR appl. in thermometry below 77K 80−66067
$NaClO_3$, Γ-irrad. defects, ^{35}Cl NQR, 77 and 300K 78−91981
$NaClO_3$, mol. torsional oscills., cooperative study by NQR 80−25244
$NaClO_3$, shift of Na NQR freq. by nonreson. RF photon dressing 78−43674
$NaClO_3$-$CsClO_3$, NQR, mag. susceptibility meas. 78−35059
$NaD_3(SeO_3)_2$, ^{23}Na second-order quadrupole shift, temp. depend. 78−15055
$NaD_3(SeO_3)_2$, ^{23}Na resonance line temp. depend., of first order quadrupole shift and spontaneous polarisation 79−8069
Na_2HAsO_4, ^{75}As NQR, phase transition mechanism 78−52375
Na_2HAsO_4, hydrogen bonded, ^{75}As NQR study 79−38399
$NaHCO_3$, ^{1}H/^{2}H quadrupole reson. freqs. detected by double reson. with level crossing 78−84497
$NaIO_4$, nuclear electric hexadecapole interactions of ^{127}I 79−1722
$Na_xIn_xSn_{1-x}S_2$, intercalation-substitution compounds, NMR study 80−44952
$Na_xIn_xSn_{1-x}S_2$, ionic conductors, ^{23}Na NMR and complex impedance meas. 79−91314
NaN_3, NMR, Na nuclear quadrupole moment, phase transition 77−73092
$NaNH_4SeO_4.2H_2O$, ferroelectric phase transition mechanism 78−31162
$NaNO_2$, ^{14}N NQR, multiple spin echoes 78−19365
$NaNO_2$, ferroelec. nuclear quadrupole coupling const. and spontaneous polarisation 80−71229
$NaNO_2$, NQR of ^{14}N at ferroelec. transition, order-disorder fluctuations 77−63311
$NaNO_2$, size effect and spin-lattice relax. of ^{14}N 80−20480
$NaReO_4$, ^{23}Na and ^{187}Re NMR and NQR temp. depend. 80−54973
$NaReO_4$, NQR 77−20745
$NaReO_4$, NQR and thermal expansion investig. 77−12229
$NaReO_4$, quadrupole coupling, cation electric field gradients 78−35060
$NaReO_4$, temp. depend. of nuclear quadrupole freq. of ^{23}Na, ^{187}Re, NMR and NQR meas. 78−95529
β-$Na_{0.33}V_2O_5$, quasi-one-dimensional conductor, NMR studies 80−93204
$Na_2ZnCl_4.3H_2O$, NQR of ^{23}Na and ^{35}Cl, single-cryst. study 78−91983
^{23}Na spin-$^3/_2$ nuclei, double quadrupole resonance 80−32634
Nb, elastically deformed, quadrupole effects, NMR line intensity *(Russian)* 78−56400
Nb_3Al:^{93}Nb, NQR spectra, NQR signal disappearance in supercond. state 78−19369
$Nb_3Al(Ga)$, NQR freq. temp. depend., supercond. transition temp. 80−93207
$NbCl_5$, anomalies of ^{93}Nb and ^{35}Cl NQR, 4.2-480K 79−99789

nuclear quadrupole resonance continued
NbD, orthorhombic β phase, ^{93}Nb Knight shift and quadrupole coupling parameters 78−19352
$NbF_5(Cl_5)$, nuclear electric hexadecapole interactions of ^{93}Nb 79−1722
Nb_3Ga:^{93}Nb, NQR spectra, NQR signal disappearance in supercond. state 78−19369
NbH, orthorhombic β phase, ^{93}Nb Knight shift and quadrupole coupling parameters 78−19352
Nb_3Ir, A-15 struct. ^{93}Nb NQR spectra 80−20496
Nb_3Os, A-15 struct. ^{93}Nb NQR spectra 80−20496
Nb_3Pt, A-15 struct. ^{93}Nb NQR spectra 80−20496
Nb_3Sb, NQR study, ^{93}Nb nuclear relax. 78−88073
Nd-Co alloys, NMR of ^{143}Nd and ^{145}Nd quadrupole interaction parameters 78−19343
O_2, in β-quinol clathrate, guest-host interaction, mag. reson. spectra 78−76346
^{17}O, NQR at natural isotope abundance, double reson. new techniques, review 80−53013
^{17}O, NQR in ice II 77−1617
^{17}O, naturally abundant, fine struct. obs. 80−75881
^{17}O nuclear quadrupole double resonance spectroscopy, line shapes and examples 80−31820
$Pb_{1-c}Li_c$ (As)(Ag)(In)(Sn)(Sb)(Te)(Au)(Tl)(Bi), liquid alloys, local fluctuations and quadrupolar relaxation 80−66060
PbI_2 intercalated with aniline, NQR meas. *(Russian)* 79−91311
PbI_2-piperidine intercalations rel. to NQR, spin-lattice relax. temp. depend. *(Russian)* 78−27108
PbI_2(2H and 4H), layer cryst., elec. field effect on NQR, elec. polarisation mechanism 77−20746
Pd, nucl. acoustic reson from 4-200K 80−25247
$PrNi_5$, metallic Van Vleck paramag., nucl. interactions, NMR meas. 80−44953
$RbAg_4I_5$, superionic conductor, evidence for first-order phase transition 78−83949
$RbBrO_3$, hexagonal modification, temp. depend. of NQR freq., interpretation of long-wave spectra 80−25243
$RbCaF_3$, cubic to tetragonal phase transition, ^{87}NMR meas. 80−7187
$RbCaF_3$, NQR obs. of struct. transition at 198K 79−65191
$RbCdCl_3$, n.q.r. spin-lattice relax. near cubic-tetragonal transition, soft modes 77−1616
$RbCuCl_3$, quasi-1-dimens., NQR obs. 80−54987
$RbCuF_3$, ^{63}Cu NQR meas. 80−50219
$RbD_3(SeO_3)_2$, ^{2}D NMR struct. anal. 80−2661
$RbD_3(SeO_3)_2$, DMR, electric quadrupole coupling, ferroelec. transition 79−91312
$RbFeCl_3$, linear chain cryst., quadrupole and mag. reson., rel. to $CsFeCl_3$ 79−38403
$RbICl_4$, ^{35}Cl NQR spectra, press. cond. temp. depend 80−20501
$RbICl_4$, NQR of ^{35}Cl, press. and temp. depend., phase transform. obs. 80−15820
$RbIO_3$, hexagonal modification, temp. depend. of NQR freq., interpretation of long-wave spectra 80−25243
$RbNiCl_3$, cryst., ^{35}Cl and ^{87}Rb NMR down to 1.3K 79−42848
Rb_2PtI_6, cubic to tetragonal phase transition data for I nucleus 79−1500
$RbReO_4$, quadrupole coupling, cation electric field gradients 78−35060
Rb_2ZnCl_4, ^{35}Cl NQR, incommensurate struct. phase transition 79−47401
Rb_2ZnCl_4, commensurate-incommensurate phase transition, ^{35}Cl NQR study 80−75966
Rb_2ZnCl_4, incommensurate phase form., domain struct. near phase transition, NQR obs. 79−33643
Rb_2ZnCl_4, incommensurate phase transitions, ^{35}Cl NQR study 80−75968
Rb_2ZnCl_4, NQR exam. of noncommensurate superstructures produced by phase transitions 79−69791
ReO_3, compressibility collapse phase transition, NQR study 80−39282
$^{99,101}RuO_2$, NQR spectroscopy 80−63664
Sb complexes, oxalate-fluoride and nitrate-fluoride cpds., NQR 77−12236
Sb complexes, $SbCl_5$.L (L=organic radical), charge transfer and quadrupole-interaction consts. calc. 77−10590
Sb complexes, $SbCl_5$.L (L=organic radical), charge transfer and charge distrib. calc. using NQR data 77−12243
Sb, nucl. spin-lattice relax., 4.2K 78−91984
Sb:^{111}Cd,In, elec. field gradient, TDPAC expts. 80−55002
$SbCl_3$, cryst. struct., Zeeman split fine struct. lines, FT NQR obs. 80−54982
$SbCl_3$, nuclear electric hexadecapole interactions of ^{123}Sb 79−1722
$^{121}Sb_2O_3$ powder, transverse chemical shift and quadrupole interaction strength 77−28479
Sb_2S_3, influence of temp. on NQR spectra of ^{121,123}Sb 78−60354
Sb_2S_3, NQR freq. of ^{121,123}Sb, temp. depend., phase transition 77−12228
Sb_2S_3, deep struct. changes, NQR obs., high-press. and temp. effects 80−54139
SbSI, tricrit. point, NQR under press. 79−38469
$ScVO_4$, ^{51}V NMR, nucl. quadrupole coupling const., chem. shift 77−90055
SmB_6, ^{11}B nucl. quadrupole interaction, NMR meas. 80−2660
Sn complex, $SnCl_4.L_2$ (L_2=organic phosphorus ligand), NQR of ^{35}Cl and ^{14}N 77−16201
Sn complexes, $SnCl_4$.L (L=organic radical), charge transfer and quadrupole-interaction consts. calc. 77−10590
$SnBr_2$, ^{81}Br NQR line width obs. 80−50219
$SnCl_2.1.5H_2O$ single cryst., ^{35}Cl NQR, cryst. struct. 80−60449
$SnCl_2.2H_2O$, ferroelec., Cl NQR study 79−38467
SnI_2, ^{127}I NQR freqs. meas. 80−58285
$SrBr_2$-H_2O, ^{79}Br NQR, cryst. struct. 78−27110
$Sr(ClO_3)_2$, mol. torsional oscills., cooperative study by NQR 80−25244
SrO-B_2O_3, ^{11}B NMR lineshape, BO_3^{-3} triangle, perfect trigonal symm. *(Korean)* 78−19367
$^{87}Sr^{2+}$, aq. ions, nucl. quadrupole relax. 78−64287
$Te(OH)_6$, ^{1}H/^{2}H quadrupole reson. freqs. detected by double reson. with level crossing 78−84497
Ti-Nb-H system, quadrupole interaction, ^{93}Nb NMR *(Russian)* 77−24761
$UNi_{5-5x}Cu_{5x}$, NMR and press. effects 80−25230
V, elastically deformed, quadrupole effects, NMR line intensity *(Russian)* 78−56400
V-CO sigma phase alloys, NMR and electric-field gradients 80−108109
V-Ni sigma phase alloys, NMR and electric-field gradients 80−108109
VB, nuclear quadrupole parameters 80−103896

nuclear quadrupole resonance continued
V_3Si, NMR of ^{51}V above and below 21K struct. transition *(Russian)* 80−34796
^{131}Xe, in poly-γ-benzyl-L-glutamate liq. crystal solution, quadrupole splitting 79−4741
$YAlO_3$:Pr, hyperfine interaction in lowest levels of $^3H_4$ and $^1D_2$ states 79−78065
$Y(ReO_4)_3.4H_2O$, ^{187}Re HQR freq. temp. depend. 80−25245
YVO_4, ^{51}V NMR, nucl. quadrupole coupling const., chem. shift 77−90055
YbB_6, ^{11}B nucl. quadrupole interaction, NMR meas. 80−2660
$YbCu_2Si_2$, interconfiguration fluctuation, NMR expts. 80−66069
$YbCu_2Si_2$, valence fluctuation and temp. depend. of Cu nuclear quadrupole interaction 80−15818
$YbNbO_4$, ^{93}Nb NQR spectra, 77 to 450K 79−38401
$YbVO_4$, ^{51}V NMR, nucl. quadrupole coupling const., chem. shift 77−90055
Zn, HCP metal, pulsed ^{67}Zn NMR studies at 4.2K 79−91315
Zn, pure NQR obs. 79−47354
$ZnBr_2$, ^{81}Br NQR line width obs. 80−50219
$ZnCl_2$, ^{35}Cl NQR freqs. meas. 80−58285
$ZnCr_xFe_{2-x}O_4$, Mossbauer spectra, quadrupole splitting, Debye temp. 80−93218
ZnI_2, ^{127}I NQR freqs. meas. 80−58285
ZrB_2, self-consistent band struct., XPS, reflectance, NQR, Hall effect and density of states meas. 80−107689
ZrB_2, single cryst., quadrupole coupling const. of ^{12}B 78−37279

nuclear radius *see nuclear size*

nuclear reaction and scattering models
see also nuclear optical model
A(p,p)X, quasi-two-body scaling appl., single scatt. model validity 79−3151
abrasion-ablation model, appl. to relativistic heavy ion collisions 79−3172
Amado 3-body model, cross section calc. of $^6Li(\tau,\tau)$ and $^6Li(\tau,t)$ 79−6616
Amado 3-body model, cross-section calc. of $^6Li(\tau,\tau)$ and $^6Li(\tau,t)$ 79−6617
Amado model, quasi-three body calc. of $^3H(p,p)$ 78−25191
Amado model for nd scatt., NN exchange cuts in second Born amplitude 77−2790
band crossing model, appl. to $^{12}C+^{16}O$ scatt. 78−89898
band crossing model, resonance and strong absorption phenomena in heavy ion scatt. 79−3165
Blanns geom. depend. hybrid model, anal. of (n,n′) cross-sections 77−26749
Brueckners R-matrix model for absorptive scatt. in $^2H(\pi,\pi)$ 77−6457
cascade evaporation model of shock wave formation in heavy ion collisions 78−33215
cascade-disintegration model, appl. to heavy-ion-nucleus interactions *(Russian)* 79−3177
classical many-body model for heavy ion collisions nuclear binding energy and density 78−66302
classical microscopic model of heavy ion reactions 78−66298
classical phenomenological model of heavy ion strongly damped collisions 77−34333
collective tube model of high energy proton scatt. on polarised nuclei 80−32273
complex nuclei reactions, TI-59 model, ang. distrib. and backangle cross section 79−54417
composite particle scatt., Saito model, generalised Levinson theorem 77−303
continuum shell model, 3-particle system, limitations in reaction theory 79−75932
continuum shell-model coupled-channel calcs., appl. to $^{15}N(p,n)$ 3-7 MeV 77−34269
core-coupling model, appl. to Pd(p,t) reacts. 77−57672
corelike potential between complex nuclei, resonating group anal. 78−4922
correlated cluster model for energetic proton inclusive spectra is p-nucleus collisions 77−71600
Coulomb-nuclear interference for high spin states 78−46097
coupled channel model, wave function orthogonality, bound state to continuum transitions 78−78335
coupled particle-vibrator model, appl. to $^{56}Fe+n$ doorway state struct. 77−88143
cumulative effects, phenomenological model for pion prod. and elastic scattering involving deuterons 78−58267
cumulative meson production processes, phenomenological model for mechanism 78−58266
deep inelastic collisions, angular momentum dissipation within a classical friction model 79−93644
deep inelastic heavy ion collisions, unified model, collectivity and statistics, coupled channel eqns. 78−66320
deuteron scattering from N-body scatt. theory, approx. three body model 79−75934
diffraction theory of charge exchange reactions, (p,n), (^3He,^3H), mean energy regions *(Russian)* 78−82352
diffusion model, with one body dissipation, γ-ray multiplicities calc. for heavy ion collisions 79−6487
diffusion model anal. of $^{130}Te+^{28}Si$ at 140 MeV 78−82382
diffusion model of heavy ion induced reacts. 78−54789
direct nucleon transfer reactions, model-independent spectroscopic information, use of spectroscopic factor and vertex constants 78−17168
direct-semidirect model, appl. to $^{88}Sr(n,\gamma_1)$ 77−23023
direct-semidirect model, refined, for fast neutron capture data anal. 77−18541
direct-semidirect model of fast neutron quadrupole radiative capture by ^{208}Pb 77−26711
doorway isobar model for $^{12}C(\pi,\pi)$ 77−10434
double folding pot. for inelastic scatt. between nuclei 80−13425
DWBA amplitude, strong absorpt. model, effect of ang. momentum depend. pots. 79−85486
DWIA applicability in nuclear struct. determ. by meson-nucleus reactions 79−85351
E1-E2 direct-semidirect model for fast nucleon radiative capture, γ ang.-distribs. 78−62536
education, compound and intermediate nuclear struct. wave packet scatt. time evolution, simple model 79−9054

nuclear reaction and scattering models continued
emulsion nuclei+p, diffractive coherent prod., inclusive and exclusive channels 78−62530
energetic heavy ion beam model for radiobiology 80−26293
exciton model, appl. to (π^-,f) 78−94042
exciton model, pre-equilib. decay of A≃200 nuclei at excitation energies to 90 MeV 77−82922
exciton model, preequilibrium reactions, angular distribs. 80−52652
exciton model, two particle reactions *(Russian)* 78−21536
exciton model of γ-emission in (N,γ) reactions 78−62539
exciton model of pre-equilib. decay, finite depth of nucl. pot. well 77−18487
exciton model of pre-equilibrium theory for nuclear reactions, master eqn. soln. 78−13050
exciton state decay time estimation *(Russian)* 77−61393
Fermi Gas model, nuclear response function and dissipation 79−40955
Fermi gas model anal. of (HI,xn) excitation functions 77−18602
few nucleon systems, resonating group model 78−29431
fireball model, pion and nucleon total differential cross-sections 78−17241
fireball model for proton inclusive spectra, heavy-ion collisions 77−6339
firestreak model calcs. for relativistic heavy-ion reactions, particle spectra 79−568
fixed scatterer models for hadron-nucleus scatt., validity 77−18484
fluctuon model of coherent fluctuations of nuclear density 79−75959
fluid dynamic relativistic model appl. to $^{20}Ne^{+}$ ^{238}U reaction 77−74877
folding study of fusion cross section and resonance in $^{12}C+^{12}C$ scatt. 79−13337
generalised Fresnel model for very heavy ion elastic scatt., rel. to optical model 78−74393
generalised Fresnel model for very heavy ion elastic scatt., dynamic polarisation effects 78−74394
generalised Fresnel model for very heavy ion elastic scatt. 78−74392
giant dipole resonance region radiative nucleon capture, expt. ang. distrib. coeffs., direct-semidirect theory 78−74354
Glauber model, implications for inelastic hadron-nucleus scatt. 79−75930
Glauber model applicability near Δ_{33} reson. in $He(\pi,\pi)He$ 77−14193
Griffin model two-body matrix element, exciton no. depend. 78−82326
hadron+nucleus high energy collisions modified cascade model, multiplicities energy depend. 79−59064
hadron-nuclear interactions, fast proton backward emission mechanism *(Russian)* 79−63706
hadron-nucleus collisions at high energies space-time model 77−67728
hadron-nucleus high energy reactions, triple pomeron in coherent processes 77−18534
hadron-nucleus interaction, multiple particle prod., absorptive part of scatt. amplitude *(Russian)* 78−17164
hadron-nucleus interactions, implications for prod. models 78−58258
hadron-nucleus interactions, secondary particle multiplicity, one-cluster model *(Russian)* 78−17165
heavy ion collision double-nova model, fragment recoil momenta 77−54255
heavy ion deep inelastic collisions, dynamic model based on linear response theory *(Russian)* 79−80954
heavy ion elastic collisions and nuclear surface diffuseness, diffraction formulae 80−47494
heavy ion fusion, evaporation model breakdown, preequilibrium α emission 78−89927
heavy ion reactions, central, spectator-participant model 80−73861
heavy ion reactions, coupled channel approx., treatment of resonances 79−9621
heavy ion reactions, parameter free model of strongly damped collisions 78−62568
heavy ion reactions, reaction types, reaction theories, review 78−74401
heavy ion reactions, two-body molecular model for resonances 79−9620
heavy ion transfer reactions, DWBA including recoil effects 77−18605
heavy ion two nucleon transfer reactions, exact four body model 77−10426
heavy ion-nucleus collisions, friction model 78−86546
heavy-ion deep inelastic collisions, classical model with friction and deformation 77−30633
heavy-ion peripheral fragmentation, direct reaction model 78−8847
heavy-ion-induced transfer reactions, effective Q-value model 79−63692
high energy heavy ion collisions, comparison of models, appl. to $U+Ne\rightarrow p+X$ 78−46088
high energy heavy ion collisions, hydrodynamic and classical microscopic descriptions 78−54791
high energy nuclear collisions, isobaric-gas model, shock waves, temp., density, pionisation 78−94022
high-energy heavy-ion collision, model 78−33207
hybrid model, geom. depend., pre-equilibrium anal. of (n,n′) 77−23026
hydrodynamical and phenomenological models for central asymmetric heavy-ion collisions, moderate energies 80−5164
inelastic collisions of light nuclei and nucleon-nucleus collisions, dynamical model *(Russian)* 80−37356
inelastic p scattering, two step process, three body model, (core+n)+p system 78−62537
interacting boson model, electron scatt. data anal., Sm-Nd region 78−62522
intermediate coupling model calcs. of Te(d,t) and (^3He,α) reacts. 77−88153
intranuclear, cascade model, anal. of 39 MeV reacts with ^{209}Bi and ^{56}Fe 78−33185
intranuclear-cascade method, applicability to nucleon reactions 79−9531
isobar, hole model of (π,π) and pion-nuclear many body problem 79−59090
isobar model, pion induced deep inelastic reacts. 78−41779
isobar model, relativistic three-body problem 77−18495
isobar model for pion induced reactions, proton spectrum 77−18617
K-matrix model, appl. to realistic heavy-ion adiabatic pots. 77−3033
K-matrix model calcs. of $^{12}C+^{12}C$ reactions at 3.2-64 MeV/nucleon 77−3034
Landau's relativistic hydrodynamical model of pp to p-nucleus multiplicity ratios 77−46169
large p_T production off nuclei, parton tubes, coherent tube model 78−21392
leading particle spectra on nuclear targets and multi-chain model 80−73829
Lee model use in pion-nucleus scatt. theory testing 80−78325

nuclear reaction and scattering models continued
light nuclei (p,π^+) reactions, π distortion effect on asymmetry 78−50176
modified quasi-deuteron model, Pb photon absorpt. data fit 79−49619
molecular orbital interpretation of $\Delta l=1\hbar$ transfer anomaly in heavy ion collisions 77−82952
multi-chain model for high energy hadron nucleus collisions 79−59042
multichannel direct resonance and heavy ion reactions, exactly solvable model *(Russian)* 79−67732
multichannel nuclear reactions, connected kernel formalism 78−46038
multiple diffraction theory for high energy hadron-nucleus scatt., correl. and isospin effects 78−94000
multiple scatt. and anal. of (p,π) 77−10393
neutron radiative capture, γ-ray ang. distrib., DSD capture model 78−89861
nucleon tunnelling model of mass diffusion in deep inelastic heavy ion collisions 78−78409
nucleus+hadron, cluster model of hadronic interactions, intermediate energy secondary nucleons prod. *(Russian)* 78−17062
nucleus-nucleus and nucleon-nucleus collision model, Glauber's theory, classical transport eqn. 79−6522
one-dimensional cascade model of interacting nuclei using Glauber theory 78−17233
one-nucleon model in DWBA, anal. of (p,π) 77−10393
opaque-nucleus model, B and Ti total proton reaction cross section predictions 78−33174
pairing vibration model with isospin, α-transfer reactions on A=40-62 nuclei 78−17242
parity dependent 78−29432
peripheral model, single-nucleon transfers due to multiply charged ions 80−22850
peripheral model for DD (e^-,$\alpha\nu$) on heavy nuclei 80−37369
pion prod. and absorption in heavy ion reactions below 500 MeV 79−40952
polarisation in heavy ion reactions, Strutinsky model, asymptotic Clebsch-Gordan coeffs. 78−74391
pole peripheral model, for (α,2α) reactions 77−6328
potential capture model, calc. of spectroscopic factors for ^{37}Cl(n,γ) 77−30583
potential model, energy dissipation heavy ions reactions 80−22849
precompound emission, exciton decay rate 77−46147
preequilibrium decay models *(Rumanian)* 80−47457
preequilibrium model for p and α emission from neutron bombarded CsI crystal 77−50139
preequilibrium model quasi-free scatt. for (N,α) reactions 77−88133
random matrix model anal. heavy ion deeply inelastic reacts. 78−33213
recent advances in neutron physics, prod., handling, detection, nuclear reactions, resonances 77−26686
relativistic nuclear collisions, inclusive ρ spectra, knock-out mech. 77−82950
relativistic stripping model in plane wave impulse approx., anal. of ^{12}C(p,π^+)^{13}C 77−325
review, hadron-nucleus interactions at high energies, phenomenological models 78−8859
semiclassical description using complex trajectories for very heavy-ion elastic scatt. 79−561
semiclassical models of $\pi^\pm$ prod. in nucleon+nuclei reactions, multiple scatt., nucleon recoil 77−2996
semiphenomenological model, unified description of reactions, states and transitions 79−75844
single-particle level density, excitation dependence of nuclear level density parameter 80−32149
solitons as model for nuclear potential 80−83081
spallation reaction, Serber's qualitative two-step model *(Japanese)* 78−74345
spin 1/2 particles, polaris. in nucl. scatt., diffr. model anal. *(Russian)* 79−89273
strength function shape from solvable model 77−302
strong absorpt. model, resonant pion-nucleus total cross-sections 77−23114
strongly absorbing nucleus, boundary conditions 79−71825
SU(6) boson model for two-nucleon transfer intensities, (t,p) appls. 78−25206
three-body model, test of coupled eqns. many body scatt. formalism 78−50139
three-body NNα model for ^{4}He(d,d)^{4}He scatt. *(French)* 77−71598
three-cluster distorted-wave methods 79−6524
three-nucleon model anal. of (p,π) 77−10393
threshold phenomena in weak coupling and memory loss models 80−106026
tube model in high-energy hadron-nucleus collisions, nucleon recoil spectra 77−61458
tube models of multiple prod. on nuclei 78−41680
unified model appl. to ^{12}C+n system 78−29437
unified weak coupling model, appl. to ^{12}C(n,n) at 0.2-5.0 MeV 77−82930
weakly absorbed particles, modified Austern-Blair theory, DWBA 80−86867
(α,2α), 90 MeV, strong absorption diffraction model, spectroscopic factors 79−22306
^{12}C+π^-, 40 GeV/c, leading particle spectrum and bremsstrahlung model *(Russian)* 78−41781
(d,p) low energy direct processes new model, ^{12}C(d,p)^{13}C appl. 77−88097
(d,p) reactions, stripping of relativistic deuterons, Glauber theory 78−94014
(d,p) reacts. at intermediate energies, triangle graph model 80−27616
(d,π) reactions, prod. cross sections near threshold, non-nucleon model 77−41976
(γ,π), improved surface prod. model including π-nucleus effects 79−85455
(n,f), nuclear constants eval. for heavy fissile nuclei using coupled channel model *(Russian)* 79−59100
(n,γ), valence model, mass range 40<A<70 79−45256
N-exchange model of p-d backward scatt. 77−18562
ND→πND, effectsof hadron formation zone on decay angle distrib. in coherent prod. on nuclei 79−36205
(p,n) scattering, charge exchange, isobaric analogue state, giant resonance effect, semimicroscopic model 78−89868
(p,X), total reaction cross sections and the matter density of finite nuclei 79−45150

nuclear reaction and scattering models continued
p elastic scattering on ^{3}He, ^{3}H, 156 MeV, differential cross section, diffr. theory of multiple scatt. 77−61404
p-nucleus high energy collisions, impact parameter anal. of multiplicity distrib. 77−79369
p-nucleus interactions, 20 to 200 GeV/c, EFC model *(Russian)* 78−46065
p-nucleus reactions, slow particle characts., relation to high energy interaction models 78−58269
p+emulsion, 400 GeV, shower particle ang. distribs. from inelastic collisions, Glauber-Gribov model *(Russian)* 78−89881
p+nucleus, theoretical models review 78−94010
pN reaction, subthreshold $\bar{p}$ production, interpretation by cumulative process 'gathering' model 78−58268
(π^+,π^+p), strong absorpt. model for π induced knockout reactions 78−74404
π or N+nucleus, intranuclear cascade model for high energy (up to 1000 GeV) reactions 78−70498
π production, multiple-collision model in relativistic nucleus-nucleus collisions 78−37365
^{238}(e,e'), scatt. from octupole band, model for nuclear surface vibrations 78−37333
Ag+α, 720 MeV, correlated energy spectra of light fragments, fireball and coalescence models 78−62555
Al+α, 720 MeV, correlated energy spectra of light fragments, fireball and coalescence models 78−62555
^{27}Al, inelastic electron scatt., charge distrib., Coriolis band mixing calc., C2 form factors 79−529
^{241}Am, neutron cross sections, 1 keV to 15 MeV, optical and stat. model calcs. 77−57655
^{197}Au+^{140}Ar, 217 MeV, deform. of double nucl. system 79−6699
^{10}B(^{14}N,^{14}N), 4.3-9.1 MeV, differential cross sections, incoming wave boundary condition model 79−22348
^{10}B(p,π^+), differential cross sections, DWBA calc. 79−85415
^{9}Be(p,^{3}H)^{7}Be, 75 MeV, continuous spectra phase space model anal. 79−76000
^{9}Be(p,^{3}He)^{7}Li, 75 MeV, continuous spectra phase space model anal. 79−76000
^{9}Be(p,α)^{6}Li, 30 MeV, continuous spectra phase space model anal. 79−76000
^{9}Be(p,α)^{6}Li, 75 MeV, continuous spectra phase space model anal. 79−76000
^{209}Bi+^{136}Xe, stochastic model for strongly damped collisions with liquid drop driving forces 78−89834
^{209}Bi(p,n) pre-compound process, 18 to 64 MeV, cross sections, hybrid models anal. 79−3140
C+π^- collision data, 40 GeV/c, comparison with Bialkowski, Chiu and Tow model 78−58305
^{12}C-^{12}C quasimolecular resonance, coupled channel anal. 78−78402
^{12}C+^{12}C, sub-Coulomb total cross section, simple pot. model of resonances 78−66303
^{12}C+^{12}C in elastic scatt., high energy, resonances obs., evidence for band crossing model 78−66305
^{12}C+^{12}C scatt., intermediate molecular resonances, band crossing model anal. 79−6655
^{12}C+^{12}c, rotational band fragmentation rotation-vibr. model 78−54665
^{12}C+^{13}C resonances, coupled channel anal. with core-exchange model 79−13338
^{12}C+emulsion, 50 GeV/c, multiple particle prod., cascade evaporation model *(Russian)* 79−22322
^{12}C(^{11}B,^{12}C)^{11}B, 28 MeV DWBA amplitude, strong absorpt. model, effect of ang. momentum depend. pots. 79−85486
^{12}C(K$^\pm$,K$^\pm$), Glauber model anal. 80−42697
^{12}C(α,α), 9-11 MeV, elastic and inelastic, resonances and ang. distribs., orthogonality condition model 79−6637
^{12}C(e,e'N), energy and ang. distribs. diffraction approx. for final state interaction *(Russian)* 77−18531
^{12}C(γ,π^0)^{12}C, 220-360 MeV, phenomenological isobar doorway model calcs., total cross section 79−525
^{12}C(γ,$\pi^\pm$), PWIA anal. 77−14108
^{12}C(p,p), elastic and inelastic scatt., 185 MeV, polarisation, diffraction model anal. 79−75943
^{13}C(p,π^-), 185 MeV, differential cross section, two-nucleon model *(Chinese)* 79−59069
^{40}Ca photonuclear reactions, differential cross section calcs., direct-semidirect model 78−33166
^{40}Ca+^{40}Ca, low impact parameters, energy dependence of fusion cross section 78−41751
^{40}Ca(K$^\pm$,K$^\pm$), Glauber model anal. 80−42697
^{40}Ca(p,p), elastic and inelastic scatt., 185 MeV, polarisation, diffraction model anal. 79−75943
^{40}Ca(p,π^+), differential cross sections, DWBA calc. 79−85415
^{48}Ca(^{3}He,t)^{48}, coupled channel calc., two-step processes, nonorthogonality corrections 77−30615
^{140}Ce(N,γ_0), 2-10 MeV, giant M1 resonance in direct-semidirect model 79−17898
^{52}Cr(d,d) and ^{52}Cr(d,p) stripping channel effect, coupled channel model, DWBA anal. 77−57676
^{133}Cs(N,γ)^{134}Cs, exciton model, γ spectra calc. 78−62539
Cu(^{16}O,^{16}O), A=63,65, 40 to 46 MeV, differential cross sections, G-matrix and adiabatic pot. models 78−78411
^{162}Dy+^{16}O, Coulomb-nuclear interference for high spin states 78−46097
^{56}Fe(n, n), up to 1 MeV, cross section by coupled channels method, simple vibrational model 78−70535
^{2}H breakup into Δ resonances, probability, isobar model, static NN-$\Delta\Delta$ mixing pot. 78−29438
^{2}H+π, elastic scatt., absorpt., model using coupled channel eqns., exact soln. 77−88176
^{2}H(n,p2n), 120 MeV, n-n scatt. length determ., Watson-Migdal model anal. 78−82339
^{2}H(p,π)^{3}H, pion prod. models for medium energies 77−18563
^{2}H(π,p)^{1}H, threshold to 3,3 resonance region, disintegration model containing absorption 77−88177
^{2}H(π,π), elastic scatt., charge exchange, deuteron disintegration, three-particle rel. eqns. 78−37381
^{3}Heπ^-→nd, ^{3}Heπ^-→n+n+p, two nucleon absorpt. model 78−41776
^{4}He(^{3}He,^{3}He)^{4}He, four body approach 79−75933
^{4}He(N,N), microscopic study using single channel resonating group method, effective nuclear potentials 79−85425
^{4}He(α,α), 5.05, 4.30 GeV/c, high energy multiple diffraction theory 78−29486

nuclear reaction and scattering models continued
^{4}He(d,d), distortion effects, orthogonality condition model 80−63190
^{4}He(γ, pnd), ^{4}He(γ,p), ^{4}He(γ,n), 60-170 MeV, quasideuteron mechanism calcs. 77−2978
^{4}He(p,p′), high energy, nonlocal imaginary pot. in one channel approx. 78−592
He(e,e), A=3 and 4, high momentum transfer, elastic struct. functions 78−62521
He(p,p), A=3,4, backward p elastic scatt. anal. using D and T exchange models 78−58270
^{86}Kr+^{197}Au, 620 MeV, diffusion model anal. 77−10427
^{6}Li(^{3}He,^{3}He^{3}H)^{3}He, Amado model appl., short-range interactions 77−6408
^{6}Li(p,p)^{6}Li, four body approach 79−75933
^{7}Li($\pi^{\pm}$,πN)^{6}Li* cross-section ratios, N charge exchange model 77−54257
^{24}Mg(^{16}O, ^{16}O′), 20-42 MeV, Coulomb-nuclear interf. effects, coupled channel calcs. 77−3040
^{26}Mg(p,n)^{26m}Al(6.35s), ground state cross section, statistical compound model 79−30827
^{15}N(α,γ)^{19}F, energy levels from α-^{15}N and t-^{16}O coupled channel orthogonality condition model 80−37326
^{15}N(p,γ), ^{16}O excited state GDR, coupled channels version of continuum shell model 79−542
^{93}Nb(n,γ)^{94}Nb, exciton model, γ spectra calc. 78−62539
Ni mass region, α transfer reactions, pairing vibr. model anal. 79−13272
^{64}Ni+^{40}Ca, 182 MeV, deep inelastic collisions, short lifetime and long lifetime regime 78−21597
^{16}O+p fragmentation reaction, 2 GeV, three-stage model anal. 79−6551
^{16}O(t,γ)^{19}F, energy levels from α-^{15}N and t-^{16}O coupled channel orthogonality condition model 80−37326
^{208}Pb(N,γ_0), 2-10 MeV, giant M1 resonance in direct-semidirect model 79−17898
^{208}Pb(N,γ), 6 to 40 MeV, dipole/quadrupole interference, direct-semidirect model, γ ang. distrib. 78−93994
^{208}Pb(n,γ), pure resonance model for fast nucleon capture 79−80936
^{208}Pb(p,γ) fast capture, direct-semidirect model excitation function calcs. 78−94004
^{208}Pb(p,p), elastic and inelastic scatt., 185 MeV, polarisation, diffraction model anal. 79−75943
^{208}Pb(p,π^+), differential cross sections, DWBA calc. 79−85415
^{108}Pd, vibr. states study, elastic and inelastic electron scatt., anharmonic vibrator model 78−62520
^{28}Si(n,γ), n and γ width correlation, valence, optical and shell model comparison 79−6606
Sn mass region, α transfer reactions, pairing vibr. model anal. 79−13272
^{120}Sn(α, p), semi-microscopic spectator model 77−26779
Sn(α,α′), even-even isotopes, nuclear struct. effects in microscopic theory 80−37391
Ta+α, 720 MeV, correlated energy spectra of light fragments, fireball and coalescence models 78−62555
^{159}Tb+^{86}Kr, 620 MeV, energy spectra, charge and ang. distribs., diffusion model 78−50202
^{50}Ti+^{32}S, diffusion model anal. of energy depend. of fission like mass distrib. 77−82949
Ti(n,n), 1-4.5 MeV, elastic inelastic, total cross sections, optical-statistical, coupled-channels models 79−539
^{238}U+^{20}Ne, 250 MeV/nucleon, comparison of macroscopic and microscopic calcs. 77−50153
^{238}U+^{20}Ne, expt. and relativistic two fluid model energy spectra 78−78298
^{238}U+^{40}Ar, Coulomb-nuclear interference for high spin states 78−46097
^{238}U+^{4}He, expt. and relativistic two fluid model energy spectra 78−78298
^{51}V(p,n), 1.56-5.53 MeV, total cross section, excitation functions, isobaric analogue resonance 78−4943
^{90}Zr(p,p), elastic and inelastic scatt., 185 MeV, polarisation, diffraction model anal. 79−75943
^{90}Zr(p,π^+), differential cross sections, DWBA calc. 79−85415

nuclear reaction and scattering theory
see also nuclear reaction and scattering models; statistical theory of nuclear reactions and scattering
1p and 2s1d shell nuclei, fusion cross sections, entrance channel versus compound nucleus limitations 80−78343
1p shell nuclei, DWBA applicability to stripping reactions, ladder diagram summing *(Russian)* 79−30818
3-body breakup, final state interaction approx. in cluster model formalism 77−18500
3-body problem with one infinite mass particle, integral and Schrodinger eqn. equivalence 80−18255
^{12}C-α-^{12}C nuclear molecular states, quantum mechanical three-body approach 79−97692
^{18}F levels, J$^{\pi}$ and ang. distribs. DWBA anal. of ^{19}F(p,d) 80−42545
^{208}Pb (N,N^1) unnatural parity state excitation, π− condensate instability proximity, DWBA 79−97660
^{2}H, isobar knock-out theory 77−18510
(γ, p) reactions at intermediate energies, Δ(1232) contrib. 77−18522
A=12-15, heavy ion induced α-transfer α-clusters, DWBA anal. 79−26454
A=16-40, α-spectroscopic factors between ground states, shell model prediction 79−13204
A=40 to 56, two-nucleon transfer reactions, coupled channel formalism for isospin depend. optical pot. 80−42609
A(a,ax)B, optimum kinematic conditions for quasi-free knock-out reactions 79−6548
A(d,π)X, relativistic energies, Glauber theory 77−30540
A(d,p)X, stripping at relativistic energies, Glauber theory 77−30540
absolute normalisation of (t,d) and (^{3}He,d) reactions, comparative DWBA anal. 77−14143
adiabatic approximation for heavy ion scatt. 78−631
Adler-Adler cross section formalism, improved resonance formula for fissile elements 78−74358
alpha cluster reactions, effective single particle operator 80−32218
alpha scatt. back-angle anomalies, S-matrix continuation to complex l-plane 77−30613
alpha-alpha interaction for coupled channels 77−18489
alpha-particle breakup on various nuclei at 140 MeV 78−46080
amorphous state analogy 79−54370
analyticity in nuclear physics, review 78−89835

nuclear reaction and scattering theory continued
angle Glauber approximation, eikonal phase function corrections 77−30525
angular-momentum dissipation in heavy-ion collisions 78−82376
antisymmetrisation, redundant solns., scatt. solns., and nonsymmetric nonlocal pots. 80−27604
antisymmetrisation effects in nuclear collisions, projection operator techniques 78−46036
asymptotic reduced α-amplitude, model calc. 77−74818
ATDHF theory 78−54710
backward maxima including exchange processes, ^{12}C(α,α) example *(Russian)* 77−74819
Baer-Kouri-Levin-Tobocman coupled eqns., exchange symmetry and kernel connectivity preservation 78−78329
Baer-Kouri-Levin-Tobocman many body scatt. theory, Feshbach projection operator method 80−508
Bencze-Redish-Sloan connected kernel eqns., new derivation method 78−78330
Bethe-Faddeev wave function generalisation to N-body clusters 77−57639
Bloch unified theory, variational principle 77−14083
book, excitation mechanics of nucleus 77−41937
Born series rearrangement in model space, resolvent operator expansion 80−13422
break up process as three body problem, Faddeev eqns. 78−89842
break-up reactions to resonant final states, appl. to ^{6}Li(p,2p)^{5}He 77−10381
breakup amplitudes, 2→3 cluster, variational principles 77−10375
breakup reactions at intermediate energy 77−14086
breakup three-body collisions, exact and approx. calcs. 77−88088
bremsstrahlung emission nuclear reaction, meas. of reaction time *(Russian)* 79−49613
central high energy heavy ion collisions, possible finite particle number effects, p spectra 80−99181
centre-of-mass effects in high-energy scatt. by light nuclei, ^{3}He charge form factor 77−26642
channel averages and energy averaged cross section relation 80−68634
channel coupling array method, optical pot. 77−18496
channel coupling equations of Bencze and Tandy, spurious soln. discussion 78−57857
channel coupling nuclear scatt. scheme, N-particle transition operators 78−569
channel-coupling-array theory, bound-state approx. effect on DWBA and multistep processes 78−568
charged particle elastic scatt., effect of Coulomb-nuclear interference on cross-section determ. 80−502
charged particle-nucleus scatt., formalism to include Coulomb interaction 77−18485
charged three body problems with Coulomb pots. 80−18256
cluster effects in scatt. reactions 77−67711
cluster knockout, quasi-free calcs. in DWIA 77−34273
cluster model approx. with antisymmetrised coupled eqns. formalism 77−2959
cluster scatt. process in (αα′), quasi-free model 77−14139
cluster spectroscopic factors for p-shell nuclear in shell-model 77−30486
cluster states in reaction theory, breakup into composite fragments 79−36207
clustering aspects of nuclear structure and nuclear reactions, review 79−3100
clusters of nuclei, quasielastic knocking on by hadrons, Young-Trayman angle *(Russian)* 78−33159
coherent pion prod. in high energy heavy ion collisions, pion laser 80−73856
coherent recoil dominance, basis for quasi two-body scaling 78−50140
collective tube model, credibility of criticism by Azimov et al., effects of target fragmentation 78−93982
colliding ion system, projectile nucleon mean free path, nuclear matter approach, Pauli blocking 80−86920
collision integral in nuclear matter at zero temperature 79−17928
collisions and microscopic theory, conference 78−563
complete fusion excitation functions, systematic semiempirical anal. with modified proximity pot. 79−6720
complete fusion systems, barrier penetration, enhanced fusion-fission yields 80−13520
complex cross sections for prod. of resonant final states 78−37324
complex nuclear collisions, quantum description of friction, phenomenological ansatz 80−18340
complex nuclear collisions, trial function regularisation and generator coord. amplitudes 77−14081
complex nuclear collisions, two-centre generator coordinate method 77−14080
complex nuclei, parity violating effects, nucleon-nucleus weak interaction 79−75833
complex particles, distorted wave anal. with finite interaction radius 79−9528
complex poles residues of outgoing Green function, eigenfunction expansion involving resonant states 77−82885
composite nuclei scatt., microscopic anal. 78−54780
composite nucleus scission, fusion and strongly damped collisions, rot. energy, boundary diffuseness 80−102224
composite particle emission in relativistic heavy ion collisions, firestreak, and coalescence model 79−80952
composite particle scatt., Saito model, generalised Levinson theorem 77−303
composite particle scattering, generator coord. method, Kohn-Hulthen variational principle 77−2957
composite particles, N-cluster dynamics and effective interaction, dynamical eqn. 80−42560
composite-particle interactions, nuclear cluster theory, computational procedures 79−13225
compound nuclear reactions, isospin mixing treatment 79−3119
compound nucleus mirror reactions, isospin mixing from Ericson fluctuations 79−22190
compound nucleus nonstatistical struct., runs tests as indicators 80−506
compound particle knock out reactions, account of residual interaction *(Russian)* 77−14090
compound-nucleus cross sections from nuclear charge-density distributions 79−9605
compressed zone evolution in high energy nuclear collisions, pion charact. 79−26447

nuclear reaction and scattering theory continued
conference on few body systems and nuclear forces, Graz, Austria (Aug. 1978) 79−80880
conference on heavy ion reaction dynamical props., Johannesburg, S.Africa (Aug. 78) 80−17715
conference on nuclear interactions, Canberra, Australia (Aug.-Sep. 1978) 80−4476
conference on nuclear physics, Mikolajki, Poland (2-14 Sept. 1979) 80−101662
connected kernel formalism 78−4921
continuous slowing down theory, appl. to low-energy neutron resonances 77−26645
continuum shell model, 3-particle system, limitations in reaction theory 79−75932
core polarisation effects in inelastic scatt. and charge exchange 77−22983
core polarisation in inelastic scatt., extension to include charge-exchange reactions 78−78359
cosmic-ray events, energy estimates 80−22647
Coulomb effects in N-particle scattering processes, channel distortion approx. 79−45222
Coulomb effects in three body reactions with two charged particles 78−78331
Coulomb energy dissipation in reactions with heavy ions 79−76014
Coulomb excitation, accuracy of WKB approx. determ. 77−65216
Coulomb excitation, classical limit S-matrix 77−3036
Coulomb excitation, effect on reaction cross section determination in heavy ion elastic scattering 79−97720
Coulomb excitation matrix elements, recurrence relations 79−89272
Coulomb fission prompt component, model including rot. states and vibr. motion 79−67783
Coulomb interaction effects on calc. of scatt. charcts. 79−9529
Coulomb interaction role intensification due to reaction mechanism 78−17174
Coulomb nuclear interference in $^{12}C+\pi^-$ and $^{16}O+\pi^\pm$ elastic scatt. around P_{33} resonance 77−23110
coupled channel Born approximation code, OUKID, finite range heavy ion direct reactions, appls. 78−89832
coupled channel calc. of direct and collective cross sections of deformed nuclei 77−26748
coupled channel Coulomb excitation, asymptotic soln. 77−46146
coupled channel multiparticle scattering theories, Green function eqns., factorisation props., spurious solns. 78−82323
coupled channel optical model calc. improvement *(Chinese)* 80−99159
coupled channel problems, with off-shell resonances 79−71823
coupled channel variational method for microscopic study of reactions between complex nuclei 79−13263
coupled channel variational method for multi-step direct nuclear reactions. I. Formalism and numerical test 78−66258
coupled channels method, separable, neutron-nucl. scatt. 77−2954
coupled eqns. many body scatt. formalism, test on three-body model 78−50139
coupled reaction channel calculations, iterative solutions, method of moments 80−18251
coupled two-body channel scatt., nonsingular integral eqn. 77−30526
coupled-channel calcs. of ^{94,96}Mo(n,n) ang. distrib. 77−26716
coupled-channel model of low energy scatt. 79−76040
Cr ^{130}Te+^{28}Si, diffusion model anal. of onset of friction 78−8848
credibility of criticism by Azimov et al., misuse of CTM 78−93980
cross section of deep inelastic collisions, general form using S-matrix theory 78−566
cross section width fluctuation factor, neutron capture, elastic and inelastic scatt. 77−34294
cross sections for ion beam anal. 80−45606
cross-section adjustment and evaluation, finite element basis in data adjustment 80−68612
DC (p,2p) reaction, three body model anal. of two step process 79−40911
decompositions into three- and four-body wave function channels 78−78333
deep inelastic collisions, parametrised S-matrix approach 80−32249
deep inelastic collisions, tunnelling effects on one-body proximity friction 79−67724
deep inelastic heavy ion collision, shape relaxation and fragment deformation 80−22683
deep inelastic heavy ion collisions, charge and mass distrib. variances, time depend. 79−97651
deep inelastic heavy ion collisions, light particle emission, dissipation mechanism 78−50191
deep inelastic heavy ion reactions, doorway mechanism 78−632
deep inelastic heavy ion reactions, fast light particles and heavy ejectile ang. correlation 80−57791
deep inelastic processes as multi-step direct reactions, (p,p′) appl. 77−26652
deep inelastic reaction, neutron excess degree of freedom relaxation model *(Chinese)* 80−102202
deep inelastic reactions, energy dissipation and angular momentum transfer 78−41679
deeply inelastic heavy ion collisions, charge transfer ang. momentum depend., fragment kinetic energies 80−47505
deeply inelastic heavy ion collisions, helicity representation, quantum mechanical cross section 80−47506
deeply inelastic heavy ion collisions, transport eqn. strong coupling effects 80−52693
deformed even-even nuclei, specific form. of nucleon-nucleus interaction, low energy 78−13077
delay effect in description of γ-α ang. correls. in (α,α') reactions *(Russian)* 77−34329
Delbruck scattering amplitudes, numerical calcs. 77−88108
deuteron breakup and stripping, three-body model 79−515
deuteron stripping and breakup, adiabatic theory 77−18512
differential cross section, empirical continuation 79−45224
differential cross section, empirical continuation into nonphysical region 79−67722
diffraction at backangles 79−17874
dipole sum rule schematical eval., collective isovector quadrupole strength 80−47428
direct nuclear reactions, few-body approaches 77−18511
direct reactions, many particle final states, DWBA theory 78−21539
direct rearrangement reactions description by coupled channel eqns. 79−89271
nuclear reaction and scattering theory continued
dissipative heavy ion collisions, transport equation for microscopic Wigner functions 79−13329
dissipative heavy-ion collisions, doorway concept and relative motion 80−86925
distorted wave series convergence, Lippmann-Schwinger eqn. 79−75942
distorted waves method, finite radius of interaction, reaction mechanisms *(Russian)* 80−52647
distribution properties of the channel interactions in N-body scattering and applications 79−45219
dominant partition method 80−47455
doorway state effect on neutron strength functions, shell model approach for 90<A<142 *(Russian)* 77−82888
doorway states, fragmented, micro-resonances, strength functions, K-matrix width 80−57754
doorway states spreading width, statistical significance, isobaric analogue states 79−93588
Doppler broadening methods comparison 77−22984
double stripping core independ. 2-nucleon transfer, Tang-Herndon effective interactions, (α,d), (t,p) 80−73836
double well-cluster shell model, spurious states of cm motion *(Chinese)* 77−14045
DWBA, simplified for heavy ion induced transfer reacts. at high energies 79−93643
DWBA approach to inelastic scatt. at medium energies 77−6380
DWBA approximate methods for (d,p) stripping reactions 77−14137
DWBA calculations for (d,^{3}He) and (d,t) reactions, normalisation and finite-range effects 77−10416
DWBA description of one- and two-proton transfer reactions, ^{16}O beam on ^{64}Ni, ^{74}Ge, ^{76}Ge 77−14178
DWBA integrals, evaluating strategies for computation 80−86863
DWBA method for heavy-ion induced transfer reactions, residual interaction 77−41995
DWBA t-matrix, semi-classical approach 78−32706
DWBA theory, ang. momentum selection rules for (p,t) reactions 77−46154
e^+e^- angular distribution of e^+e^- pairs produced by linearly polarized photons *(Russian)* 79−40904
education, multiple scattering theory, target nucleus wave function antisymmetry 77−49523
education, N-body disintegration theory, Maxwellian distrib., nuclear appls. 80−57033
education, non-Hermitean Hamiltonians, dissipative forces 77−33763
effective internuclear potential, antisymmetrisation effects 79−59085
effective internuclear potential, odd-even l-depend. 79−6450
effective potentials for heavy-ion scattering derived from channel coupling 80−57794
eigenstates calc. for system of core and two valence nucleons 80−42606
eikonal approx., electron-oriented nucleus scatt., polarisation of e^-, nuclei and emitted γ rays 78−37331
eikonal approx. and distortions in heavy particle stripping mechanism *(Russian)* 78−78337
eikonal approx. of electron scatt. by spherically symmetric nuclei 78−37330
eikonal approximation of nuclear Coulomb scatt. amplitude 78−74344
eikonal description of heavy ion scatt. 77−41938
elast. scatt. on heavy nuclei, anal. with molecular type pots. 77−18502
elastic and quasi-elastic polarised heavy ion collision theory, semi-quantal description 80−18330
elastic and transfer processes, channel coupling and nonorthogonality 77−10377
elastic deuteron-nucleus scattering, breakup corrections to spin depend. 78−58289
elastic nucleus scatt., below Coulomb barrier, effects of polarisability 77−88102
elastic projectile-nucleus scatt., optimal approx., multiple scatt. amplitudes 80−9275
elastic projectile-nucleus scattering, optical pot. reactive content, DWIA justification 79−36211
elastic scatt. of bound system on target, 3-body and eikonal formalism 77−18498
elastic scattering, semiclassical time-independ. formulation in three-dimens with complex trajectories 80−27605
elastic scattering, triangle graph decomposition, spin effects *(Russian)* 77−6331
elastic scattering between complex nuclei, barrier penetration effects, semiclassical theory 77−34339
elastic scattering cross sections with coupled channels, optical model fitting code 79−13264
elastic two-fragment collisions, multiple scatt., optical pot. and N-body approaches 79−93573
electro- and photonuclear EM sum rules 80−22810
electrodisintegration of A=3 nuclei, interaction role in final state *(Russian)* 77−74835
electron inelastic scatt. on nuclei, review 77−34289
electron pair production, cross section calc. on nuclei in range 1≤Z≤92 80−503
electron quasielastic cross section calc., using momentum depend. pot. in Fermi gas model 78−21546
electron scatt. theory, EM struct. from DWBA and other models 80−5133
electron scattering, inelastic, charge distribs. expansions for model independent anals. 77−50114
electron-nucleus quasielastic scatt., Δ(1232) contrib. 77−79366
electron-positron pair, and photon, formation from photon in nuclear field *(Russian)* 79−22267
electroproduction above pion threshold, EM interactions and mag. sum rules 80−42639
electroproduction of light fragments on nuclei, quasielastic knockout by electrons, general theory *(Russian)* 79−13276
emulsion nuclei, 50-400 GeV/c, multiparticle prod., multiple scatt. model anal. 79−67782
energy dependence structs. in reaction cross sections, molecular resonances 79−45227
entrance-channel coherence in dissipative heavy-ion collisions and compound-nucleus formation 79−49639
exact finite range calculations of light-ion induced two-neutron transfer reactions 79−63639
exact finite range DWBA and CCBA anal. of ang. distribs. from ^{62}Ni(^{16}O,^{15}N) and ^{62}Ni(^{12}C,^{11}B) 77−54249

nuclear reaction and scattering theory continued
exact finite range DWBA form factor for heavy-ion induced nuclear reactions, calc. program adaption 80−9271
exchange effects in direct reactions, antisymmetrisation and three body models 80−13446
exchange effects in elastic scatt., DWBA calcs. 78−565
exchange effects in nuclar collisions, DWBA calcs. 78−46084
exchange effects in nucleus-nucleus interactions, antisymmetrisation effects 79−36271
extrapolation of low-energy reaction cross-sections 77−2955
Faddeev approach to neutron scatt. from protons in heavy hydrocarbons in eV range 78−54728
Faddeev eqns., adiabatic limit for particle exchange, three-body scatt. 80−68613
Faddeev eqns. approx. solns., possibility of complex eigenvalues 77−9909
Faddeev generalised theory 77−18492
fast radiative capture, role of collective excitations 77−23024
Fermidynamics and time dependent Schrodinger-Hartree Fock theory 79−3105
Feshbach-Villars formalism and pion-nucleon scattering, relativistic scatt. theory, T-matrix 80−63211
few nucleon systems, 3N and 4N calcs., reviews 78−50094
few particle scatt., integral equation and resonating group methods, relation 77−18493
few-body aspects 77−26644
few-body equations, spurious solutions, numerical investigations 79−67723
few-nucleon reaction mechanism, effect of Pauli principle and channel coupling 77−65219
Feynman diagrams, nucleon identity effects 79−9530
field theoretic formalism, effects due to nucleon indistinguishability 79−75927
finite-range DWBA anal. of (α,^{6}Li) reactions on ^{12}C, ^{24}Mg,^{40}Ca 77−14142
fission, ATDHF validity 78−50149
fission, first order adiabatic approx., fission fragment excitation energy 80−32312
fission, slope constant of the exponential prompt-neutron yield formula 80−22806
fission fragment emission anisotropy, effect of spin of target nucleus *(Russian)* 77−22992
fission scission point model based on deformed shell effects 77−10455
fission trajectory calcs. basis for α-α accompanied reaction 77−34352
fluid dynamics of small finite systems, nuclear matter flow, time depend. Hartree Fock 78−46018
form factors for heavy ion one- and two-nucleon transfer reactions 77−46188
formation zones, large p_T prod. on nuclei 77−50134
four body reactions, triple ang. correl. anal., sequential decay 78−17161
four body system, decoupled Yakubovski eqn. optical pot. and physical implications 78−78334
four nucleon system, reactions and scatt. using K-matrix formalism, differential cross sections *(Russian)* 80−106027
four nucleon system two dimens. integral-equation soln. 78−41650
four particle problem in resonating group approx., integral eqns. 77−2960
four particle scatt. with three particle interactions, scatt. eqns. 79−22249
four particle systems, eigenfunction/eigenvalue problem, effective Hamiltonians in paired channels 78−13037
four particle systems, reaction dynamics 79−80905
four-body model of the four-nucleon system 79−63643
four-body system, Efimov effect and three-body effective pot. 80−86865
four-nucleon problem, microscopic K-matrix continuous spectrum *(Russian)* 77−61352
fragment elastic scattering, unitarity and optical pot. 80−106028
fragmentation, phenomenological model and experimental proofs, cross sections 79−97694
fragmentation theory, two body breakup channels in fission, fusion, heavy ion scatt. 78−46037
fragmentation theory of heavy-ion fusion reactions 77−54239
friction and nucleus-nucleus interaction pot. 78−8850
frictional effects in nuclear reactions with large scale collective motion, review 78−78336
frictional effects on post-scission dynamics and fission fragment kinetic energies 79−36225
fusion, classical model, empirical nucleus-nucleus potl. 77−74870
fusion barrier of heavy ion collisions, penetrability calc. 78−41798
fusion reactions, Woods Saxon, folding and proximity pot. anals. 79−45316
generalized Moshinsky bracket recurrence relations 79−93569
generator coordinate amplitude evaluation using spherical Bessel functions, ^{6}Li(α,α) appl. 77−54194
generator coordinate method for arbitrary cluster widths, appl. to ^{40}Ca(α, α) 77−18581
generator coordinate two-centre functions, appl. to light nuclear collisions 78−50137
giant dipole resonance, role of compound nucleus levels *(Russian)* 78−25164
giant isobaric resonances, isobar doorway model 79−85428
giant resonances in nuclear reactions, microscopic theory of intermediate struct. 80−99161
Glauber approx. corrections, nucleon-nucleus scatt., nuclear density distrib. 78−50166
Glauber calcs. of p-^{4}He scatt. near 1 GeV, filling of first minimum 77−57663
Glauber calculations of p+nucleus elastic scatt. at 1 GeV 79−13260
Glauber high-energy approx. extension to composite particles 78−82328
Glauber model anal. of hadron scatt. probe of neutron density 78−66196
Glauber model of multiple scatt., extension by means of optical potential, appl. to ^{4}He(p,p)^{4}He 77−50093
Glauber multiple scatt. theory, nuclear multiparticle reactions, eikonal model 79−505
Glauber theory, functional integral representation for high energy heavy ion scatt. 79−40945
Glauber theory of high-energy proton elastic scattering 77−41966
Glauber-Sitenko approx., fast hadron scatt. anal. *(Russian)* 78−25161
Gordon's method for nonlocal pot., off shell generalisation to van Leeuwen-Reiner eqn. 79−36206
Griffin-Hill-Wheeler spaces, 1- and 2-conjugate parameter generator states, giant resonances and scatt. 80−42618
group theory applications to nuclear reactions 77−18503

nuclear reaction and scattering theory continued
hadron+nucleus, multi-chain model, recoil nucleon effect 80−83124
hadron+nucleus interaction, Glauber theory and unitarity 77−22979
hadron+nucleus interactions, Fermilab energies, inclusive rapidity distribs., parton-cascade model 78−37252
hadron+nucleus reacts., high-energy, correlation between fast target protons and hadron+nucleon collisions 78−41681
hadron cumulative production on nuclei, mechanism *(Russian)* 77−6332
hadron-nuclei interactions, universal descript. of ang. distrib. 78−17188
hadron-nucleus collisions, bremsstrahlung analogy effects for particle prod. 77−14098
hadron-nucleus collisions, high energy, simple space time description, zero parameter model 80−47479
hadron-nucleus collisions, transverse momentum distrib. of secondary hadrons *(Russian)* 78−29444
hadron-nucleus elast. diff. cross-sect., effects of centre of mass correls. 78−93977
hadron-nucleus elastic scatt., explicit formula in eikonal approx. 80−42665
hadron-nucleus high energy reactions, multiple prod., parton-hadron cascade model *(Russian)* 78−17066
hadron-nucleus high-energy scatt., Regge theory 77−10383
hadron-nucleus inclusive inelastic scatt. in phase space, quantum theory 80−32247
hadron-nucleus interaction, normalised particle number anal. 77−61392
hadron-nucleus interactions, existence of slowly moving sources, vel. depend. frictional sources 79−6690
hadron-nucleus reactions, high energy, secondary particle multiplicity distrib. anal. *(Russian)* 79−59095
hadron-nucleus reactions, multiple production, expt. results, review *(Russian)* 79−3118
hadron-nucleus reactions, quasi-elastic cluster knock-out, multiplicities 78−46042
hadron-nucleus scatt., corrections to Glauber amplitude *(Russian)* 78−41683
hadron-nucleus scatt., Glauber model leading corrections, Watson multiple collision series summation 79−85557
hadron-nucleus scatt., multiple scattering nature, experimental test proposal 79−63702
hadron-nucleus scatt., planar diagrams and appl. of Abramovsky-Gribov-Kancheli relations *(Russian)* 79−93670
hadron-nucleus scatt., reggeon parton spacetime struct. Koplik-Mueller paradox *(Russian)* 80−42730
half-off-shell quasiphases of nonlocal interactions from on-shell phase functions 80−106023
Hamiltonian formulation of N-body theories, effective interactions and many-body corrections 79−75938
Hamiltonian model for N, π and Δ in many body problems 79−85417
Hartree-Fock scatt. formalism, nonsymmetric nonlocal pots. 78−17126
heavy ion+nucleus, orbiting quasimolecular system, nuclear-surface-wave interpretation 80−86914
heavy ion collision dynamics 79−71868
heavy ion collision polarisation, damping mechanism approach via elementary excitation modes 80−18338
heavy ion collision theory, book 77−46189
heavy ion collisions, charge equilibrium model using collective high freq. mode and quantal master eqn. 80−27667
heavy ion collisions, classical dynamical theory of transfer 78−41769
heavy ion collisions, classical microscopic description of particle cluster collisions 79−9533
heavy ion collisions, composite particle formation, direct, classical thermodynamic and quantum statistical theories 80−32297
heavy ion collisions, critical electron state wave function calc. 80−57796
heavy ion collisions, eqns. of motion in Ehrenfest's theorem 79−17916
heavy ion collisions, mass asymmetry as collective coord. in Hartree-Fock calcs. 79−17914
heavy ion collisions, mass transport theory, transport coeffs. including ang. momentum 78−58302
heavy ion collisions, microscopic transport theory, fragment shell struct. effects on mass transfer 78−58301
heavy ion collisions, nuclear level shifts, generalised relativistic Coulomb problem *(Russian)* 80−52586
heavy ion collisions, perturbed stationary state method, low energy collision and mol. resons. 80−78320
heavy ion collisions, pion spectra, Coulomb distortion in final state EM interaction 80−13497
heavy ion collisions at high energy, review of four theoretical methods based on classical approx. 79−89326
heavy ion collisions quasifree promptly emitted nucleons, prod. mechanism and cross sections 79−71863
heavy ion compound reactions, critical ang. momentum effects on high spin selectivity 79−36272
heavy ion deep inelastic collision, high lying vibrational and incoherent excitations, simultaneous treatment 79−36256
heavy ion deep inelastic collision cross sections, ang. momentum coherence 79−54451
heavy ion deep inelastic collisions, characteristic time scales 79−71869
heavy ion deep inelastic collisions, dissipative processes, Feynman's influence functional method treatment 80−57789
heavy ion deep inelastic collisions, evolution within ang. distribs. 78−86544
heavy ion deep inelastic collisions, interaction times and transport coeffs. *(Chinese)* 80−42693
heavy ion deep inelastic collisions, kinetic energy dissipation, nuclear matter density oscillations *(Russian)* 80−37397
heavy ion deep inelastic collisions, microscopic descript., excitation of surface vibr. modes 78−46085
heavy ion deep inelastic reaction well above Coulomb carrier, hydrodynamical and scatt. mechanisms 77−14174
heavy ion deep inelastic reactions, γ-ray multiplicity, partial ang. momenta *(Russian)* 80−37346
heavy ion deep inelastic reactions, charge equilibration 79−49635
heavy ion deeply inelastic collisions, phenomena, transport theoretical approach 78−46086
heavy ion direct transfer reactions, DWBA approach review 79−49614
heavy ion dynamical props. from coupled channels calcs. total, direct and fusion cross sections 79−67772
heavy ion elastic scatt., internal S-matrix dynamics and internal deflection function 80−78307
heavy ion elastic scattering, local optical potential determ., semiclassical derivation 79−59083

nuclear reaction and scattering theory continued
heavy ion fusion and damped reactions, rolling friction, nuclear pots., classical trajectories 80−78312
heavy ion fusion and deep inelastic scatt., shape degrees of freedom, classical dynamic model 80−22876
heavy ion fusion cross section, energy depend., nuclear matter density distrib., depend. 80−47519
heavy ion fusion reaction excitation function anal., nucleus-nucleus pots. 80−42728
heavy ion high energy collisions, classical microscopic calcs., 117 and 300 MeV/nucleon 77−54250
heavy ion high energy reacts., shock wave formation, cascade evaporation model 78−33215
heavy ion inclusive cross sections, collective and statistical effects, fluctuations for complex collisions 79−36258
heavy ion inclusive reactions, fragment momentum distrib., from Glauber approx. *(Chinese)* 80−99185
heavy ion induced direct reactions and scatt., multi-step processes 78−50190
heavy ion induced two nucleon transfer, exact finite range microscopic DWBA, FORTRAN program SATTNT 77−61449
heavy ion inelastic collisions, gasdynamic mechanisms *(Russian)* 77−61452
heavy ion inelastic reactions, differential cross section from helicity representation *(Russian)* 80−86924
heavy ion inelastic scatt., closed form quantal description, DWBA anal. 77−14147
heavy ion inelastic scatt., Coulomb-nuclear interf., appl. of Austern Blair theory, comparison with DWBA 77−3043
heavy ion inelastic scatt., coupled channels calcs. for direct reactions, long range Coulomb coupling 80−83117
heavy ion inelastic scatt., direct reactions, coupled channel calcs., coupled radial eqns. 80−83118
heavy ion inelastic scatt., stripping-pick-up mechanism, coupled channel theory 78−54784
heavy ion inelastic scattering, form factors 79−26458
heavy ion inner shell excitations, multistep processes, quasimolecular model, coupled channels calc. 80−9303
heavy ion intermediate energy collisions, elastic scatt., Coulomb excitation, nucleon transfer, expt. facilities, models 79−6697
heavy ion large-angle scatt., elastic cross-section, excitation functions 80−52689
heavy ion large-angle scatt., inelastic cross-section and collective state excitation 80−52690
heavy ion potential-energy curves, HF calc. 77−18606
heavy ion potentials, antisymmetrisation effects 77−18596
heavy ion quasi-fission, focusing effect, large energy loss, classical dynamic model 77−57689
heavy ion quasi-identical elastic scatt., derivation of local approx. 79−6658
heavy ion reaction, theoretical tools 77−14170
heavy ion reactions, exact finite range DWBA overlap integral parametrization 80−68693
heavy ion reactions, Hartree-Fock approx., statistical aspects 78−50193
heavy ion reactions, incident nuclei energies up to 20 MeV per nucleon 79−71865
heavy ion reactions, multiple collision model anal., at high and relativistic energies 78−86542
heavy ion reactions, phenomenological nuclear friction mechanism, particle-hole excitation, nucleon exchange *(Chinese)* 80−42694
heavy ion reactions, precompound emission inference ambiguities from excitation function anal. 79−22319
heavy ion reactions, two-particle transfer, overlap functions, DWBA anal. 80−73862
heavy ion reactions above Coulomb barrier, fast α-particle emission, anal. of radial friction 77−38296
heavy ion reacts., coherent and statistical features 78−41771
heavy ion reacts., double transfer reaction model, Buttle-Goldfarb approx. 79−6677
heavy ion reacts., transfer amplitude and ang. distribs. 79−59081
heavy ion relativistic collisions, Coulomb excitation of target and projectile, differential and total cross sections 79−54450
heavy ion relativistic collisions, pion bremsstrahlung and critical phenomena, nuclear matter phases 80−86919
heavy ion scatt., Glauber approx., validity of optical limit, higher order correction effects 77−54252
heavy ion scatt., Glauber multiple scatt. series approx. quasi elastic shadowing 79−17915
heavy ion scatt., Pauli-principle resonance effects, analytic representation 79−6659
heavy ion scatt., semi-classical description 79−71867
heavy ion scattering, angle depend. phase shifts, coupled channel formalism 80−18253
heavy ion scattering, Coulomb barrier top energies, WKB calc. 80−86918
heavy ion scattering, impact parameter representation, quantal trajectories 77−14181
heavy ion scattering, modified perturbed stationary state anal. 79−36262
heavy ion stripping and pickup reactions on closed shell nuclei, level shifts, DWBA 80−91168
heavy ion sub-Coulomb transfer reacts., DWBA analytical expressions 77−67760
heavy ion transfer reactions, closed form description based on distorted waves theory 80−68691
heavy ion transfer reactions 80−5165
heavy ion transfer reacts., nuclear wave function polarisability 78−54785
heavy ion-induced multistep multinucleon transfer reactions, grazing collisions, quantal theory 79−6698
heavy ion-nucleus reactions, deform. of intermediate double nucl. system 79−6699
heavy ion-nucleus reactions, reaction mechanism anal. using γ-ray bremsstrahlung spectra 79−76016
heavy ion-nucleus reactions, time dependent SCF theory 79−17932
heavy ions inelastic scattering from deformed light nuclei near Coulomb barrier energies 78−54796
heavy particle transfer mechanism for α backscatt. on light nuclei 77−6420
heavy recoil effects on transfer of one nucleon *(French)* 78−33115
heavy relativistic nuclei, phase shifts and scatt. cross sections *(Russian)* 79−22321
nuclear reaction and scattering theory continued
heavy-ion charge exchange and knock-out at relativistic energies, Glauber's theory 77−23101
heavy-ion collisions, classical many-body model incorporating Pauli principle 77−54236
heavy-ion collisions, compressed nuclear matter classical microscopic calc. 77−10432
heavy-ion collisions, mass exchange and ang. distrib., dynamical treatment 77−61454
heavy-ion collisions, perturbation theory of nucl. friction, strong energy damping 77−67766
heavy-ion collisions, struct. limitations of mass distrib., time depend. Hartree-Fock calc. 79−30852
heavy-ion collisions, tidal bore effect, 40-200 MeV/N 77−34331
heavy-ion collisions, transport coeffs. for asymmetric fragmentation and generalised Einstein relns. 77−3047
heavy-ion deep inelastic collisions, general form of cross-section 78−13131
heavy-ion diffuse surface nuclear and Coulomb pot. energies 77−18593
heavy-ion hydrodynamics and HF calc. comparison 77−18598
heavy-ion interaction potentials, energy density formalism using Fermi type nucleon density distrib. 77−67758
heavy-ion processes, two-centre-oscillator basis 77−26789
heavy-ion proton-proton correlations in relativistic collisions 77−88170
heavy-ion quasielastic collisions, time-depend. single particle method 77−34334
heavy-ion react., separable approx. to TDHF calcs. in 3-D 78−74320
heavy-ion reactions, phenomenological determ. of strength of dissipative forces 77−71619
heavy-ion relativistic collisions, four-channel unitary model 77−41990
heavy-ion relativistic scatt., meson and light nucl. prod. 77−71622
heavy-ion scatt., inelastic, with Coulomb interaction, soln. of coupled eqns. 77−65232
heavy-ion transfer, exact finite-range coupled-channel formalism 77−30620
heavy-ion transfer reactions, DWBA form factors 79−13322
heavy-ion two-nucleon transfer cross sections 77−14155
heavy-ion two-nucleon transfer indirect transitions, coupled channel method 77−50148
(HI,X), rare earths, deeply inelastic transfer reactions, kinematic anal. 80−99186
high energy collisions of heavy nuclei, Glauber rescatt., Reggeon field theory 78−37369
high energy cosmic nuclei+emulsion nuclei collisions, cross sections, multiplicity distribs. 78−41744
high energy hadron-nucleus collisions, book contrib. 79−21889
high energy heavy ion collisions, single nucleon knockout, DWIA formalism 80−99165
high energy inelastic scatt., non-eikonal effects 80−42608
high energy interactions of nuclei, review 79−22326
high energy nuclear collisions, nucleon correlations, classical Glauber model 79−40892
high energy scattering from a bound nucleon: unitarity and closure approximation 80−78236
high excited nuclear matter, p-wave π absorption, high energy heavy ion appls. 79−93542
high momentum behaviour constraints of inelastic amplitudes 77−79346
Humblets modified K matrix 79−22248
impulse approx. in peripheral region, appl. to π+nucleus scatt. and k-mesonic atoms 79−507
impulse approx. with nuclear current conservation, off-shell form factors 80−52632
impulse approximation calcs. of three-body final states in ^{7}Li+^{3}He, clustering in ^{7}Li 77−3023
inclusive production cross section for particle with large transverse momentum *(Russian)* 77−38216
inclusive production off nuclei, multiple scatt. theory extension 77−41869
inclusive quasielastic d prod. in heavy ion collisions, quasiclassical description 79−6695
indirect processes in inelastic excitation of low lying O+ states 77−6417
inelastic electron scatt., nuclear charge and current spatial struct. 80−5134
inelastic form factors properties from energy weighted sum rules 78−37319
inelastic nucleon scatt. anal., comparison of effective two-nucleon interactions 79−93608
inelastic scatt. interactions from realistic pots. 77−67727
inelastic scattering, nuclear field theory 78−13043
integro-differential eqn., numerical soln. of eigenvalue problems *(Russian)* 77−57641
interacting composite systems, generalised spectator expansion in multiple scatt. framework 80−27664
interaction potential between magic nuclei, Skyrme interaction energy functional, microscopic and proximity pots. 78−62556
interaction-time effects of quasifree processes 79−75863
interactions between two light nuclear systems, two-body pots. 77−18501
intermediate structs. from heavy ion excitation functions 78−13147
internuclear cascade mechanism, meson(nucleon)-nucleus high energy reactions *(Russian)* 79−80903
internuclear cascades and multiple prod. of nuclei, parton and multiperipheral models *(Russian)* 77−6330
intranuclear transport theory anal. of inclusive single particle scatt. 79−80902
inverse problem, R-matrix scatt. theory *(Russian)* 77−50092
inverse problem in finite difference approach to Schrodinger eqn. 77−54195
inverse scatt. problem, off-shell transition amplitude generation, real symmetric function 79−6431
inverse scatt. problem *(Russian)* 77−22982
ion-ion cross section, Pauli principle effects in impulse approx. 80−47500
ion-ion interaction pot., real part energy depend., antisymmetrization effects, Fermi gas model 80−83120
ion-ion interaction pots. and barriers, energy density functionals simple parametrisation 79−93658
ion-ion scattering, momentum dependence, in microscopic theory 78−41752
isobars and nuclei, N* components in meson-nucleus reactions and scatt. 79−85522
isolated doorway resonances, spreading width and branching ratios 77−57645

nuclear reaction and scattering theory continued
isospin symmetry-breaking in compound and precompound reactions 77−88087
isovector correlations, π single charge exchange reactions, in light nuclei 78−29499
K-matrix elements in terms of bar phase parameters 77−57634
K-matrix formalisms in multiparticle scatt. 77−30527
K-matrix theory, method for compensating for neglected open channels 78−13039
K-matrix theory, wave function approach 77−57637
K-matrix theory, wave function approach 77−57638
Kapur-Peierls calculations of neutron resonance reactions on light nuclei 77−50136
Kapur-Peierls resonance formalism, unitarity constraints 77−14084
kinetic energy distrib. of fission fragments, thermal fluctuation influence 80−22865
kinetic eqn. soln. for quasi-equilibrium systems, secondary nucleon energy spectra 79−75928
kinetics, quasiclassical method, and angular distribution of nucleons 80−22777
large deformations and dissipation in a random-matrix model approach for fission or colliding nuclei 80−18162
large momentum transfer reactions, density fluctuations, quark-parton mechanism *(Russian)* 79−80868
large scale collective motion in very heavy ion reactions, macroscopic description 80−5049
least squares fitting with normalisation parameters for scattering data 79−45221
Lee model use in pion-nucleus scatt. theory testing 80−78325
light heavy ion total reaction cross sections in diffraction model, resonance oscillations 80−13503
light heavy-ion systems, fusion cross section variations, nuclear proximity pot. 80−57815
light ion reactions, two step processes, effective interaction, CC and DWBA 78−54733
light nuclei, α transfer and knockout reactions, α clustering 78−41687
light nuclei, α-transfer reactions, spectroscopic factors, exact finite range DWBA anal. 80−13372
light nuclei, microscopic theory of three cluster problem 78−54707
light nuclei correlation struct. from elastic electron scatt. 77−18532
light nuclei high energy hadron scatt., complex ang. momentum theory *(Russian)* 78−46067
line shape in inelastic scatt. leading to resonant states 77−54211
Lippmann-Schwinger eqn. constraints on Born approx. applicability 79−6527
local potential models for complex nuclei scatt., appl. to α-α, ^{3}He-α and ^{16}O-^{16}O 77−34270
local Slater exchange approx. for nucleon and heavy ion scatt. 79−22309
long-range heavy-ion potential induced by multiple Coulomb excitation 80−13496
loosely bound composite particles, elastic scatt., disintegration, form factors 77−301
low energy π capture, quasideuteron absorption dominant mechanism 79−6701
low energy fission, charge distrib., quantum mechanical phenomenon of GDR 80−86945
low energy two body virtual states, role in three particle scatt. 79−17869
low-energy nucl. physics, test of elementary particle theory 78−21361
magnetic dipole and quadrupole state excitation, inelastic electron scatt., various nuclei 78−50154
magnetic substate population, heavy-ion inelastic scatt., closed formalism based on DWBA 77−6424
Majorana exchange forces contrib. to scatt. by light nuclei *(Russian)* 77−312
many body scattering, channel coupling array theory, wave function formalisms 80−78235
many particle systems, microscopic derivation of classical eqns. of motion 80−102199
many-body resonances, analytical continuation of bound states examination 79−75955
many-body scatt. theory, orthogonalised distorted waves and optical potentials 79−75940
many-body scattering, coupled channel eqns. and off shell transforms. 78−402
many-channel pot. scatt., formal series meth. *(Russian)* 77−74821
Marchenko eqn. extension to nonHermitian differential systems 80−83080
mass transport in nuclear collisions, nucleon exchange, drift and diffusion coeffs. 79−563
master equations for finite open systems, appl. to nuclear reaction theory *(Russian)* 77−34274
matrix elements between arbitrary single particle wavefunctions, generator coordinate method 80−57751
maximum polarisation for spin-1 particles 77−79355
meson exchange current effects in hadron-nucleus scatt. 79−26380
meson-nuclear physics, International Topical Conf. 77−6436
mesonic degrees of freedom, role in hadron-nucleus scatt. 79−26412
mesonic processes and quarks in nuclei 80−42564
microscopic calculation of absorption channels in pion elastic scattering from light nuclei 79−76039
microscopic calculations for ^{4}H, ^{4}Li continuum, appl. to ^{3}H(n,n), ^{3}He (p,p) 78−17114
microscopic calculations of medium corrections to pion-nuclear elastic scattering 78−78418
microscopic description, conf. 78−50136
microscopic description of nuclei collisions, GCM and RGM framework, appl. to ^{4}He+^{4}He 77−34272
microscopic ion-ion spin-orbit pot., appl. to ^{4}He+^{9}Be, and ^{40}Ca+^{13}C 78−17163
microscopic R-matrix formalism 78−54726
microscopic R-matrix theory in generator coord. basis, appl. to ^{16}O(α,α) 77−14079
microscopic theories of and nucl. motion 78−54727
minimal four body eqns. for final state amplitudes 78−66254
minimally coupled N-particle scatt. integral eqns. 77−88090
multi-channel scatt., microscopic R-matrix theory 78−13041
multi-nucleon transfer, spectroscopic factors for shell model computer codes 77−65195
multi-particle rescatt. effects, cumulative π, p, K prod. *(Russian)* 80−52638

nuclear reaction and scattering theory continued
multi-step amplitudes, variational approach, exact T-matrix and DWBA amplitude differences 79−3167
multichannel model of doorway states mixing via fine-structure states, appl. to fission isomers 77−34231
multichannel quasi-separable pot. approach to N-nucleus scatt. 78−37320
multichannel resonances, combined Hamiltonian and S-matrix methods *(Russian)* 79−63645
multichannel scattering, exact and Glauber amplitudes 80−13421
multichannel scattering, time independent theory 77−17859
multichannel scattering theory, off-shell t-matrix element calc. 79−63644
multidimensional barrier penetration and fission-widths, barrier resonance 80−13454
multihadron production in matter connection with hadron quark-glue model 79−356
multiparticle final states and power behaviour, coherent state representation in deep scatt. 78−13047
multiparticle production on nuclei, role of colour 78−93981
multiple collision models for high-energy hadron-nucleus collisions, expt. evidence against 77−50128
multiple Coulomb excitation of deformed heavy nuclei, uniform semiclassical theory 78−8840
multiple Coulomb excitation of heavy ions, semiclassical S-matrix integral representation 78−630
multiple nuclear production, short range velocity correlations *(Russian)* 77−2961
multiple scatt. from non-overlapping pots. using differential operators technique 78−82128
multiple scatt. theory, spectator expansion of full Green's operator 78−17162
multiple scattering and few-body Hamiltonian models of nuclear reactions 80−47443
multiple scattering expansion with strong three-particle correlations 79−54416
multiple scattering formalism, time depend. generalisation 78−86518
multiple scattering in hadron-nucleus interactions, enhancement of Bose-Einstein symmetrisation effects 78−58271
multiple scattering with rearrangement 79−504
multiple scattering with three-body forces 78−63
multiplicity distrib. nonlinear phenomena from high energy nucleus-nucleus collisions 79−6685
multistep compound processes, autocorrelation function, average fluctuation cross section, different theoretical approaches 80−78234
muon capture in heavy nuclei, neutron emission energy and multiplicity distribs. 77−6313
muon capture with neutron emission, 3-body decay kinematics 77−67736
muonic atoms, prompt fission, muon entrainment by fission fragment, probability *(Russian)* 80−37911
Muskhelishvili-Omnes equation and final state interactions 79−67196
N=27 nuclei levels and analogue states, DWBA anal., from (^{3}He,α) reaction 79−17808
N-body integral eqns. and orthogonality scatt. 77−17861
n-body reaction calcs., integral transform applicability 78−4920
N-body scattering equation approach using pole decomposition of Green's function 80−62540
N-body scattering theory, unified connected theory of few-body reaction mechanisms 79−71822
N-body systems, current research in N-particle scatt. 79−80906
n-body theory of reactions, decoupled Yakubovski eqn. 79−40891
N-particle scatt., dynamical eqns., for transit operators 77−18428
n-particle scatt. theory, asymptotic completeness 79−75413
natural boundary condition methods for calc. of scatt. cross section 77−6327
nearly head-on heavy ion collision, centrality parameter for intermediate energy 80−22856
neutron cross section representation in unresolved resonance region 77−23051
neutron physics, recent advances 77−26640
neutron producing reactions, kinematics 80−86862
non-Hermitian bound state formalisms based on N-body scatt. theory, quantal rules 79−75939
nonfissile nuclei, inherent inaccuracy in capture cross section calc. reactor appl. 80−22836
nonlinear dynamics reaction theory, S-matrix TDHF theory 80−86834
nonlocal Hamiltonians, scatt. solns. in terms of generalised Bessel Neumann series 80−57752
nonlocal pot. problems, physical consequences of anomalous states 79−93570
nonlocal potential scatt., phase shift and extra nodes 77−74265
nuclear collisions, relativistic, classical many-body calc. 79−17918
nuclear Dirac phenomenology, consistency with meson-nucleon interactions 80−9272
nuclear field theory and structureless particle inelastic scatt. by nuclei 78−78332
nuclear isobars elastic scatt., appl. to pion-nucleus interaction *(Russian)* 79−45297
nuclear matter, leptoproduced high energy particles, nuclear attenuation, hadronisation time 80−102182
nuclear matter overlap integral calcs. in diffuse surface model 79−17821
nuclear processes in solar atm. due to charged particles accelerated in flares 78−57527
nucleon+nucleus, inclusive fast nucleon spectra, phenomenology for weak, EM and strong processes 79−22292
nucleon density distrib., basis of electron and proton cross section calcs. 78−54738
nucleon Fermi motion in deuteron, smearing effects, (West β correction), on expt. results. 80−32107
nucleon inelastic scatt., theory of two-step processes 77−34271
nucleon-alpha particle, two-channel potl., exact method for calc. 77−18488
nucleon-nucleus cross sections, Glauber theory and N-N inelasticity 80−68669
nucleon-nucleus reactions, microscopic theory *(Russian)* 77−34290
nucleon-nucleus reactions, particle production, Fermi motion versus collective tube model 79−93659
nucleon-nucleus unstable hadron coherent prod., cross section errors from parton model 79−22253
nucleus-nucleus collision, new approach to antisymmetrisation and rearrangement 77−2956

nuclear reaction and scattering theory continued
nucleus-nucleus collisions, fragmentation velocity, source vel. mass independ. correlation 78−93979
nucleus-nucleus elastic scatt., Andreev's expansion obtained by generating function method *(Russian)* 79−89327
nucleus-nucleus interaction pot. using energy dependent delta interaction, Skyrme interaction folding 79−36269
nucleus-nucleus multiple scatt., high energies, profile function, approx. descripts. 80−106022
nucleus-nucleus pot., static polarisation effects, nuclear shapes 80−5154
nucleus-nucleus reactions, microscopic theory, RGM, GCM, OCM kernels 79−13228
nucleus-nucleus reactions, particle production, Fermi motion versus collective tube model 79−93659
nucleus-nucleus reactions, pion production, Fermi motion effects, multiplicity distribs. and inclusive cross sections 79−93622
nucleus-nucleus scattering amplitude, using Glauber-Sitenko eikonal approx. *(Russian)* 79−80953
nucleus-nucleus total cross section energy depend. 80−106071
odd-A deformed nuclei, EM and electron scatt. form factors, selection rules 79−9458
off energy two body t-matrix in the R-matrix theory *(Russian)* 80−22780
off-energy-shell generalisation 80−18257
off-energy-shell T matrix, frame depend., relativistic pot. theory 78−25159
off-shell Coulomb T-matrix, three particle eqns. with Coulomb interaction, exact soln. 80−42605
off-shell T-matrix in nuclear reactions 80−47441
off-shell transformations and wave function formalisms in many-body scattering theories 79−75937
one- and two-nucleon overlaps generated by a Sturmian method for transfer reactions 79−45220
one-nucleon transfer reactions form factors, Pauli principle *(Russian)* 77−6393
one-particle formalism in continuum approach for photonuclear cross-section calcs. 80−37355
one-particle transfer reactions, extraction of spectroscopic information *(Rumanian)* 79−17871
orthogonality effects on single nucleon ejection amplitudes in medium energy reactions 79−22251
(p,2p) reactions, intermediate energies, distorted wave impulse approx. anal. review, $^{40}Ca(p,2p)^{39}K$ illustration 78−62541
(p,t), rare earths, 18-20 MeV, Q effects on cross section, DWBA anal., A dependence 79−63675
(p,t) reactions, exact finite-range DWBA calcs. 77−71597
p-wave neutron-reduced widths, anal. 79−36242
pair rotational (vibrational) spectra formulae, branching ratio, selection rules, two particle transfer reaction *(Chinese)* 79−9448
parity nonconserving nuclear interactions and weak neutral currents, review 77−41936
parity violation in nuclear processes with polarised neutrons 79−59008
partial wave anal., method for removing ambiguities and parametrising S-matrix elements 77−14029
partial wave expansions for arbitrary spin, non-central forces 78−21535
(particle, xn) excitation functions, simple formula 78−93978
particle+gamma angular correlations in (a,bγ) type reactions, phase, sign conventions 77−26641
particle scattering from target, spin-spin interaction calcs. 78−81730
partition permuting array approach to few-body Hamiltonian models of nuclear reactions 80−86864
path integrals and time-dependent mean-field theories, many-body problem, Hartree-Fock eqns., Slater determinants 80−37342
Pauli correlations in high-energy heavy-ion collisions 78−21593
Pauli principle and absorption in heavy ion reacts. 78−50188
Pauli principle in multiple scatt. theory, exact eqns., cluster exchange 80−106024
peripheral heavy ion reactions, nucleon exchange model for nuclear alignment 79−89323
perturbative calc. of nuclear reaction cross sections, eigenchannel and Barrett-Delsanto methods 79−63638
phase-shift anal. ambiguities 77−18208
photoabsorption, shadowing effects, generalised vector dominance model 77−2976
photoeffect, simple model, various cross-sections 77−30553
photon scatt., exchange effects, scatt. amplitude and integrated photoabsorpt. cross section 77−82910
photon-nucleus scattering, photon shadowing, two component model, GVMD model 77−46159
photonuclear energy integrated cross-sections, calcs., A=2-40 77−50110
photonuclear reaction cross section, one particle in continuum approach 79−93604
photonuclear reactions, S-matrix element transformation, particle polarisation 79−89293
photonuclear reacts., coupled channels method *(Russian)* 78−50153
photonuclear resonances, energy correction for unfolded cross-section data 77−10387
photonuclear sum rule, spin current contribs., strong violations 80−18291
photoprocesses in few-nucleon systems, exchange meson currents role *(Russian)* 79−22269
photoproduction reactions, energy depend. determ. by quasimonochromatic photon beam *(Russian)* 79−75970
photospallation systematics, complementary study 78−17179
physical transition operators, off-shell continuations 77−22980
pion electroproduction from the nucleon near threshold 80−68651
pion interferometry of relativistic nuclear collisions, theory 80−32301
pion multiplicity and nonlinear effects in pion production, NN inelastic interactions *(Russian)* 80−52637
pion multiplicity in central nuclear collisions *(Russian)* 79−59079
pion photoproduction on nuclei in Δ(1236) region, nonrelativistic operator 77−41949
pion radiative capture, effective Hamiltonian *(Russian)* 77−74887
pion single-charge-exchange in isobar doorway model, comparison with $^{13}C(\pi^+,\pi^0)^{13}N$ 77−41999
pion spectrum and polariz. operator in nuclear medium in heavy nuclei collisions *(Russian)* 80−68558
pion total cross-sections, strong absorpt., N*(3,3) resonance 77−10442
pion-induced spallation cross-section, systematics 79−6716
pion-nucleon vertex function with one nucleon off shell 79−40966
pion-nucleus, elastic scatt. many-body theory 79−36279
nuclear reaction and scattering theory continued
pion-nucleus optical potl. and effective Δ-nucleus potl. in (3,3) resonance region 77−10378
pion-nucleus reactions, intermediate state of ρ-propagation in static model 79−67781
pion-nucleus s-wave amplitude, test of new threshold expansion using dispersion relns. 77−6325
pion-nucleus scatt., Δ(1232) isobar propagation in nuclear matter 77−10349
pion-nucleus scatt. amplitude determ. using derivative sum rules and dispersion relations 77−10373
pion-nucleus scatt. and absorption amplitudes, composite particle struct. 79−67778
pion-nucleus scatt. lengths, multiple scatt. theory, binding corrections 78−651
plane wave impulse approx., second-order energy depend. correction 77−22981
plane wave impulse approx. with energy independ. pseudopot., description of $^{24}Mg(p,p')$ and $^{28}Si(p,p')$ 77−61420
polarisation in elastic scatt., semiclassical approx. 79−26417
polarised spin-1 nuclei or mesons, elastic scatt., relativistic spin-1 wave eqn. EM interaction 77−50104
pole expansions for resonance functions, scatt. amplitudes and continuum states *(Russian)* 80−86871
potential scattering, distorted wave formalism, Pade approximants to K-matrix 77−10374
pre-compound decay into complex particle channels 79−6456
production processes on nuclei, helicity-flip anal. 77−82797
projectile-bound nucleon scatt., optimal approx. 79−22250
projection of ang. mom. eigenstates from two-centre generator coord. model functions 77−22912
promptly emitted particles in nuclear collisions, fusion nucleon spectra 80−42678
propagator analytical continuation for strong coupling 77−26647
proton inclusive spectra in nuclear high energy collisions 78−70557
proton scattering amplitude, physical constraints 79−71824
proton scattering at 1 GeV, reviews 79−26428
proton size folding 78−29372
proton-emulsion nuclei interactions, 70 GeV/c, rapidity intervals 78−54750
proton-induced fission, 70 to 200 MeV compound nucleus formation, fragment ang. anisotropy *(Russian)* 79−13359
proximity friction, one body, calc. of key function using Thomas Fermi approx. 78−70454
PWIA cross section for quasifree reactions, nuclear cluster struct. investigation 78−82324
QCD and short range nuclear phenomena 80−91060
quantal fluctuation squeezing, Schrodinger eqn., deep inelastic reactions 80−47444
quantum dynamical semi-groups in nucleon-nucleus scatt. 79−6595
quantum three-body problem, distorted Faddeev eqns. with coupled channel approach 80−52635
quark lattice and QCD in nuclei 80−5101
quark-parton model, hadron prod. in nucl. reaction 78−12868
quark-parton model of hadron-nucleus interaction *(Russian)* 79−22066
quasi-classical approximation for heavy ion elastic scattering *(Russian)* 79−63686
quasi-elastic direct transfer reaction to continuum states, DWBA and diffraction model 80−18277
quasi-elastic heavy ion scatt., multistep processes and interference phenomena 80−22857
quasi-elastic transfer reactions induced in ^{209}Bi targets by heavy ions, ang. distrib. anal. 79−17931
quasi-free scatt. data anal. in the impulse approx. 80−68615
quasibound state wavefunctions for particles inside Coulomb barrier, computation 77−2914
quasielastic heavy ion reaction, amplitude for transitions between molecular (two-center) channels 80−18322
R-matrix anal. of polarisation effects in ^{7}Li system 77−2968
R-matrix anal. of reactions in ^{7}Li system below 10.5 MeV 77−26751
R-matrix analysis, light element neutron cross section standards 77−23041
R-matrix and phase-shift anal. of neutron polarisation in elastic scatt. from light nuclei 77−23088
R-matrix and shell model unification, appl. to $^{12}C+n$ 78−54699
R-matrix method for nuclear reactions, errors in Tobocman's formulation 79−63642
R-matrix resonance cross-section expressions, new Kapur-Peierls type expansions 77−30528
R-matrix theory, convergence anal. of Buttle corrected, variationally corrected, and iterative R-matrix methods 79−6528
R-matrix theory, threshold cusp 79−58893
R-matrix theory for heavy ion transfer reacts. 78−13150
radial integrals with finite energy loss for Dirac-Coulomb functions 77−23000
radiative muon capture rates, maximum photon energy, sum rule correction calc. 79−6517
radiative nucleon capture, pure resonance model, direct-semidirect model, pure semidirect model 80−78257
radiative particle capture, gamma ang. distrib. theory 79−93571
Rayleigh and whispering gallery waves excited by heavy ion elastic and inelastic scatt. 80−91164
reaction duration meas. theory by shadow effect *(Russian)* 79−93572
reaction mechanisms, at low energy and near 3.3 reson. region 79−80958
rearrangement reactions, coupled channel methods, non-orthogonality effects 80−42607
rearrangement reactions, coupled reaction channels compared with coupled channels array 80−47442
recoil effect, kinematics of mol. states approach to heavy ion transfer reactions 78−62557
recoil nuclei registration in particle coherent diffractive prod. *(Russian)* 79−30810
reduced matrix eqn. for many-body scatt., symm. solns. 78−29433
redundant states, reduced potentials, and extra nodes in the radial wave function 80−42603
redundant states and Jost functions for nonlocal potentials 80−9274
relativistic continuum mechanics for heavy ion high energy collision calcs. 79−45299
relativistic heavy ion collisions, charged particle emission multiplicities and ang. correlations, firestreak models 80−18328

nuclear reaction and scattering theory continued
relativistic heavy ion collisions, d prod. mechanism, three models, fireball rate eqns. 80−63198
relativistic heavy ion collisions, effective nucleon numbers 80−13499
relativistic heavy ion collisions, exptl. results and theories 79−71871
relativistic heavy ion collisions, fragmentation cross sections, abrasion-ablation model, factorisation 80−78261
relativistic heavy ion collisions, pion volume emission from Δ (1232) decay 79−93651
relativistic heavy ion collisions, projectile fragmentation, two step abrasion-ablation model 79−97724
relativistic heavy ion peripheral collisions, charge exchange *(Russian)* 80−37398
relativistic heavy ion processes, infinite momentum frame description 79−40944
relativistic heavy ion-nucleus reactions, review, book contrib. 80−27672
relativistic heavy-ion collisions, two-pion to single-pion inclusive data ratio, pion source parameters 79−3171
relativistic nuclear collisions, K prod. in multiple collision model 80−99157
relativistic nuclear physics, collisions of relativistic ions *(Rumanian)* 78−46104
relativistic nuclei disintegration, spectator fragments distrib. 79−22261
relativistic nucleus-nucleus collisions, secondary particle multiplicity, multiple scatt. model 80−22847
relativistic particle production on nuclei at large angles, multiple interaction mech. *(Russian)* 77−74822
relativistic two-body forces in many-body systems, Weinberg and Yukawa interactions 80−32203
relativistic two-body t matrix, separable expansions to local potentials in a quasipotential approach 79−63641
renormalized plane wave-projected and Coulomb-projected T-matrices 79−17267
resonance scatt. of protons, lineshapes, ^{25}Mg(p,p′) and ^{16}N(p,p′) calcs. *(German)* 77−22989
resonance theory of potential scatt., phase shift parameters 78−16685
resonant states in the presence of Coulomb interactions, Schrodinger eqn. 80−91161
resonant subsystems in few-body theory 77−18494
resonating group method, recent investigation results, review 79−3098
resonating group method normalisation kernel, eigenvalue asymptotic expression 77−14082
resonating-group method anal. 77−82886
resonating-group method for nuclear many-body problems, review 79−9497
review of reaction theory for nuclear engineers *(Japanese)* 80−99155
RGM variational method based on GCM kernel 78−564
rotational excitation ang. momentum transfer in inelastic scatt., coupled channel and adiabatic method 77−50094
rotational states, Coulomb excitation by spherical nucleus, distortion, semiclassical model 79−67620
Rutherford scattering formula, small-angle end, for teachers 78−16608
s-d shell nuclei, semiempirical prediction of heavy ion reaction resonances 79−22256
S-matrix theory, threshold cusp 79−58893
s-wave level reson., tensor analysing power far light nuclei 77−82893
Saito potential, off-energy-shell unitarity 80−18207
scaling behaviour in inclusive backward angle prod. 78−8791
scattering amplitudes for two charged fragments 79−75936
scattering by singular potentials of the general type at high energies 80−63141
scattering in generator coord. method, appl. of variational principle with natural boundary 77−54196
scattering integral equations for distorted transition operators, N- particle scatt., DWBA 79−6532
scission region, nascent fragment bending and wriggling modes, quantum numbers 80−18285
Se(d,d), polarised deuterons, vector analysing power, coupled-channel calcs. 78−62550
second-order excitation in nucleus-nucleus interaction potential 79−36264
semiclassical approx. of Coulomb matrix elements including distorting potentials 77−57640
semiclassical approxs. for heavy-ion transfer reactions 78−94021
semiclassical Coulomb excitation theory, classical-limit S-matrix, orbital dynamics 78−33205
semileptonic weak and EM interactions, isoelastic processes, one-body density matrix formalism 77−18528
separable approx. to local interactions, exponential pot. 79−508
shadowing in electroproduction, geometrical origin, virtual photon generation 77−82913
shell model approach, elimination of spurious centre of mass resonances 79−75929
shell model continuum calcs., status and prospects 78−54698
short range correlations in nucleus-nucleus scatt. amplitude, optical phase shift expansion 78−70502
simple approximations and symmetry measures for model interactions 79−17867
single-particle basis, translation invariance in microscopic calcs. *(Russian)* 77−46149
single-particle basis and translational invariance in microscopic approach 77−14078
single-particle resonances, numerical anal. 78−29436
smooth cutoff model angular distrib., decomposition, pole contribs. 77−10376
soft hadron-nucleus reactions at high energies, theoretical model 79−17870
soft hadronic collisions and fragmentation on nucl. targets, quark dynamics 79−22063
soluble Kisslinger pot., associated Schrodinger eqn. 79−85416
solvable few-body models as tests for reaction theories 77−18497
spectral function methods, non-relativistic two-body off-shell amplitudes 77−26643
spectroscopic information from nuclear reactions: applications 79−459
spectroscopic information from nuclear reactions: theory 79−458
spectroscopic investigation of decaying states using continuum shell model 80−486
spectroscopy by continuation of polarisation observables into nonphysical region, nuclear struct. 78−78356
spherical nuclei, dipole states, transition densities and electroexcitation, GDR form factors *(Russian)* 80−52611

nuclear reaction and scattering theory continued
spherical pot., heavy charged particle scatt., Debye expansion and JWKB approx. 77−53803
spherical tensor formalism, polaris. transfer and spin correlation reactions *(Russian)* 79−59047
spin $^1/_2$ particles scattered from nuclei, beam polarisation and nucl. recoil effects 79−67738
spin polarisation analysing power in nuclear reactions, extreme values 78−37326
spin zero nuclei+polarised proton, Coulomb multiple scatt. anal. 79−22277
spin-polarisation analysing powers in nuclear reactors, M-matrix conditions 78−8787
spurious solutions in few-body equations 79−45223
statistical significance of spreading widths for doorway states, comments 80−27611
stellar environment, strong interactions and nucl. struct. 80−72765
strong coupling method reformulation on the basis of the Schwinger variational principle *(Russian)* 78−89836
strongly damped collisions, nonequilibrium process 80−18258
strongly damped heavy ion collisions, nucleon exchange as possible mechanism, semiclassical model 79−6689
strongly damped heavy-ion collisions, in microscopic calc. of kinetic-energy loss in rapid stretching 77−14167
Sturm-Liouville equation, convergence, rel. to nucleon-nucleus pot. 79−6534
Sturm-Liouville equation, math. aspects rel. to nucleon-nucleus pot. 79−6533
sub Coulomb elastic scatt., adiabatic and dynamic polarisation effects 79−97698
subCoulomb elastic heavy ion scatt., influence of low lying collective states 78−78414
sum rules in photonuclear reactions 77−79362
supercritical pomeron, parton model interpretation, appl. to scatt. off nuclei 78−41497
superheavy element prod. in compound nucleus reaction, theoretical optimisation method 78−46103
superheavy nuclei prod. in compound nucleus reactions, barriers, shapes 77−46184
symmetric very-heavy-ion reactions, compound nucleus cross-sections 77−74878
symmetry effects in heavy ion transfer reactions 77−54241
T-matrix, perturbation formalism for complex poles and widths, appl. to intermediate struct. 78−66255
t-matrix Lippmann-Schwinger type scatt. eqns., iterative soln., off shell matrix elements 80−86866
Tabakin rank-one potl. in orthogonality condition model, 3-body energy 77−18423
target nucleon+α and target nucleon+^{6}Li, pots. in microscopic model with antisymmetrisation effects 78−62516
TDHF, particles+core reduction 78−33135
TDHF approximation and exact Schrodinger dynamics, Taylor series comparison 80−42568
TDHF calcs. using separable three dimens. wavefunctions, ^{4}He+α 78−50111
theory of resonating group method and generator coordinate method, and orthogonality condition model 79−13226
thermonuclear reaction rate enhancement due to strong screening 78−13186
three body phase space distribs. 80−37393
three body problem, connected kernel method failure 80−106025
three body problem, Green function hierarchy 79−75941
three body problem with pairwise interactions, Baer-Kouri-Levin-Tobocman and Faddeev eqns. 80−99158
three body scatt., spline function moment methods 80−505
three body sequential decay processes, α-transfer reaction studies 79−6526
three cluster resonating group method, cluster struct. in light nuclei and cluster rearrangement collisions 78−54705
three nucleon, finite range microscopic form factors, zero range DWBA calcs. 79−6525
three particle systems, reaction mechanism and approx. models 79−80904
three particle systems with Coulomb interaction, scatt. and breakup eqns. exact solns. 80−504
three particles, binding energy and scatt. state calcs. using boundary condition model *(Russian)* 79−40837
three particles with Coulomb interaction, binding energy and scatt. states *(Russian)* 80−5051
three-body breakup reacts., dynamics 78−13040
three-body d+nucleus scatt. model, effects of imaginary pots. 79−9532
three-body eigen wave function of a continuous spectrum, asymptotic form 79−5994
three-body K-operators and unitary approx., appl. to (d,p) and (d,d) 77−18499
three-body Lippmann-Schwinger equations, asymptotic behaviour and soln. uniqueness 80−42604
three-body problem, relativistic description, deuteron breakup appl. 77−46156
three-body processes in the presence of coulomb forces 79−6523
three-body scatt., two pot. formula, distorted Faddeev eqns. integral form 80−57753
three-body scatt. amplitudes, appl. of contour rot. 78−567
three-body scatt. problem, cluster expansions, effective intercluster pots. 80−5082
three-nucleon elastic scatt., hyperspherical harmonics 77−57636
three-nucleon system, coherence effect, N-particle generalisation, final state interactions 78−89833
three-particle reactions with rearrangement, partial amplitude asymptotics *(Russian)* 77−74820
three-particle relativistic kinematics 80−27602
three-particle scatt., finite cross section 79−85011
three-particle scattering, subtraction techniques 78−24694
threshold phenomena, K-matrix description 79−30809
threshold phenomena in R-matrix theory 79−17865
threshold pion absorption in nuclei 78−82390
time delay of resonance wave packets, stat. model anal. 80−22802
time dependent approach to the collision of two charged composite particles 79−75935
time dependent Hartree Fock solns. for heavy ion scatt., wave packets to stationary waves 78−62558

nuclear reaction and scattering theory continued
time dependent HF method evolution, implications for heavy ion reaction calcs. 77−10424
time dependent Schrodinger eqn., alternative approx. soln. for heavy ion reactions 80−32296
time-dependent intranuclear cascade model 80−63140
time-dependent mean-field approximation for nuclear dynamical problems 80−63113
time-dependent-S-matrix Hartree-Fock theory of complex reactions 80−63112
total pion absorption cross section, A depend., proton yields 80−106081
total reaction cross sections and elastic scatt., refractive scatt. or strong absorption 79−567
trans-uranium nuclei, fission barrier and (neutron width-fission width), nucleon contents depend. *(Russian)* 80−106093
transfer induced transport in nuclear collisions 80−507
transfer reactions, 3-body with sequential decay, spectroscopic information 77−54203
transfer reactions of bound system on target, 3-body and eikonal formalism 77−18498
transition T-matrix complex widths and poles, perturbation formalism 77−26646
transparency in composite particle-nucleus reactions 80−9273
transport coefficients for deeply inelastic scattering from the Feynman path integral method 79−17922
triplet S channel, half shell function parametrisation in separable form 80−52636
truncated pion-nucleon amplitudes and pion-nucleus interactions 80−68708
two charged clusters collision, scatt. amplitudes and integral eqns. 80−68614
two cluster couplings, uniqueness of many-particle scatt. integral eqns. 78−25160
two nucleon distrib. function for two nucleon transfer, effective Hamiltonian approach 80−22778
two nucleon transfer and scatt. matrix elements from dynamic deformation theory 79−85488
two particle partial scatt. amplitude away from energy shell, asymptotic behaviour 77−6326
two step (p,d) (d,t) process, Strum-Liouville state asymptotic convergence 79−54414
two-body collisions and time dependent Hartree-Fock theory 79−36208
two-body force scatt. calculations, limitations 77−88089
two-body interaction, shell model calc. matrix elements 80−42567
two-body rearrangement collision, effect of continuum contribution 79−13262
two-body scattering in force field 79−85012
two-centre generator coordinate basis for microscopic theories 78−13038
two-centre problem with realistic potentials, single particle energies, wave functions 77−82887
two-cluster transfer reactions, in Coulomb field, classical theory 77−67757
two-nucleon transfer, ang. momentum and binding energy effects 79−59021
two-nucleon transfer, centre-of-mass corrections to overlap factors 78−13042
two-nucleon transfer form factors, Taylor-series method 77−10382
two-nucleon transfer reactions, excitation of quadrupole vibrations 79−17786
two-particle emission, appl. of exciton model *(Russian)* 77−304
two-step DWBA, energy depend. for (p,t) unnatural parity state excitations 78−70528
ultra-high energy nuclear interaction event with large transverse momentum at 445 TeV *(Chinese)* 80−105140
ultrarelativistic nuclear collisions, asymptotic hadron spectrum, hot hadronic matter 80−63118
unbound ejectile pickup reactions, finite range DWBA calcs. 79−85439
uncorrelated target, optical pot. unitary content, DWIA and Glauber theory 80−99160
unequal fragments, generator coordinate and resonating group methods 77−18490
unified description of fission and nuclear collisions *(Russian)* 78−33163
unified nuclear pot. for heavy ion elastic scatt., fission, fusion, masses and deformations 80−5189
unified theory of the nucleus, book 77−41900
uniqueness of the N-body Lippmann-Schwinger-Glockle-Tobocman equations 79−54415
unitary ang. distribs. nonconvexity and partial wave ambiguities in error affected data 79−26411
valency doorway model of neutron radiative capture, appl. to Mo isotopes 77−23021
variable amplitude nonlinear eqns. for one-dimens. scatt. 77−22431
variational principles for true three- and four-particle scatterings 80−18254
variational principles for true three- and four-particle scatterings 80−78233
variational techniques in nuclear and chemical reactions, R- and S-matrix 77−60966
very heavy ion-nucleus collisions, struct. effects in dissipative collisions 80−57795
very heavy ions with complex trajectories, elastic scatt., semiclassical anal. 80−18331
virtual excitations in the scattering of complex particles by nuclei 80−99156
virtual photon theory, validity 77−2977
virtual processes, Coulomb interaction, scope for experiments 79−9438
wave function orthogonality, bound state to continuum transitions for (Γ,p), (e,e′p), (π,N) 78−78335
wave-spreading effects in nuclear scattering at intermediate energies 80−18252
weakly absorbed particles, modified Austern-Blair theory, DWBA 80−86867
Weinberg functions, Born approx. in scattering problems, phase shift 80−32248
Wigner transform and the eikonal approximation for nonlocal potentials, inclusive scatt. 80−13423
X(a,b)Y(c)Z, ang. correlation following sequential decay 79−93645
Yukawa pot. scatt., separable expansion method, off-shell T matrix 78−93564
(α,2α), A=9, 12, 16, 20, 22 80−68629

nuclear reaction and scattering theory continued
(α, 2α) 700 MeV, cross section, effective cluster number from PWIA, momentum distrib. 79−40940
(α,2α) reacts., three-body anal. 78−13126
(α,α), 1.37-2.55 GeV, microscopic anal. 80−47490
(α,α), critical energies, ang. distrib. energy depend. semiclassical theory 79−76007
(α,α), elastic scatt. critical radius, single particle anal. 80−13490
(α,α), internal S-matrix dynamics and internal deflection function 80−78307
(α,α) elastic and inelastic, by heavy nuclei, Glauber amplitude approx. scheme 79−40939
(α,α) scatt. at high energy, appl. to Ca(α,α) at 1.4 GeV 78−66293
(α,α'X), inelastic interaction cascade model for Z=3-13, 29-82 80−106064
(α,αX), 1 GeV/N, inclusive hadron-nucleus cross-sections, multiple scatt. series 80−13519
(α, ^{3}Me), composite particle scatt. breakup mechanism 80−83105
(α, N), DWBA finite range calc. 79−9541
(α,X), 140 MeV, inclusive spectra, 'quasi-two-body scaling' and 'hot spots' 80−5142
(α,xn), 640, 710 MeV, n ang. and energy distribs., intranuclear cascade model 80−83109
α scattering from 2d-1s shell optical model and coupled-channel anal. 77−6407
α strength factors for (α,p) and heavy-ion α-transfer reactions on medium nuclei 77−18454
α-α interaction, consistent calc. by resonating group method 77−18491
α-α scattering, appl. of generator coordinate formalism 77−18584
α-decay spectroscopic factors, coupled channel problem, local pots. justification 80−47439
α-transfer, scatt. and two-nucleon transfer, surface clustering 77−10344
α-transfer reacts. between light nuclei 78−54787
α-transfer to α-decaying nuclei 77−79396
α+α scatt., exchange Coulomb kernel in resonating group formulation 79−6531
α+nucleus real pot., energy and target depend. 79−36251
(αnp) three-body elastic scatt. calc. using hyperspherical harmonics 79−63640
(d,d) breakup channel contrib. to optical pot. in 3-particle approx. 79−6630
(d,d) elastic and inelastic, diffraction scatt. theory, d dissociation and stripping reactions 79−6633
(d,^{3}He) on ^{12}C, ^{16}O, ^{24}Mg, ^{40}Ca, 29 MeV, polarised d, low lying analogue states, DWBA anal. 78−82285
(d, ^{6}Li), 54.25 MeV, α-cluster spectroscopic factors, DWBA anal. 80−52571
(d,^{6}Li), A$\sim$60,116, L=0 transitions, cross sections, microscopic anal. 80−78189
(d,np), diffraction theory calcs. 79−6537
(d,p), 12.08 MeV, ^{154}Sm, ^{166}Er, ^{170}Yb, ^{176}Yb, final nucleus level struct., DWBA anal. of ang. distribs. 79−30788
(d,p), 1.7-15 MeV, rearrangement collisions three body model, bound state approx., DWBA calcs. 79−93595
(d,p), composite particle scatt. breakup mechanism 80−83105
(d,p), role of ΔN=2 interaction, differential cross sections, DWBA anal. 80−91189
(d,p) direct reactions, multistage processes and methods 77−41974
(d,p) reactions, δ-shell method for approx. finite range DWBA calcs. 79−555
(d,p) stripping reactions, energies below Coulomb barrier 77−6394
(d,t), 12.08 MeV, ^{154}Sm, ^{166}Er, final nucleus, level struct., DWBA anal. of ang. distribs. 79−30788
(d,t), DWBA anal., form factors and d-t overlap integral S- and D-state components 80−18320
(d,t), role of ΔN=2 interaction, differential cross sections, DWBA anal. 80−91189
(d,t) anomalous transitions in rare earths, inadequacy of CCBA 78−70543
(d,t) on ^{12}C, ^{16}O, ^{24}Mg, ^{40}C, 29 MeV, polarised d, low lying analogue states, DWBA anal. 78−82285
d breakup effect on spin orbit and tensor pots. 80−32286
d stripping cross sections to a resonance, exact and DWBA anal. comparison 78−93985
d stripping reactions, Tabakin pot. calcs., differential cross sections, ang. distribs. 78−611
dnp coupling constant from ^{2}H(p,p)^{2}H data, 1.5-3 MeV, Cutkosky method 77−10404
(dx) breakup on nucleus, adiabatic treatment stripping and forbidden transition cross section 80−9299
(e,e), A=2, 3, 4, scaling laws in relativistic impulse approx. model, spin effects 80−52662
(e,e), c.m. motion effects in oscillator shell model 80−106050
(e,e), finite dimension nuclei, differential cross section static correction, shell model 79−75976
(e,e), relativistic e, helicity representation 80−5132
(e,e), virtual photon intensity and finite nuclear size effects, PWBA calcs. 79−26424
(e,e′), light and medium nuclei, high energy approx. anal., transition densities and probabilities *(Russian)* 80−63129
(e,e′), shift of quasielastic peak 79−6572
(e, e′p), eN interaction in quasifree scatt., nonrelativistic Hamiltonian through 2nd order 80−52663
(e,e'p) quasi-free scatt., spectral function, sum rule discrepancy, shell model deviation 80−42641
(e,e'π), π electromag. processes, theoretical aspects 80−22822
(γ,γ), 412, 468, 662 keV, elastic scatt. cross sections, Rayleigh scattering anal. 80−86898
(γ,n), 45-160 MeV, cross sections in quasi-deuteron model for direct reactions 80−63170
(γ,N), fine structure in ang. distrib. in giant resonance region 77−6342
(γ,π), few body pion photoprod. in Δ-resonance, region 80−42636
(γ,π), light nuclei near threshold, π mass difference effects, nuclear K-matrix 80−27674
(γ,π), π electromag. processes, theoretical aspects 80−22822
(K,K), isobar doorway model, optical pot., Λ-nuclear matter binding energy 80−106079
(K^-, π^-) on light nuclei, hypernuclear spectroscopy 78−50116
K^--nucleus reaction, in emulsion, ^{8}Li fragment energy, evaporation theory 78−62577

nuclear reaction and scattering theory continued
($\mu^{\pm}$,$\mu^{\pm\prime}$xN), A=12-203, muodisintegration cross sections, PWBA anal. 80−68650
(n, 2n) and (n, 3n) cross-sections anal., level-density parameters of A>150 nuclei 79−30824
(n,2n) excitation functions, reactions with two particles emission *(Russian)* 77−61427
(N,α), microscopic finite-range anal. 80−63181
(n,f), intermediate struct. line fitting, subthreshold fission resonances 80−102214
(n,f), near thermal, effects of phonon transfer on cross sections 78−50221
(n,γ), mechanism in 3s size resonance, s-wave radiative width partition 80−37387
(n,γ), mechanism in 3s size resonance, radiative width statistical and valence effects 80−37388
(n,γ), polarized space parity nonconservation, optical pot. and GDR parameters *(Russian)* 80−86803
(n,γ) cross sections, semi-direct model calcs., 6-15 MeV 77−23047
(n,γ) gamma ray spectra calc. 80−52620
(n,n), cross section and polarisation, Lane model extension to light nuclei 79−85449
(N,N'X), shower proton and meson transverse momenta, intranuclear cascade model 80−102185
(n,p), 14 MeV cross sections, empirical formulas 78−70517
(n,p) scatt. observables, R-matrix calc., 20-140 MeV 77−57668
(n,x) reactions on medium and heavy nuclei, models 77−26698
(n,X) X=p,2n,3n, precompound and compound emission mechanisms 80−102176
N-nucleus reacts., NN spin depend. t-matrix for intermediate energy 78−41682
n+nucleus, high momentum study, quasi-two-body scaling, differential cross sections 77−57665
N*(1688) resonance effects on nuclear reaction, NN scatt. phase parameters 80−105987
Nd S-wave scatt., dispersion relation approach to three-body systems, unitarity approx. 79−506
NNπ system, phenomenological relativistic quantum mechanics, scatt. theory 80−83082
(p,2p), backward inclusive prod. mech. probing, differential cross section 80−68668
(p,2p), distorted momentum distrib., and pp collisions, geometry choice for independent study 79−6597
(p,2p), distorted wave t-matrix anal. 78−50169
(p,2p), off shell effects using optimum geometrical conditions 79−6598
(p,2p), off-shell effects in distorted wave off shell impulse approx. 77−6376
(p,2p) coplanar symmetric reaction, impulse approx. for peak cross section 79−45257
(p,2p) DWIA calcs., N-N off shell t-matrix, optical model from N-N 77−88124
(p,2p) high-energy knockout reactions, factorisation corrections 79−17885
(p,2p) knockout, DWIA and PWA mechanisms 77−88120
(p, α) microscopic form factors, DWBA cluster form factor replacement 80−47478
(p,X), inclusive backward collision, intermediate energies, correlated nucleon clusters 79−40914
(p,d), 51.9 MeV, forbidden transition ang. distribs., CCBA and DWBA anals. 80−86848
(p,d), 52 MeV, deeply bound hole state transition strength giant resonance, DWBA anal. 80−47426
(p,d), pol. p, 65 MeV, A=12-94, differential cross sections and anal. powers, pickup 80−91172
(p,d) reactions on light nuclei, differential cross sections, peripheral and distorted wave model calcs. 79−9560
(p,Λ^0), inclusive cross section, constituent-constituent multiple scatt. model for dependence on atomic number 80−83101
(p,n), 1 GeV, A=7-212, charge exchange scatt., Glauber diffractional theory anal. *(Russian)* 80−83103
(p, n), 22.2 MeV, A=27-197, neutron spectra, direct and equilib. processes *(Russian)* 80−52648
(p,n), anomalous optical potential for sub-Coulomb barrier protons, 2 particle 1 hole states 80−105948
(p,n), pion exchange at intermediate energy 80−63179
(p,n) elastic and inelastic scatt., deformation of neutron excess, coupled channel anal. 79−93480
(p,n) quasielastic reaction, cross section and polarisation, Lane model extension to light nuclei 79−85449
(p,n) transitions to anti-analogue states, fluctuations in Lane pot. 78−8815
(p,N*), high energy reactions, Glauber scatt. theory study *(Chinese)* 79−93626
(p, p), 1 GeV, polarisation data, Glauber anal. spin-orbit parameters, matter distribs. 80−52655
(p,p), 1 GeV, polarisation features, Glauber model calcs. 79−40915
(p,p), 1 GeV elastic and inelastic scatt., diffr. minima filling mechanism *(Russian)* 80−86907
(p,p), 600, 750 MeV, polarisation and cross section, Glauber model calc., NN matrix test 80−47485
(p,p), <100 MeV, Coulomb corrections to NN coupled states, nonrelativistic scatt. theory 80−78114
(p,p), A=9 to 70, differential cross sections, struct. effects, optical and coupled channel anal. 80−47482
(p,p), cross section and polarisation, Lane model extension to light nuclei 79−85449
(p,p), elastic scattering theory, multiple scatt. test review 80−42654
(p,p), knock-on exchange, local equivalent methods 78−33184
(p,p), polarisation in elastic scatt., multiple diffraction approx. 79−97696
(p,p), small distances, new electrodynamics approach 80−63180
(p,p), statistical significance of spreading widths for doorway states, reply to comments 80−63147
(p,p) 1 GeV, Glauber theory of spin-orbit interactions 78−37336
(p,p) total cross sections, 180 to 560 MeV, Galuber model calcs. 79−40917
(p,p'), 800 MeV, cross sections, quasifree knockout mechanisms, PWIA calcs. 80−78294
(p,p'), A=6 to 208, 800 MeV, proton spectra, quasifree scatt., DWIA anal. 80−52677

nuclear reaction and scattering theory continued
(p,p'), deformed nuclei, local approx. results for exchange effects 79−452
(p,p'), direct, and multistage processes, DWBA anal. *(German)* 78−25202
(p,p'), ground state correlation, continuum spectra 78−94007
(p,p'), hadronic transition operator for collective state transition rates 79−45262
(p,p'), single neutron states, two step process and effective interaction 80−78290
(p,p'), unnatural parity states excitation, π-condensate instability effects, DWBA anal. 80−78168
(p,p') inelastic spectra in high energy continuum, single and multiple scatt. mechanisms 80−57777
(p,p') to collective states, medium energies, spin-orbit deformation from DWBA calcs. 79−9565
(p,p'd), quasifree scatt., break-up cross section at high energies 80−99174
(p,pd), (p,pt), (p,^{3}He) reactions on ^{12}C, ^{16}0, spectroscopic factors, cluster model, DWIA 77−54214
(p,π), exclusive single nucleon transfer, theoretical status 80−42652
(p,π) reactions, nucleon-nucleus distorted wave, small component role, relativistic effects 79−40919
(p,π) reactions near threshold, relativistic effects in one-nucleon model 77−34302
(p,π^-), nuclear size dependence of π^- prod., unified pattern 78−82349
(p,π^+), polarised p, 200 MeV, p distortion and asymmetries 79−22285
(p,π^+), relativistic PWIA 77−10394
(p,π^+) cross-section calcs., model relating to (π^+,π^+) cross-section 77−61422
(p,π^+) reaction anal. at momentum transfer below 600 MeV/c 77−79376
(p,t), low lying level ang. distribs., zero range DWBA anal. 79−67656
(p, t) ang. distrib., zero-range DWBA calc., volume absorptive optical pot. singular prop. 80−523
(p, t) ang. distrib. with deep minima, DWBA calcs. geometrical aspects 80−522
(p,X), 24 and 70 GeV/c, pseudorapidity distribution, energy and target depends. 80−5138
(p,X), 400 GeV/c, deuteron prod. mechanism, pick up reactions 80−83096
(p,X), high energy, Glauber anal., produced particle-A relation *(Chinese)* 80−102192
(p,X), multi-chain model, charged particle distrib. 80−83098
(p,X), pion production, Fermi motion effects, multiplicity distribs. and inclusive cross sections 79−93622
(p,X) 90 MeV, inclusive spectra, 'quasi-two-body scaling' and 'hot spots' 80−5142
(p,X) in emulsion 24 GeV, clusters in rapidity interval method, multiperipheral model 80−5135
P scatering, 0.8 to 1.5 GeV, neutron distrib. anal. 79−26429
p-nucleus, high energy reaction temp., kinematic props. of nuclear fragments 78−54761
p-nucleus, Maxwell distrib. and mass motion to account for ang. distrib. anisotropy, ~600 MeV 77−61425
p-nucleus collisions, fragmentation velocity, source vel. mass independ. correlation 78−93979
p-nucleus high-energy reactions, two-particle rapidity correlations in produced particles 77−18545
p+emulsion, 200 GeV, data anal. hydrodynamical model 79−551
p+nucleus, inclusive π prod., 0.78 to 5 GeV, relation to NN π prod. 78−78384
p+pN, 640 MeV, obs. of correl. between backward emitted protons and forward outgoing protons 79−17902
pp, low energy scatt., spin depend. EM force effects, Coulomb DWBA anal. 79−9568
pp bremsstrahlung, 730 MeV, γ-energies of <300 MeV, differential cross section 80−99108
(π^+, 2p) quasi two particle scaling, momentum distrib. from statistical model *(Russian)* 79−40968
(π,γ), cross sections from Boltzmann eqn. 79−89330
(π,γ), π electromag. processes, theoretical aspects 80−22822
(π_-, NN), low energy pion absorption, $\sigma+\omega$ model, optical pots., real ρ^2(r) pot. 80−83125
(π,π), A>2 nuclei, three rung ladder graph, singularity curves 80−32303
(π,π), Coulomb effects in pion Klein-Gordon eqn. 79−93668
(π,π), cross section calc., comparison of factorisation approx. taking account of nucleon Fermi motion 78−29497
(π,π), elastic scatt. amplitude anal., use in DWIA 79−85544
(π,π), elastic scatt. relativistic kinematics, differential cross sections 80−63210
(π,π), light nuclei near threshold, π mass difference effects, nuclear K-matrix 80−27674
(π,π), many body effects in resonant scatt. 78−94029
(π,π), many-body response problem, reaction channel m-croscopic treatment 79−85547
(π,π),(3,3) resonance region, Brown-Rho bag model descript. 80−57806
(π,π) elastic and inelastic, approx. four particle eqns. *(Russian)* 78−86554
(π,π) elastic scatt., covariant theory, first and second order optical pots. 79−85545
(π,π) elastic scatt., reaction mechanisms, structure information and neutron radii 80−42702
(π,π) single and double charge exchange in resonance region, geometrical limit 80−86930
(π^+,π^{+or0}) inelastic reactions, cross sections from Boltzmann eqn. 79−89330
($\pi^{\pm}$, $\pi^{\pm}$), slow mesons, anal. using effective quasi-potential *(Russian)* 77−34350
(π,π'), 1p shell targets, DWIA calcs., strong transitions, isospin effects 80−42708
(π,π'), particle-hole state excitation, field theory calcs. *(Russian)* 80−37318
(π, π') many body QFT framework anal., final state particle-hole correlations 80−13508
(π,π') momentum space DWIA study 79−85551
($\pi^{\pm}$,$\pi^{\pm\prime}$), π^- nuclear response enhancement, continuum effects, stretched state isospin mixing 80−86929
(π,π'), microscopic Fermi liquid approach 79−26459

nuclear reaction and scattering theory continued
(π,πN) reactions, nuclear structure effects, modified semiclassical model 77−34348
(π^+,π^+p) quasi two particle scaling, momentum distrib. from statistical model *(Russian)* 79−40968
(π,πX), multi-nucleon removal processes, reaction mechanisms 79−85520
(π,X), effective S-wave πNN interaction, effects in nuclear matter 80−105985
(π,X), reaction mechanisms, nuclear environment and models 80−42700
(π,X), total cross section treatment for (3,3) resonance region 80−42703
π-nucleus inelastic interaction, 200 GeV/c, two particle correlations *(Russian)* 78−46112
π-nucleus Low eqn., multiple scatt. effects 77−41998
π-nucleus scatt., field theoretic T-matrix 77−6324
π-nucleus scatt., Lee model evaluation of scatt. operator 79−22328
π-nucleus scatt., nonrelativistic QFT formulation, Low eqn., optical pot. definition 79−6700
πA, multiple scatt. theory *(Russian)* 79−49640
πd quasielastic and inelastic rescattering as cumulative particle prod. source *(Russian)* 79−22340
π^3He^{3}H coupling constant estimation, Chew-Low eqn. 77−3051
πN elastic scatt., nonstatic model for nuclear reactions 80−102125
πN T-matrix, off-shell model of scattering amplitude 79−414
πNN-NN coupled problem, unitary model 80−99135
πNN-NN system, coupled channel approach, coupled equations 79−85371
πnucleus scatt., nucleon Fermi motion, numerical approx. in momentum-space calc. 79−45302
ρ-meson intermediate states in πN scatt. Chew-Low theory modifications 79−479
Σ^-+nucleus low energy reactions in finite range potential model 79−85424
(t,p) stripping reactions, repulsive-core effects, Tabakin potential 77−30607
t+nucleus, form factors for two-nucleon stripping process wth Skyrme potentials, DWBA 78−58287
^{7}H(d,d), 5-45 MeV deuteron wave function asymptotic D- to S-state normalisation, anal. power 80−78304
Ag+^{20}Ne, 175 MeV, γ-ray multiplicities and energies, primary fragment angular momenta 78−46093
Al(Ne,X), 400 MeV/N, direct vs. thermal particle emission, inclusive cross sections 80−52688
Al(Ne,X), proton inclusive spectra, direct plus thermal model 80−57799
^{26}Al excited states, isobaric analogues, spins, DWBA anal. of ^{27}Al(^{3}He,α) 80−105981
^{27}Al (^{14}N, X), 70, 100 MeV, deep inelastic, charged reaction products ang. correlations, 3-body kinematics 80−5162
^{27}Al(^{20}Ne,^{12}C), 120 MeV, anal. of continuous spectra by multi-step direct reaction theory 79−45287
^{27}Al(^{20}Ne,^{16}O), 120 MeV, anal. of continuous spectra by multi-step direct reaction theory 79−45287
^{27}Al(^{3}He,^{3}He), 46 MeV, ang. distribs., optical and DWBA anal., scatt. pots. 79−556
^{27}Al(α,α), 41 MeV, elastic and inelastic, ang. distribs., optical and DWBA anal., scatt. pots. 79−556
^{27}Al(d,pX) 80 MeV, inclusive proton spectra, d break-up, DWBA anal. 80−91190
^{27}Al(e,e'), 70-340 MeV, odd parity state electroexcitation, form factors, transition probabs. 80−78208
^{27}Al(n,n), (in)elastic scatt. cross sections, duration of collision process *(Russian)* 79−80942
^{27}Al(p,α)^{24}Mg, finite-range cluster-model description, DWBA approach 80−52667
^{27}Al($\pi^\pm$,$\pi^\pm$N), 180-255 MeV, quasielastic pion scatt. coincidence expt. interpretation, impulse approx. 80−68704
Al(d,d), 4.3, 6.3, 8.9 GeV/c, secondary momentum spectra, multiple scatt. model anal. *(Russian)* 80−27650
(Ar, π^-X), 800 MeV/A, π^- energy and ang. distribs., firestreak and hard scatt. model anal. 80−13498
^{38}Ar levels, J$^\pi$ and transition strengths, DWBA anal. of ^{40}Ar(p,t) 80−47378
(^{40}Ar,X), 222-340 MeV, A=116-197, charged particle emission, early collision evolution, fission and evaporation cross sections 80−106072
^{40}Ar+^{40}Ar, 250-1000 MeV/N, intranuclear cascade calcs. for multiplicity and cross sections 80−32300
^{40}Ar(p,p), 18-44 MeV, differential cross sections, phase shift anal., energy depend. 80−47481
^{73}As bound and isobaric analogue states, spectroscopic factors, DWBA anal. of ^{72}Ge(^{3}He,d) 79−54391
^{197}Au+^{63}Cu, mass exchange and ang. distrib., dynamical treatment 77−61454
^{197}Au(^{16}O,X), colliding heavy ion interface, nucleon emission, fusion and strongly damped collisions 80−86922
^{197}Au(^{20}Ne, spallation), 8.0 GeV, cross sections and target residues, model comparison 80−68630
^{197}Au(^{6}Li, X), 75 MeV, Z=1 or 2 fast particle prod. mechanism above Coulomb barrier 80−42687
^{197}Au(α,α'), 120 MeV, isoscalar resonance excitation, low lying transitions, DWBA calc. 80−512
^{197}Au(d,pX), 80 MeV, inclusive proton spectra, d break-up, DWBA anal. 80−91190
α-particle transfer spectroscopic factors using interacting boson approx., A=44 to 68 78−78258
^{8}B β^+-decay, β-α angular correlations, final state energy depend., current test 80−102151
^{10}B levels and differential cross sections PWBA and coupled channel anal. of (α,t) 80−102121
^{10}B+^{10}B, fusion below Coulomb barrier, quantum mechanical barrier penetration model anal. 80−18361
^{10}B(d,p)^{11}B, 2.5 to 21.0 MeV, angular distrib., DWBA analysis 80−68675
^{10}B(p,π^+), 320-605 MeV, cross sections, pion exchange model anal. 80−27676
^{10}B(p,π), microscopic model anal., stripping model test for (d,p) 79−85436
^{10}B(t,d)^{11}B, 5.5 MeV, angular distrib., DWBA analysis 80−68675
^{11}B states, spectroscopic factors from DWBA anal. of ^{12}C(p,2p) 80−5057
^{11}B+^{10,11}B, fusion below Coulomb barrier, quantum mechanical barrier penetration model anal. 80−18361
nuclear reaction and scattering theory continued
^{11}B+d→3αn, 3.75 MeV, sequential decay reaction mechanism from ang. distrib. anal. 79−6631
^{11}B+p→3α and ^{10}B+d→3α reaction mechanisms, sequential decay and many-body theory 77−6362
^{12}B levels, J$^\pi$ and diff. cross sections, R-matrix anal. of ^{11}B(n,n) 80−78151
^{12}B polarisation, quantum mechanical explanation for ^{100}Mo(^{14}N,^{12}B) 79−17890
^{A}Ba, A=132, 134, 136, negative parity states, J$^\pi$, transitions, DWBA anal. of Ba(p, t) 80−86810
^{138}Ba(γ,π^-xn)La, 150-300 MeV, pion production cross sections calc. 80−9287
(^{9}Be,^{8}Be) Coulomb break up mechanism 79−36257
^{9}Be, π^+ electroprod., distorted wave impulse approx. anal. 79−17894
^{9}Be+^{4}He, microscopic ion-ion spin-orbit pot. 78−17163
^{9}Be(^{10}B,^{10}B), 9.5-14.2 MeV, ang. distribs., cross sections, elastic p transfer 80−78318
^{9}Be(d,d'), 12.8 MeV, two stage mechanism described by square Feynman diagrams *(Russian)* 79−22299
^{9}Be(e,π^+), 1848 MeV, virtual photon spectrum, virtual photon theory test 80−102183
^{9}Be(γ,π^+), 100-800 MeV, cross section, surface prod. model anal. 80−47466
^{9}Be(γ,π^+), threshold to 175 MeV, total cross sections, DWIA anal. 80−13459
^{9}Be(n,n), cross sections and polarisation from Lane model anal., multi-channel constraints 79−80914
^{9}Be(p,n), cross sections and polarisation from Lane model anal., multi-channel constraints 79−80914
^{9}Be(p,p'), 6.4 MeV, two stage mechanism described by square Feynman diagrams *(Russian)* 79−22299
^{9}Be(p,p), cross sections and polarisation from Lane model anal., multi-channel constraints 79−80914
^{9}Be(p,p) polarisation behaviour near (p,n) threshold, virtual scatt. mechanism feasibility 79−6592
^{9}Be(p,π^+), 320-605 MeV, cross sections, pion exchange model anal. 80−27676
^{10}Be levels and differential cross sections DWBA and coupled channel anal. of (α, ^{3}He) 80−102121
Bi+Xe, 1.13 GeV, deep inelastic nuclear reaction, electronic 1sσ vacancy prod., compound nucleus 80−27662
Bi(Kr,X), strongly damped collisions, classical dynamical model with shape deformation 80−27658
Bi(Xe,X), strongly damped collisions, classical dynamical model with shape deformation 80−27658
^{201}Bi (α,f), 23-140 MeV, l_{crit} from fragment ang. distribs. anal. 80−106087
^{209}Bi low lying levels and spectroscopic factors, EFR-DWBA anal. of ^{208}Pb(^{7}Li, ^{6}He) 80−32182
^{209}Bi single particle levels, ang. distribs., spectroscopic factors, DWBA anal. of ^{208}Pb(^{7}Li,^{6}Me) 80−63067
^{209}Bi(^{136}Xe,X), 940 MeV bombarding energy depend., fragment deformation, sequential fision 80−86938
^{209}Bi(^{56}Fe,X), damped collisions, fast A/Z equilibration and correlated nucleon exchange 80−86798
^{209}Bi(X,Y)^{210}Po, ^{211}At, X=^{14}N, ^{16}O, ^{19}F, ^{40}Ar, ^{40}Ca, ^{56}Fe, ^{63}Cu, 1 and 2 p transfer reactions, determ. transfer prob. 79−36274
^{209}Bi(α,^{3}He), 172.5, 140 MeV, plane wave spectator model anal. n momentum distrib. in α 79−54445
^{209}Bi(α,X), 69.2, 140 MeV, scatt. and fission reaction mechanisms, cross sections 80−18350
^{209}Bi(α,α'), 120 MeV, isoscalar resonance excitation, low lying transitions, DWBA calc. 80−512
^{209}Bi(γ,f), 40-65 MeV, absolute total photofission cross section, compound nucleus form. 80−86934
^{209}Bi(n,n), 50, 100, 200 MeV, eikonal scatt. by complex pots., cross sections 80−27643
Bi(d,d), 4.3, 6.3, 8.9 GeV/c, secondary momentum spectra, multiple scatt. model anal. *(Russian)* 80−27650
^{77}Br, level struct., l-transfers, spectroscopic factors, DWBA anal. from ^{76}Se(^{3}He,d), 41 MeV 78−86479
^{79}Br, level struct., l-transfers, spectroscopic factors, DWBA anal. from ^{78}Se(^{3}He,d), 41 MeV 78−86479
^{80}Br level struct. and transitions, DWBA anal. spectroscopic factors from ^{81}Br(p,d), 22.8 MeV 79−3084
(C, π^-X), 800 MeV/A, π^- energy and ang. distribs., firestreak and hard scatt. model anal. 80−13498
C (C,C), 800 MeV/N, high momentum nucleons from relativistic nuclear collisions, hard scatt. mechanism 79−40950
C(K$^\pm$,K$^\pm$) intermediate energy, forward scatt. amplitudes, Glauber model calcs. 79−30856
^{2}C(K$^\pm$,K$^{\pm\prime}$), 300-800 MeV, microscopic particle-hole shell model calcs., DWIA anal. 79−59091
^{A}C(p,p), A=12, 13, 0.8 GeV, elastic and inelastic, ang. distribs., states, optical and DWBA anal. 79−3154
^{12}C 2$^+$ (4.43 MeV) state, transition DWA anal. from (p,p') and (e,e') 79−67704
^{12}C (α,α), ang. distrib., microscopic anal., Pauli principle, excitation effects 78−33198
^{12}C α-decay, (d,d') excited, 4π ang. pattern meas., DWBA anal. 79−67720
^{12}C, α-transfer spectroscopic factors for O$^+$, 2$^+$ and 4$^+$ states, transitions from (d, ^{6}Li) 80−13370
^{12}C deduced levels and spectroscopic factors, ang. distribs., DWBA anal. from ^{16}O(d,^{6}Li) 80 MeV 78−94013
^{12}C, excitation cross sections induced by 1 GeV protons and electrons, Glauber theory *(Russian)* 78−41684
^{12}C, proton total cross section, 0.15 to 1 GeV, α-particle model and Glauber multiple scatt. theory 77−18538
^{12}C, π^+ electroprod., distorted wave impulse approx. anal. 79−17894
^{12}C+^{10,11}B, fusion below Coulomb barrier, quantum mechanical barrier penetration model anal. 80−18361
^{12}C+^{12}C, 250-1000 MeV/N, intranuclear cascade calcs. for multiplicity and cross sections 80−32300
^{12}C+^{12}C system, dynamical struct. change during scatt. process and mol. resonances 79−13321
^{12}C+^{12}C system, microscopic nuclear pots., elastic and inelastic channels 79−6654
^{12}C+^{12}C system, nuclear molecule microscopic description, HF and coupled channel calcs. 80−13493

nuclear reaction and scattering theory continued

$^{12}C+^{13}C$, identical core neutron transfer, coupled channel anal., form factors 79−13319
$^{12}C+^{16}O$ inelastic scatt., microscopic coupled channel calc. 78−625
$^{12}C+^{16}O$ inelastic scatt., microscopic R-matrix method anal. 79−6656
$^{12}C+^{16}O$ multichannel scatt., microscopic calcs. in generator coordinate method, spin assignments 79−564
$^{12}C+^{16}O$ system, ang. mom. projected microscopic calc. 77−14148
$^{12}C+^{6}Li(^{16}O)$ scatt., anomalous backscatt. from nonlinear Schrodinger eqn. for nuclear matter 79−6465
$^{12}C+^{6}Li\rightarrow^{4}He+^{2}H+^{12}C$, three body phase space distribs. 80−37393
$^{12}C+\gamma\rightarrow 3\alpha$, photodisintegration theory using 3α model and hyperspherical functions *(Russian)* 78−78365
$^{12}C+n$, matrix and shell model unification 78−54699
$^{12}C+\pi^-$, 40 GeV/c, effect of nucl. transparency *(Russian)* 78−54805
$^{12}C+\pi^-$, multiple scattering theory with separate treatment of proton and neutron 79−45301
$^{12}C(^{12}C,\ ^{12}C)$, shape resonance energy and widths, projection operator method 80−78255
$^{12}C(^{12}C,\gamma)$, 11.8-20.0 MeV, total cross section resonant and average behaviour 80−106069
$^{12}C(^{12}C,^{12}C')$, gross struct., barrier top resonance model calc. 80−9279
$^{12}C(^{12}C,^{12}C')$, intermediate resonance, coupled channels calcs. 80−42611
$^{12}C(^{12}C,^{12}C)$, 10-30 MeV, projection operator method, Feshbach doorways, intermediate structure 80−68695
$^{12}C(^{12}C,^{12}C)$, 10-30 MeV, molecular structure, projection operator anal., differential cross sections 80−106033
$^{12}C(^{12}C,^{12}C)$, 35-63 MeV, elastic and inelastic, cross sections, DWBA and optical anal. 79−93656
$^{12}C(^{12}C,^{12}C)$, 6-30 MeV, intermediate struct. from band crossing model, molecular resonances 79−54425
$^{12}C(^{12}C,^{12}C)$, elastic scatt., incoming wave boundary condition model calcs. 80−47504
$^{12}C(^{12}C,X)$ 93.8 MeV, $X=^{11}C,^{11}B,^{10}B$, ang. distribs. and cross sections, DWBA anal. 79−93657
$^{12}C(^{12}C,X)$ fusion cross section oscillations, overlapping compound states availability 80−9321
$^{12}C(^{12}C,\alpha)^{20}Ne$, 45 to 52 MeV, reaction mechanism, ang. momentum effects 77−38295
$^{12}C(^{12}C,p)X$, 800 MeV/N, fireball and preequilibrium cross sections, π condensation proximity influence 80−27659
$^{12}C(^{14}N,\ ^{12}C)^{14}N$, 79 and 155 MeV, DWBA calcs., recoil and sequential transfer effects 78−46090
$^{12}C(^{14}N,^{13}N)^{13}C$, 100 MeV, exact finite range CCBA anal. 79−17926
$^{12}C(^{14}N,^{13}N)^{13}C$ at high energies, simplified DWBA anal. 79−93643
$^{12}C(^{3}He,^{3}He')$, 18, 20, 24.5 MeV, differential cross sections, DWBA anal. 79−6647
$^{12}C(^{3}He,^{3}He')$, spin-flip transitions, microscopic α-spectator model 77−79400
$^{12}C(^{3}He,d)$, spectral line shape anal. 78−25203
$^{12}C(^{40}Ar,X)$, 213 MeV/N, relativistic fragmentation, microscope and macroscopic calcs., np correlation 80−13495
$^{12}C(^{40}Ca,^{46}Ca)$, 90° and 180° excitation functions energy depend., DWBA anal. 80−42582
$^{12}C(^{6}Li,^{6}Li')$, spin-flip transitions, microscopic α-spectator model 77−79400
$^{12}C(^{6}Li,d)^{16}O^*$, 18-28 MeV, configuration mixing effect and cross sections, zero range DWBA 80−42692
$^{12}C(^{6}Li,d)^{16}O\rightarrow^{12}C+\alpha$, reaction mechanism from ang. correlations, direct transfer 80−78319
$^{12}C(^{7}Li,\ ^{7}Li)$, 40 MeV, spectroscopic factors, DWBA anal. 79−75904
$^{12}C(K^-,\pi^-)_\Lambda{}^{12}C^*$, 800 MeV/c, ang. distribs. from DWIA calcs. 80−32225
$^{12}C(K^\pm,K^\pm)$, 100-1000 MeV, differential and total cross sections, nucleon motion 80−102206
$^{12}C(\alpha,\ \alpha)$, 1.37 GeV, elastic and inelastic, Glauber multiple scatt. theory 79−3161
$^{12}C(\alpha,\alpha)$, 1.37 GeV, S-matrix expansion from Glauber multiple scatt. theory 80−91191
$^{12}C(\alpha,\alpha)^{12}C$, elastic and inelastic, 1.37 GeV, multiple diffr. model, eikonalised DWIA 77−34326
$^{12}C(\alpha,\gamma)^{16}O$ cross-section, K-matrix parametrisation 77−6411
$^{12}C(d,\alpha)^{10}B(1.74\ MeV,\ T=1)$, coupled channel anal. of energy depend. isospin violation 78−70541
$^{12}C(d,d')$, spin-flip transitions, microscopic α-spectator model 77−79400
$^{12}C(d,d)$, 1.69 GeV/c, Coulomb interference region, Glauber theory anal. 80−99178
$^{12}C(d,d)$, 650 MeV, Glauber theory approx. anal. using realistic deuteron wave functions 77−46176
$^{12}C(d,d)$, 650 MeV, Glauber model calcs. for cross sections 79−13306
$^{12}C(d,n)$, spectral line shape anal. 78−25203
$^{12}C(e,\ e'p)$, eN interaction in quasifree scatt., nonrelativistic Hamiltonian through 4th order 80−47469
$^{12}C(e,e'P)^{11}B$, nonorthogonality of initial and final nucl. states *(Russian)* 78−66265
$^{12}C(e,e'p)$, 700 MeV, DWIA anal. proton spectral function 77−6353
$^{12}C(e,e'p)$, cross sections from DWIA, optical, and shell model calcs. *(Russian)* 80−32270
$^{12}C(e,e'p)^{11}B$, validity of the factorised DWIA 79−59054
$^{12}C(e,e'\pi^+)^{12}B$, near threshold, equivalent photon approx., Kroll-Ruderman term 78−13065
$^{12}C(e,e)$, electroexcitation cross sections, incoherent superposition of single nucleon processes 80−32269
$^{12}C(e,e\pi)$, total cross section from square reaction matrix element *(Russian)* 80−32271
$^{12}C(ee'd)$, electroproduction cross section, Born approx. *(Russian)* 79−26427
$^{12}C(\gamma,\pi^-)$, 160-250 MeV, total cross section from elementary Hamiltonian model 80−18292
$^{12}C(\gamma,\pi^-)$, total cross section calc. in impulse approx. 80−13458
$^{12}C(\gamma,\pi^-p)$, final state interaction, distorted and plane wave momentum distribs. 80−78275
$^{12}C(\gamma,\pi^+)^{12}C$, up to 175 MeV, total cross sections, DWIA anal. 79−59049
$^{12}C(n,n)$, 15 to 18 MeV, resonance effects 77−30591
$^{12}C(n,n)$, (in)elastic scatt. cross sections, duration of collision process *(Russian)* 79−80942
$^{12}C(p,X)$, reaction and scatt. dynamics, optical and coupled channel anal. 80−78297
$^{12}C(p,2p)$, 400 MeV, DWIA check using quasifree (p,pn) comparison 79−93621

nuclear reaction and scattering theory continued

$^{12}C(p,2p)$, asymmetric energy-sharing mode, half distorted-wave formalism, intermediate giant resonance 80−68656
$^{12}C(p,\alpha)$, 45.2 MeV, cross sections, finite range DWBA anal., cluster form factors 80−68666
$^{12}C(p,n)$, 144 MeV, charge exchange, one pion exchange and PCAC tests 80−78299
$^{12}C(p,p')$, 0.8 GeV, polarised p, spin orbit deformation effects, DWBA anal. 79−30832
$^{12}C(p,p')$, 122 MeV, level excitation, cross sections, effective NN interaction, DWIA anal. 80−78197
$^{12}C(p,p')$, 22-27 MeV, 1^+ state de-excitation γ-ray ang. distrib., tensor force effects, DWBA anal. 80−68580
$^{12}C(p,p')$, 64 MeV, direct reaction, model t-matrix test, cross section and anal. power 79−93594
$^{12}C(p,p')$, 800 MeV, multistep processes, ang. distribs., Glauber model anal. 80−47475
$^{12}C(p,p')$, non-eikonal effects in high energy inelastic scatt. 80−42608
$^{12}C(p,p')^{12}C$, PWIA anal. and bound-state momentum distribs. 78−601
$^{12}C(p,p'\gamma)$, 23.5-27 MeV, 1^+ state spin flip meas. DWBA anal., cross sections 80−68529
$^{12}C(p,p')$, 20-40 MeV, pol. p, anal. powers, imaginary spin-orbit pot., coupled channels anal. 80−102179
$^{12}C(p,p')$, polarised p, 20, 30, 40 MeV, anal. power and cross sections, spin-orbit deformation 79−75963
$^{12}C(p,p)$, below 8 MeV, iterative R-matrix in collective rot. model, phase shifts, inelasticity 79−3141
$^{12}C(p,p)$, pol. p, 14.23 MeV resonance broadening, nuclear recoil, atomic excitation effects 80−102165
$^{12}C(p,p)$, pol. p, 450-600 keV, Mott-Schwinger interaction existence, anal. power 80−22805
$^{12}C(p,p)$ dispersive effects in ground state rot. band excitation, coupled channel calcs. 79−40828
$^{12}C(p,p)$ spin 0-spin 1/2 phase shift anal. discrete ambiguities 80−18307
$^{12}C(p,p\gamma)$, bremsstrahlung cross section near 1.7 MeV resonance, Feshbach-Yennie approx. 80−42662
$^{12}C(p,pn)$, pol. nucleon quasi-elastic scatt., nuclear wave function and model tests 80−42656
$^{12}C(p,\pi^+)^{13}C$, relativistic pion stripping formalism 78−41717
$^{12}C(\pi,\ \pi)$ elastic and inelastic, nonstatic effects in isobar doorway model 79−80955
$^{12}C(\pi,X)$, Kalinkin-Shmonin model, expt. data 80−86931
$^{12}C(\pi,\gamma)$, photon spectrum from generalised Helm model 79−76023
$^{12}C(\pi,\pi')$, A* excitation, A* model unified description 80−102205
$^{12}C(\pi,\pi)$, 260, 280 MeV, elastic and inelastic differential cross sections from Glauber theory *(Chinese)* 79−59092
$^{12}C(\pi,\pi)$, 260 MeV, short range correlations from Glauber multiple diffraction theory *(Chinese)* 80−102210
$^{12}C(\pi,\pi)$, elastic and inelastic, recoil effects 79−85555
$^{12}C(\pi,\pi)$ cross section calc., comparison of factorisation approx. taking account of nucleon Fermi motion 78−29497
$^{12}C(\pi,\pi)$ elastic scatt., π^+,π^- diffr. minima differences 77−61459
$^{12}C(\pi^-,2\gamma)$, doubly radiative capture theory, branching ratio and ang. correlations 80−9314
$^{12}C(\pi^-,\pi^-)$, 40 GeV, semi-coherent elastic scatt., angular distrib. 80−68701
$^{12}C(\pi^-,\pi^\pm)X$, 40 GeV, multiparticle prod. mechanism, various model predictions 79−573
$^{12}C(\pi^+,\ \pi^+p)$, 100, 180 MeV, knock out reaction, cross section and pion distortion in DWIA 80−91167
$^{12}C(\pi^+,\pi^+)$, 49.9 MeV, differential cross sections, partial wave and optical model anal. 79−22333
$^{12}C(\pi^+,\pi^+)$, elast. and inelast. scatt., 50 MeV, ang. distrib. determ. optical model and DWBA 79−45304
$^{12}C(\pi^+d)$, DWBA cross section formula, PWBA differential cross section *(Chinese)* 80−22861
$^{12}C(\pi^\pm,\ \pi^\pm N)$, 291 MeV, quasielastic scatt., differential cross sections, Monte-Carlo data fit 80−68703
$^{12}C(\pi^\pm,\ \pi^\pm)$, model Coulomb corrections in eikonal 80−5171
$^{12}C(\pi^\pm,\pi^\pm N)$, 180-255 MeV, quasielastic pion scatt. coincidence expt. interpretation, impulse approx. 80−68704
^{13}C spectroscopic factors, cross sections DWBA anal. optical model parameters from $^{12}C(^{16}O,X)$ 80−13371
$^{13}C+^{13}C$, appl. of molecular particle core model 78−82384
$^{13}C+^{60}Ni$, one nucleon transfer, nuclear and Coulomb components 77−34340
$^{13}C+^{94}Mo$, one nucleon transfer, nuclear and Coulomb components 77−34340
$^{13}C(^{12}C,^{12}C)$, mixed parity neutron orbits, coupled channel theory with adiabatic assumption 80−9304
$^{13}C(^{12}C,^{12}C)$, molecular neutron orbit formation, $1/2^+$ state excitation, coupled channels calcs. 80−78156
$^{13}C(^{12}C,^{12}C)$ 15, 87 MeV, elastic transfer exchange amplitude, coupled reaction channel and DWBA calcs. 80−32298
$^{13}C(^{16}O,\ ^{17}O)^{12}C$, non-orthogonality of channel states 80−83115
$^{13}C(^{6}Li,\ ^{6}Li)$, 40 MeV, spectroscopic factors, DWBA anal. 79−75904
$^{13}C(^{9}Be,X)$, 11.6 MeV, p,t,d,α, ^{8}Be ang. distribs., Hauser-Feshbach and DWBA anals. 80−91193
$^{13}C(\alpha,\alpha')$, 22, 36 MeV, resonant state line shapes 80−91148
$^{13}C(d,X)$, 13 MeV, cross section, vector and power, optical model parameters, DWBA anal. 79−22301
$^{13}C(d,d')$, 12.8 MeV, two stage mechanism described by square Feynman diagrams *(Russian)* 79−22299
$^{13}C(p,\alpha)^{10}B_{g.s.}$, 65 MeV, pol. p, DWBA form factor 80−52559
$^{13}C(p,d)$, 800 MeV, cross sections, DWBA anal. 80−42667
$^{13}C(p,d)$ modified DWBA anal., optical model parameter influence on vertex consts. *(Russian)* 78−78340
$^{13}C(p,p)$, 9.1-18.4 MeV, polarised p, cross section phase-shift anal., ^{14}N possible resonances 79−6602
$^{13}C(\pi^+,\ \pi^{+or0})$, 120-226 MeV, inelastic scatt, and charge exchange, coupled channels calcs. 80−57804
$^{13}C(\pi^+,\pi^0)^{13}N$, 70-230 MeV, calc. of cross section, using multistep contributions within modified eikonal formalism 78−21609
$^{13}C(\pi^+,\pi^0)^{13}N$, two-body correlation effects 77−88178
$^{13}C(\pi^+,\pi^0)^{13}N_{g.s.}$, (3,3) resonance region, importance of two-step processes in multiple scatt. treatment 77−6464
^{14}C proton shell closure, p transition spectroscopic factors, DWBA calcs. for $(^3He,d)$, $(t,^3He)$ 79−80871
^{14}C spectroscopic factors, cross sections DWBA anal. optical model parameters from $^{12}C(^{16}O,X)$ 80−13371
$^{14}C(^{16}O,^{18}O)^{12}C$, full recoil one and two step DWBA anal. 78−70564

nuclear reaction and scattering theory continued
^{14}C(^{6}Li,^{6}He), 62 MeV, Gamow-Teller sum rules and ground state wave function 80−106073
^{14}C(^{7}Li,t)^{18}O, 20.4 MeV, FRDWBA anal. 78−82381
^{16}C mass excess and final states, DWBA anal. of ^{14}C(t,p) 23 MeV 78−78392
(^{12,13}C,X) elastic, inelastic and single nucleon transfer excitation functions optical and DWBA anal. 80−13492
Ca+Ca, classical many-body model for heavy ion collisions 80−536
Ca(Ca,X), 400 MeV, classical eqns. of motion calcs., central collisions, thermal models 80−106070
^{A}Ca(α,α'), 24,29 MeV, A=40,42,44,48 backward ang. distrib. anomaly, coupled and channel anal. 80−86911
^{A}Ca(α,α'), A=40, 42, 44, 1.37 GeV, low lying state ang. distribs., Glauber rigid body approx. 79−54394
^{A}Ca(p,p'), pol. p, A=40,48, 800 MeV, diff. cross sections, anal. powers, DWIA anals., high spin levels 80−83067
^{A}Ca(p,p), 0.6, 1 GeV, A=40,42,44,48, matter density, Glauber model anal. 79−93500
^{A}Ca($\pi^{\pm}$, $\pi^{\pm}$N), A=40, 44, 48, 291 MeV, quasielastic scatt., differential cross sections, Monte-Carlo data fit 80−68703
^{40}Ca ($\pi^{\pm}$, $\pi^{\pm}$), model Coulomb corrections in eikonal 80−5171
^{40}Ca α-spectroscopic factors, direct α-stripping, zero range DWBA anal. of ^{36}Ar(^{6}Li,d) 79−45157
^{40}Ca composite system, heavy ion resonances from ^{24}Mg+^{16}O, ^{28}Si+^{13}C 80−86874
^{40}Ca+^{13}C, microscopic ion-ion spin-orbit pot. 78−17163
^{40}Ca+^{20}Ne, 36-95 MeV, Coulomb-nuclear interference 78−50210
^{40}Ca+^{40}Ca, 3D TDHF calcs. 78−626
^{40}Ca(^{11}B,^{10}B), 51.5 MeV, n stripping, DWBA anal. with Woods-Saxon and double folding optical pots. 80−102171
^{40}Ca(^{11}B,^{12}C), 32, 68 MeV, single proton pickup, DWBA anal., optical pot. 80−106037
^{40}Ca(^{11}B,^{12}C), 51.5 MeV, p pickup, DWBA anal. with Woods-Saxon and double folding optical pots. 80−102171
^{40}Ca(^{13}C, ^{14}N)^{39}K and ^{40}Ca (^{13}C, ^{12}C)^{41}Ca, 60, 68 MeV, spin depend. effects 78−66300
^{40}Ca(^{13}C,^{14}N), 40, 68 MeV, single proton pickup, DWBA anal., optical pot. 80−106037
^{40}Ca(^{13}C,^{14}N), 50 MeV, L=1 proton pickup, ^{39}K $s_{1/2}$ and $d_{3/2}$ states, DWBA anal. 79−67734
^{40}Ca(^{13}C,^{14}N)^{39}K(3/2^{+}), CCBA fit to anomalous ang. distrib. 77−38297
^{40}Ca(^{14,15}N,^{15,16}O), 70 MeV, L=1 proton pickup, ^{39}K $s_{1/2}$ and $d_{3/2}$ states, DWBA anal. 79−67734
^{40}Ca(^{16}O,^{15}N)^{41}Sc, DWBA anal. including nuclear wave function polarisation 78−629
^{40}Ca(^{16}O,^{16}O), optical pot., nuclear matter approach, energy density matter [-] 80−83112
^{40}Ca(^{16}O,X), ion-ion interaction pot., imaginary part, effective interaction 80−68692
^{40}Ca(^{40}Ca, X), 10 MeV/N, charged particle emission Q-valve depend. 80−47503
^{40}Ca(^{40}Ca,^{40}Ca), optical pot., nuclear matter approach, energy density matter [-] 80−83112
^{40}Ca(^{7}Li,^{7}Be)^{40}K, charge exchange microscopic DWBA anal. 79−26453
^{40}Ca(^{9}Be, ^{9}Be'), 45, 60 MeV, low lying collective states, ang. distribs., DWBA double folding pot. anal. 80−78113
^{40}Ca(^{9}Be,^{9}Be'), 45, 60 MeV, 1^{-} state excitation Frahn scaling formula for cross section 80−102136
^{40}Ca(N,N), microscopic description validity 79−544
^{40}Ca(α,α), 1.37 GeV, S-matrix expansion from Glauber multiple scatt. theory 80−91191
^{40}Ca(α,αp), 96.8 MeV proton pickup by α-particles to unbound states DWBA anal. 79−22305
^{40}Ca(e,e'), quasi-elastic scatt., scaling law test, knockout process contribution 79−22274
^{40}Ca(μ,γ), photon asymmetry, O(1/m^{2}) and nuclear effects 80−78219
^{40}Ca(n,X), local approximation to a non-local potential 80−91182
^{40}Ca(p, 2p)^{39}K, 148.2 MeV, factorisation approx., energy states of ^{39}K, DWIA calcs. 78−62535
^{40}Ca(p,p'), giant resonances from antisymmetrised DWBA anal. 79−85432
^{40}Ca(p,p'), realistic complex nuclear matter t-matrix anal. Hamada-Johnston pot. 79−9564
^{40}Ca(p,π^{+})^{41}Ca, relativistic pion stripping formalism 78−41717
^{40}Ca(p,p'), DWIA test in Glauber theory, transition density 80−99173
^{40}Ca(t,p), centre of mass corrections to DWBA overlap factors 80−18319
^{40}Ca(t,p)^{42}Ca, form factors for two-nucleon stripping process wth Skyrme potentials, DWBA 78−58287
^{42}Ca(p,t) form factor, hole and continuum contribs. for pick-up reactions 80−78256
^{47}Ca high spin states through double step processes, CCBA calcs. from ^{48}Ca(^{3}He,α) 78−89797
^{48}Ca+^{3}He, 82 MeV, cross sections, (^{3}He,t) DWBA anal. 79−13310
^{48}Ca(^{16}O, ^{14}C), two nucleon sequential transfer, on-shell anal., cross sections 80−99180
^{48}Ca(^{16}O, ^{15}N), ^{15}N excitation contrib. in optical pot., DWBA grazing peak shift 80−86921
^{48}Ca(^{16}O,^{14}C)^{50}Ti, full recoil one and two step DWBA anal. 78−70564
^{48}Ca(^{16}O,^{16}O), nuclear and Coulomb components to scatt. amplitude 77−34340
^{48}Ca(^{18}O, ^{16}O), two nucleon sequential transfer, on-shell anal., cross sections 80−99180
^{48}Ca(^{18}O,^{16}O) 50 MeV, cross sections, DWBA multipole expansion calcs., form factors 79−13325
^{48}Ca(^{3}He,t), 66, 70 MeV, reaction mech. and and ^{48}Sc Gamow-Teller strength, ang. distribs. 80−42589
^{48}Ca(^{3}He,t), finite-range formalism anal. of (^{3}He,α) (α,t) sequence 78−17229
^{48}Ca(^{3}He,t)^{48}Sc, 23 MeV, finite range effects and nonorthogonality corrections in two-step processes 79−3162
^{48}Ca(p,p), 1 GeV, elastic scatt. differential cross section calc. 80−47480
^{48}Ca(p,t), (p,^{3}He)(^{3}He,t) two step process calcs., two step cross section 79−36245
^{48}Ca(t,p), exact finite range DWBA calcs., realistic triton and nuclear wave functions 80−63191
^{98}Ca(^{16}O,^{15}C), simple unitary estimate for multistep processes, cross section bounds 79−40922

nuclear reaction and scattering theory continued
C(d,d), 4.3, 6.3, 8.9 GeV/c, secondary momentum spectra, multiple scatt. model anal. *(Russian)* 80−27650
^{114}Cd(p,p'), 11 MeV, polarised p, differential cross sections, anal. powers, spin flip prob. 79−89284
^{116}Cd(^{3}He,n), second order processes in DWBA calcs. 78−46076
^{141}Ce levels, single neutron holes, spectroscopic factors, DWBA anal. of ^{142}Ce(d,t), (^{3}He,α) 79−85353
Ce(p,p') and Ce(p,t), DWBA anal., ^{138,140}Ce levels, spectroscopic factors 77−54217
^{252}Cf scission point configuration, α-ang. distrib., trajectory calcs. for LRA fission 80−83134
^{252}Cf, spontaneous ternary fission scission config. from trajectory calcs., Monte Carlo calcs. 79−6718
Cl(Ar,X), proton inclusive spectra, direct plus thermal model 80−57799
^{35}Cl+^{27}Al, deep inelastic fragment energies, rot. energy contributions 79−63697
^{A}Co, A=55,57,59,61, deduced levels, proton-hole states, semimicroscopic model from Ni(p,α) 79−45171
^{57}Co levels and analogue states, J$^{\pi}$ from DWBA anal. of ^{58}Ni(^{3}He, α) 79−63592
^{59}Co(α,xnyp), 20-172.5 MeV, cross sections excitation functions, hybrid model, preequilib. effects 80−57784
^{59}Co(e,e), magnetic e scatt., exchange current effects, plane wave Born approx. 80−78282
^{59}Co(n,2n) direct process contrib., cross section and secondary n spectrum *(Russian)* 78−78386
^{59}Co(p,X), 12-45 MeV, reaction cross section and hybrid model analysis 79−67749
^{60}Co, level struct., spectroscopic factors, DWBA anal. from ^{59}Co(d,p), 14 MeV 78−86478
C(p,π^{+}) 240 MeV inclusive pion production *(Russian)* 80−86908
C($\pi^{\pm}$, $\pi^{\pm}$X), X=He or d, 170 MeV, cross sections and ang. distribs., direct knockout mechanism *(Russian)* 80−86887
^{A}Cr(p,p), A=50, 52, 6 MeV, elastic and inelastic differential cross sections, spin flip probability *(Russian)* 80−91187
^{51}Cr levels, spectroscopic function and analogue states, PWBA anal. of ^{52}Cr(^{3}He,α) 80−68547
^{52}Cr(^{16,18}O,^{16,18}O'), 30-42 MeV, excitation function differences, optical and DWBA anals. 79−63698
^{52}Cr(d,p)^{53}Cr, Coulomb stripping, 2.12-2.48 MeV, DWBA anal., spectroscopic strengths 80−516
Cu (p,π^{+}) 240 MeV inclusive pion production *(Russian)* 80−86908
^{63}Cu levels and transition j-depend., DWBA anal. of ^{60}Ni(^{19}F, ^{16}O) 80−42542
^{63}Cu(p,p'), 40 MeV, octupole states, weak coupling model 79−93495
^{69}Cu mass excess and low lying states, DWBA anal. from ^{70}Zn(d,^{3}He) 79−6422
^{A}Dy(d,t), A=162, 164, coupled-channels Born approx. anal. 80−83104
^{A}Er(d,t), A=166, 168, coupled-channels Born approx. anal. 80−83104
^{166}Er+^{86}Kr, 5.99 MeV/N, angular-momentum dissipation in heavy-ion collisions 78−82376
^{166}Er+^{86}Kr, relaxation times in dissipative collisions, fragment deformation, classical model 79−30853
^{166}Er(e,e'), 35-350 MeV, coupled channels anal., rot. band excited states, charge densities 79−3139
^{167}Er(d,d'), 12.1 MeV, excitation of Nilsson states, Coriolis coupling 78−33190
^{A}Eu, A=144,148,150,152, ground and excited state analogues, two-phonon coupling effects from Sm(p,n) 79−89277
^{A}Eu(p,p'), A=151-3, 12 MeV, rot. states, deformation parameters, DWBA and coupled channel anal. 79−9459
^{151}Eu narrow band and pickup strength, shape coexistence from (d,t) 80−86799
^{153}Eu 5/2^{+} ground state rot. band, J$^{\pi}$, shape coexistence from (d,p) 80−86799
^{154}Eu(p,p'), 12 MeV, ground band rot. states, deformation parameters, coupled channels anal. 80−9195
^{18}F (e,e'), polarised e, parity mixing and form factors from elementary particle theory anal. 79−89233
^{18}F levels and resonances, cross sections in R-matrix formalism from ^{17}O(p,α) 80−18267
^{18}F resonances, α-widths, isospin and parity mixing, R-matrix anal. of ^{14}N(α,α) 80−91162
^{19}F level struct., ang. distribs. anal. using DWBA of ^{17}O(^{3}He,p) 80−9232
^{19}F levels, resonances and phase shifts, resonating group calcs. from ^{15}N(α,α) 80−32189
^{19}F(α,αp), 140 MeV, quasifree p knockout, spectroscopic factors, DWIA anal. 79−67650
^{19}F(d,X), X=^{7}Li, ^{7}Be, 13.6 MeV, diff. cross sections, ^{5}He cluster direct transfer *(Russian)* 80−52650
^{19}F(p,γ)^{20}Ne, giant multipole reson., microscopic theory 77−22987
^{19}F(p,p), 17.5 and 30 MeV, low lying level cross-sections, coupled-channel method 80−42649
Fe induced heavy ion reactions, 1.7 A GeV, props. of participants and spectators in non-peripheral reactions 79−49636
^{A}Fe(^{16}O, ^{12}C), 50 MeV, a=54, 56, 58, α-spectroscopic factors, DWBA anal., (^{6}Li, d) comparison 79−63585
^{A}Fe(p,X), A=54, 56, 57, 58, 12-45 MeV, reaction cross section and hybrid model analysis 79−67749
^{54}Fe(^{16,18}O,^{16,18}O'), 30-42 MeV, excitation function differences, optical and DWBA anals. 79−63698
^{54}Fe(^{3}He,p), ^{56}Co particle-hole states, T=1, zero DWBA anal. 80−78308
^{54}Fe(^{6}Li,^{6}Li), 38, 44, 50 MeV, elastic and inelastic scatt., optical model anal. and inelastic scatt. deformation lengths 79−59082
^{54}Fe(^{7}Li,^{7}Li), 36, 42, 48, MeV, elastic and inelastic scatt., optical model anal. and inelastic scatt. deformation lengths 79−59082
^{54}Fe(α,α'), coupled channels calc., capture cross section, GQR decay modes 80−27654
^{54}Fe(n,2n) direct process contrib., cross section, DWTA and DWBA anal. *(Russian)* 78−78386
^{54}Fe(p,d)^{53}Fe, 40 MeV spectroscopic factors, ang. distrib., DWBA anal. 79−22287
^{54}Fe(p,p'), 39, 62 MeV, DWBA anal., collective spectra, direct process contrib. *(Russian)* 80−13408
^{54}Fe(p,p'), pol. p, 800 MeV, diff. cross sections, anal. powers, DWIA anals. 80−83067
^{54}Fe(p,p), 5.5-6.2 MeV, resonance effects, deformation, spectroscopic factors, statistical, optical and DWBA anal. 79−6593

nuclear reaction and scattering theory continued
^{55}Fe $2p_{3/2}$ neutron orbit radius isotone shift from DWBA anal. of ^{54}Fe(t,d) 80−32172
^{55}Fe(^{52}Cr, X), entrance channel mass asymmetry effects on reaction mechanism, fission and fusion 80−106077
^{56}Fe(^{6}Li, X), 75 MeV, Z=1 or 2 fast particle prod. mechanism above Coulomb barrier 80−42687
^{56}Fe(e,α), E2 isoscalar resonance sum rule, DWBA anal. 80−68621
^{56}Fe(e,e′), 0.1-14 GeV, deep inelastic inclusive scatt. response functions and momentum distrib. 80−42640
^{56}Fe(n,2n), direct process contrib., cross section, DWTA and DWBA anal. *(Russian)* 78−78386
^{56}Fe(n,n′), 14 MeV, ang. distrib., reaction mechanism 77−26756
^{58}Fe levels, J^{π}, anal. powers and cross sections from ^{56}Fe(t,p) pol.t 80−68539
Fe(π^{+},π^{+}) elast. and inelast. scatt., 50 MeV, ang. distrib. determ. optical model and DWBA 79−45304
^{154}Gd levels, bands, J^{π}, DWBA anal. of ^{152}Gd(t,p) 80−78110
^{160}Gd(^{12}C, αxn)$^{168-x}$Er, particle fragmentation accompanied by incomplete fusion, two step model 80−86947
^{160}Gd(d,t) ^{159}Gd, coupled-channels Born approx. anal. 80−83104
Gd(d,d′), A=155, 157, 12.1 MeV, excitation of Nilsson states, Coriolis coupling 78−33190
^{A}Ge A=68,70,72,74, deformations and collective spectra, reaction mechanisms from Ge(p,t) 79−22168
^{A}Ge(^{16}O,^{16}O′), A=72, 74, 76, coupled channel anal. with double folding potential 79−45282
^{A}Ge(^{16}O,^{16}O), A=72, 74, 76, coupled channel anal. with double folding potential 79−45282
^{A}Ge(^{18}O,^{18}O), A=72, 74, 76, coupled channel anal. with double folding potential 79−45282
^{76}Ge levels, J^{π} assignments, shape transition DWBA anal. from ^{74}Ge(t,p) 79−17815
^{78}Ge level struct., J^{π} values from DWBA anal. of ^{76}Ge(t,p), 17 MeV 79−6417
^{78}Ge level struct., proposed nuclear shape transition, DWBA anal. from ^{77}Ge(t,p), 15 MeV 78−78266
^{1}H(D,2p)n, 26.5 MeV, 4 dimens. comparison with local S-wave interaction Faddeev calcs. 79−17866
^{1}H(d,d), 20 MeV, measurement on T_{21}, three nucleon Faddeev calc. comparison 79−71857
^{1}H(d,d), anal. power ang. distrib., d D-state asymptotic normalisation 79−36247
^{1}H(μ^{-},$\nu\gamma$), radiative capture relativistic calcs., rate and photon spectrum 80−68605
^{1}H(n,γ)^{2}H, relativistic invariant approach, parity violation 79−3147
^{1}H(n,γγ), cross-section calc. 77−6385
^{1}H(n,γγ), thermal, consistency between pion exchange currents and NN pot., cross sections 80−68556
^{1}H(n,n), 16.9 MeV, anal. power, F-wave contribs. 80−63158
^{1}H(n,n)p, 210-495 MeV, free elastic scatt., phase shift anal. 80−52676
^{1}H(n,p)n, pol. n,p, 50 MeV, spin correlation parameter $A_{yy}(\theta)$, phase shift anal. 80−68530
^{1}H(p,p), 6.141 MeV, anal. power, Paris pot. predictions 80−63156
^{1}H(p,p), pol.p, 9.57 MeV, spin correlation parameter, phase shift anal. 80−102112
^{1}H(p,π^{+})^{2}H, Low eqn. approx. soln., field theory propagator modification 79−85546
^{1}H(p,π^{+})^{2}H, NN pot., isobar configurations and π prod., inelastic cross sections 79−63666
^{1}H(π^{-},γγ)n, off-mass shell πN amplitude, $\pi^{0}\rightarrow\gamma\gamma$ amplitude, chiral Lagrangian model 79−93669
^{1}H(t,dn), 2.5 GeV/c, 4π geometry, pole approx. description 80−68678
^{2}H (π^{+}, π^{+}), low energies, Coulomb interaction *(Russian)* 80−83129
^{2}H breakup, new theorems concerning final state interactions *(Russian)* 77−326
^{2}H breakup induced by 22.7 MeV nucleons, calc. with separable interactions with tensor forces 77−18554
^{2}H ground state, N* configurations 77−18436
^{2}H, photonuclear sum rules and interaction effects, integrated cross-section determ. from double commutator 78−21542
^{2}H-N breakup calcs., separable interactions with P-waves and tensor forces, polarisation 77−50101
^{2}H+p, polarised projectile, parity nonconservation in low energy scatt. 78−70522
^{2}H+p(d), 6.3 GeV/c, inclusive spectra of fast p and d *(Russian)* 78−46075
^{2}H+π, coupled channel theory 78−13157
^{2}H+π, crossed pion absorpt. contrib. to scatt. length 77−10433
^{2}H(N,X) disintegration cross-section, cut-off radius in impulse approx. type models *(Russian)* 79−22276
^{2}H(α,α)^{2}H, three body calcs., Pade technique 78−46074
^{2}H(α,αn), quasi-elastic scatt., direct reaction unitarised impulse approx. 80−42674
^{2}H(α,αp), 140 MeV, quasifree p knockout, spectroscopic factors, DWIA anal. 79−67650
^{2}H(α,αp)n, 15 MeV, six-body effects, Faddeev anal. 79−76008
^{2}H(α,αp)n, 15-42 MeV, three body calc., reaction mech. 78−70546
^{2}H(α,αp)n, 42 MeV, observation and comparison to theoretical calcs. 77−82942
^{2}H(α,np)^{4}He, differential cross section and polarisation, three body model 80−47460
^{2}H(α,pα)n, 7.5-7.9 MeV, modified impulse approx. anal. 79−6648
^{2}H(d,N), 50-85 MeV, ang. distribs., PWBA anal. 79−76005
^{2}H(d,d), 50-85 MeV, ang. distribs., PWBA anal., two body final states 79−6636
^{2}H(d,d), 53, 63 GeV, inelastic intermediate state effects, Glauber multiple scatt. theory 79−36104
^{2}H(d,n), pol.d, anal. power and polarisations in R-matrix methodology, comparison with (d,p) 80−78273
^{2}H(d,p), pol.d, anal. power and polarisations in R-matrix methodology, comparison with (d,n) 80−78273
^{2}H(d,t)^{1}H, differential cross sections calc. using DWBA, distortions 78−54772
^{2}H(e,e′p), consistent nonrelativistic treatment including meson exchange currents and isobar configurations 79−40905
^{2}H(e,e), EM form factors, relativistic formulae, moment corrections 80−63075
^{2}H(e,e), EM interactions and mag. sum rules 80−42639
^{2}H(e,e), energy weighted sum rules, almost realistic NN pot. anal. *(Russian)* 80−13465

nuclear reaction and scattering theory continued
^{2}H(e,ne)^{1}H, meson exchange effects at quasi-elastic peak 77−30556
^{2}H(γ,η)^{2}H, impulse approx. calc. of elastic η photoproduction 77−14110
^{2}H(γ,n), forward angle cross section and sum rule from Siegert's theorem 79−80925
^{2}H(γ,n)p, cross section and polarisation with arbitrary number of EM multipoles 79−80923
^{2}H(γ,n)p, differential cross section and proton polarisation using supersoft core pot. 79−89287
^{2}H(γ,π^{0}), coherent photoprod., binding effects and threshold amplitude calc. 80−32264
^{2}H(γ,π^{0}), cross section and threshold effects using dynamical $\gamma N\rightarrow N\pi^{0}$ model 80−27627
^{2}H(γ,π^{+})2n cross section, threshold charged photopion prod. operator props. 79−89292
^{2}H(γ,π^{+})nn, n-n final state interaction effects 80−102181
^{2}H(γ,π), 210-700 MeV, total and differential cross sections from impulse approx. 80−68647
^{2}H(μ^{+},μ^{+})pn, Coulomb break-up amplitude in three-body scatt. theory 79−71844
^{2}H(μ^{+},μ^{+}np), ≤5 MeV, Coulomb break-up of deuteron and n-p off-shell effects 79−75777
^{2}H(n, np)n, 130 MeV, Faddeev eqn. multiple scatt. series anal. 79−97707
^{2}H(n,2n)p, inelastic scatt. mechanism at moderate energy *(Russian)* 78−41723
^{2}H(n,n), (n,p), 24 MeV, quasifree scatt., n-n effective range, Monte Carlo anal. 80−68554
^{2}H(n,n), ghost states and Pauli principle for many-body scatt. 79−76001
^{2}H(n,n), local soft core NN pots., quasiparticle formalism 79−6529
^{2}H(n,n), nonlocal nonsymmetric pot., treatment of Schrodinger eqn. 78−82325
^{2}H(n,n), quantum theory evolution law approach appl. *(Russian)* 79−80866
^{2}H(n,n), scattering in high-partial waves, on-shell theory 78−41565
^{2}H(n,n), virtual state in three nucleon system, partial wave dispersion relations 79−40920
^{2}H(n,np), at $\vartheta_{n}=0°$, collinearity effect 78−82356
^{2}H(n,p)2n, 13.98 Mev, proton spectra and n-n scatt. lengths 77−88141
^{2}H(n,pn)n, 22.7, 46.3 MeV, perturbation calcs. for realistic pots. 79−45265
^{2}H(p,2p)n, inelastic scatt. mechanism at moderate energy *(Russian)* 78−41723
^{2}H(p,2p)n, interference effects for const. NN relative energies 77−26774
^{2}H(p,γ) and ^{3}He(γ,pd) anal. using Reid soft-core pot. 77−26664
^{2}H(p,pX), 19 GeV/c, Thomas Reiche Kuhn sum rule appl., mean energy losses 80−91192
^{2}H(p,p), 600 MeV and 1 GeV, noneikonal theory 79−80930
^{2}H(p,p), back angle elastic cross sections in Kerman-Kisslinger model, inelasticity corrections 80−106060
^{2}H(p,p), Coulomb corrections near elastic threshold 77−34282
^{2}H(p,p), near threshold, on-shell two-body model 77−34283
^{2}H(p,p), tensor asymmetries, deuteron D-wave and non-eikonal effects, Glauber model 80−78296
^{2}H(p,p), theoretical anal. of nucleon-nucleon forces 79−9554
^{2}H(p,p) Glauber versus final state interaction theory, inelastic/elastic scatt. cross sections 77−57554
^{2}H(p,p) large angle elastic scatt., d form factor at large q^{2} 80−102189
^{2}H(p,p)^{2}H, determination of Coulomb corrections 77−10400
^{2}H(p,π^{+}), 400, 470, 600 MeV, microscopic model calcs., reaction cross section 79−40916
^{2}H(p,π^{+})^{3}H, 400, 470, 600 MeV, differential cross section using isobar model 80−9291
^{2}H(p,π^{+})^{3}H, NN pot., isobar configurations and π prod., inelastic cross sections 79−63666
^{2}H(π, π) 25-180 MeV, three body calc. up to (3,3) resonance, polarisations 79−40964
^{2}H(π,p)p, cross sections, Faddeev like eqns., absorption effects for scatt. 80−86928
^{2}H(π,p)p in resonance region, theoretical models 80−83123
^{2}H(π,pp), pion absorption in field theory using Low equation 79−67779
^{2}H(π,π)$_{s}$, pole terms and absorption in p-wave πd interaction 80−86932
^{2}H(π,π), 140-260 MeV, (3,3) region, tensor force, cross sections, pol. parameters 80−68641
^{2}H(π,π), 142, 180 MeV, covariant three-body calc. 77−6450
^{2}H(π,π), (3,3) resonance region, three body relativistic eqns., cross section calcs. 78−74405
^{2}H(π,π), Coulomb effects in elastic scatt., approx. treatment 79−85548
^{2}H(π,π), expt. and theoretical work, present status, model testing, πN interaction 80−42699
^{2}H(π,π), Faddeev calcs. 77−18622
^{2}H(π,π), graph summation method 77−18624
^{2}H(π,π), high energies, total cross sections from refined Glauber model 80−78322
^{2}H(π,π), high energy total cross section in Glauber model 80−18346
^{2}H(π,π), low energy scattering theory *(Russian)* 79−54460
^{2}H(π,π), medium energy elastic scatt. amplitudes, covariant multiple scatt. model convergence test 80−42710
^{2}H(π,π), modified Glauber amplitude anal., differential and total cross sections 79−22334
^{2}H(π,π), relativistic description, πN waves, NN rescatt., ρ-exchange, π absorption and emission 80−9310
^{2}H(π,π), scatt. length, exchange current contrib. 80−78328
^{2}H(π,π) elastic scatt., multiple scatt. calcs. 77−18623
^{2}H(π^{-}, π^{-}), 552 MeV/c, elastic differential cross section Glauber theory anal. *(Russian)* 80−52700
^{2}H(π^{-}, π^{-}p)n, 438 GeV/c, break up process, kinematic variables, np final state interaction *(Russian)* 80−52701
^{2}H(π^{-},nγ)n, multiple scatt. corrections, off-shell rescatt. effects, effective range 80−83127
^{2}H(π^{+}, p)p, pπ exchange current effects on pion absorption, cross section enhancement 80−57803
^{2}H(π^{+}, π^{+}), 49 MeV, P-wave dispersive contrib. π and ρ rescatt. 80−78331
^{3}H doublet scatt. length, Phillips plot, N/D input parametrisation 80−42672
^{3}H, enhancement factor calc. in photonuclear electric dipole sum rule 78−37288
^{3}H photoeffect, electric dipole sum rules 79−36231
^{3}H photoeffect, hyperspherical harmonics and elec. dipole sum rules 77−57650

nuclear reaction and scattering theory continued
^{1}H, three-particle photodisintegration, hyperspherical functions method *(Russian)* 78−589
^{1}H, total photodisintegration cross-section calc. using coupled hyperspherical harmonics 77−18525
^{1}H(e,e'p)2n, realistic NN interactions, three body variational wave functions, spectral functions 80−47470
^{1}H(n,n), scatt. length, 4-nucleon problem, integral eqn. approach 80−91183
^{1}H(n,n) differential cross section, nonrelativistic theory of four nucleon systems *(Russian)* 79−80881
^{1}H(p,γ)^{3}He, intermediate energy, ang. distribs., reaction amplitude and ^{3}He vertices 80−22835
^{1}H(p,n)^{1}He, R-matrix anal. of polarisation and analysing power 77−88142
^{1}H(π^{-},3n), final state continuum spectra, hyperspherical basis 77−26590
^{1}H($\pi^{\pm}$,$\pi^{\pm}$), 232, 252, 295 MeV/c, forward angle scatt., nuclear struct. and π reaction models 79−76032
^{4}H(α,α), intermediate energies, Glauber analysis 78−46077
^{A}H(γ,π^{0}), A=1, 2, 1-10 MeV, photoprod. yields, DWIA anal., dipole photoprod. amplitudes 80−68645
H(e^{+},e^{+})H, s-wave scatt., effective range expansion 80−47467
He+p, A=3,4, polarised projectile, parity nonconservation in low energy scatt. 78−70522
(^{3}He,^{3}He), 12-51.3 MeV, ang. distribs., S-matrix formalism frame anal., fission ingoing channel *(Russian)* 80−5152
(^{3}He,n) Coulomb stripping reaction theory 77−54232
(^{3}He,p) reactions on ^{6}Li, ^{9}Be, DWBA anal., proton polarisation, differential cross section 77−82944
(^{3}He, ^{3}He), coupled reaction channel effects on polarisation 79−85442
^{3}He (π, Γ)^{3}H, model calc. of Panofsky ratio 77−14190
^{3}He (π, π) Δ(1236) resonance region, Watson multiple scatt. series. integral eqns. 80−37402
(^{3}He, d) and (^{3}He, $\bar{d}$), stripping reactions, zero range normalization factors 79−75956
^{3}He elast. scatt. on heavy nuclei, anal. with molecular type pots. 77−18502
^{3}He, enhancement factor calc. in photonuclear electric dipole sum rule 78−37288
^{3}He, microscopic spin orbit potential, microscopic formulation inadequacies 79−26355
^{3}He photoeffect to isospin 3/2, coupled hyperspherical harmonics 78−41696
^{3}He, three-particle photodisintegration, hyperspherical functions method *(Russian)* 78−589
^{3}He(^{3}He,d^{3}He), three body break up reaction energy spectra, computer program 80−27593
^{3}He(^{3}He,p^{3}He), three body break up reaction energy spectra, computer program 80−27593
^{3}He(d,d), 0.32 MeV, continuum ambiguity in phase shift anal. 79−76006
^{3}He(d,d), 0.32-5.0 MeV, anal. power, scatt. amps., ^{5}Li states, phase shift anal. 80−47382
^{3}He(e, e), charge formfactors, second Born approx. and pole model 80−18155
^{3}He(e,e'), 0.1-14 GeV, deep inelastic inclusive scatt. response functions and momentum distrib. 80−42640
^{3}He(e,e'), nuclear high momentum components and y scaling 80−106051
^{3}He(e,e')pd, Faddeev calc., scatt. cross-sections 77−18530
^{3}He(e,e'p)d, Faddeev calc., scatt. cross-sections 77−18530
^{3}He(e,e), charge formfactors, second Born approx. and pole model 80−78133
^{3}He(γ,2p)n, 80-120 MeV, proton energy distribs., diffr. cross sections, direct breakup 80−86897
^{3}He(γ,p)^{2}H, intermediate energy, ang. distribs., reaction amplitude and ^{3}He vertices 80−22835
^{3}He(γ,pd) and ^{2}H(p,γ) anal. using Reid soft-core pots. 77−26664
^{3}He(γ,π^{0}), cross section and threshold effects using dynamical $\gamma N \rightarrow N\pi^{0}$ model 80−27627
^{3}He(γ,π^{+}) near threshold, photoprod. yield and transition matrix element 79−89291
^{3}He(γ,π^{+})^{3}H, Fermi motion and off-shell effects, impulse approx. 80−27626
^{3}He(γ,π^{+})^{3}H cross section near threshold , 80−83093
^{3}He(γ,$\pi^{\pm}$), (3,3) resonance region, nuclear wave functions, kinematics 78−78361
^{3}He(μ^{-},$\nu\gamma$), radiative capture relativistic calcs., rate and photon spectrum 80−68605
^{3}He(n,n), scatt. length, 4-nucleon problem, integral eqn. approach 80−91183
^{3}He(n,n) differential cross section, nonrelativistic theory of four nucleon systems *(Russian)* 79−80881
^{3}He(p, p), 1 GeV, differential cross section minimum, Glauber model description 79−80938
^{3}He(p,2p)^{2}H, 155 MeV, multiple scatt. diffraction theory anal. *(Russian)* 77−10408
^{3}He(p,2p)d(d*), 136 MeV, d/d* ratio, PWIA anal. 79−75999
^{3}He(p,p), 19-30 MleV, spin anal. power and phase shift anal. 79−13295
^{3}He(p,p), charge independ. R-matrix anal. of four nucleon system 79−85479
^{3}He(p,pd)p, 35 and 45 MeV, four-body break-up calcs. 77−57667
^{3}He(p,pp)d, 35 and 45 MeV, four-body, break-up calcs. 77−57667
^{3}He(p,π^{+})^{4}He, 415, 716 MeV, DWIA calcs. of differential cross-section 77−6359
^{3}He(π,π), 68-154 MeV, single and double collision differential cross section calcs. *(Russian)* 80−106083
^{3}He(π,π)^{3}He, Glauber theory calc. in (3,3)-reson. region 77−82968
^{3}He(π^{-},π^{-}), low energies, scatt. lengths and phase shift calcs., inelastic process contribs. 79−54459
^{3}He(π^{-},π^{0}), form factor sensitivity in Glauber multiple scatt. formalism 80−105964
^{3}He(π^{-},π^{0})^{3}H, Glauber theory calc. in (3,3)-reson. region 77−82968
^{3}He(π^{+},3p), final state continuum spectra, hyperspherical basis 77−26590
^{3}He($\pi^{\pm}$,$\pi^{\pm}$), 232, 252, 295 MeV/c, forward angle scatt., nuclear struct. and π reaction models 79−76032
^{3}He($\pi^{\pm}$,$\pi^{\pm}$), low energy, scatt. lengths, approx. pot. 4-body eqns. 79−76033
^{3}He(t,d)^{4}He, symmetry breakdown as cluster spatial effect 79−6619
^{4}He (p,p), effective channel approach, N* resonance effects 79−9570
nuclear reaction and scattering theory continued
^{4}He (π^{-}, π^{-}p), 5GeV/c, quasielastic scatt., cross section, form factor, final state interactions 80−99190
^{4}He deduced monopole excitation to O^{+} state DWBA anal. from (α,α') 79−22226
^{4}He photodisintegration, electric dipole transitions, photoeffect cross section 79−67742
^{4}He photodisintegration, total, dipole, and quadrupole cross sections, sum rules *(Russian)* 80−83094
^{4}He, photonuclear reaction cross-section continuum calcs. 77−71603
^{4}He, π scatt. and absorption, microscopic calc. 79−85501
^{4}He-d-d vertex constant, normalisation 77−6329
^{4}He+N, resonating-group method anal. 77−82886
^{4}He+n, below 15 MeV, R-function anal. 77−23028
^{4}He+π, effects of pion absorption 79−22341
^{4}He+π^{-}, coupled channel method, determ. of total cross sections 79−36281
^{4}He+π^{-}, multiple scattering theory with separate treatment of proton and neutron 79−45301
^{4}He+π^{-} second-order optical pot., multiple scatt. theory 77−82966
^{4}He(π, π), elastic data inconsistencies and dispersion relations above 33 resonance 80−68700
^{4}He(^{3}He,^{3}He), 60.2, 113.1 MeV, ang. distrib., optical and coupled channel anal., cross sections 80−47492
^{4}He(α,αX), 4,5 GeV/c, Thomas Reiche Kuhn sum rule appl., mean energy losses 80−91192
^{4}He(α,α), 4.32, 5.07 GeV/c, Glauber multiple scatt. theory comparisons 80−63192
^{4}He(α,α), composite particle scatt., generator coordinate and natural boundary condition methods 80−13489
^{4}He(α,α), nuclear separable plus Coulomb interaction 80−83106
^{4}He(α,α), phenomenological-potential constant, from phase shift, theory of complex orbital momentum 77−14145
^{4}He(α,n)^{7}Be meas. and α-α elastic phase-shift calcs. 77−50143
^{4}He(d,d), Glauber theory at high energy *(Russian)* 78−41732
^{4}He(d,d), noncentral forces, Pauli principle effects on d polarisation, orthogonality condition model 79−6614
^{4}He(d,d), pol. d, 12-17 MeV, differential cross sections, anal. powers, phast shift anal. 80−13449
^{4}He(d,pn)^{4}He, differential cross section and polarisation, three body model 80−47460
^{4}He(γ,X), X=p,n, 50-150 MeV, total cross sections, quasiparticle formalism calcs. 80−78277
^{4}He(γ,2n)2p, final state interaction effects, 2 nucleon photoabsorption mechanism 79−36228
^{4}He(γ,d)d, total cross-section calc. 77−18526
^{4}He(γ,pn)^{2}H, three particle photodisintegration, pole mechanism contrib. *(Russian)* 80−91176
^{4}He(γ,π^{0}), differential cross section, complex momenta theory for nondiffractive processes *(Russian)* 80−32266
^{4}He(n,X), local approximation to a non-local potential 80−91182
^{4}He(p, p), 1.05 GeV, cross sections and polarisations, correlation effects calcs. 80−57774
^{4}He(p,2p), 250, 350, 500 MeV, cross section energy depend., DWIA calcs. 80−37375
^{4}He(p,2p), pol. nucleon quasi-elastic scatt., nuclear wave function and model tests 80−42656
^{4}He(p,d), intermediate energies, pion exchange currents in DWBA anal. 80−32199
^{4}He(p,d) pickup reaction, isobar configurations and short range correlations 80−22798
^{4}He(p,d)^{3}He, 770 MeV, exact finite range DWBA, cross sections 78−70531
^{4}He(p,d)^{3}He, 770 MeV, multiple-scattering approach 80−27636
^{4}He(p,nπ^{+}), pion prod. operator non-relativistic approx. 79−85500
^{4}He(p,nπ^{+}), pion prod. operator non-relativistic approx. 80−27640
^{4}He(p,p), 0.35-23.1 GeV, differential cross section and polarisation, Glauber theory *(Chinese)* 79−49628
^{4}He(p,p), 20-55 MeV, anal. power, cross sections, phase shift anal. 79−9569
^{4}He(p,p), 45-65 MeV, phase shift anal. 80−22832
^{4}He(p,p), 68-125 MeV, resonating group anal. 77−88139
^{4}He(p,p), elastic scatt., medium energies, effective channel anal. 77−2997
^{4}He(p,p)^{4}He forward amplitude real part, 1.5-10 GeV, from dispersion relns. 77−314
^{4}He(π,πX)^{3}H, 5 GeV, nucleon isobar content in He using impulse approx. 79−36276
^{4}He(π,π), forward scatt. amplitude, imaginary part in unphysical region 77−14194
^{4}He(π,π), multiple scatt. formalism, dynamics of πN resonances 77−6447
^{4}He(π,π), multiple scatt. anal. at medium energies 77−26791
^{4}He(π,π), single scatt. optical pot., Pauli principle and binding effects on cross section 80−86933
^{4}He(π^{-},π^{-}), 51-260 MeV, dynamical and fixed scatterer approx. calcs. 78−25244
^{4}He(π^{-},π^{-})^{4}He, 51-260 MeV, nuclear-Coulomb interf. calc. using optical model phase shift anal. 77−54199
^{4}He(π^{+},π^{+}2n2p), 120-165 MeV, total cross section, multiple scatt. processes 79−85517
^{A}He(γ,π^{0}), A=3, 4, 1-10 MeV, photoprod. yields, DWIA anal., dipole photoprod. amplitudes 80−68645
^{A}He(π,π), A=3, 4, low energy scatt. length and phase calcs. 80−47508
He(e^{+},e^{+})He, s-wave scatt., effective range expansion 80−47467
He(π,π), absorpt. effects in resonance region 79−76036
^{204}Hg(^{3}He,n) 33.3 MeV, cross sections, DWBA anal. for data near Z=82 79−67733
^{62}Hi(α,^{3}He), 172.5, 140 MeV, plane wave spectator model anal. n momentum distrib. in α 79−54445
^{165}Ho, electron-oriented nucleus scatt., eikonal approx. calc. 78−37331
^{165}Ho(π,π), aligned deformed nuclei, cross sections and diffractive minima from eikonal approx. 80−22860
K(Ar,X), proton inclusive spectra, direct plus thermal model 80−57799
^{A}K, A=37,39, levels, excitation and microscopic form factors, DWBA calcs. from Ca(p,α) 80−32185
^{38}K level spectrum and (^{3}He,t) reaction mechanism from ^{38}Ar(^{3}He,t) 79−22229
^{38}K low lying 1^{+}, T=0 states, DWBA anal. of ^{40}Ca(p,^{3}He) 80−470
^{39}K $9/2^{-}$ forbidden transition, cross section CCBA anal., L=1 transitions from ^{40}Ca(^{15}N,^{16}O) 79−9507

nuclear reaction and scattering theory continued
^{39}K high spin states, J^{π} assignments, DWBA anal. of ^{41}Ca(d,α), 22 MeV, ^{39}K high spin states, J^{π} assignments, DWBA anal. 79−40851
^{42}K levels and ang. distribs., spectroscopic factors, DWBA anal. from ^{41}K(d,p) 79−17806
Kr induced deeply inelastic collisions, transport eqn. appl. 78−82380
^{139}La(n,γ), non-statistical capture, radiative widths, γ-ray doorway state model 80−37389
(^{6}Li,X), 156 MeV, projectile break up in continuous particle spectra, cross section, fragmentation 80−86889
(^{6}Li,d), A=20 to 68, DWBA reduction, ground state α-transfer strengths 80−106068
(^{6}Li,d), A~60,116, L=0 transitions, cross sections, microscopic anal. 80−78189
(^{6}Li,d) on odd A, sd shell nuclei, α-cluster spectroscopic strengths, DWBA anal. 79−3104
^{6}Li (α,α), 59 MeV, elastic and inelastic, differential cross section systematic anal. 80−22845
^{6}Li-n, R-matrix calc. of total elastic, (n,α) differential cross-sections and polarisation 77−57669
^{6}Li+d, 0.1-1.0 MeV, DWBA and R-matrix cross section anal., direct contribution 79−67758
^{6}Li+n reactions, 4.4-7.3 MeV, DWBA and optical model anal. 77−18539
^{6}Li(^{3}He, ^{3}He^{3}He)^{3}He, 45 MeV, three trion model 77−88160
^{6}Li(^{3}He, t^{3}He)^{3}He, 45 MeV, three trion model 77−88160
^{6}Li(^{3}He,^{3}H)^{6}Be, 27 MeV, comparison of experimental data and cluster and distorted wave calcs. 79−76010
^{6}Li(^{3}He,^{3}He), phase shifts, cross sections, resonating group calcs., odd-even features, resonances 80−68681
^{6}Li(^{3}He,^{3}He)^{6}Li*, 27 MeV, comparison of experimental data and cluster and distorted wave calcs. 79−76010
^{6}Li(H,ν)^{3}H^{3}H, muon capture in ditriton channel by elementary particle model 79−40907
^{6}Li(α,αp), 140 MeV, quasifree p knockout, spectroscopic factors, DWIA anal. 79−67650
^{6}Li(d,X) system, resonating group method, single channel approx., cluster states 80−57782
^{6}Li(e, e), charge formfactors, second Born approx. and pole model 80−18155
^{6}Li(e,e'), 76-141 MeV, form factors, appl. to (π^{-},γ), phenomenological model 80−83068
^{6}Li(e,e), charge formfactors, second Born approx. and pole model 80−78133
^{6}Li(e,e), electroexcitation cross sections, incoherent superposition of single nucleon processes 80−32269
^{6}Li(μ^{-},ν_{μ})^{3}H^{3}H, total and differential muon capture rates from elementary particle model 79−89297
^{6}Li(n,n), resonating group calcs. of phase shifts and cross sections 78−50168
^{6}Li(p,n), 144 MeV, charge exchange, one pion exchange and PCAC tests 80−78299
^{6}Li(p,p) 0.6, 1.04 GeV, α-d cluster model and Glauber multiple scatt. theory 79−85476
^{6}Li(p,pd), 590 MeV, α-d motion, impulse distrib., cluster momentum distrib. 80−52679
^{6}Li(p,pd), 670 MeV, large angle quasifree scatt., spectroscopic factor, momentum distrib., cluster model 80−63184
^{6}Li(p,pd)α, 156 MeV, relative wave function of d and α clusters, PWIA, DWIA anal. *(Chinese)* 79−59068
^{6}Li(p,pt)^{3}He, 1 GeV, knock-out of clusters, distorting factors, microscopic approach *(Russian)* 78−58285
^{6}Li(τ,τ)^{6}Li, 27 MeV cross-section calc. by Amado 3-body model 79−6617
^{6}Li(τ,τ)^{6}Li, 45 MeV, cross-section calc. by Amado 3-body model 79−6616
^{7}Li(α,α), low energy elastic and inelastic scatt., Pauli principle effect 78−4953
^{7}Li(d, t), 12 MeV, nuclear vertex constant in peripheral model for virtual decay ^{7}Li→α+t 80−18295
^{7}Li(d,$\alpha\alpha$)n, 2 MeV, quasi free reaction, ^{7}Li struct. 78−41727
^{7}Li(γ,π^{-}), total cross section calc. in impulse approx. 80−13458
^{7}Li(n,n')αT, three body sequential reactions, kinetics modelling 80−37371
^{7}Li(p, α), 45 MeV, nuclear vertex constant in peripheral model for virtual decay ^{7}Li→α+t 80−18295
^{7}Li(p, p'), microscopic calc. for 1/2^{-} level excitation, isoscalar quadrupole renormalisation 77−14046
^{7}Li(p,d), 800 MeV, cross sections, DWBA anal. 80−42667
^{7}Li(p,n)^{7}Be, microscopic multi-channel calcs. to 2.5 MeV c.m. 78−4934
^{7}Li(p,p)^{7}Li, microscopic multi-channel calcs. to 2.5 MeV c.m. 78−4934
^{7}Li(π^{+},π^{-})^{7}Be, distorted wave impulse calc., optical pot., multiple scatt. 78−50138
^{7}Li(t, ^{9}Li)^{1}H, near threshold anomaly, S-matrix formalism, ^{10}Li neutron binding energy *(Russian)* 80−105961
^{8}Li β^{-}-decay, β-α angular correlations, final state energy depend., current test 80−102151
^{A}Li (p, nd), A=6,7, 670 MeV, quasifree scatt., PWIA anal., cross sections 79−75985
^{A}Li, A=6,7, π^{+} electroprod., distorted wave impulse approx. anal. 79−17894
^{A}Li(πp), A=6, 7, 75, 175 MeV, diffential cross sections, reaction mechanisms 80−78332
^{A}Mg(d,^{6}Li), 80 MeV, A=24,26, α-spectroscopic factors and ang. distribs., DWBA anal. 80−99126
^{23}Mg hole states, transitions and spectroscopic factors, DWBA anal. of ^{24}Mg(p,d) 80−32161
^{23}Mg j-forbidden $^{7}/_{2}^{+}$ state excitation, CCBA calculations, two step processes from ^{24}Mg(p,d), 49.5 MeV 79−26369
^{24}Mg (α,$\alpha'\gamma$) 104 MeV, nuclear deformation from ang. correlations, coupled channel anal. 78−78301
^{24}Mg high spin states, high spin particle spectroscopy upper limits for compound reactions from ^{10}B(^{16}O,d) 79−36126
^{24}Mg+^{16}O, two step α-transfer reaction 79−76018
^{24}Mg(^{13}C,^{13}C'), 35 MeV, 2^{+} population probab., spin-flip and spin orbit pots., coupled channel anal. 80−99125
^{24}Mg(^{3}He,α)^{23}Mg, 10 MeV, ang. distribs., DWBA and CCBA calcs. with inelastic effects 77−61443
^{24}Mg(α,α'), 120 MeV, ground and gamma band excitation, coupled channel calcs. in rotational model 79−89315

nuclear reaction and scattering theory continued
^{24}Mg(α,α'), 1.37 GeV, low lying state ang. distribs., Glauber rigid body approx. 79−54394
^{24}Mg(d,d$_{1}$), vector analysing power, d$_{1}$-γ ang. correl., DWBA and CCBA anals. 77−30605
^{24}Mg(p,p'), 0.8 GeV, rot., γ and β bands, ground state deformation, DWBA, coupled channels anal. 80−9198
^{24}Mg(p,p'), 20, 40, 800 MeV, γ-vibr. band, coupled channels anal. 80−9194
^{24}Mg(p,p'), polarised p, 20.3 MeV, cross section and analysing power, DWBA and coupled channel anal. 78−82287
^{24}Mg(p,p'), 40 MeV, DWBA anal., positive parity states, transitions and giant resonance 79−6419
^{24}Mg(p,p), 18-44 MeV, differential cross sections, phase shift anal., energy depend. 80−47481
^{24}Mg(p,p), 22.5 to 28.0 MeV, differential cross sections, optical, coupled channel, core excitation anal. 79−6613
^{24}Mg($\pi^{\pm}$,$\pi^{\pm}$) 180 MeV elastic and inelastic scatt., optical model and DWBA calcs. 78−89915
^{26}Mg (α,$\alpha'\gamma$) 104 MeV, nuclear deformation from ang. correlations, coupled channel anal. 78−78301
^{26}Mg (α,α), 104 MeV, oblate-prolate effects in struct. and reactions 80−9225
^{26}Mg(^{11}B,^{10}B)^{27}Mg, 114 MeV, transfer amplitude and ang. distribs. 79−59081
^{26}Mg(^{12}C,^{12}C'), 41.3 MeV, ang. distrib. meas. and coupled channel meth. 77−65231
^{26}Mg(^{13}C, ^{12}C), ^{26}Mg(^{13}C, ^{14}C), 35 MeV, inelastic effects, DWBA, CCBA calcs. 77−3041
^{26}Mg(^{16}O, ^{14}C)^{28}Si, full recoil one and two step DWBA anal. 78−70564
^{26}Mg(p,p'), 24 MeV, rot. description of low lying states, coupled channels anal. 79−54376
^{26}Mg(p,π^{+}), isobar configuration effects, p→$\Delta^{0}\pi$ model, ang. distribs. *(Chinese)* 80−47484
^{27}Mg energy levels, spectroscopic factors, DWBA, Hauser-Feshbach anals. from ^{26}Mg(d,p) 80−52581
^{A}Mn, A=51, 53 small angle cross sections for levels, DWBA anal. from Cr(^{3}He,d) 79−22203
^{53}Mn low lying states, DWBA anal., shell model wave functions from ^{56}Fe(p,α) 80−32211
^{55}Mn transitions to low lying levels, α spectroscopic strengths, DWBA anal. 79−45156
^{A}Mo, A=98,102, anal. powers, transitions, shape coexistence states, DWBA anal. of Mo(t,p), pol.t 80−86895
^{A}Mo(d,d), A=92-100, 21.5 MeV, elastic and inelastic cross sections, coupled channel anal., deformation 79−553
^{92}Mo(^{16}O,X), entrance channel mass asymmetry effects on reaction mechanism, fission and fusion 80−106077
^{96}Mo(t,p), pol.t, cross section and anal. powers, struct. depend., DWBA anal. 80−78272
^{100}Mo(^{14}N,^{12}B), 90 meV, spin alignment of products, semi-classical model calcs. 80−73859
^{14}N 1^{+} state cross sections, effective two nucleon interaction, isovector tensor component from ^{14}C(p,n) 80−18208
^{14}N spectroscopic factors, cross sections DWBA anal. optical model parameters from ^{12}C(^{16}O,X) 80−13371
^{14}N(d, p)^{15}N, 12 to 52 MeV, stripping reaction anal., distorted wave method 79−80948
^{14}N(d,^{6}Li)^{10}B, four-nucleon pickup from ^{14}N, DWBA anal. of ang. distrib. 79−63679
^{14}N(d,p$_{0}$)^{15}N, 52 MeV, DWBA and impulse approx. anal. 77−34318
^{14}N(γ,π^{-}), DWIA anal., wave function and π optical pot. effects on cross section 80−63168
^{14}N(p,d) modified DWBA anal., optical model parameter influence on vertex consts. *(Russian)* 78−78340
^{14}N(p,n), 144 MeV, charge exchange, one pion exchange and PCAC tests 80−78299
^{14}N(p,p'), 122 MeV, level excitation, cross sections, effective NN interaction, DWIA anal. 80−78197
^{14}N(p,p'), 25-40 MeV, level cross sections, optical parameters, DWBA anal., tensor effective interaction 80−68555
^{14}N(p,pd), excitation spectrum of ^{12}C, exchange processes effect, impulse approx. 77−61405
^{15}N+X, X=^{11}B,^{12}C,^{18}O,^{13}C, deduced excited states, shell model wave functions, DWBA anal. 79−45284
^{15}N(n',n)^{15}N, continuum random phase approx. 80−27635
^{15}N(p,p), 18-44 MeV, differential cross sections, phase shift anal., energy depend. 80−47481
^{16}N ground state quadruplet, DWBA anal. of ^{14}N(t,p) 79−22200
NaF(Ne,Ne), 800 MeV/N, high momentum nucleons from relativistic nuclear collisions, hard scatt. mechanism 79−40950
Na(Ne,X), 800 MeV/N, direct vs. thermal particle emission, inclusive cross sections 80−52688
^{23}Na positive parity states ang. distrib., DWBA anal. from ^{21}Ne(^{3}He,p), 18 MeV 78−82284
^{24}Na fragment ang. and energy distribs., two-step model anal. of ^{197}Au(p,X) 80−52678
^{24}Na, level struct. and spin assignments, DWBA anal. from ^{22}Ne(^{3}He,p), 18 MeV 78−86477
^{92}Nb low lying multiplets, DWBA anal. for spectroscopic factors from ^{91}Zr(α,t) 80−57685
^{93}Nb(d,pX), 80 MeV, inclusive proton spectra, d break-up, DWBA anal. 80−91190
^{93}Nb(e,e), magnetic e scatt., exchange current effects, plane wave Born approx. 80−78282
^{97}Nb high spin analogue resonance near N=50 neutron shell, DWBA anal. of ^{96}Zr(^{3}He,d) 80−42613
^{A}Nd, A=145, 147, 149, single neutron hole states spectroscopic factors, DWBA anal. of (d,t), (^{3}He,α) 80−78109
(Ne, π^{-}X), 800 MeV/A, π^{-} energy and ang. distribs., firestreak and hard scatt. model anal. 80−13498
Ne+Ne, classical many-body model for heavy ion collisions 80−536
Ne(Ne,X), 117-800 MeV, classical eqns. of motion calcs., central collisions, thermal models 80−106070
^{20}Ne 13482 keV level, parity violating effects in two resonance interference from ^{19}F(p,α) pol. p 80−83033
^{20}Ne breakup cross section, direct mechanism, DWBA anal. of ^{40}Ca(^{20}Ne,^{16}O) 80−18276
^{20}Ne+^{208}Pb, elastic and inelastic, 131 MeV, ^{20}Ne nuclear moments from inelastic data 78−66204

nuclear reaction and scattering theory continued
^{20}Ne+^{20}Ne, 250-1000 MeV/N, intranuclear cascade calcs. for multiplicity and cross sections 80−32300
^{20}Ne+^{27}Al, deep inelastic fragment energies, rot. energy contributions 79−63697
^{20}Ne(d,d), pol. d, 10-12 MeV, cross section, coupled channel and fluctuations anal. 80−27617
^{20}Ne(e,e′α), EM induced α emission, α spectroscopic amplitudes, anal. solvable model 80−32267
^{20}Ne(γ,α), EM induced α emission, α spectroscopic amplitudes, anal. solvable model 80−32267
^{20}Ne(p,p′), differential cross-sections, analysing powers in direct reaction theory 77−65223
^{21}Ne, spectroscopic factors, pickup strengths in ^{22}Ne(^{3}He,α) at 15 MeV 79−63684
^{21}Ne states cross section, coupled channel and fluctuations anal. from ^{20}Ne(d,p) 80−27617
Ni(^{16}O,^{18}O), surface transparent pots., and CCBA anal. of diffractive behaviour 78−50206
^{A}Ni, A=60, 62, 66, levels, J^{π}, anal. powers and cross sections from Ni(t,p)pol.t 80−68539
^{A}Ni, A=64, 58, level ang. momentum and spin values, DWBA anal. from (t,d) polarised t 79−36163
^{A}Ni(e,p),(e,α), A=58, 60, 62, electrodisintegration cross sections, E1, E2 absorption, DWBA anal. 80−106052
^{A}Ni(n,n), A=58,60,62,64, 5 MeV, differential cross sections, optical, statistical and coupled channel anals. *(Russian)* 80−37377
^{A}Ni(p,xγ), 80-164 MeV, A=58, 60, 62, 64, prod. cross sections, pre-equilibrium phase 80−78301
^{57}Ni levels and analogue states, J^{π} from DWBA anal. of ^{58}Ni(^{3}He, α) 79−63592
^{58}Ni+^{16}O, 96 MeV, particle spectra for hot spot emission 79−22312
^{58}Ni(^{16}O,^{12}C), 46, 60 MeV, DWBA anal. with optical pot., ^{62}Zn levels 79−6694
^{58}Ni(^{3}He,α), 130 MeV, selected transition, DWBA anal., cross sections 80−83086
^{58}Ni(^{3}He,α)^{57}Ni, 15-205 MeV, zero-range DWBA normalisation, energy depend. 77−34280
^{58}Ni(^{6}Li,^{6}Li′), 71 MeV, excited states deformation lengths, DWBA and coupled channels anals. 80−68541
^{58}Ni(^{7}Li,^{7}Li′), 19 MeV, first 2^{+} states Coulomb-nuclear interference, optical and DWBA anal. 80−22852
^{58}Ni(α,α′) 1.37 GeV, low lying state ang. distribs., Glauber rigid body approx. 79−54394
^{58}Ni(d,α), ^{56}Co particle-hole states, T=1, zero DWBA anal. 80−78308
^{58}Ni(d,d′), 10 MeV, diff. cross sections and d-γ ang. correlations, multi-shell coupled channel calcs. 80−83064
^{58}Ni(p,d), 121 MeV, DWBA applicability test, d D-state contribs. 79−13261
^{58}Ni(p,d)^{57}Ni at 52 MeV, deuteron D-state effect, calcs. 79−54434
^{58}Ni(p,p′), 0.8 GeV, coupled channels effects 79−63669
^{58}Ni(p,p), 178 MeV, ang. distribs., cross sections and polarisation, coupled channels calcs. 79−75984
^{58}Ni(p,p), 800 MeV, elastic and inelastic, cross section, deformation lengths, optical and DWBA anals. 80−68664
^{58}Ni(p,p), 800 MeV, non-eikonal corrections to Glauber diffraction approx. 79−71851
^{58}Ni(p,p), pol. p, 40 MeV, elastic and inelastic, asymmetries and differential cross sections *(Russian)* 80−27623
^{58}Ni(π,π), 162 MeV, elastic and inelastic ang. distribs., optical and PWIA anals. 80−42706
^{60}Ni deduced levels from ^{58}Fe(^{16}O,^{14}C)^{60}Ni, DWBA anal., spectroscopic strengths 80−47380
^{60}Ni(^{13}C,^{13}C), nuclear and Coulomb components to scatt. amplitudes 77−34340
^{60}Ni(^{18}O,^{18}O′), stripping-pick-up mechanism, coupled channel theory 78−54784
^{60}Ni(p,p′), near 6 MeV, spin-flip probabilities distorted wave and statistical anal. *(Russian)* 79−80939
^{61}Ni level ang. distribs., DWBA anal. from ^{59}Ni(t,p) 79−17816
^{64}Ni(^{16}O,^{14}C)^{66}Zn, 56 MeV, full recoil one and two-step DWBA anal. 78−46091
^{64}Ni(^{18}O,^{18}O′), coupled channel anal. with double folding potential 79−45282
^{64}Ni(^{18}O,^{18}O), coupled channel anal. with double folding potential 79−45282
Ni(d,d), 13-80 MeV, second order breakup corrections in DWBA 80−86910
Ni(p,t), A=60, 62, at 27 MeV, two step processes, finite range effects 78−58281
N(π±, π$^{±}$ X), X=He or d, 170 MeV, cross sections and ang. distribs., direct knockout mechanism *(Russian)* 80−86887
^{A}O, A=17, 19, level scheme, two-step transfer contribs., coupled channel anal. from O(^{13}C,X) 80−32181
^{A}O(π^{+},π$^{−}$), A=16,18, cross section and ang. distribs., Glauber and coherent fluctuation models *(Chinese)* 80−102211
^{14}O low lying states, exact finite and zero range DWBA anal. from ^{12}C(^{3}He,n), 12-24 MeV 78−82286
(^{16}O,X), A=54-208, direct transfer to discrete and continuum states, DWBA diffraction model 80−78262
^{16}O 4^{+} state nonstatistical population in compound nucleus calcs. of ^{12}C(^{6}Li,d) 80−102137
^{16}O (α, 2α), DWIA calc., cross section and spectroscopic factors 79−63681
^{16}O, α-spectroscopic amplitudes anal. using shell model based calc. 79−13203
^{16}O form factor effects, zero range DWBA calcs. from ^{18}O(p,t) 80−491
^{16}O induced reactions in nuclear emulsions at 2.1 GeV/nucleon, multiplicity distrib. of white and grey tracks *(Spanish)* 80−47495
^{16}O levels, Hauser Feshbach and DWBA anal. α-spectroscopic strengths from ^{12}C(^{6}Li,d), 20-34 MeV 79−569
^{16}O levels and ang. distribs., ^{3}He spectroscopic strengths, Hauser-Feshbach/DWBA anals. of ^{13}C(^{6}Li,t) 80−47390
^{16}O, neutrino absorption cross-sections, <500 MeV, Helm model 77−41956
^{16}O, π^{+} electroprod., distorted wave impulse approx. anal. 79−17894
(^{16}O, X), 90, 120 MeV/N, fragmentation reaction mechanism, orbital dispersion, momentum distribs. 79−97723
^{16}O+^{11}B, 115 MeV, α-transfer, DWBA anal., spectroscopic factors 79−22311
nuclear reaction and scattering theory continued
^{16}O+^{13}C, 105 MeV, α-transfer, DWBA anal., spectroscopic factors 79−22311
^{16}O+^{16}O, 3D TDHF calcs. 78−626
^{16}O+^{16}O, fusion cross section gross struct., excitation functions, coupled channel method 80−52705
^{16}O+^{16}O, nucleon-nucleon forces and heavy-ion potentials 79−6657
^{16}O+^{16}O, nucleus-nucleus interaction and nuclear saturation props. 79−6395
^{16}O+^{16}O collisions, resonating group study, effective two-nucleon forces 79−59044
^{16}O+^{16}O elastic scattering, GCM calcs., phase shifts, ang. distribs. 77−30625
^{16}O+^{16}O system, strong damping of inner oscills., nuclear saturation props. 78−41749
^{16}O+^{20}Ne, elastic and inelastic 50 MeV, contribution of α-cluster exchange 77−10429
^{16}O+^{4}He, group theory appl. to reaction studies 80−9276
^{16}O+^{7}Li, 50, 68 MeV, α-transfer, DWBA anal., spectroscopic factors 79−22311
^{16}O+X, X=^{11}B,^{12}C,^{13}C,^{18}O, deduced excited states, shell model wave functions, DWBA anal. 79−45284
^{16}O+α nucleon exchange and backangle anomaly 79−6638
^{16}O(^{12}C,^{12}C), 18-26 MeV, molecular structure, projection operator anal., differential cross sections 80−106033
^{16}O(^{12}C,X), sub-barrier energies, fusion cross section, static and dynamic deformation effects 80−42729
^{16}O(^{16}O,^{16}O′), gross struct., barrier top resonance model calc. 80−9279
^{16}O(^{16}O,^{16}O), Coulomb field effects using generalised JWKB method 80−13504
^{16}O(^{16}O,^{16}O), elastic scatt., incoming wave boundary condition model calcs. 80−47504
^{16}O(^{16}O,^{16}O), elastic scatt., l-window formalism 80−68684
^{16}O(^{16}O,^{16}O), optical pot., nuclear matter approach, energy density matter [-] 80−83112
^{16}O(^{16}O,^{16}O), surface transparent pot. scatt. semiclassical wave propagation matrix method 79−101
^{16}O(^{3}He,p)^{18}F, 19.8 MeV DWBA anal. of exchange effects 77−46179
^{16}O(^{6}Li, d), 32 MeV, unnatural parity levels in ^{20}Na, reaction mechanisms 77−14158
^{16}O(^{6}Li,α)^{18}F, 34 MeV, DWBA anal. of exchange effects 77−46179
^{16}O(^{6}Li,d)^{20}Ne, 19.8 to 32 MeV, reaction mechanism and excitation functions 78−41757
^{16}O(K^{+},K^{+}′), plane and distorted wave impulse approx. anal., plane waves 79−9630
^{16}O(N,N), microscopic description validity 79−544
^{16}O(α,2α), determ. of spectroscopic factors by DWIA 79−6639
^{16}O(α,α′), inelastic scatt. from 8.88 MeV 2$^{−}$ state, magnitude and ang. distribs. of cross sections at 40.5 and 65 MeV 79−49631
^{16}O(α,α), 28-33.6 MeV, forward peaking variation, DWBA with optical pots., ang. distribs. 80−13488
^{16}O(α,α), microscopic R-matrix theory in generator coord. basis 77−14079
^{16}O(α,d), 1.12 MeV, forward peaking variation, DWBA with optical pots., ang. distribs. 80−13488
^{16}O(d,^{6}Li)^{12}C, 35 MeV, finite range CCBA calcs. 77−6403
^{16}O(d,X), X=d or N, elastic scatt. and stripping, three body calc. 80−91165
^{16}O(d,d), treatment as three-body problem 79−6618
^{16}O(d,p)^{17}O, channel coupling array and coupled reaction channel methods 78−8831
^{16}O(d,p)^{17}O, coupled channel variational method for multi-step direct nuclear reactions. II. Test on a (d,p) reaction 78−66259
^{16}O(e,e), T=1 level form factors, Helm model, pion photoprod. and muon capture appls. 80−52553
^{16}O(e,π^{+}), 180.4 MeV, virtual photon spectrum, virtual photon theory test 80−102183
^{16}O(γ, p), 300 to 900 MeV/c, p-shell momentum distrib. calc. 78−50151
^{16}O(γ,N), giant resonance region, features in energy depend. of ang. distrib. 77−6343
^{16}O(γ,p)^{15}N, 50 to 350 MeV, evaluation of isobar photoprod. contrib. to (γ,p) reaction 79−45245
^{16}O(γ,π^{0}) coherent photoprod. in isobar-hole formalism, DWIA comparison 79−89290
^{16}O(γ,π^{+}), 200-350 MeV, cross sections, DWIA anal. 80−106048
^{16}O(γ,π^{+}), differential cross section from elementary Hamiltonian model 80−18292
^{16}O(γ,π^{+}), threshold to 175 MeV, total cross sections, DWIA anal. 80−13459
^{16}O(γ,π), total cross section, Δ-hole states damping, π^{0},ρ exchange, Δ isobar hole model 80−91174
^{16}O(μ,ν), recoil nucleus odd and even tensor orientations, general expressions 80−13451
^{16}O(n,n), elastic cross section, microscopic calc. 80−531
^{16}O(n,n), totally microscopic description, optical pot. and many-body theory 79−546
^{16}O(p,p′^{16}O) at 27.2 MeV, 6.05 MeV 0^{+} level excit., meas. and microscopic calc. 77−26687
^{16}O(p,p′), 150 MeV, spin-orbit interaction within collective model and DWBA 79−45128
^{16}O(p,p′), giant resonances from antisymmetrised DWBA anal. 79−85432
^{16}O(p,p'), 20-40 MeV, pol. p, anal. powers, imaginary spin-orbit pot., coupled channels anal. 80−102179
^{16}O(p,p'), polarised p, 20, 30, 40 MeV, anal. power and cross sections, spin-orbit deformation 79−75963
^{16}O(p,p), nucleon distrib. in nuclei, self-consistent anal. 79−9556
^{16}O(p,p) polarised p, 800 MeV, differential cross section and anal. power, microscopic anal. 79−80915
^{16}O(π,π), binding effects in optical model with S-wave interaction 77−14196
^{16}O(π,π), T-matrix from isobar-hole model, many-body corrections, optical pot. parameter 80−9312
^{16}O(π,π), three-body model of πN interaction using finite binding pots. 80−42707
^{16}O(π^{+},π^{+}), 50 MeV, partial wave amplitude anal. 79−22335
^{16}O(π^{+},π^{+}) elast. and inelast. scatt., 50 MeV, ang. distrib. determ. optical model and DWBA 79−45304
^{16}O(π$^{±}$,π$^{±}$), Coulomb-nuclear interference, new anal. method 78−21608
^{16}O(t,p), centre of mass corrections to DWBA overlap factors 80−18319

nuclear reaction and scattering theory continued
^{17}O(^{11}B,^{8}Li), 115 MeV, shell and semiclassical reaction model anal. 80−13494
^{17}O(^{12}C,^{9}Be), 115 MeV, shell and semiclassical reaction model anal. 80−13494
^{17}O(^{13}C,^{10}B), 105 MeV, shell and semiclassical reaction model anal., ^{20}F spins 80−13494
^{17}O(^{16}O, ^{16}O), repeated neutron transfer, coupled channels anal. 78−54782
^{17}O(e,e), mag scatt., form factors, HF calcs., core polarisation effects 80−42579
^{17}O(γ,n$_0$)^{16}O, 4.3-7 MeV, resonance radiation width, channel and pot. radiative capture, R-matrix anal. 79−6567
^{17}O(γ,n), cross section, Lane-Lynn radiative capture mechanisms 80−52660
^{18}O, heavy ion excitation, single particle and core polarisation amplitude interference 80−5117
^{18}O(^{18}O, ^{16}O)^{20}O 52 MeV, microscopic anal. with DWBA calc. 79−26450
^{18}O(p,α_0)^{15}N, 6.6 to 10.4 MeV, partial wave anal. of differential cross sections 79−93609
^{18}O(p,p), 18-44 MeV, differential cross sections, phase shift anal., energy depend. 80−47481
^{18}O(p,t), exact finite range DWBA calcs., realistic triton and nuclear wave functions 80−63191
^{18}O(p,t), finite range DWBA anal. with realistic triton wave function 80−78300
^{18}O(π,π'), 164 MeV, yrast state and level excitation, DWIA calcs., shell model context 80−42526
^{18}O(π,π'), momentum space DWIA calcs., DWIA validity, shell model sensitivities 79−85553
^{18}O($\pi^{\pm}$,$\pi^{\pm}$) ^{18}O(2^+), DWIA anal. with microscopic form factors, effective charges 79−85549
^{18}O($\pi^{\pm}$,$\pi^{\pm}$), correlation effects, Glauber theory anal. 79−85514
^{20}O states below 6 MeV, J$^{\pi}$ assingments, DWBA anal. of ^{18}O(t,p) 79−22201
(^{17,18}O,^{17,18}O'), 54-69 MeV, on A=48-92, excited states and ang. distribs., DWBA anal. 79−67705
O($\pi^{\pm}$, $\pi^{\pm}$X), X=He or d, 170 MeV, cross sections and ang. distribs., direct knockout mechanism *(Russian)* 80−86887
^{A}Os, A=190,192, two-quasiproton states, level struct., DWBA anal. of Ir(t,α) 79−89237
^{A}P, A=31, 33, levels and transition j-depend., DWBA anal. for Si(^{19}F, ^{16}O) 80−42542
^{30}P high spin two nucleon states decay props. from ^{28}Si(α, dγ) 80−13402
^{30}P positive parity states, transitions and spectroscopic strengths, DWBA anal. of ^{29}Si(^{3}He,d) 80−102138
^{31}P high E$_x$ states, J$^{\pi}$, DWBA anal. ^{29}Si(^{3}He,p) 80−68536
^{31}P(^{3}He,d), 25 MeV, ^{32}S energy levels and ang. distribs., DWBA anal. 78−78265
^{31}P(d,p), 1.5-2.5 MeV, ^{32}P spectroscopic factors and level transition excitation function anal. 78−74371
Pb+O, 315 MeV, phenomenological determ. of strength of dissipative forces 77−71619
Pb(C,C), 800 MeV/N, high momentum nucleons from relativistic nuclear collisions, hard scattering mechanism 79−40950
^{A}Pb, A=205-207, neutron hole states, spectroscopic factors, DWBA anal. of Pb(^{3}He,α) 80−47352
^{A}Pb(^{3}He,n), A=204,206,208, 33.3 MeV, cross sections, DWBA anal. for data near Z=82 79−67733
^{A}Pb(α,α), A=206, 208, 120 MeV, isoscalar resonance excitation, low lying transitions, DWBA calc. 80−512
^{203}Pb multiplet struct., DWBA anal. from ^{205}Pb(p,t) 79−17784
^{207}Pb inner hole states, spectroscopic strengths DWBA anal. from ^{208}Pb(^{3}He,α) 79−17813
^{207}Pb(p,p'), 135 MeV, DWIA test 78−33186
^{208}Pb (e,e'), 2$^-$ giant resonance twist mode excitation, B(M2) values, form factors 80−78246
^{208}Pb giant monopole and quadrupole resonances, multipole excitations from (α,α')(d,d') 80−106031
^{208}Pb, high-spin states, form factors for electroexcitation 77−14116
^{208}Pb+^{16}O, classical, semiclassical and quantum mechanical scatt. and reaction calcs. 79−566
^{208}Pb+^{16}O, microscopic model anal. of fragment yields at 20 MeV/A and 2100 MeV/A 78−33214
^{208}Pb+^{208}Pb deep inelastic processes, TDHF and elementary modes of excitation 79−63695
^{208}Pb+^{20}Ne(^{40}Ar), 250-1000 MeV/N, intranuclear cascade calcs. for multiplicity and cross sections 80−32300
^{208}Pb(^{12}C, ^{11}B), 77 MeV, bound and continuum state excitation, direct and two step processes 80−63205
^{208}Pb(^{12}C, ^{11}B)^{209}Bi, DWBA anal. including nuclear wave function polarisation 78−629
^{208}Pb(^{16}O,^{12}C)^{212}Po, semiclassical anal. of α-transfer, calc. of angular distrib. 79−6672
^{208}Pb(^{16}O,^{15}N) 104, 138.5, 216.6 MeV, DWBA and optical model anal., energy dependence 78−82378
^{208}Pb(^{16}O,^{15}N) 312.6 MeV, optical model and DWBA anal., energy depend., lower energy comparison 78−82379
^{208}Pb(^{16}O,^{15}O), 312.6 MeV, optical model and DWBA anal., energy depend., lower energy comparison 78−82379
^{208}Pb(^{16}O,^{16}O'), 315 MeV, continuous spectrum and giant resonance excitation, coherent state model test 80−32252
^{208}Pb(^{16}O,^{16}O), elastic ang. distrib., nuclear contributions, Born approx. validity 79−36252
^{208}Pb(^{16}O,^{16}O) 104, 138.5, 216.6 MeV, DWBA and optical model anal., energy dependence 78−82378
^{208}Pb(^{16}O,^{18}O) 312.6 MeV, optical model and DWBA anal., energy depend., lower energy comparison 78−82379
^{208}Pb(^{16}O,^{17}O) 104, 138.5, 216.6 MeV, DWBA and optical model anal., energy dependence 78−82378
^{208}Pb(^{208}Pb, X), giant resonance polarisation pots. from nucleus-nucleus effective pot. 80−78248
^{208}Pb(^{20}Ne,X), 400 MeV/N, inclusive p, d, t, ^{3}He cross sections from sequential scatt. model 80−57792
^{208}Pb(^{3}He,^{3}He'), 108.5 MeV, giant monopole resonance, DWBA anal. 79−71828
^{208}Pb(^{86}Kr,X), 610 MeV, deep inelastic ang. momentum transfer from sequential fission fragments 80−18325
^{208}Pb(N,N), microscopic description validity 79−544

nuclear reaction and scattering theory continued
^{208}Pb(α,α'), 65 MeV, inclusive reaction, giant resonance background, heavy ion model anal. 80−5150
^{208}Pb(α,α'), 96 MeV, ang. distribs., breathing mode states, DWBA calcs. 78−50183
^{208}Pb(α,α), elastic ang. distrib., nuclear contributions, Born approx. validity 79−36252
^{208}Pb(α,αp) 96.8 MeV, proton pickup by α-particles to unbound states DWBA anal. 79−22305
^{208}Pb(d,^{6}Li) ^{204}Mg, SS MeV, levels and spectroscopic factors, α clustering, DWBA anal. 79−67694
^{208}Pb(d,p), polarised d, tensor anal. powers, sub-Coulomb stripping calc. corrections 79−80918
^{208}Pb(e,e'), 50-335 MeV, J$^{\pi}$=12$^-$, 14$^-$ high spin states, DWBA anal. 79−93490
^{208}Pb(n,γ), fast, direct-semidirect and pure resonance model calcs. 80−47486
^{208}Pb(p,d), 121 MeV, DWBA applicability test, d D-state contribs. 79−13261
^{208}Pb(p,p'), 39, 62 MeV, DWBA anal., collective spectra, direct process contrib. *(Russian)* 80−13408
^{208}Pb(p,p'), 5 to 8 MeV, hyperfine reson. struct., Feynman diagrams 79−6589
^{208}Pb(p,p'), giant resonances from antisymmetrised DWBA anal. 79−85432
^{208}Pb(p,p'), sum rule anal. of inclusive cross section 78−33183
^{208}Pb(p,p), 0.8 GeV, elastic and inelastic, ang. distribs., states, optical and DWBA anal. 79−3154
^{208}Pb(p,π), microscopic model anal., stripping model test for (d,p) 79−85436
^{208}Pb(p,t), finite range DWBA anal. with realistic triton wave function 80−78300
^{208}Pb(p,t), simple unitary estimate for multistep processes, cross section bounds 79−40922
^{208}Pb(p,t)^{206}Pb, successive and simultaneous transfer processes, on-shell, DWBA methods 78−8812
^{208}Pb(p,t)^{206}Pb(3^+), pol. p, 22 MeV, anal. power and (p,d)(d,t) sequential transfer processes 80−5119
^{208}Pb(π,π), 162 MeV, elastic and inelastic ang. distribs., optical and PWIA anals. 80−42706
^{208}Pb($\pi^{\pm}$,$\pi^{\pm}$N), 180-255 MeV, quasielastic pion scatt. coincidence expt. interpretation, impulse approx. 80−68704
^{208}Pb(t,p), centre of mass corrections to DWBA overlap factors 80−18319
Pb(n,n), 14.0-17.4 MeV, neutron polarisation, ang. depend. diffraction struct. 80−18283
^{106}Pd(t,p), pol.t, cross section and anal. powers, struct. depend., DWBA anal. 80−78272
^{110}Pd(^{208}Pb, X), equilibrium process time evolution, mass and charge distribs., energy loss 79−97725
^{118}Pd+^{118}Pd, 637 MeV time depend. Hartree-Fock-Bogoliubov calc. for fusion and subsequent ^{236}U fission 79−36265
^{153}Pm 5/2$^-$ h$_{11/2}$ dominated band, anomalous ang. distribs., CCBA calcs. for ^{154}Sm(t,α) 80−86788
^{141}Pr(n,γ), non-statistical capture, radiative widths, γ-ray doorway state model 80−37389
^{A}Pt, A=192, 194, 196, states, J$^{\pi}$, ang. distribs. and transitions, DWBA anal. of Pt(p,t) 80−468
^{A}Pt(^{3}He,n) A=194,196, 33.3 MeV, cross sections, DWBA anal. for data near Z=82 79−67733
^{194}Pt(^{16}O,^{16}O'), 7-17.5 MeV, Coulomb excitation, low lying collective state reduced matrix elements, triaxiality 78−82269
^{194}Pt(α,α'), 7-17.5 MeV, Coulomb excitation, low lying collective state reduced matrix elements, triaxiality 78−82269
^{239}Pu, deformation effects on neutron total cross-sections, adiabatic coupled-channel calc. 79−17896
^{240}Pu fission total kinetic energy release, excitation energy depend., scission point anal. of ^{241}Pu(^{3}He,αf) 80−18351
^{242}Pu(μ,f), radiationless muonic transition induced fission, fission dynamics probe, friction coeff. 80−78336
Pu(γ,γ) 12.754 MeV, Delbruck scatt., Coulomb correction terms, differential cross sections 80−27629
(^{32}S,X), A=59-89, double differential cross section, mass asymmetry, transport model 80−102203
^{32}S levels and spectroscopic factors, DWBA anal. from ^{28}Si(^{18}O,^{14}C) 79−22204
^{32}S levels and spectroscopic factors from pickup DWBA anal. of ^{33}S(^{3}He,α) 80−9235
^{32}S(d,p), DWBA anal. converging overlap integrals, stripping to decaying states 79−6530
^{32}S(γ,p$_0$), giant dipole resonance decay model, cross section and p spectrum 79−6563
^{32}S(n,γ), fast n, doorway structs. and single particle resonances, microscopic treatment 80−52646
^{32}S(n,n), 25-1100 keV, total cross section, multilevel anal., strength functions, optical parameters 80−78298
^{32}S(n,n), 5 MeV, elastic and inelastic scatt., differential cross-sections, model anal. *(Russian)* 80−42668
^{A}Sb, A=123,125,127,129, cross-sections, ang. distribs., spectroscopic factors, DWBA anal. of Te(t,α) 80−52572
^{119}Sb intrinsic high spin state population, cluster DWBA anal. of ^{116}Sn(α,p) 79−67630
Sc fragment differential ranges and energy spectra from ^{238}U(p,X), reaction mechanisms 80−42666
^{A}Sc, A=44m,46,47,48, fragment emission, two-step model applicability from ^{238}U(p,X) 80−99177
^{44}Sc, (f$_{7/2}$)^4 states populated in ^{41}Ca(α,p) 25 MeV reaction, relative transition strengths, semi-microscopic model calcs. 79−6645
^{45}Sc total neutron cross section, parametric fit, bound level parameters, spin 77−23048
^{49}Sc proton single particle states, spectroscopic factors, DWBA anal. of ^{48}Ca(d,n) 80−99118
^{74}Se transition energy correlations in γ-continuum from ^{64}Ni(^{16}O,α2n) 80−95309
^{74}Se(d,p), 6 MeV, ^{75}Se energy levels, DWBA, sum rule anals., spectroscopic factors 78−66285
^{2}Si($\pi^{\pm}$, $\pi^{\pm}$) 130, 180, 226 MeV, πN(3), region, inelastic transitions, optical and DWIA anal. 79−97677
^{A}Si(^{3}He,^{3}He), 46 MeV, A=28-30, ang. distribs., optical and DWBA anal., scatt. pots. 79−556

nuclear reaction and scattering theory continued
^{A}Si(α,α), 41 MeV, A=28-30, ang. distribs., optical and DWA anal., scatt. pots. 79−556
^{A}Si(p,p'), A=28,29,30, 51.9 MeV, blocking effect and core-excitation DWBA and optical model 78−82336
^{28}Si ($\alpha,\alpha'\gamma$) 104 MeV, nuclear deformation from ang. correlations, coupled channel anal. 78−78301
^{28}Si+^{16}O, pot. for back-angle enhanced elastic scatt. 79−40953
^{28}Si+^{20}Ne, 120 MeV, numerical anal. based on linear response theory 79−36273
^{28}Si+^{20}Ne, frictional coeffs. using linear response theory 79−13327
^{28}Si(^{10}B,^{9}Be), 59, 75, 132 MeV, l=1 transfer reaction, exact finite range DWBA anal. 79−22317
^{28}Si(^{10}B,^{9}Be), unique l=1 reaction, ang. distrib. wave number depend., 0WBA anal. 80−63204
^{28}Si(^{12}C,^{12}C'), 41.4 MeV, ang. distrib. meas. and coupled channel meth. 77−65231
^{28}Si(^{15}N,^{14}N), 44 MeV, n stripping, DWBA and coupled channel anal., two step processes 79−6552
^{28}Si(^{16}O,^{16}O), 65 MeV, elastic and inelastic, optical and coupled channels model anals. 79−45293
^{28}Si(^{16}O,^{16}O), backward angle elastic excitation function structure 79−36263
^{28}Si(^{16}O,^{16}O), elastic and inelastic, coupled channels calcs., optical pot. energy depend. 79−571
^{28}Si(^{16}O,^{16}O) gross struct. in excitation function elastic transfer amplitudes 79−36215
^{28}Si(^{18}O,^{18}O), 65 MeV, elastic and inelastic, optical and coupled channels model anals. 79−45293
^{28}Si(^{18}O,X), 56 MeV, multinucleon transfers, ang. distribs., distorted wave and shell model anal. 80−27663
^{28}Si(^{19}F,^{16}O), 60 MeV, exact finite range DWBA and CCBA calcs. 80−538
^{28}Si(^{20}Ne, X), 120 MeV, linear response theory anal., frictional coeffs. and energy dissipation 80−13502
^{28}Si(^{7}Li, ^{7}Be)^{28}Al, 36 MeV, excited states in ^{7}Be+^{28}Al system microscopic DWA anal. 77−14157
^{28}Si(^{9}Be, ^{9}Be'), 45, 60 MeV, low lying collective states, ang. distribs., DWBA double folding pot. anal. 80−78113
^{28}Si(d,^{3}He)^{27}Al, multistep processes, CCBA anal., SU(3) model 77−30609
^{28}Si(e,e'), 38.7-57.5 MeV, energy levels, isovector M1 strength, DWBA anal. 79−75847
^{28}Si(e,e'), 6^{-} T=1 resonance form factor, mag. strength quenching, meson exchange currents 80−86882
^{28}Si(n,γ), 565, 813 keV, resonance γ, spectra, valence model test 80−63124
^{28}Si(n,γ), calc. of neutron and gamma widths for ^{29}Si 3/2^{-} doorway resonances 77−26587
^{28}Si(n,γ), fast n, doorway structs. and single particle resonances, microscopic treatment 80−52646
^{28}Si(n,n), 5 MeV, elastic and inelastic scatt., differential cross-sections, model anal. *(Russian)* 80−42668
^{28}Si(n,n), core-parricle doorway states calc. 77−23003
^{28}Si(π,π'), momentum space DWIA calcs., DWIA validity, shell model sensitivities 79−85553
^{28}Si(π,π), 162 MeV, elastic and inelastic ang. distribs., optical and PWIA anals. 80−42706
^{29}Si levels, J$^{\pi}$, spectroscopic factor, DWBA anal. of ^{28}Si(^{3}He, ^{2}He) 80−86811
^{29}Si levels and ang. distribs., DWBA anal. of ^{27}Al(α,d) 80−78157
^{29}Si(^{16}O,^{17}O)^{28}Si, non-orthogonality of channel states 80−83115
^{30}Si(^{16}O,^{16}O), elastic and inelastic, 60 MeV, to 1st excited 2^{+} state, coupled channels anal. 78−82377
^{30}Si(K^{-},$\bar{K}^{0}$), 300 MeV, microscopic particle-hole shell model calcs., DWIA anal. 79−59091
^{30}Si(p,α)^{27}Al, 40.75 MeV, differential and relative cross sections, distorted wave direct pickup calcs. 78−94009
Si(π^{+},π^{+}), elast. and inelast. scatt., 50 MeV, ang. distrib. determ. optical model and DWBA 79−45304
^{A}Sm(^{20}Ne, ^{20}Ne), 70 MeV, A=148, 150, 152, Coulomb polarisation pot., coupled channel calcs. 80−22855
^{A}Sm(p,p), 1 GeV, A=152, 154, dispersive effects in ground state rot. band excitation, coupled channel calcs. 79−40828
^{144}Sm(α,α'), 96 MeV, ang. distribs., breathing mode states, DWBA calcs. 78−50183
^{148}Sm(^{18}O,^{16}O), interference effects, coupled channels calc. with BCS+RPA wavefunctions 77−26787
^{150}Sm(^{16}O,^{18}O), interference effects, coupled channels calc. with BCS+RPA wavefunctions 77−26787
^{152}Sm(^{16}O,^{16}O), 72 MeV, coupled-channels anal., nucl. excitation effects 79−26457
^{152}Sm(e,e'), 35-350 MeV, coupled channels anal., rot. band excited states, charge densities 79−3139
^{154}Sm(p,p'), 0.8 GeV, ang. distribs. and multipole moments, DWBA and coupled channel anals. 80−105969
Sm(n,n'), 7 MeV, A=148,150,152,154, differential cross sections, coupled channel anal., deform. effects 77−54219
Sn+^{18}O, 100 MeV, quasielastic collisions, time-depend. single particle method 77−34334
^{A}Sn(e,e') A=116, 120, 124, electric moment distrib., lowest lying quadrupole states excitation 79−6392
^{A}Sn(n,n'), A=116, 118, 120, 122, 11 MeV, octupole vibr. states, diff. cross section, deformation length, DWBA anal. 80−102092
^{A}Sn(p,p'), A=116, 124, 0.8 GeV, polarised p, spin orbit deformation effects, DWBA anal. 79−30832
^{118}Sn(^{7}Li,^{6}He), 48 MeV, DWBA anal. with optical model parameters, ^{119}Sb transitions 79−6688
^{118}Sn(p,t). ang. distribs. and cross sections full finite range CCBA anal. 80−5141
^{120}Sn+^{132}Xe, deeply inelastic, relative motion mass transport and dynamics 79−13320
^{120}Sn(p,n), statistical multistep direct emission, p-h and DWBA calcs. 80−106035
^{122}Sn excitation of 6^{+}, 8^{+}, 10^{+} and 9^{-} states, DWBA anal. from ^{122}Sn(p,p') and ^{124}Sn(p,t) 79−89264
^{122}Sn+^{120}Sn, 630 MeV, multipair transfer calcs. for superfluid ions, coupled channel WKB approx. 78−37373
^{124}Sn(n,n), pol. thermal, parity violation near resonance, DWBA calcs. 80−68528
nuclear reaction and scattering theory continued
^{124}Sn(p,p), threshold enhancement of parity violation, Born approx. 80−18191
Sn(d,^{6}Li)Cd, microscopic description of alpha-transfer reactions 79−6615
Sn(p,n), microscopic description 77−57670
^{87}Sr(e,e), magnetic e scatt., exchange current effects, plane wave Born approx. 80−78282
^{88}Sr(^{12}C,^{10}Be), 60 MeV, coupled channel Born approx. anal., form factors, sequential amplitudes 79−9608
^{88}Sr(n,n'), 11 MeV, octupole vibr. states, diff. cross section, deformation length, DWBA anal. 80−102092
^{181}Ta+α, 4.2 and 5.15 GeV, central nuclear collisions, pion multiplicity calc. *(Russian)* 79−59079
^{181}Ta(^{20}Ne, spallation), 8.0 GeV, cross sections and target residues, model comparison 80−68630
^{185}Ta single proton states and rot. bands, J$^{\pi}$ from ^{186}W(t,α),pol.t 80−91130
^{159}Tb(^{11}B,X), 51 MeV, fusion and deep inelastic, quantised frictional motion calcs. 80−102223
^{159}Tb(^{14}N,X), 140 MeV, incomplete fusion reactions, sum rule model 80−95332
^{93}Tc high spin analogue resonance near N=50 neutron shell, DWBA anal. of ^{92}Mo(^{3}He,d) 80−42613
^{94}Tc levels and J$^{\pi}$, coupled channel and DWBA anal. of ^{92}Mo(^{3}He,p) 79−89239
^{125}Te low lying negative parity high spin states multistep induced population from (d,t)(^{3}He,α) 80−57657
^{126}Te(^{22}Ne, ^{22}Ne'), 93.5 MeV, 2^{+} state mutual excitation and transitions 79−54404
^{126}Te(t,p), pol.t, cross section and anal. powers, struct. depend., DWBA anal. 80−78272
^{130}Te+^{28}Si, 140 MeV, diffusion model 78−82382
Th+Ar, 388 MeV, phenomenological determ. of strength of dissipative forces 77−71619
^{232}Th (^{40}Ar, X), differential cross sections calc. from random matrix model transport theory 79−49634
^{232}Th, deformation effects on neutron total cross-sections, adiabatic coupled-channel calc. 79−17896
^{232}Th three hump fission barrier, photofission cross section and half life 79−67788
^{232}Th+^{40}Ar, 288 MeV phenomenological approach to deeply inelastic collisions 79−54449
^{232}Th+^{40}Ar, 390 MeV, Z$\leq$38 products energy spectra, reaction mechanism, dynamic deformation *(Russian)* 78−89909
^{232}Th(^{3}He,n), 33.3 MeV, cross sections, DWBA anal. for data near Z=82 79−67733
^{232}Th(α,α'), 120 MeV, isoscalar giant resonances, DWBA anal. 80−42621
^{A}Ti, A=44, 48, ang. distribs. for transitions, DWBA anal., spectroscopic strengths from Ca(^{7}Li,t) 80−68584
^{A}Ti(^{7}Li,^{7}Li'), A=46,48, 17 MeV, first 2^{+} states Coulomb-nuclear interference, optical and DWBA anal. 80−22852
^{46}Ti(d,d), 7,10 MeV, ang. distribs., DWBA and Hauser Feshbach anal. 80−47377
^{47}Ti levels, DWBA and Hauser Feshbach anal., compound nucleus cross sections from ^{46}Ti(d,p) 80−47377
^{48}Ti levels and transition ang. distribs., form factors, DWBA anal. of ^{45}Sc(α,p) 79−45202
^{48}Ti(p,p), 1 GeV, elastic scatt. differential cross section calc. 80−47480
^{49}Ti(e,e), magnetic e scatt., exchange current effects, plane wave Born approx. 80−78282
^{50}Ti(α,α), 140 MeV, model independent description limits from local optical pots. 80−102196
^{51}Ti $2p_{3/2}$ neutron orbit radius isotone shift from DWBA anal. of ^{50}Ti (t,d) 80−32172
Ti(p,d), A=46,48,50, DWBA calcs., rms radius pick-up reaction cross sections 79−541
^{205}Tl, level excitation energies and ang. distribs. cluster model DWBA calcs. from ^{208}Pb(p,α) 79−17814
U(Ne,X), 250, 400 MeV/N direct vs. thermal particle emission, inclusive cross sections 80−52688
U(Ne,X), proton inclusive spectra, direct plus thermal model 80−57799
^{A}U, A=233, 235, 238, deformation effects on neutron total cross-sections, adiabatic coupled-channel calc. 79−17896
^{233}U(α,X), 28-140 MeV, scatt. and fission reaction mechanisms, cross sections 80−18350
^{235}U fission fragment thermonuclear superheavy nuclei synthesis, prod. cross sections 80−95331
^{235}U+^{235}U, classical microscopic description 77−14160
^{235}U(n,f), thermal, fragment ionisation, charge distribs., stat. and instant perturbation theory *(Russian)* 80−63219
^{235}U(n,γ), thermal, d, t, He emission probabilities from stable core model *(Russian)* 80−68713
^{238}U subbarrier photofission, cross section and half-life, double hump model 80−102217
^{238}U-^{238}U, mass transfer, quantum mech. anal. within fragmentation theory 77−82948
^{238}U+^{20}Ne, 250 MeV/nucleon, comparison of macroscopic and microscopic calcs. 77−50153
^{238}U+^{20}Ne(^{40}Ar), 250-1000 MeV/N, intranuclear cascade calcs. for multiplicity and cross sections 80−32300
^{238}U+^{238}U, deeply inelastic, relative motion mass transport and dynamics 79−13320
^{238}U+^{248}U fragmentation, superheavy element prod. due to collective mass transfer 77−337
^{238}U+^{40}Ar, 220 MeV, fissionability of target-like fragments in deep inelastic collisions, reaction mechanism 79−54455
^{238}U(^{136}Xe, ^{136}Xe), multiple Coulomb and nucl. excitation 78−21603
^{238}U(^{238}U, ^{238}U), multiple Coulomb and nucl. excitation 78−21603
^{238}U(HI,f), Coulomb fission cross sections from coupled channel calcs. 80−9319
^{238}U(Kr,Kr'), multiple Coulomb excitation, coupled eqns. soln. by iteration 79−93654
^{238}U(Pb,Pb'), multiple Coulomb excitation, coupled eqns. soln. by iteration 79−93654
^{238}U(Xe,f), depend. of Coulomb fission on nucl. struct. 78−13173
^{238}U(e,e'f), 5.5-9 MeV, fission fragment ang. distribs. DWBA anal., low lying fissioning levels 80−42713
^{238}U(n,γ), cross section and resonance shape, gas molecule vibr. effects 80−42661

nuclear reaction and scattering theory continued
^{238}U(p,p′), 22 MeV, rot. band, multipole deformation parameters from coupled channel anal. 80−13369
^{A}V(p,X), A=50, 51, 12-45 MeV, reaction cross section and hybrid model analysis 79−67749
^{49}V proton hole, analogue and high spin states, distorted wave anal. from ^{52}Cr(p,α) 79−9482
^{51}V(^{3}He,dp), ^{3}He breakup, DWBA calcs. for strongly absorptive projectiles 80−68682
^{51}V(α,t), absolute normalisation from spin depend. sum rule anal. 80−27652
^{51}V(e,e), magnetic e scatt., exchange current effects, plane wave Born approx. 80−78282
Xe induced deeply inelastic collisions, transport eqn. appl. 78−82380
^{A}Xe, A=124,126-8,130,132, levels, transitions and J$^{\pi}$ values, DWBA anal. from Te(^{3}He, n) 79−75852
^{136}Xe(n,γ), thermal, Lane-Lynn theory of direct neutron capture verification 79−36218
^{89}Y+^{40}Ar, 237 meV, γ-ray multiplicities and energies, primary fragment angular momenta 78−46093
^{90}Y low lying multiplets, DWBA anal. for spectroscopic factors from ^{91}Zr(d,^{3}He) 80−57685
^{176}Yb(p,p′), 0.8 GeV, ang. distribs. and multipole moments, DWBA and coupled channel anals. 80−105969
^{A}Zn(α,α′), 18 MeV, A=64,66,68,70, compound and precompound α emission spectra 78−82367
^{A}Zn(p,α), 12.5 MeV, A=64,66,68,70, compound and precompound α emission spectra 78−82367
^{62}Zn ang. distribs. for transitions, DWBA anal., spectroscopic strengths from ^{58}Ni(^{7}Li,t) 80−68584
^{68}Zn low lying states, S-values from DWBA anal. of ^{64}Ni(^{6}Li, d) 79−36160
Zr-region, two nucleon transfer reactions, spectroscopic amplitudes, form factors, ang. distrib. 80−22779
^{A}Zr (p,p), A=92, 94, 2-6.5 MeV, optical and Lane model anal. comparison 80−18302
^{A}Zr(p,p) A=90, 92, elastic and inelastic, 40 MeV polarised protons, cross sections and anal. power 79−54428
^{90}Zr(^{3}He,^{3}He′), 108.5 MeV, giant monopole resonance, DWBA anal. 79−71828
^{90}Zr(^{3}He,n), second order processes in DWBA calcs. 78−46076
^{90}Zr(^{6}Li,^{6}Li′), 2^{+}(2.18 MeV) and 3^{-}(2.75 MeV) states in ^{90}Zr, DWBA anal. 79−26448
^{90}Zr(^{7}Li,^{6}He)^{91}Nb, 34 MeV DWBA calcs. 79−26448
^{90}Zr(^{7}Li,^{6}Li)^{91}Zr 34 MeV, 1.21 and 2.03 MeV states, 2.19 MeV doublet in ^{91}Zr, DWBA anal. 79−26448
^{90}Zr(^{7}Li,^{7}Li′), 2^{+}(2.18 MeV) and 3^{-}(2.75 MeV) states in ^{90}Zr, DWBA anal. 79−26448
^{90}Zr(α,αp) 96.8 MeV proton pickup by α-particles to unbound states DWBA anal. 79−22305
^{90}Zr(d,p), improved coupled-channel treatment of (d,n̄) threshold effect 77−74859
^{90}Zr(e,e′), 2^{-} giant resonance twist mode excitation, B(M2) values, form factors 80−78246
^{90}Zr(γ, α), above GDR region, cross sections, DWBA anal. 80−63173
^{90}Zr(n,n′), 11 MeV, octupole vibr. states, diff. cross section, deformation length, DWBA anal. 80−102092
^{90}Zr(p,d), 121 MeV, DWBA applicability test, d D-state contribs. 79−13261
^{90}Zr(p,n), IAS transition, 18.5 to 45 MeV, microscopic model anal. 77−82927
^{90}Zr(t,p), centre of mass corrections to DWBA overlap factors 80−18319
^{90}Zr(t,p), exact finite range DWBA calcs., realistic triton and nuclear wave functions 80−63191
^{92}Zr(p,α), 35 MeV, polarised p, DWBA anal., anal. power, optical pot., J-depend. 79−3143
^{92}Zr(p,α)^{89}Y, 35 MeV, microscopic DWBA anal. of three particle transfer 79−9567
^{92}Zr(p_{pol}, A)^{89}Y, finite-range cluster-model description, DWBA approach 80−52667
^{96}Zr(t,p), 20 MeV, short range correlations with Tabakin pot. 78−13115

nuclear reactions and scattering
see also alpha particle-nucleus reactions; alpha particle-nucleus scattering; chemical effects of nuclear reactions and scattering; cosmic ray-nucleus reactions; cosmic ray-nucleus scattering; deuteron-nucleus reactions; deuteron-nucleus scattering; direct nuclear reactions and scattering; electron-nucleus reactions; electron-nucleus scattering; fission; form factors (nuclear); hadron-nucleus reactions; hadron-nucleus scattering; heavy ion-nucleus reactions; heavy ion-nucleus scattering; helium 3-nucleus reactions; helium 3-nucleus scattering; muon-nucleus reactions; muon-nucleus scattering; neutrino-nucleus reactions; neutrino-nucleus scattering; nuclear fusion; nuclear reaction and scattering theory; nuclear reactions involving few nucleon systems; nuclear resonance reactions and scattering; nuclear scattering involving few nucleon systems; nuclear spallation; nuclear spectroscopic factors; nucleosynthesis; photon-nucleus reactions; photon-nucleus scattering; polarisation in nuclear reactions and scattering; triton-nucleus reactions; triton-nucleus scattering
backward angle peaks, exchange processes, review *(Russian)* 77−79392
bibliography, recent nuclear physics expt. papers 77−41873
break-up processes in few-body systems 77−22993
break-up reactions 77−22994
charged particle induced nuclear reactions, reaction list for atomic number 1-98 77−14099
collisions and microscopic theory, conference 78−563
conference, cross sections and technology, Washington, USA (March 1975) 77−22826
conference, general congress, Societe Francaise de Physique, Toulouse, France (June 1979) 80−77536
conference on nuclear structure and reactions, clustering aspects, Winnipeg, Canada (June 1978) 79−3099
data tables, recent references May-Aug 1978 79−30773
education, scatt. simulation in one-dimens. 77−33780
energy of separation and nucl. reactions, 1977 at. mass evaluation tables 78−497
few body dynamics, conf. 77−18368
growth points in nuclear physics, book 80−94929
hadron-nuclei collisions, statistical mechanism of multiparticle prod. 77−46155

nuclear reactions and scattering continued
hadron-nucleon inelasticity coeff., high energies, A-dependence *(Russian)* 77−6166
hadron-nucleus, correl. length between created particles, multiple prod. case *(Russian)* 77−6187
hadron-nucleus, validity of fixed scatterer models 77−18484
hadron-nucleus collisions, correlations between secondaries 77−57654
hadron-nucleus collisions at 200 GeV, obs. of prompt single muons and dimuons 77−30572
hadron-nucleus collisions at high energy, expt. data review 77−50120
hadron-nucleus fast interaction, particle density fluctuations *(Russian)* 77−6167
hadron-nucleus high energy reactions, triple pomeron in coherent processes 77−18534
hadron-nucleus reactions, few nucleon systems, intermediate energies 77−79363
hadron-nucleus scatt., cluster expansion of optical potential 77−10380
high energy hadron-nucleus collisions, effective mass number 77−88135
high energy physics, conf., Schladming, Austria (Feb.-Mar., 1977) 78−8494
high-energy reactions in astrophysics, comparison of methods for cross sections calc. 78−28505
high-momentum transfer, wave function struct. at relativistic values of nucleon momenta *(Russian)* 78−89805
inclusive hadron production in high energy particle+nucleus collisions, sum rules, scaling law 77−57673
inelastic scattering excitation of giant multipole resonances 77−57593
intermediate energies, work at Saclay, facilities and expts. 77−61636
Isolde experiments, prod. of extreme neutron/proton ratio nuclei, nuclear props. study *(Danish)* 78−4972
large transverse momentum hadron prod. on nuclei 77−30461
lepton collisions, cascade model, space-time model, tests and predictions 80−68633
medium energy data library 77−18765
modern atomic and nuclear physics (book) 80−11
multiparticle production of nuclei, intranuclear cascading of secondaries 78−66262
multiple scatt. theory, coherent and incoherent particle prod. in nuclei *(Russian)* 77−216
nuclear reaction thresholds and half-life meas., computer controlled system 78−55114
nuclear structure references 1975-7 79−30772
optical model, parabolic repulsion potential for scattering of ^{6}Li and ^{9}Be by light and medium nuclei 80−22782
partition functions, astrophysical implications 79−21167
phenomenological equations for reacting fluids 78−15649
proton inclusive spectra in nuclear high energy collisions 78−70557
pycnonuclear reactions, pair correlation function in dense plasma 79−67001
review of 30 years work by Nuclear Reactions Lab. Dubna, USSR 79−36204
review of research programs at Saclay Nuclear Physics dept. *(French)* 79−437
secondary particle multiplicity distribution in nuclei, 200 and 800 GeV *(Russian)* 78−89879
secondary particles from high energy reactions, detection losses correction by generator functional technique 77−6650
solar flares, thermonuclear reactions and spallation rel. to H and He isotopic comp. 77−45266
stellar dense matter, nuclear reaction rate enhancement 79−21168
stellar nuclear reactions, possible non-thermal processes 78−20816
Sun, nuclear reactions explanation of solar neutrino flux obs. 77−74035
Swiss Physical Society, autumn sessions 78−72053
tandem accelerators and nuclear phys. conf. 78−13349
thermonuclear reaction rate, parameter-depend. integral evaluation 79−29985
thermonuclear reaction rate parameter calc. for d+^{6}Li 77−61436
thermonuclear synthesis of elements *(Russian)* 77−6341
three body sequential decay X(a,b)Y(c)Z processes, parity, spin, reaction mechs. info. from ang. correl. method 78−50222
West correction to total cross-section of scatt. from deuterons or nuclei 77−2958
(particle, xnγ), neutron multiplicity for gamma rays 80−37689
Σ^{-}-nucleus, 23 GeV/c, Y* prod. 77−50183
Ag+hadrons, 7-200 GeV/c, analogy between He isotopes and secondary particles *(Russian)* 77−3006
Be+hadron, 200 GeV, jets and single particle prod. at high p⊥ 78−45975
Br+hadrons, 7-200 GeV/c, analogy between He isotopes and secondary particles *(Russian)* 77−3006
^{3}H(x,x′y)^{3}H, existence of excited states of A=3 nuclei 79−9553
^{95}Nb(n,γ)^{95}Nb, ^{95m}Nb, cross section meas. rel. to fusion reactor design probs. 77−23060
^{208}Pb(α, α′), neutron collectivities, E2 giant resonance excitation 77−26558
Te isotopes, fission product conc., sensitivity anal. of cross section effects 78−82428

nuclear reactions involving few nucleon systems
for nuclear inelastic scattering involving few nucleon systems see "nuclear scattering involving few nucleon systems"
3-body breakup, final state interaction approx. in cluster model formalism 77−18500
3N and 4N calcs., review 78−50094
break-up reactions 77−22994
charged particle cross sections, exotic fusion fuels 77−23293
Coulomb effects in three body reactions with two charged particles 78−78331
coupling constants from dispersion anal. of N and d scatt. amplitudes, ^{6}Li-α-d, ^{4}He-d-d, ^{3}He-d-p, ^{3}H-d-n, ^{2}H-p-n 78−29399
electromagnetic reactions at intermediate enegies 77−79363
few body systems, anal. coupling constant continuation for resonance and stripping reactions *(Russian)* 80−13435
few-body problem connection with inclusive interactions 77−22760
few-nucleon reactions for A>3, coincidence expts., survey 77−18518
four nucleon system, reactions and scatt. using K-matrix formalism, differential cross sections *(Russian)* 80−106027
four nucleon system two dimens. integral-equation soln. 78−41650
four-nucleon problem, microscopic K-matrix continuous spectrum *(Russian)* 77−61352
generalized Moshinsky bracket recurrence relations 79−93569

nuclear reactions involving few nucleon systems continued
hadronic reactions at intermediate energies 77−79363
light nuclei, three and four nucleon low energy scatt. expts., review 79−80945
nuclear data needs for fission reactors, fusion reactors and safeguards programmes 77−18657
nuclear surface phenomena, Yakubovski eqn. appl. to N-body systems 79−75931
polarisation in few-body reactions 77−22995
polarisation phenomena 77−18520
reaction mechanism, effect of Pauli principle and channel coupling 77−65219
relativistic effects 77−18519
resonant subsystems in few-body theory 77−18494
resonating group model for few nucleon problems 78−29431
review of reactions involving few-nucelon systems at intermediate energies 78−13054
three body problem with energy dependent potentials 77−18413
three body vertices, few-body break-up reactions, singlet or triplet deuteron interpretations 77−82901
three particle systems, reaction mechanism and approx. models 79−80904
three particle systems with Coulomb interaction, scatt. and breakup eqns. exact solns. 80−504
three-body reactions with charged particles 79−75968
three-nucleon systems, props. and interactions 79−71805
H+p, 24 GeV, J/ψ prod. cross section 78−46055
nd, three body systems, review of recent theoretical anal. 79−80842
nd break-up, quasi-free scattering, peripherical nature 78−89726
t wave function, asymptotic normalisation 77−10384
D(d,n)^{3}He, 1.1 to 2.5 GeV/c, energy depend., cross sections, reaction mech. 78−54643
D(p,p), 630 MeV, asymmetry in scatt. polarised protons *(Russian)* 78−46064
D(p,π^+)T, 410, 605, 809 MeV, pion angular distrib. 78−29466
H+p, 200 GeV, data anal. hydrodynamical model 79−551
H+p($\pi^\pm$), 200 GeV, jet production 79−54438
^{1}H(D,2p)n, 26.5 MeV, 4 dimens. comparison with local S-wave interaction Faddeev calcs. 79−17866
^{1}H(α,^{3}He)^{2}H, 3.98 GeV/c, ang. distrib. meas., comparison with DWBA 77−61416
^{1}H(α,α'X), 1.74, 2.57 GeV, low mass πN enhancement, cross section t-depend. 80−63193
^{1}H(d,X), 3.3 GeV/c, two-nucleon mass enhancement assoc. with spectator high momentum tail in breakup 77−18569
^{1}H(d,dγ) 6.3-7.1 MeV, bremsstrahlung anomaly near breakup threshold 78−89888
^{1}H(d,pn)$_2$, 45.4 MeV, tensor anal. powers 79−85447
^{1}H(n, γ)^{2}H, 37 to 72 MeV, total cross section meas. 79−49627
^{1}H(n,d), 1.88 GeV/c, neutral missing mass, ABC effect obs., cross section 78−74364
^{1}H(n,γ), polarised neutrons, calc. of P-violating asymmetry 77−18565
^{1}H(n,γ), thermal, photon circular polarisation in parity violating capture 77−6375
^{1}H(n,γ), thermal calc. of γ-circular polarisation, p-nonconservation effects 77−18564
^{1}H(n,γ)^{2}H, 2200 m/s neutrons, capture cross section 77−74849
^{1}H(n,γ)^{2}H, relativistic invariant approach, parity violation 79−3147
^{1}H(n,$\gamma\gamma$), branching ratio meas. 77−30579
^{1}H(n,$\gamma\gamma$), cross-section calc. 77−6385
^{1}H(n,$\gamma\gamma$), thermal, consistency between pion exchange currents and NN pot., cross sections 80−68556
^{1}H(n,$\gamma\gamma$)$_2$, thermal n, cross section for two-quantum n capture 79−54439
^{1}H(n,$\gamma\gamma$)^{2}H, thermal, upper cross-section limit 77−3001
^{1}H(n,p)n, 50 MeV, polarisation parameter meas. 78−50148
^{1}H(p,eν^+)^{2}H, bounds on rate, impulse approx. 77−3000
^{1}H(p,pπ^+)n, 800 MeV, Δ^{++} prod. and cross sections 79−22294
^{1}H(p,π^+)^{2}H, NN pot., isobar configurations and π prod., inelastic cross sections 79−63666
^{1}H(t,dn), 2.5 GeV/c, 4π geometry, pole approx. description 80−68678
^{2}H breakup, 156 MeV protons, NN multiple scatt. anal. 77−18546
^{2}H breakup, 45 MeV proton induced, np final state interaction ang. distrib. 77−18552
^{2}H breakup, new theorems concerning final state interactions *(Russian)* 77−326
^{2}H breakup induced by 12.5 MeV protons, Ebenhoh code anal. 77−18547
^{2}H breakup induced by 22.7 MeV nucleons, calc. with separable interactions with tensor forces 77−18554
^{2}H breakup induced by 8.5 MeV protons, Faddeev calcs. 77−18548
^{2}H breakup using 156 MeV protons, test for special kinematic conditions 77−18551
^{2}H disintegration, proton and neutron induced, up to 50 MeV *(Russian)* 78−89848
^{2}H-N breakup calcs., separable interactions with P-waves and tensor forces, polarisation 77−50101
^{2}H+^{3}He, 22 to 53 MeV, quasifree processes 77−82903
^{2}H+nucleon, breakup reaction, off shell sensitivity, S-wave N-N interactions 78−82340
^{2}H+p, ^{2}H+n, breakup reactions, realistic nucleon-nucleon interactions 78−62526
^{2}H+p(d), 6.3 GeV/c, inclusive spectra of fast p and d *(Russian)* 78−46075
^{2}H+p(n), differential cross sections, Coulomb penetration factor in DWBA calc. *(Chinese)* 80−27603
^{2}H(^{2}H,n)^{3}He, fusion through metallic D 80−13517
^{2}H(^{2}H,n)^{4}He, muon catalysis kinetics *(Russian)* 80−91206
^{2}H(^{3}He, p), cross section meas., appl. in ion beam anal. 80−42673
^{2}H(^{3}He,^{4}He)^{1}H, 27 and 33 MeV, polarised ^{3}He beam analysing power and cross sections 79−89316
^{2}H(N,X) disintegration cross-section, cut-off radius in impulse approx. type models *(Russian)* 79−22276
^{2}H(α,^{5}an)p, 28.3 MeV, ^{5}Li (3/2$^-$) tensor polarisation 80−13450
^{2}H(α,^{5}He(g.s.))p tensor polarisation ang. distribs. from sequential decay ^{2}H(α,p)^{5}He(α)n reaction 77−82899
^{2}H(α,α)np, 20-28 MeV, total reaction cross section 79−89317
^{2}H(α,αn)^{1}H, 27.2 MeV, absolute differential cross sections 79−9599
^{2}H(α,αp)n, 15 MeV, semiphenomenological impulse approx. anal. 77−82943
^{2}H(α,αp)n, 15-42 MeV, three body calc., reaction mech. 78−70546
^{2}H(α,αp)n, 42 MeV, observation and comparison to theoretical calcs. 77−82942
^{2}H(α,pα) 22.5 MeV, tensor polarisation ang. distribs. in ^{2}H(α,^{5}He(g.s.))p 77−82899
^{2}H(α,pα)n, 18 MeV, cross section, ang. depend. meas., semiphenomenological anal. 78−58292
^{2}H(α,pα)n, 18 MeV, obs. of n-p final state interaction 77−6414
^{2}H(α,pα)n, 7.5-7.9 MeV, modified impulse approx. anal. 79−6648
^{2}H(α,pα)n, Coulomb interaction effects, ^{5}He(g.s.) resonance energy and width 77−71615
^{2}H(d,^{3}He), differential cross sections at 13.2 MeV, DWBA anal. 79−45276
^{2}H(d,^{3}He)n, 2-20 MeV collimated monoenergetic neutron beam prod. using associated particle technique 77−83418
^{2}H(d,N), 50-85 MeV, ang. distribs., PWBA anal. 79−76005
^{2}H(d,2n)2p, proposed expt. to determ. nn effective range 77−18585
^{2}H(d,2p2n), 80 MeV, PWBA, double spectator process 78−41731
^{2}H(d,d), 4.3, 6.3 and 8.9 GeV.c, struct. of secondary d spectra high momentum parts *(Russian)* 78−78394
^{2}H(d,dp)n, 50-85 MeV, p-n coincidence spectra 77−18568
^{2}H(d,n), 13.6, 24.3 MeV, 0° absolute differential cross section 80−27649
^{2}H(d,n), 18-26 MeV, differential cross sections, ang. distribs., ^{4}He broad level search 80−102117
^{2}H(d,n), 290, 460 keV, neutron polarisation, ang. depend. 80−42632
^{2}H(d,n), 50-85 MeV, ang. distribs., PWBA anal., two body final states 79−6636
^{2}H(d,n), anal. power, comparison with mirror reaction (d,p) 79−75964
^{2}H(d,n), polarised d, <5.5 MeV, comparison of analysing power with ^{2}H(d,p) 79−17911
^{2}H(d,n)^{3}He, 1.5-15.5 MeV, tensor anal. power, charge symmetry violation in mirror reaction 80−13368
^{2}H(d,n)^{3}He, 35-275 keV, neutron polarisation determ. 77−41942
^{2}H(d,n)^{3}He, 6 to 17 MeV, n prod. absolute differential cross sections 78−74373
^{2}H(d,n)^{3}He, four-body model of the four-nucleon system 79−63643
^{2}H(d,n)^{3}He, neutron polarisation meas. with Mott-Schwinger scatt. polarimeter 79−22571
^{2}H(d,n)^{3}He, struct. and form factor models in mass-3 system 79−45274
^{2}H(d,n)^{3}He, total cross-section energy depend. 78−29477
^{2}H(d,n)^{3}He source spectra, TUNL fast neutron cross section facility 77−26931
^{2}H(d,p), (d,n), 50-85 MeV cross-section meas. 79−13307
^{2}H(d,p), anal. power, comparison with mirror reaction (d,n) 79−75964
^{2}H(d,p), polarised d, <5.5 MeV, comparison of analysing power with ^{2}H(d,n) 79−17911
^{2}H(d,p)^{3}H, 13.4, 17 MeV, pol. d, anal. power direct reaction and isospin symmetries 80−515
^{2}H(d,p)^{3}H, 1.5-15.5 MeV, tensor anal. power, charge symmetry violation in mirror reaction 80−13368
^{2}H(d,p)^{3}H, cross-section anal. using four-body integral eqns. 77−18577
^{2}H(d,p)^{3}H, four-body calc. solns. 79−71855
^{2}H(d,p)^{3}H, struct. and form factor models in mass-3 system 79−45274
^{2}H(d,p)^{3}H and ^{2}H(d,n)^{3}He, comparison of analysing powers 2.5 to 11.5 MeV 79−6628
^{2}H(d,p)T, differential cross sections at 13.2 MeV, DWBA anal. 79−45276
^{2}H(d,pd)n, 12.2 MeV, collinearity condition repeat experiment 79−76004
^{2}H(d,pnd), 52 MeV, break-up mechanism 78−74375
^{2}H(d,t)^{1}H, differential cross sections calc. using DWBA, distortions 78−54772
^{2}H(n, γ), slow neutrons, mesic interaction current, isobaric resonance *(Italian)* 78−25179
^{2}H(n, $\gamma\gamma$), thermal, cross-section meas. 77−26703
^{2}H(n, nn)p, 25 MeV, neutron-neutron effective range 80−83041
^{2}H(n, np)n, 130 MeV, Faddeev eqn. multiple scatt. series anal. 79−97707
^{2}H(n, np)n, 17 to 27 MeV, neutron-neutron scattering length determination, Monte Carlo analysis 80−13476
^{2}H(n,2n)p, 21.5 MeV, quasi-free scatt. 79−75993
^{2}H(n,2n)p, in thick targets, n-n scatt. length determ., computer expt. 80−57776
^{2}H(n,2n)p, inelastic scatt. mechanism at moderate energy *(Russian)* 78−41723
^{2}H(n,γ)^{3}H, existence of excited states of A=3 nuclei 79−9553
^{2}H(n,$\gamma\gamma$), thermal, calc. of cross sections and branching ratios 77−14131
^{2}H(n,$\gamma\gamma$), three-particle calc. 77−50131
^{2}H(n,n')pn, polarised n, 14, 30 MeV, neutron analysing power 79−71835
^{2}H(n,n), nonlocal nonsymmetric pot., treatment of Schrodinger eqn. 78−82325
^{2}H(n,nn), 14.1 MeV, n-n quasifree scatt. obs. 78−82337
^{2}H(n,nn)p, 21.5 MeV, cross section, nn effective range parameter 79−67669
^{2}H(n,nn)p, neutron-neutron quasifree scatt., 14.1 MeV 77−23018
^{2}H(n,np), at ϑ_n=0°, collinearity effect 78−82356
^{2}H(n,np)n, <27 MeV, n-n scatt. length 79−17904
^{2}H(n,p2n), 120 MeV, n-n scatt. length determ., Watson-Migdal model anal. 78−82339
^{2}H(n,p)2n, 13.98 Mev, proton spectra and n-n scatt. lengths 77−88141
^{2}H(n,p)nn, 13.95 MeV, proton spectrum, neutron-neutron scatt. length 77−26704
^{2}H(n,pn)n, 22.7, 46.3 MeV, perturbation calcs. for realistic pots. 79−45265
^{2}H(n,pnn), 794 MeV, quasielastic charge exchange, modified impulse approx. 78−50173
^{2}H(n,π^-)^{3}He, 400 to 580 MeV at backward pion angles 80−73847
^{2}H(p, 2p)$_2$, 400 MeV, quasifree knockout cross sections 79−93614
^{2}H(p, dπ^+)n, 585 MeV, d momentum spectra 78−41718
^{2}H(p, pn), 400 MeV, quasifree knockout cross sections 79−93614
^{2}H(p, pn)n, 8.5 MeV, ang. distrib. of final state interaction 78−54751
^{2}H(p,Nπ)^{2}H, Deck model anal. 77−22757
^{2}H(p,X),(d,X),(α,X),(^{12}C,X), 1.55, 2.89 GeV/c, total and inelastic cross sections 79−6610
^{2}H(p,2n)n, 50 MeV, expt. and theoretical cross sections 79−75994
^{2}H(p,2p), 156 MeV, kinematic collinearity condition 77−30547
^{2}H(p,2p), 156 MeV $d^3\sigma$ and $d^4\sigma$ spectra for collinear nucleon system 78−17175
^{2}H(p,2p)n, 13.25 MeV, meas. of total breakup cross-section 77−18555

nuclear reactions involving few nucleon systems continued
^{2}H(p,2p)n, 15 MeV, polarised p, cross section in non-coplanar geometry 78−93997
^{2}H(p,2p)n, 20 MeV, cf. Faddeev eqn. calcs. 77−18549
^{2}H(p,2p)n, 22.7 MeV, proton analysing power 80−78302
^{2}H(p,2p)n, 28.5 MeV, collinearity effect 79−75995
^{2}H(p,2p)n, 28.6 MeV, breakup cross sections in collinear geometry 80−9296
^{2}H(p,2p)n, 45 MeV, sensitivity to various separable S-wave NN potentials 77−313
^{2}H(p,2p)n, 585, 800 Mev, n-p final state interactions 77−41965
^{2}H(p,2p)n, 8.5 MeV, n-p final state interaction, cross section, ang. distrib. 78−21560
^{2}H(p,2p)n, high energy, final state np interaction 77−18533
^{2}H(p,2p)n, inelastic scatt. mechanism at moderate energy *(Russian)* 78−41723
^{2}H(p,2p)n, interference effects for const. NN relative energies 77−26774
^{2}H(p,γ)^{3}He, 450, 550 MeV, differential cross sections, inverse reaction comparison 80−86904
^{2}H(p,n)2p, pol. n and p, 10.6-15.1 MeV, transverse polarisation transfer at 0° 80−42630
^{2}H(p,np)^{1}H, 1.825 GeV/c anal., Glauber theory comparison 77−71525
^{2}H(p,nπ^+), 585 MeV, differential cross sections, reaction mechanisms 79−548
^{2}H(p,p)pn, polarised p, vector anal. power in final state interaction region 79−71836
^{2}H(p,pn), 156 MeV, kinematic collinearity condition 77−30547
^{2}H(p,pn), 156 MeV $d^3\sigma$ and $d^4\sigma$ spectra for collinear nucleon system 78−17175
^{2}H(p,pn)^{1}H, 1 GeV, final-state interactions 77−82900
^{2}H(p,pn)^{1}H in relativistic description of moving composite particles 77−46156
^{2}H(p,pn)p, 15 to 156 MeV, attenuation of quasifree scatt., empirical rules 77−61415
^{2}H(p,pn)p, 1.67 GeV/c, secondary particle ang. distribs. and correlations *(Russian)* 80−27646
^{2}H(p,pp)n, 50 MeV, pp coincidence meas. 77−18556
^{2}H(p,pp)n, 6.4 to 25.8 MeV, pn final state interaction, cross sections 78−54757
^{2}H(p,π^+), 400, 470, 600 MeV, microscopic model calcs., reaction cross section 79−40916
^{2}H(p,π^+)^{3}H, NN pot., isobar configurations and π prod., inelastic cross sections 79−63666
^{2}H(p,π^+)^{3}H, studied via pp→π^+d amplitude and triangle graph 77−38265
^{2}H(p,π)^{3}H, pion prod. models for medium energies 77−18563
^{2}H(p_0,p_1,p_2)n, 156 MeV, test on p_1-n-p_2 colliniarity reson. 79−75996
^{2}H(t,n)^{4}He, 10.5 MeV polarised tritons, analysing power, polarisation function and transfer coeff. 77−10413
^{2}H(t,n)^{4}He, 7-17 MeV, absolute differential cross sections meas. 77−26780
^{3}H (p,n)^{3}He, determ. of π^3He^{3}He coupling constant from differential cross section 78−89801
^{3}H, influence of structure on cross-section of complete electrosplitting *(Russian)* 79−22272
^{3}H-n(p) phase shift, below d+d threshold, from Alt-Grassberger-Sandhas eqns. 78−41650
^{3}H+n, 14 MeV, spectra meas. 77−18558
^{3}H(^{3}He, X), 50, 65, 78 MeV, quasifree scattering and quasifree reaction processes 80−13486
^{3}H(^{3}He,^{4}He)^{2}H, excitation functions for incident energy 17 to 33 MeV 79−6640
^{3}H(^{4}He,d), reaction mechanism, effect of Pauli principle and channel coupling 77−65219
^{3}H(d, n)^{4}He, meas. of mean d interaction energy in tritiated Ti layer 79−31281
^{3}H(d,n)$_3$ pol. d, below 6.75 MeV, tensor anal. power 80−42633
^{3}H(d,n)^{4}He, 6 to 17 MeV, n prod. absolute differential cross sections 78−74373
^{3}H(d,n)^{4}He, 7-17 MeV, absolute differential cross section meas. 77−26780
^{3}H(d,n)^{4}He, 700 keV, n polarisation meas., scintillation + TOF technique 78−86538
^{3}H(d,n)^{4}He, neutron energy meas. with Si detector 80−32566
^{3}H(d,n)^{4}He, neutron fluence and energy transfer standard 80−102194
^{3}H(n,n)^{3}H, possible anomaly in backward elastic scatt. cross section near 14 MeV 78−13088
^{3}H(p,γ), 30-100 MeV, meson exchange and nucleon correlation process calcs. 79−549
^{3}H(p,γ), 6 to 16 MeV polarised protons, ^{4}He excited states 77−18559
^{3}H(p,n), 1.24, 1.8 GeV, differential cross section, spin independ. Glauber model interpretation 80−63183
^{3}H(p,n)^{3}He, 6 to 17 MeV, n prod. absolute differential cross sections 78−74373
^{3}H(p,n)^{3}He, associated particle methods for neutron flux monitoring 79−9977
^{3}H(p,n)^{3}He, coupled channels anal. of neutron polarisation 77−18560
^{3}H(p,n)^{3}He, R-matrix anal. of polarisation and analysing power 77−88142
^{3}H(p,p), 0.6 to 1.04 GeV, differential cross sections calcs. *(Russian)* 78−54763
^{3}H(π^-,3n), final state continuum spectra, hyperspherical basis 77−26590
^{3}H(t,2n)^{4}He, 30-160 keV, differential cross section measurement 78−17223
^{A}H(n,X), 60 keV-80 MeV, A=1,2,3 total cross section and scatt. length 80−99176
H(α,X), 16.5 GeV/c, inelastic cross sections, multiplicity, ang. and momentum distribs. 78−82359
H(d,2p)n, 26.5 MeV, Faddeev cross section and scatt. symmetries over 50% of total phase space 79−76003
H(d, d), 800 to 1430 keV, differential cross section meas. 79−80947
H(d,n)^{3,4}He reactions, NA-2 neutron generator, fast neutron spectrum, stilbene scintillation spectrometer meas. *(Czech)* 77−71710
H(d,p), 6.3 GeV, proton momentum spectra 79−6621
H(d,p), A=1,2, 6.3 GeV/c, p momentum spectra from d breakup 78−89887
H(d,pp)n, 12.9 MeV, differential cross-sections meas. 78−13113
^{3}He breakup, 156 MeV protons, NN multiple scatt. anal. 77−18546
^{3}He breakup induced by 156 MeV protons, pd final state interactions 77−23013

nuclear reactions involving few nucleon systems continued
^{3}He, influence of structure on cross-section of complete electrosplitting *(Russian)* 79−22272
^{3}He+^{3}He, evidence for high-energy deuterons 77−23099
^{3}He+^{3}He, possible sources of high-energy deuterons, solar neutrino problem 77−18588
^{3}He+^{3}He, quasifree processes, 50-78 MeV, cross-section meas. 77−18586
^{3}He+d breakup, quasifree processes 77−18575
^{3}He(^{2}He, ^{2}H)^{4}He, high energy deuteron prod. 79−93639
^{3}He(^{3}He, dd)pp, 50, 78 MeV, cross sections, two-spectator quasifree process 78−86539
^{3}He(^{3}He,^{2}Hνe^+)^{4}He, 11.5 MeV, search for high energy deuterons 79−76012
^{3}He(^{3}He,X) 50, 65, 78 MeV, quasifree scattering and quasifree reaction processes 80−13486
^{3}He(^{3}He,dd)pp, 50, 78 MeV, study of four body continuum 77−18587
^{3}He(^{3}He,p)^{5}Li, polarised protons, deuteron transfer obs. 77−329
^{3}He(N,πX), expt. review of π-prod. by (un)polarised nucleons on few-nucleon systems 79−80944
^{3}He(d,d)^{3}He, 0.3-8 MeV, single-level reson. and ^{5}Li parameters 77−30606
^{3}He(d,p), pol. d, below 6.75 MeV, tensor anal. power 80−42633
^{3}He(d,p), polarised d, 10-17 MeV, cross sections, vector and tensor anal. powers 79−75966
^{3}He(n, γ), 1-70 keV, effective cross sections *(Russian)* 79−30836
^{3}He(n,$\gamma\gamma$), thermal, calc. of cross sections and branching ratios 77−14131
^{3}He(p,2p)^{2}H, 155 MeV, multiple scatt. diffraction theory anal. *(Russian)* 77−10408
^{3}He(p,2p)d, 590 MeV, in noncoplanar geometry, two particle spallation, diffr. description *(Russian)* 78−33160
^{3}He(p,2p)d(d*), 136 MeV, d/d* ratio, PWIA anal. 79−75999
^{3}He(p,dp), (p,2p), and (p,pn), 156 MeV $d^3\sigma$ and $d^4\sigma$ spectra for collinear nucleon system 78−17175
^{3}He(p,dp)p, 156 MeV, p-d scatt. at small rel. energy in FSI region 79−85441
^{3}He(p,p), 0.6 to 1.04 GeV, differential cross sections calcs. *(Russian)* 78−54763
^{3}He(p,pd)p, 35 and 45 MeV, four-body break-up calcs. 77−57667
^{3}He(p,pp)d, 35 and 45 MeV, four-body, break-up calcs. 77−57667
^{3}He(p,π^+)^{4}He, 415 MeV, angular distrib., microscopic description, generalisation of (π,π) *(Chinese)* 80−63188
^{3}He(p,t)Δ^{++}, 850 MeV, search for (Δ^{++},2n) in the ^{3}He wave function 78−82345
^{3}He(π^+,3p), final state continuum spectra, hyperspherical basis 77−26590
^{3}He(t,d)^{4}He, charge asymmetry effects 79−3159
^{3}He(t,d)^{4}He, symmetry breakdown as cluster spatial effect 79−6619
^{3}He(t,d)^{4}He asymmetry, cluster model anal., isobaric analogue states 78−78389
^{4}He (^{3}He,p), 15.95 MeV (c.m.), phase shift anal., σ_r determ. 77−88159
^{4}He (α,n)^{7}Be, differential cross sections meas., 39 to 50 MeV 78−25207
^{4}He+N, potential calc. using microscopic model 77−88091
^{4}He+α, 103 MeV, exptl. study of ^{6,7}Li and ^{7}Be prod. 79−45279
^{4}He+α, 75.2 MeV, TDHF calcs. using separable three dimens. wavefunctions 78−50111
^{4}He+α break-up reactions, 130 MeV, continuous energy spectra of emitted particles 79−76013
^{4}He+n, pole positions of ^{5}He resonances, models calcs. 78−70530
^{4}He+p, 18.6 GeV/c, coherent prod. of low mass p$\pi^+\pi^-$ states 78−33175
^{4}He+p, 50 MeV, deuteron production possibilities, astrophysics importance 79−40928
^{4}He+p, 8.56 GeV/c, two pronged events, cross sections and prod. features 79−3152
^{4}He+π^-, coupled channel method, determ. of total cross sections 79−36281
^{4}He(^{3}He,α), 15.95 MeV (c.m.), phase shift anal., σ_r determ. 77−88159
^{4}He(α,n)^{7}Be, differential cross sections meas., 39 to 50 MeV 78−25207
^{4}He(α,p)^{7}Li, differential cross sections meas., 39 to 50 MeV 78−25207
^{4}He(d,p), 6.8 , 7.8 MeV, continuous proton spectra obs. 78−37352
^{4}He(d,p)^{4}He n, 15 MeV polarised deuterons, differential cross sections, vector analysing powers 78−89884
^{4}He(d,t)^{3}He, charge asymmetry effects, cluster model calc. 77−14136
^{4}He(p,^{3}He), ^{2}H, large momentum transfers, π exchange effects 80−5143
^{4}He(p,X)^{3}He, 6.85 GeV/c, inclusive angular distributions 77−74845
^{4}He(p,X)^{3}He, 6.85 GeV/c, Glauber multiple model 79−63664
^{4}He(p,2p)^{3}H, 350 and 500 MeV, energy sharing spectrum, symmetric angular distrib. 79−6582
^{4}He(p,d), intermediate energies, pion exchange currents in DWBA anal. 80−32199
^{4}He(p,d), reaction mechanism, effect of Pauli principle and channel coupling 77−65219
^{4}He(p,d)^{3}He, 275-500 MeV, large angle meas. 78−41713
^{4}He(p,d)^{3}He, 3.98 GeV/c, ang. distrib. meas., comparison with DWBA 77−61416
^{4}He(p,d)^{3}He, 770 MeV, calcs. 77−6357
^{4}He(p,d)^{3}He, 770 MeV, exact finite range DWBA, cross sections 78−70531
^{4}He(p,d)^{3}He, direct-reaction mechanisms 78−581
^{4}He(p,d)^{3}He, energy depend. and cross sections 200-500 MeV 79−13296
^{4}He(p,d)^{3}He, large momentum transfers, π exchange effects 80−5143
^{4}He(p,pn)^{3}He, ^{3}He momentum spectra determ. by cluster model interpretation 79−6577
^{4}He(t,n), R-matrix anal. of polarisation effects in ^{7}Li system 77−2968
^{4}He(t,n)^{6}Li, cross section using var. calcs. in generator coordinate method 78−13122
^{4}He(t,t)$_4$ R-matrix anal. of polarisation effects in ^{7}Li system 77−2968
^{4}He(t,t)^{4}He, cross section using var. calcs. in generator coordinate method 78−13122
^{4}He(t,t)^{4}He, elastic cross section from two-centre generator coordinate model functions 78−12994
H(n,γ), parity violation study, high-rate counting circuitry for γ-rays 78−62527
H(n, $\gamma\gamma$), thermal, cross-section meas. 77−26703
^{2}N breakup, nucleon induced, NN interaction parameters 77−18550

nuclear reactor fuel *see fission reactor fuel*

nuclear reactor instrumentation
acoustic monitoring equipment for nuclear power plants: research, development and industrial production 79−76076
activation detector ave. cross sections in ^{252}Cf benchmark field 78−82598
activation detectors for fast neutron fluence determ., radiochem. evaluation, reactor appl. *(German)* 77−34510
activation detectors for neutron flux and spectrum determination 77−71727
AGR, Central Inertial Collector for removal of spalled oxide particles from coolant 80−5231
AGR shutdown sequence equipment, use of computer based training simulator 79−89461
ampules for handling graphite specimens for irrad. in reactor core and reflector channels 77−50220
automated nondestructive assay system for Pu samples 77−61512
automatic power control of IRT-M reactor using in-core detector system 77−50264
automatic reactor regulator and xenon oscillations 79−41015
automatic stochastic data processing system for reactor monitoring 79−97962
BER II research reactor, transport capsule separation from sample containers at fast pneumatic transport systems for neutron activation analysis 77−74966
Biblis Nuclear Power Station, meas. and control system, fault statistics evaluation *(German)* 79−97819
Bohunice A-1 reactor, type E2 instrumented fuel elements *(Slovak)* 77−50260
boilers water conditions, chemical monitoring development in UK *(Russian)* 77−88217
BR3 reactor, instrumentation for continuous monitoring of primary water B content *(French)* 80−32408
burnup meter for fast reactor fuels using γ-ray spectrometer with minicomputer *(Japanese)* 77−50206
BWR, Bilibino power station, internal power-distribution monitor system 78−17341
BWR, computer based systems 80−83211
BWR, H_2 and O_2 monitoring in containment and off-gas systems 80−32414
BWR, in-service inspection and external base-line tests, instrumentation 80−784
BWR, method for detecting bypass coolant boiling 80−571
BWR, on-line core performance evaluation and operating guidance system 79−97859
BWR in-core detector noise, neutronic anal. 79−81026
BWR in-core instrument tube vibration obs. by reactor noise techniques 78−94064
BWR in-core neutron detector sensitivity to control rod vibr. using neutron noise anal. 80−57910
BWR in-core neutron flux instrumentation package 77−71641
BWR neutron noise source identification, stochastic model data anal. 78−94106
BWR neutron noise source identification from existing instrumentation 79−13483
BWR noise, response of neutron detector to local coolant void distribs. 80−683
BWR power plants, neutron flux monitor 77−14240
BWR power reactor, in-core startup system with neutron flux monitor 80−32405
BWR safety relief valve, remote set pressure verification 79−54487
BWR-4 neutron noise anal. of incore instrum. tube vibr. and impacting 79−36353
BWR-4 neutron noise analysis spectra, instrument tube flow-induced vibr. 78−94063
BWR-4 neutron noise analysis spectra characterisation 79−13482
cables insulated with Al_2O_3 and MgO, resistance to high-temp. and intense gamma radiation 78−25332
calorimeter for remote meas. of heat release from irrad. fuel rods 77−46223
calorimeters for in-core nucl. heating rates meas. 78−25279
CAMAC-controlled calibration system for nucl. reactor systems 78−37532
CANDU, development of irrad. fuel bundle counters for reactor safeguards systems 78−94119
CANDU, nuclear quality high pressure valve bellows, development, report 78−82490
CANDU 600 MW, spent fuel bundle counter, safeguard design 79−13495
CANDU distributed computer control systems 79−76105
CANDU nuclear power reactors, automated chemistry control system development 80−42738
CANDU nuclear reactors, in-situ inspection of press. tubes, nonrotating device 78−25259
CANDU self-powered flux detectors, response characts. 80−32404
CANDU-PHW, thermal neutron flux-mapping system 80−792
cavity geometry impact on power distrib. meas. with multisection ex-core detectors 79−93794
ceramic probes for meas. O_2 content in liquid sodium manufacture and props. 77−54308
class 1E electronic instruments, ageing 78−8945
class 1E reactor components radiation test facilities for LOCA anal. 79−59277
Compton recoil gamma-ray spectroscopy, current status 80−47808
computer modules, appl. to data handling, simulation, alarm anal., and safety *(German)* 79−49788
computer-based radionuclide analyzer system for nuclear power stations 79−81100
computerised reactor safety systems, design, specification and implementation 79−63783
conduction centrifugal EM pump for nuclear reactor coolants, characts., operation 78−86246
conductivity calorimeters, fission energy distrib. in fuel elements *(Czech)* 77−6492
conference, nuclear power systems, San Francisco, CA, USA (Oct. 1979) 80−56994
containment structures pressure tightness verification, pressurisation plant, data acquisition and processing *(Spanish)* 80−13775
control and instrumentation designs beyond the 1980s 80−57872
control and instrumentation test loop diagrams 80−68890

nuclear reactor instrumentation continued
control instrumentation, commissioning and maintenance experience at Rajasthan 79−89455
control rod drop damping and velocity meas. instrumentation *(German)* 80−5248
control rod reactivity meas. error analysis 79−9783
control room and desk design, alarm system, information displays 79−89462
coolant pressure boundary leakage detection system 80−63306
core monitoring system accuracy, effect of inoperable in-core detectors 79−93790
core temp. monitoring, can thermocouple distribution procedure 78−54856
count-doubling time monitor, new reactor safety circuit for low-power-level operation 79−41004
counting-Campbelling channel for in-core and out of core neutron flux meas. 80−32406
CRBRP ex-vessel transfer machine 78−8943
CRBRP mixing-tee model, vibration studies of perforated plates 79−49665
cross-correlation flow meas. error estimation and reduction 79−3194
CRT man-machine communication system in nuclear power stations 79−45364
data acquisition fast analogue scanner 77−6656
data processing system of Dungeness 'B' power station 77−67831
decentralized instrumentation and control system with bus transmission in nuclear power plants 79−97847
digital computer applications in reactor instrumentation and control 80−106134
digital computer control in Canadian nuclear plants, past performance and future outlook 78−58383
directional γ-ray detector for in-core fuel motion monitoring 78−37448
directional fully encapsulated gamma detector for in-core reactor meas. 80−63307
dosimetry using TLD and Rh activation techniques 77−50301
Dounreay Fast Reactor, instrumentation developments since 1972 80−23118
Dounreay fast reactor creep-measuring machine 77−42015
EBR II, reactor subassembly removal using gripper device 80−57942
EBR-II, Na-water, leak detection system 78−78484
EBR-II active calorimeter design improvement 79−9967
EBR-II anomalous reactivity meter 77−42114
EBR-II subassembly profilometer at HFEF 77−54299
eddy current flaw detector, nuclear reactor fuel testing appl., electrically conducting inclusions detection 77−90560
electrical isolation devices employing fiber optic cable 79−59218
electrochemical O_2 meter for meas. in liquid Na 78−58337
electron bombardment heater for heat transfer studies 77−30146
EM compatiblity and protection against EM interference 79−89465
EM instruments for use in liquid sodium, theoretical anal. 78−54857
fast flux reactor tests, neutron radiography facility 80−18371
fast reactor integral meas. consistency, cross-section adjustment 79−9867
fast reactor system, eval. of variational method for estim. of neutron detection efficiency 79−80992
fast response electrometer for pulse reactor experiments 78−70157
FBR core surveillance and protection systems *(French)* 79−76099
FBR fuel pin safety expts. at SLSF, centerline fuel thermocouple performance 80−102283
FFTF, thermal-hydraulic anal. of air dump heat exchangers 79−59146
FFTF core component meas. system 79−9728
FFTF element measuring system 79−9729
FFTF fuel failure, cover-gas monitoring system 78−4998
FFTF-type eddy-current flowmeter performance in SLSF P-series test trains 79−9669
fissile resistors, appl. to intense neutron flux pulse meas. 79−31326
fission chambers, miniature, for neutron field meas. in critical assemblies 78−82422
fission counters, performance optimisation algorithm 80−47828
fission counters of high sensitivity for use, in high gamma fields 78−8883
fission reactor safety channel system with on-line testing capability 77−65278
flowmeter, flux distortion, tests using analogue rig to simulate flow with boundary layer 78−38420
flowmeter calibration, Na-cooled reactor, signal anal. method 78−38425
flowmeters for two-phase mass flow rate meas. during LOCA blowdown phase 80−778
fluctuation-type reactor power and period meter, errors 77−54292
fluid velocity profile meas. by nonintrusive transaxial tomography 80−99268
fuel cladding, internally pressurised, instrument for strain meas. 77−65271
fuel cladding strain meas., microprocessor-controlled microwave extensometer 78−33240
fuel pin mass and heat transfer coeff. meas. by pneumatic gauging 78−58329
fuel pin simulators for thermodynamic expts. with nucl. fuel elements 80−37420
fuel recycling remote manipulation systems design and performance 77−67854
fuel rod gas pressure meas. during LOFT, sensor description 80−57876
fuel thermocouples and liquid-level probes for core monitoring 80−99239
full m-core instrumentation system, calculational verification 77−42149
full-range reactor power meas., pulsed ion chamber methodology 79−13480
fusion reactor, Doublet III, neutral beam injector system, instrumentation and control 80−99322
gain stabilized NaI(Tl) γ-ray detector, electronics, disc-based minicomputer, power shape in LWR core 78−33284
gamma densitometer meas., anal. of dynamic bias 80−27730
gamma densitometry, static error evaluation 80−27729
gamma spectroscopy on-line system, automatic sequencing using microprocessor controller 77−54393
gamma-ray densitometry, dynamic bias 80−27728
gamma-ray spectrometer, wide range Ge, for on-line meas. of reactor cooling water activity 77−65381
gamma-ray spectrum meas. inside reactor, calorimetric method 78−17293
gamma-ray threshold self-powered detector, use as reactor power monitor 77−65280

nuclear reactor instrumentation continued
gas cooled reactors, velocity flow field near moving cascade, meas. using hot wire technique 77−50195
gas tagging, analytical design for optimization of tag gas isotopic compositions 80−23026
GCR He primary coolant impurity monitor 80−32413
graphite radiation damage dosemeter, GAMIN, correlation data 78−29657
HFR at Grenoble, neutron beam installations 77−26864
high voltage instrument cables for 650°C, in-vessel breeder reactor service 80−57878
high-temperature optical void probe 79−93705
high-temperature reactor structural displacement and strain analysis by picture processing *(Japanese)* 80−78352
HTGCR fuel, electrostatic transport system for spherical particles *(German)* 77−67847
HTGR, He circulators for primary coolant cycle, developmental and performance tests 80−597
HTGR monitoring and control instrumentation, special needs 78−734
HTGR nuclear fuel microspheres, automatic particle size analyser 79−12921
HTR, fission chamber development 79−76112
HWGCR, KS-150, in-core instrumentation, neutron flux, temp. distrib. 77−83050
HWR, charact. of Pt self-powered flux detectors 77−65282
hydrodynamic testing equipment with gravitational channel for reactor core meas. *(Slovak)* 78−21625
hydrogenous neutron deectors for reactor spectrum meas. 77−71733
IAEA nuclear safety standards program for protection, electric, instrumentation systems 79−45365
IAEA safeguards, instruments and techniques for nondestructive assay 78−33302
IEEE conf., scintillation and semiconductor counters and nucl. power systems 77−54389
impurity monitoring in liquid Na, electrochemical meters 80−22886
in-cell weighing system at HFEF 77−54298
in-core meas. of energy release, computerised *(Czech)* 78−86637
in-core measuring system for VVER-440 and VVER-1000 type reactors 'INCORMER' *(Russian)* 79−30965
in-core movable neutron flux mapping computerised console development 78−13308
in-core neutron detection using mag. focused electrons, appl. to fast and thermal reactors 77−50271
in-core neutron detector using magnetically focused electrons 79−45564
in-reactor fuel-to-sheath heat transfer meas. 79−13408
in-reactor performance of surface-mounted and embedded thermocouples 79−93704
in-reactor small high temp. ionisation chamber 79−18087
in-reactor temp. meas. accuracy, thermometer construction effects 79−17969
installation for in-reactor study of creep and stress-to-rupture, plane stress mode 78−39996
International Electrotechnical Commission standards for reactor instrumentation and controls 79−45366
ionic sensors for nuclear reactor in-core temp. meas. *(Czech)* 78−32820
irradiated fuel, nondestructive devices for on-site examination 80−13699
irradiated fuel visual inspection, design of compact, portable stand 79−67912
Japanese reactor noise pattern library 79−3338
JOSEF gas filled separator, focusing and dispersive props. 77−26426
k(∞) meter for LWR spent fuel storage pools 80−37560
laboratory instructional programs in computer instrumentation at RPI 80−31472
laser scanning camera 80−52748
laser system for determ. of fission product release and distrib. in coated particles *(German)* 78−82403
leached hull monitor for determ. of transuranic content of spent reactor fuel 79−85606
leak detection system operating experience 79−9808
liquid level detector based on level sensitive transducer for PWR environment 80−57874
LMFBR, acoustic surveillance of anomalous events 78−37397
LMFBR, ANL high temp. microphones 77−46361
LMFBR, boiling stability tests on THORS Na loop 78−37396
LMFBR, Clinch River, in-core instrumentation 78−29608
LMFBR, compact Na cooled reactor, KNK-1, total and fast neutron flux meas. *(German)* 78−62591
LMFBR, coolant start of boiling detection by acoustic method 78−86646
LMFBR, fuel motion diagnostics instrumentation, evaluation with PARKA 79−45360
LMFBR, Na purification system, cold traps and plugging indicator 80−99209
LMFBR, plugging indicator, measuring accuracy 79−63732
LMFBR, safeguards system for monitoring of fissile material inventory 80−63293
LMFBR blanket assembly cooling, flow regulating device 80−23029
LMFBR coolant flow rate meas. suing electromagnetic convertor 80−73887
LMFBR coolant temp. meas. using high integrity coaxial thermocouples 80−32410
LMFBR cooling circuit, calibration of EM flowmeters by average frequency method 80−570
LMFBR core instrumentation, approach based on IR television, on-line computing, pattern recognition 77−54310
LMFBR core melt-down protection system *(Russian)* 79−76101
LMFBR core simulation, Na loop safety facility, P2 expt., LOCA, acoustic meas. 78−33264
LMFBR data multiplexing system 79−76102
LMFBR ex-vessel low level flux monitor neutron source strength determ., appl. of nuclear data 77−26865
LMFBR failed-fuel detection using gaseous fission-product detectors 79−97856
LMFBR fuel pin plenum press. transducer 78−8884
LMFBR fuel pins, computer anal. and control for nondestructive gamma scanning 79−9754
LMFBR high-temp. neutron detector test results 77−74909
LMFBR hypothetical accident, use of hodoscopes to obtain tomographic resoln. of fuel motion 79−54537
LMFBR in-core instrumentation, Na test facility 77−50196
nuclear reactor instrumentation continued
LMFBR inherent secondary shutdown assembly, hydraulic tests 79−49666
LMFBR multipin bundles, eval. of hodoscopes for fuel motion meas. 79−93780
LMFBR Na-heated steam generator, flow instability detection by noise anal. 79−97854
LMFBR reactivity surveillance using ex-core detectors 79−9802
LMFBR safety testing, scram signal generator for fluid motion monitoring 80−18551
LMFBR steam generators, safety alarm system, water leakage detection *(Czech)* 78−33268
LMFBR subassembly fault detection, microprocessor-based distributed system appl. *(Japanese)* 79−41002
LOFT drag disc turbine meter rakes for two-phase flow measurement 80−102260
LOFT reactor advanced instrumented center fuel bundle, in-reactor meas. devices for LOCA expts. 80−23024
logarithmic electrometer, for pulse-reactor expts. 78−86291
low-temp. facilities, irrad. devices, cold neutron sources *(French)* 77−131
LWBR delayed-neutron pellet assay gauge 79−54590
LWR, power distrib. monitoring using gamma thermometers 79−45368
LWR power station radioactive unplanned dischage meas. 78−89995
LWR power stations, design features and instrumentation for materials safeguards *(Russian)* 80−63278
magnetic flowmeters, bubble noise effects on output signal, Na loop test 78−91038
magnetic scattering expt., deviations from saturation 79−31355
magnetoacoustic rod position monitoring transducer system for nuclear power plant 78−33262
Magnox reactors, remote corrosion monitoring, laser based instrument 78−41822
Maine Yankee reactor protection system setpoint calc. 79−13479
malfunction detection by Dynamic Data System methodology 79−622
manipulator vehicles of Nuclear Emergency Brigade in Federal Republic of Germany 77−50315
mass flow instrumentation performance, during LOFT nonuclear test series 80−69952
master-slave manipulators and remote maintenance in nuclear research 77−71682
materials safeguarding, containment and surveillance devices 80−63349
materials safeguarding, development of containment and surveillance measures for IAEA safeguards 80−63350
materials safeguarding, fuel assembly identification using US signatures, statistical aspects 80−69620
materials safeguarding, remote-controlled and long-distance unique identification of reactor fuel elements or assemblies using US signature equipment 80−63296
materials safeguarding, VACOSS electronic sealing system 80−63348
materials safeguards, ultrasonically identified security seals for CANDU safeguard systems 80−63297
materials testing, intrareactor facility for physicomechanical props. investig. by pulsed US spectroscopic method 78−70591
melting pool surfaces, temp. meas. by ratio pyrometers 78−82471
mesh-packed cold traps for liquid Na purification, effect of shape on perform. 79−40986
meshless cold trap, performance evaluation 79−54488
microprocessor appl. 80−83147
microprocessor based operator independent reactor power monitor 79−85644
microprocessor controlled multipoint recorder with graphical video output for reactor core temperatures 80−57873
microprocessor controlled reactivity meter for real time monitoring of reactors 78−33263
mineral insulated cables performance, review *(German)* 77−6573
mixed oxide fuel, retained fission gas determ., new instrumental method 79−54477
monitor for detecting spent fuel bundle absence from position in storage basket 77−61511
multiaxis neutron diffractometer automation 80−102417
multiple fuel failure resolution with gas tagging, barycentric coordinate technique 79−13485
multiplication meter, Pu sample verification and assay appl. 78−82527
multivariable parameter meas. and display microprocessor solution 79−72221
MWR feedwater and recirculation flow, minicomputer-based digital control 80−23027
neutron 2 keV filtered beam facility 77−23346
neutron and γ-ray spectra meas. on radial shielding model of KS-150 reactor *(Slovak)* 78−21624
neutron beta-emission cable-type detector with Ag emitter, sensitivity during long service in reactor 78−86644
neutron counters, development, electron drift vel. in inert gas mixtures 80−48843
neutron detector response in water moderated reactor, influence of air bubbles 80−18442
neutron detectors for reactor control 77−54326
neutron flux, density measurements for reactor control *(German, English)* 78−17335
neutron flux density distribution meas., azimuthal-axial, at fuel element surface *(Czech)* 79−36344
neutron flux density monitor of non-flux perturbing thin foil 80−32522
neutron flux detection using self-powered Inconel-Inconel coaxial cable 80−42842
neutron flux instrumentation commissioning, EM compatibility 79−89466
neutron flux level CRT state indicator 77−79444
neutron flux meas., calculation of target and detector size in determination of 14-MeV neutron energy flux 79−97829
neutron flux meas., high temp. neutron rad. detectors and cables 79−76111
neutron flux meas., integrated cable detectors for use under flux and/or at high temperature *(French)* 79−76114
neutron flux meas., self-powered neutron detector with enriched-U emitter 79−76115
neutron flux monitoring during reactor refuelling and start-up, instrum. *(Polish)* 80−42792
neutron instrumentation for protection and control of nuclear reactors *(French)* 80−32407
neutron noise analysis techniques 77−3069

nuclear reactor instrumentation continued
neutron noise meas. technique, coupled swimming pool reactor *(French)* 77−10462
neutron radiography facility at Texas A and M Nuclear Science Centre 80−9401
neutron radiography using Birmingham dynamitron accelerator 77−81452
neutron sensor for volumetric steam content determ. 79−30904
neutron spectrometer for neutron spectra meas. in thermal reactors *(German)* 79−3282
neutron spectroscopy using miniature detectors and preamplifiers 80−47669
noise, specialists' meeting, Gatlinburg, USA, Sept. 1977 78−94057
noise analysis, Polish developments 79−3216
noise analysis by multivariate statistical pattern recognition system 77−14228
nondestructive assay instruments for Pu-U anal., in-line evaluation 79−85589
nondestructive assay of highly enriched spent fuel, using Ge(Li) detector and ^{235}U fission chambers 79−89522
nondestructive gamma-ray spectrometry method for fuel burn-up control *(Slovak)* 78−21672
nondestructive materials assay system for LASL's U recovery plant 77−42167
nuclear engineering, process instrumentation meas. 78−17447
nuclear fuel nondestructive assay techniques and instruments *(Japanese)* 77−57716
nuclear reactor vessel, recording instrument for US inspection results 79−5104
on-line alarm analysis in the hierarchical control system of the WWR-SM research reactor 79−76104
on-line radiation monitoring at fuel reprocessing plant 79−85731
on-line reactivity meter, comparison between direct and polarity correlation techniques for projected Gauss Markovian process 79−54528
operation in adverse environments, conference, London (1976) 78−189
operational and reliability experience with ractor instrumentation for AGR and magnox reactors, review 79−89453
oxide thickness in shutdown fission reactor meas., abrading system appl. 79−63720
Pakistan, transfer of control and instrumentation technology 77−65356
PBF, temp. sensitivity of Co self-powered neutron detectors under PWR conditions 78−33275
PBHTR, out-of-core instrum. for detection of spatial flux irreg. *(German)* 78−82430
period meter, digital, microprocessor controlled, hardware and software 80−63473
photographic techniques to study reactor thermodynamics and fluid dynamics *(Spanish)* 77−71635
piezoelectric transducer, appl. to fast breeder reactors 77−12314
plant diagnostics−the integrated approach 80−68899
plugging indicator, liquid Na impurity deposition rate obs. 79−13557
plugging indicator for Na impurities, meas. accuracy 78−54813
pneumo-tube on vertical channel of thermal neutron research reactor-2000 *(Russian)* 77−38332
portable digital reactivity meter for power reactors PWR, BWR appls. *(German, English)* 77−82999
portal monitors for detecting and safeguarding special nuclear materials 80−63406
post-accident filtration design for PWR and BWR containments 79−49739
power burst facility fission product detection system 79−54536
power density limitation system development 80−68884
power measurement by continuous calorimetry, automated system 78−17336
power plant, Trojan, operating and startup experience 77−65283
power plant availability improvement by surveillance techniques 79−9812
power plant control and instrumentation. [conf. Cannes, France (Apr. 1978)] 79−76096
power plants, diagnostic system using noise anal. 78−50279
power plants, practical implementation of regulatory guide 1.75, class 1E circuits 77−65345
power signal background and source strength meas. 77−57707
power spectral density signature analysis, statistical algorithm 79−624
power station, Three Mile Island, operating experience with control, instrumentation and electrical system 77−65285
pressure and temp. sensors, reactor time const. determ. by dynamic data system method 79−93750
pressure pulse sensors, calibration, indirect piezoelectric effect *(Czech)* 77−5857
pressure recorder liquid cooling pipe *(German)* 77−88218
pressure transducer response verification, testing unit and test methodology 78−13253
pressure vessels testing, strain gauges performance in pressurised water at 50°C 79−35713
primary coolant flowmeter 80−73912
primary-circuit components, surveillance of vibr. behaviour 80−790
protection system, development of integrated numerical protection system *(French)* 79−76097
protection system equipment, class 1E, qualification requirement 77−67822
Prototype Fast Reactor, instrumentation and control systems 77−67830
pulsed-neutron sources for flow measurement 79−93695
PWR, computerised axial power distrib. monitoring system 77−65279
PWR, coolant pump motors, max. freq. decay rate determ. 79−45337
PWR, core flux meas. by microprocessor based automatic flux mapping system 79−45359
PWR, digital rod position indicator system for control rod drive line dynamic characts. study 78−33265
PWR, effect of measurement conditions on the design of delayed-neutron detector units *(French)* 79−97855
PWR, equipment for the limitation of power density 80−697
PWR, ex-core neutron detectors, calc. of spatial weighting func. 79−36351
PWR, fault tolerant multiplexed control rod position detection and system 77−65281
PWR, fixed in-core gamma thermometer for neutron flux meas. 80−717
PWR, improved instrumentation and computer control systems 78−29601
PWR, on-line meas. of B concentration in water using neutron absorption method *(French)* 80−32409
nuclear reactor instrumentation continued
PWR, power monitoring, direct charge detectors appl. 78−17344
PWR, Pt-resistance thermometers, in-pile response time testing 79−59219
PWR, system for internal neutron meas. *(French)* 79−76113
PWR, thermohydraulic processes study, models and expt. instrumentation *(Hungarian)* 78−82433
PWR, Westinghouse, neutron flux mapping at low power 78−21703
PWR acoustic monitoring instrumentation 78−17309
PWR acoustic monitoring instrumentation 79−89488
PWR components, vibrations meas. using correlation techniques *(German)* 80−79247
PWR control and instrumentation *(Japanese)* 78−33271
PWR coolant two-phase flow, meas. instrumentation 80−37550
PWR ex-core ion-chamber transform and filtration methods of digitised fluctuation signals anal. 77−54312
PWR fuel assembly test instrumentation at LOFT facility 80−37551
PWR instrumentation operating experience during start-up and operation 79−89456
PWR LOCE at LOFT facility, instrument calibration for mass flow rate meas. in two-phase flow 80−37552
PWR movable in-core neutron detectors *(Japanese)* 79−26722
PWR multisection ex-core detector spatial weighting functions 79−13481
PWR neutron flux detectors, reliability tests *(French)* 80−32403
PWR power station operation in France, monitoring and control equipment eval. 79−89454
PWR primary circuit component exam., development of automatic equipment 80−13559
PWR steam generators, remote controlled TV for detection of leaking tubes *(French)* 80−791
PWR temp. sensor response time characts., estimation by noise anal. method 79−59216
PWR with wide vessel to concrete air gaps, ex-core detector sensitivity studies 80−73970
quartz, track retaining props. for high temp. in-core neutron fluence meas. 77−75032
radiation monitor for nuclear power station radioactivity meas. *(German)* 79−67876
radiological protection system installation, code of practice and design principles 79−85832
reactance oscillator for dynamic characteristics meas. in power reactors 79−89400
reactimeter, microprocessor based, nucl. engineering lab. class enhancement 80−36825
reactivity determination, pulsed neutron source technique, ZR-4 reactor appl. *(Hungarian)* 78−21673
reactivity meas. by Sjostrand method, on-line device *(Italian)* 77−38321
reactivity meter for LMFBR 80−32415
reactivity meters for monitoring extremely subcritical reactors, source analogue 77−71643
reactor diagnosis by acoustic meas. methods, magnetostrictive and piezoelec. high-temp.-resistant sensors 80−32411
reactor logic protection system using a redundant computer struct., self-checking procedures *(French)* 79−76103
reactor noise monitor, real time calc. of RMS values, av. freq. and peak freq. 79−76079
reactor portal monitors, evaluation and vulnerability anal. 79−49722
reactor protection computer systems, statistical verification of reliability 80−32417
reactor protection system, in-core power distribution synthesis from three-segment ex-core detectors 79−9865
reactor trip system, design of internal architecture for Westinghouse microprocessor-based [nuclear reactor] integrated protection system 79−76100
recoil separator, Lohengrin, ion optics, nuclear fission product spectroscopy 77−22607
refractory metals, work function, ionising radiation effects meas. method 80−6951
reliability improvements of nuclear reactor instrumentation 80−32416
remote handling system, fuel defect test loop 78−82436
remote manipulation in reactors by MA-23 bilateral servomanipulator system 77−50314
remote monitoring system for radioactive emissions of nuclear reactors 77−50307
remote multiplexing appl., functional and cost analyses review 80−52752
remote multiplexing control and safety systems evaluation 79−76109
remote multiplexing for nuclear reactor instrumentation and control circuits 80−57885
resonant US thermometer for nuclear reactor appls. 78−57948
RF local probe development for void fraction meas. 80−568
rod bundle blowdown heat transfer instrumentation, transient two-phase flow meas. 80−685
rod calorimeters using pyrolytic graphite, theoretical anal. 79−12804
rotating machines, vibration monitor using average freq. technique 79−97748
safeguarding of critical facilities to detect diversion of nuclear materials 80−68808
safeguarding on-power-fuelled reactors−instrumentation and techniques 79−26657
safeguards implementation technology in nucl. fuel cycle 78−86660
safety equipment, reliability in design 80−37555
safety related instruments qualification, impact of IEEE Std. (323-1974) 80−52753
safety-channel trip comparator, fail-safe logic elements 77−65277
seismic instrumentation for nuclear power plants in Germany, review 79−620
seismic qualification of safety-related instrumentation cabinets 80−23063
self-powered detectors for in-core reactor neutron flux meas., detector signal composition 80−32402
self-powered detectors for incore monitoring 79−45367
self-powered gamma-ray detector with directional discrimination 79−30895
self-powered neutron detectors for incore meas., comparative performance 79−45369
self-powered threshold gamma-ray detector, appl. for estimation of reactor kinetic parameters 79−59306
semiconductor detectors for neutron field investigation in critical assemblies 77−54430
semiconductor fission chambers, absolute fission ratio measurement *(Japanese)* 77−67948

nuclear reactor instrumentation continued
separator, gas-filled on-line, for neutron-rich fission products *(German)* 77−18708
signal noise, characts. and benefits, results from CANDU-BLW reactor 77−65310
solid-state track detectors for mass of temp. of neutron gas 78−66455
solid-state track recorder applications in U.S. nuclear reactor energy programs 80−95506
source level flux monitor expts. 77−54337
Spanish reactor monitoring instrumentation *(Spanish)* 77−38420
special nuclear materials, computer-based in-plant nondestructive assay instrumentation 79−9752
spent fuel bundle counter, performance study 80−23064
spent fuel bundle counter for 600 MW CANDU reactor 80−63269
spent fuel bundle counters for CANDU reactors, appl. of safeguards design principles 80−63347
spool piece, improved, for LOCE blowdown flow meas. 80−27727
steam fraction determ. in flowing air/stream mixtures by meas. of IR rad. attenuation 80−75010
subchannel void fraction by gamma scattering 80−27726
subcriticality meas. in power stressed reactors with analog reactimeter 79−97834
Super-Phenix FBR control system evaluation *(French)* 79−76106
superconducting Tokamak TF coil system, protective control features 78−62625
tagged assembly failure location analysis program 79−13486
tape-controlled remote automatic diameter meas. machine, report 78−86241
TAPIRO fast research reactor, computerised protection system 80−63308
teleoperator systems for reactor maintenance, technology assessment 80−68872
temperature meas., automatic system using platinum resist. thermometers 79−89399
temperature sensors, response time testing by noise anal. 78−13300
test gauge, operation at low multiplication 78−82526
TFTR, design calculations for A 14-MeV neutron collimator 79−59257
TFTR, neutronics anal. of neutral beam injectors 79−59261
thermal neutron radiography facility on IRT-2000 reactor 78−17286
thermal response of safety related equipment under high superheat conditions 77−46343
thermocouples, 2200°C fuel centerline for LOFT program 80−57877
thermocouples, influence in wall of directly heated test rods 79−93706
thermoelectric thermometers, readings stability in IVV-2 reactor 79−40568
thermographic imaging of fuel rods 77−42085
thermometric cell for safety studies on IRT WWER 79−97837
thin film fission thermocouples for energy deposition meas. in FBR safety expts. 80−47658
thin-film fission thermocouple detectors for reactors safety expts. 80−22987
TMI-2 accident, nuclear reactor safety, role of instrumentation and control *(Japanese)* 80−73947
Tokamak power reactor, position control and sensor requirements 78−5035
Tokamaks, magnetic divertors for impurity control 78−763
track-etch monitor for reactor power anal., evaluation 80−78418
transit time estimation, improved correlation method, coolant bubbles appl. 78−94067
TREAT, new hodoscope collimator 77−42026
TREAT reactor, acoustic monitoring of IRT-10 test 78−8944
TREAT reactor, computational method for predicting neutron hodoscope performance 79−80995
triaxial chamber use and experience at V.I. Lenin Leningrad nuclear power station 79−22377
two-phase flow system, local density measurements, side-scatter gamma technique 80−569
two-phase flows, high-intensity X-ray system for stochastic measurements 79−93791
two-phase mass flow measurement, ^{16}N tagging 79−93793
two-phase-flow instrumentation development at Brookhaven National Laboratory 80−102261
ultrasonic density meas., online system 78−718
US cross correlation flowmeter, HWR appl. 78−25283
US flowmeter for LMFBR Na flow meas. 80−32412
US flowmeter for Na flow meas. *(Japanese)* 78−78455
US leak detection for piping systems in reactor environment 77−61528
US temp. profiling system for critical heat flux meas. of nuclear reactor fuel assembly 80−37032
US thermometry appls. 80−73365
US viewing system for reactor fuel assemblies under liquid Na 80−57875
vibration and pressure transducer design for nuclear reactor environment 78−823
vibration monitor for rotating machines, ave. frequency technique 78−13299
video detection/tracking of tracer particles in model packed-bed reactor 77−42012
water-moderated water-cooled reactor, local control of loop channel energy release profile and magnitude 78−86645
X-ray optical systems, construction and appls. 79−17582
Zebra 8 assemblies, neutron spectra meas. with proton recoil counters 77−38393
Zebra multi-chamber scanning system, fission distribs. in prototype fast reactor mock-up 77−42181
Zircaloy fuel cladding, irrad. capsule design for continuously monitoring creepdown 79−54513
ZPPR at Argonne, gamma-ray response calc. for encapsulated solid-state dosimeters 77−46420
ZPPR-4 control rod worth meas. and calc. 79−9803
Be convertor/neutron counter apparatus for determ. of relative fission density release of fuel elements *(Russian)* 80−73973
^{7}Be, impurity in Li liq. in fusion reactor, control system 80−32466
$Bi_4Ge_3O_{12}$ scintillators, appl. as high energy gamma detectors 80−47827
$CaSO_4$:Dy TLD meas. of reactor thermal neutrons 78−78441
Cd rod generator of reactivity functions 77−57709
CdTe detectors, test of fuel enrichment *(Czech)* 77−50276
^{252}Cf neutron source for water-steam mixture void fraction meas. 79−26762
D_2O leak detection, on-line infrared analyzers, CANDU report 78−82038

nuclear reactor instrumentation continued
Ga and alloy high-temp. couplants for acoustic transducers 79−14195
Ge on-line, hyperpure detector, radiation monitoring system 78−37493
H detector, appl. of press. depend. of permeability in H-Ni system 77−46424
H meters, EBR-II H_2O-to-Na leak detection system 78−86760
H meters, on-line, calibration system 78−86236
H_3BO_3 concentration in primary circuit coolant, method and device for determ. *(Russian)* 77−38331
^{3}He proportional counter for fast reactor neutron field spectral charact. *(Japanese)* 78−46222
Li, liq., impurity monitoring and control system for fusion reactor 80−32465
^{6}Li sandwich counter, meas. of neutron spectra in fast neutron systems 80−27884
Na ionisation detector, aerosol effects on characts. 79−49243
Na loop, plugging meter behaviour obs., hydride and oxide deposition analysis 80−5207
Na system cold trap temperature control using resistance heater 77−57710
Na valves for advanced reactors, reliability data collection at CREDO 80−22897
Ni membrane diffusion sensor for H in liquid Na *(Japanese)* 79−49649
Ni-Mo NMP-430 tensoresistors for irradiation expts. 79−49648
^{237}Np threshold detector, subthreshold phenomena effects on nondestructive assay of reactor fuel 79−22409
O_2 activity meas. in liquid Na, development of electrolytic probes 80−18550
Pb-Bi eutectic alloy flow rate meas. apparatus 77−79412
platinum self-powered in-core detectors for PWR core power distrib. monitoring 80−73971
Pt resistance thermometer response time testing in situ 79−13484
Pt resistance thermometers, in-situ response-time testing for safety systems 79−93743
Pt self-powered detectors, neutron/gamma sensitivity 78−78557
Pt-self-powered neutron detector, temp. and radiation tests 79−81132
Rh self-powered neutron detectors, reliability anal. 79−41078
Rh-self-powered neutron detector, temp. and radiation tests 79−81132
Si sandwich surface barrier detector with ^{6}LiF radiator, neutron spectrom. 77−57807
Tm self-powered neutron detectors for power reactors 79−13607

nuclear reactor materials *see fission reactor materials*

nuclear reactor operation *see fission reactor operation*

nuclear reactor theory and design *see fission reactor theory and design*

nuclear reactors *see fission reactors*

nuclear resonance reactions and scattering
see also nuclear resonances
(3,3) reson. in $^{13}C(\pi^+,\pi^0)^{13}N$, eikonal cross-section calc. 77−18609
(3,3) reson. in $^{13}C(\pi^+,\pi^0)^{13}N$ 77−18608
(3,3) reson. in pion-nucleus collisions, nuclear density and π-N off-shell amplitude 77−3050
A=6to 14, radiative pion capture, mag. dipole resonance excitation in 1p shell nuclei 78−74408
A≤28, giant quadrupole resonance, E2 intensity distrib., from (α, α'), DWBA anal. *(Hungarian)* 80−52642
Adler-Adler cross section formalism, improved resonance formula for fissile elements 78−74358
atomic excitation effects on nuclear resonances and Q values 79−45226
average resonance neutron capture, completeness in nuclear spectroscopy 80−106006
average resonance parameter eval. and calcs., statistical model for capture process 80−18271
break-up reactions to resonant final states, appl. to $^{6}Li(p,2p)^{5}He$ 77−10381
Breit-Wigner single-level formula for cross sections, multilevel correction 78−29441
complex cross sections for prod. of resonant final states 78−37324
compound nucleus decay, failure of statistical theory, discussion of (n, γ) reactions 77−54213
continuum shell model description of resonant structures in nuclear reactions 79−13345
coupled channel Coulomb excitation, asymptotic soln. 77−46146
coupled channel problems, with off-shell resonances 79−71823
cross-section probability tables generation in unresolved resonance energy range 79−80986
direct reactions, semiclassical time-independ. formulation in three-dimens with complex trajectories 80−27605
Doppler effect calcs., resonance data set choice in unresolved resonance region, sensitivity study 80−52651
duration of reactions for strongly overlapped resonance levels *(Russian)* 78−46044
E1 giant resonances, features 77−79350
effective neutron resonance cross sections, calc. in energy and space 79−17954
energy dependence structs. in reaction cross sections, molecular resonances 79−45227
fast reactor physics, assessment of JAERI fast group constants set version 2 80−602
few body systems, anal. coupling constant continuation for resonance and stripping reactions *(Russian)* 80−13435
fission product nuclear data evaluation, cross sections up to 15 MeV, resonance parameters 77−23044
fragmented analogue states produced in proton-nucleus reactions, fine struct. anal. 77−6391
giant dipole resonance, isospin structure 77−79352
giant monopole resonance, self-consistent generator coord. method 77−2891
giant multipole reson. fragmentation over two-phonon states in spherical nuclei 78−575
giant multipole resonances, survey 77−79351
giant quadrupole capture of energetic nucleons by nuclei 77−10398
giant quadrupole resonances in light nuclei excited by α or p inelastic scatt. 78−624
giant resonance production mechanisms *(French)* 80−78243
heavy ion+nucleus, orbiting quasimolecular system, nuclear-surface-wave interpretation 80−86914
heavy ion collisions, resonance states in two-body breakup channels, theory of fragmentation 79−9619
heavy ion deep inelastic reactions, particle transfer, excitation of collective surface vibrs., in damping processes 78−70555

nuclear resonance reactions and scattering continued
heavy ion optical model, surface transparency and resonance phenomena 79−9617
heavy ion reactions, resonances, conference, Hvar, Yugoslavia (June 1977) 79−9614
heavy ion reactions, resonances, s-d nuclei with A=24 to 32 79−6403
heavy ion reactions, two-body molecular model for resonances 79−9620
heavy ion resonance reactions as orbiting cluster phenomena 80−47446
heavy-ion collision, narrow structure obs. in continuum, quasi-bound states, shell model anal. 77−14175
heavy-ion reaction intermediate struct. and nuclear reaction reson. states in continuum shell model 77−54243
Kapur-Peierls formalism, unitarity constraints 77−14084
level densities, thermodynamic temps., spin cutoff factors, nuclei with 23≤A≤40, expt. calcs. 77−30492
light heavy ion collision, resonant and non-resonant behaviour of complete fusion cross-sections 79−9625
light-nuclei, neutron resonance reactions using Kapur-Peierls formalism 77−50136
line shape in inelastic scatt. leading to resonant states 77−54211
lineshapes from reson. states in p scatt., appl. to ^{25}Mg(p,p′) and ^{16}N(p,p′) *(German)* 77−22989
multichannel direct resonance and heavy ion reactions, exactly solvable model *(Russian)* 79−67732
multichannel resonances, combined Hamiltonian and S-matrix methods *(Russian)* 79−63645
N=82 nuclei, elastic and inelastic polarised proton scatt., isobaric analogue states 77−74825
neutron cross section representation in unresolved resonance region 77−23051
neutron elastic removal cross sections, interference effect of strong scattering resonances in LMFBR 80−68658
neutron interactions with nuclei, conf. 77−23015
neutron resonance capture anal. 77−26693
neutron resonances, partial E1 radiative strength functions, shell and optical model interpretation *(Russian)* 77−82895
neutron scatt. from parity violating pot. 78−25167
nuclear continuum spectrum from disintegration by high energy particles, direct and resonant mechanisms *(Russian)* 79−30803
off-shell resons. in terms of resonant states, elastic and stripping reactions 77−65217
photo-nucleon spectra, shell and pre-equilibrium decay model of giant reson. decay *(Russian)* 78−579
photon-nucleus scatt., 5 to 30 MeV, angular distribs., polarisations, electric quadrupole scatt. in continuum 77−79359
photonuclear giant dipole resonance, isospin shift of energy 77−50111
pion+nucleus total cross-sections in (3,3) resonance region 77−10437
pion deep inelastic reacts. in isobar model 78−41779
pion total cross-sections, strong absorpt., N*(3,3) resonance 77−10442
pion-bound nucleon scatt. near 33 reson., impulse approx. 77−23108
pion-nucleus resonant total cross sections in strong absorpt. model 77−23114
pion-nucleus total cross section data from LAMPF and BNL, (3,3) resonance 77−10436
potential scattering parameters, determ. from reson. parameters 78−16685
R-matrix theory, convergence anal. of Buttle corrected, variationally corrected, and iterative R-matrix methods 79−6528
radiative capture and fission cross sections ratio meas. in reson. region 77−50175
radiative nucleon capture, pure resonance model, direct-semidirect model, pure semidirect model 80−78257
Rayleigh and Compton contribs. to nuclear resonance scattering of gamma rays, line inversion 80−39919
Rayleigh and whispering gallery waves excited by heavy ion elastic and inelastic scatt. 80−91164
recent advances in neutron physics, prod., handling, detection, nuclear reactions, resonances 77−26686
resonance analysis of neutron transmission data, least square fitting program REFIT 80−22840
resonance escape probability, Monte Carlo importance sampling technique 77−61471
s-d shell nuclei, semiempirical prediction of heavy ion reaction resonances 79−22256
s-wave level reson., tensor analysing power far light nuclei 77−82893
self shielding factors, elastic removal cross sections, strong reson. scatt. 79−13374
single-particle resonances, numerical anal. 78−29436
slowing down of resonance neutrons in matter 77−50191
statistical theory, strong absorption and the distribution of zeros of the S-matrix 79−36214
stellar interiors, effects of thermonuclear ion-electron screening, static soln. 77−29793
T-matrix, perturbation formalism for complex poles and widths, appl. to intermediate struct. 78−66255
thermonuclear reaction rate integrals, closed-form evaluation and approximation considerations 80−8535
unified model appl. to ^{12}C+n system 78−29437
widths Γ_γ anal. for several nuclei *(Russian)* 77−30561
zero-spin particle reactions, angular distrib. anal. 79−13342
(d,^{6}Li) reaction, 80 MeV, on ^{14}N, ^{16}O, ^{20}Ne, ^{24,25,26}Mg, ^{40}Ca targets, resonance-like phenomena 79−13308
d, threshold, potential resonance near top of broad barrier 79−514
(γ,γ) processes using (n,γ) photons 80−18288
(γ,γ′), spin, parity and width of resonance level 80−18287
(γ,N), fine structure in ang. distrib. in giant resonance region 77−6342
(γ,n), spin, parity and width of resonance level 80−18287
μ capture, subsequent excitations and particle emission cascade, hydrodynamical model 78−89825
(n,α) resonance neutron reactions, α-widths from statistical relationships, deviations 78−33173
(n, α) with resonance neutrons, properties of highly-excited states of nuclei *(Russian)* 80−106053
(n,γ), A=94-190, resonance capture, low lying level population fluctuations, γ-rays 80−52619
(n,γ), mechanism in 3s size resonance, s-wave radiative width partition 80−37387
(n,γ), mechanism in 3s size resonance, radiative width statistical and valence effects 80−37388
(n,γ), resonance TOF spectroscopy at Nevis Lab. 77−23073

nuclear resonance reactions and scattering continued
(n,γ) cross sections above 2.5 keV for light and closed shell nuclides, mechanisms, resonance parameters 77−23049
(n,n) resonance TOF spectroscopy at Nevis Lab. 77−23073
(n,nγ), A=19-207, neutron scattering resonance radiative widths 80−99146
(n,p) reactions on ^{6,7}Li, ^{12}C, ^{14}N, ^{16}O, ^{20}Ne, ^{27}Al, ^{209}Bi, isovector analogue giant resonances study 77−26726
NN resonances and total cross sections, expt. evidence review 80−42558
(p,γ), 50 MeV, giant dipole resonance, γ-emission spectrum from giant dipole resonance 79−59065
(p,γ) resonance broadening meas. of light ion ranges 77−69023
(p,n) reactions, alignment and decay of IAS, depend. on higher multipole contrib. 77−3003
(p,n) scattering, charge exchange, isobaric analogue state, giant resonance effect, semimicroscopic model 78−89868
(π^-,γ), absorpt. on light nuclei, resonance states 77−14189
(π^-,γ), unified description of direct and resonance processes 78−86551
(π^+,p) near (3,3) resonance region, isobar doorway model 78−41778
(π,π), phase shifts in (3,3) resonance region and diffractive nature 77−6462
(π,π) optical pot., possible local field correction from resonant scatt. cross section 79−85421
(π,πN) quasi-free scatt. in reson. region, (p,2p) comparison 77−88173
(π,πn) reaction on light nuclei near (3,3) resonance 77−14182
πA, multiple scatt. theory *(Russian)* 79−49640
^{159}Tb, 58 keV level, nuclear reson. fluorescence 78−33121
A(a,ax)B type resonance reactions, chain struct. states *(Chinese)* 80−52645
^{27}Al (p,p$_0$), elastic resonance scatt., 0.85-3.0 MeV, excitation functions 77−14121
^{27}Al bound state parity and spin assignments, level struct. from ^{26}Mg (p,γ) resonances 78−66206
^{27}Al+^{12}C, 83 MeV, giant resonance excitation 78−17235
^{27}Al(α,α′)^{27}Al, 126 MeV, GQR, DWBA anal. 77−74826
^{27}Al(d,α)^{25}Mg, 1.5-2.5 MeV, intermediate resonance widths 77−88151
^{27}Al(d,p)^{28}Al, 1.5-2.5 MeV, intermediate resonance widths 77−88151
^{27}Al(n,γ), resonance capture, ^{28}Al E1 transitions and partial radiative widths 80−52618
^{27}Al(p,α$_0$)^{24}Mg, Al conc. as a function of depth in epitaxially grown Si layers on sapphire substrates 79−4328
^{27}Al(p,α), 937 and 885 keV resonance lifetime meas. using crystal blocking technique 79−63671
^{27}Al(p,α)^{24}Mg, 1.35 to 1.46 MeV, test of detailed balance at isolated resonances and time reversibility 79−45260
^{27}Al(p,α)^{24}Mg resonance, nuclear lifetime meas. problems in single cryst. blocking expt. 77−47500
^{27}Al(p,γ), 0.5-2.1 MeV, determ. of ^{28}Si levels and resonances 78−66205
^{27}Al(p,γ)^{28}Si, 0.5 to 0.9 MeV, resonance strengths of selected resonances in s-d shell 78−66281
^{27}Al(p,γ)^{28}Si, 12917 and 12924 keV ^{28}Si level gamma-gamma directional correl. 79−536
^{27}Al(p,γ)^{28}Si, 2046 keV, gamma-ray intensity calibration standard 77−30698
^{27}Al(p,γ)^{28}Si, 2.4-2.74 MeV, γ-spectra, isobaric analogue states 77−57646
^{27}Al(p,γ)^{28}Si, expt. γ-ray yield curves from H_2^+ and H_1^0 beams, material anal. 79−3530
^{27}Al(p,γ)^{28}Si, standard resonance strength 77−30565
^{241}Am, total neutron cross section and neutron reson. parameters, 0.004 to 30 eV 77−50135
^{243}Am, total neutron cross section and neutron reson. parameters, 0.4 to 35 eV 77−46171
^{36}Ar, neutron low energy total cross-section, bound level parameters 77−23071
^{75}As(n,n′γ)^{75}As, deexcitation gammas, energy levels, branching ratios, spins, parities, excitation function meas. 78−89869
^{197}Au+^{14}N, 161 MeV, giant resonances in inelastic scatt. 78−62564
^{10}B, total neutron cross section, 90 to 420 keV 79−40913
^{10}B(^{10}B,α)^{16}O, excitation functions, resonance like structures 78−29496
^{10}B(d,α)^{8}Be(g.s.), excitation functions struct., isoscalar giant resonances in ^{12}C 78−46073
^{10}B(e,e), 140 MeV, resonances in e spectra *(Russian)* 78−78367
^{10}B(t, α)^{9}Be*($2s_{1/2}$), resonant spectra 80−22691
^{11}B, (α,γ$_0$), 15.5-19.5 MeV, excitation curve ang. distrib., cross section, ^{15}N resonances 78−94019
^{11}B+^{12}C elastic scatt., resonances 78−89901
^{11}B(γ,γ), resonance scatt., molecular orientation effects 80−78252
^{11}B(p,3α), 35.4-1500 keV, resonance cross sections, astrophysical S-factor, fusion fuel 79−36213
^{11}B(p,α)^{8}Be 6.0-18.0 MeV, isoscalar giant reson. 77−46152
^{138}Ba(n,γ), resonance n capture cross section meas. 3 to 100 keV 79−93610
^{138}Ba(p,p′), 10-11.7 Mev polarised protons scatt. at IAR 77−2991
^{9}Be+^{12}C→^{21}Ne*, different decay channels, resonance-like structures obs. 79−13333
^{9}Be(^{12}C,^{8}Be), 10-15 MeV, excitation functions and resonant enhancements 79−17881
^{9}Be(^{3}He,α)^{8}Be(O), reaction mechanism and isoscalar giant resonances in C^{12} *(French)* 78−78341
^{9}Be(α,α′), 6.5 MeV, ^{13}C, T=3/2 resonance parameters, ground state γ-decay width 79−3123
^{9}Be(α,n) 6.5 MeV, ^{13}C, T=3/2 resonance parameters, ground state γ-decay width 79−3123
^{9}Be(p,αγ)^{6}Li, 2.56 MeV, ^{10}Be 8.89 MeV reson. J$^\pi$ 77−50098
^{9}Be(p,p)^{9}Be, 2.56 MeV, ^{10}Be, 8.89 MeV reson. J$^\pi$ 77−50098
^{209}Bi+^{14}N, 161 MeV, giant resonances in inelastic scatt. 78−62564
^{209}Bi(n,γ), 2.6-901 keV, cross-sections, resonance peaks, radiative widths 77−3002
^{209}Bi(n,γ), TOF transmission spectroscopy, strength functions 77−23077
^{209}Bi(n,n), 16-18 MeV differential cross section resonant characters 79−75952
^{209}Bi(n,n) TOF transmission spectroscopy, strength functions 77−23077
^{12}C-^{12}C quasimolecular resonance, coupled channel anal. 78−78402
^{12}C-^{12}C resonances, speculation of nature, excited α-particles 79−13339
^{12}C+^{12}C, 6.25 MeV reson., J$^\pi$ determ. 77−50099
^{12}C+^{12}C, mol. resonance props. by GCM 79−13321
^{12}C+^{12}C collisions, nuclear molecules, two-centre shell model parastatistics 79−9618
^{12}C+^{12}C quasimolecular interactions, recent developments 79−9615
^{12}C+^{12}C system, 7.5 MeV, reson. spin assignment 77−14089

nuclear resonance reactions and scattering continued
$^{12}C+^{12}C$ system, inelastic scatt. and fusion cross section, folding model, resonances 79−13337
$^{12}C+^{13}C$ resonances, coupled channel anal. with core-exchange model 79−13338
$^{12}C+^{16}C$ scatt. reson. and strong absorpt. phenomena, band crossing model 79−3165
$^{12}C+^{16}O$ elastic scatt., generator coord. calc., reson. spin assignments 77−57685
$^{12}C+^{16}O$ resonances, microscopic interpretation 79−13340
$^{12}C+^{16}O$ scatt. reson. and strong absorpt. phenomena, band crossing model 79−3165
$^{12}C+^{16}O$ system, coupled channel approx., treatment of resonances 79−9621
($^{12}C+^{16}O$) system, E_{cm}=12.8 MeV resonance, spin parity determ. 79−6405
$^{12}C+^{28}Si$, 17.5 to 33 MeV, resonant backward angle elastic scatt. 78−46096
^{12}C+n, TOF transmission meas. of neutron resonances 80−37374
$^{12}C(^{12}C, ^{10}B)$ 22-42 MeV, resonances in $^{10}B+^{14}N$ and $^{12}C+^{12}C$ channels 79−80910
$^{12}C(^{12}C, \gamma)$, 11.8-20.0 MeV, total cross section resonant and average behaviour 80−106069
$^{12}C(^{12}C,^{12}C)$, 6-30 MeV, intermediate struct. from band crossing model, molecular resonances 79−54425
$^{12}C(^{12}C,^{16}O)^{8}Be$, 5.75-8.9 MeV, sub-Coulomb resonances in ^{12}C-^{12}C system 77−57688
$^{12}C(^{12}C,\alpha)$, 4-8 MeV, ^{20}Ne spin assignments for sub-Coulomb resonances 77−54245
$^{12}C(^{12}C,\alpha)^{20}Ne$, ^{24}Mg reson. J^{π}, rot.-vibr. coupling 78−491
$^{12}C(^{12}C,\alpha)^{20}Ne$, E_{cm}=6.5-12 MeV, new resonances, J^{π} determ. 77−54200
$^{12}C(^{12}C,\alpha)^{20}Ne$, resonances, existence of second $J^{\pi}=0^{+}$ reson. at high excitation energy in ^{24}Mg 78−25214
$^{12}C(^{12}C,\alpha)^{20}Ne$, resonance anomaly anal. in fluctuation theory 78−25215
$^{12}C(^{12}C,\gamma)^{24}Mg$, 5 to 11 MeV, γ yields, resonance features 78−54799
$^{12}C(^{12}C,p)^{23}Na$, schematic model for continuum resonances, shape resonance fragmentation 77−67764
$^{12}C(^{13}C,\alpha\gamma)^{21}Ne$, 13.9-15 MeV, yield curves near 14.4 MeV reson. 77−54254
$^{12}C(^{14}N,\alpha)$, 10.1-15.9 MeV, forward angle excitation function structure, nonstatistical struct. 80−86885
$^{12}C(^{15}N,\alpha)$ reson. struct. and ^{27}Al yrast levels 77−79348
$^{12}C(^{16}O, ^{12}C^{*})$, 45-53 MeV, $^{12}C^{*}$ m-substate population, spin alignment and excitation functions 80−42615
$^{12}C(^{16}O,\alpha)^{24}Mg$, population of resonant $^{12}C+^{12}C$ states 78−62563
$^{12}C(^{16}O,^{12}C_{g.s.})^{16}O^{*}$, obs. of α-doorway states 79−6662
$^{12}C(^{16}O,^{12}C^{*}_{4.4})^{16}O$, 22.7 to 33.0 MeV, excitation function enhancement for 0^{+}, 6.049 MeV ^{16}O state 78−58299
$^{12}C(^{16}O,^{16}O^{*})^{12}C^{*}$, 33-54 MeV, intermediate struct. resonances, ang. distribs., statistical anal. 78−82330
$^{12}C(^{16}O,^{16}O)$, elastic and inelastic, 23-32 MeV, strong absorption region resonances, excitation functions 80−86884
$^{12}C(^{16}O,^{16}O)^{12}C$, 15.4 to 30.9 MeV, correlation between fusion and inelastic scatt. 78−66310
$^{12}C(^{16}O,^{16}O)^{12}C$ resonant scatt., 15-30 MeV, ang. distribs., interpretation *(French)* 79−3166
$^{12}C(^{16}O,^{8}Be)$ $E_{c.m.}$=18.5-20.5 MeV, populating ^{28}S 12^{+} reson. 77−18508
$^{12}C(^{16}O,^{8}Be)^{20}Ne$, 13.5-23 MeV, excitation functions, ang. distribs. and cross sections 79−13334
$^{12}C(^{16}O,X)$, transparency to l=9 partial wave in 14.7 MeV resonance region 80−78314
$^{12}C(^{16}O,\alpha)$, J^{π} for 12.8 MeV c.m. resonance 79−59045
$^{12}C(^{16}O,\alpha)^{24}Mg$, 13.5-23 MeV, excitation functions, ang. distribs. and cross sections 79−13334
$^{12}C(^{16}O,\alpha)^{24}Mg$, 13.7, 14.2, 14.7 MeV, ang. distribs., intermediate resonance struct. 79−13331
$^{12}C(^{18}O,^{8}Be)^{22}Ne$, 15-22.5 MeV, resonance strength investig. 79−13336
$^{12}C(^{18}O,\alpha)^{26}Mg$, 15-22.5 MeV, resonance strength investig. 79−13336
$^{12}C(^{20}Ne,\alpha)^{28}Si$, energy depend., non-statistical effects 79−13332
$^{12}C(^{9}Be,^{8}Be)$, 11.4 MeV to 14.8 MeV (c.m.), search for resonances 79−45290
$^{12}C(^{9}Be,^{7}Be)$ elastic and inelastic 10-15 MeV, excitation functions and resonant enhancements 79−17881
$^{12}C(^{9}Be,\alpha)^{17}O$, 10-15 MeV, excitation functions and resonant enhancements 79−17881
$^{12}C(\alpha,\alpha)$, 150 MeV, isoscalar giant quadrupole reson. 77−307
$^{12}C(\alpha,\gamma_{n})$, excitation function meas. in vicinity of 12.44 and 13.1 MeV levels of ^{16}O 77−6413
$^{12}C(d,p)^{13}C$, 0.5 to 2.5 MeV, excitation functions and angular distribs., possible doorway state *(Chinese)* 80−68679
$^{12}C(e,e)$ 140 MeV, resonances in e spectra *(Russian)* 78−78367
$^{12}C(\gamma,p)^{11}B$, 40-120 MeV, reaction mechanism *(Russian)* 77−65221
$^{12}C(\gamma,\pi^{0})$, pionic and EM A* resonance excitation 80−91160
$^{12}C(n,n)$, 15 to 18 MeV, resonance effects 77−30591
$^{12}C(p,\gamma)$, 16-40 MeV, ^{13}N giant dipole reson. as doorway-states 77−6336
$^{12}C(p,p')$, 16-40 MeV, ^{13}N giant dipole reson. as doorway-states 77−6336
$^{12}C(p,p)$, hadron induced semicoherent scatt., excitation of $^{12}C(2^{+}$, 4.4 MeV) level 78−70569
$^{12}C(p,p)^{12}Cm$ bremsstrahlung near 1.7 MeV resonance 79−45249
$^{12}C(p,p\gamma)$, meas. of bremsstrahlung spectra to determ. reaction time delays of 10^{-20} sec. 77−6378
$^{12}C(\pi,X)$, angular distrib. of inelastic diffusion of $\pi^{\pm}$ *(French)* 80−47507
$^{12}C(\pi,\pi')$, obs. of enhanced ^{12}C excitation by inelastic π scatt. on $\pi N(3,3)$ reson. 79−17938
$^{12}C(\pi,\pi')^{12}C^{*}$, giant dipole resonance, Glauber theory 77−6467
$^{12}C(\pi,\pi)$, hadron induced semicoherent scatt., excitation of $^{12}C(2^{+}$, 4.4 MeV) level 78−70569
$^{12}C(\pi,\pi)$, many body effects in resonant scatt. 78−94029
$^{12}C(\pi,\pi)$, pionic resonance fluorescence in $\Delta(33)$ region 79−85554
$^{12}C(\pi^{+},p)^{11}C$ near (3,3) resonance region, appl. of isobar doorway model 78−41778
$^{12}C(\pi^{+},\pi^{+})$, 148 MeV, inelastic scatt., 15.1 MeV (1^{+}) state, differential cross section 78−89792
$^{12}C(t,\gamma_{0})^{15}N$, 1-3.4 MeV, giant reson. excit., J^{π},Γ assignments 77−34277
$^{12}C(\tau,d)$, 36 MeV, ^{12}C+p resonance line shapes 79−59076

nuclear resonance reactions and scattering continued
^{13}C, giant reson. isospin splitting, photonuclear and e-scatt. cross-sections 78−577
$^{13}C(^{3}He,\gamma_{2})^{16}O$, ang. distrib. and correlation meas. of 26.42 MeV resonance 77−61444
$^{13}C(\alpha,n)^{16}O$, widths of isospin forbidden decays of ^{17}O T=3/2 levels 77−6321
$^{13}C(d,\gamma_{0})^{15}N$, E_{exc}=17.7 MeV, 95° differential cross section resonance struct. 78−37351
$^{13}C(d,\gamma)$, 2.90 to 9.95 MeV, cross sections, ang. distrib. meas., ^{15}N reson. obs. 77−6395
$^{13}C(\gamma,n_{0,1})^{12}C$, 98° diffr. cross-sections, reson. due to ^{13}C level struct. 78−586
$^{13}C(\gamma,n)$ 7.6 to 41.8 MeV, photoneutron cross section meas., giant resonance isospin splitting 79−63657
$^{13}C(\pi^{+},\pi^{0})^{13}N$ in (3,3) reson. region, optical model calc. 77−18610
$^{13}C(\pi^{+},\pi^{0})^{13}N_{g.s.}$, (3,3) resonance region, importance of two-step processes in multiple scatt. treatment 77−6464
$^{13}C(\tau,d)^{13}N$, at 81.4 MeV, ang. distribs., analysis of particle inbound states 77−10418
$^{14}C(^{12}C,X)$, 40-57 MeV, strong resonant behaviour in inelastic and transfer channels, γ-yields 80−52644
$^{14}C(^{16}O,^{16}O)^{14}C$, resonance struct. at excitation energies 40-51 MeV in ^{30}Si, comparison with $^{12}C+^{18}O$ 79−13335
$^{14}C(^{16}O,^{18}O)^{12}C$, resonance struct. at excitation energies 40-51 MeV in ^{30}Si, comparison with $^{12}C+^{18}O$ 79−13335
$^{40}Ca+^{14}N$, 161 MeV, giant resonances in inelastic scatt. 78−62564
^{40}Ca+p, fine struct. levels sign meas., off-diagonal strength function, analogue state broadening theory test 78−78381
$^{40}Ca(^{12}C,^{12}C)$, 20 to 35 MeV, resonant heavy ion scatt., from s-d shell nuclei 79−67763
$^{40}Ca(^{12}C,^{12}C)$, 20-35 MeV, resonant scatt., ang. distribs., cross sections and excitation functions 79−45237
$^{40}Ca(^{3}He,^{3}He'\alpha)^{36}Ar$, 70 MeV, GQR J^{π} 77−50097
$^{40}Ca(^{3}He,^{3}He'p)^{39}K$ 70 MeV, GQR J^{π} 77−50097
$^{40}Ca(^{40}Ca,X)$, 400 MeV, fragment energy spectra struct., giant resonances, direct process 80−47452
$^{40}Ca(^{9}Be,^{9}Be)$, 20 to 35 MeV, resonant heavy ion scatt., from s-d shell nuclei 79−67763
$^{40}Ca(\alpha,2\alpha)$, 115 MeV, GQR decay spectra 77−30523
$^{40}Ca(\alpha,\alpha p)$, 115 MeV, GQR decay spectra 77−30523
$^{40}Ca(n,\gamma)$, 10 MeV polarised neutrons, ^{41}Ca giant dipole resonance 79−93620
$^{40}Ca(\pi,\pi N)$ at (3,3) reson., WKD approx. validity 77−18615
$^{40}Ca(\pi,\pi)$, pionic resonance fluorescence in $\Delta(33)$ region 79−85554
$^{42}Ca(p,p)$, 1.2 to 3.0 MeV, cross-section meas., ^{43}Sc struct. 77−6374
Ca(n,γ), E>2.5 keV, reson. parameters, odd-even effects 77−34299
Cd covered Au foils, neutron spectra determination by resonance reactions 79−93837
Cd(p,p)Cd, A=110, 112, 5-9 MeV, isobaric analogue reson., QRPA calc. 78−576
Cd(π^{-}, X), 0 MeV, A=111, 112, E2 nuclear resonance effects, γ and X-ray meas. 78−41774
^{140}Ce+n, 20-240 keV total cross section, resonance multilevel shape anal., level spacings 79−3148
$^{140}Ce(n,\gamma)$, 6.2-15.6 MeV, gamma-ray spectra, cross-section meas. 78−33176
$^{140}Ce(n,\gamma)$, resonance n capture cross section meas. 3 to 100 keV 79−93610
$^{35}Cl(p,\gamma)$, decay of first T=2 state in ^{36}Ar 77−6294
$^{35}Cl(p,\gamma)^{36}Ar$, 0.5 to 0.9 MeV, resonance strengths of selected resonances in s-d shell 78−66281
$^{243}Cm(n,f)$, thermal neutron fission cross section and fission-resonance integral 80−86942
$^{59}Co(n,\gamma)$, 2.5 keV-1 MeV, TOF capture cross-section meas. 77−30586
$^{50}Cr(p,p)$ and (p,p'), E_{p}=6 MeV, cross sections, opt. pot. parameters 78−13086
$^{52}Cr(p,\gamma)^{53}Mn$, resonant react. appl. to Cr depth distribs. 79−33011
$^{52}Cr(p,p)$ and (p,p'), E_{p}=6 MeV, cross sections, opt. pot. parameters 78−13086
$^{52}Cr(\pi,X)$, angular distrib. of inelastic diffusion of $\pi^{\pm}$ *(French)* 80−47507
Cr(n,γ), up to 600 keV, cross sections, resonance parameters, point-wise evaluation 77−23050
^{243}Cu, thermal neutron capture and fission cross sections, resonance integrals 77−67744
Cu(n,γ), 63, 5, cross-section meas., reson. parameters determ. 77−38274
Cu(n,n), A=63, 65, E=10-150 keV, total cross-sections and reson. parameters 77−38273
Cu(p, spallation), 200, 350 MeV, radioactive residual nuclei prod. cross sections at (3,3) resonance 79−3130
Cu($\pi^{\pm}$, spallation), 50-350 MeV, radioactive residual nuclei prod. cross sections at (3,3) resonance 79−3130
$^{19}F(\alpha,n)^{22}Na$, 2.3-4.7 MeV, populating ^{23}Na reson. levels 77−65199
$^{19}F(\alpha,p\gamma)^{22}Ne$, 2.3-4.7 MeV, populating ^{23}Na levels 77−65199
$^{19}F(p,\alpha)^{16}O$, 1.5 to 2 MeV, [211] quartet state in ^{20}Ne 78−46006
$^{19}F(p,\alpha\gamma)^{16}O$, 872 keV resonance, appl. of H molecular ion beams 79−36452
$^{19}F(p,\alpha\gamma)^{16}O$, reson. reaction, teaching expt. using Van de Graaff generator 77−74178
$^{19}F(p,\gamma)^{20}Ne$, giant multipole reson., microscopic theory 77−22987
Fe, total neutron cross-section, thick sample transmission meas. and resonance anal. 77−23066
Fe+n, A=54, 56, 1-70 keV, total cross section, resonance parameters *(Russian)* 78−17210
$^{A}Fe(n,\gamma)$, A=54,56,58, resonance capture, $^{55,57,59}Fe$ level schemes 79−547
^{54}Fe, high resolution total neutron cross section meas. 77−23065
$^{54}Fe(n,\gamma)$, cross section, resonance and background interference 80−18310
$^{54}Fe(n,\gamma)$ 2.5-500 keV, valence neutron capture, reson. parameters 77−57659
$^{54}Fe(p,\gamma)$, 1.5-2.9 MeV, excited levels and isobaric analogue states in ^{55}Co 77−18509
$^{54}Fe(p,p)$, 3.28-4.53 MeV, ^{55}Co IAR, J^{π} assignments 78−574
^{56}Fe, high resolution total neutron cross section meas. 77−23065
^{56}Fe partial radiation widths from neutron capture resonances, valency model calcs. 77−26707
^{56}Fe+n, 0-2.2 MeV, doorway state struct. 77−88143
$^{56}Fe(\gamma,n)$, 13.3 MeV bremsstrahlung, resonance spectrum and cross-section meas. *(Russian)* 77−6349

nuclear resonance reactions and scattering continued
^{56}Fe(n,γ)$_0$, 2.5-870 keV, resonance neutron capture study 77−2990
^{56}Fe(n,γ)^{57}Fe, high energy γ-ray transitions of ^{56}Fe resonances, E_n=7 to 70 keV 77−23081
^{57}Fe, (n,γ), cross section, 2.5-200 keV, s-wave resonances 80−18309
^{58}Fe(n,λ), resonance capture cross section s- and p-wave radiative widths 80−47476
Fe(γ,n), A=54, 56, GDR intermediate struct. in 5-26.3 MeV range 77−74824
Fe(p,γ), absolute resonance strengths meas. using separated targets 77−79374
^{74}Ge(p,p) elastic and inelastic scatt. at 3.3-5.4 MeV, IAR excit. 77−34278
^{1}H(^{15}N, αγ)^{12}C, appl. to quantitative H analyses in different materials problems 79−5196
^{1}H(^{19}F, αγ)^{16}O, appl. to quantitative H analyses in different materials problems 79−5196
^{1}H(^{19}F,αγ)^{16}O, for meas. of H depth distrib. in solid 77−81435
^{2}H(^{3}He,^{4}He)^{1}H, 27 and 33 MeV, polarised ^{3}He beam analysing power and cross sections 79−89316
^{2}H(γ,n)p, cross section asymmetry polarised photons 400 to 600 MeV, resonances *(Russian)* 79−89294
^{2}H(n, γ), slow neutrons, mesic interaction current, isobaric resonance *(Italian)* 78−25179
^{2}H(p,p), pol.p, spin rot. and depolarisation, NN amplitude double spin flip part 80−78271
^{2}H(p,p)^{2}H backward elastic scatt., resonance region, double-scatt. mechanism *(Russian)* 77−74854
^{3}H(π^-, γ)3n, rest π, resonance branching ratio, bound state upper limit 80−99162
^{4}H photodisintegration in giant resonance region 77−41944
^{3}He (π, π) Δ(1236) resonance region, Watson multiple scatt. series. integral eqns. 80−37402
^{3}He(d,d)^{3}He, 0.3-8 MeV, single-level reson. and ^{5}Li parameters 77−30606
^{4}He-^{4}He, possible ^{8}Be high-lying reson. below α-α* threshold 77−82840
^{4}He+^{4}He, reson. excit., ^{8}Be α-cluster, coupled channel calcs. 78−529
^{4}He+n, pole positions of ^{5}He resonances, models calcs. 78−70530
^{4}He(^{3}He,^{3}He), 18 to 70 MeV, differential cross-sections, resonating group method anal. 79−85482
^{4}He(^{3}He,n)^{6}Be, 38.61 MeV, ^{6}Be reson. search, solar neutrino flux importance 78−619
^{4}He(^{7}Li,γ)^{11}B, 1.68 MeV, appl. to He concentration profile determ. in materials, meas. technique 79−5200
^{4}He(d,d), 870-1430 keV, differential cross sections and resonance parameters *(Russian)* 79−59075
^{4}He(d,d)^{4}He, 6-7 MeV, polarised d, ^{6}Li 1^+ reson., analysing powers 77−88095
^{4}He(γ,P)^{3}H, 20 to 50 MeV, 2^+ resonances *(Russian)* 79−59052
^{4}He(γ,n)^{3}He, 20 to 50 MeV, 2^+ resonances *(Russian)* 79−59052
^{4}He(γ,π^0), impulse approx. for differential cross sections in resonance region *(Russian)* 78−41698
^{4}He(π,π), extraction of Breit-Wigner parameters from p-wave, isohelion existence 77−6455
Hf(γ,xn), x=1, 2; A=176, 178, 180, 8-21 MeV, GDR, neutron yields and multiplicities *(Russian)* 77−82894
^{165}Ho(γ,γ′) 8.5-11.4 MeV, elastic and Raman scatt., giant reson. struct. 77−34284
^{165}Ho(n,γ), <2 keV, spin depend. of s-wave neutron strength function 78−21562
^{138}La, thermal neutron capture cross section and reson. integral 77−6365
^{6}Li(d,α)^{4}He, 1.5-11.5 MeV, resonance behaviour, analysing powers 77−82935
^{6}Li(d,α)^{4}He, below 12 MeV, analysing powers, 8Be reson. levels 77−82936
^{6}Li(d,α)^{4}He*, 13.6 MeV, α spectra, excited state of ^{4}He, spin, parity 78−54771
^{6}Li(d,γ)^{8}Be, first T=2 state radiative width 77−14130
^{6}Li(p,2p)^{5}He, appl. of break-up reaction theory to resonant final states 77−10381
^{6}Li(t,d)^{7}Li, 0.35 to 1 MeV, resonance struct. in compound nucl. excitation curves 78−17217
^{6}Li(t,γ)^{9}Be, 0.35 to 1 MeV, resonance struct. in compound nucl. excitation curves 78−17217
^{6}Li(t,p)^{8}Li, 0.35 to 1 MeV, resonance struct. in compound nucl. excitation curves 78−17217
^{7}Li system reactions, R-matrix anal. 79−9585
^{7}Li(e,e′) at first πN resonance, cross section longitudinal and transverse components *(Russian)* 80−86901
^{7}Li(p,γ)^{8}Be, polarised p, 380-960 keV, ^{8}Be level, J^π 77−88131
^{7}Li(t,γ)^{10}Be, excitation functions and resonant struct. for 17.79 MeV state 78−13110
^{24}Mg+^{16}O system, high spin cluster-like resonances 17-31 MeV 79−6664
^{24}Mg+e, 21 to 32 MeV, E0 and E2 excitations, fission into two ^{12}Cg.s. nuclei 78−54744
^{24}Mg(^{16}O,^{12}C)^{28}Si, excitation functions for O^+ and 2^+ states of ^{28}Si 78−54800
^{24}Mg(^{16}O,^{16}O), 17-31 MeV, backward angle cross sections, resonant structure 79−30813
^{24}Mg(^{18}O, ^{14}C)^{28}Si, ground-state excitation function structure 79−63694
^{24}Mg(^{3}He,^{3}He′), giant dipole reson. excitation 77−6338
^{24}Mg(^{3}He,^{3}He), 130 MeV, giant reson. excitation, DWBA anal. 79−89319
^{24}Mg(^{3}He,t), giant dipole reson. excitation 77−6338
^{24}Mg(α, ^{12}C)^{16}O, 12.7-17.4 MeV, quasimol. resonance in excitation function, ^{12}C+^{16}O system, spins 78−54775
^{24}Mg(α,α′)^{24}Mg, 126 MeV, GQR, DWBA anal. 77−74826
^{24}Mg(α,α′)^{24}Mg, exptl. evidence of intermediate resonances, alpha-particle doorway states 79−13314
^{24}Mg(α,γ), 1.5-3.8 MeV, determ. of ^{28}Si levels and resonances 78−66205
^{24}Mg(α,p)^{27}Al, 3.38 to 3.52 MeV, test of detailed balance at isolated resonances and time reversibility 79−45260
^{24}Mg(e,e′), 6^-, T=1 reson. discovery at 15 MeV 77−41940
^{24}Mg(n,n)^{24}Mg, 0.4 to 1.8 MeV reson. level ang. momentum 77−54202
^{24}Mg(p,p′), 22.5 to 28.5 MeV, giant reson. effects 78−4923
^{24}Mg(p,p), 15 Mev, excitation functions 80−22825
^{24}Mg(p,p), 5.65-6.25 MeV, isospin-forbidden T=3/2 reson., isospin mixing 77−18507
^{24}Mg(t,^{3}He) giant dipole reson. excitation 77−6338

nuclear resonance reactions and scattering continued
^{26}Mg(p,p), 1.54-3.06 MeV, high resolution study, excited analogue states of ^{27}Mg 78−78377
Mg(n,γ), A=24, 25, 26, E=0.1-1800 keV, determ. of isobaric analogue impurities 77−6386
^{55}Mn(p,γ), ^{56}Fe isobaric analogue resonance levels, branching ratios 80−68617
Mo(n,γ), 3-90 keV, neutron reson. parameters, capture cross-sections meas. 77−6371
Mo(n,γ)^{93,99}Mo, 0-3 MeV, valence doorway model for radiative capture 77−79368
^{14}N(p,p), average geometry optical model potential, doorway state effects 77−79367
^{15}N(α,γ)^{19}F, 2.8 to 4.0 MeV, ^{19}F reson. strengths and ang. distrib. 77−65211
^{15}N(α,γ)^{19}F, 5.2 to 8.4 MeV, resonances and gamma decay schemes 78−37358
^{15}N(γ,γ), 6.324 MeV, resonance scatt. cross section temp. depend. in BN, NH_4Cl 80−57767
^{15}N(n,n)^{15}N, reson. struct. in continuum shell model, heavy-ion implications 77−54243
^{15}N(p,α) (p,αγ), 0.9-1.25 MeV, ^{16}O levels, J^π 78−509
^{15}N(p,α)^{15}N, 2.50-5.14 MeV, 3^+ ^{16}O reson. state excit. 78−580
^{15}N(p,$\gamma_{0,1,2}$), 6-22 MeV, ang. distrib. and correl. meas., ^{16}O excited state giant resonance 77−82926
^{15}N(p,γ), ^{16}O excited state GDR, coupled channels version of continuum shell model 79−542
^{15}N(p,n_0)^{15}O, 8.5-19.0 MeV, resonance struct., excitation functions, cross sections 78−50164
^{15}N(p,p)^{15}N, 2.50-5.14 MeV, 3^+ ^{16}O reson. state excit. 78−580
^{23}Na(p,γ) resonance reaction, 3906 keV, ^{24}Mg lowest T=2 state, total width 78−89870
^{23}Na(p,γ)^{24}Mg, 0.5 to 0.9 MeV, resonance strengths of selected resonances in s-d shell 78−66281
^{23}Na(p,p), (p,α), lowest T=2 level of ^{24}Mg narrow resonance, isospin forbidden particle decays 78−89871
Nd+^{12}C, 70.4 MeV, excitation of 3^- states in ^{148,150}Nd deformed nuclei 78−62559
^{142}Nd(γ,γ), 1.85-5.0 MeV, resonance fluorescence, level radiative widths, spin assignments 79−9538
^{146}Nd(γ,γ′), reson. fluoresc., J^π, M2/E1 and Γ meas. 77−26663
^{20}Ne(p,γ), depth profiling of implanted Ne 79−7621
^{20}Ne(p,γ)^{21}Na, 1.7 MeV, DSA lifetime of 2425 keV state in ^{21}Na 77−82860
^{21}Ne (p,p′γ), 0.4 to 1.6 MeV, study of resonances 77−18540
^{21}Ne(p,γ), 0.4 to 1.6 MeV, study of resonances 77−18540
^{21}Ne(p,γ)^{22}Na, γ-ray ang. distrib. and mixing ratios, analogue resons. 78−62504
^{21}Ne(p,p), 0.4 to 1.6 MeV, study of resonances 77−18540
Ne(α,α), A=20, 22, 150 MeV, isoscalar giant quadrupole reson. 77−307
Ne(p,γ), absolute resonance strengths meas. using separted targets 77−79374
^{58}Ni, ^{60}Ni partial radiation widths from neutron capture resonances, valency model calcs. 77−26707
^{58}Ni+p, K-shell X-ray photon proton coincidences, nucl. time delay 79−18281
^{58}Ni(e,e′), 40 to 75 MeV, excitation of T_0+1 giant M1 resonance 77−14118
^{58}Ni(e,e′α), electric quadrupole giant resonance α-decay *(Russian)* 79−85434
^{58}Ni(e,e′p), electric quadrupole giant reson. decay *(Russian)* 79−85434
^{58}Ni(p,γ)^{59}Cu, 3547 and 1833 keV resonances, lifetime meas. 77−26621
^{58}Ni(p,γ)^{59}Cu, γ-decay of ^{59}Cu analogue resons. 78−13005
^{58}Ni(p,p′), 5.65 to 6.13 MeV, resonance and statistical mechanisms *(Russian)* 79−80911
^{58}Ni(p,p′), 60 MeV, analysing power for excitation of giant resonance region of continuum 77−6387
^{58}Ni(p,p), elastic and inelastic scatt., 5.2 to 6.05 MeV, scatt. cross section energy depend. 79−9559
^{59}Ni, neutron cross-sections and resonance integrals 77−23072
^{60}Ni(e,e′), 40 to 60 MeV, excitation of T_0+1 giant M1 resonance 77−14118
^{60}Ni(p,γ)^{61}Cu, 1800 to 290 KeV, γ-ray spectra and j^π assignments 79−59063
^{60}Ni(p,p′), near 6 MeV, spin-flip probabilities distorted wave and statistical anal. *(Russian)* 79−80939
^{62}Ni(p,γ), study of $g_{9/2}$ isobaric analogue state in ^{63}Cu 79−22258
Ni(e,α), E2 strength in resonance regions statistical decay 80−91146
Ni(e,e′) A=58, 60, 64, isospin splitting of giant dipole resonance *(Russian)* 77−50116
^{227}Np damage track detectors, effects of subthreshold fission on neutron dose meas. 78−33375
^{237}Np(γ,γ′) 8.5-11.4 MeV, elastic and Raman scatt., giant reson. struct. 77−34284
^{A}O(π,π), 163 MeV, A=16, 18, comparison of π^+ and π^- scatt. at (3,3) resonance 78−86552
^{A}O($\pi^\pm$,$\pi^\pm$) , A=16, 18, resonance region, proton and neutron distribs. 80−91195
^{16}O+^{12}C system, exptl. survey of resonant structs. below and above Coulomb barrier 79−9616
^{16}O+^{16}O collisions, resonating group study, effective two-nucleon forces 79−59044
^{16}O+n, 3-30 MeV, TOF transmission meas. of neutron resonances 80−37374
^{16}O(^{12,13}C,αX), 140 MeV, fast α prod. and molecular resonance search 80−106066
^{16}O(^{12}C,^{12}Cα)^{12}C, 68 to 80 MeV, sequential decay via excited states in ^{16}O 78−50189
^{16}O(^{12}C,^{8}Be)^{20}Ne*, determ. of resonance struct. in ^{28}Si 79−6663
^{16}O(^{7}Li,^{3}He)^{20}F, 24 MeV, ang. distribs. of states below 6.25 MeV, gas target 78−82369
^{16}O(0^+,6.05 MeV) intermediate struct. resonances from ^{12}C(^{16}O,^{16}O′) 46 to 56 MeV 78−78410
^{16}O(α, α)^{16}O, elastic scatt. reson reaction, appl. to O determ. in Si 79−34408
^{16}O(α,α_1)^{16}O*, resonance observation of 8p-4h state in ^{20}Ne 78−50132
^{16}O(α,α′+charged particle), 155 MeV, α-decay dominance in ^{16}O isoscalar giant quadrupole resonance 78−46035
^{16}O(α,α′), 60 MeV, giant dipole and quadrupole 77−2965

nuclear resonance reactions and scattering continued
$^{16}O(\alpha,\alpha)^{16}O$, 3.045 MeV, O distrib. profiles, from emitted α-particle energy anal. 79−5213
$^{16}O(\gamma,N)$, giant resonance region, features in energy depend. of ang. distrib. 77−6343
$^{16}O(p,p')$, 45 MeV, giant dipole and quadrupole 77−2965
$^{16}O(p,p')$, microscopic anal. of doorway states in giant resonance region 77−2966
$^{16}O(p,p')^{16}O^*$, 42.5-49.3 MeV, octupole GR strength, polarised proton 77−57644
$^{16}O(p,p)$, average geometry optical model potential, doorway state effects 77−79367
$^{16}O(\pi,\gamma n)$, direct and resonance reaction unified shell model, n, γ spectra 80−52696
$^{16}O(\pi,\pi)$, pionic resonance fluorescence in $\Delta(33)$ region 79−85554
^{17}O, giant reson. isospin splitting, photonuclear cross-sections 78−577
$^{17}O(\alpha,n)$, 1.4-2.3 MeV, decay width of lowest T=3/2 level of ^{21}Ne 77−6322
$^{17}O(e,e')$, 65-168 MeV, giant resonance excitation 78−4930
$^{18}O(\alpha,\gamma)$, 0.6 to 2.3 MeV, props. of ^{22}Ne compound states, astrophys. reaction rate 78−57545
$^{18}O(\gamma,n)$ 8.0 to 41.8 MeV, photonuclear cross section meas., resonance decay branching 79−63656
$^{18}O(p,\alpha)$ 72 to 935 keV, astrophysical reaction rate, ^{19}F resonances 79−26439
$^{18}O(\pi,X)$, angular distrib. of inelastic diffusion of $\pi^{\pm}$ *(French)* 80−47507
Os(n,γ), 5-350 eV for A=187, 189, neutron reson. and spin-state determ. 77−6224
$^{31}P(d,\alpha)^{29}Si$, 1.5-2.5 MeV, intermediate resonance widths 77−88151
$^{31}P(d,p)^{32}P$, 1.5-2.5 MeV, intermediate resonance widths 77−88151
$^{31}P(p,\gamma)^{32}S$, 0.5 to 0.9 MeV, resonance strengths of selected resonances in s-d shell 78−66281
$^{31}P(p,\gamma)^{32}S$, ang. distribs. of γ-rays from decay of ^{32}S reson. states 78−13085
Pb isotopes, gamma radn. reson. scatt. 4.7-8.3 MeV 78−78362
Pb+Kr, deep inelastic collisions, excitation of nuclear surface modes 78−37374
^{207}Pb+n, 3-485 keV, ^{208}Pb resonance parameters, s-, p- and d-wave entrance channel doorway states 79−470
^{207}Pb+n, obs. of ^{208}Pb giant mag. dipole states, spin parity assignments 77−57666
$^{207}Pb(n,\gamma)$, primary E2 transitions to ^{208}Pb ground state 78−58284
$^{207}Pb(n,\gamma)$, up to 1 MeV, obs. of ^{208}Pb giant M1 fine struct. 77−79347
$^{207}Pb(n,n)^{207}Pb$, 265 keV, (s+d)-wave mixing 77−46167
^{208}Pb, finite Fermi-system theory, E1, E2, M1 resonances, γ absorpt. cross section near threshold 77−50055
$^{208}Pb+^{12}C(^{14}N)$, giant resonances, ang. distrib., inelastic scatt. 78−62564
$^{208}Pb(^3He,^3Ne)$, 130 MeV, giant reson. excitation, DWBA anal. 79−89319
$^{208}Pb(d,d')$, 24 MeV, mag. dipole states, spin, parity, transition strengths 77−14129
$^{208}Pb(e,e')$, Ex<100 MeV, giant multipole reson. electroexcitation 77−34279
$^{208}Pb(\gamma,n_{pol})$, evidence for M1 collective strength at 8-10 MeV 77−38255
$^{208}Pb(\gamma,n)$, 8 to 13 MeV, total cross section, resonance struct. 78−4928
$^{208}Pb(n,\gamma)$, fast, direct-semidirect and pure resonance model calcs. 80−47486
$^{208}Pb(n,n)$, 16-18 MeV differential cross section resonant characters 79−75952
$^{208}Pb(p,p')$, 24 MeV, mag. dipole states, spin, parity, transition strengths 77−14129
$^{208}Pb(p,p')$, 40, 45 MeV, fine struct. in giant resonance region, collective dipole spin flip excitation 78−46056
$^{208}Pb(p,p')$, 5 to 8 MeV, hyperfine reson. struct., Feynman diagrams 79−6589
$^{208}Pb(\pi,\pi)$, many body effects in resonant scatt. 78−94029
$^{209}Pb(\gamma,\pi^+)^{209}Pb$, photoprod. to single particle states 77−22998
^{106}Pd, reson. scatt. of annihilation quanta, excited state lifetime meas. *(Russian)* 77−26651
Pd(n,n'), near threshold energy for first 2^+ collective levels excitation, statistical model test 77−61408
^{147}Pm, 0.02 to 250 eV, neutron total cross section and neutron resonance parameters 79−97709
^{239}Pu(n, f), undisturbed resonance integral determ., and neutron flux meas. 80−5453
^{240}Pu resonance capture in reactor cell codes, parametric description 79−13384
^{241}Pu, evaluation of neutron cross sections in region 10^{-5} eV to 15 MeV 78−17254
$^{244}Pu(n,\gamma)$ resonance integral meas. 80−73846
Ru(n,n'), near threshold energy for first 2^+ collective levels excitation, statistical model test 77−61408
^{A}S, A=32,33,34, 0.51 to 51.9 eV neutrons, determ. of neutron scatt. lengths, absorpt. and free cross sections 79−30841
^{32}S, (π,γ), shell model anal. 78−89910
$^{32}S(^{12}C,^{12}C)$, 20 to 35 MeV, resonant heavy ion scatt., from s-d shell nuclei 79−67763
$^{32}S(^{12}C,^{12}C)$, 20-35 MeV, resonant scatt., ang. distribs., cross sections and excitation functions 79−45237
$^{32}S(^{12}C,^{12}C)$ backward angle scatt., resonant like structs. 79−17876
$^{32}S(^{9}Be,^{9}Be)$, 20 to 35 MeV, resonant heavy ion scatt., from s-d shell nuclei 79−67763
$^{32}S(\gamma,n)$, (γ,p), cross sections, ^{31}S, ^{31}P excited residual states 78−8795
$^{32}S(p,p)$, 3-3.8 MeV, isospin-forbidden T=3/2 reson., isospin mixing 77−18507
$^{32}S(\pi,\pi)$, many body effects in resonant scatt. 78−94029
$^{33}S(p,\gamma)$, 1.0, 2.0 MeV, reson. excit., Q-value *(French)* 77−26612
$^{34}S(\alpha,\Gamma)^{38}Ar$, 2-3.5 MeV, reson. levels, mixing ratio 79−71859
$^{34}S(p,p)$, 1.45-2.85 MeV, high resolution differential cross-sections 77−65222
^{45}Sc+n, total cross section, neutron resonances, thermal scatt. parameters 78−8821
^{46}Sc energy levels, resonances, spin and parity from $^{45}Sc(n,\gamma)$ 80−52673
$^{82}Se(p,p)$ elastic, inelastic 4.5-77 MeV scatt., IAS, ^{83}Se low-lying states 78−573
^{A}Si, A=28,29,30, 0.51 to 5.19 eV neutrons, determ. of neutron scatt. lengths, absorpt. and free cross sections 79−30841
^{28}Si α-doorway states in α-decay to ^{24}Mg low lying K-band 80−47438
nuclear resonance reactions and scattering continued
^{28}Si backward angle cross sections, entrance channel resonance effects from $^{24}Mg(^{16}O,^{12}C)$ 79−30813
^{28}Si+n, isobaric analogue resonances from total and differential elastic cross sections 78−41715
$^{28}Si(^{12}C,^{12}C)$, 20 to 35 MeV, resonant heavy ion scatt., from s-d shell nuclei 79−67763
$^{28}Si(^{12}C,^{12}C)$, 20-35 MeV, resonant scatt., ang. distribs., cross sections and excitation functions 79−45237
$^{28}Si(^{13}C,^{13}C)$, 20 to 35 MeV, resonant heavy ion scatt., from s-d shell nuclei 79−67763
$^{28}Si(^{13}C,^{13}C)$, 20-35 MeV, resonant scatt., ang. distribs., cross sections and excitation functions 79−45237
$^{28}Si(^{16}O,^{12}C)$, resonant like structs., forward α transfer mechanism 79−17876
$^{28}Si(^{16}O,^{16}O)^{28}Si$, 45-64 MeV elastic scatt., quasi-molecular or barrier-top resonance 79−13341
$^{28}Si(^3He,d)^{29}P$, stripping to bound and unbound states 77−82934
$^{28}Si(^{9}Be,^{9}Be)$, 20 to 35 MeV, resonant heavy ion scatt., from s-d shell nuclei 79−67763
$^{28}Si(^{9}Be,^{9}Be)$, 20-35 MeV, resonant scatt., ang. distribs., cross sections and excitation functions 79−45237
$^{28}Si(\alpha,\alpha')$ 120 MeV, giant reson. multipolarities 77−54201
$^{28}Si(\alpha,\alpha')^{28}Si$, 126 MeV, GQR, DWBA anal. 77−74826
$^{28}Si(\alpha,\alpha)$, 150 MeV, isoscalar giant quadrupole reson. 77−307
$^{28}Si(d,p)^{29}Si$, 1.8 to 3 MeV, energy behaviour of vector analysing power, intermediate resonances *(Russian)* 79−49617
$^{28}Si(n,n)$, core-parricle doorway states calc. 77−23003
$^{28}Si(n,n)$, to 4.5 MeV, s- and p- wave reson. struct., R-matrix interpretation 77−23002
$^{28}Si(n,p)$, 21.6 MeV, cross sections, proton spectra, ^{28}Al analogue dipole state 77−30571
$^{28}Si(p,\gamma)$, 1.3-2.3 MeV, resonant and direct capture, ^{29}P excitation functions and spectroscopic factors 79−80912
$^{28}Si(p,p'\gamma)^{28}Si$, 3.5-3.8 MeV, spin-flip probability in resonance region *(Russian)* 78−41725
$^{28}Si(p,p)$ 5.6-5.9 MeV, isospin-forbidden T=3/2 reson., isospin mixing 77−18507
$^{28}Si(\pi,X)$, angular distrib. of inelastic diffusion of $\pi^{\pm}$ *(French)* 80−47507
^{29}Si doorway state neutron capture, levels and γ-spectra from $^{28}Si(n,\gamma)$ 80−57729
$^{29}Si(n,\gamma)$, evidence for neutron capture through doorway states 79−17909
$^{144}Sm(\gamma,\gamma)$, resonance fluorescence up to 5 MeV 78−66263
$^{154}Sm(p,p')^{154}Sm$, 1 GeV, giant reson. excit., Glauber calc. 77−82891
$^{154}Sm(\gamma,\gamma')$, reson. fluoresc., J^π, M2/E1 and Γ meas. 77−26663
$^{A}Sn(n,\gamma)$ A=114,116,118, $^{115,117,119}Sn$ resonance meas., weak coupling model calc. for levels, J^π assignments 79−6416
$^{117}Sn(\gamma,\gamma')$, excitation of 6517 keV level, resonant scatt. 79−3135
^{120}Sn finite Fermi-system theory, E1, E2, M1 resonances, γ absorpt. cross section near threshold 77−50055
$^{120}Sn(^3He,^3He)$, 130 MeV, giant reson. excitation, DWBA anal. 79−89319
$^{120}Sn(\gamma,\gamma')$, excitation by 7310 keV level, resonant scatt. 79−3135
$^{120}Sn(\gamma,\gamma')$ nuclear resonant scatt. from 6730 keV level 79−3134
$^{120}Sn(\pi,\pi)$, many body effects in resonant scatt. 78−94029
$^{122}Sn(K^-,X)$, 0 MeV, E2 nuclear resonance effects, γ and X-ray meas. 78−41774
$^{124}Sn(e,e)$ ^{150,225}MeV giant multipole resonances, positions and half widths *(Russian)* 78−78349
$^{124}Sn(n,n)$, pol. thermal, parity violation near resonance, DWBA calcs. 80−68528
Sn(p,n) for A=117-124 at 2.6-7 MeV, p-wave size reson. optical model fit 77−30575
$^{88}Sr(\gamma,\gamma)$, 14 MeV, highly excited spin-1 resonances, spin and radiative widths 80−86876
$^{88}Sr(\gamma,\gamma)$, reson. fluoresc. yield meas. width of 1.836 MeV level determ. 77−79357
$^{88}Sr(n,\gamma)$ valence neutron capture, 3-400 keV, ^{89}Sr resonance parameters 77−2989
$^{88}Sr(p,p')^{88}Sr(2_1^+)$, 7-7.5 MeV polarised protons, scatt. at IAR 77−318
$^{181}Ta(e,e')$, 79-119 MeV, DWBA anal., giant multipole resonance parameters 77−30558
$^{181}Ta(e,e')$, giant monopole and quadrupole resonances excitation 78−17184
$^{181}Ta(n,total)$, 15 to 2030 eV resonances, time of flight spectroscopy 78−41716
^{159}Tb polarised target, transmission of polarised resonance neutrons, 20 eV to 100 keV, spins *(Russian)* 77−50138
$^{159}Tb(\gamma,\gamma')$ 8.5-11.4 MeV, elastic and Raman scatt., giant reson. struct. 77−34284
$^{159}Tb(n,\gamma)$, resonance parameters *(Russian)* 77−74850
Te, A=124, G, nucl. reson. fluoresc. vacancy cascades in mols. 77−2953
$^{232}Th(n,\gamma)$, cross-section from 2.6-800 keV 78−8807
^{44}Ti lowest T=2 state isospin forbidden γ-decay from resonances in $^{40}Ca(\alpha,\gamma)$ 79−22228
$^{234}U(n,\Gamma)$, 3 eV to 8.9 MeV, intermediate struct. 77−74895
$^{234}U(n,f)$, intermediate struct. anal. 77−79408
$^{235}U(n,\gamma f)$, X-ray prefission yield depend. on fission width 77−10453
$^{235}U(n,f)$, spins of resonances below 150 eV 77−23147
$^{235}U(n,\gamma)$ resonance capture, primary γ-transitions, parity assignments 77−26619
^{236}U, giant E2 isoscalar resonance determ. 80−27607
$^{236}U(n,\gamma)$, 30-1800 eV, cross section meas. 77−23061
$^{236}U(n,n)$, 30-1800 eV, cross section meas. 77−23061
^{238}U, energy-depend. Doppler effect calc. using collision probability method 77−57714
^{238}U neutron cross sections evaluation for incident neutron energies up to 4 keV 80−5146
^{238}U, neutron resonance parameters, transmission meas. on natural U 77−23063
^{238}U+n, Doppler effect meas. at 24 and 144 keV 79−97704
$^{238}U(e,\alpha)e'^{234}Th$ cross section, giant quadrupole resonance 78−58262
$^{238}U(n,\gamma)$, cross section and resonance shape, gas molecule vibr. effects 80−42661
$^{238}U(n,\gamma)$, p-wave assignment of resonances 77−23062
$^{238}U(n,\gamma)^{239}U$ resonance capture self-indication obs. at 77, 293 and 873K 79−9574
$^{238}U(p,p')$, isobaric analogue reson., modified KASTOR code calc. 77−14132

nuclear resonance reactions and scattering continued
^{51}V(p,n), 1.56-5.53 MeV, total cross section, excitation functions, isobaric analogue resonance 78−4943
V(p,n)^{51}Cr, 2.34 MeV, shell model anal. of analogue resonance [illegible] 14122
^{89}Y(p,p), (p,p'γ), 4.5-8.0 MeV polarised protons, IAS spectroscopy of [illegible] 61396
^{89}Y, reson. neutron capture cross-section between 2.5 and 100 keV [illegible] 82924
^{89}Y(n,γ), 6.2-15.6 MeV, gamma-ray spectra, cross-section meas. 78−33176
^{68}Zn(p,γ), 3.8 MeV, ^{69}Ga, IAR corresponding to $1/2^-$ and $9/2^+$ ^{69}Zn states 78−66257
^{70}Zr, finite Fermi system theory, E1, E2 and M1 resonances, γ absorpt. cross section near threshold 77−50055
^{90}Zr+^{12}C(^{14}N), giant resonances in inelastic scatt. 78−62564
^{90}Zr(^{3}He,^{3}He), 130 MeV, giant reson. excitation, DWBA anal. 79−89319
^{90}Zr(^{3}He,t)^{90}Nb, 130 MeV, giant Gamow-Teller resonance, T=4, T=5 components 78−46081
^{90}Zr(^{3}He,t)^{90}Nb, 18.5 MeV resonance, isovector dipole and Gamow-Teller transitions 80−86881
^{90}Zr(p,p'), polarised protons, compound nuclear contribs. to IAR inelastic decay 78−8813
^{91}Zr, 292.4 eV neutron resonance parameters, radiative and neutron widths, spin assignments 77−6369

nuclear resonances
see also isobaric analogue resonances; nuclear collective states and giant resonances
^{12}C-α-^{12}C nuclear molecular states, quantum mechanical three-body approach 79−97692
A=11, 12, energy levels, transitions and resonances, compilation 80−46743
A=184, 194, 200, 208, pygmy resonance, E1 transition probabilities, BCS wave functions, spin-isospin oscillation *(Chinese)* 80−63087
A=21-44, energy levels, excitation energies, branching and mixing ratios, lifetimes, J^π, resonances 79−13208
A=24 to 32, resonances in heavy ion reactions, semiempirical predictions 78−74307
A=60-140, spherical nuclei, two phonon admixture effect on M1 resonance *(Russian)* 80−5105
A=7-40, EM transition strength distribs. *(Russian)* 80−86855
average resonance parameter eval. and calcs., statistical model for capture process 80−18271
band crossing model, resonance and strong absorption phenomena in heavy ion scatt. 79−3165
barrier-top resonance and heavy ion reactions 77−38291
baryon resonances in nuclei, review 77−79364
break-up reactions to resonant final states, appl. to ^{6}Li(p,2p)^{5}He 77−10381
coherent production of resonances in nuclei, book contrib. 79−21889
collision duration in presence of strong overlapping resonance levels 78−17169
common doorway resonance, decay amplitude phase relation from (n,γ) reactions 80−57758
conference on heavy ion reaction dynamical props., Johannesburg, S.Africa (Aug. 78) 80−17715
conference on nuclear struct. spectroscopy and atomic nucleus struct., Tashkent (Mar. 77) 79−6470
continuous slowing down theory, appl. to low-energy neutron resonances 77−26645
continuum shell model calcs. of particle emission threshold effects, cross section, line shape of resonances 78−46014
core polarisation effects in inelastic scatt. and charge exchange 77−22983
decaying states, using Kapur-Peierls and Siegert resonant states and extended Hellmann-Feynman theorem 78−4503
doorway states, fragmented, micro-resonances, strength functions, K-matrix width 80−57754
double-beta decay, electron-neutrino pair emission via Δ(1232) resonance 78−54722
few body dynamics analytical continuation, nuclear shell model, resonances and bound states *(Russian)* 79−40860
fission resonances, spin determ. using polarised beam and target, review 77−26796
gamma-ray scattering, body Fe stores meas. technique 79−83914
heavy ion clustering aspects and nuclear quasimolecular resonances 79−6439
heavy ion fusion and transfer reactions, resonance effects 80−9283
heavy ion molecular resonances 78−13148
heavy ion reactions, coherence angle and cross section fluctuations correlation function, resonances 80−57790
heavy ion reactions, narrow resonances in continuum states 77−54240
heavy ion scatt., optical potential resonances, semiclassical method, S-matrix amplitude 79−3120
heavy ion scatt., Pauli-principle resonance effects, analytic representation 79−6659
heavy-ion scatt. band crossing model, appl. to ^{12}C+^{16}O scatt. 78−89898
high resolution proton scattering 79−45252
hypernuclei, interdisciplinary viewpoint of theories and developments *(Czech)* 80−22749
irreducible spin precession theory applied to atomic and nuclear RF spectroscopy 80−27969
isolated doorway resonances, spreading width and branching ratios 77−57645
isoscalar E1/broad resonances (T=0) 79−13250
level density of nuclei, role of collective effects and neutron resonances *(Russian)* 79−49586
light heavy ion total reaction cross sections in diffraction model, resonance oscillations 80−13503
light nuclei, E1 transitions from reson. states, probability distribs. 78−13021
many-body resonances, analytical continuation of bound states examination 79−75955
Mehta-Dyson statistics, appl. to sequences of neutron resonances 77−30543
molecular reson. in heavy-ion scatt. 78−62561
multidimensional barrier penetration and fission-widths, barrier resonance 80−13454
narrow resonances in the continuum 79−85435

nuclear resonances continued
neutron capture probabilities for thick samples at resonance energies 78−46123
neutron evaluated nuclear data files in unresolved resonance region, data representation 78−29459
neutron resonance data, statistical anal. method 80−102174
neutron resonances, nuclei from ^{64}Zn to ^{177}Hf, total α-widths 77−26708
neutron resonances, reaction mechanisms and nuclear struct. 77−26564
neutron total cross section fluctuations, shell model approach using Greens function, resonances 79−22283
Nordheim integral treatment for resonance processing, proper use 80−37427
nucleon resonances in nuclei, review 77−26563
particle-hole calc. of isobaric analogue and isovector monopole reson. 78−21537
photonuclear resonances, energy correction for unfolded cross-section data 77−10387
pigmy resonance, EM transitions, threshold states effects *(Hungarian)* 78−89818
pionic atoms, E2 nuclear resonance effects 79−76534
pole expansions for resonance functions, scatt. amplitudes and continuum states *(Russian)* 80−86871
protein-solvent systems, dynamics investigation by nucl. gamma-resonance 79−62166
RCPL1 program, calc. of Doppler broadened neutron resonance cross-sections 79−67810
recent advances in neutron physics, prod., handling, detection, nuclear reactions, resonances 77−26686
resonance widths calc. using microscopic R-matrix theory in generator coord. basis 77−14079
resonances as components of bound states 79−45239
resonant states in the presence of Coulomb interactions, Schrodinger eqn. 80−91161
resonant subsystems in few-body theory 77−18494
s-d nuclei with A=24 to 32, resonances in heavy ion reacts. 79−6403
s-wave neutron reduced widths 77−22850
sd shell nuclei, (p,γ) resonance strengths 80−22786
sd-shell nuclei heavy-ion reaction resonances, low level density regions, shell model 80−57757
single-particle resonances, numerical anal. 78−29436
spherical nuclei, M1 transition strength distrib. at high excitation energies 79−75895
spherical nuclei with pairing, M1-reson. calc. 79−6390
statistical significance of spreading widths for doorway states, comments 80−27611
stripping reactions to unbound states from p-n correlations, spin, parity and widths 78−62547
three neutron resonance, enhancement factors, forces, and binding energy 79−45230
three-particle reson., eigenvalues of Faddeev eqn. kernel determ. 77−2565
time delay of resonance wave packets, stat. model anal. 80−22802
time-dependence of reson. scatt. radiation 77−14060
total radiative width of neutron resonances *(Russian)* 79−13270
UCN, quasibound states in matter, reson. positions and widths 80−73833
unified model appl. to ^{12}C+n system 78−29437
unitary sum rules and collision time in large resonance level overlaps *(Russian)* 78−70309
Wigner's random matrix model, time reversal violation 77−30542
yrast region of rapidly rotating nuclei, instability toward nucleon emission 77−88027
α-decay lifetimes and resonance widths, comparison of calc. methods 78−78325
Δ(1232) isobar in nuclei, one-boson-exchange and straton model anal. *(Chinese)* 78−78275
Δ resonance shifts, simple model 77−82829
Δ-nuclear states excited in ^{4}He-π^- scatt. 77−88093
(e,e), low-q, A=14 nuclei, isospin T=2, 1 and 0 collective resonances, shell model 80−510
(γ,γ'), spin, parity and width of resonance level 80−18287
(γ,n), spin, parity and width of resonance level 80−18287
(γ,X), A=14 nuclei, isospin T=2, 1 and 0 collective resonances, shell model 80−510
(n,f), intermediate struct. line fitting, subthreshold fission resonances 80−102214
(n,γ), mechanism in 3s size resonance, s-wave radiative width partition 80−37387
(n,γ), mechanism in 3s size resonance, radiative width statistical and valence effects 80−37388
(N̄,X), complex shell model, narrow resonances and bound states *(Chinese)* 80−42622
^{3}n model with $^1S_0$ interaction in Faddeev eqn. framework, 3 neutron resonance 79−67680
NNN̄ system, bound and reson. states using Fadeev eqns. *(Russian)* 78−89804
(π,γ), A=14 nuclei, isospin T=2, 1 and 0 collective resonances, shell model 80−510
(π^-,γ), 1p shell nuclei, spin-dipole excitations, shell model calcs. 79−17935
π- and ρ-exchange pots., influence on mag. resonances, mag. moments, and transition probabs. 80−99133
^{8}Be, reson. levels, J^π, via ^{6}Li(d,α)^{4}He, 1.5-11.5 MeV 77−82935
^{8}Be, reson. levels , J^π via ^{6}Li(d,α) below 12 MeV 77−82936
^{A}Al, A=25,26,27 levels, resonances, γ-ray branching ratios from ^{A}Mg(p,γ) 80−86875
^{26}Al low energy resonances, decay and J^π assignments, branching ratios from ^{25}Mg(p,γ) 80−42624
^{26}Al T=1 states, resonances, J^π and transitions from ^{25}Mg(p,γ) 80−99131
^{27}Al, GQR via (α,α') scatt. at 126 MeV 77−74826
^{27}Al levels, resonances, J^π, branching and mixing ratios from ^{26}Mg(p,γ) 80−99132
^{27}Al yrast states via ^{12}C(^{12}N,α) reson. struct. 77−79348
^{27}Al(^{12}C,^{12}C), 14-25 MeV, 180° scatt. excitation function and ang. distrib. struct. 80−32253
^{241}Am, total and fission cross sections in resonance region, resonance parameters 77−23160
^{241}Am, total neutron cross-section in resonance region 77−26746
^{36}Ar, neutron low energy total cross-section, bound level parameters 77−23071

nuclear resonances continued
^{36}Ar, resonances populated in ^{24}Mg(^{12}C,α) 79−67629
^{71}As intermediate struct., resonance spin from ang. correlations of ^{70}Ge(p,p'γ) 79−67729
^{75}As, nucl. reson. fluoresc. meas., spins and level widths determ. 77−61379
^{197}Au(α,α'), 120 MeV, isoscalar resonance excitation, low lying transitions, DWBA calc. 80−512
^{10}B 1175 keV level resonance strength from ^{6}Li(α,γ) 79−45228
^{10}B, 8.89 MeV reson. J$^{\pi}$ assignments via (p,p) and (p,αγ) 2.56 MeV 77−50098
^{10}B(e,e), 140 MeV, resonances in e spectra *(Russian)* 78−78367
^{11}B (e,e') 120-250 MeV, excited state form factors, shell and diagram model anal. *(Russian)* 79−40852
^{11}B intermediate resonance and electric quadrupole transition contribution to ^{12}C(γ,pα)^{7}Li *(Russian)* 79−40896
^{12}B levels, J$^{\pi}$ and diff. cross sections, R-matrix anal. of ^{11}B(n,n) 80−78151
^{A}Ba, A=136, 138, M1 transition enhancement from neutron resonances quasiparticle-phonon model 79−9506
^{A}Ba(γ,γ) A=136-8, 1.68-5.0 MeV, nuclear resonance fluorescence, levels transitions and spins 79−6543
^{6}Be reson. search in ^{4}He(^{3}He,n)^{6}Be at 38.61 MeV, solar neutrino flux 78−619
^{6}Be system, excitation obs. in polarised (^{3}He,^{3}He) scatt. 78−78400
^{8}Be double resonance, 16.6 and 16.9 MeV levels, prod. by α+α 78−62553
^{8}Be high spatial symmetry excited states, resonances, rot. band from (d,αt), (p,αt) 80−86780
^{8}Be high-lying reson. below α-α* threshold, cluster model calc. 77−82840
^{8}Be resonant state, αα* cluster and sympletic model anal. from ^{7}Li(p,α), ^{6}Li(d,α) 79−9537
^{9}Be, 1/2^{+} resonance state at 1.68 MeV 79−6398
^{9}Be(e,e), longitudinal form factor for 1/2^{+} resonance 80−22682
^{209}Bi, reson. parameters for s and p-wave levels 78−37322
^{209}Bi(α,α'), 120 MeV, isoscalar resonance excitation, low lying transitions, DWBA calc. 80−512
CC ^{20}Ne 8^{+} level radiative width, resonance strength from ^{16}O(α,γ) 80−83065
^{11}C intermediate resonance and electric quadrupole transition contribution to ^{12}C(γ,nα) *(Russian)* 79−40896
^{11}C levels and resonance, γ-ray excitation curves from (p,αγ), (p,pγ) 80−9280
^{12}C (^{16}O, ^{16}O'), 19-23 MeV, intermediate width structs., ang. correlations, spins 80−13431
^{12}C, radiative transitions and isospin mixing 77−38242
^{12}C-^{12}C system, sub-Coulomb resonances study using ^{12}C(^{12}C,^{16}O)^{8}Be 77−57688
^{12}C+^{11}B, 9.4-17.8 MeV, excitation functions for elastic, inelastic, ^{8}Be, α exit channels, resonances 79−67731
^{12}C+^{12}C, 19.5 MeV, intermediate struct. in continuum shell model, quasi-molecular shape resonance 79−45235
^{12}C+^{12}C, overlapping 10^{+} and 12^{+} resonances near E$_{c.m.}$=18.5 MeV 77−6432
^{12}C+^{12}C, sub-Coulomb total cross section, simple pot. model of resonances 78−66303
^{12}C+^{12}C gross struct. resonances in excitation functions from ^{12}C(^{12}C, ^{10,11}B) 80−102167
^{12}C+^{12}C scatt., intermediate molecular resonances, band crossing model anal. 79−6655
^{12}C+^{12}C scatt. and fusion cross sections above Coulomb barrier, folding model, resonances 79−6687
^{12}C+^{12}C system resonant structs., J$^{\pi}$ assignments, true ^{24}Mg states from ^{12}C(^{12}C, ^{16}O) 80−99163
^{12}C+^{16}O, 22 MeV, spins of reson. assigned 78−17236
^{12}C+^{16}O, elastic scatt., simple double folded optical pot. model for resonances 79−6535
^{12}C+^{16}O, resonance at 12.8 MeV 77−46187
^{12}C+^{16}O, resonance behaviour, similarity to that in ^{12}C+^{12} 78−33210
^{12}C+^{16}O scatt., band crossing model of resonances 78−89898
^{12}C+^{28}Si, 17 to 37 MeV, inelastic and elastic backward angle scatt., surface resonances 78−37367
^{12}C(^{12}C, ^{12}C), shape resonance energy and widths, projection operator method 80−78255
^{12}C(^{12}C, ^{12}C) intermediate struct. resonances, ^{24}Mg giant isoscalar quadrupole fission/fusion doorway states 80−37410
^{12}C(^{12}C, ^{12}C)^{12}C*, 0$_2^{+}$, 3$_1^{-}$, 4$_1^{+}$ state excitation functions, resonance structures 80−42616
^{12}C(^{12}C,^{12}C'), 18.5-32.8 MeV, spin alignment and possible molecular resonances 80−86804
^{12}C(^{12}C,^{12}C'), 10-40 MeV, resonance phenomena, band crossing model appl., molecular phenomena 79−54424
^{12}C(^{12}C,^{12}C'), 14.5-32 MeV, gross structure peaks, particle-γ coincidences 79−97693
^{12}C(^{12}C,^{12}C'), gross struct., barrier top resonance model calc. 80−9279
^{12}C(^{12}C,^{12}C'), intermediate resonance, coupled channels calcs. 80−42611
^{12}C(^{12}C,^{12}C), 10-30 MeV, projection operator method, Feshbach doorways, intermediate structure 80−68695
^{12}C(^{12}C,^{12}C), 10-30 MeV, molecular structure, projection operator anal., differential cross sections 80−106033
^{12}C(^{12}C,^{12}C), 13-14.1 MeV, Coulomb barrier resonance parameter direct determ., J$^{\pi}$ assignments 80−513
^{12}C(^{12}C,α), 11-15 MeV, quasimolecular resonances 79−6544
^{12}C(^{12}C,α)^{20}Ne, 17 to 20 MeV, excitation functions, correl. resonances 77−34344
^{12}C(^{12}C,α)^{20}Ne, statistical methods for resonance detection, nonstatistical struct. 79−45238
^{12}C(^{12}C,p)^{23}Na, schematic model for continuum resonances, shape resonance fragmentation 77−67764
^{12}C(^{12}C,xα), 12-31.5 MeV, inclusive α-particle yield, resonant like structs. 80−42691
^{12}C(^{14}N,α)^{22}Na, statistical methods for resonance detection, nonstatistical struct. 79−45238
^{12}C(^{15}N,α)^{23}Na, statistical methods for resonance detection, nonstatistical struct. 79−45238
^{12}C(^{16}O, ^{16}O'), molecular resonances from coupling interactions derived by folding procedure 79−89279
^{12}C(^{16}O,^{16}O)^{12}C* (2^{+}, 4.44 MeV) mol. reson., band crossing model 78−62562
nuclear resonances continued
^{12}C(^{16}O,^{20}Ne), 10-15.5 MeV, cross sections and ang. distribs., resonances, direct and stat. anal. 79−67730
^{12}C(^{3}He,d), spectral line shape anal. 78−25203
^{12}C(α,α'), generator coordinate multichannel calc., levels and resonances 80−78149
^{12}C(α,α), 9-11 MeV, elastic and inelastic, resonances and ang. distribs., orthogonality condition model 79−6637
^{12}C(d,n), spectral line shape anal. 78−25203
^{12}C(e,e) 140 MeV, resonances in e spectra *(Russian)* 78−78367
^{12}C(n, X), compound resonance decay based on bound and metastable single nucleon states *(Russian)* 80−5107
^{12}C(p,p), pol. p, 14.23 MeV resonance broadening, nuclear recoil, atomic excitation effects 80−102165
^{12}C($\pi^{\pm}$,$\pi^{\pm}$), 162 MeV, large scale elastic and inelastic scatt. near πN(3,3) resonance 79−40961
^{13}C, TOF transmission meas. of neutron resonances 80−37374
^{13}C, T=3/2 resonance parameters, ground state γ-decay width from ^{9}Be(α,n) and ^{9}Be(α,α') 79−3123
^{13}C+^{13}C, appl. of molecular particle core model 78−82384
^{13}C(α,α'), 22, 36 MeV, resonant state line shapes 80−91148
^{13}C(γ,n), 6.5-9.3 MeV, ang. distribs., E1, M1 and E2 excitations, resonance radiative widths 80−68581
^{14}C+^{16}O scatt., molecular resonances, generator coordinate study 79−36216
^{22}C, electroexcitation of collective M1 resonances, RPA calcs. 77−46104
^{A}Ca(π,π), A=40,48, 40-241 MeV, first and second order optical pots., resonance behaviour 80−68624
^{40}Ca composite system, heavy ion resonances from ^{24}Mg+^{16}O, ^{28}Si+^{13}C 80−86874
^{40}Ca, high spin cluster like resonances obs. in ^{24}Mg+^{16}O 79−6664
^{40}Ca(^{12}C, ^{12}C), 135-150 MeV, elastic excitation function at 180°, resonance like struct. 79−9609
^{40}Ca(^{16}O,^{16}O), rot. band of molecular resonances, generator coordinate model 80−13428
^{40}Ca(^{40}Ca, ^{40}Ca), generator coordinate study, rot. band of molecular resonances 79−75948
^{40}Ca(^{40}Ca,X), deep inelastic, doubly differential cross section, spectra struct. 80−5103
^{40}Ca(α,α), 6-18 MeV, resonances, anomalous large angle scatt. and quasi-molecular states 80−27613
^{40}Ca(α,α), entrance channel resonances, backward angle scatt., elastic scatt. enhancement 80−27612
^{40}Ca(α,γ)^{44}Ti, 2.75-4.00 MeV, γ-ray ang. distrib. of reson. for spin parity values 77−65230
^{40}Ca(γ,γ), 6.95, 7.12 MeV, strengths of isospin forbidden E1 transitions 78−13059
^{40}Ca(n,γ)^{41}Ca, up to 15 MeV, higher-order processes, coupled channel treatment 77−61431
^{40}Ca(p,p'γ), 6.25 MeV, triple ang. correlation, 3^{-} exit channel, resonances, single particle states 80−68626
^{41}Ca damped reaction fragment, energy spectra struct., evaporation processes from ^{40}Ca(^{40}Ca,X) 79−93591
Cd, A=110, 112, isobaric analogue resonances, QRPA anal. of (p,p) reactions 78−576
^{104}Cd, (p,t) study at 42 MeV, hole states at high excitation 78−50158
^{111}Cd, pionic, E2 nuclear resonance effects 78−29868
^{112}Cd, kaonic, E2 nuclear resonance effects 78−29868
Cf, N=152 to 154, resonances, fission probabilities and thresholds 78−46119
^{35}Cl, negative energy resonance parameters for (n,n), (n,γ), (n,p) and (n,α) 77−23025
^{35}Cl(n,γ), slow n, 398 eV resonance J$^{\pi}$ determination 79−36147
^{36}Cl anomalous M1/E1 strength ratio and doorway states from ^{35}Cl(n,γ) 80−57730
^{245}Cm, neutron resonance parameters, neutron energies 1-30 eV range 78−17167
^{245}Cm, resonance parameters up to 30 eV, neutron transmission meas. 77−26584
^{245}Cm(n,f), cross section, 0.01 to 35 eV 78−21612
^{246}Cm, resonance parameters up to 150 eV, neutron transmission meas. 77−26584
^{248}Cm, resonance parameters up to 100 eV, neutron transmission meas. 77−26584
^{55}Co f-wave resonances, inelastic p amplitudes, analogue state spectroscopic factors from ^{54}Fe(p,p'γ) 80−47451
^{55}Co, IAR, J$^{\pi}$ via ^{54}Fe(p,p) 3.28-4.53 MeV 78−574
^{59}Co, neutron resonance spectroscopy, R-matrix anal. 78−21555
^{A}Cr(p,p), A=50, 52, 6 MeV, elastic and inelastic differential cross sections, spin flip probability *(Russian)* 80−91187
^{50}Cr(p,p'γ), 2.00-3.03 MeV, proton and γ-ray ang. distrib. meas., p-wave reson. obs. 77−41961
^{52}Cr(γ,γ), up to 12 MeV, highly excited spin-1 resonances, γ-transitions 80−13427
^{53}Cr levels, J$^{\pi}$, γ-transitions and 1626 eV resonance from ^{52}Cr(n,γ) 80−42610
^{133}Cs, neutron resonance parameters up to 400 eV 77−26581
^{133}Cs, nuclear resonance parameters, 1 to 400 eV, calc. by shape and area methods 79−30789
^{134}Cs (t$_{1/2}$=2.2 yr), neutron resonance parameters up to 400 eV 77−26581
^{134}Cs, nuclear resonance parameters, 1 to 400 eV, calc. by shape and area methods 79−30789
^{A}Cu A=29,63, Doppler shift attenuation factors, level lifetimes, resonances from Ni(p,γ) 80−57741
^{59}Cu, resonance states parameters *(Russian)* 79−80911
^{63}Cu(p,p'), 40 MeV, octupole states, weak coupling model 79−93495
Cu(π^{-}, spallation) 0.6, 0.9, 12 GeV, T=1/2 resonances, Na, Sc and Co rel. yields 80−5109
(d,p), A=88-106, pol. d, excitation curve isospin anomaly, neutron single particle resonances 80−27595
^{167}Er, s-wave resonance parameters, 5 to 130 eV, spin determ. 77−26585
^{A}Es, A=255,256, fission barrier first peak height, pot. energy surface struct. 80−42720
^{152}Eu (T$_{1/2}$=12.4 yr) neutron resonances 0 to 14 eV, radiation width, level spacings 77−26583
^{152g}Eu, neutron resonance obs. by time of flight spectroscopy, cf. ^{151}Eu and ^{153}Eu *(Russian)* 78−25120
^{18}F J$^{\pi}$=3^{-} doublet at 6241 keV, isospin mixing from (p,γ), (p,α), (α,γ) (^{14}N,α) 80−511

nuclear resonances continued
^{18}F levels and resonances, J^{π} assignments from ^{17}O(p,α), ^{17}O,(p,$p_1\gamma$), ^{17}O(p,γ) 79−9480
^{18}F levels and resonances, cross sections in R-matrix formalism from ^{17}O(p,α) 80−18267
^{18}F resonances, α-widths, isospin and parity mixing, R-matrix anal. of ^{14}N(α,α) 80−91162
^{19}F deduced resonances from ^{18}O(p,α)^{15}N reaction at stellar energies 79−26439
^{19}F levels, resonances and phase shifts, resonating group calcs. from ^{15}N(α,α) 80−32189
^{19}F resonance parameters and J^{π} values from ^{18}O(pp) polarised p 79−45232
^{19}F, resonant and bound levels, ^{18}O(p,γ) and ^{18}O(p,pγ) reactions 78−89790
^{19}F $T=^3/_2$ states resonance energy, γ-decay and J^{π}, capture strength from ^{16}O(p,γ) 79−67728
^{19}F(p,$\alpha\gamma$)^{16}O, F conc. profiles determ. in corroded MAGNOX fuel canning materials 79−92035
^{A}Fe(p,p'), A=54, 56, 6 MeV, resonances, spin flip and cross section depends., Hauser Feshbach anal. *(Russian)* 80−83084
^{54}Fe neutron capture, asymmetric s-wave reson., background interf. 78−21563
^{54}Fe(p,p), 5.5-6.2 MeV, resonance effects, deformation, spectroscopic factors, statistical, optical and DWBA anal. 79−6593
^{55}Fe resonances, levels, J^{π}, valence capture γ-ray spectrum from ^{54}Fe(n,γ) 80−86852
^{56}Fe+n, 0-2.2 MeV, doorway state struct. 77−88143
^{56}Fe(e,α), E2 isoscalar resonance sum rule, DWBA anal. 80−68621
^{56}Fe(γ,γ), up to 12 MeV, highly excited spin-1 resonances, γ-transitions 80−13427
^{56}Fe(n,γ), resonance state, partial radiation widths of high energy transitions 78−13104
^{57}Fe, 14 keV, nuclear resonance excitation by synchrotron radiation 78−78363
^{57}Fe, 14 keV state excitation by synchrotron radiation 78−25147
^{57}Fe anomalous M1/E1 strength ratio and doorway states from ^{56}Fe(n,γ) 80−57730
^{57}Fe, gamma decay of 1.167 keV $p_{1/2}$ resonance obs. in ^{56}Fe(n,γ) 77−30585
^{57}Fe(n,X) transmission data up to 400 keV, J^{π} value for resonances 80−18311
^{58}Fe+n, total cross section from 7 to 325 keV, resonance struct. anal. 78−74357
^{58}Fe(n,γ) capture and total cross section meas. below 325 keV, resonance parameters 80−18314
^{58}Fe(n,n), 0.03-500 keV, total cross section, resonance parameters and level spacings 79−6603
^{59}Fe resonances, primary γ-intensities, E1-M1 correlation from ^{58}Fe(n,γ) 80−57740
Fe(n,X), 3 eV-1 MeV transmission meas., resonance anal. 80−18316
Fe(n,γ) cross-section meas. principal resonance parameters 80−18312
^{255}Fm, fission barrier first peak height, pot. energy surface struct. 80−42720
^{156}Gd, Mehta-Dyson statistics, appl. to sequences of neutron resonances 77−30543
^{156}Gd(n,γ), up to 2.24 keV, n resonances, spectra fluctuation, statistical theory test 79−36188
^{73}Ge, 13.3 keV Mossbauer resonance, dispersive interference effects 78−25145
Ge(n,n'), 2^+ level excitation cross sections, intermediate resonances, optical model with coupled channels *(Russian)* 79−40897
^{2}H(α,αp)n, 15-42 MeV, ^{6}Li 1^+ resonance and breakup amplitude, three body model 79−75954
^{2}H(γ,n)p, cross section asymmetry polarised photons 400 to 600 MeV, resonances *(Russian)* 79−89294
^{2}H(p,p), polarised p, 316, 516 MeV, anal. powers in resonance region, backward angle scatt. 79−71834
^{A}H(π^+, π^+), A=1,2, 130-280 MeV, 180° excitation function, dibaryon resonance signals 80−68619
^{3}He(π,π), 1 GeV, backward scatt., nonstable meson-nucleon interaction cross section, resonance *(Russian)* 80−68559
^{4}He 2^+ resonance evidence at 40 MeV from ^{4}He(e,^{3}H), and ^{3}H(p,γ) 80−86880
^{4}He (p,p), effective channel approach, N* resonance effects 79−9570
^{4}He system, high spin states 78−86484
^{4}He+n, separable pot. fits to reson. parameters 78−8822
^{4}He(d,d), 4.8-6.8 MeV, ^{6}Li resonances, phase shift analysis 79−75953
^{4}He(γ,P)^{3}H, 20 to 50 MeV, 2^+ resonances *(Russian)* 79−59052
^{4}He(γ,d)^{2}H, ^{4}He elec. quadrupole reson., multipole expansion *(Russian)* 78−66264
^{4}He(n,γ)^{3}He, 20 to 50 MeV, 2^+ resonances *(Russian)* 79−59052
^{177}Hf neutron resonances, high energy γ-rays 77−22938
^{177}Hf spin 4^- resonances, intermediate substructures 77−26586
^{177}Hf(n,γ), 1-165 eV, γ-ray spectra obs., level scheme determ. 77−50130
Ho, magnetic moment of neutron resonances 77−26576
^{165}Ho(n,γ), 0 to 2 keV, neutron strength function of states with selected spin 77−26705
I β^+ decay force function resonance struct., level populations *(Russian)* 80−102154
^{127}I neutron resonance parameters, 20 eV to 2 keV 77−22897
^{192}Ir levels, resonances and low energy γ-rays from ^{191}Ir(n,γ) 80−47397
^{140}La, s- and p-wave resonances, obs. in La(n, γ) 78−17186
^{140}La, spectra from ^{139}La(n, γ) 78−17185
^{6}Li resonance effects on d-α elastic scatt. 78−46074
^{6}Li system, resonance behaviour from excitation function of ^{3}H(^{3}He,^{4}He)^{2}H reaction 79−6640
^{6}Li$_{\Lambda}$, supermultiplet struct. and decay props. of hypernuclear 1^+ resonances from (K^-,π^-) 80−78186
^{6}Li(^{3}He,^{3}He), phase shifts, cross sections, resonating group calcs., odd-even features, resonances 80−68681
Lu β^+ decay force function resonance struct., level populations *(Russian)* 80−102154
^{175}Lu, ^{176}Lu, neutron resonance parameters up to 200 eV 77−26582
^{176}Lu, reson. spins, secondary γ-transition intensity, from ^{175}Lu(n,γ) 78−21512
^{177}Lu, reson. spins secondary γ-transition intensity meas. in ^{176}Lu(n,γ) 78−21512
^{23}Mg resonances through γ-decay excitation functions from ^{12}C(^{12}C,n) 80−63148
nuclear resonances continued
^{24}Mg (α,α' ^{12}C), 120 MeV, symmetric fission, resonances and average partial widths 80−42714
^{24}Mg, existence of second $J^{\pi}=0^+$ reson. at high excitation energy, study of ^{12}C(^{12}C,α)^{20}Ne reaction 78−25214
^{24}Mg, form. in ^{12}C+^{12}C reaction at 10.5 to 15 MeV, possible rot. band 78−13134
^{24}Mg, GQR via (α,α') scatt. at 126 MeV 77−74826
^{24}Mg intermediate struct. correlations, elastic and reaction channel excitation functions from ^{12}C(^{12}C,X) 80−68625
^{24}Mg nuclear molecular resonances in ^{12}C-^{12}C system from ^{12}C(^{16}O,α), 80−13430
^{24}Mg nucleus, ^{12}C+^{12}C quasimolecular rotational band resonances *(Russian)* 79−13269
^{24}Mg radiative decays of unbound high spin states, resonance J^{π} assignment from ^{20}Ne(α,γ) 79−67701
^{24}Mg, rot. band, reson. states, J^{π} via ^{12}C+^{12}C 78−491
^{24}Mg, rot. band obs. with ^{12}C(^{12}C,α)^{20}Ne 78−12951
^{24}Mg, rotational band fragmentation and rotation-vibr. model, ^{12}C+^{12}C appl. 78−25096
^{24}Mg(^{16}O,^{16}O), 24-40 MeV, backward angles, excitation functions, ang. distribs. and resonant behaviour 80−68622
^{24}Mg(α,^{12}C)^{16}O, 22-26 MeV, intermediate resonances in ^{12}C+^{16}O system, J^{π} assignments 79−17880
^{24}Mg(α,α'), 22-26 MeV, intermediate resonances in ^{12}C+^{16}O system, J^{π} assignments 79−17880
^{24}Mg(d,n)^{25}Al, stripping reactions to unbound states from p-n correlations, spin, parity and widths 78−62547
^{51}Mn, p-wave reson. determ. from ^{50}Cr(p,p'γ) 77−41961
^{55}Mn energy level excitation curve, bound state and resonance γ-decay from ^{54}Cr(p,γ) 79−476
^{55}Mn, neutron resonance spectroscopy, R-matrix anal. 78−21555
^{55}Mn(n,γ)^{56}Mn, 2.5-600 keV, total cross section, resonance energies and capture area 79−6607
^{A}Mo(n,γ) A=98, 100 resonance parameters, capture Γ-rays and reaction mechanism 80−18272
^{98}Mo neutron resonances, spin-parity determ. using low energy γ-rays 77−26570
^{100}Mo resonances, search for valence neutron capture in 3p neutron giant resonance 77−30587
^{101}Mo levels, γ-rays and p-wave resonance partial radiative widths from ^{100}Mo(n,γ) 80−57739
^{101}Mo resonances, levels, J^{π}, level spacings, cross section from ^{100}Mo(n,γ) 79−89278
^{14}N, energy levels up to 11.05 MeV, transitions and resonance decay from ^{13}C(p,γ) 80−47376
^{14}N possible broad resonances from ^{13}C(p,p) with polarised p 79−6602
^{15}N excited states, R-matrix anal. of n polarisation in ^{14}C(p,n)and ^{11}B(α,n) 78−4937
^{15}N level excitation functions, resonance, p ang. distribs. from ^{13}C(^{3}He,p), 3.6-6.6 MeV 78−93942
^{15}N, reson. obs. using ^{13}C(d,γ) reaction 77−6395
Na, A=21, 2, 3, absolute reson. strengths meas. in Ne(p,γ), Ne(p,pγ) 77−38272
^{21}Na DSA lifetime of 2425 keV state via ^{20}Ne(p,γ)^{21}Na 1.7 MeV 77−82860
^{22}Na, resonance levels obs. in ^{20}Ne(d,p_0) 78−46072
^{23}Na levels, resonance strengths, γ-decays and level lifetimes from ^{22}Na(p,γ) 79−45229
^{23}Na resonances through γ-decay excitation functions from ^{12}C(^{12}C,p) 80−63148
^{93}Nb neutron resonances, spin and parity assignments from (n,γ) meas. 77−26569
^{93}Nb(γ,γ'), energy levels, spin and parity, 6465 KeV resonance total width 78−93940
^{143}Nd spin 3^- resonances, intermediate substructures 77−26586
^{20}Ne, sub-Coulomb resonances populated in ^{12}C(^{12}C,α), spin assignments 77−54245
^{20}Ne 13482 keV level, parity violating effects in two resonance interference from ^{19}F(p,α) pol. p 80−83033
^{20}Ne, 40 MeV excitation, ^{10}B(^{10}B,α)^{16}O, excitation functions, resonance like structures 78−29496
^{20}Ne excitation functions, resonance search from ^{10}B(^{14}N,α) 80−27614
^{20}Ne, gamma decays of some T=0, 1 and 2 states above 9.5 MeV 77−34244
^{20}Ne, intermediate resonances of quasimol. α-structure 79−6404
^{20}Ne low lying levels and intermediate structure J^{π} from ^{16}O(^{12}C, ^{8}Be) 80−102166
^{20}Ne narrow $J^{\pi}=10^+$ resonance in strong absorption region, excited states from ^{12}C(^{16}O,^{8}Be) 79−30814
^{20}Ne non-isolated resonances, excitation functions and ang. distribs. from ^{20}Na(p,α) *(Chinese)* 80−22788
^{20}Ne, resonance observation of 8p-4h state in ^{16}O(α,α_1)^{16}O* reaction 78−50132
^{20}Ne resonances, J^{π}, excitation functions and branching ratio from ^{19}F(p,γ) 80−22787
^{20}Ne resonances through γ-decay excitation functions from ^{12}C(^{12}C,α) 80−63148
^{20}Ne* low lying states and resonances, J^{π} assignments and energies from ^{12}C(^{16}O,^{8}Be) 79−93592
^{21}Ne, decay widths of lowest T=3/2 level, obs. as isospin forbidden resonance in ^{17}O(α,n) 77−6322
^{22}Ne compound states from ^{18}O(α,γ), transitions, spins, parities, astrophys. reaction rate 78−57545
^{22}Ne(γ,γ), up to 18 MeV, nuclear resonance fluorescence, states, transitions and lifetimes 79−45234
^{A}Ni(n,X) A=58, 60, transmission data, resonance anal. 80−18317
Ni(n,γ), A=58, 60, resonance state, partial radiation widths of high energy transitions 78−13104
Ni(n,γ) cross-section meas. principal resonance parameters 80−18312
^{237}Np, neutron resonance params., 8 to 250 eV 77−26709
^{238}Np levels, resonances and transitions from ^{237}Np(n,γ) 80−52589
^{15}O levels from ^{15}N(p,n_0), resonance struct., excitation functions, cross sections 78−50164
^{15}O, reson. widths and branching ratios meas. from ^{14}N(p,γ)^{15}O 77−38244
^{16}O, 3^+ reson. state, particle-hole component via (p,p) and (p,α) reactions 78−580
^{16}O α-cluster states, widths and resonances, optical model, direct transfer in ^{12}C(^{6}Li,d) 80−105975

nuclear resonances continued
^{16}O, external mixing of resonance states in continuum shell model 79−22257
^{16}O level excitation functions, resonances from ^{12}C(^{16}O,^{12}C) 80−63146
^{16}O, levels near 13 MeV via ^{15}N+p 0.9-1.25 MeV 78−509
^{16}O mag. dipole strength, M1 resonances from ^{15}N(p,γ), polarised p 79−80898
^{16}O, search for 0^+ level near 8.87 MeV 2^- level using ^{4}He(^{12}C,^{4}He) 77−88044
^{16}O+^{16}O, fusion cross section gross struct., excitation functions, coupled channel method 80−52705
^{16}O+^{28}Si, 17 to 37 MeV, inelastic and elastic backward angle scatt., surface resonances 78−37367
^{16}O(^{12,13}C,αX), 140 MeV, fast α prod. and molecular resonance search 80−106066
^{16}O(^{12}C, ^{12}C′) quasimolecular resonance, doublet like intermediate structure 79−54421
^{16}O(^{12}C,^{12}C), 18-26 MeV, molecular structure, projection operator anal., differential cross sections 80−106033
^{16}O(^{12}C,^{12}Cα)^{12}C, 68 to 80 MeV, sequential decay via excited states in ^{16}O 78−50189
^{16}O(^{16}O,^{16}O′), gross struct., barrier top resonance model calc. 80−9279
^{16}O(^{16}O,^{16}O), 10-41 MeV, molecular resonances γ-yield, band crossing model 80−106032
^{16}O(^{16}O,X), cross sections, energy dependence, nuclear molecular resonances, band crossing model 80−68686
^{16}O(γ,γ), 6.95, 7.12 MeV, strengths of isospin forbidden E1 transitions 78−13059
^{17}O levels, resonances, J^π and radiative width from ^{14}N(t,γ) 80−47389
^{17}O, TOF transmission meas. of neutron resonances 80−37374
^{17}O, widths of isospin forbidden neutron decays of T=3/2 levels, obs. in ^{13}C(α,n) 77−6321
^{17}O(γ,n_0)^{16}O, 4.3-7 MeV, resonance radiation width, channel and pot. radiative capture, R-matrix anal. 79−6567
^{17}O(γ,n), 5-33 MeV, ground state differential cross section at 98° resonances 79−89288
^{17}O(γ,n), 8.5-39.7 MeV, cross section, giant dipole and pygmy resonance decays 80−42619
Os, A=187, 189, spin-state determ. and neutron reson. via (n,γ) 5-350 eV 77−6224
^{188}Os, muonic resonance spectra, deduced isomer shifts and electric moments 80−18948
^{29}P resonance coherence widths from ^{28}Si(p,p), pol. p 80−32258
^{141}P(n,γ), resonance parameters, s-wave radiative and reduced neutron widths 80−47471
^{A}Pb(α,α), A=206, 208, 120 MeV, isoscalar resonance excitation, low lying transitions, DWBA calc. 80−512
^{206}Pb+n, 3-50 KeV, neutron resonances, J^π assignments, decay scheme 79−36217
^{207}Pb doorway resonances, M1 ground state radiative strength, level density from ^{206}Pb(n,n), (n,γ) 79−93589
^{207}Pb neutron separation energy and resonances, decay transitions from ^{206}Pb(n,γ) 79−36217
^{207}Pb p-wave resonances, enhanced primary M1 transitions from ^{206}Pb(n,γ) 80−57728
^{207}Pb+n resonances, d+s admixture 77−22899
^{208}Pb, finite Fermi-system theory, E1, E2, M1 resonances, γ absorpt. cross section near threshold 77−50055
^{208}Pb, M1 reson. states fine struct., 2p-2h states in RPA 77−22831
^{208}Pb resonance parameters, s-, p- and d-wave entrance channel doorway states from ^{207}Pb+n 79−470
^{208}Pb, search for collective M1 resonance in ^{208}Pb(γ,n_0) 77−46103
^{208}Pb(e,e′), isospin fine struct., 8-12 MeV, multipole assignment of 8.9 MeV reson. 78−13071
^{208}Pb(γ,γ), 6.92, 7.12 MeV, reson. fluoresc. meas. 78−8797
^{208}Pb(γ,n), 9.5-12 MeV, photoneutron ang. distribs., struct. below giant resonance 80−13444
^{209}Pb excited states, $3/2^-$ resonances from shell model of ^{208}Pb(n,n) 80−78240
^{209}Pb excited states and $3/2^-$ resonances, shell model, calcs. from ^{208}Pb(n,n) 80−18262
^{209}Pb reson. parameters calc. in ^{208}Pb(n,n), shell model 77−82920
^{102}Pd, (p,t) study at 42 MeV, hole states at high excitation 78−50158
^{107}Pd(n,γ) and transmission meas., level parameters 78−58277
^{147}Pm, neutron total cross sections and resonance parameters up to 400 eV 77−23020
^{240}Pu, 42.9 keV γ transition, Mossbauer reson. obs. 79−36229
^{240}Pu, reson. in isomeric and prompt fission probabilities 78−78429
^{240}Pu subbarrier resonances and fission probabilities from ^{239}Pu(d,pf) 79−13266
^{241}Pu, multilevel resonance parameters for 0.01 to 100 eV neutrons 79−36154
^{241}Pu, neutron resonances, probability table method and correlated data 79−36284
^{241}Pu, statistical anal. of reson. neutron fission cross section 77−38305
πN(3,3), obs. of enhanced ^{12}C excitation by inelastic π scatt. on πN(3,3) reson. 79−17938
^{226}Ra, total enutron cross-section up to 1 keV 77−26745
Rb odd isotopes, β^- strength functions, 'pygmy' resonances 79−93559
^{a}Ru, A=99, 101, neutron resonance mean spacings and strength functions from Ru(n,γ) *(Russian)* 79−40895
^{28}S, $J^\pi=12^+$ reson. observed in ^{12}C(^{16}O,^{8}Be) $E_{c.m.}$=18.5-20.5 MeV 77−18508
^{32}S, decay of reson. states populated in ^{31}P(p,γ) 78−13085
^{32}S resonances and excitation functions, Hauser Feshbach anal. of ^{20}Ne(^{12}C,X), X=p,d,α 80−78249
^{32}S(n,X), 2.5-1100 keV, resonance struct. from total and capture cross sections 80−42620
^{32}S(n,γ), fast n, doorway structs. and single particle resonances, microscopic treatment 80−52646
^{32}S(n,γ), single particle resonances and doorway states, K matrix formalism 80−37384
^{41}Sc 2p-1h intermediate struct. resonances, anal. powers, J^π from ^{40}Ca(p,p′γ) 80−86883
^{41}Sc, decay and partial widths of 2883 and 5037 keV levels 77−88077
^{43}Sc, resonance struct obs. in ^{42}Ca(p,γ)^{43}Sc below 2.75 MeV 78−13072
^{45}Sc resonance decays, energy levels and J_π values from ^{44}Ca (p,γ) 79−80908
^{45}Sc total neutron cross section, parametric fit, bound level parameters, spin 77−23048
^{46}Sc, s- and p-wave radiative widths obs. in ^{45}Sc(n, γ) 78−17187

nuclear resonances continued
^{48}Sc Gamow-Teller strength, ang. distribs., from ^{48}Ca (^{3}He,t) 80−42589
Se(n,n′) 2^+ level excitation cross sections, intermediate resonances, optical model with coupled channels *(Russian)* 79−40897
^{28}Si 10.9 MeV resonance, J^π assignment from ^{12}C(^{16}O,α) 79−26414
^{28}Si 10.9 MeV resonance from ^{12}C(^{16}O,α)^{24}Mg, spin, parity 78−74384
^{28}Si, 12.8 MeV resonance obs. in ^{12}C+^{16}O system 79−6405
^{28}Si alpha doorway states from ^{12}C(^{16}O,^{12}C) 80−63146
^{28}Si excitation functions, ang. distribs. and resonant behaviour from ^{24}Mg(^{16}O,^{12}C) 80−68622
^{28}Si excitation functions, ang. distribs., resonance spin assignments from ^{24}Mg(^{16}O,^{12}C) 80−68623
^{28}Si, excitation functions for O^+ and 2^+ states, meas. from ^{24}Mg(^{16}O,^{12}C) 78−54800
^{28}Si, excited levels populated in ^{27}Al(p,α)^{24}Mg at E_p=1540-2220 keV 78−17189
^{28}Si, GQR via (α,α′) scatt. at 126 MeV 77−74826
^{28}Si levels, obs. in (α,γ) and (p,γ) reacts. 78−66205
^{28}Si lowest T=2 resonance α-width, observed narrow resonances from ^{24}Mg(α,$α_0$) 79−45236
^{28}Si, obs. of α-doorway states in ^{12}C+^{16}O system 79−6662
^{28}Si p3/2 neutron resonance γ-decay, partial rad. widths from Si(n,γ) 80−52617
^{28}Si, reson. as ^{12}C+^{16}O quasimol. bands 77−79349
^{28}Si, resonance struct. determ. by ^{16}O(^{12}C,^{8}Be)^{20}Ne* reaction 79−6663
^{28}Si resonance wave functions and differential cross sections from ^{27}Al(p, n), (p, p), (p, α) 80−18261
^{28}Si resonance wave functions from differential cross sections of ^{27}Al(p,X), X=p,n,α 80−78239
^{28}Si, resonances in ^{27}Al+p⇌^{24}Mg+α, test of detailed balance at isolated resonances and time reversibility 79−45260
^{28}Si resonances obs. in ^{27}Al(p,$α_0$)^{24}Mg at 1.12-3.08 MeV 78−13091
^{28}Si, three body nuclear molecular resonances for ^{12}C-α-^{12}C 79−75949
^{28}Si+^{16}O(^{12}C), elastic scatt., 90° excitation function gross struct. 79−75950
^{28}Si(^{12}C,^{12}C), 27.8-31.5 MeV, elastic and inelastic excitation functions, fine struct., statistical anal. 80−18269
^{28}Si(^{12}C,^{12}C), entrance channel resonances, backward angle scatt., elastic scatt. enhancement 80−27612
^{28}Si(^{16}O,^{16}O), 30-32.7 MeV, elastic and inelastic excitation functions, fine struct., statistical anal. 80−18269
^{28}Si(^{16}O,^{16}O), entrance channel resonances, backward angle scatt., elastic scatt. enhancement 80−27612
^{28}Si(^{16}O,^{16}O) gross struct. in excitation function elastic transfer amplitudes 79−36215
^{28}Si(^{28}Si, ^{28}Si), 80-150 MeV, elastic and inelastic, energy depend. struct., multistep processes 79−80909
^{28}Si(e,e′), 6^- T=1 resonance form factor, mag. strength quenching, meson exchange currents 80−86882
^{28}Si(n,γ), 565, 813 keV, resonance γ, spectra, valence model test 80−63124
^{28}Si(n,γ), fast n, doorway structs. and single particle resonances, microscopic treatment 80−52646
^{28}Si(n,γ), single particle resonances and doorway states, K matrix formalism 80−37384
^{29}Si $3/2^-$ doorway resonance, calc. of neutron and gamma widths 77−26587
^{29}Si neutron resonance, γ-spectra, partial and total radiative widths from ^{28}Si(n,γ) 80−42578
^{149}Sm, neutron total cross sections and resonance parameters up to 400 eV 77−23020
Sm(p,t), even isotopes, high energy neutron pairing strength, two neutron holes, resonances 80−78116
Sn, A=114, 116, 118, 120 and 122, (p,t) study at 42 MeV, hole states at high excitation 78−50158
Sn, solid and liquid, neutron cross sections, Doppler effect meas. 80−22933
^{117}Sn, E1 and M1 photo-absorption cross section, substructure due to E1 transition and giant M1 reson. 79−40901
^{119}Sn, E1 and M1 photo-absorption cross section, substructure due to E1 transition and giant M1 reson. 79−40901
^{120}Sn finite Fermi-system theory, E1, E2, M1 resonances, γ absorpt. cross section near threshold 77−50055
^{122}Sn, kaonic, E2 nuclear resonance effects 78−29868
^{181}Ta 6.2 keV Mossbauer resonance, prep. of narrow line sources 79−76253
^{181}Ta, neutron resonances, probability table method and correlated data 79−36284
^{181}Ta(n,total), 15 to 2030 eV resonances, time of flight spectroscopy 78−41716
Tb, magnetic moment of neutron resonances 77−26576
^{159}Tb, neutron resonances, time-of-flight spectra 80−27633
^{159}Th(n,γ), 2.6-700 keV, cross-sections and resonance parameters 78−50172
^{230}Th(n,f), 0.68-1.10 MeV, fission fragment ang. distribs., resonance and moment of inertia 80−102219
^{232}Th, quadrupole photofission and role of nucl. symm. *(Russian)* 78−17258
^{A}Ti(n,γ) A=46, 47, 49, 50, 45 MeV, cross section meas., resonance parameters 80−18315
^{206}Tl resonances, neutron strength functions and radiative widths 77−22898
U, A=233, 5, statistical anal. of reson. neutron fission cross section 77−38305
^{234}U subbarrier resonances and fission probabilities from ^{233}U(d,pf) 79−13266
^{235}U(n,f), 0.001-25 keV, polarised n, spin separated cross sections, resonance struct. 79−3126
^{235}U(n,f) cross section, thermal normalization technique for meas. of neutron cross section vs. energy 79−9590
^{236}U, subbarrier resonances and fission probabilities from ^{235}U(d,pf), 11-17 MeV, ^{236}U 79−13266
^{237}U virtual photon excited state decay and total cross section of ^{238}U(e,n) 80−22757
^{238}U, capture width of 6.67 eV neutron resonance 78−50162
^{238}U, neutron resonance params. and cross sections, 9 eV to 4 keV 77−26710
^{238}U, neutron resonance parameters, time-of-flight spectroscopy 80−47375
^{238}U, neutron resonances, probability table method and correlated data 79−36284

nuclear resonances continued
^{238}U, neutron transmission, resonance meas. and anal. 79−26436
^{238}U neutron transmission meas. and resonance analysis 79−9575
^{238}U, statistical reson. parameters determ. from computer code ADDJA 77−26650
^{238}U subbarrier photofission, cross section and half-life, double hump model 80−102217
^{238}U+n, resolved resonance energies, 100 eV-170 keV 78−37339
^{238}U(n,f), 5 eV-2.5 MeV, fission cross section, fission barrier second well parameters, resonances 80−63217
^{238}U(n,f), cross section up to 6 MeV, intermediate struct. obs. 77−23161
^{238}U(n,f), second well gamma decay if subthreshold fission resonances 77−26800
^{238}U(n,γ) cross section, 5-100 keV, doorway state detection, statistical tests 79−93590
^{49}V(p,p′), 3/2$^-$ resonances, inelastic proton channel 79−93586
^{51}V, neutron resonance spectroscopy, R-matrix anal. 78−21555
^{52}V capture area, resonance parameters and mean level spacings from ^{51}V(n,γ) 79−6608
^{183}W, determ. of neutron level spins up to 400 eV *(Russian)* 79−80870
^{89}Y, high resolution neutron total cross section meas., 27-240 keV 78−25193
^{89}Y(p,γ$_0$)^{90}Zr, 14-27 MeV, E_2 and E_3 radiation anal. in direct-semidirect model 77−38266
^{90}Y, level widths and density from ^{89}Y total neutron cross section 78−70519
^{172}Yb, muonic resonance spectra, deduced isomer shifts and electric moments 80−18948
^{173}Yb(n,γ)^{174}Yb, width correlation, primary transition intensities for resons. 77−79370
^{68}Zn muonic atom, dynamical E0 excitation, E0 resonances, muonic X-rays 80−95749
^{90}Zr, finite Fermi system theory, E1, E2 and M1 resonances, γ absorpt. cross section near threshold 77−50055
^{90}Zr, neutron reson. parameters below 300 keV 78−8805
^{91}Zr, 292.4 eV neutron resonance parameters, radiative and neutron widths, spin assignments 77−6369
^{91}Zr, high resolution neutron transmission and capture 78−8806

nuclear scattering *see nuclear reactions and scattering*

nuclear scattering involving few nucleon systems
3N and 4N calcs., review 78−50094
elastic and inelastic cross sections of nD, nT, DD, DT, TT, αD, αT, phase shift anal. 77−22996
EM effects, separation, Coulomb problem 77−23014
few body systems, anal. coupling constant continuation for resonance and stripping reactions *(Russian)* 80−13435
four nucleon system, reactions and scatt. using K-matrix formalism, differential cross sections *(Russian)* 80−106027
four-nucleon problem, microscopic K-matrix continuous spectrum *(Russian)* 77−61352
generalized Moshinsky bracket recurrence relations 79−93569
integral equation and resonating group methods relation 77−18493
microscopic calculations for ^{4}H, ^{4}Li continuum, appl. to ^{3}H(n,n), ^{3}He (p,p) 78−17114
neutron-trinucleon scattering lengths, four-body model with separable NN interaction *(Ukrainian)* 77−30495
nuclear surface phenomena, Yakubovski eqn. appl. to N-body systems 79−75931
polarisation in few-body reactions 77−22995
polarised deuteron investigation of few nucleon systems 77−18578
quantum three-body problem, distorted Faddeev eqns. with coupled channel approach 80−52635
three body scatt., spline function moment methods 80−505
three particle systems with Coulomb interaction, scatt. and breakup eqns. exact solns. 80−504
three particles with Coulomb interaction, binding energy and scatt. states *(Russian)* 80−5051
three- and four-nucleon systems, computational methods, Faddeev eqn. 77−22907
three-body scatt. amplitudes, appl. of contour rot. 78−567
three-body scatt. problem, cluster expansions, effective intercluster pots. 80−5082
α-α scatt., 75.2 MeV, TDHF calcs. in 2 and 3 dimensions 78−78401
α+α scatt., exchange Coulomb kernel in resonating group formulation 79−6531
αα and NN scatt. analogies, quark struct. and clustering connections 79−6442
d-α elastic scatt., three-body calc. 78−46074
^{2}H(n,n), 2.48 and 3.28 MeV, elastic differential cross section and related phase shift analyses 79−75992
^{2}H(p,p), theoretical anal. of nucleon-nucleon forces 79−9554
Nd S-wave scatt., dispersion relation approach to three-body systems, unitarity approx. 79−506
pd, elastic scatt. analysing power meas. 78−93901
^{2}H(d,d), 5-45 MeV deuteron wave function asymptotic D- to S-state normalisation, anal. power 80−78304
^{2}H(n,p)n, 63.1 MeV, differential cross section 80−63186
H, neutron-photon multigroup cross sections for neutron energies ≤60 MeV 79−30880
^{1}H+d, polarised projectile, parity nonconservation in low energy scatt. 78−66271
^{1}H(N,N), 180° cross-sections 77−26737
^{1}H(d,d), 2 GeV, polarised d, tensor and vector asymmetries 80−9285
^{1}H(d,d), 20 MeV, measurement on T_{21}, three nucleon Faddeev calc. comparison 79−71857
^{1}H(d,d), 35, 45 MeV, d wave function D- to S-state ratio from anal. power and cross section 79−89314
^{1}H(d,d), 45.4 MeV, tensor anal. powers 79−85447
^{1}H(d,d), anal. power ang. distrib., d D-state asymptotic normalisation 79−36247
^{1}H(d,d), deuteron D-state asymptotic normalisation 79−71858
^{1}H(d,d), elastic backward scatt., GeV energies, tensor anal. power 79−80916
^{1}H(d,d), polarised d, 5-13 MeV, analysing powers 79−71833
^{1}H(d,d), polarised p and d, analysing power data 79−71830
^{1}H(d,d) 10, 20 MeV, 79−13304
^{1}H(n,n), 14.2 MeV, polarised n, analysing powers 79−71832
^{1}H(n,n), 16.9 MeV, anal. power, F-wave contribs. 80−63158
^{1}H(n,n), 180° cross sections for fast neutron meas. with counter telescopes 79−36240

nuclear scattering involving few nucleon systems continued
^{1}H(n,n), pol. n, 13.5-16.9 MeV, anal. power and spin-orbit phase parameters 80−78269
^{1}H(n,n)$_1$ pol. n, 50 MeV, anal. power 80−68639
^{1}H(n,n)^{1}H, 10 keV-20 MeV, use for neutron flux meas., proton-recoil detectors 79−9960
^{1}H(n,n)^{1}H, 325 MeV, phase shift anal. and mixing parameters 77−79277
^{1}H(n,n)^{1}H, 50 MeV polarised neutrons 77−26732
^{1}H(n,n)^{1}H, differential cross section below 30 MeV, phase shift anal. 79−9586
^{1}H(n,n)^{1}H, polarised neutron scatt. 77−26734
^{1}H(n,n)^{1}H analysing power, 14.5 MeV, Hamburg polarised neutron facility, initial expts. 77−26946
^{1}H(n,n)^{7}H, 14 MeV polarised neutrons, analysing powers 77−54210
^{1}H(n,n)p, 210-495 MeV, free elastic scatt., phase shift anal. 80−52676
^{1}H(n,p), pol. n and p, 220-495 MeV, free elastic scatt., D_t and P parameters 80−52674
^{1}H(n,p), pol. n and p, 220-495 MeV, free elastic scatt., Wolfenstein parameters R_t, A_t 80−52675
^{1}H(n,p)n, pol. n,p, 50 MeV, spin correlation parameter $A_{yy}(\theta)$, phase shift anal. 80−68530
^{1}H(p,p), 0.35-1.0 MeV, differential cross section meas. 78−78379
^{1}H(p,p), 1-3 GeV/c, pol. p, spin parameters A and A_{nn} 80−95304
^{1}H(p,p), 225, 327, 520 MeV, analysing powers 79−75961
^{1}H(p,p), 398-572 MeV, analysing power meas., EM-nuclear interf. 77−23008
^{1}H(p,p), 6.14 MeV, cross sections and anal. power for noncentral reaction 79−85444
^{1}H(p,p), 6.141 MeV, anal. power, Paris pot. predictions 80−63156
^{1}H(p,p), pol.p, 9.57 MeV, spin correlation parameter, phase shift anal. 80−102112
^{1}H(p,p) 647 and 800 MeV, absolute differential cross-section meas. 77−6390
^{2}H+^{3}He, 22 to 53 MeV, quasifree processes 77−82903
^{2}H+n, realistic nucleon-nucleon interactions 78−62526
^{2}H+p, 50 MeV polarised p scatt., analysing power meas. 77−71608
^{2}H+p, polarised projectile, parity nonconservation in low energy scatt. 78−66271
^{2}H+p, polarised projectile, parity nonconservation in low energy scatt. 78−70522
^{2}H+p(d), 6.3 GeV/c, inclusive spectra of fast p and d *(Russian)* 78−46075
^{2}H+p(p̄), high energy cross section calc. complex ang. momentum theory *(Russian)* 78−46067
^{2}H(N,N), extraction of ^{2}H wave function 77−18418
^{2}H(N,N), off-shell effects, calcs. with phase equiv. separable pots. of rank two 77−18553
^{2}H(α,α), 17.9 GeV/c, Glauber model rigid projectile approx. 79−63685
^{2}H(α,α)^{2}H, 6 to 14 MeV, cross section meas. 80−27655
^{2}H(d,d), 4.3 to 8.9 GeV, momentum spectra at 103 mrad lab. angle 79−6641
^{2}H(d,d), 50-85 MeV, ang. distribs., PWBA anal., two body final states 79−6636
^{2}H(d,d), 50-85 MeV cross-section meas. 79−13307
^{2}H(d,d), medium energy, total cross section, optical model calcs. 79−9593
^{2}H(d,d)^{2}H, four-body model of the four-nucleon system 79−63643
^{2}H(d,d)D, differential cross sections at 13.2 MeV, DWBA anal. 79−45276
^{2}H(d,n)^{3}He, 12.3 MeV, neutron spectra normalisation, differential cross-section meas. 77−88106
^{2}H(d,p)^{3}H, cross-section anal. using four-body integral eqns. 77−18577
^{2}H(d,p)T, differential cross sections at 13.2 MeV, DWBA anal. 79−45276
^{2}H(n,n′), 14.8 MeV neutrons, d break-up cross section meas. 79−80932
^{2}H(n,n), 10 MeV, differential cross section, (p,p) comparison for Coulomb force 79−71793
^{2}H(n,n), 30 MeV, plarisation asymm., analysing power 78−62538
^{2}H(n,n), 794 MeV, extreme back angle scatt. 78−50174
^{2}H(n,n), 8.05 MeV, elastic differential cross-section meas. by recoil technique 78−17207
^{2}H(n,n), (n,p), 24 MeV, quasifree scatt., n-n effective range, Monte Carlo anal. 80−68554
^{2}H(n,n), backward scattering, 200 to 800 MeV search for bump in 180° excitation function 78−62445
^{2}H(n,n), elastic scatt., perturbation calcs., Faddeev eqns., Reid soft core pot. 78−33177
^{2}H(n,n), ghost states and Pauli principle for many-body scatt. 79−76001
^{2}H(n,n), local soft core NN pots., quasiparticle formalism 79−6529
^{2}H(n,n), polarised n, anal. power predictions 79−85445
^{2}H(n,n), scattering amplitudes, 14.4 MeV Faddeev eqns. variational soln. *(Russian)* 79−85321
^{2}H(n,n), scattering in high-partial waves, on-shell theory 78−41565
^{2}H(n,n), virtual state in three nucleon system, partial wave dispersion relations 79−40920
^{2}H(n,n) 14.2 MeV, polarised n, analysing powers 79−71832
^{2}H(n,n) backward elastic scatt., 350 to 550 MeV, ang. distribs. 79−75782
^{2}H(n,n) backward elastic scatt., 200 to 800 MeV, ang. distribs. and relativistic momentum transfer variable 79−75783
^{2}H(n,n) scatt. length in $J=1/2^+$ three-N state calc. with super-soft core 77−71570
^{2}H(n,n) scattering length determination, using NN interaction radius approx. 79−6426
^{2}H(n,n)^{2}H, 14 MeV polarised neutrons, analysing powers 77−54210
^{2}H(n,n)^{2}H, 2.45 MeV, polarised n, depolarisation factor ang. distrib., phase shifts 78−78358
^{2}H(n,n)^{2}H, 2.6 MeV polarised beam, ang. variation of polarisation 77−26733
^{2}H(n,n)^{2}H, 50 MeV polarised neutrons 77−26732
^{2}H(n,n)^{2}H, polarised n, 12 MeV, analysing power, similarity with (p,p) scatt. 78−70514
^{2}H(n,n)^{2}H, polarised neutron scatt. 77−26734
^{2}H(n,n)^{2}H, sum rules linking doublet and quartet phase-shifts with ^{3}H binding *(Russian)* 77−74831
^{2}H(n,n)^{2}H analysing power, 14.5 MeV, Hamburg polarised neutron facility initial expts. 77−26946
^{2}H(p, p′) d bag, nuclear bag states containing quarks, detection 78−70465

nuclear scattering involving few nucleon systems continued
^{2}H(p,2p)n, 23, 39.5 MeV, noncoplanar reaction, breakup cross section 80−530
^{2}H(p,p′), 0.6-25 GeV, backward emitted proton inclusive spectra, short range correlation 80−32281
^{2}H(p,p), 10 MeV, differential cross section, p and d analysing powers 78−46063
^{2}H(p,p), 10 MeV, differential cross section, (n,n) comparison for Coulomb force 79−71793
^{2}H(p,p), 40-1000 MeV backward scatt., N-exchange model 77−18562
^{2}H(p,p), 600 MeV and 1 GeV, noneikonal theory 79−80930
^{2}H(p,p), 800 MeV, differential cross sections and anal. powers 80−83091
^{2}H(p,p), backscattering, large momentum transfers, π exchange effects 80−5143
^{2}H(p,p), Coulomb corrections near elastic threshold 77−34282
^{2}H(p,p), large angle scatt., cross section and anal. power 79−80917
^{2}H(p,p), near threshold, on-shell two-body model 77−34283
^{2}H(p,p), pol.p, spin rot. and depolarisation, NN amplitude double spin flip part 80−78271
^{2}H(p,p), polarised p, 14.1 MeV, analysing power 79−71831
^{2}H(p,p), polarised p, 2.5-6.5 MeV, vector and tensor anal. powers 79−63653
^{2}H(p,p), polarised p, 316, 516 MeV, anal. powers in resonance region, backward angle scatt. 79−71834
^{2}H(p,p), polarised p, medium and high energies, polarisation phenomena 79−85448
^{2}H(p,p), rank-1 pots. using shielded Coulomb pot., separable nuclear forces 79−71854
^{2}H(p,p), tensor asymmetries, deuteron D-wave and non-eikonal effects, Glauber model 80−78296
^{2}H(p,p),(n,n), precise low energy cross section meas. with polyethylene targets 78−82342
^{2}H(p,p) 17, 20, 24 MeV, polarised p and d, analysing power data 79−71830
^{2}H(p,p) cross section, d wave function with spin at light front *(Russian)* 79−85478
^{2}H(p,p) elastic backward scattering, detection of d relativistic wave function dependence on additional variable *(Russian)* 79−58973
^{2}H(p,p) Glauber versus final state interaction theory, inelastic/elastic scatt. cross sections 77−57554
^{2}H(p,p) large angle elastic scatt., d form factor at large q^2 80−102189
^{2}H(p,p)^{2}H, 1.5-3 MeV, extraction of dnp coupling constant, Cutkosky method 77−10404
^{2}H(p,p)^{2}H, 1.825 GeV/c anal., Glauber theory comparison 77−71525
^{2}H(p,p)^{2}H, determination of Coulomb corrections 77−10400
^{2}H(p,p)^{2}H, large angles, resonance one-pion-exchange model *(Russian)* 77−34306
^{2}H(p,p)^{2}H backward elastic scatt., resonance region, double-scatt. mechanism *(Russian)* 77−74854
^{2}H(p,p)np, 13-19 MeV, p energy spectrum shape 79−6594
^{2}H(p,pγ), elastic cross sections, bremasstrahlung, threshold and Coulomb effects 80−91186
^{2}H(t,n)^{4}He, 20 MeV, neutron spectra normalisation, differential cross-section meas. 77−88106
^{2}H(t,t)^{2}H, 10.5 MeV polarised tritons, analysing power meas. 77−10413
^{3}H+α, elastic scatt., orthogonality condition model derived from parity energy surfaces 78−29432
^{3}H(n,n), scatt. length, 4-nucleon problem, integral eqn. approach 80−91183
^{3}H(n,n), thermal n_t coherent scatt. length, four body problem relation 79−75997
^{3}H(n,n), zero energy total cross section and scatt. lengths 80−57778
^{3}H(n,n) coherent scatt. length meas. by neutron interferometry 79−59113
^{3}H(n,n) differential cross section, nonrelativistic theory of four nucleon systems *(Russian)* 79−80881
^{3}H(n,n)^{3}H, four-body model of the four-nucleon system 79−63643
^{3}H(n,n)^{3}H, possible anomaly in backward scatt. cross section near 14 MeV 77−6363
^{3}H(p, p), 600 MeV, Glauber formalism study *(French)* 79−93616
^{3}H(p,n)^{3}He, 13.6 MeV, neutron spectra normalisation, differential cross-section meas. 77−88106
^{3}H(p,p), 1-10 MeV, isospin splitting of 1p-1h excitation in ^{4}He 78−41622
^{3}H(p,p), 156 MeV, differential cross section, diffr. theory of multiple scatt. 77−61404
^{3}H(p,p), 1.24 GeV, differential cross section, spin independ. Glauber model interpretation 80−63183
^{3}H(p,p), 1.26-3.71 MeV polarised p, spin depend. N-N forces 79−6634
^{3}H(p,p), 4-12 MeV, Amado model quasi-three body calc. 78−25191
^{3}H(p,p), 5.8 and 6.8 MeV, phase shift anal. *(Russian)* 77−65225
^{3}H(p,p), 8 to 17.1 MeV, cf. neutron polarisation in ^{3}He(n,n) 78−25171
^{4}H(α,α) intermediate energies, Glauber analysis 78−46077
^{4}H(p,p), microscopic optical pot. calc. 79−85423
^{A}H(p,p) A=1,2, total cross sections, 180 to 560 MeV, Galuber model calcs. 79−40917
H(α,α), 4.00, 5.08. 6.90 GeV/c, cross-section meas. 77−6416
H(d,d), A=1, 2, E=52 MeV, polarised deuterons, vector analysing power 78−584
He+p, A=3,4, polarised projectile, parity nonconservation in low energy scatt. 78−66271
He+p, A=3,4, polarised projectile, parity nonconservation in low energy scatt. 78−70522
(^{3}He,^{3}He), 18-33 MeV polarised ^{3}He, ^{6}Be excitation 78−78400
^{3}He+^{3}He, quasifree processes, 50-78 MeV, cross-section meas. 77−18586
^{3}He(^{3}He, ^{3}He′), 120 MeV, continuum energy spectra bump struct., cross sections 80−83108
^{3}He(^{4}He,^{4}He)^{3}He, 20-26 MeV, elastic scatt., ang. distribs. and excitation functions *(Russian)* 77−327
^{3}He(α,α), 24.5 to 42.0 MeV, meas. of polarisation analysing power 77−3026
^{3}He(d,d), 0.32 MeV, continuum ambiguity in phase shift anal. 79−76006
^{3}He(d,d), polarised d, 10-17 MeV, cross sections, vector and tensor anal. powers 79−75966
^{3}He(d,d), polarised d, 1.5-11.5 MeV, differential cross sections and anal. powers 79−85443
^{3}He(n,n), 1-24 MeV optical model anal. 77−23027
^{3}He(n,n), 2.63 MeV polarised neutrons, asymmetry 77−26736

nuclear scattering involving few nucleon systems continued
^{3}He(n,n), 3.7-15.3 MeV, polarised n, analysing power, A=4 system neutron channels 79−75965
^{3}He(n,n), 8 to 17.1 MeV, cf. proton polarisations in ^{3}H(p,p) 78−25171
^{3}He(n,n), coherent scatt. length meas. by neutron interferometry 78−13098
^{3}He(n,n), scatt. length, 4-nucleon problem, integral eqn. approach 80−91183
^{3}He(n,n) coherent scatt. length meas. by neutron interferometry 79−59113
^{3}He(n,n) differential cross section, nonrelativistic theory of four nucleon systems *(Russian)* 79−80881
^{3}He(n,n) thermal n_t coherent scatt. length, four body problem relation 79−75997
^{3}He(p, p), 1 GeV, differential cross section minimum, Glauber model description 79−80938
^{3}He(p, p), 600 MeV, Glauber formalism study *(French)* 79−93616
^{3}He(p,p), 156 MeV, differential cross section, diffr. theory of multiple scatt. 77−61404
^{3}He(p,p), 18-48 MeV, elastic differential cross section ang. distribs., four body problem 79−75998
^{3}He(p,p), 19-30 MleV, spin anal. power and phase shift anal. 79−13295
^{3}He(p,p), 1.75 to 4.13 GeV/N, small angle scatt., Glauber model *(Russian)* 78−41726
^{3}He(p,p), 1.75 to 4.50 MeV polarised protons, analysing power meas. for ^{4}He T=1 level ordering 79−26438
^{3}He(p,p), 415-800 MeV, large angle differential cross-sections 77−30573
^{3}He(p,p), 6.8 to 16.2 MeV, optical model pot. calcs. of cross section and polarisation data 79−63672
^{3}He(p,p), charge independ. R-matrix anal. of four nucleon system 79−85479
^{3}He(p,p), forward dispersion relations and wave function models 79−75956
^{3}He(p,p), generator coord. method study of ^{4}Li 80−27581
^{3}He(p,p), pol. p, 0.3-1.0 MeV, differential cross section, anal. power, and phase shifts 80−42629
^{3}He(p,p), polarised p, 6.8-10.7 MeV, polarisation transfer coeffs. 79−17889
^{3}He(p,p), polarised p, below 6 MeV, anal. power meas. for four nucleon system levels 79−71837
^{3}He(p,p) virtual scatt. from ^{4}He+p two pronged events 79−3152
^{3}He(p,p)^{3}He, 0.02-2 eV, scatt. lengths *(Russian)* 77−61430
^{3}He(p,p)^{3}He, 2.3 to 13.6 MeV data, phase shift anal. 78−78376
^{3}He(p,p)^{3}He, 2.3 to 8.8 MeV, ang. distribs. of analysing power 78−78375
^{3}He(p,p)^{3}He, four-body calc. solns. 79−71855
^{3}He(p,p)^{3}He, four-body model of the four-nucleon system 79−63643
^{3}He(t_{pol},t)^{3}He, 9-17 MeV, analysing power, differential cross sections 77−74829
^{4}He (d,d) pol. d, 17-43 MeV, vector anal. power, highly excited six nucleon system 80−47458
^{4}He (p,p), 200, 350, 500 MeV, differential cross-section and analyzing power meas. 78−17195
^{4}He (p,p), effective channel approach, N* resonance effects 79−9570
^{4}He (p_i,p), high and intermediate energies, polarisation, research review 78−94010
^{4}He scatt. system, multichannel cluster model description 77−82902
^{4}He+α scattering, generator coord. method, Kohn-Hulthen variational principle 77−2957
^{4}He+n, 20 MeV, phase shift, resonating group method 78−50159
^{4}He+n, below 15 MeV, R-function anal. 77−23028
^{4}He+n, elastic scatt., orthogonality condition model derived from parity energy surfaces 78−29432
^{4}He+p, 8.56 GeV/c, two pronged events, cross sections and prod. features 79−3152
^{4}He+p, interaction potential from inverse scatt. problem method *(Russian)* 78−46068
^{4}He+p($\bar{p}$), high energy cross section calc. complex ang. momentum theory *(Russian)* 78−46067
^{4}He+π^-, multiple scattering theory with separate treatment of proton and neutron 79−45301
^{4}He(^{3}He,^{3}He), ^{7}Be ^{4}He+^{3}He coupling, dispersion anal. 78−89889
^{4}He(^{3}He,^{3}He), 18 to 70 MeV, differential cross-sections, resonating group method anal. 79−85482
^{4}He(^{3}He,^{3}He), 18-22 MeV, analysing power ang. distrib., differential cross sections, ^{7}Be excited state 78−46078
^{4}He(^{3}He,^{3}He)^{4}He, four body approach 79−75933
^{4}He(N,N), microscopic study using single channel resonating group method, effective nuclear potentials 79−85425
^{4}He(α,α), 5.05, 4.30 GeV/c, high energy multiple diffraction theory 78−29486
^{4}He(α,α), nuclear separable plus Coulomb interaction 80−83106
^{4}He(α,α), s-wave, Coulomb amplitudes from generator coordinate theory 80−83107
^{4}He(α,α), size change of α effect on phase shift, generator coordinate and variational methods *(Chinese)* 80−68683
^{4}He(α,α) anal. to study direct part of N-N potential 77−10420
^{4}He(d,d), cross sections and polarisation parameters, three-body NNα model *(French)* 77−71598
^{4}He(d,d), distortion effects, orthogonality condition model 80−63190
^{4}He(d,d), Faddeev Lovelace eqn. soln. 78−54767
^{4}He(d,d), Glauber theory at high energy *(Russian)* 78−41732
^{4}He(d,d), low energy, resonating group method anal. with distortion effect 80−73851
^{4}He(d,d), noncentral forces, Pauli principle effects on d polarisation, orthogonality condition model 79−6614
^{4}He(d,d), pol. d, 12-17 MeV, differential cross sections, anal. powers, phast shift anal. 80−13449
^{4}He(d,d), polarised d, 20.2 MeV, elastic scatt. tensor anal. power 79−85450
^{4}He(n,n)^{4}He, below 21 MeV, R-function and physical-state parameters 77−88105
^{4}He(p, p), 225, 327, 520 MeV, analysing powers 79−75961
^{4}He(p,p′), high energy, nonlocal imaginary pot. in one channel approx. 78−592
^{4}He(p,p), 0.35-23.1 GeV, differential cross section and polarisation, Glauber theory *(Chinese)* 79−49628
^{4}He(p,p), 0.4 GeV, nucleon-nucleon data inputs 78−74369
^{4}He(p,p), 0.5-1.7 GeV, differential cross section and polarisation meas. 79−22295

nuclear scattering involving few nucleon systems continued
^{4}He(p,p), 185 to 500 MeV, large angle cross section, analysing power 78−74363
^{4}He(p,p), 1.05 GeV, backward peak, differential cross section meas. 78−70525
^{4}He(p,p), 20-55 MeV, anal. power, cross sections, phase shift anal. 79−9569
^{4}He(p,p), 200-500 MeV, differential cross section and anal. power 80−68640
^{4}He(p,p), 2.68 GeV, elastic differential cross section 79−17900
^{4}He(p,p), 45, 52, 60, 65 Mev, cross sections and polarisation meas. 79−97706
^{4}He(p,p), 45-65 MeV, phase shift anal. 80−22832
^{4}He(p,p), 5.75 GeV, meas. of $d\sigma/dt$, $t=0.18$ to 2.2 $(GeV/c)^2$ 78−70532
^{4}He(p,p), 68-125 MeV, resonating group anal. 77−88139
^{4}He(p,p), 788 MeV, back angle diffraction struct., Dirac, eqn. optical model 80−68667
^{4}He(p,p), 788 MeV, cross section, backward diffr.-like struct. evidence 78−94008
^{4}He(p,p), differential elastic scatt. cross-section, 1 GeV protons *(Russian)* 77−79382
^{4}He(p,p), elastic scatt., medium energies, effective channel anal. 77−2997
^{4}He(p,p), elastic scatt. at medium energies, microscopic optical pots. 79−97703
^{4}He(p,p), medium energy, anal. power, relativistic optical model anal. 79−40925
^{4}He(p,p), resonance amplitudes in light nuclei 77−18561
^{4}He(p,p), total cross sections, 180 to 560 MeV, Galuber model calcs. 79−40917
^{4}He(p,p) elastic scatt., 1.05 GeV, shape around first interference minimum 77−57662
^{4}He(p,p) elastic scatt., polarisation meas. 0.56 to 1.73 GeV, $0.006\leq -t\leq 1.2$ $(GeV/c)^2$ 77−57664
^{4}He(p,p) elastic scatt. near 1 GeV, Glauber theory calcs. 77−57663
^{4}He(p,p)^{4}He, 0-18 MeV, statistical anal., data fluctuations, error estimation 78−25196
^{4}He(p,p)^{4}He, calc. with Glauber model optical potential in Schrodinger eqn. 77−50093
^{4}He(p,p)^{4}He, elastic data for 350-1150 MeV 77−61424
^{4}He(p,p)^{3}He, optical model anal. 78−78369
^{4}He(p,p)^{4}He forward amplitude real part, 1.5-10 GeV, from dispersion relns. 77−314
^{A}He(p,p), A=3,4, backscattering, large momentum transfers, π exchange effects 80−5143
^{A}He(p,p)^{A}He, A=3,4, depth profile meas. of He in Ni and Nb 79−14839
He(d, d), 9.0, 19.8 GeV/c, small angle, total and differential cross section, scatt. amplitude *(Russian)* 79−97711
H(n,p)n, 25.8, 50.9 MeV, differential cross-sections 78−600

nuclear screening
actinide ions, tetrapositive, nucl. hexadecapole antishielding factors 79−26909
additive-orbital scheme for calculating atomic and molecular polarizabilities 77−3273
alkali metal salts, NMR spectra of alkali metal nuclei, shielding and quadrupole coupling consts. 78−84487
alkali metals, Sternheimer shielding functions calcs. 79−76352
atom, electron pair prod., by intermediate and low energy photons, screening corrections 79−49991
atom, many-electron, using Slater's value of at. screening parameters 80−912
atom, sommerfeld screening parameters for $S_{1/2}$ terms in X-ray spectra 78−66495
atom, X-ray spectra, Z=13 to 103, Sommerfeld screening parameter σ_1 78−25463
atomic electron screening and correlations, effects on internal conversion coeffs. 80−18237
atomic inner shell bound-bound radiative transitions, analytical description 78−82684
atomic ions, electron impact, 1 to 100 keV, bremsstrahlung emission, theory 78−22005
atomic $np^2(n+1)s$ excited-state config. quadrupole moments, Sternheimer shielding factor, of N(P)(As)(Sb) 80−37755
atomic quadrupole shielding factors calc. using elec. field variant orbitals 80−106276
atomic screening parameters, using Hartree-Fock energy 79−6883
atoms in molecules, diamag. shieldings rel. to electronegativity 80−102524
benzene, ^{1}H chem. shift tensor, proton mag. shielding anisotropy 78−19348
bound s-state energies for exponential cosine screen Coloumb potential, Ecker-Weizel approx. 79−97965
bremsstrahlung, high frequency cross section limit for neutral ats. and ions 79−27142
bromomethane, microwave spectrum obs., B rot. and centrifugal distortion consts. 77−75135
cation radii verification using screened nucl. charge model 80−59944
closed-shell system, harmonic oscillator model for mag. props., shielding tensor 79−81299
Coulomb gas 2-D, interaction potential, screening length, critical temp. 80−62571
diamagnetic molecule, mag. susceptibility, nucl. mag. shielding, calc. methods *(German)* 78−33448
diatomic molecular orbitals, shielded, parametric shielding pots. calcs. 77−54506
diatomic molecule, nucl. spin-rot. interaction const., electron spin current contrib. 80−23441
diatomic molecule nucl. mag. shielding using LCAO MO functions and gaussian expansion 79−36548
diatomic molecules, electronic states, variable-screening method 78−25410
diatomic molecules, variable screening model 78−74587
p-diethoxybenzene, ^{13}C shielding tensors determ., by NMR from powder patterns 78−25556
dihydromuconic acid, C=C bond, ^{13}C shielding tensor, NMR meas. 78−1005
p-dimethoxybenzene, ^{13}C shielding tensors determ., by NMR from powder patterns 78−25556

nuclear screening continued
dipolar nuclear reservoir, spin-lattice relax. by chem. shielding tensor anisotropy 79−15372
energy levels of screened Coulomb potential, perturbation theory appl. 78−25406
ethane, ^{13}C NMR, density depend. mag. shielding in gas phase 77−75187
ethylene, ^{13}C NMR, density depend. mag. shielding in gas phase 77−75187
ethylene, matrix isolated, shielding tensor anisotropy, ^{13}C NMR meas. 79−59491
finite ligand size and the Sternheimer antishielding factor γ_∞ 80−103653
first row elements, ground state, self-consistent orbitals with uniform long-range behaviour 80−9485
fluoromethane, chem. shielding. mol. rot. and anharmonic vibr. 78−94258
Group IVA elements, excited states, quadrupole moments, Sternheimer shielding factors 78−82630
halides, NMR spectra of halogen nuclei, shielding and quadrupole coupling consts. 78−84487
halogens, Sternheimer shielding functions calcs. 79−76352
highly ionised atoms, dipole and quadrupole polarisabilities, extrapolation method calcs. 80−9534
hydrocarbon, ^{13}C NMR shielding constants and tensors, finite perturbation calcs. 77−27092
hydrocarbons, α-substituent effects in ^{13}C NMR, quantum chem. calcs. 78−74680
hydrocarbons, proton NMR chem. shifts, mag. shielding effect of neighbouring C atoms 77−27094
hydrogenic atom, Coulomb excitation, by heavy projectile, nucl. screening effect 78−17777
III-V phosphide semiconductors, ^{31}P nuclear mag. shielding 79−33549
induction energy between neutral spherical S-state atoms, nonexpanded multipoles 80−23485
inert gas isoelectronic series, polarisabilities and shielding factors 79−98008
inert gases, at. polarisabilities, linear and nonlinear, screening consts. effects 79−31435
ionic crystal, Sternheimer antishielding factors of F^-, Cl^-, Br^- and I^-, approx. free- and cryst.-ion pot. influence 80−39544
ionic crystals, Sternheimer quadrupole shielding-antishielding function for F^-, Cl^-, Br^-, and I^- 80−80236
itinerant-electron ferromagnet, US propag. and struct. instabilities, screening effects 77−69653
lanthanide ions, finite ligand size and Sternheimer antiscreening 79−19561
lanthanide ions, tripositive nucl. hexadecapole antishielding factors 79−26909
line broadening theory, screening process dynamics *(Russian)* 80−69988
magnetic shielding constants calc. by GIAO method using Gaussian functions 80−1001
mesonic atom and nuclear E1 transitions, dynamic electron screening 78−55260
metal, single-particle density matrix, perturbation expansion 80−54635
metallic elements, core elections, Sternheimer antishielding factors calcs. 78−21862
methane, ^{13}C NMR, density depend. mag. shielding in gas phase 77−75187
methane, ^{1}H and ^{13}C mag. shielding, He and methane intermol. effects 78−37571
methane, multipole moments and polarisabilities 79−85910
methane, NMR chem. shift., temp. depend., virial coeffs. 78−58722
methane, nucl. elec. shielding tensor calcs. 80−83296
methane, proton mag. shielding const., HF perturbation theory 78−46258
methane, rotational state, avoided-crossing molecular beam spectroscopy 80−63730
methane+Kr(Xe), ^{13}C-mag. shielding density depend. 78−9173
methyl bromide, rot. Zeeman effect 79−54909
methyl cyanide, microwave rot. spectra, mol. consts. 77−34615
methyl iodide, rot. microwave spectra, nucl. quadrupole, spin-rot. and nucl. shielding tensors 78−42040
3-methyl lumiflavin, in soln., absorpt. spectrum 80−58277
methylamine, C-N and N-H bond nucl. mag. isoscreening line diagrams 80−78555
methylchloride, high resoln. rot spectrum, spin-rotation and nucl. mag. shielding tensors 77−27054
molecular magnetic properties optimal gauge parameters, var. calcs. 77−71760
molecular multipole magnetisability, mag. shielding, multiple SCF perturbation theory 77−34549
molecule, mag. shielding, shielding anisotropies, INDO calcs. 78−21851
molecule, nuclear site symm. and nuclear mag. shielding in a uniform elec. field 79−41116
molecules, NMR, ^{13}C chem. shifts, screening constant calcs., CNDO/S method *(French)* 79−94012
muonic atom energy levels 79−76533
NMR chem. shift., temp. depend., virial coeffs. 78−58722
NMR chemical shift, nucl. other than protons, semi-empirical calcs., review 77−75188
NMR shielding constant, cusp-type anomaly in fluid crit. region 78−39411
nuclear magnetic shielding density 80−63559
open-shell ions, coupled HF calc., static dipole polarisabilities and shielding factors 79−6862
organic compounds, ^{13}C NMR, chem. shift, effective excitation energy calcs. 77−14457
α-oxalic acid.$2H_2O$, proton mag. shielding, rel. to deuterium shielding 77−77106
pair production near threshold screening effects, partial wave calc., energy shift screening theory 80−57768
paramagnetic systems, NMR shifts calc. using nonmultipole expansion method 80−2651
pionic atoms, electron screening and inner shell refilling, X-ray 80−78729
polystyrene, chem. shift, conformational struct. *(Russian)* 80−5652
polyvynylpyridines, atactic, chem. shift, conformational struct. *(Russian)* 80−5652
proton magnetic shielding, chem. substitution effect on chem. shift, LCAO perturbation method 77−68064

nuclear screening continued
pyromellitic acid dianhydride, cryst. struct., anisotropic proton mag. shielding 79−87326
radioactive atoms, hyperfine spectrosc., nucleus-electron interactions, review 79−72259
screened photoeffect cross-sections, anal. calcs. 77−10643
Slater's calculations, improved screening-loss parameter calc. 80−83271
slow heavy ion scattering, screened Coulomb pot. 77−14522
Sommerfeld screening parameters for the K level in X-ray spectra 79−68208
stellar interiors, thermonuclear ion-electron screening at all densities 77−29793
Sternheimer effect in ligand field splitting, nucl. and electronic levels 78−70757
Sternheimer shielding parameters role in core electronic and nucl. splittings 80−43106
Sternheimer valence shielding and antishielding factors for 2p and 3p ats. and ions 80−18807
supercharged nuclei, vacuum charge distrib., relativistic Thomas-Fermi approx. *(Russian)* 77−41876
technetium hexahalides, X_α-SW-calc. of chemically induced decay const. variation of ^{99m}Tc in TcO_4^- and hexahalides 79−54769
tetrafluoromethane, ^{19}F chem. shielding, depend. on internal coords. 78−5249
tetrafluoromethane, bond length and chemical shielding, NMR lineshape anal. of multispin system 80−32741
thermonuclear reaction rate enhancement due to strong screening 78−13186
thermonuclear reactions, quantum theory of screening effect in relativistic electron plasma *(Russian)* 77−17350
transition metal, d-electron contrib. to impurity screening 77−62857
2,4,6-trifluoronitrobenzene, ^{19}F shielding anisotropies, nematic phase NMR 77−27090
two-electron atom, three-body problem, Feshback-Rubinow approx., nucl. screening 77−18777
water, NMR shielding constants of ^{1}H and ^{17}O, paramag. contrib., triple perturbation theory 79−10127
XX H-X band, proton mag. shielding, linear electric field depend. 77−79545
p-xylene, ^{13}C chem. shielding tensors 78−60342
μ^+atom, e^+e^- pair prod., energy spectrum, screening effects *(Russian)* 78−55250
Ag, Sternheimer shielding functions calcs. 79−76352
Al, static quadrupole polarisability and shielding factor, Hartree-Fock calc. 78−41950
Al($^2P_{3/2}$), at. quadrupole shielding factor 79−10222
Ar, atomic polarisabilities and shielding factors, coupled HF approx. 78−22048
B and F chemical shifts, MINDO/3 in Pople's free electron model 79−93926
B^{2+}, multipole polarizabilities and shielding factors, calcs. on open shell ions 78−46263
BF_3, ^{19}F chem. shielding, depend. on internal coords. 78−5249
BH, susceptibility and mag. screening calcs. 77−57861
Ba II, ab initio calc. of isotope shifts 78−37555
Be, ground state reduced first order density matrix CI calc., mag. shielding const. and diamagnetic susceptibility 79−6872
Be^+, multipole polarizabilities and shielding factors, calcs. on open shell ions 78−46263
Bi, outer electron shielding, parity non-conserving optical rot. 79−18153
Br^-, nuclear quadrupole interaction , second-order Stark effect 78−21879
Br_2, muon stopping, diamag. shielding of muon-substituted cpds. 79−57279
^{81}Br, nucl. screening tensor from SiH_3Br microwave spectrum, 8-40 GHz 78−21916
C, CNDO/S nucl. screening const. calcs. 78−86787
CO, ^{13}C chem. shielding, temp. and internuclear distance depend. 77−75068
CO, ^{13}C NMR, density depend. mag. shielding in gas phase 77−75187
CO, chemical shielding temp. depend. 78−5250
CO group, NMR chem. shift, solvent's dielectric const. effect, mag. anisotropy 79−42847
CO, nucl. elec. shielding tensor calcs. 80−83296
CO, one-election props., SCF and CI calcs. 80−27951
CO_2, ^{13}C NMR, chem. shift., determ. of virial coeffs., rovibr. motion 78−58720
CO_2, ^{13}C NMR, density depend. mag. shielding in gas phase 77−75187
CO_2, mol. quadrupole moments, mag. shielding and spin-rot. tensors 79−22609
CO_2+Kr(Xe), ^{13}C-mag. shielding density depend. 78−9173
CS_2, mol. quadrupole moments, mag. shielding and spin-rot. tensors 79−22609
^{13}C, shielding consts. and anisotropy of NMR shielding tensor, modified CNDO/S calcs. *(French)* 80−32610
C=C bond, ^{13}C shielding tensor, NMR meas. 78−1005
Cd, nuclear quadrupole antishielding effects, ab initio theory 78−34814
Cd, quadrupole antishielding factors, Hartree-Fock perturbation theory 78−62723
$CdBr_2.4H_2O$, NMR, ^{113}Cd nucl. mag. shielding 78−68395
$CdCO_3$, NMR, ^{113}Cd nucl. mag. shielding 78−68395
$CdCl_2$, NMR, ^{113}Cd nucl. mag. shielding 78−68395
CdF_2, NMR, ^{113}Cd nucl. mag. shielding 78−68395
CdI_2, NMR, ^{113}Cd nucl. mag. shielding 78−68395
CdO, NMR, ^{113}Cd nucl. mag. shielding 78−68395
CdS, NMR, ^{113}Cd nucl. mag. shielding 78−68395
CdSe, NMR, ^{113}Cd nucl. mag. shielding 78−68395
CdTe, NMR, ^{113}Cd nucl. mag. shielding 78−68395
Ce II, isotope shift and screening, pseudo-relativistic HF calc. 78−90096
Cl, static quadrupole polarisability and shielding factor, Hartree-Fock calc. 78−41950
Cl^-, atomic core states, antishielding effects calcs. 80−83299
ClF, ^{19}F chem. shielding, temp. and internuclear distance depend. 77−75068
ClF, chemical shielding temp. depend. 78−5250
$ClHCl^-$, deuteron quadrupole coupling const., nuclear mag. shielding, geometry depend. 78−58586
Cs^+ and Cs, analytic SCF HF ground state wave function, ionis. pot., mag. props. 77−18785
$^{133}Cs^+$/Cs g-factor ratio, NMR and zeeman transition freqs. 78−17817
Cs_2 molecules, magnetic shielding studies by NMR 77−42341
nuclear screening continued
^{133}Cs salts, powders, nucl. mag. shielding and quadrupole coupling 77−90056
Cu, Sternheimer shielding functions calcs. 79−76352
$D_2^+(HD^+)$, g-factors and related mag. props., calc. theory 79−41124
F_2, ^{19}F chem. shielding, temp. and internuclear distance depend. 77−75068
F_2, chemical shielding temp. depend. 78−5250
F_2, mag. shielding and susceptibility, finite perturbation mol. orbitals calcs. 77−46513
FH, one-electron props., review of expt. and theoretical data, Hartree-Fock calcs. 77−67980
$FHCl^-$, deuteron quadrupole coupling const., nuclear mag. shielding, geometry depend. 78−58586
FHF^-, deuteron quadrupole coupling const., nuclear mag. shielding, geometry depend. 78−58586
Fe, Sternheimer shielding functions calcs. 79−76352
Fe^{3+}, quadrupole antishielding factors, Hartree-Fock perturbation theory 78−62723
H atom lattice impurity, H atom confined to spherical box with penetrable walls, Schrodinger eqn. 79−84987
H halides, spin-orbit coupling effect on proton mag. shielding 80−23440
H, multipole polaris. and shielding factors Wiener Askar perturbation treatment 77−34774
H, multipole polarisability and shielding factors, hydrodynamic analogy to quantum mech. 78−66677
H^+ chemical shifts, INDO calcs. 80−32743
H_2, harmonic oscillator model, elec. polarisability, mag. susceptibility and chem. shift tensor calcs. 79−81299
H_2, mag. field depend. orbitals for mag. screening and susceptibility of mol. 78−78611
H_2, metallic, phonons, supercond. transition, nonlinear self consistent screening approach 79−95537
H_2, nucl. mag. shielding, elec. field, accurate coupled Hartree-Fock 78−25434
H_2, precession magnetic shielding of proton, semiempirical functions 78−82654
H_2, shielding const., variable screening method 79−93932
H_2, triplet state, screening and susceptibility 79−41117
H_2-He, nucl. shielding, ab initio coupled HF calc. 79−89690
HBr, chemical shielding temp. depend. 78−5250
HBr, precession magnetic shielding of proton, semiempirical functions 78−82654
HCN Sternheimer shielding, perturbing elec. field and field gradient effects 77−88403
HCl, chemical shielding temp. depend. 78−5250
HCl, precession magnetic shielding of proton, semiempirical functions 78−82654
HCl, Sternheimer shielding, perturbing elec. field and field gradient effects 77−88403
HF, mag. field depend. orbitals for mag. screening and susceptibility of mol. 78−78611
HF, mag. shielding and susceptibility, ab initio finite perturbation calcs. using GIAOs 77−6670
HF, mol. props. internucl. separation depend., MCSCF calc. 78−70965
HF, NMR shielding consts. and mag. susceptibilities, coupled HF with extended GTO basis 80−5480
HF, precession magnetic shielding of proton, semiempirical functions 78−82654
HF_2^-, mag. shielding and susceptibility, finite perturbation mol. orbitals calcs. 77−46513
$H_2^+(HD^+)$, g-factors and related mag. props., calc. theory 79−41124
HI, precession magnetic shielding of proton, semiempirical functions 78−82654
H_2O, $(H_2O)_2$, mag. shielding rel. to hydrogen bonding 77−14348
H_2O, elec. and mag. props., equations of motion method calcs. 77−83513
H_2O, elec. and mag. props. in static fields, perturbed Hartree-Fock calcs. 78−50462
H_2O, muon stopping, diamag. shielding of muon-substituted cpds. 79−57279
H_2O, nucl. elec. shielding tensor calcs. 80−83296
H_2O, nucl. mag. shielding and susceptibility, SCF calcs. 77−14351
H_2O, one-electron props., review of expt. and theoretical data, Hartree-Fock calcs. 77−67980
H_2O powder, PMR chem. shift anisotropy, nucl. mag. screening tensor 78−17687
H_2O, proton mag. shielding const., HF perturbation theory 78−46258
HOF, nucl. mag. shielding and susceptibility, SCF calcs. 77−14351
H_2S, powder, PMR chem. shift anisotropy, nucl. mag. screening tensor 78−17687
H_2SeO_4, NMR of ^{77}Se, chemical shift and screening tensors *(Russian)* 78−64285
HT, triton-proton mag. moment ratio determ. by NMR method with 10^{-6}% accuracy *(Russian)* 77−61773
He, atomic polarisabilities and shielding factors, coupled HF approx. 78−22048
He, isoelectronic sequences, screening constants, ground and excited states 78−62701
He+CO, nuclear mag. shielding consts., interaction geometry depend., chemical shift, gauge invariant method 78−62866
HeH, HeH^+, variable screening model calcs. 78−74587
HeH^+, electronic states, variable-screening method 78−25410
^{199}Hg nuclear shielding anisotropies rel. to isotropic chem. shifts in methyl mercury compounds 77−3384
ICN, microwave spectrum, mag. hyperfine struct., I nucl. shielding tensor 78−17661
In, quadrupole antishielding factors, Hartree-Fock perturbation theory 78−62723
^{191}Ir 129 keV transition, atomic screening, time reversal violation 80−106011
Li, dipole (quadrupole) polarisabilities, shielding factors, using hydrodynamic analogy 80−52905
Li, isoelectronic sequences, screening constants, ground and excited states 78−62701
Li, multipole polarisabilities, shielding factors calc., hydrodynamic analogy to quantum mechs. 77−68134
Li^+-ligand complexes, NMR appl. ^{7}Li chemical shifts, expt. and ab initio studies 80−63670
LiH, NMR shielding consts. and mag. susceptibilities, coupled HF with extended GTO basis 80−5480

nuclear screening continued
Mg^{2+} atomic core states, antishielding effects calcs. 80−83299
MnO_4, aqueous soln., ^{55}Mn nuclear mag. shielding, NMR obs., O isotope exchange 77−10691
MoS_4^{2-}, S isotope effect on ^{95}Mo nucl. mag. shielding 77−63301
N, CNDO/S nucl. screening const. calcs. 78−86787
N containing molecules, N NMR, nuclear mag. shielding, X-ray photoelectron spectra 78−17695
N_2, cryst., screened nucl. pot. and lattice dynamics, pseudo-atom approx. 78−34575
N_2, elec. and mag. props., equations of motion method calcs. 77−83513
N_2, one-electron props., polarisabilities and polarisability derivatives, SCF and CI calcs. 80−37746
NH_3, mag. shielding consts., coupled HF perturbation theory 79−6863
NH_3, nucl. elec. shielding tensor calcs. 80−83296
NH_3, proton mag. shielding const., HF perturbation theory 78−46258
NH_4^+, Sternheimer shielding, perturbing elec. field and field gradient effects 77−88403
N_2O, ^{15}N NMR, chem. shift., determ. of virial coeffs., rovibr. motion 78−58720
^{14}N NMR chemical shift, external neat nitromethane scale 78−24834
^{14}N screening, absolute scale 78−2762
Na isoelectronic sequence, hypervirial theorem, screening parameters and oscill. strengths 79−6882
Na^+, atomic core states, antishielding effects calcs. 80−83299
Na_2 molecules, magnetic shielding studies by NMR 77−42341
Na_2+Na, spin polarisation exchange via opt. pumping, NMR 77−14452
NaK+Na, spin polarisation exchange via opt. pumping, NMR 77−14452
$(NbCl_nBr_{6-n})^-$, ^{93}Nb nucl. spin relax. and mag. shielding 78−58723
$(NbCl_nBr_{6-n})^-$ complexes in acetonitrile soln., ^{93}Nb spin relax. and mag. shielding 80−44944
Ne, atomic polarisabilities and shielding factors, coupled HF approx. 78−22048
O, CNDO/S nucl. screening const. calcs. 78−86787
OCS, mol. quadrupole moments, mag. shielding and spin-rot. tensors 79−22609
^{17}O, screening constants by CNDO/S and INDO calculations 77−46576
$PBMoO_4$, ^{207}Pb mag. shielding anisotropy, Fourier transform NMR 77−90057
PF_3, in smectic solvent, ^{31}P NMR, ^{19}F and ^{31}P mag. shielding 77−18942
PH_3, ^{31}P NMR chem. shift, virial coeff. determ. 78−58721
PH_3, NMR shielding consts. and mag. susceptibilities, coupled HF with extended GTO basis 80−5480
$P(P^+)(P^{2+})$, static quadrupole polarisability and shielding factor, Hartree-Fock calc. 78−41950
PSF_3, in orienting smectic solvent, ^{19}F and ^{31}P mag. shielding anisotropies, F-P-F bond angle 77−18942
^{31}P, nucl. mag. screening in PH_3, pseudopot. calcs. 79−6879
^{31}P, shielding consts. and anisotropy of NMR shielding tensor, modified CNDO/S calcs. *(French)* 80−32610
Pb, muonic high-lying states transitions, electron screening effects 77−34786
$PbCO_3$, ^{207}Pb mag. shielding anisotropy, Fourier transform NMR 77−90057
$PbCrO_4$, ^{207}Pb mag. shielding anisotropy, Fourier transform NMR 77−90057
$Pb(NO_3)_2$, ^{207}Pb mag. shielding anisotropy, Fourier transform NMR 77−90057
$Pb(NO_3)_2$, nucl. mag. shielding tensors of $^{207}Pb^{2+}$, NMR obs. 80−44939
$PbWO_4$, ^{207}Pb mag. shielding anisotropy, Fourier transform NMR 77−90057
Pr_3 Sternheimer shielding functions calcs. 79−76352
Pr^{3+}, correlation contributions to nuclear antiscreening factor, many-body calc. 79−56153
Pr^{3+}, nuclear quadrupole screening parameter, many-body perturbation theory calcs. 78−47751
SiF_4, ^{19}F chem. shielding, depend. on internal coords. 78−5249
SiH_3Br, rot. Zeeman effect 79−54909
$Si(Si^+)$, static quadrupole polarisability and shielding factor, Hartree-Fock calc. 78−41950
Sn, internal conversion coeffs. for inner shells of atomic ions and relativistic ionic potentials 80−68600
^{119}Sn-^{117}Sn primary isotope effect on mag. shielding, NMR of Sn cpds. 79−72338
TcO_4^-, X_α-SW-calc. of chemically induced decay const. variation of ^{99m}Tc in TcO_4^- and hexahalides 79−54769
Xe+$CO(N_2)$, ^{129}Xe chem. shielding, second virial coeff. 78−66563
^{129}Xe+nonspherical molecule, interaction pots., effect on mag. shielding, NMR meas. 77−71816
Zn, nuclear quadrupole antishielding effects, ab initio theory 78−34814
Zn, Zn^{2+}, quadrupole antishielding factors, Hartree-Fock perturbation theory 78−62723
ZnS, ^{67}Zn and ^{33}S nuclear magnetic shielding, chemical shifts and linewidths 80−60434
ZnSe, ^{67}Zn nuclear magnetic shielding, chemical shifts and linewidths 80−60434
ZnTe, ^{67}Zn nuclear magnetic shielding, chemical shifts and linewidths 80−60434
$ZrBrH_n$, (n=0.5, 1), ^{1}H NMR, shielding tensors 79−69731
$ZrClH_n$, (n=0.5, 1), ^{1}H NMR, shielding tensors 79−69731

nuclear shape
see also nuclear collective states and giant resonances; nuclear energy levels; nuclear resonances
2s-1d shell nuclei, cluster struct. and inelastic scatt. of polarised protons 79−6557
^{238}U(n,f), reactor n, shoulders in very asymmetric mass distrib., cumulative yields 79−59005
γ vibrations in permanently deformed nuclei 78−86465
A=110-210 nuclei, new parameters of deformed Woods-Saxon pot. 78−93951
A=12-240, even-even, dynamic deformation theory, B(E2) values, quadrupole and mag. moments 80−68591
A=160-180 nuclei, manifestations of oblate shapes at high spin, transition energies in yrast region 78−78249
A=190, Nilsson strength fragmentation, quadrupole and hexadecapole deformations 80−47394
A>228 odd mass nuclei, single particle states, nuclear deform. 78−12952

nuclear shape continued
actinide nuclei, cranking model, collective inertia parameters 80−57665
actinide nuclei, even-even, E_2 transitions from 2^+ state of gamma-vibrational band 80−91150
actinide nuclei quadrupole and hexadecapole deforms., model independ. parameters using Fermi distrib. 78−17096
actinides, effect of simple consistency condition on multipole moments 78−86475
actinides, level energies and B(E2) ratios of deformed even nuclei 79−13221
alpha decay theory, hindrance factors of spherical and deformed nuclei *(Russian)* 79−49612
alpha-particle energy spectrum, fission-emitted, fission-fragment shape and orientation depends. 78−74346
asymmetric deform. rot. spectra and K-mixing 77−79303
asymmetric rotator, yrast states, wobbling freq., boson representation 80−32167
axially symmetric nuclei, soln. of HF eqns. in coord. space 77−88060
backbending, effect of protons 77−82816
backbending in $^{180-182}$Os, ^{181}Re, Coriolis antipairing, rot. alignment, deform. jumps 78−70432
band structures, generalised HFB approach in intrinsic frame of reference, equilib. deformation 80−22664
binary fission saddle pints, shape parametrization for liquid-drop studies 80−106086
boson approximation for deformed nuclei *(Russian)* 77−74778
central-tensor coupled effective interaction pot., binding energy, shape, electric moment 77−14036
charge and slope polarisation of nuclei, liquid drop model anal. 79−9543
charge- and mass-density waves in finite nuclei, possible expt. test 77−54144
collective model, two-phonon states, effect of Pauli principle 80−68565
collective model for light nuclei, HF calc. shape anal. 77−41882
collective props. of nuclei deduced from electron scatt., deformed nuclei, review 78−50064
collision integral in nuclear matter at zero temperature 79−17928
complex deformed and spherical nuclei, giant resonances within quasiparticle phonon model 79−63648
compound deformed state g-factors and moments of inertia *(Russian)* 77−74757
conference on medium heavy nuclei structure, Rhodes, Greece (May 1979) 80−67935
conference on nuclear physics, Mikolajki, Poland (2-14 Sept. 1979) 80−101662
core-particle coupling models, deform., ^{185}Re, ^{75,77}Se appls. 79−450
Coulomb effect in rotating nuclei in the Thomas-Fermi approach 80−47355
cranking, microscopic derivation for nuclear systems with large angular momentum 79−40829
cranking model anal. of nuclear inertia in fission and heavy ion reacts. 78−41656
decoupling model for fission fragment transitional nuclei, odd-odd and even mass 80−78174
deep inelastic heavy ion collision, shape relaxation and fragment deformation 80−22683
deformation, large amplitude collective motion in a nontrivial schematic model 80−73816
deformation, unified microscopic description 77−79305
deformation changes rel. to α-decay rotation signatures 79−13258
deformation depend. of kinetic energy, role in calc. of collective states in Ba and Xe 77−67695
deformation energies for nuclei with different charge-to-mass ratio for fusion or binary fragmentation 79−80869
deformation energy dissipation, linear response function HF and HFB approx. 79−26366
deformation energy of nuclei, one particle spectrum, self consistent calcs., Hartree Fock variational method 78−12957
deformation energy surfaces at very high spin states, microscopic determ. 77−71560
deformation of neutron-density in inelastic scatt. 78−46000
deformation structure in light f-p shell nuclei, $^{41-44}$Ca, ^{43}Sc, ^{44}Ti calcs. 78−66228
deformations of rare earth nuclei, Skyrme-HF calcs. 78−62480
deformed and superdeformed nuclei from heavy ion reactions, α-decay amplification 80−102156
deformed even nuclei, level energies, γ transitions, moment of inertia, collective Hamiltonian 78−25133
deformed even-even nuclei, ^{152}Sm to ^{238}U, semimicroscopic calcs. of giant dipole resonances 77−50096
deformed even-even nuclei, application of SU(3) *(Bulgarian)* 79−9493
deformed even-even nuclei, specific form. of nucleon-nucleus interaction, low energy 78−13077
deformed even-even nuclei, SU_3 description of energy levels and reduced E2 transition probabilities *(Russian)* 79−13251
deformed nuclear states in yrast-band, microscopic model 79−6365
deformed nuclei, absorption of slow π^-, mesic atoms 80−78321
deformed nuclei, bandcrossing in K≠0 bands, odd-A rare earths 80−5045
deformed nuclei, constrained HF energies, two-step iterative method 80−83053
deformed nuclei, coupled rot. bands, RPA type approach 78−89775
deformed nuclei, effect on Coriolis interaction, Nilsson model and Woods-Saxon pot. calcs. 80−63071
deformed nuclei, electron scatt., elastic differential cross section calc. 77−82912
deformed nuclei, even-even, phonon space and giant resonances *(Russian)* 80−52641
deformed nuclei, existence in spherical domain 79−75829
deformed nuclei, first monopole excitation energies in systems with pairing forces 77−61364
deformed nuclei, fragmentation of single-particle states, neutron strength functions 77−6233
deformed nuclei, gaps in single-particle level scheme and backbending 78−17072
deformed nuclei, giant quadrupole reson splitting 78−4924
deformed nuclei, heavy-ion scatt., generator coord. method 78−12960
deformed nuclei, HF approach to mag. moments 78−12967
deformed nuclei, improved parametrisation of Woods-Saxon pot. 80−86823
deformed nuclei, level densities, K-band positions 77−22855

nuclear shape continued
deformed nuclei, low and high energy collective states and giant resonances, RPA calc. 79−17779
deformed nuclei, magnetic dipole γ-transitions, one particle matrix element tables 79−6472
deformed nuclei, new isovector collective modes 79−9443
deformed nuclei, pairing self-consistent description *(Russian)* 79−67646
deformed nuclei, photoreactions as struct. probe 77−2975
deformed nuclei, polarisation, and energy shifts in muonic atoms 80−86893
deformed nuclei, rot. states in Hartree-Fock-Bogoliubov approx. 77−10347
deformed nuclei, semimicroscopic description of giant octupole reson. 77−280
deformed nuclei, shell and isotope effects in neutron-nucleus interactions, review of Soviet research 79−36168
deformed nuclei, single nucleon form factor for knockout and pick-up reactions, (p,2p) calcs. 78−93999
deformed nuclei, single particle level blocking in BCS approx. 80−99117
deformed nuclei, single particle matrix elements of electric quadrupole γ-transitions 77−88072
deformed nuclei, single particle matrix elements of radiative M2-transitions, Nilsson model 80−22753
deformed nuclei, splitting of giant multipole states, vibr. pot. model 78−4893
deformed nuclei, state microscopical structure in neighbourhood of yrast line 79−45137
deformed nuclei, static isoscalar and isovector polarisability, isovector $K=\pm1^+$ modes 80−32260
deformed nuclei, surface thickness effects and multipole excitation splitting, sum rule approach 79−453
deformed nuclei, transition densities for electroexcitation 78−17183
deformed nuclei, yrast level ground state correlations, RPA anal. 80−86777
deformed nuclei calc. by HF method with Skyrme's interaction *(Russian)* 79−456
deformed nuclei energy density mass formula, approx. method, binding energy, quadrupole moments 79−13195
deformed nuclei high spin state radiative decay in Australian nuclear physics review 77−88021
deformed rare earth nuclei, bandcrossing in $K\neq0$ bands, backbending 80−9204
deformed single-particle basis for pot. energy surfaces and spectra 78−8735
density-depend. folding interactions, effect on nucl. shape 77−22871
doubly even deformed nuclei, excited states, Pauli principle effects, quasiparticle-phonon model 80−63094
doubly odd deformed nuclei, EM transitions, nanosec. lifetimes 78−62505
droplet of nucl. matter under rapid rot., anal. using Thomas-Fermi method 79−36179
E1 giant resonance of deformed nuclei in the region $150<A\leq186$ *(Russian)* 78−78348
ellipsoidal, liquid-drop model, irrotational incompressible hydrodynamic flow 80−83050
even-even and odd A nuclei, nuclear shapes and motions, review 80−5054
even-even deformed nuclei, aligned rot. of octupole vibrational states 78−12955
even-even deformed nuclei, collective $K^\pi=0^+$ states, realistic boson expansion comparison 80−5043
even-even deformed nuclei, coupled rot. bands, charge and density distribs. 78−89776
even-even deformed nuclei, giant E_λ resonances of high multipolarity, force functions 79−75944
even-even deformed nuclei, multiphonon $K^\pi=0^+$ states, matrix elements of general Hamiltonian 78−41621
even-even deformed nuclei, multiphonon $K^\pi=0^+$ states, norms 78−17089
even-even deformed nuclei, nonadiabatic effects 78−528
even-even neutron-rich fission products, de-excitation spectra, β-decay, deformation 80−78203
even-even nuclei, electric and dynamic quadrupole moments 78−66203
even-even nuclei, z=6 to 100, probable members of quasi-bands in spherical and deformed regions 80−13357
even-even nuclei with $A\approx150$, excited states calculation, phenomenological models: band-mixing, vibrational-rotational and interacting-boson model 80−22653
even-even rotating nuclei, role of pairing in deformability *(Russian)* 77−6210
even-even spherical nuclei, 2_1^+ state deformation parameter from (p,p) and EM excitation 80−27549
exact canonically conjugate momentum to the quadrupole tensor and a microscopic derivation of the nuclear collective hamiltonian 78−78251
excitation during collective deformation, time depend. Hartree Fock Bogolyubov method, fission process 78−58229
finite temperature shape transitions, stability conditions, level density, HF and HFB calcs. 79−67644
fission, most probable charge, shell and deform. effects 78−29440
fission, relaxation phenomena, collective deformation, and internal excitation energy *(Russian)* 79−80920
fission and heavy-ion reactions, deform. described by density moments 77−41883
fission dynamics effects of shell struct. and pair correl. 79−6560
fission isomers, meas. of extreme nucl. deform. *(German)* 79−40971
fission process, scission, dynamic excitation model, ^{240}Pu appl. 77−14095
fissioning nucleus, deformation process mass parameter, liquid drop model 80−102221
folded pot., effect of nucl. deform. 78−93983
form factor calc. using method of hyperspherical functions 77−18381
fp-shell nuclei, high-spin states 78−12946
governor model for asymmetric deformed nuclei, band anal. 80−86776
ground state deformation energy, rot. band inertial parameter depend. 80−18185
groundstate and β-band simultaneous description, new model 77−2898
growth points in nuclear physics, book 80−94928
Hartree Fock Bologiubov theory, appl. to light/heavy nuclei, book contrib. 79−75881
Hartree-Fock-Bogolyubov approach to nuclear band description *(Russian)* 79−3107
heated fast rotating nuclei, equilib. props. 78−70439

nuclear shape continued
heavy deformed nuclei, flow patterns for collective rotations 79−75816
heavy ion collisions, rarefaction of oblate shaped nuclear matter, hydrodynamics calcs. 78−89894
heavy ion deeply inelastic collisions, shape deformation and viscosity 78−25234
heavy ion fusion and deep inelastic scatt., shape degrees of freedom, classical dynamic model 80−22876
heavy ion induced deep inelastic transfer, decay of binary nuclear system 80−22848
heavy ion reactions, potential energy surface topography 77−330
heavy transition nuclei, self-consistent anisotropic oscill. model, shape parameters calc. 77−79306
heavy-ion collisions, in-beam gamma-ray spectroscopy, nuclear shape and reaction mechanism *(French)* 79−560
heavy-ion deep inelastic collisions, classical model with friction and deformation 77−30633
heavy-ion reactions, collective pot. energy surfaces, appl. to Ar+Ag, Kr+Cu, and Xe+Bi 78−41748
high angular momenta nuclei, backbending, yrast states, large moment of inertia band 77−14027
high excitation energies, shape changes *(German)* 79−54384
high spin effects in nuclei with proton no. 40-60, shape, deforms. 78−503
high-spin states of transitional and spherical nuclei, decoupled and strongly coupled bands 78−12939
highly deformed nuclei, inertial matrix elements by hydrodynamic calc. *(French)* 79−71838
incompressibility of nonsymmetric nuclear matter *(Russian)* 79−59030
independent particle model, forces between heavy nuclei, neck formation 78−635
inertia ellipsoid axes from hyperspheric functions method, nuclear struct. and shape *(Russian)* 79−30767
interacting boson model, sphericity 77−41902
intermediate atomic weight nuclei, 6 MeV proton scatt. anal., quadrupole deform. 78−13076
intrinsic multipole moments in deformed nuclei, correls. effects 78−29385
isospin dependence of expt. nuclear deformations 77−82817
large deformations, single particle levels, self-consistent field rearrangement, HF method 80−78107
large deformations and dissipation in a random-matrix model approach for fission or colliding nuclei 80−18162
light deformed nuclei, Skyrme interaction spin components, spectra, projected HF theory 80−73820
light deformed nuclei, stability, shape, Hartree-Fock calcs. *(Russian)* 80−52568
light nuclei, shape in translationally invariant shell model 79−26367
liquid drop deformation energy for axial symmetric nuclei 79−59022
liquid drop energy, shell correction determ. 78−12992
liquid drop model deformation energy calculation program 79−13197
low-spin low-energy phase transitions 77−22834
M1 magnetic form factor and spin oscillations 79−67652
microscopic cluster model, light nuclei as proving ground, reviews 79−3101
monopole excitations in heavy nuclei, hadron induced 78−86471
Muonic atoms, X-ray vacuum corrections, nuclear moments, transitions and deformation parameters 80−37912
muonic atoms of deformed nuclei, nuclear polarisation correction 77−23584
N=5 shell, deformed odd-neutron nuclei, band ordering and spectrum 80−83018
N=82 region, high spin isomers, deformation energy surface, shape constrained cranked HF theory 80−57666
n-deficient even-mass isotopes near Pb, yrast states, shape transitions 77−61345
near Pb region, α-decay peculiarities and shape staggering effects 79−49611
neutron excess deformation, coupled channel anal. of (p,n) elastic and inelastic scatt. 79−93480
neutron rich nuclei; β^--emitters, deformation and spectroscopy 80−78223
neutron rich transitional fission fragments, spectroscopy, 0^+ states and octupole vibrs. 80−78204
neutron strength functions in deformed nuclei, semi-microscopic approach 77−22851
Nilsson model, group theoretical treatment, deformation, pot-energy surface, oscillator shell coupling 78−33129
Nilsson states, asymptotic quantum numbers for prolate and oblate deformations 80−9226
nuclear matter overlap integral calcs. in diffuse surface model 79−17821
nuclear potentials in deformed nuclei 78−46097
nuclei far from stability, spectroscopy 77−22910
nucleon overlaps, Sturm Liouville expansions, convergence props. 78−78281
nucleus-nucleus pot., static polarisation effects, nuclear shapes 80−5154
oblate high spin isomers, pairing Hamiltonian anal. by RPA 78−12996
octupole excit. in deformed nuclei, translational invariance *(Russian)* 77−61343
octupole low-energy resonances in deformed nuclei, RPA calc. 77−82892
odd deformed nuclei, E2-transition probabilities with $\Delta K=1$ 79−6495
odd deformed nuclei, M1 transitions, one particle intranuclear conversion matrix elements 79−6473
odd nuclei, soft and deformed, rotor plus quasiparticle approach, moments, transition probabilities 80−78214
odd-A deformed nuclei, EM and electron scatt. form factors, selection rules 79−9458
odd-odd deformed nuclei, mag. props. 77−82822
one body dissipation and super viscidity of nuclei, nuclear fission, collisions and deformation 78−86501
one body nuclear dynamics, classical theory for collective motion 78−8755
one-body dissipation, general classical theory, quantal corrections 78−86494
one-body dissipation of nuclear deformation collective energy, semiclassical approx. *(Russian)* 78−86502
oscillations, radial transition density in particle-vibration coupling model, ^{208}Pb example 77−50048
oscillator basis for octupole collective motion in nuclei 78−70470
particle transfer during nuclear deformation, Hartree-Fock calcs. *(Russian)* 79−3079

nuclear shape continued
particle-vibration coupling model, octupole mode 79−17839
pear-shaped nuclei, 3-D representation of pot. energy *(French)* 79−67645
photoscattering by giant resonances in deformed nuclei, cross section determ. by semimicroscopic approach 79−9545
polarised nuclear matter, deform. of Fermi surface 78−12998
potential energy surface and collective spectra 78−86464
potential energy surfaces, folded Yukawa-plus-exponential model 80−86816
potential energy surfaces of odd-mass isotones of Tl, Au, Ir, Re 80−26867
probabilities of α-, β- and γ-transitions accompanied by changes in nuclear shape *(Russian)* 78−89820
prolate symmetry axis, rotation of nuclei at high spin states, yrast states 78−70431
proton and neutron densities, HF calc. 77−18380
proximity treatment of the interaction between deformed nuclei 78−78338
quadrupole deformation anal., collective rot. and SU(3) models 77−41880
quadrupole excitations, microscopic approach to description *(Russian)* 77−50041
quadrupole moment of heavy deformed nuclei in pseudo-SU(3) model 77−71565
quadrupole transfer strength, deformed rare-earth nuclei, heavy ion reactions 77−336
quadrupole vibration theory, potential oscillations and collective motion *(Russian)* 79−13222
quasirotational bands, spherical-deformed transition rates 78−54663
radial wave functions of valence nucleons 80−73788
radiative strength functions in spherical nuclei, giant dipole resonance influence, ^{124}Te, ^{140,142}Ce appls. 78−89774
rapidly rotating nuclei, density distrib. 78−8734
rapidly rotating nuclei, shell struct., collective motion and elastic deformation 79−71782
rare earth deformed nuclei, high spin region excited rot. bands, RPA calcs. 80−78108
rare earth even nuclei, Woods Saxon pot., very high spin Strutinsky calcs. 77−88055
rare earth nuclei, cranking model, collective inertia parameters 80−57665
rare earth nuclei, even-even, E_2 transitions from 2^+ state of gamma-vibrational band 80−91150
rare earth nuclei, modified oscillator pot. parameters, single particle levels 80−68509
rare earths, nuclear deformation, Coulomb displacement energy depend., shell model 80−102108
rare-earth nuclei transition density, ang. momentum projection corrections to rot. model 78−500
rotating nuclei, from heavy ion collision, high spin states instability against fission *(Rumanian)* 78−50150
rotating nuclei, two-phase model 78−33113
rotating nuclei deformation energy, Nilsson model dynamical moment of inertia, shell corrections *(German)* 78−82276
rotating nuclei of high and v.high nucl. spin *(German)* 78−25102
rotating toroidal nuclei, ang. mom. thresholds 78−41629
rotation, zero point energy 78−25101
rotation effects on collective props. review *(Russian)* 78−37299
rotational states, Coulomb excitation by spherical nucleus, distortion, semi-classical model 79−67620
rotational states in heavy deformed nuclei, high-spin anomaly 78−93934
scission of deformed nucleus, review of fission process 77−14096
self shape of nuclei *(Russian)* 78−29381
self-consistent field calcs., HF calcs., NN interactions, and results of appl., book contrib. 79−75880
self-consistent field rearrangement in large nuclear deformations, HF calcs. 80−18184
self-consistent treatment of interaction between shape and pairing deform. 77−71561
semiclassical interpretation of gross-shell struct. in deformed nuclei 77−82818
semiempirical nuclear level density formula with shell effects 78−82290
semimicroscopic description of nucl. states at low, intermediate and high excitation energies 78−54666
semiphenomenological model, effective deformation and elasticity parameters 79−9454
shape isomer prod. in nuclear reactions and β-decay 79−6377
shape isomers, spontaneous fission, static and decay props. and excitations, review, book contrib. 78−82402
shape meas. and collective model validity for $N \neq Z$ nuclei 78−45999
shell model, spherical vibrational and deformed rotational motion 78−50069
shell model mass formula 77−6261
shell structure, trend towards certain shapes 77−14026
single particle realistic level schemes, nuclear shell correction energies, temp. smearing method 78−17118
single particle Schrodinger fluid, nuclear fluid dynamics, shell model basis, shape distortions 79−93484
special shell structure for nuclei at high angular momenta 79−17825
spherical nuclei, fragmentation of hole states in quasiparticle-phonon model 80−83020
spherical nuclei, geminal product approx., appl. to ^{4}He, ^{16}O 78−66230
spherical nuclei, isomer and isotope shifts, theory of finite Fermi systems 80−39929
spherical nuclei, low lying states, effects of particle-particle channel residual interaction 78−12978
spherical nuclei, masses determ. by energy-density method 77−6215
spherical nuclei, nuclear mass formula, energy density functional, self-consistent calc. 78−78244
spherical nuclei, odd, l-forbidden M1 conversion transitions, penetration matrix elements 80−22763
spherical nuclei, quasi-particle theory, modification of BCS basis 80−63109
spherical nuclei, quasiparticle-phonon model, iterative method 80−68566
spherical nuclei, Te to Sm, very high spin states, deform. energy surfaces 78−50079
spherical shell model, collective features, review 78−50098
spheroidal asymmetric oscillator pot., shell model calcs. 77−74779
spin-isospin density phase in finite nuclei, strongly oblate shape 80−22746
nuclear shape continued
spontaneous fission mass parameters, cranking and hydrodynamic models, deformation depend. *(Russian)* 80−13511
spontaneously fissioning isomers, review of expt. data, equilib. quadrupole deformation parameters *(Russian)* 77−54260
state density renormalisation as function of deformation 77−6201
statically deformed nuclei, level spacing by statistical methods 79−45165
strong deformed nuclei, review 77−79308
strongly damped heavy-ion collisions, in microscopic calc. of kinetic-energy loss in rapid stretching 77−14167
strongly deformed nuclei, shortlived states, g-factor meas. method 80−52577
sudden shape transitions, pair correlation association, E2 transition rate and backbending *(Chinese)* 79−59007
supercritical nuclear composites, spontaneous vacuum decay 78−25235
superheavy element prod. in compound nucleus reaction, theoretical optimisation method 78−46103
superheavy nuclei, spontaneous fission props. for $98 \leq Z \leq 106$ and $150 \leq N \leq 164$, shell model 78−82401
surface deform. effect on form factors determ. *(Russian)* 77−46108
Thomas-Fermi approach to rotating nuclei 78−41657
Thomas-Fermi approx. extensions, finite nuclei, RMS radii 77−6256
thomas-Fermi study of nuclei at high angular momenta 78−66197
transitional nuclei, single particle and collective degrees of freedom coupling *(Russian)* 80−13345
transitional odd-man nuclei, diagonalisation of collective quadrupole Hamiltonian 77−6221
transitional odd-odd mass nuclei, gamma deformed rotor model 79−93498
transuranic nuclei, Po to Th, very high spin states, deform. energy surfaces 78−50079
triaxial nuclei, Hartree Bogoliubov predictions 78−33116
triaxial shapes in nuclei, projected HF and Hartree-Fock-Bogoliubov overlap integrals 78−78293
twist mode, appl. to ^{208}Pb 77−88037
unified model with vibrating core of variable deform., appl. to ^{21}Ne, ^{21,22}Na 77−50068
unified nuclear pot. for heavy ion elastic scatt., fission, fusion, masses and deformations 80−5189
unified pot. from liquid drop model, description of nuclear props. 79−22213
velocity fields and transition densities in nuclear collective modes 79−89255
volume and surface vibr. relations, quantum hydrodynamics 80−9227
Woods-Saxon potential spectrum, pairing force strength, Nilsson model comparison 80−57704
yrast region of rapidly rotating nuclei, instability toward nucleon emission 77−88027
yrast spectroscopy, nuclei with high angular momentum, review 78−50063
yrast traps, island of high spin isomers near N=82 78−8844
yrast traps, struct., nuclear deform. 78−21486
Z=114-126, nuclear stability reexamination using deformed Woods-Saxon pot. lifetimes level density 79−3094
Z=34-94, high spin yrast isomers and nuclear deformation 79−6369
α-cluster deformation inside light nuclei 79−17829
α-clustering and spectroscopic factors, shell effects and deformation correlations in (^{6}Li,d), (d,^{6}Li) 79−6436
α-emission probability at very high ang. momenta, shape change effects 79−89229
(d,p), effects of d deformation and D-state influence, wave functions 79−13201
(n,γ), interacting boson and Nilsson model tests, Pt-Os transition region 80−37380
np interaction and nucl. deformation 78−8748
^{194}Os, populated in ^{192}Os(2n,γ), level transitions, prolate-oblate transition 78−62540
(p,α), (t,α) reactions comparison in shape transitional region near N=90 79−540
(p,p), A=9 to 70, differential cross sections, struct. effects, optical and coupled channel anal. 80−47482
(p,p′), deformed nuclei, ground state rot. band, shape meas. and exchange contrib. 79−451
(p,p′), deformed nuclei, local approx. results for exchange effects 79−452
(p,t) reaction use for investigation of shape transition, Pt isotopes low excited states 77−54212
(π^-, X) slow pion capture in deformed nuclei, effects on high spin state excitation 80−18345
^{232}Th(α, α'), coupled channel Born anal. of deformation correl 80−5149
A=Rb, A=74-79, 90-99, direct meas. of masses, deformation onset at N=60 79−54383
^{227}Ac, 7 to 16 MeV photofission, giant resonance and nuclear deformation *(Russian)* 78−41795
Ag, deform. of ground and excited states 78−82277
^{A}Ag+^{11}B, 86 MeV, A=107, 109 79−67766
^{A}Ag+^{40}Ar, 285 MeV, A=107, 109 79−67766
^{103}Ag high spin states, bands transitions, intermediate deformation Coriolis coupling from (^{3,4}He, xnγ) 80−105944
^{109}Ag (^{40}Ar, X), α-decay amplification in superdeformed nuclei, high ang. momentum deexcitation 80−22776
Al, A=25, 27, M1, E2, transition probabilities between differently deformed states, Nilsson model 77−61376
^{24}Al, β-transitions, weak magnetism, nuclear struct., matrix elements 79−13253
^{27}Al, analogue-antianalogue M1 transitions, nucl. shape change influence 78−13006
^{27}Al, shape mixing using ang. momentum projection from Hartree-Fock intrinsic states 78−86472
^{27}Al(^{10,11}B,^{10,11}B), 41.6, 50 MeV, ang. distribs., cross sections and deformation parameters, absorption effects 79−67773
^{27}Al(α,α), x=p,d,t,h,α' and x-γ, 140 MeV, reaction mechanism characts. for deformed ^{27}Al 79−63682
^{240}Am^m, spontaneously fissioning isomer optical shift in pumped $^8S_{7/2} \rightarrow {}^{10}P_{7/2}$ transition, nuclear deformation 80−27971
^{38}Ar high spin state density, γ-decay mode, deformed states from ^{35}Cl(α,pγ) 80−32168
At high spin isomers, deformed independent particle model, yrast lines, shape 79−480
^{193,195}Au, decoupled bands and rot. alligned coupling to triaxial shape 77−65191

nuclear shape continued
Au, isotopes near A=186, competition of nucl. shape 78−17094
Au, odd isotones, deformation pot. energy from Nilsson model 80−57676
Au, odd isotopes, pot. energy surfaces and quadrupole deformation parameters, deformed basis model 79−80867
Au odd mass isotopes, odd proton effects on potl. energy surfaces 77−22877
Au odd mass isotopes, particle rotor descriptions 77−22914
^{187}Au energy states from ^{187}Hg decay, parities γ-spectra, triaxial nuclear deform. *(French)* 78−33143
^{197}Au+^{140}Ar, 217 MeV, deform. of double nucl. system 79−6699
^{197}Au(^{40}Ar,X), 240 MeV, fragment shape deformation in deep inelastic collisions 80−47365
^{10}B, energy level struct., admixed wave functions, ground state quadrupole moment, deformability 77−50054
^{10}B, triaxial deformation in shell model non-central forces, projected HF calc. 80−13367
^{11}B, determ. of hexadecapole mom. and quadrupole deform. from ^{11}Be(^{3}He, ^{3}He) 77−65229
Ba odd-mass isotopes, A=125-133, high spin level systematics and triaxial shapes 77−22838
^{A}Ba, A=142, 144, onset of deformation in neutron-rich isotopes 79−93499
^{128}Ba, level scheme, near instability against γ-deformation via ^{128}La decay 77−82806
^{129}Ba, triaxial shape and high-spin bands obs. in ^{124}Sn(^{12}C,3n) 77−34219
^{130}Ba, Wilets-Jean Hamiltonian for energy levels, transitions, moment, etc. 79−9457
^{134}Ba, reorientation effect and multiple Coulomb excitation meas. 77−61450
^{8}Be, effective nucleus eccentricity depend. on total momentum *(Russian)* 79−3078
^{9}Be deformed nucleus, continuum states in strong coupling model 80−22682
^{10}Be, triaxial deform. in 1p shell 77−46105
Bi(Kr,X), strongly damped collisions, classical dynamical model with shape deformation 80−27658
Bi(Xe,X), strongly damped collisions, classical dynamical model with shape deformation 80−27658
^{209}Bi+^{136}Xe, deep inelastic collisions, deformation role, cross sections 79−36270
^{75}Br, first 9/2^{+} state and prolate deform. from ^{75}As(α,4nγ) 78−50088
^{12}C, β-transitions, weak magnetism, nuclear struct., matrix elements 79−13253
^{12}C, monopole excitations, transition densities from simple collective model 79−40834
^{12}C, pot. and charge deform. of rot. states 77−46106
^{12}C spin-orbit force and deformation, self-consistent HF calc. 79−455
^{12}C+^{28}Si, 17 to 37 MeV, inelastic and elastic backward angle scatt., surface resonances 78−37367
^{12}C+^{6}Li(^{7}Li), 9 MeV, isotopic shape effects in elastic scatt. of aligned ions 78−89904
(^{12}C+α) system, effect of nuclear deform. on folded pot. 79−6453
^{12}C(^{16}O, ^{16}O), 35 to 50 MeV, backscatt., dynamic deformation and excitation functions, optical anal. 80−18227
^{12}C(α,α′), 38-50.5 MeV, sign of nuclear deform. from Blair phase shift 77−61439
^{13}C+^{6}Li(^{7}Li), 9 MeV, isotopic shape effects in elastic scatt. of aligned ions 78−89904
^{40}Ca, excitation of low lying collective states by (n,n′) scatt. 78−17205
^{40}Ca, magic nuclei at collective excitations, energy spectrum and shape *(Russian)* 80−106015
^{40}Ca(α,α), 20-50 MeV anomalous elast. and inelast. scatt. optical model anal. 77−88161
^{42}Ca high spin state density, γ-decay mode, deformed states from ^{39}K(α,pγ) 80−32168
^{48}Ca, nuclear incompressibility, Hartree-Fock calc. *(Russian)* 79−49577
^{208}Ca, nuclear incompressibility, Hartree-Fock calc. *(Russian)* 79−49577
Cd, even-mass, shape coexistence, quasi-rot. band 78−496
^{A}Cd, A=105,107,109,111, odd neutron deficient, rotor+particle model anal. 79−36127
^{114}Cd(p,p′), optical pot. deform. effect on analysing power and p-γ ang. correlations 79−17903
Ce, A=138,140, levels from (p,p′), (p,t) reactions, spin, parity, deform. parameters, enhancement factors 77−54217
^{140}Ce, hexadecapole motion obs. from α-scatt., EM transitions and conversion electron spectra 78−25097
^{252}Cf, empirical limitations for spontaneous fission energy dissipation, fragment deformation 79−3188
Cm, deformation energy surface, two-centre shell model calc. 77−71559
^{244}Cm, nucl. shape of first saddle point 77−74756
^{56}Co, populated in ^{54}Fe(α,pn), transition rates of high spin states 77−6301
^{59}Co, deformation effect from fast neutron transmission in 0.8 to 20 MeV range 80−57675
^{59}Co, deformation effect of aligned target, fast-neutron transmission 80−47364
^{51}Cr, EM properties, lifetimes of 749 and 777 keV levels, E2/M1 mixing ratio 80−63127
^{52}Cr(γ,γ^{1}), 35 MeV, 2^{+} state deexcitation γ-rays, differential cross sections, deformation *(Russian)* 80−13406
^{53}Cr, possible deformed 7/2^{-} states with ΔJ=1 band 79−45170
Cs, deformed nuclei, low-lying positive parity states 77−6240
Cs isotopes, strongly deformed shapes from mag. mom. and spin meas. 78−70444
^{A}Cs, A=117-124, 126, 138, 140-147, direct meas. of masses, deformation onset at N=60 79−54383
^{A}Cs, A=142, 144, 146, low lying levels, J^{π}, mixing ratios and γ-γ ang. correlations 80−102119
^{40}Cu, nuclear incompressibility, Hartree-Fock calc. *(Russian)* 79−49577
Dy deformed nuclei, particle ang. momentum alignment effects 80−68522
Dy, deformed nuclei, quasicontinuum γ-spectrum, M1, E1, E2 components 80−498
^{A}Dy, (A=151,152), high spin yrast states, γ-ray polarisation in (^{32}S,sn) reactions 80−497
^{152}Dy high spin isomers, yrast traps, oblate shape at high ang. momenta 79−97646
nuclear shape continued
^{152}Dy, yrast isomers, oblate shape, excitation energies, spin and parity 79−17795
^{152}Dy, yrast states of isomers at high angular momenta, particle-hole struct. 79−36124
^{152}Dy, yrast traps, and very high spin states, populated in (^{32}S,4nγ) 78−89778
^{152}Dy yrast traps, isomers and oblate deformations from ^{124}Te(^{32}S, 4n) 80−13362
^{153}Dy, populated in ^{153}Ho β-decay, lower excited states 80−22765
^{155}Dy, weakly deformed, isomeric 9^{+}/$_{2}$ and lowest 7^{-}/$_{2}$ states decay 79−89231
^{158}Dy collective excitations as populated in ^{158}He^{g,m} decay 78−82270
^{165}Dy, collective contributions to E1, ΔK=1 matrix elements in odd-odd deformed nuclei 79−17857
Dy(α,α′), A=156,8, E=12-13 MeV, E2, E4 transition matrix elements determ. 78−33202
Er, deformed nuclei, particle ang. momentum alignment effects 80−68522
^{A}Er (A=156,157,158), high spin yrast states, γ-ray polarisation in (^{32}S,xn) reactions 80−497
^{A}Er, A=158,160,162, high spin states and deformation, number conservation effects 79−89225
^{156}Er, nonaxial deformability of rotating nuclei in two-phase model *(Russian)* 78−46002
^{158}Er, number conservation, effect on energy spectra, deform. and B(E2) values 79−36122
^{160}Er, number conservation, effect on energy spectra, deform. and B(E2) values 79−36122
^{160}Er, produced in ^{124}Sn+^{40}Ar, γ-ray multiplicity spectra, nuclear shape at high angular momentum 78−37260
^{164}Er deformed nucleus, excited rot. bands, selfconsistent HFB treatment 80−42515
^{166}Er, non axial deformability of rotating nuclei in two-phase model *(Russian)* 78−46002
^{166}Er, Skyrme-HF calcs., deformation, electric moments, spin-orbit potentials 78−62480
^{166}Er+^{86}Kr, relaxation times in dissipative collisions, fragment deformation, classical model 79−30853
Er(α,α′), A=162, 4, E=12-13 MeV, E2, E4 transition matrix elements determ. 78−33202
^{A}Eu(p,p′), A=151-3, 12 MeV, rot. states, deformation parameters, DWBA and coupled channel anal. 79−9459
^{151}Eu, energy levels and coexistence of three shapes 77−79304
^{151}Eu narrow band and pickup strength, shape coexistence from (d,t) 80−86799
^{152}Eu doubly odd nucleus, transition probabilities and deformations, obs. in (n,γ) 79−97680
^{152}Eu, transitional nucleus, ground state rotational struct. stability 78−93929
^{153}Eu 5/2^{+} ground state rot. band, J^{π}, shape coexistence from (d,p) 80−86799
^{154}Eu(p,p′), 12 MeV, ground band rot. states, deformation parameters, coupled channels anal. 80−9195
^{19}F low lying positive parity states from rot. model, moments and deformation 79−6410
^{20}F, β-transitions, weak magnetism, nuclear struct., matrix elements 79−13253
^{54}Fe, surface structure analysis using Blair phase shifts 78−12959
^{54}Fe(p,p), 5.5-6.2 MeV, resonance effects, deformation, spectroscopic factors, statistical, optical and DWBA anal. 79−6593
^{55}Fe, possible deformed 7/2^{-} states with ΔJ=1 band 79−45170
^{56}Fe, populated in ^{54}Fe(α,pp), transition rates of high spin states 77−6301
^{56}Fe, surface structure analysis using Blair phase shifts 78−12959
^{56}Fe yrast band, coexistence of prolate and oblate shapes 78−12947
^{56}Fe(^{3}He,^{3}He), 33-83 MeV, details of nuclear surface 77−34324
^{56}Fe(p,p), 6 MeV, elastic and inelastic, quadrupole deformation, IAR excitation, optical pots. *(Russian)* 80−63149
^{58}Fe, surface structure analysis using Blair phase shifts 78−12959
^{252}Fm, pot. energy surface, liquid model, deformation energy formulae *(Chinese)* 80−102106
^{A}Ga, A=69, 71, spectroscopic factors, occupation number anomalies from Ge(d,He) 26 MeV 78−82279
^{A}Ga, A=71,73, levels, ang. distribs., spin assignments and deformation transition from Ga(t,p) 79−54392
^{A}Ga, A=73, 75, deduced levels, occupation number anomalies, spectroscopic factors from Ge(d,^{3}He) 26 MeV 78−82279
^{66}Ga deformation parameter determ. from beta decay Fermi matrix element 79−75923
Gd even nuclei, A=152-160, dynamic deform. theory, level energies B(E2) values 78−89795
Gd, isotope shifts and deform. obs. 77−65433
^{147}Gd^{m} high spin yrast trap, oblate deformation and quadrupole moment 80−32157
^{150}Gd, high spin states, pairing correlations and nuclear shape, HFB approach 80−42517
^{151}Gd shape coexistence, dynamic calculation 79−45151
^{153}Gd, weakly deformed, isomeric 9^{+}/$_{2}$ and lowest 7^{-}/$_{2}$ states decay 79−89231
^{154}Gd multiphonon vibr. bands, dynamic deformation theory 80−5035
^{154}Gd(α,α′), 11.8 MeV, charge deform. parameter determ. 78−33201
^{160}Gd(^{40}Ar, ^{40}Ar), deformed nuclei surface struct. by radial and ang. localisation 79−85362
Ge, A=70, 72 and 74, dynamic deformation theory, energy levels 78−58235
Ge isotopes, shape transition and quadrupole softness, Hartree Bogoliubov calc. 80−68527
^{A}Ge, A=68,70,72, discovery of multiple collective band struct. *(Chinese)* 79−80865
^{A}Ge A=68,70,72,74, deformations and collective spectra, reaction mechanisms from Ge(p,t) 79−22168
^{A}Ge, A=72,74,76,78, ang. distribs., levels and spin assignments, deformation transition from Ge(t,p) 79−54390
^{A}Ge(d,d) 16 MeV, A=70-74, polarised d, elastic and inelastic, levels and deformation 79−554
^{74}Ge, energy levels, shape transition from 15 MeV ^{72}Ge(t,p) study 78−93945
^{76}Ge levels, J^{π} assignments, shape transition DWBA anal. from ^{74}Ge(t,p) 79−17815

nuclear shape continued
^{73}Ge level struct., proposed nuclear shape transition, DWBA anal. from ^{77}Ge(t,p), 15 MeV 78−78266
^{2}H deformation effects in nuclear interaction, DWBA anal. *(Japanese)* 78−21575
^{2}H scattering, deformed tensor interactions, folding model 80−57783
^{4}He, monopole excitations, transition densities from simple collective model 79−40834
^{6}He, density distribution function of nucleons 80−22650
Hf-Ir, isotopes, deformation, level assignments, static moments, modified oscill. model 77−22872
^{180}Hf, nonrotational interpretation of E_4 matrix element 78−33111
Hg, 188, 186, 184, shape staggering laser spectroscopy isotope shifts 77−74755
Hg even isotopes, nonaxial deforms., odd parity states, semidecoupled model 77−34220
Hg, even-A, possible triaxial shape and phase transition, triaxial rotor model 79−93503
Hg isotopes, nuclear ground state props. via atomic spectra 77−22874
Hg, isotopes near A=186, competition of nucl. shape 78−17094
Hg, neutron deficient isotopes, nuclear shape staggering, laser spectroscopy detection 78−54680
^Hg, A=184, 186, 188, shape coexistence and energy level schemes 79−97652
^Hg, A=190-200, even, phase transition and possible triaxial shape, energy levels 80−63098
^Hg, A=198,200,202,204, reorientation effect, Coulomb excitation, oblate shapes 79−71790
^Hg, A=198-204, reorientation effect meas. on 2^+ states 78−37282
^Hg, A=200,202,204, oblate shape determ. 79−17792
^{185}Hg, nuclear shape isomerism detected by laser spectroscopy 79−49576
^{186}Hg from ^{186}Tl decay, γ, conversion electron spectra and coincidences, shape coexistence 78−25156
^{188}Hg, coexistence of spherical and deformed bands 77−6587
^{188}Hg, HF calc., shape and lowest band struct., B(E2) values 80−32148
^{194}Hg, level density calc., shell and pairing effects, deformation, excitation energy dependence 79−67662
^{197}Hg, non-axial deform. anal., $i_{13/2}$ neutron coupling to triaxial rotor and to anharmonic vibrator 77−22847
^{198}Hg, static quadrupole moment of 1st excited state 78−17095
Ho, A=161,163,165, E1 transitions, hexadecapole deforms., Nilsson model calc. 77−82861
^{165}Ho(π,π), aligned deformed nuclei, cross sections and diffractive minima from eikonal approx. 80−22860
I odd-A nuclei, deformed $9/2^+$ proton-hole states, Nilsson calc. 77−74746
^{123}I, bands and decay props., core-particle coupling and polarisation effects 80−13354
In populated in ^{111,113}Cd(p,nγ), energy levels, spins, lifetimes, shape 77−320
Ir, A=187, 189, triaxial rotor model and γ-vibr. model comparison, γ decay, level schemes 78−54695
Ir, A=191, 193, shape of stable transition nuclei, photoabsorpt. cross-sections *(Russian)* 77−79307
Ir, odd isotones, deformation pot. energy from Nilsson model 80−57676
Ir, odd isotopes, pot. energy surfaces and quadrupole deformation parameters, deformed basis model 79−80867
Ir odd mass isotopes, odd proton effects on potl. energy surfaces 77−22877
Ir odd mass isotopes, particle rotor descriptions 77−22914
^Ir, A=191,193 photoneutron yield curves, nuclear shape and giant dipole resonances, 8-21 MeV *(Russian)* 79−13268
^{185}Ir level scheme determ. from ^{185}Pt decay 77−22843
^{185}Ir levels excited in (α,xn) reactions rel. to shape of Ir nucleus 80−9231
^{187}Ir, diagonalisation of collective quadrupole Hamiltonian 77−6221
Ir(p,t)^{189,191}I, 18 MeV, ground state rot. band, 7/2 gamma vibr. levels 78−74360
Kr isotopes, changes in nuclear charge radii 79−93504
^Kr, A=74,76,78,80, discovery of multiple collective band struct. *(Chinese)* 79−80865
^{84}Kr+^{209}Bi, 712 MeV, deform. and transfer in strongly damped collisions 78−21601
La odd-A isotopes, rot. aligned coupling, ang. momentum projection 77−2921
^{6}Li ground state, double well-cluster shell model, d-cluster contraction and deform. *(Chinese)* 78−78290
^{6}Li(p,p'), 185 MeV, optical model anal. of inelastic scatt. to 1st excited state, deformation parameters 79−22300
^{7}Li, model for coupling two cluster structs., influence on shape and states 78−78288
^{7}Li(spherical) and ^{7}Li (strongly deformed), comparison of elastic scatt. from ^{58}Ni 79−6680
MO, onset of deformation at A∼100 80−73790
Mg isotopes, deformation parameters for ground state rot. band 77−316
^{24}Mg ($\alpha,\alpha'\gamma$) 104 MeV, nuclear deformation from ang. correlations, coupled channel anal. 78−78301
^{24}Mg, low lying rot. bands from extended deformation model, parity violating deformations 79−6360
^{24}Mg, low spin rotational states, energy props., extended deformation model 80−86785
^{24}Mg, monopole excitations, transition densities from simple collective model 79−40834
^{24}Mg, pot. and charge deform. of rot. states 77−46106
^{24}Mg, triaxial nuclei rots., extended cranked shape consistent oscillator model 80−102133
^{24}Mg+^{12}C(^{16,18}O) scatt., ^{24}Mg pot. quadrupole deform. length determ. 78−12963
^{24}Mg+d, 10 MeV vector polarised deuterons scatt., nuclear shape effects, optical pot., analysing power 78−54768
^{24}Mg($\alpha,\alpha_1\gamma$), 104 MeV, alpha-gamma ang. correl., quadrupole deform. 77−88155
^{24}Mg(α,α'), 38-50.5 MeV, sign of nuclear deform. from Blair phase shift 77−61439
^{24}Mg(p,p'), 0.8 GeV, rot., γ and β bands, ground state deformation, DWBA, coupled channels anal. 80−9198
^{24}Mg(p,p), 40 MeV, natural parity transitions 78−66277
^{26}Mg ($\alpha,\alpha'\gamma$) 104 MeV, nuclear deformation from ang. correlations, coupled channel anal. 78−78301
^{26}Mg (α,α), 104 MeV, oblate-prolate effects in struct. and reactions 80−9225

nuclear shape continued
^{26}Mg(^{12}C,^{12}C'), 41.3 MeV, ang. distrib. meas. to nucl. shape calcs. 77−65231
Mo even isotopes, HFB calc. of deform. due to isoscalar n-p interaction 78−74302
Mo neutron rich isotopes, excited 0 states 77−22937
^Mo, A=98,102, anal. powers, transitions, shape coexistence states, DWBA anal. of Mo(t,p), pol.t 80−86895
^Mo, A=98-110, deformation and shape transition, HFB calcs. 79−93502
^Mo(d,d), A=92-100, 21.5 MeV, elastic and inelastic cross sections, coupled channel anal., deformation 79−553
^{92}Mo(n,n), elastic and inelastic, 11 MeV, isospin effects, optical and deformation parameters 79−17794
Mo(d,d), A=92, 94, 96, 98, 100, elastic, inelastic scatt., coupled channel, optical model anal., deformation parameters 78−94017
^{12}N, β-transitions, weak magnetism, nuclear struct., matrix elements 79−13253
Na, A=21, 23, M1, E2, transition probabilities between differently deformed states, Nilsson model 77−61376
^Na, A=22, 24, β-transitions, weak magnetism, nuclear struct., matrix elements 79−13253
^Na, A=26-30, nuclear spin from NMR meas. nuclear deformation 79−10072
Nd isotopes, prolate-oblate transition from ^{128}Te(^{16}O,5nγ) 78−70438
Nd+^{12}C, 70.4 MeV, excitation of 3^- states in ^{148,150}Nd deformed nuclei 78−62559
^Nd, A=138,139, high spin states, J^π, γ-cascades and shape transition from ^{140}Ce(α, xn) 80−102090
^Nd(n,n) A=142,144,146,148,150, 7 MeV, optical pot. and deformation, cross sections 79−89230
^{142}Nd, nuclear and Coulomb deform. parameters from DWBA anal. of ^{13}C scatt. 77−3032
^{146}Nd, 7 MeV neutron elastic and inelatic scatt., diff. cross sections, deform. effects 77−26768
^{149}Nd, weakly deformed, isomeric $^{9+}/_2$ and lowest $^{7-}/_2$ states decay 79−89231
Nd(n,n) elastic and inelastic scatt. on even-A isotopes, 4.08 MeV, deformation effects 77−26715
^{20}Ne, deformed nuclei, giant multipole resonances, and transitions, microscopic theory from ^{19}F(p,γ) 79−513
^{20}Ne, deformed nucleus, quadrupole moment, HF calc. exponential convergence and acceleration 79−85367
^{20}Ne, effective nucleus eccentricity depend. on total momentum *(Russian)* 79−3078
^{20}Ne hexadecapole moments, quadrupole deformation effects, E4 effective charge, valence polarisation 80−78142
^{20}Ne, one-body density matrix determ. by iterative steepest descent approach 78−17125
^{20}Ne, pot. and charge deform. of rot. states 77−46106
^{20}Ne, quadrupole and hexadecapole deformation parameters from ^{208}Pb(^{20}Ne,^{20}Ne') 131 MeV 78−66204
^Ni(^{40}Ca, fusion), A=58, 60, 62, 113-170 MeV, fusion cross sections and excitation functions 80−32315
^{56}Ni from HI reactions, superdeformed nucleus decay, α-decay amplification 80−68608
^{58}Ni (^{7}Li, ^{7}Li), 14.22 MeV, alignment axis orientation depend. of cross section, mass quadrupole moment alignment 80−68638
^{58}Ni+^{23}Na, deformed aligned projectile ions, elastic scatt., fusion, polarisation effects 78−58303
^{58}Ni+^{6}Li(^{7}Li), 12.7 MeV, isotopic shape effects in elastic scatt. of aligned ions 78−89904
^{58}Ni(^{6}Li,^{6}Li^{2}), 71 MeV, excited states deformation lengths, DWBA and coupled channels anals. 80−68541
^{58}Ni(p,p), 800 MeV, elastic and inelastic, cross section, deformation lengths, optical and DWBA anals. 80−68664
^{60}Ni, hexadecapole motion obs. from α-scatt., EM transitions and conversion electron spectra 78−25097
^{16}O, magic nuclei at collective excitations, energy spectrum and shape *(Russian)* 80−106015
^{16}O, nuclear incompressibility, Hartree-Fock calc. *(Russian)* 79−49577
^{16}O, tetrahedral rotor behaviour, charge form factors, deformed α clusters 79−45141
^{16}O+^{12}C, fine struct. in fusion cross section 78−89928
^{16}O+^{28}Si, 17 to 37 MeV, inelastic and elastic backward angle scatt., surface resonances 78−37367
^{16}O(^{12}C,X), sub-barrier energies, fusion cross section, static and dynamic deformation effects 80−42729
^{16}O(α,α) 17 to 27 MeV, backscatt., dynamic deformation and excitation functions, optical anal. 80−18227
^{18}O 1.982 MeV state, static electric quadrupole moment determ. 77−74763
^{18}O, neutron deform. param. determ. from (π,π') scatt. 78−29502
^{18}O+$\pi^\mp$, inelastic and elastic scatt., neutron-proton radius differences and isovector deform. 79−40963
^Os, A=182, 184, 186, high spin yrast states, back-bending 80−86802
^Os(α,α') A=188,190,192, 4_3^+ level population, hexadecapole vibrs. 78−89780
^{189}Os, evidence for triaxiality 77−14035
^{192}Os(^{12}C,^{14}C)^{190}Os, 70 MeV, shape transition effect on quadrupole transfer strength 78−644
^{192}Os(p,p') and (d,d'), γ-ray spectra, energy level scheme, triaxial shape model 77−34243
^{31}P, analogue-antianalogue M1 transitions, nucl. shape change influence 78−13006
Pb, A=204,6, quadrupole moments of first excited state meas. 78−21491
^{205}Pb(d,d'), 14, 17 MeV, direct population of collective states, multiplets, deform. parameters 78−74376
^{208}Pb, neutron and nuclear matter space distribs. from (p,p) 1 GeV scatt. *(Russian)* 78−502
^{208}Pb, damping of single particle states and giant resonances 79−17782
^{208}Pb, excitation of low lying collective states by (n,n') scatt. 78−17205
^{208}Pb, isoscalar electric giant dipole resonance, from RPA calc., nuclear compressibility 78−86520
^{208}Pb+^{208}Pb, 1600 MeV, axially symmetric TDHF 78−74398
^{208}Pb(^{16}O,X), 80-313 MeV, optical model anal., dynamic shape or density changes 80−18186
Pd, even-mass isotopes, collective model with deform., vibr., rot. energy levels, B(E2) ratios 78−17120

nuclear shape continued
^{A}Pd(p,X), 6 MeV, A=102,104,106,108,110, quadrupole deformation, cross sections, direct processes, optical parameters *(Russian)* 79−67753
^{A}Pm, A=149,151, shape coexistence, deformed states from Nd decay 80−78135
^{141}Pm medium spin states, J^{π}, transitions and shape from (p,2n), (^{3}He,3n), (α,4n) 80−86779
Po high spin isomers, deformed independent particle model, yrast lines, shape 79−480
^{210}Po, excited, deformed, fission or neutron emission, shell-correction approach to nuclear densities 77−30483
^{210}Po, level density calc., shell and pairing effects, deformation, excitation energy dependence 79−67662
^{212}Po, fission excitation functions anal., shell effects at saddle point, nuclear shape 78−54737
^{139}Pr medium spin states, J^{π}, transitions and shape from (p,2n), (^{3}He,3n), (α,4n) 80−86779
Pt, A=194, 195, 196, 198, shape of stable transition nuclei, photoabsorpt. cross-sections *(Russian)* 77−79307
Pt even isotopes, nonaxial deforms., odd parity states, semidecoupled model 77−34220
Pt, isotopes near A=186, competition of nucl. shape 78−17094
Pt, prolate-oblate transition 78−62540
Pt+^{136}Xe, A=192, 194, 196, Coulomb excitation, γ softness from E2 transition strengths 77−82951
^{A}Pt, A=186,188,190, subnanosecond high spin isomers, decay chains and lifetimes from Yb(^{16,18}O, xn) 79−45140
^{A}Pt, A=192, 194, β_4 deformations, anomalous interference terms, rigid asymmetric rotor model 79−75832
^{A}Pt, A=194-8 photoneutron yield curves, nuclear shape and giant dipole resonances, 8-21 MeV *(Russian)* 79−13268
^{187}Pt→^{185}Pt, oblate to prolate transition meas. 77−22878
^{190}Pt(p,t)^{185}Pt reaction, 25 MeV ^{188}Pt states population 78−86532
^{191}Pt, non-axial deform. anal., $i_{13/2}$ neutron coupling to triaxial rotor and to anharmonic vibrator 77−22847
^{192}Pt(α,α'), 24 MeV, coupled channels anal. of ground state band, negative β_4 deformation 78−70550
^{193}Pt low lying negative parity states and shape from ^{195}Pt(p,t) 80−68540
^{194}Pt, determ. of sign of $P_3=M(0_1^+2_1^+)M(2_1^+2_2^+)M(2_2^+0_1^+)$ 79−63588
^{196}Pt, O(6) symmetry of interacting boson approx. model in shape transition 80−27550
Pu, deformation energy surface, two-centre shell model calc. 77−71559
^{239}Pu, 8-μs fission isomer, quadrupole moment 77−30484
^{239}Pu, deformation effects on neutron total cross-sections, adiabatic coupled-channel calc. 79−17896
^{239}Pu, spectroscopy in second minimum of pot. energy surface 79−30805
^{239}Pu(n,f), thermal n, fission fragment energy correlation meas., fine struct. and deformation 79−13355
^{240}Pu, hexadecapole shape isomeric state, shell correction method fission barrier calcs. 80−545
^{240}Pu, level density calc., shell and pairing effects, deformation, excitation energy dependence 79−67662
^{240}Pu, nucl. shape at first saddle point 77−74756
^{240}Pu^{m}, shape isomer, half-life and excitation function meas. *(Chinese)* 78−78253
^{A}Rb, A=77, 78, 78m, 79, 84m, nuclear spins and mag. moments, deformed shapes 79−17793
Re, A=187, 189, 191, obs. of proton hole states via (t,α) 77−88025
Re, odd isotones, deformation pot. energy from Nilsson model 80−57676
Re, odd isotopes, pot. energy surfaces and quadrupole deformation parameters, deformed basis model 79−80867
Re odd mass isotopes, odd proton effects on potl. energy surfaces 77−22877
Rn high spin isomers, deformed independent particle model, yrast lines, shape 79−480
Ru, even isotopes, potential energy surfaces and ground state equilib. deformation 80−73789
^{A}Ru, A=106, 108, levels, transitions, J^{π} and shape from Tc decay 80−57744
^{102}Ru levels populated in ^{102}Tc^{g} β^--decay 78−86513
^{32}S, 18.3 MeV vector polarised deuteron scatt. from deformed nuclei 79−6629
^{32}S deformed states, comparison of cluster and shell model wave functions 79−22187
^{32}S shape isomeric state from unconstrained variation 80−95306
^{32}S+d, 10 MeV vector polarised deuterons scatt., nuclear shape effects, optical pot., analysing power 78−54768
Se, A=76, 78, 80, 82, static quadrupole moments of first 2^+ excited states 77−65197
^{A}Se, A=70,72,74, discovery of multiple collective band struct. *(Chinese)* 79−80865
^{A}Se(p,p), A=76-82, doubly even nuclei, deformation parameters 79−97705
^{74}Se(^{16}O,^{16}O′), 33, 34 MeV, first excited state, static quadrupole moment, deformation evidence 79−17802
^{74}Se(α,α'), 7.3 MeV, first excited state, static quadrupole moment, deformation evidence 79−17802
Si, A=28, 29, 30, charge distrib. in ground, excited states via (e,e′) 18.5-117.1 MeV 77−54142
^{A}Si(^{10,11}B,^{10,11}B), 33.7, 41.6, 50 MeV, A=28,30, ang. distribs., cross sections and deformation parameters, absorption effects 79−67773
^{A}Si(p,p′), A=28,29,30, 51.9 MeV, blocking effect and core-excitation, deformation parameter 78−82336
^{27}Si, shape mixing using ang. momentum projection from Hartree-Fock intrinsic states 78−86472
^{28}Si, 2^+ 1.78 MeV state, reduced matrix element and deformation length from (^{16}O,^{16}O) 79−13317
^{28}Si ($\alpha,\alpha'\gamma$) 104 MeV, nuclear deformation from ang. correlations, coupled channel anal. 78−78301
^{28}Si (p,p'), 14-40 MeV, low lying states, optical and statistical model anals., giant resonances 79−40894
^{28}Si, appl. of theory of bi-determinantal intrinsic states 79−9484
^{28}Si, deformed nucleus, quadrupole moment, HF calc. exponential convergence and acceleration 79−85367
^{28}Si, pot. and charge deform. of rot. states 77−46106
^{28}Si, prolate and oblate intrinsic states *(French)* 78−70482
^{28}Si+^{12}C(^{16,18}O) scatt., ^{28}Si pot. quadrupole deform. length determ. 78−12963
nuclear shape continued
^{28}Si+^{20}Ne, 120 MeV, numerical anal. based on linear response theory 79−36273
^{28}Si+^{20}Ne, frictional coeffs. using linear response theory 79−13327
^{28}Si+d, 10 MeV vector polarised deuterons scatt., nuclear shape effects, optical pot., analysing power 78−54768
^{28}Si(^{12}C,^{12}C′), 41.4 MeV, ang. distrib. meas. reorientation effects 77−65231
^{28}Si($\alpha,\alpha'\gamma$), 104 MeV, ang. correl. meas., sensitivity to quadrupole deform. 78−54774
^{28}Si(p,p') 3.1-3.8 MeV, interference effects, β_2 and optical parameters 77−26685
Sm isotopes, deform. effects in neutron scatt. 77−74758
Sm isotopes, shape transition, s-d IBA model Hamiltonian struct. 80−32173
Sm+O^{16} fusion, cross sections for spherical and deformed Sm isotopes, shape effects 78−78407
^{A}Sm, A=150, 152, 154, 7 MeV neutron elastic and inelastic scatt., diff. cross sections, deformation effects 77−26768
^{A}Sm(^{16}O,X), 60-75 MeV, A=148, 150, 152, 154 deformation effects on fusion 80−18360
^{A}Sm(^{3}He, ^{3}He′), A=144, 148, 152, 154, 150, 40.9 MeV, transition cross sections, deformation parameters, coupled channels anal. 79−67640
^{A}Sm(^{40}Ar,X) A=144, 148, 154, 3.6-4.5 MeV/A, sub-barrier fusion, evaporation residue cross section, deformation 80−68718
^{A}Sm(N,N′) A=152,154, deformed nuclei struct., rot. model with optical pot., coupled channel formalism 79−3146
^{144}Sm, produced in ^{100}Mo+^{48}Ca 78−37260
^{147}Sm, deformed $1h_{11/2}$ neutron hole states 78−86466
^{148}Sm, 7 MeV neutron elastic and inelastic scatt., diff. cross sections, deform. effects 77−26768
^{150}Sm deformation, collective spectra and moments of inertia starting from nuclear force 79−17790
^{151}Sm, gamma spectra, energy levels *(Dutch)* 80−47430
^{152}Sm (n,n), 2.4-7.2 MeV, inelastic and elastic optical model and deformation parameter depend. *(Russian)* 80−13481
^{152}Sm, ground-state rot. band via electron scatt., charge distrib. 77−30475
^{154}Sm, Skyrme-HF calcs., deformation, electric moments, spin-orbit potentials 78−62480
^{154}Sm(p,p′), 35 MeV, extraction of deform. parameters 78−54755
Sm(n,n) elastic and inelastic scatt. on even-A isotopes, 4.08 MeV, deformation effects 77−26715
Sm(n,n′), 7 MeV, A=148,150,152,154, differential cross sections, coupled channel anal., deform. effects 77−54219
Sn, deform. of ground and excited states 78−82277
^{A}Sn(n,n′), A=116, 118, 120, 122, 124, 11 MeV, levels, deformation parameters, isospin effects, optical parameters 80−57679
^{A}Sn(n,n′), A=116, 118, 120, 122, 11 MeV, octupole vibr. states, diff. cross section, deformation length, DWBA anal. 80−102092
^{A}Sn(n,n), A=116,118,120,122,124, isovector deformation parameters and core polarization 79−67642
Sr, even isotopes, potential energy surfaces and ground state equilib. deformation 80−73789
^{79}Sr, mass excess values from beta and gamma spectra from ^{32}S+^{54}Fe(^{58}Ni) 80−63137
^{87}Sr(p,p′), 20.5 MeV, level scheme, ang. distribs., transitions and deformation parameter 79−22195
^{88}Sr(n,n′), 11 MeV, octupole vibr. states, diff. cross section, deformation length, DWBA anal. 80−102092
^{88}Sr(n,n), elastic and inelastic, 11 MeV, isospin effects, optical and deformation parameters 79−17794
^{98}Sr, onset of deform. anal. from ^{98}Rb decay 78−12961
^{98}Sr very low lying 0^+ state, shape coexistence bands, $T_{1/2}$, transitions from ^{98}Rb decay 80−78148
^{100}Sr ground state rot. band transitions, deformations and lifetimes from ^{100}Rb β-decay 79−93550
^{181}Ta, deformed nuclei, electron scatt., elastic differential cross section calc. 77−82912
^{A}Tb, A=149, 151, 153, 155, 157, prop. anal. on function of nuclear shape 79−75828
^{149}Tb from HI reactions, superdeformed nucleus decay, α-decay amplification 80−68608
^{153}Tb, prod. in ^{153}Dy decay, weak deform. 77−41884
Te(^{3}He,^{3}He) A=122-128, 8-18 MeV, optical model and deform. parameters 77−34221
^{A}Te, A=117,119,121, $\Delta J=1$ band structures on ns isomeric states 79−54382
^{118}Te, produced in ^{82}Se+^{40}Ar, γ-ray multiplicity spectra, nuclear shape at high angular momentum 78−37260
Te(α,α) A=122-128, 8-18 MeV, optical model and deform. parameters 77−34221
^{231}Th, asymmetrically deformed, rot. bands from ^{230}Th (n,γ) 79−3068
^{232}Th, deformation effects on neutron total cross-sections, adiabatic coupled-channel calc. 79−17896
^{232}Th+^{40}Ar, 390 MeV, Z≤38 products energy spectra, reaction mechanism, dynamic deformation *(Russian)* 78−89909
^{232}Th(γ,X) 5-18.3 MeV, photoneutron and photofission cross sections, giant resonance and deformations 80−68712
^{232}Th(γ,f), deep subthreshold photofission, double humped fission barrier anal., shape isomer 80−5179
^{232}Th(p,p′), 35 MeV, extraction of deform. parameters 78−54755
^{233}Th(N,N′), deformed nuclei struct., rot. model with optical pot., coupled channel formalism 79−3146
Ti even isotopes, deformed nuclei in Lipkin-Nogami approach, Kuo Brown effective interaction 79−59006
Tl, odd isotones, deformation pot. energy from Nilsson model 80−57676
Tl, odd isotopes, pot. energy surfaces and quadrupole deformation parameters, deformed basis model 79−80867
Tl odd mass isotopes, odd proton effects on potl. energy surfaces 77−22877
Tl odd mass isotopes, particle rotor descriptions 77−22914
^{197}Tl, diagonalisation of collective quadrupole Hamiltonian 77−6221
Tm, A=163-171, E1 transitions, hexadecapole deforms., Nilsson model calc. 77−82861
U, deformation energy surface, two-centre shell model calc. 77−71559
U spontaneously fissionable isomers, excitation by K shell e^+ annihilation, shape isomery model *(Russian)* 79−30802
^{A}U, A=232, 234, 236, octupole-octupole residual interactions and low lying 0^+ excited states 79−36136

nuclear shape continued
^{A}U, A=233, 235, 238, deformation effects on neutron total cross-sections, adiabatic coupled-channel calc. 79−17896
^{A}U(α, α′), A=234, 236, 238, coupled channel Born anal. of deformation correl 80−5149
^{A}U(γ,X), A=235, 236, 238, 5-18.3 MeV, photoneutron and photofission cross sections, giant resonance and deformations 80−68712
^{A}U(γ,f), A=235, 236, 238, deep subthreshold photofission, double humped fission barrier anal., shape isomer 80−5179
^{235}U, pot. energy surface, liquid model, deformation energy formulae *(Chinese)* 80−102106
^{235}U(n,f), thermal n, fission fragment energy correlation meas., fine struct. and deformation 79−13355
^{236}U fission isomer produced in ^{238}U(γ,2n) prod. cross sections, half life 78−46045
^{236}U fission shape isomer, γ-decay from ^{238}U(γ,2n) 80−18230
^{236}U nuclear instability and fission in strong mag. field energy level deformation *(Russian)* 79−13360
^{236}U, nuclear matter density distrib., in asymmetric two centre shell model 80−32209
^{236}U shape isomer, γ branch upper limit, γ-yields from ^{235}U(d,p) 80−99145
^{236}U shape isomer, rot. band and const. via ^{235}U(d,p) 12 MeV 77−34208
^{236}U shape isomer populated in ^{235}U(n_{th},γ), isomeric/prompt fission ratio 77−323
^{237}U shape isomer, γ-decay search, branching ratio from ^{238}U(Γ,2nγ′) 45 MeV 78−93961
^{238}U collective and deformation props., general collective model 80−86827
^{238}U deformed even-even nucleus, rot. vibr. band excitation, classical limit S-matrix 79−3067
^{238}U delayed fission cross-section for 14 MeV neutrons, shape isomer excitation 77−26808
^{238}U, muonic, non-axiality effects in quadrupole hyperfine splitting 77−46107
^{238}U shape isomeric γ-decay, in μ^- atoms, isomer lifetime 77−34245
^{238}U(^{136}Xe, ^{136}Xe), multiple Coulomb and nucl. excitation 78−21603
^{238}U(^{238}U, ^{238}U), multiple Coulomb and nucl. excitation 78−21603
^{238}U(N,N′), deformed nuclei struct., rot. model with optical pot., coupled channel formalism 79−3146
^{238}U(e,e′), 87.5 MeV, deformed fissionable nucleus, giant multipole resonances and isovector states 80−42612
^{238}U(p,p′), 22 MeV, rot. band, multipole deformation parameters from coupled channel anal. 80−13369
^{238}U(p,p′), 35 MeV, extraction of deform. parameters 78−54755
^{239}U, population in direct and collective neutron capture by ellipsoidally deformed nucleus 78−94001
^{48}V, odd-parity rotational band structure 77−46102
^{A}W(e,f), A=182,184,186, 35-55 MeV, fission barriers, pairing strength deformation depend., stat. anal. 80−57810
^{180}W, K=2$^-$ octupole alignment, ground-band angular momenta 78−78237
^{184}W(^{12}C, ^{12}C′), 70 MeV, 4$^+$ state excitation ang. distrib., hexadecapole deformation length effects 80−68521
^{185}W, beta spectrum, shape factor meas. 77−2947
Xe-Nd region, microscopic anal. of core deform. 78−74303
^{130}Xe+^{209}Bi, 1130 MeV, deform. and transfer in strongly damped collisions 78−21601
^{A}Y, A=82, 83, mass excess values from beta and gamma spectra from ^{32}S+^{54}Fe(^{58}Ni) 80−63137
^{162}Yb high spin states with Skyrme interaction, cranked Hartree-Fock calcs. 79−13189
^{168}Yb(α,α′), 12-13 MeV, E2, E4 transition matrix elements determ. 78−33202
^{170}Yb negative parity yrast band, rot. aligned n, deformation coupled bandhead from Er(α,xn) 79−93489
^{176}Yb(p,p′), 35 MeV, extraction of deform. parameters 78−54755
Zr, even isotopes, potential energy surfaces and ground state equilib. deformation 80−73789
Zr neutron rich isotopes, excited 0 states 77−22937
Zr, onset of deformation at A∼100 80−73790
^{A}Zr, A=96, 98, 100, deformation and shape transition, unified shell model 79−93502
^{90}Zr (p,p′), 0.8 GeV, low energy giant octupole resonance excitation, deformation length 79−93593
^{90}Zr, neutron and nuclear matter space distribs from (p,p) 1 GeV scatt. *(Russian)* 78−502
^{90}Zr(n,n′), 11 MeV, octupole vibr. states, diff. cross section, deformation length, DWBA anal. 80−102092
^{90}Zr(n,n), elastic and inelastic, 11 MeV, isospin effects, optical and deformation parameters 79−17794
^{96}Zr, shape transition microscopic study using shell model 79−40835
^{98}Zr, shape transition microscopic study using shell model 79−40835

nuclear shell model
0 to 300 MeV, cross sections, shell model calcs 79−93605
$1f_{7/2}$ neutron single particle energy systematics 77−30480
1p shell isotensor charge depend. contrib. to isobaric mass multiplets, shell model anal. 79−67632
3-centre shell model description of light-particle accompanied fission 77−41941
^{61}Ni multiparticle configs., transition probabilities from shell model 78−70496
^{90}Y, 1$^+$ and 0$^+$ states populated in ^{88}Sr(^{3}He,p) 78−25116
β band influence on structure of decoupled bands 78−93921
A=10-15, log ft values, spectroscopic factors calc. 77−61357
A=110-210 nuclei, new parameters of deformed Woods-Saxon pot. 78−93951
A=154, nuclear data sheets, levels, decay props., isomeric states, Nilsson orbitals 79−71781
A=16 to 28, α-structure amplitudes and shell model wavefunctions for nuclear states 79−45192
A=16 to 40, mag. moments, shell model calcs, mesonic exchange current effects, book contrib. 80−479
A=16-40, α-spectroscopic factors between ground states, shell model prediction 79−13204
A=18, shell-model interaction, convergence in reaction matrix G 78−50102
A=18, shell-model spectra, one-boson-exchange potential 80−68550

nuclear shell model continued
A=18 nuclei, negative parity spectra, phonon dynamic interaction propagator approach 78−8739
A=18 nuclei, reaction matrix calc. 77−14085
A=18 shell model spectra and 3 nucleon force 78−25124
A=18 to 22, influence of non-central interactions on 1s-0d nuclei 78−93949
A=18 to 38 nuclei, anal. of nuclear spectroscopic data 79−26381
A=190, Nilsson strength fragmentation, quadrupole and hexadecapole deformations 80−47394
A=24-28 nuclei, reliability of calculated decay props. 78−93970
A=36-39, energy levels and effective interactions from large scale shell model calcs. 79−59011
A=40 to 100, strength and radius parameters of deformed Woods-Saxon potential 79−97673
A=40-56, spectroscopy props. using pure configuration shell model *(Chinese)* 80−42584
A=41-55, charge dependent two body interactions from $1s_{7/2}$ shell displacement energies 79−67668
A=42, multiple scattering formalism for the effective interaction 80−102126
A=50 to 150, shell, dynamical deformation and interacting boson models, limitations 80−68563
A=50-57, N=28-30, effective interactions and energy spectra from shell model calc. 78−82299
A=6 extended shell-model calcs. 77−14017
A=6-14, one π exchange currents effect on partial muon capture rates 79−22239
A=6-14 nuclei, OPE current effect on allowed β-decays in the 1p shell nuclei 79−54413
A=6to 14, radiative pion capture, mag. dipole resonance excitation in 1p shell nuclei 78−74408
A=90 region, N=50, shell model calcs. 80−68564
A≤44, fp-shell nuclei struct., effect of core-excitation and α-clustering correl. 80−9245
A≥210, strength and radius parameters of deformed Woods-Saxon potential 79−97673
a giant resonance theory in the 1p1h+2p2h+continuum approximation 79−67628
actinides, effect of simple consistency condition on multipole moments 78−86475
advances in nuclear physics, clustering and self-consistent field theory, book 79−75879
algebraic approach to dynamic problems 77−18451
alpha-decay, fission method study *(French)* 79−93565
analogue energy splitting in neutronrich nucleus, isoinvariant linearisation 77−65205
analogue resonances, finite Fermi systems, polarisation effects *(Russian)* 78−46041
anaiogue states and resonances in semimicroscopic shell model *(Russian)* 80−86872
angular momentum coupling of fermions in single j-shell, orthonormalization method 78−50100
BCS approximation, application and results 79−89249
beta-decay, shell effects in gross theory 77−38251
book, collective and single-particle models 77−41904
boson model, interacting, shell-model basis, correspondence between fermion and boson states and operators 80−52593
bound state problems, scatt. theory methods, binding energies 79−17823
broken-pair approx., spectra of ^{90}Zr, ^{92}Mo, ^{94}Ru, ^{96}Pb 78−29408
Brueckner shell model for binding energies of sd-shell nuclei with realistic effective Hamiltonian 77−57594
calculation techniques *(French)* 79−45188
central NN potentials, relative motion dependent, jj and LS coupling, universal of hyperspherical functions method 77−61355
centre-of-mass motion for two unequal fragments system, harmonic oscillator shell model 79−49588
classification of states in the unitary scheme for complex nuclei and commutation properties of SU_3-irreducible ε-tensors 79−63598
closed shell nuclei, convergence studies for the one body mass radius operator 79−45146
cluster spectroscopic factors for p-shell nuclear in shell-model 77−30486
collective excited states, pairing degrees of freedom influence, shell model anal. 79−89250
collective motion, independent-particle description 77−14021
collective motion, shell model tests of interacting boson model descript. 78−78280
collective regularity, shell model appl. to microscopic description 78−50069
collective state single unperturbed level, large energy shift due to residual interaction 79−444
collectivity, shell model, SU_6(s,d) boson model, states struct., Ba, Sm appls. 78−54672
compound nucleus, giant resonances, force functions for partial E1-transitions 78−12985
compound nucleus formation cross section in heavy ion reactions, shell model calcs. 78−13132
conference on interacting bosons in nuclear physics, Erice, Italy (June '78) 80−27042
configuration mixing, Coulomb energy anomaly, inmirror nuclei 78−25099
configuration seniority spectral distribs. for mixed configs. of identical nucleons 78−70468
continuum, alternative approach to R-matrix 78−523
continuum, thermodynamical calc. of shell correction in nuclei *(Russian)* 78−29409
continuum calcs., status and prospects 78−54698
continuum effects in thermodynamical calcs. of binding energy shell corrections 77−71555
continuum shell model, 3-particle system, limitations in reaction theory 79−75932
continuum shell model, convergence problems, separation expansion and perturbative continuum treatment 79−17827
continuum shell model, recoil corrections for nucleon-nucleus scattering 78−8751
continuum shell model calcs. of particle emission threshold effects, cross section, line shape of resonances 78−46014
continuum shell model description of resonant structures in nuclear reactions 79−13345
continuum shell-model coupled-channel calcs., appl. to ^{15}N(p,n) 3-7 MeV 77−34269

nuclear shell model continued
core polarisation 77−26598
core-quasiparticle-coupling model for odd-A transitional nuclei, ^{191}Pt appl. 78−54701
correlation subsystems calc. 79−80884
Coulomb displacement energies, charge and mass number depend. in isotope shifts 78−8729
Coulomb energy anomaly and charge-dependent nuclear forces 79−58997
Coulomb excitation of sd shell nuclei, B(E2) values, lifetime meas. 78−25216
cross conjugate nuclei, correl. between g-factors of cross-conjugate pairs of states 79−460
Davidson's algorithm with and without perturbation ocrrections 80−27570
decoupled bands, perturbative anal. level energies 78−41623
deep nuclear levels, practicability of kaon probe 78−25237
deeply inelastic nucleon transfer form factors, shell model calc. 79−89265
deformation, unified microscopic description 77−79305
deformation energy of nuclei, one particle spectrum, self consistent calcs. shell corrections 78−12957
deformation structure in light f-p shell nuclei, $^{41-44}$Ca, ^{43}Sc, ^{44}Ti calcs. 78−66228
deformed independent particle model, high spin isomers in Po, At, Rn 79−480
deformed nuclei, effect on Coriolis interaction, Nilsson model and Woods-Saxon pot. calcs. 80−63071
deformed nuclei, gaps in single-particle level scheme and backbending 78−17072
deformed nuclei, improved parametrisation of Woods-Saxon pot. 80−86823
deformed nuclei, polarisation, and energy shifts in muonic atoms 80−86893
deformed nuclei, semiclassical interpretation of gross-shell struct. 77−82818
deformed nuclei, single particle matrix elements of radiative M2-transitions, Nilsson model 80−22753
degenerate, eqns. of motion method for anharmonic vibrs. 77−61356
degenerate single-particle oscillator shells, particle-vibr. coupling, exact selection rule for l-forbidden M1 transitions 78−78278
delayed neutron emission, β-strength function 77−71595
density matrix expansion in exactly solvable model, local density approx., local Fermi momentum approx. 78−50099
deuteron form factors and spectroscopic factors in heavy spherical nuclei, shell model *(Russian)* 80−63078
distribution of shell model eigenvector components, invariance props. of random matrices ensemble 78−62492
doorway state effect on neutron strength functions, shell model approach for $90<A<142$ *(Russian)* 77−82888
doorway states, energy dependence of inelastic cross-section, shell model, coupled channel anal. 80−73854
double core model for fission 77−30546
double folding pot. for inelastic scatt. between nuclei 80−13425
double well cluster shell model folding potential *(Chinese)* 80−52596
double well-cluster shell model, spurious states of cm motion during fission and heavy ion reactions *(Chinese)* 77−14045
doubly magic nuclei, Skyrme force calc. for nuclear struct. 78−49721
droplet model with shell correction for masses and radii 77−22863
effective Hamiltonian, form throughout sd shell 80−27571
effective interaction through second order for sd shell 77−54161
effective interactions, folded diagram expansion, self consistent and oscillator sd shell model spaces 78−21502
effective interactions in s-d shell, correl. coeffs. 78−4904
effective operators and the truncation of shell model configuration space 79−80885
effective operators in nuclei 78−12990
effective proton-proton interaction for $2p_{1/2}$ and $1g_{9/2}$ orbits 77−57608
effective sd-shell interaction, central and non-central components, appl. to ^{28}Si 77−54160
effective three-body interaction in ^{93}Tc, ^{93}Mo, ^{94}Ru 78−524
effective three-body interactions in $f_{7/2}$ shell 77−2920
effective two-body interaction near doubly closed shells 77−65206
eigenvalue distribution in scalar space for noninteracting and interacting bosons 80−78177
eigenvector component nongaussian distrib., statistical study 80−5077
elastic scattering of protons, ang. distrib., cross section, anomaly rel. to shell struct. of target 78−54752
electron+nucleus scattering, three body correlations, influence on charge form factor of closed shell nuclei 79−6571
empirical $(1f_{7/2})^n$ model, review 79−17826
energy dependent radial functions formalism of continuum shell model, appl. to ^{16}O+p, ^{40}Ca+p 78−25185
energy level densities, shell effects and pairing effects, SCF theory of statistical thermodynamics *(Chinese)* 80−63088
even parity states in ^{19}F, ^{21}Ne, ^{23}Na, generator coord. method, projected Hartree-Fock, and complete diagonalisation calcs. comparison 78−89796
even-even nuclei, 1^- excitations, self consistent shell model description *(Russian)* 80−13407
even-even nuclei in 2p-1f shell, binding energy, quadrupole moment, by HF calc. 79−17843
even-even rare earths, microscopic quadrupole and hexadecapole moments 80−13376
exact canonically conjugate momentum to the quadrupole tensor and a microscopic derivation of the nuclear collective hamiltonian 78−78251
exchange kernels, analytical derivation methods 79−13228
exp(S) formalism, n-body Schrodinger eqn. 77−22918
extended basis shell model, two-nucleon transfer 78−29406
$f_{7/2}$ shell nuclei, odd-A, collective bands of positive parity states 78−54677
$f_{7/2}$ shell nuclei, shell model study in pure $f_{7/2}^n$ config. 79−36162
$f_{7/2}$ shell nuclei, two-body spin-orbit coupling interaction, energy spectra *(Chinese)* 79−93531
$f_{7/2}$ shell single particle state systematics, centroid energies, Saxon-Woods pot. 79−3066
Fano effect in photonuclear reactions? 80−519
fermion system, two-body propagators with dynamic effective interactions, s-channel 77−41897
few body dynamics analytical continuation, nuclear shell model, resonances and bound states *(Russian)* 79−40860
nuclear shell model continued
field theory of collective excitations, soluble model 77−71426
finite depth potentials, shell corrections 78−58241
finite well potentials, shell correction method, appl. to ^{240}Pu nucleus 78−37298
fission barrier calculations, effect of simple consistency condition, drop model with shell corrections 77−67732
fission dynamics effects of shell struct. and pair correl. 79−6560
fission isomer properties investigation using Nilsson pot. 78−29403
fission scission point model based on deformed shell effects 77−10455
fixed J spectral distribs. in large shell model space, scalar centroids and widths 79−49581
fixed-J configuration centroids, exact calc. 79−67683
folded diagram calculation of effective charges, valence nucleon in 1s0d shell 78−4905
folded diagrams and s-d shell effective interactions, excit. spectra and ground state binding 77−79315
form factors, elastic and dynamic, with correction for motion of centre of mass *(Russian)* 78−8753
four nucleon wave functions, Taylor series method 78−66223
fractional parentage coeffs., nucl. shell model, reduced SU(3), computer program 78−50097
frictional effects in nuclear reactions with large scale collective motion, review 78−78336
fusion, power prod. in reactors, and astrophys. appl. *(Norwegian)* 79−30872
generalised Schwinger representation of fermion pairs to anharmonicity 78−89807
geometry, effect on the observed dependences in nucl. pot. 78−4900
giant dipole resonance, role of compound nucleus levels *(Russian)* 78−25164
giant dipole resonance decay, photonucleon emission in shell model 79−45233
giant dipole resonance decoupling and threshold states in schematic and shell models 80−78245
globally self-consistent, magic nuclei and spherical nuclei calculations 79−59020
gross-shell effects in the single-particle level distribution with fixed angular momentum projection *(Russian)* 79−22179
gross-shell structure in deformed oscillator pot., semiclassical anal. *(Russian)* 79−22178
Hamiltonian field theory for systems of nucleons and mesons 79−75860
Hamiltonians, semiclassical approx., spin-independ. pots. 80−32208
harmonic oscillator brackets, derivation of new expression 78−20997
Hartree-Fock self consistency and many body monopole forces 79−67685
Hartree-Fock-Bogolubov eqns., exact soln. 80−27582
heavy even-even nuclei, spectra from shell model and interacting bosons 79−6411
heavy ion collisions, microscopic transport theory, fragment shell struct. effects on mass transfer 78−58301
heavy ion reactions, cluster correlation, review, book contrib. 80−27670
heavy ion reactions, two-particle transfer, overlap functions, DWBA anal. 80−73862
heavy ion scatt., nucleon transfer in dynamical two centre shell model, mol. single particle effects 79−89325
heavy ion transfer reacts., nuclear wave function polarisability 78−54785
heavy nuclei, photoproton reaction, isospin effect 79−80926
heavy nuclei collision, independent particle model, forces between heavy nuclei 78−635
heavy spherical nuclei, choice of density depend. interaction and α-decay *(Russian)* 78−46010
heavy-ion collision, narrow structure obs. in continuum, quasi-bound states, shell model anal. 77−14175
heavy-ion reaction, cluster transfer, shell model investig. 77−14172
heavy-ion reaction, intermediate struct. and nuclear reaction reson. states in continuum shell model 77−54243
high angular momenta nuclei, shell effects on moment of inertia and level density *(Russian)* 79−67635
high-spin nuclear rotations, single particle Nilsson model 78−12943
high-spin states and shell struct. in N=Z nuclei, ^{20}Ne appl. 80−47342
high-spin states in N=28 nuclei 78−29407
highly excited nearly spherical nuclei, ang. momentum effects, backbending, yrast states 79−49566
hole spectral density in finite nuclei 79−63584
hole states, continuum shell model approach for (p,2p) and (e,e'p) reactions 79−22162
hypernuclei, interdisciplinary viewpoint of theories and developments *(Czech)* 80−22749
hyperspherical expansion, complex fro form eqns. of motion 77−22909
hyperspherical functions method, relation to shell model *(Russian)* 77−10337
identical nuclei, collisions, heavy ion real pots. *(German)* 77−57691
inner shell core struct. of nuclei from high energy electron elastic scatt. and knockout reactions 78−54739
interacting boson model, collective motion descript., shell model test 80−27542
interacting boson model, collective state description, shell model connection 80−37341
interacting boson model, collective states of even-even nuclei, shell model descript. 78−62493
interacting boson model, monopole and quadrupole pairing 80−73812
interacting boson model, shell model and microscopic nuclear struct. 80−27575
interacting boson model, shell model description 80−27574
interacting boson model, shell model fermion Hamiltonians with monopole and quadrupole pairing 80−27576
interacting boson model, shell model foundation 80−37340
inverse scatt. problem, quantum mech. systems with discrete spectra 77−78995
Ising struct. in shell-cluster model 77−26601
isobar configurations in closed shell nuclei, ^{4}He, ^{16}O calcs. 78−66226
isobaric distributions in deep inelastic reactions 80−18270
isomorphic model, appl. to nuclei ground state props. 78−78277
isomorphic model appl. to s-d shell nuclei 77−50069
isoscalar effective charges with scaling and HF wavefunctions 77−26559
j=7/2 shell, complete factorisation 77−6264
K-harmonics and shell model methods, review *(Russian)* 77−82836
K-matrix model, self-consistent appl. to finite and superheavy nuclei 77−6257

nuclear shell model continued
Kalamboukis tests of Davidson algorithm, comments, nuclear structure 80–86852
l-forbidden M1 transitions, shell effects, reduced transition probabilities 80–68894
large amplitude collective motion, semiclassical approach, degenerate shell model appl. 80–27535
level crossing effect on collective dynamics 77–50042
level density, analytic formula, shell and pairing effects 78–50092
level density, shell. struct. effect excit. energy depend. 77–79311
light nuclei, α spectroscopic factors, harmonic oscillator shell model 77–50051
in light nuclei, monograph 77–67707
light nuclei, props. from double well cluster shell model 80–27572
light nuclei, role of complicated configs. in giant resonances, continuum shell model 78–86463
light nuclei, shape in translationally invariant shell model 79–26367
light nuclei, shell and cluster struct. coexistence, review 78–50107
liquid drop energy, shell correction determ. 78–12992
low level excitation, inelastic electron scatt. *(Russian)* 78–58265
low-lying states of $1f_{7/2}$ nuclei 77–46123
magnetic dipole moments in shell model 78–82280
magnetic moment dependence on shell-model wave function in light nuclei 78–17100
many body shell model bases, normal products of commutation reln. and p-h reln. 78–66227
many-body configuration, Gaussian distrib. in nuclear spectroscopy 78–66229
mass depend. of spin-orbit splitting in A=176-208 region 78–29405
mass formula 77–6261
mass formula and mass relationships 78–25108
mean field near Fermi surface, energy dependence, single-particle quantities, Brueckner-Hartree-Fock calcs. 80–68572
medium and heavy nuclei, binding energy shell effects, universal behaviour 79–447
microscopic binding energy calcs., modified Strutinsky correction 79–67638
microscopic theory of one-body dissipation, collective motion, independ. particle model 78–54700
modified Lipkin model, orthogonal polynomial expansion for effective interactions 79–26373
multi-nucleon transfer, spectroscopic factors for shell model computer codes 77–65195
multi-nucleon transfer and direct reactions, nuclear struct., review 78–50060
N=28, odd-even effect in shell model 79–13217
N=28 isotones, effective interactions, Coulomb displacements and separation energies 78–50077
N=28 nuclei, energy spectra calc. in shell model 79–13206
N=28 region, $1f_{7/2}$ nuclei, low lying and high spin states 78–54667
N=50, odd-even effect in shell model 79–13217
N=50 isotones, effective interactions, Coulomb displacements and separation energies 78–50077
N=50 isotones, effects of $1p_{3/2}$ core excitations 79–466
N=Sl isotones, shell model calcs., energy levels, transitions and spectroscopic factors 79–63593
N=Z even-even nuclei, 2s-1d shell Hartree-Fock calcs. s-wave interaction 79–26385
N~28 nuclei, shell model study of high-spin states 79–3087
N-fermion translation invariant systems, derivation of energy lower bound models 78–65866
neutron excess nuclei, near equality of isoscalar and EM transition rates 78–8770
neutron gas, crystallisation, zero-order, Bethe-Fermi homework potential 80–63117
neutron resonances, partial E1 radiative strength functions, shell and optical model interpretation *(Russian)* 77–82895
neutron resonances, reaction mechanisms and nuclear struct. 77–26564
neutron skin, compared with droplet model theory 80–52599
neutron total cross section fluctuations, shell model approach using Greens function, resonances 79–22283
Nilsson model, (t,α) reaction, 17 MeV, proton hole states in ^{187,189,191}Re 77–88025
Nilsson model, group theoretical treatment, deformation, pot-energy surface, oscillator shell coupling 78–33129
Nilsson model description of ^{189}Os spectroscopy 77–14035
Nilsson states, asymptotic quantum numbers for prolate and oblate deformations 80–9226
non-normal parity states, 1p shell nuclei, $1\hbar\omega$ spectra 78–12977
nuclear Coulomb energy, shell model calc., pair distrib. function method 79–13183
nuclear structure, conf. 78–50059
nuclei far from stability, spectroscopy 77–22910
nucleon motion in nuclei, determ. using high energy electron induced knock-out reactions *(French)* 79–445
nucleon overlaps, Sturm Liouville expansions, convergence props. 78–78281
nucleon transfer reactions, centre-of-mass corrections to overlap factors 77–308
odd mass nuclei, $1g_{9/2}{}^{+}$ shell region, low lying states, anharmonic effects 80–57687
odd mass nuclei, 2s-1d shell, nuclear forces, energy levels 77–2917
odd-A $1f_{7/2}$ nuclei, high spin states, shell model analysis 78–62560
odd-odd fission products, level schemes, rot. bands, shell model states 80–78167
one-body Gamow Teller β-decay matrix elements for 1s-0d shell, empirical renormalisation 78–66248
optical model pot. 79–93580
optimum atomic mass formula from nuclear mass shell and parity corrections *(Russian)* 80–37902
P-shell hypernuclei, formation, γ-radiation, and spin values, shell model 79–22223
p-shell hypernuclei, shell model anal. of Λ binding energies 78–78300
p-shell hypernuclei with effective Λ-nucleon potentials, binding energy and well depth 79–36184
pairing interactions at high spin 77–54162
pairing vibration in closed-shell nuclei, RPA calc. 77–67710
particle-rotor model for ^{151}Sm transitional nucleus, neg. parity states, spectroscopic factors, B(E2) values 78–50080
pf-shell nuclei, Hermitian operator method calcs., energy levels, transitions 78–54702
photo-nucleon spectra, shell and pre-equilibrium decay model of giant reson. decay *(Russian)* 78–579
photoneutron reactions near threshold, optical model, review *(Russian)* 77–82904
photonuclear reaction mechanisms, 40 to 140 MeV, shell model based description 77–79360
photonuclear sum rules from continuum calcs., dependence on residual interactions 80–22807
pigmy resonance, EM transitions, threshold states effects *(Hungarian)* 78–89818
pion radiative capture on light nuclei, partial transitions, shell model calc. 77–57693
potential energy surfaces of odd-mass isotones of Tl, Au, Ir, Re 77–26567
prolate symmetry axis, rotation of nuclei at high spin states, yrast states 78–70431
proton pairing vibrs., p-h corrections at Z=50 77–57609
proton-neutron basis, decomposition matrix rel. to basis of specified isospin T 80–37337
proton-neutron multiplets, odd-odd nuclei, parabolic Regge trajectories, exchange of quadrupole phonon 80–52590
quadrupole moment of heavy deformed nuclei in pseudo-SU(3) model 77–71565
quadrupole moments and rms charge radii, shell model calcs. 80–47369
quasi-particle factorisation scheme, appl. to $1f_{7/2}$– shell 79–80875
quasiconfiguration approach to effective forces, appl. to $f_{7/2}$ problem 79–45187
quasispin generalisation to monopole and quadrupole pairing, interacting boson mode, shell model hamiltonians 79–80886
radial depend. of shell model pot. *(Russian)* 78–41655
rapidly rotating nuclei, high spin rot. including shell fluctuations, semiclassical description 80–47348
rapidly rotating nuclei, shell struct., collective motion and elastic deformation 79–71782
rare earth even nuclei, Woods Saxon pot., very high spin Strutinsky calcs. 77–88055
rare earth nuclei, validity of pseudo SU(3) model 77–34240
rare earths, nuclear deformation, Coulomb displacement energy depend., shell model 80–102108
reaction theory, elimination of spurious centre of mass resonances 79–75929
reaction valleys, two-centre shell model, fission and heavy-ion reactions *(Russian)* 77–82947
realistic calculations 79–17828
recoil corrections in electric gamma transitions 79–89263
recoupling coefficients of the general linear group in bases adapted to shell theories 78–77670
renormalised shell model matrix elements from nucleon-nucleon phase shifts 78–12991
residual n-p interaction in doubly odd deformed nuclei 77–14012
review 78–86493
rotating nuclei deformation energy, Nilsson model dynamical moment of inertia, shell corrections *(German)* 78–82276
rotational and intrinsic nuclear motions, semimicroscopic derivation of coupling 77–30498
rotational band termination, shell model calcs. in sd shell 80–32145
rotational collective microscopic theory in Sp(3,R) model 77–26600
sd shell nuclei; spin-tensor decomp. of effective interaction 79–93522
sd shell nuclei, effective interaction between nucleons 78–17117
sd-shell nuclei, ground state alpha cluster correl. calcs. 78–74314
sd-shell nuclei, ground-state alpha-cluster correl. 79–6402
sd-shell nuclei, large scale shell model calcs. compared with perturbation theory in SU(3) basis 77–57613
sd-shell nuclei heavy-ion reaction resonances, low level density regions, shell model 80–57757
self shape of nuclei *(Russian)* 78–29381
semiclassical approx. for spherical momentum depend. pot. 78–50101
semiempirical liquid drop model, shell correction formula 77–6267
semiempirical mass formulae, shell corrections, α-decay period estimates for heavy nuclei *(Russian)* 79–22184
semiempirical nuclear level density formula with shell effects 78–82290
semiempirical shell correction to droplet model, magic number effects 77–10339
semiempirical shell model, mass excess calc. 77–6260
seniority scheme for non-degenerate single particle orbits 78–74315
shape, reln. to shell struct. 77–14026
shell correction accuracy calc. *(Russian)* 80–37338
shell corrections to semi-empirical formulae for binding energy and radius *(Russian)* 78–78283
shell depend. level density formula 77–22849
shell effects in nuclear radii and binding energies, prediction of relative radii 79–45149
shell model calcs. A=24, mass, spectra and β decay 78–4903
shell model continuum calcs., centre of mass problems 77–82909
shell model level densities in evaporation calculations 79–45241
single particle energies, by nonhermitian potential *(Chinese)* 79–93496
single particle realistic level schemes, nuclear shell correction energies, temp. smearing method 78–17118
single particle Schrodinger fluid, nuclear fluid dynamics, shell model basis, shape distortions 79–93484
single particle states, systematics in a Woods-Saxon potential *(Rumanian)* 79–59003
single-closed shell nuclei, microscopic description of quadrupole excitations 77–41901
single-particle energy levels, shell-model anal. 78–17071
single-particle level density, excitation dependence of nuclear level density parameter, shell effects 80–32149
single-particle motion in nucleus, forces between constituent nucleons, shell model 80–47408
single-particle resonances, numerical anal. 78–29436
singular part of effective interaction, effect on perturbation theory, appl. to ^{18}O 77–6265
Skyrme tensor interaction, HF spin-orbit effects in spherical nuclei 77–61350
SL(3,R) symmetry, coupling of self-conjugate systems 79–97228
space truncation using spectral strength distrib. 78–29404
special shell structure for nuclei at high angular momenta 79–17825
spectroscopic investigation of decaying states using continuum shell model 80–486
spherical nuclei, α-decay widths calc. *(Rumanian)* 77–46145

nuclear shell model continued
spherical nuclei, absolute α-decay widths, renormalised effective interaction contrib. in shell model 79−75925
spherical nuclei, geminal product approx., appl. to ^{4}He, ^{16}O 78−66230
spherical shell model, collective features, review 78−50098
spherical shell model, renormalisation for collective model within truncated space 78−54697
spheroidal asymmetric oscillator pot., shell model calcs. 77−74779
spin orbit interaction of nucleons, relative motion dependent, universal coeffs. of hyperspherical function method 77−61354
spin rotation, high angular velocity, collective aspects of heavy ion collisions 80−78309
stability against nucleon emission in shell model 77−22969
stable odd-mass sd nuclei, EM multipole moments of ground states 80−102116
state densities, shell correction approach 77−6201
statistical, spectrum fluctuations 77−26599
strangeness exchange reactions and hypernuclear spectroscopy 79−67699
strangeness exchange reactions producing hypernuclei, shell model calcs. 78−17130
strength distributions and statistical spectroscopy, shell model comparisons 77−79323
strength functions, shell model calc. 80−32187
strong two body correlations in nuclear shell model calcs. 77−6259
Strutinsky type corrections for highly asymmetric systems 77−71576
SU(3) recoupling coeffs. 78−66050
subshell closure effects of nuclear binding energies, neutron rich nuclei 78−58230
subshells, exact eqn. for binding energy *(Russian)* 77−71575
sum rule anal. of one-nucleon transfer data on ^{41}Ca, ^{43}Ca, ^{45}Sc, ^{49}Ti, ^{51}V, shell model validity 77−67730
superfluid deformed rare earth nuclei, quasiparticle-phonon coupling, self-consistent calcs. 77−54138
superfluid nuclei, pairing correls. in excited states, low seniority shell model approx. improvement 77−54163
superfluid nuclei, quasiparticle-phonon self-consistent coupling 77−54164
superheavy elements, variations in nuclear skin thickness 77−14025
superheavy nuclei, lifetime, theoretical prediction of nonoccurrence in nature 78−662
superheavy nuclei, spontaneous fission props. for $98 \leq Z \leq 106$ and $150 \leq N \leq 164$, shell model 78−82401
superheavy nuclei stability, spin-orbit symmetry potential 78−50104
superheavy shell struct. in $250 \leq A \leq 500$ mass region 77−22833
symmetrical basis in the three-body problem *(Russian)* 79−40861
symplectic collective model, irreducible U(3) tensor interactions 80−83048
teaching, from Compton effect to quarks, at., proton, and nucl. struct. 78−24596
tensor M1 operator asymptotic cancellation, particle-vibration coupling 78−50082
ternary fission, three-centre shell model 79−36226
thermal neutron scatt., shell model formalism 78−13095
third-order effective shell-model interaction 78−50102
Thomas-Fermi, extended model, binding energies and liq. drop parameters 77−67699
threshold effects in nuclear reactions, ^{15}N(n,n) reaction *(Russian)* 77−287
total single particle energies, energy and N-averagings in shell correction method 80−22671
transitional nuclei, dynamical interplay between pairing and quadrupole modes, shell model anal. 79−89252
translation invariant, quasielastic cluster knockout theory, review, book contrib. 79−75874
translationally invariant to usual wave function transformation 77−67706
tri-diagonalisation of matrix, appl. to shell model calc. 78−58240
truncation of shell model vector space 77−286
two nucleon reduced widths, symm. two-centre shell model 80−105994
two nucleon transfer, RPA theory, pairing vibrs., and extended basis shell model 79−481
two-body interaction, shell model calc. matrix elements 80−42567
two-body shell model matrix elements by Taylor-series method 80−32212
two-body spin-orbit interaction matrix elements, shell model *(Chinese)* 80−47356
two-centre shell model, alpha decay widths calcs. 77−71593
two-nucleon reduced widths in symmetric two-centre shell model 80−32213
two-nucleon reduced widths in the asymmetric two-center shell model 80−63107
two-nucleon transfer, ang. momentum and binding energy effects 79−59021
two-particle high spin states, crude shell model location, max. spin coupling 79−22172
unified model appl. to ^{12}C+n system 78−29437
unified model with vibrating core of variable deform., appl. to ^{21}Ne, ^{21,22}Na 77−50068
valence nucleon effective interactions 80−9244
valence nucleon no. dependences of core and single particle props. 77−26596
valence nucleons, muonic atom analysis 80−27530
valence nucleons, radial wave functions 80−73788
validity, fresh look 77−22827
variational calculations in harmonic oscillator basis 77−6263
vibrational collective motion, shell model anal. using algebraic approach 78−50072
wave functions from shell and cluster model 78−29412
Woods-Saxon potential for ^{40}Ca and ^{48}Ca 80−63106
yrast region of rapidly rotating nuclei, instability toward nucleon emission 77−88027
yrast spectroscopy, nuclei with high angular momentum, review 78−50063
yrast traps, single particle calcs. for rare earth nuclei 77−88031
yrast traps, struct., nuclear deform. 78−21486
Z=114-126, nuclear stability reexamination using deformed Woods-Saxon pot. lifetimes level density 79−3094
zero point energies in two centre shell model 78−93952
(α,α), folding potentials, Woods-Saxon and squared Woods-Saxon parametrisations 80−102195
(α,^{2}He) reaction in 1p- and 2s1d-shell nuclei, A-depend. of neutron binding energy 78−74379

nuclear shell model continued
α-clustering and spectroscopic factors, shell effects and deformation correlations in (^{6}Li,d), (d,^{6}Li) 79−6436
α-nucleus separation energies, Woods-Saxon pot., A depend., closed shell effects 78−25107
α-transfer, spurious C.M. effects separation in shell nucleon configuration framework 79−45194
Δ(33) interaction with nucleus, effective shell model pot., pion scatt. test 80−32202
(e,e), ^{49}Ti, ^{51}V, ^{59}Co, ^{87}Sr, ^{93}Nb nuclei, exchange current effects, plane wave Born approx. 80−78282
(e,e), c.m. motion effects in oscillator shell model 80−106050
(e,e), finite dimension nuclei, differential cross section static correction, shell model 79−75976
(e,e), low-q, A=14 nuclei, isospin T=2, 1 and 0 collective resonances, shell model 80−510
(e,e′), 70 MeV, 1p shell nuclei, shell model cross sections, giant M2, transversal E1 resonances 80−63143
(e,e′), cross section near quasielastic maximum, shell and optical models *(Russian)* 80−91179
(e,e'p) quasi-free scatt., spectral function, sum rule discrepancy, shell model deviation 80−42641
(γ,n), valency mechanism near threshold, optical nuclear model *(Russian)* 77−6351
(γ,p) 60-100 MeV, single particle knock-out using shell model wavefunctions, mass depend. 79−13273
(γ,X), A=14 nuclei, isospin T=2, 1 and 0 collective resonances, shell model 80−510
ΛN effective potentials on p-shell hypernuclei 79−85394
ΛN weakly spin depend. pot. in p-shell hypernuclei 79−85395
(n,γ), interacting boson and Nilsson model tests, Pt-Os transition region 80−37380
($\bar{N}$,X), complex shell model, narrow resonances and bound states *(Chinese)* 80−42622
n capture abundance peak, A≈252, due to subshell effect of N=164 77−2993
n-p residual interaction effect on elastic electron scatt. by dipole giant resonance positioning 77−82914
NN I=1 scattering with one boson exchange, Bethe Salpeter eqn. 77−57455
(p,p), isobaric analogue resonances, microscopic and phenomenological parameters, S-matrix eval. methods 78−13045
(π,γ), A=14 nuclei, isospin T=2, 1 and 0 collective resonances, shell model 80−510
(π^{-},γ), 1p shell nuclei, spin-dipole excitations, shell model calcs. 79−17935
(π,π') differential cross section calculation program modification 79−54457
π condensate instability and shell effects in nuclei from ^{16}O to ^{298}114 *(Russian)* 77−50074
π-nucleus scattering, binding effects in optical pot. of pion in nucleus 78−41685
A=16, capture rates calc. for (π^{-}, γ) and (μ^{-}, ν_{μ}) reactions on ^{16}O 78−17105
Ag, deform. of ground and excited states 78−82277
Al, A=25, 27, M1, E2, transition probabilities between differently deformed states, Nilsson model 77−61376
^{24}Al, effective M3 matrix elements and transitions from shell model 80−102143
^{26}Al, sd-shell nuclei, stellar weak interaction rates, appl. to supernovae 80−82336
^{27}Al, inelastic electron scatt., charge distrib., Coriolis band mixing calc., C2 form factors 79−529
^{27}Al(γ,p)^{26}Mg, energy and angular distribution *(Korean)* 80−18289
^{243}Am(n,f), low energy, far-out asymmetric mass distrib. 80−83132
^{72}As, populated in ^{72}Ge(p,nγ), level scheme determ. 77−14032
^{76}As, level structure, transitions and J^{π}, from ^{76}Ge(p,nγ) 80−47379
^{212}At, ^{212}At^{m}, configuration mixed shell model, α-decay rate calc. 77−74814
Au, odd isotones, deformation pot. energy from Nilsson model 80−57676
Au, odd isotopes, pot. energy surfaces and quadrupole deformation parameters, deformed basis model 79−80867
Au, odd mass isotopes, $h_{9/2}$ intruder state 77−88024
^{197}Au(^{86}Kr,X), 620 MeV, independent particle-shell struct. in deep inelastic collisions 79−97726
^{8}B, isospin symmetry breaking in A=8 mirror decays 78−93973
^{10}B, EM transitions, model anal. based on [42] representation dominance 79−40880
^{10}B, energy level struct., admixed wave functions, ground state quadrupole moment, deformability 77−50054
^{10}B, triaxial deformation in shell model non-central forces, projected HF calc. 80−13367
^{11}B, +ve parity states in weak coupling model, E1 and β strengths 77−34228
^{11}B, 2α+t model, parity states, shell and cluster structs. 78−50110
^{11}B (e,e′) 120-250 MeV, excited state form factors, shell and diagram model anal. *(Russian)* 79−40852
^{11}B(p,n)^{11}C, shell model anal. of polarisation-analysing power differences 80−22804
^{125}Ba, 7/2$^{\pm}$ states, populated in ^{116}Sn(^{12}C, 3n), explained by triaxial core model 78−37258
^{126}Ba backbending, shell model calc., pair realignment and Coriolis antipairing 80−32164
^{8}Be 1^{+} and 1^{-} levels, expt. and shell model calcs. from ^{7}Li(p,γ_0) 80−63095
^{8}Be lowest negative parity state, shell and cluster model calcs. from ^{7}Li(p,p), ^{8}Be lowest negative parity state, shell and cluster model calcs. 80−18205
^{8}Be spontaneous fission pot. energy curve, cluster shell model *(Chinese)* 80−22867
^{9}Be, molecular model, n and α-particle decay widths, charge form factors 78−46015
^{9}Be, positive parity excited energy levels, three well cluster shell model study *(Chinese)* 79−93518
^{10}Be, triaxial deform. in 1p shell 77−46105
^{12}Be, Hartree-Fock calculations of nuclear bulk properties with density- and starting-energy dependent effective interaction 80−9246
^{206}Bi, high-spin states anal. from ^{205}Tl(α,3n) 78−82368
^{208}Bi, influence of nucl. polarisation on level props. 78−54686
^{209}Bi, single particle state mag. moment in large shell model space 79−45162

nuclear shell model continued
^{209}Bi(^{136}Xe,X), deeply inelastic collisions, mass transport, shell effects 80−99188
^{210}Bi, influence of nucl. polarisation on level props. 78−54686
^{80}Br, 37 keV level quadrupole moment, shell model anal. *(French)* 79−85366
^{81}Br+ν_e, 0 to 300 MeV, cross sections, shell model calcs 79−93605
C(^{16,17}O,^{16,17}O), two centre shell model, molecular single particle states at level crossings 80−47354
^{2}C($K^{\pm}$,$K^{\pm\prime}$), 300-800 MeV, microscopic particle-hole shell model calcs., DWIA anal. 79−59091
(^{12}C,X) on A=144-164, search for high spin isomeric states, shell effects 79−71784
^{12}C, ^{13}N ground states, dispersion anal. of ^{12}C+p forward scatt. 77−34297
^{12}C, centre-of-mass spuriosity in continuum shell-model calculations 80−32210
^{12}C, p and e inelastic, Glauber theory using shell model wave functions 77−46164
^{12}C, shell model proton transition densities from (e,e′) data 79−93517
^{12}C, single particle energies of closed minor shells 77−6208
^{12}C+^{12}C, 19.5 MeV, intermediate struct. in continuum shell model, quasi-molecular shape resonance 79−45235
^{12}C+n, matrix and shell model unification 78−54699
^{12}C+ν_{e^-} 0 to 300 MeV, cross sections, shell model calcs 79−93605
^{12}C(e,e′P)^{11}B, nonorthogonality of initial and final nucl. states *(Russian)* 78−66265
^{12}C(e,e′p), 700 MeV, proton spectral function, independ.-particle shell model, DWIA anal. 77−6353
^{12}C(e,e′p), cross sections from DWIA, optical, and shell model calcs. *(Russian)* 80−32270
^{12}C(e,e′p)^{11}B, cross section calc. based on shell model with residual interaction *(Russian)* 77−311
^{12}C(γ,π^-p), 340-380 MeV, quasi-free photoprod., impulse and shell model anal. *(Russian)* 80−5124
^{12}C(n,n), <17 MeV, resonating group calcs., phase shifts and differential cross sections 80−32275
^{12}C(p,^{6}Li)^{7}Be, 51.9 MeV, cluster coupling shell model 78−46058
^{12}C(π^-, γ)^{12}B*, excitation of collective states, shell model 80−22652
^{12}C(π^-p) in Δ(1232) region, differential yield, impulse and shell model anal. *(Russian)* 79−67744
^{13}C, decay props. of giant dipole reson. photoreactions anal. in continuum shell model 77−26665
^{13}C, photoexcited giant dipole resonace, continuum shell model anal. 80−18266
^{13}C-^{13}N mirror nuclei, 15.1 MeV resonance width, isospin forbidden transitions 79−13265
^{13}C+^{13}C, appl. of molecular particle core model 78−82384
^{13}C(π,π'), 162 MeV, pure n and p transitions, differential cross sections 80−5040
^{14}C, $(sd)^2$ positive-parity states, shell model calcs. 78−54674
^{14}C proton shell closure, p transition spectroscopic factors, DWBA calcs. for (^{3}He,d), (t,^{3}He) 79−80871
^{14}C($\pi\gamma$), collective resonances, A=14 isobaric states, shell model predictions 79−85386
^{15}C 0.74 MeV $5/2^+$ state g-factor, shell model interpretation from ^{3}H(^{13}C,p) 80−32176
^{16}C, $(sd)^2$ positive-parity states, shell model calcs. 78−54674
^{A}Ca, (A=43-46), pairing force, seniority number 80−27563
^{A}Ca, A=40 to 48, giant multipole resonances, mass dependence of energy weighted sums 80−63144
^{A}Ca, A=47, 49, single particle states lifetimes calcs. 80−105943
^{A}Ca= A=40, 48, Hartree-Fock calculations of nuclear bulk properties with density- and starting-energy dependent effective interaction 80−9246
^{40}Ca, 1^-, T=0 state at 6.95 MeV, isospin forbidden electroexcitation 78−25177
^{40}Ca, core polarisation J-averaged effects through 3rd order up to 10 ħω excitations 79−67671
^{40}Ca, effective convection current 79−63606
^{40}Ca, ground state energy 78−29389
^{40}Ca, pion exchange currents and nuclear charge form factors 77−10338
^{40}Ca structure, supersoft-core pot., HF approx., ground state props. 78−533
^{40}Ca$_\Lambda$, Λ particle full set of nuclear shell orbitals 79−63623
^{40}Ca+^{16}O, polarisation of single particle states, two centre shell model 77−30622
^{40}Ca+^{16}O, single-particle polarisation, two-centre shell model 78−13142
^{40}Ca(^{16}O,^{15}N)^{41}Sc, effect of polarisation of shell-model states 77−67768
^{40}Ca(α,α), giant isoscalar quadrupole resonance, α-over p-decay ratio, SU(3) and shell model 80−27608
^{41}Ca, E2 core polarisation charge, Woods-Saxon shell model compared to harmonic oscillator model 80−63072
^{41}Ca, lifetimes of excited $3/2^-$ states from ^{2}H(^{40}Ca, p) 60 MeV 78−70487
^{41}Ca, neutron empirical E2 charge from γ transition probability 78−70487
^{41}Ca, two particle-one hole states, EM transition probabilities 77−88035
^{42}Ca, collective states, quasi-degenerate intrinsic Hamiltonian, variational methods 80−68505
^{42}Ca, extended Skyrme force versus realistic interactions, effective interactions 79−54395
^{42}Ca, state calc. by shell model including $1g_{9/2}$ orbit 79−80873
^{48}Ca, single particle energies of closed minor shells 77−6208
$^{40}_{\Lambda}$Ca(k^-,π^-), energy excitation spectra, nuclear shell orbitals for Λ 79−85565
^{A}Cd, (A=106, 108, 110, 112, 114, 116, 118), so-called two phonon states, quasiparticle shell model calcs. 79−89251
^{140}Ce(e,e′), 50-92 MeV, E0, E1, E2, E3 and E4 giant resonances, cross section, shell model anal. 79−54423
^{252}Cf fission, isotopic mass dispersion discontinuity, neutron shell effect 79−45312
^{252}Cf fission, spontaneous, far-out asymmetric mass distrib. 80−83132
^{A}Cl, A=34, 38, effective M3 matrix elements and transitions from shell model 80−102143
^{34}Cl, core polarisation J-averaged effects through 3rd order up to 10 ħω excitations 79−67671
^{34}Cl, ground and excited states, shell model verification by ^{32}S(^{3}He,p)^{34}Cl cross section meas. 78−13119
^{34}Cl, produced by ^{32}S+deuteron, shell struct. effects, Fermigas model predictions 78−89882

nuclear shell model continued
^{37}Cl+ν_{e^-} 0 to 300 MeV, cross sections, shell model calcs 79−93605
^{37}Cl(ν,e^-)^{37}Ar, shell model cross section calc., appl. to cosmic ray and background elimination *(Russian)* 80−5131
Cm, deformation energy surface, two-centre shell model calc. 77−71559
^{244}Cm, nucl. shape of first saddle point 77−74756
^{246}Cm(t,p)^{248}Cm, 17 MeV, shell gap obs. 77−46174
Co isotopes, shell model 78−62479
^{55}Co, GDR, (p,γ) cross section determ. in shell model 78−78345
^{58}Co 1^+ level population, shell model calcs., (t,^{3}He) and (e,e′) comparison from ^{58}Fe(p,n) 79−9481
^{49}Cr low lying states, deformed configuration mixing shell model calcs. 77−6302
^{52}Cr, shell model study and gamma decay of isobaric analogue states 78−86492
^{52}Cr studied via (α,2nγ), high spin states, shell model calcs. 78−54675
^{54}Cr levels, transitions, $T_{1/2}$, J^π, shell model anal. from ^{51}V(α,pγ) 80−47381
^{54}Cr, proton-neutron correl., shell model for collective motion 77−79312
^{A}Cs, A=121, 123, 125, $g_{9/2}$ and $h_{11/2}$ bands 78−50067
Cu, CC ^{56}Ni core excitation effects on A=57-66 nuclei, MSDI and ASDI comparison 78−78254
Cu, isotopes, shell model calcs. of BE, spectroscopic factors and excit. energies 77−22860
^{60}Cu spin states, shell model, 6^- and 9^+ states in odd odd Cu isotopes 78−74313
^{A}Dy, A=161, 163, Nilsson state ΔN=2 mixing, rot. bands from (d,t), (d,p) 80−95295
^{151}Dy high spin yrast isomers, shell model configs. from ^{152}Gd(α,5n) and ^{130}Ce(^{18}O,3n) 79−49573
^{152}Dy, yrast states of isomers at high angular momenta, particle-hole struct. 79−36124
^{157}Er low-lying scheme determ. from ^{157}Tm decay 77−22958
^{166}Er(^{86}K,X), deep inelastic collision, charge drift and dispersion calc., thermal eqn. model based on shell model 80−57798
^{167}Er(d,d′), 12.1 MeV, excitation of Nilsson states, Coriolis coupling 78−33190
^{149}Eu, proton states and transitions shell model anal. of ^{148}Sm(α,t) 79−30781
^{152}Eu, isomeric levels and transitions, Nilsson model 80−18195
^{152}Eu, level scheme, low energy transitions, reaction data, Nilsson model interpretation 78−66215
^{155}Eu, single proton states, spins and parity, rot. bands from ^{156}Gd(t,α), ^{154}Sm(α,t) 79−30766
^{A}F, A=18, 19, E2 transition rates calc., shell model with effective interaction and charges 80−47423
^{18}F, effective interaction, nonlocal pot. reaction matrix free scatt., spectra 77−46122
^{18}F, negative parity states, dynamic interaction propagator approach 79−13191
^{18}F, semi-microscopic calc. of α-cluster states, shell model approx. 80−465
^{18}F, shell and cluster admixtures, T=0 positive parity levels, E2 rates 77−18396
^{19}F isospin mixing in yrast $I=5/2^+$ level 79−93508
^{19}F positive parity alpha clusters, Woods-Saxon well calcs. 79−26383
^{24}F, effective interactions in sd-states 77−14044
^{A}Fe, A=54-56, high spin states, energy levels, spectroscopic factors, EM props., shell model 80−47359
^{A}Fe, A=56-58, shell model calcs., static moments and EM transition rates 79−17853
^{A}Fe, A=56-60, shell struct. of collective states, level spectra 79−93494
^{56}Fe+ν_{e^-} 0 to 300 MeV, cross sections, shell model calcs 79−93605
^{52}Fe levels from ^{54}Fe(p,t), ang. distrib., spin, parity, $f_{7/2}$ shell model 78−74362
^{54}Fe, studied via (α,2nγ), high spin states, shell model calcs. 78−54675
^{54}Fe(^{3}He,p), ^{56}Co particle-hole states, T=1, zero DWBA anal. 80−78308
^{54}Fe(ρ,α)^{51}Mn, 35 MeV, nuclear struct. study 79−75980
^{56}Fe, fp shell model calcs., spectra and spectroscopic factors 80−68588
^{56}Fe, proton-neutron correl., shell model for collective motions 77−79312
^{56}Fe, shell model wave functions from ^{56}Fe(p,α) 80−32211
^{56}Fe(e,e′), Coulomb form factor for O^+→4^+ transition, collective 4^+ states, shell model 80−57664
^{56}Fe(ρ,α)^{53}Mn, 35 MeV, nuclear struct. study 79−75980
^{A}Fm(n,f), A=253, 255, 257, 259, fission mass distrib. transition, liquid drop and shell model calcs. 80−32310
^{A}Fm(sf), A=254, 256, 258, 260, fission mass distrib. transition, liquid drop and shell model calcs. 80−32310
Ga, odd, single particle and collective degrees of feedom, clustering, shell model anal. 80−68510
^{A}Ga, A=67 to 69, energy spectra, shell model calc. 79−17818
^{66}Ga high spin states, shell model interpretation from ^{64}Zn(α,pnγ) and ^{63}Cu(α,nγ) *(French)* 79−3086
^{71}Ga+ν_{e^-} 0 to 300 MeV, cross sections, shell model calcs 79−93605
^{71}Ga(ν,e^-)^{71}Ge, shell model cross section calc., appl. to cosmic ray and background elimination *(Russian)* 80−5131
^{A}Gd, A=146,147, mass and Z=64 shell closure from ^{144}Sm(^{12}C,^{9,10}Be) 80−57669
^{A}Gd, A=146.7, particle hole yrast states and Z=64 shell closure from Sm (α, xn) 79−49571
^{146}Gd region, proton subshell effects from α-decay and spectroscopy, self-consistent study 80−57748
^{150}Gd, high spin states, pairing correlations and nuclear shape, HFB approach 80−42517
Gd(d,d′), A=155, 157, 12.1 MeV, excitation of Nilsson states, Coriolis coupling 78−33190
Ge, A=64, 66, 68, 70, Lipkin-Nogami method, ground state props. 78−50103
Ge, odd, single particle and collective degrees of feedom, clustering, shell model anal. 80−68510
^{A}Ge, A=68 to 70, energy spectra, shell model calc. 79−17818
^{4}He (e,e′pp) reaction cross-section and ground state shell model calcs. *(Russian)* 80−78283
^{4}He, centre of mass spuriosity in continuum shell model calcs. 77−26597
^{4}He, giant dipole reson., shell model calcs. including noncentral forces and target recoil corrections 79−17824
^{4}He ground state wave function in translationally invariant oscillator basis 77−6262
^{4}He harmonic oscillator sum rules for photonuclear reactions, shell model, perturbative corrections 78−41692

nuclear shell model continued
^{4}He, pion exchange currents and nuclear charge form factors 77−10338
^{4}He, recoil corrected continuum shell model calcs. 79−67684
^{4}He, shell model calcs. 80−13393
^{4}He, structure in the translation-invariant oscillator basis *(Russian)* 78−25123
^{4}He(α,α), size change of α effect on phase shift, generator coordinate and variational methods *(Chinese)* 80−68683
^{4}He(γ,p), shell model continuum calcs., centre of mass problems 77−82909
^{4}He(γ,π^0), cross-sections determ., selection rules calc. 77−82905
^{6}He β-decay from three body model of A=6 system, α-N, N-N interactions 78−46032
^{6}He, density distribution function of nucleons 80−22650
$^{7}_{\Lambda}$He, prod. cross section calc., γ decay spectrum, shell model theory 78−62501
Hf-Ir, isotopes, deformation, level assignments, static moments, modified oscill. model 77−22872
Hf-Os region, high lying states, Nilsson strength fragmentation 80−42539
^{A}Hg, quadrupole moment, change between first $5/2^-$ states for A=197,199, shell model anal. 80−52576
^{194}Hg compound nucleus, fission and, n, p, ^{4}He emission ang. momentum and energy depend. 79−76045
^{194}Hg, level density calc., shell and pairing effects, deformation, excitation energy dependence 79−67662
Ho, A=161,163,165, E1 transitions, hexadecapole deforms., Nilsson model calc. 77−82861
^{A}Ho, A=153, 160, isomeric levels and transitions, Nilsson model 80−18195
^{170}Ho, 43 s and 2.76 min states, energies and intrinsic structs. 78−78321
I odd-A nuclei, deformed $9/2^+$ proton-hole states, Nilsson calc. 77−74746
Ir, odd isotones, deformation pot. energy from Nilsson model 80−57676
Ir, odd isotopes, pot. energy surfaces and quadrupole deformation parameters, deformed basis model 79−80867
^{183}Ir levels, J^{π} assignments, Nilsson states for N=105 isotones from ^{183}Pt fast β-transition 79−22206
^{38}K, effective M3 matrix elements and transitions from shell model 80−102143
^{41}K, populated by ^{38}Ar(α,pγ), levels props., shell model calc. 78−62588
^{47}K, single particle states lifetimes calcs. 80−105943
^{6}Li bound states, six body hyperspherical soln. to N-body Schrodinger eqn. 79−9490
^{6}Li, charge form factor, short range Jastrow correls. in harmonic oscillator shell model 78−70467
^{6}Li ground state, double well-cluster shell model, d-cluster contraction and deform. *(Chinese)* 78−78290
^{6}Li, RMS radii, binding energy, electric quadrupole transitions using generalised hyperspherical functions *(Russian)* 78−86469
$^{6}_{\Lambda}$Li, supermultiplet struct. and decay props. of hypernuclear 1^+ resonances from (K^-,π^-) 80−78186
^{6}Li(e,e′), 140-330 MeV, 3.65 MeV 0^+ state form factor at high momentum transfer 80−495
^{6}Li(e,e), elastic and inelastic charge form factors from shell model wave functions 80−68523
^{6}Li(γ,π^0), cross-sections determ., selection rules calc. 77−82905
^{7}Li, cluster model wave function and r.m.s. radius 78−70442
^{7}Li, cluster struct. interplay model and appl., energy levels and shell clusters 79−17842
^{7}Li, proton scatt., $3/2^-\rightarrow 1/2^-$ transition, LS coupling shell model, isoscalar quadrupole renormalisation 77−14046
^{8}Li, isospin symmetry breaking in A=8 mirror decays 78−93973
$^{7}_{\Lambda}$Li, prod. cross section calc., γ decay spectrum, shell model theory 78−62501
^{24}Mg, 1s-0d shell effective interaction, (e,e) scatt. form factor calc. 77−61400
^{24}Mg, ground state rot. bands from shell-model Hamiltonians 77−79298
^{24}Mg isoscalar quadrupole excitations in 2 centre shell model, collective approach, particle-hole excitations 79−45139
^{24}Mg, low spin rotational states, energy props., extended deformation model 80−86785
^{24}Mg, O_1^+, 2_1^+, 4_1^+ states, EM props. from large basis shell model 79−75900
^{24}Mg rotational band collectivity, shell model excitation in Sp(4, R) symmetry 80−102095
^{24}Mg states, Nilsson model spectroscopic factors, collective model rot. bands from ^{23}Na(^{3}He,d) 79−6421
^{24}Mg(p,p′), 40 MeV, DWBA anal., positive parity states, transitions and giant resonance 79−6419
^{24}Mg(p,t), CCBA anal. using shell model wave functions 77−321
^{26}Mg transition strength n and p components, $\pi^{\pm}$ inelastic scatt. comparison, shell model 80−68585
^{28}Mg, isospin forbidden β-decay 78−78315
^{53}Mn low lying states, DWBA anal., shell model wave functions from ^{56}Fe(p,α) 80−32211
^{53}Mn(ρ,α)^{52}Cr, 35 MeV, nuclear struct. study 79−75980
^{55}Mn, proton-neutron correl. shell model for collective motion 77−79312
^{57}Mn, low lying level struct. via ^{55}Mn(t,p)^{57}Mn, shell model comparison 77−74769
Mo isotopes struct., spectroscopy weak coupling approx. in shell model 79−22194
^{A}Mo, A=94, 96, 98, multiparticle states, method of generalised seniority 80−22759
^{94}Mo even parity states, shell model calc. 77−50061
^{94}Mo high spin state transitions, mixing ratios, spins, shell model calcs. from ^{94}Tc decay 79−97678
^{15}N low-lying positive parity states, Nilsson scheme from ^{14}C(^{3}He,d) 79−80871
^{15}N, photoabsorption, shell-model anal. of giant dipole state 78−29447
^{15}N+X, X=^{11}B,^{12}C,^{18}O,^{13}C, deduced excited states, shell model wave functions, DWBA anal. 79−45284
^{15}N(p,γ), ^{16}O excited state GDR, coupled channels version of continuum shell model 79−542
^{15}N(π^+,π^0)^{15}O, isobar hole model calc. of single charge exchange 79−85523
^{17}N levels and ang. distribs. meas., shell model calcs. from ^{15}N(t,p) 80−9233
Na, A=21, 23, M1, E2, transition probabilities between differently deformed states, Nilsson model 77−61376
nuclear shell model continued
^{21}Na, parity mixing matrix element using SU_3 shell model calcs. 79−9462
^{22}Na bound state lifetimes, transition strength in terms of shell model 78−93967
^{22}Na, effective interactions for dominant shell-model configurations: ds-shell example 80−32204
^{23}Na α-transfer spectroscopic factors from shell model wave functions of ^{19}F(^{6}Li,d) 79−36149
^{23}Na high spin positive parity state, approx. microscopic methods, shell model comparison 79−85352
^{23}Na, high-spin states, shell-model calc. in sd shell 77−65213
^{24}Na, effective M3 matrix elements and transitions from shell model 80−102143
Nb and Tc doubly odd isotopes, multiplet struct., ^{96}Tc nuclear struct. 78−46024
^{91}Nb from ^{89}Y(α,2nγ)^{91}Nb, high spin states, shell model structure 79−93514
^{91}Nb, level struct., $p_{3/2}$ core excitations 77−50060
^{20}Ne, 0g orbit mixing via (e,e′), one-step forbidden transition anal. 78−493
^{20}Ne, coexistence of shell struct. and cluster struct. 78−78279
^{20}Ne collective motion, B(E2) rates, algebraic formulation in symplectic shell model 80−83015
^{20}Ne, ground state rot. bands from shell-model Hamiltonians 77−79298
^{20}Ne, O_1^+, 2_1^+, 4_1^+ states, EM props. from large basis shell model 79−75900
^{20}Ne, positive parity alpha clusters, Woods-Saxon well calcs. 79−26383
^{20}Ne quadrupole transitions, electron scatt. form factors, shell model calcs. 78−62523
^{21}Ne, energy moments, sd shell realistic effective interactions, shell model spectra 80−18190
^{22}Ne(p,t), CCBA anal. using shell model wave functions 77−321
^{24}Ne, effective interactions in sd-states 77−14044
^{26}Ne, effective interactions in sd-states 77−14044
Ni, A=58. 60, 62, 64, 66, Lipkin-Nogami method, ground state props. 78−50103
Ni, CC ^{56}Ni core excitation effects on A=57-66 nuclei, MSDI and ASDI comparison 78−78254
Ni, fp shell model calcs., spectra and spectroscopic factors 80−68588
Ni isotopes, shell model calcs. of BE, spectroscopic factors and excit. energies 77−22860
^{A}Ni A=57-59, $f_{7/2}$ hole configuration effects, shell model calcs. 80−22670
^{A}Ni(e,e′), 102 MeV, A=58,60, E1-E4 giant multipole resonance comparison, shell model anal. 80−42614
^{58}Ni(d,α), ^{56}Co particle-hole states, T=1, zero DWBA anal. 80−78308
^{58}Ni(p,p), 20.4 and 30.3 MeV, elastic and inelastic scatt. multishell model description 78−86533
^{62}Ni level struct. and decay scheme, shell model calcs. from ^{59}Co(α,pγ), 10 MeV 79−3085
^{62}Ni(γ,X), 19.2-26.2 MeV, photoneutron and photoproton spectra, giant dipole resonance-decay, isospin conservation 80−13443
Ni(α,X)Zn, α spectroscopic factors in shell model 79−45158
^{252}No, high mass asymmetry distribs. in fissioning nuclei, shell effects 79−3186
^{A}Np(n,f), A=234, 235, low energy, far-out asymmetric mass distrib. 80−83132
^{A}O, A=16, 17, valence-core self-consistency, wave functions, binding energy, levels, spectra 80−63123
^{A}O, A=18, 19, E2 transition rates calc., shell model with effective interaction and charges 80−47423
^{16}O, α-spectroscopic amplitudes in shell model 77−71564
^{16}O, α-spectroscopic amplitudes anal. using shell model based calc. 79−13203
^{16}O, centre-of-mass spuriosity in continuum shell-model calculations 80−32210
^{16}O, charge distribution, orthogonal scheme model *(Russian)* 78−29382
^{16}O, external mixing of resonance states in continuum shell model 79−22257
^{16}O, Hartree-Fock calculations of nuclear bulk properties with density- and starting-energy dependent effective interaction 80−9246
^{16}O independent particle shell model momentum density distrib., short range correlations 80−78176
^{16}O, isospin forbidden 7.12 MeV E1 transition, continuum shell-model calc. 77−18472
^{16}O, pion exchange currents and nuclear charge form factors 77−10338
^{16}O, positive parity giant multipole resons., particle hole shell model 79−30811
^{16}O, rotational band collectivity, shell model excitation in Sp(4, R) symmetry 80−102095
^{16}O, shell model decomposition of core excitation states 78−50109
^{16}O+^{4}He, group theory appl. to reaction studies 80−9276
^{16}O+X, X=^{11}B,^{12}C,^{13}C,^{18}O, deduced excited states, shell model wave functions, DWBA anal. 79−45284
^{16}O+ν_e, 0 to 300 MeV, cross sections, shell model calcs 79−93605
^{16}O(α,α), giant isoscalar quadrupole resonance, α-over p-decay ratio, SU(3) and shell model 80−27608
^{16}O(γ, p), 300 to 900 MeV/c, p-shell momentum distrib. calc. 78−50151
^{16}O(γ,N), shell model calcs. with and without continuous spectrum *(Russian)* 77−2979
^{16}O(μ^-,e^-)^{16}O*, shell model anal. of μe conversion rate *(Russian)* 79−89300
^{16}O(π,γ), continuum shell model, strongly excited resonances, nucleon emission 78−94031
^{16}O(π,γn), direct and resonance reaction unified shell model, n, γ spectra 80−52696
^{16}O(π^-,γn), γ-spectrum and γ-n ang. correlation function from continuum shell model 78−86551
^{16}O(π^+,π^+), 50-340 MeV, isobar hole doorway states, collective Δ-hole states 79−85350
^{17}O in a shell model space, Q-box study 79−93530
^{17}O(^{11}B,^{8}Li), 115 MeV, shell and semiclassical reaction model anal. 80−13494
^{17}O(^{12}C,^{9}Be), 115 MeV, shell and semiclassical reaction model anal. 80−13494
^{17}O(^{13}C,^{10}B), 105 MeV, shell and semiclassical reaction model anal., ^{20}F spins 80−13494
^{18}O, effective interaction, nonlocal pot. reaction matrix free scatt., spectra 77−46122

nuclear shell model continued
^{18}O, effective interactions in sd-states 77−14044
^{18}O, $J^{\pi}=0^{+}$ system, singular part of effective shell model interaction 77−6265
^{18}O, negative parity states, dynamic interaction propagator approach 79−13191
^{18}O, transition strength n and p components, $\pi^{\pm}$ inelastic scatt. comparison, shell model 80−68585
^{18}O, two-body surface correls. in extended basis shell model 78−532
^{18}O$_2$ shell-cluster admixtures, spectra, α-widths and electric transitions 77−54136
^{18}O(π,π'), 164 MeV, yrast state and level excitation, DWIA calcs., shell model context 80−42526
^{18}O(π,π'), momentum space DWIA calcs., DWIA validity, shell model sensitivities 79−85553
^{22}O, Hartree-Fock calculations of nuclear bulk properties with density- and starting-energy dependent effective interaction 80−9246
^{193}Os level scheme and transitions, Coriolis coupled Nilsson states from ^{192}Os(n,γ) 80−57698
Pb, A=200, 202, 204, seniority four admixtures in low lying 0^{+} states 78−8741
Pb cored nuclei, high spin stater energies, quadrupole interaction, yrast traps 77−34223
^{A}Pb, A=202, 204, spectra from multistep shell model method 80−78194
^{A}Pb, A=207,209, single particle state mag. moment in large shell model space 79−45162
^{205}Pb, ^{206}Pb, cluster vibrational field coupling model description 77−57604
^{205}Pb, hole states below 2.56 MeV, spectroscopic strengths via ^{204}Pb(d,p) 77−30478
^{205}Pb, particle states via ^{204}Pb(d,p), spectroscopic factors 77−34216
^{207}Pb neutron hole states, core vibration effects, shell model energies 79−36142
^{207}Pb(p,p'), excitation of neutron-hole states, 61.2 MeV protons 78−8724
^{208}Pb and neighbouring nuclei, shell model calcs. with correlated pairs basis 80−22712
^{208}Pb, closed-shell effect on fission barriers at Z=82 and N=126 77−309
^{208}Pb, finite Fermi-system theory, E1, E2, M1 resonances, γ absorpt. cross section near threshold 77−50055
^{208}Pb shell structure, effect on magicity of superheavy nuclei 80−78175
^{208}Pb, shell-model interaction for neutron hole states 77−18446
^{208}Pb, single particle spectra, effect of core polarisation 77−2892
^{208}Pb(^{12}C,^{11}B)^{209}Bi, single-particle polarisation, two-centre shell model 78−13142
^{209}Pb excited states, $3/2^{-}$ resonances from shell model of ^{208}Pb(n,n) 80−78240
^{209}Pb excited states and $3/2^{-}$ resonances, shell model, calcs. from ^{208}Pb(n,n) 80−18262
^{209}Pb reson. parameters calc. in ^{208}Pb(n,n), shell model 77−82920
^{209}Pb unbound high spin shell model states, single nucleon states 78−25126
Pd, A=101-5, particle-core coupling, Nilsson model rot. model at intermediate deform. 77−10362
^{105}Pd, high-spin particle-core multiplets via ^{96}Zr(^{12}C,3nγ)^{105}Pd, rot. model 77−54140
^{A}Pm, A=143, 145, proton states and transitions, stripping strength, shell model anal. from Nd(^{3}He,d) 80−68508
^{A}Pm, A=143-153, odd-A, spectroscopic factors, shell model anal. from pickup and stripping reactions 80−78137
^{147}Pm proton states and transitions shell model anal. of ^{148}Sm(t,α), ^{146}Nd(^{3}He,d) 79−30781
^{209}Po, 125-neutron isotone, shell model alpha decay theory 77−18483
^{210}Po, excited, deformed, fission or neutron emission, shell-correction approach to nuclear densities 77−30483
^{210}Po, level density calc., shell and pairing effects, deformation, excitation energy dependence 79−67662
^{212}Po, fission excitation functions anal., shell effects at saddle point, nuclear shape 78−54737
^{212}Po, shell model α-spectroscopic factors 80−32245
^{142}Pr, $2^{-}\rightarrow 2^{+}$ β spectrum, shape meas. 77−50083
Pu, deformation energy surface, two-centre shell model calc. 77−71559
^{239}Pu fission, isotopic mass dispersion discontinuity, neutron shell effect 79−45312
^{239}Pu(n,f), far-out asymmetric mass distrib. 80−83132
^{240}Pu, level density calc., shell and pairing effects, deformation, excitation energy dependence 79−67662
^{240}Pu, nucl. shape at first saddle point 77−74756
^{213}Ra, 125-neutron isotone, shell model alpha decay theory 77−18483
^{87}Rb, low-lying level struct. in quasiparticle-core model 77−82825
Re, odd isotones, deformation pot. energy from Nilsson model 80−57676
Re, odd isotopes, pot. energy surfaces and quadrupole deformation parameters, deformed basis model 79−80867
^{211}Rn, 125-neutron isotone, shell model alpha decay theory 77−18483
^{212}Rn high spin isomers, excited core states coupled to valence protons 77−74745
^{212}Rn, shell model states, semiempirical calcs. half lives, mag. moments, excitation functions 80−63083
^{A}Ru, A=96, 98, 100, multiparticle states, method of generalised seniority 80−22759
^{94}Ru level structure, spin and parity, from beta decay of ^{94}Rh isomers 80−57747
^{32}S, 1s-0d shell effective interaction, (e,e) scatt. form factor calc. 77−61400
^{32}S, (π,γ), shell model anal. 78−89910
^{32}S, comparison of cluster and two-centre shell models 79−6444
^{32}S deformed states, comparison of cluster and shell model wave functions 79−22187
^{32}S, O_1^{+}, 2_1^{+}, 4_1^{+} states, EM props. from large basis shell model 79−75900
^{32}S$_{\Lambda}$, Λ particle full set of nuclear shell orbitals 79−63623
^{32}S(n,γ), non-statistical effects in shell model calcs. 80−32274
$^{32}_{\Lambda}$S(k^{-},π^{-}), energy excitation spectra, nuclear shell orbitals for Λ 79−85565
Sb, neutron rich nuclei, IBM and shell model approaches, collective modes 80−78129
^{122}Sb, low-lying state props., coupled neutron quasiparticle-proton model 77−61378
^{133}Sb, level scheme of one proton and doubly closed shell core 78−37291
Sc, A=43, 47, $d_{3/2}$ hole states, wave functions mag. moment, M2 transitions, shell model 78−17116
nuclear shell model continued
^{41}Sc, two particle-one hole states, EM transition probabilities 77−88035
^{43}Sc, state calc. by shell model including $1g_{9/2}$ orbit 79−80873
^{49}Sc, single particle states lifetimes calcs. 80−105943
^{28}Si, level props. and moment of inertia 78−29390
^{28}Si, O_1^{+}, 2_1^{+}, 4_1^{+} states, EM props. from large basis shell model 79−75900
^{28}Si, sd-shell calcs. for O^{+} states, particle-hole conjugation 77−67704
^{28}Si, spin cutoff factors, sd shell realistic effective interactions, shell model spectra 80−18190
^{28}Si+^{20}Ne, frictional coeffs. using linear response theory 79−13327
^{28}Si(^{18}O,X), 56 MeV, multinucleon transfers, ang. distribs., distorted wave and shell model anal. 80−27663
^{28}Si(α,d)^{30}P, spectroscopic factor calcs. 79−6384
^{28}Si(n,γ), n and γ width correlation, valence, optical and shell model comparison 79−6606
^{28}Si(π,π'), momentum space DWIA calcs., DWIA validity, shell model sensitivities 79−85553
^{30}Si($K^{-},\bar{K}^{0}$), 300 MeV, microscopic particle-hole shell model calcs., DWIA anal. 79−59091
^{A}Sm, A=146,147, excited states, energy levels, spin, parity, shell and cluster-vibration models, from (α,xn) and (^{3}He,xn) 80−57683
^{A}Sm(d,^{3}He)$^{A-1}$Pm, A=144,148,152,52 MeV, strong exhaustion of $1g_{9/2}$ strength by deeply-bound proton-hole states in Pm isotopes 79−45142
Sn, A=104, 106, 108, seniority four admixtures in low lying 0^{+} states 78−8741
Sn, deform. of ground and excited states 78−82277
Sn, odd isotopes, number-projected three-quasiparticle description 78−93953
Sn, odd mass isotopes, low lying negative parity states, energy levels, shell model calc. 80−5076
^{A}Sn, (A=112, 114, 116, 118, 120, 122), so-called two phonon states, quasiparticle shell model calcs. 79−89251
^{A}Sn(^{35}Cl,^{35}Cl'), 108 MeV, A=112-124 even isotopes, 2_1^{+} mag. moments and shell model struct. 80−86805
^{116}Sn particle-hole states, strength decoupling form giant dipole resonance, Gaussian force, δ-force diagonalisation 78−25125
^{120}Sn finite Fermi-system theory, E1, E2, M1 resonances, γ absorpt. cross section near threshold 77−50055
^{132}Sn, energy levels, gamma transitions, spin and parity 80−9239
^{132}Sn, exact and statistical results for multi-proton cases 78−86483
^{132}Sn region, level spectra 78−86482
^{A}Sr, A=89 to 94, struct. of states in the generalised seniority shell model 79−6408
^{90}Sr, energy spectra from nuclear shell model 79−22225
Tc, A=93-101 odd isotopes, levels, EM moments in unified model 77−82826
^{93}Tc, level struct., $p_{3/2}$ core excitations 77−50060
^{95}Tc, transition rates of even-parity states calc. 77−74806
^{96}Tc even mass odd nucleus, proton spectroscopy, from ^{95}Mo(^{3}He,d), shell model anal. 79−63573
^{99}Tc, low-lying states via ^{98}Mo(^{3}He,d)^{99}Tc, proton config. 77−22894
Te evaporation residues from (^{12}C,xnγ), and (^{40}Ar,xnγ), shell effects at high spin 79−22165
^{132}Te 2^{+} level, shell model calc., Lanczos and Householder method comparison 80−22711
^{132}Te low lying levels and EM props., shell model description 80−42549
^{232}Th fission, isotopic mass dispersion discontinuity, neutron shell effect 79−45312
^{44}Ti, α-particle spectroscopic factors, two-oscill. shell model calcs. 79−6386
^{45}Ti $d_{3/2}$ hole states, wave functions, mag. moment, M2 transitions, shell model 78−17116
^{50}Ti, shell model calcs. using surface delta interaction 78−37290
^{50}Ti, studied via (α,2nγ), high spin states, shell model calcs. 78−54675
Tl, A=185,187 isomeric decays, half-life, $h_{9/2}$ intruder state 77−26616
Tl, odd isotones, deformation pot. energy from Nilsson model 80−57676
Tl, odd isotopes, pot. energy surfaces and quadrupole deformation parameters, deformed basis model 79−80867
Tl, odd mass isotopes, $h_{9/2}$ intruder state 77−88024
^{206}Tl, influence of nucl. polarisation on level props. 78−54686
^{207}Tl, single particle state mag. moment in large shell model space 79−45162
^{208}Tl, influence of nucl. polarisation on level props. 78−54686
Tm, A=163-171, E1 transitions, hexadecapole deforms., Nilsson model calc. 77−82861
U, deformation energy surface, two-centre shell model calc. 77−71559
^{A}U fission, A=233,235,238, isotopic mass dispersion discontinuity, neutron shell effect 79−45312
^{A}U(n,f), A=235, 238, low energy, far-out asymmetric mass distrib. 80−83132
^{235}U(d,p), induced fission, subthreshold cross section meas., 2-centre shell model calc. 79−6719
^{236}U, nuclear matter density distrib., in asymmetric two centre shell model 80−32209
^{238}U, high mass asymmetry distribs. in fissioning nuclei, shell effects 79−3186
^{238}U, shell corrections for finite depth single particle potentials 79−30782
^{238}U(^{238}U,X), 7.42 MeV/N, mass transport, shell effects, anharmonic pots. 80−99187
^{238}U(^{238}U,X) deeply inelastic collisions, mass transport, shell effects 80−99188
^{238}U(^{84}Kr,X), mass fragmentation, dynamical theory, two centre shell model, binary decay process 80−68628
^{239}U, population in direct and collective neutron capture by ellipsoidally deformed nucleus 78−94001
V, A=47,59,51, spectra, e.m. moments, B(E2) and B(M1) values calc. 78−8745
^{50}V, half lives of β-decay and e^{-}-capture in $\Delta J=4$ transitions 79−22246
^{51}V high spin states, lifetimes, shell model calcs., yrast levels from ^{48}Ca(^{10}B, α3n) 79−6425
^{51}V, shell model, pairing-plus-surface-tensor interaction, energy levels, B(E2) values 78−78282
^{51}V, shell model calcs. using surface delta interaction 78−37290
^{51}V struct., pairing plus surface tensor interaction 77−18411
^{51}V(e,e'), shell model calcs., effective charges 77−26674
^{51}V(p,n)^{51}Cr, 2.34 MeV, shell model anal. of analogue resonance 77−14122
^{51}V(p,p'), 6 MeV, levels, spins and EM props., shell model anal. 80−63092

nuclear shell model continued
^{52}V, spectrum study with Kuo-Brown renormalised interaction and Vervier interaction 78−86492
^{185}W, beta spectrum, shape factor meas. 77−2947
$^{126-228}$X, primordial and other nuclei, shell model calc. 78−8752
Xe-Nd region, microscopic anal. of core deform. 78−74303
^{89}Y, level struct., $p_{3/2}$ core excitation 77−50060
^{90}Y, energy spectra from nuclear shell model 79−22225
Zn, A=60, 62, 64, 66, 68, Lipkin-Nogami method, ground state props. 78−50103
Zn, even isotopes, weak-coupling model, level struct., E2 transition rates 77−54159
Zn isotopes, A=62-68, shell model calc. 77−270
Zn to Ni even isotope transition, α-particle spectroscopic factors, shell model calcs. 79−6385
^{A}Zn, A=65 to 68, energy spectra, shell model calc. 79−17818
Zr even isotopes, quadrupole moments and E2 transition rates, broken pair approx. 80−52579
Zr even isotopes, seniority shell model, generalised approx. 79−89253
Zr-region, two nucleon transfer reactions, spectroscopic amplitudes, form factors, ang. distrib. 80−22779
^{A}Zr, A=90, 92 and 94, charge densities and single-particle structure 80−9224
^{A}Zr, A=92, 94, 96, multiparticle states, method of generalised seniority 80−22759
^{A}Zr, A=96, 98, 100, deformation and shape transition, unified shell model 79−93502
^{90}Zr, energy spectra from nuclear shell model 79−22225
^{90}Zr, finite Fermi-system theory, E1, E2, M1 resonances, γ absorpt. cross section near threshold 77−50055
^{96}Zr, shape transition microscopic study using shell model 79−40835
^{98}Zr, shape transition microscopic study using shell model 79−40835

nuclear size
$1f_{7/2}$ radii, isotope shifts from nucleon transfer reactions 77−34222
A=40-100, charge distrib. from (e,e) and muonic X-ray meas. 78−54679
A=4-16, monopole giant resonances, state density radii and compressibility using hyperspherical functions *(Russian)* 80−27615
A=4n, densities, form factors, transitions, multipole moments in s-d shell, HFC 80−37321
alkali metal radioisotopes, hyperfine spectroscopy, nucl. props. 80−57677
alpha particle-nucleus scatt., critical radii, correl. with nuclear matter distribs. 79−45148
BCS techniques applied to self-consistent shell model 79−89249
charge RMS radii mass number depend., fine struct. 78−501
compound state statistical description, single particle states, radius and excitation energy *(Russian)* 79−22180
Coulomb energies and nuclear radii in energy density formalism 77−82810
deformed nuclei calc. by HF method with Skyrme's interaction *(Russian)* 79−456
density-dependent HF description, of nuclei in rare earth and Ni regions 77−54170
doubly magic nuclei, Skyrme force calc. for nuclear struct. 78−49721
energy density formalism calcs. with Fermi type distrib. of nucleons 77−46121
even-even spherical nuclei far from stability, Hartree-Fock calc. *(Russian)* 77−41908
FCC lattice model of nuclear struct. 77−14042
form factor calc. using method of hyperspherical functions 77−18381
form factors, analytic representation and radii determ. of hadrons and light nuclei 77−30386
growth points in nuclear physics, book 80−94928
Isolde experiments, prod. of extreme neutron/proton ratio nuclei, nuclear props. study *(Danish)* 78−4972
light muonic atoms, nuclear size effects, energy levels, Lamb shift 80−14254
light natural elements, muonic X-ray transitions, nuclear charge radii 80−99589
light nuclei, hyperspherical functions for size, excited states, compressibility, binding energy 80−22679
linearised Hartree Fock model, effective charge, isoscalar nuclear shifts, rms radius ^{208}Pb, ^{90}Zr 78−25138
matter distribution in nuclei far from β stability valley, charact. features 77−64635
mean square radii, method of hyperspherical functions, contribs. of higher harmonics 77−6220
Mossbauer isomer shifts and nuclear models, book contrib. 79−85385
muonic atoms, light, finite nucl. size corrections to energy levels 79−18321
neutron density distrib., probing with hadrons 78−66196
neutron distribution in nuclei, elastic and inelastic proton scattering, review 80−22649
nuclear isotopes far off stability line, production, props., review *(Hungarian)* 79−9927
nuclear radii from total neutron cross sections, optical model calcs. 79−9455
nucleon FMS radii, neutron distrib. anal. from 0.8 to 1.5 GeV scatt. data 79−26429
nucleonic mass distrib. using mag. spectrometer *(French)* 79−449
one body mass radius operator of closed shell nuclei, convergence studies 79−45146
optical model complex pots. determ. from Reid's hard core interaction 77−88092
potential energy surfaces, folded Yukawa-plus-exponential model 80−86816
proton and neutron densities, HF calc. 77−18380
proton and neutron radii from momentum-depend. pot. approximated by Morse function 77−6190
proton RMS charge radius from ^{1}H Lamb shift meas. 77−50047
quadrupole moments and rms charge radii, shell model calcs. 80−47369
radii and masses in droplet model with shell correction 77−22863
radii of Li, Be, C, Al, Cu, Sn, Pb from π^- and p elastic scatt. meas., 30 to 50 GeV/c *(Russian)* 77−34351
radii of neutron distribs. in nuclei 78−93933
radii variation in drip line regions, energy density method 77−22876
s-d shell nuclei, RMS radii in isomorphic model 77−50069
self-consistent field calcs., HF calcs., NN interactions, and results of appl., book contrib. 79−75880

nuclear size continued
shell corrections to semi-empirical formulae for binding energy and radius *(Russian)* 78−78283
shell effects in nuclear radii and binding energies, prediction of relative radii 79−45149
shell effects in the RMS radii of the nuclear charge distributions determined by electron scattering 79−13200
shell model, globally self-consistent, magic nuclei and spherical nuclei calculations 79−59020
short-lived isotopes, laser spectroscopy in fast atomic beams and resonance cells 80−57700
single particle nuclear density struct., Hartree-Fock and model independent anal. *(Russian)* 79−80941
single-particle models, relation between average kinetic energy and mean-square radius 80−52567
single-particle motion in nucleus, forces between constituent nucleons, shell model 80−47408
spherical nuclei, isomer and isotope shifts, theory of finite Fermi systems 80−39929
spin unsaturated systems, finite range two- and three-body interactions 78−66220
statistical description of nuclear compound states, temp. Green's functions method *(Russian)* 78−17115
stellar dense matter, nuclear size effect rel. to neutron stars limiting mass 80−101611
three-body forces in 3- and 4-nucleon systems 78−29400
(e,e), A=60 region, nuclear radius, core polarisation and isotone shifts, muonic X-rays 80−22685
(e,e), virtual photon intensity and finite nuclear size effects, PWBA calcs. 79−26424
μ^- K-shell X-ray transitions in F, Na, Al, Si, P, S, K, nuclear charge radii 78−66195
neutron and matter radii from 1 GeV proton elastic scatt. amplitudes 78−70515
(p,p), polarised p, 0.8 GeV, neutron isotopic density differences and RMS radii 79−67643
(p, t) ang. distrib. with deep minima, DWBA calcs. geometrical aspects 80−522
(p,X), 5-9 GeV/c, total inelasic and knock-out cross sections, nuclear RMS radius *(Russian)* 80−32175
(p,X), nuclear size dependence of particle prod., hydrodynamical model 80−22593
(p,X), total reaction cross sections and the matter density of finite nuclei 79−45150
(π,π) elastic scatt., reaction mechanisms, structure information and neutron radii 80−42702
(π^-,X), 1.75-6.5 GeV/c, total inelasic and knock-out cross sections, nuclear RMS radius *(Russian)* 80−32175
^{36}Ar, charge distrib. via ^{36}Ar(e,e′) 65-115 MeV 77−18527
^{40}Ar, charge distrib. via ^{40}Ar(e,e′) 65-115 MeV 77−18527
Ba, radioisotopes, at. beam laser spectroscopy, hyperfine struct., nucl. moments and radii 80−57678
^{A}Ba, A=126 to 135, charge radii, mag. dipole and elec. quadrupole moment 79−72436
^{8}Be, ground state props., modified Brueckner-Bethe-Goldstone method 78−50076
^{9}Be, ground state props. for rot. band in molecular model 77−54137
^{9}Be, struct., size, quadrupole moment, generator coord. method calc. 79−71788
^{9}Be(γ,π), photoabsorption and sum rules, structure, RMS radius, polarisability and exchange parameters 80−22686
C+p, 50 to 275 GeV/c, inclusive particle prod., nuclear size depend. 77−46168
^{A}C(π^-,π^-), (A=12,13), 29.2 and 49.5 MeV, neutron radii determ. 79−97653
^{A}C$(\pi^{\pm},\pi^{\pm})$, A=12,13, 180 MeV near (3,3) reson., nuclear RMS radii determ. 79−85538
^{12}C, α-cluster model, binding energy, RMS radii, and form factors 79−75825
^{12}C, α-particle model of ground and 0^+ excited states, hyperspherical method 77−6272
^{12}C, constrained variational calcs. for binding energy and RMS radii, N*(1234) allowance 79−3074
^{12}C, ground state props., modified Brueckner-Bethe-Goldstone method 78−50076
^{12}C(^{17}O,^{16}O), single-n sub-Coulomb transfer reactions, single particle wave function RMS radius, n-excess 79−85355
^{13}C(^{16}O,^{17}O)^{12}C, sub-Coulomb, RMS radii of single-particle orbitals, neutron excess 77−333
^{13}C(^{18}O,^{19}O)^{12}C, sub-Coulomb, RMS radii of single-particle orbitals, neutron excess 77−333
Ca isotopes, nuclear rms radii using Skyrme interaction with state depend. effective mass 79−45147
Ca, stable and radioisotopes, hfs, isotope shifts, dye laser saturation spectroscopy, beam expt. 80−58169
^{A}Ca, A=40, 44, pionic X-rays and neutron radius 79−36802
^{A}Ca, A=40, 48, single particle levels, rms charge radius, Wood-Saxon pot. 80−63106
^{A}Ca, A=40,48, nuclear radii, energy density and HF-BCS methods 80−47363
^{A}Ca, A=40 to 46,48, nuclear charge distrib., from isotope shift of 6573 angstrom line 80−57674
^{A}Ca+p, A=40, 44, 48, 700 MeV, total reaction cross section meas., matter radii 79−40924
^{A}Ca(α,α), A=40, 42, 44, 48, 104 MeV, cross sections and optical pots., nuclear size 80−68524
^{A}Ca(α,α), A=40, 42, 44, 48, 104 MeV nuclear size and density distrib. from folding model anal. 80−68525
^{A}Ca$(\pi^{\pm},\pi^{\pm})$, A=40,48, 180 MeV near (3,3) reson., nuclear RMS radii determ. 79−85538
^{40}Ca, ^{48}Ca RMS radii, RPA ground state correls., isotope effect 77−6238
^{40}Ca bulk props., ground state energies and RMS charge radii 78−58242
^{40}Ca, radius difference to ^{48}Ca, from 104 MeV alpha scatt. optical model calcs. 79−454
^{40}Ca root mean square radius series 79−36146
^{41}Ca $1f_{7/2}$ neutron radial distrib., single particle, orbits, RMS radii from ^{40}Ca(^{13}C,^{12}C) 80−42532
^{41}Ca, mean square nuclear charge radius, correl. with doubly magic ^{40}Ca 79−54385

nuclear size continued
^{43}Ca, nuclear charge radius, spin, moments, by laserspectroscopy 80−18187
^{48}Ca, neutron distribution radius, Nolen Schiffer anomaly 78−93933
^{48}Ca, neutron radius determ., charge symm. 78−29380
^{48}Ca, RMS neutron and proton radii difference, from pion-nucleus data 77−10436
^{48}Ca, radius difference to ^{40}Ca, from 104 MeV alpha scatt. optical model calcs. 79−454
^{48}Ca($\pi^{\pm},\pi^{\pm}$), optical pot. ambiguities, neutron radius determ. 79−17872
Ca(p,p), A=40,48, 1 GeV, spin-effects, Coulomb interactions, Glauber theory 77−82931
Ca($\pi^{\pm},\pi^{\pm}$), 130 MeV, A=40,48, π^{+}, π^{-} cross sections, neutron radius 78−25240
Cd, A=110, 116, difference in nuclear charge radius, X-ray isotopic shift meas. 77−18382
^{A}Cd, A=110, 112, 114, 116 nuclear charge radius differences 79−26365
^{A}Cl(e, e'), 116, 194 MeV, A=35, 37, charge distrib. and RMS charge radius 80−102109
^{59}Co(e,e), valence nucleon orbit determ. 78−54669
^{52}Cr, 1f nucleon orbit RMS radii from transfer data 80−27544
^{52}Cr($\pi^{\pm},\pi^{\pm}$), 180 MeV near (3,3) reson., nuclear RMS radii determ. 79−85538
Cs, HFS, isotope shift related to nucl. charge rad. 78−78826
^{A}Cs, A=133, 137-139, hyperfine struct., isotope shifts, nuclear moments and radii, laser spectroscopy 79−10071
^{A}Cs, A=138 to 142, nucl. moments and charge radii changes from hyperfine struct. and isotope shifts 79−17804
^{55}Fe $Zp_{3/2}$ neutron orbit radius isotone shift from DWBA anal. of ^{54}Fe(t,d) 80−32172
^{2}H D-state probability measurability in meson exchange current theory, moments and RMS radius 79−89246
^{2}H(e,e), charge and structure radius, form factor and structure function *(Russian)* 79−40841
^{3}H, props. calc. by interpolation approach *(Russian)* 77−22903
^{3}H, unitary scheme model anal. with Gogny, Pires and de Tourreil interaction 79−59016
^{3}H, virtual dissociation into deuteron and neutron, mean square radius *(Russian)* 79−3092
^{4}He, bulk props., ground state energies and RMS charge radii 78−58242
^{4}He, constrained variational calcs. for binding energy and RMS radii, N*(1234) allowance 79−3074
^{4}He, ground state props., modified Brueckner-Bethe-Goldstone method 78−50076
^{4}He, nucl. binding energy, radius and charge form factor, Brueckner calcs. 79−71787
^{4}He, structure in the translation-invariant oscillator basis *(Russian)* 78−25123
^{A}Hg, A=198-202 and 204, nuclear charge radii variations from K X-ray isotope shifts 78−70441
Kr isotopes, changes in nuclear charge radii 79−93504
^{6}Li, RMS radii, binding energy, electric quadrupole transitions using generalised hyperspherical functions *(Russian)* 78−86469
^{6}Li, transition probabilities between cluster structure states and r.m.s. radius, double well-cluster model *(Chinese)* 80−63128
^{7}Li, cluster model wave function and r.m.s. radius 78−70442
^{A}Li(γ,π), A=6, 7 80−22686
^{A}Mo, A=92, 94-98, 100, muonic atom X-ray transitions, nuclear charge radii 80−27545
^{93}Nb(e,e), valence nucleon orbit determ. 78−54669
Ni mean square charge radii from isotope shifts 80−99484
^{58}Ni, nuclear radii, energy density and HF-BCS methods 80−47363
^{60}Ni, Coulomb contributions to nuclear radii and energies 80−68515
^{61}Ni, populated in ^{60}Ni(t,d), neutron orbit radius determ. 77−38217
^{A}O(π^{-},π^{-}), (A=16,18), 29.2 MeV, neutron radii determ. 79−97653
^{A}O($\pi^{\pm},\pi^{\pm}$), A=16, 18, resonance region, proton and neutron distribs. 80−91195
^{16}O, 0^{+} states, appl. of K-harmonics method 78−54685
^{16}O, bulk props., ground state energies and RMS charge radii 78−58242
^{16}O, constrained variational calcs. for binding energy and RMS radii, N*(1234) allowance 79−3074
^{16}O, contrib. of meson exchange currents to charge density and RMS radius 77−10313
^{16}O, ground state props., modified Brueckner-Bethe-Goldstone method 78−50076
^{16}O, relativistic self-consistent nuclear model, separation energy, mean square radius *(Russian)* 79−97654
^{16}O(p,p), 1 GeV, spin-effects, Coulomb interactions, Glauber theory 77−82931
^{18}O, neutron deform. param. determ. from (π,π') scatt. 78−29502
^{18}O, RMS neutron and proton radii difference, from pion-nucleus data 77−10436
^{18}O+$\pi^{\mp}$, inelastic and elastic scatt., neutron-proton radius differences and isovector deform. 79−40963
^{18}O(^{17}O,^{16}O)^{19}O, sub-Coulomb, RMS radii of single-particle orbitals, neutron excess 77−333
^{19}O($\pi^{\pm},\pi^{\pm}$), 180 MeV near (3,3) reson., nuclear RMS radii determ. 79−85538
^{28}P, nucleon unbound states, spin, parity, partial width, from ^{28}Si(d,pn) 80−102118
^{208}Pb (p,p), 1 GeV, spin-effects, Coulomb interactions, Glauber theory 77−82931
^{208}Pb, nuclear radii, energy density and HF-BCS methods 80−47363
^{208}Pb+^{12,13}C, single-n sub-Coulomb transfer reactions, single particle wave function RMS radius, n-excess 79−85355
^{208}Pb+^{16,17,18}O, single-n sub-Coulomb transfer reactions, single particle wave function RMS radius, n-excess 79−85355
Pb(α,α), 104 MeV, nucl. matter sizes and isoscalar octupole transition rate 77−6422
^{294}Pu, muonic atom direct electroprod., finite nuclear size effects *(Russian)* 80−69272
^{A}Rb, A=90-93, nucl. moment and charge radius using fast-beam laser spectroscopy 79−40839
^{89}Rb, nucl. moment and charge radius using fast-beam laser spectroscopy 79−40839
^{32}S α-cluster struct., ground and first excited states, energies, radii and moments 80−102122
^{32}S, nuclear radii, energy density and HF-BCS methods 80−47363
^{32}S, transition densities, form factors and transient radii 79−6481
nuclear size continued
^{28}Si($\pi^{\pm},\pi^{\pm}$), 180 MeV near (3,3) reson., nuclear RMS radii determ. 79 85538
^{29}Si, nucleon unbound states, spin, parity, partial width, from ^{28}Si(d,pn) 80−102118
Sm, stable even isotopes, mean-square charge radii 79−67647
^{A}Sm, A=144-154, mean square nuclear charge radius, laser atomic beam spectroscopy 80−102468
^{A}Sn (t,α), 4.75-5.25 MeV, A=112, 116, 118, 120, 124, single proton states RMS radius 80−13350
^{A}Sn, A=113,115,117,118,119,120, rms neutron orbit sizes, DWBA anal. of Sn(t,d) data 79−36145
^{A}Sn, A=116 and 124, neutron matter densities and RMS radii 78−70526
Sn(p,n), even isotopes, 4-10 MeV, cross sections, optical parameters and nuclear radius A-depend. 80−57773
Sn(p,p_0), pol.p, 6.77-8.8 MeV, cross sections, optical parameters and nuclear radius A-depend. 80−57773
Sr isotopes, $1g_{9/2}$ nucleon-transfer reactions, spectroscopic factors 78−50068
^{87}Sr 1 $g_{9/2}$ neutron distrib. radial size, states, differential cross sections from ^{86}Sr(^{18}O,^{17}O) 80−95301
^{87}Sr(e,e), valence nucleon orbit determ. 78−54669
^{232}Th(γ,X) 5-18.3 MeV, photoneutron and photofission cross sections, giant resonance and deformations 80−68712
Ti, A=46,50, neutron radius determ., charge symm. 78−29380
^{A}Ti(α,α), A=46,48,50, 140 MeV, nuclear size comparison, optical model pot. 79−17913
^{51}Ti $Zp_{3/2}$ neutron orbit radius isotone shift from DWBA anal. of ^{50}Ti (t,d) 80−32172
Ti(p,d), A=46,48,50, DWBA calcs., rms radius pick-up reaction cross sections 79−541
^{A}U(γ,X), A=235, 236, 238, 5-18.3 MeV, photoneutron and photofission cross sections, giant resonance and deformations 80−68712
^{51}V, 1f nucleon orbit RMS radii from transfer data 80−27544
^{51}V(e,e), valence nucleon orbit determ. 78−54669
W+p, 50 to 275 GeV/c, inclusive particle prod., nuclear size depend. 77−46168
Xe, MS radius from K-X-ray isotope shifts 77−23454
^{68}Zn(^{3}He,^{3}He), elastic and inelastic scatt. angular distrib. fine struct. 80−106063
^{90}Zr, nuclear radii, energy density and HF-BCS methods 80−47363
^{90}Zr, proton orbit sizes and E0 matrix element for 2 lowest 0^{+} states 80−27546
^{90}Zr(p,p), 1 GeV, spin-effects, Coulomb interactions, Glauber theory 77−82931

nuclear spallation
A=23 to 127, photospallation, 0.1 to 1 GeV, mass yield distrib. 80−73835
A=80-240 nuclei, capture of stopped π^{-}, spallation, fission, new isotope synthesis 77−6459
book, spallation reactions and their applications 77−42005
breeder system, parametric anal. 77−61585
bremsstrahlung-induced reactions in nuclei with A=27-238, 450 MeV to 2.2 GeV *(German)* 78−33164
cosmology, high-energy spallation reactions rel. to D prod. 77−33709
emulsion nuclei, cosmic ray nuclei collisions, spallations produced by 0.1 to 1 GeV/nucleon nuclei, low energy particles *(Russian)* 78−33234
fission products, transmutation by spallation and neutron reactions using linear accelerator 78−13268
fragmentation by high energy particles, status of studies *(Russian)* 77−50100
high-energy fission in astrophysics, comparison of methods for cross sections calc. 78−28505
LWR fuel enrichment by linear accelerator 79−13497
mass yield formula for intermediate energy photospallation of medium weight nuclei 78−29445
mechanism and cross sections for γ and e induced reactions, Serber's two step model *(Japanese)* 78−74345
neutron beam research, spallation neutron sources 79−9926
neutron source, alternative π, μ and ν beam prod. and uses 78−66442
nuclear energy synergetics, charact. of integrated systems 79−13382
photon induced reactions, intermediate energies, isomeric cross-section ratios 77−41954
photospallation systematics, complementary study 78−17179
pion-induced spallation cross-section, systematics 79−6716
pulsed neutrons from spallation source, thermal neutron scatt. 77−83350
pulsed spallation neutron source, accelerator, target and moderator design 77−67930
pulsed spallation neutron sources 80−27852
reactor fuel breeding using proton linear accelerator 78−29630
reactor fuel enrichment by proton accelerator 79−13498
red giants, Li synthesis by spallation reactions 77−49366
short-lived products, spectroscopy, gas-jet recoil transport 77−23338
solar flares, thermonuclear reactions and spallation rel. to H and He isotopic comp. 77−45266
St. Severin chondrite, ^{53}Mn production due to nucl. spallation, depth-depend. 80−82316
UK pulsed spallation neutron source 79−45517
yield distribution calc. method, including isomeric state effects 79−93596
d+nucleus, 3.46-10.2 GeV/c, spallation, distrib. of spectator neutrons, theory and expt. comparison *(Russian)* 78−58290
$\nu(\bar{\nu})$d$\rightarrow$np$\nu(\bar{\nu})$, weak neutral currents, (V, A) and (S,T,P) theories 78−12893
(p, spallation), 0.08-24 GeV, Ar isotopes, spallation ratios and prod. cross sections 80−9284
(p, spallation), 480 MeV, medium to heavy mass targets, deep spallation products 80−83085
(p, spallation) cross sections for medial isotope preparation 77−23052
(p,X), 0.6-21 GeV, ^{A}Rb, A=83,84,86 prod. cross sections and recoil props. 80−9295
π^{-}-nucleus, 3.9 GeV/c, backward proton emission *(Russian)* 77−38302
Ag(^{12}C, spallation), 25.2 GeV, radionuclide prod. cross sections, charge dispersions and mass yield curves 79−67735
Ag(p,X), X=N to Ar, 2.1 and 4.9 GeV, fragment energy spectra, Maxwellian functional form 78−70529
Ag(p,f), product event cross-sections at 14, 18, 23 GeV 77−10411
Ag(p, spallation), 300 GeV, radionuclide prod. cross sections, charge dispersions and mass yield curves 79−67735

nuclear spallation continued
Al+p, 82-800 MeV, production of ^{7}Be, ^{22}Na, and ^{28}Mg 77−6388
Al(p,X), X=He to Na, 2.1 and 4.9 GeV, fragment energy spectra, Maxwellian functional form 78−70529
Al(p,x), spallation by 300 GeV protons, activation cross section meas. rel. to ^{12}C(p,pn)^{11}C 79−40898
^{197}Au(^{20}Ne, spallation), 8.0 GeV, cross sections and target residues, model comparison 80−68630
^{197}Au(d,X), E_d=13.6 MeV, d breakup anal. with neutron elastic scatt. 79−9540
^{197}Au(p,X), 0.2-6.0 GeV, product cross sections, mass yields, spallation products 80−83088
^{197}Au(p,x) ^{22}Na-^{196}Au, 1-100 GeV radionuclide recoil props., fission, fragmentation and spallation 79−3149
^{197}Au($\pi^{\pm}$, spallation), 100-300 MeV, cross sections for products A=167-196 80−27619
Ba fragments, differential ranges and ang. distribs. from ^{238}U(p,X) 79−67790
C stars, low-energy spallation rel. to ^{6}Li/^{7}Li ratio 78−40927
c+n in cellulose nitrate plastic detector, spallation products 78−17198
^{12}C+α, spallation fragments 6≤A≤11 yields, nucleosynthesis interest 79−30845
^{12}C(p, spallation), Li, Be, B prod., 45-100 MeV, nucleosynthesis and space radiation effects implications 77−23053
^{36}Cl prod. in proton induced high-energy spallation, cosmic ray effects 77−61421
^{59}Co, spallation by 0.3-1.0 GeV photons, cross-sections 78−41691
C(p,X) X=He to C, 2.1 and 4.9 GeV, fragment energy spectra, Maxwellian functional form 78−70529
C(π,πp), 170 MeV, two stage and knock out contribs., π^{+},π^{-} spallation differences *(Russian)* 80−68632
^{137}Cs, 10 GeV proton spallation for transmutation of radioactive waste, calc. of transmutation number 80−13470
Cu (γ,X), 2-5 GeV, spallation 77−71604
Cu spallation by 25 GeV ^{12}C and 28 GeV protons, mass yields 77−6435
Cu+^{40}Ar spallation, 80 GeV, 35 radioactive nuclide prod. cross sections 78−66260
Cu(^{12}C, spallation), 25 GeV, mean kinetic props., momentum transfer, target recoil props. 79−3129
Cu(p, spallation), 200, 350 MeV, radioactive residual nuclei prod. cross sections at (3,3) resonance 79−3130
Cu(p, spallation), 28 GeV, mean kinetic props., momentum transfer, target recoil props. 79−3129
Cu(π^{-}, spallation) 0.6, 0.9, 12 GeV, T=1/2 resonances, Na, Sc and Co rel. yields 80−5109
Cu(π^{-}, spallation), 500, 1570 MeV, product relative yields, charge dispersion and mass yield 79−6554
Cu($\pi^{\pm}$, spallation), 50-350 MeV, radioactive residual nuclei prod. cross sections at (3,3) resonance 79−3130
D production model limitations based on high-energy neutrino background 79−44328
Fe, spallation by 0.3-1.0 GeV photons, cross-sections 78−41691
Fe+p, high energy spallation, prod. cross sections of stable, long-lived nuclides 77−2998
^{56}Fe, hadron generated cascades, energy flux absorption length, 1-20 TeV *(Russian)* 78−28468
^{3}He(p,2p)d, 590 MeV, in noncoplanar geometry, two particle spallation, diffr. description *(Russian)* 78−33160
^{4}He(α,n)^{7}Be meas. and α-α elastic phase-shift calcs. 77−50143
^{10}He isotope search in ^{232}Th target nucleus spallation *(Russian)* 80−5110
^{172}Hf production, recovery and purification for nucl. medicine use as ^{172}Lu generator 78−48893
^{123}I production from ^{123}Xe formed in spallation reactions by 660 MeV protons, medical appls. 80−85494
^{127}I(p,5n)^{123}Xe→(β)→^{123}I, yield curves for cyclotron prod. of ^{123}I 78−44611
^{6}Li, Coulomb disintegration in field of heavy target nucleus, perturbation theory 78−66319
Mg+p, 82-800 MeV, production of ^{7}Be, ^{22}Na, and ^{28}Mg 77−6388
^{52}Mn, 2-5 GeV photospallation, ratios of isomeric yields *(Russian)* 78−46047
^{55}Mn, spallation by 0.3-1.0 GeV photons, cross-sections 78−41691
^{55}Mn(γ,X), 2-5 GeV, spallation 77−71604
Mo+α, A=92,96,100, isobaric yield curves at A=72 from high energy spallation 78−25211
N+n in cellulose nitrate plastic detector, spallation products 78−17198
^{14}N+α, spallation fragments 6≤A≤11 yields, nucleosynthesis interest 79−30845
^{17}N yields from proton-nucleus collisions, isotope depend. *(Russian)* 77−61429
^{93}Nb(α, X), 15-72 MeV, excitation functions and spallation cross-sections 80−18274
^{58}Ni spallation by 1 GeV protons, reaction channels *(Russian)* 78−74370
N(π,πp), 170 MeV, two stage and knock out contribs., π^{+},π^{-} spallation differences *(Russian)* 80−68632
O+n in cellulose nitrate plastic detector, spallation products 78−17198
^{16}O+α, spallation fragments 6≤A≤11 yields, nucleosynthesis interest 79−30845
O(π,πp), 170 MeV, two stage and knock out contribs., π^{+},π^{-} spallation differences *(Russian)* 80−68632
^{239}Pu, fissile fuel preparation by spallation of ^{238}U *(Russian)* 79−22441
^{44}Sc, 2-5 GeV photospallation, ratios of isomeric yields *(Russian)* 78−46047
SiO_2+p, 82-800 MeV, production of ^{7}Be, ^{22}Na, and ^{28}Mg 77−6388
^{181}Ta(^{20}Ne, spallation), 8.0 GeV, cross sections and target residues, model comparison 80−68630
Ta(p, spallation), 1 GeV, ^{A}Lu, neutron deficient isotopes, A=157, 158, 160, 161, 163 79−75957
^{232}Th(α,x), 140 MeV, spallation and fission product yields 80−13512
^{232}Th(p, spallation), spallation cross section and recoils, range calcs. computer code MARLOWE 79−93736
^{232}Th(p,X), 10-100 MeV, spallation residue excitation functions, fissionability 80−18353
^{233}U, fissile fuel preparation by spallation of ^{232}Th *(Russian)* 79−22441
^{238}U, deuteron and proton bombardment, excitation function determ. 78−41709
^{238}U+p, 1-300 GeV, production props. of Sc nuclei 77−6389
^{238}U(p,X), 0.8-11.5 GeV, formation of A=131 isobaric nuclides 80−9293

nuclear spallation continued
^{238}U(p,X), 400 GeV/c, unusual backward enhancement in product ang. distrib. 80−514
U(p,X), X=F to Ar, 2.1 and 4.9 GeV, fragment energy spectra, Maxwellian functional form 78−70529
^{51}V, spallation by 0.3-1.0 GeV photons, cross-sections 78−41691
^{51}V(γ,X), 2-5 GeV, spallation 2-5 GeV, spallation yields 77−71604
W(p, spallation), 1 GeV, ^{A}Lu, neutron deficient isotopes, A=157, 158, 160, 161, 163 79−75957
^{123}Xe production by 1 GeV proton spallation on Cs, Ba, La 79−63676
^{125}Xe production by 1 GeV proton spallation on Cs, Ba, La 79−63676
^{A}Zr(p,4pxn)Rb, A=90, 91, 94, spallation reactions, nuclear structure influence on yields of product nuclei 80−22794
^{A}Zr(p,6pxn)Br, A=90, 91, 94, spallation reactions, nuclear structure influence on yields of product nuclei 80−22794
Zr(p,4pxn)Rb spallation reactions, 1 GeV, meas. with online mass spectrometer *(Russian)* 77−10409

nuclear spectroscopic factors
1p-shell nuclei, absolute factors from 100 MeV (p,α) reaction 77−30574
2n(p) transfer reactions from ^{10}B collisions with ^{12}C,^{14}N,^{16}O 78−50207
^{56}Fe, neutron scatt., spectroscopic factors in particle vibrator model 78−70535
å ^{2}→cc ^{2} 79−36149
A=16 to 40 nuclei, α-spectroscopic factors, shell model calcs. 79−13204
A=19-31 odd nuclei, $K^{\pi}=^{1}/_{2}^{-}$ bands, spectroscopic factors and transitions 80−32151
A=21-24, spectroscopic factors for single nucleon transfer reactions 77−71563
A=21-39 odd sd shell nuclei, ground state alpha spectroscopic strengths 79−3104
A=21-44, single particle transfer reactions 77−46109
A=44 to 68, alpha particle transfer using interacting boson approx 78−78258
A-27,31, analog factors from (d,t) and (d,^{3}He) reactions 77−54229
amplitudes from nuclear reactions, applications 79−459
amplitudes from nuclear reactions, theory 79−458
cluster effects in nuclear scattering 77−67711
cluster spectroscopic factors in the K-harmonics method 78−62512
continuum shell model of decaying states, spectroscopic amplitudes, decay widths and partial widths 80−486
deformed nuclei, approximate projection technique for EM properties calc. 79−93510
deuteron form factors and spectroscopic factors in heavy spherical nuclei, shell model *(Russian)* 80−63078
double magic nuclei, one-hole states 78−17090
double stripping core independ. 2-nucleon transfer, Tang-Herndon effective interactions, (α,d), (t,p) 80−73836
double-magic nuclei, low lying states, self consistant description *(Russian)* 78−89783
empiracal $(1f_{7/2})^{n}$ model 79−17826
even actinides, lowest 0^{+} state excitation, collective phonon state, spectroscopic factors from (p,t), (t,p) 80−13410
even actinides, two-nucleon transfer, first 0^{+} collective state excitation, spectroscopic factor *(Russian)* 80−42530
fission isomers, spectrosc. props. 80−105966
four-nucleon pickup from ^{14}N 79−63679
ground-state alpha-cluster correlation in sd-shell nuclei 78−74314
hole spectral density in finite nuclei 79−63584
inner hole state excitation in (^{3}He,α) reactions *(French)* 78−41735
isobaric analogue resonances in f-p shell nuclei, unified-model description 78−78343
light nuclei, α-spectroscopic factors 77−50051
light nuclei, neutron and deuteron scatt. amp., dispersion anal. 78−29399
multi-nucleon transfer spectroscopy in shell model 77−65195
N=27 nuclei, spectroscopic study by means of (T,α) reaction 79−17808
N=28 nuclei, high spin states, shell model study 79−3087
nucleon transfer on odd-mass nuclei, spectroscopic sums, spin depend. 79−36219
odd mass nuclei, self-consistent quasiparticle-phonon coupling 77−54164
one-particle transfer reactions, spectroscopic information source *(Rumanian)* 79−17871
(p,d), DWBA calcs. RMS radius effects 79−541
p-shell nuclei, cluster spectroscopic factors, quasielastic cluster knockout theory, review, book contrib. 79−75874
p-shell nuclei, cluster spectroscopic factors 77−30486
quadrupole vibrations in two-nucleon transfer reactions 79−17786
shell model calculations, simplified techniques *(French)* 79−45188
Skyrme-type interactions, spectroscopy of light nuclei, density dependent Hartree-Fock 80−22717
Sn Z=50 region isotopes, system struct calcs. 80−18192
spectroscopic information from angular correlations and transfer reactions 77−54203
strong absorption model for the (α,2α) reaction 79−22306
symmetry breaking in the ground state region of nuclei, statistical meas. 78−8737
two-nucleon transfer reactions, quadrupole vibr. excitation sepctroscopic factor *(Russion)* 79−30780
(α,2α), A=9, 12, 16, 20, 22 80−68629
α-decay spectroscopic factors, coupled channel problem, local pots. justification 80−47439
α-spectroscopic factors, pseudo SU(3) approx. 78−70471
(d,^{6}Li), 54.25 MeV, α-cluster spectroscopic factors, DWBA anal. 80−52571
(d,^{6}Li), A=144-238, alpha-cluster transfer from alpha-decaying nuclei 80−91166
(d,p) Coulomb stripping reactions, spectroscopic factors 77−6394
^{A}Ag A=109,111, spectroscopic factors from d(d,^{3}He) 77−18369
^{27}Al isobaric analogue resonances, spectroscopic factors and γ-rays from (p,p), (p,γ) 80−86873
^{28}Al, levels and spectroscopic factors from ^{30}Si(d,α) 78−41728
^{36}Ar relative spectroscopic factors from ^{40}Ca(d,^{6}Li) 79−93509
^{39}Ar, spectroscopic factors from ^{40}Ar(p,d) DWBA calcs. 78−17204
^{41}Ar, spectroscopic factor absolute determ. in sub-Coulomb (d,p) reaction 79−30787
^{73}As bound and isobaric analogue states, spectroscopic factors, DWBA anal. of ^{72}Ge(^{3}He,d) 79−54391
^{76}As low lying state spectroscopic factors from ^{75}As(d,p) 77−10319
^{A}B(α,^{8}Be), A=9,10, 65-72.5 MeV α-spectroscopic factors 77−6418

nuclear spectroscopic factors continued
^{10}B, α-transfer reactions, spectroscopic factors, exact finite range DWBA anal. 80−13372
^{10}B(d,p)^{11}B, 0.8 to 2.4 MeV, spectroscopic factors, reaction mechanism 79−17910
^{11}B, analogue states from ^{12}C(d,^{3}He), DWBA calcs. 78−82285
^{11}B, from ^{10}B(d,p) 1 to 2 MeV reaction 77−41977
^{11}B, positive parity states, spectroscopic factors 77−34228
^{11}B states, spectroscopic factors from DWBA anal. of ^{12}C(p,2p) 80−5057
^{138}Ba, α=spectroscopic factors from (d,^{6}Li) 77−18571
^{8}Be, multi-nucleon transfer spectroscopy from ^{12}C(p,^{6}Li) 78−46058
^{8}Be, isospin mixed states, spectroscopic factors 77−65198
^{9}Be, spectroscopic factors from (^{9}Be,^{8}Be) 78−17098
^{9}Be, spectroscopic factors from reactions on ^{29}Si and ^{41}Ca 78−70552
^{11}Be, spectroscopic factors from 25MeV ^{10}Be(d,p) reaction 79−36156
^{209}Bi levels and spectroscopic factors, ^{210}Bi(9$^-$) parentage from ^{210}Bi^m(d,t) 80−78158
^{209}Bi low lying levels and spectroscopic factors, EFR-DWBA anal. of ^{208}Pb(^{7}Li, ^{6}He) 80−32182
^{209}Bi, multiplet struct., pairing modes, role 78−12973
^{209}Bi, neutron resonance spectroscopy 78−37322
^{209}Bi single partjcle levels, ang. distribs., spectroscopic factors, DWBA anal. of ^{208}Pb(^{7}Li,^{6}Me) 80−63067
^{209}Bi(^{3}He,d), 30 MeV, effective residual interaction matrix elements, spectroscopic factors, cross sections 80−99134
^{209}Bi(α,t), 40 MeV, effective residual interaction matrix elements, spectroscopic factors, cross sections 80−99134
^{201m}Bi(t,α)^{209}Pb, single neutron states spectroscopic factors 77−34320
^{247}Bk, 1/2$^-$[521] proton orbital and stability 77−67698
^{247}Bk proton states, transitions and spectroscopic factors from (α,t), α-decay, electron capture 79−89224
^{A}Br, A=(77,79) levels and spectroscopic factors from Se(^{3}He,d) 78−86479
^{78}Br level struct. determ. from (α,nγ), (^{3}He,d) and (p,d) reacts. 79−59010
^{80}Br, level struct. spectroscopic factors in ^{81}Br(p,d) reaction 79−3084
^{A}C(α,^{8}Be), A=12,13, 65-72.5 MeV α-spectroscopic factors 77−6418
^{11}C, low lying analogue states from ^{12}C(d,t), DWBA calcs. 78−82285
^{11}C, spectroscopic factors from ^{9}Be(^{3}He,n) and Coulomb distorted wave eqns. 79−40938
^{11}C, states below 8.7MeV, DWBA calcs. 78−78396
^{12}C, α-transfer reactions, spectroscopic factors, exact finite range DWBA anal. 80−13372
^{12}C, α-transfer spectroscopic factors for O$^+$, 2$^+$ and 4$^+$ states, transitions from (d, ^{6}Li) 80−13370
^{12}C, from (p,pd), (p,pt), (p,p^{3}He) 75 MeV reactions 77−54214
^{12}C, isoscalar giant quadrupole resonances, RPA calcs., E2 strength fragmentation, spectroscopic factors 80−13437
^{12}C, spectroscopic factors energy lepend in *16*O(d,^{6}Li) 78−74372
^{12}C, spectroscopic factors from ^{12}C(d,^{6}Li) 78−94013
^{12}C(^{13}C,^{13}C), 12 MeV, ^{13}C-^{12}C+n spectroscopic factor determ. 77−65194
^{12}C(^{7}Li, ^{7}Li), 40 MeV, spectroscopic factors, DWBA anal. 79−75904
^{13}C spectroscopic factors, cross sections DWBA anal. optical model parameters from ^{12}C(^{16}O,X) 80−13371
^{13}C, spectroscopic factors from ^{11}B(^{3}He,n) and Coulomb distorted wave eqns. 79−40938
^{13}C(^{6}Li, ^{6}Li), 40 MeV, spectroscopic factors, DWBA anal. 79−75904
^{14}C proton shell closure, p transition spectroscopic factors, DWBA calcs. for (^{3}He,d), (t,^{3}He) 79−80871
^{14}C spectroscopic factors, cross sections DWBA anal. optical model parameters from ^{12}C(^{16}O,X) 80−13371
Ca isotopes, $f_{7/2}$ neutron occupancies 78−78240
^{A}Ca, (a=41,43), non-energy weighted sum rule 77−67730
^{A}Ca, A=41,43,45,49, spectroscopic factors from (d,p) *(German)* 77−18567
^{A}Ca(^{12}C,^{8}Be), (A=40,42,44,48), 45 MeV, spectroscopic factors 77−88172
^{31}Ca, low lying analogue state from ^{40}Ca(d,t), DWBA calcs. 78−82285
^{40}Ca, α-particle spectroscopic factors 79−45157
^{40}Ca, spectroscopic factors from DWBA calcs of (^{9}Be,^{8}Be) reaction 78−17239
^{40}Ca, weak s resonance γ-ray decay in negative parity low lying levels 80−27591
^{40}Ca(^{11}B,^{10}B), 51.5 MeV, n stripping, DWBA anal. with Woods-Saxon and double folding optical pots. 80−102171
^{40}Ca(^{11}B,^{12}C), 51.5 MeV, p pickup, DWBA anal. with Woods-Saxon and double folding optical pots. 80−102171
^{40}Ca(d,^{6}Li), 80 MeV, ground state α-spectroscopic factors, ^{36}Ar relative spectroscopic factors 79−93509
^{42}Ca, $(f_{7/2})^2$, $f_{7/2}p_{3/2}$, $f_{7/2}p_{1/2}$ multiplets, from ^{41}Ca(d,p) 78−74374
^{42}Ca(p,p) 0.5, 3.0 MeV, spectroscopic factors 77−6374
^{49}Ca, spectroscopic factors from ^{48}Ca(d,p) 78−78391
Cd 2_1^+ excitation, α-spectroscopic factors in IBA model from Sn(d,^{6}Li) 80−105967
Cd, α-spectroscopic factors from (d, ^{6}Li) 80−534
^{114}Cd, proton hole states from ^{115}In(d,^{3}He) 78−8829
^{A}Ce, (A=138,140), from (p,p') and (p,t) reactions 77−54227
^{A}Ce, A=140,142, α-spectroscopic factors from (d,^{6}Li) 77−18571
^{141}Ce levels, single neutron holes, spectroscopic factors, DWBA anal. of ^{142}Ce(d,t), (^{3}He,α) 79−85353
^{143}Ce quasi-$f_{7/2}$ low lying states spectroscopic factors, cluster-vibr. model from ^{142}Ce(d,p) 80−47391
^{38}Cl, from ^{37}Cl(n,γ) reaction 77−30583
^{55}Co f-wave resonances, inelastic p amplitudes, analogue state spectroscopic factors from ^{54}Fe(p,p'γ) 80−47451
^{55}Co, from 25 MeV ^{54}Fe(τ,d)^{55}Co reaction 77−88029
^{55}Co isobaric analogue resonances, J$^\pi$, partial widths and spectroscopic factors from ^{54}Fe(p,γ), (p,p') 79−85431
^{57}Co, (3/2$^+$ state), anomalous analyzing power, DWBA calc. from ^{60}Ni(p,α) 80−86894
^{59}Co, from 27.2 MeV (α,t) reaction 77−38290
^{60}Co, levels and spectroscopic factors from Co(d,p) 78−86478
^{63}Co, proton hole state determ. from ^{64}N,(d,^{3}He) 79−22163
^{49}Cr, levels and spectroscopic factors from ^{50}Cr(τ,α) 78−33199
^{50}Cr(p,p), (p,p'), 3.2 to 4.4 MeV, ^{51}Mn level study 77−54151
^{51}Cr, level struct. from ^{50}Cr(d,p) 12 MeV reaction 77−50059
^{51}Cr levels, spectroscopic function and analogue states, PWBA anal. of ^{53}Cr(^{3}He,α) 80−68547
nuclear spectroscopic factors continued
^{52}Cr(d,p)^{53}Cr, Coulomb stripping, 2.12-2.48 MeV, DWBA anal., spectroscopic strengths 80−516
^{A}Cu, (A=58-68), from shell model calcs. 77−22860
^{A}Cu, A=59,61,63,65 exact spectroscopic strengths from Ni(^{3}He,d) 77−10303
^{60}Cu, levels, spectroscopic factors from ^{60}Ni(^{3}He,t) 78−46079
^{63}Cu, proton hole state determ. from ^{64}Zn(d,^{3}He) 79−22163
^{166}Er, α-spectroscopic factors from (d,^{6}Li) 77−18571
^{167}Er, levels and spectroscopic factors from ^{168}Er(d,t) 78−17222
^{167}Er, spectroscopic factors from ^{168}Er(d,t) 79−495
^{251}Es, 1/2$^-$[521] proton orbital and stability 77−67698
^{19}F, coupled channel orthogonality condition model 80−47384
^{19}F, relative spectroscopic factors from ^{16}O(α,p) 77−14140
^{19}F, spectroscopic factors from (^{13}C,^{9}Be) 77−14033
^{19}F(α,αp), 140 MeV, quasifree p knockout, spectroscopic factors, DWIA anal. 79−67650
^{20}F, levels and spectroscopic factors from ^{19}F(d,p) 78−25118
^{A}Fe, A=54-56, high spin states, energy levels, spectroscopic factors, EM props., shell model 80−47359
^{A}Fe, A=56,57, spectroscopic factors in semi-microscopic model 77−2912
^{A}Fe(^{16}O, ^{12}C), 50 MeV, a=54, 56, 58, α-spectroscopic factors, DWBA anal., (^{6}Li, d) comparison 79−63585
^{53}Fe, from 18 MeV ^{54}Fe(^{3}He,α) reaction 77−74767
^{53}Fe, spectroscopic factors from 40MeV ^{54}Fe(p,d) reaction 79−22287
^{55}Fe levels, J$^\pi$, spectroscopic factors, DWBA anal. of ^{56}Fe(^{3}He,α) 80−99127
^{56}Fe, fp shell model calcs., spectra and spectroscopic factors 80−68588
^{A}Ga, (A=69,71,73,75), levels and spectroscopic factors from Ge(d,^{3}He) 78−82279
^{68}Ga, from ^{69}Ga(d,t) and ^{70}Ge(d,α) 77−57603
^{71}Ge, levels and spectroscopic factors from ^{68}Zn(α,nγ) 78−8742
^{71}Ge negative parity states, J$^\pi$, energy spectra and spectroscopic factors 79−59013
^{74}Ge, 26 MeV levels from As(d,^{3}He) 78−25112
^{74}Ge, from elastic and inelastic proton scatt. 77−34278
^{2}H(α,αp), 140 MeV, quasifree p knockout, spectroscopic factors, DWIA anal. 79−67650
^{3}He spectroscopic strengths from ^{13}C(^{6}Li,t) 80−47390
^{A}Ho,(A=167,169), spectroscopic factors from ^{168,170}Er(t,α) reaction 79−36155
^{A}I, (A=123,125), from (^{3}He,d) reactions 77−34230
^{A}I, A=121 to 131, comparative study of proton states excited by (α,t), (^{3}He,d) 79−63572
^{A}In, A=119, 121, unified model description, vibr. multiplet yrast struct., branching ratios 80−105953
^{39}K, low lying analogue states from ^{40}Ca(d,^{3}He), DWBA calcs. 78−82285
^{39}K states and spectroscopic strengths DWBA anal. of ^{40}Ca(^{7}Li,^{8}Be) 80−5069
^{40}K energy levels and spectroscopic strengths from ^{41}Ca(d,^{3}He) 79−89238
^{42}K, energy levels and spectroscopic factors from ^{41}K(d,p) reaction 79−17806
^{85}Kr positive-parity states calc. by quasiparticle phonon coupling 79−75845
^{85}Kr, structure information from ^{84}Kr(d,p) and ^{84}Kr(d,po) 79−471
^{6}Li, EM form factors and spectroscopic factors in phenomenological cluster models 80−496
^{6}Li, nucleon spectral function, K-harmonics calc. 79−75834
^{6}Li(α,αp), 140 MeV, quasifree p knockout, spectroscopic factors, DWIA anal. 79−67650
^{6}Li(n,γ), cross section and spectroscopic factors from direct capture pot. model 80−99171
^{6}Li(p,γ), cross section and spectroscopic factors from direct capture pot. model 80−99171
^{6}Li(p,pd), 670 MeV, large angle quasifree scatt., spectroscopic factor, momentum distrib., cluster model 80−63184
^{A}Li, (A=6,7), from 56.3 MeV (n,d) reaction 77−88140
^{175}Lu, muonic, nuclear spectroscopic ground state quadrupole moments from X-rays 79−98252
^{A}Mg(d,^{6}Li), 80 MeV, A=24, 26, ground state α-spectroscopic factors 79−93509
^{A}Mg(d,^{6}Li), 80 MeV, A=24,26, α-spectroscopic factors and ang. distribs., DWBA anal. 80−99126
^{22}Mg, 2-nucleon transfer spectroscopic amplitudes from ^{24}Mg(p,t) 77−321
^{23}Mg hole states, transitions and spectroscopic factors, DWBA anal. of ^{24}Mg(p,d) 80−32161
^{23}Mg, low lying analogue states from ^{24}Mg(d,t), DWBA calcs. 78−82285
^{24}Mg, ^{16}O+α+α cluster model, energy level structure 80−18215
^{24}Mg, from 157 MeV (p,pα) quasi-free scatt. 77−88121
^{24}Mg, K$^\pi$=0$^-$, K$^\pi$=3$^-$ bands, radiative and α-widths from (α,γ), (^{16}O,$\alpha\gamma$) 80−18173
^{25}Mg, excited states, spectroscopic factors from ^{24}Mg(d,p) 78−8826
^{26}Mg, excited states, spectroscopic factors from ^{26}Mg(p,p) 78−78377
^{26}Mg, levels and spectroscopic factors from ^{27}Al(n,d) 78−4935
^{27}Mg energy levels, spectroscopic factors, DWBA, Hauser-Feshbach anals. from ^{26}Mg(d,p) 80−52581
^{A}Mn, (A=51,3), spectroscopic factors from ^{50,52}Cr(^{3}He,d) DWBA anal. 79−22203
^{55}Mn, α-particle spectroscopic strengths 79−45156
^{A}Mo, (A=93,95), from 40 MeV ^{94,96}Mo(p,d) reaction 77−74748
^{93}Mo, shell model calcs., energy levels, transitions and spectroscopic factors 79−63593
^{A}N, (A=14,15), α-transfer spectroscopic factors 79−26454
^{A}N, (A=57-67), from shell model calcs. 77−22860
^{A}N(α,^{8}Be), A=14,15, 65-72.5 MeV α-spectroscopic factors 77−6418
^{13}N, ground state factors from p+^{12}C scatt. dispersion anal. 77−34297
^{13}N spectroscopic factors from ^{12}C(^{3}He,d) 77−10418
^{14}N, α-transfer reactions, spectroscopic factors, exact finite range DWBA anal. 80−13372
^{14}N spectroscopic factors, cross sections DWBA anal. optical model parameters from ^{12}C(^{16}O,X) 80−13371
^{15}N, low lying analogue states from ^{16}O(d,^{3}He), DWBA calcs. 78−82285
^{15}N low lying states, cross sections and anal. power, transitions, spectroscopic factors from ^{14}N(d,p), pol. d 80−32183
^{16}N, DWBA calcs from ^{17}O(d,^{3}He) 78−58288
^{23}Na, alpha spectroscopic factors from ^{19}F(^{6}Li,d) 78−82383

nuclear spectroscopic factors continued
^{23}Na, α-transfer spectroscopic factors 79−36145
^{23}Na level α-spectroscopic strengths assuming direct cluster transfer from ^{19}F(^{6}Li,d) 80−27552
^{23}Na levels and spectroscopic amplitudes, J^{π} assignments, high spin states from ^{20}Ne(α,p) 79−75848
^{23}Na, low lying analogue states from ^{24}Mg(d,^{3}He), DWBA calcs 78−82285
^{A}Nb, (A=93,5,7), quasiparticle-phonon coupling model calcs. 79−472
^{92}Nb low lying multiplets, DWBA anal. for spectroscopic factors from ^{91}Zr(α,t) 80−57685
^{92}Nb, shell model calcs., energy levels, transitions and spectroscopic factors 79−63593
^{93}Nb(^{3}He,α), 19.4 MeV, spectroscopic factors and pick-up strength 77−88154
^{A}Nd, A=142,144,146, α-spectroscopic factors from (d,^{6}Li) 77−18571
^{A}Nd, A=145, 147, 149, single neutron hole states spectroscopic factors, DWBA anal. of (d,t), (^{3}He,α) 80−78109
^{143}Nd, levels and spectroscopic factors from ^{144}Nd(d,t) 78−89791
^{20}Ne, 2-nucleon transfer spectroscopic amplitudes from ^{22}Ne(p,t) 77−321
^{20}Ne, 8p-4h O^{+} state, alpha decay, branching ratios 78−50132
^{20}Ne, alpha spectroscopic factors from ^{24}Mg(d,^{8}Li) 78−78352
^{20}Ne, α-particle spectroscopic strengths for levels up to 12.15 MeV 79−26451
^{20}Ne, α-transfer reactions, spectroscopic factors, exact finite range DWBA anal. 80−13372
^{20}Ne from ^{16}O(^{16}O,^{12}C)^{20}Ne, polarisation measurements 80−9301
^{20}Ne, spectroscopic factors from (^{13}C,^{9}Be) 77−14033
^{20}Ne(d,^{6}Li), 80 MeV, ground state α-spectroscopic factors 79−93509
^{20}Ne(e,e'α), EM induced α emission, α spectroscopic amplitudes, anal. solvable model 80−32267
^{20}Ne(γ,α), EM induced α emission, α spectroscopic amplitudes, anal. solvable model 80−32267
^{21}Ne, alpha particle spectroscopic factors in stripping reaction ^{17}O(^{6}Li,d) 79−516
^{21}Ne, spectroscopic factors, pickup strengths in ^{22}Ne(^{3}He,α) at 15 MeV 79−63684
^{22}Ne, α-spectroscopic strengths from ^{18}O(^{6}Li,d) 77−18594
Ni, α-particle spectroscopic factors 79−45158
Ni, fp shell model calcs., spectra and spectroscopic factors 80−68588
^{A}Ni, A=59,61,63,65, spectroscopic factors from (d,p) *(German)* 77−18566
^{59}Ni, spectroscopic factors in semi-microscopic model 77−2912
^{60}Ni deduced levels from ^{58}Fe(^{16}O,^{14}C)^{60}Ni, DWBA anal., spectroscopic strengths 80−47380
^{61}Ni, from ^{60}Ni(t,d) at sub-Coulomb energies 77−38217
^{62}Ni, collective states, spectroscopic factors 77−61433
^{A}O, (A=17,18), one neutron spectroscopic factors 78−54783
^{15}O, low lying analogue states from ^{16}O(d,t), DWBA calcs. 78−82285
^{16}O (α, 2α), DWIA calc., cross section and spectroscopic factors 79−63681
^{16}O, alpha particle spectroscopic factors, from ^{12}C(^{7}Li,T) 78−89896
^{16}O, alpha spectroscopic strengths from ^{12}C(^{6}Li,d) 20-34 MeV reaction 79−569
^{16}O, alpha-spectroscopic amplitude anal. 79−13203
^{16}O α-cluster states, widths and resonances, optical model, direct transfer in ^{12}C(^{6}Li,d) 80−105975
^{16}O, α-spectroscopic factors in Zuker, Buck and McCrory shell model 77−71564
^{16}O, α-transfer reactions, spectroscopic factors, exact finite range DWBA anal. 80−13372
^{16}O, configuration mixing, alpha cluster transfer 78−46004
^{16}O, DWBA calcs from ^{17}O(d,t) 78−58288
^{16}O, from 21.8 MeV ^{12}C(^{7}Li,d)^{16}O reaction 77−82880
^{16}O, from (p,pd), (p,pt), (p,p^{3}He) 75 MeV reactions 77−54214
^{16}O, inelastic form factors in K-harmonics method *(Russian)* 78−25113
^{16}O, isoscalar giant quadrupole resonances, RPA calcs., E2 strength fragmentation, spectroscopic factors 80−13437
^{16}O(α,^{8}Be), 65-72.5 Mev, α-spectroscopic factors 77−6418
^{16}O(e,e), spectroscopic amplitude determ. 80−5127
^{17}O, spectroscopic factors DWBA calcs from ^{18}O(d,t) 78−66287
^{18}O, from (d,t), (d,τ) 52 MeV reactions 77−41980
^{18}O+^{18}O, one and two neutron transfer reactions 78−8837
^{29}P, data anal. from ^{28}Si(^{3}He,d) 78−66294
^{29}P excitation functions and spectroscopic factors from ^{28}Si(p,γ) resonant and direct capture 79−80912
^{30}P positive parity states, transitions and spectroscopic strengths, DWBA anal. of ^{29}Si(^{3}He,d) 80−102138
^{32}P, levels, spectroscopic factors from ^{31}P(d,p) 78−74371
^{A}Pb, A=205-207, neutron hole states, spectroscopic factors, DWBA anal. of Pb(^{3}He,α) 80−47352
^{205}Pb, excited states, from ^{204}Pb 77−30478
^{205}Pb, from ^{204}Pb(d,p) reaction, particle states 77−34216
^{207}Pb, inner hole states, spectroscopic factors from ^{20} u8Pb(^{3}He,α) 70 MeV reaction 79−17813
^{207}Pb, T=45/2 inner hole states, spectroscopic factors from DWBA calc. 78−93928
^{208}Pb single particle and hole states, renormalisation, core polarisation, spectroscopic factors 80−57658
^{208}Pb, spectroscopic factors from DWBA calcs of (^{9}Be,^{8}Be) reaction 78−17239
^{208}Pb(^{3}He,d), 30 MeV, effective residual interaction matrix elements, spectroscopic factors, cross sections 80−99134
^{208}Pb(^{6}Li,d), 90 MeV, alpha-cluster transfer from alpha-decaying nuclei 80−91166
^{208}Pb(α,t), 40 MeV, effective residual interaction matrix elements, spectroscopic factors, cross sections 80−99134
^{208}Pb(d,^{6}Li) ^{204}Mg, SS MeV, levels and spectroscopic factors, α clustering, DWBA anal. 79−67694
^{211}Pb, spectroscopic factors from ^{210}Pb(t,d) 78−17108
^{109}Pd levels, J^{π}, transitions, unique parity states, and spectroscopic factors from ^{108}Pd(n,γ) 80−42547
^{A}Pm, A=143-153, odd-A, spectroscopic factors, shell model anal. from pickup and stripping reactions 80−78137
^{149}Pm single proton states, spin assignments, spectroscopic factors from ^{150}Sm(t,α), pol.t 80−18170
^{151}Pm single proton states, rot. bands, level J^{π} assignments, spectroscopic strengths from ^{150}Nd(^{3}He,d), and ^{152}Sm(t,α) 79−67626
^{153}Pm, structure information from ^{154}(T,α) 79−469
^{142}Pn, deduced levels, spectroscopic factors, ^{144}Sm(^{3}He,αp) 78−70451

nuclear spectroscopic factors continued
^{A}Po, (A=209,211) deduced levels, J^{π} assignments, spectroscopic factors-from stripping and pick-up reactions 79−22197
^{212}Po, shell model α-spectroscopic factors 80−32245
^{A}Pt, (A=191,193,195,197), levels, spectroscopic factors, from n pick-up reaction 78−50089
^{A}Pt, (A=193,5,7) neutron pick-up spectroscopic factors 78−8810
^{197}Pt, states and spectroscopic factors from (d,p), (d,t) and (u,γ) 78−78267
^{A}Ru, (A=101,3,5), spectroscopic factors in quesi particle-phonon coupling model 79−22231
^{A}Ru, A=97,101, spectroscopic factors from ^{96,100}Ru(d,p) 77−18570
^{32}S, levels and spectroscopic factors from ^{31}P(^{3}He,d) 78−78265
^{32}S, levels and spectroscopic factors, DWBA anal. from ^{28}Si(^{16}O,^{12}C) 79−22204
^{32}S levels and spectroscopic factors from pickup DWBA anal. of ^{33}S(^{3}He,α) 80−9235
^{34}S(p,p), 1.45-2.85 MeV, differential cross sections 77−71564
^{35}S, from ^{34}S(d,p)^{35}S 11.8 MeV reaction 77−88149
^{A}Sb, A=123,125,127,129, cross-sections, ang. distribs., spectroscopic factors, DWBA anal. of Te(t,α) 80−52572
^{116}Sb, levels and spectroscopic factors from ^{115}Sn(^{3}He,d) 78−66295
^{122}Sb, spectroscopic factors for one neutron transfer reactions 77−61378
^{127}Sb states, collective neutron excitation role, spectroscopic factors and form factors from ^{30}Te(p,α) 79−67622
^{A}Sc, A=45, 47, 49 positive parity states from Ti(d,^{3}He)Sc reactions 79−97656
^{42}Sc two particle states, spectroscopic strengths and J^{π} values from ^{41}Ca(^{3}He,d) 79−63591
^{45}Sc, from 27.2 MeV (α,t) reaction *(Russian)* 77−38290
^{45}Sc, neutron stripping and pick up, sum rule anal. 78−8828
^{45}Sc, non-energy weighted sum rule 77−67730
^{49}Sc proton single particle states, spectroscopic factors, DWBA anal. of ^{48}Ca(d,n) 80−99118
^{A}Se, (A=77,79,81,83), struct. study in Se(d,p) 78−89885
^{A}Se, A=75, 77, 79, 81, levels and ang. distribs., spectroscopic factors from Se(p, d) 80−22696
^{75}Se, levels, spectroscopic factors from ^{74}Se(d,p) 78−66285
^{80}Se(p,n)^{80}Br, isobaric resonances, spectroscopic factors 79−36212
^{A}Si, (A=29,30), spectroscopic factors from ^{26}Mg(^{14}N,^{10,11}B) 78−66299
^{28}Si, isoscalar giant quadrupole resonances, RPA calcs., E2 strength fragmentation, spectroscopic factors 80−13437
^{28}Si, spectroscopic factors from DWBA calcs of (^{9}Be,^{8}Be) reaction 78−17239
^{29}Si levels, J^{π}, spectroscopic factor, DWBA anal. of ^{28}Si(^{3}He, ^{2}He) 80−86811
^{29}Si, spectroscopic factors, short-range correlations from ^{28}Si(D,p) 78−572
^{A}Sm, A=144,148,150,154, α-spectroscopic factors from (d,^{6}Li) 77−18571
^{A}Sm, A=148, 150, 152, 154, levels, moments, isomer shifts, spectroscopic amplitudes, sixth order boson expansion 79−89242
^{151}Sm, neg. parity states, particle rotor model 78−50080
Sn 2_1^+ excitation, α-spectroscopic factors in IBA model from Te(d,^{6}Li) 80−105967
Sn, α-spectroscopic factors from (d, ^{6}Li) 80−534
Sn, odd isotopes, deeply bound hole states, gross struct. 78−93930
Sn, odd isotopes, one-nucleon transfer spectroscopic factors 78−93953
^{A}Sn, (A=115,117,118,121,123), deeply bound hole states, study in neutron pickup reactions 77−30570
^{A}Sn, A=111,115,119, neutron hole distribs., IAS and spectroscopic factors from Sn(^{3}He,γ) 80−42519
^{116}Sn+^{16}O, two proton transfer reactions 78−8836
Sr, lg$_{9/2}$ nucleon distrib. from nucleon transfer reactions 78−50068
^{A}Sr, (A=87,89), from (d,p) and (p,d) reactions 77−88150
^{89}Sr, energy levels, spectroscopic factors from ^{88}Sr(d,p) 78−66286
^{96}Tc even mass odd nucleus, proton spectroscopy, from ^{95}Mo(^{3}He,d), shell model anal. 79−63573
^{98}Tc, levels and spectroscopic factors from 99Te(p,d) 78−25183
^{98}Tc spectroscopic factors from ^{99}Tc(d,t), (p,d) 77−18370
^{131}Te γ-transitions, spectroscopic factors and reduced transition intensities from ^{130}Te(n,γ) 80−91143
^{A}Ti, A=44, 48, ang. distribs. for transitions, DWBA anal., spectroscopic strengths from Ca(^{7}Li,t) 80−68584
^{49}Ti, non-energy weighted sum rule 77−67730
^{A}Tl, (A=203,205), intermediate coupling model calcs. 77−38276
^{204}Tl neutron hole states, J^{π} and spectroscopic factors from ^{205}Tl(p,d) 80−86783
^{51}V, from 27.2 MeV (α,t) reaction *(Russian)* 77−38290
^{51}V, non-energy weighted sum rule 77−67730
^{80}Y, high resolution neutron total cross sections 78−25193
^{87}Y, spectroscopic amplitudes from isobaric analog reson. meas. 77−61396
^{90}Y low lying multiplets, DWBA anal. for spectroscopic factors from ^{91}Zr(d,^{3}He) 80−57685
^{90}Y, shell model calcs., energy levels, transitions and spectroscopic factors 79−63593
^{94}Y, deduced levels, spectroscopic factors, ^{96}Zr(^{3}He,αp) 78−70451
Zn, α-particle spectroscopic factors 79−45158
^{A}Zn, (A=68,70), 26 MeV levels from Ga(d,^{3}He) 78−25112
^{62}Zn ang. distribs. for transitions, DWBA anal., spectroscopic strengths from ^{58}Ni(^{7}Li,t) 80−68584
^{63}Zn, neutron pick-up spectroscopic factors 79−465
^{67}Zn, from ^{66}Zn(d,p) 12 MeV reaction 77−22891
^{67}Zn, negative parity states, cluster-vibration coupling 77−34206
^{68}Zn, collective states, spectroscopic factors 77−61433
^{89}Zr, deeply bound hole states, isobaric analog states 78−492
^{91}Zr, shell model calcs., energy levels, transitions and spectroscopic factors 79−63593
^{92}Zr level struct. and reduced spectroscopic factors from ^{91}Zr(d,p) 80−32192
^{95}Zr, neutron-hole strengths, isobaric analogue states 78−508

nuclear spin and parity
see also nuclear isospin
1f$_{7/2}$-shell nuclei, selective population of high-spin states in heavy ion reactions 77−18374
^{116}Xe quasi-rotational bands, levels J^{π} and $T_{1/2}$ from ^{116}Cs decay 80−83021
^{18}F levels, J^{π} and ang. distribs, DWBA anal. of ^{19}F(p,d) 80−42545
^{22}Na, resonance levels obs. in ^{20}Ne(d,p$_0$) 78−46072

nuclear spin and parity continued
^{238}Np energy level scheme determ. by Nilsson model 79−26370
^{149}U vibr. states, obs. in ^{238}U(n,γ) 78−41627
^{24}Mg radiative decays of unbound high spin states from ^{20}Ne(α,γ), ^{20}Ne(α,α′γ) 79−6484
A=105, nuclear data sheets, levels, decays and J^{π} assignments 79−93486
A=110-210 nuclei, new parameters of deformed Woods-Saxon pot. 78−93951
A=12, recoil polarisation in muon capture, arbitrary nuclear spin, form factors 79−75978
A=12 to 40, (α,^{2}He) reaction, high spin state transition cross sections in 1p and 2s1d shell 79−6644
A=144 nuclear data sheets, levels, decays and J^{π} assignments 79−93487
A=149, data sheets to August 1974 77−10305
A=159, nuclear data sheets, levels, decays, and J^{π} assignments 79−93488
A=160-180 nuclei, manifestations of oblate shapes at high spin, transition energies in yrast region 78−78249
A=16, (π^-, γ) and (μ^-, ν_μ) capture reactions on ^{16}O, positive and negative parity states construction 78−17105
A=176, data sheets to April 1976 77−10306
A=18 nuclei, negative parity spectra, phonon dynamic interaction propagator approach 78−8739
A=204, nuclear data sheets, levels, J^{π} and transitions 80−31429
A=212, nuclear data sheets, levels, J^{π}, transitions 80−31430
A=21-44, energy levels, excitation energies, branching and mixing ratios, lifetimes, J^{π}, resonances 79−13208
A=221, nuclear data sheets, levels, J^{π}, transitions 80−31431
A=225, nuclear data sheets, levels, J^{π}, transitions 80−31432
A=228 to 240 even nuclei, anharmonicity of vibr. states superfluid model 77−61340
A=237, nuclear data sheets to November 1977 78−82267
A=241, nuclear data sheets to November 1977 78−82268
A=40 to 100, strength and radius parameters of deformed Woods-Saxon potential 79−97673
A=48, nuclear data sheets, to September 1977 78−82266
A=50, nuclear data sheets 77−10304
A=58 nuclear data sheet to June 1976 77−18372
A=71 nuclear data sheets, levels, J^{π} and transitions 80−31428
A=73, nuclear data sheets, levels, J^{π} and transitions 80−101673
A=76 nuclear data sheet to June 1976 77−18373
A=77, nuclear data sheets, levels, J^{π} and transitions 80−105439
A≥210, strength and radius parameters of deformed Woods-Saxon potential 79−97673
A∼90 nuclei, isomeric states, spin polarisation, M4 transitions and giant resonances 80−63157
A = 143, nuclear data sheets, level energies, J^{π} assignments 79−30775
A = 202 nuclear data sheets, levels and transitions 79−40831
angular correlation method for parity assignments, model independ. technique 78−21827
backbending, core-particle coupling model appl. band construction 79−97645
backbending, ground state band and aligned two quasiparticle band crossing interpretation 79−22167
backbending in $^{180-182}$Os and ^{181}Re Coriolis antipairing, rot. alignment, deform. jumps 78−70432
backbending phenomena, two fluid model of nuclear rots., ^{164,166}Er, ^{166,168,170}Yb 77−50049
charged particle polarisation, methods of meas. *(Rumanian)* 79−59321
coherent parity-violation experiments with neutron beams 79−59073
coherent state model, for negative parity bands 78−89782
collective transition average lifetimes, spin (30-50) region in heavy ion-nucleus reactions 78−89822
complex nuclei, parity violating effects, nucleon-nucleus weak interaction 79−75833
compound nucleus reactions, consequences of isospin mixing 78−25168
critical opalescence, a precursor to nuclear π condensation, local spin ordering 78−82303
deep inelastic reactions, energy dissipation and angular momentum transfer 78−41679
deformation energy surfaces at very high spin states, microscopic determ. 77−71560
deformed rare earth nuclei, bandcrossing in K≠0 bands, backbending 80−9204
dense neutron and nucl. matter, spin and isospin instability 78−86474
dense neutron and nuclear matter, spin and isospin stability 80−22737
deuteron disintegration reactions on zero-isospin nuclei, strong nonconservation of isospin 78−13106
deuterons, D-state probability, review of spin, binding energy, magnetic and quadrupole moment 78−62488
dipole moment of nuclear state using transient mag. field from ion passing through ferromag. *(Dutch)* 78−29386
double crossing of ground rotational band and super band 78−45996
effective interaction calcs., symmetry coeff., isospin-spin depend. of single particle pot. compressibility, rearrangement energy 77−46126
elastic deuteron-nucleus scattering, breakup corrections to spin depend. 78−58289
elastic electron scatt. and atom parity nonconservation caused by nuclear parity violation 80−27427
even-even and odd A nuclei, nuclear shapes and motions, review 80−5054
even-even deformed nuclei, aligned rot. of octupole vibrational states 78−12955
even-even nuclei, backbending mechanism anal. *(Chinese)* 78−78247
even-even nuclei, resonance model of backbending and downbending 77−67694
even-even nuclei, z=6 to 100, probable members of quasi-bands in spherical and deformed regions 80−13357
even-even spherical nuclei, neutron strength function, spin depend., quasi-particle-phonon model *(Russian)* 80−42561
even-even transitional nuclei, bunching of spin states in γ-band, asymm. rotor model 78−62485
exchange current contribs. to parity violating elec. transitions 78−29383
exotic nuclei with isospin T>A/2, props. 77−22926
$f_{7/2}$ shell nuclei, odd-A, collective bands of positive parity states 78−54677
fast rotating nuclei, yrast traps 79−71786
fermion system, classification of states, spin 1/2, using chain of subgroups of unitary scheme 79−63597
fission, spatial parity nonconservation *(Russian)* 78−25170
nuclear spin and parity continued
fission fragment emission anisotropy, effect of spin of target nucleus *(Russian)* 77−22992
fission product spin distrib., statistical theory predictions, asymmetric fission explanation 78−70509
fission resonances, spin determ. using polarised beam and target, review 77−26796
fluctuating hyperfine field I-depend. 77−22880
four-body model of four-nucleon system, spin and isospin effects 79−71802
fp-shell nuclei, high-spin states 78−12946
giant dipole resonance, isospin structure 77−79352
giant multipole resonances, spin-isospin vibrs., spin waves, Regge poles in collective model 78−89777
Hartree Fock Bogoliubov method, high nuclear spins, quadrupole pairing, moment of inertia, yrast traps 78−54712
Hartree Fock Bologiubov theory, appl. to light/heavy nuclei, book contrib. 79−75881
Hartree-Fock-Bogolyubov approach to nuclear band description *(Russian)* 79−3107
(heavy ion, xn) reactions, higher moments of γ-ray multiplicity 77−18604
heavy ion collisions, mass transport theory, transport coeffs. including ang. momentum 78−58302
heavy ion induced transfer reactions, new methods using particle ang. correls. *(French)* 79−558
heavy ion scattering, parity depend. 78−4957
heavy-ion collisions, in-beam gamma-ray spectroscopy, nuclear shape and reaction mechanism *(French)* 79−560
heavy-ion induced fusion-evaporation, phenomenological restrictions for spin alignment attenuation factors 77−57686
heavy-ion induced reactions, dynamically deformed rot. nucleus calcs. of polarisation effects 78−25222
high angular momenta nuclei, backbending, yrast states, large moment of inertia band 77−14027
high angular momentum behaviour, transitional nuclei and backbending 79−17789
high energy nucleon-nucleus scatt., spin effects, Glauber theory multiple scatt. amplitudes *(Chinese)* 79−21979
high spin effects in nuclei with proton no. 40-60, shape, deforms. 78−503
high spin state population, compound nucleus reaction, computer code CARLA 78−89843
high spin state radiative decay in Australian nuclear physics review 77−88021
high spin states, identification method at high excitation energies 79−17788
high spin states 79−71785
high-spin isomery, heavy ion experiments at UNILAC *(German)* 78−66435
high-spin nuclear rotations, single particle Nilsson model 78−12943
high-spin selectivity in heavy-ion compound reactions, critical ang. momenta determ., spectroscopy 77−54238
high-spin states, light particle emission, deformation effects 79−22198
high-spin states, means and methods of investig. 78−86722
high-spin states, spectroscopy with heavy-ion compound reactions 77−14176
high-spin states and shell struct. in N=Z nuclei, ^{20}Ne appl. 80−47342
high-spin states of transitional and spherical nuclei, decoupled and strongly coupled bands 78−12939
hot nuclei with high angular momenta, γ-ray emission in heavy ion reactions, rot. bands 78−13133
hydrodynamical model of nuclear fluid, spin and isospin props. 78−70479
hypernuclei, produced by strangeness exchange reactions, spin-orbit term 78−17130
interacting boson model, collective states of even-even nuclei, shell model descript. 78−62493
isobaric quartets in nuclei, T=3/2 states, isobaric multiplet mass eqn. 79−93519
Isolde experiments, prod. of extreme neutron/proton ratio nuclei, nuclear props. study *(Danish)* 78−4972
isospin dependence of expt. nuclear deformations 77−82817
isospin forbidden beta decays, collective model, Fermi matrix elements, appl. to ^{8}Li, ^{134}Cs 77−67722
isospin sum rules for E2 strength distribution in 1s nuclei 77−30550
level densities, thermodynamic temps., spin cutoff factors, nuclei with 23≤A≤40, expt. calcs. 77−30492
level density depend. on spin and parity, semimicroscopic method *(Russian)* 77−34202
light deformed nuclei, Skyrme interaction spin components, spectra, projected HF theory 80−73820
light nuclei, expts. on parity mixing 78−12965
light nuclei, m-particle n-hole struct. from few nucleon transfer reactions, review 78−50062
light nuclei inelastic form factors for abnormal parity states, K-harmonic method *(Russian)* 78−25113
Lipkin model, quasi-spin pairing and struct. 79−485
long lived high spin isomers, magnetic moments, nuclear struct. *(German)* 77−82820
low energy positive parity spectra, 2ħω excitations, ang. momentum projected deformed particle-hole model calcs. 78−25119
M1 magnetic form factor and spin oscillations 79−67652
microscopic collective Hamiltonian, spin-isospin part of the matrix element 79−63609
mini-orange spectrometers, conversion electron spectroscopy 79−93864
mirror nuclei, spin and isospin distribs. in medium heavy nuclei 79−71789
moderately deformed nuclei, high-spin states studied in (heavy ion, xnγ) reaction 77−14180
Mossbauer transition characts. tabulation book contrib. 79−87364
negative parity band crossing in even-even nuclei, ^{150}Sm, ^{152}Gd, ^{156}Er, ^{238}U, Dy (A=154, 156) 78−21488
neutron elastic scattering, 11 MeV, isospin depend. of neutron-nucleus optical pot. 77−14126
neutron rich fission fragments, excited state spin assignment, various methods 80−78506
neutron scatt. from parity violating pot. 78−25167
neutron scattering theory, parity violating interaction 78−25166
neutron strength function, spin depend. *(Russian)* 78−17069

nuclear spin and parity continued
non-standard perturbation theory for Green functions, nuclear spin eqns. appl. *(Russian)* 79−45
nuclear force, parity violating, unified treatment 80−47400
nuclear matter, polarised, thermal props., temp., spin isospin and spin-isospin pressure 80−102135
nuclear matter, spin-isospin and pion condensation phase transistions, eqn. of state 80−86843
nucleon-nucleus elastic scatt., spin effects in framework of Glauber optical model 79−40909
odd A shell nuclei, positive parity states, collective bands, Hartree-Fock calcs. 79−30778
odd p-shell nuclei, lowest positive parity state from projected HF theory 79−463
odd-even staggering, Coriolis effects in particle-core coupling 79−49580
odd-odd man nuclei, decoupled and strongly coupled particles system 78−8727
optical potential of deuteron-nucleus elastic scatt., Ž.S interaction 78−41729
optimum atomic mass formula from nuclear mass shell and parity corrections *(Russian)* 80−37902
orthogonality condition model derived from parity energy surfaces, n+α, ^{3}H+α appl. 78−29432
P-shell hypernuclei, formation, γ-radiation, and spin values, shell model 79−22223
parity nonconservation, asymmetric α-emission in polarised nuclei decay 79−6379
parity nonconservation in heavy atoms and weak magnetism in neutral currents *(Russian)* 80−82932
parity violating nuclear effects, low energy anal., NN scatt. parametrisation 78−66218
parity violating one-body potl. effects 77−18383
parity violation in nuclear forces, neutron capture γ-ray expts. 80−37322
parity violation in nuclear processes with polarised neutrons 79−59008
parity-non-conserving nuclear forces, theoretical and phenomenological approach review 80−42556
partial wave expansions for arbitrary spin, non-central forces 78−21535
photonuclear giant dipole resonance, isospin shift of energy 77−50111
photonuclear reactions, differential polarisation coeffs. 78−4926
photonuclear sum rule, spin current contribs., strong violations 80−18291
polarised deuteron beam uses in nuclear structure studies 77−71612
polarised nuclear matter, binding energy, spin energies, relativistic calc. 80−102134
polarised nucleus fission, parity nonconservation mechanism, rot. state mixing *(Russian)* 80−37408
polarization in nuclear reactions, review of research at low energies *(Russian)* 78−33162
projection of wave functions on states with definite ang. momentum 78−12590
prolate symmetry axis, rotation of nuclei at high spin states, yrast states 78−70431
quadrupole pairing forces influence on backbending, cranked Hartree Fock Bogoliubov approach 78−29401
rare earths, yrast band energy calcs., exponential model with pairing attenuation, backbending 79−9446
rare-earth nuclei, back-bending phenomena, high spin states 78−74300
renormalisation of g_s factors in conversion transitions, spin-force consts. 77−61347
review, spin and moment data tables 77−22881
rotating nuclei, from heavy ion collision, high spin states instability against fission *(Rumanian)* 78−50150
rotating nuclei, selfconsistency conditions in cranked harmonic oscillator model, HF calcs. 78−58239
rotating nuclei of high and v.high nucl. spin *(German)* 78−25102
rotation effects on collective props. review *(Russian)* 78−37299
rotational states in heavy deformed nuclei, high-spin anomaly 78−93934
self consistent cranking model, anomalies 79−26382
self consistent cranking model with RPA corrections, high spin states, conservation laws 77−14047
semileptonic weak and EM interactions, (e,e) P-vibrations and state abnormal P admixtures 79−75977
shape isomers, spontaneous fission, static and decay props. and excitations, review, book contrib. 78−82402
shell model study, high-spin states in N=28 nuclei 78−29407
Skyrme's interaction, spin stability and mag. polarisability 77−2916
spectroscopy using (γ,γ') and (n,γ) scatt. 80−18287
spherical nuclei, Te to Sm, very high spin states, deform. energy surfaces 78−50079
spin, parity and spectroscopic factors of excited states populated in ^{24}Mg(d,p) 78−8826
spin and isospin stability of dense neutron and nuclear matter with hard core interaction 79−26386
spin assignments using polarised neutrons and oriented target nuclei in (n,γ) reacts. 78−29724
spin exchange and polarisation changes, RPA breakdown from HF connection 80−99142
spin giant resonance and core polarization effects, coupling term effects *(Chinese)* 80−47450
spin stability of nuclear matter and Skyrme interaction 77−54146
spin-alignment attenuation factors in mass 61-67 nuclei populated by (α, n) and (α, p) reactions 79−26390
spin-isospin density phase in finite nuclei, strongly oblate shape 80−22746
spin-isospin polarizability of nuclear matter and renormalization of weak currents 79−67697
spin-polarisation analysing powers in nuclear reactors, M-matrix conditions 78−8787
spin-rotation effects in elastic proton-nucleus scattering 79−26441
spin-zero particle reactions, critical ang. momentum effect on ang. distribs. 77−18607
stripping reactions to unbound states from p-n correlations, spin, parity and widths 78−62547
strongly deformed nuclei, shortlived states, g-factor meas. method 80−52577
SU_3 representation, maximal basis restriction 80−42552
sudden shape transitions, pair correlation association, E2 transition rate and backbending *(Chinese)* 79−59007
supermultiplet model, transformation matrices rel. to canonical basis of group SU_4 79−67693
symmetry breaking in ground state region, statistical meas. 78−8737

nuclear spin and parity continued
tensor quasiparticle interaction and spin-isospin sound in nuclear matter 79−63618
three nucleon clusters in nuclear matter, two-body force spin structure 78−17112
total γ-decay energy meas., selection of high spin nuclear states 79−26391
transuranic nuclei, Po to Th, very high spin states, deform. energy surfaces 78−50079
two-quasi particle excitations, high-spin rot. state, ang. momentum projection 78−41615
two-step DWBA, energy depend. for (p,t) unnatural parity state excitations 78−70528
wave functions, matrix elements, cranked deformed harmonic oscillator, high spin nucleus appl. 78−25131
weak interaction between nuclear particles, parity violation, review 77−6295
yrast bands of negative parity, gapless superconductivity, exactly solvable R(8) model 77−14015
yrast traps, island of high spin isomers near N=82 78−8844
yrast traps, obs. in heavy ion collisions 80−37319
yrast traps, struct., nuclear deform. 78−21486
yrast traps at very high angular momenta, microscopic description 78−70426
yrast wave function, variational principle used to solve Hartree Fock problem 79−93537
Z=34-94, high spin yrast isomers and nuclear deformation 79−6369
Z=55-63, odd proton nuclei, low lying even parity states 80−27551
zero-spin particle reactions, angular distrib. anal. 79−13342
(e,e), A=2, 3, 4, scaling laws in relativistic impulse approx. model, spin effects 80−52662
in (p,n) reactions quadrupole moment, isovector component, nuclear spin re-orientation effect 80−52573
Λ- and Σ-hypernuclei, γ-transitions, spin-orbit components of single particle pots. 80−42574
(n,2n), 14.7 eV, isomeric cross-section ratios, statistical theory, moment of inertia 79−97701
(n,f), parity violation in compound nuclei 80−47368
(n,f), themal, parity violation from opposite parity rot. states 80−95303
(n,γ), parity violation in compound nuclei 80−47368
(n,γ), polarized space parity nonconservation, optical pot. and GDR parameters *(Russian)* 80−86803
(n,γ), spin assignments using polarised beams and gamma spectroscopy 80−37323
(n,γ) reactions with polarised thermal neutrons, spin state determ. *(Dutch)* 79−22290
^{20}Ne, rotational bands 78−45993
NN parity nonconserving pot., evidence for enhanced $\Delta S=0$, $\Delta T=2$ weak interaction in nuclei 77−18419
(π,π'), collective transitions, giant resonances, isospin content and spin transfer 80−42580
^{51}Mn levels studied via high resolution proton scatt. from ^{50}Cr 77−54151
^{134}Ba level scheme obs. from ^{134}La decay 77−10360
^{8}Be, reson. levels, J^π, via ^{6}Li(d,α)^{4}He, 1.5-11.5 MeV 77−82935
^{8}Be, reson. levels , J^π via ^{6}Li(d,α) below 12 MeV 77−82936
^{230}Ac levels, J^π and transitions, Nilsson assignments from ^{230}Ra decay 80−68543
^{109,111}Ag, particle-vibr. multiplet excit. by two-neutron stripping 77−34214
Ag, A=109,111, proton hole states via ^{110,112}Cd(d,^{3}He) 50 MeV 77−18369
Ag, static mag. moments, spin, parity and excitation energy from nuclear orientation *(Dutch)* 79−80872
^{A}Ag, A=104, 106, levels, J^π, and isobaric analogue resonances from Pd(p,n) 80−32180
^{A}Ag A=99, 101, 103, levels, transitions and J^π from Cd decay, Pd(p,2nγ) 80−47383
^{103}Ag collective excitation and J^π following ^{94}Mo(^{12}C,p2nγ), rotor-plus-particle model 80−86782
^{104}Ag levels, J^π, $T_{1/2}$, bands and transitions from ^{103}Rh(α, 3nγ) 80−102093
^{105}Ag, high spin states γ-single spectra, $\gamma\gamma$ coincidence, excitation functions, ang. distrib., polarisation meas. 78−21519
^{105}Ag, high spin states populated in ^{103}Rh(α,2n) 77−22936
^{107}Ag high spin states, J^π assignments, polarisations and transitions from (^{7}Li,4nγ), (^{6}Li,3nγ) 80−27536
^{108}Ag, populated in ^{108}Pd(p,nγ), level struct., spin and parity, isomeric state lifetimes and g-factors 77−18392
^{109}Ag levels from ^{109}Pd decay, spins, γ cascades, mixing ratios 77−22930
^{110}Ag, populated in ^{110}Pd(p,nγ), level struct., spin and parity, isomeric state lifetimes and g-factors 77−18392
^{111}Ag, 376.7 keV level lifetime, shape coexistence, γ-branching 78−551
^{111}Ag, level struct. via ^{110}Pd(^{3}He,d)^{111}Ag 33.2 MeV 77−88045
^{24}Al spin assignments, from ^{24}Mg(^{3}He,t) at 38.5 MeV 77−18580
^{26}Al 1^+ T=0 states, isobaric analogue state, spin-isospin effective interaction from ^{26}Mg(p,n) 80−68553
^{26}Al excited states, isobaric analogues, spins, DWBA anal. of ^{27}Al(^{3}He,α) 80−105981
^{26}Al level anal. from ^{25}Mg(^{3}He,d)^{26}Al at 18 MeV 78−62554
^{26}Al low energy resonances, decay and J^π assignments, branching ratios from ^{25}Mg(p,γ) 80−42624
^{26}Al T=1 states, resonances, J^π and transitions from ^{25}Mg(p,γ) 80−99131
^{27}Al bound state parity and spin assignments, level struct. from ^{26}Mg (p,γ) resonances 78−66206
^{27}Al, coherence widths from ^{12}C(^{15}N,α) 78−41619
^{27}Al, J^π=5/2 state, cross section and analysing power ang. distribs. 80−18296
^{27}Al levels, resonances, J^π, branching and mixing ratios from ^{26}Mg(p,γ) 80−99132
^{27}Al, low lying states, band mixing effects, quadrupole moment 78−490
^{27}Al, spins of p-h states from analysing powers of (d,τ) reacts. 78−25111
^{28}Al levels, spins and γ-rays, multipole mixing from ^{27}Al(n,γ), pol. thermal 80−47398
^{28}Al levels, transitions and spin from ^{27}Al(n,γ), pol. Al and n 80−78153
^{28}Al, spectroscopic meas. in ^{30}Si(d,α) react. with polarised deuterons 78−41728
^{28}Al, spin-parity assignment, from ^{30}Si(d,α)^{28}Al at 8.12 MeV 77−6222

nuclear spin and parity continued
^{26}Al, $T_{1/2}$, J^{π}, levels below 5.45 MeV via ^{27}Al(d,pγ) 77−57623
^{32}Ar, high spin states from heavy-ion fusion evaporation reactions, decay schemes 77−2932
^{36}Ar, delayed proton and alpha emission, transition energies, levels, J^{π}, from ^{36}K decay 80−52629
^{38}Ar high spin states from ^{27}Al(^{14}N,2pn), decay scheme 78−25232
^{38}Ar levels, J^{π} and transition strengths, DWBA anal. of ^{40}Ar(p,t) 80−47378
^{38}Ar, model independ. J^{π} assignments from ^{24}Mg(^{16}O,2pγ) 77−18384
^{38}Ar yrast levels, J^{π} assignments, transitions, branching and mixing ratios from ^{35}Cl(α, pγ), ^{24}Mg(^{16}O, 2pγ) 79−67625
^{39}Ar, energy level spin and parity assignments, level spectroscopy from (α,nγ), (d,pγ) 78−93943
^{39}Ar low lying states from ^{37}Cl(α,d), spectra, ang. distribs., spins 78−25212
^{40}Ar, yrast levels, J^{π}, branching and mixing, via (^{16}O, 2pγ) 34 MeV 77−74759
^{40}Ar+^{58}Ni, deep inelastic collision at 280 MeV, fragment energy and spin 78−21599
^{40}Ar(α,α$_1$), 12-15 MeV, J^{π} assignments for deduced levels 79−89232
^{37,39}Ar, high-spin states of $(fp)^2$ character via (α,d) reaction 77−74865
As, neutron-deficient isotopes, nuclear spin meas. by at. beam mag. resonance 77−18386
^{A}As, A=70, 72, level scheme, transitions, J^{π} and lifetimes from Ge(p,nγ) 80−22695
^{A}As, A=71, 73, levels, J^{π}, transitions, T1/2 from Se decay, Ge(^{3}He,d), (p,xnγ) 80−57684
^{68}As β-decay, γ coincidence and singles spectra, spin, parity assignments, half-life meas. 77−79333
^{69}As positive parity states, possible rotational aligned $g_{9/2}$ proton band 78−78311
^{70}As states, excitation functions, spin and halflifes from ^{69}Ga(α,3n), ^{60}Ni(^{12}C,np), ^{63}Cu(^{10}B,2np) 79−6414
^{71}As, intermediate struct., props. 78−93948
^{71}As intermediate struct., resonance spin from ang. correlations of ^{70}Ge(p,p'γ) 79−67729
^{72}As, populated in ^{72}Ge(p,nγ), level scheme determ. 77−14032
^{74}As level structure, studied via ^{72}Ge(α,npγ), 30 to 50 MeV 77−10357
^{75}As, nucl. reson. fluoresc. meas., spins and level widths determ. 77−61379
^{75}As populated in ^{75}Se decay, E0 transitions 80−22752
^{75}As(n,n'γ)^{75}As, deexcitation gammas, energy levels, branching ratios, spins, parities, excitation function meas. 78−89869
^{76}As, level structure, transitions and J^{π}, from ^{76}Ge(p,nγ) 80−47379
^{78}As, level struct. determ. in ^{80}Se(d,α) at 16 MeV 78−8827
^{79}As levels, J^{π} and ang. distribs. from ^{76}Ge(α,p) 80−78161
At high spin isomers, deformed independent particle model, yrast lines, shape 79−480
^{206}At→^{206}Po EC-β^+ decay to Po excited levels, At spin-parity 77−79340
^{209}At high spin states from ^{206}Pb(^{6}Li, 3nγ), γ meas., neutron hole influence 77−2934
^{210}At excited states, spins, parities and rate of population from ^{210}Rn decay 79−75917
^{212}At high spin states, decay, g factor, J^{π} assignments, level energies from ^{208}Pb(^{7}Li,3n) 80−5042
^{213}At levels, J^{π}, transitions and lifetimes from ^{208}Pb(^{7}Li,X) 80−68542
^{189,191,193}Au, high-spin states, blocking effect in rot.-alignment model 77−14016
Au levels from p stripping reactions on ^{194,196,198}Pt, high spin states 78−78398
Au, short-lived isotopes, spin and mag. moment meas. from atomic-beams 77−22882
Au, spin and mag. moment, trends in neutron deficient nuclei 78−37261
Au(^{86}Kr,X), 724 MeV, deeply inelastic, ^{4}He, ^{1}H emission, fragment spin, semiempirical method 80−47366
^{A}Au A=190, 192, 194, levels, J^{π}, isomers and rot, aligned bands from Ir(α,xn) 80−9215
^{A}Au, A=193-199, positive parity states, particle-asymmetric rotor description 78−46005
^{183}Au, high-spin states anal, $h_{9/2}$ and $i_{13/2}$ bands 78−25117
^{187}Au energy states from ^{187}Hg decay, parities γ-spectra, triaxial nuclear deform. *(French)* 78−33143
^{196}Au, studied via ^{197}Au(n,2n), isomeric cross-section ratio and spin-cut-off factor 78−13096
^{198}Au, energy level spin from ^{197}Au(n,γ) with polarised n and Au 79−457
^{198}Au level spin assignments from γ ang. distrib. and circular polarisation from ^{197}Au(n,γ) 80−52570
^{10}B levels, J^{π}, ^{12}C(p,^{3}He) at 51.9 MeV 77−30566
^{10}B levels, J^{π} and ang. distribs. from ^{9}Be(^{3}He,d) 80−42546
^{10}B(d, d'), energy depend. isospin violation in 10 MeV region 77−14134
^{10}B(n,α)^{7}Li, thermal polarised n capture, P-odd asymmetry meas. *(Russian)* 80−13452
^{11}B, 2α+t model, parity states, shell and cluster structs. 78−50110
^{11}B, struct. study of 2α+t system in orthogonality condition model, level energies and parity 80−5080
^{12}B, aligned, existence of G-parity irregular induced tensor current 78−29384
^{12}B J-transfer determ. from ^{13}C(d,^{3}He), polarised d, 29 MeV 79−49579
^{12}B levels, J^{π} and diff. cross sections, R-matrix anal. of ^{11}B(n,n) 80−78151
^{12}B, spin polarisation in ^{100}Mo(^{14}N, ^{12}B), semiclassical anal. 78−33212
^{12}B spin polarisation meas. in ^{100}Mo(^{14}N,^{12}B) 77−71562
Ba odd-mass isotopes, A=125-133, high spin level systematics and triaxial shapes 77−22838
^{A}Ba, A=130, 132, 134, 136, levels and EM props., ang. momentum projected quasiboson model 80−5067
^{A}Ba, A=132, 134, 136, negative parity states, J^{π} , transitions, DWBA anal. of Ba(p, t) 80−86810
^{A}Ba, A=142, 144, onset of deformation in neutron-rich isotopes 79−93499
^{A}Ba, A=142,144,146, transition γ-γ ang. correlations, levels, J^{π}, mixing ratios 80−73823
^{A}Ba(γ,γ) A=136-8, 1.68-5.0 MeV, nuclear resonance fluorescence, levels transitions and spins 79−6543
^{125}Ba, $7/2^{\pm}$ states, populated in ^{116}Sn(^{12}C, 3n), explained by triaxial core model 78−37258
^{127}Ba high spin level structure studied via ^{118}Sn(^{12}C,3n)^{127}Ba 77−38226
^{129}Ba, excitation and props. of high-spin levels using ^{120}Sn(^{12}C,3nγ) 78−17104

nuclear spin and parity continued
^{129}Ba, struct. determ. from ^{129}La β-decay 79−22244
^{139}Ba level scheme, J^{π} and γ-transitions from ^{139}Cs β-decay 80−42590
^{142}Ba, γγ ang. correlations, levels, spins and mixing ratios from ^{142}Cs decay 80−57734
^{7}Be excited state from ^{4}He(^{3}He,^{3}He) polarised scatt. study 78−46078
^{8}Be, 3^+ doublet at 19 MeV, level-parameters, isospin mixing model 78−89789
^{8}Be, reson. level, J^{π}, via ^{7}Li (p,γ)^{8}Be 380 to 960 keV 77−88131
^{9}Be, positive parity excited energy levels, three well cluster shell model study *(Chinese)* 79−93518
^{10}Be, form. in ^{7}Li(t,γ) reaction, excitation functions and resonant struct. for 17.79 MeV state 78−13110
^{11}Be single neutron strength, levels, spin assignments, spectroscopic factors from ^{10}Be(d,p) 79−36156
^{12}Be core excited T=2 levels, spin, half life from ^{10}Be(t,p), 12 MeV 78−66210
^{203}Bi high spin states from ^{203}Tl(α,4n), lifetimes meas. 78−29485
^{205}Bi high spin states populated in Tl(α,xn), yrast states, isomers 77−30616
^{206}Bi, high-spin states anal. from ^{205}Tl(α,3n) 78−82368
^{207}Bi optical HFS intensity profile for nuclear spin determ. 77−54619
^{207}Bi, spin and parity of states with J≤21/2, ^{205}Tl(α,2n)^{207}Bi and ^{205}Tl(α,2n)^{207}Bi 78−89788
^{208}Bi isobaric analogue resonances, spin assignments, decay amplitudes from ^{207}Pb(p,p) 79−75946
^{208}Bi two-particle, two-hole configuration, levels, J^{π} and excitation energies from ^{210}Bi^{m}(p,t) 80−32190
^{209}Bi coherent scattering of polarised thermal neutrons, parity violating effects 78−29461
^{209}Bi+^{86}Kr, 610 MeV, ang. momentum transfer in deeply inelastic scatt. 77−79397
^{209}Bi(n,n), direct scatt., polarised thermal neutrons, empirical parity-violating potentials and neutron optical activity 79−59074
^{211}Bi levels, spin assignments and spectroscopic strengths from ^{210}Bi^{m}(d,p), 20 MeV 79−6418
^{12}B hypernucleus, spin determ. from $_{\Lambda}{}^{12}$B→^{12}C*+π^- 80−27589
^{A}Br level structure studied via the ^{75}AS(α, 3nγ) reaction, 30 to 55 MeV 77−54174
^{76}Br long-lived positive parity isomer from ^{75}As(α,3n) 79−54375
^{77}Br collective bands, lifetimes, spins and E2 transition probabilities from ^{64}Ni(^{16}O, 2nP) 80−13415
^{78}Br, high-spin states, from ^{77}Se(α,2np), decay into isomers 80−52569
^{78}Br level struct. determ. from (α,nγ), (^{3}He,d) and (p,d) reacts. 79−59010
^{80}Br, level struct. determ. from thermal (n,γ) meas. 78−41667
^{80}Br spin states from γ-spectra obs. in ^{80}Se(p,nγ) and ^{79}Br(n,γ) *(French)* 78−29393
^{82}Br, level struct. determ. from thermal (n,γ) meas. 78−41667
^{82}Br spin states from γ-spectra obs. in ^{82}Se(p,nγ) and ^{81}Br(n,γ) *(French)* 78−29393
^{83}Br, levels assignment, ^{83m}Se decay scheme obs. 78−17147
^{10}C levels, spin and parity, ^{12}C(p,t) and ^{12}C(p,^{3}He) comparative study 77−30566
^{12}C, 14.08 MeV level J^{π} assignment via ^{12}C(α,α')^{12}C* at 45 MeV 77−82819
^{12}C, 19.25 MeV level spin assignment from ^{11}B(p,n)^{11}C, 3-49 MeV 78−93996
^{12}C (^{16}O, ^{16}O'), 19-23 MeV, intermediate width structs., ang. correlations, spins 80−13431
^{12}C isovector M1 excitations, current and spin contribs. from (e,e'), (p,n) 80−68582
^{12}C J-transfer determ. and isospin mixing from ^{13}C(d,t) polarised d 79−49579
^{12}C, multipole elec. giant resons., anomalous parity isovector states, Coulomb excitation cross sections 79−9439
^{12}C, residual interactions, current conserving RPA calculations 80−57710
^{12}C, spin flip transition after ^{12}C(e,e'π^+)^{12}B, near threshold 78−13065
^{12}C, study of isospin mixing 77−18385
$^{12}C_{2+}$ m-state population in ^{64}Zn (^{12}C, $^{12}C_{2+}$*) 79−93521
$^{12}C_{2+}$ spin alignment using γ-decay in flight in ^{16}O(^{12}C,$^{12}C_{2+}$)^{16}O and ^{12}C(^{16}O,$^{12}C_{2+}$)^{16}O interactions 78−41767
^{12}C+^{12}C, 6.25 MeV reson., J^{π} determ. 77−50099
^{12}C+^{12}C system, 7.5 MeV, reson. spin assignment 77−14089
^{12}C+^{12}C system resonant structs., J^{π} assignments, true ^{24}Mg states from ^{12}C(^{12}C, ^{16}O) 80−99163
^{12}C+^{16}O, 22 MeV, spins of reson. assigned 78−17236
^{12}C+^{16}O elastic scatt., generator coord. calc., reson. spin assignments 77−57685
^{12}C+^{16}O multichannel scatt., microscopic calcs. in generator coordinate method, spin assignments 79−564
^{12}C(^{12}C,^{12}C'), 18.5-32.8 MeV, spin alignment and possible molecular resonances 80−86804
^{12}C(^{12}C,^{12}C), 13-14.1 MeV, Coulomb barrier resonance parameter direct determ., J^{π} assignments 80−513
^{12}C(^{12}C,^{8}Be)^{16}O(GS), excitation functions and Legendre anal. for resonance J^{π} assignments 78−78347
^{12}C(^{16}O, ^{12}C*), 45-53 MeV, ^{12}C* m-substate population, spin alignment and excitation functions 80−42615
^{12}C(^{16}O,^{12}C)^{16}O, 22.7 to 33.0 MeV, excitation function enhancement for 0^+, 6.049 MeV ^{16}O state 78−58299
^{12}C(^{16}O,^{16}O*)^{12}C*, 33-54 MeV, intermediate struct. resonances, ang. distrib. optical model fit, spin assignments 78−82330
^{12}C(^{16}O,α)$_1$, J^{π} for 12.8 MeV c.m. resonance 79−59045
^{12}C(^{16}O,α)^{24}Mg, low energy, spin and parity assignments 78−21602
^{12}C(^{6}Li,α)^{14}N(2.31 MeV), 9 to 20 MeV, isospin violation 78−41763
^{12}C(d,α)^{10}B(1.74 MeV, T=1), coupled channel anal. of energy depend. isospin violation 78−70541
^{12}C(e,e'), E2 transitions, convection currents and spin magnetisation 79−13244
^{12}C(μ^-,ν_{μ}γ)^{12}B, appl. of μ^- radiative capture to nucl. spin and isospin transitions 78−86511
^{12}C(n,n), spin-flip probability to first 2^+ level 80−78288
^{12}C(p,p') proton polarisation and natural parity level excitations *(Russian)* 80−5144
^{12}C(p,p'γ), 23.5-27 MeV, 1^+ state spin flip meas. DWBA anal., cross sections 80−68529
^{12}C(p,p'), polarised p, 20, 30, 40 MeV, anal. power and cross sections, spin-orbit deformation 79−75963

nuclear spin and parity continued
^{12}C(p,p), 14-45 MeV, differential cross section and spin-flip probabilities, giant resonances 80−73850
^{12}C($\pi^+,\pi^{+\prime}$), 100-291 MeV, cross sections and ang. distribs., spin and isospin transfer 80−52697
^{13}C, reson. struct. anal. from ^{13}C(γ,n_0)^{12}C 78−586
^{13}C, spin precession for 5/2$^+$ state, recoil in Fe 77−2904
^{13}C(γ,n), 7.6-24 MeV, photoneutron ang. distribs., level scheme and J^π assignments 80−466
^{14}C, (sd)^2 positive-parity states, shell model calcs. 78−54674
^{14}C energy levels from ^{12}C(t,p), spins, parities 78−70542
^{14}C, populated by ^{12}C(t,p)^{14}C, spin and parity of states near 10 MeV excitation in ^{14}C 78−37263
^{14}C(e,e′), 37, 50.5, 60.5 MeV, 180° scatt. cross sections, excited states, spin parity 77−30557
^{16}C, (sd)^2 positive-parity states, shell model calcs. 78−54674
^{16}C levels populated in ^{14}C(t,pγ), spin assignments 78−8830
Ca, A=38, 40, 42, level props. from Ar(^{3}He,n) reacts. 77−65227
Ca, extended Skyrme force calculation, spin instability 79−63601
^{A}Ca(p,p′), pol. p, A=40,48, 800 MeV, diff. cross sections, anal. powers, DWIA anals., high spin levels 80−83067
^{38}Ca, J^π and configuration mixing via ^{40}Ca(p,t)^{38}Ca 51.9 MeV 77−26684
^{40}Ca, ^{36}Ar+α model, energy levels, spin and parity 77−57602
^{40}Ca, GQR, J^π, via (^{3}He,^{3}Heα) and (^{3}He,^{3}He′p) 70 MeV ang. distribs. 77−50097
^{40}Ca giant resonances prod. from ^{40}Ca(^{3}He,^{3}He′)^{40}Ca*→^{36}Ar+^{4}He 79−93479
^{40}Ca, high spin cluster like resonances obs. in ^{24}Mg+^{16}O 79−6664
^{40}Ca, residual interactions, current conserving RPA calculations 80−57710
^{40}Ca, weak s resonance γ-ray decay in negative parity low lying levels 80−27591
^{40}Ca(^{13}C, ^{14}N)^{39}K and ^{40}Ca (^{13}C, ^{12}C)^{41}Ca, 60, 68 MeV, spin depend. effects 78−66300
^{40}Ca(e,e′), strong mag. dipole transition, coherent spin flip transitions, ground state correlations 79−71817
^{40}Ca(p,α), polarised p, 22.0 MeV, analysing power J dependence 79−67740
^{41}Ca, high-spin positive parity states anal. with ^{38}Ar(α,nγ)^{41}Ca 77−38224
^{41}Ca parity doublet gamma lifetimes, 3/2 levels, parity mixing from ^{40}Ca(d,pγ) 80−78209
^{41}Ca, positive parity levels via ^{40}Ca(d,p)^{41}Ca with polarised deuterons 77−6402
^{41}Ca, spin and parity from ^{38}Ar(α,nγ) angular distrib. and linear polarisation of γ 80−63079
^{41}Ca yrast states from ^{26}Mg(^{18}O, 3nγ), γ meas., spin, parity, branching and mixing 78−58250
^{42}Ca from ^{41}Ca(d,p), 11 MeV, cross section, vector analysing power, spectroscopic strengths 78−74374
^{42}Ca, high spin states from ^{39}K(α,p), lifetimes, multipole mixing ratios 78−50186
^{42}Ca high spin states from ^{28}Si(^{16}O,2pγ), γ meas. 78−89787
^{43}Ca high spin positive parity states, struct., from ^{40}Ar(α,nγ) 78−46025
^{45}Ca levels, excitation functions and J^π from ^{45}K β-decay 80−105978
^{45}Ca, nuclear charge radius, spin, moments, by laserspectroscopy 80−18187
^{47}Ca high spin states through double step processes, CCBA calcs. from ^{48}Ca(^{3}He,α) 78−89797
^{47}Ca, low-lying levels anal. in ^{48}Ca(d,t) reactions 78−13114
^{48}Ca, isospin purity violation, dominant role of noncollective monopole states 78−12964
^{49}Ca levels from ^{48}Ca(d,p), analysing power, cross section, spins, parities, spectroscopic factors 78−78391
^{107}Ca 21/2$^+$ 2679 keV three quasiparticle state, nuclear struct. of isomeric states using g-factor 77−88039
Cd, A=104 and 105, populated in α+Pd reactions, high spin states 78−62484
Cd, A=105 to 109, parity assignments from (^{16}O,xnγ) obs. 78−41630
Cd, A=106-112, L,J,π via (^{3}He,n) 25.4 MeV reaction to 0$^+$ states 77−50050
Cd, α-spectroscopic factors from (d, ^{6}Li) 80−534
Cd, isotopes A=109, 106, 105, 104, high spin states excited by (α,xnγ) *(French)* 78−29394
^{A}Cd, A=105,107,109,111, odd neutron deficient, rotor+particle model anal. 79−36127
^{A}Cd, A=107, 109, 111, from Pd(α,3nγ)Cd, high spin states obs. 80−450
^{A}Cd(n,nγ) A=114,116, energy levels, spins, and gamma-ray multipole mixing ratios investig. 80−52580
^{103}Cd levels, J^π and positive parity decoupled band, rotor anal. of ^{94}Mo(^{12}C, 3nγ) 80−102096
^{106}Cd, high-spin states via γ-spectra populated in ^{104}Pd(α,2nγ) 77−30508
^{109}Cd, 11 μs isomeric level, spin and parity determ. by ^{108}Pd(α,3n) *(French)* 78−8738
^{109}Cd, low lying level struct. via γ-γ correls. following ^{109}In decay 77−30509
^{112}Cd, negative parity yrast band, E1 transitions polarisability, quadrupole-octupole coupled vibr. system 79−484
^{114}Cd proton hole states populated in ^{115}In(d,^{3}He), DWBA anal. 78−8829
^{114}Cd(p,p′), 11 MeV, polarised p, differential cross sections, anal. powers, spin flip prob. 79−89284
Cd(n,n′γ), A=114,6, E=2.67 MeV, ang. distribs. meas., 3$^-$ octupole states anal. 77−38275
Cd(n,nγ), γ spectra and ang. distrib., ^{114,116}Cd energy levels, spins, particles 77−88070
Ce, A=136,137,138, high spin states and isomers obs. using in-beam γ-spectroscopy 78−82309
Ce, A=137, 139, high spin levels, γ spectra, hole-core coupling 77−50063
Ce, A=138,140, levels from (p,p′), (p,t) reactions, spin, parity, deform. parameters, enhancement factors 77−54217
Ce band structures populated in ^{116,118}Sn(^{18}O,3n), high spin levels, yrast cascade 78−8842
^{141}Ce, γ-decay, levels, J^π, branching via ^{140}Ce(d,pγ) 8 MeV 77−14064
^{141}Ce, spin-parity assignments from ^{140}Ce(d,p)^{141}Ce 77−38283
^{250}Cf low spin states, bandheads, J^π and transitions from ^{250} Es EC decay 80−105952
nuclear spin and parity continued
^{250}Cf two-quasiparticle states populated by ^{250}Es^m EC decay 77−46140
^{250}Cf(d,d′), 15 MeV, vibr. states, J^π and reduced transition probabilities 80−47351
Cl, A=35,36,37 high spin states from heavy-ion fusion evaporation reactions, decay schemes 77−2932
^{34}Cl, high spin negative parity states, lifetimes meas. 78−74327
^{34}Cl high spin states 78−82289
^{34}Cl, J^π, levels, mixing ratios, $T_{1/2}$ via ^{33}S(p,γ) and ^{33}S(p,p) 1.0, 2.0 MeV 77−26613
^{34}Cl negative parity high spin states, ang. distribs. and lifetimes from ^{31}P(α,n) 79−17812
^{34}Cl states populated in ^{32}S(^{3}He,p) at 18 MeV 77−88046
^{35}Cl, isobaric analogue resonances determ. from ^{34}S(p,p) meas. 77−65222
^{35}Cl, model independ. J^π assignments from ^{24}Mg(^{16}O,p$\alpha\gamma$) 77−18384
^{35}Cl, resonance level spin determ. in ^{34}S(p,γ) 79−9552
^{35}Cl(n,γ), slow n, 398 eV resonance J^π determination 79−36147
^{36}Cl, spin and parity of 3723, 4294 and 5313 keV levels 77−88038
^{37}Cl high spin state decay, spin assignments, yrast level lifetime from ^{27}Al(^{19}F,2αp), ^{27}Al(^{12}C,2p), ^{34}S(α,p) 79−6490
^{37}Cl, in-beam γ-ray spectroscopy via ^{3}H(^{35}Cl,pγ) 78−13013
^{34,35,36}Cl, high-spin states of (fp)^2 character via (α,d) reaction 77−74865
^{54}Co deduced levels, J-depend., two-step processes from ^{54}Fe(^{3}He,t) 37.7 MeV 79−6412
^{55}Co excited levels and IAS meas. with ^{54}Fe(p,γ) 77−18509
^{55}Co isobaric analogue resonances, J^π, partial widths and spectroscopic factors from ^{54}Fe(p,γ), (p,p′) 79−85431
^{55}Co, resonance decays, branching ratios and analogue resonances from ^{54}Fe(p,γ) 80−52643
^{55}Co, spectroscopic study via ^{54}Fe(^{3}He,d)^{55}Co and ^{54}Fe(τ,dp)^{54}Fe reactions 77−88029
^{56}Co, γ-ray transitions, branching ratios, spin assignments, energy level lifetimes from ^{54}Fe(^{3}He, pγ) 79−497
^{56}Co, populated in ^{54}Fe(α,pn), transition rates of high spin states 77−6301
^{57}Co, $g_{9/2}$ IAR in ^{56}Fe(p,γ) 78−70504
^{57}Co, $g_{9/2}$ isobaric analogue resonances, obs. in ^{56}De(p,γ)^{57}Co 78−82332
^{57}Co, level props. study from ^{57}Fe(τ,d) reaction, DWBA calcs. 78−93946
^{57}Co levels and analogue states, J^π from DWBA anal. of ^{58}Ni(^{3}He, α) 79−63592
^{59}Co (n, n′γ), 1.3-3.9 MeV, energy level structure and decay scheme 79−45164
^{59}Co level energies, branching ratios lifetimes and spins from (p,p′),(α,pγ) 80−63093
^{59}Co, neutron resonance spectroscopy, R-matrix anal. 78−21555
^{59}Co(n,n′γ), 1.1-3.3 MeV, level inelastic scatt. cross section, decay γ-rays, spins, branching ratio 79−6605
^{60}Co, level struct., spectroscopic factors, DWBA anal. from ^{59}Co(d,p), 14 MeV 78−86478
^{60}Co low lying states from ^{57}Fe(α,pγ), spin constraints, γ mixing ratios 78−29487
^{A}Cr(p,p′), 6 MeV, A=50, 52, p spin flip probability 79−9561
^{A}Cr(p,p), A=50, 52, 6 MeV, elastic and inelastic differential cross sections, spin flip probability *(Russian)* 80−91187
^{48}Cr, spectroscopy of high spin states 79−59032
^{49}Cr, 2432 keV state, spin-parity assignment using three Ge(Li) Compton polarimeters 77−83456
^{49}Cr energy levels, spins, parities, spectroscopic factors, from ^{50}Cr(τ,α) 78−33199
^{51}Cr, bands, levels, EM transitions, J^π, branching and mixing ratios from ^{48}Ti (γ,nγ)^{51}Cr and ^{51}V(p,nγ)^{51}Cr 80−52606
^{51}Cr, level struct. to E_x=8.1 MeV via ^{50}Cr(d,p) 77−50059
^{51}Cr populated in ^{50}Cr+polarised deuterons, D-state effects, spin assignments 77−30608
^{52}Cr, 1p5h config., high-spin neutron-hole states, EM transition rates 78−70430
^{52}Cr 4.75 MeV excited state from ^{50}V(α,d), 8$^+$ assignment 78−74380
^{52}Cr, γ-decay of analogue states obs. in ^{51}V(p,γ) 78−70503
^{52}Cr, γ-spectra, levels, J^π via α+^{50}Cr reaction 77−74794
^{52}Cr high spin states, transitions and J^π values from ^{50}Ti(α,Znγ) 80−455
^{52}Cr, high-spin states populated by ^{50}Ti(α,2nγ), assignment from spectroscopic states 77−65190
^{52}Cr studied via (α,2nγ), high spin states, shell model calcs. 78−54675
^{52}Cr, total photoneutron cross section, high resolution meas., isospin effects 78−8792
^{53}Cr, excited negative parity states to 2322 keV via (p,p′γ) and (α,$\alpha'\gamma$) 77−82851
^{53}Cr levels, J^π, γ-transitions and 1626 eV resonance from ^{52}Cr(n,γ) 80−42610
^{54}Cr levels, transitions, $T_{1/2}$, J^π, shell model anal. from ^{51}V(α,pγ) 80−47381
^{55}Cr deduced levels and spins, from ^{54}Cr(d_{pol},p), cross section and vector analysing power 80−52684
^{56}Cr, γ-ray spectroscopy of low-lying states studied via ^{54}Cr(t,pγ) 77−10358
^{57}Cr mass excess, half life, ground state spin and parity, from ^{48}Ca(^{11}B, pn) 78−70436
Cs, ground state spins, moments, charge radii by laser spectroscopy 80−78147
Cs isotopes, nucl. spins and mag. moments, atomic-beam mag. reson. expt. 78−17097
Cs isotopes, short-lived, determ. of nucl. spins by β radiation detected optical pumping 78−37262
Cs neutron rich isoptopes, nucl. spins and mag. moments 80−47367
Cs, short-lived isotopes, spin and mag. moment meas. from atomic-beams 77−22882
Cs, spin and mag. moment, trends in neutron deficient nuclei 78−37261
^{A}Cs, A=142, 144, 146, low lying levels, J^π, mixing ratios and γ-γ ang. correlations 80−102119
^{119}Cs, new isomer, I=3/2, determ. in on-line ABMR expts. 78−70444
^{119}Cs, spin of neutron deficient nucleus by β radiation detected optical pumping 78−8782
^{131}Cs populated in ^{131}Ba decay, E0 transitions 80−22752
^{139}Cs level scheme, J^π and γ-transitions from ^{139}Xe β-decay 80−42590
Cu, isotopes, shell model calcs. of BE, spectroscopic factors and excit. energies 77−22860
^{59}Cu, reson. lifetime, J, via ^{58}Ni(p,γ) 1833 and 3547 keV 77−26621
^{60}Cu spin states, shell model, 6$^-$ and 9$^+$ states in odd odd Cu isotopes 78−74313

nuclear spin and parity continued
^{61}Cu, J^{π} assignments, E1 photon strength functions, partial radiative widths 79−59063
^{62}Cu 390 keV state, ferromag. effect, spin assignment 77−2903
^{62}Cu high spin states populated in $^{60}N+\alpha$, $^{63}Cu+p$, $^{52}Cr+^{14}N$, level scheme *(French)* 78−21496
^{62}Cu, yrast states obs. in $^{60}Ni(\alpha,pn\gamma)$ and $^{63}Cu(p,pn\gamma)$ 78−12945
^{63}Cu, decay of analogues, γ-ray ang. distribs. and spins of resons. 78−13002
^{63}Cu EM decay transitions, level J^{π} assignments, level lifetimes from $(\alpha,p\gamma)$, (^{11}B, 2pγ) 79−85402
^{63}Cu, EM props., J^{π} via $(p,p'\gamma)$ 5.0 MeV 77−74800
^{63}Cu, levels, J^{π} via ^{63}Zn(d,^{3}He) polarised d, 13 MeV 77−88100
^{63}Cu(p,p′) negative parity level excitation, gamma ray obs., test for core excitation model 80−68534
^{64}Cu, γ-spectra, J^{π} assignments via $^{64}Ni(p,n\gamma)$ 2.75-3.75 MeV 77−18470
^{65}Cu, low-lying level struct. via (e,e′) 120 MeV *(Russian)* 77−74838
^{162,164}Dy, γ-mixing, J^{π} values, levels via (n,n′γ) reaction 77−74768
Dy, A=160,162,164, high spin rot. states populated in heavy ion scatt., lifetime meas. 77−30511
Dy even isotopes, aligned Stockholm band intrinsic spin I_0^{eff} 80−13363
^{A}Dy, (A=151,152), high spin yrast states, γ-ray polarisation in (^{32}S,sn) reactions 80−497
^{A}Dy, A=150, 151, 152, levels, J^{π} and transitions from Ho EC decay 79−89241
^{A}Dy, A=158, 160, high spin rot. state pairing correlation, self-consistent treatment 79−3070
^{150}Dy, high-spin isomers produced by $^{144,146}Nd(^{12}C,xn)$, gamma-ray spectra 78−50075
^{152}Dy, high spin state populations from $^{124}Sn(^{32}S,4n)$ 80−57660
^{152}Dy, yrast isomers, oblate shape, excitation energies, spin and parity 79−17795
^{152}Dy, yrast traps, and very high spin states, populated in (^{32}S,4nγ) 78−89778
^{154}Dy N=88 nuclei quasirot. bands and J^{π} from beta-decay 80−83025
^{156}Dy, collective struct., J^{π}, via (p,t) reaction below 2.3 MeV excit. 77−74747
^{156}Dy, prompt transitions multipolarities, γ and conversion electron spectra, energy level bands, spin, parity 78−8768
^{156}Dy rotational levels obs. in ^{159}Tb(p,4nγ) at 27-51 MeV 77−6199
^{158}Dy collective excitations as populated in $^{158}Ho^{g,m}$ decay 78−82270
^{161}Dy, Nilsson bands, J^{π} via (d,p), (d,t) and (n,γ) 77−34215
^{162}Dy, level scheme, γ-branchings following ^{162}Tb decay 77−34246
$^{162}Dy+^{16}O$, Coulomb-nuclear interference for high spin states 78−46097
Er, A=161,162, high ang. momentum states from $Nd+^{16,18}O$, γ decay modes from multiplicity meas. 78−29419
Er, A=164, 166, 168, 170, high spin rot. states populated in heavy ion scatt., lifetime meas. 77−30511
Er even isotopes, aligned Stockholm band intrinsic spin I_0^{eff} 80−13363
Er yrast levels, spin alignment, populated by preequilibrium $(\alpha,xn\gamma)$ reactions 80−52557
^{A}Er, (A=154,155), rotational struct. at high spins 80−457
^{A}Er (A=156,157,158), high spin yrast states, γ-ray polarisation in (^{32}S,xn) reactions 80−497
^{A}Er, A=154, 155, γ-ray spectra, ang. distrib., high spin states 79−9503
^{154}Er, high-spin states 78−29373
^{156}Er N=88 nuclei quasirot. bands and J^{π} from EC decay 80−83025
^{156}Er, negative parity yrast states, microscopic calc. 78−495
^{158}Er, high-spin yrast levels, second discontinuity obs. 77−61373
^{158}Er, second backbending using cranked Hartree-Fock-Bogoliubov method 79−13188
^{158}Er, var. calc. and HFB calc. of back-bending 77−57584
^{160}Er, produced in $^{124}Sn+^{40}Ar$, γ-ray multiplicity spectra, nuclear shape at high angular momentum 78−37260
^{163}Er, excited states populated in ^{163}Tm decay 78−17146
^{164}Er multiple high spin band struct. from $^{160}Gd(^{9}Be,5n)$, backbending 78−70429
^{167}Er, s-wave resonance parameters, 5 to 130 eV, spin determ. 77−26585
^{170}Er level struct. obs. in ^{170}Ho β^--decay 78−41675
^{172}Er levels, bands, J^{π} and transitions from ^{170}Er(t,p) 80−83038
^{256}Es 7.6 hr β-decaying high-spin isomer, discovery following ^{254}Es(t,p) 77−22964
Eu, A=149, 151, band struct. anal. with Sm(d,3nγ) at 18-25 MeV 77−41913
^{A}Eu, A=157, 159, single proton states, rot. bands, J^{π} assignments and mass from Gd(t,α) 79−45132
^{144}Eu, multiplet splitting and isomerism, J, π, T1/2 via (d,2n) and (p,n) 77−14014
^{145}Eu high spin states, J^{π} and transitions from (^{7}Li,4nγ) and (^{6}Li,3nγ) 80−47350
^{145}Eu, IAS, J^{π} via polarised proton scatt. 77−74825
^{149}Eu level structure populated in $^{150}Sm(p,2n\gamma)$, spin, parity 78−21561
$^{151}Eu(^{16}O,^{16}O'\gamma)$, 25-42 MeV, energy levels, transitions, spin assignments determ. 77−38294
^{153}Eu 5/2$^+$ ground state rot. band, J^{π}, shape coexistence from (d,p) 80−86799
^{155}Eu, single proton states, spins and parity, rot. bands from $^{156}Gd(t,\alpha)$, $^{154}Sm(\alpha,t)$ 79−30766
^{17}F 14.174 MeV T=3/2 level, spin assignment from $^{16}O(p,p')$, polarised p 79−67648
^{18}F 5$^+$ excited state from $^{16}O(\alpha,d)$ 78−58291
^{18}F, 5603 keV level, isospin mixing via (α,γ) and (p,γ) reactions 78−543
^{18}F (e,e′), polarised e, parity mixing and form factors from elementary particle theory anal. 79−89233
^{18}F isospin mixed states seen via $^{14}N(\alpha,\alpha_1)^{14}N$, 7.6 to 16.9 MeV 77−14029
^{18}F $J^{\pi}=3^-$ doublet at 6241 keV, isospin mixing from (p,γ), (p,α), (α,γ) (^{14}N,α) 80−511
^{18}F level spin, isospin and parity assignments, from $^{20}Ne(d,\alpha)$ tensor analysing power meas. 78−74305
^{18}F levels and resonances, J^{π} assignments from $^{17}O(p,\alpha)$, $^{17}O,(p,p_1\gamma)$, $^{17}O(p,\gamma)$ 79−9480
^{18}F, negative parity states, dynamic interaction propagator approach 79−13191
^{18}F resonances, α-widths, isospin and parity mixing, R-matrix anal. of $^{14}N(\alpha,\alpha)$ 80−91162
^{18}F, spin-parity assignment from $^{17}O(p,p)^{17}O$, at 1.4-3.0 MeV 78−29391
^{18}F, trinucleon cluster states, low lying negative parity states 78−29387
^{19}F 5.10 MeV level parity from $^{17}O(^{3}He,p)$ 79−45155
^{19}F, energy levels from α-^{15}N and t-^{16}O coupled channel orthogonality condition model 80−37326

nuclear spin and parity continued
^{19}F, even parity state, EM props., collective struct., generator coord. method, HF method anal. 79−89220
^{19}F even-parity states, generator coord. method, projected Hartree-Fock, and complete diagonalisation calcs. comparison 78−89796
^{19}F, high-spin negative parity states, via $^{15}N(\alpha,\gamma)^{19}F$ 77−61346
^{19}F level scheme, anal. using parity mixing 77−18387
^{19}F, level struct. J^{π}, spectroscopic factors via (^{13}C, ^{9}Be) reaction 77−14033
^{19}F level structure populated in $^{16}O(\alpha,p)$, spin, parity *(Spanish)* 77−67756
^{19}F, levels, spectroscopic factors via $^{16}O(\alpha,p)^{19}F$ 77−14140
^{19}F levels, studied via $^{19}F(p,p'\gamma)$, 5 to 9 MeV 77−297
^{19}F low lying positive parity states from rot. model, moments and deformation 79−6410
^{19}F parity mixing, approx. short-range correls. in wave function, appl. 77−285
^{19}F, parity mixing and weak parity nonconserving NN interaction 77−6223
^{19}F, produced in $^{15}N(\alpha,\gamma)^{19}F$, 5.2 to 8.4 MeV, resonances and gamma decay schemes 78−37358
^{19}F resonance parameters and J^{π} values from $^{18}O(pp)$ polarised p 79−45232
^{19}F, resonl levels from $^{15}N(\alpha,\gamma)^{19}F$, 2.8 to 4.0 MeV 77−65211
^{19}F T=$^{3}/_{2}$ states resonance energy, γ-decay and J^{π}, capture strength from $^{16}O(p,\gamma)$ 79−67728
^{20}F 2.97 MeV doublet γ-decay, J^{π} assignment from $^{11}B(^{13}C,\alpha\gamma)$ 79−6491
^{20}F energy levels populated in $^{14}N(^{7}Li,p)$, spin, parity 78−21596
^{20}F excited states from $^{16}O(^{7}Li,^{3}He)$, energies, spins 78−82369
^{20}F spins from $^{17}O(^{13}C,^{10}B)$ 80−13494
^{52}Fe, γ-spectra, levels, J^{π} via $\alpha+^{50}$Cr reaction 77−74794
^{52}Fe levels, J^{π}, via $^{54}Fe(p,t)^{52}Fe$ 52 MeV reaction 77−50058
^{52}Fe levels from ^{54}Fe(p,t), ang. distrib., spin, parity, $f_{7/2}$ shell model 78−74362
^{53}Fe, levels, J^{π}, populated via (τ,α) 18 MeV 77−74767
^{54}Fe 8$^+$ and 10$^+$ level spin assignments and lifetimes from (^{16}O,2p), (^{6}Li, pn) 80−68531
^{54}Fe high spin states, transitions and J^{π} values from $^{52}Cr(\alpha,Zn\gamma)$ 80−455
^{54}Fe, studied via $(\alpha,2n\gamma)$, high spin states, shell model calcs. 78−54675
$^{54}Fe(P,\alpha)^{51}Mn$, 21 MeV analogue state, excitation 80−13471
^{55}Fe levels, J^{π}, spectroscopic factors, DWBA anal. of $^{56}Fe(^{3}He,\alpha)$ 80−99127
^{55}Fe resonances, levels, J^{π}, valence capture γ-ray spectrum from $^{54}Fe(n,\gamma)$ 80−86852
^{56}Fe isobaric analogue resonances, γ ang. distribs., spin assignments, decay characts. 78−78342
^{56}Fe, level struct. via (^{12}C,α2p), (α,2p) and (α,α) reactions 77−67702
^{56}Fe low lying levels, J^{π}, γ-γ coincidences, internal conversion from ^{56}Co β^+-decay 80−86815
^{56}Fe, populated in $^{54}Fe(\alpha,pp)$, transition rates of high spin states 77−6301
^{56}Fe yrast band, coexistence of prolate and oblate shapes 78−12947
^{57}Fe(n,X) transmission data up to 400 keV, J^{π} value for resonances 80−18311
^{58}Fe high spin states from $^{55}Mn(d,p\gamma)$, decay props., γ-γ coincidence 78−21515
^{58}Fe levels, J^{π}, anal. powers and cross sections from $^{56}Fe(t,p)$ pol.t 80−68539
^{59}Fe deduced levels and spins, from $^{58}Fe(d_{pol},p)$, cross section and vector analysing power 80−52684
^{59}Fe, spin assignments to p-wave neutron states 77−22852
^{60}Fe, level struct., spin and parity assignments, mass excess from $^{58}Fe(t,p)$ 17 MeV 78−82288
Fr, nuclear ground state spins, at beam mag. reson. obs. 78−78257
Fr, spin and mag. moment, trends in neutron deficient nuclei 78−37261
^{213}Fr, high spin yrast states in N=126 isotones 79−45131
from $^{16}O(d,\alpha_3)$, J^{π} assignments 79−3160
^{A}Ga, A=71,73, levels, ang. distribs., spin assignments and deformation transition from Ga(t,p) 79−54392
^{65}Ga, 1.286 MeV state spin 9/2 determ. from $^{64,66}Zn(p,\gamma)$ obs. 79−63663
^{65}Ga high spin states, J^{π} and transitions, triaxial struct. from (^{12}C,αp),(^{7}Li,Zn) 80−63062
^{65}Ga, spin assignments of levels by forward-angle j dependence 78−93935
^{66}Ga high spin states, shell model interpretation from $^{64}Zn(\alpha,pn\gamma)$ and $^{63}Cu(\alpha,n\gamma)$ *(French)* 79−3086
^{67}Ga, high spin states, using $^{57}Fe(^{12}C,pn\gamma)$ at 40 MeV 79−36128
^{67}Ga, levels, branching, mixing, $T_{1/2}$, via $^{67}Zn(p,n\gamma)$ 3.6-4.3 MeV 77−34247
^{68}Ga, spectroscopy with $^{69}Ga(d,t)$ and $^{70}Ge(d,\alpha)$, DWBA 77−57603
$^{69}Ga(n,n'\gamma)$, fast n, levels, J^{π}, transitions and mixing ratios, statistical anal. *(Russian)* 80−13382
$^{69}Ga(p,p'\gamma)$, 3.0-5.1 MeV, low lying state struct., lifetimes, spin and parity 79−467
^{70}Ga, high spin levels via $^{68}Zn(\alpha,pn\gamma)^{70}Ga$ 77−30611
^{71}Ga ang. correlations, level spin assignments and multipole mixing ratios from $^{71}Zn^{m}$ decay 78−78305
^{73}Ga, levels, J^{π} and ang. distribs. from $^{70}Zn(\alpha,p)$ 80−78161
Gd, A=156, 158, high spin rot. states populated in heavy ion scatt., lifetime meas. 77−30511
^{A}Gd, A=146-7, high spin yrast traps, g-factors 79−63578
$^{A}Gd(n,\gamma)$, A=154,156-8, 2, 24 keV, resonance averaged γ-spectra, level and J^{π} appls. 80−37347
^{67}Gd, γ-spectroscopy of high-spin levels via $^{64}Zn(\alpha,p\gamma)$, $^{53}Cr(^{16}O,pn\gamma)$ 78−93960
^{145}Gd levels, J^{π} and transitions, neutron hole coupling to ^{146}Gd core from $^{144}Sm(\alpha,3n)$ 80−78164
^{146}Gd, 1579 keV state, assignment of isospin and parity, using γ-ray ang. distrib. 78−21489
^{146}Gd, 3$^-$ 1579 keV first excited state 78−41670
^{146}Gd lowest 2$^+$ state, J^{π} and transitions from ^{146}Tb decay 80−105979
^{147}Gd, high-spin states and particle-core coupling 77−26614
^{150}Gd levels and transitions, J^{π} assignments mixing ratio, nuclear orientation from ^{150}Tb decay 79−13205
^{150}Gd, negative parity yrast band, E1 transitions polarisability, quadrupole-octupole coupled vibr. system 79−484
^{150}Gd, vibr. levels anal. from ^{150}Tb decay 78−8772

nuclear spin and parity continued
^{151}Gd excited state spin assignments γ-γ ang. correlations from ^{151}Tb decay *(Russian)* 79−49597
^{151}Gd, high spin states, gamma ray and conversion electron obs., level struct. 77−46130
^{152}Gd N=88 nuclei quasirot. bands and J^{π} from EC decay and (α,xnγ) 80−83025
^{152}Gd, negative parity bands, coherent state model 78−89782
^{153}Gd γ-directional distrib., levels, spin assignments from ^{153}Tb decay 79−13241
^{154}Gd levels, bands, J^{π}, DWBA anal. of ^{152}Gd(t,p) 80−78110
^{154}Gd levels from γ ang. distribs., populated by ^{152}Sm(α,2nγ) and ^{154}Tb decay 79−442
^{158}Gd excited states from ^{157}Gd(n,γ), level struct., rot. bands, transition probabilities 78−89819
Ge excited states from ^{72,74,76}Ge(p,t), spins, parities 78−25194
Ge isotopes, using (p,t) reaction at 26 MeV incident energy 78−86480
^{A}Ge, A=66,69,70, negative parity high spin states, spin and lifetimes from HI reactions 80−73768
^{A}Ge, A=72,74,76,78, ang. distribs., levels and spin assignments, deformation transition from Ge(t,p) 79−54390
^{A}Ge(d,d) 16 MeV, A=70-74, polarised d, elastic and inelastic, levels and deformation 79−554
^{19}Ge excited state, J, mean lifetimes and transitions from ^{64}Za(^{7}Li,ph)
^{19}Ge excited state, J, mean lifetimes and transitions 80−68517
^{66}Ge levels, lifetimes, J^{π} and transitions from ^{58}Ni(^{10}B,pnγ) 80−73799
^{66}Ge states and decay scheme, polarisations J^{π} and ang. distribs. from ^{58}Ni(^{10}B,pnγ) 80−22692
^{68}Ge, energy levels populated in ^{70}Ge(p,t), 26 MeV, spin-parity assignments 77−54216
^{68}Ge, lifetimes of excited states populated in ^{58}Ni(^{12}C,2p), spins and parities of levels 78−13020
^{69}Ge excited states, lifetimes and J^{π} assignments, mixing ratios from ^{66}Zn(α,nγ) 79−63629
^{69}Ge excited states, spin and γ-decay, parity state struct. from ^{69}Ga(p,nγ) 3-5.6 MeV, ^{69}Ge excited states, spin and γ-decay, parity state struct. 79−464
^{69}Ge high spin states, J assignment, decay scheme from ^{55}Mn(^{16}O,pn) 80−68518
^{69}Ge, J^{π} assignments from (d,t) and (d,p) reacts. with polarised deuterons 78−17221
^{69}Ge, transitions, spin and parity, and mag. moments determ. from β-decay of ^{69}As 79−22245
^{70}Ge level spin and parity assignments from ^{56}Fe(^{16}O,2pγ), ^{67}Zn(α,nγ), ^{68}Zn(α,2nγ) 79−3081
^{71}Ge, J^{π} assignments from (d,t) and (d,p) reacts. with polarised deuterons 78−17221
^{71}Ge, levels, studied via ^{68}Zn(α,nγ), 8 to 10 MeV, comparison with coupling model calcs. 78−8742
^{71}Ge negative parity states, J^{π}, energy spectra and spectroscopic factors 79−59013
^{72}Ge, gamma-ray spectra, energy levels, spin and parity assignments, from ^{72}Ga beta-decay *(Korean)* 78−50128
^{72}Ge high spin levels obs. in ^{70}Zn(α,2nγ) *(French)* 79−22304
^{72}Ge levels pop. in ^{8}Zn(^{6}Li,pn), in beam gamma-ray spectroscopy 80−47343
^{72}Ge spin, parity assignments, new O^{+} states 79−63594
^{74}Ge, energy levels, shape transition from 15 MeV ^{72}Ge(t,p) study 78−93945
^{76}Ge levels, J^{π} assignments, shape transition DWBA anal. from ^{74}Ge(t,p) 79−17815
^{78}Ge level struct., J^{π} values from DWBA anal. of ^{76}Ge(t,p), 17 MeV 79−6417
^{1}H(n,γ), thermal calc. of γ-circular polarisation, p-nonconservation effects 77−18564
^{1}H(n,p)n, pol. n,p, 50 MeV, spin correlation parameter $A_{yy}(\theta)$, phase shift anal. 80−68530
^{1}H(p,p), 1-3 GeV/c, pol. p, spin parameters A and A_{nn} 80−95304
^{1}H(p,p), pol.p, 9.57 MeV, spin correlation parameter, phase shift anal. 80−102112
^{2}H propagation in nucl. matter, spin depend. of optical pot. 79−93635
^{2}H(e,e), deep inelastic scatt., P nonconservation 79−75776
^{2}H(γ,n)p, parity violation expts. review, weak NN interaction 80−73792
^{2}H(γ,π^{+})nn, photoprod. near threshold, nucleus axial props. rel. to nucleon spin-fip *(French)* 79−522
^{2}H(p,p), pol.p, spin rot. and depolarisation, NN amplitude double spin flip part 80−78271
^{3}H$_{\Lambda}$, and contrib. of spin forces to Λ-N interaction *(Russian)* 77−79319
^{A}H, A=1, 2, nuclear electric dipole moments from P nonconserving atomic transitions 80−57681
^{3}He+$\mu^{-}\rightarrow\nu_{\mu}$+^{3}H, angular correlations and capture rates, spin and isospin transitions, hyperfine effects 78−70494
^{3}He(p,p), 19-30 MleV, spin anal. power and phase shift anal. 79−13295
^{3}He(π,π), role of spin isospin effects in Δ(1236) resonance domain *(Russian)* 78−78423
^{4}He isospin splitting of 1p-1h excitation, obs. in ^{3}H(p,p) 78−41622
^{4}He level density and J^{π} calcs. 79−63596
^{4}He, low lying T=1 level ordering from p-^{3}He elastic scatt. 79−26438
^{4}He, parity mixing below 30 MeV excitation energy for ΔT=0,1 transitions 80−52604
^{4}He system, high spin states 78−86484
^{4}He, T=1 excited negative parity state struct. 80−57688
^{4}He(α,αd), 119 MeV, excited states, J^{π} and γ-ang. correlations 80−86809
^{4}He(γ,π^{0}), P-odd effects, Regge and boson pole interference *(Russian)* 79−6564
^{6}He, form. in ^{7}Li(t,α) reaction, spin assignments 78−13110
Hf isotopes from π^{-} capture, high spin states 78−54806
Hf, static mag. moments, spin, parity and excitation energy from nuclear orientation *(Dutch)* 79−80872
^{172}Hf, decoupled two-quasiparticle bands, backbending 78−4890
^{172}Hf rotation bands from ^{160}Gd(^{16}O,4n), high spin states, halflives 78−25217
^{174}Hf, angular momentum fluctuation energy in the cranking model 79−89254
^{175}Hf, three- and five-quasiparticle isomers, rotational bands and residual interactions from ^{170}Er(^{9}Be, 4n) 80−83022
^{176}Hf yrast traps, cranking Hartree Fock Bogoliubov calcs. 78−25100
^{178}Hf, yrast states struct. changes via ^{176}Yb(α,2n)^{178}Hf 77−50044
Hg, A=191,2,3,5,7,9, rot. aligned bands, high spin states, energy levels B(E2) values 78−70483

nuclear spin and parity continued
Hg even isotopes, nonaxial deforms., odd parity states, semidecoupled model 77−34220
Hg high spin states and rotation alignment in ^{198}Hg 77−57591
Hg isotopes, nuclear ground state props. via atomic spectra 77−22874
^{191}Hg^{m}, and $^{190m\text{-}185m}$Hg, nucl. spins, on-line quantum beat spectrosc. determ. 80−9562
^{196}Hg, band crossing, level scheme, J^{π} 77−65192
^{197}Hg energy levels from ^{193}Pt(α,2n), γ and conversion electron spectra, spins, parities 78−25149
^{201}Hg γ-γ directional correlations, level transitions, spin assignments, mixing ratios from ^{201}Tl decay 79−496
^{201}Hg missing $f_{5/2}$ state Coulomb excitation, level scheme, J^{π}, transitions using (α,α), (^{16}O, ^{16}O) 80−47386
^{206}Hg, obs. of excited states in (^{18}O,^{16}O) and (^{17}O,^{16}O) reactions 77−6242
^{A}Ho, A=167,169, energy levels from Er(t,α), polarised t 79−36155
^{155}Ho high spin states, lifetimes, J^{π} and rot. parameters from ^{145}Nd(^{14}N,4n) 79−85354
^{155}Ho, negative-parity bands 78−93937
^{165}Ho levels from ^{166}Er(t,α), 17 MeV polarised tritons, analysing powers, spins 78−78390
^{165}Ho+n, polarised projectile and target, spin depend. of total cross section *(Russian)* 78−17211
^{165}Ho(^{165}Ho,X), deep inelastic, spin and transferred ang. momentum alignment 80−106043
^{165}Ho(n,γ), <2 keV, spin depend. of s-wave neutron strength function 78−21562
^{165}Ho(n,n), polarised n and target 0.4-2.5 MeV, total cross section spin-spin effect 79−17899
^{166}Ho, energies of low-lying high spin levels *(Russian)* 78−89793
^{166}Ho, spin assignments to levels, using ^{165}Ho(n,γ) polarised target and projectile 79−59062
^{123,125}I, levels, J^{π}, spectroscopic factors 77−34230
I, A=123,125, level struct. from Te(^{3}He,d) 24 MeV reactions 77−50057
I energy levels, collective excitations, spin,parity, populated in ^{121,125}Sb(α,2n), γ spectra 78−4891
^{A}I, A=121 to 131, comparative study of proton states excited by (α,t), (^{3}He,d) 79−63572
^{129}I energy levels populated in ^{129}Te decay, γ spectra, coincidence spectra 77−2935
In populated in ^{111,113}Cd(p,nγ), energy levels, spins, lifetimes, shape 77−320
^{106}In, assignments via ^{106}Sn decay 78−93971
^{108}In, levels, J^{π} from ^{108}Sn decay γ- and conversion electron-spectra 77−71589
^{111}In band structure and hole-core coupling, ^{109}Ag(α,2nγ), branching and mixing ratios 78−58249
^{111}In, isospin mixing obs. in ^{110}Cd(p,p'), ^{110}Cd(p,α), ^{107}Ag(α,α') and ^{107}Ag(a,p) 77−57598
^{111}In, rotational band detect., internal conversion electron spectra from ^{111}Cd(p,nγ)^{111}In 79−6362
^{112}In, 8^{-}, 6^{+} isomeric states, $T_{1/2}$, g-factors via ^{112}Cd(p,n), ^{109}Ag(α,n) 77−10318
^{114}In isomer decay, spin, excitation function, T_{112} γ-X-ray and γ-γ coinc. 77−6312
^{115}In 597 keV level J^{π} assignment from ^{115}Cd^{g} β-decay 79−80900
^{117}In level scheme, J^{π} and transitions from ^{117}Cd isomer decay, unified model anal. 80−32193
^{A}Ir, A=189, 191, levels, J^{π}, transitions and mixing ratios from Pt decay 80−68602
^{183}Ir, high spin states of rotation aligned bands, backbending 77−30485
^{183}Ir levels, J^{π} assignments, Nilsson states for N=105 isotones from ^{183}Pt fast β-transition 79−22206
^{185}Ir, high spin states of rotation aligned bands, backbending 77−30485
^{185}Ir levels excited in (α,xn) reactions, positive parity band 80−9231
^{185}Ir levels populated in ^{185}Pt^{m+g} decay 80−9269
^{186}Ir anomalous $I^{\pi}K=5^{+}1$ ground state config. confirmation, spectroscopic quadrupole moment 79−93506
^{189}Ir low lying positive parity bands, state anomalous angular distribs. from ^{191}Ir(p,t), 34.7 MeV 78−66212
^{191}Ir, levels excited in (p,2n) and (d,3n) 79−22164
^{191}Ir low lying positive parity bands, state anomalous angular distrib. from ^{193}Ir(p,t) 34.7 MeV 78−66212
^{192}Ir β decay into ^{192}Pt 4^{+} and 3^{+} levels, spectral shapes, ground state parity 77−50086
^{A}K, A=43,44, levels, spin and parity assignments, decay scheme from ^{43,44}Ar β-decay 79−13210
^{38}K, J^{π} via ^{40}Ca (d,α)^{38}K 7.5, 7.75, 8.0 MeV polarised d near 0° 77−6401
^{39}K high spin states, J^{π} assignments, DWBA anal. of ^{41}Ca(d,α), 22 MeV,
^{39}K high spin states, J^{π} assignments, DWBA anal. 79−40851
^{39}K high spin states from ^{24}Mg(^{18}O, p2nγ), decay scheme 78−25232
^{39}K high spin states from ^{28}Si(^{16}O,αpγ), γ meas. 78−89787
^{39}K, J^{π}, hole-core wave functions via ^{39}K(α,α') 31 MeV 77−50056
^{39}K, spins of p-h states from analysing powers of (d,τ) reacts. 78−25111
^{39}K(d,α)^{37}Ar, 1.83-2.53 MeV, fluctuations analysis and spin values deduced 77−23095
^{40}K excitation energy, γ decay, of lowest T=2 state populated in ^{40}Ar(p,n) 78−8769
^{40}K, spin and mixing ratio determ. from ang. distrib. meas. 79−93551
^{40}K, yrast levels, J^{π}, branching and mixing, via (^{16}O,pnγ) 34 MeV 77−74759
^{41}K, populated by ^{38}Ar(α,pγ), levels props., shell model calc. 78−62588
^{41}K yrast states from ^{26}Mg(^{18}O, p2nγ), γ meas., spin, parity, branching and mixing 78−58250
^{41}K(p,pγ), 1.58 MeV, parity doublet gamma lifetimes, 3/2 levels, parity mixing 80−78209
^{42}K, levels, studied by ^{44}Ca(d,α)^{42}K reactions, 11 MeV, DWBA analysis 78−8723
^{42}K, yrast state J^{π} assignments via ^{26}Mg(^{18}O, pnγ) anal. at 25,34 MeV 77−57618
^{43}K high spin states, J^{π} and lifetimes from ^{40}Ar(α,pγ) 79−67621
^{44}K excited levels, J^{π}, transitions and lifetimes from ^{48}Ca(p,αn) 80−68544
^{46}K levels, J^{π} and tensor anal. powers from ^{48}Ca(d,α), pol.d 80−102113
^{A}Kr, A=74,76, rot. bands, band crossing and backbending 80−18176
^{A}Kr, A=76,78,80, yrast states and band struct., backbending from Zn(^{12}C, 2n) 80−13359
^{A}Kr, A=79, 81, high spin E2 bands, J^{π}, transitions from Ge(^{10,11}B, xγ) 80−63061

nuclear spin and parity continued
^{77}Kr, low lying state J^π assignments, anal. powers from ^{78}Kr(d,t) 79−45153
^{78}Kr high spin states from ^{65}Cu(^{16}O,p2n), band struct. 78−74387
^{79}Kr excited states, J^π assignment, transitions, level lifetimes from ^{79}Rb β^+ decay 79−17810
^{79}Kr, low lying levels from ^{79}Br(p,nγ) 80−105972
^{81}Kr levels, J^π, ICC via ^{81}Rb 77−79309
^{81}Kr levels, transitions and J^π assignments, first excited state lifetime from ^{81}Br(p,nγ) 79−75849
^{84}Kr, 1.84 μs isomeric state, g-factor meas. 78−17101
^{84}Kr levels, γ-cascades, $J^{(\pi)}$, mixing ratios and correlations from ^{84}Br decay 80−63134
^{85}Kr positive-parity states calc. by quasiparticle phonon coupling 79−75845
^{87}Kr ground state spin assignment from ^{86}Kr(d,p), polarised and unpolarised d 79−471
^{87}Kr levels in ^{86}Kr(n_{th},γ) 77−74798
^{93}Kr, γ-ray decay scheme, levels, J^π, logft values 77−54152
^{133}La level struct., parity levels, decoupled band struct. from ^{133}Ce β-decay 79−9476
^{139}La, IAS, J^π via polarised proton scatt. 77−74825
^{143}La, level scheme obs. in ^{143}Ba decay 78−50129
^{5}Li level parameters via ^{3}He(d,d)^{3}He 0.3-8 MeV 77−30606
^{6}Li+$\mu^-\rightarrow\nu_\mu$+^{6}He, angular correlations and capture rates, spin and isospin transitions, hyperfine effects 78−70494
^{6}Li+n, spin depend. capture and scatt. of slow neutrons 78−46059
^{6}Li(γ,π^+)^{6}He, photoprod. near threshold, nucleus axial props. rel. to nucleon spin-flip *(French)* 79−522
^{6}Li(n,t)^{4}He, thermal polarised n capture, P-odd asymmetry meas. *(Russian)* 80−13452
^{176}Lu, reson. spins, secondary γ-transition intensity, from ^{175}Lu(n,γ) 78−21512
^{177}Lu, reson. spins secondary γ-transition intensity meas. in ^{176}Lu(n,γ) 78−21512
^{178}Lu isomeric states and spins, transition probability from ^{181}Ta(n,α) 80−52582
^{A}Mg(p,p), A=24, 26, 6.9 GeV/c, elastic and inelastic differential cross sections, ^{26}Mg spin flip probability *(Russian)* 79−59071
^{23}Mg, even parity state, EM props., collective struct., generator coord. method, HF method anal. 79−89220
^{24}Mg, ^{16}O+α+α cluster model, energy level structure 80−18215
^{24}Mg, 11.86 MeV level, confirmation of $J^\pi=8^+$ assignment from ^{12}C(^{16}O,αγ) 42 MeV 78−70445
^{24}Mg, evidence for rotational band and its fragmentation in ^{12}C(^{12}C, α)^{20}Ne reaction 79−9449
^{24}Mg, existence of second $J^\pi=0^+$ reson. at high excitation energy, study of ^{12}C(^{12}C,α)^{20}Ne reaction 78−25214
^{24}Mg, form. in ^{12}C+^{12}C reaction at 10.5 to 15 MeV, possible rot. band 78−13134
^{24}Mg from ^{12}C(^{13}C,n), nonstatistical population of high spin states 78−74385
^{24}Mg, identification of 10^+ levels using ^{12}C(^{16}O,α) at 26.7 MeV 78−33119
^{24}Mg isovector M1 excitations, current and spin contribs. from (e,e'), (p,n) 80−68582
^{24}Mg, low lying rot. bands from extended deformation model, parity violating deformations 79−6360
^{24}Mg, mol. config. of ^{12}C+^{12}C, high spin props., Strutinsky method 78−50201
^{24}Mg, populated via ^{12}C(^{12}C,γ), resonance in γ yields, $J^\pi=2^+$ resonance 78−54799
^{24}Mg, population of high spin unnatural parity states 78−37334
^{24}Mg radiative decays of unbound high spin states, resonance J^π assignment from ^{20}Ne(α,γ) 79−67701
^{24}Mg, reson. levels, J^π, via ^{12}C(^{12}C,α)^{20}Ne, E_{cm}=6.5-12 MeV 77−54200
^{24}Mg, rot. band, reson. states, J^π via ^{12}C+^{12}C 78−491
^{24}Mg+n resonances, spin and parity values 77−6386
^{24}Mg(^{13}C,^{13}C'), 35 MeV, γ-rays and spin flip 80−18189
^{24}Mg(^{13}C,^{13}C'), 35 MeV, 2^+ population probab., spin-flip and spin orbit pots., coupled channel anal. 80−99125
^{24}Mg(α,^{12}C)^{16}O, 12.7-17.4 MeV, quasimol. resonance in excitation function, ^{12}C+^{16}O system, spins 78−54775
^{24}Mg(α,^{12}C)^{16}O, 22-26 MeV, intermediate resonances in ^{12}C+^{16}O system, J^π assignments 79−17880
^{24}Mg(α,α'), 22-26 MeV, intermediate resonances in ^{12}C+^{16}O system, J^π assignments 79−17880
^{24}Mg(α,p)^{27}Al, 25-26 MeV, high spin selectivity 77−23097
^{24}Mg(d,n)^{25}Al, stripping reactions to unbound states from p-n correlations, spin, parity and widths 78−62547
^{24}Mg(p,p'), 135 MeV, cross section, population of unnatural parity high spin states 78−54753
^{24}Mg(p,p'γ), 6.9 MeV, spin flip probability 77−88127
^{24}Mg(p,p'), 40 MeV, DWBA anal., positive parity states, transitions and giant resonance 79−6419
^{24}Mg(p,p), 14-45 MeV, differential cross section and spin-flip probabilities, giant resonances 80−73850
^{24}Mg(p,p), 40 MeV, natural parity transitions 78−66277
^{25}Mg reson. level ang. momentum via ^{24}Mg(n,n) 0.4 to 1.8 MeV 77−54202
^{26}Mg(p,p'), 6 MeV, spin-flip probability, ang. distrib., energy depend. 78−13078
^{27}Mg, excited states up to E_x=7976 keV, studied via ^{26}Mg(d,pγ) reaction 77−41981
Mn levels from ^{50,52,54}Cr(α, p), 18, 26 MeV, J-depend., spins, parities 78−78397
^{51}Mn, EM transitions, J^π, half-lives, branching and mixing ratios 77−18471
^{52}Mn, γ-spectra, levels, J^π via α+^{50}Cr reaction 77−74794
^{52}Mn, high spin state spectroscopy via ^{59}K(^{16}O,2pnγ) 37-52 MeV 77−10321
^{52}Mn, low-lying states J, γ-branching and mixing via ^{52}Cr(p,nγ) 77−14028
^{53}Mn fragmented $g_{9/2}$ isobaric analogue resonance, transitions, J^π assignments from ^{52}Cr(p,γ) 79−45240
^{53}Mn high spin states, decay scheme, J^π assignments, mixing ratios from ^{40}Ca(^{16}O, 3pγ) *(French)* 79−67627
^{54}Mn low lying 2p-4h states, J^π from tensor anal. powers of ^{56}Fe(d,α), pol.d 80−99124
^{54}Mn, populated in ^{52}Cr(α,pnγ), low lying intruder states 79−58998
nuclear spin and parity continued
^{55}Mn, energy levels, bound state mean lifetimes and spins from ^{54}Cr(p,γ) 80−42586
^{55}Mn, levels, J^π, γ-branching via (n,n'γ) 1.0-3.6 MeV 77−79310
^{55}Mn, neutron resonance spectroscopy, R-matrix anal. 78−21555
^{55}Mn(n,n'γ), 2.2-3.2 MeV energy level J^π assignments, transition branching and mixing ratios 79−40881
^{56}Mn levels, transitions and spins from ^{55}Mn(n,γ), pol. Mn and n 80−78154
^{58}Mn energy levels populated in ^{58}Fe(t,^{3}He), mass excess, spin-parity assignments 77−54230
^{60}Mn, mass and β-decay half life, ground state spin and parity 78−78317
^{92}Mo high spin states from ^{90}Zr(α,2nγ), negative parity states 78−89786
^{93}Mo, excited state lifetimes and widths populated in ^{92}Mo(γ,γ) to 5.1 MeV 77−30512
^{94}Mo, analogue resonances, direct neutron decay, anal. of ^{93}Nb(p,n)^{93}Mo data *(Russian)* 79−3128
^{94}Mo even parity states, shell model calc. 77−50061
^{94}Mo high spin state transitions, mixing ratios, spins, shell model calcs. from ^{94}Tc decay 79−97678
^{94}Mo, level spins and multiple mixing ratios from γ-γ correlation meas. 78−21517
^{98}Mo neutron resonances, spin-parity determ. using low energy γ-rays 77−26570
^{101}Mo resonances, levels, J^π, level spacings, cross section from ^{100}Mo(n,γ) 79−89278
^{93,95}Mo, transfer $\mathcal{L}$ values, spectroscopic factors, J^π via (p,d) and (d,t) 40 MeV 77−74748
^{12}N, aligned, existence of G-parity irregular induced tensor current 78−29384
^{13}N level structure via ^{12}C(p,p) scatt. with 11.5 to 18 MeV polarised beam 77−315
^{14}N 9.13 MeV state, obs. in ^{13}C(p,γ) 78−41641
^{14}N(α,γ)^{18}F, hadronic nuclear-parity violation with change of isospin, γ spectrum search 78−94018
^{14}N(d, d'), energy depend. isospin violation in 10 MeV region 77−14134
^{15}N 3/2$^-$ state spin alignment and polarisation, 1/2-spin orbit interaction from ^{27}Al, ^{88}Sr(^{16}O,^{15}N) 80−27622
^{15}N 9.155 MeV state, lifetime, cluster nature and parity from ^{12}C(^{7}Li,αγ), ^{12}C(^{6}Li,^{3}Heγ) 79−6424
^{15}N, giant reson. excitation around 17 MeV, J^π,Γ assignments 77−34277
^{15}N, obs. of high spin states in ^{12}C(^{6}Li,t) and ^{12}C(^{6}Li, ^{3}He) 78−13015
^{15}N polarisation, spin alignment and excited state ang. distrib. from ^{88}Sr(^{16}O, ^{15}N) 79−67709
^{15}N, spin assignments for giant resonances from ^{11}B(α,γ_0), 15.5-19.5 MeV 78−94019
^{15}N, spins of p-h states from analysing powers of (d,τ) reacts. 78−25111
^{15}N three particle states at high excitation energies, J^π, selective population from ^{12}C(^{7}Li, α) 80−99129
$^{15}N_{3/2}$ (6.33 MeV) state, spin alignment meas. from (^{16}O,^{15}N) using γ-recoil 79−17796
^{15}N-^{15}O, study of excited states, spin and parity *(French)* 78−33158
^{15}N+X, X=^{11}B,^{12}C,^{18}O,^{13}C, deduced excited states, shell model wave functions, DWBA anal. 79−45284
^{16}N, $J^\pi=1^-$ assignment from ^{15}N(d,p) 79−30786
^{16}N, levels at 5.5-8.5 MeV from ^{14}N(t,p) 78−66207
^{16}N levels from ^{18}O(d,α) using polarised deuterons, spin parity assignments 78−89886
^{17}N 2p-1h states from ^{15}N(t,p), spins, parities, cross sections 78−62548
^{17}N, excited states obs. in ^{18}O(t,αγ) at 3.5 MeV *(French)* 77−14031
Na neutron rich isotopes, nuclear ground state props. via laser spectroscopy 77−22875
^{A}Na, (A=21, 23), even parity state, EM props., collective struct., generator coord. method, HF method anal. 79−89220
^{A}Na, A=22,23 J^π assignments from ^{12}C(^{12}C,Xγ), X=p or d 79−45154
^{A}Na, A=26-30, nuclear spin from NMR meas. nuclear deformation 79−10072
^{22}Na, 4.52 MeV state, J^π, lifetime, via ^{12}C(^{12}C,dγ)^{22}Na 77−54147
^{22}Na, 4.77 MeV level J^π via ^{24}Mg(d,αγ)^{22}Na with tensor polarised deuterons 77−22934
^{22}Na, analogue resons., γ-ray ang. distrib. and mixing ratios in ^{21}Ne(p,γ)^{22}Na 78−62504
^{22}Na, ground state band struct., J^π, E2 transitions, $T_{1/2}$ *(French)* 77−34210
^{22}Na levels, resonances in ^{21}Ne+p reactions, 0.4 to 1.6 MeV 77−18540
^{23}Na, DWBA anal. of α-spectroscopic factors in ^{19}F(^{6}Li,d) 78−82383
^{23}Na energy levels from ^{23}Mg(d,α), spin, parity, angle-integrated cross section 78−50179
^{23}Na even parity states, generator coord. method, projected Hartree-Fock, and complete diagonalisation calcs. comparison 78−89796
^{23}Na levels, resonance strengths, γ-decays and level lifetimes from ^{22}Na(p,γ) 79−45229
^{23}Na levels and spectroscopic amplitudes, J^π assignments, high spin states from ^{20}Ne(α,p) 79−75848
^{23}Na, levels populated by ^{12}C(^{15}N,α) 78−50070
^{23}Na, spectroscopy of high-spin states in ^{12}C(^{12}C,pγ) 77−46131
^{24}Na, J^π assignments via ^{22}Ne(^{3}He,p)^{24}Na 18 MeV reaction 77−74760
^{24}Na, level struct. and spin assignments, DWBA anal. from ^{22}Ne(^{3}He,p), 18 MeV 78−86477
^{25}Na, J^π assignments from ^{23}Na(t,p) 79−6381
^{25}Na, τ, J, π, branching and mixing ratios for lowest 5 levels 77−57624
^{A}Nb, A=92, 94, γ-ray multipolarities, internal conversion coeffs., energy levels 79−63625
^{91}Nb from ^{89}Y(α,2nγ)^{91}Nb, high spin states, shell model structure 79−93514
^{92}Nb energy levels populated in ^{92}Zr (p, n), spins, parities 77−14125
^{92}Nb, γ-spectra, level and decay scheme for states to 1.6 MeV excit. 77−30504
^{92}Nb, high-spin states, EM props. via ^{88}Sr(^{7}Li, 3n)^{92}Nb 34 MeV 77−74770
^{92}Nb low lying multiplets, DWBA anal. for spectroscopic factors from ^{91}Zr(α,t) 80−57685
^{93}Nb high-spin three-quasiparticle states obs. in ^{93m} Mo decay 77−34262
^{93}Nb neutron resonances, spin and parity assignments from (n,γ) meas. 77−26569
^{93}Nb(γ,γ'), energy levels, spin and parity, 6465 KeV resonance total width 78−93940
^{94}Nb, excitation energy 979 keV 79−9551
^{94}Nb excited states from ^{94}Zr(p,nγ), spin, parity, γ-spectra 77−88125

nuclear spin and parity continued
^{94}Nb(n,γ)^{95m,g}Nb, isomeric cross section ratio 79−49623
^{97}Nb, 1251 keV level spin-parity characteristics, ^{97}Zr β-decay meas. 77−22879
^{97}Nb level structure from ^{97}Zr decay, spins, parities γ ang. correls. 78−29418
^{99}Nb, level schemes, from ^{99}Zr β-decay obs. 79−17863
^{133}Nb, high-spin levels, in-beam γ-ray spectra meas. *(French)* 77−61372
Nd, A=139, 141, high spin levels, γ spectra, hole-core coupling 77−50063
Nd isotopes, prolate-oblate transition from ^{128}Te(^{16}O,5nγ) 78−70438
^{A}Nd, A=138,139, high spin states, J$^{\pi}$, γ-cascades and shape transition from ^{140}Ce(α, xn) 80−102090
^{20}Nd, low lying positive parity states by (^{16}O-α)+(^{12}C-^{8}Be) orthogonality condition model 79−6400
^{139}Nd, N=79, states populated in ^{139}Pm decay 77−41929
^{142}Nd(γ,γ), 1.85-5.0 MeV, resonance fluorescence, level radiative widths, spin assignments 79−9538
^{143}Nd, high-spin states and particle-core coupling 77−26614
^{143}Nd, levels, J, π, via ^{142}Nd(n,γ) with E=thermal 77−10320
^{144}Nd, neg. parity states, γ-transition multipolarity 79−40882
^{146}Nd(γ,γ'), reson. fluoresc., J$^{\pi}$, M2/E1 and Γ meas. 77−26663
^{147}Nd, spin by vector analysing powers of ^{148}Nd(d,t)^{147}Nd 78−609
^{148}Nd(d,t)^{147}Nd, vector analysing powers, spin determ. of ^{147}Nd 78−609
^{151}Nd, rot. states populated through neutron capture 77−6196
Ne, low spin states populated in ^{16,18}O(^{3}He,n) 77−14141
^{A}Ne, (A=19,21) , even parity state, EM props., collective struct., generator coord. method, HF method anal. 79−89220
^{12}Ne parity mixing meas. extension review 80−73792
^{19}Ne 5.09 MeV level parity from ^{21}Ne(p,t) 79−45155
^{20}Ne, sub-Coulomb resonances populated in ^{12}C(^{12}C,α), spin assignments 77−54245
^{20}Ne 13482 keV level, parity violating effects in two resonance interference from ^{19}F(p,α) pol. p 80−83033
^{20}Ne, alpha-cluster states, spin, parity and branching ratios 78−50066
^{20}Ne continuum states, J$^{\pi}$ and branching from ^{12}C(^{12}C, αα) 80−22660
^{20}Ne, form. in ^{19}F(p,γ) reaction, 668 keV, γ-ray transitions to ground state, rel. to stellar nucleosynthesis 78−17191
^{20}Ne, gamma decays of some T=0, 1 and 2 states above 9.5 MeV 77−34244
^{20}Ne high spin states, J$^{\pi}$ and α-decay branching ratios from ^{16}O(^{12}C,^{8}Be) 80−18166
^{20}Ne high spin states, J$^{\pi}$ assignments from ^{16}O(^{6}Li,d) 80−18167
^{20}Ne high-spin states studied via α-transfer reaction ^{16}O(^{14}N,^{10}B)^{20}Ne, 155 MeV 77−14164
^{20}Ne, level struct., J$^{\pi}$, spectroscopic factors via (^{13}C,^{9}Be) reaction 77−14033
^{20}Ne levels, J$^{\pi}$, branching ratio and EM transition rates from ^{16}O+α 80−42540
^{20}Ne, levels, J$^{\pi}$ and ang. distribs. from ^{18}O(t,p) 80−18204
^{20}Ne low lying levels and intermediate structure J$^{\pi}$ from ^{16}O(^{12}C, ^{8}Be) 80−102166
^{20}Ne resonances, J$^{\pi}$, excitation functions and branching ratio from ^{19}F(p,γ) 80−22787
^{20}Ne states, J$^{\pi}$, differential cross sections and ang. distribs. from ^{16}O(α,α') 80−18203
^{20}Ne, suitability of lowest T=1 states for parity nonconservation experiments from ^{16}O(α,γ) 79−22189
^{20}Ne, unnatural parity levels at high excitation, γ spectra from ^{12}C(^{12}C, αγ) 77−2933
^{20}Ne unnatural parity levels populated in ^{16}O(^{7}Li, d), reaction mechanisms 77−14158
^{20}Ne* low lying states and resonances, J$^{\pi}$ assignments and energies from ^{12}C(^{16}O,^{8}Be) 79−93592
^{21}Ne α-spectroscopic strengths and level J$^{\pi}$ assignments from ^{17}O(^{6}Li,d) α-stripping 79−516
^{21}Ne deduced spectroscopic factors, levels and anal. powers from ^{20}Ne(d_{pol},p) 80−83087
^{21}Ne even parity states, generator coord. method, projected Hartree-Fock, and complete diagonalisation calcs. comparison 78−89796
^{21}Ne, γ-ray circular polarisation, parity mixing 78−70443
^{21}Ne low lying levels, EM transitions, 2.80 MeV 1/2$^{\pm}$ doublet parity mixing 79−9462
^{21}Ne, parity-nonconserving nucleon-nucleon pot., large parity admixtures 78−82278
^{21}Ne states, spins and rotational bands from ^{12}C(^{13}C,α) 79−75815
^{21}Ne−^{21}Na, study of excited states, spin and parity *(French)* 78−33158
^{22}Ne backbending, yrast line and rotational motion, Strutinsky method from ^{11}B+^{13}C 79−36135
^{22}Ne compound states from ^{18}O(α,γ), transitions, spins, parities, astrophys. reaction rate 78−57545
^{22}Ne levels, J$^{\pi}$, α-particle spectroscopic strengths studied via ^{18}O(^{6}Li,d) at 32 MeV 77−18594
Ni even isotopes, negative parity levels, Tam-Dancoff approx., ^{56}Ni core 79−3080
Ni isotopes, shell model calcs. of BE, spectroscopic factors and excit. energies 77−22860
Ni+^{16}O, 100 MeV, deep inelastic, γ-circular polarisation and spin orientation 79−17848
^{A}Ni, A=60, 62, 66, levels, J$^{\pi}$, anal. powers and cross sections from Ni(t,p)pol.t 80−68539
^{A}Ni, A=61-63, yrast level lifetimes and J$^{\pi}$ assignments from ^{48}Ca+^{18}O 79−9445
^{A}Ni, A=64, 58, level ang. momentum and spin values, DWBA anal. from (t,d) polarised t 79−36163
^{A}Ni(p,α) A=60,62, polarised p, 22.0 MeV, analysing power J dependence 79−67740
^{56}Ni core excitation effects on A=57-66 nuclei, MSDI and ASDI comparison 78−78254
^{57}Ni energy levels, spin and parity assignments from ^{59}Ni(p,t) 79−9475
^{57}Ni high spin yrast cascade, decay modes J assignment from ^{54}Fe(α,nγ) 80−68514
^{57}Ni levels and analogue states, J$^{\pi}$ from DWBA anal. of ^{58}Ni(^{3}He, α) 79−63592
^{58}Ni, 6.02 and 5.59 MeV state J$^{\pi}$ determ. via (α,α') and (^{6}Li,d) 77−54148
^{58}Ni(^{16}O, X), 70 MeV, compound nuclei charged particle evaporation, moment of inertia 80−57785
^{58}Ni(^{16}O,X), 100 MeV, deep inelastic, fragment spin polarisation and alignment, γ-rays 80−18284

nuclear spin and parity continued
^{60}Ni high spin states, J$^{\pi}$, $T_{1/2}$, ang. distribs. and polarisations from ^{56}Fe(^{7}Li, p2nγ) 80−99116
^{60}Ni, spin of 1.33 MeV level, anisotropy coefficients in $4^{+}\rightarrow 2^{+}\rightarrow 0^{+}$ cascade *(Spanish)* 79−89525
^{60}Ni yrast state lifetimes and parities from ^{51}V(^{12}C,2np) 79−45134
^{61}Ni, γ-spectroscopy above 2.2 MeV excit., J$^{\pi}$,T, branchings 77−54172
^{61}Ni, low-lying levels, J, B(E2), B(M1) from Coulomb excit. 77−26610
^{61}Ni, spectroscopy of levels below 2.2 MeV obs. in ^{58}F(α,nγ) 77−6289
^{64}Ni, isospin purity violation, dominant role of noncollective monopole states 78−12964
^{65}Ni, spin assignments to p-wave neutron states 77−22852
Ni(e,e') A=58, 60, 64, isospin splitting of giant dipole resonance *(Russian)* 77−50116
Ni(n,γ), A=58, 60, resonance state, partial radiation widths of high energy transitions 78−13104
^{242}Np levels, J$^{\pi}$ and transitions from ^{242}U decay 79−67664
^{243}Np energy level spin assignments and anal. power from ^{244}Pu(t,α), polarised t 79−36165
^{15}O, obs. of high spin states in ^{12}C(^{6}Li,t) and ^{12}C(^{6}Li, ^{3}He) 78−13015
^{16}O, 3^{+} reson. state, particle-hole component via (p,p) and (p,α) reactions 78−580
^{16}O, alpha-cluster states, spin, parity and branching ratios 78−50066
^{16}O high spin states, J$^{\pi}$ and α-decay branching ratios from ^{12}C(^{12}C,^{8}Be) 80−18166
^{16}O highly excited states from ^{12}C(^{6}Li,d), spin, parity, decay into α+^{12}C 77−79395
^{16}O, inelastic form factors for abnormal parity states, K-harmonic method *(Russian)* 78−25113
^{16}O, levels near 13 MeV via ^{15}N+p 0.9-1.25 MeV 78−509
^{16}O, residual interactions, current conserving RPA calculations 80−57710
^{16}O resonance, giant resonance, populated in ^{15}N(p,$\gamma_{0,1,2}$), ang. distrib., γ correl., spin assignments 77−82926
^{16}O, search for 0^{+} level near 8.87 MeV 2^{-} level using ^{4}He(^{12}C,^{4}He) 77−88044
^{16}O states, J$^{\pi}$ from ^{12}C(^{12}C, αα) 80−22660
^{16}O, T=0 pairing vibr. determ. from ^{14}N(^{3}He,p) 78−70422
^{16}O+X, X=^{11}B,^{12}C,^{13}C,^{18}O, deduced excited states, shell model wave functions, DWBA anal. 79−45284
^{16}O(p,p'), proton polarisation and natural parity level excitations *(Russian)* 80−5144
^{16}O(p,p'), 135 MeV, 4^{-} particle-hole states, J$^{\pi}$ ambiguity removal 80−5036
^{16}O(p,p'), polarised p, 20, 30, 40 MeV, anal. power and cross sections, spin-orbit deformation 79−75963
^{17}O α-cluster states, α-decay orbital momenta and parities from ^{13}C(^{6}Li,d) and α-decay *(Russian)* 78−86486
^{17}O high spin 4p-3h strength location from excited peaks of ^{13}C(^{6}Li,d),(^{7}Li,t) 79−3082
^{17}O levels, resonances, J$^{\pi}$ and radiative width from ^{14}N(t,γ) 80−47389
^{18}O, dineutron cluster states, single-channel resonating group calc., levels, J$^{\pi}$ 77−82841
^{18}O, negative parity states, dynamic interaction propagator approach 79−13191
^{18}O, trinucleon cluster states, low lying negative parity states 78−29387
^{18}O-^{18}F, study of excited states, spin and parity *(French)* 78−33158
^{19}O high spin states populated in ^{13}C(^{7}Li,p) 78−21595
^{19}O, p-γ correl. meas., form. from ^{18}O(d,p) reaction 77−10353
^{20}O states below 6 MeV, J$^{\pi}$ assingments, DWBA anal. of ^{18}O(t,p) 79−22201
Os, A=187, 189, spin-state determ. and neutron reson. via (n,γ) 5-350 eV 77−6224
Os even nuclei, spin expsn. Hamiltonian, quadrupole moments 80−5058
^{A}Os, A=188, 189, levels, J$^{\pi}$, transitions and mixing ratios from Ir decay 80−68602
^{186}Os, K=0 rot. band collective states, populated in ^{186}Ir decay 77−82803
^{186}Os, levels deduced from ^{186}Ir decay and ^{186}W,(α,4n)^{186}Os 78−86481
^{189}Os spectroscopy, Nilsson model description 77−14035
^{191}Os, energy levels and spectra from ^{190}Os(d,p), ^{192}Os(d,t), ^{190}Os(n,γ) reactions 77−41917
^{192}Os(p,p') and (d,d'), γ-ray spectra, energy level scheme with negative parity states 77−34243
^{193}Os, energy levels and spin assignments using ^{192}Os(n,γ) 79−36161
^{194}Os, obs. of levels populated in ^{192}Os(t,p) 78−50181
P, A=30, 32, high spin states from ^{16}O+^{16,18}O reactions and ^{27}Al(α,n), γ-ray meas. 78−74386
^{28}P, energy levels and spectroscopic assignments using ^{28}Si(^{3}H,t) *(French)* 79−45167
^{28}P, nucleon unbound states, spin, parity, partial width, from ^{28}Si(d,pn) 80−102118
^{28}P spin assignments from ^{28}Si(^{3}He,t) at 38.5 MeV 77−18580
^{29}P, unbound states via ^{28}Si(d,pn) 10-11.8 MeV ang. distribs., DWBA anal. 77−6236
^{30}P high spin two nucleon states decay props. from ^{28}Si(α, dγ) 80−13402
^{30}P, spin cutoff parameters, spectral distrib. calc. and meas. comparison from ^{27}Al(α,n) 79−6382
^{31}P high E_x states, J$^{\pi}$, DWBA anal. ^{29}Si(^{3}He,p) 80−68536
^{31}P states from ^{29}Si(^{3}He,p), energy levels, ang. distribs., L-values 78−82361
^{32}P, spin-parity assignments from ^{34}S(d,α)^{32}P 78−17219
^{141}PM struct. determ. from ^{141}Sm^{g} decay 77−46142
Pb, 195-203, high-spin neutron hole excitations, hole-core weak coupling 77−50062
Pb, A=200, 202, 204, seniority four admixtures in low lying 0^{+} states 78−8741
Pb cored nuclei, high spin stater energies, quadrupole interaction, yrast traps 77−34223
Pb isotopes from π^{-} capture, high spin states 78−54806
Pb, odd-A isotopes, weak coupling calc. for high spin neutron hole excitations 78−62475
Pb, strongly forbidden T1-transition, parity nonconservation *(Russian)* 77−10366
^{4}Pb, A=202, 203, 204, transfer strengths from 17.5 MeV ^{204,205,206}Pb(p,t) reaction 78−94005
^{201}Pb, nuclear spin, metastable atomic states, hyperfine struct. meas. 78−25110
^{203}Pb, nuclear spin, metastable atomic states, hyperfine struct. meas. 78−25110

nuclear spin and parity continued
^{204}Pb populated by ^{204}Bi decay, isomeric transitions, J^{π} assignments 78−50122
^{204}Pb yrast levels populated in ^{204}Hg (α,4n), spin, parity, γ spectra 78−12954
^{204}Pb(n,n'γ), 1.5-3.1 MeV, levels, J^{π}, excitation functions and mixing ratios 80−102123
^{206}Pb+n, 3-50 KeV, neutron resonances, J^{π} assignments, decay scheme 79−36217
^{207}Pb parity assignments and M1 radiative strength from ^{206}Pb(n,n) 80−52614
^{207}Pb(γ,n), 7632 keV level photoexcitation, cross section and J^{π} 80−37330
^{208}Pb 7064 keV level negative parity, EM deexcitation pattern from ^{207}Pb(d,p) 79−36148
^{208}Pb, from ^{207}Pb(n,γ), J^{π} assignments for resonances 78−58284
^{208}Pb giant magnetic dipoles states obs. in ^{207}Pb+n, spin parity assignments 77−57666
^{208}Pb, high-spin states, form factors for electroexcitation 77−14116
^{208}Pb, isospin purity violation, dominant role of noncollective monopole states 78−12964
^{208}Pb(d,d'), 24 MeV, mag. dipole states, spin, parity, transition strengths 77−14129
^{208}Pb(e,e'), 50 to 335 MeV, 12^{-} mag. spin state excitations 78−50155
^{208}Pb(γ,γ), parity of bound J=1 levels 79−22188
^{208}Pb(n,n'γ), 5.2-8.5 MeV, E1 excitations, collective states and spin assignments, statistical model anal. 79−54405
^{208}Pb(p,p'), 135 MeV, normal parity level excitation, J^{π}, differential cross sections 80−57690
^{208}Pb(p,p'), 24 MeV, mag. dipole states, spin, parity, transition strengths 77−14129
^{208}Pb(p,p'), 61.2 MeV, low lying normal parity excitations 77−74843
^{209}Pb unbound high spin shell model states, single nucleon states 78−25126
^{210}Pb levels, J^{π}, transitions and lifetimes from ^{208}Pb(^{7}Li,X) 80−68542
Pb(p,t), A=204,6,8, E=35 MeV, spectra and ang. distribs. meas. DWBA anal., sum rules 78−13101
^{108,110}Pd, particle-vibr. multiplet excit. by two-neutron stripping 77−34214
Pd, A=102,4,6, collective and two-quasiparticle excitation for Zr (^{13}C, 3nγ) 77−18601
^{104}Pd levels populated in ^{104m,g}Ag β^{+} decay , spins, parities 78−13018
^{105}Pd, from decay of ^{105m,g}Ag 78−37306
^{106}Pd energy states and J^{π} from ^{106}Ag^{m} decay 80−18197
^{106}Pd, gamma-gamma ang. correlation meas. from decay of ^{106}Rh^{g} 77−79325
^{109}Pd levels, J^{π}, transitions, unique parity states, and spectroscopic factors from ^{108}Pd(n,γ) 80−42547
^{109}Pd unique parity states, particle rotor model low spin test 79−93515
^{141}Pm medium spin states, J^{π}, transitions and shape from (p,2n), (^{3}He,3n), (α,4n) 80−86779
^{142}Pm, multiplet splitting and isomerism, J, π, T1/2 via (d,2n) and (p,n) 77−14014
^{143}Pm, IAS, J^{π} via polarised proton scatt. 77−74825
^{145}Pm level struct., J^{π} and lifetimes, cluster-vibr. model anal. of ^{146}Nd(p,2n) 80−91125
^{147}Pm, level struct. via ^{148}Nd(p,2nγ) 12.1-20.2 MeV 78−510
^{147}Pm, low-lying levels, spin-parity and multipole mixing ratios 77−88043
^{149}Pm, populated in ^{149}Nd β decay 79−63628
^{149}Pm single proton states, spin assignments, spectroscopic factors from ^{150}Sm(t,α), pol.t 80−18170
^{149}Pm→^{149}Sm, beta decay matrix elements 78−70488
^{151}Pm single proton states, rot. bands, level J^{π} assignments, spectroscopic strengths from ^{150}Nd(^{3}He,d), and ^{152}Sm(t,α) 79−67626
^{152}Pm decay, β and γ rays, spins, half lives, ^{152}Sm levels 78−542
^{153}Pm struct., spin and parity assignments, Nilsson model interpretation from ^{154}Sm(t,α) polarised t 79−469
Po high spin isomers, deformed independent particle model, yrast lines, shape 79−480
^{A}Po, A=209, 211 deduced levels, J^{π} assignments, spectroscopic factors from stripping and pickup reactions 79−22197
^{206}Po, excited levels, populated by ^{206}At EC-β^{+} decay 77−79340
^{207}Po^{m}(2.79 s), ^{207}Po^{g} decay, spin from conversion electrons meas. 78−58252
^{212}Po, isomer with spin and parity 8^{+}, α- and γ-decay 78−82283
^{212}Po, levels, J^{π}, transitions and lifetimes from ^{208}Pb+^{7}Li 80−68542
^{212}Po levels and J^{π}, weak coupling calc. using realistic matrix elements 80−5068
^{139}Pr medium spin states, J^{π}, transitions and shape from (p,2n), (^{3}He,3n), (α,4n) 80−86779
^{140}Pr isobaric analogue resonances, de-excitation cascade, K-shell ionisation, spin depend. from ^{140}Ce(p,n) 80−78202
^{141}Pr, IAS, J^{π} via polarised proton scatt. 77−74825
^{141}Pr, positive parity levels, gamma-ray yields and ang. distribs. 80−105962
^{143}Pr 351 keV level populated in ^{143}Ce 1110keV β decay, transition shape, spin, parity 77−50085
^{191,193}Pt high-spin levels via ^{190,192}Os(α,3nα), triaxial rotor model 77−34213
Pt even isotopes, nonaxial deforms., odd parity states, semidecoupled model 77−34220
Pt transient isotopes, high spin state anomalies, spherical states concept *(Russian)* 77−34217
^{A}Pt, A=191 to 197, odd, levels excited via (p,d) and (d,t) 78−50089
^{A}Pt, A=192, 194, 196, states, J^{π}, ang. distribs. and transitions, DWBA anal. of Pt(p,t) 80−468
^{181}Pt ground state spin from ^{185}Hg decay 77−22968
^{187}Pt, levels, J^{π}, $T_{1/2}$, possible E0 transitions from ^{187}Au decay *(French)* 80−32230
^{188}Pt side band, low lying and high spin states populated in ^{191}Ir(p,4nγ) 78−4936
^{191}Pt energy levels, γ and conversion electron spectra, spins, parities 78−25149
^{196}Pt level struct. and J^{π} assignments, interacting boson approx. O(6) limit from ^{195}Pt(n,γ) 79−75853
Pt(p,d)^{193,195,197}Pt, l-assignments, spectroscopic factors 78−8810
^{237}Pu fission isomers, half lives and yield ratio, statistical model anal. from ^{239}Pu(γ,Zn) 79−40885
^{239}Pu, spectroscopy in second minimum of pot. energy surface 79−30805
nuclear spin and parity continued
^{239}Pu(n,f), polarised thermal neutrons, parity nonconservation *(Russian)* 78−33232
^{239}Pu(n,f), thermal, isotopic distrib. of rare gases, proton parity effect *(French)* 77−3054
^{243}Pu, J^{π}, Nilsson and rot. bands via (n,γ), (d,p) and (d,t) 77−6202
^{214}Ra, high spin yrast states in N=126 isotones 79−45131
^{230}Ra levels, J^{π} and transitions, Nilsson assignments from ^{230}Ac decay 80−68543
Rb, ground state spins, moments, charge radii by laser spectroscopy 80−78147
Rb isotopes, short-lived, determ. of nucl. spins by β radiation detected optical pumping 78−37262
Rb neutron rich isotopes, nucl. spins and mag. moments 80−47367
Rb, short-lived isotopes, spin and mag. moment meas. from atomic-beams 77−22882
Rb, spin and mag. moment, trends in neutron deficient nuclei 78−37261
^{A}Rb, A=77, 78, 78m, 79, 84m, nuclear spins and mag. moments, deformed shapes 79−17793
^{A}Rb(n,n'γ), 550-2100 keV, A=85,87, levels, excitation functions, J^{π}, Hauser-Feshbach anal. 80−105982
^{76}Rb, spin of neutron deficient nucleus by β radiation detected optical pumping 78−8782
^{79}Rb positive parity decoupled band, levels and J^{π} from (^{9}Be,Xγ), (^{10}B,Xγ), (^{12}C,Xγ), (^{28}Si,3pγ) 79−89223
^{80}Rb, level struct., quasi-rot. bands, via ^{79}Br(α,3n) 30-55 MeV reaction 77−88028
^{83}Rb band struct., spin assignments and transitions from (^{6}Li,3n), (^{16}O,p2n), (α,2n) 80−73774
^{83}Rb high spin states, Jπ and transitions from HI and α reactions 80−105949
^{84}Rb levels from ^{85}Rb(p,d), spin and parity determ. 78−82338
^{85}Rb high spin states, yrast cascade, J^{π}, γ-transitions from ^{82}Se(Li,xnγ) 80−73775
^{85}Rb levels, J^{π} and transitions from Kr^{m,g}, Sr^{m,g} decay, cluster-vibr. model 80−78162
^{90}Rb level scheme, transitions, J^{π} assignments and internal conversion coeffs. from ^{90}Kr β-decay 79−67663
^{93}Rb, γ-ray decay scheme, levels, J^{π}, logft values 77−54152
^{A}Re, A=181, 182, 187, spin polarisation, state struct. and mag. moments in rot. model 80−18194
^{A}Re, A=181,182,187, rotational struct., spin polarization 80−83016
Rh, static mag. moments, spin, parity and excitation energy from nuclear orientation *(Dutch)* 79−80872
^{103}Rh, β-γ-γ directional correl., J^{π} determ. 77−26628
^{103}Rh level scheme from fast n scatt., γ transitions, spins, parities, cross sections 78−78374
^{105}Rh, in Fe, oriented nuclear decay, mag. moments 77−46111
^{105}Rh low-lying levels, spin and parity assignments from γ transition data 79−80897
^{105}Rh, particle-vibr. multiplet excit. by two-neutron stripping 77−34214
^{109}Rh, 79.8 sec., β-decay to ^{109}Pd, γ and γ-γ meas. 79−3116
Rn high spin isomers, deformed independent particle model, yrast lines, shape 79−480
^{210}Rn high spin states, decay and lifetimes, spin assignments from ^{204}Pb(^{9}Be,3n) 80−18168
^{212}Rn high spin isomers, excited core states coupled to valence protons 77−74745
^{212}Rn high spin isomers with core excited neutron configs. from ^{204}Hg(^{12}C, 5n) 78−54792
^{212}Rn, high spin yrast states in N=126 isotones 79−45131
Ru, A=102, 104, collective states, J, B(E2), B(E3) via (d,d') scatt. 77−26557
^{A}Ru, A=106, 108, levels, transitions, J^{π} and shape from Tc decay 80−57744
^{94}Ru level structure, spin and parity, from beta decay of ^{94}Rh isomers 80−57747
^{95}Ru level scheme, low lying states, g-factor spin, parity 77−88071
^{100}Ru, negative parity bands obs. in ^{100}Mo(α,4n)^{100}Ru 77−6291
^{100}Ru, negative parity yrast band, E1 transitions polarisability, quadrupole-octupole coupled vibr. system 79−484
^{103}Ru, level struct. from ^{103}Tc decay 79−9470
^{105}Ru, γ-γ ang. correl. meas., spin and γ-ray mixing ratios 78−21516
S, A=32, 36, mol. configs. of O+O, high spin props., Strutinsky method 78−50201
^{31}S level J^{π} assignments, transition cross section from ^{33}S(p,t) 79−67660
^{32}S energy levels, spin, parity and isospin assignments from ^{31}P(^{3}He,d) 78−78265
^{32}S levels and J^{π} from ^{32}Cl β^{+} decay 80−22772
^{32}S(n,X), 2.5-1100 keV, resonance struct. from total and capture cross sections 80−42620
^{32}S(n,n), spin-flip probability to first 2^{+} level 80−78288
^{32}S(p,p), 14-45 MeV, differential cross section and spin-flip probabilities, giant resonances 80−73850
^{33}S, excited states, ang. correl. meas. 77−38239
^{33}S, state spectroscopy via ^{30}Si(α,nγ), E1,E2, J^{π} assignments <5 MeV 77−34227
^{34}S, populated in ^{32}S(t,p) at 10 MeV 78−50180
^{35}S, obs. of IAS in ^{34}S(p,p) 77−65222
^{35}S, total ang. mom. of levels up to 5.058 MeV, obs. in ^{34}S(d,p) 77−88149
^{A}Sb, A=113,115,117,119, high spin states, J^{π} assignments, decay schemes and lifetimes from Cd(^{6}Li,3n) 79−54381
^{A}Sb, A=121,123, levels below 2 MeV, spins, transitions and mixing ratio from (p,γ), (n,n'γ) 80−32191
^{120}Sb low lying level scheme, J^{π} assignments from ^{120}Sn(p,nγ) 79−22196
^{122}Sb energy levels populated in ^{121}Sb(n,γ), spin, parity, γ and conversion electron spectra 78−54721
^{122}Sb, low-lying state props., coupled neutron quasiparticle-proton model 77−61378
^{123}Sb(γ,γ'), energy levels, spin and parity, strong M1 transitions 78−93940
^{130}Sb levels, spin-parity assignments, from ^{130}Sn β decay 77−34264
^{133}Sb, level scheme of one proton and doubly closed shell core 78−37291
^{A}Sc, A=45, 47, 49 positive parity states from Ti(d,^{3}He)Sc reactions 79−97656
^{41}Sc 2p-1h intermediate struct. resonances, anal. powers, J^{π} from ^{40}Ca(p,p'γ) 80−86883
^{41}Sc, decay and partial widths of 2883 and 5037 keV levels 77−88077
^{42}Sc, β^{+} decay, isospin symm. hindered, branching fraction 78−21526

nuclear spin and parity continued
^{42}Sc two particle states, spectroscopic strengths and J^{π} values from ^{41}Ca(^{3}He,d) 79−63591
^{43}Sc, analogue resonances and struct. props. from ^{42}Ca(p,p) at 1.2-3.0 MeV 77−6374
^{43}Sc, $J^{\pi}=19/2^{-}$ isomer, high-spin precursors, from ^{29}Si(^{16}O,pn) 80−57656
^{45}Sc levels, J^{π}, transitions and lifetimes from (p,p′)(^{3}He,^{3}He′)(α,α') 80−63091
^{45}Sc, low-lying negative parity levels, Coulomb excitation 79−93552
^{45}Sc resonance decays, energy levels and J_{π} values from ^{44}Ca (p,γ) 79−80908
^{45}Sc total neutron cross section, parametric fit, bound level parameters, spin 77−23048
^{46}Sc energy levels, resonances, spin and parity from ^{45}Sc(n,γ) 80−52673
^{46}Sc transition polarisation, levels and spin assignments from ^{45}Sc(n,γ), pol. n 80−52656
^{49}Sc isobaric analogue states and resonances, J^{π} from ^{48}Ca(p,p) 80−13426
Se even isotopes, A=76-82 level struct. from (n,n′γ) 77−34233
Se isotopes level structures from ^{76,78,80,82}Se(d,p) spins, parities, spectroscopic factors, l-values 78−89885
^{A}Se(d_{pol},d), A=76,78,80,82, 12 MeV, two-step scatt. process via $J^{\pi}=2_1^{+}$ excited states 80−57781
^{72}Se from ^{58}Ni(^{16}O, 2pγ), high spin and excitation energy regions, γ cascade 78−54795
^{72}Se, high spin and excitation regions anal., ^{58}Ni(^{16}O,2pγ) 78−25226
^{72}Se yrast states from ^{58}Ni(^{16}O,2pγ), γ spectra, lifetimes, nuclear model predictions 77−54176
^{73}Se high-spin states via ^{70}Ge(α, nγ) at 10-18 MeV 77−10324
^{74}Se level scheme, J^{π} assignments, bands and transitions from ^{60}Ni(^{16}O,2p), ^{64}Ni(^{12}C,2n) and ^{65}Cu(^{11}B,2n) 79−54393
^{76}Se high spin states, bands, J^{π}, transitions and $T_{1/2}$ from ^{71}Ga(^{7}Li,2n) 80−105951
^{79}Se high spin levels, transitions, J^{π} assignments from ^{76}Ge(α,nγ) 80−459
^{83}Se, IAS, J^{π} via ^{82}Se(p,pγ) 4.5-7.7 MeV 78−573
^{76,74}Se, 33 MeV levels, J^{π} via Se(p,t)Se 77−67700
^{25}Si(p,p), 14-45 MeV, differential cross section and spin-flip probabilities, giant resonances 80−73850
^{27}Si, γ-branchings and mixing ratios determ. from ^{24}Mg(α,nγ) 78−17224
^{28}Si 10.9 MeV resonance, J^{π} assignment from ^{12}C(^{16}O,α) 79−26414
^{28}Si 10.9 MeV resonance from ^{12}C(^{16}O,α)^{24}Mg, spin, parity 78−74384
^{28}Si, 12.8 MeV resonance obs. in ^{12}C+^{16}O system 79−6405
^{28}Si excitation functions, ang. distribs., resonance spin assignments from ^{24}Mg(^{16}O,^{12}C) 80−68623
^{28}Si, excited levels populated in ^{27}Al(p,α)^{24}Mg at E_p=1540-2220 keV 78−17189
^{28}Si, high vel. recoil in polarised Fe, transient mag. fields 77−43910
^{28}Si isovector M1 excitations, current and spin contribs. from (e,e′), (p,n) 80−68582
^{28}Si levels, obs. in (α,γ) and (p,γ) reacts. 78−66205
^{28}Si levels and J^{π} from ^{28}P β^{+} decay 80−22772
^{28}Si, population of high spin unnatural parity states 78−37334
^{28}Si resonances obs. in ^{27}Al(p,α_0)^{24}Mg at 1.12-3.08 MeV 78−13091
^{28}Si, spin cutoff factors, sd shell realistic effective interactions, shell model spectra 80−18190
^{28}Si(n,n), spin-flip probability to first 2^{+} level 80−78288
^{28}Si(p,p′), 135 MeV, cross section, population of unnatural parity high spin states 78−54753
^{28}Si(p,p), 6.9 GeV/c, elastic and inelastic differential cross sections, spin flip probability *(Russian)* 79−59071
^{29}Si, nucleon unbound states, spin, parity, partial width, from ^{28}Si(d,pn) 80−102118
^{29}Si, unbound states via ^{28}Si(d,pn) 10-11.8 MeV ang. distribs., DWBA anal. 77−6236
^{29}Si(e,e′), 63-112 MeV, ground state transitions props. and transition radii of excited levels 77−50115
Sm, A=152, 154, high spin rot. states populated in heavy ion scatt., lifetime meas. 77−30511
^{A}Sm, A=146,147, excited states, energy levels, spin, parity, shell and cluster-vibration models, from (α,xn) and (^{3}He,xn) 80−57683
^{A}Sm, A=147, 149, levels, J, γ-transitions and multipole mixing ratios, $\gamma\gamma$ correlations from Eu EC decay 80−106012
^{A}Sm, A=148,9, structural connections, levels, bands, J^{π}, transitions and mixing ratios from Nd+^{3}He(α) 79−63576
^{144}Sm, produced in ^{100}Mo+^{48}Ca 78−37260
^{144}Sm(γ,γ), resonance fluorescence up to 5 MeV 78−66263
^{145}Sm, high-spin states and particle-core coupling 77−26614
^{146}Sm levels excited by ^{146}Eu decay, spin-parity assignment *(Russian)* 77−14062
^{149}Sm 286 keV level J^{π} character from ^{149}Pm first forbidden β-decay, β-γ ang. correlation 79−49609
^{150}Sm, negative parity bands, coherent state model 78−89782
^{150}Sm, negative parity yrast band, E1 transitions polarisability, quadrupole-octupole coupled vibr. system 79−484
^{150}Sm, nucl. struct. from ^{150}Eu decay *(Japanese)* 77−41888
^{151}Sm, low energy levels, spin values, ga gamma-gamma ang. correl. meas. 77−18398
^{151}Sm transitional nucleus, neg. parity states, spectroscopic factors, B(E2) values, particle-rotor model 78−50080
^{153}Sm, spin, parity, deduced levels, using ^{150}Nd(α,n), comparison with particle-rotor model 79−58999
^{154}Sm(γ,γ'), reson. fluoresc., J^{π}, M2/E1 and Γ meas. 77−26663
Sn, A=104, 106, 108, seniority four admixtures in low lying 0^{+} states 78−8741
Sn, A=108-118, L,J,π via (^{3}He,n) 25.4 MeV reaction to 0^{+} states 77−50050
Sn, α-spectroscopic factors from (d, ^{6}Li) 80−534
Sn deeply bound hole states and isobaric analogue states populated in ^{116,118,120,124}Sn neutron pick-up reactions 77−30570
Sn, extended Skyrme force calculation, spin instability 79−63601
Sn from ^{122,124}Sn(n,γ) up to 20 keV, level schemes, spin-parity assignments, neutron separation energies 77−54215
Sn odd isotopes, A=109-117, high spin states, level schemes 78−54684
Sn, odd mass isotopes, low lying negative parity states, energy levels, shell model calc. 80−5076
Sn, single closed shell even mass nuclei, collective bands, spin, parity, from Cd(α,2nγ), γ meas. 78−54719

nuclear spin and parity continued
^{A}Sn, A=109,111,113,115,117, level scheme, J^{π} assignments, high spin states from Cd(α,xn) 79−45168
^{A}Sn, A=120,122,124,126,128, levels, transitions and J^{π} values from In isomeric decays 79−75851
^{A}Sn(n,γ) A=114,116,118, ^{115,117,119}Sn resonance meas., weak coupling model calc. for levels, J^{π} assignments 79−6416
^{A}Sn(p,p′), A=115, 117, 119, 18 MeV, state spin assignment, particle-vibr. coupling 80−32160
^{114}Sn, isospin purity violation, dominant role of noncollective monopole states 78−12964
^{115}Sn, Coulomb excit. via (^{4}He,^{4}He) and (^{16}O,^{16}O) reactions 77−67719
^{115}Sn, levels, J^{π} via ^{116}Sn(d,t)^{115}Sn 23 MeV 78−612
^{116}Sn levels, J^{π} and transitions from ^{115}Sn(n,γ) 80−52587
^{116}Sn(d,p), pol. d, 8.22 MeV, vector anal. power, p and d spin depend. effects 80−5114
^{117}Sn(n,γ)^{118}Sn, disturbance of parity in ^{118}Sn gamma decay *(Russian)* 77−3008
^{117}Sn(n,γ)^{118}Sn, parity violation obs. 78−8820
^{120}Sn 6730 keV level, spin, absorpt. cross section, from nuclear resonant scatt. 79−3134
^{121}Sn level props. determ. from ^{120}Sn+n transmission and capture gamma-ray meas. 77−3004
^{124}Sn, isospin purity violation, dominant role of noncollective monopole states 78−12964
^{124}Sn(n,n), pol. thermal, parity violation near resonance, DWBA calcs. 80−68528
^{124}Sn(p,p), threshold enhancement of parity violation, Born approx. 80−18191
^{132}Sn, doubly magic nucleus, level scheme 78−54668
^{132}Sn, energy levels, gamma transitions, spin and parity 80−9239
^{132}Sn level struct., lifetimes, γ-γ coincidences, internal conversion from ^{235}U fission 80−52584
Sn(d,t)Sn, even A=112 to 124, deeply bound hole states of odd A Sn 78−8725
^{A}Sr, A=94,96 direct and skip cascades, $\gamma\gamma$ ang. correlations, levels, mixing ratios from Rb decay 80−86851
^{83}Sr, excited states struct. ^{83}Y β^{+} decay, γ-ray coincidence meas. 77−6309
^{83}Sr high spin states, J^{π} and de-excitation from Kr(α,xn) 80−42516
^{83}Sr, high spin states and spin ordering, γ-ray excitation functions 78−66199
^{85}Sr, high spin states and spin ordering, γ-ray excitation functions 78−66199
^{87}Sr excited levels from ^{87}Rb(p,nγ), spin, parity, branching ratios, lifetimes 77−50076
^{88}Sr(γ,γ), 14 MeV, highly excited spin-1 resonances, spin and radiative widths 80−86876
^{89}Sr level transitions and spin assignments from ^{88}Sr(d,p)^{89}Sr, polarised d 78−66286
^{92}Sr $\gamma\gamma$ ang. correlations, levels, J^{π}, mixing ratios from ^{92}Rb decay 80−57725
^{93}Sr, γ-ray decay scheme, levels, J^{π}, logft values 77−54152
^{173}Ta, levels, rot. parameters, γ-mixing 77−34248
^{177}Ta, rotational struct., spin polarization 80−83016
^{177}Ta spin polarisation, state struct. and mag. moments in rot. model 80−18194
^{178}Ta 2.45 h decay, J^{π} assignment, ^{178}Hf 9^{-} to 8^{-} transition 79−45201
^{180}Ta, evidence for Gallagher-Moszkowski doublets from ^{181}Ta(p,d) reaction 78−58233
^{180}Ta, ground state spin, (p,d) cross-sections 79−26368
^{180}Ta nuclear spin and mag. dipole moment from laser resonance fluorescence 80−78143
^{182}Ta, levels, J^{π}, via 2-3 eV neutron capture γ-spectra 78−602
^{185}Ta single proton states and rot. bands, J^{π} from ^{186}W(t,α),pol.t 80−91130
^{148}Tb, high spin states, transitions J^{π} assignments from (Li,xn) and (^{10}B,xn) 79−49582
^{153}Tb excited states from Eu(α, xn), rot bands, spin, parity, γ spectra 78−62552
^{153}Tb low excited states, γ-ray angular distrib. in ^{153}Dy decay 79−6471
^{153}Tb, low excited states, lifetime meas. 79−6492
^{153}Tb, negative-parity bands 78−93937
^{153}Tb, prod. in ^{153}Dy decay, weak deform. 77−41884
^{159}Tb polarised target, transmission of polarised resonance neutrons, 20 eV to 100 keV, spins *(Russian)* 77−50138
Tc, A=94,8, levels determ. from Mo(^{3}He,t)Tc at 24 MeV 77−26778
^{A}Tc, A=94 to 98, γ-ray multipolarities, internal conversion coeffs., energy levels 79−63625
^{93}Tc $^{17}/_{2}$ isomer, parity mixing search, partial γ-decay widths from ^{63}Cu(^{32}S,2n2p), 120 MeV 78−93936
^{93}Tc $17/2^{-}$ isomer, internal conversion coeffs., parity mixing search from ^{92}Mo(α,2np) 43 MeV 78−78255
^{93}Tc, J=17/2 doublet, parity mixing, weak NN interaction 80−73791
^{94}Tc levels and J^{π}, coupled channel and DWBA anal. of ^{92}Mo(^{3}He,p) 79−89239
^{95}Tc, energy levels from ^{95}Mo(p, nγ)^{95}Tc 80−37372
^{95}Tc, high momentum states band structs. obs. in (α,2nγ) 78−33109
^{95}Tc in Fe, oriented nuclear decay, mag. moments 77−46111
^{96}Tc energy level diagram, γ transitions and parities from ^{96}Mo(p,nγ) 79−9479
^{96}Tc even mass odd nucleus, proton spectroscopy, from ^{95}Mo(^{3}He,d), shell model anal. 79−63573
^{96}Tc, high spin states, γ-energy, intensity, coincidence, ang. distrib. and electron conversion from ^{93}Nb(α,n) 80−52554
^{96}Tc low lying states, level scheme, parities, from conversion electron, γ spectra 78−46024
^{97}Tc high spin states, spins and transitions from ^{94}Zr(^{6}Li,3nγ) 80−73780
^{97}Tc levels, decay props., mixing ratios and J^{π}, from directional correlations in ^{97}Mo(p,nγ) 79−89240
^{97}Tc, spin of 785.0 keV level from γ-γ ang. correl. study 77−71584
^{98}Tc energy levels from ^{99}Tc(p,d), l-values, spectrocopic factors, parities 78−25183
^{98}Tc, excited by (d,t) and (p,d), l,J,π determ. 77−18370
^{99}Tc, 920 keV level spin, from ^{99}Mo beta decay gamma-ray obs., 0.1-1 MeV 77−54145
^{99}Tc level structure, spin-parity, from inelastic scatt. and proton stripping studies 78−8743
^{99}Tc, low-lying states via ^{98}Mo(^{3}He,d)^{99}Tc, proton config. 77−22894
^{100}Tc level scheme, transitions and J^{π} values, n binding energy from ^{99}Tc(n,γ) 79−63590

nuclear spin and parity continued
^{102}Tc deduced levels, tentative J^{π} and transitions from ^{102}Mo decay 80−52630
$^{\wedge}$Te, A=117,119,121, $\Delta J=1$ band structures on ns isomeric states 79−54382
^{118}Te, produced in ^{82}Se+^{40}Ar, γ-ray multiplicity spectra, nuclear shape at high angular momentum 78−37260
^{121}Te isomeric state, spin, lifetime and mag. moment from (α,n),(d,Zn) 80−47387
^{123}Te level scheme obs., ^{123}I decay, gamma-ray spectra meas. 77−10361
^{123}Te levels, spin assignments and E2/M1 multipole mixing ratio from ^{123}I decay 79−75836
^{124}Te, spin of 1248 keV level, meas. with Ge(Li) polarimeter 77−34530
^{125}Te level scheme obs., ^{125}Sb decay, gamma-ray spectra meas. 77−10361
^{127}Te from fission, 10^{+} isomeric state, J^{π} from deexcitation pattern, half life 80−460
^{134}Te, levels, J^{π}, 6^{+} isomer level mag. moment 77−82824
^{231}Th excited states and bands, spins, γ-transitions from ^{230}Th(n,γ) 80−57699
^{232}Th, vibr. states, Coulomb excitation 79−9432
^{232}Th+^{86}Kr, Coulomb-nuclear interference for high spin states 78−46097
^{233}Th, excited levels, using thermal and average reson. neutron capture in ^{232}Th 79−45166
Ti, A=42, 44, level props. from Ca(^{3}He,n) reacts. 77−65227
Ti, A=45-51 odd isotopes, spectra and EM transitions, spin assignments, rot. bands 77−74793
^{43}Ti positive parity states, mean lifetimes, quasirotational band from ^{40}Ca(α,n) 20 MeV 79−6415
^{44}Ti levels, lifetimes and spins meas. from ^{40}Ca(α,γ)^{44}Ti 77−79328
^{44}Ti resonance levels obs. in ^{40}Ca(α,γ) at 2.75-4.00 MeV 77−65230
^{45}Ti, 40 keV level spin and g-factor via ^{42}Ca(α,n) 77−74761
^{46}Ti deduced levels, spin assignments and γ-decay, band struct. from ^{43}Ca(α,nγ), 8-15 MeV 78−78302
^{46}Ti(α,nγ)^{49}Cr, gamma-ray ang. distrib., ang. correlation, linear polarisation and Doppler-shift attenuation meas. 77−82941
^{48}Ti high spin states, γ-decay, J^{π} assignments, lifetimes from ^{45}Sc(α,pγ) 80−13356
^{48}Ti high spin states from ^{45}Sc(α,pγ) 78−74378
^{50}Ti, 1p7h config., high-spin neutron-hole states, EM transition rates 78−70430
^{50}Ti high spin states, transitions and J^{π} values from ^{48}Ca(α,Znγ) 80−455
^{50}Ti, studied via (α,2nγ), high spin states, shell model calcs. 78−54675
^{51}Ti, populated in ^{51}Sc β-decay spin-parity values 77−6318
Tl, A=195, 197, rot. bands, high spin states 78−62476
Tl, A=201,203, levels via (d,3nγ), J^{π},$T_{1/2}$, $9/2^{-}$ band discovery 77−34207
Tl, A=208,206,204, high-spin states, α-spectra via (d,α) 80 MeV 78−504
Tl, strongly forbidden T1-transition, parity nonconservation *(Russian)* 77−10366
$^{\wedge}$Tl, A=196, 198, staggering of even and odd spin states 78−70446
^{190}Tl→^{190}Hg→^{190}Au, decay spectra and periods 77−6317
^{196}Tl high spin states, γ-decay and rot. structs. from ^{197}Au(α,5n), ^{194}Pt(^{6}Li,4n) 79−440
^{198}Tl rotational structure 77−54130
^{201}Tl levels, transitions and J^{π} assignments from ^{201}Pb decay 80−5099
^{204}Tl neutron hole states, J^{π} and spectroscopic factors from ^{205}Tl(p,d) 80−86783
^{206}Tl, isomeric yrast states obs. 77−281
Tl(n,n'γ), 1.03-2.26 MeV, ang. distribs. meas., intermediate coupling model 77−38276
^{163}Tm, high spin rot. levels, studied via ^{165}Ho(^{3}He,5n) and ^{165}Ho(α,6n) reactions 78−8722
^{167}Tm rotational bands, J^{π}, γ-transitions and branching ratios from ^{165}Ho(α,2nγ) 80−86781
^{169}Tm, studied via ^{169}Tm(^{32}S,^{32}S'γ), EM props. of ground state rot. band 78−8726
^{173}Tm level and band struct., spin assignments, ang. distribs. from ^{176}Yb(p,α), 16 MeV, ^{173}Tm level and band struct., spin assignments, ang. distribs. 79−474
^{175}Tm single proton states, rot. bands, J^{π} assignments from ^{176}Yb(t,α), pol. t 80−452
$^{\wedge}$U(n,f), A=233,235, ejection fission products angular depend. on thermally polarised neutron capture *(Russian)* 80−86941
^{233}U, high-energy spin state obs. using Coulomb excitation 78−17102
^{233}U(n,f), thermal polarised neutrons, neutron emission P-odd asymmetry *(Russian)* 80−78338
^{235}U(n,f) polarised thermal neutrons, P-odd asymm. *(Russian)* 78−33231
^{235}U, levels, J^{π}, multipolarities via (n,γ) 5-49 MeV 78−512
^{235}U(n,f), 0.001-25 keV, polarised n, spin separated cross sections, resonance struct. 79−3126
^{235}U(n,f), polarised thermal neutrons, parity nonconservation *(Russian)* 78−33232
^{235}U(n,f), quantum numbers of low-lying resonances 77−23148
^{235}U(n,f), thermal n, fission product isobaric charge distrib., parity effects 79−17791
^{235}U(n,f), thermal polarised n capture, P-odd asymmetry meas. *(Russian)* 80−13452
^{235}U(n,γ) resonance capture, primary γ-transitions, parity assignments 77−26619
^{236}U, odd-parity level at 687.59 keV, mixing ratios, half-life 77−50079
^{236}U(n,f), P-odd asymmetry in neutron emission *(Russian)* 79−89339
^{237}U levels, bands and J^{π} assignments, n binding energy from ^{236}U(n,γ) 80−5041
^{238}U, negative parity bands, coherent state model 78−89782
^{238}U+^{40}Ar, Coulomb-nuclear interference for high spin states 78−46097
^{238}U(^{136}Xe,^{136}Xe), multiple Coulomb and nucl. excitation 78−21603
^{238}U(^{238}U,^{238}U), multiple Coulomb and nucl. excitation 78−21603
^{238}U(n,γ), 2, 24 keV, resonance averaged γ-spectra, level and J^{π} appls. 80−37347
^{47}V spin values and level scheme recalc. 78−78256
^{48}V, $K^{\pi}=4^{-}$ rotational band 78−12944
^{48}V, odd-parity rotational band structure 77−46102
^{48}V spin values by atomic beam mag. resonance method 78−78256
^{49}V proton hole, analogue and high spin states, distorted wave anal. from ^{52}Cr(p,α) 79−9482
^{51}V, neutron resonance spectroscopy, R-matrix anal. 78−21555
nuclear spin and parity continued
^{51}V(p,p'), 6 MeV, levels, spins and EM props., shell model anal. 80−63092
^{52}V, spin assignments to p-wave neutron states 77−22852
^{53}V, spin-parity assignments from ^{53}Ti β-decay meas. 77−46139
W, A=178, 180, 182, high spin states, microscopic-macroscopic model 79−438
W high spin states, A=172, 174, 176, from Dy(^{16}O, xn), decoupled quasiparticle bands, backbending 78−50199
$^{\wedge}$W, A=172-175, bands and backbending, $i_{13/2}$ neutron decoupling from Dy(^{16}O,xn) 80−9212
$^{\wedge}$W, A=173, 175, high-spin states, single-particle structure 78−93922
$^{\wedge}$W, A=178, 180, 182, 184, levels and J^{π}, ang. distribs. from W(p,t) 80−78159
^{170}W, nonspherical nucleus after backbending, crit. spin rel. to angular vel., bands *(Russian)* 79−75822
^{174}W, decoupled two-quasiparticle bands, backbending 78−4890
^{178}W high spin states, yrast bands and backbending from ^{170}Er(^{12}C,4n) 80−13352
^{179}W, backbending, high spin isomer decay 78−45997
^{180}W octupole vibr. states, J^{π} and transitions from ^{180}Re decay 80−83024
^{181}W levels (neutron and collective) and J^{π}, ang. distribs. from ^{183}W(p,t) 80−78160
^{182}W high spin states, J assignments and mixing ratios from ^{182}Re isomer decay 80−42593
^{182}W, level struct. determ. from (α,2nγ) and ^{182m}Re decay 77−41914
^{183}W, determ. of neutron level spins up to 400 eV *(Russian)* 79−80870
^{186}W levels, spin-parity assignments, via ^{184}W(t,p) at 15 MeV 77−18572
^{188}W levels, spin-parity assignments, via ^{186}W(t,p) at 15 MeV 77−18572
Xe, A=118,120,122, level struct., J, π, following Cs β-decay 77−57601
$^{\wedge}$Xe, A=122,124,126,128, 0^{+} excited state spin assignments and transitions from Cs β-decay 79−67649
$^{\wedge}$Xe, A=124,126-8,130,132, levels, transitions and J^{π} values, DWBA anal. from Te(^{3}He, n) 79−75852
$^{\wedge}$Xe, A=129, 131, populated in (α,nγ), props. of low-lying levels 80−464
^{125}Xe, negative parity levels in odd-A neutron deficient isomers 79−17817
^{127}Xe level scheme from decay of ^{127}Cs 77−299
^{128}Xe levels, J^{π}, log ft values, deduced from ^{128}Cs decay 77−54189
^{129}Xe, low-lying levels determ. from Coulomb excitation and (α,n) reacts. 78−70450
^{131}Xe, low-lying levels determ. from Coulomb excitation and (α,n) reacts. 78−70450
^{131}Xe, negative parity states, nucl. orientation, γ-ray spectra of Fe:^{131}Xe 77−28487
^{132}Xe level struct., J^{π}, transitions and multipole mixing ratio from ^{132}I decay 80−91134
^{87}Y, IAS spectroscopy and compound nuclear enhancement 77−61396
^{87}Y level struct., γ-spectroscopy and J^{π} from (p,2nγ), (α,2nγ) 80−83040
^{88}Y(n,2n)^{87}Y cross sections, spin dependence and preequilibrium emission 77−30598
^{89}Y, high resolution neutron total cross section meas., 27-240 keV 78−25193
^{89}Y high spin states from γ-ang. distribs. in ^{87}Rb(α,2nγ), 30-55 MeV 78−93941
^{90}Y low lying multiplets, DWBA anal. for spectroscopic factors from ^{91}Zr(d,^{3}He) 80−57685
^{94}Y deduced levels spectroscopic factors, spin and parity from ^{96}Zr(^{3}He,αp) 39 MeV 78−70451
^{171}Y populated in ^{171}Lu decay, level scheme, γ-transitions, spin-parity assignments 77−46133
Yb, A=170,172, 174, high spin rot. states populated in heavy ion scatt., lifetime meas. 77−30511
$^{\wedge}$Yb, (A=168, 170), angular momentum fluctuation energy in the cranking model 79−89254
$^{\wedge}$Yb, A=166,168,170, Yrast band investigation, self consistent cranking model anal. 79−6367
$^{\wedge}$Yb A=172, 174, electric monopole transitions from excited $K^{\pi}=0^{+}$ levels from Yb(n,γ) 79−6486
$^{\wedge}$Yb(^{16}O,^{16}O'γ), A=168-176, even nuclei, 58-62 MeV, Coulomb excitation, vibr. and rot. states 80−32162
^{160}Yb, yrast line irregularity, backbending effect 79−30777
^{167}Yb $i_{13/2}$ band, spin alignment in the particle-rotor and cranking models 80−42536
^{167}Yb, spin and parity determ. from ^{167}Lu→^{167}Yb data, ϵ/β^{+} anomaly 79−6380
^{169}Yb γγ ang. correlations, levels and spins from ^{169}Lu decay *(Russian)* 80−83069
^{172}Yb levels, bands, J^{π} and $T_{1/2}$ from ^{170}Er(α,2n) 80−91127
^{173}Yb(n,γ), search for non statistical effects 77−30588
^{173}Yb(n,γ)^{174}Yb, width correlation, primary transition intensities for resons. 77−79370
^{175}Yb level structure, band structure and J^{π} assignments from ^{176}Yb(d,t) and ^{174}Yb(d,p) 79−40850
^{177}Yb level structure, band structure and J^{π} assignments from ^{176}Yb(d,p) 79−40850
Zn, A=66,67, level struct. determ. from ^{64}Ni(α,n), (α,2n), spin-parity assignments 77−46178
$^{\wedge}$Zn, A=64, 66 levels and primary E1 transition strength functions from Cu(p,γ) 80−91149
^{62}Zn, band mixing HF model, struct. and electromag. transitions 78−54676
^{63}Zn EM decay transitions, level J^{π} assignments, level lifetimes from (α, nγ), (^{11}B, npγ), (^{7}Li, pnγ) 79−85402
^{63}Zn level scheme, spin and parity assignments from (p,d), (p,nγ), (α,nγ), (^{12}C,pnγ) 79−465
^{63}Zn, levels, J^{π} via ^{64}Zn(d,t) 13 MeV, polarised d 77−88100
^{64}Zn, γ-ray spectroscopy from ^{61}Ni(α,nγ)^{64}Zn 78−21514
^{64}Zn, γ-ray studies of levels above 3.1 MeV 80−32238
^{64}Zn high spin states, J^{π}, $T_{1/2}$, γ-decays from (α,nγ), (^{11}B,p2nγ) 80−73767
^{64}Zn, J^{π} assignments from γ-ray linear polarisation meas. from ^{59}Co(^{7}Li,2n) 79−6383
^{64}Zn, struct. of quasi-bands from (α,nγ) and (^{11}B,p2nγ) 78−70424
^{65}Zn, high spin states obs. in (α,nγ), and (^{16}O,np) 78−13016
^{65}Zn odd-parity states from ^{62}Ni(α,nγ), γ study, energies, branching and mixing ratios, lifetimes 78−50120
^{66}Zn negative parity high spin states, spin and lifetimes from HI reactions 80−73768

nuclear spin and parity continued
^{67}Zn, γ spectroscopy of low spin states from ^{64}N(α,nγ), 8.2 MeV 78−78303
^{67}Zn, high spin states obs. in (α,nγ) 78−13016
^{67}Zn, populated in ^{64}Ni(α,n), level struct. below 2.0 MeV, γ-ray studies 78−62483
^{67}Zn, role of cluster-vibr., coupling in struct. of negative parity states 77−34206
Zr, A=86, 87, 88, high spin states 78−74383
Zr, A=90-95, levels, J^{π}, neutron-hole struct., ^{95}Zr IAS 78−508
Zr neutron deficient isotopes, studied via heavy ion induced compound reactions 77−57621
^{A}Zr(n,n′γ) 2.2-3.7 MeV, A=92, 94, level and decay scheme, J^{π} assignments 79−17850
^{89}Zr high spin states, J values, γ ang. distrib. from (α, 2nγ) and (α, nγ) 79−89217
^{89}Zr, IAS and bound hole states via ^{90}Zr(^{3}He, ^{4}He)^{89}Zr 39 MeV 78−492
^{90}Zr, isospin purity violation, dominant role of noncollective monopole states 78−12964
^{91}Zr, 292.4 eV neutron resonance parameters, radiative and neutron widths, spin assignments 77−6369
^{91}Zr, level struct. via (d,p), (p,p′) and (p,d) reactions, DWBA, CCBA anal. 77−18393
^{92}Zr levels, J^{π}, cross sections, vector anal. power, optical parameters from ^{91}Zr+pol. d 80−78268
^{92}Zr(p,α), 35 MeV, polarised p, DWBA anal., anal. power, optical pot., J-depend. 79−3143
^{96}Zr, unusually strong excitation of 1.59 MeV O^{+} state in ^{100}Mo(d, ^{6}Li) 79−49584
^{99}Zr→^{99}Nb, half life, level schemes and β-decay investigation 79−17863
^{100}Zr, levels, J^{π} via ^{100}Y β-decay 77−82878

nuclear spin-lattice relaxation
^{13}C NMR, proton-decoupled, spin-echo determ. of short T_2 values, errors, appl. to protein mobility 78−2769
α,β-β-trifluoroacetonitrile, liq.-liq. transition rel. to mol. motion, NMR study 80−70383
acetone, solid, effects of tunnelling on spin-lattice relax. of methyl protons 77−12216
acetonitrile, ^{13}C relaxation times anal. using J-diffusion model of mol. reorientation 80−87149
acetonitrile, dissolved in liq. cryst., NMR, ^{13}C, ^{14}N relax. times, temp. depend. 79−94016
acetonitrile-d_2, liq., intermol. ^{1}H spin-lattice relax. and pair-diffusion 79−99781
acetyl chloride, liq., proton spin-lattice relax., temp. depend. 78−39435
N-acetyl-D-alloisoleucine, ^{13}C NMR, soln. struct., dynamics, proton relaxation mechanisms 80−76708
N-acetyl-l-phenylalanine methyl ester, model for amino acid side chains internal motions in peptides and proteins 80−48017
acoustic, liquids 80−97128
acrylonitrile, NMR and relax. props., liq.-liq. transition rel. to mol. motion 80−70382
actinide systems, spin fluctuations effect, model approach 77−28404
actinides, spin fluctuation theory, for mag. and elec. props. 78−91869
adamantane, derivatives in solution, mol. motion and methyl group rot. barriers from ^{13}C NMR relax. times 80−74179
adamantane, NMR, spin-lattice relax., plastic-brittle phase transform. 79−95665
adamantane, proton enhanced ^{13}C NMR, T_1 value method 78−91972
adamantane powder, dipolar relaxation, short time behaviour, pulse method meas. 80−84667
adamantane-d_{16}, in soln., deuteron spin-lattice relax. time, mol. rotational correl. time 78−84491
agarose gels, $H_2{}^{17}O$ enriched, ^{17}O NMR, hydration anal. 77−81426
L-alanine, nucl. spin-lattice relax. of CH_3 and NH_3 groups 77−8440
l-alanine powder, short dipolar relaxation time meas. by saturation method 80−60441
albumin denaturation, investigation by PMR 80−3582
alcohol homologous series, $^{1}HT_1$-relax. time, paramagnetic, diamagnetic shift reagent effects *(German)* 78−43673
alcohols, liq. mol. rot., deuteron relax. obs. 77−8432
alkali chloride aqueous solutions, ^{35}Cl relax. rates of chloride ions 77−88471
alkali halides, dislocation dynamics studied by nucl. spin relax. meas. 80−108091
alkali halides, dislocation motion, nucl. spin relax. study *(Dutch)* 79−78556
alkali halides, doped, impurities effect 78−19362
alkali silicate and borate glasses, ionic motion, ^{7}Li NMR obs. 78−27107
alkali silicate glass, Li^{+} motion, ^{7}Li NMR spectra, nucl. relax. 80−34804
alkane chain internal rot. correlation times, from ^{13}C T_1 data 78−17688
p-alkanoyl-benzylidene-p′-aminoazobenzenes, liq. cryst., proton mag. relax., self-diffusion 77−84632
alkoxybenzoic acids, liq. crystal, solid phase, methyl group C_3 reorientation, proton spin relax. 77−1071
p-alkoxybenzoic acids, nematic liq. cryst., proton spin lattice relax., mol. dynamics 78−34425
p-alkoxybenzylidene-alkylanilines, solid state 78−64294
p-alkoxybenzylidene-p-n-alkylanilines, solid state, nuclear spin relax. 78−76337
p-alkoxybenzylidene-p-n-alkylanilines, thermotropic mesophases, proton spin-lattice relax. 78−91968
alkylammonium cadmium tetrachloride, struct. phase transition, PMR, spin-lattice relax. time 77−35688
alkylene diammonium cadmium tetrachloride, struct. phase transition, PMR, spin-lattice relax. time 77−35688
alternating copolymer of styrene and N-substituted maleimides, NMR relax. studies of mol. motion 77−85608
amidinium salts, ^{14}N NQR spectra, H^{+} relax. times 80−60448
amino acid side chains, internal motions in peptides and proteins, N-acetyl-l-phenylalanine methyl ester model 80−48017
amino acids, polycryst., proton mag. relax. and mol. motion 78−20139
ammonium hydrogen oxalate hemihydrate, single cryst., DNMR obs., elec. field gradients, reorientation 77−85618
ammonium ions, tunnelling, model of spin-lattice relax. time 77−63305
ammonium salts, proton spin relax. and phonons 78−84493
ammonium salts, reorientation of $NH_4{}^{+}$, PMR relax. and inelastic neutron scatt. 79−82167

nuclear spin-lattice relaxation continued
amniotic fluid, human proton relax. times in low field range, appl. to nucl. magnetography *(French)* 78−3574
amorphous state, nuclear spin lattice relax., review 79−11354
Anderson model, dynamical susceptibility of impurity electrons 77−12090
anilinium chloride, $NH_3{}^{+}$ intraionic C_3 reorientation, NMR and rot. frame expt. 79−28630
anilinium halides, and anilinium sulphate, proton mag. relax. obs. 80−34800
anisotropic overall reorientation parameters, determ. in liquid phase *(German)* 78−31121
anthracene-TCNB, 1:1 charge transfer complex, phase transition at 206K, NMR meas. 79−7690
anthraquinone, in Shpolskii matrices, triplet state spin-lattice relax. rates 78−21952
antiferromagnet, nucl. spin-lattice relax., possible magnon bottleneck 77−32283
antiferromagnet nucl. spin lattice relax., field depend. of dipolar-induced two-magnon process 78−6593
automated measurement with pulse length and phase optimisation 77−21437
azobenzenes, substituted, isotropic, nucl. spin-lattice relax. 79−23519
azoxybenzenes, substituted, isotropic, nucl. spin-lattice relax. 79−23519
benzene, cryst., press. depend. of nuclear spin-lattice relax. time 79−28635
benzene-2,5-dibromothiophene, self-association, proton mag. relax. 77−28471
benzenes, substituted, dielectric absorpt. and NMR 78−88251
benzonitrile, field depend. ^{13}C NMR spin-lattice relax. and anisotropic mag. shielding 79−76450
biological systems, hydrated, PMR spin-lattice relax. of water, cross-relax. effects 79−34496
biomembrane, water transport determ. methods *(Rumanian)* 80−94435
biomolecular components, proton relaxation; solid state, activation energies, relax. consts., 50-500K 78−68998
α-bis(N-methylsalicylaldiminato) copper II, dynamic behaviour of antiferro- to ferromagnetic transition 79−73715
α-bis (N-methylsalicylaldiminato) copper II, one-dimens. spin-$^{1}/_{2}$ Heisenberg antiferromag., high-field spin dynamics 80−71224
blood, magnetic relax. time of H_2O protons 79−11898
blood, peripheral, in cancer patients, PMR relax. times 77−86579
borate glass, Li^{+} motion, ^{7}Li NMR spectra, nucl. relax. 80−34804
9-bromo-meta-carborane, mol. reorientation, ^{1}H and ^{11}B NMR 77−16185
bromobenzenes ^{13}CBr bond, spin-spin coupling consts., correl. with C hybridisation s-character 80−34806
bromoform liquid, NMR spin-lattice relax. time 80−25232
Brownian motion and NMR spin relax., book 78−15054
2-butanol adsorption on Al_2O_3, PMR spectra 79−19457
n-,t-butanol in alkanes, molecular relaxation processes studied by ^{13}C NMR 80−63654
p-t-butyltoluene, selective deuteration, proton spin-lattice relax. 79−1721
camphene, plastic cryst., ^{13}C NMR obs. 79−95667
d-camphor, high resolution ^{13}C NMR spectra, 275 to 343K 79−56621
cancer detection by NMR, behaviour of different nuclear probes 79−62326
capronate, proton spin-lattice relaxation in various phases *(Russian)* 80−97163
carbon tetrabromide, ^{13}C NMR in liq., FCC plastic cryst. and monoclinic cryst. 79−78549
carbonyl groups, spin-lattice relax. mechanism, mathematical relaxation model *(German)* 80−80633
carborane, ortho- and para-, phase transition and mol. reorientation, isomer effects, PMR obs. 80−80628
CBOOA, with cholesterol decanoate, short range smectic A order in nematic phase, NMR meas. 77−28475
cetyliodide, cryst. phase transitions, mol. dynamics, spectroscopic and dielectric meas *(Russian)* 79−51965
charge transfer complexes, polycryst., NMR spin-lattice relax. *(French)* 77−32279
chemical fast kinetics studied by NMR, review 80−55662
chlorinated compounds, ^{13}C T_1 meas. and scalar coupling consts. 80−18945
chlorobenzene, liq., spin lattice relax. time, elec. field induced charges 80−44945
chlorobenzene-d_0, -d_1, mol. reorientation and D nucl. relax. time, temp. depend. 78−39424
3-chlorodiphenyl, in dipolar aprotic solvent, internal rot. barrier, ^{13}C T_1, obs. 78−29860
chlorofluoromethanes, liq., NMR spin-lattice and dielec. relax. 79−33604
chloroform, in isotropic MBBA, nucl. spin-lattice relax., reorientation 79−4735
chloroform, liq., crit. fluctuations, proton spin relax. obs. 78−19358
chloroform diluted in CS_2, proton transverse relax. time and reorientation of chloroform *(French)* 77−32280
chloroform-d_1, D NMR relax., in nematic liq. cryst., motion spectral densities determ. 77−63304
chloroform-hexamethylphosphoramide complex, mol. motion and assoc., PMR obs. *(French)* 78−72429
chloromethane, low density gas, proton spin-lattice relax., mol. reorientation 79−3462
chloromethylgermane, polycryst., proton spin-lattice relax. times meas. 78−39430
chloromethylsilane, polycryst., proton spin-lattice relax. times meas. 78−39430
chloromethylstannane, polycryst., proton spin-lattice relax. times meas. 78−39430
2-chloropyrimidine, CS_2 soln., mol. reorientation, ^{1}H, ^{13}C nucl. mag. relax. 78−27105
choline salts, hydration, NMR spin-lattice relax. obs. 79−87830
choline salts, mol. motion, proton spin-lattice relax. 77−59474
collagen, hydrated, PMR spin-lattice relax. of water, cross-relax. effects 79−34496
computation of T_1 from pulsed NMR data, least-squares formula 78−24837
copper benzoate, antiferromag., spin dynamics at low temp. 77−32278
copper benzoate, spin 1/2 system, one-dimensional nucl. relax. 78−39427

nuclear spin-lattice relaxation continued
correlation time calc. from nuclear mag. relax. data, computer program 78−88210
critical dynamics at phase transitions and nuclear relaxation 78−75805
cross-section calcs. averaged j_z-conserving coupled states approx. [illegible] 78−84885
crystal, anisotropy of spin-lattice relax. times 79−15374
cubic crystal, non-Arrhenius diffusional behaviour and high-field nuclear spin relax. 77−47611
CW spectroscopy, phys. chem. lab. expt. 80−17775
n-pcyanobenzylidene-p-n-octyloxyaniline, liq. cryst., proton FFT of aromatic and alkyl motions 77−15302
cyanomethane, multiple quantum coherence in dipolar relaxation measurements 79−73845
cyclodiphosphazane, cryst., NQR study, intramol. interaction geom. and CCl_3 group dynamics 79−78564
cyclohexane, FCC plastic phase, self-diffusion coefficient, 6 to −40°C, nucl. spin-lattice (spin) relax. 77−36144
cyclohexane, plastic-phase, NO-doped, heterogeneous solid soln., mag. reson. evidence 78−34449
cyclooctane, solid, NMR lineshape and spin-lattice relax. 77−24757
cyclopropane, liq., mol. dynamics, Raman and NMR studies of orientational motion 80−93296
cytochrome c_3, haeme-haeme mag. interaction, Mossbauer obs. 80−108836
d-d interaction with paramag. impurities in weak static fields, relax. theory 79−69741
cis-decalin, shift difference between chem. exchange sites using ^{13}C T_1 meas. 80−18945
decanol, dynamic mol. struct. in cyclohexane-d_{12}, ^{13}C NMR 78−33519
n-decylammonium cadmium chloride, perovskite-type layer cmpd. n-decylammonium chain dynamics 79−99313
di-(2-ethylhexyl)phthalate, ^{13}C and ^{1}H relax., reorientational correlation times 79−51869
di-t-butyl nitroxide radical, in soln., proton relax., meas. of H-bonding 78−27103
di-t-butylnitroxide radical, solid, nucl. and electron spin relax. times meas. 78−60350
diamantane, NMR meas. of mol. motion 79−42858
dibenzenechromium, cryst. and soln., dynamic struct., NMR expts. 77−15328
1,4-dibromonaphthalene, proton spin relaxation by optically excited triplet states 79−19810
dicarbonyl compounds in soln., internal motion, dielectric relax., ^{13}C NMR relax., far IR spectra 77−28517
p-dichlorobenzene, ^{35}Cl spin-lattice relaxation under press. 79−4738
o-dichlorobenzene, dil. soln. in CS_2, nucl. relax. and anisotropic mol. reorientation 79−95669
trans-1,2-dichloroethane, solid, NQR at high press., hindered rot. 79−95672
dichloromethane in nematic liq. crystal , $A_2(^{12}CH_2Cl_2)$ nuclear relax., dipole-dipole interaction 77−54567
1,8-dichlorooctane, quadrupolar relax. centres, limited spin diffusion 80 100649
2,6- dichlorophenol, soln., anisotropic reorientation, H-bonding effect, NMR obs. 79−99782
dicyanoacetylene, solns., NMR and mol. reorientation 79−73840
α,α-dideuterotetrabutylammonium iodide, in soln., deuteron spin-lattice relax. time, mol. rotational correl. time 78−84491
α,α-dideuterotetraethylammonium iodide, in soln., deuteron spin-lattice relax. time, mol. rotational correl. time 78−84491
diethyl ether, liq., spin lattice relax. time, elec. field induced charges 80−44945
1,2-difluorotetrachloroethane, mol. motions and Zeeman-quadrupole cross relax., NMR obs. 79−65751
dilute Kondo alloys, calc. of host nucl. spin-lattice relax. 78−88215
dilute paramagnet, mag. reson. linewidth due to two-particle interaction 77−90012
1,4-dimethoxy-2,6-dimethylbenzene, methyl reorientations, NMR relax. and inelastic neutron scatt. obs. 79−61253
N,N-dimethylcarbomoylchloride, chem. exchange rate by NMR method, temp. depend. 79−79243
dioxane, liq., spin lattice relax. time, elec. field induced charges 80−44945
dipalmitoyl phosphatidylcholine, gel and liquid crystalline phases, deuterium mag. resonance obs. 79−91308
dipolar nuclear reservoir, spin-lattice relax. by chem. shielding tensor anisotropy 79−15372
dipolar solid, multiple-pulse spin locking 77−20742
dipolar solids, nuclear spin-lattice relax. from hindered rot. 78−52373
dipolarly coupled spin pairs, correlation function and relaxation time, group theory approach 78−48068
dipole-dipole reservoir of nuclei in magic angle configuration 80−11286
dipole-quadrupole nuclei interaction, quasi-rigid and tumbling lattice 77−66434
dislocation dynamics investigation, theory 78−34512
dislocation motion in plastically deformed crystals, nuclear spin relaxation study *(Dutch)* 79−78556
dislocation velocity determ. by spin-lattice relax. meas., theory and expt. 77−35566
DMSO-Tl^+, spin-lattice relax., chem. shift anisotropy 79−51870
DNA, molecular motions, investigated by ^{31}P and ^{13}C NMR relaxation 80−63657
dynamic ^{13}C NMR spectroscopy, review 77−51971
EBBA, binary systems with non-nematic solutes, phase transition behaviour and ^{1}H NMR anal. 80−34174
EBBA, isotropic phase, order fluctuations, self-diffusion, and rot. motion, proton spin relax. meas. 79−87328
EBBA, liq. cryst., rapid cooling and mag. field effects on NMR relax. and thermal behaviour 79−82321
electrolyte solution, relax. of spin 1/2 nuclei of heavy atoms 77−24758
ENDOR, relax. of nuclei due to non-Kramers paramag. ions 77−69731
epoxy polymers, cured spin-spin and lattice relax., proton coupling, ^{13}C NMR obs. 80−34799
erythrocytes, bound water in frozen solns., proton mag. relax. 77−28472
ethanol, polymorphic forms, mol. motion, NMR obs. 80−88885
ethylene bromide, liq., proton spin-lattice relax., temp. depend. 78−39435
ethylene glycol, spin-lattice proton relaxation time, mol. rot. motion, kinetics 77−51984

nuclear spin-lattice relaxation continued
ethylene oxide, rot. relax., double reson. and Stark switching obs. 80−106340
eye cataractous lens, NMR study of state of water *(Hungarian)* 78−64986
eye lens, normal and senile cataractous, PMR study of state of water 78−64987
eye lenses, crystalline, of humans, fish and birds, state of water, NMR meas. 79−48212
fast inversion-recovery spin-lattice relax. time meas., systematic errors elimination 79−30516
fast inversion-recovery technique for spin-lattice relax. meas., modified version 80−77826
FCC lattice, correl. functions for simple hopping, NMR relax. times 79−95202
ferrocene, cryst. and soln., dynamic struct., NMR expts. 77−15328
ferroelectric, disorder excitation relaxation effects, phonon-excitation coupled model 78−10852
ferroelectric, order-disorder, crit. dynamics, NMR data compared with dielec. data 78−76415
ferromagnet, nucl. spin-lattice relax., possible magnon bottleneck 77−32283
ferromagnetic alloys, conc., spin fluctuations, SCR theory and CPA calcs. 78−64290
ferromagnets, homogeneous, magnon bottle neck and magnon avalanche effects, microscopic theory 79−51877
field cycling method for obs. of low temp. tunnelling in molecular solids 79−65755
Fischer-Tropsch wax, NMR investigation 80−7186
fluid near critical point, spin-lattice relaxation time 80−80630
p-fluoranil, ^{19}F NMR and spin-lattice relax. meas., pot. profile calc., mole. reorientation 80−29634
9H-fluorene, soln., correl. times from ^{13}C relax. 80−23438
fluorite lattices, $^{19}F^-$, self-diffusion, spin lattice relax., NMR techniques 80−34801
fluorobenzene, mol. reorientation and weak mol. interaction influence, ^{2}D spin-lattice relax. obs. 80−106333
2-fluoropyridine, natural abundance ^{1}H coupled ^{15}N NMR spectra, selective population transfer method 79−95682
formiate, proton spin-lattice relaxation in various phases *(Russian)* 80−97163
formic acid, liq., microdynamic behaviour, struct., nucl. spin-lattice relax. 77−76270
FT NMR meas. by variable nutation angle method 77−49757
furfuryl alcohol resins, PMR study of mol. motion 79−8062
$Ga_xAl_{1-x}As$, optically oriented electron, nuclei spin instability *(Russian)* 80−70660
glasses, nuclear quadrupole spin-lattice relax., soliton-nucl. quadrupole moment interaction, temp. depend. 80−50220
glassy polymers double NMR, appl. of cross relaxation dynamics in modulated systems 80−71242
glycerol, nucl. mag. spin relax. and high freq. motion 79−51874
glycerol-d_3(-d_4), compressed viscous liq., reorientational motion, NMR obs. 80−7183
glycine, nucl. spin-lattice relax. of CH_3 and NH_3 groups 77−8440
graphite, adsorbed methanol, proton mag. relax. times obs. 77−51590
graphite intercalation cpds. with Li, nucl. relax. times 80−44947
graphite-DNO_3, intercalation cpd., mol. dynamics 79−28631
haemoglobin in red cell suspensions, T_1 and T_2 meas. 78−80832
haemoglobin solution, proton mag. relax. meas. 77−1975
halloysite, $Al_2O_3(SiO_2)_3(H_2O)_2$, NMR study of adsorbed water, molecular motions 78−95226
heteronuclear interaction, spin-lattice relax. in lab. and rot. coord. frame 78−91979
heteronuclear system, spin diffusion, NMR 78−88213
hexafluorobenzene, cryst., press. depend. of nuclear spin-lattice relax. time 79−28635
hexafluorobenzene+bisdiphenylenephenylallyl radical, solvent effects on collisions, dynamic nucl. polaris., spin-lattice relax. 77−63303
hexamethyldialuminium, methyl group rotation and bonding, CW proton second moment and line shape studies 79−47346
hexamethylethane, ^{13}C-^{13}C dipolar interaction, NMR longit. cross relax. 80−93196
n-hexyl chain bound to macromol., ^{13}C spin-lattice relax. 77−23510
n-hexylamine-nickel di-acetylacetonate, ^{13}C nucl. spin relax., electron spin delocalisation 78−5248
n-hexylamine.Gd(FOD)$_3$, flexible chain dynamics, NMR, steric effects calcs. 77−6800
holmium ethylsulphate, pseudomagnetic moment of ^{165}Ho and spin-lattice relax. times 77−63306
homonuclear coupled spin system, inversion-recovery data anal. 79−33554
hopping among inequivalent octahedral sites in body-centred tetragonal lattice 79−1520
hopping of a pair of distinguishable particles on uniform one dimensional chain, time-dependent correlations 78−88212
hybrid relaxation and multiple pulse methods for studying chemical, physical and spin exchange 80−80629
hydrocarbon chain, gauche-trans isomerisation, ^{13}C relax. times and nucl. Overhauser enhancement model 78−33520
imidazoline nitroxide radical, H-bonding with H donors, NMR, DNP and spin lattice meas. 79−15971
inversion-recovery NMR experiments, three-parameter-nonlinear fitting procedure 77−85605
iodomethane, oriented in nematic liq. crystal, longit. NMR, relax. mech. 77−63302
ionic conductors, central component NMR relax. rates 80−29640
isopropanol, ^{13}C T_1 value temp-depend. field-depend. 79−61247
Kondo superconductor, nucl. spin-lattice relax. 78−52156
LF fluctuation, dissipation and relaxation properties, universality 80−84687
ligand bound to macromolecule, cross relax. effect on T_1 78−78723
lipid bilayers, D relax. rates and mol. dynamics 80−26206
liquid, simultaneous meas. of NOE and T_1 79−42854
liquid binary mixtures, proton mag. relax. and mol. motion 77−28471
liquid crystal, isotropic phase NMR, critical orientational order fluctuations 77−55236
liquid crystal, smectic-B, layer sliding 77−36149
liquid crystals, nematic and smectic, EPR and NMR relax., first-rank tensor component effects 78−14275

nuclear spin-lattice relaxation continued
liquid crystals, NMR spin-lattice relax. time near phase transitions 80−71222
liquid metals and alloys, nuclear quadrupole relaxation 78−15050
liquid metals and alloys, review 78−2755
liquid solution, relaxation studies in magnetic resonance spectroscopy 79−73841
liquids, translational diffusion spin relax., pair correl. functions, dynamic effects 78−68404
lithium acetate, proton relax. study of nearly free methyl rotors 78−39428
lithium oxalate hydrate, proton spin-lattice relax., 180° flips and diffusion of water mol. 77−15327
liver tissue and tumour proton mag. relaxation rel. to Fe content 79−39355
lysozyme, tryptophan residues, H exchange for D, relax., proton NMR spectra 80−35846
lysozyme spin-labelled preps., water-protein layer microstruct. study by mag. relax. 78−76980
macromolecular rotational diffusion, ^{13}C spin-lattice relax. data anal., computer program, appls. 79−95664
macromolecules, internal motion, NMR spin-lattice relax. 79−41257
magnetic props. of materials, appl. of nucl. orientation, review 80−44928
magnetic relaxation depend. on internal motion in solid, correlations 80−25239
malignant cells, evidence for a condensed phonon state 79−62214
mammalian cells, NMR relax. time meas. of bulk water 80−21454
MBBA, ^{13}C spin-lattice relax., Fourier-transform NMR, NOE 78−48064
MBBA, isotropic phase, order fluctuations, self-diffusion, and rot. motion, proton spin relax. meas. 79−87328
MBBA, liquid crystal, spin thermometric anal. of spin-lattice relax. by order director fluctuation 77−47346
MBBA, mol. dynamics near nematic-isotropic liq. cryst. transition *(Russian)* 78−84495
MBBA, nematic, freq. depend. of proton T_1, rot. diffusional mechanism interpret. 77−12219
MBBA, nematic liq. cryst., ^2H NMR, mol. order and reorientation 79−27906
MBBA, order fluctuations, self-diffusion, rot. motion, proton spin T_1 relax. 77−32285
MBBA, partially deuterated, D spin-lattice relax. 78−48070
MBBA, proton spin-lattice relax. in crit. regime 80−80631
MBBA, ring deuterated, dipolar spin system exam. 77−39533
MBBA, solid, NMR and thermal behaviour, cooling and mag. field effects 78−76336
MBBA-d_{13}, ^1H spin-lattice relaxation, intermol. and intramol. contribs. 80−75873
MBBA-d_{13}, nematic phase, mol. order and director fluctuations, ^2D NMR meas. 79−90529
MBBA-d_{13}, nematic phase, rot. frame spin-lattice relax. 80−84668
MBBA-d_8, H and D spin-lattice relax. 77−59475
measurement, variable perturbation method 80−22408
measurement method for low temps. applic. to Fe:^{60}Co 77−85596
measurement technique for slowly relaxing systems with weak NMR signals 77−49752
measurement via auto-increment cct. for digital pulse programmer 77−79134
melanostatin, correl. between X-ray struct. and conform. in soln. 77−48752
mesitylene-d_{12}, extended diffusion with internal rot., NMR test 79−31549
metal:D, dynamic quadrupole nuclear spin relax., α or α' phases 77−48085
metal, non-Arrhenius diffusion and NMR relax. relationship 78−47568
metal tritides, ^3He NMR and distrib. 78−30661
metal-H system, NMR depend. on struct., H diffusion and electronic struct., book contrib. 79−82887
methaemoglobin, solid lyophilised bovine, rot. frame proton $T_{1\rho}$ spin-lattice relax. 78−95995
methane, phase II, nuclear spin-lattice relax. and site symm. 80−97155
methane, solid, nucl. longit. relax. near rot. ordering transition 77−43896
methane, solid, rot. ordering and proton spin-lattice relax. 78−91967
methane, solid-state phase transitions, 5-80K, PMR spin-lattice relax. up to 3 kbar 77−40137
methane-Ar, liq. mixture, self-diffusion and nuclear mag. relaxation *(Russian)* 78−87799
methane-Kr mixtures, rot. self-diffusion and spin-lattice relax. *(Russian)* 79−69745
methanol, ^{13}C spin-lattice relax., cross correlation of rot. motion 79−42855
methanol-β-quinol clathrate, orientation and reorientation dynamics, dielec. and NMR obs. 79−99783
methanols, labelled, proton T_1 in presence of intramol. rots., intermol. relax. rate 80−2656
methyl acetate, liq., proton spin-lattice relax., temp. depend. 78−39435
methyl ammonium aluminium sulphate, ferroelec., proton spin-lattice relax. time anomaly 80−60440
methyl bromide, ^{13}C relaxation times anal. using J-diffusion model of mol. reorientation 80−87149
methyl bromide, liq., NMR relax., anisotropic mol. reorientation 78−2764
methyl chloride, liq., NMR spin-lattice and dielec. relax. 79−33604
methyl compounds with hindered rot. ^{13}C spin-rot. relax. times 79−50049
methyl cyanide, liq., NMR spin-lattice and dielec. relax. 79−33604
methyl group, ^2H quadrupole coupling const. by high-resolution NMR spectroscopy 78−25563
methyl group, NMR relax., spin rot. and chem. shift anisotropy effects 78−31117
methyl group, proton spin relax. due to intermol. proton coupling, reorientation 78−25564
methyl group, proton tunneling reson. at low temp. 80−108087
methyl group hinderance barrier, spin-rot. relax. times 80−53011
methyl groups, detection of proton NMR at arbitrary temps. of tunnelling system 78−39432
methyl groups, reorientation in solids, nonexponential Zeeman relax. 78−6589
methyl groups in solids, proton spin-lattice relax. mechanisms at low temp. 77−51982
methyl groups in solids, reorienting and tunnelling, spin-lattice relax. 80−50217
methyl iodide, ^{13}C relaxation times anal. using J-diffusion model of mol. reorientation 80−87149
methyl piperidines, PMR spin-lattice relax. times and lineshapes, 100-300K 77−81027
methyl protons, in solids, spin-lattice relax., torsional vibr. effects calcs. 77−16196
methyl rotator in isotropic fluid, motional asymm. determ. from ^{13}C spin dynamics 77−69718
4-methyl-2,6-ditertiarybutyl phenol, proton spin relax., 80-340K methyl rot. 79−78553
4-methyl-2,6-ditertiarybutylphenol, flip-flop motion and spin symmetry conversion of methyl groups 77−15326
4-methyl-2,6-ditertiarybutylphenol, methyl group reorientation, classical dynamics, NMR relax. and inelastic neutron scatt. 80−88066
4-methyl-2,6-ditertiarybutylphenol, proton spin-lattice relax. and activation energies of tunnelling CH_3 groups 77−48071
methyl-d groups, reorienting or tunnelling spin-lattice relax. 80−97156
3,5-methyl-pyridine, rot. pot., proton spin-lattice relax., inelastic neutron scatt. study 79−47351
methylene bromide-d_0-d_2, liq., nucl. spin-lattice relax., rot. correl. times 77−59476
methylene chloride, in EBBA-d_{23}, intermol. dipolar random field cross-relax. term obs. 80−60438
methylene chloride, liq., NMR spin-lattice and dielec. relax. 79−33604
methylene chloride, liq., proton spin-lattice relax., temp. depend. 78−39435
methylene chloride, partially deuterated, T_1 meas. and anal., −96 to 40°C 78−80237
methylene iodide, benzene soln., spin-lattice relax., struct., dynamics 77−1610
methylpyridines, rot. tunnelling, NMR relax. and inelastic neutron scatt. 79−4733
α-bis(N-methylsalicylaldiminato)-copper (II), ^1H NMR spin-lattice relax. time, spin dynamics 79−99786
methyltrifluorosilane-d_3, extended diffusion with internal rot., NMR test 79−31549
microemulsions, PMR spin-lattice relax. time meas., inversion recovery method *(French)* 78−48066
molecular crystal, p-$Cl_3P{=}NSO_2C_6H_4Cl$, quadrupole nature of spin-lattice relax. 77−59480
molecular crystals, chem. shielding, spin-lattice, quadrupole interactions, ^2D NMR spin echo spectroscopy 80−34817
molecular crystals, nucl. quadrupole relax. of I=1 nuclei 77−12247
molecular groups in solids, effect of symm.-restricted spin diffusion 78−39431
molecular medium, decay of two $^1/_2$ spins, Nakajima-Zwanzig technique 78−23361
molecular multiple internal rot., ^{13}C-{^1H} nuclear Overhauser enhancement, ^{13}C spin lattice relax. 77−479
molecular reorientation in crystal, nuclear quadrupole spin-lattice relax. 80−66062
molten salt, nucl. quadrupolar spin-lattice relax., microscopic liq. dynamics 79−91313
monovalent ions in aq. metal ion solns., ^{14}N NMR relax. 80−20481
motion induced NMR spin relax. times in low temp. HF limit 80−60443
motion of spin between two positions and magnetic relaxation 79−69742
motion-induced nuclear spin relax., orientation depend., point defect self-diffusion mechanism 77−48078
trans,trans-mucodinitrile solid, NMR relax., mol. motions between unequal pot. wells 78−19353
multiple-pulse sequence technique for NMR $T_{1\rho}$ measurements 77−85606
multiplet relaxation in anisotropic media, mag. recovery rate 78−43662
muscle, frog, spin-lattice relax. times for ^{13}C in isotope-enriched glycine 77−44605
muscle, hydrated, PMR spin-lattice relax. of water, cross-relax. effects 79−34496
muscle water proton and deuteron relax. over wide ranges of reson freqs. 77−52740
muscle water transverse and longit. NMR relax. rates 78−35810
nematic liq. crystal spin-relaxation, composite Markov process, rot. reorientation and director fluctuations 77−62471
nematic liquid crystal, low-temp., temp. depend. minima of binary mixture 78−26427
nematic liquid crystal, nuclear spin relax., translational self-diffusion 78−43670
nematic liquid crystal, orientational depend. 77−84625
nematic liquid crystal, spin-lattice relax., viscosity effects, theory 77−4574
neopentane adsorbed on graphite, quasi two-dimens. fluid, NMR 80−102525
neopentane-d_{12}, ^{13}C and ^2H spin-lattice relax. times, orientational and ang. momentum correl. times 79−33551
Ni-Pt-P, metallic glass, electronic structure, pulsed NMR study 80−75869
nitrobenzene, liq., spin lattice relax. time, elec. field induced charges 80−44945
t-nitrobutane, plastic cryst., proton spin-lattice relax. time meas. 77−90058
nitromethane, liq., NMR relax. obs. of internal mol. rot. 79−95668
nitromethane, liq., proton spin-lattice relax., temp. depend. 78−39435
nitromethane, proton spin-lattice relax. time, methyl group rot., 1 to 10K 77−48080
NMR line profile, paramagnetic ion nuclei in magnetically conc. solid, theory 80−25238
NMR spin-lattice relax., effect of correlated atomic diffusion 80−107495
NMR-NQR double resonance, two-freq. methods, resonance spectrometers 80−20512
NNR population inversion using composite sandwich 79−93197
non-Kramers paramagnetic ions, induced nuclear spin-lattice relax. calc. at low temps. 77−8442
nonadecane, mol. motion in solid, ^1H spin relax. 78−15048
norbornane, derivatives in solution, mol. motion and methyl group rot. barriers from ^{13}C NMR relax. times 80−74179
NQR pulsed panoramic RF spectrometer 77−10074
NQR spin-lattice relax. due to mol. fragments reorientation *(Russian)* 80−7189

nuclear spin-lattice relaxation continued
nuclear dipolar magnetic ordering, dipole-dipole interactions review 77−85475
nucleic acid bases, ^{14}N relax. and N-proton spin coupling, NH-proton spin-lattice relax. 80−26202
OBPA, liq. cryst., proton spin-lattice relax., freq. cut-off effect 77−20738
off-resonance nuclear spin-lattice relaxation time, pulsed NMR method for mol. motion in condensed phases 79−78554
one-dimensional charge transfer conductors, press. effects on mag. props., review 78−6505
one-dimensional hopping, moment expansions and occupancy (site) correlation functions, appl. to NMR relax. 78−55972
optimised inversion recovery spin-lattice relaxation measurements, error analysis 77−48072
organic free radicals, solid, selective pulse NMR expts. 80−60452
organic glasses, low temp. mol. mobility, NMR T_1 meas. 80−60439
organic nitriles, spin-lattice relax. times obs. *(German)* 79−47350
organic polycyclic compounds, ^{13}C NMR, spin-lattice relaxation meas., rot. barriers in hindered methyl groups 77−10689
organophosphorus compounds, liq., ^{31}P nucl. spin-lattice relax. and Overhauser effect 79−36666
oxalic acid dihydrate, PMR, water mols., reorientation 79−42856
oxalic acid dihydrate, proton spin-lattice relax., 180° flips and diffusion of water mol. 77−15327
oxalic and dihydrate, monocrystals, high resolution PMR 78−64283
PAA, isotropic, nucl. spin-lattice relax. 79−23519
PAA, methyl deuterated, dipolar spin system exam. 77−39533
PAA, nematic, freq. depend. of proton T_1, rot. diffusional mechanism interpret. 77−12219
PAA, nematic and crystalline phases, NMR and relax. 79−4740
PAA, selectively deuterated, proton spin-lattice relax. temp. freq. depend., diffusion 77−43132
PAA, smectic-C and nematic long chain homologues, H-spin-lattice relax. *(German)* 78−87610
PAA-d_6, -d_8, H and D spin-lattice relax. 77−59475
paradichlorobenzene, ^{35}Cl nucl. quadrupole spin-lattice relax. meas. 77−28469
paradichlorobenzene, NQR study of the lattice dynamics *(Russian)* 80−97160
paramagnet, conc., effect of heating of electron spin on relax. of nuclei 77−8438
paramagnetic complexes, nucl. spin-lattice relax., electron spin density matrix theory 78−13521
paramagnetic impurities in solids and liqs., theory of spin-lattice relax. due to diffusion 78−10794
paramagnetic impurity effects, statistical approach using pair probability densities 77−48081
paramagnetic impurity induced nucl. flip-flop transitions 79−47348
paramagnetic material effect on chem. shift and relax. times, mol. struct. effect 78−46373
paramagnetic metal ions as structural probes for NMR investigation of inorganic and bioinorganic compounds 78−62828
peptides, in soln., nuclear Overhanzer effect methods for total conformational anal. 79−16136
perdeuterobenzene, liquid, reorientation and spin-rotation interaction 78−39423
perfluorocyclohexane, spin-lattice relax. during pulsed spin locking 78−39425
periodically irradiated system, master eqn. 78−43664
4-phenyl n-pentyl ester, Nematel 105, nematogen, isotropic phase, Rayleigh scatt. and mol. reorientation 78−34429
phenylene sulphides, NMR relaxation for mol. motions *(German)* 80−11288
phosphate glass, Li^+ motion, ^7Li NMR spectra, nucl. relax. 80−34804
phosphatidylcholine hydration, adsorpt.-desorpt. isotherm and PMR 78−15781
phospholipid bilayer membrane, spin $^1/_2$-nuclei, in chain methylene groups 77−48767
phospholipid bilayers, struct. dynamics from deuterium spin-lattice relax. time meas. 79−79485
phosphoranes, cryst., NQR study, intramol. interaction geom. and CCl_3 group dynamics 79−78564
photoexcited molecule, exchange between triplet states with nonparallel eigenvectors 79−59374
picoline compounds, proton spin-lattice relax. time, methyl group rot., 1 to 10K 77−48080
piperazines, PMR spin-lattice relax. times and lineshapes, 100-300K 77−81027
plastic crystals, self-diffusion parameters from anal. of NMR relax data 79−42301
PMMA, isotactic, syndiotactic, ^{13}C spin-lattice relaxation times, chain config., dynamics 77−24760
PMMA, mol. motions in benzene soln., ^{13}C NMR and EPR 79−78551
PMR medical imaging, mice and phantom expts. 77−86584
PMR relaxation times vs. water content for tumour and normal tissue 77−12884
polarised β-active nuclei, cross relaxation processes 80−60431
poleythylene, linear, butane diffusion coeff., VP depend. nulc. spin echo obs. 79−38404
poly(γ-benzyl-L-glutamate), soln., rot. diffusion, ^{13}C NMR 77−75350
poly-β-benzyl-L-aspartate, soln., ^{13}C and ^1H NMR dynamic study 79−69737
poly-γ-benzyl-L-glutamate, soln., ^{13}C and ^1H NMR dynamic study 79−69737
poly-L-alanine, soln., ^{13}C NMR dynamical study 79−69737
poly-N-vinylsuccinimide, dielec. and pulsed NMR relax. glass-rubber transition, mol. motions 77−48125
poly-p-phenylene sulphide, NMR relaxation for mol. motions *(German)* 80−11288
polyacetylene and polyacetylene: AsF_5, one-dimens. spin diffusion, NMR T_1 and dynamic nuclear polarisation meas. 80−44946
polyacrylic acid:Fe^{3+}, electron state of Fe^{3+}, Mossbauer and magnetisation obs. 79−73872
polyatomic fluid, local dynamics, spectroscopic studies, summer school lecture series 80−6343
polyatomic molecules, intramolecular vibr. relax., restricted quantum exchange theory 80−63610
polybut-1-ene and but-1-ene-polypropylene copolymers in solution, ^{13}C spin-lattice relax. and mol. motions 79−95670
1,4-polybutadiene, epoxidised, ^{13}C NMR, Overhauser effect 79−51872
nuclear spin-lattice relaxation continued
polybutadiene, mol. motion in solid and soln., ^{13}C NMR relaxation meas. *(Japanese)* 80−2666
polycarbonate, magic-angle ^{13}C NMR, relax. times, motions 79−4739
polydiethylsiloxane, mol. motion, NMR spin relax. data re-interpret. 80−84664
polydimethylsiloxane proton spin-lattice relax., chain motions 78−70987
polydimethylsiloxane-bisphenol-A polycarbonate block copolymer, PMR spin diffusion effects 77−66431
polydimethylsiloxanes, partially cryst., spin diffusion rel. to nuclear spin-lattice relax. *(Russian)* 79−51878
polyethylene, chain end fixing, spin-lattice relax. time *(German)* 78−76340
polyethylene, homopolymers, copolymers and model systems, ^{13}C NMR chem. shifts and relax. times 79−72449
polyethylene, linear, ^{13}C spin-lattice relaxation 80−25235
polyethylene, linear, glass transition temp. upper limit, ^{13}C Fourier transform NMR 79−14918
polyethylene, linear, nuclear relaxation, mol. motion *(Russian)* 80−44949
polyethylene, molecular motion and spin-lattice relaxation 78−48071
polyethylene, short chain branching, ^{13}C NMR 79−33557
polyethylene, solid, multicomponent decay of nucl. magnetisation, in rot. coord. system, anal. *(Russian)* 78−27106
polyethylene, solid, nucl. spin-lattice relax. time, freq. depend. defect diffusion, 77-373K 78−72428
polyethylene melt, dynamics anal. by three components, proton relax. 79−65754
polyethylene oxide, dilute solns., mol. motion, EPR and NMR investigations 79−94863
polyethylene oxide, NMR relaxation in melt, three component model 77−55723
polyethylene oxide in benzene solns., ^1H relaxation times, intermol. interactions 77−32281
polyethylene terephthalate, NMR relax. and mol. mobility *(Russian)* 78−88219
polyfluorostyrene, para- and meta-, dil. soln., ^{19}F magnetic resonance 78−10792
polyisobutylene, ^{13}C spin-relaxation parameters rel. to effect, mol. wt., temp. 77−40146
polyisobutylene, linear, interpretation of spin relax. in terms of specific motion 79−42857
polyisobutylene, relax. modes of short range fluctuation, n.m.r. meas. 77−3502
polyisobutylene, soln., ^1H NMR relax. 77−24759
cis-polyisoprene, ^1H NMR, T_1 and T_2 meas., −50-170°C 79−69738
1,4-polyisoprene, epoxidised, ^{13}C NMR, Overhauser effect 79−51872
polymer glassy and crystalline, relax. process characterisation, ^{13}C NMR obs. 80−34802
polymer melt, NMR relaxation, mol. motion, local defect component theory 77−55722
polymers, spin-lattice parameters, rotating frame, dipolar narrowed Carr-Purcell meas. 79−47347
polymers, synthetic, dil. solns., NMR relax., review 79−89693
polymethacrylic acid, syndiotactic deuterated, aq. solns., methylene deuteron relax., freq. and temp. depend. 77−90062
polymethylacrylate, tacticity from peak-eliminated Fourier transform NMR 77−563
polypeptides, amide proton relax. 79−20502
polypropylene, amorphous, ^{13}C NMR spin-lattice relaxation times of isotactic, syndiotactic sequences 77−4572
polysaccharide gels and sols, PMR relax. times rel. to temp., pH and conc. 78−56952
polystyrene, dilute soln., ^1H mag. relax., selective inversion technique appl. 80−44957
polystyrene in dil. sol., solvent depend. of molecular motion, proton mag. relax. meas. 79−41932
polystyrene soln., macromolecular chain dynamics, C^{13} and NMR 78−55267
polystyrene soln., monosubstituted, mol. chain dynamics, NMR meas. 78−56393
polystyrene solution, conc., diffusion and NMR relax. times 77−55725
polystyrene-trans-decalin system, ^{13}C spin-lattice relax., solvent rot. diffusion 79−33556
polyurethanes, cross-linked, mol. mobility and struct., thermomechanical and NMR obs. *(Russian)* 80−69285
polyvinyl acetate-vinyl acetate, partially polymerised, ^1H-, ^{13}C-spin lattice relax. time meas. *(German)* 79−28633
population inversion, spin-lattice relax. meas., composite 180° pulse effect 80−77827
Portland cement, absorbed H_2O, pulsed NMR study 80−84665
potassium palmitate-d_{31}, spin-lattice relax., chain position and temp. depends. 78−68405
powders, high speed rot., spin diffusion, NMR spin lattice relax. obs. of D 80−66056
propanediol, behaviour of nucl. spins near highly polarised paramag. centres 77−77127
n-propylammonium chloride, NMR, spin-lattice relax., cation dynamics 79−11353
protein, proton magnetic reson. and spin diffusion 77−28470
proteins, PMR spin-lattice relax. time, role of cross-relax. 78−35800
proteins, solid, PMR spin-lattice relax., mol. dynamics 80−51041
proton spin-lattice relax. and activation energies of tunnelling CH_3 groups 77−48071
pulsed NMR spectroscopy, pulse spacing selection for increased accuracy in meas. 77−28474
pulsed spin locking, RF, spin-lattice relax. calc. model 78−39425
PVC, proton spin-lattice relax. dispersion, quadrupolar dip 77−16197
pyrazine, cryst., mol. reorientation, NMR, pot. energy calc. 78−76335
pyridine-H-bond donors, D spin-lattice relax. meas., mol. interactions anal. *(French)* 80−87151
pyrimidine, liq., nucl. relax. and mol. reorientation, nucl. Overhauser enhancement 78−60351
pyrrole, natural abundance ^1H coupled ^{15}N NMR spectra, selective population transfer method 79−95682
quadrupolar, in solids 78−39429
quadrupole mechanism, effects of self-consistency 77−55719
quadrupole spin relaxation, dynamic appl. to at. vacancy hopping 77−8436
quadrupole spin-lattice relaxation time in single crysts., orientation depend. 79−95666

nuclear spin-lattice relaxation continued
quadrupole-Zeeman cross-relax. between two nucl. spin species, appl. to difluorotetrachloroethane 79−65766
quasi one-dimensional and two-dimensional crystals, NMR relaxation time mag. field depend. *(Russian)* 79−61254
quinolinium $(TCNQ)_2$, charge transport, proton spin-lattice relaxation 80−88545
quinuclidine, plastic phase, mol. reorientations, ^1H and ^{14}N NMR relax. 79−69039
rare earth alloys, cryst. field effect on EPR and NMR 78−56391
rare earth compounds, cryst. field effects on EPR and NMR 79−4736
rare earth Cu_2Si_2, interconfiguration fluctuation system, NMR meas. 80−15817
rare earth dil. alloy, nucl. spin-lattice relax. of ^{165}Ho 78−48069
rare earth systems, NMR, EPR, and Mossbauer effect, book contribs. 80−39883
rare gas liquids, nucl. spin relax. of H_2 79−56623
relaxation time meas., simulation, systematic and random error effects 80−37062
retinal rod outer segment membranes and liposomes of extracted phospholipids, proton spin-lattice relax. rates 77−90782
ribonuclease-A, solid, PMR spin-lattice relax., mol. dynamics 80−51041
$tRNA_{yeast}^{phe}$, Fourier transform PMR in aq. soln., ^1H exchange and relax. rates meas. method 78−15049
RNA, molecular motions investigated by ^{31}P and ^{13}C NMR relaxation 80−63657
rotating coordinate system, phenomenological approach 80−39887
rotating frame, ^{13}C spin-lattice relax. using proton decoupled Fourier transform spectra, errors origin 80−18945
rotating frame relax. time for spinning sample 79−47344
rotating frame spin-lattice relax. in presence of off-reson. RF field 79−93193
rotating-frame measurement, modification of commercial spectrometer 80−22407
rotational tunnelling induced, in symmetric systems of identical nuclei *(Russian)* 78−60353
ruthenium acetylacetonate, nucl. spin-lattice relax., electron spin density matrix theory 78−13521
ruthenocene, cryst. and soln., dynamic struct., NMR expts. 77−15328
semiconductor, relaxation of nuclear spins interacting with holes 78−48073
short relaxation time measurement using CW NMR spectrometer 77−57374
simple cubic lattice, simple hopping, correlation functions, NMR relaxation rates 79−42864
single-scan Fourier transform method for T_1 determ. 77−20741
single-scan T_1 meas. using solid echoes 78−86307
small molecules in protein solns., spin-lattice relax. times, inversion recovery spin-echo sequence 80−21446
smectic liq. crystal, nuclear spin relax., effect of translational diffusion 78−63669
smectic-A liquid crystals, nucl. spin relax. by translational self diffusion 80−60442
sodium dodecyl sulphate: Gd^{3+}, micellar system, chain folding, ^{13}C NMR obs. 80−61158
sodium valerate, mesophase, self-diffusion and spin-lattice relax. 79−69008
solid, effect of crit. slowdown on NMR near second order struct. transition 79−73846
solid, motion-induced nuclear spin relaxation, temp. depend. 79−61250
solid, nucl. spin relax. by translational diffusion 77−16195
solid electrolytes and solid soln. electrodes, review 80−60432
solid polymers, NMR, review 80−88888
soliton gas, interaction with nucl. spin 79−69736
solvent-paramagnetic solute system, nucl. spin-lattice relax. times, cross-correl. method 79−95679
soya protein gels and sols, PMR relax. times rel. to temp., pH and conc. 78−56952
spin diffusion, influence on nucl. spin-lattice relax. due to impurity nuclei under magic angle conditions 78−15061
spin diffusion under magic angle conditions, calc. 78−19363
spin glasses, nuclear magnetic relaxation calcs. *(French)* 80−34797
spin pair undergoing reorientations by jumping among inequivalent sites, nucl. mag. spin relax. 79−42862
spin system kinetics for spin quantisation by strong acoustic field 78−15052
spin systems under multiple pulse NMR conditions, chem. shift relax. 80−34808
spin temperature oscillations in spin-locking expt. 79−99785
squaric acid, critical slowing down of fluctuations at phase transition, ^{13}C spin-lattice relax. 80−44948
squaric acid, dielec. const. and PMR near struct. phase transition 79−10946
statistical analysis of time data 77−20739
steady state pulse method, master eqn. for T_1 NQR determ. 80−54975
steam, supercritical, compressed, proton spin-lattice relax. time meas. 80−22403
stearate, proton spin-lattice relaxation in various phases *(Russian)* 80−97163
structural transitions, dynamic aspects, nuclear quadrupole relax. studies 78−76344
styrene, thermal polymerization, PMR obs. 80−3342
succinonitrile, plastic and liq., NMR, ^{13}C spin-lattice relax. and ^{14}N linewidth 79−24227
sulpholan, molecular solid, laboratory frame and rotating frame spin-lattice relax., pulsed NMR meas., phase transitions obs. 80−93197
superconducting dilute mag. alloys, effects of indirect coupling upon nucl. spin-lattice relax. 77−80874
superconducting state, nucl. mag. relax. rate *(Rumanian)* 78−60247
superconductor, nuclear spin relaxation rate fluctuation growth, mag. field effect 78−10606
superimposed exponentially decaying signals, computer-aided anal. technique 78−23360
superionic conducting materials, nucl. mag. relax. by paramag. impurities 79−42866
superionic conductors, mag. reson., book contrib. 80−25240
TBBA, smectic, spin-lattice relax., self-diffusion, mol. rot. 78−35055
TCNQ, salt, $Me\phi_3As(TCNQ)_2$, nonOhmic elec. cond., tunnelling model and expt. 79−99558
TCNQ complex, Adn $TCNQ_2$, nuclear-spin-lattice relaxation 80−39886
nuclear spin-lattice relaxation continued
TCNQ complexes with dipyranylidene and dithiadipyranylidene, high cond. investigs. and related props. 78−6368
TCNQ compounds, dimensionality of triplet excitons 78−91974
TCNQ salt, $(N(CH_3)_3H)(I)(TCNQ)$, proton spin-lattice and spin-spin relax. times 79−8065
TCNQ salt, pyridinium $(TCNQ)_2$, low temp. mag. phase transition, ESR study 80−25139
TCNQ salt, $Qn(TCNQ)_2$, temp. and freq. depend. of nucl. relax. rate 78−6594
TCNQ salts, NMR relax. time mag. field depend. *(Russian)* 79−61254
TCNQ salts, proton nucl. relax. meas. 80−20484
TCNQ-DIP Φ_4, electronic diffusion coeffs. in chains, proton spin-lattice relax. and dynamic nucl. polarisation 80−25241
TCNQ-HMTSeF, nucl. spin relax. obs., diffusive character of response function and interchain coupling 78−10797
TCNQ-NMP, incomplete charge transfer, NMR relax. and line-shift meas. 80−20485
TCNQ-NMP, nucl. relax. and spin dynamics 78−52370
terephthalic acid polyester in solution, ^{13}C spin relaxation study 79−87327
tert-butylchloride-d_9, extended diffusion with internal rot., NMR test 79−31549
tetraalkylammonium halides, mol. reorientation, spin lattice relax. time study 80−18875
1,2,4,5-tetrachlorobenzene, in durene host, phosphoresc., cross-relax. between spin levels 78−9186
1,2,4,5-tetrachlorobenzene, proton spin relaxation by optically excited triplet states 79−19810
tetrafluoromethane, compressed fluid ang. momentum relax., NMR 78−19354
tetrafluoromethane-inert gas, compressed fluids, ang. momentum relax., NMR 78−19355
tetrahedral four spin $^1/_2$ systems, Zeeman and tunnel system reson., coupled and uncoupled relax. 80−50214
tetrahedrally coordinated four spin 1/2 system, anisotropy of T_{1D} and $T_{1\rho}$ 79−38393
tetrahedrally coordinated four spin-1/2 system, semiclassical anal. 77−73094
tetramethyl gruop VIa cation silicon hexafluorides, ^1H and ^{19}F nucl. spin lattice relax. 78−80234
tetramethylammonium octahydrotriborate, NMR study of proton and B dynamics 80−93200
tetramethylgermanium, Zeeman spin-lattice relaxation rate maxima 80−84666
meso-tetraphenylporphine, NH H^+ tunnelling rate 80−97158
TGS, proton spin-lattice relax. time, temp. depend., near transition pt. 78−43668
TGS, spin-lattice relax. meas. of ^1H, ^{13}C, and ^{15}N near ferroelec. transition 77−1646
thermodynamic influence of spin-spin energy on cross-relax. and spin diffusion 78−76343
thermodynamics of nuclear spins 80−54964
thylakoid membranes of wheat chloroplasts, proton spin-lattice relax. time, −8°C phase transition 80−108853
time of spin-lattice relax. meas. method 77−71355
tissue, living and ischaemically damaged, longit. relax. decay 77−12895
tissue molecular dynamics and freezing phase transition studied by proton spin relax. 78−68983
tissue of newt, PMR study, blood, liver and tail samples 79−20515
TMMC, antiferromag., nuclear spin-lattice relax. by solitons 80−97159
TMMC, linear antiferromag., 3D ordering and spin correlations, mag. field effect 78−19262
TMMC, linear antiferromag., mag. field effect on nucl. spin-lattice relax. time, 2 to 4.2K 79−61255
TMMC, linear Heisenberg antiferromag., effect of mag. field on 3d ordering and spin correlations 78−68229
TMMC, spin dynamic exam., effect of mag. field at low temp. 79−73733
toluene, liq., NMR spin-lattice and dielec. relax. 79−33604
toluene-d_0, -d_1, mol. reorientation and D nucl. relax. time, temp. depend. 78−39424
transition metal complexes, vibronic coupling and spin relax. NMR decay rate study 80−18870
transition metal hydrides, proton diffusion mechanisms, NMR determ. 77−90060
translational diffusion mechanism, reciprocal-space formalism, mean-field theory 80−71208
s-triazine, mol. cryst., low temp. mol. reorientation, phase transition, ^{14}N NQR 77−36150
tribromofluoromethane, liq., ^{13}C and ^{19}F nucl. relax., ^{19}F-^{79}Br and ^{13}C-^{79}Br scalar coupling consts. 78−76330
trichloromethane in nematic liq. crystal, AX($^{13}CHCl_3$) nuclear relax., dipole-dipole interaction 77−54567
trichlorophosphazenes, ^{35}Cl NQR spectra and reorientational motion of PCl_3 group 78−25567
trichlorophosphazo compound, Cl_3P:NCCl$(CF_3)_2$, nuclear quadrupole spin-lattice relax. 80−66062
trichlorophosphazoperfluoro-1,1-dimethylethane, cryst., ^{19}F NMR and mol. mobility, fluorination influence 80−34809
1,3,5- trifluorobenzene, liq., NMR spin-lattice and dielec. relax. 79−33604
trifluorobenzene, symmetrical ^1H and ^{19}F NMR, cross relax. 79−38406
triglycine fluoroberyllate, spin-lattice relax. meas. of ^1H, ^{13}C, and ^{15}N near ferroelec. transition 77−1646
trimethylammonium cadmium chloride, $(CH_3)_3NHCdCl_3$, struct. phase transitions 79−1502
trimethylammonium cobalt chloride, low-dimensional Ising-like system, nucl. spin-lattice relax. of protons meas. 77−85609
trimethylammonium cobalt trichloride dihydrate, Ising-like system, nucl. spin-lattice relax. of ^1H and ^{35}Cl 80−29638
trimethylphosphate, plastic and hard crysts., liq., nucl. spin-lattice relax. mol. motion 78−48065
trioxane, NMR proton relax., mol. rot., rel. to polymerisation 79−73843
triphenylene, triplet state, MIDP and T-S excitation spectrosc. 79−81233
triptycene, soln., correl. times from ^{13}C relax. 80−23438
tris(3-deutero-2,4-pentadionato)aluminium, in soln., deuteron spin-lattice relax. time, mol. rotational correl. time 78−84491
tristearin irreversible liq.-liq. phase transition, ^{13}C NMR meas. 78−26681

nuclear spin-lattice relaxation continued
trithiane, NMR proton relax., mol. rot., rel. to polymerisation 79−73843
tryptophan, Fourier transform PMR in aq. soln., ^{1}H exchange and relax. rates meas. method 78−15049
TTF-CuBDT, inter- and intra-chain exchange couplings, proton spin-lattice relax. time meas. 80−71220
TTF-TCNQ, electron-electron interaction strength, electron scatt. and spin-lattice relax. data 78−30878
TTF-TCNQ, interchain tunnelling effect on nucl. spin-lattice relax. time, interchain coupling of CDW 80−20163
TTF-TCNQ, nucl. spin relax. obs., diffusive character of response function and interchain coupling 78−10797
TTF-TCNQ and related cpds., magnetic props., press. effects 77−47981
TTF-TCNQ electronic props., PMR 78−2763
tumour detection, spectrum anal. of multiple components data 78−48851
tumour-bearing mouse tissues, proton T_1 study of water coverage parameter changes 79−24953
two-band superconductor, effect of nonmag. impurit. *(Russian)* 77−51845
two-spin system, NMR relax. rate parameters, by nuclear Overhauser effect 77−69720
two-spin system in FCC cryst. and third-nearest-neighbour jumps on a SC lattice 79−15127
type I superconductor, paramagnon effect on nucl. spin-lattice relax. rate 77−32119
variable nutation WEFT, biochemical appl. 80−20482
vinyl polymer solutions, proton spin-lattice relax. and Overhauser enhancements 77−55721
water, adsorbed on cellulose, NMR relaxation times 79−78552
water, adsorbed on porous glass, proton spin-lattice relax. meas. by pulse NMR 78−84053
water, liq., NMR proton spin-lattice relax. and shear viscosity press. depend., −15 to 10°C 77−40144
water, liq., proton spin-lattice relax. by slow proton exchange 80−60437
water PMR obs. in obligately halophilic blue-green alga 79−96526
water-formic acid (acetic acid)(propionic acid)(n-butyric acid), PMR relax. obs., mol. assoc. 79−33553
Ag_3AsS_3, phase transition near critical pt., spin-lattice relax. *(Russian)* 79−38397
AgBr:Na^+(Li^+), correlated diffusion of impurities, nuclear spin relax. meas. 80−108094
$AgClO_3$, structural phase transition, ^{35}Cl NQR meas. 80−15819
AgF, diffusion, elec. cond. and ^{19}F relax. $T_{1\rho}$ meas. 80−92718
Ag_2F, NMR of ^{109}Ag and ^{19}F, modified Korringa relation in two-dimens. metal 80−93199
β-AgI, ion dynamics and transition to superionic state, nucl. spin-lattice relax. meas. 78−43179
$(AgI)_x(Ag_2O\ B_2O_3)_{1-x}$, amorphous superionic compound, ^{11}B lineshape and relaxation 80−108107
$Ag(NH_3)_2Ag(NO_3)_2$, phase transition, mol. motion, PMR obs. 78−88203
$AgNa(NO_2)_2$, ultraslow crit. dynamics of order parameter, ^{23}Na spin relax. times obs. 78−76410
$Ag_2SO_4.4NH_3$, mol. motion, proton mag. reson. 79−47349
Ag_2SbS_3, order-disorder phase transition, NQR and spin-lattice relax. expts. 78−47523
Ag_3SbS_3, pyrargyrite, order-disorder phase transition and elec. polarisation 79−38468
Al, nucl. mag. thermometry using SQUID magnetometer 77−26292
Al particles, small supercond. nuclear spin-lattice relax. meas. 80−88681
Al particles, supercond., Zeeman crit. field, NMR spin echo meas. 79−56453
Al small particle, NMR study, Knight shift, spin-lattice relax. time, supercond. effects 80−39710
Al, supercond, small particles, Josephson-coupled, local fluctuation effects 78−72308
Al, superconducting band gap anisotropy and Fermi surface anisotropy *(Spanish)* 80−84544
Al, superconducting particles, nucl. relax. and supercond. fluctuations 78−60251
Al-B, dil., diffusion of ^{12}B 79−60541
Al-Mn, dil., superconducting and normal state, ^{27}Al spin-lattice relax. rates 79−60977
Al-Mn(Cr)(V), dil., supercond., nucl. spin relax. and quasiparticle excitations 80−88680
Al-transition metal alloys, anomalous sp. ht. and nuclear spin-lattice relax. 79−46814
Al-V, dil., superconducting and normal state, ^{27}Al spin-lattice relax. rates 79−60977
$AlCl_3$, aq. soln., HCl additive effects on ^{27}Al spin-lattice relax. 80−66058
Al_2Cl_6 molten, nuclear mag. relax., mol. rot. 80−71209
β-AlO_3-$(Na,Li)_2O$, NMR, Raman and IR spectra, and X-ray diffr., heat treatment induced changes 80−107508
Al_2O_3:Cr^{3+}, corundum and ruby, ^{27}Al quadrupole, transitions, acoustic and elec. saturation 77−90071
β-Al_2O_3-$(Na,Li)_2O$, ionic motion obs. using NMR and internal friction 80−108099
β-Al_2O_3-$(Na,Li)_2O$ solid electrolyte, Li motion and activation obs. using ^{7}Li NMR 80−108100
β-Al_2O_3-H_3O^+, pulsed ^{1}H NMR study, 77 to 440K 79−87329
β-Al_2O_3-Li_2O-Na_2O, spin-lattice relaxation and Li motion 80−70451
β-Al_2O_3-NH_4^+, PMR relax. time obs. of ionic motion 80−71213
β-Al_2O_3-NH_4^+ and β″-Al_2O_3-NH_4^+-H_3O, single cryst. PMR and proton motion 80−108101
β″-Al_2O_3-Na_2O, ^{23}Na NMR obs. of ionic diffusion, 180 to 800K, attempt freq. 80−108097
β-Al_2O_3-Na_2O, ^{23}Na NQR and two-dimens. diffusion, model analysis 80−108111
β-Al_2O_3-Na_2O, ^{23}Na nucl. spin-lattice relax., barrier height distribs. and diffusion processes 77−55720
β-Al_2O_3-Na_2O, ^{27}Al NMR obs., Na motion and cond. characts. 80−108096
β-Al_2O_3-Na_2O, AC ionic cond., dielec. and NMR relax. 80−59713
β″-Al_2O_3-Na_2O, absorbed water effect on NMR lineshape and spin-lattice relax. time 80−108098
β-Al_2O_3-Na_2O, anomalous Na behaviour obs. using pulsed and CW NMR 80−108095
Ar:H_2, nuclear spin relax. of H_2, crystal field meas. 79−51875
As, amorphous and cryst., NQR for tunnelling modes and local struct. order 79−61261
As, pulsed NQR, bonding, bond angle distrib. obs. in different phases 80−54984
As, rhombohedral, nucl. quadrupole spin-lattice relax. 79−15373
As-Se-Tl system, chalcogenide glasses, NMR spin-lattice relax. time meas. 79−95671
Au-Co, liquid alloys, ^{59}Co NMR studies, nucl. relax. rates 79−95660
Au-Fe, dil., crit. dynamics 80−60325
Au-V, dil., ^{51}V CW NMR line width anal., RKKY broadening 78−15033
$AuIn_2$, pulsed NMR expts, rel. to performance as nuclear refrigerant 79−61259
B hydrides, relaxation time meas., ^{11}B NMR spectroscopy 77−32276
B_2O_3 vitreous and liq., ^{11}B NMR line shape and spin-lattice relax. meas. 77−4575
B_2S_3, vitreous and liq., ^{11}B NMR line shape and spin-lattice relax. meas. 77−4575
$Ba(ClO_3)_2.H_2O$, ^{35}Cl NQR meas. 77−66435
BaF_2, NMR relax., ionic cond. and self-diffusion 78−23362
BaF_2:K^+(La^{3+}), nuclear spin relax. orientation depend., point defect self-diffusion mechanism 77−48078
$BaFe_{12}O_{19}$, nucl. spin-lattice and spin-spin relax. in domain walls 77−69610
$^{135}Ba^{2+}$, $^{137}Ba^{2+}$, aq. ions, nucl. quadrupole relax. 78−64287
Be, electronic struct., NMR study 80−108085
BeF_2 aqueous solns., mag. and quadrupole relax. 80−71226
$Be_{1-x}Mn_x$, Be-rich, NMR and paramag. susceptibility 80−71206
BeNi, dil., electronic struct., NMR study 80−108085
$^{9}Be^{2+}$, aq. ions, nucl. quadrupole relax. 78−64287
Bi-BiI_3 mixture, molten, NMR meas. 77−51976
Bi-Mn, dil. liq. alloy, static and dynamic props. of localised Mn moments 79−82755
C_8AsF_5 intercalation compound, NMR and static mag. susceptibility meas. 78−88214
$(CH_3)_3NHCoCl_3.2H_2O$, chain ferromag. two magnon bound state, nuclear spin-lattice relax. 78−88206
CO, in He bath, NMR spin-lattice relax., coupled states ang. momentum decoupling 77−77117
^{13}C NMR, proton enhanced, T_1 value method, artifact suppression 78−91972
^{13}C NMR in solids, high-resolution 80−34802
^{13}C NMR intensity meas. technique, chem. anal. appl. 77−51981
^{13}C pulsed NMR, simultaneous T_1 and T_2 meas., Fourier transform. visualization 78−24838
^{13}C spectra, modified DEFT pulse sequence use 79−93191
^{13}C-^{1}H, spin-pair with time-dependent internuclear distance, spin-lattice relax. time 79−42862
^{13}C-enriched mols., proton relax. and nuclear Overhauser effect from NMR meas. 77−68058
$CaB_3O_4(OH)_3.2H_2O$, NMR of ^{11}B in crit. region 77−16199
CaF_2, spin diffusion under magic angle conditions, calc. 78−19363
CaF_2, spin-diffusion const. 77−66432
$Ca(NO_3)_2$ hydrous melts, proton spin relax. and mobility 77−77118
$Ca(NO_3)_2$, hydrous melts, correl. times, conc. depend., proton NMR relax. obs. 77−90059
$CaSO_4.2H_2O$, solid echo effect 77−51988
$^{43}Ca^{2+}$, aq. ions, nucl. quadrupole relax. 78−64287
Cd complex, aminoacetate, proton spin-lattice relaxation, temp. depend. 78−31119
CdI_2-Cd(I) mixture, molten, nuclear spin relax. 80−88887
$CeAl_2$, antiferromag. ordering and Kondo behaviour, ^{27}Al NQR study 80−71231
CeF_3, ^{19}F spin-lattice relax. and mag. couplings 79−65753
$Ce_2Mg_3(NO_3)_{12}.24H_2O$ demagnetization cryostats, appls. of nucl. cooling in nucl. orientation studies 79−63230
ClF, gas, rot. frame NMR, reorientational and ang. correl. times 78−78721
ClO_3F, ^{19}F NMR line shape temp. depend. and spin-lattice relax. 78−91969
$Cl_3PNPO(CCl_3)_2$, NQR spin-lattice relax. study of PCl_3 and CCl_3 group reorientation 78−2767
Co complex, $Co(NH_3)_6I_3$, phase transition investig. by NMR 77−1608
Co complex, tris(ethylenediamine)cobalt(III) ion in complex anion solns., ^{59}Co NMR relax. obs. 80−25234
Co complexes, NMR studies *(Japanese)* 79−8068
Co, HCP, NMR and nucl. relax. meas. in domain walls 77−36146
Co, NMR in paramagnetic and ferromagnetic states, crit. nucl. relax. 79−56622
Co-^{48}V, nucl. orientation of ^{48}V, γ-ray anisotropy obs. 80−97169
Co-Al system, nucl. spin relaxation exam. 79−19798
CoB, diamag., nucl. spin-lattice relax. of ^{59}Co 77−59479
$CoCl_2$, solution, spin-lattice relax. time meas. using CW NMR spectrometer 77−57374
Co(II)-containing aq. electrolyte soln., nucl. mag. relax., hydration shell *(Russian)* 80−54966
$(Co_{1-x}M_x)B$, M=Mn or Fe, paramag., spin echo NMR spectra, ferromag. transition, spin-lattice relax. 80−29645
$CoSe_2$, temp. induced local mag. moments, ^{59}Co NMR 79−65747
$CoSiF_6.6H_2O$, paramag., nucl. and electron spin lattice relax. 78−84494
Cr complex, Cr(V)-dimethylformamide, proton dynamic polaris. and relax. 78−91988
Cr complex, Cr(V)-fluoroorganics, proton and ^{19}F dynamic polaris. and relax. 78−91989
CrB_2, itinerant antiferromag., sping fluctuations, NMR study 80−108119
CrB_2, NMR of ^{11}B meas. 78−56397
$Cr_{1-x}Mo_xCo$, x≤0.25, antiferromag., nucl. mag. relax. 78−6590
$Cr_{1-x}V_x$, nucl. spin relax., spin fluctuation effect 80−34811
$Cr_{1-x}V_xCo$, mag. state of Co impurity, NMR exam. 78−27100
$Cr_{1-x}V_xCo$, x≤0.5, antiferromag., nucl. mag. relax. meas. 78−6590
Cs-Au liq. alloy, formation of localised electronic states, NMR obs. 80−93201
$CsCoCl_3$, Ising like antiferromag., mag. phase transition, ^{133}Cs NMR 80−7184
CsD_2PO_4, pseudo-one-dimensional ferroelectric transition, ^{31}P chemical shift and relaxation study 80−66123
CsD_2PO_4, pseudo-one-dimens. ferroelec. transition, DMR and relax. study 80−71223
CsH_2PO_4 and CsD_2PO_4, pseudo one-dimens. ferroelec. ordering dynamics, ^{31}P NMR study 80−75971
$CsNiCl_3$, temp. depend., anisotropic effects 78−64293

nuclear spin-lattice relaxation continued
$CsNiCl_3(F_3)$, one-dimensional anisotropic paramag., nucl. relax. rate and spin dynamics 77−69723
$CsNiF_3$, NMR and relax. exam. 78−52371
$CsPbCl_3$, n.q.r. spin-lattice relax. near cubic-tetragonal transition, soft modes 77−1616
Cs_2SO_4-$(NH_4)_2SO_4$ mixed cryst., ferroelec. transition, structural and dielec. props., proton spin-lattice relax. 78−39512
$(Cu,Zn)Cs_2(SO_4)_26(H,D)_2O$, thermal contact between nucl. Zeeman and electron dipole-dipole interaction system 77−90065
$(Cu,Zn)Cs_2(SO_4)_2.6(H,D)_2O$, proton spin-lattice relax. exam., rel. to EPR 77−90064
$(Cu,Zn)Cs_2(SO_4)_2.6(H,D)_2O$ Tutton salt, proton spin-lattice relax. time, proton conc. depend. and spin diffusion role 80−71221
Cu complex, α-CuNSal, one-dimensional $S=^1/_2$ Heisenberg system, nucl. relax. at high temp. 77−85610
Cu complex, $CuCl_2.2NC_5H_5$, spin 1/2 system, one-dimensional nucl. relax. 78−39427
Cu complex, Cu(II) dimers. temp. depend. PMR relax., singlet-triplet separation determ. 80−43073
Cu-Co, Kondo system, NMR, spin-lattice relax., impurity spin dynamics 77−69724
Cu-Cr, Kondo alloy, NMR of Cu satellites, 1 to 4K 79−73837
Cu-Cs diluted deuterated Tutton salts, electron non-Zeeman system, nuclear relaxation study 80−44951
Cu-Fe, classical Kondo system, impurity spin dynamics, NMR relax. of impurity neighbour nuclei 77−36056
Cu-Fe alloys, Kondo system, static and dynamic susceptibilities, NMR and Mossbauer spectra 77−63090
Cu-Fe dilute alloy, host NMR spin lattice relaxation 79−51873
Cu-Mn, dil., spin-glass dynamics, NMR meas. 78−31120
Cu-Mn, spin glass, ^{63}Cu NMR linewidth and relax. meas. 77−69583
Cu-Mn dilute alloys, local moment fluctuations, NMR meas. 77−63091
CuCl, molten, ionic liquid description from NMR meas. 77−24257
$CuCl_2.2NC_5H_5$, antiferromag. spin dynamics at low temp. 77−32278
$CuCr_2S_4$, ferromag., spin wave contrib. to nucl. spin-lattice relax. time meas. 77−36147
CuI, superionic, NMR relax. evidence for sublattice melting 77−15623
$CuK_2Cl_4.2H_2O$, proton spin-lattice relax. and exchange interactions, temp. depend. 79−95663
$Cu(NO_3)_2.2^1/_2H_2O$, ^1H spin-lattice relax. time, 4.2K, 5-60 kOe 79−15371
$Cu(NO_3)_2.2^1/_2H_2O$, singlet ground state system, mag. props. 80−44850
$Cu(NO_3)_2.2.5H_2O$, linear Heisenberg antiferromag., proton spin-lattice relax. times 79−61257
$Cu(NO_3)_2.2.5H_2O$, single cryst., $S=^1/_2$ alternating linear antiferromag. spin dynamics 79−51793
$CuSO_4.5H_2O$, $S=^1/_2$ antiferromag. Heisenberg chain, spin dynamics 80−11285
$CuSeO_4$, $S=^1/_2$ Heisenberg antiferromag. linear chain, proton spin-lattice relax. 78−39433
$CuSeO4.5H_2O$, S=1/2 antiferromag. chain, proton relax. near saturation field 79−15370
$CuSeO_4.5H_2O$, antiferromag. chain system, proton spin-lattice relax. near saturation field 79−61256
$CuSiF_6.6H_2O$, paramag., nucl. and electron spin lattice relax. 78−84494
Cu_3VS_4, out of equil. mixed cond., off-centre positions and order-disorder transition, ultrafast nucl. relax. obs. 80−108103
Cu_3VS_4, out of equil. mixed cond., chem. origin of mobile ions, spin-lattice relax. and NQR obs. 80−108104
n-D_2, solid, nucl. spin-lattice relax. and evidence for low temp. phase transition 79−56022
D_2O, compressed at low temp., mol. motions, spin-lattice relax., viscosity and self-diffusion 77−76287
D_2O, in lyotropic phase, spin-lattice relax. time meas., density matrix formalism 77−18944
D_2O, liq., mol. rot., deuteron relax. obs. 77−8432
D_2O, nuclear mag. relax. of deuterons at identically oriented planar interfaces 77−36148
Dy_2FeSbO_7, Dy^{3+} relax. by Mossbauer spectroscopy of ^{57}Fe 77−59494
$Dy_2Sn_2O_7$, Dy^{3+} relax. by Mossbauer spectroscopy of $^{119}Sn^m$ 77−59494
$ErRh_4B_4$, mag. supercond., NMR study of ^{11}B 80−107957
EuB_6, low temp. nucl. spin-lattice and spin-spin relax. times meas. 77−90063
Fe film, nuclear magnetisation relax. at 77 to 500K 78−60352
Fe III low-spin complexes, nucl. spin-lattice relax., electron spin density matrix theory 78−13521
Fe, nuclear orientation and NMR/ON on implanted ^{114m}In 79−47345
Fe, nuclear orientation-mag. reson. of ^{48}V 79−61288
Fe^{2+} compounds, Mossbauer spectra, spin-lattice relax. effects 80−50239
Fe:^{60}Co, accurate meas. 77−85596
Fe-^{48}V, nucl. orientation of ^{48}V, γ-ray anisotropy obs. and NMR meas. 80−97169
Fe-Co, 3d ferromagnet nuclear spin-lattice relaxation 80−80627
Fe-Co, dil., ensemble rotation concept in NMR on oriented nuclei 77−90061
$FeBO_3$, dynamic NMR frequency shift for ^{57}Fe *(Russian)* 78−43677
FeF_2:Mn, antiferromag., NMR relax., impurity bonding 80−66061
FeF_3, canted antiferromag., spin echo spectra of ^{57}Fe and ^{19}F nuclei 80−2662
$FeSO_4.n\ H_2O$ (n=1,4,5,7), Fe^{2+} ion mag. interaction with crystallisation water protons, proton NMR obs. 80−60447
$FeSiF_6.6H_2O$, paramag., nucl. and electron spin lattice relax. 78−84494
Ga, liq., nucl. acoustic reson. Knight shift, rel. to spin-lattice relax. 78−19351
Ga, liq., nuclear quadrupole relax. for ^{69}Ga, 20-150°C, calc. 77−36151
GaP:Te(S), nucl. relax. rel. to donor density 80−11284
Ge:As, NMR, conduction electrons in impurity band, metal-nonmetal transition 79−78544
H, gaseous, high-resolution mag. reson. study, 1 to 1.3K 80−95560
o-H_2 molecules in solid nonmagnetic host, nucl. spin lattice relax. times calc. 80−20483
o-H_2, nuclear spin-lattice relax. of in-plane and out-of-plane ortho-H_2 pairs 78−56394
H_2, single crystals, NMR, dynamic effects 80−107608
H_2, solid, low ortho conc., transverse and longit. relax. meas. 77−81025
H_2, solid, NMR, pulsed, linewidth transition, T_1, low ortho conc. 78−43667
o-H_2, solid, NMR relax. and libron energy 78−88204

nuclear spin-lattice relaxation continued
H_2, solid, nuclear spin-lattice relaxation, crystal and mag. field effects 79−42865
H_2, solid ortho-para mixtures, incoherent neutron scatt. 77−47304
H_2, transverse NMR low density spectrum 78−74681
p-H_2:o-H_2, solid, nuclear spin-lattice relaxation, importance of Suhl-Nakamura interaction 78−52374
H_2-N_2 mixtures, 300K, proton spin relax., single relax. time approx. 77−61766
HCl and $(HCl)_2$, matrix isolated, pulsed NMR 79−22730
HCl, in the bath, NMR spin-lattice relax., coupled states ang. momentum decoupling 77−77117
HCl, proton spin-lattice relax. time near liq.-vapour critical point 79−73842
α-$HCrO_2$, H^+ mobility investig. by nuclear relax. meas. 77−48076
HD, liq., in He bath, NMR spin-lattice relax., coupled states ang. momentum decoupling 77−77117
HD, solid, enhanced nucl. polarisation of D 77−8450
HD+He, relax. and kinetic cross-sections, DWBA calcs. 79−41782
$H_{2-n}D_nSe$(n=0, 1 and 2), ^{77}Se NMR on XL-100 spectrometer, isotope effects and spin-lattice relaxation 80−71211
$H_{0.36}MoO_3$ and $H_{1.71}MoO_3$ bronzes, NMR relax. obs. at 77<T<450K, H diffusion 80−108089
$H_{1.6}MoO_3$ bronzes, proton mobility 78−39426
HNO_3-graphite intercalation cpd., proton relax. meas., two-dimens. system model 77−51968
H_2O in biological samples, PMR, fast-exchange model interpretation via differential kinetics clarified 80−67033
H_2O, nuclear magnetic relax. of protons at identically oriented planar interfaces 77−36148
H_2O, supercooled, longit. proton relax. times, press. and temp. depend. 77−85598
H_2O:HF ice, pulsed NMR 77−28467
$H_2Os_3(CO)_{10}$, and $H_4Os_4(CO)_{12}$, polycryst., PMR chem. shift 79−95655
$H_4Ru_4(CO)_{12}$, polycryst., PMR chem. shift 79−95655
H_2S, proton spin-lattice relax. time near liq.-vapour critical point 79−73842
$HTaWO_6$, and $HTaWO_6.H_2O$ defect pyrochlores, NMR study of proton motion 79−82889
$H(UO_2P(As)O_4)4H_2O$, H motion, PMR obs. 78−80239
$H(UO_2PO_4)4H_2O$, solid, fast hydrogen ion diffusion, NMR relax. time meas. 80−2205
^1H, in ^{13}C nuclear Overhauser enhancement reduced value interpret. 77−46581
^1H-^1H spin pair with time-independent internuclear distance, spin-lattice relax. time 79−42862
^2H spin lattice relaxation, mols. with multiple internal rots., limiting behaviour 79−39356
He-H_2, rot. relax and spectral line shapes, coupled states calcs. 77−50500
^3He, adsorbed, on MgO, nucl. mag. relax. props. 80−49457
^3He, adsorbed monolayers, dipolar anisotropy effects in spin relax 77−7940
^3He adsorbed on Grafoil, nuclear spin relax. and atomic motion 79−51369
^3He adsorbed on graphite, NMR relax. times below 4.2K 78−38898
^3He adsorbed on graphite, mag. props., 2-D gas behaviour 78−47631
^3He, BCC, NMR multiple echoes, soln. of eqn. of motion of magnetisation 79−86961
^3He, BCC, Zeeman exchange cross relax. time 78−22930
^3He film, submonolayer and multilayer, adsorbed on Grafoil, pulsed NMR study 80−49456
^3He films adsorbed on Grafoil, NMR relax. times 79−28171
^3He, liq. and solid., spin polarised, thermodynamical nuclear orientation 79−46879
^3He, liquid, interface with antiferromagnet, anomalous thermal behaviour and nucl. spin relax. 79−56002
^3He liquid in contact with magnetic substrate nuclear spin relaxation 78−43200
^3He, normal, nuclear spin relax. in confined geometries 79−51372
^3He, solid, bulk and divided samples, nuclear spin-lattice relaxation meas. 78−84026
^3He, solid, mag. susceptibility meas. using double sample cell NMR technique 79−63225
^3He:^4He, HCP, solid, nucl. spin-lattice relax., ^4He impurity effects 80−88396
^3He-^4He dilute mixtures, nuclear relax. at 4K in low mag. fields 79−51365
^3He-^4He mixtures, anomalous 80−54463
^3He-^4He solid mixture, ^3He-^3He and ^3He-^4He tunnelling motions, NMR meas. 78−38908
$HfV_2H_{2.1}$, proton NMR relax. time and Knight shifts, diffusional activation energies meas., sorption props. 80−75871
Hg, liq., nuclear quadrupole relax. rate for ^{201}Hg, −35 to 80°C, calc. 77−36151
$Hg_{2.86}AsF_6$, linear chain compound NMR exam. 78−19359
In, liq., nuclear quadrupole relax. rate for ^{115}In, 170-650°C, calc. 77−36151
$In_{1-x}I_x$, molten mixture, NMR, reson. shifts, relax. rates, quadrupole relax. 80−2654
K^+ salts, diamag. ion solvation in methanol soln., NMR relax. obs. 78−56389
KB_3H_8, NMR study of proton and boron dynamics 80−71210
KCl:NH_4Cl, PMR, NH_4^+ ion proton spin-lattice relax. time temp. depend. 78−27104
$KClO_3$, NQR freq. of ^{35}Cl, temp. depend., mol. dynamics 77−12227
$K_3Co(CN)_6$, NMR spin lattice relax. of ^{59}Co rel. to $Co(CN)_6$ octahedra vibr. modes 80−39885
$K_3Co(CN)_6$, spin 7/2 system, quadrupolar relax. parameters 78−56392
$KCoF_3$, antiferromag., with residual orbital moment, nucl. mag. relax. 80−71215
$KCoF_3$, Co^{2+} spin-lattice relax. narrowing of ^{19}F NMR 77−85611
$KCoF_3$, NMR, magnon-phonon interaction contribution to nuclear spin-lattice relax. 78−88207
$KCr(SO_4)_2.12H_2O$, spin lattice relaxation, in liquid He and in vacuum 78−39434
KHF_2, nucl. spin-lattice relax. and anomalous thermal expansion meas. 77−8441
KH_2PO_4, ^{39}K spin-lattice relax. time double NMR meas. 79−47358
KH_2PO_4, paraelectric, dynamic central peak depend. on deuterium content 79−65752

nuclear spin-lattice relaxation continued
$KH_3(SeO_3)_2$, temp. and mag. field dependence of proton spin-lattice relax. time 78−23363
$K_2HgCl_4.H_2O$ proton spin-lattice relax., 180° flips and diffusion of water mol. 77−15327
$KLiSO_4$, ^7Li NMR, spin-lattice relax. *(Chinese)* 80−39884
$KMg_{1-x}Mn_xF_3$, disordered paramagnet, ^{19}F NMR study 80−71216
K_2MnF_4, nucl. spin-magnon relax. time, temp. depend., NMR study 80−25117
K_2MnF_4, ordered quadratic-layer Heisenberg antiferromag., nucl. spin-magnon relax. 80−71217
K_2MnF_4, quadratic layer antiferromag., field induced two magnon nuclear spin-lattice relax. 79−61258
$KNiF_3$, ^{19}F spin-lattice relaxation 80−93211
$KNiF_3$, spin-lattice relax. exam. 79−73838
K_2NiF_4, nucl. spin-magnon relax. time, temp. depend., NMR study 80−25117
K_2NiF_4, ordered quadratic-layer Heisenberg antiferromag., nucl. spin-magnon relax. 80−71217
K_2NiF_4, quadratic layer antiferromag., field induced two magnon nuclear spin-lattice relax. 79−61258
K_2OsCl_6, Cl NQR spectra by Fourier transform methods 80−75879
K_2OsCl_6 powder, spin-lattice relax., dynamic clustering near struct. transition 77−48079
$K_2Pt(CN)_4Br_{0.30}.3H_2O$, dynamic ^{195}Pt NMR meas. below metal-insulator transition 80−34810
K_2PtCl_6, K_2ReCl_6, K_2SnCl_6, solid state phase transitions, lattice vibr., NMR and NQR obs. 80−34814
$K_xRb_{1-x}HF_2$, nuclear spin-lattice relax. and internal motion mechanism 79−99787
K_2SiO_3 aqueous soln., ^{29}Si NMR expts. 78−15051
$KTaO_3$:Li, ferroelec. transition and atomic motions, ^7Li NMR study 80−75872
K_2TeO_3, D_2O soln., $^{123,125}Te$ Fourier transform NMR 78−15046
K_2TiF_6, anion motion and phase transition, NMR spectra 79−99788
^{83}Kr, nucl. mag. relax. meas. in gas 80−43072
La, FCC, NMR 4.2 to 296K, mag. susceptibility and sp. ht. 80−15813
La hydrides, relax. time, temp. depend. meas. by pulse NMR 78−88217
LaAg, electronic struct., NMR relax. times meas. 79−51871
$(La_{1-n}Ce_n)_3Al$, mag. impurity effects in normal and supercond. state, NMR 78−2622
$La_{1-x}Ce_xAl_2$, supercond., nucl. relax. and impurity magnetism 77−20495
LaF_3, ^{19}F NMR study, relaxation times meas. 80−108093
LaF_3, ionic transport, NMR and cond. studies 80−107555
LaF_3:Pr^{3+}, optical meas. of spin-lattice relaxation of dilute nuclei 80−93212
$(La_{1-n}Gd_n)_3Al$, mag. impurity effects in normal and supercond. state, NMR 78−2622
$La_{1-x}Gd_xAl_2$, supercond., nucl. relax. and impurity magnetism 77−20495
La_3In, mag. susceptibility and normal state NMR meas. 78−31118
$LaNi_5$-H, with small Cr additions, NMR parameters *(Russian)* 80−29637
β-$LaNi_{5-y}Al_y$ hydrides, H diffusion, NMR studies 80−15298
$LaNi_3H_x$ (x=4.7, 4.9), NMR line width, spin-lattice relaxation time temp. depend., H self-diffusion *(Russian)* 79−61248
$LaNi_5H_{6.6}$, $LaNi_5H_{6.2}$, H diffusion NMR spectra *(Russian)* 78−2287
$La_2Ni_7H_x$ (x=9.9, 11.4), NMR line width, spin-lattice relaxation time temp. depend., H self-diffusion *(Russian)* 79−61248
La_3Tl, mag. susceptibility and normal state NMR meas. 78−31118
Li, liq., nucl. spin lattice relax. of β-emitter ^8Li 77−51985
Li, thermal mixing rate calc. 78−10795
Li^+ salts, diamag. ion solvation in methanol soln., NMR relax. obs. 78−56389
Li-methylamine soln., metal-nonmetal transition, electron and nucl. spin-lattice relax. 79−87306
Li-methylamine solution, NMR investig. of metal-nonmetal transition 77−40142
LiAl, NMR relax. investig. of ^7Li self-diffusion 77−12217
α-$LiAlO_2$, NMR study of Li^+ motion 79−42863
Li_5AlO_4, α and β phases, NMR study of Li^+ motion 79−42863
β-$LiAlSiO_4$, superionic cond., Li^+ motion, order-disorder transition 77−12220
$LiBF_4$, $LiHBF_3$, spin-spin coupling and T_1 in non-aq. solns. 77−23512
LiCl, aq. soln., ^7Li spin-lattice relax. time, 5-65°C 77−48075
LiCl, aqueous, proton, deuteron and ^7Li relax. times, mol. motion obs. 79−28632
^6LiCl, aq., temp.-depend. relax. 77−1613
LiF, behaviour of nucl. spins near highly polarised paramag. centres 77−77127
LiF:Co(Mg), nucl. acoustic reson. 77−8445
LiH, F-center, dynamic and NEDOR polarisation meas. *(French)* 77−28481
LiH, solid, anion and cation diffusion, NMR relax. and linewidth obs., Schottky disorder 80−15815
α-$LiIO_3$, ^7Li NMR, spin-lattice relax., spurious reson. *(Chinese)* 80−39884
$LiIO_3$, ^7Li nuclear spin-lattice relax. meas. 78−10796
$LiIO_3$, cross relax. in two-spin system, inhomog. broadened line 78−88218
$Li_6In_2O_6$, pseudo-two-dimens. electrolytic solid, Li ion mobility, NMR study *(French)* 80−34235
Li_3N, diffusion processes and struct. NMR study 80−108090
Li_3N, ionic hopping model, NMR relax. data anal. 80−92714
Li_3N layer structure with fast ion cond., ^6Li NMR obs. of diffusion 80−108102
Li_3N, NMR exam. of ion diffusion 79−19397
$LiNH_4SO_4$, nuclear spin lattice and effective proton relaxation, phase transitions 80−54965
$LiNbO_3$:Fe, Mossbauer spectra quadrupole doublet asymmetry 80−44960
Li_7NbO_6, pseudo-two-dimens. electrolytic solid, Li ion mobility, NMR study *(French)* 80−34235
Li_xNiPS_3, antiferromag., mag. props. and ionic mobility, NMR meas. 79−24223
Li_2O, cation diffusion, NMR obs., MgO and LiF doping effects *(German)* 77−20112
$Li_2S(O)$, cation diffusion NMR investigation up to 800°C 80−108092
Li_8SnO_6, pseudo-two-dimens. electrolytic solid, Li ion mobility, NMR study *(French)* 80−34235

nuclear spin-lattice relaxation continued
$LiTmF_4$ Van Vleck paramagnet, electron and nuclear spin-lattice relaxation of Er^{3+} ions 79−95643
MBBA, solid, proton spin-lattice relaxation in metastable and stable phase 78−64286
methane, solid, librational tunnelling and proton relax. temp. 80−38969
$MgCl_2$, aq. soln., ^{25}Mg NMR, longit. relax. rates 79−91309
$Mg(NO_3)_2$, aq. soln., ^{25}Mg NMR, longit. relax. rates 79−91309
$^{25}Mg^{2+}$, aq. ions, nucl. quadrupole relax. 78−64287
Mn, antiferromagnetic, NMR exam. 77−16193
Mn-Ge, antiferromagnetic, NMR exam. 77−16193
MnB, NMR of ^{55}Mn 77−28468
$Mn(ClO_4)_2/NaClO_4$ in aq. soln., interaction between Mn^{2+} and ClO_4^-, NMR studies 80−71212
MnF_2, nuclear spin lattice relax. exam. 78−76331
MnF_2, nuclear spin-lattice relax. and magnon lifetime near spin-flop transition 77−69721
MnSi, NMR and susceptibility above T_c 78−43665
β_1-MnZn, ferromag., spin wave contrib. to nucl. spin-lattice relax. time meas. 77−36147
$Mo_{1-x}Re_xCo$, mag. state of Co impurity, NMR exam. 78−27100
$(Mo_{0.5}Ru_{0.5})_{80}P_{20}$, amorphous normal and mixed supercond. state, ^{31}P NMR 79−87193
$Mo_{1-x}V_x$, supercond., NMR and mag. susceptibility meas. 79−56388
α-N_2, solid, field depend., theory 78−68407
$(ND_4)_2BeF_4$ and $(NH_4)_2BeF_4$, incommensurate phase, ^9Be NMR study 80−75973
ND_4ClO_4, level-crossing relax. study of MD_4^+ ion tunnelling freq. 80−7185
ND_4ClO_4, librational tunnelling and proton relax. temp. 80−38969
$(ND_4)_2PbCl_6$-ND_4Cl polycryst. mixture, D spin-lattice relax. times, ND_4^+ reorientation activation energies 78−6587
$(ND_4)_2PtCl_6$, level-crossing relax. study of MD_4^+ ion tunnelling freq. 80−7185
NH_3, magnetic relaxation rates for microwave spectrum and contributions to linewidth 80−5564
NH_4, hindered rotation effects 77−8433
NH_4 salts, relaxation time of dipolar energy of proton spins 78−76333
NH_4^+, in crystal lattice, tunnelling effect on proton spin-lattice relax. time 79−61252
NH_4^+ motion in solids, nucl. spin-lattice relax. exam. 78−56388
NH_4^+, nuclear dipolar relaxation in four-spin-1/2 tetrahedral group 79−24225
$N_2H_6^{2+}$ salts, NMR spin lattice relaxation study, ^{14}N-^1H dipole-dipole contrib. to relax. 80−75878
$(NH_4)_2Al(SO_4)_2$, ^1H spin-lattice relax., 100-500K 79−38398
$NH_4Al(SO_4)_2.12H_2O$, dielectric losses, proton relaxation by NH_4^+ hopping 79−56721
NH_4BF_4, H^+ relax. and tunnelling, nucl. spin-lattice relax. obs. 79−51876
NH_4Br, anisotropy of T_{1D} and $T_{1\rho}$ 79−38393
NH_4Br, proton spin-lattice relax. time up to 2200 bar, phase transitions 77−63307
NH_4Br, proton spin-lattice relax., temp. depend. 79−42859
N_2H_5Br, mol. ion motion and barriers to rot., PMR and neutron scatt. meas. 79−24226
$(NH_4)_2Ce(NO_3)_6$, proton relax. by tunnelling at low temp. 78−43666
$(NH_4)_2Ce(NO_3)_6$, proton spin-lattice relax., temp. depend. 79−42859
NH_4Cl, anisotropy of T_{1D} and $T_{1\rho}$ 79−38393
N_2H_5Cl, mol. ion motion and barriers to rot., PMR and neutron scatt. meas. 79−24226
NH_4ClO_4, proton relax. by tunnelling at low temp. 78−43666
NH_4ClO_4, proton tunnelling frequencies from nuclear spin-lattice relaxation 78−6591
NH_4ClO_4, with 0.015% and 0.1% D, proton Zeeman relaxation 78−6592
$(NH_4)_2Cr_2O_7$, proton spin-lattice relax., temp. depend. 79−42859
$(NH_4)_2Cr_2O_7$, proton tunnelling frequencies from nuclear spin-lattice relaxation 78−6591
$(NH_4)_2GeF_6$, H^+ relax. and tunnelling, nucl. spin-lattice relax. obs. 79−51876
$(NH_4)_2GeF_6$, NMR, nuclear dipolar energy relax. 79−42853
$(NH_4)_2HAsO_4$, $(NH_4)_2HPO_4$, molecular motion, PMR meas. 77−85591
NH_4HF_2, powder, proton and fluorine 2nd moments meas., 77-395K 80−34803
$(NH_4)_2HPO_4$, NH_4^+ motions, PMR relax. times obs., 77-430K, struct. transition 77−85599
$NH_4H_2PO_4$, ^1H spin-lattice relax. in paraelec. and antiferroelec. phases 79−33555
NH_4HSO_4, NH_4^+ movement 77-388K 77−28524
$(NH_4)_3H(SO_4)_2$, movement of NH_4^+ in all phases over 77 to 388K, NMR study 77−28524
NH_4LiSO_4, ferroelec., PMR line shape and spin-lattice relax. 78−88205
$(NH_4)_2MoO_4$, ^1H spin-lattice relax., 100-500K 79−38398
$NH_4NH_2SO_3$, ^1H spin-lattice relax., 100-500K 79−38398
NH_4NO_3, proton spin-lattice relax., temp. depend. 79−42859
NH_4PF_6, H^+ relax. and tunnelling, nucl. spin-lattice relax. obs. 79−51876
$(NH_4)_2PbCl_6$, librational tunnelling and proton relax. temp. 80−38969
$(NH_4)_2ReCl_6(IrCl_6)$, proton relaxation near antiferromagnetic phase transitions 80−80640
NH_4ReO_4, PMR, NH_4^+ tunnelling, ground torsional level struct. 78−27097
NH_4ReO_4, polycryst., ^1H spin-lattice relax. by mech. sample rot. 77−16200
NH_4ReO_4, proton absorpt. lineshape and spin-lattice relax., ^{187}Re anomalous temp. depend. 78−48067
NH_4SCN, proton spin-lattice relax., temp. depend. 79−42859
$(NH_4)_2S_2O_8$, proton spin-lattice relax., temp. depend. 79−42859
$(NH_4)_2SiF_6$, cubic and trigonal, proton tunnelling frequencies from nuclear spin-lattice relaxation 78−6591
$(NH_4)_2SiF_6$, proton relax. by tunnelling at low temp. 78−43666
$(NH_4)_2SiF_6$, trigonal, proton and ^{19}F relax, 30 to 200K 77−76549
$(NH_4)_2SnCl_6$, ^1H spin-lattice relax., 100-500K 79−38398
$(NH_4)_2SnCl_6$, $^{35,37}Cl$ NQR, Raman spectra and spin lattice relax., hindered rot. 80−54974
$(NH_4)_2SnCl_6$, proton relax. by tunnelling at low temp. 78−43666
$(NH_4)_2SnCl_6$, proton tunnelling frequencies from nuclear spin-lattice relaxation 78−6591
NH_4TaWO_6, rapid ionic motion, spin-lattice and spin-spin relax. times meas. 79−38396

nuclear spin-lattice relaxation continued
$(NH_4)_2TiF_6$, ^1H-^{19}F coupled NMR, line shapes, spin-lattice relax. 79−73839
$(NH_4)_2TiF_6$, H^+ relax. and tunnelling, nucl. spin-lattice relax. obs. 79−51876
N_2O dissolved in liq. cryst., NMR, relax. times 80−25233
^{15}N, spin-lattice relax. time, quantum effect of NH_4-ion rot. 80−75875
Na^+ salts, diamag. ion solvation in methanol soln., NMR relax. obs. 78−56389
Na_2 nuclear spin polarized, comparison with ortho-para conversion rate 79−43568
$NaBD_4$, ^{11}B spin-lattice relax., struct. phase transition 78−84492
$NaBF_4$, spin-spin coupling and T_1 in non-aq. solns. 77−23512
$NaBH_4$, ^{11}B spin-lattice relax., struct. phase transition 78−84492
$NaBH_4$, $NaBD_4$, first order struct. transition, NMR meas. 78−80240
NaCl:Ca^{2+}, highly doped, aggregation of point defects, NMR and dielec. loss meas. 79−10847
NaCl:Ca^{2+}, spin-lattice relax. meas., 160 to 360°C, vacancy contrib. 77−28477
NaCl:Sr, dimer and trimer aggregate formation by NMR, ionic cond. and dielectric losses 80−15094
$NaClO_3$, ^{35}Cl NQR meas. 77−66435
$NaClO_4/Mn(ClO_4)_2$ in aq. soln., interaction between Mn^{2+} and ClO_4^-, NMR studies 80−71212
NaF(Cl), dislocation velocity determ. by nuclear spin-lattice relax. meas. 77−35566
$NaH_3(SeO_3)_2$, proton spin lattice relaxation 79−78557
$Na_xIn_xSn_{1-x}S_2$, intercalation-substitution compounds, NMR study 80−44952
$Na_xIn_xSn_{1-x}S_2$, ionic conductors, ^{23}Na NMR and complex impedance meas. 79−91314
NaN_3, NMR, Na nuclear quadrupole moment, phase transition 77−73092
$NaNO_2$, size effect and spin-lattice relax. of ^{14}N 80−20480
$NaNO_3$, ^{23}Na spin-lattice relax., orientation depend. 78−23372
$NaNO_3$, of ^{23}Na, −75.5 to +320°C *(Japanese)* 77−43897
Na_2O-B_2O_3:Cu^{2+}, Mn^{2+} glasses, Cu^{2+}-Mn^{2+} interaction studied by ESR 80−93166
$Na_2S(O)$, cation diffusion NMR investigation up to 800°C 80−108092
Na_2SiO_3 aqueous soln., ^{29}Si NMR expts. 78−15051
$Na_2Si_3O_7.xH_2O$, amorphous, pulsed NMR study 79−78555
Na_2TeO_3, D_2O soln., $^{123,125}Te$ Fourier transform NMR 78−15046
Na_xWO_3, Knight shift, spin-lattice and spin-spin relax., high press. NMR obs. 80−50211
$Na_xY_xZr_{1-x}S_2$, ionic cond. and NMR mobility obs., comp. depend. *(French)* 80−70459
$Na_3Zr_2PSi_2O_{12}$, NASICON, ^{23}Na NMR obs. of ionic diffusion, 180 to 800K 80−108097
Nb, NMR study up to 1700K, Knight shift and spin-lattice relax. time 80−2653
Nb, proton diffusion, NMR obs., 120-480K 80−34812
Nb_3Al, nuclear magnetic relaxation, near T_c *(Russian)* 79−42852
Nb_3Al, quasi-one-dimensional supercond., giant enhancement of nucl. relax. rate near T_c 78−56257
Nb_3Al:^{93}Nb, NQR spectra, NQR signal disappearance in supercond. state 78−19369
$(NbCl_nBr_{6-n})^-$, ^{93}Nb nucl. spin relax. and mag. shielding 78−58723
$(NbCl_nBr_{6-n})^-$ complexes in acetonitrile soln., ^{93}Nb spin relax. and mag. shielding 80−44944
NbS_2, intercalation with pyridine, nucl. spin-lattice relax. meas. 80−54962
Nb_3Sb, NQR study, ^{93}Nb nuclear relax. 78−88073
$NbSe_2$, 2H phase, layered type II supercond., NMR meas. 77−36024
$NbSe_2$ (2H), charge density waves state, NMR meas. 78−39421
Nb_3Sn, quasi-one-dimensional supercond., giant enhancement of nucl. relax. rate near T_c 78−56257
Nb_3Sn(Al)(Sb), NMR of ^{93}Nb and spin-lattice relax. time at low temp. 77−85388
NdF_3, ^{19}F spin-lattice relax. and mag. couplings 79−65753
Ne solid, ultraslow diffusion of ^{21}Ne, adiabatic demagnetisation in rotating reference frame 77−73095
Ni complex, hexamethylphosphorotriamide Ni (II), paramagnetic, pulsed NMR, substitution reaction *(French)* 78−10793
Ni, critical NMR obs. near mag. transition 77−81026
Ni, ferromagnetic, electronic struct. and hyperfine field of nonmag. impurities, calc. 80−70658
Ni, hyperfine fields on ^{12}B, NMR obs., near T_c 77−28476
Ni, hyperfine interactions on implanted ^{12}B, crit. behaviour near T_c 78−43663
Ni:^{12}B, NMR, crit. slowing-down at Curie temp. 77−8418
Ni:B, impurity electronic struct. calc., ^{12}B NMR data anal., magnetisation decrease 79−47046
Ni-b, hyperfine interactions from 6 to 730K, ^{12}B NMR 80−29372
Ni-Cu(Zn)(Ga)(Ge)(As)(Se)(Br)(Kr), dil., ferromagnetic, hyperfine field and relax. time obs. of impurity heavy nuclei 80−75533
Ni-P alloy, amorphous, NMR expts. and interpretation 79−8060
Ni-Pd-P, metallic glass, electronic structure, pulsed NMR study 80−75869
$Ni(NH_3)_6X_2$, (X^-=Cl^-, BF_4, ClO_4^-) spin dynamics at struct. phase transition 79−15309
NiPB amorphous alloys, ^{31}P and ^{11}B NMR near paramag.-ferromag. transition 79−33558
$Ni_{0.98}Pd_{0.02}$, dil. ferromag., nucl. mag. relax. meas. 77−16198
$NiSe_2$, paramag. props., NMR, mag. susceptibility 80−60175
$Ni_{1-x}Si_x$, electronic states of Si NMR study 80−50216
$NiSiF_6.6H_2O$, paramag., nucl. and electron spin lattice relax. 78−84494
^{61}Ni, paramag. solid and liq. phases, nucl. spin relax. and Knight shift 78−76327
P, amorphous, NMR studies 79−69740
P+Nb, dil. alloy, NMR obs. of ^{93}Nb 80−71203
PBr_3, ^{31}P scalar relax. using off-reson. RF field 79−93193
PF_3, cryst., mol. motion, ^{19}F NMR investig. 77−73093
PF_3Br_2, spin systems under multiple pulse NMR conditions, chem. shift relax. 80−34808
P_4S_3, ^{31}P NMR spectrum and spin-lattice relax. time, 77 to 500K and 7 to 25 MHz 79−8064
PbF_2, NMR relax. and self diffusion 78−80236
PbF_2, superionic, F^- motion and F sublattice melting, NMR obs. 77−43374
PbF_2:Mn, mag. tagging of ion diffusion, ^{19}F NMR meas. 80−108106
PbI_2 intercalated with aniline, NQR meas. *(Russian)* 79−91311

nuclear spin-lattice relaxation continued
PbI_2-piperidine intercalations rel. to NQR, spin-lattice relax. temp. depend. *(Russian)* 78−27108
$Pb_{1.125}Mo_6Se_{7.5}$, Chevrel phase supercond., NMR study 80−49989
$PbSnF_4$, fast ionic cond. of F^- ions, NMR study *(French)* 80−39345
Pd-Mn alloy, NMR of ^{27}Al meas. 77−12215
Pd-Ni alloy, NMR of ^{27}Al meas. 77−12215
$Pd_{0.7}$, D spin-lattice relaxation time, D quadrupole coupling, D atom diffusion 79−73844
PdCo, dil., ferromag., nucl. mag. relax. meas. 78−6590
PdF_2, motionally narrowed NMR line shapes, free-induction decay meas. 78−68406
PdH, electronic struct. and proton spin-lattice relax. calc. 78−67937
$PdH_{0.76}$, ^1H spin-lattice relax. meas. 78−43672
PdH(D), stoichiometric, ^1H and ^2D NMR, rel. to supercond. T_c 78−72430
PdH(D), superconducting, electronic spin density, isotope effects 78−39262
PdNb, dilute, NMR obs. of ^{93}Nb 80−71203
Pr $(NO_3)_3.6H_2O$, Van Vleck paramag., Orbach processes and nucl. relax. 77−8439
$PrAlO_3$, ^{27}Al NMR, electronic spin dynamics at Jahn-Teller phase transition 78−68403
PrF_3, ^{19}F spin-lattice relax. and mag. couplings 79−65753
$Pr(ReO_4)_3.4H_2O$, Van Vleck paramag., Orbach processes and nucl. relax. 77−8439
$Pr_2(SO_4)_3.8H_2O$, ^{141}Pr spin-lattice relax. time meas. 77−28478
$Pr_2(SO_4)_3.8H_2O$, Van Vleck paramag., Orbach processes and nucl. relax. 77−8439
Pt, Knight shift and spin-lattice relax., up to 1358K 78−72425
PtV, dil. alloys, NMR obs. of ^{51}V 80−71203
$RbAg_4I_5$, static and dynamic NMR effects at 208K and 122K phase transitions 80−108105
$RbCaF_3$, cubic to tetragonal phase transition, ^{87}NMR meas. 80−7187
$RbCaF_3$, cubic to tetragonal phase transition, ^{87}Rb NMR study 80−70392
$RbCdCl_3$, n.q.r. spin-lattice relax. near cubic-tetragonal transition, soft modes 77−1616
RbCl:Ag, dynamic behaviour of off-centre Ag^+ defects, NMR study 79−28634
RbCl:NH_4Cl, PMR, NH_4^+ ion proton spin-lattice relax. time temp. depend. 78−27104
$Rb_2CuBr_4.2H_2O$, dynamic props. in paramag. state, spin-lattice relax. time meas. 80−71214
RbI, press. depend. of I nucl. relax. press. induced polymorphic transform. study 79−1720
$RbMnF_3$, of ^{19}F, 0.1-3K 77−20743
Rb_2PtI_6, cryst., role of ordinary and harmonic Raman processes, ^{127}I nucl., spin-lattice relax., obs. 79−8063
Rb_2SO_4-$(NH_4)_2SO_4$ mixed cryst., ferroelec. transition, structural and dielec. props., proton spin-lattice relax. 78−39512
Rb_2ZnCl_4, incommensurate phase transition, ^{87}Rb NMR study 80−75967
Rb_2ZnCl_4, spin-lattice relax. in incommensurable phase, phason and amplitudon excitations 80−50213
SF_6, solid, NMR line shape and relax. 77−51978
Sb, NQR, nucl. spin-lattice relax., 4.2K 78−91984
$Sb_2O_{5.n}H_2O$, crystalline, ^1H NMR study of proton transport 80−60446
SbSI, tricrit. point, NQR under press. 79−38469
Sc_3In, itinerant electron ferromagnet, spin fluctuations 77−73096
Sc_3In, itinerant electron ferromag., NMR and relax. 78−6586
ScM (M=Cu, Ag, Pd, Rh, Ir, Ru), electronic struct., NMR relax. times meas. 79−51871
Se, solid, chemical shift and nucl. spin-lattice relax., high temp behaviour 80−60445
^{77}Se, FT NMR in solns., chem. shift, I_1 relax. times, NOE enhancement 78−95528
Si, nuclear spin-lattice relax. in weak mag. fields *(Russian)* 79−51879
Si, optically pumped, dynamic polarisation and mag. relax. of ^{29}Si 78−48081
Si:H film, amorphous, H-associated disorder modes, PMR spin-lattice relax. time meas. 80−93202
Si:P, electronic states, NMR of metallic and intermediate samples 79−4511
Si:S, electron-nuclear interactions during pumping, influence of mag. field 79−95378
Si-Au, solid soln., influence of precip. on relax. of ^{29}Si nucleus 80−11287
$SiCl_4$ molecule, NMR relaxation expts. to study molecular reorientation 80−63673
SiH_4, appl. of NMR field cycling method for obs. of low temp. tunnelling in molecular solids 79−65755
SiH_4, magnetisation relax., appl. of theory of spin-lattice relax. 80−50214
SiH_4, NMR linewidths and relax. times at 6.7 to 124K 77−85602
SiH_4, solid, NMR direct detection of tunnel splittings 78−56396
Si_3N_4:Fe, α- and β-phases, Mossbauer and Raman obs. of state of Fe 79−33572
SmF_3, ^{19}F spin-lattice relax. and mag. couplings 79−65753
Sn, nuclear spin-lattice relax. time meas. using SQUID magnetometer, appl. to thermometry 79−63212
Sn, supercond, small particles, Josephson-coupled, local fluctuation effects 78−72308
$SnCl_2.2H_2O$, dielectric dispersion and absorpt. and proton spin-lattice relax. at phase transition 77−8437
^{117}Sn, ^{119}Sn, low temp. NMR thermometry 80−82775
^{119}Sn NMR by pulse Fourier transform, T_1, T_2 and chem. shifts 77−55715
SrF_2:Dy^{3+}, nuclear spin-lattice relax. anisotropy, 78 to 300K 79−38395
$^{87}Sr^{2+}$, aq. ions, nucl. quadrupole relax. 78−64287
TTF-TCNQ, ^{13}C Knight shift and spin-lattice relax. meas., local susceptibility determ. 77−4571
$TTF.CuS_4C_4(CF_3)_4$, spin-Peierls system, nucl. spin-lattice relax. process 78−19361
TaH_x, H diffusion and electronic struct., pulsed NMR obs. 80−54967
TaS_2, intercalation with pyridine, nucl. spin-lattice relax. meas. 80−54962
TaS_2-NH_3 intercalation complex, press. induced diffusion effects, NMR study 79−19797
$TaS_2(NH_3)_x$, NMR spectral densities and two-dimens. diffusion 80−50215

nuclear spin-lattice relaxation continued
$TaS_2(pyridine)_{1/2}$, superconducting intercalation complex, proton spin lattice relaxation time 78−80096
Te compounds, dihalides, organometallics, ^{125}Te, ^{13}C, ^{1}H NMR spectra, nucl. coupling, exchange processes 79−95658
Te, diffusion and cond. props., NMR investigation 79−78547
Te, NMR spectrum, electron paramagnetism and atomic self-diffusion mechanism 78−72426
ThC_xN_y, NMR, Knight shift and spin-lattice relax. 80−100621
Th_4D_{15}, NMR relax. expts., diffusion processes and hyperfine fields 79−8066
Th_4H_{15}, NMR investig. of proton environment and motion 77−48077
Ti-H, H diffusion and phase consistution, V influence, proton spin-lattice relax. meas. 78−27484
Ti-H, proton spin-lattice relaxation time, band struct. 78−56395
Ti-Nb-H, proton spin-lattice relax. time, conc. depend., diffusion effects 77−4576
TiCuH, H-atom diffusion activation energy from PMR obs. 78−91978
β-$TiFeH_{1.03}$, H diffusion, NMR meas. 80−10707
$TiH_{1.45}$, PMR study of spin correl. and saturation effects 77−59477
TiH_x, H diffusion, NMR obs. 80−34813
γ-TiH_x, interstitial H diffusion mechanism, NMR spin-lattice relax. study 80−103515
$Ti_{1-x}Nb_xH_{1.94}$, electronic struct. MNR meas. 80−15439
$TiS_2(NH_3)_{1.0}$, NMR spectral densities and two-dimens. diffusion 80−50215
$TiSe_2$, electronic instability, ^{77}Se NMR 78−10790
TlBr melts, Tl doped and pure, stoichiometric, nucl. spin relax. 80−25236
TlH_2AsO_4, proton spin-lattice relax. study of structural phase transition 79−19796
$Tl_2SeAs_2Te_3$, amorphous semicond., nuclear spin-lattice relaxation by localised electronic states, modification by spin diffusion 78−52372
$^{205}Tl^+$, NMR in aq. soln., dissolved O_2 on nuclear spin relax. rate 78−19356
$^{205}Tl^+$ adsorbed on hydrated silica, NMR relax. chem. shift 78−72427
$^{205}Tl^+$ ion, solvent effects on spin-lattice relaxation time 77−48073
$TmVO_4$, enhanced nuclear cooling and spin-lattice relax. time 80−80632
$UC_{1-x}N_x$, NMR of ^{13}C and ^{15}N, 5f electrons nature, mag. susceptibility, spin fluctuations 77−20736
$UO_2(NO_3)_2$, aq. soln., pulsed NMR relax. time, ^{235}U enrichment depend. 80−2658
V-based A15 compounds, nuclear spin-lattice relax. time, electronic density of states 77−59354
V-H, NMR of anomalous diffusion of H and phase transition 77−16571
$V_{0.75-x}Ga_{0.25+x}$ ^{51}V, nucl. spin-lattice relax. time, annealing and neutron effects 79−82710
$V_{1-x}Ga_x$, nuclear spin-lattice relax. and supercond. 79−56387
V_3Ga, nuclear magnetic relaxation, near T_c *(Russian)* 79−42852
$V_3Ga(Si)$, high T_c supercond., rel. to density of states sharp struct. effect on electron-phonon coupling 78−14877
V_3Ge, A-15 cpds., nucl. mag. relax. in normal and supercond. state 80−49993
VH_x, Knight shift and spin-lattice relax. of proton NMR, local electronic environment of protons 77−16194
$V_2(Hf,Zr)$, NMR and mag. susceptibility, density of states determ. *(Russian)* 80−66053
$V_{2-x}Nb_3Hf$, NMR of ^{51}V and mag. susceptibility, 20-300K *(Russian)* 80−93192
$V_{1-x}Pt_x(Ga_x)(Si_x)$, A-15 cpds., nucl. mag. relax. in normal and supercond. state 80−49993
V_3S_4, and V_5S_8, itinerant antiferromag. spin fluctuations, NMR studies 80−93198
V_3Se_4, itinerant antiferromag., spin fluctuations, NMR study 80−75874
V_5Se_8, itinerant antiferromag., spin fluctuations, NMR study 80−75874
V_3Si, NMR meas. near struct. transform. *(Russian)* 80−44942
V_3Si, NMR of ^{51}V above and below 21K struct. transition *(Russian)* 80−34796
V_3Si, nuclear magnetic relaxation, near T_c *(Russian)* 79−42852
^{89}Y spin-spin relaxation times, pH depend. 80−66059
YbCuAl, intermediate-valent, nucl. reson. and relax. 79−78550
Zn complex, aminoacetate, proton spin-lattice relaxation, temp. depend. 78−31119
Zn, HCP metal, pulsed ^{67}Zn NMR studies at 4.2K 79−91315
Zn, liq., NMR and relax. 79−8061
Zr and its alloys, H diffusion, NMR study 80−108088
Zr-H system, low temp. NMR 78−72431
$ZrMn_2H_x$, proton NMR relax. time and Knight shifts, diffusional activation energies meas., sorption props. 80−75871
$ZrZn_2$, itinerant electron ferromag., nucl. spin-lattice relax. time meas. 77−63308

nuclear spin-spin relaxation *see spin-spin relaxation*

nuclear structure
see also form factors (nuclear); nuclear binding energy; nuclear charge; nuclear density; nuclear energy level transitions; nuclear energy levels; nuclear forces; nuclear isomerism; nuclear isospin; nuclear matter; nuclear moments; nuclear polarisation; nuclear shape; nuclear size; nuclear spectroscopic factors; nuclear spin and parity; nuclear structure theory
$\langle\Gamma_n^0\rangle$ for isotonic groups, dependences *(French)* 77−3005
A=109 nuclei, data sheets (to October 1977) 79−9441
A=110, nuclear data sheets 78−66189
A=111 nuclei, nuclear struct. data sheets to February 1979 80−9193
A=112, experimental nuclear structure data to January 1979 80−98763
A=117 nuclear struct. data sheets to June 1978 79−36130
A=123, experimental nuclear structure data to June 1979 80−94931
A=141, nuclear structure data sheets to 01 Sept. 1977 79−13184
A=141 nuclei, data sheets 79−6371
A=142, nuclear struct. data sheets to Oct. 1977 79−30769
A=145, experimental nuclear structure data to August 1979 80−94932
A=147 nuclear struct. data sheets to May 1978 79−30770
A=148 nuclei, nuclear struct. data, level props. 77−67697
A=163, nuclear data sheets to April 1979 80−98762
A=18-20, light nuclei, compilation of energy levels, nuclear struct. information 78−62478
A=194, review of struct. information to July (1977) 78−89769
A=195, nuclear data sheets to Jan. 1978 79−17781
A=195 nuclei, data sheets 79−6372
A=197 nuclei, review of nuclear struct. information 77−57585
A=198 nuclei, struct., level props., decay, review 78−17077
A=201 nuclear struct. data sheets to May 1978 79−30771
A=205 nuclei, data sheets (to November 1977) 79−9442
A=207, review of struct. information to August (1977) 78−89770
A=209, review of struct. information to September (1977) 78−89771
A=211, nuclear struct. data sheets to July 1978 79−36131
A=213, nuclear structure data sheets (July 1979) 80−67942
A=214 nuclei, struct. info., energy levels, spin, parity, decay 78−17078
A=217, nuclear structure data sheets (July 1979) 80−67943
A=218 nuclei, nuclear struct. info., energy levels, spin, parity, decay 78−17079
A=222 nuclei, nuclear struct. info., energy levels, spin, parity, decay 78−17080
A=226 nuclei, review of nuclear struct. information 77−57586
A=230 nuclei, review of nuclear struct. information 77−57587
A=232, 236, 240 nuclei, review of nuclear struct. information 77−57588
A=234 nuclei, nuclear struct. info., energy levels, spin, parity, decay 78−17081
A=238 nuclei, nuclear struct. info., energy levels, spin, parity, decay 78−17082
A=242 nuclei, nuclear struct. info., energy levels, spin, parity, decay 78−17083
A=32 to 140, nuclear struct., binding energies, dipole moments *(French)* 77−46098
A=45, nuclear data sheets 78−66187
A=47, nuclear data sheets 78−66188
A=51 nuclei, data sheets (to August 1977) 79−9440
A=52 nuclear struct. data sheets to April 1978 79−36129
A=53 nuclei, struct., level props., ENSDF data 78−17076
A=54, nuclear structure data sheets, to Dec. 1977 79−17780
A=54 nuclei, data sheets 79−6370
A=56 nuclei, nuclear struct. data, level props., from ENSDF 77−74743
A=57 nuclei, nuclear struct. data, level props., from ENSDF 77−74744
A=58 nuclear data sheet to June 1976 77−18372
A=63, nuclear structure data sheets (July 1979) 80−67941
A=70, nuclear struct. data sheets to Oct. 1977 79−30768
A=76 nuclear data sheet to June 1976 77−18373
A=84 nuclei, nuclear struct. data sheets to March 1979 80−9191
A=87 nuclei, nuclear struct. data sheets to January 1979 80−9192
anomalous nuclei, crit. charge *(Russian)* 78−8736
antineutrino probes for nuclear struct. expts. 79−531
atomic physics in nuclear experiments, conference, Haifa, Israel, Aug. 1976 78−70947
backbending even-even nuclei, particle-rotor model with VMI core *(German)* 77−6258
bibliography, recent nuclear physics expt. papers 77−41873
bound neutral nuclei, search in W fragmentation near Zn sample 77−30502
clustering aspects of nuclear struct. and nuclear forces, review 79−80887
conference on few body systems and nuclear forces, Graz, Austria (Aug. 1978) 79−80880
Conference on meson-nuclear physics, Houston, USA (Mar. 1979) 79−85489
conference on nuclear spectroscopy and structure, Alma Ata, USSR, (Mar. 78) 79−75809
conference on nuclear struct. spectroscopy and atomic nucleus struct., Tashkent (Mar. 77) 79−6470
conference on nuclear structure and reactions, clustering aspects, Winnipeg, Canada (June 1978) 79−3099
data sheets, 1978 recent references, cumulation 79−80862
data sheets, 1979 recent references, cumulation 80−94930
data sheets, recent references, Jan. to April 1979 80−5039
data tables, May to August 1979 references 80−41953
data tables, recent references May-Aug 1978 79−30773
deformed nuclei, photoreactions as struct. probe 77−2975
education, compound and intermediate nuclear struct. wave packet scatt. time evolution, simple model 79−9054
electron scatt. theory, EM struct. from DWBA and other models 80−5133
Evaluated Nuclear Structure Data File for basic and applied research 78−17544
even-even nuclei, quasi-ground, beta and gamma bands, data tables 78−82265
exotic light nuclei, with unequal numbers of protons and neutrons 78−89831
exotic nuclei with isospin T>A/2, props. 77−22926
few-body systems, photon and lepton probes 77−26591
frontiers in nuclear physics 78−70427
growth points in nuclear physics, book 80−94928
hadron-nucleus total cross-sections, moments of nucl. densities 78−78252
heavy fissile nuclei, nuclear constants estimation *(Russian)* 79−30779
heavy ion collisions, use in nuclear struct. determ. 79−54446
heavy ion induced reactions, γ-ray multiplicity, ang. momentum and struct. depend. *(Rumanian)* 78−89906
heavy-ion transfer reactions, clustering effects in nuclei 77−14171
high angular momenta, review *(German)* 79−40832
high resolution proton scattering 79−45252
high-energy elastic and inelastic scatt. by light nuclei, mechanism and struct. determ. *(French)* 79−534
hyperfine interactions, conference, Madison, NJ, USA (Jun 1977) 78−39076
intermediate energy nuclear physics, review of recent expts. 78−50061
intermediate energy reactions with photon, pion, proton, electron, kaon as struct. probes 77−88107
ion-nucleus collisions, transfer reactions, study of nuclear structure *(French)* 80−78310
light nuclei, α spectroscopic factors, harmonic oscillator shell model 77−50051
light nuclei, cluster struct., review 78−50107
lighter nuclei structure, conf., Hvar, Yugoslavia, 8-13 May 1978 78−74298
meson-nucleus reactions as determination method 79−85351
modern atomic and nuclear physics (book) 80−11
momentum wave function determ. in atomic, molecular and nuclear systems 77−88556
momentum-space wavefunctions via nucleon knockout reactions, off-shell effects 77−88122
multi-nucleon transfer and direct reactions, nuclear struct., review 78−50060

nuclear structure continued
neutral nuclei, search for existence in W+p interactions *(Czech)* 78−29454
nuclear Coulomb energy, shell model calc., pair distrib. function method 79−13183
Nuclear Data Sheets, computer-readable form 77−22828
Nuclear Data Sheets, recent references 77−71551
nuclear data table preparation 79−75812
nuclear structure, conf. 78−50059
nuclear structure references 1975-7 79−30772
nucleon motion in nuclei, determ. using high energy electron induced knock-out reactions *(French)* 79−445
nucleus as many body field system and a system with abnormal mass, charge, density and energy 78−12938
one-nucleon transfer reactions, high energy, reaction kinetics and struct. determ. *(French)* 79−535
Pauli's exclusion principle for strong interactions in hadrons, nuclei, and astrophysics 80−37206
periodic properties, stability *(Czech)* 77−50040
phase-equiv. non-local potentials 78−66224
properties from alpha scatt. studies *(Hungarian)* 80−18159
quarks and leptons, high energy and nuclear physics interface 80−41974
radioactive atoms, hyperfine spectrosc., nucleus-electron interactions, review 79−72259
relativistic nuclear physics, collisions of relativistic ions *(Rumanian)* 78−46104
review of 30 years work by Nuclear Reactions Lab. Dubna, USSR 79−36204
review of research programs at Saclay Nuclear Physics dept. *(French)* 79−437
single particle momentum states via (p,2e) knockout reactions 77−88117
spectroscopy, publications produced in USSR 80−22186
spectroscopy and heavy-ion reaction, conference, Varenna, Italy (July-August 1974) 77−14169
supernuclei containing bound states of charmed baryons, existence, decay, phys. significance 77−79320
Swiss Physical Society, autumn sessions 78−72053
valence neutron radial distrib. from elastic electron scatt. 77−57652
weak interactions in nuclei, axial polarisability 77−22924
d, D-state about 4%, appl. to reaction data anal. 78−70461
Δ(1232), momentum distrib. in nuclei 77−18444
(n,α) cross sections, 14 MeV, empirical formulae 79−63662
NN dynamics at medium energies, phase parameters, one pion exchange model 80−63102
nN inelastic scattering, shell and isotope effects, review of Soviet research 79−36168
(π,π) 80-300 MeV studies around (3,3) resonance region, review 79−85528
(π,πN) reactions, nuclear structure effects, modified semiclassical model 77−34348
π scattering by few-nucleon nuclei, diffractional approx. *(Russian)* 78−650
A=101 nuclei, nuclear struct. data sheets to May 1979 80−41954
A=103 nuclei, nuclear struct. data sheets to July 1979 80−41955
A=196 nuclei, nuclear structure data sheets to Sept. 1978 80−41956
A=200 nuclei, nuclear struct., data sheets to Nov. 1978 79−71778
A=206 nuclei, nuclear struct. data sheets to July 1978 79−71779
A=229 nuclei, nuclear struct. data sheets to March 1978 79−26361
A=233 nuclei, nuclear struct. data sheets to March 1978 79−26362
A=49 nuclei, nuclear struct. data sheets to Dec. 77 79−26360
A=62 nuclei, nuclear data sheets to August 1978 79−71777
Ag, A=107, 9, +^{86}Kr, 618 MeV, γ-ray multiplicities and angular momentum fractionation 78−37370
^{40}Ar(d, p)^{41}Ar, 1.354 MeV, spectroscopic factor comparison with isobaric analogue reson. 79−30787
^{197}Au +^{86}Kr, 618 MeV, γ-ray multiplicities and angular momentum fractionation 78−37370
^{9}Be, molecular model, n and α-particle decay widths, charge form factors 78−46015
^{9}Be, neutron spectroscopic factor from (^{9}Be,^{8}Be) reacts. 78−17098
^{71}Br, prod. in proton spallation reactions, nuclear structure influence on yields of product nuclei 80−22794
^{12}C, 3α system, resonating group method for nuclear props. 78−50108
^{12}C(e,e') nuclear struct. anal., depend. of meson exchange currents, high momentum transfer data 79−13283
^{12}C(p,pd), (p,pt), (p,pα), spectroscopic data on quasielastic ejection on nucleon clusters from 1p shell nuclei 79−80931
^{12}C→^{16}O, measurement of alpha-widths in ^{16}O relevant to astrophysics 79−6682
^{13}C-^{12}C+n spectroscopic factor determ. from ^{12}C(^{13}C,^{13}C) at 12 MeV 77−65194
^{59}Co, electron elast. scatt. cross sections, phase shift anal. and HF calcs. *(Russian)* 78−41707
Cu, A=63, 65, electron elast. scatt. cross sections, phase shift anal. and HF calcs. *(Russian)* 78−41707
^{150}Gd, compound nucleus, evaporation calcs., comparison with exptl. decay data 77−61391
^{150}Gd compound nucleus formation and decay, obs. in ^{134}Ba+^{16}O, and ^{110}Pd+^{40}Ar 77−61453
^{4}He, struct. effects on α-decay of superheavy nuclei 78−17158
He(e,e), A=3 and 4, high momentum transfer, elastic struct. functions 78−62521
^{165}Ho +^{86}Kr, 618 MeV, γ-ray multiplicities and angular momentum fractionation 78−37370
^{2}M+hadron→proton+X, polarised d, S and D wave functions, nuclear core hypothesis 78−62417
^{26}Mg(p,π$^{\pm}$), 180 MeV, effect of Δ^{++} components in nuclei 78−33181
^{14}N(p,pd), (p,pt), (p,pα), spectroscopic data on quasielastic ejection on nucleon clusters from 1p shell nuclei 79−80931
^{99}Nb, fission product of ^{235}U *(German)* 78−29395
Nd(^{16}O,^{12}C), A=142, 144, comparison of reduced widths derived from transfer reactions and α-emitters, DWBA anal. 79−6671
^{58}Ni compound nucleus in ^{54}Fe(α,p), resonance struct., α-widths 77−30617
^{60}Ni, electron elast. scatt. cross sections, phase shift anal. and HF calcs. *(Russian)* 78−41707
^{16}O, α-spectroscopic amplitudes anal. using shell model based calc. 79−13203
^{16}O, RPA calc., many-body oscills. problem 78−82298
^{16}O(^{6}Li,d)^{20}Ne, 20, 32, 38 MeV α-particle spectroscopic strength determ., DWBA anal. 79−26451

nuclear structure continued
^{16}O(p,pd), (p,pt), (p,pα), spectroscopic data on quasielastic ejection on nucleon clusters from 1p shell nuclei 79−80931
^{16}O(π^{+},π^{-}), 140 MeV, nuclear structure effects on cross section 78−17246
^{18}O(π^{+},π^{-}), 140 MeV, nuclear structure effects on cross section 78−17246
^{18}O(π^{+},π^{-})^{18}Ne, nuclear struct. effects 78−37380
(π,π), elastic and inelastic, use in nuclear struct. determ. studies, review 79−85527
^{74}Rb, prod. in proton spallation reactions, nuclear structure influence on yields of product nuclei 80−22794
^{32}S, doorway structs. in radiative capture of neutrons 79−532
^{28}Si, doorway structs. in radiative capture of neutrons 79−532
^{97}Sr, fission product of ^{235}U *(German)* 78−29395
Xe Fermi motion of nucleons via Xe+π^{+} 2.34 GeV/c p emission 77−18628
^{97}Y, fission product of ^{235}U *(German)* 78−29395
^{99}Y, fission product of ^{235}U *(German)* 78−29395
^{62}Zn compound nucleus in ^{58}Ni(α,p), resonance struct., α-widths 77−30617
^{97}Zr, fission product of ^{235}U *(German)* 78−29395
^{99}Zr, fission product of ^{235}U *(German)* 78−29395

nuclear structure theory
see also generator coordinate method; HF calculations; nuclear models; nuclear reaction and scattering theory; RPA calculations
0^{-} level positions, effects of one pion exchange 77−6232
0p shell nuclei, effective interaction spin-tensor decomposition 80−32198
γ-vibrational levels, Coriolis effects and microscopic structure 77−82809
σ-model appl. to nuclear physics in one dimension, fission, Hartree approx. 79−80890
A=12 polarised β-decay, nuclear Dirac wave function test 80−5060
A=15 mag. moments, nuclear Dirac wave function test 80−5060
A=16-58, charge, proton and neutron density distribs. calc. 80−22680
A=18, effective interaction, 2nd order core polarisation diagrams with intermediate particle states 79−45180
A=18-22, Coulomb matrix elements and energy shifts 77−10308
A=24-60, yrast lines using Strutinsky method, empirical fusion bands 80−42514
A=3, two particle orbital functional parentage coeffs. 79−63604
A=42, multiple scattering formalism for the effective interaction 80−102126
A=42 isotopic spin triplet, Coulomb energies and shifts, microscopic calcs. 80−9200
A=42 nuclei, T=1, J=0 states, Coulomb displacement energies, Hartree-Fock wave functions, charge depend. 78−89773
A=45-153, β^{+}-decay strength function maximum 79−75914
A=4-16, monopole giant resonances, state density radii and compressibility using hyperspherical functions *(Russian)* 80−27615
A=50 to 150, shell, dynamical deformation and interacting boson models, limitations 80−68563
A=60-140, spherical nuclei, two phonon admixture effect on M1 resonance *(Russian)* 80−5105
A=60-260 nuclei, violated Wigner SU(4) symmetry reconstruction from mass data *(Russian)* 80−37336
A=60-80 even-even nuclei, collective motions and band structs. 80−9202
A=90 region, core pol. effects and giant quadrupole resonances, HF and macroscopic calcs. 80−57756
abnormal nuclear states 77−22921
actinide nuclei, modified oscillator potential, dynamical moment of inertia, single particle levels 79−67637
actinide nuclei, quadrupole and hexadecapole deforms., model independ. parameters using Fermi distrib. 78−17096
adiabatic TDHF approx., mass parameters, single collective variable, theoretical aspects 80−73765
adiabatic TDHF limit versus TDHF, in soluble model of nuclear dynamics 78−50113
alternating layer spin structure, one-dimensional, localised, in nuclear system, and π^{0} condensation 78−4902
analogue resonances, finite Fermi systems, polarisation effects *(Russian)* 78−46041
analytic observables in nuclear physics 80−105993
angular momentum projection in nuclear physics 77−50066
anisotropic oscillator model with projection, pot. energy operator matrix elements *(Russian)* 79−97672
antisymmetrized n-nucleon problems, refined resonating group calcs., reduction to cluster modes 78−17123
asymmetric matter, lowest order Brueckner theory, k-matrix calc. 77−2928
asymmetric rotator, yrast states, wobbling freq., boson representation 80−32167
ATDHF theory 78−54710
average effective-interaction calcs. in HF and harmonic oscill. basis 77−57605
backbenders, rot. energy expressions and least squares fitting 80−27531
backbending, core-particle coupling model appl. band construction 79−97645
backbending, ground state band and aligned two quasiparticle band crossing interpretation 79−22167
backbending nuclei, macroscopic foundation of model *(German)* 79−54386
band level staggering in doubly-odd nuclei, evidence for predicted phase change 80−32144
BCS equations, number conserving derivation 79−75871
Bethe-Faddeev wave function generalisation to N-body clusters 77−57639
Bethe-Goldstone eqn., methods of soln. 77−18445
Bloch density for nonlocal pots., ħ-expansion partial resummation, average binding energies 80−86797
boson and fermion systems, eigenvalue spectra widths, symmetry, Wigner coeffs. 80−18213
boson expansion technique description of collective motion 77−279
bound multineutron system, 8 and 20 neutrons, existence probability 80−68570
bound neutral polyneutron systems, existence anal. HFC 78−70475
bound state problems, scattering theory calc. 79−92979
bound state wave function determination problems using momentum space singularity struct. 79−54398
bound states of 2N, 3N and 4N systems, nuclear forces 79−71800

nuclear structure theory continued
bound three and four particle systems, two particle resonance poles and energy spectra 78-41204
bound trinucleon soln. including Δ(1236) isobar effects 79-67674
bound trinucleon systems, formalism for including the Δ(1236) resonance 79-54397
Brueckner's theory of nuclear matter, external field 78-33137
Brueckner and Jastrow methods comparison 77-290
Brueckner expansion, embedding in Green's function theory for nuclear matter binding energy 79-22220
Brueckner theory, unification with HFB theory 80-105995
Brueckner theory for finite nuclei, effective particle potentials 77-6248
Brueckner-Bethe calculations of nuclear matter 80-22718
Brueckner-Bethe-Goldstone method, appl. to ^{4}He, ^{8}Be, ^{12}C and ^{16}O 78-50076
canonical transformations and Gaussian integral kernels 77-18453
central NN potentials, relative motion dependent, jj and LS coupling, universal of hyperspherical functions method 77-61355
charge-dependent three-body force with N* (1236) in the intermediate states 79-67677
Chung-Wildenthal hamiltonians in sd shell, possible unifaction, few particle spectra 79-85406
closed shell nuclei, binding energies, Sussex interaction and delta force 79-22182
closed shell nuclei, elementary excitations unified model 77-67712
cluster variational calcs. for extended nuclear systems 77-6279
clustering aspects of nuclear structure and nuclear reactions, review 79-3100
coherent rot. states, quantum flow pattern and vortex struct. 80-22656
cold nuclear matter, stationary finite amplitude motions, quantum shock waves and solitons 80-42573
collective angular momentum in classical mechanics 80-4516
collective excitation, interplay of pairing and intrinsic modes 79-36132
collective excitations of nuclei in a relativistic mean-field theory 80-95300
collective parameter dynamics, monopole vibrs., variational principles 80-95298
collective states as symmetric couplings of proton and nuetron pairs, SU(6)×SU(2) group 77-26561
complex deformed and spherical nuclei, giant resonances within quasiparticle phonon model 79-63648
compound nucleus, giant resonances, force functions for partial E1-transitions 78-12985
compound nucleus nonstatistical struct., runs tests as indicators 80-506
compound nucleus reactions, mirror channel and isospin mixing correlations 79-9488
compound state statistical description, single particle states, radius and excitation energy *(Russian)* 79-22180
compressibility of nuclear matter, density depend. of binding energy, hyperspherical functions method *(Russian)* 78-17093
conference, 11th Masurian school in nuclear physics, Mikolajki, Poland (Aug.-Sept. 1978) 79-63605
conference on medium heavy nuclei structure, Rhodes, Greece (May 1979) 80-67935
conference on neutron capture gamma ray spectroscopy, Upton, USA. (Sep. '78) 80-36780
conference on nuclear interactions, Canberra, Australia (Aug.-Sep. 1978) 80-4476
configuration mixing, Coulomb energy anomaly, inmirror nuclei 78-25099
configuration seniority spectral distribs. for mixed configs. of identical nucleons 78-70468
constrained Hartree-Fock and quasi-spin projection 80-99141
constrained Hartree-Fock Hamiltonian, simple cure to breakdown 78-536
continuum function expansion on resonance wave functions and amplitudes, nuclear struct. calcs. 79-13215
convergent algorithm, gradient method appl. 78-12987
core polarisation, multiple scatt. eqn. for two particle one hole system and generalised vertex 77-65204
core polarisation contributions to two body effective interaction, centre of mass effects 78-66219
core polarisation effects in inelastic scatt. and charge exchange 77-22983
core-quasiparticle model, odd transitional nuclei 78-12988
correlations and dipole excitations anal. 77-38230
Coulomb displacement energies, isobaric analogue resonances, TDHF calcs. 80-42518
Coulomb displacement energy, T=1/2 mirror nuclei 77-282
Coulomb displacement energy of mirror nuclei, core polarisation effect 77-50043
Coulomb effect in rotating nuclei in the Thomas-Fermi approach 80-47355
Coulomb energies and nuclear radii in energy density formalism 77-82810
Coulomb energy differences, dispersion theory using Cottingham formula 77-2895
damped oscillator approach to nuclear structure 80-27569
decoupling model for fission fragment transitional nuclei, odd-odd and even mass 80-78174
deformation of neutron-density in inelastic scatt. 78-46000
deformations of rare earth nuclei, Skyrme-HF calcs. 78-62480
deformed even-even nuclei, application of SU(3) *(Bulgarian)* 79-9493
deformed nuclei, constrained HF energies, two-step iterative method 80-83053
deformed nuclei, coupled rot. bands, RPA type approach 78-89775
deformed nuclei, even-even, phonon space and giant resonances *(Russian)* 80-52641
deformed nuclei, existence in spherical domain 79-75829
deformed nuclei, one-particle state fragmentation, general regularities *(Russian)* 78-494
deformed nuclei, pairing self-consistent description *(Russian)* 79-67646
deformed nuclei, rot. states in Hartree-Fock-Bogoliubov approx. 77-10347
deformed nuclei, single particle level blocking in BCS approx. 80-99117
deformed nuclei, state microscopical structure in neighbourhood of yrast line 79-45137
deformed nuclei energy density mass formula, approx. method, binding energy, quadrupole moments 79-13195
deformed nuclei level densities, K-band positions 77-22855
degenerate many fermion theory, cf. with perturbation theory 77-6254
degenerate many fermion theory on expS form 77-6253
dense neutron and nuclear matter, spin and isospin stability 80-22737
density fluctuations, application to scattering 79-517
density matrix , harmonic oscill. approx. 80-13391
density matrix approx. 78-33128
density matrix for arbitrary spin, equations of motion for new SU(n) parameters 80-52592
density matrix representation for higher spin systems 79-75873
density oscillations, from semi-infinite nuclear matter calc., Regge type oscillation comparison 80-57671
density-dependent Hartree-Fock and Brueckner-Hartree-Fock theories, nuclear forces, nuclear struct. *(German)* 77-82842
deuterons, current conservation and off-shell effects with arbitrary interaction 79-45183
differential operators in terms of collective and internal nucl. variables 77-71574
dilute Fermi gas, self energy, momentum distrib., and effective mass, nuclear matter 80-63119
dipole giant resonance in fissioning nuclei, microscopic calcs., excitation energies, dipole strengths, transition densities 78-29442
dipole sum rule schematical eval., collective isovector quadrupole strength 80-47428
double crossing of ground rotational band and super band 78-45996
doubly closed shell nuclei, isovector giant monopole resonances, sum rule approach 80-78244
doubly even deformed nuclei, excited states, Pauli principle effects, quasiparticle-phonon model 80-63094
dynamical Bose-Fermi supersymmetries in complex nuclei 80-57703
dynamical symmetries in nuclei 80-9249
E0 conversion, reduced probability, quadrupole moment effects 80-18235
E1 transition selection rule, light nuclei transition strengths 80-106014
E1-giant dipole resonance, strength function pygmy anomaly, nonstatistical background coupling 80-37358
effective fields on nucleus allowing 2p2h config., Green's function method eqns. 79-6361
effective form factor pot. due to unbound core after direct process, asymptotic behaviour 80-27560
effective interaction calcs., symmetry coeff., isospin-spin depend. of single particle pot. compressibility, rearrangement energy 77-46126
effective interaction constraints imposed by antisymm. and charge independ. 78-86500
effective interaction energy dependence, collective state partitioning model 77-22911
effective interactions, appl. to structure problems 77-46120
effective interactions, HF self-consistent potl. and linked valence expansions 77-6273
effective mass and exchange current effects in finite nuclei 80-78171
effective moment of inertia, effective freq. depend. in deformed oscillator basis model 79-75811
effective NN interaction and exchange current vel. depend., dipole sum rule enhancement 80-63100
effective pots., energy depend. pole expansions in 4-body integral equations 79-45178
electronuclear sum rules, generalised, from EM structure functions 78-89806
electronuclear sum rules, linear energy weighted, nuclear struct. determ. method 79-75897
electronuclear sum rules 77-82906
EM field inside the nucleus, Salam-Strathdee phase transitions, vanishing Cabibbo angle 78-37296
EM form factors asymptotic behaviour, colour quark statistics 77-10301
EM isovector form factors of bound nucleons 80-78134
energy density formalism, charge distrib. fine structure, spherical nuclei 77-6251
energy density formalism calcs. with Fermi type distrib. of nucleons 77-46121
energy weighted electronuclear sum rules, centre-of-mass corrections 80-5091
equicontinuous Schauder decomposition of nuclear spaces 79-36175
equilibration process, master eqn. and closed form approaches 80-99166
even nuclei, 2^+ excited states quadrupole moments, energy weighted sum rule appl. 80-9229
even-even deformed nuclei, collective $K^\pi=0^+$ states, realistic boson expansion comparison 80-5043
even-even deformed nuclei, coupled rot. bands, charge and density distribs. 78-89776
even-even deformed nuclei, giant E_λ resonances of high multipolarity, force functions 79-75944
even-even N=Z nuclei, generalised BCS calcs. for 2s-1d shell 78-522
even-even nuclei, excited states, angular momentum projection method, appl. to ^{162}Er 0^- band 79-3069
even-even nuclei, heavy, deformed, B(E2; $2^+ \rightarrow 0^+$) values calc. 78-74325
even-even nuclei, static quadrupole moments of arbitrary excited states, sum rule approach 80-91135
even-even nuclei, yrast band backbending mechanism criteria 80-91128
even-even nuclei in 2p-1f shell, binding energy, quadrupole moment, by HF calc. 79-17843
even-even spherical nuclei, neutron strength function, spin depend., quasiparticle-phonon model *(Russian)* 80-42561
even-odd mass difference ratio, mass and binding energy formula 80-47361
exact fermion model with monopole and quadrupole low lying collective states 79-9495
exact removal of spurious states in RPA calculations 79-22217
exchange currents, threshold π photoprod. equivalence theorem 77-79321
exchange effects, trace of energy-momentum tensor, in weakly bound states 78-37293
exchange mag. moments, meson exchange currents, field theoretical approach 80-52574
excitation, elementary modes, conference, Varenna, Italy, July-Aug. (1976) 79-17834
excitation energies, calc. by energy density method 80-47425
exotic nuclei, stability calcs. using Hartree-Fock approx. with Skyrme interaction 78-82273
extended generator coordinate method with HFB states excitation energies, B(E2) values of ^{72,74}Ge, ^{70}Zn 77-6203
extended Thomas-Fermi approx. to kinetic energy density 77-2919

nuclear structure theory continued
Faddeev-Yakubovsky equations for two distinct pairs of identical particles 77−82832
fast neutron scatt., reaction mechanisms and nucl. struct. 77−26696
fast rotating heated nuclei, collective excitation microscopic description, statistical characts. *(Russian)* 79−97649
fast rotating nuclei, harmonic oscillator approx., moments of inertia and yrast lines 79−30765
FCC lattice model of nuclear struct. 77−14042
Fermi liquid optimal correl. function in hypernetted chain approx. 77−64996
Fermi model fluid eqn. of state via lowest order constrained method 77−18443
Fermi systems, nuclear field theory, path integral techniques 78−50096
Fermi systems, semi-infinite, surface props., thickness and energy 80−52600
Fermidynamics and time dependent Schrodinger-Hartree Fock theory 79−3105
fermion system, classification of states, spin 1/2, using chain of subgroups of unitary scheme 79−63597
fermion system, two-body operators with dynamic effective interactions, t-channel 77−41898
fermion system, two-body propagations with dynamic effective interactions 77−41896
fermion system, two-body propagators with dynamic effective interactions, s-channel 77−41897
fermion system with higher symmetries, energy spectrum 77−5698
few body dynamics, conf. 77−18368
few nucleon systems, description via analytical continuation in copuling constant 77−18420
few quasi-particle components of nuclear states in quasi-particle-phonon model 79−75843
few-body systems, bound states, bridge concept 77−22927
few-nucleon systems, analytical continuation of the core constants 79−71803
few-nucleon systems, nonrelativistic dynamical eqns. and approx. methods 77−22906
feynman graphs for Jastrow wave functions 79−22210
FHNC expression for the three-body term of the kinetic energy in the Jackson-Feenberg form 79−67682
field theory, appl. to ^{209}Bi nuclear struct. 77−67692
field theory, renormalisation of single particle states 78−24926
finite Fermi system correlation energy, fast configuration interaction approach 80−22739
finite nuclei and inhomogeneous infinite systems, ground states, FHNC method extension 80−22736
fluid-dynamical approximation for finite Fermi systems 79−89259
form factor, one particle momentum distrib. 77−6206
form factor calc. using method of hyperspherical functions 77−18381
four nucleon system, nonrelativistic soluble field theoretic formalism 77−2918
four-body correl., mode-mode coupling model, light nuclei 77−10322
four-body model of four-nucleon system, spin and isospin effects 79−71802
four-body problem, configuration space approach 78−46012
four-body system, energy dependent pole approx. 79−71801
four-nucleon integral eqn. solns. using effective UPA 79−71794
Franzini-Radicati mass relationship in isobars, Wigner SU(4) supermultiplet 80−105958
functional approach to nuclear field theory, schematic model, monopole pairing, particle-hole forces 78−50095
G-matrix equation and nuclear forces 80−9242
Gamow state vectors as functionals over subspaces of the nuclear space 80−32227
Garvey-Kelson generalised mass relations *(Rumanian)* 79−75827
generalised Fermi sea for plane wave HF theory, 3-dimens. semi-realistic interactions 80−105999
generator coordinate method in natural state formalism, appl. to harmonic oscill. 77−17831
ghost elimination by inclusion of self-energy insertions in self consistent manner 77−26595
giant dipole resonance, particle-hole calcs., M1 strength 80−22785
giant dipole resonance energy calcs., pair correlations 78−93924
giant dipole resonance of deformed even-even nuclei, ^{152}Sm to ^{238}U, semimicroscopic calcs. 77−50096
giant resonance simple microscopic model *(Russian)* 78−578
giant resonances, self-consistent microscopic anal. including particle continuum 77−2896
Green function appraoch to single particle states 77−30533
ground state deformation energy, rot. band inertial parameter depend. 80−18185
ground state properties of Lipkin Meshkov Glick model using atomic coherent states, nuclear phase transitions 78−62489
ground-state proton-neutron occupancies in the f-p shell 80−13381
groundstate bands in coherent states, vibr. and rot. limits 77−82811
group symmetries in nuclear struct., book 80−41963
group theoretical approach to dynamic aspects 77−18451
hadrons, extended, second-quantisation of strongly interacting fields 80−13270
Hamiltonians, semiclassical approx., spin-independ. pots. 80−32208
hard core exponential pots., unitary pole approx. validity at positive energies 79−3093
harmonic forces, translationally invariant wave function of many-body system 77−61018
harmonic oscillator ground state, Faddeev eqn. exact soln. 80−86821
Hartree eqn., quasiclassical soliton soln., Newtonian interaction with screening 80−68569
Hartree Fock Bologiubov theory, appl. to light/heavy nuclei, book contrib. 79−75881
Hartree Fock theory, ambiguities, auxiliary pot. 78−25137
Hartree-Fock anal. of nucl. many-body problem 77−18457
Hartree-Fock and linear response, coordinate space representation and gradient iteration 80−18216
Hartree-Fock basis, unitary group decomposition of Hamiltonian operators 79−80889
Hartree-Fock calcs., fast iterative procedure 80−47414
Hartree-Fock calcs. of semi-infinite nuclear matter with complete forces (finite range and spin-orbit term) 78−86499
Hartree-Fock-Bogolubov eqns., exact soln. 80−27582
Hartree-Fock-Bogolyubov constrained eqns., soln. determ. 77−18459

nuclear structure theory continued
heated spherical nuclei, quantal model of fluctuation E2 radiation *(Russian)* 78−78306
heavy ion deep inelastic collisions, microscopic descript., excitation of surface vibr. modes 78−46085
heavy ion deeply inelastic collisions, phenomena, transport theoretical approach 78−46086
heavy ion interactions, generator coordinate method, microscopic treatment 78−66304
heavy spherical nuclei, choice of density depend. interaction and α-decay *(Russian)* 78−46010
HF, adiabatic time-depend. description of nucl. collective motion 77−74786
HF calcs., translationally invariant self-consistent field theories 77−74788
HF calcs. with effective interaction, self-consistency *(Russian)* 77−18458
HF method, projected, appl. to rotational motion in 1p-shell odd-A nuclei 77−6207
high-spin states of transitional and spherical nuclei, decoupled and strongly coupled bands 78−12939
hole excitation spectrum in finite Fermi system, many body field theory 80−102105
hole states in nuclear matter, single-particle potential 80−32150
hole theory in nonorthogonal basis 77−57606
hydrodynamic models, current density sum rule 77−79314
hypermomentum in hadron dynamics and gravit. 78−41487
hypernuclei, symmetry classification for excited states, appl. to Be isotopes *(Chinese)* 78−25144
hypernuclei excitation of unitary analogue states 78−17131
hyperspherical expansion, complex fro form eqns. of motion 77−22909
hyperspherical functions method, contrib. of higher harmonics to mean square radii 77−6220
hyperspherical functions method, relation to shell model *(Russian)* 77−10337
hyperspherical harmonics method, eqn. soln. *(Russian)* 78−41659
hyperspherical-expansion approach to bound state 77−79317
ideal fermions in boson expansions 80−42565
impure nuclear matter with Λ, binding energy, functional variational approach 80−22744
inelastic electron scatt., nuclear charge and current spatial struct. 80−5134
inertia ellipsoid axes from hyperspheric functions method, nuclear struct. and shape *(Russian)* 79−30767
inertia parameter approximations 78−50073
infinite nuclear matter, correlated basis functions method 80−22721
infinite nuclear matter ambiguities, harmonic oscillator and infinite well solns. 80−22742
interacting boson model, sphericity 77−41902
interacting boson model for collective states in even even nuclei 80−22715
internal conversion, penetration effects and nuclear structure 79−75907
intrashell quartet states, ang. momentum projection 77−10348
intrinsic multipole moments in deformed nuclei, correls. effects 78−29385
isobar admixtures in two-nucleon continuum 77−10335
isobar configurations in few nucleon systems, review 78−37294
isobar degrees of freedom, binding energy from BHF approx. 80−22734
isobar degrees of freedom in nuclear matter, binding, NN interactions and 2π exchange 80−22735
Isolde experiments, prod. of extreme neutron/proton ratio nuclei, nuclear props. study *(Danish)* 78−4972
isoscalar effective charges with scaling and HF wavefunctions 77−26559
isoscalar giant resonances and pair correlations, variational calcs. 79−75945
Jackson-Feenberg form of the kinetic energy in the chain and FHNC approximations 79−67681
Judek effect and nuclear hidden colour excitations in heavy cosmic ray-nucleus reactions 80−27567
K-harmonic model, collective monopole excitations 77−6194
K-harmonics and shell model methods, review *(Russian)* 77−82836
K-harmonics method, appl. to 0^+ states of ^{16}O 78−54685
K-harmonics method, group of canonical transformations 78−50106
K-harmonics method, higher approx. 78−78287
K-harmonics method for nuclear many body problem with two-body interaction 78−33125
K-matrix model, self-consistent appl. to finite and superheavy nuclei 77−6257
kaonic ^{12}C, coupled channel formalism, role of Λ(1405), binding effect, Pauli blocking 78−55261
large deformations, single particle levels, self-consistent field rearrangement, HF method 80−78107
large maplitude collective motion, field theory, excitation energies 80−22665
level densities, SCF approximation 77−2909
level density just above yrast line *(Chinese)* 78−86485
level density of nuclei and the superconductive-type pair interaction *(Russian)* 80−13383
light deformed nuclei, Skyrme interaction spin components, spectra, projected HF theory 80−73820
light nuclei, hyperspherical functions for size, excited states, compressibility, binding energy 80−22679
light nuclei, inelastic form factors for abnormal parity states, K-harmonic method *(Russian)* 78−25113
light nuclei, isospin mixing, charge depend. nuclear forces and Coulomb interactions 80−5056
linearly transformed energy spectra perturbation by configuration mixing 79−59034
local harmonic approach and ATDHF theory 77−71578
M1 transitions in spherical nuclei, finite Fermi systems theory *(Russian)* 77−6296
macroscopic nuclear dynamics 78−12993
magic nuclei, microscopic model incorporating 2p2h configuration *(Russian)* 80−13392
magnetic multipole interaction between two nonoverlapping charge distributions 79−89731
many body effective interaction theory problem, comparison with atoms 80−47406
many body problem, boson-fermion descript. *(Chinese)* 78−82297
many body problem in Lee model, NN scatt. and matter binding energy 80−63116

nuclear structure theory continued
many-body charge density operators, breakdown of Siegert theorem 78−29379
many-body theory, comparison of Brueckner and λ_{00} approx. 77−2929
Marchenko eqn. extension to nonHermitian differential systems 80−83080
mass and BE via HF calcs. 77−22862
mass fitting and averaging, correction due to one particle Hamiltonian symmetry *(Russian)* 80−83032
mathematical formulation in relative co-ordinates 79−30796
matrix element calc. numerical results via new approximate meth. 77−88053
matrix elements between arbitrary single particle wavefunctions, generator coordinate method 80−57751
matrix elements by method of ang. pot. functions *(Russian)* 77−46097
matter distribution in nuclei far from β stability valley, charact. features 77−64635
mean field theory of nuclear dynamics, time depend. 78−12986
medium heavy nuclei, equations of motion appl. to pairing correlations, spurious states 80−73810
medium heavy nuclei, pairing correlations, RPA ground states 79−54401
Mehta-Dyson statistics, appl. to sequences of neutron resonances 77−30543
meson exchange contrib. to ^{3}H beta decay and mag. moments of ^{3}H and ^{3}He 77−6249
meson-nuclear physics, International Topical Conf. 77−6436
meson-nucleus physics, doorway isobar theory 77−10327
mesonic processes and quarks in nuclei 80−42564
microscopic approach to description of quadrupole excitations *(Russian)* 77−50041
microscopic basis for multicluster problem, 3α system 77−18455
microscopic binding energy calcs., modified Strutinsky correction 79−67638
microscopic calculations for ^{4}H, ^{4}Li continuum, appl. to ^{3}H(n,n), ^{3}He (p,p) 78−17114
microscopic collective rot. states in Sp(3,R) model 77−26600
microscopic derivation of quantum fluctuations in nuclear reactions, collective and intrinsic state coupling 79−45138
microscopic effective interactions in correlated model space, eqn. of motion method 80−86818
microscopic nuclear Hamiltonian matrix elements in space of collective fermion states 77−88022
microscopic theories of and nucl. motion 78−54727
microscopic versus empirical effective interactions in a single j shell 80−18210
mode coupling and Dyson's finite boson expansion 78−520
modified one body nuclear dissipation 78−50071
momentum and mass distribs., form factors, short range correlation effects 80−105959
momentum dependent δ interactions for nuclear struct. calcs., ground state props. 78−74309
momentum distrib. in nucl. calc. 77−79300
monopole vibrations and effective interactions, hyperspherical model 78−58223
Monte Carlo methods in quantum many-body problems 80−22727
Moshinsky brackets, new formula, Pauli operator, oscillator wave functions 77−34239
multi-quasi-particle excitation bands, moments of inertia and blocking effect *(Chinese)* 79−49568
multiparticle cores in nuclei, matter fluctuations, binding energy, repulsion correlations 79−75864
multipole phonon states, G_2 group shift operator properties 80−99139
multipole phonon states, R(7) group shift operators 80−99140
multipole radiation theory, in senior undergraduate physics course 78−54120
multipole-phonon state classification by shift operator techniques 80−86828
multipole-phonon states, classification, quadrupole shift operator eigenvalues 80−86829
multipole-phonon states, O_1^0 quadrupole phonon eigenstates 80−86830
multiquantum excitation calculation of density distrib. and charge form factors 77−41885
muon capture, nuclear struct. aspects naive impluse approx. adequacy 79−26402
N=5 shell, deformed odd-neutron nuclei, band ordering and spectrum 80−83018
N identical particles, Rayleigh-Ritz principle complement for energy spectrum 80−5074
N-body scatt., wave function components within linked-cluster formalism 79−45040
n-fermion problem, new boson expansion, appl. to ^{4}He 78−511
N-particle system with separated collective motion, Hamiltonian *(Russian)* 77−5701
N-quadrupole and N-octupole state construction, practical method 79−75817
narrow resonances in the continuum 79−85435
neck rupture in nuclear fission, fragment kinetic energies 78−25169
neutron, alpha and nuclear matter, ground vacuum states 80−22738
neutron and nuclear matter, variational calc. models 80−22724
neutron matter, hypernetted chain calcs. with the Paris pot. 80−57714
neutron matter, pair condensation, variational theory using correlated basis functions 80−32220
neutron resonances, reaction mechanisms and nuclear struct. 77−26564
neutron rich nuclei stability, HF calcs. *(Russian)* 80−78181
neutron s-wave strength functions, odd-even fluctuations 77−22856
neutron strength function, spin depend. *(Russian)* 78−17069
neutron strength function fluctuations 77−22858
neutron strength functions in deformed nuclei, semi-microscopic approach 77−22851
neutronrich nuclei, analogue energy splitting, isoinvariant linearisation 77−65205
non-magic nuclei laser states, self-consistent theory *(Russian)* 79−9483
nonlocal continuous potentials, theory of integral operators and eigenvalue anal. 78−8274
nuclear, matter, V^8 models, variational calcs. for binding energy and density 80−42571
nuclear and neutron matter with isobars, transition pot. model, neutron stars 80−68573
nuclear critical opalescence, pion field and condensation 80−42559
nuclear Dirac phenomenology and the Λ-nucleus potential, anomalous mag. moment 80−37344
nuclear structure theory continued
nuclear far from β-stability, delayed neutron energy spectra, structure effects 80−78226
nuclear field theory, phonon renormalisation, eigeneqns. and sum rules *(Chinese)* 80−102127
nuclear field theory, schematic model functional approach, diagram rules 80−102128
nuclear forces, charge dependence and nuclear struct. effects, nuclear charge distribs. 80−32197
nuclear forces, nonrelativistic quark model study, resonating group method 80−47403
nuclear kinetics, quasiclassical method, and angular distribution of nucleons 80−22777
nuclear many-body problem as relativistic field theory 77−10336
nuclear matter, Λ^0 binding energy, many-body cluster contribs., Jastrow calc. 79−93545
nuclear matter, ν_6 semirealistic model, variational theory accuracy and convergence 80−57712
nuclear matter, abnormal occupation, two body correlations and plane wave HF energy 80−86844
nuclear matter, Brueckner Bethe and variational calcs. review, nuclear saturation problem 80−22745
nuclear matter, charge constrained coherent pion states from transversing fast nucleon 80−27585
nuclear matter, fermion hypernetted chain variational calc. 80−22725
nuclear matter, Hugenholtz Van Hove theorem and density depend. effective interactions 80−32219
nuclear matter, iterative isobar process role, effective NN interaction 80−99143
nuclear matter, N-N separable non-local interaction, single particle potential 78−58245
nuclear matter, optimised Jastrow correlations for Fermi liquids 80−32223
nuclear matter, spin-isospin and pion condensation phase transistions, eqn. of state 80−86843
nuclear matter, test of Jastrow trial wave function 77−18465
nuclear matter, three-body problem, variational and Bethe-Faddeev methods 80−27586
nuclear matter binding energy, hypernetted chain approx., impurity ground state energy 80−83055
nuclear matter binding energy expansion convergence in Brueckner-Bethe-Goldstone theory 80−488
nuclear matter binding energy from low density expansions, Brueckner-Hartree-Fock approx. 80−22720
nuclear matter equation of state, relativistic quantum field theory of neutron stars 80−5088
nuclear matter momentum distribs., single particle orbitals, Fermi hypernetted chain theory 80−86841
nuclei far from β-stability, exotic nuclei 80−5075
nucleon, bound in harmonic oscill. pot., coupled to pion field, EM struct. 78−8732
nucleon overlaps, Sturm Liouville expansions, convergence props. 78−78281
nucleon pairing and quadrupoling effects, appl. of 5D quasi-spin group 79−9494
nucleon resonances in nuclei, review 77−26563
nucleon self-energy in finite nuclei; renormalisation, nucleon-meson interaction, ^{16}O calcs. 78−17110
nucleon-nucleon interaction as derived from the De Rujula, Georgi, Glashow phenomenological quark-quark potential 80−78172
nucleon-nucleus potential at low and intermediate energy in a Dirac-Hartree model 80−5070
number operators for composite particles in nonrelativistic many-body theory 80−94982
octupole excit. in deformed nuclei, translational invariance *(Russian)* 77−61343
odd mass nuclei, $1g_{9/2}{}^+$ shell region, low lying states, anharmonic effects 80−57687
odd mass nuclei in $1f_{7/2}$, level density and spacings from resonance data anal. 80−18206
odd proton nuclei, parity nonconserving effects, phenomenological proton-nucleus weak interaction 79−40853
odd-odd deformed nuclei, ground state static moments 78−66201
odd-odd nuclei, pn multiplets x=I(I+1) energy depend., parabolic rule, nuclear states 80−13379
odd-odd nuclei, role of tensor force as an effective interaction 80−37332
odd-odd nuclei near A=50 statistical props. of low-lying 1^+ levels 77−6243
one boson exchange potentials and low energy nuclear physics *(Russian)* 77−82834
one-body dissipation, linear response approach 77−57681
one-body dissipation and nuclear dynamics, TDHF calcs. 80−52597
one-boson-exchange model including N-Δ interaction 77−18422
one-dimensional many-boson systems, with attractive delta interactions, ground state energy 80−27071
one-dimensional TDHF eqn. numerical soln. with and without collision term 80−5083
one-hole states, in double magic nuclei, form factors, spectroscopic factors, centroid energies 78−17090
open shell nuclei by seniority and reduced isospin projections 80−47415
oscillator matrix elements from NN phase shifts with short range correl. 77−271
pair correlations, isotopically invariant, generalisation of Mottelson function 79−6366
pair field of yrast state with quadrupole pairing 77−22832
pairing and intrinsic modes, ideal boson-quasiparticle space 77−18441
pairing collective degrees of freedom, Dyson-like representation of fermion space 78−25134
pairing correlation treatment, single particle levels, binding energy, spectra, branching ratios *(Chinese)* 80−102107
pairing correlations in finite nuclei including virtual mesons 77−41899
pairing Hamiltonian, charge-independ., conservation laws 78−29402
pairing motion, large amplitude, time-dependent Hartree-Fock method 78−4908
pairing properties and superconductivity, semiclassical treatment, local density approx. of nuclear gap 80−32188
pairing rotation and intrinsic Hamiltonian, RPA theory 80−57708
pairing-force interaction many-fermion system, energy calc. 78−8339
parastitistics with continuous order, nuclear appls. 77−71572
Paris NN pot. parametrisation, phase shifts, nuclear matter binding energy 80−47405

nuclear structure theory continued
parity non-conservation review 80−32207
parity violating one-body potl. effects 77−18383
partially conserved axial-vector current and model chiral field theories in nuclear physics 79−67698
particle hole calculations, centre of mass subtracted kinetic energy, ^{4}He, ^{16}O appls. 78−62491
particle-hole states, microscopic self-consistent calc., ^{16}O levels 77−67713
particle-hole type matrix elements for density-dependent interactions 79−40856
particle-number-projected mass tensor 80−9220
particle-phonon coupling, unified theory, appl. to Sb and In isotopes 77−61360
particle-vibration coupling form factor from simple model 80−57663
particle-vibrational doorway states 78−70421
path integral approach to many-nucleon systems and time-dependent Hartree-Fock 80−78180
Pauli principle and quasirotational structure of excited nuclei spectra 77−6193
Pauli principle test, particle stability e and N indistinguishability 80−105992
perturbative approximations to Bloch-Horowitz effective Hamiltonian, energies, bounds, ^{18}O calcs. 78−70466
phase transition in rotational band of excited state *(Russian)* 77−6211
pion condensate strength, upper limit from pion absorption 77−71625
pion condensation, field theoretic many-body system 80−22703
pion condensation thresholds for nuclei with A=16 to 298 77−26606
pion dispersion relation in nuclear matter 80−42572
pion-few nucleon problems, Hamiltonian approach 77−6448
pionic degrees of freedom in atomic nuclei, possible obs. in doorway states 78−74312
pionic field, isobaric excitation effects as weak axial coupling consts. 77−10328
pole expansions for resonance functions, scatt. amplitudes and continuum states *(Russian)* 80−86871
preequilibrium processes in atomic nuclei, statistical description 78−13048
progenitor sum rules, nuclear theory appl., meson+nucleon interaction, inelastic form factors 78−54690
projection of ang. mom. eigenstates from two-centre generator coord. model functions 77−22912
projection of angular momentum 77−5689
projection of wave functions on states with definite ang. momentum 78−12590
propagation by pairing and surface excitations, nuclear states description 78−46007
proton and neutron densities, HF calc. 77−18380
proton size folding 78−29372
proton-proton potential models obtained from the Virginia phase-shift analysis 80−47401
proximity forces 77−61353
pseudo Nilsson quantum numbers, goodness in asymptotic limit 80−99138
QCD phenomenology, quarks and gluons in medium energy nuclear physics 80−42563
quadrupole oscillation wave functions, multiplicity factor *(Chinese)* 80−102103
quantum number projection, general theory, particle number and ang. momentum 80−27565
quark exchange model, for nuclear binding energies 79−93533
quark lattice and QCD in nuclei 80−5101
quasi-particle theory modification in spherical nuclei, pairing model 80−105991
quasi-spin projection in an exactly soluble model 79−71812
quasibound state wavefunctions for particles inside Coulomb barrier, computation 77−2914
quasiparticle pairing at arbitrary densities, soluble model 77−6252
quasiparticle spectra near the yrast line 80−453
quasirotational bands, non-adiabatic effects 78−54663
quasispin generalisation to monopole and quadrupole pairing, interacting boson mode, shell model hamiltonians 79−80886
radiative strength distrib. with energy, E1, M1 giant resonances, particle-hole calcs. 80−37349
radii and masses in droplet model with shell correction 77−22863
radii variation in drip line regions, energy density method 77−22876
rapidly rotating nuclei, high spin rot. including shell fluctuations, semiclassical description 80−47348
rare earth nuclei, modified oscillator pot. parameters, single particle levels 80−68509
rare-earth nuclei, inertial functions of Bohr's collective Hamiltonian 77−61359
reaction G-matrix, definitions and matrix element calcs. 77−6250
reaction matrix equation, Brueckner calcs. in harmonic oscill. basis 79−59015
realistic NN pot. construction for three body systems and nuclear matter 80−22699
reality conditions for classical motions along collective paths 78−66234
recoil distance method for excited state lifetimes, zero order description corrections *(Rumanian)* 79−36198
relativistic mean field theories, correlation effects estimate 80−5073
relativistic N-N one-boson-exchange potentials with asymptotic power-law energy dependence 78−82293
relativistic two-body forces in many-body systems, Weinberg and Yukawa interactions 80−32203
renormalised shell model matrix elements from nucleon-nucleon phase shifts 78−12991
repulsive core regularisation, two-body binding energy 77−82814
resonances as components of bound states 79−45239
resonant states in the presence of Coulomb interactions, Schrodinger eqn. 80−91161
resonating group calcs. in light nuclei 78−54704
resonating group method, recent investigation results, review 79−3098
ring diagrams in nuclear matter, many-body forces contrib., ρ and π exchange 80−22740
rotation, inertial parameters in microscopic theory 80−91132
rotation, zero point energy 78−25101
rotation for low and high spin values, appl. of Peierls Yoccoz ang. mom. projection method 77−2899
rotational levels from α-nucl. folded pot. 77−67703
rotational motion, nuclear, microscopic description via SU(3) 79−36133

nuclear structure theory continued
RPA coordinate space formalism derivation, interaction strength and transform. coeffs. for Skyrme interactions 78−70473
RPA nonlinear extension, appl. to even Ni isotopes 77−61366
s-d shell effective interactions, effective single particle field sizes 79−89247
s-d shell nuclei, HF two-determinantal deformed approx. 77−18461
S-matrix pole trajectory in three neutron model 78−82296
s-shell nuclei, binding energy scheme with soft core nucleon-nucleon potential *(Russian)* 79−3077
S-wave pion-nucleus dynamics in the $\sigma+\omega$ model 79−89245
saturation in finite nuclei, nuclear matter density and binding energy 80−83029
schematic model, propagation of elementary excitations 78−33127
Schwinger's variational principle in the nuclear two-body problem and in multichannel theory 79−75868
Schwinger boson representation for the quantized rotator 78−93602
Schwinger variational principle for bound states and scatt. problems 78−16932
sd-shell levels, fixed-JT averaging method rel. to projected HF method 77−10345
second class axial vector currents with mesonic effects, beta-decay 77−30520
second class current upper limit from β-decay data 80−47404
second class currents on nuclei, effective two-body operator approach 78−54694
self consistent pseudopots. in thermodynamic limit, state depend. one body field, HF calcs. 80−83054
self-consistent calcs. of nuclear props. with phenomenological effective forces 79−22161
self-consistent calculations of nuclear properties with phenomenological effective forces, review 79−22218
self-consistent field calcs., NN interactions, and results of appl., book contrib. 79−75880
self-consistent pseudopots. in thermodynamic limit, correlation field, nuclear matter single particle orbitals 80−9253
self-consistent quasiparticle RPA in nuclear structure theory 80−86835
self-consistent Thomas Fermi method, spherical nuclei 77−57607
self-consistent WKB calculation in a model nucleus with Skyrme interaction 79−45186
semi-classical approx. to single particle and spectral density 77−26562
semi-infinite nuclear matter calc., nuclear density oscillations 80−22681
semi-infinite nuclear medium, kinetic energy density, simple approx., giant monopole resonance 80−32222
semimicroscopic method for level density calcs. *(Russian)* 77−34202
shell and cluster concepts, role of mesons, bubble nuclei 77−22827
shell corrections for highly asymmetric systems 77−71576
short-lived isotopes, laser spectroscopy in fast atomic beams and resonance cells 80−57700
short-range forces and surface tension, surface isomers 77−57596
single determinantal states, HF and energy variance minimisation methods 77−6204
single particle nuclear density struct., Hartree-Fock and model independent anal. *(Russian)* 79−80941
single particle orbitals, Coriolis attenuation problem, pairing plus recoil model 80−32159
single particle pots., Lehmann representation discrete and continuous energy spectra *(Chinese)* 80−102104
single particle states, discrete expansions of continuum wave functions, convergence props. 80−57659
single particle states in 1f 2p shell, energy calcs. 78−25098
single-particle density, decomposition in time-even and time-odd parts 78−17074
single-particle states in nuclear matter and in finite nuclei 80−78117
Skyrme forces used in self-consistent RPA calc. 77−50072
SL(3,R) symmetry, coupling of self-conjugate systems 79−97228
Slater determinant manifold curvature 79−54396
Slater determinants coupling for construction of K-harmonics, computer oriented method 77−57612
small nuclear systems, deviation from saturation, mass formula correction 79−80891
solid like aspect with alternating layer spin and π condensation 80−22733
Sp(3,R) matrix elements, recursion formula 80−62878
Sp(6,R) symmetry, α-breakup amplitudes, of giant E2 excitations in light nuclei 78−29435
spectral distrib. method for approximated level densities, validity in boson space 79−462
spectral distribution methods in effective interaction theory 78−86489
spectroscopic information from nuclear reactions: applications 79−459
spectroscopic information from nuclear reactions: theory 79−458
spherical even-even N or Z≈40, 0^+ anomalous state struct. 77−18397
spherical even-even nuclei, anharmonicity effect in many phonon states 77−61361
spherical even-even nuclei, phonon picture, n-quasi-particle collective states 77−10307
spherical nuclei, compound state γ-transitions, reduced γ-widths, Wigner stat. matrix method *(Russian)* 80−68587
spherical nuclei, Hartree-Fock-Bogolyubov calcs., D1 effective interaction, nuclear matter, binding energies 80−63105
spherical nuclei, nuclear mass formula, energy density functional, self-consistent calc. 78−78244
spin orbit interaction of nucleons, relative motion dependent, universal coeffs. of hyperspherical function method 77−61354
spin-dependent parameters in Landau-Migdal theory 77−82844
spin-unsaturated subshells and the nucleon-nucleus optical-model spin-orbit potential 80−18259
stability limits, HF calc. with Skyrme interaction 77−18377
state densities, shell correction approach 77−6201
static Hartree Fock problem, imaginary time step method 80−86832
static HF eqns., rapidly convergent direct density method 79−97674
static nuclear Laplacian force *(Bulgarian)* 78−54688
static self-consistent HF problems, alternative methods 80−68568
statistical description of nuclear compound states, temp. Green's functions method *(Russian)* 78−17115
statistical spectroscopy for nuclei in fp shell 77−6255
stellar environment, nucl. reactions and strong interactions 80−72765
strengh distributions and statistical spectroscopy, general theory 77−79322
strength function of deeply bound hole states 78−17113
strength functions for isobaric analogue resonances 78−50143

nuclear structure theory continued
strongly bound π nuclear states, vel. depend. pot. binding, pionic atoms 80-37331
Sturmian expansion method for bound state problems 80-68561
SU(4) theory, role in nuclear struct. theory 79-3097
sudden shape transitions, pair correlation association, E2 transition rate and backbending *(Chinese)* 79-59007
sum rule, cubic inverse energy-weighted and adiabatic inertial parameters in HF calcs. 77-79316
sum rules for coeffs. of fractional parentage 77-50067
sum rules for spin-dependent excitations of nuclei 79-59018
superband and ground band ang. momentum difference *(Chinese)* 80-102102
supercritical nuclei, Z>137, WKB method appl. *(Russian)* 79-49587
superdense nuclei, search for and synthesis, review of expts. and π-condensation theory 79-6463
superdense states, parameter restrictions *(Russian)* 77-61370
superheavy elements, magic numbers, energy density method 77-14059
superheavy elements, variations in nuclear skin thickness 77-14025
superheavy nuclei HF calcs. for magic numbers Z=126 and 138 77-88062
surface thickness of nuclear densities and single particle pots., self consistent study 79-85360
symmetries and nuclei 79-80883
symmetries and statistical behavior in fermion systems in nuclei 80-9248
symmetries and statistics in many-particle systems, group theory aspects 77-18452
symmetrised basis, construction for several particles *(Russian)* 79-80882
symmetry breaking in ground state region, statistical meas. 78-8737
systematics, momentum-depend. pot., approximated by Morse function 77-6190
T matrix, $^1S_0$ two-nucleon, interior wave function 77-14038
TDHF, particles+core reduction 78-33135
TDHF and functional approaches, Lipkin model 78-93957
TDHF approximation and exact Schrodinger dynamics, Taylor series comparison 80-42568
TDHF eqns. for quantum mechanical many body systems 78-78296
TDHF equations of motion for algebraic Hamiltonians in a coherent state representation 80-57709
TDHF Hamiltonian, variational derivation 79-93536
TDHF time depend. phases, TDHF variational principle 79-93535
TDHF with two-body dissipation 80-91140
TDMF phase, unique implication of variational principle 80-27583
thermodynamic functions of nuclei *(Russian)* 78-539
Thomas-Fermi approach to rot. nuclei 77-18442
Thomas-Fermi approx., classical turning point 77-71573
Thomas-Fermi approx. extensions, finite nuclei 77-6256
Thomas-Fermi kinetic-energy density with gradient corrections 80-91169
three body calc. with separable pots. for binding energy 79-45145
three body problem with three body forces, special solns. to integral eqns. 79-75869
three parameter rotational formula, physical meaning, rot. and vibr. limits 80-18157
three particle level spectrum, Thomas theorem and Efimov effect, N/D eqns. 80-42562
three particle nuclear molecular states, Schrodinger eqn., wave functions and energy spectrum *(Russian)* 78-86497
three- and four-nucleon systems, computational methods, Faddeev eqn. 77-22907
three- and four-nucleon systems, dynamical eqns. and approx. methods 77-22905
three-body force from 2π, $\pi\rho$, and 2ρ exchanges 80-78169
three-body force from kinematical effects in the three-nucleon system 80-105986
three-body problem with Bargmann potentials 78-82274
three-body problems with local potls. in coord. space 77-26594
three-body vertices with two-body techniques 77-18435
three-nucleon bound state, perturbation approach to Faddeev eqn. 78-54691
three-nucleon bound state computed with explicit $\Delta(1236)$ components 79-67673
three-nucleon system, fractional-parentage construction of wave function 77-14041
three-nucleon system, local strong and Coulomb potls. 77-18427
three-nucleon system with separable pots., EM props. 77-18437
three-nucleon systems, harmonic oscillator basis for ground-state calcs. 79-71807
threshold states in different schematic models 78-82272
time depend. Hartree eqn. quantisation, boson expansion, particle hole excitations 79-13230
time dependent Hartree eqn. quantisation, finite and infinite boson expansions 79-13231
time-dependent Hartree-Fock dynamics and phase transition in Lipkin-Meshkov-Glick model 80-52598
time-dependent mean-field approximation for nuclear dynamical problems 80-63113
time-dependent mean-field theory and quantized bound states, Lipkin model 80-63114
time-dependent-S-matrix Hartree-Fock theory of complex reactions 80-63112
total single particle energy, asymptotic form of smooth part 78-4892
transitional nuclei, single particle and collective degrees of freedom coupling *(Russian)* 80-13345
transitional odd-mass nuclei, diagonalisation of collective quadrupole Hamiltonian 77-6221
transitional odd-odd mass nuclei, strong and decoupling struct. 77-30476
translational nuclei, ang. momentum projected quasiboson states 78-41637
translationally invariant effective interactions, factorisation 77-82833
trinucleon ground state observables, new harmonic oscill. basis calc. 77-74776
trinucleon props. with one-boson exchange potls. 77-18421
triton, momentum space calculations, Faddeev bound-state eqns., binding energy 78-25122
two-body collisions and time dependent Hartree-Fock theory 79-36208
two-nucleon system, isobar configs., relativistic model 77-41894

nuclear structure theory continued
two-particle density matrix, for U(3(n-1)) states with $E_{min}+1$ in nuclei with $n \leq 16$ 78-41624
unified theory of the nucleus, book 77-41900
uniform extended Fermi medium, correlated basis functions, graphical anal., integral eqn. methods 80-22722
unitary pole expansion for hard core potentials 77-88054
unitary pole expansion for hard core pots., negative zero eigenvalues contrib. to t-matrix 80-9243
unitary scheme model anal. with Gogny, Pires and de Tourreil interaction 79-59016
variational calculation for model nuclear matter using a new integral equation method 78-82301
variational calculation in truncated bases, unbounded operators effect 80-27568
vertex constants *(Russian)* 78-33155
vibrational transitional nuclei, quasirotational states 78-12942
wave function struct. at relativistic values of nucleon momenta *(Russian)* 78-89805
wave functions, approximate short-range correls., appl. to ^{19}F parity mixing 77-285
weak, EM and strong interactions in the nucleus 80-4978
Young's diagram for nuclear excited states 80-42566
yrast band, backbending, canonical formalism *(French)* 80-52555
yrast level spacing discontinuity, rotation alignment mechanism 78-17085
yrast levels, ang.-momentum-projection from coherent phonon state 77-82808
Yukawa pot., superposition, off-shell Jost function 78-29415
Z=114-126, nuclear stability reexamination using deformed Woods-Saxon pot. lifetimes level density 79-3094
α-nucleus separation energies, Woods-Saxon pot., A depend., closed shell effects 78-25107
Δ resonance inclusion in one-boson-exchange potential, Brueckner-Hartree-Fock calcs. for ^{16}O 77-54155
Δ-Δ system, deeply bound, one boson exchange potl. model 77-30501
Δ-propagation in nuclear matter, Pauli principle effects 80-32221
(e,e'd), cross sections, short range correls. in nuclei, two body density 78-54743
μ capture by complex nuclei, universal V-A interaction, appl. to nuclear struct. studies 77-67725
(n,γ) gamma ray spectra calc. 80-52620
(n,xγ) reactions, ENDF/B prompt γ-ray evaluations, models and data 77-26753
^{3}n system, S-matrix pole trajectories 79-67679
NN dynamics at medium energies, elastic and inelastic scatt., unitary model 80-63101
NN forward scatt., two and three pion cut contribs., nucleon exchange model 80-63103
NN interaction matrix, irreducible basis of representations of group O(n-1) 77-6271
NN parity nonconserving pot., evidence for enhanced $\Delta S=0$, $\Delta T=2$ weak interaction in nuclei 77-18419
NN T-matrix, analyticity constraints 77-18408
π prod. and absorpt. in nucl. reactions, vertex function anal. 78-12989
π- and ρ-exchange pots., influence on mag. resonances, mag. moments, and transition probabs. 80-99133
πN scattering amplitude in nuclear matter, quantum field theory approach 80-42570
πNN-NN coupled systems theory, relativistic extensions 80-63104
Σ-hypernuclear state width, model estimation 80-57719
A=12, nuclear axial dipole transition moment in the sigma model for 1^+, $T=0 \rightarrow 0^+$, T=0 transition 79-45184
Ag nuclei, highly excited, disintegration, photographic emulsion, quark model theory comparison 80-68560
$^{110}Ag^m$ orientated, β-ray asymmetry, Fermi/Gamow-Teller matrix element ratio 79-93562
^{22}Al, Coulomb matrix elements and energy shifts 77-10308
As isotopes, levels and spectra from broken pair model 80-73801
^{212}At, nuclear field theory approach to alpha-decay, calc. of relative α-decay rates 79-45218
^{212}At, relative α-decay width and excited levels, nuclear field theory 80-47437
Au isotopes, statistical anal. of level schemes 77-6230
Au, odd isotopes, $9/2^-$ level excitation energy, semi-empiricle method 77-22844
Au odd mass isotopes, statistical anal. of levels 77-22842
^{A}Au A=190, 192, 194, quasi-rotation aligned bands 79-40833
^{197}Au(^{20}Ne,^{20}Ne), 90 MeV, state lifetimes, weak coupling core excitation model, translation rates 79-63630
^{197}Au(^{35}Cl,^{35}Cl), 120 MeV, state lifetimes, weak coupling core excitation model, translation rates 79-63630
^{12}B, aligned, β-ang. distrib. asymmetry coeffs., pseudotensor interaction, T=1 isospin triplet decay 80-106021
Ba isotopes, ang. momentum projected quasiboson states 78-41637
Ba isotopes, microscopic dynamic calc. of collective states 78-17075
^{A}Ba, A=130, 132, 134, 136, levels and EM props., ang. momentum projected quasiboson model 80-5067
^{8}Be, 3^+ doublet at 19 MeV, level-parameters, isospin mixing model 78-89789
^{8}Be, matrix elements of potential energy operator on generalized hyperspherical functions *(Russian)* 79-22211
^{9}Be deformed nucleus, continuum states in strong coupling model 80-22682
$^9_\Lambda$Be, Λ separation energy, hyperspherical harmonics method 79-93547
^{208}Bi, 0^+ IAS, spreading width and isospin impurity, isovector monopole state influence 80-78155
^{209}Bi, effect of pairing modes in multiplet struct. 78-12973
^{209}Bi energy and transition probability convergence in Dyson's boson expansion 80-78206
Br nuclei, highly excited, disintegration, photographic emulsion, quark model theory comparison 80-68560
^{12}C, bound-state momentum distribs. and (p,p') PWIA anal. 78-601
^{12}C, covariant optical model anal. of π elastic scatt. at 1 GeV 77-14197
^{12}C, EM and allowed weak transitions, improved impulse approx. treatment 78-41662
^{12}C M1 (15.11 MeV) form factor, evidence for nuclear pion field critical opalescence 80-32232
^{12}C M1 form factor, pion field critical opalescence, ρ role, polarisation phenomena 80-68552

nuclear structure theory continued
^{12}C, residual interactions, current conserving RPA calculations 80−57710
^{12}C(^{12}C,^{12}C'), 10-40 MeV, resonance phenomena, band crossing model appl., molecular phenomena 79−54424
^{12}C(n,n), <17 MeV, resonating group calcs., phase shifts and differential cross sections 80−32275
^{14}C$_{g.s.}$ β-decay, mesonic exchange currents, weak process microscopic treatment 80−57742
Ca, isotopic sequence charge distrib. calc. 79−85361
^{40}Ca, charge form factors of doubly closed shell nuclei 77−6274
^{40}Ca, core polarisation charge for E6 transition, Bohr Mottelson model calc. 79−36194
^{40}Ca, coupling of 4p and 4h modes 78−93926
^{40}Ca, finite nuclear props. in relativistic quantum field theory, mass and p densities 80−9219
^{40}Ca, high-spin members of 4p-4h triaxial band 77−74742
^{40}Ca, magic nuclei at collective excitations, energy spectrum and shape *(Russian)* 80−106015
^{40}Ca, residual interactions, current conserving RPA calculations 80−57710
^{40}Ca root mean square radius series 79−36146
^{40}Ca structure, supersoft-core pot., HF approx., ground state props. 78−533
Cd even-even nuclei, low lying collective states, two-photon character 80−57667
^{112}Cd, pionic atoms, dynamical nuclear polarisation, nuclear structure effects 79−94113
^{52}Cr, 1f nucleon orbit RMS radii from transfer data 80−27544
^{53}Cr, possible deformed 7/2$^-$ states with $\Delta J=1$ band 79−45170
^{A}Cu, A=65,67,68, energy levels, core coupling model calcs. 80−9238
Dy deformed nuclei, particle ang. momentum alignment effects 80−68522
Dy, $\Delta N=2$ coupling problem 80−47412
^{149}Dy, collective and noncollective excitations, Hamiltonian calc. for level density 79−36139
^{152}Dy yrast isomers, γ-rays from compound nuclei 80−86789
^{164}Dy, low lying spectra and EM transitions, level struct. in quasirotational bands 79−36141
Er, deformed nuclei, particle ang. momentum alignment effects 80−68522
^{A}Er, A=156, 164, aligned positive parity bands from rot. aligned model 80−9209
^{A}Er, A=158,160,162, high spin states and deformation, number conservation effects 79−89225
^{156}Er, negative parity yrast states, microscopic calc. 78−495
^{158}Er, high spin state anomaly, backbending 79−22173
^{58}Er moment of inertia curve behaviour in recrossing ground state band and superband 79−59001
^{158}Er, number conservation, effect on energy spectra, deform. and B(E2) values 79−36122
^{160}Er, number conservation, effect on energy spectra, deform. and B(E2) values 79−36122
^{162}Er, ang. momentum projection for rot. nuclei, numerical aspects 79−63575
^{162}Er, negative parity excited bands, exact ang. momentum and particle number projection 79−45135
^{166}Er, low lying spectra and EM transitions, level struct. in quasirotational bands 79−36141
^{169}Er γ-vibr. band, M1 admixtures in intra-band transitions 80−99149
^{55}Fe, possible deformed 7/2$^-$ states with $\Delta J=1$ band 79−45170
^{56}Fe, semi-microscopic calc. of levels, spectroscopic factors and EM props. 77−2912
^{57}Fe, semi-microscopic calc. of levels, spectroscopic factors and EM props. 77−2912
Gd, $\Delta N=2$ coupling problem 80−47412
^{A}Gd, A=154, 156, energy levels and E2 transition rates from three-band mixing model, backbending 79−67623
^{146}Gd, excitation energy of lowest 2$^+$, 3$^-$ levels, energy density method 79−3088
^{146}Gd, spherical HFB calcs. for Z=64 shell closure 80−22716
^{147}Gd, collective and noncollective excitations, Hamiltonian calc. for level density 79−36139
^{151}Gd shape coexistence, dynamic calculation 79−45151
^{154}Gd multiphonon vibr. bands, dynamic deformation theory 80−5035
Ge, even-even nuclei, γ-spectroscopy, exptl. results and models 80−68589
^{68}Ge, ground and both neutron and proton rotational aligned bands, model calcs 79−54377
^{2}H, $^{3}S_1$-$^{3}D_1$ n-p state, mixing parameter energy depend. pot. description 77−82830
^{2}H bound state, relativistic quasipot. wave eqn. soln. 80−102132
^{2}H charge operator, retardation, quasipot. eqns. and rel. corrections 80−99122
^{2}H D-state, asymptotic normalisation 78−41653
^{2}H D-state probability, three lower bounds 80−102129
^{2}H D-state probability lower bound, binding energy, quadrupole moment 80−91137
^{2}H D-state probability measurability in meson exchange current theory, moments and RMS radius 79−89246
^{2}H, EM props. in relativistic one boson exchange model 79−67678
^{2}H, EM struct. in terms of meson currents, quarks and Heitler-London-Cutkosky picture 77−10326
^{2}H ground state, N* configurations 77−18436
^{2}H magnetic moment due to two boson exchange, pseudovector πN coupling model 79−40843
^{2}H, NN realistic nonlocal pots. from inverse scatt. theory for $^{3}S_1$-$^{3}D_1$ interaction 78−41651
^{2}H nucleus wave function momentum contribution from QCD diagrams *(Russian)* 80−68562
^{2}H, quadrupole form factor and D-state probability 77−71571
^{2}H radial functions, pionic exchange current contribs. to pp$\rightarrow$^{2}He$^+\nu_e$ 77−10329
^{2}H, repulsive nonlocal potl. models 77−88050
^{2}H, two-nucleon bound state description 77−38221
^{2}H-^{3}H binding energy correlation, ^{4}He theory and Tjon line 79−89227
^{2}H(e,e), EM form factors, relativistic formulae, moment corrections 80−63075
^{2}H(e,e), form factors, tensor pol., and two-nucleon force calcs. 80−106045
^{2}H(γ,n)p, parity violation expts. review, weak NN interaction 80−73792
nuclear structure theory continued
^{3}H asymptotic normalization parameter using partial wave dispersion relation technique 79−45185
^{3}H binding energy, 3N bound state with separable interactions, Faddeev theory corrections 80−13388
^{3}H binding energy, quantum theory evolution law approach appl. *(Russian)* 79−80866
^{3}H binding energy, relativistic calc., Bethe Salpeter eqn. 80−68519
^{3}H binding energy from 1-boson exchange, n-d and n-(pn)* momentum distribs. 79−67639
^{3}H, D-state asymptotic normalisation const., Faddeev eqn. with Reid soft core pot. 79−59017
^{3}H, energy levels using ATMS method and realistic nuclear forces 80−22707
^{3}H, ground state energy, second order Brueckner-Baranger approx. 80−63082
^{3}H ground state props. from configuration space Faddeev calcs. 80−102130
^{3}H, hyperspherical approach to simple model, basis expansion 78−54693
^{3}H, influence of structure on cross-section of complete electrosplitting *(Russian)* 79−22272
^{3}H realistic wave function, energy and density distribs. 80−86794
^{3}H Sussex interaction, g-matrix and variational calcs. 79−3091
^{3}H, three-particle bound states for partly nonlocal interactions with continuum bound states 80−32206
^{3}H, three-particle system for nonlocal interactions with continuum bound states 79−75870
^{3}H wave function anal. form from Faddeev eqn., ^{3}He form factor 80−47410
^{3}H$_\Lambda$, short range repulsion, separation energy, K-harmonics calcs. 80−86846
^{3}H(π^+,π^-), 232, 252, 295 MeV/c, forward angle scatt., nuclear struct. and π reaction models 79−76032
^{A}H, A=2,3, binding energy from Brillouin-Wigner perturbation method, strong short ranged interactions 80−86796
$^{\Lambda}$^{3}H binding energy using phenomenological ΛN pots. 80−9254
$^{\Lambda}$^{3}H, ground state energy, hyperspherical harmonics method 79−93547
He neutron rich isotopes, reaction matrix calcs., stability 78−66225
^{3}He bound state, perturbation approach with Reid soft core pot. 79−67675
^{3}He change form factor, relativistic corrections for three nucleon observables 79−85383
^{3}He charge form factor, 3N bound state with separable interactions, Faddeev theory corrections 80−13388
^{3}He charge form factors at high momentum transfer, relativistic interactions, N form factors 80−32205
^{3}He Coulomb energy from configuration space Faddeev calcs. 80−102131
^{3}He, influence of structure on cross-section of complete electrosplitting *(Russian)* 79−22272
^{3}He, totally antisymmetric wave function with generalised Faddeev eqn. 80−83046
^{3}He-^{3}H nuclei; charge asymmetric energy using different OBEP models 78−70372
^{3}He^{3}Hπ coupling constant, determ. from forward dispersion relations 78−58307
^{3}He(π^+,π^-), 232, 252, 295 MeV/c, forward angle scatt., nuclear struct. and π reaction models 79−76032
^{4}He binding energy, 4-nucleon problem, integral eqn. approach 80−91183
^{4}He binding energy, Δ(3-3) effects, reaction matrix calc., Δ degrees of freedom 80−9218
^{4}He binding energy, nonrelativistic theory of four nucleon systems *(Russian)* 79−80881
^{4}He, binding energy and form factor calcs., Reid interaction 78−54678
^{4}He, charge form factors of doubly closed shell nuclei 77−6274
^{4}He, covariant optical model anal. of π elastic scatt. at 1 GeV 77−14197
^{4}He elementary diagram calcs. with truncated sums 79−85382
^{4}He, energy levels using ATMS method and realistic nuclear forces 80−22707
^{4}He, four-nucleon bound state with realistic NN interaction, hyperspherical harmonics *(Russian)* 80−83045
^{4}He, ground state energies, four order high lying contribs. 79−75850
^{4}He, ground state energy, second order Brueckner-Baranger approx. 80−63082
^{4}He isobar configurations, impulse approx. 77−46114
^{4}He, microscopic determ. of nucleon momentum distribs. 78−70428
^{4}He mixed symmetry state admixture from ^{3}He(n,γ) *(Russian)* 80−37378
^{4}He, N*-^{3}H configurations 79−17822
^{4}He nuclear charge density determ. using form factor analyticity 80−63077
^{4}He nuclear struct. calc. using gradient method of quantum mechs. 77−82831
^{4}He, parity mixing below 30 MeV excitation energy for $\Delta T=0,1$ transitions 80−52604
^{4}He, reaction matrix calc. with three and four particle correls. 77−34218
^{4}He, struct. effects on α-decay widths 78−62513
^{4}He, struct. of 2nd 0$^-$ state 78−93947
^{4}He structure based on realistic two- and three-body interactions 77−18417
^{4}He, vertex consts. calc. by method of integral equations 77−14076
^{4}He$_\Lambda$-^{4}H$_\Lambda$ binding energy difference, exact 4-body calc. 79−63622
^{4}He-d-d vertex constant, normalisation 77−6329
^{5}He$_\Lambda$, Λ-N pot. Majorana component on B$_\Lambda$ value, overbinding 80−99144
^{6}He matrix elements of potential energy operator on generalized hyperspherical functions *(Russian)* 79−22211
^{6}He$_{\Lambda\Lambda}$, $\Lambda\Lambda\alpha$ binding Feddeev's method 77−38238
^{6}He$_{\Lambda\Lambda}$, short range repulsion, separation energy, K-harmonics calcs. 80−86846
$^{\Lambda}$^{4}He-$^{\Lambda}$^{4}H binding energy difference, bound states, exact four body calc. 80−9255
^{4}He-$^{\Lambda}$^{4}H bound states using 4-body eqns. and separable pots. 79−75893
^{A}Hf, A=166, 168, 170, 172, yrast states, quadrupole moments and B(E2) values, microscopic calcs. 80−32147
^{172}Hf, negative parity excited bands, exact ang. momentum and particle number projection 79−45135
^{180}Hf band crossing and giant backbending 80−32156

nuclear structure theory continued
^{180}Hf, nonrotational interpretation of E_4 matrix element 78−33111
^{A}Hg, A = 190-200, even, phase transition and possible triaxial shape, energy levels 80−63098
^{196}Hg, energy level spectra, random-phase method calcs. 79−9469
^{A}I, bands and decay props., core-particle coupling and polarisation effects 80−13354
In isotopes, A=110, 112, 114, np coupling const. determ. 77−34205
^{A}In, A=119, 121, unified model description, vibr. multiplet yrast struct., branching ratios 80−105953
Ir, odd isotopes, 9/2 level excitation energy, semi-empiricle method 77−22844
Ir odd mass isotopes, statistical anal. of levels 77−22842
^{191}Ir, levels excited in (p,2n) and (d,3n) 79−22164
^{A}K, A=40,42, EM transitions and transition probabilities for low lying states 79−75896
^{78}Kr band struct., lifetimes and E2 transitions n-p boson model anal. from ^{65}Cu (^{16}O, 2np) 79−80863
^{6}Li, (αnp) three-body elastic scatt. calc. using hyperspherical harmonics 79−63640
^{6}Li, α-d relative wave functions using three different models 79−75872
^{6}Li bound states, six body hyperspherical soln. to N-body Schrodinger eqn. 79−9490
^{6}Li energy levels, d-α elastic scatt., three body calcs. 77−54158
^{6}Li, even parity levels, anal. using P-model *(Russian)* 79−49585
^{6}Li ground state, cluster struct. obs. in ^{6}Li(p,pα)np 77−88129
^{6}Li ground state, separable pot. three body model 78−50090
^{6}Li ground state, translationally invariant spectral function in K harmonics 79−89257
^{6}Li, hyperspherical L_m approx., nuclear forces, binding energies 78−74311
^{6}Li structure, three-body NNα model with separable interactions *(French)* 77−71598
^{6}Li(d,X) system, resonating group method, single channel approx., cluster states 80−57782
^{7}Li, ang. momentum eigenstates projection from two-centre generator coordinate model functions 78−12994
^{7}Li charge form factor with resonating group wave function, quad. moment, charge radius 80−102110
^{7}Li, projection of ang. mom. eigenstates from two-centre generator coord. model functions 77−22912
^{7}Li→αt virtual decay vertex constant from (d,t), (p,α) 80−78231
^{8}Li scattering system, microscopic multichannel cluster model calc., resonating group calc. 78−4906
^{24}Mg coherence width, intermediate structure effects from ^{23}Na(p,α)^{20}Ne 79−45133
^{24}Mg nucleus, ^{12}C+^{12}C quasimolecular rotational band resonances *(Russian)* 79−13269
^{26}Mg (α,α), 104 MeV, oblate-prolate effects in struct. and reactions 80−9225
^{32}Mg, excitation energy of lowest 2^+, 3^- levels, energy density method 79−3088
^{12}N, aligned, β-ang. distrib. asymmetry coeffs., pseudotensor interaction, T=1 isospin triplet decay 80−106021
^{14}N$_{g.s.}$ partial muon capture, mesonic exchange currents, weak process microscopic treatment 80−57742
^{A}Nb, A=90,92,94, Gamow-Teller strength distrib., RPA calcs. 80−78218
^{91}Nb, energy spectra and EM props. using broken pair model 80−499
^{91}Nb, nuclear field theory, testing and appl. 79−13214
^{93}Nb B(Eλ) transitions, quasiparticle-phonon multiplet, nuclear field theory for superfluid nuclei 80−47427
^{143}Nd, collective and noncollective excitations, Hamiltonian calc. for level density 79−36139
^{20}Ne ground state level calc., maximum method 80−73795
^{20}Ne low lying states, configuration mixing calcs. with basis states from variational method 80−22693
^{20}Ne, rot. levels from α-^{16}O folded pot. model 77−67703
^{21}Ne configuration level density calcs. using spectral distrib. expansion, operator traces 79−71791
^{21}Ne, strength function calcs. in many fermion systems, Monte-Carlo method 80−86820
Ni doubly even nuclei, eqns. of motion method, pairing correlations, ground state energies 80−52585
^{A}Ni, A=58,60,62,64, tensor open-shell RPA calcs., M2, M8 excitations 79−22216
^{58}Ni, charge density, HF calcs. from (e,e) data 79−89260
^{58}Ni, mag. quadrupole resonance, M2 strength distrib., quasiparticle-phonon model 79−75947
^{59}Ni, semi-microscopic calc. of levels, spectroscopic factors and EM props. 77−2912
^{60}Ni, Coulomb contributions to nuclear radii and energies 80−68515
O, isotopic sequence charge distrib. calc. 79−85361
^{A}O, A=16, 17, valence-core self-consistency, wave functions, binding energy, levels, spectra 80−63123
^{14}O$_{g.s.}$ β-decay, mesonic exchange currents, weak process microscopic treatment 80−57742
^{15}O, normal parity levels from P-model calcs. with realistic NN interaction *(Russian)* 80−32194
^{16}O, 0^- levels, energy shift, two channel anal. 79−75840
^{16}O, 0^+ level pot. harmonics and matrix elements, BE contrib. *(Russian)* 77−82835
^{16}O and infinite nuclear matter, mesonic and isobar degrees of freedom 79−9491
^{16}O and Sd shell nuclei, binding energy from realistic Hamiltonians and spectral distrib. theory 80−22678
^{16}O, charge form factors, of doubly closed shell nuclei 77−6274
^{16}O, covariant optical model anal. of π elastic scatt. at 1 GeV 77−14197
^{16}O, Δ(3,3) excitations and effective 3-nucleon forces 80−27561
^{16}O energy states, HF calcs. using cartesian basis wave functions 78−74319
^{16}O ground state and binding energy, microscopic calc. with realistic NW interaction *(Russian)* 80−5052
^{16}O, ground state energies, four order high lying contribs. 79−75850
^{16}O ground state energy and low odd parity states, correlated basis function method 80−57689
^{16}O ground-state energy, nonunitary model operator approach 80−83030
^{16}O, inelastic form factors for abnormal parity states, K-harmonic method *(Russian)* 78−25113
^{16}O isospin mixing matrix elements, three level model 80−78136

nuclear structure theory continued
^{16}O, longit. isoscalar electroexcitation, sum rules and mean excitation energy 78−521
^{16}O, magic nuclei at collective excitations, energy spectrum and shape *(Russian)* 80−106015
^{16}O microscopic determ. of nucleon momentum distribs. 78−70428
^{16}O, odd parity levels, correlated basis functions method 80−22721
^{16}O, pion condensation and short range correlation 77−6245
^{16}O, π bound states in finite nuclei 78−46013
^{16}O region, effect operators, number conserving set generalisation 80−42555
^{16}O, residual interactions, current conserving RPA calculations 80−57710
^{16}O two boson approach test, interacting boson approx., 0^+ and 2^+ levels 79−9489
^{16}O(π,2N), bound 2p pion absorpt., microscopic description, NN correls. 78−94030
^{17}O, energy multiple-scatt. contrib. using energy-depend. reaction matrix 77−14013
^{17}O, M3 suppression in HF theory 78−33134
^{17}O, mag. form factor, core polarisation and exchange current effects 78−46003
^{18}O 1.98 MeV 2^+ state static quadrupole moment, from nuclear sum rules 80−13374
^{18}O, struct. of negative parity states, consistency and ghost elimination 77−26595
^{188}Os, ground and γ-band level energies, B(E2) values and EM moments, triaxial description 79−36140
^{192}Os, Wilets-Jean Hamiltonian for energy levels, transitions, moment, etc. 79−9457
Pb even isotopes, two quasiparticle 2^+ state coupling to T=0 giant quadrupole resonance 80−68618
Pb region, mag. moments and M1, M2 and M4 values, self consistent calcs. 80−47371
Pb region, particle-vibration multiplet spectra, self-consistent framework 80−102089
^{208}Pb 1^+ states, fine struct., energy levels, transition probabilities, matrix diagonalised method *(Chinese)* 78−78269
^{208}Pb breathing model transition density, single particle and collective state dynamical coupling 80−106007
^{208}Pb, charge and proton distribs., single particle model 78−50074
^{208}Pb, finite nuclear props. in relativistic quantum field theory, mass and p densities 80−9219
^{208}Pb, high-spin states, form factors for electroexcitation 77−14116
^{208}Pb, isoscalar giant multipole resonances, simple macroscopic model, damping mechanisms 80−42617
^{208}Pb, longit. isoscalar electroexcitation, sum rules and mean excitation energy 78−521
^{208}Pb, mag. quadrupole resonance, M2 strength distrib., quasiparticle-phonon model 79−75947
^{208}Pb, partly self-consistent potl., charge distrib. and Fermi surface *(Russian)* 77−272
^{208}Pb region, finite Fermi systems, review 78−537
^{208}Pb region, mag. transition strength, core polarisation effects, form factor shape 80−86850
^{208}Pb single particle and hole states, renormalisation, core polarisation, spectroscopic factors 80−57658
^{208}Pb(p,p′), 135 MeV, normal parity excitations, microscopic description, NN interaction shape 80−57691
^{211}Pb, nuclear field theory, testing and appl. 79−13214
^{14}Pd, A=101, 103, 105, decoupled rotational band struct., in spherical quasiparticle theory 78−66193
^{109}Pd low spin odd parity states, rot. aligned model, Coriolis calc. of ^{108}Pd(n, γ) 80−57695
^{109}Pd unique parity levels, interacting boson approx. model test for odd-A nuclei 79−85369
^{110}Pd, pionic atoms, dynamical nuclear polarisation, nuclear structure effects 79−94113
^{149}Pm, β-decay, nucl. matrix elements, calc., γ-transitions 80−52628
^{212}Po levels and J^π, weak coupling calc. using realistic matrix elements 80−5068
^{A}Pt, A=190, 192, 194, levels and γ-transition reduced probab., interacting boson model 80−18196
^{188}Pt, ground and γ-band level energies, B(E2) values and EM moments, triaxial description 79−36140
^{196}Pt level struct. and J^π assignments, interacting boson approx. O(6) limit from ^{195}Pt(n,γ) 79−75853
^{196}Pt rotation-vibration struct., O(6) interacting boson description alternative 79−59019
^{196}Pt struct., O(6) limit, levels fed in ^{195}Pt(n,γ) 78−33110
^{97}Rh levels and γ-transitions, 3QP model anal. of ^{97}Pd β^+-decay 80−102120
^{104}Ru, pionic atoms, dynamical nuclear polarisation, nuclear structure effects 79−94113
^{32}S shape isomeric state from unconstrained variation 80−95306
^{41}Sc-^{41}Ca Coulomb energy shift of mirror nuclei, 2p-2h core excitations influence 78−12953
^{42}Sc, weak neutral current props., search for 0^- isomer using ^{42}Ca(p,n) 79−45126
Se, even-even nuclei, γ-spectroscopy, exptl. results and models 80−68589
^{A}Se, A=74, 76, vibr. states and transition from dynamic deformation theory 80−73770
^{28}Si, appl. of theory of bi-determinantal intrinsic states 79−9484
^{28}Si, generator coord. calc. 77−50073
^{28}Si, strength function calcs. in many fermion systems, Monte-Carlo method 80−86820
^{29}Si rot.-vibr. coupling effects, excitation spectrum and ang. distribs. from ^{28}Si(d, p) 80−57661
Sm, $\Delta N=2$ coupling problem 80−47412
^{A}Sm, A=148, 150, 152, 154, levels, moments, isomer shifts, spectroscopic amplitudes, sixth order boson expansion 79−89242
^{A}Sm, A=152, 154, energy levels and E2 transition rates from three-band mixing model, backbending 79−67623
^{A}Sm(N,N′) A=152,154, deformed nuclei struct., rot. model with optical pot., coupled channel formalism 79−3146
^{A}Sm(p,t), A=148, 150, 152, 154, 40 MeV, two neutron transfer strengths, IBA model predictions 79−85474
^{145}Sm, collective and noncollective excitations, Hamiltonian calc. for level density 79−36139
^{150}Sm, pionic atoms, dynamical nuclear polarisation, nuclear structure effects 79−94113

nuclear structure theory continued
^{151}Sm low energy levels from expt. and Coriolis mixing calcs. of ^{150}Sm(n,γ) 80−57697
^{154}Sm giant multipole resonance fragmentation among two-phonon states 80−18260
Sn, A=114, 6, 8, struct. of quintet states of negative parity 77−288
Sn, deep h-le state fragmentation, strength functions, giant resonances, quasiparticle phonon model 80−37320
Sn, even isotopes A=116-124, 0^+, 2^+ 4^+ states, Tamm Dancoff approx. 78−37297
Sn isotopes, levels and spectra from broken pair model 80−73801
Sn isotopes, quantum number projection, particle number projection 80−27566
^{A}Sn, A=116, 118, 120, 122, 124, 0^+, 2^+ and 4^+ states 1 number conserving approach 80−22694
^{122}Sn+^{120}Sn, 630 MeV, multipair transfer calcs. for superfluid ions, coupled channel WKB approx. 78−37373
Sn(α,α′), even-even isotopes, nuclear struct. effects in microscopic theory 80−37391
^{86}Sr, populated in ^{89}Y(p,α), DWBA microscopic anal. 78−70449
^{A}Te, A=122,124,126 yrast band double backbending, possible mechanisms *(Chinese)* 80−99120
^{126}Te, M1, giant resonance and radiative strength functions 80−57731
^{233}Th(N,N′), deformed nuclei struct., rot. model with optical pot., coupled channel formalism 79−3146
Ti even isotopes, deformed nuclei in Lipkin-Nogami approach, Kuo Brown effective interaction 79−59006
^{A}Ti, A=44, 46, 48, 52, energy levels and EM props. using classical semimicroscopic model 79−59012
^{48}Ti, (A+2)particles-2 holes excitations, interaction renormalisation 78−29375
^{48}Ti, pionic atoms, dynamical nuclear polarisation, nuclear structure effects 79−94113
Tl, odd isotopes, $9/2^-$ level excitation energy, semi-empiricle method 77−22844
Tl odd mass isotopes, statistical anal. of levels 77−22842
^{203}Tl, ^{205}Tl, core excitations to low-lying states, e.m. props., hyperfine splittings, isomer shifts 78−89794
^{1}u2C mean life, Pauli exclusion principle validity for nucleons 80−18233
^{238}U, nuclear excitation rate in high-temp. environment 78−66244
^{238}U(N,N′), deformed nuclei struct., rot. model with optical pot., coupled channel formalism 79−3146
^{46}V, weak neutral current props., search for 0^- isomer using ^{46}Ti(p,n) 79−45126
^{51}V, 1f nucleon orbit RMS radii from transfer data 80−27544
^{51}V struct., pairing plus surface tensor interaction 77−18411
W, A=178, 180, 182, high spin states, microscopic-macroscopic model 79−438
^{A}W, A=170-182, even isotopes, yrast states, spectra and quad. moments, variation formulation 80−99119
Xe isotopes, microscopic dynamic calc. of collective states 78−17075
^{133}Xe, semi-microscopic anal. by generalised vibrational intensity and selection rules and diagonalisation 77−2901
^{89}Y, energy spectra and EM props. using broken pair model 80−499
^{166}Yb, high spin state anomaly, backbending 79−22173
^{168}Yb low lying collective excitation energies calcs. at high angular momenta 79−13190
^{168}Yb, low lying spectra and EM transitions, level struct. in quasirotational bands 79−36141
Zn, even isotopes, effect of particle-vibr. coupling in nucl. struct. 78−12940
^{61}Zn states, pseudo LS coupling model 80−68548
^{62}Zn, band mixing HF model, struct. and electromag. transitions 78−54676
^{69}Zn, energy levels, core coupling model calcs. 80−9238
Zr even isotopes, quadrupole moments and E2 transition rates, broken pair approx. 80−52579
^{A}Zr, A=93, 95, $1h_{11/2}$ neutron single particle strength, quasiparticle-phonon coupling 79−89226
^{90}Zr, anal. of spectrum of transitions to low-lying 2^+ states 78−17138
^{90}Zr, mag. quadrupole resonance, M2 strength distrib., quasiparticle-phonon model 79−75947

nuclear track emulsions
400 GeV/c proton interactions, charged particle multiplicity 78−21558
α-irradiated emulsion layers, processing by iron oxalate developer *(Russian)* 78−50443
alpha naphtol, developer, use in nuclear photography 78−17490
anomalous tracks observed in uranium loaded nuclear emulsions 80−99410
automatic nuclear emulsion scanner with moving microscope 79−13595
automatic rotary diaphragm for microphotometer 80−22415
autoradiography, coating of slides with nuclear emulsions, new semiautomatic device 77−70574
autoradiography, double radionuclide methods for tissue sections or cell smears, using light microscopy 77−5113
autoradiography, increasing detect. power of type M nucl. emulsion gel 78−20269
C-jets, computer simulation using conventional particle physics 79−58990
cellulose acetate, mailed detector method for ^{226}Ra source leakage testing 77−60264
cellulose nitrate, detect. of ion beam in HV electron microscope 78−45755
cellulose nitrate, detection efficiency and alpha-particle range 77−10540
cellulose nitrate, optical contrast of alpha-particle tracks 77−6633
cellulose nitrate, solid state track detector for neutron irradiated B quantitative anal. 78−56937
cellulose nitrate emulsion, sensitivity and efficiency for α-particle detection 78−13380
cellulose nitrate emulsion for α-particle track relocalisation 78−17480
cellulose nitrate film, pinhole imaging of laser-prod. thermonucl. alpha particles 77−67934
cellulose nitrate film with thin layer of $Li_2B_4O_7$, response to neutrons 78−62677
cellulose nitrate track detector, effect of γ-radiation on bulk etching rate 80−885
cellulose nitrate track detectors, CA80-15 and LR-115, etch pits due to Rn and Tn alpha particles 78−855
characteristic curves of photographic material used in emulsion chambers 79−49905

nuclear track emulsions continued
charged particle detection by photographic recording systems, appls. 78−17527
cosmic particle dosimetry for Apollo and Apollo-Soyuz Biostack expts. 78−20288
cosmic ray, magnetic monopole candidate, reassessment of 1975 Lexan and emulsion meas. 79−3333
cosmic ray high energy interactions in emulsion stack combined with ionisation calorimeter 78−49263
cosmic ray muons, energy spectrum at sea level, 1-10 TeV, with emulsion chamber 79−25424
cosmic ray nuclei masses determ. from C, N, O energy loss parameters 78−94175
CR-39 plastic, electrochem. etching, optimum conditions 80−95505
detection and measurement of very short flight paths in nuclear emulsions 80−102389
development probability, AgBr grain diameter depend. 80−9056
diffusion of $^{241}Am^{3+}$ ions in ion-exchange membrane, autoradiographic method 78−35721
dosimeter, latent image fading, effect of dry N_2 desiccation 78−15903
dosimetry film exposure determ., comparison of X-ray fluoresc. and optical density 78−24137
electrochemical etching of fast neutron induced recoil tracks in cellulose triacetate 80−91406
electron-photon cascade energy determ., effects of optical density and energy spectrum meas. errors 79−84613
emulsion stack connected with ionis. calorimeter for high energy cosmic ray obs. 78−25386
film badge, underestimation of exposure from Am-Be neutron probe 78−15900
film dosimeter, K emulsion, characts. 78−20290
fragmentation parameters meas. in nuclear emulsions, validity 78−90017
gelatin in nuclear photoemulsion, effect of pulsed elec. field on physical and mech. props. *(Russian)* 78−869
hadron production in deep inelastic scattering of 150 GeV muons in nuclear emulsions 79−17893
heavy charged particle specific energy losses meas. using densitometric method *(Russian)* 80−63482
heavy ion physics, expt. methods for radiation detection and meas., review *(Russian)* 79−49900
heavy ion track width, Katz's theory 80−32578
heavy ion tracks, separation from background by pulsed electric field 78−17491
heavy particle track grain counting for nucl. charge determ. 78−17528
high energy physics, appl. of solid state nuclear track detector, emulsion technique 78−17501
hypernuclei studies, information on ΛN and ΛΛ interactions 77−22923
Ilford G-5, Ne, N tracks, width meas. 78−17488
intaglio imaging with nuclear particles 78−65993
ionographic detectors, identification of nuclear reactions, computation 77−3243
Kodak Type II film badges, gamma dose meas. in presence of thermal neutrons 79−39517
laser plasma, 5-20 keV X-ray emission spectrum investigation using nucl. emulsions 80−92392
latent image regression under action of pulsed electric field *(Russian)* 77−49802
lithium and ^{6}Li analysis with the nuclear track technique 80−95504
loading with thin wires 77−34520
long lived tracks, interpretation as new hadrons or background 77−23391
mica solid state particle track detectors, fission fragment ranges rel. to cryst. orientation 80−91408
microphotometer, MF-2 type, scatt. light effects on optical densities of electron-photon cascade tracks 77−61655
microscope nonachromatic objective design, for track obs. 77−400
microscope television for track detection 79−3290
multiple Coulomb scatt. of heavy ions, scatt. const. meas. 77−6636
muon deep inelastic scatt. event location 80−27906
neutrino detection, long exposures to high energy neutrinos in severe muon background 79−54744
neutrino interaction detection and analysis in photoemulsion *(Russian)* 78−41900
neutron monitor for personnel in criticality accidents, use of NTA film 77−29208
neutron personnel dosimetry using cellulose nitrate film and LiF as radiator and TLD 77−64132
neutron personnel monitoring film, Kodak NTA, energy depend. 79−100753
nitrocellulose, radiography of geological specimens for determ. of α- and fission-activity 78−20540
nuclear photoemulsion obs. at E_π=115 MeV, ang. distribs. and cross sections *(Russian)* 79−13352
nuclear physics appl., focal plane detectors 79−72191
nuclei stopping in nuclear emulsion, charge determ. 79−85363
p+emulsion, 200 GeV, star event containing single electron, charmed particle generation, anal. 77−61414
particle track detectors, trends and developments *(Hungarian)* 80−18755
personal dosimetry service testing and evaluation in 1976 in Michigan 78−53498
phosphates, uranium content, fluorimetry, comparison of results 78−20414
photodensitometry of tracks of highly ionizing particles in the cosmic rays 79−22551
photoemulsion, kaon capture, doubly charged particle yield 79−40959
photographic film dosimetry by low energy photon transmission 79−45433
photometric meas. of thin CNO particle tracks 79−76281
pion$^-$, sensitivity of personnel monitoring film 78−28079
plastic sandwich stack event, cosmic ray nucleus interpretation 78−69635
primary cosmic ray interactions with photoemulsion nuclei using satellite Intercosmos-6 *(Russian)* 78−93063
proton 400 GeV interactions 79−3145
proton interactions at 28 GeV *(Korean)* 80−18299
proton-emulsion nuclei interactions, 70 GeV/c, rapidity intervals 78−54750
pulsed electric field effect on cosmic ray detection 79−26829
recording possibilities in electron microscopic autoradiography conditions 78−17489

nuclear track emulsions continued
review of appl. in other scientific fields 79−97934
secondary ionisation, delta-ray effects 80−881
sensitivity centre variation with AgBr grain diameter 80−9055
short lifetime charm particles from ν interactions detection in nuclear emulsion 79−22539
short lived particle decay detection 79−97947
small emulsion chambers, design, scanning and energy meas. 79−59299
small emulsion chambers, materials, construction, anal. techniques, cosmic ray expt. 79−59300
small-grain development of emulsion monofilms for electron-microscope autoradiography *(Russian)* 80−297
solid state nuclear detectors for neutron yield estimation 77−10544
solid state nuclear track detectors, conf., Neuherberg/Munich, (Oct. 1976) 78−17513
solid state track detectors, critical angles for fission fragment registration 80−91407
superheavy elements, synthesis and identification 78−46239
superheavy primary cosmic ray nuclei, obs. with solid-state track detectors and X-ray films *(Japanese)* 78−61688
supralinear photographic emulsions, radiobiological aspects 80−26290
supralinearity, mimicking response of biological systems 78−20233
supralinearity and particle discrimination 77−38562
tissuelike medium α trajectory heavy secondary ion ejection 80−9466
tissuelike medium α trajectory production of δ-rays 80−9465
track struct. and particle identification 80−91383
track structure theory in radiobiology and radiation detection 78−50446
track width, filar micrometer meas. for low-energy heavy ions 80−91403
ultra heavy cosmic ray nuclei meas. 78−20596
ultraheavy cosmic ray charge determ. in emulsion, Mott cross section effects 79−18084
wire loaded, corrections for target absorpt. of charged particles 78−70695
X-ray energy distribution, plasma focussed, nuclear emulsion study 78−83620
X-ray topography, improvement of nuclear emulsion development methods 79−50940
e^+e^- early cascade development 79−89158
γ-rays, ultrahigh energy, emulsion chamber investigation *(Chinese)* 77−10525
K^- capture by emulsion nuclei, double charged particle yield *(Russian)* 78−78420
K^- reactions, 1.8 GeV/c, ^{8}Li emission 77−30637
K^- tracks, 1.5 GeV/C, fast stable particles from light emulsion nuclei, emission probabilities 78−17245
K^-+emulsion, 1.8 GeV/c, ^{8}He obs. in hammer tracks 79−6711
K^-+light emulsion nuclei, 1.5 GeV/c, K^-p and K^-n channels, probability distrib. 78−13161
K^-+photonuclear emulsion nuclei, hypernuclei in hammer-like events 78−13162
p-emulsion nucleus, expts. on particle prod., 200 to 400 GeV 77−30433
p+complex nuclei, 10 GeV, inelastic emulsion scatt., optical model anal. *(Korean)* 78−50165
p+emulsion, 400 GeV, shower particle ang. distribs. from inelastic collisions, Glauber-Gribov model *(Russian)* 78−89881
p+emulsion, 67-400 GeV, leading baryon pseudorapidity distribution, leading particle props. 79−6611
p+emulsion 400 GeV, inelastic scatt., secondary charged particle multiplicities *(Russian)* 78−89880
p+emulsion nucleus, 400 GeV, two particle correlations between produced particles *(Russian)* 79−3157
p+emulsion nucleus, 60 and 200 GeV, shower particle multiplicity distrib. parametrisations 78−62524
p+nuclear emulsion, 400 GeV nonwhite stars 78−13097
pN interaction in nuclear emulsion with single electron emission, possible charm particle prod. *(Russian)* 77−252
pp and pn inelastic interactions, 69 GeV/c 78−66161
pp→DD cross sections, Monte Carlo anal., particle lifetime for detection in emulsion 78−82229
π^- interactions, 65 GeV/C, γ quanta production 78−13160
π^--emulsion interaction, 50 GeV/c , charge particle multiplicity 78−46109
π+emulsion nucleus, 60 to 200 GeV, shower particle multiplicity distrib. parametrisations 78−62524
π^-N interactions, 50 GeV/c, inclusive charged π prod. in nuclear emulsion anal. 78−66168
Ag halide grains, photographic sensitivity and response to charged particles, interstitial generation 77−10124
Ag halide monocrystal detectors, reference listing 79−72196
Ag nuclei, highly excited, disintegration, photographic emulsion, quark model theory comparison 80−68560
AgBr detectors, preparation, sensitivity, discrimination ability 78−94169
AgBr, nucl. emulsion, latent image form., grain diameter depend. 80−9453
AgBr(^{40}Ar,X), 1.8 GeV, central collisions, Maxwell-Boltzmann distrib. anal. 78−66315
AgBr(^{4}He,X), 2.1 GeV, central collisions, Maxwell-Boltzmann distrib. anal. 78−66315
AgBr(^{16}O,X), 2.1 GeV, central collisions, Maxwell-Boltzmann distrib. anal. 78−66315
Ag(K^-,K^0), cascade hypernucleus identification in nuclear emulsion 80−52603
Ar track width determ. by photometric meas. 78−94167
Br nuclei, highly excited, disintegration, photographic emulsion, quark model theory comparison 80−68560
Br(K^-,K^0), cascade, hypernucleus identification in nuclear emulsion 80−52603
^{12}C+photoemulsion nucleus, 50 GeV/c, low energy particles in stars produced *(Russian)* 78−89907
$_\Lambda{}^{12}$C hypernucleus detection in p+emulsion nucleus, 250 GeV, Λ binding energy *(Russian)* 78−89816
He nuclei emission in 7.5 to 200 GeV hadron interactions *(Russian)* 80−9325
^{6}Li$\mu^-\rightarrow{}^3$H^{3}Hν in ^{6}Li loaded photoemulsion, secondary particles ang. distrib. and energy *(Russian)* 78−89855
^{14}N+emulsion nuclei, 2.1 GeV/nucleon interactions 77−41991
Ne, track width determ. by photometric meas. 78−94167
^{16}O induced reactions in nuclear emulsions at 2.1 GeV/nucleon, multiplicity distrib. of white and grey tracks *(Spanish)* 80−47495
^{16}O+emulsion nuclei, 150-200 MeV/nucleon interactions 77−41992

nuclear track emulsions continued
^{222}Rn gas detection using Track Etch system for U exploration 80−98488
Si(Li)-emulsion shower counter for cosmic ray electron obs. 80−58033
U glass, fission track dating, error analysis 80−95503

nucleation
see also crystal growth; crystallisation
$A+A_n\rightleftarrows A_{n+1}$*, cluster dynamics, classical trajectory study 80−3316
acetic acid vapour, homogeneous nucleation, assoc. clusters, crit. supersaturation temp. depend. 77−31762
acetylene pyrolysis, nucleation of C black particles *(French)* 79−52648
aerosol, binary homogeneous nucleation theory, limiting behaviour 78−92517
aerosol, heteromolecular nucleation and condensation, multi-dimens. theory 78−92518
aerosol, polydisperse, growth in adiabatic condensation nuclei counter, finite expansion time 79−79306
aerosol formation, growth, general dynamic eqn., H_2SO_4/H_2O aerosol simulation appl. 79−47990
aerosol formation measurements from gas in coal fired power station plumes 80−81502
aerosol formation of volatile binary solutions, ion-induced nucleation 79−47992
aerosol growth kinetics during SO_2 oxidation in atmosphere 78−96255
aerosol large particles ingestion by cloud, ice nucleation by freezing 77−37308
aerosol particle size distrib., dynamic behaviour, coagulation, condensation, nucleation and removal 78−35726
aerosols, condensation nucleus counters, comparisons, comments 77−56758
aerosols, effect on rate of new particle form. in polluted atm. 79−24926
aligned composites, in-situ growth by disproportionation of amorphous metal systems 78−72755
alkali halide, molecular processes of condensation and evaporation 79−69237
alkali halide aq. solns., homogeneous nucleation glass form., press. depend. 78−51649
alkali-halide crystals, two-dimens. nucleation and hole nucleation, mol. beam method *(German)* 80−93499
alloy, binary, quenching, cluster growth, first order phase transition, computer simulation anal. 79−34039
alloy, heterogeneous nucleation during solidification 79−28077
alloy, rapidly solidified powder, nucleation, undercooling and homogeneous struct. 79−11598
alloy decomposition kinetics, Johnson-Mehl-Avrami (JMA) formula appl. 80−16263
alloys, dislocation pile-up model, fatigue crack nucleation at intermetallic particles 79−69189
alloys, heterogeneous nucleation activity, and melting point ratio correlation 78−92255
alloys, spinodal decomposition, review 80−96657
ammonium sulphate vapour pressures, nucleation of new particles in atmosphere 79−81708
amorphous semiconductor film, laser induced nucleation, long wavelength instability 80−84126
anisotropic nuclei, kinetics of formation *(Russian)* 80−29149
anodic film form., electrode pot. variation rel. to nucleation, growth 78−68634
anthraquinone, UV light effect on nucleation during crystallisation on anthracene surface 80−75478
anthrone, UV light effect on nucleation during crystallisation on anthracene surface 80−75478
apatite crystal growth in skeletal tissues 80−94181
atmospheric gases condensation on cold metal surfaces, nucleation barrier 78−22838
atomic cluster, free energy, chem. pot. and surface energy, microscopic capillarity approx. 80−5654
attachment energy as habit controlling factor, growth models 80−59420
austenitic stainless steel, 18 Cr-11 Ni, directly aged, nucleation of $M_{23}C_6$ carbides *(Polish)* 78−52806
azo pigments, dispersions in flow system, nucleation and growth kinetics meas. 77−63967
beam-addressable optical display using supersaturated vapour photonucleation 80−4691
benzene, nucleate boiling heat transfer, press. factor 77−69080
benzoic acid, ENSH method of oriented thin film growth 79−99443
binary alloy, kinetics of nuclei coalescence by reactive diffusion *(Russian)* 79−42398
binary alloy, model quenched computer simulation of time evolution in nucleation region 79−82344
binary alloys, kinetic nucleation model 77−85118
binary liquid mixtures, spinodal decomposition, review 80−96657
binary mixture, nucleate boiling, bubble growth, saturation press.-temp. relation 77−46892
binary mixture supersaturated vapour condensation, homogeneous nucleation 78−2247
binary mixtures, liq. and solid, spinodal decomposition theory 78−71863
binary mixtures, near critical, metastable, phase separation and nucleation and drop growth, rate eqns. 80−65232
biotite, deform. and recrystallisation in Woodroffe Thrust mylonite zone 80−21739
black chrome, electroplated layer, field ion microscopy study 79−28246
boiling, conservative nature of heat transfer laws 77−24395
boiling, delayed, in nonstationary heat exchange with phase transformations *(Russian)* 78−83235
boiling, heat transfer enhancement 78−9530
boiling, heat transfer model 78−75056
boiling, nucleate, superheating, heterogeneous nucleation theory calc. 79−46170
boiling, nucleate pool, influence of surface conditions, bubble flux density 79−55379
boiling, nucleate type, boiling acoustic emission and bubble dynamics 77−46893
boiling, nucleation centres interaction, obs. technique 78−14065
boiling, of liq. film, bubble nucleation and venting 78−30153
boiling, possible mean no. of nucleation sites 77−62628
boiling, subcooled, latent heat transport contrib. 78−75046
boiling, subcooled, nucleate, mechanistic model 78−90697
boiling, transition type, in forced convective flow, boundaries meas. 79−27499

nucleation continued
boiling and bubbling heat transfer under the conditions of free and forced convection 78−90637
boiling at surface near peak heat flux, mechanism 77−75780
boiling delay, unsteady heat transfer with phase transition 80−48690
boiling heat transfer, nucleation factor 77−69079
boiling heat transfer, surface roughness effect 78−9534
boiling under reduced gravity conditions 77−4192
bone, hydroxyapatite nucleation energetics 78−40127
book, current topics in material science 80−46747
α-brass, 70:30, cold-worked, recrystallised grains nucleation on heating 80−29998
brass, 70:30, rolled, nucleation and annealing texture development 80−45320
brass, nonradial diffuse streaks and complex diffuse scatt. patterns of electrons 79−7527
bronzes, Na-W, cubic crysts., orientation relation of nucleation and growth 79−55687
bubbel nucleation in oscill. press. field 79−32216
bubble, theoretical experimental review 79−41734
bubble growth in combined gravitational and non-uniform temp. fields 78−22249
bubble growth in slow formation regime of nucleate pool boiling 78−90687
bubble homogeneous nucleation in gas-liq. soln., press., expt. and theory 78−91430
bubbles, active nucleation site spatial distrib., bubble flow density 78−71267
bulk melting, liq. phase nuclei form. 80−88304
butane drops, nucleation in flowing water 79−1099
di-butylphthalate, critical nuclei, meas. of number of mols. and surface tension from rate of nucleation 79−65293
calcium phosphates, seeded growth, effect of solid/soln. ratio, calcification 78−15303
cavity nucleation, by plastic deform. 79−29127
cavity nucleation at second phase particles in grain boundaries 78−59819
cell wall and lattice misorientation origin during deform. 80−71712
chemical system, multiple steady state, phase transform. stochastic theory, nucleation 78−53187
chemical systems, non-equilib., mol. dynamics studies of long range and short range fluctuations 80−21318
cholesteric nonanoate, isothermic crystallisation, microscopic exam. *(Polish)* 80−10651
cholesteryl caprinate spherulite growth rate and nucleation rate, optical method *(Polish)* 80−10652
classical nucleation theory, test on cryst. nucleation in Li_2O-SiO_2 glass 80−1939
classical nucleus in liq.-liq. miscibility gap, undercooling in binary system 77−28002
cloud, ice nucleation by aerosol particles 80−61864
cloud, warm cumulus, three-dimens. numerical model with microphysical processes *(Russian)* 78−88884
cloud chamber, coronal discharge effect on cloud droplet growth 77−34514
cloud chamber, low-pressure tissue-equivalent gas for α-particle tracking 80−9462
cloud chamber, thermal diffusion, continuous flow parallel plate type, analysis w.r.t. atm. water droplet growth 80−36416
cloud chamber, thermal diffusion, unsteady state, supersaturation profile 80−63449
cloud condensation nuclei counters using diffusion chambers 77−41224
cloud condensation nuclei from paper mill effluents, induced fog *(French)* 78−96270
cloud droplet growth studies, optical motion control appl. to Atmospheric Cloud Physics Laboratory 80−12634
cloud droplet nucleation, expts. with monodisperse NaCl aerosols 80−82003
cloud nucleus counter, dual-range performance 79−53543
cloud seeding, effectiveness of dry ice nucleation 79−84395
cloud seeding, Florida Area Cumulus Experiment, rainfall results, 1970-75 77−45113
cloud seeding criteria, winter orographic clouds 79−84391
cloud seeding experiment, comparison of night-time and day-time seeding 79−88441
clouds, coagulation processes, Monte Carlo simulation *(Russian)* 79−84377
clouds, ice nucleus counters 77−41225
clouds, ice-bearing cumulus evolution, numerical simulation and obs. 77−2216
clouds, minimum particle size for nucleation 78−44939
clusters in imperfect vapour, nucleation theory 77−35289
coherent phase form. at stress concentrators, effect of dislocation splitting, dislocation pile-ups, and phase elastic moduli *(Russian)* 80−49356
collective heterogeneous boiling nuclei formation, statistical dynamic model using wettability 77−89531
colloidal plasmas in space: some aspects of condensation and growth of solids 79−41795
computer simulation, of 2D nucleation models of cryst. growth 79−73116
condensation, homogeneous, cluster size distrib., stochastic model 80−22311
condensation, kinetic theory, stochastic approach *(Russian)* 77−72676
condensation from small nuclei, modified Mayer theory 80−79924
condensed system, kinetic approach to nucleation 78−51647
conference, phase transformations in metallurgy, York, England (Apr. 1979) 80−2994
continuous multi-particle crystal growth in vertical cone 77−69978
convective clouds, dry ice appls. for on-top seeding 78−73531
cordierite glass ceramics, effect of TiO_2 and ZrO_2 content on phase sequence during heat treatment 78−48381
cosmic dust, grains sudden nucleation and growth in supernova and nova ejecta 80−26941
creep damage and the remaining life concept 80−59574
criterion for dynamic recrystallisation during hot working 78−52852
critical nucleus size and work of formation calc., for nucleus at cryst. surface *(Russian)* 77−31911
critical temperature region, excluded volume interference effects 79−80553
cryogenic fluid boiling in capillary tubes, heat transfer 79−59915
cryogenic liquid, boiling, heat transfer coeffs. 78−9539

nucleation continued
crystal frequency distribution, simulation taking nuclei distrib. into account 80−100184
crystal nucleation and growth at surfaces, kinetic studies, review 78−72046
crystal nucleation and solidification, Landau theory 78−83761
crystal nucleation and symmetry, interaction pots. effect 80−34169
crystal surface nucleation growth processes, Monte Carlo simulation 77−58965
crystalline solid, secondary phase inception, Volmer-Weber-Becker-Doring theory *(Hungarian)* 79−10954
crystallisation from melt, nucleation on supercooling, inter-nuclear separation distrib. function *(German)* 77−19885
crystallisation kinetics, review, book contrib. 77−39550
crystallization centres, low frequency vibration effects on rate *(Russian)* 78−15383
cubic Kossel crystal, simple, two-dimensional nucleation rate calc. *(Italian)* 78−22675
decanoic acid, associated vapours, homogeneous nucleation 80−96638
defect clusters, nucleation and growth due to energetic particle radiation, chemical rate reaction theory, computer program 80−49263
dense fluid systems, spatial correls. effect on steady state nucleation kinetics 78−11500
diamond, nucleation and growth, 55 kbar and 1450K 79−99087
diamond, synthesis from graphite, nucleation rate 79−16032
p-dichlorobenzene, contact nucleation 77−52661
dielectric crystallisation kinetics, electric field effect, nucleation 80−19919
diethyl ether, tensile strength, expt. compared with homogeneous nucleation 77−62574
diethylene, critical nuclei, meas. of number of mols. and surface tension from rate of nucleation 79−65293
diffusion kinetics, crystallisation of salts from supersaturated solns. 79−23553
diffusion-controlled, time lag 78−47497
diffusional crystal growth mechanisms 80−3059
diphenyl methane, critical nuclei, meas. of number of mols. and surface tension from rate of nucleation 79−65293
droplet formation in supersaturated systems, reaction kinetics 77−66748
droplet growth and initial dew point temp. accuracy in cloud chamber on space shuttle 78−96268
droplet growth in nonuniform vapour 77−47563
droplets nucleation in finite systems, theory and computer simulation 80−26038
dropwise condensation and nucleation heat transfer rate, mechanism 77−4193
ductile fracture topography, geometrical contribs. and H_2 effects 79−83310
ductile intergranular fracture, discussion on mechanism 79−73250
durene, ENSH method of oriented thin film growth 79−99443
electrically charged droplets and clusters, theory 79−47985
electrochemical displacement reactions, electron microscope obs. of nucleation and growth, comparison of Cu/Fe and Cu/Al cementation systems 79−47939
electrochemical phase formation 80−55309
electrocrystallisation, nucleation, phase form., symposium, Southampton, England (Dec. 1977) 80−51942
electrocrystallisation, nucleation and growth mechanism, ohmic overpotential effects, simulation 78−51842
electrocrystallisation, nucleation and growth mechanism, ohmic overpotential effects determ. 78−51843
electrolyte, binary, cryst. growth kinetics during precipitation 80−49149
electrolytic nucleation at high supersaturation 78−61025
electron microdiffraction patterns of nucleation models, computer simulation *(French)* 77−62449
electron-hole drops formation, nucleation theories 79−33239
electron-hole plasma nucleation, time evolution 80−49616
epitaxial growth mode, numerical confirmation of Palmberg's criterion 77−11812
ethanol, nucleate boiling heat transfer, press. factor 77−69080
ethanol-water mixture, saturated, min. film boiling temp. on horiz. stainless steel and Cu surfaces 78−90692
ethyl ether, nucleation press. for bubble form., dissolved N_2 effect 77−51486
ethyl ether-N_2, bubble homogeneous nucleation in gas-liq. soln., press., expt. and theory 78−91430
ethylene glycol, critical nuclei, meas. of number of mols. and surface tension from rate of nucleation 79−65293
falling film rewetting 78−75906
fatigue crack nucleation at particles in Al alloys, computer simulation 80−100893
fatigue high temp., hold time effects, cavitation nucleation, creep interaction 78−60734
FCC crystal formation, soft-core model, geometrical anal. of crystallisation 78−42939
ferroelectrics, domain structure as outcome state for poling procedure 80−80728
film, growth mode and growth kinetics of dislocation free interfaces 77−85103
film, microporosity induced by nucleation and growth processes, TEM expt. 78−10303
film, polycryst., nodule mechanism of diffusion-induced disintegration *(Russian)* 78−51829
film, thermodynamic theory of clustering and percolation transitions 77−47697
film, ultrathin, effort of optical radiation on growth and struct. 78−72045
film defect growth and nucleation, electron microscopy and diffraction exam. *(French)* 80−59824
film deposition, adatom diffusion and capture by clusters, random-walk problem 78−2385
film growth, island growth and coalesc. stage, computer model 79−11034
film nucleation and initial stages of growth 78−75961
fine particles aggregation, mechanism and rate at uniform shear field 80−101046
first-order phase transitions, clusters, metastablility, nucleation 78−54326
Fisher's droplet model, pure filled vap.-liq. nucleation theory 77−62626
flow boiling bubble population prediction, from gas bubble nucleation expts. 78−90696

nucleation continued
fluor-richterite crystal, habit, growth in oxide-fluoride mixtures, statistical study *(German)* 78−38639
fly ash nucleation props. in coal-fired power-plant plume 79−5607
forced convection quench data rel. to steady-state nucleate boiling data 78−90995
formic acid, homogeneous nucleation in associated vapour 79−10933
fracture, ductile intergranular, problem of nucleation of voids 79−79110
free energy of formation of nucleus, influence of elec. field 77−35702
free jet, homogeneous nucleation of clusters, noncryst. struct. *(French)* 78−79760
garnet, pretransition phenomena and long-range ordering 79−99151
gas and vapour bubble nucleation on brass surface in water 78−71845
gas bubbles in solids, simultaneous hetero- and homogeneous nucleation model 80−2066
gasdynamics and homogeneous nucleation, supersonic flow with condensation 77−62292
gel, gas cavitation nuclei, physical props. of surrounding nonionic surfactants 79−100444
glass, crystallisation and nucleation of reheating 80−84078
glass ceramic, nucleation and growth studies by small angle neutron scatt. 79−32913
glass formation and effect of nucleating heterogeneities 77−11487
glass forming melts, crystn. kinetics processes 80−64905
glass forming systems, induced crystallisation, transient heterogeneous nucleation 80−64903
glass transition, soft-sphere model, mol. dynamics study 80−49343
glass-ceramics, transient heterogeneous nucleation of glass-forming systems 80−88042
glass-ceramics and photosensitive glass, microstructure rel. to properties *(German)* 80−38926
glass-forming melts, nucleation and cryst. growth 78−2016
glasses, spinodal decomposition, review 80−96657
glycerin nonadecane, critical nuclei, meas. of number of mols. and surface tension from rate of nucleation 79−65293
grain boundary, stress induced drift diffusion, appl. to creep and growth of grain boundary voids 78−72811
grain boundary crack nucleation, and growth under low cyclic stresses, dislocation mechanism 80−19811
grain boundary migration vacancy generation, and drag force 80−15090
grain boundary sliding, containing particles, during diffusional creep, dislocation bowing, dislocation loop nucleation 79−37712
grain formation by nucleation, astrophysical environment 78−16501
graphite, spatial distribution of particles in cast Fe, metallographic study 78−92419
graphite nucleation, role of pre-heat treatments *(Japanese)* 80−35220
heat transfer mechanism with boiling in narrow spaces, interferometry obs. 78−94527
heptanoic acid, associated vapours, homogeneous nucleation 80−96638
heterogeneous, application of theory of spherical film thermodynamics 77−15724
heterogeneous nucleation, appl. of thermodynamic pots. 77−7948
heterogeneous nucleation of artificially modified ice *(Russian)* 77−29395
heterogeneous nucleation systems, crit. conditions characterising formation 78−56023
heterogeneous theory, appl. to precipitate nucleation at Guinier-Preston zones 77−36509
heteromolecular, ion induced, gas to condensed state 79−41260
hexatricontane, growth kinetics of (001) faces from soln., surface nucleation effect at high supersaturation 79−52098
HOAOB, isotropic-nematic transition, supercooling and nucleation, interface dendrites 78−42896
homogeneous, and heterogeneous nucleation processes for substance of different crystn. struct. 80−49144
homogeneous, classification of spontaneous condensation processes 80−6500
homogeneous, statistical system modelling *(Russian)* 78−83934
homogeneous condensation, from supersaturated vapour, stochastic simulation 78−51657
homogeneous formation of nuclei, rate *(Russian)* 77−44500
homogeneous nucleation and growth processes, computer simulation 78−30764
homogeneous nucleation kinetics, influence of two families of analytic γ-plots 77−48392
homogeneous nucleation kinetics, steady state solns. 80−50873
homogeneous precipitation of supersaturated soln., phenomenological theory, in liquid and solid soln. 78−67833
homogeneous vapour nucleation, in carrier gas, hydrodynamic theory 79−69236
hydrocarbon vapour, spontaneous condensation in submerged turbulent jet 79−64721
ice, bacteria as biogenic sources of freezing nuclei 79−20948
ice, heterogeneous crystallisation, of supercooled water, role of adsorption 79−95125
ice, heterogeneous nucleation, lattice misfit, hydrophilic sites on hydrophobic surface 79−48530
ice, in atmosphere, bacterial sources of nuclei 77−5292
ice, in atmosphere, terrestrial and marine sources of biogenic nuclei 77−5291
ice, monolayer ledges on basal surfaces 77−35809
ice, nucleation threshold on Cu_2S, Ag_2S, Mo_2S and CdS photosensitive surfaces 77−55343
ice, on CuS aerosol prepared by burning pyrotechnic mixture, freezing temps. 78−96279
ice, on PbI_2, −10 to −25°C *(French)* 77−78301
ice, two-step nucleation 78−49094
ice crystal growth in vapour at high saturation, thermodynamic anal. 77−1088
ice crystal growth on membrane filter, vapour depletion, chamber parameters effects 79−70858
ice deposition coefficient meas., appl. to cirrus cloud seeding 77−70779
ice depositional growth, parametrisation 77−70766
ice disc growth from vapour, cryst. habit change mechanism 80−84117
ice nucleants at −1°C using bacteria 77−53221
ice nucleating materials 78−49093
ice nucleation, effect of rocket effluent 79−88446
ice nucleation by fluid-breaking metaldehyde particles *(Chinese)* 80−12468
ice nucleation by fluorophlogopite 77−87007
ice nucleation in atmosphere, natural nuclei origin 79−48531
nucleation continued
ice nucleation mechanisms of submicron aerosol particles 79−20947
ice nucleation on AgI, CNDO calc. 77−4254
ice nucleation on AgI, exptl. verification of ice-forming activity theory 80−101406
ice nucleation on AgI, influence of aerosol particle size, struct. 80−61164
ice nuclei, for weather modification, supersonic expansion method 77−29487
ice nuclei, probability of formation in supercooled water 78−3909
ice-forming nuclei and atmospheric aerosols, elemental comp. 78−3882
ice-forming nuclei surfaces, elemental comp. 78−3881
industrial crystallisation, conference, Warsaw, Poland (Sept. 1978) 80−46737
inert gas fluid, nucleation of freezing by positive ions 77−84893
ingot, heat exchange between melt stream and crystn. *(Russian)* 79−69043
inoculating seed crystal surfaces, kinetic factors 79−43119
inorganic salt hydrate melts, nucleation, thermal storage appl. 79−66417
instability zone rel. to new phase preformation and nucleation 78−10169
interface reaction const., correl. with elementary surface process 78−63683
interfacial diffusion effect on nucleation kinetics at grain and interface boundaries 77−35761
interstellar grains formation, time-depend. nucleation theory 80−26946
ion clusters in heteromolecular nucleation, steady state thermodynamic model 78−48687
ion plating, mechanisms and theory 78−11130
ion solvation, correlation of total and partial enthalpies, vel. to nucleation energy barrier 80−89514
ion-implanted bubble garnet film, vel. asymmetry during stripe head propag. 80−39834
ionic crystals, precipitation from aq. solns., induction period 80−50882
ions, mol. clustering, gaseous-condensed state, nucleation and solvation 80−28129
irradiated, numerical simulation of void nucleation 79−73208
irradiated material, heterogeneous void nucleation 77−51415
Ising single spin flip kinetic model, nucleation process computer simulation 77−62613
island films, statistical model 80−92795
isobutene, droplet nucleation from crit. gas-phase+positive ions 79−39222
isobutyric acid-water near-critical liquid mixture, nucleation 80−92664
Johnson-Mehl and cellular microstructure, comparative analysis, computer simulation 80−54392
kinetic characteristics of crystal nucleation, two-barrier thermodynamic pot., nuclei size distrib. 78−10300
kinetics, generalised theory, applic. to dil. systems and limited no. of effective single element systems 77−39663
kinetics of new phase generation resulting from chemical interaction of components in soln. *(Russian)* 78−19707
latent image formation in Ag halides, nucleation, growth and developability 79−20395
lattice gas, two-dimens., thermodynamic pot. for homogeneous nucleation 79−82326
layerwise growing crystals, face profiles calcs. 79−60290
Lennard-Jones system, cryst. nucleation kinetics 77−62615
linear hydrocarbons, cryst. nucleation and cryst.-melt interfacial tension 79−69024
liquid, boiling at wall, nucleation, influence of dissolved gases 77−76537
liquid, dielectrophoretic heat transfer 78−94874
liquid droplet nucleation, stat. mech. treatment trans.-rot. paradox 77−62625
liquid film, nucleate boiling suppression 78−75055
liquid film, with nucleate boiling, heat transfer and film breakdown 78−34122
liquid in gas, microscopic theory *(Russian)* 78−67801
liquid in gas, microscopic theory *(Russian)* 78−67802
liquid jet, burnout in nucleate boiling 78−90991
liquid metal, nucleation undercooling meas. in small drops 77−7851
liquid metallic thin film, supercooling, electron diffraction study *(French)* 79−7676
liquid microclusters, thermodynamics, size effects, theory 78−22935
liquid stability, effect of elec. field on limits 77−31764
liquid superheat and vapour subcooling, corresponding states correlation 79−32218
liquid superheat in heterogeneous nucleation on rough Cu surface 79−37146
liquid-liquid interface, nucleate boiling 78−2342
liquids, saturated, boundaries of region of existence of nucleate boiling, thin film breakdown 80−48695
LPE growth, model layer thickness calc. 79−19484
LPE growth rate calc., from GaP and GaAs LPE data 79−19485
magnetic alloy, interface behaviour 80−84913
magnetic bubble nucleation via charged walls 79−78479
magnetic transitions of first kind, nucleation centre formation 78−2683
magnetoelectric composite, growth from melt, gas bubble form. ahead of solidification front 79−29044
marine advection fog, water distrib. rel. to droplet size, salt particle nuclei 79−5570
martensite, nucleation and streaming 78−39774
martensite nucleation at dislocations, elasticity model 80−55393
martensite nucleation general concept, general concepts, FCC to HCP transform. 77−36502
martensite nucleation mechanism, kinetics 77−36504
martensitic nucleation mechanism, FCC→BCC and other martensitic transforms. 77−36503
martensitic transformation, internal stress relax. effect on microstruct. and kinetic features 77−44250
martensitic transformation, nucleation site, variation in number 77−12621
martensitic transformation, nucleation site, variation in number 77−12622
martensitic transformation, nucleation time estimate 80−29954
massive transformations, free energy, microstruct., growth and nucleation 77−4776
materials processing in space 78−35296
melting mechanism, nucleation and growth theory 77−35674
l-menthol, vap., homogeneous nucleation, high-temp. Becker-Doering theory predictions 78−67820

nucleation continued
menthol, vap. phase nucleation and growth on C, glass and fused quartz 77−7992
metal, deformed struct. role in recrystallisation nucleation, review 79−34060
metal, FCC, low stacking fault energy, nucleation phenomena 79−90681
metal, nucleation of vacancy precipitation during quenching 77−72612
metal, oriented island growth on point defects 78−87889
metal, solidifying, heterogeneous nucleation 78−39754
metal, X-ray excitation of surface plasmons on spherical voids 77−11974
metal and alloy polycrystals, internal friction amplitude depend. *(Russian)* 79−90726
metal cluster generator for gas-phase electron diffr., variation of microcryst. with size 78−63645
metal cluster growth and props., photography and catalysis appl., conf., Villeurbanne, France (Sep. '79) 80−105431
metal clusters, 2 to 500 atoms, nucleation, mass spectra 80−102596
metal colloids in ionic cryst., preparation, optical, mag. resonance, elec. props. 80−59459
metal condensation on alkali halide, nucleus saturation density and epitaxy 78−18928
metal film, nucleation controlled interaction with Si substrate, silicide form. 80−10711
metal films, nucleation on alkali halide crystals, effect of ionisation of condensing flux 80−107675
metal films, on alkali halide substrates, nucleation and growth, surface study techniques, review 80−10809
metal growth in space, theoretical models, comparison with ground expts. 78−84786
metal ion adsorption, nucleation effects *(German)* 78−68635
metal layers, underpot. deposition, mechanisms, phase transitions, nucleation 78−60590
metal silicide growth on Si 78−10230
metallic epitaxial film growth with ionised beams and surface imperfections 77−32529
metals, electrochemical nucleation, potentiostatic obs. 79−15038
metastability in kinetic spherical spin system model, nucleation appl. 78−65873
metastable state relaxation, critical point region nucleation in thermodynamic systems *(Russian)* 80−13026
methane(-ethane)(-N_2), heat transfer in nucleate boiling of liquified gases and binary mixtures *(German)* 79−18687
methanol, enantiomers, racemic mixture nucleation 78−26677
mica, deformed, syntectonic nucleation of new grains 79−65102
microcluster metastable equilib. conc., homogeneous nucleation stat. mech. in vap. 77−62627
microclusters, atomistic models, heterogeneous water nucleation on ions, free energy barrier 77−62612
microclusters, computer simulation of nucleation and thermodynamics, mol. dynamics and Monte Carlo 78−51656
microlayer, formation and evaporation, theory 78−9536
mixture, binary, nucleate boiling heat transfer, conc. depend. 78−87249
molecular dynamics of clustering near gas-liq. phase transition 78−47509
Monte Carlo simulation nucleation, comparison with normal growth theories 77−68932
myristic acid, associated vapours, homogeneous nucleation 80−96638
naphthalene, ENSH method of oriented thin film growth 79−99443
naphthalene crystal nucleation on anthracene microcrystals suspended in vapour-gas stream 80−76165
nematic-cholesteric liq. cryst. mixture, NMR, reordering, nucleation and growth model 77−72546
new phase, role of fluctuations *(Russian)* 78−18563
Nimonic PE16, He injected, bubble-void transitions in Ni ion bombard. 80−34095
Nimonic type PE-16, irradiated, numerical simulation of void nucleation 79−73208
n-nitroaniline, UV light effect on nucleation during crystallisation on anthracene surface 80−75478
Nolan-Pollak condensation nucl. counter, droplet growth rate, supersaturation 77−60480
non-spherical nuclei, nucleation kinetics, high pressure effects 80−19730
nonlinear relaxation process, nucleation in early stage, Markov process framework 78−70060
nonuniform vapour, nucleation model, cluster diffusion effects 77−4206
nonvolatile liquid, boiling, nucleation eqn. in phase space 79−27495
nuclear fuel, bubble nucleation modelling, and fission-induced re-soln. 79−71891
nuclear track detectors, X-ray anal. of microcrystallite nucleation 80−890
nucleate boiling, active sites role 77−15569
nucleate pool boiling, meas. of void frequency distribs. and profiles using neutron beams 80−27691
nucleate to film boiling transition collective phenomena, Nukiyama curve 78−9531
nucleation theory and first order phase transition dynamics near critical points 80−84284
nucleus shape depend. parameters, generalisation 78−84765
octaphenylcyclotetrasiloxane, phase behaviour and nucleation kinetics 80−29168
one-dimensional polycrystalline structure, computer simulation *(German)* 77−68935
optical glass, melting, fining, surface tension, diffusion, nucleation in microgravity 80−81016
ordered alloys with periodic struct., decomp. invest. *(Russian)* 80−93558
organic eutectics, surface nucleation parameters 79−19163
orthoferrite garnet, mag. bubble lattice nucleation obs. 78−76283
Ostwald ripening kinetics 78−2047
PAA, isotropic-nematic transition, supercooling and nucleation, interface dendrites 78−42896
n-pentane-water interface, nucleate boiling 78−2342
percolation clusters in nucleation theory 79−52785
perfluoromethylcyclohexane-methylcyclohexane, near-critical liquid mixture, nucleation 80−92664
PET, crystallization, lamellar growth kinetics and thickness 80−103266
phase boundaries in first-order phase transitions, dynamics stability 80−107403
phase transitions, kinetics 79−28075
photographic development, nucleation and growth phenomena 80−101858
PMMA sheet in methanol, pre-soak, dissolved gas content rel. to craze nucleation, creep 79−66185
poly-1-butene, sheared melts, nucleation and crystal growth meas. 79−69027
polyethylene, extended chain crystal, fine structure and nucleation mechanism 78−14287
polyethylene, flow-induced fibril form. from soln. 80−59402
polyethylene, high modulus filaments, form. from melt, cryst. nucleation effects 79−70034
polyethylene, lamellar structs. nucleated onto fibrous substrates for high modulus 78−75578
polyethylene melt, cryst. kinetics during cooling, nucleation density effect 80−100181
polyethylene terephthalate, induced crystn. on metallic nucleating particles 79−15658
trans-1,4-polyisoprene crystals, press. effect on growth rate 80−88064
polymer, mixed heterogeneous homogeneous nucleation and nonintegral exponents of time 78−55820
polymer, row nucleation, phenomenological model 78−14301
polymer crystallisation, natural and artificial heterogeneous nucleation 78−51431
polymer crystallisation, thermodynamic analysis of nucleation *(Russian)* 77−19881
polymer crystals, deform. and fracture, submicrocrack nucleation and supermod. struct. 78−52918
polymer nucleation, bundle-like and longit. growth of fibrillar crystal from flowing soln. 78−51433
polymerisation, from emulsion, homogeneous nucleation 79−29354
polypropylene, isotactic, epitaxial crystn. on alkali halide surface 78−26787
polypropylene oxide, isotactic, crystallisation, heterogeneous nucleation, interfacial energy effects 79−69023
polystyrene, isotactic, crystalline core of row structures, nucleation and growth 79−86718
polystyrene, isotactic, isothermal crystn. using SiO_2 as nucleating agent 79−24807
polystyrene, isotactic, spherulite radial growth retardation by SiO_2 nucleation 80−107066
pool boiling, bubble freq. model, surface effects 78−90651
pool boiling heat transfer including microlayer evap., model development 77−42833
pores in system with excess vacancies extraneous inclusion role in nucleation *(Russian)* 79−73164
porous anodic films on Al, nucleation and growth 78−44273
powders, rapidly solidified, nucleation, undercooling and homogeneous structs. 78−52708
pre-ice-nucleation conditions in settling cloud chamber, numerical simulation 79−79950
precipitation, orientation relationship generation 77−73275
precipitation, orientation relationship generation 77−77487
precipitation processes, study by particle site anal. 80−50883
premartensitic phenomena, nucleation, shape memory effect, review 80−3041
pretransition phenomena and long-range ordering 79−99151
proteins, effect of protein conc. and solubility on nucleation rate 78−87632
quartz, α and β phases coexistence state, elastic light scatt., birefringence 79−47412
quasi-stationary approximation of nucleation kinetics at high supersaturations on (111) faces of cryst. with diamond struct. 80−84128
quenching temperature, 0.03-1.3 MPa, base material thermal props. depend. 78−94587
rate, relationship between experimentally determined and true values 80−54343
rate of formation of condensation nuclei in two component metastable media 80−79930
recrystallisation, finely dispersed second-phase particles effect 77−8845
recrystallisation nucleation, model for strain induced grain boundary migration 79−46675
recrystallization, primary, one dimension, model considerations, nuclei start to grow simultaneously, with same rate *(German)* 79−29094
reduced gravity, solidification interface, bubble interactions 78−84787
repeated precipitation on edge dislocations, micromechanisms 78−95752
replacement free energy and nucleation rate, review 77−62611
review, fundamentals of nucleation theory *(Spanish)* 78−43101
review, nucleation 80−49143
review, nucleation theory for high and low supersaturations 80−49142
rotating thin-ring electrode, bubble nucleation 78−48664
salt nuclei, size rel. to critical supersaturation 78−44940
sapphire:Ti^{4+}, plastically deformed, precipitation hardening, TEM study 80−7592
sapphire :Ti^{4+}, deformation history effects on precipitation hardening 79−83209
second phase on screw dislocation 78−51540
secondary nucleation, formation, survival and growth of nuclei 80−50540
secondary nucleation, influence of crystal brittleness and degree of supersaturation using in growth *(Italian)* 78−23836
secondary nucleation kinetics 80−19945
secondary nucleation theory, error in surface area estimation 77−89396
secondary nuclei birth and growth rate in single-seeded batch crystalliser 78−83759
seeding, hygroscopic, in cumulus clouds, a model 79−88442
SEM with ultrahigh vacuum system for surface physics expts. 78−38925
semiconductor, electron-hole droplet nucleation and stability, hydrodynamic approach 78−72080
semiconductor epitaxial film growth with ionised beams and surface imperfections 77−32529
separate-bubble cavitation tests, nucleation meas. by Venturi tube *(French)* 79−55402
sickle haemoglobin gelation, reaction order and crit. nucleus size 78−76983
silicates, refractory, nonequilib. phases nucleation and condensation from SiO vapour 79−60497
single crystals, growth simulation 80−88069
size dependent crystal growth, new empirical kinetic equation 78−38637
size dependent growth systems, effective nucleation rate 80−38972
solid phase reactions, modelling using population balance approach 80−11874
solid-solid nucleation, kinetics for parallelepiped crit. nucleus shape 77−31773

nucleation continued
solidification in space environment, bubbles thermal migration and interaction with solidification interfaces 79−47670
solids, amorphous and crystalline, condensing from gas phase, nucleation, growth and transform. 80−24745
SOS early growth, island coalescence model 77−76704
spherulite primary nucleation, determ. from spherulite shapes in bulk samples 80−70359
spherulite primary nucleation kinetics determ. from truncation of spherulites 79−69031
spinodal decomposition *(Japanese)* 79−20026
statistical mechanical theory of the kinetics of phase transitions, review, book contrib. 80−73270
steady state process kinetics, diatomic clusters role *(Russian)* 77−31750
stearic acid homogeneous vapour phase nucleation, diffusion cloud chamber obs. 80−79923
steel, 30Kh3SNMBF, α-phase nucleation and growth, influence of supercooled austenite state *(Russian)* 77−48435
steel, alloy, Cr-C (12, 0.2 wt.%) growth of grain boundary ferrite allotriomorphs, photoemission electron microscope exam. 78−88468
steel, austenite hot deformation influence on phase transformations 80−7606
steel, austenitic stainless, grain boundary struct. changes during initial stages of recrystallisation 77−36559
steel, austenitic stainless, irrad. creep of type 316 in HVEM 80−97523
steel, austenitic stainless, NbC precipitate particle size distrib., TEM study of grain to grain variations 79−29066
steel, austenitic stainless, neutron-irradiated, gamma-alpha transformation 79−96027
steel, austenitic type 347, nucleation and growth of creep cavities 80−40513
steel, ball bearing, fatigue damage, influence of dispersed phases in martensitic matrix 80−108549
steel, C martensitic, tempering induced decomposition and segregation, atom probe study 80−3112
steel, Cr, lower bainite transform., significance of carbide precip. 80−97476
steel, Cr-W(Mo), quenched, carbide reactions during tempering 80−89229
steel, ferrite nucleation, appl. to B hardenability 78−27505
steel, hardenability, role of B and P segregation 80−97486
steel, low alloy, pearlite block, exam. of crystallographic features, formation processes *(Japanese)* 78−84799
steel, low alloy, SNCM 8, quenched, tempered, prior austenite grain size effect on stress corrosion cracks *(Japanese)* 79−66215
steel, low alloy ferritic, sub-micron cavity nucleation, SEM obs. 78−95753
steel, low C, nucleation and increase of discontinuities in environment of non-metallic inclusions *(Polish)* 79−79022
steel, Mo-Cr (3 wt.%), CrC formation in isochronal tempering, electron microscope study 80−7584
steel, Ni-B, B effect on temperability and microstructure 79−15710
steel, stainless, ferrite to austenite decomp. 80−93554
steel, stainless, He effects on microstruct. in ion-irrad. 80−29078
steel, stainless, martensite formation, in situ obs. 80−25692
steel, stainless, martensite nucleation, in situ electron microscope obs. 80−7572
steel, stainless, martensite nuclei obs., role of defects in nucleation 80−25693
steel, stainless, type 304 welded, low temp. sensitisation, nucleation of CR carbide nuclei along grain boundaries TEM, SEM study 79−38851
steel, stainless, type 304L, fast neutron irradiation, voids nucleation 79−77644
steel, stainless, type 316, irradiated, numerical simulation of void nucleation 79−73208
steel, stainless, type 316, microstruct. changes in creep ductility, SEM, TEM, optical microscopy and X-ray diffr. study 79−38927
steel, type 1045, hydrogen enhanced nucleation of microvoid as function of local plastic strain 79−79053
steel, type FV548, 1 MeV electron irradiated, influence of pre-injected He on void nucleation and growth 80−34054
steel, unkilled deep drawing sheets, influence of N content on recrystn. *(German)* 80−40376
steel, W-Cr (3 wt.%), CrC formation in isochronal tempering, electron microscope study 80−7584
step decoration on cryst. surfaces, conditions 80−15349
stereological counting measurements, use in testing growth rate theories 80−16311
stochastic process of nucleation in the early stage 79−80521
strain energy interactions, T_0 concept, sympathetic nucleation 77−73278
structural stability of isolated small particles, atomistic studies 79−77957
subcooled forced convection boiling heat transfer at subatmospheric pressure 78−94525
substitutional solid solutions, new phase nucleation mechanism 80−61135
sulphate particle formation by heteromol. nucleation and condensation in cavities 80−26183
supercooled fluid states, soft core system, mol. dynamics method 78−18565
superheated binary liquid mixtures, homogeneous nucleation of bubbles 78−67818
superheated liquid, elec. field induced nucleation, pre-nucleation relax. phenomenon 77−51489
supersaturated cooling gas, time depend. nucleation theory 78−6151
supersaturated gas condensation kinetic model, cluster nucleation assoc. and dissoc. 78−85151
supersaturated soln., shape stability of growing cylindrical particle due to diffusion and interface kinetics 80−79720
supersaturated vapour, critical clusters, theory and Monte Carlo simulation, review 80−82734
supersaturated vapour, equilib. press. depend. on nucleating drop radius 80−69960
supersaturated vapour, photonucleation 79−7682
supersaturated vapour nucleation on photoexcited mols. 77−76540
supersonic nozzle flows of condensible vapour, near-equil. heterogeneous nucleation and similarity rules 77−58759
surface nucleation, method for determining kinetic parameters 79−46980
tetracyanoethylene, oriented adsorption on KCl, LEED-AES study 77−62737
TGS, domain nucleation in AC elec. fields 80−34867
theories, review (1930 to 1960) 79−86897
nucleation continued
theory with Maxwell demons 77−85054
thermodynamic theory of nucleation on charged particles 79−39216
thermodynamics of nucleation on charged centres 79−20955
thin film condensates coalescence, influence on morphological changes, modelling 80−107676
thin film Congress Loughborough, England, (Sept. 1978) 79−77949
thin film growth, nucleation kinetics, coalesc. of mobile nuclei 80−6671
thin films, kinetics under complete condensation conditions 80−88453
thin films, precipitation and nuclei form. in presence of condensation centres, thermodynamic model 80−103594
thin films, vapour deposited, saturation cluster density, general formula 80−15408
three-dimensional epitaxial crystallite nucleation at substrate grain boundaries 77−76707
TNT, role of HNS in grain modification 79−100129
transient boiling, bubble nucleation and growth instabilities 78−90649
transient effects, leading up to nucleate boiling 78−90650
transient superheat on vertical surfaces in subcooled boiling 79−7282
transients in cryst. growth rate 80−84118
transition metal, bimetallic cluster, photoselective bimetallic aggregation, review 80−53182
triethylene glycol, critical nuclei, meas. of number of mols. and surface tension from rate of nucleation 79−65293
turbulent jet, quasi-two-dimensional description of rapid-type nucleation 77−35190
turbulent water film, with different initial flow conditions and high temp. gradients, heat transfer 78−90862
two phase alloy hardening by second phase particle coalescence 80−7591
two-dimensional, double potentiostatic step response, perturbation effects calcs. 78−51841
two-dimensional, simulation using kinetic Ising model 80−54156
unstable heat transfer conditions, free convection-film boiling transition 78−14006
V-VI-VII ferroelectric semiconductor film growth, effect of artificial nucleation centres 79−11032
vacuum condensation, in presence of inhomogeneously distributed adsorbed atoms 77−15722
vacuum condensation, saturation density of nuclei, substrate temp. depend. 78−18932
vacuum condensation of nuclei, stabilisation of sizes 79−8248
vapour bubble nuclei, stability and nucleation, effect of gases 77−31303
vapour-liquid nucleation, mol. dynamics theory 78−75803
vapour-liquid-solid growth mechanism *(Russian)* 80−107074
void nucleation, effect of mobile He 77−51405
void swelling, nucleation theory 80−65038
voids, review of diffusional growth of creep voids 78−71720
voids, simultaneous reacton of vacancies and interstitials 79−42051
volatile liquid, statistical thermodynamics of new phase form. *(Russian)* 78−18739
water, boiling, heat transfer around single nucleation site 77−24394
water, metastable states diagram and new phase nucleation probability *(Russian)* 78−95129
water, nucleate and transient boiling in narrow space between disks 77−84115
water, nucleate boiling heat transfer, press. factor 77−69080
water, nucleation on ions, molecular model 77−1222
water at interfaces, mol. struct. and dynamics 77−31873
water droplets, ebullition under steady-state superheated conditions 80−74928
water droplets, ebullition under transient superheated conditions 80−74929
water supercooled droplets, on ice substrate after low speed collision, freezing behaviour, cryst. struct. 80−29152
water vapour, condensation in presence of H_2SO_4 and HNO_3 pollutants 78−81343
water vapour, in rarefaction waves, condensation, heterogeneous nucleation 77−58731
water vapour, photoinduced nucleation 79−10934
water vapour, photoinduced nucleation expt. 80−2149
water vapour at saturation, droplet nucleation by ions, ion mobilities 79−46794
water vapour condensation in rarefaction waves, homogeneous nucleation case 77−42869
water vapour expansion with condensation, nozzle flow at high pressure 80−106828
water vapour nucleation on AgI target, mol. beam investig. 77−52212
water vapour-Ar mixture, homogeneous condensation 79−46796
water vapour-N_2 mixture, homogeneous condensation 79−46796
water-isobutyric acid (2,6-lutidine) mixtures, critically quenched, phase separation and coalescence 80−24581
water-methanol (n-propanol), binary mixtures, nucleation 80−44305
whiskers nucleation, effect of machining support surface *(Russian)* 79−65352
YIG, hot spraying to give fine, free flowing, sinterable powder 80−20865
YIG, precipitation of Fe_3O_4 78−84815
zincblende type cryst. growth, atom clustering and stacking formations on interfaces 77−19884
Ag, cluster growth and nucleation on Mo (100), UHV-SEM, AES/(RHEED or LEED) obs. comparison 78−63956
Ag, crystal (100) faces, polynuclear growth mechanism during electrocrystallisation *(German)* 78−18562
Ag epitaxial films, grain boundary struct. evolution during recrystn., interface energy effect *(Russian)* 80−15387
Ag epitaxial growth, cluster mobilities, in-situ electron microscopes obs. 80−15407
Ag, FCC, low stacking fault energy, nucleation phenomena 79−90681
Ag film, vacuum deposited onto SiO, C and mica, quantitative study of nucleation 79−77959
Ag, film growth on Si (111) 7×7, LEED, AES and UPS expts. 78−38988
Ag film growth on Si (111), nucleation and growth modes, SEM study 80−100423
Ag, grain growth in strained {110}<112> low stacking fault FCC crystals after artificial nucleation 79−91722
Ag halide emulsion crystal growth, complex solubility computation 79−83516
Ag, high purity, nucleation and twinning during recrystallization, TEM study 79−29082
Ag, oriented crystallisation on active amorphous C centres 79−7762

nucleation continued
Ag speck nucleation and phase formation in latent image 80−97716
Ag-Al (26 at.%), massive transform, $\beta \rightarrow \zeta$, crystallography and morphology 80−97475
Ag-Au, nucleation and growth on substrates 79−77956
Ag-Hg-Sn dental amalgams, non-γ_2 phase, transmission electron metallography 79−74162
AgBr layer, sensitised, topography of developed centres 80−73491
AgBr monosize emulsion growth 79−79312
AgBr:I single jet precipitation, grain growth kinetics 79−20414
AgBrI microcrystals, growth mechanisms 79−19171
AgBrI photographic emulsion prep., double-jet nucleation turbidimetry 79−100446
AgCl crystal growth in gelatin soln. 80−64942
AgCl nucleation from aqueous solns., stopped-flow UV absorption spectrophotometry 79−20413
AgI aerosol, ice forming activity, UV irrad. effect 80−71950
AgI, aerosols, ice nucleation at different supercooled fog temps. *(Russian)* 77−27983
AgI pyrotechnic nucleant characts., use in Florida Area Cumulus Expt. 79−100919
Al alloys, continuous precipitation, nucleation, spinodal decomposition 80−3061
Al, compressed, nucleation and recrystallisation study by electron microscopy and Kikuchi diffr. 79−52236
Al, deformed, nucleation and recrystallisation at second phase particles 78−6941
Al, elongated, deformed, recrystallisation, orientation relations, hard-sphere model for Rowland transform. *(French)* 77−77497
Al epitaxial films, grain boundary struct. evolution during recrystn., interface energy effect *(Russian)* 80−15387
Al film, nucleation and growth on C layers, adsorption energy and surface diffusion 79−99451
Al film, nucleation-grown, RF sputtered, Mayadas-Shatzkes cond. 77−1498
Al grain refinement, effect of Al_3Ti, TiC and B 78−52828
Al/Cu thin film couples, TEM study of intermetallic nucleation at interface 80−65305
Al-Cu (2-5 wt.%), precipitation total surface influence on resistivity *(French)* 80−71650
Al-Cu (3.5 wt.%), precip. on stationary and non-stationary grain boundaries 78−84820
Al-Cu (3.5wt.%), grain boundary precip. 78−84820
Al-Cu film bilayers, growth kinetics of θ phase, He^+ backscatt. and X-ray exam. 78−84105
Al-Mg-Si, Guinier-Preston zones, inception and effect on ageing, review *(Hungarian)* 79−11627
Al-Mg-Si, nucleation and precipitation growth on dislocations, electron microscope studies 80−3064
Al-Mg-Si alloys, ductile intergranular fracture mechanisms, void formation and nucleation 80−108578
Al-Mg-Ti-Zr alloy AL23-1, nucleating cellular dendritic crystallisation *(Russian)* 79−70055
Al-Pt (2 wt.%), rapidly solidified alloy, metastable phase formation 79−52194
Al-Si, hypereutectic silumins, P and Na modification 78−84792
Al-Si, internal friction and Si precipitate nucleation 78−60690
Al-Si alloy, effect of irrad. on the nucleation of incoherent precipitates 79−8303
Al-Ti, solid soln., unidirectionally solidified, segregation patterns revealed by etching 79−47693
Al-Ti(-Si), nucleation entropy and grain refinement 79−91627
Al-Zn, grain boundary reaction sites, determ. of struct. aspects, by electron microscopy 80−103359
Al-Zn (6.8 at.%), neutron small angle scatt., interparticle interference 77−77514
AlN, precipitation from gas phase 78−6025
Al_2O_3, influence of cooling rate on nucleation *(German)* 78−38638
Al_2O_3 ultrafine gel particle form. from NH_3-$AlCl_3$ solution 80−93807
Al_2O_3-TiO_2 powder, plasma-prepared, morphology and phase constitution 80−100833
Al_2O_3-ZrO_2 cast refractories, nucleation processes reconstruction by SEM, TEM and STEM 78−35380
$Al_2(SO_4)_3K_2SO_4.24H_2O$, secondary nucleation rate under agitation 80−50541
$Al_2(SO_4)_3(NH_4)_2SO_4$ or $AlNH_4(SO_4)_2.12H_2O$, size dependent growth systems, effective nucleation rate 80−38972
AlSb, laser pulse annealing, induced nucleation, crystal growth 80−84966
Al_2TiO_5 powders, decomposition kinetics using nucleation and growth-rate constants *(Japanese)* 80−35156
Ar, cluster formation and homogeneous nucleation, comparison of expt. and theory 80−79925
Ar in He carrier gas, nucleation in supersonic nozzle flow 78−94871
Ar, liquid, superheated, nucleation 79−23741
Ar, nonequilibrium condensation and surface tension in supersonic jet flow *(Russian)* 80−65210
Ar, nucleation, thermodynamics 78−14454
Ar phase stability boundary, nucleus surface tension rel. to surface radius of curvature 79−60603
Au, adatom beam scatt. expts. on NaCl and KBr (100) surfaces 79−77924
Au clusters, coalescence on NaCl substrates at room temp. 78−18935
Au crystallites, formation in flowing Ar system, density, size distrib. and size dispersion 78−88415
Au, effect of intermittent deposition on nucleus formation and growth on alkali halide substrates 79−23853
Au epitaxial films, grain boundary struct. evolution during recrystn., interface energy effect *(Russian)* 80−15387
Au epitaxial growth, cluster mobilities, in-situ electron microscopes obs. 80−15407
Au, epitaxial growth and nucleation on NaCl during ion bombardment 79−11024
Au epitaxial particles, high resolution dark field electron microscopy 77−85111
Au film, deposition on polymer substrates, effects of glow discharge on nucleation characts. 79−77963
Au film, early growth stages on amorphous C, cluster migration obs. 79−77964
Au film, growth kinetics of icosahedral particles *(French)* 77−24494

nucleation continued
Au, film, on sapphire substrate, nucleation, growth and postdeposition thermally induced epitaxy 79−77946
Au, film growth on mica substrate, surface defects and heterogeneous nucleation 78−47684
Au island condensate, on LiF or NaCl, nucleation kinetics, influence of ionised atoms 77−11816
Au, nucleation on NaCl from new vapour source, temporal and electron micrograph obs. 79−77954
Au, nuclei interaction on KCl (100) surface 77−89670
Au, on KCl, collective behaviour, monatomic step influence 77−15719
Au, on KCl, nucleus growth mechanism and kinetics, electron microscope obs. 77−62780
Au on NaCl:Fe(Mn), surface imperfection effects 77−15699
Au, on organic substrates, ion bombard. effects 78−75965
Au, stacking fault tetrahedra, critical nucleation temp. 78−26581
Au, VPE on NaCl, role of surface steps 78−79902
Au vacuum condensation on KCl, spatial distribution of nuclei 78−18931
Au vacuum deposited layer on KI, nucleation and growth 79−61516
Au, vacuum evaporated particle coalescence behaviour on doped alkali halides 79−77961
Au-Ag, deposition on alkali halide, kinetic nucleation model 77−85118
Au-Si contact reaction, nucleation, growth rate meas., TEM and transmission electron diffr. obs. 79−23846
B, closed system CVD, deposition rate and rate-limiting steps 80−93492
B-transition metal, amorphous thin film, crystallisation, TEM obs. 79−19483
Ba, silicates, solid state reactions, thermodynamics and kinetics *(German)* 80−76236
$BaMoO_4$, single crystals, habit modification, growth kinetics in silica gel 80−20777
BaO film on W surface, struct. of crit. nuclei in heterogeneous crystn., LEED and FEM 77−11817
BaO-SiO_2 glass ceramic, nucleation, effect of electric fields 78−83742
BaO-SiO_2 glass ceramic, growth and nucleation kinetics 80−7528
$BaTiO_3$, charges effect on form. of nucleation centres of ferroelec. phase 79−65810
$BaTiO_3$, crystallisation from melt, nucl. and final cryst. sizes 77−24951
Bi, evaporated film, nuclei size distrib. 77−11802
$6Bi_2O_3.SiO_2$, stable γ-phase cryst. form. from supercooled melt, metastable δ-phase precip., surface contamination role 79−91635
Bi_2Te_3, anodic oxide films, two-dimens. nucleation and growth 80−11807
CC GaP, improvements in synthesis, solute diffusion (SSD) growth 79−65992
CO bubbles in liq. Fe, homogeneous nucleation 77−60106
Ca metasilicate glass, crystallisation kinetics 77−11486
$CaCO_3$ crystallisation from aqueous solutions, kinetic study 80−59419
$CaCO_3$, nucleation mechanism accompanying Ostwald ripening 80−50641
$CaCO_3$, precipitation from Mg^{2+} containing soln. *(French)* 77−85915
$CaCO_3$, with perfect struct., temp. depend. of rate of twinning 80−10561
$Ca(NO_3)_2$-H_2O solns., ice I homogeneous nucleation temp., slow vitrification mechanism 78−26666
$Ca(No_3)_2$-H_2O system, induction period supercooling depend. meas. 80−19918
$Ca_{10}(PO_4)_6(OH)_2$ dissolution kinetics, nucleation-controlled 80−59659
$CaSO_4.2H_2O$, supersaturated soln., nucleation induction time 79−69042
$CaTiO_3$, crystallisation from melt, nucl. and final cryst. sizes 77−24951
Cd, epitaxial monolayer, nucleation and growth on Ge (111) 77−7986
Cd epitaxial monolayer, nucleation and growth on Ge (111), RHEED and mol. beam study 77−43447
Cd films, nucleation and growth, props. 80−29878
Cd-Zn alloys, splat-quenched, X-ray diffr., SEM and TEM study of struct. 79−66077
Cd_3As_2 films, nucleation processes, on NaCl substrates 80−59813
CdS, cryst. growth from vapour by one-dimens. nucleation on (110) singular surface, model 78−2048
CdS, epitaxial growth and nucleation, on monocrystn. ZnS, substrate real struct. influence 80−88455
CdS single cryst., vaporization and form. of negative whiskers 80−92659
Co, HCP to FCC transition, mag. domain nucleation 78−64218
Co-Ga β' quenched single crystals, annealing-out of point defects 80−55426
Co-P metallic glasses, crystn. kinetics by differential scanning calorimetry 78−91257
Co_5Sm crystals, microstruct., homogeneous precip. and nucleation 80−104160
Cu alloys, continuous precipitation, nucleation, spinodal decomposition 80−3061
Cu, cementation, characterisation of nucleation and growth from aq. soln., TEM and SEM study 79−28972
Cu crystals, two-phase, recrystn. retardation, particle size, spacing effects 80−89242
Cu, electrochem. nucleation and growth on Te and Al, TEM 80−104451
Cu, electrochem. overgrowths, role of substrate dislocations and grain boundaries in nucleation and growth 79−51454
Cu electrocrystallisation on graphite electrodes, nucleation 80−93504
Cu, electrolytic epitaxial nucleation and growth, on (111) Ag 80−104081
Cu film, polycryst., nodule mechanism of diffusion-induced disintegration *(Russian)* 78−51829
Cu, grain growth in strained {110}<112> low stacking fault FCC crystals after artificial nucleation 79−91722
Cu, horizontal plate, pool-boiling heat transfer, nucleation centre size, surface roughness 78−90652
Cu-B(25 wt.%) *(Japanese)* 80−55402
Cu-Be-Co(0.1,0.2 wt.%), discontinuous precipitation *(Japanese)* 80−55402
Cu-Cr (0.55 wt.%), crystallography of precipitates, strain field study 80−25699
Cu-Ni-Al, review 80−7564
Cu-Ti, dil. alloy, cellular precipitates, nucleation, TEM study 80−3069
β-Cu-Ti, dil. alloy, growth phenomena associated with precipitation, TEM study 80−3070
Cu-Zn (30 wt.%), rolled, electron microscope exam. of recrystallisation 78−76663
Cu-Zn-Al, memory alloy wire and ribbon reversible martensitic transformation, ageing effect, review 80−7564

nucleation continued
Cu_3Au alloy, dynamics of ordering clusters in thermal non-equilib. state 79−51257
Cu_2O, layer form. at anodic overpotential, nucleation of holes 79−61865
Cu_2O on Cu, two stage metastable and stable surface nucleation, 800-1000°C 77−70214
$CuSO_4.5H_2O$ dehydration nuclei growth rate depend. on water vapour press. 79−15986
$CuSO_4.5H_2O$, secondary nucleation and growth in a fluidized bed 80−50542
γ-Fe alloy, supersat. solid soln., recrystn. inhibition by cold rolling 77−73286
Fe alloy type G18, martensitic $\gamma \rightleftharpoons \varepsilon$ transformation, dislocation pile-ups, ε phase nucleation *(Russian)* 80−55396
Fe alloys, anisotropic precipitation struct. in external mag. field *(German)* 78−72785
Fe, BCC, void nucleation following electron irrad. 80−29054
Fe, cast, flake and nodular, heterogeneous nuclei and graphite chemistry 79−55896
Fe, cold rolled, struct., transmission Kossel patterns obs. 77−48451
Fe dissolution, morphology of differently oriented single crystal surfaces, dislocation effects *(German)* 77−9002
Fe, effect of atm. corrosion on fatigue crack nucleation and fracture surface morphology, in air and vacuum *(Japanese)* 79−8387
Fe, epitaxy on Au, growth processes, ultra high vac. in situ electron microscopy 78−30842
Fe-B metallic glasses, crystn. kinetics by differential scanning calorimetry 78−91257
Fe-C, proeutectoid ferrite nucleation kinetics at austenite grain boundaries 80−55405
Fe-C, softening of high purity Fe, by C, due to double kink nucleation *(French)* 78−84949
Fe-C (0.25 wt.%), austenitising temp. effect on proeutectoid ferrite reaction kinetics, scanning Auger microprobe exam. 78−44144
Fe-C melt, graphite cryst. growth rate rel. to supersaturation *(German)* 77−55940
Fe-C-Si, high purity, vacuum melted, nodular graphite form. 80−108452
Fe-Ga (25 at.%), precipitation *(French)* 77−70057
Fe-Mn-V-C austenitic steel, discontinuous precipitation, morphological changes 80−3078
Fe-Mo (13-20 at.%) binary alloys, spinodal decomp. on ageing, TEM and X-ray diffr. study 80−97503
Fe-N, nucleation and precipitation growth on dislocations, electron microscope studies 80−3064
Fe-N single crystals, solid soln. stress assisted nucleation of α'' precipitates 78−52810
Fe-Ni (28 at.%), martensitic transformations, Mossbauer scattering evidence of soft modes 80−93223
Fe-Ni (29 wt.%), martensite nucleation at dislocations, elasticity model 80−55393
Fe-Ni-C, martensite nucleation, tensile prestraining effect 77−8828
Fe-Ni-C (31, 0.28 wt.%), crossings of thin plate martensites, TEM obs. 80−25756
Fe-Ni-C (31.1, 0.02 wt.%), kinetics analysis of temp. rate of nucleation of a thermal martensitic transformation 79−78965
Fe-Ni-Ti alloys, high pressure effect on martensite crystal nucleation and growth *(Russian)* 78−39769
Fe-rare earth, amorphous thin film, crystallisation, TEM obs. 79−19483
Fe-Si (3 wt.%), domain wall drift due to nucleation during cyclic magnetisation 78−95461
Fe-Zn, crystallographic relations by X-ray diffr. 80−24408
$Fe_3B_7O_{13}I$, boracite single cryst., nucleation control density growth 80−80955
$Fe_{80}(C_{1-x}B_x)_{20}$ amorphous alloy, α-Fe crystn., morphology 80−70129
α-Fe_2O_3 crystal flux growth, solubility and relative supersaturation in Fe_2O_3-PbO-V_2O_5 fluxed melt system 80−64934
FeOCl-pyridine intercalate, mechanism, nucleation and diffusion 80−49420
(GaAl)As, DH laser, LPE growth, meniscus lines as nucleation sites 77−15706
$Ga_{0.9}Al_{0.1}As$, nucleation morphologies on $Ga_{0.65}Al_{0.35}As$ surfaces grown by LPE 78−15323
$Ga_{1-x}Al_xAs$-Ge, MBE of ultra thin film superlattices on GaAs substrates, TEM study 79−37932
GaN:Zn epilayers, growth parameters effect on props., device struct. 78−26975
GaSe, anodic oxide films, two-dimens. nucleation and growth 80−11807
GaSe, growth of crysts. with natural facets at large angles to layers 78−15305
$Gd_3Ga_5O_{12}$, flux growth and nucleation temp. determ. *(Chinese)* 80−60761
Ge alloys, amorphous film, crystn. transform. kinetics 78−22653
Ge, amorphous film, laser pulse annealing 80−15006
Ge, amorphous film, post nucleation growth, computer simulation 78−34729
Ge, electron-hole drops, non-isothermal nucleation 80−44514
Ge, exciton condensation, electron-hole drop investigation in UHF field, nucleation *(Russian)* 80−80193
Ge, exciton drops nucleation centres under conditions of inhomogeneous strain *(Russian)* 78−2429
Ge, laser pulse annealing, induced nucleation, crystal growth 80−84966
Ge, solid-liquid interfacial tension determ., glassy sphere nucleation by rapid cooling 77−51570
Ge, ultra-pure electron-hole drop condensation nucleation phenomena 77−47744
Ge-transition, metal planar interfaces, first phase to nucleate 77−62764
Ge_xSe_{1-x} amorphous film, photocrystallisation, elec. cond. meas. 79−32911
$Ge_{20}Se_{40}Te_{40}$ amorphous alloys, thermal crystn. study 78−26789
HNO_3-water, homogeneous nucleation, relative humidity depend. 78−71846
H_2O, condensation via rarefaction wave 78−71847
H_2O droplet growth in presence of soluble gases, expts. 80−21807
H_2O droplets, subcooled, nucleation in Ar-H_2O vapour mixture, rate const. 80−61131
H_2O-H_2SO_4, mixtures, transient nucleation, stochastic theory 77−1221
H_2O-H_2SO_4 system, nucleation, aerosol form. 77−70327
H_2O-H_2SO_4-ion aerosol particles, ultrafine, stratospheric form., ion-induced nucleation 80−72608
H_2SO_4 aerosol growth, kinetic model 77−37340
H_2SO_4, aerosols form., expt. and theory 78−96256
nucleation continued
H_2SO_4 secondary aerosol form. in urban atmosphere 77−33137
H_2SO_4-H_2O, aerosol form., nucleation calcs. 78−31709
H_2SO_4-H_2O, vapour mixture, temp. depend. of nucleation, aerosol form. 77−86350
H_2SO_4-H_2O aerosols nucleation rate in presence of ionisation source 80−104464
H_2SO_4-H_2O solution aerosol particles nucleation in stratosphere 77−56678
H_2SO_4-water, homogeneous nucleation, relative humidity depend. 78−71846
He, boiling on surfaces, heat transfer coeff. 78−9545
He, dense gas, positive ion excess, ion-induced droplets 79−14925
He liquid, transient heat transfer, static coolant 78−75049
He, nucleate pool boiling, heat flux and press. effect on heat transfer 79−14235
^{3}He, absence of BCC nucleation on Grafoil substrate, 30-320 mK 79−19422
^{3}He, solid, phase separation of dil. ^{4}He impurities 80−88393
^{3}He-^{4}He, dilute, nucleation and stratification induced by press. at low temp. *(Russian)* 78−34672
^{3}He-^{4}He, liquid, nucleation of superfluid phase transitions at container walls 79−56014
^{3}He-^{4}He liquid mixture, nucleation of superfluidity and phase separation 78−43204
^{3}He-^{4}He mixtures, liq., coherence length effects on nucleation of superfluid transitions 77−66069
^{4}He charged drops in cryogenic vap., He^+ mobility, 1.3-2.0K 79−32734
^{4}He crystals, nucleation and orientation 80−84339
^{4}He, isotopically pure superfluid, vortex nucleation 80−44378
^{4}He, liq., nucleation of freezing by positive ions 77−84893
^{4}He, solid, at Grafoil/high press. liq. ^{4}He interface 77−28062
^{4}He, solid, nucleation in Vycor under press., superfluid oscills. near melting press. 79−51388
^{4}He, superfluid, vortex nucleation inhibition by strong electric fields 80−92735
Hg, condensation, two-dimensional, on W 80−107666
HgSe, press. induced phase transitions, nucleation, resistance discontinuity 77−27996
In epitaxial growth, cluster mobilities, in-situ electron microscopes obs. 80−15407
interstitial cluster nucleation, effect of trapping at onset of irradiation 79−78974
$KAl(SO_4)_2.12H_2O$, secondary nucleation, origin, nuclei size distrib. 79−94933
$K_2Al_2(SO_4)_4.24H_2O$, growing in aqueous solution, observation of secondary nuclei production 78−68613
KCl, crystal growth rate in cooling soln., nucleation and supersaturation 77−76337
KCl crystallites, nucleation, oriented growth on amorphous SiO_2 using square-wave surface relief grating 78−47672
KCl, influence of collisions on cryst. growth and secondary nucleation under conditions of meas. crystn. 80−50544
KCl, two-dimens. nucleation rate on the (100) surfaces, mol. beam method, 289-343°C *(German)* 80−93500
KCl:Ba^{2+}, localised stress relaxation in excess vacancy system, prismatic loops *(Russian)* 80−88160
KCl:Ba(Ca)(Sr), microstruct. and hardness, impurity distrib. effects 79−24529
KCl:Pb^{2+} crystals, precipitation, density changes, nucleation mode, lattice relaxation, heat treatment 79−66066
$KClO_4$ single crystals, gel growth, temp. effects etching 79−78862
KDP, growth in soln., nucleation rate, supersaturation and temp. depend. 77−4728
KH_2PO_4 single crystal evidence for spiral growth on pyramidal faces 80−84120
KH_2PO_4, supersaturated solution, nucleation rates meas. from induction period 79−23549
K_2O-Al_2O_3-SiO_2 system, crystallisation of glasses in primary phase field of leucite 78−67658
K_xWO_3 bronze, oxidation to $K_2O(WO_3)_n$, struct. changes 78−68925
Kr, liquid, superheated, nucleation 79−23741
Li_4, plane configs., ab initio SCF calc., rel. to condensation *(French)* 77−4062
LiF, radiation induced voids, formation on dislocations 80−15159
Li_2O-$2SiO_2$ glass, DTA study, Kissinger plot 80−84084
Li_2O-SiO_2 glass, cryst. nucleation, test of classical nucleation theory 80−1939
Li_2O-SiO_2 glass, water content effect on crystal nucleation and growth 79−55670
$Li_2O.2SiO_2$ glass, kinetics of crystal nucleation, effect of Pt and other impurities 78−88440
$Li_{x+2}P_xO_{3x+1}$, polyphosphate, melting and crystallisation 80−70376
$Li_2Si_2O_5$ glass, steady state crystal nucleation rate 79−90564
$Li_2Si_2O_5$ glass, steady state crystal nucleation rate 79−90565
MgO, precipitation from gas phase 78−6025
MgO-Al_2O_3-SiO_2, melt and glass crystn. with ZrO_2-TiO_2 nucleants 77−31599
MgO-Al_2O_3-SiO_2 glass, features of crystallisation, in the presence of the thermal decomposition of tetrabutoxytitanium 78−87627
$MgSO_4.7H_2O$, cryst. regeneration and growth in contact nucleation 79−23545
$MgSO_4.7H_2O$, growing in aqueous solution, observation of secondary nuclei production 78−68613
MnAs, formation of nuclei in ferromag. paramag. transition, thermal hysteresis 79−73720
Mo, BCC, void nucleation following electron irrad. 80−29054
Mo, damage profile resulting from Ni^{2+} and He^+ ion bombardment 78−10100
Mo, film on sapphire substrate, orientational growth, epitaxial textures, nucleation textures *(Russian)* 80−75454
Mo-C dilute alloy defect cluster nucleation and growth under 1250 keV electron microscope *(Japanese)* 78−87663
Mo-Zr, heavy ion irradiated, void swelling, phase instability 80−29084
Mo-Zr, nucleation conditions, effect on formation of oxide phase during internal oxidation *(Russian)* 80−81064
$MoGe_2$-Mo diffusion couple, nucleation of $Mo_{13}Ge_{23}$ *(French)* 77−55398
N_2, heat transfer during nucleate boiling, heating wall and metallic coating thicknesses depend. 79−32210

nucleation continued
N_2, heat transfer in boiling on surface of vertical cylindrical rod 80−48706
N_2, liq., nucleate boiling heat transfer from PTFE coated surface 78−34000
N_2 pool boiling in high centrifugal accel. fields, peak nucleate boiling heat flux 79−59907
NH_3, condensation by homogeneous nucleation in supersonic nozzles 77−11230
NH_4Cl, cryst. nucleation, growth rates from organic media, outline meas. technique 79−38730
NH_4Cl, submicron particles, density, morphology 80−61166
NH_4Cl-H_2O, solidification microstructs., effect of reduced gravity 80−96632
$NH_4H_2PO_4$ single crystal evidence for spiral growth on pyramidal faces 80−84120
NO_2 in nonane, supersaturated gas, photoinduced nucleation 78−80760
NO_x^--HNO_x-H_2O clusters, gas phase, thermodynamic quantities, mass spectra obs. 80−50875
Na silicate glass temp. depend. of rate of nucleation of acicular crystals 77−19875
Na smoke particles, nucleation and growth, light scatt. study 80−35580
NaA and NaX zeolite crystals, crystn. study in presence of triethanolamine, Na_2O and SiO_2 content influence 79−65995
$NaBO_2.H_2O_2.3H_2O$, crystallisation from aq. soln., nucleation rates with surfactant 78−91276
NaCl cleavage step decoration, nucleation and growth of metallic thin films 77−69200
NaCl:Ni^{2+}, kinetics of impurity precipitation 77−69090
NaCl:Pb, precipitation of Pb impurity 78−48415
Na_2O-2CaO-3SiO_2 glass, cryst. nucleation and growth, viscosity, thermodynamic props. 80−84079
Na_2O-Al_2O_3-SiO_2, glass, nucleation, crystn., ceramic form. 80−84082
Na_2O-BaO-Al_2O_3-SiO_2, glass, nucleation, crystn., ceramic form. 80−84082
Na_2O-CaO-SiO_2 glass, water content effect on crystal nucleation and growth 79−55670
2Na_2O-CaO-3SiO_2 glass, cryst. nucleation rate, viscosity, heat treatment 80−84081
Na_2O-SiO_2:Au+CeO_2, Au particle nucleation 80−81066
$Na_2O.2SiO_2$, nucleation kinetics, temp. depend. 78−26467
Na_2SO_4 aq. soln. droplets, nucleation by $Na_2B_4O_7.10H_2O$ in emulsion *(French)* 79−1492
$Na_2S_2O_3.5H_2O$, glass transition, anal. of large stable supercooling 77−51477
Na_2SiF_6, precipitation from H_2SiF_6 soln., mechanism, kinetics, habit 77−44142
$Na_2O.3MoO_3$, nucleation of fibrillar crystals, effect of surface layer, growth on air bubbles 78−60559
$Na_2O.3MoO_3.3H_2O$, nucleation and growth from soln. 77−84682
Nb, BCC, void nucleation following electron irrad. 80−29054
Nb, film on sapphire substrate, orientational growth, epitaxial textures, nucleation textures *(Russian)* 80−75454
NbC particles, growth and dissolution, in aged and deformed austenitic stainless steel 78−39782
Nb_3Ge coevaporated film, high supercond. transition temp., nucleation and growth 80−76185
Ni (100), adsorption of O_2 and reduction of surface oxide by H_2 80−108741
Ni base superalloy, γ'-precipitation influence on recrystallisation 80−29955
Ni crystallisation, on reinforced fibres *(Russian)* 80−75455
Ni, electrochem. overgrowths, role of substrate dislocations and grain boundaries in nucleation and growth 79−51454
Ni, electroplated layer, field ion microscope study 79−28246
Ni, epitaxial growth, on NiO(100), by low pressure hydrogen reduction *(French)* 80−11578
Ni-Al alloys, effects of electron irradiation in precipitation, nucleation and dislocation loop growth, TEM study 79−42106
Ni-B film, crystn. on reinforced fibres *(Russian)* 80−75455
Ni-based superalloys, TEM obs. of cellular transformation products 80−3045
Ni-Co-Cr superalloy, powder produced, necklace struct. development 80−40395
Ni-Cr, ordering by nucleation and growth and by spinodal decomposition *(French)* 78−27471
Ni-Mn, ordering by nucleation and growth and by spinodal decomposition *(French)* 78−27471
Ni-P metallic glasses, crystn. kinetics by differential scanning calorimetry 78−91257
Ni-Ti (9.6 wt.%), mag. study on phase decomposition *(Japanese)* 80−15758
$Ni_3B_7O_{13}Br$, boracite single cryst., nucleation control density growth 80−80955
Ni_3Fe, Mossbauer spectra, order-disorder transition 78−10811
Ni_4Mo, coherent phase form. at stress concentrators *(Russian)* 80−49356
$Ni(NH_4)_2(SO_4)_2.6H_2O$, precipitation from equimolar aqueous solns., kinetics study 80−7848
$(Ni_{0.5}Pd_{0.5})_{82}P_{18}$ amorphous alloy, liquid-quenched, crystn. kinetics, nucleation 80−100176
Pb film, vacuum deposited onto SiO, C and mica, quantitative study of nucleation 79−77959
Pb, underpotential adsorption, cathodic deposition, on Ag(111) and (100) *(German)* 80−108363
Pb, variations of energy of the ⟨111⟩ torsion joint as a function of the angle of torsion in metallic seeds [dendritic structure] *(French)* 80−25682
Pb-Sn eutectic, directionally solidified, perfection and stability of lamellar struct. *(French)* 77−77468
$PbNb_2O_6$, ferroelectric thick crystals, domain formation and dislocation loops 78−60410
PbS epitaxial growth, cluster mobilities, in-situ electron microscopes obs. 80−15407
PbS(Se)(Te)-NiSb eutectic system, crystn. 79−52190
PbS(Te)-Sb eutectic system, crystn. 79−52190
$Pb_{1-x}Sn_xTe$, LPE grown heterostructures, improved nucleation and planar interface 79−95949
PbTe, continuous epitaxial film, grain size, growth cond. depend. 78−26786

nucleation continued
$Pb(Zr,Ti)O_3$, synthesis from cryochem. mixtures, chem. reacts. in sublimation drying 79−11538
Pd, epitaxial growth, cluster mobilities, in-situ electron microscopes obs. 80−15407
Pd, two-dimens. nucleus form. on Ag (111), UHV electron microscope obs. 80−10760
PuO_2-UO_2 mixed oxide fuel, plutonia particle behavior during sintering in Ar-H_2 (8%) atmosphere 79−8258
Rb, liq., cryst. nucleation and growth, mol. dynamics calcs. 79−74144
S atom nucleation particulate formation from SF_6 and SF_6-H_2 mixture photolysis 78−76836
SF_6, condensation in supersonic nozzle flow 78−34611
SF_6-Ar, condensing flow, gasdynamic and IR meas. 80−6501
SO_2, gas, photooxidation, cloud chamber obs. 79−1961
SO_2, photooxidation in gas phase, nucleation appls. 79−83479
SO_2-alkane-H_2O gaseous mixture, photoinduced nucleation and quantum yields 79−96348
SO_2+H_2O+O_2(N_2)(Ar), condensation nuclei form., ion polarity and age depend. 79−39220
SO_4^{2-} aerosol form. and growth in stratosphere 79−5604
$SSe_{22.5}$, amorphous-cryst. transition, light effect, rel. to polymer crystallisation 79−99076
Sb film on NaCl, effect of ion irradiation on form., struct. and props. 77−36408
Se film, trigonal, sputtered and evaporated nucleation and growth processes 77−31920
Se, vitreous, crystn., optical microscope obs. 77−84659
$Se_{0.95}Te_{0.05}$, glass crystallisation, effect of an alternating electric field 80−88054
$Se_{1-x}Te_x$, amorphous film, photo-crystallisation 80−59839
Se_xTe_{1-x}, growth of single crystals by Czochralski method 80−66423
Si, (111) surface structure phase transform, screw dislocations RHEED study 80−88153
Si amorphous film, crystallisation kinetics and morphology, TEM obs. 78−84093
Si, CVD, gas phase diffusion and surface reactions 79−15614
Si, CVD on SiO_2 and Si_3N_4 substrates, nucleation in SiH_4-HCl-H_2 system at high temp. 80−49538
Si, Czochralski grown crystal, O precip., nucleation behaviour and dislocation loop form. *(Japanese)* 80−59664
Si, dissolved O_2 precipitation, homogeneous nucleation 77−11695
Si epitaxial growth, nuclei spacing, activation energy 77−62770
Si, epitaxial layer, growth mechanism from ion-molecular beams 80−2299
Si epitaxial stacking fault nucleation site identification, annihilation, and suppression 77−76705
Si, heteroepitaxial early growth island morphology rel. to deposition conditions 78−6245
Si on sapphire, deposition kinetics and interface characteris. 79−28234
Si, on sapphire, early growth, models 77−24962
Si single crystal growth by heat-exchanger casting 78−11104
Si, slip dislocation nucleation during laser annealing 80−84179
Si, solid-phase epitaxial growth stages in Si(crystal)-Pd_2Si-Si(amorphous) system 77−85114
Si:H amorphous film, plasma-deposited, growth morphology and defects 80−44128
Si-Al-Al_2O_3 system, solid phase Si regrowth on sapphire 80−100413
Si-Co interface metal-semiconductor transition, rel. to first compound nucleation 80−24771
SiC, cryst. growth on oriented seeds by sublimation 78−35279
SiC, determ. of size and conc. of crit. clusters in vapour phase in homogeneous nucleation process 79−94951
SiC, epitaxial film, effect of impurities on polymorphism during growth 80−15414
α-SiC, single crysts. phase struct. rel. to heat treatment, nucleation 80−38991
SiO_2-Al_2O_3 mixture, depend. of phase comp. on nuclei available 79−11584
SiO_2-Na_2O-CaO glass, phase separation characts., melting atmosphere effect 80−44141
$SmCO_5$, etched microparticles, Barkhausen discontinuity, nucleation, and domain wall pinning 79−87288
Sn, $\alpha \rightarrow \beta$ transform., α-Sn nucleation and growth in β-Sn 78−38838
Sn, crystn., mechanism of influence of soluble impurities 78−71692
Sn droplets, on Bi, Zn and Al, heterogeneous nucleation 80−44294
Sn film, vapour-deposited on NaCl single cryst., nucleation, growth, microstruct. 78−91561
Sn polymorphic transformations ($\beta \rightarrow \alpha$), effect of impurities, exam. 80−7557
SnTe, epitaxial film, nucleation and form. of three-dimensional islands 79−65348
$SrSo_4$ epitaxy, on $BaSO_4$ from aqueous solns. mechanisms of growth 79−56093
$SrTiO_3$, crystallisation from melt, nucl. and final cryst. sizes 77−24951
steel, austenitic stainless, 18 Cr-11 Ni, effect of boron on nucleation of $M_{23}C_6$ carbides *(Polish)* 78−84808
Ta film, nucleation of α or β phase, impurity effects 77−24493
Ta, film on sapphire substrate, orientational growth, epitaxial textures, nucleation textures *(Russian)* 80−75454
Te, ENSH method of oriented thin film growth 79−99443
Te evaporated film nucleation on Au oriented islands, grain growth 78−2388
Te film, evaporated, predeposited Ag, Sn, Bi, Al and Se nucleation centres effect on grain growth 77−4739
Te, growth of single crystals by Czochralski method 80−66423
Te, vacuum deposited film, effects of electron irradiation on surface coverage *(Japanese)* 79−82477
Te, vacuum deposited on NaCl, crystallite growth and morphology, electron microscopy 80−65401
Ti, pit nucleation in bromide media, ion beam anal. 80−93683
Ti-Ag (10 to 17.5 wt.%), eutectoid system, $\beta \rightarrow \alpha_m$ transform., nucleation kinetics 80−97474
Ti-Al-Sn (5, 2.5 wt.%), annealing of near-basal hydrides 80−20989
α+β-Ti-Al-Sn-Zr-Mo-Cr, low cycle fatigue crack nucleation and early growth 79−8354
Ti-Au, (9.9 wt.%), eutectoid system, $\beta \rightarrow \alpha_m$ transform., nucleation kinetics 80−97474
Ti-Cr (15 at.%), aged omega phase, electron microscope exam. 78−72783

nucleation continued
Ti-Mo-Zr-Sn (11.5, 6.0, 4.5 wt.%) alloy, struct. as affected by processing history 80−84972
$TiAl_3$ crystals dissolution in pure Al liq., grain refinement of α-Al solid-solution by Ti addition 80−35178
TiC, W_6Co_6C cemented carbide substrates, structure, composition and hardness exam. 78−11425
TiD_2, nucleation and growth in D_3^+ implanted Ti, TEM study 80−97717
TiO_2 brookite synthesis from Ti in NaF or Ti compounds, form. mechanism *(Japanese)* 80−93529
Tl, underpotential adsorption, cathodic deposition, on Ag(111) and (100) *(German)* 80−108363
$TlAsS_2$, glass, crystallisation, effect of an alternating electric field 80−88054
UO_2, condensed vapour following core disruptive accident, particle-size distribs. using first-generation model 78−13295
V, film on sapphire substrate, orientational growth, epitaxial textures, nucleation textures *(Russian)* 80−75454
W, film on sapphire substrate, orientational growth, epitaxial textures, nucleation textures *(Russian)* 80−75454
Xe, liquid, superheated, nucleation 79−23741
$Y_{2.3}Gd_{0.6}Fe_{4.7}Al_{0.4}O_{12}$ garnet, effect of Gd on magnetite exsolution in a garnet matrix 79−11624
Zn, electrolytic deposition, on Pt single crystal spheres, critical overvoltage 80−104080
Zn film, on Cu_2O, effect of ion irradiation on form., struct. and props. 77−36408
$ZnC_2O_4.2H_2O$, crystn. kinetics by precipitation 80−50884
ZnO microcrystals, morphology, formed by Zn anodic electrocrystn. 77−80432
ZnO, precipitation from gas phase 78−6025
ZnS(Se)(Te) film, on semicond. substrates, early stages of growth, electron microscope obs. *(Russian)* 78−38976
ZnTe, epitaxial film growth initial stages 77−80707
Zr-Cr (1.9 wt.%), β-quenched and tempered, $ZrCr_2$ precipitation, TEM study 79−66062
Zr-Nb, singularities of β→ω transform. in alloy, with high content of β-stabiliser *(Russian)* 78−76644
Zr-Nb-Ge, singularities of β→ω transform. in alloy, with high content of β-stabiliser *(Russian)* 78−76644
γ-ZrH, precipitation in Zr, exam. of precipitation mechanism due to shears, electron microscope exam. 78−84809

nuclei *see nucleus*

nuclei with mass number 1 to 5
3N and 4N model systems, props., stochastic variational method 77−41891
^{2}H, isobar knock-out theory 77−18510
^{3}He(e,e'p) coincidence expt. at Saclay 600 MeV linac 79−71849
^{5}Li states, phase shift anal. of ^{3}He(d,d) 80−47382
A=2, 4, 16, photonuclear sum rule enhancement factor, Hartree Fock, Bethe-Goldstone eqns. 79−3137
A=3,4, finite nuclei, binding energy in Jastrow-Factor-Cluster method 79−49575
A=3, d+n clustering, D-state effects in (d,t) and (d,^{3}He) 79−22302
A=3, two particle orbital functional parentage coeffs. 79−63604
A=3 nuclei, charge asymm. from EM contribution to ^{3}He-^{3}H binding energy difference 78−29378
A=3 nuclei, charge asymmetry 79−71808
A=3 systems, charge form factor and bound nucleon polarisation 80−22708
A=3-4 hypernuclei, binding energy anal., Λ-N pot., scatt. length and effective range 80−9256
A=4-16, monopole giant resonances, state density radii and compressibility using hyperspherical functions *(Russian)* 80−27615
A=5 to 10 nuclei, energy levels 79−49583
A<100, average E1/M1 strength ratio 80−52621
baryon-antibaryon nuclei 80−22709
big bang, helium synthesis, neutrino flavors, and cosmological implications 80−73084
bound trinucleon systems, formalism for including the Δ(1236) resonance 79−54397
charge structure, effect of neutron charge 80−105963
energy-weighted longit. sum rule for electron-nucleus scatt. and nuclear forces 78−58238
few body systems and EM interactions, conference, Frascati, Italy (March 1978) 79−71804
few nucleon systems, 3N and 4N calcs., reviews 78−50094
few nucleon systems, e.m. processes 79−71797
few-body methods, stat. mechanics, atomic and molecular physics, nuclear N-body problem 79−85379
few-body problem, deuteron, EM effects, three body bound state, break-up reactions 79−85384
few-body quantum system stochastic variational method for all conventional N-N pots. 77−53799
few-nucleon systems studied with electromagnetic probes, future prospects 79−71809
four-nucleon problem, integral eqn. approach, pair-wise interactions *(Russian)* 77−88052
fragmentation of nucleus caused by decay of bound muon *(Russian)* 79−68333
generalised Low eqn. approach to reaction matrix 79−85491
H=3 nucleus complete electrodisintegration, interaction role in final state *(Russian)* 77−74835
hypernuclei studies in nuclear emulsions 77−22923
internal conversion coeffs. for at. numbers Z≤30 77−46136
isobar configurations in few nucleon systems, review 78−37294
microscopic calculations for ^{4}H, ^{4}Li continuum, appl. to ^{3}H(n,n), ^{3}He (p,p) 78−17114
neutronium (Z=0) bound isotopes search in high-energy proton induced fragmentation 77−22904
origin, abundances in matter-antimatter model of universe 78−45439
photofission by massive neutrinos radiative decay, rel. to cosmic abundances 79−92668
photonuclear energy integrated cross-sections, calcs., A=2-40 77−50110
polyneutron systems, search in U+p 700 MeV interactions 77−50064
potential scattering, boundary condition model, two and three nucleon problems *(Russian)* 78−86491
$p\bar{p}$ atom, ground state energy displacement *(Russian)* 79−89813

nuclei with mass number 1 to 5 continued
realistic NN pot. construction for three body systems and nuclear matter 80−22699
resonating-group method anal. 77−82886
review of reactions involving few-nucelon systems at intermediate energies 78−13054
three body systems in nuclear physics, review 78−517
three particle level spectrum, Thomas theorem and Efimov effect, N/D eqns. 80−42562
three- and four-body interaction props., hyperspherical expansion convergence *(Russian)* 78−518
three- and four-nucleon systems, dynamical eqns. and approx. methods 77−22905
three-body, two-pion exchange forces, ^{4}He calc. 77−41895
three-nucleon system, bound state calc. program PERFECT 80−13390
three-nucleon system, Faddeev eqns. perturbation, nucleon-nucleon interaction with tensor force 78−70463
three-nucleon systems, harmonic oscillator basis for ground-state calcs. 79−71807
three-nucleon systems, props. and interactions 79−71805
three-particle nucleus, virtual decay, vertex form factors *(Russian)* 77−26607
trinucleon ground state observables, new harmonic oscill. basis calc. 77−74776
trinucleon props. with one-boson exchange potls. 77−18421
triton-proton mag. moment ratio determ. by NMR method with 10^{-6}% accuracy *(Russian)* 77−61773
two-fermion system, one-boson-exchange pot. in relativistic config. space *(Russian)* 77−88051
two-nucleon system, Δ resonance, excitation spectrum 78−41649
two-nucleon system EM processes, baryon resonances 77−79364
αα and NN scatt. analogies, quark struct. and clustering connections 79−6442
(d,p), effects of d deformation and D-state influence, wave functions 79−13201
d stripping, inclusive p spectrum, d wave function behaviour 79−17884
(e,e), A=2, 3, 4, scaling laws in relativistic impulse approx. model, spin effects 80−52662
(γ,X), A=2, 3, 4, photonuclear and EM interactions 80−22816
^{1}H(n,n)^{1}H at 16.9 MeV, analysing power meas. 78−4941
^{2}H, ΔΔ content 77−22680
^{2}H(γ,π^0), near threshold, total and differential cross-sections 77−14106
^{2}H(π,π), covariant NN dynamics 77−6449
^{2}H(π,π), relativistic three-body calc. 77−74715
^{2}H(π^+,pp), pion absorpt., effect of ρπ exchange currents *(Korean)* 80−47402
H+p, 24 GeV, J/ψ prod. cross section 78−46055
^{3}n binding energy, calc. from ^{3}H, ^{3}He, ^{4}H, ^{4}He and ^{4}Li ground-state properties 80−83044
^{3}n system, bound state, Faddeev eqn. calc. 80−105989
^{3}n system, S-matrix pole trajectories 79−67679
^{4}n binding energy, calc. from ^{3}H, ^{3}He, ^{4}H, ^{4}He and ^{4}Li ground-state properties 80−83044
NN system, positions of resonances found by applying Faddeev's equations *(Russian)* 79−93529
(p,$\pi^\pm$), 320-800 MeV protons on ^{2}H to ^{10}B targets, coherent pion production *(French)* 79−533
$p\bar{p}$ annihilation, γ spectra, evidence for quasinuclear bound states 78−54642
(π,π) elastic and inelastic, approx. four particle eqns. *(Russian)* 78−86554
(π,π) elastic scatt. on light nuclei, optical pot. and scatt. amplitude model *(Russian)* 78−89918
π scattering by few-nucleon nuclei, diffractional approx. *(Russian)* 78−650
π^3He^{3}H coupling constant estimation, Chew-Low eqn. 77−3051
t→dn vertex constant from Faddeev eqn. *(Russian)* 80−83079
t formation average cross sections in (α,t) and (d,t) 80−42670
^{2}H(d,d), 5-45 MeV deuteron wave function asymptotic D- to S-state normalisation, anal. power 80−78304
^{2}H(n,p)n, 63.1 MeV, differential cross section 80−63186
^{2}H, possibility of thermonuclear fuel in relativistic plasma in B(p, 2α)α reaction *(Russian)* 80−37573
^{2}(n,2n)p, 21.5 MeV, quasi-free scatt. 79−75993
^{5}B(p,2α)α, possibility of thermonuclear fuel in relativistic plasma *(Russian)* 80−37573
^{12}C+π , multiple scattering theory with separate treatment of proton and neutron 79−45301
D, NMR in $(ND_4)_2PbCl_6$-ND_4Cl polycryst. mixture 78−6587
D, NMR of benzene and cyclohexane solubilised in hexadecytrimethylammonium bromide 78−24015
D, prod. by cosmological cosmic rays 78−12436
D-D fusion reactor, heliotron *(Japanese)* 78−54878
D-T, muon catalysed fusion for pellet ignition 77−3063
D+e scattering, neutron struct. function extraction, space-time descript. 78−62404
D+hadron, inclusive π, N spectra in high energy hadronic reactions, d fragmentation region *(Russian)* 78−54809
^{2}D, in electrolyte solns., NMR relax. *(Russian)* 78−15053
^{2}D, NQR in ice II 77−1617
D(d,n)^{3}He, 1.1 to 2.5 GeV/c, energy depend., cross sections, reaction mech. 78−54643
D(e,e'p)n, 160 to 300 MeV/c neutron-spectator impulse region *(Russian)* 77−50118
D(e,e'p)n, 500 MeV, coincidence cross section and deuteron momentum distrib. 79−67747
D(γ,ω), cross section meas., comparison with theory 78−58261
D(p,p), 630 MeV, asymmetry in scatt. polarised protons *(Russian)* 78−46064
D(p,π^+)T, 410, 605, 809 MeV, pion angular distrib. 78−29466
H, ^{2}H, ^{3}H, muon capture theory 78−553
H, A=4,3, containing charmed baryon, binding energies, lifetimes 78−89815
H, A=4,5, levels determ. from Li(^{6}Li,^{8}B) 77−46183
H, d-n or p-n, coupling constants from dispersion anal. of N and d scatt. amplitudes 78−29399
H, He, in solar cosmic rays, nuclear reactions interpretation of isotopic comp. 77−45266
H, neutron-photon multigroup cross sections for neutron energies ≤60 MeV 79−30880

nuclei with mass number 1 to 5 continued
H^+, upper limit from P- and T-violating interactions in hyperfine struct., mol. beam reson. expt. on TlF 80−53019
H^+, value from electric dipole hyperfine struct. calc. of TlF 80−53162
H+p, 200 GeV, data anal. hydrodynamical model 79−551
$H+p(\pi^{\pm})$, 200 GeV, jet production 79−54438
$H+\pi^{\pm}$, 50-30 MeV, total cross section meas. 77−6437
$H+\pi^{\pm}$, A=1,2, total cross sections, charge independ. and symm. 78−66321
$H(^{56}Fe,X)$, relativistic ^{56}Fe fragmentation, charge and mass changing cross sections 79−54453
$H(^3He,^3He)$, 33 MeV, ^3He polarisation anal. power meas. optical model anal. 77−38286
^1H, capture rate of μ^-, meas. by Saclay linac beam *(French)* 79−368
^1H coupled with ^{13}C, spinor character for spin $^1/_2$ nucleus via NMR interferometry 78−17699
^1H, double-resonance FT experiments using NMR probe double tuned matching boxes 77−45874
^1H, in electrolyte soins., NMR relax. *(Russian)* 78−15053
^1H, inverse β-decay fission $\bar{\nu}$ induced reaction cross sections 79−22273
^1H, NMR in o-$As_2B_{10}H_{10}$, mol. reorientation 77−85583
^1H, NMR in phospholipid bilayer 77−48767
^1H-^{13}C NMR in organic solids, spin decoupling dynamics 77−4582
^1H+d, 6.3 GeV/c, inclusive spectra of fast p and d *(Russian)* 78−46075
^1H+d, polarised projectile, parity nonconservation in low energy scatt. 78−66271
$^1H+\mu^- \rightarrow \nu_\mu$+n, angular correlations and capture rates, spin and isospin transitions, hyperfine effects 78−70494
$^1H(^{19}F,\alpha\gamma)^{16}O$, for meas. of H depth distrib. in solid 77−81435
^1H(D,2p)n, 26.5 MeV, 4 dimens. comparison with local S-wave interaction Faddeev calcs. 79−17866
^1H(N,N), 180° cross-sections 77−26737
$^1H(\alpha,^3He)^2H$, 3.98 GeV/c, ang. distrib. meas., comparison with DWBA 77−61416
$^1H(\alpha,\alpha'X)$, 1.74, 2.57 GeV, low mass πN enhancement, cross section t-depend. 80−63193
$^1H(\alpha,\alpha)$p, in mica, giant halos round α-emitting inclusions containing water 77−51420
^1H(d,X), 3.3 GeV/c, two-nucleon mass enhancement assoc. with spectator high momentum tail in breakup 77−18569
^1H(d,d), 2 GeV, polarised d, tensor and vector asymmetries 80−9285
^1H(d,d), 20 MeV, measurement on T_{21}, three nucleon Faddeev calc. comparison 79−71857
^1H(d,d), 35, 45 MeV, d wave function D- to S-state ratio from anal. power and cross section 79−89314
^1H(d,d), 45.4 MeV, tensor anal. powers 79−85447
^1H(d,d), anal. power ang. distrib., d D-state asymptotic normalisation 79−36247
^1H(d,d), deuteron D-state asymptotic normalisation 79−71858
^1H(d,d), elastic backward scatt., GeV energies, tensor anal. power 79−80916
^1H(d,d), polarised d, 5-13 MeV, analysing powers 79−71833
^1H(d,d), polarised p and d, analysing power data 79−71830
^1H(d,d) 10, 20 MeV, 79−13304
^1H(d,dγ) 6.3-7.1 MeV, bremsstrahlung anomaly near breakup threshold 78−89888
^1H(d,pn), 45.4 MeV, tensor anal. powers 79−85447
$^1H(\gamma,\pi^0)$, 1 to 10 MeV above threshold 79−85454
$^1H(\gamma,\pi^0)$, 290 to 360 MeV, differential cross sections in Δ(1232) region *(Russian)* 78−89852
$^1H(\gamma,\pi^0)$, polarised γ, 0.76-1.3 GeV, asymmetry meas. in photoprod. cross section *(Russian)* 79−59051
$^1H(\gamma,\pi^+)$, 3.4-18 GeV, πNN form factor and differential cross sections, one pion exchange 80−68526
$^1H(\mu^-,\nu\gamma)$, radiative capture relativistic calcs., rate and photon spectrum 80−68605
$^1H(n,\gamma)^2H$, 37 to 72 MeV, total cross section meas. 79−49627
$^1H(\bar{n},X)$, annihilation, 1.4 GeV/c, $\pi^{\pm}$, p emission angles, momentum and multiplicity distribs. 80−532
^1H(n,d), 1.88 GeV/c, neutral missing mass, ABC effect obs., cross section 78−74364
^1H(n,d)π^0, 459, 648, 802 MeV, relative diff. cross section and ang. distrib. 80−52671
$^1H(n,\gamma)$, polarised neutrons, calc. of P-violating asymmetry 77−18565
$^1H(n,\gamma)$, thermal, photon circular polarisation in parity violating capture 77−6375
$^1H(n,\gamma)$, thermal calc. of γ-circular polarisation, p-nonconservation effects 77−18564
$^1H(n,\gamma)^2H$, 2200 m/s neutrons, capture cross section 77−74849
$^1H(n,\gamma)^2H$, exchange current contribs. to parity violating elec. transitions 78−29383
$^1H(n,\gamma)^2H$, exchange current and interaction effects using unitary equivalent transforms. 79−9566
$^1H(n,\gamma)^2H$, relativistic invariant approach, parity violation 79−3147
$^1H(n,\gamma)^2H$, repulse core effect 77−38259
$^1H(n,\gamma\gamma)$, branching ratio meas. 77−30579
$^1H(n,\gamma\gamma)$, cross-section calc. 77−6385
$^1H(n,\gamma\gamma)$, thermal, consistency between pion exchange currents and NN pot., cross sections 80−68556
$^1H(n,\gamma\gamma)$, thermal n, cross section for two-quantum n capture 79−54439
$^1H(n,\gamma\gamma)^2H$, cross section upper limit 80−52683
$^1H(n,\gamma\gamma)^2H$, thermal, upper cross-section limit 77−3001
^1H(n,n), 14.2 MeV, polarised n, analysing powers 79−71832
^1H(n,n), 16.9 MeV, anal. power, F-wave contribs. 80−63158
^1H(n,n), pol. n, 13.5-16.9 MeV, anal. power and spin-orbit phase parameters 80−78269
^1H(n,n), pol. n, 50 MeV, anal. power 80−68639
$^1H(n,n)^1H$, 10 keV-20 MeV, use for neutron flux meas., proton-recoil detectors 79−9960
$^1H(n,n)^1H$, 325 MeV, phase shift anal. and mixing parameters 77−79277
$^1H(n,n)^1H$, 50 MeV polarised neutrons 77−26732
$^1H(n,n)^1H$, differential cross section below 30 MeV, phase shift anal. 79−9586
$^1H(n,n)^1H$, polarised neutron scatt. 77−26734
$^1H(n,n)^1H$ analysing power, 14.5 MeV, Hamburg polarised neutron facility, initial expts. 77−26946
$^1H(n,n)^7H$, 14 MeV polarised neutrons, analysing powers 77−54210
^1H(n,n)p, 210-495 MeV, free elastic scatt., phase shift anal. 80−52676

nuclei with mass number 1 to 5 continued
^1H(n,p), pol. n and p, 220-495 MeV, free elastic scatt., D_t and P parameters 80−52674
^1H(n,p), pol. n and p, 220-495 MeV, free elastic scatt., Wolfenstein parameters R_t, A_t 80−52675
^1H(n,p)n, pol. n,p, 50 MeV, spin correlation parameter $A_{vv}(\theta)$, phase shift anal. 80−68530
$^1H(n,\pi^0)^2H$, differential cross sections for 470-590 MeV, ang. distribs. 80−57628
$^1H(n,\pi^0)^2H$, nuclear forces charge symmetry test 80−5071
$^1H(\bar{p},X)$, elastic, inelastic and charge exchange cross sections in optical model 80−68665
$^1H(p,X),(d,X),(\alpha,X),(^{12}C,X)$, 1.55, 2.89 GeV/c, total and inelastic cross sections 79−6610
$^1H(p,e\nu^+)^2H$, bounds on rate, impulse approx. 77−3000
^1H(p,p), 0.35-1.0 MeV, differential cross section meas. 78−78379
^1H(p,p), 1-3 GeV/c, pol. p, spin parameters A and A_{nn} 80−95304
^1H(p,p), 225, 327, 520 MeV, analysing powers 79−75961
^1H(p,p), 398-572 MeV, analysing power meas., EM-nuclear interf. 77−23008
^1H(p,p), 6.14 MeV, cross sections and anal. power for noncentral reaction 79−85444
^1H(p,p), 6.141 MeV, anal. power, Paris pot. predictions 80−63156
^1H(p,p), EM effects, separation 77−23014
^1H(p,p), pol.p, 9.57 MeV, spin correlation parameter, phase shift anal. 80−102112
^1H(p,p) 647 and 800 MeV, absolute differential cross-section meas. 77−6390
$^1H(p,p)^1H$, E_n=1 MeV, cross section meas. 78−13089
$^1H(p,p\pi^+)n$, 800 MeV, Δ^{++} prod. and cross sections 79−22294
$^1H(p,\pi^+)^2H$, Low eqn. approx. soln., field theory propagator modification 79−85546
$^1H(p,\pi^+)^2H$, NN pot., isobar configurations and π prod., inelastic cross sections 79−63666
$^1H(p,\pi^+)^2H$, pol. p, total cross section, ang. distribs. and asymmetry parameters 80−63182
$^1H(p,\pi^+)pn$, polarised p, 305, 330 MeV, pion production differential cross section 79−67754
$^1H(\pi^-,X)$, 40 GeV/c, hadron emission into backward hemisphere *(Russian)* 79−59094
$^1H(\pi^-,\gamma)$, effective range theory parameters a_{nn} and r_{nn} 79−85381
$^1H(\pi^-,\gamma\gamma)$n, off-mass shell πN amplitude, $\pi^0 \rightarrow \gamma\gamma$ amplitude, chiral Lagrangian model 79−93669
$^1H(\pi^+,\pi^+\gamma)$, 269, 298, 324 MeV, radiative scatt. cross section, internal emission and recoil corrections 80−57805
^1H(t,dn), 2.5 GeV/c, 4π geometry, pole approx. description 80−68678
^2H, $^3S_1$-$^3D_1$ n-p state, mixing parameter energy depend. pot. description 77−82830
^2H (γ,π), theoretical and expt. results. 80−42698
^2H (p,p)(n,n), precise low energy cross section meas. with polyethylene targets 78−82342
^2H (π^+, π^+), low energies, Coulomb interaction *(Russian)* 80−83129
^2H asymptotic D-state normalisation from dp scatt. 79−13304
^2H, binding energy meas. *(Russian)* 79−9453
^2H bound state, relativistic quasipot. wave eqn. soln. 80−102132
^2H breakup, 156 MeV protons, NN multiple scatt. anal. 77−18546
^2H breakup, 45 MeV proton induced, np final state interaction ang. distrib. 77−18552
^2H breakup, new theorems concerning final state interactions *(Russian)* 77−326
^2H breakup induced by 12.5 MeV protons, Ebenhoh code anal. 77−18547
^2H breakup induced by 22.7 MeV nucleons, calc. with separable interactions with tensor forces 77−18554
^2H breakup induced by 8.5 MeV protons, Faddeev calcs. 77−18548
^2H breakup using 156 MeV protons, test for special kinematic conditions 77−18551
^2H charge operator, retardation, quasipot. eqns. and rel. corrections 80−99122
^2H D-state, asymptotic normalisation 78−41653
^2H D-state probability measurability in meson exchange current theory, moments and RMS radius 79−89246
^2H, D-state wave function calc. 78−8740
^2H deformation effects in nuclear interaction, DWBA anal. *(Japanese)* 78−21575
^2H disintegration, proton and neutron induced, up to 50 MeV *(Russian)* 78−89848
^2H disintegration due to weak neutral currents 79−22273
^2H, distant ENDOR obs. of partially deuterated succinic acid 80−23445
^2H, dynamic and static polarisability from Rayleigh scatt., two-photon disintegration 79−75867
^2H, Δ(1236) inobar probability is nuclear many-body system ground state 79−75859
^2H, EM form factor determ. 77−61287
^2H, EM form factor determ., relativistic impulse approx. 77−65158
^2H, EM struct. in terms of meson currents, quarks and Heitler-London-Cutkosky picture 77−10326
^2H, elastic scatt. of protons and α-particles *(Russian)* 78−21566
^2H electrodisintegration, study of e.m. processes in nuclei 79−71797
^2H form factor, relativistic effects 77−18519
^2H form factors, retardation currents, wave functions 77−34234
^2H ground state, N* configurations 77−18436
^2H γ-energy and binding energy from $^1H(n,\gamma)$ 80−52564
^2H, inverse β-decay, fission $\bar{\nu}$ induced reaction cross sections 79−22273
^2H label quantitative meas. in ^{13}C NMR 77−50456
^2H magnetic moment due to two boson exchange, pseudovector πN coupling model 79−40843
^2H, mass redeterm. 78−70434
^2H, muon capture, kinematics and dynamics 78−33151
^2H NMR, deuteron quadrupole coupling constants, determ. from natural abundance ^{13}C satellites 79−31556
^2H NMR, spontaneous polarisation of TGS, temp. depend., microscopic mechanism determ. 77−81070
^2H, NMR obs. of phase transform. in NbD_x 77−20721
^2H NMR of D_2O in lyotropic phase, T, calcs. 77−18944
^2H, NMR relax. and mol. dynamics in lipid bilayers 80−26206
^2H, NMR relax. rates in liq. nitromethane 79−95668
^2H, NN realistic nonlocal pots. from inverse scatt. theory for $^3S_1$-$^3D_1$ interaction 78−41651
^2H, NQR in high-press. forms of ice 77−90069
^2H, NQR in nematic mesophases 79−82890

nuclei with mass number 1 to 5 continued
H, neutrino-induced nucleosynthesis 77−87582
H neutron binding energy and n mass excess from ^{1}H(n,γ) 80−47362
H nucleus wave function momentum contribution from QCD diagrams *(Russian)* 80−68562
H photo- and electrodisintegration, meson exchange current and isobar config. effects 79−71840
H photodisintegration, quadrupole contrib. to cross section, isospin sum rules 77−30550
H, photodisintegration amplitudes with arbitrary number of EM multipoles 79−93437
H photodisintegration and electrodisintegration, weak interaction and P nonconservation 78−89849
H photodisintegration depend. on NN potential, 10 to 180 MeV *(Russian)* 77−6350
^{2}H, photonuclear sum rules and interaction effects, integrated cross-section determ. from double commutator 78−21542
^{3}H pionic atom, energy shift off-shell contribs., zero energy approx. validity 79−76537
^{2}H, quadrupole form factor and D-state probability 77−71571
^{2}H, quadrupole moment, calc. from D_2 elec. field gradient 79−93511
^{2}H quadrupole moment, energy depend. of NN interaction anal. 77−74775
^{2}H, quadrupole moment operator *(French)* 79−461
^{2}H quadrupole moments, $^3S_1$-$^3D_1$ and $^3D_2$ states simple pot. model 78−78271
^{2}H, quasi-elastic electron scatt., deuteron structure aspects 79−71847
^{2}H radial functions, pionic exchange current contribs. to pp→^{2}He$^+\nu_e$ 77−10329
^{2}H, relax. in nitrobenzene 77−48070
^{2}H, repulsive nonlocal potl. models 77−88050
^{2}H static moments, relativistic and exchange current corrections 79−17799
^{2}H target, expt. to observe excited states of nucleons in nuclei *(French)* 79−3179
^{2}H threshold, potential resonance near top of broad barrier 79−514
^{2}H, two-nucleon bound state description 77−38221
^{2}H wave function, from ^{2}H(N,N) scatt. and NN potential 77−18418
^{2}H-^{3}H binding energy correlation, ^{4}He theory and Tjon line 79−89227
^{2}H-N breakup calcs., separable interactions with P-waves and tensor forces, polarisation 77−50101
^{2}H^{3}Hμ→^{4}He+n+μ^-+17.6 MeV, muonic catalysis in synthesis reactions *(Russian)* 80−52706
^{2}H+^{3}He, 22 to 53 MeV, quasifree processes 77−82903
^{2}H+d, 6.3 GeV/c, inclusive spectra of fast p and d *(Russian)* 78−46075
^{2}H+n, deuteron breakup reaction, Reid soft-core pot. calcs. at 22.7 and 46.3 MeV 77−74860
^{2}H+nucleon, breakup reaction, off shell sensitivity, S-wave N-N interactions 78−82340
^{2}H+nucleon, Fermi-motion corrections 78−82348
^{2}H+p, 200, 300, 400 GeV, hadron prod. at large p_T invariant cross section 79−40926
^{2}H+p, 50 MeV polarised p scatt., analysing power meas. 77−71608
^{2}H+p, polarised projectile, parity nonconservation in low energy scatt. 78−66271
^{2}H+p, polarised projectile, parity nonconservation in low energy scatt. 78−70522
^{2}H+p(n), differential cross sections, Coulomb penetration factor in DWBA calc. *(Chinese)* 80−27603
^{2}H+p($\vec{p}$), high energy cross section calc. complex ang. momentum theory *(Russian)* 78−46067
^{2}H+π, coupled channel theory 78−13157
^{2}H+π, crossed pion absorpt. contrib. to scatt. length 77−10433
^{2}H+π, elastic scatt., absorpt., model using coupled channel eqns., exact soln. 77−88176
^{2}H+π$^-$, multiplicity distrib. data, simple non-interacting fireball model 79−3178
^{2}H+π$^-$→π^{0}nn, rest capture branching ratio, impulse approx. 78−62957
^{2}H+π$^+$, proton spectra, cross section, π. absorpt. mechs. 78−25239
^{2}H(^{20}Ne,pγ), Doppler shift attenuation lifetime meas. in ^{21}Ne 77−30513
^{2}H(^{2}H, n)^{3}H, fusion possibility in ^{2}H metallic state at low temp. 79−67806
^{2}H(^{2}H,n)^{3}He, fusion through metallic D 80−13517
^{2}H(^{2}H,p)^{3}He, appl. to effective ion temp. determ. in plasma focus *(Russian)* 79−27824
^{2}H(^{3}H,n)^{4}He, muon catalysis kinetics *(Russian)* 80−91206
^{2}H(^{3}He,^{4}He)^{1}H, 27 and 33 MeV, polarised ^{3}He beam analysing power and cross sections 79−89316
^{2}H(^{3}He,2pt), 2.2-6 MeV, A=5 levels coupled to nucl.-^{4}He*(0^+) channel 77−2906
^{2}H(^{3}He,p)α, light element profiling of tapered corrosion sections 79−92036
^{2}H(^{40}Ar,nγ)^{41}K, ^{2}H(^{40}Ar,pγ)^{41}Ar, 56 MeV, γ-decays of low-lying states in ^{41}K, ^{41}Ar obs. 77−41986
^{2}H(K^+,K^+)^{2}H, low energy, diagram formalism anal. *(Russian)* 77−26543
^{2}H(N,N), extraction of ^{2}H wave function 77−18418
^{2}H(N,N), off-shell effects, calcs. with phase equiv. separable pots. of rank two 77−18553
^{2}H(N,X) disintegration cross-section, cut-off radius in impulse approx. type models *(Russian)* 79−22276
^{2}H(α, n), 100 MeV, neutron polarisation meas. 78−70726
^{2}H(α,^{3}He(g.s.))p tensor polarisation ang. distribs. from sequential decay ^{2}H(α,p)^{3}He(α)n reaction 77−82899
^{2}H(α,^{3}Li)n, ^{3}Li tensor polarisation and cross sections 79−75967
^{2}H(α,α), 17.9 GeV/c, Glauber model rigid projectile approx. 79−63685
^{2}H(α,α)^{2}H, 6 to 14 MeV, cross section meas. 80−27655
^{2}H(α,α)np, 20-28 MeV, total reaction cross section 79−89317
^{2}H(α,αn), quasi-elastic scatt., direct reaction unitarised impulse approx. 80−42674
^{2}H(α,αn)^{1}H, 27.2 MeV, absolute differential cross sections 79−9599
^{2}H(α,αp), 140 MeV, quasifree p knockout, spectroscopic factors, DWIA anal. 79−67650
^{2}H(α,αp)n, 15 MeV, semiphenomenological impulse approx. anal. 77−82943
^{2}H(α,αp)n, 15 MeV, six-body effects, Faddeev anal. 79−76008
^{2}H(α,αp)n, 15-42 MeV, ^{6}Li 1^+ resonance and breakup amplitude, three body model 79−75954
^{2}H(α,αp)n, 15-42 MeV, three body calc., reaction mech. 78−70546

nuclei with mass number 1 to 5 continued
^{2}H(α,αp)n, 42 MeV, observation and comparison to theoretical calcs. 77−82942
^{2}H(α,n)αp, 100 MeV, differential cross-section and polarisation meas. 77−88157
^{2}H(α,np)^{4}He, differential cross section and polarisation, three body model 80−47460
^{2}H(α,pα) 22.5 MeV, tensor polarisation ang. distribs. in ^{2}H(α,^{5}He(g.s.))p 77−82899
^{2}H(α,pα)n, 18 MeV, cross section, ang. depend. meas., semiphenomenological anal. 78−58292
^{2}H(α,pα)n, 18 MeV, obs. of n-p final state interaction 77−6414
^{2}H(α,pα)n, 7.5-7.9 MeV, modified impulse approx. anal. 79−6648
^{2}H(α,pα)n, Coulomb interaction effects, ^{5}He(g.s.) resonance energy and width 77−71615
^{2}H(d,^{3}He), differential cross sections at 13.2 MeV, DWBA anal. 79−45276
^{2}H(d,^{3}He)n, 2-20 MeV collimated monoenergetic neutron beam prod. using associated particle technique 77−83418
^{2}H(d,N), 50-85 MeV, ang. distribs., PWBA anal. 79−76005
^{2}H(d,2n)2p, proposed expt. to determ. nn effective range 77−18585
^{2}H(d,2p2n), 80 MeV, PWBA, double spectator process 78−41731
^{2}H(d,d), 4.3, 6.3 and 8.9 GeV.c, struct. of secondary d spectra high momentum parts *(Russian)* 78−78394
^{2}H(d,d), 50-85 MeV, ang. distribs., PWBA anal., two body final states 79−6636
^{2}H(d,d), 50-85 MeV cross-section meas. 79−13307
^{2}H(d,d), 53, 63 GeV, inelastic intermediate state effects, Glauber multiple scatt. theory 79−36104
^{2}H(d,d), medium energy, total cross section, optical model calcs. 79−9593
^{2}H(d,d)^{2}H, four-body model of the four-nucleon system 79−63643
^{2}H(d,d)D, differential cross sections at 13.2 MeV, DWBA anal. 79−45276
^{2}H(d,dp)n, 50-85 MeV, p-n coincidence spectra 77−18568
^{2}H(d,n), 13.6, 24.3 MeV, 0° absolute differential cross section 80−27649
^{2}H(d,n), 18-26 MeV, differential cross sections, ang. distribs., ^{4}He broad level search 80−102117
^{2}H(d,n), 290, 460 keV, neutron polarisation, ang. depend. 80−42632
^{2}H(d,n), anal. power, comparison with mirror reaction (d,p) 79−75964
^{2}H(d,n), intense fast neutron beam prod. in high-press gas target 77−3201
^{2}H(d,n), pol.d, anal. power and polarisations in R-matrix methodology, comparison with (d,p) 80−78273
^{2}H(d,n), polarised d, <5.5 MeV, comparison of analysing power with ^{2}H(d,p) 79−17911
^{2}H(d,n)^{3}He, 12.3 MeV, neutron spectra normalisation, differential cross-section meas. 77−88106
^{2}H(d,n)^{3}He, 1.5-15.5 MeV, tensor anal. power, charge symmetry violation in mirror reaction 80−13368
^{2}H(d,n)^{3}He, 35-275 keV, neutron polarisation determ. 77−41942
^{2}H(d,n)^{3}He, 6 to 17 MeV, n prod. absolute differential cross sections 78−74373
^{2}H(d,n)^{3}He, four-body model of the four-nucleon system 79−63643
^{2}H(d,n)^{3}He, struct. and form factor models in mass-3 system 79−45274
^{2}H(d,n)^{3}He, total cross-section energy depend. 78−29477
^{2}H(d,p), (d,n), 50-85 MeV cross-section meas. 79−13307
^{2}H(d,p), anal. power, comparison with mirror reaction (d,n) 79−75964
^{2}H(d,p), pol.d, anal. power and polarisations in R-matrix methodology, comparison with (d,n) 80−78273
^{2}H(d,p), polarised d, <5.5 MeV, comparison of analysing power with ^{2}H(d,n) 79−17911
^{2}H(d,p)^{3}H, ^{2}H(d,n)^{3}H, analysing power meas. 78−25204
^{2}H(d,p)^{3}H, 13.4, 17 MeV, pol. d, anal. power direct reaction and isospin symmetries 80−515
^{2}H(d,p)^{3}H, 1.5-15.5 MeV, tensor anal. power, charge symmetry violation in mirror reaction 80−13368
^{2}H(d,p)^{3}H, cross-section anal. using four-body integral eqns. 77−18577
^{2}H(d,p)^{3}H, four-body calc. solns. 79−71855
^{2}H(d,p)^{3}H, four-nucleon integral eqn. solns. using effective UPA 79−71794
^{2}H(d,p)^{3}H, struct. and form factor models in mass-3 system 79−45274
^{2}H(d,pd)n, 12.2 MeV, collinearity condition repeat experiment 79−76004
^{2}H(d,pnd), 52 MeV, break-up mechanism 78−74375
^{2}H(d,t)^{1}H, differential cross sections calc. using DWBA, distortions 78−54772
^{2}H(δ,π^0), multiple scatt. contrib. to threshold photoprod. 80−73718
^{2}H(e, e′) d bag, nuclear bag states containing quarks, detection 78−70465
^{2}H(e, e)pn, polarised e, neutral weak currents, right-left asymmetry 79−80787
^{2}H(e, ep)n, spectator momentum distrib., quasielastic knockout mechanism *(Russian)* 79−30817
^{2}H(e, np), EM inelastic form factors, exchange current effects in electrodisintegration 79−93418
^{2}H(e,e′), 56.4 MeV, cross sections, form factors, meson exchange current contrib. 80−68649
^{2}H(e,e′), electrodisintegration at high energy and momentum transfer 79−6342
^{2}H(e,e′p), consistent nonrelativistic treatment including meson exchange currents and isobar configurations 79−40905
^{2}H(e,e′p), single hole state momentum distrib. 80−22674
^{2}H(e,e′p) 1180 MeV electrons, proton distribution, neutron momentum distribution *(Russian)* 80−68652
^{2}H(e,e′p)n, cross-section, neutron electric form factor 79−3138
^{2}H(e,e′p)n, recent developments in lepton scattering 79−80929
^{2}H(e,e), charge and structure radius, form factor and structure function *(Russian)* 79−40841
^{2}H(e,e), deep inelastic scatt., P nonconservation 79−75776
^{2}H(e,e), EM form factors, relativistic formulae, moment corrections 80−63075
^{2}H(e,e), EM interactions and mag. sum rules 80−42639
^{2}H(e,e), elastic and deep inelastic, nuclear matter density at large momentum transfers *(Russian)* 78−86529
^{2}H(e,e), electric and mag. scatt., tensor polarisation, mesonic exchange current effects 79−85374
^{2}H(e,e), energy weighted sum rules, almost realistic NN pot. anal. *(Russian)* 80−13465

nuclei with mass number 1 to 5 continued

^{2}H(e,e), form factors, tensor pol., and two-nucleon force calcs. 80−106045
^{2}H(e,e), quasi-elastic scatt., en coincidence, n electric form factor 79−67563
^{2}H(e,e), tensor polarisation and d wave function short range behaviour 79−40900
^{2}H(e,e), tensor polarisation and d wave function short range behaviour 79−67564
^{2}H(e,eπ), total cross section from square reaction matrix element *(Russian)* 80−32271
^{2}H(e,n)p EM sum rules, exchange currents and isobar configurations 79−93526
^{2}H(e,ne)^{1}H, meson exchange effects at quasi-elastic peak 77−30556
^{2}H(e,np), dispersion approach *(Russian)* 77−22737
^{2}H(γ, NNπ), threshold to Δ(1236) region, EM props. of NNπ system 78−41694
^{2}H(γ, pp)π^-, high momenta of emitted nucleons 78−70512
^{2}H(γ, π^-)2p, target asymmetry and effective neutron polarisation, polarised d 80−9286
^{2}H(γ, π^+)nn, excitation function, cross-section, threshold π^+ prod. 77−26670
^{2}H(γ,η)^{2}H, impulse approx. calc. of elastic η photoproduction 77−14110
^{2}H(γ,n), 20.3 MeV, linearly pol. γ, neutron yield and cross section 80−91171
^{2}H(γ,n), forward angle cross section and sum rule from Siegert's theorem 79−80925
^{2}H(γ,n)^{1}H, 400-700 MeV, p polarisation *(Russian)* 80−106046
^{2}H(γ,n)^{1}H, photodisintegration at 0° for outgoing protons 77−88109
^{2}H(γ,n)p, 375-650 MeV, proton polarisation energy depend. at CMS angle 90° *(Russian)* 80−63159
^{2}H(γ,n)p, cross section and polarisation with arbitrary number of EM multipoles 79−80923
^{2}H(γ,n)p, cross section asymmetry polarised photons 400 to 600 MeV, resonances *(Russian)* 79−89294
^{2}H(γ,n)p, differential cross section and proton polarisation using supersoft core pot. 79−89287
^{2}H(γ,n)p, parity violation expts. review, weak NN interaction 80−73792
^{2}H(γ,nnπ^+), threshold form factors 79−85453
^{2}H(γ,np), 325-725 MeV, proton polarisation anomalous struct. 77−30551
^{2}H(γ,np), <800 MeV, proton polarisation in γn$\rightarrow\pi^-$p *(Russian)* 78−41700
^{2}H(γ,np), cross-sections from 74 to 241 MeV 77−30552
^{2}H(γ,p), recent developments in lepton scattering 79−80929
^{2}H(γ,p)n, EM properties of πNN system, virtual π reabsorption 79−22109
^{2}H(γ,p)n, forward proton prod., low energy theorems 78−70510
^{2}H(γ,p)n, tensor NN force effects 77−57649
^{2}H(γ,pπ) photoexcitation in Δ(1236) region 80−22813
^{2}H(γ,π^-p)^{1}H, 250-500 MeV, Δ(1236) region, cross section 78−41693
^{2}H(γ,π^-p)^{1}H, π^--p coincidence obs., mechanism and rescatt. effects *(French)* 79−3133
^{2}H(γ,π^0), 1 to 10 MeV above threshold 79−85454
^{2}H(γ,π^0), 1-7 MeV, yield meas. 78−82333
^{2}H(γ,π^0), 450 MeV cross section asymmetry *(Russian)* 79−89171
^{2}H(γ,π^0), coherent photoprod., binding effects and threshold amplitude calc. 80−32264
^{2}H(γ,π^0), cross section and threshold effects using dynamical γN$\rightarrow$Nπ^0 model 80−27627
^{2}H(γ,π^0), impulse approx. calc. of differential cross-section 77−18524
^{2}H(γ,π^0)^{2}H, recoil deuteron polarisation statistical tensors anal. 78−74348
^{2}H(γ,π^0)^{2}H, threshold and Δ(1236) region, EM props. of πNN system 78−41695
^{2}H(γ,π^+), 1-4 MeV, cross-section meas. 78−21544
^{2}H(γ,π^+), threshold prod., excitation function 77−14105
^{2}H(γ,π^+)2n, π^+ energy spectra and emission angle *(Russian)* 79−40903
^{2}H(γ,π^+)2n, threshold to 22 MeV, bremsstrahlung yield and total cross section 80−9288
^{2}H(γ,π^+)2n cross section, threshold charged photopion prod. operator props. 79−89292
^{2}H(γ,π^+)nn, n-n final state interaction effects 80−102181
^{2}H(γ,π^+)nn, photoprod. near threshold, nucleus axial props. rel. to nucleon spin-fip *(French)* 79−522
^{2}H(γ,π^+)nn, threshold cross-section, impulse approx. 77−38256
^{2}H(γ,$\pi^\pm$), photprod. on neutrons effect of Fermi motion 78−74349
^{2}H(γ,π), 210-700 MeV, total and differential cross sections from impulse approx. 80−68647
^{2}H(γ,π), impulse approx. and π rescattering effects 77−6346
^{2}H(γ,π), threshold photoprod. cross sections, elementary nucleonic amplitudes 80−22812
^{2}H(μ,ν_μ)nn, differential spectra *(Russian)* 77−82915
^{2}H(μ^-, ν)2n, axial meson exchange currents, a_{nn} and g_p extraction 79−97658
^{2}H(μ^-, ν)2n, hard pions and axial meson exchange current effects 79−40906
^{2}H(μ^+,μ^+)pn, Coulomb break-up amplitude in three-body scatt. theory 79−71844
^{2}H(n, γ), slow neutrons, mesic interaction current, isobaric resonance *(Italian)* 78−25179
^{2}H(n, $\gamma\gamma$), thermal, cross-section meas. 77−26703
^{2}H(n, nn)p, 25 MeV, neutron-neutron effective range 80−83041
^{2}H(n, np)n, 130 MeV, Faddeev eqn. multiple scatt. series anal. 79−97707
^{2}H(n, np)n, 17 to 27 MeV, neutron-neutron scattering length determination, Monte Carlo analysis 80−13476
^{2}H(n,2n)p, in thick targets, n-n scatt. length determ., computer expt. 80−57776
^{2}H(n,γ)^{3}H, existence of excited states of A=3 nuclei 79−9553
^{2}H(n,$\gamma\gamma$), three-particle calc. 77−50131
^{2}H(n,n'), 14.8 MeV neutrons, d break-up cross section meas. 79−80932
^{2}H(n,n')pn, polarised n, 14, 30 MeV, neutron analysing power 79−71835
^{2}H(n,n), 10 MeV, differential cross section, (p,p) comparison for Coulomb force 79−71793
^{2}H(n,n), 30 MeV, plarisation asymm., analysing power 78−62538
^{2}H(n,n), 794 MeV, extreme back angle scatt. 78−50174
^{2}H(n,n), 8.05 MeV, elastic differential cross-section meas. by recoil technique 78−17207

nuclei with mass number 1 to 5 continued

^{2}H(n,n), (n,p), 24 MeV, quasifree scatt., n-n effective range, Monte Carlo anal. 80−68554
^{2}H(n,n), backward scattering, 200 to 800 MeV search for bump in 180° excitation function 78−62445
^{2}H(n,n), elastic scatt., perturbation calcs., Faddeev eqns., Reid soft core pot. 78−33177
^{2}H(n,n), ghost states and Pauli principle for many-body scatt. 79−76001
^{2}H(n,n), local soft core NN pots., quasiparticle formalism 79−6529
^{2}H(n,n), nonlocal nonsymmetric pot., treatment of Schrodinger eqn. 78−82325
^{2}H(n,n), polarised n, anal. power predictions 79−85445
^{2}H(n,n), quantum theory evolution law approach appl. *(Russian)* 79−80866
^{2}H(n,n), scattering amplitudes, 14.4 MeV Faddeev eqns. variational soln. *(Russian)* 79−85321
^{2}H(n,n), scattering in high-partial waves, on-shell theory 78−41565
^{2}H(n,n), virtual state in three nucleon system, partial wave dispersion relations 79−40920
^{2}H(n,n) 14.2 MeV, polarised n, analysing powers 79−71832
^{2}H(n,n) backward elastic scatt., 350 to 550 MeV, ang. distribs. 79−75782
^{2}H(n,n) backward elastic scatt., 200 to 800 MeV, ang. distribs. and relativistic momentum transfer variable 79−75783
^{2}H(n,n) backward scatt., relativistic effects 77−18519
^{2}H(n,n) scatt. length in $J=1/2^+$ three-N state calc. with super-soft core 77−71570
^{2}H(n,n) scattering length determination, using NN interaction radius approx. 79−6426
^{2}H(n,n)^{2}H, 12 MeV, polarised neutrons, analysing power meas. 78−33193
^{2}H(n,n)^{2}H, 14 MeV polarised neutrons, analysing powers 77−54210
^{2}H(n,n)^{2}H, 2.45 MeV, polarised n, depolarisation factor ang. distrib., phase shifts 78−78358
^{2}H(n,n)^{2}H, 2.6 MeV polarised beam, ang. variation of polarisation 77−26733
^{2}H(n,n)^{2}H, 50 MeV polarised neutrons 77−26732
^{2}H(n,n)^{2}H, polarised n, 12 MeV, analysing power, similarity with (p,p) scatt. 78−70514
^{2}H(n,n)^{2}H, polarised neutron scatt. 77−26734
^{2}H(n,n)^{2}H, sum rules linking doublet and quartet phase-shifts with ^{3}H binding *(Russian)* 77−74831
^{2}H(n,n)^{2}H analysing power, 14.5 MeV, Hamburg polarised neutron facility initial expts. 77−26946
^{2}H(n,nn), 14.1 MeV, n-n quasifree scatt. obs. 78−82337
^{2}H(n,nn)p, 21.5 MeV, cross section, nn effective range parameter 79−67669
^{2}H(n,nn)p, neutron-neutron quasifree scatt., 14.1 MeV 77−23018
^{2}H(n,np), at $\vartheta_n=0°$, collinearity effect 78−82356
^{2}H(n,np)n, <27 MeV, n-n scatt. length 79−17904
^{2}H(n,p2n), 120 MeV, n-n scatt. length determ., Watson-Migdal model anal. 78−82339
^{2}H(n,p)2n, 13.98 Mev, proton spectra and n-n scatt. lengths 77−88141
^{2}H(n,p)nn, 13.95 MeV, proton spectrum, neutron-neutron scatt. length 77−26704
^{2}H(n,pn)n, 22.7, 46.3 MeV, perturbation calcs. for realistic pots. 79−45265
^{2}H(n,pnn), 794 MeV, quasielastic charge exchange, modified impulse approx. 78−50173
^{2}H(n,π^-), 400-580 MeV, differential cross sections and ang. distribs. 80−86906
^{2}H(n,π^-)^{3}He, 400 to 580 MeV at backward pion angles 80−73847
^{2}H(ν,ν), polarised deuterons, asymmetry in emission of recoil deuterons 77−79264
^{2}H($\bar{\nu}_e$,$\bar{\nu}_e$n)p, antineutrino spectrum 80−102150
^{2}H($\bar{\nu}_e$,$\bar{\nu}_e$n)p, neutral current cross section for reactor $\bar{\nu}$ 80−5129
^{2}H(p, 2p)$_p$, 400 MeV, quasifree knockout cross sections 79−93614
^{2}H(p, dπ^+)n, 585 MeV, d momentum spectra 78−41718
^{2}H(p, n), 50 MeV, neutron polarisation meas. 78−70726
^{2}H(p, p') d bag, nuclear bag states containing quarks, detection 78−70465
^{2}H(p, pn), 400 MeV, quasifree knockout cross sections 79−93614
^{2}H(p, pn)n, 8.5 MeV, ang. distrib. of final state interaction 78−54751
^{2}H(p,Nπ)^{2}H, Deck model anal. 77−22757
^{2}H(p,2n)n, 50 MeV, expt. and theoretical cross sections 79−75994
^{2}H(p,2p), 156 MeV, kinematic collinearity condition 77−30547
^{2}H(p,2p), 156 MeV $d^3\sigma$ and $d^4\sigma$ spectra for collinear nucleon system 78−17175
^{2}H(p,2p)n, 13.25 MeV, meas. of total breakup cross-section 77−18555
^{2}H(p,2p)n, 15 MeV, polarised p, cross section in non-coplanar geometry 78−93997
^{2}H(p,2p)n, 20 MeV, cf. Faddeev eqn. calcs. 77−18549
^{2}H(p,2p)n, 23, 39.5 MeV, noncoplanar reaction, breakup cross section 80−530
^{2}H(p,2p)n, 28.5 MeV, collinearity effect 79−75995
^{2}H(p,2p)n, 28.6 MeV, breakup cross sections in collinear geometry 80−9296
^{2}H(p,2p)n, 45 MeV, sensitivity to various separable S-wave NN potentials 77−313
^{2}H(p,2p)n, 585, 800 Mev, n-p final state interactions 77−41965
^{2}H(p,2p)n, 8.5 MeV, n-p final state interaction, cross section, ang. distrib. 78−21560
^{2}H(p,2p)n, high energy, final state np interaction 77−18533
^{2}H(p,2p)n, interference effects for const. NN relative energies 77−26774
^{2}H(p,dπ^+), 800 MeV, pion prod. with spectator neutron, cross section 80−9294
^{2}H(p,γ), 7-15 MeV, polarised and unpolarised p, cross section and anal. power 79−40921
^{2}H(p,γ) and ^{3}He(γ,pd) anal. using Reid soft-core pot. 77−26664
^{2}H(p,γ)^{3}He, 450, 550 MeV, differential cross sections, inverse reaction comparison 80−86904
^{2}H(p,n)2p, pol. n and p, 10.6-15.1 MeV, transverse polarisation transfer at 0° 80−42630
^{2}H(p,np)^{1}H, 1.825 GeV/c anal., Glauber theory comparison 77−71525
^{2}H(p,nπ^+), 585 MeV, differential cross sections, reaction mechanisms 79−548
^{2}H(p,nπ)^{2}H, 800 MEV, cross-section meas. 77−6358
^{2}H(p,p'), 0.6-25 GeV, backward emitted proton inclusive spectra, short range correlation 80−32281
^{2}H(p,p), 10 MeV, differential cross section, p and d analysing powers 78−46063

nuclei with mass number 1 to 5 continued
^{2}H(p,p), 10 MeV, differential cross section, (n,n) comparison for Coulomb force 79−71793
^{2}H(p,p), 40-1000 MeV backward scatt., N-exchange model 77−18562
^{2}H(p,p), 600 MeV and 1 GeV, noneikonal theory 79−80930
^{2}H(p,p), 800 MeV, differential cross sections and anal. powers 80−83091
^{2}H(p,p), back angle elastic cross sections in Kerman-Kisslinger model, inelasticity corrections 80−106060
^{2}H(p,p), backscattering, large momentum transfers, π exchange effects 80−5143
^{2}H(p,p), Coulomb corrections near elastic threshold 77−34282
^{2}H(p,p), large angle scatt., cross section and anal. power 79−80917
^{2}H(p,p), near threshold, on-shell two-body model 77−34283
^{2}H(p,p), pol.p, spin rot. and depolarisation, NN amplitude double spin flip part 80−78271
^{2}H(p,p), polarised p, 14.1 MeV, analysing power 79−71831
^{2}H(p,p), polarised p, 2.5-6.5 MeV, vector and tensor anal. powers 79−63653
^{2}H(p,p), polarised p, 316, 516 MeV, anal. powers in resonance region, backward angle scatt. 79−71834
^{2}H(p,p), polarised p, medium and high energies, polarisation phenomena 79−85448
^{2}H(p,p), rank-1 pots. using shielded Coulomb pot., separable nuclear forces 79−71854
^{2}H(p,p), tensor asymmetries, deuteron D-wave and non-eikonal effects, Glauber model 80−78296
^{2}H(p,p) 17, 20, 24 MeV, polarised p and d, analysing power data 79−71830
^{2}H(p,p) cross section, d wave function with spin at light front *(Russian)* 79−85478
^{2}H(p,p) elastic backward scattering, detection of d relativistic wave function dependence on additional variable *(Russian)* 79−58973
^{2}H(p,p) Glauber versus final state interaction theory, inelastic/elastic scatt. cross sections 77−57554
^{2}H(p,p) large angle elastic scatt., d form factor at large q^2 80−102189
^{2}H(p,p)^{2}H, 1.5-3 MeV, extraction of dnp coupling constant, Cutkosky method 77−10404
^{2}H(p,p)^{2}H, 1.825 GeV/c anal., Glauber theory comparison 77−71525
^{2}H(p,p)^{2}H, 316, 516 MeV, backscatt. anal. power meas. 78−74368
^{2}H(p,p)^{2}H, determination of Coulomb corrections 77−10400
^{2}H(p,p)^{2}H, large angles, resonance one-pion-exchange model *(Russian)* 77−34306
^{2}H(p,p)^{2}H backward elastic scatt., resonance region, double-scatt. mechanism *(Russian)* 77−74854
^{2}H(p,p)^{3}He, four-body problem calc. 78−516
^{2}H(p,p)np, 13-19 MeV, p energy spectrum shape 79−6594
^{2}H(p,p)pn, polarised p, vector anal. power in final state interaction region 79−71836
^{2}H(p,pγ), elastic cross sections, bremasstrahlung, threshold and Coulomb effects 80−91186
^{2}H(p,pn), 156 MeV, kinematic collinearity condition 77−30547
^{2}H(p,pn), 156 MeV $d^3\sigma$ and $d^4\sigma$ spectra for collinear nucleon system 78−17175
^{2}H(p,pn), 47 MeV, excit. energy spectra, energy sharing spectra 77−50132
^{2}H(p,pn)^{1}H, 1 GeV, final-state interactions 77−82900
^{2}H(p,pn)^{1}H, 12.5 MeV, angular distrib. of p-n final state interaction 80−52672
^{2}H(p,pn)^{1}H in relativistic description of moving composite particles 77−46156
^{2}H(p,pn)p, 15 to 156 MeV, attenuation of quasifree scatt., empirical rules 77−61415
^{2}H(p,pn)p, 1.67 GeV/c, secondary particle ang. distribs. and correlations *(Russian)* 80−27646
^{2}H(p,pp)n, 50 MeV, pp coincidence meas. 77−18556
^{2}H(p,pp)n, 6.4 to 25.8 MeV, pn final state interaction, cross sections 78−54757
^{2}H(p,π^0)^{3}He, 377, 462, 576 MeV, possible forward peak in cross section 78−89874
^{2}H(p,π^0)^{3}He, (p,π^+)^{3}H, 250-800 MeV, distorted-wave impulse-approx. calc. 77−82932
^{2}H(p,π^+), 400-470 MeV, backward π differential cross sections and anal. power 80−86905
^{2}H(p,π^+), polarised p, 305, 330 MeV, pion production differential cross section 79−67754
^{2}H(p,π^+)^{3}H, 400, 470, 600 MeV, differential cross section using isobar model 80−9291
^{2}H(p,π^+)^{3}H, microscopic model using realistic nuclear wavefunctions 79−85465
^{2}H(p,π^+)^{3}H, NN pot., isobar configurations and π prod., inelastic cross sections 79−63666
^{2}H(p,π^+)^{3}H, studied via pp→π^+d amplitude and triangle graph 77−38265
^{2}H(p,π^+n)^{2}H, 585 MeV, Glauber theory, NN and NΔ amplitudes 78−62525
^{2}H(p,π)^{3}H, pion prod. models for medium energies 77−18563
^{2}H(π, π) 25-180 MeV, three body calc. up to (3,3) resonance, polarisations 79−40964
^{2}H(π,2nγ), final state interactions, n+n scatt. parameters 78−25245
^{2}H(π,nπ), total cross sections 79−85510
^{2}H(π,p)^{1}H, threshold to 3,3 resonance region, disintegration model containing absorption 77−88177
^{2}H(π,p)p, absorptive P-wave pion-nucleus optical pot. 79−22327
^{2}H(π,p)p, cross sections, Faddeev like eqns., absorption effects for scatt. 80−86928
^{2}H(π,p)p, reactive two body contrib. to pion-nucleus optical pot. 80−9313
^{2}H(π,p)p in resonance region, theoretical models 80−83123
^{2}H(π,pp), pion absorption in field theory using Low equation 79−67779
^{2}H(π,π)$_{,}$, pole terms and absorption in p-wave πd interaction 80−86932
^{2}H(π,π), 140-260 MeV, (3,3) region, tensor force, cross sections, pol. parameters 80−68641
^{2}H(π,π), 141 to 260 MeV backward elastic scatt. in (3,3) reson. region 79−85531
^{2}H(π,π), 142, 180 MeV, covariant three-body calc. 77−6450
^{2}H(π,π), 142, 256 MeV, form factor−backward scatt. correlation, tensor polarisation 80−99189
^{2}H(π,π), 343-637 MeV/c, elastic differential cross section meas. 78−50215
^{2}H(π,π), 47 MeV, differential elastic cross section 79−85530

nuclei with mass number 1 to 5 continued
^{2}H(π,π), (3,3) resonance region, three body relativistic eqns., cross section calcs. 78−74405
^{2}H(π,π), Brueckners R-matrix model for absorptive scatt. 77−6457
^{2}H(π,π), Coulomb effects in elastic scatt., approx. treatment 79−85548
^{2}H(π,π), elastic differential cross section, Faddeev calc. and π-absorption 79−75793
^{2}H(π,π), elastic scatt., charge exchange, deuteron disintegration, three-particle rel. eqns. 78−37381
^{2}H(π,π), exchange of ρ-mesons 78−21610
^{2}H(π,π), expt. and theoretical work, present status, model testing, πN interaction 80−42699
^{2}H(π,π), Faddeev calcs. 77−18622
^{2}H(π,π), graph summation method 77−18624
^{2}H(π,π), high energies, total cross sections from refined Glauber model 80−78322
^{2}H(π,π), high energy total cross section in Glauber model 80−18346
^{2}H(π,π), impulse approx. calc. of scatt. in resonance region 77−6452
^{2}H(π,π), low energy scatt. absorption effects, cross sections, Faddeev like equations 80−86928
^{2}H(π,π), low energy scattering theory *(Russian)* 79−54460
^{2}H(π,π), medium energy elastic scatt. amplitudes, covariant multiple scatt. model convergence test 80−42710
^{2}H(π,π), modified Glauber amplitude anal., differential and total cross sections 79−22334
^{2}H(π,π), multiple scatt. calc. 78−29506
^{2}H(π,π), multiple scatt. formalism 77−6451
^{2}H(π,π), NΔ interaction anal., D* model 78−29503
^{2}H(π,π), off-shell pion-nucleon amplitude multiple-scatt. calc. 77−79401
^{2}H(π,π), pion absorption effect from threshold to resonance 80−99193
^{2}H(π,π), pion-deuteron scatt. length 78−58306
^{2}H(π,π), polarised d, dibaryon resonance signals in excitation functions 80−9181
^{2}H(π,π), relativistic description, πN waves, NN rescatt., ρ-exchange, π absorption and emission 80−9310
^{2}H(π,π), relativistic Faddeev calc. 80−102066
^{2}H(π,π), scatt. length, exchange current contrib. 80−78328
^{2}H(π,π) 142 MeV, three-body calc. 78−37378
^{2}H(π,π) constrained phase anal. from NNπ system relativistic 3-body theory 77−61457
^{2}H(π,π) correction in (3,3) resonance region for differential cross section 79−97732
^{2}H(π,π) elastic scatt., multiple scatt. calcs. 77−18623
^{2}H(π,π)^{2}H, 142 MeV, elastic cross section and polarisation observables 79−75791
^{2}H(π,π)^{2}H, impulse approx., three-body helicity formalism 77−74885
^{2}H(π^-, n)n, mechanism, cross-sections, EM form factors 79−89181
^{2}H(π^-, nγ)n, n-n scatt. length from γ spectrum 78−62576
^{2}H(π^-, π^-), 552 MeV/c, elastic differential cross section Glauber theory anal. *(Russian)* 80−52700
^{2}H(π^-, π^-p)n, 438 GeV/c, break up process, kinematic variables, np final state interaction *(Russian)* 80−52701
^{2}H(π^-,nγ)n, multiple scatt. corrections, off-shell rescatt. effects, effective range 80−83127
^{2}H(π^-,π^-), 1.57, 1.66 and 1.76 GeV/c elastic hack scatt. cross section energetic shape struct. *(Russian)* 80−47510
^{2}H(π^-,π^-), 438 MeV/c, differential and total cross sections 79−76026
^{2}H(π^+, p)p, pπ exchange current effects on pion absorption, cross section enhancement 80−57803
^{2}H(π^+, π^+), 49 MeV, P-wave dispersive contrib. π and ρ rescatt. 80−78331
^{2}H(π^+,p)^{1}H, total cross section, ang. distribs. and asymmetry parameters 80−63182
^{2}H(π^+,p)p, pion absorption, absorptive P-wave pion-nucleus optical pot. 79−76031
^{2}H(π^+,p)p, pionic disintegration, absorptive π-nucleus optical pot., microscopic model 80−99191
^{2}H(π^+,pp) 40, 50 and 60 MeV, absolute differential cross sections, ang. distrib. polynomial fit 78−70571
^{2}H(π^+,π^-)X$^-$, 2.6 GeV/c, d proton screening correction and Glauber parameter 80−9175
^{2}H(π^+,π^+), 130 to 350 MeV, 180° scatt. 80−78335
^{2}H(π^+,π^+), tensor polarisation and cross section at 180° 80−5116
^{2}H($\pi^\pm$,p$\pi^\pm$), 340 MeV/c, reaction mechanisms and isospin effects 80−32306
^{2}H($\pi^\pm$,p$\pi^\pm$)n, 350 MeV break-up, differential cross sections 79−85509
^{2}H($\pi^\pm$,$\pi^\pm$), 140-260 MeV, backward scatt., differential cross sections 80−99194
^{2}H($\pi^\pm$,$\pi^\pm$), 47 MeV, elastic scatt. differential cross section 79−75794
^{2}H(t,n)^{4}He, 10.5 MeV polarised tritons, analysing power, polarisation function and transfer coeff. 77−10413
^{2}H(t,n)^{4}He, 20 MeV, neutron spectra normalisation, differential cross-section meas. 77−88106
^{2}H(t,n)^{4}He, 7-17 MeV, absolute differential cross sections meas. 77−26780
^{2}H(t,t)^{2}H, 10.5 MeV polarised tritons, analysing power meas. 77−10413
^{2}H(tμ,nμ^-)^{4}He, fusion reaction, 2 GeV energy release 78−17250
^{2}H(tμ,nμ)^{4}He, muon catalysed fusion, neutron yield, muonic molecules 80−106095
(^{3}H,^{3}H), polarised scatt., optical model parameters 78−70540
^{3}H asymptotic normalization parameter using partial wave dispersion relation technique 79−45185
^{3}H, BE in σ-model with three-body forces 77−71568
^{3}H, binding energies, three body calcs., Faddeev formalism, alpha cluster model 79−75876
^{3}H binding energy, 3N bound state with separable interactions, Faddeev theory corrections 80−13388
^{3}H binding energy, D-state percentage of deuteron, wave function shape 77−2902
^{3}H binding energy, energy depend. boundary condition model 79−13194
^{3}H binding energy, quantum theory evolution law approach appl. *(Russian)* 79−80866
^{3}H binding energy, relativistic calc., Bethe Salpeter eqn. 80−68519
^{3}H, binding energy, truncated t-matrix approx., trinucleon bound state problem 79−448
^{3}H, binding energy, unitary pole and Adhikari-Sloan expansions 78−499
^{3}H, binding energy and charge form factor, internucleon force 77−18438
^{3}H, binding energy calc., realistic nonlocal pots. from inverse scatt. theory for $^3S_1$-$^3D_1$ interaction 78−41651
^{3}H binding energy calcs., soft core potentials 77−18378

nuclei with mass number 1 to 5 continued
^{3}H binding energy from 1-boson exchange, n-d and n-(pn)* momentum distribs. 79−67639
^{3}H binding energy in J=1/2$^+$ three-N state calc. with super-soft core 77−71570
^{3}H biological half-life estimation in man, model 79−20689
^{3}H bound state for Reid soft-core pot. perturbational exact calc., binding energy 79−63602
^{3}H β-decay spectrum, $\bar{\nu}$e mass *(Russian)* 80−91159
^{3}H β-polarisation at low vel., C_V'/C_V and C_A'/C_A 77−10369
^{3}H, β-spectrum meas., refining of upper limit of $\bar{\nu}$ rest mass 78−17144
^{3}H charge form factor calc. with pair and recoil exchange currents 77−34238
^{3}H, chronic HTO exposure of rats, age effect 77−5044
^{3}H concentration measurements in nuclear power plant atmosphere, instrumentation 79−26765
^{3}H decay, electron spectra rel. to neutrino rest mass and astronomical consequences *(Russian)* 80−109575
^{3}H determination in whole-body sections by liq. scintillation counting *(German)* 77−5114
^{3}H, EM form factors, 3-nucleon wave function calc. 80−95302
^{3}H, effluent gases from nuclear power industry, ambient contamination, props. *(Spanish)* 78−61540
^{3}H electrodisintegration, quasi-elastic region, realistic interactions 79−71850
^{3}H, energy levels using ATMS method and realistic nuclear forces 80−22707
^{3}H, enhancement factor calc. in photonuclear electric dipole sum rule 78−37288
^{3}H form factor, two pion exchange charge density in static approx. 78−66222
^{3}H formation in water cooled, water moderated reactors, role of nuclear reactions 79−17970
^{3}H, ground state energy, second order Brueckner-Baranger approx. 80−63082
^{3}H ground state props. from configuration space Faddeev calcs. 80−102130
^{3}H hypernucleus, binding energy, role of spin forces in Λ-N interactions *(Russian)* 78−54718
^{3}H, influence of structure on cross-section of complete electrosplitting *(Russian)* 79−22272
^{3}H, integrated cross section for trinucleon photoeffect 78−82334
^{3}H isobaric analogue state excitation, cross section from ^{3}He(π^-, π^0) 80−42544
^{3}H, meson exchange contrib. to beta decay and mag. moment 77−6249
^{3}H, meson exchange currents, effect on charge form factors 80−105990
^{3}H model, appl. of three particle bound state eqns., binding energy 78−78276
^{3}H, muon capture 78−37314
^{3}H neutron binding energy 80−47362
^{3}H neutron binding energy from ^{1}H(n,γ) 80−52564
^{3}H ν-decay, ρ exchange current, weak axial vector current low energy theorem 79−40886
^{3}H, one-boson exchange pot., binding energy calc. 78−41652
^{3}H, one-hole states, in double magic nuclei, form factors, spectroscopic factors, centroid energies 78−17090
^{3}H, partly non-local pots. model 77−54157
^{3}H photodisintegration, quadrupole contrib. to cross section, isospin sum rules 77−30550
^{3}H photoeffect, electric dipole sum rules 79−36231
^{3}H photoeffect, hyperspherical harmonics and elec. dipole sum rules 77−57650
^{3}H, photonucl. sum rules 79−6427
^{3}H, props. calc. by interpolation approach *(Russian)* 77−22903
^{3}H realistic wave function, energy and density distribs. 80−86794
^{3}H, relativistic correction to binding energy 77−79302
^{3}H, relativistic corrections to two-body pot., binding energy 78−74301
^{3}H, semileptonic weak and EM interactions, isoelastic processes 77−18528
^{3}H Sussex interaction, g-matrix and variational calcs. 79−3091
^{3}H, three body bound states, realistic nucleon-nucleon interactions 78−62526
^{3}H, three body calc. with separable pots. for binding energy 79−45145
^{3}H, three nucleon observables with meson theoretical interactions, binding energy, form factors 79−67676
^{3}H, three-particle photodisintegration, hyperspherical functions method *(Russian)* 78−589
^{3}H, three-particle system for nonlocal interactions with continuum bound states 79−75870
^{3}H, total photodisintegration cross-section calc. using coupled hyperspherical harmonics 77−18525
^{3}H urine analysis, liq. scintillation solns. 77−9273
^{3}H wave function anal. form from Faddeev eqn., ^{3}He form factor 80−47410
$^3_\Lambda$H, and contrib. of spin forces to Λ-N interaction *(Russian)* 77−79319
$^3_\Lambda$H, charge symm. breaking, Λ separation energy in hypertriton 78−17132
$^3_\Lambda$H, charge symm. breaking considerations for hypertriton 78−17133
$^3_\Lambda$H, short range repulsion, separation energy, K-harmonics calcs. 80−86846
^{3}H-impregnated solid H_2, equilib. conc. of stored atomic H 77−46510
^{3}H-thymidine, cell survival and cytogenic responses, mammalian cells 77−5046
^{3}H+α, elastic scatt., orthogonality condition model derived from parity energy surfaces 78−29432
^{3}H+n, 14 MeV, spectra meas. 77−18558
^{3}H(^{3}He, X), 50, 65, 78 MeV, quasifree scattering and quasifree reaction processes 80−13486
^{3}H(^{3}He,^{3}He), 20-33 MeV, analysing power, differential cross section meas. 78−17227
^{3}H(^{3}He,^{4}He)^{2}H, excitation functions for incident energy 17 to 33 MeV 79−6640
^{3}H(^{4}He,d), reaction mechanism, effect of Pauli principle and channel coupling 77−65219
^{3}H(α,^{6}Li)n, 11.3-12.0 MeV, excitation functions 78−621
^{3}H(α,t)^{4}H, 11.3-12.0 MeV, excitation functions 78−621
^{3}H(α,t)n, 11.3-12.0 MeV excitation 78−621
^{3}H(d, n)^{4}He, meas. of mean d interaction energy in tritiated Ti layer 79−31281
^{3}H(d,n), pol. d, below 6.75 MeV, tensor anal. power 80−42633

nuclei with mass number 1 to 5 continued
^{3}H(d,n)^{4}He, 150 keV, vector polarised deuterons, n-p analysing power 78−62544
^{3}H(d,n)^{4}He, 6 to 17 MeV, n prod. absolute differential cross sections 78−74373
^{3}H(d,n)^{4}He, 7-17 MeV, absolute differential cross sections meas. 77−26780
^{3}H(d,n)^{4}He, 700 keV, n polarisation meas., scintillation + TOF technique 78−86538
^{3}H(d,n)^{4}He, neutron fluence and energy transfer standard 80−102194
^{3}H(e,e')nd, three-body calc. 78−33170
^{3}H(e,e'p)2n, realistic NN interactions, three body variational wave functions, spectral functions 80−47470
^{3}H(e,e'X), X=p or n, coincidence reactions, electrodisintegration cross sections 80−22823
^{3}H(e,e), many-body exchange effects, charge form factors calc. 78−33169
^{3}H(e,np), disintegration and Coulomb excitation cross sections in channelled nuclei 80−59539
^{3}H(γ,X) two- and three-body photodisintegration cross sections 80−32263
^{3}H(γ,π^0), 0-8 MeV, cross sections, taking π rescatt. amplitudes into account 78−78364
^{3}H(γ,π^0), polarisation effects 180 to 700 MeV, impulse approx. calcs. *(Russian)* 80−37368
^{3}H(γ,π^0)^{3}H, polarisation effects 180 to 700 MeV, impulse approx. calcs. *(Russian)* 80−37368
^{3}H(γ,xn), x=1 or 2, photodisintegration cross sections 80−22817
^{3}H(μ,ν)3n, transitions from bound to continuum three nucleon states 80−5128
^{3}H(n,$\gamma\gamma$), thermal, calc. of cross-sections and branching ratios 77−14131
^{3}H(n,n), scatt. length, 4-nucleon problem, integral eqn. approach 80−91183
^{3}H(n,n), thermal n_1 coherent scatt. length, four body problem relation 79−75997
^{3}H(n,n), zero energy total cross section and scatt. lengths 80−57778
^{3}H(n,n) coherent scatt. length meas. by neutron interferometry 79−59113
^{3}H(n,n) differential cross section, nonrelativistic theory of four nucleon systems *(Russian)* 79−80881
^{3}H(n,n) four-nucleon integral eqn. solns. using effective UPA 79−71794
^{3}H(n,n)^{3}H, four-body model of the four-nucleon system 79−63643
^{3}H(n,n)^{3}H, possible anomaly in backward scatt. cross section near 14 MeV 77−6363
^{3}H(n,n)^{3}H, possible anomaly in backward elastic scatt. cross section near 14 MeV 78−13088
^{3}H(p, p), 600 MeV, Glauber formalism study *(French)* 79−93616
^{3}H(p,γ), 30-100 MeV, meson exchange and nucleon correlation process calcs. 79−549
^{3}H(p,γ), 6 to 16 MeV polarised protons, ^{4}He excited states 77−18559
^{3}H(p,γ)^{3}He, intermediate energy, ang. distribs., reaction amplitude and ^{3}He vertices 80−22835
^{3}H(p,n), 1.24, 1.8 GeV, differential cross section, spin independ. Glauber model interpretation 80−63183
^{3}H(p,n)^{3}He, 13.6 MeV, neutron spectra normalisation, differential cross-section meas. 77−88106
^{3}H(p,n)^{3}He, 6 to 17 MeV, n prod. absolute differential cross sections 78−74373
^{3}H(p,n)^{3}He, coupled channels anal. of neutron polarisation 77−18560
^{3}H(p,n)^{3}He, R-matrix anal. of polarisation and analysing power 77−88142
^{3}H(p,n)^{3}He charge exchange reaction, multifold diffr. scatt. theory *(Russian)* 80−78303
^{3}H(p,p), 0.6 to 1.04 GeV, differential cross sections calcs. *(Russian)* 78−54763
^{3}H(p,p), 1-10 MeV, isospin splitting of 1p-1h excitation in ^{4}He 78−41622
^{3}H(p,p), 156 MeV, differential cross section, diffr. theory of multiple scatt. 77−61404
^{3}H(p,p), 1.24 GeV, differential cross section, spin independ. Glauber model interpretation 80−63183
^{3}H(p,p), 1.26-3.71 MeV polarised p, spin depend. N-N forces 79−6634
^{3}H(p,p), 4-12 MeV, Amado model quasi-three body calc. 78−25191
^{3}H(p,p), 5.8 and 6.8 MeV, phase shift anal. *(Russian)* 77−65225
^{3}H(p,p), 8 to 17.1 MeV, of neutron polarisation in ^{3}He(n,n) 78−25171
^{3}H(p,p) four-nucleon integral eqn. solns. using effective UPA 79−71794
^{3}H(π^-, γ)3n, rest π, resonance branching ratio, bound state upper limit 80−99162
^{3}H(π^-,3n), final state continuum spectra, hyperspherical basis 77−26590
^{3}H(π^+,γ)^{3}He 79−80959
^{3}H($\pi^\pm,\pi^0$)^{3}He, elastic scatt., charge exchange and symmetries, and ^{3}H, ^{3}He form factors meas. 79−80959
^{3}H($\pi^\pm,\pi^\pm$), 232, 252, 295 MeV/c, forward angle scatt., nuclear struct. and π reaction models 79−76032
^{3}H($\pi^\pm,\pi^\pm$), elastic scatt., charge exchange and symmetries, and ^{3}H, ^{3}He form factors meas. 79−80959
^{3}H($\pi^\pm,\pi^\mp$), 232-252 MeV charge exchange differential cross section 80−37401
^{3}H(t,2n)^{4}He, 30-160 keV, differential cross section measurement 78−17223
^{3}H(t,de$^-\bar{\nu}$)4He, 1.4 MeV, cross-section meas. 77−74861
^{4}H, cluster model, energy levels by interaction set anal. 78−25136
^{4}H, particle unstable state, study 79−93528
^{4}H photodisintegration in giant resonance region 77−41944
^{4}H(α,α) intermediate energies, Glauber analysis 78−46077
^{4}H(p,p), microscopic optical pot. calc. 79−85423
^{4}H(π,π), differential cross-sections calc. 77−6458
^{A}H, A=1, 2, nuclear electric dipole moments from P nonconserving atomic transitions 80−57681
^{A}H, A=1,2,3, ang. and vel. distribs. from Pb(α,X) *(Russian)* 80−63194
^{A}H, A=2, 3, EM sum rules, total absorption cross sections 79−71818
^{A}H, A=2,3, binding energy from Brillouin-Wigner perturbation method, strong short ranged interactions 80−86796
^{A}H(γ,π^0), A=1, 2, 1-10 MeV, photoprod. yields, DWIA anal., dipole photoprod. amplitudes 80−68645
^{A}H(n,X), 60 keV-80 MeV, A=1,2,3 total cross section and scatt. length 80−99176
^{A}H(p,p) A=1,2, total cross sections, 180 to 560 MeV, Galuber model calcs. 79−40917

nuclei with mass number 1 to 5 continued
^{1}H(p,π), A=1,2, 0.7-8 GeV, scaling and nonscaling of inclusive π prod. 79−22296
^{1}H(π,π), A=1, 2, intermediate energies, collective isobaric resonance 80−63208
^{1}H(π^{+}, π^{+}), A=1,2, 130-280 MeV, 180° excitation function, dibaryon resonance signals 80−68619
$^{4}_{\Lambda}$H→απ^{-}γ, evidence for γ transitions 79−85393
$^{3}_{\Lambda}$H binding energy using phenomenological ΛN pots. 80−9254
$^{3}_{\Lambda}$H, binding energy via rank-2, two-body pots. 77−26604
$^{3}_{\Lambda}$H, ground state energy, hyperspherical harmonics method 79−93547
$^{4}_{\Lambda}$H, γ-ray spectra of stopped K^{-} in ^{6,7}Li 79−63621
H(α,X), 16.5 GeV/c, inelastic cross sections, multiplicity, ang. and momentum distribs. 78−82359
H(α,α), 4.00, 5.08. 6.90 GeV/c, cross-section meas. 77−6416
H(d,2p)n, 26.5 MeV, Faddeev cross section and scatt. symmetries over 50% of total phase space 79−76003
H(d, d), 800 to 1430 keV, differential cross section meas. 79−80947
H(d,d), A=1, 2, E=52 MeV, polarised deuterons, vector analysing power 78−584
H(d,n)^{3,4}He reactions, NA-2 neutron generator, fast neutron spectrum, stilbene scintillation spectrometer meas. *(Czech)* 77−71710
H(d,p), 6.3 GeV, proton momentum spectra 79−6621
H(d,p), A=1,2, 6.3 GeV/c, p momentum spectra from d breakup 78−89887
H(d,pp)n, 12.9 MeV, differential cross-sections meas. 78−13113
H(e^{-},e^{-})H, s-wave scatt., effective range expansion 80−47467
He (A=3, 4), energy spectroscopy, plastic solid state nuclear track detectors 78−13377
He, A=3, 5, BE, level calcs. using new boson expansion to n-fermion problem 78−511
He, A=3,4, form factors determ. by pole and quark-counting model 77−26568
He, A=3,4, relativistic corrections to two-body pot., binding energy 78−74301
He, A=5,4, containing charmed baryon, binding energies, lifetimes 78−89815
He, d-d or d-p, coupling constants from dispersion anal. of N and d scatt. amplitudes 78−29399
He isotopes prod. cross sections in natural Mg, Al, Si, CaF_2 by 12-45 MeV protons 77−17310
He isotopes prod. in lunar materials by solar cosmic ray protons, rate calc. 77−17311
He neutron rich isotopes, reaction matrix calcs., stability 78−66225
^{3}He, nucl. mag. moment, ratio of precession freqs. of gas phase helions-proton mixture *(Russian)* 79−17803
He+nuclear emulsion, 1.05 GeV/amu, scatt. const. 78−13151
He+p, A=3,4, polarised projectile, parity nonconservation in low energy scatt. 78−66271
He+p, A=3,4, polarised projectile, parity nonconservation in low energy scatt. 78−70522
He+p, particle multiplicity correlations in streamer chamber 79−85506
He+p($\pi^{\pm}$), 1.5 to 2.5 GeV interactions in streamer chamber 79−6709
He+π, fragment and pion multiplicities 77−18620
He+π, particle multiplicity correlations in streamer chamber 79−85506
He(^{3}He,^{3}He), 33 MeV, ^{3}He polarisation anal. power meas. optical model anal. 77−38286
^{2}He, ground state level determ. 80−99136
^{2}He(e,e) energy weighted sum rules *(Russian)* 80−86900
(^{3}He,d), 70, 90, 110 MeV, projectile break-up and d continuum spectra, reaction mechanism 79−13312
^{3}He (π, Γ)^{3}H, model calc. of Panofsky ratio 77−14190
^{3}He (π, π) Δ(1236) resonance region, Watson multiple scatt. series. integral eqns. 80−37402
^{3}He and $^{3}\bar{H}e$ prod. by 200 GeV protons 79−9563
^{3}He, asymptotic normalisations for S-state wave-function component 77−74777
^{3}He, BE, 4 boson approx. and ^{4}He BE 77−61351
^{3}He, binding energies, three body calcs., Faddeev formalism, alpha cluster model 79−75876
^{3}He bound state, perturbation approach with Reid soft core pot. 79−67675
^{3}He breakup, 156 MeV protons, NN multiple scatt. anal. 77−18546
^{3}He breakup, DWBA calcs. for strongly absorptive projectiles in ^{51}V(^{3}He,dp) 80−68682
^{3}He breakup induced by 156 MeV protons, pd final state interactions 77−23013
^{3}He change form factor, relativistic corrections for three nucleon observables 79−85383
^{3}He charge form factor, 3N bound state with separable interactions, Faddeev theory corrections 80−13388
^{3}He charge form factor, internucleon force 77−18438
^{3}He, charge form factor, n+d collision anal. 77−18439
^{3}He charge form factor 79−71806
^{3}He, charge form factor calc. using centre-of-mass effects 77−26642
^{3}He charge form factor calc. with pair and recoil exchange currents 77−34238
^{3}He, charge form factor one-boson exchange pot. 78−41652
^{3}He, charge form factor with Reid soft core pot. 80−13389
^{3}He, charge form factors, recent developments in lepton scattering 79−80929
^{3}He charge form factors at high momentum transfer, relativistic interactions, N form factors 80−32205
^{3}He, Coulomb energy, charge symmetry breaking 80−27564
^{3}He Coulomb energy, quasiparticle method 77−18416
^{3}He Coulomb energy from configuration space Faddeev calcs. 80−102131
^{3}He, dM stars as interstellar source 79−48810
^{3}He, EM form factors, 3-nucleon wave function calc. 80−95302
^{3}He elastic breakup in (^{3}He,pd) 80−52685
^{3}He, elastic electron scatt. data, comparison with charge form factor calcs. 79−71848
^{3}He, enhancement factor calc. in photonuclear electric dipole sum rule 78−37288
^{3}He form factor, two pion exchange charge density in static approx. 78−66222
^{3}He form factor from ^{3}H wave function anal. form 80−47410
^{3}He, influence of structure on cross-section of complete electrosplitting *(Russian)* 79−22272
^{3}He, integrated cross section for trinucleon photoeffect 78−82334
^{3}He, isospin 1/2 three body photodisintegration suppression 79−40902

nuclei with mass number 1 to 5 continued
^{3}He, liquid, pionic K X-ray transition energies and Lorentzian widths 80−78727
^{3}He, meson exchange contrib. to mag. moment 77−6249
^{3}He, meson exchange currents, effect on charge form factors 80−105990
^{3}He, microscopic spin orbit potential, microscopic formulation inadequacies 79−26355
^{3}He, muon capture 78−37314
^{3}He, muon capture theory 78−553
^{3}He, μ-capture, total and partial capture rates 79−9522
^{3}He, nuclear charge form factor, two-boson exchange charge density π, ρ, ω exchanges 80−63073
^{3}He, one-body charge form factor computer code listing 80−57673
^{3}He Panofsky ratio meas., $\omega(\pi^{-},\pi^{0})/\omega(\pi^{-},\gamma)$ 79−76034
^{3}He photodisintegration, quadrupole contrib. to cross section, isospin sum rules 77−30550
^{3}He photoeffect to isospin 3/2, coupled hyperspherical harmonics 78−41696
^{3}He, pionic, X-ray transitions obs. 77−65549
^{3}He, prod. by cosmological cosmic rays 78−12436
^{3}He prod. in Br,Ag+p in 24 GeV/c reacts., role of pick-up processes 80−27632
^{3}He, π^{-} nonradiative absorption at rest 79−76035
^{3}He, rigorous bounds for charge densities from form factor data 80−5055
^{3}He, semileptonic weak and EM interactions, isoelastic processes 77−18528
^{3}He spectroscopic strengths from ^{13}C(^{6}Li,t) 80−47390
^{3}He target, expt. to observe excited states of nucleons in nuclei *(French)* 79−3179
^{3}He, three body bound states, realistic nucleon-nucleon interactions 78−62526
^{3}He, three body calc. with separable pots. for binding energy 79−45145
^{3}He, three-particle photodisintegration, hyperspherical functions method *(Russian)* 78−589
^{3}He, threshold pion photoproduction and radiative capture, π-^{3}He-^{3}H coupling constant 79−40962
^{3}He, totally antisymmetric wave function with generalised Faddeev eqn. 80−83046
^{3}He, trinucleon bound state problem, binding energy, form factors and mag. moment 80−22710
^{3}He trinucleon photoeffect, electric dipole transitions to isospin 1/2 trinucleon states 79−45246
^{3}He wave function, D-state component from tensor analysing power of (d, ^{3}He) reactions 78−54769
^{3}He-^{3}H binding energy difference, Coulomb energy contribution 79−491
^{3}He-^{3}H charge asymm., neutron-proton mass difference 78−70464
^{3}He-^{3}H Coulomb energy difference and charge dependent three-body force 79−45181
^{3}He-^{3}H mass difference, separation of EM contribs. 77−23014
^{3}He-^{3}H mass difference, ρ-ω mixing charge symmetry breaking force, nonlocal contribs. 78−70458
^{3}He-^{3}H nuclei; charge asymmetric energy using different OBEP models 78−70372
^{3}He+^{3}He, evidence for high-energy deuterons 77−23099
^{3}He+^{3}He, possible sources of high-energy deuterons, solar neutrino problem 77−18588
^{3}He+^{3}He, quasifree processes, 50-78 MeV, cross-section meas. 77−18586
^{3}He+^{3}He→2p+^{4}He, fusion power feasibility 77−38310
^{3}He+α scatt., exchange Coulomb kernel in resonating group formulation 79−6531
^{3}He+d breakup, quasifree processes 77−18575
^{3}He+μ^{-}→ν_{μ}+^{3}H, angular correlations and capture rates, spin and isospin transitions, hyperfine effects 78−70494
^{3}He(^{3}He, ^{2}H)^{4}He, high energy deuteron prod. 79−93639
^{3}He(^{3}He, ^{3}He′), 120 MeV, continuum energy spectra bump struct., cross sections 80−83108
^{3}He(^{3}He, dd)pp, 50, 78 MeV, cross sections, two-spectator quasifree process 78−86539
^{3}He(^{3}He,^{2}Hνe^{+})^{4}He, 11.5 MeV, search for high energy deuterons 79−76012
^{3}He(^{3}He,X) 50, 65, 78 MeV, quasifree scattering and quasifree reaction processes 80−13486
^{3}He(^{3}He,d^{3}He), three body break up reaction energy spectra, computer program 80−27593
^{3}He(^{3}He,dd)pp, 50, 78 MeV, study of four body continuum 77−18587
^{3}He(^{3}He,de$^{+}\nu$)^{4}He, 15, 25 MeV, cross-section and solar neutrino problem 77−50142
^{3}He(^{3}He,p^{3}He), three body break up reaction energy spectra, computer program 80−27593
^{3}He(^{3}He,p)^{4}He, polarisation meas. in final state interactions 77−18589
^{3}He(^{3}He,p)^{5}Li, polarised protons, deuteron transfer obs. 77−329
^{3}He(^{4}He,^{4}He)^{3}He, 20-26 MeV, elastic scatt., ang. distribs. and excitation functions *(Russian)* 77−327
^{3}He(D,p)^{4}He, appl. to effective ion temp. determ. in plasma focus *(Russian)* 79−27824
^{3}He(N,πX), expt. review of π-prod. by (un)polarised nucleons on few-nucleon systems 79−80944
^{3}He(α,α), 24.5 to 42.0 MeV, meas. of polarisation analysing power 77−3026
^{3}He(d,d), 0.32 MeV, continuum ambiguity in phase shift anal. 79−76006
^{3}He(d,d), polarised d, 10-17 MeV, cross sections, vector and tensor anal. powers 79−75966
^{3}He(d,d), polarised d, 1.5-11.5 MeV, differential cross sections and anal. powers 79−85443
^{3}He(d,d)^{3}He, 0.3-8 MeV, single-level reson. and ^{5}Li parameters 77−30606
^{3}He(d,p), 6.44 MeV polarised d, absolute standard of d vector analysing powers 77−34281
^{3}He(d,p), pol. d, below 6.75 MeV, tensor anal. power 80−42633
^{3}He(d,p), polarised d, 10-17 MeV, cross sections, vector and tensor anal. powers 79−75966
^{3}He(d,p)^{4}He, 8.5-10.5 MeV polarised deuterons, max. tensor analysing power 77−6397
^{3}He(e, e′p) electrodisintegration by 1200 MeV electrons *(Russian)* 80−37370
^{3}He(e, e), charge formfactors, second Born approx. and pole model 80−18155

nuclei with mass number 1 to 5 continued
^{3}He(e,e'), 0.1-14 GeV, deep inelastic inclusive scatt. response functions and momentum distrib. 80−42640
^{3}He(e,e'), nuclear high momentum components and y scaling 80−106051
^{3}He(e,e') 1000-1100 MeV, differential cross section for quasi-elastic scatt. *(Russian)* 78−86528
^{3}He(e,e')pd, three-body calc. 78−33170
^{3}He(e,e'p), cross-section, Fadeev technique, nucleon-nucleon interaction *(Russian)* 80−73842
^{3}He(e,e'p)^{2}H, 1.2 GeV, p angular distrib., recoil nucleus momentum distrib. *(Russian)* 79−9550
^{3}He(e,e'X), X=p or n, coincidence reactions, electrodisintegration cross sections 80−22823
^{3}He(e,e')pd, Faddeev calc., scatt. cross-sections 77−18530
^{3}He(e,e'p)d, Faddeev calc., scatt. cross-sections 77−18530
^{3}He(e,e), 29-95 MeV, RMS charge radius and charge form factor 77−57653
^{3}He(e,e), 3-15 GeV, inclusive scatt. 80−13464
^{3}He(e,e), charge density distrib., charge form factor, of ^{3}He 78−29453
^{3}He(e,e), charge formfactors, second Born approx. and pole model 80−78133
^{3}He(e,e), elastic and inelastic cross sections 40-60 Mev, possible 10 MeV state 79−40908
^{3}He(e,e), form factors and dimensional scaling quark model 78−93991
^{3}He(e,e), model depend. of charge densities 78−78248
^{3}He(e,e), relationship to ^{3}He(π^-,π^-) 80−78323
^{3}He(e,e) 170 to 750 MeV, EM structure, form factors and distribs. 77−54208
^{3}He(e,π^+)^{3}H, cross section from t recoil cross section meas. 79−6574
^{3}He(e,π^+)e't, (e,t)e'π^+ cross-sections and ang. distribs. calc. 78−21545
^{3}He(γ,2p)n, 15-50 MeV, three-body calc. with spin-depend. separable pot. 77−38257
^{3}He(γ,2p)n, 80-120 MeV, proton energy distribs., diffr. cross sections, direct breakup 80−86897
^{3}He(γ,n)$_2$ photodisintegration cross sections 80−22817
^{3}He(γ,p)^{2}H, 165 to 330 MeV, EM and pion exchange contribs. to unpolarised differential cross section 77−18521
^{3}He(γ,p)^{2}H, intermediate energy, ang. distribs., reaction amplitude and ^{3}He vertices 80−22835
^{3}He(γ,pd) and ^{2}H(p,γ) anal. using Reid soft-core pots. 77−26664
^{3}He(γ,π^0), 0-8 MeV, cross sections, taking π rescatt. amplitudes into account 78−78364
^{3}He(γ,π^0), 1 to 10 MeV above threshold 79−85454
^{3}He(γ,π^0), cross section and threshold effects using dynamical $\gamma N \rightarrow N\pi^0$ model 80−27627
^{3}He(γ,π^0), polarisation effects 180 to 700 MeV, impulse approx. calcs. *(Russian)* 80−37368
^{3}He(γ,π^0)^{3}He, polarisation effects 180 to 700 MeV, impulse approx. calcs. *(Russian)* 80−37368
^{3}He(γ,π^+) near threshold, photoprod. yield and transition matrix element 79−89291
^{3}He(γ,π^+)^{3}H, exchange current effects, two body processes 79−71839
^{3}He(γ,π^+)^{3}H, Fermi motion and off-shell effects, impulse approx. 80−27626
^{3}He(γ,π^+)^{3}H, threshold π prod., and axial vector form factor 79−574
^{3}He(γ,π^+)^{3}H, threshold form factors 79−85453
^{3}He(γ,π^+)^{3}H cross section near threshold , 80−83093
^{3}He(γ,$\pi^+\pi^-$)^{3}He, gauge-invariant one-pion-exchange model 77−18298
^{3}He(γ,$\pi^\pm$), (3,3) resonance region, nuclear wave functions, kinematics 78−78361
^{3}He(γ,π), threshold photoprod. cross sections, elementary nucleonic amplitudes 80−22812
^{3}He(μ,$\gamma\nu$), transition amplitude, PCAC tests 80−102152
^{3}He(μ^-,$\nu_\mu\gamma$)^{3}H, appl. to nuclear spin and isospin doublets 78−82320
^{3}He(μ^-,$\nu\gamma$), radiative capture relativistic calcs., rate and photon spectrum 80−68605
^{3}He(n, γ), 1-70 keV, effective cross sections *(Russian)* 79−30836
^{3}He(n,γ), thermal, effective cross section *(Russian)* 80−37378
^{3}He(n,$\gamma\gamma$), thermal, calc. of cross-sections and branching ratios 77−14131
^{3}He(n,$\gamma\gamma$), thermal neutrons, cross section and branching ratio 79−45263
^{3}He(n,n), 1-24 MeV optical model anal. 77−23027
^{3}He(n,n), 2.43, 3.0 MeV, analysing power ang. distrib. 77−30568
^{3}He(n,n), 2.63 MeV polarised neutrons, asymmetry 77−26736
^{3}He(n,n), 3.7-15.3 MeV, polarised n, analysing power, A=4 system neutron channels 79−75965
^{3}He(n,n), 8 to 17.1 MeV, cf. proton polarisation in ^{3}H(p,p) 78−25171
^{3}He(n,n), coherent scatt. length meas. by neutron interferometry 78−13098
^{3}He(n,n), scatt. length, 4-nucleon problem, integral eqn. approach 80−91183
^{3}He(n,n) coherent scatt. length meas. by neutron interferometry 79−59113
^{3}He(n,n) differential cross section, nonrelativistic theory of four nucleon systems *(Russian)* 79−80881
^{3}He(n,n) thermal n$_t$ coherent scatt. length, four body problem relation 79−75997
^{3}He(n,p) cross section standard, status 77−23040
^{3}He(n,p)^{3}H, for direct nucl. pumping of ^{3}He-Xe laser 77−71972
^{3}He(n,p)^{3}H, plasma form by reaction prods. in nuclear reactor 77−76146
^{3}He(n,p)^{3}H direct nuclear pumped laser 77−83851
^{3}He(n,p)^{3}H react., direct nuclear pumped lasers 79−31863
^{3}He(n,p)T, appl. to anal. of fusion reactor materials, archeometry, and nuclear spectroscopy 80−61200
^{3}He(p, p), 1 GeV, differential cross section minimum, Glauber model description 79−80938
^{3}He(p, p), 600 MeV, Glauber formalism study *(French)* 79−93616
^{3}He(p,2p)^{2}H, 155 MeV, multiple scatt. diffraction theory anal. *(Russian)* 77−10408
^{3}He(p,2p)d, 590 MeV, in noncoplanar geometry, two particle spallation, diffr. description *(Russian)* 78−33160
^{3}He(p,2p)d(d*), 136 MeV, d/d* ratio, PWIA anal. 79−75999
^{3}He(p,dp), (p,2p), and (p,pn), 156 MeV d$^3\sigma$ and d$^4\sigma$ spectra for collinear nucleon system 78−17175
^{3}He(p,dp)p, 156 MeV, p-d scatt. at small rel. energy in FSI region 79−85441
^{3}He(p,p), 0.6 to 1.04 GeV, differential cross sections calcs. *(Russian)* 78−54763

nuclei with mass number 1 to 5 continued
^{3}He(p,p), 156 MeV, differential cross section, diffr. theory of multiple scatt. 77−61404
^{3}He(p,p), 18-48 MeV, elastic differential cross section ang. distribs., four body problem 79−75998
^{3}He(p,p), 19-30 MleV, spin anal. power and phase shift anal. 79−13295
^{3}He(p,p), 1.75 to 4.13 GeV/N, small angle scatt., Glauber model *(Russian)* 78−41726
^{3}He(p,p), 1.75 to 4.50 MeV polarised protons, analysing power meas. for ^{4}He T=1 level ordering 79−26438
^{3}He(p,p), 415-800 MeV, large angle differential cross-sections 77−30573
^{3}He(p,p), 6.8 to 16.2 MeV, optical model pot. calcs. of cross section and polarisation data 79−63672
^{3}He(p,p), charge independ. R-matrix anal. of four nucleon system 79−85479
^{3}He(p,p), forward dispersion relations and wave function models 79−75956
^{3}He(p,p), pol. p, 0.3-1.0 MeV, differential cross section, anal. power, and phase shifts 80−42629
^{3}He(p,p), polarised p, 6.8-10.7 MeV, polarisation transfer coeffs. 79−17889
^{3}He(p,p), polarised p, below 6 MeV, anal. power meas. for four nucleon system levels 79−71837
^{3}He(p,p) virtual scatt. from ^{4}He+p two pronged events 79−3152
^{3}He(p,p)^{3}He, 0.02-2 eV, scatt. lengths *(Russian)* 77−61430
^{3}He(p,p)^{3}He, 2.3 to 13.6 MeV data, phase shift anal. 78−78376
^{3}He(p,p)^{3}He, 2.3 to 8.8 MeV, ang. distribs. of analysing power 78−78375
^{3}He(p,p)^{3}He, cross-section anal. using four-body integral eqns. 77−18577
^{3}He(p,p)^{3}He, four-body calc. solns. 79−71855
^{3}He(p,p)^{3}He, four-body model of the four-nucleon system 79−63643
^{3}He(p,p)^{3}He, four-body problem calc. 78−516
^{3}He(p,pd)p, 35 and 45 MeV, four-body break-up calcs. 77−57667
^{3}He(p,pp)d, 35 and 45 MeV, four-body, break-up calcs. 77−57667
^{3}He(p,π^+)^{4}He, 300-400 MeV, virtual pion exchange 77−74848
^{3}He(p,π^+)^{4}He, 415, 716 MeV, DWIA calcs. of differential cross-section 77−6359
^{3}He(p,π^+)^{4}He, 415, 716 MeV, differential cross-section meas. 77−6360
^{3}He(p,π^+)^{4}He, 415 MeV, angular distrib., microscopic description, generalisation of (π,π) *(Chinese)* 80−63188
^{3}He(p,t)Δ^{++}, 850 MeV, search for (Δ^{++},2n) in the ^{3}He wave function 78−82345
^{3}He(p(polarised),p)^{3}He, nuclear force and T-violation effects 78−4797
^{3}He(π,π), 1 GeV, backward scatt., nonstable meson-nucleon interaction cross section, resonance *(Russian)* 80−68559
^{3}He(π,π), 145, 180, 195 MeV, differential cross section, mesonic exchange effects, form factors, optical pot. 79−85376
^{3}He(π,π), 68-154 MeV, single and double collision differential cross section calcs. *(Russian)* 80−106083
^{3}He(π,π), elastic interactions in JINR high press. streamer chamber, triggering system 80−102400
^{3}He(π,π), elastic interactions in JINR high press. streamer chamber, selection criteria 80−102401
^{3}He(π,π), optical model calc. 77−6454
^{3}He(π,π), optical potential in momentum representation 80−78324
^{3}He(π,π), role of spin isospin effects in Δ(1236) resonance domain *(Russian)* 78−78423
^{3}He(π,π) in Δ_{33} reson. region, differential cross section, comparison with model calcs. 77−18621
^{3}He(π,π)^{3}He, Glauber theory calc. in (3,3)-reson. region 77−82968
^{3}He(π^-, π^0)^{3}H, 100 to 260 MeV optical-model calcs. 77−79403
^{3}He(π^-,γ)^{3}H, Panofsky ratio and axial vector form factor 79−574
^{3}He(π^-,γ)^{3}H, radiative capture rate and threshold π photoprod., Panofsky ratio from ^{3}He(π^-,π^0) 79−13350
^{3}He(π^-,n)^{2}H, 100, 200 and 290 MeVs differential cross sections 78−33223
^{3}He(π^-,π^-), 145, 180 and 195 MeV, relationship to ^{3}He(e,e) 80−78323
^{3}He(π^-,π^-), 68 MeV, differential cross section 78−33221
^{3}He(π^-,π^-), low energies, scatt. lengths and phase shift calcs., inelastic process contribs. 79−54459
^{3}He(π^-,π^0), form factor sensitivity in Glauber multiple scatt. formalism 80−105964
^{3}He(π^-,π^0)^{3}H, elastic scatt., charge exchange and symmetries, and ^{3}H, ^{3}He form factors meas. 79−80959
^{3}He(π^-,π^0)^{3}H, isobaric analogue state ang. distrib. 79−85508
^{3}He(π^-,π^0)^{3}H, large angle charge exchange scatt. differential cross section 79−22331
^{3}He(π^-,π^0)^{3}H, optical potential in momentum representation 80−78324
^{3}He(π^-,π^0)^{3}H, Panofsky ratio and axial vector form factor 79−574
^{3}He(π^+,3p), final state continuum spectra, hyperspherical basis 77−26590
^{3}He($\pi^\pm$,$\pi^\pm$), 100-260 MeV, optical model calc. 77−79403
^{3}He($\pi^\pm$,$\pi^\pm$), 232, 252, 295 MeV/c, forward angle scatt., nuclear struct. and π reaction models 79−76032
^{3}He($\pi^\pm$,$\pi^\pm$), elastic scatt., charge exchange and symmetries, and ^{3}H, ^{3}He form factors meas. 79−80959
^{3}He($\pi^\pm$,$\pi^\pm$), low energy, scatt. lengths, approx. pot. 4-body eqns. 79−76033
^{3}He(t,d)^{4}He, 9-17 MeV, polarised tritons, analysing-power ang. distrib. meas. 78−29481
^{3}He(t,d)^{4}He, charge asymmetry effects 79−3159
^{3}He(t,d)^{4}He, symmetry breakdown as cluster spatial effect 79−6619
^{3}He(t,d)^{4}He asymmetry, cluster model anal., isobaric analogue states 78−78389
^{3}He(t_{pol},t)^{3}He, 9-17 MeV, analysing power, differential cross sections 77−74829
^{3}He(τ,τp)d, 120 MeV, coincident energy spectra, quasi-free scatt. 79−22303
^{3}He$\pi^-\rightarrow$nd, ^{3}He$\pi^-\rightarrow$n+n+p, two nucleon absorpt. model 78−41776
^{4}He 2$^+$ resonance evidence at 40 MeV from ^{4}He(e,^{3}H), and ^{3}H(p,γ) 80−86880
^{4}He (^{3}He,p), 15.95 MeV (c.m.), phase shift anal., σ_r determ. 77−88159
^{4}He, (3+1) cluster model of the T=0 0$_2^+$ state by GCM 79−6396
^{4}He (d,d), 17-45 MeV, differential cross section and tensor and power ang. distribs. 80−42631
^{4}He (d,d), pol. d, 20 MeV, optical pot. strong tensor term, anal. powers 80−37364
^{4}He (d,d) pol. d, 17-43 MeV, vector anal. power, highly excited six nucleon system 80−47458

nuclei with mass number 1 to 5 continued
^{4}He (e,e'pp) reaction cross-section and ground state shell model calcs. *(Russian)* 80−78283
^{4}He, $(\gamma,^3H)/(\gamma,^3He)$ cross section ratio for 31-51 MeV, deduced $\sigma(\gamma,p)/(\gamma,n)$ ratio 79−67743
^{4}He (p,p), 200, 350, 500 MeV, differential cross-section and analyzing power meas. 78−17195
^{4}He (p,p), effective channel approach, N* resonance effects 79−9570
^{4}He (p_i,p), high and intermediate energies, polarisation, research review 78−94010
^{4}He (π^-, π^-p), 5GeV/c, quasielastic scatt., cross section, form factor, final state interactions 80−99190
^{4}He (π^+,$\pi^\pm$), 100-260 MeV, optical-model calc. 77−79403
^{4}He abundance and standard big-bang universe model 78−89277
^{4}He BE calc. in 4 boson approx. 77−61351
^{4}He binding energy, 4-nucleon problem, integral eqn. approach 80−91183
^{4}He binding energy, Δ(3-3) effects, reaction matrix calc., Δ degrees of freedom 80−9218
^{4}He binding energy, nonrelativistic theory of four nucleon systems *(Russian)* 79−80881
^{4}He binding energy, reaction matrix calc. with three and four particle correls. 77−34218
^{4}He, binding energy, truncated t-matrix approx., trinucleon bound state problem 79−448
^{4}He binding energy, unitary pole approx. 78−25103
^{4}He, binding energy and form factor calcs., Reid interaction 78−54678
^{4}He, binding energy calc. using Alt-Grassberger-Sandhas eqns. 78−41650
^{4}He broad level search from ^{2}H(d,n) 80−102117
^{4}He, bulk props., ground state energies and RMS charge radii 78−58242
^{4}He, centre of mass spuriosity in continuum shell model calcs. 77−26597
^{4}He charge form factors, pion exchange currents effects 77−18379
^{4}He, charge form factors of doubly closed shell nuclei 77−6274
^{4}He, closed shell nuclei, convergence studies for the one body mass radius operator 79−45146
^{4}He, constrained variational calcs. for binding energy and RMS radii, N*(1234) allowance 79−3074
^{4}He continuum, microscopic calcs., dynamical R-matrix, model for struct. and reactions 77−14043
^{4}He continuum microscopic calcs. cross sections and levels from ^{3}He+n, ^{3}H+p channels 80−57702
^{4}He, coupled channel anal. of Λ'(1405) in kaonic atoms 78−540
^{4}He deduced monopole excitation to O^+ state DWBA anal. from (α,α') 79−22226
^{4}He, effects of three body force on energy levels 78−54692
^{4}He elementary diagram calcs. with truncated sums 79−85382
^{4}He, energy levels using ATMS method and realistic nuclear forces 80−22707
^{4}He, excitation of O^+ state anal. by α-scatt. from ^{12}C, ^{13}C, ^{16}O 77−10419
^{4}He excited states obs. in ^{3}H(p,γ) induced by 6 to 16 MeV polarised protons 77−18559
^{4}He, exotic nuclei stability anal., Hartree-Fock approx. with the Skyrme interaction 78−82273
^{4}He, four-body problem unitary pole approx. calc. 78−516
^{4}He, four-nucleon bound state with realistic NN interaction, hyperspherical harmonics *(Russian)* 80−83045
^{4}He, fragmentation in nuclear emulsions at 2.1 GeV/nucleon 78−70561
^{4}He, giant dipole reson., shell model calcs. including noncentral forces and target recoil corrections 79−17824
^{4}He ground state, energy and wave function, static Hartree-Fock calcs. 80−47414
^{4}He, ground state energies, four order high lying contribs. 79−75850
^{4}He, ground state energy, second order Brueckner-Baranger approx. 80−63082
^{4}He, ground state props., modified Brueckner-Bethe-Goldstone method 78−50076
^{4}He ground state wave function in translationally invariant oscillator basis 77−6262
^{4}He, HF charge distribs. 77−14024
^{4}He harmonic oscillator sum rules for photonuclear reactions, shell model, perturbative corrections 78−41692
^{4}He isobar configurations, impulse approx. 77−46114
^{4}He, isobar configurations in closed shell nuclei 78−66226
^{4}He isospin splitting of 1p-1h excitation, obs. in ^{3}H(p,p) 78−41622
^{4}He, isotopically pure, apparatus for preparation 78−57959
^{4}He level density and J* calcs. 79−63596
^{4}He level energies, Brink's model with single-particle functions with realistic behaviour *(Russian)* 77−74785
^{4}He, low lying T=1 level ordering from p-^{3}He elastic scatt. 79−26438
^{4}He, magic nucleus, nonlocal pots., binding energies 77−41877
^{4}He magnetometer, optically pumped *(Japanese)* 80−8434
^{4}He, microscopic determ. of nucleon momentum distribs. 78−70428
^{4}He mixed symmetry state admixture from ^{3}He(n,γ) *(Russian)* 80−37378
^{4}He, monopole excitations, transition densities from simple collective model 79−40834
^{4}He, multiple scatt. effects in fast neutron polarisation expts., Monte Carlo anal. 78−13052
^{4}He muonic atom, nuclear polarisation corrections 78−22056
^{4}He, n-fermion problem new boson expansion technique 78−511
^{4}He, N*-^{3}H configurations 79−17822
^{4}He, nucl. binding energy, radius and charge form factor, Brueckner calcs. 79−71787
^{4}He nuclear charge density determ. using form factor analyticity 80−63077
^{4}He nuclear struct. calc. using gradient method of quantum mechs. 77−82831
^{4}He, one particle density distrib., nucleon density, from nuclear ellipsoid of inertia *(Russian)* 79−30784
^{4}He, parity mixing below 30 MeV excitation energy for ΔT=0,1 transitions 80−52604
^{4}He, particle hole calculations, centre of mass subtracted kinetic energy 78−62491
^{4}He, photoabsorption total cross sections 30-100 MeV *(Russian)* 78−89850
^{4}He photodisintegration, 9-dimens. space hyperspherical harmonics 79−75975
^{4}He photodisintegration, clustering effects 79−6562
nuclei with mass number 1 to 5 continued
^{4}He photodisintegration, clustering effects 79−36227
^{4}He photodisintegration, electric dipole transitions, photoeffect cross section 79−67742
^{4}He photodisintegration, pair correlation study *(Russian)* 80−86899
^{4}He photodisintegration, quadrupole contrib. to cross section, isospin sum rules 77−30550
^{4}He photodisintegration, total, dipole, and quadrupole cross sections, sum rules *(Russian)* 80−83094
^{4}He, photodisintegration down to meson prod. threshold *(Russian)* 79−13282
^{4}He, photonuclear reaction cross-section continuum calcs. 77−71603
^{4}He production, nonzero neutrino rest mass effects 80−105413
^{4}He, π scatt. and absorption, microscopic calc. 79−85501
^{4}He, π^0 coherent photoprod., screening corrections and rescatt. *(Russian)* 78−41697
^{4}He, reaction matrix equation, Brueckner calcs. in harmonic oscill. basis 79−59015
^{4}He, recent developments in lepton scattering 79−80929
^{4}He, recoil corrected continuum shell model calcs. 79−67684
^{4}He reduced widths, point approx., higher order corrections 79−13213
^{4}He, saturating effect of N*(1234) on binding 78−58231
^{4}He scatt. system, multichannel cluster model description 77−82902
^{4}He, second O^+ state, excitation energy 79−67658
^{4}He, shell model calcs. 80−13393
^{4}He, single determinantal states, HF and energy variance minimisation methods 77−6204
^{4}He, soft-core radial wave function, photo-disintegration calculation 80−18209
^{4}He, spherical nuclei, geminal product approx. 78−66230
^{4}He, struct. effects on α-decay of superheavy nuclei 78−17158
^{4}He, struct. effects on α-decay widths 78−62513
^{4}He, struct. of 2nd 0^+ state 78−93947
^{4}He structure based on realistic two- and three-body interactions 77−18417
^{4}He, structure in the translation-invariant oscillator basis *(Russian)* 78−25123
^{4}He system, high spin states 78−86484
^{4}He system, O^+ states, microscopic wave function 80−463
^{4}He, TRK dipole sum rule reevaluation including isobar effects 78−66221
^{4}He, T=1 excited negative parity state struct. 80−57688
^{4}He truncation influence, using recurrence relations for reaction matrices 79−489
^{4}He, vertex consts. calc. by method of integral equations 77−14076
$^4He_\Lambda$-$^4H_\Lambda$ binding energy difference, exact 4-body calc. 79−63622
^{4}He-^{4}He, possible ^{8}Be high-lying reson. below α-α* threshold 77−82840
^{4}He-^{4}He effective interaction, energy density formalism *(Russian)* 77−46119
^{4}He-d-d vertex constant, normalisation 77−6329
^{4}He+^{4}He, Hill-Wheeler eqn. direct soln. 78−4956
^{4}He+^{4}He, microscopic description of nuclei collisions, GCM and RGM framework 77−34272
^{4}He+^{4}He, reson. excit., ^{8}Be α-cluster, coupled channel calcs. 78−529
^{4}He+^{4}He elastic scattering, barrier penetration effects, semiclassical theory 77−34339
^{4}He+N, potential calc. using microscopic model 77−88091
^{4}He+N, resonating-group method anal. 77−82886
^{4}He+U, fireball model for proton inclusive spectra 77−6339
^{4}He+U, relativistic ions, product spectra, statistical models 78−638
^{4}He+α, 75.2 MeV, TDHF calcs. using separable three dimens. wavefunctions 78−50111
^{4}He+α break-up reactions, 130 MeV, continuous energy spectra of emitted particles 79−76013
^{4}He+α scattering, generator coord. method, Kohn-Hulthen variational principle 77−2957
^{4}He+α→^{6}He, ^{6}Li, ^{7}Li, ^{7}Be, 61.5-158.2 MeV, Li nucleosynthesis 79−17886
^{4}He+n, 20 MeV, phase shift, resonating group method 78−50159
^{4}He+n, below 15 MeV, R-function anal. 77−23028
^{4}He+n, elastic scatt., orthogonality condition model derived from parity energy surfaces 78−29432
^{4}He+n, pole positions of ^{5}He resonances, models calcs. 78−70530
^{4}He+n, separable pot. fits to reson. parameters 78−8822
^{4}He+p, 18.6 GeV/c, coherent prod. of low mass $p\pi^+\pi^-$ states 78−33175
^{4}He+p, 8.56 GeV/c, two pronged events, cross sections and prod. features 79−3152
^{4}He+p, interaction potential from inverse scatt. problem method *(Russian)* 78−46068
^{4}He+p(p̄), high energy cross section calc. complex ang. momentum theory *(Russian)* 78−46067
^{4}He+π, effects of pion absorption 79−22341
^{4}He+π^-, capture at rest, neutron energy spectrum determ. 79−6702
^{4}He+π^-, coupled channel method, determ. of total cross sections 79−36281
^{4}He+π^-, excitation of Δ-nuclear states 77−88093
^{4}He+π^-, multiple scattering theory with separate treatment of proton and neutron 79−45301
^{4}He+π^-, pion absorption, isobar formation in streamer chamber 79−85504
^{4}He+π^- second-order optical pot., multiple scatt. theory 77−82966
^{4}He+π^+, 110, 160 MeV, cross section ratio of (π^+,π^+p) to $(\pi^+,\pi^+n)+(\pi^+,\pi^0p)$ reactions 78−74403
^{4}He+$\pi^+\rightarrow\pi^+\pi^-$ppd, 1.7 GeV/c, cross section, Δ(1232) and ρ(770) resonance prod. 78−89911
^{4}He+$\pi^\pm$, proton spectra, cross section, π. absorpt. mechs. 78−25239
^{4}He* from ^{6}Li(d,α), spin, parity from α spectra and ang. distribs. 78−54771
^{4}He(π, π), elastic data inconsistencies and dispersion relations above 33 resonance 80−68700
^{4}He(^{3}He,^{3}He), ^{7}Be ^{4}He+^{3}He coupling, dispersion anal. 78−89889
^{4}He(^{3}He,^{3}He), 18 to 70 MeV, differential cross-sections, resonating group method anal. 79−85482
^{4}He(^{3}He,^{3}He), 18-22 MeV, analysing power ang. distrib., differential cross sections, ^{7}Be excited state 78−46078
^{4}He(^{3}He,^{3}He), 60.2, 113.1 MeV, ang. distrib., optical and coupled channel anal., cross sections 80−47492
^{4}He(^{3}He,^{3}He)^{4}He, four body approach 79−75933
^{4}He(^{3}He,α), 15.95 MeV (c.m.), phase shift anal., σ_r determ. 77−88159

nuclei with mass number 1 to 5 continued

^{4}He(^{3}He,n)^{6}Be, 38.61 MeV, ^{6}Be reson. search, solar neutrino flux importance 78−619
^{4}He(^{4}He,^{4}He), local pot. theory for phase shifts and reson. 77−34270
^{4}He(^{6}Li, ^{6}Li), 15.1-22.7 MeV, polarised Li, vector anal. power, spin-orbit pot. 79−67737
^{4}He(^{6}Li,γ)^{10}B, test of weak-interaction models 77−331
^{4}He(N,N), microscopic study using single channel resonating group method, effective nuclear potentials 79−85425
^{4}He(α,α), 158.2 MeV, differential cross sections, optical model anal. 79−22307
^{4}He(α,α), 17.9 GeV/c, Glauber model rigid projectile approx. 79−63685
^{4}He(α,α), 4.32, 5.07 GeV/c, Glauber multiple scatt. theory comparisons 80−63192
^{4}He(α,α), 5.05, 4.30 GeV/c, high energy multiple diffraction theory 78−29486
^{4}He(α,α), composite particle scatt., generator coordinate and natural boundary condition methods 80−13489
^{4}He(α,α), large amplitude collective motion, adiabatic TDHF calcs. 80−86786
^{4}He(α,α), natural boundary condition methods for the microscopic treatment of composite-particle scattering 79−63680
^{4}He(α,α), nuclear separable plus Coulomb interaction 80−83106
^{4}He(α,α), phenomenological-potential constant, from phase shift, theory of complex orbital momentum 77−14145
^{4}He(α,α), s-wave, Coulomb amplitudes from generator coordinate theory 80−83107
^{4}He(α,α), size change of α effect on phase shift, generator coordinate and variational methods *(Chinese)* 80−68683
^{4}He(α,α), time dependent HF calcs. reaction cross sections 79−26443
^{4}He(α,α) anal. to study direct part of N-N potential 77−10420
^{4}He(α,α) elastic scatt. 32.6 to 35.4 MeV, ^{8}Be levels by double resonance formalism 78−62553
^{4}He(α,α) microscopic optical pot. for elastic scatt. in terms of nuclear density 79−54444
^{4}He(α,αd), 119 MeV, excited states, J^π and γ-ang. correlations 80−86809
^{4}He(α,n)^{7}Be, ^{4}He(α,p)^{7}Li, α-α scatt. phase shifts, cross sections near threshold 79−3163
^{4}He(α,n)^{7}Be meas. and α-α elastic phase-shift calcs. 77−50143
^{4}He(d, n), 50 MeV, neutron polarisation meas. 78−70726
^{4}He(d,d), 4.8-6.8 MeV, ^{6}Li resonances, phase shift analysis 79−75953
^{4}He(d,d), 870-1430 keV, differential cross sections and resonance parameters *(Russian)* 79−59075
^{4}He(d,d), cross sections and polarisation parameters, three-body NNα model *(French)* 77−71598
^{4}He(d,d), distortion effects, orthogonality condition model 80−63190
^{4}He(d,d), Faddeev Lovelace eqn. soln. 78−54767
^{4}He(d,d), Glauber theory at high energy *(Russian)* 78−41732
^{4}He(d,d), low energy, resonating group method anal. with distortion effect 80−73851
^{4}He(d,d), noncentral forces, Pauli principle effects on d polarisation, orthogonality condition model 79−6614
^{4}He(d,d), pol. d, 12-17 MeV, differential cross sections, anal. powers, phast shift anal. 80−13449
^{4}He(d,d), polarised d, 20.2 MeV, elastic scatt. tensor anal. power 79−85450
^{4}He(d,d)^{4}He, 6-7 MeV, polarised d, ^{6}Li 1^+ reson., analysing powers 77−88095
^{4}He(d,n)αp, 50 MeV, differential cross-section and polarisation meas. 77−88157
^{4}He(d,p), 6.8 , 7.8 MeV, continuous proton spectra obs. 78−37352
^{4}He(d,p)^{4}He n, 15 MeV polarised deuterons, differential cross sections, vector analysing powers 78−89884
^{4}He(d,pα)n, at E_d=8.9 MeV, absolute cross-section meas. 77−34317
^{4}He(d,pn), break-up process, NN interaction, numerical calc. of cross section 77−74858
^{4}He(d,pn)^{4}He, differential cross section and polarisation, three body model 80−47460
^{4}He(d,pn)^{4}He, Faddeev eqns., separable pots., total cross sections 78−21571
^{4}He(d,t)^{3}He, charge asymmetry effects, cluster model calc. 77−14136
^{4}He(e,e′p)^{3}H, 1186 MeV, recoil nucleus momentum distrib. *(Russian)* 78−54748
^{4}He(e,e), cross section anal., nuclear charge form factor, short range correl. 78−8746
^{4}He(e,e), elastic scatt., spectroscopic information and form factors 80−9260
^{4}He(e,e), form factors and dimensional scaling quark model 78−93991
^{4}He(e,e) 170 to 750 MeV, EM structure, form factors and distribs. 77−54208
^{4}He(γ, pnd), ^{4}He(γ,p), ^{4}He(γ,n), 60-170 MeV, quasideuteron mechanism calcs. 77−2978
^{4}He(γ,P)^{3}H, 20 to 50 MeV, 2^+ resonances *(Russian)* 79−59052
^{4}He(γ,X), X=p,n, 50-150 MeV, total cross sections, quasiparticle formalism calcs. 80−78277
^{4}He(γ,2d), 30-35 MeV, 2^+ state search *(Russian)* 80−42553
^{4}He(γ,2n)2p, final state interaction effects, 2 nucleon photoabsorption mechanism 79−36228
^{4}He(γ,2np)p, total photofission theory in hyperspherical basis *(Russian)* 79−22347
^{4}He(γ,d)^{2}H, ^{4}He elec. quadrupole reson., multipole expansion *(Russian)* 78−66264
^{4}He(γ,d)d, total cross-section calc. 77−18526
^{4}He(γ,n), 30-35 MeV, 2^+ state search *(Russian)* 80−42553
^{4}He(γ,n) shell model continuum calcs., centre of mass problems 77−82909
^{4}He(γ,n)^{3}He, 20 to 50 MeV, 2^+ resonances *(Russian)* 79−59052
^{4}He(γ,n)^{3}He, electric dipole and quadrupole cross section *(Russian)* 77−6352
^{4}He(γ,p), 200-450 MeV, ang. distribs., differential and total cross sections 79−75971
^{4}He(γ,p), shell model continuum calcs., centre of mass problems 77−82909
^{4}He(γ,p)^{3}H, 165 to 330 MeV, EM and pion exchange contribs. to unpolarised differential cross section 77−18521
^{4}He(γ,pn)^{2}H, three particle photodisintegration, pole mechanism contrib. *(Russian)* 80−91176
^{4}He(γ,pn)^{2}H reaction, distribution along Treiman-Yang angle *(Russian)* 80−27628

nuclei with mass number 1 to 5 continued

^{4}He(γ,pπ$^-$), π$^-$-p coincidence obs., mechanism and rescatt. effects *(French)* 79−3133
^{4}He(γ,π^0), 1 to 10 MeV above threshold 79−85454
^{4}He(γ,π^0), cross-sections determ., selection rules calc. 77−82905
^{4}He(γ,π^0), differential cross section, complex momenta theory for nondiffractive processes *(Russian)* 80−32266
^{4}He(γ,π^0), impulse approx. for differential cross sections in resonance region *(Russian)* 78−41698
^{4}He(γ,π^0), P-odd effects, Regge and boson pole interference *(Russian)* 79−6564
^{4}He(γ,π^0), polarisation effects 180 to 700 MeV, impulse approx. calcs. *(Russian)* 80−37368
^{4}He(γ,ρ^0)^{4}He, eikonal and quasi-eikonal models in complex ang. momentum plane *(Russian)* 77−50160
^{4}He(n,X), local approximation to a non-local potential 80−91182
^{4}He(n,n), 2-5 MeV polarised neutrons, analysing powers, R-function and phase shift anal. 77−23088
^{4}He(n,n)^{4}He, below 21 MeV, R-function and physical-state parameters 77−88105
^{4}He(p, p), 1.05 GeV, cross sections and polarisations, correlation effects calcs. 80−57774
^{4}He(p, p), 225, 327, 520 MeV, analysing powers 79−75961
^{4}He(p,^{3}He), ^{2}H, large momentum transfers, π exchange effects 80−5143
^{4}He(p,X), multiple scattering theory, validity of closure approx. 79−45269
^{4}He(p,X)^{3}He, 6.85 GeV/c, inclusive angular distributions 77−74845
^{4}He(p,X)^{3}He, 6.85 GeV/c, Glauber multiple model 79−63664
^{4}He(p,2p), 250, 350, 500 MeV, cross section energy depend., DWIA calcs. 80−37375
^{4}He(p,2p), pol. nucleon quasi-elastic scatt., nuclear wave function and model tests 80−42656
^{4}He(p,2p)^{3}H, 350 and 500 MeV, energy sharing spectrum, symmetric angular distrib. 79−6582
^{4}He(p,d), intermediate energies, pion exchange currents in DWBA anal. 80−32199
^{4}He(p,d), reaction mechanism, effect of Pauli principle and channel coupling 77−65219
^{4}He(p,d) pickup reaction, isobar configurations and short range correlations 80−22798
^{4}He(p,d)^{3}He, 275-500 MeV, large angle meas. 78−41713
^{4}He(p,d)^{3}He, 3.98 GeV/c, ang. distrib. meas., comparison with DWBA 77−61416
^{4}He(p,d)^{3}He, 770 MeV, calcs. 77−6357
^{4}He(p,d)^{3}He, 770 MeV, differential cross section meas., DWBA anal. 77−46166
^{4}He(p,d)^{3}He, 770 MeV, exact finite range DWBA, cross sections 78−70531
^{4}He(p,d)^{3}He, 770 MeV, multiple-scattering approach 80−27636
^{4}He(p,d)^{3}He, direct-reaction mechanisms 78−581
^{4}He(p,d)^{3}He, energy depend. and cross sections 200-500 MeV 79−13296
^{4}He(p,d)^{3}He, large momentum transfers, π exchange effects 80−5143
^{4}He(p,nπ$^+$), 18.6 GeV, invariant mass distrib., double Regge pole model comp. 79−3144
^{4}He(p,nπ$^+$), ≃500 MeV, NNπ vertex function 79−59066
^{4}He(p,nπ$^+$), pion prod. operator non-relativistic approx. 79−85500
^{4}He(p,nπ$^+$), pion prod. operator non-relativistic approx. 80−27640
^{4}He(p,p′), high energy, nonlocal imaginary pot. in one channel approx. 78−592
^{4}He(p,p), 0.35-23.1 GeV, differential cross section and polarisation, Glauber theory *(Chinese)* 79−49628
^{4}He(p,p), 0.4 GeV, nucleon-nucleon data inputs 78−74369
^{4}He(p,p), 0.5-1.7 GeV, differential cross section and polarisation meas. 79−22295
^{4}He(p,p), 0.56-1.73 GeV, differential cross-section meas. 77−88138
^{4}He(p,p), 0.58, 1, 2.1 GeV, corrections to Glauber model calc. 77−79379
^{4}He(p,p), 185 to 500 MeV, large angle cross section, analysing power 78−74363
^{4}He(p,p), 1.05 GeV, backward peak, differential cross section meas. 78−70525
^{4}He(p,p), 20-55 MeV, anal. power, cross sections, phase shift anal. 79−9569
^{4}He(p,p), 200-500 MeV, differential cross section and anal. power 80−68640
^{4}He(p,p), 2.68 GeV, elastic differential cross section 79−17900
^{4}He(p,p), 45, 52, 60, 65 Mev, cross sections and polarisation meas. 79−97706
^{4}He(p,p), 45-65 MeV, phase shift anal. 80−22832
^{4}He(p,p), 560-1730 MeV, Dirac eqn. optical model anal. 78−29467
^{4}He(p,p), 5.75 GeV, meas. of dσ/dt, t=0.18 to 2.2 $(GeV/c)^2$ 78−70532
^{4}He(p,p), 600, 1050 MeV, optical model partial-wave anal. 77−10406
^{4}He(p,p), 68-125 MeV, resonating group anal. 77−88139
^{4}He(p,p), 788 MeV, back angle diffraction struct., Dirac, eqn. optical model 80−68667
^{4}He(p,p), 788 MeV, cross section, backward diffr.-like struct. evidence 78−94008
^{4}He(p,p), (p̄,p̄), 24, 50 GeV quasieikonal model, complex momenta theory *(Russian)* 78−29473
^{4}He(p,p), differential cross-section, multifold diffr. scatt. theory *(Russian)* 80−78303
^{4}He(p,p), differential elastic scatt. cross-section, 1 GeV protons *(Russian)* 77−79382
^{4}He(p,p), elastic scatt., medium energies, effective channel anal. 77−2997
^{4}He(p,p), elastic scatt. at medium energies, microscopic optical pots. 79−97703
^{4}He(p,p), intermediate energies, energy depend. of optical model 77−23006
^{4}He(p,p), intermediate energy, microscopic momentum space optical pot. calc. 79−71853
^{4}He(p,p), medium energy, anal. power, relativistic optical model anal. 79−40925
^{4}He(p,p), resonance amplitudes in light nuclei 77−18561
^{4}He(p,p), total cross sections, 180 to 560 MeV, Galuber model calcs. 79−40917
^{4}He(p,p) 18.6 GeV 79−3144
^{4}He(p,p) elastic scatt., 11.1-14.2 MeV, differential cross-section meas. 77−38270
^{4}He(p,p) elastic scatt., 1.05 GeV, shape around first interference minimum 77−57662

nuclei with mass number 1 to 5 continued
^{1}He(p,p) elastic scatt., polarisation meas. 0.56 to 1.73 GeV, $0.006 \leq -t \leq 1.2$ (GeV/c)^2 77−57664
^{1}He(p,p) elastic scatt. near 1 GeV, Glauber theory calcs. 77−57663
^{1}He(p,p)^{4}He, 0-18 MeV, statistical anal., data fluctuations, error estimation 78−25196
^{1}He(p,p)^{4}He, calc. with Glauber model optical potential in Schrodinger eqn. 77−50093
^{4}He(p,p)^{4}He, elastic data for 350-1150 MeV 77−61424
^{4}He(p,p)^{4}He, optical model anal. 78−78369
^{4}He(p,p)^{4}He elastic scatt., 11.93, 17.00 MeV, analysing power meas. 77−38269
^{4}He(p,p)^{4}He forward amplitude real part, 1.5-10 GeV, from dispersion relns. 77−314
^{5}He(p,pn)^{3}He, ^{3}He momentum spectra determ. by cluster model interpretation 79−6577
^{5}He(p,pπ^0), 18.6 GeV, invariant mass distrib., double Regge pole model comp. 79−3144
^{4}He(π,X), 120, 145, 165 MeV, total and differential cross sections 80−78326
^{4}He(π,πX)^{3}H, 5 GeV, nucleon isobar content in He using impulse approx. 79−36276
^{4}He(π,π), 1.12 GeV, covariant optical model, nucl. struct. calc. 77−14197
^{4}He(π,π), 24-110 MeV, optical pot., quasideuteron model calcs. 78−74406
^{4}He(π,π), 60-260 MeV, energy-independ. phase shift anal. 78−41773
^{4}He(π,π), 75-260 MeV, dibaryon contrib. to πNN cluster 79−89328
^{4}He(π,π), (3,3) region, multiple scatt. theory study by optical pot. method *(Russian)* 80−13509
^{4}He(π,π), backward dispersion relations and phase shift anal. 79−63703
^{4}He(π,π), dispersion relations for forward scatt. logarithm 78−17243
^{4}He(π,π), elastic interactions in JINR high press. streamer chamber, selection criteria 80−102401
^{4}He(π,π), exchange of ρ-mesons 78−21610
^{4}He(π,π), extraction of Breit-Wigner parameters from p-wave, isohelion existence 77−6455
^{4}He(π,π), forward scatt. amplitude, imaginary part in unphysical region 77−14194
^{4}He(π,π), low energy, first order optical pot., Pauli principle corrections, nuclear binding 80−27675
^{4}He(π,π), lowest order optical model 77−6456
^{4}He(π,π), microscopic calc. of medium corrections 78−78418
^{4}He(π,π), model which reduces to eikonal approx. 77−6444
^{4}He(π,π), multiple scatt. formalism, dynamics of πN resonances 77−6447
^{4}He(π,π), multiple scatt. anal. at medium energies 77−26791
^{4}He(π,π), optical model calc. 77−6454
^{4}He(π,π), single scatt. optical pot., Pauli principle and binding effects on cross section 80−86933
^{4}He(π,π) 28 to 260 MeV, corrections to optical potential, role of ρ^2 term 78−70574
^{4}He(π,π) in Δ_{33} reson. region, differential cross section, comparison with model calcs. 77−18621
^{4}He(π,π)^{4}He, 3,3 resonance region, Δ-isobar dynamics 77−34347
^{4}He(π,π)^{4}He, eikonal and quasi-eikonal models in complex ang. momentum plane *(Russian)* 77−50160
^{4}He(π^-,n)^{3}H, 100, 200 and 290 MeVs differential cross sections 78−33223
^{4}He(π^-,π^-X)^{3}H, 5 GeV, nucleon isobar prod. and knockout 80−42709
^{4}He(π^-,π^-), 110-260 MeV, cross section, phase shifts 78−54804
^{4}He(π^-,π^-), 1.12 GeV, multiple scatt. theory 77−6466
^{4}He(π^-,π^-), 20-280 MeV, phase shift anal. 77−18641
^{4}He(π^-,π^-), 51-260 MeV, dynamical and fixed scatterer approx. calcs. 78−25244
^{4}He(π^-,π^-), total cross section, improved optical pot., second order correction 79−22330
^{4}He(π^-,π^-)^{4}He, 51-260 MeV, nuclear-Coulomb interf. calc. using optical model phase shift anal. 77−54199
^{4}He(π^+,3p)^{1}H, 98-156 MeV, cross-section comparison with models 77−18612
^{4}He(π^+,3pn), quasideuteron absorption in non-radiative capture 79−85495
^{4}He(π^+,π^-) 4p, 1.5 to 2.0 GeV/c, cross sections, momentum spectra, ang. distrib. Δ resonances prod. 77−65237
^{4}He(π^+,π^0p), 120-165 MeV, isobaric resonance excitation, total inelastic cross section 79−85427
^{4}He(π^+,π^0p), 120-165 MeV, 3 nucleon exchange in knock-out reactions, cross sections 79−85437
^{4}He(π^+,π^0p)^{3}He, 105 to 135 MeV, cluster effects 79−85513
^{4}He(π^+,π^+2n2p), 120-165 MeV, total cross section, multiple scatt. processes 79−85517
^{4}He(π^+,π^+n), 120-165 MeV, isobaric resonance excitation, total inelastic cross section 79−85427
^{4}He(π^+,π^+n), 120-165 MeV, 3 nucleon exchange in knock-out reactions, cross sections 79−85437
^{4}He(π^+,π^+n)^{3}He, cluster effects 79−85513
^{4}He(π^+,π^+p), 120-165 MeV, isobaric resonance excitation, total inelastic cross section 79−85427
^{4}He(π^+,π^+p)^{3}H, 135 to 155 MeV, cluster effects 79−85513
^{4}He(π^+,$\pi^\pm$p), 120-165 MeV, 3 nucleon exchange in knock-out reactions, cross sections 79−85437
^{4}He($\pi^\pm$, $\pi^\pm$), resonance region, first order optical pot. calcs. 79−40957
^{4}He($\pi^\pm$,$\pi^\pm$), 30-70 MeV, backward scatt. cross-sections 77−18630
^{4}He($\pi^\pm$,$\pi^\pm$), 51 MeV, three body systems, review of recent theoretical anal. 79−80842
^{4}He($\pi^\pm$,$\pi^\pm$), differential cross section 78−33221
^{4}He($\pi^\pm$,$\pi^\mp$) double charge exchange, model development 77−54259
^{4}He($\pi^\pm$,$\pi^\mp$)4(p,n), ang. distrib. and cross-section calc. 77−23109
^{4}He(t,n), 10-11 MeV, multichannel R-matrix anal. of polarisation effects 77−2968
^{4}He(t,n)^{6}Li, cross section using var. calcs. in generator coordinate method 78−13122
^{4}He(t,t), 10-11 MeV, multichannel R-matrix anal. of polarisation effects 77−2968
^{4}He(t,t)^{4}He, cross section using var. calcs. in generator coordinate method 78−13122
^{4}He(t,t)^{4}He, elastic cross section from two-centre generator coordinate model functions 78−12994
^{5}He, 16.7 MeV states energy calc. using mixed cluster representation 80−27555

nuclei with mass number 1 to 5 continued
^{5}He, effective 3- and 4-body forces in 5 nucleon system 79−477
^{5}He energy levels deduced from d(t,t)d 80−47488
^{5}He first excited state charact. from ^{7}Li(d,$\alpha\alpha$)n 77−276
^{5}He$_\Lambda$, Λ-N pot. Majorana component on B_Λ value, overbinding 80 99144
^{5}He$_\Lambda$ hypernucleus, Friedel sum rule, hadron phys. meaning, nuclear matter density, binding energy 78−82305
^{5}He(g.s.) resonance energy and width, Coulomb interaction effects in ^{2}H(α,pα)n 77−71615
$^{\Lambda}$He, A=3, 4, charge structure, effect of neutron charge 80−105963
$^{\Lambda}$He, A=3, 4, EM sum rules, total absorption cross sections 79−71818
$^{\Lambda}$He, A=3,4, EM form factors and structure at large momentum transfer 79−67710
$^{\Lambda}$He, A=3,4, pionic, scatt. lengths and 1s width charge exchange contribs. calcs. 79−17934
$^{\Lambda}$He, A=4, 5, non-self-consistent energy calculations with a density-dependent effective interaction 79−36170
$^{\Lambda}$He(γ,π^0), A=3, 4, 1-10 MeV, photoprod. yields, DWIA anal., dipole photoprod. amplitudes 80−68645
$^{\Lambda}$He(p,p), A=3,4, backscattering, large momentum transfers, π exchange effects 80−5143
$^{\Lambda}$He(p,p)$^{\Lambda}$He, A=3,4, depth profile meas. of He in Ni and Nb 79−14839
$^{\Lambda}$He(π,π), A=3, 4, intermediate energies, collective isobaric resonance 80−63208
$^{\Lambda}$He(π,π), A=3, 4, low energy scatt. length and phase calcs. 80−47508
$^{\Lambda}$He(π^- n), A=3,4, 50-290 MeV, cross section, energy depend. 79−85521
$^{\Lambda}$He($\pi^\pm$,$\pi^\pm$), A=3,4, 260 to 310 MeV, differential cross sections 80−99192
$^{4}_{\Lambda}$He→$\alpha\pi^0\gamma$, evidence for γ transitions 79−85393
$^{4}_{\Lambda}$He, γ-ray spectra of stopped K^- in ^{6,7}Li 79−63621
$^{4}_{\Lambda}$He-$^{4}_{\Lambda}$H binding energy difference, particle mixing and charge asymmetric ΛN forces 79−75891
$^{4}_{\Lambda}$He-$^{4}_{\Lambda}$H binding energy difference, bound states, exact four body calc. 80−9255
$^{4}_{\Lambda}$He-$^{4}_{\Lambda}$H separation energy difference, Coulomb energy contribution 79−491
He(d, d), 9.0, 19.8 GeV/c, small angle, total and differential cross section, scatt. amplitude *(Russian)* 79−97711
He(e,e), A=3,4, many-body exchange effects, charge form factors calc. 78−33169
He(e,e), A=3 and 4, high momentum transfer, elastic struct. functions 78−62521
He(e^+,e^+)He, s-wave scatt., effective range expansion 80−47467
He(γ,pπ), photoexcitation in Δ(1236) region 80−22813
He(μ,μ), beam polarisation and nucl. recoil effects 79−67738
He(p,p), A=3,4, backward p elastic scatt. anal. using D and T exchange models 78−58270
He(π^-,π^-), 1.12 GeV, multiple scatt. anal., optical model potl. 77−6453
He(π,π)He, Glauber model applicability near Δ_{33} reson. region 77−14193
H(γ,π^0), near threshold photoprod. on ^{1}H and ^{2}H, cross section calcs. 78−25174
H(n,γ), parity violation study, high-rate counting circuitry for γ-rays 78−62527
H(n, $\gamma\gamma$), thermal, cross-section meas. 77−26703
H(n,n), A=2,3, differential scatt. rate distribs., multigroup rate coeffs. determ. 77−61476
H(n,n) cross section standard, status 77−23040
H(n,n)p, 27.3 MeV, neutron ang. distrib. meas. 78−62532
H(n,p)n, 25.8, 50.9 MeV, differential cross-sections 78−600
H(p, Λ^0), inclusive cross section, constituent-constituent multiple scatt. model for dependence on atomic number 80−83101
H(p,x), direct and charge transfer scattering processes, second quantisation 80−78289
H(ϕ,π^0), 350 MeV, differential cross sections 78−86527
H(π^-, $\pi^0\gamma$), Panofsky ratio meas. with TRIUMF pion^0 spectrum 77−14192
Li+$\pi^\pm$, 125 MeV, true absorpt. and scatt. 79−63705
^{4}Li, cluster model study using generator coord. method on ^{3}He+p scatt. 80−27581
^{5}Li ($3/2^-$) tensor polarisation from ^{2}H(α, αn)p 80−13450
^{5}Li, effective 3- and 4-body forces in 5 nucleon system 79−477
^{5}Li level parameters via ^{3}He(d,d)^{3}He 0.3-8 MeV 77−30606
^{6}Li(γ,π^0), cross-sections determ., selection rules calc. 77−82905
^{6}Li(n,n), differential scatt. rate distribs., multigroup rate coeffs. determ. 77−61476
^{2}M+hadron→proton+X, polarised d, S and D wave functions, nuclear core hypothesis 78−62417
^{2}M+π, resonances near ΔN threshold, Argand diagrams 78−62582
^{2}N breakup, nucleon induced, NN interaction parameters 77−18550
^{3}Ne(α,α), antisymmetrisation effects on the effective internuclear potential 79−59085
^{20}Ne+U, relativistic ions, product spectra, statisical models 78−638
^{16}O, charge form factors of doubly closed shell nuclei 77−6274

nuclei with mass number 6 to 19
1 GeV, neutron production *(Russian)* 79−85477
60 to 183 MeV, folded potentials for d intermediate channels 79−17868
^{10}B(π^-,2n), stopped pion absorption 78−25243
^{12}C(^{16}O,^{16}O), anomaly at 13.7 MeV, optical model anal. 78−21587
^{12}C($\pi^\pm$,$\pi^{\pm\prime}$), isospin mixing doublet, possible isospin mixing matrix element extraction 79−85364
^{12}C-α-^{12}C nuclear molecular states, quantum mechanical three-body approach 79−97692
^{16}O(p,p), spin orbital interaction and nucl. matter density distrib. *(Russian)* 79−22176
^{16}O+^{16}O, 3-D TDHF calcs. 78−54781
^{16}O(γ,N), photonuclear sum rules from continuum calcs., dependence on residual interactions 80−22807
^{16}O(π^+,π^+), 50 MeV, Lorentz-Lorenz effect 78−17247
^{18}F levels, J^π and ang. distribs. DWBA anal. of ^{19}F(p,d) 80−42545
^{18}O(p,p), polarised p, elastic and inelastic, 6.1-16.6 MeV, ^{19}F resonance parameters and J^π values 79−45232
(^{6}Li,^{6}Li) 50.6 MeV elastic scatt. on A=12-208 nuclei, optical model parameters 77−18592
^{6}Li(n,n), 4-7.5 MeV, differential cross section meas. 77−34313
^{9}Be(π^-,2n), stopped pion absorption 78−25243

nuclei with mass number 6 to 19 continued
A=10 to 50, m-particle n-hole struct. from few nucleon transfer reactions, review 78−50062
A=10-58, neutron separation energies, self consistent set from (n,γ) reaction 80−52563
A=11, 12, energy levels, transitions and resonances, compilation 80−46743
A=12, decay of T=1 isospin triplet, β-ray anisotropy 78−78322
A=12, recoil polarisation in muon capture, arbitrary nuclear spin, form factors 79−75978
A=12 polarised β-decay, nuclear Dirac wave function test 80−5060
A=12 to 24, nuclear cluster norm determ. using integral transform and SU(3) recoupling techniques 79−22214
A=12 to 40, (α,^{2}He) reaction, high spin state transition cross sections in 1p and 2s1d shell 79−6644
A=15 mag. moments, nuclear Dirac wave function test 80−5060
A=15-18, effective interaction from coupled cluster many-body method extension 80−22701
A=16, 17, 18 and 19, cluster struct., review 78−50107
A=16, 17 nuclei, energy levels, struct., review 77−46116
A=16 to 28, α-structure amplitudes and shell model wavefunctions for nuclear states 79−45192
A=16 to 4O, mag. moments, shell model calcs, mesonic exchange current effects, book contrib. 80−479
A=16-40, α-spectroscopic factors between ground states, shell model prediction 79−13204
A=16-58, charge, proton and neutron density distribs. calc. 80−22680
A=17 and 18, multipole matrix elements, HF calcs. 78−50098
A=18, 19, sd shell nuclei, effective interaction between nucleons 78−17117
A=18, 2p1h multiple scatt. formalism, effective interactions, energy spectra 77−67709
A=18, 3p1h multiple scatt. formalism for 2 valence nucleons, microscopic effective interaction 79−6428
A=18, α-clustering on odd-parity levels 78−74318
A=18, average effective-interaction calcs. in HF and harmonic oscill. basis 77−57605
A=18, effective interaction, 2nd order core polarisation diagrams with intermediate particle states 79−45180
A=18, multiple scattering, three-particle one-hole nuclear effective interaction 80−13384
A=18, shell-model interaction, convergence in reaction matrix G 78−50102
A=18, shell-model spectra, one-boson-exchange potential 80−68550
A=18 nuclei, importance of high lying intermediate excitations on nuclear effective interactions 78−70460
A=18 nuclei, negative parity spectra, phonon dynamic interaction propagator approach 78−8739
A=18 nuclei, reaction matrix calc. 77−14085
A=18 to 22, influence of non-central interactions on 1s-0d nuclei 78−93949
A=18-20, light nuclei, compilation of energy levels, nuclear struct. information 78−62478
A=18-22, Coulomb matrix elements and energy shifts 77−10308
A=18-38, inelastic scatt. E4 transition probabilities in the 0d, 1s shell 80−78210
A=19-31 odd nuclei, $K^\pi = {}^1/_2{}^-$ bands, spectroscopic factors and transitions 80−32151
A=2, 4, 16, photonuclear sum rule enhancement factor, Hartree Fock, Bethe-Goldstone eqns. 79−3137
A=4-16, monopole giant resonances, state density radii and compressibility using hyperspherical functions *(Russian)* 80−27615
A=5 to 10 nuclei, energy levels 79−49583
A=6 extended shell-model calcs. 77−14017
A=6 to 14 nuclei, muon capture rate calcs. 78−33150
A=6-14, one π exchange currents effect on partial muon capture rates 79−22239
A=6-14 nuclei, OPE current effect on allowed β-decays in the 1p shell nuclei 79−54413
A=6-44, gamma-ray transition strengths, data tables 80−37345
A=6to 14, radiative pion capture, mag. dipole resonance excitation in 1p shell nuclei 78−74408
A=8 fragment products from K^-+emulsion nuclei 80−52695
A=8 mirror asymmetry, existence of second class weak currents 77−6307
A=8 systems, second class current problem 77−41921
A=9 to 70, proton scatt., 14 to 45 MeV, differential cross sections 79−45273
A<100, average E1/M1 strength ratio 80−52621
A≤28, giant quadrupole resonance, E2 intensity distrib., from (α, α′), DWBA anal. *(Hungarian)* 80−52642
A≤57 nuclei, E2, M1 multipole mixing ratios 80−22751
emulsion+p, 400 GeV ang. distribs. of secondaries 79−36232
even-even nuclei, z=6 to 100, probable members of quasi-bands in spherical and deformed regions 80−13357
heavy-ion α-transfer reactions on targets A=10, 12, 14, 16 *(Japanese)* 78−4962
internal conversion coeffs. for at. numbers Z≤30 77−46136
kaonic ^{12}C, coupled channel formalism, role of Λ(1405), binding effect, Pauli blocking 78−55261
light nuclei, alpha cluster model, 3-body problem 80−32217
light nuclei, multipole giant resonances 78−86462
light nuclei, shape in translationally invariant shell model 79−26367
mirror nuclei, A=13-33, transverse photon effect 77−6229
neutronium (Z=0) bound isotopes search in high-energy proton induced fragmentation 77−22904
NMR in organic solids, spin decoupling dynamics 77−4582
non-normal parity states, 1p shell nuclei, 1ħω spectra 78−12977
nuclear photoemulsion obs. at E_π=115 MeV, ang. distribs. and cross sections *(Russian)* 79−13352
oriented nuclei, β-γ ang. correl., G-parity nonconservation 78−54723
P-shell hypernuclei, formation, γ-radiation, and spin values, shell model 79−22223
photonuclear energy integrated cross-sections, calcs., A=2-40 77−50110
prod. cross sections from shell model theory 78−62501
projectile fragmentation in nuclear emulsions at 2.1 GeV/nucleon 78−70561
props. of prompt muons prod. by 28 GeV protons 79−17906
resonating-group method anal. 77−82886
shell model calc. of log ft values and spectroscopic factors, A=10-15 77−61357

nuclei with mass number 6 to 19 continued
stable odd-mass sd nuclei, EM multipole moments of ground states 80−102116
thermonuclear reaction rate data for intermediate mass nuclei 80−31427
(α,^{2}He), 55 and 65 MeV, on 1p and 2s1d shell nuclei, A=12 to 40 78−82365
(α,n) cross-sections and α-stopping power in light elements 77−74862
Be+p, 200 GeV, d, $\bar{d}$, t, $\bar{t}$, ^{3}He, $^3\bar{H}e$ prod. 79−9563
C+p, 24 GeV, J/ψ prod. cross section 78−46055
(e,e), low-q, A=14 nuclei, isospin T=2, 1 and 0 collective resonances, shell model 80−510
(γ,Π) in nuclear matter, optical pot. and Fermi gas model, Li, Be appl. 79−36230
(γ,X), A=14 nuclei, isospin T=2, 1 and 0 collective resonances, shell model 80−510
K^0 meson production cross section *(Russian)* 78−82394
^{6}Li, d+α clusters, break up in nuclear field, ^{118}Sn+^{6}Li study 78−46092
^{6}Li(α,α), resonant-group kernel function, analytical computation 79−40941
^{6}Li(γ,π$^+$)^{6}He, cross-section determ. 77−14100
Λ nucleus, 40≥A≥12, strangeness exchange reactions, anal. 77−292
(p,p) scatt. on light nuclei, 6 MeV, optical model anal. *(Russian)* 78−25200
(p,π$^+$), 320-800 MeV protons on ^{2}H to ^{10}B targets, coherent pion production *(French)* 79−533
(π$^-$,2n), π absorption study by subsequent particle emission observation 79−85493
(π$^-$,2n) struct. and reaction information, two hole states, direct mechanism 79−85496
(π,γ), A=14 nuclei, isospin T=2, 1 and 0 collective resonances, shell model 80−510
(π$^-$,γ), 1p shell nuclei, spin-dipole excitations, shell model calcs. 79−17935
^{12}C(p,p), 11.5-18 MeV polarised protons, ang. distribs. 77−3010
^{18}O(γ,σ_0), 19-32 MeV, E1 and E2 cross section, E1-E2 phase difference 80−63172
6Li(p,n), 144 MeV, one pion exchange and PCAC expt. test 80−528
8Be, reson. levels, J^π, via 6Li(d,α)^{4}He, 1.5-11.5 MeV 77−82935
8Be, reson. levels , J^π via ^{6}Li(d,α) below 12 MeV 77−82936
^{12}(α, α), 1.37 GeV, microscopic anal. using modified Glauber model 78−617
^{16}(0$^+$)(μ,ν)^{16}N(0$^-$), one pion exchange current problem for ^{16}O(0$^+$)⇄^{16}N(0$^-$) 79−85375
A=12-15, heavy ion induced α-transfer α-clusters, DWBA anal. 79−26454
^{22}Al, Coulomb matrix elements and energy shifts 77−10308
Am-Be neutron probe, underestimation of radiation exposure by film badges 78−15900
B, 20 to 50 MeV, total reaction cross sections compared to opaque-nucleus model 78−33174
B, A=10,11, prod. by ^{12}C spallation by p and α 77−79380
B isotopes, separation using anion exchange resin *(Japanese)* 78−33625
B, muonic X-ray transitions, nuclear charge radii 80−99589
B, NQR in heteroorganic group III compounds, summary 78−25565
B, nucleosynthesis contribution from ^{16}O(p,X) 79−40978
B, primary cosmic ray nuclei, isotopic composition using nuclear emulsions 79−80155
B+^{27}Al, A=10,11, elastic scatt. quadrupole effects at 50 MeV, optical parameters 77−88169
B+P, A=10, 11, 660 MeV, H and He isotope prod. 77−18544
^{8}B β$^+$-decay, β-α angular correlations, final state energy depend., current test 80−102151
^{8}B, isospin symmetry breaking in A=8 mirror decays 78−93973
^{9}B, 17.11 MeV energy level of T=3/2 quadruplet from ^{6}Li(^{3}He,γ), ^{6}Li(^{3}He,p) 79−22193
^{9}B 17.637 MeV state form., α-α coincidence meas. from ^{6}Li(^{3}He,α)^{5}Li(GS), ^{9}B 17.637 MeV state form., α-α coincidence meas. 79−475
^{9}B complex system, excitation functions for 17.19 and 17.64 MeV levels from ^{6}Li+^{3}He 80−78188
^{9}B, energy levels anal. in ^{9}Be(p,pn)^{8}Be 78−21550
^{9}B, isospin forbidden nucleon decays of T=3/2 levels 77−6320
^{9}B(α,2α), pole peripheral model, ang. correl. functions calc. 77−6328
$^{\wedge}$B, A=10, 11, neutron-photon multigroup cross sections for neutron energies ≤60 MeV 79−30880
$^{\wedge}$B+n, A=10,11, 1.0 to 14 MeV, total cross-section meas. using ^{9}Be(d,n)^{10}B neutron source 79−22280
$^{\wedge}$B+p, A=10,11, 1 GeV, neutron production *(Russian)* 79−85477
$^{\wedge}$B(p,X), A=10, 11, 740 MeV, ^{7}Be prod. cross section for cosmic ray anal. 79−93625
$^{\wedge}$B(p,π$^+$), A=10, 11, 0.5-10 MeV, total cross sections near pion Coulomb barrier 80−32280
$^{\wedge}$B(p,π$^+$), A=10,11, 200 MeV, pion energy spectra for discrete final states, cross sections 80−106057
^{10}B 1175 keV level resonance strength from ^{6}Li(α,γ) 79−45228
^{10}B, 3590 keV excited state lifetime from ^{7}Be(p,γ) 79−9510
^{10}B, 8.89 MeV reson. J^π assignments via (p,p) and (p,αγ) 2.56 MeV 77−50098
^{10}B (α, 2α), 700 MeV, cross section, effective cluster number from PWIA, momentum distrib. 79−40940
^{10}B, α-transfer reactions, spectroscopic factors, exact finite range DWBA anal. 80−13372
^{10}B, cluster effects, low-lying states determ. 77−6228
^{10}B concentration effect on thermal neutron beam response of hamster and HeLa cells 78−73178
^{10}B, EM transitions, model anal. based on [42] representation dominance 79−40880
^{10}B, energy level struct., admixed wave functions, ground state quadrupole moment, deformability 77−50054
^{10}B, form. in ^{11}B(t,α) reaction, 0.5 to 1.25 MeV, excitation functions and ang. distribs. 78−17216
^{10}B, four-body breakup induced by 18 MeV neutrons, double final state interaction 78−17192
^{10}B levels, J^π, ^{12}C(p,^{3}He) at 51.9 MeV 77−30566
^{10}B levels, J^π and ang. distribs. from ^{9}Be(^{3}He,d) 80−42546
^{10}B levels and differential cross sections PWBA and coupled channel anal. of (α, t) 80−102121
^{10}B, neutron cross section standards, detection techniques 79−9970
^{10}B shields, transport calcs. and transmission factors for activation detectors 78−78434
^{10}B spectroscopic factor determ. using ^{14}N(d,^{6}Li)^{10}B 79−63679

nuclei with mass number 6 to 19 continued
^{10}B spectroscopic factors, ^{9}Be(^{3}He,d) with 33 MeV polarised beam 77−328
^{10}B T=1 states, γ-transition strengths, lifetimes, branching and mixing ratios from ^{6}Li(α,α) 80−27594
^{10}B, total neutron cross section, 90 to 420 keV 79−40913
^{10}B transitions and levels from ^{11}B(γ,nγ^{1}) *(Russian)* 80−13433
^{10}B, triaxial deformation in shell model non-central forces, projected HF calc. 80−13367
^{10}B+^{10}B, fusion below Coulomb barrier, quantum mechanical barrier penetration model anal. 80−18361
^{10}B+^{7}Li, 24 MeV, charged particle reaction channels, reaction mech. 78−8841
^{10}B+n, 1.5-14 MeV total cross-section meas. 77−26742
^{10}B(^{10}B,α)^{16}O, excitation functions, resonance like structures 78−29496
^{10}B(^{14}N, α)^{20}Ne reaction near Coulomb barrier, intermediate structure resonances 79−9450
^{10}B(^{14}N,^{14}N), 4.3-9.1 MeV, differential cross sections, incoming wave boundary condition model 79−22348
^{10}B(^{14}N,X), 2.9-7.5 MeV, evaporation residue and total fusion cross section 79−22348
^{10}B(^{14}N,α)^{20}Ne, 10 MeV, search for resonances 78−82385
^{10}B(^{14}N,α)^{20}Ne, highly-excited rot. band obs. in Mg 78−33218
^{10}B(^{16}O,d), 60 MeV 78−89781
^{10}B(^{3}He,^{3}He), optical potentials and volume integrals, mass and energy dep. 80−52686
^{10}B(^{3}He,pγ), 4.1 MeV, radiative transitions and isospin mixing in ^{12}C 77−38242
^{10}B(^{9}Be, X), total reaction cross sections for sub-Coulomb energies, neutron transfer reaction 79−80950
^{10}B(α,α), 5-50 MeV, optical and Inopin-Ericson model anal. 77−3025
^{10}B(α,d)^{12}C, 40 MeV, ratio of isospin forbidden/allowed yield 77−18385
^{10}B(α,n$_{0}$)^{13}N, 18-20 MeV, neutron ang. distribs. multi-nucleon transfer mechanism 77−14144
^{10}B(α,n$_{1}$)^{13}N*, 18-20 MeV, neutron ang. distribs., multi-nucleon transfer mechanism 77−14144
^{10}B(d, d′), energy depend. isospin violation in 10 MeV region 77−14134
^{10}B(d,^{2}He), 55 MeV, cross sections, ^{2}He energy spectra and ang. distribs. 80−18321
^{10}B(d,3α), 360 keV, sequential decay, absolute three-particle cross section meas. 78−17220
^{10}B(d,3α), 4.4 to 5.6 MeV, ^{12}C excited states 77−18576
^{10}B(d,α), cross-section contrib. from ^{8}Be 3^{+} states, isospin mixing model 78−89789
^{10}B(d,α)^{8}Be(g.s.), excitation functions struct., isoscalar giant resonances in ^{12}C 78−46073
^{10}B(d,ααα)^{4}He, E$_{d}$<3.4 MeV, reaction mechanism 77−6362
^{10}B(d,αα)^{4}He, Q=17.88 MeV, quasi-free effect search 78−4947
^{10}B(d,αα)α, ^{12}C excited states between 29 and 34 MeV 78−21494
^{10}B(d,p)^{11}B, 1 to 2 MeV, ang. distribs., reduction factor, spectroscopic factors 77−41977
^{10}B(d,p)^{11}B, 2.5 to 21.0 MeV, angular distrib., DWBA analysis 80−68675
^{10}B(d,p)^{11}B, E$_{d}$=0.8 to 2.4 MeV, reaction mechanism 79−17910
^{10}B(e,e′), 67-194 MeV, form factors, transitions and ground state radiative width 79−75898
^{10}B(e,e′)^{10}B, 40-61 MeV, multipolarities, transition widths 77−10356
^{10}B(e,e′p), 700 MeV, proton spectral functions, momentum distribs., DWIA anal. 78−41701
^{10}B(e,e), 140 MeV, resonances in e spectra *(Russian)* 78−78367
^{10}b(γ,d), from (e,e′d), cross section, E2 transistors giant resonance and clusters 80−63169
^{10}B(n, α)^{7}Li, tumour dose enhancement in fast neutron therapy 78−73249
^{10}B(n,^{4}He)^{7}Li, determ. of B in complex matrices from ^{4}He and ^{7}Li tracks in plastic detectors 79−18080
^{10}B(n,α$_{0}$)^{7}Li, 1-1500 keV, cross section meas. 77−26755
^{10}B(n,α$_{1}$)^{7}Li*, 0.1 to 2.0 MeV, cross section meas. 79−36237
^{10}B(n,α$_{1}$)^{7}Li*, 1-1500 keV, cross section meas. 77−26755
^{10}B(n,α), 2 and 24 keV, ang. distribs., branching ratio 79−54440
^{10}B(n,α) cross section standard, status 77−23040
^{10}B(n,α) cross section standard, R-matrix anal. 77−23041
^{10}B(n,α)^{7}Li, 10 keV to 1 MeV, review of cross section meas. 79−9587
^{10}B(n,α)^{7}Li, 13.9 MeV, differential cross sections meas. 78−78387
^{10}B(n,α)^{7}Li, appl. to anal. of fusion reactor materials, archeometry, and nuclear spectroscopy 80−61200
^{10}B(n,α)^{7}Li, for neutron activation anal. of Si:B, range distrib., IBR-30 expts. 78−11585
^{10}B(n,α)^{7}Li, radiation chemical transform. of CN^{-} by inner source 79−34341
^{10}B(n,α)^{7}Li, recoil particles, radiolysis of aq. solns., intrajectory reacts. *(French)* 77−12812
^{10}B(n,α)^{7}Li, thermal neutron flux, determ. accuracy 77−342
^{10}B(n,αγ)^{7}Li, 0.1 to 2.2 MeV, cross section determ. 79−45248
^{10}B(n,αγ)^{7}Li, 5 to 700 keV, relative cross section, ^{11}B $^{5}/_{2}^{-}$ level 78−89866
^{10}B(n,αγ)^{7}Li, relative cross section, 5 to 800 keV 77−26727
^{10}B(n,n), 4-8 MeV, differential cross section meas., struct. determ. 77−23016
^{10}B(n,n), cross sections for neutrons of 4 to 8 MeV 78−21553
^{10}B(p, π^{+})^{11}B, 140 to 200 MeV, π^{+} ang. distrib., energy depend. 79−63667
^{10}B(p,π^{+}), 320-605 MeV, cross sections, pion exchange model anal. 80−27676
^{10}B(p,π^{+}), differential cross sections, DWBA calc. 79−85415
^{10}B(p,π^{+}), near threshold, reaction energy dependence 79−85461
^{10}B(p,π^{+})^{11}B, 163 to 186 MeV, expt. and theoretical study of π^{+} prod. 79−59061
^{10}B(p,π), microscopic model anal., stripping model test for (d,p) 79−85436
^{10}B(π^{-},2n), neutron-pair emission characts., excitation energy spectra 78−13159
^{10}B(π^{-},n), single neutron emission induced by stopped π^{-} in 1p shell nuclei 79−59089
^{10}B(π^{+},π^{0}), 1st order pion-nucleus pot. calc. 77−23113
^{10}B(t,α)^{10}B, 0.5 to 1.25 MeV, excitation functions and ang. distribs. 78−17216
^{10}B(t,α)^{9}Be, 0.5 to 1.25 MeV, excitation functions and ang. distribs. 78−17216
^{10}B(t,d)^{11}B, 5.5 MeV, angular distrib., DWBA analysis 80−68675

nuclei with mass number 6 to 19 continued
^{10}B(t,p)^{12}B, 0.5 to 1.25 MeV, excitation functions and ang. distribs. 78−13109
^{11}B, $^{5}/_{2}^{-}$ level from ^{10}B(n,αγ)^{7}Li, 5 to 700 keV 78−89866
^{11}B, +ve parity states in weak coupling model, E1 and β strengths 77−34228
^{11}B, 2α+t model, parity states, shell and cluster structs. 78−50110
^{11}B, (α,γ$_{0}$), 15.5-19.5 MeV, excitation curve ang. distrib., cross section, ^{15}N resonances 78−94019
^{11}B (e,e′) 120-250 MeV, excited state form factors, shell and diagram model anal. *(Russian)* 79−40852
^{11}B, absolute excitation energy meas. using electrostatic analyser 77−30741
^{11}B analogue of ^{11}C 6478 keV state, lifetime from ^{7}Li(α,γ) 80−5092
(^{11}B, αX), 116 MeV, heavy ion-alpha in-plane correlations 80−18343
^{11}B, energy levels, using ^{10}B(p,π^{+}) 163 to 186 MeV 79−59061
^{11}B, excited states parameters from ^{7}Li(α,α)^{7}Li expt. *(French)* 79−93637
^{11}B intermediate resonance and electric quadrupole transition contribution to ^{12}C(γ,pα)^{7}Li *(Russian)* 79−40896
^{11}B, low lying analogue states, DWBA anal. from ^{12}C(d,^{3}He) 29 MeV, polarised d 78−82285
^{11}B, M2 giant resonance calcs. from (e,e′),(π^{-},γ),(μ^{-},ν) 80−22784
^{11}B, NMR, for senior level inorganic courses 78−4424
^{11}B, NMR in borate glass, fast stable analysis technique 78−6585
^{11}B, NMR in o-$As_2B_{10}H_{10}$, mol. reorientation 77−85583
^{11}B, NMR in vitreous borophosphates 77−7672
^{11}B, NMR line shape and spin-lattice relax. meas. in vitreous and liq. B_2O_3 and B_2S_3 77−4575
^{11}B, NMR lineshape in SrO-B_2O_3, BO_3^{-3} triangle, perfect trigonal symm. *(Korean)* 78−19367
^{11}B, NMR obs. of Na_2O-B_2O_3-SiO_2 glass struct. 78−38625
^{11}B, NMR of $[(B_{10}H_{12})_2Ni]^{2-}$ 79−31553
^{11}B NMR spectroscopy, biased spectral decomposition in glass 78−88198
^{11}B, neutrino-induced prod. in stellar C layer 80−82337
^{11}B non-normal parity state electroexcit. calcs., E1, M2 giant reson. 77−57643
^{11}B, projected HF calc. in intermediate coupling 77−18460
^{11}B, radiative widths meas., 2.125 to 8.92 MeV levels, intensity calibration of photon spectrum 79−13242
^{11}B, semileptonic weak and EM interactions, isoelastic processes 77−18528
^{11}B states, spectroscopic factors from DWBA anal. of ^{12}C(p,2p) 80−5057
^{11}B, struct. study of 2α+t system in orthogonality condition model, level energies and parity 80−5080
^{11}B, studied via ^{10}B(d,p)^{11}B, 1 to 2 MeV, ang. distribs., reduction factor, spectroscopic factors 77−41977
^{11}B$_{Λ}$→π^{-}+^{11}C*, produced in p+emulsion nuclei reacts. *(Russian)* 80−9297
^{11}B+^{10,11}B, fusion below Coulomb barrier, quantum mechanical barrier penetration model anal. 80−18361
^{11}B+^{12}C elastic scatt., resonances 78−89901
^{11}B+d→3αn, 3.75 MeV, sequential decay reaction mechanism from ang. distrib. anal. 79−6631
^{11}B+n, 1.5-14 MeV total cross-section meas. 77−26742
^{11}B+p→^{4}He+^{8}Be→3(^{4}He) fusion power feasibility 77−38310
^{11}B(^{14}N,^{9}Be)^{16}O, 50 MeV, reaction product spectra, non-statistical processes 77−57684
^{11}B(^{16}O,^{15}N)^{12}C, exchange effects on ang. distribs. 78−627
^{11}B(^{18}O,^{14}O)^{15}B, 96, 103 MeV mass of ^{15}B meas. 77−38219
^{11}B(^{3}He,^{3}He) 17.5 and 40.0 MeV, elast. and inelast. scatt. from ground state and low excited levels 77−65229
^{11}B(^{3}He,n)^{13}N, ang. distrib. at energies below Coulomb barrier 79−40938
^{11}B(^{3}He,n)^{13}N, Coulomb stripping reaction theory 77−54232
^{11}B(^{6}Li,^{8}B), 80,93 MeV, ^{9}Li energy levels anal. 77−46183
^{11}B(P,γ)^{12}C, radiative capture of intermediate-energy protons to high-lying states 79−36243
^{11}B(α,γ$_{0}$)^{15}N, giant dipole reson. region 77−26777
^{11}B(α,n)^{14}N, n polarisation ang. distrib., R-matrix anal., ^{15}N excited states 78−4937
^{11}B(α,p)^{14}C, 4.4-6.7 MeV, absolute differential cross-section meas. 78−46054
^{11}B(d,α$_{0}$)^{9}Be, Hauser-Feshbach statistical theory *(Spanish)* 77−67753
^{11}B(d,α)^{9}Be, non-relativistic, analytic S-matrix theory *(Spanish)* 77−67754
^{11}B(d,p)^{12}B reactions, 1.3 to 3.0 MeV, DWBA analysis of magnetic substate populations of residual nucleus 78−29480
^{11}B(e,e′), E1 transitions to unnatural parity states 80−22758
^{11}B(γ,γ), resonance scatt., molecular orientation effects 80−78252
^{11}B(γ,nγ′) 30 MeV giant dipole resonance decay, ^{10}B transitions *(Russian)* 80−13433
^{11}B(γ,p)^{10}Be, 18 to 31 MeV, photoproton spectra and ang. distrib., excited state transitions 78−13056
^{11}B(γ,π^{-})^{11}C, 142.0-169 MeV, cross-section near threshold 77−6348
^{11}B(n,α)^{8}Li, 14.4 MeV, ang. distrib., total cross sections 79−89303
^{11}B(n,α)^{8}Li, 14.4 MeV, spectra and ang. distribs., recoil nucl. transitions 78−17193
^{11}B(n,n), 4-8 MeV, differential cross section meas., struct. determ. 77−23016
^{11}B(p, n)^{11}C, steel B depth distrib. meas. using time of flight method 80−71986
^{11}B(p, p), 1 GeV, quadrupolar effect, cross sections *(Russian)* 79−30834
^{11}B(p,^{6}Li)^{6}Li, 51.9 MeV, five nucleon transfer mechanisms, DWBA calcs. 80−73845
^{11}B(p,2α)α, reaction characts., potentiality for controlled thermonuclear fusion 77−30667
^{11}B(p,3α), 35.4-1500 keV, resonance cross sections, astrophysical S-factor, fusion fuel 79−36213
^{11}B(p,3α), E$_{p}$=2 to 4 MeV, energy depend. of interference phenomena 78−13084
^{11}B(p,α)^{8}Be, continuous energy spectra of α-particles 77−30567
^{11}B(p,α)^{8}Be 6.0-18.0 MeV, isoscalar giant reson. 77−46152
^{11}B(p,αα)^{4}He, E$_{p}$>2.5 Mev, reaction mechanism 77−6362
^{11}B(p,αα)^{4}He, Q=8.68 MeV, quasi-free effect search 78−4947
^{11}B(p,γ), 163 keV, ^{12}C radiative transition and isospin mixing 77−38242
^{11}B(p,γ), 30-100 MeV, meson exchange and nucleon correlation process calcs. 79−549

nuclei with mass number 6 to 19 continued

^{11}B(p,γ), 6-23 MeV, capture to ground state and first three exited states of ^{12}C 77−74842
^{11}B(p,γ) 40,60,80 MeV, photon spectra direct reaction calc. 79−89281
^{11}B(p,n)^{11}C, 3-49 MeV, cross section, ang. distrib., ^{12}C level spin assignment 78−93996
^{11}B(p,n)^{11}C, analogue reaction at 16.3 to 26.5 MeV, polarisation transfer meas. 77−26735
^{11}B(p,n)^{11}C, shell model anal. of polarisation-analysing power differences 80−22804
^{11}B(p,p), polarisation behaviour near (p,n) threshold, virtual scatt. mechanism feasibility 79−6592
^{11}B(p,p), polarisation effects for elastic scatt. near (p,n) reaction threshold 78−13075
^{11}B(p,p)^{11}B, resonant scatt., determ. of ^{12}C analogue states 77−38260
^{12}B, aligned, β ang. distribs., second class currents 78−50126
^{12}B, aligned, β-ang. distrib. and alignment correction coeffs., axial vector currents 80−5097
^{12}B, aligned, β-ang. distrib. asymmetry coeffs., pseudotensor interaction, T=1 isospin triplet decay 80−106021
^{12}B, aligned, existence of G-parity irregular induced tensor current 78−29384
^{12}B analogue states at 4.5 MeV giant resonance region, strong spin-isospin mode, from ^{12}C(e,e'π^+) 80−78250
^{12}B average polarisation, form factors and partial capture rate from ^{12}C(μ^-,ν), polarised π^- 79−22263
^{12}B, beta decay, PCAC and vector current conservation 79−93561
^{12}B, beta-ray spectra and conserved vector current 79−54409
^{12}B, beta-spectra reanalysis, shape-factors and CVC theory 77−67724
^{12}B β^- decay, conserved vector current, elementary particle approach 78−66246
^{12}B β-decay, polarised nucleus, asymm. of β-ray ang. distrib., second class currents 77−41919
^{12}B β-decay, radiative corrections 77−38249
^{12}B, β-ray branching and $T_{1/2}$ 78−41674
^{12}B, form. in ^{10}B(t,p) reaction, 0.5 to 1.25 MeV, excitation functions and ang. distribs. 78−13109
^{12}B, hyperfine fields in ferromag. Ni, NMR obs. 77−28476
^{12}B, hyperfine interactions in Mg, decoupling by external mag. field 77−24756
^{12}B, implanted in Ni, hyperfine interactions, crit. behaviour near T_c 78−43663
^{12}B, in Mg, elec. quadrupole interactions, obs. by depolarisation due to level mixing 77−55728
^{12}B J-transfer determ. from ^{13}C(d,^{3}He), polarised d, 29 MeV 79−49579
^{12}B, mag. moment from β-ray spectra of recoil nuclei polarised by fast polarised beams 77−28502
^{12}B, meas. of weak magnetism term in β spectra 78−4917
^{12}B, NMR in Ni, hyperfine field determ. 77−8418
^{12}B polarisation, quantum mechanical explanation for ^{100}Mo(^{14}N,^{12}B) 79−17890
^{12}B, polarised, β-decay asymm., G-parity nonconservation, second class currents 77−41920
^{12}B, polarised, higher order effects in determ. of asymmetry parameters in β-decay 79−22247
^{12}B, produced in ^{12}C($\mu^-,\nu_\mu\gamma$)^{12}B, impulse approx. calc. 78−37315
^{12}B, quadrupole coupling const. in ZrB_2 single cryst. 78−37279
^{12}B, quadrupole interaction in Be, Mg and Zn 78−47750
^{12}B spin polarisation, obs. in ^{100}Mo(^{14}N,^{12}B) 79−3168
^{12}B, spin polarisation in ^{100}Mo(^{14}N,^{12}B), semiclassical anal. 78−33212
^{12}B spin polarisation in ^{100}Mo(^{14}N,^{12}B) 80−63160
^{12}B spin polarisation in ^{232}Th(^{14}N,^{12}B) 80−63161
^{12}B spin polarisation meas. in ^{100}Mo(^{14}N,^{12}B) 77−71562
^{12}B spin polarisation meas. from β-decay, product of ^{100}Mo(^{14}N,^{12}B)^{102}Ru 78−50196
^{12}B state excitation energies and widths, DWBA ang. distribs. from ^{10}B(t,p) 23 MeV 78−70544
^{12}B, weak magnetism and beta spectra 77−6314
^{12}B+^{16}O→^{16}Al, fusion cross section comparison to ^{12}Cr^{14}N→^{26}Al 79−71873
^{12}B(1$^+$,g.s.), induced pseudo-scalar coupling constant in ^{12}C(μ,ν_μ) 79−49606
^{12}B→^{12}Ce$^-\bar{\nu}_e$, data anal., second-class currents and CVC 77−82874
^{12}B→B$^-$+^{12}C, second-class current search, alignment correlation meas. by Zeeman technique 78−37313
^{12}B→β^-+^{12}C, alignment correlation meas. by Zeeman technique, vector currents and form factors 78−37312
^{13}B state excitation energies and widths, DWBA ang. distribs. from ^{11}B(t,p), 23 MeV 78−70544
^{14}B, mass excess and excited states from ^{14}C(^{14}C,^{14}B) 80−42676
^{15}B, mass excess from ^{48}Ca(^{18}O,^{15}B)^{51}V 78−70433
^{15}B mass meas. in ^{11}B(^{18}O,^{14}O)^{15}B at 96, 103 MeV 77−38219
B(e,e), A=10, 11, form factors, Hartree Fock calcs. 78−58263
Be (p, X), 2.2, 6, 8.5 GeV, p and d inclusive spectra at 162° *(Russian)* 79−97710
Be, constraints on form. from abundance in α Centauri A 77−41379
Be, double differential neutron cross sections at 5.9, 10.1, and 14.2 MeV 77−67743
Be, hypernuclei, symmetry classification for excited states *(Chinese)* 78−25144
Be, integral test of cross section, neutron leakage spectra, spherical assembly 77−23033
Be, meas. of mass no. depend of ψ photoprod. 77−26668
Be muonic X-ray transitions, nuclear charge radii 80−99589
Be, neutron diffusion in finite blocks, flux synthesis method for 3D multigroup eqn. 77−34366
Be, neutron forces in relativistic electron radiation field in crystal, channelling *(Russian)* 80−70287
Be, neutron spectra from p,d, ^{3}He collisions 80−524
Be, nucleosynthesis contribution from ^{16}O(p,X) 79−40978
Be, π^- and p elastic scatt., 30 to 50 GeV/c, nuclear radius, real/imaginary forward scatt. amplitude ratio *(Russian)* 77−34351
Be+^{40}Ar, 1.8 GeV/nucleon, central collisions, single particle inclusive spectra, associated multiplicity 79−9607
Be+d, 14-40 MeV, Monte Carlo calc. of neutron yields 79−49887
Be+hadron, 200 GeV, jets and single particle prod. at high p⊥ 78−45975
Be+p, 150 GeV, inclusive muon pair prod. parameters, statistical interpretation 79−30820
Be+p, 200 GeV/c, relative yields of $\pi^\pm$, K$^\pm$, p, $\bar{p}$ 78−93995

nuclei with mass number 6 to 19 continued

Be+p, 400 GeV/c, dihadron prod., A depend. of prod. cross sections for massive dihadron states 78−33180
Be+p, 400 GeV/c, two hadron correlation at large transverse momenta 78−46060
Be+p, 7 GeV/c hadron multiple prod. *(Russian)* 79−22298
Be+p, direct muon prod. in 70, 50 and 35 GeV collisions 77−2872
Be+p, high mass symmetric hadron and pion pair prod., scaling props. 79−22291
Be+p, high transverse momentum scatt., two particle correlations and ϕ prod., jet trigger 78−78225
Be+p collisions 400 GeV, meas. of dihadron mass continuum and search for narrow resonances 78−33178
Be+p→Λ^0(K_S^0)($\bar{\Lambda}^0$)+X, neutral strange-particle prod. by 300 GeV protons 79−17905
Be+p→p, 640 MeV, proton inclusive spectra and ang. distrib. meas. 77−67751
Be+π^-, 43 GeV/c, inclusive J/ψ prod., A-depend. 78−62581
Be+π^-, 7 GeV/c hadron multiple prod. *(Russian)* 79−22298
Be+π^+, 150 GeV, inclusive muon pair prod. parameters, statistical interpretation 79−30820
Be(^{48}Ca,X), 212 MeV/amu, neutron rich nuclide yields from ^{48}Ca fragmentation 80−27660
Be(^{56}Fe,X), relativistic ^{56}Fe fragmentation, charge and mass changing cross sections 79−54453
Be(^{3}He,n) fast neutron generation in cyclotron 77−88311
Be(K$^-$,$\rho\omega\rho$X), *(Russian)* 79−9637
^{4}Be, M2 giant resonance calcs. from (e,e'),(π^-,γ),(μ^-,ν) 80−22784
^{6}Be, α+p+p decay, α spectrum meas. 77−74813
^{6}Be, levels and parentage via (p,pn) 47 MeV reactions 77−50132
^{6}Be reson. search in ^{4}He(^{3}He,n)^{6}Be at 38.61 MeV, solar neutrino flux 78−619
^{6}Be system, excitation obs. in polarised (^{3}He,^{3}He) scatt. 78−78400
^{7}Be, ^{4}He^{3}He coupling from ^{3}He+^{4}He scattering, dispersion anal. 78−89889
^{7}Be, 477.6 keV, Analytic fitting of full-energy peaks in Ge(Li) spectra at high count rates 80−99147
^{7}Be as a tracer for helio-geophysical phenomena 80−98525
^{7}Be, cosmic ray accel. probe 78−81512
^{7}Be, cosmic-ray-produced, mean tropospheric residence time at north temperate latits. 78−85633
^{7}Be decay, radiative capture of orbital electrons, inner bremsstrahlung spectrum, decay energy 79−500
^{7}Be effective for charge exchange analogues of Gamow-Teller transitions from ^{7}Li(p,n) 80−57726
^{7}Be, electron capture decay, internal ionisation 77−18892
^{7}Be, electron capture radioactive decay probabilities in atoms and ions 79−59556
^{7}Be excitation functions from ^{6}Li(^{3}He, d) 80−18223
^{7}Be excited state from ^{4}He(^{3}He,^{3}He) polarised scatt. study 78−46078
^{7}Be, L/K capture ratio, multiconfig. Hartree-Fock calc. atomic electron correlations 78−62510
^{7}Be, lifetimes of first excited levels meas. 77−22943
^{7}Be, nucl. electron capture, inner bremsstrahlung spectrum, partial decay energy 79−6512
^{7}Be, photoprod. from target with masses <40, cross-sections 79−22268
^{7}Be, prod. by cosmological cosmic rays 78−12436
^{7}Be, prod. in ^{4}He(α,n) reactions, differential cross sections meas., 39 to 50 MeV 78−25207
^{7}Be, production in $\alpha+\alpha$ reacts. at 103 MeV 79−45279
^{7}Be(p,γ), low energy cross section from direct, capture potential model 80−102184
^{7}Be(p,γ)^{8}B, cross section, 360 keV 77−61432
^{7}Be→^{7}Li, inner bremsstrahlung spectra, disintegration energies 77−54191
^{7}Be→^{7}Li, total electron capture decay energy from inner bremsstrahlung spectrum, student experiment 78−24611
^{8}Be 1$^+$ and 1$^-$ levels, expt. and shell model calcs. from ^{7}Li(p,γ_0) 80−63095
^{8}Be, 1$^+$ reson. parameters via ^{4}He(d,d)^{4}He, 6-7 MeV 77−88095
^{8}Be, 2$^-$ threshold states 77−54150
^{8}Be, 3$^+$ doublet at 19 MeV, level-parameters, isospin mixing model 78−89789
^{8}Be, α-cluster excitation via α-α-scatt., coupled channel calcs. 78−529
^{8}Be α-cluster spectroscopic factors, DWBA anal. from (d, ^{6}Li) 80−52571
^{8}Be, α-decay, Gamov states in generator coord. method 77−14075
^{8}Be, α-particle and Sp(2,R) model connection 77−65207
^{8}Be, $\alpha\alpha^+$ rotational band existence 79−13192
^{8}Be $\alpha\alpha^*$ rot. levels search in ^{2}H(^{6}Li,α) 79−22175
^{8}Be central-tensor coupled effective interaction pot., binding energy shape, electric moment 77−14036
^{8}Be, cluster formation, multicentre variational model *(Chinese)* 78−25128
^{8}Be collective excitation spectra from generalised hyperspherical functions method *(Russian)* 80−91133
^{8}Be cross sections and ang. distribs., direct knockout model anal. of ^{12}C($\pi^+,\pi^+\alpha$) *(Russian)* 80−27620
^{8}Be double resonance, 16.6 and 16.9 MeV levels, prod. by $\alpha+\alpha$ 78−62553
^{8}Be, double well-cluster shell model, spurious states of cm motion *(Chinese)* 77−14045
^{8}Be, ΔT=1 γ-decay from 16.6-16.9 MeV states 78−8771
^{8}Be, effective nucleus eccentricity depend. on total momentum *(Russian)* 79−3078
^{8}Be, energy levels deduced from ^{6}Li(^{6}Li,$\alpha\alpha$)α reaction mechanism 80−83113
^{8}Be, excited states ang. distrib. in ^{12}C(d,^{6}Li) reaction 79−6624
^{8}Be fission mode, large amplitude collective motion, adiabatic TDHF calcs. 80−86786
^{8}Be, formation prevalence in ^{7}Li(d,$\alpha\alpha$n), 7.0 MeV 78−82357
^{8}Be, ground state props., modified Brueckner-Bethe-Goldstone method 78−50076
^{8}Be, γ-decay strength of isovector M1 transition, microscopic wave function 78−62503
^{8}Be high spatial symmetry excited states, resonances, rot. band from (d,αt), (p,αt) 80−86780
^{8}Be high-lying reson. below α-α^* threshold, cluster model calc. 77−82840
^{8}Be, highly excited $\alpha\alpha^*$ states from ^{7}Li+p and ^{6}Li+d 78−78262

nuclei with mass number 6 to 19 continued
^{8}Be isospin mixed 2^+ doublet, level parameters from ^{4}He(α,α) 80−27556
^{8}Be, isospin mixing in nuclei, matrix elements explained by Coulomb interaction 78−37264
^{8}Be, isospin mixing of states near 17 MeV, from ^{9}Be(d,t)^{8}Be and ^{8}Be(d,^{3}He)^{8}Li 77−65198
^{8}Be isovector radiative decay, E2-M1 mixing ratio, conserved vector currents from ^{4}He(α,γ) 79−6488
^{8}Be level energies, Brink's model with single-particle functions with realistic behaviour *(Russian)* 77−74785
^{8}Be, level feeding via β and γ transitions, role of spatial quantum numbers 77−67723
^{8}Be low lying states, Sp(2, R) model with generator coordinate method 79−45169
^{8}Be lowest negative parity state, shell and cluster model calcs. from ^{7}Li(p,p), ^{8}Be lowest negative parity state, shell and cluster model calcs. 80−18205
^{8}Be, lowest T=2 state isospin forbidden decays, branching ratios 79−67703
^{8}Be, matrix elements of potential energy operator on generalized hyperspherical functions *(Russian)* 79−22211
^{8}Be, obs. of 2^+ state from ^{8}Li(β)^{8}Be(α)α 78−93938
^{8}Be, Pauli-principle effects, simulation 78−8756
^{8}Be production in photonuclear reactions with E_γ=1.5 to 4.5 GeV, cross sections *(Russian)* 77−74834
^{8}Be, quasi-mol. struct. model observed from α-α scatt. 79−6397
^{8}Be, reson. level, J^π, via ^{7}Li (p,γ)^{8}Be 380 to 960 keV 77−88131
^{8}Be resonant state, $\alpha\alpha^*$ cluster and sympletic model anal. from ^{7}Li(p,α), ^{6}Li(d,α) 79−9537
^{8}Be rot. levels using α-α cluster model with effective pot. interaction 77−22915
^{8}Be, scattering system, microscopic nucl. cluster model 78−54703
^{8}Be, Skyrme-type interactions, spectroscopy of light nuclei, density dependent Hartree-Fock 80−22717
^{8}Be spectroscopic factors, ^{9}Be(^{3}He,α) with 33 MeV polarised beam 77−328
^{8}Be spontaneous fission pot. energy curve, cluster shell model *(Chinese)* 80−22867
^{8}Be* (2.9 MeV), α-α disintegration anal. 77−34352
^{8}Be(α,α)^{8}Be elastic scatt. generalised optical potentials, three-body approximation *(Russian)* 79−13313
^{8}Be(n,n)^{8}Be elastic scatt. generalised optical potentials, three-body approximation *(Russian)* 79−13313
^{8}Be(t,t)^{8}Be elastic scatt. generalised optical potentials, three-body approximation *(Russian)* 79−13313
(^{8}Be,^{8}Be) Coulomb break up mechanism 79−36257
(^{9}Be,^{9}Be), optical pot. 79−59087
^{9}Be, $1/2^-$ resonance state at 1.68 MeV 79−6398
^{9}Be, $2s_{1/2}$ state obs. in ^{10}B(t, α) 80−22691
^{9}Be (d,t), cross-section contrib. from ^{8}Be 3^+ states, isospin mixing model 78−89789
^{9}Be (n,n) 7-15 MeV, elast. and inelast. scatt. 77−34314
^{9}Be (p,π^+), 200 MeV polarised protons, differential cross sections, analysing power 78−78382
^{9}Be, α-cluster behaviour via ^{9}Be(α,α) anomalous 40 MeV effects 78−615
^{9}Be, α-cluster struct., binding energy determ., Faddeev eqn. soln. 78−41640
^{9}Be, binding energies, three body calcs., Faddeev formalism, alpha cluster model 79−75876
^{9}Be, break-up and spectroscopic factors from DWBA anal. of (^{9}Be,^{8}Be) 78−17239
^{9}Be deformed nucleus, continuum states in strong coupling model 80−22682
^{9}Be elastic scatt., 14-26 MeV, universal optical pot. determ. *(German)* 78−70552
^{9}Be, first T=3/2 states, γ-decay, branching ratios and total widths from ^{7}Li(^{3}He, pγ) 79−6489
^{9}Be, form. in ^{10}B(t,α) reaction, 0.5 to 1.25 MeV, excitation functions and ang. distribs. 78−17216
^{9}Be, form. in ^{6}Li(t,γ) reaction, 0.35 to 1 MeV, resonance struct. in compound nucl. excitation curves 78−17217
^{9}Be, HF and GCM calc. in α-cluster molecular model, ground state props. 77−54137
^{9}Be, isospin forbidden nucleon decays of T=3/2 levels 77−6320
^{9}Be low lying spectrum, 3-body molecular description, adiabatic one level approx. 80−78150
^{9}Be, molecular model, n and α-particle decay widths, charge form factors 78−46015
^{9}Be, n+α+α cluster model 79−6452
^{9}Be, neutron spectroscopic factor from (^{9}Be,^{8}Be) reacts. 78−17098
^{9}Be, photoabsorption total cross sections 30-100 MeV *(Russian)* 78−89850
^{9}Be, positive parity excited energy levels, three well cluster shell model study *(Chinese)* 79−93518
^{9}Be π capture, two-photon emission obs. 79−26460
^{9}Be, π^+ electroprod., distorted wave impulse approx. anal. 79−17894
^{9}Be quasibound states, refined resonating group calc. 77−2907
^{9}Be, quasielastic elec. scatt., final state interaction effects *(Russian)* 78−41708
^{9}Be, reactions with ^{16}O, ^{19}F, C^{12}, cross sections and optical model calcs. 78−8838
^{9}Be, struct., size, quadrupole moment, generator coord. method calc. 79−71788
^{9}Be, thick target neutron yields from (p,n) and (d,n) reacts. 77−26752
^{9}Be, three body calc. with separable pots. for binding energy 79−45145
^{9}Be, three body molecular calc. of low-lying spectrum 79−93534
^{9}Be$_\Lambda$, hypernuclear excited states in 1p shell *(Chinese)* 78−82306
^{9}Be$_\Lambda$, in ^{9}Be(K^-, π^-) strangeness exchange reaction, ang. distribs. PWIA anal. *(Chinese)* 79−80956
^{9}Be+^{12}C, 2.8-6.3 MeV, fusion and neutron transfer cross-sections 78−41746
^{9}Be+^{12}C→^{21}Ne*, different decay channels, resonance-like structures obs. 79−13333
^{9}Be+^{16}O, 3.2-14.4 MeV, excitation functions from residual nuclei gamma-ray yield 79−49599
^{9}Be+^{7}Li, 2 MeV neutron energy spectrum meas. using nuclear emulsion technique 78−62574
^{9}Be+n, 1.0 to 14 MeV, total cross-section meas. using ^{9}Be(d,n)^{10}B neutron source 79−22280
^{9}Be+n, 1.5-14 MeV, total cross-section meas. 77−26742

nuclei with mass number 6 to 19 continued
^{9}Be+n, differential elast. and inelast. scatt. 7 to 15 MeV 79−36234
^{9}Be+p, 1 GeV, neutron production *(Russian)* 79−85477
^{9}Be+p, 660 MeV, H and He isotope prod. 77−18544
^{9}Be(^{10}B,^{10}B), 9.5-14.2 MeV, ang. distribs., cross sections, elastic p transfer 80−78318
^{9}Be(^{12}C,^{8}Be), 10-15 MeV, excitation functions and resonant enhancements 79−17881
^{9}Be(^{3}He, $\alpha\alpha$)^{4}He, 2.5, 2.7 MeV, energy depend., quasifree reaction near Coulomb barrier 78−74381
^{9}Be(^{3}He, $\alpha\alpha$)^{4}He, 2.8 MeV, quasi-free and sequential processes 79−67759
^{9}Be(^{3}He,^{3}He), 46.1 MeV, absolute differential cross section, optical model anal. 79−59078
^{9}Be(^{3}He,3α), 29.6-30.5 MeV, ^{12}C excited states 77−18576
^{9}Be(^{3}He,α)^{8}Be, j-depend. of analysing powers, ^{8}Be spectroscopic factor 77−328
^{9}Be(^{3}He,α)^{8}Be(O), reaction mechanism and isoscalar giant resonances in C^{12} *(French)* 78−78341
^{9}Be(^{3}He,$\alpha\alpha$)α, ^{12}C excited states between 29 and 34 MeV 78−21494
^{9}Be(^{3}He,d)^{10}B, j-depend. of analysing powers, ^{10}B spectroscopic factors 77−328
^{9}Be(^{3}He,n)^{11}C, ang. distrib. at energies below Coulomb barrier 79−40938
^{9}Be(^{3}He,n)^{11}C, Coulomb stripping reaction theory 77−54232
^{9}Be(^{3}He,p), 14 MeV, proton polarisation, ang. distribs., differential cross section 77−82944
^{9}Be(^{6}Li,^{8}B), 80,93 MeV, ^{7}He energy levels anal. 77−46183
^{9}Be(^{7}Li,^{6}He)^{10}B, spectroscopic factors from DWBA 77−74874
^{9}Be(^{7}Li,^{6}Li)^{10}Be, spectroscopic factors from DWBA 77−74874
^{9}Be(^{9}Be, ^{9}Be), 5 to 16 MeV, absolute cross sections, optical model parameters 77−67761
^{9}Be(^{9}Be, (p, t, α)), 5 and 12 MeV, absolute differential cross sections 77−67761
^{9}Be(^{9}Be,^{9}Be) 14, 20 and 26 MeV, optical model parameters, 9 to 22 MeV excitation curves 79−26449
^{9}Be(K^-, Π^-), 720 MeV/c, Sigma hypernuclei prod., missing mass spectrum 80−57721
^{9}Be(K^-,π), narrow Σ-hypernuclear states, estimated widths, quantum number assignments 80−42576
^{9}Be(α, α'), 65 MeV, levels and differential cross sections, optical anal. 80−102121
^{9}Be(α, n), 100 MeV, neutron polarisation meas. 78−70726
^{9}Be(α,2α), 140 MeV, quasifree knockout, DWIA anal. spectroscopic factors 80−68629
^{9}Be(α,α)^{9}Be, 40 MeV, anomalous effects and cluster behaviour 78−615
^{9}Be(d,α_0)^{7}Li, 0.9 to 2.5 MeV, ang. distribs. 77−18573
^{9}Be(d,α_1)^{7}Li*, 0.9 to 2.5 MeV, ang. distribs. 77−18573
^{9}Be(d,α)^{7}Li 12.17 to 14.43 MeV, α ang. distribs., excitation functions 78−54770
^{9}Be(d,α)^{7}Li to g.s. and 1st excited state, E_d=2.25-3.1 MeV, DWBA anal. 77−30610
^{9}Be(d,d'), 12.8 MeV, two stage mechanism described by square Feynman diagrams *(Russian)* 79−22299
^{9}Be(d,d), 12.17 to 14.43 MeV, elastic and inelastic scatt., optical model anal. 78−89883
^{9}Be(d,n), secondary neutron emission characts. 79−30843
^{9}Be(d,n),(p,n), 14-23 MeV, thick target neutron yields 77−57791
^{9}Be(d,n) 83.7 MeV, 0° neutron spectra, comparison with Serber model calcs. 77−6400
^{9}Be(d,n)^{10}B use of neutrons for meas. of full cross sections *(Russian)* 80−69008
^{9}Be(d,n)^{10}Be, neutron distrib. from bombardment of thick Be target 77−83408
^{9}Be(d,p), 12 MeV polarised deuterons, analysing powers, j-mixing ratio 77−82937
^{9}Be(d,pγ)^{10}Be, 1.5 MeV, angular correlation meas. 78−94015
^{9}Be(d,t), 12 MeV polarised deuterons, analysing powers, j-mixing ratio 77−82937
^{9}Be(d,t)^{8}Be 12.17 to 14.43 MeV, t ang. distribs., excitation functions, spectroscopic factor 78−54770
^{9}Be(e,X), transverse and longit. form factors for electrodisintegration, small momentum transfer *(Russian)* 79−80927
^{9}Be(e,e'), internuclear nucleon effective mass in quasielastic scatt. *(Russian)* 79−3076
^{9}Be(e,e'p), 700 MeV, proton spectral functions, momentum distribs., DWIA anal. 78−41701
^{9}Be(e,e'p), single hole state momentum and energy distribs. 80−22674
^{9}Be(e,e'p), suppression factor, final-state interaction and cross-sections in shell model *(Russian)* 77−61401
^{9}Be(e,e'π^+), energy and ang. distribs. of πs, low lying residual states 78−54740
^{9}Be(e,e), longitudinal form factor for $1/2^+$ resonance 80−22682
^{9}Be(e,π^+), 1848 MeV, virtual photon spectrum, virtual photon theory test 80−102183
^{9}Be(e,$\pi^\pm$), 10 MeV π, of PWIA calcs. 79−93607
^{9}Be(γ,X), charged particle emission in (e,e'x) reaction, virtual phonon theory 80−13460
^{9}Be(γ,α_0)^{5}He, 18 to 26 MeV, integrated cross section 78−37327
^{9}Be(γ,γ'), 32 MeV, energy spectra, d prod. process *(Russian)* 80−91177
^{9}Be(γ,n$_0$)^{8}Be, 18 to 26 MeV, ang. distrib. and cross section 77−26662
^{9}Be(γ,n) cross section, strong coupling model 80−22682
^{9}Be(γ,n)^{8}Be, 18 to 26 MeV, integrated cross section 78−37327
^{9}Be(γ,π^+), 100-800 MeV, cross section, surface prod. model anal. 80−47466
^{9}Be(γ,π^+), threshold to 175 MeV, total cross sections, DWIA anal. 80−13459
^{9}Be(γ,π), photoabsorption and sum rules, structure, RMS radius, polarisability and exchange parameters 80−22686
^{9}Be(n, p) and ^{9}Be(n, t), 18.3 MeV, ang. distribs. 77−18539
^{9}Be(n,2n) pseudolevel eval. validation 80−22697
^{9}Be(n,n), 2-5 MeV polarised neutrons, analysing power, R-function and phase-shift anal. 77−23088
^{9}Be(n,n), cross sections and polarisation from Lane model anal., multichannel constraints 79−80914
^{9}Be(p, p), 1 GeV, quadrupolar effect, cross sections *(Russian)* 79−30834
^{9}Be(p,^{3}H)^{7}Be, 75 MeV, continuous spectra phase space model anal. 79−76000

nuclei with mass number 6 to 19 continued
^{9}Be(p,^{3}He)^{7}Li, 75 MeV, continuous spectra phase space model anal. 79−76000
^{9}Be(p,α)^{6}Li, 30 MeV, continuous spectra phase space model anal. 79−76000
^{9}Be(p,α)^{6}Li, 75 MeV, continuous spectra phase space model anal. 79−76000
^{9}Be(p,α)^{6}Li, α ang. distrib. determ. by Doppler γ-line broadening method 77−61407
^{9}Be(p,α)X, direct knockout model for fragmentation, (p,pα) predictions 80−18275
^{9}Be(p,$\alpha\gamma$)^{6}Li, 2.56 MeV, ^{10}Be 8.89 MeV reson. J$^{\pi}$ 77−50098
^{9}Be(p,d^{3}He), DWIA anal., α-spectroscopic factors, quasifree process 77−79378
^{9}Be(p,n), cross sections and polarisation from Lane model anal., multi-channel constraints 79−80914
^{9}Be(p,n) comparison of neutron spectra expt. obs. 79−59056
^{9}Be(p,p'), 6.4 MeV, two stage mechanism described by square Feynman diagrams *(Russian)* 79−22299
^{9}Be(p,p), 22-8 MeV, polarised protons, R-matrix theory 77−82921
^{9}Be(p,p), cross sections and polarisation from Lane model anal., multi-channel constraints 79−80914
^{9}Be(p,p), polarisation effects for elastic scatt. near (p,n) reaction threshold 78−13075
^{9}Be(p,p), total cross sections, 180 to 560 MeV, Galuber model calcs. 79−40917
^{9}Be(p,p)^{9}Be, 2.56 MeV, ^{10}Be, 8.89 MeV reson. J$^{\pi}$ 77−50098
^{9}Be(p,p)X, 0.8 GeV, inclusive cross sections, quasi-two-body scaling 79−3150
^{9}Be(p,pα), 100 MeV, absolute spectroscopic factors 77−30574
^{9}Be(p,pn), 47 MeV, excit. energy spectra, energy sharing spectra 77−50132
^{9}Be(p,pn)^{8}Be, 10-24 MeV, cross section, reaction mechanism, ^{9}Be level excitation 79−22284
^{9}Be(p,pn)^{8}Be, kinematically complete exam. of ^{9}B and ^{9}Be levels 78−21550
^{9}Be(p,pn)^{8}Be$_{gs}$, ^{9}Be-^{9}B isobaric doublet asymmetric excitation 77−26678
^{9}Be(p,π^{-})^{10}C, 613 MeV, residual nucleus excitation levels, cross section 78−78383
^{9}Be(p,π^{+}), 0.5-10 MeV, total cross sections near pion Coulomb barrier 80−32280
^{9}Be(p,π^{+}), 320-605 MeV, cross sections, pion exchange model anal. 80−27676
^{9}Be(p,$\pi^{\pm}$), 800 MeV, ang. distribs. 79−85463
^{9}Be(p,π), 200 MeV, proton distortion and asymmetries 79−85464
^{9}Be(π, πN), 60 and 300 MeV, γ-ray meas. 78−41780
^{9}Be(π,X), X=γ, $\gamma\gamma$, $e^{+}e^{-}$, rare pion absorption modes, theoretical and expt. results 80−42698
^{9}Be(π,π), 162 MeV elastic scatt., ang. distribs., diffraction patterns, optical model calcs. 78−58309
^{9}Be(π,π), ang. distribs., optical model calcs. 78−58308
^{9}Be(π^{-}, γ), photon spectra meas. with SIN pairspectrom. 77−10446
^{9}Be(π^{-},2n), neutron-pair emission charact., excitation energy spectra 78−13159
^{9}Be(π^{-},n), single neutron emission induced by stopped π^{-} in 1p shell nuclei 79−59089
^{9}Be($\pi^{\pm}$,$\pi^{\pm}$) elastic and inelastic quadrupole scatt., 162 MeV, rot. and optical model anal. 79−6714
^{9}Be(t,n), 1.1-1.7 MeV, neutron spectra and ang. distribs. meas. *(Russian)* 77−50140
^{9}Be(t,t)^{9}Be, 15, 17 MeV, polarised t, differential cross sections and optical model fits 78−41730
^{10}Be abundance in cosmic rays rel. to age, balloon meas. technique 77−29602
^{10}Be, abundance in galactic cosmic rays rel. to age 78−12060
^{10}Be analogue states from ^{10}B(e,e) anal. 79−75898
^{10}Be ang. distribs. to isobaric analogue states cross section ratio from ^{9}Be(p,π^{+}) 79−89274
^{10}Be, distrib. in geophysical samples, meas. using tandem van de Graaf accelerator 80−61924
^{10}Be, form. in ^{11}B(γ,p) reaction, 18 to 31 MeV, photoproton spectra and ang. distrib., excited state transitions 78−13056
^{10}Be, form. in ^{7}Li(t,γ) reaction, excitation functions and resonant struct. for 17.79 MeV state 78−13110
^{10}Be in 1000 and 5000 yr old Antarctic ice, meas. 79−2305
^{10}Be, in cosmic rays, implication for origin 79−44314
^{10}Be in marine sediments rel. to geophysical events and cosmic ray var. 79−29748
^{10}Be levels and differential cross sections DWBA and coupled channel anal. of (α, ^{3}He) 80−102121
^{10}Be, long-lived cosmogenic isotopes, cosmic-ray intensity variations 77−53361
^{10}Be near threshold state from ^{7}Li(t,^{9}Li) *(Russian)* 80−13484
^{10}Be, triaxial deform. in 1p shell 77−46105
^{10}Be$_{\Lambda\Lambda}$, four body dynamical eqns. in Faddeev-Yakubovsky formalism 80−47419
^{10}Be+^{14}N, multiparticle nuclear reactions, 9.5 MeV/nucleon, α-particle yield *(Russian)* 79−17927
^{10}Be(^{3}He,^{3}He), 46.1 MeV, absolute differential cross section, optical model anal. 79−59078
^{11}Be single neutron strength, levels, spin assignments, spectroscopic factors from ^{10}Be(d,p) 79−36156
^{11}Be state excitation energies and widths, DWBA ang. distribs. from ^{9}Be(t,p) 23 MeV 78−70544
^{11}Be(^{3}He,^{3}He), 46.1 MeV, absolute differential cross section, optical model anal. 79−59078
^{11}Be(^{3}He,n$_{0}$)^{13}N, 5-12 MeV, excitation function and ang. distrib. 77−54231
^{12}Be core excited T=2 levels, spin, half life from ^{10}Be(t,p), 12 MeV 78−66210
^{12}Be, Hartree-Fock calculations of nuclear bulk properties with density- and starting-energy dependent effective interaction 80−9246
^{12}Be mass excess and excited states from ^{10}Be(t,p) 79−22183
$^{\Lambda}_{\Lambda}$^{9}Be, binding energy calcs., clustering 79−9501
$^{\Lambda}_{\Lambda}$^{9}Be, excited states and spectra, continuum effects calcs. 80−57720
$^{\Lambda}_{\Lambda}$^{9}Be, Λ separation energy, hyperspherical harmonics method 79−93547
Be(α,n), neutron spectrum of ^{228}Ra-Be source 78−41882
Be(d,n), activation cross-section, integral tests, dosimeter appl. 80−32553
Be(d,n), stripping-theory anal. of thick-target neutron prod. 77−6600

nuclei with mass number 6 to 19 continued
Be(γ,X), photoabsorption cross-section, Levinger's factor, mass number dependence 80−63165
Be(γ,ω), cross section meas., comparison with theory 78−58261
Be(γ,p), intermediate energy bremsstrahlung, cross sections 78−13061
Be(γ,p)X, 180-420 MeV, quasifree NN system photodisintegration, p spectrum 80−106049
Be(p,X), 200, 300, 400 GeV, hadron prod. at large p_T invariant cross section 79−40926
Be(p,X), 200, 300 GeV/c direct photon prod., η/π^{0} and γ/π^{0} prod. ratios 80−27618
Be(p,X), 2.14 GeV/c, d and t quasifree knockout at 62 mrad, differential cross sections *(Russian)* 79−30819
Be(p,X), 400 GeV, p, d, t, π, ^{3}He, α backward prod., inclusive cross sections 79−85475
Be(p,X), 400 GeV, p backward prod. invariant cross section 79−93623
Be(p,X) 400 GeV, search for new massive particles 78−89877
Be(p,X), 400 GeV/c, light ion backward prod., invariant cross section 80−32279
Be(p,X), 400 GeV/c, nucleon number depend. of inclusive dihadron prod. 79−49626
Be(p,X), 400 GeV/c, two particle quantum number corrections, p$\bar{p}$ and $K^{+}K^{-}$ correlations 79−49625
Be(p,X) 70 GeV/c, $\pi^{\pm}$, $K^{\pm}$, p and $\bar{p}$ relative yields *(Russian)* 79−40930
Be(p,2π^{-}X), 28.5 GeV, fireball model comparison 79−59059
Be(p,h$^{\pm}$), 200 to 400 GeV, inclusive production of large-transverse-momentum hadrons and hadron pairs 79−89310
Be(p,$\bar{p}\pi^{-}$), 10 GeV, $\bar{p}$ weak absorpt., $\bar{p}$ and π^{-} yields *(Russian)* 79−75987
Be(p,xpX), x=1, 2, 640 MeV, energetic backward p emission, inclusive differential cross section 80−9290
Be(π^{-}, Ψ), 43 GeV, A dependence of inclusive distrib. *(Russian)* 78−45983
Be(x,x), x=$\pi^{\pm}$, $K^{\pm}$, p, $\bar{p}$ 70, 125, 175 GeV/c 80−83128
$^{\Lambda}$^{12}B hypernucleus, spin determ. from $^{\Lambda}$^{12}B→^{12}C*+π^{-} 80−27589
^{nat}U(p, α)$\alpha\alpha$, sputtering yield meas. *(Japanese)* 80−25513
(C,X), light relativistic ion-target interactions, particle emission 80−102193
C (C,C), 800 MeV/N, high momentum nucleons from relativistic nuclear collisions, hard scatt. mechanism 79−40950
C (n,n), pol. n, 16.1 MeV, differential cross section, optical model fit 80−32259
C (p, X), 2.2, 6, 8.5 GeV, p and d inclusive spectra at 162° *(Russian)* 79−97710
C (π^{-},p) 1.5-5 GeV/c, cumulative proton polarisation *(Russian)* 80−86896
C, A=12 and 14, exotic nuclei stability anal., Hartree-Fock approx. with the Skyrme interaction 78−82273
C, absorpt. of stopped π^{-}, charged particle energy spectra meas. 78−33224
C backward π^{+} prod., momentum depend., scaling, Monte Carlo calcs. 79−13305
C, beta-generated external bremsstrahlung spectra 77−57625
C degenerate core thermonuclear reaction propag., neutrino mech. *(Russian)* 79−5812
C, elastic and inelastic cross sections, 8 to 14.5 MeV 77−23091
C energy loss params., appl. on mass determ. of cosmic ray nuclei in nuclear emulsion 78−94175
C, integral test of cross section, neutron leakage spectra, spherical assembly 77−23033
C, K_{L}^{0}→K_{S}^{0} coherent regeneration, optical model calcs. 77−30427
C, K^{-} absorption at rest, study of final states containing Λ-hyperon 77−41997
C, K^{0} regeneration, Regge behaviour and nuclear effects, ω-pomeron cut 79−13347
C, laser-injector-generated, acceleration in synchrophasotron 78−29675
C, muonic X-ray transitions, nuclear charge radii 80−99589
C, μ^{-} capture, charged particle energy spectra *(Russian)* 78−89828
C, natural, total and elastic scatt. cross sections for neutron energy <5 MeV, 8.5-15 MeV, use as standard 79−9588
C, neutron elastic and inelastic scatt. cross sections, 9 to 15 MeV 77−23086
C, neutron-photon multigroup cross sections for neutron energies ≤60 MeV 79−30880
C, photonuclear cross sections in giant reson. region 78−17178
C, primary cosmic ray nuclei, isotopic composition using nuclear emulsions 79−80155
C, π^{-} and p elastic scatt., 30 to 50 GeV/c, nuclear radius, real/imaginary forward scatt. amplitude ratio *(Russian)* 77−34351
C, π^{+} absorption in flight, 80-140 MeV, absorption cross section 79−85494
C, shadowing in photon-nucleus 20 to 185 GeV total cross sections 79−30823
C+C, 800 MeV/A, wide angle inclusive proton spectra 79−40951
C+C 800 MeV/N, p and π inclusive spectra, energy and ang. distribs. 78−54790
C+K_{L}, 30 to 150 GeV, total cross sections, inelastic screening evidence 79−17936
C+K_{S}, 20 to 140 GeV, precise coherent K_{S} regeneration amplitudes 79−17937
C+K^{-} at rest, absorpt. branching fractions determ. 77−67771
C+n, 200 GeV, multiplicity distribs., target thickness effects, appl. to air shower obs. 77−50127
c+n in cellulose nitrate plastic detector, spallation products 78−17198
C+p, 28.5 GeV, prompt dimuon prod., cross section, atomic number depend., mass distrib. 78−89858
C+p, 300 GeV, nuclear fragment prod., p:d:t ratio, ^{3,4}He abundances 78−70513
C+p, 50 to 275 GeV/c, inclusive particle prod., nuclear size depend. 77−46168
C+p, 600 MeV, pion production, energy spectra, A depend. *(Russian)* 78−17213
C+p, 7 GeV/c hadron multiple prod. *(Russian)* 79−22298
C+p, C+$\pi^{\pm}$, 225 GeV/c, J/ψ and ψ(3.7) prod. study using muon pair meas. 77−57694
C+p, inelastic interactions, 6.0 GeV/c, in emulsions 78−86530
C+p(d)(α), 0.7-8 GeV, scaling and nonscaling of inclusive π prod. 79−22296
C+p(d)(α)(^{12}C), 4.2 GeV/N, multiple π^{-} prod., mean multiplicity *(Russian)* 80−27647

nuclei with mass number 6 to 19 continued
C+π, 40 to 280 MeV, second order optical pot., effect of short range correls. 78−74407
C+π^-, 3.7 GeV/c, proton spectra *(Russian)* 78−41785
C+π^-, 40 GeV/c, two-particle correls., rapidities, ang. distribs. *(Russian)* 78−17251
C+π^-, 7 GeV/c hadron multiple prod. *(Russian)* 79−22298
C+π^- collision data, 40 GeV/c, comparison with Bialkowski, Chiu and Tow model 78−58305
C+$\pi^\pm$, 125 MeV, true absorpt. and scatt. 79−63705
C+$\pi^\pm$, C+p, massive muon pair prod., test of Drell Yan model 77−57695
C_Λ, A=12,13, hypernuclear excited states in 1p shell *(Chinese)* 78−82306
C(^{12}C,X), 4.5 GeV/c, emission of short range particles (R<100 mkm) *(Russian)* 80−63202
CC ^{12}C(α, α), 1.37 GeV, elastic and inelastic, Glauber multiple scatt. theory 79−3161
C(^{56}Fe,X), relativistic ^{56}Fe fragmentation, charge and mass changing cross sections 79−54453
C(^{3}He,^{4}He)C, A=12, 13, differential cross-sections at 18, 20 and 24.5 MeV *(Russian)* 78−623
C($K^\pm$,$K^\pm$) intermediate energy, forward scatt. amplitudes, Glauber model calcs. 79−30856
C(K_L^0, K_S^0), 10-50 GeV/c, regeneration, coherent production model 78−33220
C(^{20}Ne, π^+X), 400 MeV/N, pion prod. doubly differential cross sections and ang. distrib. 80−32299
C(^{16,17}O,^{16,17}O), two centre shell model, molecular single particle states at level crossings 80−47354
^{2}C($K^\pm$,$K^{\pm\prime}$), 300-800 MeV, microscopic particle-hole shell model calcs., DWIA anal. 79−59091
^{7}C(^{3}He,^{3}He), 44.04 MeV, absolute differential cross section, optical model anal. 79−59078
^{A}C (n,n), A=12, 13, thermal neutron scatt. parameters 79−93628
^{A}C, A=12, 13, nuclear critical opalescence, M1 form factor, pion field and condensation 80−73809
^{A}C, A=13,14, M2 giant resonance calcs., from (e,e′),(π^-,γ),(μ^-,ν) 80−22784
^{A}C, A=13,14, neutron binding energy from ^{1}H(n,γ) 80−52564
^{A}C, A=13,14 neutron binding energy 80−47362
^{A}C+n, A=12,13, 1.0 to 14 MeV, total cross-section meas. using ^{9}Be(d,n)^{10}B neutron source 79−22280
^{A}C(^{16}O,X), A=12, 13 exit channel competition for some residual nucleus 80−47499
^{A}C(^{9}Be,^{9}Be) A=12, 13, 14, 20 and 26 MeV, optical model parameters 79−26449
^{A}C(p,γ), A=12, 13, isotopic anal., estimation of ^{13}C/^{12}C conc. ratio 79−48014
^{A}C(p,p), A=12, 13, 0.8 GeV, elastic and inelastic, ang. distribs., states, optical and DWBA anal. 79−3154
^{A}C(p,π^+), A=12, 13, 0.5-10 MeV, total cross sections near pion Coulomb barrier 80−32280
^{A}C(p,π^+), A=12,13, 200 MeV, pion energy spectra for discrete final states, cross sections 80−106057
^{A}C(p,$\pi^\pm$), A=12,13, 200 MeV, analogue and nonanalogue state cross sections 80−99130
^{A}C(π,π′), A=12, 13, ~180 MeV, isospin mixing, levels, excitation functions and ang. distribs. 80−42543
^{A}C(π^-,π^-), (A=12,13), 29.2 and 49.5 MeV, neutron radii determ. 79−97653
^{A}C(π^-,π^-), A=12,13, 49.5 and 29 MeV, differential cross sections 79−85534
^{A}C($\pi^\pm$,$\pi^\pm$), A=12,13, 180 MeV near (3,3) reson., nuclear RMS radii determ. 79−85538
^{10}C ang. distribs. to isobaric analogue states cross section ratio from ^{9}Be(p,π^-) 79−89274
^{10}C levels, spin and parity, ^{12}C(p,t) and ^{12}C(p,^{3}He) comparative study 77−30566
^{10}C low lying level ang. distribs., zero range DWBA anal. from ^{12}C(p,t) 79−67656
^{10}C, T=2 state total width and first excited state excitation energy 78−66211
^{11}C energy levels from ^{12}C(^{3}He,α), ang. distribs., DWBA calcs. comparison 78−78396
^{11}C, forbidden transition ang. distribs., CCBA and DWBA anals. of (p,d) 80−86848
^{11}C intermediate resonance and electric quadrupole transition contribution to ^{12}C(γ,nα) *(Russian)* 79−40896
^{11}C isotopes, production and transport system 78−46200
^{11}C labelled radiopharmaceuticals, cyclotron prod. for nuclear medicine appls. 77−44753
^{11}C levels and resonance, γ-ray excitation curves from (p,αγ), (p,pγ) 80−9280
^{11}C, low lying analogue states, DWBA anal. from ^{12}C(d,t), 29 MeV, polarised d 78−82285
^{11}C negative parity states lifetime limits and transition strengths from ^{10}B(p,γ) 80−5092
^{11}C, photoprod. from target with masses <40, cross-sections 79−22268
^{11}C prod. in ^{12}C+Ne^{10+} in polystyrene, reaction cross-section meas. 77−3035
^{11}C, production by cyclotron, biomedical appls. *(French)* 80−56216
^{11}C, semileptonic weak and EM interactions, isoelastic processes 77−18528
^{11}C spectroscopic factors, ^{12}C(^{3}He,α) with 33 MeV polarised beam 77−328
^{11}C, spectroscopic factors from ^{9}Be(^{3}He,n) ang. distrib. at energies below Coulomb barrier 79−40938
^{11}C/^{11}B, mirror level pair cross sections from ^{12}C($\pi^\pm$,πN) 79−67665
(^{12}C,X), A=12-19, total fusion cross sections and fusion barrier parameters 80−9322
^{12}C 1^+(T=1, 15.1 MeV) state excitational pionic modes, M1 form factor for (p,p′), (e,e′) 80−78195
^{12}C, 14.08 MeV level J^π assignment via ^{12}C(α,α′)^{12}C* at 45 MeV 77−82819
^{12}C, 15.1 MeV level decay branching ratios, meas. with NBS positron annihilation in flight facility 79−31306
^{12}C, 17.77 and 18.36 MeV state struct., from ^{11}B(p,p) 1.9 to 3.0 MeV R-matrix study 79−9435
^{12}C, 19.25 MeV level spin assignment from ^{11}B(p,n)^{11}C, 3-49 MeV 78−93996

nuclei with mass number 6 to 19 continued
^{12}C, 2_1^+ state, rel. depend. of transient mag. field effect, recoil in Fe 78−37285
^{12}C 2^+ (4.43 MeV) state, transition DWA anal. from (p,p′) and (e,e′) 79−67704
^{12}C 2^+ level, transverse EM form factor, convection current contrib. 80−63076
^{12}C, 2.1 GeV/nucleon, fragmentation parameters in emulsion 77−3027
^{12}C, 3 alpha force and 3α model 79−30798
^{12}C, 3-α struct. in boson model 78−17124
^{12}C, 3α model, props., stochastic variational method 77−41891
^{12}C, 3α problem calcs., multicluster model 79−3102
^{12}C 3α system, multicluster problem based on microscopic theory 77−18455
^{12}C, 3α system, resonating group method for nuclear props. 78−50108
^{12}C (^{12}C,^{12}C), molecular collective excitation theory in two centre model 79−89256
^{12}C (^{16}O,^{16}O′), 19-23 MeV, intermediate width structs., ang. correlations, spins 80−13431
^{12}C (K^+,$K^{+\prime}$)^{12}C*, DWIA, Fermi motion effect 77−54258
^{12}C (α,α), ang. distrib., microscopic anal., Pauli principle, excitation effects 78−33198
^{12}C (n,p) and (n,d) reactions, study of isovector analogue giant resonances, proton hole states 77−26726
^{12}C (π,X), X=γ, γγ, e^+e^-, rare pion absorption modes, theoretical and expt. results 80−42698
^{12}C ($\pi^\pm$, π^+d), 180 MeV, cross-section ratios 80−32308
^{12}C ($\pi^\pm$, $\pi^\pm$t), 180 MeV, cross section ratios 80−32308
^{12}C, absolute excitation energy meas. using electrostatic analyser 77−30741
^{12}C, adiabatic mass parameters, isoscalar quadrupole modes 77−14049
^{12}C, alpha cluster in Hartree Fock calcs. 80−63110
^{12}C, anologue states from reson. proton scatt. 77−38260
^{12}C, α-cluster deformation, elastic form factors of electron scatt. 79−17829
^{12}C, α-cluster model, binding energy, RMS radii, and form factors 79−75825
^{12}C α-cluster spectroscopic factors, DWBA anal. of (d, ^{6}Li) 80−52571
^{12}C, α-cluster struct., binding energy determ., Faddeev eqn. soln. 78−41640
^{12}C α-decay, (d,d′) excited, 4π ang. pattern meas., DWBA anal. 79−67720
^{12}C, α-particle model, amalgamation of two nucleon correl. into multiple scatt. process 77−54169
^{12}C, α-particle model 77−82839
^{12}C, α-particle model of ground and 0^+ excited states, hyperspherical method 77−6272
^{12}C, α-transfer reactions, spectroscopic factors, exact finite range DWBA anal. 80−13372
^{12}C, α-transfer spectroscopic factors for O^+, 2^+ and 4^+ states, transitions from (d, ^{6}Li) 80−13370
^{12}C, binding energies, three body calcs., Faddeev formalism, alpha cluster model 79−75876
^{12}C, boson 3α model and effective inter-α forces 78−66232
^{12}C, bound-state momentum distribs. and (p,p′) PWIA anal. 78−601
^{12}C, branching ratio of 7.654 MeV state meas., rate of stellar He burning 77−2941
^{12}C, β-transitions, weak magnetism, nuclear struct., matrix elements 79−13253
^{12}C, capture rate of μ^-, meas. by Saclay linac beam *(French)* 79−368
^{12}C central-tensor coupled effective interaction pot., binding energy shape, electric moment 77−14036
^{12}C, centre-of-mass spuriosity in continuum shell-model calculations 80−32210
^{12}C, charge transition density, sum rules, oscillation form factors *(Russian)* 79−22186
^{12}C, comparison of absolute cross sections for electron and photon induced reactions, DWBA calc. test 77−41958
^{12}C, constrained variational calcs. for binding energy and RMS radii, N*(1234) allowance 79−3074
^{12}C, coupled channel anal. of Λ′(1405) in kaonic atoms 78−540
^{12}C deduced levels and spectroscopic factors, ang. distribs., DWBA anal. from ^{16}O(d,^{6}Li) 80 MeV 78−94013
^{12}C, EM and allowed weak transitions, improved impulse approx. treatment 78−41662
^{12}C, Efimov state search using Ali-Bodmer α-α force and Faddeev technique 79−6420
^{12}C, elastic and inelastic scatt. of ^{10}B, ^{14}N, common optical potential 77−34276
^{12}C, elastic back angle scatt. from α-nuclei 79−6665
^{12}C, electric quadrupole strength, giant quadrupole resonance 80−52575
^{12}C energy levels from (p,d) 80−42667
^{12}C, exchange current corrections for muon partial capture rates 78−33152
^{12}C, excitation cross sections induced by 1 GeV protons and electrons, Glauber theory *(Russian)* 78−41684
^{12}C excitation spectrum from ^{14}N(p,pd), exchange processes effect, impulse approx. 77−61405
^{12}C, excited state decay, axion emission search 80−32235
^{12}C, excited state struct., anomalous α-decay props. 3-cluster GCM model 79−6399
^{12}C, excited state struct., α-particle model 80−47385
^{12}C excited states, obs. in ^{10}B(d,3α) and ^{9}Be(^{3}He,3α) 77−18576
^{12}C excited states between 29 and 34 MeV, obs. in ^{10}B(d,αα)α, and ^{9}Be(^{3}He,αα)α 78−21494
^{12}C, four-body breakup induced by 18 MeV neutrons, double final state interaction 78−17192
^{12}C gamma line Doppler broadening in ^{12}C(n,n′γ)^{12}C and ^{9}Be(α,nγ)^{12}C, 4438 keV 80−91147
^{12}C giant electric and magnetic multipole resonances, microscopic descript. 78−538
^{12}C, ground state props., modified Brueckner-Bethe-Goldstone method 78−50076
^{12}C, HF charge distribs. 77−14024
^{12}C, high energy electron and proton bombardment, in a deformed translationally invariant model 79−58996
^{12}C, inclusive proton photoprod., momentumm spectra, max. bremsstrahlung energy 2.0 to 4.5 GeV *(Russian)* 77−34287
^{12}C, internal pair emission branch of 7.65 MeV, stellar triple-α reaction 77−54183
^{12}C, inverse inertia parameter calc. 78−50073

nuclei with mass number 6 to 19 continued

^{12}C, isoscalar giant quadrupole resonance 78−78238
^{12}C, isoscalar giant quadrupole resonances, RPA calcs., E2 strength fragmentation, spectroscopic factors 80−13437
^{12}C, isoscalar giant reson. in ^{11}B(p,α)^{8}Be 6.0-18.0 MeV 77−46152
^{12}C isoscalar giant resonance from ^{10}B(d,α)^{8}Be(g.s.) excitation functions struct. 78−46073
^{12}C, isoscalar giant resonances *(French)* 78−78341
^{12}C, isospin mixing in nuclei, matrix elements explained by Coulomb interaction 78−37264
^{12}C, isospin mixing of 1^+ states 78−4898
^{12}C, isovector GQR splitting 77−22988
^{12}C isovector M1 excitations, current and spin contribs. from (e,e'), (p,n) 80−68582
^{12}C $J^\pi=0^+$ isoscalar levels, α-particle model with group theoretical methods 77−74766
^{12}C J-transfer determ. and isospin mixing from ^{13}C(d,t) polarised d 79−49579
^{12}C, K^+ interaction with nuclei 78−13165
^{12}C, kaonic, Y* resonance nonlocal effects, kaonic shifts and widths 79−7039
^{12}C, lowest T=2 state excitation energy from ^{14}C(p,t), 27.6 MeV 78−66211
^{12}C, lowest T=2 state isospin forbidden decays, branching ratios 79−67703
^{12}C M1 (15.11 MeV) form factor, evidence for nuclear pion field critical opalescence 80−32232
^{12}C M1 form factor, pion field critical opalescence, ρ role, polarisation phenomena 80−68552
^{12}C, M1 form factor, pion field, rho meson role 80−105970
^{12}C mag. transition form factors, core polarisation and exchange current effects 79−75899
^{12}C, magnetic dipole excitation in (e,e') scatt. 77−30560
^{12}C, meson dynamics in many-body calc. 77−22917
^{12}C, mixed T=0 and 1 states, isospin mixing matrix elements 78−37289
^{12}C, monopole excitations, transition densities from simple collective model 79−40834
^{12}C, multipole elec. giant resons., anomalous parity isovector states, Coulomb excitation cross sections 79−9439
^{12}C, muon capture theory 78−553
^{12}C μ capture rate, average nuclear polarisation, elementary particle approach 78−66246
^{12}C, μ^- capture reactions with ^{8}Li prod. *(Russian)* 78−54745
^{12}C negative parity states from ^{13}N isospin forbidden p decays in ^{11}B(^{3}He,np) 79−26372
^{12}C p_0 channel E2 strength from ^{11}B(p,γ) pol p. 80−22790
^{12}C, photodisintegration induced by 40 MeV γ-rays, correl. spectroscopy 77−6345
^{12}C, pion photoproduction and radiative capture 78−50213
^{12}C, pion-exchange contribs. to charge densities, HF calcs. 78−46001
^{12}C, positive-parity states, anomalous α-decay props. 78−62511
^{12}C, pot. and charge deform. of rot. states 77−46106
^{12}C, p$\pi\alpha$ penetration range, 200 MeV to 2 GeV *(French)* 78−4964
^{12}C, proton total cross section, 0.15 to 1 GeV, α-particle model and Glauber multiple scatt. theory 77−18538
^{12}C, π capture, two-photon emission obs. 79−26460
^{12}C, π^- capture, p, d and α inclusive prod. spectra 79−22338
^{12}C, π^+ absorption in flight, cross section, 91-143 MeV 80−63212
^{12}C, π^+ electroprod., distorted wave impulse approx. anal. 79−17894
^{12}C, π^+ induced two nucleon removal 78−25242
^{12}C, quasielastic π scatt., recoil proton spectra obs. 77−14198
^{12}C, quasielastic scatt. of polarised 635 MeV protons, depend. of left-right asymm. on nucl. momentum *(Russian)* 77−79384
^{12}C, radiative transitions and isospin mixing 77−38242
^{12}C relativistic ions, Coulomb disintegration into 3 α-particles, total cross section 79−40943
^{12}C, rescatt. effects in 2p bound π-absorpt. 79−36275
^{12}C, residual interactions, current conserving RPA calculations 80−57710
^{12}C, saturating effect of N*(1234) on binding 78−58231
^{12}C, shell model proton transition densities from (e,e') data 79−93517
^{12}C, single particle energies of closed minor shells 77−6208
^{12}C, Skyrme-type interactions, spectroscopy of light nuclei, density dependent Hartree-Fock 80−22717
^{12}C spin-orbit force and deformation, self-consistent HF calc. 79−455
^{12}C, spreading widths of giant reson. calc., core-coupling RPA approx. 77−74827
^{12}C struct., determ. of Brink's model parameters, calc. of binding energy, 2^+ level lifetime 79−85358
^{12}C struct. calcs. via 3α system resonating group method 78−531
^{12}C, struct. of excited states in 3-α model 77−65201
^{12}C structure, energy levels, binding energy, cluster model with varying hinge angle 78−4907
^{12}C, study of isospin mixing 77−18385
^{12}C, tetrahedral struct., quark exchanges, rotations, vibrations and binding energy 79−6459
^{12}C, three alpha struct. in Faddeev formalism 77−14048
^{12}C, three α model calcs. and O_2^+ state 79−75856
^{12}C, three α-particle model calcs., Faddeev formalism, low lying states 77−18399
^{12}C, three body calc. with separable pots. for binding energy 79−45145
^{12}C to ^{22}Ne induced nucleon transfer reactions 78−41768
^{12}C transfer spectra direct contrib. from ^{208}Pb(^{16}O,X) projectile fragmentation 80−63155
^{12}C, transition densities, form factors and transient radii 79−6481
^{12}C, vector polarised ^{6}Li elastic scatt., full optical model anal. 78−70553
^{12}C, weak hadronic form factor and recoil polarisation in muon capture 78−62508
$^{12}C_\Lambda \rightarrow \pi^- + {}^{12}$N, produced in p+emulsion nuclei reacts. *(Russian)* 80−9297
$^{12}C_1$ 3α model, composite particle interactions, Pauli principle *(Russian)* 80−18214
$^{12}C_{2+}$ m-state population in ^{64}Zn (^{12}C, $^{12}C_{2+}$*) 79−93521
^{12}C-^{12}C, excit. function struct., momentum space folding model 77−57683
^{12}C-^{12}C excit. function calc. in momentum space folding model 77−57682
^{12}C-^{12}C quasimolecular resonance, coupled channel anal. 78−78402
^{12}C-^{12}C resonances, speculation of nature, excited α-particles 79−13339
^{12}C-^{12}C scattering, fusion cross-section, folding model study, coupled channel effects 78−89893

nuclei with mass number 6 to 19 continued

^{12}C+^{10,11}B, fusion below Coulomb barrier, quantum mechanical barrier penetration model anal. 80−18361
^{12}C+^{10,11}B, sub Coulomb energy, fusion cross sections, elastic scatt., optical model anal. 77−34335
^{12}C+^{10}B, 100 MeV, 2n and 2p transfer reacts., DWBA anal. 78−50207
^{12}C+^{11}B, 116 MeV, in-plane heavy ion-alpha particle correlations 79−17921
^{12}C+^{11}B, 9.4-17.8 MeV, excitation functions for elastic, inelastic, ^{8}Be, α exit channels, resonances 79−67731
^{12}C+^{12}C, 19.5 MeV, intermediate struct. in continuum shell model, quasi-molecular shape resonance 79−45235
^{12}C+^{12}C, 250-1000 MeV/N, intranuclear cascade calcs. for multiplicity and cross sections 80−32300
^{12}C+^{12}C, 2.1 GeV/n elastic scatt., correlations 78−41761
^{12}C+^{12}C, 2.8-6.3 MeV, total fusion cross section, S-factor 80−22877
^{12}C+^{12}C, 3.2-64 MeV/nucleon, time-depend. HF calcs. 77−3034
^{12}C+^{12}C, 6.25 MeV reson., J^π determ. 77−50099
^{12}C+^{12}C, 800 MeV, p and π inclusive cross sections, non-equilibrium processes 79−40947
^{12}C+^{12}C, 800 MeV/nucleon, two-fireball model for p and π inclusive spectra 79−13323
^{12}C+^{12}C, comment on interaction phenomena 79−13315
^{12}C+^{12}C, diffuse surface nuclear and Coulomb pot. energies 77−18593
^{12}C+^{12}C, fusion reactions, Woods Saxon, folding and proximity pot. anals. 79−45316
^{12}C+^{12}C, low energy, HFB and generator coordinate self consistent microscopic approach 80−42679
^{12}C+^{12}C, mol. resonance props. by GCM 79−13321
^{12}C+^{12}C, molecular config., ^{24}Mg high spin props., Strutinsky method 78−50201
^{12}C+^{12}C, multiparticle nuclear reactions, 9.5 MeV/nucleon, α-particle yield *(Russian)* 79−17927
^{12}C+^{12}C, nuclear fragmentation at 2.1 and 1.05 GeV/N, phenomenological anal., diffractive excitation model 77−54247
^{12}C+^{12}C, optical pot. for nucleus-nucleus systems using double folding model 79−45225
^{12}C+^{12}C, partial widths of molecular resonances 78−46094
^{12}C+^{12}C, self-consistent heavy-ion potentials 77−6434
^{12}C+^{12}C, sub-Coulomb total cross section, simple pot. model of resonances 78−66303
^{12}C+^{12}C collisions, nuclear molecules, two-centre shell model parastatistics 79−9618
^{12}C+^{12}C elastic scatt., optical model anal. 77−6429
^{12}C+^{12}C elastic scatt., low partial waves 77−71620
^{12}C+^{12}C elastic scatt., induced rot., energy depend. of optical pot. real part 78−89903
^{12}C+^{12}C fusion, 2.5 to 6.2 MeV, γ-ray transitions and cross-section fluctuations 77−30628
^{12}C+^{12}C gross struct. resonances in excitation functions from ^{12}C(^{12}C, ^{10,11}B) 80−102167
^{12}C+^{12}C in elastic scatt., high energy, resonances obs., evidence for band crossing model 78−66305
^{12}C+^{12}C inelastic scatt., gross struct. origin, nonreson. diffr. model calcs. 79−30849
^{12}C+^{12}C quasimolecular interactions, recent developments 79−9615
^{12}C+^{12}C reson. at $E_{c.m.}$=19.3 MeV, high spin states in ^{23}Na and ^{23}Mg anal. 77−26579
^{12}C+^{12}C scatt., 10-20 MeV, optical model pot. 79−26456
^{12}C+^{12}C scatt., intermediate molecular resonances, band crossing model anal. 79−6655
^{12}C+^{12}C scatt. and fusion cross sections above Coulomb barrier, folding model, resonances 79−6687
^{12}C+^{12}C subCoulomb fusion cross-section, 6.5-12 MeV 77−50151
^{12}C+^{12}C system, 7.5 MeV, reson. spin assignment 77−14089
^{12}C+^{12}C system, inelastic scatt. and fusion cross section, folding model, resonances 79−13337
^{12}C+^{12}C system, microscopic nuclear pots., elastic and inelastic channels 79−6654
^{12}C+^{12}C system, molecular configuration in ^{24}Mg 79−13193
^{12}C+^{12}C system, nuclear molecule microscopic description, HF and coupled channel calcs. 80−13493
^{12}C+^{12}C system, quasimolecular states, coupled channel anal. 78−33217
^{12}C+^{12}C system resonant structs., J^π assignments, true ^{24}Mg states from ^{12}C(^{12}C, ^{16}O) 80−99163
^{12}C+^{12}C(^{16}O), elastic scatt. and fusion cross-section calc. 77−46182
^{12}C+^{12}C$\rightarrow$^{12}C(2_1^+)+^{12}C(2_1^+), 15-45 MeV, obs. of molecular resonances 77−74867
^{12}C+^{13}C, identical core neutron transfer, coupled channel anal., form factors 79−13319
^{12}C+^{13}C elastic transfer interaction, intermediate energies, n exchange cross sections 79−13318
^{12}C+^{13}C resonances, coupled channel anal. with core-exchange model 79−13338
^{12}C+^{14}N, 59, 70 MeV, radiative capture and 1-nucleon emission cross sections 79−93652
^{12}C+^{14}N fusion, 248 MeV, cross-section meas. liquid-drop limit for ^{26}Al 78−4959
^{12}C+^{14}N reactions, 53 MeV, ang. distribs., Hauser-Feshbach anal. 77−14166
^{12}C+^{16}C scatt. reson. and strong absorpt. phenomena, band crossing model 79−3165
^{12}C+^{16}O, 11 to 27 MeV, structure in gamma-ray yields 77−34250
^{12}C+^{16}O, 22 MeV, spins of reson. assigned 78−17236
^{12}C+^{16}O, 3.9-12 MeV, total fusion cross section determ. 77−42003
^{12}C+^{16}O, 8.5-12.9 MeV, oscills. in excitation function for complete fusion 77−3037
^{12}C+^{16}O, elastic scatt., simple double folded optical pot. model for resonances 79−6535
^{12}C+^{16}O, fusion cross sections, struct. in γ-ray yields 79−9626
^{12}C+^{16}O, light- and heavy-ion emission comparison 78−641
^{12}C+^{16}O, nuclear fragmentation at 2.1 and 1.05 GeV/N, phenomenological anal., diffractive excitation model 77−54247
^{12}C+^{16}O, resonance at 12.8 MeV 77−46187
^{12}C+^{16}O, resonance behaviour, similarity to that in ^{12}C+^{12} 78−33210
^{12}C+^{16}O complete fusion, partial prod. cross section for nuclides, evaporation model calcs. 79−36294
^{12}C+^{16}O elastic scatt., generator coord. calc., reson. spin assignments 77−57685
^{12}C+^{16}O elastic scatt. and total reaction cross sections near Coulomb barrier 77−54235

nuclei with mass number 6 to 19 continued
$^{12}C+^{16}O$ inelastic scatt., microscopic coupled channel calc. 78−625
$^{12}C+^{16}O$ inelastic scatt., microscopic R-matrix method anal. 79−6656
$^{12}C+^{16}O$ multichannel scatt., microscopic calcs. in generator coordinate method, spin assignments 79−564
$^{12}C+^{16}O$ resonances, microscopic double folded model 78−41754
$^{12}C+^{16}O$ resonances, microscopic interpretation 79−13340
$^{12}C+^{16}O$ scatt., band crossing model of resonances 78−89898
$^{12}C+^{16}O$ scatt. reson. and strong absorpt. phenomena, band crossing model 79−3165
$^{12}C+^{16}O$ system, ang. mom. projected microscopic calc. 77−14148
$^{12}C+^{17,18}O$, 12.6-14.0 MeV elastic scatt., ang. distribs. 78−37361
$^{12}C+^{17,18}O$ one- and many-nucleon transfer reactions at 12.6 to 14 MeV c.m. energies 78−82371
$^{12}C+^{18}O$, excitation functions for dominant fusion channels 7 to 25 MeV, obs. of regular gross struct. 79−36293
$^{12}C+^{20}Ne$, 110 MeV, complete identification of products of reaction 77−88165
$^{12}C+^{20}Ne$, 150-294 MeV, energy depend. of multinucleon transfer reacts. 79−67769
$^{12}C+^{20}Ne$, entrance channel effects coupled channel calc. 77−65235
$^{12}C+^{20}Ne$ elastic scatt., strength of absorpt. 77−3028
$^{12}C+^{27}Al$, elastic scatt. quadrupole effects at 55 MeV, optical parameters 77−88169
$^{12}C+^{28}Si$, 17 to 37 MeV, inelastic and elastic backward angle scatt., surface resonances 78−37367
$^{12}C+^{28}Si$, 17.5 to 33 MeV, resonant backward angle elastic scatt. 78−46096
$^{12}C+^{6}Li(^{16}O)$ scatt., anomalous backscatt. from nonlinear Schrodinger eqn. for nuclear matter 79−6465
$^{12}C+^{6}Li(^{7}Li)$, 9 MeV, isotopic shape effects in elastic scatt. of aligned ions 78−89904
$^{12}C+^{9}Be$, 11.4 MeV cm energy, p, d, t, α production 80−9302
$^{12}C+^{9}Be$, parabolic repulsion potential, optical model 80−22782
$^{12}C+K^{\pm}$, application of forward dispersion relns. to scatt. amplitude and length 77−18626
$^{12}C+Ne^{10+}$, in polystyrene, reaction cross-section for ^{11}C prod. 77−3035
$^{12}C+\alpha$, 100-160 MeV, $^{10,11}B$ prod., cosmic-ray propag. appl. 77−79380
$^{12}C+\alpha$, 2.5 GeV-nucleon, nuclear fragmentation meas. *(Russian)* 78−54773
$^{12}C+\alpha$, spallation fragments $6\leq A\leq 11$ yields, nucleosynthesis interest 79−30845
$^{12}C+\alpha\rightarrow 4\alpha$, multiparticle nuclear reactions, 9.5 MeV/nucleon, α-particle yield *(Russian)* 79−17927
($^{12}C+\alpha$) system, effect of nuclear deform. on folded pot. 79−6453
$^{12}C+d$, 1.1-4.6 GeV/nucleon, nuclear fragmentation meas. *(Russian)* 78−54773
$^{12}C+d$, 6.3 GeV/c, inclusive spectra of fast p and d *(Russian)* 78−46075
$^{12}C+$emulsion, 50 GeV/c, multiple particle prod., cascade evaporation model *(Russian)* 79−22322
$^{12}C+\gamma\rightarrow 3\alpha$, photodisintegration theory using 3α model and hyperspherical functions *(Russian)* 78−78365
$^{12}C+n$, 18.2 MeV, multiparticle breakup, three-α correl. spectra 77−6364
$^{12}C+n$, 1.5-14 MeV total cross-section meas. 77−26742
$^{12}C+n$, 60 kev-20 MeV, average energy per ion pair, calc. 80−22841
$^{12}C+n$, total and elastic cross sections in few MeV region 79−59057
$^{12}C+\nu$, neutral current processes in nuclei, elementary particle approach 79−93606
$^{12}C+\nu_e$, 0 to 300 MeV, cross sections, shell model calcs 79−93605
$^{12}C+p$, 1 GeV, neutron production *(Russian)* 79−85477
$^{12}C+p$, 1 GeV, prod. of Li isotopes, meas. with online mass spectrometer *(Russian)* 77−10409
$^{12}C+p$, 40, 50, 150, 600 MeV, 25 GeV, $^{10,11}B$ prod., cosmic-ray propag. appl. 77−79380
$^{12}C+p$, 4.3 GeV/c, search for d knockout 79−6580
$^{12}C+p$, 50 MeV, three particle final state *(Russian)* 78−29471
$^{12}C+p$, 62 MeV, complex particle emission, pre-equilibrium exciton model anal. 78−66280
$^{12}C+p$, 660 MeV, H and He isotope prod. 77−18544
$^{12}C+p$, 9.5 MeV, optical pot., inverse scatt. method *(Russian)* 79−552
$^{12}C+p$, secondary proton momentum spectra, 4.3 to 8.9 GeV collisions *(Russian)* 79−3039
$^{12}C+p(d)(\alpha)$, transparency in composite particle-nucleus reactions 80−9273
$^{12}C+$photoemulsion nucleus, 50 GeV/c, low energy particles in stars produced *(Russian)* 78−89907
$^{12}C+\pi$, 5 GeV/c, momentum spectra and mechanism of proton emission *(Russian)* 79−89334
$^{12}C+\pi$, 60-120 MeV, p-wave optical pot., cross sections, Chew-Low model 78−70567
$^{12}C+\pi$, Glauber theory in microscopic α-cluster model 79−13346
$^{12}C+\pi$, P-wave pion absorption on two nucleons and low-energy pion-nucleus scattering 78−78416
$^{12}C+\pi$ optical potl. at 50 MeV 77−6440
$^{12}C+\pi$ optical potl. improved calcs. 77−6334
$^{12}C+\pi^-$, 4 GeV/c, general characts. of secondary π inclusive prod. *(Russian)* 78−78421
$^{12}C+\pi^-$, 40 GeV, secondary charged particle multiplicities *(Russian)* 79−3184
$^{12}C+\pi^-$, 40 GeV/c, cross sections of Λ and K prod. *(Russian)* 77−6184
$^{12}C+\pi^-$, 40 GeV/c, effect of nucl. transparency *(Russian)* 78−54805
$^{12}C+\pi^-$, 40 GeV/c, multiplicity distribs. of secondary charged particles, Glauber model calcs. *(Russian)* 78−17252
$^{12}C+\pi^-$, 40 GeV/c, secondary charged particle inclusive spectra, $\pi^{\pm}$ struct. functions *(Russian)* 78−89921
$^{12}C+\pi^-$, 40 GeV/c, total disintegration, emission angles and momenta of fragments *(Russian)* 78−89920
$^{12}C+\pi^-$, 5 GeV/c, charged π emission space-time characts. *(Russian)* 78−78422
$^{12}C+\pi^-\rightarrow p+X$, 40 GeV/c π^- momentum *(Russian)* 79−89335
$^{12}C+\pi^+$, 50 MeV, off-shell ambiguities and phenomenological optical potentials 78−37379
$^{12}C+\pi^+$, total cross-section depend. on nuclear density and π-N off-shell amplitude near (3,3) 77−3050
$^{12}C+\pi^+(\pi^-)$ elastic and inelastic scatt. at 148 MeV 77−50159
$^{12}C+\pi^{\pm}$, proton spectra, cross section, π. absorpt. mechs. 78−25239
$^{12}C^*$ recoil momentum spectrum, Doppler broadened deexcitation γ rays from $^{14}N\ \pi^-$ capture 77−54256

nuclei with mass number 6 to 19 continued
$^{12}C(^{10}B,d)$, 20-20.5 MeV, possible selectivity 78−41764
$^{12}C(^{11}B,^{12}C)^{11}B$, 28 MeV DWBA amplitude, strong absorpt. model, effect of ang. momentum depend. pots. 79−85486
$^{12}C(^{12}C,\ ^{10}B)$ 22-42 MeV, resonances in $^{10}B+^{14}N$ and $^{12}C+^{12}C$ channels 79−80910
$^{12}C(^{12}C,\ ^{12}C)$, shape resonance energy and widths, projection operator method 80−78255
$^{12}C(^{12}C,\ ^{12}C)$ intermediate struct. resonances, ^{24}Mg giant isoscalar quadrupole fission/fusion doorway states 80−37410
$^{12}C(^{12}C,\ ^{12}C)^{12}C^*,\ 0_2^+,\ 3_1^-,\ 4_1^+$ state excitation functions, resonance structures 80−42616
$^{12}C(^{12}C,\alpha)^{20}Ne$, 6.85-15 MeV, evidence for rotational band and its fragmentation in ^{24}Mg 79−9449
$^{12}C(^{12}C,\alpha)^{20}Ne$, coupled channel approx., treatment of resonances 79−9621
$^{12}C(^{12}C,\alpha\gamma)$, 30 MeV, ^{20}Ne unnatural parity levels at high excitation 77−2933
$^{12}C(^{12}C,\gamma)$, 11.8-20.0 MeV, total cross section resonant and average behaviour 80−106069
$^{12}C(^{12}C,^{12}C')$, 10-40 MeV, resonance phenomena, band crossing model appl., molecular phenomena 79−54424
$^{12}C(^{12}C,^{12}C')$, 14.5-32 MeV, gross structure peaks, particle-γ coincidences 79−97693
$^{12}C(^{12}C,^{12}C')$, gross struct., barrier top resonance model calc. 80−9279
$^{12}C(^{12}C,^{12}C')$, intermediate resonance, coupled channels calcs. 80−42611
$^{12}C(^{12}C,^{12}C')$, 50 GeV/c, multiplicities and ang. distribs. *(Russian)* 79−22323
$^{12}C(^{12}C,^{12}C^*)^{12}C^*$, 10-15 MeV, excitation function of 4.44 MeV 2^+ ^{12}C states 77−82957
$^{12}C(^{12}C,^{12}C)$, 10-30 MeV, projection operator method, Feshbach doorways, intermediate structure 80−68695
$^{12}C(^{12}C,^{12}C)$, 10-30 MeV, molecular structure, projection operator anal., differential cross sections 80−106033
$^{12}C(^{12}C,^{12}C)$, 13-14.1 MeV, Coulomb barrier resonance parameter direct determ., J^{π} assignments 80−513
$^{12}C(^{12}C,^{12}C)$, 35-63 MeV, elastic and inelastic, cross sections, DWBA and optical anal. 79−93656
$^{12}C(^{12}C,^{12}C)$, 6-30 MeV, intermediate struct. from band crossing model, molecular resonances 79−54425
$^{12}C(^{12}C,^{12}C)$, elastic scatt., incoming wave boundary condition model calcs. 80−47504
$^{12}C(^{12}C,^{12}C)$, perturbed stationary state method, low energy collision and mol. resons. 80−78320
$^{12}C(^{12}C,^{16}O)^8Be$, 5.75-8.9 MeV, sub-Coulomb resonances in ^{12}C-^{12}C system 77−57688
$^{12}C(^{12}C,^8Be)^{16}O^*$, 78 MeV, spectroscopy of high spin states in ^{16}O 78−50066
$^{12}C(^{12}C,^8Be)^{16}O(GS)$, excitation functions and Legendre anal. for resonance J^{π} assignments 78−78347
$^{12}C(^{12}C,X)$, 27-60 MeV, evaporation residue cross sections from complete fusion, statistical anal. 79−13369
$^{12}C(^{12}C,X)$, collective potentials and inertia parameters, adiabatic time dependent HF calcs. quasimolecular resonances 80−63195
$^{12}C(^{12}C,X)$, optical potential, nuclear matter approach 80−57801
$^{12}C(^{12}C,X)$, two fireball model, pp correlations and inclusive pion spectrum 80−68694
$^{12}C(^{12}C,X)$ 93.8 MeV, X=^{11}C,^{11}B,^{10}B, ang. distribs. and cross sections, DWBA anal. 79−93657
$^{12}C(^{12}C,\alpha)$, 11-15 MeV, quasimolecular resonances 79−6544
$^{12}C(^{12}C,\alpha)$, 4-8 MeV, ^{20}Ne spin assignments for sub-Coulomb resonances 77−54245
$^{12}C(^{12}C,\alpha)$, 7-15 MeV, excitation function statistical anal., nonstatistical features 80−99167
$^{12}C(^{12}C,\alpha)^{20}Ne$, ^{24}Mg reson. J^{π}, rot.-vibr. coupling 78−491
$^{12}C(^{12}C,\alpha)^{20}Ne$, 17 to 20 MeV, excitation functions, correl. resonances 77−34344
$^{12}C(^{12}C,\alpha)^{20}Ne$, 45 to 52 MeV, reaction mechanism, ang. momentum effects 77−38295
$^{12}C(^{12}C,\alpha)^{20}Ne$, 6.85-15 MeV, rot. band in ^{24}Mg obs. 78−12951
$^{12}C(^{12}C,\alpha)^{20}Ne$, E_{cm}=6.5-12 MeV, new resonances, J^{π} determ. 77−54200
$^{12}C(^{12}C,\alpha)^{20}Ne$, evidence for rot. band in ^{24}Mg at 10.5 to 15 MeV 78−13134
$^{12}C(^{12}C,\alpha)^{20}Ne$, populates 8p-4h O^+ level, α-decay 78−50132
$^{12}C(^{12}C,\alpha)^{20}Ne$, resonance anomaly anal. in fluctuation theory 78−25215
$^{12}C(^{12}C,\alpha)^{20}Ne$, spin-zero particle reactions, critical ang. momentum effect on ang. distribs. 77−18607
$^{12}C(^{12}C,\alpha)^{20}Ne$, statistical methods for resonance detection, nonstatistical struct. 79−45238
$^{12}C(^{12}C,\alpha)^{20}Ne_{g.s.}$, overlapping 10^+ and 12^+ resonances in $^{12}C+^{12}C$ near $E_{c.m.}$=18.5 MeV 77−6432
$^{12}C(^{12}C,d)^{22}Na$, 14.3 MeV, spectra meas., ^{22}Na excitation functions determ. 77−82956
$^{12}C(^{12}C,\gamma)^{24}Mg$, 5 to 11 MeV, γ yields, resonance features 78−54799
$^{12}C(^{12}C,n)^{23}Mg$, 3.54-4.94 MeV, cross section, neutron branching ratio, stellar processes estimates 77−34336
$^{12}C(^{12}C,p)^{23}Na$, schematic model for continuum resonances, shape resonance fragmentation 77−67764
$^{12}C(^{12}C,p)X$, 800 MeV/N, fireball and preequilibrium cross sections, π condensation proximity influence 80−27659
$^{12}C(^{12}C,x\alpha)$, 12-31.5 MeV, inclusive α-particle yield, resonant like structs. 80−42691
$^{12}C(^{13}C,^{13}C)$ 4.8-9.5 MeV, cross-section at Coulomb barrier 77−14154
$^{12}C(^{13}C,^{13}C)^{12}C$, 12 MeV, accurate determ. of ^{13}C-$^{12}C+n$ spectroscopic factor 77−65194
$^{12}C(^{13}C,\alpha\gamma)^{21}Ne$, 13.9-15 MeV, yield curves near 14.4 MeV reson. 77−54254
$^{12}C(^{13}C,n)$, 13.4-15.3 MeV, nonstatistical population of ^{24}Mg high spin states 78−74385
$^{12}C(^{14}N,\ ^{12}C)^{14}N$, 79 and 155 MeV, DWBA calcs., recoil and sequential transfer effects 78−46090
$^{12}C(^{14}N,^{10}B)^{16}O$, DWBA anal., spectroscopic factors 79−6673
$^{12}C(^{14}N,^{13}N)^{13}C$, 100 MeV, exact finite range CCBA anal. 79−17926
$^{12}C(^{14}N,^{13}N)^{13}C$, exchange effects on ang. distrib. 78−627
$^{12}C(^{14}N,^{13}N)^{13}C$ at high energies, simplified DWBA anal. 79−93643
$^{12}C(^{14}N,^{6,7}Li)$, ($^{14}N,^{7,9}Be$), E=86.9, 157 MeV, spectra, ang. distribs. meas. 78−33216
$^{12}C(^{14}N,X)$, 27-60 MeV, evaporation residue cross sections from complete fusion, statistical anal. 79−13369

nuclei with mass number 6 to 19 continued
$^{12}C(^{14}N,\alpha)$, 10.1-15.9 MeV, forward angle excitation function structure, nonstatistical struct. 80−86885
$^{12}C(^{14}N,\alpha)^{22}Na$, statistical methods for resonance detection, nonstatistical struct. 79−45238
$^{12}C(^{15}N,X)$, 27-60 MeV, evaporation residue cross sections from complete fusion, statistical anal. 79−13369
$^{12}C(^{15}N,\alpha)$ reson. struct. and ^{27}Al yrast levels 77−79348
$^{12}C(^{15}N,\alpha)^{23}Na$, statistical methods for resonance detection, nonstatistical struct. 79−45238
$^{12}C(^{16}O, ^{12}C^*)$, 45-53 MeV, $^{12}C^*$ m-substate population, spin alignment and excitation functions 80−42615
$^{12}C(^{16}O, ^{16}O')$, molecular resonances from coupling interactions derived by folding procedure 79−89279
$^{12}C(^{16}O, n)^{27}Si$, 12.8 MeV resonance investig. by time-of-flight spectra and n-γ coincidence 79−9627
$^{12}C(^{16}O,^{12}C,^{12}C)\alpha$, ^{12}C-α-^{12}C chain formation, α emitted at rest search 79−45285
$^{12}C(^{16}O,^{12}C_{2+})^{16}O$, $^{12}C_{2+}$ spin alignment using γ-decay in flight 78−41767
$^{12}C(^{16}O,^{12}C_{gs})^{16}O^*$, obs. of α-doorway states 79−6662
$^{12}C(^{16}O,^{12}C^{12}C)\alpha$, 68-80 MeV, double differential cross section, Hauser-Feshbach anal. 79−63690
$^{12}C(^{16}O,^{12}C)^{16}O$, 22.7 to 33.0 MeV, excitation function enhancement for 0^+, 6.049 MeV ^{16}O state 78−58299
$^{12}C(^{16}O,^{16}O')$, 315 MeV, giant multipole resonance excitation 79−30812
$^{12}C(^{16}O,^{16}O^*)^{12}C^*$, 33-54 MeV, intermediate struct. resonances, ang. distribs., statistical anal. 78−82330
$^{12}C(^{16}O,^{16}O)$, elastic and inelastic, 23-32 MeV, strong absorption region resonances, excitation functions 80−86884
$^{12}C(^{16}O,^{16}O)^{12}C$, 15.4 to 30.9 MeV, correlation between fusion and inelastic scatt. 78−66310
$^{12}C(^{16}O,^{16}O)^{12}C$ resonant scatt., 15-30 MeV, ang. distribs., interpretation *(French)* 79−3166
$^{12}C(^{16}O,^{16}O)^{12}C$ scattering gross struct. features, optical model 77−88164
$^{12}C(^{16}O,^{16}O)^{12}C^*$ (2^+, 4.44 MeV) mol. reson., band crossing model 78−62562
$^{12}C(^{16}O,^{20}Ne)$, 10-15.5 MeV, cross sections and ang. distribs., resonances, direct and stat. anal. 79−67730
$^{12}C(^{16}O,^{20}Ne)^8Be$, 12.25 to 15.07 intermediate struct. effects 78−620
$^{12}C(^{16}O,^8Be)$ $E_{c.m.}$=18.5-20.5 MeV, populating ^{28}S 12^+ reson. 77−18508
$^{12}C(^{16}O,^8Be)^{20}Ne$, 13.5-23 MeV, excitation functions, ang. distribs. and cross sections 79−13334
$^{12}C(^{16}O,X)$, transparency to l=9 partial wave in 14.7 MeV resonance region 80−78314
$^{12}C(^{16}O,X)$ 10.5-23.3 MeV, low energy fusion cross sections 77−14152
$^{12}C(^{16}O,2p)^{26}Mg$, energy spectra and ang. distribs. meas. 77−38293
$^{12}C(^{16}O,\alpha)$, J^π for 12.8 MeV c.m. resonance 79−59045
$^{12}C(^{16}O,\alpha)^{24}Mg$, 10.9 MeV ^{28}Si resonance, spin, parity 78−74384
$^{12}C(^{16}O,\alpha)^{24}Mg$, 13.5-23 MeV, excitation functions, ang. distribs. and cross sections 79−13334
$^{12}C(^{16}O,\alpha)^{24}Mg$, 13.7, 14.2, 14.7 MeV, ang. distribs., intermediate resonance struct. 79−13331
$^{12}C(^{16}O,\alpha)^{24}Mg$, anomaly at 13.7 MeV, optical model anal. 78−21587
$^{12}C(^{16}O,\alpha)^{24}Mg$, low energy, spin and parity assignments 78−21602
$^{12}C(^{17}O,^{16}O)$, single-n sub-Coulomb transfer reactions, single particle wave function RMS radius, n-excess 79−85355
$^{12}C(^{18}O,^{16}O)$, two nucleon transfer reactions, one and two step transfer process anal. 78−82370
$^{12}C(^{18}O,^8Be)^{22}Ne$, 15-22.5 MeV, resonance strength investig. 79−13336
$^{12}C(^{18}O,\alpha)^{26}Mg$, 15-22.5 MeV, resonance strength investig. 79−13336
$^{12}C(^{20}Ne,^{20}Ne)$, back angle scatt. systematics, structured excitation functions and oscillatory ang. distribs. 80−32295
$^{12}C(^{20}Ne,\alpha)^{28}Si$, energy depend., non-statistical effects 79−13332
$^{12}C(^{24}Mg,^{24}Mg)$, back angle scatt. systematics, structured excitation functions and oscillatory ang. distribs. 80−32295
$^{12}C(^{24}Mg,X)$, 45-71 MeV, γ-ray yield functions from high spin states, comparison with $^{16}O+^{28}Si$ 79−93492
$^{12}C(^{28}Si,\alpha X)$, 87-91.5 MeV, α-HI angular correlations, excitation functions, statistical anal. 80−86915
$^{12}C(^3He, ^3He)$, 119 MeV, optical pot. parameters energy and mass depend. 80−32289
$^{12}C(^3He,^3H)$, ($^3He,^3He'$), 44 MeV, study of ^{12}N(2.43 MeV) and ^{12}C(17.77 MeV) analogue states 77−6235
$^{12}C(^3He,^3He')$, 18, 20, 24.5 MeV, differential cross sections, DWBA anal. 79−6647
$^{12}C(^3He,^3He')$, spin-flip transitions, microscopic α-spectator model 77−79400
$^{12}C(^3He,^3He)$, 20.5-33.0 MeV, energy depend. of analysing power optical model 78−17226
$^{12}C(^3He,^3He)$, 44.04 MeV, absolute differential cross section, optical model anal. 79−59078
$^{12}C(^3He,^3He)$, E2 strength distrib., giant quadrupole reson. 77−30612
$^{12}C(^3He,^3He)$, incident ion binding energy effects on scatt., qualitative anal. 79−9600
$^{12}C(^3He,^3He)$, optical potentials and volume integrals, mass and energy dep. 80−52686
$^{12}C(^3He,^3He)$ 39.7 MeV, optical pot. mass. depend. 77−34327
$^{12}C(^3He,\alpha)$, 35.6 MeV, ^{11}C energy levels, ang. distribs., DWBA calcs. comparison 78−78396
$^{12}C(^3He,\alpha)$, inner hole states excitation, DWBA anal., reaction mechanism *(French)* 78−41735
$^{12}C(^3He,\alpha)^{11}C$, 11 MeV, multistep mechanism, CCBA calcs. 78−41734
$^{12}C(^3He,\alpha)^{11}C$, j-depend. of analysing powers, ^{11}C spectroscopic factors 77−328
$^{12}C(^3He,d)$, spectral line shape anal. 78−25203
$^{12}C(^3He,d)^{13}N$, d ang. distrib. anal. in PWBA 77−74863
$^{12}C(^3He,d)^{13}N$, j-depend. of analysing powers, ^{13}N spectroscopic factors 77−328
$^{12}C(^3He,\gamma_0)^{15}O$, differential cross section in giant dipole reson. region 78−78395
$^{12}C(^3He,n)$, 12-24 MeV 78−82286
$^{12}C(^3He,p)^{14}N$, 11 to 20 MeV, nuclear alignment 77−57679
$^{12}C(^3He,pd)$, 90 MeV, angular correlations, elastic break-up of ^3He 80−52685
$^{12}C(^3He,\pi^0)$, 180, 200 MeV, inclusive neutral pion prod. cross section 77−6410
$^{12}C(^{40}Ar,X)$, 213 MeV/N, relativistic fragmentation, microscope and macroscopic calcs., np correlation 80−13495

nuclei with mass number 6 to 19 continued
$^{12}C(^{40}Ca,^{40}Ca)$, 90° and 180° excitation functions energy depend., DWBA anal. 80−42582
$^{12}C(^4He,\pi^0)$, 710 MeV, inclusive neutral pion prod. cross section 77−6410
$^{12}C(^6Li,^6Li')$, 153 MeV, isoscalar giant quadrupole resonances 80−13440
$^{12}C(^6Li,^6Li')$, spin-flip transitions, microscopic α-spectator model 77−79400
$^{12}C(^6Li,^6Li)$ 5.8, 59.8 MeV, optical pot. inner part, elastic scatt. cross section 79−3173
$^{12}C(^6Li,^6Li)^{12}C$, 20 MeV and higher, diffraction model behaviour, anomalies caused by two step-processes 79−13344
$^{12}C(^6Li,X)$, 156 MeV, projectile break up in continuous particle spectra, cross section, fragmentation 80−86889
$^{12}C(^6Li,\alpha)^{14}N$, 33 MeV, multiple reaction mech., exact finite range DWBA calcs. 78−25231
$^{12}C(^6Li,\alpha)^{14}N$, α-particle spectrum sharp lines observation, originating from ^{16}O decay *(Russian)* 78−29495
$^{12}C(^6Li,\alpha)^{14}N$, E($^6Li$)=20 MeV, using polarised ^6Li source, exact finite range DWBA anal. 78−58293
$^{12}C(^6Li,\alpha)^{14}N$(2,31 MeV), 9 to 20 MeV, isospin violation 78−41763
$^{12}C(^6Li,d)$, $^{12}C(^6Li,\alpha)$, 20 MeV, analysing powers 78−46098
$^{12}C(^6Li,d)$, ^{16}O highly excited states spin, parity, decay into A+^{12}C 77−79395
$^{12}C(^6Li,d)$, ^{16}O level configuration mixing anal., α-spectroscopic strengths 79−6683
$^{12}C(^6Li,d)^{16}O$, 20 MeV polarised ^6Li, DWBA calc. of analysing powers, O^+ g.s. and 2^+ state of ^{16}O 79−6678
$^{12}C(^6Li,d)^{16}O$, 20 MeV polarised ^6Li, DWBA calc. of analysing powers for ^{14}N 1^+ states 79−6679
$^{12}C(^6Li,d)^{16}O$, 42 MeV, α spectroscopic factors, reduced widths, stellar He burning 78−89897
$^{12}C(^6Li,d)^{16}O^*$, 18-28 MeV, configuration mixing effect and cross sections, zero range DWBA 80−42692
$^{12}C(^6Li,d)^{16}O(\alpha)^{12}C$, 35 MeV, d-$\alpha$ coincidence spectra meas. after ^{16}O break-up, α-cluster state energies 79−63688
$^{12}C(^6Li,d)^{16}O\rightarrow^{12}C+\alpha$, reaction mechanism from ang. correlations, direct transfer 80−78319
$^{12}C(^7Li, ^7Li)$, 40 MeV, spectroscopic factors, DWBA anal. 79−75904
$^{12}C(^7Li,t)^{16}O$, 17 MeV, ^{16}O states, $^{12}C+4$ particles vertex 77−14030
$^{12}C(^7Li,t)^{16}O$, 34 MeV, α spectroscopic factors and reduced widths, stellar fusion 78−89896
$^{12}C(^7Li,t)^{26}O$, Goldfarb-Buttle method *(Chinese)* 78−8834
$^{12}C(^9Be, ^8Be)^{12}C$(g.s.), 39.68, 43.75 MeV, back angle cross section enhancement, Hauser Feshbach anal. 79−89324
$^{12}C(^9Be,^8Be)$, 11.4 MeV to 14.8 MeV (c.m.), search for resonances 79−45290
$^{12}C(^9Be,^8Be)^{13}C$, 20 MeV, α-cluster transfer process contrib. 79−6668
$^{12}C(^9Be,^8Be)^{13}C$, neutron and α-particle transfer processes 79−36255
$^{12}C(^9Be,^9Be)$, ang. distrib. from pick-up model anal. *(Russian)* 80−37396
$^{12}C(^9Be,^9Be)$, cluster effects *(German)* 79−76015
$^{12}C(^9Be,^9Be)$, large angle scatt., optical model and DWBA anal. 79−36259
$^{12}C(^9Be,^9Be)$, possibility of ^3He exchange 79−6669
$^{12}C(^9Be,^9Be)$ elastic and inelastic 10-15 MeV, excitation functions and resonant enhancements 79−17881
$^{12}C(^9Be,^9Be)^{13}C_{gs}$, cluster effects *(German)* 79−76015
$^{12}C(^9Be,\alpha)^{17}O$, 10-15 MeV, excitation functions and resonant enhancements 79−17881
$^{12}C(^9Be,\alpha)^{17}O$, ang. distrib. from pick-up model anal. of cluster transfer *(Russian)* 80−37396
$^{12}C(^9Be,\alpha)^{17}O$, cluster effects *(German)* 79−76015
$^{12}C(^9Be^9Be)$ 14, 20 and 26 MeV, optical model parameters 79−26449
$^{12}C(K,K)$, appl. of forward dispersion reln. 77−14188
$^{12}C(K^0_L, K^0_S)^{12}C$, elastic regeneration, 10-50 GeV/c, differential cross section slope 78−646
$^{12}C(K^-,\pi^-)$, 390 MeV/c, formation of hypernuclear excited states 78−74402
$^{12}C(K^-,\pi^-)$, 900 MeV/c, sum rule for hypernuclear formation, distorted wave impulse approx. 78−70572
$^{12}C(K^-,\pi^-)$, relative ang. distribs. 77−14185
$^{12}C(K^-,\pi^-)$, spin orbit interactions of Λ hyperons 79−9628
$^{12}C(K^-,\pi^-)_\Lambda{}^{12}C^*$, 800 MeV/c, ang. distribs. from DWIA calcs. 80−32225
$^{12}C(K^-,\pi)$, narrow Σ-hypernuclear states, estimated widths, quantum number assignments 80−42576
$^{12}C(K^+,K^{+\prime})$, 300 MeV inclusive scatt., plane wave impulse approx. 78−50214
$^{12}C(K^+,K^{+\prime})$, form factors, cross sections, interior probing capability 80−73866
$^{12}C(K^\pm,K^\pm)$, 100-1000 MeV, differential and total cross sections, nucleon motion 80−102206
$^{12}C(K^\pm,K^\pm)$, Glauber model anal. 80−42697
$^{12}C(K^\pm,K^\pm)$, kaon-nucleus coupling const. from scatt. amplitudes 80−32304
$^{12}C(1^+)$ decay to 3 α-particles, final-state interactions, spectra calc. 77−88086
$^{12}C(a,X)$, a=p,d,^4He,^{12}C, 4.2 GeV/c, multitudes of secondary negative particles, momentum distrib. ratios *(Russian)* 80−63178
$^{12}C(\alpha,\alpha'\gamma)$ γ angular correlation function obs. *(Russian)* 79−13246
$^{12}C(\alpha,\alpha)$, 120-172.5 MeV, optical pot. uniqueness and shape 79−97719
$^{12}C(\alpha,^5He)$, 90 MeV, α-n coincidence, ^5He breakup kinematics 77−6419
$^{12}C(\alpha,^6Li)$, 46 MeV, finite range DWBA anal. 77−14142
$^{12}C(\alpha,Li^*)$, unbound Li, relative energy distrib. of correlated decay products 79−13274
$^{12}C(\alpha,2\alpha)$, 140 MeV, quasifree knockout, DWIA anal. spectroscopic factors 80−68629
$^{12}C(\alpha,2\alpha)$, pole peripheral model, ang. correl. functions calc. 77−6328
$^{12}C(\alpha,\alpha')$, 38-50.5 MeV, sign of nuclear deform. from Blair phase shift 77−61439
$^{12}C(\alpha,\alpha')$, 60 MeV, high lying continuum states, multipolarities, strengths 77−82925
$^{12}C(\alpha,\alpha')$, generator coordinate multichannel calc., levels and resonances 80−78149
$^{12}C(\alpha,\alpha')^{12}C^*$, 45 MeV, ang. correls., ^{12}C 14.08 MeV J^π assignment 77−82819
$^{12}C(\alpha,\alpha'\gamma)^{12}C$, 17.6 to 21.8 MeV 'rotation' of ang. correl. function 77−6406
$^{12}C(\alpha,\alpha)$, 150 MeV, isoscalar giant quadrupole reson. 77−307
$^{12}C(\alpha,\alpha)$, 17.9 GeV/c, Glauber model rigid projectile approx. 79−63685

nuclei with mass number 6 to 19 continued

^{12}C(α,α), 1.37 GeV, modified eikonal multiple scattering theory 78−21576
^{12}C(α,α), 1.37 GeV, S-matrix expansion from Glauber multiple scatt. theory 80−91191
^{12}C(α,α), 2$^+$ collective level excitation, microstruct. of diffr. ang. distrib. 77−61440
^{12}C(α,α), 20 to 24 MeV, optical model anal. 77−65228
^{12}C(α,α), 2.8-6.5 MeV, anal., global pot. 78−21577
^{12}C(α,α), 9-11 MeV, elastic and inelastic, resonances and ang. distribs., orthogonality condition model 79−6637
^{12}C(α,α), exchange process calc. in impulse approx. *(Russian)* 77−74819
^{12}C(α,α), excitation function anal. with allowance for exchange processes 79−9596
^{12}C(α,α), forward differential cross sections determ. using Feynman diags. 78−25210
^{12}C(α,α), generalised optical potentials 80−22781
^{12}C(α,α), generator coord. method anal. 78−12960
^{12}C(α,α), spectra and widths of quasistationary α-cluster states *(Russian)* 77−46180
^{12}C(α,α)^{12}C, differential cross section calc. with hard core potential 77−30614
^{12}C(α,α)^{12}C, elastic and inelastic, 1.37 GeV, multiple diffr. model, eikonalised DWIA 77−34326
^{12}C(α,γ$_n$), excitation function meas. in vicinity of 12.44 and 13.1 MeV levels of ^{16}O 77−6413
^{12}C(α,γ)^{16}O cross-section, K-matrix parametrisation 77−6411
^{12}C(α,p$_0$), 17.5-18.7 MeV, p ang. distribs. and integrated cross section 79−30846
^{12}C(α,p)^{15}N, 50 MeV, proton spectra, excitation of high-spin states *(Russian)* 77−6209
^{12}C(α,p)^{15}N (3/2$^-$, 6.328 MeV) transition, giant resonance effects 79−9601
^{12}C(d, d′), isospin violating direct reaction, Coulomb interaction role 80−102170
^{12}C(d,^{2}He), 55 MeV, cross sections, ^{2}He energy spectra and ang. distribs. 80−18321
^{12}C(d,α)^{10}B, 20.7 and 29 MeV, polarised deuterons 77−82938
^{12}C(d,α)^{10}B(1.74 MeV, T=1), coupled channel anal. of energy depend. isospin violation 78−70541
^{12}C(d,d′), spin-flip transitions, microscopic α-spectator model 77−79400
^{12}C(d,d′)^{12}C, 24-29 MeV, ratio of isospin forbidden/allowed yield 77−18385
^{12}C(d,d), 1.69 GeV/c, Coulomb interference region, Glauber theory anal. 80−99178
^{12}C(d,d), 650 MeV, Glauber theory approx. anal. using realistic deuteron wave functions 77−46176
^{12}C(d,d), 650 MeV, Glauber model calcs. for cross sections 79−13306
^{12}C(d,d)^{12}C, reaction mech., relation to ^{12}C(d,p), S-matrix theory, 1.63 to 2.05 MeV *(Chinese)* 78−78393
^{12}C(d,n), 6-10 MeV polarised deuterons, differential cross-section, vector analysing power 77−6398
^{12}C(d,n), diagnostic neutron spectra from deuterons 2.5, 3.0, 3.5 MeV 79−40933
^{12}C(d,n), secondary neutron emission characts. 79−30843
^{12}C(d,n), spectral line shape anal. 78−25203
^{12}C(d,np), n-p rescattering and d break-up in FSI 77−10417
^{12}C(d,p$_0$)^{13}C, proton polarisation in stripping reaction, obs. and DWBA calc. 79−30816
^{12}C(d,p)^{12}C*, reaction mech., relation to ^{12}C(d,d), S-matrix theory, 1.63 to 2.05 MeV *(Chinese)* 78−78393
^{12}C(d,p)^{13}C, 0.5 to 2.5 MeV, excitation functions and angular distribs., possible doorway state *(Chinese)* 80−68679
^{12}C(d,p)^{13}C, 1.5 to 3.0 MeV, excitation functions 79−40932
^{12}C(d,p)^{13}C, 1.58 to 3.03 MeV, calc. of differential cross sections, spectroscopic factors 77−6394
^{12}C(d,p)^{13}C, 2.64-2.82 MeV, new model calcs. for p ang. distribs. 77−88097
^{12}C(d,p)^{13}C, differential cross sections at 9.0 MeV deuteron energy, two-step processes 77−74857
^{12}C(d,p)^{13}C, light element profiling of tapered corrosion sections 79−92036
^{12}C(d,p)^{13}C* leading to unbound states, neutron form factors, coupled channel DWBA anal. 77−26775
^{12}C(e, e′p), eN interaction in quasifree scatt., nonrelativistic Hamiltonian through 4th order 80−47469
^{12}C(e, e′p), quasifree scatt., spin-orbit distortion of emerging nucleon 80−52664
^{12}C(e, π$^\pm$), 17 and 29 MeV 79−63659
^{12}C(e,e′N), energy and ang. distribs. diffraction approx. for final state interaction *(Russian)* 77−18531
^{12}C(e,e′P)^{11}B, nonorthogonality of initial and final nucl. states *(Russian)* 78−66265
^{12}C(e,e′), 12.71 MeV 0$^+$ to 1$^+$ transition, axial isoscalar neutral current, polarisation asymmetry 79−26425
^{12}C(e,e′), 500 KeV inclusive scatt., plane wave impulse approx. 78−50214
^{12}C(e,e′), comparison of inelastic electron and positron scatt. cross sections 79−49621
^{12}C(e,e′), cross sections, shadowing effect at small four momentum transfer 80−63176
^{12}C(e,e′), deep inelastic 60-130°, 160-520 MeV response function 79−13284
^{12}C(e,e′), E2 transitions, convection currents and spin magnetisation 79−13244
^{12}C(e,e′), internuclear nucleon effective mass in quasielastic scatt. *(Russian)* 79−3076
^{12}C(e,e′), role of two-particle scatt. *(Russian)* 80−91178
^{12}C(e,e′) excitation of 2$^+$ T=1 state at 16.11 MeV, radiative width, magnetisation density 78−25176
^{12}C(e,e′)^{12}C*, 4.4 MeV, transverse excitation of first excited state 77−10342
^{12}C(e,e′d), deuteron knock-out yield, contrib. to inelastic scatt. cross section *(Russian)* 80−27621
^{12}C(e,e′p), 700 MeV, DWIA anal. proton spectral function 77−6353
^{12}C(e,e′p), cross sections from DWIA, optical, and shell model calcs. *(Russian)* 80−32270
^{12}C(e,e′p), p-shell nucleon momentum distrib. determ. 78−17182
^{12}C(e,e′p)^{11}B, cross section calc. based on shell model with residual interaction *(Russian)* 77−311-

nuclei with mass number 6 to 19 continued

^{12}C(e,e′p)^{11}B, energy spectra calc. in terms of dynamic collective model *(Russian)* 78−8804
^{12}C(e,e′p)^{11}B, recoil momentum distribs., optical potential variation effects, HF calcs. 77−41955
^{12}C(e,e′π$^+$), energy and ang. distribs. of πs, low lying residual states 78−54740
^{12}C(e,e′π$^+$)^{12}B, 195 MeV, photopion cross-section determ. 78−13066
^{12}C(e,e′π$^+$)^{12}B, near threshold, equivalent photon approx., Kroll-Ruderman term 78−13065
^{12}C(e,e′πs) threshold prod. at 280 MeV, π$^+$/π$^-$ ratio 77−41957
^{12}C(e,e') nuclear struct. anal., depend. of meson exchange currents, high momentum transfer data 79−13283
^{12}C(e,e), 180° scatt., transverse inelastic form factors and spectra, collective 2$^+$ state 80−9261
^{12}C(e,e), 25-115 MeV, ground state charge distrib. and RMS charge radius 80−57672
^{12}C(e,e), charge form factors in α cluster model 79−63571
^{12}C(e,e), elastic scatt., spectroscopic information and form factors 80−9260
^{12}C(e,e), electroexcitation cross sections, incoherent superposition of single nucleon processes 80−32269
^{12}C(e,e) , 12.71 and 15.11 MeV level struct. and isospin mixing from form factors 80−32186
^{12}C(e,e) 140 MeV, resonances in e spectra *(Russian)* 78−78367
^{12}C(e,eπ), total cross section from square reaction matrix element *(Russian)* 80−32271
^{12}C(e,n)^{11}C, 30 MeV, cross section absolute meas., corresponding (γ,n) cross section 78−66270
^{12}C(e,π$^\pm$), 10 MeV π, of PWIA calcs. 79−93607
^{12}C(e,π), charged π electroprod. near threshold, data anal. 78−66266
^{12}C(ee′d), electroproduction cross section, Born approx. *(Russian)* 79−26427
^{12}C(γ, π$^-$)^{12}N$_{gs}$, threshold prod., 15.11 MeV M1 form factor 78−62519
^{12}C(γ, π$^-$p), final state interaction, plane and distorted wave momentum distrib. 80−18286
^{12}C(γ, π^{0}p), 0.7-1.65 GeV, cross section asymmetry of π^0 photoprod. *(Russian)* 80−63164
^{12}C(γ, π^{0}p), 450 MeV, pion^0 photoproduction with proton ejection 79−80921
^{12}C(γ,N), photonuclear sum rules from continuum calcs., dependence on residual interactions 80−22807
^{12}C(γ,P), up to 4.5 GeV, ang. depend. of normalised invariant cross section parameters *(Russian)* 78−17180
^{12}C(γ,2n)^{10}C, 100 to 800 MeV, yields, cross sections 77−34285
^{12}C(γ,γ), 15.11 MeV energy level excitation, branching ratio 77−30548
^{12}C(γ,γ), 23.5-39 MeV, cross sections and giant resonances, E2 strength 80−63122
^{12}C(γ,γ), 5.5-7.2 MeV, elastic differential scatt. cross section, Thomson scatt. obs. 77−74833
^{12}C(γ,γ), total photoabsorption and elastic cross sections, spectroscopic information *(Russian)* 80−83095
^{12}C(γ,γ) scatt. study of electron prod. high energy synchrotron radiation spectrum struct. 78−13062
^{12}C(γ,n)^{11}C, relativistic heavy ions, Coulomb disintegration, photodisintegration cross section *(Russian)* 78−89851
^{12}C(γ,nα)^{7}Be, electric quadrupole transition cross-sections, behind giant resonance *(Russian)* 80−78281
^{12}C(γ,p), p-shell nucleon momentum distrib. determ. 78−17182
^{12}C(γ,p), up to 0.25 GeV, from bremsstrahlung γ-quanta *(Russian)* 80−5123
^{12}C(γ,p)^{11}B, 40-120 MeV, reaction mechanism *(Russian)* 77−65221
^{12}C(γ,p)^{11}B, electric quadrupole transition cross-sections, behind giant resonance *(Russian)* 80−78281
^{12}C(γ,p)^{11}B, threshold to 120 MeV, cross section meas. *(Russian)* 78−41699
^{12}C(γ,pα)^{7}Li, electric quadrupole transition cross-sections, behind giant resonance *(Russian)* 80−78281
^{12}C(γ,π$^-$), 160-250 MeV, total cross section from elementary Hamiltonian model 80−18292
^{12}C(γ,π$^-$), (γ,π$^-$p), knockout p interaction, optical model and quasifree π photoprod. mechanism *(Russian)* 80−42638
^{12}C(γ,π$^-$), at 44.2°, inclusive reaction, pion momentum spectra 77−50109
^{12}C(γ,π$^-$), model yield calc. 77−14107
^{12}C(γ,π$^-$), near (3,3) resonance, differential cross-section meas. 77−10385
^{12}C(γ,π$^-$), threshold to 360 MeV, total cross sections in Δ region 80−13457
^{12}C(γ,π$^-$), total cross section calc. in impulse approx. 80−13458
^{12}C(γ,π$^-$)^{12}N, near threshold, total cross section 77−14104
^{12}C(γ,π$^-$)^{12}N, threshold to reson., total and differential cross sections 79−85456
^{12}C(γ,π$^-$)^{12}N, total cross-section anal. 77−14102
^{12}C(γ,π$^-$)^{12}N, total cross section calc., Δ(1232) contrib. 80−91175
^{12}C(γ,π$^-$)^{12}N$_{g.s.}$, near threshold, total cross section calc. 78−50152
^{12}C(γ,π$^-$p), 340-380 MeV, quasi-free photoprod., impulse and shell model anal. *(Russian)* 80−5124
^{12}C(γ,π$^-$p), final state interaction, distorted and plane wave momentum distribs. 80−78275
^{12}C(γ,π^0), pionic and EM A* resonance excitation 80−91160
^{12}C(γ,π^0)^{12}C, 220-360 MeV, phenomenological isobar doorway model calcs., total cross section 79−525
^{12}C(γ,π^{0}p), 0-600 MeV residual nucleus impulse *(Russian)* 79−59050
^{12}C(γ,π$^+$)^{12}B, nuclear critical opalescence study 80−105988
^{12}C(γ,π$^+$)^{12}B, spin flip transition strength 77−14103
^{12}C(γ,π$^+$)^{12}B$_{g.s.}$, 0-4 MeV, pion photoprod. cross section 80−42637
^{12}C(γ,π$^+$)^{12}C, up to 175 MeV, total cross sections, DWIA anal. 79−59049
^{12}C(γ,π$^\pm$), 300 to 850 MeV, charged pion momentum spectra 78−93987
^{12}C(γ,π$^\pm$), PWIA anal. 77−14108
^{12}C(k$^-$, π$^-$)$^{12}_{\Lambda}$C, strangeness exchange reaction, ground state ang. distrib., 11 MeV excitation 79−85560
^{12}C(k$^-$,k$^-$), 800 MeV, differential cross sections 79−85564
^{12}C(k$^-$,π$^-$)$^{12}_{\Lambda}$C, Λ-nuclear spin-orbit coupling, ΛN effective interaction 79−85562
^{12}C(μ,γ), exclusive radiative capture, axial currents and induced pseudoscalar form factors 79−97699
^{12}C(μ,ν)^{12}B, polarisation of ^{12}B, weak coupling anal. 77−88116
^{12}C(μ$^-$, ν)^{12}B, polarisation studies, muon capture, weak interaction aspects 80−68655

nuclei with mass number 6 to 19 continued
$^{12}C(\mu^-,\nu_\mu)^{12}B$, data anal., second-class currents and CVC 77−82874
$^{12}C(\mu^-,\nu_\mu)^{12}B$, Hartree Fock wavefunction, correlations, pseudoscalar coupling constant, capture rates, recoil nuclear polarisation 80−22774
$^{12}C(\mu^-,\nu_\mu\gamma)^{12}B$, appl. of μ^- radiative capture to nucl. spin and isospin transitions 78−86511
$^{12}C(\mu^-,\nu_\mu\gamma)^{12}B$, impulse approx. calc., photon asymmetry and daughter nucleus polarisation 78−37315
$^{12}C(\mu^-,\nu)^{12}B^*$, average polarisation of recoil ^{12}B in direct capture 79−93602
$^{12}C(\mu^-,\nu)^{12}B$(g.s.), qualitative meas. of longitudinal recoil polarisation 79−54429
$^{12}C(\mu^-,\nu_\mu)^{12}B$, induced tensor and pseudotensor form factors 77−38253
^{12}C(n, X), compound resonance decay based on bound and metastable single nucleon states *(Russian)* 80−5107
$^{12}C(\bar{n},X)$, annihilation, 1.4 GeV/c, $\pi^\pm$, p emission angles, momentum and multiplicity distribs. 80−532
^{12}C(n,2n)^{11}C, 23 to 34 MeV, excitation functions, statistical model anal. 77−23082
^{12}C(n,n′)C* 15.85 MeV polarised neutrons, analysing power meas. 77−2969
^{12}C(n,n), 0.2-5.0 MeV, unified weak coupling model 77−82930
^{12}C(n,n), 14.2 MeV, elastic, inelastic, backscatt. meas., optical model test 78−58275
^{12}C(n,n), 15 to 18 MeV, resonance effects 77−30591
^{12}C(n,n), 15.85 MeV polarised neutrons, analysing power meas. 77−2969
^{12}C(n,n), 8 to 14.5 MeV, differential elastic and inelastic cross-sections 78−29455
^{12}C(n,n), (in)elastic scatt. cross sections, duration of collision process *(Russian)* 79−80942
^{12}C(n,n), <17 MeV, resonating group calcs., phase shifts and differential cross sections 80−32275
^{12}C(n,n), spin-flip probability to first 2^+ level 80−78288
^{12}C(n,n)^{12}C, 1.8-4.0 MeV, R-matrix anal. 77−23038
^{12}C(n,n)^{12}C, polarised neutron scatt. 77−26734
$^{12}C(\nu,\nu')$, $(\bar{\nu},\bar{\nu}')$, 15.11 MeV state excitation, cross sections, level decay 80−9258
$^{12}C(\nu,\nu')$, test of struct. of weak neutral currents 77−14117
^{12}C(p, 2p), 400 MeV, quasifree knockout cross sections 79−93614
^{12}C(p, p), 1 GeV, quadrupolar effect, cross sections *(Russian)* 79−30834
^{12}C(p, p), 1.7-1.89 MeV, bremsstrahlung spectra, soft photon and Feshback-Yennie approx. 79−80937
^{12}C(p, p), excitation function at 14.232 MeV, proton beam energy spread determ. 78−70669
^{12}C(p, pn), 400 MeV, quasifree knockout cross sections 79−93614
^{12}C(p, spallation), Li, Be, B prod., 45-100 MeV, nucleosynthesis and space radiation effects implications 77−23053
^{12}C(p, X), 50 MeV, effective cross sections for charged particles in outgoing channel 80−18294
^{12}C(p, X), pol.p, 65 MeV, continuum spectra anal. powers 80−102178
$^{12}C(p,^3He)^{10}B$, angular distrib. exam. at 51.9 MeV 77−30566
$^{12}C(p,^6Li)^7Be$, 36 to 56.8 MeV, differential cross section meas., reaction anal. 79−85467
$^{12}C(p,^6Li)^7Be$, 51.9 MeV, cluster coupling shell model 78−46058
^{12}C(p,X), 50 MeV, effective cross sections 80−78284
^{12}C(p,X), reaction and scatt. dynamics, optical and coupled channel anal. 80−78297
^{12}C(p,X),(d,X),(α,X),(^{12}C,X), 1.55, 2.89 GeV/c, total and inelastic cross sections 79−6610
^{12}C(p,2p), 400 MeV, DWIA check using quasifree (p,pn) comparison 79−93621
^{12}C(p,2p), asymmetric energy-sharing mode, half distorted-wave formalism, intermediate giant resonance 80−68656
$^{12}C(p,2p)^{11}B$, 1 GeV, quasi-elastic multiple scatt. 78−62515
$^{12}C(p,2p)^{11}B$, single nucleon form factor between deformed nuclear states 78−93999
^{12}C(p,3p), quasielastic ejection of proton pairs at 640 MeV *(Russian)* 79−59067
^{12}C(p,α), 45.2 MeV, cross sections, finite range DWBA anal., cluster form factors 80−68666
^{12}C(p,α) for energy calib. of 14UD Pelletron accelerator at ANU 78−17449
$^{12}C(p,\alpha)^9B$, knockout mechanism 78−29474
$^{12}C(p,\alpha)^9B_{gs}$, 45.2 MeV comparison to $^{12}C(p,\alpha^*)^9B_{gs}$ 79−6586
$^{12}C(p,d^3He)$, DWIA anal., α-spectroscopic factors, quasifree process 77−79378
^{12}C(p,d), 4.3 GeV, deuteron knockout search *(Russian)* 79−3158
^{12}C(p,d) at 65 MeV, deuteron break-up effects 77−18535
$^{12}C(p,d)^{11}C$, 185 MeV, one- and two-step processes 77−38282
$^{12}C(p,d)^{11}C$, 700 MeV, transitions confirm multistep processes 78−46110
$^{12}C(p,\gamma)$, 16-40 MeV, ^{13}N giant dipole reson. as doorway-states 77−6336
$^{12}C(p,\gamma)$, direct capture to unbound states 77−61418
$^{12}C(p,\gamma)$, precise determ. of Q-value 78−17200
^{12}C(p,n), 144 MeV, charge exchange, one pion exchange and PCAC tests 80−78299
^{12}C(p,n), 144 MeV, one pion exchange and PCAC expt. test 80−528
^{12}C(p,n), 62, 120 MeV, isobaric analogue states, differential cross sections 80−18202
^{12}C(p,p′), 0.8 GeV, DWBA and coupled-channels anal. 78−74367
^{12}C(p,p′), 0.8 GeV, polarised p, spin orbit deformation effects, DWBA anal. 79−30832
^{12}C(p,p′), 1 GeV, multiple scatt. expansion 78−50156
^{12}C(p,p′), 1 GeV, proton polarisation in natural parity level excitation *(Russian)* 80−42634
^{12}C(p,p′), 122 MeV, level excitation, cross sections, effective NN interaction, DWIA anal. 80−78197
^{12}C(p,p′), 122 MeV, precritical phenomena 80−83089
^{12}C(p,p′), 16-40 MeV, ^{13}N giant dipole reson. as doorway-states 77−6336
^{12}C(p,p′), 185 MeV, elastic and inelastic scatt., proton polarisation and ang. distribs. 79−59060
^{12}C(p,p′), 22-27 MeV, 1^+ state de-excitation γ-ray ang. distrib., tensor force effects, DWBA anal. 80−68580
^{12}C(p,p′), 45, 155 MeV, high lying continuum states, multipolarities, strengths 77−82925
^{12}C(p,p′), 50, 65 MeV, isospin depend. on analysing powers 78−82343
^{12}C(p,p′), 62, 120 MeV, isobaric analogue states, differential cross sections 80−18202

nuclei with mass number 6 to 19 continued
^{12}C(p,p′), 64 MeV, direct reaction, model t-matrix test, cross section and anal. power 79−93594
^{12}C(p,p′), 800 MeV, 15.11 MeV state diff. cross section, nuclear critical opalescence search 80−105984
^{12}C(p,p′), 800 MeV, multistep processes, ang. distribs., Glauber model anal. 80−47475
^{12}C(p,p′), Glauber model, shell model wave functions, EM form factor, spin effects 77−46164
^{12}C(p,p′), pair decay of 7.65 MeV level meas. 78−29469
^{12}C(p,p′), pol. p, 800 MeV, unnatural parity states excitation, anal. powers and isospin 80−68538
^{12}C(p,p′), single proton distrib. anal. 78−603
^{12}C(p,p′), spin flip excitation of 1^+ T=0 state 78−8817
^{12}C(p,p′) proton polarisation and natural parity level excitations *(Russian)* 80−5144
^{12}C(p,p′)^{12}C, PWIA anal. and bound-state momentum distribs. 78−601
^{12}C(p,p′)^{12}C*, pol. p., 19-23 MeV, giant resonances as doorway states, virtual excitation 80−5102
^{12}C(p,p′)X, 316, 516 MeV, analysing powers at backward angles 78−46062
^{12}C(p,p′γ), 23.5-27 MeV, 1^+ state spin flip meas. DWBA anal., cross sections 80−68529
^{12}C(p,p'), 20-40 MeV, pol. p, anal. powers, imaginary spin-orbit pot., coupled channels anal. 80−102179
^{12}C(p,p'), polarised p, 20, 30, 40 MeV, anal. power and cross sections, spin-orbit deformation 79−75963
^{12}C(p,p), 0.3-2.0 MeV, level parameters ^{13}N anal. 77−3007
^{12}C(p,p), 0.8 GeV, analysing powers 78−54760
^{12}C(p,p), 0.8 GeV, ang. distrib. meas. 78−25186
^{12}C(p,p), 0.8 GeV, polarised p, differential cross section, anal. power, nuclear matter densities 79−13299
^{12}C(p,p), 1 GeV elast. and inelast. scatt. and nuclear deform., Glauber theroy 77−6377
^{12}C(p,p), 100-2200 MeV, total and reaction cross sections from optical pot. 80−18303
^{12}C(p,p), 11.5 to 18 MeV polarised beam, ^{13}N level structure 77−315
^{12}C(p,p), 14-45 MeV, differential cross section and spin-flip probabilities, giant resonances 80−73850
^{12}C(p,p), 144 MeV, elastic scatt. cross sections, optical pot. 80−42660
^{12}C(p,p), 3-61.4 MeV, α-cluster contribs., semi-classical model 79−36233
^{12}C(p,p), 3.0 MeV, elastic scattering, discrepancies from optical model, possible α-cluster struct. 78−62528
^{12}C(p,p), 40-75 MeV, polarisation meas., differential cross sections 80−52840
^{12}C(p,p), 50-160 MeV, energy depend. optical pot. 80−22830
^{12}C(p,p), 635 MeV, left-right asymmetry depend. on residual nucleus momentum *(Russian)* 78−54765
^{12}C(p,p), 6.9 GeV/c, elastic and inelastic differential cross sections *(Russian)* 79−59071
^{12}C(p,p), below 8 MeV, iterative R-matrix in collective rot. model, phase shifts, inelasticity 79−3141
^{12}C(p,p), bremsstrahlung near 1.7 MeV resonance 80−68670
^{12}C(p,p), elastic and inelastic scatt., 185 MeV, polarisation, diffraction model anal. 79−75943
^{12}C(p,p), hadron induced semicoherent scatt., excitation of $^{12}C(2^+$, 4.4 MeV) level 78−70569
^{12}C(p,p), optical potential, spin-orbit term 80−52668
^{12}C(p,p), pol. p, 14.23 MeV resonance broadening, nuclear recoil, atomic excitation effects 80−102165
^{12}C(p,p), pol. p, 450-600 keV, Mott-Schwinger interaction existence, anal. power 80−22805
^{12}C(p,p), radial sensitivity of optical pot. 80−86869
^{12}C(p,p), spin rotation angle meas. appl. to phase shifts 77−3011
^{12}C(p,p) dispersive effects in ground state rot. band excitation, coupled channel calcs. 79−40828
^{12}C(p,p) forward scatt., dispersion anal., ^{12}C and ^{13}N ground states 77−34297
^{12}C(p,p) quasielastic scatt., 635 MeV polarised protons, asymm. meas. *(Russian)* 77−74852
^{12}C(p,p) spin 0-spin 1/2 phase shift anal. discrete ambiguities 80−18307
$^{12}C(p,p)^{12}C$, 1 GeV, polarisation meas. 77−88103
$^{12}C(p,p)^{12}C$, elastic and inelastic, 1 GeV, α-particle model in Glauber multiple scatt. theory 77−30577
$^{12}C(p,p)^{12}Cm$ bremsstrahlung near 1.7 MeV resonance 79−45249
^{12}C(p,pα), 100 MeV, absolute spectroscopic factors 77−30574
^{12}C(p,pα), 600 MeV, α-cluster quasielastic knockout, expt. methods, separation energy spectra 79−13275
$^{12}C(p,p\alpha)^8Be$, DWIA calc. 77−34273
^{12}C(p,pd), ^{12}C(p,pt), $^{12}C(p,p^3He)$, 75 MeV, expt. setup, DWIA anal. 77−322
^{12}C(p,pd), (p,pt), (p,pα), spectroscopic data on quasielastic ejection on nucleon clusters from 1p shell nuclei 79−80931
$^{12}C(p,pd)^{10}B$, energy level determ. of ^{10}B at 58 MeV 79−6578
$^{12}C(p,pd)^{10}B$, quasi-elastic cluster knock out, cross section calc. 78−46042
^{12}C(p,pγ), bremsstrahlung cross section near 1.7 MeV resonance, Feshbach-Yennie approx. 80−42662
^{12}C(p,pγ), meas. of bremsstrahlung spectra to determ. reaction time delays of 10^{-20} sec. 77−6378
^{12}C(p,pn), pol. nucleon quasi-elastic scatt., nuclear wave function and model tests 80−42656
$^{12}C(p,pt)^9B$, quasi-elastic cluster knock out, cross section calc. 78−46042
^{12}C(p,px), x=d,t, ^3He, 75 MeV, spectroscopic factors, cluster model, DWIA 77−54214
$^{12}C(p,\pi^-)^{13}O$, 613 MeV, residual nucleus excitation levels, cross section 78−78383
$^{12}C(p,\pi^+)$, 185 MeV, relativistic PWIA 77−10394
$^{12}C(p,\pi^+)$, 200 MeV polarised protons, differential cross sections, analysing power 78−78382
$^{12}C(p,\pi^+)$, optical model orthogonality constraints for bound and continuum waves 79−89306
$^{12}C(p,\pi^+)^{13}C$, 185 MeV, DWBA with Kisslinger type optical pot. 78−4938
$^{12}C(p,\pi^+)^{13}C$, π distortion effect on asymmetry, polarised protons 78−50176
$^{12}C(p,\pi^+)^{13}C$, relativistic stripping model in plane wave impulse approx. 77−325
$^{12}C(p,\pi^+)^{13}C$, relativistic pion stripping formalism 78−41717
$^{12}C(p,t)^{10}C$, angular distrib. exam. at 51.9 MeV 77−30566

nuclei with mass number 6 to 19 continued
$^{12}C(\pi, 2\gamma)$, limit on $2\gamma/1\gamma$ branching ratio 77−10447
$^{12}C(\pi, \pi N)$, 60 and 300 MeV, γ-ray meas. 78−41780
$^{12}C(\pi, \pi)$ elastic and inelastic, nonstatic effects in isobar doorway model 79−80955
$^{12}C(\pi, \pi p)^{11}B$, knockout reaction, cross section ratio $\sigma(\pi^+,\pi^+p)/\sigma(\pi^-,\pi^-p)$ meas. 80−32254
$^{12}C(\pi,X)$, angular distrib. of inelastic diffusion of $\pi^{\pm}$ *(French)* 80−47507
$^{12}C(\pi,X)$, deep inelastic, π and Δ optical pot. effects, semiclassical transport model 80−52698
$^{12}C(\pi,X)$, Kalinkin-Shmonin model, expt. data 80−86931
$^{12}C(\pi,\gamma)$, photon spectrum from generalised Helm model 79−76023
$^{12}C(\pi,\gamma\gamma)X$, two-photon decay branching ratios 77−88179
$^{12}C(\pi,p)^{11}Be$, captive rate probabilities to bound states 77−18614
$^{12}C(\pi,\pi')$, 4.5 GeV/c 2^+ scatt., Glauber theory 77−88175
$^{12}C(\pi,\pi')$, A* excitation, A* model unified description 80−102205
$^{12}C(\pi,\pi')$, collective resonances 78−78415
$^{12}C(\pi,\pi')$, enhancement near (3,3) resonance 79−85535
$^{12}C(\pi,\pi')$, monopole scatt., opt. pot., coupled-channel formalism 78−94034
$^{12}C(\pi,\pi')$, obs. of enhanced ^{12}C excitation by inelastic π scatt. on πN(3,3) reson. 79−17938
$^{12}C(\pi,\pi')^{12}C^*$, giant dipole resonance, Glauber theory 77−6467
$^{12}C(\pi,\pi'\gamma)$, 30-150 MeV, calc. π-γ ang. correls. 77−10452
$^{12}C(\pi,\pi)$, 1.12 GeV, covariant optical model, nucl. struct. calc. 77−14197
$^{12}C(\pi,\pi)$, 24-110 MeV, optical pot., quasideuteron model calcs. 78−74406
$^{12}C(\pi,\pi)$, 260, 280 MeV, elastic and inelastic differential cross sections from Glauber theory *(Chinese)* 79−59092
$^{12}C(\pi,\pi)$, 260 MeV, short range correlations from Glauber multiple diffraction theory *(Chinese)* 80−102210
$^{12}C(\pi,\pi)$, doorway, isobar model 77−10434
$^{12}C(\pi,\pi)$, effects of off-shell two body amplitudes 79−85327
$^{12}C(\pi,\pi)$, elastic and inelastic, recoil effects 79−85555
$^{12}C(\pi,\pi)$, hadron induced semicoherent scatt., excitation of $^{12}C(2^+$, 4.4 MeV) level 78−70569
$^{12}C(\pi,\pi)$, intermediate energies, collective isobaric resonance 80−63208
$^{12}C(\pi,\pi)$, many body effects in resonant scatt. 78−94029
$^{12}C(\pi,\pi)$, model which reduces to eikonal approx. 77−6444
$^{12}C(\pi,\pi)$, nonlinear meson dynamics and binding corrections, optical pots. 80−106080
$^{12}C(\pi,\pi)$, pionic resonance fluorescence in Δ(33) region 79−85554
$^{12}C(\pi,\pi)$, total cross section, density distribs. and ray bending effects 80−47509
$^{12}C(\pi,\pi)$ 28 to 260 MeV, corrections to optical potential, role of ρ^2 term 78−70574
$^{12}C(\pi,\pi)$ cross section calc., comparison of factorisation approx. taking account of nucleon Fermi motion 78−29497
$^{12}C(\pi,\pi)$ elastic scatt., π^+,π^- diffr. minima differences 77−61459
$^{12}C(\pi,\pi)$ inelastic wavefunctions, optical model with Kisslinger pot. 77−18611
$^{12}C(\pi,\pi)^{12}C$, 50 MeV, optical potential with kinematic, absorption and correl. corrections 77−50157
$^{12}C(\pi\,\gamma\gamma)$, branching ratio, ang. correlation 79−85526
$^{12}C(\pi^-, 2\gamma)$, doubly radiative capture theory, branching ratio and ang. correlations 80−9314
$^{12}C(\pi^-, e^+e^-)^{12}B$, 164 MeV, estimation of cross-section *(Russian)* 79−89333
$^{12}C(\pi^-, \gamma)$, pion$^-$ radiative capture probab. *(Russian)* 80−42538
$^{12}C(\pi^-, \gamma)^{12}B^*$, excitation of collective states, shell model 80−22652
$^{12}C(\pi^-, NN)$, bound π absorpt., HF wave functions, branching ratios, ang. distrib. 78−54803
$^{12}C(\pi^-, \pi^{-\prime})$, P_{33} resonance region, elastic cross section, Coulomb nuclear interference 77−23110
$^{12}C(\pi^-, \pi^-)$, 29 MeV, differential cross section, ang. distrib. 79−3182
$^{12}C(\pi^-, X)$, 40 GeV/c, cumulative pions and nucleus total disintegration probability *(Russian)* 80−57807
$^{12}C(\pi^-, X)$, 40 GeV/c, many-nucleon interactions, secondary $\pi^{\pm}$ spectra *(Russian)* 79−97638
$^{12}C(\pi^-, X)$, (X=p, d, t, ^{3}He, ^{4}He, ^{6}Li, ^{7}Li), emitted particle energy spectrum following pion stopping 79−93666
$^{12}C(\pi^-, xn)$, single and correlated n spectroscopy, nuclear temp. 79−6713
$^{12}C(\pi^-,X)$, 40 GeV/c, hadron emission into backward hemisphere *(Russian)* 79−59094
$^{12}C(\pi^-,X)$, 40 GeV/c, $\pi^{\pm}$ rapidity distribs., fast and slow particle components *(Russian)* 79−40969
$^{12}C(\pi^-,X)$, 40 GeV/c, secondary neutron average number, charge exchange coeffs., n inelasticity coeffs. *(Russian)* 80−32132
$^{12}C(\pi^-,2n)$, neutron-pair emission characts., excitation energy spectra 78−13159
$^{12}C(\pi^-,2n)$, stopped pion absorption 78−25243
$^{12}C(\pi^-,\gamma)$, gamma-ray meas. with SIN pairspectrom. 77−10523
$^{12}C(\pi^-,n)$, single neutron emission induced by stopped π^- in 1p shell nuclei 79−59089
$^{12}C(\pi^-,n)$, stopped pion, neutron energy spectra, mean energies and multiplicities 80−9311
$^{12}C(\pi^-,nn)$ or $^{12}C(\pi^-,pn)$, rescatt. effects in stopped pion absorpt. 78−29498
$^{12}C(\pi^-,p)$, limit on pion-condensate strength 77−71625
$^{12}C(\pi^-,p)^{11}Be$, absorption at rest, expts. with pion beams of Saclay Linac *(French)* 79−572
$^{12}C(\pi^-,\pi^-)$, 40 GeV, semi-coherent elastic scatt., angular distrib. 80−68701
$^{12}C(\pi^-,\pi^-)$, 60-90 MeV, backward scatt. cross-sections 77−18630
$^{12}C(\pi^-,\pi^-)^{12}C^*$, 20 to 40 GeV/c, semicoherent elastic scatt. 80−5174
$^{12}C(\pi^-,\pi^-)^{12}C^*$, 4.5 GeV/c, gamma-ray decay obs., nucl. polarisation anal. 77−30636
$^{12}C(\pi^-,\pi^-p)^{11}B$, 170 MeV, comparison with dispersion theory calcs. *(Russian)* 77−50161
$^{12}C(\pi^-,\pi^+)X$, 40 GeV, multiparticle prod. mechanism, various model predictions 79−573
$^{12}C(\pi^-p)$ in Δ(1232) region, differential yield, impulse and shell model anal. *(Russian)* 79−67744
$^{12}C(\pi^+,\pi^+)$, 28.4, 38.6, 48.9 MeV, ang. distribs. meas. 78−41775
$^{12}C(\pi^+,\pi^+p)$, 100, 180 MeV, knock out reaction, cross section and pion distortion in DWIA 80−91167
$^{12}C(\pi^+,X)$, 85-245 MeV, true absorption and scatt. in (3,3) resonance region 80−102207

nuclei with mass number 6 to 19 continued
$^{12}C(\pi^+,2p)$, cluster effects in in-flight π^+ capture 78−89916
$^{12}C(\pi^+,\alpha\pi^+)^8Be$, 112 MeV, pole approx. anal., knock out reaction mechanism *(Russian)* 78−86553
$^{12}C(\pi^+,d)^{10}C$, PWBA differential cross section *(Chinese)* 80−27673
$^{12}C(\pi^+,d)^{10}C$, transitions to low lying states in ^{10}C 78−46110
$^{12}C(\pi^+,p^3He)$, cluster effects in in-flight π^+ capture 78−89916
$^{12}C(\pi^+,p)$, 90 and 180 MeV, ang. distrib. meas. 79−85502
$^{12}C(\pi^+,p)^{11}C$, 49.3 MeV, transitions confirm multistep processes 78−46110
$^{12}C(\pi^+,p)^{11}C$ near (3,3) resonance region, appl. of isobar doorway model 78−41778
$^{12}C(\pi^+,pd)$, cluster effects in in-flight π^+ capture 78−89916
$^{12}C(\pi^+,\pi^{+\prime})$, 100-291 MeV, cross sections and ang. distribs., spin and isospin transfer 80−52697
$^{12}C(\pi^+,\pi^{+\prime})$, 180 MeV, 1^+ T=0,1 collective states anal. 79−85540
$^{12}C(\pi^+,\pi^++p)^{11}B$, 100 MeV, cross-section meas. 78−29510
$^{12}C(\pi^+,\pi^+)$, 0-300 MeV, cross sections, pion-nucleus optical pot. including nuclear Hamiltonian 80−68706
$^{12}C(\pi^+,\pi^+)$, 148 MeV, inelastic scatt., 15.1 MeV (1^+) state, differential cross section 78−89792
$^{12}C(\pi^+,\pi^+)$, 23-35 MeV, elastic backward scatt. 79−17940
$^{12}C(\pi^+,\pi^+)$, 40 MeV, differential cross sections and strength parameters, optical model fit 80−18347
$^{12}C(\pi^+,\pi^+)$, 49.9 MeV, differential cross sections, partial wave and optical model anal. 79−22333
$^{12}C(\pi^+,\pi^+)$, 50 MeV, DWBA, calcs. 77−50156
$^{12}C(\pi^+,\pi^+)$, elast. and inelast. scatt., 50 MeV, ang. distrib. determ. optical model and DWBA 79−45304
$^{12}C(\pi^+,\pi^+)$, phase shift equivalent optical pots., π wave function constraint 79−9629
$^{12}C(\pi^+,\pi^+p)$, 100, 130 MeV, quasi-elastic scatt. cross section 80−102208
$^{12}C(\pi^+d)$, DWBA cross section formula, PWBA differential cross section *(Chinese)* 80−22861
$^{12}C(\pi^\pm,\pi^\pm N)$, 291 MeV, quasielastic scatt., differential cross sections, Monte-Carlo data fit 80−68703
$^{12}C(\pi^\pm,\pi^\pm)$, 162, 226 MeV, elastic cross sections around πN (3,3) resonance region 78−13164
$^{12}C(\pi^\pm,\pi^\pm)$, model Coulomb corrections in eikonal 80−5171
$^{12}C(\pi^\pm,\pi^\pm)$, resonance region, first order optical pot. calcs. 79−40957
$^{12}C(\pi^\pm,\pi^\pm d)$, ^{10}B, 180 MeV, isospin effects in (3/2, 3/2) resonance region 79−85365
$^{12}C(\pi^\pm,X)$, 100-250 MeV, ^{12}C production yield ratio with ^{13}C and ^{16}O 79−85516
$^{12}C(\pi^\pm,X)$, 180, 290 MeV, quasielastic scatt., differential cross section 79−85518
$^{12}C(\pi^\pm,\pi^\pm N)$, 180-255 MeV, quasielastic pion scatt. coincidence expt. interpretation, impulse approx. 80−68704
$^{12}C(\pi^\pm,\pi^{\pm\prime})$, 148 to 226 MeV, ang. distrib. around (3,3) reson. 79−85537
$^{12}C(\pi^\pm,\pi^{\pm\prime})$, 162 MeV, strongly isospin-mixed 79−93505
$^{12}C(\pi^\pm,\pi^{\pm\prime})$ local energy shift effects 79−85511
$^{12}C(\pi^\pm,\pi^\pm)$, 162 MeV, large scale elastic and inelastic scatt. near πN(3,3) resonance 79−40961
$^{12}C(\pi^\pm,\pi^\pm p)^{11}B$, 180 MeV, isospin effects in (3/2, 3/2) resonance region 79−85365
$^{12}C(\pi^\pm,\pi^\pm p)^{11}B$, 180 MeV, π^+ to π^- cross-section ratio 80−73868
$^{12}C(\pi^\pm,\pi^\pm)$, 290 MeV, double charge exchange cross sections 80−18348
$^{12}C(\pi^-,\pi^+)$, 290 MeV, inclusive double charge exchange, differential cross sections 79−93662
$^{12}C(\pi^\pm,\pi N)$, 40-600 MeV, excitation functions and absolute cross sections 80−18226
$^{12}C(\pi^\pm,\pi N)^{12}C$(4.44 and 15.11 MeV), test of outgoing nucleon analogue charge exchange 78−25238
$^{12}C(t,\gamma_0)^{15}N$, 1-3.4 MeV, giant reson. excit., J^π,Γ assignments 77−34277
$^{12}C(t,p)_0$, 18 MeV, ^{14}C energy levels, spins, parities 78−70542
$^{12}C(t,t)^{12}C$, 15, 17 MeV, polarised t, differential cross sections and optical model fits 78−41730
$^{12}C(\tau,d)$, 36 MeV, ^{12}C+p resonance line shapes 79−59076
$^{12}C(\tau,d)^{13}N$, at 81.4 MeV, ang. distribs., analysis of particle unbound states 77−10418
^{13}C, nucl. mag. relax. in 2-chloropyrimidine, CS_2 soln., mol. reorientation 78−27105
^{13}C, $^{17,18}O$, 12.6-14.0 MeV elastic scatt., ang. distribs. 78−37361
^{13}C, 1-20 ps region mean lifetime meas., high-vel. DSA method 77−65200
^{13}C (π^+,π^0), angle integrated cross section, optical pot., n and p radius differences 80−32307
^{13}C cascade hypernucleus, decay into two ordinary hypernuclei, $^{13}C\rightarrow{}^8Be+{}^5He+Q$ by $\Xi^-p\rightarrow\Lambda^0\Lambda^0$ 80−52603
^{13}C, chem. shifts, natural abundance determ. in gas phase and extrapolation from liq. phase meas. 77−88470
^{13}C, chemical shift in N-containing cpds., approx. SCF perturbation theory 77−18945
^{13}C chemical shifts, generalised gauche NMR effect 77−68056
^{13}C, chemical shifts for halomethanes 80−1002
^{13}C coupled with ^1H, spinor character for spin $^1/_2$ nucleus via NMR interferometry 78−17699
^{13}C, decay props. of giant dipole reson. photoreactions anal. in continuum shell model 77−26665
^{13}C, dynamic NMR spectroscopy 77−51971
^{13}C ESR parameters for $Ni(CO)_2^+$ complex in NiCa-Y zeolite 77−63949
^{13}C, giant quadrupole resonance blocking mechanism 80−13437
^{13}C, giant reson. isospin splitting, photonuclear and e-scatt. cross-sections 78−577
^{13}C, high-resolution NMR in liq. and plastic crysts. 79−38388
^{13}C, in methane-d_n, NMR chem. shifts, coupling consts. 78−37657
^{13}C, indirect NMR recording, mag. coherent transfer technique 77−90068
^{13}C, interacting with strongly irradiated proton system, longit. mag. relax., Overhauser enhancement 78−19377
^{13}C, Knight shift and spin-lattice relax. meas. in TTF-TCNQ 77−4571
^{13}C, liq. cryst. NMR spectra, $(CH_3)_3P$, $(CH_3)_3PO$, $(CH_3)_3PS$, $(CH_3)_3PSe$ 77−61768
^{13}C, mass spectromatic calibration of mass and neutron separation energy 78−70434
^{13}C NMR, ^2H label quantitative meas. 77−50456

nuclei with mass number 6 to 19 continued
- ^{13}C NMR, chem. shifts in carbonyl compounds, approximate SCF perturbation theory 77−6804
- ^{13}C NMR, combined ^{2}H NMR T_1 relax. times, methyl group ^{2}H quadrupole coupling const. 78−25563
- ^{13}C NMR, high-resoln. allowing spin coupling and mag. field inhomogeneity 77−20740
- ^{13}C, NMR, modified DEFT pulse sequence use 79−93191
- ^{13}C NMR, RF amplitude effects in proton-spin decoupling 77−28463
- ^{13}C NMR, selective ^{1}H decoupling in long-range ^{13}C-^{1}H coupling 77−46582
- ^{13}C, NMR data, analysis by pattern recognition 77−48059
- ^{13}C, NMR data bank, DARC PLURIDATA system 80−30298
- ^{13}C, NMR in 1,4-disubstituted benzenes, chem. shift 77−14456
- ^{13}C, NMR in β-CO self-diffusion activation parameters, press. depend. 77−69719
- ^{13}C, NMR in CH_4, C_2H_6, C_2H_4, CO and CO_2 gases, mag. shielding 77−75187
- ^{13}C, NMR in camphene plastic cryst. 79−95667
- ^{13}C NMR in copolymers, monomer unit distrib. *(Russian)* 77−46664
- ^{13}C, NMR in phospholipid bilayer 77−48767
- ^{13}C, NMR in poly-4-methyl-1-hexene, conform. 77−10801
- ^{13}C, NMR in polymethinecyanines, 78−13516
- ^{13}C, NMR in solid CO, anisotropy of chem. shift tensor 77−90054
- ^{13}C, NMR in $ThC_{1-x}N_x$ and $UC_{1-x}N_x$ 77−20736
- ^{13}C, NMR in tristearin, liq.-liq. phase transition 78−26681
- ^{13}C NMR obs., radiation-induced degradation of glycine polycryst. 78−15775
- ^{13}C, NMR obs. of adsorbed cyclopropane on Pt 77−51591
- ^{13}C, NMR of 2,2,6,6-tetramethylpiperidine nitroxide radical.alcohol complex, chem. shift 78−46366
- ^{13}C, NMR of peptides and proteins, review 78−24023
- ^{13}C NMR of proteins, review 77−86449
- ^{13}C, NMR relax. in dicarbonyl cpds., internal motion determ. 77−28517
- ^{13}C NMR relax. times, model, gauche-trans isomerising hydrocarbon chain 78−33520
- ^{13}C, NMR selective population transfer, CH fragment, appl. of density matrix formalism 78−15059
- ^{13}C NMR shielding constants and tensors in hydrocarbons, finite perturbation calcs. 77−27092
- ^{13}C NMR shifts in triscyclopentadienyl uranium chloride 77−16190
- ^{13}C, NMR spectra, ^{13}C-X coupling consts., relative signs determ. using ^{13}C satellites 79−94018
- ^{13}C, NMR spectra of isotopically enriched N-methyl formamide in isotropic and nematic phases 77−32270
- ^{13}C, NMR spectroscopy, intensity meas. technique and chem. anal. appl. 77−51981
- ^{13}C, NMR spin-lattice relaxation times in polypropylene 77−4572
- ^{13}C NMR T_1 for 3-chlorodiphenyl soln., internal rot. barrier 78−29860
- ^{13}C NMR with coherent proton decoupling, peak-height distortions within spin multiplets 79−31547
- ^{13}C NMR with off-reson. proton spin decoupling, proton chem. shift calc. methods 78−27101
- ^{13}C, n.m.r. of hen egg-white lysozyme, carboxyl group resonances 77−1978
- ^{13}C nuclear Overhauser enhancement, reduced value rel. to ^{1}H spin-lattice relax. 77−46581
- ^{13}C, photoexcited giant dipole resonace, continuum shell model anal. 80−18266
- ^{13}C, proton-coupled J spectra in pyridine 77−68063
- ^{13}C, proton-coupled J-NMR spectra of pyridine 78−17691
- ^{13}C proton-coupled NMR spin echo two dimensional J spectroscopy, suppression of ghosts 78−15057
- ^{13}C, proton-enhanced NMR of adamantane, magic-angle spinning, polarisation transfer 78−19349
- ^{13}C pulsed NMR, simultaneous T_1 and T_2 meas., Fourier transform. visualization 78−24838
- ^{13}C recoil in polarised Fe, spin precession for $5/2^+$ state, transient field 77−2904
- ^{13}C relax. in nitrobenzene 77−48070
- ^{13}C relaxation; data estimates of C-H rot. barriers, geometry effect, appl. to Δ^5-steroids 78−13626
- ^{13}C, resonances analogue to states ^{13}N level reached in ^{12}C(p,p) 78−13046
- ^{13}C satellites use in proton spectra of oriented mols. 80−18872
- ^{13}C, shielding consts. and anisotropy of NMR shielding tensor, modified CNDO/S calcs. *(French)* 80−32610
- ^{13}C shielding tensors in dimethoxybenzene, diethoxybenzene, powder pattern NMR exam. 78−25556
- ^{13}C, simultaneous multinucl. NMR by alternate scan recording of ^{31}P and ^{13}C spectra 80−26426
- ^{13}C, slow-spinning magic-angle NMR for amorphous solid 77−48068
- ^{13}C spectroscopic factors, cross sections DWBA anal. optical model parameters from ^{12}C(^{16}O,X) 80−13371
- ^{13}C, spin conversion obs. in solid $^{13}CH_3D$ 77−20731
- ^{13}C, spin-echo spectroscopy, improved techniques 77−48086
- ^{13}C spin-lattice relax., alkane chain internal rot. correlation times 78−17688
- ^{13}C, spin-lattice relax. in n-hexyl chain bound to macromol. 77−23510
- ^{13}C, spin-lattice relax. meas. in TGS near ferroelec. transition 77−1646
- ^{13}C spin-lattice relax. using proton decoupled Fourier transform spectra, errors origin 80−18945
- ^{13}C, state transition ang. distrib., optical parameters from ^{12}C(^{7}Li, ^{6}Li) 79−75904
- ^{13}C, T_1 NMR, rot. barriers of hindered methyl groups in polycyclic cpds. 77−10689
- ^{13}C, TOF transmission meas. of neutron resonances 80−37374
- ^{13}C, T=3/2 resonance parameters, ground state γ-decay width from ^{9}Be(α,n) and ^{9}Be(α,α') 79−3123
- ^{13}C, transitions from lowest T=3/2 states 77−88075
- $^{13}C_\Lambda$, in ^{13}C(K^-, π^-) strangeness exchange reaction, ang. distribs. PWIA anal. *(Chinese)* 79−80956
- $^{13}C_\Lambda$ hypernucleus, Friedel sum rule, hadron phys. meaning, nuclear matter density, binding energy 78−82305
- ^{13}C-^{12}C+n spectroscopic factor from ^{12}C(^{13}C,^{13}C)^{12}C at 12 MeV 77−65194
- ^{13}C-^{13}C dipolar satellites in ultraoriented polyethylene 77−28465
- ^{13}C-^{13}N mirror nuclei, 15.1 MeV resonance width, isospin forbidden transitions 79−13265
- ^{13}C-^{15}N spin-spin coupling consts. calcs., lone pair contribs. 77−480
- ^{13}C-^{1}H coupling constant, in cyclohexane 78−13519

nuclei with mass number 6 to 19 continued
- ^{13}C-^{1}H spin-spin coupling consts. for pyridine 78−25562
- ^{13}C-{^{1}H} off-resonance spin decoupling, variable decoupler field strength 77−67485
- ^{13}C-enriched mols., proton relax. and nuclear Overhauser effect from NMR meas. 77−68058
- ^{13}C+^{13}C, appl. of molecular particle core model 78−82384
- ^{13}C+^{16}O, excitation functions for dominant fusion channels 7 to 25 MeV, obs. of regular gross struct. 79−36293
- ^{13}C+^{17,18}O one- and many-nucleon transfer reactions at 12.6 to 14 MeV c.m. energies 78−82371
- ^{13}C+^{60}Ni, one nucleon transfer, nuclear and Coulomb components 77−34340
- ^{13}C+^{6}Li(^{7}Li), 9 MeV, isotopic shape effects in elastic scatt. of aligned ions 78−89904
- ^{13}C+^{94}Mo, one nucleon transfer, nuclear and Coulomb components 77−34340
- ^{13}C+n, 1.5 to 14 MeV total cross-section meas. 77−26742
- ^{13}C(^{12}C,^{12}C), mixed parity neutron orbits, coupled channel theory with adiabatic assumption 80−9304
- ^{13}C(^{12}C,^{12}C), molecular neutron orbit formation, $1/2^+$ state excitation, coupled channels calcs. 80−78156
- ^{13}C(^{12}C,^{12}C) 15, 87 MeV, elastic transfer exchange amplitude, coupled reaction channel and DWBA calcs. 80−32298
- ^{13}C(^{13}C,^{24}Mg), 3.05-6.88 MeV, fusion cross section energy depend., optical anal. 80−42724
- ^{13}C(^{14}N, ^{14}C)^{13}N, sub-Coulomb charge exchange *(Russian)* 78−46106
- ^{13}C(^{15}N,^{14}N)^{14}C, 30 to 45 MeV, ang. distribs., exchange symms. 77−54237
- ^{13}C(^{16}O, ^{17}O)^{12}C, non-orthogonality of channel states 80−83115
- ^{13}C(^{16}O,^{17}O)^{12}C, sub-Coulomb, RMS radii of single-particle orbitals, neutron excess 77−333
- ^{13}C(^{17}O, ^{17}O)^{13}C, 12.9, 14 MeV c.m., compound decay reaction mechanism 77−88167
- ^{13}C(^{18}O,^{19}O)^{12}C, sub-Coulomb, RMS radii of single-particle orbitals, neutron excess 77−333
- ^{13}C(^{3}He,^{3}He), optical potentials and volume integrals, mass and energy dep. 80−52686
- ^{13}C(^{3}He,γ_2)^{16}O, ang. distrib. and correlation meas. of 26.42 MeV resonance 77−61444
- ^{13}C(^{3}He,γ)^{16}O, 25 to 300 MeV, struct. in giant resonance region of ^{16}O 79−63650
- ^{13}C(^{3}He,p), 20 MeV, p ang. distrib., ^{15}N energy levels 78−21581
- ^{13}C(^{6}Li, ^{6}Li), 40 MeV, spectroscopic factors, DWBA anal. 79−75904
- ^{13}C(^{6}Li,α)^{15}N, 32 MeV, ang. distrib. meas., zero-range DWBA calc. 78−13155
- ^{13}C(^{6}Li,d) 26, 29, 34 MeV, ^{17}O α-cluster states, α-decay orbital momenta and parities *(Russian)* 78−86486
- ^{13}C(^{7}Li,p), 16 MeV, ^{19}O high spin states 78−21595
- ^{13}C(^{9}Be,^{9}Be), large angle scatt., optical model and DWBA anal. 79−36259
- ^{13}C(^{9}Be,X), 11.6 MeV, p,t,d,α, ^{8}Be ang. distribs., Hauser-Feshbach and DWBA anals. 80−91193
- ^{13}C(α,α), forward differential cross sections determ. using Feynman diags. 78−25210
- ^{13}C(α,n)^{16}O, 0.60-1.15 MeV, astrophysical appls. 77−13230
- ^{13}C(α,n)^{16}O process, 0.60 to 1.15 MeV, reaction rate 77−45300
- ^{13}C(d, ^{3}He), isospin violating direct reaction, Coulomb interaction role 80−102170
- ^{13}C(d, t), isospin violating direct reaction, Coulomb interaction role 80−102170
- ^{13}C(d,X), 13 MeV, cross section, vector and power, optical model parameters, DWBA anal. 79−22301
- ^{13}C(d,d'), 12.8 MeV, two stage mechanism described by square Feynman diagrams *(Russian)* 79−22299
- ^{13}C(d,γ_0)^{15}N, E_{exc}=17.7 MeV, 95° differential cross section resonance struct. 78−37351
- ^{13}C(γ,$n_{0,1}$)^{12}C, 98° diffr. cross-sections, reson. due to ^{13}C level struct. 78−586
- ^{13}C(γ,n), 6.5-9.3 MeV, ang. distribs., E1, M1 and E2 excitations, resonance radiative widths 80−68581
- ^{13}C(γ,n), 7.6-24 MeV, photoneutron ang. distribs., level scheme and J^π assignments 80−466
- ^{13}C(γ,n), threshold to 25 MeV, photoneutron cross-section 77−14113
- ^{13}C(γ,n) 7.6 to 41.8 MeV, photoneutron cross section meas., giant resonance isospin splitting 79−63657
- ^{13}C(γ,n)^{12}C, 24-26 MeV, photoneutron energy and ang. distribs. 77−30554
- ^{13}C(p, p), 1 GeV, quadrupolar effect, cross sections *(Russian)* 79−30834
- ^{13}C(p,α)$^{10}B_{g.s.}$, 65 MeV, pol. p, DWBA form factor 80−52559
- ^{13}C(p,d), 200, 500 MeV, differental cross section scaling, reaction mechanism 80−42625
- ^{13}C(p,d), 800 MeV, cross sections, DWBA anal. 80−42667
- ^{13}C(p,d) modified DWBA anal., optical model parameter influence on vertex consts. *(Russian)* 78−78340
- ^{13}C(p,γ), Doppler shift attenuation anal., ^{14}N unbound states 78−25184
- ^{13}C(p,γ), pol. p, 6.25-17.0 MeV, anal. power and cross section ang. distribs., E1, E2 amplitudes 80−47461
- ^{13}C(p,p), 9.1-18.4 MeV, polarised p, cross section phase-shift anal., ^{14}N possible resonances 79−6602
- ^{13}C(p,π^-), 185 MeV, differential cross section, two-nucleon model *(Chinese)* 79−59069
- ^{13}C(π, πN), 60 and 300 MeV, γ-ray meas. 78−41780
- ^{13}C(π,np)^{11}Be, capture rate probabilities to bound states 77−18614
- ^{13}C(π,π'), 162 MeV, pure n and p transitions, differential cross sections 80−5040
- ^{13}C(π,π), elastic and inelastic near πN(3.3) reson. 80−73870
- ^{13}C(π^+, π^{+or0}), 120-226 MeV, inelastic scatt, and charge exchange, coupled channels calcs. 80−57804
- ^{13}C(π^+,p), 90 and 180 MeV, ang. distrib. meas. 79−85502
- ^{13}C(π^+,π^0), 0-300 MeV, cross sections, pion-nucleus optical pot. including nuclear Hamiltonian 80−68706
- ^{13}C(π^+,π^0), 1st order pion-nucleus pot. calc. 77−23113
- ^{13}C(π^+,π^0), total cross section energy depend., first order optical pots. 79−76028
- ^{13}C(π^+,π^0)^{13}N, 70-230 MeV, calc. of cross section, using multistep contributions within modified eikonal formalism 78−21609
- ^{13}C(π^+,π^0)^{13}N, charge-exchange transition vertex, optical pot. 77−6461
- ^{13}C(π^+,π^0)^{13}N, DWIA, isovector correls. 78−29499

nuclei with mass number 6 to 19 continued
$^{13}C(\pi^+,\pi^0)^{13}N$, eikonal model cross-section calc. near (3,3) reson. 77−18609
$^{13}C(\pi^+,\pi^0)^{13}N$, Pauli and short range correlations 77−3049
$^{13}C(\pi^+,\pi^0)^{13}N$, Pauli and short range correls. near (3,3) reson. 77−18608
$^{13}C(\pi^+,\pi^0)^{13}N$, two-body correlation effects 77−88178
$^{13}C(\pi^+,\pi^0)^{13}N$ in (3,3) reson. region, optical model calc. 77−18610
$^{13}C(\pi^+,\pi^0)$ $^{13}N_{g.s.}$, (3,3) resonance region, importance of two-step processes in multiple scatt. treatment 77−6464
$^{13}C(\pi^+,\pi^0)^{13}N$, comparison with isobar doorway calcs. 77−41999
$^{13}C(\pi^+,X)$, 100-250 MeV, ^{12}C production yield ratio with ^{12}C 79−85516
$^{14}C(\pi^+,\pi^-)$, near πN (3,3) resonance, 180 MeV, collective states and cross sections 80−13507
^{14}C, $(sd)^2$ positive-parity states, shell model calcs. 78−54674
^{14}C activity and distrib. in gaseous effluents from PWRs 79−85829
^{14}C beam prod. from isotopically enriched sputter targets 80−23221
^{14}C, beam production for Munich tandem 78−90008
^{14}C, beta ray spectrum rel. to vessels for liq. scintillation spectrometers 77−26920
^{14}C β-decay surface contamination monitoring probes, comparison of response between detectors 78−25398
^{14}C, determ. of low radiocarbon activity by CO_2 absorpt. 78−74550
^{14}C determination in whole-body sections by liq. scintillation counting *(German)* 77−5114
^{14}C energy levels from $^{12}C(t,p)$, spins, parities 78−70542
^{14}C, energy states from $^{12}C(t,p)$ 23 MeV 78−78392
^{14}C fallout from nucl. weapons testing, human radiation burden 77−64091
^{14}C fallout from nucl. weapons testing, use as biological tracer 77−64162
^{14}C first excited 0^+ state, lifetime and E^0 decay from (d,p), $(^{13}C,p)$ 80−102145
^{14}C ground state excitation in $^{14}N(\gamma,\pi^-)$ at threshold 77−14109
^{14}C, high accuracy meas. by gas proportional and liq., scintillation counting 78−74544
^{14}C in groundwater, possible subsurface prod. rel. to dating 80−85690
^{14}C in wines, abundance vars. with 11-year solar cycle, (1909 to 1952) 80−109249
^{14}C liquid scintillation counting using thick-walled vials 78−857
^{14}C, liquid scintillation counting efficiency, volume and quenching effects 79−76270
^{14}C, natural beta-decay rel. to origin of biological chirality 77−86445
^{14}C, photodisintegration induced by 40 MeV γ-rays, correl. spectroscopy 77−6345
^{14}C, populated by $^{12}C(t,p)^{14}C$, spin and parity of states near 10 MeV excitation in ^{14}C 78−37263
^{14}C production by nuclear power industry 77−54367
^{14}C production in reactors and explosions, population dose, health impact 77−14274
^{14}C proton shell closure, p transition spectroscopic factors, DWBA calcs. for $(^3He,d)$, $(t,^3He)$ 79−80871
^{14}C spectroscopic factors, cross sections DWBA anal. optical model parameters from $^{12}C(^{16}O,X)$ 80−13371
^{14}C state excitation energies and widths, DWBA ang. distribs. from $^{12}C(t,p)$ 23 MeV 78−70544
$^{14}C_{g.s.}$ β-decay, mesonic exchange currents, weak process microscopic treatment 80−57742
$^{14}C+^{16}O$ scatt., molecular resonances, generator coordinate study 79−36216
$^{14}C(^{12}C,X)$, 40-57 MeV, strong resonant behaviour in inelastic and transfer channels, γ-yields 80−52644
$^{14}C(^{12}C,\alpha)^{22}Ne$, 6.1 to 9.7 MeV, excitation functions, statistical fluctuations 77−23103
$^{14}C(^{16}O,^{16}O)^{14}C$, resonance struct. at excitation energies 40-51 MeV in ^{30}Si, comparison with $^{12}C+^{18}O$ 79−13335
$^{14}C(^{16}O,^{17}O)^{13}C$, exchange effects on ang. distribs. 78−627
$^{14}C(^{16}O,^{18}O)^{12}C$, full recoil one and two step DWBA anal. 78−70564
$^{14}C(^{16}O,^{18}O)^{12}C$, resonance struct. at excitation energies 40-51 MeV in ^{30}Si, comparison with $^{12}C+^{18}O$ 79−13335
$^{14}C(^6Li,^6He)$, 62 MeV, Gamow-Teller sum rules and ground state wave function 80−106073
$^{14}C(^6Li,^6He)^{14}N$ and Gamow-Teller strength distrib. 77−6430
$^{14}C(^7Li,t)^{18}O$, 20.4 MeV, FRDWBA anal. 78−82381
$^{14}C(\alpha,\gamma)^{18}O$ and onset of core He flash in low-mass stars 80−51735
$^{14}C(e,e')$, 37, 50.5, 60.5 MeV, 180° scatt. cross sections, excited states, spin parity 77−30557
$^{14}C(p,\gamma_0)$, polarised p in giant dipole resonance region, cross sections and analysing power 78−82346
$^{14}C(p,n)^{14}N$, n polarisation ang. distrib., R-matrix anal., ^{15}N excited states 78−4937
$^{14}C(\pi\gamma)$, collective resonances, A=14 isobaric states, shell model predictions 79−85386
$^{14}C(t,p)^{16}C$, 3.02-6.1 MeV, spectroscopy of ^{16}C 78−613
$^{14}C(t,p\gamma)$, 12 MeV, ang. correls., ^{16}C levels, spin assignments 78−8830
$^{14}C\rightarrow^{14}N\ e^-\bar{\nu}_e$, rate calcs. using elementary particle and macroscopic treatments 78−29429
^{15}C 0.74 MeV $5/2^+$ state g-factor, shell model interpretation from $^3H(^{13}C,p)$ 80−32176
^{15}C beta decay transition rates and half life, ^{15}N excited states and transitions 80−18248
^{16}C, $(sd)^2$ positive-parity states, shell model calcs. 78−54674
^{16}C levels populated in $^{14}C(t,p\gamma)$, spin assignments 78−8830
^{16}C mass excess and final states, DWBA anal. of $^{14}C(t,p)$ 23 MeV 78−78392
^{16}C, spectroscopy with $^{14}C(t,p)^{16}C$ at 3.02-6.1 MeV 78−613
$^{16}C+^9Be$, parabolic repulsion potential, optical model 80−22782
^{17}C populated in $^{48}Ca(^{18}O,\ ^{17}C)$, mass excess, low lying level struct. 78−8744
^{18}C mass excess and discrete nuclear states from $^{18}O(\pi^-,\pi^+)$ 79−13196
^{22}C, electroexcitation of collective M1 resonances, RPA calcs. 77−46104
$^{23}C(d,\gamma)^{15}N$, 2.90-9.95 MeV, cross sections, ang. distrib. meas. 77−6395
^{40}Ca, charge form factors of doubly closed shell nuclei 77−6274
^{40}Ca, giant isoscalar monopole state energies in generator coordinate method 80−37317
$C(\alpha,^4He)$, A=12, 13, 55, 65 MeV, two neutron states, A-depend. of binding energy 78−74379
$C(\alpha,X)$, 16.5 GeV/c, inelastic cross sections, multiplicity, ang. and momentum distribs. 78−82359
$C(\alpha,2\alpha)$, 700 MeV, cross section, effective cluster number from PWIA, momentum distrib. 79−40940

nuclei with mass number 6 to 19 continued
$C(\alpha,\alpha')C$, A=12,13, 65 MeV, monopole excitation of ^4He, DWBA calc. 77−10419
$C(\alpha,\chi\alpha)$, 18 GeV, π multiplicity distrib. 79−97713
$C(\alpha,d)N$ for $^{12,13}C$ isotopes, 50 MeV, deuteron energy spectra *(Russian)* 77−6209
$C(\alpha,n)$, 3.6 to 8 MeV, neutron yields 79−6651
C(d,d), 4.3, 6.3, 8.9 GeV/c, secondary momentum spectra, multiple scatt. model anal. *(Russian)* 80−27650
C(d,p), 6.3 GeV, proton momentum spectra 79−6621
C(d,p), 6.3 GeV/c, p momentum spectra from d breakup 78−89887
$C(\gamma,\gamma)$, neutron capture γ-ray Rayleigh scatt. 80−52661
$C(\gamma,\omega)$, cross section meas., comparison with theory 78−58261
$_\Lambda{}^{12}C$ hypernucleus detection in p+emulsion nucleus, 250 GeV, Λ binding energy *(Russian)* 78−89816
$_\Lambda{}^{12}C$ low lying excited states, ang. distribs. from $^{12}C(K^-,\pi^-)$ 80−32226
C(n,n), 7-15 MeV elast. and inelast. scatt. 77−34314
C(n,n) cross section standard, status 77−23040
C(n,n), differential elast. and inelast. scatt. from 9-15 MeV, cross-section meas. 77−2984
C(n,n), total cross sections below 2 MeV, R-matrix fits to data 80−13466
C(p,X) *(Russian)* 80−52649
C(p,X), 400 GeV, p, d, t, π, ^3He, α backward prod., inclusive cross sections 79−85475
C(p,X), 400 GeV, p backward prod. invariant cross section 79−93623
C(p,X), 400 GeV/c, light ion backward prod., invariant cross section 80−32279
C(p,X), 400 GeV/c, multiplicity and ang. distribs. of relativistic and slow particles *(Russian)* 79−40931
C(p,X), 70 GeV/c, $\pi^\pm$, $K^\pm$, p, $\bar{p}$ prod. with p_T=0.5-2.5 GeV/c cross sections, yield ratios *(Russian)* 80−52681
C(p,X), 740 MeV, ^7Be prod. cross section for cosmic ray anal. 79−93625
C(p,X) X=He to C, 2.1 and 4.9 GeV, fragment energy spectra, Maxwellian functional form 78−70529
C(p,3p), 640 MeV, proton pair quasifree knock-out 80−22795
C(p,p), 36.2 MeV, differential cross section, asymmetries, 0 to 7° scatt. 78−94002
C(p,p), summed scattering (elastic and inelastic with no meson production), 2.1 GeV/c, asymmetry meas. *(Russian)* 79−89313
C(p,p), total cross sections, 180 to 560 MeV, Galuber model calcs. 79−40917
C(p,p'), 0.6-25 GeV, backward emitted proton inclusive spectra, short range correlation 80−32281
$C(p,\pi^+)$ 240 MeV inclusive pion production *(Russian)* 80−86908
$C(p,\pi^+)$, 400-500 MeV, cross-sections meas. 77−10392
C(p,xpX), x=1, 2, 640 MeV, energetic backward p emission, inclusive differential cross section 80−9290
$C(\pi^-,\Lambda^0)$ 2.9 GeV, production cross section of cumulative Λ^0 hyperons *(Russian)* 78−78419
$C(\pi,X)$, 125 MeV, absorption cross section in 3:3 resonance region 79−85543
$C(\pi^-,X)$, 3 GeV/c, n inclusive spectra, neutron yield *(Russian)* 80−13510
$C(\pi^-,X)$, charged heavy particle emission after pion capture *(Russian)* 80−69271
$C(\pi^+,2p)$, 112 MeV, reaction mechanism *(Russian)* 78−29508
$C(\pi,\alpha X)$, 70 MeV, α cross sections and energy spectra, intranuclear cascade calcs. 79−575
$C(\pi^-,n)$ spectrum obs. and calc. 79−17933
$C(\pi^-,\pi^\pm X)$, X=He or d, 170 MeV, cross sections and ang. distribs., direct knockout mechanism *(Russian)* 80−86887
$C(\pi^+,\pi^+d(He))$, 60 MeV, cross sections, momentum and ang. distribs. *(Russian)* 77−74888
$C(\pi,\pi p)$, 170 MeV, two stage and knock out contribs., π^+,π^- spallation differences *(Russian)* 80−68632
$C(\pi^+,\pi^0p)$ 2.0 GeV, determ. of π^0N interaction cross-section *(Russian)* 77−14199
$C(\pi^+,\pi^0p)$, 2.9 GeV charge exchange *(Russian)* 77−339
$C(\pi^+,\pi^-p)C$, 170 MeV, direct-knock-out dominant mechanism *(Russian)* 77−61460
$^{12}Cr+^{14}N\rightarrow^{26}Al$, fusion cross section comparison to $^{10}B+^{16}O\rightarrow^{26}Al$ 79−71873
C(x,x), x=$\pi^\pm$, $K^\pm$, p,$\bar{p}$, 70, 175 GeV/c 80−83128
F+n, differential cross sections for prod. of low energy photons 77−23068
F+Ne, 800 MeV/A, wide angle inclusive proton spectra 79−40951
$F(^{20}Ne,\pi^+X)$, 400 MeV/N, pion prod. doubly differential cross sections and ang. distrib. 80−32299
^9F+n, 16-22 MeV, cross sections for prompt γ, compound statistical model calcs. 79−543
^AF, A=18, 19, deduced levels and spectroscopic factors from $^{14,15}N(^{11}B,^7Li)$ 79−26454
^AF, A=18, 19, E2 transition rates calc., shell model with effective interaction and charges 80−47423
^{15}F mass excess and T=3/2 levels from $^{20}Ne(^3He,^8Li)$ 78−78264
^{15}F mass excess from $^{20}Ne(^3He,^8Li)$, 88 and 75 MeV 78−78245
^{16}F levels populated in $^{19}F(^3He,^6He)$ and $^{16}O(^3He,t)$ 78−17231
^{17}F 14.174 MeV T=3/2 level, spin assignment from $^{16}O(p,p')$, polarised p 79−67648
^{17}F, axial vector decay, exchange corrections 79−36201
^{17}F, effective charges and radial integrals calc. 78−4897
^{17}F, mag. moments, configuration mixing and meson exchange contrib. 78−17100
^{17}F, muonic, energy shifts during atomic EM cascade, and polarisability of deformed nuclei 80−86893
^{17}F, populated in $^{16}O(d,n)$, half life meas. 77−88085
^{17}F-^{17}O mirror nuclei, configuration mixing, Coulomb energy anomaly 78−25099
^{18}F 1.04 MeV state lifetime and γ-transition polarisation from $^{18}O(p,n)$ 80−106016
^{18}F, 1.08 MeV γ transition, circular polarisation affected by neutral weak currents 78−41663
^{18}F, 1.08 MeV γ transition, circular polarisation affected by neutral weak currents 79−13243
^{18}F, 4p-2H, 1^+ rot. band anal. from $^{14}N(^7Li,t)^{18}F$ 77−79299
^{18}F, 5603 keV level, isospin mixing via (α,γ) and (p,γ) reactions 78−543
^{18}F (e,e'), polarised e, parity mixing and form factors from elementary particle theory anal. 79−89233
^{18}F alpha particle cluster states, rot. bands in $^{14}N+\alpha$ model 78−8757

nuclei with mass number 6 to 19 continued
- ^{18}F compound nucleus in ^{16}O+d reactions, level characts. from vector analysing power 77−61434
- ^{18}F compound nucleus rot. band structure, ^{16}O(d,d) study with resonating group method 77−10415
- ^{18}F, effective interaction, nonlocal pot. reaction matrix free scatt., spectra 77−46122
- ^{18}F integrated cross sections to excited residual states from ^{19}F(γ,n) 80−18200
- ^{18}F ions recoiling in vacuum, mag. decoupling of hyperfine interaction 78−37270
- ^{18}F isospin mixed states seen via ^{14}N(α,α$_1$)^{14}N, 7.6 to 16.9 MeV 77−14029
- ^{18}F $J^\pi=3^-$ doublet at 6241 keV, isospin mixing from (p,γ), (p,α), (α,γ) (^{14}N,α) 80−511
- ^{18}F, $J^\pi=5^+$ excited state, populated in ^{16}O(α,d)^{18}F 78−58291
- ^{18}F labelled anhydrous fluorinating reagent preparation using cyclotron accelerated p, d, ^{3}He, or α 79−2131
- ^{18}F labelled pharmaceuticals, cyclotron prod. for nuclear medicine appls. 77−44753
- ^{18}F level spin, isospin and parity assignments, from ^{20}Ne(d,α) tensor analysing power meas. 78−74305
- ^{18}F levels and resonances, J^π assignments from ^{17}O(p,α), ^{17}O,(p,p$_1$γ), ^{17}O(p,γ) 79−9480
- ^{18}F levels and resonances, cross sections in R-matrix formalism from ^{17}O(p,α) 80−18267
- ^{18}F, levels from ^{16}O(^{3}He,p) at 18 MeV 77−34325
- ^{18}F, negative parity states, dynamic interaction propagator approach 79−13191
- ^{18}F, prep. with an electron linear accelerator, medical and biological appls. 80−98136
- ^{18}F production and yield from ^{16}O(^{3}He,p)^{18}F reaction in water 78−28065
- ^{18}F recoil labelling of chlorofluoromethanes and tetrafluoromethane 79−52732
- ^{18}F resonances, α-widths, isospin and parity mixing, R-matrix anal. of ^{14}N(α,α) 80−91162
- ^{18}F, semi-microscopic calc. of α-cluster states, shell model approx. 80−465
- ^{18}F, shell and cluster admixtures, T=0 positive parity levels, E2 rates 77−18396
- ^{18}F, spin-parity assignment from ^{17}O(p,p)^{17}O, at 1.4-3.0 MeV 78−29391
- ^{18}F, study of excited states, spin and parity *(French)* 78−33158
- ^{18}F, trinucleon cluster states, low lying negative parity states 78−29387
- ^{18}F-F$_3$COF-^{18}F radiopharmaceutical synthesis procedure 79−29619
- ^{19}F, 3907 keV state, lifetime meas. by Doppler shift attenuation method 77−88079
- ^{19}F, 5/2$_1^-$ state, precession on recoil in Fe and Ni 78−37285
- ^{19}F 5.10 MeV level parity from ^{17}O(^{3}He,p) 79−45155
- ^{19}F (n,n), thermal neutron scatt. parameters 79−93628
- ^{19}F, alpha-particle and triton cluster states anal. 77−41907
- ^{19}F, and ^{7}Li double NMR in LiF, existence of single nuclear dipolar spin temp. 78−35065
- ^{19}F, chem. shift in solids, multiple pulse zero crossing NMR technique 78−37041
- ^{19}F chemical shifts, generalised gauche NMR effect 77−68056
- ^{19}F, coupled channel orthogonality condition model 80−47384
- ^{19}F, decoupled bands and antialigned states 78−78236
- ^{19}F deduced resonances from ^{18}O(p,α)^{15}N reaction at stellar energies 79−26439
- ^{19}F, double-resonance FT experiments using NMR probe double tuned matching boxes 77−45874
- ^{19}F ENDOR, obs. of F distortion in KCdF$_3$:Mn^{2+} 78−23369
- ^{19}F, electroexcitation of ground state rotational band 78−66191
- ^{19}F, energy levels from α-^{15}N and t-^{16}O coupled channel orthogonality condition model 80−37326
- ^{19}F, even parity excited states, collective props., EM moments, generator coordinate method 78−78259
- ^{19}F, even parity state, EM props., collective struct., generator coord. method, HF method anal. 79−89220
- ^{19}F even-parity states, generator coord. method, projected Hartree-Fock, and complete diagonalisation calcs. comparison 78−89796
- ^{19}F final state selective population, triton clustering from band anal. from (^{7}Li,t), (^{6}Li,^{3}He) 80−9306
- ^{19}F, high-spin negative parity states, via ^{15}N(α,γ)^{19}F 77−61346
- ^{19}F, hyperfine interactions of fast ions recoiling in noble gases 77−18469
- ^{19}F, in K$_2$Mn$_{1-x}$Ni$_x$F$_4$, NMR exam. of magnetizations 78−10800
- ^{19}F, in KEL-F, spectrum using multiple pulse decoupling-magic angle spinning NMR probe 78−12735
- ^{19}F isomer shift in MnO, time differential PAD 77−12280
- ^{19}F isospin mixing in yrast $I=5/2^+$ level 79−93508
- ^{19}F level scheme, anal. using parity mixing 77−18387
- ^{19}F level struct., ang. distribs. anal. using DWBA of ^{17}O(^{3}He,p) 80−9232
- ^{19}F, level struct. J^π, spectroscopic factors via (^{13}C, ^{9}Be) reaction 77−14033
- ^{19}F level structure populated in ^{16}O(α,p), spin, parity *(Spanish)* 77−67756
- ^{19}F levels, resonances and phase shifts, resonating group calcs. from ^{15}N(α,α) 80−32189
- ^{19}F, levels, spectroscopic factors via ^{16}O(α,p)^{19}F 77−14140
- ^{19}F line standard, for NMR freq. sweep calibration 78−24836
- ^{19}F low lying band state lifetimes, stopping power, transition strengths from ^{15}N(α,γ) 80−42585
- ^{19}F low lying positive parity states from rot. model, moments and deformation 79−6410
- ^{19}F, low-lying excited states calc. by generator coordinate method 78−12974
- ^{19}F, mag. moments, configuration mixing and meson exchange contrib. 78−17100
- ^{19}F, NMR, Co^{2+} spin-lattice relax. narrowing in KCoF$_3$ 77−85611
- ^{19}F NMR, single cryst. ErF$_3$ determ. of ligand hyperfine field interactions 77−48067
- ^{19}F NMR chem. shifts in polar solvents, intermol. interactions 77−51975
- ^{19}F NMR imaging for biomedical application 78−20240
- ^{19}F, NMR in cholesteric liq. cryst. cholesteryl-m-fluorobenzoate 77−8429
- ^{19}F, NMR in Fe(CO)$_3$(PF$_3$)$_2$, axial and equatorial ligand interchange 77−73091
- ^{19}F NMR in LiF, thermodynamic effects of RF pulse pair on system with two spin species 77−66433

nuclei with mass number 6 to 19 continued
- ^{19}F, NMR in lithium perfluoro-octanoate-water system, liq. cryst. struct., self-diffusion 78−15036
- ^{19}F, NMR in MHF$_2$ (M=alkali metal), TlHF$_2$, SrFHF$_2$, BaFHF$_2$ 78−2753
- ^{19}F, NMR in NH$_4$HF$_2$ and (substituted) phenylamine salts 78−2754
- ^{19}F, NMR in UF$_6$, isotope enrichment 78−23364
- ^{19}F, NMR meas. in LiTmF$_4$, local mag. field at ^{19}F rel. to paramag. susceptibility *(Russian)* 77−81023
- ^{19}F NMR solvent shifts, charge transfer contribs. 77−50454
- ^{19}F, NMR spectra, fluorobenzenes, partially oriented in lyotropic liq. cryst., NMR spectra 77−68059
- ^{19}F, n.m.r. meas. in K$_2$CuF$_4$ and KCuF$_3$, hyperfine interactions of ^{19}F nuclei 77−12209
- ^{19}F neutron induced reactions, Hauser-Feshback code for cross sections 77−23045
- ^{19}F neutron scattering resonance radiative widths 80−99146
- ^{19}F, nucl. spin cooling of Tm^{2+} electron spins, in CaF$_2$:Tm^{2+} *(French)* 77−66440
- ^{19}F, nucl. spin-lattice relax. and anomalous thermal expansion meas. in KHF$_2$ 77−8441
- ^{19}F, nuclear charge radius from μ^- X-ray transitions 78−66195
- ^{19}F, nuclear dealignment of multiply ionised 3 and 6 MeV atoms recoiling in gases 80−78267
- ^{19}F, nuclear spin-lattice relax., in RbMnF$_3$, 0.1-3K 77−20743
- ^{19}F, paramag. shifts at O in CoO in NiO 78−43719
- ^{19}F parity mixing, approx. short-range correls. in wave function, appl. 77−285
- ^{19}F, parity mixing and weak parity nonconserving NN interaction 77−6223
- ^{19}F positive parity alpha clusters, Woods-Saxon well calcs. 79−26383
- ^{19}F, produced in ^{15}N(α,γ)^{19}F, 5.2 to 8.4 MeV, resonances and gamma decay schemes 78−37358
- ^{19}F, recoil-implnted, electric field gradients, via ^{9}Be(^{12}C, np)^{19}F 77−8471
- ^{19}F, reson. levels from ^{15}N(α,γ)^{19}F, 2.8 to 4.0 MeV 77−65211
- ^{19}F resonance parameters and J^π values from ^{18}O(pp) polarised p 79−45232
- ^{19}F, resonant and bound levels, ^{18}O(p,γ) and ^{18}O(p,pγ) reactions 78−89790
- ^{19}F shielding anisotropies of fluoromethanes, NMR obs. of smectic meso-phase solns. 77−34662
- ^{19}F, spectra and E1 transitions, ang. momentum projected HF and Tamm-Dancoff methods 77−54139
- ^{19}F spin-lattice relax., obs. of diffusion in LaF$_3$ 78−6180
- ^{19}F, spin-lattice relax. meas. in triglycine fluoroberyllate near ferroelec. transition 77−1646
- ^{19}F $T=^3/_2$ states resonance energy, γ-decay and J^π, capture strength from ^{16}O(p,γ) 79−67728
- ^{19}F, transition probabilities and multipole moments between states calc. by generator coordinate method 78−13022
- ^{19}F+^{12}C, 50, 63, 76 MeV, evaporation residue mass distrib. in fusion reactions anal. 77−42004
- ^{19}F+^{12}C, 92 MeV, fusion and direct reactions anal. 78−21591
- ^{19}F+^{12}C, fusion reactions, Woods Saxon, folding and proximity pot. anals. 79−45316
- ^{19}F+^{27}Al, 40, 63, 76, 92 MeV, evaporation residue mass distrib. in fusion reactions anal. 77−42004
- ^{19}F+^{28}Si spin orbit pot., single folding model and cluster model 80−9196
- ^{19}F(^{16}O,^{16}O)^{19}F, 32.0 MeV, parity-depend. optical model calc. 77−50152
- ^{19}F(^{3}He,^{6}He), 70 MeV, ^{16}F energy levels 78−17231
- ^{19}F(^{3}He,d)^{20}Ne(4$_1^+$), 0g orbit mixing and one-step forbidden transition 78−493
- ^{19}F(^{6}Li,p), 3-15 MeV, cross sections meas. 79−76017
- ^{19}F(^{6}Li,p)^{24}Na cross-section meas. 79−9611
- ^{19}F(α,αp), 140 MeV, quasifree p knockout, spectroscopic factors, DWIA anal. 79−67650
- ^{19}F(α,n)^{22}Na, 2.6-5.1 MeV, cross sections, excitation function 78−54777
- ^{19}F(α,n)^{22}Na, isoscalar M2 transition in ^{22}Na obs. 77−10363
- ^{19}F(α,p)^{22}Ne, E=5.31 MeV, 3.34 MeV lifetime meas. 77−38245
- ^{19}F(α,t), 25 MeV, DWBA anal. of triton ang. distrib. meas. 78−54776
- ^{19}F(d,X), X=^{7}Li, ^{7}Be, 13.6 MeV, diff. cross sections, ^{5}He cluster direct transfer *(Russian)* 80−52650
- ^{19}F(d,α)^{17}O, 1.8 to 3.0 MeV, vector analysing ability using polarised deuterons *(Russian)* 80−32288
- ^{19}F(d,d), elastic scatt., 1.2-2.5 MeV, exeitation functions, ang. depend., optical model anal. 79−9594
- ^{19}F(d,d), energy depend. of vector analyzing capacity, 1.8 to 3.0 MeV, 120 to 150° scatt. 79−9592
- ^{19}F(d,d)^{19}F, 1.8 to 3.0 MeV, vector analysing ability using polarised deuterons *(Russian)* 80−32288
- ^{19}F(n, α)^{16}, average cross sections in ^{235}U fission neutron spectrum 80−22828
- ^{19}F(n, p)^{19}O, average cross sections in ^{235}U fission neutron spectrum 80−22828
- ^{19}F(n̄,X), annihilation, 1.4 GeV/c, $\pi^\pm$, p emission angles, momentum and multiplicity distribs. 80−532
- ^{19}F(n,2n), 14.7-19.0 MeV, excitation functions relative to ^{56}Fe(n,p) 79−3142
- ^{19}F(n,α)^{16}N, 13.9, 15.6 MeV, differential cross-sections meas., statistical model calc. 77−41972
- ^{19}F(n,γ)^{20}F, neutron activation meas. of bone F content 77−86592
- ^{19}F(p, α)^{16}O, 12.4 to 18.0 MeV, exit channel effects 77−14124
- ^{19}F(p,α)^{16}O, 1.5 to 2 MeV, [211] quartet state in ^{20}Ne 78−46006
- ^{19}F(p,αγ), determ. of F conc. profiles in Mg alloy scales 78−88678
- ^{19}F(p,αγ)^{16}O, F conc. profiles determ. in corroded MAGNOX fuel canning materials 79−92035
- ^{19}F(p,αγ)^{16}0, reson. reaction, teaching expt. using Van de Graaff generator 77−74178
- ^{19}F(p,γ)^{20}Ne, 668 keV, γ-ray transitions to ground state, rel. to stellar nucleosynthesis 78−17191
- ^{19}F(p,γ)^{20}Ne, calculated cross sections to ground and first excited state 77−54139
- ^{19}F(p,γ)^{20}Ne, giant multipole reson., microscopic theory 77−22987
- ^{19}F(p,p′), 5.5 MeV; time differential obs. of perturbed γ linear polarisation distrib., Hanle effect 78−78360
- ^{19}F(p,p′γ), 1459→110 keV transition, E2/M1 mixing ratio 80−106013
- ^{19}F(p,p′γ)^{19}F, 5 to 9 MeV, levels, J^π, lifetimes, branching 77−297
- ^{19}F(p,p), 17.5 and 30 MeV, low lying level cross-sections, coupled-channel method 80−42649

nuclei with mass number 6 to 19 continued
^{19}F(π^-,π^- n) and (π^-,π^- p+π^0n) knockout reactions, cross sections, nucleon charge exchange model 78−25246
^{19}F(π^-,Xγ), 230 MeV reactions near Δ(1232) resonance 77−6465
^{19}F(t,p)^{21}F, 0.9 and 1.1 MeV, proton ang. distribs., possible compound nucl. form. 78−17218
^{19}F cross sections and anal. power, compound nucleus contrib. Ericson fluctuations from ^{18}O(d,p), pol. d 80−22803
^{20}F energy levels populated in ^{14}N(^{7}Li,p), spin, parity 78−21596
^{19}F, NMR in Fe(CO)$_2$(PF$_3$)$_3$, axial and equatorial ligand interchange 77−73091
^{19}Fe(p,α_0)^{16}O, 1.5 to 3.8 MeV, Hauser-Feshbach anal., level density of ^{20}Ne *(Spanish)* 77−30562
from ^{16}O(d,α_3), J$^\pi$ assignments 79−3160
He, A=8 and 10, exotic nuclei stability anal., Hartree-Fock approx. with the Skyrme interaction 78−82273
He neutron rich isotopes, reaction matrix calcs., stability 78−66225
^{4}He, pion exchange currents and nuclear charge form factors 77−10338
^{6}He, β decay cross sections 80−27880
^{6}He, β-decay, recoil ion energy spectrum anal. 78−21525
^{6}He β-decay from three body model of A=6 system, α-N, N-N interactions 78−46032
^{6}He, density distribution function of nucleons 80−22650
^{6}He, form. in ^{7}Li(t,α) reaction, possible resonant struct. 78−13110
^{6}He, G-parity nonconservation, ev ang. correlation for allowed beta-decay 78−17151
^{6}He, mass meas. from ^{7}Li(d,^{3}He)^{6}He and ^{19}F(d,^{3}He)^{18}O* reactions 78−41628
^{6}He mass six supermultiplet system anal. power from ^{9}Be(t,^{6}Li), polarised t 79−45244
^{6}He, matrix elements of potential energy operator on generalized hyperspherical functions *(Russian)* 79−22211
^{6}He state excitation energies and widths, DWBA ang. distribs. from ^{4}He(t,p), 23 MeV 78−70544
^{6}He$_{\Lambda\Lambda}$, $\Lambda\Lambda\alpha$ binding Feddeev's method 77−38238
^{6}He$_{\Lambda\Lambda}$, short range repulsion, separation energy, K-harmonics calcs. 80−86846
^{6}He$_{\Lambda\Lambda}$ hyperfragment, $\alpha\Lambda\Lambda$ model, Faddeev formalism, two-body local potentials 77−18467
^{7}He, levels determ. from ^{9}Be(^{6}Li,^{8}B) 77−46183
^{8}He, mass determ. from spectra of ^{64}Ni(^{4}He,^{8}He)^{60}Ni, and ^{64}Ni(^{4}He,^{6}He)^{62}Ni 78−25106
^{8}He obs., in hammer tracks from K$^-$+emulsion, 1.8 GeV/c 79−6711
^{A}He, A=6, 8, neutron excess isotope prod. in fragmentation reactions *(Russian)* 80−86888
^{10}He isotope search in ^{232}Th target nucleus spallation *(Russian)* 80−5110
^{17}He, prod. cross section calc., γ decay spectrum, shell model theory 78−62501
^{38}K level spectrum and (^{3}He,t) reaction mechanism from ^{38}Ar(^{3}He,t) 79−22229
^{16}L(α,d)^{18}F, 29.8 MeV, cluster form factors, DWBA calcs. 79−6643
^{16}L(d,^{6}Li)^{12}C, 50 to 80 MeV, spectroscopic factors energy depend. 79−6622
^{16}L(d,α_3)^{14}N, 6.7-12.5 MeV, differential cross sections and anal. power, ^{18}F unnatural parity states 79−3160
L(γ,X), photoabsorption cross-section, Levinger's factor, mass number dependence 80−63165
Li, A=10, 11, ground-state config. anal. 77−22859
Li, nucleosynthesis contribution from ^{16}O(p,X) 79−40978
Li nucleosynthesis from $\alpha+\alpha$ 61.5-158.2 MeV 79−17886
Li, π^- and p elastic scatt., 30 to 50 GeV/c, nuclear radius, real/imaginary forward scatt. amplitude ratio *(Russian)* 77−34351
Li+d, 40 MeV, target system neutron spectra 79−9595
Li(^{56}Fe,X), relativistic ^{56}Fe fragmentation, charge and mass changing cross sections 79−54453
Li(^{6}Li,^{8}B), 80,93 MeV, ^{4}H, ^{5}H energy levels anal. 77−46183
^{5}Li+^{3}He three-body final states, clustering in ^{7}Li, impulse approx. calcs. 77−3023
^{6}Li, α-d, coupling constants from dispersion anal. of N and d scatt. amplitudes 78−29399
(^{6}Li,^{6}Li), 30, 88 MeV, M3Y folding model eval., model independ. anal. 80−78317
(^{6}Li,X), 156 MeV, projectile break up in continuous particle spectra, cross section, fragmentation 80−86889
(^{6}Li, ^{6}Li), 99 MeV, A=12-208, ang. distribs. from double folding model pots. 80−106074
^{6}Li, ^{7}Li, prod. by cosmological cosmic rays 78−12436
^{6}Li, ^{7}Li, spallation prod. and ratio in C stars atmospheres 78−40927
^{6}Li, ^{7}Li, two and three body neutron reactions, 14.6 MeV 77−26725
^{6}Li 1$^+$ resonance in ^{2}H(α,αp), three body model 79−75954
^{6}Li, 5.36 MeV level electroexcitation form factor via ^{6}Li(e,e')^{6}Li at 40.5 and 50.5 MeV 77−54177
^{6}Li (α,α), 59 MeV, elastic and inelastic, differential cross section systematic anal. 80−22845
^{6}Li, (αnp) 3 body model using hyperspherical harmonics, bound states 78−70469
^{6}Li, (αnp) three-body elastic scatt. calc. using hyperspherical harmonics 79−63640
^{6}Li (n,n), 4-7.5 MeV, differential scatt. cross sections meas. 79−26437
^{6}Li (n,p) and (n,d) reactions, study of isovector analogue giant resonances, proton hole states 77−26726
^{6}Li, absolute cross section for (d,p), (d,α) and (d,n), E<1 MeV 78−25205
^{6}Li, absolute excitation energy meas. using electrostatic analyser 77−30741
^{6}Li, and ^{7}Li, nuclear double reson. in powdered Li metal 77−40153
^{6}Li, α-d relative wave functions using three different models 79−75872
^{6}Li, α+p+n cluster model with local interactions, Faddeev eqns., energy and charge radius calc. 79−22215
^{6}Li, α+p+n model, numerical soln. of coupled Faddeev eqns. 79−17831
^{6}Li, αnp elastic scatt., 0.2-5.0 keV, three body model, phase shift, total cross section 79−75875
^{6}Li backward π^+ prod., momentum depend., scaling, Monte Carlo calcs. 79−13305
^{6}Li, binding energies, three body calcs., Faddeev formalism, alpha cluster model 79−75876
^{6}Li bound states, six body hyperspherical soln. to N-body Schrodinger eqn. 79−9490
^{6}Li breakup by electrons, quasifree scatt., d-α vertex const. calc. 77−6354

nuclei with mass number 6 to 19 continued
^{6}Li, charge form factor, short range Jastrow correls. in harmonic oscillator shell model 78−70467
^{6}Li, charged particle induced reactions cross section meas. rel. to fusion reactor cycles 77−23297
^{6}Li, cluster formation, multicentre variational model *(Chinese)* 78−25128
^{6}Li, cluster model, resonating group, and integral eqns. approach to 6-nucleon system 79−80888
^{6}Li, cluster struct., multivalley character of isoenergetic surfaces *(Russian)* 79−26384
^{6}Li, Coulomb disintegration in field of heavy target nucleus, perturbation theory 78−66319
^{6}Li, Coulomb energy determ. from electron scatt. spectrum *(Russian)* 77−30479
^{6}Li, determ. of π^3He^{3}H coupling constant from forward dispersion relations 78−58307
^{6}Li dissociation in ^{208}Pb field 78−41770
^{6}Li, EM form factors and spectroscopic factors in phenomenological cluster models 80−496
^{6}Li, EM form factors and vertex consts. 78−12958
^{6}Li, electron excitation cross sections, short-range correlations *(Russian)* 79−36169
^{6}Li energy levels, d-α elastic scatt., three body calcs. 77−54158
^{6}Li energy levels from (p,d) 80−42667
^{6}Li, even parity levels, anal. using P-model *(Russian)* 79−49585
^{6}Li, excitation energy of second excited state meas. in (p,p') and (p,α) 77−57619
^{6}Li excited states, D(α,α)D cross-sections, α-d systems 80−47491
^{6}Li excited states, final state interactions, three-body force effects from ^{2}H(α,αp) 80−57692
^{6}Li, form factors determ. by pole and quark-counting model 77−26568
^{6}Li glass scintillators, appl. as neutron detector, problems and consequences 79−9968
^{6}Li ground state, cluster struct. obs. in ^{6}Li(p,pα)np 77−88129
^{6}Li ground state, double well-cluster shell model, d-cluster contraction and deform. *(Chinese)* 78−78290
^{6}Li ground state, separable pot. three body model 78−50090
^{6}Li ground state, translationally invariant spectral function in K harmonics 79−89257
^{6}Li, HF charge distribs. 77−14024
^{6}Li, highly excited states obs. in ^{9}Be(p,α) 77−6244
^{6}Li, hyperspherical L$_m$ approx., nuclear forces, binding energies 78−74311
^{6}Li, levels anal. from ^{3}H(^{3}He,^{3}He), 20-33 MeV 78−17227
^{6}Li low lying positive parity energy levels, effects of weak compression *(Russian)* 78−78270
^{6}Li, NMR in aq. LiCl 77−1613
^{6}Li neutron inelastic scatt. cross-sections and partial widths, calc. 78−78370
^{6}Li, neutron total cross section meas., 10 eV to 10 MeV 77−23037
^{6}Li, nucleon spectral function, K-harmonics calc. 79−75834
^{6}Li, Pauli distortion effects in folded optical pot. 79−6454
^{6}Li, production in $\alpha+\alpha$ reacts. at 103 MeV 79−45279
^{6}Li, quantitative microlocation in the brain by a (n,α) nuclear reaction 80−41353
^{6}Li, quasi α-particle photodisintegration at 35-55 MeV *(Russian)* 78−46046
^{6}Li, quasielastic elec. scatt., final state interaction effects *(Russian)* 78−41708
^{6}Li, RMS radii, binding energy, electric quadrupole transitions using generalised hyperspherical functions *(Russian)* 78−86469
^{6}Li, radiative π capture from 1s level, partial rates 79−3180
^{6}Li resonance effects on d-α elastic scatt. 78−46074
^{6}Li resonances in ^{4}He(d,d) 79−75953
^{6}Li, self-consistent desorption using four and two body substructures 79−63611
^{6}Li structure, three-body NNα model with separable interactions *(French)* 77−71598
^{6}Li system, resonance behaviour from excitation function of ^{2}H(^{3}He,^{4}He)^{2}H reaction 79−6640
^{6}Li, three body calc. with separable pots. for binding energy 79−45145
^{6}Li, three-body model of bound state struct. 79−6374
^{6}Li, three-body model using hyperspherical harmonics 78−29411
^{6}Li, total muon capture rate 79−6516
^{6}Li, transition probabilities between cluster structure states and r.m.s. radius, double well-cluster model *(Chinese)* 80−63128
^{6}Li$_\Lambda$, supermultiplet struct. and decay props. of hypernuclear 1$^+$ resonances from (K^-,π^-) 80−78186
^{6}Li-n, R-matrix calc. of total elastic, (n,α) differential cross-sections and polarisation 77−57669
^{6}Li+^{6}Li, effect on reaction rate of fusion reactor with ^{6}Li(p,α)^{3}He cycle 79−22459
^{6}Li+^{6}Li→2α+2d, double spectator poles and quasi-free inelastic scattering 79−93646
^{6}Li+^{6}Li→^{3}4He, 0.5-2.75 MeV, meas. of cross sections and fusion parameters 78−50223
^{6}Li+α system, exchange effects, resonating-group study 80−9240
^{6}Li+d, 0.1-1.0 MeV, DWBA and R-matrix cross section anal., direct contribution 79−67758
^{6}Li+d, extrapolation of low-energy reaction cross-sections 77−2955
^{6}Li+d, thermonuclear reaction rate parameters calc. 77−61436
^{6}Li+d, three body reactions, low energy, reaction mechanisms 78−13111
^{6}Li+d reactions, low-energy, CTR appl. 77−83097
^{6}Li+μ^-→ν_μ+^{6}He, angular correlations and capture rates, spin and isospin transitions, hyperfine effects 78−70494
^{6}Li+n, 12 and 20 MeV, resonating group method exam., effective internuclear potential 78−50159
^{6}Li+n, spin depend. capture and scatt. of slow neutrons 78−46059
^{6}Li+n total cross-section meas., 0.1 to 3.0 MeV 77−26740
^{6}Li(^{14}N, ^{14}N)^{6}Li, 19.5 MeV, optical model anal. *(Russian)* 77−34346
^{6}Li(^{14}N, αd)^{14}N, 19.5 MeV, disintegration mechanism *(Russian)* 77−34346
^{6}Li(^{3}He, ^{3}He^{3}He)^{3}H, 45 MeV, three trion model 77−88160
^{6}Li(^{3}He, ^{3}He^{3}He)^{3}H, 132 MeV, quasifree scatt., ^{3}He-^{3}He two body cross sections 79−76011
^{6}Li(^{3}He, ^{3}He), excitation functions 80−18223
^{6}Li(^{3}He, t^{3}He)^{3}He, 45 MeV, three trion model 77−88160
^{6}Li(^{3}He,^{3}H)^{6}Be, 27 MeV, comparison of experimental data and cluster and distorted wave calcs. 79−76010

nuclei with mass number 6 to 19 continued

^{6}Li(^{3}He,^{3}He^{3}H)^{3}He, Amado model appl., short-range interactions 77−6408
^{6}Li(^{3}He,^{3}He), 27 MeV, cross sections, three body and optical model calcs. 79−76009
^{6}Li(^{3}He,^{3}He), 44.04 MeV, absolute differential cross section, optical model anal. 79−59078
^{6}Li(^{3}He,^{3}He), phase shifts, cross sections, resonating group calcs., odd-even features, resonances 80−68681
^{6}Li(^{3}He,^{3}He)^{6}Li*, 27 MeV, comparison of experimental data and cluster and distorted wave calcs. 79−76010
^{6}Li(^{3}He,$\alpha\alpha$p), 2.5 MeV, ^{5}Li or ^{8}Be formation, direct or compound nucleus mechanism 77−57678
^{6}Li(^{3}He,d)^{7}Be, 2-6 MeV, cross section meas. rel. to fusion reactor first wall 80−13791
^{6}Li(^{3}He,p), 14 MeV, proton polarisation, ang. distribs., differential cross section 77−82944
^{6}Li(^{3}He,p)^{8}Be, 14 MeV, p-^{8}Be optical model parameters 78−25208
^{6}Li(^{3}He,p)$\alpha\alpha$, polarisation meas. in final state interactions 77−18589
^{6}Li(^{3}He,pα), 2.9 MeV, quasifree reaction, ^{2}H(^{3}He,pα) contrib., cluster motion 80−13485
^{6}Li(^{3}He,pα)α, 36 MeV, ^{5}Li breakup meas. 77−18590
^{6}Li(^{3}He,π^-), 910 MeV, π^- doubly coherent prod., inclusive π spectra 79−85481
^{6}Li(^{3}He,π^-)^{9}C, 910 MeV, doubly coherent π prod. 80−13487
^{6}Li(^{3}He,t)^{6}Be, α spectra obs. after α+p+p decay 77−74813
^{6}Li(^{6}Li, 3α), 2 MeV, DWBA anal. of direct prod. of 3 α final states 77−74882
^{6}Li(^{6}Li,^{5}He)^{7}Be, 3-15 MeV, cross sections meas. 79−76017
^{6}Li(^{6}Li,$\alpha\alpha$)α, 36 to 46 MeV, reaction mechanism 80−83113
^{6}Li(^{6}Li,αn)^{7}Be cross section, 1.6 to 5.0 MeV 77−50146
^{6}Li(H,ν)^{3}H^{3}H, muon capture in ditriton channel by elementary particle model 79−40907
^{6}Li(α, 2α) 700 MeV, cross section, effective cluster number from PWIA, momentum distrib. 79−40940
^{6}Li(α, $\chi\pi$), 18 GeV, π multiplicity distrib. 79−97713
^{6}Li(α,2α), pole peripheral model, ang. correl. functions calc. 77−6328
^{6}Li(α,α) 5-15 MeV, calc. illustrating generator coordinate amplitudes 77−54194
^{6}Li(α,α)^{6}Li, cross section using var. calcs. in generator coordinate method 78−13122
^{6}Li(α,αd)α, 42 MeV, α-α final state interaction 77−61442
^{6}Li(α,αp), 140 MeV, quasifree p knockout, spectroscopic factors, DWIA anal. 79−67650
^{6}Li(α,π^+)^{6}He, threshold prod. in α-d cluster model 77−79356
^{6}Li(d, α), polarised d, 5-10 MeV, A_y=1 and A_{yy}=1 points search 79−36223
^{6}Li(d,^{2}He), 55 MeV, cross sections, ^{2}He energy spectra and ang. distribs. 80−18321
^{6}Li(d,X) system, resonating group method, single channel approx., cluster states 80−57782
^{6}Li(d,α), 100-180 keV, low energy cross sections, astrophysical region extrapolation 80−22843
^{6}Li(d,α), cross sections, low energy extrapolation, 3 keV-1 MeV, thermonuclear reaction rate parameter 79−6635
^{6}Li(d,α)$_1$, extreme values of analysing power 77−3018
^{6}Li(d,α)^{4}He, 1.5-11.5 MeV, resonance behaviour, analysing powers 77−82935
^{6}Li(d,α)^{4}He, below 12 MeV, analysing powers, ^{8}Be reson. levels 77−82936
^{6}Li(d,α)^{4}He*, 13.6 MeV, α spectra, excited state of ^{4}He, spin, parity 78−54771
^{6}Li(d,α)α^+, 1.2-12 MeV, $\alpha\alpha^+$ rotational band existence in ^{8}Be 79−13192
^{6}Li(d,γ)^{8}Be, first T=2 state radiative width 77−14130
^{6}Li(d,n$_1$)^{7}Be*, 0.6-1.0 MeV polarised deuterons, vector and tensor analysing powers 78−4925
^{6}Li(d,n^{3}He)^{4}He, absolute and total cross sections 79−40936
^{6}Li(d,n)^{7}Be, 0.2-0.9 MeV, differential and total cross sections for neutrons 77−23096
^{6}Li(d,n)^{7}Be, 0.4-1.0 MeV cross-section meas. 79−76017
^{6}Li(d,n)^{7}Be, low energy cross section, 100-180 keV 78−4949
^{6}Li(d,p$_0$)^{7}Li, 0.6-1.0 MeV polarised deuterons, vector and tensor analyzing powers 78−4925
^{6}Li(d,p$_1$)^{7}Li*, 0.6-1.0 MeV polarised deuterons, vector and tensor analyzing powers 78−4925
^{6}Li(d,p^{3}H)^{4}He, absolute and total cross sections 79−40936
^{6}Li(d,p), 100-180 keV, low energy cross sections, astrophysical region extrapolation 80−22843
^{6}Li(d,tp)^{4}He, 0.465 MeV, quasi-free contribs. 78−614
^{6}Li(e, e), charge formfactors, second Born approx. and pole model 80−18155
^{6}Li(e,d)e'^{4}He, meas. and anal. based on α-d cluster model, ^{6}Li(γ,d)^{4}He cross-sections extracted 77−6355
^{6}Li(e,e'), 102, 123 MeV, excitation form factor, ^{3}H-^{3}He cluster model 80−78190
^{6}Li(e,e'), 140-330 MeV, 3.65 MeV 0$^+$ state form factor at high momentum transfer 80−495
^{6}Li(e,e'), 76-141 MeV, form factors, appl. to (π^-,γ), phenomenological model 80−83068
^{6}Li(e,e')^{6}Li at 40.5 and 50.5 MeV, ^{6}Li 5.36 MeV excitation form factor 77−54177
^{6}Li(e,e'd)^{4}He, ^{6}Li(e,e'τ)^{3}H, d-α cluster model anal. 77−26673
^{6}Li(e,e'd)^{4}He, p-shell nuclei electrofragmentation, Born approx. *(Russian)* 79−67746
^{6}Li(e,e), charge formfactors, second Born approx. and pole model 80−78133
^{6}Li(e,e), elastic and inelastic charge form factors from shell model wave functions 80−68523
^{6}Li(e,e), elastic scatt., spectroscopic information and form factors 80−9260
^{6}Li(e,e), electroexcitation cross sections, incoherent superposition of single nucleon processes 80−32269
^{6}Li(e,p), 16 MeV, nonexistence of 16.1 MeV state in (γ,p) cross section 79−45174
^{6}Li(γ,X), X=n,p, 10.2-15.4 MeV bremsstrahlung, photoreaction mechanisms 80−68644
^{6}Li(γ,d), from (e,e'd), cross section, E2 transistors giant resonance and clusters 80−63169
^{6}Li(γ,d)^{4}He, cross section calc. by cluster model *(Japanese)* 77−67733
^{6}Li(γ,d)^{4}He cross-sections extracted from ^{6}Li(e,d)e' ^{4}He meas. 77−6355

nuclei with mass number 6 to 19 continued

^{6}Li(γ,η), partial photoprod. cross-section calc. 77−14111
^{6}Li(γ,η)^{6}Li, E$_\gamma$=3.56 MeV, partial photoproduction cross-section calc. *(Russian)* 79−9547
^{6}Li(γ,η)^{6}Li partial cross section for photoproduction of η mesons 77−65220
^{6}Li(γ,η)^{6}Li*(3.56 MeV), partial photoproduction reactions, large momentum transfer anal., form factor choice 80−22808
^{6}Li(γ,π^0p), 0-600 MeV residual nucleus impulse *(Russian)* 79−59050
^{6}Li(γ,π^+), cross-section calc. 78−17248
^{6}Li(γ,π^+)^{6}He, analysis using current algebra model with rigid π-mesons *(Russian)* 77−14112
^{6}Li(γ,π^+)^{6}He, photoprod. near threshold, nucleus axial props. rel. to nucleon spin-flip *(French)* 79−522
^{6}Li(γ,π^+)^{6}He, threshold to 7 MeV, cross sections rel. to proton target 77−54207
^{6}Li(γ,π^0)^{6}Li*(3.56 MeV), partial photoproduction reactions, large momentum transfer anal., form factor choice 80−22808
^{6}Li(k^-,π^-)$^6_\Lambda$Li, strangeness analogue reson. 79−85566
^{6}Li(μ^-,ν_μ)^{3}H^{3}H, total and differential muon capture rates from elementary particle model 79−89297
^{6}Li(n, d)^{5}He, 6.77, 6.57 MeV, two body breakup, ang. distrib., DWBA, optical model anal. 77−18539
^{6}Li(n, p)^{6}He, 6.77-4.71 MeV, ang. distrib. excitation function, DWBA, optical model, anal. 77−18539
^{6}Li(n, t)^{4}He, 7.25-4.71 MeV, ang. distrib., excitation function, DWBA optical model anal. 77−18539
^{6}Li(n,^{3}H)^{4}He, polarised neutrons, 0.2-2.4 MeV, analysing power meas. 77−38268
^{6}Li(n,α), 2-800 keV, cross section meas. 78−70516
^{6}Li(n,α) absolute cross section meas., 964 keV 77−23035
^{6}Li(n,α) cross section standard, status 77−23040
^{6}Li(n,α) cross section standard, R-matrix anal. 77−23041
^{6}Li(n,α) T, mechanism for driving ^{6}LiD pellet to fusion temp. 79−93823
^{6}Li(n,α)^{3}H, 1-1500 keV, cross section meas. 77−26755
^{6}Li(n,α)^{3}H, 10 to 14 MeV, cross sections 77−26724
^{6}Li(n,α)^{3}H, 23 keV cross section, absolute meas., ang. distribs. 80−18305
^{6}Li(n,α)^{3}H, 25 keV, angular anisotropy, s-p wave interf. 77−23036
^{6}Li(n,α)^{3}H, 2.7 MeV triton recoil range, reaction in Li_2O single cryst. 80−63372
^{6}Li(n,α)^{3}H, 3 to 600 keV, new meas. of cross section 77−26723
^{6}Li(n,α)^{3}H, 3-800 keV, cross section meas. 78−89865
^{6}Li(n,α)^{3}H, below 100 keV, differential cross section, angular anisotropy 79−9583
^{6}Li(n,α)^{3}H, eV and keV energy range, ang. anisotropy 77−26722
^{6}Li(n,α)^{3}H, low energy, deuteron exchange mechanism, S-matrix theory 79−30840
^{6}Li(n,α)^{3}H reaction, as standard in neutron flux meas., instruments review 79−9969
^{6}Li(n,α)T, appl. to anal. of fusion reactor materials, archeometry, and nuclear spectroscopy 80−61200
^{6}Li(n,α)T cross section from 70 to 3000 keV from the ^{235}U(n,f) calibration of a thin glass scintillator 79−85471
^{6}Li(n,α)t, 2-10 MeV, absolute cross section meas., ang. distribs. 77−23059
^{6}Li(n,d)^{5}He, 56.3 MeV, ang. distrib. meas., spectroscopic factors determ. 77−88140
^{6}Li(n,γ), cross section and spectroscopic factors from direct capture pot. model 80−99171
^{6}Li(n,n), 0.1 to 3.0 MeV, cross-section meas. 77−26740
^{6}Li(n,n), 2-5 MeV polarised neutrons, analysing powers, R-function and phase shift anal. 77−23088
^{6}Li(n,n), 4-8 MeV, differential cross section meas., struct. determ. 77−23016
^{6}Li(n,n), 7 to 14 MeV, differential cross sections of elastic and inelastic scatt. 79−22279
^{6}Li(n,n), 7-15 MeV, elast. and inelast. scatt. 77−34314
^{6}Li(n,n), resonating group calcs. of phase shifts and cross sections 78−50168
^{6}Li(n,t)$_1$, 2 and 24 keV, ang. distribs. 79−54440
^{6}Li(n,t)^{4}He, 0.2-1.4 MeV polarised neutrons, analysing powers meas. 77−23074
^{6}Li(p, ^{3}He)^{4}He, 100 to 700 keV, cross sections and angular distrib. meas. 79−93618
^{6}Li(p,^{3}He), 0.1-3.0 MeV, absolute differential and total cross sections, astrophysical S-factor 80−27642
^{6}Li(p,X), 400 GeV, p, d, t, π, ^{3}He, α backward prod., inclusive cross sections 79−85475
^{6}Li(p,X), 400 GeV, p backward prod. invariant cross section 79−93623
^{6}Li(p,X), 400 GeV/c, light ion backward prod., invariant cross section 80−32279
^{6}Li(p,2p)^{5}He, appl. of break-up reaction theory to resonant final states 77−10381
^{6}Li(p,3p), quasielastic ejection of proton pairs at 640 MeV *(Russian)* 79−59067
^{6}Li(p,α)^{3}He, 1.0-2.6 MeV, cross-section meas. 77−34295
^{6}Li(p,d^{3}He), DWIA anal., α-spectroscopic factors, quasifree process 77−79378
^{6}Li(p,dπ^+)^{5}He, 800 MeV, momentum spectra enhancement 77−10395
^{6}Li(p,γ), 200-1200 keV, cross section 80−13478
^{6}Li(p,γ), cross section and spectroscopic factors from direct capture pot. model 80−99171
^{6}Li(p,n), 144 MeV, charge exchange, one pion exchange and PCAC tests 80−78299
^{6}Li(p,p'), 185 MeV, optical model anal. of inelastic scatt. to 1st excited state, deformation parameters 79−22300
^{6}Li(p,p')X, 800 MeV, cluster recoil mechanism for inclusive nuclear reactions 78−93998
^{6}Li(p,p), 144 MeV, elastic scatt. cross sections, optical pot. 80−42660
^{6}Li(p,p), 635 MeV, left-right asymmetry depend. on residual nucleus momentum *(Russian)* 78−54765
^{6}Li(p,p) 0.6, 1.04 GeV, α-d cluster model and Glauber multiple scatt. theory 79−85476
^{6}Li(p,p) quasielastic scatt., 635 MeV polarised protons, asymm. meas. *(Russian)* 77−74852
^{6}Li(p,p)^{6}Li, four body approach 79−75933
^{6}Li(p,p)X, 0.8 GeV, inclusive cross sections, quasi-two-body scaling 79−3150
^{6}Li(p,pd), 590 MeV, α-d motion, impulse distrib., cluster momentum distrib. 80−52679

nuclei with mass number 6 to 19 continued
^{6}Li(p,pd), 670 MeV, large angle quasifree scatt., spectroscopic factor, momentum distrib., cluster model 80−63184
^{6}Li(p,pd)^{4}He, results in relation to (p,2p) 800 MeV high resolution proposed studies 77−88123
^{6}Li(p,pd)α, 156 MeV, relative wave function of d and α clusters, PWIA, DWIA anal. *(Chinese)* 79−59068
^{6}Li(p,pt)^{4}He, 1 GeV, knock-out of clusters, distorting factors, microscopic approach *(Russian)* 78−58285
^{6}Li(p,π^{+})^{7}Li, 600 MeV, comparison with π,p exchange calcs. 77−79377
^{6}Li(π^{-}, γ), photon spectra meas. with SIN pairspectrom. 77−10446
^{6}Li(π^{-},n), single neutron emission induced by stopped π^{-} in 1p shell nuclei 79−59089
^{6}Li(π^{+}, 2p), 85 MeV, ang. depend. of cross section *(Russian)* 77−34349
^{6}Li(t,d)^{7}Li, 0.35 to 1 MeV, resonance struct. in compound nucl. excitation curves 78−17217
^{6}Li(t,γ)^{9}Be, 0.35 to 1 MeV, resonance struct. in compound nucl. excitation curves 78−17217
^{6}Li(t,p)^{8}Li, 0.35 to 1 MeV, resonance struct. in compound nucl. excitation curves 78−17217
^{6}Li(τ,t)^{6}Be, 27 MeV cross-section calc. by Amado 3-body model 79−6617
^{6}Li(τ,τ)^{6}Li*, 45 MeV, cross-section calc. by Amado 3-body model 79−6616
^{6}Liμ^{-}→^{3}H^{3}Hν in ^{6}Li loaded photoemulsion, secondary particles ang. distrib. and energy *(Russian)* 78−89855
^{7}Li 3/2^{-} state from ^{6}Li(n,−a) 80−18297
^{7}Li (n,n), 4-7.5 MeV, differential scatt. cross sections meas. 79−26437
^{7}Li (n,p) and (n,d) reactions, study of isovector analogue giant resonances, proton hole states 77−26726
^{7}Li ($\bar{\nu}_e$, $\bar{\nu}_e$), antineutrino spectrum 80−102150
^{7}Li (p, n), 50 MeV 78−70726
^{7}Li, abundance as constraint on universal baryon density 78−4420
^{7}Li, and ^{19}F double NMR in LiF, existence of single nuclear dipolar spin temp. 78−35065
^{7}Li, and ^{6}Li, nuclear double reson. in powdered Li metal 77−40153
^{7}Li, ang. momentum eigenstates projection from two-centre generator coordinate model functions 78−12994
^{7}Li charge form factor with resonating group wave function, quad. moment, charge radius 80−102110
^{7}Li, cluster model wave function and r.m.s. radius 78−70442
^{7}Li, cluster struct. interplay model and appl., energy levels and shell clusters 79−17842
^{7}Li, dσ(p,p'd)/dσ(p, nd), 670 MeV, cross section ratio, cluster model estimate 80−22829
^{7}Li electric quadrupole moment, from Coulomb scatt. of aligned ^{7}Li ions 80−78141
^{7}Li, electron excitation cross sections, short-range correlations *(Russian)* 79−36169
^{7}Li, energy of first 3/2^{-} excited state from S-matrix anal. from ^{6}Li(n,t)^{4}He, 0-3.9 MeV, ^{7}Li, energy of first 3/2^{-} excited state from S-matrix anal. 79−473
^{7}Li, form. in ^{6}Li(t,d) reaction, 0.35 to 1 MeV, resonance struct. in compound nucl. excitation curves 78−17217
^{7}Li, lifetimes of first excited levels meas. 77−22943
^{7}Li, M2 giant resonance calcs. from (e,e'),(π^{-},γ),(μ^{-},ν) 80−22784
^{7}Li, model for coupling two cluster structs., influence on shape and states 78−78288
^{7}Li NMR, spin-lattice relax. in $KLiSO_4$ and α-$LiIO_3$ *(Chinese)* 80−39884
^{7}Li, NMR in glasses 78−27107
^{7}Li, NMR in Li metal, thermal mixing rate calc. 78−10795
^{7}Li, NMR in $LiCuCl_3.2H_2O$ 77−48061
^{7}Li NMR in LiF, thermodynamic effects of RF pulse pair on system with two spin species 77−66433
^{7}Li, NMR in solid LiH 80−15815
^{7}Li, NMR meas. dehydration of lithium formate cryst., influence of hydrostatic press. 78−2758
^{7}Li, non-central forces and spectrum *(Russian)* 79−89243
^{7}Li, nucl. spin-lattice relax. time meas. in $LiIO_3$ 78−10796
^{7}Li nucleosynthesis in UV Ceti flares 79−30073
^{7}Li, Pauli-principle effects, simulation 78−8756
^{7}Li, photoabsorption total cross sections 30-100 MeV *(Russian)* 78−89850
^{7}Li, photodisintegration, cluster model wave function, bremsstrahlung weighted cross section 80−63163
^{7}Li, prod. in ^{4}He(α,p) reactions, differential cross sections meas., 39 to 50 MeV 78−25207
^{7}Li, production in α+α reacts. at 103 MeV 79−45279
^{7}Li, projection of ang. mom. eigenstates from two-centre generator coord. model functions 77−22912
^{7}Li, proton scatt., 3/2^{-}→1/2^{-} transition, LS coupling shell model, isoscalar quadrupole renormalisation 77−14046
^{7}Li, quadrupole moment from HFS 78−66678
^{7}Li, quasi α-particle photodisintegration at 35-55 MeV *(Russian)* 78−46046
^{7}Li, quasielastic elec. scatt., final state interaction effects *(Russian)* 78−41708
^{7}Li, spin-lattice relax. time in aq. LiCl soln., 5-65°C 77−48075
^{7}Li system, exptl. data base 79−9584
^{7}Li system, survey of recent expts. 79−9582
^{7}Li system reactions, R-matrix anal. 79−9585
^{7}Li, thick target neutron yields from (p,n) and (d,n) reacts. 77−26752
^{7}Li two centre model, Brinks α-cluster model generalisation for odd nuclei *(Russian)* 79−30797
^{7}Li, two-centre molecule-like states, generator coordinate wave function projection 78−12995
^{7}Li+^{7}Li reaction, 2 MeV, neutron energy spectrum meas. using nuclear emulsion technique 78−62573
^{7}Li+n, elast. and inelast. scatt. of 9.1±0.2 MeV neutrons, double differential cross section meas. 79−30838
^{7}Li+p, 1 GeV, neutron production *(Russian)* 79−85477
^{7}Li+π^{-}→^{4}He+^{3}n (or ^{3}He+^{4}n), search for neutron nuclei *(Russian)* 77−74889
^{7}Li(^{3}H,γ)^{10}Be, 0.4-1.1 MeV, excitation curves, ang. distribs. 78−33200
^{7}Li(^{3}He, d$_0$)^{8}Be, 1.0 to 2.5 MeV, excitation functions, ang. distribs. 77−61438
^{7}Li(^{3}He,t)^{7}Be, 2-6 MeV, cross section meas. rel. to fusion reactor first wall 80−13791
^{7}Li(K^{-}, π^{0})$_{\Lambda}$^{7}He, prod. cross sections from shell model theory 78−62501
^{7}Li(K^{-},π^{-})$_{\Lambda}$^{7}Li, prod. cross sections from shell model theory 78−62501
^{7}Li(K^{-},π^{-}γ), hypernuclear γ-ray line 78−37377
^{7}Li(K^{-},π), narrow Σ-hypernuclear states, estimated widths, quantum number assignments 80−42576
^{7}Li(α,α), low energy elastic and inelastic scatt., Pauli principle effect 78−4953
^{7}Li(α,α), microscopic study of elastic scatt. 77−88156
^{7}Li(α,α) at 2, 4 and 7 MeV, ang. distribs. calcs., 2α+t system model 78−50110
^{7}Li(α,α)^{7}Li, ^{11}B excited states parameters *(French)* 79−93637
^{7}Li(α,α)^{7}Li elastic scatt. generalised optical potentials, three-body approximation *(Russian)* 79−13313
^{7}Li(d, t), 12 MeV, nuclear vertex constant in peripheral model for virtual decay ^{7}Li→α+t 80−18295
^{7}Li(d,α$_1$)^{5}He, E$_d$=250 to 750 keV, cross section determ. in absolute current meas. reaction chamber *(French)* 78−78388
^{7}Li(d,α), 1.5-11.5 MeV, meas. of differential cross section and analysing powers 77−3017
^{7}Li(d,ααα)n, 2 MeV, quasi free reaction, ^{7}Li struct. 78−41727
^{7}Li(d,ααα)n, excitation energy and width of ^{5}He first excited state 77−276
^{7}Li(d,ααn), 7.0 MeV, prevalence of ^{8}Be formation 78−82357
^{7}Li(d,n), neutron spectra and yields from thick targets 77−30602
^{7}Li(d,n),(p,n), 14-23 MeV, thick target neutron yields 77−57791
^{7}Li(d,p), 0.7-3.4 MeV, absolute total cross section, ^{8}Li β-decay half life 80−13483
^{7}Li(e,^{3}H)^{4}He,e', 6-15 MeV, cross sections 77−26672
^{7}Li(e,X), X=^{6}He,^{6}Li, 108-198 MeV, ang. distribs. and cross sections 80−42647
^{7}Li(e,e') at first πN resonance, cross section longitudinal and transverse components *(Russian)* 80−86901
^{7}Li(γ, n)^{6}Li* (3.56 MeV), integral reaction cross section *(Russian)* 78−46048
^{7}Li(γ,γ'), 32 MeV, energy spectra, d prod. process *(Russian)* 80−91177
^{7}Li(γ,π^{-}), threshold to 360 MeV, total cross sections in Δ region 80−13457
^{7}Li(γ,π^{-}), total cross section calc. in impulse approx. 80−13458
^{7}Li(γ,t), <50 MeV, total and differential cross sections, levels, cluster model calcs. 80−32265
^{7}Li(γ,t)^{4}He, N-fold coincidences, on-line acquisition 77−79527
^{7}Li(n,d)^{6}He, 56.3 MeV, ang. distrib. meas., spectroscopic factors determ. 77−88140
^{7}Li(n,n')^{7}Li, triton-alpha disintegration of ^{7}Li 77−38279
^{7}Li(n,n')αT, three body sequential reactions, kinetics modelling 80−37371
^{7}Li(n,n'α), cross section, appl. to fusion reactor neutronics 78−62604
^{7}Li(n,n'γ), 0.57-4 MeV, cross-section meas. 77−2985
^{7}Li(n,n'γ)^{7}Li*, threshold to 5 MeV, absolute meas. of cross section 79−67751
^{7}Li(n,n'γ)^{7}Li* (0.478 MeV) cross-section meas. from 0.5 to 5.0 MeV 80−68661
^{7}Li(n,n), 4-7.5 MeV, differential cross section meas. 77−34313
^{7}Li(n,n), 4-8 MeV, differential cross section meas., struct. determ. 77−23016
^{7}Li(n,n), 7 to 14 MeV, differential cross sections of elastic and inelastic scatt. 79−22279
^{7}Li(n,n), 7-15 MeV, elast. and inelast. scatt. 77−34314
^{7}Li(n,n) elastic and inelastic, calc. excitation functions and integrated cross sections 78−86534
^{7}Li(p, α), 45 MeV, nuclear vertex constant in peripheral model for virtual decay ^{7}Li→α+t 80−18295
^{7}Li(p, n)^{7}Be, absolute yield and neutron spectra 79−40929
^{7}Li(p,α)α^{+}, 4.5-12 MeV, αα^{+} rotational band existence in ^{8}Be 79−13192
^{7}Li(p,d^{3}He), DWIA anal., α-spectroscopic factors, quasifree process 77−79378
^{7}Li(p,d), 800 MeV, cross sections, DWBA anal. 80−42667
^{7}Li(p,γ), cross-section contrib. from ^{8}Be 3^{+} states, isospin mixing model 78−89789
^{7}Li(p,γ)^{8}Be, polarised p, 380-960 keV, ^{8}Be level, J$^{\pi}$ 77−88131
^{7}Li(p,n,γ)^{7}Be, associated gamma-ray technique for neutron fluence meas. 79−9978
^{7}Li(p,n), cross-section contrib. from ^{8}Be 3^{+} states, isospin mixing model 78−89789
^{7}Li(p,n) 77−30602
^{7}Li(p,n)^{7}Be, activation and ang. distrib. meas., absolute neutron yield determ. 78−17199
^{7}Li(p,n)^{7}Be, microscopic multi-channel calcs. to 2.5 MeV c.m. 78−4934
^{7}Li(p,n)^{7}Be as therapy neutron source especially for small cyclotrons 80−26335
^{7}Li(p,n)^{7}Be neutron yield using sphere counter 77−23381
^{7}Li(p,nα), 7-10 MeV, neutron spectra meas. 77−26741
^{7}Li(p,np), 7-10 MeV, neutron spectra meas. 77−26741
^{7}Li(p,p), polarisation effects for elastic scatt. near (p,n) reaction threshold 78−13075
^{7}Li(p,p)^{7}Li, microscopic multi-channel calcs. to 2.5 MeV c.m. 78−4934
^{7}Li(p,pα), 600 MeV, quasi-electric knockout reaction, PWIA calcs. 79−6581
^{7}Li(π, πN), 60 and 300 MeV, γ-ray meas. 78−41780
^{7}Li(π,π'), 164 MeV, ang. distrib., cross sections 79−85532
^{7}Li(π,π), 164 MeV, ang. distrib., cross sections 79−85532
^{7}Li(π,π), elastic and inelastic, nuclear struct. effects in optical model 77−23112
^{7}Li(π,πn)^{6}Li, 50-290 MeV, cross-section meas. 77−6463
^{7}Li(π^{-}, γ), photon spectra meas. with SIN pairspectrom. 77−10446
^{7}Li(π^{-}, t)^{4}H, study of particle-unstable state ^{4}H, branching ratio 79−93528
^{7}Li(π^{-},X), π^{-}-capture at rest, isotopic yield distribs., T-T coincidence, ^{4}H formation 79−85497
^{7}Li(π^{-},n), single neutron emission induced by stopped π^{-} in 1p shell nuclei 79−59089
^{7}Li(π^{+}, 2p), 85 MeV, ang. depend. of cross section *(Russian)* 77−34349
^{7}Li(π^{+},2p), cluster effects in in-flight π^{+} capture 78−89916
^{7}Li(π^{+},p^{3}He), cluster effects in in-flight π^{+} capture 78−89916
^{7}Li(π^{+},pd), cluster effects in in-flight π^{+} capture 78−89916
^{7}Li(π^{+},π^{-})^{7}Be, distorted wave impulse calc., optical pot., multiple scatt. 78−50138
^{7}Li(π^{+},π^{0}), 1st order pion-nucleus pot. calc. 77−23113

nuclei with mass number 6 to 19 continued
^{7}Li(π^{+},π^{0}), 90 to 210 MeV, ^{7}Be 429 keV 1/2^{-} excited state, cross section 78−647
^{7}Li(π^{+},π^{0})^{7}Be, DWIA isovector correls. 78−29499
^{7}Li($\pi^{\pm}$,πN)^{6}Li* cross-section ratios, N charge exchange model 77−54257
^{7}Li(t, ^{9}Li)^{1}H, near threshold anomaly, S-matrix formalism, ^{10}Li neutron binding energy *(Russian)* 80−105961
^{7}Li(t,α)^{6}He, possible resonant struct. in excitation functions 78−13110
^{7}Li→α virtual decay vertex constant from (d,t), (p,α) 80−78231
^{8}Li ang. distribs. from ^{9}Be(π^{-},πN) 80−106036
^{8}Li β^{-}-decay, β-α angular correlations, final state energy depend., current test 80−102151
^{8}Li β-decay half life from ^{7}Li(d,p) 80−13483
^{8}Li, form. in ^{11}B(n,α) reaction, 14.4 MeV, spectra and ang. distribs., recoil nucl. transitions 78−17193
^{8}Li, form. in ^{6}Li(t,p) reaction, 0.35 to 1 MeV, resonance struct. in compound nucl. excitation curves 78−17217
^{8}Li, fragment energy distrib. anal. from K^{-}+nucleus reactions 78−62577
^{8}Li fragment formation in heavy emulsion nuclei (p,X) reactions *(Russian)* 79−59072
^{8}Li, in $LiTaO_3$, multiple quantum NMR transitions obs., quadrupole moment determ. 77−73090
^{8}Li, isospin forbidden beta decays, collective model, Fermi matrix elements 77−67722
^{8}Li, isospin symmetry breaking in A=8 mirror decays 78−93973
^{8}Li, mag. moment from β-ray spectra of recoil nuclei polarised by fast polarised beams 77−28502
^{8}Li nucl. spin-lattice relax. in liquid ^{7}Li, β-emission meas. 77−51985
^{8}Li, produced by K^{-} interactions with emulsion nuclei 78−17244
^{8}Li scattering system, microscopic multichannel cluster model calc., resonating group calc. 78−4906
^{8}Li state excitation energies and widths, DWBA ang. distribs. from ^{6}Li (t,p), 23 MeV 78−70544
^{8}Li, possible γ-transition from ^{9}Be(K^{-},π^{-}p) 80−106002
^{8}Li(β)^{8}Be*(α)α, obs. of ^{8}Be state at ~6 MeV 78−93938
^{8}Li→^{8}Be+β, β-decay strength calcs., microscopic continuum wave function 78−62503
^{9}Li, β decay cross sections 80−27880
^{9}Li, levels determ. from ^{11}B(^{6}Li,^{8}B) 77−46183
^{9}Li state excitation energies and widths, DWBA ang. distribs. from ^{7}Li(t,p), 23 MeV 78−70544
^{A}Li (p, nd), A=6,7, 670 MeV, quasifree scatt., PWIA anal., cross sections 79−75985
^{A}Li (π^{-},2n), A=6,7, recoil momentum, excitation energy distribs. and neutron momenta 79−67780
^{A}Li, A=6, 7, photodisintegration, particle ang. distribs., (γ,t) cross section 79−75974
^{A}Li, A=6,7, π^{+} electroprod., distorted wave impulse approx. anal. 79−17894
^{A}Li, A=7, 8, 9, 11, neutron excess isotope prod. in fragmentation reactions *(Russian)* 80−86888
^{A}Li+ν, (A=6,7), neutral current processes in nuclei, elementary particle approach 79−93606
^{A}Li(γ,π), A=6, 7 80−22686
^{A}Li(n,x), A=6, 7, 14.6 MeV, ang. distribs. and cross sections for ^{6,7}Li, ^{6}He products 80−42650
^{A}Li(p,pα), A=6,7, 600 MeV, α-cluster quasielastic knockout, expt. methods, separation energy spectra 79−13275
^{A}Li(π^{+},p), A=6,7, 75 and 175 MeV, ang. distrib. 79−85503
^{A}Li(π^{+},π^{-}), A=6, 7, 50 MeV, optical model anal., core+valence neutron model, isotopic effects 79−6715
^{A}Li(πp), A=6, 7, 75, 175 MeV, diffential cross sections, reaction mechanisms 80−78332
^{10}Li neutron binding energy from ^{7}Li(t, ^{9}Li)^{1}H *(Russian)* 80−105961
^{11}Li beta decay, γ activity 80−106018
^{11}Li, β-delayed two neutron radioactivity 80−18247
^{6,7}Li(e,e'p), suppression factor, final-state interaction and cross-sections in shell model *(Russian)* 77−61401
^{6,7}Li(n,p)^{6,7}He, 800 MeV, cross-sections 77−61423
^{6,7}Li(p,n)^{6,7}Be, 800 MeV, high-resolution n-spectra meas. 77−61423
$_{\Lambda}{}^{A}$Li, A=6,7, excited states and spectra, continuum effects calcs. 80−57720
Li(d,d), 3-10 MeV, A=6,7, differential cross section, optical model anal. 77−61435
Li(d,n), neutron spectra from thick target bombardment for therapy 78−28049
Li(e,e'p), A=6,7, 700 MeV, proton spectral functions, momentum distribs., DWIA anal. 78−41701
Li(e,e'π^{+}), A=6,7, energy and ang. distribs. of πs, low lying residual states 78−54740
Li^{7}(γ,n), photo neutron cross sections, branching ratios 77−41943
Li(γ,x), photoabsorption cross-section, Levinger's factor, mass number dependence 80−63165
$_{\Lambda\Lambda}{}^{A}$Li, A=10, 11, double hypernuclei, prod. and decay from (K^{-},X), emulsion 80−57718
Li(n,n), 14 MeV, differential cross-section meas. 77−88130
Li(p,n), neutron spectra from thick target bombardment, for therapy 78−28049
Li(p,p) summed scattering (elastic and inelastic with no meson production), 2.1 GeV/c, asymmetry meas. *(Russian)* 79−89313
Li(p,pα), A=6,7, at 100 MeV, absolute spectroscopic factors 77−30574
Li(p,pn), 47 MeV, excit. energy spectra, energy sharing spectra 77−50132
Li(π,X), 125 MeV, absorption cross section in 3:3 resonance region 79−85543
$_{\Lambda}{}^{9}$Be multiparameter variational calc., clustering in hypernuclei *(Russian)* 77−74791
N energy loss params., appl. on mass determ. of cosmic ray nuclei in nuclear emulsion 78−94175
N, muonic X-ray transitions, nuclear charge radii 80−99589
N, NMR in mols., nuclear mag. shielding 78−17695
N, neutron air transport sensitivity to nitrogen cross section uncertainties 77−23165
N, neutron scatt. and gamma-ray prod., Monte Carlo anal. 77−26682
N, recoiling in magnetised Fe, transient mag. fields 77−12263
N, stellar nucleosynthesis rel. to galaxies ages determ. 79−25728
N+n in cellulose nitrate plastic detector, spallation products 78−17198
n+nuclear emulsion, 2.1 GeV/amu, scatt. const. 78−13151
N+p, inelastic interactions, 6.0 GeV/c, in emulsions 78−86530

nuclei with mass number 6 to 19 continued
N(^{12}C,X), 4.5 GeV/c, emission of short range particles (R<100 mkm) *(Russian)* 80−63202
^{A}N (n,n), A=14, 15, thermal neutron scatt. parameters 79−93628
^{A}N, A=16,18, E1 and M2 giant resonance excitation from O(π^{-},γ) 79−89280
^{12}N 2.43 MeV level study 77−6235
^{12}N, aligned, β ang. distribs., second class currents 78−50126
^{12}N, aligned, β-ang. distrib. and alignment correction coeffs., axial vector currents 80−5097
^{12}N, aligned, β-ang. distrib. asymmetry coeffs., pseudotensor interaction, T=1 isospin triplet decay 80−106021
^{12}N, aligned, existence of G-parity irregular induced tensor current 78−29384
^{12}N, beta decay, PCAC and vector current conservation 79−93561
^{12}N, beta-ray spectra and conserved vector current 79−54409
^{12}N, beta-spectra reanalysis, shape-factors and CVC theory 77−67724
^{12}N β-decay, radiative corrections 77−38249
^{12}N, β-ray branching and $T_{1/2}$ 78−41674
^{12}N, β-transitions, weak magnetism, nuclear struct., matrix elements 79−13253
^{12}N e^{+} energy spectra, CVC hypothesis and weak magnetism 77−54190
^{12}N ground state electric quadrupole moment from ^{12}C(γ, π), ^{12}N ground state electric quadrupole moment *(Russian)* 80−42538
^{12}N, in Mg, elec. quadrupole interactions, obs. by depolarisation due to level mixing 77−55728
^{12}N, meas. of weak magnetism term in β spectra 78−4917
^{12}N, NMR in Ni, hyperfine field determ. 77−8418
^{12}N, oriented nuclei, β-γ ang. correl., G-parity nonconservation 78−54723
^{12}N, polarised, β-decay, asymm. of β-ray ang. distrib., second class currents 77−41919
^{12}N, polarised, β-decay asymm., G-parity nonconservation, second class currents 77−41920
^{12}N, polarised, higher order effects in determ. of asymmetry parameters in β-decay 79−22247
^{12}N, quadrupole interaction in Be, Mg and Zn 78−47750
^{12}N, weak magnetism and beta spectra 77−6314
^{12}N→^{12}C(g.s.), second-class axial current, meas. alignment-positron-momentum correl. 78−82317
^{12}N→^{12}Ce$^{+}\nu_e$, data anal., second-class currents and CVC 77−82874
^{13}N cpds., for environmental and biological research, cyclotron prod. 78−82551
^{13}N, giant dipole reson. excited in ^{12}C(p,γ) and ^{12}C(p,p'), doorway-states 77−6336
^{13}N giant dipole resonance population amplitude and phase, E1 reaction amps. from ^{12}C(p,γ_0), pol. p 80−63145
^{13}N ground state, dispersion anal. of ^{12}C+p forward scatt. 77−34297
^{13}N isobaric analogue state excitation, cross sections from ^{13}C(π^{+},π^{0}) 80−42544
^{13}N labelled pharmaceuticals cyclotron prod. for nuclear medicine appls. 77−44753
^{13}N, level parameters determ. from ^{12}C(p,p) at 0.3-2.0 MeV 77−3007
^{13}N level structure via ^{12}C(p,p) scatt. with 11.5 to 18 MeV polarised beam 77−315
^{13}N, production by cyclotron, biomedical appls. *(French)* 80−56216
^{13}N, quadrupole strength, from ^{12}C(p,γ)^{13}N, semi-direct capture model calcs. 80−47370
^{13}N spectroscopic factors, ^{13}C(^{3}He,d) with 33 MeV polarised beam 77−328
^{13}N, spectroscopic factors from ^{11}B(^{3}He,n) ang. distrib. at energies below Coulomb barrier 79−40938
^{13}N state transition ang. distrib., optical parameters from ^{12}C(^{7}Li, ^{6}He) 79−75904
^{13}N, transitions from lowest T=3/2 states 77−88075
$^{13}NH_3$, simultaneous prod. of ^{123}I, ^{62}Zn and $^{13}NH_3$, multitarget assembly for high energy irrad. 77−90896
^{14}N 1^{+} state cross sections, effective two nucleon interaction, isovector tensor component from ^{14}C(p,n) 80−18208
^{14}N, 2.1 GeV/nucleon, fragmentation parameters in emulsion 77−3027
^{14}N, 5.0-9.3 MeV neutron scatt., differential cross sections and neutron ang. distribs. 77−23093
^{14}N 9.13 MeV state, obs. in ^{13}C(p,γ) 78−41641
^{14}N (e,e'), 40-60 MeV, at 180°, M1 transitions and transition widths 79−49598
^{14}N (n,p) and (n,d) reactions, study of isovector analogue giant resonances, proton hole states 77−26726
^{14}N, α-transfer reactions, spectroscopic factors, exact finite range DWBA anal. 80−13372
(^{14}N, αX), 156 MeV, heavy ion-alpha in-plane correlations 80−18343
^{14}N, DSA lifetimes determ. from exptl. stopping powers 78−17142
^{14}N, energy levels up to 11.05 MeV, transitions and resonance decay from ^{13}C(p,γ) 80−47376
^{14}N, four-body breakup induced by 18 MeV neutrons, double final state interaction 78−17192
^{14}N, g-factor, lifetime meas. of 5.106 MeV 2^{-} state of ^{14}N 78−93965
^{14}N, HF charge distribs. 77−14024
^{14}N in nitroso and nitrosyl cpds., chem. shifts correl. with nuclear quadrupole coupling consts. 77−30888
^{14}N levels and excitation energies, kinematically complete investigation from ^{16}O(π^{-}, 2n) 80−99128
^{14}N, liq. cryst. in solid phase, nuclear quadrupole coupling consts. 77−8444
^{14}N, M2 giant resonance calcs. from (e,e'),(π^{-},γ),(μ^{-},ν) 80−22784
^{14}N, meas. of nucl. g-factor of 5.11 MeV 2^{-} state by recoil distance technique 78−37268
^{14}N, multiple spin echoes in pure NQR in $NaNO_2$ 78−19365
^{14}N NMR, single cryst., separation of dipolar and quadrupolar splittings, new technique 80−25217
^{14}N, NMR and quadrupole splitting of NH_4^{+}, ND_4^{+}, lyotropic mesophase 78−17690
^{14}N NMR chemical shift, external neat nitromethane scale 78−24834
^{14}N, NQR, charge transfer and distrib. in nitrile complexes, RCN...Cl-Cl^{-}, RCN...$HCCl_3$ 77−12244
^{14}N, NQR freq. in aminoarsines, aminoboranes, N-As and N-B bonds 78−25566
^{14}N, NQR in barbiturates 77−43900
^{14}N, NQR in hexomethylenetetramine complexes, pulsed apparatus 77−10075
^{14}N, NQR in KNO_2 and $CsNO_2$ at low temp. 77−12223
^{14}N, NQR in organic compounds, correl. anal. 77−12240

nuclei with mass number 6 to 19 continued

^{14}N NQR in pyrrole, ^{1}H lineshape anal. 78−6598
^{14}N, NQR in rubidium-TCNQ, Zeeman perturbation study, charge transfer 78−39438
^{14}N, NQR in Sn complex, $SnCl_4.L_2$ (L_2=organic phosphorus ligand) 77−16201
^{14}N, NQR meas. in TBBA biaxial liq. cryst. 77−32288
^{14}N, NQR meas. in thermochromic and photochromic N-salicylideneanilines 77−28480
^{14}N, NQR of substituted nitrobenzene mols., elec. field gradient of NO_2 78−21944
^{14}N quadrupole coupling consts., ab initio calcs. 80−58283
^{14}N, relax. in nitrobenzene 77−48070
^{14}N residual states, vector anal. power. optical pot. from ^{12}C(^{6}Li,α), pol. ^{6}Li 79−97697
^{14}N screening, absolute scale 78−2762
^{14}N spectroscopic factors, cross sections DWBA anal. optical model parameters from ^{12}C(^{16}O,X) 80−13371
^{14}N unbound 4_1^+, 5_1^+, 3_2^+ states from ^{13}C(p,γ), lifetimes, branching ratios 78−25184
$^{14}N_{g.s}$ partial muon capture, mesonic exchange currents, weak process microscopic treatment 80−57742
^{14}N-induced reactions energy relax. during fusion determ. by preequilib. α emission 79−26446
^{14}N+^{10}B, 100 MeV, 2n and 2p transfer reacts., DWBA anal. 78−50207
^{14}N+^{10}B, sub Coulomb energy, fusion cross section, optical model anal. 77−34335
^{14}N+^{12}C, 112 MeV, alpha clustering, multiple shape vibrs., TDHFC calcs. 79−3164
^{14}N+^{12}C, 34.1-178.1 MeV, fusion and peripheral reaction cross sections, direct yield 79−67771
^{14}N+^{12}C, direct inelastic scatt. in 3-dimens. time depend. HF scheme 79−17925
^{14}N+^{12}C, fusion reactions, Woods Saxon, folding and proximity pot. anals. 79−45316
^{14}N+^{12}C, TDHF appl. 78−54709
^{14}N+^{12}C, time-depend. Hartree-Fock calcs. 77−46125
^{14}N+^{12}C(^{16}O), 3.6-12.6 MeV, total fusion cross sections meas. 77−42002
^{14}N+^{16}O, 20-60 MeV, compound nucl. form. 78−4954
^{14}N+^{27}Al, 100 MeV, energy relaxation and mass transfer *(French)* 80−95327
^{14}N+α, spallation fragments 6≤A≤11 yields, nucleosynthesis interest 79−30845
^{14}N+emulsion nuclei, 2.1 GeV/nucleon interactions 77−41991
$^{14}N+\mu^- \rightarrow {}^{14}C+\nu_\mu$, rate calcs. using elementary particle and macroscopic treatments 78−29429
^{14}N+p, 50 MeV, three particle final state *(Russian)* 78−29471
^{14}N(^{14}N,X), 9.4-22.0 MeV, low energy fusion cross sections 77−14152
^{14}N(^{14}N,α)^{24}Mg, 10.1 MeV, Hauser-Feshbach calcs. 79−63696
^{14}N(^{3}He,p), 15 MeV, ^{16}O excited states from ang. distrib. meas. 78−89891
^{14}N(^{3}He,p)^{16}O, 10 MeV proton polarisation ang. distrib. 79−71861
^{14}N(^{6}Li,^{6}Li′), 153 MeV, isoscalar giant quadrupole resonances 80−13440
^{14}N(^{7}Li,p), 16 MeV, cross section, ^{20}F energy levels, spin, parity 78−21596
^{14}N(^{7}Li,t)^{18}F, 4p-2H, 1^+ rot. band in ^{18}F anal. 77−79299
^{14}N(α,α$_1$)^{14}, 7.6 to 16.9 MeV, study of isospin-mixed ^{18}F states 77−14029
^{14}N(α,α), 20 to 24 MeV, optical model anal. 77−65228
^{14}N(α,α), 23.7 MeV, cross sections, 20 to 170° 78−13118
^{14}N(α,d), determ. of widths of the 14.32 and 14.40 MeV levels in ^{16}O 79−93513
^{14}N(α,γ), 1.51-1.62 MeV, populating ^{18}F 5603 keV level, isospin mixing 78−543
^{14}N(α,γ)^{18}F, hadronic nuclear-parity violation with change of isospin, γ spectrum search 78−94018
^{14}N(d, α), pol. d., vector anal. capacity energy and ang. depend. 80−18281
^{14}N(d, α), pol.d, 1.5-3 MeV, vector anal. capacity for two α-particle groups 80−78266
^{14}N(d, d′)$_x$, energy depend. isospin violation in 10 MeV region 77−14134
^{14}N(d, p)^{15}N, 12 to 52 MeV, stripping reaction anal., distorted wave method 79−80948
^{14}N(d,^{6}Li), 80 MeV, DWBA calcs. spectroscopic factors 79−6623
^{14}N(d,^{6}Li), 80 MeV, resonance-like phenomena 79−13308
^{14}N(d,^{6}Li)^{10}B, 80 MeV, four-nucleon pickup from ^{14}N, spectroscopic factor determ. for ^{10}B 79−63679
^{14}N(d,α)^{12}C, search for quartet excited states in ^{16}O 77−57600
^{14}N(d,n)^{15}O, non-linear behaviour of gas targets for isotope prod. 78−25361
^{14}N(d,p$_0$)^{15}N, 52 MeV, DWBA and impulse approx. anal. 77−34318
^{14}N(d,p)^{15}N, search for quartet excited states in ^{16}O 77−57600
^{14}N(d,p)^{15}N, 0.309-0.638 MeV, differential cross-section, ang. distrib. meas. 77−6396
^{14}N(e,e′), internuclear nucleon effective mass in quasielastic scatt. *(Russian)* 79−3076
^{14}N(e,e) in storage ring, elastic form factor 80−22819
^{14}N(γ,d), from (e,e′d), cross section, E2 transistors giant resonance and clusters 80−63169
^{14}N(γ,γ′), 32 MeV, energy spectra, d prod. process *(Russian)* 80−91177
^{14}N(γ,n$_0$)^{13}N, 17 to 26 MeV, angular distrib., giant dipole resonance, single-particle nuclear model 80−52659
^{14}N(γ,pn)^{12}C, cross-section and ^{12}C distrib., quasi-deuteron mechanism 80−63166
^{14}N(γ,π$^-$), DWIA anal., wave function and π optical pot. effects on cross section 80−63168
^{14}N(γ,π$^-$)^{14}C, threshold, impulse approx. anal. 77−14109
^{14}N(γ,π$^-$)^{14}O, 145-325 MeV, Gamow-Teller suppression and M1 radiative widths 80−52609
^{14}N(γ,π$^+$), anomalous $^{14}N_{gs} \rightarrow {}^{14}C_{gs}$ transition, Kroll Ruderman terms 80−63167
^{14}N(n,2n), 14.7-19.0 MeV, excitation functions relative to ^{56}Fe(n,p) 79−3142
^{14}N(n,2n)^{13}N, meas. of total body N, interfering reactions and spatial sensitivity 77−60240
^{14}N(n,2n)^{13}N reaction for clinical total-body N meas. 79−29589
^{14}N(n,3α)t, 18.2 MeV, correlation spectra meas. 77−2992
^{14}N(n,α)^{11}B, 12-18 MeV, pickup of three nucleons, distorted wave approx. 80−22793

nuclei with mass number 6 to 19 continued

^{14}N(n,α$_1$)^{11}B, 13.9 MeV, differential cross sections meas. 78−78387
^{14}N(n,γ)$_1$, γ-ray energies, calibration standards 80−52613
^{14}N(n,γ)^{15}N, in vivo N determ. using Pu-Be sources 77−86606
^{14}N(n,p$_0$), (n,α$_0$), (n,α$_1$), 0.5 to 15 MeV, cross section meas. 79−54437
^{14}N(p, X), 50 MeV, effective cross sections for charged particles in outgoing channel 80−18294
^{14}N(p,X), 50 MeV, effective cross sections 80−78284
^{14}N(p,X)$_x$, 7.3 GeV, differential fragmentation cross sections 79−54442
^{14}N(p,α)^{12}C, light element profiling of tapered corrosion sections 79−92036
^{14}N(p,d) at 65 MeV, deuteron break-up 77−18535
^{14}N(p,d) modified DWBA anal., optical model parameter influence on vertex consts. *(Russian)* 78−78340
^{14}N(p,γ), 1.74, 2.35 MeV, lifetimes of ^{15}O bound states 77−82928
^{14}N(p,γ), 1.742 MeV, 8.92 MeV doublet and 8.98 MeV level in ^{15}O anal. 77−38243
^{14}N(p,γ)^{15}O, 3.15-3.5 MeV, ^{15}O reson. widths and branching ratios meas. 77−38244
^{14}N(p,γ)^{15}O, isotopic anal., estimation of ^{15}N/^{14}N conc. ratio 79−48014
^{14}N(p,n), 144 MeV, charge exchange, one pion exchange and PCAC tests 80−78299
^{14}N(p,n), 144 MeV, one pion exchange and PCAC expt. test 80−528
^{14}N(p,n)^{14}O, 16 MeV, protein anal. 77−81769
^{14}N(p,n)^{14}O, threshold energy 77−26625
^{14}N(p,p′), 122 MeV, level excitation, cross sections, effective NN interaction, DWIA anal. 80−78197
^{14}N(p,p′)^{14}N at E_p=21 MeV, two-step process, spin depend. interaction 79−89301
^{14}N(p,p), 144 MeV, elastic scatt. cross sections, optical pot. 80−42660
^{14}N(p,p), average geometry optical model potential, doorway state effects 77−79367
^{14}N(p,pd), (p,pt), (p,pα), spectroscopic data on quasielastic ejection on nucleon clusters from 1p shell nuclei 79−80931
^{14}N(p,pd), excitation spectrum of ^{12}C, exchange processes effect, impulse approx. 77−61405
^{14}N(p,pd)^{12}C, quasi-elastic cluster knock out, cross section calc. 78−46042
^{14}N(p,pt)^{11}C, quasi-elastic cluster knock out, cross section calc. 78−46042
^{14}N(p,π$^+$), 0.5-10 MeV, total cross sections near pion Coulomb barrier 80−32280
^{14}N(p,t)^{12}N, 52 MeV, ^{12}N 2.43 MeV level study 77−6235
^{14}N(π$^-$,2n), neutron-pair emission characts., excitation energy spectra 78−13159
^{14}N(π$^-$,2n)^{12}C, ^{12}C excitation spectrum 77−10451
^{14}N(π$^-$,n), single neutron emission induced by stopped π$^-$ in 1p shell nuclei 79−59089
^{14}N(π$^-$,n), stopped pion, neutron energy spectra, mean energies and multiplicities 80−9311
^{14}N(π$^-$,xγ), recoil momentum spectrum of ^{12}C* using deexcitation γ rays Doppler broadened 77−54256
^{14}N(ν,ν), neutral current struct. 78−66269
^{15}N 3/2$^-$ state spin alignment and polarisation, 1/2-spin orbit interaction from ^{27}Al, ^{88}Sr(^{16}O,^{15}N) 80−27622
^{15}N 6.5 MeV ions in solids, energy loss distrib. meas. 78−59845
^{15}N 9.155 MeV state, lifetime, cluster nature and parity from ^{12}C(^{7}Li,αγ), ^{12}C(^{6}Li,^{3}Heγ) 79−6424
^{15}N, anal. by proton scatt. 79−61926
^{15}N chemical shifts in pyridenes, paramag. relax. reagent effect 78−15042
^{15}N, Coulomb form factors, effects of core polarisation 77−30474
^{15}N, direct evidence for 3p-4h excitations 79−67659
^{15}N energy levels populated in ^{13}C(^{3}He,p), p ang. distrib. 78−21581
^{15}N excitation contrib. in optical pot., DWBA grazing peak shift for ^{48}Ca(^{16}O, ^{15}N) 80−86921
^{15}N excited states, R-matrix anal. of n polarisation in ^{14}C(p,n)and ^{11}B(α,n) 78−4937
^{15}N excited states and transitions from ^{15}C beta decay 80−18248
^{15}N, giant reson. excitation around 17 MeV, J^π,Γ assignments 77−34277
^{15}N giant resonance and cross sections from (γ,d) and (d,γ) pol. d 79−93587
^{15}N integrated cross sections to excited residual states from ^{19}F(γ,α) 80−18200
^{15}N, interacting with strongly irradiated proton system, longit. mag. relax., Overhauser enhancement 78−19377
^{15}N level excitation functions, resonance, p ang. distribs. from ^{13}C(^{3}He,p), 3.6-6.6 MeV 78−93942
^{15}N low lying analogue states, DWBA anal. from ^{16}O(d, ^{3}He) 29 MeV, polarised d 78−82285
^{15}N low lying states, cross sections and anal. power, transitions, spectroscopic factors from ^{14}N(d,p), pol. d 80−32183
^{15}N low-lying positive parity states, Nilsson scheme from ^{14}C(^{3}He,d) 79−80871
^{15}N low-lying states, obs. in (e,e′) scatt. 78−12976
^{15}N, mag. moments, configuration mixing and meson exchange contrib. 78−17100
^{15}N NMR chem. shift references evaluation 78−24835
^{15}N, NMR in solid N_2, anisotropy of chem. shift tensor 77−90053
^{15}N, NMR in $ThC_{1-x}N_x$ and $UC_{1-x}N_x$ 77−20736
^{15}N, NMR of bacteria, yeast and leukaemic cells 77−90742
^{15}N NMR of haemoglobin 77−90720
^{15}N, NMR signal intensity enhancement by polarisation transfer 79−94013
^{15}N, NMR spectra of isotopically enriched N-methyl formamide in isotropic and nematic phases 77−32270
^{15}N, neutron binding energy 80−47362
^{15}N, neutron binding energy from ^{1}H(n,γ) 80−52564
^{15}N, obs. of high spin states in ^{12}C(^{6}Li,t) and ^{12}C(^{6}Li, ^{3}He) 78−13015
^{15}N, one-hole states, in double magic nuclei, form factors, spectroscopic factors, centroid energies 78−17090
^{15}N, photoabsorption, shell-model anal. of giant dipole state 78−29447
^{15}N polarisation, spin alignment and excited state ang. distrib. from ^{88}Sr(^{16}O, ^{15}N) 79−67709
^{15}N, reson. obs. using ^{13}C(d,γ) reaction 77−6395
^{15}N, spin assignments for giant resonances from ^{11}B(α,γ$_0$), 15.5-19.5 MeV 78−94019
^{15}N, spin-lattice relax. meas. in TGS near ferroelec. transition 77−1646
^{15}N, spins of p-h states from (d,τ) analysing powers 78−25111

nuclei with mass number 6 to 19 continued
^{15}N states, cross sections and lifetimes, EM decay strengths from 3 and 4 particle transfers 80−9237
^{15}N, study of excited states, spin and parity *(French)* 78−33158
^{15}N three particle states at high excitation energies, J^{π}, selective population from $^{12}C(^{7}Li, \alpha)$ 80−99129
^{15}N transfer spectra direct contrib. from $^{208}Pb(^{16}O,X)$ projectile fragmentation 80−63155
$^{15}N/^{14}N$ ratio in Galaxy, interpretation of obs. 78−4356
$^{15}N_{3/2}$ (6.33 MeV) state, spin alignment meas. from $(^{16}O,^{15}N)$ using γ-recoil 79−17796
^{15}N-^{13}C spin-spin coupling consts. calcs., lone pair contribs. 77−480
^{15}N-^{13}C spin-spin coupling constants calc. using SCF and INDO method 80−32609
^{15}N-$^{1}H^{+}$ NMR, coupling consts., double reson., difference proton Fourier transform spectroscopy 79−3467
$^{15}N+X$, X=^{11}B,^{12}C,^{18}O,^{13}C, deduced excited states, shell model wave functions, DWBA anal. 79−45284
$^{15}N+n$, continuum shell model calcs. of particle emission threshold effects, cross section, line shape of resonances 78−46014
$^{15}N+p$ reactions, ^{16}O energy levels near 15 MeV excitation, R-matrix anal. 78−29460
$^{15}N(^{15}N,X)$, π^0 condensation, spin-isospin instabilities, TDHF calcs. 80−83042
$^{15}N(\alpha,\alpha)^{15}N$, backscatt., heavy particle transfer mechanism 77−6420
$^{15}N(\alpha,\alpha)$, E_{α}=16-23.7 MeV, differential cross sections, ang. distribs. and excitation functions 78−13121
$^{15}N(\alpha,\alpha)$ forward differential cross sections determ. using Feynman diags. 78−25210
$^{15}N(d,\alpha)$, E_d<3 MeV, intermediate structure 77−10412
$^{15}N(d,d)$, 1.4-2.7 MeV, excitation functions 77−23094
$^{15}N(d,p)$, 1.4-2.7 MeV, excitation functions 77−23094
$^{15}N(d,p)^{16}N$ off-shell effects 78−62545
$^{15}N(e,e')$, 52-195.3 MeV, giant resonance electroexcitation, C1, C2 strength distribs. 79−510
$^{15}N(e,e')$, excitation of energy levels 9.7 to 14.7 MeV, 60-194 MeV, EM form factor meas. 78−25175
$^{15}N(e,t_0)$, 20-25 MeV, photodisintegration and electrodisintegration 79−80922
$^{15}N(\gamma,\gamma)$, 6.324 MeV, resonance scatt. cross section temp. depend. in BN, NH_4Cl 80−57767
$^{15}N(\gamma,\gamma)$, zero point vibr. energy in BN and NH_4Cl 80−59593
$^{15}N(n,n)$ elast. and inelast. scatt. shell model anal. of threshold effects *(Russian)* 77−287
$^{15}N(n,n)^{15}N$, reson. struct. in continuum shell model, heavy-ion implications 77−54243
$^{15}N(n',n)^{15}N$, continuum random phase approx. 80−27635
$^{15}N(p,\alpha_0)^{12}C$, 93 to 418 keV, remeas. of low energy cross section, astrophys. S-factor determ. 79−63665
$^{15}N(p,\alpha)$ $(p,\alpha\gamma)$, 0.9-1.25 MeV, ^{16}O levels, J^{π} 78−509
$^{15}N(p,\alpha)^{12}C$, <1.25 MeV polarised protons, ang. distribs. 77−3009
$^{15}N(p,\alpha)^{15}N$ 2.50-5.14 MeV, 3^+ ^{16}O reson. state excit. 78−580
$^{15}N(p,\alpha\gamma)^{12}C$, isotopic anal., estimation of $^{15}N/^{12}C$ conc. ratio 79−48014
$^{15}N(p,\gamma_{0,1,2})$, 6-22 MeV, ang. distrib. and correl. meas., ^{16}O excited state giant resonance 77−82926
$^{15}N(p,\gamma)$, ^{16}O excited state GDR, coupled channels version of continuum shell model 79−542
$^{15}N(p,\gamma)$, 30-100 MeV, meson exchange and nucleon correlation process calcs. 79−549
$^{15}N(p,\gamma)^{16}O$, anal. of ^{16}O giant dipole reson. struct. 78−4942
$^{15}N(p,n_0)^{15}O$, 8.5-19.0 MeV, resonance struct., excitation functions, cross sections 78−50164
$^{15}N(p,n)$, 3.75-7.5 MeV, continuum shell-model coupled-channel calcs. 77−34269
$^{15}N(p,p)$, 18-44 MeV, differential cross sections, phase shift anal., energy depend. 80−47481
$^{15}N(p,p)^{15}N$, 2.50-5.14 MeV, 3^+ ^{16}O reson. state excit. 78−580
$^{15}N(\pi^+,\pi^0)^{15}O$, isobar hole model calc. of single charge exchange 79−85523
$^{15}N(t,p)$, 15 MeV, 2p-1h states in ^{17}N, spins parities, cross sections 78−62548
^{16}N, 1-20 ps region mean lifetime meas., high-vel. DSA method 77−65200
^{16}N, (π^-,γ) and (μ^-,ν_{μ}) capture rates, A=16 ground and excited states 78−17105
^{16}N activity from $^{16}O(n,p)^{16}N$, nuclear powered ship, computer code and expt. comparison 78−13192
^{16}N ground state quadruplet, DWBA anal. of $^{14}N(t,p)$ 79−22200
^{16}N γ-rays for activation of elements in (γ,γ') reaction 78−88689
^{16}N, $J^{\pi}=1^-$ assignment from $^{15}N(d,p)$ 79−30786
^{16}N, levels at 5.5-8.5 MeV from $^{14}N(t,p)$ 78−66207
^{16}N levels from $^{18}O(d,\alpha)$ using polarised deuterons, spin parity assignments 78−89886
^{16}N particle hole spectra, spectroscopic strengths, from $^{17}O(d,\tau)$ tan studies 78−58288
^{16}N, random phase approx. including continuum treatment 79−59024
^{16}N structure of 1^+ states populated in two nucleon transfer and ^{14}C beta decay 78−50085
^{16}N tag for water transient flow meas. 79−14504
^{16}N tagging for two-phase mass flow measurement 79−93793
$^{16}N/^{17}N$ levels in reactor, primary coolant flow rate determ. 77−65254
$^{16}N^*$ beta-decay, elementary particle treatment 78−8800
$^{16}N^*(0^-)$ beta decay, calculated decay rate 79−59036
$^{16}N(0^-)\rightarrow{}^{16}O(0^+)+\bar{\nu}e+e^-$, one pion exchange current problem for $^{16}O(0^+)\rightleftarrows{}^{16}N(0^-)$ 79−85375
$^{16}N(0^-)\rightleftharpoons{}^{16}O(0^+)\beta$-decay and μ-capture, mesonic exchange correction 78−41673
$^{16}N(p,p')^{16}N^*$, 5.7 MeV, $J^{\pi}=1^+$, line shape 77−54211
$^{16}N(p,p')^{16}N^*$ (E_x=3.226 MeV), lineshape model calc. *(German)* 77−22989
^{17}N, 1p spin-orbit splitting anal. with $^{18}O(d,\tau)$ at 52 MeV 77−41980
^{17}N 2p-1h states from $^{15}N(t,p)$, spins, parities, cross sections 78−62548
^{17}N, β-decay delayed neutron emission, ^{17}O levels, T1/2 meas. 77−18481
^{17}N, excited states obs. in $^{18}O(t,\alpha\gamma)$ at 3.5 MeV *(French)* 77−14031
^{17}N levels and ang. distribs. meas., shell model calcs. from $^{15}N(t,p)$ 80−9233
^{17}N yields from proton-nucleus collisions, isotope depend. *(Russian)* 77−61429
^{18}N, mass excess and excited states from $^{14}C(^{18}O,^{18}N)$ 80−42676

nuclei with mass number 6 to 19 continued
^{19}N, mass excess via $^{18}O(^{18}O,^{19}N)^{17}F$ 91 MeV reaction 77−74753
^{19}N, mass meas. via $^{18}O(^{18}O,^{19}N)^{17}F$ 91 MeV 77−22868
NaF+Ne, 800 MeV/N, p and π inclusive spectra, energy and ang. distribs. 78−54790
NaF+Ne, 800 MeV/N, p and π inclusive cross sections, non-equilibrium processes 79−40947
NaF+Ne, evidence for blast wave production in fireball explosions 79−49592
$N(\alpha,^2He)$, A=14, 15, 55, 65 MeV, two neutron states, A-depend. of binding energy 78−74379
Ne, low spin states populated in $^{16,18}O(^3He,n)$ 77−14141
^{16}Ne ground state masses in isospin quintet from (π^+,π^-) 80−105960
^{16}Ne mass excess and diproton decay width from $^{20}Ne(^4He,^8He)$ 117 MeV 78−78245
^{16}Ne, mass excess from π double charge exchange reactions 78−70573
^{18}Ne analogue and nonanalogue states, π double charge exchange form factors from $^{18}O(\pi^+,\pi^-)$ 80−13405
^{18}Ne cross section, excitation function and double isobaric analogue state from $^{18}O(\pi^+,\pi^-)$ 80−27596
^{18}Ne ground state obs. in $^{18}O(\pi^+,\pi^-)^{18}Ne$ at 148, 187 MeV 77−74883
^{19}Ne $3/2^+$ state config. from ang. distribs. and cross section of $^{21}Ne(p,t)$ 79−9473
^{19}Ne alpha-particle and triton cluster states anal. 77−41907
^{19}Ne, β-decay, recoil ion energy spectrum anal. 78−21525
^{19}Ne, even parity excited states, collective props., EM moments, generator coordinate method 78−78259
^{19}Ne, even parity state, EM props., collective struct., generator coord. method, HF method anal. 79−89220
^{19}Ne, final state selective population, triton clustering from band anal. from $^{16}L(^6Li,t)$ 80−9306
^{19}Ne, mean lifetimes via $^{19}F(p,n\gamma)^{19}Ne$ at 12 MeV 77−54180
^{19}Ne, spectra and E1 transitions, ang. momentum projected HF and Tamm-Dancoff methods 77−54139
$^{19}Ne\rightarrow{}^{19}F+e^++\nu$, test of time reversal symmetry 77−30521
$^{19}Ne\rightarrow{}^{19}Fe+e^++\nu_e$, limit on Fierz interference 78−560
^{20}Ne resonances, J^{π}, excitation functions and branching ratio from $^{19}F(p,\gamma)$ 80−22787
^{20}Ne unnatural parity levels populated in $^{16}O(^7Li, d)$, reaction mechanisms 77−14158
$^{20}Ne+^{12}C$ orbiting dinuclear system, inelastic scatt. cross section 80−22854
$^{20}Ne(^{12}C,^{12}C)$, symmetry and shell struct. effects on absorption, precompound states 80−27666
^{21}Ne, parity-nonconserving nucleon-nucleon pot., large parity admixtures 78−82278
^{22}Ne 3.34 MeV level lifetime meas. by Doppler-shift method, slowing down environment effect 77−38245
$^{14}Ni(e,e')$, mag. dipole and quadrupole state excitation 78−50154
$N(n,\gamma)$, 14 MeV neutron source, electron recoil spectra from gamma-rays anal. 77−26683
N(p,X), 340, 660 MeV, ang. distribs., proton quasi-elastic knockout *(Russian)* 80−52649
N(p,X), 400 GeV/c, multiplicity and ang. distribs. of relativistic and slow particles *(Russian)* 79−40931
N(p,X), 740 MeV, ^7Be prod. cross section for cosmic ray anal. 79−93625
$N(\pi^-,X)$, charged heavy particle emission after pion capture *(Russian)* 80−69271
$N(\pi^+,2p)$, 112 MeV, reaction mechanism *(Russian)* 78−29508
$N(\pi^+,\pi^+d(He))$, 60 MeV, cross sections, momentum and ang. distribs. *(Russian)* 77−74888
$N(\pi,\pi p)$, 170 MeV, two stage and knock out contribs., π^+,π^- spallation differences *(Russian)* 80−68632
$N(\pi\pm,\pi^{\pm}X)$, X=He or d, 170 MeV, cross sections and ang. distribs., direct knockout mechanism *(Russian)* 80−86887
O cross section data test using n spatial distrib. in water 78−74417
O energy loss params., appl. on mass determ. of cosmic ray nuclei in nuclear emulsion 78−94175
O Hartree Fock pot., truncated space calcs. of exact bound state energies 79−3090
O ion induced fission of nuclei from Ag to U, fragment ang. distribs. *(Russian)* 78−17264
O, isotopic sequence charge distrib. calc. 79−85361
O, μ^- capture, charged particle energy spectra *(Russian)* 78−89828
O, neutron-photon multigroup cross sections for neutron energies ≤60 MeV 79−30880
O, recoiling in magnetised Fe, transient mag. fields 77−12263
$O+^{27}Al$, total fusion cross section near Coulomb barrier 78−13141
O+n in cellulose nitrate plastic detector, spallation products 78−17198
O+nuclear emulsion, 2.1 GeV/amu, scatt. const. 78−13151
O+p, inelastic interactions, 6.0 GeV/c, in emulsions 78−86530
$O(^{12}C,^{12}C')$, 50 GeV/c, multiplicities and ang. distribs. *(Russian)* 79−22323
$O(^{12}C,X)$, 4.5 GeV/c, emission of short range particles (R<100 mkm) *(Russian)* 80−63202
$O(^3He,n)$, low spin states populated in $^{18,20}Ne$ 77−14141
^{A}O (n,n), A =16 to 18, thermal neutron scatt. parameters 79−93628
^{A}O A=16, 17, deduced levels, spectroscopic factors from $^{12,13}C(^{13}C,^9Be)$ 79−26454
^{A}O, A=16, 17, non-self-consistent energy calculations with a density-dependent effective interaction 79−36170
^{A}O, A=16, 17, valence-core self-consistency, wave functions, binding energy, levels, spectra 80−63123
^{A}O, A=17, 19, level scheme, two-step transfer contribs., coupled channel anal. from $O(^{13}C,X)$ 80−32181
^{A}O, A=18, 19, E2 transition rates calc., shell model with effective interaction and charges 80−47423
$^AO+^{12}C$, A=16,18,22 79−45316
$^AO(^{12}C,X)$, A=16,18, fusion cross sections by TDHF calcs. 79−89342
$^AO(^3He,^3He)$, A=16, 18, optical potentials and volume integrals, mass and energy dep. 80−52686
$^AO(\pi,\pi)$, 163 MeV, A=16, 18, comparison of π^+ and π^- scatt. at (3,3) resonance 78−86552
$^AO(\pi^-,\pi^-)$, (A=16,18), 29.2 MeV, neutron radii determ. 79−97653
$^AO(\pi^-,\pi^-)$, A=16,18, 29 MeV, differential cross sections 79−85534
$^AO(\pi^+,\pi^-)$, A=16,18, cross section and ang. distribs., Glauber and coherent fluctuation models *(Chinese)* 80−102211
$^AO(\pi^{\pm},\pi^{\pm})$, A=16, 18, resonance region, proton and neutron distribs. 80−91195
$^{10}O(e,e)$, charge form factors in α cluster model 79−63571

nuclei with mass number 6 to 19 continued
^{12}O ground state masses in isospin quintet from (π^+,π^-) 80−105960
^{12}O mass excess and diproton decay width from ^{16}O(^{4}He,^{8}He) 117 MeV 78−78245
^{14}O, half life determ., precision meas. 78−90043
^{14}O low lying states, exact finite and zero range DWBA anal. from ^{12}C(^{3}He,n), 12-24 MeV 78−82286
^{14}O, superallowed Fermi β-decay half lives 78−82318
^{14}O$_{g.s.}$ β-decay, mesonic exchange currents, weak process microscopic treatment 80−57742
^{14}O(β^+)^{14}N*, Q-value 77−26625
^{14}O→^{14}N e$^+\nu_e$, rate calcs. using elementary particle and macroscopic treatments 78−29429
^{15}O activation in tissue, use in radiotheraphy proton beam localisation 77−48862
^{15}O, axial vector decay, exchange corrections 79−36201
^{15}O, level scheme determ. from ^{14}N(p,γ) 77−38243
^{15}O levels from ^{15}N(p,n$_0$), resonance struct., excitation functions, cross sections 78−50164
^{15}O, lifetimes of bound states populated in ^{14}N(p,γ) 77−82928
^{15}O low lying analogue states, DWBA anal. from ^{16}O (d,t) 29 MeV, polarised d 78−82285
^{15}O, mag. moments, configuration mixing and meson exchange contrib. 78−17100
^{15}O, normal parity levels from P-model calcs. with realistic NN interaction *(Russian)* 80−32194
^{15}O, nucl. g-factor and lifetime of 5.24 MeV 5/2$^+$ level 78−37269
^{15}O, obs. of high spin states in ^{12}C(^{6}Li,t) and ^{12}C(^{6}Li, ^{3}He) 78−13015
^{15}O production, non-linear behaviour of gas targets 78−25361
^{15}O, production by cyclotron, biomedical appls. *(French)* 80−56216
^{15}O, recoils from ^{16}O(n,2n)^{15}O, labelled mol. O_2 form. 78−3359
^{15}O, reson. widths and branching ratios meas. from ^{14}N(p,γ)^{15}O 77−38244
^{15}O, study of excited states, spin and parity *(French)* 78−33158
^{15}O T=3/2 levels from ^{17}O(p,t) 78−78264
^{15}O-^{15}N, Coulomb energy anomaly and charge-dependent nuclear forces 79−58997
^{15}O-CO_2 inhalation, for left heart imaging 77−9240
(^{16}O,^{16}O), M3Y folding model eval., model independ. anal. 80−78317
(^{16}O,X), 2 GeV/N, anomalous nuclei among relativistic projectile fragments 80−106034
^{16}O, $^1S_0$ two-nucleon T matrix, interior wave function 77−14038
^{16}O, 0$^-$ levels, energy shift, two channel anal. 79−75840
^{16}O, 0$^+$ level pot. harmonics and matrix elements, BE contrib. *(Russian)* 77−82835
^{16}O, 0$^+$ states, appl. of K-harmonics method 78−54685
^{16}O, 2.1 GeV/nucleon, fragmentation parameters in emulsion 77−3027
^{16}O, 2p bound π absorpt, p-wave rescattering terms for light nuclei 78−70575
^{16}O, 3 α forces, ground state energy and form factor 80−86817
^{16}O 3$^-$→0$^+$ gamma transition from ^{12}C(^{16}O,^{16}O) 80−63125
^{16}O, 3$^+$ reson. state, particle-hole component via (p,p) and (p,α) reactions 78−580
^{16}O, 31$^-$ state, precession in Fe foil, depend. on magnetisation 78−37285
^{16}O, 4$^-$ particle-hole states, isospin mixing 80−99123
^{16}O 4$^+$ state nonstatistical population in compound nucleus calcs. of ^{12}C(^{6}Li,d) 80−102137
^{16}O, 5.0-9.3 MeV neutron scatt., differential cross sections and neutron ang. distribs. 77−23093
^{16}O (α, 2α), DWIA calc., cross section and spectroscopic factors 79−63681
^{16}O, (d,d) and (d,p) reactions, finite-range coupled-channel calcs. 77−10377
^{16}O (n,p) and (n,d) reactions, study of isovector analogue giant resonances, proton hole states 77−26726
^{16}O (p,2p) 200 MeV polarised protons, j-dependence obs. in quasifree scatt. 77−10401
^{16}O, (π^-, γ) and (μ^-, ν_μ) capture rates, A=16 ground and excited states 78−17105
^{16}O, adiabatic mass parameters, isoscalar quadrupole modes 77−14049
^{16}O, alpha width meas. in ^{12}C→^{16}O reactions relevant to astrophysics 79−6682
^{16}O, alpha-cluster states, spin, parity and branching ratios 78−50066
^{16}O and infinite nuclear matter, mesonic and isobar degrees of freedom 79−9491
^{16}O and Sd shell nuclei, binding energy from realistic Hamiltonians and spectral distrib. theory 80−22678
^{16}O, anomalous, in meteorites, prod. by explosive nucleosynthesis 79−62795
^{16}O, α-cluster deformation elastic form factors of electron scatt. 79−17829
^{16}O α-cluster levels, props., hard-core potential calcs. 77−30614
^{16}O, α-cluster model, clustering and nuclear forces in terms of quark struct. 79−6443
^{16}O, α-cluster model comparison with giant E2 excitations 78−50109
^{16}O α-cluster states, widths and resonances, optical model, direct transfer in ^{12}C(^{6}Li,d) 80−105975
^{16}O, α-spectroscopic amplitudes, jj coupling and isotopic spin formalism 77−14072
^{16}O, α-spectroscopic amplitudes in shell model 77−71564
^{16}O, α-spectroscopic amplitudes anal. using shell model based calc. 79−13203
^{16}O, α-transfer reactions, spectroscopic factors, exact finite range DWBA anal. 80−13372
^{16}O, binding energy, wave function of ground state, orthogonal schema model 79−63582
^{16}O, bound isobars Δ(1236), single particle energies, wave functions *(Chinese)* 80−52562
^{16}O, breathing mode, K-harmonics calc. 77−6200
^{16}O, Brueckner-Hartree-Fock calcs. with Δ resonance inclusion in one-boson-exchange potential 77−54155
^{16}O, Brueckner-Hartree-Fock approach, variational definition of single particle pot. 80−32170
^{16}O, bulk props., ground state energies and RMS charge radii 78−58242
^{16}O, calc. of spectrum of O$^+$ levels 79−63627
^{16}O, capture rate of μ^-, meas. by Saclay linac beam *(French)* 79−368
^{16}O, centre-of-mass spuriosity in continuum shell-model calculations 80−32210
^{16}O, charge density calcs. K_{mm} approx. 79−9456
^{16}O, charge distribution, orthogonal scheme model *(Russian)* 78−29382

nuclei with mass number 6 to 19 continued
^{16}O, charge form factors of doubly closed shell nuclei 77−6274
^{16}O charge form factors pion exchange currents effects 77−18379
^{16}O, closed shell nuclei, convergence studies for the one body mass radius operator 79−45146
^{16}O, cluster expansions for normalisation integral calc. 80−86831
^{16}O collective and giant multipole states, Brueckner RPA particle-hole state description 80−32169
^{16}O, compound particle knock out reactions, account of residual interactions *(Russian)* 77−14090
^{16}O, configuration mixing and α-cluster transfer 78−46004
^{16}O, constrained variational calcs. for binding energy and RMS radii, N*(1234) allowance 79−3074
^{16}O, contrib. of meson exchange currents to charge density and RMS radius 77−10313
^{16}O, coupled channel anal. of Λ'(1405) in kaonic atoms 78−540
^{16}O determ. of widths of 14.32 and 14.40 MeV levels from ^{14}N(α,d) 79−93513
^{16}O, dipole polarisability sum rule, HF calc., 78−21504
^{16}O, Δ(1236) inobar probability is nuclear many-body system ground state 79−75859
^{16}O, Δ(3,3) excitations and effective 3-nucleon forces 80−27561
^{16}O E1 and p_0 channel E2 strength from ^{15}N(p,γ) 80−22790
^{16}O, effective interactions, folded diagram expansion, self consistent and oscillator sd shell model spaces 78−21502
^{16}O, elastic and inelastic scatt. of ^{10}B, ^{14}N, common and optical potential 77−34276
^{16}O, electric quadrupole strength, giant quadrupole resonance 80−52575
^{16}O, energy calcs., Jastrow variational method extension, FAHT cluster expansion 80−22677
^{16}O, energy levels, ^{13}C(^{3}He,$\alpha\gamma$)^{12}C radiative capture reaction, particle-hole picture 79−9471
^{16}O energy states, HF calcs. using cartesian basis wave functions 78−74319
^{16}O, exchange current corrections for muon partial capture rates 78−33152
^{16}O excited 0$^+$ levels 80−42551
^{16}O excited state GDR from ^{15}N(p,γ), coupled channels version of continuum shell model 79−542
^{16}O excited states from ^{14}N(^{3}He,p), ang. distrib. meas. 78−89891
^{16}O excited states near 15 MeV, R-matrix anal. of ^{15}N+p reactions 78−29460
^{16}O, exotic nuclei stability anal., Hartree-Fock approx. with the Skyrme interaction 78−82273
^{16}O, external mixing of resonance states in continuum shell model 79−22257
^{16}O form factor effects, zero range DWBA calcs. from ^{18}O(p,t) 80−491
^{16}O fragmentation at intermediate energies, statistical fluctuation, fragment momentum distribs. 80−78263
^{16}O, giant dipole reson. struct. anal. from ^{15}N(p,γ)^{16}O 78−4942
^{16}O, giant dipole resonance fine struct., 5p-5h excitation model *(Chinese)* 78−82271
^{16}O, giant E1 resonance obs. in ^{15}N(p,γ_0) at 8.6-18 MeV 78−66256
^{16}O giant electric and magnetic multipole resonances, microscopic descript. 78−538
^{16}O, giant isoscalar monopole state energies in generator coordinate method 80−37317
^{16}O, giant monopole resonance widths, RPA calcs. based on Skyrme interaction 78−93984
^{16}O, giant resonances, self-consistent microscopic anal. including particle continuum 77−2896
^{16}O ground state and binding energy, microscopic calc. with realistic NW interaction *(Russian)* 80−5052
^{16}O, ground state energies, four order high lying contribs. 79−75850
^{16}O ground state energy and low odd parity states, correlated basis function method 80−57689
^{16}O, ground state props., modified Brueckner-Bethe-Goldstone method 78−50076
^{16}O ground-state energy, nonunitary model operator approach 80−83030
^{16}O, HF charge distribs. 77−14024
^{16}O, Hamiltonian matrix analysis, base model of orthogonal scheme for 0$^+$ state 79−63610
^{16}O, Hartree-Fock calculations of nuclear bulk properties with density- and starting-energy dependent effective interaction 80−9246
^{16}O high spin states, J$^\pi$ and α-decay branching ratios from ^{12}C(^{12}C,^{8}Be) 80−18166
^{16}O highly excited states from ^{12}C(^{6}Li,d), spin, parity, decay into α+^{12}C 77−79395
^{16}O, hyperfine interactions of highly stripped ions recoiling into H and He 77−22932
^{16}O independent particle shell model momentum density distrib., short range correlations 80−78176
^{16}O induced reactions in nuclear emulsions at 2.1 GeV/nucleon, multiplicity distrib. of white and grey tracks *(Spanish)* 80−47495
^{16}O, inelastic form factors for abnormal parity states, K-harmonic method *(Russian)* 78−25113
^{16}O, isobar configurations in closed shell nuclei 78−66226
^{16}O, isoscalar giant monopole vibrs., time-depend. HF calc. 77−22986
^{16}O isoscalar giant quadrupole resonance, α-decay dominance from ^{16}O(α,α'+charged particle) 78−46035
^{16}O, isoscalar giant quadrupole resonances, RPA calcs., E2 strength fragmentation, spectroscopic factors 80−13437
^{16}O, isoscalar giant resonances and Landau parameters with density-dependent effective interactions 79−71827
^{16}O, isospin forbidden 7.12 MeV E1 transition, continuum shell-model calc. 77−18472
^{16}O, isospin mixing anal. 78−8832
^{16}O, isospin mixing in 7.12 MeV 1$^-$ state 77−283
^{16}O, isospin mixing in nuclei, matrix elements explained by Coulomb interaction 78−37264
^{16}O isospin mixing matrix elements, three level model 80−78136
^{16}O isotopic anomalies in solar system, local proton irradiation model 78−93128
^{16}O, isovector GQR splitting 77−22988
^{16}O level excitation functions, resonances from ^{12}C(^{16}O,^{12}C) 80−63146
^{16}O levels, Hauser Feshbach and DWBA anal. α-spectroscopic strengths from ^{12}C(^{6}Li,d), 20-34 MeV 79−569
^{16}O levels and ang. distribs., ^{3}He spectroscopic strengths, Hauser-Feshbach/DWBA anals. of ^{13}C(^{6}Li,t) 80−47390
^{16}O, levels near 13 MeV via ^{15}N+p 0.9-1.25 MeV 78−509

nuclei with mass number 6 to 19 continued
- ^{16}O, longit. isoscalar electroexcitation, sum rules and mean excitation energy 78−521
- ^{16}O, lowest T=2 state isospin forbidden decays, branching ratios 79−67703
- ^{16}O, M2 giant resonance calcs. from (e,e'),(π^-,γ),(μ^-,ν) 80−22784
- ^{16}O mag. dipole strength, M1 resonances from ^{15}N(p,γ), polarised p 79−80898
- ^{16}O, magic nuclei at collective excitations, energy spectrum and shape *(Russian)* 80−106015
- ^{16}O, magic nucleus, nonlocal pots., binding energies 77−41877
- ^{16}O magnetic dipole strength 80−37385
- ^{16}O, meson dynamics in many-body calc. 77−22917
- ^{16}O, mesonic and isobar degrees of freedom, Brueckner Hartree Fock calc., binding energy 79−63600
- ^{16}O microscopic determ. of nucleon momentum distribs. 78−70428
- ^{16}O, mixed T=0 and 1 states, isospin mixing matrix elements 78−37289
- ^{16}O, monopole vibration damping, TDHF calcs. 80−22667
- ^{16}O, neutrino absorption cross-sections, <500 MeV, Helm model 77−41956
- ^{16}O, nuclear incompressibility, Hartree-Fock calc. *(Russian)* 79−49577
- ^{16}O, nucleon self-energy in finite nuclei; renormalisation, nucleon-meson interaction 78−17110
- ^{16}O, nucleon-nucleon scatt., correlations, short-range, with pseudopotentials 78−37225
- ^{16}O, octupole GR strength via ^{16}O(p,p')^{16}O, 42.5-49.3 MeV, polarised protons 77−57644
- ^{16}O, odd parity levels, correlated basis functions method 80−22721
- ^{16}O, one particle density distrib., nucleon density, from nuclear ellipsoid of inertia *(Russian)* 79−30784
- ^{16}O, one pion exchange effects on 0^- level positions 77−6232
- ^{16}O, oscillator matrix elements from NN phase shifts and short range correl. 77−271
- ^{16}O, parity violating alpha decay width 77−14073
- ^{16}O, particle hole calculations, centre of mass subtracted kinetic energy 78−62491
- ^{16}O particle-hole spectra, spectroscopic strengths, from ^{17}O(d,t) triton studies 78−58288
- ^{16}O, particle-hole state self-consistent calcs. 77−67713
- ^{16}O, pion condensation and short range correlation 77−6245
- ^{16}O, pion condensation effects, RPA calcs. *(Chinese)* 80−47407
- ^{16}O, pion exchange currents and nuclear charge form factors 77−10338
- ^{16}O, pion photoproduction and radiative capture 78−50213
- ^{16}O, pion-exchange contribs. to charge densities, HF calcs. 78−46001
- ^{16}O, populated in ^{12}C(^{6}Li,α)^{14}N, α-particle spectrum sharp lines observation *(Russian)* 78−29495
- ^{16}O, positive parity giant multipole resons., particle hole shell model 79−30811
- ^{16}O, π, electroproduction, near threshold, inelastic response functions 78−33172
- ^{16}O, π bound states in finite nuclei 78−46013
- ^{16}O, π^- capture reactions, neutron spectra determ. by 2 and 4 nucleon cluster expansions 79−6703
- ^{16}O, π^+ electroprod., distorted wave impulse approx. anal. 79−17894
- ^{16}O, π^+ induced four nucleon removal 78−25242
- ^{16}O, quasielastic scatt. of polarised 635 MeV protons, depend. of left-right asymm. on nucl. momentum *(Russian)* 77−79384
- ^{16}O, RPA calc., many-body oscills. problem 78−82298
- ^{16}O, random phase approx. including continuum treatment 79−59024
- ^{16}O region, E2 core-polarisation charge 77−22888
- ^{16}O region, effect operators, number conserving set generalisation 80−42555
- ^{16}O, relativistic Hartree-Fock eqns., 1 boson exchange pot., spin orbit splitting 79−3106
- ^{16}O relativistic ions, fragmentation cross-sections in CsI 77−67770
- ^{16}O, relativistic self-consistent nuclear model, separation energy, mean square radius *(Russian)* 79−97654
- ^{16}O, residual interactions, current conserving RPA calculations 80−57710
- ^{16}O residual states, vector anal. power. optical pot. from ^{12}C(^{6}Li,d), polarised ^{6}Li 79−97697
- ^{16}O resonance, giant resonance, populated in ^{15}N(p,$\gamma_{0,1,2}$), ang. distrib., γ correl., spin assignments 77−82926
- ^{16}O, rotational band collectivity, shell model excitation in Sp(4, R) symmetry 80−102095
- ^{16}O, saturating effect of N*(1234) on binding 78−58231
- ^{16}O, search for $0^-\rightarrow 0^+$ pair transition 78−86508
- ^{16}O, search for 0^+ level near 8.87 MeV 2^- level using ^{4}He(^{12}C,^{4}He) 77−88044
- ^{16}O, search for quartet excited states via ^{14}N(d,α)^{12}C and ^{14}N(d,p)^{15}N 77−57600
- ^{16}O, self consistent K-matrix model calc. 77−6257
- ^{16}O, self-consistent generator coord. for giant monopole reson. 77−2891
- ^{16}O, shell and cluster model wave functions 78−29412
- ^{16}O, single determinantal states, HF and energy variance minimisation methods 77−6204
- ^{16}O, single-particle potential, symmetry coefficient and effective mass in nuclear matter 79−13234
- ^{16}O, Skyrme-type interactions, spectroscopy of light nuclei, density dependent Hartree-Fock 80−22717
- ^{16}O, Sp(6,R) symmetry, α-breakup amplitudes, of giant E2 excitations 78−29435
- ^{16}O, spherical nuclei, geminal product approx. 78−66230
- ^{16}O, spherical nuclei, total binding energy, many body field theory 77−30482
- ^{16}O, spin-orbit coupling in relativistic Hartree model 78−8731
- ^{16}O, spreading of giant quadrupole resonance, calcs. using 2p-2h admixtures 78−21485
- ^{16}O, spreading widths of giant reson. calc., core-coupling RPA approx. 77−74827
- ^{16}O states, J^π from ^{12}C(^{12}C, $\alpha\alpha$) 80−22660
- ^{16}O states obs. in ^{12}C(^{7}Li,t), ^{12}C+4 particles vertex 77−14030
- ^{16}O, struct. in giant resonance region obs. in ^{13}C(^{3}He,γ), 25 to 30 MeV 79−63650
- ^{16}O structure, energy levels, binding energy, cluster model with varying hinge angle 78−4907
- ^{16}O T-mixed analogue states, (^{3}He,p)/(t,p) cross section ratio from ^{14}N(t,p), ^{14}N(^{3}He,p) 79−9478
- ^{16}O, T=0 pairing vibr. determ. from ^{14}N(^{3}He,p) 78−70422
- ^{16}O, tetrahedral rotor behaviour, charge form factors, deformed α clusters 79−45141

nuclei with mass number 6 to 19 continued
- ^{16}O, third order contributions to binding energy 77−30481
- ^{16}O, transient fields in magnetised Fe, g-factor meas. 77−22887
- ^{16}O two boson approach test, interacting boson approx., 0^+ and 2^+ levels 79−9489
- ^{16}O, two nucleon emission following bound pion absorption 78−82395
- ^{16}O, two-parameter nucleon density distrib., form factors calc. 77−65193
- ^{16}O, vector polarised ^{6}Li elastic scatt., full optical model anal. 78−70553
- ^{16}O, vibrating nucleus, adiabatic anal. of time-dependent HF solns. 79−40863
- ^{16}O, weak hadronic form factor and recoil polarisation in muon capture 78−62508
- ^{16}O with Reid soft core potential, effective particle potentials for Brueckner calcs. 77−6248
- (^{16}O, X), 90, 120 MeV/N, fragmentation reaction mechanism, orbital dispersion, momentum distribs. 79−97723
- ^{16}O$_\Lambda$, Λ-N residual interactions, Λ spin-orbit splitting and effective mass 80−57722
- ^{16}O-^{16}O, excit. function struct., momentum space folding model 77−57683
- ^{16}O-^{16}O excit. function calc. in momentum space folding model 77−57682
- ^{16}O+^{10}B, 100 MeV, 2n and 2p transfer reacts., DWBA anal. 78−50207
- ^{16}O+^{11}B, 115 MeV, α-transfer, DWBA anal., spectroscopic factors 79−22311
- ^{16}O+^{12}C, 15-72 MeV, gross struct. in γ-ray yields 78−78405
- ^{16}O+^{12}C, 168 MeV, inelastic scatt., folding model, macroscopic formalism, form factors 78−25227
- ^{16}O+^{12}C, 17-28 MeV, total fusion cross section, γ-ray meas. 77−14162
- ^{16}O+^{12}C, 45-80 MeV, fusion cross sections using time-of-flight technique, TDMF calcs. 78−94043
- ^{16}O+^{12}C, fine struct. in fusion cross section 78−89928
- ^{16}O+^{12}C, isobar total prod. cross-sections, target giant reson. excitation 79−85429
- ^{16}O+^{12}C elastic scatt. and total reaction cross sections near Coulomb barrier 77−54235
- ^{16}O+^{12}C scattering, l-depend. absorptive pot., long life pot. resonances 78−62570
- ^{16}O+^{12}C system, exptl. survey of resonant structs. below and above Coulomb barrier 79−9616
- ^{16}O+^{13}C, 105 MeV, α-transfer, DWBA anal., spectroscopic factors 79−22311
- ^{16}O+^{16,18}O, high spin states of ^{30,32}P, γ-ray meas. 78−74386
- ^{16}O+^{16}O, 2- and 3-dimens. time depend. HF calc. comparison 79−17948
- ^{16}O+^{16}O, 2.1 GeV/n elastic scatt., correlations 78−41761
- ^{16}O+^{16}O, 3-dimens., time depend. HF calcs. for fusion cross sections 78−66318
- ^{16}O+^{16}O, 3D TDHF calcs. 78−626
- ^{16}O+^{16}O, 35-80 MeV, fusion cross sections using time-of-flight technique, TDMF calcs. 78−94043
- ^{16}O+^{16}O, 384 MeV, alpha clustering, multiple shape vibrs., TDHFC calcs. 79−3164
- ^{16}O+^{16}O, 64, 80 MeV, fusion events, time dependent HF calcs. 79−36292
- ^{16}O+^{16}O, diffuse surface nuclear and Coulomb pot. energies 77−18593
- ^{16}O+^{16}O, direct inelastic scatt. in 3-dimens. time depend. HF scheme 79−17925
- ^{16}O+^{16}O, elastic scatt. and fusion cross-section calc. 77−46182
- ^{16}O+^{16}O, elastic scatt. excitation functions, interf. effects 77−50155
- ^{16}O+^{16}O, entrance channel effects coupled channel calc. 77−65235
- ^{16}O+^{16}O, fusion cross section gross struct., excitation functions, coupled channel method 80−52705
- ^{16}O+^{16}O, microscopic anal. of saturation effects in interactive region 78−89899
- ^{16}O+^{16}O, mol. config., ^{36}S high spin props., Strutinsky method 78−50201
- ^{16}O+^{16}O, nucleon-nucleon forces and heavy-ion potentials 79−6657
- ^{16}O+^{16}O, nucleus-nucleus interaction and nuclear saturation props. 79−6395
- ^{16}O+^{16}O, optical potential elastic scatt., energy depend., Regge pole and Coulomb amplitudes 78−25228
- ^{16}O+^{16}O, self-consistent heavy-ion potentials 77−6434
- ^{16}O+^{16}O, total fusion cross section and excitation function, statistical model anal. 79−13371
- ^{16}O+^{16}O, total fusion cross section, time depend. HF calcs. 79−17945
- ^{16}O+^{16}O collisions, 105 MeV, appl. of 3-dimens. time-depend. HF calcs. 78−66317
- ^{16}O+^{16}O collisions, resonating group study, effective two-nucleon forces 79−59044
- ^{16}O+^{16}O elastic scattering, GCM calcs., phase shifts, ang. distribs. 77−30625
- ^{16}O+^{16}O heavy ion folding potential, antisymmetrisation effects 78−94023
- ^{16}O+^{16}O inelastic scatt., gross struct. origin, nonreson. diffr. model calcs. 79−30849
- ^{16}O+^{16}O reaction cross sections, 12.5-30.5 MeV excitation functions 78−643
- ^{16}O+^{16}O scattering, generator coord. method, Kohn-Hulthen variational principle 77−2957
- ^{16}O+^{16}O system, strong damping of inner oscills., nuclear saturation props. 78−41749
- ^{16}O+^{208}Pb peripheral collisions, cross-sections meas. at 315 MeV 77−6428
- ^{16}O+^{20}Ne, elastic and inelastic 50 MeV, contribution of α-cluster exchange 77−10429
- ^{16}O+^{27}Al, 30, 40, 60, 80 MeV, evaporation residue mass distrib. in fusion reactions anal. 77−42004
- ^{16}O+^{28}Si, 17 to 37 MeV, inelastic and elastic backward angle scatt., surface resonances 78−37367
- ^{16}O+^{28}Si, 33-215 MeV, optical pots. anal. 77−41988
- ^{16}O+^{40}Ca, inelastic scatt., exit channel distorting pot., DWBA calc. 78−94025
- ^{16}O+^{4}He, 3-D TDHF calcs. 78−54781
- ^{16}O+^{4}He, group theory appl. to reaction studies 80−9276
- ^{16}O+^{58}Ni, 44.5-76.5 MeV, ^{74}Kr compound nucleus decay 77−88168
- ^{16}O+^{58}Ni, 6 MeV/N, pre-equilib. α-emission 77−82883
- ^{16}O+^{7}Li, 50, 68 MeV, α-transfer, DWBA anal., spectroscopic factors 79−22311
- ^{16}O+AgBr, 0.2, 2.0 GeV/nucleon, search for shock-wave effects 77−23102

nuclei with mass number 6 to 19 continued
^{16}O+CNO, ^{16}O+AgBr, 2 GeV/nucleon, two-proton azimuthal angle correlations 78−62572
^{16}O+X, X=^{11}B,^{12}C,^{13}C,^{18}O, deduced excited states, shell model wave functions, DWBA anal. 79−45284
^{6}O+α, spallation fragments 6≤A≤11 yields, nucleosynthesis interest 79−30845
^{16}O+α nucleon exchange and backangle anomaly 79−6638
^{16}O+α scattering generator coord. method, Kohn-Hulthen variational principle 77−2957
^{16}O+emulsion nuclei, 150-200 MeV/nucleon interactions 77−41992
^{16}O+emulsion nuclei, 75-100 MeV/N, parallel momentum distrib. 79−9613
^{16}O+γ, continuum shell model calcs. of particle emission threshold effects, cross section, line shape of resonances 78−46014
^{16}O+light ion scatt., exchange Coulomb kernel in resonating group formulation 79−6531
^{16}O+μ, total muon capture rate, Skyrme forces, closure approx., sum rule technique 78−54742
^{16}O+ν_e, 0 to 300 MeV, cross sections, shell model calcs 79−93605
^{16}O+p, 1 GeV, neutron production *(Russian)* 79−85477
^{16}O+p, 50 MeV, three particle final state *(Russian)* 78−29471
^{16}O+p, 62 MeV, complex particle emission, pre-equilibrium exciton model anal. 78−66280
^{16}O+p, energy dependent radial functions formalism of continuum shell model 78−25185
^{16}O+p fragmentation reaction, 2 GeV, three-stage model anal. 79−6551
^{16}O+p(d)(α), transparency in composite particle-nucleus reactions 80−9273
^{16}O+π, total cross section calc., complex momentum theory anal. with $\alpha_P^0>1$ *(Russian)* 79−9638
^{16}O(^{10,11}B, ^{10,11}B), 33.7-49.5 MeV, mag. distribs., ground state quadrupole moment contrib. 80−42689
^{16}O(^{12,13}C,αX), 140 MeV, fast α prod. and molecular resonance search 80−106066
^{16}O(^{12}C, ^{12}C′) quasimolecular resonance, doublet like intermediate structure 79−54421
^{16}O(^{12}C,^{12}C$_{2+}$)^{16}O, ^{12}C$_{2+}$ spin alignment using γ-decay in flight 78−41767
^{16}O(^{12}C,^{12}C), 18-26 MeV, molecular structure, projection operator anal., differential cross sections 80−106033
^{16}O(^{12}C,^{12}C), perturbed stationary state method, low energy collision and mol. resons. 80−78320
^{16}O(^{12}C,^{12}Cα)^{12}C, 68 to 80 MeV, sequential decay via excited states in ^{16}O 78−50189
^{16}O(^{12}C,^{8}Be)^{20}Ne*, 78 MeV, spectroscopy of high spin states in ^{20}Ne 78−50066
^{16}O(^{12}C,^{8}Be)^{20}Ne*, determ. of resonance struct. in ^{28}Si 79−6663
^{16}O(^{12}C,X), sub-barrier energies, fusion cross section, static and dynamic deformation effects 80−42729
^{16}O(^{12}C,α)^{24}Mg, 12.8-14.5 MeV, energy averaged ang. distribs., Hauser-Feshbach calcs. 79−22318
^{16}O(^{14}N,^{10}B)^{20}Ne, 155 MeV, direct α-transfer, high spin states in ^{20}Ne 77−14164
^{16}O(^{16}O, X), 9.3 MeV, fusion reaction residue partial prod. cross sections from γ-detection 79−67804
^{16}O(^{16}O, X), fusion limiting ang. momenta, from evaporation, mass distrib. stat. model fit 80−68714
^{16}O(^{16}O,^{12}C)^{20}Ne, angular distrib. of ^{20}Ne polarisation at 68 MeV 79−6681
^{16}O(^{16}O,^{12}C)^{20}Ne, reaction mechanism by polarisation meas. 80−9301
^{16}O(^{16}O,^{16}O′), gross struct., barrier top resonance model calc. 80−9279
^{16}O(^{16}O,^{16}O), 10-41 MeV, molecular resonances γ-yield, band crossing model 80−106032
^{16}O(^{16}O,^{16}O), Coulomb field effects using generalised JWKB method 80−13504
^{16}O(^{16}O,^{16}O), elastic scatt., incoming wave boundary condition model calcs. 80−47504
^{16}O(^{16}O,^{16}O), elastic scatt., l-window formalism 80−68684
^{16}O(^{16}O,^{16}O), optical pot., nuclear matter approach, energy density matter [-] 80−83112
^{16}O(^{16}O,^{16}O), perturbed stationary state method, low energy collision and mol. resons. 80−78320
^{16}O(^{16}O,^{16}O), quasimolecule dynamical study, L=0 to 30 phase shifts 77−26784
^{16}O(^{16}O,^{16}O), surface transparent pot. scatt. semiclassical wave propagation matrix method 79−101
^{16}O(^{16}O,^{16}O), symmetry and shell struct. effects on absorption, precompound states 80−27666
^{16}O(^{16}O,X), 30-40 MeV, complete fusion cross section, gross and intermediate width struct. 79−67808
^{16}O(^{16}O,X), 55 MeV 80−83110
^{16}O(^{16}O,X), collective potentials and inertia parameters, adiabatic time dependent HF calcs. quasimolecular resonances 80−63195
^{16}O(^{16}O,X), cross sections, energy dependence, nuclear molecular resonances, band crossing model 80−68686
^{16}O(^{16}O,X), total fusion cross sections and fusion barrier parameters 80−9322
^{16}O(^{16}O,x) reactions, time dependent HF calcs. 77−54251
^{16}O(^{27}Al,X), 105, 145 MeV, backward angle cross sections, evaporation residues, Z=6-9 yields 80−68688
^{16}O(^{28}Si,X), 55-96 MeV, γ-ray yield functions from high spin states, comparison with ^{12}C+^{24}Mg 79−93492
^{16}O(^{3}He, ^{3}He), pol. ^{3}He, 33.3 MeV, differential cross section and anal. power, optical pots. 80−42627
^{16}O(^{3}He, x), pol. ^{3}He, x=d or α, 33 MeV, anal. power and cross sections 80−42628
^{16}O(^{3}He,^{3}He), 25 MeV, macroscopic description of exchange effects 77−57635
^{16}O(^{3}He,^{3}He), 44.04 MeV, absolute differential cross section, optical model anal. 79−59078
^{16}O(^{3}He,^{3}He), E2 strength distrib., giant quadrupole reson. 77−30612
^{16}O(^{3}He,α), inner hole states excitation, DWBA anal., reaction mechanism *(French)* 78−41735
^{16}O(^{3}He,γ)^{19}He, excitation functions ^{16}O+^{3}He cluster states 79−6539
^{16}O(^{3}He,p), 18 MeV, ang. distribs., DWBA anal. 77−34325
^{16}O(^{3}He,p)^{18}F, 19.8 MeV DWBA anal. of exchange effects 77−46179
^{16}O(^{3}He,p)^{18}F and ^{16}O(^{3}He,α)^{15}O prompt reactions, lattice location meas. of O in Nb 79−86813
^{16}O(^{3}He,p)^{18}F in water, ^{18}F prod. and yield 78−28065
^{16}O(^{3}He,t), 35 MeV, ^{16}F energy levels 78−17231

nuclei with mass number 6 to 19 continued
^{16}O(^{6}Li, d), 32 MeV, unnatural parity levels in ^{20}Ne, reaction mechanisms 77−14158
^{16}O(^{6}Li,^{6}Li′), 153 MeV, isoscalar giant quadrupole resonances 80−13440
^{16}O(^{6}Li,α)^{18}F, 34 MeV, exchange effects, DWBA anal. 77−6431
^{16}O(^{6}Li,α)^{18}F, 34 MeV, DWBA anal. of exchange effects 77−46179
^{16}O(^{6}Li,d)^{20}Ne, 19.8 to 32 MeV, reaction mechanism and excitation functions 78−41757
^{16}O(^{6}Li,d)^{20}Ne, 20, 32, 38 MeV α-particle spectroscopic strength determ., DWBA anal. 79−26451
^{16}O(^{6}Li,d)^{20}Ne, 43 MeV, α spectroscopic factors, reduced widths, stellar He burning 78−89897
^{16}O(^{6}Li,d)^{20}Ne(α)^{16}O at 57.8 MeV, ^{20}Ne α-cluster struct. >30 MeV excit. *(Russian)* 77−74784
^{16}O(^{6}Li,dγ)^{20}Ne, dγ ang. correl. reaction strength comparison, DWBA anal. 79−26452
^{16}O(^{7}Li,^{3}He)^{20}F, 24 MeV, ang. distribs. of states below 6.25 MeV, gas target 78−82369
^{16}O(^{9}Be,^{5}He)^{20}Ne*, sub-Coulomb alpha transfer cross sections 80−37394
^{16}O(^{9}Be,^{9}Be) 14, 20 and 26 MeV, optical model parameters 79−26449
^{16}O(K,K′), low lying collective state selective excitation, ang. distribs. and cross sections 79−6368
^{16}O(K^-, π^-), 390 MeV/c, formation of hypernuclear excited states 78−74402
^{16}O(K^+,$K^{+\prime}$), plane and distorted wave impulse approx. anal., plane waves 79−9630
^{16}O(N,N), microscopic description validity 79−544
^{16}O(N,N)^{16}O, resonating group method with generator-coordinate technique 77−10415
^{16}O(O,C)^{20}Ne, 17 MeV, α transfer, cluster transfer process, cross sections 78−25218
^{16}O(O,Ne)^{12}C 17 MeV, α transfer, cluster transfer process, cross sections 78−25218
^{16}O(0^+,6.05 MeV) intermediate struct. resonances from ^{12}C(^{16}O,^{16}O′) 46 to 56 MeV 78−78410
^{16}O(0^+)⇄^{16}N(0^-), beta decay and muon capture rate ratio, mesonic exchange currents 80−42594
^{16}O(0^+)⇄^{16}N(0^-), nucl. wave functions and mesonic exchange currents 79−40887
^{16}O(0^+)⇄^{16}N(0^-) β decay and μ capture reactions, mesonic exchange correction 78−58257
^{16}O(α, α)^{16}O, backscatt. heavy particle transfer mechanism 77−6420
^{16}O(α, α)^{16}O, elastic scatt. reson reaction, appl. to O determ. in Si 79−34408
^{16}O(α,^{12}C), 90.3 MeV, cross sections and systematics multi-α-cluster transfer implications 80−42675
^{16}O(α,^{12}C), 90.3 MeV, multi-α-cluster transfer and direct pickup cross sections 80−57760
^{16}O(α,2α), 140 MeV, quasifree knockout, DWIA anal. spectroscopic factors 80−68629
^{16}O(α,2α), 90 MeV, strong absorption diffraction model, spectroscopic factors 79−22306
^{16}O(α,2α)^{12}C, DWIA 77−34273
^{16}O(α,α_1)^{16}O*, resonance observation of 8p-4h state in ^{20}Ne 78−50132
^{16}O(α,α'), 60 MeV, giant dipole and quadrupole 77−2965
^{16}O(α,α'), hyperfine dynamic mag. field effects 80−68689
^{16}O(α,α'), inelastic scatt. from 8.88 MeV 2^- state, magnitude and ang. distribs. of cross sections at 40.5 and 65 MeV 79−49631
^{16}O(α,α')^{16}O, 65 MeV, monopole excitation of ^{4}He, DWBA calc. 77−10419
^{16}O(α,α), 20 to 24 MeV, optical model anal. 77−65228
^{16}O(α,α), 23.7 MeV, cross sections, 20 to 170° 78−13118
^{16}O(α,α), 25 MeV, macroscopic description of exchange effects 77−57635
^{16}O(α,α), 28 to 33.6 MeV, optical potential of incident channel 78−58291
^{16}O(α,α), 28-33.6 MeV, forward peaking variation, DWBA with optical pots., ang. distribs. 80−13488
^{16}O(α,α), antisymmetrisation effects on the effective internuclear potential 79−59085
^{16}O(α,α), effect of Pauli principle on optical potl. 77−6412
^{16}O(α,α), forward differential cross sections determ. using Feynman diags. 78−25210
^{16}O(α,α), giant isoscalar quadrupole resonance, α-over p-decay ratio, SU(3) and shell model 80−27608
^{16}O(α,α), microscopic R-matrix theory in generator coord. basis 77−14079
^{16}O(α,α), spectra and widths of quasistationary α-cluster states *(Russian)* 77−46180
^{16}O(α,α)^{16}O, 20 to 25 MeV, backward angle anomaly, α-cluster states in ^{20}Ne 77−38287
^{16}O(α,α)^{16}O, 6.9-10.2 MeV, level and isospin mixing parameters 78−66292
^{16}O(α,α)^{16}O, differential cross section calc. with hard core potential 77−30614
^{16}O(α,d), 1.12 MeV, forward peaking variation, DWBA with optical pots., ang. distribs. 80−13488
^{16}O(α,d)^{18}F, 28 to 33.6 MeV, forward angle yield, optical potential of incident channel 78−58291
^{16}O(α,d)^{18}F production on SiO_2 target 79−79650
^{16}O(α,γ)^{20}Ne, 6.9-10.2 MeV, level and isospin mixing parameters 78−66292
^{16}O(α,p), 20.1 MeV, level struct. of ^{19}F, spin, parity *(Spanish)* 77−67756
^{16}O(α,p)^{19}F, 40 MeV, populating ^{19}F levels, J^π, spectroscopic factors 77−14140
^{16}O(d,^{3}He)^{15}N, 82 MeV, finite-range DWBA calcs. 77−10416
^{16}O(d,^{6}Li), 80 MeV, resonance-like phenomena 79−13308
^{16}O(d,^{6}Li)^{12}C, 35 MeV, finite range CCBA calcs. 77−6403
^{16}O(d,^{6}Li)^{12}C, 50, 65, 80 MeV, energy depend., spectroscopic factors 78−74372
^{16}O(d,^{7}Li)^{11}C, angular distribs., direct five nucleon transfer E_d=80 MeV 79−6627
^{16}O(d,X), X=d or N, elastic scatt. and stripping, three body calc. 80−91165
^{16}O(d,α_3), 6.84 MeV polarised d, absolute standard for d vector analysing powers 77−34281
^{16}O(d,α)^{14}N, 0.66 to 1.10 MeV cross section determ. for O_2 profiling 79−45275
^{16}O(d,d), <4 MeV, d polarisation, vector analysing power, level characts. of ^{18}F compound nucleus 77−61434

nuclei with mass number 6 to 19 continued

^{16}O(d,d)^{16}O, resonating group method with generator-coordinate technique 77−10415
^{16}O(d,n), ^{17}F half life meas. 77−88085
^{16}O(d,p), 12 MeV, stripping reaction differential cross section, d distortion effect *(Japanese)* 80−22796
^{16}O(d,p), <4 MeV, vector analysing power, level charact. of ^{18}F compound nucleus 77−61434
^{16}O(d,p)^{17}O, anal. using deuteron deform. effects *(Japanese)* 78−37355
^{16}O(d,p)^{17}O, channel coupling array and coupled reaction channel methods 78−8831
^{16}O(d,p)^{17}O, coupled channel variational method for multi-step direct nuclear reactions. II. Test on a (d,p) reaction 78−66259
^{16}O(e,e′), 799, 996, 1178 MeV, cross sections *(Russian)* 80−68653
^{16}O(e,e′p), polarisation effect on quasi-free electron scatt. 77−71607
^{16}O(e,e′p), single hole state momentum and energy distribs. 80−22674
^{16}O(e,e′π^+), energy and ang. distribs. of πs, low lying residual states 78−54740
^{16}O(e,e′πs) threshold prod. at 280 MeV, π^+/π^- ratio 77−41957
^{16}O(e,e′), internuclear nucleon effective mass in quasielastic scatt. *(Russian)* 79−3076
^{16}O(e,e), elastic scatt., spectroscopic information and form factors 80−9260
^{16}O(e,e), high energy differential cross sections, nucleon density distrib. 78−54738
^{16}O(e,e), spectroscopic amplitude determ. 80−5127
^{16}O(e,e), T=1 level form factors, Helm model, pion photoprod. and muon capture appls. 80−52553
^{16}O(e,π^+), 180.4 MeV, virtual photon spectrum, virtual photon theory test 80−102183
^{16}O(e,$\pi^\pm$), 10 MeV π, of PWIA calcs. 79−93607
^{16}O(e,π), charged π electroprod. near threshold data anal. 78−66266
^{16}O(γ, p), 300 to 900 MeV/c, p-shell momentum distrib. calc. 78−50151
^{16}O(γ, p)^{15}N and ^{16}O(γ, n)^{15}O, 60-300 MeV, absorpt. mech., residual nucleus form factor 78−70511
^{16}O(γ,N), giant resonance region, features in energy depend. of ang. distrib. 77−6343
^{16}O(γ,N), shell model calcs. with and without continuous spectrum *(Russian)* 77−2979
^{16}O(γ,2n)^{14}O, 100 to 800 MeV, yields, cross sections 77−34285
^{16}O(γ,γ), 6.95, 7.12 MeV, strengths of isospin forbidden E1 transitions 78−13059
^{16}O(γ,γ), total photoabsorption and elastic cross sections, spectroscopic information *(Russian)* 80−83095
^{16}O(γ,n$_0$), 21.6-25.7 MeV, ground state photoneutron polarisation ang. distrib. 80−57765
^{16}O(γ,n), 25-45 MeV, isovector giant quadrupole resonance evidence, E2 cross section 80−18268
^{16}O(γ,n) total photoneutron cross sections 80−42619
^{16}O(γ,n)^{15}O, ang. distrib. asymmetry anal. 78−25172
^{16}O(γ,n)^{15}O, relativistic heavy ions, Coulomb disintegration, photodisintegration cross section *(Russian)* 78−89851
^{16}O(γ,n)^{15}O, two-step charge exchange contrib., corrections to direct photonuclear process 78−62518
^{16}O(γ,p$_0$) 100-300 MeV, short-range, high-momentum effects 77−26667
^{16}O(γ,p), 40-105 MeV bremsstrahlung, ang. distribs. meas. 77−41945
^{16}O(γ,p), role of Δ(1232) isobar 79−85451
^{16}O(γ,p)^{15}N, 50 to 350 MeV, evaluation of isobar photoprod. contrib. to (γ,p) reaction 79−45245
^{16}O(γ,p)^{15}N, electric quadrupole transition cross-sections, behind giant resonance *(Russian)* 80−78281
^{16}O(γ,p)^{15}N up to 120 MeV, cross-sections, energy levels *(Russian)* 80−47465
^{16}O(γ,π^0) coherent photoprod. in isobar-hole formalism, DWIA comparison 79−89290
^{16}O(γ,π^0p), 0-600 MeV residual nucleus impulse *(Russian)* 79−59050
^{16}O(γ,π^+), 200-350 MeV, cross sections, DWIA anal. 80−106048
^{16}O(γ,π^+), differential cross section from elementary Hamiltonian model 80−18292
^{16}O(γ,π^+), threshold to 175 MeV, total cross sections, DWIA anal. 80−13459
^{16}O(γ,π), total cross section, Δ-hole states damping, π^0,ρ exchange, Δ isobar hole model 80−91174
^{16}O(k^-,π^-)$^{16}_{\Lambda}$O, Λ-nuclear spin-orbit coupling, ΛN effective interaction 79−85562
^{16}O(μ,γ), exclusive radiative capture, axial currents and induced pseudoscalar form factors 79−97699
^{16}O(μ,ν_μ)^{16}N*, elementary particle treatment 78−8800
^{16}O(μ,ν), recoil nucleus odd and even tensor orientations, general expressions 80−13451
^{16}O(μ,ν)^{16}N determ. of μ^- partial capture rates 79−45247
^{16}O(μ^-,e$^-$)^{16}O*, shell model anal. of μe conversion rate *(Russian)* 79−89300
^{16}O(μ^-,ν)^{16}N*(0$^-$), calculated capture rate 79−59036
^{16}O(n,2n)^{15}O, ^{15}O recoils, labelled mol. O_2 form. 78−3359
^{16}O(n,$\alpha\gamma$), 7 to 10.5 MeV, γ-ray prod. cross-section meas. 77−34315
^{16}O(n,$\alpha\gamma$), 7-10.5 MeV gamma-ray prod. cross sections meas. 78−37338
^{16}O(n,γ), thermal n, total cross section 79−54439
^{16}O(n,γ), total cross-section meas. 77−50131
^{16}O(n,$\gamma\gamma$), single-particle direct-capture calc. 77−50131
^{16}O(n,$\gamma\gamma$), thermal, calc. of cross-sections and branching ratios 77−14131
^{16}O(n,n′γ), 7 to 10.5 MeV, γ-ray prod. cross-section meas. 77−34315
^{16}O(n,n′γ), 7-10.5 MeV, gamma-ray prod. cross sections meas. 78−37338
^{16}O(n,n), 2-5 MeV polarised neutrons, analysing power, R-function and phase-shift anal. 77−23088
^{16}O(n,n), elastic cross section, microscopic calc. 80−531
^{16}O(n,n), totally microscopic description, optical pot. and many-body theory 79−546
^{16}O(n,n)^{16}O, complex-generator−corrd. technique in resonating-group calcs. 77−67705
^{16}O(n,p)^{16}N, meas. and calc. ^{16}N activity in water of nuclear powered ship 78−13192
^{16}O(n,p)^{16}N, neutron activation anal. of metals 78−15742
^{16}O(n,p)^{16}N, utilisation for monitoring 14 MeV neutron generator output 79−3287
^{16}O(n,p)^{1}u6N, 14.1 MeV, cross-section meas. *(Spanish)* 77−67738
^{16}O(p, X), 50 MeV, effective cross sections for charged particles in outgoing channel 80−18294

nuclei with mass number 6 to 19 continued

^{16}O(p,^{3}He)^{14}N(2.31 MeV), 27-30 MeV, isospin conservation 78−50170
^{16}O(p,^{6}Li)^{11}C, 51.9 Mev, five nucleon transfer mechanisms, DWBA calcs. 80−73845
^{16}O(p,X), 50 MeV, effective cross sections 80−78284
^{16}O(p,2p), 200 MeV polarised beam reaction, possible knockout polarisation 77−88099
^{16}O(p,2p), 320 MeV polarised protons, quasifree scatt., spin orbit coupling 78−66272
^{16}O(p,2p)^{15}N, 200 and 380 MeV, momentum distribs. calc. 78−54762
^{16}O(p,2p)^{15}N, single nucleon form factor between deformed nuclear states 78−93999
^{16}O(p,α), near threshold, total cross section, reaction rate, astrophys. significance 77−82929
^{16}O(p,α)^{13}N, in-cyclotron ^{13}N prod., water loop target 80−23201
^{16}O(p,p′^{16}O) at 27.2 MeV, 6.05 MeV 0$^+$ level excit., meas. and microscopic calc. 77−26687
^{16}O(p,p′), 1 GeV, proton polarisation in natural parity level excitation *(Russian)* 80−42634
^{16}O(p,p′), 135 MeV, high spin particle-hole states, 4$^-$ states 80−9217
^{16}O(p,p′), 150 MeV, spin-orbit interaction within collective model and DWBA 79−45128
^{16}O(p,p′), 25-46 MeV, effects of two-step process determ. 78−21569
^{16}O(p,p′), 40 MeV, retarded isoscalar M2 strength obs. 78−93962
^{16}O(p,p′), 45 MeV, giant dipole and quadrupole 77−2965
^{16}O(p,p′), giant resonances from antisymmetrised DWBA anal. 79−85432
^{16}O(p,p′), microscopic anal. of doorway states in giant resonance region 77−2966
^{16}O(p,p′), proton polarisation and natural parity level excitations *(Russian)* 80−5144
^{16}O(p,p′), 135 MeV, 4$^-$ particle-hole states, J$^\pi$ ambiguity removal 80−5036
^{16}O(p,p′), 20-40 MeV, pol. p, anal. powers, imaginary spin-orbit pot., coupled channels anal. 80−102179
^{16}O(p,p′), polarised p, 20, 30, 40 MeV, anal. power and cross sections, spin-orbit deformation 79−75963
^{16}O(p,p′)^{16}O*, 42.5-49.3 MeV, octupole GR strength, polarised proton 77−57644
^{16}O(p,p), 1 GeV, cross sections using nuclear densities from self-consistent methods *(Russian)* 78−41724
^{16}O(p,p), 1 GeV, Glauber approx. corrections, differential cross sections 78−50166
^{16}O(p,p), 1 GeV, spin-effects, Coulomb interactions, Glauber theory 77−82931
^{16}O(p,p), 100-2200 MeV, total and reaction cross sections from optical pot. 80−18303
^{16}O(p,p), 20-50 MeV differential cross section, polarisation ang. distrib., optical model exchange terms 80−27638
^{16}O(p,p), 49.48 MeV, elastic scattering, discrepancies from optical model, possible α-cluster struct. 78−62528
^{16}O(p,p), 50-160 MeV, energy depend. optical pot. 80−22830
^{16}O(p,p), 635 MeV, left-right asymmetry depend. on residual nucleus momentum *(Russian)* 78−54765
^{16}O(p,p), 6.9 GeV/c, differential cross section *(Russian)* 79−59071
^{16}O(p,p), average geometry optical model potential, doorway state effects 77−79367
^{16}O(p,p), high energy differential cross sections, nucleon density distrib. 78−54738
^{16}O(p,p), imaginary spin-orbit term in proton optical potential, ang. distribs. 78−58273
^{16}O(p,p), nucleon distrib. in nuclei, self-consistent anal. 79−9556
^{16}O(p,p) 25 MeV, macroscopic description of exchange effects 77−57635
^{16}O(p,p) 65 MeV polarised p, elastic and inelastic, nuclear matter distrib. 78−78297
^{16}O(p,p) polarised p, 800 MeV, differential cross section and anal. power, microscopic anal. 79−80915
^{16}O(p,pd), ^{16}O(p,pt), ^{16}O(p,p^{3}He), 75 MeV expt. setup, DWIA anal. 77−322
^{16}O(p,pd), (p,pt), (p,pα), spectroscopic data on quasielastic ejection on nucleon clusters from 1p shell nuclei 79−80931
^{16}O(p,pd)^{14}N, quasi-elastic cluster knock out, cross section calc. 78−46042
^{16}O(p,pt)^{13}N, quasi-elastic cluster knock out, cross section calc. 78−46042
^{16}O(p,px), x=d,t, ^{3}He, 75 MeV, spectroscopic factors, cluster model, DWIA 77−54214
^{16}O(p,π^+), 0.5-10 MeV, total cross sections near pion Coulomb barrier 80−32280
^{16}O(p,π^+)^{17}O, polarised protons, π distortion effect on asymmetry 78−50176
^{16}O(p,t)^{14}O(g.s.), 27-30 MeV, isospin conservation 78−50170
^{16}O(p$_{pol}$,2p), cross section, analysing power, energy sharing spectra, distorted wave impulse approx. 80−78291
^{16}O(π, $\pi^\pm$), 115, 240 MeV, cross sections, Coulomb effects 78−62579
^{16}O(π,2N), bound 2p pion absorpt., microscopic description, NN correls. 78−94030
^{16}O(π,γ), continuum shell model, strongly excited resonances, nucleon emission 78−94031
^{16}O(π,γn), direct and resonance reaction unified shell model, n, γ spectra 80−52696
^{16}O(π,π'), ~180 MeV, isospin mixing, levels, excitation functions and ang. distribs. 80−42543
^{16}O(π,π'), excitation of collective modes and high-spin states, DWA calcs. 77−10448
^{16}O(π,π), 1.12 GeV, covariant optical model, nucl. struct. calc. 77−14197
^{16}O(π,π), 40-342 MeV, second order optical pot. parameters 79−22337
^{16}O(π,π), binding effects in optical model with S-wave interaction 77−14196
^{16}O(π,π), Coulomb-nuclear interference, extracted Bethe phase 77−10441
^{16}O(π,π), intermediate energies, collective isobaric resonance 80−63208
^{16}O(π,π), nonlinear meson dynamics and binding corrections, optical pots. 80−106080
^{16}O(π,π), pionic resonance fluorescence in Δ(33) region 79−85554
^{16}O(π,π), T-matrix from isobar-hole model, many-body corrections, optical pot. parameter 80−9312
^{16}O(π,π), three-body model of πN interaction using finite binding pots. 80−42707

nuclei with mass number 6 to 19 continued

$^{16}O(\pi,\pi)$ low energy p-wave optical pot., absorptive part from isobar-hole model 79−85556
$^{16}O(\pi,\pi)$ optical pot., local field correction 80−68705
$^{16}O(\pi,\pi)^{16}O$, microscopic isobar-hole calc. doorway states 78−4965
$^{16}O(\pi,\pi p)$, 163 MeV, coincidence expt. 80−78334
$^{16}O(\pi^-,\gamma)$, photon spectra meas. with SIN pair-spectrom. 77−14191
$^{16}O(\pi^-,\gamma)$, one and two neutron emission, decay channels 79−45300
$^{16}O(\pi^-,\gamma n)$, γ-spectrum and γ-n ang. correlation function from continuum shell model 78−86551
$^{16}O(\pi^-,\gamma n)^{15}N$, information from radiative π capture coincidence spectra 78−86550
$^{16}O(\pi^-,n)$, stopped pion, neutron energy spectra, mean energies and multiplicities 80−9311
$^{16}O(\pi^-,\pi^- p)^{15}N$, 170 MeV, comparison with dispersion theory calcs. *(Russian)* 77−50161
$^{16}O(\pi^+,p)^{15}O$, 66 MeV, ang. distrib. meas. 77−10438
$^{16}O(\pi^+,p)^{15}O$, 66 MeV, $(p_{3/2})^{-1}$ and $(p_{1/2})^{-1}$ hole state excit. 77−74886
$^{16}O(\pi^+,p)^{15}O$, 66 MeV pions, expts. with pion beams of Saclay Linac *(French)* 79−572
$^{16}O(\pi^+,\pi^-)$, 240 MeV, double charge exchange cross section 79−85515
$^{16}O(\pi^+,\pi^-)$, 240 MeV, integrated and doubly differential cross sections 80−68702
$^{16}O(\pi^+,\pi^-)^{16}Ne$, 145 MeV, non-analogue π double charge exchange 77−67773
$^{16}O(\pi^+,\pi^+)$, 50 MeV, energy spectra and cross sections 78−25241
$^{16}O(\pi^+,\pi^+)$, 40 MeV, differential cross sections and strength parameters, optical model fit 80−18347
$^{16}O(\pi^+,\pi^+)$, 50 MeV, partial wave amplitude anal. 79−22335
$^{16}O(\pi^+,\pi^+)$, 50-340 MeV, isobar hole doorway states, collective Δ-hole states 79−85350
$^{16}O(\pi^+,\pi^+)$, 80-340 MeV, ang. distribs. of cross-sections determ. 78−33225
$^{16}O(\pi^+,\pi^+)$ 40 and 49.7 MeV, differential cross sections, partial wave and optical model anal. 78−70570
$^{16}O(\pi^+,\pi^+)$ elast. and inelast. scatt., 50 MeV, ang. distrib. determ. optical model and DWBA 79−45304
$^{16}O(\pi^\pm,\pi^{\pm\prime})$, P_{33} resonance region, elastic cross section, Coulomb nuclear interference 77−23110
$^{16}O(\pi^\pm,\pi^\pm)$, elastic scatt., complex amplitude anal., phase 78−62580
$^{16}O(\pi^\pm,\pi^\pm)$, resonance region, first order optical pot. calcs. 79−40957
$^{16}O(\pi^\pm,X)$, 100-250 MeV, ^{12}C production yield ratio with ^{12}C 79−85516
$^{16}O(\pi^\pm,\pi^\pm)$, Coulomb-nuclear interference, new anal. method 78−21608
$^{16}O(t,n)^{18}F$, 1.6 to 3.7 MeV, cross-section meas., O_2 dose meas. appl. *(French)* 77−29077
$^{16}O(t,n)^{18}F$, 2.73 MeV, triton recoil and ^{18}F yields 80−68677
$^{16}O(t,p)$ centre of mass corrections to DWBA overlap factors 80−18319
$^{16}O(t,p)^{18}O$, excitation curve meas., 500-1250 keV 78−37359
$^{16}O \rightarrow {}^{12}C+\alpha$, alpha spectroscopic factors, K-harmonics method 78−62512
^{17}O, 1p spin-orbit splitting anal. with $^{18}O(d,t)$ at 52 MeV 77−41980
^{17}O α-cluster states, α-decay orbital momenta and parities from $^{13}C(^6Li,d)$ and α-decay *(Russian)* 78−86486
^{17}O, charge distrib. differences between A=16, 17, and 18 isotopes 79−63583
^{17}O compound nucleus rot. band structure, ^{16}O (N,N) study with resonating-group method 77−10415
^{17}O, cross sections to ground, 0.87 and 5.09 MeV states, neutron strength from $^{16}O(d,p)$ 80−5066
^{17}O, delayed neutron emission following ^{17}N β-decay 77−18481
^{17}O, effective charges and radial integrals calc. 78−4897
^{17}O, energy multiple-scatt. contrib. using energy-depend. reaction matrix 77−14013
^{17}O, giant reson. isospin splitting, photonuclear cross-sections 78−577
^{17}O high spin 4p-3h strength location from excited peaks of $^{13}C(^6Li,d),(^7Li,t)$ 79−3082
^{17}O in a shell model space, Q-box study 79−93530
^{17}O, in $NaAuCl_4.2H_2O$, pure quadrupole double reson., fine struct. 77−63323
^{17}O levels, resonances, J^π and radiative width from $^{14}N(t,\gamma)$ 80−47389
^{17}O, M3 suppression in HF theory 78−33134
^{17}O, mag. form factor, core polarisation and exchange current effects 78−46003
^{17}O, mag. moments, configuration mixing and meson exchange contrib. 78−17100
^{17}O, muonic, energy shifts during atomic EM cascade, and polarisability of deformed nuclei 80−86893
^{17}O NMR, proton decoupling 78−2752
^{17}O, NMR in agarose gels, hydration anal. 77−81426
^{17}O, NMR in BCC Heisenberg ferromags. with $K_2CuCl_4.2H_2O$ structures 77−69725
^{17}O NMR in chlorine oxyfluorides 77−14453
^{17}O, NMR obs. of water orientation in lyotropic phases 78−27905
^{17}O, NQR in BCC Heisenberg ferromagnets with $K_2CuCl_4.2H_2O$ struct. 78−39439
^{17}O, NQR in high-press. forms of ice 77−90069
^{17}O, NQR in ice II 77−1617
^{17}O, NQR spectrum of H_2O_2 80−9620
^{17}O, neutron rich nuclei study in $^{18}O+^{207,208}Pb$ reaction 79−89322
^{17}O, produced in 3.2-14.4 MeV $^{16}O+^9Be$, gamma transitions 79−49599
^{17}O, quad. reson. fine struct. in $Ba(ClO_3)_2.H_2{}^{17}O$, DNMR 77−8453
^{17}O, screening constants by CNDO/S and INDO calculations 77−46576
^{17}O, TOF transmission meas. of neutron resonances 80−37374
^{17}O, third-order treatment of the one-body effective interaction 79−67670
^{17}O valence energies, extended multiple scatt. approach to 2p1h system 78−29396
^{17}O, widths of isospin forbidden neutron decays of T=3/2 levels, obs. in $^{13}C(\alpha,n)$ 77−6321
$^{17}O/^{18}O$ ratio in Galaxy, interpretation of obs. 78−4356
$^{17}O+^{12}C$, 14-33 MeV, max. total fusion cross section 79−22349
$^{17}O+^{13}C$, 12.9, 14 MeV c.m., compound and direct transfer, reaction mechanism 77−88167
$^{17}O(^{11}B,^8Li)$, 115 MeV, shell and semiclassical reaction model anal. 80−13494
$^{17}O(^{12}C,^9Be)$, 115 MeV, shell and semiclassical reaction model anal. 80−13494
$^{17}O(^{13}C,^{10}B)$, 105 MeV, shell and semiclassical reaction model anal., ^{20}F spins 80−13494

nuclei with mass number 6 to 19 continued

$^{17}O(^{16}O,^{16}O)$, repeated neutron transfer, coupled channels anal. 78−54782
$^{17}O(^3He,\alpha)$, 36 MeV, isospin mixing in ^{16}O determ. 78−8832
$^{17}O(^6Li,d)$, ang. distrib., cross section, ^{21}Ne low lying states, weak coupling behaviour 78−46100
$^{17}O(\alpha,\alpha)^{17}O$, backscatt., heavy particle transfer mechanism 77−6420
$^{17}O(\alpha,d)^{19}F$, 47.5 MeV, population of positive parity states, DWBA anal. 78−70548
$^{17}O(d,^3He)$, (d,t), 52 MeV, isospin mixing in ^{16}O determ 78−8832
$^{17}O(d,t)$ and (d,τ) pick-up reactions, particle-hole spectra of ^{16}O, ^{16}N, spectroscopic strengths 78−58288
$^{17}O(e,e')$, 65-168 MeV, giant resonance excitation 78−4930
$^{17}O(e,e)$, elastic and inelastic, cross sections, excited states, charge radii 78−46049
$^{17}O(e,e)$, mag scatt., form factors, HF calcs., core polarisation effects 80−42579
$^{17}O(e,e)$, transverse form factor, ground state mag. distrib. 79−63658
$^{17}O(g.s.)$, $((sd))_{5/21/2}(1p^{-2})_{01}$ component determ. from $^{17}O(^3He,p)^{19}F$ data 78−78263
$^{17}O(\gamma,n_0)^{16}O$, 4.3-7 MeV, resonance radiation width, channel and pot. radiative capture, R-matrix anal. 79−6567
$^{17}O(\gamma,n)$, 5-33 MeV, ground state differential cross section at 98° resonances 79−89288
$^{17}O(\gamma,n)$, 8.5-39.7 MeV, cross section, giant dipole and pygmy resonance decays 80−42619
$^{17}O(\gamma,n)$, cross section, Lane-Lynn radiative capture mechanisms 80−52660
$^{17}O(n,n')^{17}O$, imaginary inelastic transition form factor, microscopic theory 78−50175
$^{17}O(p,\gamma)$, 0.56 MeV, populating ^{18}F 5603 keV level, isospin mixing 78−543
$^{17}O(p,p)$, finite-range coupled-channel calcs. 77−10377
$^{17}O(p,p)^{17}O$, 1.4-3.0 MeV, spin-parity assignment in ^{18}F 78−29391
^{18}O 1.98 MeV 2^+ state static quadrupole moment, from nuclear sum rules 80−13374
^{18}O 1.982 MeV state, static electric quadrupole moment determ. 77−74763
^{18}O, 2^+ 1.98 MeV level lifetime and g-factor determ. from high velocity recoil in vacuum 77−18474
^{18}O 6p-4h states and composite spectra from $^{12}C(^{18}O,^{12}C)$ 80−63096
^{18}O alpha particle cluster states, rot. bands in $^{14}C+\alpha$ model 78−8757
^{18}O, coexistence of spherical and deformed states 77−18394
^{18}O deduced levels and ang. distribs., cross sections from $^{12}C(^7Li,p)$, 16, 18 MeV 79−6686
^{18}O, dineutron cluster states, single-channel resonating group calc., levels, J^π 77−82841
^{18}O, effective interaction, nonlocal pot. reaction matrix free scatt., spectra 77−46122
^{18}O, effective interaction, Hartree-Fock effects 78−534
^{18}O, effective interactions in d-states 77−14044
^{18}O, heavy ion excitation, single particle and core polarisation amplitude interference 80−5117
^{18}O integrated cross sections to excited residual states from $^{19}F(\gamma,p)$ 80−18200
^{18}O, $J^\pi=0^+$ system, singular part of effective shell model interaction 77−6265
^{18}O level gamma decay from $^{17}O(n,\gamma)$ 80−52623
^{18}O low excitation struct., model calcs. 78−70452
^{18}O, low-lying positive-parity states, wave functions 77−6239
^{18}O, modified HF calcs. for low-lying collective states 77−22916
^{18}O, negative parity states, dynamic interaction propagator approach 79−13191
^{18}O, perturbative approximations to Bloch-Horowitz effective Hamiltonian energies, bounds 78−70466
^{18}O probable 6p-4h states from weak coupling calcs. 79−443
^{18}O, quadrupole moment of first excited state 77−22886
^{18}O, quadrupole moment of first 2^+ state, SU(3) representation 77−46113
^{18}O, RMS neutron and proton radii difference, from pion-nucleus data 77−10436
^{18}O, spurious centre of mass effects, effects on microscopic nuclear effective interactions 78−82292
^{18}O, static quadrupole moment of first excited state, reorientation effect in Coulomb scatt. 77−82823
^{18}O struct. calcs., collective Hamiltonian approach 79−22212
^{18}O, struct. of negative parity states, consistency and ghost elimination 77−26595
^{18}O, study of excited states, spin and parity *(French)* 78−33158
^{18}O, transition strength n and p components, $\pi^\pm$ inelastic scatt. comparison, shell model 80−68585
^{18}O, trinucleon cluster states, low lying negative parity states 78−29387
^{18}O, two-body surface correls. in extended basis shell model 78−532
^{18}O wave functions appl. to $^{14}C(^7Li,t)$ 78−82381
$^{18}O/^{16}O$ ratio in precipitation over KFA Julich, (1974-1978) *(German)* 79−12227
$^{18}O/^{17}O$, abundance ratio in hot CNO nucleosynthesis 77−78767
$^{18}O_2$ shell-cluster admixtures, spectra, α-widths and electric transitions 77−54136
$^{18}O+^{12,13}C$ fusion evaporation reactions, 100 MeV, comparison of residues with statistical calcs. 78−66311
$^{18}O+^{12}C$, 10-23.6 MeV, periodic structure 78−46095
$^{18}O+^{16}O$, 10-23.6 MeV, periodic structure 78−46095
$^{18}O+^{17}O$, one and two neutron transfer reacts., 18.52 MeV 78−54783
$^{18}O+^{18}O$, elastic scatt. excitation functions, interf. effects 77−50155
$^{18}O+^{18}O$, mol. config., ^{36}S high spin props., Strutinsky method 78−50201
$^{18}O+^{18}O$, scatt. and neutron transfer reactions, excitation levels, recoil DWBA analysis 78−8837
$^{18}O+\pi^-(\pi^-)$, elastic and inelastic scatt., angular distrib., 180 MeV, comparison with ^{28}Si 78−94035
$^{18}O+\pi^\pm$, inelastic and elastic scatt., neutron-proton radius differences and isovector deform. 79−40963
$^{18}O(^{16}O,^{16}O)^{18}O$, 24, 28, 32 MeV, two-particle transfer contrib. 77−3030
$^{18}O(^{17}O,^{16}O)^{19}O$, sub-Coulomb, RMS radii of single-particle orbitals, neutron excess 77−333
$^{18}O(^{18}O,^{16}O)^{20}O$ 52 MeV, microscopic anal. with DWBA calc. 79−26450
$^{18}O(^{18}O,^{15}O)^{21}O$, 91 MeV, determ. of ^{21}O mass 78−50078

nuclei with mass number 6 to 19 continued
^{18}O(^{18}O,^{18}O), symmetry and shell struct. effects on absorption, precompound states 80−27666
^{18}O(^{18}O,^{19}N)^{17}F, 91 MeV, exotic nuclei search, ^{19}N mass 77−22868
^{18}O(^{3}He,pγ)^{20}F, 11-15 MeV, coincidence, ang. correl. and branching ratio meas. 78−13129
^{18}O(^{6}Li,d)^{22}Ne, 32 MeV, levels, J$^{\pi}$, α-particle spectroscopic strengths 77−18594
^{18}O(α,γ), 0.6 to 2.3 MeV, props. of ^{22}Ne compound states, astrophys. reaction rate 78−57545
^{18}O(α,nγ)^{21}Ne, 4.3-6.5 MeV, excitation functions meas. 78−8833
^{18}O(d,α), 8.5 to 11.3 MeV polarised deuterons, ^{16}N levels, spin parity assignments 78−89886
^{18}O(d,p)^{19}O, ^{19}O level p-γ correl. meas. 77−10353
^{18}O(d,t), 17 MeV, ^{18}O ground state wave function 78−66287
^{18}O(d,t)^{17}O, ^{18}O(d,τ)^{17}N, 52 MeV, ^{17}O, ^{17}N levels anal., 1p spin-orbit splitting 77−41980
^{18}O(e,e′), 80-165.7 MeV, giant dipole and quadrupole resonances, form factors 80−102168
^{18}O(e,e′), isovector mag. dipole and quadrupole transitions, analogues, (π γ) relation 80−106010
^{18}O(γ,n) 8.0 to 41.8 MeV, photonuclear cross section meas., resonance decay branching 79−63656
^{18}O(γ,xn) 8-33 MeV, integrated cross sections 77−10386
^{18}O(p,α$_0$)^{15}N, 6.6 to 10.4 MeV, partial wave anal. of differential cross sections 79−93609
^{18}O(p,α), 661 to 223 keV cm, cross section meas. and S-function extrapolation using R-matrix theory 78−82341
^{18}O(p,α) 72 to 935 keV, astrophysical reaction rate, ^{19}F resonances 79−26439
^{18}O(p,α)^{15}N, applic. to high temp. oxidation studies of alloys 79−87912
^{18}O(p,d) reaction at 52 MeV, ang. distrib., DWBA anal. 77−26679
^{18}O(p,γ), 630-2260 keV, γ-ray decay scheme, for ^{19}F reson. and bound levels 78−89790
^{18}O(p,γ)^{15}N prompt reactions, lattice location meas. of O in Nb 79−86813
^{18}O(p,p′γ), 3-3.5 MeV, γ-ray ang. distrib., for ^{19}F reson. and bound levels 78−89790
^{18}O(p,p), 18-44 MeV, differential cross sections, phase shift anal., energy depend. 80−47481
^{18}O(p,t), exact finite range DWBA calcs., realistic triton and nuclear wave functions 80−63191
^{18}O(p,t), finite range DWBA anal. with realistic triton wave function 80−78300
^{18}O(p,t), polarised p, 24.4 MeV, two-step reaction to unnatural parity state, anal. power 79−67739
^{18}O(p,t)^{16}O, 20 to 45 MeV, energy depend. of two-step DWBA for unnatural parity state excitations 78−70528
^{18}O(π,X), angular distrib. of inelastic diffusion of π$^{\pm}$ *(French)* 80−47507
^{18}O(π,π′), 164 MeV, yrast state and level excitation, DWIA calcs., shell model context 80−42526
^{18}O(π,π′), 230 MeV, neutron deform. param. determ. 78−29502
^{18}O(π,π′), mirror state EM decay rates, multipole matrix element isospin decomposition 79−36190
^{18}O(π,π′), momentum space DWIA calcs., DWIA validity, shell model sensitivities 79−85553
^{18}O(π$^-$, γ) photon spectra meas. with SIN pair-spectrom. 77−14191
^{18}O(π$^+$,π$^-$), 140 MeV, nuclear structure effects on cross section 78−17246
^{18}O(π$^+$,π$^-$)^{18}Na, nuclear struct. effects 78−37380
^{18}O(π$^+$,π$^-$)^{18}Ne, 148, 187 MeV, ^{18}Ne ground state obs. 77−74883
^{18}O(π$^+$,π$^-$)^{18}Ne double-charge-exchange, isobaric analogue transition 77−38300
^{18}O(π$^+$,π$^-$)^{18}Ne(GS), optical model calc. including ^{18}F intermediate state coupling, cross section 79−13349
^{18}O(π$^{\pm}$,π$^{\pm}$′), 180 MeV, ang. distrib. around (3,3) reson. 79−85537
^{18}O(π$^{\pm}$,π$^{\pm}$′) ^{18}O(2$^+$), DWIA anal. with microscopic form factors, effective charges 79−85549
^{18}O(π$^{\pm}$,π$^{\mp}$), correlation effects, Glauber theory anal. 79−85514
^{18}O(π$^{\pm}$,π$^{\pm}$) inelastic scatt., core polarisation effects from Glauber theory 79−75962
^{18}O(t,αγ)^{17}N, study of ^{17}N excited states *(French)* 77−14031
^{19}O β-decay, Fermi to Gamow Teller mixing ratio meas., ^{19}F isospin mixing 79−9520
^{19}O, energy levels, nuclear forces 77−2917
^{19}O first excited state electric moment, B(E2) transition from ^{208}Pb(^{18}O,^{18}O′) 79−67651
^{19}O high spin states populated in ^{13}C(^{7}Li,p) 78−21595
^{19}O, p-γ correl. meas., form. from ^{18}O(d,p) reaction 77−10353
^{19}O total fusion and transfer cross sections from ^{9}Be(^{18}O,X) 80−91205
^{19}O$_{\Lambda}$, pairing correlation effects *(Chinese)* 80−47420
^{19}O(π$^-$,π$^+$), 180 MeV near (3,3) reson., nuclear RMS radii determ. 79−85538
^{20}O, 4p and 6p-2h states obs. in ^{18}O(t,p) 79−40849
^{16,18}O, particle and hole clusters, many-particle clusters *(Chinese)* 77−57614
^{16,18}O+^{16,18}O, elastic scattering, symm., shell effects, absorpt. 79−562
(^{17,18}O,^{17,18}O′), 54-69 MeV, on A=48-92, excited states and ang. distribs., DWBA anal. 79−67705
O(α,^{2}He), A=16, 18, 55, 65 MeV, two neutron states, A-depend. of binding energy 78−74379
O(α,X), 16.5 GeV/c, inelastic cross sections, multiplicity, ang. and momentum distribs. 78−82359
O(α, 2α), 700 MeV, cross section, effective cluster number from PWIA, momentum distrib. 79−40940
O(α,n), exam. of neutron yield 80−86912
O(γ,X), photoabsorption cross-section, Levinger's factor, mass number dependence 80−63165
O(n,X), 14.8 MeV, γ-prod. cross section 79−49622
O(p,X), 340, 660 MeV, ang. distribs., proton quasi-elastic knockout *(Russian)* 80−52649
O(p,X), 400 GeV/c, multiplicity and ang. distribs. of relativistic and slow particles *(Russian)* 79−40931
O(p,p), total cross sections, 180 to 560 MeV, Galuber model calcs. 79−40917
O(π$^-$,X), charged heavy particle emission after pion capture *(Russian)* 80−69271
O(π$^+$,2p), 112 MeV, reaction mechanism *(Russian)* 78−29508
O(π$^-$,n) spectrum obs. and calc. 79−17933

nuclei with mass number 6 to 19 continued
O(π$^{\pm}$,π$^{\pm}$), A=16,18, elastic and inelastic scatt., energy and A-depend. 78−54802
O(π$^{\pm}$, π$^+$X), X=He or d, 170 MeV, cross sections and ang. distribs., direct knockout mechanism *(Russian)* 80−86887
O(π$^+$,π$^+$d(He)), 60 MeV, cross sections, momentum and ang. distribs. *(Russian)* 77−74888
O(π,πp), 170 MeV, two stage and knock out contribs., π$^+$,π$^-$ spallation differences *(Russian)* 80−68632
O(π$^+$,π$^+$p)O, 170 MeV, direct-knock-out dominant mechanism *(Russian)* 77−61460
(π$^-$,π$^-$) 40 GeV/c, secondary particle multiplicities as function of number of π$^-$p collisions *(Russian)* 78−89922
^{1}u2C mean life, Pauli exclusion principle validity for nucleons 80−18233
Z, from ^{12}C(^{6}Li, d)^{16}O(α)^{12}C 77−82880

nuclei with mass number 20 to 38
14.6 MeV, differential cross sections, statistical model calcs. comparison *(Russian)* 78−78385
^{23}Na(n,n′γ), populations, of half integer spin mag. substates 77−30493
^{24}Mg radiative decays of unbound high spin states from ^{20}Ne(α,γ), ^{20}Ne(α,α′γ) 79−6484
^{30}Si, compound nucleus, 40.51 MeV excitation energy in ^{14}C+^{16}O system 79−13335
(^{6}Li,^{6}Li) 50.6 MeV elastic scatt. on A=12-208 nuclei, optical model parameters 77−18592
^{4}S, A=32,34, E1 and E2 strength, E1 giant resonance decay, isospin from Si(α,γ) 79−89266
A=10 to 50, m-particle n-hole struct. from few nucleon transfer reactions, review 78−50062
A=10-58, neutron separation energies, self consistent set from (n,γ) reaction 80−52563
A=12 to 24, nuclear cluster norm determ. using integral transform and SU(3) recoupling techniques 79−22214
A=12 to 40, (α,^{2}He) reaction, high spin state transition cross sections in 1p and 2s1d shell 79−6644
A=16 system, weak nuclear form factors of 0$^+$-0$^-$ transitions, nuclear struct. effects 80−18246
A=16 to 28, α-structure amplitudes and shell model wavefunctions for nuclear states 79−45192
A=16 to 40, mag. moments, shell model calcs, mesonic exchange current effects, book contrib. 80−479
A=16-40, α-spectroscopic factors between ground states, shell model prediction 79−13204
A=16-58, charge, proton and neutron density distribs. calc. 80−22680
A=18 to 22, influence of non-central interactions on 1s-0d nuclei 78−93949
A=18-20, light nuclei, compilation of energy levels, nuclear struct. information 78−62478
A=18-22, Coulomb matrix elements and energy shifts 77−10308
A=18-38, inelastic scatt. E4 transition probabilities in the 0d, 1s shell 80−78210
A=19-31 odd nuclei, K$^{\pi}$=$^{1}/_{2}^{-}$ bands, spectroscopic factors and transitions 80−32151
A=20, 36 to 38, sd shell nuclei, effective interaction between nucleons 78−17117
A=21 to 44, spectroscopic factors for single-nucleon transfer, review 77−71563
A=21-44, energy levels, excitation energies, branching and mixing ratios, lifetimes, J$^{\pi}$, resonances 79−13208
A=24, shell model calcs. of mass spectra and β decay 78−4903
A=24 to 32, resonances in heavy ion reactions, semiempirical predictions 78−74307
A=24-28 nuclei, reliability of calculated decay props. 78−93970
A=24-60, yrast lines using Strutinsky method, empirical fusion bands 80−42514
A=32 to 140, nuclear struct., binding energies, dipole moments *(French)* 77−46098
A=36-39, energy levels and effective interactions from large scale shell model calcs. 79−59011
A=6-44, gamma-ray transition strengths, data tables 80−37345
A=9 to 70, proton scatt., 14 to 45 MeV, differential cross sections 79−45273
A<100, average E1/M1 strength ratio 80−52621
A≤28, giant quadrupole resonance, E2 intensity distrib., from (α, α′), DWBA anal. *(Hungarian)* 80−52642
A≤57 nuclei, E2, M1 multipole mixing ratios 80−22751
C Ne+$\nu_{\mu}(\bar{\nu}_{\mu})$, inclusive distrib. of produced hadrons 78−89854
comparison of cluster and two-centre shell models 79−6444
even-even nuclei, z=6 to 100, probable members of quasi-bands in spherical and deformed regions 80−13357
fission product gamma-ray and half-life 29≤A≤69, data collection 78−50134
gamma-ray internal conversion coeffs. for all at. shells, 30≤Z≤104 79−45206
internal conversion coefficients, 30≤Z≤104, Hartree-Fock-Slater model calcs. 79−36199
internal conversion coeffs. for at. numbers Z≤30 77−46136
isomeric state formation by 14.8 MeV neutrons, in ^{24}Mg, ^{27}Al 77−30604
level densities, thermodynamic temps., spin cutoff factors, nuclei with 23≤A≤40, expt. calcs. 77−30492
light nuclei, multipole giant resonances 78−86462
mirror nuclei, A=13-33, transverse photon effect 77−6229
Na(n,n), 500 to 3000 keV, high resolution differential cross-section meas. 77−30592
photonuclear energy integrated cross-sections, calcs., A=2-40 77−50110
photospallation, 0.1 to 1 GeV, mass yield distrib. 80−73835
resonances in heavy ion reactions, s-d nuclei with A=24 to 32 79−6403
S(n,n) 20, 26 MeV, Coulomb correction term to optical model pot. 77−38280
s-d shell nuclei, semiempirical prediction of heavy ion reaction resonances 79−22256
Si(n,n), 500 to 3000 keV, high resolution differential cross-section meas. 77−30592
spectroscopy of Na neutron rich isotopes, nuclear ground state props. 77−22875
stable odd-mass sd nuclei, EM multipole moments of ground states 80−102116
thermonuclear reaction rate data for intermediate mass nuclei 80−31427
two-nucleon transfer in A=21-39 T$_z$=1/2 nuclei via (p,^{3}He) and (p,t), S=1 quenching 77−14128

nuclei with mass number 20 to 38 continued
(α,^{3}He), 55 and 65 MeV, on 1p and 2s1d shell nuclei, A=12 to 40 78−82365
(α,n) cross-sections and α-stopping power in light elements 77−74862
A nucleus, 40≥A≥12, strangeness exchange reactions, anal. 77−292
(n,n'γ), A=28-152, spherically doubly even nuclei, level excitation cross sections, statistical anal. *(Russian)* 79−67707
(n,X), fast n, ^{3}He emission cross sections for A=27-115 80−13475
^{20}Ne, rotational bands 78−45993
(p,α) preformation coeffs. for mass range 27-123 77−54209
(π,Xγ) reaction at 70 MeV on s-d shell nuclei 78−29504
^{20}Ne cluster struct., rot. bands from (^{16}O-α)+(^{12}C-^{8}Be) coupled channel orthogonality condition model 79−97647
^{28}A(n,p)^{28}Mg, reactor neutron irrad., product yield 79−538
A=20,21, Preedom-Wildenthal interaction, influence of central and non-central components 79−45179
A(α,^{2}He), A=36, 38, 55, 65 MeV, two neutron states, A-depend. of binding energy 78−74379
Al, (n,xp), (n,xd) and (n,xα) reactions, 14 MeV, sub-Coulomb barrier protons 77−30597
Al ($\pi^\pm$,$\pi^\pm$), 65-215 MeV forward scatt. amplitudes 79−85533
Al, A=25, 27, M1, E2, transition probabilities between differently deformed states, Nilsson model 77−61376
Al, beta-generated external bremsstrahlung spectra 77−57625
Al bombarded by ions, Coulomb excitation of sd shell nuclei, B(E2) values, lifetime meas. 78−25216
Al, NQR in heteroorganic group III compounds, summary 78−25565
Al, nucl. electron capture, 0.43-1.71 MeV electrons 79−6513
Al, π^- and p elastic scatt., 30 to 50 GeV/c, nuclear radius, real/imaginary forward scatt. amplitude ratio *(Russian)* 77−34351
Al, reactions induced by ^{12}C and ^{19}F ions, γ-ray spectroscopy of induced activities 77−23107
Al, sensitivity of displacement per atom cross sections rel. to in-group weighting schemes 79−36236
Al+α, 720 MeV, correlated energy spectra of light fragments, fireball and coalescence models 78−62555
Al+e, 800 MeV, multicharged particle emission during nucleus disintegration 78−41702
Al+K_L, 30 to 150 GeV, total cross sections, inelastic screening evidence 79−17936
Al+K_S, 20 to 140 GeV, precise coherent K_S regeneration amplitudes 79−17937
Al+K^-, stopped kaon capture, Doppler shifted nuclear gamma rays 78−62578
Al+n, total cross section for 6 to 14 Å neutrons 77−88148
Al+p, 200 GeV, d, $\bar{d}$, t, $\bar{t}$, ^{3}He, $^3\bar{H}\bar{e}$ prod. 79−9563
Al+p, 200 GeV, data anal. hydrodynamical model 79−551
Al+p, 200 GeV/c, relative yields of $\pi^\pm$, $K^\pm$, p, $\bar{p}$ 78−93995
Al+p, 600 MeV, pion production, energy spectra, A depend. *(Russian)* 78−17213
Al+p, 7 GeV/c hadron multiple prod. *(Russian)* 79−22298
Al+p, search for massive, long-lived, fractionally charged particles produced by 300-GeV protons 79−89311
Al+p($\pi^\pm$), 200 GeV, jet production 79−54438
Al+p→p, 640 MeV, proton inclusive spectra and ang. distrib. meas. 77−67751
Al+π^-, 3.7 GeV/c, proton spectra *(Russian)* 78−41785
Al+π^-, 7 GeV/c hadron multiple prod. *(Russian)* 79−22298
Al+$\pi^\pm$, 125 MeV, true absorpt. and scatt. 79−63705
Al(Ne,X), 400 MeV/N, direct vs. thermal particle emission, inclusive cross sections 80−52688
Al(Ne,X), proton inclusive spectra, direct plus thermal model 80−57799
^{A}Al, A=24,25,26, giant M1 strength, comparison with cross sections from Mg(p,n) 80−86878
^{A}Al, A=25,26,27 levels, resonances, γ-ray branching ratios from Mg(p,γ) 80−86875
^{22}Al(π,πpγ), 190 MeV, quasi-free single nucleon removal, p and π spectra 79−85519
^{24}Al, ^{24}Al^m, decay to γ-ray and α-particle emitting ^{24}Mg states 79−49607
^{24}Al, 1^+ isomer decay 79−85414
^{24}Al, 1^+ states anal. in ^{24}Mg(^{3}He,t)^{24}Al at 44 MeV 77−79390
^{24}Al, β-transitions, weak magnetism, nuclear struct., matrix elements 79−13253
^{24}Al, effective M3 matrix elements and transitions from shell model 80−102143
^{24}Al, low-lying 1^+ state anal. in ^{24}Mg(^{3}He,t) 78−29484
^{24}Al spin assignments, from ^{24}Mg(^{3}He,t) at 38.5 MeV 77−18580
^{25}Al, T=3/2 states γ-decay, ^{24}Mg(p,γ)^{25}Al 77−26608
^{26}Al 1^+T=0 states, isobaric analogue state, spin-isospin effective interaction from ^{26}Mg(p,n) 80−68553
^{26}Al, anomalous, in meteorites, prod. by explosive nucleosynthesis 79−62795
^{26}Al, as planetoid heat source in early solar system 78−65511
^{26}Al, coherence widths, level density param. and effective moment of inertia 78−37360
^{26}Al, decay in marine sediments, meas. with cyclotron, dating technique 79−71819
^{26}Al excited states, isobaric analogues, spins, DWBA anal. of ^{27}Al(^{3}He,α) 80−105981
^{26}Al, from supernova explosion near solar system rel. to lunar interior melting 78−40849
^{26}Al, galactic source of γ-ray line emission from beta-decay 77−33692
^{26}Al, γ-ray line detect. at Earth, constraint for stellar nucleosynthesis 80−94780
^{26}Al in early solar system, fossil or fuel 77−17387
^{26}Al in primordial comet interiors, contrib. to radiogenic melting 80−67659
^{26}Al, isoscalar and isovector E2 transition matrix elements 78−25148
^{26}Al isotopic anomalies in solar system, local proton irradiation model 78−93128
^{26}Al level anal. from ^{25}Mg(^{3}He,d)^{26}Al at 18 MeV 78−62554
^{26}Al, liquid-drop limit, fusion of ^{12}C+^{14}N 78−4959
^{26}Al, long-lived cosmogenic isotopes, cosmic-ray intensity variations 77−53361
^{26}Al low energy resonances, decay and J^π assignments, branching ratios from ^{25}Mg(p,γ) 80−42624
^{26}Al nucleosynthesis, long lived nucl. isomeric states, thermalization in stars 80−85846
^{26}Al, prod. from stellar evolutionary sequence 79−5809

nuclei with mass number 20 to 38 continued
^{26}Al production at stellar core collapse from ^{26}Mg(ν_e, e$^-$) *(Russian)* 80−77285
^{26}Al production in explosive C burning 78−20814
^{26}Al, sd-shell nuclei, stellar weak interaction rates, appl. to supernovae 80−82336
^{26}Al, synthesis in explosive H burning 80−85929
^{26}Al T=1 states, resonances, J^π and transitions from ^{25}Mg(p,γ) 80−99131
^{26}Al, yield from C and Ne shells of exploding massive star 80−90406
^{26}Al/^{26}Mg isobars, separation via negative ion mass spectroscopy 80−31146
^{26}Al^{g,m} relative yields from ^{25}Mg(p,γ) reaction 79−101058
^{26}Al^m, super-allowed Fermi β decay, lifetime meas. 77−79336
^{26}Al(n,p)^{26}Mg, stellar reaction rate, rel. to ^{26}Al prod. during C burning 79−70948
^{27}Al (^{14}N, X), 70, 100 MeV, deep inelastic, charged reaction products ang. correlations, 3-body kinematics 80−5162
^{27}Al (e,α), 120 MeV, preequilibrium α-emission, α energy spectra 79−85459
^{27}Al (n,n'γ), 14.6 MeV, differential cross sections, statistical model calcs. comparison *(Russian)* 78−78385
^{27}Al (n,p) and (n,d) reactions, study of isovector analogue giant resonances, proton hole states 77−26726
^{27}Al (p,p_0), elastic resonance scatt., 0.85-3.0 MeV, excitation functions 77−14121
^{27}Al, absolute excitation energy meas. using electrostatic analyser 77−30741
^{27}Al, analogue-antianalogue M1 transitions, nucl. shape change influence 78−13006
^{27}Al bound state parity and spin assignments, level struct. from ^{26}Mg (p,γ) resonances 78−66206
^{27}Al, coherence widths from ^{12}C(^{15}N,α) 78−41619
^{27}Al excited states lifetimes, recoil-distance method 77−30510
^{27}Al, gas phase proton irradiation, condensation, isotopic anomalies generation 79−13289
^{27}Al, in aqueous soln., quadrupolar relax., formulation of relax. rate 77−85600
^{27}Al, in aqueous soln., quadrupolar relax., reorientational motion of hydration water mols. 77−85601
^{27}Al, in ruby, appl. of NMR line acoustic saturation in quantum strain detector 77−51009
^{27}Al, inclusive proton photoprod., momentum spectra, max. bremsstrahlung energy 2.0 to 4.5 GeV *(Russian)* 77−34287
^{27}Al, inelastic electron scatt., charge distrib., Coriolis band mixing calc., C2 form factors 79−529
^{27}Al isobaric analogue resonances, spectroscopic factors and γ-rays from (p,p), (p,γ) 80−86873
^{27}Al, J^π=5/2 state, cross section and analysing power ang. distribs. 80−18296
^{27}Al, levels, GDR isospin mixing via (γ,p) 28 MeV 77−74832
^{27}Al levels, resonances, J^π, branching and mixing ratios from ^{26}Mg(p,γ) 80−99132
^{27}Al, low lying states, band mixing effects, quadrupole moment 78−490
^{27}Al, NMR in MAl_2Br_2 crysts.(M=Li, Na, K, Cs, NH_4, $(CH_3)_4N$), quadrupole effect 78−6597
^{27}Al, NMR meas. in Al-Ni alloys *(French)* 77−51974
^{27}Al, NMR meas. in Pd-Mn(Fe)(Ni) alloys 77−12215
^{27}Al neutron scattering resonance radiative widths 80−99146
^{27}Al, nucl. spin-lattice relax. meas. on $(La_{1-n}Gd_n)_3Al$ and $(La_{1-n}Ce_n)_3Al$ 78−2622
^{27}Al, nuclear charge radius from μ^- X-ray transitions 78−66195
^{27}Al, obs. of two-quantum rotary echoes in multi-level NMR of alumina 77−63316
^{27}Al, photonuclear reactions, 2-4.5 GeV, residual nuclei yields *(Russian)* 77−61399
^{27}Al, pion scatt., 355 MeV, ratio of π^+ and π^- cross sections from coincidence meas. 78−29501
^{27}Al, pionic, energy and width of 3d-2p transitions *(Russian)* 78−25760
^{27}Al, pionic, Lorentz-Lorenz quadrupote term, P-wave optical pot. 79−22252
^{27}Al, π^p high energy photoproduction and electroproduction 78−21543
^{27}Al, resonance strengths from ^{26}Mg(p,γ) 80−22786
^{27}Al, shape mixing using ang. momentum projection from Hartree-Fock intrinsic states 78−86472
^{27}Al, spins of p-h states from (d,τ) analysing powers 78−25111
^{27}Al, strongly bound π-nuclear states, criticality condition, optical pot. 78−90325
^{27}Al yrast states via ^{12}C(^{12}N,α) reson. struct. 77−79348
^{27}Al^{3+}, temp. depend. curves of quadrupole interaction parameter in K and NH_4 alums 77−55727
^{27}Al+^{12}C, 107, 155, 197 MeV, evaporation residue ^{39}K, prompt γ deexcitation 78−74395
^{27}Al+^{12}C, 83 MeV, giant resonance excitation 78−17235
^{27}Al+^{12}C, complete fusion cross sections, excitation functions *(Chinese)* 78−82406
^{27}Al+^{14}N, 100 MeV, α preequilibrium decay 79−6666
^{27}Al+^{14}N, 59 MeV, radiative capture and 1-nucleon emission cross sections 79−93652
^{27}Al+^{14}N or ^{16}O, high spin states prod in ^{35,36,37}Cl and ^{37}Ar, decay schemes 77−2932
^{27}Al+^{16,18}O, 34-81 MeV, total fusion-evaporation cross sections, fusion barrier 80−5190
^{27}Al+^{16}O, 100 MeV, fragment spin orientation meas. 77−30627
^{27}Al+^{16}O, 50-65 MeV, radiative capture cross sections upper limits 79−17923
^{27}Al+^{16}O, 60-80 MeV, fusion cross-sections 77−74898
^{27}Al+^{16}O, ang. correl. in compound nucleus decay 79−36261
^{27}Al+^{16}O, fusion and reaction cross section calc. in boundary condition model 79−9656
^{27}Al+^{16}O, fusion excitation functions, dynamical model calc. 78−50224
^{27}Al+^{16}O fusion, 30-70 MeV, statistical model calcs., yrast states and continuum feeding times 79−579
^{27}Al+^{20}Ne, 120 MeV, prompt γ emission, reaction products deexcitation 78−74396
^{27}Al+^{20}Ne, 120 MeV, strongly damped collisions 77−34332
^{27}Al+^{28}Si, 72 MeV, multinucleon removal 78−41755
^{27}Al+^{32}S, 175 MeV, possible explanation for a second deep inelastic peak 79−63699
^{27}Al+d, 6.3 GeV/c, inclusive spectra of fast p and d *(Russian)* 78−46075

nuclei with mass number 20 to 38 continued

^{27}Al+d(α), 12-50 MeV, t formation average cross sections 80−42670
^{27}Al+n, 15 MeC, cross sections for emission of sub Coulomb barrier charged particles 77−23007
^{27}Al+p, 1 GeV, neutron production *(Russian)* 79−85477
^{27}Al+p, 35-100 MeV, excitation function for ^{24}Na prod. 78−74356
^{27}Al+p, 400 MeV, p-γ coincidence meas. of multinucleon removal in quasifree process 78−37342
^{27}Al+p, 62 MeV, complex particle emission, pre-equilibrium exciton model anal. 78−66280
^{27}Al+p, 660 MeV, H and He isotope prod. 77−18544
^{27}Al+π$^-$, γ-π$^-$ coincidence spectra, 190 MeV 78−89913
^{27}Al(^{10,11}B,^{10,11}B), 41.6, 50 MeV, ang. distribs., cross sections and deformation parameters, absorption effects 79−67773
^{27}Al(^{12}C,^{12}C), 14-25 MeV, 180° scatt. excitation function and ang. distrib. struct. 80−32253
^{27}Al(^{12}C,X), 71.5 MeV, deep inelastic cross sections *(Chinese)* 79−59088
^{27}Al(^{12}C,αn), high spin negative parity states in ^{34}Cl, lifetime meas. 78−74327
^{27}Al(^{14}N,2pn), ^{38}Ar high spin states, decay scheme 78−25232
^{27}Al(^{15}N,X), 27-70 MeV, complete fusion, total fusion cross section, entrance channel effects 80−68716
^{27}Al(^{16}O,^{12}Cα)^{27}Al, 65 MeV, pre-equilib. α-decay obs. 77−61390
^{27}Al(^{16}O,^{15}N), 36-53 MeV, reaction dynamic depend. of small angle cross sections 77−18600
^{27}Al(^{16}O,X), 88 MeV, inelastic scatt. and multinucleon transfer, Q-value depend. 80−42690
^{27}Al(^{20}Ne,^{12}C), 120 MeV, anal. of continuous spectra by multi-step direct reaction theory 79−45287
^{27}Al(^{20}Ne,^{16}O), 120 MeV, anal. of continuous spectra by multi-step direct reaction theory 79−45287
^{27}Al(^{28}Si,Xγ), 65-81 MeV, fusion evaporation products, reaction cross sections 79−17946
^{27}Al(^{32}S,X), 175 MeV, completely damped process, scissioning systems 79−93647
^{27}Al(^{35}Cl,^{35}Cl), 100-170 MeV, elastic scatt. ang. distrib. 78−21605
^{27}Al(^{3}He, ^{3}He), 119 MeV, optical pot. parameters energy and mass depend. 80−32289
^{27}Al(^{3}He,^{3}He), 46 MeV, ang. distribs., optical and DWBA anal., scatt. pots. 79−556
^{27}Al(^{3}He,^{3}He), optical potentials and volume integrals, mass and energy dep. 80−52686
^{27}Al(^{3}He,^{3}He) 39.7 MeV, optical pot. mass. depend. 77−34327
^{27}Al(^{3}He,α), 34.8 ± 0.3 MeV, α-particle energy spectra distrib., c.f. pree-quilibrium decay calcs. 79−9598
^{27}Al(^{6,7}Li, ^{6,7}Li), 90 MeV, real optical pot. continuous ambiguity 80−102200
^{27}Al(^{6}Li,d)^{31}P, 36 MeV, absolute cross sections, ang. distribs. 79−89321
^{27}Al(^{9}Be, ^{9}Be), 14-26 MeV, universal optical pot. 78−25219
^{27}Al(K$^-$, π$^-$), 390 MeV/c, formation of hypernuclear excited states 78−74402
^{27}Al(K$^-$,π$^-$), relative ang. distribs. 77−14185
^{27}Al(α, α), 120-172.5 MeV, optical pot. uniqueness and shape 79−97719
^{27}Al(α, p), (α, d), (α, t), 50 MeV, reaction mechanism determ. *(Russian)* 78−54778
^{27}Al(α, ^{7}Be)^{24}Na, up to 156 MeV, excitation functions 77−3021
^{27}Al(α,X), 140 MeV, nonequilibrium light charged particle yield, energy spectra and ang. distribs. 79−40942
^{27}Al(α,X), 20, 40 MeV/N, α breakup yield, fragment yield ratios 80−9300
^{27}Al(α,α′), 106, 120, 145, 172.5 MeV, giant quadrupole reson. obs. 77−6415
^{27}Al(α,α′), 145 MeV, excitation energy anal., octupole strength conc. 78−21584
^{27}Al(α,α′)^{27}Al; 126 MeV, GQR, DWBA anal. 77−74826
^{27}Al(α,α), 41 MeV, elastic and inelastic, ang. distribs., optical and DWBA anal., scatt. pots. 79−556
^{27}Al(α,α), x=p,d,t,h,α′ and x-γ, 140 MeV, reaction mechanism characts. for deformed ^{27}Al 79−63682
^{27}Al(α,d)^{29}Si, d ang. distrib. corrections for finite interaction radius 79−9597
^{27}Al(α,n), ^{30}P high spin states, recoil dist. lifetime meas. 78−74386
^{27}Al(α,t), 25 MeV, DWBA anal. of triton ang. distrib. meas. 78−54776
^{27}Al(α,t)^{28}Si, 27.2 MeV, transitions to ground and 2^+_1 states *(Russian)* 77−34328
^{27}Al(α,x), 140 MeV, mass fragment meas., reaction mechanism models 79−63683
^{27}Al(α,xp+yn), up to 156 MeV, excitation functions 77−3021
^{27}Al(α,xp), up to 156 MeV, including prod. of ^{28}Mg, excitation functions 77−3021
^{27}Al(d, ^{3}He)^{26}Mg, 12.4 MeV, tensor analysing power, D-state component in ^{3}He wave function 78−54769
^{27}Al(d,^{3}He)^{26}Mg, 12.4 MeV polarised beam, $d_{5/2}$-$d_{3/2}$ admixing in pickup strength 77−6399
^{27}Al(d,^{3}He)^{26}Mg, 12.4 MeV, tensor analysing power, ^{3}He D-state effects 78−4948
^{27}Al(d,X) 80 MeV, charged light particle spectra and ang. distribs. exciton model anal. 79−40935
^{27}Al(d,α)^{25}Mg, 1.5-2.5 MeV, intermediate resonance widths 77−88151
^{27}Al(d,α)^{25}Mg, analysing power calc., distorted wave method 77−6404
^{27}Al(d,α)^{25}Mg, nuclear microanalysis of Al impurities in Si epitaxial layers 80−61193
^{27}Al(d,d), energy depend. of vector analyzing capacity, 1.8 to 3.0 MeV, 120 to 150° scatt. 79−9592
^{27}Al(d,n), diagnostic neutron spectra from deuterons 2.5, 3.0, 3.5 MeV 79−40933
^{27}Al(d,n), secondary neutron emission characts. 79−30843
^{27}Al(d,pX), 25.5 MeV, inclusive p spectra and cross sections from d breakup 79−13303
^{27}Al(d,pX) 80 MeV, inclusive proton spectra, d break-up, DWBA anal. 80−91190
^{27}Al(d,p)^{28}Al, 1.5 to 3.0 MeV, excitation functions 79−40932
^{27}Al(d,p)^{28}Al, 1.5-2.5 MeV, intermediate resonance widths 77−88151
^{27}Al(d,p)^{28}Al, 1.58 to 3.03 MeV, calc. of differential cross sections, spectroscopic factors 77−6394
^{27}Al(d,p)^{28}Al, 3.1 MeV, high spin states of ^{28}Al anal. 77−74856
^{27}Al(d,pγ) 2.4 MeV, ^{28}Al levels, $T_{1/2}$, J^π below 5.45 MeV 77−57623
^{27}Al(e,e′), 62 to 112 MeV, form factors, ^{27}Al energy spectrum, transition probabilities 77−34288

nuclei with mass number 20 to 38 continued

^{27}Al(e,e′), 70-340 MeV, odd parity state electroexcitation, form factors, transition probabs. 80−78208
^{27}Al(e,e′), comparison of inelastic electron and positron scatt. cross sections 79 49621
^{27}Al(e,e′), cross sections, shadowing effect at small four momentum transfer 80−63176
^{27}Al(e,e′), transition widths, multipolarity assignment DWBA calc. 78−13068
^{27}Al(e,e′p) 77−10389
^{27}Al(e,e′π$^+$), energy and ang. distribs. of πs, low lying residual states 78−54740
^{27}Al(e,e′), internuclear nucleon effective mass in quasielastic scatt. *(Russian)* 79−3076
^{27}Al(e,e) multipole operators in semileptonic weak and electromagnetic interactions 80−73840
^{27}Al(e,x), electrodisintegration charged particle yield, α to t cross section ratio *(Russian)* 80−86902
^{27}Al(γ,X), 3-30 MeV, photoabsorption cross section, giant dipole resonances 80−78254
^{27}Al(γ,p), cross sections and proton energy spectra from (e,e′p) 80−13461
^{27}Al(γ,p)^{26}Mg, energy and angular distribution *(Korean)* 80−18289
^{27}Al(γ,π$^-$) and ^{27}Al(e,e′π$^+$), 130 to 580 MeV, cross sections, impulse approx., multipole decomp. 77−54206
^{27}Al(n,α), 14.7-19.0 MeV, excitation functions relative to ^{56}Fe(n,p), n flux independent ratio 79−3142
^{27}Al(n,α), 14.8 MeV, expt. and statistical model determ. of α-prod. in fusion reactors 80−95397
^{27}Al(n,α), 4.5-18.3 MeV, cross sections and excitation curves *(Chinese)* 79−49601
^{27}Al(n,α)^{24}Na, recoil escape efficiency, evaporation model, Monte Carlo calc. 79−45271
^{27}Al(n,α)^{24}Na threshold reaction cross section, ^{252}Cf source 77−23039
^{27}Al(n,d), 56.3 MeV, spectroscopic factors, ^{26}Mg levels 78−4935
^{27}Al(n,n′), 2-4.5 MeV, level excitation functions, Hauser-Feshbach-Moldauer model test 79−36238
^{27}Al(n,n′γ)^{27}Al, γ-ray prod. cross-section meas. 79−26434
^{27}Al(n,n), (in)elastic scatt. cross sections, duration of collision process *(Russian)* 79−80942
^{27}Al(n,p), 14.7-19.0 MeV, excitation functions relative to ^{56}Fe(n,p) 79−3142
^{27}Al(n,p)^{27}Mg, 12.9-15.9 MeV, reaction cross section meas. 78−37337
^{27}Al(n,p)^{27}Mg, ave. neutron activation cross sections for ^{241}Am-Be source 79−31282
^{27}Al(n,t), 14 MeV, cross sections, fast neutron reaction excitation function calc. 79−45267
^{27}Al(p, 2p)^{26}Mg, average cross section for 6 to 15 MeV *(Japanese)* 77−57656
^{27}Al(p, α)^{24}Mg, average cross section for 6 to 15 MeV *(Japanese)* 77−57656
^{27}Al(p,X), 400 GeV, absorption cross sections and multiplicity distribs., A-depend. study 79−67748
^{27}Al(p,X), 90 MeV, charged light particle energy spectra exciton and evaporation model anal. 79−40923
^{27}Al(p,α$_0$), E_p=887.8 keV, blocking lifetime meas. comparison 79−59041
^{27}Al(p,α$_0$)^{24}Mg, 1.12-3.08 MeV, ^{28}Si resonances 78−13091
^{27}Al(p,α), 937 and 885 keV resonance lifetime meas. using crystal blocking technique 79−63671
^{27}Al(p,α)^{24}Mg, E_p =1540-2220 keV, ^{28}Si, excited level obs. 78−17189
^{27}Al(p,α)^{24}Mg, finite-range cluster-model description, DWBA approach 80−52667
^{27}Al(p,α)^{24}Mg, Q-value determ. 78−66205
^{27}Al(p,α)^{24}Mg resonance, nuclear lifetime meas. problems in single cryst. blocking expt. 77−47500
^{27}Al(p,α)X, direct knockout model for fragmentation, (p,pα) predictions 80−18275
^{27}Al(p,αx), 50 MeV, pre-equilib. alpha emission 78−70518
^{27}Al(p,γ)^{28}Si, 0.5 to 0.9 MeV, resonance strengths of selected resonances in s-d shell 78−66281
^{27}Al(p,γ)^{28}Si, 12917 and 12924 keV ^{28}Si level gamma-gamma directional correl. 79−536
^{27}Al(p,γ)^{28}Si, 2046 keV, gamma-ray intensity calibration standard 77−30698
^{27}Al(p,γ)^{28}Si, 2.4-2.74 MeV, γ-spectra, isobaric analogue states 77−57646
^{27}Al(p,γ)^{28}Si, E_p=992 keV resonance, γ-ray intensity standard 78−17472
^{27}Al(p,γ)^{28}Si, radiative capture of intermediate-energy protons to high-lying states 79−36243
^{27}Al(p,γ)^{28}Si, standard resonance strength 77−30565
^{27}Al(p,n), realistic complex nuclear matter t-matrix anal. Hamada-Johnston pot. 79−9564
^{27}Al(p,n), threshold to 6.3 MeV, total n prod. cross sections, statistical model parameters, nucleosynthesis 79−9602
^{27}Al(p,n)^{27}Si, cross sections and thermonuclear reaction rates 80−73852
^{27}Al(p,n)^{27}Si, threshold energy meas. 77−79375
^{27}Al(p,n)^{27}Si, threshold energy for accelerator calibration 79−36241
^{27}Al(p,n)^{27}Si, yield and (p,n) threshold meas., detector geometry effects 77−54221
^{27}Al(p,n)^{27}Si neutron yield meas. with sphere counter 77−23381
^{27}Al(p,p), 100-2200 MeV, total and reaction cross sections from optical pot. 80−18303
^{27}Al(p,p), (p,n) threshold anomaly 78−94003
^{27}Al(p,p) 65 MeV, elastic and inelastic, polarised p, nuclear matter distrib. 78−78297
^{27}Al(p,pα), 600 MeV, α-cluster quasielastic knockout, expt. methods, separation energy spectra 79−13275
^{27}Al(p,pα), 600 MeV, quasi-electric knockout reaction, PWIA calcs. 79−6581
^{27}Al(p,x), x=α,τ,72 MeV, spectra and angular distribs. 80−68660
^{27}Al(π$^\pm$,X γ), 190, 220 MeV, multinucleon removal cross sections and γ-ray spectra, binding energy effects 79−3183
^{27}Al(π,π′p), 255 MeV, quasielastic knockout, proton yield, $\sigma(\pi^+)/\sigma(\pi^-)$ cross section ratio 80−32305
^{27}Al(π,xγ), gamma ray coincidence spectra, nuclear surface clustering evidence 79−6707
^{27}Al(π$^-$, pxγ), 300 MeV, proton-gamma ray coincidence spectra 79−6704
^{27}Al(π$^-$,Xγ) 230 MeV reactions near Δ(1232) resonance 77−6465

nuclei with mass number 20 to 38 continued
Al(π^-,π n) and (π^-,π^- p+π^0n), knockout reactions, cross sections, nucleon charge exchange model 78−25246
^{27}Al($\pi^\pm$,p), ($\pi^\pm$,d), E=100, 220 MeV p and d spectra meas. 78−648
Al(π^+,π^-N), 180-255 MeV, quasielastic pion scatt. coincidence expt. interpretation, impulse approx. 80−68704
Al($\pi^\pm$,$\pi^\pm$X), 190 MeV, multiparticle removal occurring as separate particles, cluster removal 79−85498
^{27}Al($\pi^\pm$,$\pi^\pm$xγ), 300 MeV, pion-gamma coincidence spectra 79−6705
^{27}Al(π^-,xγ), 300 MeV, gamma-ray coincidence spectra, clustering evidence 79−6706
^{28}Al analogue dipole state excitation in ^{28}Si(n,p) 77−30571
^{28}Al E1 transitions and partial radiative widths from ^{27}Al(n,γ) 80−52618
^{28}Al ground state doublet ang. distrib., direct charge exchange model anal. from ^{28}Si(^{18}O,^{18}F) 80−9307
^{28}Al, high spin states anal. in ^{27}Al(d,p) at 3.1 MeV 77−74856
^{28}Al levels, spins and γ-rays, multipole mixing from ^{27}Al(n,γ), pol. thermal 80−47398
^{28}Al levels, transitions and spin from ^{27}Al(n,γ), pol. Al and n 80−78153
^{28}Al, neutron binding energy precision meas. 80−18182
^{28}Al, spectroscopic meas. in ^{30}Si(d,α) react. with polarised deuterons 78−41728
^{28}Al, spin-parity assignment, from ^{30}Si(d,α)^{28}Al at 8.12 MeV 77−6222
^{28}Al, $T_{1/2}$, J^π, levels below 5.45 MeV via ^{27}Al(d,pγ) 77−57623
^{29}Al, mag. moment quadrupole coupling const. β-ray detected NMR in Al_2O_3 cryst. 78−37267
^{31}Al, radioactive half-life and branching ratios 79−22240
^{34}Al neutron rich nuclide, obs. in U fragmentation by 800 MeV protons 77−61419
^{35}Al observation in ^{40}Ar+^{12}C collisions at 205 MeV/nucleon 79−22314
^{26m}Al populated in ^{26}Mg(^{3}He,t), precise Q-value, β decay energy, half life 77−30618
Al(α,X) 720 MeV, nuclear fragment prod. thermodynamic evaporation and firestreak description, pre-equilibrium emission 79−54426
Al(α,X) X=p,d,t,^{3}He,^{4}He, 720 MeV, back-angle prod. of light ions, model calcs. 79−45280
Al(α, 2α), 700 MeV, cross section, effective cluster number from PWIA, momentum distrib. 79−40940
Al(α, $\chi\pi$), 18 GeV, π multiplicity distrib. 79−97713
Al(α,n), 3.6 to 8 MeV, neutron yields 79−6651
Al(d,d), 4.3, 6.3, 8.9 GeV/c, secondary momentum spectra, multiple scatt. model anal. *(Russian)* 80−27650
Al(d,p), 6.3 GeV, proton momentum spectra 79−6621
Al(d,p), 6.3 GeV/c, p momentum spectra from d breakup 78−89887
Al(γ,X), photoabsorption cross-section, Levinger's factor, mass number dependence 80−63165
Al(γ,ω), cross section meas., comparison with theory 78−58261
Al(μ^-,X) energetic charged particle spectrum, integrated yield 80−18293
Al(n,X), 14.8 MeV, γ-prod. cross section 79−49622
Al(n,n), elastic and inelastic scatt., cross sections meas. and calcs. 78−13081
Al(n,xγ)Al, E_n=5.3 MeV, γ prod. cross-section obs. 78−89863
Al(p,X), 400 GeV, p, d, t, π, ^{3}He, α backward prod., inclusive cross sections 79−85475
Al(p,X), 400 GeV, p backward prod. invariant cross section 79−93623
Al(p,X), 400 GeV/c, light ion backward prod., invariant cross section 80−32279
Al(p,X), 70 GeV/c, $\pi^\pm$, K$^\pm$, p and $\bar{p}$ relative yields *(Russian)* 79−40930
Al(p,X), 70 GeV/c, $\pi^\pm$, K$^\pm$, p, $\bar{p}$ prod. with p_T=0.5-2.5 GeV/c cross sections, yield ratios *(Russian)* 80−52681
Al(p,X), X=He to Na, 2.1 and 4.9 GeV, fragment energy spectra, Maxwellian functional form 78−70529
Al(p,d), 2.14 GeV/c, quasifree knockout at 62 mrad, differential cross sections *(Russian)* 79−30819
Al(p,n), 800 MeV, n prod. systematics, π associated cross section 79−3153
Al(p,p), 36.2 MeV, differential cross section, asymmetries, 0 to 7° scatt. 78−94002
Al(p,p), summed scattering (elastic and inelastic with no meson production), 2.1 GeV/c, asymmetry meas. *(Russian)* 79−89313
Al(p,$\bar{p}\pi^-$), 10 GeV, $\bar{p}$ weak absorpt., $\bar{p}$ and π^- yields *(Russian)* 79−75987
Al(p,x), spallation by 300 GeV protons, activation cross section meas. rel. to ^{12}C(p,pn)^{11}C 79−40898
Al(p,xpX), x=1, 2, 640 MeV, energetic backward p emission, inclusive differential cross section 80−9290
Al(π,X), 125 MeV, absorption cross section in 3:3 resonance region 79−85543
Al(π,αX), 70 MeV, α cross sections and energy spectra, intranuclear cascade calcs. 79−575
Al(x,x), x=$\pi^\pm$, K$^\pm$, p,$\bar{p}$, 70, 125, 175 GeV/c 80−83128
Ar isotopes, spallation ratios and prod. cross sections from (p, spallation) 80−9284
Ar isotopes prod. cross sections in natural Ca by 12-45 MeV protons 77−17310
Ar isotopes prod. in lunar materials by solar cosmic ray protons, rate calc. 77−17311
Ar(^{3}He,n)Ca, A=36, 38, 11.5 MeV, neutron ang. distrib. and energy spectra 77−65227
^{32}Ar ground state masses in isospin quintet from (π^+,π^-) 80−105960
^{32}Ar, high spin states from heavy-ion fusion evaporation reactions, decay schemes 77−2932
^{32}Ar, isobaric analogue states via β-delayed protons 78−558
^{35}Ar, β-decay, recoil ion energy spectrum anal. 78−21525
^{35}Ar levels, transitions and β-delayed protons from ^{35}K decay 80−91156
^{35}Ar lowest T=3/2 state excitation energy from ^{35}K decay, ^{35}Ar lowest T=3/2 state excitation energy 79−85407
^{35}Ar→^{35}Cl β^+ decay and anomalous Cabbibo angle 77−74807
^{35}Ar→^{35}Cl superallowed decay, branching ratio meas., Cabibbo angle anomaly 79−26399
^{36}Ar α-cluster spectroscopic factors, DWBA anal. of (d, ^{6}Li) 80−52571
^{36}Ar, charge distrib. via ^{36}Ar(e,e′) 65-115 MeV 77−18527
^{36}Ar deduced levels from ^{36}K beta-delayed particle emission 80−83074
^{36}Ar, delayed proton and alpha emission, transition energies, levels, J^π, from ^{36}K decay 80−52629
^{36}Ar, electric quadrupole strength, giant quadrupole resonance 80−52575
^{36}Ar, inverse inertia parameter calc. 78−50073

nuclei with mass number 20 to 38 continued
^{36}Ar, lowest T=2 state isospin forbidden decays, branching ratios 79−67703
^{36}Ar, mode-mode coupling model for four-body correl. 77−10322
^{36}Ar, neutron low energy total cross-section, bound level parameters 77−23071
^{36}Ar, obs. of decay of T=2 state in ^{35}Cl(p,γ) 77−6294
^{36}Ar relative spectroscopic factors from ^{40}Ca(d,^{6}Li) 79−93509
^{36}Ar, resonances populated in ^{24}Mg(^{12}C,α) 79−67629
^{36}Ar, separation, calc. of thermal diffusion cascade *(Rumanian)* 78−58862
^{36}Ar(^{6}Li,d)^{40}Ca, 0$^+$ levels of ^{40}Ca, DWBA calcs. with optical model parameters 78−62571
^{36}Ar(^{6}Li,d)^{40}Ca, 17 MeV, alpha transfer to 4p-4h states 78−21590
^{36}Ar(d,p), Tabakin pot. calcs., differential cross sections, ang. distribs. 78−611
^{36}Ar(e,e′), 65 to 115 MeV, low lying level struct., lifetimes 78−8798
^{36}Ar(e,e′) 65-115 MeV, charge distrib. 77−18527
^{36}Ar(n,d), 14.1 MeV, absolute ang. distrib. meas. 78−595
^{36}Ar(n,γ), valence neutron capture in s-wave capture 77−23076
^{37}Ar atomic electron correlation in M electron capture 79−63634
^{37}Ar, double internal bremsstrahlung in electron capture, ang. correl. meas. 78−25157
^{37}Ar form. from Ca in fission reactors 77−83048
^{37}Ar, implantation in Fe, perturbed ang. distrib. 78−12969
^{37}Ar, M/L capture ratio, multiconfig. Hartree-Fock calc. atomic electron correlations 78−62510
^{37}Ar, prod. in body Ca by fast neutron exposure, Ca meas. 77−5075
^{37}Ar production rate due to cosmic ray neutrinos, contrib. to solar neutrinos tests 79−16837
^{37}Ar(n,p), (n,α), thermal, cross-sections meas. 78−94012
^{38}Ar high spin state density, γ-decay mode, deformed states from ^{35}Cl(α,pγ) 80−32168
^{38}Ar high spin states from ^{27}Al(^{14}N,2pn), decay scheme 78−25232
^{38}Ar levels, J^π and transition strengths, DWBA anal. of ^{40}Ar(p,t) 80−47378
^{38}Ar, model independ. J^π assignments from ^{24}Mg(^{16}O,2pγ) 77−18384
^{38}Ar resonance strengths from ^{37}Cl(p,γ) 80−22786
^{38}Ar yrast levels, J^π assignments, transitions, branching and mixing ratios from ^{35}Cl(α, pγ), ^{24}Mg(^{16}O, 2pγ) 79−67625
^{38}Ar(^{6}Li,d), location of 0$^+$ 4p-2h and 6p-4h configs. in ^{42}Ca 78−25220
^{38}Ar(α,nγ)^{41}Ca, high-spin positive parity states of ^{41}Ca anal. 77−38224
^{38}Ar(α,pγ)^{41}K, level props. of ^{41}K below 3.3 MeV 78−62588
^{48}Ar(p,n)^{38}K^m threshold meas. using gaseous target 79−93619
^{37,39}Ar, high-spin states of (fp)^2 character via (α,d) reaction 77−74865
^{9}Be+^{12}C→^{21}Ne*, different decay channels, resonance-like structures obs. 79−13333
C, A=20, 22, 26, exotic nuclei stability anal., Hartree-Fock approx. with the Skyrme interaction 78−82273
CC ^{20}Ne 8$^+$ level radiative width, resonance strength from ^{16}O(α,γ) 80−83065
^{12}C to ^{22}Ne induced nucleon transfer reactions 78−41768
^{12}C+^{12}C, mol. resonance props. by GCM 79−13321
^{12}C+^{12}C gross struct. resonances in excitation functions from ^{12}C(^{12}C, ^{10,11}B) 80−102167
^{12}C+^{12}C system resonant structs., J^π assignments, true ^{24}Mg states from ^{12}C(^{12}C, ^{16}O) 80−99163
^{12}C(^{16}O, α), ^{24}Mg low spin resonances, excitation functions and ang. distribs. 80−63151
^{40}C(π,γX), short-range 4-N correls. 77−18613
Ca, A=40, 48, mass and neutron distribs., HF calcs. *(Russian)* 77−82815
^{36}Ca mass via ^{40}Ca(^{4}He,^{8}He), isobaric multiplet mass eqn. deviations 77−74754
^{40}Ca, shell model anal. of ground state energy 78−29389
^{40}Ca(d,^{6}Li), 80 MeV, ground state α-spectroscopic factors, ^{36}Ar relative spectroscopic factors 79−93509
^{48}Ca, neutron radius determ., charge symm. 78−29380
Cl (Ar, π^+X), 250, 400 MeV/A, pion yield near threshold 80−18344
Cl, A=35,36,37 high spin states from heavy-ion fusion evaporation reactions, decay schemes 77−2932
Cl isotopes, effect of isotopic abundance on kerma 78−29536
Cl isotopes, slow neutron scatt. 77−71610
Cl, strength function of deeply bound hole states 78−17113
Cl+Ar, 800 MeV/A, wide angle inclusive proton spectra 79−40951
Cl(Ar,X), 0.4-1.8 GeV/u, multipion prod. energy depend. 80−106065
Cl(Ar,X), 800 MeV/N, single particle spectra from high multiplicity events 80−99184
Cl(Ar,X), proton inclusive spectra, direct plus thermal model 80−57799
^{A}Cl, A=34, 38, effective M3 matrix elements and transitions from shell model 80−102143
^{A}Cl+p, A=35, 37 below 52 MeV, cross sections, excitation functions 78−89864
^{A}Cl(e, e′), 116, 194 MeV, A=35, 37, charge distrib. and RMS charge radius 80−102109
^{31}Cl, mass excess in ^{36}Ar(^{3}He,^{8}Li) 77−57595
^{32}Cl, β^+ decay, delayed particle emission, ^{32}S levels and J^π 80−22772
^{32}Cl, isobaric analogue states via ^{32}Ar β-delayed protons 78−558
^{33}Cl, NQR study of spin-spin interactions in ferroelec. phase of solid HCl 77−85612
^{34}Cl compound nucleus in ^{32}S(d,α)^{30}P, fluctuation anal. 78−46070
^{34}Cl, core polarisation J-averaged effects through 3rd order up to 10 $\hbar\omega$ excitations 79−67671
^{34}Cl, ground and excited states, shell model verification by ^{32}S(^{3}He,p)^{34}Cl cross section meas. 78−13119
^{34}Cl, high spin negative parity states, lifetimes meas. 78−74327
^{34}Cl high spin states 78−82289
^{34}Cl, J^π, levels, mixing ratios, $T_{1/2}$ via ^{33}S(p,γ) and ^{33}S(p,p) 1.0, 2.0 MeV 77−26613
^{34}Cl, levels Γ, γ-branching, $T_{1/2}$ via ^{33}S(p,γ) 1.0, 2.0 MeV *(French)* 77−26612
^{34}Cl negative parity high spin states, ang. distribs. and lifetimes from ^{31}P(α,n) 79−17812
^{34}Cl populated in ^{34}S(^{3}He,t), precise Q-value, β decay energy, half life 77−30618
^{34}Cl, produced by ^{32}S+deuteron, shell struct. effects, Fermigas model predictions 78−89882
^{34}Cl states populated in ^{32}S(^{3}He,p) at 18 MeV 77−88046
^{34}Cl superallowed beta-decay Q-value via ^{34}S(p,n) threshold meas. 77−34298
^{35}Cl, NQR in methylammonium hexahalometallates (IV) 79−95673

nuclei with mass number 20 to 38 continued
^{35}Cl, contrib. to fast neutron dose to the human body 80−51263
^{35}Cl, elec. field effect in NMR in antiferromag. $CoCl_2$ 77−28459
^{35}Cl, isobaric analogue resonances determ. from ^{34}S(p,p) meas. 77−65222
^{35}Cl, isotope effects in NQR in dichloroacetic acid-d_0, -d_1 77−46578
^{35}Cl, model independ. J^π assignments from ^{24}Mg(^{16}O,p$\alpha\gamma$) 77−18384
^{35}Cl NMR, medium effects 77−1612
^{35}Cl, NMR in $(C_nH_{2n+1}NH_3)_2CuCl_4$, nearly 2-D ferromag. 77−28455
^{35}Cl, NQR, charge transfer and distrib. in nitrile complexes, RCN...Cl-Cl$^-$, RCN...$HCCl_3$ 77−12244
^{35}Cl, NQR freq. in $AgClO_3$, temp. depend. 77−12228
^{35}Cl, NQR freq. in aminoarsines, aminoboranes, N-As and N-B bonds 78−25566
^{35}Cl, NQR in $KClO_3$, spin generator 77−10077
^{35}Cl, NQR in $KClO_3$, temp. depend. 77−12227
^{35}Cl, NQR in organic compounds, crystal splitting, bonding effects 77−12221
^{35}Cl, NQR in Sn complex, $SnCl_4.L_2$ (L_2=organic phosphorus ligand) 77−16201
^{35}Cl, NQR meas. in trichloroacetic acid-base H bonded complex 78−25555
^{35}Cl NQR spectra and reorientational motion of PCl_3 group in trichlorophosphazenes 78−25567
^{35}Cl, NQR spectra in group IV tetrachlorides 77−12231
^{35}Cl, NQR spectral parameters in ammonium hydrogen chloracetate, temp. meas. 77−13785
^{35}Cl, negative energy resonance parameters for (n,n), (n,γ), (n,p) and (n,α) 77−23025
^{35}Cl, nucl. quadrupole spin-lattice relax. meas. in paradichlorobenzene 77−28469
^{35}Cl, relax. rates in aqueous solns. of alkali chlorides 77−88471
^{35}Cl, resonance strengths from ^{34}S(p,γ) 80−22786
^{35}Cl+^{24,25,26}Mg(^{27}Al)(^{28}Si), 100-70 MeV, mass systematics of evaporation residues 77−38311
^{35}Cl+^{27}Al, 140, 150, 160, 170 MeV, deep inelastic fragment kinetic energies anal. 77−82955
^{35}Cl+^{27}Al, deep inelastic fragment energies, rot. energy contributions 79−63697
^{35}Cl(n,d), 14.1 MeV, absolute ang. distrib. meas. 78−595
^{35}Cl(n,γ), slow n, 398 eV resonance J^π determination 79−36147
^{35}Cl(n,γ)^{36}Cl, E1 and M1 radiative strength functions 78−4940
^{35}Cl(p,γ)^{36}Ar, 0.5 to 0.9 MeV, resonance strengths of selected resonances in s-d shell 78−66281
^{35}Cl(p,n)^{35}Ar, threshold energy, reln. to vanishing Cabibbo angle 78−50167
^{35}Cl(p,n)^{35}Ar threshold energy, ^{35}Ar→^{35}Cl β-decay endpoint energy 77−74807
^{35}Cl(p,p), (p,n) threshold anomaly 78−94003
^{36}Cl, 1-20 ps region mean lifetime meas., high-vel. DSA method 77−65200
^{36}Cl anomalous M1/E1 strength ratio and doorway states from ^{35}Cl(n,γ) 80−57730
^{36}Cl, beta decay, K-shell electron ejection 77−18888
^{36}Cl, Cherenkov counting using Teflon vials 78−858
^{36}Cl, g-factor determ. from perturbed ang. distribs. 78−12970
^{36}Cl in environmental water samples, anal. using electrostatic accelerator 79−20895
^{36}Cl, internal bremsstrahlung spectra, accompanying second forbidden β-decay 78−8776
^{36}Cl prod. in proton induced high-energy spallation, cosmic ray effects 77−61421
^{36}Cl, spin and parity of 3723, 4294 and 5313 keV levels 77−88038
^{37}Cl, elec. field effect in NMR in antiferromag. $CoCl_2$ 77−28459
^{37}Cl high spin state decay, spin assignments, yrast level lifetime from ^{27}Al(^{19}F,2αp), ^{27}Al(^{12}C,2p), ^{34}S(α,p) 79−6490
^{37}Cl, in-beam γ-ray spectroscopy via ^{3}H(^{35}Cl,pγ) 78−13013
^{37}Cl, isotope effects in NQR in dichloroacetic acid-d_0, -d_1 77−46578
^{37}Cl neutrino absorpt. cross-sections, rel. to Brookhaven expt. sensitivity to solar neutrinos, collapsing stars and cosmic neutrinos 78−4929
^{37}Cl, ν_e capture, statistical theory, inclusion of first forbidden transitions, cross sections 78−93990
^{37}Cl+ν_e, 0 to 300 MeV, cross sections, shell model calcs 79−93605
^{37}Cl(^{3}He,p)^{39}Ar, 17, 19 MeV, DWBA two-particle transfer anal. 77−38288
^{37}Cl(α,d), 27 MeV, spectra, ang. distribs., ^{39}Ar low lying states, spins 78−25212
^{37}Cl(α,γ), 2.9-5.2 MeV, excitation function competition cusps, Mauser-Feshbach calcs. 80−13404
^{37}Cl(d,d), 12.0 MeV, polarised deuterons, vector analysing power 77−14094
^{37}Cl(d,t)^{36}Cl, 12.0 MeV, polarised deuterons, vector analysing power 77−14094
^{37}Cl(n,d), 14.1 MeV, absolute ang. distrib. meas. 78−595
^{37}Cl(n,γ), spectroscopic factors calc. using potential capture model 77−30583
^{37}Cl(n,γ)^{38}Cl, recoil energy spectrum calcs. 78−86531
^{37}Cl(ν,e$^-$)^{37}Ar, statistical theory calc. of total capture cross section 77−88113
^{37}Cl(ν_e,e$^-$)^{37}Ar, cross-section constraints for ^{8}B solar neutrinos 77−26675
^{37}Cl(ν_e,e$^-$)^{37}Ar, rot. model for mass-37 system, cross section calcs. 77−88114
^{37}Cl(ν,e$^-$)^{37}Ar, shell model cross section calc., appl. to cosmic ray and background elimination *(Russian)* 80−5131
^{34,35,36}Cl, high-spin states of $(fp)^2$ character via (α,d) reaction 77−74865
^{35,37}Cl, NQR in $BiCl_3.GaCl_3$ complex, geom. struct. 78−25569
^{35,37}Cl(α,d), 40 MeV, populating high-spin states, L-transfer 77−74865
Cl(n,X), 14.8 MeV, γ-prod. cross section 79−49622
Cu(p,π^+), 400-500 MeV, cross-sections meas. 77−10392
^{19}F(α,n)^{22}Na, 2.3-4.7 MeV, populating ^{23}Na reson. levels 77−65199
^{19}F(α,pγ)^{22}Ne, 2.3-4.7 MeV, populating ^{23}Na levels 77−65199
^{20}F 2.97 MeV doublet γ-decay, J^π assignment from ^{11}B(^{13}C,$\alpha\gamma$) 79−6491
^{20}F, 4 to 6 MeV levels populated in ^{19}F(d,p) 78−25118
^{20}F, β-decay, recoil-order matrix elements 77−79337
^{20}F, β-γ directional correlation meas., search for second class currents 79−13245
^{20}F β-spectra, cf conserved vector current predictions 78−50131
^{20}F, β-transitions, weak magnetism, nuclear struct., matrix elements 79−13253

nuclei with mass number 20 to 38 continued
^{20}F decay, β-γ ang. correlation, second class current contrib. 79−22236
^{20}F, elec. quadrupole interaction in $KZnF_3$ cryst., NMR meas. 77−12253
^{20}F excited states from ^{16}O(^{7}Li,^{3}He), energies, spins 78−82369
^{20}F NMR in CaF_2, rel. to (n,γ) damage annealing 77−20725
^{20}F NMR_2 in CaF_2, rel. to (n,γ) damage 77−20724
^{20}F spins from ^{17}O(^{13}C,^{10}B) 80−13494
^{20}F states up to 7 MeV excitation, studied via ^{22}Ne(d,α)^{20}F 77−10414
^{20}F→^{20}Ne+e$^+$+$\bar{\nu}_e$, CVC test in $2^+\rightarrow 2^+$ transitions 79−6514
^{21}F, form. in ^{19}F(t,p) reaction, 0.9 and 1.1 MeV, proton ang. distribs., possible compound nucl. form. 78−17218
^{24}F, effective interactions in sd-states 77−14044
^{20}Fe, β-γ directional correlation, second class current 78−50127
^{A}K, A=37,39, levels, excitation and microscopic form factors, DWBA calcs. from Ca(p,α) 80 32185
^{35}K decay, ^{35}Ar levels, transitions and β-delayed protons 80−91156
^{35}K decay, ^{35}Ar lowest T=3/2 state excitation energy 79−85407
^{36}K, beta delayed emission of protons and α-particles 80−83074
^{36}K, β-decay, delayed proton and alpha emission ^{36}Ar levels, J^π, transitions 80−52629
^{37}K $(sd)^{-3}$ g.s band investigation in ^{40}Ca(p,α)^{37}K study 79−6587
^{38}K, effective M3 matrix elements and transitions from shell model 80−102143
^{38}K, J^π via ^{40}Ca (d,α)^{38}K 7.5, 7.75, 8.0 MeV polarised d near 0° 77−6401
^{38}K, lifetime and E2/M1 branching ratio of second excited state 77−34254
^{38}K low lying 1^+, T=0 states, DWBA anal. of ^{40}Ca(p,^{3}He) 80−470
^{38}K, prod. of uniform yield from ^{40}Ca(p,2pn)^{38}K using range modulator 77−40735
^{38}K^m, β and γ spectra meas., determ. of isomeric ratios *(Russian)* 77−74771
^{38}K^m superallowed Fermi β-decay half lives 78−82318
^{38}K^m→^{38}Ar, superallowed $0^+\rightarrow 0^+$ β transition, spectrum shape 78−37316
^{38m}K, end point energy of superallowed Fermi decay 78−46030
(^{6}Li,d) on odd A, sd shell nuclei, α-cluster spectroscopic strengths, DWBA anal. 79−3104
Mg, A=24, 26, cross section for prod. in Al(p, α) reaction *(Japanese)* 77−57656
Mg, A=24-26, 80 MeV, resonance-like phenomena 79−13308
Mg, α- and ^{8}Be-spectroscopic factors determ. 78−62494
Mg bombarded by ions, Coulomb excitation of sd shell nuclei, B(E2) values, lifetime meas. 78−25216
Mg, giant quadrupole resonance strength, p- and α-inelastic scatt. and α capture 78−37323
Mg isotopes, 24.2 MeV α-scatt., optical model and coupled-channel anal. 77−6407
Mg isotopes, pionic, energy and width of 3d-2p transitions *(Russian)* 78−25760
Mg, μ^- capture, charged particle energy spectra and asymmetry *(Russian)* 78−89828
Mg+^{14}N or ^{16}O, high spin states prod. in ^{35,36,37}Cl and ^{37}Ar, decay schemes 77−2932
Mg+n, transmission and (n,γ), determ. of isobaric analogue impurities 77−6386
Mg(^{9}Be,^{9}Be), 14-26 MeV, universal optical pot. 78−25219
^{A}Mg, A=24,26, second order nonspherical quadrupole phonon effects 80−86790
^{A}Mg, A=29-32, radioactive half-life and branching ratios 79−22240
^{A}Mg+p, A=24,25,26, 1 GeV, neutron production *(Russian)* 79−85477
^{A}Mg+p, A=24-26, gas phase proton irradiation, condensation, isotopic anomalies generation 79−13289
^{A}Mg(^{16}O,^{16}O), A=24, 26, 20-35 MeV cross sections and excitation functions, optical model anal. 79−93655
^{A}Mg(^{3}He,^{3}He), A=24,25,26, optical potentials and volume integrals, mass and energy dep. 80−52686
^{A}Mg(^{7}Li,^{7}Li), A=24, 26, 88 MeV, optical potentials, phenomenological and microscopic 80−52687
^{A}Mg(α,^{12}C), A=24, 26, 90.3 MeV, cross sections and systematics multi-α-cluster transfer implications 80−42675
^{A}Mg(α,^{12}C), A=24, 26, 90.3 MeV, multi-α-cluster transfer and direct pickup cross sections 80−57760
^{A}Mg(d,^{6}Li), 80 MeV, A=24, 26, ground state α-spectroscopic factors 79−93509
^{A}Mg(d,^{6}Li), 80 MeV, A=24,26, α-spectroscopic factors and ang. distribs., DWBA anal. 80−99126
^{A}Mg(d,^{6}Li), A=24-26, 80 MeV, DWBA calcs. spectroscopic factors 79−6623
^{A}Mg(p, p'), A=24, 26, isovector dipole strength excitation in giant resonance region 80−83066
^{A}Mg(p,p), A=24, 26, 6.9 GeV/c, elastic and inelastic differential cross sections, ^{26}Mg spin flip probability *(Russian)* 79−59071
^{A}Mg(p,p) A=24-26, 65 MeV polarised p, elastic and inelastic, nuclear matter distrib. 78−78297
^{20}Mg, β-delayed proton obs., mass excess of T=2 state in ^{20}Na 79−22234
^{23}Mg even parity excited states, collective props., EM moments, generator coordinate method 78−78259
^{23}Mg, even parity state, EM props., collective struct., generator coord. method, HF method anal. 79−89220
^{23}Mg, forbidden transition ang. distribs., CCBA and DWBA anals. of (p,d) 80−86848
^{23}Mg, high spin states anal., ^{12}C+^{12}C reson. at $E_{c.m.}$=19.3 MeV 77−26579
^{23}Mg hole states, transitions and spectroscopic factors, DWBA anal. of ^{24}Mg(p,d) 80−32161
^{23}Mg j-forbidden $^7/_2^+$ state excitation, CCBA calculations, two step processes from ^{24}Mg(p,d), 49.5 MeV 79−26369
^{23}Mg low lying analogue states, DWBA anal. from ^{24}Mg(d,t) 29 MeV, polarised d 78−82285
^{23}Mg, produced in 32-14.4 MeV ^{16}O+^{9}Be, gamma transitions 79−49599
^{23}Mg resonances through γ-decay excitation functions from ^{12}C(^{12}C,n) 80−63148
^{23}Mg/^{23}Na, mirror level pair cross sections from ^{24}Mg($\pi^\pm$,πN) 79−67665
^{24}Mg, ^{16}O+α+α cluster model, energy level structure 80−18215
^{24}Mg, 11.86 MeV level, confirmation of $J^\pi=8^+$ assignment from ^{12}C(^{16}O,$\alpha\gamma$) 42 MeV 78−70445

nuclei with mass number 20 to 38 continued
^{24}Mg, 1s-0d shell effective interaction, (e,e) scatt. form factor calc. 77−61400
^{24}Mg 2_1^+ state quadrupole moment from ^{208}Pb(^{24}Mg,^{24}Mg) 80−9230
^{24}Mg 2_1^+ substate parameters near Coulomb barrier from ^{12}C(^{16}O, α) 79−67657
^{24}Mg, 2^+ level, 8^+ member, radiative width meas. 77−71613
^{24}Mg, 6 MeV 4^+ state, configuration anal., electron scatt. form factors 78−25115
^{24}Mg 6_1^+ level, α and γ decays, branching ratios from ^{12}C(^{16}O,α) 79−75901
^{24}Mg (α,Li*), unbound Li, relative energy distrib. of correlated decay products 79−13274
^{24}Mg (α,α' ^{12}C), 120 MeV, symmetric fission, resonances and average partial widths 80−42714
^{24}Mg (α,$\alpha'\gamma$) 104 MeV, nuclear deformation from ang. correlations, coupled channel anal. 78−78301
^{24}Mg (γ,p), 17-30 MeV, giant dipole resonances and transitions, shell effects *(Russian)* 80−13434
^{24}Mg (n,n), thermal neutron scatt. parameters 79−93628
^{24}Mg, binding energy, rotational band energy, Brink α-cluster model 77−6195
^{24}Mg, central-tensor coupled effective interaction pot., binding energy shape, electric moment 77−14036
^{24}Mg coherence width, intermediate structure effects from ^{23}Na(p,α)^{20}Ne 79−45133
^{24}Mg continuum states, branching ratios from ^{12}C(^{16}O, $\alpha\alpha$) 80−22661
^{24}Mg Coulomb matrix elements, isospin mixing in giant dipole resonance from ^{20}Ne(α,γ) 79−93507
^{24}Mg, dipole moment using transient mag. field from ion passing through ferromag. *(Dutch)* 78−29386
^{24}Mg, electric quadrupole strength, giant quadrupole resonance 80−52575
^{24}Mg, evidence for rotational band and its fragmentation in ^{12}C(^{12}C, α)^{20}Ne reaction 79−9449
^{24}Mg, existence of second $J^\pi=0^+$ reson. at high excitation energy, study of ^{12}C(^{12}C,α)^{20}Ne reaction 78−25214
^{24}Mg first excited state static quadrupole moment, B(E2) value from ^{208}Pb(^{24}Mg,^{24}Mg) 79−45161
^{24}Mg, form. in ^{12}C+^{12}C reaction at 10.5 to 15 MeV, possible rot. band 78−13134
^{24}Mg from ^{12}C(^{13}C,n), nonstatistical population of high spin states 78−74385
^{24}Mg giant isoscalar quadrupole fission/fusion doorway states from ^{12}C(^{12}C, ^{12}C) 80−37410
^{24}Mg ground and γ-bands, direct and multistep processes from (α,^{6}He), (p,t), (^{16}O, ^{16}O) 80−102094
^{24}Mg ground state band from ^{12}C(^{12}C,X) 80−42727
^{24}Mg, ground state rot. bands from shell-model Hamiltonians 77−79298
^{24}Mg, γ-ray and α-particle emitting states form., from ^{24}Al and ^{24}Al^m decay 79−49607
^{24}Mg, HF microscopic anal. of core struct. for deformed nucleus 78−78294
^{24}Mg high spin selectivity, critical ang. momentum effects from ^{10}B(^{16}O,d) 80−13366
^{24}Mg high spin states, high spin particle spectroscopy upper limits for compound reactions from ^{10}B(^{16}O,d) 79−36126
^{24}Mg high spin states from selective compound reactions, stat. anal. from ^{10}B(^{16}O,d) 80−18180
^{24}Mg, highly-excited rot. band obs. from ^{10}B(^{14}N,α)^{20}Ne 78−33218
^{24}Mg, identification of 10^+ levels using ^{12}C(^{16}O,α) at 26.7 MeV 78−33119
^{24}Mg intermediate struct. correlations, elastic and reaction channel excitation functions from ^{12}C(^{12}C,X) 80−68625
^{24}Mg, intrashell quartet states, ang. momentum projection 77−10348
^{24}Mg isoscalar quadrupole excitations in 2 centre shell model, collective approach, particle-hole excitations 79−45139
^{24}Mg isovector M1 excitations, current and spin contribs. from (e,e'), (p,n) 80−68582
^{24}Mg, $K^\pi=0^-$, $K^\pi=3^-$ bands, radiative and α-widths from (α,γ), (^{16}O,$\alpha\gamma$) 80−18173
^{24}Mg K=2 band and alpha cluster model state point symmetry 80−105946
^{24}Mg, levels, GDR isospin mixing via (γ,α) 28 MeV 77−74832
^{24}Mg, low energy positive parity spectra, $2\hbar\omega$ excitations, ang. momentum projected deformed particle-hole model calcs. 78−25119
^{24}Mg low lying K-band from ^{28}Si α-decay 80−47438
^{24}Mg, low lying rot. bands from extended deformation model, parity violating deformations 79−6360
^{24}Mg, low spin rotational states, energy props., extended deformation model 80−86785
^{24}Mg lowest $J^\pi=0^+$, T=Z level from ^{23}Na+p reactions, narrow resonance, isospin forbidden particle decays 78−89871
^{24}Mg lowest T=2 state from ^{23}Na(p,γ), total width 78−89870
^{24}Mg, lowest T=2 state isospin forbidden decays, branching ratios 79−67703
^{24}Mg, microscopic model of 2_1^+ and 3_1^+ states, inelastic p scatt. test 79−26358
^{24}Mg, mol. config. of ^{12}C+^{12}C, high spin props., Strutinsky method 78−50201
^{24}Mg, molecular configuration 79−13193
^{24}Mg, monopole excitations, transition densities from simple collective model 79−40834
^{24}Mg, multipole mixing ratios from polarised beam γ-ray singles meas. 77−46132
^{24}Mg neutron scattering resonance radiative widths 80−99146
^{24}Mg, novel cluster model descript., ^{16}O+^{8}Be, energy levels 78−62495
^{24}Mg nuclear molecular resonances in ^{12}C-^{12}C system from ^{12}C(^{16}O,α), 80−13430
^{24}Mg nucleus, ^{12}C+^{12}C quasimolecular rotational band resonances *(Russian)* 79−13269
^{24}Mg, 0_1^+, 2_1^+, 4_1^+ states, EM props. from large basis shell model 79−75900
^{24}Mg, populated via ^{12}C(^{12}C,γ), resonance in γ yields, $J^\pi=2^+$ resonance 78−54799
^{24}Mg, population of resonant ^{12}C+^{12}C states in ^{12}C(^{16}O, α) 78−62563
^{24}Mg, pot. and charge deform. of rot. states 77−46106
^{24}Mg, produced in 3.2-14.4 MeV ^{16}O+^{9}Be, gamma transitions 79−49599
^{24}Mg radiative decays of unbound high spin states, resonance J^π assignment from ^{20}Ne(α,γ) 79−67701

nuclei with mass number 20 to 38 continued
^{24}Mg, reson. levels, J^π, via ^{12}C(^{12}C,α)^{20}Ne, E_{cm}=6.5-12 MeV 77−54200
^{24}Mg, rot. band, reson. states, J^π via ^{12}C+^{12}C 78−491
^{24}Mg, rot. band obs. with ^{12}C(^{12}C,α)^{20}Ne 78−12951
^{24}Mg rot. band termination, level lifetimes from ^{12}C(^{16}O, α) 80−18174
^{24}Mg rotational band collectivity, shell model excitation in Sp(4, R) symmetry 80−102095
^{24}Mg, rotational band fragmentation and rotation-vibr. model, ^{12}C+^{12}C appl. 78−25096
^{24}Mg, rotational band fragmentation, rotation-vibr. model 78−54665
^{24}Mg, rotational band struct., obs. in (^{3}He,^{3}He') 78−41616
^{24}Mg, Sp(6,R) symmetry, α-breakup amplitudes, of giant E2 excitations 78−29435
^{24}Mg states, Nilsson model spectroscopic factors, collective model rot. bands from ^{23}Na(^{3}He,d) 79−6421
^{24}Mg, struct. determ. from ^{16}O+α+α model 79−6401
^{24}Mg, T=2 state props., obs. in ^{23}Na(p,γ)^{24}Mg reaction 78−8767
^{24}Mg, triaxial nuclei rots., extended cranked shape consistent oscillator model 80−102133
^{24}Mg, velocity and Z-depend. of transient mag. field in Fe 77−71566
^{24}Mg yrast and high spin states up to 24 MeV, ang. distribs. from ^{10}B(^{16}O, d) 80−18175
^{24}Mg yrast line, Strutinsky type cranking calc., pairing correlation inclusion 80−13355
^{24}Mg yrast states up to 24 MeV excitation energy from ^{10}B(^{16}O,d), 60 MeV 78−89781
^{24}Mg+^{12}C, 42-84 MeV, binary fragmentation, kinematical anal. 78−25223
^{24}Mg+^{12}C, elast. and inelast. scatt. near Coulomb barrier 77−6427
^{24}Mg+^{12}C(^{16,18}O) scatt., ^{24}Mg pot. quadrupole deform. length determ. 78−12963
^{24}Mg+^{16}O, 30-81 MeV, fusion cross section, elastic scatt. ang. distrib., optical model anal. 78−78412
^{24}Mg+^{16}O, elast. and inelast. scatt. near Coulomb barrier 77−6427
^{24}Mg+^{16}O, two step α-transfer reaction 79−76018
^{24}Mg+^{18}O, 32-72 MeV, fusion cross section, elastic scatt. ang. distrib., optical model anal. 78−78412
^{24}Mg+^{7}Li inelastic scatt., 34 MeV, microscopic interpretation, double folding model 77−14156
^{24}Mg+d, 10 MeV vector polarised deuterons scatt., nuclear shape effects, optical pot., analysing power 78−54768
^{24}Mg+e, 21 to 32 MeV, E0 and E2 excitations, fission into two ^{12}Cg.s. nuclei 78−54744
^{24}Mg+p, 400 MeV, p-γ coincidence meas. of multinucleon removal in quasifree process 78−37342
^{24}Mg(p,p), (p,p'), 9.1 MeV, optical, DWBA and Hauser-Feshbach anal. 77−316
^{24}Mg(^{12}C,^{12}C), 20-36 MeV, ang. distribs., S-matrix elements, optical model parameters 79−93660
^{24}Mg(^{13}C,^{13}C'), 35 MeV, γ-rays and spin flip 80−18189
^{24}Mg(^{13}C,^{13}C'), 35 MeV, 2^+ population probab., spin-flip and spin orbit pots., coupled channel anal. 80−99125
^{24}Mg(^{16}O, ^{16}O'), 20-42 MeV, Coulomb-nuclear interf. effects, coupled channel calcs. 77−3040
^{24}Mg(^{16}O,^{16}O), 17-31 MeV, backward angle cross sections, resonant structure 79−30813
^{24}Mg(^{16}O,^{16}O), 24-40 MeV, backward angles, excitation functions, ang. distribs. and resonant behaviour 80−68622
^{24}Mg(^{16}O,^{16}Oγ), 42 MeV, ang. correl. meas. 77−41989
^{24}Mg(^{16}O^{16}O), entrance, exit and reaction channel data at backward angles 79−36254
^{24}Mg(^{18}O, ^{14}C)^{28}Si, ground-state excitation function structure 79−63694
^{24}Mg(^{18}O,^{18}O), 29, 35 MeV, coupled channel, first order DWBA, optial pot. calcs. 78−54796
^{24}Mg(^{18}O,p2nγ), ^{39}K high spin states, decay scheme 78−25232
^{24}Mg(^{32}S,^{32}Sγ)^{24}Mg, TIPAC meas. on first 2^+ states 77−67762
^{24}Mg(^{3}He,^{3}He'), giant dipole reson. excitation 77−6338
^{24}Mg(^{3}He,^{3}He), 130 MeV, elastic scatt. ang. distribs., optical model anal. 78−94020
^{24}Mg(^{3}He,^{3}He), 130 MeV, giant reson. excitation, DWBA anal. 79−89319
^{24}Mg(^{3}He,α)^{23}Mg, 10 MeV, ang. distribs., DWBA and CCBA calcs. with inelastic effects 77−61443
^{24}Mg(^{3}He,t), giant dipole reson. excitation 77−6338
^{24}Mg(^{3}He,t)^{24}Al, 38.5 MeV, spin assignments in ^{24}Al 77−18580
^{24}Mg(^{3}He,t)^{24}Al, 44 MeV, 1^+ states in Al anal. 77−79390
^{24}Mg(^{3}He,t)^{24}Al, low-lying 1^+ states of Al anal. 78−29484
^{24}Mg(α, ^{12}C)^{16}O, 12.7-17.4 MeV, quasimol. resonance in excitation function, ^{12}C+^{16}O system, spins 78−54775
^{24}Mg(α, α), 120-172.5 MeV, optical pot. uniqueness and shape 79−97719
^{24}Mg(α, n)^{27}Si, threshold to 27 MeV, excitation functions, non-statistical reaction contribs. 77−82939
^{24}Mg(α,^{12}C)^{16}O, 22-26 MeV, intermediate resonances in ^{12}C+^{16}O system, J^π assignments 79−17880
^{24}Mg(α,^{12}C)^{16}O, E_α=90 MeV, reaction mechanism 79−6646
^{24}Mg(α,^{6}Li), 46 MeV, finite range DWBA anal. 77−14142
^{24}Mg(α,$\alpha\gamma\gamma$), 104 MeV, alpha-gamma ang. correl., quadrupole deform. 77−88155
^{24}Mg(α,α'), 120 MeV, ground and gamma band excitation, coupled channel calcs. in rotational model 79−89315
^{24}Mg(α,α'), 1.37 GeV, low lying state ang. distribs., Glauber rigid body approx. 79−54394
^{24}Mg(α,α'), 22-26 MeV, intermediate resonances in ^{12}C+^{16}O system, J^π assignments 79−17880
^{24}Mg(α,α'), 28, 40 MeV, lowest 3^+ state population, compound nucleus formation 78−33197
^{24}Mg(α,α'), 38-50.5 MeV, sign of nuclear deform. from Blair phase shift 77−61439
^{24}Mg(α,α'), 65 MeV, ^{4}He deduced monopole excitation to 0^+ state DWBA anal. 79−22226
^{24}Mg(α,α'), excitation of low-lying 0^+ states, indirect processes 77−6417
^{24}Mg(α,α')^{24}Mg, 126 MeV, GQR, DWBA anal. 77−74826
^{24}Mg(α,α')^{24}Mg, 16.7-20 MeV, quasimol. intermediate resons., statistical anal. 78−41741
^{24}Mg(α,α')^{24}Mg, exptl. evidence of intermediate resonances, alpha-particle doorway states 79−13314
^{24}Mg(α,α), 2^+ collective level excitation, microstruct. of diffr. ang. distrib. 77−61440
^{24}Mg(α,n)^{27}Si, cross sections and thermonuclear reaction rates 80−73852
^{24}Mg(α,n)^{27}Si, threshold to 13.1 MeV, total cross section 78−618

nuclei with mass number 20 to 38 continued

^{24}Mg(α,nγ)^{27}Si, 12.60-16.35 MeV, ang. correl. and lifetime meas. 78−17224
^{24}Mg(α,p)^{27}Al, 25-26 MeV, high spin selectivity 77−23097
^{24}Mg(d, pγ)^{25}Mg, differential and double differential cross sections, Hauser Feshbach anal., compound nucleus 79−89282
^{24}Mg(d,^{6}Li)^{20}Ne, 28 MeV, α pick up, angular distribs. and spectroscopic factors 78−78352
^{24}Mg(d,$\alpha\gamma$)^{22}Na, 7.75 MeV, ang. correl. meas. using tensor polarised deuterons 77−22934
^{24}Mg(d,d$_1$), vector analysing power, d$_1$-γ ang. correl., DWBA and CCBA anals. 77−30605
^{24}Mg(d,d), pol.d, 20 MeV, quadrupole transition amplitudes 80−99148
^{24}Mg(d,n)^{25}Al, stripping reactions to unbound states from p-n correlations, spin, parity and widths 78−62547
^{24}Mg(d,p), 1.5-2.5 MeV, fluctuation anal., ^{25}Mg highly excited states 78−46071
^{24}Mg(d,p)^{25}Mg, 8-13 MeV, vector polarised deuterons, excitations function of cross sections 78−8826
^{24}Mg(d,p)^{25}Mg, stripping reactions to unbound states from p-n correlations, spin, parity and widths 78−62547
^{24}Mg(d,pγ)^{25}Mg, particle-gamma and gamma-gamma coincidence, energies and branching ratios 77−22892
^{24}Mg(e,e'), 6$^-$, T=1 reson. discovery at 15 MeV 77−41940
^{24}Mg(e,e), 4$_1^+$4.12 MeV and 2$_2^+$4.24 MeV level resolution, E2 and E4 form factor meas. 79−17811
^{24}Mg(e,e), charge form factors in α cluster model 79−63571
^{24}Mg(e,e), elastic scatt., spectroscopic information and form factors 80−9260
^{24}Mg(e,e) form factor calc., test of 1s-0d shell effective interactions 77−61400
^{24}Mg(γ,γ), 5.5-7.2 MeV, elastic differential scatt. cross section, Thomson scatt. obs. 77−74833
^{24}Mg(γ,p), cross sections and proton energy spectra from (e,e'p) 80−13461
^{24}Mg(γ,p), up to 0.25 GeV, from bremsstrahlung γ-quanta *(Russian)* 80−5123
^{24}Mg(n,α)^{21}Ne, near 14 MeV, differential cross sections compared to compound-nucleus theoretical results 78−37350
^{24}Mg(n,n)^{24}Mg, 0.4 to 1.8 MeV reson. level ang. momentum 77−54202
^{24}Mg(p,X), 17.5-48 MeV, proton total cross section 78−8809
^{24}Mg(p,α), near threshold, total cross section, reaction rate, astrophys. significance 77−82929
^{24}Mg(p,f), 22 to 42 MeV 79−6717
^{24}Mg(p,γ)^{25}Al, ^{25}Al T=3/2 states γ-decay 77−26608
^{24}Mg(p,p'), 0.8 GeV, rot., γ and β bands, ground state deformation, DWBA, coupled channels anal. 80−9198
^{24}Mg(p,p'), 135 MeV, cross section, population of unnatural parity high spin states 78−54753
^{24}Mg(p,p'), 135 MeV, high spin unnatural parity states, anal. 78−37334
^{24}Mg(p,p'), 135 MeV, large momentum transfer, excitation of high-spin particle-hole states in ^{24}Mg 77−61420
^{24}Mg(p,p'), 20, 40, 800 MeV, γ-vibr. band, coupled channels anal. 80−9194
^{24}Mg(p,p'), 22.5 to 28.5 MeV, giant reson. effects 78−4923
^{24}Mg(p,p'), 40 MeV, two step pickup-stripping process, negative parity states 80−32256
^{24}Mg(p,p'), polarised p, 20.3 MeV, low lying states, collective and microscopic model 78−82287
^{24}Mg(p,p') 15-35 MeV, low lying state differential cross sections, two step effects 79−89304
^{24}Mg(p,p')^{24}Mg, 20 MeV, excitation energies up to E$_x$=13.2 MeV 77−317
^{24}Mg(p,p'γ), 6.9 MeV, spin flip probability 77−88127
^{24}Mg(p,p'), 40 MeV, DWBA anal., positive parity states, transitions and giant resonance 79−6419
^{24}Mg(p,p'), 49.5 MeV, consistent folding model, HF calc. for E2, E4 transitions 79−22288
^{24}Mg(p,p') 17.5 MeV 79−22288
^{24}Mg(p,p), 14-45 MeV, differential cross section and spin-flip probabilities, giant resonances 80−73850
^{24}Mg(p,p), 15 Mev, excitation functions 80−22825
^{24}Mg(p,p), 18-44 MeV, differential cross sections, phase shift anal., energy depend. 80−47481
^{24}Mg(p,p), 22.5 to 28.0 MeV, differential cross sections, optical, coupled channel, core excitation anal. 79−6613
^{24}Mg(p,p), 40 MeV, natural parity transitions 78−66277
^{24}Mg(p,p), 5.65-6.25 MeV, isospin-forbidden T=3/2 reson., isospin mixing 77−18507
^{24}Mg(p,pα), 157 MeV, quasifree scatt., α spectroscopic factors, SU(3) predictions 77−6370
^{24}Mg(p,pα), 600 MeV, α-cluster quasielastic knockout, expt. methods, separation energy spectra 79−13275
^{24}Mg(p,pα)^{20}Ne, 157 MeV, energy spectra, SU(3) model comparison 77−88121
^{24}Mg(p,pα)^{20}Ne, DWIA calc. 77−34273
^{24}Mg(p,t), CCBA anal. using shell model wave functions 77−321
^{24}Mg($\pi^\pm$,$\pi^\pm$) 180 MeV elastic and inelastic scatt., optical model and DWBA calcs. 78−89915
^{24}Mg(t,^{3}He) giant dipole reson. excitation 77−6338
^{24}Mg(t,^{3}He)^{24}Na, 2.46 MeV state absence in ^{24}Na 77−34229
^{25}Mg (e,e) 80-215 MeV, magnetic moment form factors, M1, M3, M5 transitions 79−40844
^{25}Mg coherence moment-of-inertia from ^{12}C(^{13}C,α) 79−75815
^{25}Mg, low-lying excited states calc. by generator coordinate method 78−12974
^{25}Mg, mag. form factors calc. 79−9458
^{25}Mg total fusion and transfer cross sections from ^{9}Be(^{18}O,X) 80−91205
^{25}Mg(^{3}He,α)^{24}Mg, 9-13 MeV, excitation functions, and differential cross-sections 77−6409
^{25}Mg(^{3}He,d)^{26}Al, 18 MeV, l-assignments for ang. distrib., level J$^\pi$ information, spectroscopic strengths 78−62554
^{25}Mg(^{3}He,p)^{27}Al, 13 MeV, statistical multistep compound emission, proton spectrum fluctuations 78−37357
^{25}Mg(d,α), 12.07 to 11.57 MeV, angle-integrated cross section, ^{23}Na, spin, parity, energy levels 78−50179
^{25}Mg(e,e), 180° scatt., magnetisation distrib., mag. multipole moments 80−9228
^{25}Mg(e,e), 40-260 MeV, cross sections, Coulomb multipole moments and magnetic form factor 78−25178

nuclei with mass number 20 to 38 continued

^{25}Mg(n,α)^{22}Ne, near 14 MeV, differential cross sections compared to compound-nucleus theoretical results 78−37350
^{25}Mg(p,γ) reaction, relative yields of ^{26}Al^g and ^{26}Al^m 79−101058
^{25}Mg(p,γ)^{26}Al, reaction rate in explosive H burning 80−85929
^{25}Mg(p,λ)^{26}Al, stellar reaction rate, rel. to ^{26}Al prod. during C burning 79−70948
^{25}Mg(p,n)^{25}Al, cross sections and thermonuclear reaction rates 80−73852
^{25}Mg(p,p')^{25}Mg*, 8.8 MeV, J$^\pi$=1/2$^+$, line shape 77−54211
^{25}Mg(p,p')^{25}Mg*, E$_x$=8.838 MeV, lineshape model calc. *(German)* 77−22989
^{25}Mg(p,p)(p,p'), 9.1 MeV, optical, DWBA and Hauser-Feshbach anal. 77−316
^{25}Mg($\pi\pm$, $\pi\pm$N), 100-300 MeV, activation cross section, π^+/π^- cross section ratio 79−89329
^{26}Mg, 2$_1^+$ state quadrupole moment in band mixed HF model 80−52578
^{26}Mg ($\alpha,\alpha'\gamma$) 104 MeV, nuclear deformation from ang. correlations, coupled channel anal. 78−78301
^{26}Mg (α,α), 104 MeV, oblate-prolate effects in struct. and reactions 80 9225
^{26}Mg, energy levels anal. with ^{12}C(4u1^{6}O,2p)^{26}Mg 77−38293
^{26}Mg, GDR proton channel decay, isospin effects *(Russian)* 77−14020
^{26}Mg, isoscalar and isovector E2 transition matrix elements 78−25148
^{26}Mg, multipole mixing ratios from polarised beam γ-ray singles meas. 77−46132
^{26}Mg, spectroscopic factors, via ^{27}Al(n,d) 56.3 MeV 78−4935
^{26}Mg transition strength n and p components, $\pi^\pm$ inelastic scatt. comparison, shell model 80−68585
^{26}Mg+^{16}O, 29-81 MeV 78−78412
^{26}Mg+^{18}O, 34 MeV, yrast states in ^{41}K, ^{41}Ca, spins, parities from γ meas. 78−58250
^{26}Mg(^{11}B,^{10}B)^{27}Mg, semiclassical approxs. for heavy-ion transfer reactions 78−94021
^{26}Mg(^{11}B,^{10}B)^{27}Mg, 114 MeV, transfer amplitude and ang. distribs. 79−59081
^{26}Mg(^{11}B,^{10}Be)^{27}Al, semiclassical approxs. for heavy-ion transfer reactions 78−94021
^{26}Mg(^{11}B,^{11}B), (^{11}B,^{10}B), (^{11}B,^{10}Be), 31 MeV, optical model and DWBA anal. 77−26785
^{26}Mg(^{12}C,^{12}C'), 41.3 MeV, ang. distrib. meas. to nucl. shape calcs. 77−65231
^{26}Mg(^{136}Xe, 4n), prod. of ^{158}Dy Yrast states, lifetimes 78−54793
^{26}Mg(^{13}C, ^{12}C), ^{26}Mg(^{13}C, ^{14}C), 35 MeV, inelastic effects, DWBA, CCBA calcs. 77−3041
^{26}Mg(^{14}N, ^{10,11}B), 60-95 MeV, ^{29,30}Si states, reaction mech., spectroscopic factors 78−66299
^{26}Mg(^{16}O, ^{14}C)^{28}Si, full recoil one and two step DWBA anal. 78−70564
^{26}Mg(^{16}O, ^{16}O'), Coulomb-nuclear interf., appl. of Austern Blair theory, comparison with DWBA 77−3043
^{26}Mg(^{16}O,^{15}N), 36-53 MeV, reaction dynamic depend. of small angle cross sections 77−18600
^{26}Mg(^{16}O,X), complete fusion, 25-70 MeV evaporation residue cross section, total fusion excitation functions 79−13370
^{26}Mg(^{3}He,^{3}He'), 4$^+$ states, B(E2) values, and band mixing, rot.-vibr. model 80−83019
^{26}Mg(^{3}He,pγ)^{28}Al, 11-15 MeV, coincidence, ang. correl. and branching ratio meas. 78−13129
^{26}Mg(^{3}He,t), precise Q-value, ^{26m}Al β decay energy, half life 77−30618
^{26}Mg(α,α_1), 15 MeV, anal. of α-γ angular correlations 77−74866
^{26}Mg(α,α'), mirror state EM decay rates, multipole matrix element isospin decomposition 79−36190
^{26}Mg(α,xp), up to 156 MeV, including prod. of ^{28}Mg, excitation functions 77−3021
^{26}Mg(d,pγ)^{27}Mg, study of ^{27}Mg excited states up to E$_x$=7976 keV 77−41981
^{26}Mg(γ,n)^{25}Na, 19.5 to 27.0 MeV, giant dipole resonance decay channel determ., isospin component 79−26423
^{26}Mg(γ,p), 16-23 MeV, proton ang. distrib. meas. 77−41946
^{26}Mg(n,α)^{23}Ne, near 14 MeV, differential cross sections compared to compound-nucleus theoretical results 78−37350
^{26}Mg(p, p'), pol.p, 5.5-17.5 MeV, cross sections and anal. powers, autocorrelations 80−106042
^{26}Mg(p,n)^{26g}Al(7.3×10^5 yr), ground state cross section, statistical compound model 79−30827
^{26}Mg(p,n)^{26m}Al(6.35s), ground state cross section, statistical compound model 79−30827
^{26}Mg(p,n)^{26}Al^g, 5.2-6.9 MeV, cross section via accelerator mass spectrometry 80−99175
^{26}Mg(p,p'), 24 MeV, rot. description of low lying states, coupled channels anal. 79−54376
^{26}Mg(p,p'), 6 MeV, spin-flip probability, ang. distrib., energy depend. 78−13078
^{26}Mg(p,p')^{26}Mg, 20 MeV, excitation energies up to E$_x$=11.2 MeV 77−317
^{26}Mg(p,p), 1.54-3.06 MeV, high resolution study, excited analogue states of ^{27}Mg 78−78377
^{26}Mg(p,p), polarised protons, direct reaction contrib. in fluctuating cross sections 77−50102
^{26}Mg(p,p)(p,p'), 9.1 MeV, optical, DWBA and Hauser-Feshbach anal. 77−316
^{26}Mg(p,π^+), isobar configuration effects, p→$\Delta^0\pi$ model, ang. distribs. *(Chinese)* 80−47484
^{26}Mg(p,$\pi^\pm$), 180 MeV, effect of Δ^{++} components in nuclei 78−33181
^{26}Mg($\pi^\pm$,$\pi^{\pm\prime}$), pion spectra, absolute cross section 80−78333
^{27}Mg energy levels, spectroscopic factors, DWBA, Hauser-Feshbach anals. from ^{26}Mg(d,p) 80−52581
^{27}Mg excited analogue states high resolution study in ^{26}Mg(p,p) 78−78377
^{27}Mg, excited states up to E$_x$=7976 keV, studied via ^{26}Mg(d,pγ) reaction 77−41981
^{27}Mg(n,γ)^{28}Mg, reactor neutron irrad., product yield 79−538
^{28}Mg, differential cross sections for lowest four states from ^{26}Mg(^{18}O,^{16}O) 79−67661
^{28}Mg ΔT=1 0$^+$→0$^+$ β-decay, isospin forbidden branching ratio to ^{28}Al 79−93560
^{28}Mg, isospin forbidden β-decay 78−78315
^{28}Mg prod., life sciences appl. 78−15882
^{28}Mg, prod. by high-energy α-induced nucl. reactions on ^{27}Al and ^{26}Mg 77−3021

nuclei with mass number 20 to 38 continued
^{25}Mg producting using compact cyclotron 77−90894
^{25}Mg production with 50 MeV neutrons 77−90895
^{28}Mg radionuclide yield from ^{27}Al(α,3p) and ^{26}Mg(α,2p) 80−32290
^{29}Mg yield from ^{27}Mg(n,γ) and ^{28}Al(n,p) 79−538
^{29}Mg mass excess from ^{26}Mg(^{18}O,^{15}O) 79−3075
^{30}Mg(α,2α), 90 MeV, strong absorption diffraction model, spectroscopic factors 79−22306
^{30}Mg mass excess from ^{26}Mg(^{18}O,^{14}O) 79−3075
^{31}Mg neutron rich nuclide, obs. in U fragmentation by 800 MeV protons 77−61419
^{32}Mg, excitation energy of lowest 2^+, 3^- levels, energy density method 79−3088
^{32}Mg neutron rich nuclide, obs. in U fragmentation by 800 MeV protons 77−61419
Mg(α,^{2}He), A=24, 26, 55, 65 MeV, two neutron states, A-depend. of binding energy 78−74379
Mg(α,α′), A=24,5,6, 106, 120, 145, 172.5 MeV, giant quadrupole reson. obs. 77−6415
Mg(n,α)Ne reaction, cross sections at 14.1 and 14.7 MeV and implications for meteorites 79−96874
Mg(n,n), elastic and inelastic scatt., cross sections meas. and calcs. 78−13081
Mg(p,p), A=24, 26, 5-6 MeV, polarisation in elastic scatt., thick target method 78−13079
^{57}Mn(n,n′), 2-4.5 MeV, level excitation functions, Hauser-Feshbach-Moldauer model test 79−36238
^{19}N, neutron rich nuclei study in ^{18}O+^{207,208}Pb reaction 79−89322
^{20}N, β-decay, recoil-order matrix elements 77−79337
Na, A=21, 2, 3, absolute reson. strengths meas. in Ne(p,γ), Ne(p,pγ) 77−38272
Na, A=21, 22, unified model with vibrating core of variable deform. 77−50068
Na, A=21, 23, M1, E2, transition probabilities between differently deformed states, Nilsson model 77−61376
Na bombarded by ions, Coulomb excitation of sd shell nuclei, B(E2) values, lifetime meas. 78−25216
Na, NMR in NaN_3, phase transition 77−73092
Na neutron rich isotopes, mass meas. 77−22861
Na neutron rich isotopes, β-delayed emission of n, 2n, α, t 78−74343
Na+Ne, 800 MeV/A, wide angle inclusive proton spectra 79−40951
NaF+Ne, 800 MeV/N, p and π inclusive spectra, energy and ang. distribs. 78−54790
NaF+Ne, 800 MeV/N, p and π inclusive cross sections, non-equilibrium processes 79−40947
NaF+Ne, evidence for blast wave production in fireball explosions 79−49592
NaF(Ne,Ne), 800 MeV/N, high momentum nucleons from relativistic nuclear collisions, hard scatt. mechanism 79−40950
$NaH_3(SeO_3)_2$, high-pressure phase transform., ^{23}Na NMR obs. 77−63380
Na(Ne,X), 800 MeV/N, direct vs. thermal particle emission, inclusive cross sections 80−52688
Na(^{20}Ne,π^+), 800 MeV/N, doubly differential cross sections and ang. distribs. 80−9305
Na(^{20}Ne, π^+X), 400 MeV/N, pion prod. doubly differential cross sections and ang. distrib. 80−32299
^Na, (A=21, 23), even parity state, EM props., collective struct., generator coord. method, HF method anal. 79−89220
^Na, A=21, 23, even parity excited states, collective props., EM moments, generator coordinate method 78−78259
^Na, A=22, 24, β-transitions, weak magnetism, nuclear struct., matrix elements 79−13253
^Na, A=22,23 J^π assignments from ^{12}C(^{12}C,Xγ), X=p or d 79−45154
^Na, A=24, 25, total fusion and transfer cross sections from ^{9}Be(^{18}O,X) 80−91205
^Na, A=26-30, nuclear spin from NMR meas. nuclear deformation 79−10072
^Na, A=27-32, radioactive half-life and branching ratios 79−22240
^Na, A=30,31,32, beta-delayed two-neutron emission 80−95316
^{20}Na, β-γ directional correlation, second-class current search 77−88083
^{20}Na, β-γ directional correlation meas., search for second class currents 79−13245
^{20}Na, positron decay, β-α ang. correl. meas. 77−46138
^{21}Na DSA lifetime of 2425 keV state via ^{20}Ne(p,γ)^{21}Na 1.7 MeV 77−82860
^{21}Na deduced levels and cross sections from ^{12}C(^{12}C,t) 80−469
^{21}Na levels obs. in ^{20}Ne(p,p) with polarised protons 77−2913
^{21}Na, mag. moment and lifetime of first excited state determ. 78−550
^{21}Na, mag. moment of first excited state, time differential plunger meas. 78−37271
^{21}Na, parity mixing matrix element using SU_3 shell model calcs. 79−9462
^{21}Na, produced in ^{2}H(^{20}Ne,nγ)^{21}Na, energy level lifetime 78−41631
^{21}Na, study of excited states, spin and parity *(French)* 78−33158
^{22}Na 0^+ level mean life, isovector mag. dipole transition from ^{19}F(α,n) 80−68595
^{22}Na, 4.52 MeV state, J^π, lifetime, via ^{12}C(^{12}C,dγ)^{22}Na 77−54147
^{22}Na, 4.77 MeV level J^π via ^{24}Mg(d,αγ)^{22}Na with tensor polarised deuterons 77−22934
^{22}Na, analogue resons., γ-ray ang. distrib. and mixing ratios in ^{21}Ne(p,γ)^{22}Na 78−62504
^{22}Na, anomalous electron capture/β^+ decay ratio, second forbidden corrections 79−22238
^{22}Na bound and analogue state lifetimes, branching ratios, DSA method from ^{21}Ne(p,γ) 0.5-6.0 MeV 78−93967
^{22}Na deduced levels from ^{12}C(^{14}N,α) and ^{14}N(^{12}C,α) 78−93944
^{22}Na, EM corrections for electron capture to β^+ decay ratio 79−89269
^{22}Na, effective interactions for dominant shell-model configurations: ds-shell example 80−32204
^{22}Na, electron capture/positron emission ratio 77−30522
^{22}Na excitation functions determ. in ^{12}C(^{12}C,d)^{22}Na at 14.3 MeV 77−82956
^{22}Na excited states lifetimes, recoil-distance method 77−30510
^{22}Na, ground state band struct., J^π, E2 transitions, $T_{1/2}$ *(French)* 77−34210
^{22}Na, isoscalar M2 transition, γ-ray spectra obs. 77−10363
^{22}Na levels, resonances in ^{21}Ne+p reactions, 0.4 to 1.6 MeV 77−18540
^{22}Na, neutron absorption cross-section calc. 77−23075
^{22}Na, populated by ^{19}F(α,n), 5.5 MeV, level lifetimes, instrument testing 78−13375

nuclei with mass number 20 to 38 continued
^{22}Na, recoil-distance lifetime meas. 77−34252
^{22}Na, resonance levels obs. in ^{20}Ne(d,p_0) 78−46072
^{22}Na, thick-target yields in Mg due to proton bombardment up to 100 MeV 77−88312
^{23}Na, 14.7 MeV neutron capture cross-section measurements with activation technique 80−32282
^{23}Na, 2.8 keV and thermal neutron capture gamma-ray spectra 77−38263
^{23}Na (n,n), thermal neutron scatt. parameters 79−93628
^{23}Na α-transfer spectroscopic factors from shell model wave functions of ^{19}F(^{6}Li,d) 79−36149
^{23}Na, band mixing, E2 and M1 matrix elements *(French)* 78−45994
^{23}Na, DWBA anal. of α-spectroscopic factors in ^{19}F(^{6}Li,d) 78−82383
^{23}Na, decoupled bands and antialigned states 78−78236
^{23}Na, ENDOR, characterisation of centre involving Ce^{3+} and Na^+ in CaF_2 77−69730
^{23}Na, E1 decays, high spin state identification 77−26617
^{23}Na energy levels from ^{25}Mg(d,α), spin, parity, angle-integrated cross section 78−50179
^{23}Na even parity states, generator coord. method, projected Hartree-Fock, and complete diagonalisation calcs. comparison 78−89796
^{23}Na high spin positive parity state, approx. microscopic methods, shell model comparison 79−85352
^{23}Na high spin states, excitation functions, nonstatistical effects, Hauser-Feshbach anal. of ^{12}C(^{15}N,α) 80−106041
^{23}Na, high spin states anal., ^{12}C+^{12}C reson. at $E_{c.m.}$=19.3 MeV 77−26579
^{23}Na, high-spin states, shell-model calc. in sd shell 77−65213
^{23}Na, in electrolyte solns., NMR relax. *(Russian)* 78−15053
^{23}Na, in $NaAuCl_4.2H_2O$, pure quadrupole double reson., fine struct. 77−63323
^{23}Na level α-spectroscopic strengths assuming direct cluster transfer from ^{19}F(^{6}Li,d) 80−27552
^{23}Na levels, resonance strengths, γ-decays and level lifetimes from ^{22}Na(p,γ) 79−45229
^{23}Na levels and spectroscopic amplitudes, J^π assignments, high spin states from ^{20}Ne(α,p) 79−75848
^{23}Na, levels populated by ^{12}C(^{15}N,α) 78−50070
^{23}Na low lying analogue states, DWBA anal. from ^{24}Mg(d,^{3}He) 29 MeV, polarised d 78−82285
^{23}Na, low-lying excited states calc. by generator coordinate method 78−12974
^{23}Na NMR intensity in rat liver homogenate, effects of alkali cations 77−12893
^{23}Na, NQR in $NaD_3(SeO_3)_2$, second-order quadrupole shift, temp. depend. 78−15055
^{23}Na, nucl. spin-lattice relax. in β-Al_2O_3-Na_2O 77−55720
^{23}Na, nuclear charge radius from μ^- X-ray transitions 78−66195
^{23}Na, nuclear relax. correl. times in polymethacrylic acid 80−50212
^{23}Na, particle-rotor model with s-d shell pairing, BCS approx. 80−57705
^{23}Na positive parity states ang. distrib., DWBA anal. from ^{21}Ne(^{3}He,p), 18 MeV 78−82284
^{23}Na, produced in 32-14.4 MeV ^{16}O+^{9}Be, gamma transitions 79−49599
^{23}Na, reson. levels via ^{19}F(α,n)^{22}Na at 2.3-4.7 MeV 77−65199
^{23}Na, resonance activation neutron detector materials, uni-resonance approx. technique for higher resonance reaction rate 77−75030
^{23}Na resonances through γ-decay excitation functions from ^{12}C(^{12}C,p) 80−63148
^{23}Na, spectroscopy of high-spin states in ^{12}C(^{12}C,pγ) 77−46131
^{23}Na, spin-lattice relax. time in $NaNO_3$ *(Japanese)* 77−43897
^{23}Na, transition probabilities and multipole moments between states calc. by generator coordinate method 78−13022
^{23}Na(^{19}F,X) complete fusion, 25-70 MeV evaporation residue cross section, total fusion excitation functions 79−13370
^{23}Na(^{3}He,^{3}He), optical potentials and volume integrals, mass and energy dep. 80−52686
^{23}Na(d,^{3}He)^{22}Ne, 12.4 MeV polarised beam, $d_{5/2}$-$d_{3/2}$ admixing in pickup strength 77−6399
^{23}Na(d,p)^{24}Na, 1.5 to 3.0 MeV, excitation functions 79−40932
^{23}Na(d,p)^{24}Na, 1.58 to 3.03 MeV, calc. of differential cross sections, spectroscopic factors 77−6394
^{23}Na(n, α)^{20}F, average cross sections in ^{235}U fission neutron spectrum 80−22828
^{23}Na(n, p)^{23}Ne, average cross sections in ^{235}U fission neutron spectrum 80−22828
^{23}Na(n,Xγ), 0.2 to 20 MeV, reaction cross sections 80−99172
^{23}Na(n,2nγ), (n,n′γ), 14.6 MeV, γ-ray ang. distrib. *(Russian)* 77−88147
^{23}Na(n,α)^{20}F, 14.1 MeV, cross-section meas. *(Spanish)* 77−67738
^{23}Na(n,γ), 24-160 keV, multigroup capture cross section and self shielding factor 77−26773
^{23}Na(n,γ), absolute cross sections in keV range 77−26771
^{23}Na(n,n′γ), 0.52-4.23 MeV, cross-sections, ang. distribs., mag. substate populations meas. 78−13100
^{23}Na(n,n′γ), cross-section near threshold 78−8808
^{23}Na(p,γ) resonance reaction, 3906 keV, ^{24}Mg lowest T=2 state, total width 78−89870
^{23}Na(p,γ)^{24}Mg, 0.5 to 0.9 MeV, resonance strengths of selected resonances in s-d shell 78−66281
^{23}Na(p,n)^{23}Mg neutron yield meas. with sphere counter 77−23381
^{23}Na(p,p′)^{23}Na, 20 MeV, excitation energies up to 11.2 MeV 77−317
^{23}Na(p,p), (p,α), lowest T=2 level of ^{24}Mg narrow resonance, isospin forbidden particle decays 78−89871
^{23}Na(p,p), (p,n) threshold anomaly 78−94003
^{24}Na, effective M3 matrix elements and transitions from shell model 80−102143
^{24}Na fragment ang. and energy distribs., two-step model anal. of ^{197}Au(p,X) 80−52678
^{24}Na fragment emission excitation functions cascade-evaporation anal. from ^{197}Au(p,x), ^{197}(π^+,z) 79−6553
^{24}Na, gamma radioactive source, buildup factor determination for meas. in air *(Rumanian)* 78−49132
^{24}Na half-life determ., $T_{1/2}$=(14.964±0.015) h 80−95311
^{24}Na half-life determ. by ^{56}Mn activation and decay obs. 79−26398
^{24}Na, J^π assignments via ^{22}Ne(^{3}He,p)^{24}Na 18 MeV reaction 77−74760
^{24}Na, level struct. and spin assignments, DWBA anal. from ^{22}Ne(^{3}He,p), 18 MeV 78−86477
^{24}Na photoproduced in Cu, Ag, Au, recoil energies 77−41953
^{24}Na photoproduction from targets with A=63 to 238, mean cross sections, 400 to 1000 MeV 77−41952

nuclei with mass number 20 to 38 continued
- ^{24}Na, produced in 32-14.4 MeV ^{16}O+^{9}Be, gamma transitions 79−49599
- ^{24}Na, reported 2.46 MeV state not seen ^{24}Mg(t,^{3}He)^{24}Na 77−34229
- ^{24}Na yield from light and intermediate nuclie in 2-5 GeV photonuclear reactions *(Russian)* 77−2980
- ^{24}Na^{m}, 1^{+} isomer, mag. moment 80−32177
- ^{24}Na^{m}, polarised, β-decay asymmetry and mag. moment from Na(n,γ) 80−91157
- ^{24}Na(γ,n), 42 MeV, photoneutron flux determ. from induced activity meas. in water 78−20112
- ^{24}Na(n,n'γ), 14.6 MeV, differential cross sections, statistical model calcs. comparison *(Russian)* 78−78385
- ^{24}Na(n,np), 14.6 MeV, differential cross sections, statistical model calcs. comparison *(Russian)* 78−78385
- ^{24}Na(n,pn), 14.6 MeV, differential cross sections, statistical model calcs. comparison *(Russian)* 78−78385
- ^{25}Na, J$^{\pi}$ assignments from ^{23}Na(t,p) 79−6381
- ^{25}Na, τ, J, π, branching and mixing ratios for lowest 5 levels 77−57624
- ^{27}Na excited states and mass excess from ^{26}Mg(^{18}O,^{17}F) 79−3075
- ^{32}Na, π bound states in finite nuclei 78−46013
- ^{24m}Na, laser induced nuclear orientation 80−57680
- Na(α, 2α), 700 MeV, cross section, effective cluster number from PWIA, momentum distrib. 79−40940
- Na(n,X), 14.8 MeV, γ-prod. cross section 79−49622
- Na(n,n), elastic and inelastic scatt., cross sections meas. and calcs. 78−13081
- ^{20}Nd, low lying positive parity states by (^{16}O-α)+(^{12}C-^{8}Be) orthogonality condition model 79−6400
- Ne Coulomb excitation of sd shell nuclei, B(E2) values, bombarded by ions, Coulomb excitation of sd shell nuclei, B(E2) values, lifetime meas. 78−25216
- Ne isotopes, meas. of 280 MeV/nucleon particles with plastic detector 77−38561
- Ne isotopes prod. cross sections in natural Mg, Al, Si by 12-45 MeV protons 77−17310
- Ne isotopes prod. in lunar materials by solar cosmic ray protons, rate calc. 77−17311
- Ne, total muon capture rates using HF wave functions 80−63135
- Ne+Ne, classical many-body model for heavy ion collisions 80−536
- Ne+$\nu_{\mu}(\bar{\nu}_{\mu})$, inclusive prod. of hadrons, preliminary data 78−89853
- Ne+p, particle multiplicity correlations in streamer chamber 79−85506
- Ne+p($\pi^{\pm}$), 1.5 to 2.5 FeV interactions in stream chamber 79−6710
- Ne+π, fragment and pion multiplicities 77−18620
- Ne+π, particle multiplicity correlations in streamer chamber 79−85506
- Ne+π^{-}, 25 and 50 GeV, multiplicity of charged particles 78−62575
- Ne+W, 340 MeV/nucleon, multiplicities and ang. distrib. 79−93661
- Ne(^{6}Li,d)Mg, 32 MeV, Mg α-particle spectroscopic strengths calc. 77−41987
- Ne(Ne,X), 117-800 MeV, classical eqns. of motion calcs., central collisions, thermal models 80−106070
- ^{A}Ne, A=21, 22, 23, total fusion and transfer cross sections from ^{9}Be(^{18}O,X) 80−91205
- ^{12}Ne parity mixing meas. extension review 80−73792
- ^{12}Ne, study of excited states, spin and parity *(French)* 78−33158
- ^{19}Ne 5.09 MeV level parity from ^{21}Ne(p,t) 79−45155
- ^{20}Ne, intermediate structure resonances in ^{10}B+^{10}B near Coulomb barrier 79−9450
- ^{20}Ne, sub-Coulomb resonances populated in ^{12}C(^{12}C,α), spin assignments 77−54245
- ^{20}Ne, 0g orbit mixing via (e,e'), one-step forbidden transition anal. 78−493
- ^{20}Ne 13482 keV level, parity violating effects in two resonance interference from ^{19}F(p,α) pol. p 80−83033
- ^{20}Ne 2$^{+}\rightarrow$0^{+} transition from ^{12}C(^{16}O,^{16}O) 80−63125
- ^{20}Ne, 40 MeV excitation, ^{10}B(^{10}B,α)^{16}O, excitation functions, resonance like structures 78−29496
- ^{20}Ne, 80 MeV, resonance-like phenomena 79−13308
- ^{20}Ne (n,p) and (n,d) reactions, study of isovector analogue giant resonances, proton hole states 77−26726
- ^{20}Ne, [211] quartet state, by study of ^{19}F(p,α)^{16}O, 1.5 to 2 MeV 78−46006
- ^{20}Ne, alpha-cluster states, spin, parity and branching ratios 78−50066
- ^{20}Ne, angular distrib. of polarisation in ^{16}O(^{16}O,^{12}C)^{20}Ne at 68 MeV 79−6681
- ^{20}Ne, α decay from 8p-4h O^{+} state, branching ratios 78−50132
- ^{20}Ne, α-and ^{8}Be-spectroscopic factors determ. 78−62494
- ^{20}Ne, α-cluster deformation, elastic form factors of electron scatt. 79−17829
- ^{20}Ne α-cluster levels, props., hard-core potential calcs. 77−30614
- ^{20}Ne α-cluster spectroscopic factors, DWBA anal. of (d, ^{6}Li) 80−52571
- ^{20}Ne α-cluster states and backward angle anomaly in ^{16}O(α,α)^{16}O 77−38287
- ^{20}Ne, α-cluster struct. at excit. energy >30 MeV *(Russian)* 77−74784
- ^{20}Ne, α-decay, Gamov states in generator coord. method 77−14075
- ^{20}Ne, α-transfer reactions, spectroscopic factors, exact finite range DWBA anal. 80−13372
- ^{20}Ne, basis states generation by variational methods 78−78295
- ^{20}Ne, binding energy, rotational band energy, Brink α-cluster model 77−6195
- ^{20}Ne breakup cross section, direct mechanism, DWBA anal. of ^{40}Ca(^{20}Ne,^{16}O) 80−18276
- ^{20}Ne central-tensor coupled effective interaction pot., binding energy shape, electric moment 77−14036
- ^{20}Ne cluster struct., coupled channel orthogonality condition model, α-decay, excited states, transitions 79−97681
- ^{20}Ne, cluster struct., review 78−50107
- ^{20}Ne, cluster struct. study in ^{16}O-α+^{12}C-^{8}Be coupled channel orthogonality condition model 79−89258
- ^{20}Ne, coexistence of shell struct. and cluster struct. 78−78279
- ^{20}Ne collective motion, B(E2) rates, algebraic formulation in symplectic shell model 80−83015
- ^{20}Ne, configuration mixing and α-cluster transfer on ^{16}O 78−46004
- ^{20}Ne continuum states, J$^{\pi}$ and branching from ^{12}C(^{12}C, $\alpha\alpha$) 80−22660
- ^{20}Ne cranking model rot. behaviour from Strutinsky method 77−2894
- ^{20}Ne, deformed nuclei, giant multipole resonances, and transitions, microscopic theory from ^{19}F(p,γ) 79−513
- ^{20}Ne, deformed nucleus, quadrupole moment, HF calc. exponential convergence and acceleration 79−85367
- ^{20}Ne, dipole moment using transient mag. field from ion passing through ferromag. *(Dutch)* 78−29386
- ^{20}Ne E1 resonance from ^{19}F(p,γ) pol. p 80−22790

nuclei with mass number 20 to 38 continued
- ^{20}Ne, effective nucleus eccentricity depend. on total momentum *(Russian)* 79−3078
- ^{20}Ne, electric quadrupole strength, giant quadrupole resonance 80−52575
- ^{20}Ne excitation functions, resonance search from ^{10}B(^{14}N,α) 80−27614
- ^{20}Ne, excited states ang. distrib. in ^{24}Mg(d,^{6}Li) reaction 79−6624
- ^{20}Ne, form. in ^{19}F(p,γ) reaction, 668 keV, γ-ray transitions to ground state, rel. to stellar nucleosynthesis 78−17191
- ^{20}Ne from ^{16}O(^{16}O,^{12}C)^{20}Ne, polarisation measurements 80−9301
- ^{20}Ne, from ^{16}O(α,γ), 10.27 MeV, first T=1,2^{+} state radiative width meas. rel. to analogue β-decays 78−549
- ^{20}Ne, gamma decays of some T=0, 1 and 2 states above 9.5 MeV 77−34244
- ^{20}Ne giant E1 resonance intermediate struct. from ^{19}F(p,γ), pol. and unpol. 80−78251
- ^{20}Ne, giant multipole reson. via ^{19}F(p,γ)^{20}Ne, microscopic calc. 77−22987
- ^{20}Ne, giant multipole resonances in excited core model 77−30539
- ^{20}Ne ground state level calc., maximum method 80−73795
- ^{20}Ne, ground state rot. bands from shell-model Hamiltonians 77−79298
- ^{20}Ne, HF microscopic anal. of core struct. for deformed nucleus 78−78294
- ^{20}Ne, heavy-ion α-transfer reactions, optical parameters *(Japanese)* 78−4962
- ^{20}Ne hexadecapole moments, quadrupole deformation effects, E4 effective charge, valence polarisation 80−78142
- ^{20}Ne high spin states, J$^{\pi}$ and α-decay branching ratios from ^{16}O(^{12}C,^{8}Be) 80−18166
- ^{20}Ne high spin states, J$^{\pi}$ assignments from ^{16}O(^{6}Li,d) 80−18167
- ^{20}Ne, high-spin states and shell struct. 80−47342
- ^{20}Ne high-spin states studied via α-transfer reaction ^{16}O(^{14}N,^{10}B)^{20}Ne, 155 MeV 77−14164
- ^{20}Ne, highly excited α-unbound states, cluster model 78−634
- ^{20}Ne, intermediate resonances of quasimol. α-structure 79−6404
- ^{20}Ne, intrashell quartet states, ang. momentum projection 77−10348
- ^{20}Ne, inverse inertia parameter calc. 78−50073
- ^{20}Ne, level densities, appl. of cluster expansion theory *(Spanish)* 79−88868
- ^{20}Ne level density from Hauser-Feshbach anal. of ^{19}F(p,α_0)^{16}O, 1.5 to 3.8 MeV *(Spanish)* 77−30562
- ^{20}Ne, level struct., J$^{\pi}$, spectroscopic factors via (^{13}C,^{9}Be) reaction 77−14033
- ^{20}Ne levels, J$^{\pi}$, branching ratio and EM transition rates from ^{16}O+α 80−42540
- ^{20}Ne, levels, J$^{\pi}$ and ang. distribs. from ^{18}O(t,p) 80−18204
- ^{20}Ne levels and branching ratio from ^{12}C(^{18}O, $\alpha\alpha$) 80−22661
- ^{20}Ne, low energy positive parity spectra, 2$\hbar\omega$ excitations, ang. momentum projected deformed particle-hole model calcs. 78−25119
- ^{20}Ne low lying levels and intermediate structure J$^{\pi}$ from ^{16}O(^{12}C, ^{8}Be) 80−102166
- ^{20}Ne low lying states, configuration mixing calcs. with basis states from variational method 80−22693
- ^{20}Ne, moment of inertia from cranked HF method 80−102098
- ^{20}Ne, multipole matrix elements, HF calcs. 78−50098
- ^{20}Ne narrow J$^{\pi}$=10^{+} resonance in strong absorption region, excited states from ^{12}C(^{16}O,^{8}Be) 79−30814
- ^{20}Ne non-isolated resonances, excitation functions and ang. distribs. from ^{20}Na(p,α) *(Chinese)* 80−22788
- ^{20}Ne, nuclear current from cranked HF solns. 80−9241
- ^{20}Ne, O$_1^{+}$, 2$_1^{+}$, 4$_1^{+}$ states, EM props. from large basis shell model 79−75900
- ^{20}Ne, one-body density matrix determ. by iterative steepest descent approach 78−17125
- ^{20}Ne, positive parity alpha clusters, Woods-Saxon well calcs. 79−26383
- ^{20}Ne, possible rot. band spectrum 77−79297
- ^{20}Ne, pot. and charge deform. of rot. states 77−46106
- ^{20}Ne, produced in 3.2-14.4 MeV ^{16}O+^{9}Be, gamma transitions 79−49599
- ^{20}Ne, quadrupole and hexadecapole deformation parameters from ^{208}Pb(^{20}Ne,^{20}Ne') 131 MeV 78−66204
- ^{20}Ne quadrupole transitions, electron scatt. form factors, shell model calcs. 78−62523
- ^{20}Ne, quartet states from ^{19}F(p,α)^{16}O 80−105973
- ^{20}Ne resonances through γ-decay excitation functions from ^{12}C(^{12}C,α) 80−63148
- ^{20}Ne, rot. levels from α-^{16}O folded pot. model 77−67703
- ^{20}Ne, rotational moment of inertia, cranked HF formalism with Skyrme force 77−30477
- ^{20}Ne, Skyrme-type interactions, spectroscopy of light nuclei, density dependent Hartree-Fock 80−22717
- ^{20}Ne, Sp(6,R) symmetry, α-breakup amplitudes, of giant E2 excitations 78−29435
- ^{20}Ne, spectra and E1 transitions, ang. momentum projected HF and Tamm-Dancoff methods 77−54139
- ^{20}Ne states, J$^{\pi}$, differential cross sections and ang. distribs. from ^{16}O(α,α') 80−18203
- ^{20}Ne, strong polarisation of levels obs. in ^{16}O(^{16}O,^{12}C) reaction 78−25213
- ^{20}Ne, suitability of lowest T=1 states for parity nonconservation experiments from ^{16}O(α,γ) 79−22189
- ^{20}Ne, unnatural parity levels at high excitation, γ spectra from ^{12}C(^{12}C, $\alpha\gamma$) 77−2933
- ^{20}Ne, velocity and Z-depend. of transient mag. field in Fe 77−71566
- ^{20}Ne with backbending, first excited 4^{+} state g-factor 80−78144
- ^{20}Ne+^{12}C, 17 to 35 MeV, excitation functions, optical model anal. 78−41759
- ^{20}Ne+^{12}C, 6.3-13.8 MeV, total fusion cross section, S-factor, γ-yields 80−22877
- ^{20}Ne+^{12}C, elastic scattering, symm., shell effects, absorpt. 79−562
- ^{20}Ne+^{20}Ne, 250-1000 MeV/N, intranuclear cascade calcs. for multiplicity and cross sections 80−32300
- ^{20}Ne+^{238}U, 250 MeV/nucleon and 2.1 GeV/nucleon, relativistic fluid dynamic anal. 77−74877
- ^{20}Ne+^{27}Al, deep inelastic fragment energies, rot. energy contributions 79−63697
- ^{20}Ne+^{53}Cu, deep inelastic reaction, evaporation, energy thermalisation 78−94024
- ^{20}Ne+^{58}Ni, 164 MeV, alpha clustering, multiple shape vibrs., TDHFC calcs. 79−3164
- ^{20}Ne+Al, relativistic ions, product spectra, statistical models 78−638
- ^{20}Ne+U, fireball model for proton inclusive spectra 77−6339

nuclei with mass number 20 to 38 continued

^{20}Ne+U→^{A}Z+X, 400 MeV/nucleon, excited nuclear matter prod. 77−50154
(^{20}Ne+α) system, effect of nuclear deform. on folded pot. 79−6453
^{20}Ne+π$^-$, pion absorption, isobar formation in streamer chamber 79−85504
^{20}Ne* low lying states and resonances, J$^\pi$ assignments and energies from ^{12}C(^{16}O,^{8}Be) 79−93592
^{20}Ne(^{12}C,X), 24-42 MeV, complete fusion, total cross section, excitation function 80−68717
^{20}Ne(^{12}C,X), 66.5 MeV, evaporation residue ang. and energy distribs. from statistical model anal. 80−83110
^{20}Ne(^{20}Ne,X), 132 MeV, TDHFB calc. for total fusion cross section 80−13521
^{20}Ne(α,2α), 140 MeV, quasifree knockout, DWIA anal. spectroscopic factors 80−68629
^{20}Ne(α,2α)^{16}O, DWIA 77−34273
^{20}Ne(α,α), 20 to 24 MeV, optical model anal. 77−65228
^{20}Ne(α,γ)^{24}Mg, radiative width of 8$^+$ member of 2$^+$ band in ^{24}Mg meas. 77−71613
^{20}Ne(d,^{6}Li), 80 MeV, ground state α-spectroscopic factors 79−93509
^{20}Ne(d,^{6}Li)^{16}O, Goldfarb-Buttle method *(Chinese)* 78−8834
^{20}Ne(d,d), pol. d, 10-12 MeV, cross section, coupled channel and fluctuations anal. 80−27617
^{20}Ne(d,p$_0$)^{21}Ne, 0.5-0.662 MeV, resonance obs., ^{22}Na levels 78−46072
^{20}Ne(d,p)^{21}Ne, 0.5-0.66 MeV, proton ang. distrib., excitation function, DWBA calc. 78−29475
^{20}Ne(e,e'), E1 and E2 giant resonances excitation at 60-120 MeV 78−50144
^{20}Ne(e,e') data anal., 0g orbit mixing 78−493
^{20}Ne(e,e'α), EM induced α emission, α spectroscopic amplitudes, anal. solvable model 80−32267
^{20}Ne(e,e), charge form factors in α cluster model 79−63571
^{20}Ne(γ,α), EM induced α emission, α spectroscopic amplitudes, anal. solvable model 80−32267
^{20}Ne(γ,n) cross sections and giant resonance struct. 80−13441
^{20}Ne(p,α), near threshold, total cross section, reaction rate, astrophys. significance 77−82929
^{20}Ne(p,γ)^{21}Na, 1.7 MeV, DSA lifetime of 2425 keV state in ^{21}Na 77−82860
^{20}Ne(p,p'), differential cross-sections, analysing powers in direct reaction theory 77−65223
^{20}Ne(p,p') 24.5 MeV, consistent folding model, HF calc. for E2, E4 transitions 79−22288
^{20}Ne(p,p) 65 MeV polarised p, elastic and inelastic, nuclear matter distrib. 78−78297
^{21}Ne 2796, 1747, 2867 keV level mean lifetimes from ^{4}He(^{18}O,n) 79−93553
^{21}Ne (p,p'γ), 0.4 to 1.6 MeV, study of resonances 77−18540
^{21}Ne α-spectroscopic strengths and level J$^\pi$ assignments from ^{17}O(^{6}Li,d) α-stripping 79−516
^{21}Ne configuration level density calcs. using spectral distrib. expansion, operator traces 79−71791
^{21}Ne, decay widths of lowest T=3/2 level, obs. as isospin forbidden resonance in ^{17}O(α,n) 77−6322
^{21}Ne deduced spectroscopic factors, levels and anal. powers from ^{20}Ne(d$_{pol}$,p) 80−83087
^{21}Ne, Doppler shift attenuation lifetime meas. at high recoil velocity 77−30513
^{21}Ne, E1 decays, high spin state identification 77−26617
^{21}Ne, energy moments, sd shell realistic effective interactions, shell model spectra 80−18190
^{21}Ne, even parity excited states, collective props., EM moments, generator coordinate method 78−78259
^{21}Ne, even parity state, EM props., collective struct., generator coord. method, HF method anal. 79−89220
^{21}Ne even parity states, generator coord. method, projected Hartree-Fock, and complete diagonalisation calcs. comparison 78−89796
^{21}Ne, γ-ray circular polarisation, parity mixing 78−70443
^{21}Ne low lying states from ^{17}O(^{6}Li,d), weak coupling behaviour, ^{20}Ne+n 78−46100
^{21}Ne, low-lying excited states calc. by generator coordinate method 78−12974
^{21}Ne, mag. moment and lifetime of first excited state determ. 78−550
^{21}Ne, produced in 3.2-14.4 MeV ^{16}O+^{9}Be, gamma transitions 79−49599
^{21}Ne, recoil into vacuum g-factor meas. of 5/2$^+$ state, 0.350 MeV 78−37272
^{21}Ne, spectroscopic factors, pickup strengths in ^{22}Ne(^{3}He,α) at 15 MeV 79−63684
^{21}Ne states, spins and rotational bands from ^{12}C(^{13}C,α) 79−75815
^{21}Ne states cross section, coupled channel and fluctuations anal. from ^{20}Ne(d,p) 80−27617
^{21}Ne, strength function calcs. in many fermion systems, Monte-Carlo method 80−86820
^{21}Ne, TDPAC obs. on ions recoiling in vacuum 77−22942
^{21}Ne, transition probabilities and multipole moments between states calc. by generator coordinate method 78−13022
^{21}Ne, unified model with vibrating core of variable deform. 77−50068
^{21}Ne*, produced in ^{2}H(^{20}Ne,p)^{21}Ne*, mag. moment meas. 78−41631
^{21}Ne(^{3}He,α)^{20}Ne, large angle excitation function fluctuations, DWBA and opt. model calcs. 79−89318
^{21}Ne(p,γ), 0.4 to 1.6 MeV, study of resonances 77−18540
^{21}Ne(p,p), 0.4 to 1.6 MeV, study of resonances 77−18540
^{21}Ne(t,p)^{23}Ne, energy levels, spin, parity 77−2917
^{22}Ne 2$^+$ state excitation in ^{126}Te(^{22}Ne, ^{22}Ne') 79−54404
^{22}Ne as neutron source for solar systems s-process, difficulty 80−72926
^{22}Ne backbending, yrast line and rotational motion, Strutinsky method from ^{11}B+^{13}C 79−36135
^{22}Ne compound states from ^{18}O(α,γ), transitions, spins, parities, astrophys. reaction rate 78−57545
^{22}Ne excited states lifetimes, recoil-distance method 77−30510
^{22}Ne, first excited 2$^+$ state, mag. moment determ. 77−18388
^{22}Ne, giant multipole resonances in excited core model 77−30539
^{22}Ne, intrashell quartet states, ang. momentum projection 77−10348
^{22}Ne levels, J$^\pi$, α-particle spectroscopic strengths studied via ^{18}O(^{6}Li,d) at 32 MeV 77−18594
^{22}Ne, lifetime meas., interpretation of Z$_2$ variation in low velocity DSAM results 79−26394
^{22}Ne lifetime of 6$^+$ member of ground state band by DSAM, B(E2) values 79−26395
^{22}Ne, produced by ^{4}He(^{19}F,p)^{22}Ne, lifetime of lowest 4$^+$ state in ^{22}Ne 78−37307
^{22}Ne, recoil-distance lifteime meas. 77−34252
^{22}Ne, stopping powers of Z=10 to 18 ions, using DSAM lifetime meas. 78−47456
^{22}Ne(^{3}He,α), 15 MeV, ang. distrib. meas. for levels <10 MeV in ^{21}Ne 79−63684
^{22}Ne(^{3}He,p)^{24}Na 18 MeV, ^{24}Na J$^\pi$ assignments 77−74760
^{22}Ne(2$^+$), g-factor and τm via ^{4}He(^{19}F,pγ) 38.5 MeV 77−34224
^{22}Ne(4$_1^+$) from ^{4}He (^{19}F,pγ), lifetime meas. by high vel. coincidence DSA method 78−33148
^{22}Ne(α,nγ)^{25}Mg, particle-gamma and gamma-gamma coincidence, energies and branching ratios 77−22892
^{22}Ne(d,α)^{20}F, 10 MeV, study of ^{20}F states up to 7 MeV excitation 77−10414
^{22}Ne(e,e'), 60 to 110 MeV, spin, parity, form factor, reduced transition prob. determ. 79−63661
^{22}Ne(γ,γ), up to 18 MeV, nuclear resonance fluorescence, states, transitions and lifetimes 79−45234
^{22}Ne(p,t), CCBA anal. using shell model wave functions 77−321
^{23}Ne structure, differential cross sections from ^{27}Al (α, ^{8}B) 80−5153
^{24}Ne, effective interactions in sd-states 77−14044
^{26}Ne, effective interactions in sd-states 77−14044
^{27}Ne neutron rich nuclide, obs. in U fragmentation by 800 MeV protons 77−61419
^{28}Ne, observation in ^{40}Ar+^{12}C collisions at 205 MeV/nucleon 79−22314
Ne(α,^{2}He), A=20, 22, 55, 65 MeV, two neutron states, A-depend. of binding energy 78−74379
Ne(α,α), A=20, 22, 150 MeV, isoscalar giant quadrupole reson. 77−307
Ne(α,α), A=20,22, large angle elastic scatt., 24.6-31.7 MeV, single Regge pole anal. 78−70547
Ne(α, χπ), 18 GeV, π multiplicity distrib. 79−97713
Ne($\bar{\nu}$,p), 0.6-25 GeV, backward emitted proton inclusive spectra, short range correlation 80−32281
Ne(p,γ), absolute resonance strengths meas. using separted targets 77−79374
Ne(p,γ)Na, Ne(p,pγ)Ne, 0.5-2.0 MeV, absolute reson. strengths in ^{21,22,23}Na meas. 77−38272
O, A=22, 24, 28, exotic nuclei stability anal., Hartree-Fock approx. with the Skyrme interaction 78−82273
^{18}O(^{18}O,^{14}O)^{22}O, 100 MeV, ^{22}O mass meas. 77−22869
^{20}O, 1-20 ps region mean lifetime meas., high-vel. DSA method 77−65200
^{20}O, determ. by ^{18}O(^{18}O, ^{16}O)^{20}O reaction at 52 MeV 79−26450
^{20}O first excited state, g-factor and lifetime from ^{3}H(^{18}O, pγ) 80−102115
^{20}O states below 6 MeV, J$^\pi$ assingments, DWBA anal. of ^{18}O(t,p) 79−22201
^{21}O, mass determ. from ^{18}O(^{18}O,^{15}O) ^{21}O reaction at 91 MeV 78−50078
^{21}O, neutron rich nuclei study in ^{18}O+^{207,208}Pb reaction 79−89322
^{22}O, Hartree-Fock calculations of nuclear bulk properties with density- and starting-energy dependent effective interaction 80−9246
^{22}O, measured in ^{18}O(^{18}O,^{14}O)^{22}O 100 MeV reaction 77−22869
^{22}O, neutron rich nuclei study in ^{18}O+^{207,208}Pb reaction 79−89322
P, A=30, 32, high spin states from ^{16}O+^{16,18}O reactions and ^{27}Al(α,n), γ-ray meas. 78−74386
^{A}P, A=31, 33, levels and transition j-depend., DWBA anal. for Si(^{19}F, ^{16}O) 80−42542
^{27}P, mass excess in ^{32}S(^{3}He,^{8}Li) 77−57595
^{28}P, β$^+$ decay, delayed particle emission, ^{28}Si levels and J$^\pi$ 80−22772
^{28}P, energy levels and spectroscopic assignments using ^{28}Si(^{3}H,t) *(French)* 79−45167
^{28}P, nucleon unbound states, spin, parity, partial width, from ^{28}Si(d,pn) 80−102118
^{28}P spin assignments from ^{28}Si(^{3}He,t) at 38.5 MeV 77−18580
^{28}P, T=1 positive parity analogue states 77−34249
^{29}P, ^{3}(He,d) stripping to bound and unbound states 77−82934
^{29}P deduced levels from ^{29}S β$^+$-delayed proton decay, half life 79−22241
^{29}P, determ. of total and partial widths of unbound states 77−74802
^{29}P excitation functions and spectroscopic factors from ^{28}Si(p,γ) resonant and direct capture 79−80912
^{29}P, mag. moment from β-ray spectra of recoil nuclei polarised by fast polarised beams 77−28502
^{29}P resonance coherence widths from ^{28}Si(p,p), pol. p 80−32258
^{29}P, unbound states via ^{28}Si(d,pn) 10-11.8 MeV ang. distribs., DWBA anal. 77−6236
^{30}P, 1st excited state, α-isospin forbidden transition probability in ^{32}S(d,α) 78−89882
^{30}P, compound nucl. form. by ^{14}N+^{16}O at 20-60 MeV 78−4954
^{30}P high spin two nucleon states decay props. from ^{28}Si(α, dγ) 80−13402
^{30}P level width isospin depend., excitation functions, statistical anal. of ^{29}Si(p,α) 80−78152
^{30}P positive parity states, transitions and spectroscopic strengths, DWBA anal. of ^{29}Si(^{3}He,d) 80−102138
^{30}P, recoil-distance lifetime meas. 77−34252
^{30}P T=1 state decay, lifetimes and branching ratios, analogue E2 transitions from ^{29}Si(p,γ) 80−68598
^{31}P, 24.2 MeV α-scatt., optical model and coupled-channel anal. 77−6407
^{31}P, analogue-antianalogue M1 transitions, nucl. shape change influence 78−13006
^{31}P, chemical shift tensor meas. in KD_2PO_4, study of ferroelec. transition 77−28527
^{31}P chemical shifts, generalised gauche NMR effect 77−68056
^{31}P excited residual states from ^{32}S(γ,p) at 16-27 MeV, cross sections 78−8795
^{31}P high E$_x$ states, J$^\pi$, DWBA anal. ^{29}Si(^{3}He,p) 80−68536
^{31}P, lifetime meas., interpretation of Z$_2$ variation in low velocity DSAM results 79−26394
^{31}P, liq. cryst. NMR spectra, $(CH_3)_3P$, $(CH_3)_3PO$, $(CH_3)_3PS$, $(CH_3)_3PSe$ 77−61768
^{31}P, NMR, metabolism of aerobic Escherichia coli cells 77−90741
^{31}P NMR analysis of intact tissue 80−26432
^{31}P NMR for anal. of living tissue 77−37117
^{31}P, NMR in amorphous ferromag. $Fe_{75}P_{15}C_{10}$ 78−2770
^{31}P, NMR in $Fe(CO)_2(PF_3)_3$, axial and equatorial ligand interchange 77−73091

nuclei with mass number 20 to 38 continued
^{31}P, NMR in $Fe(CO)_3(PF_3)_2$, axial and equatorial ligand interchange 77−73091
^{31}P, NMR in metallic glass system $(Ni_xPt_{1-x})_{75}P_{25}$ 77−12211
^{31}P, NMR in phospholipids 80−5644
^{31}P NMR spectra of P_4S_9 and P_4S_{10}, cf. related cpds. 77−8427
^{31}P NMR studies of isolated rat liver cells 78−61150
^{31}P, nuclear charge radius from μ^- X-ray transitions 78−66195
^{31}P, photonuclear reactions, 2-4.5 GeV, residual nuclei yields *(Russian)* 77−61399
^{31}P, precision Doppler-shift attenuation lifetime meas. from γ-ray lineshapes 79−36195
^{31}P, resonance strengths from ^{30}Si(p,γ) 80−22786
^{31}P, scalar relax. in PBr_3, off-reson. RF field obs. 79−93193
^{31}P, shielding consts. and anisotropy of NMR shielding tensor, modified CNDO/S calcs. *(French)* 80−32610
^{31}P, simultaneous multinucl. NMR by alternate scan recording of ^{31}P and ^{13}C spectra 80−26426
^{31}P states from ^{29}Si(^{3}He,p), energy levels, ang. distribs., L-values 78−82361
^{31}P transition cross sections from ^{33}S(p,^{3}He) 79−67660
^{31}P+n, 14.1 MeV neutrons, estimated dose to bone and whole body 79−53256
^{31}P(^{6}Li,d)^{35}Cl, 36 MeV, absolute cross sections, ang. distribs. 79−89321
^{31}P(α,n), high spin negative parity states in ^{34}Cl, lifetime meas. 78−74327
^{31}P(d,α)^{29}Si, 1.5-2.5 MeV, intermediate resonance widths 77−88151
^{31}P(d,α)^{29}Si, 2-3 MeV, excitation functions and ang. distribs. 77−79386
^{31}P(d,p), (d,α), cross-section fluctuations at 150° 78−29476
^{31}P(d,p)^{32}P, 1.5-2.5 MeV, intermediate resonance widths 77−88151
^{31}P(γ,n)^{30}P, primary first-order interference in γ-activation anal. 79−16088
^{31}P(γ,x), (x=2p,2pn,3p,3pn), 75 to 640 MeV, yields and cross sections 78−37328
^{31}P(n,α), ^{28}Al, 14.7 MeV neutron cross sections 78−70520
^{31}P(p,γ)^{32}S, 0.5 to 0.9 MeV, resonance strengths of selected resonances in s-d shell 78−66281
^{31}P(p,γ)^{32}S, ang. distribs. of γ-rays from decay of ^{32}S reson. states 78−13085
^{31}P(p,γ)^{32}S resonances below E_p=1.5 MeV 77−50141
^{31}P(p,n)^{31}S, 6.38 to 13 MeV, polarised protons, β-decay asymmetry meas. 77−18482
^{31}P(p,p), 5 to 8 MeV, anomaly at (p,n) reaction threshold energy *(Russian)* 78−94011
^{31}P(p,p), 65 MeV polarised protons, asymm. in elastic and inelastic scatt. 78−54754
^{31}P(p,p), (p,n) threshold anomaly 78−94003
^{31}P(p,p) 65 MeV, elastic and inelastic, polarised p, nuclear matter distrib. 78−78297
^{31}P(t,p), two-nucleon stripping reactions with Tabakin pot. 78−21570
^{32}P, β$^-$ decay, energy spectra of positron pairs 79−6506
^{32}P, Cherenkov counting using Teflon vials 78−858
^{32}P Cherenkov effect detect. efficiency determ. by ^{60}Co external source on liq. scintillation system 78−25387
^{32}P, half-life, integrated internal bremsstrahlung intensity meas. 77−57629
^{32}P, half-life and mean beta distintegration energy determ by low-temp calorimetry 80−5094
^{32}P high-energy beta-rays, hazards to eye lens and gonads 78−65131
^{32}P spectroscopic factors and level transition excitation function anal. from ^{31}P(d,p), 1.5-2.5 MeV 78−74371
^{32}P, spin-parity assignments from ^{34}S(d,α)^{32}P 78−17219
^{32}P, transmutation doping of ^{30}Si, residual radioactivity 79−33009
^{32}P-labelled compound, radiochromatographic scanning procedure 77−9151
^{34}P, excited states and mass excess via ^{34}S(t,^{3}He)^{34}P 23.0 MeV reaction 77−34229
^{34}P ground and excited states from ^{30}Si(^{7}Li,^{3}He), mass excess, cross section 78−25230
^{34}P mass and energy levels from ^{36}S(d,α) 79−6632
P(n,n), elastic and inelastic scatt., cross sections meas. and calcs. 78−13081
S, A=32, 34, mass and neutron distribs., HF calcs. *(Russian)* 77−82815
S, A=32, 36, mol. configs. of O+O, high spin props., Strutinsky method 78−50201
S isotopes, 24.2 MeV α-scatt., optical model and coupled-channel anal. 77−6407
S isotopes, pionic, energy and width of 3d-2p transitions *(Russian)* 78−25760
S, μ^- capture, charged particle energy spectra and asymmetry *(Russian)* 78−89828
S, nuclear charge radius from μ^- X-ray transitions 78−66195
S, nucleon optical pot. anal. 77−88137
S(A,X), 1.6 GeV, in-beam transition γ-rays 79−6483
S(^{56}Fe,X), relativistic ^{56}Fe fragmentation, charge and mass changing cross sections 79−54453
^{A}S, A=32,33,34, 0.51 to 51.9 eV neutrons, determ. of neutron scatt. lengths, absorpt. and free cross sections 79−30841
^{A}S(α,α′γ), 8-9 MeV, A=32, 34, 2_1^+ state transient field g-factor meas. 79−36151
^{28}S, $J^\pi=12^+$ reson. observed in ^{12}C(^{16}O,^{8}Be) $E_{c.m.}$=18.5-20.5 MeV 77−18508
^{29}S β$^+$-delayed proton decay, half life, ^{29}P deduced levels 79−22241
^{31}S excited residual states from ^{32}S(γ,n) at 16-27 MeV, cross sections 78−8795
^{31}S level J^π assignments, transition cross section from ^{33}S(p,t) 79−67660
^{31}S, mag. dipole moment meas. using ^{31}P(p,n)^{31}S 77−18482
^{31}S, studied via ^{28}Si(^{6}Li,t)^{31}S, t-energy spectra and reaction mechanism 78−41756
^{32}S, eikonal approx. of electron scatt. by spherically symmetric nuclei 78−37330
^{32}S, 1s-0d shell effective interaction, (e,e) scatt. form factor calc. 77−61400
^{32}S (n,n), 0.6 to 3.6 MeV, excitation functions meas., optical model anal. 78−58280
^{32}S (n,pn), 14.6 MeV, differential cross sections, statistical model calcs. comparison *(Russian)* 78−78385
^{32}S (p,p), 5-6 MeV, polarisation in elastic scatt., thick target method 78−13079
^{32}S, (π,γ), shell model anal. 78−89910

nuclei with mass number 20 to 38 continued
^{32}S α-cluster struct., ground and first excited states, energies, radii and moments 80−102122
^{32}S, binding energy, Brink α-cluster model 77−6195
^{32}S, central-tensor coupled effective interaction pot., binding energy, shape, electric moment 77−14036
^{32}S compound nucleus formation and deexcitation entrance channel effects from ^{16}O+^{16}O, ^{12}C+^{20}Ne 80−549
^{32}S, contrib. to fast neutron dose to the human body 80−51263
^{32}S, cranked Hartree-Fock-Bogolyubov calcs., p,n pairing correlations 79−6460
^{32}S, decay of reson. states populated in ^{31}P(p,γ) 78−13085
^{32}S deformed states, comparison of cluster and shell model wave functions 79−22187
^{32}S, doorway structs. in radiative capture of neutrons 79−532
^{32}S, electric quadrupole strength, giant quadrupole resonance 80−52575
^{32}S energy levels and ang. distribs., DWBA anal. from ^{31}P(^{3}He, d), 25 MeV 78−78265
^{32}S, exchange current corrections for muon partial capture rates 78−33152
^{32}S, fragment shell effects in fission determ. from many nucleon correlations 78−41690
^{32}S, kaonic, Y* resonance nonlocal effects, kaonic shifts and widths 79−7039
^{32}S levels and J^π from ^{32}Cl β$^+$ decay 80−22772
^{32}S levels and spectroscopic factors, DWBA anal from ^{28}Si(^{16}O,^{12}C) 79−22204
^{32}S levels and spectroscopic factors from pickup DWBA anal. of ^{33}S(^{3}He,α) 80−9235
^{32}S, lowest T=2 state isospin forbidden decays, branching ratios 79−67703
^{32}S, neutron scatt. obs., 1-3 MeV, ang. distrib., optical model anal. 77−50125
^{32}S, nuclear radii, energy density and HF-BCS methods 80−47363
^{32}S, nuclear saturation props. 79−6395
^{32}S, O_1^+, 2_1^+, 4_1^+ states, EM props. from large basis shell model 79−75900
^{32}S, photonuclear reactions, 2-4.5 GeV, residual nuclei yields *(Russian)* 77−61399
^{32}S resonances and excitation functions, Hauser Feshbach anal. of ^{20}Ne(^{12}C,X), X=p,d,α 80−78249
^{32}S shape isomeric state from unconstrained variation 80−95306
^{32}S, transient field g-factor meas. on 2_1^+ states 78−37273
^{32}S, transition densities, form factors and transient radii 79−6481
$^{32}S_\Lambda$, Λ particle full set of nuclear shell orbitals 79−63623
^{32}S+^{24,25,26}Mg(^{27}Al)(^{28}Si) fusion reaction, 130 MeV, mass systematics of evaporation residues 77−38311
^{32}S+Mg(^{27}Al), 160 MeV, evaporation residues, isotope and element distribs. meas. 78−13153
^{32}S+d, 10 MeV vector polarised deuterons scatt., nuclear shape effects, optical pot., analysing power 78−54768
^{32}S+π$^-$, 70 MeV, modification of ISOBAR-EVA prompt-γ code 77−18616
^{32}S+π$^+$, total cross-section depend. on nuclear density and π-N off-shell amplitude near (3,3) 77−3050
^{32}S(^{12}C,^{12}C), 20 to 35 MeV, resonant heavy ion scatt., from s-d shell nuclei 79−67763
^{32}S(^{12}C,^{12}C), 20-35 MeV, resonant scatt., ang. distribs., cross sections and excitation functions 79−45237
^{32}S(^{12}C,^{12}C) backward angle scatt., resonant like structs. 79−17876
^{32}S(^{12}C,^{13}C), finite-range coupled-channel calcs. 77−10377
^{32}S(^{32}S,^{32}S), 58-130 MeV, elastic scatt., ang. distribs., excitation function, optical model anal. 77−30623
^{32}S(^{3}He,^{3}He)^{32}S, ambiguities in ^{3}He spin-orbit pot. radius, phenomenological optical-model anal. 79−36250
^{32}S(^{3}He,p), 18 MeV, spin-parity and transfer L-values for ^{34}Cl states 77−88046
^{32}S(^{3}He,p), cross section meas., verification of ^{34}Cl shell model calcs. 78−13119
^{32}S(^{9}Be,^{9}Be), 20 to 35 MeV, resonant heavy ion scatt., from s-d shell nuclei 79−67763
^{32}S(α,^{12}C), 90.3 MeV, cross sections and systematics multi-α-cluster transfer implications 80−42675
^{32}S(α,^{12}C), 90.3 MeV, multi-α-cluster transfer and direct pickup cross sections 80−57760
^{32}S(α,^{2}He), 55, 65 MeV, two neutron states, A-depend. of binding energy 78−74379
^{32}S(d,α), ang. momentum transfers, determ. using polarized beams 78−37354
^{32}S(d,α)^{30}P, 2 to 2.5 MeV, fluctuation anal., ^{24}Cl compound nucleus 78−46070
^{32}S(d,α)^{30}P, statistical fluctuations at 135°, 2.0-2.5 MeV 78−89882
^{32}S(d,d), pol.d, 20 MeV, quadrupole transition amplitudes 80−99148
^{32}S(d,p), DWBA anal. converging overlap integrals, stripping to decaying states 79−6530
^{32}S(d,p)^{33}S, excited states, ang. correl. meas. 77−38239
^{32}S(d,p)^{33}S, statistical fluctuations, at 135°, 2.0-2.5 MeV 78−89882
^{32}S(d,p)^{33}S*, 12 MeV, ratio to (n,n) cross section, DWBA anal. 77−57677
^{32}S(d,t) and (d,^{3}He), ^{31}S, ^{31}P analogue spectroscopic factors, charge asymm., DWBA anal., optimum Q-value 77−54229
^{32}S(e,e), charge form factors in α cluster model 79−63571
^{32}S(e,e), elastic scatt., spectroscopic information and form factors 80−9260
^{32}S(e,e) form factor calc., test of 1s-0d shell effective interactions 77−61400
^{32}S(γ,d), below 30 MeV, photodeuteron yield and cross section, meas. and statistical calcs. 80−63171
^{32}S(γ,n), (γ,p), cross sections, ^{31}S, ^{31}P excited residual states 78−8795
^{32}S(γ,p$_0$), giant dipole resonance decay model, cross section and p spectrum 79−6563
^{32}S(γ,p), 17-30 MeV, giant resonance p decay channel, state transition distrib. *(Russian)* 78−89840
^{32}S(γ,pn)^{30}P primary first-order interference in γ-activation anal. 79−16088
^{32}S(μ^-,e$^+$)-^{32}Si*, muon conversion search, deduced upper limit 79−13285
^{32}S(n,X), 2.5-1100 keV, resonance struct. from total and capture cross sections 80−42620
^{32}S(n,γ), fast n, doorway structs. and single particle resonances, microscopic treatment 80−52646

nuclei with mass number 20 to 38 continued
^{32}S(n,γ), non-statistical effects in shell model calcs. 80−32274
^{32}S(n,γ), single particle resonances and doorway states, K matrix formalism 80−37384
^{32}S(n,n'γ), 13.9 MeV, 2^+ (2.23 MeV) excitation, spin flip probab., deexcitation γ-rays 80−86853
^{32}S(n,n'γ), 14.6 MeV, differential cross sections, statistical model calcs. comparison *(Russian)* 78−78385
^{32}S(n,n'γ) 14.2 MeV, spin-flip probability from 2.23 MeV state 77−14123
^{32}S(n,n), 14.2 MeV, elastic, inelastic, backscatt. meas., optical model test 78−58275
^{32}S(n,n), 2-3 MeV neutrons studied using assoc. particle TOF spectrometer 80−13468
^{32}S(n,n), 21.5 MeV, optical model and coupled channel calcs. 77−26714
^{32}S(n,n), 25-1100 keV, total cross section, multilevel anal., strength functions, optical parameters 80−78298
^{32}S(n,n), 5 MeV, elastic and inelastic scatt., differential cross-sections, model anal. *(Russian)* 80−42668
^{32}S(n,n), spin-flip probability to first 2^+ level 80−78288
^{32}S(n,n) and ^{32}S(n,n') 21.5 MeV reaction, differential cross-sections, deform. parameters 77−57658
^{32}S(n,np), 14.6 MeV, differential cross sections, statistical model calcs. comparison *(Russian)* 78−78385
^{32}S(p,p), 14-45 MeV, differential cross section and spin-flip probabilities, giant resonances 80−73850
^{32}S(p,p), 3-3.8 MeV, isospin-forbidden T=3/2 reson., isospin mixing 77−18507
^{32}S(π,γX), short-range 4-N correls. 77−18613
^{32}S(π,π), many body effects in resonant scatt. 78−94029
^{32}S(π,π), total cross section, density distribs. and ray bending effects 80−47509
^{32}S(t,p), 10 MeV, DWBA anal., ^{34}S levels 78−50180
^{33}S compound nucleus from ^{31}P(d,p)^{32}P ang. distrib. DWBA anal. and level widths 78−74371
^{33}S, excited states, ang. correl. meas. 77−38239
^{33}S levels, excited by α-capture reactions 78−33124
^{33}S, state spectroscopy via ^{30}Si(α,nγ), E1,E2, J^π assignments <5 MeV 77−34227
^{33}S(p,γ), 1.0, 2.0 MeV, reson. excit., Q-value *(French)* 77−26612
^{34}S, beta, decay, half-life, mass excess meas. 77−54188
^{34}S, populated in ^{32}S(t,p) at 10 MeV 78−50180
^{34}S, transient field g-factor meas. on 2_1^+ states 78−37273
^{34}S(^{3}He,t), precise Q-value, ^{34}Cl β decay energy, half life 77−30618
^{34}S(α,Γ)^{38}Ar, 2-3.5 MeV, reson. levels, mixing ratio 79−71859
^{34}S(d,α)^{32}P, 8.25-9.50 MeV, tensor-polarised deuterons, spin-parity assignments to ^{32}P levels 78−17219
^{34}S(d,d), elast. and inelast. scatt. of 11.8 MeV polarised deuterons 78−33191
^{34}S(d,p)^{35}S, 11.8 MeV vector polarised deuterons, optical pot. 77−88149
^{34}S(γ,γ), E<18 MeV, state lifetimes, excitation energies and level cross sections 78−93966
^{34}S(p,α)^{31}P, 35.5 MeV, DWBA, coherence effects 77−38271
^{34}S(p,γ) ^{35}Cl, determ. of ^{35}Cl resonance level spin and multipolarity mixing coeff. 79−9552
^{34}S(p,γ)^{35}Cl, E_p=700 to 2100 keV, γ-ray angular distrib. 79−9466
^{34}S(p,n)^{34}Cl, threshold energy, ^{34}Cl superallowed beta-decay Q-value 77−34298
^{34}S(p,p), 1.45-2.85 MeV, high resolution differential cross-sections 77−65222
^{34}S(p,p), (p,n) threshold anomaly 78−94003
^{34}S(t,^{3}He)^{34}P, 23.0 MeV, populating ^{34}P excited states 77−34229
^{35}S, beta-decay, internal bremsstrahlung spectrum meas. 77−50089
^{35}S content of coolant gas in Windscale AGR, gas chromatographic and radiochemical anal. 78−73125
^{35}S, internal bremsstrahlung photon intensity and energy yield 78−86509
^{36}S, mode-mode coupling model for four-body correls. 77−10322
^{36}S(d,p), 3.2 MeV, proton spectra meas., ^{37}S energy level scheme *(Russian)* 78−41733
^{37}S energy level scheme from (d,p) study, proton spectra *(Russian)* 78−41733
^{37}S level scheme and excitation energies from ^{36}S(d,p) *(Russian)* 79−30790
^{38}S producting using compact cyclotron 77−90894
^{32,33,34}S(α,d), 40 MeV, populating high-spin states, L-transfer 77−74865
^{32}$_\Lambda$S(k$^-$,π$^-$), energy excitation spectra, nuclear shell orbitals for Λ 79−85565
S(d,p), A=32, 34, Tabakin pot. calcs., differential cross sections, ang. distribs. 78−611
Si (n,n), elastic and inelastic scatt., cross sections meas. and calcs. 78−13081
Si, A=28, 29, 30, charge distrib. in ground, excited states via (e,e') 18.5-117.1 MeV 77−54142
Si, A=28, 30, 34, exotic nuclei stability anal., Hartree-Fock approx. with the Skyrme interaction 78−82273
Si, bombarded by ions, Coulomb excitation of sd shell nuclei, B(E2) values, lifetime meas. 78−25216
Si isotopes, pionic, energy and width of 3d-2p transitions *(Russian)* 78−25760
Si isotopes deformed nuclei, stability, shape, Hartree-Fock calcs. *(Russian)* 80−52568
Si, neutron-photon multigroup cross sections for neutron energies ≤60 MeV 79−30880
Si, nuclear charge radius from μ$^-$ X-ray transitions 78−66195
Si, nucleon optical pot. anal. 77−88137
Si+^{16,18}O, 34-81 MeV, total fusion-evaporation cross sections, fusion barrier 80−5190
^{2}Si(π$^\pm$, π$^\pm$) 130, 180, 226 MeV, πN(3), region, inelastic transitions, optical and DWIA anal. 79−97677
^Si, A=28,29, spin cutoff parameters, spectral distrib. calc. and meas. comparison from Mg(α,n) 79−6382
^Si, A=28,29,30, 0.51 to 5.19 eV neutrons, determ. of neutron scatt. lengths, absorpt. and free cross sections 79−30841
^Si+p, A=28, 29, gas phase proton irradiation, condensation, isotopic anomalies generation 79−13289
^Si(^{10,11}B,^{10,11}B), 33.7, 41.6, 50 MeV, A=28,30, ang. distribs., cross sections and deformation parameters, absorption effects 79−67773
^Si(^{12}C,X), 20-49 MeV, A=28-30, complete fusion cross sections, excitation function weak struct. 80−5188
^Si(^{16}O,^{16}O), A=28, 30, 20-35 MeV cross sections and excitation functions, optical model anal. 79−93655
nuclei with mass number 20 to 38 continued
^Si(^{16}O,X), 21-61 MeV, A=28-30, complete fusion cross sections, excitation function weak struct. 80−5188
^Si(^{3}He,^{3}He), 46 MeV, A=28-30, ang. distribs., optical and DWBA anal., scatt. pots. 79−556
^Si(α,α), 41 MeV, A=28-30, ang. distribs., optical and DWBA anal., scatt. pots. 79−556
^Si(e,e'), 126-293 MeV, A=28,29, levels and form factors, particle-phonon coupling anal. 80−105977
^Si(n,α), 14.8 MeV, A=28-30, cross section determ. for threshold detectors 79−17907
^Si(n,p), 14.8 MeV, A=28-30, cross section determ. for threshold detectors 79−17907
^Si(p,γ)$^{A+1}$, A=28,29,30, resonance strength determ. for H burning of ^{29,30}Si in explosive C burning 79−22289
^Si(p,p'), A=28,29,30, 51.9 MeV, blocking effect and core-excitation DWBA and optical model 78−82336
^Si(p,p) A=28-30, 65 MeV, elastic and inelastic, polarised p, nuclear matter distrib. 78−78297
^{24}Si delayed-proton emitter, search in (^{3}He,3n) 60 MeV reaction 77−22970
^{24}Si ground state masses in isospin quintet from (π$^+$,π$^-$) 80−105960
^{24}Si, isobaric multiplet mass eqn., test from decay 79−40890
^{24}Si, Q value and mass excess from ^{28}Si(α,^{8}He) 80−86795
^{25}Si(p,p), 14-45 MeV, differential cross section and spin-flip probabilities, giant resonances 80−73850
^{26}Si, isoscalar and isovector E2 transition matrix elements 78−25148
^{27}Si, forbidden transition ang. distribs., CCBA and DWBA anals. of (p,d) 80−86848
^{27}Si, γ-branchings and mixing ratios determ. from ^{24}Mg(α,nγ) 78−17224
^{27}Si, levels, GDR isospin mixing via (γ,n) 28 MeV 77−74832
^{27}Si, mass excess in ^{29}Si(p,t) 77−57595
^{27}Si, shape mixing using ang. momentum projection from Hartree-Fock intrinsic states 78−86472
^{27}Si, studied via ^{24}Mg(^{6}Li,t)^{27}Si, t-energy spectra and reaction mechanism 78−41756
^{28}Si 10.9 MeV resonance, J^π assignment from ^{12}C(^{16}O,α) 79−26414
^{28}Si 10.9 MeV resonance from ^{12}C(^{16}O,α)^{24}Mg, spin, parity 78−74384
^{28}Si, 12917 and 12924 KeV level gamma-gamma directional correl. 79−536
^{28}Si 12.291 MeV level width, axial blocking meas. from ^{27}Al(p,α) 80−63086
^{28}Si, 12.44 MeV 2^+ level lifetime meas. by crystal blocking 77−34253
^{28}Si, 12.8 MeV resonance obs. in ^{12}C+^{16}O system 79−6405
^{28}Si, 17.62 and 17.71 MeV level struct. 79−9468
^{28}Si, 2^+ 1.78 MeV state, reduced matrix element and deformation length from (^{16}O,^{16}O) 79−13317
^{28}Si 4^+ state lifetime by blocking effect method from ^{27}Al(p,α) *(Russian)* 80−91152
^{28}Si 8^+ state, level systematics and energy spectra from ^{25}Mg(^{12}C,^{9}Be) 80−42528
^{28}Si, (^{16}O,^{16}O) and (^{16}O,^{12}C) reactions, finite-range coupled-channel calcs. 77−10377
^{28}Si (α,α'γ) 104 MeV, nuclear deformation from ang. correlations, coupled channel anal. 78−78301
^{28}Si (e,f), K=2 symmetry intermediate state 80−47514
^{28}Si (p, X), pol.p, 65 MeV, continuum spectra anal. powers 80−102178
^{28}Si (p,p'), 14-40 MeV, low lying states, optical and statistical model anals., giant resonances 79−40894
^{28}Si (π$^\pm$,Xγ), 190, 220 MeV, multinucleon removal cross sections and γ-ray spectra, binding energy effects 79−3183
^{28}Si alpha doorway states from ^{12}C(^{16}O,^{12}C) 80−63146
^{28}Si, appl. of theory of bi-determinantal intrinsic states 79−9484
^{28}Si α-doorway states in α-decay to ^{24}Mg low lying K-band 80−47438
^{28}Si backward angle cross sections, entrance channel resonance effects from ^{24}Mg(^{16}O,^{12}C) 79−30813
^{28}Si, binding energy, Brink α-cluster model 77−6195
^{28}Si, central-tensor coupled effective interaction pot., binding energy, shape, electric moment 77−14036
^{28}Si compound states populated in ^{27}Al(p,α), 937 and 885 keV resonance lifetime meas. using crystal blocking technique 79−63671
^{28}Si, deformed nucleus, quadrupole moment, HF calc. exponential convergence and acceleration 79−85367
^{28}Si, dipole moment using transient mag. field from ion passing through ferromag. *(Dutch)* 78−29386
^{28}Si dipole reson., effect of 2^+ core excitation 78−17166
^{28}Si, doorway structs. in radiative capture of neutrons 79−532
^{28}Si electrofission, decay to ^{12}C(2_1^+)+^{16}O(0_1^+) fragments 78−41793
^{28}Si, energy levels populated in ^{24}Mg(α,n)^{27}Si, threshold to 13.1 MeV 78−618
^{28}Si excitation functions, ang. distribs. and resonant behaviour from ^{24}Mg(^{16}O,^{12}C) 80−68622
^{28}Si excitation functions, ang. distribs., resonance spin assignments from ^{24}Mg(^{16}O,^{12}C) 80−68623
^{28}Si, excitation functions for O^+ and 2^+ states, meas. from ^{24}Mg(^{16}O,^{12}C) 78−54800
^{28}Si, excited levels populated in ^{27}Al(p,α)^{24}Mg at E_p=1540-2220 keV 78−17189
^{28}Si, fast moving ion in Fe, nature of dynamic mag. field 78−43697
^{28}Si, generator coord. calc. 77−50073
^{28}Si, giant reson. multipolarities via (α,α'), 120 MeV reactions 77−54201
^{28}Si, γ-spectra, isobaric analogue resonances via ^{27}Al(p,γ)^{28}Si 2.4-2.74 MeV 77−57646
^{28}Si HF microscopic anal. of core struct. for deformed nucleus 78−78294
^{28}Si, high vel. recoil in polarised Fe, transient mag. fields 77−43910
^{28}Si, highly excited ^{12}C-α-^{12}C molecular state, symmetrical decay *(Russian)* 80−86861
^{28}Si, inverse inertia parameter calc. 78−50073
^{28}Si, investigation of levels and resonances in ^{27}Al(p,γ) and ^{24}Mg(α,γ) 78−66205
^{28}Si, isoscalar giant quadrupole resonances, RPA calcs., E2 strength fragmentation, spectroscopic factors 80−13437
^{28}Si isovector M1 excitations, current and spin contribs. from (e,e'), (p,n) 80−68582
^{28}Si levels and J^π from ^{28}P β$^+$ decay 80−22772
^{28}Si, lifetime meas., interpretation of Z_2 variation in low velocity DSAM results 79−26394

nuclei with mass number 20 to 38 continued

^{28}Si lifetimes in selected materials, DSA study, theoretical stopping power predictions 78−74329
^{28}Si lowest T=2 resonance α-width, observed narrow resonances from ^{24}Mg(α,α_0) 79−45236
^{28}Si, lowest T=2 state isospin forbidden decays, branching ratios 79−67703
^{28}Si, mass and neutron distribs., HF calcs. *(Russian)* 77−82815
^{28}Si, microscopic model of 2_1^+ and 3_1^+ states, inelastic p scatt. test 79−26358
^{28}Si, neutron induced binary and tertiary reactions, energy distribs. of secondaries 77−23043
^{28}Si, neutron scattering resonance radiative widths 80−99146
^{28}Si, O_1^+, 2_1^+, 4_1^+ states, EM props. from large basis shell model 79−75900
^{28}Si, obs. of α-doorway states in ^{12}C+^{16}O system 79−6662
^{28}Si p3/2 neutron resonance γ-decay, partial rad. widths from Si(n,γ) 80−52617
^{28}Si, photonuclear reactions, 2-4.5 GeV, residual nuclei yields *(Russian)* 77−61399
^{28}Si, pot. and charge deform. of rot. states 77−46106
^{28}Si, precision Doppler-shift attenuation lifetime meas. from γ-ray lineshapes 79−36195
^{28}Si, prolate and oblate intrinsic states *(French)* 78−70482
^{28}Si, π bound states in finite nuclei 78−46013
^{28}Si, reson. as ^{12}C+^{16}O quasimol. bands 77−79349
^{28}Si, resonance strengths from ^{27}Al(p,γ) 80−22786
^{28}Si, resonance struct. determ. by ^{16}O(^{12}C,^{8}Be)^{20}Ne* reaction 79−6663
^{28}Si resonance wave functions and differential cross sections from ^{27}Al(p, n), (p, p), (p, α) 80−18261
^{28}Si resonance wave functions from differential cross sections of ^{27}Al(p,X), X=p,n,α 80−78239
^{28}Si, resonances in ^{27}Al+p$\rightleftharpoons^{24}$Mg+α, test of detailed balance at isolated resonances and time reversibility 79−45260
^{28}Si resonances obs. in ^{27}Al(p,α_0)^{24}Mg at 1.12-3.08 MeV 78−13091
^{28}Si, sd-shell calcs. for O^+ states, particle-hole conjugation 77−67704
^{28}Si, shell model and statistical spectroscopic anal. 78−29390
^{28}Si, Sp(6,R) symmetry, α-breakup amplitudes, of giant E2 excitations 78−29435
^{28}Si spectrum, central and noncentral components of effective sd-shell interaction 77−54160
^{28}Si, spin cutoff factors, sd shell realistic effective interactions, shell model spectra 80−18190
^{28}Si, strength function calcs. in many fermion systems, Monte-Carlo method 80−86820
^{28}Si, T=1 positive parity analogue states, lifetimes and branching ratios 77−34249
^{28}Si, three body nuclear molecular resonances for ^{12}C-α-^{12}C 79−75949
^{28}Si, three particle (^{12}C-α-^{12}C) struct., highly excited state calcs. *(Russian)* 79−3073
^{28}Si, tri-nuclear cluster state of ^{12}C-^{12}C-α 78−50189
^{28}Si, vector polarised ^{6}Li elastic scatt., full optical model anal. 78−70553
^{28}Si+^{12}C elastic scatt. ang. distribs., optical pot. 78−8855
^{28}Si+^{12}C(^{16,18}O) scatt., ^{28}Si pot. quadrupole deform. length determ. 78−12963
^{28}Si+^{16}O, 35 MeV, undamped surface waves 77−74868
^{28}Si+^{16}O, fusion oscillations, evaporation residue gamma yields, cross section 80−42725
^{28}Si+^{16}O, pot. for back-angle enhanced elastic scatt. 79−40953
^{28}Si+^{16}O elastic scatt., smooth cutoff model angular distrib. 77−10376
^{28}Si+^{16}O(^{12}C), elastic scatt., 90° excitation function gross struct. 79−75950
^{28}Si+^{20}Ne, 120 MeV, numerical anal. based on linear response theory 79−36273
^{28}Si+^{20}Ne; frictional coeffs. using linear response theory 79−13327
^{28}Si+^{28}Si fusion reaction, 117.5 MeV, mass systematics of evaporation residues 77−38311
^{28}Si+^{6}Li, parabolic repulsion potential, optical model 80−22782
^{28}Si+^{6}Li(^{9}Be)(^{12}C), fusion and strong absorption from elastic scatt. optical pot. 80−102222
^{28}Si+^{9}Be, ^{12}C, ^{14}N or ^{16,18}O, low energy elastic scatt., global optical model anal. 78−25229
^{28}Si+^{9}Be, localisation of direct reaction processes, fusion and total cross sections 78−78353
^{28}Si+d, 10 MeV vector polarised deuterons scatt., nuclear shape effects, optical pot., analysing power 78−54768
^{28}Si+n, isobaric analogue resonances from total and differential elastic cross sections 78−41715
^{28}Si+p, 400 MeV, p-γ coincidence meas. of multinucleon removal in quasifree process 78−37342
^{28}Si+π^+(π^-), elastic and inelastic scatt., angular distrib., 180 MeV, comparison with ^{18}O 78−94035
^{28}Si(^{10}B,^{9}Be), 59, 75, 132 MeV, l=1 transfer reaction, exact finite range DWBA anal. 79−22317
^{28}Si(^{10}B,^{9}Be), unique l=1 reaction, ang. distrib. wave number depend., 0WBA anal. 80−63204
^{28}Si(^{12}C, ^{12}C) elastic scatt., 135 MeV, ang. distribs., heavy-ion-like behaviour 77−79398
^{28}Si(^{12}C,^{12}C'), 41.4 MeV, ang. distrib. meas. reorientation effects 77−65231
^{28}Si(^{12}C,^{12}C), 19-48 MeV, ang. distribs., cross sections and optical parameters 80−5157
^{28}Si(^{12}C,^{12}C), 20 to 35 MeV, resonant heavy ion scatt., from s-d shell nuclei 79−67763
^{28}Si(^{12}C,^{12}C), 20-35 MeV, resonant scatt., ang. distribs., cross sections and excitation functions 79−45237
^{28}Si(^{12}C,^{12}C), 24, 29 MeV, coupled channel, first order DWBA, optical pot. calcs. 78−54796
^{28}Si(^{12}C,^{12}C), 27.8-31.5 MeV, elastic and inelastic excitation functions, fine struct., statistical anal. 80−18269
^{28}Si(^{12}C,^{12}C), entrance channel resonances, backward angle scatt., elastic scatt. enhancement 80−27612
^{28}Si(^{12}C,^{12}C), high energy heavy ion scatt., comparison with light-ion data 79−67764
^{28}Si(^{12}C,^{16}O)^{24}Mg, entrance, exit and reaction channel data at backward angles 79−36254
^{28}Si(^{13}C,^{13}C), 20 to 35 MeV, resonant heavy ion scatt., from s-d shell nuclei 79−67763
^{28}Si(^{13}C,^{13}C), 20-35 MeV, resonant scatt., ang. distribs., cross sections and excitation functions 79−45237

nuclei with mass number 20 to 38 continued

^{28}Si(^{15}N,^{14}N), 44 MeV, modified optical pot. from backward elastic scatt. 80−32255
^{28}Si(^{15}N,^{16}O), 44 MeV, p pickup, DWBA and coupled channel anal., two step processes 79−6552
^{28}Si(^{15}N,^{16}O), 44 MeV, modified optical pot. from backward elastic scatt. 80−32255
^{28}Si(^{16,18}O,^{16,18}O), near Coulomb barrier, coupled channel, first order DWBA, optical pot. calcs. 78−54796
^{28}Si(^{16}O, ^{12}C), resonant like structs., forward α transfer mechanism 79−17876
^{28}Si(^{16}O, ^{12}C)^{32}S, transitions to g.s., meas. of excitation functions 79−17920
^{28}Si(^{16}O,^{16}O), 55 MeV, Regge pole anal. using optical pots. 79−3174
^{28}Si(^{16}O,^{16}O), 142 MeV, optical model anal. of ang. distrib. meas. 78−58295
^{28}Si(^{16}O,^{16}O), 215 MeV, energy independent Woods-Saxon optical potential 77−14165
^{28}Si(^{16}O,^{16}O), 30-32.7 MeV, elastic and inelastic excitation functions, fine struct., statistical anal. 80−18269
^{28}Si(^{16}O,^{16}O), 45 to 63 MeV, energy depend. surface transparent optical pot. 78−46099
^{28}Si(^{16}O,^{16}O), 50, 55 MeV, backward angle cross section, optical model calc. 79−9610
^{28}Si(^{16}O,^{16}O), 65 MeV, elastic and inelastic, optical and coupled channels model anals. 79−45293
^{28}Si(^{16}O,^{16}O), anomalous large angle scatt., Regge pole contrib. 79−63687
^{28}Si(^{16}O,^{16}O), backward angle elastic excitation function structure 79−36263
^{28}Si(^{16}O,^{16}O), elastic and inelastic, coupled channels calcs., optical pot. energy depend. 79−571
^{28}Si(^{16}O,^{16}O), entrance channel resonances, backward angle scatt., elastic scatt. enhancement 80−27612
^{28}Si(^{16}O,^{16}O), high energy heavy ion scatt., comparison with light-ion data 79−67764
^{28}Si(^{16}O,^{16}O), parity depend. of heavy-ion optical pot. 78−74397
^{28}Si(^{16}O,^{16}O), radial sensitivity of optical pot. 80−86869
^{28}Si(^{16}O,^{16}O) 35 MeV, elastic and inelastic back angle anomalies, nuclear rainbow angle 79−13317
^{28}Si(^{16}O,^{16}O) gross struct. in excitation function elastic transfer amplitudes 79−36215
^{28}Si(^{16}O,^{16}O) optical pot. semiclassical anal. 79−17917
^{28}Si(^{16}O,^{16}O)^{28}Si, 45-64 MeV elastic scatt., quasi-molecular or barrier-top resonance 79−13341
^{28}Si(^{16}O,$\alpha p\gamma$) or (^{16}O,2pγ), high spin states, in ^{39}K and ^{42}Ca from γ meas. 78−89787
^{28}Si(^{18}O,^{17}O)^{29}Si, 50 MeV, differential cross-sections, direct one-step process 77−74828
^{28}Si(^{18}O,^{18}O), 60 MeV, optical model parameters 79−22204
^{28}Si(^{18}O,^{18}O), 65 MeV, elastic and inelastic, optical and coupled channels model anals. 79−45293
^{28}Si(^{18}O,X), 56 MeV, multinucleon transfers, ang. distribs., distorted wave and shell model anal. 80−27663
^{28}Si(^{19}F,^{16}O), 60 MeV, exact finite range DWBA and CCBA calcs. 80−538
^{28}Si(^{20}Ne, X), 120 MeV, linear response theory anal., frictional coeffs. and energy dissipation 80−13502
^{28}Si(^{28}Si, ^{28}Si), 80-150 MeV, elastic and inelastic, energy depend. struct., multistep processes 79−80909
^{28}Si(^{28}Si,X), 60 MeV, α-α correlations to probe fusion low ang. momentum window 80−106094
^{28}Si(^{28}Si,Xγ), 65-90 MeV, evaporation residues, relative production cross sections 79−45292
^{28}Si(^{32}S,X), 135 MeV, multi-particle prod., two fragment reactions, kinematical anal. 80−83111
^{28}Si(^{3}He,α) inner hole states excitation, DWBA anal., reaction mechanism *(French)* 78−41735
^{28}Si(^{3}He,d), 25 MeV, spectroscopic factors 78−66294
^{28}Si(^{3}He,d), stripping to bound and unbound states in ^{29}P 77−82934
^{28}Si(^{3}He,t)^{28}P, 38.5 MeV, spin assignments in ^{28}P 77−18580
^{28}Si(^{6}Li, ^{6}Li), 154 MeV, differential cross section ang. distrib., optical anal. 80−63201
^{28}Si(^{6}Li,^{6}Li), high energy heavy ion scatt., comparison with light-ion data 79−67764
^{28}Si(^{6}Li,^{6}Li) elastic scatt., 135 MeV, ang. distribs., light-ion-like behaviour 77−79398
^{28}Si(^{7}Li, ^{7}Be)^{28}Al, 36 MeV, excited states in ^{7}Be+^{28}Al system microscopic DWA anal. 77−14157
^{28}Si(^{9}Be, ^{9}Be'), 45, 60 MeV, low lying collective states, ang. distribs., DWBA double folding pot. anal. 80−78113
^{28}Si(^{9}Be, ^{9}Be), 45, 60 MeV cross sections, ang. distribs., Wegner plot, optical and double folding anal. 80−47497
^{28}Si(^{9}Be,^{8}Be), DWBA anal., spectroscopic factor determ. 78−17098
^{28}Si(^{9}Be,^{9}Be), 121-201.6 MeV, strong absorption dominance, global optical model anal., fusion barrier 80−83116
^{28}Si(^{9}Be,^{9}Be), 14-26 MeV, universal optical pot. 78−25219
^{28}Si(^{9}Be,^{9}Be), 20 to 35 MeV, resonant heavy ion scatt., from s-d shell nuclei 79−67763
^{28}Si(^{9}Be,^{9}Be), 20-35 MeV, resonant scatt., ang. distribs., cross sections and excitation functions 79−45237
^{28}Si(^{9}Be,^{9}Be), high energy heavy ion scatt., comparison with light-ion data 79−67764
^{28}Si(^{9}Be,X), 30-60 MeV, total fusion cross section, evaporation residues, optical model 80−78344
^{28}Si(^{9}Be,X), X=p,d,α, energy dependence, angular distrib. of spectra, optical and statistical model anal. 80−68710
^{28}Si(α, ^{12}C), 90.3 MeV, cross sections and systematics multi-α-cluster transfer implications 80−42675
^{28}Si(α,^{12}C), 90.3 MeV, multi-α-cluster transfer and direct pickup cross sections 80−57760
^{28}Si(α,^{3}He)^{29}Si, 65 MeV, spectrum ang. distrib. meas. 78−29492
^{28}Si(α,α'), 65 MeV, ^{4}He deduced monopole excitation to O^+ state DWBA anal. 79−22226
^{28}Si(α,α'), excitation of low-lying 0^+ states, indirect processes 77−6417
^{28}Si(α,α') 120 MeV, giant reson. multipolarities 77−54201
^{28}Si(α,α')^{28}Si, 126 MeV, GQR, DWBA anal. 77−74826
^{28}Si(α,α'c), c=charged particle, 150 MeV, isoscalar giant quadrupole resonance struct. 80−13438
^{28}Si(α,$\alpha'\gamma$), 104 MeV, ang. correl. meas., sensitivity to quadrupole deform. 78−54774

nuclei with mass number 20 to 38 continued

^{28}Si(α,α), 150 MeV, isoscalar giant quadrupole reson. 77−307
^{28}Si(α,α), elastic and inelastic scatt., compound nucleus contrib. anal. 78−37356
^{28}Si(α,d)^{30}P, spectroscopic factor calcs. 79−6384
^{28}Si(α,γ)^{32}S resonances below $E_α$=3.83 MeV anal. 77−50141
^{28}Si(α,n)^{31}S, cross sections and thermonuclear reaction rates 80−73852
^{28}Si(α,p)^{31}P, proton polarisation calcs., distorted wave method 77−6404
^{28}Si(d, p)^{29}Si$_{g.s.}$, 12.1 MeV, vector polarization transfer coeff., deuteron D-state effect 77−14135
^{28}Si(d,^{3}He)^{27}Al, multistep processes, CCBA anal., SU(3) model 77−30609
^{28}Si(d,α), ang. momentum transfers, determ. using polarized beams 78−37354
^{28}Si(d,d′) 6 to 10.46 MeV polarised d, study of Ericson fluctuations 78−54735
^{28}Si(d,d), 6-8 MeV, compound nuclear polarisation effects 77−3020
^{28}Si(d,d), pol.d, 20 MeV, quadrupole transition amplitudes 80−99148
^{28}Si(d,di), 20 MeV, vector polarised deuteron scatt. from deformed nuclei 79−6629
^{28}Si(d,p), 18 MeV, cross-sections calcs. from pseudopotentials, spectroscopic factors 78−572
^{28}Si(d,p), 6 to 10.46 MeV polarised d, study of Ericson fluctuations 78−54735
^{28}Si(d,p), 8.05 MeV, stripping reaction differential cross section, d distortion effect *(Japanese)* 80−22796
^{28}Si(d,p), Tabakin pot. calcs., differential cross sections, ang. distribs. 78−611
^{28}Si(d,p)^{29}Si, 12.3 MeV, tensor analysing powers 78−29479
^{28}Si(d,p)^{29}Si, 1.0 to 2.5 MeV, excitation functions and angular distribs., DWBA anal. 78−62543
^{28}Si(d,p)^{29}Si, 1.8 to 3 MeV, energy behaviour of vector analysing power, intermediate resonances *(Russian)* 79−49617
^{28}Si(d,pn), ^{29}P and ^{29}Si nucleon unbound states, spin, parity, partial width 80−102118
^{28}Si(d,pn) 10-11.8 MeV, p-n ang. correl., unbound states, DWBA anal. 77−6236
^{28}Si(d,t) and (d,^{3}He), ^{27}Si, ^{27}Al analogue spectroscopic factors, charge asymm., DWBA anal., optimum Q-value 77−54229
^{28}Si(e,e′^{16}O)^{12}C^{2+}, 23-34 MeV, ^{12}C yields and ang. distrib. meas. 77−61466
^{28}Si(e,e′), 38.7-57.5 MeV, energy levels, isovector M1 strength, DWBA anal. 79−75847
^{28}Si(e,e′), 6$^-$ T=1 resonance form factor, mag. strength quenching, meson exchange currents 80−86882
^{28}Si(e,e′), 92 MeV, E2 strength distrib., giant quadrupole 79−36192
^{28}Si(e,e′), M2 giant resonance excitation, spin-magnetism mass depend. quenching, M1 strength reduction 78−86521
^{28}Si(e,e′), mag. dipole and quadrupole state excitation 78−50154
^{28}Si(e,e), charge form factors in α cluster model 79−63571
^{28}Si(e,e), elastic scatt., spectroscopic information and form factors 80−9260
^{28}Si(e,f), alpha cluster model approach, intermediate state to ^{12}C+^{16}O 79−40972
^{28}Si(γ, p), 18.1-29 MeV, giant dipole resonance, contrib. from various configs. 80−18264
^{28}Si(γ,α)^{24}Mg, 28 MeV, cross-sections to residual excited states 77−74832
^{28}Si(γ,n)^{27}Si, 28 MeV, cross-sections to residual excited states 77−74832
^{28}Si(γ,p), 18.1-29 MeV, photoproton energy spectra, contribs. to giant dipole resonance 80−78242
^{28}Si(γ,p)^{27}Al, 28 MeV, cross-sections to residual excited states 77−74832
^{28}Si(μ$^-$, γν), γ−ν ang. correlation, pseudoscalar and tensor form factors, particle-hole model 79−13256
^{28}Si(n,γ), 565, 813 keV, resonance γ, spectra, valence model test 80−63124
^{28}Si(n,γ), calc. of neutron and gamma widths for ^{29}Si 3/2$^-$ doorway resonances 77−26587
^{28}Si(n,γ), fast n, doorway structs. and single particle resonances, microscopic treatment 80−52646
^{28}Si(n,γ), n and γ width correlation, valence, optical and shell model comparison 79−6606
^{28}Si(n,γ), single particle resonances and doorway states, K matrix formalism 80−37384
^{28}Si(n,n′γ), 13.9 MeV, spin flip probability from 1.78 MeV state, direct theory 80−9234
^{28}Si(n,n′γ), 1.96-4.15 MeV, prod. cross section for 1780 keV transition 79−59058
^{28}Si(n,n), 0.6 to 3.6 MeV, excitation functions meas., optical model anal. 78−58280
^{28}Si(n,n), 14.1 MeV, elastic and inelastic scatt., wide angular range, spin orbit interaction 78−89867
^{28}Si(n,n), 5 MeV, elastic and inelastic scatt., differential cross-sections, model anal. *(Russian)* 80−42668
^{28}Si(n,n), core-parricle doorway states calc. 77−23003
^{28}Si(n,n), spin-flip probability to first 2$^+$ level 80−78288
^{28}Si(n,n), to 4.5 MeV, s- and p- wave reson. struct., R-matrix interpretation 77−23002
^{28}Si(n,p), 21.6 MeV, cross sections, proton spectra, ^{28}Al analogue dipole state 77−30571
^{28}Si(n,p)^{28}Al, 14.1 MeV, cross-section meas *(Spanish)* 77−67738
^{28}Si(n,p)^{28}Al, ave. neutron activation cross sections for ^{241}Am-Be source 79−31282
^{28}Si(n,p)^{28}Al*, obs. of analogue dipole state 77−30596
^{28}Si(p, p′), isovector dipole strength excitation in giant resonance region 80−83066
^{28}Si(p,d) reaction at 52 MeV, ang. distrib., DWBA anal. 77−26679
^{28}Si(p,p′(d)X), pol. p, 65 MeV, anal. powers of continuum energy spectra 80−68637
^{28}Si(p,p′), 135 MeV, cross section, population of unnatural parity high spin states 78−54753
^{28}Si(p,p′), 135 MeV, high spin unnatural parity states, anal. 78−37334
^{28}Si(p,p′), 135 MeV, large momentum transfer, excitation of high-spin particle-hole states in ^{28}Si 77−61420
^{28}Si(p,p′γ)^{28}Si, 3.5-3.8 MeV, spin-flip probability in resonance region *(Russian)* 78−41725
^{28}Si(p,p′) 3.1-3.8 MeV, interference effects, $β_2$ and optical parameters 77−26685
^{28}Si(p,p), 2.0-3.8 MeV polarised protons, analysing powers meas. 77−3012

nuclei with mass number 20 to 38 continued

^{28}Si(p,p), 6.9 GeV/c, elastic and inelastic differential cross sections, spin flip probability *(Russian)* 79−59071
^{28}Si(p,p), pol. p, 12-18 MeV, cross section, anal. power and states, ^{29}P resonance coherence widths 80−32258
^{28}Si(p,p) 5.6-5.9 MeV, isospin-forbidden T=3/2 reson., isospin mixing 77−18507
^{28}Si(p,pα) 157 MeV, quasifree scatt., α spectroscopic factors, SU(3) predictions 77−6370
^{28}Si(p,pα)^{24}Mg, 157 MeV, energy spectra, SU(3) model comparison 77−88121
^{28}Si(π,X), angular distrib. of inelastic diffusion of π$^±$ *(French)* 80−47507
^{28}Si(π,γX) reaction, 70 MeV pions, expts. with pion beams of Saclay Linac *(French)* 79−572
^{28}Si(π,nγ), neutron spectra from coincidence expts. 79−85499
^{28}Si(π,π′), momentum space DWIA calcs., DWIA validity, shell model sensitivities 79−85553
^{28}Si(π,π), 162 MeV, elastic and inelastic ang. distribs., optical and PWIA anals. 80−42706
^{28}Si(π$^+$,π$^{+\prime}$), 162 MeV, high spin particle-hole state excitation 79−85541
^{28}Si(π$^±$,π$^{±\prime}$), 162 MeV, excitation of high-spin particle-hole states 79−93667
^{28}Si(π$^±$,π$^±$), 130 to 226 MeV, ang. distrib. around (3,3) reson. 79−85537
^{28}Si(π$^±$,π$^±$), 180 MeV near (3,3) reson., nuclear RMS radii determ. 79−85538
^{29}Si 3/2$^-$ doorway resonance, calc. of neutron and gamma widths 77−26587
^{29}Si 3/2$^+$ and 5/2$^+$ states population, (d,p) and (p,π$^+$) comparison 80−95307
^{29}Si, DWBA anal. of ^{9}Be elastic scatt. on various nuclei *(German)* 78−70552
^{29}Si doorway state neutron capture, levels and γ-spectra from ^{28}Si(n,γ) 80−57729
^{29}Si, ESR of paramag. centres in natural diamond 77−36132
^{29}Si excitation functions from ^{27}Al(^{3}He,p) 80−47493
^{29}Si, in compensated Si, optical polarisation, nucl. relax. effects *(Russian)* 77−43907
^{29}Si levels, J^π, spectroscopic factor, DWBA anal. of ^{28}Si(^{3}He, ^{2}He) 80−86811
^{29}Si levels and ang. distribs., DWBA anal. of ^{27}Al(α,d) 80−78157
^{29}Si, low lying energy level structure, from ^{28}Si(d_{pol},pγ) and multi-step reaction calcs. 80−68537
^{29}Si, NMR signal intensity enhancement by polarisation transfer 79−94013
^{29}Si, NMR studies of aqueous silicate solns. 78−15051
^{29}Si neutron resonance, γ-spectra, partial and total radiative widths from ^{28}Si(n,γ) 80−42578
^{29}Si, nucleon unbound states, spin, parity, partial width, from ^{28}Si(d,pn) 80−102118
^{29}Si, optical orientation in n-Si:P and its depend. on pumping light intensity *(Russian)* 77−4581
^{29}Si rot.-vibr. coupling effects, excitation spectrum and ang. distribs. from ^{28}Si(d, p) 80−57661
^{29}Si, unbound states via ^{28}Si(d,pn) 10-11.8 MeV ang. distribs., DWBA anal. 77−6236
^{29}Si(^{16}O,^{17}O)^{28}Si, non-orthogonality of channel states 80−83115
^{29}Si(^{3}He,p), 15 MeV, excitation energies and ang. distribs. below 7.2 MeV, in ^{31}P 78−82361
^{29}Si(^{6}Li,d)^{33}S, 36 MeV, absolute cross sections, ang. distribs. 79−89321
^{29}Si(d,p), 1.1-2.1 MeV, excitation functions, statistical fluctuations anal. 80−95322
^{29}Si(e,e′), 63-112 MeV, ground state transitions props. and transition radii of excited levels 77−50115
^{29}Si(n,γ), evidence for neutron capture through doorway states 79−17909
^{30}Si, 2$_1^+$ state quadrupole moment in band mixed HF model 80−52578
^{30}Si (n,γ)^{31}Si, thermal neutron cross-section determ. 80−95321
^{30}Si first excited state, static quadrupole moment from ^{208}Pb(^{30}Si,^{30}Si) 80−13373
^{30}Si, recoil-distance lifetime meas. 77−34252
^{30}Si+^{14}N, 59, 70 MeV, radiative capture and 1-nucleon emission cross sections 79−93652
^{30}Si+n→^{31}Si, residual radioactivity meas. 79−33009
^{30}Si(^{12}C,^{12}C′) 41.3 MeV, ^{30}Si angular distrib., coupled channels calc. 79−97721
^{30}Si(^{16}O,^{15}N)^{31}P, ang. distribs. anal. 77−74875
^{30}Si(^{16}O,^{16}O), elastic and inelastic, 60 MeV, to 1st excited 2$^+$ state, coupled channels anal. 78−82377
^{30}Si(^{3}He,pγ)^{32}P, 11-15 MeV, coincidence, ang. correl. and branching ratio meas. 78−13129
^{30}Si(^{7}Li,^{3}He)^{34}P, 24 MeV, spectra, ang. distribs., mass excess, cross section 78−25230
^{30}Si(K$^-$,$\bar{K}^0$), 300 MeV, microscopic particle-hole shell model calcs., DWIA anal. 79−59091
^{30}Si(d,α)^{28}Al, 8-12 MeV, polarised d, spin-parity assignments in Al 77−6222
^{30}Si(d,p), pol.d, 1.9-2.5 MeV, anal. power excitation function anomaly 80−5118
^{30}Si(γ,2p), 75 to 640 MeV, yields and cross sections 78−37328
^{30}Si(γ,p), 75-800 MeV, yield meas. by activation method 77−71605
^{30}Si(n,^{3}He)^{28}Mg, ^{28}Mg producting using compact cyclotron 77−90894
^{30}Si(n,^{3}He)^{28}Mg, ^{28}Mg production with 50 MeV neutrons 77−90895
^{30}Si(n,β)^{31}P transmutation doping 78−6107
^{30}Si(p,α)^{27}Al, 17 MeV, polarised p, cross-section and analyzing power ang. distrib. 79−54427
^{30}Si(p,α)^{27}Al, 40.75 MeV, differential and relative cross sections, distorted wave direct pickup calcs. 78−94009
^{30}Si(p,γ$_0$), polarised p in giant dipole resonance region, cross sections and analysing power 78−82346
^{30}Si(p,γ), pol.p, 6.4-15.0 MeV, cross section and anal. power ang. distribs. 80−99168
^{30}Si(p,p), 1.1-3.0 MeV, analogue reson. obs., Coulomb energies, spectroscopic factors determ. 77−2988
^{30}Si(p,p), polarised proton fluctuation expt., compound elastic enhancement factor determ. 79−519
^{32}Si Coulomb matrix elements isospin mixing in giant dipole resonance from ^{28}Si(α,γ) 79−93507

nuclei with mass number 20 to 38 continued
^{32}Si, half life determined from varved Gulf of California sediment core 80−91153
^{32}Si half life from tandem accelerator mass spectrometry 80−95313
^{32}Si half life via accelerator mass spectrometry 80−95314
^{32}Si prod. by ^{35,37}Cl+p below 52 MeV, cross sections, excitation functions 78−89864
^{37}Si, production in 263 MeV ^{40}Ar+^{238}U deep inelastic reactions 79−22324
^{28,30}Si(^{19}F,^{16}O)^{31,33}P 60 MeV, j depend., spin-orbit effects, optical pot. 77−41993
Si(α,^{2}He), A=28, 29, 55, 65 MeV, two neutron states, A-depend. of binding energy 78−74379
Si(e,e′), A=28, 29, 30, 18.5-117.1 MeV, ground, excited state charge distribs. 77−54142
Si(n,α)Mg, A=28,29, 14.1 MeV, cross sections determ. 78−37348
Si(n,γ), 3.2-15 MeV, cross-sections determ. 77−41962
Si(n,γ), A=28.9, E=31.7-67.7 keV, gamma-ray spectra, single particle effects obs. 77−6372
Si(n,n), 20, 26 MeV, Coulomb correction term to optical model pot. 77−38280
Si(n,n)Si, 11-26 MeV, optical model fit 77−79372
Si(p,p), A=28, 29, 30, 65 MeV polarised protons, asymm. in elastic and inelastic scatt. 78−54754
Si(p_{pol},p_{pol}), giant multipole resonance region, optical model anal. 80−57779
Si(π,π), 162 MeV elastic scatt., ang. distribs., diffraction patterns, optical model calcs. 78−58309
Si(π,π), ang. distribs., optical model calcs. 78−58308
Si(π^+,π^+), elast. and inelast. scatt., 50 MeV, ang. distrib. determ. optical model and DWBA 79−45304
S(μ^-, e^-), upper limit for muon-electron conversion 78−21547
S(n,γ), 3.2-15 MeV, cross-sections determ. 77−41962
S(n,γ), on-line gamma anal. using Ge detector 80−52624
S(n,n), 14.8 MeV, differential cross section absolute meas. by surface of revolution technique 77−23394
S(n,n)S, 11-26 MeV, optical model fit 77−79372
^{49}Ti(α,α') 5.2-5.8 MeV, B(E2) value meas. for 3/2$^-$ to 7/2$^-$ transition 78−82308
uncorrelated target, optical pot. unitary content, DWIA and Glauber theory from (α,α)(α,γ) 80−105947

nuclei with mass number 39 to 58
4.7-5.4 MeV, cusp behaviour of cross-section obs. 78−29470
^{40}Ar, fragmentation in collisions at 213 MeV/nucleon, energy and isotope distrib. 79−17919
^{46}Ti(n,t)^{44}Sc, 14.6 MeV, production cross sections 79−49629
(^{6}Li,^{6}Li) 50.6 MeV elastic scatt. on A=12-208 nuclei, optical model parameters 77−18592
A=10 to 50, m-particle n-hole struct. from few nucleon transfer reactions, review 78−50062
A=10-58, neutron separation energies, self consistent set from (n,γ) reaction 80−52563
A=12 to 40, (α,^{2}He) reaction, high spin state transition cross sections in 1p and 2s1d shell 79−6644
A=16 to 40, mag. moments, shell model calcs, mesonic exchange current effects, book contrib. 80−479
A=16-40, α-spectroscopic factors between ground states, shell model prediction 79−13204
A=16-58, charge, proton and neutron density distribs. calc. 80−22680
A=21 to 44, spectroscopic factors for single-nucleon transfer, review 77−71563
A=21-44, energy levels, excitation energies, branching and mixing ratios, lifetimes, J^π, resonances 79−13208
A=24-60, yrast lines using Strutinsky method, empirical fusion bands 80−42514
A=32 to 140, nuclear struct., binding energies, dipole moments *(French)* 77−46098
A=36-39, energy levels and effective interactions from large scale shell model calcs. 79−59011
A=40 to 100, strength and radius parameters of deformed Woods-Saxon potential 79−97673
A=40 to 56, two-nucleon transfer reactions, coupled channel formalism for isospin depend. optical pot. 80−42609
A=40 to 60, neutron force function, role of input states 79−9486
A=40 to 60, total photon widths in valence capture model *(French)* 77−34291
A=40-56, spectroscopy props. using pure configuration shell model *(Chinese)* 80−42584
A=40-80, yrast props. and high spin isomers, cranking plus Strutinsky formalism 80−32152
A=41-55, charge dependent two body interactions from $1f_{7/2}$ shell displacement energies 79−67668
A=42, multiple scattering formalism for the effective interaction 80−102126
A=42 isotopic spin triplet, Coulomb energies and shifts, microscopic calcs. 80−9200
A=42 nuclei, T=1, J=0 states, Coulomb displacement energies, Hartree-Fock wave functions, charge depend. 78−89773
A=44 to 58, α-particle transfer spectroscopic factors using interacting boson approx. 78−78258
A=45, nuclear data sheets 78−66187
A=45-153, β^+-decay strength function maximum 79−75914
A=46, nuclear data sheets, level struct. and decay props. 79−13185
A=47, nuclear data sheets 78−66188
A=48, nuclear data sheets, to September 1977 78−82266
A=50, nuclear data sheets 77−10304
A=50 to 89, α-particle elastic scatt., neutron shell sensitivity, optical model parameters 79−6642
A=50-57, N=28-30, effective interactions and energy spectra from shell model calc. 78−82299
A=51 nuclei, data sheets (to August 1977) 79−9440
A=52 nuclear struct. data sheets to April 1978 79−36129
A=53 nuclei, struct., level props., ENSDF data 78−17076
A=54, nuclear structure data sheets, to Dec. 1977 79−17780
A=54 nuclei, data sheets 79−6370
A=54-82, ground state transition strengths from (p,t) reactions 80−95305
A=56 nuclei, beta transition rates in hot dense stellar matter 78−73699
A=56 nuclei, nuclear struct. data, level props., from ENSDF 77−74743
A=57 nuclei, nuclear struct. data, level props., from ENSDF 77−74744

nuclei with mass number 39 to 58 continued
A=58 nuclear data sheet to June 1976 77−18372
A=6-44, gamma-ray transition strengths, data tables 80−37345
A=9 to 70, proton scatt., 14 to 45 MeV, differential cross sections 79−45273
A<100, average E1/M1 strength ratio 80−52621
A≤57 nuclei, E2, M1 multipole mixing ratios 80−22751
compound nucleus (α,p) cross-sections in Ni region, 15 and 18 MeV 77−74864
compound nucleus (p,p′) cross-sections in Ni region, 12 MeV 77−74864
cosmic rays, abundances of elements in 26≤Z≤30 interval 79−40044
even-even nuclei, 58≤A≤150, E2, M1 multipole mixing ratio, data survey 78−50118
even-even nuclei, z=6 to 100, probable members of quasi-bands in spherical and deformed regions 80−13357
fission product gamma-ray and half-life 29≤A≤69, data collection 78−50134
gamma-ray internal conversion coeffs. for all at. shells, 30≤Z≤104 79−45206
internal conversion coefficients, 30≤Z≤104, Hartree-Fock-Slater model calcs. 79−36199
isomeric A=48-50 nuclei, mag. moments and core polarisation 78−37274
level densities, thermodynamic temps., spin cutoff factors, nuclei with 23≤A≤40, expt. calcs. 77−30492
N=28, odd-even effect in shell model 79−13217
N=28 nuclei, energy spectra calc. in shell model 79−13206
N∼28 nuclei, shell model study of high-spin states 79−3087
photonuclear energy integrated cross-sections, calcs., A=2-40 77−50110
photospallation, 0.1 to 1 GeV, mass yield distrib. 80−73835
props. of prompt muons prod. by 28 GeV protons 79−17906
resonating-group method anal. 77−82886
sum rule anal. of one-nucleon transfer data on ^{41}Ca, ^{43}Ca, ^{45}Sc, ^{49}Ti, ^{51}V, shell model validity 77−67730
thermonuclear reaction rate data for intermediate mass nuclei 80−31427
(α,α'), A=40-208, low energy octupole resonances, 96 and 115 MeV 79−511
(α,^{2}He), 55 and 65 MeV, on 1p and 2s1d shell nuclei, A=12 to 40 78−82365
α surface clustering, effect of pairing and four-body interactions in 41≤A≤45 nuclei 77−10344
Λ nucleus, 40≥A≥12, strangeness exchange reactions, anal. 77−292
(n,γ), valence model, mass range 40<A<70 79−45256
(n,n′γ), A=28-152, spherically doubly even nuclei, level excitation cross sections, statistical anal. *(Russian)* 79−67707
(n,X), fast n, ^{3}He emission cross sections for A=27-115 80−13475
(p,n) excitation functions for A=45 to 80, proton optical pot. at sub-Coulomb energies 80−9292
(π^-,2n) struct. and reaction information, two hole states, direct mechanism 79−85496
(π,Xγ) reaction at 70 MeV on s-d shell nuclei 78−29504
^{51}Mn levels studied via high resolution proton scatt. from ^{50}Cr 77−54151
A=49 nuclei, nuclear struct. data sheets to Dec. 77 79−26360
^{26}Al^{m}, super-allowed Fermi β decay, lifetime meas. 77−79336
^{27}Al(^{24}Mg,αpn)^{45}Ti, ^{45}Ti $1f_{7/2}$ shell model and high spin states 78−62560
Ar isotopes, meas. of 280 MeV/nucleon particles with plastic detector 77−38561
Ar isotopes, spallation ratios and prod. cross sections from (p, spallation) 80−9284
Ar isotopes prod. cross sections in natural Ca by 12-45 MeV protons 77−17310
Ar isotopes prod. in lunar materials by solar cosmic ray protons, rate calc. 77−17311
Ar+Au, 285 MeV, ang. distrib. of fission and deep inelastic products 77−82964
Ar+Th, 388 MeV, deep inelastic reactions, double differential cross section calc. 78−8856
^{A}Ar, A=43,44, β-decay, ^{43,44}K levels, spin and parity assignments, decay scheme 79−13210
^{A}Ar, A=45,46, β-decay, ^{A}K, A=45,46, levels, lifetimes and transitions 80−42597
(^{36}Ar+α) system, effect of nuclear deform. on folded pot. 79−6453
^{38}Ar(α,pγ)^{41}K, level props. of ^{41}K below 3.3 MeV 78−62588
^{39}Ar, lifetimes of high-spin levels meas. Doppler shift technique 77−61380
^{39}Ar low lying states from ^{37}Cl(α,d), spectra, ang. distribs., spins 78−25212
^{40}Ar, implantation in Fe, perturbed ang. distrib. 78−12969
^{40}Ar, charge distrib. via ^{40}Ar(e,e′) 65-115 MeV 77−18527
^{40}Ar excitation function for ^{152,153}Er prod. from ^{118}Sn(^{40}Ar,xn) 79−22315
^{40}Ar, fission by 1 GeV protons, ang. distrib. of products *(Russian)* 77−46200
^{40}Ar, lifetime determ. using Doppler shift attenuation 79−93551
^{40}Ar, yrast levels, J^π, branching and mixing, via (^{16}O, 2pγ) 34 MeV 77−74759
^{40}Ar+^{109}Ag, 170-340 MeV, fission barriers at high ang. momenta 77−26786
^{40}Ar+^{12}C 205 MeV/nucleon, ^{28}Ne and ^{35}Al fragment obs. 79−22314
^{40}Ar+^{164}Dy, evaporation residue prod. depend. on excitation energy of compound nucl. 78−21607
^{40}Ar+^{197}Au, 217 MeV, deform. of double nucl. system 79−6699
^{40}Ar+^{208}Pb, 1.8 GeV/nucleon, appl. of multiple-collision model for pion prod. 78−37365
^{40}Ar+^{238}U, rot. excitation, Coulomb-nuclear interf. 77−14151
^{40}Ar+^{243}Am, 214-300 MeV, fusion-fission reaction, asymm. mass distrib. 77−82963
^{40}Ar+^{27}Al, 340 MeV, energy relaxation and mass transfer *(French)* 80−95327
^{40}Ar+^{40}Ar, 250-1000 MeV/N, intranuclear cascade calcs. for multiplicity and cross sections 80−32300
^{40}Ar+^{58}Ni, 280 MeV, coincidence meas. of deep inelastic collisions 78−33206
^{40}Ar+^{58}Ni, deep inelastic collision at 280 MeV, fragment energy and spin 78−21599
^{40}Ar+^{58}Ni, triple differential cross-section, dynamical model calcs. 78−50212
^{40}Ar+^{58}Ni system, high energy, compound nucleus form. and deep inelastic scatt. *(French)* 79−559

nuclei with mass number 39 to 58 continued
^{40}Ar+Au→^{A}Z+X, 500 MeV/nucleon excited nuclear matter prod. 77−50154
^{40}Ar(^{3}He,n)^{42}Ca, 11.5 MeV, neutron ang. distrib. and energy spectra 77−65227
^{40}Ar(α,α$_i$), 12-15 MeV, J$^{\pi}$ assignments for deduced levels 79−89232
^{40}Ar(α,α′), 172.5 MeV, isoscalar giant quadrupole resonance 79−45231
^{40}Ar(α,nγ), struct. of high spin positive parity states in ^{43}Ca 78−46025
^{40}Ar(α,nγ)^{43}Ca, γ-ray spectroscopy, levels and decay scheme deform. of ^{43}Ca 79−80896
^{40}Ar(α,p)^{43}K, 15 MeV, ^{43}K 738 keV state g-factor, PAC technique 77−6227
^{40}Ar(α,pγ)^{43}K, 10.4 MeV, lifetime of 738 keV level of ^{43}K, M2 transition strength meas. 77−65226
^{40}Ar(d, p)^{41}Ar, 1.354 MeV, spectroscopic factor comparison with isobaric analogue reson. 79−30787
^{40}Ar(d,d), optical model parameter investigation using 9-12 MeV polarised d 78−94016
^{40}Ar(d,p) and ^{40}Ar(d,n), lifetime meas. of ^{41}Ar, ^{41}K, by DSA method 78−78308
^{40}Ar(e,e′), 65 to 115 MeV, low lying level struct., lifetimes 78−8798
^{40}Ar(e,e′) 65-115 MeV, charge distrib. 77−18527
^{40}Ar(γ, xp yn), 9-29 MeV, cross sections in giant resonance region, particle decay modes 80−13462
^{40}Ar(γ,2p)^{38}S production on recirculatory, Ar gas target 79−88185
^{40}Ar(γ,p)^{39}Cl production on recirculatory, Ar gas target 79−88185
^{40}Ar(n, ^{3}He)^{38}S, ^{38}S producting using compact cyclotron 77−90894
^{40}Ar(p,X), 1 GeV, deep inelastic interaction, reaction product angle and energy spectra *(Russian)* 79−75988
^{40}Ar(p,d), 35 MeV, DWBA anal., spectroscopic factors 78−17204
^{40}Ar(p,n), 8.3 meV, ^{40}K excitation energy, γ decay, of lowest T=2 state 78−8769
^{40}Ar(p,p), 18-44 MeV, differential cross sections, phase shift anal., energy depend. 80−47481
^{40}Ar(p,p) 65 MeV, elastic and inelastic, polarised p, nuclear matter distrib. 78−78297
^{40}Ar(p,p)^{40}Ar, E$_p$=1 MeV, cross section meas. 78−13089
^{41}Ar dose distributions due to atm. release from HWR, including wind effects 77−14271
^{41}Ar, γ-decays of low-lying states obs. with (Ar,p), (Ar,n) 77−41986
^{41}Ar, near-stack reactor effluent dispersion studies by SF_6 tracer method 78−11992
^{41}Ar states from ^{40}Ar(d,p), lifetimes meas. by DSA method 78−78308
^{44}Ar β decay into ^{44}K, neutron rich isotopes, weak coupling predictions, γ-ray meas. 78−74336
^{45}Ar, β-decay scheme and half life, K deduced energy levels 78−78319
^{46}Ar, β-decay scheme and half life, K deduced energy levels 78−78319
^{46}Ar decay, gamma-ray spectra meas., half-life determ. 78−21513
^{37,39}Ar, high-spin states of (fp)^2 character via (α,d) reaction 77−74865
^{75}As(d,p) 11 MeV populating ^{76}As low-lying states 77−10319
^{76}As, low-lying states via ^{75}As(d,p) at 11 MeV, spectroscopic factors, DWBA anal. 77−10319
^{40}C, π, electroproduction, near threshold, inelastic response functions 78−33172
^{48}C+^{6,7}Li, population of ^{51,52}Ti, ^{52}V yrast states, mean lifetimes meas. 77−2942
Ca (p,p), 1 GeV, neutron and proton RMS radii differences in matter 79−54403
Ca, A=41 and 43, collective bands of positive parity states, HF calcs. 78−54677
Ca, A=41-44, deform. struct. in f-p shell nuclei, Nilsson model calcs. 78−66228
Ca, extended Skyrme force calculation, spin instability 79−63601
Ca isotopes, $f_{7/2}$ neutron occupancies 78−78240
Ca isotopes, neutron RMS radii from pion total cross-sections 77−57589
Ca isotopes, nuclear rms radii using Skyrme interaction with state depend. effective mass 79−45147
Ca, isotopic sequence charge distrib. calc. 79−85361
Ca, neutron-photon multigroup cross sections for neutron energies ≤60 MeV 79−30880
Ca, nucleon optical pot. anal. 77−88137
Ca, radial charge distrib. moments, ground state correlations, generator coordinate model 79−30785
Ca, shell model, core and single particle props. 77−26596
Ca stable isotopes, nucl. charge distrib. from isotope shift in Ca I resonance line 79−9461
Ca+^{40}Ar, A=42, 48, 236 MeV, fragments mass and charge distribs. in deep inelastic reactions 78−58296
Ca+Ca, classical many-body model for heavy ion collisions 80−536
Ca(A,X), 1.6 GeV, in-beam transition γ-rays 79−6483
Ca(^{12}C, ^{8}Be), 45 MeV, even isotopes A=40-48 77−88172
Ca(Ca,X), 400 MeV, classical eqns. of motion calcs., central collisions, thermal models 80−106070
Ca(^{3}He,n)Ti A=40, 42, 13 MeV, neutron ang. distrib. and energy spectra 77−65227
Ca(Li,Li), (A=40,48), 28 and 34 MeV optical model parameters 77−54248
Ca(^{32}S,^{32}S), 58-130 MeV, elastic scatt., ang. distribs., excitation function, optical model anal. 77−30623
^{40,48}Ca(^{18}O,^{17}O)^{41,49}Ca, 50 MeV, differential cross-sections, direct one-step process 77−74828
^{A}Ca, (A=43-46), pairing force, seniority number 80−27563
^{A}Ca (α,α′) A=40, 44, nuclear level mag. moments, ^{40}Ca 2_1^+ level, ^{44}Ca 3_1^- level 79−85368
^{A}Ca, A=40, 41, non-self-consistent energy calculations with a density-dependent effective interaction 79−36170
^{A}Ca, A=40, 42-44, 48, pionic X-rays, strong interaction and isotope shifts, π-nuclear optical pot. 80−53169
^{A}Ca, A=40, 44, pionic X-rays and neutron radius 79−36802
^{A}Ca A=40, 48, charge density and single particle state struct. 79−36144
^{A}Ca, A=40, 48, neutron densities and single particle struct. 80−32165
^{A}Ca, A=40, 48, nuclear matter density distrib., saturation effect, optical potential from (α,α) 80−63115
^{A}Ca, A=40, 48, single particle levels, rms charge radius, Wood-Saxon pot. 80−63106
^{A}Ca, A=40,42,44, E0 matrix elements 79−45203
^{A}Ca, A=40,48, nuclear radii, energy density and HF-BCS methods 80−47363
^{A}Ca, A=40,48, static and transition densities, self consistent RPA theory test in fast particle (p,p), (e,e) scatt. *(Russian)* 79−49604

nuclei with mass number 39 to 58 continued
^{A}Ca, A=40 to 46,48, nuclear charge distrib., from isotope shift of 6573 angstrom line 80−57674
^{A}Ca, A=40 to 48, giant multipole resonances, mass dependence of energy weighted sums 80−63144
^{A}Ca, A=41,43,45, quadrupole moments, from hyperfine struct. splitting of $4s4p^3P_1$ 80−57674
^{A}Ca, A=43, 45, spectra, particle-hole conjugation and protection theorems *(Chinese)* 80−73796
^{A}Ca, A=44,46 excited states and transition ang. distribs. from Ti(^{14}C,^{16}O) 80−95308
^{A}Ca, A=47, 49, single particle states lifetimes calcs. 80−105943
^{A}Ca+p, A=40, 44, 48, 700 MeV, total reaction cross section meas., matter radii 79−40924
^{A}Ca+p, A=40,44, 1 GeV, neutron production *(Russian)* 79−85477
^{A}Ca(^{12}C,^{12}C), A=40,42,48, 47-51 MeV, ang. distribs. optical model anal., surface transparency 79−45291
^{A}Ca(^{6}Li,^{6}Li′), A=40, 44, 48, 153 MeV, isoscalar giant quadrupole resonances 80−13440
^{A}Ca(^{7}Li,^{7}Li), A=40, 48, 88 MeV, optical potentials, phenomenological and microscopic 80−52687
^{A}Ca(α,X), 10-27 MeV, A=40,44, fusion cross sections, anomalous large angle scatt. 79−80966
^{A}Ca(α,α′), 24,29 MeV, A=40,42,44,48 backward ang. distrib. anomaly, coupled and channel anal. 80−86911
^{A}Ca(α,α′), A=40, 42, 44, 1.37 GeV, low lying state ang. distribs., Glauber rigid body approx. 79−54394
^{A}Ca(α,α), 40-62 MeV, A=40,44, elastic and inelastic, ang. distribs. and collective state excitation 79−6650
^{A}Ca(α,α), A=40, 42, 44, 48, 104 MeV, cross sections and optical pots., nuclear size 80−68524
^{A}Ca(α,α), A=40, 42, 44, 48, 104 MeV nuclear size and density distrib. from folding model anal. 80−68525
^{A}Ca(α,α), A=40, 48, 104 MeV, refined folding model validity 79−509
^{A}Ca(α,α) and (α,α′), (A=40,42,44,48), single pole dominance 77−41985
^{A}Ca(α,p)$^{A+3}$Sc, 25 MeV, population of $f_{7/2}^4$ states 79−59077
^{A}Ca(e,e′), backward scatt., A=40, 42, 44, 48, mag. dipole ground state transition search 80−106009
^{A}Ca(e,e), A=40, 48, (in)elastic scatt., self-consistent calcs. of nuclear density *(Russian)* 79−80928
^{A}Ca(e,e), A=40,42,44,48, elastic and inelastic scatt. cross-sections from Hartree-Fock densities *(Russian)* 79−13287
^{A}Ca(γ,X), A=42, 44, 48, photoneutron and photoproton cross section systematics 80−13463
^{A}Ca(p,p′), pol. p, A=40,48, 800 MeV, diff. cross sections, anal. powers, DWIA anals., high spin levels 80−83067
^{A}Ca(p,p), 0.6, 1 GeV, A=40,42,44,48, matter density, Glauber model anal. 79−93500
^{A}Ca(p,p), 30.3 MeV, A=40,44,48, cross section ratio, optical model anal. 79−54441
^{A}Ca(p,p), 800 MeV, polarised p, A=40, 42, 44, 48, differential cross sections and anal. powers 79−36244
^{A}Ca(p,p), A=40, 48, (in)elastic scatt., self-consistent calcs. of nuclear density *(Russian)* 79−80928
^{A}Ca(p,p), A=40, 48, nucleon distrib. in nuclei, self-consistent anal. 79−9556
^{A}Ca(p,p), A=40,42,44,48, elastic and inelastic scatt. cross-sections from Hartree-Fock densities *(Russian)* 79−13287
^{A}Ca(p,p), A=40,48, polarised p, 0.8 GeV, neutron isotopic density differences and RMS radii 79−67643
^{A}Ca(π,π), A=40,48, 40-241 MeV, first and second order optical pots., resonance behaviour 80−68624
^{A}Ca($\pi^{\pm}$, $\pi^{\pm}$N), A=40, 44, 48, 291 MeV, quasielastic scatt., differential cross sections, Monte-Carlo data fit 80−68703
^{A}Ca($\pi^{\pm}$,X), A=40, 44, 48, 180, 290 MeV, quasielastic scatt., differential cross section 79−85518
^{A}Ca($\pi^{\pm}$,$\pi^{\pm}$), A=40,42,44,48, 180 MeV (in)elastic scatt. differential cross-sections, Pauling blocking 79−85539
^{A}Ca($\pi^{\pm}$,$\pi^{\pm}$), A=40,48, 180 MeV near (3,3) reson., nuclear RMS radii determ. 79−85538
^{A}Ca($\pi^{\pm}$,π^{+}), A=40, 44, 48, 290 MeV, inclusive double charge exchange, differential cross sections 79−93662
^{A}Ca($\pi^{\pm}$,$\pi^{\mp}$), A=40,44,48, 290 MeV, double charge exchange cross sections 80−18348
^{A}Ca= A=40, 48, Hartree-Fock calculations of nuclear bulk properties with density- and starting-energy dependent effective interaction 80−9246
^{14}Ca, A=40,42,44,48, E0 matrix elements determ. from (e,e′) scatt. 78−33141
^{14}Ca(p,p), A=40, 42, 44, 48, 1 GeV, cross sections using nuclear densities from self-consistent methods *(Russian)* 78−41724
^{14}Ca(p,p), A=40-48, elastic scatt. cross section ratio meas. 79−93634
^{38}Ca, J$^{\pi}$ and configuration mixing via ^{40}Ca(p,t)^{38}Ca 51.9 MeV 77−26684
^{38}Ca+^{16}O, 56 MeV, nucleon transfer reactions, effective Q-value model 79−63692
^{39}Ca β-decay Gamow-Teller interaction renormalisation constant from ^{39}K(p,n) 7480-7530 keV 79−6601
^{39}Ca, forbidden transition ang. distribs., CCBA and DWBA anals. of (p,d) 80−86848
^{39}Ca low lying analogue states, DWBA anal. from ^{40}Ca, (d,t), 29 MeV, polarised d 78−82285
^{39}Ca, mag. moment from β-ray spectra of recoil nuclei polarised by fast polarised beams 77−28502
^{39}Ca/^{39}K mirror level pair cross sections from ^{40}Ca($\pi^{\pm}$,πN) 79−67665
^{39}Ca-^{39}K mirror nuclei, configuration mixing, Coulomb energy anomaly 78−25099
^{40}Ca, photonuclear reactions, 2-4.5 GeV, residual nuclei yields *(Russian)* 77−61399
^{40}Ca, ^{1}S$_0$ two-nucleon T matrix, interior wave function 77−14038
^{40}Ca, ^{36}Ar+α model, energy levels, spin and parity 77−57602
^{40}Ca, ^{48}Ca RMS radii, RPA ground state correls., isotope effect 77−6238
^{40}Ca, 0^+ levels populated in ^{36}Ar(^{6}Li,d), DWBA calcs. 78−62571
^{40}Ca, 1^-, T=0 state at 6.95 MeV, isospin forbidden electroexcitation 78−25177
^{40}Ca (α,α′), 104 MeV, giant resonance ang. distribs., L-transfer contribs. 80−27610
^{40}Ca (α,α), α-nucleus pot., microscopic calc. 78−8788
^{40}Ca (p,2p), polarised p, 200 MeV, quasi-elastic scatt., asymmetry meas. 79−67755

nuclei with mass number 39 to 58 continued

^{40}Ca (p,p), elastic scatt., polarisation and spin-orbital amplitude parameters, 1 GeV *(Russian)* 78−17208
^{40}Ca ($\pi^{\pm}$, $\pi^{\pm}$), model Coulomb corrections in eikonal 80−5171
^{40}Ca, adiabatic mass parameters, isoscalar quadrupole modes 77−14049
^{40}Ca, alpha transfer to 4p-4h states obs. in ^{36}Ar(^{6}Li,d) 78−21590
^{40}Ca, anomalously small absorption of α-particles 79−93640
^{40}Ca, α-and p-spectra from giant reson. region via ^{40}Ca(α,2α) and ^{40}Ca(α,αp) 77−30523
^{40}Ca α-spectroscopic factors, direct α-stripping, zero range DWBA anal. of ^{36}Ar(^{6}Li,d) 79−45157
^{40}Ca, branching ratio and electric, monopole strength excited in ^{40}Ca(p,p′) at 7-10 MeV 77−30505
^{40}Ca bulk props., ground state energies and RMS charge radii 78−58242
^{40}Ca, charge density calcs. K_{mm} approx. 79−9456
^{40}Ca charge form factors, pion exchange currents effects 77−18379
^{40}Ca, charge form factors of doubly closed shell nuclei 77−6274
^{40}Ca, closed shell nuclei, convergence studies for the one body mass radius operator 79−45146
^{40}Ca composite system, heavy ion resonances from ^{24}Mg+^{16}O, ^{28}Si+^{13}C 80−86874
^{40}Ca, core polarisation charge for E6 transition, Bohr Mottelson model calc. 79−36194
^{40}Ca, core polarisation J-averaged effects through 3rd order up to 10 $\hbar\omega$ excitations 79−67671
^{40}Ca, coupling of 4p and 4h modes 78−93926
^{40}Ca, deep-inelastic electron scatt. in the transverse region, 150, 200, 250 MeV 79−17895
^{40}Ca, dipole polarisability sum rule. HF calc., 78−21504
^{40}Ca, direct reactions, orbital rearrangement and energy sum rules 77−79353
^{40}Ca, effective convection current in shell model 79−63606
^{40}Ca, electric quadrupole strength, giant quadrupole resonance 80−52575
^{40}Ca, energy levels, using ^{40}Ca(p,π^{+}) 163 to 186 MeV 79−59061
^{40}Ca, exchange current corrections for muon partial capture rates 78−33152
^{40}Ca, excitation of low lying collective states by (n,n′) scatt. 78−17205
^{40}Ca, finite nuclear props. in relativistic quantum field theory, mass and p densities 80−9219
^{40}Ca, GQR, J^{π}, via (^{3}He,^{3}Heα) and (^{3}He,^{3}He′p) 70 MeV ang. distribs. 77−50097
^{40}Ca, giant dipole resonance region radiative nucleon capture, expt. ang. distrib. coeffs., direct-semidirect theory 78−74354
^{40}Ca, giant monopole resonance widths, RPA calcs. based on Skyrme interaction 78−93984
^{40}Ca giant resonances prod. from ^{40}Ca(^{3}He,^{3}He′)^{40}Ca*→^{36}Ar+^{4}He 79−93479
^{40}Ca, high spin cluster like resonances obs. in ^{24}Mg+^{16}O 79−6664
^{40}Ca, high-spin members of 4p-4h triaxial band 77−74742
^{40}Ca ions recoiling in vacuum, decoupling of hyperfine interactions 77−22931
^{40}Ca, isoscalar giant resonances and Landau parameters with density-dependent effective interactions 79−71827
^{40}Ca, lowest T=2 state isospin forbidden decays, branching ratios 79−67703
^{40}Ca, mag. moment of 3^{-} level meas. 77−10314
^{40}Ca, magic nuclei at collective excitations, energy spectrum and shape *(Russian)* 80−106015
^{40}Ca, magic nucleus, nonlocal pots., binding energies 77−41877
^{40}Ca, monopole vibration damping, TDHF calcs. 80−22667
^{40}Ca, neutron ang. distrib. following polarized muon capture, relativistic corrections 78−13063
^{40}Ca neutron induced reactions, Hauser-Feshbach code for cross sections 77−23045
^{40}Ca, nucl. effects in radiative muon capture 78−29428
^{40}Ca, nucl. mag. momen', hyperfine interaction of electron in L, M and N regimes 78−70448
^{40}Ca, nucleon-nucleon scatt., correlations, short-range, with pseudopotentials 78−37225
^{40}Ca, photo-nucleon spectra calc. in shell and pre-equilibrium model *(Russian)* 78−579
^{40}Ca photonuclear reactions, differential cross section calcs., direct-semidirect model 78−33166
^{40}Ca, pion exchange currents and nuclear charge form factors 77−10338
^{40}Ca, pion-exchange contribs. to charge densities, HF calcs. 78−46001
^{40}Ca, pionic, Lorentz-Lorenz quadrupote term, P-wave optical pot. 79−22252
^{40}Ca, polarised muon capture, direct neutron emission 77−38252
^{40}Ca, p$\pi\alpha$ penetration range, 200 MeV to 2 GeV *(French)* 78−4964
^{40}Ca, π^{-} capture, p, d and α inclusive prod. spectra 79−22338
^{40}Ca, radius difference to ^{48}Ca, from 104 MeV alpha scatt. optical model calcs. 79−454
^{40}Ca region, E2 core-polarisation charge 77−22888
^{40}Ca, relativistic Hartree-Fock eqns., 1 boson exchange pot., spin orbit splitting 79−3106
^{40}Ca, residual interactions, current conserving RPA calculations 80−57710
^{40}Ca resonance strengths from ^{39}K(p,γ) 80−22786
^{40}Ca root mean square radius series 79−36146
^{40}Ca, self consistent K-matrix model calc. 77−6257
^{40}Ca, self-consistent generator coord. for giant monopole reson. 77−2891
^{40}Ca, single determinantal states, HF and energy variance minimisation methods 77−6204
^{40}Ca, spherical nuclei, total binding energy, many body field theory 77−30482
^{40}Ca structure, supersoft-core pot., HF approx., ground state props. 78−533
^{40}Ca, two-parameter nucleon density distrib., form factors calc. 77−65193
^{40}Ca, vibrating nucleus, adiabatic anal. of time-dependent HF solns. 79−40863
^{40}Ca, weak s resonance γ-ray decay in negative parity low lying levels 80−27591
$^{40}Ca_{\Lambda}$, Λ particle full set of nuclear shell orbitals 79−63623
^{40}Ca+^{13}C, 68 MeV, inelastic scatt., anomalous L=1 ang. distrib. anal. 77−65236
^{40}Ca+^{14}N, 161 MeV, giant resonances in inelastic scatt. 78−62564
^{40}Ca+^{14}N fusion-evaporation reaction γ-ray spectroscopy study of ^{51}Mn structure 77−18471
^{40}Ca+^{16}O, 3-D TDHF calcs. 78−54781

nuclei with mass number 39 to 58 continued

^{40}Ca+^{16}O, 45-63 MeV, excitation function determ. 78−82404
^{40}Ca+^{16}O, ang. correl. in compound nucleus decay 79−36261
^{40}Ca+^{16}O, inelastic scatt., exit channel distorting pot., DWBA calc. 78−94025
^{40}Ca+^{16}O, polarisation of single particle states, two centre shell model 77−30622
^{40}Ca+^{16}O, reaction and fusion cross section calc. in boundary condition model 79−9656
^{40}Ca+^{16}O, single-particle polarisation, two-centre shell model 78−13142
^{40}Ca+^{16}O fusion-evaporation reaction, γ-ray spectroscopy study of ^{51}Mn structure 77−18471
^{40}Ca+^{20}Ne, 36-95 MeV, Coulomb-nuclear interference 78−50210
^{40}Ca+^{3}He inelastic scatt., isoscalar multipole reson. 78−66190
^{40}Ca+^{40}Ca, 2- and 3-dimens. time depend. HF calc. comparison 79−17948
^{40}Ca+^{40}Ca, 278 MeV, comparison of 2-D and 3-D TDHF 78−82386
^{40}Ca+^{40}Ca, 278 MeV, particle transfer width, 3 dimens. TDHF calcs. 78−74389
^{40}Ca+^{40}Ca, 284 MeV, energy spectra struct. obs. 78−4958
^{40}Ca+^{40}Ca, 3-D TDHF calcs. 78−54781
^{40}Ca+^{40}Ca, 3-dimens., time depend. HF calcs. for fusion cross sections 78−66318
^{40}Ca+^{40}Ca, 3D TDHF calcs. 78−626
^{40}Ca+^{40}Ca, collective modes excitation 79−54448
^{40}Ca+^{40}Ca, elastic scatt. excitation functions, interf. effects 77−50155
^{40}Ca+^{40}Ca, evaporation-residue cross-sections meas. 78−33211
^{40}Ca+^{40}Ca, low impact parameters, energy dependence of fusion cross section 78−41751
^{40}Ca+^{40}Ca, self-consistent heavy-ion potentials 77−6434
^{40}Ca+^{40}Ca, total fusion cross section, time depend. HF calcs. 79−17945
^{40}Ca+^{40}Ca strongly damped reaction, time scale 77−54244
^{40}Ca+^{6}Li, parabolic repulsion potential, optical model 80−22782
^{40}Ca+P, 100-1050 MeV, optical pot. real part, nuclear matter approach 77−82890
^{40}Ca+α, core-like pot., resonating group anal. 78−4922
^{40}Ca+n, 14.1 MeV neutrons, estimated dose to bone and whole body 79−53256
^{40}Ca+n(p), resonating-group anal. 77−6373
^{40}Ca+p, energy dependent radial functions formalism of continuum shell model 78−25185
^{40}Ca+p, fine struct. levels sign meas., off-diagonal strength function, analogue state broadening theory test 78−78381
^{40}Ca+p, optical model potential, spin-orbit component from internucleon pot. 78−46039
^{40}Ca+p(d)(α) transparency in composite particle-nucleus reactions 80−9273
^{40}Ca+$\pi^{\pm}$, multinucleon removal, prompt de-excitation γ-spectra obs. 79−6708
^{40}Ca($^{\wedge}$B,$^{\wedge}$B), A=10,11, angular distrib., Woods-Saxon and double-folding optical models 80−52691
^{40}Ca(^{11}B,^{10}B), 51.5 MeV, n stripping, DWBA anal. with Woods-Saxon and double folding optical pots. 80−102171
^{40}Ca(^{11}B,^{12}C), 32, 68 MeV, single proton pickup, DWBA anal., optical pot. 80−106037
^{40}Ca(^{11}B,^{12}C), 51.5 MeV, p pickup, DWBA anal. with Woods-Saxon and double folding optical pots. 80−102171
^{40}Ca(^{12}C,^{12}C), 135-150 MeV, elastic excitation function at 180°, resonance like struct. 79−9609
^{40}Ca(^{12}C,^{12}C), 20 to 35 MeV, resonant heavy ion scatt., from s-d shell nuclei 79−67763
^{40}Ca(^{12}C,^{12}C), 20-35 MeV, resonant scatt., ang. distribs., cross sections and excitation functions 79−45237
^{40}Ca(^{12}C,^{12}C), 80-178 MeV, backward angle excitation functions 79−36267
^{40}Ca(^{12}C,^{8}Be)^{44}Ti, 45 MeV, semiclassical analysis of α-transfer reactions, partial wave amplitudes 79−45283
^{40}Ca(^{12}C,3p)^{49}V, ^{49}V $1f_{7/2}$ shell model and high spin states 78−62560
^{40}Ca(^{13}C, ^{14}N)^{39}K and ^{40}Ca (^{13}C, ^{12}C)^{41}Ca, 60, 68 MeV, spin depend. effects 78−66300
^{40}Ca(^{13}C,^{13}C′), 108 MeV, nuclear continuum investigation 80−13506
^{40}Ca(^{13}C,^{14}N), 40, 68 MeV, single proton pickup, DWBA anal., optical pot. 80−106037
^{40}Ca(^{13}C, ^{14}N)^{39}K, sensitivity to ^{39}K+p form factor, DWBA anal. 77−34345
^{40}Ca(^{13}C,^{14}N)^{39}K, helicity flip obs. 77−74872
^{40}Ca(^{13}C, ^{14}N)^{39}K, molecular orbital interpretation of $\Delta l=1\hbar$ transfer anomaly 77−82952
^{40}Ca(^{13}C,^{14}N)^{39}K($3/2^{+}$), CCBA fit to anomalous ang. distrib. 77−38297
^{40}Ca(^{13}C,^{9}Be), 149 MeV, α-transfer cross sections, direct reaction theory anal. 79−67767
^{40}Ca(^{14}N,^{10}B), 153 MeV, α-transfer cross sections, direct reaction theory anal. 79−67767
^{40}Ca(^{14}N,2pn)^{51}Mn, ^{51}Mn $1f_{7/2}$ shell model and high spin states 78−62560
^{40}Ca(^{16}O, ^{16}O′), 60 MeV, direct reaction calcs., ang. distribs. 78−58298
^{40}Ca(^{16}O, p)^{55}Co, 39 to 89 MeV reaction cross section 80−47496
^{40}Ca(^{16}O,^{15}N)^{41}Sc, effect of polarisation of shell-model states 77−67768
^{40}Ca(^{16}O,^{15}N)^{41}Sc, DWBA anal. including nuclear wave function polarisation 78−629
^{40}Ca(^{16}O,^{16}O), 60 MeV, long range absorption and optical model effects from strong inelastic coupling 80−535
^{40}Ca(^{16}O,^{16}O), 80-178 MeV, backward angle excitation functions 79−36267
^{40}Ca(^{16}O,^{16}O), complex heavy ion optical pot., microscopic BHF derivation 80−106067
^{40}Ca(^{16}O,^{16}O), optical pot., nuclear matter approach, energy density matter [-] 80−83112
^{40}Ca(^{16}O,^{16}O), rot. band of molecular resonances, generator coordinate model 80−13428
^{40}Ca(^{16}O,X), 40-214 MeV, fusion and elastic scatt. cross sections, optical anal. 80−32314
^{40}Ca(^{16}O,X), ion-ion interaction pot., imaginary part, effective interaction 80−68692
^{40}Ca(^{17}O, ^{17}O), 61 MeV, elastic and inelastic, microscopic single folding model anal. 80−52692
^{40}Ca(^{20}Ne,^{16}O), 262 MeV, α-transfer cross sections, direct reaction theory anal. 79−67767
^{40}Ca(^{20}Ne,X), 44.1-70.4 MeV, fusion and elastic scatt. cross sections, evaporation residues 80−550

nuclei with mass number 39 to 58 continued

^{40}Ca(^{1}He, x), pol. ^{3}He, x=d or α, 33 MeV, anal. power and cross sections 80−42628

^{40}Ca(^{3}He,^{3}He′)^{40}Ca*→^{36}Ar+^{4}He, spin, parity assignments for ^{40}Ca giant resonances 79−93479

^{40}Ca(^{3}He,^{3}He′α)^{36}Ar, 70 MeV, GQR J$^{\pi}$ 77−50097

^{40}Ca(^{3}He,^{3}He′p)^{39}K 70 MeV, GQR J$^{\pi}$ 77−50097

^{40}Ca(^{3}He,^{3}He), 27-84 MeV, energy depend. of optical model param. 78−41736

^{40}Ca(^{3}He,^{3}He), 90-120 MeV, cross sections, deduced unambiguous optical pot. 79−13311

^{40}Ca(^{3}He,^{3}He), optical potentials and volume integrals, mass and energy dep. 80−52686

^{40}Ca(^{3}He,^{3}He), pol. ^{3}He, 33.3 MeV, differential cross section and anal. power, optical pots. 80−42627

^{40}Ca(^{40}Ar,^{40}Ar), 191, 236, 272 MeV, cross sections, interaction radius, Fresnel and optical model anal. 79−59084

^{40}Ca(^{40}Ar,^{40}Ar), 191, 236, 272 MeV, elastic cross sections, optical and Fresnel model anals. 80−22858

^{40}Ca(^{40}Ar,X), 191, 263, 272 MeV, strongly damped collision cross sections, product energies 80−32291

^{40}Ca(^{40}Ca, ^{40}Ca), generator coordinate study, rot. band of molecular resonances 79−75948

^{40}Ca(^{40}Ca, X), 10 MeV/N, charged particle emission Q-valve depend. 80−47503

^{40}Ca(^{40}Ca,^{40}Ca), 58-130 MeV, elastic scatt., ang. distribs., excitation function, optical model anal. 77−30623

^{40}Ca(^{40}Ca,^{40}Ca), 64-120 MeV, optical model and strong absorpt. model anal. 77−41994

^{40}Ca(^{40}Ca,^{40}Ca), optical pot., nuclear matter approach, energy density matter [-] 80−83112

^{40}Ca(^{40}Ca,X), 400 MeV, fragment energy spectra struct., giant resonances, direct process 80−47452

^{40}Ca(^{40}Ca,X), deep inelastic, doubly differential cross section, spectra struct. 80−5103

^{40}Ca(^{40}Ca,x), relativistic, compression and pion distrib., Monte Carlo calc. 80−73853

^{40}Ca(^{40}Ca,x) reactions, time dependent HF calcs. 77−54251

^{40}Ca(^{6}Li,^{6}Li), 156 MeV, refined folding model validity 79−509

^{40}Ca(^{6}Li,^{6}Li), 156 MeV, density depend. of N-N interaction 79−6660

^{40}Ca(^{6}Li,^{6}Li), 30 MeV, back-angle anomalies 78−640

^{40}Ca(^{6}Li,^{6}Li)^{40}Ca, 30 MeV, ang. distribs. for elastic and inelastic scatt. at backward angles 79−13343

^{40}Ca(^{6}Li,d)^{44}Ti, higher-order process, coupled channels calcs. 78−82327

^{40}Ca(^{7}Li,^{7}Be)^{40}K, charge exchange microscopic DWBA anal. 79−26453

^{40}Ca(^{9}Be, ^{9}Be′), 45, 60 MeV, low lying collective states, ang. distribs., DWBA double folding pot. anal. 80−78113

^{40}Ca(^{9}Be, ^{9}Be), 45, 60 MeV cross sections, ang. distribs., Wegner plot, optical and double folding anal. 80−47497

^{40}Ca(^{9}Be,^{8}Be), DWBA anal., spectroscopic factor determ. 78−17098

^{40}Ca(^{9}Be,^{9}Be′), 45, 60 MeV, 1^{-} state excitation Frahn scaling formula for cross section 80−102136

^{40}Ca(^{9}Be,^{9}Be), 14-26 MeV, universal optical pot. 78−25219

^{40}Ca(^{9}Be,^{9}Be), 20 to 35 MeV, resonant heavy ion scatt., from s-d shell nuclei 79−67763

^{40}Ca(K^{-}, π^{-}) $^{40}_{\Lambda}$Ca, possible strange giant reson. 77−82969

^{40}Ca(K^{-},π^{-}), 900 MeV/c, sum rule for hypernuclear formation, distorted wave impulse approx. 78−70572

^{40}Ca(K^{+},Kp^{+}), DWIA calc. of proton knockout as probe of deep hole states 78−13163

^{40}Ca($K^{\pm}$,$K^{\pm}$), Glauber model anal. 80−42697

^{40}Ca(N,N), microscopic description validity 79−544

^{40}Ca(α, α), (^{6}Li, ^{6}Li), velocity of refined folding model approaches 80−541

^{40}Ca(α, α), generator coordinate method for arbitrary cluster widths 77−18581

^{40}Ca(α,^{12}C), 90.3 MeV, cross sections and systematics multi-α-cluster transfer implications 80−42675

^{40}Ca(α,^{12}C), 90.3 MeV, multi-α-cluster transfer and direct pickup cross sections 80−57760

^{40}Ca(α,^{2}He), 55, 65 MeV, two neutron states, A-depend. of binding energy 78−74379

^{40}Ca(α,^{6}Li), 46 MeV, finite range DWBA anal. 77−14142

^{40}Ca(α,2α), 115 MeV, GQR decay spectra 77−30523

^{40}Ca(α,2α), 90 MeV, strong absorption diffraction model, spectroscopic factors 79−22306

^{40}Ca(α,α'), 65 MeV, ^{4}He deduced monopole excitation to O^{+} state DWBA anal. 79−22226

^{40}Ca(α,α')^{40}Ca, medium energy, DWBA calc. 77−6380

^{40}Ca(α,α), 104 MeV, optical model analysis 78−41737

^{40}Ca(α,α), 1.37 GeV, S-matrix expansion from Glauber multiple scatt. theory 80−91191

^{40}Ca(α,α), 20-50 MeV anomalous elast. and inelast. scatt. optical model anal. 77−88161

^{40}Ca(α,α), 26 to 47 MeV, large angle scatt., differential cross section 78−46082

^{40}Ca(α,α), 27-9 MeV, anomalous large-angle scatt. 77−18583

^{40}Ca(α,α), 29 MeV, optical pot., double folding model for anomalous large angle scatt. 78−70551

^{40}Ca(α,α), 36-61 MeV, large angle struct. 78−41743

^{40}Ca(α,α), 6-18 MeV, resonances, anomalous large angle scatt. and quasi-molecular states 80−27613

^{40}Ca(α,α), back-angle anomaly, RGM and GCM 78−616

^{40}Ca(α,α), backward angle anomaly, resonating group method macroscopic study 78−74382

^{40}Ca(α,α), E_{α}=27.2 MeV, ang. distrib. meas. 78−13120

^{40}Ca(α,α), entrance channel resonances, backward angle scatt., elastic scatt. enhancement 80−27612

^{40}Ca(α,α), giant isoscalar quadrupole resonance, α-over p-decay ratio, SU(3) and shell model 80−27608

^{40}Ca(α,α), optical pot., nuclear glory effect 78−21578

^{40}Ca(α,α) 140 MeV, modified optical pot., folding pots. and energy depend. 78−70549

^{40}Ca(α,α)^{40}Ca, 166 MeV, matter density determ. from model-independ. anal. 77−38285

^{40}Ca(α,α)^{40}Ca, semiclassical anal., backward glory 79−71866

^{40}Ca(α,αp), 115 MeV, GQR decay spectra 77−30523

^{40}Ca(α,αp), 96.8 MeV proton pickup by α-particles to unbound states DWBA anal. 79−22305

^{40}Ca(α,d)^{42}Sc, 40 MeV ang. distribs. meas., Sc levels anal. 78−21579

nuclei with mass number 39 to 58 continued

^{40}Ca(α,γ)^{44}Ti, 2.75-4.00 MeV, γ-ray ang. distrib. of reson. for spin parity values 77−65230

^{40}Ca(α,γ)^{44}Ti, lifetimes and spins of ^{44}Ti levels meas. 77−79328

^{40}Ca($\alpha\alpha$), <85.6 MeV, energy depend. of optical model params. 77 3024

^{40}Ca(d, d′), 108 MeV, giant monopole resonance excitation and ang. distribs. 80−102164

^{40}Ca(d,^{6}Li), 80 MeV, DWBA calcs. spectroscopic factors 79−6623

^{40}Ca(d,^{6}Li), 80 MeV, resonance-like phenomena 79−13308

^{40}Ca(d,α), ang. momentum transfers, determ. using polarized beams 78−37354

^{40}Ca(d,α)^{38}K, 7.5, 7.75, 8.0 MeV, polarised d, J$^{\pi}$ assignment 77−6401

^{40}Ca(d,d), 4.5-5.4 MeV, excited states, excitation functions and ang. distribs., statistical anal. 80−57686

^{40}Ca(d,d), energy depend. of vector analyzing capacity, 1.8 to 3.0 MeV, 120 to 150° scatt. 79−9592

^{40}Ca(d,np), n-p rescattering and d break-up in FSI 77−10417

^{40}Ca(d,p), 7 MeV, cross-sections calcs. from pseudopotentials, spectroscopic factors 78−572

^{40}Ca(d,p)^{41}Ca(J^{+}) 11.0 MeV, analysing powers, CCBA and DWBA anal. 77−6402

^{40}Ca(e,e′), microscopic model of isovector multipole giant resonances *(Russian)* 78−54747

^{40}Ca(e,e′), quasi-elastic scatt., scaling law test, knockout process contribution 79−22274

^{40}Ca(e,e′), strong mag. dipole transition, coherent spin flip transitions, ground state correlations 79−71817

^{40}Ca(e,e′p) 77−10389

^{40}Ca(e,e), 25 MeV, nucleon density distribution in nucleus 79−75831

^{40}Ca(e,e), 757.5 MeV, cross-sections meas. 78−8801

^{40}Ca(e,e), charge form factors in α cluster model 79−63571

^{40}Ca(e,e), cross sections, model independ. charge density 80−27548

^{40}Ca(e,e), elastic scatt., spectroscopic information and form factors 80−9260

^{40}Ca(e,e), high energy differential cross sections, nucleon density distrib. 78−54738

^{40}Ca(γ,γ), 6.95, 7.12 MeV, strengths of isospin forbidden E1 transitions 78−13059

^{40}Ca(γ,p), 100-750 MeV, yields and cross sections 77−41948

^{40}Ca(μ,γ), photon asymmetry, O(1/m^{2}) and nuclear effects 80−78219

^{40}Ca(μ,$\nu\nu_{\mu}$)$_{0}$ neutron longitudinal polarisation anal. 77−30559

^{40}Ca(μ,$\nu\nu$)^{39}K, neutron spectra calc. in simple-pole model 77−71606

^{40}Ca(μ,$\nu\gamma$), ^{40}K,*, 85 MeV/c, radiative capture branching ratio, photon asymm. 77−79365

^{40}Ca(n,X), local approximation to a non-local potential 80−91182

^{40}Ca(n,α)^{37}Ar, body Ca reaction due to fast neutrons, fate of ^{37}Ar 77−5075

^{40}Ca(n,α)^{37}Ar in fission reactor material Ca impurity, ^{37}Ar form. 77−83048

^{40}Ca(n,γ_{0})^{41}Ca, 6 to 13 MeV quadrupole radiation, direct-semidirect model calcs. 79−545

^{40}Ca(n,γ_{0})^{41}Ca, 8,12 MeV γ-ray ang. distrib. 78−66279

^{40}Ca(n,γ), 8-12 MeV, fast neutron gamma ray detection system 77−26925

^{40}Ca(n,γ), direct-semidirect and compound nucleus contribs. to cross sections 80−68662

^{40}Ca(n,γ), mechanism in 3s size resonance, radiative width statistical and valence effects 80−37388

^{40}Ca(n,γ)^{41}Ca, up to 15 MeV, higher-order processes, coupled channel treatment 77−61431

^{40}Ca(n,n′)^{40}Ca, imaginary inelastic transition form factor, microscopic theory 78−50175

^{40}Ca(n,n), 10 and 50 MeV, optical model real potential 78−58274

^{40}Ca(n,n), 11-26 MeV, differential cross sections, global optical model anal. 80−18298

^{40}Ca(n,n), 2-3 MeV neutrons, cross section meas. using associated particle TOF spectrometer 79−45255

^{40}Ca(n,n), optical-model real pot., nuclear matter compressibility, effect 77−74823

^{40}Ca(n,n) 2-3 MeV neutrons studied using assoc. particle TOF spectrometer 80−13468

^{40}Ca(n,t)^{38}K, 14.6 MeV neutrons, activation cross section meas. 79−45254

^{40}Ca(p, 2p)^{39}K, 148.2 MeV, factorisation approx., energy states of ^{39}K, DWIA calcs. 78−62535

^{40}Ca(p, p′), isovector dipole strength excitation in giant resonance region 80−83066

^{40}Ca(p, π^{+})^{41}Ca, 140 to 200 MeV, π^{+} ang. distrib., energy depend. 79−63667

^{40}Ca(p,^{17}Ne^{22}Na^{28}Al), 40-85 MeV, ^{24}Na yields in 'fission-like' reactions 78−598

^{40}Ca(p,X), multiple scattering theory, validity of closure approx. 79−45269

^{40}Ca(p,2p+n)^{38}K, partial-body Ca determ. in body by proton activation anal. 77−86605

^{40}Ca(p,2p), 200 MeV, cross section and asymmetry meas. 79−6583

^{40}Ca(p,2p) 200 MeV polarised p, spin-orbit effects 79−89222

^{40}Ca(p,2p)^{39}K, distorted wave impulse approx. anal. review 78−62541

^{40}Ca(p,2pn)^{38}K, prod. of uniform ^{38}K yield using range modulator 77−40735

^{40}Ca(p,2pn)^{38}K, total cross section, 20-160 MeV 78−86536

^{40}Ca(p,α), polarised p, 22.0 MeV, analysing power J dependence 79−67740

^{40}Ca(p,nπ^{+}), ≃500 MeV, NNπ vertex function 79−59066

^{40}Ca(p,p′), 25-46 MeV, effects of two-step process determ. 78−21569

^{40}Ca(p,p′), 800 MeV, high energy octupole giant resonance, ang. distribs. 80−86879

^{40}Ca(p,p′), giant resonances from antisymmetrised DWBA anal. 79−85432

^{40}Ca(p,p′), realistic complex nuclear matter t-matrix anal. Hamada-Johnston pot. 79−9564

^{40}Ca(p,p′)^{40}Ca, 185 MeV, scatt. from 3^{-} and 5^{-} states, DWIA anal. 77−18537

^{40}Ca(p,p′γ), 6.25 MeV, triple ang. correlation, 3^{-} exit channel, resonances, single particle states 80−68626

^{40}Ca(p,p), 1 GeV, Glauber approx. corrections, differential cross sections 78−50166

^{40}Ca(p,p), 1.04 GeV elastic scatt., polarisation 78−21549

^{40}Ca(p,p), 20-50 MeV differential cross section, polarisation ang. distrib., optical model exchange terms 80−27638

nuclei with mass number 39 to 58 continued
^{40}Ca(p,p), 30 MeV, optical pot. imaginary part calcs. 80−86868
^{40}Ca(p,p), 30.3 MeV, microscopic anal. 79−93631
^{40}Ca(p,p), absorbing optical pot., Coulomb correction term 80−73831
^{40}Ca(p,p), E_p=1 GeV, elastic differential cross sections 78−13082
^{40}Ca(p,p), elastic and inelastic scatt., 185 MeV, polarisation, diffraction model anal. 79−75943
^{40}Ca(p,p), elastic scatt. at medium energies, microscopic optical pots. 79−97703
^{40}Ca(p,p), high energy differential cross sections, nucleon density distrib. 78−54738
^{40}Ca(p,p), imaginary spin-orbit term in proton optical potential, ang. distribs. 78−58273
^{40}Ca(p,p), optical potential from realistic Hamada-Johnston internucleon pot., binding energy 78−54730
^{40}Ca(p,p)^{40}Ca, 1.04 GeV, nuclear matter density calc. 77−34303
^{40}Ca(p,pα), 157 MeV, quasifree scatt., α spectroscopic factors, SU(3) predictions 77−6370
^{40}Ca(p,pα), 600 MeV, α-cluster quasielastic knockout, expt. methods, separation energy spectra 79−13275
^{40}Ca(p,pα)^{36}Ar, 157 MeV, energy spectra, SU(3) model comparison 77−88121
^{40}Ca(p,π^+), 163 to 186 MeV, expt. and theoretical study of π^+ prod. 79−59061
^{40}Ca(p,π^+), differential cross sections, DWBA calc. 79−85415
^{40}Ca(p,π^+), near threshold, reaction energy dependence 79−85461
^{40}Ca(p,π^+)^{41}Ca, relativistic pion stripping formalism 78−41717
^{40}Ca(p,t)^{38}Ca 51.9 MeV and configuration mixing 77−26684
^{40}Ca(p,p′), DWIA test in Glauber theory, transition density 80−99173
^{40}Ca(π,πN) at (3,3) reson., WKD approx. validity 77−18615
^{40}Ca(π,π), nuclear matter distribs., density depend. HF anal. 79−487
^{40}Ca(π,π), pionic resonance fluorescence in Δ(33) region 79−85554
^{40}Ca(π,π)^{40}Ca, 50 MeV, optical potential with kinematic, absorption and correl. corrections 77−50157
^{40}Ca(π^-, 2n), absorpt. at rest, ^{38}K excitation spectrum and distrib. 78−66322
^{40}Ca(π^+,$\pi^{+\prime}$), 241 and 163 MeV, giant resonance studies 79−85512
^{40}Ca(π^+,$\pi^{+\prime}$), 50 MeV, energy spectra and cross sections 78−25241
^{40}Ca(π^+,π^+), 40 MeV, differential cross sections and strength parameters, optical model fit 80−18347
^{40}Ca($\pi^\pm$,$\pi^\pm$), 115, 240 MeV, cross sections, Coulomb effects 78−62579
^{40}Ca($\pi^\pm$,$\pi^\pm$), 65 MeV, ang. distrib. 79−85536
^{40}Ca($\pi^\pm$,$\pi^\pm$), 65-215 MeV forward scatt. amplitudes 79−85533
^{40}Ca($\pi^\pm$,$\pi^\pm$), elastic and inelastic scatt., energy and A-depend. 78−54802
^{40}Ca($\pi^\pm$,$\pi^\pm$), resonance region, first order optical pot. calcs. 79−40957
^{40}Ca(t,p), centre of mass corrections to DWBA overlap factors 80−18319
^{40}Ca(t,p)^{42}Ca, form factors for two-nucleon stripping process wth Skyrme potentials, DWBA 78−58287
^{40}Ca(t,p)^{42}Ca, two-nucleon stripping process with effective interactions 78−610
^{41}Ca $1f_{7/2}$ neutron radial distrib., single particle, orbits, RMS radii from ^{40}Ca(^{13}C,^{12}C) 80−42532
^{41}Ca, DWBA anal. of ^{9}Be elastic scatt. on various nuclei *(German)* 78−70552
^{41}Ca damped reaction fragment, energy spectra struct., evaporation processes from ^{40}Ca(^{40}Ca,X) 79−93591
^{41}Ca, deorientation of highly stripped ions recoiling in vacuo 78−37325
^{41}Ca, E2 core polarisation charge, Woods-Saxon shell model compared to harmonic oscillator model 80−63072
^{41}Ca E2 resonance, cross sections and γ-spectrum from ^{40}Ca(n,γ) 80−57759
^{41}Ca excited states, excitation functions and ang. distribs., statistical anal. from ^{40}Ca(d,p) 80−57686
^{41}Ca, giant dipole resonance determ. in ^{40}Ca(p,γ) 79−93620
^{41}Ca giant dipole resonance, isospin struct., direct-semidirect anal. from ^{40}K(p,γ) 80−47449
^{41}Ca, high-spin positive parity states anal. with ^{38}Ar(α,nγ)^{41}Ca 77−38224
^{41}Ca, highly stripped ions, recoiling in vacuo, γ-decays of isomeric states obs. 78−50119
^{41}Ca, lifetimes of excited $3/2^-$ states from ^{2}H(^{40}Ca, p) 60 MeV 78−70487
^{41}Ca, mean square nuclear charge radius, correl. with doubly magic ^{40}Ca 79−54385
^{41}Ca, muonic, energy shifts during atomic EM cascade, and polarisability of deformed nuclei 80−86893
^{41}Ca parity doublet gamma lifetimes, 3/2 levels, parity mixing from ^{40}Ca(d,pγ) 80−78209
^{41}Ca, positive parity levels via ^{40}Ca(d,p)^{41}Ca with polarised deuterons 77−6402
^{41}Ca, possible use for radioactive dating 79−21063
^{41}Ca, spin and parity from ^{38}Ar(α,nγ) angular distrib. and linear polarisation of γ 80−63079
^{41}Ca, transverse decoupling of hyperfine interactions in free atoms 77−18468
^{41}Ca, two particle-one hole states, EM transition probabilities 77−88035
^{41}Ca yrast states from ^{26}Mg(^{18}O, 3nγ), γ meas., spin, parity, branching and mixing 78−58250
^{41}Ca(d,p)^{42}Ca, 11 MeV, cross section, vector analysing power, spectroscopic strengths 78−74374
^{41}Ca(d,p)^{42}Ca, two-body matrix elements in fp shell 78−21574
^{42}Ca, ^{46}Ca, B(E2) transition probabilities, effective charge concept 77−18477
^{42}Ca 0^+ 4p-2h and 6p-4h configs. populated in ^{38}Ar(^{6}Li,d) 78−25220
^{42}Ca, collective states, quasi-degenerate intrinsic Hamiltonian, variational methods 80−68505
^{42}Ca, extended Skyrme force versus realistic interactions, effective interactions 79−54395
^{42}Ca from ^{41}Ca(d,p), 11 MeV, cross section, vector analysing power, spectroscopic strengths 78−74374
^{42}Ca high spin state density, γ-decay mode, deformed states from ^{39}K(α,pγ) 80−32168
^{42}Ca, high spin states from ^{39}K(α,p), lifetimes, multipole mixing ratios 78−50186
^{42}Ca high spin states from ^{28}Si(^{16}O,2pγ), γ meas. 78−89787
^{42}Ca one-nucleon transfer reactions form factors, Pauli principle *(Russian)* 77−6393
^{42}Ca, state calc. by shell model including $1g_{9/2}$ orbit 79−80873

nuclei with mass number 39 to 58 continued
^{42}Ca, two-nucleon transfer, ang. momentum and binding energy effects 79−59021
^{42}Ca, wavefunctions of O^+ states 78−74308
^{42}Ca(^{3}He,t), precise Q-value, ^{42}Sc β decay energy, half life 77−30618
^{42}Ca(α,α′), mirror state EM decay rates, multipole matrix element isospin decomposition 79−36190
^{42}Ca(α,n)^{45}Ti, 5.41-10.95 MeV, cross sections 79−85470
^{42}Ca(α,n)^{45}Ti, integral rot., hyperfine field and g-factor of Ti $3/2^+$ state 77−50052
^{42}Ca(α,n)^{45}Ti, reaction rates in stars 80−82183
^{42}Ca(n,p)^{42}K, 14.7 MeV neutron cross sections 78−70520
^{42}Ca(p,γ), 0.7-5.5 MeV, cross section and stellar nucleosynthesis reaction rates 79−13294
^{42}Ca(p,γ)^{43}Sc, 0.66-5.39 MeV, cross sections 79−85470
^{42}Ca(p,γ)^{43}Sc, reaction rates in stars 80−82183
^{42}Ca(p,p), 1.2 to 3.0 MeV, cross-section meas., ^{43}Sc struct. 77−6374
^{42}Ca(p,p), E_p=1 GeV, elastic differential cross sections 78−13082
^{42}Ca(p,t) form factor, hole and continuum contribs. for pick-up reactions 80−78256
^{43}Ca, four-particle one-hole states anal. by ^{41}K(α,d) 78−21580
^{43}Ca γ-ray spectroscopy, levels and decay scheme deform. 79−80896
^{43}Ca high spin positive parity states, struct., from ^{40}Ar(α,nγ) 78−46025
^{43}Ca, nucl. quadrupole moment, HFS in at. beam mag. reson. 79−63940
^{43}Ca(n,p)^{43}K, 14.7 MeV neutron cross sections 78−70520
^{44}Ca 3.59 MeV 0^+ state config. from ^{48}Ti(d,^{6}Li) 79−9472
^{44}Ca, γ-ray spectra from ^{43}Ca(n,γ) 77−38278
^{44}Ca, mode-mode coupling model for four-body correl. 77−10322
^{44}Ca(^{6}Li,^{6}Li), 30 MeV, back-angle anomalies 78−640
^{44}Ca(^{6}Li,^{6}Li)^{44}Ca, 30 MeV, ang. distribs. for elastic and inelastic scatt. at backward angles 79−13343
^{44}Ca(^{7}Li, ^{7}Li), 34 MeV, ang. distribs., cross sections, double folding model anal. 80−78313
^{44}Ca(^{7}Li,3np)^{47}Ti, ^{47}Ti $1f_{7/2}$ shell model and high spin states 78−62560
^{44}Ca(α,α), 36-61 MeV, large angle struct. 78−41743
^{44}Ca(α,n)^{47}Ti, integral rot., hyperfine field and g-factor of Ti $7/2^-$ state 77−50052
^{44}Ca(e,e′p), (γ,p) cross-sections determ., giant dipole reson. anal. 77−26666
^{44}Ca(n,α)^{41}Ar, 14.7 MeV neutron cross sections 78−70520
^{44}Ca(n,p)^{44}K, 14.7 MeV neutron cross sections 78−70520
^{44}Ca(p,γ)^{45}Sc, 1.62-2.18 MeV, e.m. decay of fragmented analogue states of Sc 77−2987
^{44}Ca(p,n)^{44}Sc, 4.49-7.57 MeV, cross sections 79−85470
^{44}Ca(p,n)^{44}Sc, reaction rates in stars 80−82183
^{44}Ca(p,p′γ), inelastic proton amplitudes for fragmented analogue state in ^{45}Sc 79−17882
^{44}Ca(p,p), E_p=1 GeV, elastic differential cross sections 78−13082
^{45}Ca, internal bremsstrahlung photon intensity and energy yield 78−86509
^{45}Ca levels, excitation functions and J^π from ^{45}K β-decay 80−105978
^{45}Ca$(f_{7/2})^{-3}$ configuration states via ^{48}Ca(^{3}He,^{6}He)^{45}Ca, 70 MeV 77−14034
^{47}Ca levels, spectroscopic factors and analogue states DWBA anal. from ^{48}Ca(^{3}He,α) 79−17808
^{47}Ca, low-lying levels anal. in ^{48}Ca(d,t) reactions 78−13114
^{48}Ca, and rare isotopes, beam prod. using Cs sputter source 78−29686
^{48}Ca beam prod. from isotopically enriched sputter targets 80−23221
^{48}Ca, double beta decay, electronic lepton number conservation law 78−17150
^{48}Ca fragmentation at 212 MeV/amu in Be(^{48}Ca,X) 80−27660
^{48}Ca ion beam, appl. to superheavy element synthesis 77−74881
^{48}Ca, isospin purity violation, dominant role of noncollective monopole states 78−12964
^{48}Ca, lifetime of 5147 keV, 4504 keV, levels determ. by (p,p′γ) at 28 MeV 77−79381
^{48}Ca, neutron distribution radius, Nolen Schiffer anomaly 78−93933
^{48}Ca, nuclear incompressibility, Hartree-Fock calc. *(Russian)* 79−49577
^{48}Ca, pion-exchange contribs. to charge densities, HF calcs. 78−46001
^{48}Ca, RMS neutron and proton radii difference, from pion-nucleus data 77−10436
^{48}Ca, radius difference to ^{40}Ca, from 104 MeV alpha scatt. optical model calcs. 79−454
^{48}Ca, single particle energies of closed minor shells 77−6208
^{48}Ca stable isotope tracer analysed by proton activation 77−21622
^{48}Ca, strongly bound π-nuclear states, criticality condition, optical pot. 78−90325
^{48}Ca tandem accelerated beam 77−79496
^{48}Ca+^{11}B, 25-50 MeV, yrast decay schemes of $^{54-6}$Mn, ^{56}Cr, $^{52-3}$V 77−82854
^{48}Ca+^{15}N(^{18}O) fusion-evaporation reaction, ^{59,60}Fe, ^{59,60}Co yrast decay scheme 78−13154
^{48}Ca+^{16}O 56 MeV, transitions to resolved levels, optical model parameter 78−41758
^{48}Ca+^{3}He, 82 MeV, cross sections, (^{3}He,t) DWBA anal. 79−13310
^{48}Ca+heavy ion fusion evaporation reacts., yrast decay schemes 78−66308
^{48}Ca(^{12,13}C,X), elastic, inelastic and single nucleon transfer excitation functions, ^{49}Ca levels 80−13492
^{48}Ca(^{15}N, ^{14}C)^{49}Sc, 48 MeV, DWBA anal., optical potential ambiguities 77−34341
^{48}Ca(^{16}O, ^{14}C), two nucleon sequential transfer, on-shell anal., cross sections 80−99180
^{48}Ca(^{16}O, ^{15}N), ^{15}N excitation contrib. in optical pot., DWBA grazing peak shift 80−86921
^{48}Ca(^{16}O,^{14}C), two nucleon transfer reactions, one and two step transfer process anal. 78−82370
^{48}Ca(^{16}O,^{14}C)^{50}Ti, full recoil one and two step DWBA anal. 78−70564
^{48}Ca(^{16}O,^{15}N)^{49}Sc, 56 MeV, DWBA anal., optical potential ambiguities 77−34341
^{48}Ca(^{16}O,^{16}O), 56 MeV, ang. distribs., optical potentials 77−34341
^{48}Ca(^{16}O,^{16}O), nuclear and Coulomb components to scatt. amplitude 77−34340
^{48}Ca(^{18}O, ^{16}O), two nucleon sequential transfer, on-shell anal., cross sections 80−99180
^{48}Ca(^{18}O, ^{17}C), 102 MeV, ^{17}C ions mass excess, low lying level struct. 78−8744
^{48}Ca(^{18}O,^{16}C)^{50}Ti, 102 MeV, two-proton transfer reaction 79−63700
^{48}Ca(^{18}O,^{16}O), two nucleon transfer reactions, one and two step transfer process anal. 78−82370

nuclei with mass number 39 to 58 continued

^{44}Ca(^{18}O,^{16}O) 50 MeV, cross sections, DWBA multipole expansion calcs., form factors 79−13325
^{48}Ca(^{18}O,^{18}O)^{48}Ca, cross section anal. by DWBA and CCBA 77−3046
^{48}Ca(^{19}F,^{18}O)^{49}Sc, 56 MeV, DWBA anal., optical potential ambiguities 79−14341
^{48}Ca(^{248}Cm, 2n)^{294}X$_{116}$, super-heavy elements prod. at barrier energies 79−13368
^{48}Ca(^{32}S,^{32}Si)^{48}Ti 125 MeV, double-charge-exchange reaction 79−63701
^{48}Ca(^{4}He,^{6}He)^{46}Ca, 70 MeV, evidence for $(f_{7/2})^{-3}$ configuration states in ^{45}Ca 77−14034
^{48}Ca(^{4}He,^{8}B)^{43}Cl, 74 MeV, obs. and mass excess of ^{43}Cl 77−10310
^{48}Ca(^{3}He,t), finite-range formalism anal. of (^{3}He,α) (α,t) sequence 78−17229
^{48}Ca(^{3}He,t)^{48}, coupled channel calc., two-step processes, nonorthogonality corrections 77−30615
^{48}Ca(^{3}He,t)^{48}Sc, 23 MeV, finite range effects and nonorthogonality corrections in two-step processes 79−3162
^{48}Ca(^{6}Li, ^{6}Li), (α, α), velocity of refined folding model approaches 80−541
^{48}Ca(d,p), 11.9 MeV, analysing power, cross section, ^{49}Ca levels, spins, parities, spectroscopic factors 78−78391
^{48}Ca(d,t$_0$) and (^{3}He,d), comparison with ^{40}Ca data, isotope shifts of $1f_{7/2}$ radii 77−34222
^{48}Ca(d,t)^{47}Ca, 13.5 MeV, polarised deuterons, low-lying levels in ^{47}Ca 78−13114
^{48}Ca(e,e), 757.5 MeV, elastic cross section 80−63175
^{48}Ca(n,Zn)^{47}Ca, 14.7 MeV neutron cross sections 78−70520
^{48}Ca(n,γ)^{49}Ca, neutron activation meas. of F/Ca ratio 77−86592
^{48}Ca(p, γ)^{49}Sc, 0.6-2.7 MeV, cross sections and thermonuclear reaction rates, Hauser-Feshbach calcs. 79−36239
^{48}Ca(p, n)^{48}Sc, 0.95-2.7 MeV, cross sections and thermonuclear reaction rates, Hauser-Feshbach calcs. 79−36239
^{48}Ca(p,γ), 0.76-2.20 MeV, absolute cross sections and yields, statistical model anal. 79−26432
^{48}Ca(p,$\bar{n}$), nucleon optical potential from Lane model 80−83097
^{48}Ca(p,n)^{48}Sc, 0.76-2.20 MeV, absolute cross sections and yields, statistical model anal. 79−26432
^{48}Ca(p,nx), 45 MeV, preequilib. ang. distrib., generalised exciton model 77−10407
^{48}Ca(p,p), 1 GeV, elastic scatt. differential cross section calc. 80−47480
^{48}Ca(p,p), E$_p$=1 GeV, elastic differential cross sections 78−13082
^{48}Ca(p,t), 40, 20 MeV, two step (p,d)(d,t) process, second order DWBA 78−66276
^{48}Ca(p,t), (p,^{3}He)(^{3}He,t) two step process calcs., two step cross section 79−36245
^{48}Ca(p,t)^{46}Ca, 20, 40 MeV, finite-range effect in (p,d)(d,t) process 78−74365
^{48}Ca(p,t)^{46}Ca two-step (p-d-t) process anal. 78−62534
^{48}Ca(p,t)^{46}Ca(0$^+$,g.s.), 20 and 40 MeV, two step process, deuteron break-up effect 80−73844
^{48}Ca(π,π), nuclear matter distribs., density depend. HF anal. 79−487
^{48}Ca(π^-, π^0), excitation of collective modes and high-spin states, DWA calcs. 77−10448
^{48}Ca(π^+,π^-), optical pot. ambiguities, neutron radius determ. 79−17872
^{48}Ca(t,d)^{49}Ca(g.s.), 2.5-3.5 MeV, sub-Coulomb reaction calibration 77−79387
^{48}Ca(t,p), exact finite range DWBA calcs., realistic triton and nuclear wave functions 80−63191
^{48}Ca→ ^{48}Ti+2e$^-$, neutrinoless double β decay, matrix elements and lepton conservation 77−30518
^{49}Ca levels from ^{48}Ca(d,p), analysing power, cross section, spins, parities, spectroscopic factors 78−78391
^{98}Ca(^{16}O,^{15}C), simple unitary estimate for multistep processes, cross section bounds 79−40922
$^{40}_{\Lambda}$Ca(k$^-$,π^-), energy excitation spectra, nuclear shell orbitals for Λ 79−85565
Ca(α,α), 1.37 GeV, differential cross sections meas. on A=40, 42, 44, 48 isotopes 77−41984
Ca(α,α), (α,α'), 1.4 GeV, theoretical anal. 78−66293
Ca(α,α), large angle scatt., cluster exchange and one-nucleon exchange 77−88152
Ca(α,α'), 1.37 GeV, differential cross sections meas. on A=40, 42, 44, 48 isotopes 77−41984
Ca(d,p), A=40, 48, Tabakin pot. calcs., differential cross sections, ang. distribs. 78−611
Ca(d,p)Ca, A=40, 42, 44, 48, at 2.5 MeV, spectroscopic factors *(German)* 77−18567
Ca(e,e'), A=40, 4, at 250 MeV, coupled-channel partial wave anal. 77−74837
Ca(γ,X), photoabsorption cross-section, Levinger's factor, mass number dependence 80−63165
Ca(n,γ), A=42, 44, γ circular polarisation meas. 78−62533
Ca(n,γ), E>2.5 keV, reson. parameters, odd-even effects 77−34299
Ca(n,n) 20, 26 MeV, Coulomb correction term to optical model pot. 77−38280
Ca(n,n)Ca, 11-26 MeV, optical model fit 77−79372
Ca(p,p), 1 GeV, neutron densities 78−17087
Ca(p,p), 30 MeV, A=40, 48, pick-up and inelastic scatt. contributions to p optical pot. 78−25182
Ca(p,p), A=40,48, 1 GeV, spin-effects, Coulomb interactions, Glauber theory 77−82931
Ca(p,p) for A=40,42,44,48 isotopes, 1.044 GeV, elastic and inelastic, Glauber theory anal. 77−18536
Ca(p,p), summed scattering (elastic and inelastic with no meson production), 2.1 GeV/c, asymmetry meas. *(Russian)* 79−89313
Ca(p,p'), 19 MeV, nuclear struct. anal. 78−17197
Ca(π^-,X), stopped π^-, fast $\pi^\pm$, 180, 220 MeV, interactions near Δ(1232) resonance 79−6712
Ca($\pi^\pm$,$\pi^\pm$), 130 MeV, A=40,48, π^+, π^- cross sections, neutron radius 78−25240
Ca(π^+,$\pi^{+\prime}$), 163,241 MeV, giant quadrupole resonances 79−40893
cc ^{42}K levels and ang. distribs., spectroscopic factors, DWBA anal. from ^{41}K(d,p) 79−17806
^{40}Cd(d,p)^{41}Ca, 11 MeV, effect of Skyrme type density depend. effective pots. 78−46069
^{35}Cl, NQR meas. in $NaClO_3$ and $Ba(ClO_3)_2.H_2O$ 77−66435
^{35}Cl(^{16}O,αpn)^{45}Ti, ^{45}Ti $1f_{7/2}$ shell model and high spin states 78−62560
^{39}Cl, charge state study prod. by (n,d) in liquid Ar ionization chamber *(Russian)* 80−9298
^{39}Cl excited states and transitions from ^{39}S decay 80−42595

nuclei with mass number 39 to 58 continued

^{40}Cl, charge state study prod. by (n,p) in liquid Ar ionization chamber *(Russian)* 80−9298
^{41}Cl, observation and mass excess in ^{48}Ca(^{3}He,^{8}B)^{43}Cl at 74 MeV 77−10310
Co isotopes, shell model 78−62479
Co isotopes, thick-target yields in Ni due to proton bombardment up to 100 MeV 77−88312
^{58m}Co III complexes, stability rel. to internal conversion deexcitation, inner shell ionisation 77−42361
^{A}Co, A=55,57,59,61, deduced levels, proton-hole states, semimicroscopic model from Ni(p,α) 79−45171
^{A}Co A=55,57,59,61, level direct and compound cross sections from ^{A}Ni(p,α), A=58,60,62,64 79−9474
^{54}Co deduced levels, J-depend., two-step processes from ^{54}Fe(^{3}He,t) 37.7 MeV 79−6412
^{54}Co populated in ^{54}Fe(^{3}He,t), precise Q-value, β decay energy, half life 77−30618
^{54}Co, super-allowed Fermi β decay lifetime meas. 77−79336
^{55}Co, 1 $g_{9/2}$ analogue state fragmentation using analogue resonances from ^{54}Fe (p,γ), 3450 keV 78−70506
^{55}Co, cyclotron prod. by ^{3}He bombardment of natural Fe, bleomycin complex synthesis 77−86629
^{55}Co, energy levels from Ni(p_{pol},α) 80−68663
^{55}Co excited levels and IAS meas. with ^{54}Fe(p,γ) 77−18509
^{55}Co f-wave resonances, inelastic p amplitudes, analogue state spectroscopic factors from ^{54}Fe(p,p'γ) 80−47451
^{55}Co, GDR, (p,γ) cross section determ. in shell model 78−78345
^{55}Co, γ decay and splitting of analogue states from ^{54}Fe(^{3}He,dγ) at 18 MeV 78−70505
^{55}Co, IAR, J$^\pi$ via ^{54}Fe(p,p) 3.28-4.53 MeV 78−574
^{55}Co isobaric analogue resonances, J$^\pi$, partial widths and spectroscopic factors from ^{54}Fe(p,γ), (p,p') 79−85431
^{55}Co, resonance decays, branching ratios and analogue resonances from ^{54}Fe(p,γ) 80−52643
^{55}Co, spectroscopic study via ^{54}Fe(^{3}He,d)^{55}Co and ^{54}Fe(τ,dp)^{54}Fe reactions 77−88029
^{56}Co beta decay, limit on time-reversal violation from β-γ correl. meas. 77−34261
^{56}Co β^+-decay, ^{56}Fe low lying levels, J$^\pi$, γ-γ coincidences, internal conversion 80−86815
^{56}Co, ensemble rotation concept in NMR on oriented nuclei in dil. Fe-Co alloys 77−90061
^{56}Co, gamma-ray intensities, precision meas. 80−102139
^{56}Co, γ-ray transitions, branching ratios, spin assignments, energy level lifetimes from ^{54}Fe(^{3}He, pγ) 79−497
^{56}Co, half-life meas. by counting neutrons from D(γ,n) 77−26622
^{56}Co in Type II supernovae, decay rel. to supernova light curves 80−77427
^{56}Co levels populated in ^{58}Ni(d,$\alpha\gamma$), 7 MeV, mean lifetimes 78−4950
^{56}Co particle-hole states, T=1, zero DWBA anal. of ^{54}Fe(^{3}He,p) and ^{58}Ni(d,α) 80−78308
^{56}Co, populated in ^{54}Fe(α,pn), transition rates of high spin states 77−6301
^{56}Co, relative intensities of γ-transitions meas. 79−97930
^{56}Co standard source, relative γ-ray intensities 78−55069
^{57}Co, Mossbauer spectra, interstitial trapping in neutron irradiated Al-Co alloys 77−27914
^{57}Co, (3/2$^+$ state), anomalous analyzing power, DWBA calc. from ^{60}Ni(p,α) 80−86894
^{57}Co, ensemble rotation concept in NMR on oriented nuclei in dil. Fe-Co alloys 77−90061
^{57}Co, $g_{9/2}$ IAR in ^{56}Fe(p,γ) 78−70504
^{57}Co, $g_{9/2}$ isobaric analogue resonances, obs. in ^{56}De(p,γ)^{57}Co 78−82332
^{57}Co, gamma decay of $g_{9/2}$ isobaric analog resonance 79−63674
^{57}Co in cosmic rays, abundance rel. to pre-accel. radioactive decay 79−40044
^{57}Co labelled Co(acac)$_3$, diamag., ^{57}Fe(III) species prod. by electron capture decay, spin relax. 77−63329
^{57}Co, level props. study from ^{57}Fe(τ,d) reaction, DWBA calcs. 78−93946
^{57}Co, levels anal. with ^{54}Fe(α,p) and ^{48}Ti(^{12}C,p2n) 77−46115
^{57}Co levels and analogue states, J$^\pi$ from DWBA anal. of ^{58}Ni(^{3}He, α) 79−63592
^{57}Co, Mossbauer gamma-X-ray coincidence meas. 80−14041
^{57}Co, Mossbauer spectra evidence for relax. valence emerging in NiO and CoO 77−1626
^{57}Co, radioactive decay, γ-ray energy meas. *(German)* 77−57633
^{57}Co source, quantum beats of recoil-free γ radiation 78−43748
^{57}Co state alignment, γ-transitions and ang. distribs. from ^{56}Fe(p,γ) 80−73797
^{58}Co 1$^+$ level population, shell model calcs., (t,^{3}He) and (e,e') comparison from ^{58}Fe(p,n) 79−9481
^{58}Co decay, student expt. 80−12875
^{58}Co, fine struct. of ground hole-state analogues 78−50065
^{58}Co, fragmentation of hole-state analogues 78−54731
^{58}Co, half-life determ. 77−34498
^{58}Co, level determ. in seawater 78−85608
^{58}Co-cyanocobalamin, whole-body retention in rats, age effect 77−70559
^{59}Co+n, calc. using pre-equil. statistical model code GNASH 78−4946
^{59}Co(α,t), 25 MeV, DWBA anal. of triton ang. distrib. meas. 78−54776
Cr (d,p), A=50, 52, 54, Tabakin pot. calcs., differential cross sections, ang. distribs. 78−611
Cr, A=48,50,52,54, short-range correlations and pseudopotentials, Hartree Fock Bogoliubov method 78−535
Cr, A=48-52, effective charges and E2 transitions in 1f-2p shell nuclei 78−544
Cr, A=50, 52, pf-shell nuclei, Hermitian operator method calcs., energy levels, transitions 78−54702
Cr, fluoresc. yield meas. from electron-capture decay of ^{54}Mn 78−21530
Cr isotopes, A=50-54, n-particle cross-sections from threshold −20 MeV 77−30541
Cr, K_β/K_α following K-electron capture and X-ray excitation 78−13031
Cr, neutron-photon multigroup cross sections for neutron energies ≤60 MeV 79−30880
Cr+^{14}N(^{12}C), single- and multi-nucleon transfer reactions at 60, 70 and 90 MeV 77−14146
Cr+π, 200 GeV, multiparticle production in emulsion 79−40967
Cr(^{16}O,^{16}O'γ), 36 MeV, g-factors of first 2$^+$ states in ^{50,54}Cr 78−13138
^{A}Cr (d,d), pol. d, A=52, 54, 12 MeV, cross sections, anal. powers, global optical model anal. 80−47459

nuclei with mass number 39 to 58 continued

^{A}Cr, A=49,51-53, levels, spectroscopic factors and analogue states DWBA anal. from Cr(^{3}He,α) 79−17808
^{A}Cr, A=50, 52-54, slow n-interactions, scatt. lengths, absorpt. and scatt. cross-section 78−70539
^{A}Cr(e,e), A=50,52,53,54, 226.7 MeV, charge density distrib. *(Russian)* 78−86473
^{A}Cr(n,X), A=50, 52-54, 14 MeV, X=p,n'p,α,n'α,^{3}He, production cross-sections 80−42648
^{A}Cr(n,X), A=50,52, 14.8 MeV, charged particle emission, cross section, Hauser-Feshbach anal. 79−67750
^{A}Cr(n,2n), A=50, 52, 54, 14 MeV, cross section compilation 80−91181
^{A}Cr(n,n'γ), A=50-54, 0.84-3.97 MeV, neutron inelast. scatt. cross-sections determ. 78−62529
^{A}Cr(p,n), 11.2 MeV, A=52, 53, 54, spin cut-off parameters from neutron ang. distribs. *(Russian)* 79−80940
^{A}Cr(p,p'), 6 MeV, A=50, 52, p spin flip probability 79−9561
^{A}Cr(p,p), A=50, 52, 6 MeV, elastic and inelastic differential cross sections, spin flip probability *(Russian)* 80−91187
^{47}Cr, β-decay GT matrix elements, $T_{1/2}$ 78−557
^{47}Cr, β-decay half-life and GT matrix element 77−22950
^{47}Cr, half-life and log ft to ^{47}V 77−22951
^{48}Cr high spin states, yrast levels and 6^{-} isomeric state from ^{40}Ca(^{10}B,np) 80−454
^{48}Cr, spectroscopy of high spin states 79−59032
^{49}Cr, 2432 keV state, spin-parity assignment using three Ge(Li) Compton polarimeters 77−83456
^{49}Cr, forbidden transition ang. distribs., CCBA and DWBA anals. of (p,d) 80−86848
^{49}Cr, gamma-ray ang. distrib., ang. correlation, linear polarisation and Doppler-shift attenuation meas. in ^{46}Ti(α,nγ) 77−82941
^{49}Cr ground analogue state fine struct., l=3 states differential cross section from ^{50}Cr(p,d) 80−63152
^{49}Cr levels, transitions, and Gamow-Teller matrix elements from ^{49}Mn, β^{+}-decay 80−57746
^{49}Cr low lying states, deformed configuration mixing shell model calcs. 77−6302
^{50}Cr, $1f_{7/2}$ shell isobaric analogue states, displacement energies 79−13207
^{50}Cr, selective population of high-spin states in heavy ion reactions 77−18374
^{50}Cr+^{14}N, energy dissipation as func. of angle data comparison to classical and diffusion models 78−21604
^{50}Cr+^{22}Ne, energy dissipation as func. of angle data comparison to classical and diffusion models 78−21604
^{50}Cr+^{40}Ar, 236 MeV, fragments mass and charge distribs. in deep inelastic reactions 78−58296
^{50}Cr(^{3}He, dγ)^{51}Mn, lifetimes of some low-lying l=1 states in ^{51}Mn 77−79393
^{50}Cr(^{3}He,nγ)^{52}Fe, low-lying states of ^{52}Fe 78−4952
^{50}Cr(^{3}He,pn)^{51}Mn, ^{51}Mn $1f_{7/2}$ shell model and high spin states 78−62560
^{50}Cr(^{3}He,t), precise Q-value, ^{50}Mn β decay energy, half life 77−30618
^{50}Cr(α,p)^{53}Mn, cyclotron preparation of ^{53}Mn, extraction, anal. 77−61441
^{50}Cr(d,d), 12.3 MeV polarised deuterons, precision tensor analysing power meas. 77−3019
^{50}Cr(d,p), 12.3 MeV polarised deuterons, analysing powers, ^{51}Cr spin assignments 77−30608
^{50}Cr(e,e), 227 MeV, differential cross sections, Fermi charge density distribs. *(Russian)* 78−89785
^{50}Cr(n,n) 1.5-3.0 MeV elast. and inelast. scatt., differential cross section *(Russian)* 78−25199
^{50}Cr(n,t)^{48}V, 14.6 MeV, production cross sections 79−49629
^{50}Cr(p,γ), 0.6 to 3 MeV, captive cross section, statistical theory anal. 79−9557
^{50}Cr(p,p'γ), 2.00-3.03 MeV, proton and γ-ray ang. distrib. meas., p-wave reson. obs. 77−41961
^{50}Cr(p,p), (p,p'), 3.2 to 4.4 MeV, high resolution, study of ^{51}Mn levels 77−54151
^{50}Cr(p,p) and (p,p'), E_p=6 MeV, cross sections, opt. pot. parameters 78−13086
^{50}Cr(τ,α), 16 MeV, ^{49}Cr energy levels, spins, parities, spectroscopic factors 78−33199
^{51}Cr, bands, levels, EM transitions, J^{π}, branching and mixing ratios from ^{48}Ti (γ,nγ)^{51}Cr and ^{51}V(p,nγ)^{51}Cr 80−52606
^{51}Cr, EM properties, lifetimes of 749 and 777 keV levels, E2/M1 mixing ratio 80−63127
^{51}Cr, electron dose reduction coeff., internal radionuclides, source free target, cylindrical geometry 78−92704
^{51}Cr, gamma-ray precision energy meas. 78−58533
^{51}Cr level scheme, DWBA and optical model anal. from ^{52}Cr+^{13}C 79−36159
^{51}Cr, level struct. to E_x=8.1 MeV via ^{50}Cr(d,p) 77−50059
^{51}Cr levels, spectroscopic function and analogue states, PWBA anal. of ^{52}Cr(^{3}He,α) 80−68547
^{51}Cr populated in ^{50}Cr+polarised deuterons, D-state effects, spin assignments 77−30608
^{51}Cr, strongly deformed $K^{\pi}=1/2^{-}$ bands from γ meas., level transition parameters 79−3113
$^{51}Cr_2O_7^{2-}$ tracer solution preparation *(French)* 79−29385
^{51}Cr→^{51}V, inner bremsstrahlung spectra, disintegration energies 77−54191
^{52}Cr, 1f nucleon orbit RMS radii from transfer data 80−27544
^{52}Cr, 1p5h config., high-spin neutron-hole states, EM transition rates 78−70430
^{52}Cr 4.75 MeV excited state from ^{50}V(α,d), 8^{+} assignment 78−74380
^{52}Cr, decay of highly excited nuclei following ^{48}Ti(^{18}O,^{12}C) at 120 MeV 79−45289
^{52}Cr, γ-decay of analogue states obs. in ^{51}V(p,γ) 78−70503
^{52}Cr, γ-spectra, levels, J^{π} via α+^{50}Cr reaction 77−74794
^{52}Cr high spin states, transitions and J^{π} values from ^{50}Ti(α,Z nγ) 80−455
^{52}Cr, high-spin states, populated by ^{50}Ti(α,2nγ) spectroscopic meas. 77−65190
^{52}Cr, level scheme determ. from ^{52}V γ-ray spectrum *(French)* 77−14066
^{52}Cr level structure, appl. of generator-coordinate method extension to two quasiparticle excited states 77−54153
^{52}Cr levels populated in decay of ^{52}V, ^{52}Mu^{g} and ^{52}Fe→^{52}Mn→^{52}Cr 78−21529

nuclei with mass number 39 to 58 continued

^{52}Cr, shell model study and gamma decay of isobaric analogue states 78−86492
^{52}Cr studied via (α,2nγ), high spin states, shell model calcs. 78−54675
^{52}Cr, total photoneutron cross section, high resolution meas., isospin effects 78−8792
^{52}Cr+^{12}C, 56 MeV, heavy ion fusion, evaporation model breakdown, preequilibrium α emission from ^{64}Zn 78−89927
^{52}Cr(^{12,13}C,X), elastic, inelastic and single nucleon transfer excitation functions, ^{53}Cr levels 80−13492
^{52}Cr(^{14}N,2p2nγ), 50-75 MeV, ^{62}Cu high spin states, level scheme *(French)* 78−21496
^{52}Cr(^{16,18}O,^{16,18}O'), 30-42 MeV, excitation function differences, optical and DWBA anals. 79−63698
^{52}Cr(^{3}He,d)^{53}Mn, 24,25 MeV, ^{53}Mn isobaric analogue states 77−6237
^{52}Cr(α,α'), 8-18 MeV, cross sections, search for giant dipole resonance 80−9281
^{52}Cr(α,α), 15-19 MeV, inelastic scatt. form factors, Coulomb-nuclear interference region 78−66288
^{52}Cr(α,p_0(p_1)) differential cross section in giant dipole resonance region from (e,p_0(p_1)) 79−63655
^{52}Cr(d,d), 10 MeV, polarised d elastic scatt., optical model anal. 79−36248
^{52}Cr(d,d), 7-11 MeV, coupled-channel anal. 77−18579
^{52}Cr(d,d), 7-11 MeV, stripping channel effect, coupled channel model, DWBA anal. 77−57676
^{52}Cr(d,n)^{53}Mn, cyclotron preparation of ^{53}Mn, extraction, anal. 77−61441
^{52}Cr(d,p), 7-11 MeV, coupled-channel anal. 77−18579
^{52}Cr(d,p), cross section, stripping channel effect, coupled channel model, DWBA anal. 77−57676
^{52}Cr(d,p), polarised d, obs. of D-state and compound nucleus effects 77−34319
^{52}Cr(d,p)^{53}Cr, 10 MeV polarised beam, structure of ^{53}Cr low-lying levels 77−18395
^{52}Cr(d,p)^{53}Cr, Coulomb stripping, 2.12-2.48 MeV, DWBA anal., spectroscopic strengths 80−516
^{52}Cr(d,p)^{53}Cr, deuteron break-up model anal. of cross-section, vector analysing power and angular correlation 80−27648
^{52}Cr(d,pγ), 8.0 MeV, particle-gamma correlation meas. 77−61437
^{52}Cr(e,e'), 40-110 MeV, vibr. nuclei, branching ratios 77−6356
^{52}Cr(e,e'), 90-226 MeV, excitation of low-lying states *(Russian)* 78−54746
^{52}Cr(e,p_0(p_1)), differential cross section in giant dipole resonance region 79−63655
^{52}Cr(γ,X), photoneutron and photoproton cross section systematics 80−13463
^{52}Cr(γ,γ'), 35 MeV, 2^{+} state deexcitation γ-rays, differential cross sections, deformation *(Russian)* 80−13406
^{52}Cr(γ,γ), up to 12 MeV, highly excited spin-1 resonances, γ-transitions 80−13427
^{52}Cr(n, n), 1.77 to 3 MeV, validity of Wick's inequality in the calculation of the lower limits of the differential elastic cross sections 80−5137
^{52}Cr(n,n'γ), 0.5-10 MeV, γ-ray production cross sections 77−26762
^{52}Cr(n,n), 1.5-3.0 MeV elast. and inelast. scatt., differential cross section *(Russian)* 78−25199
^{52}Cr(n,p)^{52}V, ave. neutron activation cross sections for ^{241}Am-Be source 79−31282
^{52}Cr(p,γ)^{53}Mn, resonant react. appl. to Cr depth distribs. 79−33011
^{52}Cr(p,nγ), 6.3-7.3 MeV, populating ^{52}Mn low-lying levels 77−14028
^{52}Cr(p,p'), 4.7-5.4 MeV, cusp behaviour of cross-section obs. 78−29470
^{52}Cr(p,p) and (p,p'), E_p=6 MeV, cross sections, opt. pot. parameters 78−13086
^{52}Cr(π,X), angular distrib. of inelastic diffusion of $\pi^{\pm}$ *(French)* 80−47507
^{52}Cr($\pi^{\pm}$,$\pi^{\pm\prime}$), 180 MeV, ang. distrib. around (3,3) reson. 79−85537
^{52}Cr($\pi^{\pm}$,π^{+}), 180 MeV near (3,3) reson., nuclear RMS radii determ. 79−85538
^{53}Cr, excited negative parity states to 2322 keV via (p,p'γ) and (α,$\alpha'\gamma$) 77−82851
^{53}Cr excited state lifetimes from ^{50}Ti(α,n) 79−26392
^{53}Cr levels, J^{π}, γ-transitions and 1626 eV resonance from ^{52}Cr(n,γ) 80−42610
^{53}Cr low-lying level structure via ^{52}Cr(d,p) with 10 MeV polarised beam 77−18395
^{53}Cr, possible deformed 7/2^{-} states with ΔJ=1 band 79−45170
^{53}Cr(e,e'), 90-226 MeV, excitation of low-lying states *(Russian)* 78−54746
^{53}Cr(γ,p)^{52}V, cross-section, 14.4-27 MeV, isospin splitting 80−520
^{54}Cr levels, transitions, $T_{1/2}$, J^{π}, shell model anal. from ^{51}V(α,pγ) 80−47381
^{54}Cr, proton-neutron correl., shell model for collective motion 77−79312
^{54}Cr, yrast decay schemes from ^{48}Ca+heavy ion fusion evaporation reacts. 78−66308
^{54}Cr(d,d), pol.d, 20 MeV, quadrupole transition amplitudes 80−99148
^{54}Cr(p,γ), 1.0-3.8 MeV, γ-yields, cross sections, predicted (p,n) cross section, Stat. anal. 80−5136
^{54}Cr(p,γ)^{55}Mn, 0.83-3.606 MeV, cusp in excitation function 78−66273
^{54}Cr(t,^{3}He), 23 MeV, ^{54}V energy levels, mass excess 77−54230
^{54}Cr(t,pγ)^{56}Cr, 2.9 MeV, γ-ray spectroscopy of low-lying states in ^{56}Cr 77−10358
^{55}Cr deduced levels and spins, from ^{54}Cr(d_{pol},p), cross section and vector analysing power 80−52684
^{55}Cr, half-life determ. 78−4915
^{55}Cr, yrast decay schemes from ^{48}Ca+heavy ion fusion evaporation reacts. 78−66308
^{56}Cr, γ-ray spectroscopy of low-lying states studied via ^{54}Cr(t,pγ) 77−10358
^{56}Cr, yrast decay schemes for heavy-ion fusion evaporation reactions 77−82854
^{57}Cr mass excess, half life, ground state spin and parity, from ^{48}Ca(^{11}B, pn) 78−70436
^{57}Cr, new isotopes of interest to explosive nucleosynthesis, β-decay scheme and mass determ. 79−45208
^{58}Cr, neutron rich nuclide from ^{238}U(^{40}Ar,X) at 340 MeV 80−57802
Cr(α,α), A=50,2,3, 25 MeV, back-angle elastic scatt. 77−18582
Cr(α,p), 18, 26 MeV, levels in ^{53,55,57}Mn, J-depend., spins, parities 78−78397
Cr(γ,f), max energy 580 MeV, track detector anal. 77−18640
Cr(n,X), 14.8 MeV, γ-prod. cross section 79−49622
Cr(n,γ), absolute cross sections in keV range 77−26771

nuclei with mass number 39 to 58 continued
Cr(n,γ), up to 600 keV, cross sections, resonance parameters, point-wise evaluation 77−23050
Cr(n,n′γ), 3-6 MeV, γ-ray production cross sections 77−26767
Cr(π^+, π^0), 200 MeV, deexcitation γ spectra, transitions in ^{52}Mn 78−89912
Cu, CC ^{56}Ni core excitation effects on A=57-66 nuclei, MSDI and ASDI comparison 78−78254
Cu, isotopes, shell model calcs. of BE, spectroscopic factors and excit. energies 77−22860
Cu+Cu system, high energy, compound nucleus form. and deep inelastic scatt. *(French)* 79−559
Cu+K_L, 30 to 150 GeV, total cross sections, inelastic screening evidence 79−17936
Cu+K_S, 20 to 140 GeV, precise coherent K_S regeneration amplitudes 79−17937
^{40}Cu, nuclear incompressibility, Hartree-Fock calc. *(Russian)* 79−49577
^{58}Cu, populated in Ni(π^+, π^0), deexcitation γ spectra 78−89912
^{59}Cu, γ decay and splitting of analogue states, from ^{58}Ni(^{3}He,dγ) at 18 MeV 78−70505
(Fe,X), 1.9 GeV/N, in emulsion, mean free paths, and fragmentation parameters 80−102197
Fe 79−30880
Fe, A=52, 4, effective charges and E2 transitions in 1f-2p shell nuclei 78−544
Fe, A=52,54,56,58, short-range correlations and pseudopotentials, Hartree Fock Bogoliubov method 78−535
Fe, A=54, 56, intermediate struct. via (γ,n) 5-26.3 MeV 77−74824
Fe, A=54,58, mag. moments of 2^+ first excited states, g-factors 77−88041
Fe, Co, Ni in cosmic rays, abundances rel. to time delay between nucleosynthesis and accel. 78−28455
Fe, even nuclei, systematic meas. of mag. moments of 2_1^+ states 78−54682
Fe group elements, prod. in supernova outburst *(Russian)* 80−62167
Fe, inelastic interaction with cosmic ray muons 79−84616
Fe, integral neutron capture cross sections in GCFR lattices 78−13246
Fe, integral test of cross section, neutron leakage spectra, spherical assembly 77−23033
Fe isotopes, cross sections for charged particle prod. by 14 MeV neutrons, data compilation 80−9289
Fe isotopes, density-dependent HF description 77−54170
Fe isotopes A=53-58, spectroscopic calcs. using mass independ. effective interaction, yrast levels 78−41638
Fe, K_β/K_α following K-electron capture and X-ray excitation 78−13031
Fe, muon generated cascade showers in ionisation calorimeter 79−84618
Fe nuclei in galactic cosmic rays, isotopic comp. 80−72729
Fe, photonuclear cross sections in giant reson. region 78−17178
Fe, radial charge distrib. moments, ground state correlations, generator coordinate model 79−30785
Fe, single neutron separation energies determ. from doublets 77−26566
Fe, spallation by 0.3-1.0 GeV photons, cross-sections 78−41691
Fe+Ag, hydrodynamic effects in cosmic ray nucleus-nucleus interactions 79−80176
Fe+α, 7-24 MeV, ^{59}Ni formation cross section, poss. prod. in cosmic dusts 78−78399
Fe+Br, hydrodynamic effects in cosmic ray nucleus-nucleus interactions 79−80176
Fe+cosmic ray photon, prod. of 300-1000 GeV muons, cross section, shadowing 77−64580
Fe+n, A=54, 56, 1-70 keV, total cross section, resonance parameters *(Russian)* 78−17210
Fe+p, 28.5 GeV, prompt dimuon prod., cross section, atomic number depend., mass distrib. 78−89858
Fe+p, high energy spallation, prod. cross sections of stable, long-lived nuclides 77−2998
Fe+$\pi^\pm$, 125 MeV, true absorpt. and scatt. 79−63705
Fe(^{6}Li,d)Ni, A=54,56,58, at 34 MeV, comparison with (t,p) and (^{3}He,n) reactions 77−30631
Fe(^{16}O,^{12}C), A=54,56, high excitation region of ^{58,60}Ni, two- and four-nucleon transfer spectra 79−6675
^Fe, A=54-56, high spin states, energy levels, spectroscopic factors, EM props., shell model 80−47359
^Fe, A=56-58, shell model calcs., static moments and EM transition rates 79−17853
^Fe, A=56-60, shell struct. of collective states, level spectra 79−93494
^Fe, A=57, 59, levels, J^π and transition branching ratio from Fe(n,γ) 80−105976
^Fe(^{16}O, ^{12}C), 50 MeV, a=54, 56, 58, α-spectroscopic factors, DWBA anal., (^{6}Li, d) comparison 79−63585
^Fe(^{6}Li,X) A=54,56, 10-100 MeV, fusion and nonfusion processes, cross sections 79−45315
^Fe(α,α′), A=54,58, 8-18 MeV, cross sections, search for giant dipole resonance 80−9281
^Fe(d,d), pol. d, A=54, 56, 12 MeV, cross sections, anal. powers, global optical model anal. 80−47459
^Fe(e,e), 100-275 MeV, A=54,56,57, cross sections and muonic X-ray meas., charge distrib. systematics 80−86801
^Fe(e,e), A=54,56, 226.7 MeV, charge density distrib. *(Russian)* 78−86473
^Fe(n,X), A=54,56, 14.8 MeV, charged particle emission, cross section, Hauser-Feshbach anal. 79−67750
^Fe(n,X) A=54, 56, 57, transmission and capture meas. 80−18313
^Fe(n,2n), A=54, 56, 14 MeV, cross section compilation 80−91181
^Fe(n,γ), A=54, 56, 57, mechanism in 3s size resonance, radiative width statistical and valence effects 80−37388
^Fe(n,γ), A=54,56,58, resonance capture, ^{55,57,59}Fe level schemes 79−547
^Fe(p,X), A=54, 56, 57, 58, 12-45 MeV, reaction cross section and hybrid model analysis 79−67749
^Fe(p,γ_0) A=54,56,58, polarised p in giant dipole resonance region, cross sections and analysing power 78−82346
^Fe(p,γ_0)Co, A=54,56, giant dipole resonance splitting, direct-semidirect capture model anal. 80−106055
^Fe(p,n), 11.2 MeV, A=56, 57, spin cut-off parameters from neutron ang. distribs. *(Russian)* 79−80940
^Fe(p,p′), A=54, 56, 6 MeV, resonances, spin flip and cross section depends., Hauser Feshbach anal. *(Russian)* 80−83084
^{36}Fe+ν_e, 0 to 300 MeV, cross sections, shell model calcs 79−93605
^{51}Fe, β-decay GT matrix elements, $T_{1/2}$ 78−557
^{51}Fe, β-decay half-life and GT matrix element 77−22950

nuclei with mass number 39 to 58 continued
^{52}Fe ^{M} decay, ^{52}Mn yrast state properties, transitions and decays 79−67631
^{52}Fe, $1f_{7/2}$ shell isobaric analogue states, displacement energies 79−13207
^{52}Fe, γ-spectra, levels, J^π via α+^{50}Cr reaction 77−74794
^{52}Fe levels, J^π, via ^{54}Fe(p,t)^{52}Fe 52 MeV reaction 77−50058
^{52}Fe levels from ^{54}Fe(p,t), ang. distrib., spin, parity, $f_{7/2}$ shell model 78−74362
^{52}Fe low lying level ang. distribs., zero range DWBA anal. from ^{54}Fe(p,t) 79−67656
^{52}Fe, low-lying excited states, ^{50}Cr(^{3}He,nγ)^{52}Fe reaction 78−4952
^{52}Fe yrast state properties, transitions and decays from ^{40}Ca(^{14}N,np) 79−67631
^{52}Fe→^{52}Mn^m→^{52}Cr, γ-ray spectra, ^{52}Cr levels 78−21529
^{53}Fe, levels, J^π, populated via (τ,α) 18 MeV 77−74767
^{53}Fe, levels, spectroscopic factors and analogue states DWBA anal. from ^{54}Fe(^{3}He,α) 79−17808
^{53}Fe, strongly deformed $K^\pi=1/2^-$ bands from γ meas., level transition parameters 79−3113
^{54}Fe 8^+ and 10^+ level spin assignments and lifetimes from (^{16}O,2p), (^{6}Li, pn) 80−68531
^{54}Fe (n,γ), valence neutron capture in s-wave capture 77−23076
^{54}Fe, α-cluster spectroscopic factors, DWBA anal. of (d, ^{6}Li) 80−52571
^{54}Fe B(E2) transition probabilities, effective charge concept 77−18477
^{54}Fe, high resolution total neutron cross section meas. 77−23065
^{54}Fe high spin states, transitions and J^π values from ^{52}Cr(α,Znγ) 80−455
^{54}Fe level structure, appl. of generator-coordinate method extension to two quasiparticle excited states 77−54153
^{54}Fe, mean lifetime of 6.38 MeV 8^+ state from ^{50}Cr(^{6}Li, pn) *(French)* 79−45204
^{54}Fe neutron capture, asymmetric s-wave reson., background interf. 78−21563
^{54}Fe, neutron elastic and inelastic differential scatt. cross sections, 1.5-3.0 MeV *(Russian)* 77−26688
^{54}Fe, pf-shell nuclei, Hermitian operator method calcs., energy levels, transitions 78−54702
^{54}Fe, studied via (α,2nγ), high spin states, shell model calcs. 78−54675
^{54}Fe, surface structure analysis using Blair phase shifts 78−12959
^{54}Fe^m, static moments, perturbed ang. distribs. with combined dipole and quadrupole interactions 78−62482
^{54}Fe+^{14}N(^{12}C), single- and multi-nucleon transfer reactions at 60, 70 and 90 MeV 77−14146
^{54}Fe+p, 62 MeV, complex particle emission, pre-equilibrium exciton model anal. 78−66280
^{54}Fe(^{12,13}C,X), elastic, inelastic and single nucleon transfer excitation functions, ^{55}Fe levels 80−13492
^{54}Fe(^{16,18}O,^{16,18}O′), 30-42 MeV, excitation function differences, optical and DWBA anals. 79−63698
^{54}Fe(^{16}O,^{16}O′γ), 36 MeV, g-factors of first 2^+ states in ^{54}Fe 78−13138
^{54}Fe(^{18}O,^{17}O)^{55}Fe, 50 MeV, differential cross-sections, direct one-step process 77−74828
^{54}Fe(^{3}He,p), ^{56}Co particle-hole states, T=1, zero DWBA anal. 80−78308
^{54}Fe(^{3}He,t), precise Q-value, ^{54}Co β decay energy, half life 77−30618
^{54}Fe(^{3}Hg,pγ)^{56}Co, 11-15 MeV, coincidence, ang. correl. and branching ratio meas. 78−13129
^{54}Fe(^{6}Li,^{6}Li), 38, 44, 50 MeV, elastic and inelastic scatt., optical model anal. and inelastic scatt. deformation lengths 79−59082
^{54}Fe(^{7}Li,^{7}Li), 36, 42, 48, MeV, elastic and inelastic scatt., optical model anal. and inelastic scatt. deformation lengths 79−59082
^{54}Fe(N,α)^{51}Cr, 6-10 MeV, cross-sections meas. 79−93613
^{54}Fe(P, α)^{51}Mn, 21 MeV analogue state, excitation 80−13471
^{54}Fe(α,^{8}He), 110 MeV, ^{50}Fe proton rich nucleus, Q values, mass excesses 77−88162
^{54}Fe(α,α′), coupled channels calc., capture cross section, GQR decay modes 80−27654
^{54}Fe(α,p), 12-24 MeV, high spin states in ^{57}Co anal. 77−46115
^{54}Fe(α,p), 5.3-9.06 MeV, excitation functions, resonance struct., α-widths of ^{58}Ni states 77−30617
^{54}Fe(d,d), 10 and 13 MeV, polarised d elastic scatt., optical model anal. 79−36248
^{54}Fe(γ,X), photoneutron and photoproton cross section systematics 80−13463
^{54}Fe(γ,n), cross section meas., E1 giant dipole isospin splitting 79−17892
^{54}Fe(n, 2n), 14-19 MeV, cross section meas., neutron flux 79−13291
^{54}Fe(n,2n), 14.7-19.0 MeV, excitation functions relative to ^{56}Fe(n,p), ^{53}Fe half life 79−3142
^{54}Fe(n,2n) direct process contrib., cross section, DWTA and DWBA anal. *(Russian)* 78−78386
^{54}Fe(n,γ), cross section, resonance and background interference 80−18310
^{54}Fe(n,γ) 2.5-500 keV, valence neutron capture, reson. parameters 77−57659
^{54}Fe(n,p)^{54}Mn, 6-10 MeV, cross-sections meas. 79−93613
^{54}Fe(n,p)^{54}Mn threshold reaction cross section, ^{252}Cf source 77−23039
^{54}Fe(n,t)^{52m}Mn, 14.6 MeV neutrons, activation cross section meas. 79−45254
^{54}Fe(p,α)^{51}Mn, 9 to 13 MeV, γ-ray spectroscopy study of ^{51}Mn structure 77−18471
^{54}Fe(p,α)^{51}Mn, multi-step-direct-reaction anal. 78−8818
^{54}Fe(p,d)^{53}Fe, 40 MeV spectroscopic factors, ang. distrib., DWBA anal. 79−22287
^{54}Fe(p,γ), 1.5-2.9 MeV, excited levels and isobaric analogue states in ^{55}Co 77−18509
^{54}Fe(p,p′), 39, 62 MeV, DWBA anal., collective spectra, direct process contrib. *(Russian)* 80−13408
^{54}Fe(p,p′), 62 MeV, effect of nucleon mean free paths on intranuclear cascade calc., 77−67749
^{54}Fe(p,p′), cross sections and spectra, exciton model *(Russian)* 78−21536
^{54}Fe(p,p′), pol. p, 800 MeV, diff. cross sections, anal. powers, DWIA anals. 80−83067
^{54}Fe(p,p′), testing self consistent models of collective and single particle struct. 78−82300
^{54}Fe(p,p), 3.28-4.53 MeV, ^{55}Co IAR, J^π assignments 78−574
^{54}Fe(p,p), 5.5-6.2 MeV, resonance effects, deformation, spectroscopic factors, statistical, optical and DWBA anal. 79−6593
^{54}Fe(p,p), 800 MeV, polarised differential cross sections and anal. powers, n density 79−13297

nuclei with mass number 39 to 58 continued

^{54}Fe(p,t), 45 MeV, ^{52}Fe levels, ang. distrib., spin, parity, $f_{7/2}$ shell model 78−74362
^{54}Fe(p,t)^{52}Fe, 52 MeV, ^{52}Fe levels, J^{π} 77−50058
^{54}Fe(ρ,α)^{51}Mn, 35 MeV, nuclear struct. study 79−75980
^{54}Fe(τ,α), 18 MeV, populating ^{53}Fe levels to 7.3 MeV excit. 77−74767
^{55}Fe β-decay surface contamination monitoring probes, comparison of response between detectors 78−25398
^{55}Fe deduced levels, from ^{54}Fe(d_{pol},p), cross section and vector analysing power 80−52684
^{55}Fe electron-capture decay double internal bremsstrahlung 79−63633
^{55}Fe levels, J^{π}, spectroscopic factors, DWBA anal. of ^{56}Fe(^{3}He,α) 80−99127
^{55}Fe, neutron activation product density in life expired LWR 79−9908
^{55}Fe, possible deformed $7/2^{-}$ states with $\Delta J=1$ band 79−45170
^{55}Fe resonances, levels, J^{π}, valence capture γ-ray spectrum from ^{54}Fe(n,γ) 80−86852
^{55}Fe, thick-target yields in Co due to proton bombardment up to 100 MeV 77−88312
^{55}Fe, X-ray source, parameter determ. 78−5081
^{55}Fe $2p_{3/2}$ neutron orbit radius isotone shift from DWBA anal. of ^{54}Fe(t,d) 80−32172
^{55}Fe(^{52}Cr, X), entrance channel mass asymmetry effects on reaction mechanism, fission and fusion 80−106077
(^{56}Fe,X), 0.5-2 GeV/N, on emulsion, secondary mean multiplicities and ang. distribs. *(Russian)* 80−106076
(^{56}Fe,X), 2 GeV/N, anomalous nuclei among relativistic projectile fragments 80−106034
(^{56}Fe,X), X=Al-Mn, relativistic ^{56}Fe fragmentation, charge and mass changing cross sections 79−54453
^{56}Fe, 6^{+} doublets populated in heavy-ion compound reactions, side feeding 78−13014
^{56}Fe, (α,p), (α,d) and (α,t) reactions, 50.5 MeV, particle spectra 77−6405
^{56}Fe, absolute excitation energy meas. using electrostatic analyser 77−30741
^{56}Fe, fast moving ion in Fe, nature of dynamic mag. field 78−43697
^{56}Fe, fp shell model calcs., spectra and spectroscopic factors 80−68588
^{56}Fe, hadron generated cascades, energy flux absorption length, 1-20 TeV *(Russian)* 78−28468
^{56}Fe, high resolution total neutron cross section meas. 77−23065
^{56}Fe ions relativistic nuclei stopping power, Bethe theory higher order corrections 78−78599
^{56}Fe isobaric analogue resonances corresponding to ^{56}Mn 335.5 and 340.9 keV states from ^{55}Mn(p,γ) 78−78342
^{56}Fe isobaric analogue resonance levels, branching ratios, from ^{55}Mn(p,γ) 80−68617
^{56}Fe, K^{+} interaction with nuclei 78−13165
^{56}Fe, level struct. via (^{12}C,α2p), (α,2p) and (α,α) reactions 77−67702
^{56}Fe low lying levels, J^{π}, γ-γ coincidences, internal conversion from ^{56}Co β^{+}-decay 80−86815
^{56}Fe, neutron elastic and inelastic differential scatt. cross sections, 1.5-3.0 MeV *(Russian)* 77−26688
^{56}Fe neutron induced reactions, Hauser-Feshbach code for cross sections 77−23045
^{56}Fe, neutron scattering resonance radiative widths 80−99146
^{56}Fe, nucl. level densities, using single particle states for Woods-Saxon and Nilsson potentials 78−50086
^{56}Fe, partial radiation widths from neutron capture resonances, valency model calcs. 77−26707
^{56}Fe, partition functions, astrophysical implications 79−21167
^{56}Fe, populated in ^{54}Fe(α,pp), transition rates of high spin states 77−6301
^{56}Fe, proton-neutron correl., shell model for collective motions 77−79312
^{56}Fe, radiative transitions from unbound states obs. in neutron inelastic scatt. *(Russian)* 78−41664
^{56}Fe recoil in Fe, enhanced transient fields 77−15802
^{56}Fe, recoiling in Fe, enhanced transient fields 78−37284
^{56}Fe, search for giant quadrupole resonance 80−9281
^{56}Fe, semi-microscopic calc. of levels, spectroscopic factors and EM props. 77−2912
^{56}Fe, shell model wave functions from ^{56}Fe(p,α) 80−32211
^{56}Fe, surface structure analysis using Blair phase shifts 78−12959
^{56}Fe yrast band, coexistence of prolate and oblate shapes 78−12947
^{56}Fe+^{12}C, 192 MeV, energy spectra and yields of p,d and t 78−66306
^{56}Fe+^{16}O, energy dissipation as func. of angle data comparison to classical and diffusion models 78−21604
^{56}Fe+^{238}U, 538 MeV, quasifission dominance with projectile A and Z 77−74869
^{56}Fe+^{40}Ar, 236 MeV, fragments mass and charge distribs. in deep inelastic reactions 78−58296
^{56}Fe+^{56}Fe, 8.3 MeV/amu collision, nucleon exchange and A/Z equilibration 79−76020
^{56}Fe+n, 0-2.2 MeV, doorway state struct. 77−88143
^{56}Fe+n, 16-22 MeV, cross sections for prompt γ, compound statistical model calcs. 79−543
^{56}Fe+n reactions in man, dose from 14.8 MeV 78−20275
^{56}Fe+p, 39 MeV, intranuclear cascade model 78−33185
^{56}Fe(^{13}C, 2np), ^{56}Fe(^{15}N, n2p), ^{66,68}Ga isomeric states, lifetimes, g-factors 78−33147
^{56}Fe(^{16}O, ^{16}O′), Coulomb-nuclear interf., appl. of Austern Blair theory, comparison with DWBA 77−3043
^{56}Fe(^{16}O, ^{15}N), 36-53 MeV, reaction dynamic depend. of small angle cross sections 77−18600
^{56}Fe(^{16}O, ^{16}O′)^{56}Fe, magnetic substate population, closed formalism based on DWBA 77−6424
^{56}Fe(^{16}O,X), 81 MeV, fragments in incomplete fission 77−14153
^{56}Fe(^{3}He, ^{3}He), 33-83 MeV, details of nuclear surface 77−34324
^{56}Fe(^{3}He,t)^{56}Co, ang. distrib. meas., DWBA calc. 78−29491
^{56}Fe(^{6}Li, X), 75 MeV, Z=1 or 2 fast particle prod. mechanism above Coulomb barrier 80−42687
^{56}Fe(α,α), 15-19 MeV, inelastic scatt. form factors, Coulomb-nuclear interference region 78−66288
^{56}Fe(α,α), 2^{+} collective level excitation, microstruct. of diffr. ang. distrib. 77−61440
^{56}Fe(α,γ), 4.2-7.1 MeV, reaction cross section, statistical model anal. 79−45278
^{56}Fe(e,α), E2 isoscalar resonance sum rule, DWBA anal. 80−68621
^{56}Fe(e,e′), 0.1-14 GeV, deep inelastic inclusive scatt. response functions and momentum distrib. 80−42640

nuclei with mass number 39 to 58 continued

^{56}Fe(e,e′), Coulomb form factor for $O^{+}\rightarrow 4^{+}$ transition, collective 4^{+} states, shell model 80−57664
^{56}Fe(e,e′), longitudinal and transverse inelastic response functions and cross sections 80−57771
^{56}Fe(e,e′α), 60 and 120 MeV, evidence for α-clusters 79−6569
^{56}Fe(γ,γ), up to 12 MeV, highly excited spin-1 resonances, γ-transitions 80−13427
^{56}Fe(γ,n), 13.3 MeV bremsstrahlung, resonance spectrum and cross-section meas. *(Russian)* 77−6349
^{56}Fe(n, n′), transmission of neutrons at 24.37 keV 79−54435
^{56}Fe(n, n), 1.77 to 3.0 MeV, validity of Wick's inequality in the calculation of the lower limits of the differential elastic cross sections 80−5137
^{56}Fe(n, n), up to 1 MeV, cross section by coupled channels method, simple vibrational model 78−70535
^{56}Fe(n, p), 14-19 MeV, cross section meas., neutron flux, secondary standard 79−13291
^{56}Fe(n,2n), direct process contrib., cross section, DWTA and DWBA anal. *(Russian)* 78−78386
^{56}Fe(n,2nγ),(n,n′γ), 14.6 MeV, γ-ray ang. distrib. *(Russian)* 77−88147
^{56}Fe(n,γ), 2.5-870 keV, resonance neutron capture study 77−2990
^{56}Fe(n,γ), 6-150 keV, shape anal. and width correlations 77−26766
^{56}Fe(n,γ), anal. of gamma decay of ^{57}Fe 1.167 keV $p_{1/2}$ resonance 77−30585
^{56}Fe(n,γ), resonance state, partial radiation widths of high energy transitions 78−13104
^{56}Fe(n,γ)^{57}Fe, high energy γ-ray transitions of ^{56}Fe resonances, E_n=7 to 70 keV 77−23081
^{56}Fe(n,n′), 14 MeV, ang. distrib., reaction mechanism 77−26756
^{56}Fe(n,n′), 14 MeV, γ competition in decay of unbound states 78−8811
^{56}Fe(n,n′γ), 14 MeV, ratio of γ to neutron width 77−30593
^{56}Fe(n,n′γ), 14.6 MeV, maximum excitation state γ-decay, cross section *(Russian)* 80−68586
^{56}Fe(n,n′γ), 1.57-2.8 MeV, low levels excitation *(Russian)* 78−41722
^{56}Fe(n,n′γ), up to 14.6 MeV, radiation and neutron widths for highly excited levels *(Russian)* 78−605
^{56}Fe(n,n), 14.6 MeV, radiation widths and particle widths of highly excited states, γ-transitions 79−6409
^{56}Fe(n,p)^{56}Mn, 12 to 18 MeV, cross section meas. *(Chinese)* 79−22297
^{56}Fe(n,p)^{56}Mn, 14.8 MeV, absolute cross-section meas. using on-line neutron flux monitoring system 77−34300
^{56}Fe(n,p)^{56}Mn, 14.8 MeV, cross section determ. 78−37347
^{56}Fe(n,p)^{56}Mn, 6-10 MeV, cross-sections meas. 79−93613
^{56}Fe(n,p)^{56}Mn, ave. neutron activation cross sections for ^{241}Am-Be source 79−31282
^{56}Fe(n,p)^{56}Mn, for ^{56}Mn(2.58 hr) preparation 78−50178
^{56}Fe(n,p)^{56}Mn threshold reaction cross section, ^{252}Cf source 77−23039
^{56}Fe(ν_{μ}, μ^{-}+L^{+}+L^{0})^{56}Fe neutrino-induced heavy-lepton pair production at high energies and multimuon events 79−89298
^{56}Fe(p,2n)^{55}Co carrier-free positron-emitting label for bleomycin 79−79648
^{56}Fe(p,γ)^{57}Co, 3.7 to 3.8 MeV, gamma decay of $g_{9/2}$ isobaric analog resonance 79−63674
^{56}Fe(p,p), 100-2200 MeV, total and reaction cross sections from optical pot. 80−18303
^{56}Fe(p,p), 6 MeV, elastic and inelastic, quadrupole deformation, IAR excitation, optical pots. *(Russian)* 80−63149
^{56}Fe(p,p), elastic scatt. in giant reson. region of ^{57}Co 77−18542
^{56}Fe(p,p), elastic scatt. in giant reson. region of ^{57}Co 77−18543
^{56}Fe(ρ,α)^{53}Mn, 35 MeV, nuclear struct. study 79−75980
^{56}Fe(t,p)^{58}Fe, 17 MeV, polarised triton, meas. and two-step calcs. 77−54204
^{57}Fe,, Mossbauer spectra 77−73100
^{57}Fe, 14 keV, nuclear resonance excitation by synchrotron radiation 78−78363
^{57}Fe, 14 keV state excitation by synchrotron radiation 78−25147
^{57}Fe, (n,γ), cross section, 2.5-200 keV, s-wave resonances 80−18309
^{57}Fe anomalous M1/E1 strength ratio and doorway states from ^{56}Fe(n,γ) 80−57730
^{57}Fe enriched Fe crystal, Mossbauer transition γ-quanta 77−20780
^{57}Fe, gamma decay of 1.167 keV $p_{1/2}$ resonance obs. in ^{56}Fe(n,γ) 77−30585
^{57}Fe, γ-ray emission, test of time reversal invariance 78−29421
^{57}Fe, hyperfine mag. field in $FeSn_2$, Γ-reson. spectroscopy obs. *(Russian)* 78−39486
^{57}Fe implants in Si, electric quadrupole coupling at Fe nuclei 78−27137
^{57}Fe in Ti, quadrupole interaction, Mossbauer and PAC meas. 77−48101
^{57}Fe, in Ti, V, or Cu, press. depend. of Mossbauer fraction 77−16226
^{57}Fe, isomer shift scale construction, based on nuclear gamma resonance *(Russian)* 78−35070
^{57}Fe, Mossbauer absorption line function for a polycrystalline quadrupole-split absorber situated in a large applied magnetic field 79−87340
^{57}Fe, Mossbauer effect in BCC ternary Fe alloys 77−59396
^{57}Fe, Mossbauer effect in dimethylammonium iron chloride 77−66443
^{57}Fe Mossbauer effect in $Fe_2(MoO_4)_3$ 77−48108
^{57}Fe, Mossbauer effect in Ge, appl. of in-beam implantation method 78−25372
^{57}Fe, Mossbauer effect in haemin-histidin *(Spanish)* 77−73098
^{57}Fe, Mossbauer effect in $KMnF_3$ 77−20779
^{57}Fe, Mossbauer effect in $NpFe_2Si_2$ 77−28406
^{57}Fe, Mossbauer effect in solid N_2 matrix 77−59496
^{57}Fe, Mossbauer effect in TiAl *(Russian)* 77−1621
^{57}Fe, Mossbauer emission diffr., in weakly ferromag. single cryst. $FeBO_3$ *(Russian)* 77−81038
^{57}Fe, Mossbauer expts. on optically active chiral molecules, optical activity analogy 78−27124
^{57}Fe, Mossbauer obs. in Fe (III) bis(dithiocarbamato) iodides 77−20759
^{57}Fe, Mossbauer obs. in human transferrin 77−21481
^{57}Fe, Mossbauer polarimetric resonance electron spectroscopy, theory 79−99808
^{57}Fe, Mossbauer spectra of $FeBr_2$ and FeI_2, spin ordering obs. 78−43720
^{57}Fe, Mossbauer spectra of powders, ambiguity problem *(Japanese)* 77−66449
^{57}Fe Mossbauer spectroscopy, added precision 77−88327
^{57}Fe, NMR spectra meas. in $Sm_3Fe_5O_{12}$, spin-reorientation phase transition 77−28458
^{57}Fe nuclei, spin-echo signal recording by pulse generator and fast signal averager 78−21188
^{57}Fe, resonance line shifts, double Mossbauer spectrometer 78−82560

nuclei with mass number 39 to 58 continued
^{57}Fe resonant absorber, anomalous γ-ray transmission, energy spectrum *(Russian)* 77−28501
^{57}Fe, rot. band mixing microscopic theory using modified Kuo-Brown interaction 80−68513
^{57}Fe, semi-microscopic calc. of levels, spectroscopic factors and EM props. 77−2912
^{57}Fe, yrast decay schemes from ^{48}Ca+heavy ion fusion evaporation reacts. 78−66308
^{57}Fe^{m}, Mossbauer level excitation using specific characts. of synchrotron radiation 78−66447
^{57}Fe(III) species, prod. by electron capture decay in ^{57}Co labelled Co(III) cpds. 77−63329
^{57}Fe(α,pγ), 13 MeV, ^{60}Co low lying states, spin constraints, γ mixing ratios 78−29487
^{57}Fe(n,X) transmission data up to 400 keV, J^{π} value for resonances 80−18311
^{57}Fe(p,p')^{57}Fe*, excited 5/2$^-$ state mag. moment 79−93512
^{58}Fe energy level lifetimes up to 4213 keV from ^{55}Mn(α,pγ) 79−17853
^{58}Fe high spin states from ^{55}Mn(d,pγ), decay props., γ-γ coincidence 78−21515
^{58}Fe levels, J^{π}, anal. powers and cross sections from ^{56}Fe(t,p) pol.t 80−68539
^{58}Fe, surface structure analysis using Blair phase shifts 78−12959
^{58}Fe, yrast decay schemes from ^{48}Ca+heavy ion fusion evaporation reacts. 78−66308
^{58}Fe+n, total cross section from 7 to 325 keV, resonance struct. anal. 78−74357
^{58}Fe(^{3}He,p), ^{60}Co low lying states, DWBA anal. 78−29478
^{58}Fe(^{7}Li, ^{7}Li), 34 MeV, ang. distribs., cross sections, double folding model anal. 80−78313
^{58}Fe(γ,n), near threshold, cross sections 78−13055
^{58}Fe(n,γ) capture and total cross section meas. below 325 keV, resonance parameters 80−18314
^{58}Fe(n,λ), resonance capture cross section s- and p-wave radiative widths 80−47476
^{58}Fe(n,n), 0.03-500 keV, total cross section, resonance parameters and level spacings 79−6603
^{58}Fe(t,^{3}He), 23 MeV, ^{58}Mn energy levels, mass excess, spin-parity assignments 77−54230
Fe(α, 2α), 700 MeV, cross section, effective cluster number from PWIA, momentum distrib. 79−40940
Fe(α,n), 3.6 to 8 MeV, neutron yields 79−6651
Fe(e,e), nuclear radius, core polarisation and isotone shifts, muonic X-rays 80−22685
Fe(γ,n), A=54, 56, GDR intermediate struct. in 5-26.3 MeV range 77−74824
Fe(n,X), 14.8 MeV, γ-prod. cross section 79−49622
Fe(n,X), 3 eV-1 MeV transmission meas., resonance anal. 80−18316
Fe(n,2n), displacement per atom cross section, sensitivity rel. to n ang. distrib., energy spectra 79−36236
Fe(n,2n), primary knock-on spectra, sensitivity rel. to secondary n spectra, ang. distrib. 79−36236
Fe(n,γ), 24-160 keV, multigroup capture cross section and self shielding factor 77−26773
Fe(n,γ), A=56, 58, γ circular polarisation meas. 78−62533
Fe(n,γ), absolute cross sections keV range 77−26771
Fe(n,γ) cross-section meas. principal resonance parameters 80−18312
Fe(n,γ), determ. of recoil energy and effective mass from narrow resonance line shapes 77−57660
Fe(n,γ), on-line gamma anal. using Ge detector 80−52624
Fe(n,n) 2.9 MeV, elastic differential cross section and polarisation ang. depend., statistical anal. 79−45264
Fe(n,n), elastic and inelastic scatt., cross sections meas. and calcs. 78−13081
Fe(n,n), fast neutrons, differential cross sections, optical model calcs. *(Chinese)* 79−9572
Fe(n,n), pol. n, 16.1 MeV, differential cross section, optical model fit 80−32259
Fe(n,n′ unresolved), displacement per atom cross section, sensitivity rel. to n ang. distrib., energy spectra 79−36236
Fe(n,n′ unresolved), primary knock-on spectra, sensitivity rel. to secondary n spectra, ang. distrib. 79−36236
Fe(n,n′γ), 8.5 to 14.2 MeV, differential cross section for prod. of 0.847 MeV γ-ray 77−23080
Fe(n,xn), 20.6 MeV, neutron yield cross sections and spectra *(Russian)* 80−91188
Fe(p,X), 10-60 MeV, long lived radioisotope prod. cross sections and excitation functions 79−89305
Fe(p,γ), absolute resonance strengths meas. using separated targets 77−79374
Fe(p,p), 36.2 MeV, differential cross section, asymmetries, 0 to 7° scatt. 78−94002
Fe(p,p′), A=54,6, E=17.2, 20.4, 24.6 MeV polarised protons, optical model, DWBA anal. 78−13094
Fe(p, spallation), 0.08-24 GeV, Ar isotopes, spallation ratios and prod. cross sections 80−9284
Fe(π,X), 125 MeV, absorption cross section in 3:3 resonance region 79−85543
Fe(π^+,π^+) elast. and inelast. scatt., 50 MeV, ang. distrib. determ. optical model and DWBA 79−45304
^{175}Hf, thick-target yields in Ta due to proton bombardment up to 100 MeV 77−88312
K (Ar, π^+X), 250, 400 MeV/A, pion yield near threshold 80−18344
K, A=48, 49, 50, half lives, γ meas. 78−74341
K, nuclear charge radius from μ^- X-ray transitions 78−66195
K odd isotopes, $2s_{1/2}^{-1}$ and $1d_{3/2}^{-1}$ hole state separation energies 79−67634
K, strength function of deeply bound hole states 78−17113
^{40}K, isotope relative abundance, radioactivity expt. for schools 79−21511
K+Ar, 800 MeV/A, wide angle inclusive proton spectra 79−40951
K(Ar,X), 0.4-1.8 GeV/u, multipion prod. energy depend. 80−106065
K(Ar,X), 800 MeV/N, single particle spectra from high multiplicity events 80−99184
K(Ar,X), proton inclusive spectra, direct plus thermal model 80−57799
^K, A=37,39, levels, excitation and microscopic form factors, DWBA calcs. from Ca(p,α) 80−32185
^K, A=40,42, EM transitions and transition probabilities for low lying states 79−75896
^K, A=43,44, levels, spin and parity assignments, decay scheme from ^{43,44}Ar β-decay 79−13210

nuclei with mass number 39 to 58 continued
^K, A=45,46, levels, lifetimes and transitions from Ar β-decay 80−42597
^{38}K excitation spectrum and distrib. from ^{40}Ca(π^-, 2n), absorpt. at rest 78−66322
^{39}K 9/2$^-$ forbidden transition, cross section CCBA anal., L=1 transitions from ^{40}Ca(^{15}N,^{16}O) 79−9507
^{39}K, appl. to nucleon stability tests, radiochemical and geochemical method limits 79−22093
^{39}K, charge density and single particle state struct. 79−36144
^{39}K, contrib. to fast neutron dose to the human body 80−51263
^{39}K de-excitation, continuum γ-ray emission and ang. momentum dissipation 77−6293
^{39}K, evaporation residue from ^{27}Al+^{12}C, prompt γ deexcitation 78−74395
^{39}K, giant dipole resonance region radiative nucleon capture, expt. ang. distrib. coeffs., direct-semidirect theory 78−74354
^{39}K high spin states, J^{π} assignments, DWBA anal. of ^{41}Ca(d,α), 22 MeV, ^{39}K high spin states, J^{π} assignments, DWBA anal. 79−40851
^{39}K high spin states from ^{24}Mg(^{18}O, p2nγ), decay scheme 78−25232
^{39}K high spin states from ^{28}Si(^{16}O,αpγ), γ meas. 78−89787
^{39}K in frog striated nuscle, pulsed NMR 77−16920
^{39}K, J^{π}, hole-core wave functions via ^{39}K(α,α′) 31 MeV 77−50056
^{39}K low lying analogue states, DWBA anal. from ^{40}Ca(d,^{3}He) 29 MeV, polarised d 78−82285
^{39}K, NMR obs. of struct. transitions in $Rb_xK_{1-x}MnF_3$ 77−47577
^{39}K, produced in ^{40}Ca(p, 2p), ground and excited states, DWIA calcs. 78−62535
^{39}K $s_{5/2}$ and $d_{3/2}$ states from ^{40}Ca heavy ion L=1 pickup reactions 79−67734
^{39}K, spins of p-h states from analysing powers of (d,τ) reacts. 78−25111
^{39}K states and spectroscopic strengths DWBA anal. of ^{40}Ca(^{7}Li,^{8}Be) 80−5069
^{39}K+^{14}N fusion-evaporation reaction γ-ray spectroscopy study of ^{51}Mn structure 77−18471
^{39}K(^{12}C,^{12}C), 54, 63 MeV, angular distrib., Woods-Saxon and double-folding optical models 80−52691
^{39}K(^{39}K,X), π^0 condensation, spin-isospin instabilities, TDHF calcs. 80−83042
^{39}K(α,p), 9.5, 16 MeV, ^{42}Ca high spin states, lifetimes, multipole mixing ratios 78−50186
^{39}K(d,α)^{37}Ar, 1.83-2.53 MeV, fluctuations analysis and spin values deduced 77−23095
^{39}K(e,e′), mag. dipole and quadrupole state excitation 78−50154
^{39}K(p,^{3}He), 40 MeV, DWBA anal. 78−66278
^{39}K(p,t), 40 MeV, DWBA anal. 78−66278
^{40}K, conc. in New Zealand soil, rel. to Fe, K content 77−86867
^{40}K, decay consts. for use in geochronology and cosmochronology 78−28189
^{40}K energy levels and spectroscopic strengths from ^{41}Ca(d,^{3}He) 79−89238
^{40}K excitation energy, γ decay, of lowest T=2 state populated in ^{40}Ar(p,n) 78−8769
^{40}K, g-factor determ. from perturbed ang. distribs. 78−12970
^{40}K, γ-ray energies meas. for Ge(Li) detector calibration 80−27865
^{40}K, implantation in Fe, perturbed ang. distrib. 78−12969
^{40}K, lifetime determ. using Doppler shift attenuation 79−93551
^{40}K Mossbauer isomer shifts, book contrib. 79−87363
^{40}K, naturally occurring, gamma-ray emission energies 80−52811
^{40}K, yrast levels, J^{π}, branching and mixing, via (^{16}O,pnγ) 34 MeV 77−74759
^{41}K, γ-decays of low-lying states obs. with (Ar,p), (Ar,n) 77−41986
^{41}K, highly stripped ions, recoiling in vacuo, γ-decays of isomeric states obs. 78−50119
^{41}K, implantation in Fe, perturbed ang. distrib. 78−12969
^{41}K, l-forbidden M1 decay from 1st excited state 78−13024
^{41}K nucleus 11.36 MeV analog state total angular momentum from ^{40}Ar(p,p) reaction *(Russian)* 80−102169
^{41}K states from ^{40}Ar(d,n), lifetimes meas. by DSA method 78−78308
^{41}K yrast states from ^{26}Mg(^{18}O, p2nγ), γ meas., spin, parity, branching and mixing 78−58250
^{41}K(α,d)^{43}Ca, 40 MeV, four-particle one-hole states 78−21580
^{41}K(α,n)^{44}Sc, 5-11 MeV, ^{44}Sc mean lifetimes deduced 77−6299
^{41}K(p,p′), impurity in Co, hyperfine field calc. by gamma ray ang. corr. method 78−6340
^{41}K(p,pγ), 1.58 MeV, parity doublet gamma lifetimes, 3/2 levels, parity mixing 80−78209
^{42}K, levels, studied by ^{44}Ca(d,α)^{42}K reactions, 11 MeV, DWBA analysis 78−8723
^{42}K, yrast state J^{π} assignments via ^{26}Mg(^{18}O, pnγ) anal. at 25,34 MeV 77−57618
^{43}K 738 keV state g-factor, PAC technique 77−6227
^{43}K, (7/2)$^-$ 738 keV state g-factor and lifetime 77−10367
^{43}K high spin states, J^{π} and lifetimes from ^{40}Ar(α,pγ) 79−67621
^{43}K, myocardial imaging agents comparison 77−2037
^{43}K, prod. by V target bombard. with medium energy protons, separation, medical appls. 77−81572
^{44}K excited levels, J^{π}, transitions and lifetimes from ^{48}Ca(p,αn) 80−68544
^{44}K excited states from ^{44}Kr β decay, weak coupling predictions, γ-ray meas. 78−74336
^{45}K β-decay, ^{45}Ca levels, excitation functions and J^{π} 80−105978
^{45}K deduced energy levels from ^{45}Ar decay 78−78319
^{46}K deduced energy levels from ^{46}Ar decay 78−78319
^{46}K levels, J^{π} and tensor anal. powers from ^{48}Ca(d,α), pol.d 80−102113
^{47}K, single particle states lifetimes calcs. 80−105943
^{48}K mass excess and 0.58 MeV excited state from ^{48}Ca(^{7}Li,^{7}Be), 52 MeV 79−446
^{48}K mass excess and states from ^{48}Cu(^{7}Li,^{7}Be) 80−9221
K(n,n), 14 MeV, differential cross-section meas. 77−88130
^{24}Mg(^{32}S,2αp)^{47}V, ^{47}V $1f_{7/2}$ shell model and high spin states 78−62560
^{24}Mg(^{32}S,α3p)^{49}V, ^{49}V $1f_{7/2}$ shell model and high spin states 78−62560
Mn, A=54-6, yrast decay schemes from heavy-ion fusion evaporation reactions 77−82854
Mn levels from ^{50,52,54}Cr(α, p), 18, 26 MeV, J-depend., spins, parities 78−78397
Mn photonuclear cross sections in giant reson. region 78−17178
^Mn, A=51, 53 small angle cross sections for levels, DWBA anal. from Cr(^{3}He,d) 79−22203
^{32}Mn, $1f_{7/2}$ shell isobaric analogue states, displacement energies 79−13207

nuclei with mass number 39 to 58 continued
^{49}Mn, β^+-decay superallowed branch, ^{49}Cr levels, transitions, and Gamow-Teller matrix elements 80−57746
^{50}Mn populated in ^{50}Cr(^{3}He,t), precise Q-value, β decay energy, half life 77−30618
^{51}Mn, collective bands of positive parity states, HF calcs. 78−54677
^{51}Mn, collective states from heavy ion reactions, shell model calcs. 78−62560
^{51}Mn, EM transitions, J^π, half-lives, branching and mixing ratios 77−18471
^{51}Mn, lifetimes of some low-lying l=1 states 77−79393
^{51}Mn, p-wave reson. determ. from ^{50}Cr(p,p'γ) 77−41961
^{52}Mn, ^{53}Mn, selective population of high-spin states in heavy ion reactions 77−18374
^{52}Mn, 2-5 GeV photospallation, ratios of isomeric yields *(Russian)* 78−46047
^{52}Mn, γ-spectra, levels, J^π via α+^{50}Cr reaction 77−74794
^{52}Mn half-life meas. 78−17152
^{52}Mn, high spin state spectroscopy via ^{39}K(^{16}O,2pnγ) 37-52 MeV 77−10321
^{52}Mn, low-lying states J, γ-branching and mixing via ^{52}Cr(p,nγ) 77−14028
^{52}Mn, mag. hyperfine splitting const. in Co, NMR-ON meas. 78−43651
^{52}Mn, oriented, β-decay asymm., positron ang. distrib. meas., matrix elements 77−2951
^{52}Mn populated in Cr(π^+, π^-), deexcitation γ spectra 78−89912
^{52}Mn, recoil-implanted in Au, nuclear orientation 78−43716
^{52}Mn yrast state properties, transitions and decays from ^{52}Fe ^{M} β^+-decay 79−67631
^{53}Mn fragmented $g_{9/2}$ isobaric analogue resonance, transitions, J^π assignments from ^{52}Cr(p,γ) 79−45240
^{53}Mn fragmented $g_{9/2}$ isobaric analogue resonances, γ-transitions from ^{52}Cr(p,γ) 79−85430
^{53}Mn fragmented $g_{9/2}$ isobaric analogue resonance, γ-spectra and excitation functions from ^{52}Cr(p,γ) 80−68627
^{53}Mn, γ decay and splitting of analogue states from ^{52}Cr(^{3}He,dγ) at 18 MeV 78−70505
^{53}Mn high spin states, decay scheme, J^π assignments, mixing ratios from ^{40}Ca(^{16}O, 3pγ) *(French)* 79−67627
^{53}Mn high spin states, lifetimes, shell model calcs., yrast levels from ^{48}Ca(^{16}B, 5n) 79−6425
^{53}Mn, isobaric analogue states via ^{52}Cr(^{3}He,d) and ^{52}Cr(^{3}He,dp) 77−6237
^{53}Mn level scheme, DWBA and optical model anal. from ^{52}Cr+^{13}C 79−36159
^{53}Mn lifetimes meas. from ^{50}Cr(α,pγ)^{53}Mn *(French)* 79−67711
^{53}Mn low lying states, DWBA anal., shell model wave functions from ^{56}Fe(p,α) 80−32211
^{53}Mn, preparation in cyclotron by target bombard., extraction, anal. 77−61441
^{53}Mn, spectra, particle-hole conjugation and protection theorems *(Chinese)* 80−73796
^{53}Mn(ρ,α)^{52}Cr, 35 MeV, nuclear struct. study 79−75980
^{54}Mn, electron-capture decay, K X-ray emission rate determ. 78−21530
^{54}Mn excited state lifetimes from ^{51}V(α,n) 79−26392
^{54}Mn, intruder states and configuration purity 77−38223
^{54}Mn, level determ. in seawater 78−85608
^{54}Mn low lying 2p-4h states, J^π from tensor anal. powers of ^{56}Fe(d,α), pol.d 80−99124
^{54}Mn, nuclear orientation in Ag-Mn dil. alloy 78−43713
^{54}Mn orientation in dil. Au-Mn(Cr)(Fe), spin glass state and Kondo effect 78−6514
^{54}Mn, populated in ^{52}Cr(α,pnγ), low lying intruder states 79−58998
^{55}Mn, 14.7 MeV neutron capture cross-section measurements with activation technique 80−32282
^{55}Mn (^{12}C,X), 77 MeV, fragments in incomplete fission 77−14153
^{55}Mn energy level excitation curve, bound state and resonance γ-decay from ^{54}Cr(p,γ) 79−476
^{55}Mn, energy levels, bound state mean lifetimes and spins from ^{54}Cr(p,γ) 80−42586
^{55}Mn, in $KMnO_4$, second-order quadrupole splitting, asymmetry parameter 77−63312
^{55}Mn in $MnFeO_2$, NMR freq. dynamical shift for nuclei in domain walls *(Russian)* 77−40148
^{55}Mn, levels, J^π, γ-branching via (n,n'γ) 1.0-3.6 MeV 77−79310
^{55}Mn, NMR and mag. meas. in BCC Fe-Co-Mn and Fe-Ni-Mn alloys 78−39442
^{55}Mn, NMR in Mn_4N_x 78−2768
^{55}Mn, NMR in MnO_4, O isotope effect on nuclear mag. shielding 77−10691
^{55}Mn, NMR meas., hyperfine field in weakly antiferromag. β-Mn alloys 78−39441
^{55}Mn, NMR of impurity spin in $CoCl_2.2H_2O$ 77−85613
^{55}Mn, NMR spin echo spectra in BCC ternary Fe alloys 77−59396
^{55}Mn, neutron capture cross sections, MeV region, using activation technique 78−86535
^{55}Mn, neutron resonance spectroscopy, R-matrix anal. 78−21555
^{55}Mn, nucl. quadrupole moments from laser-RF double reson. spectroscopy 80−57682
^{55}Mn, nucl. spin-lattice relax. in ferromag. β_1-MnZn 77−36147
^{55}Mn, proton-neutron correl. shell model for collective motion 77−79312
^{55}Mn, resonance activation neutron detector materials, uni-resonance approx. technique for higher resonance reaction rate 77−75030
^{55}Mn, spallation by 0.3-1.0 GeV photons, cross-sections 78−41691
^{55}Mn, spin echo form., parametric mechanism, spin dynamics *(Russian)* 78−23367
^{55}Mn, spin echo meas. in disordered $(Fe_{1-x}Mn_x)_3Al$ alloys 77−63112
^{55}Mn, temp. depend. of NMR linewidth in $RbMnF_3$ 77−63292
^{55}Mn transitions to low lying levels, α spectroscopic strengths, DWBA anal. of ^{51}V(^{6}Li,d) 79−45156
^{55}Mn(^{3}He,3n)^{55}Co, nuclear medicine appl. 80−36132
^{55}Mn(α,α), 4.5 to 7 MeV, Coulomb excitation, search for 1.29 MeV $1/2^-$ level 78−82360
^{55}Mn(α,pγ), 12 to 24 MeV, ^{58}Fe high spin states, decay props., γ-γ coincidence 78−21515
^{55}Mn(γ,X), 2-5 GeV, spallation 77−71604
^{55}Mn(γ,γ), 5.5-11.4 MeV, interference between reson. and Thomson scatt. 78−33167
^{55}Mn(γ,xn), 10-36.5 MeV, photoneutron cross sections, integrated cross sections, giant dipole resonance 79−89289

nuclei with mass number 39 to 58 continued
^{55}Mn(n,X), 14 MeV, X=p,n'p,α,n'α,^{3}He, production cross-sections 80−42648
^{55}Mn(n,2n)$_3$, 14 MeV, cross section compilation 80−91181
^{55}Mn(n,α)^{52}V, neutron activation anal., Ge(Li) and NaI(Tl) detector γ-ray spectrometer 80−78485
^{55}Mn(n,γ), absolute cross sections in keV range 77−26771
^{55}Mn(n,γ)^{56}Mn, 2.5-600 keV, total cross section, resonance energies and capture area 79−6607
^{55}Mn(n,n'γ), 1.0-3.6 MeV, γ-branching meas. 77−79310
^{55}Mn(n,n'γ), 2.2-3.2 MeV energy level J^π assignments, transition branching and mixing ratios 79−40881
^{55}Mn(n,n'γ), populations of half integer spin mag. substates 77−30493
^{55}Mn(n,t), 14 MeV, cross sections, fast neutron reaction excitation function calc. 79−45267
^{55}Mn(ν,e) ^{55}Fe, cross section calc., appl. to solar neutrino expts. interpretation *(Russian)* 77−50119
^{55}Mn(p,n)^{55}Fe, 1.35-5.42 MeV, total cross section and isobaric analogue resonances, shape anal. 79−6604
^{55}Mn(p,n)^{55}Fe, neutron polarisation at isobaric analogue resonances 78−54759
^{55}Mn(p,p), (p,p'), cross section fluctuations anal. 78−21551
^{55}Mn(t,p)^{57}Mn, exciting ^{57}Mn low lying level struct. 77−74769
^{56}Mn, gamma intensity, from ^{55}Mn(n, γ) cross-section meas., k_0 factors calcs. 79−26433
^{56}Mn levels, transitions and spins from ^{55}Mn(n,γ), pol. Mn and n 80−78154
^{56}Mn, neutron generator, prep. by ^{56}Fe(n,p)^{56}Mn 78−50178
^{57}Mn half life 78−82321
^{57}Mn levels and J^π restrictions, from ^{57}Cr β-decay 78−70436
^{57}Mn, low lying level struct. via ^{55}Mn(t,p)^{57}Mn, shell model comparison 77−74769
^{57}Mn, yrast decay schemes from ^{48}Ca+heavy ion fusion evaporation reacts. 78−66308
^{58}Mn energy levels populated in ^{58}Fe(t,^{3}He), mass excess, spin-parity assignments 77−54230
^{58}Mn, yrast decay schemes from ^{48}Ca+heavy ion fusion evaporation reacts. 78−66308
^{59}Mn, β-decay scheme, $T_{1/2}$ and mass meas., astrophysical significance 77−26635
Mn(n,γ), primary transitions using focused 24 keV filtered neutron beam 80−63436
Mn(n,n), elastic and inelastic scatt., cross sections meas. and calcs. 78−13081
Nd, A=148, 150, pionic X-rays in 4f→3d transition, neutron isotope shift 77−75347
Ni, CC ^{56}Ni core excitation effects on A=57-66 nuclei, MSDI and ASDI comparison 78−78254
Ni doubly even nuclei, eqns. of motion method, pairing correlations, ground state energies 80−52585
Ni even isotopes, negative parity levels, Tam-Dancoff approx., ^{56}Ni core 79−3080
Ni, even nuclei, systematic meas. of mag. moments of 2_1^+ states 78−54682
Ni foils, activation by p, d, ^{3}He, ^{4}He from cyclotron beam, monitoring props. investig. 77−38578
Ni, fp shell model calcs., spectra and spectroscopic factors 80−68588
Ni isotopes, (n, particle) cross section data base construction, MeV range, statistical models 77−26728
Ni isotopes, pairing-plus-quadrupole interaction anal. 77−79313
Ni isotopes, shell model calcs. of BE, spectroscopic factors and excit. energies 77−22860
Ni mean square charge radii from isotope shifts 80−99484
Ni, radial charge distrib. moments, ground state correlations, generator coordinate model 79−30785
Ni+^{12}C, 107, 155, 197 MeV, evaporation residue Se, prompt γ deexcitation 78−74395
Ni+^{16}O, 100 MeV, deep inelastic, γ-circular polarisation and spin orientation 79−17848
Ni+^{20}Ne, 164 MeV, ang. distribs., total reaction and evaporation residue cross sections 79−565
Ni+p reactions, 12 to 45 MeV, excitation functions for Cu, Ni, Co, Mn isotopes prod. 78−66283
Ni(^{35}Cl,^{35}Cl), A=58,62, 100-170 meV, elastic scatt. ang. distrib. 78−21605
Ni(^{16}O,^{16}O')N*(2^+), A=58, 60, 62 at 42 and 48 MeV, DWBA anal. 77−74876
^{A}Ni A=57-59, $f_{7/2}$ hole configuration effects, shell model calcs. 80−22670
^{A}Ni, A=58, 64, neutron densities and single particle struct. 80−32165
^{A}Ni, A=58,60, search for giant quadrupole resonance 80−9281
^{A}Ni, A=58-64 even, magnetic mom. of 2_1^+ states from (^{32}S,^{32}S') at 72 MeV 78−66202
^{A}Ni, A=64, 58, level ang. momentum and spin values, DWBA anal. from (t,d) polarised t 79−36163
^{A}Ni+^{35}Cl, A=58, 62, 155-170 MeV, fission prod. yields, ang. distribs. and mean kinetic energies 78−41790
^{A}Ni(^{3}He, ^{3}He), A=58,60,62,64, 119 MeV, optical pot. parameters energy and mass depend. 80−32289
^{A}Ni(^{3}He, p), 8, 10 MeV, A=58, 60, 62, p spectra compound nucleus contrib., odd-even effect 80−106061
^{A}Ni(^{40}Ca, fusion), A=58, 60, 62, 113-170 MeV, fusion cross sections and excitation functions 80−32315
^{A}Ni(^{7}Li, ^{7}Li), A=58, 60, 34 MeV, ang. distribs., cross sections, double folding model anal. 80−78313
^{A}Ni(d,X), A=58, 64, 7.6 GeV/c, isotopic cross section ratios, He, Li fragments isotopic effects *(Russian)* 80−63154
^{A}Ni(e,e'), 102 MeV, A=58,60, E1-E4 giant multipole resonance comparison, shell model anal. 80−42614
^{A}Ni(e,e), 100-275 MeV, A=58,60,62,64, cross sections and muonic X-ray meas., charge distrib. systematics 80−86801
^{A}Ni(e,p),(e,α), A=58, 60, 62, electrodisintegration cross sections, E1, E2 absorption, DWBA anal. 80−106052
^{A}Ni(n,X), A=58,60, 14.8 MeV, charged particle emission, cross section, Hauser-Feshbach anal. 79−67750
^{A}Ni(n,X) A=58, 60, transmission data, resonance anal. 80−18317
^{A}Ni(n,n'γ), A=58-64, <4 MeV, gamma prod. and inferred cross sections 80−525
^{A}Ni(n,n), A=58,60,62,64, 5 MeV, differential cross sections, optical, statistical and coupled channel anals. *(Russian)* 80−37377

nuclei with mass number 39 to 58 continued

^{A}Ni($n_{th}\gamma$)$^{A+1}$Ni (A=58, 60, 62, 64), γ-ray spectra, level schemes, M1 and E2 strength functions 77−57674
^{A}Ni(p,X), A=58, 64, 7.6 10 GeV/C, isotopic cross section ratios, He, Li fragments isotopic effects *(Russian)* 80−63154
^{A}Ni(p,p), 1 GeV, A=58,60,62,64, elastic and inelastic, Glauber anal., matter distribs. 79−75883
^{A}Ni(p,p), A=58,64, polarised p, 0.8 GeV, neutron isotopic density differences and RMS radii 79−67643
^{A}Ni(p,$\pi^{\pm}$), A=58, 64, 660 MeV, pion energy spectra, isotopic effects *(Russian)* 80−42669
^{A}Ni(p,xγ), 80-164 MeV, A=58, 60, 62, 64, prod. cross sections, pre-equilibrium phase 80−78301
^{A}Ni($\pi^{\pm}$,xγ), 100-200 MeV, prompt and delayed γ spectra, nuclide yields 79−22332
^{14}Ni(α, α), A=58-64, 120-172.5 MeV, optical pot. uniqueness and shape 79−97719
^{55}Ni, β-decay GT matrix elements, $T_{1/2}$ 78−557
^{55}Ni, β-decay half-life and GT matrix element 77−22950
^{55}Ni, half-life meas. 77−22951
^{56}Ni excitation functions from ^{40}Ca(^{16}O,X) fusion 80−18362
^{56}Ni formation cross section, TDMF calcs. for fusion in ^{16}O+^{40}Ca and ^{28}Si+^{28}Si 79−93676
^{56}Ni from HI reactions, superdeformed nucleus decay, α-decay amplification 80−68608
^{56}Ni, nucleosynthesis in Type I supernovae rel. to radioactive excitation source model for late time spectra 80−105264
^{56}Ni, partition functions, astrophysical implications 79−21167
^{57}Ni, cyclotron prod. by ^{3}He bombardment of natural Fe, bleomycin complex synthesis 77−86629
^{57}Ni energy levels, spin and parity assignments from ^{59}Ni(p,t) 79−9475
^{57}Ni, fine struct. of ground hole-state analogues 78−50065
^{57}Ni, fine structure of hole-state analogues, isospin mixing 80−13401
^{57}Ni high spin yrast cascade, decay modes J assignment from ^{54}Fe(α,nγ) 80−68514
^{57}Ni levels and analogue states, J^{π} from DWBA anal. of ^{58}Ni(^{3}He, α) 79−63592
^{57}Ni, mass excess determ. from ^{59}Ni(p,t)^{57}Ni and ^{58}Ni(^{3}He,α)^{57}Ni 77−18376
^{57}Ni, studied via ^{54}Fe(^{6}Li,t)^{57}Ni, t-energy spectra and reaction mechanism 78−41756
^{57}Ni, various orbit contribs. to mag. moment 78−78254
^{58}Ni, 6.02 and 5.59 MeV state J^{π} determ. via (α,α′) and (^{6}Li,d) 77−54148
^{58}Ni (^{7}Li, ^{7}Li), 14.22 MeV, alignment axis orientation depend. of cross section, mass quadrupole moment alignment 80−68638
^{58}Ni, (α,p), (α,d) and (α,t) reactions, 50.5 MeV, particle spectra 77−6405
^{58}Ni, (p, X), E_p=7.5 GeV, yields of hydrogen and helium isotopes *(Russian)* 79−93627
^{58}Ni (p,p), 1.04 GeV, elastic scatt. 78−21549
^{58}Ni (p,p) 100 MeV, systematic optical model anal. 78−66274
^{58}Ni, charge density, HF calcs. from (e,e) data 79−89260
^{58}Ni, charge density, single particle struct., using proton wave functions 78−45995
^{58}Ni, comparison of proton and electron scatt., large momentum transfer 77−38262
^{58}Ni compound nucleus decay, fusion products from ^{46}Ti+^{12}C 79−40979
^{58}Ni compound nucleus in ^{54}Fe(α,p), resonance struct., α-widths 77−30617
^{58}Ni, cross sections for charged particle prod. by 14 MeV neutrons, data compilation 80−9289
^{58}Ni, determ. of g-factor of 2_1^+ state in Fe 78−43697
^{58}Ni, elastic and inelastic neutron scatt., 1.5-3 MeV *(Russian)* 77−26689
^{58}Ni, giant electric resonances, study of ^{54}Fe(α,γ)^{58}Ni 78−41739
^{58}Ni, giant resonance αecay modes in (e,p) and (e,d) cross section study 79−17877
^{58}Ni, HFB and dynamic anal., collective motion, zero point energy correction 80−18161
^{58}Ni, isoscalar giant quadrupole reson., decay modes 79−63649
^{58}Ni, isovector M8 strength fragmentation, inelastic electron scatt. meas. 78−37305
^{58}Ni, Lipkin-Nogami method, ground state props. 78−50103
^{58}Ni, mag. quadrupole resonance, M2 strength distrib., quasiparticle-phonon model 79−75947
^{58}Ni, mean lifetime meas., 1400 to 1650 keV range, by reson. scatt. of bremsstrahlung *(French)* 79−75905
^{58}Ni, nuclear radii, energy density and HF-BCS methods 80−47363
^{58}Ni one-nucleon transfer reactions form factors, Pauli principle *(Russian)* 77−6393
^{58}Ni, partial radiation widths from neutron capture resonances, valency model calcs. 77−26707
^{58}Ni, short-range correlations and pseudopotentials, Hartree Fock Bogoliubov method for even-even isotopes 78−535
^{58}Ni spallation by 1 GeV protons, reaction channels *(Russian)* 78−74370
^{58}Ni, spherical nuclei, excitation of collective in high-energy proton interactions 78−17073
^{58}Ni, spherical nuclei, total binding energy, many body field theory 77−30482
^{58}Ni, tensor open-shell RPA calcs., M2, M8 excitations 79−22216
^{58}Ni vector polarised ^{6}Li elastic scatt., full optical model anal. 78−70553
^{58}Ni+^{11}B, 116 MeV, in-plane heavy ion-alpha particle correlations 79−17921
^{58}Ni+^{14}N, 148 MeV, 2-particle pre-emission meas. 79−93649
^{58}Ni+^{16}O, 100 MeV, γ-ray circular polarisation meas. 78−54788
^{58}Ni+^{16}O, 96 MeV, particle spectra for hot spot emission 79−22312
^{58}Ni+^{16}O, ang. correl. in compound nucleus decay 79−36261
^{58}Ni+^{16}O, deep-inelastic collisions, light particle pre-equilibrium emission 78−54786
^{58}Ni+^{16}O deep inelastic collision, hot spot particle emission 78−13152
^{58}Ni+^{16}O fusion, 30-70 MeV, statistical model calcs., yrast states and continuum feeding times 79−579
^{58}Ni+^{208}Pb(^{238}U), 7.5 MeV/amu, ang. momentum transfer in deeply inelastic collisions from exclusive sequential-fission expts. 79−76044
^{58}Ni+^{23}Na, deformed aligned projectile ions, elastic scatt., fusion, polarisation effects 78−58303
^{58}Ni+^{32}S, 110, 132 MeV, fusion evaporation residues, Monte Carlo simulation 78−41799

nuclei with mass number 39 to 58 continued

^{58}Ni+^{40}Ar, deep inelastic collision at 280 MeV, fragment energy and spin 78−21599
^{58}Ni+^{40}Ar, triple differential cross-section, dynamical model calcs. 78−50212
^{58}Ni+^{58}Ni(^{63}Cu), 290 MeV, prod. of neutron-deficient Te, I, Xe 77−88171
^{58}Ni+^{6}Li(^{7}Li), 12.7 MeV, isotopic shape effects in elastic scatt. of aligned ions 78−89904
^{58}Ni+p, 1 GeV, alpha-particle decay channels 80−22826
^{58}Ni+p, 5.65 and 6.50 MeV, compound nucleus time evolution meas. 78−50160
^{58}Ni+p, K-shell X-ray photon proton coincidences, nucl. time delay 79−18281
^{58}Ni+π, E_{π}=0, 45 MeV γ-ray spectra, prod. cross-section for residual nuclei meas. 78−649
^{58}Ni(^{12}C,2p)^{68}Ge, E=36 MeV, lifetimes of ^{68}Ge excited states 78−13020
^{58}Ni(^{16}O, 2pγ), 54.5, 59.5, 64.5 MeV high spin and excitation energy regions in ^{72}Se, γ cascade 78−54795
^{58}Ni(^{16}O, X), 70 MeV, compound nuclei charged particle evaporation, moment of inertia 80−57785
^{58}Ni(^{16}O,^{12}C), 46, 60 MeV, DWBA anal. with optical pot., ^{62}Zn levels 79−6694
^{58}Ni(^{16}O,^{16}O′), 315 MeV, giant multipole resonance excitation 79−30812
^{58}Ni(^{16}O,^{16}O), 120-215 MeV, backward angle excitation functions 79−36267
^{58}Ni(^{16}O,X), 100 MeV, deep inelastic, fragment spin polarisation and alignment, γ-rays 80−18284
^{58}Ni(^{16}O,2pγ), 40-58 MeV, γ ang. distribs., coincidences, ^{72}Se yrast states, lifetimes 77−54176
^{58}Ni(^{16}O,2pγ)^{72}Se, 54.5-64.5 MeV, high spin and excitation regions anal. 78−25226
^{58}Ni(^{18}O,^{18}O$_2$*)^{58}Ni, 79−6676
^{58}Ni(^{3}He,^{3}He), 27-84 MeV, energy depend. of optical model param. 78−41736
^{58}Ni(^{3}He,^{3}He), 90-120 MeV, cross sections, deduced unambiguous optical pot. 79−13311
^{58}Ni(^{3}He,^{3}He), optical potentials and volume integrals, mass and energy dep. 80−52686
^{58}Ni(^{3}He,^{3}He)^{58}Ni, 33.3 MeV, analysing power for polarised ^{3}He 77−67731
^{58}Ni(^{3}He,^{8}He), 75.3 MeV, cross-section meas. 77−79394
^{58}Ni(^{3}He,α), 130 MeV, selected transition, DWBA anal., cross sections 80−83086
^{58}Ni(^{3}He,α), inner hole states excitation, DWBA anal., reaction mechanism *(French)* 78−41735
^{58}Ni(^{3}He,α)^{57}Ni, 15-205 MeV, zero-range DWBA normalisation, energy depend. 77−34280
^{58}Ni(^{3}He,α)^{57}Ni, 70 MeV, mass excess of ^{57}Ni determ. 77−18376
^{58}Ni(^{3}He,d)^{59}Cu, 33.3 MeV, analysing power for polarised ^{3}He 77−67731
^{58}Ni(^{3}He,pγ)^{60}Cu, 11-15 MeV, coincidence, ang. correl. and branching ratio meas. 78−13129
^{58}Ni(^{40}Ar,X), 280 MeV, deep inelastic, light fragments, thermal equilib., ang. momentum transfer 80−63203
^{58}Ni(^{58}Ni,X), optical potential, nuclear matter approach 80−57801
^{58}Ni(^{58}Ni,xpyn), alpha decay studies of neutron deficient isotopes produced 79−93567
^{58}Ni(^{6}Li,^{6}Li′), 71 MeV, excited states deformation lengths, DWBA and coupled channels anals. 80−68541
^{58}Ni(^{6}Li,^{6}Li), elastic and inelastic, 74 MeV, folding optical model parameters 80−102201
^{58}Ni(^{6}Li,^{6}Li) scatt. of aligned spherical ^{6}Li ion c.f. strongly deformed ^{7}Li ions 79−6680
^{58}Ni(^{6}Li,d)^{62}Zn, multipole pairing states, correspondence between 2 and 4 particle transfer reactions 78−62569
^{58}Ni(^{7}Li,^{7}Li′), 19 MeV, first 2^+ states Coulomb-nuclear interference, optical and DWBA anal. 80−22852
^{58}Ni(^{9}Be,^{9}Be), 14-26 MeV, universal optical pot. 78−25219
^{58}Ni(α,^{8}He), 110 MeV, ^{54}Ni proton rich nucleus, Q values, mass excesses 77−88162
^{58}Ni(α,X), 140 MeV, nonequilibrium light charged particle yield, energy spectra and ang. distribs. 79−40942
^{58}Ni(α,X), 20, 40 MeV/N, α breakup yield, fragment yield ratios 80−9300
^{58}Ni(α,α′), 65 MeV, ^{4}He deduced monopole excitation to O^+ state DWBA anal. 79−22226
^{58}Ni(α,α′) 1.37 GeV, low lying state ang. distribs., Glauber rigid body approx. 79−54394
^{58}Ni(α,α′c), 150 MeV, c=charged particle, particle decay from isoscalar giant resonance region 80−13439
^{58}Ni(α,α), 139 MeV, optical model analysis 78−41737
^{58}Ni(α,α), 27 to 49 MeV, cross sections, optical model anal. 79−85483
^{58}Ni(α,α), <85.6 MeV, energy depend. of optical model params. 77−3024
^{58}Ni(α,α), radial sensitivity of optical pot. 80−86869
^{58}Ni(α,α) 140 MeV, modified optical pot., folding pots. and energy depend. 78−70549
^{58}Ni(α,α)^{58}Ni, 104 MeV, calc. of S-matrix oscillations and differential cross section 77−6333
^{58}Ni(α,p), 6.26-9.12 MeV, excitation functions, resonance struct., α-widths of ^{62}Zn states 77−30617
^{58}Ni(α,tp), double differential cross section, t-p ang. correlation function, direct breakup 80−22797
^{58}Ni(α-α), 50.2 MeV, composite particle optical pot. discrete ambiguities, partly Pauli-forbidden states 80−86870
^{58}Ni(d, d′), 108 MeV, giant monopole resonance excitation and ang. distribs. 80−102164
^{58}Ni(d,^{6}Li), DWBA anal., angular distrib., spectroscopic factors 79−6625
^{58}Ni(d,X), 80 MeV, charged light particle spectra and ang. distribs. exciton model anal. 79−40935
^{58}Ni(d,α), ^{56}Co particle-hole states, T=1, zero DWBA anal. 80−78308
^{58}Ni(d,αγ), 7 MeV, mean lifetimes of ^{56}Co levels 78−4950
^{58}Ni(d,d,) pol. d, 12 MeV, cross sections, anal. powers, global optical model anal. 80−47459
^{58}Ni(d,d′), 10 MeV, diff. cross sections and d-γ ang. correlations, multishell coupled channel calcs. 80−83064
^{58}Ni(d,d), 10 MeV, multishell form factors 79−93636

nuclei with mass number 39 to 58 continued
^{58}Ni(d,d), three-body model with adiabatic approx. 79−40934
^{58}Ni(d,n), secondary neutron emission charact. 79−30843
^{58}Ni(d,p)^{59}Ni, deuteron break-up model anal. of cross-section, vector analysing power and angular correlation 80−27648
^{58}Ni(e,e′), 120-264 MeV, $J^{\pi}=6^{+}$, 5.125 MeV state isoscalar character, form factors, transition strengths 80−9262
^{58}Ni(e,e′), 40 to 75 MeV, excitation of T_0+1 giant M1 resonance 77−14118
^{58}Ni(e,e′), mag. dipole and quadrupole state excitation 78−50154
^{58}Ni(e,e′) 5.125 MeV $J^{\pi}=6^{+}$ state excitation, isoscalar character 79−22227
^{58}Ni(e,e′α), electric quadrupole giant resonance α-decay *(Russian)* 79−85434
^{58}Ni(e,e′p), electric quadrupole giant reson. decay *(Russian)* 79−85434
^{58}Ni(γ,γ), M1 strength isospin splitting for dipole ang. distrib. states 80−13412
^{58}Ni(n, n), 1.77 to 3.0 MeV, validity of Wick's inequality in the calculation of the lower limits of the differential elastic cross sections 80−5137
^{58}Ni(n,X) transmission and capture data up to 120 keV 80−18311
^{58}Ni(n,2n), 13-19 MeV, neutron excitation functions, meas. by activation techniques 79−30825
^{58}Ni(n,2n), 14 MeV, cross section compilation 80−91181
^{58}Ni(n,α) thermal neutron induced charged particle spectroscopy 77−71611
^{58}Ni(n,γ), direct-semidirect and compound nucleus contribs. to cross sections 80−68662
^{58}Ni(n,γ), resonance state, partial radiation widths of high energy transitions 78−13104
^{58}Ni(n,n′γ), 0.5-10 MeV, γ-ray production cross sections 77−26762
^{58}Ni(n,p)^{58}Co, 3-4.8 MeV, cross section meas. 77−26738
^{58}Ni(n,t), 14 MeV, cross sections, fast neutron reaction excitation function calc. 79−45267
^{58}Ni(n,t)^{56}Co, 14.6 MeV, production cross sections 79−49629
^{58}Ni(p, X), pol.p, 65 MeV, continuum spectra anal. powers 80−102178
^{58}Ni(p,X), 90 MeV, charged light particle energy spectra exciton and evaporation model anal. 79−40923
^{58}Ni(p,d), 121 MeV, DWBA applicability test, d D-state contribs. 79−13261
^{58}Ni(p,d), 50 MeV, fine struct. of ground hole-state analogues 78−50065
^{58}Ni(p,d)^{57}Ni at 52 MeV, deuteron D-state effect, calcs. 79−54434
^{58}Ni(p,γ)^{59}Cu, time struct. of the $2d_{5/2}$ analogue state 79−6591
^{58}Ni(p,γ)^{59}Cu, 3547 and 1833 keV resonances, lifetime meas. 77−26621
^{58}Ni(p,γ)^{59}Cu, γ-decay of ^{59}Cu analogue resons. 78−13005
^{58}Ni(p,n), 32 MeV, cross-sections, test of forward scatt. amplitude approx. 79−6599
^{58}Ni(p,p′(d)X), pol. p, 65 MeV, anal. powers of continuum energy spectra 80−68637
^{58}Ni(p,p′), 0.8 GeV, coupled channels effects 79−63669
^{58}Ni(p,p′), 15 MeV polarised protons, surface delta description of analysing power 77−61397
^{58}Ni(p,p′), 5.65 to 6.13 MeV, resonance and statistical mechanisms *(Russian)* 79−80911
^{58}Ni(p,p′), 60 MeV, analysing power for excitation of giant resonance region of continuum 77−6387
^{58}Ni(p,p′), E=17.2, 20.4, 24.6 MeV, polarised protons, optical model, DWBA anal. 78−13094
^{58}Ni(p,p′)^{58}Ni, medium energy, DWBA calc. 77−6380
^{58}Ni(p,p), 0.8 GeV, analysing powers 78−54760
^{58}Ni(p,p), 0.8 GeV, ang. distrib. meas. 78−25186
^{58}Ni(p,p), 0.8 GeV, polarised p, differential cross section, anal. power, nuclear matter densities 79−13299
^{58}Ni(p,p), 1 GeV, Fresnel and two-body correl. effects 78−82353
^{58}Ni(p,p), 1 GeV, neutron densities 78−17087
^{58}Ni(p,p), 178 MeV, ang. distribs., cross sections and polarisation, coupled channels calcs. 79−75984
^{58}Ni(p,p), 20.4 and 30.3 MeV, elastic and inelastic scatt. multishell model description 78−86533
^{58}Ni(p,p), 5.65, 6.5 MeV, time evolution of compound elastic scatt., cryst. blocking technique 78−62531
^{58}Ni(p,p), 800 MeV, elastic and inelastic, cross section, deformation lengths, optical and DWBA anals. 80−68664
^{58}Ni(p,p), 800 MeV, non-eikonal corrections to Glauber diffraction approx. 79−71851
^{58}Ni(p,p), 800 MeV, polarised p, n density uncertainties from optical model anal. 79−22185
^{58}Ni(p,p), elastic and inelastic scatt., 5.2 to 6.05 MeV, scatt. cross section energy depend. 79−9559
^{58}Ni(p,p), inelastic and elastic scatt., 17.1-20.6 MeV, cross section fluctuations 78−58286
^{58}Ni(p,p), pol. p, 40 MeV, elastic and inelastic, asymmetries and differential cross sections *(Russian)* 80−27623
^{58}Ni(p,p)^{58}Ni, high-resolution meas. of scattering cross section, 3.0 to 4.0 MeV 77−10397
^{58}Ni(p,pα), 157 MeV, quasifree scatt., α spectroscopic factors, SU(3) predictions 77−6370
^{58}Ni(p,pα)^{54}Fe, 157 MeV, energy spectra, SU(3) model comparison 77−88121
^{58}Ni(p_{pol},α), 22 MeV, analysing power and cross sections, Co proton-hole states 80−68663
^{58}Ni(π,π), 162 MeV, elastic and inelastic ang. distribs., optical and PWIA anals. 80−42706
^{58}Ni(π,π), 162 MeV elastic scatt., ang. distribs., diffraction patterns, optical model calcs. 78−58309
^{58}Ni(π,π), ang. distribs., optical model calcs. 78−58308
^{58}Ni(t,p)^{60}Ni, 17 MeV, polarised triton, meas. and two-step calcs. 77−54204
Ni(α,^{3}He), 172.5 MeV, double-differential cross-sections determ. 78−82363
Ni(e,e′) A=58, 60, 64, isospin splitting of giant dipole resonance *(Russian)* 77−50116
Ni(γ,p), 17.5-32.0 MeV, isospin effects in decay of highly excited ^{58,60}Ni states 77−61398
Ni(n,γ), cross-section meas. principal resonance parameters 80−18312
Ni(n,γ), on-line gamma anal. using Ge detector 80−52624
Ni(p,γ)^{59,61}Cu, analogue to antianalogue M1 transitions 77−67718
Ni(p,p), 36.2 MeV, differential cross section, asymmetries, 0 to 7° scatt. 78−94002
Ni(p,p)Ni, A=58,60,62,64, at 1.047 GeV, neutron matter densities 77−54171

nuclei with mass number 39 to 58 continued
Ni(π,αX), 70 MeV, α cross sections and energy spectra, intranuclear cascade calcs. 79−575
Ni(π^{+}, π^{-}), 200 MeV, deexcitation γ spectra, transitions in ^{58,60}Cu 78−89912
(^{17,18}O,^{17,18}O′), 54-69 MeV, on A=48-92, excited states and ang. distribs., DWBA anal. 79−67705
^{39}P neutron rich nuclide, obs. in U fragmentation by 800 MeV protons 77−61419
^{40}P, production in 263 MeV ^{40}Ar+^{238}U deep inelastic reactions 79−22324
^{A}S, A=41,42, production in 263 MeV ^{40}Ar+^{238}U deep inelastic reactions 79−22324
^{32}S(n,n), 2-3 MeV neutrons, cross section meas. using associated particle TOF spectrometer 79−45255
^{39}S decay, half life, ^{39}Cl excited states and transitions 80−42595
Sc, A=43, 45, 47 and 49, collective bands of positive parity states, HF calcs. 78−54677
Sc, A=43, 47, $d_{3/2}$ hole states, wave functions mag. moment, M2 transitions, shell model 78−17116
Sc fragment differential ranges and energy spectra from ^{238}U(p,X), reaction mechanisms 80−42666
Sc, mass dependence for radiative capture of 14.1 MeV neutrons 78−13087
Sc, strength function of deeply bound hole states 78−17113
^{A}Sc, A=44,46,48, $1f_{7/2}$ shell isobaric analogue states, displacement energies 79−13207
^{A}Sc A=44,46,48, HF projection formalism, energy levels, static moments, EM transition probabilities 79−3083
^{A}Sc, A=44,46-48, fragment ang. distribs. from ^{238}U(p,X), 0.8-400 GeV 80−83099
^{A}Sc, A=44m,46,47,48, fragment emission, two-step model applicability from ^{238}U(p,X) 80−99177
^{A}Sc, A=45, 47, 49 positive parity states from Ti(d,^{3}He)Sc reactions 79−97656
^{A}Sc, A=45, 47, HF projection formalism, energy levels, EM moments, transition probabilities 79−22199
^{41}Sc 2p-1h intermediate struct. resonances, anal. powers, J^{π} from ^{40}Ca(p,p′γ) 80−86883
^{41}Sc, decay and partial widths of 2883 and 5037 keV levels 77−88077
^{41}Sc, determ. of total and partial widths of unbound states 77−74802
^{41}Sc, muonic, energy shifts during atomic EM cascade, and polarisability of deformed nuclei 80−86893
^{41}Sc resonance strengths from ^{40}Ca(p,γ) 80−22786
^{41}Sc, two particle-one hole states, EM transition probabilities 77−88035
^{41}Sc-^{41}Ca Coulomb displacement energy, HF calcs. 80−42527
^{41}Sc-^{41}Ca Coulomb energy shift of mirror nuclei, 2p-2h core excitations influence 78−12953
^{41}Sc-^{41}Ca mirror nuclei, configuration mixing, Coulomb energy anomaly 78−25099
^{42}Sc B(E2) transition probabilities, effective charge concept 77−18477
^{42}Sc, β^{+} decay, isospin symm. hindered, branching fraction 78−21526
^{42}Sc, energy levels anal. by ^{40}Ca(α,d) at 40 MeV 78−21579
^{42}Sc, ground state β-decay, weak non-analogue Fermi branch, branching ratio upper limit 78−70495
^{42}Sc populated in ^{42}Ca(^{3}He,t), precise Q-value, β decay energy, half life 77−30618
^{42}Sc two particle states, spectroscopic strengths and J^{π} values from ^{41}Ca(^{3}He,d) 79−63591
^{42}Sc, two-nucleon transfer, ang. momentum and binding energy effects 79−59021
^{42}Sc, weak neutral current props., search for 0^{-} isomer using ^{42}Ca(p,n) 79−45126
^{43}Sc, analogue resonances and struct. props. from ^{42}Ca(p,p) at 1.2-3.0 MeV 77−6374
^{43}Sc, deform. struct. in f-p shell nuclei, Nilsson model calcs. 78−66228
^{43}Sc, g-factor of $3/2^{+}$ hole state meas. in (α,p) react. 78−21492
^{43}Sc, $J^{\pi}=19/2^{-}$ isomer, high-spin precursors, from ^{29}Si(^{16}O,pn) 80−57656
^{43}Sc, mag. moments in $19/2^{-}$ state, time-differential perturbed ang. distrib. method 78−33117
^{43}Sc, resonance struct obs. in ^{42}Ca(p,γ)^{43}Sc below 2.75 MeV 78−13072
^{43}Sc, state calc. by shell model including $1g_{9/2}$ orbit 79−80873
^{44}Sc, 2-5 GeV photospallation, ratios of isomeric yields *(Russian)* 78−46047
^{44}Sc, 68 keV state, g-factor, time differential PAC meas. 78−505
^{44}Sc, $(f_{7/2})^{4}$ states populated in ^{41}Ca(α,p) 25 MeV reaction, relative transition strengths, semi-microscopic model calcs. 79−6645
^{44}Sc, electron capture to positron emission ratio, $4\pi\beta$-γ coincidence meas. 77−18479
^{44}Sc, in TiO_2, gamma-gamma directional correlation 77−20775
^{44}Sc, mean lifetimes of 1648-1768 keV levels via ^{41}K(α,n) 5-11 MeV, DSA method 77−6299
^{44}Sc, population of $f_{7/2}{}^{4}$ states in ^{41}Ca(α,p) reaction 79−59077
^{45}Sc, 0.4-22 keV neutron total cross section, deep minima 79−9591
^{45}Sc, e.m. decay of fragmental analogue states 77−2987
^{45}Sc levels, J^{π}, transitions and lifetimes from (p,p′)(^{3}He,^{3}He′)(α,α′) 80−63091
^{45}Sc, low-lying negative parity levels, Coulomb excitation 79−93552
^{45}Sc, n transfer, spectroscopic sum spin dependence for stripping and pickup 79−36219
^{45}Sc, NMR in $ScAl_2$, density of states determ. 77−63276
^{45}Sc, neutron stripping and pick-up, reanalysed data, sum rule anal. and spectroscopic factors 78−8828
^{45}Sc resonance decays, energy levels and J_{π} values from ^{44}Ca (p,γ) 79−80908
^{45}Sc, selective population of high-spin states in heavy ion reactions 77−18374
^{45}Sc total neutron cross section, parametric fit, bound level parameters, spin 77−23048
^{45}Sc+^{22}Ne, energy dissipation as func. of angle data comparison to classical and diffusion models 78−21604
^{45}Sc+n, 0.005 to 22 keV, total neutron cross section for beam filter design 78−78371
^{45}Sc+n, total cross section, neutron resonances, thermal scatt. parameters 78−8821
^{45}Sc(^{15}N,^{15}N), 47.5 MeV, ang. distribs., optical potentials 77−34341
^{45}Sc(α,α), 25 MeV, back-angle elastic scatt. 77−18582
^{45}Sc(α,α), 27-9 MeV, anomalous large-angle scatt. 77−18583
^{45}Sc(α,α), 27.2 MeV, elastic scatt. differential cross section 78−13116
^{45}Sc(α,pγ), 11 MeV, high spin states in ^{48}Ti 78−74378

nuclei with mass number 39 to 58 continued

^{43}Sc(α,t), 27.2 MeV, cross sections, optical potential, spectroscopic factors *(Russian)* 77−38290
^{43}Sc(α,xpyn), 150 MeV, fission cross sections and probabilities, isomeric yield ratio 79−45308
^{45}Sc(e,e′p), (γ,p) cross-sections determ., giant dipole reson. anal. 77−26666
^{45}Sc(n, γ), 2.5-100 keV, s- and p-wave radiative widths 78−17187
^{45}Sc(n,2n), 13-19 MeV, neutron excitation functions, meas. by activation techniques 79−30825
^{45}Sc(n,γ), mechanism in 3s size resonance, radiative width statistical and valence effects 80−37388
^{45}Sc(p, X), pol.p, 65 MeV, continuum spectra anal. powers 80−102178
^{45}Sc(p,^{17}Ne^{22}Na^{28}Al), 40-85 MeV, ^{24}Na yields in 'fission-like' reactions 78−598
^{45}Sc(p,α), 2.5-3.8 MeV, reaction rates and stellar nucleosynthesis 77−88134
^{45}Sc(p,γ), 0.7-4.2 MeV, cross section, statistical model anal., stellar interaction rate 79−17897
^{45}Sc(p,γ)^{56}Ti, stellar reaction rates 78−93090
^{45}Sc(p,n), source of monoenergetic 10-50 keV neutrons 77−54387
^{45}Sc(p,p′), 2.5-3.8 MeV, reaction rates and stellar nucleosynthesis 77−88134
^{45}Sc(π^-,X), stopped π^-, yields and γ-rays 80−86857
^{46}Sc, beta decay half life 80−47435
^{46}Sc energy levels, resonances, spin and parity from ^{45}Sc(n,γ) 80−52673
^{46}Sc, impurity in mica, neutron fluence meas. using mica as nuclear track and activation detector 78−13346
^{46}Sc level deexcitation, E1 and M1 absolute radiative widths from ^{45}Sc(n,γ) 80−52622
^{46}Sc transition polarisation, levels and spin assignments from ^{45}Sc(n,γ), pol. n 80−52656
^{47}Sc preparation in carrier-free state by ^{48}Ti(γ,p) reaction for radiopharmaceutical appls. 77−90892
^{48}Sc Gamow-Teller strength, ang. distribs., from ^{48}Ca (^{3}He,t) 80−42589
^{48}Sc spin-flip isovector giant resonance, $T_>$ Gamov-Teller strength from ^{48}Ca(p,n) 80−106019
^{49}Sc isobaric analogue states and resonances, J^π from ^{48}Ca(p,p) 80−13426
^{49}Sc, levels via ^{48}Ca(τ,d)^{49}Sc 18 MeV 77−10303
^{49}Sc, location of major $2p_{1/2}$ strength using (^{7}Li,^{6}He) react. 78−25095
^{49}Sc proton single particle states, spectroscopic factors, DWBA anal. of ^{48}Ca(d,n) 80−99118
^{49}Sc, single particle states lifetimes calcs. 80−105943
^{51}Sc β-decay to ^{51}Ti, γ-ray spectra, β branching ratios, ^{51}Ti levels 77−6318
^{46m}Sc, neutron activation analysis of rocks 79−79356
Sc(p, spallation), 0.08-24 GeV, Ar isotopes, spallation ratios and prod. cross sections 80−9284
Si, A=42, 46, 48, exotic nuclei stability anal., Hartree-Fock approx. with the Skyrme interaction 78−82273
T, A=46, 48, 50, pf-shell nuclei, Hermitian operator method calcs., energy levels, transitions 78−54702
^{48}T excited states from ^{45}Sc(A,pγ), level struct., lifetimes, from DSA and pγ coincidence meas. 78−74326
^{48}T(p,p′), 4.7-5.4 MeV, cusp behaviour of cross-section obs. 78−29470
^{46}Tc(n,p)^{46}Sc threshold reaction cross section, ^{252}Cf source 77−23039
Ti, 20 to 50 MeV, total reaction cross sections, compared to optical model prediction 78−33174
Ti, A=44,46,48,50, short-range correlations and pseudopotentials, Hartree Fock Bogoliubov method 78−535
Ti, A=44-50, effective charges and E2 transitions in 1f-2p shell nuclei 78−544
Ti, A=45 and 47, collective bands of positive parity states, HF calcs. 78−54677
Ti, A=45-51 odd isotopes, spectra and EM transitions, spin assignments, rot. bands 77−74793
Ti, A=46,50, neutron radius determ., charge symm. 78−29380
Ti, A=51, 52, mean lifetimes of yrast states populated in ^{48}Ca+Li 77−2942
Ti even isotopes, deformed nuclei in Lipkin-Nogami approach, Kuo Brown effective interaction 79−59006
Ti isotopes, neutron, capture and transmission meas., 1 to 100 keV 77−26712
Ti, K_β/K_α following K-electron capture and X-ray excitation 78−13031
Ti, single neutron separation energies determ. from doublets 77−26566
Ti(^{3}He, pxn), ^{48}V positron source prep. for annihilation radiation lineshapes, positron lifetimes meas. 80−876
Ti(^{16}O,^{15}N), A=48, 50, 36-53 MeV, reaction dynamic depend. of small angle cross sections 77−18600
Ti(^{16}O,X), 310 MeV, fusion, upper limit to compound nucleus formation 80−78315
^{A}Ti (d,d), pol. d, A=46, 48, 50, 12 MeV, cross sections, anal. powers, global optical model anal. 80−47459
^{A}Ti, A=44, 46, 48, 52, energy levels and EM props. using classical semimicroscopic model 79−59012
^{A}Ti, A=44, 48, ang. distribs. for transitions, DWBA anal., spectroscopic strengths from Ca(^{7}Li,t) 80−68584
^{A}Ti, A=44-46, 48,49, $1f_{7/2}$ shell isobaric analogue states, displacement energies 79−13207
^{A}Ti, A=45, 47, collective states from heavy ion reactions, shell model calcs. 78−62560
^{A}Ti, A=46, 48, 50, pionic X-rays, strong interaction and isotope shifts, π-nuclear optical pot. 80−53169
^{A}Ti, A=47,49, levels, spectroscopic factors and analogue states DWBA anal. from Ti(^{3}He,α) 79−17808
^{A}Ti, A=48,50, excited states and transition ang. distribs. from Cr(^{14}C,^{16}O) 80−95308
^{A}Ti(^{7}Li,^{7}Li′), A=46,48, 17 MeV, first 2^+ states Coulomb-nuclear interference, optical and DWBA anal. 80−22852
^{A}Ti(Γ,X), A=46, 48, 50, photoneutron and photoproton cross section systematics 80−13463
^{A}Ti(α,α), A=46,48,50, 140 MeV, nuclear size comparison, optical model pot. 79−17913
^{A}Ti(n,X), A=46-50, 14 MeV, X=p,n′p,α,n′α,^{3}He, production cross-sections 80−42648
^{A}Ti(n,γ), A=46 to 50, thermal capture, gamma ray spectra 79−93629
^{A}Ti(n,γ) A=46, 47, 49, 50, 45 MeV, cross section meas., resonance parameters 80−18315
^{42}Ti, ^{50}Ti B(E2) transition probabilities, effective charge concept 77−18477

nuclei with mass number 39 to 58 continued

^{42}Ti, 6_1^+ state lifetime, B(E2) value 77−82863
^{42}Ti, two-nucleon transfer, ang. momentum and binding energy effects 79−59021
^{43}Ti, lifetime and γ decay of isomeric $19/2^-$ state from ^{40}Ca(α,nγ) 20 MeV 78−70486
^{43}Ti, mag. moments in $19/2^-$ state, time-differential perturbed ang. distrib. method 78−33117
^{43}Ti positive parity states, mean lifetimes, quasirotational band from ^{40}Ca(α,n) 20 MeV 79−6415
^{44}Ti, α-particle spectroscopic factors, two-oscill. shell model calcs. 79−6386
^{44}Ti, deform. struct. in f-p shell nuclei, Nilsson model calcs. 78−66228
^{44}Ti, fp-shell nuclei struct., effect of core-excitation and α-clustering correl. 80−9245
^{44}Ti levels, lifetimes and spins meas. from ^{40}Ca(α,γ)^{44}Ti 77−79328
^{44}Ti, lowest T=2 state decay, branching ratios from ^{46}Ti(p,t) 42 MeV 78−78304
^{44}Ti lowest T=2 state isospin forbidden γ-decay from resonances in ^{40}Ca(α,γ) 79−22228
^{44}Ti, lowest T=2 state isospin forbidden decays, branching ratios 79−67703
^{44}Ti, mode-mode coupling model for four-body correl. 77−10322
^{44}Ti, yrast states as α-particle cluster states 78−33114
^{44}Ti* band crossing search, Hauser-Feshbach calcs. for ^{28}Si(^{16}O,α) 79−22174
^{45}Ti, 40 keV level spin and g-factor via ^{42}Ca(α,n) 77−74761
^{45}Ti, $5/2^-$ 40 keV level, g-factor meas. 77−57599
^{45}Ti $d_{3/2}$ hole states, wave functions, mag. moment, M2 transitions, shell model 78−17116
^{45}Ti, integral rot., hyperfine field and g-factor of $3/2^+$ state 77−50052
^{45}Ti production by proton bombardment of Sc in cyclotron 78−80966
^{45}Ti, weak E1 transitions examined using γ-ray, γ-γ coincidence and n-γ coincidence techniques 80−57724
^{46}Ti, ^{48}Ti, (n,xp), (n,xd) and (n,xα) reactions, 14 MeV, sub-Coulomb barrier protons 77−30597
^{46}Ti, ^{48}Ti, selective population of high-spin states in heavy ion reactions 77−18374
^{46}Ti (γ,N), 12-25 MeV, isospin splitting in giant dipole resonance 79−45152
^{46}Ti deduced levels, spin assignments and γ-decay, band struct. from ^{43}Ca(α,nγ), 8-15 MeV 78−78302
^{46}Ti, eikonal approx. of electron scatt. by spherically symmetric nuclei 78−37330
^{46}Ti level structure, appl. of generator-coordinate method extension to two quasiparticle excited states 77−54153
^{46}Ti, lifetime meas. by γ-γ coincidence technique following ^{40}Ar(^{9}Be,3n) 79−59318
^{46}Ti+^{12}C, 5.8 MeV/u, influence of shell effect in nuclear level densities on compound nucleus decay 79−40979
^{46}Ti+n, 15 MeV, cross sections for emission of sub Coulomb barrier charged particles 77−23007
^{46}Ti(^{3}He,t), precise Q-value, ^{46}V β decay energy, half life 77−30618
^{46}Ti(P,n)^{46}V, threshold and ^{46}V(β^+)^{46}Ti ft value 77−10371
^{46}Ti(α,nγ)^{49}Cr, gamma-ray ang. distrib., ang. correlation, linear polarisation and Doppler-shift attenuation meas. 77−82941
^{46}Ti(d,d), 10 and 13 MeV, polarised d elastic scatt., optical model anal. 79−36248
^{46}Ti(d,d), 10 MeV, optical model calc. 78−41729
^{46}Ti(d,d), 7,10 MeV, ang. distribs., DWBA and Hauser Feshbach anal. 80−47377
^{46}Ti(d,p), polarised d, obs. of D-state and compound nucleus effects 77−34319
^{46}Ti(e,e′p), (γ,p) cross-sections determ., giant dipole reson. anal. 77−26666
^{46}Ti(n,2n), 14 MeV, cross section compilation 80−91181
^{46}Ti(n,γ), γ circular polarisation meas. 78−62533
^{46}Ti(n,p), 4.5-18.3 MeV, cross sections and excitation curves *(Chinese)* 79−49601
^{47}Ti, integral rot., hyperfine-field and g-factor of $7/2^-$ state 77−50052
^{47}Ti levels, DWBA and Hauser Feshbach anal., compound nucleus cross sections from ^{46}Ti(d,p) 80−47377
^{47}Ti(α,α′), 15.35 MeV, level density parameters, statistical model anal. 78−13130
^{47}Ti(α,p), 15.35 MeV, level density parameters, statistical model anal. 78−13130
^{47}Ti(α,pγ), 10 MeV, ^{50}V excited states, lifetimes 78−21583
^{47}Ti(n,p)^{47}Sc, carrier-free radiopharmaceutical prep. with epithermal neutrons 79−79652
^{48}Ti, (A+2)particles-2 holes excitations, interaction renormalisation 78−29375
^{48}Ti, eikonal approx. of electron scatt. by spherically symmetric nuclei 78−37330
^{48}Ti high spin states, γ-decay, J^π assignments, lifetimes from ^{45}Sc(α,pγ) 80−13356
^{48}Ti high spin states from ^{45}Sc(α,pγ) 78−74378
^{48}Ti levels and transition ang. distribs., form factors, DWBA anal. of ^{45}Sc(α,p) 79−45202
^{48}Ti, neutron elastic and inelastic differential scatt. cross sections, 1.5-3.0 MeV *(Russian)* 77−26688
^{48}Ti, pionic atoms, dynamical nuclear polarisation, nuclear structure effects 79−94113
^{48}Ti, pionic atoms, E2 nuclear resonance effects 79−76534
^{48}Ti+^{16}O, 120 MeV, deep inelastic collisions, charged particle+gamma coincidences 78−74388
^{48}Ti+^{16}O, 57.74 MeC, heavy ion fusion, evaporation model breakdown, preequilibrium α emission from ^{64}Zn 78−89927
^{48}Ti+n, 15 MeV, cross sections for emission of sub Coulomb barrier charged particles 77−23007
^{48}Ti(^{12}C,p2n), 26-48 MeV, high spin states in ^{57}Co anal. 77−46115
^{48}Ti(^{16}O,^{12}C), 120 MeV, formation and decay of ^{52}Cr primary fragment 79−45289
^{48}Ti(^{16}O,^{15}N), anomalous ang. distribs., interference effects due to ^{49}V state population 79−17924
^{48}Ti(α,pnγ)^{50}V, high-spin levels obs. by in-beam γ-spectroscopic technique *(French)* 78−21572
^{48}Ti(e,e), 227 MeV, differential cross sections, Fermi charge density distribs. *(Russian)* 78−89785
^{48}Ti(e,e), elastic and inelastic scatt. cross-sections from Hartree-Fock densities *(Russian)* 79−13287

nuclei with mass number 39 to 58 continued
^{48}Ti(γ,n), 15-27.5 MeV, giant dipole resonance splitting, dynamic collective model 80−57755
^{48}Ti(γ,p), prep. of carrier-free ^{47}Sc for radiopharmaceutical appl. 77−90892
^{48}Ti(n,γ)^{49}Ti, T violation test, γ-ray directional correlation 78−62330
^{48}Ti(n,n′γ), 1.57-2.8 MeV, low levels excitation *(Russian)* 78−41722
^{48}Ti(n,p), 4.5-18.3 MeV, cross sections and excitation curves *(Chinese)* 79−49601
^{48}Ti(p,^{17}Ne^{22}Na^{28}Al), 40-85 MeV, ^{24}Na yields in 'fission-like' reactions 78−598
^{48}Ti(p,n), 4.7-5.4 MeV, cusp behaviour of cross-section obs. 78−29470
^{48}Ti(p,p), 1 GeV, cross sections using nuclear densities from self-consistent methods *(Russian)* 78−41724
^{48}Ti(p,p), 1 GeV, elastic scatt. differential cross section calc. 80−47480
^{48}Ti(p,p), 1.044 GeV, elastic and inelastic, Glauber theory anal. 77−18536
^{48}Ti(p,p), E_p=1 GeV, elastic differential cross sections 78−13082
^{48}Ti(p,p), elastic and inelastic scatt. cross-sections from Hartree-Fock densities *(Russian)* 79−13287
^{49}Ti, 3/2$^-$→7/2$^-$ 1381 keV transition, B(E2) value 78−74328
^{49}Ti, mag. form factors, core polarisation and exchange current effects 80−13409
^{49}Ti nuclear levels from n-capture γ-rays in ^{50}Ti(γ,n) 80−37327
^{49}Ti, p transfer, spectroscopic sum spin dependence for stripping and pick-up 79−36219
^{49}Ti, polarised, T violation test, γ-ray directional correlation 78−62330
^{49}Ti(e,e), cross section, $1f_{1/2}$ neutron orbit radial distrib. 79−93541
^{49}Ti(e,e), magnetic e scatt., exchange current effects, plane wave Born approx. 80−78282
^{49}Ti(γ,γ′), nuclear levels from n-capture γ-rays 80−37327
^{49}Ti(p,γ), 0.74-3.25 MeV, cross section and thermonuclear reaction rates, nucleosynthesis, IAR effects 80−102187
^{49}Ti(p,n), 0.74-3.25 MeV, cross section and thermonuclear reaction rates, nucleosynthesis 80−102187
^{50}Ti, 1p7h config., high-spin neutron-hole states, EM transition rates 78−70430
^{50}Ti high spin states, transitions and J$^\pi$ values from ^{48}Ca(α,Znγ) 80−455
^{50}Ti level structure, appl. of generator-coordinate method extension to two quasiparticle excited states 77−54153
^{50}Ti, shell model calcs. using surface delta interaction 78−37290
^{50}Ti, studied via (α,2nγ), high spin states, shell model calcs. 78−54675
^{50}Ti+^{14}N(^{12}C), single- and multi-nucleon transfer reactions at 60, 70 and 90 MeV 77−14146
^{50}Ti+^{32}S, diffusion model anal. of energy depend. of fission like mass distrib. 77−82949
^{50}Ti+^{32}S composite system, fission characts., fragment correls. 77−332
^{50}Ti+^{40}Ar, 236 MeV, fragments mass and charge distribs. in deep inelastic reactions 78−58296
^{50}Ti(^{12,13}C,X), elastic, inelastic and single nucleon transfer excitation functions, ^{49}Ti levels 80−13492
^{50}Ti(^{32}S,f), 121 to 166 MeV, heavy fragments ang. distribs., mass distribs., excitation functions 77−30642
^{50}Ti(α,α), 140 MeV, model independent description limits from local optical pots. 80−102196
^{50}Ti(γ,X), photoneutron and photoproton cross sections, giant dipole resonance isospin splitting 80−13442
^{50}Ti(γ,n$_0$), cross sections in giant dipole reson. energy range 79−89286
^{50}Ti(γ,n), cross sections in giant dipole reson. energy range 79−89286
^{51}Ti, populated in ^{51}Sc β-decay spin-parity values 77−6318
^{51}Ti $Zp_{3/2}$ neutron orbit radius isotone shift from DWBA anal. of ^{50}Ti(t,d) 80−32172
^{53}Ti, β-decay scheme, $T_{1/2}$ and mass meas., astrophysical significance 77−26635
^{53}Ti β-decay scheme 77−46139
^{53}Ti, new isotopes of interest to explosive nucleosynthesis, β-decay scheme and mass determ. 79−45208
^{54}Ti, neutron rich nuclide from ^{238}U(^{40}Ar,X) at 340 MeV 80−57802
^{nat}Ti(^{3}He, xn)^{48}Cr, production of ^{48}Cr for life sciences appls. 80−94367
Ti(αα), A=49,50, 25 MeV, back-angle elastic scatt. 77−18582
Ti(d,p)Ti, A=47, 49, 13.6 MeV differential cross-sections 77−18574
Ti(n,n), 1-4.5 MeV, elastic inelastic, total cross sections, optical-statistical, coupled-channels models 79−539
Ti(p,X) 200, 300, 400 GeV, hadron prod. at large p_T invariant cross section 79−40926
Ti(p,2π$^-$X), 28.5 GeV, fireball model comparison 79−59059
Ti(p,d), A=46,48,50, DWBA calcs., rms radius pick-up reaction cross sections 79−541
Ti(p,n), 800 MeV, n prod. systematics, π associated cross section 79−3153
Ti(p,p), 5.2-6.0 MeV, A=46,48,50, energy depend. of cross sections 77−61409
Ti(p,p), 6 MeV, A=46,48,50, cross sections, excited states, ang. distribs. 77−61410
Ti(p, spallation), 0.08-24 GeV, Ar isotopes, spallation ratios and prod. cross sections 80−9284
Ti(p,x), 13 to 45 MeV ^{48}V $^{43-48}$Sc, ^{43}K, production excitation functions, statistical equilib. calcs. 79−36220
^{46}Ti(^{3}He,^{3}He′), excitation of low-lying 0$^+$ states, indirect processes 77−6417
V, A=47, 48, 49 and 51, collective bands of positive parity states, HF calcs. 78−54677
V, A=47,59,51, spectra, e.m. moments, B(E2) and B(M1) values calc. 78−8745
V, A=47-51, effective charges and E2 transitions in 1f-2p shell nuclei 78−544
V, A=52, 3, yrast decay schemes from heavy-ion fusion evaporation reactions 77−82854
V, fast-neutron total cross-sections, 1.0-5.5 MeV 77−82923
V isotopes, A=47-51 78−25114
V, K_β/K_α following K-electron capture and X-ray excitation 78−13031
V+p, 1 to 28.5 GeV, production of 43≤A≤51 nuclides, reaction mechanisms 77−34301
^{A}V, A = 47, 49 collective states from heavy ion reactions, shell model calcs. 78−62560
^{A}V(p,X), A=50, 51, 12-45 MeV, reaction cross section and hybrid model analysis 79−67749
^{31}V level scheme, DWBA and optical model anal. from ^{52}Cr+^{13}C 79−36159
nuclei with mass number 39 to 58 continued
^{45}V level scheme, γ-rays, level lifetimes, internal conversion from ^{40}Ca(Li,xn) 80−63085
^{46}V populated in ^{46}Ti(^{3}He,t), precise Q-value, β decay energy, half life 77−30618
^{46}V, weak neutral current props., search for 0$^-$ isomer using ^{46}Ti(p,n) 79−45126
^{46}V(β$^+$)^{46}Ti, superallowed Fermi decay half-life 77−34259
^{46}V(β$^+$)^{46}Ti superallowed Fermi decay, ft value 77−10371
^{47}V 3/2$^-$ analogue state decay amplitudes, common doorway state phase relation from ^{46}Ti(p,p′γ) 79−89276
^{47}V spin values and level scheme recalc. 78−78256
^{48}V, ^{51}V, selective population of high-spin states in heavy ion reactions 77−18374
^{48}V, K$^\pi$=4$^-$ rotational band 78−12944
^{48}V, low-lying positive parity states, deformed config. mixing model 77−6198
^{48}V, odd-parity rotational band structure 77−46102
^{48}V spin values by atomic beam mag. resonance method 78−78256
^{49}V proton hole, analogue and high spin states, distorted wave anal. from ^{52}Cr(p,α) 79−9482
^{50}V(p,p′), 3/2$^-$ resonances, inelastic proton channel 79−93586
^{50}V, $1f_{7/2}$ shell isobaric analogue states, displacement energies 79−13207
^{50}V excited states populated in ^{42}Ti(α,pγ), lifetimes 78−21583
^{50}V, γ-ray spectrum from thermal neutron capture 78−21568
^{50}V, half lives of β-decay and e$^-$-capture in ΔJ=4 transitions 79−22246
^{50}V, half-life limits for β-decay and electron capture 77−79334
^{50}V, high-spin levels anal. in ^{48}Ti(α,pnγ) reaction *(French)* 78−21572
^{50}V, isobaric analogue states anal. from ^{51}V(p,d)^{50}V 78−33182
^{50}V, low temp. photonuclear nucleosynthesis in stellar H-CNO burning zones 77−13319
^{50}V, nucl. quadrupole moments from laser-RF double reson. spectroscopy 80−57682
^{50}V quadrupole moment and atomic ground state hyperfine intervals, laser spectroscopic determ. 79−89234
^{50}V(α,d), 14 MeV, ^{52}Cr 4.57 MeV excited state, 8$^+$ assignment 78−74380
^{50}V(p,α), 13.85 MeV, level density parameters, statistical model anal. 78−13130
^{51}V, 1f nucleon orbit RMS radii from transfer data 80−27544
^{51}V (^{16}O,X), 81 MeV, fragments in incomplete fission 77−14153
^{51}V, ENDOR in $KMgF_3$ and $KZnF_3$, nucl. mag. moment 79−28638
^{51}V, γ-strength function, γ-ray spectra, average resonance method from ^{50}Ti(p,γ) 80−9257
^{51}V, in MVO_3 polycryst., M=Na, Cs, NH_4, quadrupole coupling const., asymmetry parameter, chem. shift, NMR computer calcs. 78−6584
^{51}V, isospin effects in GDR region 78−78344
^{51}V, Knight shift meas. in $Nb_{1-x}V_xH_x$ 77−59471
^{51}V, mag. form factors, core polarisation and exchange current effects 80−13409
^{51}V, NMR in $(Ti_{1-x}V_x)_2O_3$ 77−66369
^{51}V, NMR in antiferromag. V_5S_8 77−36140
^{51}V, NMR in dimorphic $LaVO_4$ 77−63310
^{51}V NMR in $PrVO_4$ 77−77110
^{51}V, NMR in RVO_4(R=Sc, Y, Yb), nucl. quadrupole coupling const., chem. shift 77−90055
^{51}V, NMR in V_2O_5-MoO_3 system meas. 77−24379
^{51}V, NMR meas. in V_2Zr, V_2Hf and V_2Ta *(Russian)* 78−23359
^{51}V, neutron resonance spectroscopy, R-matrix anal. 78−21555
^{51}V π^P high energy photoproduction and electroproduction 78−21543
^{51}V, shell model, pairing-plus-surface-tensor interaction, energy levels, B(E2) values 78−78282
^{51}V, shell model calcs. using surface delta interaction 78−37290
^{51}V, spallation by 0.3-1.0 GeV photons, cross-sections 78−41691
^{51}V, Spectra, particle-hole conjugation and protection theorems *(Chinese)* 80−73796
^{51}V struct., pairing plus surface tensor interaction 77−18411
^{51}V+^{16}O, energy dissipation as func. of angle data comparison to classical and diffusion models 78−21604
^{51}V+d(α), 12-50 MeV, t formation average cross sections 80−42670
^{51}V(^{16}O, p2nγ), lifetimes of ^{64}Zn levels 78−13019
^{51}V(^{16}O,p2n), E=36-46 MeV, high-spin states in ^{64}Zn 78−33145
^{51}V(^{16}O,p2nγ)^{64}Zn, E=50 MeV, lifetimes of quasi-rotational states of ^{64}Zn 78−17140
^{51}V(^{3}He,d), (^{3}He,^{3}He), 15 MeV, ang. distribs. meas., optical model anal. 78−33192
^{51}V(^{3}He,dp), ^{3}He breakup, DWBA calcs. for strongly absorptive projectiles 80−68682
^{51}V(^{3}He,n)^{53}Mn, cyclotron preparation of ^{53}Mn, extraction, anal. 77−61441
^{51}V(^{3}He,pd), 90 MeV, angular correlations, elastic break-up of ^{3}He 80−52685
^{51}V(α,α), 27.2 MeV, elastic scatt. differential cross section 78−13116
^{51}V(α,nγ)^{54}Mn, Doppler shift attenuation meas. of ^{54}Mn excited state lifetimes 78−17141
^{51}V(α,p$_0$), differential cross section in giant dipole resonance region from (e,p$_0$) 79−63655
^{51}V(α,t), 25 MeV, DWBA anal. of triton ang. distrib. meas. 78−54776
^{51}V(α,t), 27.2 MeV, cross sections, optical potential, spectroscopic factors *(Russian)* 77−38290
^{51}V(α,t), absolute normalisation from spin depend. sum rule anal. 80−27652
^{51}V(d,^{3}He)^{50}Ti, 30-80 MeV, finite range DWBA calcs. 77−10416
^{51}V(d,^{3}He)^{50}Ti, normalisation const. from J-depend. sum rule anal. 77−34321
^{51}V(d,t)^{50}V, 80 MeV, finite-range DWBA calcs. 77−10416
^{51}V(e,e′), shell model calcs., effective charges 77−26674
^{51}V(e,e′p) 77−10389
^{51}V(e,e′π$^\pm$) and ^{51}V(γ,π$^\pm$), 130 to 580 MeV, cross sections, impulse approx., multipole decomp. 77−54206
^{51}V(e,e), mag. elastic scatt., radial distrib. of $1f_{7/2}$ proton orbit using cross sections 78−13067
^{51}V(e,e), magnetic e scatt., exchange current effects, plane wave Born approx. 80−78282
^{51}V(e,e), valence nucleon orbit determ. 78−54669
^{51}V(e,p$_0$), 15-26 MeV, differential cross section in giant dipole resonance region 79−63655
^{51}V(γ,X), 2-5 GeV, spallation 2-5 GeV, spallation yields 77−71604
^{51}V(γ,3n), cross sections at intermediate energies 78−8793
^{51}V(n,X), 14 MeV, X=p,n′p,α,n′α,^{3}He, production cross-sections 80−42648

nuclei with mass number 39 to 58 continued
^{51}V(n,α), 4.5-18.3 MeV, cross sections and excitation curves *(Chinese)* 79−49601
^{51}V(n,γ), circular polarisation, ang. distrib. meas. 80−32285
^{51}V(n,n′)^{51}V, 14.1 MeV, pre-equilib. and evaporation model anal. 77−6366
^{51}V(n,p)^{51}Ti, neutron activation anal., Ge(Li) and NaI(Tl) detector γ-ray spectrometer 80−78485
^{51}V(n,xp),(n,xα),(n,d), 15 MeV, cross-section meas. 78−50171
^{51}V(p,X), X=γ or n, 0.93-4.47 MeV, cross sections, competition effects, Hauser-Feshbach calcs. 80−91184
^{51}V(p,2p)^{50}Ti, 17 MeV, search for double-direct reaction 77−30576
^{51}V(p,d)^{50}V, 51.9 MeV, symm. pot. anal. 78−33182
^{51}V(p,n), 1.56-5.53 MeV, total cross section, excitation functions, isobaric analogue resonance 78−4943
^{51}V(p,n)^{51}Cr, 2.34 MeV, shell model anal. of analogue resonance 77−14122
^{51}V(p,n)^{51}Cr, neutron polarisation at isobaric analogue resonances 78−54759
^{51}V(p,p′), 6 MeV, levels, spins and EM props., shell model anal. 80−63092
^{51}V(π,π′γ), 200 MeV, ^{51}V levels 78−21611
^{51}V(π⁻,Xγ) 230 MeV reactions near Δ(1232) resonance 77−6465
^{52}V capture area, resonance parameters and mean level spacings from ^{51}V(n,γ) 79−6608
^{52}V, decay, γ-ray spectrum, energies and intensities, ^{52}Cr level scheme *(French)* 77−14066
^{52}V, mean lifetimes of yrast states populated in ^{48}Ca+Li 77−2942
^{52}V, spectrum study with Kuo-Brown renormalised interaction and Vervier interaction 78−86492
^{52}V, spin assignments to p-wave neutron states 77−22852
^{53}V, spin-parity assignments from ^{53}Ti β-decay meas. 77−46139
^{54}V, β-decay scheme and $T_{1/2}$ determ. 78−21528
^{54}V energy levels populated in ^{54}Cr(t,^{3}He), mass excess 77−54230
^{54}V, yrast level lifetimes and J^{π} assignments from ^{48}Ca+^{9}Be 79−9445
^{55}V β-decay scheme and $T_{1/2}$ determ., mass excess meas. 78−21528
^{55}V, new isotopes of interest to explosive nucleosynthesis, β-decay scheme and mass determ. 79−45208
^{56}V, neutron rich nuclide from ^{238}U(^{40}Ar,X) at 340 MeV 80−57802
V(α,α), A=50,1, 25 MeV, back-angle elastic scatt. 77−18582
V(n,n), elastic and inelastic scatt., cross sections meas. and calcs. 78−13081
V(p,^{17}Ne^{22}Na^{28}Al), 40-85 MeV, ^{24}Na yields in 'fission-like' reactions 78−598
Zn to Ni even isotope transition, α-particle spectroscopic factors, shell model calcs. 79−6385
^{90}Zr, self consistent K-matrix model calc. 77−6257

nuclei with mass number 59 to 89
0.6 to 3 MeV, captive cross section, statistical theory anal. 79−9557
36≤Z≤83 nuclei, neutron induced reactions, tables of cross sections and rate factors 77−46162
(^{6}Li,^{6}Li) 50.6 MeV elastic scatt. on A=12-208 nuclei, optical model parameters 77−18592
A=24-60, yrast lines using Strutinsky method, empirical fusion bands 80−42514
A=32 to 140, nuclear struct., binding energies, dipole moments *(French)* 77−46098
A=40 to 100, strength and radius parameters of deformed Woods-Saxon potential 79−97673
A=40 to 60, neutron force function, role of input states 79−9486
A=40 to 60, total photon widths in valence capture model *(French)* 77−34291
A=40-80, yrast props. and high spin isomers, cranking plus Strutinsky formalism 80−32152
A=45-153, β^{+}-decay strength function maximum 79−75914
A=50 to 89, α-particle elastic scatt., neutron shell sensitivity, optical model parameters 79−6642
A=54-82, ground state transition strengths from (p,t) reactions 80−95305
A=59 to 68, α-particle transfer spectroscopic factors using interacting boson approx. 78−78258
A=60, nuclear data sheets, levels and transitions 80−31433
A=60-140, spherical nuclei, two phonon admixture effect on M1 resonance *(Russian)* 80−5105
A=60-80 even-even nuclei, collective motions and band structs. 80−9202
A=63, nuclear structure data sheets (July 1979) 80−67941
A=64, nuclear data sheets, levels and transitions 80−31434
A=70, heavy-ion induced fission-evaporation reactions, magnetic substrate distribs., nuclear alignment 80−73857
A=70, nuclear struct. data sheets to Oct. 1977 79−30768
A=71, nuclear data sheets, levels, J^{π} and transitions 80−31428
A=72 region, evidence for coexistence of spherical and deformed states 77−6192
A=73, nuclear data sheets, levels, J^{π} and transitions 80−101673
A=75-93 fission products far from β-stability, Q_{β}-values 77−22949
A=76 nuclear data sheet to June 1976 77−18373
A=76 to 101, subshell closure effects of nuclear binding energies 78−58230
A=76-79 charge dispersion curve from ^{232}Th(p, f) 80−18349
A=77, nuclear data sheets, levels, J^{π} and transitions 80−105439
A=84 nuclei, nuclear struct. data sheets to March 1979 80−9191
A=87 nuclei, nuclear struct. data sheets to January 1979 80−9192
A=88 to 99, fission probability, applicability of conventional systematics *(Russian)* 79−54464
A=88-96, collective treatment of pairing Hamiltonian, transfer data anal. 79−13220
A=90 region, N=50, shell model calcs. 80−68564
A=9 to 70, proton scatt., 14 to 45 MeV, differential cross sections 79−45273
A<100, average E1/M1 strength ratio 80−52621
A∼90 nuclei, isomeric states, spin polarisation, M4 transitions and giant resonances 80−63157
A = 86, nuclear data sheets, level and decay schemes 79−30774
composite nucleus scission, fusion and strongly damped collisions, rot. energy, boundary diffuseness 80−102224
compound nucleus (α,p) cross-sections in Ni region, 15 and 18 MeV 77−74864
compound nucleus (p,p′) cross-sections in Ni region, 12 MeV 77−74864
cosmic rays, abundances of elements in 26≤Z≤30 interval 79−40044

nuclei with mass number 59 to 89 continued
delayed neutron spectra from precursors with A=79-130 77−82884
double-even nuclei, Ge to Sr, low-lying octupole states anal. 78−21497
even-even and odd A nuclei, nuclear shapes and motions, review 80−5054
even-even nuclei, 2_2^{+} level deexcitation *(Russian)* 77−2939
even-even nuclei, 58≤A≤150, E2, M1 multipole mixing ratio, data survey 78−50118
even-even nuclei, z=6 to 100, probable members of quasi-bands in spherical and deformed regions 80−13357
even-even spherical nuclei, 2_1^{+} state deformation parameter from (p,p) and EM excitation 80−27549
excitation functions for neutron deficient isotope form. via high-energy d-Br reactions 78−44609
fast neutron capture and activation cross section, Co, Ni, Cu, Zn targets 77−26758
fission product gamma-ray and half-life 29≤A≤69, data collection 78−50134
gamma-ray internal conversion coeffs. for all at. shells, 30≤Z≤104 79−45206
internal conversion coefficients, 30≤Z≤104, Hartree-Fock-Slater model calcs. 79−36199
Mossbauer isomer shifts, book contrib. 79−87363
odd mass nuclei, 59≤A≤149, E2, M1 multipole mixing ratios 78−4911
photospallation, 0.1 to 1 GeV, mass yield distrib. 80−73835
separated fission products with A=88-144, delayed neutron spectra 77−34268
spin-alignment attenuation factors in mass 61-67 nuclei populated by (α, n) and (α, p) reactions 79−26390
thermonuclear reaction rate data for intermediate mass nuclei 80−31427
(α,α′), A=40-208, low energy octupole resonances, 96 and 115 MeV 79−511
(d,^{6}Li), A∼60,116, L=0 transitions, cross sections, microscopic anal. 80−78189
(e,α), Z=29-79, direct and statistical effects, cross sections and ang. distribs. 79−530
(n,γ), A=75 to 103, γ-strength functions and stat. model cross section calcs. 80−52612
(n,γ), valence model, mass range 40<A<70 79−45256
(n,n′γ), A=28-152, spherically doubly even nuclei, level excitation cross sections, statistical anal. *(Russian)* 79−67707
(n,X), fast n, ^{3}He emission cross sections for A=27-115 80−13475
(p,n), 2.5-5.8 MeV, A=89-130, cross sections, sub-Coulomb proton anomalous optical pot. 80−32278
(p,n), A=89-130, sub-Coulomb protons, anomalous optical pot. 80−102191
(p,n) excitation functions for A=45 to 80, proton optical pot. at sub-Coulomb energies 80−9292
Zn isotopes, (n,p), (n,α), (n,2n) cross sections at 14.1 MeV *(Spanish)* 77−30563
^{63}Cu+^{20}Ne, 168 MeV, gamma ray multiplicity distrib. in strongly damped oscills. 79−36266
^{87}Br, delayed neutron carrier, sorption parameter determ., appl. to fuel element leak detection 79−97828
A=Rb, A=74-79, 90-99, direct meas. of masses, deformation onset at N=60 79−54383
A=62 nuclei, nuclear data sheets to August 1978 79−71777
As, β-decay energies and masses, A=80, 81, 83 77−74808
As isotopes, (n,p), (n,α),(n,2n) cross sections at 14.1 MeV *(Spanish)* 77−30563
As isotopes, A=69, 71, 73, level scheme, cf. with Alaga model 77−22835
As isotopes, levels and spectra from broken pair model 80−73801
As neutron deficient isotopes (A=68,69,70,71), production in heavy ion reactions 77−38292
As, neutron-deficient isotopes, nuclear spin meas. by at. beam mag. resonance 77−18386
As, stable isotopes, masses meas. 78−12956
^{A}As, A=69-72, $^{4}S_{3/2}$ ground state hyperfine struct. and nuclear moments 80−32853
^{A}As, A=70, 72, level scheme, transitions, J^{π} and lifetimes from Ge(p,nγ) 80−22695
^{A}As, A=71, 73, levels, J^{π}, transitions, T1/2 from Se decay, Ge(^{3}He,d), (p,xnγ) 80−57684
^{A}As, A=71,73,75, E1 γ-ray strength function from Ge(p,γ) 79−75902
^{A}As, A=73,75,77, probabilities for analogue-antianalogue transitions 79−6496
^{A}As, A=78,80,82, ground state mass meas. and excited state energies 79−63595
^{A}As, A=79,81, Q-values and mass excess from Se(d,^{3}He) 80−9222
^{A}As, A=85-7, mass chain, half lives and n-emission probabilities of delayed-n precursors 78−70497
^{68}As β-decay, γ coincidence and singles spectra, spin, parity assignments, half-life meas. 77−79333
^{69}As 1306 keV state mag. moment, g-factor, rot. aligned band 80−86807
^{69}As β-decay, struct. determ. of ^{69}Ge 79−22245
^{69}As, recoil distance level lifetime meas. from ^{16,18}O collisions 78−78311
^{70}As, hyperfine struct. investig. using at. beam mag. reson. 77−22933
^{70}As states, excitation functions, spin and halflifes from ^{69}Ga(α,3n), ^{60}Ni(^{12}C,np), ^{63}Cu(^{10}B,2np) 79−6414
^{71}As, ^{72}As, nucl. mag. moment by NMR/ON 77−12251
^{71}As, ^{73}As, quadrupole interaction of $9^{+}/2$ states in orthorhombic Ga 77−8467
^{71}As, intermediate struct., props. 78−93948
^{71}As intermediate struct., resonance spin from ang. correlations of ^{70}Ge(p,p′γ) 79−67729
^{71}As, isobaric analogue reson. through ^{70}Ge(p,p) 3.5 to 5.3 MeV study 79−75951
^{72}As, new 87 ns isomer, g-factor via ^{59}Co(^{16}O,2pn) 53-56 MeV 77−54149
^{72}As, populated in ^{72}Ge(p,nγ), level scheme determ. 77−14032
^{73}As bound and isobaric analogue states, spectroscopic factors, DWBA anal. of ^{72}Ge(^{3}He,d) 79−54391
^{73}As core-coupled states, studied via (p,t) reaction 77−54212
^{73}As, energy levels, meas. from ^{72}Ge(p,γ) 2213 keV 78−93939
^{73}As, quadrupole nucl. interactions in Ge, TDPAC meas. 77−36160
^{73}As, yields in α, d and p interactions on Ge, Ga and As 77−54223
^{74}As decay, branching ratios and $T_{1/2}$ meas., K-fluorescence yield of Ge 77−3300
^{74}As level structure, studied via ^{72}Ge(α,npγ), 30 to 50 MeV 77−10357
^{74}As, yields in α, d and p interactions on Ge, Ga and As 77−54223

nuclei with mass number 59 to 89 continued
^{75}As, level lifetimes, bremsstrahlung, reson. fluoresc. *(French)* 79−13248
^{75}As, NMR expts. on antiferroelec. $NH_4H_2AsO_4$ in paraelec. phase 77−36184
^{75}As, NQR freq. in aminoarsines, N-As bonds 78−25566
^{75}As, NQR spectral parameters in dihydrogenarsenates, temp. meas. 77−13785
^{75}As, nucl. reson. fluoresc. meas., spins and level widths determ. 77−61379
^{75}As, PAC in Gd, mag. hyperfine field determ. 77−8459
^{75}As, stopped π^- absorpt. 77−38299
^{75}As, stopped π^- absorption, in beam and activation γ-ray spectroscopy 79−40960
^{75}As, transitions populating and depopulating 279 keV level, δ(E3/M2) 77−82852
^{75}As(α, 3nγ)^{76}Br, 30 to 55 MeV, study of ^{76}Br level structure 77−54174
^{75}As(α,2n)^{77}Br production excitation curves 79−85468
^{75}As(n, γ), 1.3-2.8 MeV, ^{75}As levels determ. 77−26611
^{75}As(n,n'γ)^{75}As, deexcitation gammas, energy levels, branching ratios, spins, parities, excitation function meas. 78−89869
^{75}As(n,n), slow n coherent scatt. length, free cross section, bound states 80−86909
^{76}As, beta decay, level scheme for ^{76}Se from $\gamma\gamma$ coincidence meas. 80−22754
^{76}As, dynamic orientation in n-Si crystals, ang. momentum, forbidden β transition 79−501
^{76}As excited states, excitation functions and decays ang. distribs., cross sections from ^{76}Ge(p,nγ) *(Russian)* 80−63089
^{76}As, first forbidden β-transitions, β-γ circular polarisation correlations 79−9517
^{76}As, level structure, transitions and J$^\pi$, from ^{76}Ge(p,nγ) 80−47379
^{78}As, level struct. determ. in ^{80}Se(d,α) at 16 MeV 78−8827
^{79}As levels, J$^\pi$ and ang. distribs. from ^{76}Ge(α,p) 80−78161
^{85}As, β-decay delayed n emission, simple statistical model description 79−67714
^{85}As, β-delayed neutron decay, statistical model, Monte Carlo techniques 78−89830
^{85}As, β-strength function energy struct., effect on delayed neutron emission prob. 79−75915
^{85}As, investigation of beta-strength functions by neutron and γ-spectroscopy 79−45209
^{85}As, neutron and gamma-ray spectroscopy of delayed neutron emission 77−22973
^{85}As, shell model anal. of delayed neutron emission 77−71595
^{71,73}As, γ-spectroscopy of high-spin states via heavy-ion reactions 77−74795
As(n,n'), 14.1 MeV, precompound processes 78−13093
Br, A=80,2, energy levels anal. from Se(p,nγ) 77−71609
Br, A=87-89, delayed neutron energies delayed neutron energies 77−74816
Br, A=87-89, delayed-neutron emission probabilities 77−74817
Br, A=87-92, shell model anal. of delayed neutron emission 77−71595
Br, break-up in relativistic proton collisions, ^{4}He emission 77−10410
Br, emulsion nuclei, 28 GeV proton interactions *(Korean)* 80−18299
Br nuclei, highly excited, disintegration, photographic emulsion, quark model theory comparison 80−68560
Br series isotopes, sensitivities to various parameters, analytical evaluation 78−82424
Br+C(O), 0.2-4.2 GeV/N, compression phenomena and Mach shock waves 80−22851
Br+Fe, hydrodynamic effects in cosmic ray nucleus-nucleus interactions 79−80176
Br+p, inelastic interactions, 6.0 GeV/c, in emulsions 78−86530
Br(^{12}C,^{12}C'), 50 GeV/c, multiplicities and ang. distribs. *(Russian)* 79−22323
Br(^{12}C,X), 4.5 GeV/c, emission of short range particles (R<100 mkm) *(Russian)* 80−63202
Br(Fe,f), central collisions, nucleon characteristics, nuclear pionisation in complete fission *(Russian)* 79−80963
Br(Hl,X), 0.2-4.2 GeV/N, nonperipheral collisions, forward-backward asymmetry, compression phenomena 80−18329
Br(K^-,f), 1.8 GeV, ternary, quaternary and cascade fission 79−63708
^{79}Br(p,3n)^{77}Kr→^{77}Br production excitation curves 79−85468
^{A}Br, A=79,81, mass using spectroscopic doublet method *(Russian)* 78−86468
^{A}Br, A=85 to 89, total β-decay energies and atomic masses of neutron-rich isotopes 79−40889
^{A}Br, A=87-89, β-delayed neutron emission probabilities, half-life 80−52634
^{A}Br, A=89-91, delayed neutron emission probabilities, β-decay half-lives 80−83078
^{A}Br(p,pxn) A=79,80, 10 to 85 MeV, excitation function meas. 79−63673
^{A}Br(p,xn) A=79,80, 10 to 85 MeV, excitation function meas. 79−63673
^{70}Br, half life of Fermi superallowed β^+ activities from ^{58}Ni(^{14}N,2n) 79−9518
^{71}Br, prod. in proton spallation reactions, nuclear structure influence on yields of product nuclei 80−22794
^{73}Br, excited state lifetimes by particle X-ray coincidence technique 78−86507
^{75}Br, excitation functions for production, pot. nuclear medicine appls. 80−98135
^{75}Br, first 9/2$^+$ state and prolate deform. from ^{75}As(α,4nγ) 78−50088
^{76}Br, ^{77}Br, production from decay of cyclotron produced ^{76}Kr and ^{77}Kr 80−52799
^{76}Br, Coriolis distorted bands, common $g_{9/2}$ parentage in N=41 nuclei 80−13349
^{76}Br level structure studied via the ^{75}AS(α, 3nγ) reaction, 30 to 55 MeV 77−54174
^{76}Br long-lived positive parity isomer from ^{75}As(α,3n) 79−54375
^{76}Br, new isomeric state with half-life 1.49 sec 79−17858
^{76}Br, populated by ^{76}Se(p,nγ), level scheme 78−50091
^{76}Br production, excitation functions for neutron deficient isotope form. via high-energy d-Br reactions 78−44609
^{76}Br^{M} decay props., half life and γ-transitions, level scheme 80−83071
^{76}Br(n,p)^{76}Se, thermal energy, ^{77}Br proton branches 78−89878
^{77}Br collective bands, lifetimes, spins and E2 transition probabilities from ^{64}Ni(^{16}O, 2nP) 80−13415
^{77}Br E2 transition probabilities and mean lives from ^{64}Ni(^{16}O,2npγ) 80−13414

nuclei with mass number 59 to 89 continued
^{77}Br, level struct., l-transfers, spectroscopic factors, DWBA anal. from ^{76}Se(^{3}He,d), 41 MeV 78−86479
^{77}Br, low energy states from ^{77}Se(p,nγ)^{77}Br reaction 79−6407
^{77}Br production, excitation functions for neutron deficient isotope form. via high-energy d-Br reactions 78−44609
^{78}Br, high-spin states, from ^{77}Se(α,2np), decay into isomers 80−52569
^{78}Br, in liq. metal target, in-beam γ-NMR-PAD 77−59465
^{78}Br level struct. determ. from (α,nγ), (^{3}He,d) and (p,d) reacts. 79−59010
^{79}Br, level struct., l-transfers, spectroscopic factors, DWBA anal. from ^{78}Se(^{3}He,d), 41 MeV 78−86479
^{79}Br, NQR in $SrBr_2$-H_2O and $CaBr_2$-H_2O, cryst. struct. 78−27110
^{79}Br, NQR spectra in group IV tetrabromides 77−12231
^{79}Br+p, 24 GeV/c, in nucl. emulsion, particle emission freq. variation 78−37335
^{79}Br(^{32}S,X), 153-184 MeV, fission like processes around A_{CN}=100, mass distrib. strong change 80−9318
^{79}Br(^{32}X,X), double differential cross section, mass asymmetry, transport model 80−102203
^{79}Br(α,2n)^{81}Rb-^{81m}Kr production excitation functions and thick target yield curves 80−12253
^{79}Br(α,3n) 30-55 MeV, populating ^{80}Rb 77−88028
^{79}Br(d,pxn), excitation functions for neutron deficient isotope form. via high-energy d-Br reactions 78−44609
^{79}Br(d,xn), excitation functions for neutron deficient isotope form. via high-energy d-Br reactions 78−44609
^{79}Br(p,3n)^{77}Kr excitation function meas. 79−88191
^{79}Br(p,3n)^{77}Kr→^{77}Br$^-$ production, separation and radiopharmaceutical labelling 79−79649
^{79}Br(p,4n)^{76}Kr excitation function meas. 79−88191
^{79}Br(p,5n)^{75}Kr→^{75}Br excitation function meas. 79−88191
^{79}Br(p,p4n)^{75}Br excitation function meas. 79−88191
^{80}Br, 37 keV level quadrupole moment, shell model anal. *(French)* 79−85366
^{80}Br isobaric analogue resonances and spectroscopic factors from ^{80}Se(p,n) 79−36212
^{80}Br level struct. and transitions, DWBA anal. spectroscopic factors from ^{81}Br(p,d), 22.8 MeV 79−3084
^{80}Br, level struct. determ. from thermal (n,γ) meas. 78−41667
^{80}Br, study of excited states from ^{79}Br(n,γ) and ^{80}Se(p,nγ) *(French)* 78−29393
^{80}Br+p, 70 GeV/c, s-particles ave. multiplicity 78−21567
^{80}Br($\bar{n}$,X), annihilation, 1.4 GeV/c, $\pi^\pm$, p emission angles, momentum and multiplicity distribs. 80−532
^{81}Br NQR in MAl_2Br_7 cryst. (M=Li, Na, K, Cs, NH_4, $(CH_3)_4N$), Zeeman effect 78−6597
^{81}Br+ν_e, 0 to 300 MeV, cross sections, shell model calcs 79−93605
^{81}Br(^{3}He,3n)^{81}Rb-^{81m}Kr production excitation functions and thick target yield curves 80−12253
^{81}Br(d,pxn), excitation functions for neutron deficient isotope form. via high-energy d-Br reactions 78−44609
^{81}Br(d,xn), excitation functions for neutron deficient isotope form. via high-energy d-Br reactions 78−44609
^{81}Br(ν,e)^{81}Kr, solar neutrinos detect. possibility 77−22160
^{81}Br(p,nγ), ^{81}Kr low lying levels from γ spectra, γ-γ coincidences 78−25195
^{82}Br, level struct. determ. from thermal (n,γ) meas. 78−41667
^{82}Br, orientation in Fe 77−59486
^{82}Br, study of excited states from ^{81}Br(n,γ) and ^{82}Se(p,nγ) *(French)* 78−29393
^{83}Br, levels assignment, ^{83m}Se decay scheme obs. 78−17147
^{84}Br decay, ^{84}Kr levels, γ-cascades, J^{II}, mixing ratios and correlations 80−63134
^{87}Br, β-decay delayed n emission, simple statistical model description 79−67714
^{87}Br, β-decay into ^{87}Kr, delayed neutrons, high energy γ spectra, energy levels 78−25155
^{87}Br, β-delayed neutron decay, statistical model, Monte Carlo techniques 78−89830
^{87}Br, β-strength function energy struct., effect on delayed neutron emission prob. 79−75915
^{87}Br, investigation of beta-strength functions by neutron and γ-spectroscopy 79−45209
^{87}Br, neutron and gamma-ray spectroscopy of delayed neutron emission 77−22973
^{87}Br, prod. by radiochem. separation, for neutron decay obs. 78−70951
^{88}Br β-decay, ^{88}Kr level scheme and transitions, delayed neutrons 80−42600
^{88}Br→^{88}Kr, γ-ray spectrum, transitions 77−295
Br(α,X) 80−22851
Br(α,X), 16.5 GeV/c, inelastic cross sections, multiplicity, ang. and momentum distribs. 78−82359
Br(α,α), 12.5-15.0 MeV, total reaction cross section determ. 79−93638
Br(p,X), 400 GeV/c, multiplicity and ang. distribs. of relativistic and slow particles *(Russian)* 79−40931
Br(p,xn)^{77}Kr, prep. of carrier free ^{77}Kr using natural Br 78−29678
Br(π^-,X), charged heavy particle emission after pion capture *(Russian)* 80−69271
CC Rb cross sections and decay props. from ^{85}Rb(γ,n), ^{85}Rb(n,2n) 79−49600
Co, A=59,60, yrast decay scheme from ^{48}Ca+^{15}N(^{18}O) fusion-evaporation reactions 78−13154
Co, admissibility as alloy constituent in primary cooling circuits of HTRs *(German)* 78−25294
Co backward π^+ prod., momentum depend., scaling, Monte Carlo calcs. 79−13305
Co isotopes, shell model 78−62479
Co, mass dependence for radiative capture of 14.1 MeV neutrons 78−13087
^{A}Co, A=55,57,59,61, deduced levels, proton-hole states, semimicroscopic model from Ni(p,α) 79−45171
^{A}Co A=55,57,59,61, level direct and compound cross sections from ^{A}Ni(p,α), A=58,60,62,64 79−9474
^{59}Co, NMR spin echo spectra in BCC ternary Fe alloys 77−59396
^{59}Co (n, n'γ), 1.3-3.9 MeV, energy level structure and decay scheme 79−45164
^{59}Co, cross sections for charged particle prod. by 14 MeV neutrons, data compilation 80−9289
^{59}Co, deformation effect from fast neutron transmission in 0.8 to 20 MeV range 80−57675

nuclei with mass number 59 to 89 continued
^{59}Co, deformation effect of aligned target, fast-neutron transmission 80−47364
^{59}Co, electron elast. scatt. cross sections, phase shift anal. and HF calcs. *(Russian)* 78−41707
^{59}Co, energy levels, lifetimes, deexcitation following (n,n′γ) studies 80−83059
^{59}Co, energy levels from Ni(p_{pol},α) 80−68663
^{59}Co, isospin effects in GDR region 78−78344
^{59}Co level energies, branching ratios lifetimes and spins from (p,p′),(α,pγ) 80−63093
^{59}Co level struct., from ^{59}Fe decay γ-spectrum 77−14063
^{59}Co, mag. form factors, core polarisation and exchange current effects 80−13409
^{59}Co, mean lifetime meas., 1400 to 1650 keV range, by reson. scatt. of bremsstrahlung *(French)* 79−75905
^{59}Co, NMR and nucl. relax. time meas. in HCP CO 77−36146
^{59}Co, NMR in $(Y_{1-x}Gd_x)_2Co_{17}$ 77−20727
^{59}Co, NMR in Co_2TiAl 78−2760
^{59}Co, NMR in $CoTi_{1-x}Al_x$, form. of mag. moment of Co atom 77−43819
^{59}Co, NMR in rare earth cobaltides, R_2Co_{17} 77−20726
^{59}Co, NMR in $Y_{1-x}Dy_xCo_5$, $Y_{1-x}Ho_xCo_5$, $Y_{1-x}Gd_xCo_2$ and Y_xCo_y 77−85585
^{59}Co NMR line breadth and chemical shift data compilation *(Japanese)* 78−15045
^{59}Co, NMR obs. of anisotropic hyperfine interactions in ferromag. Co 78−43658
^{59}Co, neutron capture cross section meas. 80−5147
^{59}Co, neutron resonance spectroscopy, R-matrix anal. 78−21555
^{59}Co, nucl. level densities, using single particle states for Woods-Saxon and Nilsson potentials 78−50086
^{59}Co, nucl. spin-lattice relax. in CoB 77−59479
^{59}Co, radiative transitions from unbound states obs. in neutron inelastic scatt. *(Russian)* 78−41664
^{59}Co, spallation by 0.3-1.0 GeV photons, cross-sections 78−41691
^{59}Co, stopped π^- absorption, in beam and activation γ-ray spectroscopy 79−40960
^{59}Co+n, 16-22 MeV, cross sections for prompt γ, compound statistical model calcs. 79−543
^{59}Co+n, 8-31 MeV, spin-spin depend. of total cross section 78−17172
^{59}Co(^{16}O,^{16}O), 142 MeV, optical model anal. of ang. distrib. meas. 78−58295
^{59}Co(^{16}O,^{16}O), 36-56 MeV, cross sections, optical and double-folding model anal. 79−6693
^{59}Co(^{16}O,2pn)^{72}As, 53-56 MeV, new ^{72}As isomer spin-precession, g-factor 77−54149
^{59}Co(^{32}S,X), 153-184 MeV, fission like processes around A_{CN}=100, mass distrib. strong change 80−9318
^{59}Co(^{32}S,X), double differential cross section, mass asymmetry, transport model 80−102203
^{59}Co(^{3}He, ^{3}He), 119 MeV, optical pot. parameters energy and mass depend. 80−32289
^{59}Co(^{3}He,α), 34.8±0.3 MeV, α-particle energy spectra distrib., c.f. pre-equilibrium decay calcs. 79−9598
^{59}Co(^{7}Li,2n), E=18 MeV, high-spin states in ^{64}Zn 78−33145
^{59}Co(α, p), (A, d), (α, t), 50 MeV, reaction mechanism determ. *(Russian)* 78−54778
^{59}Co(α,n)^{62}Cu, 6-11 MeV, gamma transitions from ^{62}Cu excited levels obs. *(French)* 77−26615
^{59}Co(α,p)^{62}Ni, 6-11 MeV, ^{62}Ni energy levels determ. *(French)* 77−26615
^{59}Co(α,pγ)^{62}Ni, lifetime meas. of excited states in ^{62}Ni 79−3115
^{59}Co(α,t), 27.2 MeV, cross sections, optical potential, spectroscopic factors *(Russian)* 77−38290
^{59}Co(α,xnyp), 20-172.5 MeV, cross sections excitation functions, hybrid model, prequilib. effects 80−57784
^{59}Co(d,p), ^{60}Co low lying states, DWBA anal. 78−29478
^{59}Co(e,e), mag. elastic scatt., radial distrib. of $1f_{7/2}$ proton orbit using cross sections 78−13067
^{59}Co(e,e), magnetic e scatt., exchange current effects, plane wave Born approx. 80−78282
^{59}Co(e,e), valence nucleon orbit determ. 78−54669
^{59}Co(γ,xn), 10-36.5 MeV, photoneutron cross sections, integrated cross sections, giant dipole resonance 79−89289
^{59}Co(γ,xn), x=2,3 or 4, cross sections at intermediate energies 78−8793
^{59}Co(n,2n), 14 MeV, cross section compilation 80−91181
^{59}Co(n,2n), (n,np), (n,d), 16.2 to 21.8 MeV, γ-ray prod. cross sections 78−13080
^{59}Co(n,2n), isomeric cross-section ratio and excitation function, mixed-powder method and gamma-ray spect. 80−47472
^{59}Co(n,2n) direct process contrib., cross section and secondary n spectrum *(Russian)* 78−78386
^{59}Co(n,α), excitation function, mixed-powder method and gamma-ray spect. 80−47472
^{59}Co(n,α), thermal, isomer state excitation, relative probabilities 79−75814
^{59}Co(n,γ), 2.5 keV-1 MeV, TOF capture cross-section meas. 77−30586
^{59}Co(n,n′), 14.6 MeV, ToF spectra meas. *(Russian)* 78−41721
^{59}Co(n,n′), 2-4.5 MeV, level excitation functions, Hauser-Feshbach-Moldauer model test 79−36238
^{59}Co(n,n′), exciton neutron inelastic scatt. model *(Russian)* 78−33189
^{59}Co(n,n′γ), 1.1-3.3 MeV, level inelastic scatt. cross section, decay γ-rays, spins, branching ratio 79−6605
^{59}Co(n,n′γ), level transitions, deexcitations and lifetimes 80−18222
^{59}Co(n,n), compound nucl. effects in spin-spin cross-sections 77−10402
^{59}Co(n,n), spin-spin cross-section for polarised neutron and target, 0.4 to 30 MeV 77−26656
^{59}Co(n,t), 14 MeV, cross sections, fast neutron reaction excitation function calc. 79−45267
^{59}Co(p,X), 12-45 MeV, reaction cross section and hybrid model analysis 79−67749
^{59}Co(p,2p)^{58}Fe, 17 MeV, search for double-direct reaction 77−30576
^{59}Co(p,d), 50 MeV, fine struct. of ground hole-state analogues 78−50065
^{59}Co(p,d), fragmentation of hole-state analogues in ^{58}Co 78−54731
^{59}Co(p,γ_0), polarised p, 5.8 to 16.5 MeV, cross section and analysing power ang. distrib., model comparison 78−70533
^{59}Co(p,γ_0), polarised p in giant dipole resonance region, cross sections and analysing power 78−82346
^{59}Co(p,x), x=α, τ, 72 MeV, spectra and angular distribs. 80−68660

nuclei with mass number 59 to 89 continued
^{59}Co(π^-, xn), single and correlated n spectroscopy, nuclear temp. 79−6713
^{59}Co(π^-,X), X=d,t, ^{3}He, ^{4}He, particle emission following stopped pion absorption 80−91196
^{60}Co, 2505 keV gamma ray intensity in β-decay 79−13249
^{60}Co beam model for radiotherapy treatment planning 77−66857
^{60}Co beta decay to ^{60}Ni, 2506 to 2159 keV γ transition 77−22929
^{60}Co brachytherapy source calibration using $Fe(NH_4)_2(SO_4)_2$-benzoic acid-xylenol orange dosimeter 77−5081
^{60}Co β-decay, nuclei polarised in iron foils cooled by dilution refrigeration 77−34263
^{60}Co contamination of freshwater food chains, direct water borne contamination of organisms *(French)* 79−20688
^{60}Co, decay to ^{60}Ni, aero-phonon, $4_1^+ \rightarrow 2_2^+$ γ-ray transition 78−17136
^{60}Co, ensemble rotation concept in NMR on oriented nuclei in dil. Fe-Co alloys 77−90061
^{60}Co, exposure-rate calibration of small radioactive sources 78−41881
^{60}Co external source on liq. scintillation system for ^{32}P Cherenkov effect detect. efficiency meas. 78−25387
^{60}Co gamma active spikants in nuclear fuel for proliferation deterrence, practical aspects 79−93716
^{60}Co, gamma radioactive source, buildup factor determination for meas. in air *(Rumanian)* 78−49132
^{60}Co gamma ray sources, exposure efficiency dependence on distance, theoretical interpretation *(Czech)* 80−850
^{60}Co γ rays, backscattering atomic number depend., Monte Carlo calcs. 77−67734
^{60}Co, half-life determ. 77−34498
^{60}Co, high energy gamma spectra appl. of improved HgI_2 spectrometer 77−65378
^{60}Co, level determ. in seawater 78−85608
^{60}Co, level struct., spectroscopic factors, DWBA anal. from ^{59}Co(d,p), 14 MeV 78−86478
^{60}Co low lying states from ^{57}Fe(α,pγ), spin constraints, γ mixing ratios 78−29487
^{60}Co low lying states struct., orbital ang. momentum, spectroscopic factors 78−29478
^{60}Co, mag. hyperfine splitting const. in Co, NMR-ON meas. 78−43651
^{60}Co neutron activation, cross section for ^{63}Cu(n,α)^{60}Co 78−74359
^{60}Co, neutron scatt. cross section meas., parameters of neutron levels 80−5147
^{60}Co, nuclear orientation-pulsed NMR in Fe 77−59490
^{60}Co, oriented, β-decay asymm., positron ang. distrib. meas., matrix elements 77−2951
^{60}Co, oriented in Fe, triple pulse reson. studies 78−43675
^{60}Co oriented nuclei in Fe, radioactive detection of single- and multiple-pulse mag. reson. 77−66437
^{60}Co polarised nuclei, β-ray emission, directional distrib. and asymmetry factor 80−95315
^{60}Co, radiation sterilisation of medical products 79−49870
^{60}Co, radioactive decay, γ-ray energy meas. *(German)* 77−57633
^{60}Co, single passage NMR/ON in Fe, elec. quad. interaction 77−16204
^{60}Co, sorption from water using fibrous ionites 77−56251
^{60}Co, spin-lattice relax. meas. on Fe 77−85596
^{60}Co, $T_{1/2}$ meas. using double ionization chamber for the differential method 79−22552
^{60}Co teletherapy, IAEA-WHO dosimetry service using mailed LiF, 1970-75 survey 77−16991
^{60}Co teletherapy dosimetry, USA nationwide survey 77−56478
^{60}Co, teletherapy dosimetry, USA survey (1974-77) 79−12011
$^{60}CoCl_2$, whole-body retention in rats, age effect 77−70559
^{62}Co differential from ^{66}Zn (α, ^{8}B) 80−5153
^{63}Co, proton hole states determ. from ^{64}Ni(d,^{3}He)^{63}Co 79−22163
^{63}Co, radioactive decay scheme from ^{64}Ni(n,d), 14.3 MeV 78−46053
^{64}Co, radioactive decay scheme from ^{64}Ni(n,p), 14.3 MeV 78−46053
^{65}Co, mass excess meas. from ^{70}Zn(^{3}He,^{8}B)^{65}Co 78−93931
Co(e,e), nuclear radius, core polarisation and isotone shifts, muonic X-rays 80−22685
Co(n,n), elastic and inelastic scatt., cross sections meas. and calcs. 78−13081
Co(n,n′), 9.1 MeV, equilib., pre-equilib., direct process anal. *(Russian)* 77−46172
Co(p,^{3}He x), 72 MeV, pre-equilibrium emission *(German)* 80−68657
Co(p,X), 10-60 MeV, long lived radioisotope prod. cross sections and excitation functions 79−89305
Co(p,αx), 72 MeV, pre-equilibrium emission *(German)* 80−68657
Co(p, spallation), 0.08-24 GeV, Ar isotopes, spallation ratios and prod. cross sections 80−9284
^{59}Cr, neutron rich nuclide from ^{238}U(^{40}Ar,X) at 340 MeV 80−57802
Cu (γ,X), 2-5 GeV, spallation 77−71604
Cu (n,X) 80−68673
Cu (p, X), 2.2, 6, 8.5 GeV, p and d inclusive spectra at 162° *(Russian)* 79−97710
Cu (p,π^+) 240 MeV inclusive pion production *(Russian)* 80−86908
Cu, A=59,61,63,65, levels and spectroscopic strengths via Ni(τ,d)Cu 18 MeV, centroid energies 77−10303
Cu, A=61,63, analogue state decay modes from Ni (^{3}He,dp) 79−67702
Cu, A=63, 65, electron elast. scatt. cross sections, phase shift anal. and HF calcs. *(Russian)* 78−41707
Cu, A=64, 66, 68, 70, level schemes, mass excesses via (t,^{3}He) reactions 77−46117
Cu, beta-generated external bremsstrahlung spectra 77−57625
Cu, CC ^{56}Ni core excitation effects on A=57-66 nuclei, MSDI and ASDI comparison 78−78254
Cu foils, activation by p, d, ^{3}He, ^{4}He from cyclotron beam, monitoring props. 77−38578
Cu, isotopes, shell model calcs. of BE, spectroscopic factors and excit. energies 77−22860
Cu, K_β/K_α following K-electron capture and X-ray excitation 78−13031
Cu, nucl. electron capture, 0.43-1.71 MeV electrons 79−6513
Cu odd isotopes populated in ^{58,61}Ni(p,γ), analogue to antianalogue M1 transitions 77−67718
Cu, π^- and p elastic scatt., 30 to 50 GeV/c, nuclear radius, real/imaginary forward scatt. amplitude ratio *(Russian)* 77−34351
Cu, reactions induced by ^{12}C and ^{19}F ions, γ-ray spectroscopy of induced activities 77−23107
Cu, recoil energies of photoproduced fragments, 800 MeV bremsstrahlung 77−41953
Cu, shadowing in photon-nucleus 20 to 185 GeV total cross sections 79−30823

nuclei with mass number 59 to 89 continued

Cu, spallation by ^{40}Ar ions, 80 GeV, 35 radioactive nuclide prod. cross sections 78−66260
Cu spallation by 25 GeV ^{12}C and 28 GeV protons, mass yields 77−6435
Cu, total neutron cross-section meas. 77−74839
Cu+^{12}C, 25.2 GeV, target residue mass and charge distribs., calcs. 79−3172
Cu+^{40}Ar, 1.8 GeV/nucleon, central collisions, single particle inclusive spectra, associated multiplicity 79−9607
Cu+Ne, 800 MeV/N, p and π inclusive spectra, energy and ang. distribs. 78−54790
Cu+p, 1 GeV, neutron production *(Russian)* 79−85477
Cu+p, 1.2-4.6 MeV, (p,n) thresholds and radiative capture, A=63, 65 78−89856
Cu+p, 400 GeV, charm prod. cross section and particle lifetimes, Monte Carlo anal. 78−89679
Cu+p, 400 GeV, dimuon and trimuon prod., prompt ν source, D$\bar{\text{D}}$ prod., axions 78−89860
Cu+p, 400 GeV, prompt ν prod., axion prod. upper limit 78−89859
Cu+p, 600 MeV, pion production, energy spectra, A depend. *(Russian)* 78−17213
Cu+p, 7 GeV/c hadron multiple prod. *(Russian)* 79−22298
Cu+p, dimuon prod., struct. in Υ region near 9.5 GeV 78−17201
Cu+p, direct muon prod. in 70, 50 and 35 GeV collisions 77−2872
Cu+p→$\Lambda^0(K_S^0)(\bar{\Lambda}^0)$+X, neutral strange-particle prod. by 300 GeV protons 79−17905
Cu+p→p, 640 MeV, proton inclusive spectra and ang. distrib. meas. 77−67751
Cu+π^-, 27, 40 GeV, cross sections and differential distribs. for muon pair prod. *(Russian)* 78−89919
Cu+π^-, 3.7 GeV/c, proton spectra *(Russian)* 78−41785
Cu+π^-, 43 GeV/c, inclusive J/ψ prod., A-depend. 78−62581
Cu+π^-, 7 GeV/c hadron multiple prod. *(Russian)* 79−22298
Cu+π^-→$\mu^+\mu^-$X, 16, 22 GeV, quark annihilation model interpretation, scaling 79−36277
Cu+π^- →ψX, 16, 22 GeV, cross section, quark fusion model 79−36278
Cu(^{12}C, spallation), 25 GeV, mean kinetic props., momentum transfer, target recoil props. 79−3129
Cu(^{56}Fe,X), relativistic ^{56}Fe fragmentation, charge and mass changing cross sections 79−54453
Cu(K^-, ϕX), *(Russian)* 79−9637
Cu(^{20}Ne,π^+), 800 MeV/N, doubly differential cross sections and ang. distribs. 80−9305
Cu(^{20}Ne, π^+X), 400 MeV/N, pion prod. doubly differential cross sections and ang. distrib. 80−32299
Cu(^{16}O,^{16}O), A=63,65, 40 to 46 MeV, differential cross sections, G-matrix and adiabatic pot. models 78−78411
Cu(^{16,18}O, xn), 36 to 55 MeV, total neutron yelds, cross sections 77−14163
^{A}Cu A=29,63, Doppler shift attenuation factors, level lifetimes, resonances from Ni(p,γ) 80−57741
^{A}Cu, A=59, 61, 63, 65, f and p shell analogue resonances, γ-decay *(Russian)* 79−30800
^{A}Cu, A=61, 63, 65, nucl. level densities, using single particle states for Woods-Saxon and Nilsson potentials 78−50086
^{A}Cu, A=63,65, mean lifetime meas., 1400 to 1650 keV range, by reson. scatt. of bremsstrahlung *(French)* 79−75905
^{A}Cu, A=65,67,68, energy levels, core coupling model calcs. 80−9238
^{A}Cu(n,X), A=63,65, 14.8 MeV, charged particle emission, cross section, Hauser-Feshbach anal. 79−67750
^{A}Cu(n,α), A=63,65, 14.8 MeV, expt. and statistical model determ. of α-prod. in fusion reactors 80−95397
^{A}Cu(n,n'), A=63, 65, 2-4.5 MeV, level excitation functions, Hauser-Feshbach-Moldauer model test 79−36238
^{A}Cu(p,p), A=63,65, 100-2200 MeV, total and reaction cross sections from optical pot. 80−18303
^{59}Cu, analogue resons. excited in ^{58}Ni(p,γ), γ-decay 78−13005
^{59}Cu, determ. of total and partial widths of unbound states 77−74802
^{59}Cu, reson. lifetime, J, via ^{58}Ni(p,γ) 1833 and 3547 keV 77−26621
^{59}Cu, resonance states parameters *(Russian)* 79−80911
^{59}Cu, time struct. of the $2d_{5/2}$ analogue state 79−6591
^{59}Cu(β^+)^{59}Ni, γ-spectra and levels 77−22935
^{60}Cu levels from ^{60}Ni(^{3}He,t) 78−46079
^{60}Cu, populated in Ni(π^+, π^0), deexcitation γ spectra 78−89912
^{60}Cu spin states, shell model, 6^- and 9^+ states in odd odd Cu isotopes 78−74313
^{61}Cu analogue states, γ-ray ang. distribs. obs. 77−82848
^{61}Cu β-decay, ^{61}Ni multiparticle configs., transition probabilities from shell model 78−70496
^{61}Cu γ-cascade multiplicities, entry state depend. on excitation energy from ^{58}Ni (α,pγ), 17 and 19.5 MeV 78−82311
^{61}Cu, J^π assignments, E1 photon strength functions, partial radiative widths 79−59063
^{61}Cu, prod. yield meas. in ^{63}Cu(d,p2n), appl. to d beam monitoring 79−36249
^{62}Cu 390 keV state, ferromag. effect, spin assignment 77−2903
^{62}Cu decay to ^{62}Ni excited levels, half life, log ft *(Spanish)* 77−67716
^{62}Cu, γ-ray transitions from ^{59}Co(α,n)^{62}Cu, ^{60}Ni(^{3}He,p)^{62}Cu,^{62}Ni(p,n)^{62}Cu *(French)* 77−26615
^{62}Cu half life from ^{63}Cu(n, 2n) 79−13291
^{62}Cu high spin states populated in ^{60}N+α, ^{63}Cu+p, ^{52}Cr+^{14}N, level scheme *(French)* 78−21496
^{62}Cu, yrast states obs. in ^{60}Ni(α,pnγ) and ^{63}Cu(p,pnγ) 78−12945
^{63}Cu, ^{65}Cu, NQR spectrum of various Cu compounds 77−12235
^{63}Cu, comparison of absolute cross sections for electron and photon induced reactions, DWBA calc. test 77−41958
^{63}Cu, decay of analogues, γ-ray ang. distribs. and spins of resons. 78−13002
^{63}Cu EM decay transitions, level J^π assignments, level lifetimes from (α,pγ), (^{11}B, 2pγ) 79−85402
^{63}Cu, EM props., J^π, via (p,p'γ) 5.0 MeV 77−74800
^{63}Cu $g_{9/2}$ analogue state fragmentation from γ-transitions in ^{62}Ni(p,γ) 79−22202
^{63}Cu, $g_{9/2}$ isobaric analogue state, using ^{62}Ni(p,γ) 79−22258
^{63}Cu in Cu-Mn spin glass, NMR linewidth and relax. meas. 77−69583
^{63}Cu, inclusive proton photoprod., momentum spectra, max. bremsstrahlung energy 2.0 to 4.5 GeV *(Russian)* 77−34287
^{63}Cu, level struct. from ^{63}Cu(p,p'γ) react. 78−78378
^{63}Cu, levels, J^π via ^{64}Zn(d,^{3}He) polarised d, 13 MeV 77−88100
^{63}Cu levels, transitions and ang. distribs. from α-transfer in ^{59}Co(^{6}Li,d) 80−73798

nuclei with mass number 59 to 89 continued

^{63}Cu levels and transition j-depend., DWBA anal. of ^{60}Ni(^{19}F, ^{16}O) 80−42542
^{63}Cu low excitation states, level struct. and lifetimes from ^{60}Ni(α,pγ) 80−86813
^{63}Cu, NMR meas. in one-dimensional antiferromag. $CsCuCl_3$ 78−2756
^{63}Cu, NMR meas. of mag. transition in $Cu_{1-x}Ni_x$ system 77−32267
^{63}Cu, NMR study of local moment fluctuations in Cu-Mn dil. alloys 77−63091
^{63}Cu, NQR in Cu_2O, temp. depend. 77−12227
^{63}Cu, nucl. spin lattice relax. time meas. in Cu-Fe dil. alloys 77−4573
^{63}Cu, nucl. spin-lattice relax. in ferromag. $CuCr_2S_4$, spin wave contrib. 77−36147
^{63}Cu, paradoxical octupole-multiplet pattern 78−41617
^{63}Cu, proton hole states determ. from ^{64}Zn(d,^{3}He)^{63}Cu 79−22163
^{63}Cu, quasielastic π scatt., recoil proton spectra obs. 77−14198
^{63}Cu state alignment, γ-transitions and ang. distribs. from ^{62}Ni(p,γ) 80−73797
^{63}Cu+^{147}Au, triple differential cross-section, dynamical model calcs. 78−50212
^{63}Cu+^{197}Au, 365 MeV deep inelastic collisions, neutron multiplicity 78−645
^{63}Cu+^{197}Au, quasi-fission, 443 MeV, γ-ray multiplicity 77−34330
^{63}Cu+^{20}Ne, deep inelastic reaction, evaporation, energy thermalisation 78−94024
^{63}Cu+^{63}Cu, 450 MeV, energy spectra struct. obs. 78−4958
^{63}Cu+n, 30-150 keV, resonance parameters from total cross-section meas. 77−26739
^{63}Cu(Li,Li), 28 and 34 MeV, optical model parameters 77−54248
^{63}Cu(α,p)^{66}Zn, proton polarisation calc., distorted wave method 77−6404
^{63}Cu(d,^{3}He), 9 MeV, polarised d, tensor anal. power and D-state effects 79−85446
^{63}Cu(d,X), X=p, d, t, ^{3}He, α, 24.7 MeV continuous spectra and ang. distribs. meas. 77−3016
^{63}Cu(e,α), 100 MeV, energy spectra, ang. distribs. 77−18529
^{63}Cu(γ,n), cross-section determ., 12-25 MeV *(Russian)* 79−89295
^{63}Cu(γ,p), up to 0.25 GeV, from bremsstrahlung γ-quanta *(Russian)* 80−5123
^{63}Cu(γ,p), up to 4.5 GeV, ang. depend. of normalised invariant cross section parameters *(Russian)* 78−17180
^{63}Cu(n, 2n), 14-19 MeV, cross section meas., neutron flux, ^{62}Cu half life 79−13291
^{63}Cu(n,2n)^{62}Cu, 12.9-15.9 MeV, reaction cross section meas. 78−37337
^{63}Cu(p, 2nγ), 22-31 MeV, in beam gamma spectroscopy of ^{62}Zn 77−6297
^{63}Cu(p,3n)^{61}Zn, 30-47 MeV, cross-section meas. 78−13090
^{63}Cu(p,p'), 40 MeV, octupole states, weak coupling model 79−93495
^{63}Cu(p,p') negative parity level excitation, gamma ray obs., test for core excitation model 80−68534
^{63}Cu(p,p'γ) 5.0 MeV, ^{63}Cu EM props. 77−74800
^{63}Cu(p,pnγ), 22-28 MeV, ^{62}Cu high spin states, level scheme *(French)* 78−21496
^{64}Cu, autoionisation of K-shell following β-decay 78−13029
^{64}Cu β^- and β^+-decays, K-shell ionisation probabilities, X-ray spectra 80−42592
^{64}Cu β^- decay, K-shell autoionis. 80−956
^{64}Cu decay in Cu-Ag, electron density change 79−99519
^{64}Cu, electron density determ. in Cu-Au alloys, β-decay expts. 79−54408
^{64}Cu, extraction from reactor-irrad. α-phthalocyanine target 80−35563
^{64}Cu, γ-spectra, J^π assignments via ^{64}Ni(p,nγ) 2.75-3.75 MeV 77−18470
^{64}Cu levels and transitions, stat. anal. of ^{64}Ni(p, nγ) *(Russian)* 80−5104
^{64}Cu, prod. yield meas. in ^{63}Cu(d,p) appl. to d beam monitoring 79−36249
^{64}Cu, simultaneous prod. with ^{67}Cu and ^{67}Ga, and bleomycin labelling with ^{67}Cu or ^{64}Cu 78−28066
^{64}Cu(p,X), 400 GeV, absorption cross sections and multiplicity distribs., A-depend. study 79−67748
^{65}Cu analogue $P_{1/2}$ resonance, γ-decay and energy levels from ^{64}Ni (p, γ) 79−80907
^{65}Cu analogue resonance direct n decay, stat. anal. from ^{64}Ni(p,nγ) *(Russian)* 80−5104
^{65}Cu, isobaric analogue reson. anal., from ^{64}Ni(p,p), (p,p') 78−78351
^{65}Cu levels and transitions, γ-strength function using average resonance capture from ^{64}Ni(p,γ) 80−13411
^{65}Cu+^{86}Kr, 366-716 MeV, evaporation residue product cross sections mass-charge distrib. 79−17947
^{65}Cu+n, 30-150 keV, resonance parameters from total cross-section meas. 77−26739
^{65}Cu(^{16}O,p2n), 42-58 MeV, high spin states in ^{78}Kr, band struct. 78−74387
^{65}Cu(^{32}S,X), 153-184 MeV, fission like processes around A_{CN}=100, mass distrib. strong change 80−9318
^{65}Cu(^{32}S,X), double differential cross section, mass asymmetry, transport model 80−102203
^{65}Cu(^{63}Cu, X) fusion, 55-105 Mev, evaporation residue excitation functions 79−63710
^{65}Cu(^{7}Li,2n), 16-9 MeV, high-spin states in ^{70}Ge anal. 78−33146
^{65}Cu(α,α), 27-9 MeV, anomalous large-angle scatt. 77−18583
^{65}Cu(e,e')^{65}Cu, 120 MeV, low-lying level struct. *(Russian)* 77−74838
^{65}Cu(n, 2n), 14-19 MeV, cross section meas., neutron flux 79−13291
^{65}Cu(n, nα), 14-19 MeV, cross section meas., neutron flux 79−13291
^{65}Cu(n, p), 14-19 MeV, cross section meas., neutron flux 79−13291
^{65}Cu(p,2p)^{64}Ni, 17 MeV, search for double-direct reaction 77−30576
^{65}Cu(p,α_0)^{62}Ni, 1.1-3.6 MeV, Wigner cusps 78−41719
^{65}Cu(p,γ)^{66}Zn, 1.1-3.6 MeV, Wigner cusps 78−41719
^{65}Cu(p,n), cross sections and spectra, exciton model *(Russian)* 78−21536
^{65}Cu(p,nγ), 3.4-4.0 MeV, ^{65}Zn lifetimes 77−74804
^{65}Cu(p,p'γ), 5.25, 6.0 MeV, levels, transition energies, lifetimes, branching ratios determ. 77−41960
^{67}Cu β-decay, multiparticle configs. in ^{67}Zn 78−70496
^{67}Cu, simultaneous prod. with ^{64}Cu and ^{67}Ga, and bleomycin labelling with ^{67}Cu or ^{64}Cu 78−28066
^{69}Cu mass excess and low lying states, DWBA anal. from ^{70}Zn(d,^{3}He) 79−6422
^{69}Cu Q-values and mass excess from ^{70}Zn(d,^{3}He) 80−9222
^{69}Cu(d,n), secondary neutron emission charact. 79−30843
Cu(α, 2α), 700 MeV, cross section, effective cluster number from PWIA, momentum distrib. 79−40940

nuclei with mass number 59 to 89 continued
Cu(α,α), A=63 and 65, 48 MeV, I.L. potential depth, optical model anal. 78−50187
Cu(α, χπ), 18 GeV, π multiplicity distrib. 79−97713
Cu(α,π), 0.7-8 GeV, scaling and nonscaling of inclusive π prod. 79−22296
Cu(e,e), nuclear radius, core polarisation and isotone shifts, muonic X-rays 80−22685
Cu(γ,X), X=p,d,t,^{3}He,^{4}He, cascade-evaporation 80−57770
Cu(γ,f), max. energy 580 MeV, track detector anal. 77−18640
Cu(γ,γ), differential cross sections, 244 to 1408 keV 79−49618
Cu(γ,γ), neutron capture γ-ray Rayleigh scatt. 80−52661
Cu(γ,n) cross section discrepancies, NBS P-2 chamber calibration 77−26671
Cu(γ,ω), cross section meas., comparison with theory 78−58261
Cu(γ,π$^-$), quasifree photoprod. cross sections 79−75972
Cu(μ$^-$,X), energetic charged particle spectrum, integrated yield 80−18293
Cu(n,X), 14.8 MeV, γ-prod. cross section 79−49622
Cu(n,γ), 63, 5, cross-section meas., reson. parameters determ. 77−38274
Cu(n,γ), determ. of recoil energy and effective mass from narrow resonance line shapes 77−57660
Cu(n,γ), on-line gamma anal. using Ge detector 80−52624
Cu(n,n), 14.2 MeV, polarisation in forward angle scatt. 80−18282
Cu(n,n), 16.1 MeV, polarisation meas., optical model anal. 79−22264
Cu(n,n) 2.9 MeV, elastic differential cross section and polarisation ang. depend., statistical anal. 79−45264
Cu(n,n), A=63, 65, E=10-150 keV, total cross-sections and reson. parameters 77−38273
Cu(n,n), fast neutrons, differential cross sections, optical model calcs. *(Chinese)* 79−9572
Cu(n,n), pol. n, 16.1 MeV, differential cross section, optical model fit 80−32259
Cu(n,n′), 14.1 MeV, precompound processes 78−13093
Cu(n,nγ), 0.67-19.6 MeV, prod. cross sections, discrete and continuum γ rays 365 to 6620 keV 77−34293
Cu(n,xγ)Cu, E$_n$=5.3 MeV, γ prod. cross-section obs. 78−89863
Cu(p,X), 400 GeV, p, d, t, π, ^{3}He, α backward prod., inclusive cross sections 79−85475
Cu(p,X), 400 GeV, p backward prod. invariant cross section 79−93623
Cu(p,X), 400 GeV/c, light ion backward prod., invariant cross section 80−32279
Cu(p,X), 70 GeV/c, π$^\pm$, K$^\pm$, p and p̄ relative yields *(Russian)* 79−40930
Cu(p,X), 70 GeV/c, π$^\pm$, K$^\pm$, p, p̄ prod. with p$_T$=0.5-2.5 GeV/c cross sections, yield ratios *(Russian)* 80−52681
Cu(p,d), 2.14 GeV/c, quasifree knockout at 62 mrad, differential cross sections *(Russian)* 79−30819
Cu(p,n) 800 MeV, n prod. systematics, π associated cross section 79−3153
Cu(p,p′), 0.6-25 GeV, backward emitted proton inclusive spectra, short range correlation 80−32281
Cu(p,p̄π$^-$), 10 GeV, p̄ weak absorpt., p̄ and π$^-$ yields *(Russian)* 79−75987
Cu(p,π), 0.7-8 GeV, scaling and nonscaling of inclusive π prod. 79−22296
Cu(p, spallation), 0.08-24 GeV, Ar isotopes, spallation ratios and prod. cross sections 80−9284
Cu(p, spallation), 28 GeV, mean kinetic props., momentum transfer, target recoil props. 79−3129
Cu(p,xpX), x=1, 2, 640 MeV, energetic backward p emission, inclusive differential cross section 80−9290
Cu(π$^-$, Ψ), 43 GeV, A dependence of inclusive distrib. *(Russian)* 78−45983
Cu(π$^-$,X), 3 GeV/c, n inclusive spectra, neutron yield *(Russian)* 80−13510
Cu(π$^-$,X), stopped pions, radioactive product yields 80−83126
Cu(π$^-$,p) 1.5-5 GeV/c, cumulative proton polarisation *(Russian)* 80−86896
Cu(π$^\pm$,π$^\pm$), 65-215 MeV forward scatt. amplitudes 79−85533
Cu(π$^-$, spallation) 0.6, 0.9, 12 GeV, T=1/2 resonances, Na, Sc and Co rel. yields 80−5109
Cu(π$^-$, spallation), 500, 1570 MeV, product relative yields, charge dispersion and mass yield 79−6554
Cu(π$^\pm$, spallation), 50-350 MeV, radioactive residual nuclei prod. cross sections at (3,3) resonance 79−3130
Cu(x,x), x=π$^\pm$, K$^\pm$, p,p̄, 70, 175 GeV/c 80−83128
Fe, A=59,60, yrast decay scheme from ^{48}Ca+^{15}N(^{18}O) fusion-evaporation reaction 78−13154
Fe, high resolution fast neutron gamma-ray prod. cross sections 77−67745
Fe photonuclear process and Fe(μ,μ′) cosmic ray scatt. >200 GeV 77−23001
Fe, total neutron cross-section, thick sample transmission meas. and resonance anal. 77−23066
^{A}Fe, A=56-60, shell struct. of collective states, level spectra 79−93494
^{A}Fe, A=57, 59, levels, J$^\pi$ and transition branching ratio from Fe(n,γ) 80−105976
^{A}Fe, A=63, 64, neutron rich nuclide from ^{238}U(^{40}Ar,X) at 340 MeV 80−57802
^{58}Fe(α,nγ), 9.0 MeV, determ. of lifetime of ^{61}Ni low lying levels 77−88078
^{59}Fe β-decay, nuclei polarised in iron foils cooled by dilution refrigeration 77−34263
^{59}Fe decay, sum-coincidence γ-spectrum, ^{59}Co level struct. 77−14063
^{59}Fe deduced levels and spins, from ^{58}Fe(d$_{pol}$,p), cross section and vector analysing power 80−52684
^{59}Fe, level determ. in seawater 78−85608
^{59}Fe level scheme from ^{58}Fe(n,γ) resonance capture 79−547
^{59}Fe resonances, primary γ-intensities, E1-M1 correlation from ^{58}Fe(n,γ) 80−57740
^{59}Fe, spin assignments to p-wave neutron states 77−22852
^{60}Fe, level struct., spin and parity assignments, mass excess from ^{58}Fe(t,p) 17 MeV 78−82288
^{60}Fe struct. and new level from ^{60}Mn decay, mass excess 78−78317
^{61}Fe, radioactive decay scheme from ^{64}Ni(n,α), 14.3 MeV 78−46053
^{62}Fe mass excess from ^{64}Ni(^{18}O,^{20}Ne) at 63 MeV 77−335
^{62}Fe mass excess from ^{64}Ni(^{18}O,^{20}Ne)^{62}Fe reaction 77−41878
^{68}Fe low lying state mean lifetimes and transitions from ^{64}Zn(^{7}Li,p2n) 80−68599

nuclei with mass number 59 to 89 continued
^{61,62}Fe, mass excess via ^{64}Ni(α,^{7}Be) and ^{64}Ni(^{11}B,^{13}N)^{62}Fe resp respectively 77−74752
Fe(μ,μ′), small Q^2 and >200 GeV, implications for photonuclear process 77−23001
Fe(n,n), 500 to 3000 keV high resolution differential cross-section meas. 77−30592
Fe(n,n), MeV elastic and inelastic cross sections meas. 80−32277
Ga, A=66, 68 isomeric state from ^{56}Fe+^{13}C and ^{56}Fe+^{15}N reactions, lifetimes, g-factors 78−33147
Ga, β-decay energies and masses, A=76-79 77−74808
Ga from ^{66,68}Zn(p,γ), γ-ray ang. distrib. 78−74353
Ga isotopes, (n,p), (n,α), (n,2n) cross sections at 14.1 MeV *(Spanish)* 77−30563
Ga, NQR in heteroorganic group III compounds, summary 78−25565
Ga, odd, single particle and collective degrees of feedom, clustering, shell model anal. 80−68510
Ga, stable isotopes, masses meas. 78−12956
^{A}Ga, A=65,67, high spin states and transitions from Fe+^{12}C(^{14}N) 80−68516
^{A}Ga, A=67 to 69, energy spectra, shell model calc. 79−17818
^{A}Ga, A=69, 71, spectroscopic factors, occupation number anomalies from Ge(d,He) 26 MeV 78−82279
^{A}Ga, A=71,73, levels, ang. distribs., spin assignments and deformation transition from Ga(t,p) 79−54392
^{A}Ga, A=73, 75, deduced levels, occupation number anomalies, spectroscopic factors from Ge(d,^{3}He) 26 MeV 78−82279
^{A}Ga, A=73,75, Q-values and mass excess from Ge(d,^{3}He) 80−9222
^{A}Ga, A=79-83, β-delayed neutron emission probabilities, half-life 80−52634
^{62}Ga superallowed Fermi β$^+$ decay half life from ^{58}Li(^{6}Li,Zn) 79−54410
^{62}Ga, superallowed Fermi β-transition, half life and β-ray end point energy 78−78320
^{65}Ga, 1.286 MeV state spin 9/2 determ. from ^{64,66}Zn(p,γ) obs. 79−63663
^{65}Ga high spin states, J$^\pi$ and transitions, triaxial struct. from (^{12}C,αp),(^{7}Li,Zn) 80−63062
^{65}Ga, spin assignments of levels by forward-angle j dependence 78−93935
^{66}Ga deformation parameter determ. from beta decay Fermi matrix element 79−75923
^{66}Ga high spin states, shell model interpretation from ^{64}Zn(α,pnγ) and ^{63}Cu(α,nγ) *(French)* 79−3086
^{67}Ga β-decay, multiparticle configs. in ^{67}Zn 78−70496
^{67}Ga, electron dose reduction coeff., internal radionuclides, source free target, cylindrical geometry 78−92704
^{67}Ga γ- and X-ray emission probabilities and half-life obs. 80−32242
^{67}Ga, high spin states, using ^{57}Fe(^{12}C,pnγ) at 40 MeV 79−36128
^{67}Ga, isobaric analogue reson., statistical reaction model anal. 79−13267
^{67}Ga, levels, branching, mixing, T$_{1/2}$, via ^{67}Zn(p,nγ) 3.6-4.3 MeV 77−34247
^{67}Ga levels below 2.5 MeV populated in ^{64}Zn(α,pγ) 77−88042
^{67}Ga, simultaneous prod. with ^{64}Cu and ^{67}Cu 78−28066
^{67}Ga tumour scanning, review 77−9250
^{67}Ga-citrate, comparison with ^{203}Pb-acetate as abscess-localising agent, tissue distrib. 77−5064
^{68}Ga decay, positron polarisation, precision meas. using new polarimeter 77−46144
^{68}Ga, labelled skeletal imaging agents for position scintiography 77−9241
^{68}Ga, spectroscopy with ^{69}Ga(d,t) and ^{70}Ge(d,α), DWBA 77−57603
^{69}Ga, IAR corresponding to 1/2$^-$ and 9/2$^+$ ^{69}Zn states from ^{68}Zn(p,γ), 3.8 MeV 78−66257
^{69}Ga, nuclear quadrupole relax. rate for liq. Ga 77−36151
^{69}Ga state alignment, γ-transitions and ang. distribs. from ^{68}Zn(p,γ) 80−73797
^{69}Ga(n,n′γ), fast n, levels, J$^\pi$, transitions and mixing ratios, statistical anal. *(Russian)* 80−13382
^{69}Ga(p,p′γ), 3.0-5.1 MeV, low lying state struct., lifetimes, spin and parity 79−467
^{70}Ga, β-decay to excited states, β- and γ-ray meas. 77−41933
^{70}Ga, high spin levels via ^{68}Zn(α,pnγ)^{70}Ga 77−30611
^{71}Ga ang. correlations, level spin assignments and multipole mixing ratios from ^{71}Zn^m decay 78−78305
^{71}Ga, quad. relax. rates in liq. GaIn alloys 77−12272
^{71}Ga+$\nu_{e,}$ 0 to 300 MeV, cross sections, shell model calcs 79−93605
^{71}Ga(ν,e$^-$)^{71}Ge, proposed new expt. for solar neutrinos detect. 78−58563
^{71}Ga(ν,e)^{71}Ge, cross section calc., appl. to solar neutrino expts. interpretation *(Russian)* 77−50119
^{71}Ga(ν,e$^-$)^{71}Ge, shell model cross section calc., appl. to cosmic ray and background elimination *(Russian)* 80−5131
^{72}Ga, 3$^-$-2$^+$ first forbidden beta transitions, β-γ ang. correlation, nuclear matrix elements 80−42599
^{72}Ga half-life determ. by ^{56}Mn activation and decay obs. 79−26398
^{72}Ga→^{72}Ge, gamma and beta-ray spectra, intensities, branching ratios, spin and parity assignments *(Korean)* 78−50128
^{73}Ga, β-decay rate for estimation of ultra-high pressure 78−77927
^{73}Ga, levels, J$^\pi$ and ang. distribs. from ^{70}Zn(α,p) 80−78161
^{74}Ga, half-life of 56.5 keV level by delayed coincident summing 77−34255
^{69,71}Ga, NQR in $BiCl_3$.$GaCl_3$ complex, geom. struct. 78−25569
^{67}Gd, γ-spectroscopy of high-spin levels via ^{64}Zn(α,pγ), ^{53}Cr(^{16}O,pnγ) 78−93960
Ge, A=64, 66, 68, 70, Lipkin-Nogami method, ground state props. 78−50103
Ge, A=68, 70, lifetime meas. by DSAM, using (α, 2nγ) reaction at E$_\alpha$=30 MeV 78−8773
Ge, A=70, 72 and 74, dynamic deformation theory, energy levels 78−58235
Ge, β-decay energies and masses, A=79, 80 77−74808
Ge, doubly even nuclei, quasiparticle+phonon model calcs. 78−41626
Ge, even-even isotopes, surface transparency of optical pots., determ. from heavy ion scatt. 78−13146
Ge, even-even nuclei, γ-spectroscopy, exptl. results and models 80−68589
Ge isotopes, (n,p), (n,α), (n,2n) cross sections at 14.1 MeV *(Spanish)* 77−30563
Ge isotopes, activation cross-sections for 14.7 MeV neutrons 77−6367
Ge isotopes, shape transition and quadrupole softness, Hartree Bogoliubov calc. 80−68527

nuclei with mass number 59 to 89 continued
Ge isotopes A=68 to 78, potential energy surface and collective spectra 78−86464
Ge, odd, single particle and collective degrees of feedom, clustering, shell model anal. 80−68510
Ge, photon induced electron pair prod. cross section *(French)* 79−524
Ge, stable isotopes, masses meas. 78−12956
^{A}Ge, A=66,69,70, negative parity high spin states, spin and lifetimes from HI reactions 80−73768
^{A}Ge, A=68, 70,72,74, level excitation, n-p interaction role from α-transfer in Zn(^{6}Li,d) 80−73821
^{A}Ge, A=68,70,72, discovery of multiple collective band struct. *(Chinese)* 79−80865
^{A}Ge A=68,70,72,74, deformations and collective spectra, reaction mechanisms from Ge(p,t) 79−22168
^{A}Ge, A=68 to 70, energy spectra, shell model calc. 79−17818
^{A}Ge, A=70, 72, 74, appl. of crystal blocking technique to study highly excited nuclear continuum using (p,p′) 79−45261
^{A}Ge, A=71-74, electric quadrupole moments, nonadiabatic rot. model calcs. 79−6389
^{A}Ge, A=72, 74, 0_2^+ levels, struct. transition between N=40 and 42 from Ga(α,p) 80−73800
^{A}Ge, A=72,74,76,78, ang. distribs., levels and spin assignments, deformation transition from Ge(t,p) 79−54390
^{A}Ge+^{86}Kr, A=70, 74, 76, 50 to 120 MeV, angular momentum limits 78−25224
^{A}Ge(d,d) 16 MeV, A=70-74, polarised d, elastic and inelastic, levels and deformation 79−554
^{A}Ge(p,p), A=72,74, 100-2200 MeV, total and reaction cross sections from optical pot. 80−18303
^{A}Ge(t,p), pol.t, A=70,72, octupole oscillations modes from anal. powers, 3_1^- octupole transition 80−102142
^{19}Ge excited state, J, mean lifetimes and transitions from ^{64}Za(^{7}Li,ph) ^{19}Ge excited state, J, mean lifetimes and transitions 80−68517
^{65}Ge, delayed proton spectra, $T_{1/2}$ meas. 77−38254
^{66}Ge levels, lifetimes, J^π and transitions from ^{58}Ni(^{10}B,pnγ) 80−73799
^{66}Ge levels, lifetimes and mixing ratio, in-beam γ-spectroscopy from ^{54}Fe(^{14}N,npγ) 80−42541
^{66}Ge states and decay scheme, polarisations J^π and ang. distribs. from ^{58}Ni(^{10}B,pnγ) 80−22692
^{67}Ge excited state decay scheme, mean lifetimes from ^{64}Zn(α,nγ) 79−26393
^{67}Ge, from ^{64}Zn(α,n), coupling consts., M1, M2, E3 transitions 78−89823
^{67}Ge, mass excess and excited states from ^{70}Ge(^{3}He,^{6}He) 79−6375
^{67}Ge, mass excess and low lying states, comparison with ^{63,65}Ni, ^{65,67}Zn and ^{69}Ge, from ^{65}Zn(α,nγ) 78−66213
^{67}Ge, quadrupole interaction temp. depend. in Zn, Cd, Sn 77−12264
^{68}Ge, ground and both neutron and proton rotational aligned bands, model calcs 79−54377
^{68}Ge, lifetimes of excited states populated in ^{58}Ni(^{12}C,2p), spins and parities of levels 78−13020
^{68}Ge multiple band struct., $g_{9/2}$ orbital, level lifetimes from ^{58}Ni(^{12}C, 2p) 80−13358
^{69}Ge, alignment in Cu, temp. depend. rel. to radiation damage during PAC obs. 77−27919
^{69}Ge excited states, lifetimes and J^π assignments, mixing ratios from ^{66}Zn(α,nγ) 79−63629
^{69}Ge excited states, spin and γ-decay, parity state struct. from ^{69}Ga(p,nγ) 3-5.6 MeV, ^{69}Ge excited states, spin and γ-decay, parity state struct. 79−464
^{69}Ge high spin states, EM props., Branching and mixing ratios from ^{55}Mn(^{16}O,pn) 80−13347
^{69}Ge high spin states, J assignment, decay scheme from ^{55}Mn(^{16}O,pn) 80−68518
^{69}Ge, J^π assignments from (d,t) and (d,p) reacts. with polarised deuterons 78−17221
^{69}Ge, Knight shift in liq. Ga 77−12271
^{69}Ge level structure and lifetimes, decay through negative parity band from ^{55}Mn(^{16}O,pnγ) 79−45172
^{69}Ge, quadrupole interaction in Zn, rel. to rad. damage during PAC obs. 77−27918
^{69}Ge, quadrupole interaction in In, Sn, Sb, Tl and Bi, TDPAD expts. 78−48089
^{69}Ge, TDPAD, in Sn host lattice 78−43725
^{70}Ge, high-spin states anal. from γ-ray spectra of heavy-ion reactions 78−33146
^{70}Ge+^{32}S, 110, 132 MeV fusion evaporation residues, Monte Carlo simulation 78−41799
^{70}Ge(^{16}O,^{16}O′γ), 36 MeV, g-factors of first 2^+ states in ^{70}Ge 78−13138
^{70}Ge(α, nγ) 10-18 MeV populating ^{73}Se high-spin states 77−10324
^{70}Ge(d,t),(d,p), differential cross sections and vector analysing powers 78−17221
^{70}Ge(p,p), 3.5 to 5.3 MeV, ^{71}As, isobaric analogue reson. 79−75951
^{70}Ge(p,t), 26 MeV, t spectra, ang. distribs., ^{68}Ge energy levels, spin, parity 77−54216
^{70}Ge(p,t)^{68}Ge, 26 MeV, spectroscopy of transitional nuclei (Ge) using transfer reactions 78−86480
^{70}Ge(t,p)^{72}Ge, 15 MeV, spin, parity assignments, new O^+ states for ^{72}Ge 79−63594
^{71}Ge, in liq. metal target, in-beam γ-NMR-PAD 77−59465
^{71}Ge, energy release accompanying electron capture 78−17148
^{71}Ge, J^π assignments from (d,t) and (d,p) reacts. with polarised deuterons 78−17221
^{71}Ge, LX-, LX-coincidences during decay 78−17149
^{71}Ge, levels, studied via ^{68}Zn(α,nγ), 8 to 10 MeV, comparison with coupling model calcs. 78−8742
^{71}Ge negative parity states, J^π, energy spectra and spectroscopic factors 79−59013
^{71}Ge, radioactive decay rate in GeS and GeS_2 79−97683
^{72}Ge excitation energies, B(E2) values, extended generator coordinate method 77−6203
^{72}Ge, gamma-ray spectra, energy levels, spin and parity assignments, from ^{72}Ga beta-decay *(Korean)* 78−50128
^{72}Ge high spin levels obs. in ^{70}Zn(α,2nγ) *(French)* 79−22304
^{72}Ge levels pop. in ^{8}Zn(^{6}Li,pn), in beam gamma-ray spectroscopy 80−47343
^{72}Ge spin, parity assignments, new O^+ states 79−63594
^{72}Ge(α,npγ)^{74}As, 30 to 50 MeV, level structure of ^{74}As 77−10357
^{72}Ge(p,γ)^{73}As, 2213 keV energy levels of ^{73}As meas. 78−93939
^{72}Ge(p,nγ), 5.0-6.3 MeV, ^{72}As level scheme determ. 77−14032

nuclei with mass number 59 to 89 continued
^{72}Ge(p,t)^{70}Ge, 26 MeV, spectroscopy of transitional nuclei (Ge) using transfer reactions 78−86480
^{73}Ge, 13.3 keV Mossbauer resonance, dispersive interference effects 78−25145
^{73}Ge, Mossbauer gamma-ray detection with Si(Li) and Ge detectors 77−10530
^{73}Ge Mossbauer transition, large E2 dispersive interference 77−40158
^{74}Ge, ^{76}Ge, two-proton transfer reactions induced by 56 MeV ^{16}O beam, spectroscopic anal. 77−14178
^{74}Ge, 26 MeV levels from ^{75}As(d,^{3}He) 78−25112
^{74}Ge, energy levels, shape transition from 15 MeV ^{72}Ge(t,p) study 78−93945
^{74}Ge excitation energies, B(E2) values, extended generator coordinate method 77−6203
^{74}Ge(^{12}C,3n)^{83}Sr, high spin states and spin ordering, γ-ray excitation functions 78−66199
^{74}Ge(^{18}O,^{16}O), (^{18}O,^{17}O), (^{18}O,^{18}O), 75 MeV, ang. distrib. meas., multistep process 77−82953
^{74}Ge(^{18}O,^{16}O)^{76}Ge, coupled-channel Born approx. anal. 77−82954
^{74}Ge(^{32}S,X), 153-184 MeV, fission like processes around A_{CN}=100, mass distrib. strong change 80−9318
^{74}Ge(^{32}S,X), double differential cross section, mass asymmetry, transport model 80−102203
^{74}Ge(p,p) elastic and inelastic scatt. at 3.3-5.4 MeV, IAR excit. 77−34278
^{74}Ge(p,t)^{72}Ge, 26 MeV, spectroscopy of transitional nuclei (Ge) using transfer reactions 78−86480
^{75}Ge, beta decay of 83 min ground state, decay characts. and scheme 79−67713
^{75}Ge, via ^{74}G(p,p′) 3.3-5.4 MeV J^π, spectroscopic factors 77−34278
^{76}Ge double beta decay expt., Monte Carlo evaluation 79−49892
^{76}Ge, double β-disintegration, search for expt. evidence *(French)* 79−36202
^{76}Ge levels, J^π assignments, shape transition DWBA anal. from ^{74}Ge(t,p) 79−17815
^{76}Ge(^{12}C,3n)^{85}Sr, high spin states and spin ordering, γ-ray excitation functions 78−66199
^{76}Ge(^{16}O,^{18}O), (^{16}O,^{16}O), 77.6 MeV, ang. distrib. meas., multistep process 77−82953
^{76}Ge(^{16}O,^{18}O)^{74}Ge, coupled-channel Born approx. anal. 77−82954
^{76}Ge(^{86}Kr,xn), 314-376 MeV, γ-multiplicity meas., Er compound nucleus formation 79−89320
^{76}Ge(n,n′γ), 2.0 to 4.1 MeV, level and decay schemes 77−23092
^{76}Ge(p,t)^{74}Ge, 26 MeV, spectroscopy of transitional nuclei (Ge) using transfer reactions 78−86480
^{76}Ge(π^+ xn)$^{76-x}$As, 100, 180 MeV, product formation cross section 80−42705
^{78}Ge level struct., J^π values from DWBA anal. of ^{76}Ge(t,p), 17 MeV 79−6417
^{78}Ge level struct., proposed nuclear shape transition, DWBA anal. from ^{77}Ge(t,p), 15 MeV 78−78266
^{67,71}Ge in Zn, quadrupole interaction, TDPAC meas. 78−43740
Ge(γ,e^+e^-), cross section near threshold, atomic electron screening effects 80−78279
Ge(γ,e^+e^-), near threshold, variable energy source, total cross section *(French)* 80−37367
Ge(n,n′), 2^+ level excitation cross sections, intermediate resonances, optical model with coupled channels *(Russian)* 79−40897
Ge(p,t), 26 MeV, ^{70,72,74}Ge excited states, spins, parities 78−25194
Ge(p,t), shape transition obs. 78−25190
Ge(t,p), shape transition obs. 78−25190
^{62}Hi(α,^{3}He), 172.5, 140 MeV, plane wave spectator model anal. n momentum distrib. in α 79−54445
^{165}Ho+^{84}Kr, 714 MeV, statistical model for mass and charge distrib. 79−17929
^{77}K, cyclotron prod. for regional cerebral blood flow meas. 77−56468
Kr even isotopes, collective levels and B(E2) values, IBA calcs. 80−27539
Kr even-even isotopes, collective states and transitions, interacting boson approx. 80−73773
Kr isotopes, changes in nuclear charge radii 79−93504
Kr, release from spherical fuel elements in HTGR 77−74940
Kr series isotopes, sensitivities to various parameters, analytical evaluation 78−82424
Kr yield from ^{238}U and ^{232}Th by 14 MeV neutron fission, meas. by emanation method *(French)* 77−30640
^{A}Kr, A=74,76, rot. bands, band crossing and backbending 80−18176
^{A}Kr, A=74,76,78,80, discovery of multiple collective band struct. *(Chinese)* 79−80865
^{A}Kr, A=74-82, even-even isotopes, B(E2) values and collectivity, interacting boson approx. 80−27537
^{A}Kr, A=76,78,80, yrast states and band struct., backbending from Zn(^{12}C, 2n) 80−13359
^{A}Kr, A=78, 80, quasi-γ bands and negative parity levels from Br(p,2nγ) 80−456
^{A}Kr, A=78,80,82,83,84,86, mass using spectroscopic doublet method *(Russian)* 78−86468
^{A}Kr, A=79, 81, high spin E2 bands, J^π, transitions from Ge(^{10,11}B, xγ) 80−63061
^{A}Kr(p,p′), 51.9 MeV, A=78, 80, 82, 84, 86, 2_2^+ and 4_1^+ state excitation 79−54389
^{73}Kr, delayed proton spectra, $T_{1/2}$ meas. 77−38254
^{74}Kr, charged particle evaporation following form. from ^{58}Ni+^{16}O 80−47453
^{74}Kr, compound nucleus decay via ^{16}O + ^{58}Ni at 44.5-76.5 MeV 77−88168
^{77}Kr carrier-free isotope prod. by (p,xn) reactions on natural Br 78−29678
^{77}Kr, low lying state J^π assignments, anal. powers from ^{78}Kr(d,t) 79−45153
^{78}Kr band struct., level scheme, from γγ-coincidence from ^{65}Cu(^{16}O, 2np) 80−18177
^{78}Kr band struct., lifetimes and E2 transitions n-p boson model anal. from ^{65}Cu (^{16}O, 2np) 79−80863
^{78}Kr band structs., in-beam γ-rays from ^{68}Zn(^{12}C, 2n) 80−22672
^{78}Kr bands, lifetimes and E2 transitions from interacting boson model and (^{16}O,p2n), (^{19}Fe,α2n) 80−73771
^{78}Kr high spin levels, bands and transitions, level lifetimes from ^{68}Zn(^{12}C,Zn) 80−42525

nuclei with mass number 59 to 89 continued
^{75}Kr high spin states, transitions and lifetimes from (^{16}O,2np), (^{19}F,2nα), (^{16}O,2n), (^{12}C,2n) 80−27534
^{78}Kr high spin states from ^{65}Cu(^{16}O,p2n), band struct. 78−74387
^{79}Kr excited states, J$^{\pi}$ assignment, transitions, level lifetimes from ^{79}Rb β^{+} decay 79−17810
^{8}Kr for pulmonary ventilation and blood flow studies, prod. and imaging 77−16966
^{70}Kr, low lying levels from ^{79}Br(p,nγ) 80−105972
^{81}Kr levels, J$^{\pi}$, ICC via ^{81}Rb 77−79309
^{81}Kr levels, transitions and J$^{\pi}$ assignments, first excited state lifetime from ^{81}Br(p,nγ) 79−75849
^{81}Kr low lying states populated in ^{81}Br(p,nγ), γ spectra, γ-γ coincidences 78−25195
^{82}Kr(α,n), 14-21 MeV, in-beam γ-ray spectra, high-spin states of ^{85}Sr obs. 77−41915
^{82}Kr(d,3n)^{81}Rb, non-linear behaviour of gas targets for isotope prod. 78−25361
^{84}Kr, 1.84 μs isomeric state, g-factor meas. 78−17101
^{84}Kr excitation function for ^{152,153}Er prod. from ^{74}Ge(^{84}Kr,xn) 79−22315
^{84}Kr levels, γ-cascades, J$^{\pi}$, mixing ratios and correlations from ^{84}Br decay 80−63134
^{84}Kr+^{209}Bi, 712 MeV, deform. and transfer in strongly damped collisions 78−21601
^{84}Kr+^{209}Bi, probabilistic model for deep inelastic reactions 77−71623
^{84}Kr+n, capture cross section meas. in Triton reactor *(French)* 80−18308
^{84}Kr(α,3n), 35-45 MeV, in-beam γ-ray spectra, high-spin states of ^{85}Sr obs. 77−41915
^{85}Kr, beta dose to crit. human tumour sites 78−28074
^{85}Kr conc. determ. at high pressures using β-ray count, CaF_2 scintillation counter activated with Eu 78−13385
^{85}Kr, effluent gases from nuclear power industry, ambient contamination, props. *(Spanish)* 78−61540
^{85}Kr extraction, occupational doses in gas liquefaction industry 78−15905
^{85}Kr, gaseous, absolute counting, calibration of well-type NaI(Tl)-detector 78−9036
^{85}Kr, laboratory calibration standards preparation *(Czech)* 79−6782
^{85}Kr level struct. and spectroscopic factors from ^{84}Kr(d,p), polarised and unpolarised d 79−471
^{85}Kr positive-parity states calc. by quasiparticle phonon coupling 79−75845
^{85}Kr radioactive waste gas recovery system using cryogenic distillation 77−54331
^{85}Kr source, use for liq. phase radiation chem. 77−60091
^{85}Kr/Xe separation from nucl. engineering off-gases, low temp. distillation *(German, English)* 77−18671
^{85}Kr^{m,g} decay, ^{85}Rb levels, J$^{\pi}$ and transitions 80−78162
^{86}Kr in meteorite, s-process nucleosynthesis and s-process neutron capture time scale 80−73080
^{86}Kr ions accelerated in UNILAC, energy meas. by recoil proton technique 78−58527
^{86}Kr+^{166}Er, deep inelastic strongly damped collision, fragment isobaric distrib, statistical equilib. 79−40949
^{86}Kr+^{197}Au, 620 MeV, diffusion model anal. 77−10427
^{86}Kr(^{3}He,n), 25.4 MeV, ^{88}Sr 0^{+} states struct., subshell closure 78−21582
^{86}Kr(n_{th},γ), Q-value, ^{87}Kr levels 77−74798
^{87}Kr energy levels from ^{87}Br β-decay, delayed neutrons, high energy γ spectra 78−25155
^{87}Kr ground state spin assignment from ^{86}Kr(d,p), polarised and unpolarised d 79−471
^{87}Kr levels in ^{86}Kr(n_{th},γ) 77−74798
^{88}Kr level scheme and transitions, delayed neutrons from ^{88}Br β-decay 80−42600
^{81m}Kr, continuous carotid infusion for assessment of regional cerebral blood flow 78−20254
^{81m}Kr dosimetry for various source organ-target organ pairs 77−16989
Kr(p,X), 2-400 GeV A=3-14 fragment energy distrib. 79−17901
Kr(p,X), fragment prod. by two body breakup 79−85440
Kr(p,p'), 51.9 MeV, low-lying octupole states anal. 78−21497
Kr(p,xn)^{81,82m}Rb, ^{81,82m}Rb prod. for positron emission tomography 80−98068
$LiAl_2B4_7$, ^{81}Br NQR and ^{27}Al NMR 78−6597
(^{6}Li,d), A$\sim$60,116, L=0 transitions, cross sections, microscopic anal. 80−78189
^{59}Mn, β-decay scheme, mass, branching ratios 77−82873
^{59}Mn, new isotopes of interest to explosive nucleosynthesis β-decay scheme and mass determ. 79−45208
^{59}Mn, observation and mass excess in ^{64}Ni(^{3}He,^{8}B)^{59}Mn at 74 MeV 77−10310
^{60}Mn, mass and β-decay half life, ground state spin and parity 78−78317
^{60}Mn, new isotopes of interest to explosive nucleosynthesis, β decay scheme and mass determ. 79−45208
^{61}Mn, neutron rich nuclide from ^{238}U(^{40}Ar,X) at 340 MeV 80−57802
^{85}Mo, delayed proton spectra, $T_{1/2}$ meas. 77−38254
^{89}Mo mass excess and excited states from ^{92}Mo(^{3}He,^{6}He) 80−42531
^{89}Mo^{m} levels, transitions and half life from ^{93}Mo(p,p'3n) 80−86858
^{60}N(α,pnγ), 22-35 MeV, ^{62}Cu high spin states, level scheme *(French)* 78−21496
^{64}N(n,γ), γ circular polarisation meas. 78−62533
Nb neutron deficient isotopes, studied via heavy ion induced compound reactions 77−57621
^{89}Nb, excited states studied by (^{3}He, 3nγ) in-beam γ-ray spectroscopy 77−41983
^{89}Nb, level scheme determ. from (^{3}He,3nγ) 77−22840
Ni 79−30880
Ni (e,α), 120 MeV, preequilibrium α-emission, α energy spectra 79−85459
Ni, A=59, 61 and 63, fine struct. of ground hole-state analogues 78−50065
Ni, A=60, 62, 64, 66, Lipkin-Nogami method, ground state props. 78−50103
Ni, A=60,62,64, short range correls. and pseudopots., Hartree Fock Bogoliubov method 78−535
Ni, CC ^{56}Ni core excitation effects on A=57-66 nuclei, MSDI and ASDI comparison 78−78254
Ni doubly even nuclei, eqns. of motion method, pairing correlations, ground state energies 80−52585

nuclei with mass number 59 to 89 continued
Ni even isotopes, negative parity levels, Tam-Dancoff approx., ^{56}Ni core 79−3080
Ni even isotopes, quasiparticle RPA nonlinear generalisation for anharmonic vibr. spectra 79−63580
Ni, even-even isotopes, surface transparency of optical pots., determ. from heavy ion scatt. 78−13146
Ni giant resonances using virtual and real photons 80−22791
Ni isotopes, (n, particle) cross section data base construction, MeV range, statistical models 77−26728
Ni isotopes, cross sections for charged particle prod. by 14 MeV neutrons, data compilation 80−9289
Ni isotopes, density-dependent HF description 77−54170
Ni isotopes, pairing-plus-quadrupole interaction anal. 77−79313
Ni isotopes, shell model calcs. of BE, spectroscopic factors and excit. energies 77−22860
Ni mass region, α transfer reactions, pairing vibr. model anal. 79−13272
Ni+^{20}Ne, 164 MeV, ang. distribs., total reaction and evaporation residue cross sections 79−565
Ni+π, A=60, 2, E_{π}=0, 45 MeV γ-ray spectra, prod. cross-section for residual nuclei meas. 78−649
Ni(^{35}Cl,^{35}Cl), A=58,62, 100-170 meV, elastic scatt. ang. distrib. 78−21605
Ni(^{18}O,^{20}Ne), even Ni isotopes, 63 MeV, energy spectra, ang. distribs., spectroscopic strengths 77−335
Ni(^{16}O,^{16}O')N*(2^{+}), A=58, 60, 62 at 42 and 48 MeV, DWBA anal. 77−74876
Ni(^{16,18}O, xn), 36 to 55 MeV, total neutron yields, cross sections 77−14163
^{A}Ni A=57-59, $f_{7/2}$ hole configuration effects, shell model calcs. 80−22670
^{A}Ni, A=58, 64, neutron densities and single particle struct. 80−32165
^{A}Ni, A=58,60, search for giant quadrupole resonance 80−9281
^{A}Ni, A=58-64 even, magnetic mom. of 2_1^{+} states from (^{32}S,^{32}S') at 72 MeV 78−66202
^{A}Ni, A=60, 62, 64, determ. of g-factor of 2_1^{+} state in Fe 78−43697
^{A}Ni, A=60, 62, 66, levels, J$^{\pi}$, anal. powers and cross sections from Ni(t,p)pol.t 80−68539
^{A}Ni, A=60, 62, nucl. level densities, using single particle states for Woods-Saxon and Nilsson potentials 78−50086
^{A}Ni, A=60,61, giant resonance decay modes in (e,p), (e,α) cross section study 79−17877
^{A}Ni, A=60,62,64, tensor open-shell RPA calcs., M2, M8 excitations 79−22216
^{A}Ni, A=61, 63, fine structure of hole-state analogues, isospin mixing from (p, d) 80−13401
^{A}Ni, A=61-63, yrast level lifetimes and J$^{\pi}$ assignments from ^{48}Ca+^{18}O 79−9445
^{A}Ni, A=64, 58, level ang. momentum and spin values, DWBA anal. from (t,d) polarised t 79−36163
^{A}Ni+^{35}Cl, A=58, 62, 155-170 MeV, fission prod. yields, ang. distribs. and mean kinetic energies 78−41790
^{A}Ni(^{3}He, ^{3}He), A=58,60,62,64, 119 MeV, optical pot. parameters energy and mass depend. 80−32289
^{A}Ni(^{3}He, p), 8, 10 MeV, A=58, 60, 62, p spectra compound nucleus contrib., odd-even effect 80−106061
^{A}Ni(^{40}Ca, fusion), A=58, 60, 62, 113-170 MeV, fusion cross sections and excitation functions 80−32315
^{A}Ni(^{7}Li, ^{7}Li), A=58, 60, 34 MeV, ang. distribs., cross sections, double folding model anal. 80−78313
^{A}Ni(α,γ), A=62, 64, 4.5-8.6 MeV, excitation function competition cusps, Mauser-Feshbach calcs. 80−13404
^{A}Ni(α,n), A=62, 64, 5.3-8.7 MeV, excitation function competition cusps, Mauser-Feshbach calcs. 80−13404
^{A}Ni(d,X), A=58, 64, 7.6 GeV/c, isotopic cross section ratios, He, Li fragments isotopic effects *(Russian)* 80−63154
^{A}Ni(e,e'), 102 MeV, A=58,60, E1-E4 giant multipole resonance comparison, shell model anal. 80−42614
^{A}Ni(e,e), 100-275 MeV, A=58,60,62,64, cross sections and muonic X-ray meas., charge distrib. systematics 80−86801
^{A}Ni(e,p),(e,α), A=58, 60, 62, electrodisintegration cross sections, E1, E2 absorption, DWBA anal. 80−106052
^{A}Ni(n,X), A=58,60, 14.8 MeV, charged particle emission, cross section, Hauser-Feshbach anal. 79−67750
^{A}Ni(n,X) A=58, 60, transmission data, resonance anal. 80−18317
^{A}Ni(n,γ), A=58, 60, 61, 6-150 keV, shape anal. and width correlations 77−26766
^{A}Ni(n,n'γ), A=58-64, <4 MeV, gamma prod. and inferred cross sections 80−525
^{A}Ni(n,n), A=58,60,62,64, 5 MeV, differential cross sections, optical, statistical and coupled channel anals. *(Russian)* 80−37377
^{A}Ni($n_{th}\gamma$)$^{A+1}$Ni (A=58, 60, 62, 64), γ-ray spectra, level schemes, M1 and E2 strength functions 77−57674
^{A}Ni(p,X), A=58, 64, 7.6 10 GeV/C, isotopic cross section ratios, He, Li fragments isotopic effects *(Russian)* 80−63154
^{A}Ni(p,α), A=58, 60, 30 MeV, α-particle angular distrib. 79−6588
^{A}Ni(p,α) A=60,62, polarised p, 22.0 MeV, analysing power J dependence 79−67740
^{A}Ni(p,α)$^{A-3}$Co, A=60,62,22 MeV, analysing power meas. in L=0 transfer reactions 79−45268
^{A}Ni(p,n), 11.2 MeV, A=60, 62, spin cut-off parameters from neutron ang. distribs. *(Russian)* 79−80940
^{A}Ni(p,p), 1 GeV, A=58,60,62,64, elastic and inelastic, Glauber anal., matter distribs. 79−75883
^{A}Ni(p,p), A=58,64, polarised p, 0.8 GeV, neutron isotopic density differences and RMS radii 79−67643
^{A}Ni(p,$\pi^{\pm}$), A=58, 64, 660 MeV, pion energy spectra, isotopic effects *(Russian)* 80−42669
^{A}Ni(p,xγ), 80-164 MeV, A=58, 60, 62, 64, prod. cross sections, preequilibrium phase 80−78301
^{A}Ni(p_{pol},α), A=60, 62, 22 MeV, analysing power and cross sections, Co proton-hole states 80−68663
^{A}Ni($\pi^{\pm}$,xγ), 100-200 MeV, prompt and delayed γ spectra, nuclide yields 79−22332
^{58}Ni, GDR proton channel decay isospin effects *(Russian)* 77−14020
^{58}Ni(n,2n)^{57}Ni, cross sections determ. 79−49624
^{59}Ni, and N=29 nuclei isobaric analogue resonances in unified model description 78−78343
^{59}Ni deduced levels, from ^{58}Ni(d_{pol},p), cross section and vector analysing power 80−52684

nuclei with mass number 59 to 89 continued
- ^{59}Ni formation cross section in Fe+α at 7-24 MeV, poss. prod. in cosmic dust 78−78399
- ^{59}Ni, fragmentation of hole-state analogues 78−54731
- ^{59}Ni levels, cross section and vector anal. power, ang. distribs. from ^{58}Ni(^{7}Li,^{6}Li), pol.^{7}Li 80−106044
- ^{59}Ni, levels and new γ-transitions following ^{59}Cu(β^+)^{59}Ni 77−22935
- ^{59}Ni, neutron activation product density in life expired LWR 79−9908
- ^{59}Ni, neutron cross-sections and resonance integrals 77−23072
- ^{59}Ni, nuclear electron capture theory 77−82869
- ^{59}Ni, radiative capture of K-electrons, γ spectra anal. 77−61384
- ^{59}Ni, semi-microscopic calc. of levels, spectroscopic factors and EM props. 77−2912
- ^{59}Ni, studied via ^{56}Fe(^{6}Li,t)^{59}Ni, t-energy spectra and reaction mechanism 78−41756
- ^{59}Ni, thermal neutron induced charged particle spectroscopy 77−71611
- ^{59}Ni(n,2n), 14 MeV, cross section compilation 80−91181
- ^{59}Ni(n,α)^{56}Fe, 0.029 to 0.042 eV, cross section for He prod. 77−23079
- ^{59}Ni(p,t)^{57}Ni, 40 MeV, mass excess of ^{57}Ni determ. 77−18376
- ^{60}Ni, 1173 keV transition M3/M2 mixing ratio meas. 80−52608
- ^{60}Ni (^{12}C,2p), 30-9 MeV, high-spin states in ^{70}Ge anal. 78−33146
- ^{60}Ni, (α,p), (α,d) and (α,t) reactions, 50.5 MeV, particle spectra 77−6405
- ^{60}Ni, aero-phonon, $4_1^+ \rightarrow 2_2^+$ γ-ray transition 78−17136
- ^{60}Ni, Coulomb contributions to nuclear radii and energies 80−68515
- ^{60}Ni deduced levels from ^{58}Fe(^{16}O,^{14}C)^{60}Ni, DWBA anal., spectroscopic strengths 80−47380
- ^{60}Ni, elastic and inelastic neutron scatt., 1.5-3 MeV *(Russian)* 77−26689
- ^{60}Ni, electron elast. scatt. cross sections, phase shift anal. and HF calcs. *(Russian)* 78−41707
- ^{60}Ni, GDR proton channel decay, isospin effects *(Russian)* 77−14020
- ^{60}Ni, hexadecapole motion obs. from α-scatt., EM transitions and conversion electron spectra 78−25097
- ^{60}Ni high spin states, J^π, $T_{1/2}$, ang. distribs. and polarisations from ^{56}Fe(^{7}Li, p2nγ) 80−99116
- ^{60}Ni, intermediate structure of giant analogue reson. 78−62517
- ^{60}Ni level scheme and γ-rays from ^{59}Ni(n,γ) 80−63099
- ^{60}Ni, partial radiation widths from neutron capture resonances, valency model calcs. 77−26707
- ^{60}Ni, photon scatt., direct obs. by giant dipole reson. 78−93988
- ^{60}Ni populated in ^{60}Co beta decay, 2506 to 2159 keV γ transition 77−22929
- ^{60}Ni, spin of 1.33 MeV level, anisotropy coefficients in $4^+ \rightarrow 2^+ \rightarrow 0^+$ cascade *(Spanish)* 79−89525
- ^{60}Ni yrast state lifetimes and parities from ^{51}V(^{12}C,2np) 79−45134
- ^{60}Ni+^{12}C, energy dissipation as func. of angle data comparison to classical and diffusion models 78−21604
- ^{60}Ni+^{40}Ar, 236 MeV, fragments mass and charge distribs. in deep inelastic reactions 78−58296
- ^{60}Ni+n, total and differential cross-sections, optical-statistical and coupled-channel models 80−13472
- ^{60}Ni+p, 400 MeV, multinucleon removal in quasifree process, p-γ coincidence expt. 78−37342
- ^{60}Ni+π, 70 MeV, γ+charged particle coincidence spectroscopy, cross section, p multiplicity 78−46111
- ^{60}Ni(^{12}C,X), 77 MeV, fragments in incomplete fission 77−14153
- ^{60}Ni(^{13}C,^{13}C), nuclear and Coulomb components to scatt. amplitudes 77−34340
- ^{60}Ni(^{16}O,^{16}O), 142 MeV, optical model anal. of ang. distrib. meas. 78−58295
- ^{60}Ni(^{3} He,t), 38 MeV, ^{60} Cu energy levels, spectroscopic factors, transition amplitudes 78−46079
- ^{60}Ni(^{3}He,p)^{62}Cu, 9-11 MeV, gamma transitions from ^{62}Cu excited levels obs. *(French)* 77−26615
- ^{60}Ni(^{6}Li,X), 156 MeV, projectile break up in continuous particle spectra, cross section, fragmentation 80−86889
- ^{60}Ni(^{6}Li,d)^{64}Zn, multipole pairing states, correspondence between 2 and 4 particle transfer reactions 78−62569
- ^{60}Ni(α,2n)^{62}Zn excitation function, and prod. of ^{62}Zn-bleomycin 78−28067
- ^{60}Ni(α,2nγ), 28-35 MeV, in beam gamma spectroscopy of ^{62}Zn 77−6297
- ^{60}Ni(α,α'), 8-18 MeV, cross sections, search for giant dipole resonance 80−9281
- ^{60}Ni(α,α), 15-19 MeV, inelastic scatt. form factors, Coulomb-nuclear interference region 78−66288
- ^{60}Ni(α,α), elast. and inelast., 29-34 MeV, coupled channels anal. 78−66289
- ^{60}Ni(α,nγ)^{63}Zn, 8-16 MeV, low-lying negative parity states of ^{63}Zn anal. 78−21521
- ^{60}Ni(α,pnγ)^{62}C, mag. hyperfine interaction, ^{62}Cu 390 keV isomeric state 77−2903
- ^{60}Ni(d, d), 9, 12 MeV, polarised d, excitation functions, optical model parameters and spin-orbit pot. 79−67756
- ^{60}Ni(e,α)e'X, alpha particle spectra, statistical model calc., direct reaction component 78−41704
- ^{60}Ni(e,e'), 40 to 60 MeV, excitation of T_0+1 giant M1 resonance 77−14118
- ^{60}Ni(n,γ), resonance state, partial radiation widths of high energy transitions 78−13104
- ^{60}Ni(n,n'γ), 0.5-10 MeV, γ-ray production cross sections 77−26762
- ^{60}Ni(n,p), 14.7 MeV, cross section meas. and ENDF/V IV evaluation 79−85458
- ^{60}Ni(p,α)^{57}Co(3/2$^+$), anomalous analyzing power, DWBA calc. 80−86894
- ^{60}Ni(p,d), fragmentation of hole-state analogues in ^{59}Ni 78−54731
- ^{60}Ni(p,γ)^{61}Cu, 1800 to 290 KeV, γ-ray spectra and j^π assignments 79−59063
- ^{60}Ni(p,p'), 15 MeV polarised protons, surface delta description of analysing power 77−61397
- ^{60}Ni(p,p'), near 6 MeV, spin-flip probabilities distorted wave and statistical anal. *(Russian)* 79−80939
- ^{60}Ni(p,p), 5.65, 6.5 MeV, time evolution of compound elastic scatt., cryst. blocking technique 78−62531
- ^{60}Ni(p,p)^{60}Ni, high-resolution meas. of scattering cross section, 3.0 to 4.0 MeV 77−10397
- ^{60}Ni(π,ΓX) reactions, 70 MeV pions, expts. with pion beams of Saclay Linac *(French)* 79−572
- ^{60}Ni(t,d), sub-Coulomb region, neutron orbit radius determ. 77−38217
- ^{61}Ni, γ-spectroscopy above 2.2 MeV excit., J^π,T, branchings 77−54172

nuclei with mass number 59 to 89 continued
- ^{61}Ni level ang. distribs., DWBA anal. from ^{59}Ni(t,p) 79−17816
- ^{61}Ni low lying states, lifetime meas. using ^{58}Fe(α,nγ) 77−88078
- ^{61}Ni, low-lying levels, J, B(E2), B(M1) from Coulomb excit. 77−26610
- ^{61}Ni, Mossbauer isomer shift, book contrib. 79−87354
- ^{61}Ni, populated in ^{60}Ni(t,d), neutron orbit radius determ. 77−38217
- ^{61}Ni, spectroscopy of levels below 2.2 MeV obs. in ^{58}F(α,nγ) 77−6289
- ^{61}Ni(^{3}He,^{3}He) 39.7 MeV, optical pot. mass depend. 77−34327
- ^{61}Ni(α,X), X=p, d, t, ^{3}He, α, 35.5 MeV, continuous spectra and ang. distribs. meas. 77−3016
- ^{61}Ni(α,$\alpha\gamma$)^{61}Ni, 4.5-5.5 MeV, low-lying levels study 77−26610
- ^{61}Ni(α,nγ)^{64}Zn, 7.8 MeV, γ-ray spectroscopy Zn levels below 3.1 MeV 78−21514
- ^{61}Ni(d,^{3}He), ^{60}Co low lying states, DWBA anal. 78−29478
- ^{61}Ni(d,p), low lying ^{61}Ni collective states, spectroscopic factors 77−61433
- ^{61}Ni(n,α) thermal neutron induced charged particle spectroscopy 77−71611
- ^{61}Ni(p,pγ)^{61}Ni, 3.0-4.5 MeV, low-lying levels study 77−26610
- ^{62}Ni, 6-11 MeV, levels determ. from ^{58}Co(α,p)^{62}Ni *(French)* 77−26615
- ^{62}Ni, elastic and inelastic neutron scatt., 1.5-3 MeV *(Russian)* 77−26689
- ^{62}Ni excitation level calcs., critical comparison of several methods *(Spanish)* 79−67654
- ^{62}Ni excited levels from ^{62}Cu decay, transition energies and intensities *(Spanish)* 77−67716
- ^{62}Ni excited states from ^{59}Co(α,pγ), B(E2) values 79−3115
- ^{62}Ni level struct. and decay scheme, shell model calcs. from ^{59}Co(α,pγ), 10 MeV 79−3085
- ^{62}Ni low lying collective states populated in ^{61}N(d,p), spectroscopic factors 77−61433
- ^{62}Ni+^{35}Cl, fusion excitation functions, dynamical model calc. 78−50224
- ^{62}Ni+$\pi^\pm$ proton spectra, cross section, π. absorpt. mechs. 78−25239
- ^{62}Ni(^{12}C,^{11}B)^{63}Cu, 48 MeV, ang. distribs., exact finite range DWBA and CCBA anal., spectroscopic factors 77−54249
- ^{62}Ni(^{16}O,^{15}N), 36-53 MeV, reaction dynamic depend. of small angle cross sections 77−18600
- ^{62}Ni(^{16}O,^{15}N)^{43}Cu, 56 MeV, ang. distribs., exact finite range DWBA and CCBA anal., spectroscopic factors 77−54249
- ^{62}Ni(^{32}Cl,f), statistical anal. of excitation functions, Bohr-Wheeler and liq. drop model 78−13181
- ^{62}Ni(^{3}He,X), X=p, d, t, ^{3}He, α, 24.3 MeV, continuous spectra and ang. distribs. meas. 77−3016
- ^{62}Ni(α, nγ), 8-14 MeV, γ ray study of ^{65}Zn odd-parity states, energies, transitions 78−50120
- ^{62}Ni(α,nγ), 8.2 MeV, ^{65}Zn lifetimes 77−74804
- ^{62}Ni(d,pX), 25.5 MeV, inclusive p spectra and cross sections from d breakup 79−13303
- ^{62}Ni(γ,X), 19.2-26.2 MeV, photoneutron and photoproton spectra, giant dipole resonance-decay, isospin conservation 80−13443
- ^{62}Ni(n,α), 14.7 MeV, cross section calc., and ENDF/V IV eval. 79−85458
- ^{62}Ni(p,γ), study of $g_{9/2}$ isobaric analogue state in ^{63}Cu 79−22258
- ^{62}Ni(p,n)^{62}Cu, 5.5-7.2 MeV, gamma transitions from ^{62}Cu excited levels obs. *(French)* 77−26615
- ^{62}Ni(p,p), 20 MeV, elastic and inelastic scatt., analysing powers *(Dutch)* 78−29464
- ^{62}Ni(p,p), elastic and inelastic scatt., 5.2 to 6.05 MeV, scatt. cross section energy depend. 79−9559
- ^{62}Ni(p,p)^{62}Ni, high-resolution meas. of scattering cross section, 3.0 to. 4.0 MeV 77−10397
- ^{62}Ni($\pi^\pm$,p),(π^-,d), E=100, 220 MeV, p and d spectra meas. 78−648
- ^{63}Ni β-decay surface contamination monitoring probes, comparison of response between detectors 78−25398
- ^{64}Ni (p, X), E_p=7.5 GeV, yields of hydrogen and helium isotopes *(Russian)* 79−93627
- ^{64}Ni, elastic and inelastic scatt. of 1.5-3.0 MeV neutrons *(Russian)* 77−61428
- ^{64}Ni, fast neutron bombard., decay schemes 78−46053
- ^{64}Ni, isospin purity violation, dominant role of noncollective monopole states 78−12964
- ^{64}Ni, one- and two-proton transfer reactions induced by 56 MeV ^{16}O beam, spectroscopic anal. 77−14178
- ^{64}Ni+^{40}Ca, 182 MeV, deep inelastic collisions, short lifetime and long lifetime regime 78−21597
- ^{64}Ni(^{16}O,^{14}C)^{66}Zn, 56 MeV, full recoil one and two-step DWBA anal. 78−46091
- ^{64}Ni(^{16}O,^{14}C)^{66}Zr, 56 MeV, anal. of direct and indirect processes 77−34342
- ^{64}Ni(^{18}O,^{20}Ne)^{62}Fe, mass excess of ^{62}Fe 77−41878
- ^{64}Ni(^{3}He,^{8}B)^{59}Mn, 74 MeV, obs. and mass excess of ^{43}Cl 77−10310
- ^{64}Ni(^{3}He,^{8}He), 75.3 MeV, cross-section meas. 77−79394
- ^{64}Ni(^{4}He,^{8}He)^{60}Ni, angular distribution 78−29488
- ^{64}Ni(α,n), (α,2n), 17-25 MeV, level struct. of ^{66}Zn, ^{67}Zn determ. 77−46178
- ^{64}Ni(α,n)^{67}Zn, 6.5 to 17.0 MeV, γ ray studies of levels below 2.0 MeV in ^{67}Zn 78−62483
- ^{64}Ni(d,^{3}He)^{63}Co, proton pickup strength determ. in ^{63}Co 79−22163
- ^{64}Ni(p,p), (p,p'), 5.0-6.2 MeV, isobaric analogue reson. in ^{65}Cu anal. 78−78351
- ^{64}Ni(p,p) 800 MeV, polarised differential cross sections and anal. powers, n density 79−13297
- ^{65}Ni, spin assignments to p-wave neutron states 77−22852
- ^{65}Ni(n,γ)^{66}Ni, cross sections determ. 79−49624
- ^{67}Ni mass excess from ^{70}Zn(^{4}He,^{7}Be) pick-up reaction 79−9452
- ^{68}Ni mass excess from ^{70}Zn(^{18}O,^{20}Ne)^{68}Ni reaction 77−41878
- Ni(α,^{3}He), 172.5 MeV, double-differential cross-sections determ. 78−82363
- Ni(α,X)Zn, α spectroscopic factors in shell model 79−45158
- Ni(α,α), A=62 and 64, 48 MeV, I.L. potential depth, optical model anal. 78−50187
- Ni(α,nγ)Zn, 6.5-17 MeV, particle-vibr. coupling in ^{65,67}Zn 77−38241
- Ni(d,d), 13-80 MeV, second order breakup corrections in DWBA 80−86910
- Ni(d,p)Ni, A=58, 60, 62, 64, at 2.8 MeV, cross-sections and spectroscopic factors *(German)* 77−18566
- Ni(e,α), E2 strength in resonance regions statistical decay 80−91146
- Ni(e,e), nuclear radius, core polarisation and isotone shifts, muonic X-rays 80−22685
- Ni(e,e') A=58, 60, 64, isospin splitting of giant dipole resonance *(Russian)* 77−50116

nuclei with mass number 59 to 89 continued
Ni(n,X), 14.8 MeV, γ-prod. cross section 79−49622
Ni(n,α), cross section for 2 step reaction 77−6368
Ni(n,γ), absolute cross sections in keV range 77−26771
Ni(n,γ), primary transitions using focused 24 keV filtered neutron beam 80−63436
Ni(n,n′γ), 3-6 MeV, γ-ray prod. cross sections 77−26767
Ni(p,d), A=60, 62 and 64, 50 MeV, fine struct. of ground hole-state analogues 78−50065
Ni(p,γ)^{59,61}Cu, analogue to antianalogue M1 transitions 77−67718
Ni(p,p)Ni, A=58,60,62,64, at 1.047 GeV, neutron matter densities 77−54171
Ni(p,p′), A=60,2, E=17.2, 20.4, 24.6 MeV, polarised protons, optical model, DWBA anal. 78−13094
Ni(p, spallation), 0.08-24 GeV, Ar isotopes, spallation ratios and prod. cross sections 80−9284
Ni(p,t), A=60, 62, at 27 MeV, two step processes, finite range effects 78−58281
(^{17,18}O,^{17,18}O′), 54-69 MeV, on A=48-92, excited states and ang. distribs., DWBA anal. 79−67705
^{208}Pb(π^+,$\pi^{+\prime}$), 50 MeV, energy spectra and cross sections 78−25241
Rb (n,2n) react. cross sections at 14.8 MeV 78−74355
Rb, fission fragment, delayed neutron branches from γ-spectroscopy 80−78230
Rb, fission products, precise Q_β values *(German)* 80−37354
Rb, ground state spins, moments, charge radii by laser spectroscopy 80−78147
Rb, isotope, neutron deficient, supermultiplet mass predictions 79−85359
Rb isotopes, delayed neutron Pn-values, beta+neutron+gamma decay modes 77−26639
Rb isotopic distrib. anal., for ^{11}B and ^{22}Ne-induced fission of ^{238}U 77−18634
Rb isotopic distrib. meas. for ^{11}B and ^{22}Ne-induced fission of ^{238}U 77−18633
Rb neutron deficient isotopes, mass meas. 77−22861
Rb neutron deficient isotopes, beta-decay energies and masses 77−22946
Rb neutron deficient radioisotope selective production in (α,xn) reacts. *(Croatian)* 78−44608
Rb neutron rich isotopes, nucl. spins and mag. moments 80−47367
Rb, neutron rich isotopes, $Q_\beta$and direct mass meas. 80−78132
Rb odd isotopes, β^- strength functions, 'pygmy' resonances 79−93559
Rb odd-even isotopes, collective states and transitions, interacting boson approx. 80−73773
Rb relative and independ. fission yields from ^{235}U(n,f) 80−27679
Rb relative independ. yield from ^{232}Th(p,f) 80−102218
Rb, short-lived isotopes, spin and mag. moment meas. from atomic-beams 77−22882
Rb, spin and mag. moment, trends in neutron deficient nuclei 78−37261
^{A}Rb, A=77, 78, 78m, 79, 84m, nuclear spins and mag. moments, deformed shapes 79−17793
^{A}Rb, A=79, 81, decoupled $g_{9/2}$ bands, level lifetimes and E2 transitons from (^{16}O, 2n)(^{19}F, p2n) 80−73772
^{A}Rb, A=83,84,86 prod. cross sections and recoil props. from (p,X) 80−9295
^{A}Rb, A=85,87, mass using spectroscopic doublet method *(Russian)* 78−86468
^{A}Rb, A=88, 90-93, gaseous fission products, β-decay energies 79−9519
^{A}Rb, A=88-94, beta endpoint energy measurements 78−93975
^{A}Rb(n,n′γ), 550-2100 keV, A=85,87, levels, excitation functions, J^π, Hauser-Feshbach anal. 80−105982
^{74}Rb, N=Z nucleus with T=1, $I^\pi=0^+$, half life 77−26627
^{74}Rb, prod. in proton spallation reactions, nuclear structure influence on yields of product nuclei 80−22794
^{74}Rb, Z=N nuclide, superallowed beta decay meas. 77−22952
^{76}Rb, short-lived, determ. of nucl. spins by β radiation detected optical pumping 78−37262
^{76}Rb, spin of neutron deficient nucleus by β radiation detected optical pumping 78−8782
^{78}Rb band struct. and level scheme from ^{64}Zn(^{16}O,np) 79−54380
^{78}Rb β-decay half lives of isomeric and ground state from (^{16}O,3n) 80−27534
^{79}Rb β^+ decay, ^{79}Kr excited states, J^π assignment, transitions, level lifetimes 79−17810
^{79}Rb positive parity decoupled band, levels and J^π from (^{9}Be,Xγ), (^{10}B,Xγ), (^{12}C,Xγ), (^{28}Si,3pγ) 79−89223
^{80}Rb, level struct., quasi-rot. bands, via ^{79}Br(α,3n) 30-55 MeV reaction 77−88028
^{81}Rb, β^+-EC decay, $T_{1/2}$, ^{81}Kr levels 77−79309
^{81}Rb, myocardial imaging agents comparison 77−2037
^{81}Rb production, non-linear behaviour of gas targets 78−25361
^{81}Rb/^{81}Kr labelled pharmaceuticals, cyclotron production for nuclear medicine appls. 77−44753
^{81}Rb-^{81}Kr generators, aspects of production, elution and automation, medical appls. 80−61696
^{82}Rb generators for imaging studies, ion exchange resin comparison 77−21626
^{82}Rb, half life meas. 79−17861
^{82}Rb, level structure, gamma angular and time distribs. from ^{81}Br(α,3n) 80−52583
^{83}Rb, implantation in Fe and Ni, Mossbauer obs. 77−24765
^{83}Rb band struct., spin assignments and transitions from (^{6}Li,3n), (^{16}O,p2n), (α,2n) 80−73774
^{83}Rb, half-life meas. 77−34257
^{83}Rb high spin states, Jπ and transitions from HI and α reactions 80−105949
^{83}Rb high spin states, positive and negative parity bands from (^{6}Li, 3n), (α, 2n) 80−18178
^{84}Rb, half-life meas. 77−34257
^{84}Rb levels from ^{85}Rb(p,d), spin and parity determ. 78−82338
^{84}Rb radioactive target, search for (n_{th},p) and (n_{th},α) reactions 77−23010
^{85}Rb high spin states, yrast cascade, J^π, γ-transitions from ^{82}Se(Li,xnγ) 80−73775
^{85}Rb levels, J^π and transitions from $Kr^{m,g}$, $Sr^{m,g}$ decay, cluster-vibr. model 80−78162
^{85}Rb, proton induced nuclear reactions, excitation functions, medical appls. 80−78286
^{85}Rb, single-particle estimate of γ-γ transition probability 78−13023
^{85}Rb, two-quantum γ-γ decay of 514 keV excited state 78−13009
^{85}Rb(^{32}S, Ẑ), double differential cross section, mass asymmetry, transport model 80−102203
nuclei with mass number 59 to 89 continued
^{85}Rb(^{32}S,X), 153-184 MeV, fission like processes around A_{CN}=100, mass distrib. strong change 80−9318
^{85}Rb(n,2n), 14.6 MeV cross-section meas. 79−59055
^{85}Rb(p,d), level location, spin and parity determ. in ^{84}Rb 78−82338
^{87}Rb, decay constant determ., Rb-Sr dating appl. 78−29424
^{87}Rb, decay consts. for use in geochronology and cosmochronology 78−28189
^{87}Rb, half-life determ. by absolute counting 77−26943
^{87}Rb, low-lying level struct. in quasiparticle-core model 77−82825
^{87}Rb, NMR obs. of struct. transitions in $Rb_xK_{1-x}MnF_3$ 77−47577
^{87}Rb(ν,e)^{87}Sr, cross section calc., appl. to solar neutrino interpretation *(Russian)* 77−50119
^{87}Rb(p,nγ), 3.8 MeV ^{87}Sr excited levels, spin, parity, branching ratios, lifetimes 77−50076
^{87}Rb→^{87}Sr+neutrals, nucleon charge conservation, improved test 80−5098
^{88}Rb decay, γ-ray energy meas. 79−22530
^{88}Rb→^{88}Sr, Gamow-Teller β-transition, matrix elements and log ft values calc. 78−21531
^{89}Rb, nucl. moment and charge radius using fast-beam laser spectroscopy 79−40839
^{89}Rb, structure in beta strength function 79−93564
^{85}Rh, form. in β-decay of ^{85}Sr, γ-ray weak transitions, intensities 77−79326
^{87}SR(e,e) elastic mag. scatt., 175 to 300 MeV, $1g_{9/2}$ neutron radial distrib. 77−57652
^{135}Sb, delayed neutron emission to excited states in ^{134}Te 77−14077
Se (d,p), 12.5 MeV, ^{77,79,81,83}Se level struct., spins, parities, cross section, vector analysing power 78−89885
Se, A=75, 77, nuclear deformations, core-particle coupling model 79−450
Se, A=76, 78, 80, 82, static quadrupole moments of first 2^+ excited states 77−65197
Se, circular polarisation of muonic K_α X-rays 78−9284
Se enriched even isotopes, neutron elastic and inelastic scatt., symmetry effects 77−26757
Se, evaporation residue from Ni+$^{12}C_2$, prompt γ deexcitation 78−74395
Se, even-even isotopes, first excited $0^{+\prime}$ states, energy systematics 78−54683
Se, even-even nuclei, γ-spectroscopy, exptl. results and models 80−68589
Se, experimental Q_β-values A=85, 86, experimental Q_β-values 78−93974
Se isotopes, (n,p), (n,α), (n,2n) cross sections at 14.1 MeV *(Spanish)* 77−30563
Se isotopes, excited states struct., energy systematics 78−54687
Se neutron deficient isotopes (A=68,69,70,71), production in heavy-ion reactions 77−38292
Se series isotopes, sensitivities to various parameters, analytical evaluation 78−82424
Se, stable isotopes, masses meas. 78−12956
Se+p→^{77}Br, production excitation curves 79−85468
Se(^{86}Kr,xnγ), Yb nuclei at high ang. momentum, moment of inertia from γ spectra 78−13135
^{A}Se (A=85-8), fission product, γ-spectra, half-life meas. 77−38240
^{A}Se, A=70,72,74, discovery of multiple collective band struct. *(Chinese)* 79−80865
^{A}Se, A=74, 76, vibr. states and transition from dynamic deformation theory 80−73770
^{A}Se, A=75, 77, 79, 81, levels and ang. distribs., spectroscopic factors from Se(p, d) 80−22696
^{A}Se(d,d), A=76, 78, 80, 82, pol. d, 12 MeV, cross sections, anal. powers, global optical model anal. 80−47459
^{A}Se(d_{pol},d), A=76,78,80,82, 12 MeV, two-step scatt. process via $J^\pi=2_1^+$ excited states 80−57781
^{A}Se(n,n), A=76-78, 80, 82, slow n coherent scatt. length, free cross section, bound states 80−86909
^{A}Se(p,p), A=76-82, doubly even nuclei, deformation parameters 79−97705
^{A}Se(t,^{3}He)^{A}As, A=78,80,82, ground state mass meas. and excited state energies of ^{A}As 79−63595
^{69}Se, delayed proton spectra, $T_{1/2}$ meas. 77−38254
^{69}Se, decay, T=1/2 β-delayed proton precursor 77−88082
^{69}Se, delayed proton decay 77−22971
^{70}Se de-excitation, continuum γ-ray emission and ang. momentum dissipation 77−6293
^{72}Se from ^{58}Ni(^{16}O, 2pγ), high spin and excitation energy regions, γ cascade 78−54795
^{72}Se, high spin and excitation regions anal., ^{58}Ni(^{16}O,2pγ) 78−25226
^{72}Se recoil distance level lifetime meas. from ^{58}Ni(^{16}O,2p) 78−78311
^{72}Se side band struct., negative parity states and transitions from ^{58}Ni(^{16}O,2p) 80−73769
^{72}Se yrast states from ^{58}Ni(^{16}O,2pγ), γ spectra, lifetimes, nuclear model predictions 77−54176
^{73}Se, excitation functions for production using ^{72}Ge(^{3}He,Zn)^{73}Se reaction 79−39501
^{73}Se high-spin states via ^{70}Ge(α, nγ) at 10-18 MeV 77−10324
^{73}Se, yield for various reactions and chem. processing 80−36131
^{74}Se, collective excitations in the interacting boson model *(Russian)* 80−5044
^{74}Se level scheme, J^π assignments, bands and transitions from ^{60}Ni(^{16}O,2p), ^{64}Ni(^{12}C,2n) and ^{65}Cu(^{11}B,2n) 79−54393
^{74}Se quasi-γ bands and negative parity levels from ^{75}As(p,2nγ) 80−456
^{74}Se transition energy correlations in γ-continuum from ^{64}Ni(^{16}O,α2n) 80−95309
^{74}Se(^{16}O,^{16}O′), 33, 34 MeV, first excited state, static quadrupole moment, deformation evidence 79−17802
^{74}Se(α,α′), 7.3 MeV, first excited state, static quadrupole moment, deformation evidence 79−17802
^{74}Se(d,p), 6 MeV, ^{75}Se energy levels, DWBA, sum rule anals., spectroscopic factors 78−66285
^{75}Se, decay, electric monopole transitions 80−22752
^{75}Se decay, gamma transitions 78−13008
^{75}Se energy levels from ^{74}Se(d,p), DWBA, sum rule anals., spectroscopic factors 78−66285
^{75}Se, whole body retention following intravenous injection as selenomethionine 77−90904
^{75}Se-selenomethionine pancreatic scanning, review 77−9237
^{76}Se high spin states, bands, J^π, transitions and $T_{1/2}$ from ^{71}Ga(^{7}Li,2n) 80−105951
^{76}Se, level scheme from γγ coincidence meas. of ^{76}As decay 80−22754

nuclei with mass number 59 to 89 continued
^{76}Se(p,nγ)^{76}Br, 5.8 to 6.8 MeV, level scheme deduced for ^{76}Br 78−50091
^{76}Se(π^-,xn)$^{76-x}$As, 100, 180 MeV, product formation cross section 80−42705
^{77}Se NMR Knight shift, in n-CdSe impurity carrier wavefunction 78−35049
^{77}Se, NMR meas. on layered supercond. $NbSe_2$ in 2H phase 77−36024
^{79}Se, 96 keV transition, conversion coeff., γ-spectrum 80−63131
^{79}Se high spin levels, transitions, J^π assignments from ^{76}Ge(α,nγ) 80−459
^{79}Se, level structure study via ^{80}Se(p,d)^{79}Se 78−93993
^{82}Se, fast moving ion in Fe and Gd, nature of dynamic mag. field 78−43697
^{82}Se(^{40}Ar,xnγ), shell effects at high spin in the γ-continuum from Te evaporation residues 79−22165
^{82}Se(p,p) elastic, inelastic 4.5-77 MeV scatt., IAS, ^{83}Se low-lying states 78−573
^{83}Se, IAS, J^π via ^{82}Se(p,pγ) 4.5-7.7 MeV 78−573
^{83m}Se, decay scheme refinement, ^{83}Br levels 78−17147
^{76,74}Se, 33 MeV levels, J^π via Se(p,t)Se 77−67700
^{78,76}Se(p,t)^{76,74}Se, 33 MeV, J^π, level assignments to 4.64 MeV 77−67700
Se(d,d), 12 MeV polarised deuterons, shell closure effects 77−38281
Se(d,d), polarised deuterons, vector analysing power, optical model calcs. 78−62550
Se(γ,f), max. energy 580 MeV, track detector anal. 77−18640
Se(n,n)Se, A=76, 78, 80, 82, 6-10 MeV, isospin and strong coupling effects 77−6383
Se(n,n′) 2^+ level excitation cross sections, intermediate resonances, optical model with coupled channels *(Russian)* 79−40897
Se(n,n′γ), 2.0 to 4.1 MeV, even A=76-82 isotopes level struct. 77−34233
Se(n,n′γ), even-A isotopes, 2.0 to 4.1 MeV, level and decay schemes 77−23092
Se(p,nγ)Br, A=80,2, energy levels of Br anal. 77−71609
^{A}Sm, A=150, 152, E2:M1 multipole mixing ratio, sign change in A=150 region 80−493
Sr, even isotopes, potential energy surfaces and ground state equilib. deformation 80−73789
Sr, fission products, precise Q_β values *(German)* 80−37354
Sr isotopes, $1g_{9/2}$ nucleon-transfer reactions, nucleon radical distrib. 78−50068
Sr, mass dependence for radiative capture of 14.1 MeV neutrons 78−13087
Sr(^{12}C,X) 3, 12.6 GeV, in-beam transition γ-rays 79−6483
^{A}Sr, A=80,82,84-86, levels and transitions from Kr(^{3}He,n) 80−18201
^{A}Sr, A=81, 83, yrast and high spin states of neutron deficient isotopes from Kr(α,xn) 80−73776
^{A}Sr, A=89 to 94, struct. of states in the generalised seniority shell model 79−6408
^{77}Sr, delayed proton spectra, $T_{1/2}$ meas. 77−38254
^{79}Sr, mass excess values from beta and gamma spectra from ^{32}S+^{54}Fe(^{58}Ni) 80−63137
^{80}Sr ground state mass from Kr(^{3}He,n) 80−18201
^{82}Sr, half life meas. 79−17861
^{83}Sr, excited states struct. ^{83}Y β^+ decay, γ-ray coincidence meas. 77−6309
^{83}Sr high spin states, J^π and de-excitation from Kr(α,xn) 80−42516
^{83}Sr, high spin states and spin ordering, γ-ray excitation functions 78−66199
^{83}Sr levels from ^{84}Sr(^{3}He,α α), 18 MeV, DWBA calcs. using optical model 78−41738
^{84}Sr quasi-γ bands and negative parity levels from ^{85}Rb(p,2nγ) 80−456
^{84}Sr(α,nγ), 16.7 MeV, high spin states in ^{87}Zr 78−74383
^{84}Sr(α,p), 18 MeV, low-lying states of ^{87}Y anal. 78−17228
^{85}Sr, 514.0 keV, Analytic fitting of full-energy peaks in Ge(Li) spectra at high count rates 80−99147
^{85}Sr, β-decay, γ-ray weak transitions, intensities 77−79326
^{85}Sr, decay to ^{85}Rb, two-quantum γ-γ decay of 514 keV excited state 78−13009
^{85}Sr, electron capture decay, K X-ray emission probability, half-life, decay scheme 79−17862
^{85}Sr, high spin states and spin ordering, γ-ray excitation functions 78−66199
^{85}Sr, high-spin states obs. from ^{82}Kr(α,n) and ^{84}Kr(α,3n) 77−41915
^{85}Sr, lifetime DSA meas. in ^{85}Rb(p,nγ) 79−36196
^{85}Sr radioisotope activities, quantitative analysis, gamma-ray spectrometry 77−18734
^{85}Sr^{m,g} decay, ^{85}Rb levels, J^π and transitions 80−78162
^{86}Sr, 8^+ state, nucl. g-factor and nucl. spin relax. in Kr 77−22884
^{86}Sr, populated in ^{89}Y(p,α), DWBA microscopic anal. 78−70449
^{86}Sr(^{3}He,α)^{85}Sr, transfer reactions, nucl. struct. obs. 77−46118
^{86}Sr(d,α)^{84}Rb, nuclear structure determ. 77−46118
^{86}Sr(d,p)^{87}Sr, transfer reactions, nucl. struct. obs. 77−46118
^{86}Sr(n,t)^{84}Rb, 14.6 MeV neutrons, activation cross section meas. 79−45254
^{87}Sr 1 $g_{9/2}$ neutron distrib. radial size, states, differential cross sections from ^{86}Sr(^{18}O,^{17}O) 80−95301
^{87}Sr excited levels from ^{87}Rb(p,nγ), spin, parity, branching ratios, lifetimes 77−50076
^{87}Sr, mag. form factors, core polarisation and exchange current effects 80−13409
^{87}Sr produced in ^{88}Sr(p,d), two step processes, excitation of core coupled states 77−88150
^{87}Sr(e,e), magnetic e scatt., exchange current effects, plane wave Born approx. 80−78282
^{87}Sr(e,e), valence nucleon orbit determ. 78−54669
^{87}Sr(n,γ), 2, 24 keV, level struct. of ^{38}Sr 77−30584
^{87}Sr(p,p′), 20.5 MeV, level scheme, ang. distribs., transitions and deformation parameter 79−22195
^{88}Sr, charge distrib., self consistent calc. *(Russian)* 77−38234
^{88}Sr, giant dipole resonance region radiative nucleon capture, expt. ang. distrib. coeffs., direct-semidirect theory 78−74354
^{88}Sr, M1 transitions, theory of finite Fermi systems *(Russian)* 77−6296
^{88}Sr populated in ^{86}Kr(^{3}He,n), subshell closure, 0^+ states 78−21582
^{88}Sr(^{12}C,^{10}Be), 60 MeV, coupled channel Born approx. anal., form factors, sequential amplitudes 79−9608
^{88}Sr(^{3}He,n), 25.4 MeV, ang. distrib. meas. 77−3022
^{88}Sr(d,α)^{86}Rb, transfer reactions, nucl. struct. obs. 77−46118
^{88}Sr(d,p), pol. d, excitation curve isospin anomaly, neutron single particle resonances 80−27595

nuclei with mass number 59 to 89 continued
^{88}Sr(e,e), 200 MeV, nucleon density distribution in nucleus 79−75831
^{88}Sr(e,e), 400 MeV, charge density distrib. variations 79−75830
^{88}Sr(γ,γ), 14 MeV, highly excited spin-1 resonances, spin and radiative widths 80−86876
^{88}Sr(γ,γ), reson. fluoresc. yield meas. width of 1.836 MeV level determ. 77−79357
^{88}Sr(n,γ_1), ang. distrib. anal. in generalised direct-semidirect model 77−23023
^{88}Sr(n,γ), 2, 24 keV level struct. of ^{89}Sr 77−30584
^{88}Sr(n,γ), 7-11 MeV ang. distrib. from fast capture 78−54758
^{88}Sr(n,γ) valence neutron capture, 3-400 keV, ^{89}Sr resonance parameters 77−2989
^{88}Sr(n,n′), 11 MeV, octupole vibr. states, diff. cross section, deformation length, DWBA anal. 80−102092
^{88}Sr(n,n), elastic and inelastic, 11 MeV, isospin effects, optical and deformation parameters 79−17794
^{88}Sr(p,γ_0), polarised p in giant dipole resonance region, cross sections and analysing power 78−82346
^{88}Sr(p,p′)^{88}Sr(2_1^+), 7-7.5 MeV polarised protons, scatt. at IAR 77−318
^{88}Sr(p,p), polarised protons, direct reaction contrib. in fluctuating cross sections 77−50102
^{89}Sr level transitions and spin assignments from ^{88}Sr(d,p)^{89}Sr, polarised d 78−66286
^{89}Sr produced in ^{88}Sr(d,p), two step processes, excitation of core coupled states 77−88150
^{89}Sr, radiochem. determ., error anal. comparison of methods 77−16873
^{89}Sr, soil analysis using total sample decomp. 80−35808
Sr(α,2nγ), 28, 35 MeV, high spin states in ^{86,88}Zr 78−74383
Ta photodisintegration yields, 600 to 1300 MeV, cross sections *(Russian)* 77−50112
W photodisintegration yields, 600 to 1300 MeV, cross sections, photo- to electro-yield ratio *(Russian)* 77−50112
Xe induced deeply inelastic collisions, transport eqn. appl. 78−82380
Y, fission products, precise Q_β values *(German)* 80−37354
Y isotopes, Hauser Feshbach calcs., of neutron cross sections 80−22839
^{A}Y, A=82, 83, mass excess values from beta and gamma spectra from ^{32}S+^{54}Fe(^{58}Ni) 80−63137
^{A}Y, A=85,87,89, E1 γ-ray strength function from Sr(p,γ) 79−75902
^{A}Y^{m,g}, A=86, 87, isomeric yield ratios and γ-spectra from ^{93}Nb(π^-,X) 80−86857
^{59}Y(n,γ), thermal, isomer state excitation, relative probabilities 79−75814
^{80}Y, fast neutron capture and the microscopic isovector optical potential 79−63668
^{83}Y β^+-decay, ^{83}Sr nucl. energy levels, γ-ray coincidence meas. 77−6309
^{86}Y, DPAC in Ni, mag. hyperfine field determ. 77−8458
^{87}Y, IAS spectroscopy and compound nuclear enhancement 77−61396
^{87}Y level struct., γ-spectroscopy and J^π from (p,2nγ), (α,2nγ) 80−83040
^{87}Y, low-lying states anal. in ^{84}Sr(α,p) at 18 MeV 78−17228
^{87}Y^m, hyperfine interactions in Al, Au, and Fe, nuclear orientation meas. 78−43715
^{87}Y^m orientation meas. in Al and Au hosts, mag. moment of $9/2^+$ isomeric state 78−41632
^{88}Y 14 ms 8^+ isomeric state, g-factor from ^{87}Rb(α,3n) 80−63080
^{88}Y, gamma-ray intensities, precision meas. 80−102139
^{88}Y solution, standardisation using efficiency extrapolation method, β-γ coincidence meas. 78−21832
^{88}Y(n,2n)^{87}Y cross sections, spin dependence and preequilibrium emission 77−30598
^{89}Y, 14.7 MeV neutron capture cross-section measurements with activation technique 80−32282
^{89}Y, 6.2-15.6 MeV, gamma-ray spectra, cross-section meas. 78−33176
^{89}Y (p,p′), 62 MeV, effect of nucleon mean free paths on intranuclear cascade calc. 77−67749
^{89}Y, energy spectra and EM props. using broken pair model 80−499
^{89}Y excited state ang. distrib. from ^{88}Sr(^{16}O, ^{15}N) 79−67709
^{89}Y, first four energy levels, from ^{92}Zr(p̄,α)^{89}Y reaction *(French)* 79−75981
^{89}Y, giant dipole resonance region radiative nucleon capture, expt. ang. distrib. coeffs., direct-semidirect theory 78−74354
^{89}Y, giant reson. pionic excitation 80−73834
^{89}Y, high resolution neutron total cross section meas., 27-240 keV 78−25193
^{89}Y high spin states and decay scheme from ^{87}Rb(α,2nγ) 80−32166
^{89}Y high spin states from γ-ang. distribs. in ^{87}Rb(α,2nγ), 30-55 MeV 78−93941
^{89}Y in $Y(NO_3)_3$, YCl_3 and $Y(ClO_4)_3$ aqueous solns., NMR study 77−24754
^{89}Y, isomeric state formation by 14.8 MeV neutrons 77−30604
^{89}Y, reson. neutron capture cross-section between 2.5 and 100 keV 77−82924
^{89}Y, spin-spin relax. times in solns. 80−2657
^{89}Y, total neutron cross section, 0.3 to 9.0 MeV 78−70519
^{89}Y, total neutron cross-section, 0.3-9.0 MeV, fluctuation anal. 77−23030
^{89}Y+^{40}Ar, 237 meV, γ-ray multiplicities and energies, primary fragment angular momenta 78−46093
^{89}Y+p, 62 MeV, complex particle emission, pre-equilibrium exciton model anal. 78−66280
^{89}Y(^{32}S,X), double differential cross section, mass asymmetry, transport model 80−102203
^{89}Y(^{3}He, ^{3}He), 119 MeV, optical pot. parameters energy and mass depend. 80−32289
^{89}Y(^{3}He, 3nγ), 20-28 MeV, in-beam γ-ray spectroscopy, ^{89}Nb levels determ. 77−41983
^{89}Y(^{40}Ar,X), 237 MeV, ang. momentum transfer in deep inelastic reactions 80−5156
^{89}Y(α,2nγ)^{91}Nb, g-factor of $21/2^+$ state in ^{91}Nb 77−30487
^{89}Y(α,2nγ)^{91}Nb at 24.0, 35.7 MeV, high spin states in ^{91}Nb 79−93514
^{89}Y(e,e′), 92.5 MeV, giant reson. and bound collective states 78−13070
^{89}Y(e,e′π^+), energy and ang. distribs. of πs, low lying residual states 78−54740
^{89}Y(n,2n)^{88}Y, preequilibrium emission effects 77−30598
^{89}Y(n,γ), 7-11 MeV ang. distrib. from fast capture 78−54758
^{89}Y(n,γ), direct-semidirect and compound nucleus contribs. to cross sections 80−68662
^{89}Y(n,n′), 2-4.5 MeV, level excitation functions, Hauser-Feshbach-Moldauer model test 79−36238
^{89}Y(n,n′), calc. of fluctuation compound nucleus cross sections 77−23029

nuclei with mass number 59 to 89 continued
^{89}Y(n,t)^{87m}Sr, 14.6 MeV neutrons, activation cross section meas. 79 48264
^{89}Y(p,γ_0)^{90}Zr, 14-27 MeV, E_2 and E_3 radiation anal. in direct-semidirect model 77−38266
^{89}Y(p,n), sub-Coulomb optical pot. 80−102190
^{89}Y(p,p'), two stage processes in direct reactions *(Dutch)* 78−29439
^{89}Y(p,p), 0.8 GeV, elastic and inelastic, differential cross sections, relativistic optical model anal. 79−45270
^{89}Y(p,p), 185 MeV, ang. distribs., polarisation, cross section, optical pot. 78−89873
^{89}Y(p,p), 65 MeV polarised protons, asymm. in elastic and inelastic scatt. 78−54754
^{89}Y(π, π^1), 163, 240 MeV, giant resonance pionic excitation 80−52561
^{88m}Y, nuclear spin relax. in liq. Rb 77−12270
^{70}Yb L-shell X-ray emission spectrum investigation 77−3297
^{89}Yb(^{32}S,X), 153-184 MeV, fission like processes around A_{CN}=100, mass distrib. strong change 80−9318
^{89}Yb(p,2nγ), 22.7 MeV, high spin states of ^{88}Zr 78−74383
^{89}Yb(p,p), 20 MeV, elastic and inelastic scatt., analysing powers *(Dutch)* 78−29464
Y(n,n'), 9.1 MeV, equilib., pre-equilib., direct process anal. *(Russian)* 77−46172
Zn, A=60, 62, 64, 66, 68, Lipkin-Nogami method, ground state props. 78−50103
Zn, A=64, 66, 68 transition charge density, and radius to collective states via (e,e') 77−50077
Zn, A=65,7, particle-vibr. coupling among positive parity states 77−38241
Zn, A=66,67, level struct. determ. from ^{64}Ni(α,n), (α,2n), spin-parity assignments 77−46178
Zn, β-decay energies and masses, A=75-78 77−74808
Zn, doubly even nuclei, quasiparticle+phonon model calcs. 78−41626
Zn, even isotopes, effect of particle-vibr. coupling in nucl. struct. 78−12940
Zn even isotopes, fast neutron elastic and inelastic scatt. cross sections *(Russian)* 77−74853
Zn, even isotopes, weak-coupling model, level struct., E2 transition rates 77−54159
Zn even isotopes in cluster-vibr. model, energy spectra, EM props. 78−54708
Zn, even nuclei, systematic meas. of mag. moments of 2_1^+ states 78−54682
Zn isotopes, A=62-68, shell model calc. 77−270
Zn isotopes, density-dependent HF description 77−54170
Zn, K_β/K_α following K-electron capture and X-ray excitation 78−13031
Zn, radial charge distrib. moments, ground state correlations, generator coordinate model 79−30785
Zn, single neutron separation energies determ. from doublets 77−26566
Zn, stable isotopes, masses meas. 78−12956
Zn to Ni even isotope transition, α-particle spectroscopic factors, shell model calcs. 79−6385
Zn+d production of ^{64}Cu, ^{64}Cu and ^{67}Ga and bleomycin labelling with ^{67}Cu or ^{64}Cu 78−28066
Zn(Li,Li) (A=64,68), 28 and 34 MeV, optical model parameters 77−54248
Zn(^{16,18}O, xn), 36 to 55 MeV, total neutron yields, cross sections 77−14163
^Zn, A=64, 66, 68, 70, transient mag. field g-factor meas. 79−67653
^Zn, A=64, 66 levels and primary E1 transition strength functions from Cu(p,γ) 80−91149
^Zn, A=65 to 68, energy spectra, shell model calc. 79−17818
^Zn(α, α'), A=64, 66, 129 MeV, isoscalar giant monopole resonances, nuclear incompressibility 80−83083
^Zn(α,α'), 18 MeV, A=64,66,68,70, compound and precompound α emission spectra 78−82367
^Zn(e,e), 100-275 MeV, A=64,66,68,70, cross sections and muonic X-ray meas., charge distrib. systematics 80−86801
^Zn(p,α), 12.5 MeV, A=64,66,68,70, compound and precompound α emission spectra 78−82367
^Zn(p,γ), A=64, 66, $g_{9/2}$ isobaric analogue resonances 79−63663
^Zn(p,p), A=66,68, 20-50 MeV differential cross section, polarisation ang. distrib., optical model exchange terms 80−27638
^{60}Zn level determ. from ^{58}Ni(^{12}C,^{10}Be) of 77 MeV 79−26371
^{61}Zn ground state mass determ. from ^{64}Zn(^{3}He,^{6}He) 70 MeV, mass excess calc. 79−26371
^{61}Zn level determ. from ^{58}Ni(^{12}C,^{9}Be) at 77 MeV 79−26371
^{61}Zn states, pseudo LS coupling model 80−68548
^{61}Zn, studied via ^{58}Ni(^{6}Li,t)^{61}Zn, mass, t-energy spectra and reaction mechanism 78−41756
^{62}Zn ang. distribs. for transitions, DWBA anal., spectroscopic strengths from ^{58}Ni(^{7}Li,t) 80−68584
^{62}Zn, band mixing HF model, struct. and electromag. transitions 78−54676
^{62}Zn compound nucleus in ^{58}Ni(α,p), resonance struct., α-widths 77−30617
^{62}Zn, in beam gamma spectroscopy using ^{63}Cu(p,2nγ), ^{60}Ni(α,2nγ) 77−6297
^{62}Zn levels from ^{58}Ni(^{16}O,^{12}C) 79−6694
^{62}Zn production and bleomycin labelling, excitation function for ^{60}Ni(α,2n)^{62}Zn 78−28067
^{62}Zn, simultaneous prod. of ^{123}I, ^{62}Zn and $^{13}NH_3$, multitarget assembly for high energy irrad. 77−90896
^{62}Zn yrast states, possible decay scheme from ^{40}Ca(^{28}Si,α2pγ) 79−54379
^{63}Zn, 5/2$^-$ 193 keV level, γ-ray ang. distrib. integral rot. 77−41912
^{63}Zn EM decay transitions, level J$^\pi$ assignments, level lifetimes from (α, nγ), (^{11}B, npγ), (^{7}Li, pnγ) 79−85402
^{63}Zn level scheme, spin and parity assignments from (p,d), (p,nγ), (α,nγ), (^{12}C,pnγ) 79−465
^{63}Zn, levels, J$^\pi$ via ^{64}Zn(d,t) 13 MeV, polarised d 77−88100
^{63}Zn, low-lying negative parity states anal. by ^{60}Ni(α,nγ) ^{63}Zn 78−21521
^{64}Zn (d,^{3}He), polarised d, 13 MeV, vector analysing power, ^{63}Cu levels deduced 77−88100
^{64}Zn, electroexcitation of giant multipole reson. *(Russian)* 78−58264
^{64}Zn, electron excitation of giant multipolar resonances *(Russian)* 78−8802
^{64}Zn, γ-ray spectroscopy and role of $g_{9/2}$ orbital 78−33142
^{64}Zn, γ-ray spectroscopy from ^{61}Ni(α,nγ)^{64}Zn 78−21514
^{64}Zn, γ-ray studies of levels above 3.1 MeV 80−32238

nuclei with mass number 59 to 89 continued
^{64}Zn high spin states, J$^\pi$, $T_{1/2}$, γ-decays from (α,nγ), (^{11}B,p2nγ) 80−73767
^{64}Zn, high-spin states anal. from heavy-ion reactions 78−33145
^{64}Zn, J$^\pi$ assignments from γ-ray linear polarisation meas. from ^{59}Co(^{7}Li,2n) 79−6383
^{64}Zn, lifetimes of levels populated in ^{51}V(^{18}O, p2nγ) 78−13019
^{64}Zn, quasi-rotational states populated in ^{51}V(^{16}O,p2nγ), lifetimes and effective population times 78−17140
^{64}Zn, search for giant quadrupole resonance 80−9281
^{64}Zn, struct. of quasi-bands from (α,nγ) and (^{11}B,p2nγ) 78−70424
^{64}Zn(α,α), 15-19 MeV, inelastic scatt. form factors, Coulomb-nuclear interference region 78−66288
^{64}Zn(d,^{3}He)^{63}Cu, 13 MeV, polarised d, tensor analysing powers 77−88101
^{64}Zn(d,^{3}He)^{63}Cu, proton pickup strength determ. in ^{63}Cu 79−22163
^{64}Zn(d,^{6}Li), 55 MeV, cluster model DWBA anal. 78−21573
^{64}Zn(d,d), polarised d, 13 MeV, optical model parameters, vector analysing power 77−88100
^{64}Zn(d,t), polarised d, 13 MeV, vector analysing power, ^{63}Zn levels deduced 77−88100
^{64}Zn(d,t)^{63}Zn, 13 MeV, polarised d, tensor analysing powers 77−88101
^{64}Zn(γ, n)^{63}Zn, giant dipole reson. isospin splitting, reaction cross section *(Russian)* 78−46040
^{64}Zn(γ,n), photoneutron energy spectra and intermediate struct. of the giant dipole reson. *(Russian)* 79−22270
^{64}Zn(p,p'), 15 MeV polarised protons, surface delta description of analysing power 77−61397
^{65}Zn dosimetry and permissible body burden 77−56474
^{65}Zn, EC decay rate determ. using X-ray gamma-ray summing 77−57804
^{65}Zn, EM transition probabilities, lifetimes, weak coupling model 77−74804
^{65}Zn, electron capture/positron emission ratio 77−30522
^{65}Zn gamma intensity, from ^{64}Zn(n, γ) cross-section meas., k_0 factors calcs. 79−26433
^{65}Zn, γ-ray spectroscopy and role of $g_{9/2}$ orbital 78−33142
^{65}Zn, high spin states obs. in (α,nγ), and (^{16}O,np) 78−13016
^{65}Zn, impurity in plastic, neutron fluence meas. using plastic as nuclear track and activation detector 78−13346
^{65}Zn intermediate nucl., 37.4 excitation 77−3016
^{65}Zn odd-parity states from ^{62}Ni(α,nγ), γ study, energies, branching and mixing ratios, lifetimes 78−50120
^{66}Zn negative parity high spin states, spin and lifetimes from HI reactions 80−73768
^{66}Zn* composite particle emission, ang.-distribs., exciton-coalescence model from (d,X), (^{3}He,X), (α,X) 80−78265
^{66}Zn(α,2α), 90 MeV, strong absorption diffraction model, spectroscopic factors 79−22306
^{66}Zn(d,p)^{67}Zn, 12 MeV, levels, ang. distribs., spectroscopic factors meas. 77−22891
^{67}Zn 9/2$^+$ quadrupole moments, evaluation using antishielded field gradients 78−51951
^{67}Zn, alignment in Cu, temp. depend. rel. to radiation damage during PAC obs. 77−27919
^{67}Zn, appl. to Mossbauer meas. of gravitational red shift 78−24905
^{67}Zn, Coulomb excitation, gamma-ray spectra 79−9434
^{67}Zn, excited state lifetime, DSA meas. *(Russian)* 78−41668
^{67}Zn, γ spectroscopy of low spin states from ^{64}N(α,nγ), 8.2 MeV 78−78303
^{67}Zn, high spin states obs. in (α,nγ) 78−13016
^{67}Zn, Mossbauer effect 77−55737
^{67}Zn, Mossbauer obs. of quadrupole interaction in Zn metal 78−27120
^{67}Zn, populated in ^{64}Ni(α,n), level struct. below 2.0 MeV, γ-ray studies 78−62483
^{67}Zn, role of cluster-vibr., coupling in struct. of negative parity states 77−34206
^{67}Zn(α,f), 140 MeV, fission cross sections and probabilities, isomeric yield ratio 79−45308
^{67}Zn(d,p), low lying ^{68}Zn collective states, spectroscopic factors 77−61433
^{67}Zn(d,p)^{68}Zn, 12.3 MeV, tensor analysing powers 78−29479
^{68}Zn, 26 MeV levels from ^{69,71}Ga(d,^{3}He) 78−25112
^{68}Zn low lying collective states populated in ^{67}Zn(d,p), spectroscopic factors 77−61433
^{68}Zn low lying states, S-values from DWBA anal. of ^{64}Ni(^{6}Li, d) 79−36160
^{68}Zn muonic atom, dynamical E0 excitation, E0 resonances, muonic X-rays 80−95749
^{68}Zn(^{3}He,^{3}He), elastic and inelastic scatt. angular distrib. fine struct. 80−106063
^{68}Zn(^{6}Li,pn) in beam gamma-ray spectroscopy of ^{72}Ge levels 80−47343
^{68}Zn(α,α), 2$^+$ collective level excitation, microstruct. of diffr. ang. distrib. 77−61440
^{68}Zn(α,α), 38 MeV, correls. of optical pot. parameters for elastic scatt. 78−13117
^{68}Zn(α,pnγ)^{70}Ga, high spin levels of ^{70}Ga 77−30611
^{68}Zn(d,d), 10 and 12 MeV, polarised d elastic scatt., optical model anal. 79−36248
^{68}Zn(γ,p), 75-800 MeV, yield meas. by activation method 77−71605
^{69}Zn, energy levels, core coupling model calcs. 80−9238
^{69}Zn^m, nuclear quadrupole alignment 78−48090
^{70}Zn, 26 MeV levels from ^{69,71}Ga(d,^{4}He) 78−25112
^{70}Zn excitation energies, B(E2) values, extended generator coordinate method 77−6203
^{70}Zn, lifetime meas. by DSAM, using (α, 2nγ) reaction at E_α=30 MeV 78−8773
^{70}Zn(^{18}O,^{20}Ne)^{68}Ni, mass excess of ^{68}Ni 77−41878
^{70}Zn(p,p'), 3.825 MeV, E0 transition probability for 0_1^+-0^+ transition 77−41963
^{71}Zn^m decay, ^{71}Ga ang. correlations, level spin assignments and multipole mixing ratios 78−78305
^{73}Zn$_{g.s}$ spin from Ga(t,p) 79−54392
^{69m}Zn dosimetry, and permissible body burden 77−56474
^{69m}Zn, nucl. orient. in Zn metal, EFG 77−59492
Zn(α,α), A=64 and 66, 48 MeV, I.L. potential depth, optical model anal. 78−50187
Zn(α,p), A=64-70 even, 18 MeV, compound and pre-compound processes 77−34296
Zn(d,d), A=66, 67, 12.3 MeV polarised deuterons, precision tensor analysing power meas. 77−3019

nuclei with mass number 59 to 89 continued
Zn(e,e), nuclear radius, core polarisation and isotone shifts, muonic X-rays 80−22685
Zn(e,e') A=64, 66, 68' 100-275 MeV, levels, transition charge density 77−50077
Zn(γ,γ), 2754 keV photon Delbruck scatt. 79−67741
Zn(p,X), A=64, 66, 68, 17.5-48 MeV, proton total cross section 78−8809
Zn(p,γ)^{67,69}Ga, 3 MeV, γ-ray ang. distrib. 78−74353
Zn(p,p'), A=64-70 even, 12.5 MeV, compound and pre-compound processes 77−34296
Zr, A=86, 87, 88, high spin states 78−74383
Zr neutron deficient isotopes, studied via heavy ion induced compound reactions 77−57621
Zr-region, two nucleon transfer reactions, spectroscopic amplitudes, form factors, ang. distrib. 80−22779
^{A}Zr(n,γ), A=64, 66, 67, 68, 70, 2.8-500 keV, capture cross sections 80−57780
^{81}Zr, delayed proton spectra, $T_{1/2}$ meas. 77−38254
^{85}Zr yrast and high spin states of neutron deficient isotopes from Sr(α,xn) 80−73776
^{86}Zr, populated in ^{73}Ge(^{16}O,3n), lifetime meas. by Doppler shift method 78−25152
^{87}Zr, in-beam γ-ray spectroscopy of excited states 79−17852
^{88}Zr, spallogenic, radiochem. separation for photoneutron source 77−14296
^{88}Zr transitions and high spin states above 8^+ isomer, ^{86}Sr(α, 2nγ)^{88}Zr 79−40848
^{89}Zr allowed β-decay, K-electron capture/e^+ emission ratios 79−93557
^{89}Zr, electron capture decay lifetime in $BaTiO_3$, $PbZrO_3$ and ZrO_2 77−28523
^{89}Zr, electron capture to positron emission ratios determ. 77−18896
^{89}Zr, fine struct. of ground hole-state analogues 78−50065
^{89}Zr high spin states, J values, γ ang. distrib. from (α, 2nγ) and (α, nγ) 79−89217
^{89}Zr, IAS and bound hole states via ^{90}Zr(^{3}He, ^{4}He)^{89}Zr 39 MeV 78−492
^{85g}Zr→^{85}Y decay scheme, half life 77−34258

nuclei with mass number 90 to 149
36≤Z≤83 nuclei, neutron induced reactions, tables of cross sections and rate factors 77−46162
107<A<143, isomeric ratios for (n,2n) reactions at 14.8 MeV 78−13073
^{116}Sn(d,d), polarised d, 8.22 MeV, anal. power 80−5114
^{121}Sb, Mossbauer spectra in Sb-containing glasses 77−20764
^{145}Sm neutron separation and level exciton (n,γ) and (d,p) correlations 80−22756
^{147}Nd, level scheme from (n,γ) meas. 77−34232
^{148}Pm^{m,g} isomeric pair prod., in (d,2n), (p,n) and (α,pn) reacts. 77−88144
^{149}Nd, level scheme from (n,γ) meas. 77−34232
(^{6}Li,^{6}Li) 50.6 MeV elastic scatt. on A=12-208 nuclei, optical model parameters 77−18592
^{90}Y, 1^+ and 0^+ states populated in ^{88}Sr(^{3}He,p) 78−25116
A=105, nuclear data sheets, levels, decays and J^π assignments 79−93486
A=109 nuclei, data sheets (to October 1977) 79−9441
A=110, nuclear data sheets 78−66189
A=110 to 120, shell corrections to semi-empirical formulae for binding energy and radius *(Russian)* 78−78283
A=110-210 nuclei, new parameters of deformed Woods-Saxon pot. 78−93951
A=111 nuclei, nuclear struct. data sheets to February 1979 80−9193
A=112, experimental nuclear structure data to January 1979 80−98763
A=116-140 fission products far from β-stability, Q_β-values 77−22949
A=117 nuclear struct. data sheets to June 1978 79−36130
A=119, nuclear data sheets, level and decay props. 79−71780
A=120-150, levels and EM props., recent results 80−68592
A=121 nuclear data sheets, level schemes and decay properties 79−75818
A=123, experimental nuclear structure data to June 1979 80−94931
A=131 isobaric nuclides, formation in ^{238}U(p,X) 80−9293
A=134-144, fission yields from spectroscopic meas., γ-branching and half-lives 80−78213
A=135-143, odd A fission products, delayed n, decay studies and Q_β meas. 80−78227
A=136 nuclear data sheets, level schemes and decay props. 79−75819
A=140, nuclear data sheets, levels and transitions 80−31435
A=141, nuclear structure data sheets to 01 Sept. 1977 79−13184
A=141 nuclei, data sheets 79−6371
A=142, nuclear struct. data sheets to Oct. 1977 79−30769
A=144 nuclear data sheets, levels, decays and J^π assignments 79−93487
A=144 to 147 short-lived fission products, β-decay energies 77−22948
A=145, experimental nuclear structure data to August 1979 80−94932
A=147 nuclear struct. data sheets to May 1978 79−30770
A=148 nuclei, nuclear struct. data, level props. 77−67697
A=149, data sheets to August 1974 77−10305
A=149-155, systematics of α-particle energies of isotopes, N=84-87, 59≤Z≤76 *(Russian)* 77−14071
A=32 to 140, nuclear struct., binding energies, dipole moments *(French)* 77−46098
A=40 to 100, strength and radius parameters of deformed Woods-Saxon potential 79−97673
A=45-153, β^+-decay strength function maximum 79−75914
A=60-140, spherical nuclei, two phonon admixture effect on M1 resonance *(Russian)* 80−5105
A=75-93 fission products far from β-stability, Q_β-values 77−22949
A=76 to 101, subshell closure effects of nuclear binding energies 78−58230
A=88 to 99, fission probability, applicability of conventional systematics *(Russian)* 79−54464
A=88-96, collective treatment of pairing Hamiltonian, transfer data anal. 79−13220
A=90 region, core pol. effects and giant quadrupole resonances, HF and macroscopic calcs. 80−57756
A=90 region, N=50, shell model calcs. 80−68564
A=90 to 101 short-lived fission products, β-decay energies 77−22948
A=90 to 160 fission product neutron capture cross-section adjustment based on integral meas. 79−9578
A<100, average E1/M1 strength ratio 80−52621

nuclei with mass number 90 to 149 continued
A∼150, yrast states, deformed oscillator Hamiltonian calcs. 80−78126
A∼150 transitional region, collective props., interacting boson model 80−27538
A∼90 nuclei, isomeric states, spin polarisation, M4 transitions and giant resonances 80−63157
A = 143, nuclear data sheets, level energies, J^π assignments 79−30775
Ce, A=136, 137, 138, from (α,xn) reactions, high spin states and isomers obs. using in-beam γ-spectroscopy 78−82309
charge radii and binding energy per nucleon, linear relationship evidence 80−68520
Cr ^{130}Te+^{28}Si, diffusion model anal. of onset of friction 78−8848
deformed rare earth nuclei, bandcrossing in K≠0 bands, backbending 80−9204
delayed neutron spectra from precursors with A=79-130 77−82884
doorway state effect on neutron strength functions, shell model approach for 90<A<142 *(Russian)* 77−82888
doubly even nuclei, yrast band B(E2) values, hydrodynamical model and CAP effect 80−86793
emulsion+p, 400 GeV ang. distribs. of secondaries 79−36232
even actinides, two-nucleon transfer, first 0^+ collective state excitation, spectroscopic factor *(Russian)* 80−42530
even-even neutron-rich fission products, de-excitation spectra, β-decay, deformation 80−78203
even-even nuclei, 2_2^+ level deexcitation *(Russian)* 77−2939
even-even nuclei, 58≤A≤150, E2, M1 multipole mixing ratio, data survey 78−50118
even-even nuclei, z=6 to 100, probable members of quasi-bands in spherical and deformed regions 80−13357
even-even rare earths, microscopic quadrupole and hexadecapole moments 80−13376
even-even spherical nuclei, 2_1^+ state deformation parameter from (p,p) and EM excitation 80−27549
fission products yield from ^{239}Pu(n,f) 80−27678
(HI,X), rare earths, deeply inelastic transfer reactions, kinematic anal. 80−99186
high angular momentum fusion compound nucleus deexcitation, high spin states, rare earths 80−9259
high spin effects in nuclei with proton no. 40-60, shape, deforms. 78−503
internal conversion coefficients, 30≤Z≤104, Hartree-Fock-Slater model calcs. 79−36199
life sciences appl. 78−15882
magic and doubly magic nuclei, A=129, 131, 133 chains, 0^+ states, spectroscopy 80−78165
multipole excitation of doubly-open shell spherical nuclei 78−21507
N=50, odd-even effect in shell model 79−13217
N=50 isotones, transition probabilities, $1p_{3/2}$ and $0f_{5/2}$ hole excitation effects 80−47431
N=82 nuclei, elastic and inelastic polarised proton scatt., isobaric analogue states 77−74825
N=82 region, high spin isomers, cranked HF calcs., deformation shapes, excitation energies 80−99121
N=82 region, high spin isomers, deformation energy surface, shape constrained cranked HF theory 80−57666
N=83, odd-even nuclei, callective and noncollective excitations 79−36134
neutron-rich nuclei in A∼100 region, decay props. 77−22961
odd-odd fission products, level schemes, rot. bands, shell model states 80−78167
pairing correlation for fast rot. nuclei 78−78284
photospallation, 0.1 to 1 GeV, mass yield distrib. 80−73835
quadrupole collective model with γ-independ. pot. energy surface 77−61363
rapid automated nuclear chemistry, short lived fission products, reactor safety 80−81353
rare earth deformed nuclei, high spin region excited rot. bands, RPA calcs. 80−78108
rare earth metals, Mossbauer isomer shifts, book contrib. 79−87361
rare earth nuclei, high spin states from (HI, xn) reactions, discrete γ-transitions 80−5050
rare earth nuclei, modified oscillator pot. parameters, single particle levels 80−68509
rare earth nuclei, validity of pseudo SU(3) model 77−34240
rare earth nuclei, yrast traps, single particle effects 77−88031
rare earths, nuclear deformation, Coulomb displacement energy depend., shell model 80−102108
rare earths, pairing energy, single particle levels and interaction matrix elements 78−8721
rare earths, yrast band energy calcs., exponential model with pairing attenuation, backbending 79−9446
rare-earth isotopes, neutron deficient, β-decay and delayed protons 77−22953
rare-earth nuclei, back-bending phenomena, high spin states 78−74300
Sb, A=111, 3, 5, excited states anal. with Sn(p,2nγ)Sb 77−2911
separated fission products with A=88-144, delayed neutron spectra 77−34268
Sn Z=50 region isotopes, system struct calcs. 80−18192
spherical nuclei, Te to Sm, very high spin states, deform. energy surfaces 78−50079
vibration and rot. inertial functions, microscopic calc. for barium region 77−18448
Z=37-43, neutron rich fission products, mass energy surface, decay props. 80−78228
Z=50, p-h corrections to proton pairing vibrs. 77−57609
Z=55-63, odd proton nuclei, low lying even parity states 80−27551
(α,α'), A=40-208, low energy octupole resonances, 96 and 115 MeV 79−511
(d,^{6}Li), A∼60,116, L=0 transitions, cross sections, microscopic anal. 80−78189
(e,α), Z=29-79, direct and statistical effects, cross sections and ang. distribs. 79−530
(^{3}He,n), 25.4 MeV, N=82 nuclei, n ang. distrib., transitions, vibr. band search 79−63574
(n,γ), A=75 to 103, γ-strength functions and stat. model cross section calcs. 80−52612
(n,γ), A=94-190, resonance capture, low lying level population fluctuations, γ-rays 80−52619
(n,n), A=90 region, elastic, inelastic and total cross section, statistical model calcs. 80−68674

nuclei with mass number 90 to 149 continued
(n,n'γ), A=28-152, spherically doubly even nuclei, level excitation cross sections, statistical anal. *(Russian)* 79−67707
(n,X), fast n, ^{3}He emission cross sections for A=27-115 80−13475
(p,α) preformation coeffs. for mass range 27-123 77−54209
(p,n), 2.5-5.8 MeV, A=89-130, cross sections, sub-Coulomb proton anomalous optical pot. 80−32278
(p,n), A=89-130, anomalous optical pot. for sub-Coulomb protons 80−102190
(p,n), A=89-130, sub-Coulomb protons, anomalous optical pot. 80−102191
(p,n), A=90 region, reaction cross section, statistical model calcs. 80−68674
(p,n), anomalous optical potential for sub-Coulomb barrier protons, 2 particle 1 hole states 80−105948
(π$^-$,xnyp), E=0, medium nuclei in Z≃50 region, isomer yield ratios 77−71624
^{118}Sn+^{6}Li, α and d energy spectra, break up of ^{6}Li d+α clusters in nuclear field 78−46092
^{99}Tc^m compounds, chemically induced decay constant variation 78−93968
^{A}Si(d,X), A=112, 124, 7.6 GeV/C, isotopic cross section ratios, He, Li fragments isotopic effects *(Russian)* 80−63154
^{116}Sn(p,p), 0.8 GeV polarised p, differential cross section and analysing power data anal. 78−70526
^{134}Ba level scheme obs. from ^{134}La decay 77−10360
^{129}Xe, chem. shift in NO gas, chem. shielding 77−6706
^{127}I(p,xn) and ^{127}I(p,pxn), excitation functions, yields for ^{123}Xe prod. 78−594
^{105}→^{105}Pd, polarised nuclei, ^{105}Rh mag. moment, E2/M1 mixing ratios 77−6315
A=Rb, A=74-79, 90-99, direct meas. of masses, deformation onset at N=60 79−54383
A=101 nuclei, nuclear struct. data sheets to May 1979 80−41954
A=103 nuclei, nuclear struct. data sheets to July 1979 80−41955
^{109,111}Ag, particle-vibr. multiplet excit. by two-neutron stripping 77−34214
Ag (^{9}Be, ^{9}Be), 14-26 MeV, universal optical pot. 78−25219
Ag (α,x), 0.2-4.2 GeV/N, compression phenomena and Mach shock waves 80−22851
Ag (p,X), 400 GeV/c, multiplicity and ang. distribs. of relativistic and slow particles *(Russian)* 79−40931
Ag (π,αX), 70 MeV, α cross sections and energy spectra, intranuclear cascade calcs. 79−575
Ag, A=107, 9, +^{86}Kr, 618 MeV, γ-ray multiplicities and angular momentum fractionation 78−37370
Ag, A=109,111, proton hole states via ^{110,112}Cd(d,^{3}He) 50 MeV 77−18369
Ag, beta-generated external bremsstrahlung spectra 77−57625
Ag break-up in relativistic proton collisions, ^{4}He emission 77−10410
Ag, deform. of ground and excited states 78−82277
Ag, emulsion nuclei, 28 GeV proton interactions *(Korean)* 80−18299
Ag nuclei, highly excited, disintegration, photographic emulsion, quark model theory comparison 80−68560
Ag, odd-mass isotopes, 9/2$^+$→7/2$^+$ transitions, transition probabilities, half-lives 77−18475
Ag, proton-induced fission at 400 GeV, ternary to binary event ratio 78−13170
Ag, recoil energies of photoproduced ^{24}Na, 800 MeV bremsstrahlung 77−41953
Ag, resonance neutron self shielding factors, expts. and calcs. 77−42008
Ag, static mag. moments, spin, parity and excitation energy from nuclear orientation *(Dutch)* 79−80872
Ag+^{12}C, 25.2 GeV, target residue mass and charge distribs., calcs. 79−3172
Ag+^{20}Ne, 175 MeV, γ-ray multiplicities and energies, primary fragment angular momenta 78−46093
Ag+^{40}Ar, 340 MeV, binary aspects, particle multiplicities of fragments 78−70554
Ag+^{40}Ar deep inelastic reactions, γ-ray polarisation meas., neg. deflection angles 78−8845
Ag+^{40}Ar(^{86}Kr), γ-ray circular polarisation meas. 78−54788
Ag+^{84,86}Kr, 7.2 MeV/nucleon, nuclear relaxation phenomena, diffusion, orbiting 77−34338
Ag+^{9}Be, breakup of ^{9}Be in Coulomb field 78−50203
Ag+α, 720 MeV, correlated energy spectra of light fragments, fireball and coalescence models 78−62555
Ag+C, Ag+O, rarefaction of oblate shaped nuclear matter, hydrodynamics calcs. 78−89894
Ag+C(O), 0.2-4.2 GeV/N, compression phenomena and Mach shock waves 80−22851
Ag+Fe, hydrodynamic effects in cosmic ray nucleus-nucleus interactions 79−80176
Ag+Ne, 175 MeV, ang. mom. transfer meas. 77−30626
Ag+p, 1 to 28.5 GeV, production of 43≤A≤51 nuclides, reaction mechanisms 77−34301
Ag+p, 200 GeV, data anal. hydrodynamical model 79−551
Ag+p, 300 MeV, 450 MeV, 24 GeV, cross-section meas. 77−67740
Ag+p, 300 MeV, heavy fragment evaporation yields 79−6584
Ag+p, inelastic interactions, 6.0 GeV/c, in emulsions 78−86530
Ag(^{12}C, ^{12}C'), 50 GeV/c, multiplicities and ang. distribs. *(Russian)* 79−22323
Ag(^{12}C,X), 4.5 GeV/c, emission of short range particles (R<100 mkm) *(Russian)* 80−63202
Ag(^{12}C, spallation), 25.2 GeV, radionuclide prod. cross sections, charge dispersions and mass yield curves 79−67735
Ag(^{56}Fe,X), relativistic ^{56}Fe fragmentation, charge and mass changing cross sections 79−54453
Ag(Fe,f), central collisions, nucleon characteristics, nuclear pionisation in complete fission *(Russian)* 79−80963
Ag(K$^-$,f), 1.8 GeV, ternary, quaternary and cascade fission 79−63708
^{A}Ag, A=104, 106, levels, J$^\pi$, and isobaric analogue resonances from Pd(p,n) 80−32180
^{A}Ag, A=104,104m, characts. of the excited levels of ^{104}Pd 79−9515
^{A}Ag, A=105, 107, 109, 111, isomeric transition internal conversion, γ-transition energies and e intensities 79−6503
^{A}Ag, A=105,107, positive parity band, mixing and branching ratios lifetimes from (^{16}O,2np)(^{14}N,3n) 80−9197
^{A}Ag, A=105-109, negative parity states, vibr. versus rot. descriptions 80−73781

nuclei with mass number 90 to 149 continued
^{A}Ag, A=105-109, negative parity states, EM props. from particle-asymmetric rotor model 80−102097
^{A}Ag, A=113, 115, β-decay, ^{113,115}Cd low lying 7/2$^-$ state lifetime, triaxial rotor interpretation 80−47432
^{A}Ag, A=97, 98 and 99^{g,m} decay spectral meas. 78−93976
^{A}Ag A=99, 101, 103, levels, transitions and J$^\pi$ from Cd decay, Pd(p,2nγ) 80−47383
^{A}Ag+^{11}B, 86 MeV, A=107, 109 79−67766
^{A}Ag+^{40}Ar, 285 MeV, A=107, 109 79−67766
^{A}Ag(^{63}Cu,X)Y, A=107, 109, new Ir, Os and Re isotopes 78−70563
^{A}Ag(^{86}Kr, X), A=107, 109, γ-ray multiplicities from diffusion model with one body dissipation 79−6487
^{A}Ag(^{86}Kr,X), A=107,109, 620 Mev, deep inelastic scatt., ang. momentum transfer, γ-ray multiplicities 80−27665
^{A}Ag(p,n), A=107,109, 2.0-6.7 MeV, cross sections, Hauser-Feshbach optical calcs. for p absorption systematics 80−47483
^{A}Ag(p,p), A=107,109, 2.0-6.7 MeV, cross sections, Hauser-Feshbach optical calcs. for p absorption systematics 80−47483
^{100}Ag^{g,m} decay, ^{100}Pd levels and γ-transitions 80−83077
^{101}Ag, T$_{1/2}$ meas., decay scheme, ^{101}Pd levels 78−37311
^{103}Ag collective excitation and J$^\pi$ following ^{94}Mo(^{12}C,p2nγ), rotor-plus-particle model 80−86782
^{103}Ag high spin states, bands transitions, intermediate deformation Coriolis coupling from (^{3,4}He, xnγ) 80−105944
^{103}Ag levels and spectra from ^{103}Cd decay 79−22235
^{103}Ag→^{103}Pd, β-ground state feedings and branchings 80−102147
^{104}Ag, β$^+$ decay, ^{104}Pd energy levels, spins, parities 78−13018
^{104}Ag levels, J$^\pi$, T$_{1/2}$, bands and transitions from ^{103}Rh(α, 3nγ) 80−102093
^{105}Ag absolute transition probabilities from 53.2 keV level, half-life 79−49605
^{105}Ag β decay, ^{105}Pd level scheme 77−82849
^{105}Ag decay, energy levels, spin, parities, of populated ^{105}Pd states 78−37306
^{105}Ag decay, γ-ray spectra, γ-γ coincidence and ang. correl. meas. 78−13007
^{105}Ag, excited level struct. and transitions populated by decay of ^{105}Cd 79−97655
^{105}Ag, γ-transitions, level scheme via (p,nγ) reaction *(Russian)* 77−74801
^{105}Ag high spin states and bands, g-factor and isomeric state from ^{103}Rh(α, 2nγ) 79−36125
^{105}Ag, high spin states γ-single spectra, γγ coincidence, excitation functions, ang. distrib., polarisation meas. 78−21519
^{105}Ag, high spin states populated in ^{103}Rh(α,2n) 77−22936
^{106}Ag low-lying excited states from ^{103}Rh(α,nγ) and ^{104}Pd(α,pnγ) 80−57693
^{106}Ag^m, L/K ratios, Q-value 78−29426
^{106}Ag^m, mag. moment determ. from orientation meas. 77−10315
^{106}Ag^m decay, IC and γ-rays, ^{106}Pd energy states and J$^\pi$ 80−18197
^{107}Ag, comparison of absolute cross sections for electron and photon induced reactions, DWBA calc. test 77−41958
^{107}Ag high spin states, J$^\pi$ assignments, polarisations and transitions from (^{7}Li,4nγ), (^{6}Li,3nγ) 80−27536
^{107}Ag+^{11}B, deep inelastic transfer, decay of binary nuclear system 80−22848
^{107}Ag+^{40}Ar, deep inelastic transfer, decay of binary nuclear system 80−22848
^{107}Ag+p, 24 GeV/c, in nucl. emulsion, particle emission freq. variation 78−37335
^{107}Ag(α,f), 640MeV 80−95329
^{107}Ag(e,α), 100 MeV, energy spectra, cross sections 77−18529
^{107}Ag(n,2n), 14.6 MeV, cross-section meas. 79−59055
^{107}Ag(n,γ), cross sections for prod. of ^{108}Ag^m 79−29625
^{107}Ag(n,γ)^{108}Ag, coincidence meas. of low-lying states of 215.38 keV 78−12975
^{107}Ag(n,γ)^{108}Ag^m, in stainless-steel structure of high-power nuclear reactors 80−42747
^{107}Ag(n,n), 0.25-4.5 MeV, total, elastic and inelastic cross sections, optical-statistical anal. 80−27639
^{107}Ag(p,αX), 20-45 MeV, α spectra, exciton model anal. 80−18306
^{107}Ag(p,α), 20 to 44 MeV, energy spectra and α-particle angular distrib. 79−49630
^{107}Ag(p,n)^{107}Cd, preequilib. emission of neutrons, ang. distrib. 78−62542
^{108}Ag, form. in ^{107}Ag(n,γ) reaction, isomeric level scheme at 215.38 keV 78−12975
^{108}Ag levels and γ-transitions, population-spin correlation from ^{107}Ag(n,γ) 80−63097
^{108}Ag, low-lying states and state distrib. following ^{107}Ag(n,γ) 78−50084
^{108}Ag, populated in ^{108}Pd(p,nγ) level struct. 77−18392
^{108}Ag transition multipolarity and conversion electrons from ^{107}Ag(n,e$^-$) 80−52627
^{108}Ag^m, neutron cross-section for production from ^{107}Ag 79−29625
^{108}Ag^m, prod. in nuclear reactors by thermal neutron capture in stainless-steel structure 80−42747
^{108}Ag^m (127 yr.), K-electron capture probability, ^{108}Ag-^{108}Pd ground state mass difference 79−59038
^{108}Ag+p, 70 GeV/c central collisions, s-particles ave. multiplicity 78−21567
^{109}Ag (^{40}Ar, X), α-decay amplification in superdeformed nuclei, high ang. momentum deexcitation 80−22776
^{109}Ag, internal conversion of high-multipolarity transition 77−2945
^{109}Ag levels from ^{109}Pd decay, spins, γ cascades, mixing ratios 77−22930
^{109}Ag, NMR in solns. of Ag salts in organic solvents 77−16191
^{109}Ag^m decay, double K-shell vacancy creation per internal conversion 79−45212
^{109}Ag+^{11}B, deep inelastic transfer, decay of binary nuclear system 80−22848
^{109}Ag+^{40}Ar, 170-340 MeV, fission barriers at high ang. momenta 77−26786
^{109}Ag+^{40}Ar, 197 MeV, evaporation residue cross section calc. 78−50146
^{109}Ag+^{40}Ar, deep inelastic transfer, decay of binary nuclear system 80−22848
^{109}Ag+^{40}Ar, fusion excitation functions, dynamical model calc. 78−50224
^{109}Ag+^{40}Ar, reaction and fusion cross section calc. in boundary condition model 79−9656
^{109}Ag+^{86}Kr, 366-716 MeV, evaporation residue product cross sections 79−17947

nuclei with mass number 90 to 149 continued
^{109}Ag(^{40}Ar,X), fusion reactions, charge density asymmetry liquid drop model 80−63220
^{109}Ag(α,2nγ), γ studies, ^{111}In level struct., spin, parity 78−58249
^{109}Ag(p,n)^{109}Cd, 6 and 7 MeV, neutron spectra meas. *(Russian)* 78−54764
^{109}Ag(p,p′), pol.p, 6.06 MeV, anal. powers, large absorption pot., optical model 80−83092
^{110}Ag 118.718 keV isomer, low lying states and transitions, coincidence study from ^{109}Ag(n,γ) 80−73806
^{110}Ag, decay period, least square fitting, pocket calculator program with variable precision 80−67976
^{110}Ag low lying states, decay scheme and $T_{1/2}$ from ^{109}Ag(n,γ) 80−47393
^{110}Ag low-lying levels, from ^{109}Ag(n,γ) obs. 80−47422
^{110}Ag, populated in ^{110}Pd(p,nγ), level struct. 77−18392
^{110}Ag^{m} oriented, T-reversal test and struct. study 78−86505
^{110}Ag^{m} cascade decay, γ-γ linear polarisation direction correls., Ge detectors *(Japanese)* 78−41903
^{110}Ag^{m} decay, precise γ-ray spectroscopy 78−58251
^{110}Ag^{m} disintegration, scheme of ^{110}Cd *(French)* 78−58248
^{110}Ag^{m} orientated, β-ray asymmetry, Fermi/Gamow-Teller matrix element ratio 79−93562
^{111}Ag, 376.7 keV level lifetime, shape coexistence, γ-branching 78−551
^{111}Ag, absolute yields in ^{238}U neutron induced fission 79−49642
^{111}Ag, excited state lifetimes, γγ ang. correls. 77−6298
^{111}Ag, level scheme, daughter 74 s ^{111m}Ag to ^{111}Cd decay scheme 78−541
^{111}Ag, level struct. via ^{110}Pd(^{3}He,d)^{111}Ag 33.2 MeV 77−88045
^{111}Ag, production by ^{239}Pu fission, absolute yields 77−50167
^{113}Ag, 5.3 h decay scheme, ^{113}Cd level scheme 78−46028
^{115}Ag, 20 min decay scheme, ^{115}Cd level scheme 78−46029
^{122}Ag decay, struct. of neutron rich even-even Cd nuclei 78−66249
^{108m}Ag, γ-ray energies meas. for Ge(Li) detector calibration 80−27865
^{110m}Ag, fission product, amount in burnt-up HTR fuel *(German)* 78−25298
^{110m}Ag fission product, release from coated fuel particles in HTR, diffusion process 77−88228
^{110m}Ag, fission product release from HTGR 77−74939
^{110m}Ag, gamma transitions to ^{110}Cd 79−85401
^{110m}Ag, gamma-ray intensities, precision meas. 80−102139
^{110m}Ag release from coated particle fuel in HTR 77−74936
Ag(α,X), 16.5 GeV/c, inelastic cross sections, multiplicity, ang. and momentum distribs. 78−82359
Ag(α,X), 720 MeV, nuclear fragment prod. thermodynamic evaporation and firestreak description, pre-equilibrium emission 79−54426
Ag(α,X) X=p,d,t,^{3}He,^{4}He, 720 MeV, back-angle prod. of light ions, model calcs. 79−45280
Ag(α,f), fission fragments tracklength and ang. distribs., fission moment of inertia 77−50182
Ag(γ,X), X=p,d,t,^{3}He,^{4}He, cascade-evaporation 80−57770
Ag(γ,f), max. energy 580 MeV, track detector anal. 77−18640
Ag(γ,γ), 412, 468, 662 keV, elastic scatt. cross sections, Rayleigh scattering anal. 80−86898
Ag(γ,ω), cross section meas., comparison with theory 78−58261
Ag(n,γ), cross-section determ. by Fe filtered beam TOF method 77−23078
Ag(n,n′), 14.1 MeV, precompound processes 78−13093
Ag(p,X), X=N to Ar, 2.1 and 4.9 GeV, fragment energy spectra, Maxwellian functional form 78−70529
Ag(p,α)X, direct knockout model for fragmentation, (p,pα) predictions 80−18275
Ag(p,f), 1 GeV, binary fission, possible mass instability of correlated fragments 80−83133
Ag(p,f), 600 MeV, binary fission process 77−3060
Ag(p,f), 600 MeV, fragment energies, cross sections level density and barrier heights 80−42723
Ag(p,f), 600 MeV, mass yields in binary fission 78−8819
Ag(p,f), product event cross-sections at 14, 18, 23 GeV 77−10411
Ag(p, spallation), 300 GeV, radionuclide prod. cross sections, charge dispersions and mass yield curves 79−67735
Ag(π^-,X), charged heavy particle emission after pion capture *(Russian)* 80−69271
Ar(HI,X) 0.2-4.2 GeV/N, nonperipheral collisions, forward-backward asymmetry, compression phenomena 80−18329
Au+^{86}Kr, 724 MeV, coincidence meas., pre-equilibrium α-emission 78−33208
Ba, A=117, 119, 121, delayed proton emitters, positron-proton coincidence meas. 78−78326
Ba, A=134-138, average neutron cross sections, statistical and optical model calcs. 78−29458
Ba, A=144, 145, short lived fission product, $Q_{\bar{\beta}}$-value 78−37317
Ba and rare-earth neutron deficient isotopes, β^+ strength $T_{1/2}$, X-ray, γ-ray spectra 77−34260
Ba, charge radii and binding energy per nucleon, linear relationship evidence 80−68520
Ba fragments, differential ranges and ang. distribs. from ^{238}U(p,X) 79−67790
Ba isotopes, ang. momentum projected quasiboson states 78−41637
Ba isotopes, collective states, soln. of Schrodinger eqn. with Bohr Hamiltonian 77−67695
Ba isotopes, microscopic dynamic calc. of collective states 78−17075
Ba isotopes, neutron deficient, β-decay and delayed protons 77−22953
Ba isotopes, uptake and retention of ^{133}Ba and ^{140}Ba-^{140}La in mouse tissues, eye and skeleton doses 77−9276
Ba, neutron deficient, charge radii, moments, transitions and isomers, atomic beam laser spectroscopy 80−102141
Ba, neutron rich nuclei from N=82, energy level systematics 77−22896
Ba odd neutron isotopes, microscopic struct. of low lying collective excited states *(Japanese)* 79−3065
Ba odd-mass isotopes, A=125-133, high spin level systematics and triaxial shapes 77−22838
Ba, radioisotopes, at. beam laser spectroscopy, hyperfine struct., nucl. moments and radii 80−57678
Ba, shell model, SU_6(s,d) boson model, collective states struct. 78−54672
^{A}Ba,(A=134-138), quadrupole moments and change in mean square radii of charge distrib. 79−50154
^{A}Ba, A=122-125, low energy γ-data, β decay probabilities 79−499
^{A}Ba, A=126 to 135, charge radii, mag. dipole and elec. quadrupole moment 79−72436

nuclei with mass number 90 to 149 continued
^{A}Ba A=128, 131, 133, charge radii and nuclear moments 79−9460
^{A}Ba, A=130, 132, 134, 136, levels and EM props., ang. momentum projected quasiboson model 80−5067
^{A}Ba, A=131,133, l-forbidden M1 transitions, energy level lifetime meas. from La decay *(Russian)* 79−49603
^{A}Ba, A=132, 134, 136, negative parity states, J^{π}, transitions, DWBA anal. of Ba(p, t) 80−86810
^{A}Ba, A=134 to 138, 135, sensibility anal. of effect of key parameters of fission prod. conc. 79−30870
^{A}Ba, A=135,137, Coulomb excitation, transition probabilities, γ-rays and level collectivity from (^{16}O,^{16}O′), (α,α′) 80−78201
^{A}Ba, A=136, 138, M1 transition enhancement from neutron resonances quasiparticle-phonon model 79−9506
^{A}Ba, A=142, 144, onset of deformation in neutron-rich isotopes 79−93499
^{A}Ba, A=142,144,146, transition γ-γ ang. correlations, levels, J^{π}, mixing ratios 80−73823
^{A}Ba, A=143,146, expt. β-decay energy of neutron-rich nuclides 79−30808
^{A}Ba, A=143 to 148, β-decay half life meas. 79−67718
^{A}Ba, A=144 to 147, β-decay half life determ. 78−78318
^{A}Ba(γ,γ) A=136-8, 1.68-5.0 MeV, nuclear resonance fluorescence, levels transitions and spins 79−6543
^{123}Ba, high spin levels and bands from ^{114}Sn(^{12}C, 3n)^{123} Ba 79−45127
^{125}Ba, 7/2$^{\pm}$ states, populated in ^{116}Sn(^{12}C, 3n), explained by triaxial core model 78−37258
^{126}Ba backbending, shell model calc., pair realignment and Coriolis antipairing 80−32164
^{126}Ba, backbending and E2 transition strengths of yrast states 79−26363
^{126}Ba→^{126}Cs→^{126}Xe, meas. of decay spectra 77−6316
^{127}Ba high spin level structure studied via ^{118}Sn(^{12}C,3n)^{127}Ba 77−38226
^{128}Ba, charge radius determ. using Doppler free laser spectroscopy 77−71558
^{128}Ba, level scheme, near instability against γ-deformation via ^{128}La decay 77−82806
^{129}Ba, excitation and props. of high-spin levels using ^{120}Sn(^{12}C,3nγ) 78−17104
^{129}Ba, γ-ray linear polarisation meas. from ^{120}Sn(^{12}C,3n) 78−50121
^{129}Ba, struct. determ. from ^{129}La β-decay 79−22244
^{129}Ba, triaxial shape and high-spin bands obs. in ^{124}Sn(^{12}C,3n) 77−34219
^{131}Ba decay, ^{131}Cs level struct. obs. 77−10359
^{131}Ba, decay, electric monopole transitions 80−22752
^{131}Ba decay, gamma-ray spectra of ^{131}Cs 79−85400
^{131}Ba, L/K and M/L capture ratios 78−29425
^{131}Ba, magnetic mom. and charge determ. using Doppler free laser spectroscopy 77−71558
^{133}Ba, 12.34 keV M1 transition 80−106004
^{133}Ba decay data and standardisation 77−88081
^{134}Ba, inversion of 0^+ phonon states and γ softness 77−10364
^{134}Ba, reorientation effect and multiple Coulomb excitation meas. 77−61450
^{134}Ba+^{16}O, compound nucleus, ^{150}Gd, deexcitation, evaporation calcs. comparison with exptl. decay data 77−61391
^{134}Ba+^{16}O, formation and decay of ^{150}Gd compound nucleus 77−61453
^{135}Ba, nucl. mag. moments and ratios of quadrupole moments, NMR spectroscopy 77−73088
^{135}Ba, nucl. quadrupole moment, calc. using NQR, HFS and fine struct. data 78−50081
^{135}Ba^{m} yield in ^{133}Cs(α,pn) and ^{139}La(p,αn) reactions, depend. on energy of bombarding energy 80−5151
^{135}Ba(α,α′), 8-10 MeV Coulomb excitation, reduced E2 transition probabilities 78−13127
^{136}Ba, mag. moment of 2140.2 keV 5$^-$ state 79−59009
^{136}Ba(n,2n)^{135}Ba^{m}, 14.2 MeV, neutron activation cross sections 80−91180
^{137}Ba, nucl. mag. moments and ratios of quadrupole moments, NMR spectroscopy 77−73088
^{137}Ba, nucl. quadrupole moment, calc. using NQR, HFS and fine struct. data 78−50081
^{138}Ba, 14.7 MeV neutron capture cross-section measurements with activation technique 80−32282
^{138}Ba, 6^+ state, nucl. g-factor and nucl. spin relax. in Xe 77−22884
^{138}Ba, E(1) and E(2) transitions via (γ, γ) at E<5 MeV 77−74797
^{138}Ba+α, closed shell 82 neutron nucleus, B(E2)-values 78−66296
^{138}Ba(d,^{6}Li), 35 MeV, ang. distrib. meas., deduced α-particle spectroscopic factors, reduced widths, decay lifetimes 77−18571
^{138}Ba(d,γ), 5-26 MeV, experimental and calc. compound nucleus cross sections 79−76002
^{138}Ba(d,p), below and near Coulomb barrier 78−29483
^{138}Ba(γ,γ), E<MeV, E(1) and E(2) transitions 77−74797
^{138}Ba(γ,n), E1 and M1 radiative strength functions 77−22999
^{138}Ba(γ,π xn)La, 150-300 MeV, pion production cross sections calc. 80−9287
^{138}Ba(n,2n)^{137}Ba^{m}, (14.2±0.2) MeV, activation cross sections, Ge(Li) meas. 79−22278
^{138}Ba(n,α)^{135}Xe^{m,g}, 14.2 MeV, neutron activation cross sections 80−91180
^{138}Ba(n,γ), 30 keV, capture cross sections, stellar nucleosynthesis 80−42663
^{138}Ba(n,γ), resonance n capture cross section meas. 3 to 100 keV 79−93610
^{138}Ba(n,p), 14.2 MeV, neutron activation cross sections 80−91180
^{138}Ba(p,p′), 10-11.7 Mev polarised protons scatt. at IAR 77−2991
^{139}Ba β$^-$ decay into ^{139}La, γ-rays, energy levels 78−70492
^{139}Ba, first order forbidden β-decay, quasi-particle-phonon interaction calcs. 79−9514
^{139}Ba, fractional independent yield and γ-activity from ^{249}Cf(n,f) 79−89337
^{139}Ba, γ-ray emission profitabilities and half-life obs. 80−57723
^{139}Ba level scheme, J^{π} and γ-transitions from ^{139}Cs β-decay 80−42590
^{139}Ba reduced normalisation from ^{138}Ba(d,p) 78−86522
^{140}Ba, fission product, γ-ray emission probability 77−82862
^{140}Ba, fractional cumulative yield from ^{245}Cm(n,f) 80−63074
^{140}Ba, production by ^{239}Pu fission, absolute yields 77−50167
^{140}Ba, radioactive fallout in air and rain, results to end of 1977 78−82535
^{142}Ba, γγ ang. correlations, levels, spins and mixing ratios from ^{142}Cs decay 80−57734
^{143}Ba decay to ^{143}La, β-branching and log ft values 78−50129

nuclei with mass number 90 to 149 continued
^{143}Ba, nuclear spectroscopy of neutron rich A=143 nuclei 79−59039
^{144}Ba, beta and gamma spectra, level scheme 77−22962
^{145}Ba, fission product, β-decay anal. 78−78323
^{147}Ba, neutron rich nucleus identification, $T_{1/2}$ meas. 77−26633
^{148}Ba, neutron rich nucleus identification, $T_{1/2}$ meas. 77−26633
^{133m}Ba production for medical purposes by ^{133}Cs(d,2n)^{133m}Ba 77−60251
^{137m}Ba, internal conversion decay, double K-hole creation 77−18887
Ba(γ,γ), 412, 468, 662 keV, elastic scatt. cross sections, Rayleigh scattering anal. 80−86898
Ba(γ,γ')$_M$, 7.28, 7.63 MeV, ^{209}Bi, ^{139}La energy level anal. 78−13058
Ba(p,X)^{M}Xe (M=124-136), excitation functions, 38-600 MeV, lunar samples appl. 77−57661
^{209}Bi+^{136}Xe, 1130 MeV, statistical model for mass and charge distrib. 79−17929
^{209}Bi(n,2n)^{208}Bi, 14.1 MeV, ang. and spectral distribs. 78−82354
Br, isomer ratios in fission fragments at high excitation 80−32261
^{A}Br, A=89-91, delayed neutron emission probabilities, β-decay half-lives 80−83078
^{90}Br, experimental Q_β-values 78−93974
^{92}Br mass chain, half lives and n-emission probabilities of delayed-n precursors 78−70497
(^{12}C,X) on A=144-164, search for high spin isomeric states, shell effects 79−71784
^{107}Ca 21/2$^+$ 2679 keV three quasiparticle state, nuclear struct. of isomeric states using g-factor 77−88039
^{107,109}Cd in Ag, spin rotation amplitude, temp. depend. 78−43738
^{110,112}Cd(d,^{3}He) 50 MeV, populating Ag proton hole states 77−18369
Cd 2_1^+ excitation, α-spectroscopic factors in IBA model from Sn(d,^{6}Li) 80−105967
Cd, A=104 and 105, populated in α+Pd reactions, high spin states 78−62484
Cd, A=105 to 109, parity assignments from (^{16}O,xnγ) obs. 78−41630
Cd, A=106-112, L,J,π via (^{3}He,n) 25.4 MeV reaction to 0^+ states 77−50050
Cd, A=106-116, Q_{2+} mass depend. via Cd(α,α') and Cd(^{16}O,^{16}O') 77−18390
Cd, A=110, 112, isobaric analogue resonances, QRPA anal. of (p,p) reactions 78−576
Cd, A=110, 116, difference in nuclear charge radius, X-ray isotopic shift meas. 77−18382
Cd, A=110-116, charge distrib., self consistent calc. *(Russian)* 77−38234
Cd, A=97, 99, β delayed proton emission, spectra, branching ratio, half life 78−86517
Cd, α-spectroscopic factors from (d, ^{6}Li) 80−534
Cd covered U-mica system, neutron dosimetric meas. using fission fragment track technique 78−13347
Cd decay and half life, ^{A}Ag A=99, 101, 103, levels, transitions and J$^\pi$ 80−47383
Cd, even isotopes, effect of residual interaction in particle-particle channel on low-lying states 78−21503
Cd, even nuclei, systematic meas. of mag. moments of 2_1^+ states 78−54682
Cd even-even nuclei, low lying collective states, two-photon character 80−57667
Cd, even-mass, B(E2) and Q(2_1^+) via (e,e') 68, 112 MeV scatt. 77−71585
Cd, even-mass, shape coexistence, quasi-rot. band 78−496
Cd even-mass isotopes, vibr. excitations 77−54129
Cd, isotopes A=109, 106, 105, 104, high spin states excited by (α,xnγ) *(French)* 78−29394
Cd, multipole-multipole interaction in particle-particle channel 79−6364
Cd, neutron capture gamma spectra, for neutron thermometry 79−30837
Cd, quadrupole moments of first excited states of even isotopes 78−17099
Cd stable even-A isotopes 106-116, neutron capture resonance parameters and cross sections 78−50161
Cd stable isotopes, yields in ^{235}U(n_{th},f) and ^{239}Pu(n_{th},f) in symm. region 77−34358
Cd:^{113}Sn, quadrupole interaction temp. depend. 77−8469
Cd+p, 7 GeV/c hadron multiple prod. *(Russian)* 79−22298
Cd+π$^-$, 7 GeV/c hadron multiple prod. *(Russian)* 79−22298
^{1}Cd, A=113, 115 from ^{113,115}Ag β-decay 80−47432
^{A}Cd, (A=106, 108, 110, 112, 114, 116, 118), so-called two phonon states, quasiparticle shell model calcs. 79−89251
^{A}Cd, A=104-116, low lying level scheme, mass excess from Cd(p,t) 80−73807
^{A}Cd, A=105,107,109,111, odd neutron deficient, rotor+particle model anal. 79−36127
^{A}Cd, A=107, 109, 111, from Pd(α,3nγ)Cd, high spin states obs. 80−450
^{A}Cd, A=110, 112, 114, 116 nuclear charge radius differences 79−26365
^{A}Cd, A=111,112, pionic atoms, E2 nuclear resonance effects 79−76534
^{A}Cd, A=111,115, deeply bound hole state transition strength giant resonance, DWBA anal. of (p,d) 80−47426
^{A}Cd, A=111-115, electric quadrupole moments, nonadiabatic rot. model calcs. 79−6389
^{A}Cd, A=112, 114, 0_2^+ and 0_3^+ states, E0, E2 transitions and collectivity 80−102144
^{A}Cd, A=98,102,106,110, deformation energy curves, HF calc. with Skyrme effective force 79−36127
^{A}Cd, static quadrupole moments determ. for A=111, 113, 115 78−37281
^{A}Cd(^{16}O,^{16}O'), 44 MeV, A=112, 114, 0_2^+, 0_3^+ state collectivity, E0 and E2 decay, $T_{1/2}$ 80−73784
^{A}Cd(^{63}Cu,X)Y, A=106, 108, 110, new Ir, Os and Re isotopes 78−70563
^{A}Cd(n,nγ) A=114,116, energy levels, spins, and gamma-ray multipole mixing ratios investig. 80−52580
^{A}Cd(p,t), A=106, 104, at high excitation, observation of hole states 78−25187
^{100}Cd(d,p), pol. d, excitation curve isospin anomaly, neutron single particle resonances 80−27595
^{103}Cd decay, ^{103}Ag levels and spectra 79−22235
^{103}Cd levels, J$^\pi$ and positive parity decoupled band, rotor anal. of ^{94}Mo(^{12}C, 3nγ) 80−102096
^{103}Cd levels and spectra from ^{103}In decay 79−22235
^{103}Cd→^{103}Ag, β-ground state feedings and branchings 80−102147
^{104}Cd, (p,t) study at 42 MeV, hole states at high excitation 78−50158
nuclei with mass number 90 to 149 continued
^{104}Cd, $\beta^+/(EC+\beta^+)$ probability ratio, EC decay energies, mass excesses 80−27543
^{104}Cd quasirot. ground state band and γ-transition from ^{102}Pd(α,2nγ) 80−105955
^{105}Cd decay, ^{105}Ag, excited level struct. and transitions 79−97655
^{106}Cd collective and yrast levels, γ-transitions, 2 quasiparticle+rotor model from (heavy ion, xnγ) 79−22169
^{106}Cd, high-spin states via γ-spectra populated in ^{104}Pd(α,2nγ) 77−30508
^{106}Cd, total neutron cross section meas. below 1.5 keV 77−26743
^{106}Cd(n,t)Ag, 14.6 MeV, production cross sections 79−49629
^{106}Cd(p,p'), 10, 12 MeV, compound nucleus lifetime by X-ray spectroscopy 80−22831
^{107}Cd, g-factor of 845.6 keV state, differential PAC 77−6225
^{107}Cd, heavy ion nucl. alignment, recoil in vac., time-differential meas. 78−37304
^{107}Cd, quadrupole interaction of $11^-/2$ states in Cd 77−8468
^{108}Cd levels from ^{96}Zr(^{16}O, 4nγ), γ meas., decay scheme, band struct. 78−66301
^{109}Cd, 11 μs isomeric level, spin and parity determ. by ^{108}Pd(α,3n) *(French)* 78−8738
^{109}Cd β-decay surface contamination monitoring probes, comparison of response between detectors 78−25398
^{109}Cd, correlated radiation damage in Ag, TDPAC 78−43739
^{109}Cd decay, double K-shell vacancy creation per internal conversion 79−45212
^{109}Cd, double K-shell vacancy creation probability 77−54182
^{109}Cd EC decay data revision 80−5095
^{109}Cd, gamma-ray precision energy meas. 78−58533
^{109}Cd, LX-, LX-coincidences during decay 78−17149
^{109}Cd, low lying level struct. via γ-γ correls. following ^{109}In decay 77−30509
^{109}Cd nuclear transformation rate meas. using 4π proportional counter 78−21826
^{109}Cd, production in nuclear reactors by neutron irrad. of ^{107}Ag 80−52798
^{109}Cd(n,α), thermal, cross-sections meas. 78−94012
^{110}Cd, collective excitations in the interacting boson model *(Russian)* 80−5044
^{110}Cd, γ-ray spectra using coincidence and sum method *(French)* 78−62675
^{110}Cd level scheme from ^{110}Ag^m *(French)* 78−58248
^{110}Cd, n spectra of isobaric analogue resonance decay from ^{109}Ag(p,n)^{109}Cd *(Russian)* 78−89841
^{110}Cd, O^+ bands from cluster-vibration coupling, semimicroscopic mechanism for band mixing 79−36121
^{110}Cd, recoiling in Fe, enhanced transient fields 78−37284
^{110}Cd, transition determ. in ^{110}Ag^m spectroscopy 78−58251
^{110}Cd(n,n'γ), fast reactor neutrons, γ-ray ang. distrib. 77−6287
^{110}Cd(p,γ), γ-22 MeV differential cross-section meas. 79−93617
^{110}Cd(p,n)^{110m,g}In, anal. of isomer ratios in preequilibrium statistical model 77−6361
^{111}Cd, 1330 keV level excitation cross section from positron annihilation 80−68583
^{111}Cd $5/2^+$ quadrupole moments, evaluation using antishielded field gradients 78−51951
^{111}Cd, elec. field gradient in Zn and Sn hosts, press. depend., TDPAC expts. 78−48092
^{111}Cd, elec. quadrupole moment from elec. field gradients of trans-dimethyl organometallic moieties 80−29371
^{111}Cd, excitation by photon less positron annhilation, isomeric γ-transitions *(Russian)* 80−5089
^{111}Cd, hyperfine field in Heusler alloys, TDPAC meas. 78−43705
^{111}Cd, hyperfine field polarisation in Dy, TDPAC 77−73106
^{111}Cd, hyperfine interaction in Ag, dose-rate depend. and annealing props. rel. to PAC obs. 77−27920
^{111}Cd in Ag-Sn, electric quadrupole interaction, time depend. PAC 77−16229
^{111}Cd in antiferromag. transition metal salts, hyperfine fields, PAC meas. 77−48104
^{111}Cd, in Be, quadrupole interaction, temp. depend., TDPAC obs. 77−20772
^{111}Cd in RIn_3, RSn_3, quadrupole coupling consts. and valence states, PAC meas. 77−48102
^{111}Cd, mag. hyperfine field in $Ni_{1+x}MnSb$, TDPAC obs. 78−43709
^{111}Cd, nucl. orientation coeffs. with axially symm. elec. field gradient 80−97168
^{111}Cd, PAC in liq. In and In-Bi alloys 77−4584
^{111}Cd, PAC meas. for recoil damage in InSb and InP 77−89484
^{111}Cd, pionic, E2 nuclear resonance effects 78−29868
^{111}Cd, quad. interac. temp. depend. in Sb 77−59487
^{111}Cd, quad. interac. temp. depend. in Te 77−63324
^{111}Cd, quadrupole hyperfine interaction in Cd, effect of radiation defect annealing 78−43741
^{111}Cd, quadrupole interaction in Be, temp. depend. 77−8466
^{111}Cd, quadrupole interaction in Pd rel. to radiation damage during DPAD expts. 77−27917
^{111}Cd, TDPAC in dilute Ag-Cu(Sn) alloys, EFGs at impurities 77−16213
^{111}Cd, TDPAC meas. in Ag_xCd_y, Ag_xAl_y, Ag_xZn_y 77−28492
^{111}Cd^m, nuclear orientation in Zn and Be, 245 keV state quadrupole moment, half-life 80−37324
^{111}Cd(γ,γ), isomeric states excitation, integral cross sections 80−27528
^{111}Cd(n,γ), meas. of absolute partial p-wave capture cross-section 77−34307
^{111}Cd(n,n')^{111m}Cd, 13-17 MeV, cross section meas. by activation method 78−46057
^{111}Cd(p,nγ)^{111}In, E_p=6 MeV, γ-ray spectra and ^{111}In level scheme 78−13083
^{112}Cd, $0_1^+ \rightarrow 0^+$ elec. monopole transition in low-lying ^{112}Cd levels prod. in ^{112}I decay 79−54406
^{112}Cd, E0 transition from o_1^+ state following ^{112}In beta decay 80−68578
^{112}Cd, negative parity yrast band, E1 transitions polarisability, quadrupole-octupole coupled vibr. system 79−484
^{112}Cd, pionic atoms, dynamical nuclear polarisation, nuclear structure effects 79−94113
^{112}Cd, pionic E2 nuclear resonance effects 78−29868
^{112}Cd(n,2n), 13-18 MeV, compound nucleus and precompound emission models 77−74841
^{112}Cd(n,n'γ), fast reactor neutrons, γ-ray ang. distrib. 77−6287

nuclei with mass number 90 to 149 continued
^{112}Cd(n,p)^{112}Ag, 13-17 MeV, cross section meas. by activation method 78−46057
^{112}Cd(p,α)^{109}Ag, 22 MeV, analysing power, J-depend., DWBA 78−70523
^{112}Cd(p,n)^{112m,g}In, anal. of isomer ratios in preequilibrium statistical model 77−6361
^{112}Cd(p,p′), 30 MeV polarised proton inelastic scatt., phonon states 77−2982
^{113}Cd, level scheme from ^{113}Ag 5.3 h β-decay 78−46028
^{113}Cd(n,γ), meas. of absolute partial p-wave capture cross-section 77−34307
^{113}Cd(p,n), 11.2 MeV, spin cut-off parameters from neutron ang. distribs. *(Russian)* 79−80940
^{114}Cd, neutron binding energy precision meas. 80−18182
^{114}Cd proton hole states populated in ^{115}In(d,^{3}He), DWBA anal. 78−8829
^{114}Cd, total neutron cross section meas. below 1.5 keV 77−26743
^{114}Cd(α,α) (elast. and inelast.), 21 MeV, Coulomb-nuclear interference calcs. 79−26444
^{114}Cd(e,e′), 40-110 MeV, vibr. nuclei, branching ratios 77−6356
^{114}Cd(n,e^{+}e^{-}), thermal 77−26624
^{114}Cd(n,t)^{112}Ag, 14.6 MeV neutrons, activation cross section meas. 79−45254
^{114}Cd(p,p′), 11 MeV, polarised p, differential cross sections, anal. powers, spin flip prob. 79−89284
^{114}Cd(p,p′), optical pot. deform. effect on analysing power and p-γ ang. correlations 79−17903
^{115}Cd, level scheme from ^{115}Ag 20 min decay 78−46029
^{115}Cd^{g} 852 keV first forbidden β-transition, ^{115}In 597 keV level J$^{\pi}$ assignment 79−80900
^{115}Cd^{m,g}, decay to ^{115}In, decay scheme, unified model description of odd mass In nuclei 78−66251
^{116}Cd(^{16}O,^{16}O′γ), 33 MeV, quadrupole moments determ. 77−41887
^{116}Cd(^{3}He,n), second order processes in DWBA calcs. 78−46076
^{116}Cd(α,α′γ), 8.5 MeV, quadrupole moments determ. 77−41887
^{116}Cd(d,n)^{117m,g}In, excitation functions 78−13105
^{116}Cd(p,p′γ), 5-20 MeV, lowest 3^{-} collective level identification from decay excitation function 79−9444
^{116}Cd(p,t), 22 MeV, polarised p, anal. power systematic nuclear struct. depend. 79−22265
^{117}Cd isomer decay, ^{117}In level scheme, J$^{\pi}$ and transitions 80−32193
^{122}Cd, struct. determ. from ^{122}Ag β-decay 78−66249
^{126}Cd, mass separated, decay scheme and half life, ^{126}In levels 79−3117
^{133}Cd NMR Knight shift, in n-CdSe impurity carrier wavefunction 78−35049
^{119g,m}Cd, decay schemes, half-lives, excited levels 77−296
Cd(α,2nγ), 17-33 MeV, ^{112,114,116,118}Sn collective bands, spin, parity, γ meas. 78−54719
Cd(d,xn), $E_d \leq 27.5$ MeV, cross sections for form. of ^{114m}In and ^{116m}In 80−13482
Cd(e,e′) for even-mass isotopes, 68, 112 MeV, B(E2) and Q(2_1^+) 77−71585
Cd(γ,γ), 412, 468, 662 keV, elastic scatt. cross sections, Rayleigh scattering anal. 80−86898
Cd(γ,γ) differential cross sections, 244 to 1408 keV 79−49618
Cd(γ,γ′), 7.28, 7.63 MeV, ^{209}Bi, ^{139}La energy level anal. 78−13058
Cd(γ,n), photoneutron Q-value determinations using monochromatic photons 79−22271
Cd(n,n′γ), A=114,6, E=2.67 MeV, ang. distribs. meas., 3^{-} octupole states anal. 77−38275
Cd(n,nγ), γ spectra and ang. distrib., ^{114,116}Cd energy levels, spins, particles 77−88070
Cd(p,nγ), ^{111,113}In energy levels, spins, lifetimes, Hauser-Feshbach anal. 77−320
Cd(p,p)Cd, A=110, 112, 5-9 MeV, isobaric analogue reson., QRPA calc. 78−576
Cd(π^{-}, X), 0 MeV, A=111, 112, E2 nuclear resonance effects, γ and X-ray meas. 78−41774
Ce (n,2n) react. cross sections at 14.8 MeV 78−74355
Ce, A=137, 139, high spin levels, γ spectra, hole-core coupling 77−50063
Ce, A=140,142, radiative strength functions in spherical nuclei, giant dipole resonance influence 78−89774
Ce, A=145, 147, 148, short lived fission product, Q_β-value 78−37317
Ce band structures populated in ^{116,118}Sn(^{16}O,3n), high spin levels, yrast cascade 78−8842
Ce, fast neutron capture and the microscopic isovector optical potential 79−63668
Ce isotopes, half-life meas. 77−6311
Ce isotopes, neutron rich, decay properties 78−13032
^{A}Ce, A=124-127, half lives, low energy γ-data, β decay probabilities 79−499
^{A}Ce(n,γ), A=140, 142, 30 keV, capture cross sections, stellar nucleosynthesis 80−42663
^{133}Ce, 5-h isomer β-decay, ^{133}La level struct., parity levels, decoupled band struct. 79−9476
^{134}Ce, γ-ray emission, excited levels of ^{134}La determ. 77−6290
^{135}Ce, yrast cascade dipole component from ^{122}Sn(^{16}O,4n) 80−9266
^{136}Ce, 10^{+} isomeric states, systematic behaviour 79−30791
^{138}Ce, ^{139}Ce, high-spin states, lifetime meas. using (α,xn) reactions 77−18476
^{138}Ce(^{37}Fe,X), fusion reactions, charge density asymmetry liquid drop model 80−63220
^{139}Ce, half-life determ. 77−34498
^{139}Ce→^{139}La, internat. comparison of activity meas. March 1976 79−13613
^{140}Ce, 6.2-15.6 MeV, gamma-ray spectra, cross-section meas. 78−33176
^{140}Ce γ-spectra, E1 and M1 hindrance factors from ^{143}Nd(n,γα) 80−37386
^{140}Ce, hexadecapole motion obs. from α-scatt., EM transitions and conversion electron spectra 78−25097
^{140}Ce, M1 transitions, theory of finite Fermi systems *(Russian)* 77−6296
^{140}Ce+α, closed shell 82 neutron nucleus, B(E2)-values 78−66296
^{140}Ce+n, 20-240 keV total cross section, resonance multilevel shape anal., level spacings 79−3148
^{140}Ce(N,γ$_0$), 2-10 MeV, giant M1 resonance in direct-semidirect model 79−17898
^{140}Ce(d,p), below and near Coulomb barrier 78−29483

nuclei with mass number 90 to 149 continued
^{140}Ce(d,p)^{141}Ce, 17 MeV, spectra and ang. distrib. obs., DWBA anal. 77−38283
^{140}Ce(e,e′), 50-92 MeV, E0, E1, E2, E3 and E4 giant resonances, cross section, shell model anal. 79−54423
^{140}Ce(e,e′), giant dipole resonance, E1 form factor and breathing mode existence 79−3125
^{140}Ce(γ,n) E1 and M1 radiative strength functions 77−22999
^{140}Ce(n,γ), resonance n capture cross section meas. 3 to 100 keV 79−93610
^{140}Ce(p,X), 17.5-48 MeV, proton total cross section 78−8809
^{140}Ce(p,p′), 30 MeV, DWBA, Ce levels, spin, parity, deform. parameters, enhancement factors 77−54217
^{141}Ce collective M1 excitation effects on γ-ang. distribs., direct semidirect model of ^{140}Ce(n,γ) 80−57733
^{141}Ce decay, internal conversion coefficient, efficiency extrapolation technique 79−30806
^{141}Ce, γ-decay, levels, J$^{\pi}$, branching via ^{140}Ce(d,pγ) 8 MeV 77−14064
^{141}Ce, half-life determ. 77−34498
^{141}Ce levels, single neutron holes, spectroscopic factors, DWBA anal. of ^{142}Ce(d,t), (^{3}He,α) 79−85353
^{141}Ce reduced normalisation from ^{140}Ce(d,p) 78−86522
^{141}Ce, spin-parity assignments from ^{140}Ce(d,p)^{141}Ce 77−38283
^{142}Ce(α,2n)^{144}Nd, high-spin states of ^{144}Nd anal. 77−82940
^{143}Ce, 1404 keV beta transition, spectral shape, ^{143}Pr 57 keV state 78−74339
^{143}Ce quasi-$f_{7/2}$ low lying states spectroscopic factors, cluster-vibr. model from ^{142}Ce(d,p) 80−47391
^{143}Ce, shape of 1110 keV β transition to ^{143}Pr 351 keV level, spin, parity 77−50085
^{144}Ce, 0^{-}→0^{+} beta transition spectral shape anal. 77−38246
^{144}Ce, 284.3 D, decay scheme, energy levels and transitions in ^{144}Pr 77−14070
^{144}Ce, e-γ and e-e coincidences, improved detection system 80−52605
^{144}Ce gamma active spikants in nuclear fuel for proliferation deterrence, practical aspects 79−93716
^{144}Ce, gamma-ray precision energy meas. 78−58533
^{144}Ce in low level radioactive liquid waste, chem. treatments, removal efficiencies 77−54351
^{144}Ce level scheme determ. 77−22962
^{144}Ce levels from ^{144}La decay 80−13417
^{144}Ce, low energy conversion lines resolution using fast discriminator cct. 80−5450
^{144}Ce photoneutron sources, determ. of standard neutron yield, influence of bremsstrahlung 79−72177
^{145}Ce, fission product, β-decay anal. 78−78323
^{149}Ce, β-decay half life meas. 79−67718
^{149}Ce, fission product, γ-spectra, half-life meas. 77−38240
^{139m}Ce, internal conversion of N=81 isotones 78−13027
Ce(d,^{6}Li), (A=140, 142), 35 MeV, ang. distrib. meas., deduced α-particle spectroscopic factors, reduced widths, decay lifetimes 77−18571
Ce(γ,γ), 2754 keV photon Delbruck scatt. 79−67741
Ce(γ,γ′), 7.28, 7.63 MeV, ^{209}Bi, ^{139}La energy level anal. 78−13058
Ce(γ,n), 30 to 140 MeV, partial photoneutron cross section, total cross section approx. 80−22809
Ce(n,n′) 1.8 meV to 1.8 eV, total neutron cross-section meas. using TOF spectrometry 79−85466
Ce(p,t), 30 MeV, DWBA, ^{138,140}Ce levels, spin, parity, enhancement factors 77−54217
^{252}Cf, spontaneous fission product charge distrib. 78−13176
^{137}Co, gamma radioactive source, buildup factor determination for meas. in air *(Rumanian)* 78−49132
^{141}Cr(γ,γ′), 7.28, 7.63 MeV, ^{209}Bi, ^{139}La energy level anal. 78−13058
Cs, A=114-118, neutron deficient isotopes, half lives, β^{+},γ, delayed p and α meas. 78−70489
Cs, A=116-120, spectra of delayed protons and α-particles in β^{+} decay *(Russian)* 78−46034
Cs, A=118,120,122, ground isomeric states, β-decay, $T_{1/2}$, γ- and CE-spectra 77−57601
Cs, A=119, 121, 123, 125, deformed 9/2^{+} proton hole states 78−41620
Cs, A=134, 137, distrib. in Peach Bottom HTGR primary coolant circuit 78−13275
Cs, A=141-145, delayed-neutron emission probabilities 77−74817
Cs β-decay, ^{A}Xe, A=122,124,126,128, 0^{+} excited state spin assignments and transitions 79−67649
Cs, deformed nuclei, low-lying positive parity states 77−6240
Cs, fission fragment, delayed neutron branches from γ-spectroscopy 80−78230
Cs, fission product, release and diffusion in fuel elements *(German)* 78−25298
Cs, ground state spins, moments, charge radii by laser spectroscopy 80−78147
Cs isotope, neutron deficient, supermultiplet mass predictions 79−85359
Cs isotopes, delayed neutron Pn-values, beta+neutron+gamma decay modes 77−26639
Cs isotopes, nucl. spins and mag. moments, atomic-beam mag. reson. expt. 78−17097
Cs isotopes, strongly deformed shapes from mag. mom. and spin meas. 78−70444
Cs isotopes decay, Xe level schemes and quasi-rotational bands 77−22839
Cs isotopic distrib. anal., for ^{11}B and ^{22}Ne-induced fission of ^{238}U 77−18634
Cs isotopic distrib. meas. for ^{11}B and ^{22}Ne-induced fission of ^{238}U 77−18633
Cs, low-lying collective states anal. 77−88030
Cs neutron deficient isotopes, beta-decay energies and masses 77−22946
Cs neutron deficient isotopes, beta-decay, Xe low lying levels 77−22947
Cs neutron rich isoptopes, nucl. spins and mag. moments 80−47367
Cs, neutron rich isotopes, $Q_\beta$and direct mass meas. 80−78132
Cs precursors, half lives and delayed neutron emission probabilities 79−49610
Cs radioisotopes, hyperfine spectroscopy, nucl. charge radius, ground and isomeric states 80−57677
Cs relative and independ. fission yields from ^{235}U(n,f) 80−27679
Cs relative independ. yield from ^{232}Th(p,f) 80−102218
Cs release and transport in coated HTGR fuel particles 77−74935
Cs release in Biso-coated HTR fuel particles 77−79441
Cs, short-lived isotopes, spin and mag. moment meas. from atomic-beams 77−22882
Cs, spin and mag. moment, trends in neutron deficient nuclei 78−37261

nuclei with mass number 90 to 149 continued
Cs transport and isotopic fractional in fuel rods 78−82453
Cs, A=117-124, 126, 138, 140-147, direct meas. of masses, deformation onset at N=60 79−54383
Cs, A=119, 121, 123, 125, collective props. and level schemes from (^{10}B,p2n), (^{14}N,3n) (^{10}B,3n) 79−22171
Cs, A=119-133 odd isotopes, collective props., bands and transitions from heavy ion reactions 80−68512
Cs, A=121, 123, 125, $g_{9/2}$ and $h_{11/2}$ bands 78−50067
Cs A=127, 129, 131, 133, high spin state and collective properties from (^{10}B, 3n), (α, 2n) (^{6}Li, 3n) 79−22170
Cs, A=133, 137-139, hyperfine struct., isotope shifts, nuclear moments and radii, laser spectroscopy 79−10071
Cs, A=133 to 137, sensibility anal. of effect of key parameters of fission prod. conc. 79−30870
Cs, A=138 to 142, nucl. moments and charge radii changes from hyperfine struct. and isotope shifts 79−17804
Cs, A=139-144, beta endpoint energy measurements 78−93975
Cs, A=141-145, β-delayed neutron emission probabilities, half-life 80−52634
Cs, A=142, 144, 146, low lying levels, J^π, mixing ratios and γ-γ ang. correlations 80−102119
Cs, A=142-146, β-decay half life meas. 79−67718
Cs, A=144-147, β-decay half life determ. 78−78318
Cs, A=147, 148, $T_{1/2}$ determ. 79−9524
^{114}Cs β-decay, half life and branching ratio, ^{114}Xe excited states and γ-rays 80−47436
^{114}Cs, neutron deficient isotopes from ^{58}Ni(^{58}Ni,xpyn), alpha decay studies 79−93567
^{116}Cs decay, ^{116}Xe quasi-rotational bands, levels J^π and $T_{1/2}$ 80−83021
^{116}Cs, delayed particle emission in β^+ decay 78−8778
^{118}Cs, delayed particle emission in β^- decay 78−8778
^{119}Cs, new isomer, I=3/2, determ. in on-line ABMR expts. 78−70444
^{119}Cs, short-lived, determ. of nucl. spins by β radiation detected optical pumping 78−37262
^{119}Cs, spin of neutron deficient nucleus by β radiation detected optical pumping 78−8782
^{120}Cs, mag. mom. determ. in on-line ABMR expts. 78−70444
^{123}Cs, decoupled band obs. by in-beam γ-ray spectra of ^{115}In(^{12}C,4n) 78−21520
^{123}Cs(^{123m}Cs), gamma and conversion electron radiation 80−106017
^{123}Cs→^{123}Xe→^{123}I, generator prod. for radiopharmaceutical appls., high energy alpha reactions 77−37053
^{124}Cs, β-decay, ^{124}Xe level struct. 78−13033
^{124}Cs, β-decay props. of collective 1^+ states 78−13028
^{126}Cs, β-decay props. of collective 1^+ states 78−13028
^{126}Cs, EC and β^+-decay, exam. of Xe nuclear level struct. 78−21498
^{127}Cs, 66-keV decay, $T_{1/2}$, K conversion coeff. 77−54184
^{127}Cs collective quadrupole dynamics, band struct., transitions, collective model anal. from ^{127}I(α,4n) 80−78112
^{127}Cs production for radiopharmaceutical appls., high energy alpha reactions 77−37053
^{127}Cs, yield in I irrad. by α-particles 79−67760
^{127}Cs→^{127}Xe, study of γ-rays, ^{127}Xe level scheme 77−299
^{128}Cs decay, ^{128}Xe, collective excitations obs. 79−45143
^{128}Cs→^{128}Xe, ^{128}Xe levels, spin-parity assignments, log ft values 77−54189
^{129}Cs 11/2$^-$ isomer, g-factor and lifetime in CsI cubic environment from ^{127}I(α,2n) 79−6394
^{129}Cs, band struct., in-beam γ-ray spectroscopy after (γ,2n) reaction 78−4951
^{129}Cs, β decay, ^{129}Xe population, energy level scheme, γ spectra meas. 77−2936
^{129}Cs decay, ^{129}Xe excited state lifetimes, γ-transitions 80−78205
^{129}Cs, implantation into Fe, Mossbauer obs. 77−20753
^{129}Cs, myocardial imaging agents comparison 77−2037
^{129}Cs, yield in I irrad. by α-particles 79−67760
^{131}Cs, 133.5 keV state, electric quadrupole interaction 80−32228
^{131}Cs, level struct. obs. from ^{131}Ba decay 77−10359
^{132}Cs radioactive target, search for (n_{th},p) and (n_{th},α) reactions 77−23010
^{132}Cs(n,α), thermal, cross-sections meas. 78−94012
^{133}Cs, 161 keV transition M1-E2 mixing ratio and nucl. struct. parameter 78−74332
^{133}Cs, excited levels lifetime meas. using retarded coincidence method *(French)* 78−62507
^{133}Cs, Mossbauer isomer shifts, book contrib. 79−87363
^{133}Cs, NMR in ferroelectric CsH_2PO_4 78−15034
^{133}Cs, NMR in nearly one-dimensional antiferromag. system $CsNiBr_3$ 77−77041
^{133}Cs, neutron resonance parameters up to 400 eV 77−26581
^{133}Cs, nuclear resonance parameters, 1 to 400 eV, calc. by shape and area methods 79−30789
^{133}Cs, quadrupole interaction of 81 keV state in Te 78−48088
^{133}Cs salts, powders, nucl. mag. shielding and quadrupole coupling 77−90056
^{133}Cs+n, CsI crystal bombardment, p and α emission spectra, yields, preequilib. mech. 77−50139
^{133}Cs(^{3}He, 3n)^{133}La, band struct., in-beam γ-ray spectroscopy 78−4951
^{133}Cs(N,γ)^{134}Cs, exciton model, γ spectra calc. 78−62539
^{133}Cs(α,2n)^{135}La, band struct. of ^{135}La, in-beam γ-ray spectroscopy 78−4951
^{133}Cs(α,α′), 161 keV state magnetic moment and B(E2) values, Coulomb excitation 79−45159
^{133}Cs(α,pn)^{135m}Ba, ^{135m}Ba yield depend. on energy of bombarding particle 80−5151
^{133}Cs(d,2n)^{133m}Ba, thick-target yield for ^{133m}Ba prod. for medical use 77−60251
^{133}Cs(n,γ)^{134}Cs, E_n=14.1 MeV, γ emission exciton model *(Russian)* 79−13302
^{133}Cs(n,n′γ), level scheme and deexcitation of excited ^{133}Cs levels 78−13004
^{133}Cs(p,pxn), 550 MeV, cross-sections meas. and Monte Carlo calcs. 77−41969
^{133}Cs(p,xn) 550 MeV, cross-sections meas. and Monte Carlo calcs. 77−41969
^{134}Cs 176.403 keV isomer, populating γ-rays, low lying levels from ^{133}Cs(n,γ), ^{134}Cs 176.403 keV isomer, populating γ-rays, low lying levels 80−78200
^{134}Cs ($t_{1/2}$=2.2 yr), neutron resonance parameters up to 400 eV 77−26581
nuclei with mass number 90 to 149 continued
^{134}Cs, activity meas. 79−59292
^{134}Cs, as potential radiotherapy radionuclide, prod. and decay scheme 77−90875
^{134}Cs, fission products in low-enriched (Pu,U)O_2 fuel assemblies profiles of activity ratios 77−57713
^{134}Cs, for treatment of cervical cancer, isodose curves 77−90876
^{134}Cs, gamma-ray intensities, precision meas. 80−102139
^{134}Cs, half-life, gamma-spectrometric determ. 78−93972
^{134}Cs, isospin forbidden beta decays, collective model, Fermi matrix elements 77−67722
^{134}Cs, nuclear resonance parameters, 1 to 400 eV, calc. by shape and area methods 79−30789
^{134}Cs, radionuclide determ. in coastal marine sediments and seawater 79−88370
^{134}Cs, sorption from water using fibrous ionites 77−56251
^{134}Cs, standardisation (1977) AECL 78−25371
^{134}Cs/^{137}Cs activity ratio, spent fuel assembly 78−82487
^{136}Cs, fractional independent yield form ^{238}U photofussion with bremsstrahlung 79−36283
^{137}Cs, 10 GeV proton spallation for transmutation of radioactive waste, calc. of transmutation number 80−13470
^{137}Cs, activities in water entering N.North Sea 79−16520
^{137}Cs, anal. of IAR in ^{136}Xe(p,p_1) at 11.82 MeV 78−66282
^{137}Cs, beta-decay, internal bremsstrahlung meas. 77−79338
^{137}Cs body burden in Japanese from 1967 to 1975 77−9283
^{137}Cs brachytherapy source calibration using Fe$(NH_4)_2(SO_4)_2$-benzoic acid-xylenol orange dosimeter 77−5081
^{137}Cs β-decay, β_1 component discrepancies for β- spectrum 79−75918
^{137}Cs concentration determ. in LMFBR Na heat carrier 79−41043
^{137}Cs contamination of external-radiation doses in USSR territory 78−86698
^{137}Cs decay determ. by β-ray spectrometry 79−26397
^{137}Cs, distrib. in fuel elements of Peach Bottom HTGR 78−13274
^{137}Cs distribution in watersheds of Eastern USA 77−25701
^{137}Cs distributions effects on γ-intensity in γ scan method for reactor fuel bundle *(Japanese)* 79−36342
^{137}Cs excited levels from ^{137}Xe β decay, γ spectra, coincidences, branching, logft values 77−54186
^{137}Cs, exposure-rate calibration of small radioactive sources 78−41881
^{137}Cs fission product release from HTGR 77−74939
^{137}Cs, fission products in low-enriched (Pu,U)O_2 fuel assemblies profiles of activity ratios 77−57713
^{137}Cs, gamma source, Poisson and Brockwell-Moyal freq. distribs., χ-square test 80−5430
^{137}Cs gamma-ray spectra of spherical reactor fuel elements, burn-up determ. *(German)* 78−25299
^{137}Cs γ rays, backscattering, atomic number depend., Monte Carlo calcs. 77−67734
^{137}Cs in low level radioactive liquid waste, chem. treatments, removal efficiencies 77−54351
^{137}Cs, narrowly collimated γ-ray sources, radiation fields in Al and H_2O *(Russian)* 77−30549
^{137}Cs, radioactive decay, γ-ray energy meas. *(German)* 77−57633
^{137}Cs, radioactive fallout in air and rain, results to end of 1977 78−82535
^{137}Cs, radionuclide determ. in coastal marine sediments and seawater 79−88370
^{137}Cs, removal from nuclear power station liquid waste by zeolite 79−6749
^{137}Cs, rotational invariance in beta-ray ang. distrib. 78−66252
^{137}Cs source for computerised tomography 77−60239
^{137}Cs standardisation by 4π(PC)-γ efficiency tracing method 79−13577
^{137}Cs $T_{1/2}$ determ. using new specific activity meas. 78−70714
^{137}Cs to ^{131}I fractional release ratio from breached fission fuel elements 78−21713
^{137}Cs transmutation in fussion reactor imploding liner blanket 78−17420
^{137}Cs-^{137m}Ba generator, for nucl. medicine, preparation by ion exchange chromatography 78−28071
^{138}Cs, independent isomeric yield ratio from spontaneous fission of ^{252}Cf 79−22342
^{139}Cs β-decay, ^{139}Ba level scheme, J^π and γ-transitions 80−42590
^{139}Cs level scheme, J^π and γ-transitions from ^{139}Xe β-decay 80−42590
^{142}Cs decay, ^{142}Ba, γγ ang. correlations, levels, spins and mixing ratios 80−57734
^{143}Cs, delayed neutrons, energy spectra 80−99153
^{143}Cs, nuclear spectroscopy of neutron rich A=143 nuclei 79−59039
^{144}Cs, beta and gamma spectra, level scheme 77−22962
^{145}Cs, mass chain, half lives and n-emission probabilities of delayed-n precursors 78−70497
^{147}Cs, unambiguous identification of neutron-rich isotope 78−78318
^{134m}Cs, myocardial imaging in humans 77−16964
Dy A=148, 149, deduced levels from ^{148,149}Ho β-decay 79−36166
^{147}Dy charge states and charge distrib. from ^{113}Cd(^{40}Ar,6n) *(Russian)* 79−40840
^{148}Dy, p single particle states and pairing force calcs., high spin states 80−42522
^{148}Dy$_{82}$ 10^+ isomer, $\pi h_{11/2}$ effective E2 charge 78−93964
^{149}Dy, 27/2$^-$ three-particle isomer on ^{146}Gd doubly closed shell nucleus 77−22895
^{116}Er in Fe, Ni, hyperfine interaction, Mossbauer spectra 77−48105
^{154}Er, high-spin yrast states, lifetime meas. using recoil-distance method 79−40884
^{167}Er(n,p)^{167}Ho, (14.2±0.2) MeV, activation cross sections, Ge(Li) meas. 79−22278
Eu, A=147, 149, 151, band struct. obs. via heavy-ion reactions 77−82855
Eu, A=149, 151, band struct. anal. with Sm(d,3nγ) at 18-25 MeV 77−41913
Eu, A=144,148,150,152, ground and excited state analogues, two-phonon coupling effects from Sm(p,n) 79−89277
Eu, A=145, 147, 149, mag. moments of 11/2$^-$ states 79−40846
Eu EC decay, A=147, 149, ^{147,149}Sm levels, J, γ-transitions and multipole mixing ratios, γγ correlations 80−106012
Eu, transitions in ^{147}Gd decay 79−6475
^{143}Eu^m, decay obs., struct. determ. 78−50130
^{144}Eu, multiplet splitting and isomerism, J, π, T1/2 via (d,2n) and (p,n) 77−14014
^{145}Eu high spin and isomeric states, transitions, weak coupling from ^{144}Sm(α,2npγ) 80−13348

nuclei with mass number 90 to 149 continued

^{145}Eu high spin core coupled states and transitions from ^{142}Nd(^{6}Li, 3nγ) 80−42520

^{145}Eu high spin levels, isomers and in-beam γ-spectroscopy from ^{144}Sm(α,2np) 80−78124

^{145}Eu high spin states, J^{π} and transitions from (^{7}Li,4nγ) and (^{6}Li,3nγ) 80−47350

^{145}Eu, IAS, J^{π} via polarised proton scatt. 77−74825

^{145}Eu level and transition effects on ^{145}Gd decay anomalies 80−32244

^{146}Eu 9^{+} isomer, γ-decay, high spin particle-hole multiplet population from ^{147}Sm(p,2n) 80−63066

^{146}Eu decay, spin-parity assignment of ^{146}Sm levels *(Russian)* 77−14062

^{147}Eu populated in ^{147}Gd decay, γ-ray spectra obs. at small-source detector distance *(Russian)* 79−93520

^{148}Eu decay, ^{148}Sm energy levels, struct. interpretation from boson expansion model *(Russian)* 78−78261

^{149}Eu level structure populated in ^{150}Sm(p,2nγ), spin, parity 78−21561

^{149}Eu, proton states and transitions shell model anal. of ^{148}Sm(α,t) 79−30781

^{141g}Eu, ^{141m}Eu β-decay props., J^{π}, decay energy, $T_{1/2}$ 77−82876

Ga isotopes, independ. yield in ^{238}U(p,f) 78−13171

^{A}Gd A=144,146,147,148, high spin isomer g-factors yrast traps from (^{28}Si,^{28}Si′), (α,α′) 80−78146

^{A}Gd, A=146, 147, g-factors of yrast states 79−17800

^{A}Gd, A=146,147, mass and Z=64 shell closure from ^{144}Sm(^{12}C,^{9,10}Be) 80−57669

^{A}Gd, A=146-7, high spin yrast traps, g-factors 79−63578

^{A}Gd, A=146.7, particle hole yrast states and Z=64 shell closure from Sm (α, xn) 79−49571

^{A}Gd, A=150-156, E2:M1 multipole mixing ratio, sign change in A=150 region 80−493

^{142}Gd, populated in (α,6n), ground state bands obs. 77−2938

^{143}Gd^{m+g}, β^{+} and EC decay 78−50130

^{144}Gd level scheme, delayed transitions, in-beam study from ^{144}Sm(α,4nγ) 79−17809

^{145}Gd EC/β^{+}-decay branching ratio anomalies, ^{145}Eu level and transition effects 80−32244

^{145}Gd, ε/β^{+} anomalous values, reinvestigation 77−79332

^{145}Gd levels, J^{π} and transitions, neutron hole coupling to ^{146}Gd core from ^{144}Sm(α,3n) 80−78164

^{145}Gd→^{145}Eu, weak interaction treatment, modifications to Re/R$_{\beta+}$ ratio from finite size and Coulomb corrections 77−46143

^{146}Gd, 1579 keV state, assignment of isospin and parity, using γ-ray ang. distrib. 78−21489

^{146}Gd, 3^{-} 1579 keV first excited state 78−41670

^{146}Gd decay, γ- and internal conversion electron spectra 79−75916

^{146}Gd, excitation energy of lowest 2^{+}, 3^{-} levels, energy density method 79−3088

^{146}Gd, high multiplicity yrast isomers prod. in (α,xn) reactions 78−41666

^{146}Gd lowest 2^{+} state, J^{π} and transitions from ^{146}Tb decay 80−105979

^{146}Gd, lowest 2^{+} state and energy gap at Z=64 78−82310

^{146}Gd, mag. moments of isomeric states 79−40847

^{146}Gd, O_2^{+} state EM decay, $T_{1/2}$ and monopole strength 80−95310

^{146}Gd, p single particle states and pairing force calcs., high spin states 80−42522

^{146}Gd region, proton subshell effects from α-decay and spectroscopy, self-consistent study 80−57748

^{146}Gd, spherical HFB calcs. for Z=64 shell closure 80−22716

^{147}Gd, high-spin states and particle-core coupling 77−26614

^{147}Gd^{m} high spin yrast trap, oblate deformation and quadrupole moment 80−32157

^{147}Gd→^{147}Eu decay, γ-ray spectra obs. at small-source detector distance *(Russian)* 79−93520

^{149}Gd level scheme and transitions from ^{149}Tb^{g} electron capture 79−9477

^{A}Ho, A=148, 149, identification and β-decay from ^{144}Sm+^{10}B, ^{148,149}Dy levels 79−36166

^{149}Ho low lying yrast states from ^{122}Te(^{32}S,X), ^{121}Sb(^{32}S,X) 80−91151

^{123,125}I, levels, J^{π}, spectroscopic factors 77−34230

^{137,138}I, delayed-neutron emission probabilities 77−74817

I, 123≤A≤133, coupled quadrupole model, spectra, B(E2), B(M1), moments calcs. 77−82837

I, A=110-114, neutron-deficient, prod. in ^{58}Ni+^{58}Ni(^{63}Cu) at 290 MeV 77−88171

I, A=117-127, odd, collective props. determ. 77−46124

I, A=123,125, level struct. from Te(^{3}He,d) 24 MeV reactions 77−50057

I, A=124, 6, nucl. reson. fluoresc. in ^{124}Te and ^{126}Te 77−2953

I, A=129, 131, 132, PAC obs. of quadrupole interaction in Te, Zn, and Cd 78−48087

I β^{+} decay force function resonance struct., level populations *(Russian)* 80−102154

I energy levels, collective excitations, spin,parity, populated in ^{121,123}Sb(α,2n), γ spectra 78−4891

I isotopes 121, 123, 125, rotational bands meas. 77−22837

I, low-lying collective states anal. 77−88030

I odd-A nuclei, deformed 9/2^{+} proton-hole states, Nilsson calc. 77−74746

I, odd-mass nuclei, 9/2^{+} bands, deformed states 78−17106

I prod. relative thresholds from fusion and transfer induced fission in ^{238}U(^{40}Ar,f) 79−9640

I-plasminogen, ^{123}I or ^{131}I evaluation as imaging agent for pre-existing thrombi 77−21610

^{A}I, A=110-113, neutron deficient isotopes from ^{58}Ni(^{58}Ni,xpyn), alpha decay studies 79−93567

^{A}I, A=115-127 odd isotopes, collective props., bands and transitions from heavy ion reactions 80−68512

^{A}I, A=121, 123, 125, mass excesses, ^{121}I energy levels from Te(^{3}He,d) and Te(α,t) 78−78246

^{A}I, A=121, 123 and 125, cyclotron prod. by ^{127}I(p,xn)Xe→(β)→I reactions, yield curves 78−44611

^{A}I, A=121 to 131, comparative study of proton states excited by (α,t), (^{3}He,d) 79−63572

^{A}I, A=123, 125, mag. moments and polarisation NMR on oriented nuclei 79−75836

^{A}I, A=127, 129, 130, 131, sensibility anal. of the effect of key parameters on fission prod. conc. 79−36290

^{A}I, A=127, 129, Mossbauer isomer shifts, book contrib. 79−87360

^{A}I, A=131-135, gamma spectra of radioiodines in reactor coolant 79−9732

nuclei with mass number 90 to 149 continued

^{A}I, A=131-135, rapid determ. of reactor coolant contamination 79−9733

^{A}I, A=133, 135, sensibility anal. of effect of key parameters of fission prod. conc. 79−30870

^{A}I, A=137-139, β-delayed neutron emission probabilities, half-life 80−52634

^{A}I, A=139-141, delayed neutron emission probabilities, β-decay half-lives 80−83078

^{113}I decay, ang. correl. meas in ^{113}Xe 77−6292

^{115}I(n,γ), average activation cross sections in ^{252}Cf spontaneous fission neutron field 79−30830

^{121}I mass excess, energy levels and single particle strength distrib. from ^{120}Te (^{3}He,d) 80−5053

^{121}I single particle strength distrib., determ. from ^{120}Te(^{3}He,d) 78−70423

^{123}I, absorbed dose to thyroid from radioiodine impurities 77−29207

^{123}I, bands and decay props., core-particle coupling and polarisation effects 80−13354

^{123}I, carrier-free, prod. from ^{127}I(p,5n)^{123}Xe using in-beam collection of ^{123}Xe 78−44610

^{123}I, carrier-free iodide generated from ^{123}Xe, kit prep. and quality control 77−29205

^{123}I, coincidence-counting assays 77−14320

^{123}I decay, ^{123}Te levels, spin assignments and E2/M1 multipole mixing ratio 79−75836

^{123}I decay, gamma-ray spectra, ^{123}Te level scheme obs. 77−10361

^{123}I imaging with scintillation camera, detect. performance and quality factor 77−40743

^{123}I, isomer shift calibration of ^{29}I and ^{127}I, lifetime variations in electron capture decay 80−39925

^{123}I labelled pharmaceuticals, cyclotron production for nuclear medicine appls. 77−44753

^{123}I, large scale prod. from flowing liq. target using ^{127}I(p,5n)^{123}Xe reaction 77−29203

^{123}I, mass. meas., ground state Q-value of ^{123}Te (^{3}He,d) 78−4896

^{123}I, prep. from gaseous TeF$_6$, nuclear medicine appl. *(French)* 80−98137

^{123}I preparation as iodide for synthesis of radiodiagnostic agents, use of compact cyclotron 77−21627

^{123}I prod. from ^{127}I(p,5n)^{123}Xe→^{123}I, at 58 MeV 80−94369

^{123}I, prod. using 6 MeV Van de Graaff accelerator 79−53243

^{123}I, prod. via ^{124}Xe(n,2n)^{123}Xe reaction in nucl. reactor, for nucl. medicine 77−2051

^{123}I, prod. via ^{127}I(p,5n)^{123}Xe reaction, excitation function 77−2981

^{123}I product radionuclidic purity and quality, comments from ^{124}Te(p,2n) 79−29621

^{123}I product radionuclidic purity using ^{124}Te(p,2n), reply 79−29622

^{123}I production by ^{124}Te(p,2n) reaction, new approach to target chem. 77−60250

^{123}I production for radiopharmaceuticals, excitation functions and target enrichment vs. radionuclidic purity 77−60252

^{123}I production from ^{123}Xe formed in spallation reactions by 660 MeV protons, medical appls. 80−85494

^{123}I production in cyclotron by ^{124}Te(p,2n)^{123}I, improved targetry and radiochem. 78−28064

^{123}I, simultaneous prod. of ^{123}I, ^{62}Zn and ^{13}NH$_3$, multitarget assembly for high energy irrad. 77−90896

^{123}I source sumpeak calibration absolute activity 77−57785

^{123}I two-crystal coincidence counting 78−13394

^{123}I-hexadecenoic acid, exptl. basis for myocardial imaging 77−16970

^{124}I production in cyclotron by ^{124}Te(p,n)^{124}I, improved targetry and radiochem. 78−28064

^{125}I β-decay surface contamination monitoring probes, comparison of response between detectors 78−25398

^{125}I, electron capture decay lifetime, calibration of Mossbauer isomer shift of ^{127}I and ^{129}I 80−39922

^{125}I implantation into Ge, Mossbauer obs. 77−20758

^{125}I in partially blocked thyroid of rats, testis damage 78−3565

^{125}I iodination for immunoassay, thyroid uptake and film badge monitoring of workers 77−13013

^{125}I, Mossbauer spectra in iodobenzoic and iodohippuric acids 77−12241

^{125}I source activity calculation from counting rates in single and coincidence photopeaks 78−13371

^{125}I surface contamination meas., due to medical use of ^{125}I sources, detectors sensitivity comparison *(Czech)* 79−34673

^{125}I therapy, RBE of soft X-rays 78−7405

^{125}I thyrotoxicosis management, dosimetry, radiobiology, clinical aspects 77−2048

^{125}I toxicity in cultured mammalian cell, primary site for division delay 77−52851

^{125}I-UdR effect on division in Chinese hamster cells 77−29179

^{125}I-iododeoxyuridine, cell survival and cytogenic responses, mammalian cells 77−5046

^{125}I-iododeoxyuridine, effect of ^{125}I-decay, mol. consequences of Auger effect 77−4982

5-^{125}I-iododeoxyuridine as prototype for radionuclide therapy with Auger emitters 77−29186

^{125}I-iodoproflavine binding with DNA, double strand break induction 78−20145

^{125}I+methane, γ irrad. effects on organic iodide form. and decomp. *(Japanese)* 77−81418

^{126}I β-decay, 0^{+} states of ^{126} Te anal. 77−74810

^{127}I, 14.7 MeV neutron capture cross-section measurements with activation technique 80−32282

^{127}I, 24 keV neutron capture cross section meas. with Fe-filtered neutron beam 79−40910

^{127}I 57.6 keV level half-life meas., β-γ delayed coincidences 77−6300

^{127}I γ cascade following ^{127}Te decay, 360.3-57.6 keV γ-γ directional correl. 78−25151

^{127}I, NQR in complex iodomercuroates 77−12230

^{127}I, NQR in iodobenzoic and iodohippuric acids 77−12241

^{127}I, NQR spectra in complex and simple iodates 77−12234

^{127}I, NQR spectra in group IV tetraiodides 77−12231

^{127}I, neutron capture cross sections, MeV region, using activation technique 78−86535

^{127}I neutron resonance parameters, 20 eV to 2 keV 77−22897

^{127}I, nuclear spin echo in CsI, magnetoacoustic excitation *(Russian)* 77−4578

^{127}I+n, CsI crystal bombardment, p and α emission spectra, yields, preequilib. mech. 77−50139

nuclei with mass number 90 to 149 continued
^{127}I(α,2n)^{129}Cs, band struct. of ^{129}Cs, in-beam γ-ray spectroscopy 78-4951
^{127}I(n,2n), ^{126}I, 14.1 MeV, ang. and spectral distribs. 78-82354
^{127}I(n,2n), 4.5-18.3 MeV, cross sections and excitation curves *(Chinese)* 79-49601
^{127}I(n,γ), cross-section determ. by Fe filtered beam TOF method 77-23078
^{127}I(n,γ) cross section 77-23032
^{127}I(n,γ)^{128}I fission products in fast reactors, effective cross sections calc. *(Dutch)* 79-537
^{127}I(n,n'γ), 3, 14 MeV, 57 and 202 keV γ-ray prod. cross section 79-67706
^{127}I(n,n'γ), fast n,γ-ang. distribs., level ang. momenta 80-18224
^{127}I(p,5n)^{123}Xe, ^{123}I prod., excitation function 77-2981
^{127}I(p,5n)^{123}Xe, for large scale ^{123}I prod. from flowing liq. target 77-29203
^{127}I(p,5n)^{123}Xe$\rightarrow$^{123}I statistical model based computation 79-26416
^{127}I(p,5n)^{123}Xe$\rightarrow$^{123}I$^-$ production, separation and radiopharmaceutical labelling 79-79649
^{127}I(p,n)^{127}Xe statistical model based computation 79-26416
^{127}I(p,p), 100-2200 MeV, total and reaction cross sections from optical pot. 80-18303
^{127}I(p,xn)Xe$\rightarrow$(β)$\rightarrow$I reactions, yield curves for cyclotron prod. of ^{123}I, ^{125}I and ^{121}I 78-44611
^{128}I decay ^{128}Xe, collective excitations obs. 79-45143
^{128}I, on-line data acquisition system for monitoring high resolution multi-dimensional spectra 78-58567
^{129}I coincidence counting, efficiency extrapolation technique, methane 4π counter efficiency 77-88354
^{129}I, CrI_3 ferromagnetic, origin of magnetic hyperfine field transferred 78-92000
^{129}I, distrib. in irrad. UO_2 pellets, neutron activation anal. *(German)* 77-16880
^{129}I energy levels populated in ^{129}Te decay, γ spectra, coincidence spectra 77-2935
^{129}I, γ-ray and X-ray radiation, internal conversion coeff. 79-6499
^{129}I in transition metals, calibration of Mossbauer isomer shift 80-20520
^{129}I, internal conversion electron and Mossbauer spectra, calibration of isomer shift 80-39921
^{129}I, Mossbauer obs. in Fe (III) bis(dithiocarbamato) iodides 77-20759
^{129}I time depend. quadrupole interactions, γ-γ correlations from ^{129}Te^{m+g} decay 80-78145
$^{129}I_2$ radioisotope detection in nuclear fuel cycle, intracavity selective absorpt. analysis 78-46182
^{131}I contamination in eluate of ^{99}Mo-^{99m}Tc generators loaded with (n,γ)-prod ^{99}Mo 77-5079
^{131}I decay in 3-iodotyrosine, intramolecular effects 77-36870
^{131}I, effect of small amounts on ^{99m}Tc detect. by scintillation camera 77-16972
^{131}I, environmental, in vivo thyroid monitoring 77-9264
^{131}I, gamma radioactive source, buildup factor determination for meas. in air *(Rumanian)* 78-49132
^{131}I in tissue, specific energy calc. in accordance with crit. cell concept 77-2031
^{131}I, in vivo whole-body counter calibration for quantiative retention estimation 78-3579
^{131}I, radiation exposure dose determ., hot particle model 78-82520
^{131}I, radioactive fallout in air and rain, results to end of 1977 78-82535
^{131}I recovery and trapping, in sublimation separation of ^{99}Mo from neutron irrad. 77-9257
^{131}I, reduced normalisation of isobaric analogue resonances from ^{131}Te(p,p) 78-86522
^{131}I therapy of hyperthyroidism, gonadal dose and genetic significance 77-5082
^{131}I transport from pasture to milk, modelling Dresden-Monticello data 79-88203
^{131}I-hippurate uptake, external monitoring for renal blood flow meas. 77-2036
^{131}I-tetracycline, prep. and stability 77-29204
^{132}I 3^+ and 1^+ state electric and mag. moments 79-63587
^{132}I decay ^{132}Xe level struct., J^π, transitions and multipole mixing ratio 80-91134
^{132}I isomer and gamma-ray spectrum from ^{133}Cs(π^-,p) 80-78199
^{132}I isotope, doubly odd, quadrupole moments, PAC meas. 78-37280
^{133}I, β decay, ^{133}Xe population, energy level scheme, γ spectra meas. 77-2936
^{133}I yield and γ-ray spectra from ^{133}Cs(π^-,p) 80-86857
^{134}I fractional independ. yield from ^{238}U(γ,f) 80-57814
^{134}I yield from ^{237}Np(n,f) 80-86935
^{135}I, fractional cumulative yields in ^{252}Cf SF 78-41791
^{135}I, fractional cumulative yield from ^{245}Cm(n,f) 80-63074
^{136}I β-decay, ^{136}Xe levels anal. neutron particle-hole states 77-74811
^{136}I, isomeric ratio, γ-spectra thermal neutron and 3 MeV fission of ^{235}U *(French)* 80-68709
^{136}I level scheme via ^{135}Te (20.9 s) β decay 77-82877
^{137}I beta delayed neutrons, ^{137}Xe neutron unbound states, high energy X-rays 80-86856
^{137}I, β-decay delayed n emission, simple statistical model description 79-67714
^{137}I, β-delayed neutron decay, statistical model, Monte Carlo techniques 78-89830
^{137}I, delayed neutron energies 77-74816
^{137}I, investigation of beta-strength functions by neutron and γ-spectroscopy 79-45209
^{137}I, neutron and gamma-ray spectroscopy of delayed neutron emission 77-22973
^{137}I, shell model anal. of delayed neutron emission 77-71595
^{138}I, β-decay scheme, population of ^{137}Xe and ^{138}Xe levels, delayed neutron obs. 80-27600
^{132m}I, ^{134m}I, isomer yield ratios in ^{235}U(n,f) 77-38306
I(γ,γ), 2754 keV photon Delbruck scatt. 79-67741
I(n,n) 2.9 MeV, elastic differential cross section and polarisation ang. depend., statistical anal. 79-45264
I(n,n), pol. n, 16.1 MeV, differential cross section, optical model fit 80-32259
In, A=109, 110, 111, low temp. orientation, γ-ray spectra 77-79327
In, A=113m, 115m, cross-section of inelastic neutron acceleration 78-17196

nuclei with mass number 90 to 149 continued
In isomeric decays, ^{A}Sn, A=120,122,124,126,128, levels, transitions and J^π values 79-75851
In isotopes, A=110, 112, 114, np coupling const. determ. 77-34205
In isotopes, independ. yield in ^{238}U(p,f) 78-13171
In isotopes, unified theory of particle-phonon coupling 77-61360
In light isotopes, decay study with LISOL on-line mass separator 77-23361
In, NQR in heteroorganic group III compounds, summary 78-25565
In, odd-mass isotopes, positive parity bands in deformed and spherical representation 78-21495
In, photonuclear cross sections in giant reson. region 78-17178
In populated in ^{111,113}Cd(p,nγ), energy levels, spins, lifetimes, shape 77-320
In relative independ. yield from ^{232}Th(p,f) 80-102218
In+p, 1 to 28.5 GeV, production of 43$\leq$A$\leq$51 nuclides, reaction mechanisms 77-34301
^{A}In, A=104, 106, β-decay half lives and decay schemes 78-74333
^{A}In, A=109,110, nucl. g-factor NMR-ON meas. on Fe-In alloys 78-37275
^{A}In, A=113, 115, excitation by photon less positron annhilation, isomeric γ-transitions *(Russian)* 80-5089
^{A}In, A=113,115, mean lifetime meas., 1400 to 1650 keV range, by reson. scatt. of bremsstrahlung *(French)* 79-75905
^{A}In, A=119, 121, unified model description, vibr. multiplet yrast struct., branching ratios 80-105953
^{A}In, A=120-129, total β-decay energies and masses of strongly neutron rich isotopes 78-86512
^{A}In, A=127-132, β-delayed neutron emission probabilities, half-life 80-52634
^{A}In(n,n'), A=113,115, average activation cross sections in ^{252}Cf spontaneous fission neutron field 79-30830
^{12}In, β-decay obs., decay scheme, half-lives 79-45207
^{103}In decay, ^{103}Cd levels and spectra 79-22235
^{106}In level scheme via ^{106}Sn decay 78-93971
^{107}In nucleus and K shell excitation, lifetime meas. from ^{106}Cd(p,p')^{106}Cd 80-63130
^{108}In high spin struct., in-beam spectroscopy, conversion electrons from ^{98}Mo(^{14}N,4nγ) 80-73782
^{108}In, level scheme determ. from ^{108}Sn decay and ^{108}Cd(p,n) 78-41636
^{108}In, levels, J^π from ^{108}Sn decay γ- and conversion electron-spectra 77-71589
^{109}In high spin states, γ-transitions, ang. distribs. from ^{108}Cd(α,2np) 80-73783
^{109}In high spin states, transitions, isomeric state, negative parity bands from ^{107}Ag(α, 2nγ) 80-451
^{109}In, levels and transitions obs. in ^{107}Ag(α,2n) 77-22836
^{110}In, nucl. orientation, nucl. mag. moment, γ-ray spectra of Fe:^{110}In 77-28485
^{111}In, ^{113}In^m, electron dose reduction coeff., internal radionuclides, source free target, cylindrical geometry 78-92704
^{111}In $21/2^+$ isomeric state g-factor and relaxation time from ^{109}Ag(α,2nγ) 80-73794
^{111}In at active site of bovine carbonic anhydrase, γ-ray perturbed directional correl. obs. of conform. change 79-83700
^{111}In band structure and hole-core coupling, ^{109}Ag(α,2nγ), branching and mixing ratios 78-58249
^{111}In, DPAC obs. of elec. field gradient in radiation damaged Cu 78-43727
^{111}In, ion implantation damage, in Ni 77-59052
^{111}In, isospin mixing obs. in ^{110}Cd(p,p'), ^{110}Cd(p,α), ^{107}Ag(α,α') and ^{107}Ag(α,p) 77-57598
^{111}In, nucl. orientation coeffs., nucl. mag. moment 80-97168
^{111}In, populated in ^{111}Cd(p,nγ), γ-ray spectra, level scheme 78-13083
^{111}In, rotational band detect., internal conversion electron spectra from ^{111}Cd(p,nγ)^{111}In 79-6362
^{111}In-^{109}In mass difference from Q values of Cd(^{3}He,d) 80-63069
^{112}In, 8^-, 6^+ isomeric states, $T_{1/2}$, g-factors via ^{112}Cd(p,n), ^{109}Ag(α,n) 77-10318
^{112}In, half-lives and mag. moments of two high spin states, γ-ray spectra 77-22940
^{112}In low lying levels, transitions, $T_{1/2}$, multipolarities and mixing ratios from ^{112}Cd(p,nγ) 80-68545
^{113}In decay to ^{113}In, decay scheme, unified model description of odd mass In nuclei 78-66251
^{113}In, internal conversion of high-multipolarity transition 77-2945
^{113}In levels, from decay of ^{113}Sn 77-38247
^{113}In, nucl. levels, mean life determination by reson. fluoresc. under bremsstrahlung bombardment *(French)* 77-54179
^{113}In, unified model description of odd mass In nuclei 78-66251
^{113}In(α, 2nγ)^{115}Sb, 20-30 MeV, high-spin states in ^{115}Sb anal. 77-41982
^{114}In, deeply bound hole state transition strength giant resonance, DWBA anal. of (p,d) 80-47426
^{114}In, internal conversion on outer electron shells, 191 keV E4 transition 80-42587
^{114}In isomer decay, spin, excitation function, T_{112} γ-X-ray and γ-γ coinc. 77-6312
^{114}In^m, nuclear quadrupole alignment 78-48090
^{115}In, 24 keV neutron capture cross section meas. with Fe-filtered neutron beam 79-40910
^{115}In 597 keV level J^π assignment from ^{115}Cd^g β-decay 79-80900
^{115}In (^{12}C,X), 69.0, 83.0, 117.0 MeV, ang. distribs. for target residues 77-50150
^{115}In (^{14}N,X), 130, 97 MeV, ang. distribs. for target residues 77-50150
^{115}In, β^- decay spectrum, measured $T_{1/2}$, E_β 79-40888
^{115}In, conc. and temp. depend. nucl. relax. in liq. In-Sn(Pb) alloys 78-19357
^{115}In, elec. quadrupole moment from elec. field gradients of trans-dimethyl organometallic moieties 80-29371
^{115}In, isomeric state formation by 14.8 MeV neutrons 77-30604
^{115}In, K-shell positron annihilation, excitation of nucleus *(Russian)* 78-33171
^{115}In, Knight shift and quadrupole interaction in InBi 77-55717
^{115}In, neutron capture cross sections, MeV region, using activation technique 78-86535
^{115}In nuclear quadrupole coupling for organoindium cpds., additive calcs. 77-50453
^{115}In, nuclear quadrupole relax. rate for liq. In 77-36151
^{115}In, π^- capture, p, d and α inclusive prod. spectra 79-22338
^{115}In, thickness depend. of total and capture cross section 77-26747
^{115}In unified model description of odd mass In nuclei 78-66251

nuclei with mass number 90 to 149 continued
^{115}In^{m}, nuclear excitation by e^+ annihilation with K-shell electrons 79−22230
^{115}In(^{12}C,4n)^{123}Cs, in-beam γ-ray spectroscopy, decoupled band in ^{123}Cs obs. 78−21520
^{115}In(d,^{3}He), 50 MeV, proton hole states in ^{114}Cd, DWBA anal. 78−8829
^{115}In(γ,γ')^{115m}In, appearance energies of In complex cpds. determ. 78−8794
^{115}In(γ,γ), isomeric states excitation, integral cross sections 80−27528
^{115}In(n,γ), cross section, statistical theory anal., radiative strength functions *(Russian)* 78−17212
^{115}In(n,γ), effective cross section dependence on thermal neutron temp. 80−547
^{115}In(n,γ), population of ^{116}In low-lying levels 77−30589
^{115}In(n,γ)^{116m}In, 14.7 MeV, cross-section meas. with improved activation technique 77−50133
^{115}In(n,n'), cross section meas. using proton recoil detector with CsI(Tl) scintillator 79−54433
^{115}In(n,n')^{115m}In, 0.335 to 14.74 MeV, excitation curve 77−23084
^{115}In(n,n')^{115m}In, threshold to 4.1 MeV, excitation function by activation technique 78−78372
^{115}In(n,n')^{115m}In integral cross section ratio meas. using ^{235}U(n_{th},f) neutron spectrum 77−23130
^{115}In(νe^-)^{115}Sn*, scintillator for solar neutrino spectroscopy at low energies 78−73639
^{115}In(p,γ) γ-22 MeV differential cross-section meas. 79−93617
^{115}In(p,n), 11.2 MeV, spin cut-off parameters from neutron ang. distribs. *(Russian)* 79−80940
^{115}In(p,n), 2.0-6.7 MeV, cross sections, Hauser-Feshbach optical calcs. for p absorption systematics 80−47483
^{115}In(p,p), 2.0-6.7 MeV, cross sections, Hauser-Feshbach optical calcs. for p absorption systematics 80−47483
^{117}In level scheme, J^π and transitions from ^{117}Cd isomer decay, unified model anal. 80−32193
^{117}In, quadrupole interaction in Sn, temp. depend. 77−8470
^{118}In^{g} decay scheme, excited states of ^{118}Sn 77−54187
^{120}In, β-decay, half life and decay schemes, ^{120}Sn level struct. 78−86510
^{122}In, states and masses determ. from (t,^{3}He) 78−66290
^{124}In, states and masses determ. from (t,^{3}He) 78−66290
^{126}In levels from ^{126}Cd β-decay 79−3117
^{128}In yield from symmetrical fission at 15 MeV, delayed neutron yield *(Russian)* 79−22266
^{113m}In eluates from ^{113}Sn generator, monitoring Zr and ^{113}Sn breakthrough 77−5078
^{113m}In generator with modified silica gel column 77−90897
^{114m}In, K-shell internal conversion, $K\alpha_1$ hypersatellite line energies, intensities 77−18885
^{114m}In, prod. in Cd(d,xn) reactions, $E_d \leq 27.5$ MeV, cross sections 80−13482
^{114m}In-EDTA complex, method of determ., use as tracer in hydrology 77−73458
^{115m}In specific activity determination, for nuclear accident dosimetry 79−3248
^{116m}In, prod. in Cd(d,xn) reactions, $E_d \leq 27.5$ MeV, cross sections 80−13482
^{119g,m}In, decay schemes, half-lives, excited levels 77−296
In(γ,γ), neutron capture γ-ray Rayleigh scatt. 80−52661
In(γ,n), photoneutron Q-value determinations using monochromatic photons 79−22271
In(n,n), 2.5 MeV, small angle scatt., cross section, asymm. 78−74361
Kr, A=90, 91, ^{232}Th fission products, yields, γ-ray spectra 78−74410
Kr induced deeply inelastic collisions, transport eqn. appl. 78−82380
Kr isotopes, A=88 to 91, decay rate determ. for ground state beta-branching 77−26634
^{A}Kr, A=88-93, gaseous fission products, β-decay energies 79−9519
^{90}Kr β-decay, ^{90}Rb level scheme, transitions, J^π assignments and internal conversion coeffs. 79−67663
^{93}Kr, experimental Q_β-values 78−93974
^{93}Kr, γ-ray decay scheme, levels, J^π, logft values 77−54152
^{138,139}La, Fourier transform NMR 80−57354
La, A=144, 145, 147, short lived fission product, Q_β-value 78−37317
La, A=144-6, β-decay, γ-ray singles and coincidence meas. 78−4913
La, low-lying collective states anal. 77−88030
La odd-A isotopes, rot. aligned coupling, ang. momentum projection 77−2921
^{138}La/^{139}La nuclear electric quadrupole moment ratio, laser RF double reson. obs. 80−23447
^{A}La, A=123-125,127, half lives and low energy γ-ray data, β-decay probabilities 79−499
^{A}La, A=125, 127, collective props., bands and transitions from heavy ion reactions 80−68512
^{A}La A=131,133, decay, ^{131,133}Ba l-forbidden M1 transitions, energy level lifetime meas. *(Russian)* 79−49603
^{A}La, A=144-149, β-decay half life meas. 79−67718
^{125}La $27/2^+$ 2737 keV three quasiparticle state, nuclear struct. of isomeric states using g-factor 77−88039
^{128}La decay scheme populating ^{128}Ba levels 77−82806
^{129}La β-decay, struct. of ^{129}Ba 79−22244
^{131}La→ ^{131} decay scheme, γ, X-ray and conversion electron spectra *(Russian)* 80−32241
^{133}La, band struct., in-beam γ-ray spectroscopy after (^{3}He,3n) reaction 78−4951
^{134}La decay, ^{134}Ba level scheme obs. 77−10360
^{134}La, half-life meas. 77−6311
^{134}La levels anal. using decay of ^{134}Ce 77−6290
^{135}La, band struct., in-beam γ-ray spectroscopy after (α,2n) reaction 78−4951
^{137}La, Mossbauer effect in CeO_2-$LaCrO_3$ and CeO_2-La_2O_3 78−27121
^{137}La, possibility of obs. of Mossbauer effect 78−39457
^{138}La, low temp. photonuclear nucleosynthesis in stellar H-CNO burning zones 77−13319
^{138}La, magnetic moment of the first excited state, meas. using TDPAD 79−63589
^{138}La, naturally occurring, gamma-ray emission energies 80−52811
^{138}La, nucl. mag. moments and ratios of quadrupole moments, NMR spectroscopy 77−73088
^{138}La, radioactive decay meas., half life, γ energies 80−13418
^{138}La, thermal neutron capture cross section and reson. integral 77−6365
^{139}La, 166 keV hindered M1 transition, internal conversion, algorithm for data anal. 77−46137

nuclei with mass number 90 to 149 continued
^{139}La, ENDOR in $LaCl_3$:Gd^{3+} 77−20749
^{139}La from ^{139}Ba β^- decay, γ-rays, energy levels 78−70492
^{139}La, IAS, J^π via polarised proton scatt. 77−74825
^{139}La, level props., Coulomb excitation obs. 80−13378
^{139}La, NMR in dimorphic $LaVO_4$ 77−63310
^{139}La, NMR in $La_{1-x}Gd_x(Zn,Ag)$ 78−15038
^{139}La, nucl. mag. moments and ratios of quadrupole moments, NMR spectroscopy 77−73088
^{139}La, nucl. relax. and impurity magnetism in supercond. $La_{1-x}Gd_xAl_2$ and $La_{1-x}Ce_xAl_2$ 77−20495
^{139}La, nuclear structure effect on internal conversion of l-forbidden transitions 79−63632
^{139}La, reduced normalisation of isobaric analogue resonances from ^{139}Ba(p,p) 78−86522
^{139}La(^{86}Kr, X), TDHF fusion calcs., fusion cross sections 80−37409
^{139}La(^{86}Kr,X), 505, 610, 710 MeV, TDHF calcs., fusion behaviour 80−9323
^{139}La(^{86}Kr,X), 505, 610 and 710 MeV, elastic and deeply inelastic reactions, optical model anal. 78−66316
^{139}La(e,e'p), $f_{7/2}$ ground isobaric analogue resonance, proton decay mode 78−29450
^{139}La(e,p), 15-25 MeV, T_0+1 giant dipole resonance and characteristic decay mode 80−78247
^{139}La(γ,γ'), 7.28, 7.63 MeV, energy levels anal. 78−13058
^{139}La(n, γ), 10-70 keV, gamma-ray transitions 78−17185
^{139}La(n, γ), 2.5-90 keV, s- and p-wave resons. 78−17186
^{139}La(n,γ), non-statistical capture, radiative widths, γ-ray doorway state model 80−37389
^{139}La(n,μ), 14.1 MeV, gamma emission from pre-equilibrium exciton model 79−75960
^{139}La(n,t)^{137m}Ba, 14.6 MeV neutrons, activation cross section meas. 79−45254
^{139}La(p,αn)^{135m}Ba, ^{135m}Ba yield depend. on energy of bombarding particle 80−5151
^{139}La(p,f), 600 MeV, fragment energies, cross sections level density and barrier heights 80−42723
^{140}La, beta decay half life 80−47435
^{140}La, fission product, γ-ray emission probability 77−82862
^{140}La γ-ray intensities, meas. with coaxial Ge(Li) detector *(French)* 78−58534
^{140}La half-life determ. by ^{56}Mn activation and decay obs. 79−26398
^{141}La, γ-γ coincidence and elec. conversion meas. 79−13252
^{142}La, fractional independent yield and γ-activity from ^{249}Cf(n,f) 79−89337
^{143}La, decay, gamma-ray spectra *(French)* 77−30517
^{143}La, gamma-ray spectra, half-life 77−82859
^{143}La, level scheme obs. in ^{143}Ba decay 78−50129
^{143}La, nuclear spectroscopy of neutron rich A=143 nuclei 79−59039
^{144}La, beta and gamma spectra, level scheme 77−22962
^{144}La, radioactive decay meas., half life, ^{144}Ce levels 80−13417
^{145}La, fission product, β-decay anal. 78−78323
^{146}La, expt. β-decay energy of neutron-rich nuclides 79−30808
La(p,f), 600 MeV, mass yields in binary fission 78−8819
(^{6}Li,d), A∼60,116, L=0 transitions, cross sections, microscopic anal. 80−78189
MO, onset of deformation at A∼100 80−73790
^{148}m, struct. anal. from decay of ^{148}Pm, ^{148m}Pm gamma-ray spectra 77−67717
Mo, A=103-5, half-lives and γ-ray energies of short-lived isotopes following ^{235}U fission 78−17137
Mo, A=92-100, charge distrib., self consistent calc. *(Russian)* 77−38234
Mo, A=94-100, B(E2; $0^+ \rightarrow 2^+$) via ^{4}He and ^{16}O scatt. 77−6226
Mo, A=94-100 static quadrupole moment determ. from α- and ^{16}O-scatt. 77−6226
Mo, A=95, 97, nucl. acoustic reson. determ. of electronic contrib. to elec. field gradient tensor in Mo 78−48059
Mo, activation in cyclotron by p, d, α, ^{3}He 79−30839
Mo even isotopes, HFB calc. of deform. due to isoscalar n-p interaction 78−74302
Mo, even-even isotopes, first excited $0^{+\prime}$ states, energy systematics 78−54683
Mo, γ-ray attenuation meas. using Ge(Li) detector 78−17539
Mo isotopes struct., spectroscopy weak coupling approx. in shell model 79−22194
Mo neutron rich isotopes, excited 0 states 77−22937
Mo, proton, deuteron, α-particle, bombardment, yields of Tc isotopes, energy depend. 77−23098
Mo, reactions induced by ^{12}C and ^{19}F ions, γ-ray spectroscopy of induced activities 77−23107
Mo stable isotope eval., 5 keV-5 meV neutrons, rel. to reactor structural steel 80−13620
Mo+α, A=92,96,100, isobaric yield curves at A=72 from high energy spallation 78−25211
Mo+n, 1.6×10^{-3} to 10 eV, total cross section, raactor structural material 78−46052
Mo(A=94, 95, 96), nuclear reson. fluoresc., line profiles, level lifetimes 77−71586
Mo(^{3}He,n), 25.4 MeV, ang. distrib. meas. 77−3022
Mo(^{3}He,t)Tc, A=94,98, E=24 MeV, levels of ^{94}Tc, ^{98}Tc determ. 77−26778
Mo(^{3}He, xn)^{97}Ru, in compact cyclotron, ^{97}Ru chem. separation 77−37054
Mo(^{16}O, ^{16}O') A=94-100, 36 MeV, static quadrupole moment determ. 77−6226
^{A}Mo (e,α), A=92, 94, 120 MeV, preequilibrium α-emission, α energy spectra 79−85459
^{A}Mo, A=103, 104, ^{252}Cf fission fragment β-decay, X-ray-β particle coincidence technique 80−74094
^{A}Mo, A=92, 94-98, 100, muonic atom X-ray transitions, nuclear charge radii 80−27545
^{A}Mo, A=92, 95, 96, 97, 98, 100, (n,p), (n,n'p), (n,α), (n,n'α), (n,^{3}He) prod. cross sections at 14 MeV 80−93829
^{A}Mo, A=94, 96, 98, multiparticle states, method of generalised seniority 80−22759
^{A}Mo, A=94,97 deeply bound hole state transition strength giant resonance, DWBA anal. of (p,d) 80−47426
^{A}Mo, A=95, 97, nucl. quadrupole moments from laser-RF double reson. spectroscopy 80−57682

nuclei with mass number 90 to 149 continued
^Mo, A=98,102, anal. powers, transitions, shape coexistence states, DWBA anal. of Mo(t,p), pol.t 80−86895
^Mo, A=98-110, deformation and shape transition, HFB calcs. 79−93502
^Mo+^{86}Kr, A=92, 98, deep inelastic reactions, fast collective mode, quantal fluctations 79−67636
^Mo(^{3}He,^{3}He′), A=92,94,96,98,100, 110 MeV, giant quadrupole resonance isotopic depend. 80−9282
^Mo(d,d), A=92-100, 21.5 MeV, elastic and inelastic cross sections, coupled channel anal., deformation 79−553
^Mo(n,2n), A=92, 100, 14 MeV, cross section compilation 80−91181
^Mo(n,γ) A=98, 100 resonance parameters, capture Γ-rays and reaction mechanism 80−18272
^Mo(n,n) A=92,96,98,100, E_n=7 to 26 MeV, determ. optical model pot. parameters 79−22286
^Mo(p,n), 5.82 to 6.14 MeV, A=94 to 98, γ-ray multipolarities, internal conversion coeffs., energy levels 79−63625
^Mo(p,n), A=94-96, 98, 1.7-6.7 MeV, total cross sections, p strength functions, optical model anal. 80−18301
^Mo(p,p′), (A=92,94), 20 MeV, polarisation effects on nuclear excited states *(Russian)* 80−27645
^{91}Mo, fine struct. of ground hole-state analogues 78−50065
^{92}Mo, broken-pair approx. to seniority shell model 78−29408
^{92}Mo, elastic and inelastic scatt. of 30 MeV polarised protons 77−23004
^{92}Mo energy levels calc. from two-body effective parameters 77−57608
^{92}Mo high spin states from ^{90}Zr(α,2nγ), negative parity states 78−89786
^{92}Mo in beam γ-spectroscopy, level, lifetimes and excitation functions from ^{90}Zr(α,Zn) 79−13240
^{92}Mo, mag. moments of 8^+ and 11^- states anomalous orbital magnetism 79−6391
^{92}Mo, populated in heavy ion reactions, mag. moments, proton core polarisation 78−21598
^{92}Mo(^{16}O,X), entrance channel mass asymmetry effects on reaction mechanism, fission and fusion 80−106077
^{92}Mo(N,N)^{92}Mo, optical model anal. 80−47473
^{92}Mo(α,nγ), ^{95}Ru level scheme, low lying states, g-factor 77−88071
^{92}Mo(d,n)^{93m,g}Tc, excitation functions and yields 77−41975
^{92}Mo(d,p), pol. d, excitation curve isospin anomaly, neutron single particle resonances 80−27595
^{92}Mo(e,e), 302 MeV, nucleon density distribution in nucleus 79−75831
^{92}Mo(γ,γ), to 5.1 MeV, excited state lifetimes 77−30512
^{92}Mo(n,n′), 11 MeV, isospin effects cf. with direct reaction theory 77−34312
^{92}Mo(n,n′), isospin dependence of expt. nuclear deformations 77−82817
^{92}Mo(n,n), 7-26 MeV, differential cross sections, global optical model anal. 80−18298
^{92}Mo(n,n), elastic and inelastic, 11 MeV, isospin effects, optical and deformation parameters 79−17794
^{92}Mo(n,t)^{90}Nb, 14.6 MeV, production cross sections 79−49629
^{92}Mo(p,d), 50 MeV, fine struct. of ground hole-state analogues 78−50065
^{92}Mo(p,p′), time development function at isobaric analogue resonances, compound nuclear level decays 79−3124
^{92}Mo(π^+,π^+), 180 MeV, octupole transitions 79−85542
^{93}Mo decay schemes, lifetimes, expt., theory *(French)* 77−293
^{93}Mo, effective three-body interaction 78−524
^{93}Mo excited state lifetimes, delayed coincidences method 77−6298
^{93}Mo, excited state lifetimes and widths populated in ^{92}Mo(γ,γ) to 5.1 MeV 77−30512
^{93}Mo, shell model calcs., energy levels, transitions and spectroscopic factors 79−63593
^{93}Mo^m, low temp. nucl. orientation, γ-ray spectra 77−79327
^{94}Mo, analogue resonances, direct neutron decay, anal. of ^{93}Nb(p,n)^{93}Mo data *(Russian)* 79−3128
^{94}Mo, direct neutron decay of analogue resonances 80−22824
^{94}Mo even parity states, shell model calc. 77−50061
^{94}Mo high spin state transitions, mixing ratios, spins, shell model calcs. from ^{94}Tc decay 79−97678
^{94}Mo, level spins and multiple mixing ratios from γ-γ correlation meas. 78−21517
^{94}Mo(d,2n)^{94m,g}Tc, excitation functions and yields 77−41975
^{94}Mo(n,n)^{94}Mo, ang. distribs., 5.1 to 8.0 MeV, comparison with coupled channel and spherical optical model calcs. 77−26716
^{94}Mo(p,γ), 4.4 MeV, γ-ray multipolarities, internal conversion coeffs., energy levels 79−63625
^{95}Mo, ^{97}Mo, Fourier transform NMR, chem. shifts and Larmor freqs. *(German)* 77−59473
^{95}Mo, first excited $3/2^+$ state, g-factor determ. 77−26574
^{95}Mo, levels, B(E2), B(M1), branching ratios populated in ^{95}Tc^{m,g} decay 77−82856
^{95}Mo, NMR, identification of $MoO_{4-n}S_n^{2-}$ in aqueous soln. 77−48069
^{95}Mo, NMR meas. in $Sn_{0.5}Eu_{0.5}Mo_6S_8$ 77−43782
^{95}Mo, nucl. mag. shielding in MoS_4^{2-}, S isotope effect 77−63301
^{95}Mo(^{3}He,d), 33.6 MeV, proton spectroscopy of ^{96}Tc, shell model anal. 79−63573
^{96}Mo vibration-rotation struct. and yrast levels from variable moment of inertia model 80−73778
^{96}Mo(n,n)^{96}Mo, ang. distribs., 5.1 to 8.0 MeV, comparison with coupled channel and spherical optical model calcs. 77−26716
^{96}Mo(p,γ), 3.9 MeV, γ-ray multipolarities, internal conversion coeffs., energy levels 79−63625
^{96}Mo(t,p), pol.t, cross section and anal. powers, struct. depend., DWBA anal. 80−78272
^{98}Mo neutron resonances, spin-parity determ. using low energy γ-rays 77−26570
^{98}Mo static quadrupole moment of first 2^+ state from (α,α′), (^{16}O,^{16}O′) 80−5061
^{98}Mo(α,α′), 8 MeV, multiple Coulomb excitation, fast $2^+ \rightarrow 0^{+\prime}$ transition 79−17846
^{98}Mo(^{3}He,d)^{99}Tc level struct., spin-parity assignments 78−8743
^{98}Mo(^{3}He,d)^{99}Tc at 18 MeV populating low-lying states 77−22894
^{98}Mo(d,n), secondary neutron emission characts. 79−30843
^{98}Mo(d,n)^{99m}Tc, excitation functions and yields 77−41975
^{98}Mo(d,p), (d,n), (d,α), activation analysis, excitation functions 80−22842
^{98}Mo(d,p)^{99}Mo, excitation functions and yields, <13 MeV 78−37353
^{98}Mo(p,α)^{95}Nb, nuclear structure determ. 77−46118
^{99}Mo, absolute yields in ^{238}U neutron induced fission 79−49642
^{99}Mo beta decay, gamma-ray obs., 0.1-1 MeV, ^{99}Tc 920 keV level spin 77−54145

nuclei with mass number 90 to 149 continued
^{99}Mo, cyclotron production, excitation functions, thick target yields 77−46170
^{99}Mo effective activation cross section from (n,γ) reaction *(Japanese)* 79−97702
^{99}Mo first excited state g factor from ^{96}Zr(α,n) and ^{98}Mo(d,p) 79−17801
^{99}Mo fission product, sequential cation-exchange separation from neutron irrad., U_3O_8 77−90898
^{99}Mo isobaric analogue resonances, activation analysis, excitation functions of ^{98}Mo+d reactions 80−22842
^{99}Mo, levels and gamma decay scheme obs. in ^{98}Mo(n,γ) 77−30580
^{99}Mo, production as generator for ^{99m}Tc 78−37353
^{99}Mo, production by ^{239}Pu fission, absolute yields 77−50167
^{99}Mo, radiochemical characts. and role in nucl. fuel reprocessing, review *(Czech)* 78−82496
^{99}Mo separation from ^{131}I and ^{103}Ru uranium fission products 77−25297
^{99}Mo separation from neutron irradiated ^{235}U, HNO_3 soln., S collector 77−42161
^{99}Mo separation from neutron irrad. UO_2 by vacuum sublimation 77−90893
^{99}Mo, short lived isomers from photonuclear reactions, internal conversion coeffs. 78−37308
^{99}Mo, sublimation separation from neutron irrad. UO_2 77−9257
^{99}Mo-^{99m}Tc generators with (n,γ)-prod. ^{99}Mo, eluate contamination from ^{131}I, ^{103}Ru and ^{239}Np 77−5079
^{99}Mo-^{99m}Tc multiload generator, Multigen, prep. and testing 77−16982
^{100}Mo,(d,p)^{101}Mo excitation functions and yields, <13 MeV 78−37353
^{100}Mo resonances, search for valence neutron capture in 3p neutron giant resonance 77−30587
^{100}Mo+^{100}Mo→^{200}Po, two dimensional fusion barrier, penetrability calc. 78−41798
^{100}Mo+p, cyclotron production of ^{99}Mo, ^{99m}Tc, excitation functions, target yields 77−46170
^{100}Mo(^{12}C,^{10}Be)^{102}Ru, 48 MeV, anal. of direct and indirect processes 77−34342
^{100}Mo(^{14}N,^{12}B), ^{12}B polarisation, quantum mechanical explanation 79−17890
^{100}Mo(^{14}N,^{12}B), 200 MeV, ^{12}B spin polarisation in deep inelastic collision 80−63160
^{100}Mo(^{14}N,^{12}B), 90 meV, spin alignment of products, semi-classical model calcs. 80−73859
^{100}Mo(^{14}N,^{12}B)^{102}Ru, 90 and 125 MeV, spin polarisation of ^{12}B 78−50196
^{100}Mo(^{16}O,^{16}O′γ), 33 MeV, quadrupole moments determ. 77−41887
^{100}Mo(α,4n)^{100}Ru, 45 MeV, negative parity bands obs. in ^{100}Ru 77−6291
^{100}Mo(α,α′γ), 8.5 MeV, quadrupole moments determ. 77−41887
^{100}Mo(d,n)^{100}Mo(d,n)^{101}Tc, excitation functions and yields 77−41975
^{100}Mo(γ,n)^{99}Mo^{m1,m2,g}, isomeric cross section ratios 78−29448
^{100}Mo(n,n′γ), fast n, gamma transitions, level energies and scheme 80−73822
^{100}Mo(p,α)^{97}Nb, transfer reactions, nucl. struct. obs. 77−46118
^{100}Mo(p,p′), 6.975 MeV, E0 transition probability for 0_1^+-0^+ transition 77−41963
^{101}Mo levels, γ-rays and p-wave resonance partial radiative widths from ^{100}Mo(n,γ) 80−57739
^{101}Mo, levels and gamma decay scheme obs. in ^{100}Mo(n,γ) 77−30580
^{101}Mo resonances, levels, J^π, level spacings, cross section from ^{100}Mo(n,γ) 79−89278
^{102}Mo, β-decay, T1/2, ^{102}Tc deduced levels, tentative J^π and transitions 80−52630
^{102}Mo fission product decay, ^{102}Tc decay scheme and γ-intensities 80−78229
^{104}Mo, first excited 0^+ state, $E0^2/E2^+$ ratio 79−17819
^{91g}Mo, ^{91m}Mo, decay anal., half-life meas., γ-γ coincidences 77−2937
^{93m}Mo, nucl. g-factor NMR-ON meas. on Fe-Mo alloys 78−37275
^{93m}Mo→^{93}Nb, high-spin three-quasiparticle states of ^{93}Nb 77−34262
^{93,95}Mo, transfer $\mathcal{L}$ values, spectroscopic factors, J^π via (p,d) and (d,t) 40 MeV 77−74748
Mo(α,α′) A=94-100, 8 MeV, static quadrupole moment determ. 77−6226
Mo(α, xn)^{97}Ru, in compact cyclotron, ^{97}Ru chem. separation 77−37054
Mo(d,α)Nb, on natural Mo, A=92,94,97,98, up to 13 MeV, excitation functions and yields 77−82933
Mo(d,d), A=92, 94, 96, 98, 100, elastic, inelastic scatt., coupled channel, optical model anal., deformation parameters 78−94017
Mo(γ,γ), 2754 keV photon Delbruck scatt. 79−67741
Mo(n,X), 2 keV-20 MeV cross sections, coherent optical and statistical model calcs. 80−18318
Mo(n,γ), 24 keV cross-sections meas., A=92-98 77−57671
Mo(n,γ), 3-90 keV, neutron reson. parameters, capture cross-sections meas. 77−6371
Mo(n,γ), determ. of recoil energy and effective mass from narrow resonance line shapes 77−57660
Mo(n,γ), valency doorway model 77−23021
Mo(n,γ)^{93,99}Mo, 0-3 MeV, valence doorway model for radiative capture 77−79368
Mo(n,n), unified optical model anal., Lane model breakdowns 79−17873
Mo(ν,γ), 1.17 and 1.33 MeV, cross-sections 79−75973
Mo(p,p), unified optical model anal., Lane model breakdowns 79−17873
Mo(p,p′γ), odd isotopes, excited d-states from analogue resonances and p-γ correlations 80−68546
Nb, A=90, 92, short lived isomers from photonuclear reactions, internal conversion coeffs. 78−37308
Nb and Tc doubly odd isotopes, multiplet struct., ^{96}Tc nuclear struct. 78−46024
Nb, α-particle bombardment, yields of Tc isotopes, energy depend. 77−23098
Nb fast neutron capture and activation cross sections 77−26758
Nb, high spin negative parity states from cluster vibration coupling model 79−75823
Nb integral test of cross section, neutron leakage spectra, spherical assembly 77−23033
Nb isotopes, A=95, 97, 99, beta-decay schemes, level struct. 77−26631
Nb+Nb, 67 MeV, Doppler shift and anisotropy of quasimolecular X-rays 77−3048
Nb+$\pi^\pm$, 125 MeV, true absorpt. and scatt. 79−63705
^Nb, A=90,91,94 neutron spectra, level density, direct processes from Zr(p,n) *(Russian)* 79−67666

nuclei with mass number 90 to 149 continued
^{A}Nb, A=90,92,94, Gamow-Teller strength distrib., RPA calcs. 80−78218
^{A}Nb, A=92, 94, γ-ray multipolarities, internal conversion coeffs., energy levels 79−63625
^{A}Nb, A=93,95,97, quasiparticle-phonon coupling model calcs. levels, transitions and spectroscopic factors 79−472
^{A}Nb, nucl. g-factor, A=90, 92 m, NMR-ON meas. on Fe-Nb alloys 78−37275
^{90}Nb, mag. hyperfine splitting const. in Co, NMR-ON meas. 78−43651
^{90}Nb, decay rate perturbation by implantation in metals 77−22944
^{90}Nb giant particle hole resonances, Gamow-Teller strength from ^{90}Zr(p,n) 80−86877
^{90}Nb isovector resonance analogues, Gamow-Teller transition from ^{90}Zr(^{3}He,t) 79−9539
^{91}Nb, 17^{-}/2 state, g-factor meas. 80−32179
^{91}Nb 21/2^{+} state, lifetime, g-factor meas. 77−30487
^{91}Nb, 3.8 μs isomeric state, mag. moment, TDPAD meas. 78−41634
^{91}Nb analogue state decay modes from ^{90}Zr (^{3}He,dp) 79−67702
^{91}Nb, energy spectra and EM props. using broken pair model 80−499
^{91}Nb from ^{89}Y(α,2nγ)^{91}Nb, high spin states, shell model structure 79−93514
^{91}Nb, level struct., $p_{3/2}$ core excitations 77−50060
^{91}Nb, nuclear field theory, testing and appl. 79−13214
^{91}Nb, populated in heavy ion reactions, mag. moments, proton core polarisation 78−21598
^{91}Nb, struct. anal. from ^{91}Zr(p,nγ) at 3.5-4.8 MeV 78−13011
^{91}Nb, two-body effective parameters calc., energy levels 77−57608
^{92}Nb energy levels populated in ^{92}Zr (p, n), spins, parities 77−14125
^{92}Nb, γ-spectra, level and decay scheme for states to 1.6 MeV excit. 77−30504
^{92}Nb, half life determ. by gamma spectroscopy, comparison of ^{92}Nb, ^{94}Nb activities and abundances 78−29423
^{92}Nb, high-spin states, EM props. via ^{88}Sr(^{7}Li, 3n)^{92}Nb 34 MeV 77−74770
^{92}Nb low lying multiplets, DWBA anal. for spectroscopic factors from ^{91}Zr(α,t) 80−57685
^{92}Nb, shell model calcs., energy levels, transitions and spectroscopic factors 79−63593
^{92}Nb^{g}, cross-section and half-life from ^{93}Nb(n,2n), 14.8 MeV 78−70491
^{93}Nb, 1 quasiparticle 2 phonon multiplet, microscopic quasiparticle cluster phonon coupling model 77−2908
^{93}Nb, 24 keV, neutron capture cross section meas. with Fe-filtered neutron beam 79−40910
^{93}Nb (e,e), 80-215 MeV, magnetic moment form factors, M1, M3, M5 transitions 79−40844
^{93}Nb, (n,n′) and (n,2n) reactions, two-particle emission in terms of exciton model *(Russian)* 77−304
^{93}Nb, (n,n), 14.6 MeV, radiation widths and particle widths of highly excited states, γ-transitions 79−6409
^{93}Nb, (n,p), (n,n'p), (n,α), (n,n'α), (n,^{3}He) prod. cross sections at 14 MeV 80−93829
^{93}Nb B(Eλ) transitions, quasiparticle-phonon multiplet, nuclear field theory for superfluid nuclei 80−47427
^{93}Nb high-spin three-quasiparticle states obs. in ^{93m} Mo decay 77−34262
^{93}Nb, Knight shift and quadrupole coupling parameters in orthorhombic β phase NbH and NbD 78−19352
^{93}Nb, mag. form factors, core polarisation and exchange current effects 80−13409
^{93}Nb, NMR meas. in $Nb_{1-xv}V_{xv}H_{x}$ 77−59471
^{93}Nb, NMR obs. of phase transform. in NbD_{x} 77−20721
^{93}Nb neutron resonances, spin and parity assignments from (n,γ) meas. 77−26569
^{93}Nb, quadrupole interaction in Ti-Nb-H system *(Russian)* 77−24761
^{93}Nb, total muon capture rate, quenching of Cabibbo angle 79−22232
^{93}Nb^{m}, γ-ray transitions of isomeric level, K-conversion coeff., exchange effects 77−6304
^{93}Nb+^{16}O, 50-65 MeV, radiative capture cross sections upper limits 79−17923
^{93}Nb+d(α), 12-50 MeV, t formation average cross sections 80−42670
^{93}Nb(^{14}N,X), 210 MeV, deep inelastic, particle-particle correlations for Li, Be, B, C 80−63206
^{93}Nb(^{3}He,α), 19.5 MeV, ^{92}Nb levels determ. 77−88154
^{93}Nb(^{63}Cu,F), (^{63}Cu,X), 280 MeV deep inelastic collisions, mass and KE distrib. 77−26783
^{93}Nb(α, X), 15-72 MeV, excitation functions and spallation cross-sections 80−18274
^{93}Nb(α,2n), 23-7 MeV, proton-neutron excitations in high-spin states of ^{95}Tc 78−17225
^{93}Nb(α,n)^{96}Tc 10.8, 14.0 MeV populating ^{96}Tc low-lying levels 77−2931
^{93}Nb(d,pX), 25.5 MeV, inclusive p spectra and cross sections from d breakup 79−13303
^{93}Nb(d,pX), 80 MeV, inclusive proton spectra, d break-up, DWBA anal. 80−91190
^{93}Nb(e,e), 180° scatt., magnetisation distrib., mag. multipole moments 80−9228
^{93}Nb(e,e), magnetic e scatt., exchange current effects, plane wave Born approx. 80−78282
^{93}Nb(e,e), valence nucleon orbit determ. 78−54669
^{93}Nb(γ,γ′), energy levels, spin and parity, 6465 KeV resonance total width 78−93940
^{93}Nb(n,2n), 13-19 MeV, neutron excitation functions, meas. by activation techniques 79−30825
^{93}Nb(n,2n), 14 MeV, cross section compilation 80−91181
^{93}Nb(n,2n)^{92m}Nb react. cross section meas., 14-19 MeV 78−93992
^{93}Nb(n,γ), 14.1 MeV, gamma emission from pre-equilibrium exciton model 79−75960
^{93}Nb(n,γ), cross-section below 3 MeV, coherent optical and statistical model calcs. 77−26713
^{93}Nb(n,γ), cross-section determ. by Fe filtered beam TOF method 77−23078
^{93}Nb(n,γ)^{94}Nb, E_{n}=14.1 MeV, γ emission exciton model *(Russian)* 79−13302
^{93}Nb(n,γ)^{94}Nb, exciton model, γ spectra calc. 78−62539
^{93}Nb(n,n′), exciton, neutron inelastic scatt. model *(Russian)* 78−33189
^{93}Nb(n,n′)^{93m}Nb, fast neutron flux determ. by ^{93m}Nb disintegration rate meas., X-ray emission *(German)* 77−38579
^{93}Nb(n,n′γ), 1.3-2.7 MeV, energy levels, decay scheme, de-excitation gammas 78−41710
^{93}Nb(n,n′γ), (n,γn′), 14.6 MeV, differential cross sections from nγ coincidence spectra anal. *(Russian)* 78−17209
nuclei with mass number 90 to 149 continued
^{93}Nb(n,n′γ), up to 14.6 MeV, radiation and neutron widths for highly excited levels *(Russian)* 78−605
^{93}Nb(n,t), 14 MeV, cross sections, fast neutron reaction excitation function calc. 79−45267
^{93}Nb(n,xp),(n,xα),(n,d), 15 MeV, cross-section meas. 78−50171
^{93}Nb(p, X), pol.p, 65 MeV, continuum spectra anal. powers 80−102178
^{93}Nb(p,αX), 20-45 MeV, α spectra, exciton model anal. 80−18306
^{93}Nb(p,α), 20 to 44 MeV, energy spectra and α-particle angular distrib. 79−49630
^{93}Nb(p,n)^{93}Mo, direct neutron decay of analogue resonances of ^{94}Mo 80−22824
^{94}Nb excited states from ^{94}Zr(p,nγ), spin, parity, γ-spectra 77−88125
^{94}Nb level density, neutron spectra and ang. distribs. nonequilib. processes from ^{94}Zr(p,n) *(Russian)* 80−37376
^{94}Nb, spin parity determ., excitation energy 979 keV 79−9551
^{94}Nb(n,γ)^{95m,g}Nb, isomeric cross section ratio 79−49623
^{95}Nb, beta decay, K-shell electron ejection 77−18888
^{95}Nb, K-shell autoionisation in β-decay 77−298
^{95}Nb, NMR in Fe 77−59482
^{95}Nb(n,γ)^{95}Nb, ^{95m}Nb, cross section meas. rel. to fusion reactor design probs. 77−23060
^{97}Nb, 1251 keV level spin-parity characteristics, ^{97}Zr β-decay meas. 77−22879
^{97}Nb high spin analogue resonance near N=50 neutron shell, DWBA anal. of ^{96}Zr(^{3}He,d) 80−42613
^{97}Nb, independent yields from thermal neutron induced fission, radiochem. obs. 78−54807
^{97}Nb level structure from ^{97}Zr decay, spins, parities γ ang. correls. 78−29418
^{98}Nb, 51 min, independent yields from thermal neutron induced fission, radiochem. obs. 78−54807
^{99}Nb fission product, nuclear struct. *(German)* 78−29395
^{99}Nb, level schemes, from ^{99}Zr β-decay obs. 79−17863
^{100}Nb mass and excited states from ^{100}Mo(t,^{3}He) 79−63581
^{103}Nb, experimental Q_{β}-values 78−93974
^{133}Nb, high-spin levels, in-beam γ-ray spectra meas. *(French)* 77−61372
^{90m}Nb, decay rate perturbation by implantation in metals 78−21524
^{93m}Nb activity measurement, determ of fast neutron fluence in power reactors *(German)* 77−34371
^{93m}Nb, gamma-emission from 30 keV level *(French)* 77−57617
^{93m}Nb, radioactive decay period meas. *(French)* 77−79341
^{92,94}Nb production in Earth crust by cosmic-ray muons 77−49045
Nb(γ,n), photoneutron Q-value determinations using monochromatic photons 79−22271
Nb(n,n′), 14.1 MeV, precompound processes 78−13093
Nb(n,n′), 9.1 MeV, equilib., pre-equilib., direct process anal. *(Russian)* 77−46172
Nb(π,X), 125 MeV, absorption cross section in 3:3 resonance region 79−85543
Nd (n,2n) react. cross sections at 14.8 MeV 78−74355
Nd, A=139, 141, high spin levels, γ spectra, hole-core coupling 77−50063
Nd decay, ^{A}Pm, A=149,151, shape coexistence, deformed states 80−78135
Nd, even-even, E2 transition probabilities from multiple Coulomb excitation, IBA comparison 80−78212
Nd isotopes, determ. in nuclear fuels as burnup indicator, separation, mass spectrometric method 77−44553
Nd isotopes, prolate-oblate transition from ^{128}Te(^{16}O,5nγ) 78−70438
Nd, N=85 isotones, bands and transitions from α and HI excitation, in-beam study 80−78123
Nd odd isotopes, $1h_{11/2}{}^{-1}$ neutron state strength distrib. 77−46100
Nd(^{12}C,^{12}C), A=143-150 even isotopes, multistep effects in elast. and inelast. scatt. at 70.4 MeV 78−17240
Nd(^{16}O,^{12}C), A=142, 144, comparison of reduced widths derived from transfer reactions and α-emitters, DWBA anal. 79−6671
Nd(^{16}O,^{16}O), 40-48 MeV, even nuclei, 2^{+} state E2 transition probabilities and quadrupole moments 80−18234
^{A}Nd, A=138,139, high spin states, isomers and γ-cascade from ^{140}Cd(α, xzn) 80−78120
^{A}Nd, A=138,139, high spin states, J$^{\pi}$, γ-cascades and shape transition from ^{140}Ce(α, xn) 80−102090
^{A}Nd, A=142,144,146,148, fast neutron radiative capture cross sections, 5 to 350 keV *(Russian)* 78−33188
^{A}Nd, A=145, 147, 149, single neutron hole states spectroscopic factors, DWBA anal. of (d,t), (^{3}He,α) 80−78109
^{A}Nd+n, A=143,145, capture cross section meas. in Triton reactor *(French)* 80−18308
^{A}Nd(^{32}S,^{33}S^{1}), 56 MeV, A=144,146,148, first excited 2^{+} state mag. moment meas. 79−17798
^{A}Nd(^{6}Li,xnypγ), A=142, 146, 150, 54-99 MeV, determ. of cross sections 78−66307
^{A}Nd(n,n) A=142,144,146,148,150, 7 MeV, optical pot. and deformation, cross sections 79−89230
^{133}Nd, high spin states, negative parity level band based $h_{11/2}$ state from ^{116}Sn(^{20}Ne, 3n) 79−75813
^{138}Nd, 10^{+} isomeric states, systematic behaviour 79−30791
^{139}Nd, N=79, states populated in ^{139}Pm decay 77−41929
^{140}Nd ns isomers and yrast isomers, γ-transitions from ^{128}Te(^{16}O,4n) 80−78121
^{141}Nd, ^{142}Nd, high-spin states, lifetime meas. using (α,xn) reactions 77−18476
^{141}Nd, level struct. determ. from (d,t) at 17 MeV and (^{3}He,α) at 24 MeV 77−41979
^{142}Nd, nuclear and Coulomb deform. parameters from DWBA anal. of ^{13}C scatt. 77−3032
^{142}Nd+α, closed shell 82 neutron nucleus, B(E2)-value 78−66296
^{142}Nd(^{16}O, ^{14}C), 104 MeV, two proton transfer between pairing rot. states 77−10430
^{142}Nd(^{3}He,α), 24 MeV, levels in ^{141}Nd anal., DWBA calc. 77−41979
^{142}Nd(^{84}Kr,X), fusion reactions, charge density asymmetry liquid drop model 80−63220
^{142}Nd(d,p), below and near Coulomb barrier 78−29483
^{142}Nd(d,t), 17 MeV, levels in ^{141}Nd anal., DWBA calc. 77−41979
^{142}Nd(e,e′p), spectra and ang. distribs. meas., $T_{>}$ giant reson. anal. 78−13069
^{142}Nd(γ,γ), 1.85-5.0 MeV, resonance fluorescence, level radiative widths, spin assignments 79−9538
^{142}Nd(n,γ)^{143}Nd, E=thermal, ^{143}Nd levels, J, π 77−10320

nuclei with mass number 90 to 149 continued
^{141}Nd, from ^{144}Nd(d,t)^{141}Nd, nuclear levels, intermediate coupling unified model calcs. 78−89791
^{141}Nd, high-spin states and particle-core coupling 77−26614
^{141}Nd, levels, J, π, via ^{142}Nd(n,γ) with E=thermal 77−10320
^{141}Nd reduced normalisation from ^{142}Nd(d,p) 78−86522
^{141}Nd spin 3 resonances, intermediate substructures 77−26586
^{143}Nd(n,α), studied with intense neutron spectrometer 77−23364
^{143}Nd(n,α), thermal cross-sections 78−4932
^{143}Nd(n,α)^{140}Cd, thermal neutrons, partial cross-section 78−608
^{143}Nd(n,α)^{140}Ce, reaction mechanism 79−9558
^{143}Nd(n,γ)^{144}Nd, ^{144}Nd excited states, level scheme extension 77−6231
^{143}Nd(n,γα)^{140}Ce, thermal neutrons, partial cross-section 78−608
^{144}Nd capture states partial α-decay widths from ^{143}Nd(n,γα) 80−37328
^{144}Nd excited state charact., level scheme extension 77−6231
^{144}Nd, excited states calculation, phenomenological models: band-mixing, vibrational-rotational and interacting-boson model 80−22653
^{144}Nd, high-spin states anal. from ^{142}Ce (α,2n)^{144}Nd 77−82940
^{144}Nd, level props. from ^{143}Nd(d,p) and ^{146}Nd(p,t) 77−6241
^{144}Nd levels and transitions, γ-ray spectra from ^{144}Pr^{m}β-decay *(French)* 80−18250
^{144}Nd, neg. parity states, γ-transition multipolarity 79−40882
^{144}Nd(^{12}C,^{14}C)^{142}Nd, 78 MeV, Coulomb excitation effect 77−46186
^{144}Nd(^{61}Ni,X), fusion reactions, charge density asymmetry liquid drop model 80−63220
^{144}Nd(n,γ), 0.04 to 11 keV, reson. γ-ray anal. 78−8823
^{145}Nd energy levels from ^{144}Nd(d,p) and ^{146}Nd(d,t), DWBA calcs. 80−68533
^{145}Nd level scheme from ^{144}Nd(n,γ) 78−8823
^{145}Nd(p,p), (p,p′), 8.7-10.3 MeV, isobaric analogue reson. and seniority model 77−57642
^{146}Nd, 7 MeV neutron elastic and inelastic scatt., diff. cross sections, deformation effects 77−26768
^{146}Nd, from ^{146}Pr decay, level props., 104 γ-ray transitions 78−86476
^{146}Nd(^{16}O,X), 142 MeV, narrow window for incomplete fusion 80−95325
^{146}Nd(γ,γ′), reson. fluoresc., J^{π}, M2/E1 and Γ meas. 77−26663
^{147}Nd, beta decay, ^{147}Pm γγ cascade angular correlations 79−63624
^{147}Nd, beta spectrum, hard component 80−22769
^{147}Nd, β decay, ^{147}Pm level scheme 80−83073
^{147}Nd β-decay, ^{147}Pm energy levels and γ-ray transitions E2/M1 mixing ratio 79−67655
^{147}Nd decay, ^{147}Pm levels, transitions, γγ-coincidences and IC electrons 80−18243
^{147}Nd, energy levels anal. from ^{148}Nd(d,t)^{147}Nd 78−507
^{147}Nd low spin states ns lifetimes, particle rotor model interpretation from ^{146}Nd(d,pγ) 80−78207
^{147}Nd, production by ^{239}Pu fission, absolute yields 77−50167
^{147}Nd, spin by vector analysing powers of ^{148}Nd(d,t)^{147}Nd 78−609
^{148}Nd, appl. to burnup determ. of U and (Th, U) fuels 78−82459
^{148}Nd from ^{148}Pr β-decay, low lying energy levels, quasi band description 80−5096
^{148}Nd ions recoiling in vac. or low press. He, nuclear deorientation, perturbation mech. model 77−50105
^{148}Nd, vibrational states, B(E2) branding rates and interband transitions, pairing plus quadrupole calcs. 80−78127
^{148}Nd+^{12}C, 70.4 MeV, excitation of 3^{-} states in deformed nuclei 78−62559
^{148}Nd+^{19}F, 166 MeV, massive transfer accompanying proton, dueteron and triton emission 79−93648
^{148}Nd(^{16,18}O, xnγ), 69-78 MeV, ^{161,162}Er high ang. momentum states, γ decay modes from multiplicity meas. 78−29419
^{148}Nd(^{18}O,4n)^{162}Er, γ mulitplicities, side feeding pattern, Monte Carlo calc. 79−578
^{148}Nd(α,3nγ)^{149}Sm, 35-45 MeV, collective band struct. of ^{149}Sm anal. 77−61342
^{148}Nd(d,t)^{147}Nd, energy levels of ^{147}Nd 78−507
^{148}Nd(d,t)^{147}Nd, vector analysing powers, spin determ. of ^{147}Nd 78−609
^{148}Nd(n,γ)^{149}Nd→^{149}Pm, energy levels 80−27592
^{148}Nd(p,2nγ), 12.1-20.2 MeV, γ-spectra, deduced ^{147}Pm level struct. 78−510
^{149}Nd, level struct. determ. from decay of ^{149}Pr 77−71591
^{149}Nd, weakly deformed, isomeric $^{9+}/_{2}$ and lowest $^{7-}/_{2}$ states decay 79−89231
^{149}Nd→^{149}Pm, energy level study 80−27592
^{149}Nd→^{149}Pm, γ-ray spectra and Pm level scheme 79−63628
^{141m}Nd, internal conversion of N=81 isotones 78−13027
Nd(d,^{6}Li) (A=142, 144, 146), 35 MeV, ang. distrib. meas., deduced α-particle spectroscopic factors, reduced widths, decay lifetimes 77−18571
Nd(γ,γ), 2754 keV photon Delbruck scatt. 79−67741
Nd(n,2n), A=142, 148, 14.6 MeV, activation cross section 77−88128
Nd(n,n) elastic and inelastic scatt. on even-A isotopes, 4.08 MeV, deformation effects 77−26715
^{237}Np(n,f), thermal neutron sub-barrier fission ^{134}I and ^{135}Xe yields 80−86935
(^{17,18}O,^{17,18}O′), 54-69 MeV, on A=48-92, excited states and ang. distribs., DWBA anal. 79−67705
^{141}PM struct. determ. from ^{141}Sm^{g} decay 77−46142
^{141}PR(e,e′p), $f_{7/2}$ ground isobaric analogue resonance, proton decay mode 78−29450
^{141}P(n,γ), resonance parameters, s-wave radiative and reduced neutron widths 80−47471
^{96}Pb, broken-pair approx. to seniority shell model 78−29408
^{105}Pb, level scheme, from nuclear reactions and ^{105}Ag β decay 77−82849
^{207}Pb, mag. shielding anisotropy in lead compounds, Fourier transform NMR 77−90057
^{208}Pb(^{6}Li, αp), 22.2 and 23.0 MeV, break-up near Coulomb barrier 78−636
^{208}Pb(^{6}Li,αd), 22.2 and 23.0 MeV, break-up near Coulomb barrier 78−636
^{108,110}Pd, particle-vibr. multiplet excit. by two-neutron stripping 77−34214
Pd, A=101-5, particle-core coupling, Nilsson model rot. model at intermediate deform. 77−10362
Pd, A=102,4,6, collective and two-quasiparticle excitation for Zr (^{13}C, 3nγ) 77−18601
Pd, circular polarisation of muonic $K_{α}$ X-rays 78−9284
Pd, even isotopes, low lying collective states, IBA 80−27540
Pd, even-even, collective states, B(E2), branching ratios and moments, boson expansion method 80−102099

nuclei with mass number 90 to 149 continued
Pd, even-mass isotopes, collective model with deform., vibr., rot. energy levels, B(E2) ratios 78−17120
Pd isotope cumulative yields, cumulative yields of Ru and Pd isotopes 79−576
Pd, quadrupole moments of first excited states of even isotopes 78−17099
^Pd (n,γ), A=104, 105, 106, 108, 110, cross sections above 2.6 keV 79−80933
^Pd, A=106, 108, collective excitations in the interacting boson model *(Russian)* 80−5044
^Pd(p,X), 6 MeV, A=102,104,106,108,110, quadrupole deformation, cross sections, direct processes, optical parameters *(Russian)* 79−67753
^Pd(p,t), A=104, 102, at high excitation, observation of hole states 78−25187
^Pd(p,t), A=104, 110, 22 MeV, polarised p, anal. power systematic nuclear struct. depend. 79−22265
^{14}Pd, A=101, 103, 105, decoupled rotational band struct., in spherical quasiparticle theory 78−66193
^{97}Pd $β^{+}$-decay, ^{97}Rh levels and γ-transitions, 3QP model anal. 80−102120
^{99}Pd level scheme, γ-ray cascade, studied via heavy-ion reactions 77−30506
^{100}Pd levels and γ-transitions from ^{100}Ag^{g,m} decay 80−83077
^{101}Pd, level struct. obs. in ^{101}Ag β-decay 78−37311
^{101}Pd nonyrast rotational states, transitions, $T_{1/2}$, branching and mixing ratios from ^{92}Zr(^{12}C,3n) 80−105950
^{102}Pd, 1592 keV E0 transition $T_{1/2}$ meas. using e-γ coincidence 80−22762
^{102}Pd, (p,t) study at 42 MeV, hole states at high excitation 78−50158
^{102}Pd, meas. of $Q(2_1^+)$ by reorientation precession technique 78−12971
^{102}Pd(α,2nγ)^{104}Cd, high-spin states in ^{104,105}Cd anal. 78−62484
^{102}Pd(α,nγ)^{105}Cd, high-spin states in ^{104,105}Cd anal. 78−62484
^{102}Pd(n,2n), 13-18 MeV, compound nucleus and precompound emission models 77−74841
^{102}Pd(n,t)^{100}Rh, 14.6 MeV, production cross sections 79−49629
^{102}Pd(p,p′:γ,γ), population of low spin levels, level scheme 79−36153
^{102}Pd(p,p′γ), 8 MeV, ang. correl. meas. to determ. level scheme 78−21559
^{102}Pd(p,p′γ), long lived O^{+} state, E0 transitions 80−73804
^{103}Pd decay, 357 keV γ:K X-ray abundance ratio obs. 79−498
^{103}Pd, K-electron capture decay, double K-shell vacancy creation 80−22773
^{104}Pd decoupled band behaviour, Coriolis decoupling 77−6205
^{104}Pd levels populated in ^{104m,g}Ag $β^{+}$ decay , spins, parities 78−13018
^{104}Pd, meas. of $Q(2_1^+)$ by reorientation precession technique 78−12971
^{104}Pd(^{6}Li,xnypγ), 54-99 MeV, breakup, fusion-evaporation and pre-equilib. nucleon emission 78−17238
^{104}Pd(α,3nγ)^{105}Cd, high-spin states in ^{104,105}Cd anal. 78−62484
^{105}Pd, 20 eV to 200 keV neutron capture cross sections 77−26759
^{105}Pd E2/M1 mixing ratios from decay of polarised ^{105}Rh 77−6315
^{105}Pd, high-spin particle-core multiplets via ^{96}Zr(^{12}C,3nγ)^{105}Pd, rot. model 77−54140
^{105}Pd levels with large spin, γ spectra 79−6478
^{105}Pd muonic X-rays, nuclear charge parameters, quadrupole moments 78−29377
^{105}Pd(^{3}He,^{3}He) 39.7 MeV, optical pot. mass depend. 77−34327
^{105}Pd(n,p)^{105}Rh, 13-17 MeV, cross section meas. by activation method 78−46057
^{105}Pd(p,nγ)^{105}Ag, γ-spectra, level scheme *(Russian)* 77−74801
^{106}Pd, E0 transition from 0_1^+ state following ^{106}Rh beta decay 80−68578
^{106}Pd energy states and J^{π} from ^{106}Ag^{m} decay 80−18197
^{106}Pd, excited states and transitions from decay of ^{106}Rh^{g} 77−79324
^{106}Pd, gamma-gamma ang. correlation meas. from decay of ^{106}Rh^{g} 77−79325
^{106}Pd, γ-γ directional correlations, mixing ratios 77−82853
^{106}Pd levels and E0 transitions from ^{106}Ru β-decay 79−75894
^{106}Pd, reson. scatt. of annihilation quanta, excited state lifetime meas. *(Russian)* 77−26651
^{106}Pd(^{6}Li,xnypγ), 54-99 MeV, breakup, fusion-evaporation and pre-equilib. nucleon emission 78−17238
^{106}Pd(p,t), 30 MeV, core-coupling model 77−57672
^{106}Pd(t,p), pol.t, cross section and anal. powers, struct. depend., DWBA anal. 80−78272
^{107}Pd fission product neutron capture and total cross-section obs. 79−9573
^{107}Pd(n,γ) and transmission meas., level parameters 78−58277
^{108}Pd, repulsive P-wave interaction, nucl reson. meas. 77−14195
^{108}Pd, vibr. states study, elastic and inelastic electron scatt., anharmonic vibrator model 78−62520
^{108}Pd(p,nγ)^{108}Ag, E_p2.6-3.95 MeV, level struct. of ^{108}Ag 77−18392
^{108}Pd(p,t), 30 MeV, core-coupling model 77−57672
^{109}Pd, ^{238}U fission product, gamma-ray spectra, half-life determ. 77−50084
^{109}Pd decay, double K-shell vacancy creation per internal conversion 79−45212
^{109}Pd, energy levels determ. from decay of ^{109}Rh 78−25154
^{109}Pd, level structure and half life 77−82827
^{109}Pd levels, J^{π}, transitions, unique parity states, and spectroscopic factors from ^{108}Pd(n,γ) 80−42547
^{109}Pd low spin odd parity levels, γ-rays, particle-rotor comparison from ^{108}Pd(n,γ) 80−73805
^{109}Pd low spin odd parity states, rot. aligned model, Coriolis calc. of ^{108}Pd(n, γ) 80−57695
^{109}Pd unique parity levels, interacting boson approx. model test for odd-A nuclei 79−85369
^{109}Pd unique parity states, particle rotor model low spin test 79−93515
^{110}Pd, pionic atoms, dynamical nuclear polarisation, nuclear structure effects 79−94113
^{110}Pd, pionic atoms, E2 nuclear resonance effects 79−76534
^{110}Pd, repulsive P-wave interaction, nucl. reson. meas. 77−14195
^{110}Pd+^{40}Ar, compound nucleus ^{150}Gd, deexcitation, evaporation calcs., comparison with exptl. decay data 77−61391
^{110}Pd+^{40}Ar, formation and decay of ^{150}Gd compound nucleus 77−61453
^{110}Pd(^{12}C,xnγ), shell effects at high spin in the γ-continuum from Te evaporation residues 79−22165
^{110}Pd(^{208}Pb, X), 1.18-1.28 GeV, charge equilib. time scale, relaxation time 80−18188
^{110}Pd(^{208}Pb, X), equilibrium process time evolution, mass and charge distribs., energy loss 79−97725

nuclei with mass number 90 to 149 continued
- ^{110}Pd(^{208}Pb,X), 1.2 GeV, central collisions, neutron rich nucleon flow, mass, charge and energy 80−18337
- ^{110}Pd(^{3}He,d)^{111}Ag, 33.2 MeV, ^{111}Ag level struct. 77−88045
- ^{110}Pd(^{63}Cu,X)Y, new Ir, Os and Re isotopes 78−70563
- ^{110}Pd(e,e′), 40-110 MeV, vibr. nuclei, branching ratios 77−6356
- ^{110}Pd(n,2n), 13-18 MeV, compound nucleus and precompound emission models 77−74841
- ^{110}Pd(p,nγ)^{110}Ag, E_p=2.6-3.95 MeV, level struct. of ^{110}Ag 77−18392
- ^{110}Pd(p,t)^{108}Pd(2_1^+), analysing power difference from ^{110}Pd(p,t)^{108}Pd(2_1^+) 78−37341
- ^{111}Pd, isomer decay populating ^{111}Ag levels 78−551
- ^{111}Pd^{g,m}, γ-ray decay, ^{111g}Pd half-life, ^{111}Ag levels and decay 78−541
- ^{112}Pd, ^{238}U fission product, gamma-ray spectra, half-life determ. 77−50084
- ^{118}Pd+^{118}Pd, 637 MeV time depend. Hartree-Fock-Bogoliubov calc. for fusion and subsequent ^{236}U fission 79−36265
- ^{109g}Pd, gamma-ray decay, gamma-gamma coincidences 78−29417
- Pd(n,n′), near threshold energy for first 2^+ collective levels excitation, statistical model test 77−61408
- Pd(p,t)Pd, A=104, 108, 110, at 52 MeV, direct and indirect interf. 77−54220
- Pm, A=143, 144, 145, ICC, γ-spectra, multipolarities for low-lying levels 77−50081
- Pm, A=147, 149, 151, from (p,α), (t,α) reactions, cross sections, reaction mechs. 79−540
- ^Pm, A=143, 145, proton states and transitions, stripping strength, shell model anal. from Nd(^{3}He,d) 80−68508
- ^Pm, A=143-153, odd-A, spectroscopic factors, shell model anal. from pickup and stripping reactions 80−78137
- ^Pm, A=147,149,151 single proton hole states in pickup reactions from Sm(p,α) 80−78128
- ^Pm, A=149,151, shape coexistence, deformed states from Nd decay 80−78135
- ^{52}Pm, strong exhaustion of deeply-bound proton hole states 79−45142
- ^{139}Pm decay, states in N=79 ^{139}Nd 77−41929
- ^{141}Pm medium spin states, J^π, transitions and shape from (p,2n), (^{3}He,3n), (α,4n) 80−86779
- ^{142}Pm, multiplet splitting and isomerism, J, π, T1/2 via (d,2n) and (p,n) 77−14014
- ^{143}Pm high spin states, J^π, transitions, isomer g-factors from (d,2N), (α,2N) 80−32154
- ^{143}Pm, IAS, J^π via polarised proton scatt. 77−74825
- ^{143}Pm, p single particle states and pairing force calcs., low lying levels 80−42522
- ^{143}Pm reduced normalisation of isobaric analogue resonances from ^{143}Nd(p,p) 78−86522
- ^{145}Pm, form. in electron capture decay of ^{145}Sm, γ-transition decay rate and intensities 78−13030
- ^{145}Pm level struct., J^π and lifetimes, cluster-vibr. model anal. of ^{146}Nd(p,2n) 80−91125
- ^{145}Pm, low-lying levels anal. using ^{145}Sm decay 78−29420
- ^{147}Pm, 0.02 to 250 eV, neutron total cross section and neutron resonance parameters 79−97709
- ^{147}Pm, beta-ray dose rates in skin, conversion from values meas. in air 77−16996
- ^{147}Pm, β-decay, branching ratio and K-shell autoionisation 80−42598
- ^{147}Pm β-decay surface contamination monitoring probes, comparison of response between detectors 78−25398
- ^{147}Pm decay, K-orbital shake off electrons and X-ray spectra 77−46141
- ^{147}Pm, emitted β-ray polarisation 79−85412
- ^{147}Pm energy levels and γ-ray transitions E2/M1 mixing ratio from ^{147}Nd β-decay 79−67655
- ^{147}Pm, γ-γ cascades angular correlations in ^{147}Nd beta decay 79−63624
- ^{147}Pm, in-vivo measurement by phoswich detector 78−28087
- ^{147}Pm, internal bremsstrahlung photon intensity and energy yield 78−86509
- ^{147}Pm, level scheme and transitions following ^{147}Nd 80−83073
- ^{147}Pm, level struct. via ^{148}Nd(p,2nγ) 12.1-20.2 MeV 78−510
- ^{147}Pm levels, transitions, γγ-coincidences and IC electrons from ^{147}Nd decay 80−18243
- ^{147}Pm, low-lying levels, spin-parity and multipole mixing ratios 77−88043
- ^{147}Pm, neutron total cross sections and resonance parameters up to 400 eV 77−23020
- ^{147}Pm proton states and transitions shell model anal. of ^{148}Sm(t,α), ^{146}Nd(^{3}He,d) 79−30781
- ^{148}Pm, ^{148m}Pm decay, struct. of ^{148}Sm determ. 77−67717
- ^{148}Pm, isomeric yield ratio in fission of ^{236}U compound nucleus 77−82975
- ^{149}Pm, β^- decay, ^{149}Sm level scheme 80−22750
- ^{149}Pm, β-decay, nucl. matrix elements, calc., γ-transitions 80−52628
- ^{149}Pm, energy levels from ^{149}Nd beta decay 80−27592
- ^{149}Pm first forbidden β-decay, β-γ ang. correlation, ^{149}Sm 286 keV level J^π character 79−49609
- ^{149}Pm high spin states and bands, rot. description and in-beam study from ^{150}Nd(p,2nγ) 80−32153
- ^{149}Pm levels, bands, transitions, in-beam spectroscopy, particle-rotor anal. from ^{150}Nd(p,2nγ) 80−78125
- ^{149}Pm, populated in ^{149}Nd β decay 79−63628
- ^{149}Pm, shape factor anal. of β-transitions 78−21532
- ^{149}Pm single proton states, spin assignments, spectroscopic factors from ^{150}Sm(t,α), pol.t 80−18170
- ^{149}Pm→^{149}Sm, beta decay matrix elements 78−70488
- ^{148m,148g}Pm, independent form. cross-section from ^{232}Th by ^{4}He ion induced fission 78−33228
- ^{148m}Pm, ^{148g}Pm, ^{146}Pm, independ. yields from ^{233}U(n,f) and ^{235}U(n,f) 77−79407
- Pr, low-lying collective states anal. 77−88030
- Pr, mass dependence for radiative capture of 14.1 MeV neutrons 78−13087
- Pr+n, neutron spin states amplitudes and scatt. cross sections 77−23019
- ^{139}Pr isomeric $11/2^-$ state, half-life, g-factor, and nuclear orientation relaxation from ^{140}Ce(p,2nγ) 79−75837
- ^{139}Pr medium spin states, J^π, transitions and shape from (p,2n), (^{3}He,3n), (α,4n) 80−86779
- ^{140}Pr, deeply bound hole state transition strength giant resonance, DWBA anal. of (p,d) 80−47426
- ^{140}Pr isobaric analogue resonances, de-excitation cascade, K-shell ionisation, spin depend. from ^{140}Ce(p,n) 80−78202
- ^{140}Pr, $P_K/P_{\beta+}$ ratio for allowed decay 77−61386

nuclei with mass number 90 to 149 continued
- ^{141}Pr, double K-hole creation in 145 keV internal conversion 77−18823
- ^{141}Pr, IAS, J^π via polarised proton scatt. 77−74825
- ^{141}Pr, ICC, γ-spectra, multipolarities for low-lying levels 77−50081
- ^{141}Pr, internal conversion decay, double K-hole creation 77−18887
- ^{141}Pr, NMR freq. shifts in PrN and PrSb 77−85595
- ^{141}Pr NMR in $PrVO_4$ 77−77110
- ^{141}Pr, natural line shape of giant dipole resonance 77−88096
- ^{141}Pr, neutron capture cross section and transmission TOF meas. 79−67752
- ^{141}Pr, nucl. spin-lattice relax. time meas. in $Pr_2(SO_4)_3.8H_2O$ 77−28478
- ^{141}Pr, nuclear structure effect on internal conversion of l-forbidden transitions 79−63632
- ^{141}Pr, positive parity levels, gamma-ray yields and ang. distribs. 80−105962
- ^{141}Pr reduced normalisation of isobaric analogue resonances from ^{141}Ce(p,p) 78−86522
- ^{141}Pr+^{35}Cl, 135-170 MeV, evaporation residue excitation functions 77−88166
- ^{141}Pr+^{35}Cl, 155-170 MeV, fission prod. yields, ang. distribs. and mean kinetic energies 78−41790
- ^{141}Pr+n, spherical optical model anal., fast neutron differential elastic scatt. and total cross sections 78−46051
- ^{141}Pr(^{35}Cl,^{35}Cl), 100-170 MeV, elastic scatt. ang. distrib. 78−21605
- ^{141}Pr(^{35}Cl,f), statistical anal. of excitation functions, Bohr-Wheeler and liq. drop model 78−13181
- ^{141}Pr(e,p), 15-25 MeV, T_0+1 giant dipole resonance and characteristic decay mode 80−78247
- ^{141}Pr(n,γ), circular polarisation, ang. distrib. meas. 80−32285
- ^{141}Pr(n,γ), non-statistical capture, radiative widths, γ-ray doorway state model 80−37389
- ^{142}Pr, $2^-\rightarrow 2^+$ β spectrum, shape meas. 77−50083
- ^{143}Pr 351 keV level populated in ^{143}Ce 1110keV β decay, transition shape, spin, parity 77−50085
- ^{143}Pr, 57 keV state, from ^{143}Ce 1404 keV beta transition spectrum shape 78−74339
- ^{143}Pr in Ce, $Ce(NO_3)_3$ soln., mag. dipole moment of 57 keV state, PAC meas. 77−46110
- ^{143}Pr, internal bremsstrahlung 77−82879
- ^{144}Pr, 935 keV beta transition, spectrum shape 78−4918
- ^{144}Pr, high energy β spectrum investig., $^{144}Ce0^-\rightarrow 0^+$ beta transition spectral shape anal. 77−38246
- ^{144}Pr levels and transitions, studied via ^{144}Ce decay 77−14070
- $^{144}Pr^m$β-decay, ^{144}Nd levels and transitions, γ-ray spectra *(French)* 80−18250
- ^{145}Pr, level schemes determ. from β-decay of A=145 nuclei 78−78323
- ^{146}Pr β-decay, ^{146}Nd level scheme and transitions 78−86476
- ^{146}Pr→^{146}Nd, decay scheme and energy levels, log ft values 78−4912
- ^{148}Pr, β^- decay scheme and $T_{1/2}$ determ. using γ coincidence counting techniques 79−93558
- ^{148}Pr β-decay to ^{148}Nd, γ-spectra energy levels, isomerism 80−5096
- ^{148}Pr, short lived fission product, Q_β-value 78−37317
- ^{149}Pr decay, β-branching and log ft values determ. 77−71591
- ^{149}Pr, fission product, γ-spectra, half-life meas. 77−38240
- Pr(γ,n) cross section discrepancies, NBS P-2 chamber calibration 77−26671
- Rb, A=92, 97, delayed-neutron emission probabilities 77−74817
- Rb, A=92-97, delayed neutron energies 77−74816
- Rb decay, ^Sr, A=98, 100 rot. struct. sudden onset, gamma transitions 80−73777
- Rb decay, ^{94,96}Sr direct and skip cascades, γγ ang. correlations, levels, mixing ratios 80−86851
- Rb isotopes, A=88 to 91, decay rate determ. for ground state beta-branching 77−26634
- Rb neutron rich isotopes, nucl. spins and mag. moments 80−47367
- Rb odd isotopes, β^- strength functions, 'pygmy' resonances 79−93559
- Rb precursors, half lives and delayed neutron emission probabilities 79−49610
- ^Rb, A=90 to 99, structure in beta strength function 79−93564
- ^Rb, A=90-93, nucl. moment and charge radius using fast-beam laser spectroscopy 79−40839
- ^Rb, A=91, 93, 94, short-lived, determ. of nucl. spins by β radiation detected optical pumping 78−37262
- ^Rb, A=91 to 98, β-decay half life meas. 79−67718
- ^Rb, A=92-96, β-delayed neutron emission probabilities, half-life 80−52634
- ^Rb, A=93,94,95, delayed neutrons, energy spectra 80−99153
- ^Rb, A=96,98, β-decay schemes and total energies, mass excess and separation energies 80−27601
- ^Rb, A=96 to 100, half-lives and neutron emission probabilities in neutron rich isotopes 79−17864
- ^Rb, A=96-98. β-decay half life determ. 78−78318
- ^{90}Rb, β,γ, conversion electron spectra obs. 77−71583
- ^{90}Rb, independent isomeric yield ratio from spontaneous fission of ^{252}Cf 79−22342
- ^{90}Rb level scheme, transitions, J^π assignments and internal conversion coeffs. from ^{90}Kr β-decay 79−67663
- ^{92}Rb decay, ^{92}Sr γγ ang. correlations, levels, J^π, mixing ratios 80−57725
- ^{93}Rb, γ-ray decay scheme, levels, J^π, logft values 77−54152
- ^{94}Rb β-delayed n decay, ^{93}Sr excited state depopulation γ-rays, n coincidence 80−52631
- ^{98}Rb decay, ^{98}Sr very low lying 0^+ state, shape coexistence bands, $T_{1/2}$, transitions 80−78148
- ^{98}Rb, γ spectra and coincidence meas., deform. in ^{98}Sr anal. 78−12961
- ^{100}Rb β-decay, ^{100}Sr ground state rot. band transitions, deformations and lifetimes 79−93550
- Rh, A=108-111, prod. by fission of ^{235}U, ^{238}U, ^{239}Pu, ^{249}Cf, separation, identification 78−89924
- Rh, static mag. moments, spin, parity and excitation energy from nuclear orientation *(Dutch)* 79−80872
- ^{94}Rh decay, $T_{1/2}$ ^{94}Ru levels and γ-transitions 80−18244
- ^{94}Rh, γ-spectrum and half-lives 80−83062
- ^{97}Rh levels and γ-transitions, 3QP model anal. of ^{97}Pd β^+-decay 80−102120
- ^{99}Rh γ-ray cascade, obs. in ^{90}Zr+^{12}C, and ^{91}Zr+^{11}B 78−41762
- ^{99}Rh isomer, ($T_{1/2}$=4.5 hr.), decay, anticoincidence and integral coincidence spectra meas. 79−6479
- ^{99}Rh, possible high-spin cascade obs. in heavy ion reactions 77−30506
- ^{100}Rh, γ-ray spectrum and ang. γγ correlations, ^{100}Ru level struct. study 79−6510

nuclei with mass number 90 to 149 continued
^{100}Rh, in Be, quadrupole interaction, temp. depend., TDPAC obs. 77−20772
^{100}Rh, lifetime measurements in excited states 79−63631
^{100}Rh, quadrupole interaction in Be, temp. depend. 77−8466
^{100}Rh short lived isomer, decay scheme from (α,pn), (p,n) and (p,3n) 79−75920
^{101}Rh, 20 eV to 200 keV neutron capture cross sections 77−26759
^{103}Rh, (α,p), (α,d) and (α,t) reactions, 50.5 MeV, particle spectra 77−6405
^{103}Rh, β-γ-γ directional correl., J^{π} determ. 77−26628
^{103}Rh E2/M1 mixing ratios from decay of polarised ^{103}Ru 77−6315
^{103}Rh, neutron capture cross sections, 0.5 to 3.0 MeV 79−40912
^{103}Rh, neutron elastic and inelastic cross sections up to 1500 keV, γ-ray transitions, 40 keV isomeric state 77−23089
^{103}Rh, nucl. levels, mean life determination by reson. fluoresc. under bremsstrahlung bombardment *(French)* 77−54179
^{103}Rh, quadrupole moments of $3/2^-$ and $5/2^-$ states, reorientation precession meas. 77−2905
^{103}Rh(e,e′), 350-800 keV, isomer Coulomb excitation cross sections 80−22659
^{103}Rh(n,γ), absolute cross sections in keV range 77−26771
^{103}Rh(n,γ), cross-sections above 2.6 keV 80−32276
^{103}Rh(n,n′)^{103M}Rh reaction rate, absolute calibration 79−85875
^{103}Rh(n,n(γ)), 0.2-2 MeV, ^{103}Rh level scheme, branching ratios, spins, parities, cross sections 78−78374
^{103}Rh(p,n), sub-Coulomb optical pot. 80−102190
^{104}Rh(n,γ), 0.5-3.0 MeV, γ-spectra strength functions 80−32240
^{105}Rh E2/M1 mixing ratios from decay of polarised ^{105}Ru 77−6315
^{105}Rh gamma transitions, directional correl., multiple mixing ratios 79−80897
^{105}Rh in Fe, oriented nuclear decay, mag. moments 77−46111
^{105}Rh, particle-vibr. multiplet excit. by two-neutron stripping 77−34214
^{106}Rh, orientation and mag. moment in Fe 77−85623
^{106}Rh^{g}, decay, excited states and transitions in ^{106}Pd 77−79324
^{106}Rh^{g}, decay, gamma-gamma ang. correlation meas. in ^{106}Pd 77−79325
^{108}Rh, level structure and half life 77−82827
^{109}Rh, 79.8 sec., β-decay to ^{109}Pd, γ and γ-γ meas. 79−3116
^{109}Rh, half-life and decay props. 78−25154
^{101m}Rh, cyclotron prod. through natural precursor ^{101}Pd 77−52875
^{103m}Rh in Fe, γ-detected NMR of 40 keV metastable state, 0.5 to 14 kG external fields 77−59499
Rh(α,^{5}He), 90 MeV, α-n coincidence, ^{5}He breakup kinematics 77−6419
^{102,104}Ru(d,d′) 12 MeV, collective excit., J, B(E2), B(E3) 77−26557
Ru, A=102, 104, collective states, J, B(E2), B(E3) via (d,d′) scatt. 77−26557
Ru, A=99, 101, hyperfine struct. and nucl. moments determ. 77−26575
Ru, even isotopes, low lying collective states, IBA 80−27540
Ru, even isotopes, potential energy surfaces and ground state equilib. deformation 80−73789
Ru, even-even, collective states, B(E2), branching ratios and moments, boson expansion method 80−102099
Ru isotope cumulative yields, cumulative yields of Ru and Pd isotopes 79−576
Ru isotopes, A=107-113, prod. by fission of ^{235}U, ^{238}U, ^{239}Pu, ^{249}Cf, separation, identification 78−89924
Ru isotopic axial distributions in EBR II (U, Pu)O_2 failed fuel pins, γ-scanning determ. 78−687
Ru, quadrupole moments of first excited states of even isotopes 78−17099
Ru short lived isotopes, γ-spectra, gas phase fast separation 77−23582
^{A}Ru, A=101, 103, 105, quasiparticle-phonon coupling model, spectra, moments and transitions 79−22231
^{A}Ru, A=104,106,108, level scheme and transitions, collective model anal. of Tc decay 80−78166
^{A}Ru, A=106, 108, levels, transitions, J^{π} and shape from Tc decay 80−57744
^{A}Ru, A=96, 98, 100, multiparticle states, method of generalised seniority 80−22759
^{a}Ru, A=99, 101, neutron resonance mean spacings and strength functions from Ru(n,γ) *(Russian)* 79−40895
^{A}Ru, first excited 2^+ states, quadrupole moments meas. for A=96, 100 and 104 78−78260
^{A}Ru(^{16}O,^{16}O′), 36-45 MeV, A=96, 98, 100, 102, 104, first 2^+ excited state quadrupole moment 80−47374
^{A}Ru(α,α′), 8.5-9.5 MeV, A=96, 98, 100, 102, 104, first 2^+ excited state quadrupole moment 80−47374
^{A}Ru(n,γ), A=100-104, cross-sections above 2.6 keV 80−32276
^{A}Ru(p,p′γ), A=96, 98, 5-8 MeV, level schemes, transitions, vibr. state, mixing ratios 80−18199
^{94}Ru, broken-pair approx. to seniority shell model 78−29408
^{94}Ru, effective three-body interaction 78−524
^{94}Ru level structure, spin and parity, from beta decay of ^{94}Rh isomers 80−57747
^{94}Ru levels and γ-transitions from ^{94}Rh decay 80−18244
^{94}Ru, populated in heavy ion reactions, mag. moments, proton core polarisation 78−21598
^{95}Ru level scheme, low lying states, g-factor spin, parity 77−88071
^{96}Ru(d,p), 16 MeV, spectra and ang. distribs. meas., ^{97}Ru levels anal. 77−38284
^{96}Ru(d,p)^{97}Ru, 11.5 MeV, study of states in ^{97}Ru 77−18570
^{97}Ru, ^{10}Ru states, studied via ^{96,100}Ru(d,p) reactions at 11.5 MeV 77−18570
^{97}Ru 2.9 day decay, γ-γ correls. from ^{97}Tc 785 keV 77−54178
^{97}Ru ground state g-factor, relaxation time 80−83036
^{97}Ru high spin states, band like structs., transitions from ^{88}Sr(^{12}C,3nγ) 80−73779
^{97}Ru levels anal. with ^{96}Ru(d,p) at 16 MeV 77−38284
^{97}Ru populated in ^{88}Sr(^{13}C, 3nγ), band-like structures 80−32146
^{97}Ru preparation using compact cyclotron, chem. separation 77−37054
^{97}Ru→^{97}Tc, polarised nuclei ^{97}Ru mag. moment, E2/M1 mixing ratios 77−6315
^{99}Ru decay scheme from ^{99}Tc^{m} β-decay 80−42596
^{99}Ru, hyperfine field in Rh_2MnSn, TDPAC expt. 78−43708
^{99}Ru, Mossbauer spectra meas. in $La_xSr_{1-x}RuO_3$ and $La_xCa_{1-x}RuO_3$ 77−48107
^{100}Ru, negative parity bands obs. in ^{100}Mo(α,4n)^{100}Ru 77−6291
^{100}Ru, negative parity yrast band, E1 transitions polarisability, quadrupole-octupole coupled vibr. system 79−484
^{101}Ru(d,p)^{101}Ru, 11.5 MeV, study of states in ^{97}Ru 77−18570

nuclei with mass number 90 to 149 continued
^{100}Ru(p,t), 22 MeV, polarised p, anal. power systematic nuclear struct. depend. 79−22265
^{101}Ru, short lived isomers from photonuclear reactions, internal conversion coeffs. 78−37308
^{102}Ru 2^+ state quadrupole moment, reorientation effects and multiple Coulomb excitation from (α,α), (^{16}O,^{16}O) 80−5063
^{102}Ru levels populated in ^{102}Tc^{g} β$^-$-decay 78−86513
^{102}Ru(^{16}O,^{16}O), 38-42 MeV, Coulomb excitation, 2^+ state electric quadrupole moment 80−73793
^{102}Ru(^{3}He,n), 25.4 MeV, ang. distrib. meas. 77−3022
^{102}Ru(α,α), 8.5, 9.0 MeV, Coulomb excitation, 2^+ state electric quadrupole moment 80−73793
^{102}Ru(γ,p)^{101}Tc^{m,g}, isomeric cross section ratios 78−29448
^{103}Ru contamination in eluate of ^{99}Mo-^{99m}Tc generators loaded with (n,γ)-prod ^{99}Mo 77−5079
^{103}Ru, gamma-ray precision energy meas. 78−58533
^{103}Ru, in sublimation separation of ^{99}Mo from neutron irrad. UO_2 77−9257
^{103}Ru, level scheme determ. from ^{103}Tc β-decay 79−85413
^{103}Ru, levels and gamma decay scheme obs. in ^{102}Ru(n,γ) 77−30580
^{103}Ru→^{103}Rh, polarised nuclei, ^{103}Ru mag. moment, E2/M1 mixing ratios 77−6315
^{104}Ru level energies, B(E2) ratio, mixing ratios, γ-ang. correlations, from ^{104}Tc β-decay 79−493
^{104}Ru, level scheme determ., β$^-$ and γ-activities of ^{104}Tc 78−82313
^{104}Ru, pionic atoms, dynamical nuclear polarisation, nuclear structure effects 79−94113
^{104}Ru, pionic atoms, E2 nuclear resonance effects 79−76534
^{105}Ru, γ-γ ang. correl. meas., spin and γ-ray mixing ratios 78−21516
^{105}Ru, level and γ-decay scheme determ. 78−82312
^{105}Ru, levels and gamma decay scheme obs. in ^{104}Ru(n,γ) 77−30580
^{105}Ru→^{105}Rh, polarised nuclei, ^{105}Ru mag. moment, E2/M1 mixing ratios 77−6315
^{106}Ru 512 keV γ-ray, precise meas., Ge(Li) detector, comparison with positron annihilation radiation standard 77−6610
^{106}Ru β-decay, e$^+$ spectra, ^{106}Pd levels and E0 transitions 79−75894
^{106}Ru gamma active spikants in nuclear fuel for proliferation deterrence, practical aspects 79−93716
^{106}Ru in low level radioactive liquid waste, chem. treatments, removal efficiencies 77−54351
^{106}Ru photoneutron sources, determ. of standard neutron yield, influence of bremsstrahlung 79−72177
^{106}Ru, products, in low-enriched (Pu,U)O_2 fuel assemblies profiles of activity ratios 77−57713
^{93g}Ru, ^{93m}Ru, decay anal., half-life meas., γ-γ coincidences 77−2937
Ru(n,γ) cross sections for ^{101,102,104}Ru 77−23032
Ru(n,n′), near threshold energy for first 2^+ collective levels excitation, statistical model test 77−61408
S6, A=120, 122, 3^+ isomeric states quadrupole moments, (p,n) excited, TDPAD method 78−41635
Sb, A=108,109,110, gamma-ray meas., decay scheme calc. 77−18473
Sb, A=115, 117, $11/2^-$ isomeric states, half-life, and g-factor 78−33122
Sb, A=127-33, fission fragments, partial level schemes determ. 78−29392
Sb, A=128,130,131,134, total β decay energies, mass excesses, β-γ coincidence study 77−82870
Sb, A=131, 133 prod. by ^{232}Th reactor induced fission, yield, radiochem. separation, anal. 78−89923
Sb isomer ratio, high spin trapping from (α,xn)(α, pn) 80−22655
Sb, isomer ratios in fission fragments at high excitation 80−32261
Sb isotopes, fission product conc., sensitivity anal. of various key parameter effects 78−82428
Sb isotopes, unified theory of particle-phonon coupling 77−61360
Sb, mass dependence for radiative capture of 14.1 MeV neutrons 78−13087
Sb, neutron rich isotopes, half-lives, fission yields, and neutron emission probabilities 77−67721
Sb, neutron rich nuclei, IBM and shell model approaches, collective modes 80−78129
Sb, odd-mass nuclei, $9/2^+$ bands, deformed states 78−17106
^{A}Sb, A=113,115,117,119, high spin states, J^{π} assignments, decay schemes and lifetimes from Cd(^{6}Li,3n) 79−54381
^{A}Sb, A=113-175, odd isotopes, collective props., bands and transitions from heavy ion reactions 80−68512
^{A}Sb, A=115, 117, M2, E3 transition reduced matrix elements, EM core polarisation 79−17847
^{A}Sb, A=119,122, level density, neutron spectra and ang. distribs. nonequilib. processes from Sn(p,n) *(Russian)* 80−37376
^{A}Sb, A=121, 123, elec. and mag. hfs. 79−10224
^{A}Sb, A=121,123, levels below 2 MeV, spins, transitions and mixing ratio from (p,γ), (n,n′γ) 80−32191
^{A}Sb, A=123,125,127,129, cross-sections, ang. distribs., spectroscopic factors, DWBA anal. of Te(t,α) 80−52572
^{A}Sb, A=134,135, β-delayed neutron emission probabilities, half-life 80−52634
^{A}Sb, A=135-6, mass chain, half lives and n-emission probabilities of delayed-n precursors 78−70497
^{A}Sb(n,2n), A=121,123, 12.8-18.1 MeV, activation cross sections 80−47477
^{A}Sb(n,2n) A=121, 123, 14 MeV neutron activation cross sections meas. c.f. statistical theory estimates 79−13300
^{A}Sb(n,p), A=121, 123, 14 MeV neutron activation cross sections meas. c.f. statistical theory estimates 79−13300
^{112}Sb, ^{114}Sb, 8$^-$ states, half-life and mag. moment, γ-ray spectra 77−22941
^{113}Sb, 15 MeV excitation, average nucl. lifetime determ. 80−43164
^{113}Sb mean nuclear lifetime from X-ray spectrum in ^{112}Sn(p,p′) 80−9267
^{114}Sb, 8$^-$, 210 μs state, mag. moment, PAC of liq. Sn:^{114}Sb 77−26609
^{114}Sb, quadrupole relax. in liq. Sn 77−16215
^{115}Sb g-factor of $19/2^-$ and $11/2^-$ isomers from ^{115}In(α,4n) 79−40845
^{115}Sb, g-factor of $19/2^-$ isomeric state, time differential perturbed ang. distrib. method 79−22192
^{115}Sb, high-spin states anal., ^{113}In(α,2nγ) at 20-30 MeV 77−41982
^{117}Sb, levels studied via ^{116}Sn(^{16}O,^{15}N)^{117}Sb, ang. distrib. anal. of 64 MeV reacts. 78−8836
^{117}Sb, nucle. spin relax. in liq. In-Te alloys 77−52004
^{117}Sb, spin relax. in liq. In-Sb alloys 77−16216
^{118}Sb beta-decay, study of ^{118}Sn excited states 77−54187

nuclei with mass number 90 to 149 continued
^{119}Sb, decay schemes, lifetimes, expt., theory *(French)* 77−293
^{119}Sb, γ-γ and γ-e directional correls. following ^{119m}Te decay, branching ratios 78−546
^{119}Sb, implantation into Si, Mossbauer obs. 77−20757
^{119}Sb intrinsic high spin state population, cluster DWBA anal. of ^{116}Sn(α,p) 79−67630
^{119}Sb, low-lying states obs. in decay of ^{119m}Te 77−50088
^{120}Sb low lying level scheme, J$^{\pi}$ assignments from ^{120}Sn(p,nγ) 79−22196
^{120}Sb, nuclear alignment in Sn, temp. depend. 78−41720
^{121}Sb, ^{123}Sb, NQR freq. in Sb_2S_3, temp. depend. 77−12228
^{121}Sb, ^{123}Sb, NQR of Sb oxalate-fluoride and nitrate-fluoride complexes 77−12236
^{121}Sb, elec. quadrupole moment from elec. field gradients of trans-dimethyl organometallic moieties 80−29371
^{121}Sb, in $V_{2-x}Sb_xO_4$, Mossbauer spectra, defect struct. exam. 78−18635
^{121}Sb, Mossbauer isomer shifts, book contrib. 79−87360
^{121}Sb, Mossbauer spectra, large anisotropy in mag. hyperfine field in Mn_2Sb 77−73101
^{121}Sb, nucl. level lifetimes by bremsstrahlung reson. fluoresc. *(French)* 79−13247
^{121}Sb, positive parity levels, Coulomb excitation obs. 78−21522
^{121}Sb(d,2n)^{121m,g}Te, 4-24 MeV, yield meas. 78−37349
^{121}Sb(n,γ), γ and conversion electron spectra, ^{122}Sb energy level scheme 78−54721
^{121}Sb(p,n)^{121m,g}Te, 4-24 MeV, yield meas. 78−37349
^{122}Sb, 2$^-$(1.41 MeV β$^-$)2$^+$ negatron decay, numerical values of matrix elements 77−41925
^{122}Sb, 5$^+$ isomeric state, mag. moment determ. from ^{122}Sn(d,2n)^{122}Sb 78−21493
^{122}Sb, 5$^+$ state, mag. moment, g-factor meas. 77−71567
^{122}Sb energy levels populated in ^{121}Sb(n,γ), spin, parity, γ and conversion electron spectra 78−54721
^{122}Sb, low-lying state props., coupled neutron quasiparticle-proton model 77−61378
^{122}Sb(2$^-$)→^{122}Te(2$^+$), comparison with pairing-plus-quadrupole model 77−10370
^{122}Sb→^{122}Te second 2$^+$ excited state, β-γ ang. correls., β-ray spectrum shape 77−38250
^{123}Sb, nucl. level lifetimes by bremsstrahlung reson. fluoresc. *(French)* 79−13247
^{123}Sb populated in ^{123}Sn^m decay, γ-ray, X-ray and electron spectra 77−88073
^{123}Sb, positive parity levels, Coulomb excitation obs. 78−21522
^{123}Sb(d,2n)^{123m}Te, 4-24 MeV, yield meas. 78−37349
^{123}Sb(γ,γ'), energy levels, spin and parity, strong M1 transitions 78−93940
^{123}Sb(p,n)^{123m}Te, 4-24 MeV, yield meas. 78−37349
^{124}Sb, beta-decay to ^{124}Te, level struct. determ. 79−54387
^{124}Sb, first forbidden β-transitions, β-γ circular polarisation correlations 79−9517
^{124}Sb(n,γ)^{125}Sb, reactor neutron capture cross section of 60.3-day ^{124}Sb 80−13469
^{125}Sb decay, gamma-ray spectra, ^{125}Te level scheme obs. 77−10361
^{125}Sb high spin levels, gamma transition energies and intensities from ^{125}Sn^g decay 80−73819
^{125}Sb, in HCl solns., valency states investig., radioanal. tracer preparation, stability 77−63943
^{125}Sb in Pd_2MnSb, orientation meas. with ^{125}Te Mossbauer effect 77−55713
^{125}Sb, radioactive decay, ^{125}Te levels form. *(French)* 77−65202
^{125}Sb, reduced normalisation of isobaric analogue resonances from ^{125}Sn(p,p) 78−86522
^{125}Sb, via nuclear orientation Mossbauer meas. 77−55713
^{125}Sb→^{125}Te, γ-ray spectra of ^{125}Te 79−71816
^{127}Sb, sensibility anal. of the effect of key parameters on fission prod. conc. 79−36290
^{127}Sb states, collective neutron excitation role, spectroscopic factors and form factors from ^{30}Te(p,α) 79−67622
^{130}Sb levels, spin-parity assignments, from ^{130}Sn β decay 77−34264
^{131}Sb partial level scheme from ^{131}Sn beta decaying isomer, γ spectra 77−50091
^{132}Sb, doubly closed shell nuclide, β-spectra, total binding energy determ. 77−50046
^{133}Sb, level scheme of one proton and doubly closed shell core 78−37291
^{134}Sb, expt. β-decay energy of neutron-rich nuclides 79−30808
^{135}Sb, β-decay delayed n emission, simple statistical model description 79−67714
^{135}Sb, β-delayed neutron decay, statistical model, Monte Carlo techniques 78−89830
^{135}Sb, β-strength function energy struct., effect on delayed neutron emission prob. 79−75915
^{135}Sb, delayed neutron emission to excited states in ^{134}Te 77−14077
^{135}Sb, investigation of beta-strength functions by neutron and γ-spectroscopy 79−45209
^{135}Sb, neutron and gamma-ray spectroscopy of delayed neutron emission 77−22973
^{135}Sb, shell model anal. of delayed neutron emission 77−71595
Sb(α,2nγ), collective excitations in ^{123,125}I, spin, parity, level schemes 78−4891
Sb(γ,n), photoneutron Q-value determinations using monochromatic photons 79−22271
Sb(n,γ) determ. of recoil energy and effective mass from narrow resonance line shapes 77−57660
Sb(t,α), A=121, 123, α-particle ang. distrib. at 12 MeV, DWBA anal. 78−62546
^{90}Si transmutation in fusion reactors 79−26559
Sm equilibrium and pre-equilibrium decay, α-multiplicities, energies and entry lines from ^{150}Nd(α,xn) 79−93549
Sm, even isotopes, n ang. distrib., transitions, vibr. band search from Nd(^{3}He,n) 79−63574
Sm isotopes, A=148,152,154, 16 MeV, coherent optical model analysis 77−26750
Sm isotopes, deform. effects in neutron scatt. 77−74758
Sm odd isotopes, $1h_{11/2}^{-1}$ neutron state strength distrib. 77−46100
Sm, stable even isotopes, mean-square charge radii 79−67647
Sm+^{12}C, population of ^{154}Er, high-spin states 78−29373
Sm(^{3}He,^{3}He'), 53 MeV, even A=144-154, DWBA anal. of ang. distribs. 78−17230
Sm(^{16}O, ^{14}C) A=144, 148, 152, 104 MeV, two proton transfer between pairing rot. states 77−10430

nuclei with mass number 90 to 149 continued
Sm, A=144,148, fast neutron radiative capture cross sections, 5 to 350 keV *(Russian)* 78−33188
Sm, A=144-154, mean square nuclear charge radius, laser atomic beam spectroscopy 80−102468
Sm, A=144-154, nuclear charge density and quadrupole moments from muonic X-rays 79−40838
Sm, A=146,147, excited states, energy levels, spin, parity, shell and cluster-vibration models, from (α,xn) and (^{3}He,xn) 80−57683
Sm, A=147, 149, levels, J, γ-transitions and multipole mixing ratios, γγ correlations from Eu EC decay 80−106012
Sm, A=148, 150, 152, 154, levels, moments, isomer shifts, spectroscopic amplitudes, sixth order boson expansion 79−89242
Sm, A=148, 150, 152, 154, 156, excited states of transitional region nuclei, rot. bands *(Russian)* 80−52556
Sm, A=148,9, structural connections, levels, bands, J$^{\pi}$, transitions and mixing ratios from Nd+^{3}He(α) 79−63576
Sm+^{20}Ne, A=148, 150, 152, 70 MeV, Coulomb absorpt. obs. 78−70558
Sm(^{16}O,X), 60-75 MeV, A=148, 150, 152, 154 deformation effects on fusion 80−18360
Sm(^{16}O,X), 60-75 MeV, A=148,150,152,154, fusion cross section, evaporation residues 80−83137
Sm(^{20}Ne, ^{20}Ne), 70 MeV, A=148, 150, 152, Coulomb polarisation pot., coupled channel calcs. 80−22855
Sm(^{3}He, ^{3}He^1), A=144, 148, 152, 154, 150, 40.9 MeV, transition cross sections, deformation parameters, coupled channels anal. 79−67640
Sm(^{40}Ar,X) A=144, 148, 154, 3.6-4.5 MeV/A, sub-barrier fusion, evaporation residue cross section, deformation 80−68718
Sm(^{86}Kr,X), A=144, 154, 490 MeV, transfer reactions and associated γ-multiplicity moments 80−18342
Sm(p,p'), A=144,154, 67 MeV, giant isoscalar monopole resonance excitation 79−22259
Sm(p,t), A=148, 150, 152, 154, 40 MeV, two neutron transfer strengths, IBA model predictions 79−85474
^{140}Sm, 10$^+$ isomeric states, systematic behaviour 79−30791
^{140}Sm, populated in (α,α4n), ground state bands obs. 77−2938
^{141}Sm, M4 11/2$^-$→3/2$^+$ transition, level energy 77−10365
^{141}Sm^g decay scheme, ^{141}Pm level struct. 77−46142
^{142}Sm isomers, lifetimes and transitions from ^{142}Nd(α,4n) 80−78122
^{142}Sm ns isomers and yrast isomers, γ-transitions from (^{24}Mg,4n), (^{19}F,4n) 80−78121
^{143}Sm, T$_>$ hole analogue states, p decay, deduced states and p branching ratio 78−70451
^{144}Sm, isoscalar breathing mode state obs. in (α,α') scatt. at 96 MeV 78−17086
^{144}Sm, p single particle states and pairing force calcs., high spin states 80−42522
^{144}Sm, produced in ^{100}Mo+^{48}Ca 78−37260
^{144}Sm+^{86}Kr, 490 MeV, γ-ray multiplicity moments 78−54798
^{144}Sm+α, closed shell 82 neutron nucleus, B(E2)-value 78−66296
^{144}Sm(^{10}B,4n), ^{148}Tb high spin states, γ-ray and electron meas. 79−49582
^{144}Sm(^{13}C,^{13}C'), 108 MeV, nuclear continuum investigation 80−13506
^{144}Sm(Li,xn) ^{148}Tb high spin states, γ-ray and electron meas. 79−49582
^{144}Sm(α,α'), 96 MeV, ang. distribs., breathing mode states, DWBA calcs. 78−50183
^{144}Sm(γ,γ), resonance fluorescence up to 5 MeV 78−66263
^{144}Sm(n,γ), resonance and thermal n, γ-spectra, recent expt. review, non-statistical effects 80−37383
^{145}Sm decay, low-lying levels of ^{145}Pm anal. 78−29420
^{145}Sm, electron capture decay to ^{145}Pm, γ-transition decay rate and intensities 78−13030
^{145}Sm, electron capture decay, internal bremsstrahlung 78−13035
^{145}Sm, excited state lifetimes γγ ang. correls. 77−6298
^{145}Sm, high-spin states and particle-core coupling 77−26614
^{145}Sm primary γ-rays, direct capture and neutron separation energy, (d,p),(n,γ) correlation 80−57738
^{146}Sm, high spin states and transitions from ^{146}Nd(α,4n) 79−6423
^{146}Sm levels excited by ^{146}Eu decay, spin-parity assignment *(Russian)* 77−14062
^{147}Sm, deformed $1h_{11/2}$ neutron hole states 78−86466
^{147}Sm+n, capture cross section meas. in Triton reactor *(French)* 80−18308
^{147}Sm(n, α)^{144}Nd, 12 to 18 MeV, energy and angular distribution of α-particles, statistical, pre-equilibrium and knock-on models 80−13477
^{147}Sm(n,α)^{144}Nd, 12.4 to 18.2 MeV, energy spectra, ang. distrib., statistical, preequilib., knock-on models anal. 77−26731
^{147}Sm(n,α)^{144}Nd, 2 keV, statistical model anal. 80−102186
^{147}Sm(p,p), (p,p'), 7.5-10.8 MeV, isobaric analogue reson. and seniority model 77−57642
^{148}Sm, 7 MeV neutron elastic and inelastic scatt., diff. cross sections, deformation effects 77−26768
^{148}Sm compound states partial α-widths, α-spectra of ^{147}Sm(n,α) 80−47392
^{148}Sm levels from ^{148}Eu decay, struct. interpretation from boson expansion model *(Russian)* 78−78261
^{148}Sm+^{63}Cu, ^{56}Fe, evolution from deep inelastic transfer to quasi-fission characts. 77−18595
^{148}Sm(^{18}O,^{16}O), interference effects, coupled channels calc. with BCS+RPA wavefunctions 77−26787
^{148}Sm(^{18}O,^{16}O)^{150}Sm, 2_1^+ ang. distributions, shape difference between pick-up and stripping reaction 78−33209
^{148}Sm(α,xn)^{146}Gd, high multiplicity yrast isomers prod. 78−41666
^{148}Sm(n,n'), 7 MeV, differential cross sections, coupled channel anal., deform. effects 77−54219
^{148}Sm(n,n), (n,n'), (n,n'γ), E=2.47 MeV, collective excitations obs. 78−33187
^{149}Sm 286 keV level J$^{\pi}$ character from ^{149}Pm first forbidden β-decay, β-γ ang. correlation 79−49609
^{149}Sm, γ-γ ang. correl. meas., transition multipolarities, multipole mixing ratios 77−41910
^{149}Sm, level scheme following ^{149}Pm β$^-$ decay 80−22750
^{149}Sm, neutron total cross sections and resonance parameters up to 400 eV 77−23020
^{149}Sm(α,xn)^{147}Gd, high multiplicity yrast isomers prod. 78−41666
^{149}Sm(n,γ)^{150}Sm, neutron capture γ-ray spectra calcs. 78−94006
^{150}Sm, calc. of ^{149}Sm(n,γ) spectra 78−94006
^{152}Sm+^{14}N, 135, 165 MeV, massive transfer accompanying proton, deuteron and triton emission 79−93648
^{154}Sm+^{14}N, 135, 165 MeV, massive transfer accompanying proton, deuteron and triton emission 79−93648

nuclei with mass number 90 to 149 continued
Sm(d,^{6}Li) (A=144, 148, 150, 154), 35 MeV, ang. distrib. meas., deduced α-particle spectroscopic factors, reduced widths, decay lifetimes 77−18871
Sm(n,γ) A=147, 149, cross section, statistical theory anal., radiative strength functions *(Russian)* 78−17212
Sm(n,n) elastic and inelastic scatt. on even-A isotopes, 4.08 MeV, deformation effects 77−26715
Sm(p,t), even isotopes, high energy neutron pairing strength, two neutron holes, resonances 80−78116
Sn 2_1^+ excitation, α-spectroscopic factors in IBA model from Te(d,^{6}Li) 80−105967
Sn (^{35}Cl,^{35}Cl), A=116,120,124, 100-170 MeV, elastic scatt. ang. distrib. 78−21605
Sn, A=104, 106, 108, seniority four admixtures in low lying 0^+ states 78−8741
Sn, A=108-118, L,J,π via (^{3}He,n) 25.4 MeV reaction to 0^+ states 77−50050
Sn, A=112-124, charge distrib., self consistent calc. *(Russian)* 77−38234
Sn, A=114, 116, 118, 120 and 122, (p,t) study at 42 MeV, hole states at high excitation 78−50158
Sn, A=114, 6, 8, struct. of quintet states of negative parity 77−288
Sn, A=116, 120, density of states of spherical nuclei calc. 78−513
Sn, A=127 to 131, total β decay energies, mass excesses, β-γ coincidence study 77−82870
Sn, A=131, 132 prod. by ^{232}Th reactor induced fission, yield, radiochem. separation, anal. 78−89923
Sn, α-spectroscopic factors from (d, ^{6}Li) 80−534
Sn, deep h-le state fragmentation, strength functions, giant resonances, quasiparticle phonon model 80−37320
Sn, deep hole states observed in particle transfer reactions 80−68511
Sn, deform. of ground and excited states 78−82277
Sn, even isotopes, collective states and transitions from simple phenomenological model 80−73787
Sn, even isotopes A=116-124, 0^+, 2^+ 4^+ states, Tamm Dancoff approx. 78−37297
Sn, extended Skyrme force calculation, spin instability 79−63601
Sn, internal conversion coeffs. for inner shells of atomic ions and relativistic ionic potentials 80−68600
Sn isotopes, fission product conc., sensitivity anal. of various key parameter effects 78−82428
Sn isotopes, levels and spectra from broken pair model 80−73801
Sn isotopes, M1 transitions, theory of finite Fermi systems *(Russian)* 77−6296
Sn isotopes, quantum number projection, particle number projection 80−27566
Sn isotopes, relation between interacting boson approx. and quasiparticle formalism 80−32216
Sn mass region, α transfer reactions, pairing vibr. model anal. 79−13272
Sn Mossbauer isomer shifts, book contrib. 79−87359
Sn, neutron cross section, filtered neutron beam technique, Doppler effect 80−52670
Sn, neutron pickup reactions, deeply bound hole states, isobaric analogue states in ^{115,117,119,123}Sn 77−30570
Sn, nucl. electron capture, 0.43-1.71 MeV electrons 79−6513
Sn odd isotopes, A=109-117, high spin states, level schemes 78−54684
Sn odd isotopes, spreading widths of deep lying hole states 78−29388
Sn, odd mass isotopes, low lying negative parity states, energy levels, shell model calc. 80−5076
Sn odd-mass isotopes, hole-state analogues, line broadening and Coulomb displacement energies 80−52560
Sn, photoactivation by 42 MeV bremsstrahlung, gamma transition energies and line intensities 78−13057
Sn, π^- and p elastic scatt., 30 to 50 GeV/c, nuclear radius, real/imaginary forward scatt. amplitude ratio *(Russian)* 77−34351
Sn, seniority breaking; centroid energy, partial width and mixing parameter calcs. 78−70468
Sn, simple configurations in capture states 77−22939
Sn, single closed shell even mass nuclei, collective bands, spin, parity, from Cd(α,2nγ), γ meas. 78−54719
Sn stable isotopes, yields in ^{235}U(n_{th},f) and ^{239}Pu(n_{th},f) in symm. region 77−34358
Sn+K_L, 30 to 150 GeV, total cross sections, inelastic screening evidence 79−17936
Sn+K_S, 20 to 140 GeV, precise coherent K_S regeneration amplitudes 79−17937
Sn+p, Sn+$\pi^\pm$, 225 GeV/c, J/ψ and ψ′(3.7) prod. study using muon pair meas. 77−57694
Sn+$\pi^\pm$, Sn+p, massive muon pair prod., test of Drell Yan model 77−57695
Sn(^{3}He, n), 25.4 MeV, ang. distribs., ^{114,118,120,122,126}Te deduced levels 78−89890
Sn(^{3}He,t), 45.9 MeV, IAS, Coulomb displacement energies 77−6337
Sn(^{16}O,3n)^{131,129}Ce, band structs., high spin levels, yrast cascades 78−8842
Sn(^{16}O, 4nγ), 76 MeV, lifetimes of yrast states of even Ce nuclei 78−21589
^Sn, (A=112, 114, 116, 118, 120, 122), so-called two phonon states, quasiparticle shell model calcs. 79−89251
^Sn (t,α), 4.75-5.25 MeV, A=112, 116, 118, 120, 124, single proton states RMS radius 80−13350
^Sn, A=106,108, $\beta^+/(EC+\beta^+)$ probability ratio, EC decay energies, mass excesses 80−27543
^Sn, A=106-108, yrast levels and transitions from ^{54}Fe(^{58}Ni, X) 80−105957
^Sn, A=108 to 126, quasi-particle coupling to pairing and quadrupole vibrs. 79−54373
^Sn, A=109,111,113,115,117, level scheme, J^π assignments, high spin states from Cd(α,xn) 79−45168
^Sn, A=111,115,119, neutron hole distribs., IAS and spectroscopic factors from Sn(^{3}He,γ) 80−42519
^Sn, A=112, 114, 116, 118, positive parity band heads, excitation energies and transitions from Cd(α, 2nγ) 79−45136
^Sn, A=112-124 even isotopes, 0^+ state collectivity, E0 and E2 transition rates 80−73785
^Sn, A=113, 115, 117, 119, deeply bound hole state struct. from (^{3}He,α) 78−93930
^Sn, A=113,115,117,118,119,120, rms neutron orbit sizes, DWBA anal. of Sn(t,d) data 79−36145

nuclei with mass number 90 to 149 continued
^Sn, A=116, 118, 120, 122, 124, 0^+, 2^+ and 4^+ states 1 number conserving approach 80−22694
^Sn, A=116, 124, neutron densities and single particle struct. 80−32165
^Sn, A=118,120,122, deep hole states, excitation energies and ang. distribs. from Sn(p,t) 80−86792
^Sn, A=120,122,124,126,128, levels, transitions and J^π values from In isomeric decays 79−75851
^Sn, even A=116, to 124, $2_2^+ \rightarrow 2_1^+$ energy level transitions in (n,n′γ) reaction, pair interaction effects *(Russian)* 79−3114
^Sn+^{35}Cl, A=112, 116, 120, 124, 155-170 MeV, fission prod. yields, ang. distribs. and mean kinetic energies 78−41790
^Sn+^{40}Ar, A=122, 124, 50 to 120 MeV, angular momentum limits 78−25224
^Sn+p, A=116,124, 1 GeV, neutron production *(Russian)* 79−85477
^Sn(^{35}Cl,^{35}Cl′), 108 MeV, A=112-124 even isotopes, 2_1^+ mag. moments and shell model struct. 80−86805
^Sn(^{40}Ar, xn), (A=116, 120, 122, 124), 161-236 MeV, γ-multiplicity meas., Er compound nucleus formation 79−89320
^Sn(d,^{6}Li)^{108}Cd, even A=112 to 124 spectra for E_d=33 MeV 79−6626
^Sn(e,e′) A=116, 120, 124, electric moment distrib., lowest lying quadrupole states excitation 79−6392
^Sn(n,γ) A=114,116,118, ^{115,117,119}Sn resonance meas., weak coupling model calc. for levels, J^π assignments 79−6416
^Sn(n,n′), A=116, 118, 120, 122, 124, 11 MeV, levels, deformation parameters, isospin effects, optical parameters 80−57679
^Sn(n,n′), A=116, 118, 120, 122, 11 MeV, octupole vibr. states, diff. cross section, deformation length, DWBA anal. 80−102092
^Sn(n,n), 11-26 MeV, A=116, 118, 120, 122, 124, differential and total cross sections, optical pots. 80−78293
^Sn(n,n), A=116,118,120,122,124, isovector deformation parameters and core polarization 79−67642
^Sn(n,n) A=116, 124, 11, 24 KeV, differential cross sections, global optical model anal. 80−18298
^Sn(p,X), A=112, 124, 7.6, 10 GeV/C, isotopic cross section ratios, He, Li fragments isotopic effects *(Russian)* 80−63154
^Sn(p,n), A=112, 116, 124, 35.3 MeV cross-sections, test of forward scatt. amplitude approx. 79−6599
^Sn(p,p′), A=115, 117, 119, 18 MeV, state spin assignment, particle-vibr. coupling 80−32160
^Sn(p,p′), A=116, 124, 0.8 GeV, polarised p, spin orbit deformation effects, DWBA anal. 79−30832
^Sn(p,p), A=116, 120, 4-9 MeV, proton optical pot. low energy behaviour 79−85469
^Sn(p,p), A=116,124, polarised p, 0.8 GeV, neutron isotopic density differences and RMS radii 79−67643
^Sn(p,p) A=116, 124, 800 MeV, polarised p, n density uncertainties from optical model anal. 79−22185
^Sn(p,$\pi^\pm$), A=112, 124, 660 MeV, pion energy spectra, isotopic effects *(Russian)* 80−42669
^Sn(p,t), 52 MeV, A=117,119, angle integrated cross sections, blocking effect ^{115,117}Sn transition strengths 79−89307
^Sn(p,t), A=122, 120, 124, 116, 118, at high excitation, observation of hole states 78−25187
^{106}Sn decay, ^{106}In level scheme determ. 78−93971
^{106}Sn excited states from ^{106}Co (^{3}He,3n), coincidence experiments 80−52607
^{108}Sn, electron capture decay to ^{108}In, level scheme 77−71589
^{109}Sn, mass excess and excited states from ^{112}Sn(^{3}He,^{6}He) 79−6375
^{110}Sn, level struct. determ. from decay of ^{110}Sb 77−18473
^{112}Sn 6^+ isomeric state g-factor and relaxation time from Cd(α,2nγ) 80−73794
^{112}Sn, determ. of multipole mixture values in $2_2^+ \rightarrow 2_1^+$ transitions *(Russian)* 79−89268
^{112}Sn+^{32}S fusion, 160 MeV, mass, velocity, angular and charge state distribs. 78−82405
^{112}Sn+^{35}Cl, 135-170 MeV, evaporation residue excitation functions 77−88166
^{112}Sn(^{3}He,α), 34.8±0.3 MeV, α-particle energy spectra distrib., c.f. preequilibrium decay calcs. 79−9598
^{112}Sn(A,n)^{115}Te, nuclear alignment of ^{115}Te temp. depend. 78−41720
^{112}Sn(p,p′), 20.51, 25.0 MeV, energy levels, excitation functions and ang. distribs. 80−32184
^{113}Sn, chem. effect on electron capture probability and decay const. 79−54412
^{113}Sn, correlated radiation damage in Ag, TDPAC 78−43739
^{113}Sn, decay, electron capture probability 77−67720
^{113}Sn, decay to levels of ^{113}In 77−38247
^{113}Sn-^{113m}In generator, monitoring Zr and ^{113}Sn breakthrough in ^{113m}In eluates 77−5078
^{114}Sn, determ. of multipole mixture values in $2_2^+ \rightarrow 2_1^+$ transitions *(Russian)* 79−89268
^{114}Sn, isospin purity violation, dominant role of noncollective monopole states 78−12964
^{115}Sn, Coulomb excit. via (^{4}He,^{4}He) and (^{16}O,^{16}O) reactions 77−67719
^{115}Sn, fine struct. in deeply bound hole states 77−41874
^{115}Sn, levels, J^π via ^{116}Sn(d,t)^{115}Sn 23 MeV 78−612
^{115}Sn, neutron spectra from ^{115}In(p,n) *(Russian)* 79−9579
^{115}Sn, quad. relax. rates in liq. GaIn alloys 77−12272
^{115}Sn, spin relax. in liq. In-Sb alloys 77−16216
^{115}Sn weak coupling neutron hole states from ^{116}Sn(^{3}He,α) 80−73786
^{115}Sn(^{3}He,d), 28.4 MeV, ^{116}Sn state excitation energies, and partial half lives, spectroscopic factors 78−66295
^{116}Sn, collective states and E0, E2 transition rates 79−17787
^{116}Sn, level density with schematic forces 78−41639
^{116}Sn levels, J^π and transitions from ^{115}Sn(n,γ) 80−52587
^{116}Sn, levels studied via ^{116}Sn(^{16}O,^{16}O) and ^{116}Sn(^{16}O,^{16}O′) ang. distrib. anal. of 64 MeV reacts. 78−8836
^{116}Sn particle-hole states, strength decoupling form giant dipole resonance, Gaussian force, δ-force diagonalisation 78−25125
^{116}Sn, π content of ground and low-lying states 77−38225
^{116}Sn, state excitation energies and partial half lives from ^{115}Sn(^{3}He,d), 28.4 MeV 78−66295
^{116}Sn+^{35}Cl, fusion excitation functions, dynamical model calc. 78−50224
^{116}Sn(^{12}C, 3nγ), 45-55 MeV, collective excitations in ^{125}Ba 78−37258
^{116}Sn(^{20}Ne, 3n)^{133}Nd, study of high spin states in ^{133}Nd *(French)* 77−61372
^{116}Sn(^{32}Cl,f), statistical anal. of excitation functions, Bohr-Wheeler and liq. drop model 78−13181

nuclei with mass number 90 to 149 continued

^{116}Sn(^{3}He,^{3}He), 90-120 MeV, cross sections, deduced unambiguous optical pot. 79−13311
^{116}Sn(^{40}Ar,X), 222-340 MeV, charged particle emission, early collision evolution, fission and evaporation cross sections 80−106072
^{116}Sn(^{40}Ar,X) 187, 222, 340 MeV, fusion cross sections, direct and evaporative p and α prod., evaporation, fission 80−13518
^{116}Sn(α,α'), 96, 129 MeV, giant resonance excitation, isoscalar breathing mode state, nuclear incompressibility 80−68620
^{116}Sn(d,p), pol. d, 8.22 MeV, vector anal. power, p and d spin depend. effects 80−5114
^{116}Sn(d,t), fine struct. in deeply bound hole states in ^{115}Sn 77−41874
^{116}Sn(d,t)^{115}Sn, 23 MeV, populating ^{115}Sn levels to 4 MeV excit. 78−612
^{116}Sn(e,e'), 40-110 MeV, vibr. nuclei, branching ratios 77−6356
^{116}Sn(p,α)^{113}In, 22 MeV, analysing power, J-depend., DWBA 78−70523
^{116}Sn(p,p'), 800 MeV, high energy octupole giant resonance, ang. distribs. 80−86879
^{116}Sn(p,t), 20 MeV, two step (p,d)(d,t) process, second order DWBA 78−66276
^{116}Sn(p,t)^{114}Sn, 20 MeV, finite-range effect in (p,d)(d,t) process 78−74365
^{117}Sn, level density with schematic forces 78−41639
^{117}Sn, substructure in radiative strength function using quasiparticle-phonon nucl. model 79−40901
^{117}Sn^m, E5 transition, branching ratio from ^{120}Sn(p,3np) 79−45200
^{117}Sn(γ,γ'), excitation of 6517 keV level, resonant scatt. 79−3135
^{117}Sn(n,γ)^{118}Sn, disturbance of parity in ^{118}Sn gamma decay *(Russian)* 77−3008
^{117}Sn(n,γ)^{118}Sn, parity violation obs. 78−8820
^{117}Sn(p,d), polarised p, 12.9 MeV, anal. power 80−5114
^{117}Sn(p,p), polarised p, 12.9 MeV, anal. power 80−5114
^{118}Sn (^{6}Li,αd), 22.2 and 23.0 MeV, break-up near Coulomb barrier 78−636
^{118}Sn excited states, studied via β-decay of ^{118g}In and ^{118}Sb 77−54187
^{118}Sn, inclusive proton photoprod., momentum spectra, max. bremsstrahlung energy 2.0 to 4.5 GeV *(Russian)* 77−34287
^{118}Sn(^{12}C,3n)^{127}Ba, high spin level structure in ^{127}Ba 77−38226
^{118}Sn(^{18}O,^{16}O)^{120}Sn, 53 to 62 MeV, optimum Q value at the Coulomb barrier 78−78413
^{118}Sn(^{3}He,α), inner hole states excitation, DWBA anal., reaction mechanism *(French)* 78−41735
^{118}Sn(^{6}Li, αp), 22.2 and 23.0 MeV, break-up near Coulomb barrier 78−636
^{118}Sn(^{6}Li,^{6}Li'), 153 MeV, isoscalar giant quadrupole resonances 80−13440
^{118}Sn(^{7}Li,^{7}Li), 48 MeV, optical model parameters for DWBA anal. 79−6688
^{118}Sn(e,e), 225 MeV, nucleon density distribution in nucleus 79−75831
^{118}Sn(γ,p), up to 0.25 GeV, from bremsstrahlung γ-quanta *(Russian)* 80−5123
^{118}Sn(γ,p)^{117}In, 150 to 750 MeV, reaction cross section 78−37329
^{118}Sn(p,αX), 20-45 MeV, α spectra, exciton model anal. 80−18306
^{118}Sn(p,α), 20 to 44 MeV, energy spectra and α-particle angular distrib. 79−49630
^{118}Sn(p,α)^{115}In, 20 MeV polarised protons, DWBA calcs. 78−41714
^{118}Sn(p,t), 22 MeV, polarised p, anal. power systematic nuclear struct. depend. 79−22265
^{118}Sn(p,t). ang. distribs. and cross sections full finite range CCBA anal. 80−5141
^{119}Sn, hyperfine mag. field in $FeSn_2$, γ-reson. spectroscopy obs. *(Russian)* 78−39486
^{119}Sn, 23.87 keV level half-life 80−47433
^{119}Sn elec. quadrupole moment from elec. field gradients of trans-dimethyl organometallic moieties 80−29371
^{119}Sn, electron scatt. in solids, effective range, Mossbauer obs. 77−63345
^{119}Sn, hyperfine field in Rh_2MnSn, Mossbauer expt. 78−43708
^{119}Sn impurity atoms in Pd-Fe(Co), Mossbauer effect under pressure, and hyperfine mag. field model *(Russian)* 77−55742
^{119}Sn in Fe_3O_4, Mn_3O_4 and Co_3O_4, field exam. by Mossbauer meas. 77−69753
^{119}Sn, in SnI_4 cryst., dynamical props. by Mossbauer spectroscopy 77−59495
^{119}Sn, in SnTe, temp.-depend. isomer shift of Mossbauer line 77−8457
^{119}Sn isomer shift calibration const. 77−28496
^{119}Sn, magnetic moment, of $I=+^3/_2$ level *(Russian)* 78−50083
^{119}Sn, Mossbauer effect in Au, Pd, and Pt matrices 78−15080
^{119}Sn, Mossbauer effect meas. in supercond. $Eu_zSn_{1-z}Mo_6S_y$ 77−69447
^{119}Sn, Mossbauer obs. of hyperfine interactions in MnSb 77−40160
^{119}Sn, Mossbauer spectra 77−73100
^{119}Sn, Mossbauer spectra of β-Mn-Fe-Sn alloys, weak itinerant electron antiferromagnetism 77−36158
^{119}Sn NMR by pulse Fourier transform, T_1, T_2 and chem. shifts 77−55715
^{119}Sn resonance from inert gas matrix, Mossbauer isomer shift calibration 77−46530
^{119}Sn, resonance line shifts, double Mossbauer spectrometer 78−82560
^{119}Sn, substructure in radiative strength function using quasiparticle-phonon nucl. model 79−40901
^{119}Sn^m, Mossbauer spectroscopy of $Dy_2Sn_2O_7$, hyperfine interaction and Dy^{3+} relax. 77−59494
^{119}Sn(d,pX), 25.5 MeV, inclusive p spectra and cross sections from d breakup 79−13303
^{119}Sn(d,t), 6 MeV, polarised d, tensor anal. power and D-state effects 79−85446
^{119}Sn(γ,n), giant mag. dipole resonance location, photoneutron polarisation method 80−37357
^{119}Sn(p,X), 400 GeV, absorption cross sections and multiplicity distribs., A-depend. study 79−67748
^{119}Sn(p,n')^{119}Sb, 17-19 MeV, analogue state excitation and decay 79−6542
^{119}Sn(p,n)^{119}Sb, 16-20 MeV, isobaric analogue state, ang. distrib. meas. 78−29468
^{119}Sn(π^-,π^-), smooth cutoff model angular distrib. 77−10376
^{11x}Sn, (x=3-6,8) quad. moment, γ-ray spectra of Cd:Sn 77−26571
^{120}Sn, 62 MeV, complex particle emission, pre-equilibrium exciton model anal. 78−66280
^{120}Sn finite Fermi-system theory, E1, E2, M1 resonances, γ absorpt. cross section near threshold 77−50055
^{120}Sn, giant multipole reson. fragmentation over two-phonon states 78−575

nuclei with mass number 90 to 149 continued

^{120}Sn γ-spectra, E1 and M1 hindrance factors from ^{123}Te(n,γα) 80−37386
^{120}Sn, level struct. from ^{120}In β-decay 78−86510
^{120}Sn, nuclear K-X-ray satellites, Z=50-83, by α-bombard., 17.5-22.5 MeV 80−42984
^{120}Sn, spherical nuclei, excitation of collective states in high-energy proton interactions 78−17073
^{120}Sn+^{132}Xe, deeply inelastic, relative motion mass transport and dynamics 79−13320
^{120}Sn+^{35}Cl, 135-170 MeV, evaporation residue excitation functions 77−88166
^{120}Sn+^{86}Kr, 5.99 MeV/N, are γ-ray multiplicity 78−82375
^{120}Sn+n, transmission and capture γ-ray meas., ^{121}Sn props. 77−3004
^{120}Sn+p, exciton model of pre-equilib. decay 77−18487
^{120}Sn(^{120}Sn,^{118}Sn), semiclassical description of two nucleon transfer in superfluid nuclei, nuclear Josephson effect 79−45296
^{120}Sn(^{12}C,3nγ)^{129}Ba, E=45-54 MeV, excitation of high-spin levels in ^{129}Ba 78−17104
^{120}Sn(^{3}He,^{3}He), 130 MeV, elastic scatt. ang. distribs., optical model anal. 78−94020
^{120}Sn(^{3}He,^{3}He), 130 MeV, giant reson. excitation, DWBA anal. 79−89319
^{120}Sn(^{40}Ar,X), deeply inelastic collisions, form factors, microscopic calcs. 80−18339
^{120}Sn(^{6}Li,X), 156 MeV, projectile break up in continuous particle spectra, cross section, fragmentation 80−86889
^{120}Sn(α, p), semi-microscopic spectator model 77−26779
^{120}Sn(α,f), 140 MeV, fission cross sections and probabilities, isomeric yield ratio 79−45308
^{120}Sn(d, d'), 108 MeV, giant monopole resonance excitation and ang. distribs. 80−102164
^{120}Sn(γ,γ'), excitation by 7310 keV level, resonant scatt. 79−3135
^{120}Sn(γ,γ') nuclear resonant scatt. from 6730 keV level 79−3134
^{120}Sn(p,n), statistical multistep direct emission, p-h and DWBA calcs. 80−106035
^{120}Sn(p,n)^{120}Sb, nuclear alignment of ^{120}Sb temp. depend. 78−41720
^{120}Sn(p,nx), 45 MeV, preequilib. ang. distrib., generalised exciton model 77−10407
^{120}Sn(p,p) 100 MeV, systematic optical model anal. 78−66274
^{120}Sn(π,π), many body effects in resonant scatt. 78−94029
^{120}Sn(π,π), total cross section, density distribs. and ray bending effects 80−47509
^{121}Sn level props. determ. from ^{120}Sn+n transmission and capture gamma-ray meas. 77−3004
^{121}Sn, liquid scintillation counting for activation analysis of biological samples at nanogram level 78−3693
^{121}Sn$^m\rightarrow{}^{121}$Sn$^g\rightarrow{}^{121}$Sb, branching fraction, K-shell IC coeff. 78−82319
^{122}Sn excitation of 6^+, 8^+, 10^+ and 9^- states, DWBA anal. from ^{122}Sn(p,p') and ^{124}Sn(p,t) 79−89264
^{122}Sn, kaonic, E2 nuclear resonance effects 78−29868
^{122}Sn+^{120}Sn, 630 MeV, multipair transfer calcs. for superfluid ions, coupled channel WKB approx. 78−37373
^{122}Sn(^{40}Ar,4n)^{158}Er, high-spin yrast levels in ^{158}Er, second discontinuity obs. 77−61373
^{122}Sn(K^-, X), 0 MeV, E2 nuclear resonance effects, γ and X-ray meas. 78−41774
^{122}Sn(d,2n)^{122}Sb, ^{122}Sb 5^+ state mag. moment and g-factor 77−71567
^{122}Sn(d,2n)^{122}Sb, ^{122}Sb 5^+ isomeric state mag. moment determ. 78−21493
^{122}Sn(d,d), 15 MeV, optical model calc. 78−41729
^{122}Sn(p,n), 11.2 MeV, spin cut-off parameters from neutron ang. distribs. *(Russian)* 79−80940
^{123}Sn(p,p), 20 MeV, elastic and inelastic scatt., analysing powers *(Dutch)* 78−29464
^{123}Sn, deeply bound hole state transition strength giant resonance, DWBA anal. of (p,d) 80−47426
^{123}Sn^m decay scheme, γ-ray, X-ray and electron spectra, ^{123}Sb transitions 77−88073
^{124}Sn, electron excitation of giant multipolar resonances *(Russian)* 78−8802
^{124}Sn, inelast. ^{3}He and α-particle scatt., ang. distrib. meas. and DWBA anal. 78−13125
^{124}Sn, isospin purity violation, dominant role of noncollective monopole states 78−12964
^{124}Sn+^{86}Kr, 440 and 720 MeV, energy division versus mass of strongly damped products 78−54797
^{124}Sn(^{32}S,xn), continuum γ rays, linear polarisation, feeding high spin yrast states in ^{151,2}Dy 80−497
^{124}Sn(^{3}He,^{3}He) (elast. and inelast.), 14.35 MeV, Coulomb-nuclear interference calcs. 79−26444
^{124}Sn(^{3}He,α), inner hole states excitation, DWBA anal., reaction mechanism *(French)* 78−41735
^{124}Sn(^{40}Ar,xn)Er, 161-236 MeV, pre-equilibrium neutron emission 79−3169
^{124}Sn(^{6}Li,^{6}Li), elastic and inelastic, 74 MeV, folding optical model parameters 80−102201
^{124}Sn(^{86}Kr,X), deep inelastic, final and primary yields and dispersions, statistical anal. 79−54452
^{124}Sn(α,α), optical model parametrization, cross section, energy depend. 78−33196
^{124}Sn(α,α) (elast. and inelast.), 19.5 MeV, Coulomb-nuclear interference calcs. 79−26444
^{124}Sn(d,p), below and near Coulomb barrier 78−29483
^{124}Sn(e,e) ^{150,225}MeV giant multipole resonances, positions and half widths *(Russian)* 78−78349
^{124}Sn(n,n), pol. thermal, parity violation near resonance, DWBA calcs. 80−68528
^{124}Sn(p,p), 0.8 GeV polarised p, differential cross section and analysing power data anal. 78−70526
^{124}Sn(p,p), threshold enhancement of parity violation, Born approx. 80−18191
^{125}Sn reduced normalisation from ^{124}Sn(d,p) 78−86522
^{125}Sn, ^{125}Sb high spin levels, gamma transition energies and intensities 80−73819
^{130}Sn$\rightarrow{}^{130}$Sb, decay scheme, log ft values, spin-parity assignments 77−34264
^{131}Sn beta decaying isomer, ^{131}Sb partial level scheme, half life 77−50091
^{131}Sn, expt. β-decay energy of neutron-rich nuclides 79−30808

nuclei with mass number 90 to 149 continued
^{132}Sn, doubly closed shell nuclide, β-spectra, total binding energy determ. 77−50046
^{132}Sn, doubly magic, RPA calc. of level scheme 78−50087
^{132}Sn, doubly magic nucleus, level scheme 78−54668
^{132}Sn, energy levels, gamma transitions, spin and parity 80−9239
^{132}Sn, exact and statistical results for multi-proton cases 78−86483
^{132}Sn level struct., lifetimes, γ-γ coincidences, internal conversion from ^{235}U fission 80−52584
^{132}Sn levels, isomers, lifetimes and transition probabilities from fission 80−78163
^{132}Sn region, level spectra, shell model anal. 78−86482
^{117m}Sn, half-life and γ-ray intensities 78−4916
^{119m}Sn, $Ba^{119m}SnO_3$ Mossbauer source, resonant self-absorpt. correction 77−28498
^{119m}Sn half-life, by X- and γ-ray intensity meas. 77−26620
^{119m}Sn, Mossbauer obs. of radiation-induced migration in Si 77−15462
Sn(α,α'), even-even isotopes, nuclear struct. effects in microscopic theory 80 37391
Sn(d, ^{6}Li)Cd, alpha-cluster pickup reactions, spectroscopic factors and reduced widths 80−534
Sn(d,^{6}Li)Cd, microscopic description of alpha-transfer reactions 79−6615
Sn(d,t)Sn, even A=112 to 124, deeply bound hole states of odd A Sn 78−8725
Sn(γ,γ), 2754 keV photon Delbruck scatt. 79−67741
Sn(γ, n), 30 to 140 MeV, partial photoneutron cross section, total cross section approx. 80−22809
Sn(n,γ), up to 20 keV, ^{123,125}Sn level schemes, spin-parity assignments, neutron separation energies 77−54215
Sn(n,n') (A=118,120,122,124), isospin dependence of expt. nuclear deformations 77−82817
Sn(p,X), 70 GeV/c, $\pi^{\pm}$, $K^{\pm}$, p, $\bar{p}$ prod. with p_T=0.5-2.5 GeV/c cross sections, yield ratios *(Russian)* 80−52681
Sn(p,2nγ)Sb, A=111, 3, 5, excited states of Sb anal. 77−2911
Sn(p,n), 3-7 MeV, competition of gamma ray and neutron emission 77−23022
Sn(p,n), 4 to 10 MeV polarised protons, optical model parameters 77−2972
Sn(p,n) (A=112,116,124), 22.8 MeV, ang. distribs. to isobaric analogue states, nuclear matter distrib. 77−10405
Sn(p,n), even isotopes, 4-10 MeV, cross sections, optical parameters and nuclear radius A-depend. 80−57773
Sn(p,n) for A=117-124 at 2.6-7 MeV, p-wave size reson. optical model fit 77−30575
Sn(p,n), microscopic description 77−57670
Sn(p,n)Sb, A=115-120, between analogue states via (p,p) and (p,n$\bar{p}$) anal. 77−88132
Sn(p,n)Sb reson. reaction, direct neutron decay of isobaric anal. reson. *(Russian)* 77−88145
Sn(p,n)^{116,118}Sb, threshold region, thick-target cross sections, statistical theory, Q values 77−54218
Sn(p,n$\bar{p}$)Sn, A=115-120, 14-18 MeV, IAS, p branching ratios 77−88132
Sn(p,p), 8.8 MeV polarised protons, optical model parameters 77−2972
Sn(p,p_0), pol.p, 6.77-8.8 MeV, cross sections, optical parameters and nuclear radius A-depend. 80−57773
Sn(p,p)Sn, A=115-120, 14-18 MeV, optical model parameters, (p,n) analogue state reaction relevance 77−88132
Sn(p,t), bump at 8-9 MeV excitation 78−74366
Sn($\pi^{\pm}$,$\pi^{\pm}$), 65-215 MeV forward scatt. amplitudes 79−85533
Sn(t,p), A=116, 118, two-nucleon stripping reactions with Tabakin pot. 78−21570
Sn(x,x), x=$\pi^{\pm}$, $K^{\pm}$, p,$\bar{p}$, 70, 175 GeV/c 80−83128
So(n,2n), A=121,3, cross-section meas., isomeric ratio calc. *(Spanish)* 77−67739
Sr, high spin negative parity states from cluster vibration coupling model 79−75823
Sr isotopes, A=95, 97, 99, beta-decay schemes, level struct. 77−26631
Sr isotopes with A=96, 98, 100, decay scheme, level scheme of Y 77−26632
^{A}Sr, A=89 to 94, struct. of states in the generalised seniority shell model 79−6408
^{A}Sr, A=94,96 direct and skip cascades, $\gamma\gamma$ ang. correlations, levels, mixing ratios from Rb decay 80−86851
^{A}Sr, A=94 to 98, β-decay half life meas. 79−67718
^{A}Sr, A=96,98, β-decay schemes and total energies, mass excess and separation energies 80−27601
^{A}Sr, A=96-98, β-decay half life determ. 78−78318
^{A}Sr, A=98, 100 rot. struct. sudden onset, gamma transitions from Rb decay 80−73777
^{90}Sr β-decay surface contamination monitoring probes, comparison of response between detectors 78−25398
^{90}Sr, conc. and distrib. in N.Atlantic surface water 78−65345
^{90}Sr contamination of external-radiation doses in USSR territory 78−86698
^{90}Sr effects, vasoformative non-osteogenic sarcomas of bone-marrow stroma 77−12964
^{90}Sr, energy spectra from nuclear shell model 79−22225
^{90}Sr fusion reactor transmutation waste management program effectiveness 77−34460
^{90}Sr in low level radioactive liquid waste, chem. treatments, removal efficiencies 77−54351
^{90}Sr, leaching behaviour in cement composites 78−37416
^{90}Sr, level struct. determ. from decay of ^{90}Rb 77−71583
^{90}Sr photoneutron sources, determ. of standard neutron yield, influence of bremsstrahlung 79−72177
^{90}Sr, radioactive fallout in air and rain, results to end of 1977 78−82535
^{90}Sr, radiochem. determ., error anal. comparison of methods 77−16873
^{90}Sr, soil analysis using total sample decomp. 80−35808
^{90}Sr, transmutation in fusion reactor imploding liner blanket 78−17420
^{90}Sr-^{90}Y beta source absorbed dose, thermolum. dosimetry, appl. to dating 77−90911
^{90}Sr-^{90}Y high-energy beta-rays, hazards to eye lens and gonads 78−65131
^{90}Sr+^{90}Y, beta-ray dose rates in skin, conversion from values meas. in air 77−16996
^{90}Sr+^{90}Y bremsstrahlung efficiency for humans, ^{90}Sr body content determ. 77−2061
^{91}Sr, decay scheme, gamma-ray spectra 77−71587
nuclei with mass number 90 to 149 continued
^{92}Sr $\gamma\gamma$ ang. correlations, levels, J^{π}, mixing ratios from ^{92}Rb decay 80−57725
^{93}Sr excited state depopulation γ-rays, n coincidence from ^{94}Rb β-delayed n decay 80−52631
^{93}Sr, γ-ray decay scheme, levels, J^{π}, logft values 77−54152
^{93}Sr neutron binding energy from transitions and β-delayd neutron defined level correspondences 80−63070
^{97}Sr fission product, nuclear struct. *(German)* 78−29395
^{98}Sr, onset of deform. anal. from ^{98}Rb decay 78−12961
^{98}Sr very low lying 0^+ state, shape coexistence bands, $T_{1/2}$, transitions from ^{98}Rb decay 80−78148
^{100}Sr ground state rot. band transitions, deformations and lifetimes from ^{100}Rb β-decay 79−93550
^{181}Ta, quadrupole interaction in Be, temp. depend. 77−8466
^{181}Ta(n,2n)^{180}Ta^{m}, (14.2±0.2) MeV, activation cross sections, Ge(Li) meas. 79−22278
^{A}Tb, A=147, 148, high spin particle-hole states, octupole M2/E3 isomers from ^{151}Eu(α,xn) 80−18171
^{146}Tb decay and T1/2, ^{146}Gd lowest 2^+ state, J^{π} and transitions 80−105979
^{147}Tb, p single particle states and pairing force calcs., low lying levels 80 −42522
^{148}Tb, high spin states, transitions J^{π} assignments from (Li,xn) and (^{10}B,xn) 79−49582
^{149}Tb compound nucleus, statistical model de-excitation calcs. 78−50146
^{149}Tb from HI reactions, superdeformed nucleus decay, α-decay amplification 80−68608
^{149}Tb, high spin states obs. 80−18158
^{149}Tb, lifetimes of low-lying levels *(Russian)* 78−46027
^{149}Tb, prop. anal. on function of nuclear shape 79−75828
^{149g}Tb production in deep inelastic transfer reactions, fragment ang. momentum in (^{40}Ar,X) (^{63}Cu,X) 79−30854
Tc, A=93, 94, 95, 96, 99m, cyclotron production, excitation functions, thick target yields 77−46170
Tc, A=93, 94, 95, low temp. nucl. orientation, γ-ray spectra 77−79327
Tc, A=93-101 odd isotopes, levels, EM moments in unified model 77−82826
Tc, A=94,8, levels determ. from Mo(^{3}He,t)Tc at 24 MeV 77−26778
Tc, A=98, 100, 101, short lived isomers from photonuclear reactions, internal conversion coeffs. 78−37308
Tc decay, ^{104,106,108}Ru level scheme and transitions, collective model anal. 80−78166
Tc decay ^{106,108}Ru levels, transitions, J^{π} and shape 80−57744
Tc, high spin negative parity states from cluster vibration coupling model 79−75823
Tc isotopes, yield from irrad. of Mo and Nb targets 77−23098
^{A}Tc, A=93-95, nucl. g-factor NMR-ON meas. on Fe-Tc alloys 78−37275
^{A}Tc, A=93-96, excitation functions and isomer ratios from ^{93}Nb(α,xn) (x=1 to 4) 80−492
^{A}Tc, A=94 to 98, γ-ray multipolarities, internal conversion coeffs., energy levels 79−63625
^{93}Tc $^{17}/_{2}$ isomer, parity mixing search, partial γ-decay widths from ^{65}Cu(^{32}S,2n2p), 120 MeV 78−93936
^{93}Tc, ^{94}Tc, mag. moment determ., γ-ray spectra of Fe:^{93,94}Tc 77−28484
^{93}Tc 17/2$^-$ isomer, internal conversion coeffs., parity mixing search from ^{92}Mo(α,2np) 43 MeV 78−78255
^{93}Tc, effective three-body interaction 78−524
^{93}Tc, g.m, γ-ray spectra 79−6476
^{93}Tc high spin analogue resonance near N=50 neutron shell, DWBA anal. of ^{92}Mo(^{3}He,d) 80−42613
^{93}Tc, J=17/2 doublet, parity mixing, weak NN interaction 80−73791
^{93}Tc, level struct., $p_{3/2}$ core excitations 77−50060
^{93}Tc, populated in heavy ion reactions, mag. moments, proton core polarisation 78−21598
^{93}Tc^{m+g}, decay schemes, lifetimes, expt., theory *(French)* 77−293
^{94}Tc decay, ^{94}Mo high spin state transitions, mixing ratios, spins, shell model calcs. 79−97678
^{94}Tc levels and J^{π}, coupled channel and DWBA anal. of ^{92}Mo(^{3}He,p) 79−89239
^{95}Tc, 1 quasiparticle 2 phonon multiplet, microscopic quasiparticle cluster phonon coupling model 77−2908
^{95}Tc, energy levels from ^{95}Mo(p, nγ)^{95}Tc 80−37372
^{95}Tc, high momentum states band structs. obs. in (α,2nγ) 78−33109
^{95}Tc, high spin states, coupled proton-neutron excitations 78−17225
^{95}Tc in Fe, oriented nuclear decay, mag. moments 77−46111
^{95}Tc, transition rates of even-parity states calc. 77−74806
^{95}Tc^{m,g} decay populating ^{95}Mo levels, cluster-vibr. model 77−82856
^{96}Tc, as pertechnetate and erythrocyte label, dosimetry rel. to use in humans *(French)* 77−90909
^{96}Tc energy level diagram, γ transitions and parities from ^{96}Mo(p,nγ) 79−9479
^{96}Tc even mass odd nucleus, proton spectroscopy, from ^{95}Mo(^{3}He,d), shell model anal. 79−63573
^{96}Tc, high spin states, γ-energy, intensity, coincidence, ang. distrib. and electron conversion from ^{93}Nb(α,n) 80−52554
^{96}Tc low lying states, level scheme, parities, from conversion electron, γ spectra 78−46024
^{96}Tc, low-lying levels, γ-transitions via ^{93}Nb(α,n)^{96}Tc 10.8, 14.0 MeV 77−2931
^{97}Tc E2/M1 mixing from 785 keV ^{97}Tc γ-γ correl. 77−54178
^{97}Tc E2/M1 mixing ratios from decay of polarised ^{97}Ru 77−6315
^{97}Tc, energy levels, low-lying, decay properties 80−63084
^{97}Tc excited state lifetimes, delayed coincidences method 77−6298
^{97}Tc, γ-γ ang. correl. study, E2/M1 mixing ratios, transition strengths 77−71584
^{97}Tc high spin states, spins and transitions from ^{94}Zr(^{6}Li,3nγ) 80−73780
^{97}Tc, K-capture probability for β-transition to 216 and 324 keV levels 79−6511
^{97}Tc levels, decay props., mixing ratios and J^{π}, from directional correlations in ^{97}Mo(p,nγ) 79−89240
^{98}Tc 14 μs isomer, low lying levels and transitions from ^{98}Mo(p,n) 80−73802
^{98}Tc energy levels from ^{99}Tc(p,d), l-values, spectrocopic factors, parities 78−25183
^{98}Tc, excited by (d,t) and (p,d), l,J,π determ. 77−18370
^{98}Tc, lifetimes of isomeric states from ^{98}Mo(p,n), 4-5 MeV 78−82314
^{98}Tc, low-lying levels obs. in ^{98}Mo(p,n) 77−88076
^{99}Tc, 920 keV level spin, from ^{99}Mo beta decay gamma-ray obs., 0.1-1 MeV 77−54145

nuclei with mass number 90 to 149 continued
^{99}Tc, β-decay, branching ratio and K-shell autoionisation 80−42598
^{99}Tc level structure, spin-parity, from inelastic scatt. and proton stripping studies 78−8743
^{99}Tc, low-lying states via ^{98}Mo(^{3}He,d)^{99}Tc, proton config. 77−22894
^{99}Tc, neutron capture cross section meas. up to 80 keV 78−25197
^{99}Tc, radiochemical characts. and role in nucl. fuel reprocessing, review *(Czech)* 78−82496
^{99}Tc, reduction and sorption in granitic bedrock, biological hazard estimation 79−79415
^{99}Tc, rotational invariance in beta-ray ang. distrib. 78−66252
^{99}Tc^{m}, β-decay rate for estimation of ultra-high pressure 78−77927
^{99}Tc^{m}, electron dose reduction coeff., internal radionuclides, source free target, cylindrical geometry 78−92704
^{99}Tc^{m}, $T_{1/2}$ meas. using double ionization chamber for the differential method 79−22552
^{99}Tc^{m} β-decay, β-branching, ^{99}Ru decay scheme 80−42596
^{99}Tc^{m} decay constant, chemical state effect 80−42591
^{98}Tc+n, capture cross section meas. in Triton reactor *(French)* 80−18308
^{99}Tc(d,d′), 17.2 MeV, level struct., spin-parity assignments 78−8743
^{99}Tc(d,t), 15,19 MeV, ^{98}Tc excit. in 0.43-1.32 MeV range 77−18370
^{99}Tc(p,d), 15,19 MeV, ^{98}Tc excit. in 0.43-1.32 MeV range 77−18370
^{99}Tc(p,d), 22.9 MeV, ^{98}Tc energy levels, l-values, spectroscopic factors, parities 78−25183
^{100}Tc internal conversion, isomeric level half life from ^{100}Mo(p,n), 3.7 MeV 78−78313
^{100}Tc level scheme, transitions and J^{π} values, n binding energy from ^{99}Tc(n,γ) 79−63590
^{100}Tc low lying and isomeric levels, transitions and mean lines from ^{100}Mo(p,nγ) 80−42548
^{100}Tc μs isomers, isomeric transitions and mean lives from ^{100}Mo(p,n) 80−73803
^{100}Tc, struct. anal. by (n,γ) reactions in Grenoble High Flux Reactor 77−34310
^{102}Tc decay scheme and γ-intensities from ^{102}Mo fission product decay 80−78229
^{102}Tc deduced levels, tentative J^{π} and transitions from ^{102}Mo decay 80−52630
^{102}Tc^{g}, β^{-} decay, deduced ^{102}Ru levels 78−86513
^{103}Tc, β-decay, ^{103}Ru level scheme determ. 79−85413
^{103}Tc, decay scheme to ^{103}Ru 79−9470
^{103}Tc, experimental Q_{β}-values 78−93974
^{104}Tc, β^{-}decay, γ-spectra, ^{104}Ru level scheme determ. 78−82313
^{91g}Tc, ^{91m}Tc, decay anal. half-life meas., γ-γ coincidences 77−2937
^{95m}Tc, as pertechnetate and erythrocyte label, dosimetry rel. to use in humans *(French)* 77−90909
^{95m}Tc labelled bone imaging agent, biological half-life determ. 77−16961
^{95m}Tc→^{95g}Mo, K capture branching ratio 77−6308
^{99m}Tc, bone imaging agents, biological half-life determ. using ^{95m}Tc as substitute 77−16961
^{99m}Tc detection by scintillation camera, effect of small amounts of ^{131}I 77−16972
^{99m}Tc generators, comparison of weekly and biweekly systems rel. to radiation safety 77−2049
^{99m}Tc, in hexahalogen complexes, decay const. determ. 80−106020
^{99m}Tc intravenous isotope method for regional cerebral blood flow and vol. meas. 77−86610
^{99m}Tc, production from ^{99}Mo 78−37353
^{99m}Tc, supercond. effect on decay rate, lattice consts., transition temp. 78−41671
^{99m}Tc, use for organ imaging and radiopharmaceuticals 78−61241
^{99m}Tc, X_{α}-SW-calc. of chemically induced decay constant variation of Tc in TcO_4^- and hexahalides 79−54769
^{99m}Tc-DTPA entrapped in liposomes, as scanning agent, organ distrib. in mice and dogs 77−16969
^{99m}Tc-HEDP, quantitative evaluation of rheumatoid arthritic activity 78−20255
^{99m}Tc-$NaTcO_4$ imaging, for diagnosis for deep-vein thrombosis 77−16971
^{99m}Tc-diethyl-acetanilido-iminodiacetate, evaluation as hepatobiliary reagent 77−90874
^{99m}Tc-glucoheptonate, use in brain tumour detect. 78−20253
^{99m}Tc-pyrophosphate, myocardial dosimetry for infarct imaging 77−40771
$^{99m}TcO_4$, radiation damage to mouse testis cells 78−24103
Te, A=108-110, neutron-deficient, prod. in ^{58}Ni+^{58}Ni(^{63}Cu) at 290 MeV 77−88171
Te, A=124, G, nucl. reson. fluoresc. vacancy cascades in mols. 77−2953
Te, A=134,135, total β decay energies, mass excesses, β-γ coincidence study 77−82870
Te evaporation residues from (^{12}C,xnγ), and (^{40}Ar,xnγ), shell effects at high spin 79−22165
Te, even isotopes, effect of residual interaction in particle-particle channel on low-lying states 78−21503
Te isomer ratio, high spin trapping from Sn(α,3n) 80−22655
Te isotopes, fission product conc., sensitivity anal. of various key parameter effects 78−82428
Te levels from ^{112,116,118,120,124}Sn(^{3}He, n) reactions, ang. distribs. 78−89890
Te odd neutron isotopes, microscopic struct. of low lying collective excited states *(Japanese)* 79−3065
^{123,125}Te, Fourier transform NMR, K_2TeO_3, Na_2TeO_3 in D_2O soln. 78−15046
Te^{m+g}, A=113,115,119, decay schemes, lifetimes, expt., theory *(French)* 77−293
Te(^{40}Ar,xnγ), Yb nuclei at high ang. momentum, moment of inertia from γ spectra 78−13135
Te(^{3}He,^{3}He), A=122, 124, 19.52 MeV populating I levels 77−34230
Te(^{3}He,^{3}He) A=122-128, 8-18 MeV, optical model and deform. parameters 77−34221
Te(^{3}He,α), 20 MeV, A=122, 124, 126, ang. distrib. anal. 77−88153
Te(^{3}He,d), A=122, 124, 19.52 MeV, populating I levels 77−34230
Te(^{3}He,t), 45.9 MeV, IAS, Coulomb displacement energies 77−6337
Te(^{3}He, xn)^{125}Xe, prod. of ^{125}Xe for medical use using natural Te 78−3604
^{A}Te (A=135-7), fission product, γ-spectra, half-life meas. 77−38240
^{A}Te, A=107-110, neutron deficient isotopes from ^{58}Ni(^{58}Ni,xpyn), alpha decay studies 79−93567
^{A}Te, A=117, 119, 121, collective excitations, high spin states and transitions from (α, Zn)(d, Zn)(^{3}He, 3n) 80−13346

nuclei with mass number 90 to 149 continued
^{A}Te, A=117,119,121, ΔJ=1 band structures on ns isomeric states 79−54382
^{A}Te, A=122,124,126 yrast band double backbending, possible mechanisms *(Chinese)* 80−99120
^{A}Te, A=127, 129, 131, ground state mag. moments 80−5059
^{A}Te, A=127m, 128, 129m, 130, 131m, 132, sensibility anal. of the effect of key parameters on fission prod. conc. 79−36290
^{A}Te, A=135,136, expt. β-decay energy of neutron-rich nuclides 79−30808
^{A}Te^{m}, A=125, 127, 129, 11/2^{-} isomeric state magnetic moments 80−42537
^{A}Te(^{3}He,^{3}He) A=122, 124 (elast. and inelast.), 12.5 to 21 MeV, Coulomb-nuclear interference calcs. 79−26444
^{A}Te(^{3}He,d)I, 36 MeV, A=120 to 130, comparative study of $^{121\ to\ 131}$I proton states 79−63572
^{A}Te(α,α) A=122,124 (elast. and inelast.), 19.3 MeV, Coulomb-nuclear interference calcs. 79−26444
^{A}Te(α,t)I, 36 MeV, A=124 to 130, comparative study of $^{121\ to\ 131}$I proton states 79−63572
^{A}Te(p,t) A=122, 128, 22 MeV, polarised p, anal. power systematic nuclear struct. depend. 79−22265
^{m}Te, A=125,127,129, internal conversion of M4 transitions at 109.27, 88.26, 105.50 keV 77−65214
^{115}Te, nuclear alignment in Sn, temp. depend 78−41720
^{118}Te, levels studied via ^{116}Sn(^{16}O,^{14}C)^{118}Te, ang. distrib. anal. of 64 MeV reacts. 78−8836
^{118}Te, produced in ^{82}Se+^{40}Ar, γ-ray multiplicity spectra, nuclear shape at high angular momentum 78−37260
^{119}Te, implantation into Si, Mossbauer obs. 77−20757
^{120}Te quasi-rot. band based on proton 4p-2h state, level scheme, transitions from ^{118}Sn(α,2nγ) 80−78119
^{120}Te(d,p)^{121}Te, energy levels spectroscopy of ^{121}Te 77−41973
^{121}Te isomeric state, spin, lifetime and mag. moment from (α,n),(d,Zn) 80−47387
^{122}Te, backscatt. of ^{4}He, ^{14}N, ^{16}O, and ^{18}O, reorientation effect meas. 78−50209
^{122}Te, inelast. ^{3}He and α-particle scatt., ang. distrib. meas. and DWBA anal. 78−13125
^{122}Te on Au target fabrication for cyclotron isotope prod. 77−83406
^{122}Te(^{3}He,d), ^{125}I mass meas. from ground state Q-value 78−4896
^{123}Te level scheme obs., ^{123}I decay, gamma-ray spectra meas. 77−10361
^{123}Te levels, spin assignments and E2/M1 multipole mixing ratio from ^{123}I decay 79−75836
^{123}Te(d,p)^{124}Te, energy levels spectroscopy of ^{124}Te 77−41973
^{124}Te, giant multipole reson. fragmentation over two-phonon states in spherical nuclei 78−575
^{124}Te (p,n)^{124}I, excitation functions and target enrichment vs. nuclidic purity 77−60252
^{124}Te capture states partial α-decay widths from ^{123}Te(n,$\gamma\alpha$) 80−37328
^{124}Te, energy levels spectroscopy by ^{123}Te(d,p)^{124}Te 77−41973
^{124}Te, inelast. ^{3}He and α-particle scatt., ang. distrib. meas. and DWBA anal. 78−13125
^{124}Te, level struct. determ. from ^{124}Sb beta-decay 79−54387
^{124}Te, radiative strength functions in spherical nuclei, giant dipole resonance influence 78−89774
^{124}Te, spin of 1248 keV level, meas. with Ge(Li) polarimeter 77−34530
^{124}Te^{M}, internal conversion in valence shell for M1 and M4 transitions, effect of chemical environment 78−33149
^{124}Te(^{12}C,^{14}C)^{122}Te, 70 MeV, optical model parameters, CCBA anal. 77−18591
^{124}Te(d,t), 10 MeV, ang. distrib. anal. 77−88153
^{124}Te(p,2n)^{123}I, excitation functions and target enrichment vs. radionuclidic purity 77−60252
^{124}Te(p,2n)^{123}I, improved targetry and radiochem. for ^{123}I prod. 78−28064
^{124}Te(p,2n)^{123}I, new approach to target chem. for ^{123}I prod. 77−60250
^{124}Te(p,2n)^{123}I statistical model based computation 79−26416
^{124}Te(p,n)^{124}I, improved targetry and radiochem. for ^{124}I prod. 78−28064
^{125}Te, 109 keV transition, K-conversion coeff. determ. 78−552
^{125}Te, 9/2^{-} 321 keV level, quad. moment from PAC of implanted Te metal 77−28488
^{125}Te enriched Te, nucl. spin-lattice relaxation and Knight shift, high temp. behaviour 77−1614
^{125}Te, hyperfine field in PdMnSb, Mossbauer expts., compared with Jena-Geldart model 78−43707
^{125}Te, implantation into Ge, Mossbauer obs. 77−20758
^{125}Te, level scheme, from radioactive decay of ^{125}Sb *(French)* 77−65202
^{125}Te level scheme obs., ^{125}Sb decay, gamma-ray spectra meas. 77−10361
^{125}Te, levels and transitions following decay of ^{125}Sb 79−71816
^{125}Te low lying negative parity high spin states multistep induced population from (d,t)(^{3}He,α) 80−57657
^{125}Te, Mossbauer isomer shift meas. in ZnTe, CdTe and HgTe 77−16233
^{125}Te, Mossbauer isomer shifts, book contrib. 79−87360
^{125}Te, NMR orbital shifts in Te compounds, depend. on ionicity and local struct. 77−32273
^{125}Te, theory of nucl. elec. field gradient 77−55736
^{125}Te, via ^{125}Sb nuclear orientation Mossbauer meas. 77−55713
^{125}Te(n,γ), 2, 24 keV, ^{126}Te level struct. 77−34308
^{126}Te, 0^{+} states populated by β-decay of ^{126}I 77−74810
^{126}Te, level struct. obs. in ^{125}Te(n,γ) 77−34308
^{126}Te, M1, giant resonance and radiative strength functions 80−57731
^{126}Te(^{22}Ne, ^{22}Ne′), 93.5 MeV, 2^{+} state mutual excitation and transitions 79−54404
^{126}Te(p,n), $2_2{}^{+}\rightarrow 2_1{}^{+}$ transition multipole mixing ratio 80−78198
^{126}Te(t,p), pol.t, cross section and anal. powers, struct. depend., DWBA anal. 80−78272
^{127}Te decay, ^{127}I γ cascade, 360.3-57.6 keV γ-γ directional correl. 78−25151
^{127}Te, energy levels spectroscopy by ^{120}Te(d,p)^{121}Te 77−41973
^{128}Te backscatt. of ^{4}He, ^{14}N, ^{16}O, and ^{18}O, reorientation effect meas. 78−50209
^{128}Te $\beta\beta$ decay ratio of ^{128}Te/^{130}Te half lives 78−66250
^{129}Te, deeply bound hole state transition strength giant resonance, DWBA anal. of (p,d) 80−47426
^{129}Te, implantation into Fe and Ni, Mossbauer obs. 77−20756
^{129}Te^{m,g} decay, ^{129}I energy levels, γ spectra, coincidence spectra 77−2935

nuclei with mass number 90 to 149 continued
^{129}Te^{m+g} decay, ^{129}I time depend. quadrupole interactions, γ-γ correlations 80−78145
^{130}Te double β-decay, lepton charge conservation *(Russian)* 80−102153
^{130}Te, N stability, geochem. test independ. of decay mode 78−8667
^{130}Te+^{16}O, 90 MeV, mechanism of four nucleon transfers in heavy-ion reactions 79−6674
^{130}Te+^{28}Si, 140 MeV, diffusion model 78−82382
^{130}Te(^{32}S,xn), continuum γ rays, linear polarisation, feeding high spin yrast states in $^{156-8}$Er 80−497
^{130}Te(^{40}Ar,xnγ), angular momentum effects in pre-equilibrium processes 78−50208
^{130}Te(d,p), below and near Coulomb barrier 78−29483
^{130}Te(γ,p), 75-800 MeV, yield meas. by activation method 77−71605
^{130}Te(n,γ), resonance and thermal n, γ-spectra, recent expt. review, non-statistical effects 80−37383
^{130}Te(n,t)^{128g}Sb, 14.6 MeV neutrons, activation cross section meas. 79−45254
^{131}Te γ-transitions, spectroscopic factors and reduced transition intensities from ^{130}Te(n,γ) 80−91143
^{131}Te reduced normalisation from ^{130}Te(d,p) 78−86522
^{132}Te 2^+ level, shell model calc., Lanczos and Householder method comparison 80−22711
^{132}Te, fission product, sequential cation-exchange separation from neutron irrad. U_3O_8 77−90898
^{132}Te from fission, 10^+ isomeric state, J^π from deexcitation pattern, half life 80−460
^{132}Te, in sublimation separation of ^{99}Mo from neutron irrad. UO_2 77−9257
^{132}Te low lying levels and EM props., shell model description 80−42549
^{134}Te, levels, J^π, 6^+ isomer level mag. moment 77−82824
^{136}Te (20.9 s), ^{136}I level scheme 77−82877
^{119m}Te decay, population, ^{119}Sb levels, γ-γ and γ-e correls. 78−546
^{119m}Te, electron capture decay, γ-ray spectra, ^{119}Sb level scheme determ. 77−50088
^{119m}Te, mag. moment, nucl. orientation, γ-ray spectra of Fe:^{119m}Te 77−28486
^{123m}Te, yields in Sb bombardment by protons and deuterons 78−37349
^{121m,g}Te, yields in Sb bombardment by protons and deuterons 78−37349
Te(α,α) A=122-128, 8-18 MeV, optical model and deform. parameters 77−34221
Te(α,f), fission fragments tracklength and ang. distribs., fission moment of inertia 77−50182
Te(α, xn)^{125}Xe, prod. of ^{125}Xe for medical use using natural Te 78−3604
Te(d, ^{6}Li)Sn, alpha-cluster pickup reactions, spectroscopic factors and reduced widths 80−534
Te(γ,f), max. energy 580 MeV, track detector anal. 77−18640
Te(n,n′), A=124-130, scattering cross sections and optical model 78−4944
Te(n,n′γ), A=124-130, gamma-ray ang. distribs. 77−34316
Te(t,p), SU(6) boson model for two-nucleon transfer intensities 78−25206
^{129}Tm, implantation in Fe below 5K, in situ Mossbauer obs. 77−20754
^{184}W(^{12}C,^{12}C)^{184}W, 70 MeV, Coulomb inelastic effects 77−30629
^{184}W(^{18}O,^{18}O)^{184}W, 90 MeV, Coulomb inelastic effects 77−30629
Xe, A=118,120,122, level struct., J, π, following Cs β-decay 77−57601
Xe, A=126-132 even nuclei, gyromagnetic ratios of 1st 2^+ states 78−12966
Xe, A=131-135, fine structure of yields 78−86560
Xe, A=139, 140, ^{232}Th fission products, yields, γ-ray spectra 78−74410
Xe, from ^{248}Cm spontaneous fission, rel. to origin of carbonaceous chondrite fission Xe 77−37581
Xe in radionuclide ventilation studies, clinical comparison of ^{127}Xe and ^{133}Xe 77−86594
Xe isotope shifts of 1s electron in K-X-rays following electron capture 77−23454
Xe isotopes, A=118, 120, 122, level schemes and quasi-rotational bands 77−22839
Xe isotopes, collective states, soln. of Schrodinger eqn. with Bohr Hamiltonian 77−67695
Xe isotopes, microscopic dynamic calc. of collective states 78−17075
Xe isotopes, yrast levels, ang.-momentum-projection from coherent phonon state 77−82808
Xe, isotopic yield in photofission of ^{237}Np and ^{235}U 77−54265
Xe levels, beta decay of neutron deficient Cs isotopes 77−22947
Xe levels populated in ^{129}Cs, ^{133}I β decay energy level scheme, γ spectra meas. 77−2936
Xe, neutron rich nuclei from N=82, energy level systematics 77−22896
Xe, odd neutron isotopes, microscopic struct. of low lying collective excited states *(Japanese)* 79−3065
Xe prod. cross sections with protons of 320-590 MeV, nuclear medicine appl. 80−36133
Xe, prod. from natural ^{238}U fission, determ., extraction from granite 78−96216
Xe relative cumulative yields, fine struct. peak from ^{237}Np(n,f) *(Russian)* 79−30868
Xe release from spherical fuel elements in HTGR 77−74940
Xe yield from ^{238}U and ^{232}Th by 14 MeV neutron fission, meas. by emanation method *(French)* 77−30640
Xe/Kr separation from nucl. engineering off-gases, low-temp. distillation *(German, English)* 77−18671
Xe-Nd region, microscopic anal. of core deform. 78−74303
Xe+π, 2.34-10.0 GeV, π^0 and proton characteristics *(Russian)* 77−3052
Xe+π^-, 3.2 GeV/c, π^0, η, ω, f meson prod. determ. of meson-N total cross sections *(Russian)* 79−22122
Xe+π^-, π^0 prod. anal., possible existence of abnormal nuclear density 77−54143
Xe+π^- 3.2 GeV/c, intermediate Δ^- prod. in π^0 and η prod. *(Russian)* 79−36280
Xe+π^- inclusive K^0-meson production cross section *(Russian)* 78−82394
Xe+π^+→p+..., 2.34 GeV/c, proton angular distrib., shock-wave effect *(Russian)* 77−38304
^Xe, A=111-113, neutron deficient isotopes from ^{58}Ni(^{58}Ni,xpyn), alpha decay studies 79−93567
^Xe, A=112,113, neutron deficient isotopes, new island of α-emission 79−6521
^Xe, A=113,5, β-delayed p and α branch ratio, fluctuation function role 79−71820

nuclei with mass number 90 to 149 continued
^Xe, A=122,124,126,128, 0^+ excited state spin assignments and transitions from Cs β-decay 79−67649
^Xe, A=124,126-8,130,132, levels, transitions and J^π values, DWBA anal. from Te(^{3}He, n) 79−75852
^Xe, A=126, 128, 130, Wilets-Jean Hamiltonian for energy levels, transitions, moment, etc. 79−9457
^Xe, A=128 to 132, 129m, 131m, 133m, sensibility anal. of the effect of key parameters on fission prod. conc. 79−36290
^Xe, A=129, 131, Mossbauer isomer shifts, book contrib. 79−87360
^Xe, A=129, 131, populated in (α,nγ), props. of low-lying levels 80−464
^Xe, A=133 to 136, sensibility anal. of effect of key parameters of fission prod. conc. 79−30870
^Xe(n,α), A=125,127, thermal, cross-sections meas. 78−94012
^{114}Xe excited states and γ-rays from ^{114}Cs β-decay 80−47436
^{114}Xe, neutron-deficient, prod. in ^{58}Ni+^{58}Ni(^{63}Cu) at 290 MeV 77−88171
^{116}Xe level scheme and yrast band, in-beam γ-study from ^{106}Cd(^{12}C, 2n) 80−13360
^{116}Xe quasi-rotational bands, levels J^π and $T_{1/2}$ from ^{116}Cs decay 80−83021
^{118}Xe, decay investig. using mass separator on-line with synchrocyclotron 78−17139
^{119}Xe, decay investig. using mass separator on-line with synchrocyclotron 78−17139
^{123}Xe production by 1 GeV proton spallation on Cs, Ba, La 79−63676
^{123}Xe production for radiopharmaceutical appls., high energy alpha reactions 77−37053
^{123}Xe production in ^{127}I(p,xn) and ^{127}I(p,pxn) reactions 78−594
^{123}Xe-^{123}I generator production for radiopharmaceutical appls., high energy alpha reactions 77−37053
^{124}Xe, energy level scheme, ^{124}Cs decay 78−13033
^{124}Xe, level struct. exam. using β^+-decay of Cs 78−21498
^{124}Xe(n,2n)^{123}Xe, ^{123}I prod. in nucl. reactor, for nucl. medicine 77−2051
^{125}Xe $11/2^-$→$9/2^-$ transition in odd parity band from ^{124}Te(α, 3n) 80−9203
^{125}Xe, negative parity levels in odd-A neutron deficient isomers 79−17817
^{125}Xe odd and even parity band structs., level lifetimes from ^{125}Te(^{3}He,3nγ) 80−27533
^{125}Xe production by 1 GeV proton spallation on Cs, Ba, La 79−63676
^{125}Xe production for medical use by ^{3}He bombardment of natural Te 78−3604
^{126}Xe, 2_2^+→2_1^+ transition multipole mixing ratio 80−78198
^{126}Xe, first 2^+ excited state g-factor 77−18389
^{126}Xe, level struct. exam. using β^+-decay of Cs 78−21498
^{127}Xe decay, absolute gamma-ray intensities 78−548
^{127}Xe level scheme from decay of ^{127}Cs 77−299
^{127}Xe radioactive target, search for (n_{th},p) and (n_{th},α) reactions 77−23010
^{128}Xe, collective excitations obs. following decay of ^{128}Cs and ^{128}I 79−45143
^{128}Xe levels, J^π, log ft values, deduced from ^{128}Cs decay 77−54189
^{129}Xe, chem. shift in CH_4, CF_6 and SiF_4, chem. shielding 77−6707
^{129}Xe, excited state lifetimes by delayed coincidence method 80−18231
^{129}Xe excited state lifetimes, γ-transitions from ^{129}Cs decay 80−78205
^{129}Xe, implantation in Fe, NMR/ON 77−20723
^{129}Xe, low-lying levels determ. from Coulomb excitation and (α,n) reacts. 78−70450
^{129}Xe; implantation in Fe, Mossbauer, NO and NMR/ON obs. 77−20755
^{130}Xe+^{209}Bi, 1130 MeV, deform. and transfer in strongly damped collisions 78−21601
^{131}Xe, ang. correl. meas. of γ-γ cascades from ^{131}I decay 77−6292
^{131}Xe, in poly-γ-benzyl-L-glutamate liq. crystal solution, quadrupole splitting 79−4741
^{131}Xe, low-lying levels determ. from Coulomb excitation and (α,n) reacts. 78−70450
^{131}Xe, negative parity states, nucl. orientation, γ-ray spectra of Fe:^{131}Xe 77−28487
^{132}Xe level struct., J^π, transitions and multipole mixing ratio from ^{132}I decay 80−91134
^{132}Xe levels, from ^{132}I β-decay 79−9521
^{132}Xe+^{56}Fe, 5.73 MeV/u, reaction mechanism, evidence for new type of strongly damped collisions 79−13328
^{133}Xe, gaseous, absolute counting, calibration of well-type NaI(Tl)-detector 78−9036
^{133}Xe intravenous isotope method for regional cerebral blood flow and vol. meas. 77−86610
^{133}Xe, laboratory calibration standards preparation *(Czech)* 79−6782
^{133}Xe, nuclear moments and optical isotope shift 78−33118
^{133}Xe, semi-microscopic anal. by generalised vibrational intensity and selection rules and diagonalisation 77−2901
^{135}Xe, direct meas. of absolute and fractional independ. yields from ^{238}U(γ,f) 80−78341
^{135}Xe, poisoning of IRT reactor, optimisation of operation regime *(Russian)* 80−37473
^{136}Xe, neutron particle-hole states determ. from ^{136}I β-decay 77−74811
^{136}Xe+^{209}Bi, 1130 MeV, very heavy-ion collision mechanisms 78−89905
^{136}Xe+^{238}U, nuclear Coulomb excitation, inner shell ionisation and internal conversion, quasimol. formation 78−94026
^{136}Xe+Th(Au)(Al), 624 MeV, internal pair conversion positron spectra 77−67769
^{136}Xe(n,γ), resonance and thermal n, γ-spectra, recent expt. review, non-statistical effects 80−37383
^{136}Xe(n,γ), thermal, Lane-Lynn theory of direct neutron capture verification 79−36218
^{136}Xe(n,γ)^{137}Xe, determ. of neutron binding energy of ^{137}Xe 77−41879
^{136}Xe(n_{th},γ)^{137}Xe, spectra meas., ^{137}Xe level and decay scheme 78−13102
^{137}Xe β decay into ^{137}Cs, γ spectra, coincidences, excited levels, branching logft values 77−54186
^{137}Xe level and decay scheme from ^{136}Xe(n_{th},γ) 78−13102
^{137}Xe low lying state parentage coeffs., anal. of ^{136}Xe(p,p^1) 78−66282
^{137}Xe neutron binding energy, determ. from ^{136}Xe(n,γ) 77−41879
^{137}Xe neutron unbound states, high energy X-rays from ^{137}I decay 80−86856
^{137}Xe, populated in ^{138}I β-decay, delayed neutrons feeding excited states obs. 80−27600

nuclei with mass number 90 to 149 continued
^{137}Xe(p,p$_1$), 10.26 to 11.82 MeV, anal. by ^{137}Cs analogue resonance and parentage coeffs. in ^{137}Xe states 78−66282
^{138}Xe+^{181}Ta, deep inelastic transfer, decay of binary nuclear system 80−22848
^{139}Xe β-decay, ^{139}Cs level scheme, J$^\pi$ and γ-transitions 80−42590
^{139}Xe, populated in ^{138}I β-decay, level scheme 80−27600
^{140}Xe, μ-mesic conversion of γ-rays 77−82865
^{129m}Xe implanted in diamond, lattice location, combined Mossbauer and IPAC meas. 78−43733
^{129m}Xe, Mossbauer effect in ferromagnetic, hyperfine field determ. 77−8460
Xe(p,X) 10-400 GeV A=3-14 fragment energy distrib. 79−17901
Xe(p,X), fragment prod. by two body breakup 79−85440
Xe(π$^-$, Λ^0) 2.9 GeV, production cross section of cumulative Λ^0 hyperons *(Russian)* 78−78419
Xe(π,X), 2.34 to 9 GeV/c, multiple particle prod. and hadron formation time *(Russian)* 79−80957
Xe(π,p), E$_\pi$=2.34 and 3.5 GeV/c, energy and angular distrib. obs. *(Russian)* 79−9633
Xe(π$^+$,pX), 2.34 GeV/c, gauge props. of proton emission *(Russian)* 77−38303
Xe(π$^+$,pπ^0), E$_\pi$=2.34 GeV/c, momentum distrib. function estimate for internuclear nucleons *(Russian)* 79−9634
Xe(π$^+$,π^{0}p) 2.9 GeV, determ. of π^{0}N interaction cross-section *(Russian)* 77−14199
Xe(π$^+$,π^{0}p), 2.9 GeV charge exchange *(Russian)* 77−339
Y isotopes, A=95, 97, 99, beta-decay schemes, level struct. 77−26631
Y isotopes with A=96, 98, 100, decay scheme, level scheme of Zr 77−26632
Y, mass dependence for radiative capture of 14.1 MeV neutrons 78−13087
^{A}Y, A=96 to 98, β-decay half life meas. 79−67718
^{89}Y gamma transitions, microscopic finite-range anal. of ^{92}Zr(p,α) 80−63181
^{89}Y, level struct., p$_{3/2}$ core excitation 77−50060
^{90}Y, 7$^+$ to 2$^-$E5 transition probability 78−66243
^{90}Y β decay surface contamination monitoring probes, comparison of response between detectors 78−25398
^{90}Y electrosorption on anodically polarised Pt surface 79−52684
^{90}Y, energy spectra from nuclear shell model 79−22225
^{90}Y internal bremsstrahlung, evidence for detour transitions in β-decay processes 78−66247
^{90}Y, level widths and density from ^{89}Y total neutron cross section 78−70519
^{90}Y low lying multiplets, DWBA anal. for spectroscopic factors from ^{91}Zr(d,^{3}He) 80−57685
^{90}Y, non-ionic, migration through sand column *(Japanese)* 77−944
^{90}Y, shell model calcs., energy levels, transitions and spectroscopic factors 79−63593
^{90}Y(^{90}Sr) beta scintillation counting, improved method with reusable phosphors 78−9024
^{91}Y, beta ray generated bremsstrahlung yield consts. 80−42588
^{93}Y(p,n), sub-Coulomb optical pot. 80−102190
^{94}Y deduced levels spectroscopic factors, spin and parity from ^{96}Zr(^{3}He,αp) 39 MeV 78−70451
^{96}Y from ^{235}U fission, spectroscopic meas. *(German)* 77−67726
^{97}Y fission product, nuclear struct. *(German)* 78−29395
^{98}Y, β-decay, level scheme of ^{98}Zr determ. 77−41934
^{98}Y from ^{235}U fission, spectroscopic meas. *(German)* 77−67726
^{98}Y^g, β-decay schemes and total energies, mass excess and separation energies 80−27601
^{99}Y fission product, nuclear struct. *(German)* 78−29395
^{99}Y→^{99}Zr, half life and beta decay investigation 79−17863
^{100}Y β-decay, T$_{1/2}$, γ-spectra, low lying O$^+$ state in ^{100}Zr 77−82878
^{100}Y, fission product, γ-spectra, half-life meas. 77−38240
^{90m}Y, ^{90g}Y decays, weak β transitions, γ-ray emission 77−34265
^{91}Ze primary γ-rays and binding energies from ^{90}Zr(n,γ) 80−52566
Zr (^{13}C, 3nγ), 45-56 MeV, collective and two-quasiparticle excitation in Pd 77−18601
Zr (n,2n) react. cross sections at 14.8 MeV 78−74355
Zr, A=90-95, levels, J$^\pi$, neutron-hole struct., ^{93}Zr IAS 78−508
Zr, A=90-96, charge distrib., self consistent calc. *(Russian)* 77−38234
Zr, deep hole states observed in particle transfer reactions 80−68511
Zr, even isotopes, potential energy surfaces and ground state equilib. deformation 80−73789
Zr even isotopes, quadrupole moments and E2 transition rates, broken pair approx. 80−52579
Zr even isotopes, seniority shell model, generalised approx. 79−89253
Zr, high spin negative parity states from cluster vibration coupling model 79−75823
Zr isotopes, A=95, 97, 99 beta-decay schemes, level struct. 77−26631
Zr isotopes, Hauser Feshbach calcs., of neutron cross sections 80−22839
Zr, isotopes, neutron separation energies, (d,t) reactions *(German)* 77−57592
Zr level scheme from Y β-decay 77−26632
Zr neutron rich isotopes, excited 0 states 77−22937
Zr neutron separation energies from (d,t) and (d,p) reactions 80−47489
Zr, onset of deformation at A∼100 80−73790
Zr-region, two nucleon transfer reactions, spectroscopic amplitudes, form factors, ang. distrib. 80−22779
Zr+d, excitation functions and thick target yields 78−50182
Zr(^{3}He, ^{4}He), A=91-96, E=39 MeV, Zr levels, J$^\pi$, ^{95}Zr IAS 78−508
Zr(^{3}He,n), 25.4 MeV, ang. distrib. meas. 77−3022
Zr(Li,Li) (A=90,91), 28 and 34 MeV, optical model parameters 77−54248
^{A}Zr (p,p), A=92, 94, 2-6.5 MeV, optical and Lane model anal. comparison 80−18302
^{A}Zr, A=90, 92 and 94, charge densities and single-particle structure 80−9224
^{A}Zr, A=91, 92, 94, binding energy and primary γ-ray intensities from Zr(n,γ) 80−52565
^{A}Zr, A=92, 94, 96, multiparticle states, method of generalised seniority 80−22759
^{A}Zr, A=92, 96, first excited 0$^+$ state transition strength from (^{6}Li,^{8}B), (d,^{6}Li) correlation 80−78260
^{A}Zr, A=93, 95, 1h$_{11/2}$ neutron single particle strength, quasiparticle-phonon coupling 79−89226
^{A}Zr, A=96, 98, 100, deformation and shape transition, unified shell model 79−93502

nuclei with mass number 90 to 149 continued
^{A}Zr(^{35}Cl,^{35}Cl′), 90 MeV, A=92, 94, 2$_1^+$ levels mag. moments 80−105968
^{A}Zr(^{3}He, ^{3}He), A=90,92, 119 MeV, optical pot. parameters energy and mass depend. 80−32289
^{A}Zr(d,p), pol. d, A=90,91, excitation curve isospin anomaly, neutron single particle resonances 80−27595
^{A}Zr(n,n′γ), A=92, 94, 3-6 MeV, γ-ray production cross sections 77−26767
^{A}Zr(n,n′γ) 2.2-3.7 MeV, A=92, 94, level and decay scheme, J$^\pi$ assignments 79−17850
^{A}Zr(p,n), 11.2 MeV, A=90, 91, 94, spin cut-off parameters from neutron ang. distribs. *(Russian)* 79−80940
^{A}Zr(p,n), 5.055, 5.27 MeV, A=92, 94, γ-ray multipolarities, internal conversion coeffs., energy levels 79−63625
^{A}Zr(p,n), A=92, 94, 1.7-6.7 MeV, total cross sections, p strength functions, optical model anal. 80−18301
^{A}Zr(p,p′), (A=90,92), 20 MeV, polarisation effects on nuclear excited states *(Russian)* 80−27645
^{A}Zr(p,p′), A=94,96, 11.2-13.4 MeV, anal. power and excitation function T$^>$ fluctuations 80−42626
^{A}Zr(p,p) A=90, 92, elastic and inelastic, 40 MeV polarised protons, cross sections and anal. power 79−54428
^{40}Zr(α, α), energy depend. of phenomenological optical pot. 79−97717
^{90}Zr, 1 GeV, Glauber approx. corrections, differential cross sections 78−50166
^{90}Zr (α,α) 40 to 140 MeV, modified optical pot., folding pots. and energy depend. 78−70549
^{90}Zr, (d,d) and (d,p) reactions, finite-range coupled-channel calcs. 77−10377
^{90}Zr (p, p′), 57.5 MeV, polarised p, low lying level and giant resonance excitation 79−36157
^{90}Zr (p,p′), 0.8 GeV, low energy giant octupole resonance excitation, deformation length 79−93593
^{90}Zr (p,p) 100 MeV, systematic optical model anal. 78−66274
^{90}Zr (p,π$^+$), 180 MeV, ang. distribs., discrete states, differential cross section 79−13298
^{90}Zr, anal. of spectrum of transitions to low-lying 2$^+$ states 78−17138
^{90}Zr, broken-pair approx. to seniority shell model 78−29408
^{90}Zr, E1 γ-ray strength function from ^{89}Y(p,γ) 79−75902
^{90}Zr, elastic and inelastic scatt. of 30 MeV polarised protons 77−23004
^{90}Zr, energy spectra from nuclear shell model 79−22225
^{90}Zr, finite Fermi-system theory, E1, E2, M1 resonances, γ absorpt. cross section near threshold 77−50055
^{90}Zr, giant electric and magnetic multipole resonances, microscopic descript. 78−538
^{90}Zr, giant multipole reson. fragmentation over two-phonon states 78−575
^{90}Zr, giant resonance levels, study by proton and electron scatt. *(Russian)* 79−3127
^{90}Zr, γγ directional correl. meas. 78−33144
^{90}Zr, intermediate structure of giant analogue reson. 78−62517
^{90}Zr, isospin purity violation, dominant role of noncollective monopole states 78−12964
^{90}Zr, linearised Hartree Fock model, effective charge, isoscalar nuclear shifts, rms radius 78−25138
^{90}Zr, M1 transitions, theory of finite Fermi systems *(Russian)* 77−6296
^{90}Zr, mag. quadrupole resonance, M2 strength distrib., quasiparticle-phonon model 79−75947
^{90}Zr, neutron absorpt. cross section, optical pot. imag. part 79−9536
^{90}Zr neutron absorption, multipole giant resonance contrib. to optical pot. imaginary part 80−18263
^{90}Zr, neutron and nuclear matter space distribs from (p,p) 1 GeV scatt. *(Russian)* 78−502
^{90}Zr, neutron reson. parameters below 300 keV 78−8805
^{90}Zr, nuclear radii, energy density and HF-BCS methods 80−47363
^{90}Zr, pion-exchange contribs. to charge densities, HF calcs. 78−46001
^{90}Zr, populated in heavy ion reactions, mag. moments, proton core polarisation 78−21598
^{90}Zr, proton orbit sizes and E0 matrix element for 2 lowest 0$^+$ states 80−27546
^{90}Zr, self-consistent generator coord. for giant monopole reson. 77−2891
^{90}Zr, spherical nuclei, excitation of collective states in high-energy proton interactions 78−17073
^{90}Zr, static and transition densities, self consistent RPA theory test in fast (p,p), (e,e) scatt. *(Russian)* 79−49604
^{90}Zr, two-body effective parameters calcs., energy levels 77−57608
^{90}Zr+^{12}C, 56 MeV, assignment of γ-ray cascade to ^{99}Rh 78−41762
^{90}Zr+^{12}C(^{14}N), giant resonances in inelastic scatt. 78−62564
^{90}Zr+^{208}Pb(^{238}U), 7.5 MeV/amu, ang. momentum transfer in deeply inelastic collisions from exclusive sequential-fission expts. 79−76044
^{90}Zr+^{86}Kr, 366-716 MeV, evaporation residue product cross sections 79−17947
^{90}Zr(^{13}C,^{13}C′), 108 MeV, nuclear continuum investigation 80−13506
^{90}Zr(^{16}O,^{14}C), 80 MeV, coupled channel Born approx. anal., form factors, sequential amplitudes 79−9608
^{90}Zr(^{3}He, ^{4}He)^{89}Zr, 39 MeV, ^{89}Zr IAS and bound hole states 78−492
^{90}Zr(^{3}He,^{3}He′), 108.5 MeV, giant monopole resonance, DWBA anal. 79−71828
^{90}Zr(^{3}He,^{3}He), 130 MeV, elastic scatt. ang. distribs., optical model anal. 78−94020
^{90}Zr(^{3}He,^{3}He), 130 MeV, giant reson. excitation, DWBA anal. 79−89319
^{90}Zr(^{3}He,^{3}He), 90-120 MeV, cross sections, deduced unambiguous optical pot. 79−13311
^{90}Zr(^{3}He,α), inner hole states excitation, DWBA anal., reaction mechanism *(French)* 78−41735
^{90}Zr(^{3}He,n), second order processes in DWBA calcs. 78−46076
^{90}Zr(^{3}He,pd), 90 MeV, angular correlations, elastic break-up of ^{3}He 80−52685
^{90}Zr(^{3}He,t)^{90}Nb, 130 MeV, giant Gamow-Teller resonance, T=4, T=5 components 78−46081
^{90}Zr(^{3}He,t)^{90}Nb, 18.5 MeV resonance, isovector dipole and Gamow-Teller transitions 80−86881
^{90}Zr(^{3}He,t)^{90}Nb, 80 MeV, Gamow-Teller M1 state excitation 78−50184
^{90}Zr(^{6}Li,^{6}Li′), 153 MeV, isoscalar giant quadrupole resonances 80−13440
^{90}Zr(^{6}Li,^{6}Li′), 2$^+$(2.18 MeV) and 3$^-$(2.75 MeV) states in ^{90}Zr, DWBA anal. 79−26448
^{90}Zr(^{6}Li,^{6}Li′), 74 MeV, excitation of giant quadrupole reson. 78−8854

nuclei with mass number 90 to 149 continued
^{90}Zr(^{6}Li,^{6}Li), elastic and inelastic, 74 MeV, folding optical model parameters 80−102201
^{90}Zr(^{6}Li,^{6}Li) 34 MeV, optical model anal. 79−26448
^{90}Zr(^{6}Li,X), 156 MeV, projectile break up in continuous particle spectra, cross section, fragmentation 80−86889
^{90}Zr(^{7}Li,^{6}He)^{91}Nb, 34 MeV DWBA calcs. 79−26448
^{90}Zr(^{7}Li,^{6}Li)^{91}Zr 34 MeV, 1.21 and 2.03 MeV states, 2.19 MeV doublet in ^{91}Zr, DWBA anal. 79−26448
^{90}Zr(^{7}Li,^{7}Li′), 2^+ (2.18 MeV) and 3^- (2.75 MeV) states in ^{90}Zr, DWBA anal. 79−26448
^{90}Zr(^{7}Li,^{7}Li) 34 MeV, optical model anal. 79−26448
^{90}Zr(α,X), 140 MeV, nonequilibrium light charged particle yield, energy spectra and ang. distribs. 79−40942
^{90}Zr(α,X), 20, 40 MeV/N, α breakup yield, fragment yield ratios 80−9300
^{90}Zr(α,2nγ), 28 MeV, high spin states above 8^+ isomer in ^{92}Mo 78−89786
^{90}Zr(α,α′), 65 MeV, ^{4}He deduced monopole excitation to O^+ state DWBA anal. 79−22226
^{90}Zr(α,α′), 96, 129 MeV, giant resonance excitation, isoscalar breathing mode state, nuclear incompressibility 80−68620
^{90}Zr(α,α), E=26.2-166 MeV, antisymmetrisation effects, α pot., form factor, optical model anal. 78−82366
^{90}Zr(α,α), form factor, coupling between real and imaginary optical potential 80−68680
^{90}Zr(α,αp) 96.8 MeV proton pickup by α-particles to unbound states DWBA anal. 79−22305
^{90}Zr(d, d'), 108 MeV, giant monopole resonance excitation and ang. distribs. 80−102164
^{90}Zr(d, d), 10, 11, 12 MeV, polarised d, excitation functions, optical model parameters and spin-orbit pot. 79−67756
^{90}Zr(d,X), 70 MeV, charged light particle spectra and ang. distribs. exciton model anal. 79−40935
^{90}Zr(d,d), 10 and 12 MeV, polarised d elastic scatt., optical model anal. 79−36248
^{90}Zr(d,d), 10 and 15 MeV, optical model calc. 78−41729
^{90}Zr(d,p), improved coupled-channel treatment of (d,n̄) threshold effect 77−74859
^{90}Zr(d,p)^{91}Zr, 12.3 MeV, tensor analysing powers 78−29479
^{90}Zr(d,p)^{91}Zr, 5.5 MeV, effects of d D state determ. 77−67752
^{90}Zr(e,e′), 2^- giant resonance twist mode excitation, B(M2) values, form factors 80−78246
^{90}Zr(e,e′), M2 giant resonance excitation, spin-magnetism mass depend. quenching, M1 strength reduction 78−86521
^{90}Zr(e,e′), mag. dipole and quadrupole state excitation 78−50154
^{90}Zr(e,e), 302 MeV, nucleon density distribution in nucleus 79−75831
^{90}Zr(e,e), (in)elastic scatt., self-consistent calcs. of nuclear density *(Russian)* 79−80928
^{90}Zr(γ, α), above GDR region, cross sections, DWBA anal. 80−63173
^{90}Zr(γ,α) statistical and pre-equilibrium cross sections and multipolarities from (e,α) 80−68646
^{90}Zr(n,X), 10-20 MeV, multipole giant resonance contrib. to optical pot. imaginary part 80−78241
^{90}Zr(n,γ) ^{91}Zr, thermal neutron reactions, γ-ray line obs. 78−17190
^{90}Zr(n,n′), 11 MeV, isospin effects, cf. with direct reaction theory 77−34312
^{90}Zr(n,n′), 11 MeV, octupole vibr. states, diff. cross section, deformation length, DWBA anal. 80−102092
^{90}Zr(n,n), 11 MeV, differential cross sections, global optical model anal. 80−18298
^{90}Zr(n,n), elastic and inelastic, 11 MeV, isospin effects, optical and deformation parameters 79−17794
^{90}Zr(p,X), 90 MeV, charged light particle energy spectra exciton and evaporation model anal. 79−40923
^{90}Zr(p,d), 121 MeV, DWBA applicability test, d D-state contribs. 79−13261
^{90}Zr(p,d), 50 MeV, fine struct. of ground hole-state analogues 78−50065
^{90}Zr(p,n), IAS transition, 18.5 to 45 MeV, microscopic model anal. 77−82927
^{90}Zr(p,n̄), nucleon optical potential from Lane model 80−83097
^{90}Zr(p,nx), 45 MeV, preequilib. ang. distrib., generalised exciton model 77−10407
^{90}Zr(p,p′), polarised protons, compound nuclear contribs. to IAR inelastic decay 78−8813
^{90}Zr(p,p), 0.8 GeV, analysing powers 78−54760
^{90}Zr(p,p), 0.8 GeV, elastic and inelastic, differential cross sections, relativistic optical model anal. 79−45270
^{90}Zr(p,p), 0.8 GeV, polarised p, differential cross section, anal. power, nuclear matter densities 79−13299
^{90}Zr(p,p), 1 GeV, spin-effects, Coulomb interactions, Glauber theory 77−82931
^{90}Zr(p,p), 4.5-9 MeV polarised protons, reaction cross-section near (p,n) threshold 77−3015
^{90}Zr(p,p), 65 MeV polarised protons, asymm. in elastic and inelastic scatt. 78−54754
^{90}Zr(p,p), 800 MeV, polarised p, n density uncertainties from optical model anal. 79−22185
^{90}Zr(p,p), (in)elastic scatt., self-consistent calcs. of nuclear density *(Russian)* 79−80928
^{90}Zr(p,p), elastic and inelastic scatt., 185 MeV, polarisation, diffraction model anal. 79−75943
^{90}Zr(p,p), polarised protons, direct reaction contrib. in fluctuating cross sections 77−50102
^{90}Zr(p,p), spin orbital interaction and nucl. matter density distrib. *(Russian)* 79−22176
^{90}Zr(p,p)^{90}Zr, 1 GeV, neutron and nuclear matter space distribs. *(Russian)* 78−502
^{90}Zr(p,π^+), differential cross sections, DWBA calc. 79−85415
^{90}Zr(p,π^+)^{91}Zr, 160 MeV, ang. distributions 78−37345
^{90}Zr(p,x), x=α,π, 72 MeV, spectra and angular distribs. 80−68660
^{90}Zr(π,π′), 226 MeV, giant reson. examination 80−73871
^{90}Zr(π,π)^{90}Zr, 50 MeV, optical potential with kinematic, absorption and correl. corrections 77−50157
^{90}Zr(π^+,π^+′), 241 and 163 MeV, giant resonance studies 79−85512
^{90}Zr(π^+,π^+), 40 MeV, differential cross sections and strength parameters, optical model fit 80−18347
^{90}Zr(t,p), centre of mass corrections to DWBA overlap factors 80−18319
^{90}Zr(t,p), exact finite range DWBA calcs., realistic triton and nuclear wave functions 80−63191

nuclei with mass number 90 to 149 continued
^{91}Zr, 292.4 eV neutron resonance parameters, radiative and neutron widths, spin assignments 77−6369
^{91}Zr, high resolution neutron transmission and capture 78−8806
^{91}Zr, level struct. via (d,p), (p,p′) and (p,d) reactions, DWBA, CCBA anal. 77−18393
^{91}Zr, nuclear reson. fluoresc., γ-ray spectra 78−588
^{91}Zr, populated in thermal neutron radiative capture reactions, γ-ray line obs. 78−17190
^{91}Zr, shell model calcs., energy levels, transitions and spectroscopic factors 79−63593
^{91}Zr+^{11}B, 40 MeV, assignment of γ-ray cascade to ^{99}Rh 78−41762
^{91}Zr(^{6}Li,^{6}Li) 34 MeV, optical model anal. 79−26448
^{91}Zr(d,t), 6 MeV, polarised d, tensor anal. power and D-state effects 79−85446
^{91}Zr(p,nγ), 3.5-4.8 MeV, ^{91}Nb lifetimes, branching ratios, multipole mixing ratios 78−13011
^{92}Zr, elastic and inelastic scatt. of 30 MeV polarised protons 77−23004
^{92}Zr, gamma-gamma directional correl. study 78−29422
^{92}Zr level struct. and reduced spectroscopic factors from ^{91}Zr(d,p) 80−32192
^{92}Zr levels, J^π, cross sections, vector anal. power, optical parameters from ^{91}Zr+pol. d 80−78268
^{92}Zr, neutron binding energy precision meas. 80−18182
^{92}Zr(N,N)^{92}Zr, optical model anal. 80−47473
^{92}Zr(n,γ)^{93}Zr, thermal neutron reactions, γ-ray line obs. 78−17190
^{92}Zr(n,n′γ), 1.57-2.8 MeV, low levels excitation *(Russian)* 78−41722
^{92}Zr(p, n), 4.25-5.30 MeV, ^{92}Nb energy levels, spins, parities 77−14125
^{92}Zr(p,α), 35 MeV, polarised p, DWBA anal., anal. power, optical pot., j-depend. 79−3143
^{92}Zr(p̄,α)^{89}Y, 35 MeV, analysing power study *(French)* 79−75981
^{92}Zr(p,α)^{89}Y, 35 MeV, microscopic DWBA anal. of three particle transfer 79−9567
^{92}Zr(p,p′), 40 MeV polarised protons, 2^+ states excitation 79−6600
^{92}Zr(p_{pol}, A)^{89}Y, finite-range cluster-model description, DWBA approach 80−52667
^{93}Zr, populated in thermal neutron radiative capture reactions, γ-ray line obs. 78−17190
^{94}Zr, 2^+ state, recoiling in Fe, enhanced transient fields 78−37284
^{94}Zr+^{16}O, 140, 315 and 33600 MeV, isotope yields and cross sections 77−14161
^{94}Zr+^{16}O, 140 and 315 MeV, energy depend. of heavy ion peripheral reactions 78−74399
^{94}Zr+^{22}Ne, 174 MeV, energy spectra and prod. cross sections for Be, B, C, N, O *(Russian)* 77−23105
^{94}Zr(n,α)^{91}Sr, fast n, fission spectrum averaged cross section 80−63177
^{94}Zr(n,γ)^{95}Zr, thermal neutron reactions, γ-ray line obs. 78−17190
^{94}Zr(n,n′γ), 1.57-2.8 MeV, low levels excitation *(Russian)* 78−41722
^{94}Zr(p,nγ), 1.7-30 MeV, ^{94} Nb excited states, spin, parity, γ-spectra 77−88125
^{95}Zr from Chinese atmospheric thermonuclear explosions, appl. to stratospheric transport parametrisation 79−2342
^{95}Zr, gamma intensity, from ^{94}Zr(n, γ) cross-section meas., k_0 factors calcs. 79−26433
^{95}Zr, populated in thermal neutron radiative capture reactions, γ-ray line obs. 78−17190
^{96}Zr, shape transition microscopic study using shell model 79−40835
^{96}Zr, unusually strong excitation of 1.59 MeV O^+ state in ^{100}Mo(d, ^{6}Li) 79−49584
^{96}Zr(^{16}O, 4nγ), 56 MeV, γ yields, polarisations, ang. distribs., ^{108}Cd decay scheme 78−66301
^{96}Zr(n,γ)^{97}Zr, thermal neutron reactions, γ-ray line obs. 78−17190
^{96}Zr(t,p), 20 MeV, short range correlations with Tabakin pot. 78−13115
^{96}Zr(t,p), two-nucleon stripping reactions with Tabakin pot. 78−21570
^{97}Zr β decay into ^{97}Nb, level struct., spins, parities, from γ ang. correls. 78−29418
^{97}Zr, β-γ ang. correlation, ^{97}Nb 1251 keV level investig. 77−22879
^{97}Zr fission product, nuclear struct. *(German)* 78−29395
^{97}Zr, gamma intensity, from ^{96}Zr(n, γ) cross-section meas., k_0 factors calcs. 79−26433
^{97}Zr, populated in thermal neutron radiative capture reactions, γ-ray line obs. 78−17190
^{97}Zr, $T_>$ hole analogue states, p decay, deduced states and p branching ratio 78−70451
^{98}Zr, level scheme determ. from β-decay of ^{98}Y 77−41934
^{98}Zr, shape transition microscopic study using shell model 79−40835
^{99}Zr fission product, nuclear struct. *(German)* 78−29395
^{99}Zr→^{99}Nb, half life, level schemes and β-decay investigation 79−17863
^{100}Zr, confirmation of 331 keV 0^+ state 78−41643
^{100}Zr, fission product, γ-spectra, half-life meas. 77−38240
^{100}Zr, lifetime meas. of 331.3 keV 0_2^+ state 78−21523
Zr(α,α), A=90, 92, optical model parametrization, cross section, energy depend. 78−33196
Zr(α,α), A=90,2, E=40-120 MeV, form factors, optical model anal. 78−13123
Zr(n,γ), (n,X), A=92,94, 2-120 keV, total and capture cross-sections meas. 77−2986
Zr(p,4pxn)Rb spallation reactions, 1 GeV, meas. with online mass spectrometer *(Russian)* 77−10409
Zr(p,p′γ), odd isotopes, excited d-states from analogue resonances and p-γ correlations 80−68546

nuclei with mass number 150 to 189
2_γ^+ level depopulation, reduced quadrupole transition probabilities, neutron-proton mass deformation difference 77−34203
36≤Z≤83 nuclei, neutron induced reactions, tables of cross sections and rate factors 77−46162
^{150}Sm(^{16}O,^{18}O)^{148}Sm, 2_1^+ ang. distributions, shape difference between pickup and stripping reaction 78−33209
^{173}Lu decay scheme determ. 77−82868
^{181}Ta(n,γ), γ-ray spectral shape depend. on n energy diverging interval size 78−78373
(^{6}Li,^{6}Li) 50.6 MeV elastic scatt. on A=12-208 nuclei, optical model parameters 77−18592
^{A}Er, A=156, 160, yrast level population, decay, and lifetimes from Sn(^{40}Ar, 4n), ^{A}Er, A=156, 160, yrast level population, decay, and lifetimes *(Russian)* 79−97648
γ-ray multiplicities meas. at beam energies 40 to 140 MeV 78−21585
A=110-210 nuclei, new parameters of deformed Woods-Saxon pot. 78−93951
A=120-150, levels and EM props., recent results 80−68592

nuclei with mass number 150 to 189 continued
A=149-155, systematics of α-particle energies of isotopes, N=84-87, $59 \leq Z \leq 76$ *(Russian)* 77−14071
A=152-238 fissility behaviour irregularity with respect to Z^2/A *(Russian)* 77−23121
A=154, nuclear data sheets, levels, decay props., isomeric states, Nilsson orbitals 79−71781
A=158-176, 'extension of variable moment of inertia model to high spins', comments 80−86791
A=159, nuclear data sheets, levels, decays, and J^π assignments 79−93488
A=160-180 nuclei, manifestations of oblate shapes at high spin, transition energies in yrast region 78−78249
A=163, nuclear data sheets to April 1979 80−98762
A=167-196, product cross sections from $^{197}Au(\pi^\pm$, spallation) 80−27619
A=170-212 nuclei, 20-60 MeV ^3He ion induced fission, effective momenta of inertia *(Russian)* 77−34360
A=174 to 188, shell corrections to semi-empirical formulae for binding energy and radius *(Russian)* 78−78283
A=176, data sheets to April 1976 77−10306
A=187-199 odd-A nuclei, structure and formation of rot. bands based on intruder orbitals 77−22829
A=45-153, β^+-decay strength function maximum 79−75914
A=90 to 160 fission product neutron capture cross-section adjustment based on integral meas. 79−9578
A~150, yrast states, deformed oscillator Hamiltonian calcs. 80−78126
A~150 transitional region, collective props., interacting boson model 80−27538
axially symmetric rare earths, mag. moments, current densities in projected HF approach 79−89236
$C^{152}Sm(^{16}O,^{16}O)$, 72 MeV, coupled-channels anal., nucl. excitation effects 79−26457
(d,3nγ), A=159-181, delayed feeding $T_{1/2}$, rot. band transitions 77−34211
data sheets for A=184 nuclei 78−12948
deformation energy surfaces at very high spin states, microscopic determ. 77−71560
deformed nuclei, one-particle state fragmentation, general regularities *(Russian)* 78−494
deformed rare earth nuclei, bandcrossing in $K \neq 0$ bands, backbending 80−9204
doubly even nuclei, yrast band B(E2) values, hydrodynamical model and CAP effect 80−86793
E1 giant resonance of deformed nuclei in the region $150 < A \leq 186$ *(Russian)* 78−78348
E2, M1 multipole mixing ratios in odd-mass nuclei, A>150 77−30503
E_2-transition probabilities and Davydov-Rostovsky model 78−74330
even actinides, two-nucleon transfer, first 0^+ collective state excitation, spectroscopic factor *(Russian)* 80−42530
even-even deformed nuclei, RPA calcs. of giant quadrupole resonances *(Russian)* 77−50045
even-even nuclei, $58 \leq A \leq 150$, E2, M1 multipole mixing ratio, data survey 78−50118
even-even rare earths, microscopic quadrupole and hexadecapole moments 80−13376
fission induced by 1 GeV protons, mass and energy distribs. meas. 77−71627
ground state rot. band transitions and delayed feeding via (d,3n) for A=158-180 77−34211
(HI,X), rare earths, deeply inelastic transfer reactions, kinematic anal. 80−99186
high angular momentum fusion compound nucleus deexcitation, high spin states, rare earths 80−9259
high spin effects in nuclei with proton no. 40-60, shape, deforms. 78−503
inclusive production of large-transverse-momentum hadrons and hadron pairs 79−89310
multipole excitation of doubly-open shell spherical nuclei 78−21507
N=5 shell, deformed odd-neutron nuclei, band ordering and spectrum 80−83018
N=82 region, high spin isomers, cranked HF calcs., deformation shapes, excitation energies 80−99121
N=82 region, high spin isomers, deformation energy surface, shape constrained cranked HF theory 80−57666
N=82-86, high spin isomers, gamma spectroscopy 80−47358
n-deficient even-mass isotopes near Pb, yrast states, shape transitions 77−61345
near Pb region, α-decay peculiarities and shape staggering effects 79−49611
odd-mass deformed nuclei, absolute EM transition probabilities *(Russian)* 77−34251
odd-mass isotones potential energy surfaces 77−26567
pre-Actinide W-Bi nuclei, (p,f) 24-30 MeV meas., fission barriers *(Russian)* 77−82978
preactinide nuclei Hf-Bi, fission via (α,f) 20-50 MeV 77−18637
props. of prompt muons prod. by 28 GeV protons 79−17906
rare earth anomalous (d,t) transitions, inadequacy of CCBA 78−70543
rare earth deformed nuclei, high spin region excited rot. bands, RPA calcs. 80−78108
rare earth metals, Mossbauer isomer shifts, book contrib. 79−87361
rare earth nuclei, density-dependent HF description 77−54170
rare earth nuclei, high spin states from (HI, xn) reactions, discrete γ-transitions 80−5050
rare earth nuclei, modified oscillator pot. parameters, single particle levels 80−68509
rare earth nuclei, validity of pseudo SU(3) model 77−34240
rare earth nuclei, yrast traps, single particle effects 77−88031
rare earth nuclei (d,t) reactions, band heads, two-step process 78−62551
rare earths, nuclear deformation, Coulomb displacement energy depend., shell model 80−102108
rare earths, pairing energy, single particle levels and interaction matrix elements 78−8721
rare earths, yrast band energy calcs., exponential model with pairing attenuation, backbending 79−9446
rare-earth nuclei, back-bending phenomena, high spin states 78−74300
recoil shadow method in-beam spectroscopy of low energy conversion electrons 78−33372
spherical nuclei, Te to Sm, very high spin states, deform. energy surfaces 78−50079

nuclei with mass number 150 to 189 continued
superfluid deformed rare earth nuclei, quasiparticle-phonon coupling, self-consistent calcs. 77−54138
VV ^{173}Yb, e.m. consts. of lower rot. bands determ. 77−82802
Z=55-63, odd proton nuclei, low lying even parity states 80−27551
(α,α'), A=40-208, low energy octupole resonances, 96 and 115 MeV 79−511
(e,α), Z=29-79, direct and statistical effects, cross sections and ang. distribs. 79−530
(γ,X), A=154-209, 7-20 MeV, total photoabsorption cross section 80−57766
(n,γ), A=94-190, resonance capture, low lying level population fluctuations, γ-rays 80−52619
(n,n'γ), A=28-152, spherically doubly even nuclei, level excitation cross sections, statistical anal. *(Russian)* 79−67707
(p, spallation), 480 MeV, medium to heavy mass targets, deep spallation products 80−83085
W+p, 24 GeV, J/ψ prod. cross section 78−46055
^{159}Tb, 58 keV level, nuclear reson. fluorescence 78−33121
^{161}Dy, in Gd_2O_4, and Gd, TDPAC meas. 78−10809
^{181}Ta 79−40910
^{152}(n,n) elastic and inelastic 1.7, 2.75 MeV, cross sections 79−75839
Au, A=189, 191, 193, level schemes, gamma spectroscopy of high-spin states 77−22848
Au isotopes, A=184-197, β^+-decay, single particle and collective degrees of freedom 77−22956
Au, isotopes near A=186, competition of nucl. shape 78−17094
Au, odd isotopes, negative-parity level props. 78−17103
Au odd-mass isotopes, $9/2^-$ level excitation energies, estimates 77−275
^{A}Au, A=181, 182, alpha decay, half lives, decay energies and branching ratios 79−45215
^{A}Au, A=189, 191, 193, high spin states and transitions, isomeric states from Ir(α,xnγ) 80−5038
^{A}Au, A=189, 193, 195, particle-asymmetric rotor description of $h_{11/2}$ levels system 78−70425
^{185}Au, collective band structure from $^{175}Lu+^{16}O$, $^{170}Yb+^{19}F$, $^{165}Ho+^{24}Mg$ reactions 79−22166
^{185}Au, high-spin states anal. $h_{9/2}$ and $i_{13/2}$ bands 78−25117
^{187}Au decay, ^{187}Pt, levels, J^π, $T_{1/2}$, possible E0 transitions *(French)* 80−32230
^{187}Au energy states from ^{187}Hg decay, parities γ-spectra, triaxial nuclear deform. *(French)* 78−33143
^{189}Au, γ-ray ang. distrib. meas., particle-hole symm. 77−88074
^{197}Au natural line shape of giant dipole resonance 77−88096
$^{197}Au+^{32}S$, 373 MeV, in-plane ang. correls. between α and residue heavy ions 78−46101
$^{197}Au(n,\gamma)$, cross section, statistical theory anal., radiative strength functions *(Russian)* 78−17212
^{198}Au gamma-ray strength functions from spectrum fitting method from $^{197}Au(n,\gamma)$ 80−52616
^{A}Ba($^{32}S,^{32}S'$), A=130, 132, 134, 136, 72-80 MeV, 2_1^+ state mag. moments 80−47373
^{188}Bi alpha decay half lives 80−57749
CC ^{158}Dy high spin states B(E2) values, IBA model test from $^{26}Ng(^{136}Xe, 4n)$ CC ^{158}Dy high spin states B(E2) values, IBA model test 80−27541
CC ^{168}Er high intrinsic excitation levels, γ-decay props. from $^{167}Er(n,\gamma)$ 80−52588
(^{12}C,X) on A=144-164, search for high spin isomeric states, shell effects 79−71784
cc ^{160}Tm doubly odd deformed nucleus, excited states and state lifetimes from ^{160}Yb decay 79−13209
^{A}Cd($^{32}S,^{32}S'$), A=106, 108, 110, 112, 114, 116, 72-80 MeV, 2_1^+ state mag. moments 80−47373
^{156}Ce, fission product, γ-spectra, half-life meas. 77−38240
^{158}Cy, double crossing of ground rotational band and super band 78−45996
$^{162,164}Dy$, γ-mixing, J^π values, levels via (n,n'γ) reaction 77−74768
$^{162,164}Dy$(n,n'γ) 1.5-2.4 MeV, ang. distribs., Dy levels, J^π, γ-branching 77−74768
Dy (A=154, 156), negative parity band crossing in even-even nuclei 78−21488
Dy (p,t), 18-20 MeV, Q effects on cross section, DWBA anal., A dependence 79−63675
Dy, A=160,162,164, high spin rot. states populated in heavy ion scatt., lifetime meas. 77−30511
Dy atom K-shell ionisation and X-rays from $^{158}Gd(\alpha$,xn) 79−93960
Dy deformed nuclei, particle ang. momentum alignment effects 80−68522
Dy, deformed nuclei, quasicontinuum γ-spectrum, M1, E1, E2 components 80−498
Dy, $\Delta N=2$ coupling problem 80−47412
Dy equilibrium and pre-equilibrium decay, α-multiplicities, energies and entry lines from $^{160}Gd(\alpha$,xn) 79−93549
Dy even isotopes, aligned Stockholm band intrinsic spin I_0^{eff} 80−13363
Dy, high spin isomer α-decay search 80−102158
Dy K-shell internal conversion yields, gamma transition multipolarities from (α,xn), (^{12}C,xn) 80−78215
Dy, N=85 isotones, bands and transitions from α and HI excitation, in-beam study 80−78123
Dy, odd mass isotopes, rot. excitations anal. 77−82813
Dy, quadrupole moment calc. using HF method *(Russian)* 80−13375
Dy(^{40}Ar, xn)Po, 160-270 MeV, excitation functions, statistical model calcs. 77−3042
Dy(^3He,d) 46.5 MeV, A=162,164, form factor effects 77−14138
Dy(^3He,d), (α,t), ^{A}Ho single proton states, A=157, 159, 161, 163 78−489
Dy(^{16}O, xn), 70-110 MeV, high spin states in $^{172,174,176}W$, decoupled quasiparticle bands, backbending 78−50199
^{A}Dy, (A=151,152), high spin yrast states, γ-ray polarisation in (^{32}S,sn) reactions 80−497
^{A}Dy, A=150, 151, 152, levels, J^π and transitions from Ho EC decay 79−89241
^{A}Dy, A=152, 153, isomeric states and complex band structs. from Nd(^{12}C, xnγ), Gd(α, xnγ) 79−67624
^{A}Dy, A=156-164, deformation hexadecapole moments, Hartree-Fock calcs. *(Russian)* 80−63081
^{A}Dy, A=158, 160, high spin rot. state pairing correlation, self-consistent treatment 79−3070
^{A}Dy A=158,160, quasi-continuum γ-ray cascades, neutron drip line from $^{160}Gd(\alpha$, xn) 79−75903

nuclei with mass number 150 to 189 continued

$^{\wedge}$Dy, A=161, 163, Nilsson state $\Delta N=2$ mixing, rot. bands from (d,t), (d,p) 80−95295
$^{\wedge}$Dy A=162, 164, gamma to ground band transitions, γ-γ directional correlations from (n,γ) 80−68579
$^{\wedge}$Dy(α,α), A=161,163, 9.0-13.5 MeV, B(E2) values, rigid rotor model validity 79−494
$^{\wedge}$Dy(d,t), A=162, 164, coupled-channels Born approx. anal. 80−83104
^{150}Dy, high-spin isomers produced by ^{144,146}Nd(^{12}C,xn), gamma-ray spectra 78−50075
^{151}Dy decay, ^{151}Tb lower excited state lifetimes, ^{151m}Tb isomer 79−75919
^{151}Dy high spin states, isomers, α-decays and yrast sequence from (^{32}S,3n), (^{18}N,4n) 79−93493
^{151}Dy high spin yrast isomers, shell model configs. from ^{152}Gd(α,5n) and ^{136}Ce(^{18}O,3n) 79−49573
^{151}Dy levels, bands and transitions, in-beam γ-rays from ^{142}Nd(^{12}C,3nγ) 80−458
^{152}Dy 60 ns isomer deexcitation E2 x- (orΔ) transition, half life, $\gamma\gamma$-coincidence from ^{152}Gd(α,4n) 80−86859
^{152}Dy, collective bands and absence of yrast traps 80−9207
^{152}Dy continuum γ-ray multipolarity by linear polarisation meas. from ^{140}Ce(^{16}O,4n) 79−85408
^{152}Dy high spin isomeric states, g-factors from ^{140}Ce(^{16}O, 4n) 80−13377
^{152}Dy high spin isomers, yrast traps, oblate shape at high ang. momenta 79−97646
^{152}Dy high spin isomers, yrast states and level lifetimes from (^{15}N, 4n), (^{16}O, 4n) 80−13361
^{152}Dy, high spin state populations from ^{124}Sn(^{32}S,4n) 80−57660
^{152}Dy high spin struct., in beam γ meas. from (^{15}N, 4n), (^{16}O, 4n) 80−18179
^{152}Dy, high-spin isomer at high excitation energy obs. in ^{154}Gd(α,6n) 77−22841
^{152}Dy, rotation along axis of symmetry 80−448
^{152}Dy yrast continuum γ-ray multipolarity via polarisation meas. from ^{140}Ce(^{16}O,4n) 80−9264
^{152}Dy yrast isomers, γ-rays from compound nuclei 80−86789
^{152}Dy, yrast isomers, oblate shape, excitation energies, spin and parity 79−17795
^{152}Dy yrast line single particle nature at high ang. momentum from Sn(^{32,34}S, 4n) 79−71783
^{152}Dy, yrast states of isomers at high angular momenta, particle-hole struct. 79−36124
^{152}Dy, yrast traps, and very high spin states, populated in (^{32}S,4nγ) 78−89778
^{152}Dy yrast traps, isomers and oblate deformations from ^{124}Te(^{32}S, 4n) 80−13362
^{153}Dy β-decay to ^{153}Tb, decay scheme, weak deform. in ^{153}Tb 77−41884
^{153}Dy, populated by ^{144}Nd(^{12}C,3n), 59 MeV, level lifetimes, instrument testing 78−13375
^{153}Dy, populated in ^{153}Ho β-decay, lower excited states 80−22765
^{153}Dy→^{153}Tb mass difference from β^+ spectrum *(Russian)* 79−13257
^{154}Dy, ^{156}Dy backbending from band crossing 77−14022
^{154}Dy N=88 nuclei quasirot. bands and J^{π} from beta-decay 80−83025
^{155}Dy, weakly deformed, isomeric $^{9+}/_2$ and lowest $^{7-}/_2$ states decay 79−89231
^{156}Dy (p,t), 29.9 MeV, possible two-phonon $\beta\gamma$ vibr. 77−14018
^{156}Dy, collective struct., J^{π}, via (p,t) reaction below 2.3 MeV excit. 77−74747
^{156}Dy, gamma-band anomalous behaviour 77−82812
^{156}Dy high spin states, γ-ang. distribs., lifetimes and feeding times from ^{148}Nd(^{12}C, 5n) 80−13364
^{156}Dy high spin states lifetimes and feeding times, quadrupole moments from ^{24}Mg(^{136}Xe,4n) 80−32239
^{156}Dy, prompt transitions multipolarities, γ and conversion electron spectra, energy level bands, spin, parity 78−8768
^{156}Dy rotational levels obs. in ^{159}Tb(p,4nγ) at 27-51 MeV 77−6199
^{156}Dy, superband 78−29374
^{156}Dy, superband in backbending, band-mixing model 77−34209
^{157}Dy, β band influence on structure of decoupled bands 78−93921
^{157}Dy, decoupled bands, perturbative anal. level energies 78−41623
^{158}Dy band side feeding pattern and γ-multiplicities, statistical model from ^{26}Mg(^{136}Xe, 4n) 79−75821
^{158}Dy collective excitations as populated in ^{158}He$^{g.m}$ decay 78−82270
^{158}Dy γ-spectrum from ^{158}Gd(α,4n), 40 MeV, fusion and neutron evaporation, ^{158}Dy γ-spectrum 79−36291
^{158}Dy, Yrast states from heavy ion collisions, lifetimes 78−54793
^{158}Dy(p,t)^{156}Dy, 29.9 MeV, populating levels below 2.3 MeV, collective struct. 77−74747
^{159}Dy evaluation for transmission imaging and bone mineral anal. 77−48861
^{159}Dy, lifetimes of low excited states, delayed e-γ and $\gamma\gamma$ coincidences *(Russian)* 80−68596
^{159}Dy, yrast-band of odd nuclei 80−22651
^{160}Dy anomalous γ-L X-ray directional correlations from ^{160}Tb decay 80−52610
^{160}Dy, γ transitions following ^{160}Tb decay 80−83060
^{160}Dy, γ-ray intensity and ang. correl. meas. 77−10354
^{160}Dy γ-spectrum from ^{160}Gd(α,4n) 40, 49 MeV, fusion and neutron evaporation 79−36291
^{160}Dy, hyperfine interaction of Γ_8 quartet, Mossbauer expt. 78−43718
^{160}Dy, meas. of 1178-87 keV cascade ang. correl. function 77−14061
^{161}Dy, E0, E2 and E4 charge moment determ., using muonic atoms 78−21490
^{161}Dy, hyperfine parameters for C_2 and C_{3i} site symmetries, Mossbauer obs. 77−20770
^{161}Dy, lifetimes of low excited states, delayed e-γ and $\gamma\gamma$ coincidences *(Russian)* 80−68596
^{161}Dy, Nilsson bands, J^{π} via (d,p), (d,t) and (n,γ) 77−34215
^{162}Dy, intraband transition rates in gamma vibr. bands 78−45992
^{162}Dy, level scheme, γ-branchings following ^{162}Tb decay 77−34246
^{162}Dy rotational states lifetime meas. using ^{162}Dy(^{40}Ar,^{40}Ar'γ) 78−50123
^{162}Dy, static quadrupole moments of arbitrary excited states, sum rule approach 80−91135
^{162}Dy+^{16}O, Coulomb-nuclear interference for high spin states 78−46097
^{162}Dy(^{136}Xe,^{136}Xe'), 547, 612 MeV, high spin state energies and reduced transition probabilities 80−18232
^{162}Dy(n,n'γ), study of ^{162}Dy levels up to 2 MeV 77−6285
^{162}Dy(p, α), statistical direct reaction model calc. 79−80913
^{163}Dy(α,α'), E2 and E4 transition moments, rotational states 78−41740

nuclei with mass number 150 to 189 continued

^{164}Dy, in neutron-irrad. Al_2O_3, β-decay, electron slowing-down flux spectrum 78−10108
^{164}Dy, low lying spectra and EM transitions, level struct. in quasirotational bands 79−36141
^{164}Dy multipole mixing in γ to ground bands from ^{163}Dy(n,γ) 80−52615
^{164}Dy, recoil distance meas. of lifetimes of rotational states 78−66242
^{164}Dy+n, capture cross section meas. in Triton reactor *(French)* 80−18308
^{164}Dy(^{32}S,^{32}S'γ), recoil distance lifetimes of ground state bands 78−8774
^{164}Dy(^{40}Ar,X), 222-340 MeV, charged particle emission, early collision evolution, fission and evaporation cross sections 80−106072
^{164}Dy(^{40}Ar,X) 222, 340 MeV, fusion cross sections, direct and evaporative p and α prod., evaporation, fission 80−13518
^{164}Dy(^{40}Ar,xn)$^{204-x}$Po, $4\leq X\leq 9$, absolute cross sections and excitation function meas. 79−13330
^{164}Dy(α,α'), 11.5-12 MeV, E_2 and E_3 transition strengths meas. 77−26618
^{164}Dy(α,xnγ), x=6-11, 120 MeV, pre-equilibrium n emission, deexcitation mechanism 79−93641
^{164}Dy(n,γ), thermal, isomer state excitation, relative probabilities 79−75814
^{164}Dy(n,n'γ), γ spectrum, level populations 77−61406
^{165}Dy, collective contributions to E1, $\Delta K=1$ matrix elements in odd-odd deformed nuclei 79−17857
^{165}Dy, γdecays obs., ^{165}Ho level determ. *(French)* 77−274
^{165}Dy, neutron binding energy precision meas. 80−18182
^{166}Dy decay, ^{166}Ho low lying levels and transitions, 54.24 keV level mag. moment 80−13380
^{167}Dy, β^- decay, level scheme of ^{167}Ho obs. 77−26580
Dy(α,α'), A=156,8, E=12-13 MeV, E2, E4 transition matrix elements determ. 78−33202
Dy(α, xn γ) equilib. and pre-equilib. reactions, ang. momentum transfer, ground state bands 79−45277
Dy(α, xn γ)Er, 90 MeV, preequilibrium and equilibrium de-excitation processes 78−50185
Dy(n,α)Gd, A=161, 163, at 14.1 and 18.2 MeV, α-emission energy spectra 77−65224
$^{\wedge}$ER, A=167,168, absolute atomic masses 79−89228
Er *(Russian)* 80−13375
Er (p,t), 18-20 MeV, Q effects on cross section, DWBA anal., A dependence 79−63675
Er, A=158, 160, 162, backbending even-even nuclei, particle-rotor model with VMI core *(German)* 77−6258
Er, A=161,162, high ang. momentum states from Nd+^{16,18}O, γ decay modes from multiplicity meas. 78−29419
Er, A=162, 164, 166, (α,2nγ) studies of vibr. and other side bands 77−2893
Er, A=164, 166, 168, 170, high spin rot. states populated in heavy ion scatt., lifetime meas. 77−30511
Er, A=164, 166, backbending phenomena, two fluid model of nuclear rots. 77−50049
Er, deformed nuclei, particle ang. momentum alignment effects 80−68522
Er even isotopes, aligned Stockholm band intrinsic spin I_0^{eff} 80−13363
Er γ-multiplicities and cross sections, neutron evaporation from ^{130}Te(^{32}S,X), (^{16,18}O,X) 80−73824
Er, high spin isomer α-decay search 80−102158
Er production in $^{\wedge}$Ge+^{86}Kr, A=70, 74, 76, and $^{\wedge}$Sn+^{40}Ar, A=122, 124, 50 to 120 MeV, angular momentum limits 78−25224
Er rotational nuclei, transition energy correlations, very high ang. momentum 80−86787
Er yrast levels, spin alignment, populated by preequilibrium (α,xnγ) reactions 80−52557
Er+n (A=162-170), (n,α), (n,t), (n,np), (n,nd), (n,p), (n,2n) reaction cross sections 78−82350
$^{\wedge}$Er,A=166,168,170, fast neutron radiative capture cross sections, 5 to 350 keV *(Russian)* 78−33188
$^{\wedge}$Er, (A=154,155), rotational struct. at high spins 80−457
$^{\wedge}$Er (A=156,157,158), high spin yrast states, γ-ray polarisation in (^{32}S,xn) reactions 80−497
$^{\wedge}$Er, A=154, 155, γ-ray spectra, ang. distrib., high spin states 79−9503
$^{\wedge}$Er, A=156, 164, aligned positive parity bands from rot. aligned model 80−9209
$^{\wedge}$Er, A=156-162, transitions from ^{158}Gd+^{12}C fusion 79−580
$^{\wedge}$Er, A=158,160,162, high spin states and deformation, number conservation effects 79−89225
$^{\wedge}$Er, A=159,160, energy levels, deexcitation γ-rays, g-factors and hyperfine interaction from ^{28}Si(^{136}Xe, xn) 80−102114
$^{\wedge}$Er, A=162-170, deformation hexadecapole moments, Hartree-Fock calcs. *(Russian)* 80−63081
$^{\wedge}$Er, A=166-170, α-particle Coulomb excitation of octupole vibr. states 78−41618
$^{\wedge}$Er+n, (A=166-170), strength functions and scatt. lengths from total and scatt. cross sections 77−26706
$^{\wedge}$Er(d,t), A=166, 168, coupled-channels Born approx. anal. 80−83104
$^{\wedge}$Er(p, α), A=166,168, statistical direct reaction model calc. 79−80913
^{153}Er 360 ns yrast trap, γ transitions and lifetimes from ^{144}Sm(^{12}C,3n) 80−9205
^{154}Er, collective bands and absence of yrast traps 80−9207
^{154}Er, high-spin states 78−29373
^{154}Er yrast cascade to spin 36, side feeding, energy, multipolarity irregularities from (^{16}O, 4n), (^{64}Ni, 4n) 79−36191
^{154}Er yrast trap and transitions, decay scheme from (^{64}Ni,4n), (^{16}O,4n) 80−9206
^{155}Er, backbending effects via (^{12}C, xn) excit. 77−71556
^{156}Er decoupled band behaviour, Coriolis decoupling 77−6205
^{156}Er, level struct. determ. in ^{156}Tm (β^++EC) decay 77−22957
^{156}Er N=88 nuclei quasirot. bands and J^{π} from EC decay 80−83025
^{156}Er, negative parity band crossing in even-even nuclei 78−21488
^{156}Er, negative parity yrast states, microscopic calc. 78−495
^{156}Er, nonaxial deformability of rotating nuclei in two-phase model *(Russian)* 78−46002
^{156}Er, rotating nuclei, two-phase model 78−33113
^{157}Er, ^{155}Er nucl. energy levels from obs. of ^{157}Tm, ^{155}Tm decay *(French)* 77−57630
^{157}Er, lifetimes of excited states, delayed e-γ coincidences *(Russian)* 80−68597
^{157}Er low-lying scheme determ. from ^{157}Tm decay 77−22958
^{158}Er, anomalous rotational bands−a model of a soft rotor coupled with $i_{13/2}$ particles 79−85356

nuclei with mass number 150 to 189 continued
^{158}Er, back-bending phenomenal, rotating potential *(Chinese)* 80−47357
^{158}Er, double crossing of ground rotational band and super band 78−45996
^{158}Er, Hartree Fock Bogoliubov method, high nuclear spins, quadrupole pairing, moment of inertia, yrast traps 78−54712
^{158}Er, high spin state anomaly, backbending 79−22173
^{158}Er, high-spin yrast levels, second discontinuity obs. 77−61373
^{158}Er, level struct. determ. in ^{156}Tm (β^++EC) decay 77−22957
^{158}Er, moment of inertia anomaly at ang. momentum of 26 to 30 78−62496
^{158}Er moment of inertia curve behaviour in recrossing ground state band and superband 79−59001
^{158}Er, number conservation, effect on energy spectra, deform. and B(E2) values 79−36122
^{158}Er, second backbending using cranked Hartree-Fock-Bogoliubov method 79−13188
^{158}Er, var. calc. and HFB calc. of back-bending 77−57584
^{159}Er decay populating ^{159}Ho levels, γ-singles and electron conversion spectra 78−547
^{159}Er, decoupled bands, perturbative anal. level energies 78−41623
^{160}Er continuum γ-ray multipolarity by linear polarisation meas. from ^{148}Nd(^{16}O,4n), yrast levels 79−85408
^{160}Er high spin yrast states and transitions from ^{152}Sm(^{13}C,5n) 80−9208
^{160}Er, number conservation, effect on energy spectra, deform. and B(E2) values 79−36122
^{160}Er, produced in ^{124}Sn+^{40}Ar, γ-ray multiplicity spectra, nuclear shape at high angular momentum 78−37260
^{162}Er 0$^-$ band, angular momentum projection method for even-even nuclei excited states 79−3069
^{162}Er, ang. momentum projection for rot. nuclei, numerical aspects 79−63575
^{162}Er compound nucleus fission at high ang. momentum, fragments from ^{30}Si(^{132}Xe,f) 80−99196
^{162}Er, energy levels determ. from ^{165}Ho(p,4nγ) obs. 77−61348
^{162}Er energy spectrum anomalies, rot. bands, cranking model with Hartree-Fock-Bogolubov theory 79−3064
^{162}Er, microscopic calc. of high-spin rot. states 78−8730
^{162}Er, negative parity excited bands, exact ang. momentum and particle number projection 79−45135
^{163}Er, excited states populated in ^{163}Tm decay 78−17146
^{163}Er level struct., DWBA anal. of ang. distribs. from ^{166}Er(d,t) 79−30788
^{164}Er deformed nucleus, excited rot. bands, selfconsistent HFB treatment 80−42515
^{164}Er high spin props. in multiple band crossing region from (^{18}O,4nγ), (α,4nγ), (^{136}Xe,^{136}Xeγ) 80−83023
^{164}Er multiple high spin band struct. from ^{160}Gd(^{9}Be,5n), backbending 78−70429
^{164}Er, populated via ^{150}Nd(^{18}O,4n)^{164}Er, multiple band crossings 78−37257
^{164}Er, rot. bands calc. from Hartree-Fock-Bogolyubov eqn. 77−18459
^{164}Er rot. states, HF and HFB self consistent calc. with Skyrme interaction 80−22662
^{164}Er, two-fluid model of nuclear rotations and surface vibrations, energy levels 78−62474
^{164}Er(^{3}He,3n), gamma deexcitation mechanism of rot. levels 79−26442
^{164}Er(α,2n), gamma deexcitation mechanism of rot. levels 79−26442
^{165}Er decay parameters and whole-body dose, for radioisotope scanning 77−70529
^{166}Er, 2-quasiparticle states obs. 80−18198
^{166}Er (α,α'), 11.5-12 MeV, E_2 and E_3 transition strength meas. 77−26618
^{166}Er, collective props., HF calcs., review 78−50064
^{166}Er, Coulomb excitation with ^{4}He and ^{16}O ions 78−8839
^{166}Er, giant dipole resonances of deformed even-even nuclei, semimicroscopic calcs. 77−50096
^{166}Er, level population by radioactive decay of ^{166}Ho *(French)* 78−545
^{166}Er, level population from ^{166}Tm decay 79−93556
^{166}Er, low lying spectra and EM transitions, level struct. in quasirotational bands 79−36141
^{166}Er, non axial deformability of rotating nuclei in two-phase model *(Russian)* 78−46002
^{166}Er, rotating nuclei, two-phase model 78−33113
^{166}Er, Skyrme-HF calcs., deformation, electric moments, spin-orbit potentials 78−62480
^{166}Er, spin dependence of E2/M1 admixtures 77−6192
^{166}Er transverse form factors from projected HF approach 80−105965
^{166}Er+^{86}Kr, 515 MeV, deep inelastic collisions, angular momentum dissipation within a classical friction model 79−93644
^{166}Er+^{86}Kr, 5.99 MeV/N, are γ-ray multiplicity 78−82375
^{166}Er+^{86}Kr, 602 MeV, neutron emission in strongly damped collisions 78−82373
^{166}Er+^{86}Kr, deep inelastic strongly damped collision, fragment isobaric distrib. statistical equilib. 79−40949
^{166}Er+^{86}Kr, relaxation times in dissipative collisions, fragment deformation, classical model 79−30853
^{166}Er(^{4}He,xn$\alpha\gamma$), angular momentum effects in pre-equilibrium processes 78−50208
^{166}Er(^{4}He,xnγ), angular momentum effects in pre-equilibrium processes 78−50208
^{166}Er(^{86}K,X), deep inelastic collision, charge drift and dispersion calc., thermal eqn. model based on shell model 80−57798
^{166}Er(^{86}Kr, X), 600 MeV, deeply inelastic, alignment of transferred ang. momentum, discrete γ-ray ang. correlations 80−47498
^{166}Er(^{86}Kr,X), 12.1 MeV/u, dynamical splitting of projectilelike fragments 80−42685
^{166}Er(^{86}Kr,X), 5.1-7.9 MeV/N, deep inelastic neutron emission, pre-equilibrium effects search 80−63200
^{166}Er(^{86}Kr,X), 8.18 MeV/amu, energy loss and nucleon exchange 80−18323
^{166}Er(^{86}Kr,X), statistical fluctuations in dissipative collisions, multidifferential cross sections 80−37399
^{166}Er(^{86}Kr,X) 6-8 MeV, dynamic equilib. process observables, energy dissipation, mass, ang. momentum 80−18336
^{166}Er(α,α'), 11.25 to 12 MeV, elec. moment, charge deform. parameters 77−54233
^{166}Er(d,^{6}Li), 35 MeV, ang. distrib. meas., deduced α-particle spectroscopic factors, reduced widths, decay lifetimes 77−18571
^{166}Er(e,e'), 35-350 MeV, coupled channels anal., rot. band excited states, charge densities 79−3139

nuclei with mass number 150 to 189 continued
^{166}Er(γ,γ'), 14.4-16.6 MeV, γ-vibr. band head transitions, dynamic collective model 80−57662
^{166}Er(γ,γ), 15 MeV, elastic and nuclear Raman scatt. 80−22811
^{166}Er(p, X), pol.p, 65 MeV, continuum spectra anal. powers 80−102178
^{166}Er(t,α), 17 MeV polarised tritons, ^{165}Ho levels, analysing powers, spins 78−78390
^{167}Er level struct., DWBA anal. of ang. distribs. from ^{166}Er(d,p) 79−30788
^{167}Er levels and transitions, spectroscopic factor bombarding energy depend. from ^{168}Er(d,t), 9-15 MeV 79−495
^{167}Er, s-wave resonance parameters, 5 to 130 eV, spin determ. 77−26585
^{167}Er(α,α), 9.0-13.5 MeV, B(E2) values, rigid rotor model validity 79−494
^{167}Er(α,α), E2 and E4 transition moments, rotational states 78−41740
^{167}Er(d,d'), 12.1 MeV, excitation of Nilsson states, Coriolis coupling 78−33190
^{168}Er, $2_\gamma \rightarrow 2_g$ transition, band mixing, electric monopole contrib. 77−2940
^{168}Er, 80 and 1094 keV states, g-factors from ang. correlation methods 80−83035
^{168}Er γ-vibr. band, M1 admixtures in intra-band transitions 80−99149
^{168}Er, intraband transition rates in gamma vibr. bands 78−45992
^{168}Er, neutron binding energy precision meas. 80−18182
^{168}Er(d,t)^{167}Er, 17 MeV, DWBA anal. of ang. distribs. 78−17222
^{168}Er(d,t)^{167}Er, 17 MeV, band heads, two-step process 78−62551
^{169}Er, β-decay half-life, γ-ray spectra 77−79330
^{169}Er, internal bremsstrahlung photon intensity and energy yield 78−86509
^{170}Er level struct. obs. in ^{170}Ho β^--decay 78−41675
^{170}Er(^{32}S,^{32}S'γ), recoil distance lifetimes of ground state bands 78−8774
^{172}Er levels, bands, J^π and transitions from ^{170}Er(t,p) 80−83038
Er(α,α'), A=162, 4, E=12-13 MeV, E2, E4 transition matrix elements determ. 78−33202
Eu, A=153,155, from (p,α), (t,α) reactions, cross sections, reaction mechs. 79−540
Eu(^{16}O, xn), ^{162,164,165}Lu prod., γ transitions, half-lives determ. 78−62509
^Eu (n,X), A=153, 154, 155, total neutron cross sections, effect on reactor characts. 80−32284
^Eu, A=144,148,150,152, ground and excited state analogues, two-phonon coupling effects from Sm(p,n) 79−89277
^Eu, A=151, 152, 153, 154, 155, excited states of transitional region nuclei, rot. bands *(Russian)* 80−52556
^Eu, A=152,154, gamma-ray intensities, precision meas. 80−102140
^Eu, A=153,155, single proton hole states in pickup reactions from (p,α) 80−78128
^Eu, A=157, 159, single proton states, rot. bands, J^π assignments and mass from Gd(t,α) 79−45132
^Eu β-decay, A=152, 154, $^{152, 154}$Gd negative parity states and β-γ-γ correlations 79−97676
^Eu+n, (A=151, 153), strength functions and scatt. lengths from total and scatt. cross sections 77−26706
^Eu(N, γ), A=151, 153, cross sections, time of flight spectra, scintillation detectors 80−27634
^Eu(p,p'), A=151-3, 12 MeV, rot. states, deformation parameters, DWBA and coupled channel anal. 79−9459
^{51}Eu(p,pxn), x=2-5, up to Ep=52 MeV, excitation functions 77−38261
^{150}Eu decay, ^{150}Sm nucl. struct. determ. *(Japanese)* 77−41888
^{151}Eu, ^{153}Eu, 20 eV to 200 keV neutron capture cross section 77−26759
^{151}Eu, energy levels and coexistence of three shapes 77−79304
^{151}Eu level scheme from excitation functions, rotor and interacting boson anals. from ^{152}Sm(p,2nγ) 79−45163
^{151}Eu, Mossbaeur obs. of hyperfine interactions in Eu intermetallic cpds. 78−43714
^{151}Eu, Mossbauer effect in $Eu_xSr_{1-x}S$, $Eu_xSr_{1-x}SO_4$, and Eu_xCa_{1-x} 78−14971
^{151}Eu, Mossbauer effect meas. in supercond. $Eu_ySn_{1-y}Mo_6S_y$ 77−69447
^{151}Eu, Mossbauer spectra in $Sn_{0.5}Eu_{0.5}Mo_6S_8$ 77−43782
^{151}Eu, Mossbauer spectra of EuTe, press. up to 60 kbar 77−63181
^{151}Eu, Mossbauer spectra of EuO-RN solid solns., (R=Nd,Eu,Gd) 78−6610
^{151}Eu narrow band and pickup strength, shape coexistence from (d,t) 80−86799
^{151}Eu, neutron capture cross section, E_n=0.1-100 keV, reson. parameters 77−50121
^{151}Eu(^{16}O,^{16}O'γ), 25-42 MeV, energy levels, transitions, spin assignments determ. 77−38294
^{151}Eu(n,α)^{148}Pm, α spectra and ang. distribs. calc., statistical knock-on-model 77−79371
^{151}Eu(p,xn), x=1,3-6, up to Ep=52 MeV, excitation functions 77−38261
^{152}Eu 89.8488 keV isomeric state feeding, delayed coincidence meas., level scheme from ^{151}Eu(n,γ) 80−63126
^{152}Eu ($T_{1/2}$=12.4 yr) neutron resonances 0 to 14 eV, radiation width, level spacings 77−26583
^{152}Eu, conversion electron spectra meas. with Si(Li) detector 79−36460
^{152}Eu, decay, gamma transitions and probabilities of beta transitions 80−22768
^{152}Eu doubly odd nucleus, transition probabilities and deformations, obs. in (n,γ) 79−97680
^{152}Eu, intercomparison of gamma ray emission rate meas., using Ge spectrometers 78−82568
^{152}Eu, isomeric levels and transitions, Nilsson model 80−18195
^{152}Eu, isomeric state struct. 80−83017
^{152}Eu, K-forbidden beta transition, spectral shape anal. 78−74335
^{152}Eu, level scheme, low energy transitions, reaction data, Nilsson model interpretation 78−66215
^{152}Eu, radioactive decay, γ-ray energy meas. *(German)* 77−57633
^{152}Eu sources, international comparison of γ-ray emission rate meas. using Ge spectrom. 79−22529
^{152}Eu, transitional nucleus, ground state rotational struct. stability 78−93929
^{152}Eu, X-ray emission probabilities per decay 80−14027
^{152}Eu^m (n,n'), thermal neutron acceleration by isomeric nuclei *(Russian)* 80−52680
^{153}Eu 5/2$^+$ ground state rot. band, J^π, shape coexistence from (d,p) 80−86799
^{153}Eu, EM transitions, multipole, internal conversion coeffs. *(Russian)* 80−63121
^{153}Eu, Mossbauer effect in $SmFe_2(Co_2)(Ni_2)$ 77−63338

nuclei with mass number 150 to 189 continued

^{151}Eu, neutron capture cross section, E_n=0.1-100 keV, reson. parameters 77-50121
^{151}Eu, quadrupole moment effect on internal conversion coeff. *(Russian)* 77-82867
^{151}Eu+n, capture cross section meas. in Triton reactor *(French)* 80-18308
^{151}Eu(n,X), gamma transitions and band levels *(Russian)* 79-67700
^{151}Eu(n,γ)^{152}Eu, thermal, ^{154}Eu level scheme 77-61374
^{151}Eu(p,xn)$_x$ x=1,3,5 up to Ep=52 MeV, excitation functions 77-38261
^{151}Eu(t,α)^{150}Sm, level population 77-67755
^{154}Eu, 3$^-$ $\rightarrow$ 2$^+$ β transition, shape anal. 77-30516
^{154}Eu decay, γ-ray transitions anal. 77-65212
^{154}Eu, level scheme, populated by thermal neutron capture, conversion electron spectra 77-61374
^{154}Eu low lying levels, bands, transitions from ^{153}Eu(n,γ) 80-57694
^{154}Eu(p,p'), 12 MeV, ground band rot. states, deformation parameters, coupled channels anal. 80-9195
^{155}Eu, single proton states, spins and parity, rot. bands from ^{156}Gd(t,α), ^{154}Sm(α,t) 79-30766
^{156}Eu decay, γ-γ directional correls., ^{156}Gd transitions from second K$^\pi$=0$^+$ band 78-25150
^{156}Eu$\rightarrow$ ^{156}Gd, elec. monopole transitions from excited 0$^+$ states in ^{156}Gd 77-18478
^{150m}Eu, 35.8 y, decay coincidence study, ^{150}Sm levels 77-82858
^{152g}Eu, neutron resonance obs. by time of flight spectroscopy, cf. ^{151}Eu and ^{153}Eu *(Russian)* 78-25120
Eu(α, 2n) and (α, 4n), ^{153}Tb excited states, rot. bands, spin, parity 78-62552
Eu(n,γ), A=151, 153, cross section, statistical theory anal., radiative strength functions *(Russian)* 78-17212
Eu(n,γ), separated isotopes, integral capture cross section meas. in CFRMF 77-26760
^{160}Ga(^{12}C,α), 7.5 to 16.7 MeV/A, incomplete fusion reactions, crit. ang. momentum anal. of excitation functions 79-71862
^{154,156}Gd, pairing-plus-quadrupole calcs. 77-82807
Gd (A=154-156), collective properties 77-6192
Gd (p,t), 18-20 MeV, Q effects on cross section, DWBA anal., A dependence 79-63675
Gd, A=156, 158, high spin rot. states populated in heavy ion scatt., lifetime meas. 77-30511
Gd, ΔN=2 coupling problem 80-47412
Gd even nuclei, A=152-160, dynamic deform. theory, level energies B(E2) values 78-89795
Gd, high spin isomer α-decay search 80-102158
Gd, isotope shifts and deform. obs. 77-65433
Gd, N=85 isotones, bands and transitions from α and HI excitation, in-beam study 80-78123
Gd, quadrupole moment calc. using HF method *(Russian)* 80-13375
$^{154-160}$Gd, vibrational state B(E2), B(E3) via (α,α')Coulomb excit. 77-74803
$^{154-160}$Gd(α,α'), 11-17 MeV Coulomb excit. of vibrational levels 77-74803
Gd(^{35}Cl,^{35}Cl'γ), A=154, 6, 132-43 MeV, lifetime meas. of high spin states 78-13140
^{A}Gd, A=152, 154, 156, 158, excited states of transitional region nuclei, rot. bands *(Russian)* 80-52556
^{A}Gd, A=152, 154, γ-transition energy and intensity meas. from Eu decay 80-73818
^{A}Gd A=152, 154, negative parity states and β-γ-γ correlations from Eu β-decay 79-97676
^{A}Gd, A=152-160, deformation hexadecapole moments, Hartree-Fock calcs. *(Russian)* 80-63081
^{A}Gd, A=154, 156, energy levels and E2 transition rates from three-band mixing model, backbending 79-67623
^{A}Gd, A=156,158,160, fast neutron radiative capture cross sections, 5 to 350 keV *(Russian)* 78-33188
^{A}Gd+α, A=154,160, reaction cross section meas., in beam γ-spectrometric technique 79-26445
^{A}Gd(n,γ), A=154,156-8, 2, 24 keV, resonance averaged γ-spectra, level and J$^\pi$ appls. 80-37347
^{150}Gd, collective bands and absence of yrast traps 80-9207
^{150}Gd, compound nucleus, evaporation calcs., comparison with exptl. decay data 77-61391
^{150}Gd compound nucleus formation and decay, obs. in ^{134}Ba+^{16}O, and ^{110}Pd+^{40}Ar 77-61453
^{150}Gd, high spin states, pairing correlations and nuclear shape, HFB approach 80-42517
^{150}Gd levels and transitions, J$^\pi$ assignments mixing ratio, nuclear orientation from ^{150}Tb decay 79-13205
^{150}Gd negative parity yrast states, obs. in (α,xn) and ^{150}Tb decay 77-88033
^{150}Gd, negative parity yrast band, E1 transitions polarisability, quadrupole-octupole coupled vibr. system 79-484
^{150}Gd, vibr. levels anal. from ^{150}Tb decay 78-8772
^{151}Gd, 108 and 395 keV levels, mag. moments and half-lives, PAC 77-22883
^{151}Gd excited state spin assignments γ-γ ang. correlations from ^{151}Tb decay *(Russian)* 79-49597
^{151}Gd, high spin states, gamma ray and conversion electron obs., level struct. 77-46130
^{151}Gd shape coexistence, dynamic calculation 79-45151
^{152}Gd β- and octupole bands, downbending moments of inertia from ^{150}Sm(α, 2n) 80-91131
^{152}Gd N=88 nuclei quasirot. bands and J$^\pi$ from EC decay and (α,xnγ) 80-83025
^{152}Gd, negative parity band crossing in even-even nuclei 78-21488
^{152}Gd, negative parity bands, coherent state model 78-89782
^{152}Gd, populated in ^{152}Eu decay, gamma transition and IC 80-22768
^{152}Gd, vibrational states, B(E2) branding rates and interband transitions, pairing plus quadrupole calcs. 80-78127
^{152}Gd(α,3nγ)^{153}Dy, 35-45 MeV, collective band struct. of ^{153}Dy anal. 77-61342
^{153}Gd γ-directional distrib., levels, spin assignments from ^{153}Tb decay 79-13241
^{153}Gd levels and γ-ray spectra from ^{152}Gd(n, γ) 80-57736
^{153}Gd, mag. moment meas. of 129.2 keV 77-82850
^{153}Gd, use in tissue lipid content analysis by photon absorpt. 78-28041
^{153}Gd, weakly deformed, isomeric $^{9^+}/_2$ and lowest $^{7^-}/_2$ states decay 79-89231

nuclei with mass number 150 to 189 continued

^{154}Gd, 2$^+$ rot. states, time integral perturbed angular correl., meas. method 77-9154
^{154}Gd (α, xn), 47-130 MeV, reaction cross section 80-22844
^{154}Gd (α,xn), deformed Dy quasicontinuum spectrum, M1, E1, E2 components 80-498
^{154}Gd, backbending from band crossing 77-14022
^{154}Gd, elec. monopole and quadrupole matrix elements for the K$^\pi$=0$^+$ bands 77-57626
^{154}Gd, γ-γ directional correls., coincidence meas. 77-65212
^{154}Gd levels, bands, J$^\pi$, DWBA anal. of ^{152}Gd(t,p) 80-78110
^{154}Gd multiphonon vibr. bands, dynamic deformation theory 80-5035
^{154}Gd, two-fluid model of nuclear rotations and surface vibrations, energy levels 78-62474
^{154}Gd(α,α'), 11.8 MeV, charge deform. parameter determ. 78-33201
^{155}Gd, β band influence on structure of decoupled bands 78-93921
^{155}Gd, K X-ray intensity following thermal neutron capture 77-26691
^{155}Gd, Mossbauer obs. of transferred hyperfine interactions in $Gd_xY_{1-x}Co_2$ 77-63339
^{155}Gd, Mossbauer spectroscopy of mag. ordering in $Gd_xCe_{1-x}Ru_2$ 78-27139
^{155}Gd, nuclear moments of 86.54 keV state, Mossbauer meas. 77-85635
^{155}Gd, vibr. state, level scheme, γ and conversion electron spectra from ^{154}Gd(n,γ) 80-57696
^{155}Gd(α,α), 9.0-13.5 MeV, B(E2) values, rigid rotor model validity 79-494
^{156}Gd, collective props., HF calcs., review 78-50064
^{156}Gd, elec. monopole transitions from excited 0$^+$ states, ^{156}Eu decay obs. 77-18478
^{156}Gd, excited states calculation, phenomenological models: band-mixing, vibrational-rotational and interacting-boson model 80-22653
^{156}Gd, Mehta-Dyson statistics, appl. to sequences of neutron resonances 77-30543
^{156}Gd transitions from second K$^\pi$=0$^+$ band following ^{156}Eu decay, branching, mixing ratios 78-25150
^{156}Gd(α,α'), 11.25 to 12 MeV, elec. moments, charge deform. parameters 77-54233
^{156}Gd(n,γ), up to 2.24 keV, n resonances, spectra fluctuation, statistical theory test 79-36188
^{157}Gd(n,γ), γ and conversion electron spectra, ^{158}Gd collective bands 78-89819
^{158}Gd, excited states calculation, phenomenological models: band-mixing, vibrational-rotational and interacting-boson model 80-22653
^{158}Gd excited states from ^{157}Gd(n,γ), level struct., rot. bands, transition probabilities 78-89819
^{158}Gd+^{12}C, 112-164.7 MeV, fusion pre-equilibrium effects, $^{170-x}$Yb, $^{166-x}$Er, x=4-10, transitions 79-580
^{158}Gd+^{12}C, 152 MeV, fusion pre-equilib. particle emission 79-581
^{158}Gd+n, capture cross section meas. in Triton reactor *(French)* 80-18308
^{158}Gd(p,n)^{158}Tb, 7.4 MeV, equilib. and nonequilib. contribs. 78-21565
^{160}Gd, giant dipole resonances of deformed even-even nuclei semimicroscopic calcs. 77-50096
^{160}Gd(^{12}C, αxn)$^{168-x}$Er, particle fragmentation accompanied by incomplete fusion, two step model 80-86947
^{160}Gd(^{12}C,2α), 7.5 to 16.7 MeV/A, incomplete fusion reactions, crit. ang. momentum anal. of excitation functions 79-71862
^{160}Gd(^{12}C,xα), 120, 200 MeV, average α-multiplicities, incomplete fusion and breakup 80-27661
^{160}Gd(^{12}C,xαyn), 90-200 MeV, incomplete fusion, fast α prod. absolute cross sections 80-18359
^{160}Gd(^{16}O,4n), ^{172}Hf high spin states, two-quasiparticle struct. 78-25217
^{160}Gd(^{40}Ar, ^{40}Ar), deformed nuclei surface struct. by radial and ang. localisation 79-85362
^{160}Gd(^{9}Be,5n), 59 MeV, multiple high spin band struct. in ^{164}Er, backbending 78-70429
^{160}Gd(α,xn), 47-130 MeV, reaction cross section 80-22844
^{160}Gd(α,xnγ), compound and precompound γ-ray entry lines from measured multiplicities and energies 79-6649
^{160}Gd(d,t) ^{159}Gd, coupled-channels Born approx. anal. 80-83104
^{160}Gd(n,2n), 14.6 MeV, activation cross section 77-88128
Gd(α,α'), 11.5-12 MeV, E_2 and E_3 transition strengths meas. 77-26618
Gd(α,α'), 11.8 MeV, A=154, 156, electric quadrupole and hexadecapole moments, charge deform. parameters 77-30489
Gd(α,α'), A=154,156,158,160, E2 and E4 reduced matrix elements 78-29490
Gd(α, xn)Dy, K-shell ionisation cross-sections meas. 80-78687
Gd(d,d'), A=155, 157, 12.1 MeV, excitation of Nilsson states, Coriolis coupling 78-33190
Gd(p,α)^{153,155}Eu, 17 MeV, direct and sequential reaction mechs., (t,α) comparison 79-540
He, A=157, 159, 161, 163, single proton states, Dy(^{3}He,d) and Dy(α,t) reactions 78-489
Hf (A=176-180), collective properties 77-6192
Hf (p,t), 18-20 MeV, Q effects on cross section, DWBA anal., A dependence 79-63675
Hf, A=166, 168, 170, yrast feeding and lifetimes via Sn(Ti,4n) 195, 198 MeV 77-50078
Hf, alpha decay studies of the isotope 79-63636
Hf isotopes from π^- capture, high spin states 78-54806
Hf, quadrupole moment calc. using HF method *(Russian)* 80-13375
Hf region, long lived high spin isomers, magnetic moments, nuclear struct. *(German)* 77-82820
Hf, static mag. moments, spin, parity and excitation energy from nuclear orientation *(Dutch)* 79-80872
Hf-Ir, isotopes, deformation, level assignments, static moments, modified oscill. model 77-22872
Hf-Os region, high lying states, Nilsson strength fragmentation 80-42539
$^{176-180}$Hf, vibrational state B(E2), B(E3) via (α,α')Coulomb excit. 77-74803
$^{176-180}$Hf(α,α'), 11-17 MeV Coulomb excit. of vibrational levels 77-74803
^{A}Hf, A=166, 168, 170, 172, yrast states, quadrupole moments and B(E2) values, microscopic calcs. 80-32147
^{A}Hf, A=171, 173, three quasiparticle isomers and rot. bands 79-26354
^{A}Hf, A=172-180, prolate isotopes, Yrast traps using cranked modified oscillator pot. 78-93923
^{A}Hf, A=176-180, deformation hexadecapole moments, Hartree-Fock calcs. *(Russian)* 80-63081
^{A}Hf, A=179,180, absolute atomic masses 79-89228

nuclei with mass number 150 to 189 continued
^{A}Hf(HI,xn), A=170-173, two and three quasiparticle isomers, rot. bands, decays and lifetimes 80−9211
^{A}Hf(n,nγ), 2.75 MeV, A=180,178,176, levels and excitation cross sections 79−75839
^{A}Hf(p, α), A=176,178,180, statistical direct reaction model calc. 79−80913
^{171}Hf, hindered electric dipole transitions and lifetimes from (HI,xn) reactions 80−9263
^{171}Hf one- and three-quasiparticle states, high spin rot. bands from (^{16}O,5n), (^{13}C,4n) 80−18163
^{172}Hf, decoupled two-quasiparticle bands, backbending 78−4890
^{172}Hf EC decay, ^{172}Lu levels, transitions and J^{π} values 80−18249
^{172}Hf, gamma-ray spectra of ^{172}Yb, excited level struct. 78−33140
^{172}Hf, negative parity excited bands, exact ang. momentum and particle number projection 79−45135
^{172}Hf production, recovery and purification for nucl. medicine use as ^{172}Lu generator 78−48893
^{172}Hf rotation bands from ^{160}Gd(^{16}O,4n), high spin states, halflives 78−25217
^{172}Hf yrast band and high spin states, $22^{+}\rightarrow 20^{+}$ transition, band crossing from ^{160}Gd(^{16}O,4n) 80−42523
^{174}Hf, angular momentum fluctuation energy in the cranking model 79−89254
^{174}Hf, approximate ang. momentum projection from cranked HFB wave functions, yrast energies 79−30776
^{174}Hf, double crossing of ground rotational band and super band 78−45996
^{174}Hf, microscopic calc. of high-spin rot. states 78−8730
^{174}Hf(^{3}He,3n), gamma deexcitation mechanism of rot. levels 79−26442
^{174}Hf(α,2n), gamma deexcitation mechanism of rot. levels 79−26442
^{175}Hf, β band influence on structure of decoupled bands 78−93921
^{175}Hf multi-quasiparticle states and bands, isomeric states, lifetimes from ^{170}Er(^{9}Be,4n) 80−9213
^{175}Hf, thick-target yields in Ta due to proton bombardment up to 100 MeV 77−88312
^{175}Hf, three- and five-quasiparticle isomers, rotational bands and residual interactions from ^{170}Er(^{9}Be, 4n) 80−83022
^{176}Hf, ground rotational band level energies calc. 78−45996
^{176}Hf yrast traps, cranking Hartree Fock Bogoliubov calcs. 78−25100
^{177}Hf, hyperfine field polarisation in Dy and Gd, IPAC 77−73106
^{177}Hf neutron resonances, high energy γ-rays 77−22938
^{177}Hf, nucl. quadrupole moment determ. 77−83520
^{177}Hf spin 4^{-} resonances, intermediate substructures 77−26586
^{177}Hf(n,α) α-decay of highly excited states of deformed nuclei *(Russian)* 79−9526
^{177}Hf(n,γ), 1-165 eV, γ-ray spectra obs., level scheme determ. 77−50130
^{178}Hf, 2^{+}-0^{+} transitions, mean square nuclear charge radius change, Mossbauer expt. 78−25109
^{178}Hf 9^{-} to 8^{-} transition from ^{178}Ta 2.45 h decay 79−45201
^{178}Hf, energy levels, K-forbidden decays, M4 decay of yrast state 80−68506
^{178}Hf, g-factor for K=6, $J^{\pi}=6^{+}$ isomer, perturbed ang. distrib. meas. 78−37277
^{178}Hf, giant dipole resonances of deformed even-even nuclei, semimicroscopic calcs. 77−50096
^{178}Hf, yrast states struct. changes via ^{176}Yb(α,2n)^{178}Hf 77−50044
^{178}Hf(n,α), 14.8 MeV, energy spectra, statistical model anal. 77−10396
^{179}Hf energy levels from decay of ^{179}Lu 77−54185
^{179}Hf, isomeric state formation by 14.8 MeV neutrons 77−30604
^{179}Hf, nucl. quadrupole moment determ. 77−83520
^{180}Hf band crossing and giant backbending 80−32156
^{180}Hf, internal conversion coeff., penetration effect 79−6500
^{180}Hf, nonrotational interpretation of E_4 matrix element 78−33111
^{180}Hf, polarisation of internal conversion electron calc. 78−50125
^{180}Hf(α,2nγ), 26 MeV, rot. and intrinsic struct. of ^{182}W determ. 77−41914
^{180}Hf(α,α′), 21, 24 MeV, ang. distrib. meas., sensitivity to excited-state quadrupole moments 77−88158
^{180}Hf(n,α), 14.8 MeV, energy spectra, statistical model anal. 77−10396
^{180}Hf(n,α), thermal cross-sections 78−4932
^{180}Hf(n_{th}, α), cross section 78−66284
^{181}Hf, decay, perturbed γγ directional correlations, complex chem. 77−36774
Hf(α,α′), A=176,8,180, E2 and E4 reduced matrix elements 78−29490
Hf(γ,xn), x=1, 2; A=176, 178, 180, 8-21 MeV, GDR, neutron yields and multiplicities *(Russian)* 77−82894
Hf(n,n′γ), 2.75 MeV, direct excitation of some collective levels 77−26720
Hg, 188, 186, 184, shape staggering laser spectroscopy isotope shifts 77−74755
Hg isotopes, A=184-197, β^{+}-decay, single particle and collective degrees of freedom 77−22956
Hg isotopes, nuclear ground state props. via atomic spectra 77−22874
Hg, isotopes near A=186, competition of nucl. shape 78−17094
Hg, neutron deficient isotopes, nuclear shape staggering, laser spectroscopy detection 78−54680
^{A}Hg, A=177-183, 188, alpha decay, half lives, decay energies and branching ratios 79−45215
^{A}Hg, A=181-185, α-decay, Pt rot. states and moments of inertia staggering 78−89779
^{A}Hg, A=182-184, alpha decay branching ratio 80−57749
^{A}Hg, A=184, 186, 188, shape coexistence and energy level schemes 79−97652
^{180}Hg, $T_{1/2}$=3s decay chain, on-line γ-ray spectroscopy 78−13034
^{184}Hg, excited deformed band, shape isomerism anal. 77−6234
^{184}Hg→^{184}Au decay, energy levels and lifetimes *(French)* 78−41661
^{185}Hg decay, ^{181}Pt ground state spin 77−22968
^{185}Hg, nuclear shape isomerism detected by laser spectroscopy 79−49576
^{185}Hg^{m}, and $^{186m-191m}$Hg, nucl. spins, on-line quantum beat spectrosc. determ. 80−9562
^{186}Hg from ^{186}Tl decay, γ, conversion electron spectra and coincidences, shape coexistence 78−25156
^{187}Hg decay, ^{187}Au energy states, parities, γ spectra, triaxial nuclear deform. *(French)* 78−33143
^{188}Hg, coexistence of spherical and deformed bands 77−6587
^{188}Hg, HF calc., shape and lowest band struct., B(E2) values 80−32148
Ho, A=161,163,165, E1 transitions, hexadecapole deforms., Nilsson model calc. 77−82861
Ho, A=163,165, collective state form factor effects in Dy(^{3}He,d) at 46.5 MeV 77−14138

nuclei with mass number 150 to 189 continued
Ho, doubly odd deformed nuclei, EM transitions, nanosec. lifetimes 78−62505
Ho fast neutron capture and activation cross sections 77−26758
Ho, high spin isomer α-decay search 80−102158
Ho, magnetic moment of neutron resonances 77−26576
Ho, mass dependence for radiative capture of 14.1 MeV neutrons 78−13087
Ho+n, neutron spin states amplitudes and scatt. cross sections 77−23019
^{A}Ho, A=150, 151, 152, high spin isomer EC, ^{150,151,152}Dy levels, J^{π} and transitions 79−89241
^{A}Ho, A=153, 160, isomeric levels and transitions, Nilsson model 80−18195
^{A}Ho, A=167,169, energy levels from Er(t,α), polarised t 79−36155
^{152}Ho α-decay and branching ratio 79−89241
^{153}Ho→^{153}Dy, decay scheme, lifetimes 80−22765
^{155}Ho high spin states, lifetimes, J^{π} and rot. parameters from ^{145}Nd(^{14}N,4n) 79−85354
^{155}Ho, negative-parity bands 78−93937
^{157}Ho, lifetimes of excited states, delayed e-γ coincidences *(Russian)* 80−68597
^{157}Ho→^{157}Dy decay, internal conversion electron spectra and eγ coincidences *(Russian)* 80−68604
^{158}Ho, isomeric state and rotational band meas. in ^{159}Tb(α,5n) and ^{160}Dy(p,3n) 77−2890
^{159}Ho energy levels from ^{159}Tb(α,4nγ)^{159}Ho and ^{159}Tb(^{3}He,3nγ)^{159}Ho 77−26556
^{159}Ho, level scheme, γ-singles, conversion electron spectra via ^{159}Er decay 78−547
^{159}Ho, level scheme determ. from (^{3}He,3nγ) 77−22840
^{165}Ho, electron-oriented nucleus scatt., eikonal approx. calc. 78−37331
^{165}Ho + ^{86}Kr, 618 MeV, γ-ray multiplicities and angular momentum fractionation 78−37370
^{165}Ho, 24 keV neutron capture cross section meas. with Fe-filtered neutron beam 79−40910
^{165}Ho, aligned, pion cross-section meas. in (3,3) reson. region 78−29507
^{165}Ho, deformed nuclei, electron scatt., elastic differential cross section calc. 77−82912
^{165}Ho, excited state lifetimes, delayed coincidences method 77−6298
^{165}Ho level scheme determ. *(French)* 77−274
^{165}Ho levels from ^{166}Er(t,α), 17 MeV polarised tritons, analysing powers, spins 78−78390
^{165}Ho, NMR obs. of transferred hyperfine interactions in $Gd_xY_{1-x}Co_2$ 77−63339
^{165}Ho natural line shape of giant dipole resonance 77−88096
^{165}Ho, nuclear K-X-ray satellites, Z=50-83, by α-bombard., 17.5-22.5 MeV 80−42984
^{165}Ho, pseudomagnetic moment and spin-lattice relax. in holmium ethylsulphate 77−63306
^{165}Ho transverse form factors from projected HF approach 80−105965
^{165}Ho+^{56}Fe, 8.3 MeV/amu collision, nucleon exchange and A/Z equilibration 79−76020
^{165}Ho+^{84}Kr, damped collision, interaction time 78−637
^{165}Ho+n, polarised projectile and target, spin depend. of total cross section *(Russian)* 78−17211
^{165}Ho+n, strength functions and scatt. lengths from total and scatt. cross sections 77−26706
^{165}Ho(^{165}Ho,X), deep inelastic, spin and transferred ang. momentum alignment 80−106043
^{165}Ho(^{56}Fe, xn HI), 8.5 MeV/u, damped collision α- and n-emission, n multiplicities 79−93653
^{165}Ho(^{86}Kr,X), 620 Mev, deep inelastic scatt., ang. momentum transfer, γ-ray multiplicities 80−27665
^{165}Ho(^{86}Kr X), γ-ray multiplicities from diffusion model with one body dissipation 79−6487
^{165}Ho(α,2n)^{167}Tm, levels and transitions 80−73766
^{165}Ho(e,α), 100 MeV, energy spectra, cross sections 77−18529
^{165}Ho(e,e), polarised target, as possible test for charge density waves in finite nuclei 77−54144
^{165}Ho(γ,γ′) 8.5-11.4 MeV, elastic and Raman scatt., giant reson. struct. 77−34284
^{165}Ho(n,γ), 0 to 2 keV, neutron strength function of states with selected spin 77−26705
^{165}Ho(n,γ), <2 keV, spin depend. of s-wave neutron strength function 78−21562
^{165}Ho(n,γ), cross-section determ. by Fe filtered beam TOF method 77−23078
^{165}Ho(n,γ), polarised neutron capture by polarised nucleus, assignment of spins to ^{166}Ho levels 79−59062
^{165}Ho(n,n), 1 and 2 MeV, oriented nuclei, deformation effect meas., coupled-channel calc. 77−65218
^{165}Ho(n,n), polarised n and target 0.4-2.5 MeV, total cross section spin-spin effect 79−17899
^{165}Ho(p, X), pol.p, 65 MeV, continuum spectra anal. powers 80−102178
^{165}Ho(p, xnyp γ), 60 MeV, preequilibrium and equilibrium de-excitation processes 78−50185
^{165}Ho(p,4nγ), 30-51 MeV, energy levels of ^{162}Er 77−61348
^{165}Ho(p,αX), 20-45 MeV, α spectra, exciton model anal. 80−18306
^{165}Ho(p,α), 20 to 44 MeV, energy spectra and α-particle angular distrib. 79−49630
^{165}Ho(p,xn), 30-51 MeV, energy levels of ^{162}Er 77−61348
^{165}Ho(p,xnypγ), 60 MeV, n and γ energies and ang. distribs. 78−89872
^{165}Ho(π,π), aligned deformed nuclei, cross sections and diffractive minima from eikonal approx. 80−22860
^{165}Ho(π^{-},X), 175 MeV/c, monopole and quadrupole strong interaction effects in pionic atoms 78−41777
^{165}Ho(π^{-},xn), two-nucleon absorpt. mechanism calc. 77−18618
^{166}Ho, beta decay 77−6310
^{166}Ho electrosorption on anodically polarised Pt surface 79−52684
^{166}Ho, energies of low-lying high spin levels *(Russian)* 78−89793
^{166}Ho, internal hyperfine field obs. using β-γ directional correl. 80−32229
^{166}Ho low lying levels and transitions, 54.24 keV level mag. moment from ^{166}Dy decay 80−13380
^{166}Ho, radioactive decay, ^{166}Er level population *(French)* 78−545
^{166}Ho, spin assignments to levels, using ^{165}Ho(n,γ) polarised target and projectile 79−59062
^{166}Ho^{m} in ^{165}Ho, gamma-ray emission from oriented nuclei in multiaxis nucl. spin system 79−82905
^{166}Ho^{m} in $HoVO_4$, nuclear orientation study below 1K 80−88899

nuclei with mass number 150 to 189 continued
^{165}Ho, level scheme determ. from β^- decay of ^{167}Dy 77−26580
^{170}Ho, 43 s and 2.76 min states, energies and intrinsic structs. 78−78321
^{170}Ho β -decay, $T_{1/2}$ meas., ^{170}Er level struct. 78−41675
^{166m}Ho, relative intensities of gamma-rays 78−46201
Ho(n,n), 2.5 MeV, small angle scatt., cross section, asymm. 78−74361
Ho(π^+,π^-), 65-215 MeV forward scatt. amplitudes 79−85533
^{115}In, 24.3 keV neutron activation cross sections with Fe filter technique 77−26763
^{186,188}Ir in Re crystal, electric quadrupole orientation, elec. field gradient 80−78140
Ir, A=187, 189, triaxial rotor model and γ-vibr. model comparison, γ decay, level schemes 78−54695
Ir decay, oriented nuclei, ^{188,189}Os levels, J^π, transitions and mixing ratios 80−68602
Ir, odd isotopes, negative-parity level props. 78−17103
Ir odd-mass isotopes, $9/2^-$ level excitation energies, estimates 77−275
^{A}Ir, A=168-170, new isotopes from ^{63}Cu induced reactions 78−70563
^{A}Ir, A=169, 170, evidence for existence from ^{93}Nb+^{84}Kr collisions 79−503
^{A}Ir, A=187, 189, 191, 193, positive parity states, particle asymmetric rotor descriptions 79−49572
^{A}Ir, A=189, 191, levels, J^π, transitions and mixing ratios from Pt decay 80−68602
^{170}Ir, prod. in Cu induced reacts., decay characteristics 77−82961
^{181}Ir, γ-ray spectra, half-life, decay scheme 78−41672
^{183}Ir, high spin states of rotation aligned bands, backbending 77−30485
^{183}Ir levels, J^π assignments, Nilsson states for N=105 isotones from ^{183}Pt fast β-transition 79−22206
^{185}Ir, high spin states of rotation aligned bands, backbending 77−30485
^{185}Ir level scheme determ. from ^{185}Pt decay 77−22843
^{185}Ir levels excited in (α,xn) reactions 80−9231
^{185}Ir levels populated in ^{185}Pt^{m+g} decay 80−9269
^{186}Ir anomalous $I^\pi K=5^+1$ ground state config. confirmation, spectroscopic quadrupole moment 79−93506
^{186}Ir decay into ^{186}Os, K=0 rot. band collective states 77−82803
^{187}Ir, diagonalisation of collective quadrupole Hamiltonian 77−6221
^{188}Ir level scheme and transitions from ^{188}Pt electron capture 79−22237
^{189}Ir from (p,t) at 18 MeV, ground state rot. band, 7/2 gamma vibr. levels 78−74360
Lu, A=162,4,5, from Eu(^{16}O, xn), gamma transitions, half-lives anal. 78−62509
Lu β^+ decay force function resonance struct., level populations *(Russian)* 80−102154
^{A}Lu, A=158, 159, alpha decay and gamma transitions 80−73827
^{A}Lu, A=160-163, decay and $T_{1/2}$, $^{160-163}$Yb transitions 80−102146
^{A}Lu, A=169 to 172, internal conversion electron reference lines, energy value refinement 79−75908
^{A}Lu A=171, 173, Nilsson state transitions from 1/2 life, Coriolis coupling matrix from Yb(p,n), 13 MeV 79−6485
^{A}Lu, neutron deficient isotopes, A=157, 158, 160, 161, 163 from W or Ta p spallation 79−75957
^{A}Lu(n,γ), A=175,176, 30 keV, capture cross sections, stellar nucleosynthesis, ^{176}Lu cosmic clock 80−42663
^{157}Lu, short lived α emitter, α energy, $T_{1/2}$ and branching ratio 80−501
^{164}Lu, β-decay , half-life, populating ^{164}Yb levels 77−82805
^{167}Lu intrinsic and rotational levels, obs. in (^{3}He,5n), (α,6n) and (p,4n) 77−88026
^{169}Lu allowed hindered β^+ decay, ^{169}Yb $^7/_2{}^+$[404]→$^7/_2{}^+$[633] transition ft value 80−102148
^{169}Lu decay, ^{169}Yb $\gamma\gamma$ ang. correlations, levels and spins *(Russian)* 80−83069
^{169}Lu, internal conversion electron spectrum E_γ<100 keV, ^{169}Yb ground state population probability 79−6497
^{169}Lu, positron decay spectrum 79−6504
^{169}Lu, radioactive decay, gamma ray and conversion electron spectra 80−22766
^{169}Lu, radioactive decay scheme 80−22767
^{170}Lu→^{170}Hf, beta decay, reduced transition probabilities 77−22945
^{171}Lu decay, ^{171}Yb level scheme, γ-transitions, spin-parity assignments 77−46133
^{171}Lu, positron decay 79−6505
^{172}Lu decay, identification of γ-spectra unplaced energies by delayed coincidence meas. 80−78221
^{172}Lu, decay scheme, γ-ray, conversion electron spectra 79−75913
^{172}Lu, gamma-ray spectra of ^{172}Yb, excited level struct. 78−33140
^{172}Lu generator, ^{172}Hf production, recovery and purification for nucl. medicine use 78−48893
^{172}Lu, γ-ray spectrum anal. 77−82847
^{172}Lu, internal conversion electron spectra 79−75906
^{172}Lu levels, transitions and J^π values from ^{172}Hf EC decay 80−18249
^{172}Lu, radioactive decay, γ-ray spectra, internal conversion electron spectra 79−75912
^{173}Lu→^{173}Yb e.m. consts. of lower rot. bands of ^{173}Yb determ. 77−82802
^{174}Lu isomeric levels, γ-spectra, T 1/2 and decay modes from ^{176}Yb(p,3n) 80−99151
^{174}Lu, populated by ^{176}Lu (p,t)^{174}Lu, energy levels and rotational bands 78−37346
^{175}Lu, ^{176}Lu, neutron resonance parameters up to 200 eV 77−26582
^{175}Lu delayed transitions from ^{176}Yb(p,3n) 80−99151
^{175}Lu, level schemes from ^{176}Yb(p,xnγ) and ^{176}Yb(d,xnγ) reaction 79−75838
^{175}Lu, muonic, nuclear spectroscopic ground state quadrupole moments from X-rays 79−98252
^{175}Lu, nuclear rot. band energies *(Russian)* 78−54720
^{175}Lu, quadrupole moment effect on internal conversion coeff. *(Russian)* 77−82867
^{175}Lu+^{12}C, 78 MeV, fission fragment angular distrib., shape of saddle point of compound nucleus *(Chinese)* 78−78427
^{175}Lu+^{19}F, 142 MeV fission ^{1}H and ^{4}He emission from ^{194}Hg compound nucleus 78−50220
^{175}Lu(^{12}C,f), fission probability calc., α emission and evaporation effects 78−657
^{175}Lu(α,α), 9.0-13.5 MeV, B(E2) values, rigid rotor model validity 79−494
^{175}Lu(γ,γ'), elastic and Raman scatt. at 8.5-11.4 MeV, GDR parameters 78−587
^{175}Lu(π^-,X), 230 MeV/c, monopole and quadrupole strong interaction effects in pionic atoms 78−41777
^{176}Lu β-decay half life 80−52633

nuclei with mass number 150 to 189 continued
^{176}Lu deformed odd-odd nucleus, γ transition probabilities, rot. band mixing 77−61375
^{176}Lu, K X-ray intensity following thermal neutron capture 77−26691
^{176}Lu, level schemes from ^{176}Yb(p,xnγ) and ^{176}Yb(d,xnγ) reactions 79−75838
^{176}Lu, reson. spins, secondary γ-transition intensity, from ^{175}Lu(n,γ) 78−21512
^{176}Lu(n,γ), effective cross section dependence on thermal neutron temp. 80−547
^{177}Lu, reson. spins secondary γ-transition intensity meas. in ^{176}Lu(n,γ) 78−21512
^{177}Lu, 150 keV state, mag. dipole moment, TDPAC 77−41886
^{177}Lu decay, beta spectral shapes 78−74337
^{177}Lu, excited state lifetimes by delayed coincidence method 80−18231
^{177}Lu excited state lifetimes, γ-transitions from β-decay transitions 80−78205
^{177}Lu, nuclear quadrupole alignment 78−48090
^{178}Lu isomeric states and spins, transition probability from ^{181}Ta(n,α) 80−52582
^{179}Lu β-decay, level struct. of ^{179}Hf 77−54185
^{176m}Lu, electron capture meas. *(German)* 78−33153
Nd decay, ^{A}Pm, A=149,151, shape coexistence, deformed states 80−78135
Nd, even-even, E2 transition probabilities from multiple Coulomb excitation, IBA comparison 80−78212
Nd(^{12}C,^{12}C), A=143-150 even isotopes, multistep effects in elast. and inelast. scatt. at 70.4 MeV 78−17240
Nd(^{16}O,^{16}O), 40-48 MeV, even nuclei, 2^+ state E2 transition probabilities and quadrupole moments 80−18234
^{A}Nd(^{6}Li,xnypγ), A=142, 146, 150, 54-99 MeV, determ. of cross sections 78−66307
^{A}Nd(n,n) A=142,144,146,148,150, 7 MeV, optical pot. and deformation, cross sections 79−89230
^{150}Nd, Doppler shift meas. of ground state bands using ^{150}Nd(^{40}Ar,^{40}Ar'γ) 78−50124
^{150}Nd, fast neutron radiative capture cross sections, 5 to 350 keV *(Russian)* 78−33188
^{150}Nd, vibr. bands, population by ^{150}Pr decay 78−89817
^{150}Nd+^{12}C, 70.4 MeV, excitation of 3^- states in deformed nuclei 78−62559
^{150}Nd+^{150}Nd→^{300}120, effect of nuclear force finite range on fission and heavy-ion reactions 78−13180
^{150}Nd+^{20}Ne, 128 to 172 MeV, γ-ray multiplicities in evaporation residues 77−14065
^{150}Nd+^{20}Ne, 174.8 MeV, fusion, pre-equilib. particle emission 79−581
^{150}Nd+^{20}Ne, 175 MeV, cross sections and energy spectra 78−41760
^{150}Nd(^{16,18}O, xnγ), 69-78 MeV, ^{161,162}Er high ang. momentum states, γ decay modes from multiplicity meas. 78−29419
^{150}Nd(^{16}O,4n)^{162}Er, γ multiplicities, side feeding pattern, Monte Carlo calc. 79−578
^{150}Nd(^{20}Ne, xnγ), multipolarities of yrast and statistical cascades, total γ conversion coeff. 78−70484
^{150}Nd(^{20}Ne,X), 115, 130 MeV, γ-continuum multiplicity distrib., yrast bump 80−9265
^{150}Nd(^{20}Ne,xn$\alpha\gamma$), angular momentum effects in pre-equilibrium processes 78−50208
^{150}Nd(^{20}Ne,xnγ), angular momentum effects in pre-equilibrium processes 78−50208
^{150}Nd(α,4n)^{150}Sm, 45 MeV, yrast bands in Sm anal. in interacting boson approx. 78−13124
^{150}Nd(α,α'), 11.5 MeV, electric quadrupole and hexadecapole moments, charge deform. parameters 77−30489
^{150}Nd(α,α'), 11.5-12 MEV, e_2 and E_3 transition strengths meas. 77−26618
^{150}Nd(α,n)^{153}Sm, 14 to 22 MeV, theoretical and expt. study of ^{153}Sm 79−58999
^{150}Nd(e,e'), possible $K^\pi=0$ octupole band, e scatt. form factors 79−9447
^{150}Nd(n,2n), 14.6 MeV, activation cross section 77−88128
^{150}Nd(n,γ), ^{151}Nd rot. states, spin, parity, γ-rays, conversion electrons meas. 77−6196
^{151}Nd, level scheme from (n,γ) meas. 77−34232
^{151}Nd, rot. states populated through neutron capture 77−6196
^{180}Nd(^{12}C,xn), deformed Dy quasicontinuum spectrum, M1, E1, E2 components 80−498
Nd(n,n) elastic and inelastic scatt. on even-A isotopes, 4.08 MeV, deformation effects 77−26715
Os, A=150-2, backbending, Coriolis antipairing, rot. alignment, deform. jumps 78−70432
Os, A=187, 189, spin-state determ. and neutron reson. via (n,γ) 5-350 eV 77−6224
^{A}Os, A=165-168, new isotopes from ^{63}Cu induced reactions 78−70563
^{A}Os, A=169, 170, α-branching ratios 79−503
^{A}Os, A=182, 184, 186, high spin yrast states, back-bending 80−86802
^{A}Os, A=186, 188, 190, 192, rigid asymmetric rotor model descript., E2 and E4 props. 80−13403
^{A}Os, A=186, 188, 7^- isomeric state lifetime from W(α,2nγ) 79−17854
^{A}Os, A=186,188, levels and transitions from Re decay, triaxial rotor model 80−91155
^{A}Os, A=186-194, collective levels, transitions, mag. and quadrupole moments, boson expansion theory 80−105954
^{A}Os, A=188, 189, levels, J^π, transitions and mixing ratios from Ir decay 80−68602
^{A}Os, A=189,190, absolute atomic masses 79−89228
^{A}Os(α,α') A=188,190,192, $4_3{}^+$ level population, hexadecapole vibrs. 78−89780
^{A}Os(γ,xn), 7-30 MeV, A=186,188-190,192, photoneutron cross section and giant resonances 79−54422
^{A}Os(n,γ), A=186-188, 2.6-800 keV, capture Maxwellian cross sections, galactic nucleosynthesis 80−42664
^{A}Os(t,p), 15 MeV, A=188,190,192, cross section meas., DWBA calcs. 78−50181
^{171}Os, alpha decay, half lives, decay energies and branching ratios 79−45215
^{177}Os→^{177}Re decay scheme, lower excited states of ^{177}Re obs. 78−17145
^{179}Os→^{179}Re decay scheme, lower excited states of ^{179}Re obs. 78−17145
^{183}Os, K-isomer populations, (p,xnγ), (He,xnγ) reaction study 78−93927
^{183}Os $9/2^+$ [624] ground state g-factor from NMR 80−83037
^{185}Os, γ-ray spectra obs., first forbidden beta decay anal. 78−559

nuclei with mass number 150 to 189 continued

^{186}Os, ^{187}Os neutron capture cross section ratios, E_n=25 keV age of universe 77−6384
^{186}Os, 2^+-0^+ transitions, mean square nuclear charge radius change, Mossbauer expt. 78−25109
^{186}Os, electromagnetic moments from muonic X-rays 78−12972
^{186}Os, K=0 rot. band collective states, populated in ^{186}Ir decay 77−82803
^{186}Os, levels deduced from ^{186}Ir decay and ^{186}W,(α,4n)^{186}Os 78−86481
^{188}Os, electromagnetic moments from muonic X-rays 78−12972
^{188}Os, ground and γ-band level energies, B(E2) values and EM moments, triaxial description 79−36140
^{188}Os, hyperfine interaction in Gd, PAC expts. 78−48102
^{188}Os, muonic resonance spectra, deduced isomer shifts and electric moments 80−18948
^{188}Os(d,p)^{189}Os, 12 MeV, ^{189}Os spectroscopy, Nilsson model, triaxiality 77−14035
^{188}Os(n_{th},γ), ^{189}Os spectroscopy, Nilsson model, triaxiality 77−14035
^{189}Os, level scheme from ^{189}Re beta-decay 79−54388
^{189}Os, nuclear excitation by electron transition, (NEET) 77−34256
^{189}Os spectroscopy, Nilsson model description, triaxiality 77−14035
^{189}Os(α,2n), 23-27 MeV, ^{191}Pt level scheme, γ, conversion electron spectra, spins, parities 78−25149
^{189}Os(e,e′), 72-100 keV, nucl. excitation by electron transition 78−41703
^{189}Os(t, α)^{188}Re, 15.1 MeV, ^{188}Re energy level obs. 80−47487
Os(γ,xn), photoneutron cross section, bremsstrahlung yield curves 78−17176
Os(n,γ), 5-350 eV for A=187, 189, neutron reson. and spin-state determ. 77−6224
^{A}Pb, A=183,184, alpha decay half lives 80−57749
^{184}Pb isotope identification from Sm(^{40}Ca,xn) 80−32302
^{A}Pd(^{32}S,^{32}S′), A=102, 104, 106, 108, 110, 72-80 MeV, 2_1^+ state mag. moments 80−47373
Pm, A=147, 149, 151, from (p,α), (t,α) reactions, cross sections, reaction mechs. 79−540
^{A}Pm, A=143-153, odd-A, spectroscopic factors, shell model anal. from pickup and stripping reactions 80−78137
^{A}Pm, A=144,148, strong exhaustion of deeply-bound proton hole states 79−45142
^{A}Pm, A=147,149,151 single proton hole states in pickup reactions from Sm(p,α) 80−78128
^{A}Pm, A=149,151, shape coexistence, deformed states from Nd decay 80−78135
^{150}Pm, decay, ^{150}Sm nucl. struct. determ. *(Japanese)* 77−41889
^{150}Pm, fractional independent yield from ^{238}U photofission with bremsstrahlung 79−36283
^{151}Pm, excited state lifetimes, delayed coincidences method 77−6298
^{151}Pm level scheme in low excitation region <1 MeV 77−54173
^{151}Pm single proton states, rot. bands, level J^π assignments, spectroscopic strengths from ^{150}Nd(^{3}He,d), and ^{152}Sm(t,α) 79−67626
^{151}Pm→^{151}Sm, β-decay, level scheme of ^{151}Sm 77−74792
^{152}Pm decay, β and γ rays, spins, half lives, ^{152}Sm levels 78−542
^{153}Pm 5/2$^-$ $h_{11/2}$ dominated band, anomalous ang. distribs., CCBA calcs. for ^{154}Sm(t,α) 80−86788
^{153}Pm struct., spin and parity assignments, Nilsson model interpretation from ^{154}Sm(t,α) polarised t 79−469
^{150}Pr decay into ^{150}Nd vibr. levels 78−89817
^{150}Pr, fission product, γ-spectra, half-life meas. 77−38240
Pt, A=187, 189, 191, low-temp. orientation studies, mag. moment and E2/M1 ratios in daughters 77−22889
Pt decay, oriented nuclei, ^{189,191}Ir levels, J^π, transitions and mixing ratios 80−68602
Pt, isotopes near A=186, competition of nucl. shape 78−17094
Pt rot. states and moments of inertia staggering from ^{A}Hg, A=181-185 α-decay 78−89779
^{A}Pt, A=173-179, 188, alpha decay, half lives, decay energies and branching ratios, rot. struct. 79−45215
^{A}Pt, A=178,179, alpha decay branching ratio 80−57749
^{A}Pt, A=186,188,190, subnanosecond high spin isomers, decay chains and lifetimes from Yb(^{16,18}O, xn) 79−45140
^{A}Pt, A=188-198 collective levels, transitions, mag. and quadrupole moments, boson expansion theory 80−105954
^{181}Pt ground state spin from ^{185}Hg decay 77−22968
^{182}Pt, low-energy collective states 77−22846
^{183}Pt fast β-transition, ^{183}Ir levels, J^π assignments, Nilsson states for N=105 isotones 79−22206
^{185}Pt^{m+g} decay, population of ^{185}Ir levels 80−9269
^{186}Pt, energy level scheme 79−97652
^{187}Pt, levels, J^π, $T_{1/2}$, possible E0 transitions from ^{187}Au decay *(French)* 80−32230
^{187}Pt→^{185}Pt, oblate to prolate transition meas. 77−22878
^{188}Pt α-decay energy and branching ratio 79−22237
^{188}Pt decay, ^{188}Ir level scheme and transitions 79−22237
^{188}Pt, energy level scheme 79−97652
^{188}Pt, ground and γ-band level energies, B(E2) values and EM moments, triaxial description 79−36140
^{188}Pt side band, low lying and high spin states populated in ^{191}Ir(p,4nγ) 78−4936
Re, A=183, 184, 186, 188, nuclear quadrupole alignment in Re single cryst. at low temp. 78−48091
Re, A=187, 189, 191, obs. of proton hole states via (t,α) 77−88025
Re, alpha decay studies of the isotope 79−63636
Re, doubly odd deformed nuclei, EM transitions, nanosec. lifetimes 78−62505
Re isotopes, $T_{1/2}$ determ. for β-decay using moving tape apparatus 77−65411
Re, odd isotones, deformation pot. energy from Nilsson model 80−57676
Re, odd isotopes, pot. energy surfaces and quadrupole deformation parameters, deformed basis model 79−80867
Re, p bombardment 15-160 MeV, long lived isotope prod., high temp. graphite thickness gauge calibration 77−23054
Re, photofission cross section, 220-550 MeV, coherent electron bremsstrahlung beam 79−13353
^{A}Re, A=166, 167, 168, evidence for existence from ^{93}Nb+^{84}Kr and ^{89}Y+^{84}Kr collisions 79−503
^{A}Re, A=168 and 169, new isotopes from ^{63}Cu induced reactions 78−70563
^{A}Re, A=181, 182, 187, magnetic moments meas. by PAC 80−22688
^{A}Re, A=181, 182, 187, spin polarisation, state struct. and mag. moments in rot. model 80−18194
^{A}Re, A=181,182,187, rotational struct., spin polarization 80−83016

nuclei with mass number 150 to 189 continued

^{A}Re, A=183,184, nuclear K-X-ray satellites, Z=50-83, decay scheme 80−42984
^{172}Re, isomeric states, γ-ray transition 79−9433
^{177}Re, populated in decay of Os isotopes, lower excited state obs. 78−17145
^{179}Re, populated in decay of Os isotopes, lower excited state obs. 78−17145
^{180}Re decay, ^{180}W octupole vibr. states, J^π and transitions 80−83024
^{181}Re, backbending, Coriolis antipairing, rot. alignment, deform. jumps 78−70432
^{181}Re states and transitions, rot. bands and Nilsson states from ^{181}Ta(^{3}He,3nγ) 79−36152
^{182}Re, cryonuclear physics for radioactive decay studies *(Dutch)* 78−29416
^{182}Re isomer decay mag. moment, ^{182}W high spin states, J assignments and mixing ratios 80−42593
^{183}Re, elec. quadrupole moment of 514 Nilsson state, TDPAC meas. 78−37276
^{183}Re, γ-ray spectra obs., first forbidden beta decay anal. 78−559
^{184}Re decay, energies, relative intensities, of conversion electrons and γ rays 77−61381
^{185}Re, ^{187}Re, NQR freq. in NH_4ReO_4, temp. depend. 77−12228
^{185}Re nuclear deformations, core-particle coupling model 79−450
^{185}Re/^{187}Re quadrupole moment ratio 79−9465
^{186}Re→^{186}Os beta decay, absolute log ft values, beta spectra, directional correlation coeff. and WS potential parameters calc. *(Rumanian)* 78−82316
^{187}Re, 206 keV state, g-factor, time differential PAC meas. 78−505
^{187}Re, 36.23 keV transition, penetration coeff. and mixing ratio determ. 77−50080
^{187}Re, decay const. determ. from ^{187}Re-^{187}Os systematics in meteorites 80−41778
^{187}Re low lying level struct. and transitions, E2/E1 mixing ratios from ^{187}W decay 80−27557
^{187}Re(n,γ), thermal, isomer state excitation, relative probabilities 79−75814
^{188}Re, energy levels obs., form. by ^{189}Os(t, α)^{188}Re 80−47487
^{188}Re, first forbidden 1.98 MeV beta decay, matrix elements 77−61385
^{189}Re, beta-decay, ^{189}Os scheme 79−54388
^{182m}Re β-decay, rot. and intrinsic struct. of ^{182}W determ. 77−41914
Sm (n,2n) react. cross sections at 14.8 MeV 78−74355
Sm (p,t), 18-20 MeV, Q effects on cross section, DWBA anal., A dependence 79−63675
Sm, A=152, 154, electric quadrupole and hexadecapole moments, charge deform. parameters, Coulomb excitation expts. 77−30489
Sm, A=152, 154, high spin rot. states populated in heavy ion scatt., lifetime meas. 77−30511
Sm, deep hole states observed in particle transfer reactions 80−68511
Sm, ΔN=2 coupling problem 80−47412
Sm equilibrium and pre-equilibrium decay, α-multiplicities, energies and entry lines from ^{150}Nd(α,xn) 79−93549
Sm, fission, proton induced, 1 GeV, cross section *(Russian)* 78−94041
Sm, ion recoiling into gas and vac., hyperfine field and correl. time meas. 78−66240
Sm isotopes, A=148,152,154, 16 MeV, coherent optical model analysis 77−26750
Sm isotopes, deform. effects in neutron scatt. 77−74758
Sm isotopes, shape transition, s-d IBA model Hamiltonian struct. 80−32173
Sm odd isotopes, $1h_{11/2}^{-1}$ neutron state strength distrib. 77−46100
Sm, shell model, SU_6(s,d) boson model, collective states struct. 78−54672
Sm, stable even isotopes, mean-square charge radii 79−67647
Sm+O^{16} fusion, cross sections for spherical and deformed Sm isotopes, shape effects 78−78407
Sm(^{3}He,^{3}He′), 53 MeV, even A=144-154, DWBA anal. of ang. distribs. 78−17230
^{A}Sm, A=144-154, mean square nuclear charge radius, laser atomic beam spectroscopy 80−102468
^{A}Sm, A=144-154, nuclear charge density and quadrupole moments from muonic X-rays 79−40838
^{A}Sm, A=148, 150, 152, 154, levels, moments, isomer shifts, spectroscopic amplitudes, sixth order boson expansion 79−89242
^{A}Sm, A=148, 150, 152, 154, 156, excited states of transitional region nuclei, rot. bands *(Russian)* 80−52556
^{A}Sm, A=150, 152, 154, 7 MeV neutron elastic and inelastic scatt., diff. cross sections, deformation effects 77−26768
^{A}Sm, A=150, 152, muonic, X-ray spectra meas. and anal., charge radii, multipole moments 79−3600
^{A}Sm, A=150,152,154, fast neutron radiative capture cross sections, 5 to 350 keV *(Russian)* 78−33188
^{A}Sm, A=152, 154, energy levels and E2 transition rates from three-band mixing model, backbending 79−67623
^{A}Sm+^{20}Ne, A=148, 150, 152, 70 MeV, Coulomb absorpt. obs. 78−70558
^{A}Sm(^{16}O,^{16}O′), A=150, 152, hyperfine dynamic mag. field effects 80−68689
^{A}Sm(^{16}O,X), 60-75 MeV, A=148, 150, 152, 154 deformation effects on fusion 80−18360
^{A}Sm(^{16}O,X), 60-75 MeV, A=148,150,152,154, fusion cross section, evaporation residues 80−83137
^{A}Sm(^{20}Ne, ^{20}Ne), 70 MeV, A=148, 150, 152, Coulomb polarisation pot., coupled channel calcs. 80−22855
^{A}Sm(^{32}S,^{32}S′), A=150, 152, hyperfine dynamic mag. field effects 80−68689
^{A}Sm(^{3}He, ^{3}He′), A=144, 148, 152, 154, 150, 40.9 MeV, transition cross sections, deformation parameters, coupled channels anal. 79−67640
^{A}Sm(^{40}Ar,X) A=144, 148, 154, 3.6-4.5 MeV/A, sub-barrier fusion, evaporation residue cross section, deformation 80−68718
^{A}Sm(^{86}Kr,X), A=144, 154, 490 MeV, transfer reactions and associated γ-multiplicity moments 80−18342
^{A}Sm(N,N′) A=152,154, deformed nuclei struct., rot. model with optical pot., coupled channel formalism 79−3146
^{A}Sm(n,nγ), 2.75 MeV, A=150,152,154, levels and excitation cross sections 79−75839
^{A}Sm(p,p′), A=144,154, 67 MeV, giant isoscalar monopole resonance excitation 79−22259
^{A}Sm(p,p), 1 GeV, A=152, 154, dispersive effects in ground state rot. band excitation, coupled channel calcs. 79−40828

nuclei with mass number 150 to 189 continued
^{150}Sm(p,t), A=148, 150, 152, 154, 40 MeV, two neutron transfer strengths, IBA model predictions 79−85474
^{150}Sm deformation, collective spectra and moments of inertia starting from nuclear force 79−17790
^{150}Sm, excited states calculation, phenomenological models: band-mixing, vibrational-rotational and interacting-boson model 80−22653
^{150}Sm, γ-spectra, levels in ^{150m}Eu, 35.8 y decay 77−82858
^{150}Sm γ-spectra from ^{150}Nd(α,4n), 45 MeV, fusion and neutron evaporation 79−36291
^{150}Sm, negative parity band crossing in even-even nuclei 78−21488
^{150}Sm, negative parity bands, coherent state model 78−89782
^{150}Sm, negative parity yrast band, E1 transitions polarisability, quadrupole-octupole coupled vibr. system 79−484
^{150}Sm, nucl. struct. from ^{150}Eu decay *(Japanese)* 77−41888
^{150}Sm, nucl. struct. from ^{150}Pm decay *(Japanese)* 77−41889
^{150}Sm, nucl. struct. from Coulomb excitation *(Japanese)* 77−41890
^{150}Sm, pionic atoms, dynamical nuclear polarisation, nuclear structure effects 79−94113
^{150}Sm, pionic atoms, E2 nuclear resonance effects 79−76534
^{150}Sm, vibrational states, B(E2) branding rates and interband transitions, pairing plus quadrupole calcs. 80−78127
^{150}Sm, yrast bands anal. from ^{150}Nd(α,4n), interacting boson approx. 78−13124
^{150}Sm(^{12}C,^{14}C), 2_1^+ ang. distributions, shape difference between pickup and stripping reaction 78−33209
^{150}Sm(^{16}O,^{18}O), interference effects, coupled channels calc. with BCS+RPA wavefunctions 77−26787
^{150}Sm(^{16}O,xnγ), Yb nuclei at high ang. momentum, moment of inertia from γ spectra 78−13135
^{150}Sm(^{6}Li,xnypγ), 54-99 MeV, determ. of cross sections 78−66307
^{150}Sm(α,3nγ)^{151}Gd, 35-45 MeV, collective band struct. of ^{151}Gd anal. 77−61342
^{150}Sm(p,2nγ), 18-26 MeV, level struct. of ^{149}Eu, spin, parity 78−21561
^{151}Sm, β-decay, branching ratio and K-shell autoionisation 80−42598
^{151}Sm, gamma spectra, energy levels *(Dutch)* 80−47430
^{151}Sm, low energy levels, spin values, ga gamma-gamma ang. correl. meas. 77−18398
^{151}Sm low energy levels from expt. and Coriolis mixing calcs. of ^{150}Sm(n,γ) 80−57697
^{151}Sm, populated in ^{151}Pm decay, level scheme, γ-ray spectra 77−74792
^{151}Sm, struct. determ. from gamma ray spectra in (n,γ) 77−22853
^{151}Sm, transition probabilities determ. 77−79329
^{151}Sm transitional nucleus, neg. parity states, spectroscopic factors, B(E2) values, particle-rotor model 78−50080
^{152}Sm, 2^+ rot. states, time integral, perturbed angular correl., meas. method 77−9154
^{152}Sm (^{16}O, ^{14}C), 104 MeV, two proton transfer between pairing rot. states 77−10430
^{152}Sm (n,n), 2.4-7.2 MeV, inelastic and elastic optical model and deformation parameter depend. *(Russian)* 80−13481
^{152}Sm, collective props., HF calcs., review 78−50064
^{152}Sm, giant dipole resonances of deformed even-even nuclei ^{152}Sm to ^{238}U, microscopic calcs. 77−50096
^{152}Sm, giant resonance excitation by (e,e′) at 60-105 MeV, DWBA analysis *(Russian)* 78−41686
^{152}Sm ground and γ-bands, direct and multistep processes from (α,^{6}He), (p,t), (^{16}O,^{18}O) 80−102094
^{152}Sm, ground-state rot. band via electron scatt., charge distrib. 77−30475
^{152}Sm, γ-transition energy and intensity meas. from ^{152}Eu decay 80−73818
^{152}Sm, HF one body density for core and valence nucleons 78−78294
^{152}Sm, level population by (t,α) reaction 77−67755
^{152}Sm levels populated in ^{152}Pm decay, γ spectra 78−542
^{152}Sm, populated in ^{152}Eu decay, gamma transitions and IC 80−22768
^{152}Sm, static quadrupole moments of arbitrary excited states, sum rule approach 80−91135
^{152}Sm(^{35}Cl,^{35}Cl′γ), 132-43 MeV, lifetime meas. of high spin states 78−13140
^{152}Sm(^{3}He,3n), gamma deexcitation mechanism of rot. levels 79−26442
^{152}Sm(α,2n), gamma deexcitation mechanism of rot. levels 79−26442
^{152}Sm(e,e′), 251.5 MeV exciting ground-state rot. band 77−30475
^{152}Sm(e,e′), 35-350 MeV, coupled channels anal., rot. band excited states, charge densities 79−3139
^{152}Sm(n,n′γ), 1.0-2.75 MeV, statistical model deviations *(Russian)* 77−26690
^{152}Sm(n,n′γ), 2.5 MeV, direct excitation of rotational levels 77−30594
^{152}Sm(n,n′γ), 2.75 MeV, direct excitation of some collective levels 77−26720
^{152}Sm(n,n′γ) spectra and ang. distribs. anomalous excitation *(Russian)* 77−54224
^{152}Sm(n,n'γ), 2.5 MeV, rot. level direct excit. 77−14127
^{153}Sm level struct., DWBA anal. of ang. distribs. from ^{154}Sm(d,t) 79−30788
^{153}Sm, production by ^{239}Pu fission, absolute yields 77−50167
^{153}Sm, radioactive decay, γ-ray energy meas. *(German)* 77−57633
^{153}Sm, reactor prod. of curie strength photon beam 78−86709
^{153}Sm, spin, parity, deduced levels, using ^{150}Nd(α,n), comparison with particle-rotor model 79−58999
^{154}Sm (p,p′)^{154}Sm, 1 GeV, giant reson. excit., Glauber calc. 77−82891
^{154}Sm, giant multipole reson. fragmentation among two-phonon states 80−78238
^{154}Sm giant multipole resonance fragmentation among two-phonon states 80−18260
^{154}Sm, Skyrme-HF calcs., deformation, electric moments, spin-orbit potentials 78−62480
^{154}Sm, strength functions for transitions to $I^\pi=2^+$ states 78−86519
^{154}Sm(^{12}C,^{14}C)^{152}Sm, 65 MeV, ground-state rot. band ang. distribs., quadrupole transfer strength 77−336
^{154}Sm(^{16}O,X), 153 MeV, angular momentum transfer in incomplete-fusion reactions 80−9320
^{154}Sm(^{40}Ar,X), 222, 340 MeV, fusion cross sections, direct and evaporative p and α prod., evaporation, fission 80−13518
^{154}Sm(^{40}Ar,X), 222-340 MeV, charged particle emission, early collision evolution, fission and evaporation cross sections 80−106072
^{154}Sm(α,α), 50 MeV, long range absorption and optical model effects from strong inelastic coupling 80−535
^{154}Sm(γ,γ′), reson. fluoresc., J^π, M2/E1 and Γ meas. 77−26663
^{154}Sm(n,2n), 14.6 MeV, activation cross section 77−88128

nuclei with mass number 150 to 189 continued
^{154}Sm(p,p′), 0.8 GeV, ang. distribs. and multipole moments, DWBA and coupled channel anals. 80−105969
^{154}Sm(p,p′), 35 MeV, extraction of deform. parameters 78−54755
^{154}Sm(p,p′), 35 MeV, ground state rot. band and multipole moment 80−32178
^{154}Sm(p,p'), 1 GeV, possibility of observing giant resonances with high multipolarities *(Russian)* 78−78350
^{155}Sm, level struct., DWBA anal. of ang. distribs. from ^{154}Sm(d,p) 79−30788
Sm(α,α′), 11.25 to 12 MeV, a=152,156, elec. moments, charge deform. parameters 77−54233
Sm(α,α′), 11.5-12 MeV, E_2 and E_3 transition strengths meas. 77−26618
Sm(d,^{6}Li) (A=144, 148, 150, 154), 35 MeV, ang. distrib. meas., deduced α-particle spectroscopic factors, reduced widths, decay lifetimes 77−18571
Sm(n,n), (n,n′), (n,n′Γ), A=150,2, E=2.47 MeV, collective excitations obs. 78−33187
Sm(n,n′), 7 MeV, A=150,152,154, differential cross sections, coupled channel anal., deform. effects 77−54219
Sm(p,α)^{147,149,151}Pm, 17 MeV, direct and sequential reaction mechs., (t,α) comparison 79−540
Sm(t,p), SU(6) boson model for two-nucleon transfer intensities 78−25206
^{127}T, 24.3 keV neutron activation cross sections with Fe filter technique 77−26763
Ta (γ,γ), 2.754 MeV, elastic scatt. diffr. cross section, Rayleigh, Thomson, Delbruck scatt. interference 79−528
Ta, alpha decay studies of the isotope 79−63636
Ta backward π^+ prod., momentum depend., scaling, Monte Carlo calcs. 79−13305
Ta, doubly odd deformed nuclei, EM transitions, nanosec. lifetimes 78−62505
Ta fast neutron capture and activation cross sections 77−26758
Ta, γ-ray attenuation meas. using Ge(Li) detector 78−17539
Ta, mass dependence for radiative capture of 14.1 MeV neutrons 78−13087
Ta, meas. of mass no. depend. of ψ photoprod. 77−26668
Ta, photofission cross section, 220-550 MeV, coherent electron bremsstrahlung beam 79−13353
Ta, reactions induced by ^{12}C and ^{19}F ions, γ-ray spectroscopy of induced activities 77−23107
Ta+α, 720 MeV, correlated energy spectra of light fragments, fireball and coalescence models 78−62555
Ta+n, differential cross sections for prod. of low energy photons 77−23068
Ta+p, 300 MeV, 450 MeV, 24 GeV, cross-section meas. 77−67740
Ta+p(K^-), 28.5 (12.6) GeV/c, backward particle emission, energy depend. 78−25236
Ta+p(d)(α)(^{12}C), 4.2 GeV/N, multiple π^- prod., mean multiplicity *(Russian)* 80−27647
Ta+p→p+X, backward inclusive scattering of polarised protons 78−17206
Ta(A,X), 720 MeV, nuclear fragment prod. thermodynamic evaporation and firestreak description, pre-equilibrium emission 79−54426
Ta(C,Z), 4.2 GeV.c^{-1}, inelastic cross section meas. and multiplicities obs. *(Russian)* 79−9580
Ta(^{56}Fe,X), relativistic ^{56}Fe fragmentation, charge and mass changing cross sections 79−54453
^{166}Ta, isotope identification in ^{159}Tb(^{16}O,9n) reaction, half-life and decay scheme 77−79331
^{173}Ta, levels, rot. parameters, γ-mixing 77−34248
^{176}Ta, decay of four-particle isomer 78−70481
^{176}Ta, isomeric states and rot. struct. anal., in-beam γ-ray spectroscopy 78−78312
^{177}Ta, γ-transition $55/22^+ \rightarrow 77/22^+$, E2/M1 mixing, μ determ., $T_{1/2}$ 77−10355
^{177}Ta, magnetic moments meas. by PAC 80−22688
^{177}Ta, rotational struct., spin polarization 80−83016
^{177}Ta spin polarisation, state struct. and mag. moments in rot model 80−18194
^{178}Ta 2.45 h decay, J^π assignment, ^{178}Hf 9 to 8^- transition 79−45201
^{178}Ta level properties, rot. bands, transitions and level lifetimes from ^{176}Lu(α, 2n), ^{178}Hf(d, 2n), ^{178}Hf(p, n) 79−36158
^{178}Ta, nucl. orientation in Fe 78−39412
^{180}Ta, evidence for Gallagher-Moszkowski doublets from ^{181}Ta(p,d) reaction 78−58233
^{180}Ta, ground state spin, (p,d) cross-sections 79−26368
^{180}Ta, low temp. photonuclear nucleosynthesis in stellar H-CNO burning zones 77−13319
^{180}Ta mass, 10^{13} y naturally occurring isomer state 80−57670
^{180}Ta nuclear spin and mag. dipole moment from laser resonance fluorescence 80−78143
^{180}Ta, radioactive decay and half-life of naturally occurring isotope 77−61377
^{180}Ta^m, β^- and EC branching ratios, K-internal conversion coeff., γ-intensities, T 1/2 80−68601
^{181}Ta, 133-482 keV cascade, effect of source preparation technique on differential ang. correl. 77−71711
^{181}Ta, 136 keV level, g-factor meas. 79−6387
^{181}Ta, 6.2 keV level, Mossbauer spectroscopy, source prep. 78−25373
^{181}Ta 6.2 keV Mossbauer resonance, prep. of narrow line sources 79−76253
^{181}Ta, anomalous M1-conversion, 482-keV transition, penetration parameter meas. 77−61382
^{181}Ta, appl. to Mossbauer meas. of gravitational red shift 78−24905
^{181}Ta, collective props., HF calcs., review 78−50064
^{181}Ta, DPAC in K_3HfF_7 77−32299
^{181}Ta, deformed nuclei, electron scatt., elastic differential cross section calc. 77−82912
^{181}Ta, EFG in HfV_2O_4, temp. depend., TDPAC 77−59488
^{181}Ta, elec. quadrupole interactions in 482-keV level, meas. using Ge detector 79−40842
^{181}Ta, fission, proton induced, 1 GeV, cross section *(Russian)* 78−94041
^{181}Ta, freq. modulation of 6.2 keV Mossbauer states 79−13202
^{181}Ta, ground state rotational band, electroexcitation 78−33168
^{181}Ta, in Be, quadrupole interaction, temp. depend., TDPAC obs. 77−20772
^{181}Ta, isomer shifts of 6.2 keV γ-rays, book contrib. 79−87358
^{181}Ta, mag. form factors calc. 79−9458

nuclei with mass number 150 to 189 continued
^{181}Ta, Mossbauer gamma-ray detection with Si(Li) and Ge detectors 77−10530
^{181}Ta, Mossbauer transition in Ta at 6.2 keV and high temps. 77−12269
^{181}Ta, neutron resonances, probability table method and correlated data 79−36284
^{181}Ta, nuclear K-X-ray satellites, Z=50-83, by α-bombard, 17.5-22.5 MeV 80−42984
^{181}Ta, PAC obs. of crit. behaviour of Ni-Ta system 78−43723
^{181}Ta, pion$^-$ capture, high spin states and neutron multiplicities meas. 78−54806
^{181}Ta, pionic X-rays, effective quadrupole moment determ. 78−66200
^{181}Ta, radial charge parameters, quadrupole moment, from muonic atom transitions 77−34226
^{181}Ta, TDPAC determ. of hyperfine critical exponents in HfNi 77−8465
^{181}Ta transverse form factors from projected HF approach 80−105965
^{181}Ta+^{12}C, 4.2 GeV/N, identical pion$^-$ interference effect, generation range determ. *(Russian)* 80−42695
^{181}Ta+^{12}C, 78 MeV, fission fragment angular distrib., shape of saddle point of compound nucleus *(Chinese)* 78−78427
^{181}Ta+^{138}Xe, deep inelastic transfer, decay of binary nuclear system 80−22848
^{181}Ta+^{16}O, elastic scatt. transfer reactions, fission, total cross sections, optical model parameters 77−54246
^{181}Ta+^{20}Ne, 8.0 GeV, target residue mass, charge distrib. determ. 79−17930
^{181}Ta+^{40}Ar, deep inelastic transfer, decay of binary nuclear system 80−22848
^{181}Ta+^{86}Kr, 620 MeV, charge and ang. distribs., kinetic energy spectra, of deeply inelastic fragments 78−25221
^{181}Ta+^{86}Kr, deep inelastic transfer, decay of binary nuclear system 80−22848
^{181}Ta+α, 4.2 and 5.15 GeV, central nuclear collisions, pion multiplicity calc. *(Russian)* 79−59079
^{181}Ta+p, 1 GeV, neutron production *(Russian)* 79−85477
^{181}Ta+π$^{\pm}$, proton spectra, cross section, π. absorpt. mechs. 78−25239
^{181}Ta(^{136}Xe,X), 1120 MeV, energy, angular, charge distribs. meas. 77−3029
^{181}Ta(^{14}N,X), 85-115 MeV, cross sections, preequilibrium α-particle emission 80−42680
^{181}Ta(^{20}Ne, spallation), 8.0 GeV, cross sections and target residues, model comparison 80−68630
^{181}Ta(^{6}Li,xn), 75, 85, and 95 MeV, K X-ray multiplicity 79−76019
^{181}Ta(^{84}Kr,^{84}Kr′γ), 348 MeV, ground-state rotational band obs. 77−6197
^{181}Ta(a,X), a=p,d,^{4}He, ^{12}C, 4.2 GeV/c, multitudes of secondary negative particles, momentum distrib. ratios *(Russian)* 80−63178
^{181}Ta(d,n), secondary neutron emission characts. 79−30843
^{181}Ta(d,pX) 25.5 MeV, inclusive p spectra and cross sections from d breakup 79−13303
^{181}Ta(e,α), 100 MeV, energy spectra, cross sections 77−18529
^{181}Ta(e,e′), 79-119 MeV, DWBA anal., giant multipole resonance parameters 77−30558
^{181}Ta(e,e′), giant monopole and quadrupole resonances excitation 78−17184
^{181}Ta(γ,X), 3-30 MeV, photoabsorption cross section, giant dipole resonances 80−78254
^{181}Ta(γ,γ′)^{181}Ta, elastic and Raman scatt. at 8.5-11.4 MeV, GDR parameters 78−587
^{181}Ta(γ,γ), 6.84-11.39 MeV, Rayleigh and Delbruck scatt. destructive interference, cross sections 79−6566
^{181}Ta(γ,γ), 9 MeV, Delbruck amplitude contrib. determ. 77−41947
^{181}Ta(γ,n) photoneutron absorpt. cross section meas. 20.9 to 837.8 keV *(German)* 80−5122
^{181}Ta(n,2n), 14.6 MeV, cross-section meas. 79−59055
^{181}Ta(n,2n)^{180}Ta^{m}, 14.68 MeV, cross section 80−68659
^{181}Ta(n,α), thermal, isomer state excitation, relative probabilities 79−75814
^{181}Ta(n,γ), 2-3 eV, γ-spectra, energy levels, J$^{\pi}$ 78−602
^{181}Ta(n,γ), 30 keV, capture cross sections, stellar nucleosynthesis 80−42663
^{181}Ta(n,γ), cross section, statistical theory anal., radiative strength functions *(Russian)* 78−17212
^{181}Ta(n,n′)^{181}Ta, 9.1 MeV, CC neutron spectra and angular distrib. meas. *(Russian)* 78−25198
^{181}Ta(n,total), 15 to 2030 eV resonances, time of flight spectroscopy 78−41716
^{181}Ta(n_{th}, α), cross section 78−66284
^{181}Ta(p,X), 20-48 MeV, proton total reaction cross section 79−80934
^{181}Ta(p,4n)^{178}W radionuclide production and purification 80−12252
^{181}Ta(p,d), evidence for Gallagher-Moszkowski doublets in ^{180}Ta 78−58233
^{181}Ta(p,n), 11.2 MeV, spin cut-off parameters from neutron ang. distribs. *(Russian)* 79−80940
^{181}Ta(p,n)^{181}W, 10.2 MeV, CC neutron spectra and angular distrib. meas. *(Russian)* 78−25198
^{181}Ta(p,n)^{181}W, multi-step compound and direct reactions, statistical theory 80−57761
^{181}Ta(p,p′)X, 800 MeV, cluster recoil mechanism for inclusive nuclear reactions 78−93998
^{181}Ta(p,p)X, 0.8 GeV, inclusive cross sections, quasi-two-body scaling 79−3150
^{181}Ta(π$^{\pm}$,p), (π$^{\pm}$,d), E=100, 220 MeV, p and d spectra meas. 78−648
^{182}Ta β-decay, ^{182}W 100 keV E2-transition, L-subshell internal conversion coeff. 79−75909
^{182}Ta, configuration mixing in positive parity states 77−22854
^{182}Ta decay, K-conversion coeff. of γ-rays above 800 keV 77−14069
^{182}Ta, decay scheme, conversion electron spectra, K-line transitions 78−13025
^{182}Ta deformed odd-odd nucleus, γ transition probabilities, rot. band mixing 77−61375
^{182}Ta, Fe-Ta, nuclear mag. moment, NMR-ON study 80−78139
^{182}Ta, levels, J$^{\pi}$, via 2-3 eV neutron capture γ-spectra 78−602
^{182}Ta rot. bands, bandheads and decay data from ^{181}Ta(n,γ) 79−93491
^{185}Ta single proton states and rot. bands, J$^{\pi}$ from ^{186}W(t,α),pol.t 80−91130
Ta(α,X) X=p,d,t,^{3}He,^{4}He, 720 MeV, back-angle prod. of light ions, model calcs. 79−45280
Ta(γ,γ), 1.17 and 1.33 MeV, cross-sections 79−75973
Ta(γ,γ), differential cross sections, 244 to 1408 keV 79−49618
Ta(γ,γ), neutron capture γ-ray Rayleigh scatt. 80−52661

nuclei with mass number 150 to 189 continued
Ta(γ,n), 30 to 140 MeV, partial photoneutron cross section, total cross section approx. 80−22809
Ta(γ,n), photoneutron Q-value determinations using monochromatic photons 79−22271
Ta(n,X), slow and ultracold total and inelastic cross sections 80−68673
Ta(n,γ), absolute cross sections in keV range 77−26771
Ta(n,γ), separated isotopes, integral capture cross section meas. in CFRMF 77−26760
Ta(p,X), 400 GeV, p, d, t, π, ^{3}He, α backward prod., inclusive cross sections 79−85475
Ta(p,X), 400 GeV, p backward prod. invariant cross section 79−93623
Ta(p,X), 400 GeV/c, light ion backward prod., invariant cross section 80−32279
Ta(p,p′), 0.6-25 GeV, backward emitted proton inclusive spectra, short range correlation 80−32281
Ta(p, xn), 23 MeV, n energy distribs. *(Russian)* 78−86537
Ta(π$^-$,X), stopped pions, radioactive product yields 80−83126
Tb, doubly odd deformed nuclei, EM transitions, nanosec. lifetimes 78−62505
Tb, high spin isomer α-decay search 80−102158
Tb, magnetic moment of neutron resonances 77−26576
Tb+n, neutron spin states amplitudes and scatt. cross sections 77−23019
^{A}Tb, A=151, 153, 155, 157, prop. anal. on function of nuclear shape 79−75828
^{150}Tb, β-decay, ^{150}Gd vibr. levels anal. 78−8772
^{150}Tb decay, ^{150}Gd levels and transitions, J$^{\pi}$ assignments mixing ratio, nuclear orientation 79−13205
^{151}Tb 11/2 isomer, high spin few-particle states, in beam study from (^{3}He,3n) and (α,4n) 79−17805
^{151}Tb decay, ^{151}Gd excited state spin assignments γ-γ ang. correlations *(Russian)* 79−49597
^{151}Tb lower excited state lifetimes, ^{151m}Tb isomer from ^{151}Dy decay 79−75919
^{151}Tb, positron decay, γ-ray coincidence spectra 79−9513
^{153}Tb decay, ^{153}Gd γ-directional distrib., levels, spin assignments 79−13241
^{153}Tb excited states from Eu(α, xn), rot. bands, spin, parity, γ spectra 78−62552
^{153}Tb, fission barrier at 28.5 MeV 80−91202
^{153}Tb low excited states, γ-ray angular distrib. in ^{153}Dy decay 79−6471
^{153}Tb, low excited states, lifetime meas. 79−6492
^{153}Tb, meas. of positron spectrum 79−6509
^{153}Tb, negative-parity bands 78−93937
^{153}Tb, prod. in ^{153}Dy decay, weak deform. 77−41884
^{154}Tb, beta-decay, ^{154}Gd matrix elements determ. 77−57626
^{155}Tb, excited state lifetimes 79−6494
^{155}Tb, oriented in Gd, γ-decay ang. distrib., hyperfine splitting, moment and mixing ratios 79−45242
^{156}Tb, orientation in Gd matrix, γ-ray ang. distrib. anisotropy meas. 79−59031
^{159}Tb, neutron resonances, time-of-flight spectra 80−27633
^{159}Tb polarised target, transmission of polarised resonance neutrons, 20 eV to 100 keV, spins *(Russian)* 77−50138
^{159}Tb, transmission of polarised resonance neutrons through polarised target, 20-100 keV 77−26657
^{159}Tb transverse form factors from projected HF approach 80−105965
^{159}Tb+^{86}Kr, 620 MeV, energy spectra, charge and ang. distribs., diffusion model 78−50202
^{159}Tb(^{11}B,X), 51 MeV, fusion and deep inelastic, quantised frictional motion calcs. 80−102223
^{159}Tb(^{14}N,X), 140 MeV, incomplete fusion reactions, sum rule model 80−95332
^{159}Tb(^{14}N,X), 85-115 MeV, cross sections, preequilibrium α-particle emission 80−42680
^{159}Tb(^{14}N,X), 95 MeV, fast α-particle ang. distribs. 80−63207
^{159}Tb(^{14}N,αxn), 95 MeV, γ-multiplicities following fast α-emission 79−67770
^{159}Tb(^{16}O,9n)^{166}Ta, isotope identification, half-life and decay scheme 77−79331
^{159}Tb(^{40}Ar,X), 273 MeV, complete fusion and charge transfer reactions 79−45314
^{159}Tb(e,α), 100 MeV, energy spectra, cross sections 77−18529
^{159}Tb(γ,γ′) 8.5-11.4 MeV, elastic and Raman scatt., giant reson. struct. 77−34284
^{159}Tb(n,γ), resonance parameters *(Russian)* 77−74850
^{159}Tb(n,γ)^{160}Tb, E$_n$=14.1 MeV, γ emission exciton model *(Russian)* 79−13302
^{159}Tb(p,X), 20-48 MeV, proton total reaction cross section 79−80934
^{159}Tb(p,4nγ), 27-51 MeV, ^{156}Dy rotational levels 77−6199
^{159}Tb(p,f), 600 MeV, binary fission process 77−3060
^{159}Tb(p,f), 600 MeV, fragment energies, cross sections level density and barrier heights 80−42723
^{160}Tb β-decay, oriented nuclei, γ transitions multipole mixing parameters 80−18240
^{160}Tb, β-decay in $TbSi_2$, electronic config. of ^{160}Dy ion produced 79−59340
^{160}Tb decay, ^{160}Dy anomalous γ-L X-ray directional correlations 80−52610
^{160}Tb, perturbed ang. correl. determ. by one ang. meas. 79−17851
^{160}Tb→^{160}Dy, A_2^{β} ang. correl. coeff., β-γ-γ ang. correl. studies 79−13255
^{160}Tb→^{160}Dy, γ-transitions and angular distributions 80−83060
^{162}Tb β-decay, γ-spectra, $T_{1/2}$, deduced ^{162}Dy levels 77−34246
Tb(p,f), 600 MeV, mass yields in binary fission 78−8819
^{159}Th(n,γ), 2.6-700 keV, cross-sections and resonance parameters 78−50172
Tl, A=185,187 isomeric decays, half-life, $h_{9/2}$ intruder state 77−26616
Tl isotopes, A=184-197, β$^+$-decay, single particle and collective degrees of freedom 77−22956
^{184}Tl, half-life 79−97652
^{184}Tl, energy level struct. of ^{184}Hg anal. 77−6234
^{186}Tl, α-decay, half-life meas. 77−79343
^{186}Tl decay, γ, conversion electron spectra and coincidences, ^{186}Hg bands, shape coexistence 78−25156
^{186}Tl, isomer and ground state half-lifes 79−97652
^{188}Tl, half-life 79−97652
^{189}Tl→^{189}Hg→^{189}Au, gamma spectra, ^{189}Au shape coexistence 77−6587
Tm, A=163-171, E1 transitions, hexadecapole deforms., Nilsson model calc. 77−82861

nuclei with mass number 150 to 189 continued
Tm, doubly odd deformed nuclei, EM transitions, nanosec. lifetimes 78−62505
Tm self-powered neutron detectors for power reactors 79−13607
Tm+n, neutron spin states amplitudes and scatt. cross sections 77−23019
^{153}Tm, short lived α emitter, α energy, $T_{1/2}$ and branching ratio 80−501
^{156}Tm, (β^++EC), level struct. of ^{156}Er 77−22957
^{157}Tm→^{157}Er, Nilsson model anal. of low-lying scheme 77−22958
^{158}Tm, (β^++EC), level struct. of ^{158}Er 77−22957
^{163}Tm decay, ^{163}Er excited state obs. 78−17146
^{163}Tm, high spin rot. levels, studied via ^{165}Ho(^{3}He,5n) and ^{165}Ho(α,6n) reactions 78−8722
^{165}Tm, levels excited by β-decay of ^{165}Yb 78−74334
^{166}Tm decay, ^{166}Er level population 79−93556
^{167}Tm, energy level scheme from ^{165}Ho(α,2nγ) *(German)* 80−68576
^{167}Tm, levels and transitions from ^{165}Ho(α,2n) 80−73766
^{167}Tm rotational bands, J^π, γ-transitions and branching ratios from ^{165}Ho(α,2nγ) 80−86781
^{167}Tm(HI,xnγ), ang. distrib., multipolarities *(French)* 80−68575
^{169}Tm, 316 keV state, g-factor 79−63586
^{169}Tm, anisotropic ang. correlation between γ-rays and K X-rays following internal conversion 77−6305
^{169}Tm, excited state lifetime meas. 80−32237
^{169}Tm, γ-ray transitions for level struct., obs. in ^{169}Yb electron capture decay 78−82307
^{169}Tm, high resolution meas. of anisotropic directional correl. between γ-rays and KX rays 80−32243
^{169}Tm, Mossbauer expts. in ^{3}He-^{4}He dilution refrigeration 78−27127
^{169}Tm, NMR in $LiTmF_4$, compared with cryst. field calcs. 77−12213
^{169}Tm, neutron capture cross sections, 0.5 to 3.0 MeV 79−40912
^{169}Tm, nuclear acoustic reson. in $TmVO_4$-type crysts. 77−24753
^{169}Tm, nuclear K-X-ray satellites, Z=50-83, by α-bombard., 17.5-22.5 MeV 80−42984
^{169}Tm, studied via ^{169}Tm(^{32}S,^{32}S'γ), EM props. of ground state rot. band 78−8726
^{169}Tm+^{12}C, 78 MeV, fission fragment angular distrib., shape of saddle point of compound nucleus *(Chinese)* 78−78427
^{169}Tm+n, strength functions and scatt. lengths from total and scatt. cross sections 77−26706
^{169}Tm(^{14}N,X) 85-115 MeV, cross sections, preequilibrium α-particle emission 80−42680
^{169}Tm(e,α), 100 MeV, energy spectra, ang. distribs. 77−18529
^{169}Tm(n,γ), capture cross section from 10^{-5} eV to 2×10^7 eV, statistical model 80−63189
^{169}Tm(p,αX), 20-45 MeV, α spectra, exciton model anal. 80−18306
^{169}Tm(p,α), 20 to 44 MeV, energy spectra and α-particle angular distrib. 79−49630
^{169}Tm(p,n), cross sections and spectra, exciton model *(Russian)* 78−21536
^{170}Tm, beta decay form factors coeffs. calc. *(Rumanian)* 79−80899
^{170}Tm gamma-ray strength functions from spectrum fitting method from ^{169}Tm(n,γ) 80−52616
^{170}Tm, precise γ-ray energies from radioactive decay 79−45525
^{170}Tm(n,γ), 0.5-3.0 MeV, γ-spectra strength functions 80−32240
^{171}Tm, 635.4 keV level props., mag. moment from γ ang. correl. meas. 78−13017
^{171}Tm, g factor of 635.4 keV level meas. 77−10316
^{175}Tm single proton states, rot. bands, J^π assignments from ^{176}Yb(t,α), pol. t 80−452
Tm(n,n') 1.8 meV to 1.8 eV, total neutron cross-section meas. using TOF spectrometry 79−85466
W, A=174, 175, from (^{16}O, xn), γ continuum spectra, yrast cascades, dipole component 78−54794
W, A=178, 180, 182, high spin states, microscopic-macroscopic model 79−438
W, A=182, 180, 178, pair excitations via (p,t) 21 MeV reaction 77−88032
W, activation in cyclotron by p, d, α, ^{3}He 79−30839
W, alpha decay studies of the isotope 79−63636
W even nuclei, pairing phonons or SU(3) bosons 79−93532
W high spin states, A=172, 174, 176, from Dy(^{16}O, xn), decoupled quasiparticle bands, backbending 78−50199
W isotopes, A=172-176, high spin states and backbending 77−34204
W isotopes, A=182, 184, 186, Coulomb excitation with ^{4}He and ^{16}O ions 78−8839
W, photofission cross section, 220-550 MeV, coherent electron bremsstrahlung beam 79−13353
W, produced in (^{16}O,xn) 78−37371
W, quadrupole moment calc. using HF method *(Russian)* 80−13375
W+Ne, 340 MeV/nucleon, multiplicities and ang. distrib. 79−93661
W+O, fission lifetime distrib. and probability estimates 78−659
W+p, 25 GeV, antiproton prod., flux optimisation using hadron cascade calcs. 77−83411
W+p, 28.5 GeV, prompt dimuon prod., cross section, atomic number depend., mass distrib. 78−89858
W+p, 400 GeV/c, dihadron prod., A depend. of prod. cross sections for massive dihadron states 78−33180
W+p, 400 GeV/c, dimuon mass spectrum, Υ signals 78−89857
W+p, 50 to 275 GeV/c, inclusive particle prod., nuclear size depend. 77−46168
W+p→muons, 28.5 GeV, large transverse momenta, μ polarisation meas. 77−71542
W+π, 200 GeV, multiparticle production in emulsion 79−40967
W+π^-, 43 GeV/c, inclusive J/ψ prod., A-depend. 78−62581
W(^{16}O,^{16}O'), 53, 4 MeV, quadrupole moment determ. 78−12968
$^{\wedge}$W (^{84}Kr,^{84}Kr'γ) A=183, 184, 186, 340 MeV, Coulomb excitation, energy levels and bands 79−63577
$^{\wedge}$W, A=170-182, even isotopes, yrast states, spectra and quad. moments, variation formulation 80−99119
$^{\wedge}$W, A=172-175, bands and backbending, $i_{13/2}$ neutron decoupling from Dy(^{16}O,xn) 80−9212
$^{\wedge}$W, A=173, 175, hindered electric dipole transitions and lifetimes from (HI,xn) reactions 80−9263
$^{\wedge}$W, A=174, 175 quasicontinuum γ-rays yrast cascade dipole component, moment of inertia from Dy(^{16}O, xnγ) 80−47424
$^{\wedge}$W, A=178, 180, 182, 184, levels and J^π, ang. distribs. from W(p,t) 80−78159
$^{\wedge}$W, A=182-186, deformation hexadecapole moments, Hartree-Fock calcs. *(Russian)* 80−63081

nuclei with mass number 150 to 189 continued
$^{\wedge}$W, A=184, 186, rigid asymmetric rotor model descript., E2 and E4 props. 80−13403
$^{\wedge}$W(^{12}C,f), A=182, 183, 184, 186, 80 to 115 MeV, lifetime meas. by crystal-blocking tech. 80−91198
$^{\wedge}$W(^{16}O,f), A=182, 183, 184, 186, 80 to 115 MeV, lifetime meas. by crystal-blocking tech. 80−91198
$^{\wedge}$W(^{19}F,f), A=182, 183, 184, 186, 80 to 115 MeV, lifetime meas. by crystal-blocking tech. 80−91198
$^{\wedge}$W(α,f) (A=182 to 186), 41 and 65 MeV, cross section, fragment mass distrib. 77−38307
$^{\wedge}$W(e,f), A=182,184,186, 35-55 MeV, fission barriers, pairing strength deformation depend., stat. anal. 80−57810
$^{\wedge}$W(n,nγ), 2.75 MeV, A=182,184,186, levels and excitation cross sections 79−75839
^{134}W, E1+M2+E3 multipolarity mixtures 536.7 and 920.9 γ-transition 79−6474
^{170}W, nonspherical nucleus after backbending, crit. spin rel. to angular vel., bands *(Russian)* 79−75822
^{174}W, decoupled two-quasiparticle bands, backbending 78−4890
^{178}W high spin rot. levels and bands from ^{177}Hf(α,3nγ) 79−26359
^{178}W high spin states, yrast bands and backbending from ^{170}Er(^{12}C,4n) 80−13352
^{179}W, backbending, high spin isomer decay 78−45997
^{180}W ground and $K=2^-$ octupole band ang. momenta coupling, lifetimes from ^{181}Ta(p,2nγ) 80−9214
^{180}W, $K=2^-$ octupole alignment, ground-band angular momenta 78−78237
^{180}W octupole vibr. states, J^π and transitions from ^{180}Re decay 80−83024
^{180}W, rot. and vibr. bands, γ-vibr. band, metastable state half life from ^{181}Ta(p,2nγ) 79−54378
^{181}W electron capture decay, ^{181}Ta L X-ray spectrum, L_1 subshell yield 79−49608
^{181}W, level absolute density from n spectra, statistical anal. of ^{181}Ta (p, n) *(Russian)* 79−97657
^{181}W level density, n spectra and ang. correls., direct and nonequilib. processes from ^{181}Ta(p,n) *(Russian)* 80−68631
^{181}W levels (neutron and collective) and J^π, ang. distribs. from ^{183}W(p,t) 80−78160
^{182}W 100 keV E2-transition, L-subshell internal conversion coeff. from ^{182}Ta decay 79−75909
^{182}W, 2^+-0^+ transitions, mean square nuclear charge radius change, Mossbauer expt. 78−25109
^{182}W high spin states, J assignments and mixing ratios from ^{182}Re isomer decay 80−42593
^{182}W, level struct. determ. from (α,2nγ) and ^{182m}Re decay 77−41914
^{182}W, Mossbauer lineshape, dispersion amplitudes 78−25146
^{182}W, reson. γ-quanta absorption and emission probabilities *(Russian)* 78−23383
^{182}W+^{12}C, 98 MeV, fission, ^{1}H and ^{4}He emission from ^{194}Hg compound nucleus 78−50220
^{182}W(^{12}C,^{14}C)^{180}W, 70 MeV, ground-state rot. band ang. distribs., quadrupole transfer strength 77−336
^{182}W(^{12}C,X) 77-167 MeV, fusion cross sections, direct and evaporative p and α prod., evaporation, fission 80−13518
^{182}W(^{12}C,f), fission probability calc., α emission and evaporation effects 78−657
^{182}W(^{20}Ne,xn)Po, neutron deficient isotope prod. 78−8835
^{183}W, determ. of neutron level spins up to 400 eV *(Russian)* 79−80870
^{183}W(α,α'), 15 MeV, level and band Coulomb excitation, B(E2) values 80−32233
^{184}W, 1285 keV 5^- state struct. anal. 79−9467
^{184}W (n,n'γ), fast n, level struct. and populations, γ-transitions 79−75841
^{184}W, pygmy resonance, E1 transition probabilities, BCS wave functions, spin-isospin oscillation *(Chinese)* 80−63087
^{184}W, quadrupole mom. of second 2^+ state 77−30490
^{184}W, T-invariance violation, test in 922 keV γ-ray 77−71581
^{184}W(^{12}C,^{12}C'), 70 MeV, 4^+ state excitation ang. distrib., hexadecapole deformation length effects 80−68521
^{184}W(^{18}O, ^{18}O), polarisation by Coulomb excitation in closed formalism 78−37376
^{184}W(^{20}Ne,Xn)-$^{204-x}$Po, $4\leq X\leq 9$, absolute cross sections and excitation function meas. 79−13330
^{184}W(p,X), 400 GeV, absorption cross sections and multiplicity distribs., A-depend. study 79−67748
^{184}W(t,p)^{186}W, 15 MeV, study of levels, spin-parity assignments 77−18572
^{185}W, beta spectrum, shape factor meas. 77−2947
^{186}W, giant dipole resonances of deformed even-even nuclei, semimicroscopic calcs. 77−50096
^{186}W, 14.7 MeV neutron capture cross-section measurements with activation technique 80−32282
^{186}W levels, spin-parity assignments, via ^{184}W(t,p) at 15 MeV 77−18572
^{186}W, neutron capture cross sections, MeV region, using activation technique 78−86535
^{186}W quadrupole mom. of second 2^+ state 77−30490
^{186}W, resonance activation neutron detector materials, uni-resonance approx. technique for higher resonance reaction rate 77−75030
^{186}W+^{86}Kr, cross-sections for fusion, quasifission and deep inelastic collisions *(Russian)* 78−54801
^{186}W(^{12}C,^{14}C)^{184}W, 70 MeV, ground-state rot. band ang. distribs., quadrupole transfer strength 77−336
^{186}W(n,n'γ), fast n, level struct. and populations, γ-transitions 79−75842
^{186}W(t,p)^{188}W, 15 MeV, study of levels, spin-parity assignments 77−18572
^{187}W, absorpt., distrib. and milk secretion by dairy cow 77−9281
^{187}W decay, ^{187}Re low lying level struct. and transitions, E2/E1 mixing ratios 80−27557
^{187}W, p and α interactions, 2 to 5 GeV/nucleon, multiplicities of secondary particles *(Russian)* 78−46066
^{188}W levels, spin-parity assignments, via ^{186}W(t,p) at 15 MeV 77−18572
W(α,α'), 13.5 MeV, anal. of deexcitation γ-rays, quadrupole moment determ. 78−12968
W(α,α'e$^+$e$^-$), 1.0-2.5 MeV, e$^+$e$^-$ pair prod. search 80−27637
W(γ,γ), 412, 468, 662 keV, elastic scatt. cross sections, Rayleigh scattering anal. 80−86898
W(n,n), pol. n, 16.1 MeV, differential cross section, optical model fit 80−32259

nuclei with mass number 150 to 189 continued
W(n,n'γ), 2.75 MeV, direct excitation of some collective levels 77−26720
W(p,X), 10-60 MeV, long lived radioisotope prod. cross sections and excitation functions 79−89305
W(p,X) 200, 300, 400 GeV, hadron prod. at large p_T invariant cross section 79−40926
W(p,X), 400 GeV, particle mean multiplicities 80−13473
W(p,2π X), 28.5 GeV, fireball model comparison 79−59059
W(p,n), 800 MeV, n prod. systematics π associated cross section 79−3153
W(p,p'e^+e^-), 1.0-2.5 MeV, e^+e^- pair prod. search 80−27637
W(p,t)W, A=182, 180, 178, at 21 MeV, pair excitations 77−88032
W(π^-, Ψ), 43 GeV, A dependence of inclusive distrib. *(Russian)* 78−45983
^{132}Xe+n, capture cross section meas. in Triton reactor *(French)* 80−18308
^{171}Y populated in ^{171}Lu decay, level scheme, γ-transitions, spin-parity assignments 77−46133
^{169,175}Yb electrosorption on anodically polarised Pt surface 79−52684
Yb (p,t), 18-20 MeV, Q effects on cross section, DWBA anal., A dependence 79−63675
Yb, A=153-158, neutron deficient isotopes, daughter products, α-decay, halflives 78−21533
Yb, A=163, 165, 167, backbending of rotational bands 78−8728
Yb, A=164,5, from Lu decay, level schemes determ. 78−62509
Yb, A=166,168,170, backbending phenomena, two fluid model of nuclear rots. 77−50049
Yb, A=169, 170, moments of inertia of excited bands, even-odd difference *(Chinese)* 78−498
Yb, A=170,172, 174, high spin rot. states populated in heavy ion scatt., lifetime meas. 77−30511
Yb, A=172,174,176, Mossbauer effect in Yb cpds., appl. of in-beam implantation method 78−25372
Yb, fission, proton induced, 1 GeV, cross section *(Russian)* 78−94041
Yb, quadrupole moment calc. using HF method *(Russian)* 80−13375
Yb with high angular momentum from heavy ion reactions, moment of inertial using γ-spectra 78−13135
^{A}Yb, (A=168, 170), angular momentum fluctuation energy in the cranking model 79−89254
^{A}Yb, A=158, 159, alpha decay and gamma transitions 80−73827
^{A}Yb, A=160, 161, backbending, multiple band crossing freq. and alignment from Sm(^{16}O,3n) 80−47347
^{A}Yb A=160-163, γ-transitions from Lu decay 80−102146
^{A}Yb, A=160-166, transitions from ^{158}Gd+^{12}C fusion 79−580
^{A}Yb, A=161, 162, 166, yrast cascade dipole component from Sm(^{16}O,4n) 80−9266
^{A}Yb, A=163, 165 level schemes and backbending behaviour of neutron deficient isotopes 79−40836
^{A}Yb, A=164, 166, high spin yrast states and transitions from Gd(^{13}C,5n) 80−9208
^{A}Yb, A=166, 168, 170, backbending and moment of inertia in HFB cranking method 80−42521
^{A}Yb, A=166,168,170, Yrast band investigation, self consistent cranking model anal. 79−6367
^{A}Yb, A=168, 170, approximate ang. momentum projection from cranked HFB wave functions, yrast energies 79−30776
^{A}Yb, A=168-176, deformation hexadecapole moments, Hartree-Fock calcs. *(Russian)* 80−63081
^{A}Yb, A=169-x, γ de-excitation and ang. momentum distribs. after fast α-emission from ^{159}Tb(^{14}N,αxn) 80−18228
^{A}Yb A=172, 174, electric monopole transitions from excited $K^\pi=0^+$ levels from Yb(n,γ) 79−6486
^{A}Yb(^{16}O,^{16}O'γ), A=168-176, even nuclei, 58-62 MeV, Coulomb excitation, vibr. and rot. states 80−32162
^{A}Yb(^{40}Ca,^{40}Ca'), A=170,172,174, 168 MeV, rotational g-factor meas. using transient field interactions 80−18193
^{159}Yb, identification 77−50075
^{160}Yb decay, cc ^{160}Tm doubly odd deformed nucleus, excited states and state lifetimes 79−13209
^{160}Yb double backbending and rot. states, HFB cranking model anal. 80−32155
^{160}Yb yrast levels, 2nd and 3rd backbending, cranked HFB calcs. 80−63064
^{160}Yb, yrast line irregularity, backbending effect 79−30777
^{161}Yb from (^{16}O, xn), γ continuum spectra, yrast cascades, dipole component 78−54794
^{161}Yb, produced in (^{16}O, xn), γ-ray spectra, dipole moment in yrast cascade 78−37371
^{161}Yb quasicontinuum γ-rays yrast cascade dipole component, moment of inertia from Sm (^{16}O, xnγ) 80−47424
^{162}Yb high spin states, HF self consistent calc. with Skyrme interaction, cranking approach 80−9210
^{162}Yb high spin states with Skyrme interaction, cranked Hartree-Fock calcs. 79−13189
^{162}Yb rot. states, HF and HFB self consistent calc. with Skyrme interaction 80−22662
^{164}Yb, levels populated in ^{164}Lu decay, band struct. 77−82805
^{165}Yb, beta-decay to ^{175}Tm, γ-ray and conversion electron spectra 78−74334
^{166}Yb, backbending even-even nuclei, particle-rotor model with VMI core *(German)* 77−6258
^{166}Yb, high spin state anomaly, backbending 79−22173
^{166}Yb multiple band crossing, (gSS'S''S'') system gamma correlation patterns 80−106008
^{167}Yb $i_{13/2}$ band, spin alignment in the particle-rotor and cranking models 80−42536
^{167}Yb, spin and parity determ. from ^{167}Lu→^{167}Yb data, ε/β^+ anomaly 79−6380
^{167}Yb→^{167}Tm mass difference, from positron spectrum, level transition branching ratio 79−6376
^{168}Yb low lying collective excitation energies calcs. at high angular momenta 79−13190
^{168}Yb, low lying spectra and EM transitions, level struct. in quasirotational bands 79−36141
^{168}Yb, microscopic calc. of high-spin rot. states 78−8730
^{168}Yb, rot. bands calc. from Hartree-Fock-Bogolyubov eqn. 77−18459
^{168}Yb, two-fluid model of nuclear rotations and surface vibrations, energy levels 78−62474
^{168}Yb(α,α'), 12-13 MeV, E2, E4 transition matrix elements determ. 78−33202

nuclei with mass number 150 to 189 continued
^{169}Yb $^7/_2^+$[404]→$^7/_2^+$[633] transition ft value from ^{169}Lu allowed hindered β^+ decay 80−102148
^{169}Yb, conversion electron spectrum below 300 keV 77−6303
^{169}Yb, double K-shell vacancy creation by internal conversion, X-ray obs. 77−57627
^{169}Yb, E2 transitions in rot. bands, partial probability calcs. 79−75835
^{169}Yb, electron dose reduction coeff., internal radionuclides, source free target, cylindrical geometry 78−92704
^{169}Yb γγ ang. correlations, levels and spins from ^{169}Lu decay *(Russian)* 80−83069
^{169}Yb in Fe, lattice location and hyperfine field, PAC meas. 77−48100
^{169}Yb, K-shell internal conversion, $K\alpha_1$ hypersatellite line energies, intensities 77−18885
^{169}Yb, populated in ^{169}Lu decay, meas. of γ-ray and conversion electron spectra 80−22766
^{169}Yb populated in ^{169}Lu decay, γ-ray and conversion electron spectra 80−22767
^{169}Yb, precise γ-ray energies from radioactive decay 79−45525
^{170}Yb, giant dipole resonances of deformed even-even nuclei, semimicroscopic calcs. 77−50096
^{170}Yb, Mossbauer relax. spectrum in $Cs_2NaYbCl_6$ 78−27141
^{170}Yb, Mossbauer spectroscopy, fast γ-ray detection systems 78−25376
^{170}Yb negative parity yrast band, rot. aligned n, deformation coupled bandhead from Er(α,xn) 79−93489
^{170}Yb(n,γ), 10-70 keV capture cross-section 80−27631
^{170}Yb(p,α)^{167}Tm, α spectra and ang. distribs. calc., statistical knock-on model 77−79371
^{171}Yb, EM transitions, mixing of states having different quantum numbers 79−6493
^{171}Yb level struct., DWBA anal. of ang. distribs. from ^{170}Yb(d,p) 79−30788
^{172}Yb, gamma ray spectra, β-decay of ^{172}Hf and ^{172}Lu 78−33140
^{172}Yb levels, bands, J^π and $T_{1/2}$ from ^{170}Er(α,2n) 80−91127
^{172}Yb, muonic resonance spectra, deduced isomer shifts and electric moments 80−18948
^{172}Yb octupole band, particle vibrational alignment from ^{170}Er (α,2n) 80−13351
^{172}Yb(d,p)^{173}Yb, 14 MeV, proton spectra and ang. distrib. meas. level struct. determ. 78−29482
^{172}Yb(t,p)^{174}Yb, 15 MeV, pairing vibr. character of 1494 keV 0^+ state in ^{174}Yb 77−18572
^{173}Yb, γ-transitions from 7/2, 7/2$^-$ [514] 636 keV level 80−78187
^{173}Yb, high field nucl. relax. in dil Au-Yb alloy, anisotropic cond. electron exchange 77−8434
^{173}Yb M1 transitions from 636 keV level, multipole mixture parameters, penetration effect 80−18220
^{173}Yb(n,γ), search for non statistical effects 77−30588
^{173}Yb(n,γ)^{174}Yb, width correlation, primary transition intensities for resons. 77−79370
^{174}Yb, pairing vibr. character of 1494 keV 0^+ state via ^{172}Yb(t,p), 15 MeV 77−18572
^{174}Yb(^{12}C,f), fission probability calc., α emission and evaporation effects 78−657
^{174}Yb(^{32}S,^{32}S'γ), recoil distance lifetimes of ground state bands 78−8774
^{174}Yb(^{40}Ar, xn)Ra and ^{174}Yb(^{40}Ar, pxn)Fr, 160-270 MeV, excitation functions, statistical models calcs. 77−3042
^{174}Yb(d,t)^{173}Yb, 14 MeV, proton spectra and ang. distrib. meas. level struct. determ. 78−29482
^{175}Yb level structure, band structure and J^π assignments from ^{176}Yb(d,t) and ^{174}Yb(d,p) 79−40850
^{176}Yb, collective props., HF calcs., review 78−50064
^{176}Yb(α,α), rot. state excitation, coupled-channel and adiabatic calc. 77−50094
^{176}Yb(d,xnγ), 14 MeV, gamma-ray spectra *(Russian)* 78−54720
^{176}Yb(d,xnγ), 14 MeV, γ-ray spectra angular distribs. and γγ coincidences 79−75838
^{176}Yb(n,2n), 14.6 MeV, activation cross section 77−88128
^{176}Yb(p,p'), 0.8 GeV, ang. distribs. and multipole moments, DWBA and coupled channel anals. 80−105969
^{176}Yb(p,p'), 35 MeV, extraction of deform. parameters 78−54755
^{176}Yb(p,p'), 35 MeV, ground state rot. band and multipole moment 80−32178
^{176}Yb(p,xnγ), 66 MeV, γ-ray spectra angular distribs. and γγ coincidences 79−75838
^{176}Yb(p,xnγ), 6.6 MeV gamma-ray spectra *(Russian)* 78−54720
^{177}Yb level struct., DWBA anal. of ang. distribs. from ^{176}Yb(d,p) 79−30788
^{177}Yb level structure, band structure and J^π assignments from ^{176}Yb(d,p) 79−40850
^{195}Yb, matrix elements in 7/2$^-$-9/2$^+$ beta-decay 77−41932

nuclei with mass number 190 to 219
2_γ^+ level depopulation, reduced quadrupole transition probabilities, neutron-proton mass deformation difference 77−34203
36≤Z≤83 nuclei, neutron induced reactions, tables of cross sections and rate factors 77−46162
^{208}Pb (N,N^1) unnatural parity state excitation, π− condensate instability proximity, DWBA 79−97660
^{209}Bi(α,f), search for near threshold asymmetrical fission *(Russian)* 78−33233
^{222}Rn released by uranium tailings piles, potential population dose 79−85824
(^{6}Li,^{6}Li) 50.6 MeV elastic scatt. on A=12-208 nuclei, optical model parameters 77−18592
A=110-210 nuclei, new parameters of deformed Woods-Saxon pot. 78−93951
A=152-238 fissility behaviour irregularity with respect to Z^2/A *(Russian)* 77−23121
A=167-196, product cross sections from ^{197}Au($\pi^\pm$, spallation) 80−27619
A=170-212 nuclei, 20-60 MeV ^{3}He ion induced fission, effective momenta of inertia *(Russian)* 77−34360
A=187-199 odd-A nuclei, structure and formation of rot. bands based on intruder orbitals 77−22829
A=190, Nilsson strength fragmentation, quadrupole and hexadecapole deformations 80−47394
A=194, review of struct. information to July (1977) 78−89769
A=195, nuclear data sheets to Jan. 1978 79−17781
A=195 nuclei, data sheets 79−6372
A=197 nuclei, review of nuclear struct. information 77−57585

nuclei with mass number 190 to 219 continued
A=198 nuclei, struct., level props., decay, review 78−17077
A=199, nuclear level scheme data sheets, decay scheme 79−13186
A=200 region, macroscopic fission barriers, isospin depend., liquid drop model 80−57811
A=201 nuclear struct. data sheets to May 1978 79−30771
A=203, nuclear data sheets, level struct., decay schemes 79−13187
A=204, nuclear data sheets, levels, J^{π} and transitions 80−31429
A=205 nuclei, data sheets (to November 1977) 79−9442
A=207, review of struct. information to August (1977) 78−89770
A=209, review of struct. information to September (1977) 78−89771
A=211, nuclear struct. data sheets to July 1978 79−36131
A=212, nuclear data sheets, levels, J^{π}, transitions 80−31430
A=213, nuclear structure data sheets (July 1979) 80−67942
A=214 nuclei, struct. info., energy levels, spin, parity, decay 78−17078
A=215, nuclear data sheets, decay characteristics and level struct. 78−58224
A=217, nuclear structure data sheets (July 1979) 80−67943
A=218 nuclei, nuclear struct. info., energy levels, spin, parity, decay 78−17079
A=219, nuclear data sheets, decay characts. and level struct. 78−58225
A≤208, pygmy resonance, E1 transition probabilities, BCS wave functions, spin-isospin oscillation *(Chinese)* 80−63087
A = 202 nuclear data sheets, levels and transitions 79−40831
compound nuclei prod. in (HI, xn), lifetimes with account of fission process *(Russian)* 78−25233
double magic nuclei, self consistent description of low lying collective states *(Russian)* 78−89783
E2, M1 multipole mixing ratios in odd-mass nuclei, A>150 77−30503
E_2-transition probabilities and Davydov-Rostovsky model 78−74330
effective residual interaction matrix elements, spectroscopic factors, cross sections 80−99134
even-even and odd A nuclei, nuclear shapes and motions, review 80−5054
even-even nuclei, 2_2^+ level deexcitation *(Russian)* 77−2939
even-even nuclei, E_2 transitions from 2^+ state of gamma-vibrational band 80−91150
fission induced by 1 GeV protons, mass and energy distribs. meas. 77−71627
g-factor measurement using heavy-ion induced reactions 77−26572
ground-state correlations observable in hard heavy-ion reactions 78−78406
heavy nuclei, fission process gamma ray analysis *(Rumanian)* 79−40973
isomeric state formation by 14.8 MeV neutrons in Tl, Pb, Bi 77−30604
magnetic dipole transitions near ^{208}Pb 79−6393
multipole excitation of doubly-open shell spherical nuclei 78−21507
near Pb region, α-decay peculiarities and shape staggering effects 79−49611
odd-mass isotones potential energy surfaces 77−26567
optical model parametrization, cross section, energy depend. 78−33196
pre-Actinide W-Bi nuclei, (p,f) 24-30 MeV meas., fission barriers *(Russian)* 77−82978
preactinide nuclei, fission excitation functions and fission barrier height, liquid drop model 80−47513
preactinide nuclei Hf-Bi, fission via (α,f) 20-50 MeV 77−18637
Pt(t,α), A=194, 196, population of Ir, A=193, 195, proton states 78−33123
rare earths, pairing energy, single particle levels and interaction matrix elements 78−8721
transuranic nuclei, Po to Th, very high spin states, deform. energy surfaces 78−50079
(α,α'), A=40-208, low energy octupole resonances, 96 and 115 MeV 79−511
(e,α), Z=29-79, direct and statistical effects, cross sections and ang. distribs. 79−530
(γ,X), A=154-209, 7-20 MeV, total photoabsorption cross section 80−57766
(n,γ), A=94-190, resonance capture, low lying level population fluctuations, γ-rays 80−52619
(n,γ), interacting boson and Nilsson model tests, Pt-Os transition region 80−37380
^{194}Os, populated in ^{192}Os(2n,γ), level transitions, prolate-oblate transition 78−62540
(p, spallation), 480 MeV, medium to heavy mass targets, deep spallation products 80−83085
Tl(γ,γ), 4.5 MeV to neutron emission threshold, strengths in energy levels 79−36164
^{206} Pb, cluster vibrational field coupling model description 77−57604
^{208} Pb+p, 100-1050 MeV, optical pot. real part, nuclear matter approach 77−82890
90 MeV, α-n coincidence ^{5}He breakup kinematics 77−6419
^{208}(N,γ), pol. N, anal. power and giant multipole resonances, direct-semidirect model 80−18265
^{207}(e,e′), transverse scatt. amplitude suppression, form factors, neutron hole states 80−91129
A=196 nuclei, nuclear structure data sheets to Sept. 1978 80−41956
A=200 nuclei, nuclear struct., data sheets to Nov. 1978 79−71778
A=206 nuclei, nuclear struct. data sheets to July 1978 79−71779
^Ac, A=209-214, 216, deduced mass from Fr direct mass meas. 80−78130
At high spin isomers, deformed independent particle model, yrast lines, shape 79−480
At isotopes production in ^{209}Bi+^{12}C, excitation functions *(Chinese)* 78−82387
^At, A=198m,198g,199, alpha branching ratios 80−99154
^At, A=200-206, 208, deduced mass from Fr direct mass meas. 80−78130
^At, A=207-211, quasielastic transfer reaction excitation function for ^{209}Bi+heavy ion 79−3176
^At, A=209, 210, production by photospallation of ^{232}Th and ^{238}U 80−52797
^{205}At mass distribution width for fission and quasifission from Re+^{20}Ne and ^{165}Mo+^{40}Av 79−63707
^{207}At, g-factor of $25/2^+$ isomeric state, evidence for neutron excitation 78−70447
^{208}At energy levels and transitions, IC electrons from ^{208}Rn decay 80−18242
^{209}At, gamma-ray spectra, produced by ^{209}Bi(^{3}He, 3nγ)^{209}At, 28 and 26 MeV 78−74377
^{209}At, γ-transition, multipolaritis, level scheme following ^{208}Rn decay 80−83072
nuclei with mass number 190 to 219 continued
^{209}At high spin states from ^{206}Pb(^{6}Li, 3nγ), γ meas., neutron hole influence 77−2934
^{210}At excited states, spins, parities and rate of population from ^{210} Rn decay 79−75917
^{210}At, isomeric 19^+ state, isospin depend. in two-particle core polarisation 78−21499
^{211}At half life, branching ratio of electron capture and α decay modes 78−58253
^{211}At heavy product range and ang. distrib. from ^{209}Bi(HI,X) 80−83119
^{212}At, ^{212}At^m, configuration mixed shell model, α-decay rate calc. 77−74814
^{212}At excitation functions and isomer ratios from ^{209}Bi(α,n) 80−83039
^{212}At high spin states, decay, g factor, J^{π} assignments, level energies from ^{208}Pb(^{7}Li,3n) 80−5042
^{212}At, nuclear field theory approach to alpha-decay, calc. of relative α-decay rates 79−45218
^{212}At, relative α-decay width and excited levels, nuclear field theory 80−47437
^{213}At levels, J^{π}, transitions and lifetimes from ^{208}Pb(^{7}Li,X) 80−68542
^{189,191,193}Au, high-spin states, blocking effect in rot.-alignment model 77−14016
^{193,195}Au, decoupled bands and rot. alligned coupling to triaxial shape 77−65191
Au, 380 MeV, binary decay induced by K^- 79−93671
Au (π,αX), 70 MeV, α cross sections and energy spectra, intranuclear cascade calcs. 79−575
Au, A=189, 191, 193, level schemes, gamma spectroscopy of high-spin states 77−22848
Au, A=191,3, γ-ray ang. distrib. meas., particle-hole symm. 77−88074
Au, binary fission characts. induced by α-particle bombardment of 0.65 to 4.12 GeV 78−13169
Au, eikonal approx. of electron scatt. by spherically symmetric nuclei 78−37330
Au fast neutron capture and activation cross sections 77−26758
Au fragmentation by π^+ and protons, excitation function for ^{24}Na prod. 77−38301
Au isotopes, A=184-197, β^+-decay, single particle and collective degrees of freedom 77−22956
Au isotopes, statistical anal. of level schemes 77−6230
Au levels from p stripping reactions on ^{194,196,198}Pt, high spin states 78−78398
Au, odd isotones, deformation pot. energy from Nilsson model 80−57676
Au, odd isotopes, negative-parity level props. 78−17103
Au, odd isotopes, pot. energy surfaces and quadrupole deformation parameters, deformed basis model 79−80867
Au, odd mass isotopes, $h_{9/2}$ intruder state 77−88024
Au odd-mass isotopes, $9/2^-$ level excitation energies, estimates 77−275
Au, photofission induced by 220-500 MeV coherent beam 77−3056
Au, photonuclear cross-sections in giant reson. region 78−17178
Au, proton-induced fission at 400 GeV, ternary to binary event ratio 78−13170
Au, recoil energies of photoproduced ^{24}Na, 800 MeV bremsstrahlung 77−41953
Au, resonance neutron self shielding factors, expts. and calcs. 77−42008
Au, short-lived isotopes, spin and mag. moment meas. from atomic-beams 77−22882
Au, spin and mag. moment, trends in neutron deficient nuclei 78−37261
Au+^{12}C, 25 GeV, momentum transfer to target fragmentation products 79−6691
Au+^{12}C, 25.2 GeV, target residue mass and charge distribs. 77−74873
Au+O, fission lifetime distrib. and probability estimates 78−659
Au+p, 300 MeV, 450 MeV, 24 GeV, cross section meas. 77−67740
Au(HI,X,), fission fragment backscattering corrections to absolute fission counting rate measurements 80−68685
Au(^{86}Kr,X), 724 MeV, deeply inelastic, ^{4}He, ^{1}H emission, fragment spin, semiempirical method 80−47366
^Au, A=189, 191, 193, high spin states and transitions, isomeric states from Ir(α,xnγ) 80−5038
^Au, A=189, 193, 195, particle-asymmetric rotor description of $h_{11/2}$ levels system 78−70425
^Au A=190, 192, 194, levels, J^{π}, isomers and rot, aligned bands from Ir(α,xn) 80−9215
^Au A=190, 192, 194, quasi-rotation aligned bands 79−40833
^Au, A=193-199, positive parity states, particle-asymmetric rotor description 78−46005
^{147}Au(^{40}Ar, f), 340 MeV, H and He emission, rapid energy equilib., to ang. distribs. 80−86936
^{197}Au(n,γ)^{198}Au integral cross section ratio meas. using ^{235}U(n_{th},f) neutron spectrum 77−23130
^{190}Au, obs. of rotation aligned bands 79−17783
^{191}Au, monopole conversion, magnetic dipole transitions, latent penetration effect 79−9464
^{192}Au, obs. of rotation aligned bands 79−17783
^{193}Au, intermediate coupling vibr. models 77−22845
^{193}Au levels, three holes cluster vibr. and particle asymmetric rotor descriptions 80−57668
^{193}Au positron spectra, Fermi-Kuri diags. 77−22960
^{194}Au decay scheme, γ-spectrum, low-intensity transitions and level energies of ^{194}Pt 78−13003
^{194}Au, isomeric states anal. conversion electron and γ-ray spectra from ^{194}Pt(p,n) and ^{195}Pt(p,2n) 77−71582
^{194}Au, obs. of rotation aligned bands 79−17783
^{195}Au decay, K-shell capture fractions, internal conversion electrons, coincidence techniques 80−57743
^{195}Au, intermediate coupling vibr. models 77−22845
^{196}Au energy levels and Q-value from ^{197}Au(γ,n) 80−37329
^{196}Au, fission, proton induced, 1 GeV, cross section *(Russian)* 78−94041
^{196}Au, L/K, M/L electron-capture ratio determ., derivation of exchange and overlap corrections 79−22233
^{196}Au, studied via ^{197}Au(n,2n), isomeric cross-section ratio and spin-cut-off factor 78−13096
^{197}Au, isomer shift obs. of charge density perturbations in Au alloys 77−20771
^{197}Au +^{86}Kr, 618 MeV, γ-ray multiplicities and angular momentum fractionation 78−37370
^{197}Au, 14.7 MeV neutron capture cross-section measurements with activation technique 80−32282
^{197}Au, 16 MeV, coherent optical model analysis 77−26750

nuclei with mass number 190 to 219 continued

^{197}Au, 24.3 keV neutron activation cross sections with Fe filter technique 77−26763
^{197}Au, 62 MeV, complex particle emission, pre-equilibrium exciton model anal. 78−66280
^{197}Au (^{9}Be, ^{9}Be), 14-26 MeV, universal optical pot. 78−25219
^{197}Au, (α,p), (α,d) and (α,t) reactions, 50.5 MeV, particle spectra 77−6405
^{197}Au (e,α), 120 MeV, preequilibrium α-emission, α energy spectra 79−85459
^{197}Au ($\pi\pm$,$\pi\pm$N), 100-300 MeV, activation cross section, π^+/π^- cross section ratio 79−89329
^{197}Au, hyperfine interaction in Gd, Mossbauer obs. 77−20773
^{197}Au, Mossbauer effect in Au, Pd, and Pt matrices 78−15080
^{197}Au, Mossbauer effect in rare earth ferromagnets 77−8463
^{197}Au Mossbauer spectroscopy, integrating counting technique 78−25377
^{197}Au, neutron capture cross section ratios in range 10 to 90 keV 78−50163
^{197}Au, neutron capture cross sections, MeV region, using activation technique 78−86535
^{197}Au, neutron capture cross sections, 0.5 to 3.0 MeV 79−40912
^{197}Au, nuclear K-X-ray satellites, Z=50-83, by α-bombard, 17.5-22.5 MeV 80−42984
^{197}Au, resonance activation neutron detector materials, uni-resonance approx. technique for higher resonance reaction rate 77−75030
^{197}Au, stopped π^- absorpt. 77−38299
^{197}Au, stopped π^- absorption, in beam and activation γ-ray spectroscopy 79−40960
^{197}Au+^{12}C, 25.2 GeV, target residue mass and charge distribs., calcs. 79−3172
^{197}Au+^{12}C, 78 MeV, fission fragment angular distrib., shape of saddle point of compound nucleus *(Chinese)* 78−78427
^{197}Au+^{132}Xe, 7.5 MeV/amu ions, neutron multiplicities as func. of total energy loss 78−21606
^{197}Au+^{136}Xe, 1064 MeV, fragment spin orientation from continuum γ-ray anisotropy meas. 80−22853
^{197}Au+^{136}Xe, 979 MeV, quasi-fission, charge and ang. distribs., secondary fission of products 77−46193
^{197}Au+^{136}Xe, recoil range distribs. of heavy mass products in deep inelastic reacts. 78−66309
^{197}Au+^{140}Ar, 217 MeV, deform. of double nucl. system 79−6699
^{197}Au+^{14}N, 161 MeV, giant resonances in inelastic scatt. 78−62564
^{197}Au+^{16}O, 140, 315 and 33600 MeV, isotope yields and cross-sections 77−14161
^{197}Au+^{16}O, 140 and 315 MeV, energy depend. of heavy ion peripheral reactions 78−74399
^{197}Au+^{40}Ar, 217 MeV, fusion and deep inelastic collision, charge and mass anal. 77−82959
^{197}Au+^{40}Ar, 220 MeV, nucleon transfer reactions *(Russian)* 78−33219
^{197}Au+^{40}Ar, deep inelastic reactions, isotopic distribs., n excess degree of freedom relaxation 80−9308
^{197}Au+^{63}Cu, mass exchange and ang. distrib., dynamical treatment 77−61454
^{197}Au+^{63}Cu, quasifission, strongly damped collisions, 365, 443 MeV, mass and kinetic energy distribs. 77−34337
^{197}Au+^{63}Cu, triple differential cross-section, dynamical model calcs. 78−50212
^{197}Au+^{63}Cu quasi-fission, 443 MeV, γ-ray multiplicity 77−34330
^{197}Au+^{6}Li, 75 MeV, γ-rays form α and d fragment transfer 78−86545
^{197}Au+^{86}Kr, 620 MeV, diffusion model anal. 77−10427
^{197}Au+^{9}Be, breakup of ^{9}Be in Coulomb field 78−50203
^{197}Au+Ar, 183-248 MeV, fusion and deep inleastic collision, influence of bombarding energy 77−82958
^{197}Au+Kr, recoil range distribs. of heavy mass products in deep inelastic reacts. 78−66309
^{197}Au+d(α), 12-50 MeV, t formation average cross sections 80−42670
^{197}Au+n, strength functions and scatt. lengths from total and scatt. cross sections 77−26706
^{197}Au+p, 10-90 MeV, exciton model, pre-equilibrium decay calcs., excitation functions 77−82922
^{197}Au+p, 11.5, 300 GeV, formation cross sections for nuclides ^{22}Na to ^{196}Au 77−2999
^{197}Au(^{A}Xe,X), A=129, 132, 136, damped collision, proton and neutron exchange correlations 80−18335
^{197}Au(^{A}Xe,X), A=129, 132, 136, <787 MeV, light and heavy fragment N/Z ratios 80−32292
^{197}Au(^{132}Xe,X), damped collisions, charge distrib. second moments and giant El quantal fluctuations 80−27547
^{197}Au(^{132}Xe,X), neutron multiplicities 80−57797
^{197}Au(^{14}N,X), 85-115 MeV, cross sections, preequilibrium α-particle emission 80−42680
^{197}Au(^{14}N,n), DWBA anal. above Coulomb barrier 80−86917
^{197}Au(^{16}O,Cα), ang. correlations between react. products 78−8849
^{197}Au(^{16}O,X), colliding heavy ion interface, nucleon emission, fusion and strongly damped collisions 80−86922
^{197}Au(^{16}O,p)X, 315 MeV, high energy p emission, fireball and preequilibrium anals. 80−91194
^{197}Au(^{19}F,^{12}B), 186 MeV, deeply inelastic, direct processes and continuum cross sections 79−80951
^{197}Au(^{20}Ne, spallation), 8.0 GeV, cross sections and target residues, model comparison 80−68630
^{197}Au(^{20}Ne,^{20}Ne), 90 MeV, state lifetimes, weak coupling core excitation model, translation rates 79−63630
^{197}Au(^{20}Ne,X), 110 MeV, C, N, and O isotopic yields and energy spectra meas. *(Russian)* 79−9612
^{197}Au(^{20}Ne,X), exactly central heavy-ion collisions by nuclear hydrodynamics 80−68690
^{197}Au(^{22}Ne, f), 178 MeV, α-particles and fission fragments, spectra and cross sections *(Russian)* 80−91203
^{197}Au(^{22}Ne,αX), 178 MeV, max. α-particle energy at forward angles 80−68698
^{197}Au(^{32}S,X), 373 MeV, α and heavy ion out-of-plane correlations 79−76021
^{197}Au(^{35}Cl,^{35}Cl), 120 MeV, state lifetimes, weak coupling core excitation model, translation rates 79−63630
^{197}Au(^{3}He, 3nγ), 24-28 MeV, level struct. in ^{197}Al anal. 77−46177
^{197}Au(^{3}He,^{3}He) 39.7 MeV, optical pot. mass depend. 77−34327
^{197}Au(^{40}Ar, X), deep inelastic reaction, neutron excess degree of freedom relaxation model *(Chinese)* 80−102202
^{197}Au(^{40}Ar,X), 222, 340 MeV, fusion cross sections, direct and evaporative p and α prod., evaporation, fission 80−13518

nuclei with mass number 190 to 219 continued

^{197}Au(^{40}Ar,X), 222-340 MeV, charged particle emission, early collision evolution, fission and evaporation cross sections 80−106072
^{197}Au(^{40}Ar,X), 240 MeV, fragment shape deformation in deep inelastic collisions 80−47365
^{197}Au(^{40}Ar,X) 259 MeV, differential recoil range distributions, large contrib. of deep inelastic processes 78−70565
^{197}Au(^{63}Cu,X), 400 MeV, neutron multiplicity in deep inelastic collisions 80−18324
^{197}Au(^{63}Cu,X), 9.6 MeV/A, quasi elastic, deep inelastic and fission like ang. distribs. 80−18334
^{197}Au(^{6}Li, X), 75 MeV, Z=1 or 2 fast particle prod. mechanism above Coulomb barrier 80−42687
^{197}Au(^{6}Li, xn+yp), 48-156 MeV, excitation functions 77−18603
^{197}Au(^{6}Li,xn), 75, 85, and 95 MeV, K X-ray multiplicity 79−76019
^{197}Au(^{7}Li,α)^{200}Hg, 12 to 20 MeV excitation, ang. distrib. of evaporation residues, determ. of Γ_n/Γ_f 77−61451
^{197}Au(^{84}Kr,X), 9.6 MeV/A, quasi elastic, deep inelastic and fission like ang. distribs. 80−18334
^{197}Au(^{86}Kr, X), 730 MeV, heavy fragment coincidences, sequential fission probability 79−22316
^{197}Au(^{86}Kr, X), γ-ray multiplicities from diffusion model with one body dissipation 79−6487
^{197}Au(^{86}Kr, Z_3f), 618 MeV, ang. momentum depolarisation, sequential fission 78−62585
^{197}Au(^{86}Kr,X), 620 MeV, independent particle-shell struct. in deep inelastic collisions 79−97726
^{197}Au(^{86}Kr,X), 620 Mev, deep inelastic scatt., ang. momentum transfer, γ-ray multiplicities 80−27665
^{197}Au(^{86}Kr,X) 612 MeV, γ-ray circular polarisation 80−13453
^{197}Au(^{86}Kr,Z) 620 MeV, diffusive relax. along mass asymmetry coord. 77−50149
^{197}Au(HI,X), 60-120 MeV complete fusion cross sections from fission fragment ang. distrib. 80−13516
^{197}Au(α, 3n)^{198}Tl, 30 to 55 MeV, study of ^{198}Tl rotational structure 77−54130
^{197}Au(α, p), (α, d), (α, t), 50 MeV, reaction mechanism determ. *(Russian)* 78−54778
^{197}Au(α,α'), 120 MeV, isoscalar resonance excitation, low lying transitions, DWBA calc. 80−512
^{197}Au(α,α'), 120 MeV, new giant resonance at 80 A $^{1/3}$ MeV 77−41939
^{197}Au(α,α), 24 MeV, total reaction cross section 78−25209
^{197}Au(α,f), 140 MeV, fission cross sections and probabilities, isomeric yield ratio 79−45308
^{197}Au(α,f), 640MeV 80−95329
^{197}Au(d,X), E_d=13.6 MeV, d breakup anal. with neutron elastic scatt. 79−9540
^{197}Au(d,f), 2.1 GeV, binary and ternary fission kinetics *(French)* 78−70577
^{197}Au(d,f), 80 MeV, post neutron emission fission products 80−83136
^{197}Au(d,γ), 5-26 MeV, experimental and calc. compound nucleus cross sections 79−76002
^{197}Au(d,pX), 80 MeV, inclusive proton spectra, d break-up, DWBA anal. 80−91190
^{197}Au(d,pn), E_d=13.6 MeV, disintegration reactions, isotopic effects 78−13108
^{197}Au(d,pn) 13.6 MeV disintegration, neutron elastic scatt. effect *(Russian)* 77−34322
^{197}Au(e,xn), 37 to 147 MeV, cross sections, giant dipole reson. 79−89296
^{197}Au(γ,π^-), cross sections for ^{197}Hg^{g,m} states 79−9548
^{197}Au(γ,π^-xn), threshold to 750 MeV, activation method determ. of yields, and expt. mean cross sections 79−54430
^{197}Au(n,γ), 10-500 keV, absolute cross sections 77−26772
^{197}Au(n,γ), average activation cross sections in ^{252}Cf spontaneous fission neutron field 79−30830
^{197}Au(n,γ), cross section meas. using large Gd loaded liquid scintillator 78−25380
^{197}Au(n,γ), cross-section determ. by Fe filtered beam TOF method 77−23078
^{197}Au(n,γ), effective cross section dependence on thermal neutron temp. 80−547
^{197}Au(n,γ) standard reaction, Monte Carlo simulation of cross section fluctuations 77−61461
^{197}Au(n,n')^{197m}Au, E_n=3 and 14.1 MeV, form. cross sections of short-lived isomer, cyclic activation technique 80−32283
^{197}Au(n,n')^{197}Au, pre-equilib. and evaporation model anal. 77−6366
^{197}Au(n,xn), 20.6 MeV, neutron yield cross sections and spectra *(Russian)* 80−91188
^{197}Au(p,^{3}He x), 72 MeV, pre-equilibrium emission *(German)* 80−68657
^{197}Au(p,X), 0.2-6.0 GeV, product cross sections, mass yields, spallation products 80−83088
^{197}Au(p,X), 20-48 MeV, proton total reaction cross section 79−80934
^{197}Au(p,X)^{149}Tb, target fragmentation momentum transfer, collective tube model, collectivity effects 80−37359
^{197}Au(p,αx), 72 MeV, pre-equilibrium α-emission 79−26440
^{197}Au(p,αx), 72 MeV, pre-equilibrium emission *(German)* 80−68657
^{197}Au(p,f), 1 GeV, fission fragment ang. correlation, kinematically different events search *(Russian)* 79−59103
^{197}Au(p,n), 11.2 MeV, spin cut-off parameters from neutron ang. distribs. *(Russian)* 79−80940
^{197}Au(p,n)^{197}Hg, preequilib. emission of neutrons, ang. distrib. 78−62542
^{197}Au(p,x), x=α, π, 72 MeV, spectra and angular distribs. 80−68660
^{197}Au(p,x) ^{22}Na-^{196}Au, 1-100 GeV radionuclide recoil props., fission, fragmentation and spallation 79−3149
^{197}Au(p,xn)$^{198-x}$Hg, excitation function meas., for ^{194}Hg half-life determ. 79−45214
^{197}Au(π^-, xn), single and correlated n spectroscopy, nuclear temp. 79−6713
^{197}Au(π^-,X), X=d,t, ^{3}He, ^{4}He, particle emission following stopped pion absorption 80−91196
^{197}Au($\pi^\pm$,x), 176-368 MeV, ^{24}Na fragment emission excitation functions cascade-evaporation anal. 79−6553
^{198}Au, 411 keV transition energy, absolute meas. rel. to He-Ne laser freq. *(Czech)* 80−22755
^{198}Au, energy level spin from ^{197}Au(n,γ) with polarised n and Au 79−457
^{198}Au level spin assignments from γ ang. distrib. and circular polarisation from ^{197}Au(n,γ) 80−52570
^{198}Au, populated in ^{198}Au(n,γ), high energy transitions 80−22878

nuclei with mass number 190 to 219 continued
Au, radioactive decay, γ-ray energy meas. *(German)* 77−57633
Au, redetermination of γ-ray standards between 0.1 and 1.0 MeV 78−37472
Au(n,γ), 0.5-3.0 MeV, γ-spectra strength functions 80−32240
Au, carrier-free extraction from neutron-irradiated ^{198}Pt, medical appls. 79−2130
Au, NMR/ON in Fe, quad. interaction, orbital mag. hyperfine field 77−12250
Au, populated in ^{198}Au(n,γ), high energy transitions 80−22878
Au, evidence for existence, β-decay to ^{201}Hg 79−63635
Au(α,f) 0.65, 1.74, 4.12 GeV, and using polycarbonate detector 78−13178
Au(α,f), fission fragments tracklength and ang. distribs., fission moment of inertia 77−50182
Au(γ,X), X=p,d,t,^{3}He,^{4}He, cascade-evaporation 80−57770
Au(γ,f), 140 to 1000 MeV, energy depend. of nuclear fissility 77−82971
Au(γ,f), max. energy 580 MeV, track detector anal. 77−18640
Au(γ,n), photoneutron Q-value determinations using monochromatic photons 79−22271
Au(γ,ω), cross section meas., comparison with theory 78−58261
Au(n,γ) cross section standard, status 77−23040
Au(n,γ), neutron capture cross section standards, review 79−9589
Au(p,d), 2.14 GeV/c, quasifree knockout at 62 mrad, differential cross sections *(Russian)* 79−30819
Au(p,p̄π$^-$), 10 GeV, p̄ weak absorpt., p̄ and π$^-$ yields *(Russian)* 79−75987
Au(π$^-$,X), stopped π$^-$ capture, product nuclei distribs., isomeric yield ratios, neutron multiplicity 77−18625
^{209}Be(^{136}Xe,X), statistical fluctuations in dissipative collisions, multidifferential cross sections 80−37399
Bi (d,p), 6.3 GeV/c, p momentum spectra from d breakup 78−89887
Bi (γ,f), 140 to 1000 MeV, energy depend. of nuclear fissility 77−82971
Bi, A=206, 208, 211, two-particle states anal. 77−38289
Bi, binary fission characts. induced by α-particle bombardment of 0.65 to 4.12 GeV 78−13169
Bi isotopes, neutron deficient, anal. of α decay in terms of surface probabilities of α-particle formation *(Russian)* 79−9527
Bi, photofission induced by 220-500 MeV coherent beam 77−3056
Bi, π$^-$ absorption *(Russian)* 78−46115
Bi+π$^\pm$, 125 MeV, true absorpt. and scatt. 79−63705
Bi+Xe, 1130 MeV, parameter free model of strongly damped collisions 78−62568
Bi+Xe, 1.13 GeV, deep inelastic nuclear reaction, electronic 1sσ vacancy prod., compound nucleus 80−27662
Bi(Kr,X), strongly damped collisions, classical dynamical model with shape deformation 80−27658
Bi(Xe,X), strongly damped collisions, classical dynamical model with shape deformation 80−27658
Bi, A=196-202, 204, deduced mass from Fr direct mass meas. 80−78130
^{194}Bi→^{194}Pb, $T_{1/2}$ meas. and ^{194}Pb excited level scheme determ. 77−6306
^{196}Bi→^{196}Pb, $T_{1/2}$ meas. and ^{196}Pb excited level scheme determ. 77−6306
^{201}Bi (α,f), 23-140 MeV, l_{crit} from fragment ang. distribs. anal. 80−106087
^{203}Bi high spin states from ^{203}Tl(α,4n), lifetimes meas. 78−29485
^{204}Bi, decay scheme 78−50122
^{204}Bi excited states, γ rays, conversion electrons and γγ coincidences from ^{204}Po, EC 80−18241
^{205}Bi high spin states populated in Tl(α,xn), yrast states, isomers 77−30616
^{206}Bi decay, ^{206}Pb γγ directional correlations, multipole mixing ratios, transition strength limits 80−86849
^{206}Bi, decay investig. from nuclear orientation of ^{206}Bi in Ni 77−41911
^{206}Bi, high-spin states anal. from ^{205}Tl(α,3n) 78−82368
^{206}Bi, mass excess calc. from Pd(α,d)Bi 77−10312
^{206}Bi, nucl. orientation in ferromag. BiMn 78−13010
^{206}Bi, nuclear orientation in Ni for ^{206}Pb decay investig. 77−41911
^{207}Bi $3p_{1/2}$ isobaric analogue resonance from ^{206}Pb(p,p_0), polarised p, analysing power 78−78346
^{207}Bi, decay, time differential perturbed ang. γ-γ correl. meas. 78−17134
^{207}Bi EC decay, ^{207}Pb, 569.65-1063.63 keV cascade γ-γ ang. correl. meas. 80−86847
^{207}Bi, gamma-ray intensities, precision meas. 80−102139
^{207}Bi, gamma-ray transitions following electron capture, 1.44 and 1.46 MeV γ-rays 79−85399
^{207}Bi, γ-γ coincidence spectra, Ge(Li) detect. 77−2930
^{207}Bi, γ-γ directional correls., mag. perturbation obs. 77−74796
^{207}Bi, half life determ. from ^{211}At and ^{207}Po decays 78−58253
^{207}Bi high spin states, level decays, three particle interactions from ^{205}Tl(α,2n), ^{208}Pb(d,3n) 79−49567
^{207}Bi, mag. relax. in liq. Tl and Pb, TDPAC 77−16217
^{207}Bi, nucl. orientation in ferromag. BiMn 78−13010
^{207}Bi optical HFS intensity profile for nuclear spin determ. 77−54619
^{207}Bi, spin and parity of states with J≤21/2, ^{205}Tl(α,2n)^{207}Bi and ^{205}Tl(α,2n)^{207}Bi 78−89788
^{208}Bi, 0$^+$ IAS, spreading width and isospin impurity, isovector monopole state influence 80−78155
^{208}Bi $3p_{1/2}$ isobaric analogue resonance from ^{207}Pb(p,p_0) analysing power, polarised p 78−78346
^{208}Bi, influence of nucl. polarisation on level props. 78−54686
^{208}Bi isobaric analogue resonances, spin assignments, decay amplitudes from ^{207}Pb(p,p) 79−75946
^{208}Bi M1 isobaric analogue resonances and giant spinflip resonances from ^{208}Pb(p,n) 80−106030
^{208}Bi two-particle, two-hole configuration, levels, J$^\pi$ and excitation energies from ^{210}Bi^m(p,t) 80−32190
^{208}Bi(1+), β-decay to ^{208}Pb(0+), collective particle-hole states 77−61388
^{208}Bi(d,f), 2.1 GeV, binary and ternary fission kinetics *(French)* 78−70577
^{209}Bi, conc. and temp. depend. nucl. relax. in liq. Bi-Sn(Pb) alloys 78−19357
^{209}Bi, 62 MeV, complex particle emission, pre-equilibrium exciton model anal. 78−66280
^{209}Bi (n, xnf), fission high energy neutrons *(Russian)* 80−106091
^{209}Bi (n,3n)^{207}Bi, 14 MeV, cross section determ. 78−50177

nuclei with mass number 190 to 219 continued
^{209}Bi (n,p) and (n,d) reactions, study of isovector analogue giant resonances, proton hole states 77−26726
^{209}Bi, charge distrib. from elastic electron scatt. and muonic X-ray data anal. 78−54681
^{209}Bi coherent scattering of polarised thermal neutrons, parity violating effects 78−29461
^{209}Bi EM props. of particle vibration coupling states from ^{208}Pb(^{7}Li, ^{4}He 2nγ) 78−70485
^{209}Bi, effect of pairing modes in multiplet struct. 78−12973
^{209}Bi energy and transition probability convergence in Dyson's boson expansion 80−78206
^{209}Bi, fission, proton induced, 1 GeV, cross section *(Russian)* 78−94041
^{209}Bi from ^{208}Bd(d,nγ), half life of 2442.8 keV lowest 2p 1h state 78−74331
^{209}Bi, levels, ground state widths via reson. fluoresc. 77−74799
^{209}Bi levels and spectroscopic factors, ^{210}Bi(9$^-$) parentage from ^{210}Bi^m(d,t) 80−78158
^{209}Bi low lying levels and spectroscopic factors, EFR-DWBA anal. of ^{208}Pb(^{7}Li, ^{6}He) 80−32182
^{209}Bi, mag. moments and core polarisation blocking 77−26573
^{209}Bi, NQR in $BiCl_3.GaCl_3$ complex, geom. struct. 78−25569
^{209}Bi, neutron elastic and inelastic differential scatt. cross sections, 1.5-3.0 MeV *(Russian)* 77−26688
^{209}Bi, particle-vibr. model 78−519
^{209}Bi, pion$^-$ capture, high spin states and neutron multiplicities meas. 78−54806
^{209}Bi, π$^-$ capture, p, d and α inclusive prod. spectra 79−22338
^{209}Bi, Q value via ^{210}Po E2 transitions 77−14068
^{209}Bi reduced normalisation of isobaric analogue resonances from ^{209}Pb (p,p) 78−86522
^{209}Bi, reson. parameters for s and p-wave levels 78−37322
^{209}Bi single particle levels, ang. distribs., spectroscopic factors, DWBA anal. of ^{208}Pb(^{7}Li,^{6}Me) 80−63067
^{209}Bi, stopped π$^-$ absorption, in beam and activation γ-ray spectroscopy 79−40960
^{209}Bi structure, appl. of nuclear field theory 77−67692
^{209}Bi/^{208}Pb isotone pair, charge distrib. polarisation from e$^-$ scatt. and muonic X-ray data consistency 77−22873
^{209}Bi+^{12}C, 78 MeV, fission fragment angular distrib., shape of saddle point of compound nucleus *(Chinese)* 78−78427
^{209}Bi+^{12}C, complete fusion cross sections, excitation functions *(Chinese)* 78−82406
^{209}Bi+^{12}C, reaction mechanisms above Coulomb barrier, semi-classical anal. *(Chinese)* 79−22320
^{209}Bi+^{12}C reaction, fission product charge distrib., 40 to 66 MeV 77−79406
^{209}Bi+^{136}Xe, 1130 MeV, differential cross section calc., statistical model 78−50192
^{209}Bi+^{136}Xe, 1130 MeV, very heavy-ion collision mechanisms 78−89905
^{209}Bi+^{136}Xe, damped collision, interaction time 78−637
^{209}Bi+^{136}Xe, deep inelastic collisions, deformation role, cross sections 79−36270
^{209}Bi+^{136}Xe, stochastic model for strongly damped collisions with liquid drop driving forces 78−89834
^{209}Bi+^{14}N, 161 MeV, giant resonances in inelastic scatt. 78−62564
^{209}Bi+^{14}N, 85 and 95 MeV, preequilibrium α spectra, statistical treatment 78−41750
^{209}Bi+^{14}N, ang. distrib. anal. for quasi-elastic transfer reactions 79−17931
^{209}Bi+^{16}O, ang. distrib. anal. for quasi-elastic transfer reactions 79−17931
^{209}Bi+^{19}F, ang. distrib. anal. for quasi-elastic transfer reactions 79−17931
^{209}Bi+^{40}Ar, ang. distrib. anal. for quasi-elastic transfer reactions 79−17931
^{209}Bi+^{40}Ca, ang. distrib. anal. for quasi-elastic transfer reactions 79−17931
^{209}Bi+^{56}Fe, 8.3 MeV/amu collision, nucleon exchange and A/Z equilibration 79−76020
^{209}Bi+^{84}Kr, 600 MeV, differential cross section calc., statistical model 78−50192
^{209}Bi+^{84}Kr, 600 MeV, strongly damped collisions, time-depend. mean field theory 78−82374
^{209}Bi+^{86}Kr, 610 MeV, ang. momentum transfer in deeply inelastic scatt. 77−79397
^{209}Bi+C^{13}C, 60-72 MeV, excitation functions for Fr and At isotope prod. *(Chinese)* 78−82387
^{209}Bi+d, 6.3 GeV/c, inclusive spectra of fast p and d *(Russian)* 78−46075
^{209}Bi+p, 39 MeV, intranuclear cascade model 78−33185
^{209}Bi+p, nucleon losses on high-energy fission 78−46120
^{209}Bi(^{12}C,f), mass distrib. of fission fragments determ. *(Chinese)* 78−86558
^{209}Bi(^{136}Xe,X), 940 MeV bombarding energy depend., fragment deformation, sequential fision 80−86938
^{209}Bi(^{136}Xe,X), deeply inelastic collisions, mass transport, shell effects 80−99188
^{209}Bi(^{14}N,X), 85-115 MeV, cross sections, preequilibrium α-particle emission 80−42680
^{209}Bi(^{16}O,^{12}C), 93 MeV, α-transfer reactions 79−67762
^{209}Bi(^{16}O,^{12}C)^{213}At, 93 MeV, comparison with α-decay data 77−334
^{209}Bi(^{3}He, 3nγ)^{209}At, gamma-ray spectra of ^{209}At, 26 and 28 MeV 78−74377
^{209}Bi(^{3}He,d), 30 MeV, effective residual interaction matrix elements, spectroscopic factors, cross sections 80−99134
^{209}Bi(^{48}Ca, X), fusion reactions from Cf and Fm integral yields, statistical model anal. *(Russian)* 79−97740
^{209}Bi(^{56}Fe,X), 464 MeV, damped collision, actinide spontaneous fission activities 80−86937
^{209}Bi(^{56}Fe,X), damped collisions, fast A/Z equilibration and correlated nucleon exchange 80−86798
^{209}Bi(^{6}Li,X), 60-156 MeV, break-up fragment transfer, cross sections, recoil ranges 80−13491
^{209}Bi(^{7}Li,5n)^{211}Rn, 38-60 MeV, excitation function 80−95323
^{209}Bi(^{84}Kr, X), TDHF fusion calcs., fusion cross sections 80−37409
^{209}Bi(^{86}Kr, f), 610 MeV, deeply inelastic, Q and Z depend. of ang. momentum transfer 79−67786
^{209}Bi(HI,X), 60-120 MeV complete fusion cross sections from fission fragment ang. distrib. 80−13516

nuclei with mass number 190 to 219 continued
^{209}Bi(HI,X), quasi-elastic transfer, heavy product range and ang. distrib. 80−83119
^{209}Bi(X,Y)^{210}Po, ^{211}At, X=^{14}N, ^{16}O, ^{19}F, ^{40}Ar, ^{40}Ca, ^{56}Fe, ^{63}Cu, 1 and 2 p transfer reactions, determ. transfer prob. 79−36274
^{209}Bi(α,^{3}He), 172.5, 140 MeV, plane wave spectator model anal. n momentum distrib. in α 79−54445
^{209}Bi(α,X), 140 MeV, nonequilibrium light charged particle yield, energy spectra and ang. distribs. 79−40942
^{209}Bi(α,X), 20, 40 MeV/N, α breakup yield, fragment yield ratios 80−9300
^{209}Bi(α,X), 69.2, 140 MeV, scatt. and fission reaction mechanisms, cross sections 80−18350
^{209}Bi(α,α'), 120 MeV, isoscalar resonance excitation, low lying transitions, DWBA calc. 80−512
^{209}Bi(α,α'), 120 MeV, new giant resonance at 80 $A^{-1/3}$ MeV 77−41939
^{209}Bi(α,α), 24 MeV, total reaction cross section 78−25209
^{209}Bi(α,f), 640MeV 80−95329
^{209}Bi(α,t), 40 MeV, effective residual interaction matrix elements, spectroscopic factors, cross sections 80−99134
^{209}Bi(e,f), 110 MeV electrons, mass and kinetic energy distribs. 79−93672
^{209}Bi(γ, γ), reson. fluoresc. meas., levels, ground state widths 77−74799
^{209}Bi(γ,X), 3-30 MeV, photoabsorption cross section, giant dipole resonances 80−78254
^{209}Bi(γ,3n)^{206}Bi, photon activation anal. 78−85273
^{209}Bi(γ,f), 40-65 MeV, absolute total photofission cross section, compound nucleus form. 80−86934
^{209}Bi(γ,f), bremsstrahlung of 600 MeV max. energy, fragment energy correl. meas. 77−71630
^{209}Bi(γ,γ'), 7.28, 7.63 MeV, energy levels anal. 78−13058
^{209}Bi(γ,γ), 4.5 MeV to neutron emission threshold, strengths in energy levels 79−36164
^{209}Bi(γ,γ) 2.754 MeV photons, Delbruck scatt., differential cross section meas. 79−26422
^{209}Bi(γ,xn), x=2,3 or 4, cross sections at intermediate energies 78−8793
^{209}Bi(n,^{3}He)^{207}Tl, 14 MeV, cross section determ. 78−50177
^{209}Bi(n,2n), 14.1 MeV, pre-equilib. contributions, neutron yields and energy spectra, statistical model calcs. 77−50126
^{209}Bi(n,α)^{206m}Tl, 14 MeV, cross section determ. 78−50177
^{209}Bi(n,γ), 2.6-901 keV, cross-sections, resonance peaks, radiative widths 77−3002
^{209}Bi(n,γ), 4.9-8.0 MeV, γ-ray prod. cross-section meas. 77−38264
^{209}Bi(n,γ), TOF transmission spectroscopy, strength functions 77−23077
^{209}Bi(n,n'), 2-4.5 MeV, level excitation functions, Hauser-Feshbach-Moldauer model test 79−36238
^{209}Bi(n,n), 0.6 to 1.0 MeV, optical model params. 78−21557
^{209}Bi(n,n), 16-18 MeV differential cross section resonant characters 79−75952
^{209}Bi(n,n), 1.2 to 4.5 MeV total and differential cross sections 80−86903
^{209}Bi(n,n), 50, 100, 200 MeV, eikonal scatt. by complex pots., cross sections 80−27643
^{209}Bi(n,n), direct scatt., polarised thermal neutrons, empirical parity-violating potentials and neutron optical activity 79−59074
^{209}Bi(n,n) TOF transmission spectroscopy, strength functions 77−23077
^{209}Bi(n,t), 14 MeV, cross sections, fast neutron reaction excitation function calc. 79−45267
^{209}Bi(n,xn), 20.6 MeV, neutron yield cross sections and spectra *(Russian)* 80−91188
^{209}Bi(n_{th}, α), cross section 78−66284
^{209}Bi(p, X), pol.p, 65 MeV, continuum spectra anal. powers 80−102178
^{209}Bi(p,X), 90 MeV, charged light particle energy spectra exciton and evaporation model anal. 79−40923
^{209}Bi(p,X) *(Russian)* 79−80964
^{209}Bi(p,n) pre-compound process, 18 to 64 MeV, cross sections, hybrid models anal. 79−3140
^{209}Bi(p,n)^{209}Po, preequilib. emission of neutrons, ang. distrib. 78−62542
^{209}Bi(p,p'(d)X), pol. p, 65 MeV, anal. powers of continuum energy spectra 80−68637
^{209}Bi→Pb, electron capture decay, LL-vacancy production by KLl Auger transitions 77−18832
^{210}Bi, β-decay, extended Siegert theorem 77−41924
^{210}Bi β-decay, longitudinal polarisation of electrons at 900 keV, precision meas. 77−71592
^{210}Bi, influence of nucl. polarisation on level props. 78−54686
^{210}Bi, magnetic moment and beta-decay 77−41926
^{210}Bi, quasielastic transfer reaction excitation function for ^{209}Bi+heavy ion 79−3176
^{210}Bi, spectrum anal. from ^{208}Pb(α,d) at 33 and 48 MeV 78−82364
^{210}Bi→^{210}Po→^{206}Pb, decay chain, L-shell ionisation investig., X-ray emission during β, α decay 77−18891
^{211}Bi, 410 keV state single particle component determ. from DWBA anal. of (α,p) reacts. 77−88034
^{211}Bi levels, spin assignments and spectroscopic strengths from ^{210}Bi^{m}(d,p), 20 MeV 79−6418
^{212}Bi, isomeric states from α-activities 78−82282
^{212}Bi, selective separation from ^{228}Th source 77−40566
^{214}Bi, conc. in basement lab., working levels 77−40797
^{214}Bi, meas. of low conc. in air 78−28308
^{210m}Bi(t,α)^{209}Pb, 20 MeV, cross-section meas., ^{209}Pb levels 77−34320
Bi(α,f), 0.65, 1.74, 4.12 GeV, and using polycarbonate detector 78−13178
Bi(d,d), 4.3, 6.3, 8.9 GeV/c, secondary momentum spectra, multiple scatt. model anal. *(Russian)* 80−27650
Bi(d,p), 6.3 GeV, proton momentum spectra 79−6621
Bi(γ,n) cross section discrepancies, NBS P-2 chamber calibration 77−26671
Bi(γ,n), photoneutron Q-value determinations using monochromatic photons 79−22271
Bi(n,n), 10 MeV, neutron polarisation meas. at small angles 77−3014
Bi(n,n), 10.4 MeV, polarised neutrons, analysing power 77−30545
Bi(n,n), 2.5 MeV, small angle scatt., cross section, asymm. 78−74361
Bi(n,n), elastic and inelastic scatt., cross sections meas. and calcs. 78−13081
Bi(π,X), 125 MeV, absorption cross section in 3:3 resonance region 79−85543
^{208}Ca, nuclear incompressibility, Hartree-Fock calc. *(Russian)* 79−49577
Eu, A=149, 151, band struct. anal. with Sm(d,3nγ) at 18-25 MeV 77−41913

nuclei with mass number 190 to 219 continued
Fr isotopes production in ^{209}Bi+^{12}C, excitation functions *(Chinese)* 78−82387
Fr, nuclear ground state spins, at beam mag. reson. obs. 78−78257
^{A}Fr, A=201-203, alpha decay, branching ratios, mass excess and half life 80−99154
^{A}Fr, A=204-210, 212, 224-228, direct mass meas. 80−78130
^{213}Fr, high spin yrast states in N=126 isotones 79−45131
^{213}Fr, Knight shift in Tl, PAC 77−12275
^{160}Gd(α,4n)^{160}Dy, quasi-continuum transitions multipolarities from ICC 77−82945
Hf-Ir, isotopes, deformation, level assignments, static moments, modified oscill. model 77−22872
Hf-Os region, high lying states, Nilsson strength fragmentation 80−42539
Hg, A=191,2,3,5,7,9, rot. aligned bands, high spin states, energy levels B(E2) values 78−70483
Hg, A=199, 197, 5/2$^-$ state halflife and mag. moments 78−506
Hg even isotopes, nonaxial deforms., odd parity states, semidecoupled model 77−34220
Hg, even-A, possible triaxial shape and phase transition, triaxial rotor model 79−93503
Hg high spin states and rotation alignment in ^{198}Hg 77−57591
Hg isotope shifts, odd-even staggering, Coriolis effects in particle-core coupling 79−49580
Hg isotopes, A=184-197, β^+-decay, single particle and collective degrees of freedom 77−22956
Hg, neutron capture gamma spectra, for neutron thermometry 79−30837
Hg, neutron deficient isotopes, nuclear shape staggering, laser spectroscopy detection 78−54680
Hg, nuclear magnetic moment ratio of odd isotopes *(French)* 77−75081
Hg, positive-parity states, Coriolis antipairing effect, deformed-rotor model 78−12950
Hg, total neutron cross section meas., 4.5×10^{-4} to 10 eV, TOF method 77−14120
^{A}Hg, A=190-200, even, phase transition and possible triaxial shape, energy levels 80−63098
^{A}Hg, A=193, 195-198, electric quadrupole moments, nonadiabatic rot. model calcs. 79−6389
^{A}Hg, A=198, 200, rigid asymmetric rotor model descript., E2 and E4 props. 80−13403
^{A}Hg, A=198,200,202,204, reorientation effect, Coulomb excitation, oblate shapes 79−71790
^{A}Hg, A=198-202,204, muonic X-ray transitions, nuclear state quadrupole moments and charge distrib. 79−41253
^{A}Hg, A=198-202 and 204, nuclear charge radii variations from K X-ray isotope shifts 78−70441
^{A}Hg, A=198-204, reorientation effect meas. on 2$^+$ states 78−37282
^{A}Hg, A=200,202,204, oblate shape determ. 79−17792
^{A}Hg, quadrupole moment, change between first 5/2$^-$ states for A=197,199, shell model anal. 80−52576
^{A}Hg(α,α'), A=198, 200, 204, 16-27 MeV backward scatt., collective states 80−13365
^{A}Hg(α,f) (A=198 to 204), 41 and 65 MeV, cross section, fragment mass distrib. 77−38307
^{190}Hg, 21 ns isomer $(\nu i_{13/2})^2$ interpretation from g-factor meas. 80−105945
^{191}Hg positron spectra, Fermi-Kuri diags. 77−22960
^{191}Hg^{m}, and $^{190m1-185m}$Hg, nucl. spins, on-line quantum beat spectrosc. determ. 80−9562
^{194}Hg, α evaporation spectrum 80−68715
^{194}Hg compound nucleus, fission, ^{1}H and ^{4}He emission 78−50220
^{194}Hg compound nucleus, fission and, n, p, ^{4}He emission ang. momentum and energy depend. 79−76045
^{194}Hg, half life determ. 79−45214
^{194}Hg, level density calc., shell and pairing effects, deformation, excitation energy dependence 79−67662
^{195}Hg level scheme and transitions, band population from ^{195}Tl (1.13 h) decay 79−17807
^{196}Hg, band crossing, level scheme, J$^{\pi}$ 77−65192
^{197}Hg (64 h) decay γ intensities, obs. 79−75922
^{197}Hg energy levels from ^{195}Pt(α,2n), γ and conversion electron spectra, spins, parities 78−25149
^{197}Hg level scheme and transitions from ^{197}Tl electron capture 79−67719
^{197}Hg, non-axial deform. anal., $i_{13/2}$ neutron coupling to triaxial rotor and to anharmonic vibrator 77−22847
^{197}Hg, quadrupole interaction and lattice location in Be 78−48086
^{197}Hg, quadrupole moment of 5/2$^-$ 134 keV state 77−34225
^{197}Hg source for Mossbauer studies 79−26796
^{197}Hg, TDPAC and Mossbauer obs. of quadrupole interactions of Au in Be 78−43726
^{198}Hg, implantation in Fe, combined lattice-location hyperfine-interaction expt. 77−20752
^{198}Hg, static quadrupole moment of 1st excited state 78−17095
^{199}Hg, internal conversion coeffs., HF calcs. and expts. 77−57628
^{199}Hg, K X-ray intensity following thermal neutron capture 77−26691
^{199}Hg, Mossbauer spectroscopy, fast γ-ray detection system 78−25376
^{199}Hg nuclear shielding anisotropies rel. to isotropic chem. shifts in methyl mercury compounds 77−3384
^{200}Hg, neutron binding energy precision meas. 80−18182
^{201}Hg γ-γ directional correlations, level transitions, spin assignments, mixing ratios from ^{201}Tl decay 79−496
^{201}Hg missing $f_{5/2}$ state Coulomb excitation, level scheme, J$^{\pi}$, transitions using (α,α), (^{16}O, ^{16}O) 80−47386
^{201}Hg, nuclear quadrupole relax. rate for liq. Hg 77−36151
^{202}Hg, transfer strengths from 17.5 MeV ^{204}Hg(p,t) reaction 78−94005
^{202}Hg+p, 10-90 MeV, exciton model, pre-equilibrium decay calcs., excitation functions 77−82922
^{202}Hg(α,3nγ), 38.2 MeV, γ-spectra obs., ^{203}Pb decay scheme determ. 78−29489
^{203}Hg, gamma-ray precision energy meas. 78−58533
^{203}Hg nuclei, optically pumped, anharmonic mag. resonance phenomena 79−94015
^{204}Hg (α,4n), yrast levels in ^{204}Pb, spin, parity, γ spectra 78−12954
^{204}Hg(^{13}C, 5n), ^{212}Rn high spin isomers, excited core states coupled to valence protons 77−74745
^{204}Hg(^{13}C, 5n), ^{212}Rn high spin isomers with core excited neutron configs. 78−54792
^{204}Hg(^{3}He,n) 33.3 MeV, cross sections, DWBA anal. for data near Z=82 79−67733

nuclei with mass number 190 to 219 continued
^{204}Hg(t,p), 17 MeV, neutron pairing vibr. in ^{206}Hg 78−62549
^{206}Hg excited states from ^{204}Hg (t,p), neutron pairing vibr. 78−62549
^{196}Hg, obs. of excited states in (^{18}O,^{16}O) and (^{17}O,^{16}O) reactions 78−6242
^{197m}Hg, anomalous K/L conversion coefficients 77−26623
Hg(γ,γ), 4.5 MeV to neutron emission threshold, strengths in energy levels 79−36164
Hg(n,n), 2.5 MeV, small angle scatt., cross section, asymm. 78−74361
Hg(n,n) 2.9 MeV, elastic differential cross section and polarisation ang. depend., statistical anal. 79−45264
Hg(n,n), pol. n, 16.1 MeV, differential cross section, optical model fit 80−32259
Hg(π^-,X), stopped π^- capture, product nuclei distribs., isomeric yield ratios, neutron multiplicity 77−18625
Ir, A=191, 193, hyperfine struct. of low lying fine struct. levels, hyperfine anomaly, electronic g-factor 78−66214
Ir, A=191, 193, shape of stable transition nuclei, photoabsorpt. cross-sections *(Russian)* 77−79307
Ir, A=193, 195, proton states, populated via Pt(t,α), A=194, 196 78−33123
Ir, odd isotones, deformation pot. energy from Nilsson model 80−57676
Ir, odd isotopes, negative-parity level props. 78−17103
Ir, odd isotopes, pot. energy surfaces and quadrupole deformation parameters, deformed basis model 79−80867
Ir odd-mass isotopes, 9/2$^-$ level excitation energies, estimates 77−275
Ir+^{20}Ne, 200 MeV, yields of neutron-deficient isotopes of Fr and Rn *(Russian)* 77−23104
^Ir, A=187, 189, 191, 193, positive parity states, particle asymmetric rotor descriptions 79−49572
^Ir, A=189, 191, levels, J$^\pi$, transitions and mixing ratios from Pt decay 80−68602
^Ir, A=191,193 photoneutron yield curves, nuclear shape and giant dipole resonances, 8-21 MeV *(Russian)* 79−13268
^{189}Ir low lying positive parity bands, state anomalous angular distribs. 78−66212
^{190}Ir in Re crystal, elec. quadrupole orientation, elec. field gradient 80−78140
^{191}Ir 129 keV transition, atomic screening, time reversal violation 80−106011
^{191}Ir, excited nuclei mean precession time depend. on γ-spectral width, g-factors *(Russian)* 80−78211
^{191}Ir from (p,t) at 18 MeV, ground state rot. band, 7/2 gamma vibr. levels 78−74360
^{191}Ir γ transition, time reversal like phase shift between competing multipoles 79−30801
^{191}Ir, levels excited in (p,2n) and (d,3n) 79−22164
^{191}Ir low lying positive parity bands, state anomalous angular distrib. 78−66212
^{191}Ir(^{6}Li, xn+yp), 48-156 MeV, excitation functions 77−18603
^{191}Ir(d,2n), 13 MeV, ^{191}Pt level scheme, γ, conversion electron spectra, spins, parities 78−25149
^{191}Ir(n,γ), thermal, isomer state excitation, relative probabilities 79−75814
^{191}Ir(p,4nγ), 38 MeV, low lying and high spin states in ^{188}Pt side band 78−4936
^{191}Ir(p,n), 10 MeV, ^{191}Pt level scheme, γ, conversion electron spectra, spins, parities 78−25149
^{192}Ir β decay into ^{192}Pt 4$^+$ and 3$^+$ levels, spectral shapes, ground state parity 77−50086
^{192}Ir β decay into ^{192}Pt 3$^+$ and 4$_1^+$ states, lifetime meas. by β-γ coincidence 78−25153
^{192}Ir, gamma-ray intensities, precision meas. 80−102140
^{192}Ir ground state spectroscopic quadrupole moment, g-factor, hyperfine quadrupole splitting 79−89235
^{192}Ir, interstitial radiation therapy, Angiocath afterloading technique 77−13002
^{192}Ir levels, resonances and low energy γ-rays from ^{191}Ir(n,γ) 80−47397
^{192}Ir, NMR/ON in Ni, resonant freq. shift with applied field 77−28462
^{192}Ir, redetermination of γ-ray standards between 0.1 and 1.0 MeV 78−37472
^{192}Ir, specific γ-ray constant and exposure rate constant 79−36187
^{193}Ir, muonic, mag. hyperfine anomaly 77−83768
^{193}Ir, neutron capture cross sections, 0.5 to 3.0 MeV 79−40912
^{193}Ir(^{6}Li, xn+yp), 48-156 MeV, excitation functions 77−18603
^{194}Ir decay, ^{194}Pt level scheme 77−2900
^{194}Ir, spectral shapes of 1$^-$→2$^+$ and 1$^-$→0$^+$ beta transitions 77−30515
^{197}Ir decay studies, prod. in fast neutron reactions 77−23011
Ir(p,t)^{189,191}I, 18 MeV, ground state rot. band, 7/2 gamma vibr. levels 78−74360
Ir(t,α)Os, A=191,193, 15 MeV, possible excit. of hexadecapole vibrs. 77−26560
Os, A=190, 192, possible hexadecapole vibrs. via Ir(t,α)Os 15 MeV reactions 77−26560
Os even nuclei, spin expsn. Hamiltonian, quadrupole moments 80−5058
Os even-even isotopes, excitation energies and EM props. from interacting boson model 80−106005
Os, O(6)→rotor transition, interacting boson approx. model, levels and transitions 79−13224
^Os, A=186, 188, 190, 192, rigid asymmetric rotor model descript., E2 and E4 props. 80−13403
^Os, A=186-194, collective levels, transitions, mag. and quadrupole moments, boson expansion theory 80−105954
^Os, A=189,190, absolute atomic masses 79−89228
^Os, A=190,192, two-quasiproton states, level struct., DWBA anal. of Ir(t,α) 79−89237
^Os, A=191,193, ground state spectroscopic quadrupole moment meas. 80−27553
^Os(α,α′) A=188,190,192, 4$_3^+$ level population, hexadecapole vibrs. 78−89780
^Os(γ,xn), 7-30 MeV, A=186,188-190,192, photoneutron cross section and giant resonances 79−54422
^Os(t,p), 15 MeV, A=188,190,192, cross section meas., DWBA calcs. 78−50181
^{190}Os, collective states and static quadrupole moment, boson expansion theory 80−47346
^{190}Os, electromagnetic moments from muonic X-rays 78−12972
^{190}Os levels and γ-ray transitions, (n,γ) and (n,e$^-$) reactions 79−36189
^{190}Os(d,t)^{189}Os, 12 MeV, ^{189}Os spectroscopy, Nilsson model, triaxiality 77−14035

nuclei with mass number 190 to 219 continued
^{190}Os(n,n′)^{190m}Os, 13-17 MeV, cross section meas. by activation method 78−46057
^{191}Os, energy levels and spectra from ^{190}Os(d,p), ^{192}Os(d,t), ^{190}Os(n,γ) reactions 77−41917
^{191}Os, K-shell internal conversion, Kα$_1$ hypersatellite line energies, intensities 77−18885
^{191}Os, Nilsson model strength fragmentation obs. in ^{190}Os(n,γ) 77−74844
^{192}Os, electromagnetic moments from muonic X-rays 78−12972
^{192}Os level scheme and rot. bands, from ^{191}Os(n,γ), interacting boson approx. anal. 79−6413
^{192}Os, muonic, dynamic hyperfine effect, model independ. anal. 78−22057
^{192}Os, Wilets-Jean Hamiltonian for energy levels, transitions, moment, etc. 79−9457
^{192}Os(^{12}C,^{14}C)^{190}Os, 70 MeV, shape transition effect on quadrupole transfer strength 78−644
^{192}Os(2n,γ)^{194}Os, level transitions, prolate-oblate transition 78−62540
^{192}Os(d,p)^{193}Os, ^{193}Os energy levels, neutron separation energy 78−41642
^{192}Os(n,2n), 13-18 MeV, compound nucleus and precompound emission models 77−74841
^{192}Os(n,3n), 13-18 MeV, compound nucleus and precompound emission models 77−74841
^{192}Os(n,γ)^{193}Os, ^{193}Os energy levels, neutron separation energy 78−41642
^{192}Os(p,p′) and (d,d′), γ-ray spectra, energy level scheme 77−34243
^{193}Os, energy levels and spin assignments using ^{192}Os(n,γ) 79−36161
^{193}Os, energy levels investig. using ^{192}Os(d,p)^{193}Os and ^{192}Os(n,γ)^{193}Os reactions 78−41642
^{193}Os level scheme and transitions, Coriolis coupled Nilsson states from ^{192}Os(n,γ) 80−57698
^{194}Os beta decay, X-ray/gamma relative intensities, L$_1$ subshell yields 78−4919
^{194}Os, obs. of levels populated in ^{192}Os(t,p) 78−50181
^{196}Os, T$_{1/2}$ and partial decay scheme 78−21527
Os(γ,xn), photoneutron cross section, bremsstrahlung yield curves 78−17176
Os(t,p), 17 MeV, two neutron transfer strength, O(6) limiting symmetry in IBA, Pt comparison 80−32287
^Pa, A=215-218, 222, α-decay half life and energies from ^{151}Ta+^{40}Ar and ^{184}W+^{40}Ar 79−45216
^Pa, A=215-218, deduced mass from Fr direct mass meas. 80−78130
^{206,207,208}Pb levels, ground state widths via reson. fluoresc. 77−74799
^{206,207,208}Pb(γ, γ), reson. fluoresc. meas., levels, ground state widths 77−74799
Pb, 1$^+$ state and effective g-factor anal. 77−74764
Pb, 195-203, high-spin neutron hole excitations, hole-core weak coupling 77−50062
Pb, 380 MeV, binary decay induced by K$^-$ 79−93671
Pb (γ,γ), 344-1408 keV ^{152}Eu γ rays, differential cross sections 80−99170
Pb (p, X), 2.2, 6, 8.5 GeV, p and d inclusive spectra at 162° *(Russian)* 79−97710
Pb, A=193, 5, 7, 9, high-spin states anal. by heavy ion reactions 78−21500
Pb, A=194, 196, 198, 12$^+$ isomeric states, T$_{1/2}$, g-factor 77−74762
Pb, A=200, 202, 204, seniority four admixtures in low lying 0$^+$ states 78−8741
Pb, A=204,6, quadrupole moments of first excited state meas. 78−21491
Pb, A=204-208, charge distrib. from elastic electron scatt. and muonic X-ray data anal. 78−54681
Pb, A=206, 208, fission, proton induced, 1 GeV, cross section *(Russian)* 78−94041
Pb, beta-generated external bremsstrahlung spectra 77−57625
Pb, binary fission characts. induced by α-particle bombardment of 0.65 to 4.12 GeV 78−13169
Pb cored nuclei, high spin stater energies, quadrupole interaction, yrast traps 77−34223
Pb, diffraction scatt. of nucleons, polarisation determ. *(Russian)* 79−89285
Pb, dosimetric data and metabolic model 77−29206
Pb even isotopes, two quasiparticle 2$^+$ state coupling to T=0 giant quadrupole resonance 80−68618
Pb, γ-ray attenuation meas. using Ge(Li) detector 78−17539
Pb isotopes, gamma radn. reson. scatt. 4.7-8.3 MeV 78−78362
Pb isotopes, M1 transitions, theory of finite Fermi systems *(Russian)* 77−6296
Pb isotopes, occupation number calc., pair correlations 79−30783
Pb isotopes from π^- capture, high spin states 78−54806
Pb, multiple scatt. of cosmic ray muons at sea level, 230 MeV/c 78−7850
Pb, multiple scatt. of cosmic ray muons at sea level, anomalous scatt. distrib. 78−7851
Pb muonic isotopes, A=204, 206, 207, 208, nuclear polarisation energy shifts, RPA calcs. 78−94334
Pb, nucl. electron capture, 0.43-1.71 MeV electrons 79−6513
Pb, odd-A isotopes, weak coupling calc. for high spin neutron hole excitations 78−62475
Pb pairing vibr. band, microscopic struct. and wave functions from (p,t), (t,p) 80−91126
Pb, photofission induced by 220-500 MeV coherent beam 77−3056
Pb, π^- absorption *(Russian)* 78−46115
Pb, π^- and p elastic scatt., 30 to 50 GeV/c, nuclear radius, real/imaginary forward scatt. amplitude ratio *(Russian)* 77−34351
Pb region, even-odd nuclei, EM moments and transitions 77−88040
Pb region, forbidden charge exchange collective modes, β- and γ-decay processes 80−86784
Pb region, mag. moments and M1, M2 and M4 values, self consistent calcs. 80−47371
Pb region, particle-vibration multiplet spectra, self-consistent framework 80−102089
Pb region long lived high spin isomers, magnetic moments, nuclear struct. *(German)* 77−82820
Pb, seniority breaking; centroid energy, partial width and mixing parameter calcs. 78−70468
Pb, shadowing in photon-nucleus 20 to 185 GeV total cross sections 79−30823

nuclei with mass number 190 to 219 continued
Pb, strongly forbidden T1-transition, parity nonconservation *(Russian)* 77−10366
Pb targets, possibilities for producing super-heavy elements Z>102, new projectiles *(Russian)* 78−86548
Pb targets for superheavy element synthesis 77−82960
Pb, total photonucl. absorpt. cross sections, 25-106 MeV 79−6565
Pb+^{12}C, 25.2 GeV, target residue mass and charge distribs. 77−74873
Pb+^{14}N, 75.6 to 96.6 MeV, fission fragment angular distrib., shape of saddle point of compound nucleus *(Chinese)* 78−78427
Pb+^{14}N, complete fusion cross sections, excitation functions *(Chinese)* 78−82406
Pb+Ar, 4-17 GeV, search for ultradense nuclei 77−3044
Pb+Ar, 800 MeV/A, wide angle inclusive proton spectra 79−40951
Pb+C, 800 MeV/A, wide angle inclusive proton spectra 79−40951
Pb+C, Pb+Ne, 800 MeV/N, p and π inclusive spectra, energy and ang. distribs. 78−54790
Pb+e^+, 0.5-3.5 GeV positron initiated showers, test of cosmic ray shower calcs. 78−37332
Pb+heavy ion hard reaction, ground state correlations from liquid drop model 79−22308
Pb+K_L, 30 to 150 GeV, total cross sections, inelastic screening evidence 79−17936
Pb+K_S, 20 to 140 GeV, precise coherent K_S regeneration amplitudes 79−17937
Pb+Kr, deep inelastic collisions, excitation of nuclear surface modes 78−37374
Pb+Ne, 800 MeV/A, wide angle inclusive proton spectra 79−40951
Pb+p, 1 GeV, neutron production *(Russian)* 79−85477
Pb+p, 1 to 28.5 GeV, production of 43≤A≤51 nuclides, reaction mechanisms 77−34301
Pb+p, 3.6 GeV, emitted proton vel. spectra max. *(Russian)* 79−9571
Pb+p, 600 MeV, pion production, energy spectra, A depend. *(Russian)* 78−17213
Pb+p, 7 GeV/c hadron multiple prod. *(Russian)* 79−22298
Pb+p→$\Lambda^0(K_S^0)(\bar{\Lambda}^0)$+X, neutral strange-particle prod. by 300 GeV protons 79−17905
Pb+p→p, 640 MeV, proton inclusive spectra and ang. distrib. meas. 77−67751
Pb+Pb(U), positron prod. 78−50197
Pb+Pb(U), positron prod. in heavy ion collisions 78−50198
Pb+π^-, 3.7 GeV/c, proton spectra *(Russian)* 78−41785
Pb+π^-, 7 GeV/c hadron multiple prod. *(Russian)* 79−22298
Pb+U, 750 MeV, classical model, kinetic energy, ang. distribs., instantaneous fission fragments 78−13185
Pb(Ar,X), 800 MeV/N, single particle spectra from high multiplicity events 80−99184
Pb(C,C), 800 MeV/N, high momentum nucleons from relativistic nuclear collisions, hard scattering mechanism 79−40950
Pb(^{12}C,^{12}C'), A=204,206,208, 60 MeV, quadrupole moment and B(E3) values 79−17797
Pb(^{12}C,X), 1-2 GeV/n, central collision threshold phenomena, pion prod. 80−95326
Pb(^{12}C,X) 3.6 GeV proton emission invariant cross sections *(Russian)* 80−13500
Pb(^{56}Fe,X), relativistic ^{56}Fe fragmentation, charge and mass changing cross sections 79−54453
Pb(^{20}Ne,π^+), 800 MeV/N, doubly differential cross sections and ang. distribs. 80−9305
Pb(^{20}Ne, π^+X), 400 MeV/N, pion prod. doubly differential cross sections and ang. distrib. 80−32299
Pb(^{16}O,^{12}C)Po (A_{Pb}=204,207,208), 93 MeV, comparison with α-decay data 77−334
Pb(^{16}O,^{16}O'), A=204,206,208, 52 MeV, quadrupole moment and B(E3) values 79−17797
Pb(Xe,X), deep inelastic, δ-electron emission, reaction time effects 80−32293
^{4}Pb, A=202, 203, 204, transfer strengths from 17.5 MeV ^{204,205,206}Pb(p,t) reaction 78−94005
$^\wedge$Pb, A=190,192, level scheme, γ-branching, ^{192m}Pb half life from Gd+^{40}Ar and ^{182}W+^{16}O 79−75854
$^\wedge$Pb, A=197, 198, low energy γ-transitions and level lifetimes from ^{186}W(^{16}O, xn) 80−18221
$^\wedge$Pb, A=197,198, low energy γ-transitions 80−83058
$^\wedge$Pb, A=200,206, 12^+ isomer states, quadrupole moments 80−27554
$^\wedge$Pb, A=202, 204, spectra from multistep shell model method 80−78194
$^\wedge$Pb, A=205-207, neutron hole states, spectroscopic factors, DWBA anal. of Pb(^{3}He,α) 80−47352
$^\wedge$Pb, A=206-209, nuclear K-X-ray satellites, Z=50-83, by α-bombard., 17.5-22.5 MeV 80−42984
$^\wedge$Pb, A=207,209, single particle state mag. moment in large shell model space 79−45162
$^\wedge$Pb(^{18}O,X), (A=207, 208), (X=^{17}O, ^{19}N, ^{21}O, ^{22}O), 93 MeV, light neutron rich nuclei study 79−89322
$^\wedge$Pb(^{3}He,n), A=204,206,208, 33.3 MeV, cross sections, DWBA anal. for data near Z=82 79−67733
$^\wedge$Pb(α,α'), A=204, 206, 208, 16-27 MeV backward scatt., collective states 80−13365
$^\wedge$Pb(α,α), A=206, 208, 120 MeV, isoscalar resonance excitation, low lying transitions, DWBA calc. 80−512
$^\wedge$Pb(e,e'), A=204, 206-208, levels and inelastic cross sections 80−22698
$^\wedge$Pb(γ,γ), A=206-8, 4.5 MeV to neutron emission threshold, strengths in energy levels 79−36164
$^\wedge$Pb(γ,n), A=206, 208, levels using tagged photons 80−23245
$^\wedge$Pb(γ,n), A=206,207,208, photoneutron Q-value determinations using monochromatic photons 79−22271
$^\wedge$Pb(n,γ), A=204, 206-8, sub- and super-barrier fission, results interpretation 79−67784
^{192}Pb anomalous α-decay rate 79−67721
^{193}Pb, identification and decay 77−6587
^{194}Pb, excited level scheme from ^{194}Bi decay 77−6306
^{196}Pb, excited level schemes from ^{196}Bi decay 77−6306
^{197}Pb isomers, half lives and decay 79−36197
^{198}Pb, E2 transition probability and effective charge for neutron $i_{13/2}$ subshell 78−78309
^{199}Pb, level scheme from ^{199}Bi decay 78−78316
^{200}Pb, obs. of levels in ^{198}Hg(α,2n) 78−66192
^{201}Pb decay, ^{201}Tl levels, transitions and J^π assignments 80−5099
^{201}Pb, level scheme from ^{201}Bi decay 78−78316
^{201}Pb, nuclear spin, metastable atomic states, hyperfine struct. meas. 78−25110
nuclei with mass number 190 to 219 continued
^{201}Pb→^{201}Tl following ^{203}Tl(p,3n) or ^{205}Tl(p,5n), E_p=15 to 60 MeV, yields and excitation functions 79−5369
^{202}Pb, 4_1^+ state g-factor 77−30491
^{203}Pb, 480 ms isomeric $29/2^-$ state, decay scheme 77−22893
^{203}Pb, electron dose reduction coeff., internal radionuclides, source free target, cylindrical geometry 78−92704
^{203}Pb, high-spin level struct. determ. from ^{202}Hg(α,3nγ) at 38.2 MeV 78−29489
^{203}Pb in-beam electron conversion from high spin states from ^{204}Hg(α,5n) 79−93554
^{203}Pb multiplet struct., DWBA anal. from ^{205}Pb(p,t) 79−17784
^{203}Pb, nuclear spin, metastable atomic states, hyperfine struct. meas. 78−25110
^{203}Pb production by proton reactions on natural Tl 79−88184
^{203}Pb-acetate, tissue distrib., comparison with ^{67}Ga citrate as abscess-localising agent 77−5064
^{204}Pb, muonic, first excited 2^+ state, isomer shift of E2 transition 80−99150
^{204}Pb populated by ^{204}Bi decay, isomeric transitions, J^π assignments 78−50122
^{204}Pb yrast levels populated in ^{204}Hg (α,4n), spin, parity, γ spectra 78−12954
^{204}Pb(d,p), 13.0-20.0 MeV, populating ^{205}Pb hole states below MeV 2.56 77−30478
^{204}Pb(d,p) 13.0 MeV, populating ^{205}Pb particle states 77−34216
^{204}Pb(n,n')^{204}Pb, meas. of lead content of metal fragments 79−52850
^{204}Pb(n,n'γ), 1.5-3.1 MeV, levels, J^π, excitation functions and mixing ratios 80−102123
^{205}Pb, cluster vibrational field coupling model description 77−57604
^{205}Pb, decay, orbital electron capture ratios 77−18894
^{205}Pb decay, orbital electron capture ratios, half-life 78−74340
^{205}Pb, hole states below 2.56 MeV, spectroscopic strengths via ^{204}Pb(d,p) 77−30478
^{205}Pb multipole resonance E1-E2 and E1-M1 interference from ^{206}Pb(γ,n) 80−32251
^{205}Pb, particle states via ^{204}Pb(d,p), spectroscopic factors 77−34216
^{205}Pb(d,d'), 14, 17 MeV, direct population of collective states, multiplets, deform. parameters 78−74376
^{205}Pb(t,p)^{207}Pb preliminary results using reactor produced ^{205}Pb 77−22990
^{206}Pb, effect of renormalisation of effective interaction on ground state wave functions *(Russian)* 77−284
^{206}Pb γγ directional correlations, multipole mixing ratios, transition strength limits from ^{206}Bi decay 80−86849
^{206}Pb, half-lives of two-neutron-hole 0_2^+ state 77−10323
^{206}Pb, level scheme including conversion electrons ≲40 eV 78−21518
^{206}Pb low lying level ang. distribs., zero range DWBA anal. from ^{208}Pb(p,t) 79−67656
^{206}Pb, population of 0^+, alpha-decay of ^{210}Po 80−22775
^{206}Pb proton pairing vibr. obs., using (^{3}He,n) reaction of 33.3 MeV 78−13128
^{206}Pb+n, 3-50 KeV, neutron resonances, J^π assignments, decay scheme 79−36217
^{206}Pb(^{40}Ar,2n)^{244}Fm, fusion reactions near Coulomb barrier, optical pot. parameter determ. 79−30874
^{206}Pb(^{6}Li, 3nγ), 29-34 MeV, ^{209}At high spin states, neutron hole influence 77−2934
^{206}Pb(α,α'), 120 MeV, new giant resonance at 80 $A^{-1/3}$ MeV 77−41939
^{206}Pb(α,α), 24 MeV, total reaction cross section 78−25209
^{206}Pb(n,γ), direct-semidirect and compound nucleus contribs. to cross sections 80−68662
^{206}Pb(n,n), 15-18 MeV, total cross section 79−75990
^{206}Pb(n,p), energy dependence, 13.4-20.3 MeV rel. to exciton model calc. 79−75989
^{206}Pb(t,p), two-nucleon stripping reactions with Tabakin pot. 78−21570
^{207}Pb, 569.6 keV level, half-life meas. 78−55090
^{207}Pb 569.65-1063.63 keV cascade, γ-γ ang. correl. meas. from ^{207}Bi decay 80−86847
^{207}Pb doorway resonances, M1 ground state radiative strength, level density from ^{206}Pb(n,n), (n,γ) 79−93589
^{207}Pb, γ-γ directional correls. in ^{207}Bi decay, mag. perturbation obs. 77−74796
^{207}Pb inner hole states, spectroscopic strengths DWBA anal. from ^{208}Pb(^{3}He,α) 79−17813
^{207}Pb isobar-like isospin forbidden state excitation from ^{206}Pb(n,p) *(Russian)* 79−75855
^{207}Pb, muonic, octupole doublet isomer shifts, octupole vibrs. 80−95750
^{207}Pb muonic isomer shifts, neutron hole anomalous moment contribs. 80−78728
^{207}Pb neutron hole states, core vibration effects, shell model energies 79−36142
^{207}Pb, neutron scattering resonance radiative widths 80−99146
^{207}Pb neutron separation energy and resonances, decay transitions from ^{206}Pb(n,γ) 79−36217
^{207}Pb p-wave resonances, enhanced primary M1 transitions from ^{206}Pb(n,γ) 80−57728
^{207}Pb parity assignments and M1 radiative strength from ^{206}Pb(n,n) 80−52614
^{207}Pb, T=45/2 isobaric analogue state obs. in ^{208}Pb(^{3}He,α)^{207}Pb 78−93928
^{207}Pb+e, high resolution inelastic scatt. cross sections, induced charge of neutron, form factors 78−78366
^{207}Pb+n, obs. of ^{208}Pb giant mag. dipole states, spin parity assignments 77−57666
^{207}Pb+n resonances, d+s admixture 77−22899
^{207}Pb+p, 70 GeV/c, s-particles ave. multiplicity 78−21567
^{207}Pb(^{40}Ar,3n)^{244}Fm 79−30874
^{207}Pb(α,f), 640MeV 80−95329
^{207}Pb(d,f), 2.1 GeV, binary and ternary fission kinetics *(French)* 78−70577
^{207}Pb(d,pn), E_d=13.6 MeV, disintegration reactions, isotopic effects 78−13108
^{207}Pb(d,pn) 13.6 MeV disintegration neutron elastic scatt. effect *(Russian)* 77−34323
^{207}Pb(e,e), magnetisation distrib. from elastic mag. form factors, core polarisation, exchange currents 80−47372
^{207}Pb(γ,n), 7632 keV level photoexcitation, cross section and J^π 80−37330
^{207}Pb(γ,n), new 86 keV neutron source 79−704
^{207}Pb(n,γ), primary E2 transitions to ^{208}Pb ground state 78−58284

nuclei with mass number 190 to 219 continued
^{209}Pb(n,γ), up to 1 MeV, obs. of ^{208}Pb giant M1 fine struct. 77−79347
^{209}Pb(n,n'), 2-4.5 MeV, level excitation functions, Hauser-Feshbach-Moldauer model test 79−36238
^{209}Pb(n,n)^{209}Pb, 265 keV, (s+d)-wave mixing 77−46167
^{209}Pb(n,p) reaction, isobar analogue state excitation *(Russian)* 80−102124
^{209}Pb(p,p'), 135 MeV, DWIA test 78−33186
^{209}Pb, alpha-particle vibr. states, obs. in ^{204}Hg(^{16}O,^{12}C) 77−38218
^{209}Pb, neutron and nuclear matter space distribs. from (p,p) 1 GeV scatt. *(Russian)* 78−502
^{209}Pb, π bound states in finite nuclei 78−46013
^{209}Pb 1^+ states, fine struct., energy levels, transition probabilities, matrix diagonalised method *(Chinese)* 78−78269
^{209}Pb 7064 keV level negative parity, EM deexcitation pattern from ^{209}Pb(d,p) 79−36148
^{208}Pb (^{16}O, X), 84, 92 MeV, total reaction cross section fragmentation 79−67775
^{208}Pb (^{208}Pb,f) 1539 MeV, exam. of four-pronged double sequential fission events using mica track detectors 80−95328
^{208}Pb (Ar, π X), 1.8 GeV/nucleon, fireball model calc. of π-multiplicity distribs. 78−37366
^{208}Pb (Ar, π^+ X), 250, 400 MeV/A, pion yield near threshold 80−18344
^{208}Pb (α,α'), 100-172 MeV, giant monopole resonance evidence from strong energy depend. 80−13432
^{208}Pb (e,e'), 2^- giant resonance twist mode excitation, B(M2) values, form factors 80−78246
^{208}Pb (e,e), 502 MeV, high-momentum-transfer, charge-density distrib. anal. 77−38258
^{208}Pb (n,Zn) direct process contrib. n angular correlations *(Russian)* 78−78386
^{208}Pb (n,p), energy dependence, 13.4-20.3 MeV rel. to exciton model calc. 79−75989
^{208}Pb (p,p'), 635 Mell protons, meas. of energy spectra of secondary protons 79−97708
^{208}Pb (p,p), 1 GeV, spin-effects, Coulomb interactions, Glauber theory 77−82931
^{208}Pb (p,p), 1.04 GeV elastic scatt., polarisation 78−21549
^{208}Pb (p,p) elastic scatt., polarisation and spin-orbital amplitude parameters, 1 GeV *(Russian)* 78−17208
^{208}Pb (π^-,π^-), 29 MeV, elastic differential cross-section 79−71872
^{208}Pb and neighbouring nuclei, shell model calcs. with correlated pairs basis 80−22712
^{208}Pb breathing model transition density, single particle and collective state dynamical coupling 80−106007
^{208}Pb, charge and proton distribs., single particle model 78−50074
^{208}Pb, charge distrib. polarisation from e^- scatt. and muonic X-ray data consistency 77−22873
^{208}Pb, closed-shell effect on fission barriers at Z=82 and N=126 77−309
^{208}Pb compound nucleus, γ-decay spectral function depend. on ang. momentum *(Russian)* 78−86467
^{208}Pb core with valence nucleon or hole, mag. props., exchange currents, electron scatt. 80−22689
^{208}Pb, core-coupling RPA calcs. of NGR, electric multipole strength fragmentation 78−50142
^{208}Pb, damping of single particle states and giant resonances 79−17782
^{208}Pb, eikonal anal. of high energy proton and electron scatt. *(Russian)* 77−22908
^{208}Pb, eikonal approx. of electron scatt. by spherically symmetric nuclei 78−37330
^{208}Pb, energy of two-phonon α-vibration 77−14019
^{208}Pb, excitation of low lying collective states by (n,n') scatt. 78−17205
^{208}Pb, excitations, EM transitions in renormalised RPA 77−82857
^{208}Pb, fast neutron capture and the microscopic isovector optical potential 79−63668
^{208}Pb, fast neutron quadrupole radiative capture, direct-semidirect model 77−26711
^{208}Pb, fast neutron scatt. and capture, microscopic isovector optical pot. test 80−52682
^{208}Pb, fine struct. of M1 giant resonance obs. in ^{207}Pb(n,γ) 77−79347
^{208}Pb, finite Fermi-system theory, E1, E2, M1 resonances, γ absorpt. cross section near threshold 77−50055
^{208}Pb, finite nuclear props. in relativistic quantum field theory, mass and p densities 80−9219
^{208}Pb, from ^{207}Pb(n,γ), primary E2 transitions to ground state 78−58284
^{208}Pb, giant dipole resonance struct. 77−88023
^{208}Pb giant electric and magnetic multipole resonances, microscopic descript. 78−538
^{208}Pb, giant M1 resonance near 8 MeV 79−6541
^{208}Pb giant magnetic dipoles states obs. in ^{207}Pb+n, spin parity assignments 77−57666
^{208}Pb giant monopole and quadrupole resonances, multipole excitations from (α,α')(d,d') 80−106031
^{208}Pb, giant monopole reson struct. 78−82331
^{208}Pb, giant multipole reson. electroexcitation 77−34279
^{208}Pb, giant resonances, self-consistent microscopic anal. including particle continuum 77−2896
^{208}Pb, high-spin states, form factors for electroexcitation 77−14116
^{208}Pb, inclusive proton photoprod., momentum spectra, max. bremsstrahlung energy 2.0 to 4.5 GeV *(Russian)* 77−34287
^{208}Pb, intermediate structure of giant analogue reson. 78−62517
^{208}Pb, isobaric analogue states, effects of Coulomb isospin coupling, random-phase method *(Russian)* 80−86808
^{208}Pb, isoscalar breathing mode state obs. in (α,α') scatt. at 96 MeV 78−17086
^{208}Pb, isoscalar electric giant dipole resonance, from RPA calc., nuclear compressibility 78−86520
^{208}Pb, isoscalar giant multipole resonances, simple macroscopic model, damping mechanisms 80−42617
^{208}Pb isoscalar giant reson., decay scheme 80−9277
^{208}Pb, isospin purity violation, dominant role of noncollective monopole states 78−12964
^{208}Pb, K^+ interaction with nuclei 78−13165
^{208}Pb, linearised Hartree Fock model, effective charge, isoscalar nuclear shifts, rms radius 78−25138
^{208}Pb, longit. isoscalar electroexcitation, sum rules and mean excitation energy 78−521
^{208}Pb M1,E1,M2,E2 localised γ-ray strengths from ^{207}Pb(n,γ) 80−37350
^{208}Pb, M1 collective strength, evidence from ^{208}Pb(γ,n_{pol}) 77−38255
^{208}Pb, M1 reson. states fine struct., 2p-2h states in RPA 77−22831

nuclei with mass number 190 to 219 continued
^{208}Pb, mag. moment, M1 transition probabilities, one pion exchange calcs. 79−9463
^{208}Pb, mag. quadrupole resonance, M2 strength distrib., quasiparticle-phonon model 79−75947
^{208}Pb, magnetic high spin states, microscopic struct. 80−95297
^{208}Pb magnetic susceptibility and M1 transitions, nuclear interaction role 79−45160
^{208}Pb, mode coupling theory for two particle-two hole states 77−6214
^{208}Pb, monopole excitations in heavy nuclei, hadron induced 78−86471
^{208}Pb, monopole giant resonances, position and width 77−82896
^{208}Pb monopole vibr. vel. field, asymptotic form 80−78115
^{208}Pb, muonic, isomer shift of 2.61 MeV gamma transition 77−38753
^{208}Pb, neutron and proton surface thickness, HF calcs. 77−71557
^{208}Pb, neutron densities and single particle struct. 80−32165
^{208}Pb, neutron elastic and inelastic cross sections, 2.5 MeV, comparison with optical model 77−30595
^{208}Pb, nuclear radii, energy density and HF-BCS methods 80−47363
^{208}Pb, partly self-consistent potl., charge distrib. and Fermi surface *(Russian)* 77−272
^{208}Pb, photonuclear induced high multipole giant reson., Australian nuclear physics review 77−88021
^{208}Pb, pion scatt., 355 MeV, ratio of π^+ and π^- cross sections from coincidence meas. 78−29501
^{208}Pb, pion-exchange contribs. to charge densities, HF calcs. 78−46001
^{208}Pb, quadrupole moment of 3^- excited state 77−38222
^{208}Pb, quasielastic π scatt., recoil proton spectra obs. 77−14198
^{208}Pb region, effective interaction and energy spectra 78−25121
^{208}Pb region, finite Fermi systems, review 78−537
^{208}Pb region, mag. transition strength, core polarisation effects, form factor shape 80−86850
^{208}Pb resonance parameters, s-, p- and d-wave entrance channel doorway states from ^{207}Pb+n 79−470
^{208}Pb, search for collective M1 resonance in ^{208}Pb(γ,n_0) 77−46103
^{208}Pb, self consistent K-matrix model calc. 77−6257
^{208}Pb, self-consistent generator coord. for giant monopole reson. 77−2891
^{208}Pb shape oscillations, radial transition density in particle-vibration coupling model 77−50048
^{208}Pb shell structure, effect on magicity of superheavy nuclei 80−78175
^{208}Pb, shell-model interaction for neutron hole states 77−18446
^{208}Pb single particle and hole states, renormalisation, core polarisation, spectroscopic factors 80−57658
^{208}Pb, single particle spectra, effect of core polarisation 77−2892
^{208}Pb, static and transition densities, self consistent RPA theory test in fast (p,p), (e,e) scatt. *(Russian)* 79−49604
^{208}Pb, Thomas-Fermi model 78−8747
^{208}Pb, twist mode 77−88037
^{208}Pb-^{208}Bi, statistical role of β^- strength function 77−22955
^{208}Pb+^{110}Pd, 1.2 GeV, neutron rich nucleon flow in central heavy ion collisions 79−36268
^{208}Pb+^{12,13}C, single-n sub-Coulomb transfer reactions, single particle wave function RMS radius, n-excess 79−85355
^{208}Pb+^{12}C, 25.2 GeV, target residue mass and charge distribs., calcs. 79−3172
^{208}Pb+^{12}C, 96 MeV, inelastic scatt., folding model, macroscopic formalism, form factors 78−25227
^{208}Pb+^{12}C(^{14}N), giant resonances, ang. distrib., inelastic scatt. 78−62564
^{208}Pb+^{136}Xe, 800 MeV, charge and mass transfer near Coulomb barrier 79−22325
^{208}Pb+^{136}Xe, double octupole phonon excitation, coupled channel WKB approx. 78−4960
^{208}Pb+^{16,17,18}O, single-n sub-Coulomb transfer reactions, single particle wave function RMS radius, n-excess 79−85355
^{208}Pb+^{16}O, 140, 315 and 33600 MeV, isotope yields and cross-sections 77−14161
^{208}Pb+^{16}O, 140 and 315 MeV, energy depend. of heavy ion peripheral reactions 78−74399
^{208}Pb+^{16}O, 20 MeV/A, nucleon motion effect on energy spectra and ang. distribs. 78−4971
^{208}Pb+^{16}O, classical, semiclassical and quantum mechanical scatt. and reaction calcs. 79−566
^{208}Pb+^{16}O, elastic scatt., transfer reactions, fission, total cross sections, optical model parameters 77−54246
^{208}Pb+^{16}O, microscopic model anal. of fragment yields at 20 MeV/A and 2100 MeV/A 78−33214
^{208}Pb+^{16}O peripheral collisions, cross-sections meas. at 315 MeV 77−6428
^{208}Pb+^{208}Pb, 14 GeV, nonnuclear positrons creation 79−30847
^{208}Pb+^{208}Pb, 1600 MeV, axially symmetric TDHF 78−74398
^{208}Pb+^{208}Pb, 7.4 MeV, time depend. Hartree Fock theory test 79−49591
^{208}Pb+^{208}Pb, positron form. 78−62873
^{208}Pb+^{208}Pb deep inelastic processes, TDHF and elementary modes of excitation 79−63695
^{208}Pb+^{20}Ne(^{40}Ar), 250-1000 MeV/N, intranuclear cascade calcs. for multiplicity and cross sections. 80−32300
^{208}Pb+^{40}Ca, 255, 300 MeV, lowered fusion cross section 78−41797
^{208}Pb+^{48}Ca mass distribs. of fission fragments meas. 77−71621
^{208}Pb+^{58}Ni(^{90}Zr), fission phenomena in deep inelastic collisions 80−5186
^{208}Pb+^{6}Li, Coulomb and nucl. excitation in ^{6}Li dissociation 78−41770
^{208}Pb+^{84}Kr, 494 MeV, strongly damped collisions, time-depend. mean field theory 78−82374
^{208}Pb+^{84}Kr, 500 and 700 MeV, differential cross section calc., statistical model 78−50192
^{208}Pb+^{86}Kr, 469 MeV, search for superheavy nuclei, Z>106, lifetimes >2 ps 78−46102
^{208}Pb(^{12}C, ^{12}C'), 200 MeV, evidence for giant quadrupole excitation 79−49637
^{208}Pb(^{12}C,^{11}B), 77 MeV, bound and continuum state excitation, direct and two step processes 80−63205
^{208}Pb(^{12}C,^{11}B), 77-116 MeV, cross-section meas., DWBA anal. 77−6433
^{208}Pb(^{12}C,^{11}B)^{209}Bi, DWBA anal. including nuclear wave function polarisation 78−629
^{208}Pb(^{12}C,^{11}B)^{209}Bi, single-particle polarisation, two-centre shell model 78−13142
^{208}Pb(^{12}C,^{13}C), 77-116 MeV, cross-section meas., DWBA anal. 77−6433
^{208}Pb(^{12}C,^{14}C), 77-116 MeV, cross-section meas., DWBA anal. 77−6433

nuclei with mass number 190 to 219 continued
^{208}Pb(^{136}Xe,X), 1120 MeV, energy, angular, charge distribs. meas. 77-3029
^{208}Pb(^{136}Xe,X), 7 MeV/u, composite system lifetime from δ-electron distrib., sticking times 80-540
^{208}Pb(^{136}Xe,X)Y, 470 MeV, search for delayed fission products from superheavy nuclei 78-70562
^{208}Pb(^{13}C,^{13}C'), 108 MeV, nuclear continuum investigation 80-13506
^{208}Pb(^{14}N,^{14}N'), 266 MeV, giant resonance excitation 80-78253
^{208}Pb(^{16}O,^{16}O), elastic scatt., exponential optical pots. 80-42681
^{208}Pb(^{16}O,^{12}C), 93 MeV, α-transfer reactions 79-67762
^{208}Pb(^{16}O,^{12}C)^{212}Po, semiclassical anal. of α-transfer, calc. of angular distrib. 79-6672
^{208}Pb(^{16}O,^{12}C)^{212}Po and α-decay, comparison for α-transfer reaction mechanism 79-6652
^{208}Pb(^{16}O,^{12}C)^{212}Po, 93 MeV, semiclassical analysis of α-transfer reactions, partial wave amplitudes 79-45283
^{208}Pb(^{16}O,^{15}N), 104-312 MeV, fragment emission at high energies, Q value effects 79-6653
^{208}Pb(^{16}O,^{15}N), 312.6 MeV, DWBA anal. of cross-section energy depend. 77-30630
^{208}Pb(^{16}O,^{15}N) 104, 138.5, 216.6 MeV, DWBA and optical model anal., energy dependence 78-82378
^{208}Pb(^{16}O,^{15}N) 312.6 MeV, optical model and DWBA anal., energy depend., lower energy comparison 78-82379
^{208}Pb(^{16}O,^{15}N)^{209}Bi, heavy ion research with cyclotrons 79-54447
^{208}Pb(^{16}O,^{15}O), 312.6 MeV, optical model and DWBA anal., energy depend., lower energy comparison 78-82379
^{208}Pb(^{16}O,^{16}O'), 315 MeV, giant multipole resonance excitation 79-30812
^{208}Pb(^{16}O,^{16}O'), 315 MeV, continuous spectrum and giant resonance excitation, coherent state model test 80-32252
^{208}Pb(^{16}O,^{16}O), 312.6 MeV, DWBA anal. of cross-section energy depend. 77-30630
^{208}Pb(^{16}O,^{16}O), elastic ang. distrib., nuclear contributions, Born approx. validity 79-36252
^{208}Pb(^{16}O,^{16}O) 104, 138.5, 216.6 MeV, DWBA and optical model anal., energy dependence 78-82378
^{208}Pb(^{16}O,^{16}O) 312.6 MeV, optical model and DWBA anal., energy depend., lower energy comparison 78-82379
^{208}Pb(^{16}O,^{17}O) 104, 138.5, 216.6 MeV, DWBA and optical model anal., energy dependence 78-82378
^{208}Pb(^{18}O,^{16}O)^{206}Pb, 69-73 MeV, 2 neutron transfer mechanism 78-89900
^{208}Pb(^{16}O,Cα), ang. correlations between react. products 78-8849
^{208}Pb(^{16}O,X), 80-313 MeV, optical model anal., dynamic shape or density changes 80-18186
^{208}Pb(^{18}O,^{18}O*)^{208}Pb, quadrupole moment of first excited state of ^{18}O determ. 77-22886
^{208}Pb(^{208}Pb, HI), 7-7.5 MeV/N, product energy and element distrib., fission probab., energy losses 80-86916
^{208}Pb(^{208}Pb, X), giant resonance polarisation pots. from nucleus-nucleus effective pot. 80-78248
^{208}Pb(^{208}Pb,X), exactly central heavy-ion collisions by nuclear hydrodynamics 80-68690
^{208}Pb(^{20}Ne,X), 400 MeV/N, inclusive p, d, t, ^{3}He cross sections from sequential scatt. model 80-57792
^{208}Pb(^{3}He,^{3}He'), 108.5 MeV, giant monopole resonance, DWBA anal. 79-71828
^{208}Pb(^{3}He,^{3}He), 130 MeV, elastic scatt. ang. distribs., optical model anal. 78-94020
^{208}Pb(^{3}He,^{3}Ne), 130 MeV, giant reson. excitation, DWBA anal. 79-89319
^{208}Pb(^{3}He,α), inner hole states excitation, DWBA anal., reaction mechanism *(French)* 78-41735
^{208}Pb(^{3}He,α)^{207}Pb, 70 MeV, deephole states, $T_>$=45/2 components 78-82362
^{208}Pb(^{3}He,d), 30 MeV, effective residual interaction matrix elements, spectroscopic factors, cross sections 80-99134
^{208}Pb(^{3}He,π^0), 200 MeV, inclusive neutral pion prod. cross section 77-6410
^{208}Pb(^{3}He,t)^{208}Bi, 80 MeV, Gamow-Teller M1 state excitation 78-50184
^{208}Pb(^{40,48}Ca, ^{40,48}Ca), dist. of closest approach for classical Rutherford scatt. 78-78404
^{208}Pb(^{40,48}Ca, ^{40,48}Ca), optical model anal., strong absorption radius *(Russian)* 80-68697
^{208}Pb(^{40}Ar, ^{40}Ar), 302 MeV 78-78404
^{208}Pb(^{40}Ar, ^{40}Ar), optical model anal., strong absorption radius *(Russian)* 80-68697
^{208}Pb(^{40}Ar, πX), 1.8 GeV/nucleon, appl. of multiple-collision model for pion prod. 78-37365
^{208}Pb(^{40}Ar,X), deeply inelastic collisions, form factors, microscopic calcs. 80-18339
^{208}Pb(^{48}Ca, X), fusion reactions from Cf and Fm integral yields, statistical model anal. *(Russian)* 79-97740
^{208}Pb(^{48}Ti, ^{48}Ti), 252 MeV 78-78404
^{208}Pb(^{48}Ti, ^{48}Ti), optical model anal., strong absorption radius *(Russian)* 80-68697
^{208}Pb(^{49}Ca,Xn), excitation functions for compound-nucleus and transfer reactions of magic nuclei 79-22310
^{208}Pb(^{6}Li,^{6}Li')^{208}Pb, 156 MeV, giant quadrupole reson. excitation 77-67767
^{208}Pb(^{6}Li,^{6}Li), elastic and inelastic, 74 MeV, folding optical model parameters 80-102201
^{208}Pb(^{6}Li,X), 156 MeV, projectile break up in continuous particle spectra, cross section, fragmentation 80-86889
^{208}Pb(^{6}Li,X), 60-156 MeV, break-up fragment transfer, cross sections, recoil ranges 80-13491
^{208}Pb(^{6}Li,d), 90 MeV, alpha-cluster transfer from alpha-decaying nuclei 80-91166
^{208}Pb(^{6}Li,xn), 75, 85, and 95 MeV, K X-ray multiplicity 79-76019
^{208}Pb(^{86}Kr,X), 610 MeV, deep inelastic ang. momentum transfer from sequential fission fragments 80-18325
^{208}Pb(N, γ_0), γ-ray ang. distribs., giant E3 resonances, direct-semidirect model 79-67727
^{208}Pb(N,N), <30 MeV, microscopic optical pot. in nuclear struct. approach, HF field 80-527
^{208}Pb(N,N), microscopic description validity 79-544
^{208}Pb(N,γ_0), 2-10 MeV, giant M1 resonance in direct-semidirect model 79-17898

nuclei with mass number 190 to 219 continued
^{208}Pb(N,γ), 6 to 40 MeV, dipole/quadrupole interference, direct-semidirect model, γ ang. distrib. 78-93994
^{208}Pb(α, α'), neutron collectivities, E2 giant resonance excitation 77-26558
^{208}Pb(α,4n), 41-51 MeV, yrast states in ^{208}Po anal. 78-78307
^{208}Pb(α,α'), 120 MeV, new giant resonance at 80 A$^{-1/3}$ MeV 77-41939
^{208}Pb(α,α'), 65 MeV, inclusive reaction, giant resonance background, heavy ion model anal. 80-5150
^{208}Pb(α,α'), 96 MeV, ang. distribs., breathing mode states, DWBA calcs. 78-50183
^{208}Pb(α,α'), levels, B(E3), transition density and nuclear pot., folding model anal. 80-86812
^{208}Pb(α,α'), RPA calcs., existence of breathing mode 78-25163
^{208}Pb(α,α), 104 MeV, optical model analysis 78-41737
^{208}Pb(α,α), 172 MeV, giant resonance structures 80-91163
^{208}Pb(α,α), 172 MeV, strongly excited giant monopole resonance 80-18273
^{208}Pb(α,α), 20 to 26 MeV, total reaction cross section meas. 78-25209
^{208}Pb(α,α), elastic ang. distrib., nuclear contributions, Born approx. validity 79-36252
^{208}Pb(α,αp) 96.8 MeV, proton pickup by α-particles to unbound states DWBA anal. 79-22305
^{208}Pb(α,d)^{210}Bi, 33 and 48 MeV, two-step contrib. in two-nucleon transfer reactions 78-82364
^{208}Pb(d, d'), 108 MeV, giant monopole resonance excitation and ang. distribs. 80-102164
^{208}Pb(d,^{6}Li) ^{204}Mg, SS MeV, levels and spectroscopic factors, α clustering, DWBA anal. 79-67694
^{208}Pb(d,X), 70 MeV, charged light particle spectra and ang. distribs. exciton model anal. 79-40935
^{208}Pb(d,3n)^{207}Bi, spin and parity assignment of ^{207}Bi levels 78-89788
^{208}Pb(d,d'), 24 MeV, mag. dipole states, spin, parity, transition strengths 77-14129
^{208}Pb(d,d'), RPA calcs., existence of breathing mode 78-25163
^{208}Pb(d,n), secondary neutron emission characts. 79-30843
^{208}Pb(d,nγ), half life of ^{209}Bi 2442.8 keV lowest 2p 1h state 78-74331
^{208}Pb(d,p), below and near Coulomb barrier 78-29483
^{208}Pb(d,p), polarised d, tensor anal. powers, sub-Coulomb stripping calc. corrections 79-80918
^{208}Pb(d,p), tensor analyzing power, deuteron wave functions 80-99137
^{208}Pb(d,p)^{209}Pb, 12.3 MeV, tensor analysing powers 78-29479
^{208}Pb(d,pn), E_d=13.6 MeV, disintegration reactions, isotopic effects 78-13108
^{208}Pb(d,pn) 13.6 MeV disintegration, neutron elastic scatt. effect *(Russian)* 77-34322
^{208}Pb(d,pn) 13.6 MeV disintegration, neutron elastic scatt. effect *(Russian)* 77-34323
^{208}Pb(d,t), 10 MeV, polarised d, tensor anal. power and D-state effects 79-85446
^{208}Pb(e,e'), E2 transitions of fragmented isoscalar quadrupole giant resonance 80-22758
^{208}Pb(e,e'), 50 and 63.5 MeV, mag. quadrupole strength fragmentation 78-41705
^{208}Pb(e,e'), 50 to 335 MeV, 12 mag. spin state excitations 78-50155
^{208}Pb(e,e'), 50-335 MeV, J^π=12$^-$, 14$^-$ high spin states, DWBA anal. 79-93490
^{208}Pb(e,e'), 60 MeV, backward scatt., 2$\hbar\omega$ M1 excitation search 80-32234
^{208}Pb(e,e'), 70-335 MeV, natural parity high spin state excitation 80-63060
^{208}Pb(e,e'), Ex<100 MeV, giant multipole reson. electroexcitation 77-34279
^{208}Pb(e,e'), giant multipole resonance excitation, particle-hole interaction 80-22789
^{208}Pb(e,e'), isospin fine struct., 8-12 MeV, multipole assignment of 8.9 MeV reson. 78-13071
^{208}Pb(e,e'), M2 giant resonance excitation, spin-magnetism mass depend. quenching, M1 strength reduction 78-86521
^{208}Pb(e,e'), mag. dipole and quadrupole state excitation 78-50154
^{208}Pb(e,e'), RPA calcs., existence of breathing mode 78-25163
^{208}Pb(e,e'), form factors of states with spin up to J=10 obs. 77-310
^{208}Pb(e,e), 250 MeV, nucleon density distribution in nucleus 79-75831
^{208}Pb(e,e), 502 MeV, charge density distrib. variations 79-75830
^{208}Pb(e,e), (in)elastic scatt., self-consistent calcs. of nuclear density *(Russian)* 79-80928
^{208}Pb(γ,γ), 6.92, 7.12 MeV, reson. fluoresc. meas. 78-8797
^{208}Pb(γ,γ), mean polarisation meas. of 4843 keV 78-29446
^{208}Pb(γ,γ), parity of bound J=1 levels 79-22188
^{208}Pb(γ,n_{pol}), evidence for M1 collective strength at 8-10 MeV 77-38255
^{208}Pb(γ,n), 7.4-8.4 MeV, cross section, E1 and M1 transitions, collective and giant M1 resonance 79-89267
^{208}Pb(γ,n), 8 to 13 MeV, total cross section, resonance struct. 78-4928
^{208}Pb(γ,n), 9.5-12 MeV, photoneutron ang. distribs., struct. below giant resonance 80-13444
^{208}Pb(γ,n), polarimeter for threshold photoneutron spectroscopy 77-30739
^{208}Pb(γ,n), s-d wave admixture in ^{207}Pb+n system 77-30555
^{208}Pb(γ,n) giant mag. dipole resonance location, photoneutron polarisation method 80-37357
^{208}Pb(γ,p), up to 0.25 GeV, from bremsstrahlung γ-quanta *(Russian)* 80-5123
^{208}Pb(γ,p), up to 4.5 GeV, ang. depend. of normalised invariant cross section parameters *(Russian)* 78-17180
^{208}Pb(μ^-,ν), RPA calc. of partial and total capture rates 78-74409
^{208}Pb(n,γ), 4.9-8.0 MeV, γ-ray prod. cross-section meas. 77-38264
^{208}Pb(n,γ), fast, direct-semidirect and pure resonance model calcs. 80-47486
^{208}Pb(n,γ), pure resonance model for fast nucleon capture 79-80936
^{208}Pb(n,γ)^{209}Pb, 11 MeV, gamma-ray spectra, role of two-particle one-hole states 77-26764
^{208}Pb(n,γ)^{209}Pb, dipole centre and giant quadrupole capture, cross sections calc. 77-10398
^{208}Pb(n,$\gamma\gamma$), thermal, calc. of cross-sections and branching ratios 77-14131
^{208}Pb(n,n'γ), 5.2-8.5 MeV, E1 excitations, collective states and spin assignments, statistical model anal. 79-54405
^{208}Pb(n,n), ^{209}Pb reson. parameters calc., shell model 77-82920
^{208}Pb(n,n), 16-18 MeV differential cross section resonant characters 79-75952

nuclei with mass number 190 to 219 continued

^{208}Pb(n,n), 7-26 MeV, differential cross sections, global optical model anal. 80 - 18298
^{208}Pb(n,n), (n,n'), 7-26 MeV, optical model anal. 78-37340
^{208}Pb(p, γ), γ ang. distrib., isovector giant quadrupole resonance, direct-semidirect model 79-63647
^{208}Pb(p,P'), pol. p, 9, 10 MeV, vol. integrals for optical pots., real symmetry pot. 80-42659
^{208}Pb(p,d), 121 MeV, DWBA applicability test, d D-state contribs. 79-13261
^{208}Pb(p,d), two stage processes in direct reactions *(Dutch)* 78-29439
^{208}Pb(p,γ), γ-ray ang. distribs. asymmetry effects through IAR, direct-semidirect model 80-42581
^{208}Pb(p,γ) fast capture, direct-semidirect model excitation function calcs. 78-94004
^{208}Pb(p,$\bar{n}$), nucleon optical potential from Lane model 80-83097
^{208}Pb(p,nx), 45 MeV, preequilib. ang. distrib., generalised exciton model 77 - 10407
^{208}Pb(p,p'), 135 MeV, normal parity level excitation, J^{π}, differential cross sections 80-57690
^{208}Pb(p,p'), 135 MeV, normal parity excitations, microscopic description, NN interaction shape 80-57691
^{208}Pb(p,p'), 24 MeV, mag. dipole states, spin, parity, transition strengths 77-14129
^{208}Pb(p,p'), 39, 62 MeV, DWBA anal., collective spectra, direct process contrib. *(Russian)* 80-13408
^{208}Pb(p,p'), 40, 45 MeV, fine struct. in giant resonance region, collective dipole spin flip excitation 78-46056
^{208}Pb(p,p'), 5 to 8 MeV, hyperfine reson. struct., Feynman diagrams 79-6589
^{208}Pb(p,p'), 61.2 MeV, low lying normal parity excitations 77-74843
^{208}Pb(p,p'), 800 MeV, high energy octupole giant resonance, ang. distribs. 80-86879
^{208}Pb(p,p'), giant resonances from antisymmetrised DWBA anal. 79-85432
^{208}Pb(p,p'), precritical behaviour in pionlike excited states in nuclear matter 79-49593
^{208}Pb(p,p'), sum rule anal. of inclusive cross section 78-33183
^{208}Pb(p,p')^{208}Pb, medium energy, DWBA calc. 77-6380
^{208}Pb(p,p), 0.8 GeV, analysing powers 78-54760
^{208}Pb(p,p), 0.8 GeV, ang. distrib. meas. 78-25186
^{208}Pb(p,p), 0.8 GeV, cross sections, optical anal. np RMS radius difference, Δr_{np} 80-63187
^{208}Pb(p,p), 0.8 GeV, elastic and inelastic, ang. distribs., states, optical and DWBA anal. 79-3154
^{208}Pb(p,p), 0.8 GeV, polarised p, differential cross section, anal. power, nuclear matter densities 79-13299
^{208}Pb(p,p), 1 GeV, cross sections using nuclear densities from self-consistent methods *(Russian)* 78-41724
^{208}Pb(p,p), 1 GeV, Fresnel and two-body correl. effects 78-82353
^{208}Pb(p,p), 100-2200 MeV, total and reaction cross sections from optical pot. 80-18303
^{208}Pb(p,p), 20-50 MeV differential cross section, polarisation ang. distrib., optical model exchange terms 80-27638
^{208}Pb(p,p), 30 MeV, optical pot. imaginary part calcs. 80-86868
^{208}Pb(p,p), 30 MeV, pick-up and inelasti scatt. contribution to p optical pot. 78-25182
^{208}Pb(p,p), 800 MeV, polarised p, n density uncertainties from optical model anal. 79-22185
^{208}Pb(p,p), (in)elastic scatt., self-consistent calcs. of nuclear density *(Russian)* 79-80928
^{208}Pb(p,p), elastic and inelastic scatt., 185 MeV, polarisation, diffraction model anal. 79-75943
^{208}Pb(p,p), nucleon distrib. in nuclei, self-consistent anal. 79-9556
^{208}Pb(p,p), polarised p, 0.8 GeV, neutron isotopic density differences and RMS radii 79-67643
^{208}Pb(p,p) 100 MeV, systematic optical model anal. 78-66274
^{208}Pb(p,p)^{208}Pb, 1 GeV, neutron and nuclear matter space distribs. *(Russian)* 78-502
^{208}Pb(p,π^+), 180 MeV, ang. distribs., discrete states, differential cross section 79-13298
^{208}Pb(p,π^+), differential cross sections, DWBA calc. 79-85415
^{208}Pb(p,π^+)^{209}Pb, 160 MeV, ang. distributions 78-37345
^{208}Pb(p,$\pi^{\pm}$), semiclassical models, multiple scatt., nucleon recoil effects 77-2996
^{208}Pb(p,π), microscopic model anal., stripping model test for (d,p) 79-85436
^{208}Pb(p,t), finite range DWBA anal. with realistic triton wave function 80-78300
^{208}Pb(p,t), simple unitary estimate for multistep processes, cross section bounds 79-40922
^{208}Pb(p,t)^{206}Pb, successive and simultaneous transfer processes, on-shell, DWBA methods 78-8812
^{208}Pb(p,t)^{206}Pb, unnatural parity transitions, finite range DWBA anal. 77-67750
^{208}Pb(p,t)^{206}Pb(3^+), pol. p, 22 MeV, anal. power and (p,d)(d,t) sequential transfer processes 80-5119
^{208}Pb(p,x), x=α, τ, 72 MeV, spectra and angular distribs. 80-68660
^{208}Pb(π,π'p), 255 MeV, quasielastic knockout, proton yield, $\sigma(\pi^+)/\sigma(\pi^-)$ cross section ratio 80-32305
^{208}Pb(π,π), 162 MeV, elastic and inelastic ang. distribs., optical and PWIA anals. 80-42706
^{208}Pb(π,π), 162 MeV elastic scatt., ang. distribs., diffraction patterns, optical model calcs. 78-58309
^{208}Pb(π,π), ang. distribs., optical model calcs. 78-58308
^{208}Pb(π,π), many body effects in resonant scatt. 78-94029
^{208}Pb(π,π), total cross section, density distribs. and ray bending effects 80-47509
^{208}Pb(π,π)^{208}Pb, 50 MeV, optical potential with kinematic, absorption and correl. corrections 77-50157
^{208}Pb(π^-,^{4}n), 120 MeV, tetraneutron possible existence, cross section and lifetime bounds 79-40958
^{208}Pb(π^-,γ), RPA calc. of partial and total capture rates 78-74409
^{208}Pb(π^+,π^+), 40 MeV, differential cross sections and strength parameters, optical model fit 80-18347
^{208}Pb($\pi^{\pm}$,$\pi^{\pm}$N), 180-255 MeV, quasielastic pion scatt. coincidence expt. interpretation, impulse approx. 80-68704
^{208}Pb($\pi^{\pm}$,$\pi^{\pm}$), 80, 116 MeV, elastic and inelastic, optical and collective model anal. 79-22329
^{208}Pb($\pi^{\pm}$,$\pi^{\pm}$), elastic and inelastic scatt., energy and A-depend. 78-54802

nuclei with mass number 190 to 219 continued

^{208}Pb(t,p), centre of mass corrections to DWBA overlap factors 80 - 18319
^{209}Pb excited states, $3/2^-$ resonances from shell model of ^{208}Pb(n,n) 80 78240
^{209}Pb excited states and $3/2^-$ resonances, shell model, calcs. from ^{208}Pb(n,n) 80-18262
^{209}Pb levels obs. in ^{210m}Bi(t,α) 77-34320
^{209}Pb reduced normalisation from ^{208}Pb(d,p) 78-86522
^{209}Pb reson. parameters calc. in ^{208}Pb(n,n), shell model 77-82920
^{209}Pb unbound high spin shell model states, single nucleon states 78-25126
^{209}Pb(γ,π^+)^{209}Pb, photoprod. to single particle states 77-22998
^{210}Pb, atmospheric fluxes determ. from soil profiles 79-2346
^{210}Pb, balance in Long Island Sound 79-20861
^{210}Pb determination in sediment core from ocean floor off Californian coast 80-72101
^{210}Pb, energy level spectra, random-phase method calcs. 79-9469
^{210}Pb, from ^{222}Rn released by uranium tailings piles, potential population dose 79-85824
^{210}Pb from nucl. explosions in environment 78-21774
^{210}Pb ground state decay 80-47429
^{210}Pb levels, J^{π}, transitions and lifetimes from ^{208}Pb(^{7}Li,X) 80-68542
^{210}Pb meas. for uranium prospecting 79-53573
^{210}Pb, radionuclide determ. in coastal marine sediments and seawater 79-88370
^{210}Pb(t,d), Pauli principle effects in ^{211}Pb levels 78-17108
^{211}Pb, nuclear field theory, testing and appl. 79-13214
^{211}Pb, Pauli principle effects on level spectrum, ^{210}Pb(t,d) spectroscopic factors 78-17108
^{212}Pb inhaled body burden calibration, general phantom procedure 77-64138
^{212}Pb ion clearance from rabbit bronchial epithelium to blood 77-86641
^{212}Pb, selective separation from ^{228}Th source 77-40566
^{214}Pb, conc. in basement lab., working levels 77-40797
^{214}Pb, meas. of low conc. in air 78-28308
Pb(α,X), 3.6 GeV proton emission invariant cross sections *(Russian)* 80-13500
Pb(α,X), 3.6 GeV/N, secondary particle ang. and vel. distribs., π,p,d,t prod. *(Russian)* 80-63194
Pb(α, 2α), 700 MeV, cross section, effective cluster number from PWIA, momentum distrib. 79-40940
Pb(α,α), 104 MeV, A=204,206,208, neutron density RMS radii 78-17088
Pb(α,α), 104 MeV, nucl. matter sizes and isoscalar octupole transition rate 77-6422
Pb(α,α'), A=204,206,208, 13.8 MeV, quadrupole moment and B(E3) values 79-17797
Pb(α, $\chi\pi$), 18 GeV, π multiplicity distrib. 79-97713
Pb(α,d)Bi, 48 MeV, spectra and ang. distrib. obs., Bi two-particle states anal. 77-38289
Pb(α,f), 0.65, 1.74, 4.12 GeV, and using polycarbonate detector 78-13178
Pb(α,f), 0.65, 1.74, 4.12 GeV, fission fragment recoil characts. 78-89925
Pb(α, p), 3.6 GeV, max. in p ang. distrib. *(Russian)* 79-36253
Pb(d,α)Tl, A=208,206,204 at 80 MeV, high-spin states, α-spectra 78-504
Pb(e,e'f), 28-44 MeV, anomalous reson. struct. obs. 77-82972
Pb(γ,f), 140 to 1000 MeV, energy depend. of nuclear fissility 77-82971
Pb(γ,γ) 1.17 and 1.33 MeV, cross-sections 79-75973
Pb(γ,γ), 6.84-11.39 MeV, Rayleigh and Delbruck scatt. destructive interference, cross sections 79-6566
Pb(γ,γ), differential cross sections, 244 to 1408 keV 79-49618
Pb(γ, n), 30 to 140 MeV, partial photoneutron cross section, total cross section approx. 80-22809
Pb(γ,n) cross section discrepancies, NBS P-2 chamber calibration 77-26671
Pb(γ,$\pi^{\pm}$), quasifree photoprod. cross sections 79-75972
Pb(μ^-,X), energetic charged particle spectrum, integrated yield 80-18293
Pb(n,X), 14.8 MeV, γ-prod. cross section 79-49622
Pb(n,n) 0.6-2.2 MeV small angle scatt., differential cross sections ang. depend. 79-85472
Pb(n,n), 10 MeV, neutron polarisation meas. at small angles 77-3014
Pb(n,n), 10.4 MeV, polarised neutrons, analysing power 77-30545
Pb(n,n), 13.7-15 MeV, differential cross section energy depend., meas. and optical model 80-18304
Pb(n,n), 14.0-17.4 MeV, neutron polarisation, ang. depend. diffraction struct. 80-18283
Pb(n,n), 14.2 MeV, polarisation in forward angle scatt. 80-18282
Pb(n,n), 16.1 MeV, polarisation meas., optical model anal. 79-22264
Pb(n,n), 2.9 MeV, elastic differential cross section and polarisation ang. depend., statistical anal. 79-45264
Pb(n,n), 7-14 MeV, absolute cross sections for small-angle elastic scatt. 77-26769
Pb(n,n), A=206,207,208, 0.6 to 1.0 MeV, optical model params. 78-21557
Pb(n,n), elastic and inelastic scatt., cross sections meas. and calcs. 78-13081
Pb(n,n), fast neutrons, differential cross sections, optical model calcs. *(Chinese)* 79-9572
Pb(n,n), pol. n, 16.1 MeV, differential cross section, optical model fit 80-32259
Pb(p,X), 400 GeV/c, nucleon number depend. of inclusive dihadron prod. 79-49626
Pb(p,X), 70 GeV/c, $\pi^{\pm}$, $K^{\pm}$, p, $\bar{p}$ prod. with p_T=0.5-2.5 GeV/c cross sections, yield ratios *(Russian)* 80-52681
Pb(p,d), 9 GeV, nuclear emulsion expt. 80-78292
Pb(p,n), 800 MeV, n prod. systematics π associated cross section 79-3153
Pb(p,n), A=207,8, proton decay of isobaric analogues of ground states 77-26692
Pb(p,t), A=204,6,8, E=35 MeV, spectra and ang. distribs. meas. DWBA anal., sum rules 78-13101
Pb(p,xpX), x=1, 2, 640 MeV, energetic backward p emission, inclusive differential cross section 80-9290
Pb(π^-,X), 3 GeV/c, n inclusive spectra, neutron yield *(Russian)* 80-13510
Pb(π^-,p) 1.5-5 GeV/c, cumulative proton polarisation *(Russian)* 80-86896

nuclei with mass number 190 to 219 continued
Pb($\pi^{\pm}$,$\pi^{\pm}$), 65-215 MeV forward scatt. amplitudes 79−85533
Pb(t,α), polarised t_2 proton hole states in ^{203,205,207}Tl obs. 77−41978
Pb(x,x), x=$\pi^{\pm}$, $K^{\pm}$, p,$\bar{p}$, 70, 125, 175 GeV/c 80−83128
Pd(α,d)Bi, 48 MeV, mass excess of Bi calc. 77−10312
Po, A=202-210, isomeric levels, g, $T_{1/2}$ 77−14068
Po fission products mass, charge, kinetic energy distribs., scission point model based on deformed shell effects 77−10455
Po high spin isomers, deformed independent particle model, yrast lines, shape 79−480
Po in mica, anomalous haloes origin 79−44186
Po isotopes, alpha-decay theory 77−61389
Po light isotopes, α-decay width calcs., Feshbach theory 78−89829
Po, neutron deficient isotope prod. in ^{182}W(^{20}Ne,xn) reactions 78−8835
^Po, A=209, 211 deduced levels, J^{π} assignments, spectroscopic factors from stripping and pickup reactions 79−22197
^{199}Po charge states and charge distrib. from ^{164}Dy(^{40}Ar,5n) *(Russian)* 79−40840
^{204}Po, compound nucleus decay, excitation function meas. of ^{164}Dy(^{40}Ar,xn) and ^{184}W(^{20}Ne,xn) 79−13330
^{204}Po, EC, ^{204}Bi excited states, γ rays, conversion electrons and $\gamma\gamma$ coincidences 80−18241
^{204}Po, γ-rays, conversion electron spectra, $\gamma\gamma$ coincidences 80−83061
^{206}Po, excited levels, populated by ^{206}At EC-β^+ decay 77−79340
^{207}Po half life, charact. γ meas. 78−58253
^{207}Po^m(2.79 s), ^{207}Po^g decay, spin from conversion electrons meas. 78−58252
^{208}Po, half-lives of two-neutron-hole 0_2^+ state 77−10323
^{208}Po, perturbed angular distribution in Pb, temp. depend. 78−43735
^{208}Po, yrast two proton-two neutron hole states 78−78307
^{209}Po, 125-neutron isotone, shell model alpha decay theory 77−18483
^{209}Po, 31/2$^-$ isomeric state, g-factor meas. 77−10317
^{210}Po activity in Indian tobacco, meas. and lung dose calc. 77−9224
^{210}Po, alpha-decay, population of 0^+ of ^{206}Pb 80−22775
^{210}Po, α-decay inner shell ionis., L-electron-alpha ang. correlation 77−34267
^{210}Po, α-spectrometric dating method, appl. to sediments 78−28350
^{210}Po contamination of surfaces, removal coeff. determ. 79−26769
^{210}Po effect of renormalisation of effective interaction on ground state wave functions *(Russian)* 77−284
^{210}Po, excited, deformed, fission or neutron emission, shell-correction approach to nuclear densities 77−30483
^{210}Po heavy product range and ang. distrib. from ^{209}Bi(HI,X) 80−83119
^{210}Po, inner shell electron ejection in α-decay 77−79342
^{210}Po intake through damaged skin and efficiency of methods preventing absorpt. 77−25561
^{210}Po, level density calc., shell and pairing effects, deformation, excitation energy dependence 79−67662
^{210}Po, nucl. alpha decay, electron inner shell vacancy creation, semi quantal approach 80−68607
^{210}Po, perturbed γ-ray angular distrib. temp. depend., radiation damage effects 78−43736
^{210}Po, quasielastic transfer reaction excitation function for ^{209}Bi+heavy ion 79−3176
^{211}Po excitation functions and isomer ratios from ^{208}Pb(α,n) and ^{209}Bi(α,np) 80−83039
^{212}Po excitation functions and isomer ratios from ^{209}Bi(α,p) 80−83039
^{212}Po, fission excitation functions anal., shell effects at saddle point, nuclear shape 78−54737
^{212}Po, isomer with spin and parity 8^+, α- and γ-decay 78−82283
^{212}Po, levels, J^{π}, transitions and lifetimes from ^{208}Pb+^{7}Li 80−68542
^{212}Po levels and J^{π}, weak coupling calc. using realistic matrix elements 80−5068
^{212}Po, shell model α-spectroscopic factors 80−32245
^{212}Po, surface α-clustering and α-decays 79−75926
^{214}Po, half life of α-emitting excited 0^+ state 79−45205
^{215}Po, excited states, half-life meas. *(French)* 79−97679
^{216}Po, selective separation from ^{228}Th source 77−40566
^{216}Po→^{212}Pb, obs. of collective states fed by weak α-transitions 78−8786
^{218}Po, conc. in basement lab., working levels 77−40797
^{218}Po, meas. of low conc. in air 78−28308
^{191,193}Pt high-spin levels via ^{190,192}Os(α,3nα), triaxial rotor model 77−34213
Pt, A=187, 189, 191, low-temp. orientation studies, mag. moment and E2/M1 ratios in daughters 77−22889
Pt, A=192, 194, 2^+, 3^+ states via (α,α') Coulomb excit. 78−622
Pt, A=194, 195, 196, 198, shape of stable transition nuclei, photoabsorpt. cross-sections *(Russian)* 77−79307
Pt decay, oriented nuclei, ^{189,191}Ir levels, J^{π}, transitions and mixing ratios 80−68602
Pt even isotopes, nonaxial deforms., odd parity states, semidecoupled model 77−34220
Pt, even mass, ground and gamma band EM transition rates, asymmetric rotor model 80−32231
Pt even-even isotopes, excitation energies and EM props. from interacting boson model 80−106005
Pt isotopes, use of (p,t) reaction to study low lying states 77−54212
Pt, O(6)→rotor transition, interacting boson approx. model, levels and transitions 79−13224
Pt, photofission induced by 220-500 MeV coherent beam 77−3056
Pt, positive-parity states, Coriolis antipairing effect, deformed-rotor model 78−12950
Pt, prolate-oblate transition 78−62540
Pt transient isotopes, high spin state anomalies, spherical states concept *(Russian)* 77−34217
Pt-Os transition region, interacting boson approx. model 79−6435
Pt+^{136}Xe, A=192, 194, 196, Coulomb excitation, γ softness from E2 transition strengths 77−82951
Pt+K^- interactions, 12 GeV/c, Λ^0 prod., search for di-hyperon resonance 77−82970
Pt+p, 4-18 GeV, Υ'' prod., search for new narrow resons. 79−30833
Pt+p, dimuon prod., struct. in Υ region near 9.5 GeV 78−17201
Pt+p→$\mu^+\mu^-$+anything, massive lepton pair prod., Υ family 78−78368
Pt(^{3}He,4n), Hg isotopes, level energies, B(E2) values, rot. aligned bands 78−70483
Pt(^{3}He,d), A=194, 196, 198, 41.2 MeV, stripping strength, Au excitation energies, high spin states 78−78398
^Pt, A=186,188,190, subnanosecond high spin isomers, decay chains and lifetimes from Yb(^{16,18}O, xn) 79−45140
^Pt, A=188-198 collective levels, transitions, mag. and quadrupole moments, boson expansion theory 80−105954

nuclei with mass number 190 to 219 continued
^Pt, A=190, 192, 194, levels and γ-transition reduced probab., interacting boson model 80−18196
^Pt, A=190,192,194, state struct. in interacting boson model 80−83047
^Pt, A=190-193, lifetimes of rotation-aligned states 78−93969
^Pt, A=191 to 197, odd, levels excited via (p,d) and (d,t) 78−50089
^Pt, A=192, 194, 196, rigid asymmetric rotor model descript., E2 and E4 props. 80−13403
^Pt, A=192, 194, 196, states, J^{π}, ang. distribs. and transitions, DWBA anal. of Pt(p,t) 80−468
^Pt, A=192, 194, β_4 deformations, anomalous interference terms, rigid asymmetric rotor model 79−75832
^Pt, A=194-8 photoneutron yield curves, nuclear shape and giant dipole resonances, 8-21 MeV *(Russian)* 79−13268
^Pt(^{3}He,n) A=194,196, 33.3 MeV, cross sections, DWBA anal. for data near Z=82 79−67733
^Pt(^{6}Li,xn), A=194, 198, 75, 85, and 95 MeV, K X-ray multiplicity 79−76019
^{190}Pt, collective excitations in the interacting boson model *(Russian)* 80−5044
^{190}Pt(p,t)^{185}Pt reaction, 25 MeV ^{188}Pt states population 78−86532
^{191}Pt, core-quasiparticle-coupling model for odd-A transitional nuclei 78−54701
^{191}Pt energy levels, γ and conversion electron spectra, spins, parities 78−25149
^{191}Pt, non-axial deform. anal., $i_{13/2}$ neutron coupling to triaxial rotor and to anharmonic vibrator 77−22847
^{192}Pt 3^+ and 4_1^+ states from ^{192}Ir β decay, lifetime meas. by β-γ coincidence 78−25153
^{192}Pt 4^+ and 3^+ levels populated in ^{192}Ir β decay, spectral shapes, quadrupole vibr. levels 77−50086
^{192}Pt, Coulomb excited, transition probabilities 78−62506
^{192}Pt, lifetimes of first four excited states 77−294
^{192}Pt, lifetimes of ground-band states, B(E2) values, (Ar,Ar'γ) reaction 77−54181
^{192}Pt(Ar,Ar'γ), 149 MeV, lifetimes of ^{192}Pt ground-band states 77−54181
^{192}Pt(α,α'), 24 MeV, α-angular distrib. for 0^+, 2^+, $2^{+\prime}$, 4^+, $4^{+\prime}$ and 3^- state excitation 78−70550
^{193}Pt low lying negative parity states and shape from ^{195}Pt(p,t) 80−68540
^{194}Pt, Coulomb excitation, low lying collective state reduced matrix elements, triaxiality 78−82269
^{194}Pt, determ. of sign of $P_3=M(0_1^+2_1^+)M(2_1^+2_2^+)M(2_2^+0_1^+)$ 79−63588
^{194}Pt, level energies, ^{194}Au γ-spectrum obs. 78−13003
^{194}Pt, lifetimes of ground-band states, B(E2) values, (Ar,Ar'γ) reaction 77−54181
^{194}Pt, populated in ^{194}Ir decay, level scheme determ. 77−2900
^{194}Pt, static quadrupole moments of arbitrary excited states, sum rule approach 80−91135
^{194}Pt+^{136}Xe, multiple Coulomb excitation, E2 transition probabilities of ^{194}Pt 78−4961
^{194}Pt(^{12}C,^{12}C), 78 MeV, elastic and inelastic differential cross section, triaxial rotor anal. 79−63689
^{194}Pt(Ar,Ar'γ), 149 MeV, lifetimes of ^{194}Pt ground-band states 77−54181
^{194}Pt(p,n), conversion electron and γ-ray spectra, isomeric states in ^{194}Au anal. 77−71582
^{195}Pt, Mossbauer lineshape, dispersion amplitudes 78−25146
^{195}Pt, NMR in metallic glass system $(Ni_xPt_{1-x})_{75}P_{25}$ 77−12211
^{195}Pt^m, internal conversion coeffs., meas. of s-electron densities at nucleus in Pt metal 78−27140
^{195}Pt(α,2n), 23-27 MeV, ^{197}Hg level schemes, γ and conversion electron spectra, spins, parities 78−25149
^{195}Pt(p,2n), conversion electron and γ-ray spectra, isomeric states in ^{194}Au anal. 77−71582
^{195}Pt(p,p'), single proton distrib. anal. 78−603
^{196}Pt (^{20}Ne, ^{20}Ne'), excited states, lifetime meas. using recoil-distance method 80−13413
^{196}Pt (^{58}Ni, ^{58}Ni'), excited states, lifetime meas. using recoil-distance method 80−13413
^{196}Pt, collective states and static quadrupole moment, boson expansion theory 80−47346
^{196}Pt level struct. and J^{π} assignments, interacting boson approx. O(6) limit from ^{195}Pt(n,γ) 79−75853
^{196}Pt negative parity states in partially decoupled bands, γ-transitions from ^{195}Pt(n,γ) 80−47360
^{196}Pt, O(6) symmetry of interacting boson approx. model in shape transition 80−27550
^{196}Pt rotation-vibration struct., O(6) interacting boson description alternative 79−59019
^{196}Pt struct., O(6) limit, levels fed in ^{195}Pt(n,γ) 78−33110
^{197}Pt states populated by (d,p), (d,t) and (n,γ) reactions 78−78267
^{200}Pt decay studies, prod. in fast neutron reactions 77−23011
^{193m}Pt decay, K-shell conversion coeff. of 135.5 keV, M4 transition 77−2944
Pt(α,α')Pt, 14.9 MeV, A=192, 194, 2^+ and 3^+ state Coulomb excit. 78−622
Pt(α,d), A=194, 196, 198, 35.1 MeV, stripping strength, Au excitation energies, high spin states 78−78398
Pt(α,xn), Hg isotopes, level energies, B(E2) values, rot. aligned bands 78−70483
Pt(γ,f), 140 to 1000 MeV, energy depend. of nuclear fissility 77−82971
Pt(γ,γ), 412, 468, 662 keV, elastic scatt. cross sections, Rayleigh scattering anal. 80−86898
Pt(p,d)^{193,195,197}Pt, l-assignments, spectroscopic factors 78−8810
Pt(π^-,X), stopped π^- capture, product nuclei distribs., isomeric yield ratio, neutron multiplicity 77−18625
Pt(t,p), 17 MeV, two neutron transfer strength, O(6) limiting symmetry in IBA, Os comparison 80−32287
Ra A (^{218}Po) adsorption to monodispersed aerosol 80−32535
^{214}Ra, high spin yrast states in N=126 isotones 79−45131
^{213m}Ra, 2.1 msec. isomer, gamma and alpha decay meas. 77−14067
Re, A=187, 189, 191, obs. of proton hole states via (t,α) 77−88025
Rn decay products, concs. in mine air 77−9280
Rn isotopes, A=205, 206, 207, in flight mass separation of fusion recoils 78−25381
^{199}Rn and ^{199}Rn^m alpha decay signatures from ^{169}Tm(^{35}Cl,5n) 80−68610
^{208}Rn decay, ^{208}At energy levels and transitions, IC electrons 80−18242
^{208}Rn→^{208}At, γ-ray, conversion electron spectra 80−83072

nuclei with mass number 190 to 219 continued
^{210}Rn decay, ^{210}At excited states, spins, parities and rate of population 79−75917
^{210}Rn high spin states, decay and lifetimes, spin assignments from ^{204}Pb(^{9}Be,3n) 80−18168
^{211}Rn, 125-neutron isotone, shell model alpha decay theory 77−18483
^{211}Rn heavy product range and ang. distrib. from ^{209}Bi(Hl,X) 80−83119
^{211}Rn, production by photospallation of ^{232}Th and ^{238}U 80−52797
^{211}Rn, quasielastic transfer reaction excitation function for ^{209}Bi+heavy ion 79−3176
^{212}Rn high spin isomers, excited core states coupled to valence protons 77−74745
^{212}Rn high spin isomers with core excited neutron configs. from ^{204}Hg(^{12}C, 5n) 78−54792
^{212}Rn, high spin yrast states in N=126 isotones 79−45131
^{212}Rn, Knight shift and absolute mag. moment meas. 78−37278
^{212}Rn, shell model states, semiempirical calcs. half lives, mag. moments, excitation functions 80−63083
Sm(d,3nγ)Eu, 18-25 MeV, band struct. in ^{149,151}Eu determ. 77−41913
^{199}Sn, Mossbauer effect thermometer, rel. to Cu nuclear susceptibility thermometer, 6 mk to 1K 79−35737
$^{\wedge}$Th, A=212, 213, 214, decay energies and half lives from ^{176}Hf(^{40}Ar,X) 80−47440
Tl, A=195, 197, rot. bands, high spin states 78−62476
Tl, A=201,203, levels via (d,3nγ), J^{π},$T_{1/2}$, $9/2^{-}$ band discovery 77−34207
Tl, A=203,5,7, proton hole states obs. with Pb(t,α) 77−41978
Tl, A=205,203, charge distrib. from elastic electron scatt. and muonic X-ray data anal. 78−54681
Tl, A=208,206,204, high-spin states, α-spectra via (d,α) 80 MeV 78−504
Tl isotopes, A=184-197, β^{+}-decay, single particle and collective degrees of freedom 77−22956
Tl, mass dependence for radiative capture of 14.1 MeV neutrons 78−13087
Tl, odd isotones, deformation pot. energy from Nilsson model 80−57676
Tl, odd isotopes, negative-parity level props. 78−17103
Tl, odd isotopes, pot. energy surfaces and quadrupole deformation parameters, deformed basis model 79−80867
Tl, odd mass isotopes, $h_{9/2}$ intruder state 77−88024
Tl odd-mass isotopes, $9/2^{-}$ level excitation energies, estimates 77−275
Tl, π^{-} absorption *(Russian)* 78−46115
Tl region, particle rotor model for doubly odd transitional nuclei 79−13223
Tl, strongly forbidden T1-transition, parity nonconservation *(Russian)* 77−10366
Tl yield during proton and deuteron irradiation of Hg 78−2174
$^{\wedge}$Tl, A=196, 198, staggering of even and odd spin states 78−70446
$^{\wedge}$Tl, A=199, 200 cross section and excitation function statistical anal. from ^{197}Au(α,xn) *(Rumanian)* 80−22846
$^{\wedge}$Tl, A=203, 205, excited state g-factor from Tl(^{40}Ca, ^{40}Ca′γ) 79−22191
$^{\wedge}$Tl(^{48}Ca, X), A=203, 205, fusion reactions from Cf and Fm integral yields, statistical model anal. *(Russian)* 79−97740
^{190}Tl→^{190}Hg→^{190}Au, decay spectra and periods 77−6317
^{192}Tl high spin band struct. and transitions, isomeric state from ^{181}Ta(^{16,18}O,xnγ) 80−47353
^{193}Tl level structure, studied via decay ^{193}Pb→^{193}Tl 77−6587
^{194}Tl high spin states, excitation functions, $I^{\pi}=8^{-}$ isomeric state from ^{181}Ta(^{18}O,5n) 80−32163
^{195}Tl (1.13 h) decay, ^{195}Hg level scheme and transitions, band population 79−17807
^{196}Tl high spin states, γ-decay and rot. structs. from ^{197}Au(α,5n), ^{194}Pt(^{6}Li,4n) 79−440
^{197}Tl decay, half life and decay scheme, ^{197}Hg level scheme and transitions 79−67719
^{197}Tl, deduced mass from Fr direct mass meas. 80−78130
^{197}Tl, diagonalisation of collective quadrupole Hamiltonian 77−6221
^{197}Tl, level scheme determ. from (^{3}He,3nγ) 77−22840
^{197}Tl, levels determ. from ^{197}Au(^{3}He, 3nγ) at 24-28 MeV 77−46177
^{198}Tl rotational structure, studied via ^{197}Au(α,3n) using in beam γ-ray spectroscopy 77−54130
^{199}Tl, production by ^{197}Au(α, 2n) reaction, medical appls. 80−51245
^{201}Tl core-coupled states, studied via (p,t) reaction 77−54212
^{201}Tl dosimetry, nuclide parameters and S factors 77−13011
^{201}Tl from Tl(p,xn)^{201}Pb→^{201}Tl, E_p=15 to 60 MeV, yields and excitation functions 79−5369
^{201}Tl γ- and X-ray emission probabilities and half-life obs. 80−32242
^{201}Tl, human distrib. and phys. imaging props. 77−37042
^{201}Tl levels, transitions and J^{π} assignments from ^{201}Pb decay 80−5099
^{201}Tl, myocardial imaging agents comparison 77−2037
^{201}Tl production by proton reactions on natural Tl 79−88184
^{201}Tl, production in neutron therapy cyclotron idle beam using Tl(d,xn) 79−20669
^{202}Tl quadrupole relax. in liq. Hg 77−16215
^{203}Tl, ^{205}Tl, core excitations to low-lying states, e.m. props., hyperfine splittings, isomer shifts 78−89794
^{203}Tl core-coupled states, studied via (p,t) reaction 77−54212
^{203}Tl, nuclear structure effect on internal conversion of l-forbidden transitions 79−63632
^{203}Tl(α,4n), 46-55 MeV, ^{203}Bi high spin states, halflives 78−29485
^{203}Tl(p,3n)^{201}Pb→^{201}Tl, E_p=15 to 60 MeV, yields and excitation functions 79−5369
^{204}Tl, beta ray generated bremsstrahlung yield consts. 80−42588
^{204}Tl, beta-ray dose rates in skin, conversion from values meas. in air 77−16996
^{204}Tl, beta-transition, spectral shape, small-order deviation 78−74338
^{204}Tl, β-decay, branching ratio and K-shell autoionisation 80−42598
^{204}Tl β-decay, K-shell autoionisation accompanying internal bremsstrahlung 80−57745
^{204}Tl β-decay surface contamination monitoring probes, comparison of response between detectors 78−25398
^{204}Tl first forbidden K-capture decay, internal bremsstrahlung spectra 79−45213
^{204}Tl neutron hole states, J^{π} and spectroscopic factors from ^{205}Tl(p,d) 80−86783
^{204}Tl^{+}, diffusion in KCl, transmutation effect 77−89589
^{205}Tl, electric dipole interaction energy from electric dipole hyperfine struct. calc. of TlF 80−53162
^{205}Tl, level excitation energies and ang. distribs. cluster model DWBA calcs. from ^{208}Pb(p,α) 79−17814

nuclei with mass number 190 to 219 continued
^{205}Tl, NMR of Tl borate, germanate and silicate glasses 77−59470
^{205}Tl transition strengths from ^{208}Pb(p,α) 79−13271
^{205}Tl^{+}, NMR in aq. soln., dissolved O_2 on nuclear spin relax. rate 78−19356
^{205}Tl^{+} ion, solvent effects on spin-lattice relaxation time 77−48073
^{205}Tl(D,e^{-})^{205m}Pb, ^{205}Pb assay in Tl minerals for solar neutrino flux determ., proposed expt. 77−5447
^{205}Tl(α,2n)^{207}Bi, spin and parity assignment of ^{207}Bi levels 78−89788
^{205}Tl(α,3n), 35-51 MeV, ^{206}Bi high-spin states anal. 78−82368
^{205}Tl(n,t)^{203}Hg, 14.6 MeV neutrons, activation cross section meas. 79−45254
^{205}Tl(p,5n)^{201}Pb→^{201}Tl, E_p=15 to 60 MeV, yields and excitation functions 79−5369
^{205}Tl(p,5n)^{201}Pb→^{201}Tl, yields and excitation functions for Pb radioactivities, medical appls. 80−67249
^{206}Tl, excitation of 12^{-} isomeric state in Bi(n,α) at 14 MeV, half life 78−70453
^{206}Tl, influence of nucl. polarisation on level props. 78−54686
^{206}Tl, isomeric yrast states obs. 77−281
^{206}Tl resonances, neutron strength functions and radiative widths 77−22898
^{207}Tl, single particle state mag. moment in large shell model space 79−45162
^{208}Tl, influence of nucl. polarisation on level props. 78−54686
^{208}Tl photon measurement, in general phantom procedure for calibrating inhaled ^{212}Pb body burdens 77−64138
^{208}Tl, selective separation from ^{228}Th source 77−40566
Tl(α,xn)^{205}Bi, population of high spin states, γ and conversion electron spectra 77−30616
Tl(γ,n), photoneutron Q-value determinations using monochromatic photons 79−22271
Tl(n,n′γ), 1.03-2.26 MeV, ang. distribs. meas., intermediate coupling model 77−38276

nuclei with mass number 220 or higher
228≤A≤248 even-even deformed nuclei, RPA calcs. of giant quadrupole resonances *(Russian)* 77−50045
^{220}Rn, ^{222}Rn, PAC in Fe, combined elec. quad. and mag. interaction 77−16214
^{238}U(n,f), reactor n, shoulders in very asymmetric mass distrib., cumulative yields 79−59005
^{239}Pu(n,f), thermal, fission product yield 80−27678
^{239}U vibr. states, obs. in ^{238}U(n,γ) 78−41627
^{241}Am, medical and industrial sources and applications 77−26915
^{252}103, SF, $T_{1/2}$ meas. 77−6468
^{253}103, SF, $T_{1/2}$ meas. 77−6468
^{257}105, SF, $T_{1/2}$ meas. 77−6468
^{261}107, SF, $T_{1/2}$ meas. 77−6468
A=152-238 fissility behaviour irregularity with respect to Z^2/A *(Russian)* 77−23121
A=221, nuclear data sheets, levels, J^{π}, transitions 80−31431
A=222 nuclei, nuclear struct. info., energy levels, spin, parity, decay 78−17080
A=223, nuclear data sheets, decay characts. and level struct. 78−58226
A=225, nuclear data sheets, levels, J^{π}, transitions 80−31432
A=225-253, fission probability, applicability of conventional systematics *(Russian)* 79−54464
A=226 nuclei, review of nuclear struct. information 77−57586
A=227, nuclear data sheets, decay characts. and level struct. 78−58227
A=228 to 240 even nuclei, anharmonicity of vibr. states superfluid model 77−61340
A=230 nuclei, review of nuclear struct. information 77−57587
A=230 to 254 nuclei semi-microscopic calcs. of level density *(Russian)* 77−277
A=231-251, density-depend. delta interaction, pairing matrix elements 77−10334
A=232 nuclei, review of nuclear struct. information 77−57588
A=234 nuclei, nuclear struct. info., energy levels, spin, parity, decay 78−17081
A=235, 238, meas. of α-values in BOR-60 reactor core 79−97830
A=236 nuclei, review of nuclear struct. information 77−57588
A=237, nuclear data sheets to November 1977 78−82267
A=238 nuclei, nuclear struct. info., energy levels, spin, parity, decay 78−17082
A=240 nuclei, review of nuclear struct. information 77−57588
A=241, nuclear data sheets to November 1977 78−82268
A=242 nuclei, nuclear struct. info., energy levels, spin, parity, decay 78−17083
A<500, magicity, extrapolation of ^{208}Pb Woods-Saxon potential parameters 80−78175
A>228 odd mass nuclei, single particle states, nuclear deform. 78−12952
A≥210, strength and radius parameters of deformed Woods-Saxon potential 79−97673
A≈252, n-capture abundance peak, due to subshell effect of N=164 77−2993
actinide fission product X-rays in micas, comparison with superheavy elements K- and L-shell ionisation estimates 77−50581
actinide nuclei, fission width calc. using doorway state approach 79−13278
actinide nuclei, modified oscillator potential, dynamical moment of inertia, single particle levels 79−67637
actinide nuclei, photo- and electro-fission cross sections and yields, giant resonances 80−5187
actinide nuclei, statistical aspects in fission mechanism 77−14097
actinide nuclei, subthreshold photofission yields, data anal. 78−82400
actinide partitioning from high-level radioactive wastes, arguments against 77−61570
actinide separation from high-level waste, nuclear transmutation 77−61569
actinide series neutron-induced-fission systematics in MeV region 77−67778
actinides, effect of simple consistency condition on multipole moments 78−86475
actinides, fission through double-humped barrier excitation energy 10-35 MeV 78−583
actinides, level energies and B(E2) ratios of deformed even nuclei 79−13221
actinoid element alpha-decay, current state of results 78−17159

nuclei with mass number 220 or higher continued
CANDU-PHW, neutron group cross sections in resolved resonance region calcs. 80−13573
compound nuclei, Z=98, 100, 102, statistical description of (heavy ion, xn) cross section *(Russian)* 78−86549
compound nuclei prod. in (HI, xn), lifetimes with account of fission process *(Russian)* 78−25233
compound nucleus lifetime using shadow effect in $^{238}U(^{27}Al,f)$ *(Russian)* 78−86563
data sheets for A=231, 235, 239 nuclei 78−12949
delayed fission produced in synthesis induced by heavy-ion beams and neutron currents *(Russian)* 79−89341
E2,M1 multipole mixing ratios in odd-mass nuclei, A>150 77−30503
E_2-transition probabilities and Davydov-Rostovsky model 78−74330
even actinides, lowest 0^+ state excitation, collective phonon state, spectroscopic factors from (p,t), (t,p) 80−13410
even-even actinide nuclei, fission barriers, Strutinsky method with dynamic fission paths 77−71602
even-even nuclei, E_2 transitions from 2^+ state of gamma-vibrational band 80−91150
fissile isotopes, thermal parameters, proposed reevaluation 77−23135
fission induced by 1 GeV protons, mass and energy distribs. meas. 77−71627
fission isomers, spectrosc. props. 80−105966
fission product ENDF/B data, processed, rapid spectral and decay heat calcs. 79−67797
fissionable nuclei A=232 to 252, systemization of relative yields of retarded neutrons 79−40974
heavy and superheavy elements Dubna programme on synthesis and search 77−23570
heavy atoms, P-odd effect suppression in unified gauge theory, l-N scatt. P-odd asymmetry *(Russian)* 77−61300
heavy element decay data, reactor related calcs., current status 79−97772
heavy fissile nuclei, nuclear constants estimation *(Russian)* 79−30779
heavy isotope reactivity coeffs., in fast neutron critical assemblies 79−63742
heavy nuclei, fission process gamma ray analysis *(Rumanian)* 79−40973
independent particle model, forces between heavy nuclei 78−635
magicity of superheavy nuclei, extrapolation of ^{208}Pb Woods-Saxon potential parameters up to A=500 80−78175
multigroup time-dependent delayed γ-spectra from fission and activation 78−13184
oxide fuels, irrad. behaviour, chemical process, densification, corrosion *(Japanese)* 77−83033
prediction of fission-product mass yields and related parameters 79−30862
PWR, Pu isotope calcs. for steady-state core anal. 79−59126
rare earths, pairing energy, single particle levels and interaction matrix elements 78−8721
spontaneous fission half lives, odd A nuclei, Z≥96 78−86556
spontaneously fissioning isomers, review of expt. data, equilib. quadrupole deformation parameters *(Russian)* 77−54260
superheavy region, neutron drip line, energy density mass formula extrapolation 78−93932
superheavy shell struct. in 250≤A≤500 mass region 77−22833
trans-uranium nuclei, fission barrier and (neutron width-fission width), nucleon contents depend. *(Russian)* 80−106093
transplutonium element symposium, Baden-Baden, Germany (September 1975) 77−28974
transplutonium elements, excited quasiparticle states of odd mass deformed nuclei 77−26565
transuranic aerosols, online high sensitivity measurement system 77−65334
transuranic analysis requirements, suitability of current and methods 79−96400
transuranic nuclei, Po to Th, very high spin states, deform. energy surfaces 78−50079
transuranic transport from environment to man modelling 79−96669
transuranics, spontaneous fission, (3Z-A) depend. of prompt-neutron yield 79−67799
transuranium isomers, spontaneous fission, review of exptl. work 77−79405
transuranium nuclides, production in reactor, yields, nuclide fractional concs. determ. 77−63986
U enrichment, gas centrifuge with differential rot. 77−54363
U isotopes, sensitivities to cross sections, decay constants flux and time, analytical evaluation 78−82427
volatile superheavy elements, synthesis and identification in heavy-ion reactions 79−45288
Z=103, 105, 107 element prod. from heavy ion fusion, cross sections from statistical model 80−32313
Z=126, even-A, ternary fission rates calc. 77−54264
(n,f) simulated cross sections for exotic actinide nuclei 80−544
$^{232}Th(\alpha, \alpha')$, coupled channel Born anal. of deformation correl 80−5149
$^{232}U(\alpha,f)$, 640MeV 80−95329
$^{235}U(n,f)$, thermal to 1.75 MeV, energy spectra and yields of alpha-particles 77−26805
^{248}Cm, spontaneous fission Xe and Kr daughter isotope ratios 80−63215
^{252}Cf, spontaneous fission, neutron emission 80−37405
$^{262}105$ spontaneous fission half life from $Bk(^{18}O,5n)$ *(Russian)* 79−59101
$^{263}106$, spontaneous fission half life from $^{249}Cf(^{18}O, 4n)$ *(Russian)* 79−59101
$^{298}114$, HF calcs. of fragment KE and neutron multiplicity 77−30635
A=229 nuclei, nuclear struct. data sheets to March 1978 79−26361
A=233 nuclei, nuclear struct. data sheets to March 1978 79−26362
Ac, A=229, 231, levels via (t,α) 15 MeV 77−74749
^{227}Ac, 7 to 16 MeV photofission, giant resonance and nuclear deformation *(Russian)* 78−41795
^{227}Ac fission expt. data, review *(Russian)* 79−49641
^{227}Ac, high pressure meas. of gamma transitions 80−18225
^{227}Ac levels and bands from ^{231}Pa α-decay 79−45217
^{230}Ac decay, ^{230}Ra levels, J^π and transitions, Nilsson assignments 80−68543
^{230}Ac, identification and β-decay meas. 77−22963
^{230}Ac levels, J^π and transitions, Nilsson assignments from ^{230}Ra decay 80−68543
^{230}Ac, prod., decay characts. 78−54724

nuclei with mass number 220 or higher continued
Am, 240-3, spontaneous fission, conversion electron spectra obs. 77−82864
Am (A-241, 243), neutron induced fission rate meas. in Zebra 77−57698
Am, A=241,3, neutron capture cross-sections 77−61469
Am, A=242, 243, quadrupole moment effect on internal conversion coeff. *(Russian)* 77−82867
Am, A=244, 5, fission probabilities and barrier parameters calc. 77−79409
Am isotopes, sensitivities to cross sections, decay constants flux and time, analytical evaluation 78−82427
Am isotopes (241, 243) separation, chemical treatment of irrad. targets *(French)* 77−26883
Am isotopes depositional history in S.Greenland firn layers 77−86953
Am-Be neutron probe, underestimation of radiation exposure by film badges 78−15900
^{A}Am, A=240, 242, 244, energy levels from deuteron-induced neutron transfer 77−26578
^{A}Am, A=240,244 actinide spontaneous fission activities from $^{209}Bi(^{56}Fe,X)$ 80−86937
$^{A}Am(\gamma,\delta)$ 7-26 MeV, A=241,243, photofission cross section in E1 giant resonance region *(Russian)* 80−5182
$^{A}Am(\gamma,n)$, 10-80 MeV, A=241, 243, delayed/prompt fission yield ratio, cross section, isomer prod. 79−80924
$^{A}Am(n,f)$, thermal, sub-barrier fission fragment energy correlations for A=241, 243 80−42715
^{231}Am alpha decay, ^{237}Np γ-ray transitions *(French)* 79−492
^{232}Am α-decay, absolute γ yields 78−86516
^{239}Am statistical model anal. of fission isomer production from $(^4He,xn)$ 78−66326
$^{240}Am^m$, spontaneously fissioning isomer optical shift in pumped $^8S_{7/2}\rightarrow{}^{10}P_{7/2}$ transition, nuclear deformation 80−27971
^{241}Am, 0.5 to 25 MeV, total neutron cross section determ. 79−30831
^{241}Am (n,f), 2.5 MeV neutrons, absolute cross section meas. (1.98±0.07 b) 80−73872
^{241}Am, activities in water entering N.North Sea 79−16520
^{241}Am, alpha, X-ray, gamma-ray and neutron sources for medical use *(French)* 77−42205
^{241}Am and $Pu/^{241}Am$ ratios, environment meas. using X-ray spectrometry 77−60265
^{241}Am, α-decay, e^+e^- pair production probability determ. 78−50133
^{241}Am, α-decay, pair production probability estimate 78−13036
^{241}Am, α-decay low-energy γ-radiation *(French)* 78−74342
^{241}Am, conc. in thermonuclear test debris, collected near Bikini Atoll 78−96103
^{241}Am, fission cross section meas. 79−85569
^{241}Am, gamma ray spectra of reactor fuels 80−42577
^{241}Am, in vivo meas. at CRNL 77−77993
^{241}Am, isotope composition tables for isotopes produced in CANDU reactors 78−29564
^{241}Am, neutron cross sections, 1 keV to 15 MeV, optical and stat. model calcs. 77−57655
^{241}Am, neutron emission probability in $Np(^4He,nx)$, fissionability energy depend. determ. 78−655
^{241}Am, photofission yields of bremsstrahlung γ *(Russian)* 79−9647
^{241}Am, radioactive decay, 59.5 keV photon yield 77−6588
^{241}Am sealed source for smoke detection *(French)* 77−42204
^{241}Am soil concs., in situ gamma anal. and sampling data comparison, Nevada 77−64143
^{241}Am, thermal cross sections and resonance integrals of fission and capture 77−71629
^{241}Am, total and fission cross sections in resonance region, resonance parameters 77−23160
^{241}Am, total neutron cross section and neutron reson. parameters, 0.004 to 30 eV 77−50135
^{241}Am, total neutron cross-section in resonance region 77−26746
^{241}Am-^{239}Pu monitor for in situ soil surface and pond bottom assay 77−9546
^{241}Am-Be neutron spectrum, (n,p) reaction average cross-sections 80−22827
$^{241}Am(\alpha,n)$, neutron yield in AmO_2 79−17912
$^{241}Am(\gamma,f)$, 15 to 1300 MeV, cross sections meas. *(Russian)* 77−6473
$^{241}Am(n,f)$, 14.8 MeV, cross-section meas. using mica track detectors 80−95330
$^{241}Am(n,f)$, 14.8 MeV, mass yield distrib., and absolute fission yield, isomer ratios 80−18352
$^{241}Am(n,f)$ 100 eV to 5.3 MeV, fission cross-section meas. rel. to ^{235}U 79−85567
$^{241}Am(n,f)/^{239}Pu(n,f)$, 0.13 to 7.0 MeV neutrons, fission cross section ratio meas. 79−97738
$^{241}Am(n,\gamma)$ cross section meas., thermal to 350 keV 77−23034
$^{241}Am(n,\gamma)^{242m}Am$, γ-quanta in population of spontaneously fissile isomer *(Russian)* 79−30835
$^{242}Am^m$, from $^{243}Am(\gamma,n)$, spontaneously fissioning isomer, searches for long-lived excited states 78−86561
^{242}Am, mag. dipole moment-atomic electron satellite states, influence on E0 conversion 80−18236
^{242}Am, reduced E0 conversion due to mag. moment effects 80−83034
$^{242}Am^m$ activity measurement by ^{242}Cm daughter decay meas. after separation with different radiochem. yields 78−78596
^{243}Am, absolute yields of 43.5, 74.7 and 117.8 keV photons 80−32568
^{243}Am half life and α-activity 80−102159
^{243}Am, thermal cross sections and resonance integrals of fission and capture 77−71629
^{243}Am, total neutron cross section and neutron reson. parameters, 0.4 to 35 eV 77−46171
$^{243}Am(^{40}Ar,f)$, product mass distribs., shell effect manifestation 79−93673
$^{243}Am(^{49}Ca,xn)$, production of superheavy elements with A=114-116 78−29493
$^{243}Am(\alpha,f)$, fragment mass distrib., and yield, statistical anal. *(Russian)* 80−5183
$^{243}Am(\gamma,f)$, 15 to 1300 MeV, cross sections meas. *(Russian)* 77−6473
$^{243}Am(n,f)$, low energy, far-out asymmetric mass distrib. 80−83132
$^{243}Am(n,f)$, thermal neutron induced fission cross section 80−37403
^{244}Am decay, relative probability of electron capture 78−17153
^{245}Am, high pressure meas. of gamma transitions 80−18225
Bk, A=245-9, fission probabilities and barrier parameters calc. 77−79409

nuclei with mass number 220 or higher continued
^{A}Bk, A=240, 242, electron capture, delayed fission prob. and fission barrier height *(Russian)* 80−42722
^{242}Bk electron capture half life and α-branching ratio from ^{238}U+^{10}B, ^{235}U+^{11}B, ^{232}Th+N 79−67716
^{247}Bk, proton orbital 1/2 [521] obs., stability of superheavy elements 77−67698
^{247}Bk proton states, transitions and spectroscopic factors from (α,t), α-decay, electron capture 79−89224
^{248}Bk, 23.7 h, spectroscopic studies 78−78314
^{249}Bk neutron total cross-section obs., 0.005 to 1000 eV 79−9577
^{249}Bk, thermal cross sections and resonance integrals of fission and capture 77−71629
^{249}Bk(n,f) cross section between 0.7 and 3.0 MeV 77−50170
^{250}Bk, β$^-$ decay, half life and ^{250}Cf energy levels, bands and transitions 79−22205
^{251}Bk level structure from ^{251}Cm beta decay 79−36200
Ca+Ar, 4-17 GeV, search for ultradense nuclei 77−3044
Cf, fission products mass, charge, kinetic energy distribs., scission-point model based on deformed shell effects 77−10455
Cf, HF calcs. of fragment KE and neutron multiplicity 77−30635
Cf, N=152 to 154, resonances, fission probabilities and thresholds 78−46119
Cf, neutron irradiation separation and α-spectra identification of ^{253}Es 78−17435
Cf, splitting of cold and hot nuclei *(Russian)* 78−29516
^{A}Cf, A-234,238, actinide spontaneous fission activities from ^{209}Bi(^{56}Fe, X) 80−86937
^{A}Cf, A=244, 248, fission barrier heights from β-delayed fission, β-strength functions struct. 80−5184
^{A}Cf, A=250, 252, 254, spontaneous fission fragment kinetic energy and neutron multiplicity meas. 80−42717
^{252}Cf spontaneous fission neutron spectrum 77−50166
^{246}Cf, α-decay meas., daughter energy levels *(Russian)* 77−82882
^{247}Cf decay, ^{247}Bk proton states, transitions and spectroscopic factors 79−89224
^{249}Cf, thermal cross sections and resonance integrals of fission and capture 77−71629
^{249}Cf(n,f), separation, identification of Ru, Rh isotopes 78−89924
^{249}Cf(n,f), thermal., yields of isotopes of Nb, I and Cs, charge distrib. 78−41789
^{249}Cf(n,f) thermal n, ^{139}Ba and ^{142}La fractional independent yield and γ-activity 79−89337
^{250}Cf E0 transitions and excited 0$^+$ states from ^{250}Es decay 79−45173
^{250}Cf energy levels, bands and transitions from ^{250}Bk, β$^-$ decay 79−22205
^{250}Cf low spin states, bandheads, J$^\pi$ and transitions from ^{250} Es EC decay 80−105952
^{250}Cf, spontaneous fission, mass distrib., radiochem. and γ-ray spectrometric meas. 77−67775
^{250}Cf, spontaneous fission Xe and Kr daughter isotope ratios 80−63215
^{250}Cf two-quasiparticle states populated by ^{250}Es^m EC decay 77−46140
^{250}Cf(d,d′), 15 MeV, vibr. states, J$^\pi$ and reduced transition probabilities 80−47351
^{252}Cf α and fission fragment radiation, effect on Pt alloy 78−86601
^{252}Cf based borehole logging system, delayed neutron activation anal. method for uranium 79−53569
^{252}Cf brachytheraphy source calibration using $Fe(NH_4)_2(SO_4)_2$-benzoic acid-xylenol orange dosimeter 77−5081
^{252}Cf, density-dependent HF description 77−54170
^{252}Cf effective half-life 77−22966
^{252}Cf, empirical limitations for spontaneous fission energy dissipation, fragment deformation 79−3188
^{252}Cf fission, isotopic mass dispersion discontinuity, neutron shell effect 79−45312
^{252}Cf fission, meas. of $\bar{\nu}$ and η, Mn bath systematic effects 77−23132
^{252}Cf fission, n angular distrib., 0 to 30° *(Russian)* 78−86564
^{252}Cf fission, neutron deficient fragments, search for positron activity *(Russian)* 80−63218
^{252}Cf fission, scission point config., α-particle trajectories 77−82974
^{252}Cf fission, search for abnormal energy release reln. to superdense nuclei *(Russian)* 79−89340
^{252}Cf fission, spontaneous, far-out asymmetric mass distrib. 80−83132
^{252}Cf fission fragment hard β-radiation 79−45306
^{252}Cf fission fragment tracks in quartz glass, electron microscope obs. 78−17526
^{252}Cf fission neutron, transmission through various shields, dose equivelent meas. 77−61620
^{252}Cf, fission neutron spectra Maxwellian temp. 77−26811
^{252}Cf fission neutron TOF spectrum fine struct. 77−88182
^{252}Cf fission products, g-factors of isomeric states 77−22890
^{252}Cf fission products, masses, β decay energies, halflives, He Jet TOF mass spectrometer meas. 77−23355
^{252}Cf fission source, ionisation characts. of electron oscillating ion source coupled to He-jet skimmer system 78−70661
^{252}Cf fission source, undergraduate laboratory expts. 77−382
^{252}Cf fission-neutron spectrum unfolding experiment 80−13514
^{252}Cf for interstitial radiotherapy implantations, clinical study 78−11722
^{252}Cf in radiotherapy, RBE-dose rate relationships 77−5030
^{252}Cf in radiotherapy, RBE vs. dose-rate relationships 77−9222
^{252}Cf, low-intensity source for neutron activation analysis 77−16885
^{252}Cf, mass distribution of fragments from spontaneous fission *(Russian)* 78−29517
^{252}Cf, medical and industrial sources and applications 77−26915
^{252}Cf, neutron activation anal. of Constantinian coins 78−350
^{252}Cf, neutron radiography, use of TV imaging techniques 78−60922
^{252}Cf neutron source, optimum design for subcritical neutron multiplier 79−59290
^{252}Cf neutron source for water-steam mixture void fraction meas. 79−26762
^{252}Cf neutron sources, appls. of activation anal., review 80−18728
^{252}Cf neutron sources, high-intensity, remote fabrication and calibration equipment and techniques 77−54388
^{252}Cf, positron activity of fission fragments *(Russian)* 77−6474
^{252}Cf, radiotherapy shielding, comparison of photoneutron and ^{252}Cf neutron spectra 79−59273
^{252}Cf radiotherapy source dosimetry, appl. of liq.-dielec. ionisation chamber 77−13009
^{252}Cf, SF, charge distrib., determ. of fractional cumulative yields of ^{134}Te and ^{135}I 78−41791
nuclei with mass number 220 or higher continued
^{252}Cf scission point configuration, α-ang. distrib., trajectory calcs. for LRA fission 80−83134
^{252}Cf sealed source for medical and industrial applications *(French)* 77−42204
^{252}Cf source with high emission, n and γ dosimetry, safety *(Czech)* 78−33296
^{252}Cf spontaneous fission, average neutron yield, Monte Carlo anal. of a direct meas. 77−50180
^{252}Cf, spontaneous fission, charge distrib. 79−97735
^{252}Cf spontaneous fission, element yields from X-ray multiplicities meas. 77−26812
^{252}Cf spontaneous fission, element yields from meas. X-ray multiplicities 77−50179
^{252}Cf spontaneous fission, forward-backward anisotropy of prompt neutron emission 78−25254
^{252}Cf, spontaneous fission, fragment ranges and kinetic energies in Al 78−94037
^{252}Cf, spontaneous fission, fragment slowing in gases 80−22875
^{252}Cf spontaneous fission, fission product β spectra *(Russian)* 80−91204
^{252}Cf spontaneous fission, Maxwellian reference description of fission spectrum shape 77−23129
^{252}Cf spontaneous fission, meas. of fission neutron spectra 80−22873
^{252}Cf spontaneous fission, neutron energy distrib. *(Hungarian)* 77−23116
^{252}Cf, spontaneous fission, neutron spectra and no. depend. on fragment mass and kinetic energy *(Russian)* 77−46197
^{252}Cf spontaneous fission, neutron spectrum 79−9654
^{252}Cf spontaneous fission, neutron yields *(Russian)* 79−80965
^{252}Cf spontaneous fission, prompt element yields determ. from X-ray multiplicities 77−30643
^{252}Cf spontaneous fission, proton origin 77−38309
^{252}Cf, spontaneous fission, prompt γ-ray multiplicity distribs. 77−50174
^{252}Cf spontaneous fission, prompt neutrons and fission fragments *(Russian)* 79−40976
^{252}Cf spontaneous fission, prompt γ-ray differential angular distrib. 80−102220
^{252}Cf spontaneous fission, review of meas. of average number of neutrons emitted per fission 79−9652
^{252}Cf spontaneous fission, search for low energy delayed neutrons *(Russian)* 77−34359
^{252}Cf spontaneous fission, symm. and asymm., fragment yields, β-decay chain lengths *(Russian)* 77−50181
^{252}Cf, spontaneous fission, scission point configuration, evaluation anal. 80−37361
^{252}Cf, spontaneous fission, yields and isomer ratio in A=134 chain 78−41786
^{252}Cf, spontaneous fission ^{90}Rb and ^{138}Cs independent isomeric yield ratio 79−22342
^{252}Cf spontaneous fission beta, positron, prompt gamma events, superhigh density nuclei formation *(Russian)* 78−17263
^{252}Cf, spontaneous fission determ. of heavy-ion interaction pot. *(Russian)* 78−41765
^{252}Cf spontaneous fission fragments, neutron emission fine struct. 77−26794
^{252}Cf spontaneous fission neutron source, enhancement by ^{238}U surrounding cylinder, determination of $\nu\sigma_f$ 77−6594
^{252}Cf, spontaneous fission neutron spectrum meas. using ^{6}Li spectrom. 78−17477
^{252}Cf spontaneous fission neutron spectrum meas. 79−9653
^{252}Cf spontaneous fission neutron number absolute meas. 79−9642
^{252}Cf, spontaneous fission product charge distrib. 78−13176
^{252}Cf spontaneous fission spectrum irrad. facility for neutron reaction rate meas. 77−14294
^{252}Cf, spontaneous ternary fission, multiplicity distrib. of prompt γ rays 78−21615
^{252}Cf, spontaneous ternary fission scission config. from trajectory calcs., Monte Carlo calcs. 79−6718
^{252}Cf, standard spectrum, status report 77−23017
^{252}Cf, status, application and prospects 77−26914
^{252}Cf, sub Cd thermal neutron fluxes in H_2O near the source 79−698
^{252}Cf, third IAEA evaluation of 2200 m/s, 20°C Maxwellian neutron data 77−23136
^{252}Cf, use for brachytherapy 78−20272
^{252}Cf wire neutron source distrib., meas. by autoradiography 77−61643
^{252}Cf-^{235}U subcritical multiplier, computer-controlled cyclic activation anal. 79−11865
^{252}Cf(n,f), fast reactor neutrons, effective cross section meas. 77−23119
^{252}Cf(n,γ), neutron capture gamma expt. equipment designs 80−52832
^{252}Cf(sf), energy dissipation in fission, comments 80−42719
^{252}Cf(sf), neutron yield dependence on fragment mass 79−67787
^{252}Cf(sf), scission, energy dissipation magnitude during descent from saddle point 80−42718
^{254}Cf spontaneous fission, neutron-rich fragments, even-even products 80−78342
^{254}Cf(Sf), neutron yield dependence on fragment mass 79−67787
^{256}Cf, spontaneous fission, fission barriers and products 80−18355
^{256}Cf spontaneous fission, mass and kinetic energy distribs. from ^{254}Cf(t,p) 80−47518
Cm, deformation energy surface, two-centre shell model calc. 77−71559
Cm fission products mass, charge, kinetic energy distribs., scission-point model based on deformed shell effects 77−10455
Cm isotopes, quadrupole and hexadecapole deforms., model independ. parameters using Fermi distrib. 78−17096
Cm isotopes (242, 244, 248) separation, chemical treatment of irrad. targets *(French)* 77−26883
Cm(^{48}Ca,xn), production of superheavy elements with A=114-116 78−29493
^{A}Cm, A=246,248, fission isomer rot. spectra $I^2(I+1)^2$ correction 80−18229
^{A}Cm(n,f), A=224,246, 0.3-45 MeV, near threshold fission cross section, energy depend. *(Russian)* 80−37406
^{240}Cm, fission barrier heights from β-delayed fission, β-strength functions struct. 80−5184
^{242}Cm, α-activity, half-life 77−54193
^{242}Cm decay meas., determ. of ^{242}Am^m activity after separation with different radiochem. yields 78−78596
^{242}Cm, isotope composition tables for isotopes produced in CANDU reactors 78−29564
^{242}Cm levels via ^{246}Cf α-decay *(Russian)* 77−82882

nuclei with mass number 220 or higher continued
^{242}Cm, spontaneous fission, prompt neutron multiplicity distrib. meas. 80−83131
^{243}Cm, spontaneous fission cross-section meas. with hemispherical plate ionisation chamber 77−26810
^{243}Cm(n,f), thermal neutron fission cross section and fission-resonance integral 80−86942
^{244}Cm, fast neutron cross-sections 78−21556
^{244}Cm, neutron induced fission rate meas. in Zebra 77−57698
^{244}Cm, nucl. shape of first saddle point 77−74756
^{245}Cm (n,f), thermal, charge distrib., ^{135}I and ^{190}Ba fractional cumulative yields 80−63074
^{245}Cm decay, ^{241}Pu level structure and γ-transitions 80−105980
^{245}Cm, from ^{249}Cf α-decay, γ-spectra and internal conversion spectra 79−6477
^{245}Cm, neutron resonance parameters, neutron energies 1-30 eV range 78−17167
^{245}Cm, resonance parameters up to 30 eV, neutron transmission meas. 77−26584
^{245}Cm, spontaneous fission cross-section meas. with hemispherical plate ionisation chamber 77−26810
^{245}Cm, thermal cross sections and resonance integrals of fission and capture 77−71629
^{245}Cm(n,f), cross section, 0.01 to 35 eV 78−21612
^{245}Cm(n,f), neutron yield dependence on fragment mass 79−67787
^{245}Cm(n,f), thermal neutron fission, kinetic energy distribs. determ. 78−658
^{245}Cm(n,f), thermal neutron induced fission, mass yield obs. 80−32309
^{246}Cm, resonance parameters up to 150 eV, neutron transmission meas. 77−26584
^{246}Cm(t,p)^{248}Cm, 17 MeV, shell gap obs. 77−46174
^{248}Cm, α-decay meas., daughter energy levels *(Russian)* 77−82882
^{248}Cm, in Fe matrix, effective mag. fields, PAC obs. *(Russian)* 77−4593
^{248}Cm, resonance parameters up to 100 eV, neutron transmission meas. 77−26584
^{248}Cm, spontaneous fission, mass distrib., radiochem. and γ-spectrometric meas. 77−67775
^{248}Cm spontaneous fission, Xe isotope comp. rel. to carbonaceous chondrite fission Xe 77−37581
^{248}Cm, Xe and Kr induced fission at Coulomb energies 77−61467
^{248}Cm+^{48}Ca, 267 MeV, search for superheavy elements 77−74871
^{248}Cm+^{48}Ca, search for volatile superheavy elements 78−94027
^{248}Cm+^{48}Ca superheavy element prod., radiochem. separation 78−74390
^{248}Cm(^{238}U,X), 7.5 MeV/amu, three particle exclusive meas. for exit channels fission fragment ang. distrib. 80−13513
^{249}Cm excited and single particle states, γ-transitions from ^{248}Cm(n,γ) 80−47399
^{251}Cm beta decay, ^{251}Bk level struct. 79−36200
^{243}Cu, thermal neutron capture and fission cross sections, resonance integrals 77−67744
^{243}Cu, simulated neutron irradiation damage, He ion implantation 78−79648
^{251}ES decay, ^{247}Bk proton states, transitions and spectroscopic factors 79−89224
Er, neutron-deficient isotope, yield meas. from Ir+^{20}Ne at 200 MeV *(Russian)* 77−23104
Es, A=249-51, fission probabilities and barrier parameters calc. 77−79409
^{A}Es, A=244, 246, 248, electron capture, delayed fission prob. and fission barrier height *(Russian)* 80−42722
^{A}Es, A=255,256, fission barrier first peak height, pot. energy surface struct. 80−42720
^{250}Es decay, ^{250}Cf E0 transitions and excited 0^{+} states 79−45173
^{250}Es EC decay, ^{250}Cf low spin states, bandheads, J$^{\pi}$ and transitions 80−105952
^{250}Es^{m} EC decay, ^{250}Cf two-quasiparticle states 77−46140
^{251}Es level struct. and p states, level transitions from ^{250}Cf(α,t) and ^{251}Fm decay 78−78268
^{251}Es, proton orbital 1/2 [521] obs., stability of superheavy elements 77−67698
^{252}Es, half-life, γ-ray decay obs. 78−4914
^{253}Es, coupled-channel α-decay theory 78−17156
^{253}Es, separation and α-spectra identification following neutron irradiation of Cf 78−17435
^{254}Es fission coincidence data from d, t, and ^{3}He induced reactions 80−42720
^{254}Es(n,f), neutron yield dependence on fragment mass 79−67787
^{254}Es(t,p), 16 MeV, prod. and discovery of ^{256}Es 7.6 hr β-decaying high-spin isomer 77−22964
Eu, enriched isotopes, EBR-II irrad., integral cross sections 79−67843
Fm fission products mass, charge, kinetic energy distribs., scission-point model based on deformed shell effects 77−10455
Fm, HF calcs. of fragment KE and neutron multiplicity 77−30635
^{A}Fm, A=242-246, actinide spontaneous fission activities from ^{209}Bi(^{56}Fe, X) 80−86937
^{A}Fm, A=258, 259, spontaneous fission, fission barriers and products 80−18355
^{A}Fm(n,f), A=253, 255, 257, 259, fission mass distrib. transition, liquid drop and shell model calcs. 80−32310
^{A}Fm(sf), A=254, 256, 258, 260, fission mass distrib. transition, liquid drop and shell model calcs. 80−32310
^{248}Fm, fission barrier heights from β-delayed fission, β-strength functions struct. 80−5184
^{252}Fm, fission process, dynamic aspects, nuclear mass parameter, action integral minimisation 78−62586
^{252}Fm, pot. energy surface, liquid model, deformation energy formulae *(Chinese)* 80−102106
^{254}Fm spontaneous fission, distrib. of mass, KE and neutron yield 78−17257
^{255}Fm, coupled-channel α-decay theory 78−17156
^{255}Fm, fission barrier first peak height, pot. energy surface struct. 80−42720
^{256}Fm(sf), neutron yield dependence on fragment mass 79−67787
^{257}Fm, spontaneous fission fragment kinetic energy and neutron multiplicity meas. 80−42717
^{258}Fm, nuclear pressure and fission fragment mass distrib. 80−18356
^{258}Fm spontaneous fission, mass and kinetic energy distribs. from ^{258}Md^{m} decay 80−47518
^{259}Fm spontaneous fission, $T_{1/2}$ and kinetic energies from ^{257}Fm(t,p) 80−47517

nuclei with mass number 220 or higher continued
Fr, nuclear ground state spins, at beam mag. reson. obs. 78−78257
Fr, spin and mag. moment, trends in neutron deficient nuclei 78−37261
^{A}Fr, A=204-210, 212, 224-228, direct mass meas. 80−78130
^{212}Fr in liq. ^{203}Tl, $(h_{9/2})^{n}$ proton states, Knight shifts and absolute mag. moments 77−82821
^{224}Fr→^{224}Ra, γrays, internal conversion, eγ coincidence spectra meas. 80−78216
H isotopes, quadrupole and hexadecapole deforms., model independ. parameters using Fermi distrib. 78−17096
^{191}Ir(n,γ), development of high intensity ^{192}Ir gamma-ray radiographic source 77−2715
^{192}Ir high intensity gamma-ray radiographic source development 77−2715
^{A}Md, A=248, 250, electron capture, delayed fission prob. and fission barrier height *(Russian)* 80−42722
^{258}Md isomer, EC decay, ^{258}Fm spontaneous fission, mass and kinetic energy distribs. 80−47518
Nd, enriched isotopes, EBR-II irrad., integral cross sections 79−67843
No, HF calcs. of fragment KE and neutron multiplicity 77−30635
^{252}No, high mass asymmetry distribs. in fissioning nuclei, shell effects 79−3186
^{252}No production, heavy ion complete fusion cross sections 79−67803
^{252}No spontaneous fission, fragment mass and kinetic energy distribs. 77−46194
Np isotopes, sensitivities to cross sections, decay constants flux and time, analytical evaluation 78−82427
^{A}Np(n,f), A=234, 235, low energy, far-out asymmetric mass distrib. 80−83132
^{227}Np damage track detectors, effects of subthreshold fission on neutron dose meas. 78−33375
^{235}Np deduced levels and Nilsson band configurations from ^{234}U(^{3}He,d) and ^{234}U(α,t) 79−468
^{235}Np, fission lifetime from ^{235}U(d,f) reaction 80−63216
^{237}Np (n,f), 3 eV to 2 MeV, cross-section meas. 77−3058
^{237}Np, absolute fast neutron fission cross sections 79−13366
^{237}Np absolute fission rate in spherical fusion blanket assemblies 77−67871
^{237}Np α-decay, ^{233}Pa excited level scheme and γ-transitions 79−80876
^{237}Np, criticality anal., possible utilisation in fission reactors 80−621
^{237}Np electron transition excitation following K-shell photoionisation, deexcitation γ-rays 80−78196
^{237}Np, energy levels from ^{241}Am α-decay, γ transitions 79−6480
^{237}Np fission, appl. as neutron dosimeter for personnel 79−13539
^{237}Np fission and capture cross sections in GCFR neutron spectra 80−37404
^{237}Np, fission rates measured in graphite-reflected lithium assembly, nonelastic neutron anisotropy effect 78−29511
^{237}Np, gamma ray spectra of reactor fuels 80−42577
^{237}Np, gamma-ray spectra following ^{231}Am α-decay *(French)* 79−492
^{237}Np, isotope composition tables for isotopes produced in CANDU reactors 78−29564
^{237}Np level scheme, α-decay of ^{241}Am *(French)* 78−74342
^{237}Np, lifetime of 60 keV state, undergraduate expt. 79−20
^{237}Np, Mossbauer effect in $NpCo_2Si_2$ and $NpFe_2Si_2$ 77−28406
^{237}Np, Mossbauer isomer shifts, book, contrib. 79−87362
^{237}Np, Mossbauer lineshape, dispersion amplitudes 78−25146
^{237}Np, Mossbauer spectroscopy, fast γ-ray detection system 78−25376
^{237}Np, muonic, n emission from radiationless muonic transitions and μ capture 79−3599
^{237}Np muonic, prompt fission, fragment atomic muon capture 80−95312
^{237}Np, neutron induced fission, appl. to dosimetry 78−89984
^{237}Np, neutron resonance params., 8 to 250 eV 77−26709
^{237}Np, nuclear excitation by electron transition (NEET) 77−34256
^{237}Np, quasi-stationary state decay through two bump barrier *(Russian)* 80−13420
^{237}Np, relative yields of Xe isotopes 77−54265
^{237}Np, spontaneous fission, prediction of fission-product mass yields and related parameters 79−30862
^{237}Np threshold detector, subthreshold phenomena effects on nondestructive assay of reactor fuel 79−22409
^{237}Np(^{4}He,f), (^{4}He,n), (^{4}He,2n), E=17.5-22.5 MeV excitation function meas. 78−656
^{237}Np(α,f), fragment mass distrib., and yield, statistical anal. *(Russian)* 80−5183
^{237}Np(d,p) 12 MeV, ^{238}Np energy level scheme determ. by Nilsson model 79−26370
^{237}Np(e,e'f), 20-120 MeV, electrofission cross section, E1, E2 strengths 78−13174
^{237}Np(e,f), 10-34 MeV, electrofission cross section, E2 transition mode and giant resonances 80−106084
^{237}Np(e,f), 110 MeV electrons, mass and kinetic energy distribs. 79−93672
^{237}Np(γ,γ') 8.5-11.4 MeV, elastic and Raman scatt., giant reson. struct. 77−34284
^{237}Np(n,f), 14.7 MeV, Xe relative cumulative yields, fine struct. peak *(Russian)* 79−30868
^{237}Np(n,f), ave. no. of neutrons/fission meas. 78−41792
^{237}Np(n,f), cross section, barrier heights, widths, intermediate structure theory 77−34357
^{237}Np(n,f), fission cross sections, use as standards in MeV region 79−13362
^{237}Np(n,f), intermediate struct. line fitting, subthreshold fission resonances 80−102214
^{237}Np(n,f), thermal neutron sub-barrier fission ^{134}I and ^{135}Xe yields 80−86935
^{237}Np(n,f), thermal to 14.7 MeV, statistical theory calcs. 77−23137
^{237}Np(n,f), thermal-neutron sub-barrier fission 77−74891
^{237}Np(n,f) cross section in ^{252}Cf spectrum, integral test for evaluated data 77−23134
^{237}Np(n,f) integral cross section ratio meas. using ^{235}N(n_{th},f) neutron spectrum 77−23130
^{237}Np(n,f)/^{239}Pu(n,f), 0.13 to 7.0 MeV neutrons, fission cross section ratio meas. 79−97738
^{237}Np(n,γ), meas. of delayed γγ coinc., search for ^{238}Np shape isomer *(Russian)* 77−324
^{237}Np(n,γ) 25 to 650 keV and 2600 to 5500 keV, ^{238}Np energy level scheme determ. by Nilsson model 79−26370
^{237}Np(nth, f), sub-barrier fission, fragment energy correl. meas. 78−21614
^{237}Np(p,f), 11-26 MeV, product yield 80−91197

nuclei with mass number 220 or higher continued
^{238}Np energy level scheme determ. by Nilsson model 79−26370
^{238}Np levels, resonances and transitions from ^{237}Np(n,γ) 80−52589
^{238}Np(n,f), subthreshold fission, fine struct. resonances anal. 78−652
^{238}Np(n,f) near threshold cross-sections 77−65240
^{239}Np, absolute meas. of branching ratio for the 277.6 keV line 80−86854
^{239}Np contamination in eluate of ^{99}Mo-^{99m}Tc generators loaded with (n,γ)-prod ^{99}Mo 77−5079
^{240}Np, high pressure meas. of gamma transitions 80−18225
^{242}Np β-decay, half life, ^{242}Pu level scheme 79−67664
^{242}Np levels, J^{π} and transitions from ^{242}U decay 79−67664
^{243}Np energy level spin assignments and anal. power from ^{244}Pu(t,α), polarised t 79−36165
^{237m}Np fission isomer from ^{238}U(p,2n), statistical model anal., fission to γ branching ratio 78−25256
Np(α,xn) ^{241}Am, neutron emission probability and fissionability energy depend. 78−655
^{190}Os, identification and β-decay meas. 77−22963
Pa, A=233, 235, 237, levels via (t,α) 15 MeV 77−74749
^Pa, A=215-218, 222, α-decay half life and energies from ^{151}Ta+^{40}Ar and ^{184}W+^{40}Ar 79−45216
^Pa, A=236, 238, β strength function struct., influence on β-delayed fission 78−89826
^Pa, A=236, 238, strength function of β-transitions 80−22764
^{231}Pa α-decay, γ-rays and internal conversion spectrum, ^{227}Ac levels and bands 79−45217
^{231}Pa, calc. of critical mass and radius by three group diffusion theory 79−13419
^{231}Pa, high pressure meas. of gamma transitions 80−18225
^{231}Pa spontaneous fission, prediction of fission-product mass yields and related parameters 79−30862
^{231}Pa(n,f), fission spectrum averaged cross section 78−70576
^{231}Pa(n,f), thermal to 14.7 MeV, statistical theory calcs. 77−23137
^{231}Pa(n,f), thermal-neutron sub-barrier fission 77−74891
^{231}Pa(n,f) sub-barrier fission, fragment mass and kinetic energy distribs. 79−17942
^{231}Pa(n,f) thermal neutron-induced fission cross-section 79−30859
^{233}Pa anal. power for spin states from ^{234}U(t,α), polarised t 79−36165
^{233}Pa decay emission probability of 312 keV gamma-ray 79−59035
^{233}Pa excited level scheme and γ-transitions from ^{237}Np α-decay 79−80876
^{233}Pa, high pressure meas. of gamma transitions 80−18225
^{233}Pa removal from ^{237}Np by coprecipitation with MnO_2 or sorption on silica gel 79−52733
^{233}Pa(n,f), cross sections, semi-empirical formula 80−22864
^{234}Pa isomers from ^{234}Th β⁻ decay, low energy γ-spectrum 78−70493
^{236}Pa, β-delayed fission, search *(Russian)* 78−46033
^{238}Pa, β-delayed fission, search *(Russian)* 78−46033
Pb, Rayleigh and Delbruck scatt., 6.8-11.4 MeV 77−26669
^{208}Pb(^{48}Ca,γ), nuclear pressure and fission fragment mass distrib. 80−18356
^{208}Pb(d,p)^{209}Pb, 9.0 MeV, effects of d D state determ. 77−67752
^{208}Pb(n,n′), 26 MeV, isospin effects, cf. with direct reaction theory 77−34312
^{239,240}Pu, conc. in thermonuclear test debris, collected near Bikini Atoll 78−96103
Pu (A=239-242), neutron induced fission rate meas. in Zebra 77−57698
Pu (n,F) thermal, rare gas yields, odd-even effect *(French)* 77−50172
Pu, A=235, 237, statistical model anal. of fission isomer production from (^{4}He,xn) 78−66326
Pu, A=238, 239, neutron emission probability in U(^{4}He,xn), fissionability energy depend. determ. 78−655
Pu, A=239, 241, delayed neutron parameters selection for reactor calcs. *(Slovak)* 78−21534
Pu, A=239, 241, fission probability, Γ_n/Γ_f ratio struct. 78−37382
Pu, A=239, 241, spontaneous fission, conversion electron spectra obs. 77−82864
Pu, alpha-energy and mass analyses, using single sample mount 78−15744
Pu as energy resource, availability, health hazards, nuclear weapon proliferation 77−46286
Pu, decontamination, sorption and distillation methods, review *(Czech)* 78−82496
Pu, deformation energy surface, two-centre shell model calc. 77−71559
Pu, even isotopes, $K=0^+$, 0^- bands, energies, inverse moments of inertia 80−63063
Pu extraction-spectrophotometric determination in spent fuel of first Czechoslovakian nuclear power station *(Czech)* 77−3105
Pu FBR fission yield, burnup determ. in mixed oxide fuels 77−23138
Pu, fission cross section calculations 77−26661
Pu fission cross section trend, 3-5 MeV, statistical model description 77−23126
Pu fuel lattice, cluster-type, thermal-neutron behaviour 77−61477
Pu, fume aerosols, aerodynamic and dissolution behaviour of laser-ignited droplets 79−13438
Pu isotope ratios, γ-ray spectrometric determ. 77−6518
Pu isotopes, ENDF/B-4 cross sections, integral data 77−23200
Pu isotopes, in vivo meas. at CRNL 77−77993
Pu isotopes, quadrupole and hexadecapole deforms., model independ. parameters using Fermi distrib. 78−17096
Pu isotopes, sensitivities to cross sections, decay constants flux and time, analytical evaluation 78−82427
Pu isotopes depositional history in S.Greenland firn layers 77−86953
Pu, K-absorption edge energy, accurate determ. using γ attenuation 77−59642
Pu, large samples, thermal-neutron coincidence counting 78−82444
Pu, multigroup time-dependent delayed γ-spectra from fission and activation 78−13184
Pu, N=150 and 152, fission probabilities and thresholds 78−46119
Pu^{239}, product separation asymmetry in fission by slow polarised neutrons *(Russian)* 80−106088
Pu/^{241}Am ratios, environmental meas. using X-ray spectrometry 77−60265
Pu-Th-U, neutron group cross sections in resolved resonance region calcs. 80−13573
Pu+U mixed oxide aqueous solns., limiting critical concs., multiplication factor 77−26859
PuO_2/UO_2 fuelled assemblies, integral meas. of effective delayed neutron fraction in FTR SNEAK 77−6497

nuclei with mass number 220 or higher continued
^{4}Pu(n,f) A=239,242,244, 14.8 MeV, cross-section meas. using mica track detectors 80−95330
^Pu (A=238, 239+240), activities in water entering N.North Sea 79−16520
^Pu, A=238,240, fission isomer rot. spectra $I^2(I+1)^2$ correction 80−18229
^Pu, A=238 to 241, gamma ray spectra of reactor fuels 80−42577
^Pu, A=239, 241, 2200 m/s and 20°C Maxwellian neutron data 79−9651
^Pu, A=239,242, muonic, prompt fission, fragment atomic muon capture 80−95312
^Pu, A=240, 242, neutron capture cross section ratios in range 10 to 90 keV 78−50163
^Pu, muonic, A=239, 242, n emission from radiationless muonic transitions and μ capture 79−3599
^Pu/^{235}U, A=240, 242, fission cross section ratio meas. 0.127 to 7.4 MeV 80−5180
^Pu(n,f), A=239, 242, 0.1 to 10 MeV fission cross section rel. to ^{235}U 79−13354
^Pu(n,f), A=239.241, nuclear constants eval. for heavy fissile nuclei using nuclear models *(Russian)* 79−59100
^Pu(n,f), A=240, 242, 244, 0.1 to 30 MeV, cross-sections rel. to ^{235}U 78−50217
^Pu(n,f), fission product decay heat calc. by summation method, appl. to FBR 79−30863
^Pu(n,f) A=240,241, 14.8 MeV, meas. of reaction parameters using solid state nuclear track detectors 80−91201
^{230}Pu(n,f), fission-fragment yields of neutron fission in FBR 80−83102
^{232}Pu, fission barrier determ., from β-delayed fission 78−29518
^{232}Pu, fission barrier heights from β-delayed fission, β-strength functions struct. 80−5184
^{236}Pu, 40 ps fission isomer quadrupole moment 77−50053
^{237}Pu , half-life determ. by gamma counting in NaI(Tl) 78−8775
^{237}Pu α-decay, ^{233}U levels, bandheads, total α-branching and transitions 79−93516
^{237}Pu fission isomers, half lives and yield ratio, statistical model anal. from ^{239}Pu(γ,Zn) 79−40885
^{237}Pu fission single particle isomers, half lives and isomeric ratio from ^{239}Pu(γ,2n) 80−18181
^{237}Pu gamma-emitting isotope, prep. of tracer by ^{238}U(^{3}He,4n) 77−34497
^{238}Pu, α-activity, half-life 77−54193
^{238}Pu for cardiac pacemakers, radioactive controls *(French)* 77−44752
^{238}Pu fuel form facility at Savannah River Plant 79−9846
^{238}Pu fuelled cardiac pacemaker, evaluation *(French)* 77−44833
^{238}Pu half-life determ. 77−22965
^{238}Pu, in Fe matrix, effective mag. fields, PAC obs. *(Russian)* 77−4593
^{238}Pu, isotope composition tables for isotopes produced in CANDU reactors 78−29564
^{238}Pu, medical and industrial sources and applications 77−26915
^{238}Pu production, chemical treatment of Np targets *(French)* 77−42201
^{238}Pu production from target elements based on MgO and NpO_2 *(French)* 77−42199
^{238}Pu production from targets in Celestin reactors, medical use *(French)* 77−42200
^{238}Pu sealed source for medical and industrial applications *(French)* 77−42204
^{238}Pu separation, chemical treatment of irrad. targets *(French)* 77−26883
^{238}Pu, sources for cardiac pacemakers, manufacture and safety tests *(French)* 77−44751
^{238}Pu, spontaneous fission decay const. meas. 77−23149
^{238}Pu(n,f), intermediate struct. line fitting, subthreshold fission resonances 80−102214
^{239}Pu, 8-μs fission isomer, quadrupole moment 77−30484
^{239}Pu (n,f), 10 eV-100 keV, fission cross section 80−27681
^{239}Pu, absolute fission yield meas. by track-etch-cum-γ-spectrometry method 80−27859
^{239}Pu aerosol, characterisation inside safety enclosures of mixed oxide fuel fabrication facility 79−13501
^{239}Pu alpha particle tracks on polycarbonate foils 79−76310
^{239}Pu alpha particles, internal source microdosimetry 78−3615
^{239}Pu, α-decay half-life by two independent methods 77−82881
^{239}Pu, calorimetric determ. of half-life 79−26405
^{239}Pu, capture/fission cross-section ratio meas., 0.007 eV-12 keV 77−54266
^{239}Pu critical sphere, k_{eff} sensitivity to fission and inelastic scatt. spectra 77−23198
^{239}Pu, cross sections for α-decay and neutron induced fission *(Russian)* 79−17944
^{239}Pu, deformation effects on neutron total cross-sections, adiabatic coupled-channel calc. 79−17896
^{239}Pu dosimetry in bone 77−16993
^{239}Pu, e and $\bar{\nu}$ energy spectra from fission fragments *(Russian)* 77−23120
^{239}Pu, endosteal cell dose and relative distrib. factors compared to ^{226}Ra 78−96091
^{239}Pu, fast fission, product decay-heat calc. 77−61464
^{239}Pu fission, isotopic mass dispersion discontinuity, neutron shell effect 79−45312
^{239}Pu fission, testing of ENDF/B-IV Th data in GCFR lattice 79−67836
^{239}Pu fission isomers produced in ^{240}Pu(n,2n), half lives 77−30641
^{239}Pu, fission product beta decay, $\bar{\nu}$ spectra 80−102150
^{239}Pu fission products γ-ray and photoneutron spectra 77−23127
^{239}Pu, fission rate, absolute meas. 79−63678
^{239}Pu, giant resonance in total photoabsorpt. cross section 77−6347
^{239}Pu, half life determ. by isotope dilution mass spectroscopy of ^{235}U 79−26409
^{239}Pu half life meas. by calorimetry, mass spectrometry and α-particle counting 79−26403
^{239}Pu, half-life determ. from α-emission rates 79−26407
^{239}Pu, half-life determ. specific activity meas., mass spectroscopy of ^{235}U daughter growth 79−26408
^{239}Pu, half-life determ. using isotope dilution mass spectroscopy and α-specific activity meas. 79−26410
^{239}Pu, high pressure meas. of gamma transitions 80−18225
^{239}Pu, highly deformed, muonic X-rays, nuclear charge distrib., elec. quadrupole moment 78−70440

nuclei with mass number 220 or higher continued
^{239}Pu in tissue, specific energy calc. in accordance with crit. cell concept 77−2031
^{239}Pu, infinite multiplication factors, neutron captures and fission, rel. to GCFR parameters 78−33245
^{239}Pu, integral neutron capture cross sections in GCFR lattices 78−13246
^{239}Pu, irradiated in BOR-60 reactor, fission yields 79−17971
^{239}Pu, isotope composition tables for isotopes produced in CANDU reactors 78−29564
^{239}Pu localisation in bone using neutron-induced autoradiography 77−40773
^{239}Pu, mass distribution of fragments in neutron induced fission *(Russian)* 78−29517
^{239}Pu, meas. of α-values in BOR-60 reactor core 79−97830
^{239}Pu muonic atom, n emission, bound μ influence on fission barrier 78−89845
^{239}Pu neutron data evaluation for ENDF/B-V 78−25288
^{239}Pu neutron data reevaluation for Nuclear Data Library KEDAK-3 77−23042
^{239}Pu, P-odd asymmetry accompanying fission by polarised thermal neutrinos *(Russian)* 77−82977
^{239}Pu, prep. and chem. charact. for half-life meas. 79−26404
^{239}Pu, prompt-neutron fission spectrum, Maxwellian and Watt distribs. 77−50177
^{239}Pu soil concs., in situ gamma anal. and sampling data comparison, Nevada 77−64143
^{239}Pu, specific power and half-life, calorimetric determ. 79−26406
^{239}Pu, spectroscopy in second minimum of pot. energy surface 79−30805
^{239}Pu, subparticle formation expt. by α-decay 79−6520
^{239}Pu, σ_c/σ_f ratio meas. in BFS critical assemblies 79−97737
^{239}Pu, $\sigma(n,\gamma)/\sigma(n,f)$ estimate based on expt. data up to 1977 79−89312
^{239}Pu thermal fission, prompt neutrons and fission fragments *(Russian)* 79−40976
^{239}Pu thermal fission afterheat, sensitivity to errors in fission product data 77−26841
^{239}Pu, thermal neutron-induced fission, ^{96}Nb and ^{98}Nb yields 78−54807
^{239}Pu, third IAEA evaluation of 2200 m/s, 20°C Maxwellian neutron data 77−23136
^{239}Pu to ^{235}U fission cross-section ratio from 0.001-30 MeV 77−26807
^{239}Pu, total muon capture rate, quenching of Cabibbo angle 79−22232
^{239}Pu, total muon-capture rate meas. 77−79335
^{239}Pu, transition effects in total photoabsorpt. cross section 77−46160
^{239}Pu uptake by pea plants 77−9282
^{239}Pu, use in weapons and energy prod., radiological hazards, security 77−10492
^{239}Pu/^{235}U, (n,f) ratio meas. in range 1 keV-30 MeV 78−46118
^{239}Pu-^{241}Am monitor for in situ soil surface and pond bottom assay 77−9546
^{239}Pu-Be source, neutron spectra calc. 77−18725
$^{239}PuO_2$, inhaled, biochem. effects on lung lipids 77−25510
$^{239}PuO_2$ high-fired particles, inhalation carcinogenesis in rats 77−21576
^{239}Pu+n, 13.9, 14.6 MeV, absolute neutron fission cross sections, associated particle method 78−89926
^{239}Pu+n, 14 MeV interactions, neutron and γ-ray spectra meas. 79−93612
^{239}Pu+n, ratio between capture and fission cross sections up to 30 keV 78−70538
^{239}Pu(α,α), 19-27 MeV, differential cross section, transmission coeffs. for fission cross section *(Russian)* 79−67800
^{239}Pu(α,f), 19-27 MeV, integral and differential cross sections, anisotropy energy depend. *(Russian)* 80−37407
^{239}Pu(d,p), 4.0-6.2 MeV, reson. in fission probabilities of ^{240}Pu 78−78429
^{239}Pu(γ,f), 15-55 MeV, photofission symmetric and asymmetric yields 80−83135
^{239}Pu(γ,f), asymmetry depend. on bremsstrahlung energy maxima 77−23117
^{239}Pu(n, f), 0.024 to 7.4 MeV fission cross section ^{235}U/^{239}Pu ratio 79−40975
^{239}Pu(n, f), undisturbed resonance integral determ., and neutron flux meas. 80−5453
^{239}Pu(n,X), nuclear reaction statistical model parameters *(Russian)* 80−18280
^{239}Pu(n,X), thermal n, gamma spectra from capture, fission and fission products 80−37352
^{239}Pu(n,f), 0.005-0.4 eV, fission fragment average kinetic energies in resonance region 80−18358
^{239}Pu(n,f), 0.1-1 Mev, light charged particle emission, saddle point states 79−22343
^{239}Pu(n,f), 0.10-2.07 MeV, meas. of prompt fission neutron spectra 77−23146
^{239}Pu(n,f), 0.3 eV resonance energy, mass distrib. of products 78−70578
^{239}Pu(n,f), 1 keV to 1 MeV, cross-section meas., ratio to ^{235}U 77−23144
^{239}Pu(n,f), 100 keV-1 MeV, light charged particle yields 77−71631
^{239}Pu(n,f), 2-144 keV, cross-section meas. 77−26813
^{239}Pu(n,f), 2-144 keV, cross-sections meas. 77−26814
^{239}Pu(n,f), 35 to 1500 keV, near equilib. delayed neutron energy spectra 77−34354
^{239}Pu(n,f), abs. meas. of fission cross-sections with photoneutron sources 79−30860
^{239}Pu(n,f), comparison exptl. cross section meas. methods 77−23157
^{239}Pu(n,f), cross section, parameter testing in statistical model *(Russian)* 80−52653
^{239}Pu(n,f), cross sections for ^{252}Cf neutrons 78−25258
^{239}Pu(n,f), cross-section, 2, 24, 55, 144 keV neutron 78−17262
^{239}Pu(n,f), cumulative yields of Ru and Pd isotopes 79−576
^{239}Pu(n,f), effective cross section dependence on thermal neutron temp. 80−547
^{239}Pu(n,f), far-out asymmetric mass distrib. 80−83132
^{239}Pu(n,f), fission cross-section averaged over ^{252}Cf neutron spectrum 79−30861
^{239}Pu(n,f), fission neutron spectra, TOF meas. 78−17476
^{239}Pu(n,f), low energy, fission widths, channel charact. 78−29515
^{239}Pu(n,f), polarised thermal neutrons, parity nonconservation *(Russian)* 78−33232
^{239}Pu(n,f), separation, identification of Ru, Rh isotopes 78−89924
^{239}Pu(n,f), statistical model anal. mass yield 77−26797
^{239}Pu(n,f), sub MeV neutrons, equilib. delayed neutron energy spectra meas. 77−38308

nuclei with mass number 220 or higher continued
^{239}Pu(n,f), $\sigma_f(^{239}Pu)/\sigma_f(^{235}U)$ meas., neutron energies 0.27-9.85 MeV 78−660
^{239}Pu(n,f), thermal, correlation for independent fission prod. yield uncertainties 78−50216
^{239}Pu(n,f), thermal, isotopic distrib. of rare gases, proton parity effect *(French)* 77−3054
^{239}Pu(n,f), thermal n, fission fragment energy correlation meas., fine struct. and deformation 79−13355
^{239}Pu(n,f), thermal n, reactor $\bar{\nu}$ and e spectra calc. 79−67791
^{239}Pu(n,f) 80−37405
^{239}Pu(n,f) 0.009-0.6 eV cross-section, Westcott factor 80−546
^{239}Pu(n,f) absolute yields and group constants of delayed neutrons in fast fission using Viper 77−54261
^{239}Pu(n,f) cross section in ^{252}Cf spectrum, integral test for evaluated data 77−23134
^{239}Pu(n,f) integral cross section ratio meas. using $^{235}U(n_{th},f)$ neutron spectrum 77−23130
^{239}Pu(n,γ), comparison of exptl. cross section meas. methods 77−23157
^{239}Pu(n,γ), thermal, fission product $\bar{\nu}_e$ spectrum, β-decay characts. 80−78340
^{239}Pu(n,n′), 3-5 MeV, fission isomer prod. 77−61462
^{239}Pu(n,t), absolute yields of ^{99}Mo, ^{111}Ag, ^{140}Ba, ^{147}Nd, ^{153}Sm 77−50167
$^{239}Pu(n_{th},f)$, yields of Cd and Sn isotopes, symm. region 77−34358
^{240}Pu, 42.9 keV γ transition, Mossbauer reson. obs. 79−36229
^{240}Pu, 50 to 250 keV, cross-section ratios c.f. ^{197}Au 79−22281
^{240}Pu, appl. of shell correction method for finite well potentials 78−37298
^{240}Pu at very high spins, double-humped fission barrier anal. 78−4970
^{240}Pu, α-decay meas., daughter energy levels *(Russian)* 77−82882
^{240}Pu, dynamic excitation model of fission process, scission 77−14095
^{240}Pu, effect on neutron lifetime in nuclear explosives 79−13531
^{240}Pu fission, dynamic excitation and collective energy, quasiparticles 79−67792
^{240}Pu fission, thermal neutron induced, average angular momenta of even-even fragments 78−86525
^{240}Pu fission total kinetic energy release, excitation energy depend., scission point anal. of ^{241}Pu(^{3}He,αf) 80−18351
^{240}Pu, half life and specific activity by α-counting 79−502
^{240}Pu, hexadecapole shape isomeric state, shell correction method fission barrier calcs. 80−545
^{240}Pu, in Fe matrix, effective mag. fields, PAC obs. *(Russian)* 77−4593
^{240}Pu, isotope composition tables for isotopes produced in CANDU reactors 78−29564
^{240}Pu, level density calc., shell and pairing effects, deformation, excitation energy dependence 79−67662
^{240}Pu levels via ^{236}U α-decay *(Russian)* 77−82882
^{240}Pu, mass distribution of fragments from spontaneous fission *(Russian)* 78−29517
^{240}Pu, moments of inertia of fissioning isomers, cranking model 78−74299
^{240}Pu, nucl. shape at first saddle point 77−74756
^{240}Pu passive assay by neutron detection, theoretical response of counters 79−22570
^{240}Pu, radial depend. of shell model pot. *(Russian)* 78−41655
^{240}Pu, reson. in isomeric and prompt fission probabilities 78−78429
^{240}Pu resonance capture in reactor cell codes, parametric description 79−13384
^{240}Pu, rotational band struct. in deformed doubly even nuclei, two fluid model 77−10341
^{240}Pu subbarrier resonances and fission probabilities from ^{239}Pu(d,pf) 79−13266
^{240}Pu-fission, P-odd neutron emission asymmetry *(Russian)* 78−74413
$^{240}Pu^m$, shape isomer, half-life and excitation function meas. *(Chinese)* 78−78253
^{240}Pu(n,2n), ^{239}Pu fission isomers, half lives 77−30641
^{240}Pu(n,f), 14.8 MeV, products from ^{66}Ni to ^{169}Er, mass distrib., total chain yields 78−25255
^{240}Pu(n,f), 500-10000 eV, subthreshold fission structure 77−23143
^{240}Pu(n,f), cross section, barrier heights, widths, intermediate structure theory 77−34357
^{240}Pu(n,f), mass yield distrib. and absolute fission yields 79−13356
^{240}Pu(n,f) 10 to 250 keV, subthreshold neutron fission cross section meas. 79−22344
^{240}Pu(n,γ), average cross section from 200 eV to 350 keV 77−50129
^{240}Pu(n,γ) cross section meas., thermal to 350 keV 77−23034
^{241}Pu compound nucleus lifetime by the shadow effect in ^{238}U(^{3}He,f) *(Russian)* 78−86562
^{241}Pu dosimetry, applicability of methods used for ^{239}Pu alphas 77−90906
^{241}Pu, evaluation of neutron cross sections in region 10^{-5} eV to 15 MeV 78−17254
^{241}Pu half life from α-spectrometry and ^{241}Am ingrowth 80−68609
^{241}Pu half-live determ. by mass spectrometry 80−78232
^{241}Pu isomeric state non-existence 80−105983
^{241}Pu, isotope composition tables for isotopes produced in CANDU reactors 78−29564
^{241}Pu level structure and γ-transitions from ^{245}Cm decay 80−105980
^{241}Pu, multilevel resonance parameters for 0.01 to 100 eV neutrons 79−36154
^{241}Pu, neutron capture and fission cross sections, 0.01 eV-30 keV 78−29512
^{241}Pu, neutron resonances, probability table method and correlated data 79−36284
^{241}Pu, statistical anal. of reson. neutron fission cross section 77−38305
^{241}Pu, third IAEA evaluation of 2200 m/s, 20°C Maxwellian neutron data 77−23136
^{241}Pu(n, f) thermal-neutron fission, determ. of cumulative fission yields 79−54462
^{241}Pu(n,f), 0.01-50 eV, fission cross-section, Westcott g_f factors 77−23153
^{241}Pu(n,f), thermal neutron fission, kinetic energy distribs. determ. 78−658
^{241}Pu(n,f) 1 keV to 30 MeV neutrons, cross section meas. rel. to ^{235}U 79−36286
^{241}Pu(n,f) fission cross section meas., 8 eV to 70 keV 77−50168
^{241}Pu(n,f) thermal, correlation for independent fission prod. yield uncertainties 78−50216
^{241}Pu(n,γ) cross section meas., thermal to 350 keV 77−23034
^{242}Pu, 50 to 250 keV, cross-section ratios c.f. ^{197}Au 79−22281

nuclei with mass number 220 or higher continued
^{242}Pu half life relative to ^{238,239}Pu, α-activity and atom ratios 80−5100
^{242}Pu, half-life meas. 78−17154
^{242}Pu halflife from precise low-temp. heat capacity meas. on PuF_3, PuF_4, PuO_2 77−2952
^{242}Pu, isotope composition tables for isotopes produced in CANDU reactors 78−29564
^{242}Pu, isotope form. calc., effect of reactor characts. 79−26489
^{242}Pu level scheme from ^{242}Np β-decay 79−67664
^{242}Pu, neutron capture cross-section, 5-70 keV 77−23055
^{242}Pu, radiative capture cross section for fast neutrons 78−82351
^{242}Pu to ^{253}Es, multigroup neutron cross sections 77−26754
^{242}Pu+n, 10 keV-20 MeV, ENDF/B-V cross sections 80−22837
^{242}Pu(^{48}Ca,xn), production of superheavy elements with A=114-116 78−29493
^{242}Pu(α,f), fragment mass distrib., and yield, statistical anal. *(Russian)* 80−5183
^{242}Pu(d,p)^{243}Pu, populating Nilsson and rot. levels 77−6202
^{242}Pu(d,t)^{243}Pu, populating Nilsson and rot. levels 77−6202
^{242}Pu(μ,f), radiationless muonic transition induced fission, fission dynamics probe, friction coeff. 80−78336
^{242}Pu(n,f), cross section, barrier heights, widths, intermediate structure theory 77−34357
^{242}Pu(n,γ)^{243}Pu, populating Nilsson and rot. levels 77−6202
^{243}Pu, J^{π}, Nilsson and rot. bands via (n,γ), (d,p) and (d,t) 77−6202
^{243}Pu(n,f) near threshold cross-section calcs. 77−65240
^{244}Pu, existence in early solar system 77−29663
^{244}Pu fast neutron fission cross-section 77−18636
^{244}Pu levels via ^{248}Cm α-decay *(Russian)* 77−82882
^{244}Pu, production of haloes in minerals, role of fission alpha particles 77−29300
^{244}Pu, Xe and Kr induced fission at Coulomb barrier energies 77−61467
^{244}Pu(n,2n)^{243}Pu, E_n=14 MeV, search for finite isomer 77−54222
^{244}Pu(n,γ) resonance integral meas. 80−73846
^{246}Pu excited states, mass excess and shell gap, L=0 transition from ^{244}Pu(t,p) 80−9236
^{293}Pu, polymeric, effects on erythrocyte survival in mice 77−9227
^{294}Pu, muonic atom direct electroprod., finite nuclear size effects *(Russian)* 80−69272
Pu(α,n), determination system by passive neutron counting 79−40985
Pu(γ,γ) 12.754 MeV, Delbruck scatt., Coulomb correction terms, differential cross sections 80−27629
Pu(n,f), 0-18 MeV, prompt neutron spectrum, evaporation model *(Chinese)* 80−42721
Pu(n,f), A=240, 241, 242, cross-sections meas. in range 0.001-30 MeV 77−26809
Pu(n,f), A=241, 243, subthreshold fission, fine struct. resonances anal. 78−652
Pu(n,f), delayed neutron spectra from thermal- and fast-neutron fission, reactor calcs. 77−34355
Pu(n,f), thermal to 14.7 MeV, statistical theory calcs. 77−23137
^{226,228}Ra in humans, radiation induced malignancies 78−96075
Ra, even isotopes, $K=0^+$, 0^- bands, energies, inverse moments of inertia 80−63063
Ra, fission products mass, charge, kinetic energy distribs., scission-point model based on deformed shell effects 77−10455
Ra, osteosarcomogenic effectiveness of ^{224}Ra and ^{226}Ra in mice 77−86560
^{214}Ra in liq. ^{206}Rb, $(h_{9/2})^n$ proton states, Knight shifts and absolute mag. moments 77−82821
^{223}Ra decay chain, precise γ-ray spectroscopy 77−54175
^{223}Ra, excited states, half-life meas. *(French)* 79−97679
^{224}Ra and daughters, radioactive props. and biological behaviour 78−96090
^{224}Ra and thorotrast radiobiological significance 78−96076
^{224}Ra biological effects, conf., Alta, USA (July 1974) 78−96068
^{224}Ra effects on osteocytes from mouse proximal tibial metaphysis, early ultrastruct. changes 77−37020
^{224}Ra, endosteal cell dose and relative distrib. factors compared to ^{226}Ra 78−96091
^{224}Ra, hyperfine field determ. in ferromagnet 77−85622
^{224}Ra injections into humans, soft-tissue effects 78−96070
^{224}Ra injections into humans, skeletal effects 78−96071
^{224}Ra preparation, for ankylosing spondylitis therapy 78−96089
^{224}Ra, short-lived α-emitter, late effects after incorporation in mice 78−96069
^{224}Ra usage in radiotherapy and radiobiology, brief history 78−96085
^{224}Ra use in treatment of ankylosing spondylitis and rheumatoid synovitis 78−96086
^{225}Ra rotational band level diagram from α-decay and conversion electrons 80−18156
^{226}Ra (n_{th},f), upper bound to cross-section determ. *(Russian)* 77−14201
^{226}Ra background levels in lower troposphere from coal burning 77−37361
^{226}Ra brachytherapy source calibration using $Fe(NH_4)_2(SO_4)_2$-benzoic acid-xylenol orange dosimeter 77−5081
^{226}Ra, conc. in New Zealand soil, rel. to Fe, K content 77−86867
^{226}Ra decay chain, γ-ray energies meas. for Ge(Li) detector calibration 80−27865
^{226}Ra, determ. in environmental samples by ^{222}Rn separation, integral counting methods 77−63988
^{226}Ra determination in water, sampling and meas. methods 77−9278
^{226}Ra dosimetry in bone 77−16993
^{226}Ra, exposure-rate calibration of small radioactive sources 78−41881
^{226}Ra fission expt. data, review *(Russian)* 79−49641
^{226}Ra, hyperfine field determ. in ferromagnet 77−85622
^{226}Ra leaching from contaminated soils, investigation of Ra bearing soils from Port Hope, Ontario 79−20900
^{226}Ra leaching from fossil bones 78−58562
^{226}Ra levels from ^{230}Th α decay, search for $K^{\pi}=0^+$ excited states 78−86504
^{226}Ra, radionuclide determ. in coastal marine sediments and seawater 79−88370
^{226}Ra source leakage testing by mailed track detector method 77−60264
^{226}Ra, total enutron cross-section up to 1 keV 77−26745
^{226}Ra(p,f), 12 MeV, prompt neutron energy distrib. meas. 78−13182
^{226}Ra(p,f), 12 MeV, prompt γ-ray spectra meas. 78−13183
^{228}Ra, radionuclide determ. in coastal marine sediments and seawater 79−88370
^{228}Ra-^{228}Ac decay and ^{228}Th decay chain, gamma ray energies 79−85857

nuclei with mass number 220 or higher continued
^{228}Ra-Be (α,n) source, neutron spectrum calc. from angular distrib. and cross-section data 78−41882
^{230}Ra decay, ^{230}Ac levels, J^{π} and transitions, Nilsson assignments 80−68543
^{230}Ra, identification and β-decay meas. 77−22963
^{230}Ra levels, J^{π} and transitions, Nilsson assignments from ^{230}Ac decay 80 68543
^{230}Ra, prod., decay characts. 78−54724
Rn, A-220, 2, α-particle meas. by solid-state track detectors 78−25396
Rn alpha particle etch pits in CA80-15 and LR-115 cellulose nitrate track detectors 78−855
Rn and Tn, air concentration in dwelling places *(Hungarian)* 77−78409
Rn detection, effect of humidity 77−6647
Rn, even isotopes, $K=0^+$, 0^- bands, energies, inverse moments of inertia 80−63063
Rn high spin isomers, deformed independent particle model, yrast lines, shape 79−480
Rn, isotope separation by barrier technique, U prospecting appl. 78−21770
Rn, neutron-deficient isotope, yield meas. from Ir+^{20}Ne at 200 MeV *(Russian)* 77−23104
^{220}Rn, decay products, diffusion coeffs. in air and Ar 79−90366
^{220}Rn decay products attachment to flowing aerosols using centrifuge 80−61167
^{221}Rn, decay scheme, α-, β-, γ-spectra meas. 79−6507
^{222}Rn, and its descendants, radioactivity in low atmosphere, pollution-dust dynamics *(Rumanian)* 80−12524
^{222}Rn concentrations in water, rapid meas. with commercial liq. scintillation counter 78−28339
^{222}Rn content in air, diffusion in lower atm., U deposits prospecting appl. *(Spanish)* 77−78303
^{222}Rn daughter conc., meas. sensitivity computer optimisation 78−49126
^{222}Rn daughter dose estimates from area sources 78−94151
^{222}Rn daughters emission and enrichments from Etna volcanic magma 77−21736
^{222}Rn, decay products, diffusion coeffs. in air and Ar 79−90366
^{222}Rn determination in air and water, sampling and meas. methods 77−9278
^{222}Rn flux measurement using charcoal canister 77−6646
^{222}Rn implanted in Cu, Si and SiO_2, TIPAC meas. 78−43732
^{222}Rn meas. for uranium prospecting 79−53573
^{222}Rn, meas. of concs. in Earth using nuclear track technique 79−53574
^{222}Rn, passive environmental monitor based on exoelectron dosimeter 78−82523
^{222}Rn, props. and behaviour of short lived daughter nuclides in the atmos. *(Japanese)* 80−72339
^{222}Rn, release to atm. due to UK coal combustion, annual rate of release determ. 80−17143
^{222}Rn released by uranium tailings piles, potential population dose 79−85824
^{224}Rn→^{224}Fr±^{224}Ra, γ−rays, internal conversion, eγ coincidence spectra meas. 80−78216
^{224}Rn→^{224}Fr→^{224}Ra decay, γ-rays IC electrons and eγ coincidences 80−18239
Sm, enriched isotopes, EBR-II irrad., integral cross sections 79−67843
^{159}Tb(^{14}N,αxn)$^{169-x}$Yb, 95 MeV, γ-ray identification 77−57697
Th, 380 MeV, binary decay induced by K^- 79−93671
Th, even isotopes, $K=0^+$, 0^- bands, energies, inverse moments of inertia 80−63063
Th, fast neutron total cross section, 0.1 to 5.0 MeV 78−58278
Th isotopes, evidence for triple humped fission barrier *(French)* 79−520
Th isotopes, quadrupole and hexadecapole deforms., model independ. parameters using Fermi distrib. 78−17096
Th, K^- meson induced fission at 700 MeV/c, fragment mass distrib. 78−13168
Th, metal rods, neutron capture, effective resonance integral meas. 77−71653
Th, neutron absorption cross section shape near thermal energy 77−46204
Th, neutron total cross-section meas. near 24 keV 78−29456
^{232}Th fission by 14 MeV neutrons, rare gas yields measured by emanation method *(French)* 77−30640
Th-^{233}U data for thermal reactor, integral testing 79−67833
Th-mica system, neutron dosimetric meas. using fission fragment track technique 78−13347
Th-U, neutron group cross sections in resolved resonance region calcs. 80−13573
Th-U-Pu, neutron group cross sections in resolved resonance region calcs. 80−13573
Th+Ar, 388 MeV, deep inelastic reactions, double differential cross section calc. 78−8856
Th+π^-, neutron multiplicity distrib. *(Russian)* 78−41783
Th(^{40,44,48}Ca,f), isotope and mass distribs. of fragments *(Russian)* 77−74897
^{A}Th (A=230,232), fission penetrabilities, three-hump model of fission barrier 79−26419
^{A}Th, A=231, 233, vibr. band systematics, excitation energies and rot. parameters 79−36137
^{232}Th(n,f), 1 eV-100 keV, subthreshold fission widths 77−26798
^{227}Th, short-lived α-emitter, late effects after incorporation in mice 78−96069
^{228}Th decay, γ-ray and internal conversion intensities 78−41669
^{228}Th, high pressure meas. of gamma transitions 80−18225
^{228}Th, precise γ-ray energy meas. with Ge(Li) detectors 78−13376
^{228}Th source, selective separation of ^{212}Bi 77−40566
^{229}Th levels from γ-spectra following ^{233}U decay 77−26636
^{230}Th alpha-decay half life from specific activity method 80−102157
^{230}Th α-decay, search for the $K^{\pi}=0^+$ excited states in ^{226}Ra 78−86504
^{230}Th, precise γ-ray energy meas. with Ge(Li) detectors 78−13376
^{230}Th, total neutron cross-sections in thermal energy region 77−26745
^{230}Th(d,p), 17 MeV, form-factor and multistep effects 77−79388
^{230}Th(n,f), 0.68-1.10 MeV, fission fragment ang. distribs., resonance and moment of inertia 80−102219
^{230}Th(n,γ), 680-1050 keV, fission barriers and cross sections, fragment ang. distribs. 80−18357
^{231}Th, asymmetrically deformed, rot. bands from ^{230}Th (n,γ) 79−3068
^{231}Th β decay and ^{235}U α decay, γ-radiation study, energy level scheme *(Russian)* 78−17160
^{231}Th excited states and bands, spins, γ-transitions from ^{230}Th(n,γ) 80−57699

nuclei with mass number 220 or higher continued
^{231}Th, L2/L3 vacancy ratio for internal conversion by γ-X-ray coincidence technique *(Spanish)* 79−97682
^{231}Th, levels via ^{230}Th(d,p) 17 MeV 77−79388
^{231}Th, rotational band level diagram from α-decay and γ-transitions 80−18156
^{232}Th, ^{4}He ion-induced fission, ^{148m}Pm, ^{148g}Pm independent form. cross-sections 78−33228
^{232}Th, 24 keV neutron capture cross section meas. with Fe-filtered neutron beam 79−40910
^{232}Th (^{40}Ar, X), differential cross sections calc. from random matrix model transport theory 79−49634
^{232}Th (^{7}Li,α)^{235}Pa, 12 to 20 MeV excitation, ang. distrib. of evaporation residues, determ. of Γ_n/Γ_f 77−61451
^{232}Th (e, f), 7-65 MeV, absolute electrofission cross sections, fragment ang. distribs. 80−5185
^{232}Th (γ, f), deep subbarrier photofission ang. anisotropy from fragment ang. distrib. *(Russian)* 79−97739
^{232}Th (n,2n)^{233}Th, testing of ENDF/B-IV Th data in GCFR lattice 79−67836
^{232}Th absolute fission rate in spherical fusion blanket assemblies 77−67871
^{232}Th, α-decay half-life, liq. scintillator expt. for students 78−12496
^{232}Th, collective props., HF calcs., review 78−50064
^{232}Th, conc. in New Zealand soil, rel. to Fe, K content 77−86867
^{232}Th, decay consts. for use in geochronology and cosmochronology 78−28189
^{232}Th, deformation effects on neutron total cross-sections, adiabatic coupled-channel calc. 79−17896
^{232}Th, delayed neutron parameters selection for reactor calcs. *(Slovak)* 78−21534
^{232}Th, effect of isomer shelf in photofission cross sections *(Russian)* 79−9648
^{232}Th fast fission yield of tritium, implications for FBRs 77−46195
^{232}Th fission, isotopic mass dispersion discontinuity, neutron shell effect 79−45312
^{232}Th, fission, proton induced, 1 GeV, cross section *(Russian)* 78−94041
^{232}Th, fission barrier heights from β-delayed fission, β-strength functions struct. 80−5184
^{232}Th, fission rates measured in graphite-reflected lithium assembly, nonelastic neutron anisotropy effect 78−29511
^{232}Th fuel, conversion and fission yield, irradiation expt. 78−86609
^{232}Th, giant dipole resonances of deformed even-even nuclei, semimicroscopic calcs. 77−50096
^{232}Th, giant resonance in total photoabsorpt. cross section 77−6347
^{232}Th, highly deformed, muonic X-rays, nuclear charge distrib., elec. quadrupole moment 78−70440
^{232}Th, in aq. soln., assay by pulsed neutron interrogation 78−68966
^{232}Th, induced fission in natural systems, radiochem. obs. 78−4966
^{232}Th level structure and decay parameters from (n,n′) and (n,n′γ) meas. 77−30494
^{232}Th, mirror hybrid reactors 80−42860
^{232}Th, muonic, μ induced prompt fission, fate of the μ 78−86557
^{232}Th, muonic, n emission from radiationless muonic transitions and μ capture 79−3599
^{232}Th muonic atom, n emission, bound μ influence on fission barrier 78−89845
^{232}Th, μ capture rate in the fission mode, μ lifetime 78−89827
^{232}Th, neutron cross section meas. 80−526
^{232}Th neutron cross sections, optical and statistical model calcs., reactor appls. 77−54227
^{232}Th neutron cross sections calc. for inelastic scatt., radiative capture and (n, 2n) 79−30829
^{232}Th, neutron elastic and inelastic cross sections, 2.5 MeV, comparison with optical model 77−30595
^{232}Th, photofission, determ. of neutron multiplicities 80−32311
^{232}Th, quadrupole photofission and role of nucl. symm. *(Russian)* 78−17258
^{232}Th, rotational band struct. in deformed doubly even nuclei, two fluid model 77−10341
^{232}Th, status of nuclear data 79−67793
^{232}Th, subCoulomb fission induced by Xe and Kr, excitation functions 77−3061
^{232}Th subthreshold photofission 78−66323
^{232}Th target nucleus spallation, ^{10}He isotope search *(Russian)* 80−5110
^{232}Th, thermal Westcott g-factor meas. 78−37287
^{232}Th three hump fission barrier, photofission cross section and half life 79−67788
^{232}Th, total muon-capture rate meas. 77−79335
^{232}Th, transition effects in total photoabsorpt. cross section 77−46160
^{232}Th, vibr. states, Coulomb excitation 79−9432
^{232}Th, Xe and Kr induced fission at Coulomb energies 77−61467
^{232}Th/^{238}U neutron capture cross section ratio, direct determ. for reactor lattices 77−50137
^{232}Th-^{238}U containing lattices, direct meas. of relative capture rates 77−61403
^{232}Th+^{12}C, 78 MeV, fission fragment angular distrib., shape of saddle point of compound nucleus *(Chinese)* 78−78427
^{232}Th+^{16}O, 140, 315 and 33600 MeV, isotope yields and cross sections 77−14161
^{232}Th+^{16}O, 140 and 315 MeV, energy depend. of heavy ion peripheral reactions 78−74399
^{232}Th+^{16}0, fission following transfer below Coulomb barrier 79−22346
^{232}Th+^{19}F, fission following transfer below Coulomb barrier 79−22346
^{232}Th+^{22}Ne, 172 MeV, energy spectra and isotope prod. with 4≤Z≤9 77−57680
^{232}Th+^{40}Ar, 213 MeV/A, complex fragment emission study 79−6667
^{232}Th+^{40}Ar, 288 MeV phenomenological approach to deeply inelastic collisions 79−54449
^{232}Th+^{40}Ar, 388 MeV, differential cross section calc., statistical model 78−50192
^{232}Th+^{40}Ar, 390 MeV, Z≤38 products energy spectra, reaction mechanism, dynamic deformation *(Russian)* 78−89909
^{232}Th+^{40}Ar(^{63}Cu), deep inelastic reactions, isotopic distribs., n excess degree of freedom relaxation 80−9308
^{232}Th+^{86}Kr, Coulomb-nuclear interference for high spin states 78−46097
^{232}Th+α, 19.8 to 27.2 MeV, elastic scatt. or capture and fission, optical model pots. 77−88181
^{232}Th+n, 0.1-18 eV, neutron total cross section determ. 80−22838

nuclei with mass number 220 or higher continued
^{232}Th+n, 14 MeV interactions, neutron and γ-ray spectra meas 79−93612
^{232}Th+n, strength functions and scatt. lengths from total and scatt. cross sections 77−26706
^{232}Th(^{14}B,^{12}B), 129 MeV, ^{12}B spin polarisation 80−63161
^{232}Th(^{16}O,X), (X=^{16}N,^{15}N,^{14}C,^{13}C,^{12}C or ^{11}B), surprisal anal., maximal entropy condition, Q-value depend. 79−9606
^{232}Th(^{16}O,γ), transfer induced fission, excitation functions and cross sections 80−13515
^{232}Th(^{19}F,γ), transfer induced fission, excitation functions and cross sections 80−13515
^{232}Th(^{3}He,n), 33.3 MeV, cross sections, DWBA anal. for data near Z=82 79−67733
^{232}Th(^{40}Ar, X), deep inelastic reaction, neutron excess degree of freedom relaxation model *(Chinese)* 80−102202
^{232}Th(^{63}Cu, X), deep inelastic reaction, neutron excess degree of freedom relaxation model *(Chinese)* 80−102202
^{232}Th(α,X), 140 MeV, nonequilibrium light charged particle yield, energy spectra and ang. distribs. 79−40942
^{232}Th(α,α′), 120 MeV, isoscalar giant resonances, DWBA anal. 80−42621
^{232}Th(α,α′f), total kinetic energy release 80−27682
^{232}Th(α,f), 19-27 MeV, integral and differential cross sections, anisotropy energy depend. *(Russian)* 80−37407
^{232}Th(α,f), 25.8-41.4 MeV, fragment ang. momentum determ. 77−82975
^{232}Th(α,x), 140 MeV, spallation and fission product yields 80−13512
^{232}Th(d,X), 70 MeV, charged light particle spectra and ang. distribs. exciton anal. 79−40935
^{232}Th(d,2n)^{232}Pa, 10-26 MeV, excitation function meas. 77−79391
^{232}Th(d,f), 2.1 GeV, binary and ternary fission kinetics *(French)* 78−70577
^{232}Th(d,t)^{231}Th, 17 MeV, form-factor and multistep effects 77−79388
^{232}Th(e,e′f), 20-120 MeV, electrofission cross section, E1, E2 strengths 78−13174
^{232}Th(e,f), 110 MeV electrons, mass and kinetic energy distribs. 79−93672
^{232}Th(γ,X) 5-18.3 MeV, photoneutron and photofission cross sections, giant resonance and deformations 80−68712
^{232}Th(γ,f), 15-55 MeV, photofission symmetric and asymmetric yields 80−83135
^{232}Th(γ,f), 9, 15, 38 MeV peak bremsstrahlung 78−33229
^{232}Th(γ,f), bremsstrahlung of 600 MeV max. energy, fragment energy correl. meas. 77−71630
^{232}Th(γ,f), deep subthreshold photofission, double humped fission barrier anal., shape isomer 80−5179
^{232}Th(γ,f), fission-neutron and fragment ang. distrib. 77−65239
^{232}Th(γ,f), sub-barrier photofission, triple humped fission barrier profile 78−58311
^{232}Th(γ,γ) 2.754 MeV photons, Delbruck scatt., differential cross section meas. 79−26422
^{232}Th(n,2n), 13-18 MeV, cross sections, pre-equilibrium contrib. 79−45258
^{232}Th(n,2n), ratio to (n,γ) in fast reactor, direct meas. 80−102233
^{232}Th(n,2pn), ^{230}Ra and Ac prod. 78−54724
^{232}Th(n,f), 0.1-30 MeV, subthreshold cross-section meas. 77−74894
^{232}Th(n,f), 1 eV to 20 keV, cross section meas. 79−67794
^{232}Th(n,f), 14.8 MeV, peak to valley ratio of mass distribs. 77−26801
^{232}Th(n,f), 1.35-2.1 MeV, $\bar{\nu}p$ values 77−74893
^{232}Th(n,f), 1.35-5.3 MeV, yields and kinetic energies, vibrational states 79−45307
^{232}Th(n,f), 1.38 MeV, prediction of fission-product mass yields and related parameters 79−30862
^{232}Th(n,f), 1.55-3 MeV, mass asymm., ang. anisotropy of fragments *(Russian)* 78−17265
^{232}Th(n,f), 2-8 MeV, fission product yields and mass distribs. 80−86939
^{232}Th(n,f), 35 to 1500 keV, near equilib. delayed neutron energy spectra 77−34354
^{232}Th(n,f), barriers of emitted fragments, fission asymm. *(Russian)* 77−10459
^{232}Th(n,f), cross section up to 6 MeV, rotational states obs., fragment ang. anisotropy 77−23161
^{232}Th(n,f), cross sections, semi-empirical formula 80−22864
^{232}Th(n,f), fast neutrons, delayed neutron spectra, reactor calcs. 77−34355
^{232}Th(n,f), fast neutrons, fission product mass distribs. 77−74896
^{232}Th(n,f), fission fragment ang. distribs., triplet-humped fission barrier 77−74892
^{232}Th(n,f), fission spectrum averaged cross section 78−17253
^{232}Th(n,f), prompt-neutron ang. distrib. 77−65238
^{232}Th(n,f), studied with intense neutron spectrometer 77−23364
^{232}Th(n,f), thermal to 14.7 MeV, statistical theory calcs. 77−23137
^{232}Th(n,f), thermal-neutron sub-barrier fission 77−74891
^{232}Th(n,f), yield meas. of Kr, Xe, Sn, Sb, proton odd-even and neutron shell effect 77−82976
^{232}Th(n,f), yields of ^{131,132}Sn, $^{131-133}$Sb isotopes determ. 78−89923
^{232}Th(n,f) cross-section meas., rotational bands 77−26803
^{232}Th(n,f) Kr and Xe isotope yields 78−74410
^{232}Th(n,γ), cross-section from 2.6-800 keV 78−8807
^{232}Th(n,γ), effective cross section dependence on thermal neutron temp. 80−547
^{232}Th(n,γ), ratio to (n,2n) in fast reactor, direct meas. 80−102233
^{232}Th(n,γ) uncertainty file, for sensitivity anal. of fast reactor system 79−67835
^{232}Th(n,γ)^{232}Th, testing of ENDF/B-IV Th data in GCFR lattice 79−67836
^{232}Th(p, f), 35-85 MeV, light mass nuclide charge dispersion curves for A=76-79 80−18349
^{232}Th(p, spallation), spallation cross section and recoils, range calcs. computer code MARLOWE 79−93736
^{232}Th(p,X), 10-100 MeV, spallation residue excitation functions, fissionability 80−18353
^{232}Th(p,f), 28 GeV, charge dispersion, mass yields 77−3062
^{232}Th(p,f), 29-97 MeV, Rb, In and Cs relative independ. yields, charge division 80−102218
^{232}Th(p,f), 4-7 MeV, cross sections *(Russian)* 78−41794
^{232}Th(p,f), 9.5-17 MeV, symmetric to asymmetric mass ratios for fragments 80−5178
^{232}Th(p,p′), 35 MeV, extraction of deform. parameters 78−54755
^{232}Th(p,p′), 35 MeV, ground state rot. band and multipole moment 80−32178

nuclei with mass number 220 or higher continued
Th(p,p'f), 52.5 MeV, fission probability 80−99195
Th(p,x), x=α, π, 72 MeV, spectra and angular distribs. 80−68660
Th(π⁻, f), resting pions, delayed fission search *(Russian)* 80−52704
Th, excited levels, using thermal and average reson. neutron capture in ^{231}Th 79−45166
^{232}Th, moment of inertia in shape isomeric deform., from ^{232}Th(n,f) 77−23161
^{232}Th neutron cross sections, optical and statistical model calcs., reactor appls. 77−54227
^{232}Th, vibrational states determ. following (n,e⁻) 77−30514
^{232}Th(N,N'), deformed nuclei struct., rot. model with optical pot., coupled channel formalism 79−3146
^{232}Th(α,α') 120 MeV, isoscalar giant quadrupole resonance fission decay channel inhibition 79−54419
^{232}Th(n,f), 1.2-2.3 MeV, transition state effect on fragment KE *(Russian)* 78−661
^{234}Th, anomaly in fission penetrability through a triple humped pot. barrier 79−3132
^{234}Th β⁻ decay into ^{234}Pa isomers, low energy γ-spectrum 78−70493
^{234}Th fission, three-hump pot. barrier 77−18635
^{234}Th, JWKB approximation for multiple-humped fission barriers 78−585
^{234}Th, penetration through three peaks barrier, semiclassical approx. *(Russian)* 79−9544
^{234}Th, separation from natural U by extraction column chromatography using TnOA and filter paper 79−43659
Th(α,f), 0.65, 1.74, 4.12 GeV, fission fragment recoil characts. 78−89925
Th(α,f), 0.65-4.11 GeV, cross sections for binary and ternary fission 77−3055
Tn alpha particle etch pits in CA80-15 and LR-115 cellulose nitrate track detectors 78−855
^{235,238}U(n,f), fast neutrons, fission product mass distribs. fission product mass distribs. 77−74896
U, 380 MeV, binary decay induced by K⁻ 79−93671
U (M,f), muon excitation probabilities, muonic atoms, Schrodinger eqn. 80−47515
U, A=233, 235, 238, delayed neutron parameters selection for reactor calcs. *(Slovak)* 78−21534
U, A=234,238, giant dipole resonances of deformed even-even nuclei, semimicroscopic calcs. 77−50096
U, A=235, 238, fission, proton induced, 1 GeV, cross section *(Russian)* 78−94041
U, A=235, 238, highly deformed, muonic X-rays, nuclear charge distrib., elec. quadrupole moment 78−70440
U, A=235, 8, total muon-capture rate meas. 77−79335
U anal. of natural waters by fission tracks 78−82587
U analysis in phosphate fertilisers and other materials using liq. scintillation spectrometry 78−53280
U and daughter prods., conc. in fossil bones from N. Greece, γ-spectroscopy, activation anal. 77−60161
U, decontamination, sorption and distillation methods, review *(Czech)* 78−82496
U, deformation energy surface, two-centre shell model calc. 77−71559
U enriching gas centrifuge cascade, reflux effect, enrichment enhancement control 77−54346
U, even isotopes, K=0⁺, 0⁻ bands, energies, inverse moments of inertia 80−63063
U FBR fission yield, burnup determ. in mixed oxide fuels 77−23138
U, fission cross section calculations 77−26661
U fission cross section trend, 3-5 MeV, statistical model description 77−23126
U fission products γ-ray and photoneutron spectra 77−23127
U fission products mass, charge, kinetic energy distribs., scission-point model based on deformed shell effects 77−10455
U gamma abundances 77−65270
U isotopes, ENDF/B-4 cross sections, integral data 77−23200
U isotopes (234, 237) separation, chemical treatment of irrad. targets *(French)* 77−26883
U, K⁻ meson induced fission at 700 MeV/c, fragment mass distrib. 78−13168
U linear polarisation of elastically scatt. γ-rays of 279 and 662 keV 77−6344
U mill tailings, radiological criteria 78−82480
U mills, radioactivity release meas. 78−82479
U mine radon control research 78−82525
U mineral deposits, criticality study using ore model *(Spanish)* 77−70655
U minerals, Pu content, ore model calcs. comparison with expt. *(Spanish)* 77−70654
U, proton-induced fission at 400 GeV, ternary to binary event ratio 78−13170
U, Pu fission by thermal neutrons, HIAWATHA, fission-fragment recoil mass spectrometer 78−16892
U, Rayleigh and Delbruck scatt., 6.8-11.4 MeV 77−26669
U spontaneously fissionable isomers, excitation by K shell e⁺ annihilation, shape isomery model *(Russian)* 79−30802
U^{233}, product separation asymmetry in fission by slow polarised neutrons *(Russian)* 80−106088
^{238}U fission by 14 MeV neutrons, rare gas yields measured by emanation method *(French)* 77−30640
U-mica system, neutron dosimetric meas. using fission fragment track technique 78−13347
U-Th, neutron group cross sections in resolved resonance region calcs. 80−13573
U+^{12}C, 25.2 GeV, large collision residues and fission 77−71618
U+^{136}Xe, 1080 MeV, reaction mechanisms obs. with mica detectors 77−79399
U+^{136}Xe, search for superheavy elements 79−6692
U+^{20}Ne, 250 and 400 MeV nucleon^{-1}, inclusive proton production, classical many-body calc. 79−17918
U+^{20}Ne, quark matter, signature in nuclear fireball model 80−37395
U+^{20}Ne, relativistic nuclear collisions, inclusive ρ spectra, knock-out mech. 77−82950
U+^{4}He, relativistic nuclear collisions, inclusive ρ spectra, knock-out mech. 77−82950
U+^{4}He(^{20}Ne) fireball model for proton inclusive spectra 77−6339
U+^{84}Kr, 800 MeV, reaction mechanisms obs. with mica detectors 77−79399
U+Ar, 4-17 GeV, search for ultradense nuclei 77−3044

nuclei with mass number 220 or higher continued
U+Kr, solid state detector investigs. *(German)* 77−14321
U+Ne→p+X, high energy heavy ion collisions, comparison of models 78−46088
U+p, 1 to 28.5 GeV production of 43≤A≤51 nuclides, reaction mechanisms 77−34301
U+p, 7 GeV/c hadron multiple prod. *(Russian)* 79−22298
U+p, 700 MeV, search for polyneutron systems 77−50064
U+p, fragmentation, 800 MeV beam, obs. of new nuclides ^{27}Ne, ^{31}Mg, ^{32}Mg, ^{34}Al, ^{39}P 77−61419
U+p, particle-stable neutral nuclei prod. search, multi-GeV energies 78−25189
U+Pb, 750 MeV, classical model, kinetic energy, ang. distribs., instantaneous fission fragments 78−13185
U+π⁻, 7 GeV/c hadron multiple prod. *(Russian)* 79−22298
U+U, positron prod. 78−50197
U+U, positron prod. in heavy ion collisions 78−50198
U+U high energy nuclear collisions, large baryon densities prod. 78−86540
U(^{40,44,48}Ca,f), isotope and mass distribs. of fragments *(Russian)* 77−74897
U(^{56}Fe,X), relativistic ^{56}Fe fragmentation, charge and mass changing cross sections 79−54453
U(^{3}He, f), 530 MeV, cross section meas. by glass solid state track detectors 78−13179
U(Ne,X), 250, 400, 800 MeV/N, nuclear matter collective sideward flow, nuclear fluid dynamics 80−57715
U(Ne,X), 250, 400 MeV/N direct vs. thermal particle emission, inclusive cross sections 80−52688
U(Ne,X), proton inclusive spectra, direct plus thermal model 80−57799
U(Ne,n)X, 337 MeV/N inclusive double differential neutron prod. cross sections 80−32294
UO_2/PuO_2 fuelled assemblies, integral meas. of effective delayed neutron fractions in FTR SNEAK 77−6497
UO_2(α,n), 3.6 to 8 MeV, neutron yields 79−6651
U(^{208}Pb, f), 1535 MeV, direct evidence for multiple sequential fission 79−30866
U(^{238}U, f), 1785 MeV, direct evidence for multiple sequential fission 79−30866
U(Xe,f), Coulomb fission problem, uniform semi-classical approach to forbidden transitions 79−36287
^{A}U, A=232, 234, 236, octupole-octupole residual interactions and low lying 0⁺ excited states 79−36136
^{A}U, A=233, 235, 238, deformation effects on neutron total cross-sections, adiabatic coupled-channel calc. 79−17896
^{A}U, A=235, 236, 238, determ. of neutron multiplicities 80−32311
^{A}U, A=235, 238, muonic, n emission from radiationless muonic transitions and μ capture 79−3599
^{A}U, A=235, 238, relative probabilities of photofission by bremmstrahlung γ *(Russian)* 79−9646
^{A}U A=235, 239, vibr. band systematics, excitation energies and rot. parameters 79−36137
^{A}U, A=235,238, fission product beta decay, ν̄ spectra 80−102150
^{A}U, A=236, 238, strength function of β-transitions, probability of delayed fission 80−22764
^{A}U, A=236,238, fission isomer rot. spectra $I^2(I+1)^2$ correction 80−18229
^{A}U, A=237,238, nuclear excitation rate for low lying states, e and γ induced transitions 79−17856
^{A}U fission, A=233,235,238, isotopic mass dispersion discontinuity, neutron shell effect 79−45312
^{A}U^{m}, A=236,238, isomeric to prompt fission ratios; fission fragments from (d,pf), (d,pnf) 80−86940
^{A}U(^{4}He,xn) A=233-235, x=1-4, cross sections, fission evaporation competition in Pu isotopes 78−66325
^{A}U(α, α'), A=234, 236, 238, coupled channel Born anal. of deformation correl 80−5149
^{A}U(α,f), A=235,238, 19-27 MeV, integral and differential cross sections, anisotropy energy depend. *(Russian)* 80−37407
^{A}U(d,f), A=235, 238, 2.1 GeV, binary and ternary fission kinetics *(French)* 78−70577
^{A}U(γ, f), A=236, 238, deep subbarrier photofission ang. anisotropy from fragment ang. distrib. *(Russian)* 79−97739
^{A}U(γ,X), A=235, 236, 238, 5-18.3 MeV, photoneutron and photofission cross sections, giant resonance and deformations 80−68712
^{A}U(γ,f), A=235, 236, 238, deep subthreshold photofission, double humped fission barrier anal., shape isomer 80−5179
^{A}U(γ,f), A=235,238, 15-55 MeV, photofission symmetric and asymmetric yields 80−83135
^{A}U(μ,f), A=235,238, prompt and delayed fission, absolute yields and lifetimes 80−78337
^{A}U(n,X), A=233, 235, thermal n, gamma spectra from capture, fission and fission products 80−37352
^{A}U(n,f), A=233,235, ejection fission products angular depend. on thermally polarised neutron capture *(Russian)* 80−86941
^{A}U(n,f), A=235, 238, fission-fragment yields of neutron fission in FBR 80−83102
^{A}U(n,f), A=235, 238, low energy, far-out asymmetric mass distrib. 80−83132
^{A}U(n,f) A=232 to 236, 238, prediction of fission-product mass yields and related parameters 79−30862
^{A}U(u,f), A=233, 235, cumulative yields of Ru and Pd isotopes 79−576
^{230}U decay chain, γ-ray single and coincidence meas., internal conversion spectra obs. 77−6319
^{230}U, production, tracer appls., α-spectra 77−61644
^{232}U electrodeposited sources, ejection of α-recoil atoms 78−50426
^{232}U half-life from specific and relative activity methods 80−9270
^{232}U, high pressure meas. of gamma transitions 80−18225
^{232}U high spin states and ground state rot. band from ^{232}Th(α,4nγ) 80−47349
^{232}U(n,f), fission product mass distrib. 79−67789
^{232}U(n,f), reactor neutron fission, kinetic energy distribs. determ. 78−658
^{232}U→^{212}Pb decay chain, obs. of collective states fed by weak α-transitions 78−8786
^{233}U alpha-decay, γ-spectra and ^{229}Th levels 77−26636
^{233}U content in ThO_2 determ. *(Spanish)* 77−70637
^{233}U cross sections, evaluation of ENDF/B-IV and Hansen-Roach cross sections 78−29550
^{233}U, excited octupole states in odd U isotopes, vibr. states, deuteron scatt., 13.1 MeV 77−46099

nuclei with mass number 220 or higher continued
^{233}U fission by polarised neutrons, P odd asymmetry of emitted fragments *(Russian)* 80−18354
^{233}U, gamma ray spectra of reactor fuels 80−42577
^{233}U, half-life determ. 80−57750
^{233}U, high-energy spin state obs. using Coulomb excitation 78−17102
^{233}U levels, bandheads, total α-branching and transitions from ^{237}Pu α-decay 79−93516
^{233}U, monopole conversion, magnetic dipole transitions, latent penetration effect 79−9464
^{233}U neutron cross sections, optical and statistical model calcs., reactor appls. 77−54227
^{233}U neutron-induced reaction, data eval. including $\bar{\nu}_p$ and fission spectrum 79−67795
^{233}U, prompt-fission-neutron spectra 79−67793
^{233}U, states excited by ^{234}U(d,t) and ^{234}U(^{3}He,α) 78−66208
^{233}U, statistical anal. of reson. neutron fission cross section 77−38305
^{233}U, thermal neutron fission with alpha-particle emission *(Russian)* 77−46198
^{233}U, thermal neutron-induced fission, ^{96}Nb and ^{98}Nb yields 78−54807
^{233}U, third IAEA evaluation of 2200 m/s, 20°C Maxwellian neutron data 77−23136
^{233}U, total neutron cross section meas., 40 keV to 4.5 MeV 79−13293
^{233}U/^{232}Th metal fuel, irradiation expt. 78−86610
^{233}U/^{235}U, (n,f) ratio meas. in range 1 keV-30 MeV 78−46118
^{233}U-Th fuel cycle, fast reactor system, sensitivity anal. 79−67835
^{233}U-Th fuel cycle, review of fast integral data 79−67834
^{233}U+n, strength functions and scatt. lengths from total and scatt. cross sections 77−26706
^{233}U(α,X), 28-140 MeV, scatt. and fission reaction mechanisms, cross sections 80−18350
^{233}U(d,d′), multipolarities and reduced transition probabilities 78−17215
^{233}U(d,pf), fission fragment energy-velocity correlation meas. 79−45309
^{233}U(γ,f) asymmetry depend. on bremsstrahlung energy maxima 77−23117
^{233}U(n, f), 0.02-7.4 MeV, fission cross section ratio to ^{235}U 79−45313
^{233}U(n,f), ^{148m}Pm, ^{148g}Pm and ^{146}Pm independ. yields 77−79407
^{233}U(n,f), effective cross section dependence on thermal neutron temp. 80−547
^{233}U(n,f), energy depend. of η^{233}U in 0.02 to 1.00 eV region 77−23118
^{233}U(n,f), fission neutron spectra, TOF meas. 78−17476
^{233}U(n,f), statistical model anal. of mass yield 77−26797
^{233}U(n,f), thermal, correlation for independent fission prod. yield uncertainties 78−50216
^{233}U(n,f), thermal polarised neutrons, neutron emission P-odd asymmetry *(Russian)* 80−78338
^{233}U(n,f) polarised thermal neutrons, P-odd asymm. *(Russian)* 78−33231
^{233}U(n,t), thermal, Mn bath meas. of η_{2200}, Monte-Carlo anal. 77−23142
^{233}U(n_{th},f), fission neutrons per absorption, Monte Carlo anal. of meas. 77−23141
^{233}U(ρ,f), alpha-particle angular and energy spectra, cross-section anisotropy 80−57809
^{234}U, 1.0015 MeV gamma spectroscopy for U determ. in environmental samples 77−1954
^{234}U α-particle spectrum meas. with p-Si detector *(Bulgarian)* 78−82592
^{234}U fission, thermal neutron induced, average angular momenta of even-even fragments 78−86525
^{234}U subbarrier resonances and fission probabilities from ^{233}U(d,pf) 79−13266
^{234}U under barrier photofission, 4-5.7 MeV, fragment ang. distribs. *(Russian)* 80−106090
^{234}U(n, f), 3 eV to 8.9 MeV, intermediate struct. 77−74895
^{234}U(n,f), cross section rel. to ^{235}U in 2-3 MeV region 78−21613
^{234}U(n,f), intermediate struct. anal. 77−79408
^{234}U(n,f), intermediate struct. line fitting, subthreshold fission resonances 80−102214
^{234}U(n,γ)^{235}U, 5-49 MeV, low-spin states 78−512
^{235}U, ^{238}U, absolute fast neutron fission cross sections 79−13366
^{235}U (n, f), thermal neutron fission, time-depend. delayed neutron group yields 79−54463
^{235}U (n,f), fission by fast neutrons, fragment K X-ray spectra, $\bar{\nu}$ energy depend. in heat balance method 78−17260
^{235}U absolute fission rate in spherical fusion blanket assemblies 77−67871
^{235}U, absolute fission yield meas. by track-etch-cum-γ-spectrometry method 80−27859
^{235}U α decay and ^{231}Th β decay, γ-radiation study, energy level scheme *(Russian)* 78−17160
^{235}U, capture to fission ratio determ. from low energy gamma-ray meas. 77−23152
^{235}U, capture to fission ratio in range 10-500 keV 77−26804
^{235}U content in enriched samples, fission track registration technique, solid state detectors 77−56291
^{235}U, cross sections for α-decay and neutron induced fission *(Russian)* 79−17944
^{235}U, cross-section from anal. of BNL exponential expts. with ENDF/B-IV data 78−13218
^{235}U, decay product radioactive accumulation, FORTRAN program 80−68611
^{235}U, delayed neutron groups from thermal fission 79−30864
^{235}U, e and $\bar{\nu}$ energy spectra from fission fragments *(Russian)* 77−23120
^{235}U, excited octupole states in odd U isotopes, vibr. states, deuteron scatt., 13.1 MeV 77−46099
^{235}U fission cross section for Na-Be photoneutrons 77−23159
^{235}U fission fragment thermonuclear superheavy nuclei synthesis, prod. cross sections 80−95331
^{235}U fission fragments, internal conversion cascading 78−94036
^{235}U fission fragments and fission neutrons, reliability of use in simulating neutron irradiation 79−42113
^{235}U, fission probability, Γ_n/Γ_f ratio struct. 78−37382
^{235}U, fission product mass distrib. from 25 MeV bremsstrahlung irradiation 78−13175
^{235}U, fission rate meas. with Makrofol solid state track recorder 78−13396
^{235}U, fission rates measured in graphite-reflected lithium assembly, nonelastic neutron anisotropy effect 78−29511
^{235}U, fission to capture ratios in range 0.2-15.0 keV 77−3057

nuclei with mass number 220 or higher continued
^{235}U foil, sputtered, energy spectrum, fission track technique 78−68593
^{235}U, fragmentation, HF calcs., neutron multiplicities and fragment KE 77−30635
^{235}U, giant resonance in total photoabsorpt. cross section 77−6347
^{235}U, impurity in mica, neutron fluence meas. using mica as nuclear track and activation detector 78−13346
^{235}U, in aq. soln., assay by pulsed neutron interrogation 78−68966
^{235}U, induced fission, in UO_2 mineral deposit *(Spanish)* 78−44823
^{235}U internal conversion from 1/2$^+$ isomeric state, U^{4+} electron configuration 80−58146
^{235}U, irradiated in BOR-60 reactor, fission yields 79−17971
^{235}U, isotope composition tables for isotopes produced in CANDU reactors 78−29564
^{235}U, isotope dilution mass spectroscopy for ^{239}Pu half-life determ. 79−26409
^{235}U, K-shell positron annihilation, excitation of nucleus *(Russian)* 78−33171
^{235}U, levels, J$^\pi$, multipolarities via (n,γ) 5-49 MeV 78−512
^{235}U, mass distribution of fragments in neutron induced fission *(Russian)* 78−29517
^{235}U, mass spectroscopy of growth for determ. of ^{239}Pu half-life 79−26408
^{235}U, muonic, fission studies, target preparation 80−23217
^{235}U, neutron induced fission cross section, 0.008 eV to 30 keV 77−50165
^{235}U, pot. energy surface, liquid model, deformation energy formulae *(Chinese)* 80−102106
^{235}U, process control analysis in U-Al alloy components during fuel element manuf. 79−85720
^{235}U, prompt-fission-neutron spectra 79−67793
^{235}U, quadrupole moment effect on internal conversion coeff. *(Russian)* 77−82867
^{235}U, radioactive series decay, computer simulation 80−102160
^{235}U, relative yields of Xe isotopes 77−54265
^{235}U spheres, storage array, reactivity enhancement 77−57756
^{235}U, spontaneous to induced ratio, B and Li impurity effects 79−45305
^{235}U, statistical anal. of reson. neutron fission cross section 77−38305
^{235}U, subthreshold photofission 78−66323
^{235}U, σ_c/σ_f ratio meas. in BFS critical assemblies 79−97737
^{235}U, thermal fission, product decay-heat calc. 77−61464
^{235}U thermal fission afterheat, sensitivity to errors in fission product data 77−26841
^{235}U thermal fission product long-term activity meas. and calc. 79−9644
^{235}U, thermal n induced ternary fission, α energy and ang. distribs. 79−22345
^{235}U, thermal neutron fission with alpha-particle emission *(Russian)* 77−46198
^{235}U, thermal neutron induced fission, isomer yield ratios of ^{132m}I and ^{134m}I 77−38306
^{235}U, thermal neutron irrad., fission product decay power calc. 80−22868
^{235}U, thermal neutron-induced fission, ^{96}Nb and ^{98}Nb yields 78−54807
^{235}U, thermal-neutron induced fission, scission point configuration determ. 77−82973
^{235}U, thermal-neutron-induced microscopic approach to statistical theory *(Chinese)* 78−86559
^{235}U, third IAEA evaluation of 2200 m/s, 20°C Maxwellian neutron data 77−23136
^{235}U, total muon capture rate, quenching of Cabibbo angle 79−22232
^{235}U, transition effects in total photoabsorpt. cross section 77−46160
^{235}U vibrational and single particle states from ^{234}U(n,γ) 79−36123
$^{235}U^M$ prod. by nuclear excitation by electron transition in plasma 80−22668
$^{235}U^m$, highly converted nuclear transitions, electronic bridge theory appl. 79−67708
$^{235}UO_2$, visualisation of fissionable radionuclides in rat lung using neutron-induced autoradiography 78−28055
^{235}U+^{235}U, classical microscopic description 77−14160
^{235}U+n, 13.9, 14.6 MeV, absolute neutron fission cross sections, associated particle method 78−89926
^{235}U+n, 14 MeV interactions, neutron and γ-ray spectra meas. 79−93612
^{235}U(1/2$^+$; 73 eV) isomer *(Russian)* 79−9511
^{235}U(α,α), 19-27 MeV, differential cross section, transmission coeffs. for fission cross section *(Russian)* 79−67800
^{235}U(d,d′), 13.1 MeV multipolarities and reduced transition probabilities 78−17215
^{235}U(d,pf), 23 MeV, total KE release 78−78426
^{235}U(e,f), 110 MeV electrons, mass and kinetic energy distribs. 79−93672
^{235}U(γ, f), 12-70 MeV bremsstrahlung, product yields and γ-spectra 80−42716
^{235}U(γ,f), 20 MeV, long range α-particle spectrum 80−47516
^{235}U(γ,f), 25 MeV bremsstrahlung, neutron emission curve 77−10457
^{235}U(γ,f), ang. distrib. of fragments *(Russian)* 78−54808
^{235}U(n, f) 0.024 to 7.4 MeV fission cross section ^{235}U/^{239}Pu ratio 79−40975
^{235}U(n, γf), X-ray prefission yield depend. on fission width 77−10453
^{235}U(n,2n), threshold to 13 MeV, cross section meas. by Gd loaded liquid scintillator 80−52669
^{235}U(n,8), fission cross-section for 2200 m/s neutrons 79−17943
^{235}U(n,α), thermal, α-particle spectra 78−78425
^{235}U(n,α), thermal fission neutron spectrum 80−42712
^{235}U(n,f), ^{148m}Pm, ^{148g}Pm and ^{146}Pm independ. yields 77−79407
^{235}U(n,f), 0.001-25 keV, polarised n, spin separated cross sections, resonance struct. 79−3126
^{235}U(n,f), 0.1 to 10 MeV fission cross section rel. to ^{239}Pu and ^{242}Pu 79−13354
^{235}U(n,f), 0.1-20 MeV neutron fission cross section 79−9655
^{235}U(n,f), 0.10-2.07 MeV, meas. of prompt fission neutron spectra 77−23146
^{235}U(n,f), 0.2 to 1.4 MeV, average number of prompt neutrons 77−23140
^{235}U(n,f), 0.3-10 MeV, cross-section meas. 77−26806
^{235}U(n,f), 0.3-12.5 MeV, fission cross-sections meas. 78−46117
^{235}U(n,f), 0.3-1.4 MeV, energy depend of fission fragment anisotropy 79−80962
^{235}U(n,f), 0.5 MeV, prompt neutron spectrum meas., TOF techniques 77−34356
^{235}U(n,f), 0.52 MeV, prompt neutron spectra meas. 77−23158

nuclei with mass number 220 or higher continued
^{235}U(n,f), 0.6, 7 MeV, fission neutron spectra meas. 80−22872
^{235}U(n,f), 1 keV to 30 MeV neutrons, cross section meas. rel. to ^{241}Pu 79−36286
^{235}U(n,f), 2-144 keV, cross-section meas. 77−26813
^{235}U(n,f), 2-144 keV, cross-sections meas. 77−26814
^{235}U(n,f), 550 keV, correlated fragments, 4-param. (E,ν) meas. 77−26802
^{235}U(n,f), 6-9 MeV, fission product yields 78−66324
^{235}U(n,f), abs. meas. of fission cross-sections with photoneutron sources 79−30860
^{235}U(n,f), ang. distrib. of fission fragments 78−37383
^{235}U(n,f), cross section sensitivity anal. of fission rates in graphite reflected Li assembly 78−46166
^{235}U(n,f), cross sections for ^{252}Cf neutrons 78−25258
^{235}U(n,f), cross-section, 2, 24, 55, 144 keV neutrons 78−17262
^{235}U(n,f), cross-section below 1 keV 78−4969
^{235}U(n,f), effective cross section dependence on thermal neutron temp. 80−547
^{235}U(n,f), energy depend. of cross section, 0.8-20 MeV 77−23156
^{235}U(n,f), fission cross-section averaged over ^{252}Cf neutron spectrum 79−30861
^{235}U(n,f), fission fragment average kinetic energies in resonance region 80−18358
^{235}U(n,f), fission fragments with high KE, mass separation based on TOF spectra 78−46209
^{235}U(n,f), fission neutron spectra, TOF meas. 78−17476
^{235}U(n,f), intermediate struct. in keV cross-section 77−23154
^{235}U(n,f), light particle yields and spectra 77−50173
^{235}U(n,f), neutron spectrum of thermal fission 79−97736
^{235}U(n,f), nuclear constants eval. for heavy fissile nuclei using nuclear models *(Russian)* 79−59100
^{235}U(n,f), polarised thermal neutrons, parity nonconservation *(Russian)* 78−33232
^{235}U(n,f), quantum numbers of low-lying resonances 77−23148
^{235}U(n,f), reconciliation of $\bar{\nu}_p$ meas. 77−67776
^{235}U(n,f), sensitivity of decay power to uncertainties in estimated decay data 80−22932
^{235}U(n,f), separation, identification of Ru, Rh isotopes 78−89924
^{235}U(n,f), spins of resonances below 150 eV 77−23147
^{235}U(n,f), subthreshold fission, fine struct. resonances anal. 78−652
^{235}U(n,f), symmetric fission, proton scatt. by fission fragments in neck area 80−83130
^{235}U(n,f), $\sigma_f(^{239}Pu)/\sigma_f(^{235}U)$ meas., neutron energies 0.27-9.85 MeV 78−660
^{235}U(n,f), thermal, appl. of $\bar{\nu}$ constraint to fission product yields 80−22874
^{235}U(n,f), thermal, α-particle spectra 78−78425
^{235}U(n,f), thermal, charge and mass yields of light fission products 77−23122
^{235}U(n,f), thermal, charge distrib. of fission products 77−23123
^{235}U(n,f), thermal, correlation for independent fission prod. yield uncertainties 78−50216
^{235}U(n,f), thermal, discrete neutron emission probability 78−25257
^{235}U(n,f), thermal, fission product decay spectra calcs., comparison with expt. results 79−93674
^{235}U(n,f), thermal, fragment ionisation, charge distribs., stat. and instant perturbation theory *(Russian)* 80−63219
^{235}U(n,f), thermal, Rb and Cs relative and independ. fission yields 80−27679
^{235}U(n,f), thermal fission, fission product decay heat evaluation by least-squares method 79−30865
^{235}U(n,f), thermal n, fission fragment energy correlation meas., fine struct. and deformation 79−13355
^{235}U(n,f), thermal n, max. energy dissipation 79−89338
^{235}U(n,f), thermal neutron induced fission, nuclear charge distribution in fission products 80−57808
^{235}U(n,f), thermal to 15 MeV, total delayed neutron yield calcs., energy depend. 77−34353
^{235}U(n,f), time correlated associated particle method, CAMAC experiment 80−52702
^{235}U(n,f),absolute yields and group constants of delayed neutrons in fast fission using Viper 77−54261
^{235}U(n,f) 3.5 MeV, fragment X-rays 77−18638
^{235}U(n,f) absolute cross section, ^{252}Cf neutron source 77−23133
^{235}U(n,f) cross section, 1 keV to 1 MeV 77−23139
^{235}U(n,f) cross section, thermal normalization technique for meas. of neutron cross section vs. energy 79−9590
^{235}U(n,f) cross section in ^{252}Cf spectrum, integral test for evaluated data 77−23134
^{235}U(n,f) cross section in range 0.2-8.2 MeV 78−654
^{235}U(n,f) cross section standard, status 77−23040
^{235}U(n,f) fission cross section standard, propagation of uncertainties, critical benchmark meas. 79−13361
^{235}U(n,f) fission rates, interlaboratory comparison in Mol-ΣΣ field 77−23131
^{235}U(n,f) half-lives and γ-ray energies of short-lived isotopes of Mo 78−17137
^{235}U(n,f) integral cross section ratio meas. using ^{235}U(n_{th},f) neutron spectrum 77−23130
^{235}U(n,f) near threshold cross-section calcs. 77−65240
^{235}U(n,f) self-shielded fission rates, 0.464-2150 eV 79−59096
^{235}U(n,f) standard reaction, Monte Carlo simulation of cross section fluctuations 77−61461
^{235}U(n,f) sub-barrier fission, fragment mass and kinetic energy distribs. 79−17942
^{235}U(n,f) thermal n, reactor $\bar{\nu}$ and e spectra calc. 79−67791
^{235}U(n,f) up to 36 keV, statistical anal., cross sections, intermediate struct. 78−653
^{235}U(n,γ), 10-500 keV, capture to fission ratio, double humped fission barrier parameters 79−89336
^{235}U(n,γ), thermal, d, t, He emission probabilities from stable core model *(Russian)* 80−68713
^{235}U(n,γ), thermal, fission product $\bar{\nu}_e$ spectrum, β-decay characts. 80−78340
^{235}U(n,γ), thermal, shape isomer in ^{236}U, isomeric/prompt fission ratio 77−323
^{235}U(n,γ) resonance capture, primary γ-transitions, parity assignments 77−26619
^{235}U(n,γ)^{236}U, gamma-ray spectra study *(Russian)* 77−6392
^{235}U(n,γf), X-ray yield fluctuations, γ-transitions in ^{236}U 80−106085

nuclei with mass number 220 or higher continued
^{235}U(n,t), statistical model anal. of mass yield 77−26797
^{235}U(n,t), thermal, Mn bath meas. of η_{2200}, Monte-Carlo anal. 77−23142
^{235}U(n_{th},f), charge distrib. of products in mass chains 79 to 100 77−10456
^{235}U(n_{th},f), fission fragment yield distribs., excitation energy depend. 78−50218
^{235}U(n_{th},f), fission neutrons per absorption, Monte Carlo anal. of meas. 77−23141
^{235}U(n_{th},f), fragment-mass depend. of fission neutron spectrum, TOF method 78−82398
^{235}U(n_{th},f), investigation of conversion electrons in range 150 to 1500 keV *(Russian)* 77−10458
^{235}U(n_{th},f), Maxwellian reference description of fission spectrum shape 77−23129
^{235}U(n_{th},f), neutrons ang. correl., multiplicity 79−3187
^{235}U(n_{th},f), statistical approach to scission mechanism 77−18631
^{235}U(n_{th},f), yields of Cd and Sn isotopes, symm. region 77−34358
^{235}U(n_{th},f) ionic charge distrib., effect of internal conversion 78−78428
^{235}U(n_{th},f) mass yields, direct physical meas. using recoil mass spectrometer 77−50178
^{235}U(n_{th},f) nuclide yields, direct physical meas. 79−9641
^{235}U(nth, f), above-the-barrier fission, fragment energy correl. meas. 78−21614
^{235}U(p,f), 13.7-14.2 MeV, isobaric analogue resonances, fission width 78−21616
^{236}U, isotope composition tables for isotopes produced in CANDU reactors 78−29564
^{236}U activity meas. in UO_2 mineral deposit *(Spanish)* 78−44822
^{236}U, as extinct natural parent of Th, premature falsification of correct theory 79−30186
^{236}U compound nucleus, lifetime meas. by means of shadow effect 77−50171
^{236}U, effect of nuclear force finite range on fission and heavy-ion reactions 78−13180
^{236}U fission, potential energy surface depend. on neck-in and asymmetric fragmentation 77−54262
^{236}U fission, quasistatic scission configurations obtained from long range particle accompanied fission distributions 78−74411
^{236}U fission, thermal neutron induced, average angular momenta of even-even fragments 78−86525
^{236}U fission, time depend. Hartree-Fock-Bogoliubov calc. 79−36265
^{236}U fission, two parameter study, fragment mass and energy, thin film scintillators 79−13357
^{236}U fission isomer produced in ^{238}U(γ,2n) prod. cross sections, half life 78−46045
^{236}U fission path, zero point energies in two centre shell model 78−93952
^{236}U fission shape isomer, γ-decay from ^{238}U(γ,2n) 80−18230
^{236}U fission total kinetic energy release from ^{235}U (d,pf) 80−27682
^{236}U, giant E2 isoscalar resonance determ. 80−27607
^{236}U γ-transitions from ^{235}U(n,γf) 80−106085
^{236}U in LWR spent fuel, recycling in enriching plant 77−18684
^{236}U, induced fission dynamics 78−66261
^{236}U isomeric and prompt fission, nuclear superfluidity evidence from ^{235}U(d,pf) 80−68711
^{236}U low lying levels from 4^- isomer decay in (n,e), (n,γ) 80−47396
^{236}U, moments of inertia of fissioning isomers, cranking model 78−74299
^{236}U, neutron capture, scattering and total cross section, 30-1800 eV range 77−23061
^{236}U nuclear instability and fission in strong mag. field energy level deformation *(Russian)* 79−13360
^{236}U, nuclear matter density distrib., in asymmetric two centre shell model 80−32209
^{236}U, nuclear pressure and fission fragment mass distrib. 80−18356
^{236}U, odd-parity level at 687.59 keV, mixing ratios, half-life 77−50079
^{236}U, photofission, deep sub-barrier anomalies 77−65241
^{236}U, prod. in lunar materials by solar cosmic ray protons, rate calc. 77−17311
^{236}U shape isomer, γ branch upper limit, γ-yields from ^{235}U(d,p) 80−99145
^{236}U shape isomer, rot. band and const. via ^{235}U(d,p) 12 MeV 77−34208
^{236}U shape isomer populated in ^{235}U(n_{th},γ), isomeric/prompt fission ratio 77−323
^{236}U, subbarrier resonances and fission probabilities from ^{235}U(d,pf), 11-17 MeV, ^{236}U 79−13266
^{236}U two-peaked fission barrier penetrability, quasiclassical approximation *(Russian)* 79−13280
^{236}U* (6.4 MeV) ternary fission, fragment-mass yield curve, nucleon-parity type distribs. 77−67774
^{236}U* fission fragment charge distrib. in statistical model *(Russian)* 79−59102
^{236}U(^{7}Li,α)^{239}Np, 12 to 20 MeV excitation, ang. distrib. of evaporation residues, determ. of Γ_n/Γ_f 77−61451
^{236}U(α,α'f), total kinetic energy release 80−27682
^{236}U(γ,f), 5.2-6.4 MeV, ang. distrib. and yields of fission fragments 77−3059
^{236}U(n,f), cross section rel. to ^{235}U in 2-3 MeV region 78−21613
^{236}U(n,f), fast n, fragment mass and kinetic energy distribs. *(Russian)* 80−5181
^{236}U(n,f), P-odd asymmetry in neutron emission *(Russian)* 79−89339
^{236}U(p,t), cranking model anal., validity 77−18517
^{237}U levels, bands and J^π assignments, n binding energy from ^{236}U(n,γ) 80−5041
^{237}U shape isomer, γ-decay search, branching ratio from ^{238}U(Γ,2nγ') 45 MeV 78−93961
^{237}U virtual photon excited state decay and total cross section of ^{238}U(e,n) 80−22757
^{238}U, ^{235}U, decay consts. for use in geochronology and cosmochronology 78−28189
^{238}U, 0.9-2.7 MeV neutron elastic and inelastic diff. cross sections for scatt. from ground, 45, 148 keV states 77−26770
^{238}U + ^{16}O, 20 MeV/nucleon, peripheral collisions, incomplete momentum transfer 79−30848
^{238}U, 24 keV, neutron capture cross section meas. with Fe-filtered neutron beam 79−40910
^{238}U, 24.3 keV neutron activation cross sections with Fe filter technique 77−26763

nuclei with mass number 220 or higher continued
^{238}U (^{6}Li, ^{6}Li'f), 150 MeV, isoscalar giant resonance struct. 79−89275
^{238}U (^{84}Kr, X), 522 MeV, heavy reaction product ang. distribs. and integral cross sections 79−49638
^{238}U (e, f), 7-65 MeV, absolute electrofission cross sections, fragment ang. distribs. 80−5185
^{238}U (μ^-,f), fission product mass distrib., fission probability, radiochem. investigation 78−29514
^{238}U (n,n), 0.9-3.1 MeV, elastic and inelastic cross-sections meas. 79−26435
^{238}U, (p,f), 1 GeV, fission fragment ang. correlation, kinematically different events search *(Russian)* 79−59103
^{238}U absolute fission rate in spherical fusion blanket assemblies 77−67871
^{238}U, anal. of Rb and Cs isotopic distrib. in ^{11}B and ^{22}Ne-induced fission 77−18634
^{238}U asymmetrical fission, consistent two-centre model *(Russian)* 77−2974
^{238}U, capture width of 6.67 eV neutron resonance 78−50162
^{238}U collective and deformation props., general collective model 80−86827
^{238}U, collective props., HF calcs., review 78−50064
^{238}U, conc. in New Zealand soil, rel. to Fe, K content 77−86867
^{238}U, cross-section from anal. of BNL exponential expts. with ENDF/B-IV data 78−13218
^{238}U, decay product radioactive accumulation, FORTRAN program 80−68611
^{238}U, deep subthreshold photofission using 3.8 to 5.7 MeV γ-rays 78−41787
^{238}U deformed even-even nucleus, rot. vibr. band excitation, classical limit S-matrix 79−3067
^{238}U delayed fission cross-section for 14 MeV neutrons, shape isomer excitation 77−26808
^{238}U, density-dependent HF description 77−54170
^{238}U, deuteron and proton bombardment, excitation function determ. 78−41709
^{238}U Doppler effect obs. in advanced fuels critical assemblies 79−9739
^{238}U, Doppler reactivity worth meas. in GCFR critical assemblies 77−54336
^{238}U electrofission, 6-60 MeV, relative E1 contrib. 77−6471
^{238}U, energy-depend. Doppler effect calc. using collision probability method 77−57714
^{238}U, evaluation for ENDF/B-V 78−25289
^{238}U, fast fission, product decay-heat calc. 77−61464
^{238}U fast fission yield of tritium, implications for FBRs 77−46195
^{238}U fast neutron capture and activation cross section 77−26758
^{238}U fast-neutron fission, calculated fission product yields 79−67796
^{238}U filtered beam of 186 eV neutrons, development 77−88318
^{238}U fission, 14 MeV neutron induced, neutron emission and energetics 77−46192
^{238}U fission, pot.-energy surface calc. 77−61465
^{238}U, fission product mass. distrib. from 25 MeV bremsstrahlung irradiation 78−13175
^{238}U, fission rate meas. with Makrofol solid state track recorder 78−13396
^{238}U, fission rates measured in graphite-reflected lithium assembly, nonelastic neutron anisotropy effect 78−29511
^{238}U fueled fusion fission hybrid blanket, data deficiencies weighting functions, neutron source effects 77−23295
^{238}U, giant resonance in total photoabsorpt. cross section 77−6347
^{238}U, ground rotational band level energies calc. 78−45996
^{238}U, high mass asymmetry distribs. in fissioning nuclei, shell effects 79−3186
^{238}U, infinite multiplication factors, neutron captures and fission, rel. to GFR parameters 78−33245
^{238}U, integral neutron spectrum meas. to test ENDF/B-IV data 77−26825
^{238}U, meas. of Cd ratio of neutron capture rates in slightly ^{235}U enriched fuel, systematic errors 78−8901
^{238}U, meas. of Rb and Cs isotopic distrib. in ^{11}B and ^{22}Ne-induced fission 77−18633
^{238}U, microscopic calc. of high-spin rot. states 78−8730
^{238}U, mirror hybrid reactors 80−42860
^{238}U, muonic, fission studies, target preparation 80−23217
^{238}U, muonic, μ induced prompt fission, fate of the μ 78−86557
^{238}U, muonic, non-axiality effects in quadrupole hyperfine splitting 77−46107
^{238}U, muonic fission and electron decay 77−38754
^{238}U, μ capture rate in the fission mode, μ lifetime 78−89827
^{238}U, natural spontaneous fission, Xe prod., determ., extraction from granite 78−96216
^{238}U, negative parity band crossing in even-even nuclei 78−21488
^{238}U, negative parity bands, coherent state model 78−89782
^{238}U, neutron capture cross section representation, TRX-2 lattice param. sensitivity 78−25275
^{238}U, neutron capture cross section ratios in range 10 to 90 keV 78−50163
^{238}U, neutron capture cross-section below 100 eV meas. 77−26680
^{238}U, neutron cross section integral meas., interactive graphic techniques 78−29457
^{238}U neutron cross sections evaluation for incident neutron energies up to 4 keV 80−5146
^{238}U neutron data reevaluation for Nuclear Data Library KEDAK-3 77−23042
^{238}U, neutron elastic and inelastic ang. distribs., 1.1 to 3.1 MeV, to ground state rot. band 77−26717
^{238}U, neutron elastic and inelastic cross section meas., 100 to 150 keV 77−26718
^{238}U, neutron elastic and inelastic cross sections, 2.5 MeV, comparison with optical model 77−30595
^{238}U, neutron induced fission rate meas. in Zebra 77−57698
^{238}U, neutron induced fission, ^{99}Mo and ^{111}Ag absolute yields 79−49642
^{238}U, neutron resonance parameters, transmission meas. on natural U 77−23063
^{238}U, neutron resonance params. and cross sections, 9 eV to 4 keV 77−26710
^{238}U, neutron resonance parameters, time-of-flight spectroscopy 80−47375
^{238}U, neutron resonances, probability table method and correlated data 79−36284
^{238}U, neutron transmission, resonance meas. and anal. 79−26436

nuclei with mass number 220 or higher continued
^{238}U, neutron transmission meas. and anal. 77−26823
^{238}U neutron transmission meas. and resonance analysis 79−9575
^{238}U, nuclear excitation rate in high-temp. environment 78−66244
^{238}U photofission, 20-60 MeV 77−6471
^{238}U, photofission, deep sub-barrier anomalies 77−65241
^{238}U, photofission products, ang. distrib., isomeric shelf region *(Russian)* 77−6475
^{238}U, photofission with bremsstrahlung, charge distrib., fractional independent yields 79−36283
^{238}U prompt fission, prompt neutron multiplicity distribs. *(Russian)* 77−340
^{238}U, proton-induced fission, asymm. region, nucl. charge distrib. 78−4967
^{238}U pulsed sphere meas., neutron emission spectra rel. to fusion-fission blanket calcs. 77−23298
^{238}U, radioactive series decay, computer simulation 80−102160
^{238}U shape isomeric γ-decay, in μ^- atoms, isomer lifetime 77−34245
^{238}U, shell corrections for finite depth single particle potentials 79−30782
^{238}U source enhancement of ^{252}Cf spontaneous fission neutrons, determination of $\nu\sigma_f$ 77−6594
^{238}U, spontaneous emission of heavy ions, half-life of process 77−74815
^{238}U, spontaneous fission, conversion electron spectra obs. 77−82864
^{238}U, spontaneous fission, constant of disintegration meas. *(Portuguese)* 79−36282
^{238}U, spontaneous fission, half life and fragment kinetic energy meas. using cylindrical ionisation chamber 78−86555
^{238}U, spontaneous fission, in UO_2 mineral deposit *(Spanish)* 78−44823
^{238}U, spontaneous fission, prediction of fission-product mass yields and related parameters 79−30862
^{238}U, spontaneous fission decay const., calibration of fission track dating parameters 77−41207
^{238}U, stat. model calcs. of neutron capture gamma-ray spectra 77−67742
^{238}U, statistical reson. parameters determ. from computer code ADDJA 77−26650
^{238}U, strength functions for transitions to $I^\pi K=2^+0$, 2^+1, 2^+2 and $I^\pi=2^+$ states 78−86519
^{238}U, struct. in sequence of s-wave levels 77−22857
^{238}U, subCoulomb fission induced by Xe and Kr, excitation functions 77−3061
^{238}U, subbarrier photofission, differential cross section 78−41796
^{238}U subbarrier photofission, cross section and half-life, double hump model 80−102217
^{238}U target for pulsed spallation neutron source, design 77−67930
^{238}U thin self supporting foils 80−9440
^{238}U total neutron cross section, ENDF/B-IV representation 77−2983
^{238}U, transition effects in total photoabsorpt. cross section 77−46160
^{238}U, Weale expt. calc. using modified ENDF/B-IV cross sections 79−17908
^{238}U, Xe and Kr induced fission at Coulomb barrier energies 77−61467
^{238}U, Xe-induced Coulomb fission, rotation-vibration model for target nucleus 79−13367
^{238}U/^{235}U (n,f) cross-section ratio meas., 600 keV-22 MeV 77−23145
^{238}U/^{235}U fission cross section ratio, 2 to 25 MeV, high resolution meas. 77−50176
^{238}U-^{235}U, 800 MeV, possibility of detecting superheavy quasimolecules 77−14149
^{238}U-^{238}U, mass transfer, quantum mech. anal. within fragmentation theory 77−82948
^{238}U+^{A}Xe, A=129, 132, 136, sub-Coulomb transfer and fission, cross sections 79−67802
^{238}U+^{12}C, 25.2 GeV, target residue mass and charge distribs., calcs. 79−3172
^{238}U+^{12}C, 78 MeV, fission fragment angular distrib., shape of saddle point of compound nucleus *(Chinese)* 78−78427
^{238}U+^{136}Xe, 4.5-5.9 MeV/N excitation functions and ang. distrib. meas. 77−82965
^{238}U+^{136}Xe, isotope prod. cross-sections *(Russian)* 77−74879
^{238}U+^{16}O, threshold pion prod., calc. of effective NN collision cross sections 77−46185
^{238}U+^{208}Pb, 14 GeV, nonnuclear positrons creation 79−30847
^{238}U+^{20}Ne, 250 MeV/nucleon, comparison of macroscopic and microscopic calcs. 77−50153
^{238}U+^{20}Ne, expt. and relativistic two fluid model energy spectra 78−78298
^{238}U+^{20}Ne(^{40}Ar), 250-1000 MeV/N, intranuclear cascade calcs. for multiplicity and cross sections 80−32300
^{238}U+^{238}U, 14 GeV, nonnuclear positrons creation 79−30847
^{238}U+^{238}U, 1766 MeV, charge, kinetic energy and ang. distrib. of reaction products 79−26455
^{238}U+^{238}U, 1785 MeV, cross sections, charge and mass distribs. of products 78−78408
^{238}U+^{238}U, 7.42 MeV/nucleon, charge, energy and ang. distribs. of prods. 78−8846
^{238}U+^{238}U, 7.5 MeV/u, theoretical estimates for transuranium element prod. in heavy ion collisions 79−54454
^{238}U+^{238}U, deeply inelastic, relative motion mass transport and dynamics 79−13320
^{238}U+^{238}U (^{136}Xe), nuclear Coulomb excitation, inner shell ionisation and internal conversion, quasimol. formation 78−94026
^{238}U+^{238}U fragmentation, superheavy element prod. due to collective mass transfer 77−337
^{238}U+^{32}S(^{40}Ar), deep inelastic reactions, isotopic distribs., n excess degree of freedom relaxation 80−9308
^{238}U+^{40}Ar, 220 MeV, fissionability of target-like fragments in deep inelastic collisions, reaction mechanism 79−54455
^{238}U+^{40}Ar, 263 MeV, ^{37}Si, ^{40}P, ^{41}S, ^{42}S neutron rich nuclide prod. 79−22324
^{238}U+^{40}Ar, Coulomb-nuclear interference for high spin states 78−46097
^{238}U+^{40}Ar, cross-sections for fusion, quasifission and deep inelastic collisions *(Russian)* 78−54801
^{238}U+^{4}He, expt. and relativistic two fluid model energy spectra 78−78298
^{238}U+^{58}Ni(^{90}Zr), fission phenomena in deep inelastic collisions 80−5186
^{238}U+^{84}Kr, 605 MeV, quasi-fission reaction, mass-yield distrib. theory 77−42001
^{238}U+^{86}Kr, recoil range distribs. of heavy mass products in deep inelastic reacts. 78−66309
^{238}U+N, 14 MeV interactions, neutron and γ-ray spectra meas. 79−93612

nuclei with mass number 220 or higher continued
^{238}U+n, 13.9, 14.6 MeV, absolute neutron fission cross sections, associated particle method 78−89926
^{238}U+n, 2.47 MeV, energy spectra and ang. distrib. of neutrons 79−40927
^{238}U+n, Doppler effect meas. at 24 and 144 keV 79−97704
^{238}U+n, resolved resonance energies, 100 eV-170 keV 78−37339
^{238}U+p, 0.8-11.5 GeV, energy depend. of Sc fragment ang. distribs. 78 70527
^{238}U+p, 1-300 GeV, production props. of Sc nuclei 77−6389
^{238}U+p, nucleon losses on high-energy fission *(Russian)* 78−46120
^{238}U(^{12}C,f), (^{18}O,f), (^{22}Ne,f), effective widths of excited state meas. by shadow effect *(Russian)* 77−46196
^{238}U(^{12}C,f), mass distrib. of fission fragments determ. *(Chinese)* 78−86558
^{238}U(^{136}Xe, ^{136}Xe), multiple Coulomb and nucl. excitation 78−21603
^{238}U(^{16}O,f) 20 MeV/N, light particle spectra in central and peripheral collisions 80−5177
^{238}U(^{16}O,x), x=p,d,t, 315 MeV, energy spectra in coalescence model 80−99183
^{238}U(^{184}W, f), Coulomb fission excitation function, cross section 80−5176
^{238}U(^{238}U, ^{238}U), multiple Coulomb and nucl. excitation 78−21603
^{238}U(^{238}U,X), 7.42 MeV/u, charge, kinetic energy and ang. distribs. of products 80−539
^{238}U(^{238}U,X), 7.42 MeV/N, mass transport, shell effects, anharmonic pots. 80−99187
^{238}U(^{238}U,X), 7.5 MeV/amu, three particle exclusive meas. for exit channels fission fragment ang. distrib. 80−13513
^{238}U(^{238}U,X), 7.5 MeV/A, 3-dimens. TDHF-BCS model calcs., possible fission 80−52694
^{238}U(^{238}U,X), damped collision, proton and neutron exchange correlations 80−18335
^{238}U(^{238}U,X) deeply inelastic collisions, mass transport, shell effects 80−99188
^{238}U(^{238}U,f), 1785 MeV, exam. of multiprong events due to multiple sequential fission using solid state track detectors 80−91199
^{238}U(^{27}Al,f) 169, 190, 227 MeV, Z=105 compound nucleus lifetime using shadow effect *(Russian)* 78−86563
^{238}U(^{32}S, X), deep inelastic reaction, neutron excess degree of freedom relaxation model *(Chinese)* 80−102202
^{238}U(^{3}He,4n)^{237}Pu, prep. of gamma-emitting tracer 77−34497
^{238}U(^{3}He,f), ^{241}Pu compound nucleus lifetime by the shadow effect *(Russian)* 78−86562
^{238}U(^{40}Ar, X), 263 MeV, deep inelastic reaction, neutron excess degree of freedom relaxation model *(Chinese)* 80−102202
^{238}U(^{40}Ar,X), 237, 250 MeV, differential recoil range distributions, large contrib. of deep inelastic processes 78−70565
^{238}U(^{40}Ar,X), 340 MeV, production of neutron rich nuclides ^{54}Ti, ^{56}V, ^{58,59}Cr, ^{61}Mn, ^{63,64}Fe 80−57802
^{238}U(^{40}Ar,f), 212-340 MeV, I prod. relative thresholds from fusion and transfer induced fission 79−9640
^{238}U(^{48}Ca,X), 276 MeV, differential recoil range distributions, large contrib. of deep inelastic processes 78−70565
^{238}U(^{48}Ca,γ), nuclear pressure and fission fragment mass distrib. 80−18356
^{238}U(^{56}Fe,X), 538 MeV, binary coincident fragments, fragment mass and energy, fission following fusion 80−548
^{238}U(^{63,65}Cu,x), 9.6 MeV/nucleon, search for superheavy elements 77−34343
^{238}U(^{84}Kr,X), mass fragmentation, dynamical theory, two centre shell model, binary decay process 80−68628
^{238}U(^{84}Kr,f), 806 MeV, exam. of multiprong events due to multiple sequential fission using solid state track detectors 80−91199
^{238}U(^{86}Kr,X), 730 MeV, transferred ang. momentum for fission and projectile like fragments 79−93675
^{238}U(HI,f), Coulomb fission cross sections from coupled channel calcs. 80−9319
^{238}U(Kr,Kr'), multiple Coulomb excitation, coupled eqns. soln. by iteration 79−93654
^{238}U(N,N'), deformed nuclei struct., rot. model with optical pot., coupled channel formalism 79−3146
^{238}U(N,γ), neutron capture rate, absolute meas. 79−63678
^{238}U(P,X), 11.5 GeV, heavy fragment energies and masses, reaction mechanism 80−5140
^{238}U(Pb,Pb'), multiple Coulomb excitation, coupled eqns. soln. by iteration 79−93654
^{238}U(Xe,f), depend. of Coulomb fission on nucl. struct. 78−13173
^{238}U(α,f), 100-1000 MeV, resonance production 80−52658
^{238}U(α,f), 140 MeV, fission cross sections and probabilities, isomeric yield ratio 79−45308
^{238}U(α,f), 23 to 115 MeV, interpretation of fragment anisotropies 77−30644
^{238}U(α,f), 640MeV 80−95329
^{238}U(α,f), fragment mass distrib., and yield, statistical anal. *(Russian)* 80−5183
^{238}U(α,xnf), 50 MeV, post and prefission neutron meas. 79−76042
^{238}U(d,d)^{238}U, 17 MeV elastic and inelastic scatt., nuclear-Coulomb interf., optical pot. 77−79389
^{238}U(d,pf), E_d=12 MeV, fission probability, energy depend. 77−71628
^{238}U(d,pn), quadrupole moment of 200 ns isomer in ^{238}U 79−71856
^{238}U(e,α)^{234}Th, cross section, α-spectra, γ-spectra of ^{234}Th decay 78−58262
^{238}U(e,e'), 87.5 MeV, deformed fissionable nucleus, giant multipole resonances and isovector states 80−42612
^{238}U(e,e') scatt. from octupole band, model for nuclear surface vibrations 78−37333
^{238}U(e,e'α), 13.1 MeV, cross section in giant quadrupole resonance region 79−6573
^{238}U(e,e'f), 20-120 MeV, electrofission cross section, E1, E2 strengths 78−13174
^{238}U(e,e'f), 5.5-28.3 MeV, E2 isoscalar giant resonance in photofission cross section 79−512
^{238}U(e,e'n)^{237}U, 6-25 MeV, transition multipolarities 78−590
^{238}U(e,e'f), 5.5-9 MeV, fission fragment ang. distribs. DWBA anal., low lying fissioning levels 80−42713
^{238}U(e,f), 110 MeV electrons, mass and kinetic energy distribs. 79−93672
^{238}U(e,p), 40 MeV, p spectra, deduced ternary fission cross section 79−9549
^{238}U(γ,2n), ^{236}U fission isomer, cross section, half life 78−46045

nuclei with mass number 220 or higher continued
^{238}U(γ,α), 15.5 MeV, cross section upper limit 79−85457
^{238}U(γ,α), 9 MeV, cross section upper limit 79−85458
^{238}U(γ,f), ^{135}Xe, direct meas. of absolute and fractional independ. yields 80−78341
^{238}U(γ,f), 12-70 MeV bremsstrahlung, cumulative and fractional product yields for A=128-136 79−36288
^{238}U(γ,f), 12-70 MeV bremsstrahlung, fragment mass and energy distribs. 80−27680
^{238}U(γ,f), 15 to 1300 MeV, cross sections meas. *(Russian)* 77−6473
^{238}U(γ,f), 20 MeV, fission product yields, charge distrib. 80−42533
^{238}U(γ,f), 25 MeV bremsstrahlung neutron emission curve 77−10457
^{238}U(γ,f), bremsstrahlung of 600 MeV fragment energy correl. meas. max. energy 77−71630
^{238}U(γ,f), delayed neutron energy spectrum 77−23155
^{238}U(γ,f), neutron capture γ-rays, $\Gamma_{n\gamma}/\Gamma_f$ meas. 80−57813
^{238}U(γ,f), neutron capture γ-rays, ^{131g}I fractional independ. yield 80−57814
^{238}U(γ,f) fission-neutron and fragment ang. distrib. 77−65239
^{238}U(γ,γ), 15 MeV, elastic and nuclear Raman scatt. 80−22811
^{238}U(γ,γ), 6.84-11.39 MeV, Rayleigh and Delbruck scatt. destructive interference, cross sections 79−6566
^{238}U(γ,γ) 7.9, 9.0 MeV, differential cross section, Delbruck scatt., Coulomb correction effect 79−3136
^{238}U(n,2n), 13-18 MeV, cross sections, pre-equilibrium contrib. 79−45258
^{238}U(n,2n) reactions and fission rates, E_n=14.9 MeV, effect of Fe shielding, hybrid reactor situation 77−50122
^{238}U(n,2n)^{237}U, 13 to 18 MeV, excitation functions, statistical model anal. 77−23082
^{238}U(n,2n)^{237}U, meas. of average cross section by anion exchange method 79−30828
^{238}U(n,2nf), 13.5-17.5 MeV, fragment anisotropy 77−54263
^{238}U(n,αn'), 14.7 MeV, cross section, possible contrib. to (γ,α) 79−85458
^{238}U(n,f), 0.10-2.07 MeV, meas. of prompt fission neutron spectra 77−23146
^{238}U(n,f), 0.3-10 MeV, cross-section meas. 77−26806
^{238}U(n,f), 0.3-12.5 MeV, fission cross-sections meas. 78−46117
^{238}U(n,f), 14.5 MeV, neutron emission, mass distrib. and energetics 80−47512
^{238}U(n,f), 1.5-7.7 MeV, mass yield curves 78−41788
^{238}U(n,f), 1.52 MeV, mass yield distrib. meas. 77−67777
^{238}U(n,f), 1.8-16.8 MeV, fission fragment energy spectra using glass sandwich detectors 78−82399
^{238}U(n,f), 5 eV-2.5 MeV, fission cross section, fission barrier second well parameters, resonances 80−63217
^{238}U(n,f), 5 eV-5 keV, sub-barrier fission 77−23151
^{238}U(n,f), 6-9 MeV, fission product yields 78−66324
^{238}U(n,f), 7 MeV, fission neutron spectra meas. 80−22872
^{238}U(n,f), absolute yields and group constants of delayed neutrons in fast fission Viper 77−54261
^{238}U(n,f), cross section sensitivity anal. of fission rates in graphite reflected Li assembly 78−46166
^{238}U(n,f), cross section up to 6 MeV, intermediate struct. obs., fragment ang. anisotropy 77−23161
^{238}U(n,f), fission cross sections, use as standards in MeV region 79−13362
^{238}U(n,f), fission product decay heat calc. by summation method, appl. to FBR 79−30863
^{238}U(n,f), prompt-neutron ang. distrib. 77−65238
^{238}U(n,f), second well gamma decay if subthreshold fission resonances 77−26800
^{238}U(n,f), separation, identification of Ru, Rh isotopes 78−89924
^{238}U(n,f), studied with intense neutron spectrometer 77−23364
^{238}U(n,f), subthreshold cross-section, high resolution meas. 77−26799
^{238}U(n,f) cross section in ^{252}Cf spectrum, integral test for evaluated data 77−23134
^{238}U(n,f) cross section meas., 3 eV-100 keV 77−26793
^{238}U(n,f) fast neutron fission yield determ. 79−40970
^{238}U(n,f) fission rates, interlaboratory comparison in Mol-ΣΣ field 77−23131
^{238}U(n,f) integral cross section ratio meas. using ^{235}U(n_{th},f) neutron spectrum 77−23130
^{238}U(n,f) subthreshold fission cross section, 0.6 to 100 keV, barrier parameters 77−50169
^{238}U(n,γ), 2, 24 keV, resonance averaged γ-spectra, level and J^π appls. 80−37347
^{238}U(n,γ), 20-550 keV, cross section meas. 77−23056
^{238}U(n,γ), absolute cross sections in keV range 77−26771
^{238}U(n,γ), coupled channel calc. of direct and collective cross sections of deformed nuclei 77−26748
^{238}U(n,γ), cross section and resonance shape, gas molecule vibr. effects 80−42661
^{238}U(n,γ), cross section meas. using large Gd loaded liquid scintillator 78−25380
^{238}U(n,γ), cross-section determ. by Fe filtered beam TOF method 77−23078
^{238}U(n,γ), effective cross section dependence on thermal neutron temp. 80−547
^{238}U(n,γ), L100 eV cross-section and resonance parameters 77−34309
^{238}U(n,γ), p-wave assignment of resonances 77−23062
^{238}U(n,γ), statistical anal. of intermediate struct. in cross-section 77−23057
^{238}U(n,γ) cross section, 5-100 keV, doorway state detection, statistical tests 79−93590
^{238}U(n,γ)^{239}U resonance capture self-indication obs. at 77, 293 and 873K 79−9574
^{238}U(n,n'), 0.3 to 3.0 MeV, ground state rot. band excitation 77−23085
^{238}U(n,n'), 0.9 to 3.1 MeV ang. distribs. and cross sections 79−9576
^{238}U(n,n'), cross section param. from optical model anal. 78−21557
^{238}U(n,n'α), 14.7 MeV, cross section upper limit 79−85457
^{238}U(n,n'γ), 1.06 MeV, cross sections and γ spectra for various energy levels *(Russian)* 79−40883
^{238}U(n,n'γ) cross section estimates 77−57675
^{238}U(n,n'γ) technique for study of levels near 1 MeV 77−26719
^{238}U(n,n), 0.6-2.2 MeV small angle scatt., differential cross sections ang. depend. 79−85472
^{238}U(n,n), elastic and inelastic scatt. cross sections at 144 keV 78−21554

nuclei with mass number 220 or higher continued
^{238}U(n,n)^{238}U, differential elastic and inelastic cross sections at 144 keV 78−4945
^{238}U(p,X), 0.8-11.5 GeV, formation of A=131 isobaric nuclides 80−9293
^{238}U(p,X), 0.8-400 GeV, Sc fragment differential ranges and energy spectra 80−42666
^{238}U(p,X), 0.8-400 GeV 80−83099
^{238}U(p,X), 400 GeV/c, unusual backward enhancement in product ang. distrib. 80−514
^{238}U(p,X) *(Russian)* 79−80964
^{238}U(p,2n), production of ^{237m}Np fission isomer, statistical model anal. 78−25256
^{238}U(p,f), 11-29 GeV, three dimens. charge dispersion curves, isobaric yields 80−102111
^{238}U(p,f), 11.5 GeV, He and heavy fragment energy and ang. correlation 79−45310
^{238}U(p,f), 30-98.6 MeV, independ. yield of In and Ga isotopes 78−13171
^{238}U(p,f), 35-85 MeV, nuclear charge dispersion in light mass region 78−8864
^{238}U(p,f), 4-7 MeV, cross sections *(Russian)* 78−41794
^{238}U(p,f), 9.5-17 MeV, symmetric to asymmetric mass ratios for fragments 80−5178
^{238}U(p,f) 12 MeV, estimation of neutron yield from individual fragment in medium-excitation fission 80−542
^{238}U(p,nf), multiple scatt. effect due to filling in of blocking patterns 78−21617
^{238}U(p,p′), 22 MeV, rot. band, multipole deformation parameters from coupled channel anal. 80−13369
^{238}U(p,p′), 35 MeV, extraction of deform. parameters 78−54755
^{238}U(p,p′), 35 MeV, ground state rot. band and multipole moment 80−32178
^{238}U(p,p′), isobaric analogue reson., modified KASTOR code calc. 77−14132
^{238}U(p,t), 1 GeV, meas. of total fission cross-section *(Russian)* 77−341
^{238}U(p,t), 400 GeV, ang. distrib. of Sc fragments in thick targets 77−6472
^{238}U(p,xn), 800 MeV, neutron spectra meas., check on flux calcs. 77−23349
^{238}U(p,xnf), lifetime of second chance fission at threshold, in UO_2 single cryst. 78−17259
^{238}U(π^-, f), resting pions, delayed fission search *(Russian)* 80−52704
^{238}U(t,pf), fission probability, fragment ang. distrib. meas. *(Russian)* 77−46199
^{239}U, energy level assignments from ^{238}U(d,p) at 12 MeV 78−66209
^{239}U, fission induced by ^{238}U(d,p), subthreshold cross section meas., 2-centre shell model calc. 79−6719
^{239}U, neutron binding energy precision meas. 80−18182
^{239}U, population in direct and collective neutron capture by ellipsoidally deformed nucleus 78−94001
^{239}U second-chance fission decay times from crystal blocking in ^{238}U(n,f) 79−85568
^{239}U, struct. anal. by (n,γ) reactions in Grenoble High Flux Reactor 77−34310
^{240}U, fission probability, fragment ang. distrib. meas. in ^{238}U(t,pf) *(Russian)* 77−46199
^{242}U β-decay, half-life, ^{242}Np levels, J^π and transitions 79−67664
U(α,^{3}He), 90 MeV, α-n coincidence, ^{5}He breakup kinematics 77−6419
U(α,f), 0.65, 1.74, 4.12 GeV, fission fragment recoil characts. 78−89925
U(α,f), 0.65-4.11 GeV, cross sections for binary and ternary fission 77−3055
U(α,xn) ^{238,239}Pu, neutron emission probability and fissionability energy depend. 78−655
U(γ,f), 5.2-6.4 MeV, A=234, 236, 238, doubly even isotopes, ang. distribs., fragment yields 78−50219
U(γ,f) A=235,238, 25 MeV bremsstrahlung, prod. yields, mass chains, charge distribs. 77−6470
U(γ,f), max. energy 580 MeV, track detector anal. 77−18640
U(γ,γ), 0.1-1.5 MeV, Delbruck and Rayleigh scatt., differential cross sections 80−102180
U(γ,γ), 2.75 MeV, Delbruck theory, multiphoton exchange 78−8796
U(γ,γ), 412, 468, 662 keV, elastic scatt. cross sections, Rayleigh scattering anal. 80−86898
U(γ,γ), neutron capture γ-ray Rayleigh scatt. 80−52661
U(γ,n), 30 to 140 MeV, partial photoneutron cross section, total cross section approx. 80−22809
U(μf), emission of conversion μ in radiation free fission *(Russian)* 78−62587
U(n,f), 0-18 MeV, prompt neutron spectrum, evaporation model *(Chinese)* 80−42721
U(n,f), 1 to 7 MeV, ratio of ^{238}U and ^{235}U cross sections 79−30867
U(n,f), A=233,235,238, 35 to 1500 keV, near equilib. delayed neutron energy spectrum 77−34354
U(n,f), A=233-238, cross-sections meas., 0.1-30 MeV 77−23150
U(n,f), A=234,6,8, 0.1-30 MeV, fission cross-sections relative to ^{235}U 77−61463
U(n,f) A=235,238, sub MeV neutrons, equilib. delayed neutron energy spectra meas. 77−38308
U(n,f), delayed neutron spectra from thermal- and fast-neutron fission, reactor calcs. 77−34355
U(n,f) fission cross section ratio of ^{235}U to ^{238}U for 0.1 to 25 MeV neutrons 79−36285
U(n,f), heavier rare earths separation by radiochem. method 79−67785
U(n,f), thermal to 14.7 MeV, statistical theory calcs. 77−23137
U(n_{th},f), A=233,5, isomeric yield ratio of ^{148}Pm meas. 77−82975
U(n,n), 2.5 MeV, small angle scatt., cross section, asymm. 78−74361
U(n,n), 7-14 MeV, absolute cross sections for small-angle elastic scatt. 77−26769
U(n,n), small-angle scatt., possible test of neutron electric polarisability 77−22674
U(p,X), X=F to Ar, 2.1 and 4.9 GeV, fragment energy spectra, Maxwellian functional form 78−70529
U(p,f) 300 to 660 MeV protons, neutron multiplication 79−59099
U(p,f), 600 MeV, fragment energies, cross sections level density and barrier heights 80−42723
U(p,n), 800 MeV, n prod. systematics π associated cross section 79−3153
U(π^-,X), 3 GeV/c, n inclusive spectra, neutron yield *(Russian)* 80−13510
^{190}W, identification and β-decay meas. 77−22963

nuclei with mass number 220 or higher continued
^{111}^{276}X synthesis search in ^{231}Pa(^{48}Ca, 3n) *(Russian)* 79−40954
^{112}^{279}X synthesis search in ^{233}U(^{48}Ca,Zn) *(Russian)* 79−40954

nucleic acids *see macromolecules*

nucleon interactions *see hyperon-nucleon interactions; kaon-nucleon interactions; lepton-nucleon interactions; muon-nucleon interactions; neutrino-nucleon interactions; nucleon-nucleon interactions; nucleon-nucleus reactions; photon-nucleon interactions; pion-nucleon interactions*

nucleon-nucleon interactions
see also nucleon-nucleon scattering; proton-proton interactions
2N interaction, light front field theory treatment, using $\phi^2\phi_0$ theory 79−67579
(π,π'), inelastic scatt. in Fermi liquid, nucleon-nucleon interaction effects 80−22862
amorphous state analogy 79−54370
annihilation widths and displacement of quasinuclear levels, bonded channel model *(Russian)* 78−464
attractive retarded effect of one boson exchange pot. on NN scatt. 77−2859
background scattering 77−22753
backward production on nuclei and the tube model, comments 80−52544
bag-model, interquark interaction effects 77−30315
baryon+antibaryon bound states, NN̄, quasinuclear levels, annihilation, influence of decay channels, multichannel model 79−2912
baryonium and dibaryon, quark shell model 78−41479
Bethe Salpeter equation for I=1 NN scatt. with one boson exchange 77−57455
central NN potentials, relative motion dependent, jj and LS coupling, universal of hyperspherical functions method 77−61355
chiral symm. and NN interactions dispersion relation anal. 78−66048
chiral symmetry and the NN interaction, book contrib. 79−97669
conference on few body systems and nuclear forces, Graz, Austria (Aug. 1978) 79−67567
conference on few body systems and nuclear forces, Graz, Austria (Aug. 1978) 79−80880
Conference on meson-nuclear physics, Houston, USA (Mar. 1979) 79−85489
constituent quark model and production of particles from nuclear targets 80−380
cosmic ray, role of clusters in multiple pion prod. 77−34199
cosmic ray clusters, size and mass determ. NN interactions 77−71548
cosmic rays, E>2 TeV, inelastic cross section *(Russian)* 77−78589
coupling const. singular points for approx. Bethe-Salpeter eqns., with a nonlocal pseudopotential 78−25062
cross-sections related by sum rules, pomeron hypothesis, heavy-quark channels and threshold predictions 78−89755
diffraction dissociation, Deck-model baryon-exchange contribs. 77−49933
dipole interaction between nucleons, steps in binding energy and mag. moment energy *(German)* 78−74306
direct muon production at 1.9 GeV longitudinal polarisation meas. *(Russian)* 79−3038
dispersion relation anal., of NN and NN̄ scatt. 78−62337
divergent perturbation and partial wave expansions in scatt. theory, summation methods 79−67485
dressing the nucleon propagator, nested bubbles approx. in Bethe Salpeter eqn. 77−6032
dynamical mechanism, modified Duller-Walker approach 77−13982
education, Schrodinger eqn. solns. using approximate nucleon-nucleon and Λ-nucleon pots. 80−62429
effective 2-body pot. in nuclear matter 78−54714
effective NN interaction, long range components, configuration mixing 78−41646
effective NN interaction and exchange current vel. depend., dipole sum rule enhancement 80−63100
electromagnetic contrib. to NN interaction, one photon exchange helicity amplitudes 78−17040
EM pot. between nucleons, anomalous mag. moments and orbit-orbit interaction 79−93524
f-meson-other field strong gravitational coupling, effect on nuclear force in nucleon-nucleon interactions 78−514
field theoretical approach with stress on OBE pot. *(German)* 78−78203
finite state interactions *(Russian)* 78−33080
hadron interactions, effective radius quantum number depend., quark sum rules *(Russian)* 80−102062
half shell t-matrix parametrisation for delineated two-body bound state 77−18407
hard (soft) core pots., isobaric analogue resons. widths, FPT and ACCBA anal. 77−18404
hard core as relativistic effect 77−87994
hard-core systems, bound states and scatt., for teaching 78−41115
heavy ion+nucleus reactions, friction force, gas kinetic model 77−30621
heavy ion two nucleon transfer reactions, exact four body model 77−10426
heavy meson exchange effect on $^1D_2$ and $^3F_3$ N-N partial waves, dibaryon resonances 80−105874
heavy-ion optical pot. real part, new effective N-N interaction in folding model 77−18505
high density matter, relativisitc quantum many-body problem 78−4909
high energy particle-nucleus interactions, discussion 79−30858
inclusive charge exchange, parameter-free model 77−18336
inclusive hadron production in high energy particle+nucleus collisions, sum rules, scaling law 77−57673
inclusive hadroproduction of μ pairs, 39.5 GeV/c $\pi^\pm$, $K^\pm$, p, p̄ beams on Cu target 78−62470
inclusive pion production, low transverse momentum distrib., cluster model 77−67684
inclusive production of hadrons in high energy nucleus+nucleus collisions, scaling laws 78−33204
inclusive production of non-zero charm meson in central region, quark model *(Russian)* 77−14008
intermediate energy range, phase shift anal. 78−62428
isobar pot. and NΔρ-vertex 78−66140
isobars, transition potentials, short-range repulsion 77−34235
J/Ψ production in NN interactions, failure of Drell-Yan parton model 79−89106
kinematic singularity free helicity amplitudes, crossing matrix anal. props. 80−95285
lepton-hadron relation and the nucleon-nucleon potential 79−22207
long range NN interaction, axial polarisability, two pion exchange 78−29397

nucleon-nucleon interactions continued
longitudinal polarisation of direct muons with $p_\perp = 1.9$ GeV/c 79−9411
low energy expts. 78−62419
low multiplicity events, scaling and multiperipheral testing at cosmic ray energies 77−18342
low-energy pot., Regge-pole theory 78−45889
low-energy semi-phenomenological model, Nπ coupling const. *(French)* 77−18311
many body effective interaction theory problem, comparison with atoms 80−47406
matrix, irreducible basis of representations of group O(n-1) 77−6271
meson exchange 80−32195
meson exchanges and finite Fermi system theory 77−74774
meson field theory, generalised one-boson-exchange pot. 78−66096
meson field theory, one-boson-exchange model 78−66216
mesonic aspects, dynamical calcs. 77−10330
modified Duller-Walker approach, cosmic ray energy, 100-10000 GeV 78−49261
multihadron systems, NN pot., nonrelativistic covariant theory 78−70456
multiperipheral n-particle prod., KNO scaling deviation at high energies *(Russian)* 77−34141
multiplicity behaviour in ultrahigh energy interactions (10^{12} eV) 78−70415
multiplicity distributions of very high energy, universality hypothesis 77−26550
N resonances in NN interaction 78−25066
NN annihilation cross section at nonrelativistic energies *(Russian)* 78−33079
(non)conservation of isospin, parity, charge conjugation, and time reversal invariance in intermediate energy phys. 79−80772
nonrelativistic 1-boson exchange potentials based on generalised meson field theory 78−70459
nonrelativistic QCD, short range NN interaction 80−32200
nuclear collisions, pion multiplicity and nonlinear effects in pion production, NN inelastic interactions *(Russian)* 80−52637
nuclear forces, nonrelativistic quark model study, resonating group method 80−47403
nuclear form factor behaviour at high transferred momenta 79−9485
nuclear matter energy calc. with state depend. correls. and semirealistic N-N pot. 77−88066
OBEP, nonstatic with retardation, vel. depend. tensor pot. 77−88065
one boson exchange model, OZI rule, nucleon-nucleon-boson coupling 80−32066
one-boson exchange, dispersion relation and multichannel approaches 77−22759
one-boson-exchange-potential model of baryon-baryon scatt. 80−13295
P-violating interaction in Bars-Halpern-Yoshimura gauge model 77−22758
Paris NN pot. parametrisation, phase shifts, nuclear matter binding energy 80−47405
Paris nucleon-nucleon potential, book contrib. 79−97665
parity violating internucleon potential due to vector meson exchange, asymptotically free theories 77−10210
parity violating NN interactions, review of ab initio calc. problems 78−62327
parity violating nuclear effects, low energy anal., NN scatt. parametrisation 78−66218
parity violating terms in nuclear EM operators and struct. effects 79−6482
parity violation in neutron-proton capture 77−46165
parity-violating vector-meson-exchange internucleon potential, weak nuclear processes, modified factorisation approach 77−30418
phase shift analysis *(Rumanian)* 78−45942
phase shift parameters, 0 to 800 MeV (in)elastic scatt., survey 79−80837
phase shifts, mixing parameters, T=1 spin-spin pot. and T=0 central/tensor pot., discussion 79−80838
photoemulsion+p, 400 GeV/c, decay of short lived charmed particles produced *(Russian)* 79−3022
pion production in semi-inclusive reactions at 1000 GeV, scaling phenomena 79−22157
potentials, approximate relativistic Hamiltonians for interacting particles 77−13897
proton beam dump expt. at CERN SPS, obs. of excess ν_e, $\bar{\nu}_e$ events 78−45978
proton interactions, beam dump expt. at CERN SPS 78−45979
proton-emulsion collisions, 67 to 400 GeV/c, energy independence, pseudorapidity distribs. for shower particles 79−75808
QCD, transverse momentum distribs. of μ pairs from pN interactions, p-nucleus study 78−62375
quark MIT bag model anal. 79−80806
quark-gluon interaction in pN collisions, dimuon prod. at large transverse momenta 78−29355
radius perturbation theory, appl. to NN system and pionic atoms 78−21007
realistic NN pot. construction for three body systems and nuclear matter 80−22699
realistic nonlocal pots. from inverse scatt. theory for $^3S_1$-$^3D_1$ interaction 78−41651
recoil effects in microscopic description of inelastic scatt. 77−71465
Regge pole model, NN pots., one boson exchange, coupling consts. masses 78−70346
Regge trajectory scheme and di-baryon resonances 77−67633
Reid soft core potential, low-rank separable matrix formalism 80−22704
relativistic effects on the two-nucleon and nuclear matter systems 79−89261
relativistic N-N one-boson-exchange potentials with asymptotic power-law energy dependence 78−82293
resonance-nucleon and particle beam-nucleon scatt. cross sections *(Russian)* 80−32115
resonances due to annihilation, baryonium states, many channel N/D method 78−66143
s-channel helicity conservation at γV,γγ and NN vertices, vanishing of spin-zero covariant coupling 79−40691
S-wave π production, off shell effects, field theoretic model 78−70566
self-consistent field calcs., HF calcs., NN interactions, and results of appl., book contrib. 79−75880
separable nucleon-nucleon potentials and minimal relativity 80−27495
short range interactions, approximation by separable interactions of simple analytic form 79−85284
nucleon-nucleon interactions continued
short-range repulsion, gauge theory of coloured quarks 78−12880
solitary wave exchange in NN pots. 78−70457
sphericity of 24 GeV/c interactions 79−71767
spin depend. at 6 GeV determ. 78−66139
spin orbit interaction of nucleons, relative motion dependent, universal coeffs. of hyperspherical function method 77−61354
T=1 phase shifts, imaginary components, effect on spin depend. cross sections 79−36092
tensor force and d(γ,p)n forward p prod. 77−57649
time reversal noninvariant NN potential in two nucleon system 79−54352
total cross sections, medium energy dynamics, OPE three-body theory 78−25064
trinucleon bound state using Paris pot., binding energy and form factors 78−89803
TRIUMF and SIN experimental programs, E<1 GeV 79−63501
two body problem solution, NN interaction with separable pots., models, computer calcs. *(German)* 77−54156
two nuclear polynomial solitary wave exchange pots. 78−58202
two nucleon interaction, charge asymmetry, radiative corrections 79−89161
two-nucleon pot. and meson physics, nucleon-nucleon interactions, review 78−89802
unitary pole expansion, physical basis 77−18406
valence nucleon effective interactions 80−9244
variational matrix Pade approximants, NN dynamics 78−62427
weak coupling constant magnitude, anal. of ^{41}K data, CVC hypothesis *(Russian)* 77−6144
Weinberg model, NN parity-violating π-exchange pot. 77−65133
$C^+(2.26)$ search in 45 GeV/c neutron beam, C^+ hadronic and semileptonic decay *(Russian)* 79−22145
D(1865) charmed meson hadronic prod., cross section limits from pN 79−89211
Δ(1236) effect on imaginary component of NN phase shifts 78−70398
ηN→charged particles, 200 GeV, coherent tube model 79−49554
J/Ψ prod., valence- and sea-quark distribs., deep inelastic scatt. and Drell-Yan processes 79−13069
muons pair generation, nucleon cascade role 80−91120
μ prompt prod. in high p_T 400 GeV proton interactions, polarisation 77−13991
μ^+ direct prod. in pN interactions, longit. polarisation meas. 77−2995
N→πN, diffraction dissociation, two-component model 79−3037
n+N→(n*→Λkπ)X, 45 GeV, decay prob. 77−82795
n+nucleus, diffractive prod. of $p\pi^-$ systems, 8 to 24 GeV/c, cross sections 78−41711
n+nucleus, high momentum study, quasi-two-body scaling, differential cross sections 77−57665
N*N, total cross sections of diffractively produced nucleon excitations 78−21481
nd→$(p\pi^-)$d, 26.6 GeV/c coherent interaction, peripherality of nucleon diffr. dissoc. 79−45108
nd→$(p\pi^-)$d, diffr. dissoc. and interactions of diffractive produced systems 79−45107
nd→nnp, 21.5 MeV, quasi-free scatt. 79−75993
NΔ non-static interaction models, s-wave amplitudes and cross sections 79−67667
NN, 10^{12} eV, rapidity gap distrib., Snider multiperipheral cluster model 80−73757
NN̄, high-spin states, strong tensor forces 78−66146
NN, NN̄ helicity non-flip forward scatt. amplitude 78−21447
NN̄, nonrelativistic scatt. review 78−25065
N̄N, OBE pot. calc., bound state and reson. energies, widths in 1.6 to 2.7 GeV range 77−49931
NN̄, relativistic interacting system, eqn. of state using Regge-type interaction amplitude *(Russian)* 77−79032
NN̄, resonances and bound states, multichannel N/D formulation 80−78087
NN→(Nπ)N, mass-slope correl. in Reggeised Deck model 77−22712
NN→(Nπ)N, nucleon exchange, decay ang. depend., high energy nucleon diffr. dissoc. 77−79284
NN→(Nπ)(Nπ), double diffractive dissociation of nucleons, complex ang. momentum theory anal. *(Russian)* 79−54354
nn→$(p\pi^-)(p\pi^-)$, double diffraction dissociation process in deuteron colliding beams 77−13994
NN̄→(π, ρ, ω, f), statistical model 80−102028
NN̄ annihilation, level widths in coupled-channel problem *(Russian)* 79−93476
NN̄ annihilation diagrams, simple model, nonperturbative calcs. 79−67578
N̄N→$B_i\pi$, B_i are N̄N quasinuclei 80−57624
NN charge symmetry breaking, nn and pp scatt. length difference, meson mixing 80−13325
NN collisions, lepton pair prod., γγ background of Drell-Yan process 79−13057
NN collisions around 10 TeV, nucleon fragmentation by diffr. rel. to high-energy γ-quantum prod. 79−80174
NN→Δ(1236)Δ(1236), 4-25 GeV/c, Reggeised absorption model 77−6170
nn exclusive double diffraction dissociation at CERN ISR 79−9412
NN→γX, off-shell effects in the nucleon-nucleon system 79−80839
nN in nuclei, 200 GeV/c, inclusive backward prod., collective tube model 80−47338
NN inelastic interactions, ~10^{12} eV, depend. of cluster size and clustering on inelasticity 79−63566
nn interaction, effective radius determ. using three nucleon motion for nuclear forces 79−6426
NN̄ interaction, low energy, meson exchange forces, one boson exchange potential, dual quark models 78−62444
NN interaction in pion exchange, nuclear matter and pion condensation, review 80−42557
N̄N interaction information from antiprotonic atoms strong interaction effects 77−18402
NN→l^+l^-X, A depend. of lepton pair prod. on atomic nuclei *(Russian)* 79−49562
NN→μ+anything, 70 GeV, muon polarisation meas. *(Russian)* 77−6185
NN→NΔ, multiple pion exchange in nonstatic theory 77−34236
NN→NN(NNπ), isobar and peripheral model anal., and unified theory 79−80841
NN→NNπ, anal. via nonrelativistic field theory with HBE 79−85317

nucleon-nucleon interactions continued
NN→NNπ, effect of π-baryon from factors on ang. depend. of cross sections 79−85318
NN→NNπ, isovector exchange, comparison with πN elastic scatt. 78−37189
NN→NNπ, lowest order Feynman diagram calc. 79−63508
NN→NNπ, polarization analysis of reactions with four spin-1/2 particles 80−86745
NN→N(Nπ) diffractive dissociation process, one pion Regge-pole exchange amplitude *(Russian)* 80−42491
N̄N→N̄πN, 9 GeV/c, isospin cross sections, differential anal. 80−431
N̄N→pions, direct channel scheme based on statistical bootstrap, low-energy region 78−12924
N̄N potential, imaginary part 80−32118
NN potential, meson field theory two-pion exchange anal. 77−208
NN potential short range behaviour with the quark model 80−47409
nN→p̄ppX, narrow struct. in p̄p mass spectrum, threshold to 2700 MeV/c^2 79−63511
nn→π⁻d, matrix element for s-wave pion prod. 77−6142
nn→π⁻d, π-production amplitude mass extrapolation 77−74709
NN→πX, expt. review of π-prod. by (un)polarised nucleons on few-nucleon systems 79−80944
N̄N→πn, parametrisation of branching ratios 79−26341
N̄N→ππ, off-shell terms of πN scatt. matrix 80−73739
N̄N→ππ, ρ EM polarisabilities difference contribs. 79−3023
N̄N→ππ⁻, $Q^2\bar{Q}^2$ resonances using MIT bag and ^{3}Po models 78−58171
N̄N→πππ, fifth order perturbation theory prod. amplitudes, isobar model 77−54088
NN resonances and total cross sections, expt. evidence review 80−42558
nn scattering, ∼100 eV, ang. distrib., very light pseudoscalar boson exchange 78−62454
NN scattering in nonAbelian gauge theory, π-, ρ-, and ω-exchange, scalar Pade approx. 79−67573
NN short range interaction, six quark symmetry props., nucleon colour mag. attraction *(Russian)* 80−42411
N̄N system, effects of annihilation on resonances 79−58949
N̄N system, single γ and π emission rates, meson quantum number assignments 78−78208
NN two body systems, polarisation phenomena, 6 MeV/c to 150 GeV/c, QCD anal. 79−80840
NN̄→X, nuclear size dependence of particle prod., hydrodynamical model 80−22593
NNN̄ system, bound and reson. states using Fadeev eqns. *(Russian)* 78−89804
NNπ partial violating amplitude, short distance effects, PCAC 77−57557
Np→(Nπ)p, diffraction dissociation, absorptive effects 80−5009
Np→(Nπ)p, double peripheral description in diffraction model 78−58204
np→dπ⁰, charge symmetry violation, symmetry breaking mechanism 79−85313
ν production, prompt sources, and axion decays and interactions, pN beam-dump experiment 80−63028
p(p̄)N, 50-200 GeV/c, multiparticle production, multiplicities, cross sections and ang. distribs. 80−86768
p(p̄)N, ψ hadronic prod., lepton pair ang. distribs., cross section χ contribution 80−42487
p-emulsion nucleus, expts. on particle prod., 200 to 400 GeV 77−30433
p-nucleus, 20 to 200 GeV, secondary particle multiplicity distribs. charcts. *(Russian)* 77−74740
p-nucleus, 300 GeV/c, multiphoton events distribs. 77−10283
p-nucleus collision, prompt μ prod., multiple prod. model based on lepton-hadron relation 78−29362
p-nucleus collisions, direct muon prod. 77−2872
p+A→p+anything, A=C, Al, Ti, Cu, Cd, Pb, inclusive backward emission of protons, 1.5 to 9.0 GeV *(Russian)* 77−10278
p+Be, 400 GeV, meas. of polarisations of Λ⁰, Λ̄⁰ prod. 78−82253
p+Be(Cu)(Pb), 300 GeV, inclusive prod. of Λ⁰ hyperons 78−37253
p+Be→e⁺e⁻X, 30 GeV, J/ψ prod. and decay into e⁺e⁻ 77−57570
p+Cu, 300, 400 GeV, prod. of massive μ pairs 77−6379
p+emulsion, 400 GeV/c, neutral charmed particle, direct obs. of pair decay 79−85299
p+emulsion, 400 GeV/c, observation of short lived charm particles *(Russian)* 79−22144
p+emulsion nuclei, 300, 400 GeV, search for short lived charmed particles 77−50023
p+emulsion nuclei diffractive coherent prod., inclusive and exclusive channels 78−62530
p+Fe→μ⁺μ⁻+anything, enhancement in μ pair mass spectrum at 9.5 GeV, ϒ prod. 79−432
p+N, in W, Fe, C, props. of prompt muons prod. by 28 GeV protons 79−17906
p+N→Λ⁰(K_S^0)(Λ̄⁰)+X, in Be, Cu, Pb, neutral strange-particle prod. by 300 GeV protons 79−17905
p+N→μ⁻μ⁺X, 400 GeV, charged gluon effects, broken colour gauge model study 79−49473
pC→p(pol.)X, 100 to 400 GeV, proton polarisation in inclusive processes 79−58983
pd→tπ⁺, 750 MeV, T=1 NN phase shifts and total cross section 80−22630
pN, 100-GeV/c, charged-particle multiplicity distribs. 78−33101
pn, 195 GeV/c, inclusive π^+/π^- ratio and quark distributions 79−54367
pn, 195 GeV/c, single particle inclusive distribs. 79−75804
p̄N, 1.6 GeV/c, search for direct single electron production 77−49994
pN, 22.6 GeV in emulsion, cluster size in pionisation region 80−78099
pN, 22.8 GeV, cluster production, two-particle correlations 79−63550
pN, 28 GeV in Cu, prompt neutrinos and penetrating particles 80−47336
pN, 29.4 GeV, Σ and Ξ prod. ratios 80−42457
pN, 300 GeV, quark fragmentation functions in additive model 80−37222
pN, 400 GeV, azimuthal asymmetry, cluster model anal. 79−63547
pN, 400 GeV, in emulsion, two-particle rapidity correlation 80−63054
pN, 400 GeV, prompt single muon prod., charm prod. cross section 79−80855
pN, 400 GeV, rapidity gap correlations, Chew-Pignotti multiperipheral model 79−93471
pN, 400 GeV, study in nuclear photoemulsion *(Russian)* 79−93475
pN, 400 GeV/c in emulsion, ang. and rapidity distribs. 80−32140
pN, 67 GeV, multiperipheral cluster production 80−73689
pN, 67 GeV, rapidity dispersion and cluster production 80−78104
nucleon-nucleon interactions continued
pN, 67 GeV/c, in Be, Al, Cu, inclusive $\pi^\pm$, $K^\pm$, p, p̄ prod. cross sections *(Russian)* 80−86769
pN, 67 GeV/c, nuclear targets, $\pi^\pm$, $K^\pm$, p,p̄ yields *(Russian)* 80−68501
pN, 70 GeV in emulsion, pion cluster obs. 80−86762
PN, 70 GeV/c, inelastic interaction, planarity effect at accelerator energy 80−83006
pN, 70 GeV/c, multiparticle prod., principal axis variable anal. 79−36116
pn, charged secondary prod. 69 GeV/c^{-1}, transverse and rapidity distribs. 79−9409
pN, dilepton production by pol. protons, parity violating, asymmetry, Weinberg-Salam calcs. 80−42488
pN, μ pair prod., QCD predictions for zero and nonzero rapidities 78−89674
pN, nuclear targets, $p\pi^+\pi^-$ systems in coherent and incoherent collisions, 18.6 GeV/c 77−41866
pN, p̄N, 200 GeV/c, dimuon prod. cross section, Drell-Yan predictions, struct. functions 80−37300
pN, p̄N, ψ hadronic production, gluon contrib. in QCD framework 78−78139
pN, W boson and lepton pair prod. off nuclei, cross section enhancement 80−5014
p̄n annihilation, 5.55 GeV/c, meson resonance prod. and transverse spectra 79−93450
pN→charm particles, obs. in high resolution streamer chamber 80−73742
pN collision, 70 GeV/c, evidence for weak decay of new short-lived particle *(Russian)* 77−74728
pN dilepton prod. quark-parton distribs., Drell-Yan model 79−17752
pn→$\Delta^{++}\Delta^-$, quasi eikonal model anal., πP cut contribution, enhancement coefficients *(Russian)* 79−40798
pN→hadron shower, charm-pair production effects 80−73748
pN high-energy collision yields, evidence for composite quark model *(Russian)* 79−9636
pN in emulsion, 200, 400 GeV/c, multiparticle prod., azimuthal and rapidity effects 80−63035
pN in Fe, 400 GeV/c, bottom meson prod. search in multimuon final states 80−47334
pN in Fe, 400 GeV/c, ψ(3100) prod. 80−57650
pN in nuclei, 2.2, 6, 8.5 GeV, p and d inclusive spectra at 162° *(Russian)* 79−97710
p̄n interactions, 100 GeV/c, topological cross sections 79−54366
pN interactions, 400 GeV, D-prod., muon polarisation meas. 78−70413
Pn→l^+l^-X, scaling predictions, Drell-Yan model 80−73756
pN→lῑX, quark structure functions for hadrons, Drell-Yan model anal. 78−21476
pN→Λ⁰Λ̄⁰, 300 GeV, inclusive prod., triple-Regge behaviour 77−61328
pN→Λ⁰X, 28.5 GeV/c, Λ⁰ polarisation 80−32137
pN→Λ⁰X, inclusive cross section, constituent-constituent multiple scatt. model for dependence on atomic number 80−83101
pN→Λ⁰X, Λ⁰ polarisation and quark prod. mechanisms 79−63542
pN→$\mu^+\mu^-$X, 225 GeV/c, muon pair prod., qq̄ annihilation model 79−63552
pN→$\mu^+\mu^-$X, determ. of parton sea 78−29304
pN→μX, 350 GeV p-Fe collisions, prompt muon prod. rate 80−37311
pN→NNf⁰, 7-24 GeV, isospin anal. 77−46083
pN→NNπ, 6 to 1480 GeV, cross channel isospin amplitudes 78−45964
pN→NNρ, 7-24 GeV, isospin anal. 77−46083
p̄N→N̄(Nπ)$_{I=1/2}$, 5.7 GeV.c ρ exchange contrib., cross channel isospin amplitude anal. 78−45938
pN→NπΔ(1236) above 6 GeV, crossed channel isospin amplitude anal. 79−6346
pn→pX, 195 GeV/c, hierarchy of mean multiplicities 79−36112
pN→pX, 28.3 GeV/c, Pt target, polarisation of inclusively produced protons at p_T=1.5 GeV/c 78−93917
pN→pnπ⁺ (and similar), Δ(1236) isobar prod. 78−21443
pn→pπ⁺π⁻n, isobar prod. in proton diffractive dissociation *(Russian)* 79−80836
pN→π⁻X, 3.95 to 9.7 GeV/c, inclusive π⁻ prod. below 62 mrad *(Russian)* 79−49538
pN→π⁻pX , 9 GeV/c, inclusive π⁻p prod. below 188 mrad *(Russian)* 79−49538
pN→π⁰X, 200-400 GeV/c, inclusive π⁰ prod. over large X_T and X_F ranges 80−37310
p̄N→πX, intermediate p̄ contrib. to backward π prod. *(Russian)* 80−13326
pN→ψ(3.1)+X dimens. regularisation anal. 77−41812
$p^\pm N\to\mu^+\mu^-N$, 225 GeV/c, muon pair prod., 2 to 11 GeV/c^2, differential cross section 79−67612
π condensation in neutron matter, N-N interaction, critical density 80−57711
πN single and double diffractive prod., monopole transitions and slope-mass relation 77−38152
πNN vertex function, dispersion theory calc. 77−57509
$\pi^+\pi^-$ atomic bound states and ππ scatt. lengths in H_2 gas target, X-ray spectra 77−27206
ππNN̄ partial-wave amplitudes, interior dispersion relations 77−82758
ρ-meson exchange and reln. between pion-nucleus and NN interaction 77−10331
Be+p, 400 GeV/c, two hadron correlation at large transverse momenta 78−46060
Cu+p, dimuon prod., struct. in ϒ region near 9.5 GeV 78−17201
Cu+p collisions, 400 GeV, prompt ν prod. 78−46061
pN, 350 GeV in Ne, $D^\pm$ prod. cross section and lifetime 80−68494
pN→K_s^0, 300 GeV, inclusive prod., triple-Regge behaviour 77−61328
Pt+p, dimuon prod., struct. in ϒ region near 9.5 GeV 78−17201

nucleon-nucleon scattering
see also neutron-proton scattering; nucleon-nucleon interactions; proton-proton scattering
amplitude models, rel. to excitation of nucl. levels with anomalous parity by medium and high-energy nucleons *(Russian)* 77−79383
amplitude reconstruction at 6 GeV/c, current status and future meas. 77−49996
amplitude recovery from high energy nucleon-nucleus scatt., γ-transition data *(Russian)* 77−74855
bounds on the moduli for scatt. amplitudes 80−86742
bremsstrahlung amplitude, sensitivity of observables to short and intermediate distance wavefunctions 78−62449

nucleon-nucleon scattering continued
bremsstrahlung expts. review, comparison of results with theory 78-62447
Chou-Yang model and s-channel helicity conservation 79-63449
compilation of coupling constants and low-energy parameters 79-22159
conference, Vancouver, Canada, (July 1977) 78-62418
constituent description, spin-correl. meas., reaction mechanisms, QCD instanton effects 79-89180
correlations, short-range, with pseudopotentials 78-37225
Coulomb-nuclear interference polarisation in high energy large momentum transfer hadron reactions 77-79282
coupled equations for NN, NΔ, πd, NN scatt. above π prod. threshold 79-89244
deuteron breakup by nucleons, 15 to 156 MeV, attenuation of quasifree scatt., empirical rules 77-61415
dibaryon resonances in NN scatt. 80-57605
dynamics, new approach, hadron physics basis 77-18412
effective interaction in the Blankenbecler-Sugar equation in ϕ^3 theory 79-21914
eikonal description of nucleon-nucleon elastic polarisation data 77-13948
elastic scattering, optimal complete and optimal sufficient sets of expts. 79-85324
elastic scattering in spontaneously broken gauge field theory 79-36091
elementary particle scattering, phenomenological approach to the inverse problem 79-49498
hard-core systems, bound states and scatt., for teaching 78-41115
high energy elastic and inelastic scatt., review of phenomenology 77-30441
high-energy, effect of anomalous mag. moments in quantum field theory 78-465
I=1 NN amplitudes struct. at 6 GeV/c 78-70395
impact parameter representation, taking into account spin, isospin and Pauli principle 78-58198
intranuclear cascade calcs., influence of mean free path parameter 78-93958
inverse scatt. problem, potential-less approach *(Russian)* 79-85320
isospin-zero phase shift solution, NN scatt. at 325 MeV 78-50044
kinematic formalism 78-21463
large angle elastic scatt., spin depend., quark confinement short distance behaviour 79-97598
large momentum transfer polarised reaction as test of strong interaction T invariance 77-30402
low energy expts. 78-62419
low-energy, charge symmetry breaking forces, heavy nuclei binding energies 77-88047
many body problem in Lee model, NN scatt. and matter binding energy 80-63116
meson field theory, generalised one-boson-exchange pot. 78-66096
Morse function off-shell K-matrix, computation method 78-74164
multiple pion exchange in nonstatic theory 77-34236
non-iterative diagrams, role 79-67576
nonlinear chiral dynamics, one-loop approx. *(Ukrainian)* 78-460
nuclear isospin nonconservation using relativistic formalism in NN interaction 79-9500
nucleon-proton, high energy, review 77-257
parity violating observables in low energy np scatt. 78-50045
phase shift anal., K-matrix, optimal polynomial theory 78-62426
phase shift analysis *(Rumanian)* 78-45942
phase shift parameters, 0 to 800 MeV (in)elastic scatt., survey 79-80837
phase shifts, calc. using Blankenbecler-Sugar eqn. 79-67580
phase shifts, mixing parameters, T=1 spin-spin pot. and T=0 central/tensor pot., discussion 79-80838
phase shifts and resonances, coupled channel effects 79-67574
polarisation in elastic scatt., 6 to 45 GeV/c, eikonal description 77-30405
polarised NN scatt., weak neutral current models 78-41562
potential models, high-energy phase shifts and off-shell react. matrices 78-45936
pseudoresonance Argand loops *(Russian)* 79-9354
quasifree scatt. using cyclotron and D_2O target 77-34525
radiative corrections, tables 79-26335
resonance degrees of freedom in the two-nucleon system 80-5072
Saito potential, off-energy-shell unitarity 80-18207
scattering params. for separable potls. with Coulomb interaction 77-18425
small angle, appl. of eikonal vector meson exchange theory 78-17052
spin correlation parameters, implications for quark-quark interactions 79-13049
spin dependence, quark exchange evidence 80-102074
spin effects, QCD quark and gluon interactions 80-22577
spin structure and polarising power 79-67568
spin-orbit interaction model, polarisation and spin correl., elastic NN scatt. 77-30404
spin-polarisation meas., anal. 79-63505
SU(2)×SU(2) chiral symmetric Lagrangian description of low energy πN and NN scatt. 79-26251
total cross sections, medium energy dynamics, OPE three-body theory 78-25064
TRIUMF and SIN experimental programs, E<1 GeV 79-63501
two component Pomeron, πN, kN, NN forward scatt. amplitudes 80-37245
αα and NN scatt. analogies, quark struct. and clustering connections 79-6442
d double scattering on H target, d alignment, spin struct. of NN amplitude 78-45937
dd, 4.3, 6.3 and 8.9 GeV/c, struct. of secondary d spectra high momentum parts *(Russian)* 78-78394
dd, elastic scatt. $\sqrt{s}$=53 GeV, narrow min, and inelastic shadow effects, Glauber theory 78-89740
dd collisions, 4.3, 6.3, 8.9 GeV/c, d spectra high momentum struct., multiple NN scatt. model 78-89727
dd elastic scatt., 53, 63 GeV, inelastic intermediate state effects, Glauber multiple scatt. theory 79-36104
dN relativistic scattering, elastic and inelastic form factors 79-30752
dp, 800 to 1430 keV, differential cross section meas. 79-80947
Δ(1226) resonance effects 77-14051
Δ(1236) resonance, effect on NN scatt., nuclear and neutron matter 77-41909

nucleon-nucleon scattering continued
γNN→γNN forward scatt. amplitude and generalised optical theorem, dispersion relations 79-93446
n-hadron amplitudes from p-hadron and d-hadron amplitudes in Glauber-model 77-22803
n-n scatt. length from ^{2}H(n,np)n 79-17904
N-N singlet even pot. from inverse scatt. problem algebraic method 77-18315
nd, backward elastic scatt., 350 to 550 MeV, ang. distribs. 79-75782
nd, local soft core NN pots., quasiparticle formalism 79-6529
nd, polarisation effects in 3-body system 79-80946
Nd, three and four nucleon low energy scatt. expts., review 79-80945
nd, three body systems, review of recent theoretical anal. 79-80842
nd, three-body Amado-Lovelace eqn. at positive energies, anal. soln. 78-16938
Nd→(Nπ)d, ISR energies, single and coherent nucleon diffraction dissociation 80-22640
nd backward elastic scatt., 200 to 800 MeV, ang. distribs. and relativistic momentum transfer variable 79-75783
nd backward scattering, 200 to 800 MeV search for bump in 180° excitation function 78-62445
nd break-up, quasi-free scattering, peripherical nature 78-89726
nd quartet scatt., many-body theory *(Russian)* 77-38190
Nd S-wave scatt., dispersion relation approach to three-body systems, unitarity approx. 79-506
nd scatt., at d breakup energy, boundary condition method 79-22127
NN̄, nonrelativistic scatt. review 78-25065
NN̄, $Q^2\bar{Q}^2$ resonances using MIT bag and ^{3}Po models 78-58171
NN dynamics at medium energies, elastic and inelastic scatt., unitary model 80-63101
NN dynamics at medium energies, phase parameters, one pion exchange model 80-63102
nn effective range parameters from pp scatt. potls., effect of deuteron and cut off constraints 77-6246
NN elastic scatt., spin struct. interpretation, polarising power 79-85342
NN elastic scatt. with one boson exchange, Bethe-Salpeter eqn. 80-42485
NN forward scatt., two and three pion cut contribs., nucleon exchange model 80-63103
NN inelastic processes, SU(3) breaking, N(1688), Λ(1815) and Σ(1915) states 77-71526
NN large angle elastic scatt., spin correlation asymmetries, partons and coloured quarks 79-63411
NN large angle elastic scatt., spin-spin asymmetries and flavour depend., quark interchange 80-86743
NN̄ low-energy reson. in OBEP anal. 77-26539
NN̄→N̄N, differential cross-section zeros, S(1936) meson J^{PC} assignment 77-49998
NN potential from Regge pole theory in momentum space, S-matrix theory formalism 79-67525
NN potential from Regge pole theory, pseudoscalar meson potentials, M/E factor 79-67526
NN potentials, based on meson exchange, discussion and appl. to nuclear matter 79-80815
N̄N potentials for bound and scattering states 80-47323
nn quasifree scatt., 14.1 MeV, in ^{2}H(n,nn)p 77-23018
nn quasifree scatt. in cyclotrons 79-26342
NN̄ resonance, Goldberger-Treiman relation corrections 78-463
NN scattering, role of noniterative π exchange in nuclear matter 79-40857
NN scattering in the nonrelativistic quark model, total elastic cross section *(Russian)* 80-68475
nn scattering length, from proton spectrum of ^{2}H(n,p)nn at 14 MeV 77-26704
NN spin-polarisation meas. 78-74272
NN̄ system, quasi-nuclear over-threshold resonance, annihilation effects *(Russian)* 80-27521
NNπ amplitudes, parity violating, QCD calc. in Weinberg-Salam model and SU(4) flavour symmetry breaking 79-67520
Np→(Nπ)p, double peripheral description in diffraction model 78-58204
np charge exchange amplitudes, Regge behaviour of imaginary parts, polarisation 77-38145
p+α, elastic scatt. of intermediate energies, polarisation, momentum transfer effects 77-30408
pd, polarisation effects in 3-body system 79-80946
pd, three body systems, review of recent theoretical anal. 79-80842
pN, 2-15 GeV/c, in Ge, Si, influence of channelling on scattering 80-73729
p̄N, 70, 125, 175 GeV/c in Be, C, Al, Cu, Sn, Pb nuclei 80-83128
pN, high energy polarised scatt. particle struct. studies, book 80-41952
pn, topological cross section and charged secondary ang. distrib. at 69.0 GeV/c 78-78219
pn foward scatt. amplitude real to imaginary part ratio using Glauber approach 78-70410
pN scatt., 6 GeV/c, polarised beam, P-violation, longit. asymmetry meas. 79-63500
nd, 2.48 and 3.28 MeV, elastic differential cross section and related phase shift analyses 79-75992

nucleon-nucleus reactions
for inelastic nucleon-nucleus scattering, see "nucleon-nucleus scattering" see also neutron-nucleus reactions; nucleon-nucleon interactions; proton-nucleus reactions
atmospheric nucleon and charged pion unidirectional diffusion eqns. 78-57417
backward current effect at energies >1 TeV, cross section, ang. distrib., multiplicity *(Russian)* 77-74851
Bethe-Goldstone eqn., nucl. matter, nucleon optical pot. anal. 78-12981
CERN School of Physics, Austerlitz-Zeist, Holland (June 1978) 79-30857
cluster production in hadron-nucleus interaction at cosmic-ray energies 80-13467
complex momenta eikonal approx., hadron-nucleus collisions at asymptotically high energies *(Russian)* 78-74294
cross sections, Glauber theory and N-N inelasticity 80-68669
cumulative meson production processes, phenomenological model for mechanism 78-58266
deformed even-even nuclei, specific form. of nucleon-nucleus interaction, low energy 78-13077
double differential cross-section, analytic expression 78-8825

nucleon-nucleus reactions continued
exciton model of γ-emission in (N,γ) reactions 78−62539
formation zones, large p_T prod. on nuclei 77−50134
four particle systems, reaction dynamics 79−80905
giant quadrupole capture of energetic nucleons by nuclei 77−10398
hadron+nucleus cross-section, energy depend., multiplicity, scaling violation model *(Russian)* 79−22350
hadron+nucleus high energy collisions modified cascade model, multiplicities energy depend. 79−59064
hadron multiproduction on nuclei, nature of pomeron 77−87955
hadron-nucleus collisions at high energies, simple collective effects model *(Russian)* 78−89809
hadron-nucleus high energy collisions, two-particle correlations, cluster cascade model 79−49615
hadron-nucleus interactions, existence of slowly moving sources, vel. depend. frictional sources 79−6690
hadron-nucleus reactions, multiple production, expt. results, review *(Russian)* 79−3118
Hamada-Johnston interaction, nucleon optical pot. 78−12982
high energy, cumulative pion prod., inelastic rescatt. contrib., statistical bootstrap model *(Russian)* 78−54766
high momentum nucleons in nuclear matter, quasi-two-body scaling, differential cross sections 77−57665
inclusive fast nucleon spectra, phenomenology for weak, EM and strong processes 79−22292
inelastic collisions of light nuclei and nucleon-nucleus collisions, dynamical model *(Russian)* 80−37356
internuclear cascade mechanism, meson(nucleon)-nucleus high energy reactions *(Russian)* 79−80903
intranuclear cascade model for high energy (up to 1000 GeV) reactions 78−70498
intranuclear-cascade method, applicability to nucleon reactions 79−9531
microscopic theory based on Lippmann-Schwinger eqn. and projection operators method *(Russian)* 77−34290
momentum space method for hadronic atoms including relativistic hadron-nucleus reactions 79−872
multi-chain model for high energy hadron nucleus collisions 79−59042
multi-nucleon transfer and direct reactions, nuclear struct., review 78−50060
multiplicity of particles produced in hadron-nucleus high-energy interactions 78−4933
(N,α) reactions, preequilibrium model quasi-free scatt. for (N,α) reactions 77−88133
n-quasiparticle excited nucleus, pre-compound and compound systems decay 77−26654
nuclear matter, charge constrained coherent pion states from transversing fast nucleon 80−27585
off energy two body t-matrix in the R-matrix theory *(Russian)* 80−22780
optical model, for total cross-section, 180-1600 MeV 79−6538
optical model potential, spin-orbit component from internucleon pot., ^{40}Ca+p appl. 78−46039
optical nucleon-nucleus potential *(Russian)* 78−37321
optical potential from realistic Hamada-Johnston internucleon pot., binding energy 78−54730
particle production, Fermi motion versus collective tube model 79−93659
pion cumulative production in hadron-nucleus collisions *(Russian)* 78−607
pre-equilibrium calc. of nuclear spectra 77−22991
quark-parton model, relation between low mass dimuon and meson prods. 78−41477
relativistic hadron+nucleus reactions, degree of collectivisation 79−40956
relativistic nucleon-nucleus collisions, superdense matter eqn. of state *(Russian)* 78−606
resonant scatt., spectra of unbound levels 77−23005
secondary particle correl., N-nucleus interactions, 10^{12} eV 78−66178
target nucleon+α and target nucleon+^{6}Li, pots. in microscopic model with antisymmetrisation effects 78−62516
total reaction cross sections, microscopic description 80−95318
(N, α), DWBA finite range calc. 79−9541
(N,α) knock on reactions, final nucleus polarisation, polarised N capture 78−74352
(N,N′X), shower proton and meson transverse momenta, intranuclear cascade model 80−102185
(N,X), complex shell model, narrow resonances and bound states *(Chinese)* 80−42622
ND→πND, effectsof hadron formation zone on decay angle distrib. in coherent prod. on nuclei 79−36205
NN spin depend. t-matrix for intermediate energy reacts. 78−41682
π cumulative prod., cluster model 77−41968
π production, relativistic nucleon interactions *(Russian)* 78−25201
π production by nucleons on light nuclei, estimate of energy consumption *(Russian)* 79−80943
^{2}H breakup, NN interaction parameters 77−18550
^{2}H breakup induced by 22.7 MeV nucleons, calc. with separable interactions with tensor forces 77−18554
^{2}H-N breakup calcs., separable interactions with P-waves and tensor forces, polarisation 77−50101
^{2}H+nucleon, breakup reaction, off shell sensitivity, S-wave N-N interactions 78−82340
^{2}H+nucleon, Fermi-motion corrections 78−82348
^{2}H+p(n), differential cross sections, Coulomb penetration factor in DWBA calc. *(Chinese)* 80−27603
^{2}H(N,N′), three and four nucleon low energy scatt. expts., review 79−80945
^{2}H(N,X) disintegration cross-section, cut-off radius in impulse approx. type models *(Russian)* 79−22276
^{3}He(N,πX), expt. review of π-prod. by (un)polarised nucleons on few-nucleon systems 79−80944
^{4}He+N, potential calc. using microscopic model 77−88091
(N,X), disintegration by high energy nucleons, α-prod. mechanism from pre-equilibrium fluctuations *(Russian)* 80−106059

nucleon-nucleus scattering
see also neutron-nucleus scattering; nucleon-nucleon scattering; proton-nucleus scattering
1f-shell nuclides, optical pot. imag. part, isotopic features 79−9535
^{208}Pb (N,N^1) unnatural parity state excitation, π− condensate instability proximity, DWBA 79−97660
bremsstrahlung, soft photon, in pot. model 77−6381
cosmic-ray inelastic scatt. cross-section meas. 77−61413
deformed even-even nuclei, specific form. of nucleon-nucleus interaction, low energy 78−13077
eikonal model of hadronic matter distribution of particles and nuclei 79−26317
elastic scatt. at medium energies, microscopic optical pots. 79−97703
excitation of levels with anomalous parity, rel. to models of nucleon-nucleon amplitudes *(Russian)* 77−79383
Glauber approx. corrections, nucleon-nucleus scatt., nuclear density distrib. 78−50166
hadron-nucleus scatt., optical treatment in terms of scatt. amplitudes 78−89838
high energy, study of NN amplitude, γ-transition data *(Russian)* 77−74855
high energy nucleon-nucleus scatt., spin effects, Glauber theory multiple scatt. amplitudes *(Chinese)* 79−21979
high-energy, Glauber's theory, classical transport eqn. 79−6522
inelastic, leading to resonant states, line shape parameter 77−54211
inelastic, theory of two-step processes 77−34271
inelastic differential cross section, π-condensation instability of nuclei *(Russian)* 77−61426
inelastic nucleon scatt. anal., comparison of effective two-nucleon interactions 79−93608
inelastic scattering, evidence for giant resonances 79−17883
Levinson theorem, standard optical pots., nucleon+nucleus scatt. phases *(Russian)* 78−17214
local Slater exchange approx. for nucleon and heavy ion scatt. 79−22309
multichannel quasi-separable pot. approach 78−37320
multiple scatt., closure correction in second-order optical potential 78−50141
nuclei with nuclear matter t-matrices 79−93577
nucleon optical pot., spin-orbit term 80−27606
optical model, for total cross-section, 180-1600 MeV 79−6538
optical nucleon-nucleus potential *(Russian)* 78−37321
optical pot., three-body approach 77−18506
optical potential, exchange term and effect of odd forces 78−70500
quantum dynamical semi-groups in nucleon-nucleus scatt. 79−6595
recoil corrections in continuum shell model 78−8751
single scattering optical model, three body approach, appl. to nucleon+nucleus scatt. 78−25162
spin effects in framework of Glauber optical model 79−40909
three-body Bethe-Faddeev equations and single-particle potentials in nuclei 79−97684
two-channel optical model of high energy hadron-nucleus collisions 79−36210
Δ(33) interaction with nucleus, effective shell model pot., pion scatt. test 80−32202
Ca, nucleon optical pot. anal. 77−88137
^{40}Ca+N, resonating-group method anal. 77−82886
^{40}Ca+n(p), resonating-group anal. 77−6373
^{40}Ca(N,N), microscopic description validity 79−544
^{2}H(N,N), extraction of ^{2}H wave function 77−18418
^{2}H(N,N), off-shell effects, calcs. with phase equiv. separable pots. of rank two 77−18553
^{2}H(n,n′), 14.8 MeV neutrons, d break-up cross section meas. 79−80932
^{4}He+N, resonating-group method anal. 77−82886
^{4}He+n, elastic scatt., orthogonality condition model derived from parity energy surfaces 78−29432
^{4}He(N,N), microscopic study using single channel resonating group method, effective nuclear potentials 79−85425
^{92}Mo(N,N)^{92}Mo, optical model anal. 80−47473
^{92}Mo(n,n), elastic and inelastic, 11 MeV, isospin effects, optical and deformation parameters 79−17794
^{16}O+N, resonating-group method anal. 77−82886
^{16}O(N,N), microscopic description validity 79−544
^{208}Pb(N,N), <30 MeV, microscopic optical pot. in nuclear struct. approach, HF field 80−527
^{208}Pb(N,N), microscopic description validity 79−544
S, nucleon optical pot. anal. 77−88137
Si, nucleon optical pot. anal. 77−88137
^{90}Zr(n,n), elastic and inelastic, 11 MeV, isospin effects, optical and deformation parameters 79−17794
^{92}Zr(N,N)^{92}Zr, optical model anal. 80−47473

nucleon scattering *see hyperon-nucleon scattering; kaon-nucleon scattering; lepton-nucleon scattering; muon-nucleon scattering; neutrino-nucleon scattering; nucleon-nucleon scattering; nucleon-nucleus scattering; photon-nucleon scattering; pion-nucleon scattering*

nucleons
see also neutrons; protons
charge radii, parton model 80−91064
chiral substructure, parton model 77−41787
constituent quarks and deviations from Bjorken scaling 77−6089
decay, symmetry relations, effective Hamiltonian and inclusive decay rates, kinship hypothesis 80−78060
dimensions, mass, elec. and mag. moments *(French)* 80−13305
elastic form factor, exclusive and almost exclusive process asymptotic behaviour, renormalisation group 80−42464
EM form factor of nucleon is time domain *(Russian)* 78−78183
EM form factors, πN S-matrix inelast. effects in sideways dispersion relns. 78−82212
EM form factors and radii 77−2837
EM mass difference to π in Nambu-Jona-Lasinio model 79−93415
EM mass differences, quark behaviour 79−58941
EM mass shifts, asymptotic bounds and causality conditions 80−73704
EM polarisabilities from γN scatt., $\pi^0\to 2\gamma$, $\eta^0\to 2\gamma$ decay rates 77−18289
EM probes of nucleons, photo- and electro-excitation, quark model anal. of nucleon struct. 79−49520
EM radii of nucleon *(Russian)* 77−74687
EM structure, ψ(3.1) in VDM of nucleon form factors 78−50034
form factor, isovector, meson field theory, pseudoscalar πN interaction 80−62986
form factor, isovector, via $\pi^- p\to e^+e^- n$ 275 MeV *(Russian)* 77−82764
form factors, core model asymptotic behaviour, polarised struct. function 77−6086
form factors, dispersion theory, review 77−34155
form factors, dispersion theory anal. of $\pi^- p\to e^+e^- n$ cross sections *(Russian)* 77−10253
form factors, spectra representation *(Russian)* 78−93881

nucleons continued
form factors, weak, asymptotic behaviour within QCD dipole and triple-pole formulae 80−62987
form factors at $t=9.58$ GeV^2 from $\psi\rightarrow p\bar{p}$ data 77−6118
gas, weakly degenerate, virial coeffs., eqn. of state, species concentrations 77−13688
isoscalar axial-vector current between nucleon states 79−93316
isovector form factors, dispersion theory calc. of inelastic contrib. 77−13950
magnetic moment, gluon exchange corrections in MIT bag model 77−26528
polarisabilities α,β and deep inelastic e-N scatt. 77−49966
polarisabilities of hadrons, quark models 77−82703
properties in relativistic quark model with strong binding 80−102023
QCD running coupling const., nonperturbative determ., N struct. functions 79−75726
quark effective-bare mass distinction 78−12866
quark model of nucleons, ground state wave functions, O(3)×SU(6) symmetry 78−62352
stability testing, radiochemical and geochemical method limits 79−22093
struct. functions, $(1-x_s)^4$ behaviour 78−74227
structure function, quark and gluon moments, gauge theory 78−50036
structure function determination from μN inclusive scatt. meas. 80−42472
structure function Q^2-depend. in quark-gluon system 78−66088
structure functions, Bethe-Salpeter eqn. approx. soln. in quark-gluon model 77−54080
structure functions, overview of measurable types 80−73706
SU(5) grand unification, nucleon lifetime, bag model calc. 80−52450
valence gluons, existence in nucleons 79−13029
wave function, three relativistic quarks bound state on light cone *(Russian)* 77−6085
N structure function model from hard consistent quark interactions, scaling violations 80−86719
N-N* EM transition form factors 77−22735
NΔ system, theoretical investigation of bound states and resonances 79−75749
p-n mass difference, anal. of expt. data, scaling violation and renormalised struct. functions 79−97628

nucleosynthesis
^{260}104, detection methods, comparison of reactions ^{246}Cm+^{18}O, ^{248}Cm+^{16}O, ^{249}Bk+^{15}N 77−23106
^{260}104, synthesis by ^{249}Bk(^{15}N,4n) 79−30850
anomalous nuclei, primordial synthesis 80−46719
Ap stars, review of obs. and possible nucl. reactions *(Russian)* 78−20843
Ap stars, U/Th ratio, r-process nucleosynthesis 77−33508
beta transition rates in hot dense stellar matter 78−73699
big bang, lifetime and mass constraints of heavy lepton neutrinos 79−40308
big bang nucleosynthesis, cosmology and neutrino physics constraints 79−30154
big-bang model and ^{4}He abundance, review, book contrib. 78−89277
big-bang nucleosynthesis with nonzero lepton numbers 78−16583
bypassed elements, neutrino induced prod. 77−45408
charged particles, experimental nuclear astrophysics, review 79−25471
clustering in charged particle reactions 79−5744
CNO abundances in red giant envelopes 77−29825
composite particle formation in explosive nucleosynthesis 78−69678
core He flash and C and CH star origins 78−4190
cosmic ray isotopic composition, review 78−20599
cosmic ray source material synthesis, evidence from Ne, Mg and Si isotopes meas. 80−51631
cosmic rays, time delay between nucleosynthesis and accel. to relativistic energies 78−28455
cosmic rays and solar system material, origin of elements just beyond Fe 77−70952
cosmological, conventional and unconventional 80−46722
cosmological and stellar nucleosynthesis, review 80−62359
cosmological He and D abundances 80−62356
cosmology, general relativity, big bang model, nucleosynthesis, scale covariant theory, review 78−73789
D-D cross sections for thermonuclear synthesis 80−18608
Dirac cosmology, onset of galactic nucleosynthesis, and age of Universe 77−13514
dynamical r-process, nuclei far from β-stability 77−26004
early solar system, isotopic anomalies and proton irradiation 77−49317
early universe, nonlinear primordial fluctuations rel. to nucleosynthesis 79−25773
elements origin and evolution 78−32619
explosive nucleosynthesis, accelerator expts. and theory 77−71110
explosive nucleosynthesis, massive star evolution preceding and during supernova, element abundances *(German)* 79−44469
explosive nucleosynthesis, rel. to Al/Fe ratio in metal-poor-stars 78−57549
explosive r process cooling process 78−69791
galactic ^{4}He and heavy elements enrichment by stellar nucleosynthesis 78−28657
galactic chemical evolution rel. to stellar evolution and nucleosynthesis 80−67847
galactic evolution and nucleocosmochronology 77−29918
galactic nucleosynthesis, rel. to metal-poor stars O abundances 80−36610
galaxy chemical evolution, O and N abundance 80−46680
Galaxy nucleosynthesis history, chemical comp. of old halo stars 78−65616
Gamow Teller giant resonance struct., consequences for delayed neutron spectra and nucleosynthesis 77−2950
HD 76932, subgiant halo star, chem. comp. rel. to nucleosynthesis 78−81626
heavy and neutron-rich elements synthesis by rapid neutron capture process 78−77488
heavy and superheavy elements Dubna programme on synthesis and search 77−23570
heavy element, origin in star development supernovae and galactic matter *(German)* 79−44468
heavy element nucleosynthesis, current astrophysical theory review 77−29644
heavy element origin, supernova model, r- and s-processes 77−56825
heavy element synthesis and β-strength function shape 79−66918
high-luminosity stars, nucleosynthesis during thermal pulses rel. to surface comp. 78−40917
hot CNO nucleosynthesis, ^{18}O/^{17}O abundance ratio 77−78767
hydrostatic C burning, estimates using ^{12}C(^{12}C,n)^{23}Mg neutron branching meas. 77−34336
isotopic anomalies from neutron reactions during stellar explosive C burning 80−12651
K-captured isotopes content calc. in galactic cosmic rays 79−80114
light element abundances, galactic evolution and universal baryon density 79−40302
light element production by neutrinos emitted by collapsing stellar cores 79−21173
light element reactions in stars 80−101585
light element synthesis in big bang Universe 79−9044
light elements formation, thermal cycle, isotopic abundances problem *(French)* 78−96574
long neutron capture chains, abundances evaluation method 78−45216
main sequence stars, element abundance regularities rel. to nucleosynthesis *(Russian)* 77−45431
massive stars, bulk yields of nucleosynthesis 78−36552
massive stars, effects of binary evolution on heavy elements prod. 80−46534
massive stars, neutron capture nucleosynthesis in He burning codes 78−4195
massive stars and metal production 80−51741
massive stars nucleosynthesis, effect of mass loss on chemical yields 80−36614
massive stars nucleosynthesis, mass loss effects and critical rates for Wolf-Rayet stars 79−101138
massive stars presupernova evolution 79−16930
matter distribution in nuclei far from β stability valley, charact. features 77−64635
maximum isotope abundance correl. 78−45219
meteorites, isotope abundance anomalies, astrophysical implications 80−46511
Murchison meteorite, inert gases as possible relics of s-process nucleosynthesis 79−21243
N132D, supernova remnant in LMC, O/H ratios rel. to supernova nucleosynthesis 78−93345
neutrino cosmology, open universe with neutrino and graviton dominance 77−17731
neutrino number constraints in big-bang theory 79−62940
neutrino-induced nucleosynthesis, appl. to D and p-process nuclei 77−87582
neutron capture cross sections, 25 keV, evidence for slow nucleosynthesis 79−45259
neutron star matter, nucleosynthesis during decompression 77−33544
neutron stars, nonequilibrium shells, role in X-ray emission and nucleosynthesis, review 80−67774
neutron stars, nuclear fusion and C flashes 78−93293
neutron-rich Si burning, nucleosynthesis equilib. processes 79−62816
NGC 7027, planetary nebula, evidence for CNO and 3 α processing of nebular material 80−82459
noble gases isotopic anaomalies in Murchison meteorite, evidence for stellar condensates 80−41772
novae, CNO nucleosynthesis 77−87452
novae, explosive hot CNO-Ne cycle H burning rel. to abundances 79−44489
nuclear and differentiated abundance patterns 77−9656
nuclear astrophysics, introduction to form. and evolution of matter in Universe, book 80−105447
nucleocosmochronology, model, r-process elements discrete addition to presolar cloud 78−4121
occurrence in exploding supernova inner shells 79−62860
p-nuclei, low-temp. photonuclear nucleosynthesis in degenerate H burning zones rel. to novae 78−57540
p-process isotopes nucleosynthetic origin in supernova explosions 78−57541
p-process odd-A abundances and Sr isotopic anomalies 78−93101
Planck's constant, time invariance 78−93556
pregalactic H-He stars formation and nucleosynthesis 77−71157
primordial, limits on props. of massive neutral leptons 78−57438
primordial black holes, upper bound on number density calc. 78−65649
primordial black holes and big bang nucleosynthesis *(Russian)* 79−17151
primordial He production within scale covariant cosmology 80−105412
probability games, modelling stellar evolution and fusion 80−77590
pycno-nuclear reaction rate in stars 78−61724
r-nuclei prod. sites in Galaxy 80−72932
r-process, astrophysical, implications of fission mass distrib. 78−93204
r-process, rel. to origin of cosmic rays with $Z\geq 60$ 78−40782
r-process abundance peak, $A\approx 252$, due to subshell effect of $N=164$ 77−2993
r-process and r-cooling process, nuclear fissions 79−16816
r-process nuclei, isotopic anomalies 79−5740
r-process nucleosynthesis, required conditions 79−44459
r-process nucleosynthesis, supernovae mass range 79−5844
r-process seed nuclei prod. at low densities and temps. 77−64742
reaction rates for (p,n) and (α,n) 79−9602
reactions producing D, T, and ^{3}He in advanced stellar evolution, cross sections 80−56815
red giants, Li synthesis by spallation reactions 77−49366
resonant thermonuclear reaction rate integrals, closed-form evaluation and approximation considerations 80−8535
s-process, difficulty with ^{22}Ne as neutron source 80−72926
s-process, pulsed neutron flux effects 78−20812
s-process, Xe and Kr isotopic abundances 79−5739
s-process abundance evolution in galactic disc 77−13449
s-process and nuclear correction factor for Re/Os cosmochronology 80−17485
s-process calcs. and Ba II stars 80−56824
s-process element prod. in deeply mixed convective envelopes of red giant stars 77−33470
s-process elements in Ba star HR 774, Reticon spectra 79−25594
s-process isotopes, nonthermal isomeric branching, importance of long-lived states 78−7983
s-process neutron capture by ^{208}Pb at stellar temps. 78−4196
s-process nucleosynthesis, effects of unthermalised isomeric states and time-varying neutron flux on branching ratios 80−90410

nucleosynthesis continued
s-process nucleosynthesis, neutron capture time scale from s-process Kr in meteorite 80−73080
s-process nucleosynthesis, thermally pulsing stars 78−4193
s-process nucleosynthesis and stellar mixing 77−33466
s-process nucleosynthesis in giant stars, implications of Ti isotopic abundance ratios 80−26840
s-process nucleosynthesis in U Aquarii, rel. to extraordinary comp. 80−17588
s-process studies, exact soln. for unbranched network 78−28649
S-type stars, CeO band identification, new s-process mol. 77−33488
slow novae, Z=0.03 envelope model evolution rel. to CNO isotopic ratios 78−32468
solar system ^{16}O and ^{26}Al isotopic anomalies, local proton irradiation model 78−93128
solar system abundances of nuclides and nuclear structure 77−82130
star, explosive alpha-capturing reactions 79−44470
stars, Fe peak elements nucleosynthesis during C core thermonuclear explosion 78−36558
stars, lifetimes and abundance ratios in chemical evolution 79−53801
stellar, A>20 nuclei in advanced stellar evolution and supernovae 80−41817
stellar C-O cores, Urca neutrino loss rates 78−20813
stellar CNO isotope nucleosynthesis 77−87383
stellar CNO nucleosynthesis, cross section meas. 77−87382
stellar collapsed core, neutrino prod. of bypassed isotopes, neutrinos role in nucleosynthesis 79−40182
stellar cores, detonation formation 77−45398
stellar evolution, review of recent exptl. research 78−4100
stellar explosive nucleosynthesis, rel. to meteoritic isotopic anomalies 79−62795
stellar He burning shells, explosive neutron processing rel. to meteoritic abundance anomalies 79−58302
stellar interior, C burning products at const. temp. *(Russian)* 78−61722
stellar interiors, s-process during thermal pulses of He shell burning 78−28668
stellar nucleosynthesis, cosmochronology after Allende 80−4462
stellar nucleosynthesis, effect of mass loss by stellar wind on Galaxy chemical enrichment 80−41814
stellar nucleosynthesis in irregular and blue compact galaxies, rel. to chemical comp. and evolution 80−36711
stellar Si burning, $^{45}Sc(p,p')$ and $^{45}Sc(p,\alpha)$ rates meas. 77−88134
strong lined elliptical galaxies, overabundances of Na and Mg heavy isotopes 77−13464
superheavy element synthesis in fusion reactions, failure 79−45317
superheavy elements, possibility of occurrence in nature 78−20407
supernova explosions, presolar grains and meteorites isotopic anomalies 78−20845
supernova nucleosynthesis mechanisms 77−87463
supernovae, ^{56}Co synthesis from light curves analytic solns. 80−77427
supernovae, Fe group elements prod. through e-process nucleosynthesis, relative abundances *(Russian)* 80−62167
supernovae, He-driven r-process, rel. to solar system isotopic anomalies 78−57567
supernovae nucleosynthesis, implications for solar system origin 80−17509
supernovae nucleosynthesis, rel. to Ap and Am stars comp. anomalies origin 79−35277
thermonuclear astrophysics, element abundances rel. to nucleosynthesis *(Italian)* 79−53715
thermonuclear flashes on accreting neutron stars 80−31321
transuranic elements, heavy-ion reaction with stable Pb isotopes 77−26790
transuranium elements, z>100, stability *(Czech)* 77−50040
Tycho supernova, Type I supernova, nucleosynthesis rel. to remnant elemental abundancies 80−46635
ultraheavy cosmic-rays rel. to r-process models 78−49250
(α,n), A=88 to 124, reaction rates of reaction important to nucleosynthesis 79−45253
β^+ nuclei, thermally induced particle emission as possible formation process 77−6340
(n,γ) for A=138-181, stellar nucleosynthesis and s-process neutron flux 80−42663
(p,n), A=88 to 124, reaction rates of reaction important to nucleosynthesis 79−45253
Al isotopes, yield from C and Ne zones of massive star supernova 80−90406
^{26}Al in stars, long lived nucl. isomeric states, thermalization 80−85846
^{26}Al nucleosynthesis, astrophysical aspects of $^{25}Mg(p,\gamma)$ 80−42624
^{26}Al, prod. from stellar evolutionary sequence 79−5809
^{26}Al production during C burning, stellar rates, calc. 79−70948
^{26}Al production in explosive C burning 78−20814
^{26}Al, solar system synthesis limits from carbonaceous chondrites B concs. 79−16897
^{26}Al, synthesis in explosive H burning 80−85929
$^{26}Al^{g,m}$ relative yields from $^{25}Mg(p,\gamma)$ reaction 79−101058
$^{27}Al(p,n)^{27}Si$, cross sections and thermonuclear reaction rates 80−73852
Ar, galactic nucleosynthesis rel. to low Ar abundances in three halo planetary nebulae 80−82443
B, nucleosynthesis contribution from $^{16}O(p,X)$ 79−40978
^{11}B, neutrino-induced prod. in stellar C layer 80−82337
Ba abundance implications in metal rich Ba II stars 79−71024
Be, nucleosynthesis contribution from $^{16}O(p,X)$ 79−40978
C,N,O, stellar nucleosynthesis rel. to galactic obs. of CNO isotopes 78−4356
C burning in electron-degenerate stellar core, thermal oscills. 79−21269
C degenerate core thermonuclear reaction propag., neutrino mech. *(Russian)* 79−5812
C detonation supernova models, lower mass limit 79−17053
C shell burning to Fe core collapse, evolution of 15 M⊙ star 80−72937
C shell flash in 9 M⊙ star 78−89170
C stars, low-energy spallation rel. to $^6Li/^7Li$ ratio 78−40927
CNO cycles in stellar nucleosynthesis 77−87381
CNO isotope importance in astrophysics 77−87263
CNO isotopes in astrophysics, conf. Grenoble, France, 1976, Aug. 77−87262
CNO nuclides, prod. in mixed-up main-sequence stars 77−33475
CNO processing in stellar envelopes, isotopes origin and isotopic ratios evolution 78−93201
^{12}C, internal pair emission branch of 7.65 MeV, stellar triple-α reaction 77−54183
nucleosynthesis continued
$^{12}C+\alpha$, spallation fragments $6\leq A\leq 11$ yields, nucleosynthesis interest 79−30845
^{12}C(p, spallation), Li, Be, B prod., 45-100 MeV, nucleosynthesis implications 77−23053
^{13}C, ^{15}N, nucleosynthesis rel. to isotopic abundance vars. in interstellar HCN 77−53657
$^{13}C(\alpha,n)^{16}O$, 0.60-1.15 MeV, astrophysical appls. 77−13230
$^{13}C(\alpha,n)^{16}O$ process, 0.60 to 1.15 MeV, reaction rate 77−45300
Ca and Mg isotopic anomalies and lack of ^{26}Al in Allende meteorite unsual inclusion 79−40142
$^{42}Ca(p,\gamma)$, 0.7-5.5 MeV, cross section and stellar nucleosynthesis reaction rates 79−13294
^{53}Cr, new isotopes of interest to explosive nucleosynthesis, β-decay scheme and mass determ. 79−45208
D formation by nonequilib. processes 77−53423
D production model limitations based on high-energy neutrino background 79−44328
^{253}Es, separation and α-spectra identification following neutron irradiation of Cf 78−17435
Fe abundance in solar system rel. to nucleosynthesis 77−53435
Fe, nucleosynthesis rel. to galactic cosmic ray Fe nuclei isotopic comp. 80 - 72729
^{259}Fm prod. in ^{257}Fm (t,p) half-life and fission mass distrib. meas. 77−26776
H and He flashes in envelopes of accreting neutron stars 80−67772
H burning, intermediate nuclei behaviour in stellar interiors 78−45218
H burning in C-O dwarf degenerate envelope *(Russian)* 80−17585
H burning of $^{29,30}Si$ in explosive C burning 79−22289
H burning thermonuclear reactions, pp chain and CNO cycle 77−22202
$^1H+^2H$ burning star hypothesis for Jupiter 77−13282
He, C-O dwarf degenerate envelope *(Russian)* 80−17585
He core flash, convection efficiency and mixing possibilities 79−48774
He core flash onset and $^{14}C(\alpha,\gamma)^{18}O$ in low-mass stars 80−51735
He flash and convection in stellar cores 78−89191
He flash in stars with shell energy sources 78−89169
He, increasing galactic content rel. to chemical enrichment of disc dwarfs 79−88733
He, primordial nucleosynthesis rel. to Dirac Large Numbers Hypothesis 79−92900
He shell burning, thermal pulses in accreting white dwarf 80−22009
He shell flashes in red supergiants, convective penetrations and observable effects 80−51755
He-burning flashes on accreting neutron star, X-ray burst source model 79−17008
He-burning in core of massive stars 78−93207
K, Ar, interstellar, supernova nucleosynthesis rel. to isotopic anomalies 78−28761
^{138}La, low temp. photonuclear nucleosynthesis in stellar H-CNO burning zones 77−13319
Li, Be, B, cosmic-ray nucleosynthesis and extragalactic matter local infall rate 79−17084
Li, from $\alpha+\alpha$ obs. at 61.5-158.2 MeV 79−17886
Li in weak G-band stars, spallative origin 80−51752
Li, nucleosynthesis contribution from $^{16}O(p,X)$ 79−40978
Li production by weak G-band stars, results from abundance meas. 80−41819
$^6Li(d,n)^7Be$, low energy cross section, 100-180 keV 78−4949
^7Li nucleosynthesis in UV Ceti flares 79−30073
^7Li, prod. in nova explosions 78−57555
Mg isotopes, yield from C and Ne zones of massive star supernova 80−90406
Mg, stellar nucleosynthesis rel. to isotopic abundances in G and K dwarf stars 80−51757
$^{24}Mg(\alpha,n)^{27}Si$, cross sections and thermonuclear reaction rates 80−73852
$^{25}Mg(p,n)^{25}Al$, cross sections and thermonuclear reaction rates 80−73852
$^{26}Mg(p,n)^{26g}Al(7.3\times10^5$ yr), ground state cross section, statistical compound model 79−30827
$^{26}Mg(p,n)^{26m}Al(6.35s)$, ground state cross section, statistical compound model 79−30827
^{55}Mn, β-decay scheme, $T_{1/2}$ and mass meas., astrophysical significance 77−26635
^{59}Mn, new isotopes of interest to explosive nucleosynthesis β-decay scheme and mass determ. 79−45208
^{60}Mn, new isotopes of interest to explosive nucleosynthesis, β decay scheme and mass determ. 79−45208
N, in planetary nebula in irregular galaxy NGC 6822, abundance and nucleosynthesis 80−41867
N, stellar nucleosynthesis rel. to galaxies ages determ. 79−25728
$^{14}N+\alpha$, spallation fragments $6\leq A\leq 11$ yields, nucleosynthesis interest 79−30845
^{15}N, galactic evolution 77−87264
Na in M13 red giants 80−82439
Ne explosive burning in supernovae isotope production 80−94780
Ne-E, anomalous meteoritic Ne component, thermonuclear origin, supernova models 78−45292
^{20}Ne, form. in $^{19}F(p,\gamma)$ reaction, 668 keV, γ-ray transitions to ground state, rel. to stellar nucleosynthesis 78−17191
^{22}Ne and ^{26}Al nucleosynthesis in novae and supernovae outbursts 80−62143
^{22}Ne anomalous abundance in Orgueil meteorite, evidence for presolar grains 80−41773
^{56}Ni, nucleosynthesis in Type I supernovae rel. to radioactive excitation source model for late time spectra 80−105264
O, enrichment rate in Galaxy determ. from planetary nebulae O/H ratios age depend. 80−105328
O, in supernova remnant in NGC 4449, abundance rel. to nucleosynthesis 80−56895
$^{16}O+\alpha$, spallation fragments $6\leq A\leq 11$ yields, nucleosynthesis interest 79−30845
$^{A}Os(n,\gamma)$, A=186-188, 2.6-800 keV, capture Maxwellian cross sections, galactic nucleosynthesis 80−42664
Sc production in stars, $^{42}Ca(p,\gamma)$ and $^{44}Ca(p,n)$ reaction rates 80−82183
$^{45}Sc(p,\gamma)^{46}Ti$, stellar reaction rates 78−93090
$^{28}Si(\alpha,n)^{31}S$, cross sections and thermonuclear reaction rates 80−73852
^{180}Ta, low temp. photonuclear nucleosynthesis in stellar H-CNO burning zones 77−13319
Te, Xe and Kr isotopes in Allende meteorite, record of nucleosynthesis 79−40147
^{45}Ti production in star, $^{42}Ca(\alpha,n)$ reaction rate 80−82183

nucleosynthesis continued
^{49}Ti(p,γ), 0.74-3.25 MeV, cross section and thermonuclear reaction rates, nucleosynthesis, IAR effects 80−102187
^{50}Ti(p,n), 0.74-3.25 MeV, cross section and thermonuclear reaction rates, nucleosynthesis 80−102187
^{51}Ti, β-decay scheme, $T_{1/2}$ and mass meas., astrophysical significance 77−26635
^{51}Ti, new isotopes of interest to explosive nucleosynthesis, β-decay scheme and mass determ. 79−45208
^{51}V, low temp. photonuclear nucleosynthesis in stellar H-CNO burning zones 77−13319
^{51}V, new isotopes of interest to explosive nucleosynthesis, β-decay scheme and mass determ. 79−45208
Xe, isotopic anomalous in Allende meteorite, rel. to ^{184}Os/^{190}Os ratio 77−45368
Zr, isotopic composition, at. wt., rock standards, chondrite composition 79−3591

nucleus
see also hypernuclei; nuclei with mass number 150 to 189; nuclei with mass number 190 to 219; nuclei with mass number 1 to 5; nuclei with mass number 20 to 38; nuclei with mass number 220 or higher; nuclei with mass number 39 to 58; nuclei with mass number 59 to 89; nuclei with mass number 6 to 19; nuclei with mass number 90 to 149
No entries

number theory
see also digital arithmetic
education, Fibonacci numbers, recurrence relation soln., combinatorics function anal. 80−51988
gaussian sum, appl. to deterministic phase shifter design 77−14676
history, manuscripts of Nathaniel Torporley and Thomas Harriot 77−82357
unitary group representations, appl., book 79−30198

numerical analysis
see also approximation theory; curve fitting; difference equations; error analysis; finite element analysis; function approximation; function evaluation; functional analysis; functional equations; interpolation; iterative methods; Monte Carlo methods
13 GK model, numerical results for Couette, Poiseuille and thermal creep flow between parallel plates 79−77057
Abel integral eqn., numerical soln., optical diagnostics of axisymmetrical objects 79−7488
Abel integral eqn. inversion in astrophysical problems 80−26732
ablating plane (axisymmetric) body, turbulent boundary layer with neg. press. gradient 78−79389
absorbing boundary conditions for num. simulation of waves 77−87638
accelerating two-phase nozzle/diffuser flows, virtual mass effects on numerical stability 80−92204
accretion onto binary stars, numerical simulation 79−21358
acoustic noise sources, time delay bias errors in estimating frequency response and coherence functions 79−18614
acoustic radiation in 3-D, integral soln. techniques 77−68293
acoustic wave propag. in fibrous absorber, numerical results for elementary cells model *(German)* 77−802
aerodynamic wave drag, nonplanar singularity distribs., Hayes' algorithm extension 77−84271
aerodynamics, discrete vortices method and multidimensional singular integral eqns. theory 80−19421
aerofoil in unsteady airstream, two-dimens. viscous flow, numerical predictions 78−75166
aerofoil in unsteady viscous flow, numerical soln. procedures 78−75165
aerofoil with jet flap, incompressible flow past 78−59414
air, dissociated, hypersonic flow over blunt axisymmetric body, nonsteady heat exchange 79−37319
air cushion system, plenum, duct effects on heave stability 79−17202
air pollution, photochemical, potential form. in United Kingdom, numerical estimation method. 80−76682
air pollution episodes in Venetian region, real-time forecasting via advection-diffusion model 80−77096
air pollution episodes in Venetian region, real-time forecasting via Kalman predictor 80−82046
air temperature, five-day average, forecasting, combined technique improvement 79−29817
air-H_2O injection into permeable bed for underground coal gasification, numerical model 80−30359
air-water bubbly mixtures, press. wave propag. *(French)* 78−22402
airdroplet flight in air, drift loss from spray cooling pond, numerical estimation 80−19471
alloy melt, impurity conc. field model, growth by Czochralski method *(Russian)* 80−75191
alloy melt, temperature distribution during cryst. growth by Czochralski method *(Russian)* 80−75192
amplified spontaneous emission in spherical and disk-shaped laser media 80−1177
Anderson transition, numerical methods 79−60767
anelastic deformation, generalised representation by num. sol. of initial boundary value problems *(German)* 79−12610
anisotropic Milne's problem, soln. using H-functions 77−53840
antenna and scattering problems of complicated structures, mathematical methods *(German)* 79−76559
antenna radiation field, soln. as initial value problem *(Chinese)* 78−9294
applied mathematics and mechanics, conf., Giaz, Austria, Apr. 1976 *(German, English, French)* 77−67284
arbitrarily shaped body, integral approach to acoustics prediction 77−84040
Archaean tectonism, numerical models of vertical tectonism in greenstone belts 80−81861
at-power reactor noise, second-order coherent functions 78−94070
N.Atlantic waters integral circulation, numerical calc. 78−3811
atmosphere, middle, numerical model of zonal mean circulation 80−109218
atmosphere, urban, numerical simulation of mixing depths 80−105024
atmosphere, vertical diffusion study using airborne gas-chromatography and numerical modelling 78−69435
atmosphere baroclinic instability, numerical modelling *(Russian)* 78−44922
atmosphere circulation over oceans in equatorial latits., numerical calc. 78−92949
atmosphere frontal waves development, numerical simulation accounting for mountain ridges effect *(Russian)* 78−53701

numerical analysis continued
atmosphere fronts dynamics, numerical modelling *(Russian)* 77−64370
atmosphere numerical model, modified forward- backward scheme for two-grid-interval noise 80−26575
atmosphere O_3 production transport and distribution, numerical simulations with global general circulation model 80−56544
atmosphere O_3 profile, determ. from outgoing thermal radiation 78−92945
atmosphere spectral energetics, determ. via numerical filtering anal. 80−26577
atmosphere temperature regime, numerical model *(Russian)* 77−64368
atmosphere thermals, laboratory and numerical models rel. to self-similarity soln. 80−109228
atmosphere zonal circulation model, numerical expts. *(Russian)* 78−81295
atmospheric diffusion, steady state 3-D model, numerical anal. *(Japanese)* 79−79984
atmospheric diffusion, steady state model, effect of terrain 79−92582
atmospheric fronts, numerical investigation of motion employing two-layer model *(Russian)* 77−53109
atmospheric movements, spatial problem on influence of orography with Coriolis force included *(Russian)* 80−94565
atmospheric pollution, photochemical numerical model 80−40943
atom+diatom, sudden approx. of Cross, computational tests, cross section factorisation, scatt. phenomena 80−58352
atom+molecule, rotational inelastic scattering, effect of interaction pot. 79−59533
atom models, ionisation time depend. under intense EM fields 80−32683
atomic electron scattering, matrix variational calc. 79−59577
atomic photoionisation, many-body perturb. calcs. 79−59406
atomic resonant states, wavefunctions of complex coord. method 80−106282
auroral arcs global formation, numerical simulation 80−67446
autoresonant acceleration, numerical simulation of cyclotron waves 79−72022
axisymmetric flow, centreline formulation in numerical computation 79−41671
axisymmetric plastic deformation, slip line model *(Russian)* 78−83261
backscattered EM field from random surface, horizontally polarised, Kirchhoff approx. 79−7061
band struck. in 1-D, continued fraction approach 80−6694
Baneberry nucl. explosion, numerical simulation 80−841
bar (tube), compressible, combined loading, elastic-plastic problem 78−63311
beam, flexural vibrs., method of asymptotic expansions *(French)* 78−51112
beam bending, effect of secondary terms 78−79237
beam bunch effects in the circular isochronous cyclotron 79−54716
beam dynamic loading, large elastic-plastic deform., numerical anal., expt. meas. 78−1574
beam formation, eccentric, error anal. 79−3920
beam-like lattice trusses, prediction of thermoelastic and free vibration responses 80−14566
beams, dynamic plastic response, rotatory inertia and transverse shear effects 80−5947
Benjamin-Ono equation, N-soliton soln. 79−92929
Bessel functions, $J_n(z)$, $Y_n(z)$, $H_n^{(2)}$ and $H_n^{(2)}(z)$ calc., of integer order and complex argument 79−63004
best fit strain tensors method for stress computation in two material elastic media 77−46910
binary alloys, two phase region calcs. in solidifying melt *(Russian)* 80−65195
black holes, stationary accretion disc, numerical anal. of struct. 79−17015
blade to blade flow, anal. with Thomas algorithm 78−24669
blast wave, variable energy, perturbation solns. 78−51192
block composite algorithms of Newton-delayed chaotic relaxation type *(French)* 77−26151
blood flow in heart, flow pattern anal. 78−15854
blunt body, boundary and wake, supersonic viscous gas flow, numerical soln. 80−38441
blunt body, unsteady supersonic flow, grid characteristic method 80−38442
Boltzman equation, Gauss-Hermite quadrature procedures comparison for soln. of nonlinear BGK eqn. 77−49692
Boltzmann eqn., collision integrals, rigorous soln. of relaxation phase *(Russian)* 78−8231
Boltzmann equation, nonlinear, exact solns. 78−12656
Boltzmann linearised eqn. with long range pots., numerical anal. 77−35168
boundary layer eqns. soln. by inverse series method 79−41662
boundary layer flow, unsteady past wavelike bulge on flat plate, num. soln. of Navier-Stokes eqns. 77−58644
boundary layer flow, weakly separated zones *(French)* 77−72276
boundary layer on heated plate, numerical results 79−10545
boundary layer turbulence, velocity profile calc. by Du Fort Frankel scheme 79−94600
boundary-layer flows from fixed to moving surfaces, gap effects 79−14377
boundary-value problems 77−67257
box sections, interactive buckling anal. using dynamic relaxation 77−72202
branched cracks in 2-D, numerical soln. 79−46269
branched torsional systems with multiple junctions, free and forced vibrs. 77−31248
bubble dynamics, quantitative study appl. *(Italian)* 78−22403
bubble nonequilibrium collapse, heat transfer effects 79−98794
buoyancy dominated wall diffusion flames, numerical model 77−68710
Burgers' equation for nonlinear shallow water waves, Galerkin method soln., expansion of B-splines 78−87352
BWR boiling noise, local and global component obs. and calc. 78−94066
BWR LOCA, numerical simulation of hydrodynamic impact loads on cylinders 79−36350
calculus with appls. and computing, book 77−34
cantilever beam, minimum mass struct., axial vibrs., numerical determ. 79−10519
cantilevers, neutrally buoyant inflatable, free vibration in ocean environment 79−14333
capillary-porous bodies, heat and moisture transfer, analytical formulae 78−67013
Cartesian model, viscous boundary layer flow over topography 78−92904

numerical analysis continued
cascade, with large-deflection oscills., unsteady aerofoil theory, numerical soln. *(Japanese)* 78−67211
catastrophe theory, symmetry and higher order cuspoids 78−62079
Cauchy integral-equation method, steady water wave problem numerical soln. 79−10574
cavitation bubble collapse, num. simulation 77−58747
cavitation gas bubble in compressible liquid, influence of inhomogeneous sound field on motion 80−6131
cavities, advanced numerical anal. of 2-D time depend. free convection 80−43704
celestrial mechanics, rectilinear isosceles restricted problem, numerical study 80−4242
ceramics, fracture-mirror boundary formation, criteria 80−70297
chain of coupled nonlinear oscillators, large amplitude motion, numerical study 79−25993
channel contour construction, transforming supersonic flow cross-section 79−37349
channel with blocked branch, laminar flow, nonregular domain transformation into rectangular domain 80−64635
charge bunch radiation losses in pill-box resonator, time domain numerical computations of EM fields 79−31781
charged particle transport theory, discrete and continuous interactions 79−55467
chemical kinetics, eigenvalue and eigenfunction anal. of Kramer's theory 79−29330
chemical kinetics, sensitivity analysis, numerical Green's function procedure 79−100334
chemical kinetics equations, numerical solns., stiffness 78−48624
chemical reaction, multistable, separatrices calc. 79−16033
chemically reactive flow, kinetics, stiff ordinary differential eqns. numerical soln. 78−48631
chemically reactive flow characts., simultaneous heat-mass transfer *(Japanese)* 78−22431
chemically reactive flow in porous catalyst, conc. and temp. profiles, computation method 79−86523
Cholesky-conjugate gradient method, incomplete, for iterative soln. of systems of linear eqns. 78−28932
circular bar in elastic half-space, longitudinal harmonic excitation 79−10518
circular cylindrical shells, integral calc. involving characteristic beam functions 78−63359
circular elastic-plastic plates, numerical anal. under press. and temp. cycles 78−30199
circular plate, finite amplitude vibr. 78−30214
circumferential edge-crack in cylindrical cavity, stress anal. 77−80116
clamped rectangular orthotropic plates, natural freqs. of vibr. upper and lower bounds 78−83284
clamped rectangular plates, bending anal. 77−68435
classical and special relativistic physics arithmetic models formulation 78−86130
classical vibr. anal. by pseudoinverse 77−72232
closed-end cylindrical shell under line load along a generator, elastic anal. based on discrete element method and Vlasov eqns. 80−69675
clouds numerical models, methods of parametrisation of condensation process *(Russian)* 78−16091
clusters of galaxies, numerical models for X-ray line emissions 78−8149
CO_2-laser, numerical soln. to nonlinear rate eqns. of population level density *(Bulgarian)* 78−33720
coefficients of series expansions, computation through pattern recognition 77−71199
coiled tubes, laminar flow and heat transfer, efficient numerical procedure 80−64633
colliding gas-slurry jets, dispersed material motion, numerical anal. *(Russian)* 79−32653
combustion and non-combustion flow fields with swirl, numerical anal. 79−98821
complex Gauchy type singular integral eqn., curvilinear crack anal. 79−37246
complex variables method for soln. of large nonlinear differential eqns. systems 78−62062
composite, laminate, crack normal to interface, impact response 80−14628
composite, layered, Love wave diffr. by stress-free crack in plane interface 80−33501
composite materials, heat cond., numerical method calcs. 78−94522
composite media, self-consistent field approx. for elastic props. 78−51078
compressed air energy storage, anal. of moist air cycling in porous rock reservoirs 80−30575
compressible fluid flow through annular orifices, computer-aided numerical anal. 80−87806
Compton effect, multiple scatt. corrections, error bounds 78−16959
computational atomic and molecular physics, conf., Nottingham, England, (Sept. 1978) 79−59567
computational methods in physics, computer appls. 80−62456
computer graphics for numerical analysis tuition 78−81817
condensation, filmwise, onto vertical fluted plate 78−94552
conducting gas flow in high current electric arcs, calc. methods and numerical anal. 79−90478
conductivity equations, conductometric probe analysis, field disturbances in conducting fluid modelling *(Russian)* 78−231
conference, computation fluid dynamics, Rhode-Saint-Genese, Belgium (March 1977) 77−80134
conference, numerical treatment of differential equations, Oberwolfach, Germany (Dec. 1977) 79−92930
connectivity theory, boundary element methods systematic formulation 79−63035
continuity eqn. review of numerical solns. 77−26153
control jets, gasdynamic features, 3-D subsonic and supersonic flows 80−6112
convection, free, in saturated porous medium boundary layer with lateral mass flux 79−27689
convection, free, laminar, three-dimens., about surface, numerical anal., visualisation *(French)* 78−87343
convection, natural, from vert. DC current-heated plate, linear stability anal. 78−90873
convection, natural, laminar, enclosure with heat source and sink on horiz. boundary 78−90882
convection, natural, three-dimens. analysis in inclined channel with square cross section 80−14546
numerical analysis continued
convection, turbulent, numerical models based on unsteady Navier-Stokes eqns. 80−38415
convection about permeable cylinder 79−98723
convection by motile particles, two dimensional numerical study 77−56399
convection problems, numerical results, truncation errors 79−10447
convective heating of concave bodies in high speed rarefied gases 79−1214
convergence conditions for particle in cell method *(Russian)* 79−76567
corner, three-dimens., Navier-Stokes eqn. soln., numerical code 78−30314
Coulomb excitation functions, numerical calc. of limiting props. 79−9604
Coulomb off shell two body amplitudes, numerical computation 80−46858
coupled-evolutional system, variational calc. of vibr., appl. to ARIANE launcher *(French)* 77−72234
crack, in semiinfinite thermoelastic solid with heated boundary 78−55610
crack branching, asymmetric, plane stressed and loaded plate 78−59344
crack extension angle, influence of specimen's geometry 80−99965
crack problems, exact linear elastic solutions for Mode I, II and III loading 78−34072
cracks, curvilinear, star-shaped array in infinite isotropic elastic medium 78−55609
critical phenomena, renormalisation group theory, numerical method for calc. of free energy and correl. length of generalised Ising model 80−4664
cross flow heat exchanger effectiveness 78−90645
crossblow, by cone over thread, numerical solution *(Russian)* 78−55612
cruciform section optical fibre in single material 77−39046
crystal defect clusters coupling, in linear chain 79−51144
crystal growth, cubic, from soln., numerical soln. 80−88074
crystal growth, cylindrical pores growth, numerical calcs. 80−92471
crystallisation, directed, 2-D approx., numerical soln. 80−15021
cumulative ionisation of transparent dielectrics by strong light pulse, numerical soln. *(Russian)* 77−28667
current generation by RF travelling waves in tokamaks, numerical anal. 80−1800
current loop radiation pattern in inhomogeneous plasma column 77−76102
curvilinear shock wave smearing in particle in cell method calcs. 79−64693
cylinder, circ., impulsively started from rest, heat transfer, numerical anal. 80−10248
cylinder, hollow with internal circular crack, axially symmetric torsion determ., numerical results for boundary value anal. 80−64456
cylinder, in viscous fluid impulsive translation, numerical computation method 78−5727
cylinder, infinite, solid, diametrically opposite conc. load deform. and stress 78−63287
cylinder, transient thermal stresses due to arbitrary heat supply, 3-D anal. 79−46215
cylinder array, convective mass transfer with surface reaction 78−79369
cylindric flow in tubes, temp. distrib. *(German)* 77−31391
cylindrical bar in tension, necking, num. anal. 79−90147
cylindrical implosion, flow development, numerical anal. 79−4040
cylindrical parabolic focusing collector for distributed-collector solar power system 79−62108
cylindrical shells, vibr. anal. by finite element formulation 78−34048
cylindrical shells containing turbulent flowing fluid, numerical anal. 77−72291
depolarization correction for Coulomb lattice sums 79−10829
derivatives computation from equally spaced data, rainfall rate determ. 77−49125
design of transonic cascades 79−10585
detonations, sound ranging in atmosphere, anal. problems 79−94393
diatomic molecules, vibrational transitions dipole matrix elements, numerical calc. 80−95594
dielectric inhomogeneous medium, refractive index profile determ. from inverse scattering 78−58914
dielectric relaxation, Williams-Watts type, normalised complex permittivity, num. table 80−7287
differential eqns., ordinary, with numerous discontinuities, integration 79−21535
differential eqns. of mechanics, collocation and finite element methods 77−71198
differential equations, numerical integration methods, conservation props. 78−45464
differential fourth order systems near bifurcation, numerical anal. 78−24653
diffraction at shadow boundaries and transition regions, spectral domain formulation 77−75381
diffraction on transparent structures, soln. using integral equations method *(Russian)* 77−68154
diffused optical waveguide numerical analysis and applications 78−1377
diffusion, approx. soln., linear programming, regularisation 78−32775
diffusion equation, numerical integration using time level schemes 79−2609
diffusion in nonuniform multicomponent system with multidimensional regions *(Russian)* 79−12743
direct correlation function of liq. from Ornstein-Zernicke eqn. 77−47314
discharge, axially symmetric, narrow, at high overvoltage, computer simulation 79−19101
discharges in gases, pulsed, theoretical and expt. study 80−92416
discrete kinetic theory, maths. and numerical aspects, Couette flow appls. 80−19413
discrete ordinates transport problems on large scale, numerical methods efficiency 79−85099
dissipative dynamical systems, ergodic problem, numerical approach 79−88878
dissipative systems, numerical expts. on trajectory instabilities trajectory instabilities 78−41235
dissociation effects on reflected shock wave and unsteady thermal boundary layer, anal. *(Japanese)* 78−5733
double stars, rectilinear trajectories calc., appl. to h 5094, effects of erroneous positions *(French)* 78−20857
drag on a sphere moving axially in a long rotating container 79−50734
drift-Alfven waves in a sheared magnetic field, numerical anal. 79−94788

numerical analysis continued
drift-diffusion problem with special boundary conditions, numerical soln. by integral eqns. 77−76591
duct, curved transition type, three-dimens. turbulent subsonic flow calc. 80−38498
duct, plane, with sudden expansion, aerodynamics 79−94722
duct flow development, step-by-step anal. for laminar flow 80−64634
duct noise radiation, aircraft turbojet and turbofan engines 80−23834
duct with abrupt enlargement, transonic flow, self-excited oscills., model calcs. 80−28522
dye laser, N_2 laser-pumped, subns. relax. oscills. 78−82959
dynamic substructure analyses with simplified computation 79−81716
dynamical astronomy numerical simulation, new Runge-Kutta algorithms 79−12387
dynamical systems with extremely heterogeneous inertia props., Lagrangian eqns. of motion analysis 77−53775
Earth crust structure, investigation via seismic reverberation 79−66820
Earth dipole electrical soundings, perpendicular, numerical procedure for direct interpretation 79−34732
Earth EM sounding, boundary conditions for EM field above two-dimensional inhomogeneous struct. 80−85595
Earth EM sounding, transients from two horizontal thin conducting strata *(Russian)* 78−40485
Earth gravitational field, regularising algorithm for numerical model construction *(Russian)* 77−44899
Earth gravity field, numerical development of spherical functions *(German)* 78−61311
earth mantle connection, numerical anal. 80−51371
eddy-currents induced within a metal cylinder by parallel ACs *(Polish)* 78−78856
EEG signals with changing spectra, anal. using Kalman estimator 78−24167
eigenvalue systems of second order differential eqns., numerical soln., matching method 78−8232
elastic anisotropic media, stress anal. by integral eqn. method 77−72176
elastic behaviour conoid, cylindrical shell retaining walls 78−5655
elastic body containing fine inclusion system in single plane *(Russian)* 78−34017
elastic dissimilar semiinfinite strips, different widths, plane symmetric contact problem 78−55615
elastic field outside ellipsoidal inclusion 78−55566
elastic half-space transient motion, numerical inversion method *(Russian)* 77−54877
elastic linear collisions, dynamic solns., for teaching 80−17769
elastic long thin profiled strips, numerical soln. *(French)* 77−72182
elastic plug in elastic region contact problem, using Fourier integrals, quadrature method 77−53747
elastic singularity anal., boundary integral eqn. 77−68426
elastic structures, force method of anal. 79−18689
elastic thin strip, transversally loaded, elastic waves propagation solution, by physical discretisation 77−50943
elastic waveguides with elliptical cross-section, mode-matching method 79−23109
elasticity, linear theory of, shift function derivation 78−4484
elasticity, mixed boundary value problems, numerical scheme 78−26038
elasticity, mixed-boundary value problems, numerical scheme 77−68432
elastico-viscous liquid flow in axisymmetric pipe of slowly varying cross-section 80−83774
elastodynamics, numerical boundary integral eqn. method 79−63036
elastoplasticity, 2-D, boundary element method, initial stress approach 80−74762
electrochemical flux equations, solns. with variable diffusion coeff. and transference number 78−48666
electromagnetic fields, Green function selection and effects on matrix condition 80−14271
electromagnetics, use of total scalar pot. in numerical soln. 79−31764
electron beam, relativistic, fields excited near plane magnetoedielectric slab 80−18986
electron beam, relativistic, radially inhomogeneous, unneutralised, linear theory 79−50201
electron beam stabilised discharge in flowing medium, numerical calc. 78−94943
electron repulsion integrals, computation involving Gaussian basis functions 78−58572
electron ring accelerators, electron-ion instability, numerical anal. of nonlinear effects 79−54622
electron scattering, low energy, R-matrix calc. from H, H_2, N_2, He 79−59571
electrons, field-accelerated, in dry air and pure O_2, macroscopic props. comparison *(French)* 80−59161
ellipsoidal inclusions in anisotropic material, numerical evaluation of stresses and strains 77−68410
elliptic partial differential equations, nonlinear, approx. soln. by mesh refinement and local inversion 77−26160
elliptic plates on elastic foundation, anal. of large deflections 77−50914
elliptic type equations, num. soln. of mixed boundary-value problem *(Russian)* 77−67243
EM cascade eqns., numerical integration, results for air, Cu, Pb and Fe 78−20602
EM diffraction, three dimensional *(French)* 78−29883
EM field analysis, numerical techniques for conformal transformation 78−74816
EM fields, real eigenfunction expansion for symmetric complex operators 77−71906
EM remote sensing of inhomogeneities in ground 80−77165
EM scattering by multiple rectangular cylinders, numerical anal. 78−62992
EM scattering from corrugated conducting surfaces with inhomogeneous surface impedance, anal. 78−62987
EM wave diffr. by unidirectionally cond. strip, transform and Wiener-Hopf techniques 78−58883
EM wave diffraction by arbitrary complex aperture in conductive screen 79−45893
EM wave diffraction by open cylindrical surfaces 78−58890
EM wave propagation, book 79−72469
EM wave reflection and refraction by plane boundary of nonlinear medium 78−78866
EM wave scatt., smoothing process on mode-matching method 78−58886
EM wave scatt. by plane grating in homogeneous medium, point matching method 78−1132
EM wave scatt. from dielectric infinite cylinders 77−31050

numerical analysis continued
EM wave scatt. on symmetric cylindrical conductor, mode-matching method calc., smoothing process 78−58887
endochronic theory of viscoplasticity, steady waves in impacted plate, Al numerical calc. 78−83282
engine, internal-combustion, heat exchange, b.c.s of 1st kind determ. from b.c.s of 2nd kind, numerical method *(Russian)* 79−68554
entrainment from body surface under convective aerodynamic heating, numerical soln. 79−81949
EPR spectra, significance plots use 80−22409
evolution eqns. and non-classical variational problems 77−67258
exponential integrals, general method for accurate numerical evaluation 78−36
exterior Neumann problem, numerical soln. using double layer potl. 77−67287
external disturbance transformation into boundary layer waves 80−28523
extremum position and confidence limits, determ. of absorpt. max. in wide bands 80−22188
fast Fourier transforms, numerical integration of macroscopic semiconductor equations, applications *(German)* 77−69319
fatigue results, numerical expressions *(Japanese)* 80−62455
FBR safety calculations, numerical mixing errors in Eulerian calculations of coupled thermohydrodynamic motions 80−47553
FBR thermal hydraulics, sensitivity theory for general systems of nonlinear equations 80−86954
ferrofluid, helical flow with heat cond. between coaxial porous tubes 79−23371
fibrous composite, thermal crack propagation anal. 80−10205
finite difference numerical solns 78−9661
fins, extended surface array, heat flow evaluation, efficient algorithm 78−90635
fission reactor LOCA, AA 80−18528
fission reactor loss-of-coolant accident, 3-dimens. flow with multiple interfaces 79−41024
flame front, laminar, hydrodynamic instability, numerical solns. 78−51254
flexible structures, dynamic simulation by substructure synthesis 80−87733
flexural deformation of structural anisotropic domes composed of cylindrical shells 80−19260
flood and tidal flows, network hydraulic model 79−12162
flow, Ekman boundary layer, incompressible, nonlinear stability, numerical soln. 80−38378
flow, in annulus, axial, numerical stability anal. 78−83363
flow, in pipe, turbulent, perturbed by sudden enlargement 80−19354
flow, in two-dimens. channel, turbulent, with separation 80−19356
flow, inviscid, hyperbolic, computational algorithms tests 80−27140
flow, laminar, of binary mixture, in channel, with wall vapour-ice transition 79−94617
flow, new viscous-inviscid interaction method 79−1154
flow, over blunt nosed body, laminar or turbulent, heat transfer and curvature effects, numerical soln. 79−1173
flow, past arbitrary body, unsteady, inviscid incompressible, numerical soln. 80−28509
flow, rarefied, hypersonic, on wedge *(Japanese)* 79−32580
flow, rotating, nonstationary eqns. soln., appl. to flow between discs 80−28516
flow, rough-wall incompressible boundary layer, calc. model 79−1165
flow, separating incompressible laminar boundary layer, over smooth step of small height 80−19325
flow, unsteady, transitional and turbulent boundary layers, expt. and calc. methods *(French)* 78−75125
flow, unsteady, viscous, separated, laminar, numerical modelling 78−46933
flow, variable-property, in curvilinear orthogonal coords., numerical calc. 79−44746
flow, viscous, time-dependent, integral representation approach to simulation 80−38375
flow about arbitrary 2-dimens. boundary, implicit finite difference simulation 78−94628
flow around sphere, laminar, photographic-tracer film, vel. profile anal. 79−50698
flow between concentric rot. spheres, nonlinear, axisymmetric 80−19412
flow between porous walls of different permeability, quasilinearisation soln. 79−55415
flow between two counter rotating infinite plane discs, numerical soln. by multiple shooting 78−42621
flow boiling anal., numerical standards 77−79448
flow boundary layer, stochastic model of fluctuations 78−90818
flow in irregular geometries, numerical method calcs. 78−94522
flow in Laval nozzle, two-phase, direct problem, numerical soln. 78−63475
flow of purely viscous non-Newtonian fluid, Rayleigh problem, pseudosimilarity soln. *(German)* 79−37364
flow of second order fluid in curved annulus 79−72915
flow on flat plate with chem. surface reaction, mass transfer *(German)* 79−72961
flow through porous media, 2-D nonisothermal filtration 80−6137
flow through porous media, flow parameters, potential distrib. *(German)* 77−11260
flows with higher-order eqns., MacCormack's method extension 79−3987
fluid acoustic wave scatt. by temp. and vel. inhomogeneities 79−50491
fluid bidimensional flow past symmetric profile 77−60942
fluid dynamics, conf., Enschede, Netherlands (July 1976) 77−54953
fluid dynamics, macroscopic relativistic approach to numerical simulation 79−9122
fluid dynamics, viscoelastic boundary layer flow, second order, at stagnation point, heat transfer 80−103025
fluid-solid dynamic interactions and wave forces, numerical treatment 79−3944
fluid-structure coupling problem soln. using boundary-integral eqn. method 77−54920
fluidised bed reactor, solid-circulation model, steady-state multiplicity 79−86524
fluorescent dye medium, short laser pulse superposition, numerical anal. 79−31891
formaldehyde($-d_1$, d_2), and isotopic forms, microwave spectrum, ν_4-ν_6 vibr. states Coriolis reson. 78−82719
Fourier analysis of difference schemes for Laplace eqn. in rot. symm. system 78−77677

numerical analysis continued
Fourier and Bessel transforms in logarithmic variables 79−9089
Fourier transformation of data sampled at unequal intervals 78−69697
fracture analysis, 2D linear, elastic, finite element anal. vs. the edge function method 80−99963
fracture dynamics, in glass fibre reinforced plastics 80−100906
fracture initiation, numerical anal. 77−75861
frame structs., large deflection anal. by fictitious forces 78−83249
Fredholm non-singular eqns., numerical soln. 78−16630
freezing, multidimensional problems in arbitrary domains, numerical method 78−90693
fuel droplet, burning anal., quasisteady model *(Japanese)* 79−32712
fuel pin rupture in FBR, implicit compact difference method for solving linearized fuel sweepout equations 79−89355
fusion plasma, Lawson criterion for impurity losses, energy balance eq. *(Korean)* 78−17414
fusion reactor, toroidal device with nonplanar mag. axis, magnet and coil engineering 78−55009
fusion reactor inertially confined plasma, charged particle energy deposition 77−83081
fusion reactor Li blanket models, Monte-Carlo and discrete ordinates calcs. *(German)* 77−83096
fusion reactor neutronics, anisotropic neutron transport calc. using scatt. kernel without polynomial expansion 79−67936
fusion-fission hybrid blanket designs, accidental criticality 78−778
galactic cosmic ray modulation, numerical models of particle drift effect on cosmic ray transport 80−31180
galactic dynamo, numerical models 79−40262
galaxies of Local Group, numerical expts. on gravit. encounters 77−57098
galaxies redshift, numerical simulation test of cluster effect on Hubble Modulus 79−2569
galaxies spiral structure, variability in numerical models 79−25725
galaxy models, numerical orbit computation algorithms comparison 79−12497
galaxy triaxial model, nonexistence of three-dimensional tube orbits around intermediate axis 80−22046
Galileo's two bodies falling through air, numerical anal. for teaching 80−17755
gas, rotating, convective instability in gravitational field 79−27642
gas, with variable physical props., pipe flow, turbulent momentum and heat transfer calc. 78−90869
gas bubble motion in power-law fluid, heat and mass transfer with chemical reaction 79−77227
gas centrifuge, numerical anal. of weakly compressible rotating flows 80−47726
gas dynamics, self-adapted algorithms 80−38432
gas flow, high-temp., heating of graphite body, numerical soln. 79−37318
gas flow, viscous, heat-conducting, compressible *(German)* 77−11217
gas mixture, binary, spherical expansion into flooded space, components separation 79−81948
gas mixtures, removal of condensing component by suction through porous walls 79−98787
gas-liquid two-phase flow, similarity criteria and fundamental eqns. 79−98784
gas-vapour droplets, nonuniform mixture, acoustic wave attenuation 78−83154
gasdynamic lasers, improved perform. by selective thermal pumping 79−31858
Gauss-Hermite integration for periodic crack stress fields 77−39260
Gaussian circular jet with normal impingement, velocity field 77−47057
Gaussian field optical heterodyne detection, S/N ratio 79−13912
Gaussian integrals, evaluation by backwards recursion or Taylor expansion 80−31488
gausson collisions, logarithmic nonlinear Schrodinger eqn. solns., resonance energy interval 78−89357
generalised stress intensity factors, numerical determ. method, crack problem appl. 79−72851
generalised stress intensity factors, numerical eval. using Lobatto-Jacobi numerical integration rule 79−3921
long geodesics computation on ellipsoid through Gaussian quadrature 79−100806
geodesy, azimuth soln. for nearly antipodal geodesic when azimuth is nearly 90° 77−60335
geodesy, sequential solns. with bandtype system of obs. eqns. 78−65169
geology, adequacy of non-metric data 78−81413
geophysical field data, objective anal. 79−12321
geophysical prospecting, galvanic effects calc. via method of sub-areas 80−56348
geopotential field numerical analysis using meteorological information 78−7814
geothermal reservoir, effect of magma dike intrusion on free convection 78−7599
geothermal steam pipeline network, numerical simulation 80−40822
Gironde estuary vertical circulation, real time two-dimensional model *(French)* 79−62519
glass system, layered, thermal radiative props. for solar diffuse radiation flux 79−94473
glow discharge, positive column analysis, oxygen 79−55577
gravity 5° mean anomalies, recovery from ATS 6/Geos 3 satellite to satellite range-rate obs. 80−41366
grey medium between concentric cylinders, 2 dimens. radiative equilib. 78−42523
Griffin-Hill-Wheeler eqn., solvable model 78−50105
groundwater two-dimensional flow, calculation methods 79−100875
Gulf of Guinea, simple upwelling model 78−88837
Hamiltonian, Henon-Heiles, survey and applications to related examples 80−8917
Hamiltonian eigenvalues in Weyl correspondence limit, Turschner's formula 79−84988
Hankel transforms, related, of orders 0 and 1, numerical integration by adaptive digital filtering, FORTRAN IV algorithms 79−92599
harmonic oscillator Schrodinger eqn. numerical soln., teaching aid 78−8188
HDR, numerical investigation of radial mixing capabilities in strongly buoyancy-influenced vertical, turbulent channel flows 79−93751
hear conduction, transient, accuracy, stability and oscills., calc. methods 78−94516
heart valves, blood flow, vortex-grid method 80−41105
heat and moisture conductor problems 79−90113

numerical analysis continued
heat conduction, nonlinear problems, method of successive intervals 77−42694
heat conduction, transient, integral method 77−39192
heat conduction eqn., inverse, boundary conditions recovery, using Cauchy soln. and regularising algorithms 78−26016
heat conduction equation, unsteady, numerical soln. characts. at early times 78−79185
heat conduction inverse problems, uniqueness theorems 77−42691
heat conduction nonlinear inverse problem, regularised numerical soln. 77−42693
heat equation involving moving phase boundaries, analytic soln. 78−90694
heat exchanger, tubular bundle type, with longit. drive, forced turbulent convection *(French)* 79−86333
heat exchanger optimisation 79−3895
heat radiation, two-dimens. isotropic scatt. in semiinfinite medium 78−42521
heat recuperator, packed bed, heat transfer meas. 78−5742
heat transfer, conjugate, numerical method calcs. 78−94522
heat transfer in packed bed heat recuperators, precision anal. 77−75974
heavy particle scatt. in solids, classical deflection ang. using Brinkman pot., numerical calc. 80−11525
heavy-ion superconducting linac, alternating phase focusing 77−3194
heavy-ion superconducting linac, design of re-entrant cavities 77−6580
helical springs, numerical soln. of dynamic response 78−67026
Helmholtz equation in optics, numerical soln. 78−90357
Helmholtz-eqn., eigenvalues by boundary integral eqn.-finite element method 77−71195
hermitian matrix, large, eigenvectors determ., new approach 77−37717
HF elastic surface wave propagation on cylindrical obects 77−24472
hierarchical model ϵ-expansion, numerical test of Borel summability 78−12650
highly oscillatory functions, numerical integration 77−13593
highly prestressed anisotropic plates, numerical perturbation technique 78−18214
horizontal falling wire, max. strain due to instantaneous avert of its ends 80−28418
HWR, Wolsung power reactor, D_2O moderated, temp. coeff. of reactivity, numerical calcs. 78−54818
hydrodynamic neutral stability curves, analytic approach, book contrib. 80−1529
hydrodynamic stability computation, algorithm construction 80−19329
hydrodynamic stability problems, computer program for testing linear stability of vel. profiles 77−54975
hydroelastic shell opening in fluid flow numerical soln. *(Ukrainian)* 79−50592
hydrology, modified Richards' eqn., oscill. of numerical soln. 78−81243
hydrology, soil water flow modelling, finite difference and Galerkin techniques 78−81249
hypersonic boundary layer eqns. including chemical reactions, numerical error control, book contrib. 80−1699
ideal gas in ejector nozzles, theory of combined flow of high/low pressure streams 80−6123
image two-dimensional reconstruction algorithms 77−82379
impacted solids, compression and shear wave propag., modelling 80−83755
implicit difference procedure for multiphase laminar flow with heat conduction *(German)* 77−15110
incompressible three-dimensional internal flows, finite difference soln. of Navier-Stokes eqns. 77−58795
incompressible viscous fluid, entrance region heat transfer in plane Couette flow, num. procedure 77−15020
incorrectly stated problems, soln. method 79−90111
indentation, dynamic, of elastic half-space by rigid punch, numerical method 78−1612
inelastic deformation, stiff constitutive models, numerical integration 80−96208
inelastic numerical analysis for quasistatic and dynamic problems 80−19233
infinite elastic thick plate, axially symmetric loading, numerical method *(Japanese)* 78−9568
ingots, cooling regime in conditions of minimal thermal stress, modelling *(Russian)* 80−65194
inhomogeneous materials, elastic deform. under multiaxial stress, analytical relations 80−44247
inner planets orbits, numerical integration rel. to motions of perihelia 80−67531
integral computation over sphere, summation formula 79−29689
integral eqn., improvement of Sastry's method by Richardson's extrapolation 78−28924
integral eqns., singular 78−32661
integral eqns. in which boundary values and solns. defined on different curves 77−68428
integral equation, dynamic temperature meas. data recovery 77−5839
integral transforms, numerical inversions 77−67259
integration, one-step methods, quadrature formulae *(Russian)* 77−37747
integration for viscous dissipation effect on nonlinear convection at high Rayleigh number 77−54994
intensity distribution inside absorbing-isotropically scatt. semiinfinite medium 78−32335
interactive teaching package 80−86058
internal waves, nonlinear, stationary, in shallow seas, anal. for Baltic Sea 80−17292
interstellar clouds fragmentation, three-dimensional hydrodynamical calcs. 80−62236
interstellar contracting CO clouds, fragmentation 80−67838
interstellar cylindrical clouds, two-dimensional collapse calcs. 79−40247
interstellar nonrotating magnetic gas clouds collapse, numerical calcs. 80−105299
interstellar turbulent 80−56910
intracavity absorpt. spectroscopy, short pumping pulses and restricted mode competition 77−82607
invariant imbedding eqns. in general geometries 79−76050
inverse coeff. problems, soln. by regularisation method using spline functions 79−88797
inverse logarithmic-potential problem for contact surface, solvability in finite form 77−82025
inverse magnetic problem for inductive magnetisation and palaeomagnetic sounding, numerical soln. *(Russian)* 79−34747

numerical analysis continued
inverse problems, method of soln. 77−41465
inversion of Laplace transform and Fredholm integral eqns., eigenvalues and eigenfunctions 78−81800
ionosphere, chemistry and transport processes, numerical modelling 78−49202
ionosphere electron density profile parameters estimation from VLF propag. data, effectiveness 79−53614
ionosphere modification, numerical simulation of artificially created equatorial spread-F 78−88972
ionosphere negative storms, numerical simulation using observed neutral comp. data 79−25393
ionosphere observations, numerical simulation rel. to thermospheric quantities determ. 77−53268
ionosphere plasma conductivity, limits of applicability of formulae of mean free path theory 77−60512
isentropic compression, initially uniform medium, time reverse method *(French)* 79−23295
isothermal horizontal circular cylinder, laminar free convection, thick boundary layer 80−64566
isotope centrifuge, effect of thermal convection on separative power, numerical anal. 78−58500
isotope separation, binary gas mixture, convection-diffusion eqn. soln. for centrifuge axisymm. vel. field 78−17434
jet, axisymmetric, counterflow problem, num. soln. procedure 77−58757
jet, axisymmetric free shear flow with Reynolds stress closure 80−19469
jet, liq., breakup, 3-d perturbation Cosserat soln. 79−32615
Joukowski airfoil, unsteady viscous flow, bound-vorticity distrib., numerical anal. 78−51169
Jupiter-Saturn-Sun systems, long-term numerical solns. 78−24450
Kalman filter technique, neutron flux distrib., optimal allocation of in-core detectors 78−54839
Keplerian systems, numerical simulations of collisional evolution 80−109342
Korteweg de Vries eqn., similarity soln. and related Painleve transcendent 78−49674
Korteweg-de Vries-Burgers equation, time evolution, stability, of shock soln. 77−37743
L^2 discretisation of atomic and mol. electronic continua 79−59425
Lagrangian hydrodynamics meshes, discrete rezoning algorithm, hot interacting bubbles calcs. 78−42628
Lake Suwa, wind driven currents, obs., numerical calcs. *(Japanese)* 77−37254
lakewide wind-driven circulation, numerical models 77−37243
laminar boundary layer, optimal control by wall suction or blowing 79−1242
laminar boundary layer, solution of the Falkner-Skan equation by quasi-linearization 79−1156
laminar boundary layer flow, three-dimens., soln. using method of integral relations 77−58645
laminar boundary layer on moving surface under combined action of free and forced convection *(Ukrainian)* 79−50695
laminar boundary layers, nonsimilar incompressible heat transfer analysis using method of strained coords. 77−42811
laminar boundary layers in incompressible micropolar fluids 77−80140
laminar channel flow, entry region and numerical soln. for square channel 77−84325
laminar compressible MHD boundary layer flow, effect on heat transfer 79−14489
laminar film condensation inside tubes, with noncondensable gas 79−14234
laminar incompressible flow in straight polar ducts 78−22424
laminar separated flow between periodically varied walls, num. simulation using perturbated primitive variables method 77−54971
laminar stationary 2D viscous duct flow, generalised Prandtl eqns., soln. methods 78−5726
laminar trailing edge stall, triple-deck eqns. num. soln. 77−55020
laminar vapour-air mixture flow, around circ. cyl. with vapour desublimation, numerical anal. *(Russian)* 79−60051
Lane-Emden eqn. of index 5, geometric technique for M-solns. 78−61851
Langmuir probe characteristics at low plasma densities 78−63592
Langmuir waves, modulated, nonlinear Landau damping effect 78−81849
Laplace eqn., half plane representations and harmonic continuation 77−22391
Laplace operator on spherical domain, fundamental eigenvalue numerical determ. 77−87628
large chemical kinetic systems, functional group anal. 78−48626
large strain inelastic anal., dynamic problems 80−38278
large wavelength convection rolls low Prandtl number fluids 79−27643
laser, solid, nonlinear limitation for fine-scale self-focusing 79−23032
laser with saturable absorber, stationary state, nondiffusive approx. 80−19076
latent heat solar energy storage system, heat transfer eqns., numerical soln. 80−55926
layerwise growing crystals, face profiles calcs. 79−60290
left ventricular cineangiograms, computing techniques wall movement 77−90891
lighning return stroke channel, transmission line model, computer soln. 78−85644
limit analysis in continuum mechanics, nonlinear optimisation problems, numerical methods 79−2628
linear elastostatics, combined boundary integral eqn./finite element anal. of cracks 77−72178
linear elliptic PDE, numerical soln. 79−97187
linear inference and underparameterised models, geophysical appls. 78−49000
linear time dependent partial differential eqns., solns. by Laplace transform and FFT 78−57763
liquid layers, immiscible, Kelvin-Helmholtz instability, nonlinear wave packets 79−46289
liquid phase crater profile calc., formed by conc. heat source *(Russian)* 77−72131
LMFBR, 300 MWe, $^{\wedge}$Pu, A=239, 240, 241, burnup characts. 3-D numerical anal. 79−22371
LMFBR reactor vessel, buoyancy induced flow redistrib. 78−8887
LOCA in water reactors, reversal of laminar flow in circular pipe 78−50271
localized dynamic contact on structs. anal. by matched asymptotic expansions 79−7342
numerical analysis continued
Lorenz model, chaos and limit cycles 78−57787
Lotka-Volterra eqns. with stochastic approx., numerical soln. 80−8912
LWR fuel pin modelling 77−74916
magnetic dipole surrounded by infinitely conducting medium appl., exact solutions *(Russian)* 79−77174
magnetic domain wall mass at high vel., numerical anal. 80−11217
magnetic domain wall motion, one-dimensional, under biased in-plane field numerical anal. 79−15321
magnetic film, micromagnetic dynamics in domain walls, numerical model 78−72382
magnetic flexible disc/head interface interaction analysis 80−92093
magnetically confined plasma, numerical computation of MHD flow in Scyllac 77−80282
magnetosphere plasma sheet, particle dynamics 79−66879
magnetosphere time-dependent heat energy eqns., numerical soln. 80−21875
magnetotelluric sounding, fields of vertical mag. dipole over vertically inhomogeneous Earth 79−34736
major planets motion, numerical study 79−92657
many body perturbation calculations and coupled electron pair models 79−59363
many body perturbation expansion, fourth order linked diagrams for quadruply-excited states 79−59364
Mars atmosphere, numerical circulation model with topography for S.Hemisphere 77−5480
Mars polar cap winds, numerical model 79−96942
master equation, exact solutions in terms of continued fractions 79−88882
materials testing, strip with semicircular notches, tensile load conditions at end, interf. effects obs. 80−64455
maximum likelihood method, for galaxies distrib. determ. in clusters 80−56954
Maxwellian distribution, numerical aspects 79−54034
mechanical contact, cylindrical shell, liquid and gas, breakaway from solid lodgement *(Russian)* 80−87744
mechanical system, randomly loaded, crossing probabilities, numerical anal. *(German)* 80−96186
mechanics, computational methods of treating nonlinear and special linear problems 77−74226
melt/solid segregation, numerical treatment rel. to eucrites and Earth low rel. zone 79−40144
metal, strength, long-term charact. interpolation calc. using generalized curves and computer 77−86121
metal forming, limit anal. appl., book contrib. 78−11140
metal plate transient temperature field in active thermal test methods, calc. 77−75775
metallic media, varying loads, elevated temp. inelastic anal. using state variable theories 78−83264
metals, creep anal. using boundary integral eqn. method 79−46231
meteorology, numerical modelling of the atmosphere, review 79−44234
method of characteristics with fixed net appl. to slowly-varying nonstationary flows calc. *(German)* 79−5515
MHD, unsteady thermal boundary layer problem, numerical treatment 80−92227
MHD axial flow in triangular pipe, finite difference method 78−59498
MHD channel, frame type, optimal selection of frame and transverse cross section form 78−91164
mHD flow past a semi-infinite flat plate with heat transfer, exact numerical solns. of boundary layer similarity eqns. 80−83861
MHD instabilities, large computational programs, comparative numerical studies, Tokamaks 78−79425
MHD nozzle flow, secondary flow, axisymmetric elec. current 78−79381
micromagnetism, numerical calcs. 80−11222
microwave cavity containing dielec. sample, num. soln. of charact. eqn. *(French)* 78−13649
migmatite rise, numerical expts. based on continuum dynamics 80−51381
molecular collision problems, modified amplitude density func. anal. 79−6987
molecular dynamic simulation, event scheduling 80−49069
molecular inelastic collisions, rot. and vibr. inelasticity, cross section calc. 79−59542
molecule, diamagnetic, NMR shielding tensor and mag. susceptibility tensor, current density calc., appl. to H_2 *(German)* 79−76445
molecules resonant states, wavefunctions of complex coord. method 80−106282
monodimensional Poiseuille and thermal creep flows, rigorous constructive soln. 78−30319
monsoon circulations simulation 80−21812
mooring cable in nonuniform stream, equilib. shape and tension *(French)* 78−63277
MOS capacitor formed over p-on-n semiconductor structure, G-V charcts. 80−100532
multi-frequency EM system, numerical modelling 80−56623
multi-part mixed boundary value problems, numerical solns. 77−68430
multicomponent spectra, resolution by multiple regression and linear programming 79−74443
multidimensional body, radiative-convective heating, unsteady temp. calc. method 78−90640
multidimensional unsteady laminar flames, scaling transformations for numerical computations 80−19522
multimeron field configurations, numerical computation 79−258
multimode optical fibres, impulse response calculations 80−74486
multinephron kidney equations, numerical soln. 79−83822
multiple quadratic regressions, programmable desk calculators in the laboratory 80−42048
multiply-charged plasma, temp. kinetics and population levels *(Russian)* 80−106952
muonic atom, heavy, $1s_{1/2}$ levels, self-energy corrections 78−55262
N-level atomic system interaction with quantised EM field, algorithm for numerical calcs. 79−64187
N-two level atoms, interaction with radiation field in restricted rotating wave approx., numerical anal. 80−5714
natural convection in closed cavity, numerical technique 79−10446
natural convection in horizontal cylinders, asymmetric boundary conditions, numerical anal. 77−39282
natural convection in horizontal cylindrical annulus 79−81880
natural convection over confined horizontal plate heated from below *(German)* 77−72134
Navier's eqn. soln. in cylindrical coords. 79−44744

numerical analysis continued
Navier-Stokes eqn., successive approx. solns. 78−51144
Navier-Stokes eqns., bluff body aerodynamics, numerical simulation methods 78−75115
Navier-Stokes eqns., numerical solutions, accuracy of finite difference schemes 79−92946
Navier-Stokes eqns., viscous incompressible liquid flow in plane channel 80−23985
Navier-Stokes eqns. for viscous and potential flow about arbitrary 2-D bodies 77−65730
Navier-Stokes equation, incompressible, soln. using primitive variables 80−6017
Navier-Stokes equations, compressible, num. soln. at high Reynolds no., blunt body problems applic. 77−55019
Navier-Stokes equations, numerical soln. fourth+second order method *(French)* 77−75869
Navier-Stokes equations, theory and numerical analysis, book 78−77721
Navier-Stokes equations, two-dimens., num. soln. at high Reynolds no. 77−58637
Navier-Stokes equations, two-dimens., num. soln. procedure for treating unsteady flow about arbitrary shaped bodies 77−54960
Navier-Stokes equations *(Chinese)* 79−32433
Navier-Stokes equations for low viscosity flow, hydrid vortex-ADI soln. 79−68718
Navier-Stokes initial value problem approx. soln., incompressible boundary-free flow 78−57788
Navier-Stokes stationary 2-D eqns. in parabolic form, optimal control *(French)* 77−72321
Navier-Stokes stationary evolution approx., numerical method for 2-D viscous flow calc. *(Ukrainian)* 78−65778
near-critical fluids in turbulent flow through tubes, heat transfer num. prediction method 77−42832
neuron hydrodynamics, creeping flow investigation 77−5019
neutral atom+H^+ calculation of certain second Born integrals 79−59578
neutral atom electron impact, calculation of certain second Born integrals 79−59578
neutral gas diffusion in nonuniform chemically reactive atmosphere, three-dimensional time depend. modelling 79−66846
neutrino transport calcs. using neutron transport methods 77−87377
neutron diffusion calcs., appl. to reactor design and anal. 77−79427
neutron diffusion scheme, new brief three-dimens. calcs., BWR core 77−42014
neutron flux depression factor determ. by integral transform method 78−50233
neutron flux distributions in nuclear reactors, improved response matrix method calcs. 77−34363
neutron multigroup discrete ordinates transport eqns., computational efficiency of numerical methods 79−80970
neutron slowing down and transport in medium of const. cross-section 78−33235
neutron transport, critical slab reactor with finite reflector problem soln. 77−65251
neutron transport, double P_L eqns. for sphere, series soln. 78−13187
neutron transport, multidimensional, transverse leakage approx. 78−29531
neutron transport, one-dimens. transport equation soln., local separation of angle and energy 77−65248
neutron transport eqn., factorised kernels and DKPL soln. 79−80968
neutron transport equation for slabs, power series solns. comparison 78−13190
neutron transport integral eqn. soln. 77−3066
neutron transport theory, F_N method, appl. and numerical results 79−30878
neutron transport theory, homogeneous cylinder, numerical anal. 79−17953
NMR of ^{11}B in borate glass, fast stable analysis technique 78−6585
noise propagation around thin half-plane, numerical calc. 78−9486
non-linear viscoelastic behaviour, numerical anal. 78−59318
non-Newtonian flow of a liquid with an anisotropic viscosity tensor: internal effects 80−83820
non-Newtonian liquid, heat flux from nonisothermal surfaces to gradient flows *(Russian)* 79−68767
non-reactive heavy particle collision calculations, review 79−59541
nonequilibrium, plasma MHD generator, diagonal type, 2-D anal. 78−30491
nonequilibrium MHD duct with resistive electrodes, computer simulation, performance charcts. calc. 77−72509
nonisoplanatic spectral instruments, num. correction of images formed 80−249
nonlinear elastic continuum, comparison of Runge-Kutta-Nystrom method and Newmark method *(German)* 78−87273
nonlinear elastic systems, incremental approach to the solution of snapping and buckling problems 79−76975
nonlinear elasticity, boundary value problems, numerical anal. 79−92945
nonlinear eqns. of axisymmetric surfaces of revolution *(Russian)* 78−81838
nonlinear heat conduction efficient soln. method using modified Crank Nicolson method 80−1402
nonlinear internal waves, turbulence, numerical anal. 80−14721
nonlinear lattice, computational methods for dispersion, betatron functions, closed orbit distortion 79−68028
nonlinear monotonic functions with selectable intervals, constitutive eqns. appl. 79−46230
nonlinear plate and shell theory problems soln. 77−53784
nonlinear problems anal. using combined finite element-boundary integral eqn. method 77−72156
nonlinear resonant propagation of two concomitant optical pulses interacting with three-level atomic system, num. modelling 80−9942
nonlinear structural eigenvalue calcs., mode finding 78−51102
nonlinear thermal bending of shallow sandwich shells and flat plates 80−5936
nonlinear transforms, quantitative universality, recursive mechanism 79−2604
nonlinear viscoelasticity, a method of successive approxs., based on nonlinear correspondence principal 80−5953
nonlinear wave propagation, spectral and pseudospectral methods, turbulent sound wave appl. 77−5672
nonstationary interaction of opposite waves in quadratically nonlinear medium−numerical experiment *(Russian)* 78−83026

numerical analysis continued
nonstationary two-stage axisymmetric escape of gas into a submerged space 79−77200
nonstationary viscous flow of thermally conductive gas around semi-infinite plate, numerical anal. 80−6104
W. North Atlantic Ocean circulation, quasi-geostrophic simulations comparison with primitive eqn. results 79−48493
nozzle, critical air flow, heat transfer, numerical study 79−98778
nozzle, heat transfer of transonic air flow 79−1230
nuclear power plant piping systems under seismic motion, method of residues 77−3182
nuclear reactor, LMFBR, HCDA, Eulerian computer code anal., primary system response 77−3127
nuclear reactor, nonlinear structural dynamics of fuel elements, press. pulses, struct. models, expt. verification 77−3125
nuclear reactor, transient critical flow analysis in nodalised system 77−65258
nuclear reactor nodal fluxes determination using approx. analytical method 77−65261
nuclear reactor pin bundle, two-phase flow, eqns. of motion 78−86570
nuclear reactor rewetting process, exptl. and numerical anal. 77−46243
nucleation theory, time depend., supersaturated cooling gas 78−6151
objective analysis technique, for three-dimensional urban-scale wind fields construction 80−101407
ocean, underwater light field fluctuations under rough sea surface, numerical modelling *(Russian)* 77−33090
ocean, wind driven, new class of steady solns. to wind-driven ocean problem 80−85667
ocean coastal zone, stratified water circulation forecasting for water quality management planning 79−5543
ocean continental shelf circulation, diagnostic model 78−85581
ocean deep-water channel flow, rotating hydraulics theory 80−94539
ocean density profile remote sensing by acoustic pulses, numerical algorithm 77−70893
ocean solitary Rossby waves over variable relief, numerical expts. rel. to stability 80−101372
ocean surface intrusions, fronts and internal waves, numerical study 79−2262
ocean synoptical eddies, numerical scheme *(Russian)* 78−81190
ocean trapped waves, adaptive wavenumber-frequency spectrum analysis *(Russian)* 78−81189
oceanic circulation around New Zealand, numerical model 80−72538
oceanic mesoscale eddies generation, numerical simulations with two and three layer quasigeostrophic models 79−57950
oceanography, diffusion parameterisation of mesoscale eddy effects from numerical expt. 79−48508
one-dimensional, in continua, non-propagative modes *(Japanese)* 80−4539
one-group transport theory, benchmark solns. of multimedia problems 79−85581
optical data processor, representation and implementation 78−78947
optical noise filter with two aperture stops *(Japanese)* 77−14812
optical strip line, theory and numerical anal. 77−79956
optimum filter for image restoration *(Ukrainian)* 78−55308
orbital transfer, optimal, low-thrust, limited power, elliptical orbits 78−4087
ordinary differential eqns., suppression of inherent instabilities in initial value methods 79−9090
ordinary fourth order differential eqn., numerical soln., convergence 77−87636
orthotropic cantilever beams, Rayleigh-Ritz determ. of upper and lower bounds 78−59298
orthotropic plate bending anal. with identification method 78−26071
orthotropic plates, clamped or supported, random vibrs. 78−51104
overdetermined systems of linear eqns., partially regulated solns. 79−66825
oxidation kinetics, C by CO_2 in Fe-C melts *(Russian)* 80−40680
N.Pacific Ocean, numerical simulation of anomalies, model and mean state 79−48494
Painleve second transcendent, numerical and asymptotic approx. 78−49675
parabolic boundary value problem 78−28925
parabolic free boundary problem, numerical soln. via Newton's method 80−69632
parabolic initial-value problems, numerical soln. using Volterra integral eqns. 77−68437
parabolic marching problems, edge-corrected linearisation technique 77−89081
parabolic partial differential equations, operator compact implicit soln. methods 78−89348
Paris differential eqn. for fatigue cracks, numerical calc. of eqn. parameters 78−63384
partial differential equations, time-varying, numerical solns. 78−45463
particle size distribution of particles obtained by suspension polymerisation, eval. using Coulter Counter data 80−76564
path integrals covariant interpretation, nonlinear pt. transformations 79−84945
PB-HTGR, control-rod induced flux perturbations, numerical anal. using out-of-force instrumentation *(German)* 80−83179
PBR using OTTO scheme, numerical anal. of fuel cycle including ^{236}U isotope separation *(German)* 77−83030
percolation problem, Hausdorff dimension of largest cluster and backbone, numerical estimates 79−97316
periodic curvilinear cracks in isotropic medium, integral eqn. soln. 78−51118
periodic object single sideband Fresnel diffr. pattern studies 80−106440
permeable boundaries in multidimensional unsteady flow 80−38490
permeable plate, numerical anal. of turbulent boundary layers 78−67186
permeable shells with pole hole, pot. nonseparational inviscid flow *(Russian)* 77−75972
perturbed motion stability anal. *(Russian)* 78−16640
perturbed oscillator energies, numerical calc. method 79−58580
perturbed Stormer problem, long periodic solns. families 80−17440
piecewise linear elastic-plastic analysis 79−55331
pigment-antioxidant interaction, numerical analysis in polymers 79−39136
pipe, asymmetrically heated, turbulent transport and thermal diffusivities 80−64636
pipe flow, laminar with nonlinear wall heat fluxes, axial cond. 79−27636
pipe flow, thermal entry length problem, numerical soln. *(German)* 78−83494

numerical analysis continued
pipeline nonlinear anal. by potential minimisation 77−68552
pipes, hydraulic, with nonlinear boundaries, transient waves 80−43722
pipes, turbulence and heat exchange 80−24094
planar wave diffr., soln. from knife-edge grid with complex period struct. 79−72467
plane bending-and-torque supporting grids, numerical plastic collapse anal. 79−68594
plane crack, in infinite solid, stress intensity factor under normal pressure 79−72855
plane elastostatics, numerical props. of integral eqns. describing boundary value problems 78−34013
plane wave scatt. from dielectric cylinders 79−55057
planetary boundary layer equations soln. using sensitivity analysis 77−54957
planetary figures, hydrostatic equilib. eqn. numerical soln. 79−62773
planetary jet stream in atmosphere, hydrodynamical model of inner struct. *(Russian)* 77−64371
planetary system accumulation model, numerical expts. results *(Russian)* 80−8557
plasma, current-driven drift-wave eigenmodes, stability criteria 79−32769
plasma equilibrium in toroid, computational method, book 79−14601
plasma simulation spatial grid effects reduction using higher order multipoles and splines 78−91148
plasma trans-relativistic shock relations, numerical solns. 80−31202
plasticity theory, recent contributions 77−50925
plate, circ., thin, elastic, containing Griffith crack, in infinite elastic medium, stress distrib. 79−32374
plate, circular, with annular circle constraints, vibrs. and buckling 79−98652
plate, complex shape, temp. field during welding with moving heat source *(Russian)* 79−68553
plate, elastic, infinite, thick, fixed, subject to axially symmetric load, numerical stress anal. *(Japanese)* 79−50600
plate, infinite, with circular disc, tensile and compressive stress problems 80−38255
plate, melting, inverse heat cond. problem soln. 79−37112
plate bending, numerical soln. by general boundary integral formulation 80−1422
plate stability, numerical anal. *(Russian)* 79−3935
plate with circular hole under dynamic loading, comparison of deform. and flow theories 79−23228
plates, annular, dynamic stability numerical soln. *(Polish)* 80−10173
plates, appl. of improved collocation techniques 77−68434
plates, prestressed, numerical-perturbation technique for transverse vibrs. 77−27486
plates, thick, thermally loaded, 3-D anal. 80−33459
plates and shallow shells, approx. methods for linear and nonlinear anal. 78−51101
plume, above vert. heated plate, development of wall and free types 78−90881
pneumodynamics, enforced smoothing techniques for recovering dV_A/dQ distribs. 79−43946
point reactor kinetics equations soln. using Taylor series methods 78−13201
Poiseuille flow, at large Reynolds numbers, Navier-Stokes eqn. soln. *(Russian)* 78−59364
Poiseuille flow, plane, horiz., rot., stability, effect of Coriolis force 78−67203
Poisson's equation for isolated source distribs., computer soln. using finite mesh, Green's function 78−35
pollution modelling, numerical estimation of unknown parameters *(Japanese)* 80−89702
polymer, collapsing, self-interacting self-avoiding walk model, phase transition 77−38755
polymer chain, infinite, trigonometric series evaluation 79−7041
polymer flow in channels of noncircular cross-section 77−7451
polymer melt, viscosity, normal stress coeffs. determ. method *(German)* 79−7360
polymer solution, flexible mols., dynamic intrinsic viscosity, hydrodynamic interaction 78−47548
polynomials, series conversion by five term recurrence formula 77−13594
porous bed, transient non-Darcy gas flow 78−47033
potential fields, two-dimensional, singular points determ. *(Russian)* 79−39925
potential fields extrapolation numerical techniques *(Russian)* 79−74988
potential flow about boundary shape, method of singularity with spline fit distrib. 78−22324
potential scatt., inverse problem at fixed energy 78−41203
potential theory, higher-order approximations for integral eqns. 79−22877
potentials with Coulomb tails, eigenenergy calc. 79−58560
precession injection cyclotron, high quality beams 79−54617
precipitation over Central Europe, large-scale field components extraction for forecasting purposes 78−92940
pressure between elastic bodies having a slender area of contact and arbitrary profiles 79−64596
pressurised cylindrical shell with clamped crack, stress intensity factors 77−80119
problems in unbounded regions, use of coord. transforms in numerical solns. 78−8219
protostellar envelopes of masses 3 M⊙ and 10 M⊙, struct. and hydrodynamic evolution 80−36616
pseudoplastic fluid, flowing upward in vert. heated tube, variable physical props. 78−90945
pulsatile flow of blood through tube containing rigid and distensible sections, num. soln. technique 77−56419
PWR, sensitivity of emergency core coolant bypass and lower plenum refill to scale size and plenum press. 79−97827
pyrolysis of solid particle, cyclic dynamics 79−47897
quadrature formulae, error term evaluation 79−30207
quantum pendulum under periodic perturbation, stochastic behaviour 80−8834
quantum scattering theory, R-matrix propagation methods in inelastic and reactive collisions 79−59534
quantum three particle system, action-angle variables 80−95708
quasi-one dimensional steady compressible flow, time marching finite area calc. 79−81912
numerical analysis continued
quasi-one-dimensional flow equations, exterior differential form represent. *(Japanese)* 78−8243
radial deformation of nonhomogeneous spherically anisotropic media 77−11128
radial vane grids, laminar flow, numerical calcs. *(German)* 78−90824
radiant heat exchange modelling in rectangular chamber with attenuating medium 80−33433
radiation transfer eqn. in spherical geometry, numerical soln. 80−90329
radiative transfer, transient temp. of body, surface radiation and convection 77−80054
radiative transfer in diatomic gas, vibr. nonequil., probabilistic modelling 80−33434
radiative transfer in nonplane geometry media, approx. and num. methods of eqns. soln. 80−33431
radiative-convective heat transfer, numerical methods 78−94577
radionuclide movement from hypothetical nuclear waste repository 80−16853
radiowave propagation, numerical approximations of Sommerfeld integral for fast convergence 78−66727
random generation of rough surfaces, numerical procedure 78−62060
rapidly rotating gases, thermally-driven axially antisymm. geostrophic flows, flow field calc. 79−90259
rarefied binary gas mixture, two-dimens. channel flow, separation phenomena, num. soln. 77−58740
rarefied gas dynamics projection and variational methods 80−6189
reactive molecular collision calculations, review 79−61851
reactor kinetics, higher order prompt jump approx. 78−50238
reactor kinetics eqns., appl. of higher order prompt-jump approx. 78−74422
recirculating laminar flow between shrouded rotating disks, num. soln. 79−64667
rectangular bars and plates, thick, HF flexural vibr. 79−18779
rectangular plate, supported at arbitrary number of points, modal constraint method 80−23947
rectangular plates, semi-analytic solution for free vibr. 79−18778
rectangular plates, vibrations and buckling anal. *(Japanese)* 77−80084
rectangular surface embedded in uniform subsonic flow, stability 77−80178
recurrence formulas for phases and amplitudes of free wave spherical functions 78−56
recursive multichannel max. entropy spectral estimation 78−53735
reduced wave equation, exterior problems, numerical solns. 78−89351
Reggeon field theory, critical exponents calc. by convergent numerical method 77−45991
regularised long wave equation, anelastic collision of solitary waves, numerical anal. 78−77724
regularised long wave equation, solitary wave solns. 77−13616
relativistic atomic structure calculations, review 79−59379
relativistic electron Coulomb scatt., approx. to cos γ 78−28962
renal counterflow systems, numerical solution of differential equations 78−92662
response matrix doubling eqns. for currents calc. in infinte rod for nuclear reactor 77−65263
response matrix doubling equations for particle distribs. calcs. improved formulations 77−6480
reverberation chamber LF sound power injection analysis and response averaging 78−42496
Reynolds equation at very low spacing, compressible, numerical soln., factored implicit scheme, mag. recording appl. 80−92183
Riccati equations, numerical algorithm for reducing order *(Russian)* 77−49583
rivers, stable numerical model of local scour 77−21809
road traffic noise with interrupted flow, prediction eqns. derivation 77−62106
rock specimens impulse response estimation, numerical method and appl. to laboratory data 79−80049
rocks, hot, dry, hydraulically fractured linearly expanding cracks, eqns. *(Japanese)* 79−34809
rod impact, numerical soln. using Volterra integral eqns. 77−68437
rods, natural twist, influence on oscillations *(Russian)* 79−76996
rotating disc with axisymmetric surface heat source distrib., in laminar flow, heat transfer 79−46314
rotating fluid, trapped oscillations, viscous effects, num. simulation 77−55015
rotating fluid dynamics, review *(French)* 78−30300
rotational flow, analytic solutions to nonlinear eqns. 78−1670
rotationally symmetric periodic electrostatic focusing system field distrib. 79−76574
Saint Venants eqns., three point weighted scheme for numerical soln. 78−30356
saturated-unsaturated flow in deformable porous media, theory 77−91181
SAW interdigital transducers, quasi-static anal. using Green's function method 80−69621
scattering by lossy dielectric wedge, numerical soln. 77−19144
Schrodinger eqn. with central potls. and positive energies, approx. soln. through continued fractions 77−17852
Schrodinger eqn. with discontinuous pots., global trial functions 77−30035
Schrodinger equation, generalisations of finite element and R-matrix methods 78−24676
Schrodinger equation, solution by hand-held calculator using Euler method of numerical integration 80−52052
Schrodinger equation, time-depend., explicit integration method 78−57805
Schrodinger operator, interaction of type $\lambda x^2/(1+gx^2)$ 79−91
Schrodinger time depend. eqn., solutions comparison 78−12596
sea ice, dynamic thermodynamic model 80−51432
second-order perturb. theory of distrib. of materials throughout radiation protective shield 79−54608
second-order-smooth plane sign-alternating contours 79−32678
seismic boundary images, reconstruction using numerical models *(Russian)* 79−39923
seismic observations digital processing, steady numerical solns. *(Russian)* 79−53317
seismic reflection data, numerical inversion method 77−21915
seismic transverse waves in rocks, numerical anal. rel. to waves identification 77−21682
semi-infinite crack tips, practical evaluation of stress intensity factors 80−99962

numerical analysis continued
separated flows, three-dimens., with vortex filaments, num. simulation 77−58706
separated high Reynolds number flow past a corner, numerical solns. 79−81855
shallow shell theory, series representation of fundamental solution 79−10468
shearing flow over wavy boundary, heat, mass, momentum transfer, turbulence model 78−87335
shell, cylindrical, ribbed, with rectangular holes, design for stability in moment precritical state *(Ukrainian)* 77−50938
shells, circular cylindrical, with longitudinal interior partitions, free vibrs. 79−18776
shells of revolution, thin, numerical anal. thermal stress relief 77−89041
shock layer, hypersonic, vibr. nonequilib., near stagnation streamline, low Reynolds no. flow 78−87417
silica gel regeneration by adiabatic desorption mathematical model 79−1967
simplex method solution of inverse ionospheric problem 80−26619
simply supported plate, obtuse corner, numerical modeling 79−32243
simultaneous melting and evaporation due to heat source *(German)* 78−59282
sintered composite-liq. metal interaction, mass transfer eqn. approx. soln. 78−67262
sintering, final stage, steady state diffusion models, testing of models by numerical simulation 79−4428
sinusoidal complex object with a small phase modulation, Fresnel diffr. patterns, self-imaging 80−43256
size variation technique for diffusion coeff. determ. 78−83991
skew crack propagation, induced dynamic stresses, numerical soln. 79−1137
soft materials, reinforcement effect of strain gauge, numerical anal. 79−72864
soft sphere viscosity, numerical calc. using discrete hydrodynamics 79−90505
soil gas fluxes determination, chamber methods numerical evaluation 79−16700
soil hydraulic conductivity, numerical calc. from suction press.-moisture retention relation *(German)* 79−2297
soil mechanics, classical numerical models *(French)* 77−72261
solar cells, 3-D modelling of comb-shaped cells 80−50973
solar central receiver system, flux density integral for reflected sunlight, numerical anal. 80−93863
solar corona quasi-static loops, numerical modelling with uniform energy input 80−21958
solar electrons-interplanetary plasma wave interaction, numerical anal. 78−7853
solar energy thermal storage, numerical simulation of energy transfer by conduction and radiation *(French)* 79−24916
solar heating of buildings, numerical simulation of thermal performance 80−66942
solar heating of buildings calc., transient thermal flux model 79−62144
solar heating system components, optimal insulation, numerical sensitivity anal. 80−35745
solar model, constant mass, differentially rotating gaseous polytropes configurations 80−82338
solar stills, design and thermodynamic parameters, numerical anal. 80−55914
solar system formation, numerical expts. on planetesimal aggregation 78−69713
solid-state diffusion from a limited source 80−70444
solidification, numerical treatment of axisymmetrical conduction phase change 79−33073
soliton interaction dynamics and nontopological stability in nonlinear model of complex scalar field 80−101719
solitons, numerical studies, historical review 79−75367
space probe or meteorite reentry, mass loss and shape change with radiative heating 80−31198
spark in focused laser beam, and continuous optical discharge, numerical study 79−14632
spectral line formation in axisymmetric moving envelopes, numerical method and appl. to YY Orionis stars 80−41813
Spencer-Lewis eqn., orders of scatt. soln. 79−85098
spent nuclear fuel storage, supercriticality through optimum moderation 80−57896
spiral galaxies, non-linear corrugation waves numerical computations 80−67859
stability problem, lateral, with free-flying column, asymptotic solns. 79−14242
stagnation boundary layer response to change in external velocity 79−64648
star cluster models dynamical evolution, early stages 79−8958
star clusters, evolution, Fokker-Planck eqn. numerical integration 80−36675
star escape from isolated clusters, numerical methods *(Polish)* 80−26922
star formation process simulation, hydrostatic models evolution *(Polish)* 80−21998
star formation rate in external galaxies, numerical simulation 77−45555
stars, rigidly rotating, secular instabilities in general relativity, numerical results 80−4342
state of art survey, book 78−20953
stationary random fields, statistical inference 77−64930
steady flow between a rotating and a porous stationary disc in the presence of transverse magnetic field 78−79382
steam generators, steady 2-dimens. two-phase flow and heat transfer calc. 79−1237
steel, welded-joints, H_2 induced cracking, S content effect 80−97562
steel welds, bead-on-plate, H_2 diffusion and trapping 80−96697
Stefan multiphase problem, numerical algorithm 78−33989
stellar adiabatic non-radial oscillations with moderate or large l, numerical anal. 80−56819
stellar degenerate C core, numerical calcs. of thermonuclear explosion 78−36558
stellar structure, appl. of strained coordinate method in rot. main-sequence stars 77−56910
stellarator toroidal field production by modular systems 80−10441
stiff differential eqns. of chemical kinetics 79−15960
stiffened plate struct., nonlinear anal. by combined Rayleigh-Ritz-finite element method 77−72162

numerical analysis continued
Stirling cycle machine anal. using nodal anal. techniques, review 80−30532
Stirling heat engine design, isothermal second order calc. method 80−30533
stochastic transition, determination method 79−71366
Stokes flow, numerical soln., appl. to interacting spheres 78−22407
Stokes flow ellipsoid of min. drag, limited by cylindrical front *(French)* 79−53982
storm surges in Sea of Azov, two-dimensional numerical calc. 78−96231
straight long rod, dynamical buckling under hammering 79−7312
stratified fluid, internal wave solitons, numerical computation 78−59410
stratified shear flows over long obstacle, numerical method 77−33157
stratosphere, wave-mean flow interaction rel. to sudden warmings, numerical model 77−5297
stratosphere photochemical-radiative damping and instability, numerical results 78−81286
streaming, of vel. and temp., in oscill. boundary layers 78−83358
stress analysis, elastic half space containing embedded rigid block 80−23890
stress analysis of cylindircal shell with rigid circular inclusion 79−14267
stress singularity at the corner of a wedge-shaped crack or inclusion 79−46268
stress waves in heterogeneous media, Laplace transform inversion 77−80103
string response to accelerating mass 77−50875
structural damping constant evaluation by time series analysis 78−46902
structural dynamics, polynomials and variational methods 77−68393
structural dynamics, system identification by pseudoinverse 77−72232
structural elements, thin-walled, temp. fields calc., algorithm 79−37114
subduction zone, thermal model with dehydration in downgoing slab 79−79784
suction effects on shock wave-boundary layer interaction, numerical Navier-Stokes soln. 79−1243
summation of partial wave expansions in scatt. by long range pots. 79−41239
supercritical accretion discs winds struct. and appearance, numerical models 80−21984
superfluorescence, oscill., quantum statistics 79−917
supernova blast wave, Lagrangian coordinate transforms. in self-similar model 77−57072
superradiance, spatial variation with time, numerical anal. *(Russian)* 80−78821
supersonic blunt body flow of viscous perfect gas and nonequilib. gas mixture 80−28578
supersonic flow, linearised, improved higher-order panel method 80−6082
supersonic flow, steady two- and three-dimensional, shock discontinuities detection method 77−58736
supersonic flow, wake of axisymmetric body, ideal gas, numerical anal. 78−59420
supersonic flow about elliptic cones with large semiaxis ratio, num. soln. method 77−58729
supersonic flow around blunt bodies with combined cross sections, num. comput. 77−58728
supersonic inlet, flowfield computation using bicharacteristics method with shock wave fitting 80−38443
supersonic laminar boundary layer separations, quasi-3-dimens. 78−46995
surface loads, reciprocating dynamic stresses produced in elastic half space 78−9562
surveying, collocation with help of Gaussian algorithm *(German)* 79−79730
suspension, conc., of aggregable particles, viscosity calc. 79−7362
suspension deposition in entrance of a diffuser, electrostatic and gravitational effects, laminar flow 80−14785
suspensions, deposition in channel entrance, combined influence of diffusion, electricity and gravity 80−1674
swirling jets, confined, axisymmetric viscous incompressible flow, numerical prediction 77−84286
symmetric gas jet, flow computation *(Russian)* 79−37374
synchrotron radiation, angular and spectral distrib., modified Bessel functions of fractional order 80−91738
T-junction laminar flow, partially elliptic flow numerical calcs., recirculation 80−64632
Takagi-Taupin equations, boundary conditions in numerical integration, appl. to Bragg and Laue cases 80−1886
Taylor vortices, finite difference numerical computation 77−62259
tensile test for sheet metals 77−86101
texture analysis, numerical calc. of generalised spherical harmonic function *(French)* 78−18484
thermal conductivity, three-dimensional solution for arbitrary shape bodies 77−75774
thermal conductivity inverse problems *(Ukrainian)* 79−41560
thermal consts. determ., inverse heat cond. problem soln. 79−37142
thermal convection, partial spectral expansions 79−32193
thermal convection in closed gas centrifuge, eigenvector soln. of linearised eqns. 80−83797
thermal defectoscopy, two-dimensional numerical soln. with convective heat loss 77−81378
thermal imaging scanners, mirror rotation axis optimisation 80−86426
thermal-ignition analysis in boundary-layer flows 79−64800
thermoelasticity, advanced boundary integral eqn. method 77−72175
thermoelasticity anisotropic 3-D problems, numerical projective method 77−68436
thermoelastoplastic solution for a circular solid cylinder subjected to heating and cooling 80−5952
thermoelectric coolers, numerical anal. of transient behaviour 78−21140
thermoluminescence data anal., for quasicontinuous activation energy distrib. 77−52189
thermoplastic sheet, extruded, thickness adjustment and cooling between calender rolls 79−68597
thermorheological problems, numerical soln. 78−13910
thin crystals, surface state calc. 78−14778
thin elastic plates, nonlinear vibr. 78−1593
thin wire antenna coupling with human body 77−21563
thinwall framed beam, numerical integration of differential eqns. 77−19520
three-dimensional potential fields conversion and pseudo-gravit. field computation 77−82026

numerical analysis continued
three-impulse min.-time orbital transfer generation, numerical method 78−73607
tidal propag. equations, finite difference and analytical methods 79−12134
Tokamak, effect of fuel pellet injection velocity on energy parameters 80−32490
Tokamak, electrostatic drift waves, numerical anal. of instability and transport 80−48871
Tokamak machines, eddy currents, numerical and exptl. anal. 78−66374
Tokamaks, high-β, MHD stability limits 80−28643
torsion of connected bars *(German)* 78−34024
torsion of rectangular bars, appl. of improved collocation techniques 77−68434
torsional vibrs. of spherical shell, numerical results 78−59322
transformation groups for resolution of partial differential eqns., appl. to gravity, quantum mech. and heat transfer *(French)* 79−49099
transient aquifers, modified optimisation method for parameters estimation 78−61462
transient elasto-dynamic response of circular crack in thick plate under torsion 80−5993
transient heat conduction, Laplace transform and boundary integral eqn. 77−72129
transonic flow, bow shocks comput. method 77−55027
transonic flow, implicit approximate-factorisation schemes 78−94759
transonic flow, steady three-dimensional, finite vol. soln. of Euler eqns. 77−55028
transonic flow, unsteady, implicit shock-fitting computational scheme 78−94763
transonic flow over two-element airfoil systems, num. comput. of inviscid irrot. flow eqns. 77−55026
transonic free jet, overexpanded two-dimens., eqns. formulation and soln. method 80−6109
transonic small-disturbance theory, leading-edge singularity, num. integration methods eval. 80−6080
transport calculations in cylindrical geometry 79−58655
transport coeff. numerical simulation of meas. by correlation method 78−8364
transport processes, two-group problems with anisotropic scatt., closed-form solns. 78−4569
transversely isotropic medium with cylindrical cavity and external crack, stress distrib. 78−79259
trend analysis and interpolation theory, geophysical appl. 77−45684
tridimensional numerical calc. of magnetic fields using summation method *(German)* 80−106414
truss struct., accurate nonlinear anal. 79−90159
tsunami, island of Hawaii, 1979 November 25, numerical anal. by finite-element method 80−72449
tsunamis, transform. in coastal zone 78−77192
tube extensions, perforated and flared, reflection of step-wavefronts rel. to railway tunnels 79−14426
tube/fluid vibrations, effects of fluid viscosity 79−3967
turbine cascade flow, surface-oriented coords. in num. simulation 77−55018
turbulence, isotropic, energy spectral density calc. 79−86410
turbulence computation, bispectral meas. 80−38382
turbulent boundary layer, compressible, extended mixing length appls. 78−94655
turbulent boundary layer, nominally steady, two-dimens., vel. and temp. profile prediction method 80−1624
turbulent boundary layer near corner 77−47000
turbulent boundary layer-transonic shock wave interaction, integral computation method 79−1213
turbulent electron beam plasma interactions, PN calc., numerical anal. 79−14560
turbulent flow, annular, with inner cylinder rot., computation 80−1544
turbulent flow, numerical simulation of large eddies 78−9628
turbulent flow in pipes, numerical anal. by finite element method 78−18341
turbulent liquid, coherent struct.-caused mass transfer at wall, numerical computation 78−59379
turbulent shear flow, large eddy simulation 80−38390
turbulent shear flow computation, Navier-Stokes eqns., Reynolds stress modelling 78−46955
turbulent transport eqns. soln. by accurate numerical method 80−28498
turbulent two-dimens. recirculating flow, numerical model calcs. 80−19358
two dimensional fluid transient analysis, nearcharacteristics method 78−89349
two-dimensional fluid motions induced by motile particles, convection field and geotactic components 77−55080
two-dimensional multiply connected regions of arbitrary shape and boundary conditions, temp. field calc. 79−86317
two-dimensional turbulence in square region, inviscid Navier-Stokes eqn. calcs. 78−16656
two-fluid stratified layers in trapezoidal channel, nonuniform steady flow *(Rumanian)* 79−14452
two-junction Josephson interferometer, reson. phenomena, anal. 78−47910
two-phase boundary layer, successive approx. method 79−32647
two-phase flow, semi-implicit two-fluid calculational methods 80−103066
two-phase flow, two-fluid model calculations, stability problems 80−19489
two-phase reacting flow, heterogeneous, balance eqns. and soln., interior ballistic phenomena modelling 79−94737
two-phase recirculating flow, num. calc. procedure 77−55081
two-phase unsteady 1-D flow, numerical soln. of eqns. *(French)* 77−68665
underwater sound, Gaussian quadrature ranges with observed sound-speed profiles 77−46851
underwater spark induced axisymmetry unsteady motion betweeen shock wave front and contact surface *(Russian)* 79−77323
underwater wide-angle acoustic field in ocean with range-depend. vel. profiles 77−79993
unsteady aerodynamic modelling for arbitrary motions 80−19433
unsteady comp. laminar boundary layer flow, num. anal. 79−94586
unsteady flow fields with detonation, num. modelling 77−55107
unsteady flow in open channels, num. analysis method, teaching aid paper 77−29972
unsteady high Reynolds number flows, inclusion of vorticity 78−75151
numerical analysis continued
unsteady imcompressible laminar boundary layers around impulsively started cylinders *(French)* 79−72876
unsteady MHD eqn. solns., for explosion in non-homogeneous media, num. anal. 79−64778
unsteady mixed convection heat transfer from a horizontal circular cylinder 79−81879
unsteady subsonic and supersonic pot. aerodynamics for complex config. aircraft 77−72320
upper atmosphere hydrodynamical accelerator, numerical modelling *(Russian)* 78−16225
US signals, physiological measurements and numerical analysis 77−86577
uterine deformation during labour, thin shell model and kinematic analysis 79−2090
vapour pressure, constrained fitting of limited data 78−34615
Varshni V and Lennard-Jones pots., 3rd order WKBJ eigenvalues 79−6982
Venus rotation, possible dynamical evolution since formation 80−56742
vertical cones in laminar free convection, integral method 79−81881
vibration analysis of two-layered beam, with unconstrained viscoelastic layer damping *(Japanese)* 80−5968
vibrations, transverse, of rectangular plates subject to in-plane normal and shear forces, transverse vibrs. 79−14314
vibrations of thin shells, large amplitude flexural, effect of median surface curvature 79−18780
vibrations source characteristics, placed in liq. layer *(Russian)* 78−75154
visco-plastic approach to plasticity and creep problems, involving geom. nonlinearities 78−26050
viscoelasticity, nonlinear, stress relaxation, Volterra integral equation, numerical analysis 80−53646
viscoelasticity differential eqn. method approximation, for solving dynamic viscoelastic problems 80−14585
viscoelasticity equations, methods for numerical soln. 77−89042
viscoplastic medium, flow between two noncoaxial circular cylinders under pure shear 80−99938
viscous flow, 2nd order upwind scheme critique 78−94744
viscous flow equations num. soln. using integral represents. 77−54966
viscous flow past circular cylinder, two coord. systems description 77−58643
viscous gas flow computation, grid point condensation, high-order schemes 80−36866
viscous transonic cascade flows around airfoil, coord. system for numerical calcs. 78−42627
VLF signals, numerical study of satellite reception using waveguide concepts 80−90282
volcanology, lava lake cooling model, numerical analysis method 77−64247
volume phase holograms, non-sinusoidal high order modes 80−102665
von Mises and Coulomb materials, two dimens. deform., numerical appl. of limits anal. 77−54899
vortices, in mixing layer, numerical simulation 78−90853
vorticity, chordwise variation, approx. for use in panel methods 78−18306
wake, of circ. cylinders, in nearly homogeneous turbulent stream 79−1197
wall with one-way heat flow, vertical inclined cavity stack 79−3899
water wave initial value problem *(German)* 79−77155
wave, periodic, long, deform. over gently sloping bottom 78−90921
wave diffraction theory, infinite systems of eqns. *(Ukrainian)* 79−49060
wave propagation, weak, in elastic-plastic and elastic viscoplastic solids with interfaces, Al calcs. 78−18216
wave propagation in inhomogeneous media, determ. of structure from plane wave reflection response, numerical approx. 80−73183
wave propagation in inhomogeneous media, determ. of structure from plane wave reflection response, direct problem 80−77628
waveguide characteristics, of gradient-index fibres *(German)* 78−5550
waveguides, two parallel thin-film 80−106626
weather forecasting, assessment of model initial conditions using satellite imagery 80−31084
weather forecasting, short-range, effect of subjectively enhancing initial vorticity field 80−82008
weather modification due to waste heat release from large dry cooling towers 79−84471
Weibull distrib. function for analysis of data obtained by accelerated tests *(Spanish)* 79−54113
Wendroff type discrete inequalities and their applications 80−17786
whirlwind, ring-shaped, onset caused by rising air in stratified atmosphere *(Russian)* 78−77298
width of Lorentzian convoluted with Gaussian 77−79528
wing, 3-dimens. boundary layer calc. method 80−1622
wing, supersonic gas flow, numerical method and routine 80−38440
X-ray small angle scattering, slit-height exact soln., arbitrary slit transmission functions 78−42853
X-ray tube rotating anodes, temp. distrib. of compound anodes 78−62285
$\pi\pi$ elastic scatt. at complex energies, stable unbiased analytic extrapolation 79−13155
CO, vibrational transitions dipole matrix elements, numerical calc. 80−95594
CO_2, viscous hypersonic flow over blunted cone 79−77171
CO_2-N_2-He, vol. discharge, negative ions effect 80−14956
Co complex, $\Lambda(+)[Co(en)_3]^{3+}$, quadrupole transition circ. dichroism, production mechanism 79−3428
GaAs forward-biased diode structures based on direct gap semiconds. 79−65542
H embrittlement, trap theory 80−89325
H II regions gas dynamics, two-dimensional axisymmetric calcs. 80−12791
H_2^+, ground state energy inverse power expansion of two proton distances 79−97976
H_2-O_2 reaction boundary layer, math. model *(German)* 77−35253
HF chemical lasers, numerical anal. of laser generation conditions 80−9872
H_2NO, hyperfine coupling const. calc., double perturb. theory and CI methods 79−59362
H_2O, energy levels, triat. large amplitude vibrs. model appl. 80−23392
H_2SO_4 aerosol growth, kinetic model 77−37340
He, doubly excited states classification, for intermediate quantum nos. 79−10046

numerical analysis continued
He-Xe 3.51 μ laser mode competition in axial mag. field 80−63974
He+charged particle, Glauber scatt. amplitude, numerical method in Lommel function 79−22795
He(2^3S)+H(D), Penning and assoc. ionis. cross sections, vel. depend. 79−22815
KH_2PO_4, variational treatment of proton-photon system 78−88261
N glow discharge, volt-ampere charact. in gas flow *(Russian)* 80−106991
N_2 high intensity arc anode region, temp., current density, flow field, numerical anal. 78−9827
$N_2O/N_2/H_2O$, CW gasdynamic laser, numerical anal. 78−29935
N_2O_4, dissociating, turbulent pipe flow, heat transfer, resistance 78−91026
Na vapour bubble growth in superheated liquid, numerical anal. 78−29576
NaCl gas-droplet counterflow heat exchanger, numerical model *(French)* 80−61396
O_2 quenching effect in tunable dye lasers 79−72564
OH, chemiluminesc., form. from O+ethylene, mechanism, rate const., mathematical model calcs. 78−48655
Si:B redistribution after oxidation, integro-differential eqn. 77−76453
^{238}U, single charged, numerical anal. of longitudinal motion of 9.5 GeV 79−54737
X+F_2→XF+F (X=Mu, H, D, T), quasiclassical smooth sampling study of threshold behaviour 79−61852

numerical control
see also computerised numerical control; digital control; machine tools
diamond turning system evolution 80−1369
insulin/glucose transfer regulation for diabetics, user programmable system *(French)* 79−39614
radiotelescope, solar *(Czech)* 79−44371
radome and backstructure design improvements 78−57449
ruling engine development, for stigmatic concave grating *(Japanese)* 77−19464
Nd:glass laser with numerical programmed control *(Russian)* 80−91811

numerical methods
see also convergence of numerical methods; predictor-corrector methods
ablating body shape, numerical soln. method *(Russian)* 78−75134
accurate space derivative method, global numerical differentiation by compact polynomial splines 77−13597
acoustic interaction with ocean bottom, plane wave reflection loss model 79−10425
acoustic radiation problem, Schenck numerical method *(French)* 80−69589
acoustic wave propagation, in nonuniform ducts, wave-envelope technique 78−9464
acoustical ducted noise source, numerical spatial marching techniques for prediction of press. distribs. 79−46098
acoustics, evaluation of singular integrals in interface separation, new quadrature formulae 80−74559
acousto-structural vibrations, approx. numerical soln. 79−3841
addition formulae for two-point boundary systems 79−71235
advanced continuous fluid Eulerian comput. scheme for flows with large density gradients 77−46236
aerodynamic design, wind tunnel tests and numerical methods compared 77−27635
aerodynamics, one-dimensional unsteady flow, hyperbolic initial-boundary value problems solution *(German)* 80−6095
aerodynamics, transonic axisymmetric flow past slender body of revolution, integral equation method 80−74910
aerofoil, two-dimens., in incompressible flow, unsteady motion 78−67171
air, temperature, five-day average low and high temp. anomalies forecasting procedure 78−92938
algorithm for calc. of impurity concentration from sheet resistivity and sheet Hall coefficient data 80−70246
algorithm for numerical soln. of critical buckling 78−83275
alpha particle orbits in radially nonuniform slender plasma column, multigroup rep. 80−53921
Anderson localisation, statistical fluctuations in numerical approx. methods 79−6056
anisotropic transport calc., selection of angular quadrature 77−37828
annular plates, nonsymmetric postbuckling behaviour, numerical analysis 80−102968
antennas and propagation, symposium, Amherst (1976) 77−14633
apodizing filters for optimum Sparrow resolution in coherent systems with annular aperture 80−53435
applications of integral equations in particle-size statistics 78−62050
applied modelling, conf., Southampton, England (July 1977) 78−77285
approximate integral method, anal. of boundary layers on cylinder *(Russian)* 79−77062
artificial satellite motion, error evaluation, averaging method for canonical eqns. *(French)* 77−67028
artificial satellite motion, error evaluation, averaging method for canonical eqns. *(French)* 77−67029
astronomy, numerical integration of stellar orbits 79−21361
atmosphere models, advection in flux formulations for variable grid models 77−29380
Atmospheric Cloud Physics Laboratory simulation, vorticity transport eqn. solns. 80−94690
atmospheric modelling, spectral-transform method 77−37342
atmospheric numerical model *(French)* 80−21814
automated ship routing appl., meteorological surveillance 79−84390
baroclinic oceans, semi-implicit numerical model 77−29316
beam structures, thermally induced vibrations and heat conduction problem, numerical method 80−64427
beams, frames, arches, axisymmetric shells, finite element anal., Newton Raphson method, nonlinear equilib. eqns. 78−22282
bifurcation theory, applic. to premixed laminar flame modelling 80−16681
Blasius profile, eigenvalues determ. using Riccati transform. method 77−65731
blood flow through deforming tube, numerical soln. 80−104614
bluff-body flame-stabiliser flow modelling 77−72367
Boltzmann eqn., numerical method of soln., weakly ionised heterogeneous gas 77−49693
bordering functions based interpolation method 78−81816
bordering functions based numerical method 78−81815
Borel-type sums in scatt. theory, computation method 78−57823

numerical methods continued
boundary element methods, direct and indirect, formal equivalence 78−81814
boundary element methods, using weighted residual techniques potential problems and engineering appl. 78−36803
boundary elements method for fluid flow differential eqn. solution 78−90821
boundary integral eqn. method, anisotropic 3-D stress anal. 78−90714
boundary integral eqn. method, anisotropic point load solns. 77−68431
boundary integral eqn. method, appl. to creep of metals 79−46231
boundary integral eqn. method for 3-D thermoelasticity 78−5657
boundary integral eqn. methods, advanced appl. 78−42531
boundary integral eqn./finite element anal. of cracked solids 77−72178
boundary integral equation method for nonlinear free surface flow anal. 78−92850
boundary integral method, cf. finite element method 77−67250
boundary layer, laminar separation, from upstream-moving wall 78−13989
boundary layer, stability theory, high viscous eigenstates 77−907
boundary layers, book contrib. 78−59369
boundary layers beneath pot. vortex, finite-difference schemes 77−14982
boundary-integral method, appl. to plates of arbitrary plan form 77−72155
boundary-value problems in quantum mechanics and quantum field theory 77−2526
boundary-value problems solution, using patched variational principles, appl. to elliptic and mixed elliptic and hyperbolic problems 77−89144
bounded metalworking process, iterative numerical anal. technique 79−83212
bubble cavitation problem, numerical soln. 78−79347
bubbly, two-phase mixtures, numerical anal. of press. transients by explicit-implicit method 78−34185
Calvin photosynthesis cycle parameter identification 79−92186
cantilever beam axial vibration, min. mass structures determ. 78−63278
cardiac muscle model activation parameter behaviour, numerical study 78−11686
cascade flow, transonic anal., by conformal mapping and relax. techniques 77−75934
Cauchy problem for Laplace's eqn., solution approximation 77−78966
cavitation bubble, implosion, near solid boundary or free surface *(French)* 77−55056
celestial mechanics, mathematical methods, conf., Oberwolfach, Germany (Aug. 75) 77−25916
celestial mechanics, planetary motion, Taylor-Steffensen series appl. *(Russian)* 78−49352
celestial mechanics, regularised numerical method based on Taylor-Steffensen power series *(Russian)* 78−49300
celestial mechanics, satellite motion prediction by extrapolation methods *(Russian)* 78−49299
cell collocation method in continuum mechanics 78−77711
channel flow, convective vel. to wall press. fluctuations, numerical simulation 78−94829
characteristics method for unsteady two-dimensional subsonic, transonic and supersonic flow calcs. 77−55021
chemical kinetics, modelling, numerical method based on Taylor series expansion 78−48629
chemical laser, steady state operating charact. calc. 77−19241
chemically reacting flows in porous media, numerical solns. 80−43801
chemically reactive boundary layer problems with relaxation processes, Enskog-Chapman method modification *(Russian)* 80−19523
chemically reactive flow, stiff boundary valued problems in kinetics and diffusion, numerical methods 79−86525
Cholesky factorization of stiffness matrix, method for updating factorization 78−16623
CIDNP, numerical methods, model depend. 78−13530
circulation models, numerical integration method for improving soln. stability 78−69118
classical dynamics systems, stochastic props., numerical methods reliability, time averages 78−41151
cloud seeding, num. simulation technique 79−84519
coarse mesh flux expansion method, anal. of space-time effects in large LWR cores 77−67794
coarse-mesh eqns. for the numerical soln. of 2nd-order transport eqn. 80−47527
cold sheet rolling, thermoviscoelastic problem 77−39236
collocation method, appl. to boundary-value problems in applied mechanics 77−68434
colloidal spherical particle, numerical method for electrophoretic mobility determ. allowing for polarisation 77−25269
combined finite element/characteristics methods for dam porous media unsteady flow calc. 78−91012
compact finite-difference methods and boundary conditions 77−49582
complete EM field of dielectric lossy fibre excited by dipole source, numerical calc. 80−43427
complex Airy functions, evaluation algorithm 79−58562
composite body, heat conductance, combined numerical method 78−63261
composite slab with variable cond., transient heat cond. anal. using collocation method 80−10106
compressible hodograph eqn., numerical soln. 78−51179
conductivity, profile determ. by time domain reflectometry, inhomogeneous media 79−36820
conformal mapping and transform. of hydrodynamic coeffs. of heaving cylinders 79−3988
conformal transformations combined with numerical techniques, with applications to coupled-bar problems 80−83538
consistent homogenization procedure to obtain few-group cell parameters, appl. to neutron transport 79−85586
contact stress problems, counterformal, improved numerical method and program 79−41632
contour integral method for computation of singularity intensities in elasticity 77−72180
convection, natural, in closed container, numerical simulation 78−46969
convection, three-dimensional, natural, in box 78−5743
convection single-mode equations, numerical solns. 77−27530
convection theory, numerical methods 78−89058
convective coupled heat transfer, Nusselt no. computation, laminar fluid film 78−59398
convective difference schemes and Hermite interpolation 77−68368
convective diffusion eqn. computer soln. for electrochem. cell 77−16830

numerical methods continued
convective dispersive equation, movement of chemical pollutants in groundwater 80−16855
coupled-channel Schrodinger eqn. bound states, renormalised Numerov method 79−13627
crack stress intensity factor determ., using numerical method *(Italian)* 80−14625
cracks, plane elasticity, curvilinear crack edges concentrated forces and edge dislocations, numerical soln. 80−58970
creep, numerical solution methods 80−14582
creeping flow in closed cylindrical cavity, numerical calculation 80−16976
crystal growth, diffusive, numerical soln. accounting for growth rate and surface tension anisotropy 80−33912
curved rectangular conductor magnetic field calc. 77−61895
curvilinear domains, quadratures *(Russian)* 79−63006
cylindrical media, radiative transfer eqn. 78−5642
cylindrical plasma filament under axisymmetric perturbation 80−106853
cylindrical shell modal velocities, numerical fluid loading coeffs. 77−5669
deconvolution method for X-ray spectra from hot plasma 80−54030
Delbruck scattering amplitudes, numerical calcs. 77−88108
design optimisation of reinforced plastic cylindrical shell under dynamic loading 79−59935
dielectrics containing impurities, carrier distribs. and currents, numerical simulation *(French)* 80−70718
differential areas method for density of state calcs. 79−82508
differential equation solution, computer-aided linear physical systems analysis, with periodic inputs 79−51
differential equations, second order, without first derivatives, fourth-order numerical method 80−86107
differential equations, second-order, degenerative, boundary-value problem solution, asymptotic expansion *(German)* 80−32
differential equations solution, free boundary conditions *(German)* 80−35
differential equations solution, generalised splines and linear multistage formulae *(German)* 80−34
differential equations solution, Navier-Stokes, using finite difference procedure, unsteady leading edge separation bubble calc. 77−72317
differential quadrature, appl. to transient nonlinear diffusion 78−16755
diffraction problems at smooth unbounded wavy surfaces in inhomogeneous medium, direct method *(Russian)* 79−75363
diffusion eqn., multi-dimensional parabolic free surface problems, alternating direction method 77−37826
diffusion kinetics, crystallisation of salts from supersaturated solns. 79−23553
dilute alloys solidification, numerical soln. model 79−69228
direct methods for solving discrete Poisson eqns. 79−58536
direct pot. method for plane elastostatics, polynomial approx. 77−72177
direct reduction method, transfer theory soln. 80−22309
Dirichlet problem, Fourier transform technique for boundary condition of infinitely long strip 77−45679
Dirichlet problem for semilinear eqn. $\Delta^k u = f$ on a disc, approx. techniques 79−40377
discharges between plane parallel electrodes, axial and radial development, computation 77−19794
discrete ordinates method for neutron scatt. in anisotropic medium 79−85579
discrete systems, conservative dynamic, K-Quotient for determ. of upper bound 79−18777
dispersion of equal spheres, random, average nearest-neighbour spacing 79−58639
displacement incrementation in nonlinear structural analysis by self-correcting method 77−14932
dissipation integral calculation method for boundary layer turbulence calcs. *(German)* 79−86418
distributed parameter system control, conference, Coventry (1977) 79−3897
drift wave equations, numerical solution by invariant bedding 80−10374
dynamic indentation of elastic plate by rigid punch, numerical soln. 79−14260
dynamical grid method for time-dependent simulations of axisymmetric instabilities in tokamaks 79−10702
dynamical meteorology, numerical modelling, applications to weather-forecasting 79−84459
earthquake, theory of fault rupture propagation 80−104910
eddy current problems, three dimensional, network analogy *(Japanese)* 79−81325
eddy-current problems, including moving Fe parts, numerical soln. 78−90340
edge function method, appl. to elastostatics 77−68427
edge-function method, vibr. anal. of elastic plates and shells 77−72231
education, iterative soln. for square-well pot. eigenvalues, pocket calculator 77−33778
effective implicit time integration in analysis of fluid-structure problems 80−92040
eigenvalue perturbation theory, remarkable examples 78−93558
eigenvalue problems for integro-differential eqn. of nuclear theory *(Russian)* 77−57641
Einstein's field eqns. on curved background metric, approximation method 78−109
elastic coefficients, independent 4th-order for all cryst. classes, numerical methods anal. 79−69219
elastic cylinder with inserts and holes, torsion problem, integral eqn. soln. method 80−106717
elastic plate, infinite, concentrated load, stress. anal., numerical method *(Japanese)* 78−22273
elastic prismatic bar, with rigid ends, lower and upper bounds for torsional rigidity 80−48568
elastic shells, thin, doubly curved, numerical integration of triangular finite element 80−92044
elastic structural stability anal., num. methods 79−94489
elastic wave propag. anal. in rods due to impact 79−32352
elastic-perfectly plastic von Mises material, accuracies of numerical soln. constitutive eqns. 78−59315
elastic-plastic problems, supplementary strain method, appl. 80−96205
elastic-plastic thermal stress problem, soln. 77−3742
elasticity, anisotropic, stress concentration around holes, formulation of problems 79−64509
elastohydrodynamic problems for rough bodies with non-Newtonian lubrications *(Ukrainian)* 80−24054
numerical methods continued
elastostatics, linear, boundary-integral approach for mixed boundary-value problems 79−64508
electric dipole fields in conducting media, calc. by numerical methods 80−18957
electric field behaviour near singular points in composite dielectric arrangements, charge simulation method 79−31763
electrical and magnetic fields computation, using ELMAG program system *(German)* 77−3516
electrochemical diffusion, boundary value problems, orthogonal collocation calcs. 78−40053
electron beam, relativistic, high-current, in microwave linear accelerator, transient behaviour 80−32541
electrostatic field solution, two-dimensional, using Sander's function 79−878
elliptic partial differential eqns., numerical methods evaluated 78−65756
elliptic systems and numerical transforms. 78−65780
EM field problems having irregular boundaries, direct noniterative numerical soln. using network analogues 80−95766
EM fields analysis, stationary, by Trefftz's method, using quasiharmonic polynomials *(German)* 79−27128
EM radiation scattering by dielectric spheroids and ellipsoids, integral eqn. soln. 78−85622
EM waves diffraction at surfaces with inhomogeneous admittance 80−69296
EPR and saturation transfer EPR, fast computation, master supermatrix eqn. soln. 78−62213
EPR and saturation transfer EPR, fast computation, perturbation approach 78−62212
errors calc., dynamic, in linear conversion 77−5796
Euler equation solver, axisymm., implicit, unsteady, appl. to solar wind flow past planets 78−96370
Euler-Maclaurin summation rule, anal. of unsteady thermal stress problems 80−48580
Eulerian computation technique for domains with moving boundaries 77−53779
Eulerian method for numerical anal. of LMFBR HCDA fuel-coolant interaction 80−68733
exponential box scheme for boundary layers with blowing 79−1240
exponential fitting, method of characts., one-dimens. unsteady non-equilib. flow 78−49648
exterior linear elliptic problem, numerical method, appl. to 2-dimens. wave resistance 80−28485
Fabry-Perot interferometer data inversion algorithm 79−75604
Faddeev equations, generalised, for many-cluster problems 77−88058
Fermat number transform for microwave holography data processing 80−43298
Feynman diagram amplitudes in cross section calcs., computer code 79−13094
field problem computation for undergraduate teaching 77−10803
finite difference method, flow between rot. discs, central source 77−42849
finite difference method, pollution advection eqn. 77−13118
finite element Galerkin method for groundwater flow calc. 78−89320
finite geometry effects in scatt. expts., numerical integration method 78−82596
finite-difference method, to determine coupled power eqn. of step index fibre optics 77−54791
finite-size particle method, numerical criteria to test real system equivalence 77−11393
fins, nonlinear problems, 1-D conduction, initial value problem 80−83726
first-order differential eqns., common derviation of averaging method and two-timescale method 78−85835
fission gas behaviour model, intragranular, nonequilibrium behaviour, numerical integration 80−32345
fission reactor digital simulator software development, kinetic equations integration, numerical solution method 80−68901
flow, nonadiabatic, of compressible gas in tube, eqns. system numerical integration *(Russian)* 78−83427
flow, rot., between rot. and static discs, with radial flow, numerical method 78−59403
flow, two-dimens. boundary layer, viscous-inviscid flow matching, transonic and supersonic flow *(French)* 78−79334
flow boundary-value problems three-dimensional region elliptic transformation 78−55624
flow in curved tube, finite difference anal. method 80−106846
flow phenomena within vortex sink rate sensor, numerical study 78−63436
flow reversal and separation at unsteady boundary layers 78−75163
flow through duct, compressible and laminar 79−4030
fluid, classical, transport coeffs. computation by cell hydrodynamics 78−38600
fluid bifurcation phenomena numerical anal. *(French)* 80−19319
fluid dynamic problems solution, blast loading on three-dimensional structures 77−68624
fluid dynamics, 2-D two-phase flows of nucleating and wet steam, time-marching method 80−69906
fluid dynamics, book 77−57201
fluid dynamics, conf., Enschede, Netherlands (July 1976) 77−54953
fluid dynamics, conference, Tbilisi, USSR (June 1978) 80−17717
fluid dynamics, drop coagulation in cross-over pipe flows of wet steam 80−74982
fluid dynamics, Navier-Stokes equations, finite element soln., applied to blood flow 80−94269
fluid dynamics, numerical simulation 80−17805
fluid dynamics, truncation error estimation due to upstream differencing, consistency check 79−23294
fluid dynamics, viscous flows with no-slip walls, incompressible Navier-Stokes eqn., pseudospectral method 80−69924
fluid flow, numerical methods comparison 79−9123
fluid mechanics, boundary element methods versus finite elements 78−73860
fluid mechanics, num. methods and associated problems, book contrib. 77−89087
fluidised bed, numerical soln. to 20 unsteady diffusion eqn. for vortex flow 77−84320
fluids with dipolar interactions, boundary conditions for numerical simulation, book contrib. 79−60247
Fokker-Planck equatn. solutn. 80−18622
Fourier transform, numerical evaluation method 79−17194

numerical methods continued
fourth-order method for laminar or turbulent boundary layer eqns. 79−1174
full-field numerical differentiation 79−59922
fusion reactor blankets, MHD coolant flows, 3-D model 80−23119
Galerkin method, appl. to hydraulic anal. of turbulent flow around LMFBR fuel rod 79−30893
Galerkin method, fluid flow appl. 79−9118
Galerkin method, modified, for sound propag. in ducts 79−10423
Galerkin method for elliptic and parabolic eqns., interior penalty procedures 77−33847
Galerkin methods applied to some model equations for non-linear dispersive waves 79−53985
GARNET, graphic analysis of resources by numerical evaluation techniques 78−20525
gas dynamics, numerical investigation by net-characteristic method 80−19420
gas dynamics, partial ionis. computation method 78−38447
gas flow in catalytic convertor, numerical soln. 78−67281
gas flows, selfgravitating, thermodynamic processes and radiation, numerical method 80−14848
gas model of rigid spheres, Boltzmann eqn., eigenvalues eigenfunctions of Hilbert operator 77−26250
Gauss' principle of least constraint, appl. to dynamical systems 77−17811
generator coordinate method 78−29731
geometrical optics teaching to engineers, matrix algebra methods 80−62415
geophysical inverse problems, resolution anal. for discrete systems 78−49153
geosphere transport model for WIPP site, radioactive waste repository 80−16854
geostationary satellites, methods for numerical integration of eqns. of motion 78−69659
global element method, appl. in discontinuous nuclear pot. calc. 79−3089
glow discharge, reaction oscills. freq. eqn. derivation, expt. and numerical calc. 77−1027
gravity theoretical formula, Taylor expansion for reference ellipsoid 79−100807
grid points condensation in process of solving and using high order schemes in numerical integration of viscous gas flows *(Russian)* 78−59363
groundwater two-dimensional unconfined saturated flow, boundary integral solns. 78−77291
gyroscopic structure synthesis, Rayleigh-Ritz approach 79−18695
Hartree-Fock wave function, numerical technique overcoming exchange blowup 80−9485
heat cond., cylindrical inverse transient, numerical soln. 77−6501
heat conduction in complex bodies 78−59263
heat conduction transient, two-dimens., crit. time step for finite element solns. 78−71260
heat exchanger fouling data analysis, for geothermal power plant appl., use of multivariate regression technique 79−52880
heat exchangers, approx. of dynamics of method of weighted residuals *(Japanese)* 78−67024
heat transfer, fast nonstationary processes, characteristic method calcs. 80−83796
heat transfer and evaporation from cooled surfaces, nonlinear eqns. numerical soln. *(German)* 80−58893
heat transfer optimal control problem, finite element and conjugate grad. methods 80−19220
Heisenberg model, specific heat, high-temp. expansions, numerical investigation *(German)* 77−59420
Helmholtz equation eigenvalues calc., using simplified integral equation method 77−78964
Helmholtz equation for region with corners, boundary distribution soln. method 79−58532
Helmholtz equation for two dimens. polygonal regions, numerical soln. method 79−63005
Helmholtz homogeneous equation, numerical soln. methods *(German)* 78−90337
high temp., transport process soln. 80−19559
higher order panel method for general analysis and design appl. in subsonic flow 77−55022
higher-order monotonic convective difference schemes 77−13597
holographic numerical optical processor configurations 80−48194
holographic reconstruction, two dimens. Fourier transforms 78−1180
hybrid integral eqn. method, appl. to ship waves 79−32540
hybrid random choice method for viscous boundary layer 80−38461
hybrid-stress models for elastic-plastic analysis by the initial-stress approach 79−32288
hydrodynamic boundary layer for even symmetrical channels appl. *(Bulgarian)* 77−80131
hydrodynamic stability problems with time-depend. boundary conditions, numerical simulation methods, review 80−19411
hyperbolic partial differential equations linear system, numerical soln., boundary methods accuracy 77−67245
hyperbolic systems, high-order methods, dynamic problems 80−68033
hyperelastic compressible medium with cylindrical cavity, finite dynamic expansion under sudden press. 78−79213
hypersonic flow, nonequilibrium gas mixtures past blunt bodies, Navier-Stokes equation *(Russian)* 79−18909
hypersonic viscous shock-layer equation, method for successive approximations for integration *(Russian)* 78−59421
imaging system shading effects and countermeasures 78−78922
impact of cylindrical shell on surface of compressible fluid *(Russian)* 80−87746
impact of spherical shell on surface of compressible fluid *(Russian)* 80−87747
implicit marching method, highly viscous chemical laser nozzles flow, two dimens. Navier Stokes eqns. 78−63506
impulse load effects, EPIC-3 code anal. 80−19293
incompressible finite elasticity, method for numerical soln. of problems *(French)* 80−42062
incompressible viscous flow, numerical methods *(Chinese)* 77−82395
incremental formulation in nonlinear mechanics, large strain elasto-plasticity 78−77692
inductor-screen-ingot systems, EM fields calcs. *(Russian)* 77−46671
inhomogeneous planar waveguide, propag. charact. of guided waves, numerical method 79−76554

numerical methods continued
integral coarse mesh diffusion method appl. to reactor transients with feedback 79−85585
integral eqn. method, anal. of stress conc. problems in cylindrical shells 77−75806
integral eqn. method for potential problems with source function not located on boundary 78−24643
integral eqn. methods, calc. of elastic and viscoplastic stress conc. *(French)* 77−72194
integral eqns. solution, book 78−41143
integral equation approach to numerical soln. of axisymm. elasticity problems 77−22421
integral equations with kernels containing poles, interpolative technique, numerical solns. 78−41141
integral method for plane stress and strain problems 77−68433
integral soln. techniques, appl. to 3-D acoustic radiation problems 77−68293
integral transform numerical inversion, appl. 77−78967
integration by SNIFF self-adaptive algorithm 77−67261
integration formulas, asymptotic behaviour of coeffs. *(French)* 77−37742
integration of Cartesian eqns. of motion, holonomic constraints 77−27804
integration of harmonic motion differential eqns., programmable calculator, teaching appl. 78−86083
integration over solid angle and vol. of Brillouin zone, any crystal symm. 77−27843
internal friction measurement in solid metal via inverted torsion pendulum *(French)* 79−18847
internal stresses, calc. with integration methods, X-ray stress meas. 79−32415
invariant submersions, soln. of axisymmetric problem of elasticity of theory *(Ukrainian)* 79−97200
inviscid barotropic vorticity eqn., soln. by finite difference, finite element and pseudospectral method 80−43687
ionisation in rapidly changing plasma, numerical integration of ionisation rate eqns. 78−55734
IR radiation spectral absorptance and transmittance, accurate modelling technique 78−91062
Ising square frustration model, numerical study of ground state correl. 80−34638
isotropic thin shells with circular hole, stress state, numerical investigation 80−48586
jet flow, under gravity integral equation method of soln. 80−59093
jets, confined, flow pattern and turbulence quantities prediction *(Japanese)* 79−18923
Klein-Gordon nonlinear equation, numerical soln. 78−89352
Korteweg-de Vries equation, numerical methods of solution, difference and transform schemes, accuracy 80−46833
Kramers-Kronig transforms, Fourier method numerical soln. by computer 78−2825
Lagrangian method for transonic flow Euler eqns. 80−38435
Lagrangian-Eulerian method for anal. of slug impact and coolant spillage in fast breeder reactor 79−30993
lake vertical temp. profile determ. by one-dimensional heat transfer eqn. soln. 78−77290
lakes, unsteady flow, numerical model validation 80−72559
laminar and turbulent flow, conf., Swansea, Wales, July 1978 79−1155
laminar flow in vertical tubes, free convection effects 78−5722
laminar incompressible boundary layer eqns. finite element soln. 78−79304
Lanczos method, method of moments, tri-diagonalisation of a matrix 78−58240
Laplace's equation, numerical soln. by integral eqn. method without Green's function 79−12564
large field problem soln. by extended Kinzel sectioning method 77−27228
large-area solar cell electrical characterisation accuracy 79−96454
lifting surface integral eqn. solution *(Russian)* 78−73836
light beam focusing optimisation, in moving nonlinear media, using gradient method 80−106578
linear elliptic and parabolic partial differential eqns. with boundary singularities, numerical soln. 78−41142
linear equations of thermoanemometry, numerical method of soln. 77−84352
linear response theory and area preserving mappings, review 78−62174
liquid crystal, two dimensional model, structure, transition to smectic and cryst. phases 77−7857
liquid leveling, numerical soln. 77−14974
LMFBR, neutron streaming through control rod followers, diffusion coeff. by numerical integration 80−13636
long-wave hologram point-object reconstructed image field intensity distrb. 79−55093
LPE layer growth from undercooled melts, numerical model 80−6665
Lubatto-Jacobi numerical integration rule, for generalised stress intensity factors, numerical eval. using 79−3921
lumped parameter finite difference algorithm, for inverse heat cond. ablation problems 78−94508
lung numerical modelling, human 78−80911
mag. trap, axially symmetric, finite $\beta(\ll 1)$, collisionless plasma *(Russian)* 77−3971
magnetic domain wall motion, one-dimens., static in-plane field-biased, dynamic charcts. *(Japanese)* 79−73767
magnetic field computation, by Schwarz-Christoffel mapping function numerical integration *(German)* 79−89826
magnetic fields, inhomogeneous medium, numerical calc. 79−72454
magnetostatic equations, axially symmetrical, solution by difference methods 77−50585
matrix congruent numbers note 78−54147
matrix exponential method, dynamic response via digital simulation 77−72149
matrix function approximate factorisation algorithm 80−68022
matrix Riccati eqn., quasi-linearisation, iterative approx. 78−57871
matrix Riccati equation, numerical soln. method *(Russian)* 79−25822
matrix-scaling technique, transient struct. response anal. 77−72148
maximum entropy method confidence limits 80−22284
mechanical vibration problems, two dimensional *(French)* 78−59337
Mellin transform expressed as two sided Laplace transform, numerical inversion 78−77694
melt, temp. field calc. by numerical implicit method 80−44342
membrane dynamic equation solving, practical algorithm 78−77038

numerical methods continued
metals, metallic deformation, improved boundary-integral eqn. calc. method 80−28437
method of generalised coords. in fluid mechanics 77−75877
method of moments, approx. solns. of random linear integral eqns. 77−64934
method of singularities, appl. to boundary-value problems 77−67254
MHD equations, nonzero div B, effect on numerical soln. 80−69939
MHD laminar flow, longitudinal dynamic effects determination, appl. *(Rumanian)* 80−64792
micropolar elasticity, 3-D finite element approach to static and dynamic problems 78−34014
microtron electromagnet optimum shape, computer numerical anal. 77−18718
mixed explicit-implicit splitting method for compressible Navier-Stokes equations 77−58715
model conduction problem, MacCormacks time-splitting technique stability anal. 79−55361
models of tide and surge propag. as aid to navigation 79−12121
molecular electron elastic scatt., vibronic effects 78−9249
molecular wavefunctions, Schrodinger eqn. random walk soln., electron spin effects 77−18780
molecule, electronic struct., numeric MCSCF method, unicentre expansion 79−45623
molecule-molecule reaction, ergodic energy transfer, vibr. quantisation effects 78−85137
MOS structure concentration profile numerical evaluation *(Slovak)* 80−65690
moving grids construction methods for fluid dynamics problems with strong deforms. 77−54961
multi-dimensional solidification, dominated by thermal cond., similarity calc. method 80−38243
multicompartment system simulation 80−55976
multidimensional reactor dynamics equation, fast factorization and exponential transform. procedures 78−17303
multidimensional singular integral eqns., numerical methods, anal. of elastic solids 77−17818
multilayer cylindrical parts, residual stresses determ. 80−96206
natural three-dimensional convection, strongly implicit algorithms 80−33422
Navier-Stokes eqn., nonstationary, soln., numerical stability of ADI scheme *(French)* 78−87325
Navier-Stokes eqns., 2D and 3D viscous flows 77−89082
Navier-Stokes eqns., rotational flow avoidance, solns. *(German)* 80−59057
Navier-Stokes eqns., soln. by efficient numerical method 78−9619
Navier-Stokes eqns. for rotating flow above rotating disc, non-unique solns. 77−47020
Navier-Stokes equation soln. method, finite element anal., 2D unsteady viscous flow 77−89088
Navier-Stokes equations, implicit-explicit soln. method 78−83354
Navier-Stokes equations, two dimensional, numerical soln. methods *(Russian)* 80−101718
Navier-Stokes equations for low viscosity flow, hydrid vortex-ADI soln. 79−68718
Navier-Stokes equations for turbulent and transition flows, num. soln. methods 77−54979
Navier-Stokes equations solution method for viscous effects in transonic flow 77−55023
neutron transport theory, recent work at LASL 78−13195
neutron transport theory, spatial approximation methods for the S_N equations in x, y geometry 80−47525
neutron transport theory code, automated approach to quantitative error anal. 77−67788
Newman's numerical technique for boundary value problem solns. 79−40352
Newton's method, appl. to renal network flows 77−16945
Newton's method, nerve impulse local existence 78−96045
Newton method with mesh refinements for nonlinear two-point boundary value problem 78−36809
Newton-Raphson algorithm, soln. of Hartree-Fock eqn. *(Russian)* 77−49584
Newton-Raphson method, appl. to soln. for azimuth of nearly antipodal geodesic 77−60335
noise, combined structural-acoustic system, modal synthesis, LF props. 77−88980
non-Newtonian pipe flow, viscosity-shear rate depend., computer method 77−15066
nonaxisymmetric flow problems, computational technique 79−55419
nondissipative medium, boundary problem soln. with surface discontinuity *(Russian)* 80−101716
nonlinear autoregressive processes 78−24642
nonlinear flexural oscillations of orthotropic shallow spherical shells 79−3939
nonlinear instabilities, filtering in fluid dynamic eqns. 79−41667
nonlinear medium, mag. field calc. by differential grid method *(Ukrainian)* 80−4555
nonlinear shell theory, numerical method *(Russian)* 78−34006
nonmetrical method for paired comparisons *(Japanese)* 78−77833
nonNewtonian duct flow, wall heat transfer in entrance region 79−4049
Norsett methods for implicit time integration of partial differential eqns. 77−82376
nuclear facility, optimisation of radiation detector position and number 78−55043
nuclear reactor, LMFBR, HCDA, structural response calcs., methods, codes development 77−3126
nuclear reactor dynamic structural anal., comparative evaluation 77−3091
nuclear reactor dynamics, numerical integration using real integrating factors 80−68730
nuclear reactor thermal channel gap heat transfer calc. 78−21630
numerical anal. in applied engineering science (conf. May 1977) 77−67249
numerical expts. relevant to the drought in England and Wales, 1975-6 period 78−88889
numerical generation of boundary fitted curvilinear coord. systems on fields containing 2-D bodies, TOMCAT code 77−64941
numerical simulation of fluid motion, conf., Melbourne, Australia (1976) 79−9116
numerical solution of a class of integral equations arising in two-dimensional aerodynamics 78−62086

numerical methods continued
Numerov for Schrodinger equation roundoff error anal. 79−2643
Numerov scheme for Schrodinger eqn. soln. 80−52046
ocean waves generation, propagation and dissipation spectral simulation model 80−31060
oceanographic circulation partial differential equatns. solution 80−21864
operator eqns., solution by numerical means 79−84936
optical fibre mode-coupling phenomena anal. using matrix method, accuracy 80−23803
optical processing systems, seminar, Huntsville, USA (May 1979) 80−46732
optical temp. meas. evaluation by computer 78−91150
optical waveguide transmission parameters, numerical computation 77−42605
optimal control, problems with constraints, transformation methods of an exponential function type 78−12541
optimal control of 1-D linear distributed parameter systems with cost functionals 78−59257
optimal numerical filters fitted for noise damping, atm. circulation simulation appl. 78−92997
orthogonal collocation method, appl. to heat conduction problems 78−33990
orthogonal function expansion technique for electron transport Monte Carlo calcs. 77−26248
oscillators, nonlinear stochastic, triangular wave, optimally controlled, Weiner process and Poisson process, numerical studies 80−52128
oscillators with nonlinear restoring forces, first passage failure probability calc. 78−42562
over-wing-blowing configurations, aerodynamic characts. determ. 78−5774
panel method, improved high-order, for linearised supersonic flow 80−6082
parabolic method for soln. of compressible Navier-Stokes eqns. 77−58716
parabolic partial differential equatn. TEDDY2 program package 79−2613
parallel jets systems, aerodynamics calc. *(Bulgarian)* 80−28543
parametric acoustic source, numerical method for nearfield calc. 78−63221
partial and ordinary differential eqns. solns. new techniques reduce work involved 79−75326
periodic Green's function, solution electric potential problems, appl. 77−82370
perturbative numerical methods, local and accumulated truncation methods 80−62536
perturbed primitive variables method for simulation of laminar separated flow between periodically varied walls 77−54971
phase-integral calc. of quantal matrix elements, numerical method 77−49622
photoelectron spectra of cryst. solids, numerical integration within linear analytic approx. 78−60545
photogrammetry, orientation, triangulation and digitisation 78−36312
plane elastostatic boundary value problems, integral operators, eigenvalue num. calc. 80−36848
plasma, diagnostics, axial symmetry, error estimate of optical methods 77−84500
plasma, submillimetre diagnostics, active, of Ar arc, data numerical anal. 80−48979
plasma, theta-pinch implosion, numerical models including classical and anomalous transport 77−24139
plasma hybrid simulations of quasineutral phenomena 78−67403
plasma MHD, toroidal axisymmetric config., vacuum potential energy change, spectral codes 80−87869
plastic flow pattern smoothing 80−7625
plate, simply supported, shear and bending moments by hydrodynamic analogy, results 79−64524
plates, thin, converged stress solns. by extended field method 80−38306
point-like nuclear reactor neutron kinetics solns. using numerical method *(Italian)* 78−58324
Poiseuille flow, compound matrix method 80−57096
Poisson's equation, linear and nonlinear numerical solution including spatially variable dielectric const. 80−6825
Poisson eqn. soln. by successive overrelaxation technique, optimisation hazard 78−81813
Poisson equation solver for potential and press. fields on staggered grid with obstacles 77−54959
Poisson summation formula, generalisations 80−4565
polyatomic molecule, dissoc., natural collision coords. 78−44373
polymer chain, elasticity for different vibr. modes, algorithm 78−66696
polymer rod, fluid-permeable, longit. stability during creep 79−57066
polymers, linear and ring, intrinsic viscosities, perturbation calc. 79−55914
potential flow, approx. numerical solns. 78−79293
potential problem, numerical soln. by integral eqns. without Green's functions 77−26162
potential problems, numerical solution, integral equations without Green's function 78−20950
potential problems, two-dimens., numerical soln. by boundary integral eqn. method 79−58533
protostar formation, physical and numerical problems 77−29800
pseudospectral dispersion model, inter grid sources representation 79−12259
pulsar magnetosphere numerical modelling 77−29871
quadrature formula, integration of highly oscillatory functions 77−13593
quasilinear partial differential eqns. soln comparison 77−2523
radial coupled equation solution, fast numerical method, applic. to collision processes 77−14545
radial Schrodinger equation, numerical anal. technique 79−67191
radiation field of extended rectangular source, numerical integration 78−66424
radiative transfer in rectangular enclosures, six-flux model evaluation 80−1415
radiative transmission function, exponential-sum fitting 77−70995
radioactive waste migration, groundwater environment, hydrodynamic dispersion in transport models 80−17146
random choice method for gas dynamics problems soln. 77−55106
random choice soln. of nonlinear hyperbolic systems of conservation laws 77−7362
random vortex methods for two dimens. large Reynolds number flow, errors 78−42614

numerical methods continued
randomly rotating rigid body, computation of functionals over sample paths 77−74212
Rayleigh-Ritz method, appl. to clamped rectangular orthotropic plates, natural freqs. of vibr. upper and lower bounds 78−83284
Rayleigh-Ritz method for sedimentology partial differential eqns. soln. 78−92878
reactivity measurement by inverse kinetic method 79−63752
reactor shielding materials, Pb and steel, Γ leakage spectra, computer calcs. 78−58350
regenerative heat exchanger high temp. behaviour, numerical model 77−62140
response matrix eqns., properties 77−67795
restricted withdrawal of vertical cylinders from quiescent liquids, numerical treatment 77−72756
retina of Limulus, spatially synchronised oscillatory response theory 78−73158
Riccati method for difficult eigenvalue problems 77−64937
Riccati transforms., eigenfunctions of linear differential eqns. with separated boundary conditions 77−64936
RISM equation, soln. for diat. symmetric mols. 79−90508
Ritz-Galerkin method appl. to shells of revolution *(Russian)* 77−80062
river/atmosphere time dependent, single dimensional heat exchange, appl. *(Bulgarian)* 78−57221
Roberts, min. degree algorithm appl. 78−89311
rod, expanding, conductive heat transfer computation, fast numerical technique 78−75029
rotating polytropes, hydrostatic equilibria 79−80300
rotational flow, steady and unsteady, fluid in finite cylindrical container 80−14708
rotational transonic flow and inviscid potential computation by quasi-natural numerical methods 79−64666
Runge-Kutta generalised method for first order differential eqns. *(German)* 77−22400
Schrodinger eqn., time depend., explicit integration method, comment 79−72224
Schrodinger eqn. exponential-fitting methods 78−49694
Schrodinger eqn. for one-dimens. harmonic oscillator 77−71230
Schrodinger eqn. with double-minimum potential, numerical integration 78−58573
Schrodinger equation, applications of perturbation theory to numerical integration methods 80−12926
Schrodinger equation, one-dimensional eigenvalue problem, bound state solns. 78−20992
screen acoustic impedance evaluation 78−13831
seismic dispersion curves, methods of computing partial derivatives 77−37149
sensitivity theory for general systems of nonlinear equations 80−86954
separated flows, upwind and central difference schemes 80−28539
separated-sector cyclotron, mag. field meas. processing methods 79−68037
series truncation for second order nonlinear differential equation 79−4019
shakedown analysis, circular plates subjected to press. and temp. cycles 77−3749
shallow water circulation studies in Brazil, numerical model 78−77286
shear stress distribution caused by transverse force, rails of DIN 15087E *(German)* 79−61647
shell, thin walled axisymmetric, elastic deformation, nonlinear numerical anal. method *(French)* 79−41584
shell enclosures, temp. distrib. calcs. under thermal radiation, numerical calcs. 80−38241
shells of revolution, plastic, limit anal., lower bound numerical method 78−63337
shock wave diffraction on plane with semicircular cylindrical roughness, numerical integration *(Ukrainian)* 80−22201
single-step, anal. by approx. of exponential function 80−94950
singularity computations 77−67251
slotted boundary machine field soln., conformal transformation and integral methods 79−41272
slurry flow, confined, mean vel. field skewness computation 78−63481
solid particle systems, high Reynolds numbers, mass transfer, Karman-Pohlhausen method 80−79378
soliton perturbations and nonlinear focusing, anal. method for fluid dynamics 79−75369
sonic boom, nonlinear propag., including asymm. effects, numerical soln. program 77−72326
space truss analysis in post-buckling range in dual load method 80−38298
spectral coefficient error numerical calc. 79−75571
speech intelligibility in auditorium, computer evaluation *(French)* 79−37095
spherical bubble growth in uniformly ultraheated liquid 78−1550
spherical triangles, numerically stable computation *(German)* 78−88793
spherical waves focusing and reflection in gas *(Russian)* 77−7501
spherical X-ray wave, dynamic diffr. theory, numerical results 80−38867
spinning shells, Magnus characts., empirical calc. method 78−26072
spinning yawed axisymmetric body, three-dimens. flow 80−38422
spinor Bethe Salpeter and Goldstein eqns., fermion-boson coupling, numerical soln. 78−86400
split operator finite difference anal. of laminar flame 78−51252
splitting schemes for numerical soln. of two-dimens. Vlasov eqn. 78−67310
stability of explicit-implicit mesh partitions in time integration 79−1101
static field problems, numerical soln. algorithms 80−95757
statically stressed fluid, transition to turbulence, inverted bifurcation 77−7370
stationary satellite eqns. of motion integrating methods *(Japanese)* 78−85837
statistical particle-in-cell method for num. investig. of rarefied gas flows 77−55043
steady-state laminar flow in turbulence amplifier, integration *(Bulgarian)* 80−106779
Stefan problem, one-dimens., modified variable time step method 80−102960
stellar convection phenomena numerical simulations 77−29789
stellarator, MHD equilibrium and stability of plasma in toroidal geometry, 3-D computer code 80−70041
stenosed tube, numerical solns. of Navier Stokes problems 80−16975
Stirling cycle analysis, accuracy evaluation 79−48170
numerical methods continued
Stokes phenomenon associated with differential eqns., numerical investigation 77−41464
Stokes problem, second-order difference scheme 80−90678
Stokes stream function, direct soln. method 80−64
stress anal., experimental numerical hybrid technique 79−32419
stress anal. in 3-D, numerical-experimental hybrid technique 78−22265
stress-strain state of rotating shell for random loading, net-point and orthogonal die methods *(Russian)* 80−90676
string vibrations numerical study by physical discretisation 78−45480
structure frequency analysis by integrated force method 79−18692
subsonic aircraft, aerodynamic forces for aeroelastic anal., doublet-lattice method *(Italian)* 79−41598
subsonic flow, diverging, stability aspects, time-dependent method 80−74906
subsurface nuclear waste disposal, groundwater modelling 80−16852
summed progressing wave formalism for initial value problem calcs. 80−92039
supersonic flow, nonstationary separation of laminar boundary layer, numerical method *(Russian)* 79−14425
supersonic laminar viscous flow, partial differential eqns., separation 80−24062
supersonic viscous flows, interactive numerical calc. procedure 77−31326
surface area calc. by gas adsorption, progammable calculator appl. 78 15706
surface integral calc. in numerical investigation of 3D fields *(Russian)* 79−64143
surface integral method, appl. to elastic strip with periodically spaced holes 77−50911
surface integration, expressions for element base area unified with integration formulas 79−53967
surface scatt., electric field integral eqn. formulation 77−38784
thermal conduction, nonstationary, in composite bodies, numerical simulation *(Russian)* 80−92016
thermal problems, nonhomogeneous, and Stefan single-phase problem in arbitrary domains 80−79102
thermal problems, one-dimens., with phase change, efficient numerical technique 78−59270
thermocouple measurements, pulsed, computation method *(German)* 79−21749
Thomas-Fermi-Dirac eqn., diat . systems, accurate numerical soln. 77−50358
three dimensional electrostatic fields calculation using multipoles *(German)* 77−75358
three dimensional laminar flow in curved pipes, Navier-Stokes eqn. numerical soln. technique 79−10611
three-dimensional magnetostatic problem soln. using scalar potentials 79−41271
Tikhonov regularizing algorithm for nonlinear inverse heat cond. problem 80−23862
time independent ionisation structure, radiation heated plasma, numerical methods 79−7470
tomography, thorax 3D reconstruction, ultra-high speed, parallel processing computers appl. 79−48338
toroidal diffuse equilib. config., pinches, Tokamak 78−30471
toroidal pinch equil. config., nonlinear operator eqn., optimisation soln. 78−59649
torsion, axially symmetric twisted linear elastic body, numerical method for soln. 77−75802
torsion problem for elastic cylinder with holes, integral eqn. method soln. 80−36849
transcendental equations, for Fraunhofer diffraction, numerical soln. method 77−33750
transient coaxial entry tube flows, numerical program 77−15117
transient heat conduction, soln. by ADI methods in r-θ geometry 79−14203
transient laser radiation, stochastic process near an instability point, numerical solution 80−23658
transient natural convection in rectangular enclosures, numerical anal. 79−77111
transient thermal stress problems, numerical anal. method 79−72810
transmission line modelling of diffusion 79−26011
transonic axisymmetric pot. flow around inlets, Cartesian mesh soln. 77−72323
transonic flow, far-field matching method 78−26146
transonic flow numerical calculation methods and problems, review 77−58723
transonic flow past swept wing, solutn. by finite volume method 80−19431
transonic unsteady flow anal., mixed kernel function approach 78−71360
transport, problems, estimation of moments 77−71281
transverse isotropic inelastic work hardening constitutive model, numerical implementation 78−42547
triangular finite elements and numerical integration 78−33
truncation method, stability of solns. in electrodynamics *(Ukrainian)* 80−31532
turbulence model development expts. with numerical simulations 77−27551
turbulent boundary layer on a moving surface, integral and numerical methods 78−63421
turbulent diffusion, nonlinear integrodifferential eqn., numerical soln. 78−38306
turbulent flow, press. fluctuation spectrum, elastic boundary compliance effect 78−63422
turbulent flow, similar solutions, computation method 77−89102
turbulent friction factor, calc. by TI-57, binary-search method 80−83788
two-dimensional gas flow model, comparison of two methods of computation *(Russian)* 78−59413
two-dimensional rotational flow, large Reynolds no., numerical calc., discrete vortices with random walk 77−31312
two-dimensional wave propagation, method of characteristics 78−73863
two-layer shallow water flow, internal and surface waves, numerical anal. 80−19472
two-phase flows, particle interaction, obs. and calc. 79−72875
two-phase Stefan problem, numerical anal. by variational inequalities 79−82315
two-point boundary value problems, accurate method 79−88795
ultrarelativistic beam anlaysis assuming classical ideal-gas statistics, algorithm 78−63003
undergraduate teaching field problems, computer programs 77−10804

numerical methods continued
unhomogeneous bars, normal mode response, stress anal. by boundary operator method 80−19239
unsteady airloads on oscill. wings and bodies 78−71354
unsteady squeezing of viscous fluid from tube 79−90296
US Doppler signal time-domain frequency analyser, numerical assessment 79−92314
vapour pressure critical exponent optimal determ. 79−51271
vertical jet under gravity, Riemann-Hilbert problem, numerical soln. 80−36858
vibrating plates, reposing on springs, numerical solutions and eigenvalues *(French)* 78−79245
vibrating system solution, linear, damped, of finite degrees of freedom 78−24656
vibration problems, Zienkiewicz four-time-level scheme for numerical integration 78−1594
vibration problems of continuous systems, discrete models 77−89057
vibrational analysis, of thin cylindrical shell 80−5969
viscoelastic rod analysis, using Boltzmann-Volterre memory theory, second-order approximate solution *(Russian)* 78−87278
viscous flow, non-Navier Stokes computations, parabolic and thin layer approx. 80−48666
viscous flow over flat plate, comput. method developments 77−54970
Vlasov eqn., splitting scheme for numerical soln. 77−68745
Vlasov eqn., two-dimens., multistep technique for numerical soln. 77−27648
Vlasov eqn. for mag. plasma, numerical integration 77−68744
Vlasov equation, two dimens., numerical soln., multistep technique 78−1795
vortex sheet roll up, appl. of Cloud in Cell technique 79−64670
vorticity eqn., three-dimensions, conservative form, numerical soln. 77−55011
water, boundary conditions for numerical simulation, book contrib. 79−60247
water wave diffr. and radn., numerical methods, book contrib. 78−59412
waveguide theory, cylindrical inhomogeneity in homogeneous medium of infinite extent, guided EM field computation 80−14274
wavelength calculation, selected coord. method using Chebyshev integration formulae, tristimulus values *(German)* 77−82586
weather, numerical prediction review 78−69393
weather forecasting, atmospheric prediction models, computing and numerical methods 80−77095
weather forecasting, determ. of boundary layer orography and turbulence-induced vertical currents 78−96278
weighted-residual for discrete ordinate neutron transport partial differential equations soln. 79−6725
wind tunnel, wall interference, two-dimens., correction method, examples *(French)* 78−67293
wind tunnel testing, conference, Rhode-St-Genese (1976) 77−27634
wind-driven water waves, numerical model calcs. 77−922
work hardening-recovery type constitutive eqns., numerical integration, improved method 78−6949
XPS Mg Kα radiation excited, X-ray satellite line removal 77−77343
yrast-band of odd nuclei 80−22651
Zienkienicz three and four time level schemes, appl. to integration of parabolic eqns. 79−2609
np scatt., two-channel Jost matrix construction on second-order S-matrix *(Russian)* 79−9294
Θ_3^4 quantum field theory, numerical methods, anharmonic oscillator approx. 80−52390
Al billet, hot extrusion, nonsteady state temp. distrib., numerical method 80−60886
Ar laminar stream, electric arc gas heater, numerical calc. of arc parameters *(Russian)* 77−58911
H+positron, S-wave scatt., lowest reson. calc. 78−37743
H_2(HD), rot. levels and consts., nonadiabatic corrections 77−18906
He, plasma, afterglow and inertial expansion, numerical soln. of relax. kinetics 77−27769
He plasma-electron beam, electron cyclotron instability, nonlinear time development, k-spectrum 77−76210
^{3}He, superfluid B phase, spin wave breathers, double sine-Gordon equations 80−15329
In, liquid, diffusion coeff. determ. of P, mathematical model, numerical method 79−23754
LiH, numerical calc. of one-electron props. from SCF-Xα-SW calcs. 77−6688
NaCl, adsorption of Ar and Kr, energy distrib. using numerical algorithm HILDA 77−55443

numerical methods, convergence *see convergence of numerical methods*

nuvistors
No entries

Nyquist criterion
see also Nyquist diagrams
optical channel conditioning against intersymbol interference and timing errors *(Italian)* 77−23622
plasma cyclotron instability with anisotropic kinetic temp., Nyquist diagrams *(Chinese)* 80−28627
stability anal. by finite element method 78−29543

Nyquist diagrams
see also Nyquist criterion
nonconservative system resonance, modal analysis 78−42557
nonlinear materials, dynamic testing using harmonic excitation, jump phenomena 78−51141
room impulse response on speech signals 79−86294

Nyquist noise *see thermal noise*

observability
biological compartmental systems, multi-input and multi-output, controllability, observability and structural identifiability 78−76978
biological compartmental systems analysis, computer program 77−40625
cancer cell cycle kinetics, flow microfluorometric DNA distribution representation 77−21669
marine boundary layer microwave sensing, estimation techniques 79−74993

occultations
5AO 158687 by Uranus ring system struct. from photoelec. obs. 80−77348
13 Egeria, occultation of SAO 92603, photoelectric obs. rel. to minor planet possible satellite 80−46460
1980, British Astronomical Association Handbook 79−96893
Abell 401 galaxy cluster, lunar occultation rel. to diffuse X-ray emission model 79−25736
Abell cluster, lunar occultation obs. at 327 MHz, survey 80−73052
AGK3 +0°1022 by Juno, obs. 80−26773
AGK+19°0599 65 Cybele, 1979 October 18, obs. using photoelectric photometer *(Chinese)* 80−105172
AO 0235+164, BL Lacertae object, lunar occultation obs. rel. to radio halo struct. 78−4386
asteroids, dates for occultations during 1978 78−20718
atmosphere occultation meas. using monoaxial controlled solar pointer *(Japanese)* 78−32312
BD−15° 3969 by Uranus rings (1977 December 23), obs. 78−89118
Be stars, emission shell diameter meas. possibility by lunar occultation method 80−56839
bright galaxies, radio obs. of lunar occultations, spectra and struct. 79−9005
4C 03.59, BL Lacertae object, lunar occultation obs. rel. to radio halo struct. 78−4386
3C radiosources, lunar occultation obs. at 327 MHz 77−45588
β Capricorni, 1977 October 20 lunar occultation results 79−44523
β Capricorni, triple star, fundamental parameters from occultation astrometry and spectroscopy 79−40216
β Centauri, by Earth, satellite obs., atm. O_3 density meas. 77−53259
β Centauri, by Earth's atmosphere, O_3 and Cl meas. by OAO 3 77−9580
Ceres, occultations of stars during 1979/1980 apparition, predictions 79−62785
γ Ceti by 6 Hebe, obs. rel. to asteroid dimensions 79−92694
γ Ceti by asteroid 6 Hebe, 1977, Mar. 77−33407
Charon (1978 P 1), occultation on 1980 April 6 probable 80−67651
Charon (1978 P 1), probable stellar occultation, 1980 April 6, min. dia. 80−62071
Comet Kohler (1977m), occultation of 70 Ophiuchi, prediction 78−7930
composite spectrum stars susceptible to lunar occultation, identification list of 68 stars 80−26908
Crab Nebula, by Moon, 1974, Sept., 180 and 1646 MHz obs. 77−26043
Crab Nebula, by Moon, struct. determ. at 327 MHz 78−12339
Crab Nebula, by solar corona, Faraday rot. obs., coronal electron density and mag. fields meas. 77−45593
Crab Nebula, by solar corona, obs. of linear polarisation at 7.2 cm 77−60837
Crab Nebula, lunar occultation obs. at 114 and 26.3 MHz, small-scale struct. 80−46627
Crab Nebula, lunar occultation obs. at decametre wavelengths 80−62248
Crab nebula, polarised radioemission occultation by solar corona during weak solar activity *(Russian)* 78−77527
Crab Nebula X-ray source by Moon, balloon obs. *(Japanese)* 77−82319
Crab pulsar, by Moon, pulsed X-ray emission obs. 78−8032
65 Cybele, occultation of AGK3+19°599, 1979 October 17, obs. 80−31237
Earth, by Moon, determ. of terrestrial kilometric radiation spatial struct. 77−25873
15 Eunomia, close approaches to SAO stars, occultation prediction accuracy 79−30003
15 Eunomia, occultation of ζ Cancri on 1978 January 19, further predictions 78−20714
Galilean satellites mutual occultations, ephemerides correction rel. to Jupiter oblateness 77−29715
Ganymede, stellar occultation obs. by Voyager 1 rel. to exospheric atmosphere 80−26792
ε Geminorum, by Mars, 1976, April 8, atm. temp. var. *(French)* 77−53449
ε Geminorum, by Mars, evidence for atm. tides 77−37550
ε Geminorum, by Mars, evidence for waves or turbulence inplanetary atm. 79−53748
ε Geminorum, by Mars, obs. at Princeton 78−57482
ε Geminorum, by Mars, photometric obs. 77−91527
ε Geminorum, by Mars, planetary atm. temp. struct. determ. 77−87306
ε Geminorum, by Mars, planetary upper atm. temp. struct. determ. 79−53749
ε Geminorum, by Mars, struct. and extinction of Martian upper atm. 78−7898
ε Geminorum, by Mars (1976 April 8), preliminary results 77−37545
ε Geminorum, by Mars on 1976, April 8th, theory of light curve 77−53567
ε Geminorum by Mars, atmospheric oblateness determ. for planet 77−5483
ε Geminorum by Mars, McDonald Observatory obs. 77−60702
ε Geminorum by Mars, obs. from C.E. Kenneth Mees Observatory 78−53853
ε Geminorum by Mars, planetary atmosphere temp. profile determ. 79−2508
grazing occultations of α Tauri during 1979 visible from Scandinavia *(Swedish)* 78−69656
GX9+1, by Moon, position determ. 77−45612
6 Hebe, occultation of γ Ceti AB on 1977 March 5, predictions 77−29702
6 Hebe, size from 1977 March 5 γ Ceti A occultation obs. 78−53856
Helios probes by Sun, deflection of polarized microwave radiation 78−53818
532 Herculina, occultation of SAO 120774, discovery of 1978 (532) 1 possible satellite 78−69734
532 Herculina, satellite detect from occultation obs. 80−67629
Hyades, lunar occultations, 1978 September 22 reappearance events 79−40185
Iapetus, radius from 1974 March 30 lunar occultation 78−36505
Juno, occultation of AGK3 +0°1022 re-analyzed 80−41757
Jupiter, satellites, diameters from lunar occultation meas. 78−45272
Jupiter's satellites, mutual phenomena (1973 Sept.-1974 Jan.) 79−40129
Jupiter inner satellites, mutual eclipses and occultations in 1979, ephemerides 78−53866
Kepler's supernova remnant, by Moon, struct. determ. at 327 MHz 78−12339
late-type stars, angular diameters from lunar occultations 79−44475
late-type stars, by Moon, ang. dias. determ. 77−74048
υ Leonis (SAO 138298), angular diameter from lunar occultation obs. 78−45332
π Leonis by Moon, angular diam. obs. 77−33493
lunar, appl. of deconvolutation method 80−105174
lunar, comparison of profiles of Watts and Weimer *(French)* 77−41330

occultations continued
lunar occulation events, 1974 to 1977, photoelectric obs. summary 79−88642
lunar occultation of Venus 80−67605
lunar occultation technique appl., limiting ang. resolution calc. 77−87272
lunar occultations, obs. at Sydney Observatory during (1974-1976) 78−69658
lunar occultations, photoelec. obs., stellar disc brightness distrib. determ. 79−35146
lunar occultations, photoelec. obs. 79−5819
lunar occultations, photoelectric obs. at Dominion Astrophysical Observatory (DAO) 79−75198
lunar occultations, photoelectric obs. at McDonald Observatory 77−2331
lunar occultations, reaction times in obs. *(French)* 79−88607
lunar occultations during 1943-74, anal., rel. to Brown's theory, FK4 right ascension system and Watt's charts corrections 79−48696
lunar occultations from University of Illinois Prairie Observatory (1977-1978) 80−105148
lunar occultations of Hyades, photoelec. obs. 80−72921
lunar occultations of OTL radio sources at 327 MHz, position and struct. determ. 80−73060
lunar occultations of OTL radio sources at 327 MHz, position and struct. 80−73061
lunar occultations of OTL radiosources, position and struct. determ. from 327 MHz obs. 80−73062
lunar occultations of point-like X-ray sources, anal. for source positions 79−88567
lunar occultations of stars, 1969-72, Sofia Observatory obs. 79−29979
lunar occultations of stars, diameter meas., photoelec. obs. 80−72920
lunar occultations of stars, double and multiple stars obs. 78−4079
lunar occultations of stars, stellar ang. diameters determ. 79−30054
lunar occultations of stars, summary of obs. 78−7982
lunar occultations scans, object shape retrieval from new algorithm 80−105149
Mariner 10 by Venus, pressure-temp. profile obs. 78−28563
Mariner 10 radio occultation by Venus, atmospheric profile statistical and computational uncertainties 79−96938
Mars, conjunctions with ε Cancri in Praesepe (1950-2000 period) 77−91460
Mars, radio occultation meas. of surface atmospheric pressure, Viking 1 lander verification 77−22129
18 Melpomene, occultation of SAO 114159; discovery of 1978 (18) 1 possible satellite 79−16870
18 Melpomene, occultation of SAO 114159, secondary extinction event obs. rel. to 1978 (18) 1, possible satellite 80−56749
18 Melpomene, occultation of SAO 114159 on 1978 Dec. 11, revision obs. 79−12423
9 Metis occultation of SAO 80950, Guianan obs. 80−31236
Moon, marginal zone, absolute elevations from stellar occultations 80−62047
Moon, Watts datum centre determ. rel. to lunar centre of mass 77−71020
Neptune, 1980 February 10, no occultation event, revised calcs. 80−26805
Neptune, appulses of 12th and 13th magnitude stars (early 1978) 78−16347
Neptune, stellar occultation obs. (1980 August 21) 80−109395
Neptune by Jupiter, 1613 January 4, prediction rel. to obs. by Galileo 80−105485
optical lunar occultation meas., statistically rigorous reduction 78−73650
χ^1 Orionis (SAO 077705), by Moon, ang. dia. meas. 78−20825
Pallas, 1978 May 29 occultation of SAO 85009, diameter determ. 79−44400
Pallas, occultation of SAO 120836, 1973 February 6, reliability of obs. 80−46460
photoelectric obs., diffraction, stellar diameters and double stars 78−7866
photoelectric observing, techniques and apparatus 78−4117
photometric data acquisition system, microprocessor control 77−49311
Pioneer 10 and 11 by Jupiter and Saturn, radio signals spectral broadening by planetary ionospheres 80−109391
Pioneer Venus occultation experiment, radio science data generation 80−67492
TX Piscium, disc brightness distrib. and envelope obs. from lunar occultation meas. 80−67725
PKS 2025−15, by Comet Kohoutek (1973 XII), vars. rel. to tail plasma irregularities 77−13285
planet diamter meas. by occultation obs., teaching expt. 78−12457
planetary atmosphere HF radio occultation meas., phase screen concept 80−56735
planetary atmosphere studies by occultations, wavelength depend. of turbulence effects on refr. angles 79−48697
planetary atmospheres, power spectra of phase and intensity fluctuations, turbulence effects 79−40104
planetary atmospheres, turbulence detect. from spacecraft radio signal occultation 80−94734
planetary atmospheres, turbulence effects on profiles from Doppler meas. of occultations 79−2498
planetary atmospheres, turbulence effects on profiles from intensity meas. of occultations 79−2499
planetary nebulae by Moon, radio continuum obs. and electron temps. 78−41027
planetary occultations, turbulence effects on radio propag. 78−85871
planetary occultations, wave optics of central spot 77−67053
planets, atmosphere exponential turbulence and light bending during oscillation 80−17513
planets, by eclipsed Moon, 100 BC to 3000 AD period 77−49319
planets, mutual occultations in AD 1557 to 2230 period 79−88611
Pluto, appulse on 1980 Qpril 6, no occultation from S.England 80−67650
Pluto, no occultation of star on 1980 April, 6 ephemeris 80−62070
PSR 0525+21 occulted by solar corona, Faraday rot. at 1720 MHz 80−46526
radio sources, use of lunar occultations as ang. struct. investigation technique 78−65712
radiosource angular struct. determ., lunar occultation technique 77−13249
radiosource occultation obs. and near-surface lunar plasma 80−8559
radiosources, by comet tails, refr., comet plasma density determ. 79−53773
occultations continued
S255, H II region, by Moon, CO emission small-scale struct. obs. 80−46637
AQ Sagittarii, C star, ang. dia. from lunar occultation meas. 80−22008
ξSagittarii, lunar grazing occultation, 1974, October 21 obs. 77−33368
ξ^2 Sagittarii by Moon, angular diam. obs. 77−33493
SAO 114159 by 18 Melpomene, photoelectric obs. 79−12420
SAO 158687, by Uranus, 1977 March 10, obs. at Tokyo Astron. Obs. 78−61716
SAO 158687, by Uranus, 1977 March 10, rings discovery 78−69743
SAO 158687, by Uranus, 1977 March 10 77−87322
SAO 158687, by Uranus, estimation of true external errors of Tokyo meridian circle obs. 78−28487
SAO 158687, by Uranus (1977 Mar. 10) 77−22044
SAO 158687, by Uranus and satellite belt 77−29718
SAO 158687, by Uranus rings, 1977 March 10, photoelec. obs. 79−30007
SAO 158687, by Uranus rings, 1977 March 10, photoelec. obs. and anal. *(Chinese)* 78−69657
SAO 158687, by Uranus rings 1978 April 10, rings, radii and widths calc. 79−8878
SAO 158687, by Uranus satellite rings 77−37568
SAO 158687, occultation by Uranus ring system, obs. at Perth and Mauritius 77−67068
SAO 158687 by Uranian rings (1977 March 10) 78−89117
SAO 158687 by Uranus, 1977, Mar. 77−33407
SAO 158687 by Uranus, obs. rel. to planet upper atmosphere temp. struct. 79−62791
SAO 158687 by Uranus, obs. rel. to Uranian upper atmosphere struct. 80−17547
SAO 159250 by 16 Psyche on 1978 Feb. 25, details 78−16332
SAO 206553 by 704 Interamnia on 1978 April 28, details 78−16332
SAO 75392 by 78 Diana, 1980 September 4, predicted central path revision 80−101547
SAO 85009, by Pallas, 1978 May 29, corrected prediction, photoelec. obs. 78−57430
SAO 85009, by Pallas on 1978, May 29, revised position 78−12080
SAO 85009, by Pallas on 1978 May 29, prediction 78−53861
SAO 97745, by 15 Eunomia, visibility track 78−12081
SAO 99401, by Pallas on 1977, July 8 77−53460
satellite solar occultation experiment, appl. to remote sensing of middle atmospheric aerosol 80−109269
satellites of Jupiter and Saturn, eclipses and occultations *(Swedish)* 79−92695
Saturn, astrometric results from 1974 lunar occultations of satellites 78−36506
Saturn, by Moon, normal reflectances of Rhea, Titan and Iapetus 78−85897
Saturn, upper neutral atm. and ionosphere, vertical struct., Pioneer 11 radius occultation obs. 80−82293
Saturn ring A profile from stellar occultations 79−35187
Saturn satellites, mutual eclipses and occultations in 1979-1980, ephemerides 78−53868
β Scorpii, by Jupiter and Io, de Sitter theory rel. to Jupiter oblateness 77−29715
β Scorpii, by Moon, magnitude estimates, for multiple star system 77−87472
β Scorpii, by Moon, magnitude estimates for multiple star system 77−87471
β Scorpii, by Moon, occultation astrometry 78−57583
β Scorpii by Jupiter, turbulent atmosphere obs. 77−37562
solar occultation method for stratospheric aerosol meas. 77−45090
space vehicles by turbulent planetary atmospheres, effects of inhomogeneous background on radiation propag. 78−69679
spacecraft deep radio occultations and evolute flashes, planetary atms. struct. determ. 79−53731
star by Earth, stratospheric balloon meas., ceiling altitude var. compensation *(French)* 78−11947
stars, by asteroids, satellites discovery 80−4286
stars, by Earth, spacecraft obs., tropopause height determ. 77−2280
stars, by Moon, new technique for photoelec. obs. by dark limb reappearances 78−4115
stars, by Neptune, predictions for 1978-80 period 78−40868
stars, by planetary atms., turbulence effects on refr. angles 78−61773
stars, by turbulent planetary atms., wave-optical theory 78−61772
stars, by Uranus' rings, existence of rings confirmation and radii calc. 78−53872
stars, by Uranus rings, 1977-80 period, S/N ratios 78−32392
stars, predictions for 1977 September and October *(French)* 77−87241
stars and planets, by Moon, obs. at Cracow in 1974-75 period 77−33363
stars by Moon, 1965-71 events recorded at Poltava *(Russian)* 78−4083
stars by Moon (1943 to 1971), catalogue 79−88606
stars by planets, effects of photon noise and initial conditions 78−28530
stars by rings of Uranus, 1977-1980, colours and magnitudes 78−16277
stars by rings of Uranus, predictions for (1977-1980) 78−16343
stars by turbulent planetary atmospheres, effects of inhomogeneous background on radiation propag. 78−69679
stationary occultations of extrasolar planets, direct imaging with space telescope 78−85858
stellar occultation by Charon (1978 P 1) light curve obs. and implications 80−94754
stellar occultation by minor planet satellites 80−94741
stellar occultation TV scanning, image freq. limitation *(French)* 79−58264
stellar occultations by 216 Kleopatra, 1980 October 10 and November 21, implications of photometric meas. of dia. and shape 80−94743
stellar occultations by turbulent atmospheres, heuristic scatt. model 77−37534
stellar systems, detection by lunar occultation method 79−44542
γ Tauri, ang. diameter determ. from lunar occultation obs. 80−62119
α and θ^1 Tauri, diameters from Hyades lunar occultations 79−75253
θ^1 Tauri, double star, lunar occultation obs. 79−67052
α Tauri (Aldebaran), angular diameter from lunar occultation 79−40185
α Tauri (Aldebaran), radius from 1978 Aug. 26 occultation fast photometry 79−67005
technique for stratosphere minor gases determ. *(Russian)* 79−25342
turbulence effects on atmospheric profiles derived from radio occultations 77−60696
TV camera appl. for lunar occultations *(French)* 79−58263
Uranus, by Moon, 1977 February 10, radius, limb darkening and polar brightening at 6900 Å 80−17545

occultations continued
Uranus, new satellite occultation of SAO 158687, Kavalur obs. 77−53473
Uranus, satellite rings, KAO obs. of SAO 158687 occultation 77−53471
Uranus, satellite rings, Perth Observatory obs. of SAO 158687 occultation 77−53472
Uranus, satellite rings occultation of SAO 158687, discovery accounts 77−74009
Uranus and rings, obs. of stellar occultation, (1980 August 15 to 16) 80−98610
Uranus occultation of faint blue star on 1977, Aug. 26 77−53470
Uranus occultation of SAO158687, obs. possibilities in methane bands 77−29719
Uranus occultation of SAO 158687, obs. rel. to upper atmosphere mean temp. and temp. vars. 80−46477
Uranus occultation of SAO 158687, planetary radius and ellipticity determ. 80−67648
Uranus occultation of SAO 158687 on 1977, March 10, predictions 77−29717
Uranus ring occultation possibilities for two faint 11-12 mag. stars 77−56875
Uranus rings, stellar occultation predictions for December 77−82161
Uranus satellite belt, numbers and positions from SAO 158687 occultation 77−33408
Uranus satellite rings, identifications and sizes from SAO 158687 occultation by 77−45358
Uranus stellar occultation, 1980 August 15 to 16, reality of additional occultations questioned 80−109396
γ^2 Velorum, by Earth, upper atm. H_2 and O_2 densities meas. by Copernicus satellite 77−9579
Venera 9 and 10 satellites, Venus atmosphere radio occultation and surface bistatic radiolocation 79−48698
Venera 9 and 10 satellites by Venus, atmosphere sounding during radio occultation 80−101543
Venera-10 by Sun, plasma turbulence and vel. *(Russian)* 77−91504
Veneras 9, 10, dual-freq. radio occultation expts. rel. to Venus daytime ionosphere profiles 79−96939
Venus, liquid content of lower clouds, Mariner 10 radio occultation data 79−40106
Venus, nightside ionosphere, Pioneer orbiter radio occultations 80−46441
Venus, polar ionosphere, Pioneer orbiter radio occultations, electron density 79−48706
Venus atmosphere, model from radio, radar and occultation obs. 80−46420
4 Vesta, predictions for 1980 January 24 lunar occultation 79−84728
Viking by solar corona, radio obs. at 1976 Mars solar conjunction 78−20789
Viking orbiter by Mars, radio occultation meas. of atmosphere and topography 78−20687
Viking orbiters, radio occultation meas. of Mars atmosphere and topography and atmosphere 80−72836
ψ Virginis (SAO 139033), by Moon, ang. dia. meas. 78−20825
Voyager 1, radio occultation by Jupiter and atmosphere and ionosphere preliminary profiles 80−26791
Voyager 2 by solar corona, 1979 August, signals ang. and spectral broadening 80−51639
Voyager 2 occultation of Jupiter, ionosphere struct. from radio obs. 80−77337
X-ray source lunar occultation dates during next decade 77−33697
X-ray sources, point-like, positions determ., lunar occultations optimisation 79−92652
X-ray sources occultations by Moon, first and last dates (1980 to 1985) 80−77513

ocean water *see seawater*

ocean waves
12 m discus and NOMAD buoy hull transfer function computations 80−46303
acoustic propagation through internal waves, refractive index modulation, parabolic moment eqns. 80−83698
acoustic reflected and lateral waves for Sommerfeld model 77−11074
acoustic remote sensing of surface waves, theory 80−12564
acoustic wave propag. in frozen random media 77−50814
aerodynamic drag of sea surface, role of high freq. gravity waves 80−26536
Agulhas Current, giant waves 77−13085
Agulhas Current, long-wave disturbances due to topographically induced changes in coastal inertial jet 80−72545
air flow separation over water waves 77−11208
air-sea interface, momentum flux determ., wind-wave interaction method 77−33130
air-water exchange reactions, wind-wave interactions *(Dutch)* 78−3785
airflow above waves, numerical simulation *(Russian)* 80−4076
N.America west coast, sea level alongshore correl., seasonal vars. 78−73381
annual Rossby wave in tropical N.Pacific Ocean, obs. 80−51421
Antarctic Polar Front Zone, fine structure rel. to internal waves 79−2254
N.Atlantic, internal wavefield-mean flow interaction 80−36309
Atlantic, internal waves and sound scatt. layers in thermocline 79−2285
Atlantic Ocean, internal Kelvin wave rel. to upwelling in Gulf of Guinea 78−88837
N.Atlantic Ocean, waves rel. to Palisades microseisms source location 78−85495
atmosphere-ocean interaction, sea waves influence on wind profile 78−92895
E.Australian coast, wind stress generation of shelf waves 77−37234
axisymmetric disturbances, evolution in fluid *(Russian)* 79−34848
axisymmetric ocean model, wave energy dissipation, frictional bottom effects 79−79846
Baltic Sea, density and vel. fields fine struct. calc. 79−2279
Baltic Sea, two-dimensional seiches theory 80−8323
baroclinic Rossby waves, instability, energetics in two-layer ocean 79−57938
baroclinic Rossby waves asymptotic behaviour taking into account Earth's curvature 80−8321
baroclinic Rossby waves generation by meteorological forces 77−86916
baroclinic Rossby waves in flow with vertical shear *(Russian)* 78−85602
barotropic and baroclinic Rossby waves in rotating two-layer fluid, interactions and instabilities 79−57955

ocean waves continued
barotropic continental shelf waves, bottom friction effect 79−48509
barotropic nondivergent shelf waves on Ghana continental shelf 78−44837
barotropic Rossby wave leading to anticyclonic vortex formation *(Russian)* 79−100859
barotropic Rossby wave stability in baroclinic ocean 79−16508
barotropic Rossby waves asymptotic anal., with Earth curvature allowance 79−53361
barotropic topographic Rossby waves, nonlinear theory 77−78207
barotropic waves, large amplitude, interaction with ambient shear flow, critical modes 77−80175
bars, shallow profile coastal, calcs., choice of wave parameters *(Russian)* 79−88330
bars, wave-formed, sedimentation and equilib., review 79−92521
W.Bay of Bengal, wave characts. during southwest monsoon of 1978 80−109152
beach, long-period waves 77−21780
beach, uniform bore, surf and run-up 80−21779
Benguela Current, anomalously high waves region 80−51434
beta dispersion of inertial waves 79−70810
bidimensional surface waves, periodic correlational random field model *(Russian)* 78−20430
Black Sea, power spectra *(Russian)* 79−34835
Bombay High area, winter swells 78−32112
book 78−57219
bottom boundary layer, mass transport by gravity waves *(Russian)* 78−16036
bottom waves in rotating stratified fluid 79−2274
boundary current flow along continental margin, lee waves assoc. with topographic irregularity 80−72539
boundary-forced planetary waves, model mid-ocean response to strong current variability 80−72541
bounded water bodies finite amplitude waves, dynamics study 78−77273
breaking wave effects on power plant intakes *(Italian)* 80−109148
breaking waves, review 77−64310
broken ice effects on ship waves *(Russian)* 78−65326
buoy for measurement ocean waves 80−85772
buoy wave data analyses noise correction functions and error sources 80−46302
S.California, wave parameterisations rel. to beach changes statistical prediction 80−98305
capillary and gravity wave development in two-layer fluid *(Russian)* 80−12421
capillary wave slope meas., using laser optical instrument 78−36173
capillary waves, interaction between current and wave decay 77−62265
capillary waves, laser probe for 2D wave slope spectra meas. 77−60472
capillary-gravity waves in two-layer fluid *(Russian)* 79−39733
capillary-gravity waves on ocean bottom, development and stability *(Russian)* 78−16033
Caspian Sea, spatial struct. of storm waves *(Russian)* 79−29790
Caspian Sea shallow areas, wind waves freq. spectra *(Russian)* 79−16477
cliff erosion, wave induced rel. to erosive force of waves 78−20388
closed basin with topography, normal Rossby modes 78−73385
cnoidal internal wave breaking in horizontally inhomogeneous ocean *(Russian)* 77−64301
coastal, near breakwater, physical and numerical modelling 80−51401
coastal trapped long waves, obs. off United States west coast 78−44854
coastal trapped long waves, wind forced 77−70673
coastal trapped waves, anal. and numerical calc. by inverse iteration 78−69360
coastal trapped waves at low latitudes in a stratified ocean 80−90097
coastal wavestaff system 80−46324
coastal zone, arrested topographic waves 78−69359
coastal zone, wave setup and backwash due to local thermal wind-field disturbances 80−36371
coastal-trapped waves in continuously stratified ocean 77−41045
coastal-trapped waves in upwelling frontal zone 80−104975
continental shelf barotropic topographic Rossby waves, transmission and decay 77−2176
continental shelf dynamics and topographically trapped coastal waves 78−16057
continental shelf wave side band instability and long wave resonance 78−16030
continental shelf waves, effects of bottom topography and coastline alongshore vars. 77−41046
continental shelf waves, effects of variable Coriolis parameter, coastline curvature and bottom topography 78−3775
continental shelf waves, generation by alongshore vars. in bottom topography 80−51424
continental shelf waves, scatt. by isolated topographic irregularities 80−51423
continental shelf waves, scattering by longshore bottom topography vars. 80−67376
continental shelf waves (trapped), recent advances 80−98348
continental shelf waves in sheared barotropic boundary current 77−86918
correlation function and averaged power of radar signals reflected from sea waviness 80−46190
current, nonlinear waves guided by curl *(French)* 77−91137
current finestructure and moored current meter meas. of internal waves 78−44828
currents, temperature and tides low freq. fluctuations near Peru coast 79−79858
currents and sea levels poleward propag. perturbs. along Peru coast 79−34841
currents and waves interaction with rough bottom 79−70808
cylindrical solitary waves in variable depth water 78−40578
data acquisition on Norwegian continental shelf 79−12120
data buoy wave meas. system malfunction detection 80−46304
data buoy wideband wave directional spectra, real-time telemetry 80−46305
deep ocean, internal waves rel. to bottom boundary layer short-term variability 79−2269
deep ocean internal waves, dynamics 80−26517
density anomalies, large-scale, Rossby waves model and non-linear evolution *(Russian)* 79−16479
density-stratified ocean, perturbation method appl. to internal waves theory 77−49070
detection and direction meas. via microwave radars 79−5685

ocean waves continued
detection by microwave radar, gravity-capillary wave modulation 78−77333
development from periodic disturbances in non-uniform fluid, surface tension effect *(Russian)* 78−77253
diffraction by 3-D bodies, hybrid element method 78−38344
direction determ. in coastal waters 79−5642
direction sensing using solid-state water current meter 79−21070
directional wave spectra from discus buoy, data processing 79−16723
directional wave spectra meas. from fixed platforms 79−16724
directional wave spectra monitoring horizontal-spar buoy, design 79−21083
directional wave spectra routine meas. system, from discus buoys 79−16722
directional wave spectrum, new meas. method, description 79−16706
directional wave spectrum, new meas. method, lab. wind waves meas. 79−16707
directional wind wave spectrum meas., role of dispersion reln. 79−20860
directions, meas. by single wave follower buoy 79−5664
discus buoy wave spectra, comparison of buoy-fixed and vertically stabilised accelerometers 79−5678
dissipation and forces on perforated caisson breakwater 77−73760
disturbances 78−32209
Doppler scattering of EM waves by ripples due to acoustic and capillary waves 78−3807
Douglas Channel, Canada, waves in Kitimat Inlet generated by submarine slide 80−51417
drag coefficent vars. for air flow above water waves 79−44232
Eady waves, effects of vertical eddy viscosity 80−51404
edge wave excitation on beaches 77−29317
edge wave in stratified sea with sloping bottom *(French)* 80−31045
edge waves, wavelengths rel. to shoreline periodicities 80−12375
edge waves on complex beach profile, theory 80−31025
edge waves over trench-ridge topography adjoining straight coastline 78−44838
Ekman layer, stationary transport generated by waves *(Russian)* 80−17276
electric generator, wave activated, design 79−20866
electrokinetic phenomena assoc. with wave motion 78−69351
EM field vars. 78−44834
EM wave scattering theories, review 78−77243
energy absorption fundamentals 79−43726
energy conversion techniques and subsystems 80−45627
energy extraction, system optimization by diffraction theory 79−20867
energy transfers across air-water interface at high wind speeds, effect of spray 78−85574
episodic waves, exptl. and theoretical studies 78−61433
equatorial Kelvin and inertio-gravity waves in zonal shear flow 80−26520
equatorial shelf waves on exponential shelf profile 79−16496
equatorial topographic long-period waves, theory 78−92835
equatorial trapped waves, vertical eigenvalue problem 80−56477
equatorial undercurrent effect on equatorial waves 80−26519
equatorial waves, evidence for continuous wave spectrum in Indian Ocean 80−98331
equatorial waves, zonal boundary effects 78−85586
erodable base, bottom vel. and scouring 78−49029
estuary amplification of periodic and unsteady waves *(Russian)* 77−60405
evanescent internal waves in rotating stratified liquid *(French)* 78−38356
fetch and wind speed rel. to radar backscatter 78−77247
fine struct. of hydrophysical fields, nonlinear internal wave theory 78−3796
finite-amplitude, on nonuniform currents 78−40583
Florida current, wind forced continental shelf waves 77−73758
Florida Straits, continental shelf waves 77−2177
forced along continental shelf waves on an f-plane 77−2175
forced response of submarine detection system 77−72220
forced wave motion, influence of stratified currents with vel. shear *(Russian)* 78−77255
forced waves, review 78−73401
forces on floating or submerged bodies, sand bars, wave power machines appls. 77−13090
forces on sinusoidally oscillating cylinder, parametric study 79−32547
forecasting 79−66710
forecasting and physic, JONSWAP *(German)* 78−3783
forecasting for offshore operations 79−2353
forecasting service, pot. benefits case study anal. 78−77357
free and forced edge waves, finite amplitude effects 78−79330
free Rossby waves in bounded basin 79−12124
frequency spectra and wavenumbers meas. method by recorder array *(Russian)* 80−109266
frontal wave action on sandy beach, dynamic profile equilib. *(Russian)* 79−88331
generation, propagation and dissipation spectral simulation model 80−31060
generation by landslide in bay, simulation 78−92879
generation of stationary flow in boundary layer *(Russian)* 79−39731
geomag. fields, towed magnetometer investigation 80−3923
geomagnetic variations, analogue model 77−49003
geostrophic fronts, bores, breaking and blocking waves 80−104967
Ghana shelf fortnightly wave, characts. 80−26515
glaciers, floating, vibr. excitation by waves rel. to iceberg calving 78−81197
gravity and Rossby waves dispersion relations 79−2280
gravity wave critical level flow, viscous stabilization 77−45074
gravity wave growth by modulated wind stress 77−17119
gravity wave interference with EM current meter recordings 77−78456
gravity wave-critical level interaction, nonlinear model 79−1205
gravity wave-current interaction, energy propag. stopping 77−47029
gravity wave-stream function relationships, variation approach 80−36318
gravity waves, air-water interface effects 79−57947
gravity waves, deep water almost-highest, matching and anal. extn. 78−46991
gravity waves, directional spectra, remote sensing by microwave radar 78−57364
gravity waves, finite amplitude, in deep water, instabilities, superharmonics 78−38349
gravity waves, finite amplitude, in deep water, instabilities, subharmonics 78−38350

ocean waves continued
gravity waves, growth and equilib. in wind-wave tank 78−1679
gravity waves, long period, on beach, generalised KdV-eqn., soln. 78−92844
gravity waves, one-dimens., finite-element and finite-difference techniques comparison 79−18902
gravity waves, shape and breaking in stratified shear flow 78−34147
gravity waves, Stokes' coeff., new relns. 79−41698
gravity waves, two-dimens., finite-element and finite-difference techniques comparison 79−18903
gravity waves and turbulence strong interaction *(Russian)* 77−81904
gravity waves in water of variable depth 79−48514
gravity waves propag. over permeable bed *(Polish)* 78−38353
groups of waves, vels. and refr. laws verification 78−85575
growth and decay of 80 m waves, radar obs. 80−98344
Gulf of Alaska SeaSat Experiment synthetic aperture radar wave imagery 80−46199
Gulf Stream, fronts and wave disturbances compared with atmospheric jet stream 79−2268
Gulf Stream, Site D, Rossby wave obs. 78−3806
Gulf Stream surface waves, radar obs. program 80−85679
harbour channels, Galerkin finite element analysis 79−2286
harbour water levels, wave setup 80−67377
harbour wave pattern, model with directional wave spectra *(Polish)* 80−17288
harbour with large mouth, wave-induced oscills. 78−85604
Hawaii tsunami simulation, open boundary reflection interference 80−17232
heat exchange between sea and atmosphere *(Russian)* 80−56479
height and celerity obs. in surf zone 77−45012
height and dominant wavelength obtained from Geos-3 altimeter study 80−4024
height and period characts. off Mangalore, India 78−36185
height and period meas. at Digha, W. Bengal, rel. to coastal erosion 79−96764
height and spectrum remote obs. by HF skywave radar technique 80−90241
height directional spectral props., HF radio obs. 78−77241
height distrib. of waves, nonlinearity and finite band width 80−76993
height meas. using Geos 3 radar altimeter 79−16481
height meas. with satellite radar altimeter 79−44253
height measurements using GEOS 3 radar altimeter data 80−8452
height nondirectional spectrum from inversion of HF sea-echo Doppler spectrum 78−16203
heights, meas. by high resolution pulse-limited radar altimeter 78−81172
heights and periods, statistical distrib. 77−45006
heights and wind speed from Geos 3 data 80−4079
HF radar Doppler spectrum, anal. for ocean surface currents mapping 80−94626
high frequency internal waves in upper thermocline during GATE 79−57939
high sea state, wave height measurements from Geos-3 radar altimeter data, aircraft and ship data−a comparison 80−4025
high-amplitude waves, representation by stream function *(French)* 80−76986
high-frequency internal waves, obs. at ocean station P (Oregon coast) 80−98330
hindcasting appl. to engineering activities 78−69493
hurricane Camille, wind speed and direction, ocean wave height and barometric press. meas. 78−36254
Hurricane Eloise (1975), wave meas. by ocean data buoys 78−77302
hurricane over Arabian Sea, surface wind and sea waves 77−53159
hydrodynamic instability, expt. studies 79−53354
Iberian basin, internal tidal waves spatial characts. *(Russian)* 77−81906
ice covered areas, three-dimensional gravitationally-elastic, gravitationally-capillary surface waves *(Russian)* 79−32537
ice covered sea, flow vel. and ice thickness effects on unsteady waves *(Russian)* 78−65324
imaging and wavelength meas. by aerial photography 80−46323
immersed parallel-plate duct, wave tank expts. 79−52873
Indian Ocean, tidal period waves *(Russian)* 77−60419
induced atmospheric mag. field attenuation 77−13058
infrasound generated by waves, and propag. through atmos. 79−74960
interaction with arbitrary cross section cylinder barrier 79−25261
interaction with atmospheric sound waves, model *(Russian)* 80−12402
interactions in stratified media *(Russian)* 77−11231
interference, rel. to lower thermosphere heating by acoustic waves dissipation 77−53266
internal gravity wave generation in geostrophic current by atmospheric pressure disturbances *(Russian)* 79−100853
internal gravity wave packet modulation, reson. with mean motion 78−5761
internal gravity waves, mass and momentum diffusion 77−13086
internal gravity waves, rel. to low-freq. acoustic fluctuations 77−50809
internal gravity waves, shear instability *(Russian)* 78−69352
internal gravity waves, short-period, nonstationary features rel. to thermocline oscills. *(Russian)* 78−16024
internal gravity waves, wave breaking and fine struct. in deep ocean, meas. and models 78−85578
internal gravity waves, weakly-nonlinear, in stratified fluid of finite depth 79−77148
internal gravity waves in accelerating shear flow 79−32628
internal linear strongly vertically trapped waves 77−49069
internal nonlinear gravity-inertial waves in stably stratified layer 77−21785
internal nonlinear waves in stratified fluid in closed basin 78−75159
internal nonstationary waves, periodic pressure generated *(Russian)* 77−60406
internal ocean waves, book contrib., review 80−21781
internal ship waves, development caused by shifting press. in multi-layer fluid *(Russian)* 78−77256
internal short-period waves generation by shear flow instability 79−2273
internal slightly nonlinear nonstationary waves in deep ocean 78−44869
internal slip waves development, three-layer model *(Russian)* 78−65323
internal solitary waves moving over two-dimens. topography, fission and disintegration 79−79857
internal solitary waves near turning point 80−46188
internal solitary waves prod. by tidal flow over three-dimens. ridge, ocean appl. 79−46332
internal solitons in Andaman Sea, and interaction with surface waves 80−104994

ocean waves continued
internal tidal oscills. spatial characts. from temp. meas. 78−61434
internal unsteady waves generated by basin bottom pulse displacements *(Russian)* 79−39737
internal wave climate near NW.African coast during JOINT-I 79−20840
internal wave dispersion, clustering characts. *(Russian)* 77−73754
internal wave effect on surface gravity wave spectrum *(Russian)* 80−21776
internal wave field, equilib. mechanisms 78−44852
internal wave field, vertical coherence from towed sensors 80−36310
internal wave generation by advecting atmospheric fields 77−53066
internal wave generation by random wind wave field *(Russian)* 77−60383
internal wave groups, near-surface, in deep ocean, acoustic obs. during GATE 78−81177
internal wave induced finestructure, separation from intrusive fine struct. 79−48502
internal wave obs. by Skylab 78−3801
internal wave obs. with airborne synthetic aperture imaging radar 77−17110
internal wave packets propagation speed rel. to upper mixed layer heat storage, inference from Landsat data 79−100869
internal wave refraction in S.China Sea, satellite obs. 77−64298
internal wave spectra, temp. and current contamination 78−40564
internal wave spectra analytical representation 77−41056
internal wave spectra and vertical fine structure *(Russian)* 78−85595
internal wave surface effects, LANDSAT and ship obs. 77−5215
internal wave trapping by submarine canyons 77−9436
internal wave variability during IWEX (Internal Wave Experiment) 79−57957
internal wave vertical velocities obs. by free-fall vehicle 79−57942
internal waves, acoustic reverberation data 80−41562
internal waves, Cauchy problem, similarity solns. *(Russian)* 78−96221
internal waves, damping in ocean with rough bottom *(Russian)* 78−24293
internal waves, effect on surface wind waves, expt. with ship 78−40562
internal waves, effect on surface wind waves, theory 78−40563
internal waves, Gaussianity 77−60386
internal waves, generated by local disturbances in stratified fluid *(Russian)* 79−16480
internal waves, Hamiltonian formalism *(Russian)* 79−34833
internal waves, induced acoustic phase fluctuations 77−7240
internal waves, influence of horizontal density diffusion vertical var. *(Russian)* 79−39738
internal waves, mixed layer induced vels. 78−73395
internal waves, radiation by sources in exponentially stratified flow *(Russian)* 77−64300
internal waves, relationship with wind field variability 80−31052
internal waves, reson. interaction 77−45010
internal waves, resulting free surface vibrs. exptl. investigation *(Russian)* 79−16478
internal waves, scatt. of sound 79−14141
internal waves, shear distortion of orbital vels. 77−78208
internal waves, spatial spectra autoregression evaluations using reference sensor *(Russian)* 78−61578
internal waves, temp. field fine structure influence *(Russian)* 78−36182
internal waves, weak turbulence theory *(Russian)* 77−33089
internal waves, weakly nonlinear systems, props., discussion 78−93535
internal waves, wind-generated, exptl. study *(French)* 79−62518
internal waves, with horiz. varying Brunt-Vaisala freq. *(Russian)* 80−104965
internal waves and mesoscale eddies, weak interaction 77−9433
internal waves and sound-scattering layers depth fluctuations 77−78214
internal waves and temp. finestructure discrimination 77−60389
internal waves and turbulence rel. to ocean fine structure *(Russian)* 78−85596
internal waves at interface of two water media of different densities *(Polish)* 78−38352
internal waves generated by travelling disturbance *(Russian)* 78−16031
internal waves impingement onto moving mixed surface layer 78−24298
internal waves in Arctic fjord, effect on waters mixing 79−48504
internal waves interaction with small-scale surface turbulence *(Russian)* 78−44845
internal waves meas. with electrical contact device 80−12566
internal waves near inertial freq., vertical polarisation and energy flux 77−45015
internal waves on deep-stepped marine struct. 79−57943
internal waves rel. to ocean surface intrusions and fronts, numerical study 79−2262
internal waves spatial structure, vertical vars. 77−21786
internal waves stochastic models, acoustically relevant statistics 77−46854
internal waves with nonstationary shear, hydrodynamical instability *(Russian)* 78−7650
inviscid barotropic vorticity eqn., soln. by finite difference, finite element and pseudospectral method 80−43687
Isaacs wave-energy pump, field tests around Hawaii 79−57354
island and harbour diffr. of waves, integral formulation of Helmholtz eqn. 80−81919
isolated two-dimensional strongly nonlinear Rossby waves in barotropic ocean 78−44868
Kelvin and Poincare waves, multiple scatt. by irregular coastline 78−57216
Kelvin wave, rel. to equatorial adjustment in E Atlantic Ocean 78−88836
Kelvin wave in NE. Pacific 79−79849
Kelvin wave propag. in var. depth basin 79−12123
Kelvin waves, wind-generated linear and nonlinear, along irregular coastline 78−11908
Kelvin waves in equatorial region, affecting currents 80−98337
Kelvin waves propag., effects of longshore varying topography and coastline 78−92826
Kelvin-Helmholtz billows, finite amplitude, evolution 78−81293
Kelvin-Helmoltz waves, wind interaction 77−78189
Knight Inlet, British Columbia, lee wave prod. from stratified flow interaction with sill 80−101368
Korteweg-de Vries eqn. for nonstationary internal waves in inhomogeneous ocean *(Russian)* 77−45003
Krishnapatnam nearshore zone, wave conditions and wave-induced longshore currents 80−41449
ocean waves continued
Laccadive Sea (Lakshadweep), wave characts. 80−109151
large amplitude water wave digital simulation by finite element method 78−92851
layered medium disturbed by internal waves, statistical props. 78−22359
light intensity fluctuations refl. by sinusoidal waves *(Russian)* 77−13080
linearly stratified fluid, gravitational collapse of mixed region 80−33653
long and short surface waves interaction 77−41049
long barotropic waves and storm surges, model of W. coast of Norway 80−81907
long internal Rossby waves, nonlinear propag. 80−81896
long surface waves in canals, bays and oceans, linear transport methods 78−40573
long wave deformation over seamount *(Russian)* 79−39732
long waves, effects on wind boundary layer and ripple slope statistics 77−45005
long waves, propag. over water of slowly varying depth 77−49073
long waves, scattering at estuaries bordering continental shelf 77−78191
long waves energetics in rotating variable depth basin 79−20850
long waves scattering at mouth of estuaries bordered by continental shelf 77−9442
long-period gravity waves in ice-covered sea 80−67372
low-angle backscatter of microwave radar, long-period feature origin 78−57218
Mach reflection from wall *(Polish)* 77−70684
Madras coastal zone, sea level, tides and waves 77−41038
magnetic field from sea waves, exptl. obs. results 79−53350
magnetic fields, induced, analogue model study for nonuniform depths and sea-land interfaces 79−66807
magnetic gradient fluctuations caused by internal waves 80−56491
magnetic gradients from ocean waves, meas. using supercond. mag. gradiometer 79−29867
main waves generated by tropical hurricane, calcs. *(Russian)* 78−16021
Mangalore Harbour, wave heights and periods 79−100850
marginal ice zone, wave decay, inverted echo sounding from submarine 78−49025
Marineland, Florida, in situ and remotely sensed waves 78−77248
mass transport by waves in turbulent bottom boundary layer 78−3797
mass transport in deep-water waves 79−79856
mass transport velocity in progressive gravity waves, double boundary layer model 77−78217
Massachusetts Bay, tidally generated internal wave packets 79−44190
maximum height of wind waves, theory 80−41458
measurement, analogue spectrum analyser system for operational buoys 79−5662
measurement, optimum conversion of information to digital form 79−29903
measurement and data anal., by Naval Coastal Systems Center (NCSC) environmental measuring system 80−12570
measurement by offshore industry 78−69492
measurement of short gravity waves from platform, using TV camera 80−98335
meter for inshore wavemetering, with radiotransmission of data 80−101460
microscale sensing array meas. 78−85720
microseism generation mechanism from sea floor obs. off Shikotan Island 78−73319
microwave emission at 37 GHz, wind effects 80−12414
microwave scatter and sea state estimation, ocean wave models 78−77244
microwave scattering *(Russian)* 77−5210
minimum wind stress for wave inception 78−57285
mixed fluid, nonlinear internal wave formation from gravitational collapse 80−33619
model of ocean-atmos. interaction, in hamiltonian formalism *(Russian)* 80−104964
modulation characteristics of surface waves 80−51416
momentum flux and wave spectra, air-sea interaction obs. of Long Island, New York 80−26513
monochromatic waves, obliquely incident on plane beach, instabilities 80−17275
monomolecular slicks drift response to wind and wave action 78−69364
multi-component wave data, directional spectra extraction var. technique 80−26637
near-surface inertial oscillations in current records 80−109157
non-rigid bed, water wave attenuation 80−69851
non-stationary capillary-gravity waves in a shear flow *(Russian)* 79−34849
nonadiabatic wave energy transport and trapping *(Russian)* 78−65328
nonlinear, dynamic properties stochastic modelling 79−23332
nonlinear baroclinic waves, exptl. study of instability and mode selection in large basis 80−85669
nonlinear deep water gravity waves, random inhomogeneous field evolution 80−69857
nonlinear energy transfer in a narrow gravity-wave spectrum 79−100873
nonlinear free surface flow digital simulation by boundary integral eqn. method 78−92850
nonlinear internal motion in open sea, obs. using range-gated Doppler sonar 80−51422
nonlinear internal wave interactions, Langevin techniques appl. 80−67371
nonlinear internal waves in a rotating ocean 80−26534
nonlinear resonant excitation of a long and narrow bay 79−34847
nonlinear Rossby waves on large scale current, mesoscale eddies 77−64313
nonlinear stationary internal and surface waves in shallow seas, propag. 80−17292
nonlinear stationary waves *(Russian)* 77−81905
nonlinear theory, spectral anal. 77−17141
nonlinear transfers between sea waves 78−81176
nonlinear wave packets propagation, finite depth effects 79−48510
nonlinear waves, probabilistic description 80−76997
nonlinear waves in closed basin, random behaviour 80−26557
nonlinear wind-wave system, model and expt. 79−34846
nonlinearity of waves in presence of light wind *(Russian)* 80−109165
North Sea, microwave meas. using SLAR 78−77245
North Sea, surface wave refraction 77−91152
North Sea, wave height statistics using hindcast wave data 80−17273
North Sea and River Thames, surge and tide interaction 78−96219
North sea wave ht. during gale, prediction formulae 80−98346

ocean waves continued
Norwegian Sea, thermocline oscills. struct. 79−20854
oblique reflection from vertical wall *(Italian)* 77−78185
ocean test structure for wave force meas., improved platform design [Ocean Test Structure] 79−12306
ocean wind wave analysis instruments 80−26640
oil on sea surface, thermal radioemission spectral characts. 80−85686
oil thickness on wavy water surface, light sensitive gauge 79−8720
Onslow Bay, eastern USA, existence of continental shelf waves 80−72529
Oregon continental shelf and slope, internal waves rel. to barotropic and baroclinic tides 80−72543
Oregon-Washington continental shelf, barotropic response hindcast during 1972 summer 79−48497
oscillating water column wave-energy device 79−39274
oscillations, wave-induced, in harbours of variable depth 79−4023
tropical N. Pacific, annual forcing of baroclinic long waves, bathythermograph obs. 77−60392
Pacific, E.equatorial, long waves obs. in geostationary satellite IR images 78−24308
E.Pacific, equatorial long waves from deep current meas. 77−5216
N. Pacific, long-wave disturbances of dynamic height 77−60391
N.W.Pacific, temp. fluctuations in internal gravity waves freq. range 77−49081
NW Pacific, wind-wave tropical cyclone model, parametrisation characts. 78−24301
Pacific equatorial countercurrent lateral oscills. 79−16500
NW.Pacific Ocean, edge waves obs. *(Russian)* 78−44841
Pacific Ocean, equatorial, propagating forced wave rel. to 14°C isotherm slope annual var. 80−72537
N Pacific Ocean, large-scale waves rel to temp. anomalies vertical struct. 78−73394
NW.Pacific ocean continental shelf waves rel. to sea level low-freq. vars. 80−101415
pack ice attenuation of waves 80−36332
Paradip Port, India, wave characts. 80−41450
parametric wave prediction model 77−60398
parametrical wave prediction model 80−17272
patterns under Hurricane Gloria, obs. with airborne synthetic-aperture radar 78−44873
period and height forecasting at Digha, India 77−53064
periodic long wave deformation, over gently sloping bottom 78−90921
periodically rough water surface, thermal radiation critical phenomena *(Russian)* 78−81188
phase velocity, propagation direction 80−28521
plane waves, group vel. in inhomogeneous media *(Russian)* 78−5755
planetary waves, second class wave props. *(French)* 78−65337
porous elastic bed response to water waves 78−67208
power spectrum obs. in open ocean with cloverleaf buoy 80−104976
pressure on vertical walls *(Chinese)* 80−79342
propagating inertial and internal waves, refl. at rigid boundary rel. to induced drift currents 80−51403
propagation in random media, oceanic appls. 79−5987
propagation on large-scale currents over gently sloping sea bed 78−40582
propagation over deformable sea floor 79−57966
propagation over flat porous bed, radiation-type boundary condition 78−44851
propagation over soft mud bottom, two-layer fluid model 79−79862
propagation over source 78−83416
propagation theories for water waves, variational principles 80−24043
radar and Doppler effect, meas. of wave height, length and velocity, OREME project *(French)* 80−94625
radar backscatter from water waves, induced current effects on microwave backscatter, expt. 77−25688
radar data processing 78−77335
radar echoes of second order from ocean waves, first inversion 78−49032
radar imaging, synthetic aperture technique 78−77334
radar imaging of ocean surface, SAR method 80−77173
radar impulse reflection from nonlinear random sea 80−12416
radar measurement, theory and HF and microwave techniques 78−81418
radar monitoring, ground wave and sky wave sensing techniques 80−109256
radar profilometry for wave height, airborne method 80−85771
radar remote sensing, minimisation of ionospheric disturbance 80−21857
radar returns from rough sea 80−51408
random field fluctuations of near-water atm. layer and upper ocean layer, linear filtration errors 80−12425
random gravity wave field, directional energy distrib. influence on dispersion relation 77−86921
random gravity wave in deep water, statistical pressure props. 77−2155
random gravity wave mathematical representation 80−46198
random wave fluid, wave groups presence modelling 79−2245
recording of waves and current 78−61610
reef effects, model study 80−4043
reflection and refraction by shear currents 78−32117
reflection of radar signal from sea surface, spatial intensity fluctuations 80−109170
refraction, coastal, for flat inclined ocean bottom *(Russian)* 77−33084
refraction, lab. expts. 78−38355
refraction by circular island, model 80−36316
refraction rel. to sediment transport along Indian west coast 77−91145
remote sensing in Irish and Celtic Seas using MF radar 79−16725
rip currents on open coastline, wave-current interaction models 79−34839
ripple growth to swell, ang. momentum conservation explanation 80−56478
ripple induced bed roughness, effect on surface waves attenuation *(Polish)* 79−25262
ripples on carrier waves, distrib. and steepness 80−72548
Ross Ice Shelf, ocean tides and waves 79−88364
Rossby wave form. from disturbances in non stationary barotropic flow *(Russian)* 80−104963
Rossby wave interaction with zonal flow *(Russian)* 80−104982
Rossby wave interactions and stability in rot. two-layer fluid on β-plane 80−10257
Rossby wave propagation, effect of bottom relief random inhomogeneity 80−85676
Rossby waves, effects of vertical eddy viscosity 80−51404
Rossby waves, long period oscills., book contrib. 78−61435
ocean waves continued
Rossby waves, rel. to nonlinear energy and enstrophy transfers in realistically stratified ocean 80−101370
Rossby waves, strongly nonlinear, on large-scale current 77−78206
Rossby waves, topographically induced, laboratory expts. and theory 77−64289
Rossby waves in a baroclinic ocean, exact soln. *(Russian)* 80−21775
Rossby waves in rot. two-layer fluid on β-plane, reson. interactions 79−77145
Rossby waves stability in baroclinic ocean 78−3788
rotating channel with arbitrary end wall, Kelvin wave reflection 78−5751
rotating fluids, Rossby and Kelvin waves, open boundary conditions 80−61810
rotating stratified fluid, an exact soln. for edge waves 80−4038
rotating stratified fluid, internal and inertial waves 78−67245
rough sea surface rel. to underwater light field fluctuations *(Russian)* 78−36183
roughness probability density function determination, from Geos-3 altimeter data 79−100852
Rudnaya Bay, Sea of Japan, layer of storm network of sediments 79−2224
sand barrier beach shoreline accumulative section, protective dune ridge morphodynamics *(Russian)* 80−36287
sand barrier beach shoreline transit section, protective dune ridge morphodynamics *(Russian)* 80−36286
sand tracer dispersion under progressive water waves, laboratory and field obs. 80−46170
sand transport due to near-bottom orbital motion 80−98306
sand waves on shelf of tidal sea 79−12313
scalar spectra estimation by maximum entropy method 79−74900
sea ice, ocean waves SAR imaging 79−5496
Sea of Azov, storm surges calc. 78−96231
sea state, influence on marine geoid spectrum 80−3904
sea state, significant wave height extracted by algorithms 80−4023
sea state, surface roughness slope density calcs. from Geos-3 data 80−4022
sea state rel. to Beaufort scale 79−2354
sea surface roughness, rel. to mean wind speeds and turbulence at coastal site and offshore location 80−98406
sea surface roughness, rel. to spatial struct. of underwater light-field fluctuations *(Russian)* 78−53656
sea surface slope distrib. function determ. from Sun glitter, accuracy *(Russian)* 80−94611
sea surface stress measurements 79−66701
sea surface wave development, mean wind direction influence 79−48511
sea-echo Doppler spectra, sample-averaged, accuracy of parameter extraction 80−51561
SEASAT altimeter wave height comparisons 80−46201
seashore effect on breaking waves, deterministic description *(French)* 79−66707
self-focusing of waves on deep water surface *(Russian)* 80−94536
semidiurnal internal waves in Polygon-70 test area of Atlantic, spatial characts. 80−31051
set-down beneath wave groups, harbour resonance 77−25692
shallow water, propag. modelling criteria, appl. to tsunamis 78−26132
shallow water areas, tidal wave spectrum structure, theoretical analysis 77−37217
shallow water wave, refr. in presence of current 80−85680
shallow water wave equation model, finite element tidal computations 79−84282
shallow water waves in rot. basin, integral formulation 80−81920
shear current, wave action and set-down 78−90920
shelf waves, nonlinear generation 78−40587
shelf waves, resonance near islands 78−40588
shelf waves, resonant interactions with wind-generated effects 78−44835
shelf waves and mean currents, nonlinear aspects 78−40589
shelf waves diffraction by irregular coastline 78−40586
shelf waves in presence of sheared geostrophic current 78−40590
shelf-wave island resonance, radial barriers effect 79−57948
shoaling region, obs. of press. and vel. in 10 m-1 m depth region 80−76994
shoaling waves, breaking invariants 78−85577
shoaling waves, coherent microwave backscatter modulation 78−57212
shoaling waves, numerical soln. of exact eqns. 78−40579
shock waves, interaction with free surface 79−2287
shore platform formation on SE. coast of Izu peninsula, Japan 78−81147
short gravity waves, phase speeds of upwind and downwind travelling waves 80−98332
short gravity waves in finite depth waters, wave packet instability 80−81908
short gravity-capillary waves modulation by longer-scale periodic flows 80−57106
short period internal waves, spatial spectrum 78−3800
short pulse radar ocean wave sensing, preliminary results 80−46315
short surface wave transformation by inhomogeneous currents *(Russian)* 77−73753
short wave modulation by long waves, laboratory expt. 78−77249
short-fetch wind waves, near-surface Lagrangian wind and current vectors 80−72553
short-period internal wave generation mechanism *(Russian)* 78−81196
significant wave height, comments on airborne profilometer problems 80−4026
sill fjord, vertical diffusion driven by internal waves 77−2178
slope determ. from surface photographs 79−16680
small scale turbulence spectra, anal. *(Russian)* 79−88360
solitary Rossby waves in two-layer system, theory 80−17293
solitary Rossby waves over variable relief, stability, analytical theory 80−101371
solitary Rossby waves over variable relief, stability, numerical expts. 80−101372
solitary wave, diffraction by circular island in ocean, shallow-water theory *(French)* 80−83803
sound and infrasound prod. by nonlinearly interacting surface waves 77−11069
sound propagation coupled power equations for cylindrically spreading waves 77−23796
sound scattering by large sea surface inhomogeneities, phase function shape in shadowing conditions *(Russian)* 80−94530
Southern Ocean, long waves 78−40591

ocean waves continued
spatial internal wave generated by moving disturbances, development *(Russian)* 78−77251
spatially growing baroclinic waves 77−17120
spectra, remote meas., two-freq. microwave technique 78−77336
spectral decomposition of short gravity wave systems 80−36319
spectral energy density evolution of wave packets *(Russian)* 78−65327
spectral energy transfer from surface waves to internal waves, oceanic main thermocline 79−70812
spectral model, verification results using wave height study 80−4027
spectrum, dimensionless freq. spectrum *(German)* 77−86907
stable baroclinic Rossby wave propag. through mean shear flow 80−81895
standing equatorial wave modes, in bounded oceanic basins 80−51420
standing surface waves, double boundary layers 77−25694
stationary nonlinear waves in stratified rot. fluid, periodic solns., solitary waves *(Russian)* 79−7378
stationary surface and internal waves generated by baric disturbances in flow with vel. shear *(Russian)* 78−77252
stationary temperature boundary layers generation by surface waves *(Russian)* 80−1611
steady rotating flow over topography, steady β-plane channel, quasi-linear theory 80−92159
steep gravity waves in water of arbitrary uniform depth 77−70683
storm wave heights, statistical distrib. 78−73390
storm waves, rel. between heights and periods *(French)* 77−2157
stratified bottom boundary layer, wave-induced mass transport 79−2282
stratified fluid density interface, wind-wave interaction 77−62291
stratified ocean, influence of rot. on surface gravity and internal waves 79−2281
stratified ocean, vertical struct. of oscills., numerical calc. 79−39751
stratified ocean of finite depth, water wave problem, Green's function soln. 79−48489
stratified rotating liquid, waves energy relations *(Russian)* 77−27575
subsea sensor on offshore mooring platform, for wave anal. 80−26641
subsurface bubble clouds caused by breaking waves 80−46185
subtidal sea level fluctuations, rel. to atm. forcing, North Carolina coast 79−16498
successive wave heights, statistical relations 78−73396
sunlight fluctuations spatial and temporal correlation 80−94533
surf, atmospheric elec. space charge generation 78−36235
surf and run-up 78−40581
surf beat, prod. by edge waves 78−73380
surf zone, breaking wave energetics 80−12415
surf zone, hydrodynamic instability as mechanism for horizontal gyres form. 79−2244
surface and internal gravity waves coupling 77−923
surface and internal waves, adaptive spectral anal. *(Russian)* 77−29475
surface characteristics affecting acoustic scatt. 80−46194
surface distortion analysis, laser beam spreading 80−8332
surface drift currents, new model, nonlinear eqns. appl. 79−53353
surface drift induced by wind and waves 80−81914
surface film temp. fluctuations due to waves thinning viscous layer 80−109158
surface gravity wave, wind-wave generation, bispectral contrib. 78−49033
surface gravity waves, low freq. noise prod. in deep ocean 78−81184
surface gravity waves, nonlinear theory, derivations 77−60387
surface gravity waves, nonlinear theory, interp. and appls. 77−60388
surface gravity waves, triple roots and curved caustics 78−40584
surface gravity waves diffraction, ray methods 78−40574
surface gravity waves during Tropical Storm Delia, directional spectra and kinematics 79−48506
surface reflection by underwater ridges 80−4034
surface ripples, simple model 77−37230
surface roughness estimation using linear FM signal *(Russian)* 78−77353
surface wave imaging, synthetic aperture radar mechanism 79−5651
surface wave power resource estimate 77−41062
surface wave prediction model for varying wind fields 80−12408
surface wave propag. in channel connecting sea and lagoon 78−85605
surface waves, energy transfer to sediment motion 78−73389
surface waves, generation by sound *(Russian)* 77−46841
surface waves, remote sensing using one and two freq. microwave techniques 80−94622
surface waves, turbulent atm. boundary layer development *(Russian)* 79−16476
surface waves, wind-generated in deep water, Rayleigh method *(Russian)* 78−36178
surface waves diffraction and refraction computation, using finite and infinite elements, structures loading at sea calc. 77−81910
surface waves generated by shallow underwater explosions 79−2288
surface waves height meas., new acoustical methods 79−1276
surface waves incident on submerged circ. sill 78−1677
surface waves mean height determ. method 77−21928
surface waves meas., using resistance wave gauge, accuracy and calibration 80−24110
surface waves on viscous fluid of variable depth 77−11210
surface waves resonance generation by cold atm. fronts *(Russian)* 77−29309
surface wind wave related turbulence meas. by impellor current meter array 80−46301
surge and tide propag., numerical models as aid to navigation 79−12121
surge wave height determination, graphical method 80−56485
swell decay in shallow water, ang. momentum conservation explanation 80−56478
swell waves, causing press. perturbs. in atm. surface layer *(Russian)* 78−65362
swell waves at St. Helena related to distant storms 78−20432
swell waves forecasting from typical swell fields 79−39754
symmetric finite-amplitude rotational waves, streamfunction soln. 77−41044
synthetic aperture radar imageries, comparison with surface truth 79−5497
synthetic aperture radar imagery rel. to surface structure 80−46197
synthetic aperture radar imaging, focusing effects 78−40555
temperature and salinity self-similar distrib. in upper thermocline *(Russian)* 79−16474
temperature waves at wavy air-water interface 78−57213
three-layer flow, explosive reson. wave interactions 79−64680
tidal frequency waves, submerged elliptic ridge effects 78−69358

ocean waves continued
tidal sand waves study in White Sea 79−2218
tidal wave in Venice Lagoon, kinematic mathematical model *(Italian)* 79−16471
tidal wave profile distortion on entering river *(Russian)* 77−17115
tidal waves in channel, energy dissipation due to bottom friction and eddy losses 80−31058
tidal waves in estuaries, explicit finite-element formulation *(German)* 78−94755
tidal waves in rivers and estuaries, finite element models 79−53370
tidal-period internal waves in Indian Ocean equatorial zone 80−85677
tide and surge interaction in semi-infinite uniform channel, North Sea appl. 79−25251
tide waves in channel, bottom friction in perturbation method 80−98354
topographic planetary waves, resonant interactions, continuously stratified fluid 78−36186
topographic Rossby waves, mean flow generation 79−96800
topographic Rossby waves, nonlinear theory 78−3795
topographic Rossby waves generated off continental shelf, kinetic energy on shelf 80−51425
topographic Rossby waves off E. Australia, shelf circulation identification and role 80−26518
transient development of waves created against a vertical cliff 80−72530
transient waves generated by a moving oscillatory pressure on a sloping beach 80−56476
trapped coastal waves on equatorial beta plane 79−20846
trapped edge waves in presence of irregular coastline 78−44853
trapped waves, adaptive wavenumber-frequency spectrum analysis *(Russian)* 78−81189
trapping with shore absorption, decay rate and resonant response 79−34845
travel against wind, HF radar obs. 78−77242
travelling long waves in basin *(Russian)* 77−60404
trench waves theory of propag. and obs. off Japan and Chile 80−72547
tsunami, 1978 June 12, Miyagi Prefecture, Japan *(Japanese)* 80−41401
tsunami, damping in stratified ocean with rough bottom *(Russian)* 80−21651
tsunami, due to Izu-Oshima-kinkai earthquake, Jan. 1978, source mechanism 80−41393
tsunami, generation and propag., simulation using shallow water eqns. 80−41407
tsunami, island of Hawaii, 1979 November 25, numerical anal. by finite-element method 80−72449
tsunami, response of bay water *(Japanese)* 80−41399
tsunami, warning system based on sub-oceanic Rayleigh wave amplitudes 77−81806
tsunami accompanying Tonankai earthquake of 1944, source model *(Japanese)* 80−67344
tsunami along Mie coast, central Japan, 1707 and 1854 records *(Japanese)* 80−41402
tsunami associated with Ansei earthquake, 1854 Dec. 23, Japan *(Japanese)* 77−41001
tsunami at Oshima (W.Hokkaido), 1741 August 29, religious monuments *(Japanese)* 80−67345
tsunami caused by Izu-Oshima-kinkai earthquake, Jan. 1978, source mechanism *(Japanese)* 80−41392
tsunami data, estimation of magnitude of great earthquakes, 1837-1974 period 79−79745
tsunami earthquakes and subduction processes near deep-sea trenches 79−84155
tsunami from Sanriku earthquake, 1933 March 2, initial motion rel. to dislocation model 80−31000
tsunami generation and propag. in ocean with real bathymetry, numerical simulation 78−40576
tsunami generation by 1973 June 17 earthquake in Lesser Kurile Ridge region 77−53001
tsunami height rel. to earthquake mag., empirical relation 80−94461
tsunami inundation heights in 1703 and 1923 on South-Kanto coast, Japan *(Japanese)* 77−2121
tsunami long wave propagation analysis, finite element method appl. 78−92849
tsunami magnitude and wave source regions, N.E.Japan, 1611-1901 period *(Japanese)* 77−2122
tsunami prediction, overview and recommendations 79−8703
tsunami prediction and magnitude, coastal radar system appl. 80−82101
tsunami propagation, nonlinear dissipation effects *(Russian)* 79−8639
tsunami response for island system and surrounding underwater topography, calc. 77−86919
tsunami risk, estimation via stochastic model 77−21685
tsunami solitary wave, height vars. in near-shore zone 79−16507
tsunami source model from fault parameters, reliability 79−44128
tsunami type plane wave, Coriolis force effect *(Russian)* 78−77193
tsunami type waves propag. in coastal zone, dispersion and nonlinearity effects *(Russian)* 78−65325
tsunami wave generation by finite bottom displacement *(Russian)* 80−109113
tsunami wave heights along S.Boso Peninsula, Japan *(Japanese)* 77−64210
tsunami wave propagation, finite element method appl. 78−92848
tsunami with Miyagiken-oki 1978 June 12 earthquake *(Japanese)* 80−41400
tsunamis, historical, in Japan Sea, behaviour and source areas 78−65198
tsunamis, large, occurring off Sanriku district coast, simulations *(Japanese)* 78−65199
tsunamis, local behaviour 78−40577
tsunamis, Nankaido, Japan, historical monuments, inundation heights rel. to 1946 tsunami *(Japanese)* 79−70751
tsunamis, theoretical research, obs. in Japan 78−40575
tsunamis, transform. in coastal zone 78−77192
tsunamis effects at coastal sites due to offshore faulting, appl. to Israel 78−69300
tsunamis from large thrust earthquakes, implications for fore arc basins development 79−57905
tsunamis in Kanto, 1677 and 1703, behaviour along Kujukuri-hama coast from old monuments *(Japanese)* 80−67339
tsunamis interaction with Hawaiian Islands, finite element numerical model 78−69361
tsunamis inundation in Kochi Prefecture, Japan, numerical expts. *(Japanese)* 78−96150
tsunamis of 1707 and 1854 along Shizuoko coast, Japan, field surveys *(Japanese)* 78−96149

ocean waves continued
tsunamis propag. from sources off N.E.Japan Pacific coast *(Japanese)* 78−11813
tsunamis propagation, finite difference simulation, book contrib. 80−3956
two layer shear flow, radiation field and baroclinic eddy development in β-plane 79−81897
two-dimensional boundary-value problems of small amplitude waves in finite water depth, num. analysis method 77−9444
underwater sound, influence of internal waves on propag. 77−14837
underwater sound, phase modulation by internal wave vertical vel. 77−46852
underwater sound, simulation of phase modulation of first-mode directional internal wave 77−62089
uniform depth ocean, energy transmission by surface waves through an opening 80−61811
unsteady gravity wave dissipation *(Russian)* 77−78194
unsteady internal wave generation by periodic pressures *(Russian)* 79−100854
unsteady ship waves *(Russian)* 78−16032
unsteady wave development, surface tension effect *(Russian)* 79−100856
unsteady waves from initial, periodic and travelling disturbances, asymptotic anal. *(Russian)* 78−77254
upper ocean inertial oscills. radiation damping, wind mixed layer turbulence 79−39730
variable depth, conf., Canberra, Australia (July 1976) 78−40572
varying depth, classical problems 78−38354
velocities and refr. laws of wave groups, comment 79−70811
velocity, of wind driven waves *(French)* 79−8636
Venice lagoon inlets, maximum waves forecasts computation *(Italian)* 77−37205
vertical diffusion driving mechanism in Oslofjord, tidal origins 80−26531
wave crest height, distrib. of max. values 80−76999
wave energy convertor array power available 78−81216
wave-current random interactions in water of varying depth 77−37238
wave-wave interactions near shore 78−40580
wavenumber spectrum, effects on laser beam refl. from sea surface 80−31121
wavepower review 77−81919
whitecaps and sea state rel. to wind vel. and atmospheric surface layer stability 80−72554
wind driven capillary waves meas. in wave tank, rel. to ocean 79−64673
wind energy transfer to near-inertial waves, calc. 80−4017
wind generated capillary waves, spectral charact. 80−59059
wind generated surface waves, optical meas. technique 77−29503
wind generated wave damping in medium with natural turbulence *(Russian)* 77−41058
wind generated waves, harbour theory based on ray methods 78−69354
wind stress and roughness length over breaking waves 78−24299
wind stress over sea surface for short fetches *(German)* 79−29808
wind wave elevation sensor array system 80−46322
wind wave energy spectrum, spectral-correl. anal. *(Russian)* 77−73752
wind wave generation, Phillips-Miles theory 78−79328
wind wave generation in sea of finite depth 77−64314
wind wave generation on currents, lab. investig. *(Russian)* 77−91143
wind wave phase velocity, laboratory expts. 80−98350
wind waves, components in spectrum of temp. fluctuations in sea upper layer *(Russian)* 78−53655
wind waves, directional slope and curvature distribs. 77−31316
wind waves, EM fluctuations induced on deep sea floor 78−40561
wind waves, high-freq. spectra meas. in presence of currents in shallow sea 80−31053
wind waves, influence on bulk evaporation coeffs., isotopic method determ. 78−85576
wind waves, influence on wind drag coeffs. for marine regime 79−5494
wind waves, long-term parameter distrib. function 78−81202
wind waves, meas. via GOES-reporting waverider buoy 79−5663
wind waves, numerical model 77−922
wind waves, statistical model for groups 80−12409
wind waves calc. 79−14418
wind waves data, appl. to climatic comparisons of estimated and measured winds from ships 80−105020
wind waves generation theory, dynamical eqns. *(Russian)* 78−44840
wind waves growth and var. for weak wind, linear theory *(Russian)* 79−16475
wind waves growth stochastic form. 79−16499
wind waves in finite water depth, freq. spectra *(Russian)* 78−44843
wind waves in shallow water, statistical model *(Polish)* 79−25260
wind waves in stationary regime on deep water, statistical props. *(Italian)* 79−100839
wind waves problems, similarity theory appl. *(Polish)* 77−21795
wind-driven wave parameters determ. at automated buoy stations 79−21064
wind-generated sea waves, interaction with tidal currents 80−51428
wind-generated surface waves, elevation, vel. and accel. statistical distrib. 77−25695
wind-generated surface waves, HF spectrum meas. 78−44857
wind-generated water waves, spatial correls. rel. to freq. independent phase vels. 80−98333
wind-generated wave profile, transform. of wind vel. profiles and drift current *(Russian)* 78−61429
wind-generated waves, airflow separation 77−70734
wind-generated waves, power spectrum, wave height calc. *(German)* 77−17137
wind-generated waves obs. on variable current 77−41053
wind-induced, exptl. investig. of freq. spectrum components dispersion ratio *(Russian)* 79−10581
wind-ruffled sea, sunlight glitter pattern, time-averaged intensity calcs., oil pollution detect. appl. 79−53349
wind-wave height max. in storm, determ. 79−12125
wind-wave interaction, two-layer flow, numerical simulation 78−92823
wind-wave layer, temp. fluctuations *(Russian)* 80−51410
wind-wave tank, microscopic and macroscopic surface structs. growth and decay rates 80−48726

oceanic crust
abyssal regions, gigantic accumulative relief forms 77−21759
Acoustically-Navigated Geological Undersea Surveyor, for Mid-Atlantic Ridge appl. 80−4120
active margin, gravity and struct., British Columbia and Washington 79−92516
active margins 78−57191
Adak Canyon region, central Aleutians, seismicity and tectonics 80−61772
Aegean Sea, crustal struct. from deep seismic sounding 77−64239
Afar triangle, seafloor spreading obs. during November 1978 fissure eruption 79−57912
W.Africa continental margin, Late Quaternary sedimentation 77−21753
W.Africa continental margin, subsidence and uplift, DSDP Leg 41 geological results 77−21754
southern Africa continental margins, continental breakup and deep crustal struct. 77−21742
Agulhas Basin of S.Atlantic, seafloor spreading history, geomag. study 80−21696
SWAlaksa, episodic accretion and plutonism 80−101346
Alboran Sea, crustal seismic profiles 78−61370
Aleutian crustal section, fine struct. from seismic proifle 77−33017
Aleutian Ridge explosive volcanism episodes 78−53636
central Aleutians, ocean bottom seismograph meas. 80−89978
amphibolite facies, Chenaillet Massif, Hautes Alpes, France, example 78−65304
ancient oceanic lithosphere, mag. props. as alteration indicators, Othris ophiolite example 80−8297
Andaman Sea crust, seismotectonics and tectonic history 80−8283
apparent seismic velocity meas. rel. to struct. 77−2117
Arabian Sea, acoustic vel. of sedimentary rock beneath fan 80−72488
Arabian Sea, DSDP Site 220, Fe, Mn and Ti distrib. 77−73708
Arakapas fault belt, Troodos Massif, Cyprus, metallogenesis along fossil oceanic fracture zone 79−29769
Arctic Basin, detailed aeromag. survey, rel. to tectonic evolution 79−70746
Arctic basin, seismic and gravity profiles 77−33030
Arctic Ocean, Alpha Ridge is not spreading centre 79−48455
Arctic Ocean, bathymetry and sea-floor features morphology 79−48453
Arctic Ocean, heat flow north of 60°N 79−48438
Arctic Ocean, mag. anomalies rel. to evolution 79−48398
Arctic Ocean, sediment thicknesses and upper mantle temps. from magnetotelluric soundings 79−48454
Arctic Ocean Basin, form. by circum-Arctic plate accretion and Pacific plate fragments isolation 80−98294
Arctic Ocean bathymetry at latitudes north of 85°N 78−3756
Argentine Basin bottom relief 77−21712
Argo Abyssal Plain, mag. anomalies, bathymetry and seismic struct. 79−29741
aseismic ridges, isostasy anal. 80−3971
aseismic ridges, origin rel. to mantle plumes 77−91081
aseismic ridges, subsidence 77−37162
NE Atlantic, basalts from Great Meteor and Josephine seamounts, K-Ar ages 77−9399
E.Atlantic, Cretaceous black shale, thermal alteration by basaltic intrusions in E.Atlantic 78−61396
S.Atlantic, evolutionary history from deep sea drilling results 77−21756
Atlantic, graben development assoc. with initial rifting 77−21721
N.Atlantic, granite cliff exposure 77−5180
E.Atlantic, heat flow correl. with crustal age and tectonic province 77−86839
Atlantic, Holocene sediments thickness in bottom deposits 79−2216
NW Atlantic, lithospheric elec. resistivity struct. 77−2100
N.Atlantic, mag. anomalies 77−49001
E.Equatorial Atlantic, magnetic anomalies, Jurassic spreading and reversals 77−64253
Atlantic, MODE-I region bathymetry 77−56615
N.E.Atlantic, rifting and subsidence on continental margins 77−73713
N.Atlantic, struct. and age off S.E.Greenland continental margin 77−33014
Equatorial Atlantic, tectonic fabric rel. to adjoining continental margins struct. 77−21695
NE.Atlantic, upper crustal struct., seismic study 80−61784
N.Atlantic, upper igneous crust and Layer 2 porosity estimates 78−53629
Atlantic, vertical tectonic movements during Mesozoic-Cenozoic period 79−2210
equatorial Atlantic (7 to 10°N), fracture zones lithospheric struct. *(Russian)* 80−104932
N.Atlantic basalt geochemistry rel. to mantle heterogeneity 79−29745
Atlantic continental margins and deep sea Late Quaternary sedimentation 77−21751
N Atlantic continental slope, submarine canyons and valleys origin and development 77−21713
N.Atlantic crustal structure, deep drilling results 80−26478
Atlantic fracture zones in equator region, gravimetric model 80−72483
N.Atlantic Mesoic crust reconstruction 80−51365
Atlantic mid-oceanic ridge, axial temp. profile and crustal struct. 80−26476
NE Atlantic Ocean, bathymetry of continental margin around British Isles 80−12372
S.Atlantic Ocean, Cretaceous, study of clay minerals and organic matter *(French)* 79−84220
S Atlantic Ocean, depositional history during last 125 million years 78−44798
Atlantic Ocean, history of growth and topography of ocean bottom 80−3993
S.Atlantic Ocean, palaeoenvironment of anaerobic sediments in Late Mesozoic 77−17074
Atlantic Ocean south of Bermuda, geophys. survey within Mesozoic mag. anomaly sequence 80−26492
S.Atlantic oceanic crust in Mesozoic and subsequent evolution, mag. and gravity data 80−21699
Mid Atlantic plate boundary between Iceland and Azores, seismicity and earthquakes 79−88266
N.Atlantic recent sediments, volcanism effects on mineral comp. 78−44802
N.Atlantic region, gravity anomalies, regional elevation and deep struct. 79−16421
Mid Atlantic Ridge, 22 to 30°N, magmatic process var. and upper mantle heterogeneity 79−88334
Mid Atlantic Ridge, 45°N, seismic vel. struct. of crust 79−25214
Mid Atlantic Ridge, central part morphostruct. 79−44170
Mid-Atlantic Ridge, DSDP site 395, gypsum and halite 79−34796

oceanic crust continued
Mid Atlantic Ridge, palaeomag. studies, direct test of Vine-Matthews hypothesis 79−34734
Mid Atlantic Ridge, rift zone morphometric characts. 79−44171
Mid Atlantic Ridge, spatial-spectral anal. of rift zone relief 78−96190
mid-Atlantic ridge at 23°N, crust at DSDP hole 396B, logging 79−48451
Mid Atlantic Ridge crest, geological and geophys. investigations 80−8284
Mid-Atlantic Ridge crest topography 79−34797
Mid-Atlantic Ridge. Eocene limestones and tectonics 79−12106
Atlantic salt deposits distrib. 77−21752
Atlantic S.E. of Azores, crustal struct. rel. to mag. anomalies and bathymetry 80−51384
N Atlantic subduction directions and evolution of Caledonides 77−2135
Atlantic type continental margins, struct. from geophysical meas. 77−21702
Atlantic-type continental shelves, major synchronous events 77−21720
Atlantic-type geosynclines, metastable phase transition models 79−20822
Atlantis II Deep, geothermal brine system 80−94526
Atlantis II Deep geothermal system, changing hydrothermal activity 78−85532
back-arc basins, asymmetric spreading 80−85636
back-arc convection and marginal basin formation 79−25219
back-arc opening and subduction mode 79−70778
central Baffin Bay, sea-floor spreading 80−51373
Baffin Bay continental margin and Lancaster Sound, seismic refr. meas., continental/oceanic crust boundary determ. 78−20368
Baltic Sea, continuous underwater gamma-survey 80−12377
Banda Sea, seismic refr. expt., crustal struct. 78−73335
Barents Sea, morphostructural map of SE region 78−3749
Barents Sea, shelf relief, morphotectonics and evolution 79−2222
basalt, erupted at Reykjanes Ridge crest, vesicularity 78−73351
basalt, hydrothermal alteration by seawater, chemical exchange exptl. results 79−20828
basalt, Pb isotope comp., rel. to mantle evolution 78−65217
basalt, U exchange during low-temp. alteration, isotopic evidence 79−29744
basalt magnetic properties rel. to crust and upper mantle struct. and development 79−79816
basalt-seawater alteration reactions, studies via dynamic hydrothermal experimental system 79−5686
basalt-seawater reactions chemical exchange, Fe, Mn, and S species results 80−17294
basaltic and gabbroic rocks from W. Mariana basin and Mariana trench 78−65254
basaltic bodies, flow and emplacement direction from mag. susceptibility anisotropy meas. 79−29766
basaltic pillars, in collapsed lava pools on deep ocean floor 80−3991
basaltic volcanism rel. to mid-ocean ridges thermal struct. and kinematics 78−77210
basalts, deep sea, statistical anal. of clinopyroxenes 78−88828
basalts, deep sea, trace element distrib. pattern, neutron activation anal., rel. to genesis 78−11879
basalts, differential Sm/Nd evolution 78−61391
basalts, elec. resistivity meas. 80−21713
basalts, from N Pacific, mag. props. rel. to Pacific plate tectonics 78−40543
basalts, from Pacific Ocean Basin, Sr isotope comp. rel. to mantle comp. 78−65218
basalts, hydrothermal alteration by seawater at high temp. 78−69327
basalts, noble gas abundance patterns controlling factors 78−65220
basalts, trace element mobility during hydrothermal alteration 78−69328
basalts, variations in $^{143}Nd/^{144}Nd$ and $^{87}Sr/^{86}Sr$ ratios 77−29295
basalts, viscous remanent mag. characts. 78−85540
basalts and ferromanganese deposits, Pb, Nd and Sr isotope comp. 78−61395
basalts from DSDP Leg 37 and FAMOUS area, compositional and petrogenetic comparisons 77−91077
basalts from DSDP Leg 37 cores, Pb and U isotopes 77−91123
basalts from Nazca Plate, mag. props. and opaque mineralogy 78−20396
basalts from Project FAMOUS area, petrogenesis from 0 to 15 kbars exptl. study 79−29768
basalts geochemistry from back-arc spreading centre, East Scotia Sea 80−3989
basins, Arctic and N.Atlantic, devel. connection with N.E. Asia plate tectonics 80−85637
bathymetric charts construction aboard ship, efficient method 78−45029
bathymetry and heat flow vars. with age 77−33051
bathymetry profiles, flattening by radiogenic heating in convecting mantle 80−85642
Bay of Islands ophiolite complex, Newfoundland, seismic vel. struct 80−21688
Beaufort Sea area, earthquake data, tectonic setting and stress study 80−3931
Bengal fan, aeromagnetic anomalies 77−73632
Benin Gulf, Africa, oceanic fracture zones rel. to cratonic lineaments 77−21693
Bering Island, tectonic struct. of mountainous region 80−90045
Bering Sea, crustal heat flow and tectonic explanation 80−109123
Betts Cove type oceanic crust and S.Quebec ophiolites 77−81885
Black Sea, Upper Quaternary deep-sea sediments stratigraphy 79−20811
Black Sea basin, crustal struct. from Love and Rayleigh waves dispersion *(Russian)* 78−28192
Black Sea basin formation *(German)* 78−3737
Black Sea continental platform, seismic prospecting method appl. *(Rumanian)* 78−20564
Black Sea Pleistocene clay sediments, physical and mechanical props. 78−3755
Black Sea transverse rise, geological and geophysical data 78−3754
Blake Escarpment, ocean geoid estimation using Geos 3 satellite altimetry data 80−3902
Blanco fracture zone, microearthquakes location determ. using sonobuoy arrays 78−40504
block ridges, gravity field 77−81780
borehole magnetometer data interpretation 80−21625
bottom relief description using spatial correl. function 77−21760
Bouvet triple junction, S.Atlantic Ocean, geochem. and petrology of dredged basalts 78−11877
Brazil, Uruguay and Argentina continental margin geology and tectonics, rel. to S.Atlantic opening 77−21704

oceanic crust continued
S Brazil intracratonic and marginal basins tectonic evolution 77−21743
Brazilian marginal basins, evolutionary stages 77−21699
Brunhes epoch deep sea sediment core palaeomagnetic intensity variation 77−32995
calcareous ooze and chalk, Ontong Java Plateau, W Pacific, sound vel., sonobuoy data 78−40542
Cambrian greenstone belts, Australia, marginal sea crust slices in Lachlan Fold Belt 79−29765
Campbell Plateau and Lord Howe Rise, plate tectonics of SE.Gondwanaland 80−17244
Canadian continental margins, evolution and geophys. features 80−8274
Canadian hotspot under young submarine volcano J. Tuzo Wilson 77−37165
Canary Islands, age and crustal struct. 80−67355
Cape Verde archipelago, underlying crustal struct. from seismic, mag. and gravity data 77−17052
carbonate breccia beds, submarine, depositional model 79−84259
NW Caribbean, submarine morphology off N.Honduras 77−9398
Caribbean plate evolution and buoyant ocean floor 78−96183
E.Caribbean Sea floor, heat flow meas. 79−39683
Caribbean Sea floor, sedimentary cover struct. and thickness *(Russian)* 78−77212
Caribbean seismic network, preliminary results 80−61771
Caroline Plate, petrochem. of troughs and crustal accretion 80−12385
Cayman Trough, mag. anomalies inversion and sea floor spreading 79−34789
Cayman Trough, rock and palaeomagnetic evidence for spreading centre 79−84215
Cenozoic explosive volcanism recorded in deep sea cores, tectonic effects, climatic implications 77−49052
central anomaly magnetization high and sea floor spreading, comments 77−5133
Ceylon-Cocos Zone, thermal regime and nascent island arc 80−56418
Chagos-Laccadive Ridge, earthquake swarm and tectonic implications 79−16395
Charlie Fracture Zone, relationship to continental crust NE of Newfoundland 77−25664
S.China Sea, 1965 October 7, intraplate thrust earthquake 80−26461
Coast Range Complex, British Columbia, heat generation 77−17050
Cocos Plate, lower oceanic crust fine struct. 79−88337
N.Cocos plate, seismic waves vels. in lower crust and upper mantle 79−57858
Colombia basin, Caribbean Sea, crustal struct. from profiler-sonobuoy meas. 78−28198
Concepcion Bank, off Morocco, crustal struct., tectonic unit of volcanic origin 79−39689
continental crust rel. to ocean and margin formation 78−11851
continental margin basins, sediment loading and lithosphere flexure 77−21717
continental margins, stress state 78−3742
continental shelf, possibility of geoelec. mapping 78−57341
continuous seismic profiling, diffr. waves travel time curves 78−3725
convective heat transfer model for lithospheric thinning and crustal uplift 79−84199
converging plates, island arc curvature rel. to convergence vel. and subduction angle 78−81128
converted shear waves trapped in sediment layer ocean bottom seismometers and surface buoy meas. 78−44776
Coral Sea basin tectonic evolution from marine mag. anomaly data 80−21698
Cretaceous deep-sea basalts, $^{40}Ar/^{36}Ar$ for trapped mantle gases 79−16423
Cretaceous mid-ocean ridge basalt (MORB), Nd and Sr isotopic comps. and rare earth element abundances 80−94520
Cuvier Basin, off W.Australia, crust form. by rifting, seismic study 80−12368
Cyprus, ophiolitic sulphide ore deposits prod. by hydrothermal convection 79−29761
deep sea cores sedimentation rates determ. by fission/alpha track counting 78−61392
Deep Sea Drilling Project after ten years 78−73518
deep sea drilling project Glomar Challenger, international phase *(German)* 77−70837
Deep Sea Drilling Project Leg 37-1974, conference Edmonton, Canada, (May, 9176) 77−91069
Deep Sea Drilling Project of Scripps Institution of Oceanography, results 78−69464
deep sea sediment cores, Au, Pd, Ir, Mn sources, neutron activation anal. 80−17247
deep sea sedimentary sections, recycling 78−32059
deep seismic profiling, using refl. meas. *(Russian)* 79−39966
deep seismic sounding system 77−87083
deep structure to NW of Cape Verde Islands 79−2201
deep water surveying, new techniques 78−85730
deep-sea basalts, clinopyroxenes chemistry statistical anal. 80−41437
deep-sea basalts, He and Xe as measure of magmatic differentiation 80−31040
deep-sea cherts and porcelanites, mineralogy of silica phases 77−86856
deep-sea hydrothermal site on strike-slip fault, discovery 80−21710
deep-sea micronodules, near 14 Å mineral of birnessite group 79−74892
deep-sea sediment core, thermoluminesc. dating 79−74871
Dellwood knolls, role in triple junction tectonics off northern Vancouver Island 80−90067
depth anomalies, depend. on latitude and plate motion 78−28215
deviatoric stresses and earthquake occurrence at outer rise of oceanic trenches 79−84196
Djibouti Republic, magnetic anomaly map and tectonic interpretation 80−61753
DSDP interstitial waters, Ca and Mg profiles 77−5177
DSDP Leg 34 basalt, clay mineral form. 79−29767
DSDP Leg 35, Bellingshausen Abyssal Plain, interstitial water profiles and diagenetic reactions 77−5178
DSDP Leg 37, U concs. rel. to oceanic crust form. 77−91075
DSDP Leg 37 basalts, oxide microstructs. and mag. props. 77−91108
DSDP Leg 37 basalts, trace elements and petrogenesis 77−91076
DSDP Leg 37 cores, Pb concs. and isotropic comp. 77−91074
DSDP Leg 37 rock magnetisation and palaeomag. field intensity meas. 77−90996
DSDP Leg 55 rel. to hot-spots and seamount chains in Pacific 78−57184

oceanic crust continued
DSDP site 332, basalts geochemical characts. and evolution 77−91126
Early Cretaceous remanent spreading centre in central Pacific Basin 80−21706
East Pacific Rise, 9° to 12°S, anal. of fast-spreading ridge crest 77−33039
East Pacific Rise at 21°N, hydrothermal activity and crestal struct. 78−28216
East Pacific Rise at 31°S, local axial migration and spreading rate variations 77−29274
Easter volcanic chain, S.E.Pacific, mantle hot line 77−70628
electrical resistivity models, based on lab. meas. of basalts and gabbros 79−29703
Eltanin fault zone, Pacific Ocean, crustal struct. from petrographic data 80−12376
EM response of conducting sphere in two-layer conductor 78−15961
EM waves, lateral-wave propag. in oceanic lithosphere 79−92482
Emperor Seamounts, confirmed extension of Hawaiian volcanic chain *(German)* 78−96189
English Channel, deep structs. and mag. anomalies, possible hidden suture NW of Brittany 78−61397
evolution, East Pacific Rise crest model from seismic refr. data 77−17054
evolution, model constraints, implications and inferences 77−17055
Explorer ridge, marine deep seismic sounding survey 77−17048
Explorer ridge, off W.Canada, marine geophys. survey 79−25224
Explorer Ridge (NE Pacific), crustal struct. from marine deep seismic sounding survey 79−39684
extension behind island arcs and motions rel. to hot spots 79−20796
Falkland escarpment and Agulhas fracture zone, boundary between oceanic and continental basement 77−21700
Falkland-Agulhas Fracture Zone, ridge-crest offset history 80−26490
flexural rigidity and uplifted atolls 78−53630
Florida Straits, appl. of new methods in hydrographic survey 78−81450
fore-arc basins off S.America, seismic reflection profiles 77−44943
fracture zones, geoid anomalies rel. to oceanic lithosphere thickness 79−88231
fracture zones, vertical tectonism 78−53638
fracture zones and deep crustal sections, problems 77−9397
gabbro, dredged, mag. props. and marine mag. anomalies source 79−16437
Galapagos hot spot, bathymetry, magnetic anomalies and basalt magnetization 77−5132
Galapagos hotspot, spreading centre jumps and subaxial asthenosphere flow 77−33042
Galapagos Inner Rift, 86°10′W, struct. and tectonics 79−79808
Galapagos Islands, t, spreading centre jumps 80−104877
Galapagos Rift, hydrothermal Mn 77−86939
Galapagos Rift, hydrothermal plumes obs. 77−64258
Galapagos Rift, mantle He in hydrothermal plumes 77−64259
Galapagos Rift, submarine thermal springs 80−8295
Galapagos Rift at 86°W, regional morphological and struct. anal. 80−26491
Galapagos Rift at 86°W, rift valley sheet flows, collapse pits and lava lakes 80−21708
Galapagos Rift at 86°W, sealed topography and magmatic episodes 80−21681
Galapagos Rift at 86°W, volcanism struct. and evolution of rift valley 80−21707
Galapagos Rift hydrothermal fields, struct. and morphology of seafloor 80−72489
Galapagos Rift hydrothermal mounds, obs. with DSRV Alvin and detailed heat flow studies 80−51383
Galapagos Rift mounds, deep tow hydrothermal obs. 78−11871
Galapagos Rise hot spring field, radionuclide ratios rel. to clam growth rate determ. 79−84300
Galapagos spreading centre, hydrothermal deposits and assoc. basement rocks 79−29750
Galapagos Spreading Centre, hydrothermal source of suspended Mn 79−39699
Galapagos spreading centre, volcanic rock differentiation trends 80−104937
gamma-spectrometric surveying problems 79−2390
geochemical classification of radiolarian cherts and siliceous sediments *(French)* 78−96319
geochemical var. of basalts from Mid-Atlantic Ridge in central N.Atlantic 79−39675
geochemistry, automated X-ray spectrometer appl. 79−16711
geoid anomalies and lithospheric thickness 79−84077
geomagnetic anomaly of spreading centre, modelling of reversal boundary 80−109098
geomagnetic provinces boundary determ. method 77−64480
geomagnetism, induction model for sea-floor coast effect in H-polarisation 77−2104
geomorphology of sea floor and glacial morphogenesis of W.Spitsbergen underwater margins 80−26494
Gettysburg Bank, N.Atlantic Ocean, K-Ar data for age and evolution 79−88322
Gilbert Islands region, sedimentary mantle and basement struct. 79−2219
Goban Spur, SW of Ireland, continental fault pattern, seismic reflection study 77−78152
Gorda Ridge spreading centre, active faulting meas. by sonobuoy array 78−85494
Gorringe Bank, oceanic mantle and crust, geological survey 78−53632
Gran Canaria/Tenerife mag. discordance rel. to NW.African continental margin form. 78−85478
Grand Banks and J-anomaly ridge, geological comparison 78−15983
Greater Antilles, downthrust oceanic crust melting as source of Late Cretaceous granodiorites 79−57927
Guaymas Basin, Gulf of California, heat flow at spreading centres 80−41411
Guaymas Basin spreading axis, high-temp. hydrothermal deposit 80−101355
Gulf of Aden, mag. survey, seafloor spreading phases determ. 78−32049
Gulf of Aden and Afar, mag. anomaly map and plate tectonics 80−56364
central Gulf of California, heat flow meas. 80−3968
Gulf of California transform fault aftershock sequences, sonobuoy and teleseismic study 77−25651

oceanic crust continued
Gulf of Kutch, geomorphology, sediment and tectonic instability origin 80−76960
W.Gulf of Mexico, sedimentary section, multichannel seismic refl. results 77−21749
Gulf of Oman, gas hydrate layers trapping free gas 79−29746
Gulf of Oman, seismic bright spots, possible gas reservoirs 78−32057
Gulf of Papua, crustal struct. from seismic data 80−72459
Gulf of Valencia, W.Mediterranean, aeromagnetic survey *(French)* 77−29243
H-polarisation induction over ocean edge coupled to mantle by conducting crust 77−48994
Hawaiian Archipelago, lithosphere flexure model 79−20785
Hawaiian Island chain, volcanism linear migration from Kauai shield-building volcanism age 80−36281
Hawaiian Islands, isostasy and lithosphere flexure 80−26485
Hawaiian tholeiitic submarine basalts, volatile abundances 79−34795
Hawaiian-Emperor seamount chain, geoid heights derived from Geos 3 altimeter data 80−3899
heat flow, composite trans-Atlantic profile between 20°S and 35°S 77−86827
heat flow meas. over E Canada continental margins 77−5144
heat flow through floor of Scotia, S.Atlantic and Weddell Seas 80−94491
Hebridean continental margin, seismic evidence for Mesozoic age sedimentary troughs 78−53643
Hellenic trench system, subduction to transform motion, Seabeam survey 80−8285
Hercynian Ocean northern margin, sedimentary facies and basin subsidence 77−21725
Hess Rise, W.Pacific, volcanic rocks petrology 80−90026
high velocity layer, vel. indicating garnet comp. 80−17251
hot spring created by drill hole 80−55951
hydrothermal alteration age 79−34798
hydrothermal convection at slow-spreading mid-ocean ridges 79−88340
hydrothermal deposits on Mid-Atlantic Ridge FAMOUS area 78−65259
hydrothermal mounds near Galapagos Rift, chemistry 79−29739
Iceland, coastal shelf and slope, central volcanoes 77−73698
Iceland, crust of oceanic affinity, borehole results 80−8264
Iceland, melting of plagiogranites in oceanic layer rel. to rhyolites generation 77−86885
Iceland, sea floor morphology and mag. anomalies N of Iceland 80−89953
Iceland area, obs. of sea floor morphology and struct. south and west of Iceland 80−90068
Iceland Plateau, deep crust and mantle struct. from surface waves dispersion 80−41413
Iceland position and plate tectonics 77−33041
W.Iceland shelf, central volcanoes, magnetic and gravity evidence 77−37180
S.Iceland shelf, marine magnetic survey 77−37128
Iceland-Faeroe Ridge, crustal struct. 80−90016
Iceland-Faeroe Rise, magmatic rocks 77−78155
igneous rocks, $^{40}Ar/^{39}Ar$ studies 79−53325
inclined seismic zones rel. to age-length depend. of subducting margin 78−57175
Indian, bottom sediments geochem. studies 79−20808
Indian, deep-sea sedimentation, lithologic and palaeomag. study 79−20810
Indian, magmatic rocks, petrographic study 79−20807
Indian Ocean, anomalous geomag. field, statistical model 77−78105
E.Indian Ocean, clay minerals distrib. in sediments 79−44172
Indian Ocean, heat transfer through floor 77−86833
N.W.Indian Ocean, mag. inhomogeneity of basin floors 77−49002
W.Indian Ocean, mantle uplifted block 79−25228
Indian Ocean, model of evolution rel. to breakup of Gondwanaland 80−41428
Indian Ocean, seafloor spreading history 80−61790
E.Indian Ocean, volcanoclastic material in Quaternary deposits 77−78154
Indian Ocean and surrounding areas, contemporaneous tectonic events 77−64256
Indian Ocean floor, geothermal convection through oceanic crust and sediments 79−79812
S.W.Indian Ocean Ridge, sea-floor spreading and Africa-Antarctica present relative motion 77−29272
Indian Ocean sediments, seismic vels. meas. by sonobuoy 77−86852
NW Indian Ocean structures, crustal density section construction *(Russian)* 79−48431
Indian Ocean triple junction region, microseismicity 78−32020
SE.Indian Ridge, seafloor mag. anomalies rel. to chem. of mid-ocean ridge basalt 80−109102
Indo-Australian plate, deformed oceanic crust rel. to plate internal deform. 80−109134
induced electrical currents below ocean bottom with vertical water flow 80−104863
inter-arc basins, kinematic model 78−81127
interior structure *(Russian)* 79−100822
intraplate seismicity on bathymetric features, 1968 Emperor Trough earthquake 80−30997
Ionian Sea, Medina rise and Cyrene seamount *(Italian)* 79−16433
Ireland to Spain continental slope morphology 78−96191
island arcs, tectonic flow 79−25223
isostasy at midocean ridge crests 80−31022
Jan Mayen fracture zone, Norwegian Sea, seismicity map 77−78127
Jan Mayen Ridge, Cepan 1 1975 survey 78−96184
Japan trench, microearthquake activity in oceanic lithosphere off Sanriku 77−81803
Japan-Bonin trench, crustal and upper mantle changes 80−72466
Juan de Fuca and Explorer Ridges, recent plate interactions, model 77−66900
Juan de Fuca plate aseismic subduction, geodetic evidence 79−84209
Juan de Fuca plate movements 79−44162
Juan de Fuca ridge, heat flow meas., evidence for hydrothermal circulation 78−28197
Juan de Fuca Ridge crest, E.Pacific, tectonic topography compensation 80−56448
Juan de Fuca ridge system, heat flow meas., water circulation 80−72468
Juan de Fuca spreading centre tectonics, propagating rift model and pseudofaults 78−32046

oceanic crust continued
Juan de Fuca-Gorda Ridge area, mag. anomalies and basalt comp. 77−29242
Jurassic seafloor, Point Sal, California, rare earth and trace element geochem. 78−32094
Kamchatka basin, W.Bering Sea, seismic refr. meas. 77−17053
Kane fracture zone in western Central Atlantic Ocean 77−5170
Kane Fracture Zone of Atlantic, seismic study of crust struct. 80−104936
Kane fracture zone of central Atlantic 80−21668
Kerguelen Islands area, geoid determined from Geos 3 altimeter data correl. with sea bottom topography 80−3900
King's Trough, NE.Atlantic Ocean, struct. from bathymetric, seismic and gravity data 78−49005
Kuril-Kamchatka trench, seismic study of crust 80−89982
Kurile trench-Hokkaido rise system, flexure profile by plate model 80−72482
Labrador Sea and North Atlantic evolution 78−28210
Laccadive Ridge, DSDP Site 219 results 77−73707
Laccadive uplifting zone, crustal struct., gravity field modelling *(Russian)* 80−3966
late stage development of mature Atlantic-type continental margins 79−20786
Lau Basin, magnetic anomalies and crustal dilation 77−5131
layer 2, geochemistry of secondary minerals in basalts from (DSDP Leg 37) 77−91127
layer 2, low-temp. seawater-basalt interaction rel. to S distrib. 80−41432
layer 2 basalts, occurrence of TRM questioned 78−65279
layer 2 basalts DSDP Leg 37, low-temp. fluid alteration 77−91102
layer 2 magnetisation, results from DSDP (Leg 37) 77−91071
Lesser Antilles island arc, crustal struct., seismic refr. expt. 79−84139
lithosphere age-dependent subduction beneath western South America 79−2211
lithosphere flexure and uplifted atolls, comment 80−26486
lithosphere generation, rel. to upper mantle origin of ophiolite suites 78−65311
lithosphere isostasy, anal. for Hawaiian-Emperor seamount chain 79−39688
lithosphere mechanical behaviour, implications of two earthquakes seaward of Tonga Trench 79−16405
lithosphere rheological models 77−21716
lithosphere stress, from calcs. on Icelandic thermal area rock stress 80−90012
lithosphere thermal structure rel. to ridge-crest and transform earthquakes source parameters 79−88265
lithospheric formation, thermal boundary layer 77−73696
lithospheric plates underthrusting zone, oceanic sediments subduction mechanism 77−53030
lithospheric thinning, hot spots and island subsidence 78−53631
Lomonosov Ridge Experiment (Lorex 79) in Arctic Ocean 80−77120
Lord Howe Rise and SE.Australian margin, rift valley breaching 78−96179
magma mixing at mid-ocean ridges, DSDP data 78−77209
magma mixing at mid-ocean ridges, evidence from Mid Atlantic Ridge basalts 79−88335
magma series erupted in different marine tectonic settings, trace element anal. 80−21667
magnetic anomalies, validity of geological interpretations 77−60348
magnetic anomalies of seafloor spreading rel. to geochemistry 80−56345
magnetic anomalies recorded during deep-water mag. surveys, statistical anal. 80−36233
magnetic polarity record questioned by Arizona reversal chronology 80−72419
magnetic properties, DSDP Leg 34 results from Nazca plate 77−17024
magnetic records rel. to sea floor spreading 77−9337
magnetic signal, simulation of long-term changes 77−90995
magnetisation, review 77−2088
magnetized layer, lower bound on thickness 78−28162
Marcus-Necker Ridge, volcanic rocks comp. and stages of development 80−36282
marginal and interarc basins, volcanic evolution 80−8271
marginal basins, diffuse magnetic anomalies and their tectonic and petrologic significance 78−32064
marginal basins, formation rel. to relative plate motions 80−41427
Mariana Trough, back arc spreading characts. 78−53640
Marianas trench, Pacific Ocean, basic and ultrabasic rocks 77−21757
marine Bouger gravity calc. using processing density concept 79−74829
marine geology and geophysics, 1967-77 review 77−64260
marine geomagnetism, plate tectonics, plate boundaries and mag. field reversals *(French)* 79−66621
marine magnetic anomalies, source shape and nature 77−17021
marine magnetic anomalies origin, implications of palaeomagnetism of Thetford Mines ophiolites, Quebec 80−61757
marine refraction seismology, interpretation techniques 77−64230
marine sediments, mag. stratigraphy using susceptibility meas. 79−84520
marine sediments, seismic vel., density and attenuation models from multibounce phases 79−57864
marine seismic survey off Canada west coast, crustal struct. 79−100820
massive sulphide ores genesis, geothermal model from altered volcanic rocks geochemistry at Matagami, Quebec 78−77231
E.Mediterranean, deep struct. and tectonics 78−69309
Mediterranean and marginal seas origin 78−69322
Mediterranean interarc basins, comparison of Tyrrhenian and Pannonian basins 77−13075
Mediterranean region, struct. and tectonics, conf., Haifa, Israel (Aug.-Sep. 1976) 78−69306
E Mediterranean regional vertical tectonics from gravity obs. 77−5172
S.Mediterranean Ridge sand, petrographic analysis 79−70782
Mediterranean Sea, fossilised death valley *(German)* 79−57913
Melanesia Basin deep-sea sediments, palaeomag., polarity reversals 78−36102
membrane stresses near mid-ocean ridge−transform intersections 79−20784
Mesozoic sea floor off Dronning Maud Land, Antarctica, magnetic mapping 78−3715
metagabbronorite from DSDP hole 334, high-temp. deform. and recrysts. near Mid-Atlantic Ridge 77−91125
microearthquake location using max. likelihood processor 77−17033
microearthquakes near St. Paul's Fracture Zone, depth determ., lithosphere thickness 78−48980
oceanic crust continued
microseism generation mechanism from sea floor obs. off Shikotan Island 78−73319
Mid Atlantic Ridge, FAMOUS area, petrogenesis of basalts 78−11891
Mid Atlantic Ridge, geophysical significance of plagiogranite 78−16007
Mid Atlantic Ridge, long-range sonar study and tectonic implications 77−33049
Mid Atlantic Ridge, metamorphic mineral data of dredged metabasalt block 77−64279
Mid Atlantic Ridge, SW of Azores, deep seismic sounding results 78−3747
Mid Atlantic Ridge and Kurchatov Fracture Zone, sonar obs. 78−28214
Mid Atlantic Ridge crest at 26°N, magnetic anomaly patterns, spreading rate 77−32991
Mid Atlantic Ridge near 45°N, ocean bottom seismograph obs. 78−11875
Mid Atlantic Rift Valley, basaltic rocks from FAMOUS area, petrological diversity and structural setting 77−78150
mid ocean ridge median valleys, faulting 77−44964
Mid-Atlantic Ridge, FAMOUS area basalt glasses regional var. and petrogenesis 80−31041
Mid-Atlantic Ridge, geology of submarine hydrothermal field at 26°N latit. 80−85641
Mid-Atlantic Ridge, median valley model from gravity obs. 80−90071
Mid-Atlantic Ridge, oblique intersection with Charlie-Gibbs transform fault 79−84212
Mid-Atlantic Ridge, radiocarbon and ^{210}Pb distribs. in deep-sea sediment cores 77−37179
Mid-Atlantic Ridge, struct. at 45°N 78−73332
Mid-Atlantic Ridge, sulphides in DSDP Leg 37 drill core 77−91122
Mid-Atlantic Ridge (7 to 9°N), deep crustal architecture in Vernadsky fracture zone *(Russian)* 79−96747
Mid-Atlantic Ridge at 37°N, geophysical anomalies in DSDP Leg 37 drilling arcs 77−91070
Mid-Atlantic Ridge basalts, geochem. variation along length of ridge 80−90027
Mid-Atlantic Ridge basalts from DSDP sites 332 and 335, petrology and alteration 77−91124
Mid-Atlantic Ridge crest at 37°N, crustal struct. 77−9378
Mid-Atlantic Ridge mafic and ultramafic rocks, Pd, Ir and Au contents 77−91073
Mid-Atlantic Ridge N of Azores crust and upper mantle struct. 77−73691
Mid-Atlnatic Ridge, ocean-bottom seismograph obs. near 45°N, results 78−96157
Mid-Cayman Rise spreading centre, basalt glasses geochemical var. and petrogenesis 80−101364
mid-ocean ridge basalt, composition restrictions, fluid dynamical model 80−90025
mid-ocean ridge basalts, density var. rel. to magma mixing and primitive lavas scarcity 80−56460
mid-ocean ridge spreading rate, petrological evidence 80−109135
mid-ocean ridge system, thermal struct. rel. to global sea-level changes 79−29743
mid-ocean ridges, estimators for heat flow and deep rock props. 77−86843
mid-ocean ridges, spreading rate rel. to oblique spreading, model 79−34786
mid-oceanic ridge axes, topography and tectonics from fluid dynamic models 80−41433
mid-plate hot-spot swells, thermal origin 79−8619
Middle America Trench offshore Guatemala, seismic refr. and refl. meas. 80−26493
Middle-America Trench, visual obs. of sea-floor subduction line 77−66902
midocean ridge, existence of mantle double partial melt zone 80−104940
midocean ridge basalts, source evolution from Bay of Islands ophiolite complex Nd and Sr isotopic study 80−85651
midocean ridge hydrothermal systems, hot water egress thermal constraints 79−39700
mineral deposits, prospecting, extraction, X-ray spectrometric anal. *(German)* 78−20551
minerals, metal-rich deposits in oceanic lithosphere, origin 78−53634
minerals exploration, Mobile Initial Condition Indicator approach 79−5687
Mount Carmel, struct. and extension into E.Mediterranean, marine geophys. survey 77−33026
Mozambique Basin, Mesozoic magnetic lineations 79−66608
Mozambique Channel, crustal struct., seismology study 80−51362
Narmada-Son lineament, extension towards Murray Ridge 78−15985
Nauru Basin, trace element abundances in basalts 80−94499
Nazca plate, finite element modelling of stresses 79−20802
Nazca plate off S. Peru, crustal model from ocean bottom seismometer obs. 78−32032
New England Seamounts, submersible observations 78−20383
New Hebrides arc, tidal tilt from localized ocean loading 80−98211
New Hebrides arc-trench system, structure 80−72465
New Hebrides island arc, tectonic troughs form. mechanisms 78−73349
New Hebrides trench, subduction rate rel. to lithospheric bulge 77−53029
W.Newfoundland, ^{40}Ar/^{39}Ar ages and ophiolite obduction 77−33034
Newfoundland, Bay of Islands ophiolite complex, oceanic crust exposure 78−40506
NE Newfoundland, geophysical and geological trends on continental shelf 77−5145
Newfoundland Ridge, seismic structure, nature of crust, oceanic origin 79−25211
Ninetyeast Ridge, seismic sounding with bottom seismographs and air guns 78−3748
Ninetyeast Ridge area, seismicity and tectonics, Indian plate internal deform. 78−73343
Nootka Fault Zone, new plate boundary off W.Canada 79−92518
North American Atlantic continental margin, rapid Cretaceous subsidence and sedimentation 77−21722
North American Atlantic continental margin, sedimentary basins 77−25666
W.North Atlantic Ocean, sediment cores laboratory and in situ compressional wave vel. meas. 79−57866
N.Norway, continental margin crustal struct. and tectonic history 80−51360

oceanic crust continued
Norwegian-Greenland basin continental slope, submarine canyons and valleys origin and development 77−21713
Norwegian-Greenland sea, thermal evolution in sea floor spreading model 80−56427
ocean-floor metamorphism, rel. to seismic layering and magnetism 77−13068
Okhotsk and Japan Seas abyssal depressions, struct. and origin 77−37168
Okhotsk Sea deep basin, seismic study of crust 80−89982
Ontong Java and Manihiki Pacific oceanic plateaus, seismic struct. 80−21680
ophiolite complex of Point Sal, California, seismic vel. struct. 80−109110
ophiolite complexes, effects of alteration on NRM and implications for oceanic crust 78−65280
ophiolite complexes, evidence for past magnetism 80−109092
ophiolite complexes limitations as models for mag. layer of oceanic lithosphere 78−81145
ophiolite nappes emplacement, Mesozoic-Cenozoic examples 77−41012
ophiolite petrogenesis in oceanic crust, Nd and Sr isotope study 80−61782
ophiolites, Chilean, hydrothermal metamorphism vars., ocean floor metamorphism implications 79−88354
ophiolites, identification in oceanic crust 78−81117
ophiolites, seismic vels. and oceanic crustal struct. 78−77226
ophiolites of S Quebec, oceanic crust of Betts Cove type *(French)* 79−57923
ophiolitic peridotites structures, role of young lithosphere thrusting in subduction zones 80−56446
ophiolitic rocks tectonic emplacement in Precambrian Mona Complex, Anglesey 79−8631
origin by gross modification of continental crust, seismic evidence 80−89997
orogenic lherzolite petrogenesis in oceanic crust, Nd and Sr isotope study 80−61782
outer rise of oceanic trench, dynamic support 78−81116
Owen Basin, Arabian SE margin, and Owen Fracture Zone evolution 79−84217
Owen fracture zone, NW Indian Ocean, ultramafics petrology rel. to nature of oceanic upper mantle 80−94519
P-wave teleseismic delay times in major oceanic fracture zone 79−70754
Pacific, compressional wave anisotropy 77−17040
Pacific, continuous seismic profiling, sedimentary mantle struct. and comp. 79−20806
Pacific, crustal struct. in Marcus Island area 79−53331
Pacific, dissection of ocean floor 77−21711
S.Pacific, DSDP site 284, Late Cainozoic isotopic history 79−48516
Pacific, eastern central region, sea floor relief from side-scan sonar obs. 78−36142
N Pacific, eddies generated by seamounts 78−69367
W Pacific, evolutionary history 77−44965
S.W.Pacific, gravity anomalies and main tectonic units 77−17078
W.Pacific, HF P_n and S_n phases obs. at great distances, spectral anal. 78−77195
W.Pacific, high freq. P_n and S_n phases 77−86799
Pacific, Love and Rayleigh seismic wave attenuation in 15-100 s periods 77−9353
W. central Pacific, Mesozoic evolution 77−44953
S.Pacific, neoformation and weathering of assoc. volcanosedimentary levels *(French)* 78−73353
N. central Pacific, ocean floor magnetotelluric sounding 77−86772
N.Pacific, sediment core geotechnical and mineralogical props., appl. to coastal site for simulation *(French)* 79−34800
W.Pacific, struct. from seismic surfaces waves freq.-filter anal. 79−48573
N.E.Pacific and Alaska, plate tectonics and palaeomagnetism 77−91092
Central Pacific Basin, $^{40}Ar/^{39}Ar$ ages of diabase sill and basalt, rel. to ocean floor history 77−66897
SW.Pacific basin, reverberant subbottom layers distrib. 80−8290
Pacific crust surface wave dispersion 77−56604
W Pacific guyots, $^{40}Ar/^{39}Ar$ ages and evolution 78−11876
Pacific island and seamount ages rel. to volcanic chains origin 77−64242
W.Pacific island arcs, $^{87}Sr/^{86}Sr$ ratio in volcanic rocks 77−33031
Pacific lithosphere, flexure seaward of Bonin and Mariana trenches 79−57903
W.Pacific marginal basins, sea floor spreading evidence 77−37177
N.Pacific Mn nodule area, Recent metalliferous sediments 77−17076
Pacific Ocean, box cores from Ontong-Java Plateau, radiometric obs. 80−61793
Pacific Ocean, deep EM sounding near Californian coast, interpretation 77−9383
Pacific Ocean, Pn waves propag. rel. to lower lithosphere struct. 80−26459
Pacific Ocean, Sb in metalliferous sediments 77−78156
Pacific Ocean basin, volcanic history since Jurassic, crustal loading study 80−46165
Pacific Ocean bottom sediments, interstitial waters B content 80−36289
Pacific Ocean crust, seismic props. of layer 2A 77−29260
NW.Pacific oriented sedimentary cores, geomag. polarity transitions meas. 79−88243
Pacific plate, central stress fields delineated by linear volcanic chains 77−17068
E.Pacific Rise, 9°N, transitional basalts and tholeiites 79−84218
E.Pacific Rise, equatorial, regional shape and tectonics 78−44800
E.Pacific Rise, hot springs and geophysical expts. 80−101360
E.Pacific Rise, hydrothermal heat flux of black smoker vents 80−94488
E Pacific Rise, massive deep-sea sulphide ore deposits discovery 79−34799
E.Pacific Rise, metalliferous sediments and Fe-Mn concretions, magneto-mineralogical study 79−62481
E.Pacific Rise, metalliferous sediments three-dimensional distrib. 80−21705
E.Pacific Rise, P accumulation rates in metalliferous sediments 77−60364
E.Pacific Rise, picrite analysis 79−79810
E.Pacific Rise, struct. of crust, volcanism periodicity and magma flow 80−17243
E.Pacific Rise, sulphide deposits obs., near 21°N 80−101361
E.Pacific Rise, synthetic seismic profile 79−12095
E.Pacific Rise, young cratered volcanoes pairs 80−12374

oceanic crust continued
E.Pacific Rise−Galapagos Rise system, geophysical surveys results 78−73331
E.Pacific Rise crest, crustal struct. vars. from seismic travel time inversion 77−60357
E.Pacific Rise crest structure from multichannel seismic reflection 78−40523
E.Pacific Rise evolution between 3-13°S since Middle Miocene 78−88813
E.Pacific Rise geothermal system, physical limits on geothermal fluid temp. and role of adiabatic expansion 80−101362
E.Pacific Rise near 3°25′S, structural geomorphology of fast-spreading rise crest 78−44799
Pacific sea-floor topography and isostatic compensation mechanism (Hawaii region) 80−104945
Pacific subduction zones, great earthquakes recurrence 77−17045
N.Pacific subduction zones, plate effects 77−37176
Pacific-Nazca plate boundary, fast slipping transform fault zone near-bottom reconnaissance 79−25226
palaeobathymetry of spreading ridge crests rel. to age of ocean basins 77−29282
Palaeogene komatiites from Gorgona Island 79−44168
Papua New Guinea-Solomon Islands region, 1964-1973 earthquakes, seismotectonics 80−8270
Parece Vela Basin, E.Philippine Sea, evolution and chronology 80−41431
parental magma for ocean floor basalts, MgO content 79−44155
Peruvian continental margin, Andean geosynclinal pair 77−21724
Philippine Sea origin and development, ^{40}Ar-^{39}Ar ages from DSDP Leg 31 77−64254
Philippine Sea plate, lateral structural variations, surface wave anal. 77−33024
pillow lava, spreading cracks props. 79−79780
piston core behaviour recording device 78−20532
plate bending at trenches, mechanical models constraints from earthquakes 80−41426
plate motions driven by lithospheric thickening and subducted slabs 79−8622
plate-stress rel. to mantle circulation with partial shallow return flow rel. to oceanic plates 78−40520
Prince Edward fracture zone and Mozambique basin evolution, S.W.Indian Ocean 77−17077
Puerto Rico Trench origin and gravity anomalies 78−11861
random magnetisation, effect on coherence of short-wavelength marine mag. anomalies 80−36225
Rayleigh wave dispersion along Reykjanes Ridge rel. to lithosphere age 79−88267
Rayleigh waves, group vel. distribs. and upper mantle models, Pacific Ocean *(Japanese)* 79−70747
Red Sea, basalts rel. to $^3He/^4He$ ratio in brines 77−25693
Red Sea, crustal age and extent 77−29284
Red Sea opening with two poles of rotation, comments 77−5171
refractory megacrysts and Mg-rich melt inclusions in spinel in oceanic tholeiites 78−32060
reversal transition widths and fast spreading centres 77−17022
Reykjanes Ridge, crustal struct. at 63°N from seismic meas. 79−66661
Reykjanes Ridge, crustal struct. from seismic refr. 80−90020
Reykjanes Ridge, heat flow survey, age and heat flow relation 79−79768
Reykjanes Ridge, mid-Atlantic 59½°N, seismic crustal struct. 80−56423
Reykjanes Ridge, near-bottom geophysical traverse 78−65253
Reykjanes Ridge, new heat flow obs. 80−90011
Reykjanes Ridge, Profile I on SE. flank, seismic struct., RRISP 80−90019
Reykjanes Ridge, SE.flank, lithosphere evolution, seismic surface wave study 80−90022
Reykjanes Ridge crest, morphology near 62°N 80−90070
Reykjanes Ridge crest, rifted and nonrifted regions transition 79−88338
Reykjanes Ridge crest studied by surface waves with an earthquake-pair technique 80−90021
Reykjanes Ridge Iceland Seismic Experiment (RRISP 77), for crust struct. 80−90017
Reykjanes Ridge Iceland Seismic Project 1977, first results 79−57889
Reykjanes Ridge south of 60°N, evolution between 40 and 12 Myr before present 80−90069
ridge basalts, trace elements, rel. to mantle comp. 78−65219
ridge crest hot springs, obs. and implications 80−98304
ridge crests, hydrothermal activity rel. to ocean major and minor elements balance, Galapagos data 80−41459
ridge crests, metal-rich deposits form. 80−41430
ridge crests, thermally expanded, gravity signatures 79−66604
ridge migration and asymmetric sea floor spreading 78−11858
ridge system, volume changes rel. to secular changes in continents marine inundation 78−3735
rift valley formation over oceanic ridge, upwelling flow model of topographic profile *(Chinese)* 80−8280
rift-transform struct. of seafloor ridge system, thermal convection and tidal bulge formation 77−64252
rifted ocean ridges, evolution 79−34787
rifted oceanic ridges, comparison with ophiolitic breccias in E. Ligurian Apennines 77−86881
rifting and subduction causes, appl. to Atlantic margin of Brazil 78−3743
Rio Grande rise volcanic rocks, petrology 77−81866
Rivera-Tamayo oceanic fractures, ocean bed renewal, photographic/seismographic obs. *(French)* 79−74887
Rockall Bank, N.Atlantic, seismic struct., synthetic reconstruction 80−21670
Rockall Trough near-bottom traverse, hydrographic and geological inferences 79−62483
Romanche fracture zone, equatorial Atlantic, Neogene crustal emersion and subsidence 78−11857
S-wave velocity versus depth in marine sediments 77−17034
Scotia Arc evolution rel. to SW Gondwanaland reconstruction 77−33043
E.Scotia Sea, back-arc basin, volatiles in submarine volcanic rock 80−67353
Scotia Sea Island arc and back arc tholeiites, geochemical study 78−11872
sea floor roughness rel. to mesoscale ocean dynamics 79−84216
sea floor spreading, deep subduction and plate motion 78−88810
sea mounts, S.Indian Ocean, gravity models *(French)* 79−74884

oceanic crust continued
Sea of Japan, geomorphological struct. and development of central bays 77 – 49088
Sea of Japan, terrigenous and volcanogenic deep sea bottom sediments chem. comp. 77 – 21758
sea-floor basalt, rare earth elements behavior during weathering 79 – 57910
sea-floor topography, tectonic model using vol. expansion coeff. 80 – 90072
sea-mount loads affecting crust, isostatic compensation and geoid anomalies 80 – 109132
seafloor spreading, south of Agulhas Fracture Zone 78 – 24277
seawater-saturated ocean crust and oceanic island basalts, elec. props. freq. spectrum 79 – 25229
sediment model, elastic wave propag. 77 – 44966
sedimentary basins, thermal and subsidence history 78 – 49010
sedimentary basins of continental margin and craton, conf., Durham, England (Apr. 1976) 77 – 21715
sedimentary basins subsidence mechanisms, review 77 – 21746
sedimentary sea bottoms, machine classification 79 – 92626
sediments, acoustic wave vel. attenuation and refl., math. model 77 – 91104
sediments, neutron activated, gamma-ray scanning for elemental profile distribs. 77 – 17079
sediments, reflected and scatt. US waves, granulometric mode determ. *(French)* 78 – 92815
sediments containing gas hydrates, thermal cond. and acoustic wave vel. meas. 79 – 79819
sediments from DSDP Site 219, trace elements partition patterns 78 – 36143
seismic and magnetic obs. off SW Indian coast 77 – 41018
seismic internal vels. in crustal layers from sonobuoy records of mantle reflections 78 – 28184
seismic Lg phase search 79 – 25203
seismic long range explosion expt., preliminary report 77 – 73679
seismic low velocity layer at base of crust 77 – 37164
seismic Rayleigh waves of period 50 seconds, group vel. distrib. in Pacific Ocean 78 – 65197
seismic shear velocity struct., porosity and petrology 80 – 72473
seismic sounding of ocean crust, suppression of sea-floor multiples 80 – 90231
seismic surface waves azimuthal anisotropy, physical model 78 – 65186
seismic vel. evolution 79 – 5457
seismic velocity structure below Hawaii island from local earthquake data 79 – 84195
seismic wave field assoc. with fine structured Moho in continents and oceans 80 – 12361
seismic waveform synthesis, generalized ray and reflectivity methods comparison 79 – 84501
seismograph records, computer processing method 80 – 85605
seismological techniques, two-chip multichannel methods 80 – 56632
seismometer stationed on ocean bed, self-contained unit with mag. recorder *(Russian)* 80 – 36410
Seychelles-Mauritius Plateau, mag. anomalies, sediment thickness 78 – 3750
shear wave travel time residuals from oceanic earthquakes 77 – 64224
Shikoku Basin, off-ridge volcanism and seafloor spreading 78 – 65256
Sierra Leone Rise, equatorial Atlantic, alkali-rich volcanics 79 – 2215
silicic lithology of spreading ridge, late-magma vap. transport of K 80 – 81877
Siqueiros transform fault and East Pacific Rise, basalt petrology and chemistry 77 – 33050
Snares and Auckland Is., Campbell Plateau, radiometric ages 77 – 29281
Somali Basin, seismic profiling and bottom topography, possible fracture zone 78 – 28213
source-span-sink thermal models of arcs and ridges 78 – 32040
South China Sea basin, crustal struct. from profiler-sonobuoy meas. 80 – 8291
South Sandwich Islands, seismicity 78 – 7582
Southern Africa continental margin, sedimentary basin form. processes 77 – 21723
spreading, driving mechanism 79 – 100824
spreading centre processes, qualitative models including hydrothermal penetration 77 – 33045
spreading centres, hydrothermal stress drops and convective patterns 79 – 88339
spreading centres, perpendicularity to transform faults questioned 78 – 24276
spreading ridge subduction, thermal effects 79 – 88321
spreading ridges, crests palaeobathymetry rel. to ocean basin ages and latit. 78 – 11869
spreading ridges, upper mantle partial melting 78 – 65237
spreading ridges in young oceans, model with thick oceanic crust at continental boundary 79 – 79781
St. Helena Is., seamount age and bathometry 79 – 16436
stratigraphy of deep sediments rel. to Eemian interglacial 79 – 29770
stress accumulation in lithosphere 77 – 17071
structure, composition and origin 77 – 29268
structure from refraction expts. 80 – 3952
structure from seismic surface wave obs. 78 – 73323
subducted oceanic lithosphere, age rel. to interarc spreading and cordilleran tectonics alternates 79 – 29732
subduction, thermodynamic consequences of minerals dehydration, high press. and temp. 78 – 69301
subduction shear zones in Tonga and Mariana systems, stress and temp. 79 – 8620
submarine basalts, sea water weathering effect on K-Ar age 77 – 86830
submarine canyon heads, relief development processes, Black Sea 78 – 44803
submarine canyons as internal wave traps 77 – 9436
submarine faulting and ringing P-waves 79 – 84158
submarine geothermal resources, seafloor spreading centres and volcanic areas 77 – 37171
submarine lithosphere, geophys., geochem. and petrological model 80 – 3994
submarine pillow basalts, seafloor weathering effects on geomag. palaeointensities determ. 80 – 3927
subsurface layered media parameters, estimation using linearised multiple refl. model 79 – 5691
Suiko seamount, Emperor seamount chain, palaeomagnetism and relation to Hawaiian hot spot 78 – 57162
oceanic crust continued
Sunda and Banda Arcs, seismic studies of crustal struct. 77 – 70622
Sunda trench and forearc basin, seismic study 80 – 72470
surface deformation, gravity anomalies and mantle convection 77 – 44893
surface heat flow, geotherms and lithospheric thickness regional var. 77 – 53025
surface wave anelastic attenuation lateral var. across Pacific 79 – 84123
surface waves anomalous propagation in Barents Sea, from NORSAR data 79 – 25202
suture zone complexities, review 77 – 66904
synthetic seismograms from model ocean bottoms 79 – 48420
Tamayo transform fault, E.Pacific Rise, deep tow study 80 – 51361
Tanzawa plutonic complex, Japan K, Rb, Sr in granitic and gabbroic rocks 77 – 17100
Tasman Sea evolution, marine magnetic data 78 – 11870
tectonic plate subduction zone seismicity, Makran coast, Iran 80 – 85635
tectonics, ocean bed relief rel. lithosphere development *(Russian)* 79 – 88333
Tethyan oceanic crust evolution during Mesozoic, rel. to N.W.Syrian ophiolites 77 – 81896
thermal conductivity meas., pulse-probe method 79 – 53533
thermal evolution of ocean ridge, affected by spreading rate 80 – 56424
thermal evolution of passive continental margin 80 – 56427
thinning of low-vel. layer across Kurile-Japan trench 79 – 79782
tholeiitic basalts, rare earth elements behaviour during submarine weathering 78 – 73369
tidal deformation of sea floor and continents, ocean tides effects *(Russian)* 77 – 29308
Timor Trough and Australia, facies rel. to topographic wave migration during past 3 million years 78 – 49018
Tonga-Lau system, deep collision of subducted lithospheric plates 79 – 29736
topographically driven subcritical hydrothermal convection 80 – 101345
topography of ocean bottom rel. to lithosphere viscosity 77 – 64250
trace element geochem. of peridotite-gabbro-basalt suite, DSDP Leg 37 site 79 – 34793
transform earthquakes, source parameters rel. to plate vel. and transform length 78 – 53620
Transkei Basin, seismic refraction obs. 78 – 11831
trench outer rise width, model of crust thickness as function of age 80 – 56426
trenches maximum depths in world ocean 79 – 2220
Troodos ophiolite metamorphism, implications for marine mag. anomalies 80 – 81812
Tyrrhenian Sea, basalt geochemistry 79 – 53329
Tyrrhenian Sea floor, tholeiitic basalts 78 – 11873
Tyrrhenian Sea rifting, Rayleigh wave dispersion evidence 80 – 56445
Uordan-Dead Sea rift, crust and upper mantle seismic study, transition towards Mediterranean Sea 79 – 79766
upper crust formation model based on ophiolite data 77 – 60358
upper crustal structure from variable angle seismic reflection-refraction profiles 79 – 70761
NW USA, evolution from oceanic to continental crust 77 – 86847
volcanic material alteration in marine sediments, SE.Pacific Ocean 80 – 3990
Walvis Ridge, compensation mechanism 80 – 94448
Walvis Ridge, lithospheric struct. from Rayleigh wave dispersion 80 – 41412
Walvis Ridge, S. Atlantic, gravity anomalies and origin 80 – 21682
Walvis Ridge, S.E.Atlantic Ocean, morphology of S.W. region 77 – 64262
Walvis Ridge, seismic refr. obs., crust and mantle struct. 77 – 78153
water waves propagation over deformable sea floor 79 – 57966
Watkins seamount, Pacific Ocean, Cretaceous origin, palaeomagnetic obs. 80 – 104874
Weddel Sea, geomagnetic, bathymetric and seismic obs. of crust 80 – 104929
Willaumez-Manus Rise, Papua New Guinea, origin 79 – 88329
world distrib. of sutures, continental collision 77 – 66905
Yermak hot spot in Arctic Basin, magnetic and bathymetric evidence 79 – 88313
zone regining below lithospheric plates, steady state astheriosphere model 79 – 88326
zoned steady-state magma chamber comp. var., evidence from Mid Atlantic Ridge 79 – 88336
^{40}Ar-^{39}Ar geochronological studies on submarine rocks from W.Pacific 77 – 17075
Fe-Mn deposits on abyssal sea floor, geochem. 79 – 12107
Mn concretion growth rates, nonradiometric considerations 78 – 61393
Mn nodule, sediment-water interface and submergence dynamics 78 – 28217
Mn nodule mining and processing with nuclear meas. 77 – 4975
Mn nodules, accumulation rates from alpha track method 78 – 7610
Mn nodules, deep-sea, Ni and Cu accumulation as essential elements in 10-Å manganite 79 – 66674
Mn nodules, from Pacific Ocean growth rates from U series and hydration-rind dating 77 – 29280
Mn nodules, mineralogy and comp. changes from long-term seafloor mineral exposure expts. 79 – 5471
Mn nodules, on deep ocean floor struct., composition, economic pot. 79 – 29747
O isotopes exchange with seawater, results from (DSDP Leg 37) 77 – 91072
$^{87}Sr/^{86}Sr$ ratios of interstitital waters from DSPD sites rel. to sediment geochem. 79 – 34794
U abundance, heat flow implications, basalt fission track anal. 80 – 8287
U distribution and evolution in oceanic lithosphere 79 – 84226

oceanographic equipment
see also oceanographic techniques; water pollution detection and control
4 kHz seismic profiling system 77 – 2140
12 m discus and NOMAD buoy hull transfer function computations 80 – 46303
32 kW Doppler sonar for ocean internal wave meas. 80 – 46296
35 mm camera systems for deep sea appls. 78 – 4003
A/D convertor, two-phase, processes small analogue signals *(German)* 78 – 61572
Aanderaa current meter, shallow-water meas. accuracy 77 – 5378
Aanderaa Ni-coated current meter, pressure-induced direction error 80 – 4121

oceanographic equipment continued
Aanderaa thermistor chains, solar radiation effects on ocean temp. meas. *(French)* 79−62611
acoustic communications system for small submersible, design 79−5666
acoustic current meter for measuring mean current or flow *(German)* 80−77163
acoustic data buoy, microprocessor controlled, underwater signals processing 79−21024
acoustic impedance transducer, for in situ meas. of marine sediments 78−9519
acoustic pinger modification to transmit water temp. data 79−39895
acoustic reflection profile display using dot matrix plotter with minicomputer 77−9548
Acoustically-Navigated Geological Undersea Surveyor, for Mid-Atlantic Ridge appl. 80−4120
advanced instrumentation system, St. Croix, USVI 80−67427
Air Droppable Random Access Measurement System buoy sea ice tracking 77−5363
air-dropped expendable bathythermographs, mesoscale oceanographic mapping 80−101457
air-sea interaction buoy, instrumentation and data acquisition 79−66813
air-sea interaction buoy performance 79−70894
airborne expendable bathythermograph 77−2262
amperometric membrane probes, modified, for free and total residual Cl determ. in saline cooling waters 80−82112
analogue wave spectrum analyser system for operational buoys 79−5662
anchor releases, dual mode and timed electrolytic devices 78−40693
APODAS ocean profiling automatic data acquisition system *(Japanese)* 80−85769
automated profiling water quality sensing system 78−45052
automatic buoy systems, centre for data collection and processing *(Russian)* 77−78427
automatic measuring stations, testing experiences 78−96317
automatic oceanographic profiling and transmission system 77−41231
automatic sampling buoy for accumulation of dissolved and particulate organic material in seawater 78−49149
Batfish active towed body system development 77−5374
bathometer sonde for seawater temp. and salinity meas. 77−78480
bathythermograph systems, new techniques 77−17221
bead thermistors for temperature measurement *(German)* 77−21920
Benthic Untethered Multipurpose Platform for underwater acoustic TV 80−46319
Bermuda Eleuthera Acoustic Range environmental meas. buoy 77−41229
bottom seismograph using digital telemetry and floating-point conversion 77−41197
buoy for data acquisition, using Meteostat data transmission *(German)* 80−90224
buoy for robot stations deployment from ships in strong current regions 79−39984
buoy wave data analyses noise correction functions and error sources 80−46302
buoys, electronics and telemetry, developments 79−5659
buoys, environmental data acquisition 78−36287
buoys and platforms, zero-freq. hydrodynamic coeffs. 77−89219
cable length, vel. and tension meas, using DBS-2 remote counting block 79−12314
coastal water pollution monitoring, meas. and sampling techniques 79−12137
coastal wavestaff system 80−46324
compact current meter moorings, design and preliminary results 79−88482
conductivity meas. instrument, development and operational experience 79−74970
conductivity meter for in situ ocean meas., development, testing and calibration 79−5671
conductivity/temperature/pressure profiler errors 77−5377
conical porthole, deep-water, deformation effect on optical characteristics 79−76859
controllable real-time data collection system for coastal oceanography 77−5329
CTD systems, intercomparison of methods, analysis and results *(Russian)* 78−85725
current direction vanes, response charact. affecting design and use 77−64447
current followers, determ. of Lagrangian deformations 77−2276
current meters, for continental shelf deployment, development and testing 79−5674
current sensors, EM- and acoustic-types, performance assessment 79−25345
current velocity reversible sensors charact. *(Russian)* 78−65429
data acquisition system, low power, microprocessor controlled *(Italian)* 77−82068
data buoy DB1, source of meteorological data for UK 79−21079
data buoy wave meas. system malfunction detection 80−46304
data buoy wideband wave directional spectra, real-time telemetry 80−46305
data buoys, environmental data quality estimates 77−5364
data buoys, meas. of Hurricane Eloise (1975) 78−77302
data logger for recording slow sea oscillations, solid-state 80−36414
deep ocean current meas. system 77−5382
deep ocean release mechanism for instrument packages 78−12021
deep ocean technology, development in USA 77−78477
deep sea floor mapping instrumentation 77−5358
deep sea temp. and pressure sensor for tidal meas. 77−37424
deep sea tide gauge, qualification of quartz pressure sensor *(German)* 79−74980
deep seismic sounding, automation of obs. and processing of ocean-bottom seismograph recordings 78−57339
deep submergence vehicle development and reliability 77−5376
deep towed seismic profiling system, multichannel hydrophone array, sub-bottom oceanic structure study appl. 80−26550
deep-sea instrument float, evaluation of Isopar-M, press.-vol. isotherms 77−25786
deep-tow and digital techniques 77−73882
differential spectrophotometer for hydro-optical studies 78−3997
digital survey fathometer, providing chart display and digital output 79−5665
digitizer for use with pulsed depth sounders 79−21065
directional wave spectra monitoring horizontal-spar buoy, design 79−21083
oceanographic equipment continued
directional wave spectra routine meas. system, from discus buoys 79−16722
discus buoy wave spectra, comparison of buoy-fixed and vertically stabilised accelerometers 79−5678
discus hulled wave measuring buoy 77−91316
diver-operable multiwavelength spectroradiometer 80−90251
Doppler sonar, range-gated, obs. of strongly nonlinear internal motion in open sea 80−51422
Doppler sonar ocean current profiles 80−46311
drift buoys, deployed by aircraft and satellite tracked, operational test 80−90242
drift buoys, drogued, appl. to coastal flow meas. in N.Gulf of Alaska 80−51431
drifting buoys, appl. to ocean data collection 79−5668
Drifting Oceanographic Profile Buoy with minimum vertical motion 80−46306
Duing profiling current meter and White Horse acoustic sounder comparison 79−21041
dynamic hydrothermal experimental system, for seawater-basalt reactions study 79−5686
EhMIT submerged current meter for meas. in tropical Atlantic *(Russian)* 79−100978
electric conductivity meters with automatic correction of charact., seawater appl. *(Russian)* 78−65426
electric field measuring system, equivalent base for rectangular fairing *(Russian)* 79−34988
electric intensity vector direction determ. device *(Russian)* 77−60490
electrical conductivity probe, for meas. in stratified NaCl solns. 77−52718
electronic timer for oceanological instruments, ±3 sec/day accuracy 77−49190
EM velocity profiler based on geomag. induction principles 78−61569
EM water current nonlinearity and sensitivity 77−5383
errors in profiling instruments, analysis 80−8445
estuarine current meter data acquisition microcomputer system 80−46265
expendable bathythermograph digital recording and display system 80−46318
flume on rotating platform, for wind-generated internal waves exptl. study *(French)* 79−62518
fluorometer for underwater detection of rhodamine dye tracer 78−36313
free fall oceanographic instruments, design 77−41227
free vehicle grab respirometer for deep-sea sediments O_2 uptake and nutrient exchange meas. 80−3564
free-fall, wing stabilised vehicles, design considerations 77−56741
free-fall instrumemts, position determ. using acoustic navigation system 77−29490
frequency tracker for laser Doppler anemometry, soil or sand erosion appl., lab. expt. 79−72968
geomagnetic electro-kinetograph for surface current meas. *(French)* 79−29778
GOES-reporting waverider buoy 79−5663
graphic system for space-time series processing and anal. 78−3998
Great Lakes coastal waters, thermal plume meas. systems 78−44891
HF radar system, for ocean surface currents mapping 80−94626
holographic microvelocimeter, ocean particle dynamics meas. 80−12567
hydrocom, underwater communications, non-acoustic long distance system appl. 79−5667
hydrophysical apparatus, channels with automatic transfer function correction *(Russian)* 78−16193
imaging systems in water, point and beam spread functions 78−5426
inertial sighting system, airborne, appl. to coastal water surface currents obs. 78−73384
instrument testing, need for national programme 77−21924
instrumentation, problems and development 79−12308
integral thermotome for water layer temp. meas. 79−29908
integrating float, lag effects on water flow vels. integration 78−93012
integrating optics and sonar for deeply towed vehicle 78−45045
intelligent terminals and calculators, as alternative to minicomputer systems 80−12553
internal wave obs. temperature measurement array 77−5380
international standards for oceanographic instrumentation 78−45043
Inverted Echo Sounder for ocean thermal structural variations and currents 80−46312
Kiel multi-purpose sea probe microprocessor-based data acquisition system *(German)* 78−85701
laser fluorosensor performance, sea-state effect 78−92990
laser probe, for 2D wave slope spectra meas. of ocean capillary waves 77−60472
laser sand detector to discriminate between bubbles and sand 79−58109
laser sounding method and equipment for water absorpt. and attenuation coeffs. meas. *(Russian)* 79−34998
laser technology, blue-green sources for ocean optics 77−78458
laser velocimeters appl. to ocean meas. 78−36325
LED marine beam transmittance meter 77−70870
LEO I submersible reliability and safety 77−5373
lidar, scanning bathymetric system for nautical, near-shore charting 80−8463
lidar system, airborne, bathymetric and fluorescing modes 78−57370
lidar system, airborne, near-shore charting laser bathymetry 78−57371
lift bag, salvage device for deep ocean 80−82107
long tow-wire complex vibration obs. and empirical drag law 80−46309
magnetometer for sea floor temporal mag. variation meas. 80−51581
magnetometer for ULF-ELF geomag. fluctuations 80−77152
manned underwater laboratories for marine biology, geology, phys. and chem. research 77−21929
mareograph well type selection from charact. eqn. *(Polish)* 77−70871
marine spring gravimeter, GMN automatic equipment *(Russian)* 77−45197
metal-film temp. and vel. sensors and self-propelled research vehicle stability evaluation for ocean turbulence meas. 79−5672
meteorological drifting buoy, development 79−5661
MF/HF backscatter radar for sea surface meas. *(Japanese)* 78−16210
microcomputer based ocean observation system 79−16677
microcystis removal ship, Seimei, Japan *(Japanese)* 77−56753
microprocessor based real time oceanographic data acquisition and processing 79−16676
microprocessor-assisted flow-through anodic stripping voltammeter 78−36324
microprocessor-based instrument for seawater charact. meas. 80−67440

oceanographic equipment continued
microprocessor-based particle data collection system 78−36323
microscale sensing array 78−85720
microwave radars, appls. to ocean wave detect. and direction meas. 79−5685
microwave radars, one and two freq., appl. to sea surface remote sensing 80−94622
microwave radiometers, ice movement measurement *(Danish)* 80−26624
microwave remote sensing instruments, Seasat, history 80−94678
microwave scattering signature of ocean surface, aircraft AAFE RADSCAT scatterometer 77−25790
Mobile Initial Condition Indicator, submersible, dynamic approach to marine exploration 79−5687
monitoring stations in Arabian Gulf, computer control 79−8728
moored acoustic buoy system (MABS) 77−49187
Moored Acoustic Buoy System suspended Kevlar array technology 80−43572
moored buoy system design for shallow waters 78−36319
moored current meters, meas. intercomparisons, review 78−45050
multi-frequency microwave radiometer system for oceanography, performance evaluation 78−81417
multibeam sonar systems, data flow requirements 77−3697
multichannel complex for hydrophysical data conversion for computer anal. *(Russian)* 78−65427
multichannel electrooptical turbidity meter 80−67423
multichannel wide-range oceanographic sonar 80−46295
multifunctional programming unit for self-contained oceanographic instruments 79−2391
Naval Coastal Systems Center (NCSC) environmental measuring system 80−12570
near-bottom quantitative seismic profiler 78−16196
near-surface moored current meters, comparison 77−33206
near-surface temp. meas., distributed instrum. profiling sensors 77−82071
neutron tubes, appl. to sea water chlorinity determ. under natural conditions *(Russian)* 78−77360
ocean test structure for wave force meas., improved platform design [Ocean Test Structure] 79−12306
ocean wind wave elevation sensor array system 80−46322
oceanographic research shipboard minicomputers appl. 79−53562
oceanographic research techniques used in survey ships *(French)* 78−65434
Oceans '77, conf., Los Angeles, USA (Oct. 77) 78−36193
oceans '78, ocean challenge, conference (Washington, DC, USA, 1978, September 6 to 8) 79−5658
offshore geotechnical instrumentation, sea floor structure testing appl. 79−12302
optical incoherent sources for deep ocean waters, discharge spectral emission 77−82043
optical transmitter-receiver system, nearly coaxial, limiting detect. range through water 77−78461
PAG-5 air and marine proton magnetometer *(Russian)* 77−60489
photoelectric sensor chlorophyll simulator, oceanic photosynthesis in situ quantum efficiency determ. 79−39760
photometer for deep-sea work, using acoustic telemetering 80−98460
photon scalar irradiance meter, rel. to energy evaluation for photosynthesis in sea 79−79436
phototransducer drift effects on obs. of underwater light field fluctuations *(Russian)* 78−65409
piezoelectric transducer, for mobile sand grains underwater detect. 78−96192
PISCES submersible scientific equipment and data acquisition system 77−5381
Pisces submersible vehicles, first expts. in Black Sea 79−44267
Pisces-A submersible manned research complex 79−44266
piston core behaviour recording device 78−20532
pneumopress, for extracting interstitial water from marine sediments 80−26643
pollution monitoring system, automatic, shipboard, oil conc. 78−53662
polymers for undersea environment high temp./press. materials test 78−3213
portable acoustic tracking system, for underwater construction teams tracking 79−3874
pressure tolerant electronic systems 80−46317
pressure tolerant electronics, appls. 78−45056
pressure vessel for trapping deep-sea animals, simply actuated closure 78−3821
probe for surface layer elec. cond. meas. 79−2392
propeller speed meter charact. *(Russian)* 79−39903
propeller Vector Measuring Current Meter development 80−46313
proton magnetometers, calc. method of EMF for sensors precession signal *(Russian)* 78−65428
Pull-Up Shallow Water Seismometer design and appls. 78−45025
pulse compression radar scatterometer system, expt. 77−29483
punched tape data recorder for F5080 freq. meter, oceanological appl. 77−49175
pyranometers for underwater total radiant energy flux meas. 77−9524
R/V Athena, high speed ship for towing research 77−41213
radar, surface contour, airborne, computer-controlled 79−80063
radar altimeter height and timing bias report 80−46326
radio buoy for tracking oil slicks 78−45034
radio-controlled meas. system used in shallow water 78−77354
radiocommunication buoy, antennas and operating freqs. *(Russian)* 80−109253
radiometer, microwave, multichannel scanning, for Nimbus-G and SeaSat-A 77−29625
radiotelemetering meas. system for buoy testing *(Russian)* 78−16192
range resolved Brillouin scattering using pulsed laser 80−38055
recording inclinometers for deep ocean current meas. 78−45054
reference electrode for automated in situ hydrochemical meas. *(Russian)* 78−65430
remote platform data acquisition and control by minicomputer 77−5330
remote sensing of sea surface, instrument charact. in presence of basic noise *(Russian)* 80−109267
remote sounding instruments, quasi-optimum operating functions *(Russian)* 78−77362
remotely controlled profiling system for shallow water 78−36328
research ship, integrated, with data acquisition and processing systems 79−34969
resources and meas. techniques, conference, San Diego (1979) 80−41943
robot submarine with computer control 77−5375

oceanographic equipment continued
salinity/temperature sensor chain for estuarine meas. 79−5670
sampler-degasser, hermetically sealed, for study of dissolved gases in seawater 77−49191
satellite remote sensing system, USA proposal (NOSS) for 1986 launch 80−105088
Savonius rotor current meter, calibration eqns. 77−33205
'Scalar' oceanographic probe, information exchange with 'Minsk-22' computer *(Russian)* 78−77363
scanning sensor for real-time optical mapping 80−8464
scatterometer, pulse compression system, experimental study 77−17240
scatterometer, satellite- and aircraft-borne, optimization of charact. for investigating underlying surfaces 80−67436
scatterometer, surface wind speed meas. using SeaSat-A 77−29626
scatterometer, surface-based, for Arctic sea ice meas. 79−92544
sea level recorder for tectonic studies 77−45175
sea surface contour airborne radar as remote sensing instrument 80−51562
sea-floor mapping in real time, sonar-microprocessor equipment 80−26646
sea-floor pressure recorder 77−73864
seafloor earthquake meas. system, development 79−5689
Seasat radar altimeter, initial performance assessment 80−94679
SEASAT radar altimeter, resolution capability preliminary estimates 80−72645
Seasat radioaltimeter, sensor file algorithms 80−94680
Seasat scanning multichannel microwave radiometer, antenna pattern corrections 80−94683
Seasat scanning multichannel microwave radiometer, calibration algorithm development 80−94682
Seasat scanning multichannel microwave radiometer, description and performance 80−94681
SeaSat scanning multichannel microwave radiometer 80−46248
Seasat scatterometer, evaluation 80−94684
Seasat scatterometer, scattering coeff. algorithm 80−94685
Seasat synthetic aperture radar system 80−94686
Seasat visible and IR radiometer 80−94687
Seasat-1, first ocean observation satellite, appl. to marine research from outer space *(German)* 79−74979
Seasat-A, experimental oceanographic satellite 78−77455
SEASAT-A satellite microwave scatterometer for wind sensing 77−5417
SEASAT-A satellite radar altimeter design 77−5415
SEASAT-A satellite scanning multichannel microwave radiometer 77−5416
SEASAT-A satellite scatterometer (SASS), data regional integration, validation and appl. 79−5680
SEASAT-A satellite synthetic aperture radar 77−5418
SeaTrak Data Processor, surface data reduction system for current meter 78−45042
seawater attenuation matrix photometer *(Russian)* 77−78453
sediment free-fall penetrometer with Doppler telemetry 80−46320
sediment geotechnical prop. determ., instrumentation problems 79−12304
sediment movement and associated hydraulic conditions remote monitoring instrument 77−37421
sediment transport, instrument system for studies on continental shelf 79−58113
seismic reflection data acquisition using extended arrays 78−77340
seismograph observation system for ocean-bottom investigations *(Japanese)* 80−94615
seismometer hydrophones for deep ocean bottom deployment 80−51582
semisubmersible stable platform 'Kaimalino', design 77−5350
shipboard subsystem, operation peculiarities of Minsk 22 computer *(Russian)* 78−16165
shipborne automatic data collection, GRAD system 77−78428
short range precision navigation and tracking system using PLL 78−53742
side looking sonar for sand wave study in White Sea 78−3999
side scan sonar surveys, tow line depth increase 77−64490
silt-salinity-depth profiling instrument 79−88493
sofar floats for POLYMODE 78−45047
solid-state water current meter for wave direction sensing 79−21070
sonar, deterministic and random error model of multibeam hydrographic system 79−3873
sonar, fibre optic system, geological and hydrographic survey applications 78−88947
sonar, signal processing algorithms soln. with multi-microprocessor network 78−45044
sonar, towed type, portable, for ocean acoustic meas., features 78−69550
sonar systems, underwater electric cable terminations 78−45041
Spar Buoy Oceanographic Telemetry System 80−46307
Spar Buoy Oceanographic Telemetry System software engineering 80−46308
spectrometer for underwater gamma surveying, calibration 79−21066
splash down programmer unit for bathythermographic appl. 77−56759
stable platform, for microscale studies of vel., temp. and cond. 79−5669
sub-bottom profiling sonar, using nonlinear sound source 77−45198
submarine quantum irradiance and photoperiod meter, with digital recording 80−98474
submerged cylinders, forced oscills. test in water 78−5728
submerged self-contained buoy station, expt. launchings 80−26642
submersible data acquisition system SCRIBE 80−46266
submersibles, 1977 review 78−69499
submersibles, manned, for deep-sea research 77−9556
submersibles for research work, remotely operated vehicles 80−82105
submersibles for underwater research, commercially available vessels 80−82104
surface currents mapped by coastal HF radar system 78−28351
surface following data buoy DB1 rel. to drifting float displacements 79−2394
surface meteorological buoy and aircraft VHF link 80−46298
surface wave slope meter, fast response instrument, wind-wave moments meas. 78−45012
survey instrumentation, requirements and appls. 79−84508
survey vessels, multiple use 79−53561
synchronous spot-scanned underwater viewing system 77−21934
synthetic-aperture radar, surface imaging appls. 78−81445
telemetering offshore oceanographic buoy, new mooring design 79−5660
telemetry data buoy for coastal operation 78−36320
temperature-depth profiles system, solid state memories 78−24383
Tethered Remote Operated Vehicle for Arctic seafloor studies 78−61576

oceanographic equipment continued
thermal energy conversion plant, 100 MW, systems aspects 78−96235
thermistors, glass rod type dynamic response 80−90243
thermistors, spectral response characts. 78−20533
tide gauge for shallow-water, fast-response characts. 80−26639
tide gauging, automatic network 79−5692
tiltmeter, appl. to ice shelves tidal flexure meas. 80−31050
tow system with depth control, hydrographic and current meas. 80−17403
towed hydrophone location system 79−2401
towed instruments carrier, for hydrophysical research 80−36423
transducer array for acoustic holography *(Japanese)* 77−80029
transmissometer for profiling and moored observations in water 80−8462
transparency meter, Se photocell device, for biological activity 80−8442
triaxial acoustic current meter for small-scale ocean turbulence resolution 77−41232
turbid water, instrument ot meas. light absorpt. coeff. 80−82076
TV camera, pressure tolerant, small, features 78−32243
TV underwater viewing system, optical design 77−78459
two-stage mooring design and performance test 77−5365
undersea acoustic transponders, locations optimal estimation 79−5684
undersea stereoscopic television appls. 79−5677
underwater acoustic pulse compression system, signal processing methods 80−56630
underwater lens system, metrical fundamentals 77−78457
underwater offshore acoustic test range construction 79−16720
underwater radiance scanner, design and implementation 78−61609
underwater real-time communications, non-acoustic long-distance system appl. 79−5667
underwater robot/manipulator, development 78−77356
underwater temperature meas. thermistor chain 77−5379
underwater towed EM source for geophys. exploration 79−5676
underwater towed EM source for geophysical exploration 79−74971
underwater winch system for meas. of seawater physical props. *(German)* 78−69491
US, temperature-depth profile measuring system, expt. *(Japanese)* 77−70864
US abatement of fouling on glass in oceanographic sensors *(German)* 77−5342
US current meter, used for data acquisition, high sensitivity 77−41211
USSR Hydrometeorological Service, automation of data collection and processing 79−34994
Vaisala-Brunt frequency vertical fine struct. meas. in Mediterranean Sea 80−26537
vector averaging current meters, moored, for vertical temp. gradients meas. 80−12561
velocity meas. sonar system, transfer function model 77−7275
velocity sensor, calibration equipment and technique, oceanographic appls. 80−8447
velocity sensor for three-dimensional turbulence meas. 80−46314
versatile oceanographic data-logger 80−46264
vibrosource, characts. in liq. layer 79−81905
visible and infrared imaging radiometers for ocean observations 78−69536
Visible and Infrared Radiometer evaluation from SeaSat-A surface temp. obs. 80−46325
vortex amplifiers, two-stage shear-modulated hydraulic 77−53237
wave analysis instruments 80−26640
wave data analyser system for buoys 77−5362
wave energy convertor array, available wind-wave power 78−81216
wave follower buoy, wave direction meas. technique 79−5664
wave follower system, electromech., for wind-wave tank probe control 78−85734
wave height barometric sensor 77−78487
wave height sensor, buoy-mounted barometric pressure instrument 78−36321
wave recorder/perspectometer, statistical estimation of wind wave elements 77−78478
wave sensor array, high resolution, for wave directional spectra meas. in nearshore zone 78−36329
wave spectral density meas. with analogue filtering 77−41230
wavemeter for inshore zone, with radiotransmission of data 80−101460
waves measurement, precise electronic instrument 78−86294
wind-wave tank, microscopic and macroscopic surface structs. growth and decay rates 80−48726
Work Systems Package for deep ocean studies 77−33215
X-ray spectrometer, automated, anal. of large samples in geochem. oceanography 79−16711
YVETTE, free-fall shear profiler 80−31124
γ-ray field of seawater, meas. method *(Russian)* 80−109268
Na-selective electrodes in marine geochemical studies 79−12312
Nd:YAG Q-switched laser for bathymetry 80−8461

oceanographic techniques
see also oceanographic equipment; water pollution detection and control
35 mm camera systems for deep sea appls. 78−4003
acoustic bottom loss measurement using multipath resolution 79−5652
acoustic imaging, appl. to New England shelf-slope water mass surfaces 78−3784
acoustic methods *(Russian)* 77−25798
acoustic ocean bottom reflection data processing by digital deconvolution 77−33223
acoustic reflection profile display using dot matrix plotter with minicomputer 77−9548
acoustic remote sensing of high-frequency internal waves 80−41562
acoustic sounding of ocean-bottom subsurface layered media, spatial parameter estimation 80−77134
acoustic stratigraphy of carbonate sediments, fine scale detail 80−21709
acoustic tomography, for large scale monitoring 80−4119
acoustics, book 79−57970
acoustics for sediment suspensions and shallow thermoclines 77−9523
active microwave sensing of surface phenomena *(Japanese)* 78−16215
active nuclear methods appl. to seawater density and elements conc. determ. *(Russian)* 79−39902
adaptive spectral analysis of surface and internal waves *(Russian)* 77−29475
air-water interface, microwave detect. of adsorpt. and spreading films 79−5690
airborne bathymetric charting using pulsed blue-green lasers 77−29447
airborne synthetic aperture imaging radar for internal wave obs. 77−17110

oceanographic techniques continued
aircraft appl. to radiooceanography, inherent problems 77−17241
aircraft monitoring of ocean thermal structure and currents, NORPAX project 79−84517
Alboran Sea, mesoscale oceanic vortex, drifting buoy and satellite meas. *(French)* 79−16473
algorithm for processing of observational series, ocean currents appl. *(Russian)* 78−65421
Arabian Gulf, comprehensive oceanographic monitoring programme 79−8728
Arctic Ocean ice characteristics meas. by microwave scatterometry 79−84298
Arctic sea ice, layered struct. study by radar sounding *(Russian)* 78−16023
Arctic sea ice, surface-based radar scatterometer results 79−92544
artificial satellite laser ranging, oceanographic appls. 77−64484
artificial upwelling induced by ocean currents, theory and expt. 78−81217
backscattered sea return studies with CW dual-freq. X-band radar 77−17232
bathymetric charts construction aboard ship, efficient method 78−45029
bathymetry, deterministic and random error model of multibeam hydrographic sonar system 79−3873
bathymetry, high resolution for seabed flatness analyses, use of resobath system 77−21921
bathythermograph systems, new techniques 77−17221
beach processes study using luminescent tagged sands, Cuba north coast 77−64264
beam-limited target-referenced radar limitations 77−41194
Beer's law analysis, phytoplankton photosynthesis, daylight irradiance meas. 77−21800
biological life forms recording, using CCD colour TV camera 80−51301
Black Sea water, chemical anal. method and F content 78−32118
Butterworth low-pass filter, oceanographic data appl. 79−16704
Central American seas, waters geostrophic circulation calc. 78−92842
chemical tracer studies, implications of multiple components transport through thermohaline diffusive interfaces 80−12396
chlorophyll a analysis, using aircraft multispectral scanners 80−77164
climatology, hydrology, atmospheric research and meteorology from space, conference, Ajaccio, Corsica (1979 November 12 to 16) 80−62397
coastal pollution, monitoring by neutron activation analysis 77−41068
coastal radar system appl. to tsunami prediction and magnitude 80−82101
coastal water pollution monitoring, meas. and sampling techniques 79−12137
code delta-modulation for standard hydrophysical information compression *(Russian)* 78−65432
colorimetry using Technicon Autoanalyzer II, systematic absorbance errors 79−21802
computer contouring method using digital filter, bathymetry appl. 79−39894
conservation calculations in natural coordinates, example from Baltic Sea 80−51433
Continental Shelf sediment sonar signal processing 78−61622
continental shelf surface currents charting by aerial tracking of dye emitting radio beacons 79−5675
continuous seismic profiling, diffr. waves travel time curves 78−3725
coral and shell dating 80−12434
correlation and spectral analysis, appl. to hydrometeorologic elements in coastal zone *(Russian)* 78−77258
cosmogenic and artificial radioisotopes distrib. in ocean, turbulent exchange intensity determ. *(Russian)* 79−39744
crustal seismograph records, computer processing method 80−85605
CTD systems, intercomparison of methods, analysis and results *(Russian)* 78−85725
current determination by beta spiral method, vertical mixing effect 80−98459
current determination by obs. of induced EM fields, theory 80−61805
current meas., surface following data buoy DB1 rel. to drifting float displacements 79−2394
current meas. by Lagrangian drifting buoys 78−45049
current meas. methods, comparison *(Russian)* 78−81439
current meas. near ocean surface, general problems, review 78−45048
current meas. on continental margins and deep ocean 79−12315
current meter data, graphic presentation 78−45055
current monitoring using acoustic techniques 78−11907
current parameters meas. from drifting ship 77−49189
current pattern determination by aerial photography of markers 80−98483
current velocity profiler based on geomag. induction principles 78−61569
currents, calc. method using generalised formulae *(Russian)* 77−60481
currents tracking, results from satellite-tracked drifters between Africa and Antarctica 78−73376
data and information services, changes and challenges 78−69463
data objective anal. and classification 78−36318
data processing and analysis, in oceanographic research 80−94605
deep sea drilling project Glomar Challenger, international phase *(German)* 77−70837
deep sea temp. and pressure sensor for tidal meas. and calibration techniques 77−37424
deep seismic profiling, Atlantic Ocean, automatic processing of bottom seismograph records 78−45030
deep seismic sounding, automation of obs. and processing of ocean-bottom seismograph recordings 78−57339
deep water surveying, new techniques 78−85730
density and current data assimilation *(Russian)* 79−100977
density profile remote sensing by acoustic pulses, numerical algorithm 77−70893
density profile remote sensing pulses, numerical algorithm 78−20429
depth control of towed submersibles by variable body forces 77−91315
depth measurement using airborne pulsed Ne laser system 80−61908
depth sounding using airborne laser land profiler 78−49173
digitising error from period and freq. counting techniques 78−61570
directional gravity wave spectra and surface currents, remote sensing with dual freq. radar 78−96323
directional sea spectrum determ. using HF Doppler radar techniques 77−17229
directional sea wave spectrum determ. using HF Doppler radar techniques 77−29476
directional spectra extraction from multi-component wave data, var. technique 80−26637

oceanographic techniques continued
directional wave spectra from discus buoy, data processing 79−16723
directional wave spectra meas. from fixed platforms 79−16724
directional wave spectrum, new meas. method, description 79−16706
directional wave spectrum, new meas. method, lab. wind waves meas. 79−16707
dissolved O determ., comparison of polarographic electrode and Winkler tritration determ. 77−70848
diving physiology research facility 80−82106
drift buoys, deployed by aircraft and satellite tracked, operational test 80−90242
dual frequency correlation radar measurements of height statistics of ocean waves 77−17236
dye-buoy remote sensing of coastal circulation 78−65438
dynamic ocean data, acquisition and display by portable real-time minicomputer system 80−12552
dynamics investigation, realisation of four dimensional topographic reference system 78−77176
echo sounders, magnetostriction effects appl. *(German)* 78−23311
eddy detection scheme 79−96834
eddy models, environmental effect prediction anal. 80−4146
electric field meas., baseless method *(Russian)* 79−39900
electric field meas., dielectric plate in const. current flow *(Russian)* 77−65813
electric field measurement, EM phenomena accompanying movement of current fairing in sea water *(Russian)* 78−77361
element abundance charts, construction method for tropical Atlantic *(Russian)* 77−60485
EM current meter recordings, anal. of gravity wave interference 77−78456
EM sounding of sea ice, visit to Arctic and Antarctic Research Institute, Leningrad 80−4504
enhanced IR satellite imagery for sea ice and surface temp. meas. 77−37422
environmental data files, quick guide 80−12551
Eotvos effect variations allowance in gravimetric studies, data processing 79−74969
equatorial currents, strength monitoring from XBT sections and sea level obs. 78−73383
estuarine fronts remote sensing, behaviour study, pollutant effects 77−78470
estuarine hydrography and sedimentation, measurement techniques, book 80−36788
estuarine sediments, heavy metal pollution detection 78−73546
estuary mapping, classification algorithms for Landsat data 78−40567
expendable bathythermograph data correction for salinity effects, Gulf Stream rings dynamic heights calc. 78−49151
finite element methods for flow anal., book contrib. 79−32522
flat finite wave tank radiometric measurements, 3-dimensional vector modelling and restoration 77−17238
flow measurement 78−32260
fluctuating current meas. by acoustic current meter *(German)* 80−77163
frazil ice conc. meas. system using laser Doppler velocimeter 77−25796
freely sinking probe horizontal velocity meas. interpretation 80−46321
gamma-spectrometric surveying problems 79−2390
Gauss-Markov models of ocean currents for error analysis of inertial navigation system 80−36411
geomagnetic depth sounding using sea floor magnetometer system 80−51581
geomagnetic provinces boundary determ. method 77−64480
Geos 3 altimetry, anal. for regional sea surface model in Tasman and Coral seas 80−3903
geostrophic ocean currents determ. independently of reference level, inverse technique 80−51574
Gulf Stream, large-scale frontal study using Geos 3 radar altimeter data 79−5488
Gulf Stream kinematics inferred from satellite tracked drifter 77−17246
Gulf Stream ring tracking with buoyant SOFAR floats 77−17245
Gulf Stream ring tracking with free drifting surface buoy 78−7769
Gulf Stream surface waves, radar obs. program 80−85679
heat storage in oceanic upper mixed layer, inference from Landsat data 79−100869
heat transfer meas. in boundary layer, radio thermal microwave systems appl. 79−84546
heavy metal sedimentation rate in Saanich Inlet, British Columbia, ^{210}Pb technique 78−32063
heavy metals, distrib. and speciation in aquatic systems, analytical techniques 78−69390
HF radar sea-echo Doppler spectra, extraction of wave height and period 77−78474
HF radio scatter appl. to sea studies 77−17230
HF sea-echo Doppler spectra, statistics 77−17231
HF sky wave radar remote sensing of sea state, minimisation of ionospheric disturbance 80−21857
horizontal mixing measurement, Hay-Pasquill method testing in Baltic Sea 80−17290
hydrocarbon pollution detection, caution on use of Niskin sampling bottles 78−45039
hydrocom, underwater communications, non-acoustic long distance system appl. 79−5667
hydrodynamical fields time variability, anal. methods *(Russian)* 78−65424
hydrographic charting by multispectral and ocean colour scanners 77−5368
hydrographic charts preparation, appl. of LANDSAT MSS imagery 79−29894
hydrographic surveying, new methods appl. in Florida Straits 78−81450
hydrophysical information separation from satellite data *(Russian)* 79−39899
hydrophysical nonstationary processes, real time digital filtration *(Russian)* 78−65425
hydrophysical polygons, dynamic-stochastic approach to anal. of density field obs. *(Russian)* 79−8707
hydrophysical research using inert gases dissolved in seawater *(Russian)* 77−60425
ice, dielectric relax. meas. by blocking layer method 80−103914
ice forecasts for Arctic seas, practical appls. 78−96230
ice sheet radio-echo study method 77−5212
ice shelves tidal flexure measurement, near tiltmeter appl. 80−31050
ice strength meas., in situ tests 77−37423
oceanographic techniques continued
iceberg sounding by impulse radar 78−24388
iceberg volume meas. using photogrammetric techniques 77−82048
icebergs drift in Grand Banks, meas. techniques 78−81200
icebergs underwater profiling using unmanned submersibles, echo sounder and scanning sonar 79−5673
immersed object EM signature determ., modified physical optics technique 77−5372
induced-current effects on microwave backscatter 77−17111
industrial waste dumping, dispersion meas. technique 78−44884
information collection, processing and anal., automation on small-computer base 80−101439
internal waves meas. with electrical contact device 80−12566
inverted echo sounders, for meas. thermocline depth vars., MODE results 77−87108
IR radiometry and visible spectrometry 78−69535
irradiance attenuation coefficient in a stratified ocean, meas. technique 80−98325
isolation of humic substances and alcohol soluble organic matter 77−64448
isotopes for oceanographic investigations *(Russian)* 77−60486
isotopic generators appl. *(Spanish)* 78−15922
Jamaica Bay, NY, estuarine P model parameter estimation 77−21777
land-to-seafloor EM transmissions in 0.1-15 Hz band 78−93008
Langevin techniques for describing nonlinear internal wave interactions 80−67371
laser bathymetry, airborne, environmental subtraction technique 78−57372
laser bathymetry, near-shore charting appl. 78−57371
laser bathymetry for near-shore charting appl., preliminary field test results 79−5679
laser optical instrument, for capillary wave slope meas. 78−36173
laser sounding method and equipment for water absorpt. and attenuation coeffs. meas. *(Russian)* 79−34998
laser velocimeters appl. to ocean meas. 78−36325
lidar appls. *(Russian)* 79−39975
Light-Behind Camera photography for sea floor mapping 77−5359
long range acoustic propagation meas., fronts identification 79−66705
low temperature skin-layer, investigation via satellite IR photography *(Russian)* 78−36180
M_2 tide parameters from satellite orbit perturbations 77−33093
magnetic sounding, deep sea, effects of EM field of current of finite width 79−53351
magnetic stratigraphy of sediments using susceptibility meas. 79−84520
magnetotelluric sounding, effect of non-uniform ocean depths on wave-induced mag. fields 79−66807
manned underwater laboratories for marine biology, geology, phys. and chem. research 77−21929
mapping using observational data *(Russian)* 80−17416
mareograph well type selection from charact. eqn. *(Polish)* 77−70871
marine currents determination, magnetostatics problems in electrodynamics of sea *(Russian)* 78−77259
marine drilling contamination, seawater Ba content as pollution indicator 77−2180
marine environment monitoring through sedimentation 77−29319
marine geophysical surveying, new techniques appl. 79−53560
marine geophysical surveys, trackline crossover differences as accuracy indication 79−39893
marine hydrosol scattering meas. by submerged laser nephelometer *(Russian)* 77−60418
marine minerals exploration, Mobile Initial Condition Indicator approach 79−5687
marine mining, environmental effect meas. 79−12305
marine modelling (vol.6 of 'The Sea') 78−16047
marine particulate plume density and distrib., acoustic assessment 80−45843
marine photography and side-scan sonar image processing 77−5357
marine pollution, data collection 80−3545
marine proton magnetometer, optimum towing conditions 79−2393
marine research from outer space, take-off of first ocean observation satellite *(German)* 79−74979
marine sediments, correl. between geotechnical and acoustic props. bottom refl. coeff. meas. near sea floor 79−96756
marine sediments diffusion coefficients determ., resistivity techniques validity 79−92601
marine sediments probed by acoustic array, penetration conditions *(French)* 80−33324
marine seismic surveying, potential efficiency of shot grouping *(Russian)* 78−40702
measurement capability improvement using advanced engineering technology 79−12303
Mellor-Durbin theory, appl. to marine thermocline evolution 80−4041
metrology, system of provisions for hydroaero-physical measurements 79−16709
microscale studies of vel., temp. and cond., stable platform development 79−5669
microwave holographic imaging of water waves 78−37861
microwave meas. of ice and seawater reflectance, at 100, 140 and 180 GHz 79−84552
microwave radiometry, appl. to ocean temp. and salinity meas. 78−81416
microwave radiometry, appl. to sea-ice meas. in Arctic Basin 78−81174
microwave radiometry, oceanographic appls. review 78−81415
microwave radiometry of sea temp., obs. at 2.65 Ghz at Chesapeake Bay 77−29314
microwave remote sensing, radiative transfer eqns. 80−21855
microwave remote sensing 80−56612
microwave remote sensing technology for marine oil pollution surveillance *(Japanese)* 80−76685
microwave scanning radiometry, appls. 78−73551
microwave scanning radiometry 78−73550
microwave scattering signature of ocean, aircraft measurements 77−17112
microwave scattering signature of ocean surface, aircraft meas. 77−25790
microwave sensing of marine boundary layer, estimation techniques 79−74993
microwave sensors in satellites appl., passive and active 79−80060
Mikhail Lomonosov, research vessel, review of 20 years of scientific results *(Russian)* 78−69485
mining, position location system 78−45046

oceanographic techniques continued
moored instruments for meas. in permanently ice-covered waters 78−49150
mooring monitoring, acoustic phase tracking technique 78−30138
multichannel remote meas. of sea surface microwave radiation spectrum *(Russian)* 78−65420
multiradionuclide analysis of coastal marine sediments and seawater 79−88370
nautical, near-shore charting, laser appls. 80−8463
nearshore bathymetry using remote multispectral imaging 78−45053
neutron activation anal., trace metal distrib. in Atlantic Ocean 78−85745
neutron activation analysis, of deep ocean sediments *(Russian)* 79−29888
neutron-activation method, applicability to sea water current vel. studies *(Russian)* 78−77358
nitrate determ. in estuarine waters, UV absorption technique 79−16719
non-tidal water level, meteorological effects at Leeville and Lafitte, USA 77−41244
nonlinear programming method for extreme tidal sea level calc. 77−78479
nonstationary random processes, simulation and prediction *(Russian)* 77−60408
nuclear power station thermal plume monitoring by drogues 77−3192
numerical models for synoptic prediction of currents and temp./salinity structure 77−5213
ocean bottom magnetic field meas. with superconducting magnetometer 77−87102
ocean wave geomag. fields, towed magnetometer investigation 80−3923
oceanic thermal fronts off Korea, DMSP IR detection 77−21796
Oceans '77, conf., Los Angeles, USA (Oct. 77) 78−36193
oceans '77, conference, Los Angeles, CA, (17-19 October, 1977) 78−45040
offshore environmental monitoring program for proposed nuclear power plant in Islote, Puerto Rico 78−11917
offshore shoal positioning using LANDSAT imagery 77−73883
oil, remote characterisation by time-resolved laser fluorosensors, lab. expt. 78−73097
oil contaminations on sea surface, radar detect. *(Russian)* 77−49089
oil polluted sea surface, atmosphere-ocean system apparent contrast 79−25265
oil pollution indicator, ocean wave effects on remote sensing ability, model study 77−17255
oil slicks, use of FFT in evaluation of laser Raman and fluoresc. decay times 78−81444
oil spill remote detection by laser radar 79−25332
oil spill trajectory modelling, advancements 79−5509
oil spills remote detection using laser-excited Raman backscatt. and backscatt. fluoresc. 78−32242
optical interferometry, water vertical density structure meas. *(Russian)* 80−51569
optical measurement of wind-driven water surface waves 77−29503
N.Pacific Ocean current, vel. field diagnostic calc. comparison with obs. *(Russian)* 78−61428
pack ice, struct. determ. via ocean waves SAR imaging 79−5496
palaeogeographic reconstruction, H_2S levels stagnation coeff. appl. 80−36291
palaeosalinity determ. from sediments B abundance, implications of B loss from seashells 77−78204
palaeotemperatures, from SiO_2 O isotopes in diatoms, 20000 yr record in deep-sea sediments 78−32247
parametrical wave prediction model 80−17272
particle dynamics meas. using holographic microvelocimeter 80−12567
passive radiometry of ocean, radio meteorology colloquium, Victoria, British Columbia, Canada (1978 June 14 to 21) 80−46724
petroleum oil pollution at sea, detection by CO_2 laser radar 77−91324
petroleum products content determ. in oil slicks on sea surface 77−64330
PFM fibre-optic video transmission to and from undersea vehicles 80−46310
photopeak processing method for gamma-spectra *(Russian)* 77−60487
phytoplankton remote sensing from satellite, atm. optical props. 80−77105
pollutant detection, appl. summing luminescence spectrometer with polychromator and spatial filter 77−74517
pollution, technique for estimating long-term conc. of conservative substances discharged into ocean 78−44885
Project Kiwi One, S.Pacific Ocean acoustic cross-section 80−36330
pulse compression radar scatterometer system, expt. 77−29483
R/V Athena, high speed ship for towing research 77−41213
radar, pulsed sea surface wind speed and significant wave height meas. 77−29477
radar, synthetic aperture imaging of ocean waves, focusing effects 78−40555
radar altimetry for remote sensing of ocean surface circulation 80−46189
radar imaging of ocean surface waves, models 77−17237
radar imaging of ocean surface waves, models 77−25689
radar imaging of the ocean surface 78−77334
radar measurement of wind and waves, HF and microwave techniques 78−81418
radar remote sensing of sea state, HF sea-echo Doppler spectra statistical props. 77−29312
radar remote sensing techniques, review 79−12294
radar scatterometer discrimination of sea ice types 77−41198
radio and heat location, inverse problem soln. *(Russian)* 78−65419
radio interferometer techniques, appl. to oceanographic meas. 79−53559
radio meas. of sea roughness at Ukrainian Academy of Sciences 77−29313
radio observations, appl. to polar regions 78−81419
radio oceanography, short bibliography of Russian literature 78−77338
radio oceanography using aircraft, inherent problems 77−25792
radio techniques, contribs. to large-scale oceanography 78−77337
radiocarbon dating of sediments by benzene variant method aboard ships 80−85770
radioisotopic methods for studying organic matter in photic layer *(Russian)* 77−60427
radionavigation systems appl., available systems survey, modes and accuracy 80−36408
radionuclides, artificial and natural, tracers of large-scale ocean circulation *(Russian)* 79−39742

oceanographic techniques continued
radiothermal location, inverse problem soln. method *(Russian)* 78−16188
random hydrophysical processes, quantification *(Russian)* 78−77359
remote acoustic monitoring appl. to natural suspensates and slope/shelf water intrusions 79−2241
remote data access system aspects 77−41172
remote pollution detection by laser-induced luminesc. techniques 78−81442
remote sensing, appls. to oceanography and sea ice 80−77176
remote sensing, atmospheric effects on refl. solar radiation field *(Russian)* 77−33086
remote sensing, marine environment charact. *(Japanese)* 77−5339
remote sensing, ocean surveillance by US Coast Guard 78−45004
remote sensing, particulate Fe mapping in ocean acid waste dump 80−56497
remote sensing, Space Shuttle prospects 79−58225
remote sensing, utility of polarised visible radiation 79−5498
remote sensing for, water depth and bottom features mapping 78−40673
remote sensing of atmosphere, land and sea props. 78−93015
remote sensing of ocean color 80−8460
remote sensing of ocean colour 77−78460
remote sensing of ocean surface topography using elevations from GEOS-3 altimeter 79−39882
remote sensing of optical props. in continuously stratified waters 78−77331
remote sensing of sea-state and surface winds in Irish and Celtic seas using MF radar 79−16725
remote sensing of surface currents, recent progress 77−87114
remote sensing techniques used by US coastguard 79−34991
remote temperature sounding in thin surface layer *(Russian)* 80−4138
research techniques used in survey ships *(French)* 78−65434
retrieval-time data generation 77−5354
rough surface average impulse response, appl. to satellite radar altimetry 77 17235
RPV, high-altitude, for environmental appls. 80−17470
saline environmental waters, anal. via IR relative refl. and complex refr. index 77−45013
saline water trace element analysis problems 78−45051
salinity in-situ measurement, Practical Salinity Scale 1978 80−67419
salinity measurement, elec. cond. obs., temp. and conc. depend. 80−67421
salinity of standard seawater, elec. cond. compared to KCl soln. 80−67420
salinity of standard seawater, elec. cond. obs. 80−72647
salinity of standard seawater, elec.cond./salinity/temp. relations 80−67422
salt analysis of seawater by neutron activation *(Russian)* 79−39898
salt water analysis, Schales and mercuric nitrate methods *(French)* 77−78432
sand grains, mobile, underwater detect. 78−96192
sand waves, computing methods 79−12313
satellite altimeter data analysis, role of orbit determ. 78−77177
satellite imagery of ocean, atm. effects removal 78−73521
satellite IR imagery, shelf sea fronts adjustments obs. 79−92545
satellite IR pictures, automatic digital techniques for oceanic features enhancement and extraction 79−5682
satellite ocean-related imagery, appls. programme 79−5681
sea bed mapping by acoustic method, signal processing technique *(Dutch)* 77−64478
sea depth, coding via sedimentary deposits *(Russian)* 80−17383
sea floor mapping on Mid-Atlantic Ridge, integrated approach 77−5360
sea floor relief mapping considerations 80−46169
sea foam produced by storms, microwave remote sensing of storm intensity 80−41528
sea ice, airborne laser profiles, interactive correction and anal. system 79−25338
sea ice, microwave remote sensing in AIDJEX main expt. 78−81173
sea ice, sidescan sonar imagery, Arctic Ocean 79−25339
sea ice age category differentiation through location and temp. observations using microwaves 80−67380
sea ice internal forces, local values determ. from mean stresses 80−31056
sea ice/lake SAR L-band imagery computer processing 78−36311
sea level nonperiodic oscills. calc., spectral method for deriving regression eqns. 78−7660
sea level vars. monitoring, Pacific Ocean appl. 79−100840
sea roughness investigations, radiophysical, Ukrainian Academy of Sciences 77−17233
sea state, significant wave height extracted by algorithms 80−4023
sea state and wind sensing by HF skywave radar 78−24396
sea state estimation, ocean wave models and microwave scatter 78−77244
sea state radar monitoring, ground wave and sky wave sensing techniques 80−109256
sea surface charact. rel. to radar returns at near-vertical sighting angles 79−57969
sea surface inhomogeneities sensing via sound scatt., phase function shape in shadowing conditions *(Russian)* 80−94530
sea surface slope distrib. function determ. from Sun glitter, accuracy *(Russian)* 80−94611
sea surface temp., atmospheric effects elimination for remote sensing *(Russian)* 78−96311
sea surface temperature, radiometric observations at 2.65 GHz, atmospheric and surface corrections, Chesapeake Bay 77−17114
sea surface temperature measurement, Noaa 4 satellite and Aries airborne radiometer results comparison 79−62517
sea surface topography, altimeter data analysis by sequential filter 80−4145
sea surface topography obs. with Geos 3 altimeter data 80−3908
sea surface waves, remote sensing using one and two freq. microwave techniques 80−94622
sea surface waves mean height determ. method 77−21928
sea surface wind speed and significant wave height meas. using short pulse radar 77−17234
sea suspended material and chlorophyll conc., estimation from outgoing radiation spectrum meas. from helicopter 80−36333
sea temp. vertical distrib., modelling and prediction on expedition *(Russian)* 78−16190
sea water, dielectric permeability calc. *(Russian)* 78−77261

oceanographic techniques continued
sea water chlorinity determination, appl. to gamma-radiation from neutrons radiative capture *(Russian)* 78−77360
sea wave meas. using HF radio scatter 77−25789
sea wave space and time structure measurement from Doppler frequency shift 77−29482
sea waves measurement, optimum conversion of information to digital form 79−29903
sea waves recording and analysis *(Italian)* 77−29458
sea-echo Doppler radar, accuracy of parameter extraction 80−51561
sea-surface temperatures in tropical Pacific, satellite determ. and climatological usefulness 80−31044
sea-wave space and time params. determ. from freq. characts. of RF signal scattered by sea 77−17239
seafloor instrumentation systems, multifunctional, USA's offshore instrumentation program 79−53584
seafloor minerals, long-term exposure expts. rel. to Mn nodules mineralogy and comp. changes 79−5471
SEASAT, ocean wave and wind obs., appls. to offshore oil, gas and mining industries 79−80044
SEASAT program, Canadian participation 78−20535
SEASAT synthetic aperture microwave-imaging radar expt., overview 80−46267
SEASAT-A satellite ocean surface truth expts. 77−5419
SEASAT-A satellite project, instrumentation and appl. 79−84496
seawater, computerised high-precision titrations of major constituents 77−66926
seawater, elec. cond. and salinity, temp. and press. depend. obs. 80−67368
seawater, optical anisotropy coeff., temp. fluctuation, optical meas. method 78−69488
seawater, trace element estimation using radioactive ^{14}C *(Dutch)* 77−29459
seawater bromide determ. using bromide ion-selective electrodes 78−3996
seawater characteristics meas. at depths >10 km in Marianas Trench, Pacific Ocean 78−61423
seawater chlorinity and salinity determ., possible use of neutron methods *(Russian)* 78−65422
seawater complex permittivity meas. at microwave, method 77−45184
seawater density determ., possible use of beta-emitting radioisotopes *(Russian)* 78−65423
seawater density determ. using gamma radiation *(Russian)* 77−82037
seawater elec. cond. meas., var. with temp. 78−20531
seawater electrical conductivity compared to KCl standard solution, salinity scales 80−72646
seawater inherent optical props. rel. to Secchi depth 79−16472
seawater purification, method for obtaining Si-free and PO_4-free water 78−3817
seawater radioactivity, calc. in advected water masses *(Russian)* 78−77275
seawater salinity and density from gamma-ray attenuation *(Russian)* 79−39897
sediment, ^{230}Th age, α-scintillation counting method 80−72636
sediment classification by seismic reflectivity meas. 77−5370
sediment classification using broadband deep towed seismic system data 79−16721
sediment trap arrays recovery, appl. of timed electrolytic anchor release 78−40693
sedimentary sea bottoms, machine classification 79−92626
sedimentation rates determ. by nondestructive gamma-gamma coincidence spectrometry 78−85709
sediments, acoustic anisotropy due to overburden press. 80−56455
sediments, neutron activated, gamma-ray scanning for elemental profile distribs. 77−17079
seismic and side-scan sonar images, recording, signal amplitude preservation 78−36326
seismic exploration, review 77−41196
seismic profiling, continuous, with two receiver systems, effective vels. determ. 80−31150
Seto Inland Sea hydraulic model tidal flow pattern anal. *(Japanese)* 78−36314
sewage sludge tracking, using 200 kHz acoustic echo sounder 77−2182
shallow-water mineral exploration by controlled-source audiomagnetotellurics and resistivity profiling 77−5356
shelf sediments, rapidly accumulating, sonobuoy study 79−21042
shorefast sea ice melting study using multispectral LANDSAT data 77−78522
short arc adjustment model technique for oceanic geoid determination, satellite altimetry 80−21830
short pulse radar ocean wave sensing, preliminary results 80−46315
side scan sonar, review 77−70866
side-scan sonar, Pacific Ocean floor relief meas. 78−36142
side-scan sonar with selective textural enhancement 77−5371
signal processing, for precise ocean bottom mapping 77−2272
small-scale turbulence and stratification study, via towed instruments carrier 80−36423
solid-state imaging devices, conference, San Diego (1977) 78−66944
sonar, narrow beam scanning, ocean bottom profiling 79−88509
sonar, side looking, picture improvement 79−84516
sonar, water pollutant detection, diffusion and scattering theory *(Italian)* 77−91335
sonar methods for remote exploration of oceanic internal structure *(French)* 79−44274
sonobuoy position meas., sound speed adaptive estimation 79−72773
sound ray paths plotting in potential layer from bathythermograms 77−41037
sound velocity field fine struct. meas. method 77−64479
statistical prediction, appl. to beach changes in S.California 80−98305
storm zone location methods using radiothermal remote meas. *(Russian)* 78−16189
Strait of Magellan, tidal currents monitoring by onshore elec. field recording 77−87107
structural functions appl. to study of hydrophys. fields *(Russian)* 79−39901
submarine radiometry and physical environment monitoring, educational project 79−12555
submarine sediments, automatic recognition by sonoprobe survey, acoustic reflection pattern model *(Japanese)* 80−85776
subsurface temp. remote sensing using laser Raman backscatter 77−78434
oceanographic techniques continued
subsurface water temperature and salinity remote sensing by Raman scatt. 79−80036
sulphate determ. in seawater, indirect anals. by atomic absorpt. 80−89556
surface chlorophyll concentration obs. from high altitude 77−4976
surface current mapping by Coastal Ocean Dynamics Radar 80−46316
surface current probes, rapid method for data recovery 79−84518
surface currents and gravity waves, directional spectra, remote sensing by microwave radar 78−57364
surface currents mapping, HF radar system appl. 80−94626
surface imaging, spaceborne SAR, phase and Doppler errors 77−2323
surface parameters, retrieval from scanning multichannel microwave radiometer obs. 80−90261
surface phenomena measurement using lasers *(Japanese)* 79−16716
surface radiation budget calc. methods, evaluation *(Russian)* 77−29494
surface radiation budget calc. methods compared *(Russian)* 77−29495
surface roughness estimation using linear FM signal *(Russian)* 78−77353
surface roughness probability density function determination, from Geos-3 altimeter data 79−100852
surface temp. determ., satellite data processing *(Russian)* 80−17417
surface temp. meas. from meteorological satellite images 79−100990
surface temperature measurements, derivation from Meteosat image data 80−76985
surface temperature remote sensing by satellite appl. to advection in Peru Current 78−16029
surface UV reflectance meas. from airborne platform, techniques and instrumentation 80−98453
surface water, global radioactive contamination levels determ., math. method 78−7816
surface water, remotely sensed by microwave radiometry 80−36428
surface wave imaging, synthetic aperture radar mechanism 79−5651
surface waves height meas., new acoustical methods 79−1276
surface waves meas., using resistance wave gauge, accuracy and calibration 80−24110
surface wind field mapping, high-resolution, skywave radar 77−17159
surface wind wave related turbulence meas. by impellor current meter array 80−46301
surge wave height determination, graphical method 80−56485
surveillance by electric and magnetic sensing systems 78−69538
suspended sediment conc. meas. with sampling bottles accumulators 79−53552
suspended solids measurement, test of diffuse reflectance models 80−8453
swathe imaging using synthetic aperture radar 79−84506
swell waves forecasting from typical swell fields 79−39754
synthetic aperture radar imagery, random phase changes effects 77−25793
synthetic aperture radar imagery formation, effects of random phase changes 77−17242
synthetic aperture radar imagery of ocean waves, comparison with surface truth 79−5497
synthetic aperture radar imagery rel. to surface structure 80−46197
synthetic aperture radar underwater mapping, array processing 78−69549
synthetic-aperture radar, tutorial review, ocean surface imaging appls. 78−81445
Tampa Bay bottom configuration and environmental studies, photogrammetric method 77−87124
temperature by coral Sr/Ca ratio 80−12568
temperature determination by remote sounding, aerosol attenuation effects on accuracy *(Russian)* 78−81430
temperature gradient meas. in sea, anal. of two methods 80−31149
temperature measurements with Aanderaa thermistor chains, solar radiation effects *(French)* 79−62611
temperature microstructure low noise temperature microstructure low noise meas. with thermistors meas. with thermistors 79−58104
thermoanemometry, appl. to currents meas. on Baltic Sea coast *(German)* 80−101373
thermocline, depth determ. via sonar *(Russian)* 77−13132
thermocouple arrays for vertical temperature gradients horizontal var. meas. 78−61571
tidal currents, meas. by two-site HF Doppler radar system by using two-site HF 80−72533
tidal periodic flow anal. by finite element perturbation method 77−70690
tides, oceanic and shallow water, spectral method of computation *(French)* 78−28321
tides, spectral modelling, finite element method, appl. to M_2 tide in English Channel 78−61579
tides mapping with satellites, computer simulation 79−39880
trace element detection by activation analysis *(French)* 77−41067
trace element meas. by neutron activation and atomic absorption methods *(French)* 77−41238
turbulence breakdown coefficient determ., influence of data treatment technique *(Russian)* 78−7690
turbulence meas. near seabed, digitisation and record length selection 80−104971
underwater acoustic communications, swept carrier method for multipath interference suppression 79−3835
underwater acoustic pulse compression system, signal processing methods 80−56630
underwater acoustic signals, freq. shift arrival time determ. 79−3875
underwater camera data correl. and interpretation, systems approach 79−5688
underwater chlorophyll *a* fluorescence sensing, sunlight penetration depth estimation 79−79874
underwater explosions, scaling law for shock waves 77−14838
underwater explosions, source depth determ. from spectra obs. at long ranges 77−7243
underwater in-situ soil testing, direct and indirect methods, trends 79−12307
underwater light field fluctuations under rough sea surface, numerical modelling *(Russian)* 77−33090
underwater offshore acoustic test range construction 79−16720
underwater sound, CW phase fluctuation spectra rel. to ocean processes determ. 77−46850
underwater surveys by submersibles, acoustic navigation system 79−5683
unsteady waves from initial, periodic and travelling disturbances, asymptotic anal. *(Russian)* 78−77254

oceanographic techniques continued
US scattering method for small-scale turbulence study 80−26540
USA coastal zone water quality monitoring, aircraft vs. spacecraft 77−78233
Vaisala-Brunt frequency vertical fine struct. meas. in Mediterranean Sea 80−26537
velocity calc., improved Stommel-Schott method 80−41561
velocity determination from hydrographic data 80−17415
velocity sensor, calibration equipment and technique, oceanographic appls. 80−8447
vertical eddy viscosity coeff. determ. method comparison 80−98326
waste drift, satellite and current drogue studies 78−3824
water classification using solar radiation spectral attenuation meas. 79−12127
water line survey by photogrammetric methods 79−25185
water penetration imagery, surface/depth data separation by multispectral scanning 78−69539
water pollution detection by X-ray fluoresc. anal. of environmental samples, book 77−41217
water quality instrumentation system test 77−41066
water tracing using fluorescent dyes, evaluation 77−64493
water transparency, in situ meas. 79−25355
water waves, wind-generated, spatial correls. rel. to freq. independent phase vels. 80−98333
wave analysis, using subsurface sensor on offshore mooring platform 80−26641
wave and current data acquisition on Norwegian continental shelf 79−12120
wave and current recording 78−61610
wave and swell forecasting for North Sea 78−7658
wave data from synthetic aperture radar, processing 78−77335
wave detection by microwave radar, gravity-capillary wave modulation 78−77333
wave direction, meas. by single wave follower buoy 79−5664
wave direction determ. in coastal waters 79−5642
wave direction sensing using solid-state water current meter 79−21070
wave forecasting service, pot. benefits case study anal. 78−77357
wave frequency spectra and wavenumbers meas. method by recorder array *(Russian)* 80−109266
wave height determ. by synthetic aperture radar imagery 77−70845
wave height meas. using Geos 3 radar altimeter 79−16481
wave height meas. with satellite radar altimeter 79−44253
wave height measurement by radar, airborne method 80−85771
wave height measurements using GEOS 3 radar altimeter data 80−8452
wave height profiling, depth sounding, laser beam reflection method, sea surface wavenumber effects 80−31121
wave height statistics, dual freq. correl. radar meas. 77−29478
wave heights, meas. by high resolution pulse-limited radar altimeter 78−81172
wave imaging and wavelength meas. by aerial photography 80−46323
wave meas. by offshore industry 78−69492
wave measurement, analogue spectrum analyser system for operational buoys 79−5662
wave measurement, via GOES-reporting waverider buoy 79−5663
wave measurement with spar buoy 80−85772
wave obs. using Loran-A (1.85 MHz) radio wave backscatter Doppler shift *(Japanese)* 78−85737
wave phase velocity measurement method, TV meas. of refl. sky radiance 80−98335
wave slope determ. from surface photographs 79−16680
wave spectra, remote meas., two-freq. microwave technique 78−77336
wave spectra derivation by integral inversion of second order radar echoes 77−78475
wave structure, radar imaging method using SAR 80−77173
waveheight nondirectional spectrum from inversion of HF sea-echo Doppler spectrum 78−16203
waves, detect. and direction meas. via microwave radars 79−5685
waves, HF skywave radar technique for height and spectrum 80−90241
wind field mapping using satellite scatterometer on Seasat-A 78−73529
wind fields, high resolution mapping using skywave radar 77−29480
wind speed and stress estimation from ambient noise meas. 79−74963
wind speed meas. using HF skywave radar sea scatter 77−29481
wind-driven wave parameters determ. at automated buoy stations 79−21064
Woodhead seabed drifters, acoustic tracking 77−5366
X-ray fluorescence analysis, of ferromanganese nodules and marine sediments, use of semiconductor detectors *(Russian)* 79−29887
B, inorganic, determ. in coastal waters, appl. to St. Lawrence Estuary *(French)* 78−77274
CO_2 partial pressure in seawater, shipboard meas. 77−2263
Ce determination method for marine sediments 80−104543
^{134}Cs and ^{137}Cs as tracers in water and sediments 80−3541
^{137}Cs conc. meas., sorbent props. *(Russian)* 79−39763
$^{137}Cs/^{134}Cs$ radioisotopes in seawater, Cs-selective resin determ. 80−94137
^{3}H, environmental anal. by mass spectrometric meas. of ^{3}He 77−9447
$^{3}H/^{3}He$ dating as meas. of O_2 utilisation rates, appl. to Sargasso Sea 77−56654
^{222}Rn potential appl. as tracer in ocean hydrophys. studies *(Russian)* 79−39745
^{222}Rn tracer measurement in aqueous samples by decay product filtration 77−60476
Se (−II,0), -(IV) and -(VI) composition of water, by gas chromatography method 80−81928
SiO_2, dissolved, natural oceanic circulation tracer, Yucatan Strait 78−44830
U extraction from natural seawater, by sorption techniques 79−29902
V determ. in sea and surface water, preconc. on charcoal, neutron activation anal. 77−44549
V pollution, low level meas. 77−41239

oceanography
see also ocean waves; seawater; sediments; tides
abyssal fan sediment in Arabian Sea, acoustic velocity 80−72488
abyssal marine sediment, organic ^{14}C activity 79−16434
abyssal marine sediments, biological stirring, dissolved and adsorbed materials redistrib. 78−69321
abyssal shear zone east of Newfoundland Ridge, temp., salinity and nephel meas. 78−73386
abyssal water masses form. and interleaving off Wilkes Land, Antarctica 78−81180

oceanography continued
academic research institutions, research activity planning *(Russian)* 77−78202
accelerating flow horizontal divergence, turning vorticity eqn. anal. 80−77013
acid waste dump, particulate Fe mapping 80−56497
acoustic ambient noise levels meas., Cochin backwaters 79−25256
acoustic backscattering from discrete targets at 87.5 kHz 78−87181
acoustic field radial spatial coherence from near ocean surface source 78−30117
acoustic forward reflection from rough sea surface statistical anal. 78−50983
acoustic interaction with ocean bottom, plane wave reflection loss model 79−10425
acoustic long range propag. in oceans, signal speed variations 78−50984
acoustic motional source transfer function characts., ocean profile anal. appl. 78−66982
acoustic narrow-band signals and noise amplitude fluctuations in sea 78−9479
acoustic normal mode amplitudes in random ocean, statistical theory 78−50981
acoustic parabolic wave theories and applications 80−51436
acoustic powerful signals propag., approx. eqns. *(Russian)* 79−98526
acoustic propag., long range, statistical anal. of signal intensity 78−90569
acoustic propagation in deep ocean, effect of currents and tidally varying sound speed 77−79995
acoustic propagation paths to Midway Is., using shallow explosion sources 79−41496
acoustic radiated noise meas. from data buoys and cycloidal propellers 78−33960
acoustic reflectivity and attenuation, near-bottom obs. at 4 kHz 77−2140
acoustic reflectivity of sea-floor 80−98302
acoustic reverberation spectral rel. to remote detect. of turbulence 78−38124
acoustic scattering layer, comp. estimation 77−86909
acoustic sidebands from CW sources towed in deep ocean 78−50985
acoustic sidebands obs. in CW tones received at long ranges 77−7244
acoustic signal coherence limits in random ocean environment 80−46193
acoustic signals scatt. by locally irradiated sea surface, amplitude fluctuations *(Russian)* 79−29777
acoustic subbottom data analysis through simulation, theoretical vertical and lateral model 80−74571
acoustic surface backscattering, diffr., refl., and interf. at near grazing and near normal incidence 78−90570
acoustic transmission in isospeed channel, effect of random ocean current 78−13840
acoustic transmission rel. to finestructure meas. 77−64311
acoustic velocity profile, horizontal range, and travel time series expansions 78−5604
acoustics, book 79−57970
acoustics, two-point coherence function models with inhomogeneous background and anisotropy 80−81922
active layer, temp. and turbulent energy dissipation, model *(Russian)* 79−100857
active layer evolution, mathematical model *(Russian)* 79−100858
active layer vertical structure 79−44194
active ocean layer, integral model *(Russian)* 78−7649
active ocean layer, numerical modelling *(Russian)* 78−32110
admixture diffusion in vortex flow 79−2277
Adriatic Sea, active sonar detection range, refraction effects *(Croatian)* 79−57945
N.Adriatic Sea, bora driven circulation 78−40556
Adriatic Sea, chem. parameters, spring and winter time obs. 80−41447
N.Adriatic Sea, Green's function of Laplace's tidal eqn. 80−17291
N.Adriatic Sea, max. sea level, extreme values *(Italian)* 77−53061
Adriatic Sea, meteorology contrib. to high tides prediction 77−86906
Adriatic Sea, southern wind induced surges, numerical model 77−53059
N.Adriatic Sea, trace element analysis of seawater and sediment by neutron activation 77−21801
advective mixed-layer model with imposed surface heating and wind stress 80−12395
Aegean basin, hydrodynamic eqns., numerical solns. 78−65317
Aegean Sea, Cu, As and Hg conc. determ. 79−2292
Aegean Sea, spectral anal. of tidal data 77−86905
aerobic pelagic sediments, denitrification 78−77214
aerosol distributions in maritime air, IR scatt. coeffs. 77−45050
aerosol particles production, as atmospheric Cu source 79−58050
NW.Africa, upwelling, C isotopic evidence in sediments 78−65334
N.W.Africa continental slope, tidal current field 77−37214
W. African continental shelf, suspended particle mineralogy and transport in water masses 77−81900
N.W.African continental shelf, wind, current and temp. meas. 77−86923
African upwelling region, light scatt. obs., suspended particle meas. 79−5483
NW African upwelling region, local and mesoscale influences on nutrient variability 79−57971
NW.African upwelling region, sea surface temp. and salinity meas., 1971-72 winter 78−44827
NW African upwelling region near Cabo Corveiro, upwelling obs. 77−60379
Agulhas Current, giant waves 77−13085
Agulhas Current, obs. in 1969 March 79−5485
Agulhas Current, obs. of advecting meander 79−100851
Agulhas Current, satellite IR images, circulation modes 79−5484
Agulhas Current, topographically induced changes in struct. of inertial coastal jet 80−72545
Agulhas Current and Agulhas Return Current, drift of satellite-tracked buoy 79−74895
Agulhas Current during northeast monsoon 77−17126
air flow above water waves, numerical model 77−81912
air flow separation over water waves 77−11208
air layer near water surface, diurnal characts., equatorial region, GATE meas. 78−61527
air-sea energy transfer and tropical atm. struct. 77−2203
air-sea exchange of heat and water, model 80−61809
air-sea heat and moisture exchange during stormy weather 77−78375
air-sea interaction, mean wind speeds and turbulence at coastal site and offshore location 80−98406
air-sea interaction model 79−79969

oceanography continued
air-sea interface, CO_2 flux meas., eddy correl. method 79−25303
air-sea interface, gas transfer 77−91154
air-sea interface, heat and momentum flux in const. flux layer, from temp. meas. 78−44899
air-sea interface, latent and sensible heat flux calc., AMTEX-74 77−91224
air-sea interface, momentum flux determ., wind-wave interaction method 77−33130
air-sea interface, oceanic variability obs. during Project BOMEX 78−69362
air-sea sensible and latent heat transfer coeffs., meas. 200 km from land 80−72552
air-water exchange reactions, wind-wave interactions *(Dutch)* 78−3785
air-water interface, aqueous sublayer thickness determ. 77−60395
air-water interface, energy transfers at high wind speeds, effect of spray 78−85574
Alaskan continental shelf, sea ice ridging 80−12410
Albian open seaway between northern and southern proto-Atlantic 78−40538
Alboran Sea, mesoscale oceanic vortex, drifting buoy and satellite meas. *(French)* 79−16473
Alboran Sea frontal system, XBT data for 1976 Nov. and 1977 March period 79−2256
Alboran Sea gyre, laboratory simulation 79−100846
ambient air/water interface, frictional coefficient at low wind strength, obs. *(French)* 78−16020
ambient sea noise directionality, meas. and processing techniques 78−16025
ancient ocean composition, $^{87}Sr/^{86}Sr$, Jurassic to Pleistocene, Israel groundwater obs. 80−61804
ancient shorelines from stone rosettes 80−26489
Andaman Sea, hydrological charact. during late winter season 77−91148
Antarctic Bottom Water, near-zero production 78−11903
Antarctic circumpolar current, Drake Passage space and time fluctuations 77−78205
Antarctic Circumpolar Current, geotrophic barotropic volume transport 80−36305
Antarctic Circumpolar Current S of Australia, cyclonic eddy obs. from R/V Professor Zubov 79−48500
Antarctic Circumpolar current struct. and transport at Drake Passage 78−44848
W Antarctic ice sheet, radio-echo layers and recent stability 77−5212
W.Antarctic ice streams rel. to global climatic stability 77−64321
Antarctic intermediate waters distrib. charact. in world ocean 79−2271
Antarctic Ocean, interdisciplinary studies 78−11915
Antarctic Ocean, new research results *(German)* 79−62520
circum-Antarctic Ocean, rel. to Cenozoic evolution of Antarctic glaciation and global palaeoceanography 78−16063
Antarctic ocean, topographic effects in rapidly rot. flow over transverse ridge 78−28245
Antarctic Polar Front anatomy in Drake Passage 79−39723
Antarctic Polar Front Zone, climatic charact. 79−2358
Antarctic Polar Front Zone, fine structure rel. to internal waves 79−2254
Antarctic Polar Front Zone in W.Scotia Sea, 1975 summer obs. 77−86914
Antarctic Polar Frontal Zone from Australia from Drake Passage, thermal struct. 78−44850
Antarctic waters, effect of glacial weathering on Antarctic waters silica budget 78−20436
anticyclonic eddy off W.Austalian coast, trapping of drifting buoys 78−44832
aocustic coherent ray propagation through Gulf Stream ring 78−11906
aqueous heavy metals, adsorption on inorganic minerals 78−49006
Arab Gulf, transparency, thermal stratification, salinity gradient, and pH-values of water samples 79−5489
Arabian Gulf, comprehensive oceanographic monitoring programme 79−8728
Arabian Sea, denitrification rate 78−85606
Arabian Sea, hydrochem. and hydrographic features of northern basin 77−41059
Arabian Sea, inorganic N system equilib. 77−41060
Arabian Sea, inorganic phosphate distrib. during SW monsoon season 77−41061
N.Arabian Sea, light transmission charact. 77−91144
Arabian Sea, N. and E. Basins, chemistry 77−73764
Arabian Sea, petroleum hydrocarbon conc. in shelf regions and adjacent waters 79−48190
Arabian Sea, suspended matter distrib. on Indian shelf 77−73765
Arabian Sea, temp. and salinity fine struct. obs. 79−25257
Arabian Sea, upper layers temp. distrib., ISMEX-73 data 77−53065
Arabian Sea, wind stress, sensible and latent heat fluxes, ISMEX-73 data 78−85627
Arabian Sea cooling, heat budget, feedback with atm. circulation 80−104979
Arabian Sea near Persian Gulf inlet, vert. thermohaline struct. fluctuation 80−76991
Arabian Sea surface temp. anomaly effects on Indian summer monsoon 77−49120
arbitrary continuously stratified environments, propagated, reflected and transmitted acoustic waves 78−13829
central Arctic, young sea ice, energy exchange 78−85584
Arctic Alaska coast, fast ice, crystal c-axis alignment 80−67375
Arctic and Antarctic, Soviet oceanological research 79−39756
Arctic basin, drifting sea ice, deformation *(Russian)* 78−7652
Arctic Basin, ice movements, external factors 80−26541
Arctic Basin, plane nonstationary model of wind-driven circulation 77−21789
Arctic Basin, sea-ice conc. and multiyear ice fraction time depend. 78−81174
Arctic fjord, mixing 79−48504
Arctic ice cover, attenuation of 8 and 20 cm EM waves 80−67379
Arctic ice cover evolution rel. to climatic changes 79−29781
Arctic Ice Dynamic Joint Experiment 77−33190
Arctic ice pack heat and mass balance 79−39750
Arctic layered finestructure, acoustic variability, 10 to 60 kHz 79−90060
Arctic leads, atmos. boundary layer turbulence spectra obs. 80−56588

oceanography continued
Arctic Ocean, Alpha Ridge bathymetry rel. to spreading centre hypothesis 79−48455
Arctic Ocean, bathymetry and sea-floor features morphology 79−48453
W. Arctic Ocean, ice pack, rectilinear leads and internal motions 77−37208
Arctic Ocean, late Wurm ice sheet rel. to N.Hemisphere glaciation 77−45132
Arctic Ocean, sea ice decay following CO_2-induced atmospheric temp. rise 80−61802
Arctic Ocean, sediment thicknesses and upper mantle temps. from magnetotelluric soundings 79−48454
Arctic Ocean and East Greenland Current surface water T conc. 77−5230
Arctic Ocean circulation, numerical simulation 77−2165
Arctic Ocean sea ice, snow and ice cover conditions 80−26547
Arctic Ocean sediments, ^{10}Be deposition rate 77−81865
Arctic oceanic loading tide and Earth tide at Spitsbergen 77−9318
Arctic sea ice, 1953-77 period fluctuations 80−36314
Arctic sea ice, compressive strength and stress relax. meas. *(Japanese)* 77−81916
Arctic sea ice, flexural strength meas. *(Japanese)* 77−81915
Arctic sea ice, layered struct. study by radar sounding *(Russian)* 78−16023
Arctic sea ice, surface layer induced thermal stress state meas. *(Japanese)* 77−81917
Arctic sea ice, surface-based radar scatterometer results 79−92544
Arctic sea ice, water drag 77−21781
arctic sea ice extent rel. to interannual atmospheric var. 80−41501
Arctic seas, ice forecasts and practical appls. 78−96230
Arctic seas, surge level oscills. in shelf zones 80−77012
artificial upwelling induced by ocean currents, theory and expt. 78−81217
Atlantic, ^{14}C pollution from nucl. weapons tests 80−89683
Atlantic, abrasion as source of sedimentary material, shore erosion 79−2217
NWAtlantic, absolute vel. calc. 80−41561
SW.Atlantic, abyssal circulation increase during Late Pliocene rel. to global climatic cooling 78−40645
NW.Atlantic, acoustic transmission over long distance 80−90091
N.Atlantic, active layer thermal struct., synoptical variability *(Russian)* 80−109169
E.Atlantic, aeolian dusts and biogenic lipids in marine environment 77−64327
Atlantic, anomalous bottom water south of Grand Banks due to turbidity current activity 80−4042
S.Atlantic, Antarctic Intermediate Water, modal props. 80−36306
NE Atlantic, basalts from Great Meteor and Josephine seamounts, K-Ar ages 77−9399
W tropical Atlantic, bioluminescent field intensity *(Russian)* 78−65341
SW Atlantic, charact. and circulation 77−64306
N.Atlantic, conditions in Jasin observation area *(Russian)* 80−109167
NE tropical Atlantic, current data *(Russian)* 80−17378
N.Atlantic, current heat transport across 25°N latitude 80−94537
tropical Atlantic, current meas. with EhMIT meter *(Russian)* 79−100978
Atlantic, current vars. in equatorial regions 77−78210
Atlantic, current vel. spectra and horizontal eddy viscosity 77−49080
Atlantic, current-temp. profiles in equatorial counter current 77−70676
N.Atlantic, deep water formation during last ice age 80−94535
Atlantic, dynamics of equatorial zone currents *(Russian)* 77−41035
Atlantic, equatorial, chemistry, biology and particulate matter vertical flux 77−78225
Atlantic, equatorial, I distrib. in upper layers 77−60422
Atlantic, equatorial undercurrent at 30°W, seasonal variation 80−90090
N.Atlantic, fluid-parcel vels. and paths calc. with aid of diagnostic models 79−29780
S.Atlantic, glacial and interglacial oceanographic conditions from $CaCO_3$ and radiolarian distribs. 80−72556
N.Atlantic, gravimetric geoid confirmation of sea surface topography by Skylab 77−17014
Atlantic, Halifax-Bermuda section, particulate organic C and N variability 77−64326
E. centralAtlantic, horizontal temp. in upper ocean layer *(Russian)* 80−17283
NE tropical Atlantic, hydrochemical structure *(Russian)* 80−17284
N.Atlantic, iceberg fluctuations *(German)* 78−49038
N.Atlantic, improved ocean tide models rel. to tidal loading in Nova Scotia 78−92821
N.Atlantic, internal wavefield-mean flow interaction 80−36309
E.Equatorial Atlantic, Jurassic sea-floor spreading 77−64253
NW Atlantic, large scale variations in temp./salinity fine structure 77−56639
NW.Atlantic, M_2 tide and Nova Scotia crustal struct. from tilt and gravity obs. 78−40464
NW.Atlantic, main pycnocline potential energy, dynamic height and salinity 80−85672
N.Atlantic, main thermocline large-scale depth perturbs., obs. 78−24302
Atlantic, main thermocline props. 79−57960
N. Atlantic, mesoscale currents calc. from Polygon 70 hydrological obs. *(Russian)* 77−49071
NE Atlantic, mesoscale eddies, drifting buoy expt. 78−73397
N Atlantic, mesoscale motions near deep western boundary, MODE data 79−74894
N.Atlantic, Mesozoic and Cainozoic, calcareous sediments depth distrib. 80−81866
central Atlantic, meteorology in mesoscale vortex area *(Russian)* 78−85658
N.Atlantic, middepth circulation and salinity field 79−16482
N.Atlantic, midocean geostrophic vorticity balance 80−90096
N.Atlantic, mixing in Bermuda, Sargasso and Gulf Stream regions 80−98343
NW Atlantic, Mn micronodule morphology and chemistry 80−81869
Atlantic, MODE-I region bathymetry 77−56615
NW Atlantic, moored obs. of semidiurnal internal tide 77−60421
Atlantic, NE of Cape Hatteras, Gulf Stream shift effects on circulation 77−9432
Atlantic, nonlinear P-V-T props. effects on pot. energy distrib. 78−49024
N.Atlantic, ocean temps. correl. with European Grosswetterlagen temporal vars. 79−58081

oceanography continued
tropical Atlantic, optical structure, temporal var. *(Russian)* 79−39735
N.Atlantic, palaeocirculation, benthic forminifera, and ^{18}O 79−92548
NE.Atlantic, palaeohydrology *(French)* 78−65343
N. Atlantic, Pliocene ocean climate, planktonic foraminifera record 77−17206
N Atlantic, potential energy maxima in tropical and subtropical regions 78−3774
N.Atlantic, pressure field along W. margin 80−12412
N Atlantic, quasi-biennial cycles of water temp. fluctuations rel. to weather 79−53357
S.Atlantic, R/V Mikhail Lomonosov 32nd cruise results *(Russian)* 79−100862
S.Atlantic, radiation attenuation rel. to phytoplankton *(Russian)* 79−39762
NE.Atlantic, salinity and O_2 distrib., influence of Southern Atlantic Central Water 78−49028
Atlantic, S.anticyclonic gyre, optical structure *(Russian)* 79−100866
N.Atlantic, sea surface temp. response to atm. forcing 78−73399
N.Atlantic, sea surface temp. year to year changes, (1948 to 1974) 80−67367
N.Atlantic, sea-air large-scale interaction, thermodynamics 78−3786
Atlantic, semidiurnal atm. press. wave seasonal var., Polygon-70 region 77−64390
Atlantic, semidiurnal temp. fluctuations horizontal coherence, Polygon-70 *(Russian)* 78−44844
Atlantic, struct. of large-scale circulation 77−78221
Atlantic, subantarctic intermediate water *(Russian)* 79−100865
N.Atlantic, subpolar warmth during icesheet growth 79−66711
NW.Atlantic, surface temp. features, 1975-7, satellite obs. 80−51412
Atlantic, surface topography spatial inhomogeneities 77−21790
Atlantic, surface water circulation, diagnostic computation 77−78211
Atlantic, temp. microstruct. obs. in equator region 80−98340
NE tropicalAtlantic, thermohaline structure *(Russian)* 80−17281
N.Atlantic, transient response, model studies 80−12405
tropical Atlantic, transparency at 30 m depth *(Russian)* 77−64307
Atlantic, tropical, currents vertical struct. parametrisation 77−64317
Atlantic, tropical, large-scale current struct., GATE meas. 79−53355
Atlantic, tropical, mass flux divergence of deep currents *(Russian)* 78−7651
Atlantic, tropical, vertical current struct., average systems of orthogonal functions 79−53356
Atlantic, turbidity distrib. 77−56634
central Atlantic, two-degree discontinuity 77−56633
equatorial Atlantic, upwelling rate from bomb-produced ^{14}C distrib. 79−39726
Atlantic, Vema Channel, Antarctic bottom water fluctuations effects of sediments 77−81903
NE Atlantic, volume scatt. strength obs. at 2 kHz 77−11073
N Atlantic, western subtropical regions, methane distrib. in near-surface waters 77−60423
NE.Atlantic, wind and ocean circulation, climatic var., Little Ice Age 80−8422
N.Atlantic, wind stress affecting large scale density struct. *(Russian)* 80−76989
S.Atlantic anticyclonic gyre, hydrometeorological conditions *(Russian)* 79−100863
S.Atlantic anticyclonic gyre, thermohaline structure and dynamics of upper layer *(Russian)* 79−100864
Mid-Atlantic Bight, coastal longshore pressure gradient 80−12411
S.Atlantic Bight, Hg flux meas. 80−4046
S. Mid-Atlantic Bight, LF current var. 80−81909
Mid-Atlantic Bight, mean circulation 80−36317
N. Mid-Atlantic Bight, NE. drift 78−40566
Atlantic bottom topography and magnetic field of elevated area *(Russian)* 78−85531
N.Atlantic central water, vertical mixing due to salt fingers 78−85571
Atlantic coastal waters, optical coherence loss meas. 80−8333
Atlantic coastline, behaviour in Landes and Basque regions *(French)* 80−76987
Atlantic continental margins and deep sea Late Quaternary sedimentation 77−21751
mid-Atlantic continental shelf, bottom current and sediment movement 79−57964
Atlantic continental shelf circulation from Capes May to Hatteras 77−37224
N.Atlantic deep water, ^{14}C age 79−84285
N.Atlantic deep water, production since Miocene, sediment evidence 80−46186
Atlantic dry weight of suspended particulate matter 77−5233
NE.Atlantic during Cainozoic, O and C isotopes at DSDP sites 78−96239
Atlantic Eurafrican continental margin, glacial eastern boundary current 78−81179
N.Atlantic general circulation west of 50°W, determ. by inverse method 79−74901
Atlantic GEOSECS expedition, Ba profiles 77−81918
N.Atlantic internal wave field, geographical variability 77−2154
N Atlantic marine aerosol, chemical relationships 77−53136
N.Atlantic mid-depth circulation, Mediterranean contrib. to Norwegian-Greenland Sea 80−81899
Atlantic near Gibraltar, O and phosphate distribs. *(Russian)* 78−16058
tropical Atlantic near W.Africa coast, optical studies *(Russian)* 80−17285
Atlantic nuclear waste disposal site, radionuclide redistrib. 80−85309
E.Atlantic Ocean, 23°N to 47°N, dissolved Cu concs. 77−5239
S. Atlantic Ocean, bathymetry, rel. to seafloor spreading south of Agulhas Fracture Zone 78−24277
NE Atlantic Ocean, bathymetry of continental margin around British Isles 80−12372
S. Atlantic Ocean, crustal heat flow profile rel. to hydrothermal circulation 77−86827
Atlantic Ocean, cyclic currents system as plane vortex with elliptical nucleus 77−53466
N.Atlantic Ocean, deep western boundary current core, ^{3}H conc. obs. 80−101380
S Atlantic Ocean, depositional history during last 125 million years 78−44798
N.Atlantic Ocean, detailed gravimetric geoid 79−62422
W.Atlantic Ocean, equatorial, subthermocline countercurrents 80−51426
E Atlantic Ocean, equatorial adjustment 78−88836

oceanography continued
N.Atlantic Ocean, geology and bathymetry rel. to Palisdaes microseismic sources 78−85495
Atlantic Ocean, history of growth and topography of ocean bottom 80−3993
NW.Atlantic Ocean, oceanic geoid and tides derived from Geos 3 satellite data 80−3901
Central Atlantic Ocean, results of underwater irradiance meas. *(Russian)* 78−77257
Atlantic Ocean, river sediment supply 79−12157
S.Atlantic Ocean, sea water hydroptic struct. variability *(Russian)* 78−77262
N.Atlantic Ocean, September-October 1976, sea temps. rel. to British wet spell 77−45124
Atlantic Ocean, spatial charact. of semidiurnal internal waves in Polygon-70 test area 80−31051
NW.Atlantic Ocean, sterol geochemistry of sediments 79−74885
N.Atlantic Ocean, tropical, atmospheric aerosols water-soluble K, Ca and Mg contents 80−72598
Atlantic Ocean, Upper Cretaceous palaeogeography rel. to Benue Trough stratigraphic evolution 79−2230
Atlantic Ocean palaeobathymetry from Jurassic to present 78−20387
Atlantic Ocean surface temp., empirical orthogonal analysis 77−86934
N.Atlantic region, gravity anomalies, regional elevation and deep struct. 79−16421
N.Atlantic rel. to Antarctic glaciation and eutrophication 80−61812
Mid-Atlantic Ridge crest at 26°N, near bottom water temp. anomalies 79−34831
Atlantic S.E. of Azores, crustal struct. rel. to mag. anomalies and bathymetry 80−51384
N.Atlantic sea surface temp. fluctuations at tidal frequencies 77−2170
Atlantic seasonal thermocline, turbulent mixing and vertical temp. structure *(Russian)* 78−85597
E. equatorial Atlantic sediments, pore water metal concs. 80−101358
E. equatorial Atlantic sediments, pore water metals concs. 80−101358
Atlantic shallow water off Argentinian coast, bottom reverberation-derived scattering strengths 78−65321
Middle Atlantic Shelf, long-term current and temp. obs. 79−70806
Middle Atlantic Shelf, seasonal drift 77−64292
Atlantic shelf-boundary tidal meas. between Ireland and Norway 77−37220
N. Atlantic subtropical convergence, deep mesoscale eddies influence on sea surface temp. 77−41052
N.Atlantic subtropical gyre, beta spiral 80−101367
Atlantic surface aerosols in Cape Verde Is., physical and chemical props. 78−85640
tropical Atlantic surface atm. and oceanic circulation patterns assoc. with Subsaharan weather anomalies 79−5587
N.Atlantic surface water, T and ^{90}Sr conc. and distrib. 78−65345
N.Atlantic temp. fluctuations rel. to European large scale weather pattern *(German)* 78−85660
Atlantic tropical ocean temp. anomaly, atmospheric response 77−17187
N Atlantic water columns, trichlorofluoromethane (F-11) exploratory anals. 78−88847
Atlantic waters, As and Sb content *(Russian)* 77−60428
N.Atlantic waters integral circulation, numerical calc. 78−3811
Atlantis II Deep, geothermal brine system 80−94526
Atlantis II Deep geothermal system, changing hydrothermal activity 78−85532
atmosphere heat exchange with ocean, influence of waves *(Russian)* 80−56479
atmosphere-ocean coupled model, ocean role in global climate 79−53507
atmosphere-ocean heat balance over northern hemisphere, annual cycle 77−41040
atmosphere-ocean interaction parametrisation for storm conditions, atm. circulation models appl. *(Russian)* 78−65359
atmosphere-ocean interactions along North American west coast, 1965-69 period, preliminary anal. 78−61508
atmosphere-ocean momentum, heat and H_2O vapour fluxes, meas. methods 78−32213
atmosphere-ocean system, interannual variability 79−2330
atmosphere-ocean system models, max. attainable forecasting accuracy 80−82036
atmosphere/ocean ranked interaction on sub-semidiurnal time scales *(Russian)* 78−77260
atmospheric boundary layer, heat transfer with ocean, reef effects, AMTEX 1975 obs. 80−26567
atmospheric boundary layer, turbulence meas. distortion caused by rolling ship 78−3805
atmospheric shortwave and longwave radiative flux, mid-ocean obs. 80−12547
attenuation of surface generated noise received deep in the ocean 78−90573
E.Australian coast, wind stress generation of shelf waves 77−37234
W.Australian Current, eddy struct. 78−44829
E.Australian Current, evidence for flow separation 80−109160
Australian region, Oligocene unconformities rel. to eustatic sea level vars. 78−73370
authigenic silicate minerals in marine sediments and oceanic Mg budget 77−86858
axisymmetric disturbances, evolution in fluid *(Russian)* 79−34848
Azov Sea, USSR, hummocking of floating ice, distrib. 80−26549
backscattering of sound by the sea surface under shadowing conditions 78−94473
Baffin Bay, oil seepage from seabed during 1976, August 80−12400
Baffin Bay-Labrador Sea evolution rel. to Early Tertiary lava flows from Greenland 77−17020
Bahamas, intense mesoscale eddy containing Mediterranean water 79−74902
Baie des Chaleurs, Gulf of St. Lawrence, sediments distrib. and depositional history 77−64257
Baja California coast, sea level vars. and currents 80−36321
Baltic, surge of saline water from North Sea *(Russian)* 77−53070
Baltic and North Sea water exchange, barotropic model wind effects 77−73742
E Baltic coast littoral drift regime and dynamics *(Russian)* 78−36147
SE.Baltic coast transit section, suspended load composition in calm and storm *(Russian)* 80−67360
Baltic coastal shelf suspended drift quantitative distribution *(Russian)* 78−49011
SE.Baltic inshore wave deformation peculiarities *(Russian)* 78−36188

oceanography continued
Baltic Sea, density and vel. fields fine struct. calc. 79−2279
Baltic Sea, density meas. 77−56635
Baltic Sea, diffusion of dye, expt. 79−2276
Baltic Sea, estuary region, suspension distrib. under river drifts influence *(Russian)* 80−98345
Baltic Sea, influence on atmospheric heat and moisture balance and climate 77−87057
Baltic Sea, mixing in thermocline and halocline layers 78−40571
Baltic Sea, P, N and organically bound C conc. annual vars. 77−49084
Baltic Sea, salt transports determ. from conservation calculations in natural coordinates 80−51433
Baltic Sea, small-scale temp. inhomogeneities 79−2275
Baltic Sea, summer circulation calc. 77−21791
Baltic Sea, surface salinity, mean annual var. *(German)* 79−62521
Baltic Sea, two-dimensional seiches theory 80−8323
Baltic Sea, water balance study, International Hydrological Program 78−7661
Baltic Sea, water temp. stratification in offshore zone 78−3792
SW Baltic Sea, wind-driven circulations 79−5490
Baltic Sea Basin, suspended matter, quantitative distrib. and comp. 77−21783
Baltic sea circulation under action of southwest winds 79−44198
Baltic Sea coast, currents meas. via thermoanemometry *(German)* 80−101373
Baltic Sea coast sedimentary material differentiation *(Russian)* 80−104951
Baltic Sea ferromanganese concretions, trace metal distrib. rel. to accretion rates 77−81864
Baltic Sea horizontal mixing, Lagrangian and Eulerian meas. 80−17290
Baltic Sea inshore waters, light scatt. matrices *(Russian)* 77−29311
Baltic Sea region, evaporation-precipitation during IHP 78−44865
Baltic Sea sedimentation, role of river suspensions *(Russian)* 78−7616
Baltic Sea sediments, organic acids 78−49007
Baltic Sea Upper Quaternary sediments, physical props. 78−3753
SE.Baltic shore development due to hydrotechnical constructions *(Russian)* 78−36145
SE.Baltic shore zone dynamic classification *(Russian)* 78−36146
SE Baltic shore zone subdivision into lithomorphodynamic sections *(Russian)* 78−36148
SE.Baltic storm surge peculiarities of water level *(Russian)* 78−36189
E.Baltic upper shelf suspended matter distribution and structure *(Russian)* 78−36187
Baltimore Canyon, submarine mass-wasting of sediments 80−101354
banded salt finger structure, form. 78−85570
Barbados, Late Pleistocene coral terraces and O isotope stratigraphy 77−78182
Barents Sea, EM field of electrical currents in sea bottom and shore 80−104864
Barents Sea, topographically controlled Oceanic Polar Front 79−2253
Barents Sea sediments, continuous seismic profiling with two receiver systems 80−31150
baroclinic instability in two-layer current model, beta effect influence *(Russian)* 78−44842
baroclinic instability of integral circulation in open ocean 78−3789
baroclinic nonlinear response to moving hurricane, model 79−16497
baroclinic ocean, integral stream function and pot. energy determ. 78−3808
baroclinic ocean circulation, numerical model *(Russian)* 77−81907
baroclinic ocean dynamics, asymptotic state *(Russian)* 80−94531
baroclinic ocean temp. model *(Russian)* 77−73749
baroclinic oceans, semi-implicit numerical model 77−29316
baroclinic synoptic eddies, evolution model *(Russian)* 78−85599
baroclinic world ocean, numerical dynamic model 79−29782
barotropic currents over anisotropic bottom topography, nonlinear theory 78−44867
barotropic motion over continental shelf, bottom friction effect 79−48509
barotropic nonlinear motion above irregular topography, spectral theory 79−16493
barotropic ocean response to moving hurricane 78−36191
barotropic vorticity equation, new class of steady solns. 80−85667
barrier island breach morphology and dynamics, study in stability 80−12371
barrier island configuration, coastal currents altering shape 80−17289
barrier island migration computer simulation 78−20384
barrier islands, global distrib. in terms of tectonic setting 79−2214
barrier reef and lagoon, Guadeloupe Island, geomorphology and sediments *(French)* 79−29749
Barrow Canyon flow, simultaneous current and temp. meas. 77−2156
bars, longitudinal axis when formed at a shore inlet within a contour *(Russian)* 79−92522
bars, shallow profile coastal, calcs., choice of wave parameters *(Russian)* 79−88330
basin response to fluctuating winds and mesoscale motions 79−57965
Bass Strait, Australia, turbulent fluxes meas. 78−69357
bathymetrically trapped current ring obs. in Bering Sea 78−44863
Bay of Bengal, nutrients and dissolved O_2 relationship rel. to water masses classification 79−48517
Bay of Bengal, total N and P determ. 78−81213
Bay of Bengal, tropical cyclone generated surges, numerical model 80−81923
W.Bay of Bengal, wave characts. during southwest monsoon of 1978 80−109152
Bay of Fundy, Canada, bedforms and hydraulic stability in tidal environment 78−88814
bay water response to tsunami *(Japanese)* 80−41399
bays, landslide wave generation digital simulation by Galerkin finite element method 78−92879
beach changes in S.California, statistical prediction 80−98305
beach configurations, seasonal patterns and sediment transport 80−31026
beach deposits sedimentary material differentiation and bedding form. dynamico 80−26496
beach erosion prediction rel. to rising water level 77−91150
beach sediments, Mahalanobis' D^2 distance appl. *(Portuguese)* 78−61388
beach slope sand granulometric composition variations during wave cycle *(Russian)* 78−15991
beaches, transport props. and particle shape characts., Fourier analysis *(Japanese)* 79−88506

oceanography continued
Beaufort Sea, August ice cover vars. rel. to mesoscale weather conditions 80−101366
Beaufort Sea, environmental risk of oil spills, management tool 77−81920
Beaufort Sea ice movements, 1973-1975, determ. by ERTS imagery 77−45011
bed scallops and ripples formed by flowing water, size and origin 79−27628
Bellingham Bay, Washington, Hg loss rate from contaminated estuarine sediments 80−85310
Benard convection, very viscous fluid, theory 80−10236
Benguela Current, anomalously high waves region 80−51434
S.Benguela Current, upwelling site, wind effects and biology 80−104987
Benguela upwelling system off N.Namibia, late Miocene origin, sediment evidence 80−104993
benthic boundary layer physical problems 79−53352
benthic fauna Ca CO_3 shells in hydrothermal area, O isotope study 80−109173
benthic ocean, flow structs. 80−72532
Bering, Chukchi and East Siberian Seas, mean sea level vars. 77−17144
E.Bering Sea, haline front overlying continental slope 79−2251
Bering Sea, hydrographic features of deep water 80−31061
Bering Sea, medium-scale features obs. along seasonal ice edge 78−3778
E.Bering Sea, structural front in ice free conditions 80−8317
E.Bering Sea, summer 1976 heat budget 78−85583
Bering Sea shelf sediments, denitrification estimates 80−12433
Bermuda, Late Pleistocene sea level vars. 78−73400
Bermuda geomorphology, results from satellite imagery 79−5470
beta spiral and absolute vel. field determ. from hydrographic station data 77−64297
beta spirals and absolute velocities in different oceans 79−66702
Bight of Abaco, Bahamas, algorithmic tidal study, expt. and harmonic anal. 80−8319
Bight of Abaco, Bahamas, tidal model comparison with data 80−4035
biological desertification 79−5500
bioluminescence field meas. by moving linear sensor 79−20732
Black Sea, Cu and Zn behaviour in H_2S zone 79−20864
Black Sea, dark lamina form. in sediments, photosynthetic bacteria mass mortality mechanism 78−88815
Black Sea, dynamic characts. of compensation currents in littoral zone 77−70688
Black Sea, evolution to present state 78−92839
Black Sea, H_2S and O_2 zone boundaries rel. to water mass dynamics *(Russian)* 80−12435
Black Sea, large rockslide formations rel. to Cenozoic sedimentation 78−3751
Black Sea, quantitative distrib. of suspended matter 78−3818
Black Sea, shelf bathymetry *(Rumanian)* 78−20391
Black Sea, U anomaly in sediments, accumulation mechanism 77−91105
Black Sea, vertical transport and diffusivity *(Russian)* 79−39740
Black Sea, water stratification characts. in Bosporus region 77−78212
Black Sea and Bay of Biscay, grain size and mineral comp. of shelf sediments 79−20812
Black Sea continental slope, Cretaceous rock outcrops 79−44173
Black Sea sediment cores, organic geochemistry 78−49040
Black Sea shelf, temps., air and water vels., salinity *(Russian)* 77−91142
Black Sea upper layers, temp./salinity anal. of seasonal vars. *(Russian)* 78−77264
Black Sea water and sediments, stanol/stenol ratio control process 79−92549
Blake Escarpment, ocean geoid estimation using Geos 3 satellite altimetry data 80−3902
Blake-Bahama Outer Ridge, bottom boundary layer, speed and temp. obs. 80−101374
blast wave propagation in stratified ocean, theory *(Russian)* 80−81904
Bombay coast region, water pollution physicochemical studies 80−104522
Bombay Harbour sediments, elemental concs. 77−73709
Bombay High area, winter swells 78−32112
Bombay High area swells due to storms in Arabian Sea 79−100845
Bonin trench, bathymetry rel. to lithosphere seaward flexure 79−57903
bore motion over sloping beach, approx. anal. 77−17121
bottom boundary layer, struct. and dynamics 79−20842
bottom boundary layer of deep ocean, short-term variability 79−2269
bottom input impedance meas., particle vel. hydrophone appls. 78−94475
bottom layering influence on reflected FM signal characts. 78−50991
bottom nepheloid layers and bottom mixed layers, obs. on continental shelf off Oregon 78−16027
bottom profile form. mechanism under translational flow 79−29751
bottom reflection loss for a class of marine sediments, effects of density gradients 78−55498
bottom reflectivity at low freqs. 78−40559
bottom relief, random inhomogeneities, effect on Rossby wave propag. 80−85676
bottom reverberations picked up by hydroacoustic dipoles, spatial correlation functions *(Russian)* 78−53659
bottom surface layer and atm. surface layer, turbulence spectra similarity scaling 78−44860
bottom topography, convex and concave effects on drift circulation *(Polish)* 78−3771
bottom water transport through SW Indian Ridge 78−81178
boundaries, visible and invisible, in ocean, ocean fronts, seasonal movements *(Russian)* 79−84296
boundary current flow along continental margin, effect of localised topographic irregularity 80−72539
boundary layer, diurnal temp. cycle 78−20434
boundary layer, sodar echoes at Miyakojima Is., AMTEX 77−21843
boundary layer in cooling water, thermal state during transition from free to forced convection *(Russian)* 78−81192
boundary layer mixing, reinterpretation of entrainment process in laboratory expts. 80−51405
boundary layer turbulent transport 77−17131
boundary mixing in deep ocean, evidence from salinity and pot. temp. profiles 78−73388
boundary-forced planetary waves, model mid-ocean response to strong current variability 80−72541
bounded skewed shear flow, tensor form of bulk dispersion coeff. 78−73393

oceanography continued
Boussinesq turbulence, statistical theory, appl. to thermocline erosion 80−48713
Bowen ratio and surface temp. over sea surface 77−60400
Bransfield Strait, basin waters renewal by local convection 78−92831
N.Brazil continental margin, sedimentation 77−21748
Brazil Current circulation and vol. transport 78−85564
Brazil-Falkland current interface, SKYLAB MSS data analysis 78−65339
Bristol Bay, Alaska, finestructure 78−20425
Bristol Bay, Alaska, lateral water mass interaction study 80−26521
Bristol Channel, tidal regime by numerical model 80−85670
Bristol Channel tides, analytical wedge model 80−85671
British coastal waters, photosynthesis inhibition by Zn pollution 79−24921
British Isles region, EM induction by analogue model 80−56368
buoyant surface discharge and small scale oceanic fronts, numerical study 77−53067
cabbelling at thermohaline fronts 79−34844
Calangute beach, Goa, sediment transport and rip currents 77−73755
calcite, skeletal, dissolution in deep sea, rate control 79−20817
calcite dissolution by fossil fuel CO_2, effect of sediment mixing 78−81212
S California Bight, inshore circulation (1974-1977) 80−98327
California coast, 1941-1978, land and sea level changes 80−21610
California coast, warm water patches rel. to marine fog and fog-stratus systems form. 80−77060
S California coastal waters, Ba as pot. indicator of marine drilling contamination 77−2180
California Current, nutrient upwelling, satellite thermal imagery and chem. anal. 80−101379
California Current during last 8000 years, model reconstruction 80−41457
California Current eddy formation 77−53072
California Current System 80−72555
California undercurrent over continental slope off Oregon 78−57214
California Undercurrent stability off Vancouver Island 78−44859
E.Canadian Arctic, sea ice meltwater, isotope study 80−77002
Canaries Current eastern branch, tidal component *(Russian)* 78−77263
Cap Leucate, Gulf of Lions, Mediterranean, sea-shore circulation 77−37227
Cape Basin, S. Atlantic, scour and deposition at Walvis Ridge base 77−91103
Cape Blanc, Canary current upwelling region, current profiles 77−21779
capillary wave slope meas., using laser optical instrument 78−36173
carbonates in deep sea rel. to deglaciation preservation spike in pteropods and foraminifera 77−86853
careers 79−80393
Cariaco Trench, seawater temp. salinity and chemistry 80−98359
NW.Caribbean, methane content of deep water indicating seepage 80−81924
NW Caribbean, submarine morphology off N.Honduras 77−9398
Caribbean, surface salinity and dissolved silicate, Amazon River effects 79−39722
Caribbean deep water turnover from ^{14}C meas. 77−5229
Caribbean Sea, ^{90}Sr meas., vertical transport of admixtures determ. 79−53362
Caribbean Sea, thermohaline staircase and vertical mixing in the thermocline 77−64293
Caribbean Sea floor, sedimentary cover struct. and thickness *(Russian)* 78−77212
Caribbean-Atlantic water exchange through Anegada-Jungfern passage 77−21778
E.Carribean, deep water silicate content distrib. 80−76984
Caspian Sea, advective heat transport 77−78213
Caspian Sea, temp. fine struct. meas. *(Russian)* 78−73379
catastrophic chemical events, ^{34}S rises 77−56645
early Cenozoic Atlantic Ocean, calcareous plankton palaeobiography and climatic fluctuations 78−16143
Cenozoic oceanic sedimentation rates for Atlantic, Indian and Pacific Oceans 77−91107
Central American seas, waters geostrophic circulation 78−92842
chemical composition determ., active nuclear methods appl. *(Russian)* 79−39902
chemical composition of surface microlayer *(Russian)* 80−104998
chemical exchange across sediment-water interface 79−5505
chemical fields dynamic equilib. and balance anal. 77−64328
chemical speciation of Cd, Cu, Pb and Zn in mixed freshwater, seawater and brine solns. 78−20409
chemistry, major and minor elements balances, role of ridge crest hydrothermal activity from Galapagos data 80−41459
chemistry, role of ridge crest hot springs 80−98304
Chesapeake Bay, abnormal US attenuation 77−29315
Chesapeake Bay, subtidal sea level var., rel. to atm. forcing 80−26530
Chesapeake Bay, water surface laser radar refl. as function of wind speed 77−41034
Chesapeake Bay, winter 1975 wind-driven circulation 80−36313
Chesapeake Bay and Potomac River, nontidal variability, nonlocal atm. forcing 78−92829
N.Chesapeake Bay estuary, agglomerated suspended sediments microstruct. 79−53336
Chesapeake Bay sediment, time depend. transport, temp. and chloride obs. 80−81863
Chile, Quaternary sea level fluctuations 78−44980
China, Tsingtao Institute of Oceanology, visit report 78−61562
chlorophyll, gradient map from high-altitude ocean colour scanner data 80−26551
chlorophyll content airborne meas. under cloudy sky, Gulf of Guinea appl. 79−25359
chlorophyll gradient maps from U-2 aircraft platform over Pacific and Atlantic 80−101385
Chukchi Sea, Atlantic water obs. on shelf 77−9438
NE.Chukchi Sea, coastal currents obs. 78−32107
Chukchi Sea, temp. fine structure near sea ice margin 79−57961
circulation, composite Eulerian-Lagrangian model 78−44870
circulation, dynamical method and barotropic vel. 77−78218
circulation, hyperbolic partial differential equatns. numerical solution 80−21864
circulation, MHD effects in electrolytes as model *(Russian)* 78−40610
circulation, modelling expts. 79−57952
oceanography continued
circulation and hydrographic struct. over Ghana continental shelf during 1974 upwelling 77−41048
circulation and hydrography in power plant vicinity 77−41039
circulation at high latitudes over S.Atlantic and S.W.Indian oceans 77−91204
circulation calc. using numerical Euler-Lagrange model *(Russian)* 77−33092
circulation due to zonal wind stress, spin-up of stratified ocean 80−81900
circulation in world ocean, vertical component *(Russian)* 77−78195
circulation of Cayman Sea and Gulf of Mexico, rel. to local wind stress curl 79−48495
circulation studies and use of tracers 78−16053
circulation variations near Cape of Good Hope 78−3812
circumarctic ocean temp. linked with low level cloud, climatic change study 77−29415
cliff erosion, wave induced rel. to erosive force of waves 78−20388
cliff waves, transient development of waves created against a vertical cliff 80−72530
climatic effects of oceans, feedback effects rel. to quasi-cycles in meteorology 80−109239
climatic warming effect on W.Antarctic ice sheet 79−34864
closed basin with topography, normal Rossby modes 78−73385
coastal areas, depositional props. of flocculated fine sediments 77−21807
coastal boundary layer with friction, wind stress forcing, time depend. model 79−34861
coastal circulation, sewage outfall siting with dye-buoy remote sensing 78−65438
coastal circulation and wind-induced currents, review, book contrib. 80−98357
coastal current driven by wind, transient state 80−51439
coastal current observations 79−100868
coastal currents, probability distrib. of concentrations in wake of continuous point source 77−17133
coastal currents and pollution, satellite, aircraft and drogue studies 77−37206
coastal currents vertical structure 77−29305
coastal erosion in Florida 79−57911
coastal flooding assoc. with probable maximum hurricane 79−20941
coastal inlet water temp. change due to artificial heat input 79−16506
coastal surface water temp., spatial var. during upwelling 80−36322
coastal upwelling, effects of longshore varying topography and coastline 78−92826
coastal upwelling, semidiurnal internal tide var. along Oregon coast 77−37223
coastal upwelling frontogenesis, simulation, isopycnic coord. model 79−34843
coastal upwelling off Oregon, Cyclesonde obs. 77−2179
coastal upwelling onset, nonlinear model 78−92825
coastal upwelling region off Oregon, vertical and cross-shelf flow meas. 80−12397
coastal water lateral movement rel. to vertical diffusion 77−66925
coastal water surface currents, obs. using airborne inertial sighting system 78−73384
coastal waters sensitivity to anthropogenic trace metal emissions 79−43796
coastal zone, electric fields induced by sea currents *(Russian)* 79−39736
coastal zone, indicators of long-term var. of hydrometeorologic elements *(Russian)* 78−77258
coastal zone, neighbour diffusivity *(German)* 77−70668
coastal zone, statistical forecasting of local thermal wind-field disturbances freq. 80−36371
coastal zone, stratified water circulation forecasting for water quality management planning 79−5543
coastal zone of non-uniform sea, wind effect on steady circulation *(Russian)* 78−16038
coastal zone thermal wedge dynamics *(Russian)* 78−81205
coastal zone utilisation, appl. of ocean data and information services 78−69463
coastlines, geometric objects with fractional dimension, book contrib. 77−87640
Cochin backwater, India, estuarine water, particulate heavy metal content 80−7964
Cochin backwaters, India, organic pollution effects on hydrographic features 77−91156
Cochin backwaters, industrial pollution, impact on water quality and hydrographic features 80−76668
Cochin Harbour, India, seasonal vars. of hydrographic conditions 77−91149
Cochin Harbour, siltation in outer channel, tidal streams and longshore currents 78−36144
Cochin Harbour mouth, India, hydrographic characts. and tidal prism 80−41452
cold film calc. from diurnal temp. vars. 79−20855
cold skin layer, heat transfer through surface *(Russian)* 80−104985
colour of ocean, Monte Carlo model including atm. and ocean scatt., absorpt. 78−61421
computer model for generating World ocean sound velocity profile 80−87624
concentration probabilities from stationary point source of passive admixture *(Russian)* 77−78231
conference, April 1980, Birmingham, England 80−56474
conference, computing methods in applied sciences, Le Chesnay, France (Dec. 1975) 77−33846
conference, on climatology, hydrology, atmospheric research and meteorology from space, Ajaccio, Corsica (1979 November 12 to 16) 80−62397
connected basin natural oscillation, theory 80−61806
continental margin sedimentation, computer simulation 78−15998
continental shelf, geostrophic current computation 77−37232
continental shelf, physical var. 77−37213
continental shelf, simple theoretical model of flow from estuary 78−49030
continental shelf circulation, diagnostic model 78−85581
continental shelf circulation, effects of buoyancy flux 80−72540
continental shelf currents during tropical storm Delia 78−7655
continental shelf currents of Pacific NW, use of spin-up model 80−98338
continental shelf dynamics and topographically trapped coastal waves 78−16057

oceanography continued
continental shelf fronts, mixing model and motions 79−2258
continental shelf off Sierra Leone and Liberia, mesoscale flow anomalies 80−26524
continental shelf sediment transport, turning effect in bottom boundary layers 77−37235
continental shelf sediment transport modelling 78−15995
continental shelf south of Cape Hatteras, flushing by Gulf Stream 78−81183
continental shelf waters, kinetic energy from topographic Rossby waves generated off shelf 80−51425
continental shelf wave on boundary current, model 80−77072
continental shelf waves, generation by alongshore vars. in bottom topography 80−51424
continental shelf waves, scatt. by isolated topographic irregularities 80−51423
convection, simple theoretical and expt. study, geophysical appl. and analogies 80−24018
convection under ice sheet floating on warm salty water 77−70677
convective flow structure in stratified liquid after lateral heating *(Russian)* 77−11232
convective instability of stably stratified water 77−86913
lower Cook Inlet, Alaska, spring-summer 1973 conditions 79−16484
cool surface water pools assoc. with mesoscale downdraughts, GATE results 78−69365
coral C isotope composition, rel. to environmental factors 80−46202
coral growth rate (1944-74) and O and C isotope record 79−62524
coral reef epifauna, susceptibility to UV irrad. 80−98037
coral reef water, O isotope composition rel. to evaporation and precipitation 80−46202
coral reefs, area and contribs. to global oceanic processes and resources 78−57220
cosmogenic isotopes, vertical turbulent diffusion 80−12428
coupled ocean-atmosphere expt., ocean response, rel. to climate 80−12430
Cretaceous plankton species extinction due to comet impact 80−76977
Cretaceous-Tertiary boundary, plankton extinction and geochem. indicating extraterrestrial event 80−76976
Cromwell current meandering Pacific Ocean 79−2283
Cumbarjua Canal, Goa, India, hydrographic conditions and flow pattern 77−91146
current, nonlinear waves guided by curl *(French)* 77−91137
current and temp. moored meas., geostrophic comparisons, Mid-Ocean Dynamics Expt. 77−81901
current determination by beta spiral method, vertical mixing effect 80−98459
current finestructure and moored current meter meas. of internal waves 78−44828
current flow and drifter motion, random walk model 77−66923
current flow theory, three-dimens. case 80−104990
current flow theory, three-dimens. case 80−104991
current flowing over continental shelf edge, shear layers 80−81903
current large scale stability, deep layer and bottom topography influence 80−77004
current meas. on continental margins and deep ocean 79−12315
current pattern determination by aerial photography of markers 80−98483
current regime in Gulf of Kutch, NW.India 78−36184
current ring detachment and recomb. with Kuroshio meander 78−81198
current spectra interpretation, dynamical hypotheses testing 79−21045
current spectra interpretation, three-dimens. vector time series kinematics 79−21044
current structure function for intermittent turbulence *(Russian)* 78−32109
current tracer float trajectories, kinematic model 80−85682
current velocities, spectral anal. of vector time series 79−39757
current velocity profiler based on geomag. induction principles 78−61569
currents, calc. using spline polynomials 79−2284
currents, comparison of two diagnostic calc. methods *(Russian)* 77−81908
currents, idealised, mixed instability parameter obs. 80−98329
currents, synoptic-scale, numerical model 80−12424
currents, wind driven in deep water inshore region 80−81925
currents and mesoscale eddies, spatial and temporal var. 78−77240
currents and sea levels poleward propag. perturbs. along Peru coast 79−34841
currents and temp./salinity structure, numerical models for synoptic prediction 77−5213
currents and waves interaction with rough bottom 79−70808
currents and winds off Oregon Coast, rotary cross-bispectra and energy transfer functions 78−44858
currents between Africa and Antarctica, results from satellite-tracked drifters 78−73376
currents generated by heat and momentum fluxes through surface, numerical simulation 80−26535
currents in mid-ocean, geostrophic balance 80−17268
currents in synoptic eddy, periodic components *(Russian)* 78−85593
currents measurement, appl. of SeaTrak Data Processor surface data reduction system 78−45042
currents produced by bottom topography, model, numerical soln. 77−64315
currents stability in eddy-resolving general circulation models 79−16492
cyclonic mini-eddy obs. near Blake Escarpment, W. Atlantic 77−9437
cyclonic rings, water transformation, warm saline water/cooler fresher water mixing 78−44861
data collection and requirements for coastal and offshore structure study 79−12272
data collection in North Sea *(Dutch)* 79−96827
deep Antarctic convection near Maud Rise 79−20844
deep currents calc. near equator *(Russian)* 78−65330
deep ocean, fine struct., internal gravity waves and wave breaking meas. and models 78−85578
Deep Ocean Mining Environment Study phase I and II, prospect 78−16164
deep ocean technology, development in USA 77−78477
deep passages, excess bottom ^{222}Rn distrib. 79−16514
deep sea, fine-grained sediment laminations, origin, model 78−77213
deep sea carbonates, thickness and ^{14}C age of mixed layer 79−29742
deep sea cherts, stable isotope geochem. 77−5182
deep sea disturbance due to surface storm, persistant nature *(Russian)* 80−81921
deep sea floor surveys, integrating optics and sonar 78−45045
deep sea mixing models, vertical and isopycnal mixing 80−76992
deep sea sediments, benthic mixing study using radioactive tracers 80−8294
deep sea waste disposal *(German)* 78−24311
deep synoptic eddy zone, structure of homogeneous layer *(Russian)* 78−85601
deep water circulation reversibility in world ocean *(Russian)* 78−65329
deep-sea cores, ^{231}Pa dating via ^{227}Th counting 78−32238
deep-sea micronodules, near 14 Å mineral of birnessite group 79−74892
deep-sea sediment magnetic spherules, ^{40}K/^{41}K ratio rel. to possible meteorite origin 78−11874
deep-sea sedimentation, time scales and dynamic models 78−15988
deep-sea sediments, unmixing of O isotope record rel. to deglacial meltwater spike 78−3746
deep-water channel flow, rotating hydraulics theory 80−94539
Delmarva coast, USA, shoreline periodicity and offshore shoals 80−56457
Denmark Strait, temp. gradient microstruct., 1973 obs. 80−77003
Denmark Strait, upper layer temp. and salinity *(Russian)* 77−60413
Denmark Strait overflow, contrib. to deep N.Atlantic 80−85665
density fields in world ocean 79−44195
density fronts, effects on coastal pollutants 78−7659
density jump layer, solns. for spatial internal waves generated by moving disturbances *(Russian)* 78−77251
density large-scale anomalies, non-linear evolution *(Russian)* 79−16479
density stratification importance to bottom boundary layers over continental margins 77−86931
density-stratified ocean, perturbation method appl. to internal waves theory 77−49070
depth simulation, analogue/hybrid technique 80−36336
descriptive physical oceanography, 3rd edition of book 79−100872
detritus sedimentation, rel. to atm. CO_2 from burning wood 78−81368
developing turbulent surface shear layer model 80−12417
diagnostic current calcs., monotonic difference schemes *(Russian)* 77−73748
diatom biomass, short-period climatic fluctuations effects 77−49087
diffuse irradiance refl., two flow model of ocean 77−29301
diffuse radiation emerging from semi-infinite medium, intensity accounting for inner refl. *(Russian)* 79−8637
diffuse reflectance, effects of chlorophyll a fluorescence at 685 nm 79−66700
diffusion diagrams, scale-dependent diffusion modeling 77−56640
dimethyl sulphide, biologically prod., contrib. to global S cycle 77−70786
double-diffusive intrusions into density gradient, microstruct. 78−85569
Drake Passage, 1975 currents and temps. 80−36307
Drake Passage, Antarctic polar frontal zone variability during summer (1976-1977) 78−85579
Drake Passage, Antarctica, polar front motions in horizontal temp. gradients 80−4037
Drake Passage, cyclonic ring formation at polar front 77−17140
Drake Passage, deep flow variability from current meas. 78−44849
Drake Passage, satellite obs. of polar front 77−81902
Drake Passage, summer current meas. 78−7657
Drake Passage, temp. and flow spatial scales 80−101376
dredger spoil, dumping ground obs., motion of fine particles with current 80−17287
drift, wind-induced, implications of results for contained water bodies 79−48512
drift buoys, deployed by aircraft and satellite tracked, operational test 80−90242
drift current/slope current interaction 80−21780
drift currents, induced by propagating inertial and internal waves refl. at rigid boundary 80−51403
drift ice, sea floor scouring 78−92822
drift-slope current interaction, Conf., Tokyo, Japan (May 1979) 80−31411
drift-slope current interaction 80−36334
drifter data analysis, sampling rate and random position error effects 80−26527
drifting sea ice, inertial period motions *(Japanese)* 80−36327
drought in California and western Europe, 1976, atm. and oceanographic factors 79−48560
DSDP Leg 37, S isotope comps. of sulphide and sulphate minerals 77−91101
dynamic response of ocean to atmospheric disturbances 77−13084
dynamics and distrib. of water masses off S.American coast, biogeographic aspects 79−53363
dynamics investigation, realisation of four dimensional topographic reference system 78−77176
dynamics of upper ocean, equilib. Langmuir circulation model 80−101381
Earth annual wobble, affected by wind stressed sea level 80−36221
Earth rotation variability, meteorological and oceanic causes and consequences 77−56571
earthquake wave propag. along seafloor, theory 80−81843
East Australian Current, surface jet, undercurrents and low Richardson number obs. 80−104978
East Australian current anticyclonic eddy struct. 77−17134
East Australian Current eddy, sound propag. 78−65322
ecological disturbances caused by coastal pollution source, math. model 77−78232
ecological significance of solar UV radiation 80−45974
eddies and the general circulation of model gyres 80−56490
eddy, deformed, with varying Coriolis force 79−66708
eddy diffusion, explicit scale-depend. coeffs. 78−67191
eddy diffusion effects on western coast boundary layer struct. 77−17142
eddy effect on inertial oscillations 77−33082
eddy effects on sound transmission 78−11905
eddy fields in N.Atlantic and N.Pacific oceans, geographic vars. 77−9431
eddy formations, hydrochemistry *(Russian)* 78−81215
education, acoustical propag. in ocean, appl. of parabolic approx. 79−25794
educational courses evaluation for marine science 78−53657
Ekman layer, exchange of momentum, estimation methods 80−98326
Ekman pumping to geostrophic flow, water mass props. determ. 80−56489
El Nino, 1972, sea level vars. 78−44847

oceanography continued
El Nino, 1975, biological consequences 77−41063
El Nino, numerical simulation 77−17123
El Nino, response of eastern tropical Pacific to interior wind stress changes 77−17124
El Nino, verification of theories 78−24294
El Nino 1976, sea surface topography response 80−81913
electric currents, induction at short periods rel. to horizontal field vars. in Indian peninsula 77−86773
electric currents induced in insulated oceans 80−51407
electrodynamics of sea, magnetostatics problems and appl. to water masses movement *(Russian)* 78−77259
Elefsis Bay, Greece, O-deficient and organic C fields expansion 79−84299
element residence time in sea, confusion of mathematical notation 77−86937
EM field, of ocean current of finite width 79−53351
EM field of nonstationary marine currents, theory 78−44833
EM fields induced by synoptic currents, theory 80−61805
EM induction, in arbitrarily shape oceans of finite conductivity 79−16371
EM induction coast effect, soln. in thin variable integrated cond. sheet model 79−16372
EM induction for island-continent ocean channels, analogue model 77−9336
EM induction for island-continent ocean channels, analogue model study for H-polarisation 77−81795
EM induction in arbitrarily shaped infinitely conducting oceans 78−61318
EM induction in ocean, Sq-induced current around land mass 80−72413
EM induction of oceans affecting Sq field variations in IGY 80−72428
EM induction over perfectly conducting ocean edge, H-polarisation 77−44912
EM short-range propag. in shallow sea, expressions for horizontal elec. dipole 79−48515
EM sounding, analogue model meas. for horizontal mag. dipole embedded in conducting medium 79−12068
Emerald Basin, Nova Scotia, post-glacial palaeo-oceanography 77−5218
empirical orthogonal functions, stability 77−67224
energy dissipation adjacent to island, meas. 78−85573
energy generation by moving atmospheric press. disturbance *(Russian)* 77−33087
energy sources and their exploitation 80−89588
engineering under Arctic conditions, conference (Fairbanks, Alaska, August 1975) 77−37236
E England coast, storm surge (1978 January 11 to 12) 80−12419
English Channel, 1974 September 2, storm surge 78−88895
English Channel, actinide concs. and transfer into S.North Sea 79−48519
English Channel, coastal water trace element meas. methods *(French)* 77−41238
English Channel, hydraulic model of nonlinear tidal deformations in shallow water 77−37218
English Channel, quarter-diurnal tide 78−61424
English Channel M_4 tide derived from nonlinear numerial model of M_2 tide 78−49027
enhanced pole tide rel. to Chandler wobble period and damping 80−21778
environmental electromagnetic simulator 77−73894
environmental impact due to Cu mining activities, Chile 79−12140
environmental pollution by nuclear fission products 78−85607
equatorial, response to periodic monsoon winds 78−3773
equatorial baroclinic layer dynamics *(Russian)* 77−60403
equatorial counter-current formation *(Russian)* 78−16035
equatorial countercurrent, baroclinic model *(Russian)* 77−78196
equatorial current generation 80−67374
equatorial current system, non-linear theory 80−104988
equatorial current system, non-linear theory 80−104989
equatorial motions, Laplace's tidal eqn. asymptotic eigensolns. 77−33166
equatorial ocean, zonal internal waves, math. model *(Russian)* 79−12119
equatorial trapped waves, vertical eigenvalue problem 80−56477
equatorial undercurrent, dynamics 80−72558
Equatorial Undercurrent, salinity max, use for estimating nutrient enrichment and primary prod. 79−84283
equatorial undercurrent in baroclinic ocean *(Russian)* 77−41036
equatorial undercurrent of Atlantic, near-surface layer changes 80−81901
equatorial undercurrents, meas. in W.Indian Ocean 77−29306
estuaries, ^{18}O distrib. 80−26532
estuaries, contaminants, long-term dispersion 77−78229
estuaries, control of stratification in almost-enclosed regions 79−46358
estuaries, hydrodynamic model using smooth elements, accuracy 80−98356
estuaries, nontidal, hydrographic network changes under influence of natural factors and water management measures 79−29792
estuaries, stratified turbulent flow, finite element method appl. 78−90964
estuaries, two dimensional, approx. solution to obtain the streamfunction 78−81187
estuaries, very low salinity regions, chemical and biological reaction sites 78−81199
estuaries and harbours, three-layer circulations 77−86922
estuaries description, theoretical framework 77−66924
estuaries of variable breadth and depth tidally induced residual currents 80−72544
estuarine and coastal waters, suspended particles surface charge 80−36331
estuarine environment, natural suspended matter flocculation and electro-kinetic pot. *(French)* 80−61817
estuarine environments, Cu inorganic speciation 78−69371
estuarine flow, nonlinear partial differential eqn., finite element anal. *(Japanese)* 78−8233
estuarine mixing, dissolved humic acids and Fe removal 79−34830
estuarine mixing, flocculation of dissolved Fe, Mn, Al, Cu, Ni, Co and Cd 79−29774
estuarine mixing implications of Fe, Mn and organic material dissolved in river water 80−17296
estuarine Mn distributions, effect of rapid precip. of river water dissolved Mn 79−62516

oceanography continued
estuarine surface microlayer and trace metal cycling in salt marsh 79−57984
estuarine tidal front, trace metal enhancements in biotic and abiotic components 79−2265
estuarine water-quality model in an oscillating constant-volume reference frame 79−34871
estuarine waters, behaviour of trace chem. constituents 79−16512
estuary, Jamaica Bay, New York, dissolved O modelling 77−17146
estuary, mass and salt transfers and halocline depths 77−29322
estuary, spread of river jet, models 80−98353
estuary, tidal and thermal propag., numerical model 79−12133
estuary, tidal two-dimensional hydrodynamic digital simulation by finite element method 78−92846
estuary, volatile petroleum hydrocarbons contrib. to organic C budget 79−70473
estuary, well mixed, buoyancy effects on longitudinal dispersion 80−85681
estuary amplification of periodic and unsteady waves *(Russian)* 77−60405
estuary circulation (partially mixed), two-dimens. model 80−109161
estuary models of Tampa Bay, Florida, comparison 78−77269
estuary pollution model development, wind and freshwater flow influence 78−81207
estuary proportioning with sinusoidal tidal wave *(Italian)* 79−20839
estuary sediment containing lead pollution, rel. to flood control measures, California 80−76670
estuary unsteady-state two-dimensional salinity intrusion model 78−77271
estuary water quality management for P treatment 77−21823
estuary water quality models, finite difference and finite element methods 78−77375
estuary with uniform reversing tidal flow, suspended sediment model 78−7648
Eurasia continental shelf, postglacial transgressions from slope of abrasional-accumulative surfaces 79−20813
N.W.Europe, marine tides and crustal struct. interaction with Earth tide 77−86739
eustatic sea level changes and continental platform subsidence mechanisms 77−21718
evaporation, bulk coeffs. depend. on air-water interfacial conditions, isotopic method determ. 78−85576
evolution of interior, atm., ocean, Viking mission Mars information, appl. to Earth 77−78709
explosive accoustic waves, empirical and theoretical laws comparison *(Russian)* 80−109150
Faroe-Shetland Channel, N.Scotland, continental slope flow 77−9435
field data, objective anal. 79−12321
fine suspended particles, removal mechanisms and residence times 78−32106
finestructure, wave-induced and intrusive structs. separation 79−48502
finite depth stratified flow over topography on a beta-plane 80−6128
fjord, Norway, wind-driven circulation 79−20848
fjords, fronts in surface waters 79−57953
fjords, horizontal temp. and density gradients 78−24303
Flandrian sea level changes in Thames Estuary, implications for land subsidence in England and Wales 78−24304
flood and tidal flows, network hydraulic model 79−12162
flood basalt isotopic abundances of Nd and Sr, Earth struct. models 80−72475
E.Florida coast, Gulf Stream boundary eddies 80−85673
W.Florida continental shelf, LF current obs. 77−37233
Florida continental shelf, near bottom vel. and temp. profiles, Cyclesonde meas. 77−9439
Florida continental shelf, rain-formed mixed layer 80−36323
W.Florida continental shelf waters, response to cold front passage 77−37225
Florida Current, fluctuations during 1970 summer 77−73744
Florida current, wind forced continental shelf waves 77−73758
Florida Current and Antilles, Current spires of particulate material 79−16502
Florida Current transport, fluctuations at periods between tidal and two weeks 80−72551
Florida Gulf outer continental shelf, oil spill simulation 78−73406
Florida Straits, continental shelf waves 77−2177
Florida Straits, seabed sediments, current-induced movements 79−79807
flow, vel. determ. from hydrographic data 80−17415
fluctuating stratified ocean, sound propagation, comments 77−11075
fluid dynamical systems, statistical anal. and prediction 78−11901
fluid dynamics, specialist symposium, (Munich, 6 to 9 September 1977) 79−57951
fluid dynamics, use of similarity theory in Soviet work *(Russian)* 78−16174
fluid motion within ellipsoidal cavity, influence of Coriolis force field *(Russian)* 78−81296
foam formations, spectral characts. of microwave thermal emission, sea surface simulation *(Russian)* 78−69353
foam produced by storms, microwave remote sensing of storm intensity 80−41528
forced plume characteristics 78−18286
forecasting of average air temp., underlying ocean surface influence 79−29827
formaldehyde, in marine air and rainwater, wet season obs. 80−85703
frazil ice conc. meas. system using laser Doppler velocimeter 77−25796
free convection development in upper quasi-homogeneous oceanic layer *(Russian)* 77−21784
free surface vibrations caused by internal waves, experimental investigation *(Russian)* 79−16478
frequency modulation model for surface reflection of CW tone 78−83161
frequency spread of backscattered sound, facet model for rough sea surface 78−87184
fresh water and heat flux determ. from atm. obs. 80−104986
frontal circulation due to cabbeling and double diffusion 79−2263
frontal generation, mixing and mutual intrusion mechanism model 80−26522
frontal zones, light scatt. obs. 79−2266
frontogenesis of upper ocean, scalar redistribution 80−104992
fronts, Chapman conf. (New Orleans, 1977 October) 79−2246
fronts identification by long range acoustic propagation meas. 79−66705
Galapagos Rift, hydrothermal plumes obs. 77−64258

oceanography continued
Galapagos Rift, mantle He in hydrothermal plumes 77−64259
Galapagos Rift hydrothermal fields, struct. and morphology of seafloor 80−72489
Galapagos sea floor sediments, hydrothermal mounds, stratigraphy and chem. 80−26497
Galapagos submarine hydrothermal water excess ^{3}He and ^{4}He 78−40593
gamma radiation field of seawater and atm. surface layer rel. to cosmic ray neutrons *(Russian)* 79−39746
Garonne-Gironde river estuary system, radioactive tracing of physio-chemical behaviour of Zn $(OH)_2$ *(French)* 80−7994
GATE, 1974 field project 77−2247
GATE, introduction 77−2246
GATE acoustic echo sounder, preliminary results 77−33080
general circulation models 78−16048
general circulation of idealized oceanic gyre, primitive eqn. simulation 77−70671
geoid spectrum from altimetry 80−3904
geological oceanography, book 78−92845
geomagnetic coast effect, review 80−94458
geomagnetic field effects on charged particles in ocean *(Russian)* 77−60416
geomagnetic lunar daily var. at Alibag, oceanic and ionospheric dynamos contrib. 80−26444
geomagnetic variations causing water motion, theory 80−104962
Georgia shelf, current, temp. and coastal sea level response to atm. and Gulf Stream forcing 79−70804
Geos 3 project, review 80−4224
geostrophic adjustment in sea straits and wide estuaries, two-layer system 79−48503
geostrophic currents, relative press. topography and relative vel., calc. accuracy 79−39758
geostrophic flow over shallow topography 80−90120
geostrophic motion of stratified fluid above uneven bottom *(Russian)* 77−91140
geostrophic ocean currents determ. independently of reference level, inverse technique 80−51574
German Bight, airborne and ground data, Geoscientific Airborne Remote Sensing Programme *(German)* 80−67412
German Bight, geoid determ. by gravimetric levelling *(German)* 78−3813
Gironde estuary, solid pollutant dispersion analysis 77−41069
Gironde estuary, turbidity max., numerical simulation *(French)* 79−79869
Gironde estuary vertical circulation, real time two-dimensional model *(French)* 79−62519
Gironde inlet and Pertuis of Maumusson, estuarine waters seaward dispersion, remote sensing study *(French)* 80−8324
glacial oscillations global mass and energy requirements, rel. to mean ocean temp. oscills. 77−78404
glaciers-ocean-atmosphere global system, numerical modelling 79−84469
global air-sea interactions rel. to climate formation 78−16142
global changes in postglacial sea level: a numerical calculation 79−2289
global circulation in two-layer ocean model 77−53071
global data analysis 78−65316
global heat budget for tropical Atlantic and E. Pacific 77−86935
global mass and energy requirements for glacial oscills. rel. to mean ocean temp. oscills. 78−81351
global ocean tide model 77−37239
global problems of fluid dynamics 78−96173
global sea pollution, ecological aspects 78−3826
global sea-level changes, history rel. to Earth thermal struct. 79−29743
global temperature distribution, rel. to Earth heat balance annual var. 78−73300
global tides, geopotential effects 77−21787
Global Weather Experiment, observational phase through first special observing period 80−51543
Glomar Challenger drilling ship, experience and prospects 80−21711
gravity anomalies in N.Atlantic and Indian Oceans, recovery from Geos 3 altimetry data 80−3905
gravity current head dynamics, mixing and Kelvin-Helmholtz billows 79−37368
gravity surface waves, tsunami wavelength, wave equation soln. 78−90927
gravity wave-critical level interaction 79−88427
Great Barrier Reef, general nature and environment, 1973 expedition 79−84221
Great Barrier Reef, geological history and structure from seismic profile 79−84222
Great Barrier Reef, Holocene sea level changes, interpretation of 1973 Expedition results 79−84294
Great Barrier Reef, Holocene sea level changes, interpretation rel. to hydro-isostatic flexure 79−84295
Great Barrier Reef Holocene sea level changes, introduction 79−84293
E.Greenland Polar Front, submarine transects 80−85662
Greenland Sea, LF sound propag. in marginal ice zone 78−85567
Guacanayabo Bay, Cuba, tectonic processes rel. to Holocene sedimentation 78−3752
Guaymas Basin, ^{3}He meas. rel. to mantle volatiles injections in Gulf of California 80−85640
Guinea Current upwelling 78−24306
Guinea Gulf northern coast, sea temp. and level, Msf tide propag. 80−4033
Guld Stream, structure and mechanisms *(French)* 77−73763
Gulf of Alaska, coastal circulation, precipitation and runoff effects 80−36312
N.Gulf of Alaska, coastal flow from dynamic topography and satellite-tracked drogued drift buoys 80−51431
NE.Gulf of Alaska, continental shelf bottom press. and current anal. 80−8318
Gulf of Alaska, ocean temp. distrib. 77−60393
NE Gulf of Alaska, processes affecting suspended matter distrib. and transport 80−12398
NE.Gulf of Alaska continental shelf, wind, current and bottom pressure 77−25741
Gulf of Alaska SeaSat Experiment 14.6 GHz scatterometer surface wind obs. 80−46200
Gulf of Alaska SeaSat Experiment synthetic aperture radar wave imagery 80−46199
Gulf of Cadiz, Mediterranean outflow, vel. shear in deep steps 80−85663

oceanography continued
central Gulf of California, thermal waters discharges rel. to terrestrial heat flow meas. 80−3968
Gulf of California, upwelling rel. to ^{32}Si supply and radioactive half life determ. 80−91153
Gulf of Elat (Aqaba), seasonal temp. and salinity vars. 80−31047
Gulf of Gdansk, lithodynamical processes, theoretical anal. and scale model tests *(Polish)* 78−40540
Gulf of Genova, effect of low freq. winds on sea level and currents 80−8322
Gulf of Guinea, seasonal coastal upwelling, generation 79−100847
Gulf of Guinea, simple upwelling model 78−88837
Gulf of Guinea seasonal upwelling due to remote forcing 79−79860
Gulf of Kutch, element distrib. in sediments 79−48450
Gulf of Kutch, sediment distrib. in high energy tide dominated environment 79−48448
Gulf of Lions, surface currents, spatial structure *(Russian)* 80−17277
Gulf of Lions, turbulent surface layer structure during Mistral *(Russian)* 79−39734
Gulf of Lions, wind-induced upwellings 79−79870
Gulf of Maine, winter circulation, cooling and water mass formation 78−92832
W.Gulf of Maine winter circulation current and press. obs. 80−51430
W Gulf of Mexico, ^{90}Sr in water, coral, hermit crabs and molluscs 77−81590
N.Gulf of Mexico, anoxic hypersaline basin 77−86936
Gulf of Mexico, anticyclonic current patterns temporal var. 78−32114
Gulf of Mexico, aromatic hydrocarbons concs. in seawater at proposed deepwater port sites 78−44880
Gulf of Mexico, Ba non-conservative behaviour during mixing of Mississippi River and marine waters 78−32120
E. Gulf of Mexico, black magnetic spherule fallout rel. to micrometeorite studies 77−37242
Gulf of Mexico, Loop Current, laboratory simulation expts. 80−77006
NW Gulf of Mexico, near-bottom cross-shelf currents, response to wind forcing 78−3780
Gulf of Mexico, near-surface temporal var. of ^{228}Pa 79−66713
Gulf of Mexico, particle size distrib. of suspended matter in deep water 78−36177
Gulf of Mexico, surface water circulation, 1973-7 obs. 80−51415
NE.Gulf of Mexico, winter surface thermal patterns 79−2248
Gulf of Mexico and Caribbean Sea bottom press. obs. 78−36175
Gulf of Mexico circulation from estimated dynamic height fields 79−79854
W.Gulf of Oman, bathymetry rel. to tectonics 80−8279
gulf of St. Lawrence, buoyancy driven current system, mixing and circulation 80−90095
Gulf of St. Lawrence, wind-driven inertial currents in Magdalen Shallows 79−20845
Gulf of St. Lawrence and estuary, geochem. of Zn, Cu and Pb in sediments 78−92855
Gulf of Suez, possible water-layer seismic multiple refls. and head waves 80−56400
Gulf of Thailand, currents and particulate matter movements 77−49090
Gulf Stream, ^{14}C concs. in Florida annual coral rings 79−16513
Gulf Stream, anticyclonic eddy obs. in slope water aboard CGC Evergreen 80−72546
Gulf Stream, cyclonic rings, potential energy distribution 77−56651
Gulf Stream, deflection by bottom feature off Charleston, S.Carolina 79−53365
Gulf Stream, fronts and wave disturbances compared with atmospheric jet stream 79−2268
Gulf Stream, Hg distrib. 80−7965
Gulf Stream, inertia and vertical friction 77−64323
Gulf Stream, kinetic energy exchange 77−56641
Gulf Stream, large-scale frontal study using Geos 3 radar altimeter data 79−5488
Gulf Stream, propag. and evolution of cyclonic rings 80−81911
Gulf Stream, Site D, Rossby wave obs. 78−3806
Gulf stream, surface boundaries measured by Geos 3 radar altimiting and IR data 80−4021
Gulf Stream, vel. fluctuations during Late Cenozoic rel. to climate 80−12432
Gulf Stream, vertical temp. gradient struct. 77−45007
Gulf Stream and mid-ocean eddy numerical simulation 77−70672
Gulf Stream and the north east Atlantic temperature anomaly *(German)* 80−85684
Gulf Stream and Western Boundary Undercurrent crossover near Cape Hatteras 77−60381
Gulf Stream anticyclonic eddy, energy in eddy 80−85683
Gulf Stream branching region, current obs. 80−98339
Gulf Stream channel line, oscills. as functions of atmospheric circulation type 78−92841
Gulf Stream cold core ring, observed formation 78−44862
Gulf Stream cold eddy, NOAA satellite and ship data 77−2171
Gulf Stream cyclonic eddies, Sargasso Sea hydrology *(Russian)* 78−85589
Gulf Stream cyclonic ring, 'Allen', 1976-7 obs. 80−51413
Gulf Stream cyclonic ring decay, entrainment and diffusion model 77−86929
Gulf Stream east side, cold eddy studies using satellite and ship data 79−48501
Gulf Stream eddies, detection scheme 79−96834
Gulf Stream eddy-induced water exchange in mid-Atlantic bight 77−86928
Gulf stream frontal zone thermohaline struct., comparison with Kuroshio 80−85678
Gulf Stream intensification after 1976-77 winter 78−11910
Gulf Stream intrusion into S.Atlantic Bight shelf waters 78−32108
Gulf Stream meanders, effects on New England fishing grounds 78−36195
Gulf Stream meanders, GOES IR meas., time series anal. 79−34842
Gulf Stream meanders along continental margin 79−70803
Gulf Stream north wall, sound speed structure across anticyclonic eddy 79−2257
Gulf Stream perturbations by Atlantis II Seamount 77−2163
Gulf Stream position changes rel. to atmos. press. fields 80−98352
Gulf Stream ring, coalescence with Gulf Stream off Cape Hatteras 79−79872
Gulf stream ring frontal zone, asymmetric disturbances obs. 79−2267
Gulf Stream ring tracking with free drifting surface buoy 78−7769

oceanography continued
Gulf Stream ring trajectories, obs. in 1976-8 period 80−98342
Gulf Stream rings, distrib., number and movement 78−24297
Gulf Stream Rings, linear quasigeostrophic dynamics appl. 77−86917
Gulf Stream rings distrib. and number, 1975 spring period 79−39725
Gulf Stream rings dynamic heights calc. from corrected expendable bathythermograph data 78−49151
Gulf Stream roughness var. from radar cross section obs. 78−36194
Gulf Stream seaward deflection; bottom topography effects 80−36308
Gulf Stream-slope water boundary, low-salinity water transport 77−86912
H-polarisation induction over ocean edge coupled to mantle by conducting crust 77−48994
Haicheng Earthquake, 1975, precursory sea level changes *(Chinese)* 80−51331
harbour channels, Galerkin finite element analysis 79−2286
harbour resonance rel. to nonlinear excitation of long narrow bay 79−34847
harbour with large mouth, wave-induced oscills. 78−85604
Hawaiian-Emperor seamount chain, geoid heights derived from Geos 3 altimeter data 80−3899
Hawaiian-Emperor seamount chain, gravity and bathymetry rel. to oceanic lithosphere isostasy 79−39688
heat balance of upper ocean under light winds 78−69355
heat budget of upper ocean under light winds 77−41055
heat flux, effect on wintertime of W. Europe 80−26542
heat or salt flux across diffusive interface in presence of externally imposed turbulence 77−41057
heat storage in oceanic upper mixed layer, inference from Landsat data 79−100869
heavy metal sedimentation rate in Saanich Inlet, British Columbia, ^{210}Pb technique 78−32063
W. Hellenic Trench, high sedimentation rates and variable dispersal patterns 78−57193
N.hemisphere, sea surface temps. assoc. with poor summers in British Isles 80−109241
HF radio obs. of wave height, surface winds and currents 78−77241
high-latitude N Atlantic, Late Quaternary surface ocean kinematics and climatic change 78−16026
high-level radioactive waste, ultimate disposal on seabed, rel. to oceanographic circulation 78−13273
Holocene eustatic sea level change, British Isles 78−65333
Holocene sea level transgression in Fujian S.China seaboard *(Chinese)* 79−96765
Holocene sea levels, 8000 yr. record rel. to palaeoclimatology 77−78401
Holocene sea levels high stands, NW.Pacific 79−25259
horizontal advection of temp. for low freq. motions 77−56638
horizontal circulation in World Ocean *(Russian)* 78−16034
horizontal current, mesoscale horizontal turbulence problem *(Russian)* 79−39741
horizontal density diffusion vertical var. influence on internal waves *(Russian)* 79−39738
horizontal divergence and voriticity from vel. and temp. meas., MODE region 78−3772
horizontal turbulence, spectral struct. 78−3790
horizontally heated rotating fluid, spatial oscillations 77−55004
hot spring created by drill hole 80−55951
Hudson Bay, spring break-up of estuaries 78−11930
Hudson estuary, Ba and ^{226}Ra desorption from river-borne sediments 79−79877
Hudson Estuary, salinity and temp. distrib. 77−17136
Hudson River estuary, ^{222}Rn distrib. and transport across sediment-water interface 78−16064
Humboldt Bay, California, offshore current meas. rel. to proposed outfall 78−44876
Huntec Seabed Project for shelf sediment mapping 77−13130
hurricane boundary layer response to sea surface temp. changes, model 79−53439
hurricane Camille, wind speed and direction, ocean wave height and barometric press. meas. 78−36254
hurricane over Arabian Sea, surface wind and sea waves 77−53159
hurricane sea surface wind speed, L-band radar backscatt. obs. 80−56561
hydrodynamic friction-layer instability rel. to Langmuir circulation 78−92840
hydrodynamic instability, expt. studies 79−53354
hydrodynamic model of upper ocean frontal dynamics, development and anal. 80−4028
hydrodynamic model of upper ocean frontal dynamics 80−4029
hydrodynamic sea model, 3-D, variable vertical eddy viscosity, finite element anal. 80−85661
hydrodynamic system simulation programs 77−21799
hydrodynamics, relative diffusion meas. at small scales 78−88838
hydrometeorology, USSR research vessels, information acquisition and processing *(Russian)* 77−21909
hydrophone array response calc. errors due to two dimensional beam pattern assumption 78−66972
hydrosols. refr. index and turbidity effects on solar radn. flux in atm.-ocean system 77−64303
hydrothermal sulphide deposits in Cyprus, ^{87}Sr enrichment confirms ore form. by circulating seawater 77−81887
Iapetus Ocean, eustatic events and pelagic sedimentation during Ordovician and Silurian 79−29776
Iberian basin, internal tidal waves spatial characts. *(Russian)* 77−81906
ice, initial forms, microwave refr. index and absorpt. 78−49036
ice, melting in sea water, model, Antarctic ice shelf and iceberg appl. 80−4036
ice age climate and sea level at ~95000 BP 80−51444
ice cover, drifting, relationship between mean stresses and internal forces local values 80−31056
ice cover, flexural-gravity wave development, longitudinal tension effects *(Russian)* 79−100855
ice cover dynamics averaged eqns., asymm. internal stress tensor *(Russian)* 77−81909
ice cover nonuniform thickness effects on navigability 77−78222
ice crystal orientation along Arctic Ocean margins 79−16486
ice drift, numerical modelling *(Russian)* 77−13081
ice field off Okhotsk Sea coast of Hokkaido, divergence and rot. meas. *(Japanese)* 78−96223
ice from glaciers, melting process *(German)* 80−33606
ice in Gulf of Bothnia, flexural waves meas. *(Japanese)* 78−96225

oceanography continued
ice mapping and drift meas. using aircraft synthetic aperture radar images 79−70809
ice shelves, floating, tidal flexure cracks, fracture mechanics 78−69368
ice shelves tidal flexure, meas. by tiltmeter 80−31050
icebergs, calving from floating glaciers by vibrating mechanism 78−81197
icebergs, drift in Grand Banks 78−81200
icebergs, melting in environment with salinity gradient, rel. to fresh water supply 78−24305
Iceland-Faroe Ridge, eddies and meanders rel. to polar front 80−81898
India, continental shelf sediments, carbonate fraction 77−73711
India, recent shelf sediments, Fe partition patterns 77−73710
India, W. coast sediment U isotope ratios 77−41020
India, W. continental shelf, $CaCO_3$, Mg^{2+}, and Ca^{2+} content 80−8289
India, W. continential shelf, marine sediment P_2O_5 content 80−8288
W.India coast, upwelling, geopotential anomaly study 80−56482
W.India continental shelf, topography and sediments 80−56454
Indian, equatorial, ^{137}Cs radiotracer study *(Russian)* 79−39743
Indian, equatorial currents during NE.monsoon 79−2270
Indian, geostrophic currents obs. in Antarctic zone 77−64319
W.Indian, hydrological characts. and transequatorial transport 77−91147
Indian, numerical calc. of stationary large-scale circulation *(Russian)* 79−39739
Indian, palaeotemps. during Brunhes epoch from sediment core study 80−12429
Indian, sea levels in western equatorial region rel. to tides, meteorology and ocean circulation 80−4018
Indian, solar radiation penetration calc. 79−2278
Indian, surface temp. anomaly patterns effect on summer monsoon circulation, NCAR model 78−40634
N.Indian, tidal charts 78−32115
Indian and Antarctic, chem. of particulate matter 79−57973
Indian coast, Paradip port sediment movements 77−73712
Indian continental shelf, distrib. patterns of Al, Ti, Mn, Cu and Ni in sediments 79−25225
W Indian Ocean, 1975-1976 equatorial current obs. 80−104974
equatorial Indian Ocean, ^{137}Cs distrib. in upper layer *(Russian)* 77−60426
W.Indian Ocean, clay mineralogy and sedimentation 77−29279
E.Indian Ocean, deep western boundary current 77−56652
N.Indian Ocean, dissolved petroleum content 80−98361
SW Indian Ocean, drift obs. from Nimbus VI satellite-tracked buoys 78−20426
Indian Ocean, ecologic and palaeoclimatic implications of vars. of O. universa 77−9445
NW.Indian Ocean, eddy in Somali Basin associated with monsoon 80−51414
W.Indian Ocean, equatorial currents meas. 80−12427
Indian Ocean, evidence for continuous spectrum of equatorial waves 80−98331
Indian Ocean, modelling of equatorial currents variability caused by monsoons *(Russian)* 78−44839
Indian Ocean, modern and ice-age surface water zonal temp.-anomaly maps 80−77007
Indian Ocean, MUSSON-77 expt. results 80−81926
Indian Ocean, Pacific water incursion 79−16511
Indian Ocean, surface temp. rel. to Indian summer monsoon intensity 80−90121
Indian Ocean, tidal period waves *(Russian)* 77−60419
Indian Ocean middle latitudes, Subtropical Convergence fluctuations and Quaternary climates 77−13087
Indian Ocean response to change of monsoon *(German)* 77−17138
mid-Indian Ocean Ridge and Marie Celeste Fracture Zone, metal accumulation rates 77−33052
Indian rivers, chemical and sediment load input into world oceans 79−34870
Indian summer monsoon, interaction with ocean 77−56650
Indonesia, palaeobathymetry from sedimentology of Nias Island Neogene trench-slope deposits 80−104950
induced electric currents, effect on mag. bays observed at coastal observatory 78−65462
induced electric fields, coastal edge corrections calc. 79−25253
industrial waste dumping, dispersion meas. technique 78−44884
inert gases dissolved in seawater rel. to hydrophysical studies *(Russian)* 77−60425
inertial oscillations of current vel. and temp. *(Russian)* 77−33088
infinite β-plane ocean model, response to atmospheric forcing 80−4031
information processing system, AOIPS 77−78519
infrasonic sea noise, meas. and experimental problems 78−11902
injection events in ocean history 79−16515
inshore and offshore profile, statistical determination 80−56458
inshore submarine slope cross-profile changes and littoral drift balance *(Russian)* 78−15989
insolation estimation over ocean, clear and cloudy skies 77−87023
instrumentation needs for ocean biology 79−12049
interaction with atmosphere, expt. study North Pacific, NORPAX 77−56649
interglacial episode termination and Wilson Antarctic surge hypothesis 78−53669
internal currents, struct., kineticity effects 77−68570
internal solitary waves in stratified flows, cubic and quadratic nonlinearity 80−69856
internal tidal oscills. spatial characts. from temp. meas. 78−61434
internal wave spectra and vertical fine structure *(Russian)* 78−85595
internal waves, high-frequency, obs. at ocean station P (Oregon coast) 80−98330
internal waves, relationship with wind field variability 80−31052
internal waves causing geomagnetic gradient fluctuations 80−56491
internally heated rotating annulus, axisymmetric states 77−45157
Intertropical Atlantic, sea temp. cycle in upper layers *(French)* 78−96227
introductory dynamic oceanography, book 80−4044
Ionian Sea, Medina rise and Cyrene seamount *(Italian)* 79−16433
Ionian Sea, oceanic front obs. during early winter (1970) 77−45008
Ionian Sea, sapropel distrib. and E.Mediterranean Sea late Quaternary palaeoceanography 78−73350
ionic exchanges at water-sediment interface in Norwegian Sea and Intertropical Atlantic *(French)* 79−62523
Ipanema pier studies of sea bottom dynamics *(Portuguese)* 78−61389
IR radiation brightness at crossing of sea horizon *(Russian)* 77−29438

oceanography continued
IR refractive effects close to ocean surface 79−96763
Irish and Celtic Seas, tidal dynamics 79−25254
Irish Sea, density currents from 3-dim. model 78−7647
irradiance attenuation coefficient in a stratified ocean, meas. technique 80−98325
irradiance meas. in upper layer 78−44864
Israel coast, nearshore sediment pollution by trace metals derived from sewage effluent 78−44882
NW.Italy, sea level and current fluctuations along coast 79−100848
NW.Italy coastal waters, oceanographic conditions during 1977 spring 79−34827
ITCZ, near-surface oceanic layer var. during GATE 78−96228
Japan and Izu-Bonin Islands junction, bathymetry rel. to gravity meas. 77−78085
Java, East China and South China Seas, seawater optical props. 77−21792
Jervis Inlet, British Columbia, sediment-water exchange rel. to Mn deposition and nodule growth 78−96187
Joint Air-Sea Interaction (JASIN) Experiment 1978, general review 80−4113
JOINT-I expedition of Coastal Upwelling Ecosystems Analysis program 77−60470
JONSWAP 1973, surface wave prediction model for varying wind fields 80−12408
Kamchatka Current, satellite obs. of eddies 78−81182
Kandalaksha Bay, White Sea, crystalline basement struct. from seismoacoustic profiling 77−86854
Kara and Barents Seas, mean sea level vars. 1936-74 period 77−64320
Kerch Strait, Black Sea, current vel. calc. 77−78219
Kerguelen Islands area, geoid determ. from Geos 3 altimeter data 80−3900
kinetic energy dissipation field, struct. in Atlantic and Indian Oceans *(Russian)* 77−13082
Korean Peninsula, DMSP detection of oceanic thermal fronts 77−21796
Krishnapatnam nearshore zone, wave conditions and wave-induced longshore currents 80−41449
Kuril Trench, topographic profiles rel. to lithosphere elastic-perfectly plastic bending 78−73341
Kuroshio, temp. field fine structure *(Russian)* 77−91141
Kuroshio current, anomalous cyclonic meander (winter of 1978) 80−109171
Kuroshio current, Izu Ridge bottom effect on current dynamics 80−90099
Kuroshio current, mesoscale cellular convection during AMTEX 75, DMSP imagery 77−78322
Kuroshio current frontal zone thermohaline struct., comparison with Gulf Stream 80−85678
Kuroshio Extension vicinity, mesoscale thermal variability 79−16501
Kuroshio in East China Sea, variations of surface velocity from (1965-75) *(Chinese)* 80−31049
Kuroshio jet current system region, density field calc. 78−92843
Kuroshio meander, theory, comment 79−57944
Kuroshio meander, theory 80−4019
Kuroshio region, interannual variability of oceanological conditions 79−2272
Kuroshio Western Boundary Current tracking, by Nimbus 6 satellite 78−36190
Kuroshio with and without cold water mass south of Enshunada, characteristic features 79−20859
Kuwait, marine pollution 79−5510
Labrador Current, direct vel. obs. 80−101378
Labrador Shelf, early deglaciation 79−79891
Laccadive Sea, chemical oceanography 80−104995
Laccadive Sea, trace metals concs. 80−104997
Laccadive Sea (Lakshadweep), physical charact. 80−104966
Laccadive Sea (Lakshadweep), wave charact. 80−109151
Laccadive Sea waters, total Hg concs. 80−104996
Lagrangian current vectors very close to short-fetch windswept sea surface 80−72553
land and sea surface temp. fields, seasonal vars., NOAA 5 satellite IR obs. 78−85676
land-to-seafloor EM transmissions in 0.1-15 Hz band 78−93008
LANDSAT Data Collection Platform for surface hydrography 77−49174
Langmuir circulations, controlled laboratory expts. 79−23330
Langmuir circulations, generation by instability mechanism 77−64304
Langmuir circulations and wind drift currents, Langmuir vortices, struct. 77−49074
large-scale circulation, diagnostic calcs. 78−16056
laser propagation in marine boundary layer, turbulence effects 77−45156
laser propagation in water, multiple scattering effects *(Japanese)* 78−78915
Late Quaternary sea levels, central British Columbia coastal area 78−73377
Late Quaternary sedimentation on W.African continental margin 77−21753
Late Wisconsin flood into Gulf of Mexico 79−29775
lateral mixing of water masses 78−3781
Laurentian Channel and W Grand Banks, relict iceberg furrows 77−5206
law of the sea, impact on marine research 77−64308
law of the sea, Third UN Conf., impact on marine research 77−64309
layered fine-structure form. and destruction by double-diffusive processes 77−29303
layered medium disturbed by internal waves, statistical props. 78−22359
Leningrad storm surges, shallow water eqn. soln., hydrodynamic method *(Russian)* 77−29318
S.Lesser Antilles, mesoscale circulation 80−90094
LF acoustic multipath fluctuations, statistical anal. 78−90571
LF sound absorpt. rel. to temp., pH, B conc. and pressure 78−40560
LF sound propag., bottom roughness effects 79−41501
light attenuation, in situ meas. *(German)* 79−39749
light attenuation field description, analytical method 77−78455
light diffusion in sea, radiance distrib. 77−78216
light scattering effects in deep water *(Russian)* 79−34850
light scattering matrix of hydrosol, influence of form of scatt. particles *(Russian)* 78−5420
light scattering of layer, affected by underlying surface *(Russian)* 80−12403

oceanography continued
Ligurian continental shelf, and current autumnal data series anal. 80−85675
Ligurian Sea, free oscill. correl. with meteorological perturbations 79−34826
Ligurian Sea, uninodal free oscillations, obs. at Genoa 78−65318
linear prediction models, review 80−56590
lipid composition of marine aerosols, sea surface microlayer and subsurface water 80−17297
liquid phase mass transfer coeffs. at natural air-water interfaces 79−20922
lithodynamics, contact zone concept 79−12129
littoral alterations, Messina coastline, Sicily *(Italian)* 79−5469
Liverpool Bay, surface circulation 77−17139
localised vortex evolution *(Russian)* 79−100842
Lomonosov Ridge Experiment (Lorex 79) in Arctic Ocean 80−77120
S.Long Island, New York, Holocene submergence history 79−74881
Long Island Sound, ^{210}Pb balance 79−20861
Long Island Sound, obs. of motion field of Connecticut River plume 77−33111
longshore currents in Gulf of Mexico, due to hurricanes Anita and Babe 80−76998
longshore currents on fringe of Hurricane Anita, Gulf of Mexico 79−34837
longshore movement of water, Texas gulf coast 80−76995
longshore pressure gradients caused by offshore wind 80−67370
longshore sediment transport and sediment budget for Malpeque barrier system, Gulf of St. Lawrence 78−36140
longshore sediment transport by tidal current, outside surf zone 80−76961
longshore variations in longshore currents 78−7645
Loop Current winter intrusions 78−40569
Louisiana Bight, inertial currents over inner shelf near 30°N 79−20849
low frequency noise in deep ocean, prod. by surface waves 78−81184
low temperature skin-layer, hydrodynamic model *(Russian)* 78−36180
Lower Palaeozoic black shales rel. to geologic-oceanographic model 78−61436
Lower Strathearn, Scotland, sea-level changes of early Flandrian 80−56484
lowest sea level in Late Pleistocene on East China Sea continental shelf *(Chinese)* 79−79867
Loyality Islands uplift rates, ^{230}Th/^{234}U dating of raised coral terraces 78−73347
lunar and solar tide generating potentials, spectroscopy, rel. to ocean tide features 77−86904
lunar O_1 tide, contrib. to geomag. lunar daily var. at Alibag 80−56355
lunar semidiurnal oceanic and atmospheric tides, interfacial effects 79−100871
M_2 and S_2 tides calc. for world oceans from tidal potential 79−39752
M_2 ocean tide parameters and Moon's meas. longit. decel. from artificial satellite orbit data 80−31048
M_2 tide parameters from satellite orbit perturbations 77−33093
Madras coastal zone, sea level, tides and waves 77−41038
magnetic field from sea waves, exptl. obs. results 79−53350
magnetic fields induced by ocean waves, model study for non-uniform depths 79−66807
magnetic records rel. to sea floor spreading 77−9337
magnetotelluric investigations, tidal currents effects 77−78095
Mandovi estuary, circulation and sedimentation rel. to Aguada bar 77−73756
Mangalore coast, India, 1976-7 nearshore water conditions 80−8315
old Mangalore Port, India, sediment transport and siltation of navigational channel 80−56488
old Mangalore port, seasonal vars. in estuarine and oceanic waters hydrographic conditions 80−41451
Manning's roughness coeffs. for open estuarial river system 79−79897
Mariana trench, bathymetry rel. to lithosphere seaward flexure 79−57903
Marianas Trench, Pacific Ocean, water charact. meas. at depths >10 km 78−61423
marine aerosols, ^{55}Fe and stable Fe forms and availability 79−12241
marine aerosols influx into atmosphere, influence of coastal-zone physicogeographic conditions 79−29818
marine air temp. sensor error analysis 77−78437
marine atmosphere, circulation in equatorial latits. 78−92949
marine atmosphere, elec. field short-period fluctuations 79−39816
marine atmosphere, ocean as source or sink of reactive trace gases 78−3894
marine atmosphere, results of Complex Atmospheric Energetics Experiment (CAENEX) 78−3904
marine atmosphere, SO_2 meas. at concs. lower than ppb 78−81340
marine atmosphere particulate matter, organic C conc. and particle size distrib. 78−32139
marine boundary delineation, geodetic aspects *(German)* 77−91155
marine circulation three-dimensional modelling 78−77267
marine geodesy, geometrical problems *(German)* 78−3709
marine gravity modelling, considerations of indirect effect (geoid undulation effect) 80−3907
marine inundation of USSR and N.America during Phanerozoic, secular changes 78−3735
marine mineral suspensates and geochemical exploration 78−88936
marine modelling (vol.6 of 'The Sea') 78−16047
marine plankton, C isotope ratio rel. to surface water masses 79−29783
marine research and deep sea mining freedom 77−91274
marine research in China 77−64312
marine sediment, quantitative investigation by neutron activation anal. *(Russian)* 78−92814
marine sediment deposition rate and sulphate reduction 78−53642
marine sediments, sulphate reduction and methanogenesis 78−49009
marine thermocline evolution, study using Mellor-Durbin theory 80−4041
marine waste disposal information reliability 79−12275
Marion Island, former sea levels in S.Atlantic 80−77008
Marshall Island, nucl. test site ^{113}Cd^{m}, in marine organisms and sediment 80−109174
Martinique Beach, Nova Scotia, nearshore currents and beach topography 78−7646
mass transport by waves in turbulent bottom boundary layer 78−3797
mass transport velocity in progressive gravity waves, double boundary layer model 77−78217

oceanography continued
Massachusetts Bay, LF currents rel. to Merrimack River spring runoff 77−37228
Massachusetts Bay, tidally generated internal wave packets 79−44190
Math Modelsea Project, Belgian coast, silt suspension turbulent boundary layer, steady state model 78−28242
mean sea level, meas. using radio interferometer techniques 79−53559
mean sea level rise (1891-1960) *(Italian)* 77−53060
measured data quantification 79−12274
E.Mediterranean, during glacial max., surface temp. and salinity from foraminifera in sediments 80−41456
W.Mediterranean, energy budget *(Spanish)* 78−88846
W.Mediterranean, gravity and bathymetry rel. to tectonics 77−32973
Mediterranean, horizontal Quaternary shorelines 79−66676
W. Mediterranean, O and phosphate distribs. *(Russian)* 78−16058
E.Mediterranean, post-glacial deep water stagnation 79−53366
E.Mediterranean, stationary currents, computation 79−12126
Mediterranean, steady state model of upper mixed layer in Bay of Calvi 78−32116
Mediterranean Action Plan 79−62156
Mediterranean circulation, var. due to river diversion 80−77014
Mediterranean circulation in Sicily and Sardinian straits region 80−72527
Mediterranean deep water formation baroclinic instability and oceanic eddies 78−96229
Mediterranean harbour tidal harmonic constants 80−41448
Mediterranean outflow, deep circulation in Gulf of Cadiz 80−17270
Mediterranean outflow, vel. shear in deep steps 80−85663
Mediterranean outflow mixing 80−17269
Mediterranean Outflow region, salt finger obs. 77−2166
Mediterranean region, Holocene eustatic changes and coastal tectonics, crustal consumption 78−81201
Mediterranean salinity crisis, desiccated deep basin model 77−56644
Mediterranean Sea, eustatic sea variation in last 2000 yr. 77−17117
Mediterranean Sea, glacial palaeo-oceanography 79−16505
Mediterranean Sea, heat and water budgets, dependence on climate and Atlantic waters 79−84291
Mediterranean Sea, hydrological regime during glacial periods *(French)* 80−4040
Mediterranean Sea, Messinian salinity crisis and late Miocene eustatic changes in world ocean 77−91151
E.Mediterranean Sea, periodic freshwater flooding and stagnation during Late Quaternary 79−25263
Mediterranean Sea, petroleum aggregates distrib. in hyponeustal zone 77−49085
E.Mediterranean Sea, surface palaeotemps. record from long deep sea core 78−57294
E.Mediterranean Sea, T and O_2 profiles 80−17298
Mediterranean Sea, temp. inversions in intermediate layers in western basin *(German)* 79−100844
E.Mediterranean sediments, heavy metal content, off Lebanon coast 80−97830
Mediterranean surface water oil pollution, 1974 meas. *(Russian)* 77−60430
Mediterranean undercurrent variability in Gulf of Cadiz 77−2164
MEDOC, mechanisms for mixing and spreading phases 77−2161
Mersey estuary, H_2S effect on methyl Hg in sediments 79−2295
mesoscale circulation features, objective anal., MODE data 77−29304
mesoscale current velocity field, Polygon 70 area 79−20853
mesoscale dynamics rel. to sea floor roughness 79−84216
mesoscale eddies, influence on sea surface temp. *(Russian)* 78−81191
mesoscale eddies generation, numerical simulations with two and three layer quasigeostrophic models 79−57950
mesoscale eddies in mid-ocean, simulated dynamic balances, model 80−26525
mesoscale eddies role in general circulation, wind driven model 79−16491
mesoscale eddy generation, available potential energy *(Russian)* 78−85598
mesoscale energy radiation in mid-ocean 77−78187
mesoscale flow over bottom topography 79−57968
Mesoscale horizontal turbulence *(Russian)* 80−12423
mesoscale motion in western North Atlantic Ocean, space and time scales 78−49035
mesoscale motions, fluctuating winds as energy source 78−40625
mesoscale synoptic eddy, POLYMODE results for NW Atlantic *(Russian)* 78−85588
mesoscale synoptic eddy area, temp. field fine structure *(Russian)* 78−81195
mesoscale thermoclinicity anal., example from tropical thermocline during GATE 79−88359
mesoscale topography effects on stability and growth rate of two-layer model 78−44836
mesoscale warm core closed eddies form. off SE.Australian coast 78−24296
Messina Strait, tidal currents 80−81917
Messina Strait, tidal currents 80−81918
Messinian salinity crisis, evidence of Late Miocene eustatic changes in world ocean 78−61432
metalliferous sediment components, microprobe study 79−34792
metals fate in ocean, ^{210}Pb as tracer 78−11914
metasomatic garnets, low-temperature, in marine sediments, paragenesis 77−86857
meteoroid ablation spheres in abyssal clay 80−46500
meteorological tide, energy transfer from atmos. to ocean *(Russian)* 80−76988
Mezen' Bay (White Sea), marine tides EM fields 78−73378
microbubbles, in situ acoustic meas. 77−37207
microcomputer applications 78−36322
microstructure, transport processes and mixing 77−60420
microwave brightness temp. distrib. over Bay of Bengal using SAMIR Satellite Microwave Radiometer data at 19 and 22 GHz 80−104980
microwave emissivity of sea surface, roughened by wind 80−46184
microwave radiation spectrum of sea surface from multichannel remote meas. *(Russian)* 78−65420
microwave radiometric determ. of wind speed at ocean surface, Bering Sea Expedition 77−17158
microwave radiometry, oceanographic appls. review 78−81415
microwave sea backscatter intermittency at extreme grazing angles, model 78−24307
oceanography continued
Mid Atlantic Ridge near 37°N, infrasonic noise from shipping and seismic sources 77−25691
Mid-Atlantic Ridge at 37°N, bathymetry of DSDP Leg 37 drilling area 77−91070
Mid-Ocean Dynamics Experiment, mesoscale eddies study 79−57941
Mid-Ocean Dynamics Experiment maps, geostrophic streamfunction 77−41042
Mid-Ocean Dynamics Experiment maps, potential vorticity and conservation 77−41043
mid-ocean eddies and weathership records 77−64294
mid-ocean thermocline regime 77−2168
Middle Atlantic Bight, ocean tides and weather induced pressure fluctuations 77−81911
midocean mesoscale eddies, numerical model rel. to MODE obs. 78−49023
midocean ridge hydrothermal systems, hot water egress thermal constraints 79−39700
Mikhail Lomonosov, research vessel, review of 20 years of scientific results *(Russian)* 78−69485
Minch waters and sediments, Windscale effluent 77−91158
Late Miocene, water depths shallowing rel. to C isotope stratigraphy in New Zealand marine sediments 80−26479
Late Miocene-Pliocene eustatic event, correl. with phosphatic nodule beds in Victoria 79−12105
Miramichi estuary, New Brunswick, tidal current control of submarine morphology 78−36174
Mississippi Pascagoula Estuary water quality planning using Gauss-Seidel iterative technique 78−73402
Mississippi River delta, inner shelf temp. and salinity structure 77−37229
mixed layer, deepening rate model *(Russian)* 78−24292
mixed layer, generalised bulk model 77−17129
mixed layer, growth in turbulent stably stratified fluid 79−55358
mixed layer, temp. gradient struct. and Batchelor spectrum 80−77000
mixed layer, vels. induced by internal waves 78−73395
mixed layer evolution, laboratory investigation in homogeneous fluid *(Russian)* 80−94529
mixed layer model capable of simulating cyclic states 77−86926
mixing, effects of eddies and islands 78−85572
mixing and oceanic productivity 79−57972
mixing at oceanic front interface, interleaving process accompanying density difference 80−72525
mixing mechanism in upper ocean, Langmuir circulation instability 80−104970
mixing spreading in stratified fluids, analogue in rot. fluids 79−57949
Mobile Bay, Alabama, LANDSAT Data Collection Platform for surface hydrography 77−49174
Mobile Bay, Alabama, sea truth and environmental charact. study using ERTS-1 data collection platform 77−70687
MODE eddy XBT meas. of thermal gradients 77−70681
MODE meas. of horizontal divergence 77−91139
molecular boundary layer struct. over sea *(German)* 77−86989
monochromatic waves, obliquely incident on plane beach, instabilities 80−17275
Monterey Bay, optical props., spectral values 80−8327
Moro Gulf, Philippines, bathymetric and seismic evidence for subduction zone south of Mindanao 79−44117
multi-layer fluid flow, effect of shifting press. on internal ship waves *(Russian)* 78−77256
multilevel and multilayer models, coincidence of eqns. and computations *(German)* 77−56696
multipath acoustic propagation with moving source 77−23795
multiple water reflections recorded at ocean bottom 78−57331
Narara Bet, Gulf of Kutch, coastal currents, temp. and salinity 80−76990
narrow jets in zonal ocean, model 79−2264
NASA Earth and ocean dynamics programme 77−56733
natural reservoirs, average age rel. to average transit time 78−81239
navigation problems in oceanographic research *(Russian)* 80−17286
near-surface current measurement from a surface following data buoy 79−84290
near-surface inertial oscillations in current records 80−109157
near-surface mixing layer, microstruct. in stable heating conditions 78−85568
nearshore circulations finite element modelling 78−77270
nearshore currents off Long Island 77−9441
nearshore currents off Long Island rel. to sea level slope 77−45014
net long wave radiation from oceans 77−17118
Netherlands coastal waters, transit time distrib. 78−65336
Neva Bay, Leningrad, modelling of dynamic transport of pollutants 77−78220
New England continental shelf, winter hydrography and currents 77−37226
New England shelf, stability of shelf water/slope water front 79−2260
New England shelf-slope water mass interfaces, acoustic imaging 78−3784
New Jersey coast, dynamical analysis of currents 79−57962
New South Wales coast, supply of sand from Hunter River 78−16066
New York Bight, ^{228}Th-^{228}Ra radioactive disequilib. rel. to coastal pollution 79−29784
New Zealand region, oceanic circulation numerical model 80−72538
Newfoundland, depositional environments and benthos of the continental slope and rise 80−3987
Newfoundland Bank, seasonal var. of transparency *(Russian)* 79−100861
Newfoundland fjords, gravel clasts rel. to glacial erosion of bedrock 77−17148
Nile Delta, inner shelf sediment types and deposition 79−79868
NOAA spacecraft high resolution imagery data 77−78389
non-linear small-scale sea-air interaction parameterisation, effects of ice cover *(Russian)* 77−53068
nonlinear coastal and equatorial jets, theory 80−51427
nonlinear internal motion in open sea, obs. using range-gated Doppler sonar 80−51422
nonstationary random processes, simulation and prediction *(Russian)* 77−60408
W. North Atlantic circulation, quasi-geostrophic simulations comparison with primitive eqn. results 79−48493
North Atlantic Drift, decline rel. to rapid ice-sheet growth and last glaciation initiation 80−51530

oceanography continued
North Sea, $^{18}O/^{16}O$ ratio of dissolved O during 1976 Fladenground Expt. 78−73404
N.North Sea, actinide activities in inflowing water 79−16520
North Sea, circulation driven by wind, Norwegian Trench influence 80−98355
North Sea, M_2 tidal elevations and currents, hydrodynamic model 80−104973
North Sea, mathematical and numerical hydrodynamic models 77−37216
North Sea, microwave meas. using SLAR 78−77245
North Sea, nested model with shallow coastal area resolution 77−37212
North Sea, residual flows and elevations in southern region 78−16045
North Sea, sea surface temp. year to year changes, (1948 to 1974) 80−67367
North Sea, surface film, 13.9 GHz radar backscatter cross section meas. 79−39764
North Sea, surface wave refraction 77−91152
North Sea, Tertiary period O isotope palaeotemps. 78−88903
North Sea, wind fields during gales 78−96272
North Sea and River Thames, surge and tide interaction 78−96219
North Sea floor, lunar type features explanation 80−31028
North Sea surface topography, SeaSat-1 expt. geodetic aspects *(German)* 80−81805
North Sea water circulation finite element simulation 77−2162
W.Norway coast, long barotropic waves and storm surges, model 80−81907
Norway current synoptic variability 79−20852
Norwegian coastal current in Skagerrak, deep countercurrent existence 79−79873
Norwegian continental shelf, topographically trapped vortex 80−31046
Norwegian Current, evidence for baroclinic instability 77−60385
Norwegian Current low freq. fluctuations, horizontal wavelength and energy interaction terms 80−101375
Norwegian Sea, chlorofluoromethane depth profiles 78−73405
Norwegian Sea, circulation numerical model 77−29321
Norwegian Sea, currents kinematics and struct. 79−44193
Norwegian Sea pycnocline, apparent vertical eddy diffusion rates from T vertical distrib. 78−81185
Nova Scotia slope water, interleaving at subsurface front 78−85585
nuclear, detonation waves, initiation and propagation conditions 79−93834
numerical Euler-Lagrange model of currents in heterogeneous ocean *(Russian)* 77−13079
numerical modelling appls., conf., Southampton, England (July 1977) 78−77285
ocean atmosphere system, sea foam effect on albedo 77−81899
ocean basins, primordial, form. 79−20770
ocean chemistry, effects of changes on biological evolution 77−56653
ocean hydrodynamics, 7th Liege Colloquium (1975, May 5-9) 77−37211
ocean surface, heat flow conditioned by wind pulsations *(Russian)* 77−60414
ocean thermal energy conversion (OTEC), emerging programme of significance to marine community 78−44875
ocean-atmosphere climate model, large-scale long-term interactions 78−7750
ocean-atmosphere coupled model, atmospheric feedback 80−12500
ocean-atmosphere coupled model, tropical sea surface temp. anomaly effect 80−12418
ocean-atmosphere interface, coupled energy transfer, turbulent and radiative 79−2290
ocean-atmosphere system, spectral struct. of refl. solar radiation field *(Russian)* 77−33086
ocean-coast model, EM response to E-polarisation induction 78−61321
oceanic fronts, optical and particulate matter properties 80−51418
oceanic geoid., satellite obs. 77−25635
Oceans 1976 conference, Washington (Sept 1976) 77−5241
Oceans '77, conf., Los Angeles, USA (Oct. 77) 78−36193
oceans '77, conference, Los Angeles, CA, (17-19 October, 1977) 78−45040
oceans '78, ocean challenge, conference (Washington, DC, USA, 1978, September 6 to 8) 79−5658
offshore environmental and platform data processing from Norwegian continental shelf 79−12273
oil film pollution, retardation of O_2 exchange with atmos. 80−109175
oil patch probable movement from Bombay High region 78−81219
oil pollution on sea surface, effect on radio location signals *(Russian)* 77−78230
oil slicks on sea surface, petroleum products content determ. 77−64330
oil spill, dynamics in fractured ice field in Buzzards Bay, Massachusetts 78−40596
oil-rich layer at 200 metre depth, obs. in N.Atlantic and Carribean 80−56498
Okhotsk Sea, clay minerals distrib. in recent sediments 79−20804
Okhotsk Sea coast of Hokkaido in winter, ocean currents *(Japanese)* 80−36326
old Mangalore port, India, channel siltation study 80−77005
open channel, two-dimensional tidal propagation model, difficulties 78−77272
optical and hydrologic characts. correl. 77−78215
optical depths, effective IR, of clear ocean 79−8635
optical fields, constructed using probability theory *(Russian)* 80−109164
optical image resolution limitation imposed by random medium 78−37813
optical propagation in turbulent water, refr. index spectrum of temp. or salinity fluctuations 79−5487
optical properties, one parameter characterisation for remote sensing 78−7644
optically thick media, asymptotic radiance and polarisation 77−21776
Orca Basin brines and sediments, C isotope comps. 79−88369
Oregon coast, inertial oscills. from current meter data 77−41047
Oregon coastal upwelling system, vertical vel. profiles 77−60382
Oregon continental shelf, current fluctuations, seasonal differences 79−16483
Oregon continental shelf currents, spring transition 80−41453
Oregon continental shelf region, momentum, vorticity and mass balance 78−69356
Oregon Inlet, N.Carolina, coastal upwelling, exchange through Barrier Is. Inlet 77−60401
Oregon shelf, bottom mixed layer variability 79−74896

oceanography continued
Oregon shelf, fine scale temp. struct. in bottom mixed layer 77−33081
Oregon-Washington continental shelf, barotropic response hindcast during 1972 summer 79−48497
organic C, dissolved and particulate, in marine environment, stable C isotope comp. 79−20862
origin, rel. to Earth early history 79−20739
origin of the oceans *(Russian)* 80−81857
oscillatory flow, time averaged drag on obstacle or sea floor 77−65748
oscillatory ice states in water internally heated and cooled from above 77−73759
oscillatory motion around bottom ripples, theory *(Polish)* 77−70686
Oslofjord, vertical diffusion driving mechanism, internal tidal waves, model 80−26531
Otway coast evolution from Last Interglacial to Present 78−20390
Otway region, S.W.Victoria, conf. (Melbourne, 1975 October 9) 78−20415
equatorial Pacific, 1976 El Nino, sea surface topography response 80−81913
S.Pacific, ^{210}Po and ^{210}Pb distrib. in ocean water profiles 77−5225
tropical N. Pacific, annual forcing of baroclinic long waves, bathythermograph obs. 77−60392
SE.Pacific, Antarctic Intermediate Water, modal props. 80−36306
Pacific, bottom boundary layer currents, E. tropical region 80−109154
NE.Pacific, C, N and P particulate fluxes in upper water column 79−88368
Pacific, Cd distrib. in bottom sediments surface layer 79−20809
NE.Pacific, Columbia River discharge effect on radioactivity field *(Russian)* 79−39761
Pacific, cotidal charts near Hawaii using f-plane solns. 77−60394
tropical Pacific, coupled air-sea model 79−16581
NW.Pacific, current vels. and density models *(Russian)* 79−100860
S.Pacific, deep density-depth curve shapes 77−86915
NE.Pacific, depth depend. of ambient noise 78−88840
N Pacific, dissolved Ca and alkalinity distribs 80−90100
N.Pacific, dissolved Cu distrib. 78−32119
S.Pacific, DSDP site 284, Late Cainozoic isotopic history 79−48516
S.E.Pacific, DSDP Site 319, metalliferous sedimentation history 78−7611
Pacific, eastern tropical region, acoustic vol. reverberation, rel. to oceanographic features 78−36176
N Pacific, eddies generated by seamounts 78−69367
Pacific, E.equatorial, long waves obs. in geostationary satellite IR images 78−24308
E.Pacific, equatorial long waves from deep current meas. 77−5216
N.Pacific, finestructure and microstructure during passage of mild storm 77−2167
central N. Pacific, finestructure spectra from main thermocline 77−60390
central N.Pacific, frontogenesis and frontolysis rates, 1976-7 winter 79−2250
Pacific, geographic variation of LF sound absorption 79−44189
N.Pacific, heat flux vars. rel. to Kuroshio, 1956-64 period 78−28240
Pacific, horizontal circulation calc. 77−49075
S.Pacific, hydroclimatic anomalies 78−65335
Pacific, integral circulation calc., accounting for discharge *(Russian)* 77−78197
N. Pacific, interior midlatit., main thermocline seasonal cycle, wind driven model expt. 79−48499
Pacific, irradiance and beam transmittance meas. 79−48491
SE.Pacific, isohaline thermoclines 79−79865
N Pacific, large scale longitudinal surface temp. variations 77−70675
N. Pacific, long-wave disturbances of dynamic height 77−60391
W. central Pacific, Mesozoic evolution 77−44953
N.Pacific, mid-depth circulation 79−79851
N. Pacific, midlatitudes, zonal variability in eddy energy distrib. 77−60397
NE.Pacific, Mn distrib. 80−101384
tropical N.Pacific, N_2O in O_2 min., consumption during denitrification 79−5501
NE.Pacific, near surface circulation 79−79850
N. Pacific, near-surface currents vars. during POLE Expt. 78−92834
Pacific, O distrib. 77−25696
NE.Pacific, ocean surface heat loss in cyclone regions 80−77009
midlatitude N. Pacific, optimum oceanographic network design 80−36315
NE.Pacific, quality of sea surface temp. and salinity meas. 79−79853
Pacific, satellite obs. of mesoscale eddy dynamics in E tropical regions 78−24295
Pacific, sea level vars. monitoring 79−100840
N.Pacific, sea surface temp. anomalies 78−81204
N.Pacific, sea surface temp. anomaly gradient rel. to mid-tropospheric circulation 80−85674
Pacific, sea surface temp. anomaly periods rel. to tropical easterly atm. waves 77−78309
Pacific, sea surface temp. correl. with atm. CO_2 77−29307
N.Pacific, sea surface temp. meas., 1976-77, from Nimbus 6 satellite 79−20841
N.Pacific, sea surface temp. rel. to California rainfall 77−91239
NE.Pacific, shallow salinity min. in winter 79−79861
N.Pacific, size distrib. of suspended particles in surface water 80−4047
N.Pacific, small-scale mixing intensity vars. in main thermocline 77−86925
Pacific, sound diffusion loss in stratified channel 77−11072
Pacific, stationary circulation energetics, numerical expt. 79−53360
N Pacific, subarctic fronts struct. and response to atm. forcing 78−44846
N Pacific, subsurface hydrography from radiolarian distribs. 77−33095
SW.Pacific, surface salinity fluctuations, 1956-73 period 79−79863
NW.Pacific, surface temp. fronts variability, satellite obs. 80−90092
N.Pacific, synoptic obs. of Kuroshio and Oyashio fronts 78−32113
NE. Pacific, temp. anomalies, 1966-74 period, gridded by objective anal. 78−92830
tropical N.Pacific, temp. fine structure 79−16485
N.W.Pacific, temp. fluctuations in internal gravity waves freq. range 77−49081
Pacific, temperature-salinity curves and appl. to dynamic height comp. 77−2172
tropical Pacific, trace gases, ITCZ and ocean currents 80−41509
N.Pacific, trace metal vertical profiles 80−67381
Pacific, trade wind field annual and interannual vars. 77−2206

oceanography continued
Pacific, transition zone between intermediate water masses, temp. salinity curves 78−3791
NE Pacific, VLF attenuation from deep-water ambient noise field meas. 77−11070
E Pacific, volume scatt. layers in tropical regions 77−2181
N.Pacific, wind drag and relative separations of undrogued drifters 79−79866
NW Pacific, wind-wave tropical cyclone model, parametrisation charact. 78−24301
NE.Pacific, Zn conc. 78−36200
Pacific, zonal currents struct. in western equatorial region 77−49079
E.Pacific and equatorial Atlantic, hemispheric asymm. of heat budget 78−40570
N.Pacific and N.Atlantic, wind field temporal and spatial scales 79−79942
N.Pacific Basin, numerical simulation studies of oceanic anomalies, model and mean state 79−48494
Pacific basin, sedimentation rates and sea levels 79−88365
N.Pacific Basin, simulation studies for oceanic anomalies, atm.-ocean link 80−8316
N.Pacific Cenozoic sedimentation history 80−31027
N.Pacific Central environment at 35°N, phys. chem., biological charact. 80−76983
Pacific coast of Japan, charact. of throat sections of bays *(Japanese)* 77−78192
N.Pacific current, vel. field mesostruct. 77−64316
N.Pacific deep sea sediments, ^{26}Al activity rel. to prod. by cosmic rays in atm. 77−5181
Pacific equatorial countercurrent lateral oscills. 79−16500
Pacific equatorial zone, cruise of the Akademik Vernadsky *(Russian)* 77−78203
W.Pacific equatorial zone, current meas. *(Russian)* 78−16044
Pacific equatorial zone, water transparency *(Russian)* 78−16043
E.Pacific Hess Deep, rapidly-formed ferromanganese deposit on basaltic glass 77−29283
N.Pacific mesoscale phenomena, oceanographic model and acoustic survey comparison 80−46195
Pacific N. Equatorial Countercurrent, Sverdrup transports 80−67369
S.Pacific Ocean, acoustic cross-section (Project Kiwi One) 80−36330
Pacific Ocean, annual var. in slope of 14°C isotherm along equator 80−72537
E. Pacific Ocean, atmospheric Aitken nuclei concs. 77−37305
Pacific Ocean, barotropic and baroclinic tides over continental slope and shelf off Oregon 80−72543
Pacific Ocean, bathymetry rel. to roll cell mantle convection under Pacific plate 78−73345
tropical Pacific Ocean, climatological usefulness of satellite-determined sea-surface temps. 80−31044
Pacific Ocean, currents rel. to coastal California late Quaternary climate 78−57293
Pacific Ocean, December sea surface temps. correl. with spring rains in California 80−77064
Pacific Ocean, early Pliocene deep thermal struct. 80−56492
NW.Pacific Ocean, edge waves obs. *(Russian)* 78−44841
Pacific Ocean, equatorial, temp. fine struct. obs. 80−98336
Pacific Ocean, equatorial currents strength monitoring from XBT sections and sea level obs. 78−73383
Pacific Ocean, Mn distrib. 80−56494
N.Pacific Ocean, regional depend. of low-freq. acoustic attenuation 77−62090
NW.Pacific Ocean, relation between atmospheric press. and sea level 80−101415
Pacific Ocean, seawater circulation and convective heat loss on E.Pacific Rise and Galapagos Rise 78−73331
Pacific Ocean, T transport models source function 78−32122
Pacific Ocean, telluric current channelling rel. to EM induction in Vancouver Island region 80−56356
N Pacific Ocean, temp. anomalies vertical struct. 78−73394
N.Pacific Ocean, tropical, annual Rossby wave obs. 80−51421
E.Pacific Ocean, tropical, N_2O meas. in sea water and marine air 80−94542
N.Pacific Ocean, west, depth, var. of temp., salinity and sound vel. meridional gradients 80−51429
Pacific Ocean bottom sediments, interstitial waters B content 80−36289
N.Pacific Ocean current, vel. field diagnostic calc. comparison with obs. *(Russian)* 78−61428
Pacific Ocean sediments, ^{10}Be dating compared with palaeomagnetic ages 78−32058
N Pacific Ocean waters, density 78−73391
Pacific Ocean waters, nitrate N distrib. 80−31065
Pacific Pleistocenes palaeoclimatic stratigraphies, comparative anal. of results 78−57295
E.Pacific Rise, hydrothermal heat flux of black smoker vents 80−94488
E.Pacific Rise, hydrothermal vents on seabed issuing H_2 and methane 80−41422
Pacific sea-floor topography and isostatic compensation mechanism (Hawaii region) 80−104945
E. equatorial Pacific sediments, pore water nutrients and carbonate 80−101357
Pacific subantarctic section of Southern Ocean, counterclockwise circulation 78−20427
NW.Pacific subtropical front during 1954-74 period 79−2249
N.W.Pacific surface currents 80−26548
Pacific surface layer, radioactive admixture spreading studies *(Russian)* 77−60488
N.Pacific surface temp. anomalies, atm. general circulation model response 79−53431
Pacific surface temps., empirical orthogonal function anal. 77−17127
tropical Pacific thermocline displacement, simple Ekman-type model 79−48498
pack ice, drift observed using radar buoys *(Japanese)* 78−96224
pack ice, kinematic eddy viscosity *(Japanese)* 77−81913
packice drift, oceanic boundary layer effect, model 80−26528
palaeo-oceans and continental drift *(Russian)* 77−25672
palaeoceanography, Santa Barbara Basin sediments, Radiolaria study 79−84297
palaeocirculation, influence of plate tectonics 77−45017
palaeocirculation, models for Cretaceous and Permian *(Russian)* 77−29320
oceanography continued
palaeoclimatology, water temps. determ. from larval bivalve shell morphometry 79−53510
palaeocontinental slopes of East Coast Geosyncline, Canadian Atlantic Margin 78−36141
palaeocurrent indicators in deep-sea sediments 80−3992
palaeozoic sequences palaeobathymetric anal., rel. to basin tectonics 78−69341
Panama Basin, bottom water inflow 78−44826
Par River estuary, India, pollution transport and abatement methods 80−104521
Paradip Port, India, wave charact. 80−41450
particles suspension in turbulence, small sphere motion in rot. vel. field 77−58771
particulate matter suspended in water, vol. scatt. function at near-forward angles 78−55299
particulate trace metals transport by bubbles in open ocean 79−57940
passive radiometry of ocean, radio meteorology colloquium, Victoria, British Columbia, Canada (1978 June 14 to 21) 80−46724
penetrative convection model, appls. to atmopshere, ocean and laboratory expts. *(Russian)* 78−24335
Pentland Firth, anomalous tidal flow from cable voltage meas. 79−44191
Persian Gulf and approaches, oil pollution, 1978 obs. 80−105000
Peru coastal upwelling region, denitrification and H_2S 77−78226
Peru coastal waters, nitrate and static stability 79−74899
Peru Current, advection obs. by satellite 78−16029
Peru-Chile undercurrent, southernmost extension 80−85664
Peruvian upwelling system near 15°S, circulation 80−101377
phosphorite nodules on sea floor off Peru and Chile, U isotopes 78−7612
photic layer, organic matter studies, radioisotopic methods appl. *(Russian)* 77−60427
photosynthesis, in situ quantum efficiency determ. using photoelec. sensor chlorophyll simulator 79−39760
physical and biological sciences, conf., Japan (Mar. 1979) 80−17714
physical fields, optimum reconstruction *(Russian)* 77−60410
physics of atmosphere and ocean and weather prediction *(Russian)* 77−21774
phytoplankton, as source of atmospheric ice nuclei 77−5291
phytoplankton passive remote sensing via chlorophyll α fluoresc. 77−86938
plane periodic flow, post-critical regime construction *(Russian)* 78−34109
planetary boundary layer, wind driven current, temp. profile, model 80−26526
planetary fluids, displacement and rectification 77−45002
plastic debris floating in Mediterranean 80−104999
Pliocene and Pleistocene sea levels, rel. to Barents Ice Sheet and glaciations 78−57227
Pliocene eustasy, rel. to onset of sand barrier form. in Gippsland, Victoria 79−74886
Po delta, coastal current flows, mathematical model *(Italian)* 77−70667
polar regions, radio obs. appls. 78−81419
pole tide induced by Chandler wobble, tidal admittance 77−9443
poleward heat flux, by ocean gyre 80−85668
pollutant dispersal and deposition, Th isotope analogue expts. to simulate coast region 80−81927
pollutant dispersion from point source with and without chem. reaction in semi-bounded waters 77−64329
pollutant dispersion in oscillatory fluid flow 78−44881
polluter discriminant analysis using statistics data base 77−5244
pollution, dynamically passive impurity propag. in sea surface layer 80−31063
pollution, technique for estimating long-term conc. of conservative substances discharged into ocean 78−44885
pollution dispersion-convection equation, soln. for bay with currents 77−91157
pollution patches evolution modelling for southern North Sea 77−45018
pollution simulation, higher accuracy predictor-corrector method 79−66431
Polygon-70 in Atlantic Ocean, internal tidal structure *(Russian)* 80−51411
postglacial sea level changes, W.Newfoundland, rel. to ^{14}C age of Robinson's Head moraine 78−20401
prebiotic oceans, soluble organic matter scavenging 77−64436
Precambrian geologic history 77−2131
Precambrian sea, solution photochemistry, inverse segregation and banded Fe formations 79−20863
Providence River, Narragansett Bay, nontidal flow, stochastic approach to estuarine circulation 77−17132
Puget Sound, Fe geochemistry 78−69370
pulse diffusion in densely distributed scatterers 79−3632
qausigeostrophic flow above sloping boundaries 79−66703
quarter-diurnal tides loading effects by Ligurian Sea 78−61308
quasi-isothermic layer and thermocline, model of active ocean layer *(Russian)* 80−109163
quasigeostrophic motions of first kind, classification 78−3787
quasihomogeneous layer form., dynamic model 79−20851
quasihomogeneous layer form 79−53358
radar returns from sea ice, freq. charact. *(Japanese)* 80−36328
radar sea return backscattering CW dual-freq. X-band radar studies 77−25687
radiance distrib. over ruffled sea, glitter, sky and ocean contribs. 77−21902
radiation balance of ocean-atmosphere system *(Russian)* 77−78200
radiation field in semi-infinite medium with internal radiation sources *(Russian)* 77−29437
radiative transfer, absorpt. and scatt. props. determ. 77−9430
radiative transfer eqn. for scattering layer with extended scattering indicatrix *(Russian)* 78−40660
radio and heat location, inverse problem soln. *(Russian)* 78−65419
radio obs. and equipment, colloquium (Hamburg 1976 Sept. 29-Oct. 6) 78−77239
radio oceanography, short bibliography of Russian literature 78−77338
radioactive waste disposal and deep sea biology 79−29638
radioactive waste disposal into deep ocean, hazard assessment 77−88233
radioactivity-salinity correlation *(Russian)* 77−78199
radiometry, multi-frequency radiometer system performance evaluation 78−81417
radionavigation with global Omega system, hydrophysical research appls. *(Russian)* 80−17418

oceanography continued
radionuclide adsorption on hydrated MnO, ^{137}Cs and ^{90}Sr 78−3822
radionuclide distributions in oceans and marine sediments from nuclear weapons testing 78−13344
rain mixing with near-surface water 79−53371
Rayleigh-Jeffreys convective stability problem with temp. and salinity gradients *(Russian)* 78−14012
reciprocal acoustic transmission, midocean current monitoring appl. 78−11907
recycling flow over bottom topography in a rotating annulus 78−90916
Red Sea, temp. and salinity meas., warm and hot brines 79−20856
Red Sea brine, thiocyanate detect. and implications 79−57975
Red Sea brines origin, new isotopic evidence 78−96236
reflectance of flat ocean in zero water depth limit 77−41032
reflecting sea surroundings, IR contrasts 77−5211
refractive index microstruct. from diffusive and turbulent ocean mixing 80−56486
refractive index temp. struct. parameter estimation over ocean 77−41033
regional sea surface model in Tasman and Coral seas, Geos 3 altimeter data anal. 80−3903
remote sensing, LANDSAT and SEASAT data acquisition 79−12309
remote sensing applications 77−56655
remote sensing appls. to ocean surveillance, AGARD lecture series, Oslo (3-4 October 1977) 78−69534
research aspects *(Dutch)* 77−64299
research institute structure and purposes *(Russian)* 77−57147
research trends and costs prediction *(Russian)* 78−16042
research under CNEXO, Oceanological Centre of Brittany facilities *(French)* 79−8697
residence times of trace metals, river discharge effects 77−78228
residual circulation, topographic generation by oscillatory tidal currents 79−57954
resonance oscillations in closed L-shaped channel, appl. to harbour 77−78190
resources and meas. techniques, conference, San Diego (1979) 80−41943
Rio Grande Rise, marine sediments and erosional canyons of late Cainozoic 80−56456
rip currents on open coastline, wave-current interaction models 79−34839
ripple formation, growth and decay in oscillatory flow *(Polish)* 79−25227
ripples, wind-generated, gravity waves effects, Doppler meas. 77−62264
Rockall Trough near-bottom traverse, hydrographic and geological inferences 79−62483
Rosenstiel School of Marine and Atmospheric Science, University of Miami, review 80−8755
Ross Ice Shelf, circulation and melting 79−88363
Ross Ice Shelf (Antarctica), basal freezing, confirmed by core drilling 80−101393
Ross Ice Shelf project, circulation and melting 79−88366
Ross Ice Shelf Project ice hole 79−88371
Ross Ice Shelf sea temperatures 79−88362
Rossby wave, critical layer evolution 78−79329
Rossby wave interaction with zonal flow *(Russian)* 80−104982
rotating annulus experiment, Rossby regime *(Japanese)* 79−66709
rotating channel flow, hydraulic control theory 77−56642
rotating fluid, vortices formation near reson. for elastoid-inertia waves 80−12473
rotating stratified fluid, an exact soln. for edge waves 80−4038
rotating stratified fluid, parallel shear flow, baroclinic and barotropic instability 80−98328
rotating two-layer fluid, barotropic and baroclinic Rossby waves interactions and instabilities 79−57955
rough sea surface reflected acoustic signal and sea wave spectrum 78−94474
rough sea surface rel. to underwater light field fluctuations *(Russian)* 78−36183
Saanich Inlet, British Columbia, dissolved N_2O consumption in anoxic basin 78−40594
Saguenay fjord, distrib. of size spectra of suspended particles *(French)* 79−92543
Saguenay Fjord, suspended particulate matter geochemistry 78−92852
lower Saint Lawrence estuary, sediments of Rimouski shelf region 79−62530
W.Sakhalin shelf, NW.Pacific, Faye-Bouguer anomalies 77−32975
salinity calc. in estuary, semiempirical turbulence theory appl. 79−57967
salinity field, vertical restructuring in world ocean 79−39755
salinity field statistics 79−16510
salinity finestructure generation by vertical diffusion 77−70680
salt fingers, supercritical, growth rate 79−88358
salt fingers spectral signature 77−25686
saltwater-ice system, differentially heated, Arctic Ocean model 78−20435
sandy beach dynamic profile equilib. in frontal wave action *(Russian)* 79−88331
Sargasso Sea, comparison of cyclonic ring structures 79−79855
NW.Sargasso Sea, effects of 1976 to 1977 winter cooling 78−28243
Sargasso Sea, hydro-optical study *(Russian)* 78−85594
Sargasso Sea, internal wave field, vertical coherence 80−36310
NESargasso Sea, large cold core cyclonic current rings 78−49031
Sargasso Sea, narrow warm water tongue intrusion obs. using satellite and in situ data 78−73382
Sargasso Sea, optical props. of seawater *(Russian)* 80−94532
Sargasso Sea, optical transfer function meas. 80−8328
Sargasso Sea, POLYMODE area, O_2 conc. rel. to eddy dynamics 80−85685
Sargasso Sea, surface height vars. from Geos-3 altimetry obs. 80−104969
Sargasso Sea, surface mixing layers 80−81906
Sargasso Sea and tropical Atlantic, hydroptic obs. *(Russian)* 79−39748
satellite data availability from Environmental Data Service 78−36288
satellite remote sensing appls. 77−25788
scalar quantity, conservative, undergoing advection, time depend. 79−48507
Scotia Sea, Antarctica Convergence position rel. to maximum ice extent on island groups 78−20450
Scotia Sea, gradient currents, water circulation 78−3798
Scotian Shelf, hydrocarbons in surface sediments 78−49008
Scotian shelf (N.Atlantic Ocean), wind-induced sea level changes 80−72531

oceanography continued
Scotian Shelf edge, low-freq. momentum, heat, salt and nutrients fluxes 79−2242
Scripps Institution of Oceanography, research projects and education review 78−69464
sea bed movement effect on submarine cables, between St. Margarets Bay and La Paune 78−15992
sea bottom, mass transfer, horizontally 2D bodies effect 78−11909
sea breeze over gulf or lake, numerical model 77−49115
sea breeze rel. to pollution over gulf region 78−11977
sea echo radar spectra resolution limitation inferred from ionospheric Doppler broadening 78−81489
sea floods in United States and their management 77−41073
sea floor analysis with deep tow techniques 78−33942
sea gravimeter trials on Halifax Test Range, NW.Atlantic 77−2267
sea ice, brine drainage and convection 79−57963
sea ice, Danish studies using Landsat and airborne sensor data 80−94527
sea ice, dynamic thermodynamic model 80−51432
sea ice, effect on internal wave development *(Russian)* 77−78193
sea ice, EM sounding by Arctic and Antarctic Research Institute, Leningrad 80−4504
sea ice, EM wave scattering from slightly rough boundary 78−77266
sea ice, long range forecasting for north coast of Alaska 77−2174
sea ice, low-salinity, radiometer studies 78−81175
sea ice, microwave remote sensing in AIDJEX main expt. 78−81173
sea ice, ocean waves SAR imaging 79−5496
sea ice, radar anisotropy due to horizontal c axes preferred aximuthal orientation 79−34836
sea ice, US vel. meas. 77−33094
sea ice and glacial development in Late Cainozoic N.Hemisphere 80−90098
sea ice and open water in Bering Strait, radar monitoring 77−87100
sea ice apparent viscosity seasonal vars., drift models 77−33085
sea ice chemistry 79−12128
sea ice deformation, viscous law as stochastic average of plasticity 78−16028
sea ice dynamics in Arctic (May 1975), simulation 78−36192
sea ice formation, assoc. heat and salt transfer 77−64324
sea ice large-scale numerical model 79−48490
sea ice near Showa Station, Antarctica, physical props. *(Japanese)* 78−96226
sea ice pressure ridges, statistical distrib. 79−79847
sea ice seasonal change model 77−17128
sea ice structure, effects of artificial inclusion *(Japanese)* 78−88844
sea ice underside, geometrical roughness props. 80−98334
sea ice-ocean temp. oscillator model, nonlinear analysis 80−12413
sea level, abrupt height changes across fracture zones rel. to lithosphere thickness 79−88231
sea level, bottom pressure and geostrophic adjustment 77−37215
sea level, interstadial, of −40 m at 30000 yr BP, $^{230}Th/^{234}U$ age support 79−16504
sea level, Pleistocene, record in S.Australian beach ridges rel. to Milankovitch theory of ice ages 80−98307
sea level−air temperature correlations near a coastal zone 79−12122
sea level along west coast of N.America, alongshore correl. vars. 78−73381
sea level and glacial isostatic adjustment 79−20800
sea level change, $CaCO_3$ prod. and coral reef growth 77−49086
sea level changes before and after 1961 and 1968 earthquakes at Hyuganada, Japan 77−17042
sea level changes due to West Antarctic ice sheet fluctuations 77−86933
sea level changes of N.Sea (1780-1980), German Bight 80−90089
sea level during ice age, and Antarctic ice surge theory 80−51525
sea level during last 18000 years, retreat of Antarctic ice sheet 80−41455
sea level in Late Pleistocene, USA Atlantic shoreline sediments 80−26543
sea level nonperiodic vars. of synoptic freq. on tidal sea shelf *(Russian)* 78−65320
sea level oscillations, low-freq. wind-induced, along N.America east coast 79−84286
sea level position 140000-75000 BP, Barbados model error 77−21794
sea level pressure anomalies predictability over N.Pacific Ocean 78−92905
sea level response to polar movements 78−53608
sea level transients, obs. by Geos 3 coincident orbits 80−72535
sea level var., Phanerozoic history and climatic instabilities 77−66981
sea level variations along Arctic coast *(Russian)* 78−92838
sea level variations around British Isles, (1960-1975), multiple regression anal. 80−109149
sea level variations in NW Mediterranean during Roman times 77−13088
sea level vars. determ. from marsh foraminifera vertical zonations 78−44866
sea level vars. rel. to contemporary crustal movements in Canada 80−8273
sea levels versus groundwater variations rel. to mammalian extinctions 78−36215
sea model, 3-D numerical, Galerkin method with polynomial basis set 80−72524
sea motion study in Eastern Frisian Is. and sandbanks *(German)* 77−2158
Sea of Azov, O isotope comp. of seawater 77−49083
Sea of Azov, seawater self-purification from pollutants 77−53076
Sea of Azov, storm surges calc. 78−96231
Sea of Marmara sediment evidence for Late Quaternary water exchange 80−81916
Sea of Okhotsk, water-soluble gases conc. meas. 79−2291
sea salt aerosol, atmospheric temp. sensors contamination 80−82095
sea spray, contrib. to S and trace elements in South American continental aerosol 78−57245
sea straits, laboratory models 77−64305
sea surface, atm. scatt. of refl. solar radiation *(Russian)* 77−29435
sea surface, light intensity fluctuations refl. by sinusoidal waves *(Russian)* 77−13080
sea surface and atmosphere radio brightness temp. meas. from satellite *(Russian)* 77−60407
sea surface deviations from geoid, effect on geoid computation 77−64177

oceanography continued
sea surface evaporation ducts, polarisation depend. of transient signals 78−57269
sea surface layer temperature gradient, depend. on wind stress and total heat flux 77−60378
sea surface moisture-flux parametrisation 77−73788
sea surface oil pollution detect. by lidar *(Russian)* 77−45019
sea surface radiobrightness temp. from satellite sounding *(Russian)* 77−60412
sea surface scattering theory for large incident angles 77−86911
sea surface signal interpretation and energy transfer calc. 78−28241
sea surface temp. anomaly generation rel. to atm. storms 79−39721
sea surface temp. meas., comparison of obs. in NE.Pacific Ocean 78−92837
sea surface temp. obs. during 1952-65 period is N Pacific 77−41054
sea surface temperature, 8-13 μm satellite meas. interpretation 77−17145
sea surface temperature, Noaa 4 satellite and Aries airborne radiometer meas. comparison 79−62517
sea surface temperature, response to vars. in atmospheric wind forcing 79−48505
sea surface temperature (SST), NOAA-4 data time series anal. 79−53364
sea surface temperature and rainfall correls. during GATE 79−79864
sea surface temperature anomalies, linear theory of atm. response 77−78308
sea surface temperature anomalies and thermocline variability, stochastic climate model appl. 78−3918
sea surface temperature anomalies rel. to atm. surface press. anomalies 78−49034
sea surface temperature contouring, appls. of satellite ocean-related imagery programme 79−5681
sea surface temperature correl. with rainfall in N.E.Brazil 77−29398
sea surface temperature deviation at very low wind speeds 77−78224
sea surface temperatures, features enhancement on satellite IR pictures by digital techniques 79−5682
sea surface temperatures in shallow seas, 18.6 year cycle due to tidal mixing vars. 78−73387
sea surface tension variability with mean wind speed 78−7656
sea surface topography, altimeter data analysis by sequential filter 80−4145
sea surface topography, computations and obs. comparison 78−77250
sea surface topography and ocean geoid, Geos 3 investigation 80−3906
sea surface topography obs. with Geos 3 altimeter data 80−3908
sea surface ULF/ELF fields generated by submerged magnetic dipoles 77−6973
sea surface vertical heat fluxes, N.hemisphere distribs. computed by bulk method 79−96804
sea temp., salinity and winds, SKYLAB 1.4 GHz radiometric meas. 78−65338
sea use plan concepts and criteria 80−46203
sea water freezing, induced haline convection expts. *(Japanese)* 78−88843
sea-air CO_2 flux meas., eddy correl. method 78−32191
sea-air heat and moisture exchange, zonally averaged model *(Russian)* 77−17161
sea-air interface fluxes of sensible heat and moisture, parameterization 77−41041
sea-air small-scale interaction, heat exchange estimates 78−3810
sea-atmosphere heat-transfer expts. *(Russian)* 78−81206
sea-floor topography, tectonic model using vol. expansion coeff. 80−90072
sea-level lowering during Illinoian glaciation, Bahama 'blue hole' 80−72557
sea-surface microlayer, ^{210}Pb and ^{210}Po enrichment obs. 80−56496
seal level records, noise reduction, for crustal vertical movement detect. 79−2395
SEASAT A and spaceborne oceanography 79−66907
Seasat-A, data processing and distrib. 78−45005
SEASAT-A satellite project 77−5414
seasonal circulation long-term average for Atlantic and Arctic Oceans boundary regions 79−44197
seasonal temp. var., model *(Russian)* 77−60402
seasonal thermocline, one-dimens. models 78−16050
seasonal thermocline, temp. field fine structure *(Russian)* 80−17278
seasonal thermocline, vertical structure of temp. field *(Russian)* 78−85596
seasonal thermocline models, dissipation effect 80−4030
seawater, transfer matrix elements of scattering medium *(Russian)* 78−36181
seawater-clay suspension, turbulent boundary layer 79−20858
sediment ^{230}Th dating technique, by α-scintillation counting 80−72636
sediment climate record, diatomaceous sediments of Gulf of California 80−98351
sediment heat flow, equatorial Indian Ocean 80−76958
sediment layer growth and diffusional flux 77−33047
sediment mixing and accumulation, near-shore, fallout radionuclide tracer obs. 80−81864
sediment movement behaviour, current, wave and wind effects *(French)* 77−78151
sediment O_2 penetration at coastal site 80−104952
sediment of continental shelf, anomalous declination due to slumping 80−76964
sediment transport near ocean bed, theoretical flow models 78−15996
sediment-water chem. exchange traced by ^{222}Rn obs. 80−101386
sedimentation rates and organic matter chemical reactions in ocean 77−64325
sediments, acoustic anisotropy due to overburden press. 80−56455
sediments, in situ acoustic impedance meas. method 78−9519
sediments, occurrence of inositol isomers 77−5240
sediments, presence of azaarenes 77−37181
sediments anoxic pore waters, effects of oxidation during sampling on silicate content 78−61394
sediments grain size distrib. along underwater slope of S.Sakhalin Island 77−64265
sediments interstitial waters, dissolved organic matter nature and reactions 78−49039
sediments of deep-sea, ^{14}C age and vertical mixing 80−81865
seismic T waves from Tonga earthquake (June 1977), human perception on Tahiti 80−61769

oceanography continued
semiclosed water basin, eigenoscillations, hydrodynamic models, appl. to Ligurian Sea 78−3782
sensible heat flux from ocean to atm. in extratropical synoptic-scale systems 77−78223
Sepik River coast, Papua New Guinea, trace gases and breezes 78−85642
Severn estuary, seasonal and spring neap tidal depend. of axial dispersion coeffs. 80−94534
shallow circular basins, oscillation simulation 77−70678
shallow ocean water, Naval Research 79−25258
shallow sea, drift-gradient current vertical structure, model 80−77010
shallow sea, three-dimens. numerical model of tidal motion 77−37219
shallow sea thermal structure, during heating and storms *(Russian)* 80−56480
shallow seas, dynamics, coastal jet conceptual model 78−16051
shallow seas, hydrodynamic model of marine circulation and dispersion of pollutants 77−37241
shallow seas, mean circulation 77−9440
shallow seas mean circulation, comment 79−84287
shallow sound, energy balance and wind effects 79−2243
shallow water basin, wind-driven current, eddy viscosity, bottom friction 78−65319
shallow water horizontal spatial coherence meas. 78−5605
shallow water sound propag. overlying consolidated bottom 77−816
shallow water with moving boundaries, finite element method appl. 78−92847
shallow-water sound propagation 79−5493
shear diffusion two-layer model 78−20428
shear flow/topography interaction, in homogeneous rot. fluid 79−55354
shelf circulation, vertical structure 80−36320
shelf sea fronts adjustments, results from satellite IR imagery 79−92545
shelf seas around British Isles, tidal fronts 79−2259
shelf sediments off Bombay, geochem. study 79−48449
shelf water/slope water front in Middle Atlantic, summertime synoptic var. 80−12407
shelf-wave island resonance, radial barriers effect 79−57948
shelf/slope water front, double diffusion, fine structure instabilities 79−16488
shelly beaches, Victoria, Australia 79−92525
Shinnecock Inlet, radiometric sea surface temp. distrib. 80−41454
shore platform formation on SE. coast of Izu peninsula, Japan 78−81147
shoreline changes due to dredged holes, math. and lab. models *(Japanese)* 78−11878
shoreline erosion, Croatan and Pamlico Sounds, N.Carolina, LANDSAT imagery appl. 79−39701
shoreline evolution, beach sand transport modelling 78−15993
shoreline forms and dynamics of USA Atlantic coast 77−91106
shoreline periodicities, spectral anal. rel. to edge waves 80−12375
shoreline run-up spectra, universal form 77−78188
S.Sicily coast, power spectral anal. of 'Marrubbio' phenomenon 77−53062
silica, biogenic, dissolution in deep sea, rate control 79−20817
sill fjord, vertical diffusion driven by internal waves 77−2178
silt suspension turbulent boundary layer, steady state model 78−28242
Simpson Lagoon, Arctic Ocean, wind and current patterns 77−37237
skin temperature, effects of clouds, hydrodynamic model *(Russian)* 78−65331
slope currents on a rotating globe 79−100867
slope/shelf water intrusions, obs. via remote acoustic monitoring 79−2241
small scale turbulence spectra, anal. *(Russian)* 79−88360
small-scale turbulence and stratification study, via towed instruments carrier 80−36423
solar radiation, received daily sums and daytime var. *(Russian)* 79−34922
solitary Rossby waves in two-layer system, theory 80−17293
solitary Rossby waves over variable relief, stability, analytical theory 80−101371
solitary Rossby waves over variable relief, stability, numerical expts. 80−101372
Somali Current, eddy form., wind effects model 80−26523
Somali Current, large scale eddies 77−53063
Somali Current, meas. during SW monsoon (Aug. 1975) 77−91153
Somali Current, numerical model during southwest monsoon 77−17125
Somali Current, remote forcing, cross-equatorial inertial jets model 79−88357
Somali Current generation, equatorially trapped waves 77−56636
Somali Current source region, temp. and current meas. during monsoon reversal 78−92833
sound, spatial noise spectrum meas. in ocean for small observation baseline 80−102902
sound attenuation and seawater bulk viscosity, Be and B influence 77−3696
sound backscattering by disturbed sea surface 77−11077
Sound of Swina, scale model tests of flow *(Polish)* 77−70685
sound propag. loss in stochastic environment 78−9478
sound propagation, modified phase integral approx. for ray tracing technique 77−7241
sound propagation in shallow water under downward refr. conditions 77−34983
sound propagation in turbulent ocean, nature of fluctuations 79−7250
sound propagation in turbulent ocean, nature of fluctuations 79−7249
sound propagation vel. depend. on elec. cond., temp. and hydrostatic press. *(Russian)* 78−65332
sound pulse generation by explosion, region of nonlinear effects 80−56493
sound reflection from bottom, nonparametric estimation of plane wave refl. coeff. 79−7252
sound refraction by sediments, for sonar studies 80−81902
sound scattering at rough boundary, interaction models 79−7247
sound scattering by large sea surface inhomogeneities, phase function shape in shadowing conditions *(Russian)* 80−94530
sound source motion effects on total acoustic field, isospeed channel appl. 77−7242
sound speed in seawater at high press., meas. 78−13837
sound speed profiles, observed appl. to Gaussian quadrature ranges 77−46851
sound transmission from air into rough ocean, expt. 77−11071

oceanography continued
South Australian gulfs, tides and currents, math. models, finite difference techniques 79−12130
Southern Hemisphere oceans, mean annual poleward energy transports 80−51406
Southern Hemisphere oceans, poleward heat fluxes 79−48496
Southern Ocean, large-scale relative dynamic topography 78−85580
Southern Ocean, long waves 78−40591
Southern Ocean, meso-scale dynamics 80−94525
Southern Ocean, nonbiogenic fixed N from Antarctic ice sheet, ecological implications 78−32129
Southern Ocean, wind stress and bottom topography effects in two layer model 78−81181
spacecraft for ocean science 77−5335
Spanish Sahara const., effect of arid climate and upwelling on sediments 77−60380
Spit of Kursiu Nerija, morphodynamical characteristics of protectional dune ridge *(Russian)* 78−20389
spray in atmospheric surface layer, lab. and oceanic results 79−70844
spreading ridges crests, latit.-depth and age-depth relations 78−11869
St. Helena Is., seamount age and bathometry 79−16436
St Kilda shelf, tidal regime, press. gradient obs. 80−85666
St. Lawrence, estuarine front, tide-induced 77−37209
St. Lawrence Estuary, inorganic B content determ. *(French)* 78−77274
St. Lawrence estuary, tidally-generated residual motion 80−94541
St. Lawrence Estuary turbidity maximum, sediment, salinity, suspended matter study 80−4015
St. Lawrence Gulf, Mn-rich suspended particulate matter 78−11911
stability of geophysical flows 79−70884
stable jet modes, eddy and mean flow interaction 79−16490
stable wind-driven currents in two-layer ocean at equator, theory *(Russian)* 78−61427
standing equatorial wave modes, in bounded oceanic basins 80−51420
stationary currents, theory 78−81203
stationary jet current, particle motion calc. 78−3809
stationary longshore wind-driven current, tideless sea offshore zone 78−3804
statistical charact. of underwater illumination *(Russian)* 78−7653
steady coastal upwelling, nonlinear inertial model 78−92824
stepwise stratified ocean, temp. gradient meas. methods 80−31149
stochastic ray tracing in ocean waveguide 77−3694
Stokes' drift in presence of oscillatory and residual currents, theory 80−17267
storm microseisms form. conditions on Shikotan Island, 1974 Feb. 8-11 period 77−53004
storm surge prediction at Milford Haven, wind-induced motion models 79−66743
storm surge simulation expts. 78−16052
storm surge theory, in stratified sea 80−51437
storm surges prediction on east coast of India 78−85566
storm-induced mixed-layer deepening, obs. and simulation 79−20843
Strait of Georgia, British Columbia, current oscillations 78−40585
Strait of Malacca, late Pleistocene and Holocene sea level changes 79−48513
Strait of Sicily, hydrophys. charcts. periodic fluctuations 79−20857
straits and wide estuaries, geostrophic adjustment, theory and lab. expt. 79−20847
Straits of Dover, ocean colour and sea surface temp., remote meas. *(French)* 78−96238
Straits of Kerch, water exchange calcs. 80−26545
Straits of Malacca, radioactivity in marine environment 79−12135
stratified and mixed coastal water models 78−77268
stratified and rotating fluids, review of selected aspects 77−68660
stratified boundary layer under ice, turbulence calc. 77−49077
stratified currents with vel. shear, influence on forced wave motion *(Russian)* 78−77255
stratified flow around three-dimens. barrier 80−48769
stratified fluid, flow over obstacle *(Russian)* 78−24291
stratified fluid density interface, wind-wave interaction 77−62291
stratified inlet, anal. of wind influence on surface layer 77−41051
stratified inlet, obs. of wind influence on surface layer 77−41050
stratified motionless ocean with topography, spin-up 77−91138
stratified ocean, nonlinear energy and enstrophy transfers 80−101370
stratified ocean, vertical struct. of oscills., numerical calc. 79−39751
stratified ocean under stationary tropical cyclone, energetics *(Russian)* 80−61808
stratified rotating fluid, vortex created by mass transfer 80−12401
stratified turbulent upper mixed layer, struct. determ. 80−104972
subarctic water mass intrusions at OWS November 79−2252
submarine basalts, sea water weathering effect on K-Ar age 77−86830
submarine cables voltage daily vars. at tidal freqs., due to induced oceanic elec. fields 77−86753
submarine landslides, North American east coast and upper rise 79−20815
submarine quantum irradiance and photoperiod, digital recording using self-contained instrument 80−98474
subsea permafrost heat and mass transport processes, mol. diffusion and consequences anal. 79−2302
subtidal sea level fluctuations, rel. to atm. forcing, North Carolina coast 79−16498
Subtropical Convergence, models of diffusive-advective balance 77−56637
subtropical convergence south of Australia, buoy and ship obs. 78−92836
subtropical convergence zone, motions and surface features 79−2255
subtropical front zone N. of Hawaii, wintertime circulation 80−109155
sunlight fluctuations spatial and temporal correlation 80−94533
supertanker radiated noise spectra in deep ocean, origin 78−33959
surf zone, hydrodynamic instability as mechanism for horizontal gyres form. 79−2244
surface, turbulent Ekman layer evolution 80−76996
surface absorption of short-wave radiation and albedo *(Russian)* 77−60415
surface buoyancy flux anomalies, geostrophic eddy generation 80−81912
surface characteristics, remote sensing via Seasat-A experimental oceanographic satellite 78−77455
surface circulation, remote sensing with radar altimetry 80−46189
surface circulation and the distribution of pelagic tar and plastic 80−16856
surface cooling, under free and forced convection regimes *(Russian)* 78−36179

oceanography continued
surface current meas. using geomagnetic electro-kinetograph *(French)* 79−29778
surface currents due to atmos. disturbances of large-scale 80−109159
surface currents mapping, HF radar system appl. 80−94626
surface drift current speed and direction calc., geostrophic wind factor 78−61422
surface drift induced by wind and waves 80−81914
surface drift velocities 78−3779
surface effective radiation calc. *(Russian)* 78−16040
surface EM wave excitation 79−13893
surface emission temps. from DMSP 77−70682
surface features interpretation on hand-held photographs from Apollo-Soyuz Test Project 79−25360
surface film temp. fluctuations due to waves thinning viscous layer 80−109158
surface heat loss in cyclone regions 80−77009
surface instrusions, fronts and internal waves, numerical study 79−2262
surface layer, dye plumes diffusion, expt. 78−44871
surface layer elec. cond. meas. using surfacing probe 79−2392
surface layer rel. to atmospheric temp. and humidity *(Russian)* 80−17282
surface layer thermal struct. and atmospheric heat exchange *(Russian)* 77−73751
surface layers, explosive pulse propag. 79−94395
surface mixed layer, calc. of temp. discontinuity layer bedding *(Russian)* 80−109166
surface mixed layer, catastrophic mixing events obs. 79−16503
surface mixed layer, climatological numerical model, comments 77−86927
surface mixed layer, climatological numerical models 77−2159
surface mixed layer, energy and momentum transfer by wind 78−44856
surface mixed layer, turbulent energy budget 80−72526
surface mixed layer, vel. fluctuations scaling 77−45009
surface mixed layer, vertical and horizontal heat transfer 79−25252
surface mixed layer dynamics 78−44855
surface mixing role in ocean thermal struct. seasonal variation 77−2160
surface ocean current response to wind, quadratic and linear laws 80−26529
surface pattern morphogenesis and catastrophe theory 77−5217
surface radiation from normal and dusty oceanic atmosphere *(Russian)* 77−60409
surface reverberation model 77−34984
surface roughness rel. to air flow *(Russian)* 77−70669
surface seasonal temp. var. and mixed layer thickness 80−77011
surface temp., canonical correl. method study 80−26593
surface temp. fronts, environmental satellite survey 79−2247
surface temp. relation to thermocline structure 80−98347
surface temperature, isotope selective CO_2 interchange affecting trees rings 80−61814
surface temperature max. of eastern N.Pacific in winter 79−39724
surface temperature measurements, derivation from Meteosat image data 80−76985
surface temperature of sea near Azores, thermal dispersion, math. model *(French)* 77−64290
surface temperature rel. to cloud shadows 77−86930
surface temperature var., effect on atm. general circulation model 80−90122
surface thermal balance components distrib. during GATE 79−39759
surface thermal state, appl. in five-day average air temp. forecasting technique 79−29817
surface to bottom fronts, wind effects 79−2261
surface turbulent layer, seasonal var. simulation *(Russian)* 78−96220
surface UV reflectance, meas. from airborne platform 80−98453
surface water temperature, annual development in Panama Gulf and coast *(French)* 77−17109
surface water temperature natural vars. during Project BOMEX, model simulations 78−69363
surface wave propag. in channel connecting sea and lagoon 78−85605
surface waves, energy transfer to sediment motion 78−73389
surface wind and pressure fields during TROPEX-72 near Equator 77−37320
surface wind obs., SeaSat scatterometer/scanning radiometer/altimeter comparison 80−46249
surface wind speed meas. from HF sea scatter by skywave radar 77−17160
surface wind-driven flow 80−46187
surfactants affecting temp. of skin-layer, for oil slick studies *(Russian)* 80−109172
suspended clastic material, movement over shore slope under storm conditions 79−2223
suspended matter distrib. from radiation attenuation index *(Russian)* 79−39747
suspended particle size distrib. shape stability in Baltic sea 79−79876
suspended particles, rel. to chem. processes in Atlantic and Pacific oceans 78−36201
suspended particles vertical struct. and size distrib. during upwelling season off Oregon 78−85563
suspended particulate matter, chemistry, bottom sediment resuspension 79−12136
suspended sediment conc. and fluid vel. near-bottom meas., Long Island inner shelf 79−34838
suspensates, distribs. and active resuspension meas. via remote acoustic monitoring 79−2241
Sverdrup transport and ocean circulation 80−36324
symmetric instability of stratified geostrophic flow 80−98425
synoptic disturbances, evolution *(Russian)* 80−12422
synoptic eddies, Atlantic polygon 70 studies 80−26544
synoptic eddies, numerical model *(Russian)* 80−81905
synoptic eddies, remote sensing data *(Russian)* 80−12420
synoptic eddies 79−5491
synoptic eddy, current meas. *(Russian)* 78−85590
synoptic eddy area, temp. disturbances, vertical structure *(Russian)* 78−85600
synoptic eddy charcts., variability *(Russian)* 80−17280
synoptic scale processes effects on equatorial surface air layer meteorological variables 77−70689
synoptic variation of current and density fields, non-linear model *(Russian)* 80−104984
synoptical disturbance in baroclinic ocean, two-layer model *(Russian)* 80−109162

oceanography continued
synoptical eddies, numerical scheme *(Russian)* 78−81190
synoptical eddies, of the POLYMODE program *(Russian)* 80−104981
tabular iceberg, off Newfoundland Grand Banks, deterioration 77−56646
TAG Hydrothermal Field, metal-enriched sediments 79−20805
Tampa Bay bottom configuration and environmental studies, photogrammetric method 77−87124
Taranto Gulf, water mass var. and geostrophic circulation 77−53058
Tasman Sea, biological productivity of warm-core eddy 80−61816
Tasman Sea, frontal jet near Norfolk Ridge, NW of New Zealand 77−9434
S.Tasman Sea, LF acoustic propag. meas., Project TASMAN TWO 78−11904
S.Tasman Sea, temp. microstruct. effects on LF sound propag. 77−86910
technology development and oil extraction 77−70691
temperature, model of annual var. and appl. to study of climate 78−20433
temperature and salinity self-similar distrib. in upper thermocline *(Russian)* 79−16474
temperature field, transformation after passage of tropical cyclone *(Russian)* 77−53069
temperature field space/time struct. during NORPAX POLE expt. 78−3777
temperature finestructure and microstructure obs. in coastal upwelling region during variable winds 79−66704
temperature fluctuations, small-scale, in upper ocean layer, statistical regularities *(Russian)* 80−94528
temperature fluctuations spectrum in sea upper layer, wind waves components *(Russian)* 78−53655
temperature gradient spectra in vertical direction, scaling theory 80−77001
temperature measurements with Aanderaa thermistor chains, solar radiation effects *(French)* 79−62611
temperature of Atlantic and Pacific rel. to tropospheric mean temp. 77−33168
temperature vertical gradients, meas. via moored vector averaging current meters 80−12561
temperature-depth profiles, recording via solid-state memories 78−24383
temperature-salinity curve, relation to global heat transport and atmospheric water transports 80−72534
Texas continental shelf and slope, light hydrocarbons in Recent sediments 79−2213
Thailand, water pollution problems 78−88853
thermal anomalies, large-scale, form. and evolution, dynamical-numerical study 79−79852
thermal anomalies numerical study with dynamic model 80−17271
thermal boundary layer near air-water interface, fine struct. *(Russian)* 78−22332
thermal energy, conversion to electricity *(French)* 80−21389
thermal energy conversion plant design, oceanographic data interpretation 78−44874
thermal radiation, critical phenomena for periodically rough water surface *(Russian)* 78−81188
thermal radio emission from exponential slab, sea ice appl. 78−28244
thermal response to strong atm. forcing, events characts. 78−92827
thermal response to strong atm. forcing, one-dimens. mixing processes 78−92828
thermal structure and current, aircraft monitoring, NORPAX project 79−84517
thermal wedge, effects of tidal flow on position of upper surface *(Russian)* 78−16046
thermocline, small-scale turbulence *(Russian)* 80−61807
thermocline affecting vertical distrib. of oscills. *(Russian)* 80−21777
thermocline and mixed layer, model of seasonal evolution 80−26546
thermocline approx., discontinuity surface in active ocean layer *(Russian)* 78−16037
thermocline depth variations meas. with inverted echo sounders, MODE results 77−87108
thermocline disturbance evolution, theory *(Russian)* 80−104983
thermocline model *(Russian)* 80−51409
thermocline response to transient atmos. forcing, N.Pacific (1976-8) 80−109156
thermocline structure, non-stationary two-parameter model 80−101382
thermodynamic fields fine struct., statistical anal. *(Russian)* 77−33091
thermohaline and wind circulation in two-dimens. dynamical model *(Russian)* 78−40557
thermohaline diffusive interfaces, multiple components transport 80−12396
thermohaline intrusions lie across isopycnals 79−84289
thermohaline structure of water masses in vortex formation *(Russian)* 78−85592
three dimensional sound ray paths in basins, troughs and near seamounts using ray invariants 78−30113
tidal area, respiratory electron transport system activity vars., Dutch Wadden Sea 78−73403
tidal behaviour, internal surface, two-layered basin *(Japanese)* 78−11912
tidal currents calc. in homogeneous estuaries 78−7654
tidal dissipation, astronomical, geophys. and oceanographic consequences 78−20431
tidal flow in channel, modelling using turbulence energy closure scheme 79−79859
tidal flows, turbulence in depth-limited boundary layer 80−12406
tidal interaction with ice shelves 77−86902
tidal interactions in region of large bottom slope, NW Africa, JOINT-1 obs. 80−4016
tidal model of N.W.European continental shelf 77−37221
tidal phenomena, calc. using acoustic and vibr. techniques *(German)* 78−69366
tidal power schemes of West Bengal, siltation estimation 80−31059
tidal sea level extremes calc. using nonlinear programming method 77−78479
tide and solid Earth gravity tide interaction, Ross Sea area, Antarctica 77−86903
tide-generating currents, oscillating, three-dimensional structure 80−72542
tide-induced residual current, numerical model verification 77−86920
tides, analysis methods 77−87080
tides, effects on M_2 gravity tides in Japan 77−60342
oceanography continued
tides, model showing geometry effect 79−92546
tides, modelling, shelf effects parameterisation, S. Atlantic appl. *(Russian)* 79−100843
tides, periodic flow anal., using finite element perturbation method 78−24290
tides, satellite-derived parameters, lunar tidal accel. determ. 78−73662
tides, self-consistent equilib. model 78−96218
tides, semidiurnal waves determ. via. obs. of artificial satellites trajectories *(French)* 79−8634
tides, shallow water, three-dimens. nonlinear model *(Chinese)* 78−24309
tides and storm surges, three-dimens. non-linear numerical model 77−37240
tides effect on tidal gravity vars. 79−53359
tides effects on artificial satellite orbits 77−87243
time-varying shallow water channel weighting function meas. 78−5606
Tiros-N environmental spacecraft series launching 79−29973
Tokyo Bay, central Japan, recent sea level vars. from geological formations and basal topography 78−44818
topographic effect on deep circulation and abyssal O_2 distrib. 79−16494
topographically generated eddies 77−2153
trace constituents transfer past air-sea interface 79−62544
transparency field, statistical relationships with hydrological and biological characts. *(Russian)* 79−88361
trench waves theory of propag. and obs. off Japan and Chile 80−72547
trenches maximum depths in world ocean 79−2220
tropical Atlantic Ocean, coeffs. of mechanical resistance law for trade winds 77−45066
tropical circulation, modelling 78−16055
tropical cyclone surge model, finite difference method 79−12132
tropical cyclone-ocean model, mutual response 80−4032
tropical ocean and atmosphere, heat budget estimate 80−104968
tropical ocean meteorology, conference (London, 21-25 August 1978) 79−88458
tropical oceans, marine boundary layer 79−88460
tropical regions, oceanic and continental climates during ice age, simulation 78−16144
tropical storm freqs. rel. to sea surface temps. 77−91226
tropical waves 79−74945
Tunis Strait area, carbonate system elements 77−53075
turbid estuarine waters, optics, approxs. and appls. 79−66712
turbidity current flow, computer simulation 78−15997
turbidity current head motion *(Japanese)* 79−34852
turbulence, intermittent, statistical anal. *(Russian)* 77−29310
turbulence, small-scale, horizontal struct. statistical characts. *(Russian)* 80−4020
turbulence, small-scale, in upper layer 77−64318
turbulence, small-scale, statistical patterns 78−3802
turbulence, small-scale, study by acoustic scatt. method 80−26540
turbulence and air-sea interactions 78−92953
turbulence breakdown coefficient determ., influence of data treatment technique *(Russian)* 78−7690
turbulence generation, conditions and efficiency *(Russian)* 78−16022
turbulence in upper layer, numerical calc. 77−49076
turbulence meas., metal-film temp. and vel. sensors and self-propelled research vehicle stability evaluation 79−5672
turbulence meas. near seabed, digitisation and record length selection 80−104971
turbulence stratification and vertical current vel. gradients vars. in Strait of Tunis 80−26539
turbulence vertical struct. characts. 80−12426
turbulent air-water mass transfer under varied stratification conditions 79−84389
turbulent billows, splitting into two layers 79−79991
turbulent bottom layer beneath waves, residual flow and boundary shear stress 78−24300
turbulent boundary layer, penetrative convection regime, entrainment rate *(Russian)* 78−69401
turbulent boundary layer development in stratified fluid *(Russian)* 78−63477
turbulent boundary layer under pack ice 77−17130
turbulent diffusion, initial and boundary value problem *(German)* 77−86908
turbulent diffusion in vertical direction, estimation from dissipation obs. 80−98341
turbulent Ekman bottom boundary layer, effect of diurnal tidal currents 80−104977
turbulent Ekman layer, struct. of homogeneous ocean surface layer 80−51438
turbulent exchange intensity determ. from cosmogenic and artificial radioisotopes distrib. *(Russian)* 79−39744
turbulent free convection, characts., lab. visualisation expt. 79−18888
turbulent interface layers, theory 78−71323
turbulent layer self-similar development in homogeneous fluid 79−44196
turbulent spot in stably stratified fluid, dynamics *(Russian)* 78−40558
turbulent structure of bottom boundary layer in tidal current 79−84284
two-layer model, surface tension effect on development of waves from periodic disturbances *(Russian)* 78−77253
two-layer quasi-geostrophic turbulence, simple special case 78−81186
two-layer stratified ocean, internal waves generated by local disturbances *(Russian)* 79−16480
two-layer transport capacity of a constriction, barotropic current fluctuations 77−60396
typhoon havens research program at the Naval Environmental Prediction Research Facility 79−5616
typhoon Tess wake vertical struct. in upper layer of Pacific Ocean 80−26538
ULF/ELF EM fields generated above finite depth sea by submerged vertical mag. dipole 79−48400
undergraduate preparation for career in physical oceanography 79−12554
undersea transmission characts. of laser beam in Tago Bay, Japan 77−21782
underwater acoustics, research programmes in USSR 79−64382
underwater acoustics, use of angle-depth diagram 77−11067
underwater ambient noise, statistical anal. 77−79996
underwater cusps, rare form of shallow water bottom relief 77−86855
underwater explosions as acoustic sources, distrib. of measured bubble pulse periods 79−5495
underwater explosive sources, model evaluation and data interpretation 77−11068

oceanography continued
underwater illumination fluctuations, nonstatistical model *(Russian)* 77—21773
underwater irradiance in Norwegian and Barents Sea, relation to water temp. 80—31055
underwater irradiances on horizontal surfaces, effects of clouds on diurnal var. 80—72549
underwater laser beam transmission characts. in Tago Bay *(Japanese)* 77—21797
underwater light field, scatt. light influence anal. 77—64322
underwater light field fluctuations, numerical modelling *(Russian)* 78—32111
underwater light field fluctuations obs., effects of phototransducer drift *(Russian)* 78—65409
underwater light field fluctuations under rough sea surface, numerical modelling *(Russian)* 77—33090
underwater light field radiance fluctuations, expt. meas. *(Russian)* 78—88839
underwater light in NE.Atlantic, obs. using new photometer in deep sea 80—98460
underwater light-field fluctuations, experimental studies of spatial struct. *(Russian)* 78—53656
underwater sound, absorption, chemical relaxation involving Mg and carbonic acid 79—68466
underwater sound, amplitude and phase fluctuation periods for long-range propag. 77—50808
underwater sound, analysis of acoustical effects of receiver and source motions at short ranges in deep ocean channel 80—10063
underwater sound, attenuation of surface-generated noise received deep 78—9481
underwater sound, backscattering spectra of preserved zooplankton 77—79994
underwater sound, bottom refl. coeff. rel. to negative bottom loss and critical-angle shift 77—46853
underwater sound, calcs. of acoustic transmission through eddies 80—64264
underwater sound, comparison of two normal-mode solns. based on different branch cuts 77—84044
underwater sound, compressional wave attenuation in deep ocean sediments 80—79033
underwater sound, computations of strength and diffraction parameters for real and canonical oceans 80—33320
underwater sound, connection between small-waveheight solns. of ocean surface scatt. problem 78—13839
underwater sound, correlation measurement of reflection coeff. from bottom and surface of ocean 80—58848
underwater sound, correlation of bottom-reflected pseudonoise signals with transmitted signal 80—58846
underwater sound, correlation of pseudonoise signals in reflection from layered ocean bottom 80—87626
underwater sound, coupled mode analysis of multiple rough surface scattering 79—98527
underwater sound, CW phase fluctuation spectra rel. to ocean processes determ. 77—46850
underwater sound, deep ocean LF attenuation data, review 80—33318
underwater sound, derivation of wave eqn. in inhomogeneous ocean 80—33313
underwater sound, Doppler effects for randomly moving scatterers and platforms 77—62093
underwater sound, effects of class of random currents on transmission in channel with linear sound speed 80—87621
underwater sound, effects of tidally varying sound speed on propag. over sloping ocean bottom 80—10062
underwater sound, experimental studies of attenuation in sediments 80—10067
underwater sound, fluctuations in reciprocal acoustic transmission in midocean environment 80—10069
underwater sound, forward surface freq. spreading, physical models 79—14145
underwater sound, horizontal acoustic refraction through ocean mesoscale eddies and fronts 80—96085
underwater sound, hydrophone shadowing by seamounts 80—33308
underwater sound, influence of cyclonic eddies on short-range transmission 80—33316
underwater sound, influence of range dependence of ocean bottom on adiabatic approximation 80—10066
underwater sound, LF propag. off Mission Beach, California 80—79035
underwater sound, l.f. transverse to propag. direction 77—818
underwater sound, mesoscale variations in deep sound channel and effects on LF propag. 79—98529
underwater sound, mode interactions in isovelocity ocean of uniformly varying depth 80—33321
underwater sound, multipath anal. of explosive source signals 80—79034
underwater sound, ocean bottom loss and mode attenuation per cycle 79—90061
underwater sound, ocean bottom reverberation meas. at low grazing angles 79—14143
underwater sound, ocean temporal fluctuations rel. to general source extraction problem 77—84043
underwater sound, pH depend. of low-freq. absorpt. in ocean 77—84052
underwater sound, phase modulation by internal wave vertical vel. 77—46852
underwater sound, plane-wave reflection loss model including sediment rigidity 80—33311
underwater sound, point source transmission of broadband sound through sinusoidal ocean surface 79—14142
underwater sound, ratio of compressional wave vel. to shear wave vel. and Poisson's ratios in sediments and rocks 80—12404
underwater sound, ray theory model of acoustic interaction with ocean bottom 79—98532
underwater sound, scattering by internal waves 79—14141
underwater sound, sediment rigidity effect on ocean bottom reflection loss in typical deep sea sediment 80—96083
underwater sound, shallow-water propag. over low-velocity bottom 80—74579
underwater sound, simplified calculation of ray-phase perturbations due to ocean-environmental variations 80—64266
underwater sound, simulation of phase modulation of first-mode directional internal wave 77—62089
underwater sound, space scales of reflected signal fluctuations 79—90066

oceanography continued
underwater sound, stability and identification of acoustic multipaths 80—83697
underwater sound, stochastic internal-wave model for deep moving ocean 80—64267
underwater sound, velocity gradients in marine sediments 79—68465
underwater sound, viscous attenuation in high-porosity marine sediments 80—74577
underwater sound, volume scattering strengths and zooplankton distributions at acoustic frequencies between 0.5 and 3 MHz 80—33317
underwater sound, wide-angle field in ocean with range-depend. vel. profiles 77—79993
underwater sound 80—33312
underwater sound amplitude fluctuations due to temp. microstructure 80—19140
underwater sound channels, ray calcs. using pocket programmable calculator and Incomplete Beta Function 79—68467
underwater sound fields, sound propagation in an ocean shelf zone of arbitrary profile 78—90576
underwater sound in North Pacific, variation of vertical directionality of noise with depth 80—19130
underwater sound in randomly fluctuating oceans, modelling of propag. using radiation transport eqn. 79—90062
underwater sound in range-dependent ocean, examination of multipath processes within context of adiabatic mode theory 80—19134
underwater sound in refractive channels, bottom loss effects in diffusion loss 78—9482
underwater sound in upward-refr. ocean, sideband struct. prod. by refr. at rough surface 77—46847
underwater sound propag. adiabatic mode theory in range dependent environment 78—55497
underwater sound propag. in wedge-shaped ocean with penetrable bottom 80—74578
underwater sound scattering by marine organisms, review 80—64269
underwater sound scattering from marine organisms, appl. of fluid sphere theory 77—46846
underwater sound scattering from oceanographic microstructure, detection with large aperture array 79—98530
underwater sound speed profile, modification to improve accuracy of parabolic eqn. technique 78—1480
underwater sound transmission in deep ocean, anal. of source-motion effects 77—62088
underwater sound transmission through fluctuating ocean, book 79—86286
underwater visibility basic controlling parameters 78—36196
United States, average geopotential sea level series 78—57215
unsteady currents, dynamics 78—16054
upper layer, conc. and size distrib. of wind-produced air bubbles 77—17143
upper layer, mesoscale horizontal temp. and salinity inhomogeneities 77—78209
upper layer thermal struct. seasonal var. 77—21788
upper ocean, spatial variability, influence on ocean acoustics 80—51435
upper ocean frontal regime, microstructure and fine structure 79—16487
upper ocean layer, global freshening during deglaciation 78—53658
upper ocean layer, modelling 79—84292
upper ocean layer structure 79—16509
upper ocean layers, thermal and dynamic structure *(French)* 79—84288
upper ocean temperature and salinity structure, obs. during POLE expt. 80—72536
upwelling, dynamic data acquisition and display by portable real-time minicomputer system 80—12552
upwelling along edge of Arctic ice pack 79—92547
upwelling in stratified ocean due to melting of glacier ice 80—81897
upwelling off SW.India coast 80—56481
upwelling over shelf break, theory 80—72550
upwelling processes during last 75000 years, rel. to southern trade winds 78—57217
Urazoko Bay, ^{60}Co radioecology, levels in sargassoes and marine sediments 77—9448
US appl. to studies of small-scale turbulence *(Russian)* 77—78201
US National Shoreline Erosion Control Demonstration Program, review 78—16163
U.S. oceanographic research vessel fleet 77—91325
US scatt. spectral struct. from random sea surface 78—63225
Vaisala-Brunt frequency vertical fine struct. meas. in Mediterranean Sea 80—26537
Vancouver Island region, terrestrial EM induction 80—104879
vector averaging current meter records from MODE-1 central mooring, correction 77—64295
Vellar estuary, Fe precipitation, conc. determ. 80—77015
velocity estimation from hydrographic data 79—21040
velocity profiles through main thermocline 77—17135
velocity shear flow, surface and internal waves generated by baric disturbances *(Russian)* 78—77252
Vema Channel, abyssal hydrography, nephelometry, currents and benthic boundary layer struct. 77—17116
Vema Channel, increased transport of Antarctic Bottom Water during last ice age 77—21798
Venice, sea-lagoon exchange in modified tide regime 80—12431
Venice historical centre, high water and sea defences, implications of altimetry surveys *(Italian)* 77—86740
Venice Lagoon, hydrodynamic numerical modelling 79—34832
Venice lagoon inlets, maximum waves forecasts computation *(Italian)* 77—37205
vertical buoyancy flux, atmospherically induced 80—4039
vertical current struct. based on dynamicostochastic model *(Russian)* 77—78198
vertical diffusion of density in great ocean depths 77—29302
vertical diffusion of radioactive admixture *(Russian)* 77—60417
vertical eddy diffusion rel. to buoyancy gradient in the deep sea 77—5207
vertical eddy viscosity, effects on Rossby and Eady waves 80—51404
vertical fine struct. of hydrophysical fields 78—3793
vertical mixing and chimney-like formations 80—36311
vertical natural laminar convection flows in cold water, buoyancy force reversals 80—59034
vertical struct. of ocean currents rel. to frequency *(Russian)* 77—45004
vertical temperature gradients horizontal var. meas. by thermocouple arrays 78—61571

oceanography continued
Vienna Standard Mean Ocean Water (V-SMOW) stable isotopes meas. standard 78−32246
Virgin Islands, vertical current profiles and Richardson no. meas. 80−67378
Virginia Beach, Virginia, coastal currents and assoc. sand stream 78−73392
Visakhapatnam coast, Bay of Bengal, clay sediments derived from inland sediments 80−76959
Visakhapatnam coast, temp. and salinity of coastal waters 77−73757
viscous fluid one dimens. motion, friction effects, appl. to seiches 77−49068
visible light refl. and scatt., utility of polarisation in oceanographic remote sensing 79−5498
volume scatt. and biological content from sea bottom echo fluctuations 78−50990
vortex formation, dynamical structure *(Russian)* 78−85591
vortex formation from barotropic Rossby wave *(Russian)* 79−100859
vortex ripples 77−27544
vortices, evolution of isolated nonlinear examples 80−81910
vortices, topographically bound, theory 79−57956
vortices on sphere, two-dimens. hydrodynamics *(Russian)* 79−32529
Walvis Bay, methane prod. 78−28246
Wanganella Bank area, ocean dynamical conditions off E.Australia *(Russian)* 80−109168
warm and cold core rings, struct., simple model 79−57959
warm core ring birth and death 79−57958
warm front, oceanic, propagation, theory with appl. to Sagami Bay Kyucho phenomenon 80−94538
warm wavy surface, lab. study of evaporation 77−86924
waste disposal studies, strategies and tools 79−12138
water cooling through free surface, critical value of boundary Rayleigh number *(Russian)* 78−61426
water current velocity, determ. via neutron-activation method *(Russian)* 78−77358
water density vertical struct. influence on dynamics of small basins, Adriatic Sea appl. 78−53654
water density vertical vars., review of math. models 78−49022
water masses advection, radioactivity and salinity changes *(Russian)* 78−77275
water movement and induced electrical currents in ocean bottom 80−104863
water surface IR emissivity, vars. *(Russian)* 77−60384
water surfaces cooling, impact of atmospheric CO_2 79−92569
water transport, large-scale, determ. from radionuclide obs. *(Russian)* 79−39742
water vapour transport from Atlantic and Pacific Oceans, rel. to S.America water balance 79−29820
Weddel Sea continental slope mixing 77−73745
Weddell gyre 80−81894
Weddell Sea, bottom water origin, chem. tracer considerations 80−76982
Weddell Sea, bottom water variability 80−67366
Weddell Sea, fine structure meas. in temp.-compensated halocline 80−67373
Weddell Sea, geophysical studies (1978 Jan./Feb.) *(German, English)* 78−96188
Weddell Sea, tidal currents in central region 78−44831
Weddell Sea, upwelling prod. by melting icebergs 77−56647
Weddell Sea and Drake Passage currents, boundary region 77−78186
Weddell Sea drift ice, pushed north by barrier winds 80−26514
West Flower Gardens coral reef, effect on waves 80−4043
Western Port, Victoria, tidal embayment, dynamics and sediments 79−100841
wetland mapping in New Jersey and New York 78−77265
White Sea, periodic forms of bottom relief on shelf 78−44804
whitecaps and sea state rel. to wind vel. and atmospheric surface layer stability 80−72554
wide ocean current, EM field for arbitrary direction of permanent mag. field 79−57946
wind dispersion ellipticity over ocean surface, N. Atlantic example 78−61528
wind drag coefficients for marine regime, shipboard evaluations 79−5494
wind drift currents, Langmuir circulation, theory and averaged current 77−37210
wind driven currents, regression coeffs. and bottom stress anal. 80−8320
wind effects on sea state near Belgian coast *(French)* 78−65372
wind generated gravity waves, saturation range in freq. spectrum 77−60399
wind induced Ekman boundary layer, realistic model 77−70674
wind mixed layer deepening theory *(Russian)* 79−8638
wind speed in surface, microwave radiometric meas. during BESEX 77−29479
wind stress and roughness length over breaking waves 78−24299
wind stress coefficient over water surfaces, new evaluation 80−72603
wind stress over North America eastern continental shelf 78−3776
wind vertical profile fine structure over sea in near-shore zone 77−60445
wind waves, high-freq. spectra meas. in presence of currents in shallow sea 80−31053
wind waves data, appl. to climatic comparisons of estimated and measured winds from ships 80−105020
wind-driven circulation, effects of bottom topography *(Polish)* 77−73743
wind-driven circulation, finite element anal. 80−56487
wind-driven circulation in homogeneous ocean with islands and depressions 78−3799
wind-driven currents in ocean with bottom friction 77−13089
wind-driven currents on the continential shelf, review, book contrib. 80−98358
wind-driven depth-dependent upwelling circulation on continental shelf, model 79−16495
wind-driven equatorial currents in two-layer ocean *(Russian)* 79−25255
wind-driven flow in zonal channel, with stratification and bottom topography 80−51402
wind-driven Langmuir circulations, laboratory studies in wave tank 78−85582
wind-driven quasigeostrophic water movements near fast ice edges 78−49026
wind-generated sea waves, interaction with tidal currents 80−51428
wind-induced current flow in upper Hudson Shelf Valley 79−34840

oceanography continued
wind-induced heat and mass transfer over large bodies of water 77−11186
wind-ruffled sea, isophotes of sunlight glitter 77−45001
wind-wave layer, temp. fluctuations *(Russian)* 80−51410
wind-wave tank, microscopic and macroscopic surface structs. growth and decay rates 80−48726
Windward Passage sill, bathymetric chart 77−56616
Winyah Bay estuary, S.Carolina, ^{226}Ra behaviour meas. 80−98360
world ocean, normal modes, finite-element barotropic model 79−16489
world ocean, water mass model 79−79848
World Ocean, waters heat and salt content 80−31054
Yarra River estuary, dissolved I 79−34855
Yellow Sea, palaeogeographical environment evolution since Late Pleistocene *(Chinese)* 79−96766
Yermak hot spot in Arctic Basin, magnetic and bathymetric evidence 79−88313
Yucatan Current formation, summer 1971 obs. 77−2169
Yucatan Strait, deep currents obs. 79−48492
Yucatan Strait and Gulf of Mexico dissolved SiO_2 as natural circulation tracer 78−44830
zonal equatorial currents, instabilities and meridional profile 78−85587
zonal geostrophic flow, stability model *(Russian)* 77−73750
zonal two-layer current stability, charact. functions 77−49078
Zuari estuary, Goa, India, environmental parameters monitoring 78−81214
Zubov, Nikolai Nikolaevich (1885-1960), oceanologist *(Russian)* 78−86101
Al concentration and distrib., control by biological activity 78−61437
Al content controlled by inorganic processes 80−61815
^{241}Am, concs. in sediments from coastal basins off California and Mexico 80−98303
As distrib. and speciation in natural waters and marine algae 78−81210
^{10}Be in ocean surface layer, conc. and residence time 79−66714
^{10}Be var. in deep sea sediments, critical evaluation 78−7615
Br/Cl ratio in Bay of Bengal 79−25267
C reservoir changes rel. to atm. CO_2 78−57278
CO_2 atmospheric, fossil fuel generated, models for ocean uptake 79−88031
CO_2 cycling in environment, non-proportionality between flux and reservoir content 80−46261
CO_2, from fossil fuel burning, climatic effects, proposed CO_2 disposal in deep ocean 78−57301
CO_2 from fossil fuel burning, deep-sea injections and atmospheric response 80−31090
CO_2, future atm. level prediction using atm. and ocean models 78−61549
CO_2 gas seep from seabed, Norton Sound, Alaska 80−67361
CO_2 in atmospheric, $^{13}C/^{12}C$ vars. in last 22 yrs. role of ocean 80−104530
CO_2 increase rel. to future climate, coupled atm.-ocean model 79−58082
CO_3^{2-} sediments, Lawson's Bay area, Indian east coast, origin 79−25266
$C0_2$ solution in ocean surface waters, role of homogeneous buffer factor 80−21783
Ca^{2+} in seawater 80−31064
$CaCO_3$ and organic C, decomposition in deep oceans 79−25270
$CaCO_3$ dissolution in deep sea sediments, rel. to palaeoceanographic reconstruction 79−25269
$CaCO_3$ dissolution rates in deep ocean, in situ expt. in N.Atlantic 79−34853
$CaCO_3$ production of mare incognitum, upper windward reef slope, Enewetak Atoll 78−7662
Cl, Br content, origin by continuous mantle fluxing 78−65342
^{242}Cm conc. supported by ^{242m}Am 77−49091
Cu compounds, identification and determ. by chromatographic-at. spectrosc. method 78−68972
Cu-Ni enriched ferromanganese nodules and assoc. crusts from Bauer Basin, NW. Nazca Plate 77−86851
Fe, removal mechanism in estuaries 78−20437
Fe-Mn nodules from Pacific Ocean, sorption processes 79−16435
H_2 conc. in near-surface air and dissolved in seawater, tropical N.Atlantic 79−39729
H_2 dissolved in N.Atlantic surface water, interchange with air 80−77057
H_3BO_3 evaporation from seawater, major source of atm. B 79−2293
H_2S levels, stagnation coeff. and appl. in palaeogeographic reconstruction 80−36291
Hg, average future content of world's oceans 79−8687
Hg conc. determ. in Arabian Sea waters 79−25268
Hg, in fish and waters of Irish Sea and other United Kingdom fishing grounds 78−36204
Hg in surface waters in seas around the UK 78−7664
Mn, hydrothermal, in deep sea, scavenging residence time and $Mn/^3He$ relationships 78−32121
Mn nodule mining, environmental effects 77−33096
Mn nodule origin *(Russian)* 80−81868
Mn nodules, deep sea, from Pacific Ocean, Pt conc. determ. *(German)* 79−44169
Mn nodules, deep-sea, diagenetic features, X-ray spectral and SEM anal. 79−16099
Mn nodules, deep-sea, diffusion-controlled growth model 79−2212
Mn nodules, geological history 77−25674
Mn nodules, isotopic and elemental composition, U, Pa, Th, radiochem. anal., Suiko Seamount, N.Pacific 78−77215
Mn nodules, maintenance at surface by bioturbation of infauna 80−101359
Mn nodules, quant. distrib. and metal content *(Japanese)* 80−8292
Mn nodules from N equatorial Pacific, post-depositional internal metal enrichment processes 79−34791
Mn nodulus and micronodules of NW.Atlantic, rare earth element study 80−46167
N compounds exchange between ocean-atmosphere-continent system 78−3794
NO_3^-, PO_4^{3-}, $Si(OH)_4$, ratios in Moroccan upwelling region 80−4045
N_2O composition of Pacific surface water 80−51519
N_2O prod. in ocean, Atlantic and Pacific meas. 79−48518
Nd isotopic composition of sediments of different oceans 80−21704
O, in palaeoaquatic environment 78−44879
O isotope record in Pleistocene coral, Barbados, West Indies 79−66675
O isotopes exchange with oceanic crust, results from (DSDP Leg 37) 77−91072

oceanography continued
O_2, dissolved, distrib. in world ocean, numerical simulation 79−53367
O_2 singlet in natural waters 77−56659
^{18}O in equatorial Pacific core, glacial time scales and climate 80−21817
^{18}O stratigraphy in deep-sea sediments, evidence for deglacial meltwater effect 78−85530
P control in estuaries, parallel shooting models, Corpus Christi Bay (Texas) and Jamaica Bay (New York) appls. 79−57521
Pb in hydrosphere, global and regional distrib. 79−16517
^{210}Pb, ^{210}Po, concs., physico-chem. states and residence times in marine and estuarine waters 78−11913
Pu accidental release at Thule, Greenland, environmental behaviour 77−56656
^{241}Pu, concs. in sediments from coastal basins off California and Mexico 80−98303
^{226}Ra source, flux from estuarine and continental shelf sediments 78−32061
^{222}Rn evasion rates in Atlantic and Pacific, Geosecs determ. 79−79875
S compounds, reduced, emission from open oceans 79−70805
^{90}Sr and T in N.Pacific surface water during 1974, conc. meas. 80−26181
^{90}Sr diffusion from instantaneous point source in ocean, numerical calc. *(Russian)* 78−69372
T distribution in Weddell Sea water masses 79−39728
U, conc. and distrib. in marine basalts rel. to marine chemistry 77−81886
V air pollution transport from urban to remote marine areas 77−37355
OCR *see optical character recognition*
octet theory *see SU_3 theory*
ODMR *see microwave-optical double resonance*
oecology *see ecology*
OH -centres
quartz fibre, ESR and IR obs. of microinhomogeneities 77−8401
AgCl:OH , dielec. meas., defect reorientation 77−19947
KBr, diffusion of Br_2, 375 to 600°C, obs. using OH^- centre decomp. 77−43378
KBr(Cl):OH , cc U_2 to H_2O^- defects conversion after UV photodecomp. 80−107230
KI:OH , HF phonon studies under uniaxial stress 79−83002
LiF:Mg, X-irrad., colour centres, ESR and UV asborpt. meas. 80−108069
$LiNbO_3$, effect on dielec. and optical props. of single crysts. 77−12327
ZnO:Cu, H(D), IR absorpt. line spectra, OH and OD vibr., optical excitation 79−15498
ZnO:Cu, H(D), OH and OD centres, IR-active absorpt. line spectra 79−15496
ohmic contacts
1/f noise intensity and contact resistance analysis 77−62982
ceramic-In (In alloy), low resistance 77−1483
diamond, ion implantation method for n-type contacts *(Czech)* 77−1414
electrical characteristics, interfacial reaction effects, book contrib. 79−1623
electron microscopic observations of metal-semicond. contacts, new phases struct. 78−34899
n-GaAs, Au-SnNi-Au ohmic contacts low temp. alloying electroplated layers, expt. 78−35319
n-GaAs-Ge laser alloying to from ohmic contacts 80−58546
glasses, contact influence on AC cond. 78−76076
hot minority carrier effects on thermoEMF and photovoltage 77−15956
III-V semiconds., ohmic contacts *(Japanese)* 78−47869
III-V semiconductors, MBE developments in device fabrication 79−78902
laser CVD, film physical props. and applications 80−93493
metal-n-type semiconductor contact with shallow n^+-surface layer 79−38164
metal-semiconductor ohmic contact props., factors affecting contact resistance of semiconductors, theoretical model 80−60076
metal-semiconductor with graded amorphous-cryst. junction, model 77−76923
MIS structure with two ohmic contacts, thermodepolarisation charge and change of effective charge *(Russian)* 78−52093
MOS with resistive gate electrode, CV characts., losses and phase shifts 78−80057
n-n homojunction, calc. of free carrier density profile in a semicond. near ohmic contact 80−70810
n-p junctions, determ. of transport parameters of minority carriers using electron microscope 80−65665
Schottky barrier ohmic contacts, recomb. beneath, and adjacent oxide covered regions 79−47164
semiconductor device contact form. by ionised-cluster beam deposition 77−32528
n^+-Si-Al ohmic contacts, metallisation structs. for very shallow n^+/p junctions 80−60084
space charge limited current with diffusion theory, for exponential trap distribution 80−10992
sputter-etch plus evaporated film technique for inexpensive, reliable contacts to Si devices 78−23165
thin film technology, appls. in energy, optics, and electronics, review 80−78932
transient response when operated in two-carrier regime, avalanche injection model 77−55607
transition metal phosphate glasses, ohmic contact and dielectric. relax. 79−65795
transition metal silicides, refractory for ICs, review 80−100820
transmission line model, meas. of specific contact resistance of ohmic contacts 80−70826
Ag-In_2S_3-Si layered struct., Hall effect, I-V characts., surface states *(Russian)* 80−97001
Ag-In-Ge alloyed contacts to GaAs 79−78174
Al, for n-type Si, current load capacity meas. *(Czech)* 77−89846
Al-In_2S_3-Si layered struct., Hall effect, I-V characts., surface states *(Russian)* 80−97001
Al-Pd_2Si contacts on Si, elec. and structural characterisation 77−43695
Al-Si(Ge) eutectic alloys in screened ohmic contacts for solar cells 80−94090
n-$Al_xGa_{1-x}As$, Au-based ohmic contacts TEM obs. 80−34509
$Al_xGa_{1-x}Sb$-Pd contacts, struct., preparation elec. props. 80−65684
$Al_xGa_{1-x}Sb$-Pd contacts, band gap depend. of barrier height 80−65685
a-As_2Se_3-metal system, time-resolved dark injection 79−91139
Au, for n-type Si, current load capacity meas. *(Czech)* 77−89846
ohmic contacts continued
Au-Ge contacts on GaAs, SEM and TEM obs. of struct. 80−100522
Au-Ge contacts to n-GaAs layers with SiO_2 overlayer, ohmic props. 80−2467
Au-Ge film, evaporated, for ohmic contacts to GaAs, compositional stratification, effect of source material impurities 79−77951
Au-Ge ohmic contacts, laser alloying on GaAs 79−73583
Au-Ge-Ni metallisation scheme used for alloyed contacts to GaAs 77−43726
Au-polyacetylene, electrical properties of polyacetylene films *(Japanese)* 80−96888
B single crystals, contacts from Ni and Pd electrodeposition 77−44177
$BaTiO_3$, noble metal contact using In_2O_3 layer 79−42638
n-$BaTiO_3$, ohmic contact form. 80−92969
$BaTiO_3$:Nb, elec. props., contact material influence 80−70848
C-polyacetylene, electrical properties of polyacetylene films *(Japanese)* 80−96888
CdS sputtered film with In contact, electrophysical props. *(Russian)* 79−42642
CdS-Al, ohmic contact stability improved by annealing 78−6443
CdS-In, by electrolytic deposition 77−8194
CdSe sputtered film with In contact, electrophysical props. *(Russian)* 79−42642
p-CdTe with Pd and Pt, I-V characts., temp. depend. of cond., activation energy 78−39211
$Ga_{1-x}Al_xAs$, ohmic contacts, metallisation systems 80−25010
GaAs, alloying with Au and Au alloy ohmic contact metallisations, SEM and optical study 80−70820
n-GaAs, AuGe contact formation 78−76146
GaAs, chem. etched surface, Auger characterisation 77−25169
GaAs DH laser, alloying of ohmic contacts, Nd:YAG laser irrad. 80−43357
GaAs devices, ohmic contacts using epitaxial Ge films 78−88027
GaAs devices ohmic contact fabrication using epitaxial Ge films 78−47871
n-GaAs, epitaxial, thermoelec. power, temp. depend. in mm wavelength range 79−23996
GaAs epitaxial layer, AuGe ohmic contact production by laser alloying 78−88026
n-GaAs epitaxial layers, alloyed in As_2 beam, metal-Ga contacts 79−95495
GaAs large-grained solar cell film recrystallisation 79−38737
GaAs, laser-annealed ohmic contacts for microwave devices 79−73584
n-GaAs nonalloyed ohmic contacts of TiPtAu by pulse-electron-beam annealed Se implants 80−2466
GaAs, ohmic contact form. to n- and p-type samples by MBE, characts. 79−47159
n-GaAs planar contacts formation and elec. props., on basis of Au and Au-Ge alloys 79−15223
GaAs, review of ohmic contacts fabrication 80−49901
n-GaAs, smooth and continuous ohmic contacts using epitaxial Ge films alloyed with Ni 78−68086
n-GaAs, study of ohmic contacts 80−60083
GaAs transferred electron devices, ohmic contacts 78−52082
n- GaAs, ultra low resistance 80−20307
GaAs:Cr, Se layers, ion implanted, ohmic contact form., contact resist. meas. 79−91158
GaAs:Se ohmic contacts, pulsed electron beam annealing donor density, mobility 80−65678
n-GaAs:Sn, heavily doped, nonalloyed ohmic contact form. by MBE and metallisation 79−7895
n-GaAs:Sn, nonalloyed and in situ Ohmic contacts for FETs 79−56307
GaAs:Te, ion implanted, ohmic contacts produced by laser-annealing 79−73585
GaAs:Te-implanted by laser-annealing, ohmic contacts 79−19658
GaAs:Zn, high surface conc. Zn diffusion for good ohmic contact 77−11575
GaAs/Au-Ge/Au structure, ohmic contact behaviour, alloying time effect 79−19659
GaAs/In-Ge-Ag, semiconductor surface condition, effect on ohmic contact barrier height 77−4435
GaAs/metal contacts, recent developments in investigations of preparation and props. *(French)* 80−107909
GaAs-insulator interface, elec. props. 78−95370
GaAs-metal contacts, use of Ga to eliminate large As loss peaks 80−80370
GaAs-metal ohmic contacts, solid phase epitaxy formation, AES and channelling meas. 79−60658
n-$GaAs_{0.6}P_{0.4}$, reproducible ohmic contacts 79−73587
GaInAsP, rectifying and ohmic contacts 80−80376
p-$Ga_xIn_{1-x}PyAs_{1-y}$/Au-Zn, specific contact resist. 80−84509
GaP, Be-Au and Si-Au contacts, metallurgical struct. 77−1485
GaP, comparison of contact resistances of Au-Zn, Au-Zn-Sb, Au-Ge-Ni and Au-Ge-Ni-Sb alloyed contacts 80−70825
GaP-Pd contact system, low temp. alloyed contact formation 80−100519
HgCdTe, 0.1 eV photodetector performance, geometrical enhancement 77−32040
HgI_2, soft γ-ray detector fabrication and props. 77−3208
In electrodeposition on Si from glycerine soln., rapid method 77−32534
In-CdS-In structure, volt-ampere characts., carrier tunnelling emission *(Russian)* 80−49914
In-CdS-In(Te) contacts, ohmic nature, monitoring method 77−39935
p-InP, ohmic contact using Be-Au metallisation, low contact resist. 80−65677
InP, ohmic contacts by thin film epitaxy, Gunn oscill. appl. 79−38159
p-InP/In-Zn(Cd) contact evaluation 77−24619
InP-Ag contact fabrication by at. beam epitaxy of metal, elec. props. 77−59691
p-InP-Cd(Zn), ohmic contact formation on InP by laser photochemical doping 80−80369
InP-Cu contact system, low temp. alloyed contact formation 80−100519
InP-metal, elec. and metallurgical props., heat treatment effects 80−34514
InSb surface, Cu deposition, ohmic contact formation, SEM obs. 77−51817
InSb-Au contact system, low temp. alloyed contact formation 80−100519
InSb-Cu non-rectifying contacts by immersion plating 78−30984
Mo-Si sputtered contacts, contact resistance 80−92970
Ni/Au-Ge/GaAs alloyed contacts, prep. by LPE of GaAs from Au-Ge-Ni melts 77−77437

ohmic contacts continued
Ni/Au-Ge/GaAs contact system, alloying behaviour, microprobe AES and X-ray diffr. 80−54548
Ni-Ge-Au evaporated contacts on GaAs, TEM obs. 80−75449
Ni-Si:As(Sb), implanted dopant redistrib. after silicide form., appl. to ohmic contacts 79−37729
Ni_xSi, for n-type Si, current load capacity meas. *(Czech)* 77−89846
Pd-Si:As(Sb), implanted dopant redistrib. after silicide form., appl. to ohmic contacts 79−37729
Pt-Si contact, annealed in H_2 ambient, elec. props. 78−64110
Pt-Si:As, silicide form. during laser irrad., p-n junctions and ohmic contacts 80−84397
Pt-Si:As(Sb), implanted dopant redistrib. after silicide form., appl. to ohmic contacts 79−37729
PtSi film formation by ion sputtering and annealing, form. and exam. problems 80−100782
n-Si, bipolar ohmic contact with macroscopic recomb. centres. 80−80379
Si, laser assisted doping, ohmic contacts and p-n junction form. 78−79621
n-Si, low noise ohmic contact prep., transport props. 77−43723
Si, moderately doped, ohmic contact electron emission, quantum calc. 78−68087
p-Si, ohmic contact formation method 78−76137
Si solar cells, all-plate low cost contact system 80−93992
Si solar cells with fire through contacts printed on anti-reflection coating 80−93993
Si, two carrier operation 77−43716
a-Si:H sputtered films, ohmic contacts by H depletion, H diffusion 80−34511
n-Si:Re diode photocapacitance spectra, Re centre dissociation 79−90997
p-Si-Al, ohmic contacts, Si dissoln. and recrystn. effects, computer calc. 80−103749
Si-Ge junction, Si monocryst. and Ge film, elec. props. 79−51660
Si_3N_4 antireflection coating for solar cells, reactive plasma process for forming metal grid patterns 80−93990
Si_2Te_3, passivated single cryst., elec. conductivity 78−95299
WSi_2 film, FET gate electrode, oxidation mechanism, SiO_2 overlayer formation 78−76773
ZnS, high-resist., optical transmission, thermal processing effects, rel. to contact fabrication 77−63431
ZnS, low resistivity, noise characts. and contact resistance 78−14827
ZnSe, low resistance ohmic contacts using In-Ga liquid alloy, LED fabrication appl. 80−70823
ZnTe single crystal, Schottky-barrier diodes and ohmic contacts props. 80−96987

ohmmeters
see also electric resistance measurement
AC, for electrode impedance measurements 79−67342
capacitance/resistance meter, cct. *(Spanish)* 79−88946
CRT tester based on ohmmeter and adapter 79−35711
DC, pointer-type, 1 to 100 kΩ, using mass produced milliammeter *(Czech)* 79−97405
dermal-resistance meter with high resolution *(German)* 79−84031
digital microhmmeter, Sefelec RCNF-1, characts. *(French)* 77−53953
gigaohmmeter, electronic, with controllable threshold sensitivity 78−74024
high electrical resistance measurement, review of accuracy and sensitivity of various instruments and techniques 80−57331
linear analogue circuits, design, review 78−37031
linear scale, employing integrated operational amplifier *(Czech)* 77−61093
low impedance instrument using 1 KHz source *(German)* 77−13767
maintenance, renovation and repair procedures for multimeters including Avo model 8 79−35795
megohmmeter with op. amp. for liquid level meas. and regulation *(Rumanian)* 79−40532
new checking method for instruments having both uniform and non-uniform scales 80−62654
nonlinear analogue ohmmeter circuits 77−26335
percentage ohmmeter, wide-range, for resistive transducers 78−239
relative-error determination in instrument checking 80−17961
semi-precision linear ohmmeter, four decade ranges, 2% full scale accuracy 80−95109
teraohmmeter, 30 μΩ to 300 GΩ range, portable 79−17441
three-terminal ohmmeter 80−57333
transistorised, reading range extension using op. amp. *(French)* 80−42207
very high resistance measurement, meas. device using operational amplifiers 80−42240

oil circuit breakers
see also insulating oils
high-voltage, low-noise, meas. of impulse sound levels, comparison with SF_6 type *(German)* 79−94401

oil refining
air pollution data obtained near refineries, interpretation via pollution roses 78−81379
crude, heating in tube furnaces anal. 79−18972
enhanced recovery, role of coalescence phenomena and interfacial rheological props. 79−61840
hydrocracking of Athabasca bitumen, thermal, recycle-gas purity effect obs., on product yields and qualities 79−52866
micellar/polymer enhanced oil recovery, mobility control 79−61841
pollution monitoring in petroleum refinery 77−41163
process heat from nuclear steam supply systems, appl. to prod. and treatment of liquid and gaseous prime movers *(German)* 79−87944
recovery processes 79−61839
shale, jet fuels production, by surface and in situ technology 79−48048
shale oil prerefining, in situ, hydrotreatment at 1500 and 2200 psig 79−48047
shale oils comparison, from five different sources, w.r.t. boiling-point composition, elemental content and physical properties 79−48050
unleaded petrol, improving octane rating using gasohol 80−30329

oil technology
see also oil refining
Arctic oil spillage response techniques 80−46204
continuous oil-in-water meas. by towed fluorometer 80−45846
crude oil classification via computerised gas chromatograph mass spectrometry 77−81456
energy conversion, Conf., San Diego, CA, USA (Aug 1978) 79−48038
extractors, windmills appl. in rural India 79−70419

oil technology continued
fuel oil, S content determination using X-ray fluorescence spectrometry 78−61122
in situ oil shale technological developments, review 80−30354
instrumentation 79−34982
laser-induced surface depressions in heavy hydrocarbons, self-holograms 78−82927
marine sample petroleum analysis by gas chromatography and mass spectrometry 77−4977
Ninian Field drilling platform construction, assoc. weather forecasting 80−41522
North Sea and Baltic pollution, natural and man-made influences *(German)* 79−5508
ocean technology development and oil extraction 77−70691
offshore environment, meteorological sensors operation 79−70866
offshore operations, LEO I submersible reliability and safety 77−5373
oil shales of Green River, USA, thermal decomposition rel. to elec. cond. obs. 80−104495
polymer solution flow in porous media, oil extraction appl. 79−68802
prospecting, new seismic reflection techniques 78−73541
recovery from Utah tar sand deposit, by in situ combustion 79−48046
reserves and resources, production and transport problems *(German)* 80−26102
resources in US, estimation of undiscovered sites 80−21361
sea and beach persistent oil spill identification methods 80−90101
seismic prospecting techniques for oil resources *(French, English)* 80−21362
shale, in-situ oil recovery projects 79−87953
shale, Michigan Antrim, simulated in situ retorting 79−87954
shale, true in situ fracturing 79−87955
shale extraction in situ retort utilising fusion reactor 80−108780
shale oil, in situ retorts, computer simulation of ignition with hot inert gas 80−30356
shale oil extraction using nucl. heat sources, feasibility 77−34422
shale oil in situ extraction processes, US DOE 1979 R and D program 80−40812
shale research outlook 79−87952
shale resource development, Colorado's Green River Formation, vertical modified in-situ processes 79−48049
shale retort dispersion, effect of particle size distrib. and flow nonuniformities 80−28560
shale retort flow nonuniformities c.f. numerical predictions 80−28492
shale retorts, multi-dimens. simulation of flow nonuniformities in fissured porous media 80−28559
shales, review of thermophysical properties 79−100479
sonic interface detection for multiproduct liquid transportation by pipeline, developments 80−33382
speckle interferometric meas. method appl. to oil instrumentation *(French)* 77−71365
subsurface EM techniques for oil exploration 77−17263
undersea resources and related topics, world-wide survey 80−35622
world oil resource estimates (1949-79) *(French, English)* 80−21365

oiling (lubrication) *see lubrication*

oils, insulating *see insulating oils*

omega mesons
ϕ-ω mixing and violation of Okubo-Zweig-Iizuka rule 77−87948
asymptotic SU_5 and a new mass constraint for the ω, ϕ, ψ and Υ mesons 79−36001
backward prod., baryon exchange dip and parton effects 78−17030
charmed quark content determ. 77−71511
compilation study of unused data 77−65188
Dalitz arrays from $K^-p \rightarrow \pi^+\pi^-\pi^0\Lambda$ 80−105924
DCI vector meson resonances, $q\bar{q}$ excitation explanation using quark pair creation model 78−70342
decay of $\rho'(1275)$ vector meson nonet 77−79267
dual unitarisation, renormalisation of trajectories with zero quantum numbers 78−21400
$e^+e^- \rightarrow \pi^+\pi^-(\pi^0\omega)$, $\rho'(1250)$ description, EM form factors, bound states, N/D method *(Russian)* 80−42465
estimate of ω, ϕ and baryonium mixing at $t \approx 0$ 79−40814
exchange, lepton-hadron relation and the nucleon-nucleon potential 79−22207
inclusive prod. in $\bar{p}p$ interactions in 9.1 GeV/c 79−6355
Klein paradox and the mass spectra of the neutral vector mesons 79−26299
lepton pair width regularity of vector mesons, ρ, ω, ϕ, ψ and γ 79−63472
mass formulae for series 77−22714
mass of radial excitation, quark confinement potential calcs. 78−93860
masses in QCD lattice gauge theory 80−4928
meson-baryon interactions, comparative study of ρ^0, ω, $K^{*0}(890)$ and $\bar{K}^{*0}(890)$ production 78−58200
nuclear forces, ω meson contrib., field theory model 77−74772
photoproduction on D, Be, C, Al, Cu, Ag, Au, cross sections 78−58261
pion form factor, ω and ϕ effects G-parity violation 79−35963
QCD and resonance physics, appl. of sum rules to ρ-ω mixing 79−22060
QCD and resonance physics, appl. of sum rules to reson. props. of mesons 79−22059
QCD spectrum calcs. in lattice gauge theory using Wilson's fermion method, ω mass 79−367
radiative decay effect on pp bremsstrahlung at 158-400 MeV 77−74706
radiative decays anal., ω' meson at 1.2 GeV 77−46045
size in quark multiple scatt. model 79−54349
vector meson radiative decay evaluation in spectrum generating SU_4 scheme 79−54342
$\delta(980) \rightarrow \omega\gamma$, radiative decay width using a vector dominance model 78−82205
e^+e^- annihilations, radial excitations of ρ, ω, ϕ mesons 78−4866
$e^+e^- \rightarrow$hadrons, QCD perturbation theory sum rule, ρ, ω and ϕ mesons 79−85268
$e^+e^- \rightarrow \omega\rightarrow\pi^+\pi^-\pi^0$, 1.55 GeV 80−82984
$e^+e^- \rightarrow \pi^+\pi^-\pi^0$, 750-1100 MeV, ω and ϕ meson interference 80−105910
$ep \rightarrow ep\omega$, prod. by virtual photons, ω prod. to ρ^0 prod. ratio 79−6344
$ep \rightarrow \omega p$, ω prod. by virtual photon, ang. distrib., cross section 77−61302
$\eta\gamma$ decays of ρ^0, ω and ϕ, widths 77−22736
$\gamma \rightarrow \pi\omega$, transition and π form factors, p'(1200) resonance *(Russian)* 79−22098
$\gamma d \rightarrow d\omega$ or $pn\omega$, 3.9 GeV, cross sections, A_2 exchange amplitude 77−34168
γN, 7.5-10.5 GeV, inelastic ω and ρ^+ prod. 78−45930

omega mesons continued
$\gamma N \rightarrow \omega\Delta$, pion exchange mechanism anal. 77−82750
γp, 46-180 GeV, ω-meson photoprod. cross section, $\omega\gamma$ coupling constant 80−13319
$\gamma p \rightarrow pe^+e^-$, prod. of ρ, ω, ϕ anal. 78−50037
K_1^0-K_S^0 transmission regeneration on deuterons and neutrons, 10 to 50 GeV/c 80−4985
K^0N interaction, 10 to 50 GeV/c, residue of partial W amplitudes *(Russian)* 78−41590
K^-p, 32 GeV/c, vector and tensor meson prod., with quark model anal. 79−80854
K^-p, η and ω prod. at 10 and 16 GeV/c 77−34191
$K^-p \rightarrow \rho^- \Sigma^+(1385)$, $\phi\Sigma^0(1385)$, $\omega A(1520)$ or 0(1520), cross sections, momentum transfer 77−71531
$K^-p \rightarrow \Sigma^- \pi^+\omega$, 4.2 GeV/c, B (1235) backward prod., $\pi^+\omega$ mass enhancement 78−89736
$K_1 p \rightarrow K_S p$, 5 to 10 GeV, differential cross-section, ω Regge trajectory 80−22637
$K_1 p \rightarrow K_S p$ 30 to 130 GeV/c, coherent K_S regeneration amplitude, ω exchange 79−30754
$\mu^+\mu^-$ pair system, meson reson., leptonic decay *(Russian)* 77−67646
$\bar{N}N \rightarrow (\pi, \rho, \omega, f)$, statistical model 80−102028
NN scattering in nonAbelian gauge theory, π-, ρ-, and ω-exchange, scalar Pade approx. 79−67573
ω, photoproduction at high energy, parton model, γ hadronic props. 78−74266
$\omega(1670) \rightarrow B\pi$, decay mode cross section from K^-p backward prod. 80−37257
$\omega \rightarrow 2\pi$, nonet mixing and gluon effects in current quark framework 79−80799
$\omega \rightarrow 3\pi$, decay width for $V \rightarrow 3\pi$ in Bethe Salpeter model 79−58955
$\omega \rightarrow \eta\gamma$, decay rates calc. SU(3) theory 78−58181
$\omega \rightarrow \eta\gamma$, radiative decay width determ. 78−467
$\omega \rightarrow \eta\pi\gamma$, three body decay width 79−36083
$\omega \rightarrow \pi^0\gamma$ in reaction $\pi^-p \rightarrow \omega n$, $\omega \rightarrow \pi^0\gamma$, $\pi^0 \rightarrow 2\gamma$, differential cross sections 79−93464
$\omega \rightarrow \pi^0\mu^+\mu^-$, branching ratio determ., dis. in π^-p collisions 79−67556
$\omega \rightarrow \pi^0\mu^+\mu^-$ decay, mass spectrum and branching ratio *(Russian)* 79−67546
$\omega \rightarrow \pi + \gamma$, radiative decay in the MIT bag model 78−66110
$\omega \rightarrow \pi\gamma$, nonet symmetry scheme 79−63480
$\omega \rightarrow \pi\gamma$, radiative decays, final state interaction, π rescatt. *(Russian)* 78−89710
$\omega \rightarrow \pi\gamma$, suppression factors for VMD couplings calc., duality constraint anal. 77−13960
ω radiative decay, contrib. to pp bremsstrahlung field theoretic calc. 78−62451
ω-f exchange degeneracy, anal. of Pomeron-f complex 78−483
ω-ϕ-baryonium mixing model 80−32072
ω^0, backward ω^0 and η^0 prod. in π^-p interactions at 9 and 12 GeV/c 79−45100
$\omega^0 \rightarrow e^+e^-$, obs. in 4.0 GeV/c π^+p interactions 77−38199
ω', suppressed hadronic decay suppressed hadronic decay and particle degeneracies and particle degeneracies 77−74684
$\omega'(1675)$, prod. in $\pi^+p \rightarrow \Delta^{++}\pi^+\pi^-\pi^0$ 78−37241
$\omega'(1.78)$ vector meson props., quark model, VDM 77−54103
ω' meson at 1.2 GeV, radiative decays of vector mesons anal. 77−46045
$\omega' \rightarrow \omega\pi\pi$, current algebra techniques, pole plus remainder model, chiral symmetry breaking and QCD 80−62972
ω^*-ϕ^* interference in multi π prod., origin of Iizuka-Zweig-Okubo rule violation 78−70324
$\omega \rightleftharpoons \rho^0$, effects of EM mixing on pn mass difference *(Russian)* 78−74255
$\bar{p}d \rightarrow p_s\pi^+\pi^-\pi^-\pi^0$, 0.4 to 0.9 GeV/c, meson resonance production 79−93447
$\bar{p}n$ annihilation, 5.55 GeV/c, meson resonance prod. and transverse spectra 79−93450
pp, 200 GeV/c in Be, inclusive ω prod. at large p_T, η' prod. upper limit 80−52547
pp, 400 GeV/c, inclusive and semiinclusive prod. of π^0, K_s^0, Λ^0, $\bar{\Lambda}^0$, Σ^0, $\bar{\Sigma}^0$, η^0, ω^0 79−93472
pp, ISR energies, inclusive high p_T ω^0 and η' prod. 80−42504
$\bar{p}p$ annihilation, low energy, prompt e^+e^-, ω^0 and η^0 prod., inclusive prod. rates 80−42506
pp bremsstrahlung, ω radiative decay contrib. 78−70386
$pp \rightarrow e^+e^-X$, 53 and 63 GeV, prod. of high transverse momentum low mass e^-e^+ pairs 79−54365
$\bar{p}p$ inclusive prod. of $\pi^-, \eta, \rho^0, \omega, f$, mesons at 0.7 GeV/c 77−65170
$\bar{p}p \rightarrow \omega^0\rho^0$, 1950 MeV/$c^2$, coupling with $\bar{p}p \rightarrow 5\pi$ 80−27517
$pp \rightarrow ppX$, cross sections at ISR energies, ρ, ω, A_2 and f meson prod. 79−40815
ϕ-ω mass mixing sign from gluonic annihilation model, OZI rule violation 79−71722
ϕ-ω mixing, Okubo-Zweig-Iizuka rule, unitary constraints on resonance mixing 79−22024
$\pi^-N \rightarrow \rho^0(\omega)X$ at 40 GeV/c, cross sections 77−18359
$\pi\omega$ channel effect on π form factor at $s < (m_0 + m_\pi)^2$ 77−2838
$\pi\omega$ meson exchange contribution to NN interaction 77−18401
$\pi\omega \rightarrow \pi\omega$, $\rho'(1250)$ meson and two channel $\pi\pi$, $\pi\omega$ problem, N/D method *(Russian)* 80−37297
π^-p inclusive interactions, ρ^0, ω, f-mesons prod. cross section *(Russian)* 78−33098
π^-p interactions, 15 GeV/c, vector meson prod., polarisation props. 78−37251
$\pi^-p \rightarrow n\pi^-\pi^+\pi^0$, 12 GeV/c, ω prod., differential cross section, baryon exchange 79−423
$\pi^-p \rightarrow \omega n$, 15-40 GeV/c, cross sections and density matrix elements *(Russian)* 80−37302
$\pi^-p \rightarrow \omega n$, 20-200 GeV/c, prod. cross section, Regge formalism test 77−26546
$\pi^-p \rightarrow \omega n$, 6 GeV/s, abnormal polarisation effect in Ar, two-Reggeon exchange model *(Russian)* 77−10282
$\pi^-p \rightarrow \omega n$, c.m. momentum 40 to 200 MeV/c, cross section meas. 79−75789
$\pi^-p \rightarrow \omega n$, Reggeon cuts and reaction description *(Russian)* 78−45947
$\pi^-p \rightarrow \omega\pi^-p$, 11.2 GeV/c, partial wave anal. of g-meson prod. 78−78220
$\pi^-p \rightarrow \pi^-\pi^-\pi^+\pi^0p$, 11.2 GeV/c, anal. of $\omega\pi^-$ system prod. 77−88012
$\pi^-p \rightarrow \pi^+\pi^-\pi^0n$, 12, 15 GeV/c, prod. of A_2^0 (1310) and ω^* (1675) 78−74283
$\pi^+p \rightarrow (\rho^0, \omega)\Delta^{++}(1238)$, $q_L = 7.1$ GeV/c, role of new exchanges *(Russian)* 79−54355
omega mesons continued
$\pi^+p \rightarrow \omega\Delta^{++}$, positivity conditions in joint vector-meson Δ prod. 77−13975
$\pi^+p \rightarrow \omega\Delta^{++}(1236)$ 16 GeV/c, cross-sections, spin-density matrix elements 77−10284
$\pi^\pm p$, η and ω prod. at 10 and 16 GeV/c 77−34191
$\pi\pi \rightarrow \pi\omega$, $\rho'(1250)$ meson and two channel $\pi\pi$, $\pi\omega$ problem, N/D method *(Russian)* 80−37297
$\pi\pi\pi$ system, relativistic dynamics in ω channel 78−21360
ρ/ω amplitude ratio for radiative decay, sea quark γ emission 79−63440
ρ-ω interference in $K^-p \rightarrow \pi^+\pi^-(\Lambda, \Sigma^0)$ at 4.2 GeV/c 77−30429
ρ-ω mixing, quark mass differences 80−37243
ρ-ω mixing charge symmetry breaking force, nonlocal contribs., ^{3}He-^{3}H mass difference 78−70458
ρ^0-ω mixing, sign of single particle exchange nucleon force, charge asymm. pot. 77−88048
$\tau \rightarrow \nu\pi\omega$, decay width and form factor calc. using vector dominance hypothesis *(Russian)* 80−47271
w+baryonium mixing, dual S-matrix approach to baryonium 80−52526
Be(K^-,$\rho\omega\rho$X), *(Russian)* 79−9637
$\mu^+\rho$ scattering, exclusive vector meson prod. ρ, ρ^0 and ω cross sections 79−49528
Xe+π^-, 3.2 GeV/c, π^0, η, ω, f meson prod. determ. of meson-N total cross sections *(Russian)* 79−22122

omegatrons *see cyclotrons*

on-off control
see also bang-bang control
3 m parabolic dish heliostat system design, fabrication and testing 79−62111
analytical graphite furnace power supply control to allow interruption of analytical cycle 77−21432
fission reactor zonal control systems, analysis 77−71680

one-dimensional conductivity
A15 compounds as Jahn-Teller systems, multiple band electron-phonon transport theory 80−24902
alkali metal tetracyanoplatinate (FHF), one-dimens. conductors, IR spectra 77−77184
alloy transfer matrix approx., dispersion relations and transport props. 79−42524
Anderson model, one dimensional site disordered lattice, AC conductivity 78−84199
anomalies due to two mechanisms of electron phonon interaction *(Russian)* 80−34430
anomalous frequency-dependent conductivity in disordered one-dimensional systems 79−46834
antiferromagnetic Hubbard chain, interband absorpt., Peierls dimerisation, excitonic effects 80−25072
bilinear organic addition compound, cryst. struct. and cond., rel. to lateral elastic interaction between chains 77−39827
bis(tetrathiotetracene) triiodide, 1-D organic metal, cryst. struct. 77−59000
bis(tetrathiotetracene)triiodide, low temp. metallic cond. 77−24550
bis(tetrathiotetracene)triiodide, struct., reson. Raman spectra 78−66556
broken strand model for dielec. const. and elec. cond. 79−87088
calculation method, taking into account both forward and backward scatt. *(Russian)* 77−4327
CDW, one-dimensional, commensurability pinning versus impurity pinning 79−11075
CDW commensurate-incommensurate phase transition, 1-D electron-phonon system 78−14682
CDW condensates, soliton pair creation and low temp. elec. cond. 79−4550
CDW condensates in two and three space dimensions, nonlinear conduction mechs. 79−60807
CDW distorted linear chain, electronic response and longit. phonons 79−11074
CDW dynamics in one-dimens. cond. chain array, long-range Coulomb effects 78−47717
CDW in random pot., large dielec. susceptibility and diffuse X-ray pattern *(Russian)* 77−69264
CDW ordering in chain conductors 78−79731
CDW sliding in periodic and disordered lattices, pinning 78−14717
CDW structure, incommensurate, phase fluctuations, Coulomb effects and long-range order 77−43524
CDW systems, ϕ-particle model 79−82537
charge density wave condensate high freq. cond. at low temps. 79−95392
charge density wave system, props. 78−75796
charge density waves, impurity pinning 80−6819
charge line, lattice, dispersion relation using hydrodynamic eqns. of motion 77−69260
charge transfer complexes, refl. spectra, excitons 79−47477
charge transfer conductors, press. effects on mag. props., review 78−6505
charge transfer molecular crystal, electronic transport mechanisms 78−6370
charge transfer salts, soliton model for dielectric permeability 80−40036
charge-transfer solid, quasitone dimens., Hall effect and transverse mobility 77−4326
cobalt platino-oxalate, one-dimens. conductors, prep., struct. and elec. cond. 80−24900
collective excitation of CDW 78−18981
commensurate CDW system, lattice dynamics and elec. props. 79−38057
conference, Dubrovnik, Yugoslavia, (Sep. 1978) 80−12853
conjugated one-dimensional system optical nonlinearities 77−50714
copper platino-oxalate, one-dimens. conductors, prep., struct. and elec. cond. 80−24900
Coulomb gas in strong mag. field analogy with electron gas with backward scatt. 80−24817
coupled fields in one dimension: cross-over from a continuous symmetry to a discrete one 78−87758
coupled incommensurate charge density waves, 3D ordering, mean field theory calcs. 80−107719
Curie constant discontinuity explained as lateral alignment of paramag. domain tips 77−16035
DBTTF$(BF_4)_{0.8}$, new conducting compound, synthesis, elec. and mag. props. 79−28341
$(DBTTF)_{2.67}SnCl_6$, Peierls transition, fluctuations effect *(Russian)* 79−60809

one-dimensional conductivity continued
delocalisation and superalternation effects in nonlinear susceptibilities 77−11840
DEM(TCNQ)$_2$, ESR study 80−97127
dibenzotetrathiafulvalene cation radical salts, cryst. struct. by X-ray anal., rel. to elec. props. 80−24436
1,4-dibromonaphthalene, k-k scatt., exciton dephasing time-resolved phosphoresc. obs. 80−11458
3,3′-diethyl-2,2′-selenacyanine-[TCNQ]$_2$, elec. cond., and quasi-two-dimensional mag. props. 78−6564
dimerized interrupted strand model, optical absorption 77−16271
dimerized organic linear chain conductor, electron mol. vibr. coupling consts. 78−14686
disordered one-dimens. metal, with half-filled band *(Russian)* 77−80769
disordered one-dimensional conductors, elec. props., coherence length, impurity effects 80−24903
disordered one-dimensional conductors, interacting electron thermodynamics *(Russian)* 80−54679
disordered one-dimensional conductors, resistance fluctuations. 80−80256
disordered quasi-one-dimensional materials, review 78−6361
disordered quasi-one-dimensional systems with electron correlation, electronic properties 78−87966
disordered systems, AC hopping cond., cluster approx. 79−95379
disordered systems, one dimensional, electron transmission and wave propagation 80−24907
disordered systems, one dimensional nonvanishing zero temp. static cond. 80−29396
distorted one dimensional system with bond disorder, electron density of states, CPA calcs. 80−24778
distorted one-dimensional electron system, dynamical elec. cond. calc. 80−59962
dynamic correlations, in one-dimensional system with short-range attraction 77−4281
dynamic Peierls instability, mean-field model, CDW soln. 77−47748
electron density of states, influence of disorder 77−28091
electron gas, 1-dimens., with backward scatt., excitation spectrum 77−39793
electron gas, one dimensional, dynamic interaction screening, spin and charge density wave instabilities 80−24819
electron gas, quasi-one-dimensional, pair correl. function and plasmon dispersion curve 77−62851
electron gas with backward scatt., scale invariant characteristic energy 77−31927
electron spin relaxation, temp. depend., Peierls fluctuations, EPR meas. 79−73802
electron-electron interactions in physics of one dimensional conductors 80−24895
electron-electron scattering in quasi-one dimens. metals 80−10957
electron-phonon interaction, matrix element calculation, phase transition 78−79703
electron-phonon interaction, quasiparticle approach 77−20305
electron-phonon system, dynamics, Frohlich model 77−15781
electron-phonon system, renormalisation *(Russian)* 78−43314
electronic density of states, disorder and single electron spectrum, in linear chain *(Russian)* 78−56060
energy and charge transport theory *(German)* 80−15506
excitonic insulator, quasi-one-dimens. 79−90966
Fermi gas, one dimensional with backward scatt., gap renormalisation 80−24818
Fermi gas, one-dimensional theory, correlation functions 80−22278
Fermi gas model of one-dimensional conductors, review 79−47090
Fermi gas model with two charact. energies, scaling theory 78−6287
Fermi one dimensional gas with long range potential, renormalisation group, exchange, Umklapp interactions 80−2351
fermion system, cluster expansion methods and thermodynamics 78−6289
fermion system, thermodynamics by cluster expansions 77−41535
ferricyanide, X-ray spectral study of electronic struct. 77−28652
ferrocyanide, X-ray spectral study of electronic struct. 77−28652
filament, condenson energy and mass 78−91637
frequency dependent conductivity, theory of many-body effects 80−44575
Frohlich collective mode and dielectric permittivity *(Russian)* 77−89722
Frohlich conductivity and complete pinning of superstruct. *(Russian)* 77−55518
Frohlich conductivity in fluctuation region 78−84203
Frohlich model, incommensurate, displacement correlation of classical ions of one-dimensional metal 77−39641
Frohlich model dynamics, Green's function anal. 80−20170
FTF-TCNQ, libron freqs., temp. and press. effect 79−86860
graphite intercalation compounds, electronic props. in dil. limit 77−47714
harmonic microwave mixing in periodic potentials, stochastic theory 79−65460
high temperature structural instability in quasi-one dimens. conductor 77−8032
HMTSF-TCNQ, metallic state at He temps., elec. props. and band struct. 79−65462
HMTSF-TCNQ, obs. of the de Haas-Shubnikov oscills. 78−84201
HMTSF-TNAP, microwave cond. at 35 GHz 80−24963
HMTSF-TNAP, organic low temp. cond. 78−43368
HMTSF-TNAP, transport props. 80−20165
HMTTF-TCNQ, quasi-one dimensional conductor, sp, ht. 79−55897
hollandite, one dimensional ionic and solitary wave conduction 79−23954
hollandites, cryst. growth and structural props. 80−89129
hopping conduction and diffusion, theory 78−6355
hopping conduction in quasi 1-D disordered compound 78−10425
hopping conductivity, effect of impurities, current saturation 77−72856
hopping conductivity, one-dimensional bond percolation model 80−103655
Hubbard chain, low-density, intraband absorption 77−24809
Hubbard chain, optical spectrum 78−10920
Hubbard model, one-dimens., extended, $2k_F$ and $4k_F$ correl. functions, computer renormalisation group calcs., appl. to one-dimens. conductors 80−54625
Hubbard model, one-dimensional, antiferromag. and Peierls instability 78−23233
Hubbard model, phase transition due to CDW *(Russian)* 79−4526
Hubbard model, thermoelectric power near atomic line 79−47086
impurity effect on electron pairing *(Russian)* 77−11903
impurity effects, interchain interaction 78−72138

one-dimensional conductivity continued
impurity effects on ordered phases 80−24905
impurity pinning in single chain, CDW dynamics 78−47716
impurity scattering effect on electron pairing 78−60112
incommensurate CDW 80−20174
incommensurate Frohlich model, displacement correl. of classical ions 78−6291
incommensurate lattices, statics and dynamics 79−23913
incommensurate linear conductor, IR absorpt. peak theory 77−43991
incommensurate Peierls-Frohlich system, fluctuation cond., Green's function calc. 80−24886
incommensurate phase transitions, exptl. studies of soft phonons 78−75798
incommensurate sliding CDW 80−20156
infrared problems and phase transitions of continuous order in low-dimens. systems 78−6286
inorganic compounds, modulated structs., formation and nature 79−94968
instability due to electron-phonon interaction 79−99536
interchain coupling, role in linear conductors 77−47751
interchannel Coulomb interaction, in pseudo one-dimens. metal 77−1387
intra-site vibration effects on elec. cond. in disordered Hubbard model 80−107775
inverse localisation length, numerical studies 80−80257
ion-radical compounds, microscopic parameters 79−78025
IR absorption, amplitude and phase mode dynamics 77−16313
IR and Raman activity 78−60441
IR properties of linear conductor, diagrammatic calc. of IR props. 77−32374
Landau model, anisotropic one dimens., correl. length complex order parameter amplitude fluctuation effect 80−46995
Landauer generalised formula 80−103680
lattice stability, phonon dispersion, Kohn anomaly 80−96603
libron effects on electron spectrum, theory 80−96854
linear chain crysts. containing impurities, Peierls instability and supercond. *(Chinese)* 79−51486
linear chain system, exciton model of supercond. 78−6476
linear conductor, CDWs and impurity effects 80−59967
linear conductor, dynamical aspects of fluctuations 79−33715
linear conductor, interchain coupling role 78−6294
linear molecular crystal, mixing of Frenkel excitons and ionic excited states 77−15771
linear-chain conductors review 80−24887
Lloyd's disorder model in one dimension, elec. cond. 79−60779
low-dimensional crystals, excitonic superfluidity 78−6359
low-dimensional materials, cond. temp. depend., metal-insulator transition, supercond. and semicond. behaviour 79−95391
Luttinger model, quasiclassical random pot., effect on electron correlation in one dimens. system 78−39047
magnesium platino-oxalate, one-dimens. conductors, prep., struct. and elec. cond. 80−24900
magnetic field effect on generalised susceptibilities, transition to Peierls state *(Russian)* 77−80750
magnetic transition in one-dimens. electron system with attractive interaction in mag. field 80−7072
metal, ideal resist. in one dimension 77−32002
metal, one- and two-dimens., periodic lattice distortion and CDWs 79−60678
metal, one-dimens., electron interaction effect on Peierls instability *(Russian)* 79−51490
metal, phonon drag and sliding CDW 80−20173
metal, quasi one dimensional, Peierls instability criterion *(Russian)* 77−89516
metal, quasi-one-dimensional, elec. resist. due to electron-electron scatt. 79−4549
metal, quasionedimensional, effect of small mag. impurities on conductivity *(Russian)* 77−4328
metallic chains, weakly coupled, Ginzburg-Landau theory 78−60068
metallic crystals, low-dimensional, excitonic 'superfluidity' 77−20248
metallic filaments, Tomonaga-Luttinger model, quasi-1D generalisation *(Russian)* 79−51560
metals, charge density wave effects, review 79−78085
microwave permittivity measurement techniques 78−10825
mixed donor-acceptor stacks, mag. gap and partial charge transfer, VB calc. 78−76008
molecular crystal, quasi-one-dimensional, exciton wave scatt. by impurity 79−78012
molecular crystals, effects of impurity scatt. and transport topology on trapping, Frenkel excitons 78−95263
molecular crystals, electronic struct., mol. orbital theory 80−54588
narrow band quasi-one-dimensional metals, exchange-correlation effects on plasmons and on CDW instability 80−44525
nickel phthalocyanine iodide, single-cryst. elec. cond., low-dimens. mol. metals 78−76057
NMP-TCNQ, low temp. specific heat 78−52297
NMP-TCNQ, magnetic susceptibility and chem. pot. of two-site Hubbard Hamiltonian 77−47963
NMP-TCNQ, partial charge transfer effect, one dimensional disordered Hubbard model study 80−70687
NMP-TCNQ, X-ray diffuse scatt., and cond. study 80−49701
NMP-TCNQ epitaxial film, oriented, prep. by vacuum evaporation and properties obs. 79−15040
NMR relax. time mag. field depend. *(Russian)* 79−61254
nomadic polarisation in quasi-one-dimens. solids 77−63357
non-conducting chain systems, 3-d Coulomb coupling and charge ordering 78−18980
nonconducting linear chain systems, 3D Coulomb coupling and charge ordering 78−60075
nonlinear one-dimens. Hamiltonian dynamics for lattice distortion 80−20171
nonlinear response of some simple quantum systems 77−49620
nonlinear transport due to bound quantum solitons 79−51558
nonlinear transport due to bound quantum solitons 79−78089
one dimensional conductors, Fermi gas model, reviews 79−78083
one dimensional Fermi gas model in relation to spin and field theoretical models 80−24816
one-dimensional complex order parameter model, mol. dynamics 78−34787
one-dimensional conductors, conductivity peaks, Peierls transitions *(Russian)* 80−49700

one-dimensional conductivity continued
one-dimensional homonuclear molecular systems, nature of energy gap 79−11063
one-dimensional Hubbard model, Friedel oscills. around a nonmagnetic impurity 80−25073
one-dimensional metallic systems, theory of structural phase transitions 78−38830
one-dimensional metals, Peierls and CDW transition *(Chinese)* 79−51502
one-dimensional systems, electron trapping and transport by supersonic solitons 78−72139
one-dimensional systems, exchange effects in plasmon dispersion 79−60741
optical properties of one-dimensional conductors, review 80−45106
order-disorder transitions, static precursor nuclei, anomalies in high temp. superconductors, ferroelectrics, organic conductors 78−10165
organic charge transfer crystals, transport props., phase transitions, mol. dynamic *(German)* 80−39507
organic charge transfer salts, cond. meas., polycryst. techniques 78−43365
organic conductors, Fano anti-resonance and IR props. 79−15465
organic conductors, quasi one-dimensional, low temp. mag. susceptibility 80−93069
organic conductors and semiconductors, conf., Siofok, Hungary (Sept. 1976) 78−6284
organic conductors and semiconductors, electronic structure 79−35496
organic donor-acceptor compounds, incomplete charge transfer stability 78−30883
organic materials, electron-electron scatt. 80−107776
organic materials metallic state at He temps. 79−65462
organic metals, transport theory, electron-phonon scatt. 80−20161
organic semiconductors, resonant states, mag. excitations and impurities 80−24839
organic solid state chemistry, conf., Waltham, USA (June 1978) 79−46990
organic solids, dimer level splitting, hopping integral calc. using PPP Hamiltonian 80−24890
orientational metal-insulator phase transitions in quadrupolar strands with itinerant electrons 80−15455
partly charged organic solids, mol. energies calcs. 79−55694
Peierls dielectric, one dimensional, selftrapped excitations in Peierls-Frohlich state *(Russian)* 80−54678
Peierls distortion due to electron-electron interaction 79−33251
Peierls instability, dynamics, structural energy, pseudopot. calc. 80−54676
Peierls instability, lattice distortion, Kolmogorov Arnold Moser theorems, appl. to struct. problems in condensed matter 80−59878
Peierls instability, with arbitrary bandfilling 80−59968
Peierls instability and superconductivity, possibility of coexistence 78−31028
Peierls instability in nearly free electron model with nonlinear screening 77−4304
Peierls phase transition, fermion-boson system 79−60806
Peierls transition, electron-spin coupling, relative importance 79−28280
Peierls transition, Frohlich model, one-dimens., CDW stability, electron-phonon coupling 80−65452
Peierls transition, interchain bandwidth effect at low temp. 78−10352
Peierls transition temp. and 0K energy gap, mean field theory calc. 80−24782
Peierls-Frohlich dielectric, metallic screening, with pinning to impurities at finite temps. *(Russian)* 79−56208
Peierls-Frohlich state, cond., Umklapp processes *(Russian)* 79−38059
Peierls-Frolich state, impurity pinning of charge density wave 78−6298
phase ordering in quasione-dimensional system, phase ordering *(Japanese)* 80−2352
phase transition in quasi-1D system, 1D correlations effect 77−24526
phenomenological equations of motion for electrons, phonons and librons 80−10955
phonon drag conductivity in Frohlich Peierls phase, effect of impurities 78−60114
phonon dynamics 78−79704
phonons, dispersionless, effect on electron localisation and diffusion kinetics *(Russian)* 77−32005
phonons effect on localisation and electrocond. 78−6362
photoemission from organic mol. crysts., book contrib. 80−16158
phthalocyanines, partially oxidised, highly conductive molecular solids 77−47800
plasmon dispersion in one-dimensional systems, exchange effects 78−91628
poly-p-phenylene, charge transfer complexes, elec. cond. 79−91031
polyacetylene: Br(Cl)(I)(AsF_5) electrical conductivity, metal-to-insulator transition 78−10525
polyacetylene:AsF_5, X-ray absorpt. meas. of mol. struct., orientation and charge transfer 80−25486
polyacetylene, semiconducting and metallic, thermoelec. props. 80−40884
polyacetylene and derivatives, chemically doped, elec., chem. and phys. props. 80−24912
polyacetylene conductivity mechanism, Peierls phase one dimensional cond. *(Russian)* 80−88546
polyacetylene film, doped, transport props. 80−24913
polyacetylene film, partially oriented, anisotropic elec. cond., quasi-one-dimens. behaviour of fully oriented doped material 80−11112
polyacetylene pure and doped films, anisotropic optical properties 78−92137
polyacetylenes, hologenated, quasi-one-dimensional, high-cond., prep. *(Czech)* 79−28340
polycrystal, isotropic, rigorous bounds on conductivity 78−68022
polydiacetylene, cryst., one-dimens. conjugated semicond., vibronic coupling, Fano interference effects 80−34939
polydiacetylene, single cryst. piezomodulated and specular refl. spectra 77−20869
polyene chain, collective excitations and optical absorpt. 79−47019
polymer-bridged metal complex, props. of model system, MO theory 79−90940
pseudo-one-dimensional system, Ginzburg-Landau theory of phase transitions 77−15529
pyrene-TCNE, vapour-grown cryst., transit-time meas. of photocarriers 78−39149
quantum particle in one-dimensional potentials with incommensurate periods 80−34345
quantum solitons, in 1-dimens. electron gas 77−39792
one-dimensional conductivity continued
quantum solitons in one-dimensional conductors 78−6285
quasi one dimensional organic materials, microwave cond., dielectric const. *(Hungarian)* 78−26850
quasi one-dimensional charge transfer salts, soliton model for dielec. permeability 79−91338
quasi one-dimensional conductor, CDW onset and pinning 80−70690
quasi one-dimensional electron-lattice system, Peierls-Frohlich correl. 79−60810
quasi one-dimensional metal, cond. at T=0 *(Russian)* 77−28169
quasi one-dimensional metal, crit. temp. for phase transition *(Russian)* 79−78253
quasi one-dimensional spin lattice coupled system, collective modes 80−24896
quasi-one dimensional metals, variation function in theory 79−23887
quasi-one dimensional organic systems, ESR 78−52358
quasi-one-dimensional CDW systems, commensurability pinning of fluctuation cond. 80−75555
quasi-one-dimensional conductor, chiral charge density waves form. 78−6302
quasi-one-dimensional conductor, high temp. struct. instability, tight-binding approx. and fluctuation model 78−6292
quasi-one-dimensional conductors, alloys, Peiels distortion 80−59965
quasi-one-dimensional conductors, impurity effect on phase transitions 78−6297
quasi-one-dimensional conductors, order in coupled metallic chains problem 78−6358
quasi-one-dimensional electron gas with strong on site interactions 77−4306
quasi-one-dimensional electron systems, effect of interchain electron transfer on phase transition 78−51911
quasi-one-dimensional electron-lattice system, three dimensional CDW ordering temp. 78−23037
quasi-one-dimensional electron-phonon system, electron jump effect on phase tansition *(Russian)* 80−92673
quasi-one-dimensional metal, longitudinal cond. at finite temp. 78−2473
quasi-one-dimensional metal, theory of cond. 78−2472
quasi-one-dimensional metal systems with random impurities, cond. at T=0 78−6360
quasi-one-dimensional metallic system, effect of one-dimensional correlations on phase transition 77−24525
quasi-one-dimensional metallic system, phase transitions problem, Gorkov-Dzyaloshinskii model 78−6296
quasi-one-dimensional metallic systems, crit. behaviour, Ginzburg-Landau theory 79−56147
quasi-one-dimensional model with long range interaction, coupled Tomonaga chain, exact soln. 80−96856
quasi-one-dimensional organic conductor, chem. trends and stabilisation of nearly one-dimens. state, review 78−10328
quasi-one-dimensional systems, charge distrib. and lattice distortion 78−6317
quasi-one-dimensional systems, free energy of Ginzburg-Landau field, equiv. Hamiltonian 78−6293
quasi-one-dimensional systems, Peierls transition, possible pairing of spatially separated electrons and holes 79−15085
quasi-one-dimensional systems, three-dimens. ordering in system of weakly coupled chains 78−6295
quinolinium $(TCNQ)_2$, charge transport, proton spin-lattice relaxation 80−88545
random potential, one dimens., density of states *(Russian)* 77−85127
review 78−60070
rubidium platino-oxalate, one-dimens. conductors, prep., struct. and elec. cond. 80−24900
scaling hypothesis appls. *(Russian)* 77−72857
semiconductor, layered compound, collective electron cond. in strong mag. field 79−42525
sine-Gordon chain, cond., finite damping correction 80−46993
sliding Frohlich waves, lack of superconducting behaviour 78−10378
soliton pair creation by elec. fields in CDW condensates 77−69309
spin-Peierls transition in mag. field, phonon freq., Heisenberg model calcs. 80−25151
static conductivity at finite temp. *(Russian)* 78−10428
strongly disordered conductor, localisation of electrons *(Russian)* 79−78046
strongly interacting system, Efetov Larkin model 78−6288
structural aspects, book contrib. 78−10429
structural Peierls transition in quasi-one-dimensional systems with anisotropic electronic and elastic properties 79−7671
superconducting order and CDW coexistence, Peierls instability *(Russian)* 77−69445
superconducting transition in quasi-one-dimens. conductor, impurity effect 77−15986
superconducting transition temp., tunnelling amp. depend. 79−42683
superconductivity, response functions, from renormalisation group theory 80−54829
superionic conductor, correls. among mobile ions role, microscopic model 80−107534
symmetry, role on props. of quasi-one dimensional systems 80−24916
systems with half-filled zone, singularity of electronic density of states due to impurities 78−6254
$TCNQ_2$-TEA, quasi 1-D cryst., interaction between electronic and vibr. states 77−52102
$TCNQ^x$, (x=0, −1, −2), elec. dipole polarisability, π-electronic components, SCF calcs. *(Russian)* 78−84204
TCNQ, dimer gas model 78−87926
TCNQ, elect. struct. determ., CNDO parametrisation and UPS data 77−1350
TCNQ, electron mobilities from 210 to 350K using transverse photocond. meas. 79−19618
TCNQ, electron- and phonon-polaron effects in valence and cond. bands 77−76757
TCNQ, exciton surface polaritons at room temp. 79−47476
TCNQ, generalised Wigner lattices and band motion effects 80−24815
TCNQ, infinite stacks, all valence electron band struct. 78−39001
TCNQ, lattice softening mechanism 80−6481
TCNQ, lattice vibrs., temp. depend., NQR obs. 79−38402
TCNQ, optical IR antireson. absorption, charact. rel. to cryst. parameters 77−77183
TCNQ, Raman scatt. and charge transfer 77−69817
TCNQ, resonance Raman spectra 79−56787

one-dimensional conductivity continued
TCNQ, salt, $(NMe_3H)(I)(TCNQ)$, semicond. 'metal-like' complex, optical props. 79−95761
TCNQ, salt, DBTTF-TCNQ, elec. resistivity and thermoelec. power meas. 80−20193
TCNQ, salt, $Me\phi_3As(TCNQ)_2$, nonOhmic elec. cond., tunnelling model and expt. 79−99558
TCNQ, single crystal, exciton surface polaritons, attenuated total reflection spectra 79−91460
$(TCNQ)_2$ MEM, crystal struct. of 1:2 complex, at −160°C 78−10031
$(TCNQ)_2$TEA, refl. spectra 77−90154
$(TCNQ)_5^{2-}(DBzPE)^{2+}$, cryst. struct., elec. cond. and thermoelec. power 77−72606
$(TCNQ)_5^{4-}(DEPA)_2^{4+}$, cryst. struct., elec. and mag. props. 77−72605
$(TCNQ)(TTF)_{1-x}$-$(TSeF)_x$, quasi 1-D metal, mag. susceptibility, temp. depend. 77−8267
TCNQ addition compounds, high-temp. cond. and impurity bridge struct. 77−15838
TCNQ alkali salt, spin-Peierls transition 80−29395
TCNQ alkali salts, charge transfer enhanced IR absorpt. spectra 77−28558
TCNQ alkaline salts, phase transitions, vibronic intensity enhanced IR spectra 78−23441
TCNQ and its salts, XPS meas. surface effects 78−11075
TCNQ anion radical charge transfer salts, semiconducting behaviour 79−11118
TCNQ bipyridine salt, single cryst. cond. for symm. and asymm. donors 77−32003
TCNQ charge transfer complexes, elec. cond. 79−38058
TCNQ complex, $(C_{13}H_{21}N_2S_2)^+(C_{12}H_4N_4)_2$, cryst. and mol. struct. 77−62514
TCNQ complex, Adn $TCNQ_2$, nuclear-spin-lattice relaxation 80−39886
TCNQ complex, [1,2-bis(1-benzyl-4-pyridinio)ethane]$^{24}(TCNQ)_5^{2-}$, cryst. struct. and elec. cond. 79−19236
TCNQ complex formed from cation (methyl-l-N-ethyl benzimidazolium)$^+$ conductivity transition 80−10954
TCNQ complex salts, mag. props., ESR meas. 79−56603
TCNQ complex salts, optical absorption spectra 79−15486
TCNQ complex salts, temp. depend. of elec. cond., CPA approach 77−8078
TCNQ complex salts, with pyridinium cations, cond. and structural studies 79−87087
TCNQ complex with 5-phenyl-[1-thiol]-3-selenol-2-thione, charge-transfer salt, cryst. and mol. struct. 80−33986
TCNQ complexes, elec. resist. and thermoelec. power meas. 80−107777
TCNQ complexes, low temp. sp. ht. 77−51514
TCNQ complexes, Qn$(TCNQ)_2$, NMePh.TCNQ, and Li^+TCNQ^-, extrinsic and intrinsic mag. susceptibility 78−43556
TCNQ complexes with dipyranylidene and dithiadipyranylidene, high cond. investigs. and related props. 78−6368
TCNQ complexes with ferrocenes, charge transfer type, struct. and mag. props. 80−24439
TCNQ complexes with N-methyl derivatives of pyridine, cond. and thermoelec. power meas., band model anal. 80−10952
TCNQ compounds, dimensionality of triplet excitons 78−91974
TCNQ derivatives, substituted, org. cond. with low-symmetric acceptors, cond. behaviour rel. to cryst. struct. 78−6365
TCNQ ion-radical polymeric salts prep. and props. *(Russian)* 78−76061
TCNQ ion-radical salts, strain sensitivity 79−65461
TCNQ polycation salts, elec. cond. and chemical stability 79−83456
TCNQ salt, 1,1′-diethyl-2,2′-cyanine-$[TCNQ]_2$, electric and mag. props. 79−42523
TCNQ salt, 1-ethyl-3′-methyl-2,2′-quinoselenacyanine-$(TCNQ)_2$, EPR linewidth, angular and temp. depend. 78−76313
TCNQ salt, 3,3′-diethyl-6,6′-dimethyl-2,2′-thiacyanine-$(TCNQ)_2$ EPR linewidth, angular and temp. depend. 78−76313
TCNQ salt, (1,2,-bis(di-n-alkyl-4-pyridinium) ethene)$^{2+}$ $(TCNQ)_x^{2-}$, cryst. struct. and elec. props. 79−56209
TCNQ salt, (1,3,-bis(di-n-alkyl-4-pyridinium) propane)$^{2+}$ $(TCNQ)_x^{2-}$, cryst. struct. and elec. props. 79−56209
TCNQ salt, $(DEPE)^{2+}(TCNQ)_4^{2-}$, elec. and mag. props. of two crystallographic form 77−28166
TCNQ salt, $(DEPE)^{2+}(TCNQ)_4^{2-}$, elec. props., semicond. and metallic phases 78−34826
TCNQ salt, $(DEPE)^{2+}$ $(TCNQ)_4^{2-}$, semicond. form., cryst. struct., X-ray diffr. meas. 77−4094
TCNQ salt, (DEPE)$(TCNQ)_4$, elec. props., semicond. behaviour obs., no stable metallic state 77−51772
TCNQ salt, $(MeI\text{-}NEtBz)^+(TCNQ)_2^-$ 79−47087
TCNQ salt, $(N(CH_3)_3H)(I)(TCNQ)$, elastic props., semicond. transitions 79−95072
TCNQ salt, $(N(CH_3)_3H)(I)(TCNQ)$, proton spin-lattice and spin-spin relax. times 79−8065
TCNQ salt, (N-methylphenazinium)$_x$(phenazine)$_{1-x}$, 1 band filling, carrier mogility and disorder effects 80−24904
TCNQ salt, $(NMe_3H)(I)(TCNQ)$, one-dimens. semicond. with metal-like cond. 80−24909
TCNQ salt, $(NMP)_{0.5}$(phenazine)$_{0.5}$ TCNQ, transport props. 80−24891
TCNQ salt, $(NMP)_x(Phen)_{1-x}(TCNQ)$, band filling and disorder 78−87968
TCNQ salt, $(TMA^+)_3(I_3^-)(TCNQ^-)_2(TCNQ^0)$, struct., phys. props. and lattice distortion evidence 78−6305
TCNQ salt, $(TSeF)_x(TTF)_{1-x}$-TCNQ, struct., elec. and mag. props., review 80−20158
TCNQ salt, acridinium $(TCNQ)_2$ low temp. heat capacity, Debye temp. 80−2180
TCNQ salt, acridizinium, one-dimens. cond., permittivity 25 to 60 GHz, 4.2K 78−88248
TCNQ salt, Ag.TCNQ, cryst. struct. 80−70186
TCNQ salt, alkali transition metal, elec. cond. and phase transition 78−43370
TCNQ salt, Cu-TCNQ thin film between Cu and Al electrodes, elec. switching and memory phenomena 79−65562
TCNQ salt, DECA $(TCNQ)_2$, struct., phys. props. and irreversible phase transition 78−6273
TCNQ salt, dibenzo-TTF-$TCNQCl_2$, one-dimens. mag. semicond., mag. and elec. props. 80−88601
TCNQ salt, HFTTF-TCNQ, phase transitions, calorimetry study 79−51253
TCNQ salt, HMTSeF-TCNQ, Hall effect, temp. and press. depend. 77−35929
one-dimensional conductivity continued
TCNQ salt, HMTSF-TCNQ, lattice phase transitions and conduct. anomalies obs. 77−1226
TCNQ salt, HMTTF-TCNQ, electron-electron interactions, mag. susceptibility and optical reflectivity 77−81104
TCNQ salt, HMTTF-TCNQ, Madelung energy, intermol. charge transfer, 1-dimens. disorder 79−7572
TCNQ salt, HMTTF-TCNQ, metallic organic charge transfer complex, chemical prep. and phys. props. 78−2471
TCNQ salt, HMTTF-TCNQ, quasi-one-dimensional organic conductor, mag. susceptibility meas. 78−6508
TCNQ salt, HMTTF-TCNQ, sp. ht., 30 to 80K 80−24614
TCNQ salt, HMTTF-TCNQ, structure, metallic cond. and thermopower 77−8080
TCNQ salt, HMTTF-TCNQ, three-dimens. ordering, Ginzburg-Landau model for Peierls instability 80−20160
TCNQ salt, K^+TCNQ^-, cryst. struct. above and below 122°C transition 77−35541
TCNQ salt, K^+TCNQ^-, spin polarised band struct., effective Coulomb repulsion 77−15734
TCNQ salt, K^+TCNQ^-, temp. depend. of dynamic nucl. polarisation enhancement of protons 78−6601
TCNQ salt, K-TCNQ, ^{14}N NQR temp. depend. rel. to Peierls transition 79−82892
TCNQ salt, K-TCNQ, cryst. struct. *(French)* 78−43006
TCNQ salt, K-TCNQ, energy gap, electron-phonon interaction, IR spectrum 78−15167
TCNQ salt, K-TCNQ, high and low temp. phases, dielec. const. 80−34844
TCNQ salt, MeDABCO$(TCNQ)_2$, elec. cond. and IR and visible spectra meas. 79−42526
TCNQ salt, MeDABCO$(TCNQ)_2$, optical, elec., and mag. props. 80−65539
TCNQ salt, MEM$(TCNQ)_2$, dielec. const. obs., DC and microwave cond. obs. 80−59963
TCNQ salt, MEM$(TCNQ)_2$, phase transition electronic struct. interpretation 80−24781
TCNQ salt, MEM$(TCNQ)_2$, phase transitions, elec. cond., ESR, mag. susceptibility study 80−24981
TCNQ salt, Mn$(TCNQ)_2$, mag. props. 77−85558
TCNQ salt, MTPA $(TCNQ)_2$, IR refl., dielec. function and cond. 80−34924
TCNQ salt, N,N′-di(n-propyl)-4,4′-bipyridylium^{2+}(7,7,8,8,-$TCNQ)_4^{2-}$, cryst. struct., elec. props. 79−27971
TCNQ salt, N-propyl-quinolinium$(TCNQ)_2$, defect conc. depend. phase transition 80−44577
TCNQ salt, NMeQn$(TCNQ)_2$, phase transition, role of acetonitrile solvent 78−60119
TCNQ salt., NMeQn$(TCNQ)_2$, role of solvent in phase transition, thermal anal. and transport props. 79−33312
TCNQ salt, $NMP_{0.63}$phenazine$_{0.37}$TCNQ, mag. susceptibility, 0.03-4.2K 80−25191
TCNQ salt, NMP-TCNQ, realisation of disordered Hubbard model, dielec. props. 78−79917
TCNQ salt, NMP-TCNQ, X-ray diffuse scatt. rel. to charge transfer 77−80496
TCNQ salt, NPQn $(TCNQ)_2$, neutron irrad. induced defect concentration depend. phase transition 80−29449
TCNQ salt, pyridine $(TCNQ)_2$, phase transition at 80K investig. and interpret. 78−6530
TCNQ salt, pyridinium $(TCNQ)_2$, low temp. mag. phase transition, ESR study 80−25139
TCNQ salt, Qn$(TCNQ)_2$, decrease of electronic coherence length by impurities 79−69501
TCNQ salt, Qn$(TCNQ)_2$, defect depend. of dielec. permeability and cond. 79−78608
TCNQ salt, Qn$(TCNQ)_2$, defect depend. of dielec. permeability and conductivity 79−91340
TCNQ salt, Qn$(TCNQ)_2$, non-Ohmic cond. 80−20169
TCNQ salt, Qn$(TCNQ)_2$, non-ohmic elec. cond. 79−4553
TCNQ salt, Qn$(TCNQ)_2$, nonlinear electric field depend. 79−78088
TCNQ salt, Qn$(TCNQ)_2$, nonlinear transport 79−87089
TCNQ salt, Qn$(TCNQ)_2$, organic transfer salt, impurity effects on cond. 77−76799
TCNQ salt, Qn$(TCNQ)_2$, phase transition, paramag. shifts and PMR line width *(Russian)* 77−43892
TCNQ salt, Qn$(TCNQ)_2$, temp. and freq. depend. of nucl. relax. rate 78−6594
TCNQ salt, Qn$(TCNQ)_2$, thermoelec. power and cond., large Coulomb repulsion model 80−24893
TCNQ salt, Qn $(TCNQ)_2$, configurational entropy, thermoelec. power meas. 80−34432
TCNQ salt, quinilinium, one-dimens. cond., permittivity 25 to 60 GHz, 4.2K 78−88248
TCNQ salt, quinolinium, electron spin location, elec., mag., and thermal props. 80−25189
TCNQ salt, quinolinium $(TCNQ)_2$, mag. chain double resonance study, deuteration 80−25250
TCNQ salt, quinolinium $(TCNQ)_2$, random-exchange Heisenberg antiferromag. chain, sp. ht., 0.07-5K 78−14976
TCNQ salt, quinolinium $(TCNQ)_2$, transport props. 80−24891
TCNQ salt, Rb_2TCNQ_3, cryst. struct. refinement 78−55859
TCNQ salt, Rb-TCNQ, electronic spin-lattice relax. time 77−51939
TCNQ salt, TEA $(TCNQ)_2$, anomalous conductivity, conductivity transitions 80−15508
TCNQ salt, tetramethylhexamethylenediammonium-TCNQ-iodine, elec. and mag. props., struct., specific heat 80−24898
TCNQ salt, TMPD-TCNQ , mag. excitation gap attributed to spin polarisation instability 78−31086
TCNQ salt, TMTSF-DMTCNQ, cond. and thermopower meas. 80−20165
TCNQ salt, TMTSF-DMTCNQ, mag. susceptibility meas. under press. 80−29521
TCNQ salt, TMTSF-DMTCNQ, metallic state at low temp. under pressure 79−91033
TCNQ salt, TMTSF-TCNQ, microwave cond. at 35 GHz 80−24963
TCNQ salt, TMTTF-TCNQ, mag. gaps, EPR meas. 77−8390
TCNQ salt, TSeF-TCNQ, CDWs, X-ray study 79−28301
TCNQ salt, TSeF-TCNQ, doped with TTF-TCNQ, phase transitions 77−80732

one-dimensional conductivity continued
TCNQ salt, TSeF-TCNQ, electrical conductivity, press. depend. 77−51729
TCNQ salt, TSeF-TCNQ, nonlinear transport in pinched one-dimensional CDW system 77−89754
TCNQ salt, TSeF-TCNQ, Peierls transition and CDW ordering, X-ray study 80−20101
TCNQ salt, TSeF-TCNQ, short-range ordering investigated by XDE 80−59652
TCNQ salt, [1,2-di(N-methyl-4-pyridinium)ethane]$^{2+}$(7,7,8,8-TCNQ)$_4^{2-}$, struct. and elec. cond. 77−80491
TCNQ salt, [1,3-di(N-pyridinium)propane]$^{2+}$(7,7,8,8,TCNQ)$_4^{2-}$, struct. and elec. cond. 77−80492
TCNQ salt, [1,4-di(N-quinolinium-methyl)benzene]$^{2+}$ (TCNQ)$_3^{2-}$, cryst. struct., elec. anisotropy 77−35542
TCNQ salt films, textured TCNQ and NMP-TCNQ, cond. and dielec. props. 77−51733
TCNQ salt in aqueous media, electrochem. behavior 80−6976
TCNQ salt QCTCNQ, strong Coulomb correlations 79−56203
TCNQ salt with MDCA cation, first order phase transition 79−73122
TCNQ salts, (N-methyl pyridine) (TCNQ)$_2$, struct. and cond., 280 to 340K 79−23955
TCNQ salts, aminopyridinium (TCNQ)$_2$, elec. and mag. props., 4.2 to 300K 80−24889
TCNQ salts, anomalous infra-red activity and the determination of electron-molecular vibration coupling constants 80−25389
TCNQ salts, charge transfer and cond. 80−20164
TCNQ salts, charge transfer and ionic bonding 77−39558
TCNQ salts, complex, optical absorption meas. 79−4824
TCNQ salts, complex, with aromatic donors, interchain coupling and disorder 78−6314
TCNQ salts, complex, with symmetric and asymmetric donors, transport and mag. props. 78−6315
TCNQ salts, conducting, Raman spectra, estimation of degree of charge transfer from vibrational frequencies 80−50344
TCNQ salts, crystallisation versus electrical conductivity 80−92885
TCNQ salts, direct current conductivity and thermo-electric force, 4-400K *(Hungarian)* 79−56251
TCNQ salts, elec. and optical props. 79−73498
TCNQ salts, elec. cond. spectrum fine struct. 80−96884
TCNQ salts, electron arrangement in ground state, optical spectra interpretation 78−47715
TCNQ salts, electron localized and band motion, IR spectra 77−66487
TCNQ salts, electron tunnelling 78−47769
TCNQ salts, electron-vibrational interaction consts. 79−28054
TCNQ salts, ETPP (TCNQ)$_2$ and DEPE (TCNQ)$_4$, thermoelec. power 80−59966
TCNQ salts, hexamethylenetetraheterofulvalene donors in systematic mol. modifications 78−91680
TCNQ salts, ionene polycation-TCNQ salts, elec. cond. rel. to polycation struct. 80−34428
TCNQ salts, IR, X-ray electron spectra, tetrathiotetracene (TCNQ)$_2$ cond. investig. 77−44005
TCNQ salts, K(TCNQ), Ba(TCNQ)$_2$ and Ca(TCNQ)$_2$, electronic absorpt. spectra, vibronic struct., charge transfer bands 79−24331
TCNQ salts, lattice vibr. freezing, Kohn anomalies, lattice struct. 77−15401
TCNQ salts, microdomain model for struct. rel. to cond. 77−11902
TCNQ salts, Mn(TCNQ)$_2$ and hydrates, mag. and elec. props. 79−82767
TCNQ salts, model, 3D Coulomb coupling and charge ordering 78−60075
TCNQ salts, model for cond. 78−10426
TCNQ salts, modulated struct., dynamical processes, X-ray and neutron scatt. 79−95155
TCNQ salts, n-methylacridium (TCNQ)$_2$, 2,2'bipyridinium (TCNQ)$_2$ and Qn(TCNQ)$_2$, with asymmetric donors, mag. susceptibility, 0.035-4.2K 80−25190
TCNQ salts, NMR relax. time mag. field depend. *(Russian)* 79−61254
TCNQ salts, polymer composites, elec. cond. 80−20157
TCNQ salts, Qn(TCNQ)$_2$, NMeAd(TCNQ)$_2$, dielec. const. and cond. 78−79985
TCNQ salts, Qn(TCNQ)$_2$ and Cs$_2$(TCNQ)$_3$, surface magnetism obs. 78−6561
TCNQ salts, Qn(TCNQ)$_2$ and Cs(TCNQ)$_3$, surface magnetism 78−2703
TCNQ salts, Qn(TCNQ)$_2$ and NMeAd(TCNQ)$_2$, dielec. const. and elec. cond. 78−60116
TCNQ salts, Qn(TCNQ)$_2$ impurity effects on electronic coherence length 79−73500
TCNQ salts, quasi-one-dimensional, Wigner cryst. model 78−47273
TCNQ salts, simple, triplet exciton obs. by ESR 78−10373
TCNQ salts, sp. ht. meas., 0.2-300K, extended Hubbard model *(French)* 77−35710
TCNQ salts, spin density distribs., estimation from EPR fine struct. and cryst. data 79−11347
TCNQ salts, surface magnetism, magnetisation field curves meas. 77−59428
TCNQ salts, thermoelec. power, two-band model 79−4551
TCNQ salts, TSF-TCNQ, and HMTSF-TCNQ, low temp. fast neutron irradiation, elec. cond. meas. 80−59964
TCNQ salts, with disorder, singularities in density of electronic states 77−8006
TCNQ salts 78−6356
TCNQ salts of 1:1 stoichiometry, kinetic models of form. 79−46596
TCNQ salts of ionene polymers containing triethylenediammonium or 4,4'-bipyridilium ring, chem. struct. correl. with cond. 79−91032
TCNQ salts organic semiconducting polymers, electron transfer mechanisms 79−42544
TCNQ salts with alkali metals, intensities of IR absorpt., electronic transfer magnitude 78−6691
TCNQ salts with alkali metals, optical absorpt. spectra of small particles 78−19505
TCNQ salts with asymmetric donors, mag. susceptibility 78−60264
TCNQ salts with asymmetric donors, transport props. 78−60115
TCNQ salts with asymmetric donors, transport props. 79−23953
TCNQ salts with heterocyclic amines and hydroquinone form. via redox reaction 80−26013
TCNQ salts with NMP and Rb, elec. cond., temp. and press. depend. *(Japanese)* 78−43366
one-dimensional conductivity continued
TCNQ solt, CS$_2$(TCNQ)$_3$, cond. and thermopower meas., deep level acceptor model 79−42529
TCNQ-ϕ_4DTP, chemisorbed O$_2$ effects on mag. susceptibility 80−15679
TCNQ-bipyridinium salt, chain stabilisation, cond. enhancement 78−51978
TCNQ-coronene complexes, spectra, stoichiometry 78−23435
TCNQ-HMTSeF, large Hall effect obs. below room temp. 78−6364
TCNQ-HMTSeF, nucl. spin relax. obs., diffusive character of response function and interchain coupling 78−10797
TCNQ-HMTSeF, polarised single cryst. reflectance obs. and one-dimens. behaviour interpret. 78−6690
TCNQ-HMTSeF, X-ray diffuse scatt., one-dimens. distortion in phonon spectrum and interpret. 78−10144
TCNQ-HMTSF, de Haas-Shubnikov oscills. 80−10956
TCNQ-HMTSF, irrad. effects on resist. 21K 78−60113
TCNQ-HMTTF, metallic state stabilisation at low temp. under press. 78−30911
TCNQ-HMTTF, struct. evidence of CDW 78−51912
TCNQ-K, X-ray exam. of phase transitions 78−55933
TCNQ-M$_2$P charge transfer complex, triplet spin excitons, EPR spectra 78−80192
TCNQ-Na, X-ray exam. of phase transitions 78−55933
TCNQ-NMP, disordered, paramag. susceptibility 78−10645
TCNQ-NMP, elec. cond. temp. depend. 77−85203
TCNQ-NMP, metal-insulator transition theory based on generalised Hubbard model 78−18966
TCNQ-NMP, nucl. relax. and spin dynamics 78−52370
TCNQ-NMP, reduced Coulomb repulsion, intrachain and interchain polarisation 77−85162
TCNQ-NMP, transport props. 80−24891
TCNQ-perylene, electronic absorpt. spectra, vibronic struct., charge transfer bands 79−24331
TCNQ-potassium, dynamic nucl. polarisation exam., temp. depend. 78−39447
TCNQ-pyrene complex, evaporated layers and single crysts., photocond. *(Russian)* 78−6416
TCNQ-Rb, X-ray exam. of phase transitions 78−55933
TCNQ-TMTSF, conducting salt, cryst. and mol. struct. 77−24307
TCNQ-TMTTF, conducting salt, cryst. and mol. struct. 77−24308
TCNQ-TMTTF phases comparison with TTF-TCNQ, ESR 77−40116
TCNQ-TSeF:TCNQ-M, thermopower determ. 78−47772
TCNQ-TSeF, crit. behaviour at electronically driven struct., phase transition 77−80767
TCNQ-TSef, Drude optical edge, press. depend. 79−19882
TCNQ-TSeF, mag. suscept. meas. 78−56287
TCNQ-TSeF, model for phase transition and low-temp. phase 77−47734
TCNQ-TTF, chemisorbed O$_2$ effects on mag. susceptibility 80−15679
TEA(TCNQ)$_2$, elec. cond. and thermoelec. power under hydrostatic press. 80−11024
tetracyanoplatinates, quasi 1d anion deficient, elec. and struct. props. 80−103683
tetramethyltetrathiofulvalene salts, complexes with anisotropic props. *(French)* 77−69307
tetraphenyldithiadipyranylidene-iodine, synthesis and cond. props. 80−24910
tetraphenyldithiapyranylidene triiodides, elec. cond. and thermoelec. power 79−56207
tetraselenatetracene bromide complex, optical props. 78−6680
tetraselenatetracene cation radical salts, cryst. struct. by X-ray anal., rel. to elec. props. 80−24436
tetraselenotetracene bromide, positive microwave dielectric const. 78−47771
tetraselenotetracene chloride, struct. and props., no metal-dielec. transition *(Russian)* 77−59281
tetraselenotetracene iodides, struct. and physical props., DC electrical cond. and EPR linewidth meas. 80−103312
tetraselentetracene chloride, elec. cond. below 1K *(Russian)* 80−6820
tetrathiofulvalene-based salts, isomorphous series systematic investig. of solid-state props. 77−55517
tetrathiotetracene iodide, positive microwave dielectric const. 78−47771
tetrathiotetracene salts, IR, X-ray electron spectra, tetrathiotetracene (TCNQ)$_2$ cond. investig. 77−44005
tetrathiotetracenenickel bis(ethylene-1,2-dithiolene), one-dimens. cond., preparation and props. 77−85201
tetrazaporphin, coord. polymer with transition metal, one-dimens. conductor, band struct., EHT theory 79−90941
(TETTF)(TCNQ)$_2$, charge transfer complex, phys. props. and phase transition 78−64032
theoretical aspects 78−10422
thermopower in quasi-one-dimensional conductors 79−65463
three-dimensional organic chain conductors, one-dimensionalisation by impurities 78−91681
TMBP.HCNB and TMBTP.HCNB complexes, elec. and mag. props. 78−6512
(TMTSF)$_2$PF$_6$, ESR g-factor, linewidth, spin susceptibility, metal-insulator transition 80−103887
(TMTSF)$_2$PF$_6$, one dimens. conductor, superconds., resist. meas. and mag. field effects *(French)* 80−44753
(TMTSF)$_2$PF$_6$, organic one-dimensional superconductor, transition temp. 80−44754
(TMTSF)$_2$PF$_6$, quasi-dimens. cond., diamagnetic AC susceptibility 80−103781
(TMTSF)$_2$PF$_6$ (AsF$_6$), linear-chain conductor, semicond.-metal transition in small elec. field 80−103730
(TMTSF)$_2$X, (X=PF$_6^-$, AsF$_6^-$, SbF$_6^-$, BF$_4^-$, NO$_3^-$) highly conducting salts, props. 80−59969
TMTSF-DMTCNQ, cryst. and mol. struct. 78−63742
TMTSF-DMTCNQ, metallic state at low temp. under press. *(French)* 79−82579
TMTSF-DMTCNQ, role of individual stacks in phase transition 79−73307
(TMTTF)$_2$BF$_4$, organic conductor, cryst. struct. *(French)* 78−26556
(TMTTF)$_2$Br, cryst. struct. *(French)* 78−34503
TMTTF salts, (TMTTF)$_2$-X, (X=BF$_4^-$, ClO$_4^-$, SCN$^-$, PF$_6^-$, Br$^-$), physical props. 79−47085
TMTTF-TCNQ, quasi one-dimens. conductor, diffusive hopping, theory 80−54677
TMTTF-TCNQ crystals grown from several organic solvents 80−25544
Tomonaga model, correlation function 77−1342
Tomonaga model, response function calc. method 80−22279

one-dimensional conductivity continued
transition metal complex, linear chain type, synthesis 78−6047
transition metal dichalcogenides, periodic lattice distortions, charge density waves 79−82536
transition metal mixed valence complexes, quasi-one-dimens., elec. props. at ultrahigh press. 78−2470
transport processes, isothermal method for static cond. of electrons 80−29373
trapping behaviour, theoretical study 80−80258
$(TSeF)_x(TTF)_{1-x}(TCNQ)$, interstack hybridisation role in metal-insulator transition temp. determ. 78−6304
$(TSeF)_x(TTF)_{1-x}TCNQ$, struct., cond., phase transitions 78−47770
TSeF salts, mol. props., one-dimens. cond. salts form. 78−6363
TSeF-TCNQ, Ginzburg-Landau model for metal-insulator transition 78−6301
TSeF-TCNQ, Kohn anomaly of metallic state, X-ray diffuse scatt. meas. 80−19887
TSeF-TCNQ, nonlinear electronic transport, microwave harmonic mixing obs. 80−20168
TSeF-TCNQ, resist., crit. behaviour anisotropy 78−10430
TSeF-TCNQ, X-ray diffuse scatt., one-dimens. distortion in phonon spectrum and interpret. 78−10144
TSet, resonance Raman spectra 79−56787
$TSeT\text{-}I_2$, physical props., elec. cond. 80−24908
$TSeTBr_{0.5}$, phase transition, mag. props., thermal capacity and cond. *(Russian)* 79−99537
αTTF:Br, transport and mag. props., effect of doping 80−24934
$TTF_{0.4}TSeF_{0.6}$-TCNQ, $2k_F$ and $4k_F$ CDWs, X-ray study 80−65474
$TTF_{0.97}Se_{0.03}$-TCNQ, Peierls-superlattices and soft phonon anomalies, X-ray scatt. meas. 78−75795
TTF, $TseF_{1-x}TCNQ$ solid soln., DC conductivity, struct. 78−10423
TTF, infinite stacks, all valence electron band struct. 78−39001
TTF, origin of Raman spectrum instability 79−15456
$TTF(Br)_{0.7}$, EPR temp. depend., metal-insulator transition 77−43863
$TTF(I)_{0.71}$, EPR temp. depend., metal-insulator transition 77−43863
$TTF(I)_{0.71}$, physical props., Fermi energy scaling of metal-insulator transition temp. 77−8081
TTF(MBDT) spin-Peierls transition, mag. exchange interactions, mag. props. 80−25138
$TTF(SCN)_{0.54}$, physical props., Fermi energy scaling of metal-insulator transition temp. 77−8081
$TTF(SCN)_{0.588}$, Peierls instability, strain coupled charge density waves, X-ray scatt. obs. 78−79949
$TTF(SeCN)_{0.54}$, physical props., Fermi energy scaling of metal-insulator transition temp. 77−8081
$(TTF)_{12}(SCN)_7$ charge-transfer salt, elec., mag. and optical props. 77−43575
$(TTF)_{12}(SeCN)_7$, charge-transfer salt, elec., mag. and optical props. 77−43575
$(TTF)_7I_5$, superstruct. modulation, X-ray obs. 78−14333
$(TTF)Cl_x$, disorder transition, cond. decrease and commensurate charge density waves 80−70153
$(TTF)CuS_4C_4(CF_3)_4$, spin Peierls system, mag. field effects 80−7123
TTF and $(TTF)_7I_5$, Raman scatt. and charge transfer 77−69817
TTF and TTN derivatives, quasi-one-dimens. cond., phys. and electronic props. 78−6366
TTF conducting salts, ESR of itinerant spins 77−66424
TTF halides, spin-lattice relax. 78−88190
TTF-Cu bis-dithiolene, dimer, mol. displacements at 4.2K 80−10539
TTF-d_0, -d_4, IR and Raman spectra, vibr. assignments 78−23436
TTF-DETCNQ, heat capacity, elec. cond., cryst. struct., metal-insulator transition 77−8077
TTF-DETCNQ, metal-insulator transition, struct., elect. cond. and sp. ht. expts. 78−14662
TTF-halides, conductors with chain struct., lattice phonons and distortions, incommensurability transitions 80−24549
TTF-SCN, quasi one-dimens. conductor, CDW phase transform., X-ray scatt. study 80−24594
TTF-TCNQ, optical evidence for Coulomb interactions, review 78−6704
TTF-TCNQ:TCNQ-M, thermopower determ. 78−47772
TTF-TCNQ, 1:1 complex, atom-atom approx. and lattice energies 79−7568
TTF-TCNQ, $4k_F$ anomaly, density correlation of classical dimensional electron gas 77−80744
TTF-TCNQ, $4k_F$ anomaly, explanation 77−35875
TTF-TCNQ, 53 and 38K transitions, mag. and elec. props. meas., doping effect 77−66159
TTF-TCNQ, ^{15}N, ^2H isotope labelled, IR, Raman spectra, mol. vibrs., electron-phonon interactions 77−69835
TTF-TCNQ, anal. of harmonic microwave mixing 80−44635
TTF-TCNQ, and related 1D conductors, temp. depend. microwave dielec. const. 77−31967
TTF-TCNQ, and related compounds, low temp. irrad. effects 80−24906
TTF-TCNQ, and related cpds., elastoresistivity by strain gauge technique 80−24892
TTF-TCNQ, and related cpds., partial charge transfer and CDW modulation 79−95349
TTF-TCNQ, and Se analogues, microwave conductivity meas. by coaxial resonator technique 77−4384
TTF-TCNQ, anharmonic effects of phonons with Kohn anomalies 77−1197
TTF-TCNQ, anharmonic effects on resistivity 78−84202
TTF-TCNQ, anharmonic props., temp. (press.) depend., rel. to naphthalene and anthracene 80−15200
TTF-TCNQ, anisotropic cond., X-ray effects 80−96855
TTF-TCNQ, band struct., Fermi surface and density of states, LCAO calc. 78−60048
TTF-TCNQ, band struct., soft phonon instability 77−72821
TTF-TCNQ, CDW and phase transition exam. 78−6283
TTF-TCNQ, CDW instability, classical vs. crit. behaviour 78−39041
TTF-TCNQ, charge transfer change with press. 80−39564
TTF-TCNQ, collective-mode conductivity in metallic phase 78−64031
TTF-TCNQ, commensurate ordering 77−7829
TTF-TCNQ, cond. in phase transition region 80−24979
TTF-TCNQ, conductivity and dielec. permeability, freq. depend. 78−79984
TTF-TCNQ, conductivity model 79−51557
TTF-TCNQ, const. vol. resist., linear temp. depend. 78−51977
TTF-TCNQ, controlled defects effect on microwave cond. and dielec. function 80−24885
TTF-TCNQ, core exciton exam. by inelastic electron scatt. 77−4296

one-dimensional conductivity continued
TTF-TCNQ, coupled Peierl's systems, model, phase transitions 77−69230
TTF-TCNQ, covalon conduction 78−10427
TTF-TCNQ, crit. behaviour at electronically driven struct. phase transition 77−80767
TTF-TCNQ, crit. behaviour near 53K phase transition, Ginzburg-Landau theory 79−33249
TTF-TCNQ, crit. behaviour near 53K transition, generalised Ginzburg-Landau theory 79−56147
TTF-TCNQ, crystal, Raman scattering 78−80356
TTF-TCNQ, delocalisation in organic molecular conductors 79−78086
TTF-TCNQ, deuterated, compressibility under hydrostatic press., neutron diffr. meas. 78−2197
TTF-TCNQ, deuterated, phase transition exam. by elastic neutron scatt. 77−4194
TTF-TCNQ, dimers and trimers, Xα scattered wave calc. 78−10326
TTF-TCNQ, Drude optical edge, press. depend. 79−19882
TTF-TCNQ, dynamic nucl. polarisation exam., temp. depend. 78−39447
TTF-TCNQ, elastic neutron scatt. evidence for charge transfer change at high power 80−2163
TTF-TCNQ, elastic- and inelastic-neutron scatt. study 79−69208
TTF-TCNQ, elec. cond., role of librations 79−19580
TTF-TCNQ, elec. cond., SEM technique 80−86507
TTF-TCNQ, elec. cond. and spin susceptibility, press. and temp. depend. 80−24894
TTF-TCNQ, elec. resist., electron-phonon scatt. 80−92884
TTF-TCNQ, electron-electron interaction as source of metallic resist. 80−20162
TTF-TCNQ, electron-electron interaction strength, electron scatt. and spin-lattice relax. data 78−30878
TTF-TCNQ, electron-molecular distortion coupling near Peierls transition, IR spectra obs. 80−25390
TTF-TCNQ, electronic props., connection between theory and expt. 79−19581
TTF-TCNQ, electronic props. and comparison with $(SN)_x$, review 78−6306
TTF-TCNQ, electronic spin-lattice relax. time 77−51939
TTF-TCNQ, electronic struct. near Fermi level, tunnelling spectra 77−85126
TTF-TCNQ, energy gaps, far IR photocond. meas. 77−32004
TTF-TCNQ, enhancement of mag. susceptibility by Coulomb correlations 77−77023
TTF-TCNQ, enthalpy of sublimation and vapour press. meas. 80−92661
TTF-TCNQ, exchange effects in plasmon dispersion 78−91628
TTF-TCNQ, fluctuation cond. and commensurability pinning 80−34429
TTF-TCNQ, Hall mobility using Faraday rot. method at 9.3 GHz 77−47801
TTF-TCNQ, implications of amplitude solitons in incommensurate Peierls systems 80−92841
TTF-TCNQ, impurity effects on CDW fluctuations 80−44576
TTF-TCNQ, inelastic neutron scatt., re-examination 78−30721
TTF-TCNQ, interchain tunnelling effect on nucl. spin-lattice relax. time, interchain coupling of CDW 80−20163
TTF-TCNQ, interpretation of the $2k_f$ and $4k_f$ X-ray scatt. 77−63487
TTF-TCNQ, IR absorption peak theory 77−43991
TTF-TCNQ, IR reflectance in conducting phase 80−25388
TTF-TCNQ, irradiated, IR reflectance, optical and low-freq. transport comparison 79−51961
TTF-TCNQ, isotope effect on Peierls transition temp. 78−43367
TTF-TCNQ, isotope effect on Peierls transition temp. 78−43369
TTF-TCNQ, Kohn anomalies, phonon dispersion curves, neutron scatt. 78−10133
TTF-TCNQ, Kohn anomaly, electron-mol. vibr. coupling 77−31734
TTF-TCNQ, Kohn anomaly, electron-phonon coupling, neutron scatt. 77−7812
TTF-TCNQ, Kohn anomaly and Peierls-type transition, X-ray obs. 78−14435
TTF-TCNQ, Landau theory of phase transitions 78−30914
TTF-TCNQ, Landau theory of phase transitions 80−92666
TTF-TCNQ, lattice distortion, displacive transform., Landau theory 77−31743
TTF-TCNQ, lattice distortion, displacive transform., Landau theory 77−84879
TTF-TCNQ, lattice phase transitions and cond. anomalies obs. 77−1226
TTF-TCNQ, linear CDW, melting of phase locking *(Japanese)* 77−43522
TTF-TCNQ, low temp. fast neutron irradiation, elec. cond. meas. 80−59964
TTF-TCNQ, low. temp. phase stochastic theory of nonlinear DC cond. 77−80768
TTF-TCNQ, low temp. phase transitions, elastic neutron scatt. obs. 78−14464
TTF-TCNQ, Madelung energy, electronic struct. *(Russian)* 78−6253
TTF-TCNQ, mag. suscept. meas. 78−56287
TTF-TCNQ, Matthiessen's rule, effective defect resistivity 80−6821
TTF-TCNQ, metallic cond., nonlinear amplitude-phase interaction 80−88490
TTF-TCNQ, metallic cond. press. depend., single particle phonon scatt. description 79−69503
TTF-TCNQ, metallic conductivity press. depend. thermal expansion effects 79−69502
TTF-TCNQ, metallic conductivity temp. depend. 78−6357
TTF-TCNQ, microwave eddy currents and EPR 77−80996
TTF-TCNQ, mixed valency in organic crystals *(Japanese)* 79−78051
TTF-TCNQ, modulated phases in terms of four-and five-dimens. superspace groups 78−47310
TTF-TCNQ, mol. core excitons, high energy electron inelastic-scatt. spectra 77−69235
TTF-TCNQ, molecular coordination along stacking directions 79−47031
TTF-TCNQ, near commensurability, longit. cond. meas. and X-ray scatt. 79−78084
TTF-TCNQ, neutron and X-ray diffuse scatt., phase transitions, one-dimens. behaviour and interpret. 78−10381
TTF-TCNQ, new transition *(French)* 77−59263
TTF-TCNQ, non-linear elec. transport by pinned CDW 80−20172
TTF-TCNQ, non-ohmic conductivity, bion dissociation interpretation 79−63048
TTF-TCNQ, nonbonding intermolecular forces 80−83443
TTF-TCNQ, nonlinear electronic transport, microwave harmonic mixing obs. 80−20168

one-dimensional conductivity continued
TTF-TCNQ, nonlinear transport at low temp. 77−8079
TTF-TCNQ, nucl. spin relax. obs., diffusive character of response function and interchain coupling 78−10797
TTF-TCNQ, one-dimensional conductor, fluctuation conductivity in high press. phase 79−91034
TTF-TCNQ, ordering types below 54K, perp. phase depend. 78−6300
TTF-TCNQ, organic metal, Van der Waals donor stacking 80−15037
TTF-TCNQ, origin of Raman spectrum instability 79−15456
TTF-TCNQ, Peierls instability and consequences 78−6303
TTF-TCNQ, Peierls transition, photocond. meas., absorption coeffs. above gap 78−72198
TTF-TCNQ, Peierls-superlattices and soft phonon anomalies, X-ray scatt. meas. 78−75795
TTF-TCNQ, periodic lattice distortions, charge density waves 79−82536
TTF-TCNQ, phase transition model, interchain coupling of CDW 77−76558
TTF-TCNQ, phase transitions, thermoelec. power meas. 79−65464
TTF-TCNQ, phase transitions and CDW state, controlled disorder effects 80−15507
TTF-TCNQ, phase transitions and CDW state, induced defect depend., transport and mag. studies 80−24980
TTF-TCNQ, phason and metal-insulator microdomain model, Young's modulus temp. depend. anal. 77−31964
TTF-TCNQ, phason instability at 49K phase transition 77− 4303
TTF-TCNQ, phonon anomalies and superstructures, Peierls transition, X-ray diffuse scatt. obs. 77−27962
TTF-TCNQ, phonon dispersion and Kohn anomaly, inelastic neutron scatt. 77−1196
TTF-TCNQ, phonon dispersion curve meas., Peierls transition exam. 78−10134
TTF-TCNQ, physical properties, reviews *(Japanese)* 80−24883
TTF-TCNQ, physical props., Fermi energy scaling of metal-insulator transition temp. 77−8081
TTF-TCNQ, plasmon spectrum, tight binding model 78−84158
TTF-TCNQ, positive microwave dielectric const. 78−47771
TTF-TCNQ, possible Lifshitz point, struct. transitions exam. 78−2423
TTF-TCNQ, pure and irrad. crystal, nonlinear transport at low temp. 79−4552
TTF-TCNQ, quasi one-dimensional low temp. mag. susceptibility 80−93069
TTF-TCNQ, Raman scatt. and charge transfer 77−69817
TTF-TCNQ, Raman scattering 78−80355
TTF-TCNQ, resist., crit. behaviour anisotropy 78−10430
TTF-TCNQ, review 78−60070
TTF-TCNQ, segregated stack stability 78−55831
TTF-TCNQ, self-energy calcs. 79−4499
TTF-TCNQ, short-range and long-range order of phason clusters 77−35874
TTF-TCNQ, single cryst., mag. susceptibility in phase transition region, two-gap model 78−6511
TTF-TCNQ, sound vel. in a a dand b directions, 0-300K 77−84851
TTF-TCNQ, sp. ht. meas., phase transition obs. at 46K 77−43326
TTF-TCNQ, spin susceptibility below 53K, compared with elec. cond. data 77−43865
TTF-TCNQ, spin waves, scatt. at $4k_F$, spin-Peierls fluctuations 78−72093
TTF-TCNQ, struct. phase transitions, coupled phasons model 78−83942
TTF-TCNQ, struct. rel. to quasi one-dimensional elec. props. 78−14716
TTF-TCNQ, surface magnetism 78−2703
TTF-TCNQ, surface magnetism obs. 78−6561
TTF-TCNQ, symmetry changes and phase transitions 78−6299
TTF-TCNQ, TCNQ and TTF bandwidths, extended Huckel and CNDO/2 calcs. 79−7771
TTF-TCNQ, temp. depend. of dynamic nucl. polarisation enhancement of protons 78−6601
TTF-TCNQ, temp. depend. of phonon frequencies at constant vol. 80−10616
TTF-TCNQ, theory of structural phase transitions 78−38831
TTF-TCNQ, thermal cond. above and below Peierls transition, electronic and lattice contribs. 79−95394
TTF-TCNQ, three dimensional ordering 77−59087
TTF-TCNQ, two-chain Fermi gas, response behaviour 80−2381
TTF-TCNQ, two-chain inverted band model 78−6313
TTF-TCNQ, vaporisation. mass spectroscopy 77−1224
TTF-TCNQ, X-ray, neutron scattering, low temp. modulated lattice, 3D modulated lattice 78−10033
TTF-TCNQ, X-ray exam. of $2k_F$ and $4k_F$ anomalies 78−10162
TTF-TCNQ, X-ray irrad., transverse cond. 80−6432
TTF-TCNQ, XPS, surface electronic struct. 78−52627
TTF-TCNQ, Young's modulus, temp. depend., rel. to transition points 77−15475
TTF-TCNQ and related compounds, cryst. struct., organisation, dimensionality, interchain disorder 80−19790
TTF-TCNQ and related cpds., elastoresistivity 79−23956
TTF-TCNQ and related cpds., magnetic props., press. effects 77−47981
TTF-TCNQ complex, trans-diethyl-dimethyl TTF-TCNQ, one-dimens. cond. 80−96853
TTF-TCNQ complex *(Japanese)* 77−1412
TTF-TCNQ complex salt press. dependence elec. cond. at low temps. *(Japanese)* 79−87090
TTF-TCNQ complexes, charge transfer, X-ray photoelectron spectra determ. 77−73210
TTF-TCNQ crystal, antiferroelec. ordering of electronic polarisation, simple model anal. 78−92028
TTF-TCNQ crystal, charge transfer, dipolar polaris. binding energy 77−80754
TTF-TCNQ crystals, X-ray topographic study of cryst. perfection 80−96525
TTF-TCNQ derivations, transport props., reflectance spectra 78−91683
TTF-TCNQ electronic props., PMR 78−2763
TTF-TCNQ family, donor stack dominance of transport props. 80−20166
TTF-TCNQ film, energy loss spectra of low energy electrons 78−19116
TTF-TCNQ film, mag. field effects on IR spectra *(French)* 77−48260
TTF-TCNQ film on KBr, IR spectra in mag. field 77−16310
TTF-TCNQ low temp. mag. susceptibility, neutron irrad. effects 80−60311
TTF-TCNQ phase transition, press. depend., longitudinal lockin, stacking axis resistivity meas. 78−47520
TTF-TCNQ powders, phase transition obs. in sp. ht. data 77−89539

one-dimensional conductivity continued
TTF-TCNQ salts, self-consistent continued-fraction theory of cond. 79−69482
TTF-TCNQ series, cryst. struct., elec. cond., and EPR meas., steric factor effects 80−19789
TTF-TCNQ type organic metals, study of interstack interactions 79−47089
TTF-TCNQ type salt, trimethylene-TTF-TCNQ, unsymmetric cation, phys. props. 78−76059
TTF-TCNQ-d_8, large single cryst. platelet growth by diffusion method 78−3010
TTF-TNCQ, mobility due to mol. optical phonon scatt. 77−85202
TTFCuBDT, spin-Peierls transition in spin 1/2 Heisenberg chains, RPA calcs. 80−25150
TTF.$PtS_4C_4(CF_3)_4$, quasi-one-dimensional cpd., exchange, thermal and mag. study 78−68209
TTG-BDT(Cu), giant struct. distortion, high speed photography obs. 78−43121
TTSeF-2,5-dimethyl TCNQ, donor and acceptor stack stability against Peierls distortion 78−51979
$TTT_{1.2}NiS_4C_4H_4$, quasi-one-dimensional cond., cryst., mag. and elec. props. 78−10424
$TTT_2^+.I_3^-$, cryst. and mol. struct. by X-ray study 79−51096
TTT_2-$(I_3)_{1+x}$, physical props., elec., mag. and optical meas. 80−24908
$TTT_2I_{1.5-x}Br_x$, chem. impurities and neutron irrad. induced defects, effects on DC cond. 80−49699
$TTT_2I_{3+\delta}$, thermoelec. power and metal-semicond. transition 80−34431
TTT_2I_3, charge transfer salt, Coulomb effects, Madelung energy calcs. 80−19747
TTT_2I_3, charge transfer salt, Coulomb effects 79−28308
TTT_2I_3, charge transfer salt, Coulomb effects 79−46599
TTT_2I_3, chem. impurities and neutron irrad. induced defects, effects on DC cond. 80−49699
TTT_2I_3, quasi one-dimens. organic metal, elec. cond. and thermoelec. power 80−24899
$TTT_2I_xBr_{3-x}$, charge transfer complex, optical and elec. props. 79−4554
TTT, donor-acceptor system, physico-chemical studies *(Hungarian)* 80−75554
TTT, resonance Raman spectra 79−56787
$(TTT)_2I_{3+\delta}$, struct., X-ray diffuse scatt. study 80−24437
$(TTT)_2I_{3+\delta}$, 1 dimens. conducting chains, supercond. fluctuations 78−39099
$(TTT)_2I_{3+x}$, three-dimensional organic chain conductors, one-dimensionalisation by impurities 78−91681
$(TTT)_2I_3$, metal-insulator phase transition, elec. cond. and mag. susceptibility meas. 78−14719
$(TTT)_2I_3$, optical, spin-reson., magnetoresist. study, nature of ground state 78−68023
$(TTT)_2I_3$ quasi-one-dimensional organic metal, effects of disorder on cond. and thermoelec. power 79−56206
TTT cation radical salts, cryst. struct. by X-ray anal., rel. to elec. props. 80−24436
TTT cation-radial salts, new class of quasi-one-dimens. org. cond. 78−6367
TTT-$(I_3)_{0.5}$, one-dimens. metal, mag. susceptibility, elec. resist., thermopower meas. 78−87967
TTT-$I_{1.6}$, dimensionality and disorder 77−66160
TTT-I_c, direct current conductivity and thermo-electric force, 4-400K *(Hungarian)* 79−56251
$TTTI_xBr_{1.5-x}$, optical and transport props. 80−24911
two level commensurability in one-dimensional Peierls system *(Russian)* 80−70688
two-band system, coexistence of dielec. and supercond. ordering 80−10853
valence bond theory of narrow band conductors 80−24777
variational solution of sine-Gordon theory and Luther-Emery backward scatt. model for one-dimens. systems 79−40447
weakly coupled 1-D metallic chains, phase transition *(Russian)* 77−31946
zero energy state, nearest neighbour off-diagonal disorder, fluctuations and localisation 77−35883
Ba_xI_y cyclodextrin, quasi-one-dimens. cpd., synthesis, elec. and mag. props. 80−2380
$Co_{0.83}(Pt(C_2O_4)_2).6H_2O$, cond., dielec. const., microwave obs. 80−44636
$Co_{0.83}[Pt(C_2O_4)_2].6H_2O$, quasi-one-dimens. conductor, Peierls distortion and superlattice, X-ray study 80−29397
$Cs_2(Pt(CN)_4)Cl_{0.3}$, elec. cond., 300-40K, 3-dimens. ordering temp. 79−78087
$Cs_{1.75}(Pt(CN)_4).1.5H_2O$, 1-D cond., IR spectra 77−85703
$Cs_2[Pt(CN)_4](FHF)_{0.39}$, one-dimensional elec. cond. 79−69504
$Cs_{1.75}[Pt(CN)_4].xH_2O$, one-dimensional, X-ray diffuse scatt. meas. 77−19937
Cu-Pt complex, $[Cu\ (C_2N_2H_8)_2][Pt(C_2O_4)_2]$, cryst. struct. determ. 77−4072
Fe_xI_y cyclodextrin, quasi-one-dimens. cpd., synthesis, elec. and mag. props. 80−2380
Ge bicrystal, transition from 2-dimens. cond. *(Russian)* 79−56273
HMTSF-TNAP, elec. cond. under press. 78−84200
$Hg_{2.86}AsF_6$, elec. cond., pseudo-one dimens. 77−20304
$Hg_{2.86}AsF_6$, linear chain, anomalous low temp. sp. ht. 78−14476
$Hg_{2.86}AsF_6$, thermopower, temp. depend. 79−65465
$Hg_{2.91}AsF_6$, elec. cond., pseudo-one dimens. 77−20304
Hg_3AsF_6, one dimensional conductor *(Japanese)* 79−73499
$Hg_{3-\delta}AsF_6$, linear chain compound, mag. field induced residual resist., anisotropic supercond. 80−24897
$Hg_{3-\delta}AsF_6$, low-temp. sp. ht., lattice dynamics, 1- to 3-dimens. crossover 79−86864
$Hg_{3-\delta}AsF_6$, one dimens. fluctuations and chain ordering transform 80−24593
$Hg_{3-\delta}AsF_6$, one dimensional phonons and chain ordering 80−24544
$Hg_{3-\delta}AsF_6$, one-dimens. phonons and phase-ordering phase transition, neutron scatt. expts. 78−26644
$Hg_{3-\delta}AsF_6$, one-dimens. fluctuations and chain ordering transform., neutron scatt. calc. 78−59923
$Hg_{3-\delta}AsF_6$, quasi one-dimensional, anomalous magnetoresistance 80−24884
$Hg_{3-\delta}AsF_6$, quasi-one-dimens., mag. field induced residual resistivity 79−1596
$Hg_{3-x}AsF_6$, incommensurate chain compound, anisotropic Knight shift, spin-spin interactions 78−80233

one-dimensional conductivity continued
$Hg_{3-x}AsF_6$, linear chain metallic cpd., square Fermi surface model for conduction 80−6822
$Hg_{3-x}AsF_6$, phase-ordering phase transition, elastic neutron scatt. obs. 79−33087
$Hg_{3-x}AsF_6$, thermopower, phonon drag 79−65466
$Hy_{2.86}AsF_6$ linear chain cpd., metallic, anomalous elec. props. 77−51731
$K_xAl_xTi_{8-x}O_{16}$, $1.6 \leq x \leq 2.0$, dielec. response in freq. range 10^{-3} to 10^6 Hz 79−65785
$KLi(Pt(CN)_4).2H_2O$, cryst. struct., polarised emission obs. 78−52538
$K_{1.54}Mg_{0.77}Ti_{7.23}O_{16}$, one-dimens. superionic cond., ionic order, defect cond. 78−87815
$K_{1.54}Mg_{0.77}Ti_{7.23}O_{16}$, hollandite, one-dimens. superionic cond., transport model 80−107529
$K_xMg_{x/2}Ti_{8-x/2}O_{16}$ $1.6 \leq x \leq 2.0$, dielec. response in freq. range 10^{-3} to 10^6 Hz 79−65785
$K_{1.75}Pt(CN)_4$. $1.5H_2O$, quasi 1D metals, electric conductivity meas., semiconductor-metal transition 79−99538
$K_2Pt(CN)_4$, quasi-one-dimens. Peierls system, phonon dispersion and neutron scatt., calc. 80−24550
$K_2Pt(CN)_4Br_{0.3}2.6H_2O$ crystal, quasi-one-dimensional, optical consts. and dielec. permittivity dispersion 77−1695
$K_2Pt(CN)_4Br_{0.3}3H_2O$ incommensurate linear conductors correlation length in 77−80745
$K_2Pt(CN)_4Br_{0.3}3.2H_2O$, linear conductor, dynamical aspects of fluctuations 79−33715
$K_2Pt(CN)_4Br_{0.3}3.2H_2O$, linear cond., ^{195}Pt NMR evidence of low lying non-linear excitation 80−44933
$K_2Pt(CN)_4Br_{0.3} \times 3H_2O$, struct., neutron determ., Peierls distortion 79−46640
$K_2Pt(CN)_4Br_{0.3} \times 3.2D_2O$, Kohn anomaly in longit. acoustic phonon 77−7812
$K_2Pt(CN)_4Br_{0.3}.2.7D_2O$, under hydrostatic press., compressibility, neutron diffr. 79−46742
$K_2Pt(CN)_4Br_{0.3}.3H_2O$, IR absorption peak theory 77−43991
$K_2Pt(CN)_4Br_{0.3}.3H_2O$, lattice softening, temp. depend. of elastic consts., US meas. 78−14432
$K_2Pt(CN)_4Br_{0.3}.3H_2O$, struct. rel. to quasi one-dimensional elec. props. 78−14716
$K_2Pt(CN)_4Br_{0.3}.3H_2O$, one-dimensional cond., phys. props. *(Japanese)* 78−30916
$K_2Pt(CN)_4Br_{0.3}.3H_2O$, review 78−60070
$K_2Pt(CN)_4Br_{0.3}.3H_2O$, one-dimens. cond. transition, spin suscept. and DC cond. temp. depends. 78−84198
$K_2Pt(CN)_4Br_{0.3}.3H_2O$, specific heat, 0.75 to 25.7K 78−87795
$K_2Pt(CN)_4Br_{0.3}.3H_2O$, specific heat and ferroelastic behaviour 78−91447
$K_2Pt(CN)_4Br_{0.3}.3H_2O$, Krogmann salt, non-empirical localised orbital cal. of electronic struct. 78−91636
$K_2Pt(CN)_4Br_{0.3}.3H_2O$, quasi-one-dimens. conductor, Br^- distrib. long-range Coulomb interaction, effect on structure and CDW 79−7591
$K_2Pt(CN)_4Br_{0.3}.3H_2O$, quasi one-dimens. conductor, EPR linewidth 80−54938
$K_2Pt(CN)_4Br_{0.3}.3.2D_2O$, lattice dynamics, neutron scatt. expts. 78−14412
$K_2Pt(CN)_4Br_{0.3}.3.2D_2O$, dynamic struct. factor, inelastic neutron scatt. study 79−42185
$K_2Pt(CN)_4Br_{0.3}.3.2H_2O$, Kohn anomalies, phonon dispersion curves, neutron scatt. 78−10133
$K_2Pt(CN)_4Br_{0.3}.xH_2O$, conductivity and optical refl. depend. on water content 77−39828
$K_2Pt(CN)_4Br_{0.3}.xH_2O$, one-dimensional cond., effects of dehydration on mag. props. 77−85549
$K_2Pt(CN)_4Br_{0.3}.xH_2O$, dynamical props. near Peierls instability, neutron scatt.. 78−14436
$K_2Pt(CN)_4Cl_{0.3}(Br_{0.3}).3H_2O$, struct., single cryst. neutron diffr. expts. 78−14321
$K_{1.75}Pt(CN)_4 1.5H_20$, anomalous elec. cond. 79−47088
$K_{1.75}Pt(CN)_4 \times 1.5H_2O$, struct., neutron determ., Peierls distortion 79−46640
$K_{1.75}(Pt(CN)_4).1.5H_2O$, 1-D cond., IR spectra 77−85703
$K_{1.75}Pt(CN)_4.1.5H_2O$, struct., single cryst. neutron diffr. expts. 78−14321
$K_{1.75}Pt(CN)_4.1.5H_2O$, Pt chain distortion, X-ray obs. 78−14322
$K_{1.75}Pt(CN)_4.1.5H_2O$, Raman scatt. and luminesc. studies 80−25394
$K_{1.6}Pt(C_2O_4)_2 \times 1.2H_2O$, sinusoidally modulated structure 77−84730
$K_{1.6}Pt(C_2O_4)_2 \times 1.2H_2O$, struct., neutron determ. 79−46640
$K_xPt(C_2O_4)_2.nH_2O$, chem. analysis and elec. cond. meas. 78−76060
$K_2[Pt(CN)_4]Br_{0.3}.3H_2O$, high press. structs. and phase transitions 80−107423
$K_{1.75}[Pt(CN)_4]1.5H_20$, elec. cond. studies, Peierls transition 80−24901
$K_{1.75}[Pt(CN_4)].xH_2O$, one-dimensional, X-ray diffuse scatt. meas. 77−19937
$LiAlSiO_4$, β-eucryptite one-dimens. fast ion cond., temp. depend. of cryst. struct. 80−107191
β-$LiAlSiO_4$, eucryptite, one-dimensional ionic conductor, neutron scatt. study 80−49361
$Mg_{0.82}Pt(C_2O_4)_2 \times 5.3H_2O$, struct., neutron determ. 79−46640
$(NH_4)_2[Pt(CN)_4]Cl_{0.42}.3H_2O$ quasi one dimensional conductor, physical props., cond. freq. depend. 79−95393
$Na_{0.33}V_2O_5$, quasi-one-dimensional conductor, anisotropic cond. meas., 18-400K 77−85204
β-$Na_{0.33}V_2O_5$, quasi-one-dimensional conductor, NMR studies 80−93204
NbI_4, metallic state, resistivity anomaly 79−15136
NbI_4, quasi-one dimens., press.-induced metal-insulator transition 78−43447
NbS_3, transport props. 80−20175
$NbS_3(Se_3)$, Peierls distortion, electron diffr. obs. 80−39503
$NbS_3(Se_3)$, phase transitions and elec. props. 80−20178
$NbSe_2$ (2H), intercalated with TCNQ, elec. resistivity temp. behaviour anomaly *(Russian)* 80−10953
$NbSe_2$:Fe (2H), pure and doped, magnetoresist. and elec. resist. temp. depend. rel. to CDW form. 80−44574
$NbSe_3$ and $Nb_{1-x}Ta_xSe_3$, thermoelec. power meas., 10-300K 80−20177
$NbSe_3$, CDW form., non-linear props., temp. and press. depend. 80−49753
$NbSe_3$, CDW linear chain metal, two band model in ohmic region 79−38056
$NbSe_3$, CDW noise, temp. and freq. depend. 80−103681
$NbSe_3$, chain-like compound, low temp. phase transition 78−80088
$NbSe_3$, cond., Frohlich mode motion *(Russian)* 79−95395

one-dimensional conductivity continued
$NbSe_3$, conductivity anisotropy and transverse magnetoresistance 79−38055
$NbSe_3$, depinning props. of lower CDW, weak pinning model *(French)* 80−70630
$NbSe_3$, elec. field depend. thermopower 79−56204
$NbSe_3$, elec. resist. anomalies down to 7 mK associated with CDWs 79−60811
$NbSe_3$, Fermi surface, press. effects, Shubnikov-de Haas effect meas. at 1.5K 80−20068
$NbSe_3$, fibrous struct., comparison with $NbSe_2$ 78−14715
$NbSe_3$, Frohlich sliding mode, nonlinear resist. and noise 79−60808
$NbSe_3$ interference effects of CDW motions 80−88544
$NbSe_3$, linear chain metal, anomalous transport props. 78−14718
$NbSe_3$, linear-chain metal, Hall effect meas. 78−76058
$NbSe_3$, metallic, non-ohmic cond., CDW pinning 80−39563
$NbSe_3$, non-Ohmic conduction, depinning of charge density waves 79−65459
$NbSe_3$, quasi one-dimens. conductor, CDW phase transform., X-ray scatt. study 80−24594
$NbSe_3$, transport props. 80−20175
$NbSe_3$, two band model and galvanomagnetic study 80−20176
$NbSe_3$:Ta, elec. cond., anomalous, and microwave absorpt. 79−42527
Ni complex, (1,4,5,8,9,12,13,16-octamethyltetradbenzporphinato nickel) $^{+?}$ $(I_3^-)_y$, atomic limit of Hubbard model and polarons 80−39860
Pt chain compounds, one dimens. conductors, Fermi wavevector determ., X-ray scatt. obs. 80−44187
Pt complex, $(C(NH_2)_3)_2Pt(CN)_4Br_{0.23}.H_2O$, pseudo-one-dimens. cpd., solitary wave excitations, and cryst. struct. 78−6307
Pt complex, $[C(NH_2)_3]_2[Pt(CV)_4]Br_{0.23}.H_2O$, one-dimensional, X-ray diffuse scatt. meas. 77−19937
Pt complex, bis(1,2-benzoquinonedioximato)platinum(II), intrinsic elec. cond. 78−6377
Pt complex, KCP, periodic lattice distortions, charge density waves 79−82536
Pt complex, $Mg_{0.82}Pt(C_2O_4)_2.xH_2O$, X-ray diffuse scatt., 1-D Peierls-Kohn anomaly and struct. transforms. 78−14680
Pt complexes, cyano and cyanohalide hydrates, IR absorpt. spectra 77−6771
Pt complexes, pressure effect obs. 77−35930
$Pt_6(NH_3)_{10}Cl_{10}(HSO_4)_4$, chain struct. and elec. cond. 78−2469
$Rb_{1.75}Pt(CN)_4$. $1.5H_2O$, quasi 1D metals, electric conductivity meas., semiconductor-metal transition 79−99538
$Rb_{1.75}(Pt(CN)_4).1.5H_2O$, 1-D cond., IR spectra 77−85703
$Rb_2[Pt(CN)_4](FHF)_{0.40}$, one-dimensional elec. cond. 79−69504
$Rb_{1.75}[Pt(CN)_4].xH_2O$, one-dimensional, X-ray diffuse scatt. meas. 77−19937
$(SN)_x$, 1-D chain, ab initio treatment, HF LCAO calc. 77−1349
$(SN)_x$, acoustic phonons, inelastic neutron scatt. obs. 78−6136
$(SN)_x$, brominated, struct. and elec. props. 80−24914
$(SN)_x$ chain, isolated, effect of $(SCH_2)_2$ impurities, on electronic props., EHT calcs. 79−15067
$(SN)_x$ cryst., synthesis and elec. cond. *(Japanese)* 77−69308
$(SN)_x$, electrical cond. at high press., scatt., evidence for semimetallic band struct. 77−43573
$(SN)_x$, electron tunnelling, absence of supercond. energy gap 78−47769
$(SN)_x$, electronic props., ab initio LCAO HF orbital calc. 77−51635
$(SN)_x$, electronic props. and comparison with TTF-TCNQ, review 78−6306
$(SN)_x$, electronic struct., X-ray and UV photoemission obs., OPW and pseudopot. calcs. 78−6832
$(SN)_x$, electronic struct. by extended tight-binding method, comparison with S_2N_2 precursor 77−76722
$(SN)_x$, electronic struct. and opt. props. 78−6256
$(SN)_x$, epitaxial film, elec. resist., 0.03-8.9K, possible supercond. 77−15970
$(SN)_x$ film, evaporated on low temp. substrate, elec. cond. 77−63003
$(SN)_x$ film, Hall effect, elec. cond. and magnetoresist. meas. 78−84314
$(SN)_x$ film and crystal, acoustic and optical phonons, Raman, i.r. and transmission spectra 77−4642
$(SN)_x$, fluctuation induced cond. and dimensionality 77−28167
$(SN)_x$ halogenated derivatives, cond. and magnetoresist., 4.2-300K 80−24915
$(SN)_x$, intrinsic cond. anisotropy from galvanomag. effect obs. 78−6369
$(SN)_x$, lattice and electronic sp. ht. contribs. density of states 77−43344
$(SN)_x$, mol. cluster and band struct. calc. 77−8004
$(SN)_x$, neutron and heavy ion bombard., effect on elec. cond. along chain axis 78−56136
$(SN)_x$, one-dimens. supercond. mechanism *(Chinese)* 79−47189
$(SN)_x$, polycryst. films, single crysts., UPS, valence band struct. 77−69967
$(SN)_x$ polymer, Be_2 doped, influence of halogen on elec. and optical props. *(Japanese)* 79−51559
$(SN)_x$ polymer, quasi-one-dimens. and metallic behaviour *(Japanese)* 77−43577
$(SN)_x$, polymerisation, EPR obs. 79−73800
$(SN)_x$, preparation and properties 78−27389
$(SN)_x$, quantum chem. calcs. of electronic struct. 78−6257
$(SN)_x$, quasi-one-dimens., theoretical group anal. of electron spectrum 79−82511
$(SN)_x$, single cryst., elec. anisotropy, polarised refl. spectra 77−36264
$(SN)_x$ single crystal, transverse magnetoresistance 78−72140
$(SN)_x$ single crystals, galvanomag. effects 79−19582
$(SN)_x$, supercond., fluctuation cond., crit. mag. fields 80−39712
$(SN)_x$, supercond. props., review 78−6474
$(SN)_x$, supercond. props., press. depend., up to 9.5 kbar 78−68106
$(SN)_x$, temp.-depend. of elec. resist. and mag. susceptibility, density of states determ. 77−51877
$(SN)_x$, tensile and piezoresist. expts. 78−15447
$(SN)_x$, thermoelec. power, 0.1 to 4.2K, phonon drag contrib. and supercond. transition 79−56356
$(SN)_x$, uniaxial stress effect on room temp. elec. cond. 77−39826
$(SN)_x$, vaporisation, mass spectroscopy 77−1224
$(SN)_x$:Br, ion implantation effect on elec. props. 80−65026
$(SN)_x$:Br, X-ray absorpt. meas. of mol. struct., orientation and charge transfer 80−25486
$(SNBr_{0.4})_x$, $(SNI_{0.02})_x$, $(SN[ICl]_{0.01})_x$, influence of halogen on DC conductivity and magnetoresist. 78−91682
$(SNBr_{0.4})_x$, DC resistivity, temp. depend. 77−59349
$(Sn)_x$, superconducting polymer, elec. cond., heat capacity and optical props. 80−7028

one-dimensional conductivity continued
TCNQ ion-radical salts, struct. disorder 79−99885
TCNQ salt, TEA(TCNQ)$_2$, Hall effect and thermopower sign anomaly 79−56205
TCNQ salt, TSeF-TCNQ, anal. of harmonic microwave mixing 80−44635
TCNQ salts, bond lengths and charge transfer *(French)* 77−80493
TCNQ salts, $Cs_2(TCNQ)_3$, quasi-one-dimens., IR spectra, electron-vibr. interaction 78−88309
TCNQ salts, mag. props. 77−43869
TCNQ salts, Qn(TCNQ)$_2$ and N-propyl-Qn(TCNQ)$_2$, low temp. mag. susceptibility, neutron irrad. effects 80−60311
$(TSeT)_2Cl$ complex, phase transform. under press., cond. *(Russian)* 80−92674
$(TSeT)_2Cl$, metallic phases 80−20159
TTF-TCNQ, ^{13}C Knight shift and spin-lattice relax. meas., local susceptibility determ. 77−4571
TTF-TCNQ, cond. and longitudinal sound attenuation above Peierls transition point 77−28168
TTF-TCNQ, const. volume resistivity anomalous behaviour 80−103682
TTF-TCNQ, DC Hall effect meas. 77−89753
TTF-TCNQ, irradiated, libron and phonon equilibration, resistivity meas. 79−42530
TTF-TCNQ, nonlinear transport in pinched one-dimensional CDW system 77−89754
TTF-TCNQ, one-dimens. supercond. mechanism *(Chinese)* 79−47189
TTF-TCNQ, pure and irrad., nonlinear transport, ESR study, 1.2-4.2K 80−20167
TTF-TCNQ, transport props. of dynamically disordered chains 78−72137
TTF-TCNQ, transverse acoustic mode, inelastic neutron scatt. meas. 77−47526
TTF-TCNQ , elec. props. in high temp. regime, effect of controlled disorder 78−30912
TTF-TCNQ single crystal, nonlinear electronic transport, microwave harmonic mixing 78−91684
$TTF.CuS_4C_4(CF_3)_4$, spin-Peierls system, nucl. spin-lattice relax. process 78−19361
TTT_2I_3, neutron irrad. induced defects and chemical impurity effects on DC cond. 80−39565
TaS_3, CDW state, Raman spectroscopy obs. 78−60439
TaS_3, one-dimensional compound, phase anal., X-ray and elec. meas 79−51086
TaS_3, transport props. 80−20175
$TaS_3(Se_3)$, phase transitions and elec. props. 80−20178
$TaSe_3$, chain-like compound, low temp. phase transition 78−80088
$TaSe_3$, fibrous struct., comparison with $TaSe_2$ 78−14715
$TaSe_3$, transport props. 80−20175
$Tl_2Mo_6Se_6$, one dimensional supercond. crystal struct., resist. and upper crit. field 80−50016
V_3Si, quasi-one-dimens. band struct. 78−19596
ZrS_3, quasi one-dimens. semicond., elec. transport props. 80−107790
one-dimensional conductors *see one-dimensional conductivity*
online literature searching *see information retrieval*
online operation
used for systems software in online and real-time systems but for hardware aspects see real-time systems
see also interactive systems; real-time systems
air pollution automatic monitoring network, statistical approach to online control 77−41164
biological STEM, low-dose, using digital data processing system 78−24203
biological STEM, on-line data processing system 78−24202
chemical on-stream analysers development 77−66778
COSMOS plate-measuring machine, online control software 77−64652
display aid for bubble chamber film automatic meas. 78−5098
ECG, His bundle activity noninvasive recording 77−13023
electrochemical system, LF impedance meas. technique using on-line computer 80−57339
fissile material inventory and criticality control system, INMACS 79−89486
gas chromatography-mass spectrometry data system, research-oriented, principles and applics. 80−40770
image restoration and manipulation using minicomputer 77−34831
Ionospheric Sounding Satellite control, online tracking system *(Japanese)* 77−78608
LMFBR refuelling scheme optimisation by man machine interactive method 77−67826
magnetic torque curve analysis, online microprocessor system 78−254
Nancay radioheliograph, Mark II, on-line data reduction methods 78−28517
NMR in undergrad. instruction, general purpose microcomputers use for hypothetical spectra synthesis 80−42009
paediatric radioluscent bone length meas. 78−48891
particle size distribution meas., online stroboscopic microscope apparatus 80−101783
particle-particle correlation experiment, on-line four parameter anal. system *(Chinese)* 80−42910
pulmonary gas exchange data online acquisition system 78−28100
PWR differential rod worth and feedback coeff. online estimation system 79−9798
PWR power plant, vibr. and press. signals, information for online vibr. monitoring system 77−18674
radio astronomy, online interference-excising correlator 79−75110
sensor cleaning 78−77883
shade monitor, strip materials 79−30526
spectrophotometer (UR-20), data handling attachment 77−26409
spectroscopic data, optical multichannel vidicon spectrometric detector appl. 78−74077
spectroscopic data base system status 80−104475
steel, cold rolled strip, surface defects, online automatic system, design study 79−34231
STEM coupling to small computer 79−54235
vectorcardiographic analysis microprocessors and instrumentation 78−36020
West German LWR primary system online surveillance 79−3217
wind energy conversion system control, performance in turbulent wind environment 79−48069
online programming *see interactive programming*
Onsager relations *see thermodynamics*
Onsager theory of dielectrics *see dielectric properties of substances*
opacimeters *see turbidimetry*
opalescence
see also critical opalescence
depolarising optical system characterisation by automated ellipsometer 78−32855
glass, opalescing, visible light scattering, angular depend. of intensity, correction for attenuation 79−4814
$LiTaO_3$ glass-ceramics, transparent fabrication by crystn. of aluminosilicate glasses 77−59734
$MgO-Al_2O_3-SiO_2$, metastable liq. phase separation region, electron microscope exam. 78−88451
VO_2, light scatt. near semicond.-metal phase transition 78−60414
OPDAR *see optical radar*
operating amplifiers *see operational amplifiers*
operating systems (computers)
see also distributed processing; supervisory and executive programs
CERN computing school, La Grande Motte, France (1976) 77−65414
Intel 8080A, X-ray emission analyser, materials testing *(Hungarian)* 79−43522
microprocessor multiple arrays, operating systems for nuclear diagnostic system 79−49918
minicomputer high-level languages and real-time operating systems for scientific instrumentation 79−12778
Minsk 22 interrupts *(Russian)* 78−16165
multiprocessor based data acquisition system, design 79−89556
nerve fibre counting by pipeline multiminicomputer image processing 80−109013
RSX-11M appl. to X-ray diffr. and fluoresc. anal. 80−322
operational amplifiers
108 op amp radiation hardening by modified processing, failure anal. 77−18751
AC mutual inductance bridge, mag. susceptibility meas. appl. 78−89508
acoustic temp. indicator, consisting of temp. sensitive resistor and operational amplifiers *(Spanish)* 80−13061
capacitance meas. instrument appl., with direct indication, for 10pF to 10μF range *(German)* 77−146
compensation densitometer servosystem using integrated operational amplifiers 78−89525
computing amplifier calculating logarithm of a ratio 78−4600
DC current meter appl., with automatic drift compensation, for 10^{-12} to 10^{-6} A, neutron flux detection appl. *(Czech)* 78−883
ECG amplifier with automatic lead switching 78−28106
electrochemical analysis, use of operational amplifiers 80−21335
eye long-term growth and shortsightedness model 79−83768
high-gain, narrow-band, amplifier using active filters for ionosphere measurement 77−56760
high-gain amplifier circuit for Se photocells 78−4679
ion cyclotron double resonance expts., oscillator coupling elimination 77−67530
LM3900, wideband nuclear radiation monitor appl., cct. 78−78591
logarithmic converters and amplifiers, principle and appl. *(German)* 79−9233
low-noise, for biological amplifier, 24-channel, head-mounted 77−40807
magnetic field sweeper and recorder drive for de Haas-van Alphen type phenomena 77−67474
megohmmeter with op. amp. for liquid level meas. and regulation *(Rumanian)* 79−40532
mutual inductance bridge using operational amplifiers 78−54407
Norton amplifier level control, liquid nitrogen for parametric amp. using diode 78−29121
ohmmeter appl., linear scale *(Czech)* 77−61093
ohmmeter reading range extension using noninverting op. amp. *(French)* 80−42207
optical isolation amplifier, for current meas. in 10^{-11} to 10^{-6} A range 77−67473
pH meter circuit 79−21735
photoconduction decays, fast, measurement, DC-10 MHz low noise amplifier system 80−57326
photodiode sensor, camera shutter control appl. *(German)* 80−52341
potentiostat principles and construction *(Dutch)* 77−77856
proportional temperature controller, using IC sensor diode and operational amplifiers 79−75515
refractometer, photoelectric appl. 77−53971
review, operational amplifier behaviour 80−67959
skin conductance meas. IC operational amplifier cct. 77−25566
small active resistance and inductance meas. AC bridge 78−86299
strain gauge bridge networks, characteristics *(German)* 77−71311
strain gauge using integrated operational amplifier 79−75522
temperature-to-time convertor applic. 77−26290
thermistor temperature indication linearizing circuits 79−49230
thermoelectric transistor thermometer composed of thermocouple, transistor thermometer, operational amplifier *(Japanese)* 78−45625
TV optical operational amplifier 79−94327
two-channel amplifier section with common negative feedback loop 78−9042
vented box loudspeaker analogue model 80−92015
voltage waveform peak and trough precision detector 77−87792
voltmeter, high-Z input, 10 mV to 400 V 79−80646
voltmeter auxiliary equipment appl., for low voltage meas. in high ohmic circuits *(Czech)* 78−4664
Wheatstone bridge fed from a bilateral constant current source using electronic amplifier 80−57338
zone refiner, electron beam, emission current control cct. 78−6844
operations analysis *see operations research*
operations research
see also critical path analysis; decision theory and analysis; forecasting theory; game theory; mathematical programming; PERT; scheduling
fuzzy set theoretic approach to systems analysis 78−17352
nondestructive inspection parameters optimisation 77−90548
nuclear fuel cycle management, interdisciplinary approach in education and research activities 77−38433
nuclear fuel drum storage capacity computation via inventory model 79−9776
optical element production start up, operational control optimisation 78−18078
operator training *see training*
optic mode of crystals *see lattice dynamics*
optical aberrations *see aberrations*

optical activity *see optical rotation*

optical auroras *see aurora*

optical character recognition
see also character recognition equipment
automatic recognition of printed characters, heuristic algorithm, optical reading machine parameters *(French)* 77−48933
Chinese character recognition with real time optical correlator 78−29904
coherent OCR system using spatial light modulator *(Japanese)* 80−14291
development trends *(Czech)* 80−14457
Dreyfus file optical writing appraisal 78−37821
handprinted character, field effect method and angle-distance distribution method combination *(Japanese)* 78−9342
handwriting, linear prediction of optical parameters *(French)* 79−3640
Hebraic ancient handwritten characters, coherent and incoherent averaging 78−37820
holographic filter appl. *(German)* 77−88668
holographic pattern recognition of the Korean alphabet using matched spatial filters *(Korean)* 79−22920
holography technique appl., using optical spatial filter *(Japanese)* 80−5699
hybrid method, suboptimal statistical transform *(French)* 77−46703
hybrid optical-digital image processing, appl. to handwriting and aerial photos 77−68178
hybrid system, optical directional filter for two-dimensional patterns, coherent light, white light appl. *(German)* 77−83819
image classification by orthogonalised spatial filtering 77−50635
Korean alphabets holographic pattern recognition, discrimination enhancement using phase modulated matched filters 80−95854
microscope image histological specimens traced on optical mark recognition computer cards, quantitative analysis appl. 77−81612
optimised filter 80−95837
picture enhancement and stroke-width standardisation algorithm 77−38822
print contrast measurement 77−34045
reading machine, multifont adaptable automatic, for blind people 80−104814
scan system for encoding and tabulation of visually scored sleep data 80−8197
signal and image processing, conference, San Diego (1977) 78−74853
spatial filter correlator, coherent optical matched, for microfilm data base word recognition 80−43279
spatial filtering with light beam deflection 78−1370
spectral intensity filtering for image recognition 78−46529
systems based on nonredundant correlation meas. 79−94162
universal product code symbol scanning, error modes and probabilities 77−621

optical coherent transients
see also photon echo
atomic systems, coherent transients theorem 80−99808
atoms, two photon excitation, time depend. emitted light spectra, perturbation theory 80−63605
coherent optical spectroscopy, transient effects, theory 77−49780
duryal radical in durene matrix, optical coherent transient spectra 79−76764
flame spectroscopy 79−39147
free electron laser, coherent dynamics with arbitrary magnet geometry 80−83581
free electron laser, coherent transients, laser lethargy and coherence brightening 79−94204
free induction decay, of mols. undergoing radiative and radiationless relax. 78−83040
free-induction decay, 100 ps time scale, laser freq. switching method 80−19074
gaussian beam resonator, optical nutation 80−99807
generation by electro-optical laser modulator 80−102776
laser freq. switching 79−46014
laser nonlinear spectroscopy polaris. selective optical heterodyne detection 79−58798
laser saturation spectroscopy, time-resolved, free induction decay of two-level resonances 80−102775
many-pulsed excitation of optical coherent responses under large inhomogeneous line broadening *(Russian)* 80−48358
methyl iodide mol. nonlinear resonant interaction with pulsed subMM radiation *(Russian)* 80−99523
millimetric/submillimetric coherent transient spectroscopy 80−58651
molecular gas, optical nutation in standing wave, Rabi oscillations *(French)* 79−31999
multilevel molecular system, coherent pulse propag. effects 80−9968
naphthalene:pentacene, picosec. optical coherence obs. 80−14400
napthalene:pentacene, zero-phonon transition bottlenecks, photon echo detect. 80−33092
nutational photon echo 80−28283
particle motion effect on transient optical phenomena 80−1283
pentacene, intersystem crossing and internal conversion rates, fluoresc. transient and optical FID spectrosc. 79−81229
pentacene in p-terphenyl, free induction decay by extracavity laser freq. switching 78−79076
photon echoes, picosec., stimulated from accumulated grating 80−33092
quantum systems, at. or spin two level, reson. EM wave excitation, free induction decay oscills. 80−63562
rotary echoes, Bloch eqns. perturbative solns. 80−43407
ruby, coherent transients obs. by Stark switching with narrow optical hole burning 78−37947
ruby, optical free induction decay modulation and absorpt. line struct. due to superhyperfine interaction 80−33091
semiconductor, nonlinear coherence phenomena in exciton region 80−99806
semiconductors, two-photon nutation of coherent biexcitons 80−80191
spatial gratings, transient light-induced, by successive optical coherent pulses 80−64115
spectroscopy, superhigh resolution, using coherent phenomena 80−22445
subnanosecond optical free-induction decay with novel laser freq. shifting 80−38075
T_2 as collision time, dephasing time, or reciprocal linewidth, for teaching 80−27075
tetramethyl pyrazine in durene, phosphorescent mols., quantum beats in triplet states 80−58312
three-level medium, coherent transient pulse propag. in two-photon reson. 77−79904

optical coherent transients continued
three-level molecular system, cooperative evolution, transient effects of dephasing and relax. 80−28184
time-correlated picosecond laser pulses generation, rapid sampling of optical relax. phenomena 80−9969
time-resolved laser saturation spectroscopy and coherent transients survey 80−9965
transient phenomena, two-photon *(Japanese)* 79−36966
transients by laser freq. switching 78−66873
two-level atomic system, superfluoresc. fluctuations 80−23651
two-level system, backward photon echo and free induction decay generation 80−99805
CO_2, 30 ps laser pulse generation by free induction decay 77−14738
H_2O, relaxation by IR and microwave coherent transients 80−28092
I_2, coherent optical transients and optical dephasing in mol. collisions 80−9966
I_2, polarisation switching obs. 79−81492
$KCl:KReO_4$, CO_2 pulse generation by free induction decay 80−53388
$KCl:KReO_4$ free induction decay generation of ultrashort CO_2 pulses 80−74444
$LaCl_3:Pr^{3+}$, coherent transients by optical phase switching 80−95962
$LaF_3:Pr^{3+}$, optical free induction decay exam. of dephasing time 77−3637
$LaF_3:Pr^{3+}$, optical free induction decay meas. of low temp. dephasing 79−46009
$LaF_3:Pr^{3+}$, optical transition, spin decoupling and magic angle line narrowing 80−28286
$LaF_3:Pr^{3+}$, pseudo-Stark effect meas. using population hole burning and optical free-induction decay 79−24292
$LaF_3:Pr^{3+}$, ultraslow optical dephasing 80−58648
$LaF_3:Pr^{3+}$, ultraslow opt. dephasing at 2K 80−91864
NH_3, relaxation by IR and microwave coherent transients 80−28092
NH_3, transverse relax. time, T_2, of inversion doublets from free induction decay 80−58281
NH_3, two-photon coherent transients, expts. 80−19073
$^{15}NH_3$, modulated coherent Raman beats 80−23464
Na, D_1-line optical coherent transients by laser frequency switching: subnanosecond studies 79−46014
Na, mag. field quantum beats in two-photon free-induction decay 79−13692
Na, two-photon transition, distinction of competing processes in nonlinear resonant freq. mixing 80−33080
Na vapour, Zeeman coherence, transient and stationary, polarisation spectroscopy 80−58212
O_2, relaxation by IR and microwave coherent transients 80−28092
OCS, relaxation by IR and microwave coherent transients 80−28092
SF_6, model system, coherent pulse propag. effects 80−9968
SF_6, nonradiative collisionless dephasing rate, two-photon coherent transient meas. 80−14176
SmI, Zeeman coherence, transient and stationary, polarisation spectroscopy 80−58212

optical collimators
alignment techniques by optical means 80−1341
analytical ultracentrifuge appl. *(German)* 79−71443
anti-Gaussian collimating lens, intensity uniformity 77−7167
apochromatic collimator design for MTF evaluation 77−79946
asymmetric fiber power splitter 80−83661
Auger camera collimator selection for ^{67}Ga imaging 79−57764
autocollimation apparatus to test manufacturing quality of aspherical mirror profile 80−10053
autocollimation instrument for checking angles and pyramidicity of AR-90° prisms during manufacturing process 80−87570
autocollimator, photo-electric, calibration with laser interferometer system and microcomputer 80−1304
autocollimator development 78−71220
autocollimator used for alignment of end standards of length for calibration 79−54094
automatic collimator used in X-ray comparator for meas. cutoff angle of piezoelec. quartz wafers 80−105755
automodulation collimator, for X-ray astronomy *(Russian)* 80−62018
bent glass optics 78−45767
centering devices, vertical collimators, for geodetic appl. 78−13807
computerised tomography, EMI first generation scanner, dose rel. to collimator geometry 79−74760
echelette reflection characteristics in polarized radiation for an autocollimation setup 79−3787
error compensators, calc. procedure 80−28296
focusing, critical auto-collimation technique modification 78−42424
frustrated total internal reflection element, adjustable as a function of the incidence angle of highly collimated light beams 80−96022
interference mirror coating thickness meas. equipment 79−35676
laser collimation and focusing at given distance *(Russian)* 78−29959
laser tracking system testing by 1 m unobscured IR collimator 80−78991
meniscus collimator viewfinder, optimisation of mirror light transmission coeffs. 80−74469
modulating anticollimator for low and medium energy gamma-ray telescope *(Russian)* 79−16832
modulation-interference spectrum analyser 77−79161
monochromatic MTF computation program 80−14451
monochromators with off-axis mirrors, distortion and split-image curvature 78−59141
moving atmosphere simulation by rotating phase plate 80−79021
myocardial imaging using ^{201}Tl, collimator evaluation 79−34657
nonconcentric bispherical mirror objective, collimating props., ray path calcs. 78−90492
nuclear imaging using multi-slice fan beam collimators 79−44993
optical attenuator, for TEM_{00} mode laser beam, using collimators and iris diaphragm *(Japanese)* 79−98378
optoelectronic goniometers, linearity and sensitivity ranges increase 80−23786
photoelectric autocollimator detector with short time const. 77−7206
polyhedral prisms checking instrument, using photoelectric autocollimator 77−7221
prism glass reflecting angle testing in autocollimation modes 78−71194
radiography, wire-wound multi-aperture collimators 79−35911
radioisotope imaging, optimal collimator design parameters for dynamic spatial resolution 80−17087
roof and other prisms, MTF tests 80−69571
scintiallation camera collimators, point spread function study 79−35910

optical collimators continued
scintigraphy, bar-phantom image distortion by collimator 79−100722
scintillation camera/high energy collimator system, misleading results with a bar phantom image 80−12237
shearing plate for collimating system alignment 78−79126
sighting telescope and autocollimator, general-purpose optical string 79−81510
single element gradient index collimator design 78−9426
Space Telescope pointing control fine guidance subsystem design 80−82201
telescopes PPS 12 78−94423
telescopic collimating system, laser radiation directivity pattern axis spatial location 80−102748
universal optical string for surface coaxiality and linearity meas. 77−26269
vacuum collimator for UV studies, using two-mirror Cassegrain type objective 79−7219
vacuum UV monochro-collimator *(Japanese)* 77−73957
visual telescope light scatt. factor meas. apparatus 79−27365
waveguide optical collimator, Luneberg lenses with plane connecting waveguides 79−68446
X-ray diagnostic equipment, method and algorithm for adjusting 80−30852
X-ray scanning modulation collimator instrument for HEAO-A satellite 77−71003
H_2 maser frequency standard, stabilised using multitube collimator 80−91769

optical communication
see also optical links
1 Gb/s laser space communication system 77−7213
2 km 20 Mb/s optical fibre transmission system 78−42437
6.3 Mb/s optical fibre communication for power system protection and control 78−1423
400 Mb/s optical transmission expts. 77−88954
advancements, comparison with microwave communication 79−81546
aerospace systems and electronics, IEEE conference, Washington D.C., USA, 26-29 Sept (1976) 77−5420
amplitude modulated laser beam prog. in random inhomogeneous medium, phase fluctuation anal. 78−87017
analogue fibre optics data communication system, high resolution 77−46810
analogue signals, using optical waveguides, transceiver transducers *(German)* 78−1333
analogue video transmission feasibility using laser diode, over 30 km at 1.3 μm 80−58737
atmospheric laser communication line, error probability 77−14731
atmospheric scintillation effect on capacity of polarisation and amplitude modulated links 77−75428
atmospheric turbulence effect on imaging and optical communication, book contrib. 79−34960
atmospheric UV propagation and optical communications range 77−79770
background noise due to solar radiation scatt. from gradient particulate atm. 79−62576
binary optical communication system, atm. scintillation effects 77−71943
book, optics and information theory 78−5435
cable systems, for information transmission *(German)* 77−88942
channel and photodetector array, computer simulation 77−71944
channel conditioning against intersymbol interference and timing errors *(Italian)* 77−23622
channel displacement and diffusion coefficient determ. *(Russian)* 79−98303
coherent differential reception of optical signals *(Russian)* 77−87835
conference, Amsterdam, Netherlands (Sep. 1979) 80−46733
conference, Munich (1977) *(German)* 78−33854
conference on laser and fibre-optics communications, San Diego, CA, USA, Aug. (1978) 79−86203
conference on optical fibre communication, Washington, DC, USA (Mar. 1979) 79−46058
coupling system, LED to fibre, efficiency increase using facet radiator *(Japanese)* 77−79938
data transmission performance study in optical fibre communication system 78−38028
detection theory, quantum problems 77−42488
development trends, integrated optics vs. integrable optics 77−65643
development trends *(Czech)* 80−14457
digital, problems arising in system development 79−3806
digital 1.12 Gbit/s fibre system, optimum repeater parameter calcs. *(German)* 78−37989
digital fibre optical communication system, average error probability calc. 80−53228
digital laser communication systems, acousto-optical multiplexing and demultiplexing techniques for multigigabits/sec transmission 79−86132
digital systems, optical fibre cable, technological advances *(French)* 77−11020
diode laser communications for remote utility meter reading 79−86195
direct detection binary PPM system, photoelectron counter dead time effect 77−54796
discrete PPM signal reception accuracy *(Russian)* 79−94171
dispersive multimode fibre, optimum index profiles for digital communication 77−7192
distribution path arrangement into branch optical fibres *(German)* 78−79111
electro-optics, conference, Utrecht, Netherlands (Oct. 1978) 80−31420
ELOS system using atmospheric scattering from marine aerosols 79−29862
error probability anal. of digital fibre optic communication systems 78−46775
error probability calc. in communication channel with intersymbol interf. 80−53227
evolution and development trends, comprehensive survey 79−23065
extended-line-of-sight optical communication approaches 77−19187
extraterrestrial laser signals detect. likelihood, instrumentation 80−4276
fibre, development, advantages and applications 80−53410
fibre, potential and research in Denmark *(Danish)* 78−9440
fibre, research and development review 77−65629
fibre application to existing communication systems *(German)* 78−33887
fibre cable attenuation and input and output efficiency 80−14469
fibre cable transmission and strength improvement technology 80−28347

optical communication continued
fibre communication advances, materials and techniques 80−102853
fibre communication and integrated optics 78−87159
fibre communication applications, trends and implications 80−33211
fibre communication systems, military 77−88923
fibre communication technology and interactive component functions *(German)* 79−10391
fibre communications development and need for standardisation *(Italian)* 79−23066
fibre communications history and prospects 80−9994
fibre communications system operating at 44.7 Mb/s, devices and perform. 77−27382
fibre digital communications, PAM-PPM signalling format 79−27190
fibre lightguides, materials properties, review 77−3666
fibre optic and other systems *(Japanese)* 79−68438
fibre optic cable design and manufacture 77−54780
fibre optic communication, progress review of fibre design, low-loss and low-dispersion *(German)* 80−28325
fibre optic communications, fibre prod. and PO experimental link 79−37015
fibre optic systems, analytical review including survey of commercial systems 80−74489
fibre optic systems, development during next decade 80−1329
fibre optic systems, digital, error probability with inter-symbol interference and additive noise 79−89855
fibre optic systems 79−72676
fibre optic telecommunication appls. 80−1330
fibre optic transmission system, BPO installation, feasibility trials 77−72072
fibre optic VSB-FDM system for video trunking, CATV appl., transmission performance 77−62054
fibre optic waveguides, maximum information capacity derivation 77−39027
fibre optics, practical problems *(Swedish)* 78−25988
fibre optics appl., 1979 status and development trends 80−53408
fibre optics for military appls., review and assessment 78−42438
fibre optics market in Japan 79−32044
fibre optics systems, components operation and technical data *(Hungarian)* 79−18514
fibre system design charts 79−7200
fibre systems, Australian development, PCM transmission and FDM telephony 77−65630
fibre systems analysis, digital 77−65631
fibre technology and information transmission props. *(German)* 80−10010
fibre telecommunication, propag. mechanism and characts. 78−22213
fibre transmission, applications and cable techniques *(Japanese)* 80−87493
fibre transmission between 0.8 and 1.4 micron 78−37990
fibre transmission experiment, 800 M/bs, using single-mode fibre 77−88917
fibre transmission experiments, 100 Mb/s and 400 Mb/s PCM signals 77−88918
fibre transmission expts. at 34 Mb/s with HDB3 line code 80−64198
fibre transmission in TE_{01} mode 80−53432
fibre transmission lines, systems aspects 77−54792
fibre transmission technology, single mode systems in 1.0 to 1.8 μm region, review 80−38105
fibre-optic appls., techniques and predictions 80−87472
fibre-optic communication and integrated-optics sources *(Italian)* 79−94371
fibre-optic communication system performance at 1.55 μm with single-longitudinal-mode laser 80−87556
fibre-optic communication systems, book 80−73117
fibre-optic communication systems, devices and ccts., book 80−38123
fibre-optic communication systems for electric power companies 78−1422
fibre-optic communication technology status *(German)* 78−90512
fibre-optic component availability 78−18048
fibre-optic data bus system design and implementation 77−7017
fibre-optic digital transmission, shot noise probability distribution function 78−50717
fibre-optic system appls., review of benefits 80−43480
fibre-optic systems, future developments, impact on 'next generation' of electronic equipment, data ring concept 80−102808
fibre-optic systems, future in telecommunication networks 78−22214
fibre-optic systems, modal noise in multimode systems 79−46083
fibre-optic telecommunication principles and practice *(French)* 78−55463
fibre-optic transmission by laser diode analogue baseband modulation 80−58738
fibre-optic transmission technique status in Germany 78−1416
fibre-optical, propagation principles *(German)* 79−81529
fibre-optics communications requirements and system aspects 77−68268
fibres, low loss, for optical communication *(Japanese)* 78−79135
fibres application, current technology *(German)* 78−22210
fundamentals *(Japanese)* 79−27400
future developments *(Japanese)* 79−27410
glass fibre development, with attenuation less than 5 db/km *(German)* 77−34940
glass fibre development and prospects 78−9453
glass fibres, description and appl. *(Dutch)* 77−11036
glass fibres and laser appl., development *(Italian)* 77−773
glass fibres appl., system components construction and operation *(German)* 79−18553
glass fibres for, colloquium, London, England (Jan. 1979) 80−67930
glass-fibre optical communication systems 77−50762
graded index fibre, expt., 1.12 Gbits/s PCM 77−83967
guided wave acoustooptics, fundamental principles and wideband appls. 79−37038
guided wave optical systems and devices, conf. Washington DC, USA, 1978, Mar. 79−37031
guided wave optics, appls. review 79−37054
heterodyne receiver output signal dependence on angle of incidence 79−45910
heterodyne receivers for atmospheric optical communications 80−58663
high capacity telephone cable, repeaters, cable, Hitchin to Stevenage *(German)* 77−72079
high-speed optical systems at 0.85 μm, modal noise and optical feedback 80−87323

optical communication continued
historical and technical features review, future prospects *(Japanese)* 80−99863
hybrid systems, integrated optics using thin film micro-optics 77−11051
ideal light source for communication channel, high information rate 77−3541
image transmission by modulation spectroscopy *(French)* 77−14663
Infinite dimensional filtering problems in optical communication systems 78−66779
information, message and signal concepts *(German)* 78−46525
information processing using guided wave opt. communication systems 79−36852
information transmission methods, survey *(German)* 78−13804
integrated optic appls., future trends 79−37053
integrated optical circuit and hybrid fibre optic advances 77−75716
integrated optical circuits appl. *(Italian)* 78−55467
integrated optics, colloquium, London, England (May 1980) 80−79008
integrated optics, development wideband repeater 77−14813
integrated optics and single mode fibre optics 78−42469
integrated optics in fibre communication systems, introduction 80−79009
integrated optics techniques for fibre-optic communications *(German)* 78−38069
intensity fluctuations of optical carrier, turbulent atm. influence *(German)* 79−89861
interferometric system, large path diff., nonparallel light *(French)* 77−75668
International Microwave Symposium, San Diego, Calif., USA (June 1977) 78−5478
interoffice trunking exptl. optical fibre communication system 77−19454
intersymbol interference and transmission medium instability for fibre system 77−65638
interval modulation semiconductor laser communication system 78−9331
laser and electro-optical systems, conf., San Diego, CA, USA (Feb. 1980) 80−62392
laser applications *(Japanese)* 77−68269
laser communication systems, transmission of information in the optical waveband, book 79−3645
laser engineering and appls., conf., Washington, USA (May-June 1979) 80−1216
laser modulator for HF laser communication links 80−48311
laser PCM, injection laser radiation, optimal conditions 79−59733
laser pointing and tracking through air-sea interface 77−79776
laser propagation statistics in Montreal area 80−4099
laser space communication, 1 Gb/s 77−88831
LED analogue video signal transmission, LED linearisation by predistortion 78−37993
LED optical fibre system, source-drive optimisation 77−11007
light guide data transmission, review *(German)* 80−95996
light scattering by clouds, Mie formalism 77−88651
light wave transmission technology, survey 79−55213
light-wave propagation communication, glass fibres, attenuation characts. *(German)* 80−95997
lightguide theory and its implications in manufacturing 80−64186
long wavelengths beyond 2 microns *(Japanese)* 80−106469
LW fibre-optic, InGaAsP/InP lasers and detectors 80−9885
matrix transforming incoherent optical system, using extended lens-array 79−7086
military fibre-optic communication systems progress 78−1425
monomode waveguides developments 80−48404
multilevel signals in digital optical-fibre communications 79−22900
multimode digital system wavelength multiplexing constraints in 850 nm region 80−63942
multimode fibres, step-index, for experimental optical fibre transmission system 79−32059
multimode optical fibres, power attenuation, pulse distortion, electromagnetic wave propagation eqns. *(Italian)* 77−79930
multiplexing, large path-difference white-light interferometry *(French)* 77−10842
naval appls. using atmospheric, space and underwater optical communications 79−86133
noise immunity of optical signal reception with unstable modulator characts. 78−46690
optical fibre communication, conference, Paris, France, Sept. (1976) 77−11016
optical fibre transmission, conference, Williamsburg (1977) 78−1382
optical fibre transmission characteristics measurement appl. 80−53409
optimum wavelength laser, using GaAsSb 77−7086
optoelectronic Si devices for optical signal processing and communications 79−37056
parallel plane diffr. grating with periodic structure, diffr. of plane wave 80−102620
PCM optical fibre communication system numerical aperture optimisation *(German)* 78−38017
PCM with envelope modulation, pulse detection characteristics 77−11010
perceptual coding in the cosing transform domain 80−102635
photoacoustic spectroscopy appl. *(French)* 78−48143
photocounting communication analysis, optimum photon detect. 78−27956
photoelectron counting distributions of laser light signal through turbulent atm. *(Japanese)* 77−50711
photoelectron statistics, book 78−25842
photon counting limits in optical channels, signal amplification 79−50234
plane wave pulses, random media propagation 78−9324
polarization modulated light, freq. mixing detection using periodic analyzers 78−5433
public telecommunication network, future of optical fibres 77−11022
quantum communication theory, appl. of generalised quantum meas. theory 78−13668
quantum effects in communication theory 80−1147
quantum-information theory, expressions for Shannon quantity of information 79−55075
regenerative fibre-optic transmission system supervisory line codes *(German)* 78−33884
research review from different countries *(Japanese)* 79−27409
seawater transmission props. for underwater laser communication 80−33069
Second European Conference on Optical Fibre Communication, September 1976, review *(Italian)* 78−5552
semiconductor lasers, recent progress, review 78−17938
optical communication continued
signal detection characteristics, evolution of influence of destabilising factors 80−9825
signal discrete reception in turbulent atm. 78−73511
signal quantisation, for photon and field channels 77−42493
simulation 77−54675
single mode fibres, optical communication techniques *(German)* 80−102811
single-fibre optical systems, efficient power combiner for multiplexing multiple sources 78−18039
single-mode fibre cabling for low-loss communication 80−53467
single-threshold detection of random signal in noise, appl. to optical communications 79−18353
source bandwidth limit 77−61918
space laser communication, efficient appl. of low power Nd:YAG laser 77−75567
status and prospects *(German)* 78−33855
step index fibre including gap, impulse response 80−83675
sub-optimal graded index optical fibre analysis using perturbation calculus 80−87480
superconducting machine temperature telemetry via optical channel *(Russian)* 78−57966
supervisory/service channel for fibre optic transmission systems 80−95803
systems and applications 77−88916
systems aspects of optical-fibre communications 77−7016
systems theory concepts, electronic analogy *(German)* 77−3542
telephone service in Chicago (USA) 78−5574
three-layer waveguides for wideband optical communication lines 80−28310
timing error tolerant waveforms in optical fibre systems 80−14293
timing recovery in data transmission 77−79768
tracking system for space laser communication 80−33068
training, educational course status and effectiveness 80−62413
transmission system design, influence of optical component baseband frequency response 78−1415
transmission system planning *(French)* 80−87551
turbulent atmosphere, phase distortion compensation efficiency 78−1177
two-photon coherent states, quantum meas. realisable with photoemissive detectors 80−53220
using two-photon laser, optimum control of quantum noise 78−71049
UK optical fibre communication system feasibility trials *(German)* 78−33877
undersea transmission characts. of laser beam in Tago Bay, Japan 77−21782
underwater laser beam transmission characts. in Tago Bay *(Japanese)* 77−21797
unit core cable structure design, fabrication and characterisation 79−37030
wavefront sensing using white light sources 80−1146
waveguide, errors in determ. of output signal parameters 78−1365
wavelength selection for transhorizon optical communication 79−7088
white light, information processing and transmission 80−95833

optical communication equipment
see also optical waveguides
1×2 optical switch using new type of pentagonal prism switch, for optical fibres 80−64148
5 Gbit/s multiplexer, for optical fibre communication system 78−18044
400 MHz SAW timing filter for optical fibre transmission 79−50415
800 Mb/s fibre transmission test using low-loss and low-dispersion single-mode cable 80−10001
access couplers for single strand systems 80−58766
acousto-optic planar guided-wave Bragg modulators, integrated optic communication appls. 80−38131
acousto-optical multiplexer for fibre-optical systems 77−27370
acousto-optics, guided-wave, with appls. to wideband communications and signal processing, progress review 80−58801
acoustooptical multiplexer/demultiplexer terminals, appl. to laser communication system, expt. results 78−25959
adaptive optical systems, speckle effects 77−19410
amplifier based on resonant tunnelling between passive and active optical waveguides 79−59838
antennas focused at finite distances, angle-distance pattern 78−33842
avalanche, photodiodes for 400 MHz communication systems, construction and characts. 77−11011
avalanche photodiode, double epitaxial, for optical fibre communications 77−54782
avalanche photodiode detectors, 1.0 to 1.4 μm region, for high data rate fibre optic systems 79−54188
avalanche photodiode receiver sensitivity, specification and testing *(German)* 78−38015
avalanche Si photodiode receiver, for fibre-optic transmission systems 77−19455
averaged threshold receiver for lognormal atm. channel 78−13788
bandwidth of distorted multimode waveguides excited by laser sources 80−43436
beam splitter lightwave fibre tap, use in source stabilisation 78−79105
beam splitters for optical heterodyne receivers 79−18528
bidirectional coupler for duplex transmission on single optical fibre 79−37032
binary phase gratings for fibre-optic communications 80−64201
bistable optical device, transient response and applications 80−33214
bistable optical device development from integrated two-arm interferometer, appls. *(French)* 80−69555
buried heterostructure laser, sinusoidal modulation characts. 78−87054
buried-heterostructure laser packaging for wideband optical transmission systems 78−74920
bypass switch for fibre-optic data bus systems 80−99826
cable design considering structural imperfection 80−64184
cable developments, optical links appl. *(Japanese)* 79−27405
cables, connections and optical transmitters for optical fibre transmission systems *(German)* 80−99839
cabling technology, recent trends 79−3781
channel filter for fibre transmission systems, wavelength multiplexing 77−34950
characts. and appl. survey *(Flemish)* 80−5836
chirped-grating multiplexers in dielectric waveguides 77−58445
circulator, polarization-independent, configuration method 80−38095
circulator for optical fibre transmission, using Faraday rotator and Glan-Taylor prisms 80−23769

optical communication equipment continued
coated optical fibre cable unit, internal stress due to compressive loads, optimum design 80−58717
coherent laser detection system, radiation effects analysis 78−30056
components development *(German)* 79−81563
components for optical communication systems, review 80−87539
compound optical crosspoint with low crosstalk, using $LiTaO_3$ 78−33915
concentric connector for step index multimode fibres *(Japanese)* 78−90504
connector, low loss index matched optical connector 80−48452
CW injection lasers and LEDs 77−7210
data bus, eight-terminal optical fibre, using T-couplers 78−59129
data bus, glass fibre branch couplers, digital data transmission *(German)* 79−89999
data bus system with planar access coupler, optimized layout 78−33823
data bus system with single multimode fibres, planar coupler 77−79927
data bus T-system, single multimode fibre, based on access coupler 78−46810
data buses, angle optical fibre, signal distribution systems and crosstalk isolation 79−3802
data highway junctions and systems 77−39097
data transmitter, laser and LED comparison *(German)* 80−14432
data-bus system paired optical-fibre switch 80−23791
demultiplexer, low-loss optical, for wavelength division multiplexing systems, 0.8 μm region 79−98463
demultiplexer, using coupling between nonidentical waveguides 79−10380
demultiplexer, using diffraction grating, for FDM fibre transmission system 80−5845
demultiplexer for wavelength division multiplexing system 79−64309
demultiplexer using concave grating, 0.7 to 0.9 μm, expt. results 80−38099
demultiplexer using Si echelette grating 80−53422
development, present state *(Italian)* 79−10398
DH injection laser with coherent light injection, modulation behaviour 78−55352
DH photodiodes, diffusion limited transient response 80−70809
digital transmission appl., components manufacturers and selection *(French)* 79−94333
diode circuit for high bit rate pulse regeneration and injection laser modulation 77−79935
diode lasers as transmitter source in optical communication, modulation, power consumption, optical links 80−102807
diode twin-guide laser, narrow radiation angle for optical fibre coupling 78−46628
directional coupler, interference filter all-fibre for wavelength division multiplexing 80−91900
directional filter structure and characteristics for bidirectional transmission 80−58734
diversity arrays for optical communications through atmospheric turbulence 79−86263
economic advantages of using optical links, compared with wire cable 79−10385
electro-optic multimode time division multiplex device 77−79958
electro-optic multiplexer system for multimode fibre data communications 79−18510
electro-optical broadband travelling wave modulator, expt. design principle 78−94438
electro-optical channel waveguide switch for computer communication bus 80−9987
electro-optical devices for multimode optical switching 79−76882
electro-optical multiplexer for large-numerical-aperture low-loss fibres 77−83993
electro-optical transceivers, optical analogue communication systems *(German)* 78−1333
electrooptic diffraction modulator, large-aperature 80−33179
electrooptical oscillator, integrated cutoff modulation 80−48424
encoding-decoding optical fibre network 78−25963
equaliser, nonlinear, with shaping filter 78−30052
fabrication and coupling of fibres and cables *(French)* 79−68447
fail-safe fibre optics data bus using active electrooptic mirror terminals 79−23053
far IR receiver optical preamplifier 77−39068
fibre, data bus systems appl. 78−25949
fibre, modal noise, dependence on source coherence and fibre length 80−48402
fibre, single-mode systems, instability due to interference and polarization effects 80−58774
fibre 4 μm band communication, devices and materials 78−94441
fibre cable, measurement calc. of stranding pitch using stranded wire theory 80−10036
fibre cable reliability, deterioration factors, splice point reliability, coating materials, static fatigue life *(Japanese)* 80−99848
fibre cable study by CCITT 79−90031
fibre cable testing, for lightwave communications systems 80−102865
fibre cables, design, manufacture, laying and jointing *(Italian)* 80−99838
fibre communication, elimination of polarisation in optical isolators 80−5844
fibre communication development trends, review 80−69521
fibre communication devices, directional couplers, atennuators, switches development 79−3782
fibre communication receivers 80−43460
fibre communication system components, state-of-the-art survey *(German)* 80−69538
fibre communication system design study 78−50908
fibre communication systems, computer design aids 80−28350
fibre communication systems process in past three years *(Polish)* 78−87152
fibre data bus, active fail-safe terminal 78−55438
fibre data collection highway with piezoelectric phase modulators 77−39098
fibre devices, demountable connector, fibre switch, and fanout couplers 78−74989
fibre endface preparation by AC discharge heating and stretching 80−64232
fibre laser-amplifier, coupled-mode theory 78−66848
fibre materials suitable for communication appls. 79−46061
fibre optic, research status in France 77−46814
fibre optic communication cable, commercial development review 80−1331

optical communication equipment continued
fibre optic communication repeater design, high impedance input, equalisation cct. *(Italian)* 77−50758
fibre optic communication sources, detectors and circuits 77−27374
fibre optic communication systems, components, design considerations, economic trends and applications 79−23083
fibre optic communication systems, sources and detectors 78−42412
fibre optic communication systems, utilisation of optoelectronic devices 80−1328
fibre optic communications, prospects for 1 to 1.6 μm spectral range use 80−102848
fibre optic connectors, update on standardisation 80−5830
fibre optic data transmission technology, advantages over elec. cable 77−7196
fibre optic equipment, USA military development, review 79−46060
fibre optic sheets fabricated by selective photopolymerization 79−55235
fibre optic signal transmission appls. *(German)* 80−69517
fibre optic systems progress over ten years and prototype systems charcts. 78−55456
fibre optic telecommunications systems, book 80−86049
fibre optic wideband transmission systems, losses due to joints *(German)* 79−64325
fibre optical communication devices 77−58446
fibre optics, practical problems *(Swedish)* 78−25988
fibre optics, research and technology 78−87151
fibre optics, research status in USA 77−46813
fibre optics, transmitter and coupling techniques *(German)* 77−11008
fibre optics appl. to digital transmission, commercial components survey *(French)* 79−90007
fibre optics systems, research in USA 77−27363
fibre PCM repeaters with low power requirements, design and operation *(German)* 80−28315
fibre preform manufacture using modified CVD process 80−64228
fibre splicing and connection techniques *(Italian)* 80−38097
fibre switch, single-mode, optimised design 80−106607
fibre switch driven by $Pb(Zr,Ti)O_3$ bimorph 79−18502
fibre systems for civil telecommunications, state-of-the-art review 78−25979
fibre systems for telecommunications 80−91906
fibre systems receiver design, review 78−30077
fibre tapping element with low insertion loss 79−76826
fibre transmission line structures, transducers, couplers and connectors *(French)* 79−89998
fibre transmission systems, active and passive devices 80−43463
fibre transmission systems, charcts. and component manufacture *(French)* 79−68448
fibre transmission systems and components 79−10384
fibre voice transmission using unmodulated transmission of AF, telephone terminal sets *(German)* 80−28314
fibre-based system, for analogue data transmission *(German)* 80−23781
fibre-optic Bell System Chicago installation 78−42434
fibre-optic communication in industry, appls., glass fibre props., connectors 80−87550
fibre-optic communication receiver designs 77−68281
fibre-optic communication systems, book 80−73117
fibre-optic communications source and detector props. and performance 78−22212
fibre-optic system repeater error rate calc. approaches compared 77−54672
fibre-optic transmission system, semiconductor device reliability tests 80−58573
fibres, connectors, light sources and receivers, review *(French)* 79−46044
fibres, light sources, coupling units, receivers, production and use for optical transmission systems *(German)* 79−36994
fibres, structural characteristics, CVD fabrication 79−59806
fibres and components, development and performance 80−53411
FM wide-band system using optical techniques 79−64308
focal plane design and optimal processing for scattered optical fields 78−78935
frequency multiplexing source with monolithically integrated DFB lasers 77−34958
frequency-channel multiplexer and four-channel integrated-optics coupler 80−91936
GaAs laser diodes for optical communication transmission *(German)* 80−28252
glass and plastic fibre charcts. and interconnection requirements 80−69513
glass fibre communication: introductory review, status and development *(German)* 79−89997
glass fibre experimental cable, used between telephone exchanges by German Post Office *(German)* 79−64326
glass fibre link, semiconductor junction lasers ageing and modulation *(German)* 79−32042
glass fibre long wavelength optical communication, materials and devices, review 80−99854
glass fibres used for optical transmission systems *(German)* 80−69516
graded index rod lens applications in optical fibre communications 80−14485
guided-wave optics, design of devices, laser beams in thin transparent films 79−64337
Gunn device, planar, high-bit-rate pulse regeneration and modulation of injection lasers 79−59731
heterodyne receiver arrays in turbulent atm., joint signal current probability distrib. 79−81368
heterojunction lasers, for fibre optic data systems 79−55149
high concurrency data bus using arrays of optical emitters and detectors 79−76805
high-density low-loss optical fibre unit and cable 80−53468
hybrid bistable optical devices, transient response 79−59803
hybrid p-i-n photodiode-FET preamplifier design for digital optical receivers *(German)* 78−33878
III-V semiconductor emitters and detectors for 1.0-1.6 μ fibre-optic communications 80−10007
injection laser, optimum pulsed pumping conditions, for communications appls. 77−75525
injection laser automatic level control by optoelectronic feedback *(German)* 78−33883
injection laser diodes for fibre optic communication 78−33751
injection laser quantum noise in optical fibre communication systems 80−48259

optical communication equipment continued
injection laser sources for fibre optic communications, design 79−31923
injection laser transmitter module, emitter unit, driving and control circuits *(French)* 78−46636
injection lasers, directly modulated, suppression of reson. in light output 78−66853
integrated branching filter using three-dimens. input waveguide, nonradiative condition 80−38130
integrated optical communication components in III-V semiconductor technology, overview 80−79012
integrated optical device for lightwave communications and data processing systems 79−37052
integrated optical devices, present status 77−46822
integrated optical mixer in waveguide based on phase diffr. gratings, for multichannel optical communication lines 79−18554
integrated optical switch, polarization-independent, for use with single-mode optical fibres 79−37059
integrated optics demultiplexer with matrix of Si waveguide photodetectors 79−32095
integrated optics in later generation systems 80−43487
integrated optics switch, total internal refl., theoretical evaluation 79−18551
integrated optoelectronic Si devices, optical signal processing and communications, fibre-channel waveguide coupled 79−59847
interferometric system, large path diff., nonparallel light *(French)* 77−75668
IR emitting diodes and injection lasers, optical communication appls. 80−58563
IR laser for optical fibre communication 77−88745
IR multipurpose communications transmitters 78−30053
IR torch using semiconductor DH laser diode 77−39101
junction laser transmitter, output stability, beam displacement and front/back mistracking effects 78−79059
kinematic-optical projection for high-density optical information transmission *(German)* 79−72678
laser beam combined with optical antennas, parameters optimisation 79−81475
laser beam deflector, electromechanical, for data transmission through free atmosphere *(German)* 80−38053
laser communication of sound, positional modulation, for undergraduates 78−12498
laser communication system, using US light modulator, for teachers 79−40321
laser digital communication system, 100 Mb/s, optical receiver and pulse generator *(Russian)* 79−94170
laser diode, hermetic packaged lens-coupled for wideband fibre-optic transmission 79−45970
laser diode and transmitter unit lifetime tests *(German)* 78−37883
laser diode appl., TJS, single-mode oscill. with low threshold currents 80−14355
laser diode characterisation, for multichannel applic. 78−87165
laser diode degradation modes and accelerated life tests 78−1233
laser diode fabrication reproducibility *(French)* 78−42357
laser diode module description and performance 80−64069
laser diodes for fibre communications, characteristics and state of art *(Italian)* 80−58569
laser diodes in optical transmitters, switching dynamics and noise *(German)* 79−89919
laser engineering advances, conf., San Diego, CA, USA (Aug. 1977) 78−59017
laser level-control circuit for high-bit-rate system using slope detector 79−18430
laser source, He-Ne, using cold-cathode plasma, educational demonstrations and experiments appl. 78−45448
laser-driver module, temperature-compensated, using Si bipolar transistor 79−45971
laser-fibre transverse coupling and front-mirror monitoring for feedback control of laser transmitters 80−33151
lasers for fibre-optic transmission systems 77−19342
LED, as semiconductor junction transceiver, for fibre optic communication 78−42410
LED, freq. response as function of design parameters for GaAs-(Ga,Al)As DH structure 77−79941
LED, GaAlAs, high efficiency, long-lived 77−79940
LED, with self-aligned sphere lens, for efficient coupling to optical fibres 77−79939
LED's, DH, second harmonic distortion prediction 78−18058
LED coupling to optical fibre, efficiency 80−48416
LED coupling to optical fibres improved by facet radiator 78−90520
lens, gradient-index rod, appl. in optical fibre communication systems 80−69488
lens guide, low-loss image transmission 80−91872
light sources, detectors, laser appl. *(Japanese)* 79−27406
lightguide fibre, prototype drawing fascility 80−64229
lightguide fibre testing 80−64230
lightguide lines appls. in telecommunication *(Polish)* 78−79132
lightwave sources and detectors 80−64068
linearised LED and laser transmitters, for analogue fibre optical systems 78−46818
liquid crystal fibre optic switch, adjustable access coupler 79−64334
log-normal device optimal burn-in time 80−58743
long-wavelength optical communication laser diodes and LED, 1 μm range 80−48448
long-wavelength single-mode fibre transmission systems 80−58773
low-loss single-mode fibre connectors, detachable 79−27382
LW receivers using avalanche photodiodes 80−10043
matrix switch, low-loss 4×4, for fibre-optic communication 79−76823
matrix switching network for fibre-optic communication 80−58735
measuring equipment for fibre optics *(German)* 79−32043
mechanical multimode one-to-many fibre-optic switch 79−76814
metal-Ge Schottky barrier quantum detectors, optoelectronic props. 80−13146
micro-optic devices for coupling/branching in fibre optic communications 79−55211
micro-optic directional coupler, aberration losses 80−48395
microoptic devices for optical communications 79−76840
microoptic grating multiplexers, optical isolators, fibre-optic communication applications 80−48408
mode scrambler for optical fibres 77−58436
modem ccts. *(Japanese)* 79−27407
optical communication equipment continued
modular light guide system, 5 MHz to 10 MHz bandwidth, features *(German)* 79−76865
modulator, 1 Gb/s 77−79965
monolithically integrated optical repeater, fabrication and charact. 80−28353
monomode optical fibre bandwidth limitations and bend losses 80−87553
multi-gigahertz modulation concepts, for CO_2 laser communications 77−3681
multichannel IR receiver performance 79−76596
multimode 3×2 fibre optical matrix switch 80−58764
multimode fibre couplers for data bus systems 78−74970
multimode fibre systems, low loss 4×4 switching network 80−58718
multimode integrated optics, modified thick film technology 79−32093
multimode optical fibre systems, microoptic passive devices, review 79−72700
multimode telecommunications fibre scatt., geometrical analysis 77−23748
multiplexer for multimode fibre transmission system 77−88935
multiplexer for multimode fibre transmission systems 77−83960
multiplexer using blazed grating, 1.1 to 1.5 μm, for WDM transmission system 80−38100
multiplexer/demultiplexer, low-loss, using interf. filters 80−58728
multiplexers/demultiplexers for single-fibre WDM transmission 80−43475
multiwavelength monolithic integrated fibre-optic terminal development 80−33243
n^+-p-π-p^+, epitaxial Si diode for optical fibre communication at 800 to 900 nm 77−79961
near IR (1 to 2 μm) optical communications, colloquium, London, England (May 1980) 80−86040
near IR Faraday rotation isolators 78−18042
Network 2000, use of optical communication technology 80−1306
noise immunity of digital optical communication lines receiving wholly coded messages *(Russian)* 78−87020
nonblocking 8×8 optical matrix switch for fibre-optic communication 80−74485
nonlinear distortions and noise in optical communication systems due to fibre connectors 80−96001
OCCULT laser system operating in marine boundary layer 78−5565
optical ccts. design *(Japanese)* 79−27408
optical communication testbed 78−33925
optical fibre sources and detectors *(Italian)* 80−69390
optical fibre transmission systems *(Japanese)* 79−27401
optical fibres, manufacture, silica production process, connection methods, applications *(Italian)* 77−3647
optical fibres, progress and components, review *(French)* 80−69524
optical fibres and terminal components, by Swiss firm CAbloptic AG *(German, French)* 79−90005
optical waveguide charact. review 79−41455
optoelectronic devices development 80−91902
p-i-n photodetector, Au-diffused, for freq. multiplexing optical fibre system 77−88914
p-i-n photodetector under transient conditions, simulation and expts. 79−58793
p-i-n/FET hybrid optical receiver 80−33158
passive couplers for appl. in fibre optic systems 80−91903
photodetector low-noise amplifiers using J-FETs for optical fibre receivers 78−37997
photodetectors, for optical fibre communication *(Japanese)* 80−78977
photodetectors, highspeed, performance testing 79−26129
photodetectors, pin- and avalanche diodes, charact. *(Swedish)* 78−89545
photodiode detector for optical cable, optimal filter struct. and charact. 78−18067
photodiode detector for optical fibre communication *(German)* 78−33874
photoelectron counter, dead time effect on direct detection binary PPM system 77−54796
photomixer, wide bandwidth, HgCdTe diode 77−3682
photon detectors *(Czech)* 79−50396
planar fan-out structure for multimode glass fibres 79−76845
planar optical branching elements for multimode fibre transition systems 79−94351
plastic fibre-optic assemblies 80−14433
pulse interval modulation for optical fibre communication system 78−50917
pulsed light source with thin-film modulator, fabrication and charact. 80−43467
pulsed-light detector for checking optical cables 78−54455
radiation coloration and bleaching of Schott optical glasses temp., time depend. 77−19981
reach-through photodiodes, Si, avalanche buildup time 77−15892
receiver, separation elements of radiation flux *(Rumanian)* 79−90027
receiver design, optimisation in terms of excess noise factors dependence on avalanche gains 77−792
receiver noise analysis, time-domain impulse response technique 77−68280
receivers, direct detection, performance for intensity subcarrier FSK 77−39033
receivers, phase compensation type 78−1329
receiving optical antenna, angle-distance sensitivity variation anal. 78−33841
reciever charact., influence on optical fibre system performance 77−83984
reed-type routeing switch for multimode optical fibres 80−53463
repeater, fibre optic, low-power (0.5 W) design 78−22195
repeater, multistage, consisting of nonlinear amplifiers and saturable absorbers 79−59772
repeater for fibre link, low noise regeneration 78−66920
research in Japan 77−75677
review of market trends and products 80−28319
rod lens analysis and application to optical fibre communications 80−87549
Second European Conference on Optical Fibre Communication, September 1976, review *(Italian)* 78−5552
self-imaging multiplexer and branching couplers 80−106629
semiconductor devices for fibre transmission systems, reliability tests 80−43464
semiconductor junction laser module for optical fibre communications, temp. compensation 80−5757

optical communication equipment continued
semiconductor junction lasers, simultaneous feedback control of bias and modulation currents for injection lasers 80−43332
semiconductor laser, electrooptically tuned external-cavity CW, FM optical communication appl. 80−14351
semiconductor laser, GaAs-$Al_xGa_{1-x}As$ DH 77−50684
semiconductor laser, pattern effect minimization at high-rate pulse modulation 80−19059
semiconductor laser diodes, present status and technology *(German)* 80−58561
semiconductor laser intrinsic noise in optical communication systems 80−69394
semiconductor laser modulation, non-linear distortion, communication systems appl. *(German)* 80−69395
semiconductor laser sources for coherent optical-fibre systems 80−64159
semiconductor light source for fibre optical communication 80−58653
semiconductor light sources for optical fibre transmission 77−54777
semiconductor pulsed laser communications 79−22972
semiconductor SiO_2 insulated laser, device params. determining system performance 77−10949
semiconductor stripe laser high-speed modulation, noise, and nearfield meas. *(German)* 78−37923
signal receivers, optimal and nonoptimal, logical structs. efficiency comparison, simulation *(Russian)* 78−71041
single fibre connectors and cable splice hardware, optical coupling theory 80−64187
single fibre separate connector, for optical fibre data transmission, loss factors 77−88939
single mode fibre optical data bus with star couplers 80−64199
single multimode optical fibre communication directional couplers *(German)* 78−33873
single-strand fibre couplers 77−68283
slip-ring for transmission of transducer signals 78−13814
solar pumped laser for space communications 78−46645
space laser communications K-Rb arc lamp development 78−46646
space laser communications system, evaluation of optical coatings required for components 79−86248
stabilised photoreceiver unit 77−39038
standardisation of components, EIA P-6 committee 80−1352
standardisation of components, military appl. 78−30083
standards for fibre optics 79−14101
star couplers for single multimode fibre communication systems *(German)* 78−33872
star repeaters for fibre optic links 77−34934
submarine cable using glass fibre, expt. cable *(German)* 80−58711
superluminescent diode source for fibre-optic systems *(German)* 78−38013
switch, 3×3, using single-mode waveguides in electrooptical material 78−55470
switch, four-way optical fibre, mechanically operated 80−53464
switch, moving fibre, using V-grooved connecting device 79−18509
switch array, mirror-type, integrated on $LiNbO_3$ substrate 79−27436
switch constructed of graded-index rod lenses, for multimode fibre systems 79−27439
switch with high reproducibility for optical fibre transmission 79−64329
switches, optically controlled, for integrated optics and fibre optics appl. 79−37057
tapping elements, beam splitter design, for graded index optical fibres 79−72701
tapping elements, beam splitter design, for optical fibres 79−72702
TDM pulse analogue modulation, diode laser nonlinearity 78−55455
transmission devices, including laser optical modulators and solid-state techniques *(Spanish)* 79−23079
transmission equipment for field demonstration 77−7209
transmitters for fibre communication systems 80−43459
transmitting and receiving devices, laser light and fibre optics techniques *(German)* 80−5827
US Bragg cell, standing wave, appl. to laser communication system, theory 78−25958
US Bragg cell, standing wave, appl. to laser communication system, expt. results 78−25959
waveguide 4×4 switching network 77−3683
waveguide gas lasers, miniaturised 79−31936
waveguide modulator for fibre transmission systems, temperature stabilized *(Japanese)* 79−27391
waveguide modulator for single-mode optical fibre transmission system, temp. stabilized 79−41450
waveguides, manufacture, CAD, doped deposited SiO_2, optical fibres *(Italian)* 77−19385
waveguides development strategy, Poland *(Polish)* 80−48438
waveguides technology, components and systems *(German)* 80−33168
wavelength division multiplexer using optical fibre pieces 80−91917
wavelength division multiplexing technology status and prospects 80−64203
wavelength division multiplexing transmission technology 80−58727
wavelength multiplexer, single-mode-fibre 80−102816
wavelength-division multiplexer for 1-1.4 μm spectral region 78−55451
weak optical signal meas. in strong interference *(German)* 77−65623
wideband 1064 nm laser communications detector evaluation 77−18097
wideband ambiguity function generator with Doppler compensation 78−78936
wideband thin film modulators and switches, for optical communication 78−63206
Y-branch for optical communication networks and measuring equipment *(German)* 78−66918
(Al,Ga)As, high radiance DH LED design for fibre optical communication 77−79963
(Al,Ga)As LEDs, high-radiance double-heterostructure for optical fibre links 78−37991
(Al,Ga)As long-lived DH injection lasers for fibre optic communication, degradation exam. 78−50778
AlGaAs DH laser preamplifier to improve optical receiver sensitivity 80−53316
(AlGa)As oxide-defined strip lasers, self-sustained oscillations, ageing effects, appl. to communication systems 80−32991
AlGaAs-GaAs lasers for optical fibre transmission, defects and degradation 79−41382
$Al_{0.5}Ga_{0.5}As$-GaAs heterojunction phototransistors, growth by metalorganic vapour deposition 79−67380
CC GaInAs-InP injection lasers with longer wavelengths for optical fibre communications, review *(Japanese)* 78−25892

optical communication equipment continued
CO_2 10.6 μm laser, freq. modulation and demodulation 80−43378
(Ga,In)(As,P) DH lasers, 1.55 μm, low-threshold current densities 80−1221
GaAlAs DH injection laser transmitter, for long distance fibre optics communication 78−42355
(GaAl)As DH stripe contact injection lasers, local attached data fibre link appls. 80−19044
GaAlAs LED sources for fibre optic transmission, linearity improvement using phase-shift-modulation technique 77−19403
GaAlAs laser diode, for heterodyne communication systems, high frequency stability 80−99727
GaAlAs laser transmitter for optical fibre communication, features 78−90423
GaAlAs laser transmitters using optical tap for feedback control, output power stability 79−64241
(GaAl)As lasers, low threshold proton isolated, spectral and transient response 78−87052
(GaAl)As-GaAs narrow stripe laser, improved optical communication system performance 80−102733
$Ga_{1-x}Al_xAs$ buried heterostructure lasers for analogue communication 80−48297
$Ga_{1-x}Al_xAs$ feedback-stabilised injection laser for fibre-optic data transmission 77−19343
$Ga_{1-x}Al_xAs$ junction-up TJS laser electron injection efficiency improvement 80−48300
$Ga_{1-x}Al_xAs$:GaAs LED 640 mbit/s PCM optical fibre source, expt. 78−37998
$Ga_{1-x}Al_xAs$-GaAs narrow stripe laser for improved communication performance 80−48299
$Ga_xAl_{x-1}As$ laser, SiO_2 insulated, CW, 3-5 mW output 77−3656
GaAs DH injection laser, modulation behaviour, appl. in high bit-rate fibre optical communications 78−1281
GaAs DH laser/fibre transmission system modulation and injection 77−50764
GaAs diode laser in communication system using PPM methods *(Rumanian)* 77−68260
GaAs double and narrow stripe laser structures 80−64062
GaAs, high speed DH superluminescent diodes, modulation characts. 77−54783
GaAs homojunction LED signal source for fibre-optic communication 78−1413
GaAs LED modulation bandwidth, influence of inhomogeneous current density distrib. 80−9993
GaAs LEDs, high speed, optical transmitter appl. 78−33844
GaAs laser diodes, digital modulation *(German)* 78−37919
GaAs laser source package for multichannel optical links 78−1266
GaAs MESFET, optical detector appl., sensitive high-speed device 80−13143
GaAs-(GaAl)As laser, SiO_2 stripe geometry, for wide band optical communication systems 78−42358
GaAs-$Al_xGa_{1-x}As$ buried-heterostructure laser, wideband optical sources *(German)* 78−37904
GaAs-AlGaAs high-radiance LED for optical communication systems, power and modulation bandwidth 78−42416
GaAs-$Ga_{1-x}Al_xAs$, DH laser, characts. exam. for communication appl. 78−37891
GaAs-$Ga_{1-x}Al_xAs$ DH strip CW laser for optical transmission *(German)* 77−68222
GaAs-$Ga_{1-x}Al_xAs$ double heterostructure LED and injection laser transmitters 77−68282
GaAs-$Ga_{1-x}Al_xAs$ DH LED, for optical fibre communication *(Japanese)* 80−78976
GaAs-$Ga_xAl_{1-x}As$ CW stripe geometry laser fabrication and performance 77−38933
GaAs-GaAlAs, injection laser and MESFET monolithic integration on GaAs substrate 79−64242
GaAs-GaAlAs injection laser sources, for fibre optic communications 78−46637
GaAs-GaAlAs laser, optical repeater using PFM at 1 GHz 79−98395
GaAs-GaAlAs laser, practical appls. 80−1212
$GaAs_{1-x}Sb_x$ photodiode structures, current-voltage characts., photo-EMF spectra 80−29472
GaInAs, efficient photodiode for near IR detection 78−16848
$Ga_{0.47}In_{0.53}As$, photodetector applications 80−95140
$Ga_{0.7}In_{0.3}As$ photodiodes, fibre optic appls. 79−40613
GaInAsP LEDs, 1.3-1.6 μm, appl. in long haul high data rate fibre optic communication systems 80−102854
GaInAsP/InP DH lasers, direct modulation charact. meas. by sharp pulse method 80−1245
GaInAsP/InP optical sources for 1.2 to 1.4 μm wavelength region, growth and props. 79−90023
GaInAsP-InP, broad-area and stripe-geom. DH laser, for fibre optic communication 78−42356
GaInAsP-InP DH lasers, for fibre optic communications 79−31924
GaInAsP-InP lasers and detectors, for fibre optic communications at 1.0-1.6 μm 79−3803
GaInAsP-InP lasers and detectors, 1.1 to 1.3 μm, fibre optics appls. 80−14360
$Ga_{1-x}In_xAs_{1-y}P_y$-InP DH lasers, 1000-hour CW operation 78−1265
He-Ne mode locked laser for very wide band communication system 78−17994
Hg cell, enhanced Faraday effect for reversible depolarisation, communication scrambling appl. 77−42596
InGaAs/InP p-i-n small area photodiodes, fabrication, characts. and performance in 274 Mb/s receivers at 1.31 microns 80−53415
$In_{0.53}Ga_{0.47}As$ p-i-n photodiode-FET photoreceiver for 1.0 to 1.7 μm wavelength optical fibre communications systems 80−58794
InGaAsP, 1.3 μm LED, for high-bit-rate fibre data link 78−46825
InGaAsP buried stripe laser, modulation characts. at high data rates 79−98418
InGaAsP, high radiance CW LEDs emitting at 1.30 μm 78−22196
InGaAsP IR heterojunction photodiode detector 79−21813
InGaAsP InP DH lasers, optical power and wavelength stabilisation 80−38036
InGaAsP laser, single-mode CW ridge waveguide, emitting at 1.55 micron for optical fibre links 80−9883
InGaAsP photodetector, improved two wavelength demultiplexing 80−58795
InGaAsP quaternary alloy IR heterojunction detectors, props. 79−2823

optical communication equipment continued
InGaAsP/InP heterostruct. lasers as optical source, CW operation at room temp. 80−1220
InGaAsP/InP injection lasers for long wavelength (1.1 to 1.6 μm) optical communication 80−58582
InGaAsP-InP dual wavelength LED 80−15589
InGaAsP-InP:Mg LEDS, for high-bit-rate optical communication systems 80−5823
$In_{1-x}Ga_xAs_yP_{1-y}$ DH lasers for 1.3 and 1.5 μm optical fibre communications 80−91817
K vapour arc lamp, as optical pump source in Nd:YAG space communications laser 79−86261
$LiNbO_3$ total internal reflection diffraction modulator/deflector performance 77−42628
$LiNbO_3$-Ge acoustooptic modulator *(Japanese)* 80−69542
$LiNdP_4O_{12}$ electroluminescent diode pumped miniaturized laser for optical transmission system 79−41395
$LiNdP_4O_{12}$ miniaturised lasers for optical communication systems *(Japanese)* 79−27278
$LiTaO_3$ total internal diffraction modulator/deflector performance 77−42628
Nd compound optically pumped miniature lasers, for fibre optical communication system 78−50786
Nd lasers appl., characts. *(German)* 78−37902
Nd^{3+} ion miniature phosphate glass lasers with high ion concentration 80−19038
Nd:YAG laser, appl. in space communications 78−28483
Nd:YAG laser, Kr-pumped for space optical communications 77−19328
Nd:YAG laser, pumped by Kr arc lamp, conductive cooling, for space operation 77−88775
PLZT ceramic, modulator for optical communication 80−78964
Rb cell, enhanced Faraday effect for reversible depolarisation, communication scrambling appl. 77−42596
SiO_2-GeO_2/SiO_2 load bearing optical cable, geophys. appls. 80−91923
Xe short-arc lamp, current modulated, arc forms and instability 80−96399
YIG, computer optical isolator for near IR region 78−83104

optical constants
see also light absorption; reflectivity; refractive index
absorbing film on non-absorbing substrate, optical consts. calc. 77−11041
absorbing films, optical parameters determ. by ellipsometry 80−254
absorbing material optical consts., transmission interferometry meas. on medium-thickness films 79−78768
absorbing materials, optical consts. determ. using Fresnel formulae approximations 80−88946
absorbing substances, optical consts. determ at elevated temps. *(Russian)* 77−90122
absorption coefficient, optical, absolute meas., photoacoustic spectroscopy 80−82828
absorption coefficients at 632.8 nm, intracavity laser meas. 78−8454
absorption measurement, optical materials, real time holographic interferometry 80−83569
achromatic antireflection coatings, thin-layer, layer thickness calcs. 80−87468
actinides and their fluorides, interband, collective and atomic (p,d) excitations, Z-160 eV, fast EELS 80−93443
adatom-surface interaction, polarisation energy from opt. data 77−72792
alkali and alkali earth metal metaphosphate glasses exam. of temp. dependence of thermooptical const. 78−88286
alloys, substitutionally disordered, optical cond., intraband transitions 80−103933
anisotropic crystal, refl. spectra, phase difference determ., Fresnel formula validity 77−43956
anthracene, O-O exciton absorption bands, thermomodulation study 78−39563
apochromat optical glass development status and prospects 79−27348
atmospheric aerosol species optical consts. rel. to radiation balance determ. 77−17163
atmospheric aerosols microphysical parameters from complex optical meas. *(Russian)* 77−13123
ATR meas., 2-polarisation method, accuracy, optimisation 78−45673
attenuated total reflection, optical consts. determ. *(Spanish)* 77−69788
benzene, optical consts. determ. from IR absorpt. spectra *(Spanish)* 77−69787
biological materials, VUV and visible obs. 80−30762
bulk materials, low optical absorpt. coeffs. meas., adiabatic laser calorimetry with long rod samples 79−2804
cadmium arachidate monolayer on Au, surface plasma reson., optical consts. 77−90210
calculation from frustrated total internal reflection meas. 79−33658
calculation from IR absorpt. expt. data *(Spanish)* 77−69787
canted magnetic structured materials, exciton spectra, optical props. 80−70622
cermet film, as solar selective absorbers, production, struct. and optical props. 79−29485
cermet film, dense, regular, optical props., rel. to appl. as selective solar absorber 79−79408
cermet film granular media, dielectric function theory, permittivity, percolation transport props. 80−88498
chalcogenide glasses, O-free, cooling rate influence on optical consts. 80−88952
chalcopyrite crystals, temp. depend. Sellmeier coeffs. and coherence lengths 79−76752
composite material, complex dielectric const., bounds 80−108170
conjugate Fourier series approach to optical data analysis 78−90378
diamond, electric quadrupole sum rules rel. to optical consts. 79−38036
dielectic-semiconductor systems, immersion ellipsometric obs. *(Russian)* 79−15548
electrode surface, anisotropy of optical props. 80−60534
epoxy, clear, refr. index and extinction coeff. meas. 79−18492
far IR research, Rubens era (1892-1925) 78−4454
ferroelectric crystal, absorpt. coeff. calc., Green functions method 78−10851
ferromagnetic semiconductors, free carrier absorpt. of radiation 80−97227
fibrous materials, IR emittance 79−95189
film, computational algorithm for optical consts. determ. 78−72617
film, optical const. determ. from meas. of normal incidence reflectance and transmittance 77−85825

optical constants continued
film, optical consts., thickness and surface roughness determ., technique and appl. to AlN *(German)* 77−41670
film thickness and optical consts., spectrophotometer meas., computer program evaluation *(French)* 77−13808
films, optical constants, reflection spectra by Kramers Kronig method 80−76099
Fourier series algorithm 77−85679
glasses, gradient composition, optical props. 80−88947
graphite grains, interstellar, IR optical consts. rel. to temp. 78−12324
Green's function of optically anisotropic media *(German)* 80−93255
heavy water, 6-450 cm^{-1}, 19°C 78−6649
heavy water, 70 to 450 cm^{-1}, reflection dispersive Fourier transform spectrometric obs. 77−40203
heavy water, optical consts., absorpt. and refr. index 0.1 Å-1 m 78−48139
high-temperature determination method 77−85680
ice-crystal fog, aerodynamic and opt. props. 77−90648
III-V semiconductors, oxide film growth, optical props. *(German)* 78−34730
inhomogeneous optically anisotropic media, parameters by photoelec. polarimeter 77−74486
isotropic layers, thin, with rough boundary surfaces, refl. and transmission factors *(German)* 78−90354
Kramers-Kronig analysis *(Russian)* 80−80740
laser annealing, optical constants, ellipsometry observation 80−34024
laser window materials, optical suitability 77−58361
LED, using Si, photovoltaic cell, absolute spectral sensitivity calibration, radiometry, photometry *(Chinese)* 80−86367
leucosapphire, spectral absorpt. coeff., 1800K 78−27252
Lorenz-Lorentz relation, series expansion 77−40199
magnetic electron lenses, optical parameter formulae *(Chinese)* 77−88633
matching methods determ. 77−85682
measurement at two incidence angle values 80−101831
measurement method using polarised light refl. coeffs., accuracy 80−73423
measurement of films, by light intensity ratios 77−2678
measurement of magneto-optic rotation and ellipticity, spinning analyser ellipsometer *(Japanese)* 80−73419
metal, highly reflecting, determ. of IR optical constants by surface plasmon excitation 78−76418
metal, O_2 diffusion and dissolution effects on optical props. in radiative heating, appl. to Ti 79−65884
metal optical constants meas., simple polarimetric method *(French)* 77−45880
metal oxide film, optical and diffusion consts. meas., dynamic method *(Russian)* 78−43950
metal oxide layers, heterogeneous, optical consts., Garnett's theory calcs. *(Russian)* 78−23427
metallic films, determ. from Abeles formulae for reflectance, transmittance 78−15240
metals, IR optical consts., meas. by self-radiation method 80−84710
$MgSiO_3$, Mg_2SiO_4, vapour condensed, mid IR optical props. 80−31337
micellar solution, micellisation kinetics, pressure-jump and stopped-flow methods 80−45564
minerals optical constants, derivation from measured reflectances, errors in two-media method 79−58100
modulation spectroscopy, anal. of Kramers-Kronig relations 78−23423
multilayers, ultrathin, optical characts. 80−104005
narrow band interference filter, spectral transmission curve meas. 78−297
oil, optical characts., 0.4-15 μm, rel. to ocean pollution and photosynthesis suppression 79−52968
oil droplets, motion and optical props. by interf. method 78−67893
optical fibre parameter measurement using optical time domain reflectometer 80−58755
optical glass, absorption coeff. determ., refl. losses role 77−72100
optical glasses, development and manufacturing processes 80−53393
organic bases, biologically important, and derivatives, optical crystallograhpic props. 78−3449
organic liquid, optical anisotropy, determ. from refr. index, Rayleigh's const. and depolarisation *(French)* 77−59548
organic semiconductor film, optical consts. by refl. and transmission, errors 77−16414
organic uniaxial films, optical consts. and thickness determ. by modified ellipsometry 79−91512
phase boundary, Fresnel refl. coeffs., optical thickness *(German)* 77−69794
photothermal deflection technique for absorpt. meas. in optically thin media, thermal lens effect comparison 80−105717
plane parallel slab, optical const. determ. methods 80−60531
plastics, filled and reinforced, optical const. determ. 78−19472
Poley absorption magnitude 77−24813
polyethylene terephthalate, film, optical consts., frustrated total internal refl. obs. 77−55763
quartz, far IR ordinary-ray optical constants 80−45025
quartz, nonlinear polarisation plane rotation due to ruby laser irrad. *(Russian)* 80−53390
quartz high-transmittance antirefl. film, vacuum-etched 80−74449
rare earth vanadates, electron energy loss spectra, primary excitation processes in cathodolum. 79−11490
rare earths and their oxides and fluorides, interband, collective and atomic (p,d) excitations, Z-160 eV, fast EELS 80−93443
real thin films, optical consts. determ. 78−35213
reflection spectroscopy, causality calcs. optical consts. determ. as function of wavelength 78−32887
Rochelle salt, optical characteristics in UV region *(Russian)* 78−84550
ruby, spectral absorpt. coeff., 1800K 78−27252
semiconductor, optical absorpt. coeff. and minority-carrier diffusion length, differential photocurrent method of meas. 80−96896
semiconductor, optical props. with electron temp. superlattice *(Russian)* 80−34879
semiconductor epitaxial film optical constants meas. by far IR ellipsometry 78−93753
semiconductor film, transparent substrate, optical props. rel. to interference and surface unevenness 77−77310
semiconductor films, polycryst., grain boundary effects 80−80890
semiconductor-insulator system, contact interaction mechanism, optical props. 78−88375
sheet with chipped surface, spectral transmission curve meas. 78−297

optical constants continued
smokes, atmospheric, optical probing, homogeneous particle model appl. *(Russian)* 78−77328
soil-derived atmospheric dusts, particle absorption contributions to mass extinction coefficients 80−61896
solid with thermal or static disorder, optical props. 79−42936
Spectrofloat glass, theoretical anal. of optical transmission and refl. props. 77−90120
sphericity standards, interferometric meas. *(German)* 80−87569
steel, austenitic stainless, Mo-bearing, ellipsometric meas. of passive films, optical constants *(Japanese)* 78−85041
steel, stainless 18-8, ellipsometric meas. of optical const. and thickness of passive film 77−21326
substrate, surface quality determ. by optical reflectance methods 78−43862
surface anisotropy measurement by ellipsometry 78−56452
surface films and bulk material, optical props. meas. using ellipsometry, review 79−44926
surface films and film growth meas., ellipsometry appl. 78−39619
surfaces, optical examination and monitoring, review 79−67375
TCNQ, salt, $(NMe_3H)(I)(TCNQ)$, semicond. 'metal-like' complex, optical props. 79−95761
TCNQ salt, K^+TCNQ^- particles, light scatt., absorpt. spectra 79−24332
TGFB, IR spectra and optical consts. *(French)* 79−95748
TGFB, optical props. in 5 to 22 eV region, reflectance spectra 79−33652
TGFB, refl. spectra 4-22 eV, optical consts. 79−4821
TGS, optical props. in 5 to 22 eV region, reflectance spectra 79−33652
TGS, refl. spectra 4-22 eV, optical consts. 79−4821
thermoregulating plasma coatings, UV irrad. influence on optical parameters *(Russian)* 80−40259
thin film, optical characterisation *(French)* 79−11402
thin films, unbacked, optical constants by transmission interferometry 79−78778
thin surface layers, thickness and optical consts. using surface plasmon excitation 79−47533
transition metal, optical consts. 12 to 24 μm, anomalous skin effect region 77−20842
transition metal dichalcogenides, layer type, reflectivity meas., 6-40 eV 77−55801
transition metals, BCC, films, vac. evaporated, optical cond. 80−76100
TTF-I_n, single cryst. optical props., polarised specular reflectance meas. 77−12400
twisted nematic display with cholesteric dopant, transmission characteristic temp. depend. compensation 80−103934
urethane elastomers, rheo-optical const., Young's modulus *(Polish)* 79−70108
valence electrons, finite energy, f-sum rules 78−88276
water, 6-450 cm^{-1}, 19°C 78−6649
water, absorption coefficient at 488 and 541.5 nm, adiabatic laser calorimetry 77−73123
water, optical consts., absorpt. and refr. index 0.1 Å-1 m 78−48139
water 70 to 450 cm^{-1}, reflection dispersive Fourier transform spectrometric obs. 77−40203
water optical constant submillimetric wave meas. 79−33656
zero-gap semicond., IR absorption coeff., theoretical anal. 80−20641
Ag (111) surface, Ar ion bombardment, effect on struct. and reactivity, optical consts. calc. 77−59192
Ag, ellipsoidal small particle assembly absorption spectra, optical model *(Russian)* 78−60483
Ag film, ellipsometric response to CO adsorption 80−103571
Ag film, optical props., inverse problem of phenomenological theory 79−43053
Ag foil, interface with liq., oxide props., refl. and scatt. light spectroscopy 80−60702
Ag weakly modulated surface, light diffr. 77−31132
Ag-MgF_2 layered system, optical excitation of surface plasma waves 78−6803
Ag-MgF_2-Ag layered system bounding dielec., ATR ang. spectra, assoc. reson. EM oscills. 79−15541
Ag_3AsS_3, proustite, reflectivity and optical constants at 80K and 300K from 18 to 700 μm *(French)* 77−36235
AgI film, light-induced changes, ellipsometric meas. 78−56537
β-AgI thin film, exciton spectrum 80−55216
Ag_2S, film, optical characterisation, inversion method 78−11008
Al oxide anodic film, colloidal metal, origin of colour, optical props. meas. 78−68571
$(Al_{0.42}Ga_{0.58})As$, LPE grown layer, optical absorpt. coeff. meas. 78−6801
Al_2O_3, optical consts., high temp. determ. 77−85680
Al_2O_3, transparent hot-pressed, transparent and translucent properties 80−60533
Al_2O_3-Au cermet, optical constants, incl. proximity effects 78−56446
An, optical constant meas., 100 to 1000 eV using transmission gratings 80−93258
As, rhombohedral, electronic struct. and optical props. var. with internal displacement parameter 79−60702
As_2S_3, amorphous thin films resonant Raman scattering 78−68505
As_2S_3 evaporated film, optical props., depend. on light exposure and heat cycling 78−68572
As_2S_3 film, amorphous, opt. const. changes under illumination 77−77316
As_2S_3 film optical constants, wedged-film meas. 79−14066
As_3Se_2 chalcogenide semicond. film, thermoptical transitions with photostructural transformations *(Russian)* 80−16016
Au film, ellipsometric obs. of optical props., rel. to surface roughness 79−78776
Au film, evap., temp. change and gas adsorpt. effect on opt. consts., ellipsometric obs. *(German)* 80−89081
Au film, on α-quartz substrate, optical consts. evaluation from surface polariton dispersion 78−48249
Au film, optical characterisation, inversion method 78−11008
Au film, optical consts. meas. via automatic ellipsometer without phase plate 77−53970
Au film on Ag, optical constants, 4000-6000 Å, using surface plasmon optical excitation 77−69925
Au, optical consts., dispersion, temp. depend., Kramers-Kronig calcs. *(Russian)* 77−69796
Au, optical consts. direct determ., d absorpt., reflectivity 77−69791
Au, transmission interferometry, refr. index and extinction coeff. 77−69790
Au-dielectric cermets, optical constants, incl. proximity effects 78−56446

optical constants continued
Au-WO_3 electrochromic cermets, resist. and optical density meas. 79−8201
AuCu, optical constants direct determination, d absorpt., reflectivity 77−69791
B:H amorphous films, optical band gap, thermal treatment effect 80−93415
Ba film, semitransparent, opt. props. in 2-5.6 eV range, electronic transitions, thickness depend. *(French)* 80−108289
$BaTiO_3$, UV refl. spectra, optical consts. 0 to 32 eV Kramer-Kronig anal., band struct. calcs. 78−43903
$BeSO_4.4H_2O$, SHG at 2660 angstroms 78−90451
Bi film, ellipsometric obs. of optical props. 79−78776
Bi film, optical, magneto-optical and struct. props. 77−1664
Bi film, optical props., inverse problem of phenomenological theory 79−43053
$Bi_{12}GeO_{20}$, reflectivity spectrum and band struct. 79−47474
BiI_3, layered single crystal, band-edge excitons, optical constant meas. *(Russian)* 77−90171
$Bi_8T_7S_5$, thin crystal, optical consts. from transmissivity spectra, classical oscillator anal. 77−1748
$Bi_2(Te_{1-x}S_x)_3$ film, optical consts. meas., Shamir-Graff method evaluation 80−11489
C, amorphous grains, extinction coeffs., 0.21-340 μm, lab. meas. rel. to interstellar grains 80−73020
CC GaAs, n- and p-types, optical consts., 2.5-3.5 eV, normal incidence reflectance meas. 79−15428
CO_2-He-N_2, absorpt. coeff. for 10.6 μm CO_2 laser radiation, 295 to 650 K 80−92252
Ca film, optical consts. meas., 2 to 5.6 eV *(French)* 78−52586
$CaEuAl_3O_7$, mechanism of solid-phase reactions of formation and physicochem. props. 77−52622
CaF_2, optical props. of cation colloidal particles 78−23503
$CdGeAs_2$ crystals, Bridgman grown, optical props. rel. to O_2 content of starting materials 80−81213
$CdIn_2S_4$, reflectivity obs. 78−84549
CdS, highly excited semicond., linear optical response, electron-hole liq. 79−51980
CdS, reson. dispersion of Brillouin shift 78−35160
CdSe(Te), laser calorimetric meas. of two-photon absorpt. coeffs. at 1.06 μm 79−44934
CdTe, optical absorpt. coefficient, photovoltaic determ. 77−39890
Co film, optical props. by self-consistent photometric technique 80−55217
Co, optical consts. and electronic charcts., 20 to 1750°C 79−38516
Co, thin films, optical and magneto-optical permittivities 80−66163
$Co_{1-x}Fe_xSi$, elec. and optical props. 80−49740
Cr, fine particle solar absorber, effective medium theory 80−21396
Cr-Co (4 wt.%) alloy, antiferromag. transitions effect on opt. props. 77−12371
CrO_2, optical conductivities and dielec. functions in 0.2-6 eV range, rel. to band struct. 79−42938
CrSb, optical props., 0.05 to 5 eV 77−48194
Cr_7Te_8 film, optical and magneto-optical props., appl. as storage medium 78−23545
Cu film, optical consts. deduced from surface EM wave propag. 80−60697
Cu film, pure and CO covered, optical consts., ellipsometry meas. 79−78645
Cu, optical consts. direct determ., d absorpt., reflectivity 77−69791
Cu-Sn(Al)(Ga) reflecting surface absorpt. coeffs. at 10.6 μm 80−95984
CuCl, optical consts. in exciton absorption region, spectral depend. *(Russian)* 77−81125
CuCl vapour laser, output power limiting processes 80−91776
$CuFeS_2$ single crystal, optical reflectivity spectrum 80−40129
Cu_2S, film preparation for solar cells, elec., optical, struct. props. 78−76602
Cu_2S-CdS solar cells, optical absorption coefficient changes in Cu_2S 80−93980
$CuSO_4$, single cryst., IR optical consts., comparison with soln. 77−66470
D_3 Rydberg states, spectroscopic B_0 consts. 80−74109
$Eu_{0.14}Si_{0.31}O_{0.55}$, insulating amorphous mag., optical, mag., and magneto-optical props. 79−61344
Fe, passive film form. in phosphate soln., intensity-following ellipsometry study 80−104345
Fe, temp. depend., 20, 1400 and 1600°C 79−87412
Fe-Co alloys, optical and spectrosc. props. *(Russian)* 78−72529
Fe-Cr alloys, in acid and neutral solns., thickness and optical constants of passive and transpassive films 80−66698
$Fe_{80}B_{20}$, metallic glass, optical and magneto-optical props. 80−84728
$FeBr_2$, Faraday rotation in pulsed mag. field, linear absorpt. const. 80−45041
$FeGe_2$, Fe_2Ge, optical consts., electron energy loss spectra meas. 77−90121
FeO, ultrathin homogeneous absorbing films, ellipsometric nucl. microanalysis data analysis *(French)* 78−11011
$Fe_{1-x}O$, IR reflectivity obs. 77−43996
Fe_2O_3, haematite, anal. of refl. spectrum by Kramers-Kronig relations 80−16058
Fe_3O_4, magnetite, optical props. in IR 80−97271
Ga film, optical props., 2-15 eV 77−77308
Ga, optical properties in 0.3 to 5 eV range 78−31196
GaAs, absorption coefficients, method of meas. 78−83048
GaAs, ellipsometry of dielectric films on 79−69894
GaAs, opt. consts. in 0.6 to 4.2 eV range 79−51928
GaAs, optical conductivity, constants, refractivity from IR absorption spectra 78−43873
GaAs, oxide film, microscopy with an ellipsometric arrangement 80−17998
GaAs, reflection spectra, optical consts. *(Russian)* 79−38571
ε-GaAse, optical consts. for ⊥ and ∥ light polarisation, reflectivity, interf. meas. 77−52077
Gd, ferromag., magneto-optical reson., optical consts. determ. 78−6657
Gd, optical constants, reflectance meas. *(French)* 78−2869
Gd, polarimetric meas., mag. ordering effects 78−15184
Ge, dielectric const. associated with direct interband transitions 77−20817
Ge, electric quadrupole sum rules rel. to optical consts. 79−38036
Ge film, amorphous and crystalline, optical props. 77−16412
Ge, film, optical characterisation, inversion method 78−11008
Ge, rough surface, polarisation angles, ellipsometric meas. 78−56449

optical constants continued
$Ge_{0.3}As_{0.2}Se_{0.5}$, IR optic materials, characteristics *(German)* 80−38081
GeS_2, IR optic materials, characteristics *(German)* 80−38081
GeSe, amorphous film, optical properties 78−39620
$GeSe_2$ amorphous film, laser induced oscillatory phenomena 80−84711
$GeSe_2$, IR and Raman spectra 78−95585
p-GeTe, reflectance, and thermorefl. spectra 80−80814
H_3, Rydberg states, spectroscopic B_0 consts. 80−74109
H_2O, liquid, far IR optical consts. meas. with optically pumped laser 80−40082
Hg drop, optical consts. meas. from Hg-air interface, ellipsometry at spherical object 79−61326
Hg/Xe films, optical study of metal-insulator transition 79−65947
Hg-As-S-I system, glasses, optical and acousto-optical props. 78−83053
In-Bi, single crystal, vacuum UV optical props. 77−1697
In_2O_3, elec. conducting film on glass substrate, measurement of optical constants and thickness 78−60525
InP, reflection spectra, optical functions, exciton peaks *(Russian)* 80−50372
InSe, optical props. from 2-25 eV 80−29760
In_2SnO_3 film, effect of ambient atmosphere during annealing, elec. props. 80−97510
K smoke particles, optical props. 480 to 620 nm, rel. light scatt. cross sections meas. 80−97293
KCl coloured crystal, susceptibility variation calculations 80−55055
K_2CrO_4, vibr. spectra, dispersion anal. 79−8147
$KNdP_4O_{12}$, laser emission cross sections, fluorescence spectra, radiative lifetimes, quantum efficiency 80−23694
$K_2Pt(CN)_4Br_{0.3}2.6H_2O$ crystal, quasi-one-dimensional, optical consts. and dielec. permittivity dispersion 77−1695
Kr, solid, reflectivity, Kromers-Kronig anal. 77−73122
LaB_6 film, prep. by electron beam evaporation, and optical and elec. props. 80−20793
Li deposits, Kramers-Kronig anal., 0.5-10.7 eV 77−40201
$LiIO_3$, second harmonic optical coeffs. based on highly deformed oxygen-octahedra model of $(IO_3)^{-1}$ *(Chinese)* 77−75608
$LiN_2H_5BeF_4$, linear and nonlinear optical props. *(French)* 78−33778
$LiNbO_3$, optical consts. determ. by background stimulated Raman scatt. 80−48336
$LiNdP_4O_{12}$, laser emission cross sections, fluorescence spectra, radiative lifetimes, quantum efficiency 80−23694
Mn film, optical, magneto-optical and struct. props. 77−1664
$MnAu_2$, optical consts., 0.5-3.5 eV, intra-and interband absorpt. *(French)* 78−10916
MnBi film, optical, magneto-optical and struct. props. 77−1664
MnSb, optical props., 0.05 to 5 eV 77−48194
$MnSe_2$, IR lattice vibrs., dielectric dispersion 79−28735
MnTe, optical props. and electronic struct. 78−6682
MoO_2, optical conductivities and dielec. functions in 0.2-6 eV range, rel. to band struct. 79−42938
$MoS_2(Se_2)(Te_2)(2H)$ polytypes, Kramers-Kronig anal. of reflectivity spectra, 0-30 eV, band model 79−51976
NH_3 solid film, absorpt. coeffs. determ. 50 to 7000 cm^{-1} 80−97356
NH_4Br, thermorefl. spectra, band energy anal. 77−12402
NH_4Cl, thermorefl. spectra, band energy anal. 77−12402
NH_4I, thermorefl. spectra, band energy anal. 77−12402
$(NH_4)_2SO_4$, aqueous solns. and cryst., optical consts. meas. rel. to atm. aerosol props. 77−52034
Na, IR and optical props., surface-plasmon-mediated absorpt. mechanism 80−93308
NaCl surface with adsorbed water layer, absorpt. and thickness meas. 80−16001
$NaNdP_4O_{12}$, laser emission cross sections, fluorescence spectra, radiative lifetimes, quantum efficiency 80−23694
Na_2O-CaO-SiO_2 glass, mm wavelength absorpt. 79−82978
$Na_2O.Al_2O_3.10TiO_2$, crystallized bronze, chem. comp., morphology, optical and thermal props. *(Japanese)* 80−16172
Na_2S, dielectric const., transverse and longitudinal optical mode, static dielectric const., effective charge 79−73892
$NaSbSe_2$ films, struct., photoelec. and opt. props. 78−51834
Na_xWO_3, optical props. 79−38515
Nb, bulk, optical props., 6.6 to 23 eV 79−4815
NbN, opt. consts. and physicochem. spectra 77−85677
Ni, corrosion and passivation in phosphate soln., pH depend., ellipsometric study 80−104448
Ni, electronic structure and optical consts. by inelastic electron scatt. 80−7451
Ni film, evaporated, chemisorpt. of CO, ellipsometric investig. *(German)* 80−61156
Ni, optical constants at high temp. 79−24281
Ni, optical consts., influence of temp. and relation to bandstruct. 80−25403
Ni, optical spectrum, anomalous temp. depend. around T_c, band struct. 80−40128
β'-NiAl, electronic struct. and optical props. 80−97228
NiAs, optical props., 0.05-5 eV 77−48194
Ni_5Ge_3, amorphous and cryst. films, opt. props. in interband absorpt. region 80−66315
Ni_5Ge_3, amorphous-crystalline transition, opt. and elec. charact. *(Russian)* 77−85191
NiSb, optical props., 0.05 to 5 eV 77−48194
Ni(100) platelet surface optical and magneto-optic consts. 78−15151
PbI_2, complex dielectric and optical consts., ellipsometric determ. 78−23425
PbI_2, film, spectral depend. of optical consts. on fundamental absorption edge *(Russian)* 77−16415
$PbMoO_4$, Faraday rotation, interband optical transitions *(Russian)* 80−55071
PbSe:Tl, high temp. elec. and optical props., impurity states 79−60854
PbTe film, optical consts., support roughness effect 80−2882
Pb_xTe_{1-x} film, optical consts. calc. 77−11041
$Pd_{81}S_{19}$ and $Pd_{84}Si_{16}$, metallic glasses, optical refl. spectra and optical consts. 79−87464
PrB_6 film, prep. by electron beam evaporation, and optical and elec. props. 80−20793
PtO film, electrochemically formed, anisotropy of optical constants, reflection spectroscopy and Kramers-Kronig analysis 77−32456
$(SN)_x$, epitaxial, optical props. and plasmon dispersion, from electron energy loss spectra 77−35882
SbI_3, refl. spectra of cryst., 300-800nm, and derived optical consts. 79−87456

optical constants continued
Sb_2S_3, anisotropic cryst., optical const. determ., reflected-light polarisation 77−43960
SbSBr glass, IR reflectivity spectra 80−71403
Sb_2Te_3, semiconductor, optical props. determ. via Kramers-Kronig transform. 77−8537
Sc, interband, collective and atomic (p,d) excitations, Z-160 eV, fast EELS 80−93443
Sc_2O_3, interband, collective and atomic (p,d) excitations, Z-160 eV, fast EELS 80−93443
Se, A1 type metallic phase, optical consts. and refl. 77−32455
Se films, optical constants in visible region 80−97360
Se, threads in natural mordenite channels, optical absorpt., cond. *(Russian)* 80−89022
$SeOCl_2$:Pr^{3+}(Nd^{3+})(Er^{3+}), $SbCl_5$ acidified, Racah and Judd-Ofelt parameters in laser liqs. 80−106516
Si, amorphous and cryst., optical absorpt. at $\lambda = 1.06$ μm, temp. depend. 79−82939
Si amorphous sputtered film, solar energy selective absorber, spectral emissivity 78−83045
Si, interband and free carrier absorpt. consts. at high-level photoinjection 79−38514
Si, optical constants, heavily doped crystals, Kramers-Kronig analysis 77−85676
Si, rough surface, polarisation angles, ellipsometric meas. 78−56449
Si surface, influence of mech. treatment, charact. by ellipsometry 78−15141
$Si_{1-x}Au_x$, amorphous films, IR absorpt. spectra 80−16034
SiC, semiconductor, optical props. determ. via Kramers-Kronig transform. 77−8537
Si_3N_4-SiO_2, double dielec. layer on Si substrate, ellipsometric parameter meas. methodology 77−63474
SiO_2, chem. bond and rel. props. 77−43199
SiO_2 deposited on Ge, optical constants, reflection spectra by Kramers Kronig method 80−76099
SiO_2 film on Cu substrate, surface EM wave absorpt., optical consts. *(Russian)* 80−108216
SiO_2 films on Si, ellipsometric spectra, thickness determ. *(Chinese)* 80−86379
SiO_2 glasses, opt. consts. in IR and vacuum UV 78−27238
SiO_2 thin thermally grown oxide layers etching in HCl, ellipsometric control of Si surface form. *(Russian)* 80−104315
SiO_2-Al_2O_3-B_2O_3-LiO_2 ($LiO_2.Na_2O$) (Na_2O) glass exam. of optical props. 78−88277
SmB_6 film, prep. by electron beam evaporation, and optical and elec. props. 80−20793
Sn film, white, optical props. between 2-15 eV 78−19584
Sn, liq., optical props., 0.62-3.7 eV 80−75996
Sn-Au(Cu), amorphous film, optical props. 79−69895
SnO_2, elec. conducting film on glass substrate, measurement of optical constants and thickness 78−60525
SnO_2, film, optical characterisation, inversion method 78−11008
SrF_2, optical props. of cation colloidal particles 78−23503
$SrTiO_3$, absorption coeff., reflectivity, 293-853K 78−64342
$SrTiO_3$, UV refl. spectra, optical consts. 0 to 32 eV Kramer-Kronig anal., band struct. calcs. 78−43903
Ta film, optical const. var. with struct., ellipsometric meas. 77−63478
TaO_x film, optical const. var. with struct., ellipsometric meas. 77−63478
Te, synthetic, optical props. in visible spectrum and microhardness meas. *(French)* 77−28590
Ti, electropolished, optical props. from 1.8 to 3 eV 80−85088
Ti, substrate for thin oxide film, determ. by ellipsometric method *(Russian)* 77−81164
Ti-Ni, martensite transform. B2-B19′, optical props. and electron struct. *(Russian)* 80−34878
TiN, opt. consts. and physicochem. spectra 77−85677
TiO_2 anodic film, optical indices as function of crystallisation 77−66552
TiO_2 film on Ti, simultaneous determ. of optical indices of film and substrate by statistical anal. 77−20946
TiO_2 layers, activated reactive evaporation and absorpt. indices 80−97363
TiO_2:Cu, anodic, effect of Cu on optical props., rel. to possible appl. in solar energy conversion 80−16115
TiO_2-SiO_2, semicond. glass, optical props. 78−60412
TiO_x-Ti selective solar absorber, optical props. and heat resist. 79−65951
Ti_2O_3, optical consts., polarisation dependent reflectivity 78−52531
TlCl-TlBr mixed crystal, reflectivity spectra meas. 77−85743
$TlGaTe_2$, $TlInTe_2$, and $TlInSe_2$, IR refl. spectra 80−60605
Tm, polycryst., optical props., temp. depend., photocond., relaxation parameters 78−84603
UO_2, 5f-magnetic semiconductor, spectroscopic data, review 80−97299
UO_2, liquid, reactor safety research, laser experiments *(German)* 80−42787
VN, opt. consts. and physicochem. spectra 77−85677
V_2O_5, low dislocation density cryst. growth, opt. props. 77−63551
W, optical consts., dispersion, temp. depend., Kramers-Kronig calcs. *(Russian)* 77−69796
WO_2, optical conductivities and dielec. functions in 0.2-6 eV range, rel. to band struct. 79−42938
WO_3, optical props. 79−38515
Xe, liq., UV reflection spectra, density depend., excitonic band evolution 77−77246
Y film prepared in ultrahigh vac., optical meas. 6 to 14 eV 79−78767
Y, interband, collective and atomic (p,d) excitations, Z-160 eV, fast EELS 80−93443
$YAlO_3$, reflection spectra, Kramers-Kronig anal. of optical charcts. 79−8161
Y_2O_3, interband, collective and atomic (p,d) excitations, Z-160 eV, fast EELS 80−93443
$ZnIn_2S_4$, fund. optical consts., Kramers-Kronig analysis, reflectivity spectra 78−39573
$ZnIn_2S_4$ layered semiconductor, fundamental optical constants, experimental result analysis 79−56757
ZnO, ellipsometric spectroscopy of nonpolar $(1\bar{1}00)$ surface 79−33651
ZnS, linear electrooptic coeff. dispersion 80−71380
Zr, X-ray anomalous dispersion corrections using scanning interferometer 77−48274
ZrN, opt. consts. and physicochem. spectra 77−85677

optical couplers
2 km 20 Mb/s optical fibre transmission system 78−42437
4 port and 8 port kaleidoscope micro-optic star coupler for optical fibres 80−58681
16-channel star coupler for fibre optic data links 80−43450
35 Mb/s optical fibre cable transmission using IR LED optocouplers 80−34156
44.7 Mb/s fibre optic transmission system expts. 78−1420
access, with single-strand multimode fibre waveguides, fabrication 77−7176
access couplers for single strand systems 80−58766
access port for multimode optical fibres 79−50430
acoustooptic hydrophone, coupled waveguide, using intensity modulation 80−14431
adjustable branching coupler/attenuator, for multimode single fibre systems 78−46808
adjustable single-fibre connector and output monitor *(German)* 78−38011
advantages of design with optoelectronic couplers *(Rumanian)* 80−33165
altitudinal alignment in fibre end-butt coupling, using two-dimens. Si grooves 78−87148
asymmetric T-couplers for fibre optic data buses 80−102809
beam scattering at multilayered dielectric structures, with planar grating 77−42630
bench, automated scanning, optical coupling loss investigations 78−83124
bidirectional central couplers, for links with fibre bundles 78−46809
bidirectional coupler for duplex transmission on single optical fibre 79−37032
bidirectional fibre-optic data bus with T-couplers 77−19451
bidirectional optical systems, Rayleigh backscatt. freq. depend. 80−69511
binary phase gratings for fibre-optic communications 80−64201
birefringent prism couplers, for thin film optical waveguides 78−55468
bistable switch, based on waveguide coupler, exam. 78−38086
bitaper star couplers with up to 100 fibre channels 79−76824
blazed dielectric gratings, Bragg-reflection approach 79−1013
blazed dielectric gratings with high beam coupling efficiencies 80−64211
blazed replica grating coupler for optical waveguides, design and fabrication 77−88972
blazed waveguide corrugations, loss coeffs. 77−34948
Bragg effect waveguide coupler analysis 78−33827
Bragg switch, thin film 78−38088
branch, for multimode optical fibre system 78−46831
branching waveguide directional coupler, for GaAs-GaAlAs injection laser 78−38047
broad band grating filters for thin film waveguides 77−83962
cable connectors, losses, overlap design 77−7182
cable splicing, injection-moulded plastic connector 77−11054
capacitive mesh output couplers for optically pumped far IR mol. lasers 78−74916
channel waveguide coupling with fibres on Si substrate 78−46761
channel waveguide double-pole double-throw switch/coupler, using total internal refl. 78−71233
channel waveguide on Si to fibre optical coupling 77−88915
channel waveguides, single-mode, prism coupling efficiency meas. 80−99878
channel waveguides and directional couplers with graded-index profile, analysis 79−81542
'Chirped' grating coupler: a holographic approach 79−76854
chirped-grating output couplers in dielec. waveguides 77−39021
codirectional coupled waves representation 78−1150
codirectionally coupled waveguides with weighted coupling, filter charcts. 79−23068
coherent mode coupling at waveguide bends 78−38060
communication, conference, Amsterdam, Netherlands (Sep. 1979) 80−46733
communication technology state of art *(Czech)* 78−5575
compact optical directional coupler design and test results 78−1410
compensating fibre splice technique 77−42603
components for optical communication systems, review 80−87539
compound optical crosspoint with low crosstalk, using $LiTaO_3$ 78−33915
connector, 2 male plugs and central lens receptacle, 10 min. field installation, less than 1 dB loss 80−43470
connectors used in fibre optic transmission systems *(German)* 79−55205
contradirectional frequency-selective couplers for guided-wave optics 80−102803
corrugated dielectric waveguide, radiation loss calcs. 79−41461
corrugated waveguides and lasers, improved coupled mode analysis 78−46842
corrugated waveguides and lasers, improved coupled mode analysis for TM mode 78−83117
coupling efficiency analysis, single fibre connector design appl. 78−46766
coupling methods for semiconductors junction lasers and optical fibres, survey *(German)* 77−75674
curved dielectric waveguides, coupling characteristics, coupled-mode equations 80−48455
cylindrical light pipe coupling, design 77−7187
data bus system optical coupler with light conducting fibres *(German)* 80−43438
data bus system with planar access coupler, optimized layout 78−33823
data bus T-system, single multimode fibre, based on access coupler 78−46810
data collection line coupling methods *(German)* 77−62062
data communication field optical fibre appl. *(Italian)* 79−50388
data highway Y-junctions and connectors 77−39097
demountable for optical fibre communication systems 78−74989
demountable moulded optical-fibre connectors using rods and balls 79−64323
demountable multiple connector with precise V-grooved Si 79−76822
demountable optical connectors 79−32041
demountable optical fibre connector design and fabrication *(German)* 78−38010
design, manufacture and appl., by Swiss firm CAbloptic AG *(German, French)* 79−90005
DH injection laser coupling to optical fibre waveguide 78−33851
dielectric gratings for beam couplers, network methods for integrated optics 78−38070

optical couplers continued
diffraction optical coupling, heteroepitaxial GaAs-AlAs film waveguide 77−11045
diffused waveguide to GaAlAs DH laser diode coupling calcs., Gaussian beam model 79−94372
diffused waveguide tunnel excitation and emission 78−59146
digital transmission appl., components manufacturers and selection *(French)* 79−94333
diode laser output stabilization by bevelled-end fibre coupling 80−91806
diode-laser-fibre coupling, effects of fibre propagation loss 80−74484
directional, coupling length adjustment by loading a metal film 79−23055
directional, dielectric multilayered filters, wave division multiplex system appl. 79−94365
directional, distributed capacitance of planar electrodes 77−27387
directional, fabricated in TiO_2 diffused $LiNbO_3$, phase tuning 77−75680
directional, integrated, operation and manufacture *(German)* 77−75673
directional, with variable spacing, closed form solns. 78−46759
directional 1-D planar confined coupler, anal. 78−38027
directional coupler, interference filter all-fibre for wavelength division multiplexing 80−91900
directional coupler, made from plane gyroscopic, anisotropic light guides 79−18547
directional coupler, phase tuning by photostructural effect of chalcogenide glass film 77−83963
directional coupler, phase tuning using bias voltage 77−10999
directional coupler as 2×2 switch, coupling length adjustment 79−94370
directional coupler as waveguide tap with infinitesimal insertion loss 80−99883
directional coupler for fibre transmission system *(Japanese)* 80−58693
directional coupler for multimode fibres 77−3649
directional coupler phase tuning by chalcogenide glass film loading 78−1373
directional coupler switch, electrooptic, used as amplitude modulator, exam. 78−42467
directional coupler theory, accuracy in fibre or integrated optics appls. 79−3810
directional coupler with lapped multimode fibres, charcts. 80−91892
directional couplers, parameter meas. using radiation patterns 79−3771
directional couplers with graded index profile, variational analysis 80−96037
directional couplers with weighted coupling 80−9992
directional coupling device of two glass prisms, geometrical optics *(German)* 79−18524
disc waveguide, coupled power theorem and orthogonality relations 78−38003
double eccentric connectors for fibres 77−58442
dual three-rod connector for single fibre optics 79−36987
duplex fibre-optic cable interconnection system 78−46801
efficiency of LED-fibre-coupling system increase, using facet radiator *(Japanese)* 77−79938
electro-optical waveguide 3×3 switch, tuning and control theory 79−41458
encircling coupling *(French)* 79−41433
end fire coupling between fibres and diffused channel waveguides 77−79922
end-fire coupling between optical fibres and diffused channel waveguides 79−86252
endface, low-loss, monomode, butt, lens and taper types *(German)* 79−3795
endoscope with rigid to flexible imaging multifibre coupling, MTF 79−23052
evanescent wave coupling in fibre optic connectors 79−72668
fabrication using splicing technique, characteristics *(Japanese)* 80−87508
facet radiator improves efficiency of LED coupling to optical fibres 78−90520
fact directional coupler switch/modulators, novel ps optical pulse sampling method 80−58784
far IR laser hybrid output couplers, metal mesh dielectric mirror design and fabrication 80−58554
fiber array, end preparation and fusion splicing with CO_2 laser 80−10051
fiber-optic safety closure with deflector 80−53425
fibre, charcts. and technology for connector engineers 78−94440
fibre, coupling loss calculation using geometric optics method 78−42406
fibre, data bus systems appl. 78−25949
fibre, double-core single-mode, as directional coupler 80−106597
fibre, fusion splices by discharge heating 78−75007
fibre, graded-index, high index hemispherical microlens tip melt fabrication for coupling to GaAlAs laser 80−69506
fibre, joint and connector losses *(French)* 78−55464
fibre, modal noise, dependence on source coherence and fibre length 80−48402
fibre, single mode, hemispherical microlens tip fabrication for high efficiency coupling to InGaAsP laser 80−69505
fibre, theory and design 80−38122
fibre angular scrambling star couplers 80−53465
fibre array connector holding fixture 79−55241
fibre attenuation meas., backscatter method modified for endfire launching *(German)* 78−33868
fibre bundle termination, hot crimping method with metal ferrule 77−88912
fibre butt coupling in aligned vee-grooves 80−53429
fibre butt end alignment connector 79−76834
fibre butt-joining to Ti-diffused $LiNbO_3$ waveguide 79−76812
fibre cable and chuck connector optical and mech. props. *(German)* 78−33862
fibre cable corrector for multifibre cables *(French)* 78−42425
fibre cables, connections and optical transmitters *(German)* 80−99839
fibre cables connections, in-the-field 80−69545
fibre coaxial alignment system 79−37022
fibre communication devices, directional couplers, atennuators, switches development 79−3782
fibre concentric connector, step index multimode fibres appl. *(Japanese)* 78−90504
fibre connector, charcts. 78−63177
fibre connector, damage-free using Selfoc lens 78−46829
fibre connector, design and fabrication 77−88921
fibre connector, epoxyless, for single-fibre cables 79−86253
fibre connector, plastic materials in development *(French)* 79−55236

optical couplers continued
fibre connector for keyboard lens finger detection 80−19095
fibre connector loss evaluation by backscattering 80−58721
fibre connector plugs, angular misalignment precise meas. 78−46770
fibre connector technology, multimode, single-mode 80−87511
fibre connector technology 79−68439
fibre connector using low-loss lens system 78−79107
fibre connector with less than 0.5 dB loss with monofibres *(French)* 79−37008
fibre connectors, developments 78−46784
fibre connectors, hot forming versus epoxy bonding of bundles, single fibre techniques 78−42482
fibre connectors, low cost resilient alignment method 78−71230
fibre connectors, low-loss low-cost systems 79−27381
fibre connectors, minimisation of modal noise 79−90004
fibre connectors, nonlinear distortions and noise in optical communication systems 80−96001
fibre connectors, splices and couplers, design principles 80−58765
fibre connectors, theoretical possibilities based on calculated effect of tolerances *(German)* 79−27394
fibre connectors, wavelength dependent transmission loss 80−5825
fibre connectors alignment accuracy, influence of fibre tolerances 79−41441
fibre connectors and preparation procedures to minimise losses 77−14803
fibre connectors developments, standardised, for mass production *(French)* 79−86257
fibre coupling, simple permanent connection method for single-mode fibres 77−72097
fibre coupling alignment by fully automatic system 77−79949
fibre coupling using graded-index rod lenses 80−91891
fibre coupling with Lambertian source, using spherical lens, coupling efficiency calc. *(Japanese)* 78−42407
fibre demountable connector, triple-ball connector using fibre-bead location 80−43431
fibre demountable connector using injection-moulded thermoplastics 80−53472
fibre fabrication, attenuation, packaging and interconnection properties 77−27373
fibre fusion splicing set 79−27383
fibre interconnection components 78−46812
fibre joining *(Norwegian)* 79−1008
fibre joining technique and LED fibre coupling, effects of parameters *(German)* 78−63191
fibre jointing techniques and connections to communication equipment *(Norwegian)* 80−64179
fibre lightguide cable connectors, Si chips manufacture for fibre alignment 80−64188
fibre lightguide connector with spring clip 80−23802
fibre manufacturing, cabling and splicing, developments in Japan 78−59124
fibre multimode access coupler, fabrication method 80−87478
fibre optic connection systems standardisation 79−68440
fibre optic connector, epoxyless, for single fibre cable 79−37040
fibre optic connector design eliminating tolerance effects 78−46803
fibre optic connector system characteristics, aerospace user's viewpoint 78−46804
fibre optic connectors, 1978 technology state and development trends 79−41442
fibre optic connectors, 1979 design approaches 80−43437
fibre optic connectors, precision and stability developments 80−69523
fibre optic connectors, review 79−46075
fibre optic connectors, update on standardisation 80−5830
fibre optic connectors developments, cancellation of coupling mismatches 80−1332
fibre optic coupler use 80−28344
fibre optic coupling using tapered microlens, high efficiency *(Korean)* 80−43449
fibre optic data distribution system using variable tap ratio couplers 77−83953
fibre optic interconnection, using compound-lens devices, telephone links appl. 80−74493
fibre optic multimode planar coupler device, formation using ion-exchange process 79−50429
fibre optic packaging concept, interconnection system 79−90026
fibre optic processor serial interconnect system 78−1426
fibre optic rotation sensor, all-waveguide configuration, key element tests 80−58796
fibre optic source and coupling techniques *(German)* 77−19404
fibre optic structures, multimode coupling 79−37033
fibre optic system design and component selection 80−58767
fibre optic transmission, LED coupling fine adjustment *(French)* 79−94332
fibre optical coupling components 77−79957
fibre optics, transmitter and fibre-fibre coupling techniques *(German)* 77−11008
fibre optics communications, 1979 status and development trends 80−53408
fibre optics connectors, 1977 state of art and development trends 77−83971
fibre optics for military appls., review and assessment 78−42438
fibre optics systems, technology and components *(Hungarian)* 78−66900
fibre optics technology and connector systems, marketing 80−69522
fibre rod lens connector design and applications 80−53473
fibre Si array connector with low splice loss 78−55441
fibre splice, elastic-tube 80−87527
fibre splice delay distortion characteristics, shuttle pulse meas. 77−19457
fibre splice insertion loss meas., backscattering method 80−58720
fibre splice loss, Gaussian power model 78−46828
fibre splices, delay distortion characts. 77−34933
fibre splices, loss and output numerical aperture meas. 78−42403
fibre splices, parabolic-profile, loss model 79−23058
fibre splicing, connecting and sheath jointing *(Japanese)* 80−87497
fibre splicing and connecting 79−41436
fibre splicing techniques 78−79147
fibre splicing using low MP glass solder 79−55252
fibre splicing using self-aligning ceramic capillary 79−76829
fibre system connectors 78−42414
fibre taper couplers, diameter and slope meas. 77−88905
fibre tapered sections, ray trajectories, taper coupler design 79−18508
fibre tapping element with low insertion loss 79−76826

optical couplers continued
fibre to fibre coupling loss due to displacement, separation, misalignment, automatic measuring technique 79−32036
fibre to indiffused waveguide, single mode coupling 77−34959
fibre transmission line structures, transducers, couplers and connectors *(French)* 79−89998
fibre transmission system, component specifications 78−59157
fibre waveguide coupling and transmission characts. 78−79121
fibre waveguide coupling characts. 78−59156
fibre Y-branch, low-loss 80−10004
fibre-access, planar star and fused-tapered, for multiterminal data-distribution systems 79−50428
fibre-bundle holographic coupler, expt. 78−42419
fibre-optic 10 dB directional coupler 77−19452
fibre-optic area-ratio couplers for distributed data-processing equipment interconnection 79−50431
fibre-optic array splicing with etched Si chips 78−55440
fibre-optic cable and interconnection considerations and tradeoffs 79−94363
fibre-optic communication in industry, appls., glass fibre props., connectors 80−87550
fibre-optic communication systems, measurement techniques for passive optical components 80−1354
fibre-optic connector design, using resilient alignment mechanisms 80−48399
fibre-optic connector manufacture and insertion loss 79−90035
fibre-optic connector with centring rollers for tapered collet 79−37004
fibre-optic connector with fibre surrounded by resilient ferrule 79−98489
fibre-optic coupling techniques *(German)* 80−28330
fibre-optic crossbar switch 80−74497
fibre-optic directional coupler developments and applications 79−94330
fibre-optic integral data source/receiver package 78−63179
fibre-optic interconnection design and performance 80−14436
fibre-optic interconnection techniques 79−23059
fibre-optic link, splice loss evaluation by means of the back-scattering technique 79−98478
fibre-optic male connector with friction insert, ferrule and retainer 80−78968
fibre-optic planar multimode coupling structure fabrication by ion exchange 80−64233
fibre-optic rotational coupler development 77−72089
fibre-optic switch, single-throw, single-pole 79−37001
fibre-optic systems, single-mode, connector and laser module as interconnecting device between fibre and laser diode 79−50422
fibre-optic technology for interconnection designers 78−46800
fibre-optic terminal and connector construction 78−59136
fibre-photodiode alignment by etched Si structure 80−53430
fibre-to-fibre connections, technology review 78−9459
fibres, connectors, light sources and receivers, review *(French)* 79−46044
fibres, multimode, power coupling, theory 78−33893
fibres termination, silica, plastic-clad, by stripping and recladding with fluorine based copolymer 79−41466
film waveguide spectrum analyser with prism coupling 77−62071
fluoromethane TEM_{00} far IR laser with integrated pump laser, metal mesh output coupler 80−58578
focusing diffraction grating, for integrated optics, holographic production *(Russian)* 77−84009
four-channel integrated-optics coupler and frequency-channel multiplexer 80−91936
fused biconical tapered couplers, full duplex optical transmission 78−1341
future trends and problems 80−28319
GaAs homojunction rib waveguide directional coupler switch 80−69554
Gaussian beams, waveguided, coupled by misaligned or curved grating effect 80−33228
glass fibre branch couplers for optical data bus *(German)* 79−89999
glass fibre cable jointing methods *(Swedish)* 78−90525
glass fibre system techniques *(Dutch)* 77−75689
glass-fibre waveguides, dependence of overall losses on coupling-in angle of radiation 79−98504
graded index fibre, connectors and splices, transmission loss estimation 79−18550
graded index fibres, for matching injection lasers to optical fibres 79−32069
graded-index waveguide coupling and matched joining, coherent states and light propag. 80−102625
grating coupler, chirped and curved, for focusing beam 80−78979
grating coupler fabrication in waveguide photoresist. *(Czech)* 80−28354
grating couplers, anal. and design 78−1320
grating single beam coupler with large grating periodicity 77−39114
grooved chips, for fibre-optic array splice improvement 77−19456
heterostructures for integrated optics 77−39112
HF acousto-optic mode conversion and deflection 77−54776
high efficiency single mode fibre/channel waveguide flip-chip coupling 80−58799
hologram recorded with guided wave evanescent field, as grating coupler 77−10869
holograms as optical branching elements 77−10870
holographic couplers for optical fibre bundles 78−25839
holographic elements for practical fibre bundle couplers 78−46550
holographic gratings as beam-couplers and splitters 78−25821
horn for mode coupling in waveguides 78−1434
horn structures for integrated optics, coupling efficiencies 77−34964
horn-shaped coupling structures and linear waveguides fabrication 77−23782
hybrid fibre optic/electrical connector, environmentally sealed, multispin, cylindrical 79−41457
incoherent light efficient coupling into optical fibres and bundles 78−83074
industrial appls., specifications *(Swedish)* 77−775
injection heterolaser coupling into fibre waveguide, operation regime influence on efficiency 79−59834
injection laser diode coupling to planar waveguide 80−33245
injection laser/optical waveguide connection module 78−59023
integrated and guided-wave optics, conference, Incline Village, NV, USA, January 1980 80−58772
integrated bistable optical multivibrator using electro-optically controlled directional coupler switches 80−19111
integrated directional coupler modulator, 1 Gbit/s 80−38125

optical couplers continued
integrated directional coupler switches, modulators and filters using $\Delta\beta$ reversal techniques, review 80−38132
integrated optical device for Hadamard transformation 78−22221
integrated optical prism-waveguide dual coupler theory and exptl. performance 80−33236
integrated optical switch, optically controlled two channel, based on directional coupler 78−83116
integrated optics, double diffraction grating coupler with high efficiency 79−3812
integrated optics, high density multichannel waveguides with integrated couplers 77−794
integrated optics, theory of coupling to waveguides with linearly tapered horns 78−33917
integrated optics endfire coupler efficiency calc. and expt. 80−102863
integrated optics high quantum efficiency waveguide coupled photodetectors on Si substrate 80−58805
integrated optics tapered beam to film couplers, coupler eqns. 78−55472
integrated optics using periodic structures 77−39109
interconnecting fibre optics 80−69514
interconnection components for optical waveguide cables, SIECOR system 79−3804
interconnection of fibres and cables 78−46785
interferometer matching and coupling to plane wave limited by pinhole 79−75575
interferometer using modular holographic elements 77−61116
interferometric fabrication of diffraction grating and optical waveguide coupler 78−1440
IR emitting diodes, high radiance, analysis of radiation coupling into optical fibre 80−14473
joining optical fibres *(Japanese)* 79−27404
laser coupled output, importance on intracavity effects *(Chinese)* 79−64269
laser diode coupling to parabolic-index fibres 78−94435
laser diode end-fire coupling into $LiNbO_3$:Ti waveguides 79−94368
laser diode-optical fibre interconnection *(Danish)* 77−88911
laser diode-to-diffused waveguide coupling efficiency, waveguide mode asymm. effects 80−9990
laser light source for spectroscopy, far-IR, using set of mirrors and lenses 80−73481
laser to fibre hybrid coupler with cylindrical lens 77−75661
laser-fibre coupling with optical transition structures 78−42449
laser-fibre transverse coupling and front-mirror monitoring for feedback control of laser transmitters 80−33151
laser-waveguide transition coupling struct. fabrication 78−38029
laser/optical fibre using cylindrical lens and Selfoc lens combination 77−79931
LED's chalcogenide glass radiator bonded, with optical guide struct., efficient coupling to optical fibres 77−39043
LED coupling to optical fibres, truncated spherical lens efficiency 79−76813
linearly tapered directional analytic solns. 77−779
liquid crystal fibre optic switch, adjustable access coupler 79−64334
low loss, for coupling LED to fibre-optic system 80−91907
low loss access coupler for multimode fibre distrib. networks 77−72063
low-loss single-mode fibre connectors, detachable 79−27382
Luneberg lens for laser diode coupling to graded-index fibre *(German)* 78−33875
mass spectrometer, ion-cyclotron reson. type, optically-coupled feedback emission current regulator 77−61150
Michelson output coupler with one-dimensional grid, for optically pumped near MM laser 80−58555
micro-optic devices for coupling/branching in fibre optic communications 79−55211
micro-optic directional coupler, aberration losses 80−48395
microlenses to improve LED-to-fibre optical coupling and alignment tolerance 80−19088
microoptic devices for optical communications 79−76840
mode coupling between two connected multimode parabolic-index optical waveguides 79−94353
mode filters using coupling between two nonidentical waveguides 78−46757
modulator, coupled waveguide *(Japanese)* 78−46789
modulator, coupled waveguide with pn-junction, strip loaded channel waveguide, design 78−46843
modulator, coupled-waveguide, with Schottky contacts 79−23093
modulator switch, balanced bridge, using Ti-diffused $LiNbO_3$ strip waveguides 78−63201
modulator using electro-optic phase shifter pair with optical waveguide couplers 78−66952
monolithic laser-waveguide coupling by evanescent fields 77−39110
monomode fibers developments, for optical communications 80−48404
moulded multifibre connectors using rectangular multirod arrangement 80−58685
multichannel fibre cables, star and access couplers 77−88922
multichannel GaAs laser array output synchronisation 78−42417
multifibre cable structure, jointing procedure *(French)* 78−42459
multifunction integrated optic device with mag. alterable phase grating 77−11048
multimode coupling structure of two parallel parabolic index waveguides, exact analysis 79−90013
multimode electro-optic guiding for single fibre data links, system design 78−38065
multimode fibre branch fabrication 77−88955
multimode fibre coupler, simplified theory 77−68259
multimode fibre coupler for optical data bus systems 78−1414
multimode fibre couplers, structure anal. 78−63198
multimode fibre couplers for data bus systems 78−74970
multimode fibre detachable connectors fabricated with self-aligning jig 79−27384
multimode fibre directional coupler 79−37002
multimode fibre joints, design, error tolerance evaluation method 78−9436
multimode fibre optics coupler with low insertion loss 79−10379
multimode fibres, coupling efficiency in joints evaluation 78−66894
multimode fibres, multiple fibre connectors 77−3669
multimode glass fibres 80−48405
multimode graded index fibre, detachable connector 79−37039
multimode graded-index optical waveguide detachable connector 78−46830
multimode inhomogeneous fibre couplers 79−41430
optical couplers continued
multimode optical fibre coupling to single-mode waveguide 79−98485
multimode optical fibre fabrication, 3 dB low loss 78−37976
multimode optical systems-power coupling between waveguides 78−42473
multimode single fibres, low-loss Y coupler 79−23061
multimode W-type fibres, steady-state characts. 80−5818
multiple fibre end fire coupling with single-mode channel waveguides 79−7230
multiport coupling between single mode fibres and indiffused channel waveguides 78−38061
narrowband optical wave filter with stacked directional coupler 79−7226
nematic liquid crystal adjustable access couplers for fibre-optic switching 80−33217
nonlinear coherent coupler, new optical logic device 80−58630
nonreciprocal, using magnetooptic crystal 79−76872
nonreciprocal optical IC mode convertor analysis 77−84010
offset waveguides, length optimisation of S-shaped transition 78−38059
optical fibre, for demountable connector 78−30065
optical fibre cable, operational, installation underground *(German)* 79−3783
optical fibre connectors, retention grooves 77−19399
optical fibre splicing by butt-joint method, multi-glass-rod optical-fibre splicers made by drawing technique 80−53413
optical fibre transmission, conference, Williamsburg (1977) 78−1382
optical waveguides, development *(German)* 77−42613
optimisation in fibre optic union for repeater spacing *(Italian)* 78−79117
parabolic coupling horns, design 77−11002
parallel end-butt coupling for optical ICs 77−58488
passive components for integrated-optics signal processing 80−48466
passive devices for appl. in fibre optic systems 80−91903
periodic corrugated waveguides, grating coupled radiation and distrib. feedback 78−59161
periodic modulation of propag. consts., coupling coeff. modification 77−72092
phase diffraction grating as laser beam coupler, radiation parameters monitoring 80−10033
phase mismatched optical waveguides, high efficiency coupling 79−94339
phase-frequency response of diffraction coupling between two optical waveguides *(Russian)* 79−3778
photopolymerisation formed intersection, higher refr. index, without light leak 77−58489
pigtailing electro-optical sources and detectors 79−36998
planar coupler for data bus system with single multimode fibres 77−79927
planar coupler in data bus system with single multimode fibres 77−11024
planar input/output for multimode optical fibres, thick film technology appl. 79−72703
planar multimode couplers for fibre optics 79−18531
planar optical branching elements for multimode fibre transition systems 79−94351
planar optical waveguide interconnection method 80−58671
planar star coupler design for fibre optic systems 80−74474
planar star coupler for multimode fibres 80−99828
planar waveguide blazed dielectric diffraction gratings, anal. and design 80−58779
planar waveguides, method for efficient interconnection 77−19393
planar waveguides and fibres, book 78−42426
plastic film, interconnections in thin-film guided-wave optics 77−58487
plug and socket connectors, ruby jewel, for single glass fibres *(German)* 79−46039
plug fibre-fibre dismantleable connector *(German)* 77−54800
polarisation-independent optical circulator coupled with multimode fibres 80−43430
polarisation-independent optical directional coupler switch using weighted coupling 80−28352
polarisation-independent optical switch using weighted directional coupler 80−58798
power coupling efficiency, generalised scatt. matrices theory 77−27350
prism, symmetrical, as input coupler for integrated optics 79−10412
prism coupler, EM theory, tutorial approach *(French)* 77−37694
prism coupler fabrication technique 80−83685
prism coupler for optical waveguides 78−94431
prism coupling efficiency optimisation for surface IR wave excitation 77−75708
prism coupling into clad uniform optical waveguides 80−96003
prism coupling into optical waveguide second harmonic generation 80−102763
prism or grating couplers, determ. of ray directions coupled out of waveguides 79−59841
prism waveguide input-output coupler, high efficiency, analysis 79−98468
prism-waveguide coupling efficiency for waveguides with arbitrary refr. index profile, WKB approx. 79−7231
properties and appl. *(Swedish)* 77−774
quartz waveguide coupling, for IR expts. 77−34938
quasilinearly tapered couplers, weighted coupling strength 80−83674
rectangular light pipes of different dimens., coupling efficiency 77−7186
reed type routing switch for multimode optical fibres 79−72704
reliability, test results *(Swedish)* 77−776
rib waveguide switches with MOS electrooptic control, monolithic integrated optics in GaAs-$Al_xGa_{1-x}As$ 78−87168
ribbon-splicing injection-moulded connector with Si chip insert 78−1412
rotation-splice tapered fibre star coupler directivity and mode dependence 80−58748
S-shaped transition between offset straight waveguides, length optimisation 78−46838
scattering matrix and radiation characts. of junction between monomode waveguides 77−34946
self coupling phenomena of GaAlAs laser caused by optical fibre 78−55355
self-centring technique for mounting microsphere coupling lens on fibre 80−74517
self-imaging multiplexer and branching couplers 80−106629
semiconductor DFB laser excited by electron beam, radiation coupling out 79−90038
semiconductor laser array, output coupling with fibre optic tapes 79−10319

optical couplers continued
semiconductor laser beam coupling efficiency into fibre, matching element misalignment influence 80−48432
semiconductor laser coupling to thin film or fibre waveguide 77−19426
semiconductor laser efficient coupling into tapered hemispherical end single-mode fibre 80−99827
semiconductor laser optical isolator in laser-to-fibre coupling module 80−48267
semiconductor laser to rectangular dielectric waveguide, coupling efficiency anal. 77−23767
semiconductor laser to single-mode fibre coupler, cylindrical lens method 79−76807
semiconductor lasers, optically coupled, transient stimulated emission 77−23678
semiconductor source matching to thin-film planar and stripe waveguides 80−64174
shape memory effect alloy connector for optical fibres 80−53475
silicone rubber, room temp. vulcanising, as optical element coupler 77−39002
single fibre connector, design considerations 79−1010
single fibre connectors and cable splice hardware, optical coupling theory 80−64187
single fibre low loss connectors, low cost 79−68434
single fibre multichannel environmental connector, design and perform. considerations 78−71229
single fibre multichannel environmental connector, design and perform. 78−90508
single fibre optic cable connector losses 78−46802
single fibre optic connector design and development 80−53474
single fibre optic moulded connector and encapsulated connectorised devices 78−1409
single fibre optical systems, connection methods 78−46783
single fibre separate connector, for optical fibre data transmission, loss factors 77−88939
single mode coupling problems, fibre and integrated optics, for optical communication 78−42469
single mode fibre coupling structure fabrication 78−33899
single mode fibre coupling to semiconductor laser, fibre strength tests 78−33900
single mode fibre network, coupling and integrated optical switches 78−59159
single mode fibre optic system coupling techniques 78−33901
single mode fibre optical data bus with star couplers 80−64199
single mode fibre pickoff coupler 77−783
single mode grating coupling between thin-film and fibre optical waveguides 79−1012
single mode optical fibre connectors, low loss 79−81557
single multimode optical fibre communication directional couplers *(German)* 78−33873
single-fibre connectors, demountable, loss meas. 78−94433
single-fibre separable connector insertion loss characteristics 77−23770
single-mode fibre, jointing loss 78−25964
single-mode fibre coupling to single-mode Ti diffused $LiNbO_3$ waveguide 79−81547
single-mode fibre integrated optics systems, coupling methods, review 78−59162
single-mode fibre joint losses calc. 78−74980
single-mode fibre low-loss connectors 78−87139
single-mode fibre multiterminal star directional coupler 79−98473
single-mode fibre optic directional coupler, fabrication and characts. 80−58683
single-mode fibre optical power divider, encapsulated etching technique 79−27420
single-mode fibre tapered velocity coupler performance 79−55246
single-mode fibres and integrated optical components, novel method of coupling, appls. 80−43442
single-mode optical fibre coupling techniques using microscopic lenses 80−53462
single-mode optical fibres, 1.3 μm, ceramic capillary connector with 0.3 dB loss 80−23778
single-mode optical-waveguide fibre coupler 78−74973
single-strand fibre couplers 77−68283
slab waveguide star coupler for multimode optical fibres 80−87491
slab-type directional coupler with activated rhodamine 6G top layer, amplified oscill. 80−99718
slab-type waveguides, mode coupling via dichroic absorpt. of M centres 80−33178
snap connector for monofibre opt. cable 80−106609
soda lime glass, Ag^+ ion exchanged, planar optical waveguide, manufacturing tolerances 78−71212
spherical base prism, optical waveguide systems appl. 77−83985
spherical end faced coupling fibre fabrication by selective etching/melting 80−53492
splice loss in single-mode fibres using Gaussian field approx. 79−94354
splicing, end to end optical fibre waveguides appl. *(German)* 77−19416
standards for fibre optics 79−14101
star coupler, unidirectional, for single-fibre distrib. systems 78−25980
star coupler fabrication using Tl ion exchange process 79−46031
star couplers, low-loss refl. type, for optical-fibre distrib. systems 80−1301
star couplers for single multimode fibre communication systems *(German)* 78−33872
star couplers using fused biconically tapered multimode fibres 78−55443
star repeaters for fibre optic links 77−34934
step-index multi-mode fibre connector for experimental transmission system 79−32060
stepped switched optical directional couplers with unequal section lengths 80−33235
stigmatically focusing grating coupler 79−59842
strip waveguide directional coupler, leaky-wave 78−38058
strongly coupled parallel slab waveguides, coupling coeffs. 78−1356
subpicosecond gate, velocity-matched directional coupler 80−74512
surface, low-loss, design for coupling planar and strip waveguides *(German)* 78−87157
surface EM wave launching at edge of metal film 78−43945
surface polariton generation through grating couplers 77−85153
survey, coupling parameters and techniques *(German)* 80−38108
switch operation, exam. by fluorescence method 78−38049
T-coupler for multimode optical fibres 78−42457
T-couplers, for eight-terminal fibre optics data bus 78−59129

optical couplers continued
taper couplers utilizing SiO_2, photolithographic fabrication processing sequence 79−41464
taper ended multimode fibre efficient power coupling with multiheterojunction LED 79−32052
taper-ended multimode fibre used for efficient power coupling between laser and fibre 77−3657
tapered block coupling and mode conversion in integrated optics for coupling between substrates 79−50442
tapered coupler, coupled-mode eqns., parabolic cylinder functions 77−46821
tapered coupling problems, use of Bloch vector model 78−22219
tapered edge waveguide, radiation coupling 77−14810
tapered gap prism couplers for high index materials 77−72091
tapered gap prism coupling to diffused $LiNbO_3$ waveguides 80−78967
tapered horn shaped channel waveguide coupling 77−42619
tapered velocity coupler application, freq. discrimination 78−38057
tapered waveguides, permitting efficient fiber to waveguide coupling 79−50376
TE-TM mode splitter for optical waveguides, glass comp., r.f. sputtered fabrication 78−46841
tee-coupler for single-mode fibres 80−10000
thick film optical waveguide integration with fibre-optic connectors 80−33246
thin film optical coupling to fibre 78−87167
thin film slab-type directional coupler covered with high-index absorbing material, damped oscill. 80−91908
thin film waveguide, mode conversion by two-stage coupling process 79−32034
thin-film optical waveguides coupling *(Polish)* 78−33849
thin-film periodic structures, optoelectronic devices appls. *(Polish)* 78−50947
three-fibre optical interconnection for interface loss reduction 78−94439
three-waveguide system, interference effects on couplings 80−78969
transition fibre fabrication for coupling fibres to integrated optical films 77−39061
transition fibre production for coupling DH lasers to single mode fibre 77−39062
transmission-line cable joining device 79−68433
transmissive star coupler for single fibre cables, mixer rod power distrib. inhomogeneities 78−46832
transverse light coupling, from GaAs laser into optical fibres 78−18045
triple ball connector, for optical fibres 78−13795
tunable coupler filter, composed of coupled nonidentical $LiNbO_3$ strip waveguides, description 78−38083
tunable optical waveguide directional coupler filter 78−79144
tunable switched directional couplers of two thin film waveguides using SAW 78−75003
twisted elliptical optical fibre, polarisation coupling 80−99831
two-way transmission expts. over single fibre at same wavelength using micro-optic 3 dB couplers 78−55450
volume diffraction gratings with inclined layers in thin-film optical waveguides, coupling efficiency 79−90028
water surface EM wave excitation 79−13893
waveguide 4×4 switching network 77−3683
waveguide components and systems *(German)* 80−33168
waveguide tapers, multimode coupling and transmission characts. 79−27378
waveguide tapers for optical coupling of optical fibres, appls. *(German)* 80−38107
welded optical fibre signal splitter 80−102814
wideband thin film modulators and switches, for optical communication 78−63206
AlGaAs-GaAs DH lasers, coupling efficiency between gain-induced guides 79−23094
As-Se-S-Ge chalcogenide glass films, appls. to passive optical waveguide components 79−37048
As_2S_3 amorphous film waveguide and grating coupler 80−53448
As_2S_3 focusing diffraction grating with const. spacing 79−23096
As_2S_3 polyethersulphone sandwich ribbon fibre for coupling high refractive index integrated optics 79−32089
GaAlAs laser coupling to fibre, high efficiency 77−7173
$(Ga_{1-x}Al_x)As$ LOC DBR laser integration with p-n junction detector 78−38066
$Ga_{1-x}Al_xAs$ Schottky directional coupler switch, construction and operation 78−25960
$Ga_{1-x}Al_xAs$-GaAs injection laser, branching waveguide coupler fabrication by LPE 78−63202
GaAs DH laser/fibre transmission system modulation and injection 77−50764
GaAs directional couplers and electrooptic switches, wavelength depend. 78−79143
GaAs, directional-coupler switch with stepped $\Delta\beta$ reversal 77−79968
GaAs directional-coupler switch with stepped $\Delta\beta$ reversal 77−88962
GaAs electro-optic rib waveguide directional-coupler switch with stepped $\Delta\beta$ Schottky electrodes 79−98507
GaAs film optical components, prep. by MBE using Si shadow masking technique 80−28358
GaAs integrated LED/sphere-lens source for optical fibres, coupling efficiency calcs. 80−43433
GaAs laser array to channel groove waveguide coupling prism 78−38067
GaAs layer grown by MBE 79−76878
GaAs, p^+-n -n-n^+ electro-optical directional-coupler switch 77−7217
GaAs p-n-i-n^+ semi-insulating struct. as integrated optical coupler 80−64212
GaAs rib-waveguide directional-coupler switch with Schottky barriers 78−63204
GaAs:Zn waveguide, light coupling at fundamental absorption edge 79−23082
GaAs/AlGaAs integrated twin guide injection lasers prepared by LPE, coupling coeff. and coupling length meas. 79−81458
GaAs-(GaAl)As DH injection laser with pillbox resonator, coupling with straight waveguide 80−58581
$LiNbO_3$, channel waveguide to single-mode fibre high-efficiency flip-chip coupling 80−99833
$LiNbO_3$ corrugated optical waveguide, electrooptic scanning of coupled light 78−38050
$LiNbO_3$, electro-optical modulator/switch, switched directional coupler principle 77−7191
$LiNbO_3$ optical waveguide, beam-to-waveguide coupler 79−90003
$LiNbO_3$, Ti diffused, optical directional couplers, characts. 80−33145

optical couplers continued
$LiNbO_3$, Ti diffused optical waveguides, efficient prism-coupling 79-46089
$LiNbO_3$ Ti-diffused optical waveguide coupled to GaAlAs DH laser, anal. 80-58706
$LiNbO_3$ waveguide, corrugated, electro-optic scanning of light diffr. from grating output coupler 78-63172
$LiNbO_3$ waveguide modulators and switches, Ti-diffused, fabrication on directional coupler principle 80-83678
$LiNbO_3$:Ti, coupled waveguided TE/TM mode splitter 80-64142
$LiNbO_3$:Ti, two mode waveguide coupler electrooptical switch 77-83961
$LiNbO_3$:Ti optical waveguide electrooptic devices, polarisation independ. directional coupler switch 80-58783
$LiNbO_3$:Ti planar waveguide, edge coupling to GaAlAs DH laser diode 80-87559
$LiNbO_3$:Ti waveguide directional coupler type modulator 78-66951
$LiNbO_3$:Ti waveguide directional coupler switches, optically-induced cross-talk 80-48417
Si alignment chips for optical fibre cable connector 78-1411
Si connector parameters charcts. 80-69544
Si Fabry-Perot couplers for optically pumped far IR lasers 80-69404
$SrTiO_3$ prism coupler for $LiNbO_3$ integrated optics very high throughput damage resistant waveguide modulator 80-58788

optical design techniques
see also optical instruments
3 m parabolic dish heliostat system design, fabrication and testing 79-62111
aberrated pupils, apodisation, anal. 79-98298
ACCOS V, commercially available optical design and anal. program 79-86230
ACCOS V program for diffraction evaluation of general optical systems 79-86231
achromatic doublet design 78-71183
achromatic low refl. and beamsplitting coating synthesis 79-98496
achromatic metal-dielectric mirror coating, computer synthesis 78-46750
achromatized wedge scanner design 77-88948
acousto-optic deflector, anal. and design of flat transducer array 79-18527
acousto-optic modulator, wide bandwidth, design procedure 78-5569
active optical systems, real-time control over optical wave fronts 78-71187
advances and problems 79-36975
airport control tower cab, optical design 80-58661
antireflection coating, linear programming 78-5537
antireflection coating, three layer 78-9423
antireflection coating, three-layer, refractive index optimum combination 80-28306
antireflection coating, two given wavelength, design method 78-59102
antireflection coating, two-layer, error considerations in design 80-74477
antireflection coating synthesis by direct search method 79-10400
antireflection coatings, three layer 77-50775
antireflection coatings, two-wavelength, two or three layer, design 78-25943
antireflection coatings 77-83948
aperiodic spacious objects imaging, influence of AF sinusoidal phase deformations of wavefront *(Czech)* 80-14290
aperture shaping, diffracted energy spatial distrib. control, computer analysis 78-59152
aplanatic optical system containing two aspheric surfaces, design 79-81500
aplanatic two mirror telescope from near-normal to grazing incidence, comparative performance anal. 80-58654
aplanatic waxicon insensitive to tilt errors, for high power laser beam transport 80-74460
apochromat, four-lens three-colour, glass selection for design 78-13783
apochromatic collimator design for MTF evaluation 77-79946
apochromatic glass pair dispersion coeff. selection 79-72657
aspheric optics developments and appl. 80-5813
aspheric reflecting systems, geometrical design 80-38083
aspheric surfaces, two axis, design 79-86245
aspherical area shape predeterm. method *(German)* 80-28294
astronomical lightweight mirrors of glass, economical construction *(French)* 77-17370
astronomical optical surface control, Hartmann method, use of splines 79-35149
astronomical telescope design and construction technology 80-31211
astronomy, extreme values algorithm for automatic design *(Chinese)* 80-8544
automatic lens design, pseudo-second-derivative matrix computation 79-14077
automtic optical plumbline requirements and design *(German)* 77-70877
axially mobile mirror components design *(Russian)* 77-54769
baffle edge design using optical black coating 78-59154
beam expander telescope design utilizing fast spherical primaries 79-66921
beam sampling mirror gratings, optimal design 77-14791
beam splitters, non-polarizing, design 78-83110
beam splitters, variable ratio, for high energy glass laser systems 79-45952
biaxial translation stage, kinematic design 77-161
binocular models, charcts. and design features, review 80-74468
biocular magnifier design for display system viewing 79-27361
CAD, conf., San Diego, CA, USA (Aug. 1978) 79-86228
calculator techniques, for desk and pocket calculators 78-71181
camera design miniaturisation 79-26153
Cassegrain telescope design and tolerancing optimisation 80-82199
catadioptric objective, development *(German)* 80-102796
catoptric objective design, testing *(German)* 80-53400
caustic point displacement due to generalised bending, third-order approx. 80-83656
caustic surface calcs. in geom. optics, analytical illum. monitoring 77-3643
chromatic aberration first-order theory, secondary spectrum correction with common glasses 78-90382
chromatic aberrations of real rays, role of each lens in optical system 80-102655
chromatism transverse, effect on transfer charcts. of optical systems 79-908

optical design techniques continued
COCHISE: laboratory spectroscopic studies of atmospheric phenomena with high sensitivity cryogenic instrumentation 80-95166
collimator, single element gradient index design 78-9426
collimator monochromatic MTF computation program 80-14451
compact four-mirror optical system 79-23049
compact Gaussian relations for n-component optical systems 79-14082
complex optical system design, factor analysis methods 79-81509
compound catadioptric telescopes with all spherical surfaces 78-69682
compound parabolic concentrator, derivation of 79-72651
compound parabolic concentrator photovoltaic solar collector design 79-61998
computer optics 79-94322
computer optimisation program 77-54766
computer programs for optical design 79-36977
computer-aided, optimisation and interactive graphics improvements 80-78933
condenser synthesis, astigmatism-free, using spherical mirrors 78-50887
conic reflectors, basic props. of meridional and sagittal caustics 78-25948
conic reflectors, meridional caustics 77-72044
contemporary optical design, aspects 80-23766
continuous zoom forward-looking IR optical system design and implementation 79-23046
Cooke triplet, air-spaced anastigmatic quadruplet design 80-1291
Cooke triplet derivative of five-element config., design 80-33111
coronagraph diffraction limit problems and design approaches 80-82200
corrector lens for color television tube 79-86243
cost reduction in manufacturing 80-1361
coupling reflector, involute-related, for flash lamp pumped laser systems 78-90425
curved Fresnel surface, primary aberration contribs. 79-13913
decentered concave mirror in three-mirror concentric objective, for astigmatism correction 78-46749
deformable mirror design and resonance damping 79-59794
dichroic beam splitters, high-performance, for DF chem. lasers 80-95932
dichroic multilayer mirror for 16 μm region, design and fabrication 80-5808
dielectric multilayer systems for optical appls., computer program synthesis *(German)* 78-46788
dielectric semitransparent wide-band mirror, synthesis method 78-13785
diffraction gratings, review of Japanese research 80-10018
diffraction point spread function second moment as image quality criterion 80-9818
diffuse light collection onto extended absorber, mirror designs 78-22186
diffuse reflectors, light collection and dissemination 80-83658
diffuse system design, optimum conditions, appl. to optical system 78-50886
digital image processing, architectural breakthroughs 80-63939
double Gauss basic lenses, design *(German)* 80-53398
doublet, single-radius, paraxial properties and errors correction *(Czech)* 79-76791
eccentric system, paraxial approx. 79-98459
edge filters for phase contrast imagery, theoretical design 79-86250
education program, desktop computer appl. 79-84922
EKTRAMAX camera lens design and performance 80-77894
elastic tools for finishing optical components with noncircular cylindrical surfaces 80-28368
element fabrication and assembly, centration errors 80-9980
ellipsometer, self-nulling stepping-motor driven, design and performance 78-54440
equivalent concentric systems *(Russian)* 77-64659
eyepieces, imaginary front focal planes, negative collection lens, design considerations 80-64139
Fabry-Perot interferometer, wavefront form. by multilayered dielec. mirror 78-54449
factor analysis methods for designing complicated optical systems 80-28303
fibre, single mode, dispersion charcts., correlation between numerical prediction and meas. 80-91890
fibre, single-mode, ultra-low-loss, optimised structure for fabrication 80-99843
fibre endoscope one-component objective dimensional design *(Russian)* 78-69228
fibre optic rotation sensor, all-waveguide configuration, key element tests 80-58796
fibre optic sensor for photoelectric recording, design 80-28338
fibre optic system design and component selection 80-58767
fibres, multimode, step-index and graded-index, design method based on transmission charcts. 79-55233
fibres, of graded-index glass, for optical communications, light propag. props. 78-83106
film structure, electric field and absorption distributions 77-601
filter, narrow bandpass, for far IR, using double half wave designs 80-33173
filter design, global optimisation methods appl. 79-59840
filter design using image admittances 79-76801
first surface simplified aspherising procedure *(Russian)* 78-63013
five-component wide-angle pancratic objective design 78-71190
flat-field spectrograph design, holographic grating appl. 80-68264
flexible fibre light-guides, viewing instrum. appls. 80-87545
flexible high-resolution film recording system design 80-102828
flux concentrators, approach to ideality 78-66885
focus determ. for lens tolerancing computer program 79-86240
focusing system design for single mode laser 77-7109
forward-looking IR type optical system design programs 79-23047
four-colour thin apochromat design 79-27364
four-element lens systems of Cooke-triplet family design considerations 80-57404
Fourier optical evaluation techniques, user oriented 79-86131
Fourier transform lens, design and structural charcts. *(Chinese)* 79-45911
Fresnel lens, colour-corrected linear convex, for solar concentration 80-45640
Fresnel lens design, construction and performance as solar concentrator 79-62121
Fresnel lens optical design and utilisation, advantages and limitations 80-78936
Fresnel rhomb design, TI 58/59 program 79-32040
fundamental chromatism coefficients 78-1317

optical design techniques continued
Gaussian optics parameters, HP-67 calculator program 80−106439
general optical concentrator, max. radiant power density at receiver 80−102794
generalised ray tracing, caustic surfaces, bending and merit function for optical design 80−102612
geodesic aspherical perfect lens, general sol. for integrated optics 80−10049
geodesic lens, aberration corrected, for integrated optics circuits 78−38074
geodesic lens, axially symmetric, geometrical theory 80−33238
geodesic lenses, aberration-corrected rounded edge, profile calcs. 80−10048
geodesic lenses, axially symmetric, design parameters 78−83114
geodesic lenses, spherical aberration correction and fabrication tolerances 79−27435
glass selection for lens design 79−81496
gradient index imaging lens and system status 80−14420
gradient index imaging system theory 80−14294
gradient index optical elements and system design 80−106594
gradient index optical imaging systems, topical meeting, Rochester, USA (May 1979) 80−12851
gradient index spherical lens design for selfcoupled optical pickup system 80−14427
gradient-index imaging, theory 80−69331
gradient-index optics: a review 80−69478
graphical ray tracing for conic surfaces 80−5683
high performance system development and design at Carl Zeiss Jena works *(German)* 80−58660
high-volume optical component tolerance/specification relationship 80−48383
hologram achromatic lens system, design using ray tautochronism principle 79−3759
holographic, scanning system, lens design for hologram generation 78−50742
holographic concave grating design 80−1153
holographic elements, axisymmetrical, third order aberrations 80−69341
holographic elements as lenses, optical system design 78−9425
holographic grating, concave, imaging props. *(Japanese)* 78−37971
holographic gratings, design considerations *(Japanese)* 79−45914
holographic gratings update 79−7202
holographic lens design techniques, 488 nm construction, 633 nm read out 79−89866
holographic lens system, method for wave aberrations calc. 80−28175
holographic memory, optical arrangements, generalised design method 79−7098
holographic optical element, mathematical equivalence with ultra-high index lens 79−59653
holographic optical element design and construction 78−55315
holographic optical element design using analogous lens model 78−58955
holographic optical elements, third-order aberration theory and generalised aplanatic condition 80−74314
holographic scanner, two-dimens., design considerations 78−46535
holographic visor helmet-mounted display, optical design 79−86149
hyperboloid lens manufacturing technique 80−96039
hyperchromatic lens, expressions for first order chromatic aberrations 80−91879
ideal cylindrical radiation transformers and concentrators, symm. and asymm. forms 79−55200
ideal image-forming flux concentrator design 79−55201
illuminants which give prescribed tristimulus values to given object colours, design technique *(Japanese)* 78−94420
illumination distribution calc. in image plane 77−31125
illumination system, optical design 80−64135
image, dissector tubes, echelle spectrographs, design considerations 80−91918
imaging method for data processors, lens system design 77−27261
infinitely-thin-component optical system design principle 79−76794
inhomogeneous planar dielec. waveguides for integrated optics structs., synthesis *(Russian)* 80−38135
instrument design, partial coherence effects 80−78767
instrument optics design from basic elements 77−58418
integrated grating circuit for guided-beam multiple division fabricated by electron-beam direct writing 80−91934
integrated optic spectrum analyser design and fabrication 79−72720
integrated optical spectral analyser design and fabrication 79−50445
integrated optics techniques for fibre-optic communications *(German)* 78−38069
interference coating, theoretical design, with two narrow spectral transmission bands *(Russian)* 79−72666
interference coating, with narrow reflection bands, design *(Russian)* 80−43472
interference coatings, design, specified characts. 79−3786
interference coatings, synthesis, nonlocal computer method 77−50761
interference filter, V(λ), design appl. to visual system MTF evaluation 79−76843
interference filters, multilayer, design method 80−48396
interference polarizers on plane-parallel substrates 80−1336
interference spectrometer, high resolution, appl. to study of laser modal configuration *(Spanish)* 80−86458
interferometer, double-beam, computer analysis program 79−71520
interferometer design for high vibration environment 80−95131
interferometer spectrometers, field-widened 80−95146
ion commercial laser systems, design and manufacture 78−59046
IR coating nonuniformity effect on precision optical systems, compensation by auxiliary laser 80−78926
IR cryogenic sensors, CAD and evaluation 79−85184
IR heat trap field optics, compact lens-mirror system 78−55422
IR imaging and missile-borne tracker optics, selection guidelines 79−23050
IR lens system, large diameter, for pyroelec. vidicon 80−19086
IR multidetector spectrometer for atm. temp. sounding 79−25365
IR optical systems design, future computer program requirements 79−86260
IR scanning system modular design, assembly and alignment 80−78989
Keplerian binoculars with erecting lens system 79−72662
large azimuthal telescope major system design 78−73640
laser beam expander design corrected for Petzval curvature 80−74461
laser beam mode phase compensation, optimization techniques 78−1291
laser beam refraction at spherical surface, distortion, geometrical optics calc. 80−95929

optical design techniques continued
laser beam steerer-expander, two-mirror system design 79−18460
laser beam steerer-expander device, two-mirror afocal telescope design 78−46700
laser diffraction-limited system, resolution, intensity, and power distribution 77−58425
laser Doppler velocimeter, optimal geometrical design 79−64268
laser far IR waveguide cavities, coherently pumped, geometrical design criteria 77−54739
laser focusing objectives, flare image danger reduction 79−22997
laser fusion reactors, optical design, focusing optics 78−82518
laser galvanometer scanning system, CAD 77−58475
laser integration into optical systems, Nd:YAG laser 80−78887
laser interferometer optical component parameter optimisation 77−67493
laser multielement resonant reflector design, temp. and wavelength depend. props. 78−17945
laser pump system, analytical theory 80−106540
laser radar simulator for low scatter characts., three-mirror design 78−59118
laser scanning components and techniques, conference, San Diego (1976) 77−58474
laser scanning system design, stable fixed freq. 77−58478
lens, analytic merit function based on Buchdahl's aberration coeffs. 77−755
lens, aspheric, stigmatic, for ruby or He-Ne laser, CAD *(Czech)* 78−55427
lens, double Gaussian objective, design *(German)* 80−64134
lens, graded index, design using refr. index reconstruction method 77−39013
lens, gradient-index spherical, design for optical pickup systems 80−69483
lens, high aperture, for laser plasma compression expt. 79−14076
lens, intensity fluctuations in turbulent atmosphere, with (without) central screening 79−7080
lens, multi-element, defective surfaces, tilt meas. 78−66886
lens, photographic gradient singlet, design techniques based on total aberrations 80−69479
lens, standard reference, for MTF equipment testing in IR 78−50898
lens, three-element, optimisation by damped minimum method *(German)* 77−23726
lens aberration weighted coeffs., belastung (strain) indicator of optical system correctability 77−46783
lens CAD, three-lens zoom system 80−43424
lens centring monitors design, using variable parameter system *(Russian)* 78−50883
lens compensators for testing concave mirrors of astron. telescopes, design 80−28305
lens cost/tolerance relationship 79−81507
lens design, automatic, algorithm for accelerating convergence 80−38085
lens design, least squares fitting of Zernike's polynomials to wave aberration function 80−83660
lens design and ghost focus problem in fusion lasers 79−86247
lens design and testing for laser systems, assets and liabilities 78−46753
lens design code, CLIMB, using Monte Carlo sampling 77−3642
lens design computer programs, intercomparison 79−86234
lens design for laser beam shaping 78−13781
lens design intermediate phase approximation systems *(Hungarian)* 79−89982
lens design merit functions, RMS image spot size and RMS optical path difference 78−46743
lens design optimisation, Version 14 program 78−90488
lens design parameters, 35 mm format enlarging lenses, survey 80−13168
lens design principles 78−50888
lens design program 79−86233
lens design using cylindrical refractive index distribution *(Russian)* 78−74962
lens design with simultaneous image spot, optical path difference, diffraction MTF and Seidel abberation minimisation 80−74459
lens design without a computer 79−86235
lens optimisation using Walsh functions, FEE-based criterion 78−79097
lens paraxial eqn. dimensional analysis 80−74462
lens solution for flat-field telecentric scanning lenses 77−58424
lens system design, initial phase significance *(Hungarian)* 78−50881
lens system design with extended depth of focus, Version 14 optimisation program 78−90489
lens tolerancing, statistical approach 79−86238
lens-array illumination system, size calc. 78−59110
lens-hologram optical system, monochromatic aberrations 79−3760
lenses, laser compression expts., design principles, geometrical optics theorem appl. 79−55203
lenses, standard reference, for assessment of OTF meas. equipment 78−50897
lensless scanning telescope, MTF 80−58655
less design, applied optics conf., Oakland, CA, USA (May-June 1980) 80−101661
linear Fresnel lens with grooves of finite size, solar radiation concentration 80−106592
low-inertia scanner selection 77−58476
low-loss graded-index fibre, 3 km and 10 km preform design and modified CVD method 80−58746
luminaire with mirror cylindrical surfaces design using luminous flux balance method *(Russian)* 78−63166
luminaire with paraboloid reflectors, design, cylindrical luminous body dimensions calc. *(Russian)* 78−63165
Luneburg guided-wave optical thin-film lens, fabrication technique and props. 80−33223
machine shop operations 80−96045
Marechal evaluation of Strehl definition, Dini expansion of wave aberration function 78−71043
matrix transforming incoherent optical system, using extended lens-array 79−7086
matrix treatment of primary aberrations, for optical system design 77−50622
measuring instrument standardisation 77−71357
membrane mirrors for image compensation system, performance and manufacture 77−42587
meniscus collimator viewfinder, optimisation of mirror light transmission coeffs. 80−74469
merit function, diffr. based, for automatic lens design *(Chinese)* 80−5809

optical design techniques continued
merit function, optical tolerancing 77−756
metal mirror design and mounting specifications 80−48388
metal optics, reflective system specifications 80−48387
metal-dielectric thin film coatings, designing, applications 78−30042
microdensitometry, linear, sensor optics design 80−62710
microobjectives, reflected light, image glare coeff. depend. on design parameters 80−28302
microscope, phase-locked interf., design and construction 78−49894
microscope scanning stage, motion rectilinearity determ., method and device 80−10055
minicomputer optical design and analysis program 79−14075
mirror, asymmetric, with thin absorbing film, design 80−69493
mirror compensator of image surface curvature for system centering 77−72053
mirror surface, high power optical damage threshold elevation by hypervapotron cooling 79−23002
mirror systems, coupling props. determ. 80−53396
mirror-prism system transformations by biquaternions *(Russian)* 78−55426
mirrors, dielectric mutltilayer, reflectance under slight absorpt. conditions 80−83655
modular optical design, control of fifth-order aberrations 79−55199
monochromator design rel. to stray light 79−32056
monomode fibre design, power containment 77−72057
movie recorder, high speed, human factor problems in artistic design 77−30212
MTF tolerancing computer program 80−78934
multi-layer system, using equivalent films and graphical aids *(Czech)* 78−90486
multidielectric spectral filters, synthesis and realisation *(French)* 78−74998
multilayer 532/1064 nm laser reflector damage resistance improvement by non-λ/4 design 79−14019
multilayer antireflection coatings, all-dielec. Fabry-Perot interf. filters, optimisation parameters 79−41432
multilayer antireflection coatings 78−33797
multilayer coating design achieving a broadband 90° phase shift 80−102801
multilayer coating design with reduced elec. field intensity 77−72046
multilayer filter, automatic design method 77−58449
multilayer highly reflective coating design for wideband 90° phase shift 80−74464
multilayer interference filter, design and construction 79−46052
multilayer mirrors, high refl. at fundamental, second and third harmonic laser wavelengths 78−90490
multilayer nonabsorbent coating reflectivity computation program 80−28293
multilayer polariser, design, prep. and optical characterisation 79−76866
multilayer synthesis computations, use of Fourier coeffs. 78−90509
multilayer synthesis program, Fourier transform model 79−7196
multilayers, polarisation avoidance or enhancement 80−43255
multimode graded index fibre parameter optimisation, design considerations 80−102804
multiple-pass Raman gain cell 80−48334
multiple-plate glass systems, spectral directional radiation characts. prediction 78−74956
multispectral scanner, high resolution, for Earth obs., optical design 80−82174
Nanjing lightweight 4 m telescope design and construction 80−105162
night vision goggles, military low-cost, design and development 80−78990
noise in optical instruments, stray light reduction, space appls. 78−59153
non-coaxial aspherical IR optical system, automatic design *(Chinese)* 80−5810
nonaligned systems, off-centre aberrations 79−10263
nonconcentric bispherical mirror objective, collimating props., ray path calcs. 78−90492
nonimaging concentrator design as second stages with image-forming first-stage concentrators 80−50933
nonimaging concentrators, two-dimens., with refracting optics 79−81504
nonimaging concentrators and geometrical vector flux 79−72650
nonimaging concentrators for solar energy, design principles, geometrical optics theorem appl. 79−55203
nonimaging solar concentrator design, cavity enhancement by controlled directional scattering 80−45631
nonlinear optical processing, half-tone screen design methods 79−98294
nonreciprocal integrated optical devices, design considerations 77−793
null Ronchi grating from spot diagrams 78−5548
objective, 3-mirror design, optical scheme 78−55431
objective, concentric, longitudinal spherical aberrations calc. method *(Russian)* 78−71184
objective, four lens, corrections of third-order monochromatic aberrations 78−87123
objective decentring modulus, probability density distrib. calc. 79−76798
objective design with reduced secondary spectrum 77−7172
objective lens, three-component, with telecentric ray paths and lengthened rear section 77−54771
objective lens manufacturing, present status and future prospects 79−94323
ocular design, new type, experiences from common ocular testing 79−18501
oculars of optical sights, for target and hunting guns 77−58419
on-axis system, OTF rapid calc. using Tchebycheff polynomial orthogonal props. 78−90386
optical diode to enforce one-direction travelling wave operation 80−69427
optical glass, refr. index tables and calcs. for optical designer 80−83650
optical tolerance, glass and plastics comparison 79−59780
optimised spheric and aspheric optical systems for thermal IR 79−86244
opto-mechanical instruments developments *(Hungarian)* 78−50952
OTF calculation using gaussian quadrature, rel. to lens system design 78−90383
pancratic apochromatic objectives, variable focal length, design 80−53404
pancratic objectives, aberration stabilisation during focusing 80−102799
pancratic sights for sporting and hunting guns, design 78−71192
pancratic system with mechanical compensation, design *(Russian)* 78−37961
pancratic telephoto lens, design and optical characts. 79−6207
parabolic mirrors, fast off-axis, design and fabrication 78−46741
optical design techniques continued
paraboloid epimirror for microscope illuminator, design 80−28304
paraxial air angles between cemented surfaces, calc. 79−76799
paraxial optical systems, nomographic diagrams for design and anal. 80−48377
paraxial solves in lens design, ACCOS V program style 79−86229
penta mirror assembly, fabrication and performance description 79−81505
periscope, rearview, using two concave cylindrical mirrors, design 78−71178
photocopier lens array design, Wood lens and gradient index fibre comparison 80−14479
photographic gradient singlet, total aberrations 80−13177
photographic lens design, new developments and trends at Zeiss 80−62746
photographic lenses for low cost high production, design example 79−85193
photographic objective axial ray bundles achromatisation and Staeble-Ligotsky isoplanasie condition *(Russian)* 78−65988
pinhole camera graphic design 79−35863
planar star coupler design for fibre optic systems 80−74474
plane mirror system synthesis using biquaternions 80−9982
plane parallel lenses, prep., theory 79−3761
plane transmission diffraction grating in convergent beam 79−72693
plano-cylindrical Fresnel plastic lens, design and performance analysis as solar collector 80−53403
plastic birefringent filters, design, construction and system appls. 78−50943
plastic lenses, aspherical-surface, for large screen TV, optical design and evaluation 80−78937
plastic optical component specification 80−48362
plastic optics, design patterns 79−32009
plastics optical systems, moulded, development and appl. 78−87119
point eikonal coeffs. calc. from angle eikonal coeffs. 77−34817
polariser, thin film, design and fabrication 79−37010
practical IR optics, conference, Los Angeles, USA (Jan. 1978) 79−23085
principal surface design of lenses and mirrors, for laser focusing optics 77−3641
prism dimensional design, rhombic *(Czech)* 80−74494
prisms dimensional design, rhombic, with and without computer *(Czech)* 80−53431
production cost reduction appl. of CAD 79−86239
projection system wide-aperture condenser design 78−55430
proximate ray tracing and wave aberration coeffs. 77−597
radial refractive index gradient optical element, off-axis aberrations 80−14423
ray trace program, TI59 calculator 79−32023
ray trace program for TI-59 calculator with PC100A printer 79−89985
ray tracing, generalised, caustic surfaces 79−23043
ray tracing algorithm for programmable pocket calculator 79−81508
ray tracing through tilted and decentred optical surfaces, computer program 80−33120
receiver, separation elements of radiation flux *(Rumanian)* 79−90027
recording refractometer for optical glasses, 300 to 2600 nm range 80−57363
reference mirror for alignment of optical instruments 80−10054
reflecting interferometer design with predetermined characteristics *(Russian)* 79−93206
reflecting optical system, seventh order design 80−48378
reflecting telescope design, appl. of plate diagram 79−94321
reflection interference filters, using props. of absorbing multilayers 79−7207
reflection polarisers and analysers in vac. UV, design criteria 78−55424
reflective and catadioptric systems 79−86242
reflective Schmidt anastigmat telescopes with pseudo-flat 77−29649
reflector computation *(German)* 78−55429
reflector design, rotationally symmetrical, with aid of physical model *(Slovak)* 80−38088
reflector form for uniform irrad. field on receiver surface 78−90480
reflector geometrical optics design using complex coordinates 77−19380
reflex cameras, lens-array focusing system tests 80−86479
refractive null corrector design for testing aspheric surfaces 77−19377
reimaging system, out-of-field radiation analysis 78−59117
relay, system design, secondary colour reduction 78−83067
relay optical system, derivation and appl. of Gaussian design relationships 78−94424
schlieren 80−87544
schlieren system, refractive index gradient, chromatic variation meas. technique 80−74471
Schmidt-Cassegrain system, optical figuring 79−46025
scintillation counting, liq., unified approach to counting process, optimising optical design 77−3241
secondary spectrum correction with normal glass 77−62032
sensor system simulation elements and techniques 79−76851
Seya-Namioka monochromators, automatic design of holographic gratings 79−10390
simplified optical system design using graphs 80−48379
sine condition derivation via Fourier optics 79−98297
single lens, longitudinal-chromatic and spherical aberrations, ray-tracing method estimation 78−1311
skew ray tracing with the TI-59, programmable calculator 80−48141
solar concentrating collector optical efficiency, heat loss coeff. and heat removal factors 79−100483
solar concentrating props. of truncated hexagonal, pyramidal and circular cones 78−83062
solar concentrators, design variables, optical efficiency, heat loss coefficient and heat removal factor 80−7927
solar energy, photo-optical instrumentation, [Conf. San Diego, CA, USA Aug. 1978] 80−7926
solar energy collectors, flat plate, efficient optical window design 79−83628
solar energy collectors, flat-plate, optical valve design 79−81506
solar energy concentrator, paraboloidal mirror and parabolotoric focone 78−90478
solar energy concentrators, design methods analysis and classification 78−83063
solar energy concentrators, low cost-low ratio systems design 80−7928
solar ideal concentrator, for finite sources and restricted exit angles 77−7168
solar ideal flux concentrator design with reflector gaps 78−66880

optical design techniques continued
solar radiation simulator, non-axial type, reflector profile calc. *(Russian)* 78−63169
solar simulator design for testing solar collectors 80−50996
solar tower concept, ray trace approach 78−5571
solar two-dimensional concentrators for inhomogeneous media, design procedure 78−63167
solar wideband selective absorbers, optimum design 79−3793
spectacle lens design, computation of unwanted sphere and cylinder in periphery 78−48928
spectral instrument CAD status and prospects 79−44939
spectrometer for prime focus of parabolic mirror, new design *(Chinese)* 79−80226
spectrophotometer, UV-visible, high throughput, optical and optomechanical design 80−95155
spot diagram automatic computation and plotting program 79−72645
square Fresnel lens design for illuminating circular solar cells 78−79099
stack of dielectric layers, Fourier description of analysis and synthesis operations 78−94449
standing wave and pellicle, proposed design for very large space telescopes 79−92672
star simulator design 78−85814
stigmats using two curved Fresnel surfaces 80−38084
strain and centering sensitivity computation in paraxial region *(German)* 79−55202
stray light calculations, surface refl. models 78−58905
stray light problems in optical systems, conf., Reston, VA., USA (Apr. 1977) 78−59112
stray light reduction from optical components 78−59114
stray light suppression in optical systems, optical design, computer analysis 78−59113
stray radiation analysis using first-order deterministic APART program 78−59116
stray radiation rejection capabilities of optical systems, GUERAP II program analysis 78−59115
submarine periscope optical design for laser rangefinding compatibility 80−78987
submillimetre-wave optical design approach 79−32048
superachromatic triplets, design method 80−64133
superachromatization, glass combination selection 78−1315
surface configuration control by conc. loads applic., mirrors case 79−94317
surface configuration control of nonuniformly heated shells, actuators effectiveness 79−94318
surface errors rel. to optical performance, effect of mid- and high-spatial freqs. 79−59789
surface scattering rel. to microroughness, surface transfer function 78−58917
system and component specifications, seminar, Washington, USA (Apr. 1979) 80−46731
system planning and design, w.r.t. primary aberrations *(Italian)* 80−69490
system tolerancing, encircled energy performance prediction 80−78935
systems engineering, seminar, San Diego, CA, USA (Aug. 1979) 80−77541
systems engineering approach to optical design, fabrication and operation 80−95986
systems integration and optical design, conference, Reston, VA, USA (Apr. 1977) 78−50783
table telescope, 10 m segmented-mirror 80−105163
tapered light guide condenser design approach 80−33218
target and hunting gun optical sights 79−72664
teardrop-shaped diaphragm, light aperture profile calc. 77−75693
telephoto apochromat lenses, design 80−31924
telephoto lens design, two-component, with positive Petzval coefficient 79−71557
telescope, altazimuth mounted, primary mirror deflection and stress anal. 80−58659
telescope, AZT-24, design formulas for construction elements 79−35133
telescope, four-mirror unobscured anastigmatic, with all-spherical surfaces 78−57439
telescope, large aperture, for near IR imaging onto detector array 77−2339
telescope, three-mirror, design and optimisation 78−90476
telescope, two-mirror objective systems, field lens group corrector 80−78945
telescope secondary mirror, flexure, elasticity theory *(French)* 77−14789
telescope system, IR Galilean, attachment for information scanning device, aberrations 78−46751
telescopes, 25 m equivalent aperture, optical and IR, design concepts 80−82203
thermal blooming cell design for use in evaluating adaptive optics 80−102780
thin film external resonator for optimum SHG 79−18485
thin three lens cemented components, performance calc. 77−75652
three lens cemented objectives, spherical aberration correction 77−88894
three-layer equivalent film design 78−66884
three-lens cemented component calcs., reduced secondary spectrum 80−102800
threehedral reflecting prisms with two reflections, new design *(Czech)* 78−66913
tolerance sensitivities inclusion in merit function for lens optimisation 79−86236
tolerancing plan activities and documents 80−48382
tolerancing procedure based on MTF, lens appl. 79−86237
toroidal holographic gratings, design and performance *(Japanese)* 79−27412
transformation of vectors by system of three plane mirrors 77−75654
two-component pancratic systems containing mirrors, paraxial calc. 79−72661
two-lens afocal compensators in high-resolution lens objectives, design 80−33125
two-mirror anastigmatic telescopes, designs 77−60611
two-mirror corrector, well baffled, for parabolic telescope mirror 77−62030
two-mirror grazing incidence telescopes with one conical surface 79−84673
two-mirror pancratic system, extraneous image plane highlights elimination 80−87467
underwater TV viewing system, lens design 77−78459
unity-magnification projection system characteristics 79−27367

optical design techniques continued
unstable confocal resonators, operating point choice 79−59727
unstable optical resonators with tilted spherical mirrors, design eqns. 78−74930
UV high-resolution optical telescope design 80−90335
variable-focus objectives, use of aspherical surfaces 80−33124
varifocal compensated lens for flow cells irrad. 79−27357
vector transformation by system of four plane mirrors 80−9981
visual optical system specification and test procedures 80−48385
visual optical systems, aberration tolerances 77−73529
visual system quantitative tolerance specification and standard development 80−48384
wavefront aberration difference function, variance 77−3543
wavefront aberration polynomial, calc. 80−102614
waveguide, variable refractive index, self-focusing 79−7208
waveguides with prescribed propag. consts., design 80−48419
wavelength division multiplexing technology status and prospects 80−64203
waxicon design and fabrication 78−5543
wedge scanner, achromatisation 77−7205
wedge scanner, design 77−39058
well-baffled axially symmetric system design program GOSBOP 80−78940
wide angle lens family design 79−85194
wide angle system with corrected distortion 77−75653
wide field of view high resolution reflecting optics, design techniques 79−86241
wideband archival optical storage technology assessment 80−43283
with equal optical thicknesses of layers, theoretical design, dielectric interference film, with equal optical thicknesses of layers, theoretical design *(Russian)* 80−43471
Wolter lens component replication 80−95972
zoom and multiconfiguration optimization using the indices of refraction to represent zoom modes 79−86232
zoom lens, aperture diagram *(German)* 77−39016
zoom lens, Delano and aperture diagram *(German)* 78−13779
zoom lens, Delano diagram *(German)* 77−18117
zoom lens design by pocket calculator 78−55423
zoom lens system design and manufacture 80−68288
zoom null lens design for optical component and system testing 80−23811
zoom projection lens, optical level system, paraxial characts. 80−53399
AlGaAs DH laser epilayer struct. optimization for integrated optical circuits 80−99879
CO_2, 100 kJ laser, optical design and components 78−82990
CO_2 laser fusion systems, optical design approach for design and assembly 79−86193
CO_2 laser fusion system optical design and analysis 80−74391
Ge-SiO multilayer edge filter design, 3.2 to 4.9 μm range 78−87131
He-Ne laser model LG-10, design *(Rumanian)* 80−87407
$LiNbO_3$:Ti branching optical waveguide, mode coupling 80−69518
Nd:glass laser output, passive-mode locked, resonator length effect 78−79044
Nd:glass laser system, multichannel, for fusion experiments, model 80−58557
PbF_2-Na_3AlF_6, semitransparent wide band dielectric mirror synthesis using dispersive and absorbing materials 79−89986
Sb_2O_3-MgF_2, semitransparent wide band dielectric mirror synthesis using dispersive and absorbing materials 79−89986
SiO_2-Si, film-substrate, single reflection retarders for different Hg spectral lines 78−79122
TeO_2 monocrystal acousto-optical deflector design and testing *(Russian)* 79−98460
TlI/KCl/TlI low absorpt. antireflection coatings for KCl surfaces 80−38078

optical detection of ENDOR *see ENDOR; optical double resonance*

optical detection of magnetic resonance (EPR) *see microwave-optical double resonance*

optical detection of magnetic resonance (radiofrequency) *see magnetic double resonance; optical double resonance*

optical dispersion
see also optical constants
45 Mb/s fibre-optic transmission system performance 77−27376
achromatism of optical wedge of holographic elements *(Russian)* 78−13787
acrylic moulding formulations, optical and mech. props. 80−106582
active waveguide analysis, general approach 78−74991
aerosols, multiple scatt. theory for spherical particles *(Russian)* 80−94599
alpha-power graded-core fibre dispersion, closed-form approximation 80−1320
amplitude-phase holograms, optical parameter dispersion 80−58481
anharmonic oscillator model for dispersive optical bistability 80−58623
anisotropic channel waveguides, modal fields 77−65625
anomalous dispersion by band shift method, interference max. position 79−75578
anomalous dispersion meas. using 4-beam Rozhdestvenskii interferometer 80−68245
anomalous dispersion measurements with Michelson-type interferometers *(Russian)* 79−93211
anomalous dispersion near absorpt. line, meas. using interference fringes shift 77−34033
anthracene, total reflection spectra, site shift surface exciton dispersion 77−77233
apochromatic glass pair dispersion coeff. selection 79−72657
atmosphere, multiple scatt. theory for dispersive media with spherical particles *(Russian)* 80−94599
atmospheric dispersion effects on compensated imaging 77−42501
atmospheric dispersion minimisation, correctors for compensated imaging 77−46695
atmospheric turbulence sensor using atm. dispersion 77−45204
atomic absorption spectra, anomalous dispersion meas. by interference fringe shift 77−71891
beam broadening in randomly inhomogeneous cloudy aerosol medium *(Russian)* 78−58911
bistability, absorptive and dispersive, in Fabry-Perot and ring-cavity geometries 80−95942
bistability, beyond mean-field theory 80−43408
bistability through nonlinear dispersion and absorpt. 79−76653

optical dispersion continued
boundary between homogeneous media, dispersion zone *(Russian)* 77−79744
boundary conditions in crystal optics with spatial dispersion 78−92040
Brewster cases, generalised interface with uniaxial media, dispersion rels. *(German)* 80−5682
cable, meas. methods and faults location *(German)* 79−14097
chalcogenide glass Z 79−14063
chalcopyrite type ternary crystals, IR dispersion *(Russian)* 78−76451
chirped pulse, compression, in dispersive media 78−33669
chloroform molecule, liq. phase, Faraday rot. dispersion near vibr. reson. 79−91413
chlorophyll, a and b, lowest singlet-singlet transition, solvent effects 79−24952
cholesteric liquid crystal, spatial dispersion effect on optical props. 79−99844
cholesteryl pelargonate, optical dispersion 79−64990
continuous wavelength interferometry for measuring dispersion of complex refractive index 80−22423
convex dielectric thin film fibre optical modes, conformal mapping 77−83996
crystal surface, light interaction effects and spatial dispersion role *(Russian)* 78−23481
cylindrical waveguide wideband modulator, parameter optimisation *(Russian)* 79−94344
dielectric coating, highly dispersive artificial dielectric utilising metal spheres 80−5690
dielectric film, reflectivity, polariton standing-wave struct. as test of boundary conditions for spatial dispersion theories 79−4865
dielectric slab, spatial theory of dispersion, models 79−73891
dielectric slab and fibre waveguides, dispersion props. approximate formula 79−55217
dielectric sphere, Mie theory with spatial dispersion 79−98284
dielectric thin film stack, control by stationary ratio method, refractive index dispersion influence *(French)* 80−60693
dielectric waveguide hybrid and transverse mode dispersion calc. *(Russian)* 80−99857
dielectric waveguides, dispersion props., approx. formulas 80−14444
dielectrics, highly transparent, refr. index dispersion 79−72635
diffraction in dispersive media, system theoretical approach 79−98272
diffused channel waveguides, dispersion characts. 77−778
distributed-feedback waveguide structure, dispersion characts. 78−66949
Doppler-free two-photon dispersion problem 80−106562
double-beam interferometer, achromatic fringe pattern anomalies 79−49278
dye laser cavity, pulsed, concave grating for beam expansion and spectral dispersion 79−59721
elliptical multimode fibres, whispering and bouncing mode evaluation 80−10015
exciton resonance region, energy density and flux 78−48201
Fabry-Perot cavity, dispersive optical bistability 80−78889
far IR absorbent solid dispersive reflection meas., using Fourier spectrometer and cryostat 79−30580
far IR transparent solid dispersive transmission meas., using Fourier spectrometer 79−30581
Faraday rotation and dispersion associated with point-imperfections 78−19449
ferromagnetic helical structures, magnetooptic light interaction 79−65843
ferromagnetic medium, magnetised, unattenuated refracted wave propag., optical modulation appl. *(Russian)* 78−25774
fibre, 137 Mb/s data link using LEDs, material dispersion limited operation 77−88908
fibre, basic terms, properties, uses *(Dutch)* 80−64166
fibre, graded index, wavelength depend. of modal dispersion 78−63173
fibre, low-loss graded index, produced by double crucible technique 80−48449
fibre, M-like refractive index distrib., light pulse dispersion 78−71225
fibre, modal caustics and dispersion mechanism 78−33895
fibre, modal dispersion of power-law profiles with tails 80−95991
fibre, multimode, graded-index, influence of central depression on dispersion characts. 77−68264
fibre, multimode, loss and mode-conversion parameter meas. principle 78−22192
fibre, multimode, optimum operating wavelength for chromatic equalisation 78−25965
fibre, multimode with different refractive index distribs., material dispersion characts. *(Italian)* 78−50902
fibre, parabolic index, modal dispersion characteristics, lossy cladding effect 79−18515
fibre, PCVD, dispersion measurement by mode-locked synchronously-pumped dye laser 80−64191
fibre, profile dispersion meas. technique 77−39031
fibre, pulse broadening, inter- and intramodal dispersion 78−5547
fibre, pulse compression obs. 77−68262
fibre, refractive profile distortion and dispersion, group delay calc. 78−55433
fibre, single mode, dispersion characts., correlation between numerical prediction and meas. 80−91890
fibre, step-index, pulse dispersion, neutron irrad. effects 80−91897
fibre, zero material dispersion wavelength determ. by pulse delay meas. 78−1322
fibre, zero total dispersion in step-index monomode fibres at 1.3 and 1.55 micron 79−68428
fibre attenuation and dispersion meas. techniques and interpretation pitfalls 78−1399
fibre attenuation and pulse dispersion due to neutron irrad. 80−58730
fibre attenuation meas. techniques *(Italian)* 78−50903
fibre characteristic parameters and production methods, data transmission application *(French)* 79−90000
fibre dispersion investigation, scanning technique 79−76852
fibre dispersion meas. with Nd:YAG laser at 1.06 to 1.6 μm 80−87555
fibre dispersion measurement, nonreciprocity noise in fibre gyroscopes 80−1346
fibre inhomogeneous dispersion, direct meas. method 78−1400
fibre loss, dispersion and polarisation meas. by acousto-optical tunable filter 80−102855
fibre material dispersion meas. 78−63174
fibre material dispersion meas. by baseband modulated envelope detection 78−1368
fibre minimal dispersion refractive index profiles 79−98469
optical dispersion continued
fibre optic acoustical detector probe 80−91916
fibre optic measurement system based on near IR SiO_2 fibre Raman laser 79−23070
fibre optic waveguides, maximum information capacity derivation 77−39027
fibre optical cable, buried, transmission characts. meas. *(German)* 78−33865
fibre second generation systems, 1300 to 1600 nm 80−64163
fibre single mode characterisation by LP_{11} mode radiation pattern 80−23790
fibre technology and information transmission props. *(German)* 80−10010
fibre time-dispersion meas. by near and far-field scanning technique 78−74978
fibre transmission, dispersion, and strength characteristics 79−37021
fibre transmission between 0.8 and 1.4 micron 78−37990
fibre waveguide, chromatic dispersion effect on pulses of arbitrary coherence 80−1317
fibre waveguide mode properties, computation by propagating beam method 80−69502
fibre wavelength dispersion, difference method measurement 78−37974
fibre zero dispersion wavelength, pulse delay meas. 78−30064
fibre-optic cable manufacture, testing, and installation *(German)* 78−33863
fibre-optic cable pulse dispersion and attenuation meas. *(German)* 78−33859
fibre-optic communication system performance at 1.55 μm with single-longitudinal-mode laser 80−87556
fibre-optic index-difference dispersion and bending loss/wavelength relationships 78−1367
fibres, dispersion minimisation in single-mode fibres between 1.3 μm and 1.7 μm 79−76832
fibres, dispersion-free single-mode fibre in 1.5 μm wavelength region 79−76831
fibres, double-mode, meas. of propag. characts. and zero intermodal dispersion 79−46079
fibres, graded index CVD fabricated fibres, dispersion with finite number of layers 79−3769
fibres, graded-index fibre cables, transmission meas. in 1.2 to 1.6 μm range 80−10037
fibres, gradient index, pulse dispersion calc. *(German)* 78−50920
fibres, min. dispersion at 1.55 micron for single-mode step-index fibres 80−10006
fibres, modal dispersion with composite α-profile graded-index core 80−9998
fibres, mode dispersion, material dispersion and profile dispersion in graded-index single-mode fibres 80−14443
fibres, pulse distortion at wavelength of dispersion min. 78−22187
fibres, single- and multimode, fundamental mode signal transmission 78−42442
fibres, single-mode, wavelength dispersion characts. *(Japanese)* 80−33162
fibres, single-mode dispersion-free long-span, pulse broadening meas. 80−53417
fibres, truncated index with minimum mode dispersion, anal. 78−38000
fibres, zero total dispersion in graded-index single-mode fibres 79−76830
fibres for communication, fibre technology and props. *(German)* 79−81564
fibres with arbitrary index profile, pulse propag. and dispersion 80−78984
film, van der Waals interactions, dispersion depend., semiempirical anal. from Lifshitz theory 77−15728
film waveguide spectrum analyser with prism coupling 77−62071
Fizeau effect, theory, expt., and Zeeman meas., for teaching 78−24597
flat dielectric optical waveguide synthesis, inverse Sturm-Liouville problem soln. 79−7215
fluorophosphate glasses with silicofluorides, optical props. 77−72040
FM mode locked laser, dispersion effect 80−74406
focused light ATR method, appl. to guided waves on grating 78−74992
four layer waveguide, with metal buffer, guided modes 78−87136
four-photon processes stimulated by fluctuating pump in dispersive medium 79−23017
Fourier interferograms, dispersive two-beam, computation 79−97424
Fourier transform spectrometry, dispersive, bibliography 79−58806
Fourier transform spectrometry with liquid cells of varying thickness and temp. 77−38039
Fraunhofer diffraction of Gaussian beam at a straight edge 80−53205
frequency-modulation spectroscopy: a new method for measuring weak absorptions and dispersions 80−42262
gas DFB laser waveguide precision calc. and pulse energy obs. 80−58577
gas lasers, mode interactions in longit. mag. field, active medium dispersion effects 80−63967
gases, stimulated Raman scatt. second Stokes component, dispersion effects 80−91857
glass, birefringence dispersion, meas. with Babinet compensator using white light 78−27177
glass, high GeO_2, zero material dispersion wavelength and waveguide props. 80−58733
glass CVD fibres with axial refractive index dip, dispersion meas. *(German)* 78−33857
glass fibre cables for field trials, meas. methods *(German)* 78−50922
glass fibre performance specification for optical communication *(Dutch)* 78−83112
glass fibre waveguide, transmission props., theory *(Swedish)* 78−90525
glass fibre waveguides, light propagation, dispersion properties *(German)* 79−89996
glass fibres with dominant material dispersion, pulse broadening and distortion, wavelength depend. 79−10394
glass film and shell wall thickness meas., white light interferometric meas., dispersion effect 80−4757
graded index fibre, profile dispersion effects on transmission bandwidths 78−22198
graded index fibre propag., impulse response, expt. and theory 78−90496
graded single-mode optical fibres 79−59810
graded-index fibre material dispersion evaluation using nanosecond pulse radiator 79−81520
graded-index fibres, near-optimum, pulse broadening, dispersion characts. 79−7213

optical dispersion continued
graded-index fibres, nonlinear profile dispersion aids optimisation 77−68265
graded-index optical fibre intermodal dispersion, frequency-domain meas. 80−58729
graded-index optical fibres, compensation of profile dispersion 80−1316
grating monochromator, Cary principle for determining dynamic dispersion 80−58666
grating pair, strongly dispersive, compression of freq. chirped optical pulses 79−50373
grazing light ray refraction in dispersion zone above optically homogeneous media interface 80−74297
group velocity and energy density, monochromatic wave dispersion depend., for teaching 78−25792
homogeneously broadened medium, absorption spectra of optical bistability with dispersion 80−102757
homogeneously broadened medium, dispersive bistability 79−50355
homogeneously broadened medium with dispersion, optical bistability 80−83630
image processing in incoherent light 80−87339
infrared microwaveguides with a mode-guiding layer of chalcogenide glass 80−28329
inhomogeneous mutlimode dielectric fibre waveguide analysis 79−59833
inhomogeneous planar dielec. waveguides for integrated optics structs., synthesis *(Russian)* 80−38135
injection laser quantum noise in optical fibre communication systems 80−48259
IR and FIR tunable coherent sources utilising modulational instability 80−95967
IR dispersion crystal-crystal filters, effect of particle size, layer thickness and vol. conc. on transmission *(Russian)* 77−27369
IR dispersion filters, crystal-air, spectral charact. *(Russian)* 78−5581
IR reflection spectrum, dispersion formula fitting, Kramers-Kronig anal. 80−50311
isomeric molecular states generated by polarised light, Mossbauer resonance obs. 77−20781
Kramers-Heisenberg dispersion formula, Dirac transformation generalisation 78−16960
lightguide theory and its implications in manufacturing 80−64186
liquid, pure, organic and inorganic, Verdet consts., pulsed mag. field meas. 80−16012
lithium formate, and deuterated parametric light scatt., refr. index dispersion 77−90150
long-span single-mode fibre, pulse broadening around material-dispersion-free wavelength 78−71215
low-loss multimode optical fibre characterisation for nuclear diagnostics 80−78501
macromolecular conformation under press., optical rotatory dispersion meas. method 77−48984
magneto-optical linear and nonlinear effects, general system 77−52058
magnetoreflectance, inverse 1st moment, normal refl.-weighted magnetorefl., dispersion theoretic derivation 78−76436
material dispersion meas. in lightguide glasses 78−55447
microscopical and Ewald dynamical diffraction theories, refl. and transmission, spatial dispersive dielec. slab 80−83548
mineral crystals, dispersion meas. via spindle stage data anal. 78−85702
modal dispersion in fibres with any numerical aperture and profile dispersion 77−23746
modal dispersion in optical fibres with any numerical aperture and doping profile 78−1391
modal dispersion in optical fibres with strong mode coupling 79−27399
modulation phase fluctuation dispersion in turbulent atmosphere *(Russian)* 79−98277
modulator, dispersive using Stark effect system, for optical pulse compression 77−54793
molecular lasers, laser pumping, dispersion 80−87375
monochromator interdependent parameters and performance tradeoffs 79−90006
monoclinic crystal, refl. spectra dispersion anal. 79−99877
monomode fibre dispersion and bandwidth meas. by mode-locked Q-switched Nd:YAG laser 80−91933
monomode fibre dispersion minimum 79−64310
monomode fibre total dispersion and loss minima 80−91929
monomode optical fibre bandwidth limitations and bend losses 80−87553
monomode optical fibre design and fabrication for submerged cable applications 80−91932
monomode optical fibre dimensions, dispersion, and losses *(German)* 78−33866
multimode and single-mode optical fibre guides with rectangular cores 80−33220
multimode fibre, ring shaped and graded index with central dip, dispersion evaluation 78−42455
multimode fibre links, intermodal dispersion reduction by mode-delay equalising methods 80−48400
multimode fibre with refr. index gradient distrib., pulse dispersion 80−10022
multimode fibres, dispersion charact. from baseband freq. response meas. using InGaAsP laser beam 80−1308
multimode fibres, mode dispersion charact. with polynomial refractive index profile 78−74999
multimode fibres of arbitrary refr. index profile, pulse dispersion 80−74475
multimode fibres with polynomial refr. index profile, mode dispersion and minimisation *(Japanese)* 79−50408
multimode graded index fibres, minimum total dispersion 78−22203
multimode graded-index fibres, dispersion calc. by propag. beam method 79−98465
multimode optical fibre, freq. domain dispersion meas. 77−14792
multimode optical fibre dispersion rel. to wavelength, frequency-domain meas. 78−1401
multimode step-index fibres, effect of waveguide struct. on material dispersion meas. 80−1311
multiphonon effects on dispersion, Faraday rot., associated with point imperfections 78−43839
multiple-α index profile analysis, pulse dispersion calc. 79−50371
narrowband optical wave filter with stacked directional coupler 79−7226
nonlinear optical phase conjugation, compensation for channel dispersion 79−45993
nonstationary interaction of opposite waves in quadratically nonlinear medium−numerical experiment *(Russian)* 78−83026

optical dispersion continued
normal reflectance of conductors and insulators, dispersion relations and sum rules 80−29706
opaque solid, dispersive Fourier transform. meas. at 6K 79−2841
optical bistability dispersion effect, master eqn. generalisation 79−31845
optical bistability in dispersive and absorptive media 79−14025
optical fibre, coherence propagation obs. 77−46816
optical fibre, graded index, intermodal dispersion meas. 80−38115
optical fibre, high bandwidth graded-index, propag. consts. meas. related to material props. 80−38103
optical fibre, measurement of attenuation and dispersion 80−33185
optical fibre, pulse delay meas. in zero material dispersion region 78−33822
optical fibre, soliton pulse propag. 80−58759
optical fibre, step or graded index, refr. index dip effect on propag. 78−18053
optical fibre, vapour-oxidation fabricated, refractive index modulation, pulse dispersion 80−58756
optical fibre transmission meas. technique using time dispersion of Cerenkov radiation 78−5557
optical fibres, material dispersion 79−27377
optical fibres, total dispersion in step-index monomode fibres 79−68427
optical radiation pressure meas. in dispersive media refractive index depend. 78−33665
particle size distribution, spectral transparency method, improvements 80−86254
periodically stratified absorbing medium, splitting of energy flux *(German)* 77−3534
phonon-assisted radiative electronic transitions 79−24348
phosphate glasses, opt. and thermo-opt. props., calc. from chem. comp. 79−65826
photographic layer, effects of dispersion indicatrix on obs. of radiant energy *(Russian)* 79−58821
physical and chemical processes study using nonresonant light beam *(Spanish)* 79−23394
piezoelectric cubic single crystal stimulated Raman effect, coupled waves dispersion *(German)* 79−36963
planar optical elements, dispersion props. 79−3811
planar waveguides, with exponential variation of refractive index, pulse dispersion 77−11027
plane transmission diffraction grating in convergent beam 79−72693
plane wave intensity fluctuations in turbulent medium *(Russian)* 78−1156
plane-parallel plate, with spatial dispersion, light refl. and transmission coeffs. 80−88951
polymer mixtures, IR difference spectra, dispersion effects 79−96379
poly[(R)-oxypropylene], opt. rot. dispersion and vac. UV circular dichroism 80−40084
predisperser for large plane-grating spectrograph 80−73477
prism anamorphic system, for Gaussian beam expander 79−3716
prism beam expander for dye laser, dispersion 78−17968
prism beam expander in N_2 laser pumped dye laser, prism material dispersion 79−27285
prism used as beam expander in N_2 laser pumped dye laser, dispersion 78−74924
pulse dispersion in a clad lens-like medium 80−53445
pulse dispersion test bench for optical fibre characterisation 77−50778
quartz glass fibre waveguides, material dispersion meas. 79−18545
quasioptics in anisotropic and dispersive media 80−91943
radiation fluctuations from light source 80−95857
radiation pressure in dispersive medium, photon momentum, drag 78−33666
Raman oscillator, two-mode fibre, group velocity matching 78−25925
randomly scattering light absorbing media, scale models and transmissive similarity 79−55061
rectangular core fibre optic waveguide, dispersive props. 80−64172
reflection spectra, Kramers-Kronig anal. with preliminary dispersion anal. 78−49915
refractive index calcs. of optical materials, 0.365-2.6μm spectral region 80−87444
repeater section lengths rel. to transmitter power and fibre dispersion *(German)* 78−38012
ring cavity, dispersive bistability in homogeneously broadened systems 80−14306
ring index fibres, dispersion equalisation 79−32046
ring laser gyro, anomalous dispersion and gas flow effects 79−98430
ring laser gyro, dispersion and gas flow effects 80−1267
ring laser props., optical elements with mag. circular dichroism 79−31951
rough surface, far field polychromatic speckle, external angular dispersion effect 78−22086
Rozhdestvensky interferometer with nonequal arms for anomalous dispersion measurements by the interference fringe shift *(Russian)* 78−279
ruby, Cr^{3+} ion doped, R-line region, absorpt. spectrum, dispersion rel. to mag. field 80−2732
scanning interferometer designs for Fourier spectroscopy 79−75612
scattered radiation spatial structure statistical charact., optical thickness, particle conc. depend. 80−5694
self pulsing in dispersive optical bistability in ring cavity 80−78890
self-filtering S-type strip waveguides 80−33219
Selfoc conventional fibres, pulse dispersion meas. 79−64305
semiconductor, carrier relaxation time anisotropy effect on free carrier dispersion studies 80−84474
semiconductors, role of excitons in dispersion effects, band gap determ. 79−65393
semiconductors with diamond and zinc-blende struct., refractive index dispersion 79−24280
shadow methods for studying turbulence using reflection from a mirror in the medium 80−95801
silica binary comp. fibres, refr. index and profile dispersion meas. 77−19388
silica-plastic fibres, propag. charact. and fabrication for short-medium distance appls. 78−66892
silicate glass, Li_2O and Na_2O effect on thermo-optic props. 78−18029
silicate glass, single mode optical fibre, at zero dispersion wavelength, •xam. 78−38043
single mode fibre, wavelength dispersion meas. 77−39032
single mode fibre 1.1-1.3 μm dispersion meas. by pulse synchronisation 80−64192
single model fibres, polarisation mode dispersion 78−79128

optical dispersion continued
single-mode fibre, 14 km long, with low attenuation at 1.2 to 1.32 μm, MCVD fabrication 80−53461
single-mode fibre, pulse spreading due to third-order dispersion 79−50370
single-mode fibre pulse spreading due to third-order dispersion, optical source bandwidth effect 79−81523
single-mode fibres, axial refr. index dip effect on zero total dispersion wavelength 80−78962
single-mode fibres, pulse distortion, Gaussian pulse propag. theory 80−78956
single-mode fibres, tailoring zero chromatic dispersion into 1.5-1.6 μ low-loss spectral region 79−64320
single-mode optical fibres, bandwidths with AM and intensity modulation 79−81560
single-mode step-index fibre, minimum dispersion 79−89992
six-level atomic medium, self-focusing of two intense monochromatic waves *(Russian)* 78−25932
slab waveguide, TE Mode dispersion rel. to DH semiconductor lasers 80−91886
sodium nitroprusside, isomeric molecular states generated by polarised light, Mossbauer resonance obs. 77−20781
spatially dispersive crystal, formally closed soln. 78−84545
spatially dispersive crystal, reflectivity and transmittivity 80−99604
spatially dispersive media, generalised Kramers-Kronig formula, vac. polarisation tensor 77−17798
spatially dispersive media, optical boundary value problem 80−45024
spatially dispersive medium, exciton polaritons, absorption theory 80−54618
spatially dispersive medium, transient optical response 77−69792
spliced graded-index fibres, 11.7 km link, measured and predicted transmission characts. 80−14454
steel, stainless, hard, and mild, optical constant dispersion and emissivity, up to 900K 78−52464
stellar spectrography with crossed dispersion 78−49337
step-index fibres, multimode silicone-clad, mode dispersion 80−33142
step-index monomode fibre, mode dispersion anal. of approx. for propag. const. 80−1307
step-index single-mode fibres, zero-mode dispersion 78−87141
stimulated Raman emission in single-mode fibres by Nd:YAG laser pumping in low-dispersion region at 1.3 μm 80−64100
stripline waveguides, dispersion characts. and radiation fields 80−64155
surface wave propag., influence of bulk losses and bulk dispersion 78−33892
surface waves, interface with uniaxial media, dispersion rels. *(German)* 80−5682
switching in dispersive optical bistability, anomalous behaviour 80−23740
TGFB, dispersion and temp. depend. of refr. index *(Russian)* 77−66472
TGS, dispersion and temp. depend. of refr. index *(Russian)* 77−66472
thin film rib waveguide, numerical anal. by mode-matching method 80−48421
thin pigment films, by perturbed total internal refl. spectroscopy *(Russian)* 77−52197
thin-film strip waveguide on dielectric substrate, optical dispersion 80−53478
three-level molecular laser pumping and dispersion eqns. 80−69384
m-toluylenediamine, quadratic optical susceptibility dispersion 79−18477
transient nonlinear interactions of opposed waves, fluctuations 77−62011
transition metal complexes, octahedral, optical rot. dispersion theory 77−77164
transparent molecular systems, optical dispersion, polarised light, depend. on coherence, radiation field 78−5294
trapezoidal cross-section dielectric waveguides, mode dispersion by effective-index method 80−9999
trichloracetonitrile, IR dispersion, complex refractive index and permittivity, time correl. function 80−45057
two dimensional dispersion relations, phase problem appl. 80−102631
underground optical cable transmission meas. 78−50942
uniaxial noncentrosymmetric crysts. with intersecting dispersion curves, external actions effect 78−84552
vacuum-dielectric interface, spatial dispersion and optical props. 77−69793
visibility, definition, confirmation using marine optics data 80−23633
water optical constant submillimetric wave meas. 79−33656
water-methanol(ethanol)(acetic acid), liq., Verdet const., pulsed mag. field meas. 80−16012
waveguide, trapezoidal-cross-section ridge, dispersion characts. 77−88909
waveguide, wavelength dispersion 80−91887
waveguide and material dispersion interdepend. 79−98470
waveguide mode with arbitrary anisotropy, dispersion relation 80−5840
waveguides, optical, nonlinear pulse propag. theory 80−83669
waveguides with low pulse dispersion over extended spectral range 78−55448
wavelength dispersion of optical fibres directly measured by 'difference method' in 0.8-1.6 μm range 79−50395
Ag film, reflection coeff. minima and surface plasma wave dispersion curve comparison *(French)* 78−80429
Al film, enhanced mirror, high-rate sputtering, reflectance and dispersion 77−42636
$Al_xGa_{1-x}P$, solid solutions, refr. index dispersion characts. *(Russian)* 77−81080
$Al(PO_3)_3$-BaF_2-Al_3 glasses, opt. props., group I-III fluorides effect 80−66143
$Al(PO_3)_3$-NaF-LiF glasses, mixed-alkali effect 80−19715
Ar, third harmonic generation, bandwidth limitations in Lyman-α vicinity 79−81482
As_2S_3, two photon light absorpt. dispersion, induced linear light absorpt. *(Russian)* 80−66231
B_2O_3-SiO_2 and GeO_2-B_2O_3-SiO_2 graded index profiles, intermodal dispersion props. 78−71204
$Ba_2NaNb_5O_{15}$, dispersion of quadratic optical susceptibility *(Russian)* 77−3635
BaO-M_xO_y-B_2O_3 glass, UV absorpt., inherent absorpt. wavelength and oscill. strength, cation effects 78−80374
$Ba_{0.25}Sr_{0.75}Nb_2O_6$, quadratic susceptibility dispersion meas., oscillator model including structure 78−59078
$Bi_{12}GeO_{20}$, piezo- and thermo-optical props., dispersion theories and models 79−56764
$CaCO_3$, calcite, quadrupole nonlinear coeff. dispersion meas. 78−37943
optical dispersion continued
Cd, gas, refraction, determ. by phase vel. matching method *(Russian)* 78−30406
$CdGeP_2$ thermo-optic coefficient, dispersion 80−71396
p-CdP_2, Faraday rot., inherent optical activity dispersion *(Russian)* 78−35119
CdP_2, two-photon light absorpt. dispersion, allowed-forbidden transition *(Russian)* 78−15193
CdS, strain- and electro-gyration, polarised light dispersion curve pseudocrossing 77−36196
CdS thermo-optic coefficient, dispersion 80−71396
CdSe thermo-optic coefficient, dispersion 80−71396
$CdTiO_3$, refl. and absorpt. coeffs. 3-3.5 eV, and refr. index dispersion *(Russian)* 78−39561
Co film, linear mag. birefr. dispersion 77−69807
CuCl, anomalously slow group velocity of upper branch polariton 80−10893
$CuGaS_2$ thermo-optic coefficient, dispersion 80−71396
$(Er,Tb,Gd_3)Fe_5O_{12}$ plate, pseudouniaxial, domain struct., magneto-optical obs. 80−11221
$EuO_{1-\delta}$, thin film, Faraday effect dispersion and transmission, 0.5-1.1 μ, 20.4 and 77K, anion vacancies 79−19945
Fe film, linear mag. birefr. dispersion 77−69807
Fe, optical constant dispersion and emissivity, up to 900K 78−52464
GaAs, calc. using dispersion relations, Velicky's method *(Spanish)* 77−90119
GaAs lasers, comments on host dispersion in ultra-short pulse generation 80−64024
GaAs, nonlinear optical susceptibility and dispersion, electro-optic meas. 77−23707
GaAs, nonlinear refractive index dispersion at helium temp. 78−2820
GaAs, refr. index and induced birefringence dispersion 80−2717
GaP, nonlinear optical susceptibility and dispersion, electro-optic meas. 77−23707
GaS, infrared optical props., polarisation depend., vibr. modes 80−100658
GaSe, Faraday rot. near absorpt. edge, optical dispersion meas. 80−80757
Gd-La alloy, optical freq. cond. in 0.5-3.1 eV range, paramag.-ferromag. transition 80−29761
$Gd_3Ga_5O_{12}$, opt. dispersion 78−64343
Ge-As-Se IR transmitting glass composition, prep. and props. 80−69474
GeO_2 doped glass for optical fibres, wavelength dispersive props. 79−3774
GeO_2 doped gradient optical fibres, pulse dispersion *(German)* 80−74496
GeO_2-B_2O_3-SiO_2, glass fibre, pulse transmission meas. of zero material dispersion 77−88937
H_2, gas, refractivity and dispersion in visible and IR regions 78−34258
HF in absorption, anomalous dispersion meas. 80−95881
He-Ne ring laser beat frequency deviation rel. to dispersion and modulation 79−68410
HfO_2 single crystals, Y_2O_3 stabilised, optical props., impurities and annealing conditions influence 79−52399
Hg_2Cl_2, cryst., birefringence and dichroism, 200-500 nm and far IR 78−27257
$K_2Ba(NO_2)_4$, new ferroelastic, phase transitions, optical and electrical props. 79−55887
$KTaO_3$, dielec. response temp. depend. meas., dispersive Fourier transform spectroscopy 79−15449
Kr, third harmonic generation, bandwidth limitations in Lyman-α vicinity 79−81482
Kr-Ar, phase matched, generation of Lyman-α radiation 80−91845
Kr-Xe, phase matched, generation of Lyman-α radiation 80−91845
β-LiAl, optical dispersion, room temp. reflectance spectra 80−66195
$LiAlSi_2O_6$, IR refl. spectra dispersion anal. 79−99877
$LiIO_3$, dispersion of cubic nonlinear susceptibility meas. 79−76747
$LiNbO_3$, dispersion of quadratic optical susceptibility *(Russian)* 77−3635
$LiNbO_3$ waveguide, diffused, 2nd harmonic generation 79−14041
$LiNbO_3$:Ti, graded-index optical waveguides, mode dispersion characts. 79−3770
$LiTaO_3$, far IR complex refl. coeff. and refr. index, dispersive Fourier transform meas. 79−2841
$LiTaO_3$, quadratic optical susceptibility dispersion crystal struct. 79−18478
Na vapour, reson. refr. and dispersion, appl. to flow visualisation 79−41790
Na vapour doublet, dispersion free point, cooperative phased-array radiation 80−53352
Ni film, linear mag. birefr. dispersion 77−69807
PbI_2, excitons in spatially dispersive medium, absorption theory 80−54618
$PbMg_{1/3}Nb_{2/3}O_3$, vibr. spectrum and dispersion of optical consts., coexisting ferro- and paraelec. phases 77−63422
PbSnTe, optical dielectric const. variation with carrier conc. 80−84709
β′-PdIn, electrical resistance, mag. susceptibility and IR freq. dispersion *(Russian)* 80−107759
phosphate glass, Li_2O and Na_2O effect on thermo-optic props. 78−18029
Rb vapour, Doppler-free two-photon dispersion and optical bistability 80−95940
p-Si, heavily doped contact layers on IR detectors, IR transmissivity 80−108190
n-SiC (6H), doping effect on birefingence dispersion, effective electron mass 79−69807
Si_3N_4, film, absorption, refr. index, freq. dispersion 78−48248
SiO_2, fused, refractive index dispersion, thermal history depend. 80−25331
SiO_2 single-mode optical fibre, wavelength dispersion characts. in low-loss region 80−53423
SiO_2:Ge single-mode fibres, dispersion meas., pulse synchronisation technique 80−48410
SiO_2:GeO_2 optical fibres, definitive profile-dispersion data over extended wavelength range 79−76828
SiO_2:Ge(P) fibres, pulse delay meas. in zero-material-dispersion region 78−46769
SiO_2-B_2O_3(P_2O_5)(GeO_2), wavelength dispersive props. and composition in optical fibres 78−33793
SiO_2-based single mode optical fibres, dispersion minimisation 80−9997
SiO_2-K_2O-Na_2O-BaO-SrO-ZnO glass, props. optimisation 79−91611

optical dispersion continued
$TlSbS_2$, single cryst., spectral transmission distrib., polaris. effect, refractivity, dispersion 77−59551
Xe, refraction, determ. by phase vel. matching method *(Russian)* 78−30406
Xe, third harmonic generation, bandwidth limitations in Lyman-α vicinity 79−81482
Xe-Ar, 3547 to 1182 Å conversion efficiency limited by Kerr-induced dispersion 78−37940
$ZnGeP_2$ thermo-optic coefficient, dispersion 80−71396
ZnP_2, two-photon light absorpt. dispersion, allowed-forbidden transition *(Russian)* 78−15193
ZnS, linear electrooptic coeff. dispersion 80−71380
ZnSe, reson. Brillouin scatt., dispersion curves, piezobirefringence anal., electronic state lifetime broadening effects 79−61390
Zns film, dispersion characts. in vis. spectrum 77−59629
ZrO, single crystals, Y_2O_3 stabilised, optical props., impurities and annealing conditions influence 79−52399

optical double resonance
see also microwave-optical double resonance
absorption spectra in optical triple resonance 80−38069
acetic acid, active medium of optically pumped submm laser, double reson. 79−18215
acetyl cyanide-d_1, microwave-microwave double reson., r_s, r_0-struct. 78−13491
alkali metal vapour, optically pumped, longit. relax. in hyperfine states 77−57908
anthracene: phenazine, optical nuclear polarisation, 1.4 to 300K *(German)* 77−63321
aromatic molecules in cryst. lattice, phosphoresc. intensity and optical nuclear polarisation, level anticrossing effects 78−91992
atom, AC Stark effect, fluoresc., in modulated laser beams, two-photon stepwise excitation 80−42989
atom, AC Stark splitting in doubly reson, three-photon ionisation, nonmonochromatic field 78−94220
atom, spin-1/2, general higher-order effects of freq. shifts in optical-RF double reson. 78−21884
atom, two- and three-level, transition in stochastic field, saturation and Stark splitting 80−9546
atomic and laser spectroscopy, book 77−79554
Autler-Townes doublet asymmetry, fluctuating laser fields 79−98125
benzophenone, high resolution ODMR and optically detected ENDOR 79−19811
benzophenone $^3(n,\pi^*)$, and isotopic forms, in 4,4′-dibromodiphenylether, level anticrossings, ODMR obs. 78−2772
biacetyl, IR/UV double resonance, fluoresc. and phosphoresc. obs. 77−6810
tris(2,2′-bipyridine) ruthenium(II) cation, IR-optical double reson. and thermal modulation spectra 78−25576
p-bromochlorobenzene, T_1 states, zero-field ODMR, MIDP and phosphorescence excitation spectra 80−74191
camphor separated optical isomers, inverted IR Lamb dips, IR-RF double reson. obs. 78−21951
conference on optical techniques in mag. reson. spectroscopy, Dublin, Ireland (Aug. 1977). 78−43683
diatomic molecules, sub-Doppler laser spectrosc. 80−52320
p-dibromobenzene, T_1 states, zero-field ODMR, MIDP and phosphorescence excitation spectra 80−74191
p-dibromobenzene crystal nucl. spin polarisation cross. relax. study 80−29647
1,4-dibromonaphthalene, proton spin relaxation by optically excited triplet states 79−19810
p-dichlorobenzene, in p-dibromobenzene, optical detection of Cl NQR in mag. field 80−50228
p-dichlorobenzene, optically detected X-band ENDOR of excited triplet state 79−18221
p-dichlorobenzene, triplet state symmetry, geometry, ODMR, ENDOR obs. 79−18214
Doppler-free double resonance Stark spectroscopy, using acousto-optic modulator 79−44935
Doppler-free optical double reson. spectroscopy using single-freq. laser and modulation sidebands 80−68274
ethylene, IR double reson. obs., external-resonator controlled Raman laser pumped by CW CO laser 80−9624
fluorene:acridine (phenazine)(anthracene), optical nuclear polarisation, non-crossing rule, guest-host complex 77−42339
fluorene, optical polarisation of H nuclei, 4.2K *(Russian)* 77−12255
fluoromethane, $^{13}CH_3F$ and $^{12}CH_3F$, vibr. energy transfer between ortho- and para-mols. *(Russian)* 78−29845
fluoromethane, -^{12}C (-^{13}C), Doppler-free optical double reson. spectroscopy using single-freq. laser and modulation sidebands 80−68274
fluoromethane, gas, optical rotary saturation 79−27338
fluoromethane, in Kr matrix, vibr. relax., IR double reson. 77−79635
fluoromethane, in liq. O_2(Ar), vibr. energy relax. obs. 78−5208
fluoromethane+Ar, vibr. time depend. on equilib. and vibr. temps. *(Russian)* 79−27071
fluoromethane-^{12}C+fluoromethane-^{13}C, vibr. energy transfer, IR double resonance monitor 77−61833
fluoromethane-d_0, -d_1, vibr. relax. in matrix, rot. effects, double reson. obs. 78−46375
fluoromethane-d_2, matrix isolated, vibr. energy transfer at low temps. 80−37860
fluoromethane-d_3, vibr. energy transfer at low temps., inert gas and N_2 matrix obs. 80−9706
formaldehyde, four-level system, time-resolved microwave double reson. 79−59493
formaldehyde-d_2 733 μm line, Autler-Townes effect in laser interacting with RF field 80−53269
formaldehyde-d_2 vapour, IR-UV double resonance 80−43078
formaldehyde-d (d_2) submillimetre lasers, optically pumped, assignment of laser lines 80−58513
free radicals, spectroscopy, review, book contrib. 77−38653
glyoxal, singlet-triplet coupling, double reson. and level-anticrossing spectroscopy 80−48053
halo-alkanes, IR-microwave double resonance, book contrib. 80−54997
hexafluorobenzene, IR multiphoton excitation, vibr. energy redistrib. and hot band spectrum 80−95656
ion, electromagnetically confined, laser cooled, double resonance and optical pumping 80−87155
IR-microwave double resonance, appl. to propynal and NH_3 78−86902

optical double resonance continued
laser-induced line shifts and double-quantum Lamb dips 78−86825
laser-RF double reson. spectroscopy of nucl. quadrupole moments, ^{55}Mn and ^{50}V appls. 80−57682
lifetime meas. in atoms, mols., ions 77−30832
maser, three-level, collisional relax. times 78−13675
methane+methyl fluoride, intermol. vibr. energy transfer, double reson. investig. *(Russian)* 77−61839
methane-d_1, dipole moment, rot. depend., IR-IR double reson. obs. 79−81298
methane-d, Doppler-free optical double reson. spectroscopy using single-freq. laser and modulation sidebands 80−68274
1,6-methano-[10]-annulene, vapour phase 79−54976
methanol, collision-induced rot. energy transfer, M-resolved microwave double reson. 79−6955
methanol, double resonance Stark spectrosc., Doppler-free, using acousto-optic modulator 79−44935
methanol, optical-optical double reson., CO stretching band origin, assignments 79−31864
methyl alcohol, IR-microwave double reson., CO_2 laser pumped 79−64024
methyl alcohol, IR-microwave double reson. of mol. 79−64023
methyl alcohol submm wave laser, optically pumped, intracavity double resonance obs. 80−58522
methylimine, double resonance Stark spectrosc., Doppler-free, using acousto-optic modulator 79−44935
microwave double resonance, collision induced transition meas. 79−58764
microwave spectroscopy, modern aspects, book 80−51973
modern aspects, theoretical and expt. considerations, book contrib. 80−54997
molecular crystals, triply-excited impurity centres, effect of acoustic wave on phosphorescence 78−27115
molecular spectroscopy, IR laser cavity, IR-RF double reson. techniques, book contrib. 78−9278
molecule, r.f.-mm wave double resonance, hyperfine struct. 77−457
multiphoton excited molecules, double reson. spectroscopy 78−82060
NMR under optical pumping conditions 80−25253
non-Lorentzian laser lineshape and reversed peak asymmetry in double optical reson. 80−69443
nonlinear resonant propagation of two concomitant optical pulses interacting with three-level atomic system, num. modelling 80−9942
optical multistability, light self-modulation in double resonance *(Russian)* 80−106560
optical nuclear polarisation, field and orientation depend., non-crossing rule, perturbation anal. 77−42337
optical nuclear polarisation, the non-crossing rule, electronic relax. perturbation anal. 77−42338
optical-microwave double reson., theory for optical detection 77−3349
1,6-oxido-[10]-annulene, vapour phase 79−54976
perturbed band spectrum, extra lines, assignment using power-broadened line widths 79−18213
polyatomic compounds, vibr. relax., IR band line shape obs. 79−54879
propynal, energy dispersion and relax., laser IR-visible double reson. 80−48023
propynal, energy dispersion and relax., laser IR/visible double reson. obs. 80−53028
propynal, internal energy distrib., collisional effects, IR-vis. double reson. obs. 80−14159
propynal, IR-microwave double reson., rot.-vibr. transitions, microwave assignment, mol. consts. 78−86902
propynal, IR-microwave double reson. and two-photon expts. 80−83396
quinoxaline, optically detected X-band ENDOR of excited triplet state 79−18221
quinoxaline, triplet state symmetry, geometry, ODMR, ENDOR obs. 79−18214
resonance scattering methods in atomic spectroscopy 80−53167
resonant transitions in strong chaotic fields, saturation and Stark splitting 79−72542
RF saturation spectroscopy, optical nucl. polarisation detect., excited state NMR and ESR transition mechanisms 80−54995
rhodopsin physicochem. mechanism for mag. field detect. by birds 77−52811
semiconductor, dynamic polarisation of nuclei due to optical orientation of conduction electrons 78−19376
semiconductor, luminesc. polarisation jumps and oscills. *(Russian)* 77−85619
semiconductor, optical orientation and spin system cooling *(Russian)* 78−88229
semiconductor, two-phonon Raman scatt. by longitudinal optical phonons, double reson. 77−24852
semiconductor, violation of σH invariance accompanying optical orientation of spin *(Russian)* 78−35068
semiconductors, spin orientation by optical pumping, review 79−38410
Stark spectroscopy, Doppler-free using modulation sidebands 77−58051
Stark splitting, optical dynamic, Zeeman degeneracy 80−37774
sub-Doppler technique, appl. to small mols. 80−52339
submillimetre laser molecules, Stark and ODR spectroscopy 79−31864
subnatural linewidth spectra by optical double reson. with two-photon pumping 80−74200
subpicosecond spectroscopy, tunable probe, spectral dynamics 80−23429
1,2,4,5-tetrachlorobenzene, proton spin relaxation by optically excited triplet states 79−19810
1,2,4,5-tetrachlorobenzene, triplet excitons, ESR and ODMR 78−43681
thioformaldehyde, double resonance Stark spectrosc., Doppler-free, using acousto-optic modulator 79−44935
three-level atom, optical double reson., QED eqns. 77−10652
three-level atom in high photon density, theory 79−68206
three-level system, double reson., superposition of adiabatic state theory 78−78734
three-level system, double-reson. self-induced transparency, numerical integration 80−28288
triatomic molecules, sub-Doppler laser spectrosc. 80−52320
trifluorobronomethane, $CF_3{}^{79}Br$, precision IR spectra from IR-microwave double reson. 77−14428
trifluoroiodomethane, double resonance Stark spectrosc., Doppler-free, using acousto-optic modulator 79−44935
triple optical reson. in crystal, weak absorpt. struct. in IR field 77−24808
tryptophan, triplet state, zero-field splittings, wavelength depend. 78−43680

optical double resonance continued
two-level system, optical rotary saturation 78−13770
two-photon light shift and two-photon Lamb dips 79−36591
vibration relaxation time measurement, by coherent Raman-induced IR fluoresc. 79−7038
AgCl(:AgBr), intrinsic ODMR spectrum mechanism, doping effect 78−43682
$Al_{0.25}Ga_{0.75}As$, optically oriented electron, nuclear spin systems, local anisotropy effects on states, resonances *(Russian)* 78−43679
Ba^+ confined in RF quadrupole trap, optical detection 77−75096
BaO, $C^1\Sigma^+$-level, perturbation, extra lines, assignment 79−18213
BaO, lowest triplet state, photoluminesc. optical-optical double reson. obs. 79−68254
BaO, optical-optical double reson. of excited states, Parkinson band system 78−70857
$BaO+Ar(CO_2)$, in Ar flame, rot. and translational relax. by sub-Doppler optical-optical double reson. 80−95583
CO, collision-induced reorientation, direct meas. by IR double reson. 80−32800
CO, highly excited vibr. states, double quantum V-V transitions *(French)* 77−61837
CO, near resonant V-V transfer rates for high-lying vibr. states 79−3536
CO, rot. population transfer, IR laser double reson. expt. 78−50566
$CO_2+H_2(CO_2)(Ne)(NH_3)(CH_3F)$, rot. transfer collisions, momentum transfer distributions 77−523
CaCl, $E^2\Sigma$-$B^2\Sigma$ system, rot. anal., optical-optical double reson. obs., using two dye lasers 78−70855
CaCl, laser excitation and ODR spectra 78−82757
CaF, $^2\Sigma$ ground state, laser-RF double reson. spectrosc. 80−69171
Cd, Stark interaction in nspz$^3P_1$ levels, optical double resonance obs. 79−63941
ClO_2, laser-microwave double reson. of ν_1 band 80−48022
Cs vapour, general higher-order effects of freq. shifts in optical-RF double reson. 78−21884
FCN, IR-microwave double reson. and double photon transitions, HF Stark effect 77−14464
GaAlAs, luminescence circular polarisation, electron optical orientation resonant variation *(Russian)* 80−84782
GaAs:Al, optical detection of NQR 79−69752
GaAs-AlAs mixed crystal, optical obs. of multiple-photon absorpt. NMR *(Russian)* 77−90073
GeH_4, Doppler-free optical double reson. spectroscopy using single-freq. laser and modulation sidebands 80−68274
GeH_4, IR-microwave double reson., rot. assignments 77−75190
HCl, liq., vibr. relax., IR double reson. 80−95712
HDO, beam maser double reson., hyperfine struct. D quadrupole coupling 77−65493
HF, rot. relax., IR double reson. obs. 77−10740
HNO $\tilde{A}^1A''$ excited state dipole moment, optical-optical double reson. Stark spectrosc. obs. 80−106337
He-Ne laser, double reson., RF mag. field strength and g-value depend. *(Japanese)* 78−9359
$^{199}Hg^+$, hyperfine separation of ground-state, optical double-reson. 78−78828
I, chemical generation of population inversion between spin-orbit states 78−17767
KCl, distant F-centre pairs, ODNMR 78−68414
KCl, F centre pairs, ODMR, close and distant pairs 78−43691
$^{138}La/^{139}La$ nuclear electric quadrupole moment ratio, laser RF double reson. obs. 80−23447
$LaF_3:Pr^{3+}$, $^1D_2$ metastable state, hyperfine splittings, enhanced and saturated absorpt. spectra 78−43694
$LaF_3:Pr^{3+}$, 2K, optically detected coherent transients in nuclear hyperfine levels 79−19806
$LaF_3:Pr^{3+}$, hyperfine splitting of $^1D_2$ metastable state, RF optical double reson. 78−35067
$LaF_3:Pr^{3+}$, nuclear quadrupole interaction, optical-RF double reson. meas. of ground electronic state 77−48092
$LaF_3:Pr^{3+}$, spectroscopic and relaxation character of $^3P_0$-$^3H_4$ transition, photon echo 80−39897
Li_2, gerade excited electronic states, pulsed optical-optical double reson. spectroscopy, laser medium 79−81220
Li_2, optical-optical double reson., $^1\Sigma_g^+$ state mil. consts. 80−53027
N_2^++He, N_2^+ selectively excited, collisional deactivation 80−83338
NH_3, IR-microwave double reson., rot. and vibr. relax., inversion layers 78−86902
NH_3, IR-microwave double resonance, book contrib. 80−54997
NH_3, molecular beam, IR-IR double reson., laser spectroscopic method appl. 79−68243
NH_3, time-resolved four-level double-reson. signal, coherent transients effects 78−78732
$^{15}NH_3$, IR-IR double resonance, ν_2 vibr. state, electric dipole moment 77−83626
NH_3+H_2O, collision-induced energy transfer, IR-microwave double reson. obs. 78−42171
NO, selectively excited rovibrational states, multiphoton ionisation spectra 80−69202
NO, $X^2\Pi$ state, vibr. relax., IR-UV double reson. obs. 80−106338
NO_2, IR-optical double reson., fluoresc. obs., high-energy vibr. levels 78−55188
NO_2, optical RF double reson. showing nonstationary state 79−59492
$^{15}NH_3$, Doppler-free optical double reson. spectroscopy using single-freq. laser and modulation sidebands 80−68274
$^{15}NH_3$, $\nu_2R(2,0)$ line freq. coincidence with R(42) CO_2 laser line collisional relax., double reson. obs. 77−46562
Na atomic beam, Autler-Townes effect in double optical resonance 78−66499
Na, Autler-Townes effect in two-step optical resonance 77−38648
^{23}Na, S states, HFS optical double-reson. techniques 77−68023
Ne, $2p^53p$ config., Lande factors, double reson. meas. *(French)* 78−9113
Ne, optical-optical double reson., $2p_4$ and $2s_2$ level g_J-values by mode crossing 77−50411
OCS, M-resolved rot. Stark levels, four-level microwave-microwave double reson., collision induced 77−10696
OCS mixtures, rot. energy collisional transfer, M-depend., microwave double reson. 78−46435
OCS+methanol (H_2)(He), collisional rot. energy transfer, microwave-microwave double reson. obs. 77−19016
PH_3, Doppler-free optical double reson. spectroscopy using single-freq. laser and modulation sidebands 80−68274
POF_3, IR rot.-vibr. spectrum, mol. consts., laser Stark spectroscopy obs. 78−33508
Pr, metastable, F=7⇌6 Hfs, laser-RF double reson. spectroscopy 80−58170
Rb, optical pumped magnetometer *(Japanese)* 79−21790
SF_6, dynamics of 10.4 μm absorption, vibr. bath model 78−17666
SF_6, high-resolution transient double IR reson. 77−88477
SF_6, highly excited, time-resolved IR absorpt. obs. 80−9666
SF_6, IR absorpt. of highly vibr. excited mols., double reson. meas. 78−37662
SF_6, IR double reson. with tunable diode laser 80−14160
SF_6, IR double resonance, V-V energy transfer from ν_3 mode 77−482
SF_6, IR double resonance and energy transfer obs. 77−58105
SF_6, in cryogenic liqs., vibr. kinetics, IR spectrosc. obs. 79−18182
SF_6, laser-irrad., high-resolution double-reson. spectroscopy, collisionless multiphoton dissoc. 80−9623
SF_6, multiple-photon excited, double reson. spectroscopy 80−53030
SF_6, multiple-photon two-freq. IR laser pumping, optoacoustic spectroscopy 79−36717
SF_6, vibr. relax., 150 to 320K, IR double reson. study *(Russian)* 78−86899
SF_6, vibrationally excited, collisionless intramolecular energy transfer 78−37663
Sf_6, IR-IR double reson. following IR laser excitation, ν_3 mode 79−54872
Si, compensated, ^{29}Si dynamic polarisation by optical pumping in weak mag. field *(Russian)* 77−40152
Si, compensated, ^{29}Si nuclei optical polarisation, nucl. relax. effects *(Russian)* 77−43907
Si, nuclear polarisation due to optical pumping, weak mag. field *(Russian)* 79−19805
Si, optically pumped, distrib. of polarisation of electrons and nuclei 77−59485
Si:P, spin relax. time of electrons determ., dynamic polarisation of ^{29}Si nuclei 77−55730
SiH_4, Doppler-free optical double reson. spectroscopy using single-freq. laser and modulation sidebands 80−68274
Sm, and isotopes, hfs, laser-RF double reson. spectroscopy 80−58170
Sm, excited states hyperfine struct., isotope shifts, laser-RF double reson. obs. 79−41140
U, 4 eV odd levels, hyperfine struct., double reson. spectrosc. 79−81171
UF_6, vibr. excitation kinetics, IR-UV reson. methods 79−45739
^{235}U, ground and 1st excited states, hfs, laser fluoresc. and laser-RF double reson. spectroscopy 80−58170
^{235}U, ground-state hyperfine structure high-precision meas. by laser-RF double reson. 79−26942
^{235}U, high precision meas. of hyperfine struct. of 620 cm^{-1} atomic level 79−45660
V, hyperfine struct., laser-RF double-reson. obs. 79−41141
Yb, $4f^{14}6s6p$ $^3P_1$ and $^1P_1$ levels, Stark effect, tensor polarisabilities 80−87080
Zn, Stark interaction in nspz$^3P_1$ levels, optical double resonance obs. 79−63941
ZnS:In, recombination emission by optically detected magnetic resonance 80−66272

optical elements
see also diffraction gratings; fibre optics; mirrors; monochromators; optical collimators; optical fibres; optical films; optical filters; optical isolators; optical modulation; optical prisms; optical waveguides; optical zone plates
achromatic interference polarisers *(Russian)* 78−71227
achromatic low refl. and beamsplitting coating synthesis 79−98496
achromatic quarter wave plates within second order term *(French)* 79−72675
achromatized wedge scanner design 77−88948
acousto-optical x,y deflector with 32×32 positions resolution 79−72683
adaptive, membrane mirror performance 77−46782
adaptive optical components, seminar, Washington USA (Apr. 1979) 80−31421
adverse environment effects conf., San Diego, USA (Aug. 1977) 78−82976
alkaline earth fluorides, UV window and coating materials, two-photon absorpt. coeffs. 79−59734
antireflection coatings for optical components, using materials with refr. index 1.7-2.0 79−72656
aperture shaping, diffracted energy spatial distrib. control, computer analysis 78−59152
aspheric, testing in reflected light using blazed synthetic holograms 80−91881
aspheric element generation by sputtering techniques 78−59168
aspherical, manufacturing and testing techniques development, use of computer *(Italian)* 80−48467
aspherical surfaces, holographic methods of testing, review 80−33257
attenuator, variable, for use in single-mode fibre transmission systems 80−99821
attenuator, wedged-plate, computer-controllable 80−99819
attenuator metrological certification methods 80−91941
autocollimators, instrum. for checking 80−77832
axicon measn axial image 79−81499
axicon polarisation effects 79−45900
Babinet compensator, appl. in optical testing 80−33251
Babinet compensator, quantitative test for concave aspheric surfaces 79−98512
baffle edge design using optical black coating 78−59154
baffle materials, IR bidirectional refl. distrib. function meas. 78−58012
beam divider and mirror expt., amplitude correlation mehtod for optical polarisation meas. 80−53206
beam scanner with parallel displacement *(Russian)* 77−34929
beam splitter, birefringent, polarisation-independent 80−5814
beam splitter, position in Michelson interferometer, form. of bands of equal thickness 80−52298
beam splitter, self-supporting thin-film, for far IR interferometers 78−275
beam splitter, variable-ratio, reflection prism, use in holography *(Spanish)* 77−88945
beam splitter and reflection reducing coatings on ZnSe for 3-14 μm 79−76811
beam splitter lightwave fibre tap, use in source stabilisation 78−79105
beam splitter of variable ratio 79−40078

optical elements continued
beam splitter using diffr. grating combination, for Michelson interferometer 78−70205
beam splitter using variable thickness film, for integrated optics 77−65626
beam splitters, design of high efficiency for two beam IR interferometer 78−30093
beam splitters, multilayer polarised light, laboratory and factory testing 79−27428
beam splitters, non-polarizing, design 78−83110
beam splitters, variable ratio, for high energy glass laser systems 79−45952
beam splitters for optical heterodyne receivers 79−18528
beam splitting device for use with smoke chamber ray optics demonstrations 80−67990
beamsplitter choice for minimum exposure time in photoresist holography 79−59655
beamsplitter using ultrathin metal grids, polishing technique to improve reflectivity 78−55459
beamsplitters, beam inherent parameters analysis 79−36999
birefringent, rotating, and achromatic quarter wave plates, appl. to ellipsometry and photoelasticimetry *(French)* 80−14278
birefringent element, analogue, built from polarising wide field Michelson interferometer 80−91895
bistable optical devices: an overview 80−58625
bistable optical devices, overshoot switching 80−58776
blinds with internal diaphragms, light-blocking effectiveness 79−50405
Bragg reflector, nonuniform, almost periodic, perturbation anal. 77−27356
Brewster angle light trap 77−88897
camera lens shutters, friction coefficient nonreproducibility evaluation 80−62765
camera window for aerial photography large interferometer for testing 78−13821
chalcogenide glass films, kinoform optical elements and integrated optics elements prod. 77−75634
chalcogenide glass films, opt. inform. recording uses 77−75633
chemically unstable glass components, protection from biological overgrowths 78−59107
circular plate, optical hot spot, thermal stresses 77−11044
circulator, polarization-independent, configuration method 80−38095
cleaning techniques for optical surfaces 79−46093
compensator retardation determ. 79−26107
component manufacture and evaluation, seminar, Los Angeles, USA (Jan. 1979) 80−12850
component polishing process modelling *(German)* 80−87565
conference, polarised light, San Diego, Calif., USA (Aug. 1976) 77−45881
conference on optical coatings, Washington, USA (March 1978) 79−46028
conical porthole, deep-water, deformation effect on optical characteristics 79−76859
contact problems in optical surface shaping 80−74540
contamination modelling, photometric characts. estimation 80−48429
corrector element finite size rel. to wavefront compensation error 77−46693
covered groove, optical surface wave scatt. and refl. 77−75707
cube beamsplitters polarisation sensitivity, reduction by hybrid metal-dielec. coating 77−83981
damage-resistant components for 2-5 μm laser systems 77−19282
deflecting system, 3-slit, for isotopic spectral anal. 79−37005
delay line, multiple refl. in spherical resonator 77−27368
diamond turning, technology developments, appls. 77−27400
diaphragm shape selection for shadow photometry of gas flow 77−35270
dichroic beam splitters, high-performance, for DF chem. lasers 80−95932
dielectric multilayer systems for optical appls., computer program synthesis *(German)* 78−46788
dielectric thin film multilayer systems, polarisation effects and use in laser physics *(German)* 78−33912
diffraction correlators invariant to optical element shifts 80−106471
diffuser, weak, speckle pattern, spherical aberration effect 80−87476
diffuser for Fourier transform hologram recording 80−43285
diffuser with pseudorandom phase sequence [hologram recording] 80−14298
discrete component Sagnac optical rate sensor, error sources 80−1342
dust deflection from optical components by 20 kV negative potential 79−76888
dye, bleachable no.3955, relax. time meas., laser passive shutter appl. 80−23759
elastic parallelogram mechanism 78−16859
elastic tools for finishing optical components with noncircular cylindrical surfaces 80−28368
electrically heated window, thermal distortion 77−34952
electro-optic reflector, controlled, temp. fields, thermal distortions 80−96021
electromechanical shutter, constructional details 79−68435
electrostatic protection technique for optical components in dusty environments 80−58657
elliptic polarisation, Stokes parameters, vector trihedron, optical element evaluation 80−53209
elliptic retarder, expt. method for optical parameters determ. 77−88941
epoxy replication, materials, techniques and appls. 77−27401
fabrication and assembly, centration errors 80−9980
fabrication by diamond turning 79−76899
Fabry-Perot bistable devices, as optical switch, limiter or memory element 77−88931
Fabry-Perot cavity containing ruby, optical bistability and differential gain, 85 to 296K 77−39025
Fabry-Perot resonator, bistable, use as optical switch, limiter or memory element 77−39024
far IR diagnostic quartz beam splitters 77−39470
fibre optic element end forming of optical precision surfaces 77−50779
fibre optic rotation sensor, all-waveguide configuration, key element tests 80−58796
fibre type light protecting shield 78−18066
fibre type light shield with absorbing cladding, Fraunhofer diffr. 78−90521
fibre-optic polariser, in-line, formation and props. 80−106603
fine wire free standing grids for mm and sub mm waves 78−5559
flatness, interferometric examination techniques 80−69498
optical elements continued
fluorescent shutter, fast, liquid cryst., based on guest-host interaction 78−83092
focal plane camera shutters with independent curtain movements 78−29195
frequency shifter for heterodyne interferometers, using multiple rotating polarisation retarders 79−6167
frustrated total internal reflection element, adjustable as a function of the incidence angle of highly collimated light beams 80−96022
giant pulse ruby laser, spring-loaded partial kinematic mount, precise alignment of optical components 80−74518
glass, for high-performance optical components 79−36968
glass capillary array, window for vac. UV 79−89990
glass interferometer rod, inhomogeneity rel. to tempering 77−34919
glass windows in hydrostatic press. vessels 79−90016
gradient index optical elements and system design 80−106594
gradient-index imaging, theory 80−69331
grid polarisers for IR Fourier spectrometers 80−105724
grids of fine W wire, production, use in IR spectroscopy, polarization interferometry 80−9052
guided-beam splitter, refl. meas., fabrication method 80−74473
half-screen, shadow cast when illuminated by Gaussian beam, props. 80−28156
high speed rot. mech. shutter design for pre-pulse protection 80−96032
high-energy, IR laser component optical characterisation techniques 80−14347
high-volume optical component tolerance/specification relationship 80−48383
holographic, third-order aberration theory and generalised aplanatic condition 80−74314
holographic beam scanner using auxiliary reflector 77−83951
holographic beam splitter form. in optoelectronic holographic memory system 78−17882
holographic elements, axisymmetrical, third order aberrations 80−69341
holographic elements as lenses, optical system design 78−9425
holographic generation expt. arrangement 77−83966
holographic optical element design and construction 78−55315
holographic optical elements for incoherent polychromatic imaging 80−69349
image spot energy flux density distrib. for diffuse-reflection device 77−34923
imaging polarizer with spherical mirrors for VUV radiation 80−48375
information processing system parameters rel. to optical element characteristics 79−72510
integrated optical device used as switch, amplifier, limiter and memory logic element 79−32090
integrated optical functional elements based on holographic gratings in As_2S_3 film waveguides 77−79972
integrated polariser, reduced cladding-medium, fabricated in ion-exchanged guides 80−14489
interference beam splitters for 10.6 μm wavelength 79−55225
interference filter polychromator 77−72061
interference polarisers for lasers, development 78−83108
interference polarizer with large entrance aperture, characts. 80−43453
interference polarizers on plane-parallel substrates 80−1336
IR coating for high energy laser reflector and window 79−45951
IR elements, adsorbed water effect on laser breakdown threshold 77−79886
IR laser window material extrinsic absorption 79−14049
IR laser window material refractive props., temp. depend. 79−14052
IR multicomponent systems, fabrication 77−27402
IR optics elements, breakdown dynamics near surface in gaseous media 79−45986
IR polariser grid prod. process *(Russian)* 78−46795
IR segmented composite window design 80−106621
IR transparent materials and components 77−19374
IR window, large aperture, interferometric meas. 79−85170
IR window coatings, new materials 77−50736
IR window rain erosion resistant antireflective coatings 78−83050
iris diaphragm with straight leaf edge, mechanism accuracy 80−28337
large optical component antireflection and protective coatings 79−72660
Large optical component grinding and polishing condition selection 79−81579
large optical components for high-power lasers, refl. and transmission meas. 79−44927
laser anemometer elements, Gaussian beam transform. 79−45991
laser beam simple submicrosecond optical chopper 80−14373
laser damage mechanisms 78−83016
laser driven subnanosecond blast shutter 77−79842
laser heated IR windows, interferometric meas. 77−46748
laser induced damage in optical materials, symposium, Boulder, USA (Sep. 1978) 80−31417
laser mirror and window absorption, reflection and transmission obs. at 10.6 μm 79−14014
laser optical component props. depend. on material flow props. *(Russian)* 80−38047
laser polarisation rotator, broad band, using successive refls. from 4 mirrors 79−981
laser single crystal windows, stress-induced birefr. elimination 77−88818
laser window, elec. fields and power dissipation at oblique incidence 77−46746
laser window and rod critical orientations for stress-induced depolarisation elimination 79−14054
laser window degradation interactions and impurity clustering effects 79−14050
laser window materials, pulsed HF-DF laser damage 79−14011
laser window materials stress birefr. elimination 77−58362
lens guide, low-loss image transmission 80−91872
light pipe device for obtaining reference beam with single far IR spectrometer or interferometer 77−38035
light shutter array, large area electronically controllable, using polyvinylidene fluoride bimorph vanes 80−58696
linear compensator for beams path difference, opt. polarisation method of stress testing 79−93204
liquid optical element for image stabilisation 78−55462
machined part flatness and parallelism meas., contactless interferometric method 78−21208
matching focons, optical props. 79−27168
MBBA liquid crystal wedge as a polarizing element and its use in shearing interferometry 80−53444

optical elements continued
Mellin transformation, one dimensional, performed by single element coherent optical processor 79−50231
metal IR window materials, diamond machinability 78−5586
mica phase retardation plate, cleaving and optical meas. method 79−64364
moving-condenser electrodynamic unit, for fast scanning microspectroscopy 77−5903
multilayer beamsplitter coatings, accelerated fabrication method 80−102873
Mylar beam splitter efficiency in far IR interferometer 78−55434
near perfect optical square fabrication 79−72721
noise in optical instruments, stray light reduction, space appls. 78−59153
nonlinear coherent coupler, new optical logic device 80−58630
nonplanar wire polarisers for far IR 79−36989
objective decentring modulus, probability density distrib. calc. 79−76798
one-dimensional linear coherent processing by single optical element 79−94165
opaque optical components' parallelism meas. 79−81549
opticomechanical convertor, small-holes dia. meas. 80−77750
passive planar optical element construction from thin film optical waveguides 79−27440
passive shutters for ruby laser, use of KS glasses for generating subnanosec. pulses 80−102728
phase anisotropy, temp. depend., intracavity method, meas. 80−78931
phase imaging systems, chromaticity, luminous efficiency 78−33824
phase plates for laser beam compensation 77−42556
phase shifter, broadband, for two beam interferometer 78−37968
phase-rotating plate, smooth transverse intensity distrib. form. in light beam 79−59837
photographic shutters, efficiency rel. to picture quality 77−74531
picosecond laser pulse length meas. using fast optical shutter and echelette grating 79−64266
piezoelectric bimorph plate, adaptive optical element analysis 79−50389
plasma shutter, for Nova laser fusion reactor 78−66854
plasma shutter, self-triggered, for laser beam switching 77−58367
plasma shutter for CO_2 laser, transmission cut-off time depend. on breakdown intensity 80−6259
plastic optical component specification 80−48362
plastic optical components, flexible rapid curing abrasion resistant coated film 78−66890
plastic optics, components 79−32010
plastic optics, design patterns 79−32009
plastic optics for optoelectronics, moulding techniques for single, multielement systems 78−63210
Pockels double shutter in ruby laser with active phasing of spectrum *(Russian)* 79−98419
polarisation beam splitters for F II-centre laser pumping 79−45960
polarisation rotator, tunable damage-resistant, for UV and visible laser radiation 77−83964
polariser, dichroic I, for liquid crystal display 77−46807
polariser, rotating triple-reflection, for UV discharge lamps in photoelectron spectroscopy 78−94443
polariser, thin film, design and fabrication 79−37010
polariser + crystal plate + analyser system, passage of light 80−10023
polarising beam splitter, film coatings, cemented cube 77−19422
polarising optical components for high power glass laser systems 77−46727
polarizer, matching type to applic. 78−18051
polaroids for sub-mm. range based on dichroic crystals 78−5555
polishing defects obs. by etching 77−75724
polishing simulation calc. and results *(German)* 80−87566
polychromators and spatial filtering for summing luminescence spectrometer 77−74517
precision optical element testing by phase meas. interferometry 80−74520
production quality trends and limits 80−69566
production technology advances, seminar, London, England (April 1979) 80−67938
quartz:Ge attenuator for 0.25 to 1 μm band, with attenuation coeff. up to 10^5 80−48415
quartz plate standard for precision polarimeter, systematic errors *(German)* 78−16832
radial refractive index gradient optical element, off-axis aberrations 80−14423
reflection polarisers for vacuum UV, design and performance 78−33801
reflector, 90 degrees, ray transfer matrix 80−33184
refractive index gradient tolerance in optical elements 78−71179
replication for laser components 79−55253
ring laser props., optical elements with mag. circular dichroism 79−31951
rising-sun reticle, error signal rel. to target position 79−81548
rod, tapered gradient-index, geometrical optics 80−69322
rotating shutter, for Nova laser fusion reactor 78−66854
scanning multiple aperture for image restoration, coeffs. determ. 77−71930
Schmidt corrector plate replication, testing and performance calc. 78−66967
Schmidt corrector plate replication 78−66966
shaded circular apertures, encircled energy in diffr. pattern, superresolving and apodising props. 80−95787
shutter, controllable phototropic, synchronization of single pulse ruby laser 80−23699
shutter, drum or sector wheel, accuracy, specification 77−30210
shutter, heat resistant, for laser beam energy distrib. meas. 77−58369
shutter, psec time scale, using thin foil irradiated by laser beam 78−1350
soft aperture, laser beam radial intensity distrib. form. 77−7110
soft diaphragms, prepared by induced absorption method at 1.06 micron in CaF_2 78−5477
spectral shared aperture beam splitter for high-energy laser systems 80−14477
spectral slit, digitally controlled 77−34035
stray light reduction from optical components 78−59114
surface contract interaction zone, thickness calc. and distance meas. methodology *(Russian)* 80−99889
surface evaluation techniques 79−46094
surface light scattering rel. to microtopographic features 79−59639
switch, fast IR, for ultrafast photography, with 10.6 μm radiation 78−38035
optical elements continued
system and component specifications, seminar, Washington, USA (Apr. 1979) 80−46731
tapered gradient index rod, geometrical optics and imaging props. 80−14280
tapping elements with thin-film beam splitters directly applied to optical fibre endfaces, fabrication 79−37016
teardrop-shaped diaphragm, light aperture profile calc. 77−75693
thermal failures in long and short laser pulse regimes 77−19281
tools for quick precision alignment of interferometric equipment 80−73429
transmissive optics for high power CO_2 lasers 78−79057
triple grating polychromator for Thomson scatt. 77−43059
tuning fork choppers, stable sinusoidal driver circuit 79−90017
two coord. deflector, anisotropic diffraction and wide band scatt. 80−91920
ultrafast optical Kerr shutter, photography and signal sampling appls., book contrib. 77−31140
UV laser window material absorption obs. 79−14012
UV polariser, coating materials *(Russian)* 77−34928
visual instruments, optical component contamination, effect on visibility of extended objects 80−64137
volume reflecting grating parameters determ. for freq. selective optical elements *(Russian)* 80−74492
wedge scanner, design 77−39058
wedges as flux modulators 77−27355
welded optical fibre signal splitter 80−102814
wide aperture optical shutter with saturating filter at 1.06 μm 80−53457
window, laser damage threshold at 10.6 μm, up to 10^{10} W/cm^2 77−50707
window design for flat-plate solar energy collectors 79−83628
window for metallic He cryostat 77−33996
window interferogram evaluation method 77−84011
window materials for CO_2 lasers, optical suitability 77−58361
window photobleaching of H_2 lamp, radiation coloration removal 79−72698
windows, laser damage thresholds, 10.6 μm 77−50708
windows for Big European Bubble Chamber 78−17483
windows of high-press. chamber, strain determ. by holographic interferometry and finite element anal. 77−26323
wire grid polarisers, new optical model 79−902
Y-branch for optical communication networks and measuring equipment *(German)* 78−66918
BaF_2, single cryst. windows for high power lasers, stress-induced birefr. elimination 77−88818
CO_2 laser Gemini fusion system optical performance 80−74392
CS_2 optical shutter, time resolution, group velocity dispersion and beam geom. effects 77−58452
$CaCO_3$ calcite linear polarizer, role in laser technology 80−64165
CaF_2 ⟨111⟩ oriented windows, optical distortion coeffs. at chem. laser wavelengths 79−94269
CaF_2 laser window surface O_2 detection by X-ray photoelectron spectroscopy 79−14056
CaF_2, press-forged laser window, polishing, cleaning and grinding 79−59849
CaF_2, window for optical high press. cell at high temp., characts. *(German)* 80−47999
CdTe single crystal IR window for CO_2 laser 77−75566
Ge optical windows, contaminated by NH_3, CO_2, CO, HCl, methane, cryocooled, IR transmission 79−32007
Ge transparent IR window design for uniform pressure loading 79−23088
InSb-NiSb eutectic, struct. and optical props., IR polariser appl. 80−45078
KCl IR window material, polish layer effect, ellipsometric meas. 78−55419
KCl window with antirefl. coating, laser damage at 10.6 μm 77−61992
KCl:Eu IR laser window lattice equilibrium obs. 79−14055
$LiYF_4$, UV window and coating materials, two-photon absorpt. coeffs. 79−59734
$MgFl_2$ windows, vacuum sealing 78−94457
NaCl 46 cm window optical evaluation facility 80−74526
NaCl Czochralski crystal growth for large CO_2 laser windows 80−74525
NaCl large window continuous polishing 80−74527
NaCl Polytran laser windows, for CO_2 lasers, fusion appls. 78−59067
NaCl window production for Antares CO_2 laser system 80−74524
PLZT electrooptic shutters as thermal/flash protective devices 77−46808
Si, beam extinguishment device, without scatter 78−87126
Si beam splitter for CdSe optical parametric oscillator 77−88851
SiO_2-Si, film-substrate, single reflection retarders for different Hg spectral lines 78−79122
SiO_2-Si film-substrate refl. polariser, operation at Hg spectral lines 77−75655
SrF_2, press-forged laser window, polishing, cleaning and grinding 79−59849
TeO_2 two coord. deflector, anisotropic diffraction and wide band scatt. 80−91920
TlCl component antireflection coating 79−27346
W wire grids, FIR performance and appl. 80−10012
ZnS CVD IR window, optical and physical characteristics 80−106620
ZnS CVD window, IR lattice absorption, phonon assigments and image spoiling 80−33104
ZnS CVD windows for forward looking IR radar systems 78−46816
ZnS/ZnSe composite window, erosion-resistant, fabriction and evaluation 78−71211
ZnSe laser window, laser induced thermal stresses 77−46747
ZnSe laser windows, AR coated, photoacoustic chopping freq. studies using CO_2 laser 80−83629
ZnSe laser windows, photoacoustic signal var. with chopping freq. 80−75309
ZnSe/water, interface, laser-induced damage in ZnSe 80−102746

optical fibres
1.5 Mb/s bipolar signal coding and decoding optical fibre link 77−27343
1.6 km half-duplex optical data link 80−14470
2.1 km optical cable link installation, TV and telephonic transmission expt. *(German)* 78−33890
2 km 20 Mb/s optical fibre transmission system 78−42437
2 Mb/s transmission link for industry *(French)* 77−10843

optical fibres continued
4 port and 8 port kaleidoscope micro-optic star coupler for optical fibres 80−58681
5 km fibre-optic data transmission link 77−65622
6.3 Mb/s optical fibre communication for power system protection and control 78−1423
6-fibre cable with polyurethane covered steel wire central support, optical links appl. 80−43470
7-core, construction and transmission props. 79−46077
8.448 Mb/s optical cable feasibility trial *(German)* 78−33888
9 km fibre-optic telephone transmission system 78−42435
10 Mb/s short-distance fibre-optic data bus 77−68276
16 and 32 Mb/s optical data links 77−68275
16 and 32 Mb/s short-haul high-performance optical data links 78−1421
30.4 km graded index vapour-phase axial deposited fibre, props. 80−64149
32 km optical fibre transmission with data-rate-transparent repeaters 79−76875
32 Mb/s step-index optical fibre repeater equaliser *(German)* 78−33881
32Mb/s optical fibre transmission system planning and expt. 78−1418
35 Mb/s optical fibre cable transmission using IR LED optocouplers 80−33156
44.7 Mb/s fibre optic transmission system expts. 78−1420
45 Mb/s fibre-optic transmission system performance 77−27376
100 μm-core, low-loss, large numerical aperture waveguide for data processing appls. 79−50426
100 Gbit/s transmission rate, expt., review *(French)* 80−69525
140 Mb/s fibre-optic field demonstration system *(German)* 78−33889
140 Mb/s optical fibre transmission system 78−42436
140 Mbit/s feasibility trial over 5.75 km for main telecommunication network use 78−30076
400 Mb/s optical fibre communications, integrating and transimpedance front end performance comparison *(German)* 78−33879
400 Mb/s optical transmission expts. 77−88954
400 MHz SAW timing filter for optical fibre transmission 79−50415
400Mb/s SELFOC fibre transmission system expt. 78−1419
800 Mb/s fibre transmission test using low-loss and low-dispersion single-mode cable 80−10001
800 Mbit/s digital transmission expt. *(Japanese)* 80−33164
800 Mbit/s optical transmission experiments with dispersion-free fibres at 1.5 μm 80−58680
absolute power meas. thermistor sensor 78−65971
absorption and scatt. losses in optical fibres, calorimetric meas. 78−46790
absorption coefficient measurement by calorimetric techniques *(Dutch)* 79−76774
AC cataphoresis meas. techniques and apparatus 79−8442
access couplers for single strand systems 80−58766
acoustic modulation of light propagation 80−33209
acoustic sensor, single optical fibre interferometric 78−38161
acoustic sensor using fibre coil 77−72119
acoustical detector probe 80−91916
acrylic coating, surface tension effects 80−53487
adjustable single-fibre connector and output monitor *(German)* 78−38011
air-pollution monitoring fibre network system for wide area by optical absorption method 80−10002
alignment chuck, light transmission characteristic testing appl. 78−30090
alignment tool 80−23814
alkali boroaluminosilicate system, self-focusing fibres with aperture of 0.18 80−87548
alkali germanoscilicate glasses, water extraction for making graded index optical fibres 80−28361
alkali halides, polycrystalline, use as IR optical waveguide fibres 80−58750
alkali lime germanosilicate GRIN fibre prep., losses and geometrical props. 80−69560
alkali-$PbSiO_3$ optical fibres, high aperture, double-crucible preparation 78−1450
alpha-power graded-core fibre dispersion, closed-form approximation 80−1320
altitudinal alignment in fibre end-butt coupling, using two-dimens. Si grooves 78−87148
amplitude and group delay distortion meas. using link analyser 78−66940
analog modulation of light-emitting diodes for optical fiber *(Japanese)* 78−90516
analogue and digital communication systems charqcts., and state of development *(German)* 79−999
analogue fibre optic commandable communication system, 650 MHz 78−46819
analogue fibre optical systems, linearised LED and laser transmitters 78−46818
analogue fibre optics data communication system, high resolution 77−46810
analogue transmission, transceiver transducers, PAL TV transmission *(German)* 78−1333
analogue video transmission feasibility using laser diode, over 30 km at 1.3 μm 80−58737
analogue/digital communication system with 5 MHz bandwidth *(German)* 78−30062
analyser, separation elements of radiation flux *(Rumanian)* 79−90027
analysis using scalar approximation technique, accuracy 80−58703
angular pattern display using TV camera 78−33820
angular scrambling star couplers 80−53465
anisotropy effects in inhomogeneous fibres 78−1360
application to existing communication systems *(German)* 78−33887
applications as transmission medium, review 80−14456
applications outside data transmission and communication, review 80−74482
applications to military and industrial systems 78−38021
arbitrary index profile, formula for TE_{01} cutoff freq. 80−48418
arbitrary refractive index profile fibre, light backscatt., uniform approx. approach 79−14100
arbitrary-index profile fibres, bending loss of propag. modes 78−66896
arc fusion splicing of low-loss single-mode fibres 80−53489
arc splicing unit *(German)* 80−19115
area-ratio couplers for distributed data-processing equipment interconnection 79−50431
army communication systems appl., tactical command posts 78−55452
array connector holding fixture 79−55241
optical fibres continued
array splicing with etched Si chips 78−55440
asymmetric fiber power splitter 80−83661
asymmetric T-couplers for fibre optic data buses 80−102809
asymptotic theory at high frequencies of fibre with arbitrary cross section 79−1006
attenuation, bandwidth, and refractive index meas. methods compared 80−64190
attenuation, continuous meas. during manuf. 77−19400
attenuation, drawing conditions influence, expt. 78−68667
attenuation and dispersion meas. techniques and interpretation pitfalls 78−1399
attenuation and pulse dispersion due to neutron irrad. 80−58730
attenuation charact. meas. by backscatter technique *(Italian)* 80−106600
attenuation characteristics obs., by improved backscattering technique 77−75669
attenuation meas., backscatter method modified for endfire launching *(German)* 78−33868
attenuation meas. instrument 78−59138
attenuation meas. techniques *(Italian)* 78−50903
attenuation measurement, numerical aperture depend. spectral loss 78−66942
attenuation measurement *(German)* 79−76864
attenuation measurement by backscattering method, effect of noise 80−102824
attenuation measurement comparison among USA manufacturers 80−58747
attenuation measurements performed by backscattering technique 80−64152
attenuator, variable, for use in single-mode fibre transmission systems 80−99821
automated measurement system for 78−50909
automatic measurement dimensional nonuniformities, refractive index profiles 79−18541
automatic measurement fibre parameters *(Japanese)* 78−37982
avionic multiterminal data link, fibre-optic interconnection system 78−46805
axial refractive index depression in modified CVD preforms and fibres, interf. microscopy obs. 80−1319
backscatter attenuation measurements, optimised technique 80−53447
backscatter meas. theory *(German)* 80−91921
backscattering meas. using first positive system N_2 laser 78−59020
backscattering measurements, separation of power decay from imperfection contribution 79−76827
backscattering method for attenuation and connection insertion loss meas, anal. 80−58675
backscattering technique, appl. in fibre diagnostics and attenuation meas. 80−33188
band-pass attenuator 79−37003
bandwidth and backscatter measurements, review 79−64356
bandwidth change under production process and splicing *(German)* 78−33858
bandwidth determination in time domain, OTF meas., laser diode source evaluation 80−79002
bandwidth improvement due to modified CVD method *(German)* 77−54787
bandwidth limitation of system with linear intensity modulation 78−1339
bandwidth limitations due to harmonic distortion in single-mode optical fibers 79−64335
bandwidth of distorted multimode waveguides excited by laser sources 80−43436
bandwidth of multimode fibres, calc. from refr. index profile meas. 80−5817
bandwidth of single-mode fibre with AM and intensity modulation, anal. 79−81560
bandwidth spectrum of multimode fibres, depend. on refr. index profile 80−9985
bandwidth-limited operation of nonideal graded-index fibres to increase max. possible length 79−46037
baseband frequency measurement, interpretation 78−46777
basic principles and appls. *(Norwegian)* 77−72078
basic properties of multimode, single-mode, graded-index fibres *(Czech)* 79−81551
basic theory 79−32037
beam divergence on output, reduction mechanisms *(Russian)* 78−59148
beam propagation through lenslike medium of complex permittivity 77−11009
beam splitter lightwave fibre tap, use in source stabilisation 78−79105
beam to fibre coupling with low standing wave ratio 80−99822
Bell System Chicago installation 78−42434
bend loss radiation 80−33187
bend radiation calc., WKB method 78−59130
bend radiation calculation 77−46817
bent multimode waveguide, loss calcs., geometric optics method 79−37013
bent step index fibre, optical power flow 78−30092
bent step index multimode fibre, mode conversion 77−782
benzil cored fibres, void-free cryst. growth, X-ray diffr. and optical microscopy study 80−71586
bidirectional, Rayleigh scattering freq. depend. meas. 79−64317
bidirectional central couplers, for links with fibre bundles 78−46809
bidirectional coupler for duplex transmission on single optical fibre 79−37032
bidirectional fibre-optic data bus with T-couplers 77−19451
bidirectional optical systems, Rayleigh backscatt. freq. depend. 80−69511
binary phase gratings for fibre-optic communications 80−64201
birefringence, automated measurement system 79−64352
birefringence due to core ellipticity in single-mode fibres 79−68442
birefringence in fibres with elliptical cross-section 79−59816
birefringence in slightly elliptical fibres 80−106602
birefringent, Faraday rotation 80−58672
birefringent single mode fibres, linear polarisation 79−10382
bistable optical fibre switch, construction and performance 80−95994
bitaper star couplers with up to 100 fibre channels 79−76824
book, current topics in material science 80−46747
borosilicate glass single-polarisation single-mode fibres 80−64205
borosilicate optical waveguide glass, B content determ. using nuclear track counting 80−95969
BPO transmission system, feasibility trials 77−72072

optical fibres continued
Bragg cylindrical fibres, confined lossless optical propag. 78−38062
Bragg fibres, theory 79−10389
Bragg reflectors, narrow band, in optical fibres 78−79130
branch, distribution path arrangement in optical communication systems *(German)* 78−79111
branch, for multimode optical fibre system 78−46831
branching, 1:1 branch using graded-index rods, expt. 78−13811
break testing by interferometry, comparison of breaking methods 77−58491
breaking strain, estimation for long lengths of fibres 78−30060
breaking tool 78−5585
Brillouin optical fibre ring oscillator 78−1275
British Post Office optical-fibre field tests *(German)* 79−10395
broadband dual-mode, design considerations 78−94437
broadband dual-mode fibre with identical group velocities *(Japanese)* 79−59819
broadband signal response 78−33818
bundle cables termination and interconnection, use of portable tools 77−79977
bundle termination, hot crimping method with metal ferrule, glass bead 77−88912
bundles and single fibres, appls. *(Japanese)* 80−78998
buried optical cable transmission characteristics meas. *(German)* 78−33865
butt coupling in aligned vee-grooves 80−53429
butt end alignment connector 79−76834
butt-joining to Ti-diffused $LiNbO_3$ waveguide 79−76812
cable, design, performance and development projections, review 79−46069
cable, mechanical and optical properties *(Japanese)* 77−19395
cable and chuck connector optical and mech. props. *(German)* 78−33862
cable and interconnection considerations and tradeoffs 79−94363
cable attenuation and input and output efficiency 80−14469
cable connector for multifibre cables *(French)* 78−42425
cable connectors, losses, overlap design 77−7182
cable connectors, Si chips manufacture for fibre alignment 80−64188
cable construction, installation, and testing 78−46797
cable construction and jointing 77−72075
cable data highway and branch circuit 77−19453
cable design, splicing and interconnection system developments 78−42431
cable design 78−66916
cable design and manufacture 77−54780
cable design considering structural imperfection 80−64184
cable development, robust, installation and jointing development and experience 78−9460
cable developments, optical links appl. *(Japanese)* 79−27405
cable formats and construction techniques *(German)* 79−55206
cable installation methods to prevent cable damage, guidelines 78−1326
cable links field trials *(German)* 79−7206
cable pulse dispersion and attenuation meas. *(German)* 78−33859
cable reliability, deterioration factors, splice point reliability, coating materials, static fatigue life *(Japanese)* 80−99848
cable selection considerations 77−54779
cable specifications, fibre optic cable selection problem 80−28320
cable splicing, injection-moulded plastic connector 77−11054
cable stress during manufacture and installation 79−37024
cable structure, jointing procedure *(French)* 78−42459
cable structure design *(Japanese)* 79−59821
cable study by CCITT 79−90031
cable termination methods 80−53419
cable transmission and strength improvement technology 80−28347
cable units for use in ocean, design rel. to stresses 78−42439
cable vibration characteristics, fibre strain and optical loss meas. 80−99870
cabled fibre, temp. effect on transmission loss and pulse delay distortion 78−1407
cables, concatenated, connectorized, transmission losses 79−46071
cables, design, manufacture, laying and jointing *(Italian)* 80−99838
cables, historical development *(Japanese)* 80−87494
cables, longitudinal stress in fibres due to twisting in manufacture, anal. 78−30048
cables, measurement of longitudinal internal stress 79−64350
cables, origin of temp. dependence of attenuation 79−46073
cables, structure design, compressive loads and internal stress determination 79−59829
cables connections, in-the-field 80−69545
cables design and testing, w.r.t. stress-strain behaviour 80−69551
cables using reverse-lay unit-core struct., with attenuation <3 dB/km 79−46072
cables with spacers, transmission characts. and mechanical props. 79−46070
Canadian 50 km fibre-optic trunking system 79−76818
Canadian government research, role and development in communications 80−43481
capillary tubing delay lines for operation at 20 MHz 80−74654
CATV Dial-a-Program system using fibre optics, field trial in Holland 79−10262
caustic patterns for melt zones in solidified glass samples, asymmetric cases 79−22893
caustic patterns for melt zones in solidified glass samples, symmetric cases 79−22892
channel filter for fibre transmission systems, wavelength multiplexing 77−34950
channel waveguide coupling with fibres on Si substrate 78−46761
characterisation techniques compared 80−64202
characteristic modes of arbitrary profile 79−72684
characteristic parameters and production methods, data transmission application *(French)* 79−90000
characteristics and manufacture in France *(French)* 78−71201
characteristics and technology for connector engineers 78−94440
characteristics meas. using digital methods *(French)* 79−90011
characteristics measurement using optical bench equipment 80−58695
characteristics measurements, review 80−43458
chemical incompatibility of core and cladding glasses 77−75694
chemical purity in glass fibres for communication appl. 79−41437
chromatic signal distortion depend. on coherence of optical carrier 80−1317
circular arc, meridional rays, geometrical optics *(German)* 77−39048

optical fibres continued
circularly curved graded index fibre, optical beam propag. 78−25973
circulator for optical fibre transmission, using Faraday rotator and Glan-Taylor prisms 80−23769
civil and military communications prototype systems 77−27375
civil telecommunications use of optical fibre systems, state-of-the-art review 78−25979
clad, excitation by cylindrical Gaussian beam 77−42608
clad optical fibres, nondestructive interferometric meas. of α and Δ 77−84013
clad parabolic-index square-law, perturbation anal. 80−33190
clad with Teflonlike plastic coating, press. sensitivity 80−33149
clad-glass fibres, thermal stresses 80−107360
cladded fibres, inhomogeneous wave propag. 79−81531
cladded multimode, laser excitation 77−62061
cladding composition effect on stress corrosion and fatigue 77−3664
classification, transmission modes and principles 80−43428
cleaving, hand held tool 77−88907
coated, reliability testing *(Japanese)* 79−59822
coated, research on reliability of mechanical and transmission characts. 79−55234
coated, strain-induced excess loss 79−50418
coated fibre and cable unit structure optimisation 80−53466
coated optical fibre cable unit, internal stress due to compressive loads, optimum design 80−58717
coated single-mode, bending losses 78−71209
coated with UV curable epoxy acrylate, long-term mech. behaviour 78−95802
coating, secondary, rel. to transmission loss 80−58704
coating application using cylindrical bore dies, theoretical anal. of coating thickness and experimental comparison 79−46095
coating concentricity improvement by tapered nozzles *(German)* 78−38095
coating concentricity meas. and anal. 77−88898
coating structure for microbending loss minimisation 80−28346
coating technique improvement 78−5593
coating technology, overview 80−58828
coating with conical shape applicator 80−58820
coating with Ni film, on line magnetron sputtering, mechanical properties improvement 79−72723
coatings, UV-cured epoxy-acrylate, chemistry and application 78−1444
coatings centering by monitoring forward scattering patterns 80−64146
coaxial alignment system 79−37022
coherent, with dielectric core cladding, transverse and hybrid modes structure 79−14091
coloration reduction in P doped low absorpt. loss fibres 77−83968
colour multiplexing FDM 79−72677
colour multiplexing in fibre waveguide links 78−42444
coming of age of technology for telecommunication 79−98487
commercial aspects of glass-fibre technology *(German)* 79−10396
commercial developments, 1978 state of art 79−3776
commercially available, survey of characts. 77−83983
communication, components development *(German)* 79−81563
communication, conference, Amsterdam, Netherlands (Sep. 1979) 80−46733
communication, fibre cabling, light source and receiver technology, review 78−59125
communication, historical and technical features review, future prospects *(Japanese)* 80−99863
communication, research status in France 77−46814
communication, research status in USA 77−46813
communication advancements, comparison with microwave communication 79−81546
communication advances, materials and techniques 80−102853
communication appl., 1979 status and development trends 80−53408
communication appl., potential and research in Denmark *(Danish)* 78−9440
communication application, current technology *(German)* 78−22210
communication applications, in future telecommunication networks 78−22214
communication applications, microoptic grating multiplexers, optical isolators 80−48408
communication applications, trends and implications 80−33211
communication cable, commercial development review 80−1331
communication cable manufacture 80−23794
communication cables, measurement of baseband transfer function 80−1355
communication conference, Munich (1977) *(German)* 78−33854
communication development trends, review 80−69521
communication developments in Australia, PCM transmission and FDM telephony 77−65630
communication device research in Japan 77−75677
communication devices, review 77−58446
communication fibre endface preparation by AC discharge heating and stretching 80−64232
communication fibre waveguide fabrication techniques 80−1322
communication fibres and components, development and performance 80−53411
communication for military appls., review and assessment 78−42438
communication line with spectral multiplexing in 1.3 μm region 80−74504
communication lines, optoelectric systems on injection lasers 78−42464
communication lines, use of semicond. lasers and avalanche photodiodes 78−46793
communication link, 140 Mbit, experimental using GaAs laser transmitter *(French)* 78−30088
communication link, 500 MHz, using injection laser diode 77−75704
communication link, 5 Gbit/s multiplexer 78−18044
communication link, experimental loop system field trial 79−72707
communication link, long distance, injection laser transmitter appl. 78−42355
communication link between computer units, using LED-photodiode pair 78−71224
communication link component selection considerations 77−72088
communication links development in Canada, w.r.t. economics 78−42408
communication LM Ericsson system *(Swedish)* 79−55210
communication methods and field trial in Singapore 79−94361
communication receiver designs 77−68281
communication receivers 80−43460
communication sources, detectors and circuits 77−27374

optical fibres continued
communication system, A-7 ALOFT economic analysis, EM interf. and pulse tests 78−42448
communication system, cost model 78−42447
communication system, data transmission performances study 78−38028
communication system, engineering techniques for fibre optics 78−50929
communication system, interferometric with fibre link *(French)* 77−75668
communication system, measuring equipment for testing cables 79−32061
communication system appls., review of benefits 80−43480
communication system components, state-of-the-art survey *(German)* 80−69538
communication system components, USA military developments, review 79−46060
communication system components charact. and appl. *(Flemish)* 80−5836
communication system design study 78−50908
communication system performance, influence of receiver charact. 77−83984
communication system performance at 1.55 μm with single-longitudinal-mode laser 80−87556
communication system transmitters 80−43459
communication system using solid state stoichiometric Nd compound lasers 78−50786
communication system with thin-film modulator 79−10407
communication systems, analytical review including survey of commercial systems 80−74489
communication systems, book 80−73117
communication systems, charact. and component manufacture *(French)* 79−68448
communication systems, components, design considerations, economic trends and applications 79−23083
communication systems, computer design aids 80−28350
communication systems, development during next decade 80−1329
communication systems, development of fibres 80−53458
communication systems, devices and ccts., book 80−38123
communication systems, elimination of polarisation depend. in optical isolators 80−5844
communication systems, low noise regeneration using optical repeaters 78−66920
communication systems, measurement techniques for passive optical components 80−1354
communication systems, military 77−88923
communication systems, optoelectronic devices, review 79−76858
communication systems, Soviet studies *(German)* 78−25972
communication systems, use of integrated optics 80−43487
communication systems, world-wide survey 79−46059
communication systems *(Japanese)* 79−68438
communication systems analysis, digital 77−65631
communication systems appl., research and development review 77−65629
communication systems for electric power companies 78−1422
communication systems in Japan 78−46815
communication systems progress in past three years *(Polish)* 78−87152
communication systems progress over ten years and prototype systems charact. 78−55456
communication technology and interactive component functions *(German)* 79−10391
communication technology state of art *(Czech)* 78−5575
communication technology status *(German)* 78−90512
communications, fibre prod. and PO experimental link 79−37015
communications, progress review of fibre design, low-loss and low-dispersion *(German)* 80−28325
communications, prospects for 1 to 1.6 μm spectral range use 80−102848
communications applications 77−46819
communications appls., advantages and costs, introduction 78−33910
communications appls., techniques and predictions 80−87472
communications conf., EUROCON, Venice, 1977, May 78−53552
communications development and need for standardisation *(Italian)* 79−23066
communications history and prospects 80−9994
communications in industry, appls., glass fibre props., connectors 80−87550
communications link, 500 MHz injection laser diode 77−79964
communications requirements and system aspects 77−68268
communications research and technology, fibre optics 78−87151
communications source and detector props. and performance 78−22212
communications system, installation in Chicago, USA *(German)* 78−38006
communications systems, review of worldwide development 80−43468
communications technology *(German)* 79−41449
communications using optical fibres, fibre technology and props. *(German)* 79−81564
compact optical directional coupler design and test results 78−1410
compensating fibre splice technique 77−42603
complete EM field of dielectric lossy fibre excited by dipole source, numerical calc. 80−43427
component availability 78−18048
component developments 80−1356
components for optical communication systems, review 80−87539
components selection for optical links in 1979 year of fibre optics *(French)* 79−37009
compound glass, manufacturing process and fundamental charact. *(Japanese)* 80−99865
compound glass, nylon-covered, reliability and verification tests and results *(Japanese)* 80−99866
compound glass, total and scatt. loss coefficient meas. 80−69536
compound glass fibres, mode-dependent effects, total loss decomposition, absorpt. and scatt. losses 80−53437
compound glass rod absorption coeff. calorimetry 80−106631
for computing system interfaces 77−68278
concatenated fibre-optic cable, cumulative baseband frequency response models 80−78983
concentric connector for step index multimode fibre, communication systems, appl. *(Japanese)* 78−90504
concentric-core, for provision of 2 low-loss channels within single fibre 79−46081
conference, basic optical props. of materials, Gaithersburg, MD, USA (May 1980) 80−101668
conference, optical fibres and integrated optics, London, England (May 1977) 78−38063
conference, Reston, VA, USA, (Mar 1976) 77−46811
conference on laser and fibre-optics communications, San Diego, CA, USA, Aug. (1978) 79−86203
conference on measurement techniques for optical fibre systems, London, England (May 1979) 79−64348
conference on optical fibre communication, Washington, DC, USA (Mar. 1979) 79−46058
conical SELFOC fibres, third order aberration coeffs., gradient-index lens design 77−27357
connection loss, meas. method using steady-state power distrib. 79−46084
connection systems standardisation 79−68440
connections end to end, jointing instructions *(Swedish)* 79−68430
connector, charact. 78−63177
connector, damage-free, using Selfoc lens 78−46829
connector, low loss index matched optical connector 80−48452
connector design, using resilient alignment mechanisms 80−48399
connector design eliminating tolerance effects 78−46803
connector for keyboard lens finger detection 80−19095
connector for single-mode fibres, low-loss detachable *(Japanese)* 80−33163
connector for step-index multi-mode fibres, for experimental transmission systems 79−32060
connector loss evaluation by backscattering 80−58721
connector plugs, angular misalignment precise meas. 78−46770
connector system characteristics, aerospace user's viewpoint 78−46804
connector technology 79−68439
connector using low-loss lens system 78−79107
connector with centring rollers for tapered collet 79−37004
connector with fibre surrounded by resilient ferrule 79−98489
connector with less than 0.5 dB loss with monofibres *(French)* 79−37008
connectors, 1977 state of the art and development trends 77−83971
connectors, developments 78−46784
connectors, dismantleable plug connectors for single fibres *(German)* 77−54800
connectors, light sources and receivers for fibre optics, review *(French)* 79−46044
connectors, low cost resilient alignment method 78−71230
connectors, low-loss low-cost systems 79−27381
connectors, low-loss single-mode fibre connectors, detachable 79−27382
connectors, minimisation of modal noise 79−90004
connectors, nonlinear distortions and noise in optical communication systems 80−96001
connectors, retention grooves 77−19399
connectors, review 79−46075
connectors, single- and multi-fibre, basic construction *(Japanese)* 80−87509
connectors, splices and couplers, design principles 80−58765
connectors, triple ball connector, demountable 78−30065
connectors, update on standardisation 80−5830
connectors, wavelength dependent transmission loss 80−5825
connectors 1979 design approaches 80−43437
connectors alignment accuracy, influence of fibre tolerances 79−41441
connectors developments, cancellation of coupling mismatches 80−1332
connectors developments, standardised, for mass production *(French)* 79−86257
connectors in optical fibre systems 78−42414
connectors technology, 1978 state of art and development trends 79−41442
connectors theory and design 80−38122
connectors used in fibre optic transmission systems *(German)* 79−55205
contemporary optics, book 79−81353
control appls., using bidirectional optical-fibre transmission system *(Japanese)* 78−66917
controlled fusion expt. shielding and earth loop elimination 80−74007
convertors, O/E and E/O, connected to both ends of optical fibre giving low-loss, broad band, non-inductive line *(Japanese)* 80−87510
convex dielectric thin film fibre optical modes, conformal mapping 77−83996
cooling, convective, during high speed coating 80−23815
cost considerations 78−1389
cost models for A-7 aircraft ALOFT project 78−59131
coupled diode lasers, LF noise meas. 80−58542
coupled-mode theory of fibre laser-amplifier 78−66848
coupler, fabrication using splicing technique, characteristics *(Japanese)* 80−87508
coupler, low loss, for coupling LED to fibre-optic system 80−91907
coupler, multimode 3 dB low loss, fabrication 78−37976
couplers, fibre optics applications 80−28344
couplers, planar star and fused-tapered, for multiterminal data-distribution systems 79−50428
couplers, theoretical possibilities based on calculated effect of tolerances *(German)* 79−27394
coupling, fibre-to-fibre, technology review 78−9459
coupling, LED with self-aligned sphere lens 77−79939
coupling alignment by fully automatic system 77−79949
coupling and transmission charact. 78−79121
coupling and transmitting techniques *(Dutch)* 77−75689
coupling between single-mode fibres and integrated optical components, novel method and appls. 80−43442
coupling components for single optical fibers 77−79957
coupling efficiency analysis, single fibre connector design appl. 78−46766
coupling efficiency and surface damage threshold for giant and free-running laser pulses 80−33212
coupling efficiency of semicond. laser beam into fibre, matching element misalignment influence 80−48432
coupling from semicond. laser to single-mode fibres, cylindrical lens method 79−76807
coupling from thin film to fibre 78−87167
coupling length due to random bending in multimode optical fibres 78−63195
coupling light efficiency, from GaAs laser diodes into parabolic-index fibres 78−94435
coupling loss due to displacement, separation, misalignment, automatic measuring technique 79−32036

optical fibres continued
coupling methods, optical fibre waveguides, transmission systems appl. *(German)* 77−19416
coupling methods in single mode fibre integrated optics systems, review 78−59162
coupling of light from Lambertian source, using spherical lens, coupling efficiency calc. *(Japanese)* 78−42407
coupling of semiconductor lasers, efficient coupling using taper-ended multimode optical fibres 77−3657
coupling of single-mode fibres, simple method for permanent connection 77−72097
coupling parameters and techniques, survey *(German)* 80−38108
coupling techniques *(German)* 80−28330
coupling to As_2S_3 radiator bonded LED's with optical guide struct. 77−39043
coupling to channel waveguides on Si 77−88915
coupling to GaAlAs laser, high efficiency 77−7173
coupling to high index optical waveguide, method 77−19393
coupling to semiconductor laser using cylindrical Selfoc lens combination 77−79931
coupling using fibre fusion splicing set 79−27383
coupling using graded-index rod lenses 80−91891
coupling using tapered microlens, high efficiency *(Korean)* 80−43449
crosstalk between light pipes, mode theory 77−785
crosstalk in bidirectional fibre, review 78−66901
crosstalk meas. for end-to-end cross coupled fibre link 78−90502
cruciform section optical fibre in single material 77−39046
current measurement appl. 80−96015
curved, intensity modulation of transmitted light, coupled-mode theory 77−75672
curved, single mode, radiation of discrete beams 78−18041
curved graded-index fibres as image relays, aberrations 79−55219
curved multimode waveguide, geometrical optics shape of nonmeridional rays *(German)* 78−5566
curved single-mode fibre, field deformation 78−37972
curved single-mode fibres, discrete beams of radiation, anal. 77−75671
curved single-mode fibres, propag. characts. 78−66934
curved single-mode fibres radiation loss, meas. 78−74984
curved step index fibre, integrals 78−1340
cutoff wavelength meas. method for HE_{21}-, TE_{01}-, TM_{01}-modes 79−76820
cutting tool 80−1360
cutting tool 80−33255
cutting tool and automatic splicing machine 80−87575
cutting using handheld tool, flat-surface waveguide ends preparation 79−37062
cutting with hot metal wire 77−19462
CVD, high deposition rate method using He gas 77−11055
CVD fabricated, abrupt central dip in refractive index 78−22217
CVD fibre, long length strength 80−58752
CVD fibres having surface compression, fatigue characts. 79−46064
CVD modified system for optical fibre fabrication, computer-aided *(Japanese)* 79−59852
CVD-fabricated with refractive index dip on fibre axis 77−11004
cylindrical, mono-mode, multi-mode and Selfoc types, props. comparisons 77−31127
cylindrical fibre with symmetric index distrib., matrix analysis 77−84001
cylindrical optical fibre transmission and guided mode behaviour 80−28348
data and telemetry links 79−27390
data bus, eight-terminal optical fibre, using T-couplers 78−59129
data bus system design and implementation 77−7017
data bus system optical coupler with light conducting fibres *(German)* 80−43438
data bus system with single multimode fibres, planar coupler 77−79927
data bus systems appl. 78−25949
data bus T-system, single multimode fibre, based on access coupler 78−46810
data buses, angle optical fibre, signal distribution systems and crosstalk isolation 79−3802
data collection highway with piezoelectric phase modulators 77−39098
data collection line coupling methods *(German)* 77−62062
data communication field optical fibre appl. *(Italian)* 79−50388
data communication technology using low-loss fibres *(German)* 77−46800
data communications appls. 79−72676
data distribution system using variable tap ratio couplers 77−83953
data link, 137 Mb/s, using LEDs, material dispersion limited operation 77−88908
data link, fibre optics, radiation testing, degradation, transient outage time performance 77−19405
data link, high bit rate, using InGaAsP 1.3 μm LED 78−46825
data link components, ccts. 78−30054
data transmission, principle and methods 79−10393
data transmission, using inexpensive fibre links 78−42413
data transmission links *(Danish)* 80−10009
data transmission principle *(German)* 79−81529
data transmission systems, single fibre separate connectors, loss factors 77−88939
data transmission systems appl., in defence 77−75670
data transmission systems for plasma diagnostics 80−79571
data transmission technology, advantages over elec. cable 77−7196
data-bus system paired optical-fibre switch 80−23791
defects, on-site location and transmission loss eval. 79−3801
defence applications of fibre optics in UK 78−42440
deformation of cable sheath by bending in plastic range, loss anal. 80−43477
delay distortion characts. of fibre splices 77−34933
delay line stability, pulse delay in jacketed, unjacketed fibres, stress and temp. depend. 79−55232
delay lines, for pulse coding 77−83970
delta measurement by refr. index tuning 78−13792
demand explosion, review 77−46812
demountable connector using injection-moulded thermoplastics 80−53472
demountable moulded optical-fibre connectors using rods and balls 79−64323
demountable multiple connector with precise V-grooved Si 79−76822
demountable optical fibre connector design and fabrication *(German)* 78−38010
demountable triple ball connector 78−13795
demultiplexer for wavelength division multiplexing system 79−64309
optical fibres continued
design, mech. props. and performance tests and practical applications *(Japanese)* 80−99867
design considerations, short distance communication system appl. *(Italian)* 77−42601
design considerations using commercial fibres 77−19421
deterioration due to US cleaning 78−33821
development, advantages and applications 80−53410
development, present state *(Italian)* 79−10398
development for long wavelengths *(Danish)* 80−14434
development in fibre technology for 850 nm utilization *(Polish)* 79−76857
development of basic units for PCM transmission *(Dutch)* 79−68365
development trends, integrated optics vs. integrable optics 77−65643
devices and materials for 4 μm-band communication 78−94441
devices for communication systems, demountable connector, fibre switch, and fanout couplers 78−74989
DH injection laser coupling to optical fibre waveguide 78−33851
diallyl isophthalate-methyl methacrylate copolymer, light focusing rod prep. by copolymerisation, refractive index distrib. const. *(Japanese)* 79−46042
diameter checking, laser interference method 78−18080
diameter meas., high speed noncontact light scatt. technique 77−83956
diameter meas. using computerised forward scattered light system 78−62176
diameter meas. using microprocessor based system 78−1443
diameter meas. with He-Ne laser 79−97352
diameter measurement and characterisation system, high speed 77−88920
diameter measurement using fast Fourier transform 80−91894
dielectric, of noncircular cross sections, fundamental mode propagation computing 79−76874
dielectric fibre guides, nonspectral field representations 78−79116
dielectric slab and fibre waveguides, dispersion props. approximate formula 79−55217
dielectric tube waveguide, cutoff freqs. derivation under weak guidance 78−18059
dielectric waveguide hybrid and transverse mode dispersion calc. *(Russian)* 80−99857
differential delay time relationship with propagation mode number study by effecting selective mode excitation *(Japanese)* 80−87504
differential group delay in graded-index fibres, wavelength dependence and appl. to fibre-link characterization 79−50440
differential interferometry, optical characteristics determination 80−48397
differential mode delay rel. to refr. index profile, geometrical optics treatment 80−69529
differential wave attenuation in graded-index fibres, observation using OTDR 79−46085
diffraction of light by laterally illuminated optical fibres 78−50915
digital data bus interconnect system techniques 78−13793
digital data transmission, design criteria and experimental results *(Rumanian)* 78−46791
digital fibre optical communication system, average error probability calc. 80−53228
digital fibre-optic transmission system average error probability 77−27380
digital optical fibre communication link for 1 Gbit/s *(German)* 79−81565
digital optical fibre system, 4-level, using LED, meas. at 68 Mbit/s 80−1313
digital system, error probability with inter-symbol interference and additive noise 79−89855
digital techniques for evaluation of optical fibres 79−94346
digital transmission, shot noise probability distribution function 78−50717
digital transmission appl., commercial components survey *(French)* 79−90007
digital transmission appl., components manufacturers and selection *(French)* 79−94333
digital transmission error probability, quantum noise effects *(Italian)* 77−23623
digital transmission for wavelengths beyond 1 μm, silica fibre waveguides 78−50907
digital transmission system, 2 km, for field use at 20 Mb/s 78−38064
digital transmission system, expt. 78−66943
digital transmission systems, optical fibre cable, technological advances *(French)* 77−11020
m-dinitrobenzene, electrooptic cryst., growth in monomode optical fibres 80−55288
m-dinitrobenzene cored fibres, void-free cryst. growth, X-ray diffr. and optical microscopy study 80−71586
diode-laser-fibre coupling, effects of fibre propagation loss 80−74484
direct picture transmission in single optical fibre, restoration with holographic filters 79−89871
direction coupler, interference filter all-fibre for wavelength division multiplexing 80−91900
directional coupler, 10 dB 77−19452
directional coupler developments and applications 79−94330
directional coupler theory, accuracy in fibre or integrated optics appls. 79−3810
directional coupler with lapped multimode fibres, characts. 80−91892
directional filter structure and characteristics for bidirectional transmission 80−58734
discrete radiation from curved single-mode fibres, comparison of theories 78−33847
dispersion, waveguide and material, interdepend. 79−98470
dispersion characts. from baseband freq. response meas. using InGaAsP laser beam 80−1308
dispersion meas. with Nd:YAG laser at 1.06 to 1.6 μm 80−87555
dispersion measurement, by coherence propagation obs. 77−46816
dispersion measurement by mode-locked synchronously-pumped dye laser 80−64191
dispersion minimisation in single-mode fibres between 1.3 μm and 1.7 μm 79−76832
dispersion-free single-mode fibre in 1.5 μm wavelength region 79−76831
dispersion-free single-mode fibre transmission experiments up to 1.6 Gbit/s 79−59812
dispersive, multimode, optimum index profile 77−23757
dispersive multimode fibre, optimum index profiles for digital communication 77−7192

optical fibres continued
distortion of light pulse, method using interference of exciting laser beam 79−3788
distortionless propagation of 5 psec-wide pulses in km-length optical fibres 79−94358
distributed microcomputer control system for high-energy gas-laser facility 77−61975
doped silica glass, ultimate low transmission loss window in IR region 77−11023
doped-silica optical fibres, nuclear radiation effects 80−33172
double eccentric connectors 77−58442
double layer, pulse response due to boundary inhomogeneities between core and jacket 78−30089
double-core single-mode, as directional coupler 80−106597
double-mode, meas. of propag. characts. and zero intermodal dispersion 79−46079
double-mode, propag. characts. 80−99834
doubly clad, excitation by misaligned Gaussian beams 78−74972
doubly clad W-type, microbending losses 77−88899
doubly clad W-type, range of monomode operation 79−7212
drawing, by different heating methods, cooling rates 80−66538
drawing, semi-automatic machine development 79−27449
drawing, split beam CO_2 laser heat source 77−19465
drawing facility for lightguide fibres 80−64229
drawing from compound glasses, using double-crucible and glass-plastic methods 79−3815
drawing of seven optical fibres simultaneously from a double crucible 78−33920
drawing of smooth fibres, diameter control improvements 78−1445
drawing out from blanks, high temperature resistance oven 80−74491
drawing process, control of fibre diameter 79−50468
drawing process, diameter control 78−13794
drawing process control, optimisation theory appl. 79−90039
drawing technique for bundle of 19 fibres drawn from double crucible 78−55480
drawing techniques, 1 km length fabrication 79−18557
drawing techniques, effect of thermal fluctuations *(Japanese)* 78−37980
drawing techniques for plastic-clad and doped-deposited silica fibres 79−37066
drawing using laser, galvanometer beam-scanning rotating lens system 79−41463
dual beam fibre optic time-of-flight spectrometer 80−52347
dual three-rod connector for single fibre optics 79−36987
dual-mode fibre, spatial technique for modal delay difference meas. 80−78950
duplex fibre-optic cable interconnection system 78−46801
dynamic fatigue and strength degradation 80−58719
economic advantages of using optical links, compared with wire cable 79−10385
electro-optical devices for multimode optical switching 79−76882
electro-optical multiplexer for large-numerical-aperture low-loss fibres 77−83993
electronic interconnection system design 80−5828
electrooptic polarisation switch for multimode fibres 77−27335
electrostatic fibre holder 77−72095
elliptical, unclad, refractive index and ellipticity meas. 77−14797
elliptical dielectric waveguides, higher-mode cutoff 80−43432
elliptical dielectric waveguides, higher-mode cutoff conditions 79−98479
elliptical fibres, near-field correction factor 80−87490
elliptical multimode fibres, leaky ray correction factors 80−87487
elliptical multimode fibres, whispering and bouncing mode evaluation 80−10015
elliptical selectively excited, near-field distrib. 80−48401
elliptical square-law medium, astigmatic Gaussian beams 78−94427
elliptical step-index, tunnelling-radiating effect 80−58714
elliptical step-index multimode fibre, rays and modes 80−14442
elliptically clad borosilicate single-mode, strain birefringence 80−33148
encoding-decoding fibre network 78−25963
end face cut prep. and inspection techniques, review 80−74483
end face quality check 80−64164
end fire coupling between fibres and diffused channel waveguides 77−79922
end fracture torsion effects 79−76802
end preparation and fusion splicing of fibre array with CO_2 laser 80−10051
end preparation using CO_2 laser 78−55478
end-fire coupling between optical fibres and diffused channel waveguides 79−86252
epoxyless connector, for single fibre cable 79−37040
equaliser with shaping filter, nonlinear, optical communications appl. 78−30052
equalising and nonequalising optical fibre system repeaters, comparison 77−3655
error probability anal. of digital fibre optic communication systems 78−46775
error probability calc. in communication channel with intersymbol interf. 80−53227
evaluation of normalised cutoff frequencies in radially inhomogeneous fibres, perturbation theory 80−43434
evanescent wave coupling in fibre optic connectors 79−72668
excess loss increase mechanism of jacketed fibers at low temperature 80−83682
excitation by lenses 79−32057
excitation by partially coherent sources, geometric optics theory 77−79948
excitation by polychromatic partially coherent sources 77−31131
expanding horizons, appls. and advantages 78−46782
experimental 140 Mbit/s optical fibre transmission system, preliminary test results 77−68261
experimental link operating at 140 Mb/s 78−1321
fabrication, attenuation, packaging and interconnection properties 77−27373
fabrication, low OH content, vapour phase axial deposition method 78−83125
fabrication, vapour-phase axial deposition, simultaneous dehydration with consolidation 80−23780
fabrication and construction of secondary coating for optimised design *(Japanese)* 80−87567
fabrication and coupling of fibres and cables *(French)* 79−68447
fabrication and drawing processes 78−90532
fabrication by improved CVD method 77−79976
fabrication by improved CVD method 78−1448
fabrication by isothermal plasma-activated CVD *(German)* 78−33928
fabrication by vapour phase axial deposition, 1.3 μm, low-loss and wide bandwidth 80−38136
fabrication method *(Japanese)* 79−27448
fabrication processes and transmission characts. *(Japanese)* 80−87496
fabrication study for long wavelength region *(Japanese)* 80−87499
fabrication using phase separation and leaching method *(French)* 80−106623
fail-safe fibre optics data bus using active electrooptic mirror terminals 79−23053
Faraday effect in single-mode optical fibre using injection DH laser light source 80−48245
fatigue characts. improvement, using surface compression cladding 80−69549
fatigue strength, environmental and temp. effects 78−46835
fatigue strength and flaw size distribution for strong fibres 77−11056
fatigue strength meas. of screen tested fibres 80−19098
fault detection using optimal time domain reflectometer 79−54173
fault location and backscattering meas. 80−64183
fiber-optic measurements, using standards and instruments 80−74488
fibre connectors, hot forming versus epoxy bonding of bundles, single fibre techniques 78−42482
fibre data transmission system, operational 18-channel 78−46823
fibre laser gyroscopes 77−46728
fibre optic connectors, precision and stability developments 80−69523
fibre optics in telephone carrier systems 79−81528
fibre preform, high silica, continuous fabrication process, for step index fibres and graded index fibres *(Japanese)* 78−37978
fibre-optic communications components and systems 77−50752
fibre-photodiode alignment by etched Si structure 80−53430
Fibredyne systems for passive or semipassive fibre-optic sensors 78−71206
field distribution in square law medium for incident Gaussian beam 78−74840
field distribution of a point source inside a lossy optical fibre 80−10044
field measurement of splice loss applying backscattering method 80−19091
field plotting of optical fields using single-mode optical fibre 78−30097
field trial, Bell Telephones Chicago test, results *(German)* 78−74990
filament waveguides for signal transmission in far IR region *(Czech)* 80−96017
filled 10-fibre cable, epoxy/fibreglass central strength member, optical links appl. 80−43470
filled cable for telephone trunk system, viscous polyurethane filling 79−72708
film deposition on fibre end, thickness monitoring with optical time-domain reflectometer 79−55254
filter, single mode fibre birefringent 80−58713
finite difference methods for propag. parameters calc. *(Russian)* 80−64189
flexible, glass and polymer types, manufacture *(German)* 79−27393
floating zone crystal growth for IR optical waveguides 80−79019
fluidised bed probing using optical fibres 80−19533
FM analogue signal transmission system, advantages *(German)* 80−58679
FM transmission system, laser-diode noise 79−45968
formation from tubular blank, process optimisation 77−75719
formation of microcapillary by pulling from billet, azimuthal asymmetry effects, theory 78−87172
four-wave mixing, image phase compensation and real-time holography 78−63039
fractographic anal. of fracture surface, after proof stressing, SEM exam. 78−38093
fracture behaviour and strength, investigated using fracture mechanics *(Japanese)* 79−59817
fracture strength and degradation factors 78−1383
fracture stress and mirror size obs. 79−37020
fracture surface anal. 80−58754
Fraunhofer diffraction by bundled fiber-optical waveguides 78−25978
frequency response meas., combined time/frequency domain technique 79−76809
full duplex transmission link over single strand optical fibre 78−1341
full-duplex single-strand multimode system, max. achievable crosstalk isolation 78−50923
fundamental mode propag. on fibres of arbitrary cross section 80−43443
furnace drawn, tensile strength 80−58751
furnace drawn silica fibres, contamination reduction 78−33918
fused silica, GeO_2-, P_2O_5-, B_2O_3-doped, IR characts. *(Japanese)* 78−37981
fused silica fibre link from telescope to spectrograph, operation and prospects 79−53721
fusing of data highway junctions 77−39097
fusion splices by discharge heating 78−75007
fusion splices for single-mode optical fibres 78−83126
fusion splicing machine for optical fibres 80−74516
fusion-spliced optical fibres, tensile strength 78−87140
fusion-welded optical fibre splice loss expts. 79−37023
future developments, impact on 'next generation' of electronic equipment, data ring concept 80−102808
gamma irradiated, radii and refr. index changes 80−1338
gamma radiation-induced optical loss, spectral dependence, 0.45-1.75 μm region 79−50421
gamma-irradiated, differential interferometric meas. of refr. index changes 80−78952
gas-dielectric fibre, wave conversion in irregular portion 80−74500
Gaussian beam scattering characts. at dielec. media interface 78−42275
Gaussian pulse transmission through monomode fibres, source linewidth effect 78−83073
geometric perturbation detection, fibre radius meas. method 77−42592
geometrical and optical parameter meas., laser method 77−18062
geometry specifications rel. to measured fibre statistics 79−27371
germanosilicate, single polarisation, strain birefringence 80−1314
glass, 672 digital voice channel communication system 77−14662
glass, analogue data transmission system *(German)* 80−23781
glass, complex transfer function determ., test *(German)* 77−27366
glass, epoxy-acrylate coated, strength and static fatigue 78−1386
glass, flaw generation and strength, dust particle effects 77−23741
glass, for communications, colloquium, London, England (Jan. 1979) 80−67930

optical fibres continued
glass, for optical waveguide communication, state-of-the-art review 77-62052
glass, low-loss, for optical communication, fabrication technologies state of art 79-10420
glass, multicomponent fibres prep. with high numerical aperture 78-55445
glass, multimode, light propagation calc. *(German)* 77-62070
glass, phase separated, opt. props. of elongated phases 78-27179
glass, production methods for optical communications *(German)* 80-23813
glass, similarities with waveguide transmission, scalar approx. *(German)* 77-34942
glass, smooth fracture faces manufacture using incandescent wire 78-38098
glass, tensile strength testing, Weibull statistics 78-59128
glass, UV-cured, epoxy-acrylate coated, environmental effect on long-term strength 78-5582
glass absorption filters with bandpass characts. for green region *(German)* 77-34943
glass and plastic fibre characts. and interconnection requirements 80-69513
glass assessment, low absorption coeff. meas., calorimetric method 77-58405
glass core/polymer cladding, high numerical aperture 80-96024
glass CVD fibres with axial refractive index dip, dispersion meas. *(German)* 78-33857
glass fibers, production for fibre optics, exam. *(Polish)* 78-83130
glass fibre, continuous coating applicator 77-3659
glass fibre, forming process, characts., anal. techniques 80-58827
glass fibre, loss, mechanically induced periodic bends effect 77-3668
glass fibre, strengthening by molecular stuffing 80-58830
glass fibre, vapour phase materials and processes, review 80-58825
glass fibre attenuation characts., light-wave propag. communication *(German)* 80-95997
glass fibre branch couplers for optical data bus *(German)* 79-89999
glass fibre cables for field trials, meas. methods *(German)* 78-50922
glass fibre communication: introductory review, status and development *(German)* 79-89997
glass fibre cutting device *(Italian)* 78-50951
glass fibre development, large-core, for military appls. 80-48451
glass fibre development and prospects 78-9453
glass fibre drawing, fluid-dynamic stability analysis 77-11053
glass fibre drawing process, characterization and control 80-58826
glass fibre drawing process, extensional instabilities 80-89258
glass fibre experimental cable, used between telephone exchanges by German Post Office *(German)* 79-64326
glass fibre for optical communications, statistics of tensile strength *(German)* 80-38121
glass fibre long wavelength optical communication, materials and devices, review 80-99854
glass fibre manufacture, double-crucible and plasma methods 77-50763
glass fibre manufacture using CVD *(German)* 78-33933
glass fibre optical channel for nanosecond pulse transmission 77-62064
glass fibre optical waveguides, materials systems, fabrication and charact. 77-19394
glass fibre performance specification for optical communication *(Dutch)* 78-83112
glass fibre preforms, elastic stresses 79-64343
glass fibre properties for information transmission *(German)* 78-9439
glass fibre refractive index profile meas. using interf. microscope with freq. shift 80-64175
glass fibre thickness meas. and control system in production *(German)* 80-10052
glass fibre waveguide, γ-irrad., reversible optical bleaching of induced absorpt. 80-14462
glass fibre waveguide, losses below 1 dB/km 78-50936
glass fibre waveguide, transmission props., theory *(Swedish)* 78-90525
glass fibre waveguide drawing using CO_2 lasers 79-59857
glass fibre waveguides, light propagation, dispersion properties *(German)* 79-89996
glass fibre waveguides fabrication, mech. props. 77-23766
glass fibreguides, for lighwave communication, fabrication and characterisation 80-50586
glass fibres, fatigue failure prediction, appl. of fracture mech. theory 79-998
glass fibres, fatigue failure probability 79-32045
glass fibres, flaw generation by indentation fracture technique 80-81156
glass fibres, multicomponent and high SiO_2, thermal variation of attenuation 79-50390
glass fibres, tensile strength and fatigue 77-3662
glass fibres for optical data transmission *(Dutch)* 77-11036
glass fibres from a single material 78-33897
glass fibres used for optical transmission systems *(German)* 80-69516
glass fibres with dominant material dispersion, pulse broadening and distortion, wavelength depend. 79-10394
glass optical waveguide fibres, propagation theory, review 79-90015
glass systems used for optical fibres, diffusion kinetics 79-90040
glass-clad optical waveguides, ionizing radiation effects, temp. depend. 79-18519
glass-fibre optical communication systems 77-50762
glass-fibre waveguides, dependence of overall losses on coupling-in angle of radiation 79-98504
graded core W-type fibre and its propagation characteristics 80-1334
graded fibres, mode propag. time calc. using multimode theory *(German)* 80-58710
graded fibres with non-circular index contours, core fields 80-14455
graded glass fibre, effect of shape of refractive index profile, on distortion 80-33197
graded index, 0.95 Gbit/s PRS signals regeneration after transmission over 0.91 km of fibre, regeneration cct. 79-59807
graded index, baseband freq. response meas. 79-41439
graded index, connectors and splices, transmission loss estimation 79-18550
graded index, fabrication techniques on MCVD method *(Japanese)* 79-59851
graded index, fabrication techniques using MCVD and refractive index profile control 79-59856
graded index, for matching injection lasers to optical fibres 79-32069
graded index, Gaussian approx. of fundamental modes 78-66907
graded index, guided modes, asymptotic theory 78-9447

optical fibres continued
graded index, high index hemispherical microlens tip melt fabrication for coupling to GaAlAs laser 80-69506
graded index, impulse response based on mode coupling coefficient 80-58705
graded index, intermodal dispersion meas. 80-38115
graded index, low temp. dependence of loss increase due to nylon jacket shrinkage, optimum cable unit 80-64182
graded index, M-like refractive index distrib., light pulse dispersion 78-71225
graded index, minimum impulse response 77-68258
graded index, mode coupling due to perturbation of index profile 80-106598
graded index, profile, dispersion effects on transmission bandwidths 78-22198
graded index, selective mode excitation 78-37970
graded index, soln. of wave eqns. using modal approach 79-36995
graded index, transmission characts. computation 78-42454
graded index, wave eqn. for propag. fields 80-58757
graded index, wavelength depend. of modal dispersion 78-63173
graded index, with GeO_2-P_2O_5-SiO_2 core, prep. by modified CVD technique 77-88910
graded index and step index design, practical problems *(Swedish)* 78-25988
graded index CVD fabricated fibres, dispersion with finite number of layers 79-3769
graded index diameter determ. from backward scattered pattern 80-5820
graded index fibre, error estimates fo first order WKB calc. method 80-87488
graded index fibre, light pulse propag. *(Czech)* 79-98501
graded index fibre, new form of characteristic eqn. *(Italian)* 78-50901
graded index fibre, optical communication expt., 1.12 Gbits/s PCM 77-83967
graded index fibre, random bends, variational soln. of power flow equation 79-18549
graded index fibre cable links installed in operational ducts, transmission meas. 78-50928
graded index fibre cable transmission performance in operational ducts *(German)* 78-33864
graded index fibre optical loss meas. using dummy fibre 80-5819
graded index fibre propag., impulse response, expt. and theory 78-90496
graded index fibres, excitation of bound and tunnelling rays 79-55218
graded index fibres guided propag., asymptotic theory of inhomogeneous waves 78-66941
graded index fibres made by vapour phase axial deposition, refr. index profile 80-48477
graded index fibres optical loss, influence of fibre structure, expt. 78-33846
graded index fibres with mode scramblers, spliced, OTF 78-33832
graded index low-loss fibres for wavelengths beyond 1 μm 79-50383
graded index multimode fibres, cladding loss effect 78-50927
graded index P_2O_5 doped CVD fabricated silica fibres, reduction of OH-ion conc. 80-1310
graded index radially inhomogeneous single mode fibre, cut off freq. calc. 77-19401
graded index rod lens applications in optical fibre communications 80-14485
graded index single-mode fibres, spot size profile independent representation, determ. 79-50380
graded index waveguide, pulse broadening, cladding effect 77-79924
graded index waveguide problem soln., comparison of wave and ray techniques 78-59140
graded monomode fibres and planar waveguides, analytical characterisation 80-43435
graded noncircular multimode, attenuation const. of leaky modes 80-33160
graded noncircular multimode fibres, leaky modes, analytical ray theory 80-33192
graded refractive index optical fibre process 79-76836
graded single-mode fibres, dispersion 79-59810
graded weakly guiding fibres, fundamental HE_{11} modes 80-43444
graded-core, propagation characts., numerical description 77-23758
graded-index, advances in production using phase-separable glasses 79-50465
graded-index, cables, transmission expts., 1.2-1.6 μm wavelength range 80-102813
graded-index, compensation of profile dispersion 80-1316
graded-index, differential mode attenuation meas. 78-71198
graded-index, exact field expressions for guided modes 78-74977
graded-index, for optical transmission system field trial, investigation of MCVD and VAD processes 80-43462
graded-index, for transmission, optimum design of fibre struct. 79-46080
graded-index, fundamental mode microbending loss 77-23762
graded-index, geometric optics approach to light acceptance and propag. 77-23756
graded-index, light propag., Helmholtz eqn. soln. 79-27372
graded-index, manufacture, double-crucible method 80-83688
graded-index, mode eigenfunction computation propagating beam method 80-95988
graded-index, multimode, differential mode delay and attenuation meas., optimal excitation calc. 80-99842
graded-index, multimode, interconnection 79-90037
graded-index, optical loss meas. in the field 80-102851
graded-index, partially excited, pulse dispersion 77-11033
graded-index, propag. consts. and group delays 80-23770
graded-index, propag. consts. and group delays of guided modes 79-98464
graded-index, semiconductor laser sources for coherent optical-fibre systems 80-64159
graded-index, spliced, leaky modes effect 77-39022
graded-index, tunnelling rays in pulse propag. 78-18057
graded-index, with near parabolic-index profiles, mode dispersion 79-76873
graded-index, with refractive index bump, pulse response and microbending losses 77-42602
graded-index curved media, generalised Fresnel power transmission coefficients 80-102815
graded-index fibre, spatial degree of coherence 80-53441

optical fibres continued
graded-index fibre cables, transmission meas. in 1.2 to 1.6 μm range 80−10037
graded-index fibre differential mode attenuation meas. 78−1403
graded-index fibre excited by step-index fibre, baseband freq. response 80−99829
graded-index fibre link, baseband bandwidth estimation for spliced system, empirical formula 80−53460
graded-index fibre material dispersion evaluation using nanosecond pulse radiator 79−81520
graded-index fibre modal power distrib. determ. from near-field patterns 79−81518
graded-index fibre propag., ray optics approach 79−76849
graded-index fibre transmission characteristic computation 80−1321
graded-index fibre vapour-phase axial deposition method, fibre characteristics 80−58824
graded-index fibre with polynomial-profile core, propag. constants of guided modes 80−10005
graded-index fibres, analytical relations between model power distrib. and near-field intensity 80−9995
graded-index fibres, evanescent theory and perturbation theory comparison 79−32033
graded-index fibres, mode analysis using scalar wave eqn. and direct numerical integration 80−78971
graded-index fibres, near-optimum, pulse broadening 79−7213
graded-index fibres, nonlinear profile dispersion aids optimisation 77−68265
graded-index fibres, refracting leaky rays 78−79103
graded-index fibres, transmission charact. 78−66938
graded-index fibres for optical transmission system, investigation of MCVD and VAD methods *(Japanese)* 80−58692
graded-index glass fibres for optical communication, light propag. props. 78−83106
graded-index monomode fibres with elliptical cross-section, birefringence 80−53416
graded-index multilayer low-pulse-dispersion fibre with medium numerical aperture, fabrication 77−79937
graded-index multimode, distortion of light signals 80−19092
graded-index multimode, non-repeatered 50 km transmission experiment using low-loss optical fibres 78−79108
graded-index multimode fibres, bandwidth charact., appl. on long-haul transmission systems 80−64180
graded-index multimode fibres, dispersion calc. by propag. beam method 79−98465
graded-index multimode fibres, launch depend. loss in short lengths 78−90495
graded-index multimode fibres, transmission charact., expt. 78−66937
graded-index non-circular fibres, ray theory 79−55229
graded-index noncircular fibres, geometric optics analysis 79−55231
graded-index optical fibre bandwidth factors and progress 78−1390
graded-index optical fibre intermodal dispersion, frequency-domain meas. 80−58729
graded-index optical fibres, ray optical paths and relative delays, calcs. 79−89987
graded-index preform refr. index ratio and gradient profile determ. from laser beam refr. 79−81519
graded-index single-mode, expt. characterisation using far-field radiation pattern meas. 80−64150
graded-index slab and fibre waveguides, bent, power attenuation 78−87134
graded-index VAD fibres, transmission loss meas. using laser diodes 80−87486
graded-index waveguide coupling and matched joining, coherent states and light propag. 80−102625
graded-index with non-power-law refractive profiles, group delay calc. 77−14796
graded-index with polynomial profiles, propag. charact. 80−38118
gradient index, refr. index profile influence on transmission quality 78−42453
gradient refractive index fibres, optical charact. 77−787
gradient-index, numerical analysis of waveguide characteristics *(German)* 78−5550
gradient-index fibre array, appl. in copying machine 80−69500
gradient-index fibre array, unevenness of illuminance 80−69482
gradient-index fibre lens, radiometric props. 80−69481
gradient-index light-focusing, image enhancement 80−69501
GRIN, leaky modes, WKB method 77−7180
grinding and polishing productivity, diameter depend. 77−62067
grooved chips, for fibre-optic array splice improvement 77−19456
group delay differences in waveguides with graded index profiles *(German)* 78−50906
guided wave optical systems and devices, conf. Washington DC, USA, 1978, Mar. 79−37031
guided-wave optical systems and devices, seminar, Washington, USA (April 1979) 80−31418
gyroscope, based on Sagnac effect, background and development *(German)* 80−48431
half-duplex optical transmission link using LED source-detector scheme 78−71214
heat transfer in laser drawing 79−94377
helically deformed optical fibre, radiation loss calcs. 77−786
hermetic seal, fibreguide to metal, using Cu tube component 78−83120
hermetic seal, optical fibre-to-metal, construction 78−83078
heterojunction lasers for fibre optic appls., technological advances 79−36933
high bandwidth graded-index, propag. consts. meas. related to material props. 80−38103
high capacity communications system operating at 44.7 Mb/s, devices and perform. 77−27382
high capacity telephone link, fibre cable, Hitchin to Stevenage, 140 Mbits/s *(German)* 77−72079
high density, parallel transmission system for data transmission *(Japanese)* 80−87507
High Density Connector Interface, fibre optic link 80−91901
high numerical aperture multicomponent glass fibres 80−78949
high quality optical fibre cable for telecommunication 79−37029
high speed signal processing, optical and acoustic integration 78−51012
high strength hermetically sealed metal coated fibres, expt. 78−66929
high tensile strength, furnace drawing method 78−68666
high tensile strength, prep. using thermosetting plastic coating, expt. 78−63211

optical fibres continued
high-density low-loss optical fibre unit and cable 80−53468
high-speed drawing effect on optical-fibre losses 79−14095
high-speed optical systems at 0.85 μm, modal noise and optical feedback 80−87323
high-strength fibre production and prooftesting 80−64204
high-temperature fatigue strength and OH stress-induced corrosion 78−1387
hollow light guides, dielectric-type, light transmission characteristics, minimum losses *(Russian)* 79−98503
hologram recording, Fourier high-data-density, using glass fibres 79−10271
holograms as optical branching elements 77−10870
holographic appl., exit and radiation, reference and/or illuminating wave 78−17884
holographic coupler for optical-fibre-bundles expt. 78−42419
holographic couplers for optical fibre bundles 78−25839
holographic elements for practical fibre bundle couplers 78−46550
homogeneous, large aperture bundle tied by helix of metal or glass filament, light propag. anal. 78−87154
homogeneous optical fibres with deformed boundaries, modal anal. 79−59824
hybrid digital optical fibre transmission system, terminal equipment and reshaping/regenerative repeaters *(German)* 78−33880
hybrid fibre optic/electrical connector, environmentally sealed, multispin, cylindrical 79−41457
hydrophone, optical, for sonar, development 79−3832
hydrophone sensitivity anal. 79−14191
hydrophone using high-linearity multimode optical fibre sensor 79−68429
hydrophones, comments on mechanism of transduction 80−58882
illuminating fibre bundles, improved charact. due to glasses type VS 1637 and VO 720 80−102844
image and hologram transmission by 1D fibre tape, using chromatic encoding *(French)* 79−3785
image transmission and resolving power of fibre bundle *(Korean)* 79−14102
imaging multifibre misalignment MTF 79−14093
imaging plastic focusing fibre with parabolic refractive index distribution 77−19437
imaging properties, parabolic index glass rods and fibres 77−42599
immersed in high-index surrounding medium, attenuation 77−42614
impulse response meas., refined deconvolution technique 79−55242
impulse response measurement system, time domain technique 77−19406
impulse response of nearly parabolic fibres, evaluation 77−39055
impulse response of self-focusing fibre 77−42593
incoherent light efficient coupling into optical fibres and bundles 78−83074
incoherent optical power launching limits 78−63193
index profile data assessment method 78−71205
index profile measurement of single-mode fibres by scattering pattern method 78−66935
index profile measurement using transverse interferogram, accuracy 78−66931
index profile measurements of fibres and their evaluation 80−87538
index profiling by video analysis of interference fringes 78−55460
index-difference dispersion and bending loss/wavelength relationships 78−1367
index-matching fluids for long wavelength (1.2-1.6 micron) fibre-optic appls. 80−99841
industrial appl., IR LED and optical cables improvements 78−59123
industrial fibre-optic data link integrated components 79−10392
information transmission, development since 1966, review *(German)* 77−50760
information transmission systems *(German)* 77−88942
inhomogeneities, detect. by double-shearing interference microscopy *(French)* 77−54819
inhomogeneous circular waveguide, asymptotic eigenvalues 80−53442
inhomogeneous dielectric fibres transversely indicent beam wave scatt. 80−96004
inhomogeneous dispersion, direct meas. method 78−1400
inhomogeneous mutlimode dielectric fibre waveguide analysis 79−59833
injection heterolaser coupling into fibre waveguide, operation regime influence on efficiency 79−59834
injection laser diode, single freq., for integrated optics and fibre optic appls. 80−1237
insertion loss measuring set for field use 79−64357
insertion loss meter and reflectometry of prepared fibre ends 79−64358
instrumentation appl. survey 80−83665
integral data source/receiver package 78−63179
integrated and guided-wave optics, conference, Incline Village, NV, USA, January 1980 80−58772
integrated fibre-optic subsystems, progress in development and appls. 79−46068
integrated LED/sphere-lens source for optical fibres, coupling efficiency calcs. 80−43433
integrated optical communication, hybrid fibre optic advances 77−75716
integrated optical switch, polarization-independent, for use with single-mode optical fibres 79−37059
integrated optical switch for fibre data transmission system 77−27384
integrated optics techniques for fibre-optic communications *(German)* 78−38069
integrated optoelectronic Si devices, optical signal processing and communications, fibre-channel waveguide coupled 79−59847
intensity profile distortion, due to index profile determ., near field method 78−37977
interconnecting fibre optics 80−69514
interconnection advantages over conventional cabling 78−9442
interconnection components 78−46812
interconnection components for optical waveguide cables, SIECOR system 79−3804
interconnection design and performance 80−14436
interconnection of fibres and cables 78−46785
interconnection techniques 79−23059
interconnection using compound-lens devices, telephone links appl. 80−74493
interference filters, optical props. determ., via matrix method *(French)* 78−30070
interference fringe visibility, effect of guide length in coherent light 77−34932
interference of two beams from two fibres, fringe visibility 78−33828

optical fibres continued
interference pattern generated by side-illuminated optical fibres, observations 78−50914
interferometer, two-beam, and beamsplitter 77−87811
intermode phase scanning for recovering phase-modulated signals on multimode optical fibres 80−58682
International wire and cable symposium, Cherry Hill USA (Nov. 1978) 79−37018
interoffice trunk fibre-optic experimental transmission system 77−54795
interoffice trunking exptl. optical fibre communication system 77−19454
intersymbol interference and transmission medium instability for fibre system 77−65638
introduction to theory and applications, book 80−90617
ion-exchanged glass, diffusion coeffs. of Tl^+ ions 77−89583
IR and FIR tunable coherent sources utilising modulational instability 80−95967
IR coating nonuniformity effect on precision optical systems, compensation by auxiliary laser 80−78926
IR emitting diodes, high radiance, analysis of radiation coupling into optical fibre 80−14473
IR materials, high transparency, state of the art 77−27326
IR spectra, doped, nondoped fused silica, 3 to 25 μm 79−18537
IR waveguides, development for fibre and integrated optics 79−98491
irradiated by γ-rays, damage recovery by annealing 79−23078
isolator for communication systems, 0.8 μm band 79−50424
Italian local digital network applicability of optical cables *(German)* 78−33886
jacket eccentricity tolerance criteria *(German)* 78−38008
jacketed, hydraulic pressure depend. of losses 78−63175
jacketed, transmission loss 79−1011
jacketed and cabled optical fibre low-temp. attenuation increase 80−58732
jacketed fibres, thermal characts. of phase shift 80−58670
jacketed optical fibre residual stress diagnosis, pulse delay technique 80−53469
Japanese market 79−32044
jelly-filled optical fibre cable fabrication and characteristics 80−53490
joining by arc welding, practical machine for splicing in field 79−50450
joining of optical fibres *(Norwegian)* 79−1008
joining technique and LED fibre coupling, effects of parameters *(German)* 78−63191
joining techniques *(Japanese)* 79−27404
joint and connector losses *(French)* 78−55464
joint loss, effect of system parameters 79−50435
joint loss measurements with OTDR 79−64354
jointing by plastic tape wrapping *(German)* 78−38096
jointing losses causes and reduction *(Norwegian)* 77−14801
jointing techniques and connections to communication equipment *(Norwegian)* 80−64179
laminated fibre ribbon for optical communication cables 77−3653
large core broadband fibre design 78−30075
large-core high numerical aperture fibres for data-link appls. 77−39028
laser array packaged with fibre lightguide array on Si substrate 78−46611
laser array source package with fibre lightguides 77−84007
laser beam transmission through fibre light guide, spatial coherence 78−71133
laser diode, hermetic packaged lens-coupled, for wideband transmission 79−45970
laser diode interconnection *(Danish)* 77−88911
laser diodes for fibre communications, characteristics and state of art *(Italian)* 80−58569
laser drawing limitations 78−1447
laser engineering advances, conf., San Diego, CA, USA (Aug. 1977) 78−59017
laser radiation action on fibre optic components 77−7108
laser sinusoidal modulation for fibre meas., 9 MHz to 1.1 GHz, using GaAs laser 77−10966
laser splicing, thermal conditions 78−13820
laser to fibre hybrid coupler with cylindrical lens 77−75661
laser triggering through fiber optics of a low jitter spark gap 80−107000
laser-fibre coupling with optical transition structures 78−42449
laser-fibre transverse coupling and front-mirror monitoring for feedback control of laser transmitters 80−33151
launching and coupling losses, determ. using geometrical optics method 78−42406
launching and propagation of light in optical fibres 80−69504
leakage induced by non-destructive methods in fibre link 78−42450
leaky mode behaviour, with non-circularly refractive index profile 77−62045
leaky mode correction, near square law fibres 77−79934
LED and laser source and Si photodetector development 78−42430
LED communication system, source-drive optimisation 77−11007
LED coupling to optical fibres, truncated spherical lens efficiency 79−76813
LED design for compatibility 77−79932
LED reference channel nonlinearities, power coupling into optical fibres 79−78158
length influence on total losses 79−59836
lens, plastic focusing, change of ref. index profile during heat treatment process in fabricating 78−83091
lenslike fibres, density-matrix method applied to mode coupling 80−78970
less coefficients of 10^{-5} cm^{-1}, attainment, lecture 78−25991
light distribution, irradiance patterns, over endface or cross section 78−63181
light feedback suppression, from optical fibre into diode laser 79−1004
light field wave front correction, emitted from fibre lightguide *(Ukrainian)* 78−83081
light focusing glass fibres, characts. and appls. *(Hungarian)* 77−784
light guide data transmission, review *(German)* 80−95996
light propagation, basic terms, properties, uses *(Dutch)* 80−64166
light propagation, review of analytic methods of study *(French)* 79−90001
light scattering, core-cladding interface effects 77−75692
light source coherence meas. and fibre modal noise simulation by Michelson interferometer 80−48324
light sources and detectors *(Italian)* 80−69390
light transmission, fibre production methods, transmission line structures details *(French)* 79−89998
optical fibres continued
light transmission mechanism in optical fibres, communications appl. 80−43469
light velocity fibre optic wink-around expt. 80−90628
light wave transmission technology, survey 79−55213
lightguide connector with spring clip 80−23802
lightguide lines appls. in telecommunication *(Polish)* 78−79132
lightguide theory and its implications in manufacturing 80−64186
lightning stroke current meas. using optical fibre cable and optoelectronic conversion, rocket launched 78−92930
line image transmission through single fibre using spectral instrums. 80 102820
linear power response 77−54790
link for Command and Control System 280 78−42445
link systems, UK expts. 78−42462
links in space and ground-based, review of NASA tasks 78−42441
liquid core, polarisation props., bending effect 77−58440
liquid core hollow quartz fibre, stimulated Raman scatt. 78−30087
liquid crystal electro-optic switch, four-port, for unpolarized fibre light 80−58715
liquid crystal fibre optic switch, adjustable access coupler 79−64334
liquid-crystal optical fibre temp. probe rel. to thermometry and dosimetry of heat 80−98204
local distribution fibre-optic cable system 77−68277
local normal modes, superlocal modes, ideal modes 80−14466
long fibre, mirror and hollow dielec. lightguides, photometric characts. 80−33201
long fibre lightguide limiting aperture angle and props. 79−72692
long length for communications cable, proof testing 77−54818
long lengths fabrication, improved CVD method 78−33922
long step-index fibres, propagation model 77−19390
long with random inhomogeneities, output pulse shape 79−3791
long-distance graded-index fibre bandwidth estimation 80−58742
long-haul communications optical fibre fault location method 80−64193
long-span single-mode fibre, pulse broadening around material-dispersion-free wavelength 78−71215
long-span single-mode fibre transmission characts. in long wavelength regions 80−99850
long-wavelength single-mode fibre transmission systems 80−58773
loose tube packaging, fibre buckling obs. 78−25962
loss, dispersion and polarisation meas. by acousto-optical tunable filter 80−102855
loss and output numerical aperture meas. of fibre splices 78−42403
loss estimation using backscatter technique, time domain reflectometry theoretical assumptions 80−74508
loss increase due to stranding in optical cables 80−38117
loss meas. of multi-mode fibres, non-destructive method 80−69550
loss measurement using enhanced sensitivity nondestructive method 78−66895
loss mechanisms, separation by graphical method 77−14806
loss model for parabolic-profile fibre splices 79−23058
losses, spectral and length-depend. attenuation meas. using two-channel backscatter anal. 80−33159
losses, steady-state, fibre with random nearest-neighbour coupling 77−27338
losses due to fibre cross section variations 78−71226
losses rel. to glass imperfections 77−88949
lossless fibres, mode power fluctuation smoothing, source bandwidth 77−3667
lossy fibre propagation, leaky-mode radiation field computation *(German)* 78−33867
lossy fibres, coupled power eqns. 79−10376
low loss, for optical communication *(Japanese)* 78−79135
low loss, properties and appl. *(Japanese)* 78−46779
low loss, wideband near IR continuum generation (0.7-2.1 μm) 79−23064
low loss access coupler for multimode fibre distrib. networks 77−72063
low loss fibre optical cable 79−18546
low loss multicomponent glass fibre preparation *(Japanese)* 79−3814
low loss optical fibre waveguide, ionizing radiation effect on attenuation 80−38112
low loss optical fibre waveguide, radiation induced transmission loss behaviour, review 80−38111
low loss single mode, fabrication of GeO_2 doped silica core fibres, telecommun. appl. 79−18556
low loss waveguide, transient radiation effects 78−30055
low V-number,, secondary maxima in far-field radiation pattern 80−33182
low-aberration focusing fibre, optimum diffusion exchange and heat treatment 78−1378
low-dose radiation damage growth and decay obs. 78−1398
low-level-light detector used for checking optical cables 78−54455
low-loss, manufacturing technology 77−65632
low-loss, multi-mode cable technology, recent trends 79−3781
low-loss compound-glass optical fibre 78−13798
low-loss graded index, produced by double crucible technique 80−48449
low-loss graded-index fibre, 3 km and 10 km preform design and modified CVD method 80−58746
low-loss high-numerical-aperture, fabrication by vapour-phase axial deposition 80−1315
low-loss multi-component glass fibre preparation 79−46049
low-loss multimode optical fibre characterisation for nuclear diagnostics 80−78501
low-loss optical fibre evolution 80−69532
low-loss optical fibre production with high numerical aperture 80−48450
low-loss single-mode fibres, elliptical and circular core, laser gyro appl. 80−1344
low-loss SPDT fibre-optic switch 79−41445
low-loss transmission achievement and utilisation 77−27381
low-OH-content fibres, transmission-loss characts. over 0.5 to 2.5 μm range 79−59830
low-V optical fibre with dip in refractive index, perturbation theory 79−37012
luminescence meas. in inaccessible or hazardous locations using bifurcated fibre luminometer 80−62712
Luneberg lens for laser diode coupling to graded-index fibre *(German)* 78−33875
LW communication, InGaAsP/InP lasers and detectors 80−9885
Mach-Zehnder interferometric waveguide modulator, polarization-independent operation 79−18552
male connector with friction insert, ferrule and retainer 80−78968

optical fibres continued
manufacture, properties, optical links appl. 80−23793
manufacture, silica production process, connection methods, applications *(Italian)* 77−3647
manufacturing, cabling and splicing, developments in Japan 78−59124
manufacturing processes, status report 77−46815
manufacturing processes *(Japanese)* 79−27403
market trends, applications, performance charact. and prices 80−91904
market trends, worldwide 80−58699
matched filters, using optical delay line provide encoding or decoding structures 78−74983
matching of semiconductor sources to thin-film planar and stripe waveguides 80−64174
materal dispersion measurement by FM radar method 77−88919
material characteristics, waveguide design and manufacturing tolerances 78−59156
material dispersion 79−27377
material dispersion meas. 78−63174
material dispersion meas. by baseband modulated envelope detection 78−1368
material dispersion meas. in lightguide glasses 78−55447
material selection criteria for $\lambda > 1.8$ μm 80−87554
materials and construction processes, progress review 79−50459
materials properties, review 77−3666
materials suitable for communication appls. 79−46061
matrix switch, low-loss 4×4, for fibre-optic communication 79−76823
matrix switching network for fibre-optic communication 80−58735
maximum information capacity derivation 77−39027
MCVD fibre fabrication system design 79−55255
measurement of attenuation, numerical aperture and input-output radiation profile 80−33186
measurement of attenuation and dispersion 80−33185
measurement of optical fibre waveguides characteristics 78−59143
measurement of refractive-index profiles in optical-fibre preforms by spatial-filtering technique 80−48403
measurement procedure quality, standards 80−1351
and measurement technique *(Japanese)* 78−22200
measurement techniques for optical fibre specification 80−95998
measurement techniques for physical charact. 80−1353
measurement techniques for transmission loss and refractive index distribution *(Japanese)* 80−87498
measuring equipment for experimental multimode fibre transmission system *(Japanese)* 78−90506
measuring equipment for optical communications *(German)* 79−32043
mechanical and optical props. reproducibility, modified CVD prep. 80−69535
mechanical deformation meas. by light scatt. method 80−14452
mechanical multimode one-to-many fibre-optic switch 79−76814
mechanical performance characterisation methods *(German)* 78−33870
mechanical reliability, brittle failure 80−79001
mechanical reliability 80−91909
mechanical strength, fast fracture and time depend. strength meas. 77−46818
mechanical strength, fractographical analysis, review *(Japanese)* 80−35319
mechanical strength reinforcing and reliability improvement methods of fabrication *(Japanese)* 80−87568
mechanical stress effect on transmission charact. of clad fibre 78−5579
mechanical stresses effect on transmission 80−10032
mechanical testing, optical degradation under tensile stress, fatigue, defects *(French)* 77−72074
mechanical testing of fibres and cables 80−3285
mechanically operated four-way optical fibre switch 80−53464
medium and long distance digital optical fibre communication systems 78−50941
medium loss fibres and cables, research developments 77−42621
medium-loss high-numerical-aperture fibre 77−39095
medium-range data transmission optical cables 77−39096
metal coating, for strengthening and surface protection 78−30103
metal shielded optical fibre transmission characteristics 78−1369
metal-coated, high-strength, advances in reduction in microbending loss 79−46066
metal-free cables for wide temp. range appl. 80−23795
micro-light guide photometry of biological tissues 80−46005
micro-optic devices for coupling/branching in fibre optic communications 79−55211
microbend charact. and mech. prop. for design, applicational examples *(Japanese)* 80−87500
microbending eqns., exact time-dependent, solns. 80−87530
microbending loss evaluation, arbitrary-index single mode fibres 80−48411
microbending loss evaluation, core index profile effects arbitrary-index single mode optical fibres 80−48412
microbending loss measurement method 79−72709
microbending losses in fibre waveguides and cables, depend. on numerical aperture 80−96025
microbending theory, principal mode numbers use 78−94434
microdistortion, perturbation effect on transmission attenuation 77−72069
microhardness, surface orientation and prod. conditions depend. 77−62051
microlenses to improve LED-to-fibre optical coupling and alignment tolerance 80−19088
microoptic devices for optical communications 79−76840
as microphonic instrumentation transducers 77−17970
military aeronautic application *(French)* 78−46813
military avionics interconnection fibre-optic data bus 78−46806
military communication systems development 78−59158
military communications appl., local distribution systems, use of plastic clad/fused silica fibre 78−9457
military fibre-optic communication systems progress 78−1425
military optical fibre communications 78−42433
minimal dispersion refractive index profiles 79−98469
minimum dispersion at 1.55 micron for single-mode step-index fibres 80−10006
modal caustics and dispersion mechanism 78−33895
modal delay calc. method for fibres with arbitrary refractive index 79−46038
modal dispersion in fibres with any numerical aperture and profile dispersion 77−23746
optical fibres continued
modal dispersion in optical fibres with any numerical aperture and doping profile 78−1391
modal dispersion in optical fibres with strong mode coupling 79−27399
modal dispersion of power-law profiles with tails 80−95991
modal dispersion with composite α-profile graded-index core 80−9998
modal excitation by partially coherent sources 77−790
modal filters, effects on loss measurements 79−50439
modal noise, dependence on source coherence and fibre length 80−48402
modal noise anal. and meas. 80−10003
modal noise in multimode systems 79−46083
modal power distribution determination 78−87162
modal properties of dielec. waveguide, one dimens. wave eqn. analysis 79−27398
modal treatment of fibre with modified hyperbolic secant index distrib. 79−90010
mode analyser using refraction from oblique section 77−88952
mode conversion analysis by diffraction theory 77−83999
mode conversion caused by splices of graded index fibres 80−1340
mode coupling between two connected multimode parabolic-index optical waveguides 79−94353
mode coupling coeffs. determ. using fibre resonator 78−5560
mode coupling in multimode fibres, techniques and formulation 78−66902
mode coupling in small-core diameter circ. dielec. fibre *(Korean)* 79−23072
mode cutoff freqs. formula for fibre with arbitrary refr. index profile 79−55244
mode derivation 78−63180
mode dispersion, material dispersion and profile dispersion in graded-index single-mode fibres 80−14443
mode elimination in fibre loss measurement 79−50375
mode excitation by Lambertian and totally incoherent sources 78−63182
mode excitation by laser diode *(German)* 78−50921
mode excitation calc., extended two-dimensional theory *(French)* 78−5546
mode mixing effects caused by sheathing and multistranding 79−18506
mode properties, computation by propagating beam method 80−69502
mode scrambler charact. from speckle contrast 79−98283
mode scrambler for optical fibres 77−58436
mode scrambler for use in bandwidth measurements 79−50438
mode-coupled multimode, baseband transmission theory based on scattering matrix 80−14468
mode-coupled multimode, coupling length estimation 78−66933
mode-coupled multimode fibre transfer function 79−10409
mode-coupled multimode W-fibre, analytical anal., scattering matrix method 80−99872
mode-coupling mechanisms in optical fibre, quantitative estimations 79−27380
mode-mixing in optical fibres 79−46034
modes of propagation, in uniform and imperfect guides, statistical analysis *(French)* 77−79914
modular cables, composite strain analysis 79−64351
modular light guide system, 5 MHz to 10 MHz bandwidth, features *(German)* 79−76865
modulation bandwidth of superluminescent diodes for optical fibre transmission 79−36993
moisture effect on fracture strength 79−37019
monofibre cable, snap connector 80−106609
monomode, baseband response function 79−50434
monomode, fabrication, characterization and cabling for transmission in 1.2-1.6 μm range 80−10042
monomode, optical communications developments 80−48404
monomode, step discontinuity radiation charact., anal. 77−62047
monomode, with sinusoidally perturbed core, spectral excess attenuation 77−42600
monomode fibre design, power containment 77−72057
monomode fibre dispersion and bandwidth meas. by mode-locked Q-switched Nd:YAG laser 80−91933
monomode fibre dispersion minimum 79−64310
monomode fibre refractive index profile meas., near-field technique 80−91931
monomode fibre total dispersion and loss minima 80−91929
monomode fibres, novel method for transmitting images 80−69512
monomode optical fibre bandwidth limitations and bend losses 80−87553
monomode optical fibre design and fabrication for submerged cable applications 80−91932
monomode optical fibre dimensions, dispersion, and losses *(German)* 78−33866
moulded multifibre connectors using rectangular multirod arrangement 80−58685
MTF of multimode fibre guides 79−7199
multichannel fibre cables, star and access couplers 77−88922
multichannel fibre optic sonar link 78−42446
multichannel GaAs laser array output synchronisation 78−42417
multicomponent glass, profile synthesis 77−27333
multicomponent high NA, preparation using PbO, La_2O_3 and BaO *(Japanese)* 79−59853
multicore, high density, design and manufacture, charact. *(Japanese)* 80−87501
multifibre splicing and butting developments *(Japanese)* 80−87502
multilayer multimode optical fibre, ray theory, optimal distrib. of refractive index 80−87489
multilayered, fibres, pulse broadening 80−83676
multilayered dielectric, W type structures, optical transmission props. 77−42615
multilayered waveguide, attenuation and tunnelling coeffs. for leaky rays 78−38002
multilevel signals in digital optical-fibre communications 79−22900
multimodal double-layer with random axial bends, losses 79−90025
multimodal optical fibre, excitation anal. by ray optic method 79−81550
multimode, anal. of propag. charact. and field distribs. in guided modes, review 80−43441
multimode, backward stimulated Raman scattering 78−87128
multimode, band widening by means of mode convertors 77−83995
multimode, band-widening by mode filters, with external higher-index surrounding 77−62048
multimode, basic transmission characteristics 79−18538
multimode, beam evolution 78−42443
multimode, CAD of optimum refractive index profile 77−14802
multimode, comparison of impulse response calc. and meas. 79−81517

optical fibres continued
multimode, coupling efficiency in joints evaluation 78−66894
multimode, directional coupler 77−3649
multimode, effect of cladding radius 78−30050
multimode, effect of microbending on light propag. *(French)* 80−53406
multimode, energy description of propagation of monochromatic radiation 80−38116
multimode, excess loss caused by lossy outer layer, optical links appl. 79−18540
multimode, excess loss caused by lossy outer layer 77−58434
multimode, finite cladding radius effects 78−66893
multimode, finite-bandwidth propag. 78−42456
multimode, freq. depend. of modal noise, speckle theory 80−102817
multimode, freq. domain dispersion meas. 77−14792
multimode, freq. response meas, wavelength depend. 77−27341
multimode, frequency characts. 80−58669
multimode, graded index, mode conversion coeff. meas. method 80−99820
multimode, graded-index, influence of central depression on dispersion characts. 77−68264
multimode, graded-index, side launch excitation of selected modes 79−10378
multimode, graded-index fibre, low-pass filter characts. 77−23759
multimode, group delay derivation 77−75688
multimode, group delay meas. using swept frequency tech. *(Japanese)* 78−37984
multimode, Hamiltonian techniques appl. *(French)* 77−79917
multimode, impulse response calculation 80−74486
multimode, incoherently illuminated, spatial correlation of field intensity 77−14795
multimode, integrated optical appls. 78−87169
multimode, irregular, ray statistics *(Russian)* 77−88913
multimode, irregular, with fluctuation focusing, ray calcs. of power loss 80−33195
multimode, loss and mode-conversion parameter meas. principle 78−22192
multimode, loss mechanisms of leaky skew rays 77−39054
multimode, loss mechanisms of leaky skew rays 78−46768
multimode, mode conversion coeffs. and mode dependent losses meas. 79−10377
multimode, mode conversion coeffs. meas. 80−53433
multimode, mode coupling coeff. meas. 79−27370
multimode, mode dispersion characts. with polynomial refractive index profile 78−74999
multimode, mode-coupling phenomena anal. using matrix method, accuracy 80−23803
multimode, modulation transfer function 78−55442
multimode, numerical evaluation of impulse response 78−59127
multimode, nylon buffering effects 78−71207
multimode, off-axis speckle contrast of transmitted laser light 78−90513
multimode, optical characts. meas. by backscatt. 80−23801
multimode, optimum operating wavelength for chromatic equalisation 78−25965
multimode, optimum refr. index distrib., vector wave anal. 78−63183
multimode, parallel-beam impulse response, numerical results 77−39056
multimode, planar input/output couplers, thick film technology appl. 79−72703
multimode, power attenuation, pulse distortion, electromagnetic wave propagation eqns. *(Italian)* 77−79930
multimode, power coupling, theory 78−33893
multimode, power loss caused by random mode coupling 78−18046
multimode, principles and performance of tapping elements 80−48405
multimode, propagation modelling, effects of mode conversion due to microbends *(French)* 77−23760
multimode, reed type routing switch, features 79−72704
multimode, refr. index profile meas. 77−11034
multimode, reln. between differential mode delay and deviation from optimum refractive index profile 79−18512
multimode, ring shaped and graded index with central dip, dispersion evaluation 78−42455
multimode, scattering and absorption losses, approx. theory 77−27339
multimode, slab waveguide star coupler 80−87491
multimode, speckle contrast of transmitted laser light 77−62057
multimode, speckle pattern visibility of transmitted light 77−19413
multimode, splice loss and mode conversion 80−99830
multimode, splicing method using elec. arc 77−27391
multimode, step index, transmission characteristics *(Japanese)* 78−37988
multimode, step or graded index, ray analysis *(French)* 77−79915
multimode, step-index and graded-index, design method based on transmission characts. 79−55233
multimode, structural design and determination of repeater spacing in digital transmission systems *(Japanese)* 79−59820
multimode, theory of light propagation 78−30051
multimode, transmission characteristics *(Japanese)* 78−37985
multimode, transmission characts., two-mode waveguide model 78−83085
multimode, transmission characts. *(German)* 78−30069
multimode, transmission characts. of microwave-modulated radiation 78−25985
multimode, transmission loss due to lossy cladding layer *(Japanese)* 78−37986
multimode, transmission props. and theory *(Japanese)* 80−87495
multimode, truncated Gaussian beam propag. 78−90510
multimode, universal tunnelling coeff. 78−66922
multimode, used in submarine cables, optical loss change caused by hydraulic pressure 79−41440
multimode, wavelength depend. propag. 78−38018
multimode, wavelength multiplexing 77−79926
multimode 3×2 fibre optical matrix switch 80−58764
multimode access coupler, fabrication method 80−87478
multimode access port 79−50430
multimode and single-mode connector technology 80−87511
multimode and single-mode optical fibre guides with rectangular cores 80−33220
multimode average intensity distrib. of laser light far-field radiation patterns at end face 80−53459
multimode delay compensation in fibres with profile distortions 80−33143
multimode electro-optic guiding for single fibre data links, system design 78−38065

optical fibres continued
multimode fibre, optimum index profile w.r.t. mode coupling 78−18054
multimode fibre, pass band depend. on excitation conditions 80−48433
multimode fibre bandwidth computation from measured index profiles 80−58740
multimode fibre branch fabrication 77−88955
multimode fibre communication systems, low loss 4×4 switching network 80−58718
multimode fibre communication systems, optical switch 79−27439
multimode fibre communications, electro-optic multiplexer system 79−18510
multimode fibre coupler, simplified theory 77−68259
multimode fibre coupler for optical data bus systems 78−1414
multimode fibre couplers for data bus systems 78−74970
multimode fibre data bus systems, optical bypass switch 80−99826
multimode fibre detachable connectors fabricated with self-aligning jig 79−27384
multimode fibre directional coupler 79−37002
multimode fibre lightguide, coherent light modulation 80−91926
multimode fibre link, modal noise 80−87536
multimode fibre links, intermodal dispersion reduction by mode-delay equalising methods 80−48400
multimode fibre optic interferometry, applications 80−86387
multimode fibre optic switching devices, computational approach to predict optical behaviour 79−59845
multimode fibre optical equaliser conversion function 77−23747
multimode fibre optical pulse delay and broadening 77−83998
multimode fibre optics coupler with low insertion loss 79−10379
multimode fibre optimum refractive index profiles 80−14435
multimode fibre routeing reed switch improvement 80−53463
multimode fibre structures, coupling 79−37033
multimode fibre transition systems, improved planar optical branching elements 79−94351
multimode fibre transmission system, optical multiplexer 77−83960
multimode fibre transmission system, optical multiplexer 77−88935
multimode fibre with refr. index gradient distrib., pulse dispersion 80−10022
multimode fibre with z-depend. α-value, impulse response 79−81521
multimode fibres, arbitrary index profile, propag. mode anal. using ray optics adiabatic approx. 80−53418
multimode fibres, cladding influence on light attenuation 79−76855
multimode fibres, mode conversion coeff. meas. *(Portuguese)* 80−23797
multimode fibres, multiple fibre connectors 77−3669
multimode fibres, pulse propag. 77−789
multimode fibres, recent advances in production 78−30096
multimode fibres, step-index, for experimental optical fibre transmission system 79−32059
multimode fibres, tapping element 77−3670
multimode fibres of arbitrary refr. index profile, pulse dispersion 80−74475
multimode fibres with index profiles varying along length, pulse propag. 80−87534
multimode fibres with mode mixing, pulse broadening 79−81516
multimode fibres with polynomial refr. index profile, mode dispersion and minimisation *(Japanese)* 79−50408
multimode focusing fibre with random bends, optical power loss 79−7214
multimode graded fibre, near and far field power distribs. 78−1337
multimode graded index, prepared by modified CVD, reproducibility 78−90531
multimode graded index fibre, detachable connector 79−37039
multimode graded index fibre parameter optimisation, design considerations 80−102804
multimode graded index fibres, group delay times of skew rays 77−34949
multimode graded index fibres, minimum total dispersion 78−22203
multimode graded profile, characteristic eqn., WKB method *(Italian)* 78−83080
multimode graded-index, near field intensity and modal power distribution 80−102810
multimode graded-index, observation of tubular modes 80−99840
multimode graded-index optical waveguide detachable connector 78−46830
multimode GRIN fibre, power launching theory 77−7179
multimode inhomogeneous fibre couplers 79−41430
multimode irregular focusing with random ellipticity, light propag. 80−74501
multimode joint designs, error tolerance evaluation method 78−9436
multimode lightguide, time dependent propag. 78−13801
multimode localised index gradient fibre, parallel beam analysis 77−46801
multimode optical fibre bandwidth computation from refractive index profiles 79−76815
multimode optical fibre coupling to single-mode waveguide 79−98485
multimode optical fibre dispersion rel. to wavelength, frequency-domain meas. 78−1401
multimode optical fibre incoherent chirp pulse transmission 78−1374
multimode optical fibre phase modulators and discriminators, theory 78−55446
multimode optical fibre phase modulators and discriminators, expts. 78−55449
multimode optical fibre systems, microoptic passive devices, review 79−72700
multimode optical fibre transmission, perturbation soln. 78−1380
multimode optical fibre wavelength-filtering effects 80−58731
multimode optical fibres, fusion splicing using gas flame heat source, development of splicing machine 80−102866
multimode randomly bent fibres, ray theory of impulse response 78−22208
multimode self-focusing fibre, mode excitation and impulse response *(Japanese)* 78−83107
multimode single fibre systems, appl. of adjustable branching coupler/attenuator 78−46808
multimode single fibres, low-loss Y coupler 79−23061
multimode square-law fibres, microbending loss, ray theory 77−42604
multimode step index, baseband frequency response measurements, mode scrambler technique *(Japanese)* 78−37983
multimode step index, effect of waveguide struct. on material dispersion meas. 80−1311
multimode step index, input beam width influence on bandwidth 77−11028

optical fibres continued
multimode step index fibre, excess loss, due to outer layer 77−58441
multimode step index fibre, excess loss due to outer layer 78−9430
multimode step-index, baseband freq. response meas. using mode scrambler 77−19402
multimode step-index, forward and backward stimulated Raman scatt. 80−58639
multimode step-index fibre, far field radiation pattern, cladding modes effect 78−79101
multimode step-index fibre, OTF, geometrical optics calc. 77−65637
multimode step-index waveguides, leaky modes and rays 78−74979
multimode structs., planar coupler devices, formation using ion-exchange process 79−50429
multimode telecommunications fibre scatt., geometrical analysis 77−23748
multimode three-layer fibre waveguides, mode attenuation 79−59835
multimode W-type, baseband signal frequency response 77−83969
multimode W-type fibre, periodi bending loss 79−76848
multimode W-type fibre transmission charact., intermediate layer effect 78−90497
multimode W-type fibres, power flow numerical soln. 80−78955
multimode W-type fibres, steady-state charact. 80−5818
multimode W-type optical fibre launching and connection characteristics 78−1376
multimode with different refractive index distribs., material dispersion charact. *(Italian)* 78−50902
multipath time dispersion theory of optical network 78−22207
multiple fibre end fire coupling with single-mode channel waveguides 79−7230
multiple-α index profile analysis 79−50371
multiple-α index profiles 79−46078
multiplex transmission, wavelength-division, over multimode optical fibres, edge interference filters design 80−83677
multiplexer/demultiplexer, low-loss, using interf. filters 80−58728
multiply reflected Gaussian beams in circular cross section 79−18343
multiport coupling between single mode fibres and indiffused channel waveguides 78−38061
multiposition optical-fibre switch 79−41438
multireflection optical multi/demultiplexer using interference filters 79−76821
multiterminal data system for aircraft, based on time division multiplexing 78−46811
multiterminal fibre systems 78−87147
multiwavelength monolithic integrated fibre-optic terminal development 80−33243
mutliplexers, micro-optic grating, for fibre-optic communication systems 79−50423
narrow band high power laser radiation transmission through fibres, nonlinear optical processes 80−53443
near IR (1 to 2 μm) optical communications, colloquium, London, England (May 1980) 80−86040
near square law type, propag. consts. perturbation anal. 78−33891
near-field scanning technique resolution limit *(German)* 78−33856
nematic liquid crystal adjustable access couplers for fibre-optic switching 80−33217
Network 2000, use of optical communication technology 80−1306
neutron and gamma induced transient absorpt. and luminesc. 80−58763
neutron irradiated, optical absorpt. spectra 0.7 to 1.1 μm 80−58762
noise, modal, suppression by dithering laser's operating point 79−94357
non-circular graded index fibres, leaky modes 79−1003
nonblocking 8×8 optical matrix switch for fibre-optic communication 80−74485
noncircular core single-mode fibres, polarisation charact. 78−94430
noncircular cross section, perturbation approx. for propag. charact. 78−71195
noncircular preforms, nondestructive index profile meas. 79−14105
nondestructive index profile meas. of elliptical optical fibre or preform 79−64322
nonlinear effects, appl. to active and passive device fabrication 80−58638
nonlinear equalisation by shaping filter *(German)* 78−33882
nonlinear pulse propagation 79−18536
nonmeridional rays in multimode optical waveguides, transmission characts., multimode propag. *(German)* 77−54799
nuclear radiation effects 79−27413
number of gaps allowable 79−14110
nylon-jacketed optical fibre with silicone buffer layer 77−27345
onboard data bus systems, for electrical control TDM signals *(German)* 78−25968
operational 1.8 km fibre cable, installation *(German)* 79−3783
optical communication system 80−91906
optical communication systems, problems arising in development 79−3806
optical fibre, graded index, differential mode attenuation meas. 78−13797
optical fibre, index profile meas., nondestructive 78−13796
optical fibre, index profile meas. from transaxial topography, optical method *(French)* 78−66778
optical fibre appl. to transmission of solar radiation 77−3663
optical fibre colour multiplexing 79−72677
optical fibre communication, conference, Paris, France, Sept. (1976) 77−11016
optical fibre data link, integrated industrial, circuit and system considerations 78−46817
optical fibre transmission, conference, Williamsburg (1977) 78−1382
optical power meter for fibre-optic appls. 78−93746
optical switches for integrated optics and fibre optics appls. 79−37057
optical time domain reflectometry 77−84014
optical time domain reflectometry by photon counting 80−95122
optical transmission equipment for field demonstration 77−7209
optical waveguides, manufacturing techniques *(Italian)* 77−19385
optimisation in fibre optic union for repeater spacing *(Italian)* 78−79117
optimum parameter determ. 78−38023
optimum repeater parameter calcs. of 1.12 Gbits/sec system *(German)* 78−37989
optimum wavelength laser, using GaAsSb 77−7086
optoacoustic effect observation using piezoceramic transducer 80−48423
optoelectronic devices development 80−91902
optoelectronic devices facilitate fibre optic communication systems 80−1328

optical fibres continued
OTF, indirect tests, simplified procedure 79−50386
OTF measurement method *(French)* 78−42458
packaging concept, interconnection system 79−90026
packaging in loose fitting tubes of orientated polymer 78−1338
paper tape data transmission, wavelength multiplexing 80−43454
parabolic, mode depend. attenuation 77−72059
parabolic fibre cutoffs 78−13800
parabolic index, helical bends, theory based on geometrical optics 77−88951
parabolic index, modal dispersion characteristics, lossy cladding effect 79−18515
parabolic index, selective excitation by Gaussian beams 80−95992
parabolic index, with periodic bends, attenuation 80−74481
parabolic index fibres, light propag. along helical bends 77−7183
parabolic index fibres, LP_{nn}-mode excitation by Gaussian TEM_{00}-beams, power coupling coeff. 80−78958
parabolic index profile, guided modes 77−39041
parabolic-index, vector wave asymptotic eigenvalues in inhomogeneous circular waveguide 80−96010
parabolic-index core and homogeneous cladding, guided waves anal. 77 11013
parabolic-index core fibres with homogeneous cladding, guided modes 79−76853
parabolic-index fibre modes, propag. charact., linearly polarised approx. 80−78972
parabolic-index fibres, single mode, step-mode and multimode, microbending losses 77−3654
parabolic-index multimode, mode power distribution meas. method 80−14439
parabolic-index slabs and fibres with bent axes, radiation losses 78−46758
parabolic-profile splices with unequal core diameters, transmission vs transverse offset 77−3652
parallel image transmission by single fibre 78−71216
parallel optical fibre channels, pulse skew model 77−68279
parameter characterisation techniques, comparison 80−64147
parameter measurement using optical time domain reflectometer 80−58755
parameter specifications for optical waveguides, manufacturing processes 80−96041
parameters, optical, measurement techniques 79−46076
partial coherence propag. 77−72070
passive couplers for appl in fibre optic systems 80−91903
PCM optical fibre communication system numerical aperture optimisation *(German)* 78−38017
PCM repeaters with low power requirements, design and operation *(German)* 80−28315
periodic fibre waveguide, mode coupling, appl. to DFB laser 77−27348
perturbation theory of fibres with power-law core profile 79−7211
phase discriminator using fibre delay line elements, operating principles 79−18507
phase modulation of coherent light using HF sound 78−87142
phosphate glass, transparent in UV region, manufacturing 78−87113
phosphosilicate glass cored fibre CVD production 77−39120
phosphosilicate glass fibre waveguide, possibility of near IR operation 78−50935
photobleaching of radiation-induced losses in optical fibres 79−94356
photodetector low-noise amplifiers using J-FETs for optical fibre receivers 78−37997
photodiode detector for optical fibre communication *(German)* 78−33874
photosensitivity in fibre waveguide, appl. to refl. filter fabrication 78−63171
pictorial image transmission by single optical fibre by 1-D scanning 79−7229
picture direct transmission via single optical fibre 80−106628
piezo-optical effects due to thermal stresses 80−87519
pigtailing electro-optical sources and detectors 79−36998
planar fan-out structure for multimode glass fibres 79−76845
planar multimode couplers for fibre optics 79−18531
planar multimode coupling structure fabrication by ion exchange 80−64233
planar star coupler design for fibre optic systems 80−74474
planar star coupler for multimode fibres 80−99828
planar waveguides and fibres, book 78−42426
plasma activated CVD, influence of substrate temp. 80−48475
plasma augmented vapour deposition 80−69561
plastic, ductile, with improved visible and IR transmission 79−3800
plastic, multiwavelength laser illuminators for colour distortion compensation 77−58435
plastic, polystyrene core material, 140 dB/km transmission loss at 670 nm 80−19093
plastic clad SiO_2 fibre gamma-ray irradiated, signal level depend. of recovery rate 79−36997
plastic coated fused silica, dynamic fatigue data reliability 78−87166
plastic coatings, geometrical uniformity 77−27342
plastic fibre bending effect on transmission props. 77−39053
plastic fibre-optic assemblies 80−14433
plastic fibre-optic waveguide, effect of ionising radiation on optical attenuation 78−63170
plastic focusing fibre for imaging appls., fabrication and charact. 77−62040
plastic light focusing fibre, heat drawing process prep. 77−14815
plastic materials in development *(French)* 79−55236
plastic primary coating materials, tensile strength and reliability tests *(Japanese)* 79−59818
plastic rod, prep. by photocopolymerisation of MMA-VB 77−11000
plastic-coated, fused silica, ageing and static fatigue 79−46067
pluse widening 79−72674
PMMA-d_8 ductile plastic optical fibre cables with improved visible and IR transmission 78−46834
polarisation effects in short length, single mode fibres 78−71203
polarisation optical time domain reflectometry, optical fibre technique 80−78959
polarisation preservation in optical fibre waveguides with elliptical cores 79−64324
polarisation props., characterisation using automatic birefringence measurement system 79−93205
polarisation rotator, birefr. single mode optical fibre 79−76808
polarisation-conversion wavelength-selective fibre switches 80−58736

optical fibres continued
polarisation-independent optical circulator coupled with multimode fibres 80−43430
polymer clad, for communication use, improvement and appl. 80−69546
polymer clad SiO_2 fibre, ionizing radiation effect on attenuation 78−42405
polymer lightguide, light propag., nonlinearity, quasi-optical approx. 80−99837
polymer lightguide attenuation coeffs. meas., data anal., accuracy 79−1005
polymer protective coatings for glass fibres, materials and techniques 80−33252
polymeric coatings, Bell Labs activities 78−1388
polystyrene, and copolymers, spectral characts. 80−14461
power attenuation calc., in bent multimode step index slab and fibre waveguides 78−25961
power distrib. measurement method without need for scanning 79−50437
power divider, single-model, fabrication using encapsulated etching technique 79−50433
power from LED calc. *(Swedish)* 79−55208
power launching analysis in multimode opt. waveguide with graded refractive index, appl. 78−46767
power radiated from weakly guiding fibre, vol. current and coupled mode theories 77−72058
power station fibre-optic system installation 79−37028
power-law graded-index, core/cladding power distrib., propag. const. and group delay 80−48420
power-law refractive index profile, scalar modal eigenvalues and group delays 80−28322
preform, refractive index profile and cross-sectional geometry meas. method 80−91893
preform core diameter and Ge doping profile meas., X-ray nondestructive method 80−64231
preform diagnostics, nondestructive noncontacting method 79−27376
preform fabrication in axial direction by vapour phase axial deposition, continuous process 80−43473
preform index profiling, automatic nondestructive focusing method 79−50448
preform manufacture using modified CVD process 80−64228
preform rod, refractive index profile meas. by transverse differential interferogram 80−64141
preforms, axially nonsymmetric refr. index distrib., nondestructive meas. 80−106601
preforms, nondestructive struct. meas. with photoelastic effect 79−86255
preforms, refractive index distribution measurement using X-ray absorption measurements *(Japanese)* 80−87506
preforms produced at high rates by particulate-deposition methods 79−50461
preparation by Ar plasma augmented vapour deposition 80−48478
preparation methods and performance factors 80−69557
preparation using RF plasma deposition 78−55479
principle parameters for communication systems *(Italian)* 80−58694
processing techniques, review 79−50460
processor serial interconnect system 78−1426
production and use for optical transmission systems *(German)* 79−36994
profile dispersion meas. technique 77−39031
progress and components, review *(French)* 80−69524
progress in optical waveguide process and materials, review 80−23768
proof-tester for optical glass fibres 80−53412
propagation, ray approach *(French)* 77−79916
propagation characteristic analysis 78−87160
propagation characteristics of near square law fibres, perturbation analysis 78−22202
propagation theories, results from International workshop Lannion, Sept. 1976 *(French)* 77−11018
propagation theory *(Czech)* 78−74997
properties, signal to noise ratio, freq. response, dispersion effects, communication system design appl. 78−9435
properties including attenuation, dispersion, numerical aperture 79−90036
properties of multimode, monomode fibres for communication systems *(German)* 79−37000
public telecommunication network, future of optical fibres 77−11022
pulse broadening, inter- and intramodal dispersion 78−5547
pulse compression obs. after transmission through fibre 77−68262
pulse delay meas. in zero material dispersion region 78−33822
pulse dispersion in gradient index fibres, calc. *(German)* 78−50920
pulse dispersion test bench for optical fibre characterisation 77−50778
pulse distortion at wavelength of dispersion min. 78−22187
pulse interval modulation for optical fibre communication system 78−50917
pulse interval modulation optical fibre communication system field expt. 78−1424
pulse propagation and dispersion in fibres with arbitrary index profile 80−78984
pulse transmission, direct modulation by semicond. laser *(Japanese)* 79−41402
pulsed optical signal deform. in multimode fibres 79−98492
pure and doped silica, intrinisc attenuation 77−65633
PWM multilevel pulse transmission, theory and expt. 79−55078
quantitative mode anal. and excitation condition meas. 79−18517
quartz, CVE process refractive index profile, liquid doping *(German)* 77−62050
quartz, stimulated Raman scatt., Stokes components recording opposite to pump wave 80−106569
quartz cylindrical fibres in regular struct., multiple frustrated total internal refl. calc. 78−83094
quartz fibres, liquid core tetrachloroethylene filled, transmission loss meas. at 3.39 μm 79−81532
quartz glass, Ge and B dopants, OH impurities, preform material and fibre optic waveguide struct. 80−64173
quartz glass, hydroxyl-free, for low-loss fibre waveguides, γ-irrad. effects 78−13773
quartz glass fibre waveguides, low-loss, radiation-optical stability 79−64345
quartz glass fibre waveguides, material dispersion meas. 79−18545
quartz glass fibres, B and P radial doping profiles 77−50771
quartz-glass large-diameter core and polymer cladding, prod. technology, low losses 80−14463

optical fibres continued
quasiparabolic index profile, propag. characts., perturbation anal. *(French)* 80−33189
radial refractive index profile determ. 78−59137
radially inhomogeneous, vectorial wave anal. using finite elements method 78−37999
radially inhomogeneous waveguide modes, vector wave characts. 80−78960
radially stratified fibres, 4×4 matrix method for propag. characts. calc. 77−34931
radiation damage, nuclear pulsed thermal radiation effects, hardening techniques 80−33170
radiation from bends, volume-current method 79−94336
radiation from optical waveguides: leaky-mode interpretation 79−32039
radiation induced transmission loss in optical materials 79−94306
radiation loss caused by discontinuities in dielectric slab waveguide, anal. 79−7227
radiation response of optical fibre waveguides in 0.4 to 1.7 μ region 79−18518
radiometer light pipes for Pioneer Venus, faceting 77−84012
radiometer optical lens replacement for industrial contactless process temp. meas. 78−49828
Raman fibre optic tunable laser 77−14721
Raman laser, fibre optic, freq. spectrum and temporal behaviour 77−61965
Raman oscillator, tunable 1.1 μm fibre 78−1242
Raman oscillator, tunable multiple Stokes CW fibre 77−88786
Raman oscillator, two-mode fibre, group velocity matching 78−25925
Raman oscillators and nonlinear effects 77−88854
Raman ring laser 79−22981
Raman scatt., guiding structs. effects on spontaneous and stimulated emission 80−58636
Raman scatt. in long low loss fibres, model 78−55410
Raman spectrometer, slitless optical fibre, with concave holographic grating 77−71380
Raman spectrum, polymer cladding effect 78−30073
random gradient, partially coherent optical wave excitation 77−23761
random mode coupling in fibre waveguide, ray theory 77−788
random mode coupling in fibre waveguide, ray theory for graded fibres 77−3535
random-bend loss in single-mode and parabolic-index multimode fibre cables 80−78951
randomly bent multimode fibres, ray theory 78−79129
randomly distorted multimode, propag. theory, step index fibres *(French)* 80−74470
randomly gradient fibres with irregular bends, optical mode propagation and scattering 78−1325
ray statistics of multimodal optical fibres 78−94450
ray theory for randomly bent optical fibres 78−66921
ray tracing in general nonhomogenous cylindrical medium 79−94335
rays, modes and beams in fibre waveguides 77−34945
receiver design for optical fibre communication systems, review 78−30077
rectangular and circular fibre cutting machine 78−33932
rectangular core fibre optic waveguide, dispersive props. 80−64172
rectangular core optical fibres, guided wave propag. anal. 79−81556
rectangular cored multilayer fibre 80−83667
reflected and backscatt. power meas. from fibre end, time domain reflectometer 78−70177
refracted near-field scanning, calibration technique 80−99823
refractive index automatic profiling 78−46836
refractive index change due to external forces 78−74971
refractive index determ., focusing method 79−27374
refractive index dip effect on propag. in step or graded index fibres 78−18053
refractive index dip removal by etching method 79−14120
refractive index distribution for prescribed two-dimens. ray path. 79−59633
refractive index matching fluids for long wavelength fibre-optic appl. 80−69470
refractive index meas., automatic nondestructive index profiling of whole fibre samples 79−81527
refractive index measurement, methods and results 77−83965
refractive index measurement *(Japanese)* 80−10020
refractive index near-field profiling methods, detail resolution 78−42451
refractive index profile, effect on fibre bandwidth 80−23773
refractive index profile, Marcatili condition derivation and interpretation 78−22193
refractive index profile calc. from transverse interf. patterns 78−74967
refractive index profile determ. by spatial filtering 78−33829
refractive index profile determ. from diffr. pattern 78−25953
refractive index profile distortion, stress-induced 80−91889
refractive index profile distortion due to thermal stresses 80−58726
refractive index profile meas., nondestructive transverse interference method 78−38024
refractive index profile meas., Q-fibre method 78−66939
refractive index profile meas., scatt. pattern method 77−7178
refractive index profile meas. technique 78−42452
refractive index profile measurement 77−27340
refractive index profile measurement using thick samples, interf. pattern 77−61111
refractive index profile microdensitometry 80−106632
refractive index profile models 80−14453
refractive index profile nondestructive determ., backward light scatt. method 79−64306
refractive index profile nondestructive determ., fast Fourier transform method 79−64307
refractive index profile optimisation for broadband multimode fibres 78−66932
refractive index profile synthesis using algorithm for inverse Sturm-Liouville problem 80−28351
refractive index profiles, appl. of refracted near-field meas. technique 79−37014
refractive index profiles, focusing method for nondestructive meas. 79−27375
refractive index profiling, new interferometric method 79−76816
refractive index profiling methods 78−79118
refractive index profiling using video-based system 78−79104
refractive profile distortion and dispersion, group delay calc. 78−55433
refractive-index profile, nondestructive determ. using forward light scatt. method 79−23060

optical fibres continued
refractive-index profile and cross-sectional geometry of preform, nondestructive determ. 80−1312
refractive-index profile meas., scanning optical microscope 80−87535
refractive-index profile measurement of optical fibre preform 79−59815
refractive-index profile of preforms, measurement using focusing technique 79−50464
refractive-index profiles, estimation using parallel-beam excitation method 79−23062
refractometry by interference microscopy, simplified method 79−18504
regenerative fibre-optic transmission system supervisory line codes *(German)* 78−33884
reinforcement, primary coat using modified silicone, transmission characts 80−38098
reinforcement of optical fibre waveguide cables *(German)* 78−33861
remote control system for 1.5 MeV heavy-ion fusion preaccelerator 80−73993
remote detection of CARS employing fibre optic guides 80−9984
repeater, low-power (0.5 W) design 78−22195
repeater bypass DPDT switch 79−98484
repeater design, high impedance input, equalisation cct. *(Italian)* 77−50758
repeater error rate calc. approaches compared 77−54672
repeater section lengths rel. to transmitter power and fibre dispersion *(German)* 78−38012
research and development, advances, conf., Kingston, RI, USA (June 1978) 80−57005
research projects at IROE Institute (Firenze) *(Italian)* 80−56668
resin protective coating performance evaluation, UV cured 80−69547
resin-coated optical fibre, tensile strength tests *(German)* 78−33871
review of fibre waveguides, book contrib. 77−31141
review of market trends and products 80−28319
ribbon cable cutting tool 80−19113
ribbon cable sheath 79−7203
ribbon splicing with vacuum-assisted injection mould 80−53491
ribbon-splicing injection-moulded connector with Si chip insert 78−1412
ribbons, loss meas. using calorimetry 78−87127
ribbons and cables manufacture, mech. props. 78−90533
ring index fibres, dispersion equalisation 79−32046
ring interferometer, using optical fibre of 950 m length 77−37969
rod lens analysis and application to optical fibre communications 80−87549
rod lens connector design and applications 80−53473
rod preform of SiO_2 based fibre waveguide, optical meas. of OH ion distrib. 78−87130
rod-in-tube fabricated optical fibre characteristics 80−87574
rod-in-tube method, modified, for low-loss silica fibres manufacture *(Japanese)* 80−33253
rotating optical fibre ring interferometer, Fresnel-Fizeau effect 78−4685
rotation-splice tapered fibre star coupler directivity and mode dependence 80−58748
rotational coupler development 77−72089
round, transmission props. of radial offsets, EM analysis 79−81566
route bandwidth prediction statistical model 77−62046
ruby, sapphire-clad, single-crystal, growth by floating-zone technique 77−90268
rugged fibre-optic cable manufacture, testing, and installation *(German)* 78−33863
rupture stress rel. to ageing *(German)* 78−38009
safety, minimum obs. distance 77−83955
safety aspects of LED- and laser-fed cables 78−74968
safety aspects of LED- and laser-fed cables 78−74969
sandwich ribbon, measurement of polarisation props. using He-Ne laser 79−64353
sandwich ribbon fibres for hybrid integration in high-index materials 80−79013
sandwich-ribbon, near-field intensity patterns of mixed modes 77−62073
sandwich-ribbon optical fibre, near-field intensity patterns of mixed modes 77−62073
scalar approximation accuracy 79−81561
scalar Helmholtz eqn. *(German)* 78−50919
scattering, ray theory 80−69528
scattering angular depend. and polarisation rotation, Brillouin and Rayleigh scatt. meas. 78−30085
scattering loss dependence on launching condition, lossy-layer model 78−5577
scattering of light in optical waveguides 79−10375
scintillator-fibre optic system, for high bandwidth radiation diagnostics 78−46820
second generation systems, 1300 to 1600 nm 80−64163
selection criteria, practical approach to purchasing 80−91912
self coupling phenomena of GaAlAs laser caused by optical fibre 78−55355
self focusing, rectangular and Gaussian pulse propag. 78−33831
self-centring technique for mounting microsphere coupling lens on fibre 80−74517
self-focusing, matching elements calc. 80−28339
Selfoc conically graded medium, aberration anal. 80−1142
Selfoc conventional fibres, pulse dispersion meas. 79−64305
SELFOC dielectric waveguide, signal distortions 77−75699
SELFOC fibre, non-Gaussian laser beam propag. 78−1335
SELFOC fibre 400 Mb/s optical transmission system 78−1353
Selfoc-type, Fourier hologram recording appl. 80−95850
semi-automatic machine for hot splicing glass fibres for optical communication 80−23818
semiconductor junction lasers ageing and modulation *(German)* 79−32042
semiconductor junction lasers as sender elements, coupling techniques *(German)* 77−75674
semiconductor laser array, output coupling with fibre optic tapes 79−10319
semiconductor laser couple, lasing spectra 80−1202
semiconductor laser radn. coupling 77−19426
semiconductor light sources for optical fibre transmission 77−54777
sensitivity analysis of waveguides dimensional tolerances 79−76833
shape-memory effect alloy connector 80−53475
sheathed fibres, excess loss due to coated resin shrinking at low temp. 80−43476
short distance application in Italy, review 79−50369
short fibre, leaky modes effect on response 78−9449
short single-mode optical fibre polarisation effects 78−1393
optical fibres continued
short-range fibre optics 78−46786
short-range optical fibre system applications *(German)* 78−33885
side illuminated, noncircular cross section effect on forward scatt. pattern 80−33150
signal polarisation statistical meas. 80−99877
signal processing, fibre and integrated optics techniques 77−27379
signal processing fibre and integrated optical devices 79−76887
signal transfer properties influenced by stress birefringence, multimode fibres *(German)* 77−62044
signal transmission, fundamental mode, in single- and multimode fibres 78−42442
signal transmission appls. *(German)* 80−69517
silica, ageing polymer-coated fused specimens in pH solns., tensile strength and dynamic fatigue 79−46063
silica, contamination with furnace drawing, losses 77−42634
silica, epoxy acrylate coated, tensile strength >500 ksi, km length prod. 77−11052
silica, furnace drawn, tensile strengths >3.5 GN/m^2 in 1 km lengths 78−87135
silica, fused, strength increase by polyethylene coating 77−23768
silica, fused, surface flaws obs., fracture strength 77−14793
silica, laser drawn, coated, tensile strengths >3.5 GN/m^2 in 3 km lengths 78−87138
silica, LED and laser sources for 1.0 to 1.2 μm emission, review 77−38894
silica, low loss, pure, with silicone cladding, manufacture techniques 77−65619
silica, plastic clad, stress, strain and optical transmission data 79−1009
silica, stimulated Raman emission, 1-1.3 μm source 77−42568
silica based optical fibre dopants for 1 to 1.8 μm communications 80−91930
silica binary comp. fibres, refr. index and profile dispersion meas. 77−19388
silica fibre, high efficiency tunable CW Raman oscillator 77−14773
silica fibre, plastic coated, furnace drawing technique *(Italian)* 78−55475
silica glass, phosphorus containing, optical absorp. characts. of hydroxyl radicals 77−14800
silica multimode fibre waveguide, cascade stimulated Raman scatt. 77−62008
silica optical fibres, large core polymer clad, electron-beam and γ-ray effects 80−33171
silica with silicone resin coating, microbending effect on attenuation anal. *(Italian)* 78−55432
silica-plastic fibres, propag. characts. and fabrication for short-medium distance appls. 78−66892
silicate glass, optical loss, effect of manufacturing conditions 77−21085
silicate glass, single mode optical fibre, at zero dispersion wavelength, exam. 78−38043
silicone and glass clad compound glass optical fibre comparison 80−69533
silicone double-layer coating with double cone nozzle in-line with optical fibre drawing 80−53488
silicone resin clad fibre technology, optical and mech. props. 80−28349
silicone-clad silica fibres, length dependence of characts. 79−64319
silicone-clad silica low-loss fibre radiation response obs. 78−1397
singl-mode, low-loss detachable connector 79−90022
single fibre connector, design considerations 79−1010
single fibre connectors and cable splice hardware, optical coupling theory 80−64187
single fibre low loss connectors, low cost 79−68434
single fibre multichannel environmental connector, design and perform. considerations 78−71229
single fibre multichannel environmental connector, design and perform. 78−90508
single fibre optic cable connector losses 78−46802
single fibre optic connector design and development 80−53474
single fibre optic moulded connector and encapsulated connectorised devices 78−1409
single fibre optical systems, connection methods 78−46783
single layer, dimensions and refractive index meas. 77−79952
single material fibre, with two support slabs of different thickness, modal anal. 79−23084
single mode, anal. of propag. characts. and field distribs. in guided modes, review 80−43441
single mode, bending induced birefringence 80−87537
single mode, dispersion characts., correlation between numerical prediction and meas. 80−91890
single mode, homogeneous CVD fabrication and characterisation 80−69562
single mode, jointing loss 78−25964
single mode, low loss splicing technique 78−1442
single mode, measurement of wavelength dispersion in 0.8 to 1.6 μm range 79−90020
single mode, mormalised freq. meas. 77−23749
single mode, normalised freq., depend. of splice losses 78−55444
single mode, polarisation and magnetooptic props., expt. meas. 78−33830
single mode, preparation and transmission properties 80−33204
single mode, pulse fluctuations, propagation 80−87475
single mode, random bend losses, power spectrum estimation from spectral losses 78−87143
single mode, realisation using dielectric-tube waveguide with outer higher-index cladding, transmission characts. 77−42606
single mode, refr. index profile meas. by refl. method 78−46756
single mode, refractive index profile meas., focusing method 80−33144
single mode, stress birefringence 77−68263
single mode and graded-index multimode fibre cable random bend losses 80−58741
single mode coupling of fibre to indiffused waveguide 77−34959
single mode CVD fibre, bend-induced birefringence obs. 80−58723
single mode fibre, 800 Mbit/s transmission expt. 78−30058
single mode fibre, wavelength dispersion meas. 77−39032
single mode fibre 1.1-1.3 μm dispersion meas. by pulse synchronisation 80−64192
single mode fibre analysis and fabrication for low polarisation birefringence 80−58722
single mode fibre cable, 4.15 km, interf. and polarisation characts. using AlGaAs laser 79−81535

optical fibres continued
single mode fibre characterisation by LP_{11} mode radiation pattern 80−23790
single mode fibre coupling structure fabrication 78−33899
single mode fibre coupling to semiconductor laser, fibre strength tests 78−33900
single mode fibre for current meas. system, birefr. induced by bends and twists 80−99832
single mode fibre near- and far-field characteristics, profile-independent representation 80−58739
single mode fibre optic system coupling techniques 78−33901
single mode fibre optical data bus with star couplers 80−64199
single mode fibre optics and integrated optics, for optical communication 78−42469
single mode fibre pickoff coupler 77−783
single mode fibre polarisation stabilisation 80−58724
single mode fibre transmission characts. and refr. index profile meas. from exit radiation pattern 80−9986
single mode fibres, core-cladding concentricity meas. 78−33848
single mode fibres, noncircular core influence on polarisation performance 78−37973
single mode fibres, optical communication techniques *(German)* 80−102811
single mode fibres, ultra-low-loss, prep. of long lengths 79−76893
single mode fibres, very low loss, 1.5 μm transmission expts. 79−50385
single mode fibres for optical field mapping, interf. technique 78−74966
single mode grating coupling between thin-film and fibre optical waveguides 79−1012
single mode inhomogeneous fibre problems, scalar wave approach 79−64312
single mode network, coupling and integrated optical switches 78−59159
single mode optical fibre, polarisation modulation 80−64176
single mode optical fibre connectors, low loss 79−81557
single mode optical fibre polarisation stabilisation 80−33154
single model fibres, polarisation mode dispersion 78−79128
single multimode fibres, optical planar coupler in data bus system 77−11024
single multimode optical fibre communication directional couplers *(German)* 78−33873
single-fibre optical systems, efficient power combiner for multiplexing multiple sources 78−18039
single-fibre separable connector insertion loss characteristics 77−23770
single-mode, backscattering method analysis 80−106610
single-mode, Brillouin spectrum 79−46032
single-mode, characterisation factor 78−22189
single-mode, connector and laser module as interconnecting device between fibre and laser diode 79−50422
single-mode, curvature and microbending losses 79−27418
single-mode, cutoff wavelength meas., using refracted power technique 80−99844
single-mode, dependence of optical losses on bending effects 79−50417
single-mode, effect of dip in refractive index on cut-off freq. 77−39029
single-mode, electro-optical polarisation control 80−91899
single-mode, evolution and polarisation 78−9432
single-mode, exit-end reflection and transmission module, theory *(Japanese)* 79−98474
single-mode, fabrication by VAD 80−83687
single-mode, fabrication for 1.5 wavelength region 80−106627
single-mode, for ring interferometer, Fresnel drag 79−37035
single-mode, fractional wave devices and polarisation controllers 80−106606
single-mode, fusion splice loss anal. 80−64181
single-mode, hemispherical microlens tip fabrication for high efficiency coupling to InGaAsP laser 80−69505
single-mode, large-freq.-shifted three-way mixing in low dispersion wavelength region 80−99792
single-mode, low-loss, for 1.55 μm operation *(Japanese)* 80−33161
single-mode, misalignment and bend losses 79−10411
single-mode, mode shift at bend anal. 78−22191
single-mode, normal acoustic modes and Brillouin scatt. 79−76760
single-mode, numerical aperture effects on optical and mechanical props. 80−69548
single-mode, pressure sensitivity meas. and limitation 80−106605
single-mode, pulse distortion, Gaussian pulse propag. theory 80−78956
single-mode, pulse distortion due to microbending calc. 77−14798
single-mode, simplified parameter based anal. 80−69507
single-mode, single-polarisation, with refractive-index pits on both sides of core 80−99846
single-mode, splicing and bending losses 79−18505
single-mode, splicing method based on discharge fusion 79−90021
single-mode, splicing method based on discharge fusion *(Japanese)* 80−28317
single-mode, subjected to tensile stress, polarisation performance 79−59808
single-mode, suitable parameter determ. 79−27387
single-mode, ultra-low-loss, optimised structure for fabrication 80−99843
single-mode, VAD, long-length, polarisation characts. 80−106604
single-mode, wavelength dispersion characts. *(Japanese)* 80−33162
single-mode, with ultra-low loss in 1.55 μm region 79−90018
single-mode and multimode, automatic geometric meas. 79−36988
single-mode cable, evaluation of characts. *(Japanese)* 80−28316
single-mode dispersion-free long-span fibres, pulse broadening meas. 80−53417
single-mode fibre, 14 km long, with low attenuation at 1.2 to 1.32 μm, MCVD fabrication 80−53461
single-mode fibre, pulse spreading due to third-order dispersion 79−50370
single-mode fibre, wavefront distortion compensation in thick inhomogeneous medium 80−102762
single-mode fibre birefringence and optical activity obs. 78−1394
single-mode fibre cable, cabling and splicing loss increase characts. 79−81522
single-mode fibre cable, evaluation of loss increase characts. 79−90019
single-mode fibre cabling for low-loss communication 80−53467
single-mode fibre coupling to single-mode Ti diffused $LiNbO_3$ waveguide 79−81547
single-mode fibre joint losses calc. 78−74980
single-mode fibre lightguide, phase of coherent signal, temp. and stress effects 80−33208
single-mode fibre low-loss connectors 78−87139
optical fibres continued
single-mode fibre low-loss splicing by tapered butt joint method 79−50409
single-mode fibre multiterminal star directional coupler 79−98473
single-mode fibre optic directional coupler 80−58683
single-mode fibre optical power divider, encapsulated etching technique 79−27420
single-mode fibre pulse spreading due to third-order dispersion, optical source bandwidth effect 79−81523
single-mode fibre tapered velocity coupler performance 79−55246
single-mode fibre to $LiNbO_3$ channel waveguide high-efficiency flip-chip coupling 80−99833
single-mode fibre with refr. index dip, wave propag. 78−63194
single-mode fibre/channel waveguide flip-chip coupling, high efficiency 80−58799
single-mode fibres, axial refr. index dip effect on zero total dispersion wavelength 80−78962
single-mode fibres, simplified bending loss formula 79−59800
single-mode fibres, simulation of near field using microwave model 79−59825
single-mode fibres, tailoring zero chromatic dispersion into 1.5-1.6 μ low-loss spectral region 79−64320
single-mode limit with arbitrary refractive-index profile, formula 78−46771
single-mode low-birefringence fibres, prep. and polarisation characts. 79−7195
single-mode low-loss fibres, high-speed optical pulse transmission expt. at 1.29μm 79−23067
single-mode low-loss fibres fabrication with GeO_2-doped SiO_2 cores by CVD 77−39030
single-mode low-loss silica fibre prep., 10 km long 80−48476
single-mode optical fibre coupling techniques using microscopic lenses 80−53462
single-mode optical fibre microbending loss and pulse distortion analysis 78−1395
single-mode optical fibre phase modulators, pressure sensitivity meas. 79−7205
single-mode optical fibres, 1.3 μm, ceramic capillary connector with 0.3 dB loss 80−23778
single-mode optical fibres, backscattering signal anal. utilising wave optics approach 80−64151
single-mode optical fibres with different B_2O_3-SiO_2 compositions 78−1392
single-mode optical waveguides with inhomogeneous index variations 79−76804
single-mode optical-waveguide fibre coupler 78−74973
single-mode propag. in 2-mode region using mode filter 79−76825
single-mode radially inhomogeneous fibre, propag. modes 78−22206
single-mode splices, loss anal. 77−75667
single-mode step-index fibre, minimum dispersion 79−89992
single-mode step-index fibres, practical microbending loss formula 79−81534
single-mode systems, instability due to interference and polarization effects 80−58774
single-mode tube waveguide with outer higher-index cladding, far-field radiation pattern 79−90033
single-polarisation, slab model, strain birefr. 79−50381
single-polarisation single-mode, exposed cladding fabrication 80−58725
single-strand fibre couplers 77−68283
single-strand multimode fibre waveguides, access coupler fabrication 77−7176
singly and doubly clad fibres with bends, excess losses 79−14104
sinusoidal microbending loss of HE_{11}-mode in step-index fibres 78−79109
slab waveguide model, modified zigzag ray model 77−39035
slicing by collapsed glass sleeve *(German)* 78−38097
slit light guide design, fibre optics *(German)* 80−53420
snap-in fibre-optic aligners 80−1325
soda lime silica glass fibres, low OH content, low loss 78−37975
solar irradiance meas. using optical fibres and Si detectors 79−100960
soliton pulse propag. 80−58759
solitons in the theory of guided lightwaves 80−58760
source and coupling techniques *(German)* 77−19404
source and detector choice guidelines 78−50905
spark-induced fracture for low-loss joints prep. 78−1441
spatial coherence and modal struct. 80−87531
spectral loss meas., automated 79−23074
spherical end faced coupling fibre fabrication by selective etching/melting 80−53492
spherical surface, coupling to LED, efficiency 80−48416
spherical-ended fibre, efficient coupling to LED, geometrical optics. anal. 78−83086
splice, elastic-tube 80−87527
splice delay distortion characteristics, shuttle pulse meas. 77−19457
splice insertion loss meas., backscattering method 80−58720
splice loss, Gaussian power model 78−46828
splice loss evaluation by means of the back-scattering technique 79−98478
splice loss evaluation for arbitrary-index profile fibres 78−90499
splice loss in single-mode fibres using Gaussian field approx. 79−94354
splice loss/mode conversion relationship in graded index fibre 79−64321
splice machine, semi-automatic, for multimode fibres *(Japanese)* 79−59854
splice methods for cables *(Japanese)* 80−58690
spliced graded-index fibres, 11.7 km link, measured and predicted transmission characts. 80−14454
spliced graded-index multimode fibres, wavelength depend. 79−72672
splices, observation of cascade effect 79−50436
splices, offset and tilt loss 77−3651
splicing, arc fusion, protection and reliability 80−69565
splicing, connecting and sheath jointing *(Japanese)* 80−87497
splicing and connecting 79−41436
splicing and connection techniques *(Italian)* 80−38097
splicing and sheath jointing expts. 80−23806
splicing by butt-joint method, multi-glass-rod optical-fibre splicers made by drawing technique 80−53413
splicing characteristics and techniques 78−46798
splicing technique for multifibre cables using slippery fibre holder 79−50471
splicing techniques 78−79147
splicing techniques and strategies affecting cable design 78−1408

optical fibres continued
splicing techniques for compound glass and silica optical fibres *(Japanese)* 80−99890
splicing techniques for multiple units cable structure *(French)* 77−11021
splicing tools for field applications *(Japanese)* 80−87503
splicing using low MP glass solder 79−55252
splicing using self-aligning ceramic capillary 79−76829
splicing with low-power CO_2 laser 77−72098
spring steel cutter for glass fibres 80−48468
standardisation of components, EIA P-6 committee 80−1352
standardisation of components, military appl. 78−30083
standards for fibre optics 79−14101
star coupler, unidirectional, for single-fibre distrib. systems 78−25980
star couplers, low-loss refl. type, for optical-fibre distrib. systems 80−1301
star couplers for single multimode fibre communication systems *(German)* 78−33872
star couplers using fused biconically tapered multimode fibres 78−55443
star repeaters for fibre optic links 77−34934
star simulator lightguide test instrument and method 79−27422
step discontinuity, radiation loss 77−42588
step index, coupled power eqns. numerical soln. 77−54791
step index, graded index, dispersion investigation, scanning technique 79−76852
step index, mode conversion due to scattering from off-axis inhomogeneity, Green's function analysis 80−10045
step index, refractive index and radius ratio determ. from backscatt. light 78−30049
step index, scattering from arbitrarily located inhomogeneity 78−87161
step index fibre, Lambertian source, impulse response 78−33819
step index fibre, pulse widths, Goos-Hanchen shift effects 77−83952
step index fibre excited by Lambertian source, impulse response 77−62041
step index fibre including gap, impulse response 80−83675
step index fibres, splice losses, break angle depend. 77−83954
step index multimode, transmission characteristics investigation 79−18539
step index multimode fibres 2R repeater hybrid digital transmission system appl. *(Japanese)* 78−90505
step index single mode fibre, far field distrib., asymptotic expression 77−75658
step index W-fibre, excitation and splicing 79−98477
step-index, curved, field distribs. of natural modes 77−79936
step-index, excess loss dependence on parameters, expt. 78−66936
step-index, low-loss, fabrication using modified rod-in-tube method with surface treatment 79−50467
step-index, modal-noise probability distrib. meas. and anal. 80−99859
step-index, mode conversion and radiation losses due to bending 77−11032
step-index, nearly elliptical, with high eccentricity, fabrication for studying modes 80−95989
step-index, pulse dispersion, neutron irrad. effects 80−91897
step-index fibre, scattering from arbitarily located off-axis inhomogeneity 80−58702
step-index fibre baseband equalisation 78−1371
step-index fibres, multimode silicone-clad, mode dispersion 80−33142
step-index fibres, pulse responses investig. using WKB approx. 80−91898
step-index fibres with microbending, bandwidth 80−23775
step-index monomode fibre, mode dispersion anal. of approx. for propag. const. 80−1307
step-index multimode, analogue transmission system optimum receiver considerations 79−68449
step-index multimode, curvature distrib. and mode conversion due to mode scrambler *(Japanese)* 79−98500
step-index multimode, experimental optical communication system appl. *(Japanese)* 78−90503
step-index multimode guide, optical diffusion coefficients 77−11031
step-index multimode optical fibre fundamental mode meas. 79−46051
step-index optical fibre, scatt. from off-axis inhomogeneity, radiation loss 80−43446
step-index optical fibre, scattering and guided mode conversion due to spherical object, theoretical anal. 80−64153
step-index optical fibre and cable transmission characteristics 78−1404
step-index optimal fibre, scatt. and mode conversion of guided modes by spherical object 79−81558
step-index single-mode fibres, birefringence in limit of weak guidance and slight ellipticity 80−1309
step-index single-mode fibres, zero-mode dispersion 78−87141
stepping motor microprocessor controller for 100 kJ CO_2 laser beam alignment system 77−54035
stimulated Raman emission in single-mode fibres by Nd:YAG laser pumping in low-dispersion region at 1.3 μm 80−64100
stimulated Raman scatt., backscatter in an optical fibre 80−64109
stimulated Raman scatt. dynamics, Stokes components recording opposite to pump wave 80−106569
stimulated Raman scattering, cascade effects *(Russian)* 77−23714
stimulated Raman scattering, quasicompensated losses 77−14811
stimulated Raman scattering, three-wave, rel. to fibre characts. *(French)* 80−78902
stimulated Raman scattering dynamics by Stokes component detect. 80−14394
strain measurement in coated optical fibres and cables using resistance wire 80−23804
stranding pitch, numerical calc. using stranded wire theory 80−10036
strength, statistical data, graphical and analytic statistical model depiction 77−83975
strength and fracture behaviour 79−59828
strength distribution description using upper and lower limits 80−53470
strength testing, tensile, extrapolation of short length test results 78−9456
strength tests, pulling machine construction 78−33931
stress corrosion susceptibility constant, meas. 80−66680
stress-optical degradation obs. 78−1402
structural characteristics, CVD fabrication process, transmission properties 79−59806
sub-optimal graded index optical fibre analysis using perturbation calculus 80−87480
submarine cable using glass fibre, expt. cable *(German)* 80−58711
submarine optical fibre cable unit design and test results 78−46799
subpicosecond response meas. 80−78961
substrate tube diameter control during MCVD preform preparation 79−50463
sum frequency generation of visible light, Q-switched mode-locked Nd:YAG laser excitation 80−43399
supervisory/service channel for fibre optic transmission systems 80−95803
surface compressive strength, increase after ageing under load 79−46065
surface defects, influence on fractive strength *(Japanese)* 78−37987
surface wave propag., influence of bulk losses and bulk dispersion 78−33892
switch, for single-mode fibre, optimised design 80−106607
switch, moving fibre, using V-grooved connecting device 79−18509
switch, single-throw, single-pole 79−37001
switch driven by $Pb(Zr,Ti)O_3$ bimorph 79−18502
switch with electrostatic deflection cantilever 80−53427
switch with high reproducibility 79−64329
switches for fault terminal isolation 78−46833
switching, 1×2 optical switch using new type of pentagonal prism 80−64148
system design and component selection 80−58767
system design charts 79−7200
systems and field trials, review 80−58700
T-coupler for multimode optical fibres 78−42457
tactical rugged lightweight fibre-optic cable performance 79−37025
tap for feedback control of GaAlAs laser transmitters, output power stabilities 79−64241
tape twist induced stress estimation and reduction by pretwisting 80−53471
taper couplers, diameter and slope meas. 77−88905
taper ended multimode fibre efficient power coupling with multihetero-junction LED 79−32052
tapered cylindrical optical fibre, radiation characts. 79−10388
tapered fibre coupler for optical pulse backscatter meas. 77−7212
tapered hemispherical end single-mode fibre, efficient coupling from semicond. laser 80−99827
tapered parabolic-index fibre waveguide 79−76803
tapered sections, ray trajectories 79−18508
tapered waveguides, permitting efficient fiber to waveguide coupling 79−50376
tapping element with low insertion loss 79−76826
tapping elements, beam splitter design, for graded index optical fibres 79−72701
tapping elements, beam splitter design 79−72702
tapping elements with thin-film beam splitters directly applied to optical fibre endfaces, fabrication 79−37016
technology and appl., by Swiss firm CAbloptic AG *(German, French)* 79−90005
technology and components of fibre optics systems *(Hungarian)* 78−66900
technology and connector systems, marketing 80−69522
technology and information transmission props. *(German)* 80−10010
technology for interconnection designers 78−46800
tee-coupler for single-mode fibres 80−10000
Telecom Australia optical fibre communications, fibre research and measurement technique developments 80−43456
telecommunication, propag. mechanism and characts. 78−22213
telecommunication appl., development *(Italian)* 77−773
telecommunication applications 78−42432
telecommunication appls. of fibre optic systems 80−1330
telecommunication appls. principal problems 78−63196
telecommunication cable comprising 48 fibres, design and characts. *(Japanese)* 80−58688
telecommunication cable comprising 8 fibres, design and characts. *(Japanese)* 80−58689
telecommunication line, long-distance, operating at 1.3 μm 79−64346
telecommunication links, current progress reviewed 77−50753
telecommunication network, role of fibre optics 80−43484
telecommunication principles and practice *(French)* 78−55463
telecommunication system components, status of development 80−43485
telecommunication system developments 80−58678
telecommunication transmission systems *(Japanese)* 79−27401
telecommunications, comparative assessment of requirements and available systems *(French)* 78−42422
telecommunications appl. 80−87482
telecommunications systems, book 80−86049
telemetry system for EM probe, microwave radiation effects obs. appl. 78−15859
telephone carrier system appl., T1 PCM, fibre cable development 78−9458
telephone carrier systems 78−42463
telephone installation, Las Vegas, 4.5 km fibre optic cable 78−46822
telephone systems, fibre links in Europe 78−46781
temperature effect on fibre transmission 79−18511
temperature effects on transmission in lightguides 79−76817
temporal frequency dependence of modal noise in fibres [optical] 80−58687
tensile and fatigue strength 77−7211
tensile performance of packaged fibres 79−55212
tensile strength, effect of drawing conditions on fibres pulled in graphite furnace 79−50469
tensile strength, preparation conditions influence 80−33205
tensile strength and static fatigue, analysis using Weibull distribution for optimum design 80−85011
tensile strength distrib. and gauge length extrapolation 78−9434
tensile strength of glass fibres 79−46062
tensile strength testing 78−42481
tensile tester, for long optical fibres 78−83123
tensile testing machine 77−3687
tension-coiled single-mode fibres, high birefr. 80−99858
terminal and connector construction 78−59136
test equipment, BPO, view of likely requirements 79−64349
testing, backscattering method, compact optical test unit *(German)* 78−30098
testing of fibre cable for lightwave communications systems 80−102865
testing of lightguide cable 80−64230
testing using digital processing oscilloscope 78−22188
tetrachloroethylene filled optical fibre, transmission properties, compatible LED, optical link appl. 77−39060
theory, basic principles and equations, multimode and single-mode fibre characteristics 80−43457

optical fibres continued
theory, review 78−1351
thick film optical waveguide integration with fibre-optic connectors 80−33246
three-fibre optical interconnection for interface loss reduction 78−94439
three-layer quasisingle-mode fibre waveguides, data transmission 79−94360
time-dispersion meas. by near and far-field scanning technique 78−74978
time-domain reflectometer for attenuation measurement and fault location 79−64355
time-domain reflectometer with gated photomultiplier receiver, fibre break detection appl. 77−65620
timing error tolerant waveforms in optical fibre systems 80−14293
tip lens fabrication and smoothing 78−33923
total dispersion in step-index monomode fibres 79−68427
total loss spectra, precise meas., automatic meas. system 80−64169
training, educational course status and effectiveness 80−62413
transfer function meas., baseband frequency response *(French)* 77−79919
transfer function meas., swept-frequency technique 78−1375
transit time profiles of bent fibre bundles 77−88944
transition fibre fabrication for coupling fibres to integrated optical films 77−39061
transition fibre production for coupling DH lasers to single mode fibre 77−39062
transmission, applications and cable techniques *(Japanese)* 80−87493
transmission, dispersion, and strength characteristics 79−37021
transmission application, American view *(German)* 78−33845
transmission between 0.8 and 1.4 micron 78−37990
transmission cables, history and basic principles 80−69543
transmission capability expansion 78−66914
transmission characteristic meas. by digital processing oscilloscope 79−12787
transmission characteristics, long fibre, pulse circulation meas. 77−79925
transmission characteristics *(Japanese)* 79−27402
transmission characteristics measurement using backscatter technique, power decay separation from fibre imperfection contribution appl. 80−53409
transmission characteristics of mode-coupled graded-index multimode optical fibers 78−90526
transmission characts., meas. methods *(French)* 77−11019
transmission characts. meas. by computerised signal processing system 79−76876
transmission characts. of graded-index fibres with lossy outer layer 78−55437
transmission characts. of optical waveguides with periodic external force 80−99873
transmission design analysis *(Spanish)* 79−94349
transmission devices, including laser optical modulators and solid-state techniques *(Spanish)* 79−23079
transmission error investigation, receiver circuits *(Italian)* 77−54775
transmission experiment, 800 Mb/s, using single-mode fibre 77−88917
transmission experiment, 800 Mbit/sec at 1.05 μm 78−83075
transmission experiments, 100 Mb/s and 400 Mb/s PCM signals 77−88918
transmission expts. at 1.3 μm wavelength *(Japanese)* 80−28318
transmission expts. at 34 Mb/s with HDB3 line code 80−64198
transmission expts. for 100 Mb/s and 400 Mb/s PCM signals 78−1323
transmission in TE_{01} mode 80−53432
transmission line, bandwidth ultimate performance, lecture 78−25992
transmission lines, $Al_xGa_{1-x}As$ injection laser as transmitter 77−7134
transmission lines, energy loss due to optical correction of time distortions 79−50394
transmission lines, systems aspects 77−54792
transmission lines, use of microoptical switches 78−38085
transmission link technology 78−46772
transmission loss and pulse delay distortion before and after cabling 78−1406
transmission loss characteristics, low OH content optical fibres *(Japanese)* 79−64327
transmission loss characteristics of optical fibres under hydrostatic pressure 80−99869
transmission losses due to offset, end separation and angular misalignment 78−71202
transmission meas. technique using time dispersion of Cerenkov radiation 78−5557
transmission meas. without disturbing integrity 77−72076
transmission of 565 Mbit/s signals on coaxial cables and optical waveguides 80−43483
transmission of communications, laser light and fibre optics techniques *(German)* 80−5827
transmission performance, costs, fabrication 77−11017
transmission problems *(French)* 77−79918
transmission properties *(Czech)* 80−1305
transmission properties meas. 77−11006
transmission props. *(Japanese)* 78−90517
transmission system, component specifications 78−59157
transmission system, investigation of active and passive devices *(Japanese)* 80−58693
transmission system, radiation hardened, 400 MHz bandwidth, linear response 77−23750
transmission system, single-mode, temp. stabilized optical modulator 79−41450
transmission system, UK Post Office feasibility trial 78−1417
transmission system at 1.32 μm using CW Nd:YAG laser 79−94331
transmission system filtering prism *(Japanese)* 78−9441
transmission system in low-loss 1.0 to 1.4 μm wavelength region 77−11030
transmission system planning *(French)* 80−87551
transmission systems, 1.2-1.5 μm, economic evaluations and forecasts 80−87533
transmission systems, active and passive devices 80−43463
transmission systems, components construction and function *(German)* 79−10386
transmission systems, development progress 80−43482
transmission systems, reliability tests on optical semiconductor devices 80−43464
transmission systems and components 79−10384
transmission systems comparsion, 0.8 to 1.4 μm 78−46824
transmission systems design 78−1352
optical fibres continued
transmission systems using optical fibres, cables and connections *(German)* 80−99839
transmission technique status in Germany 78−1416
transmission technology, progress review 78−1330
transmission technology, single mode systems in 1.0 to 1.8 μm region, review 80−38105
transmissions, optical, timing extraction 79−10397
transmissive star coupler for single fibre cables, mixer rod power distrib. inhomogeneities 78−46832
transmittance of fibre lightguides, approx. calc. 79−55228
transmitter and coupling techniques *(German)* 77−11008
transverse light coupling, from GaAs laser 78−18045
trifluoroethyl methacrylate vinyl chlorobenzoate copolymer light focusing rod, photocopolymerisation temp. effect *(Japanese)* 79−46043
triple-ball connector using fibre-bead location 80−43431
truncated parabolic-index, with minimum mode dispersion, anal. 78−38000
tunnelling ray attenuation, generalised parameters 78−66908
TV signals two-way optical transmission using single optical fibre 79−27419
twisted elliptical optical fibre, polarisation coupling 80−99831
twisted single-mode fibres, polarisation optics 79−81524
two-beam interferometry using tapered optical fibres *(Japanese)* 77−49767
two-dimensional fibres, microbending theory, role of nonadjacent mode coupling 79−27415
two-layer elliptical fibre waveguides, first higher-mode cutoff 80−58684
two-mode, mode dispersion free charact., group delay times 79−27396
two-mode, temporal spreading of pulse 80−33183
two-mode fibre with near optimum index-profile, transmission charact. meas. 80−96000
two-phase flow, high-temperature optical void probe 79−93705
two-way transmission expts. over single fibre at same wavelength using micro-optic 3 dB couplers 78−55450
types, charact. and fabrication for communication appl., designer's viewpoint 77−46788
UK optical fibre communication system feasibility trials *(German)* 78−33877
UK Post Office junction and trunk network applications for optical fibre systems *(German)* 78−38016
ultimate low-loss single-mode fibre with 0.20 dB/km loss at 1.55 micron 79−36996
ultra wide bandwidth, fabrication by vapour axial deposition method 80−69508
ultratrace impurities determ., and behaviour during production by CVD process *(Japanese)* 80−87505
unclad, backscattered light, approx. ray theory 77−7177
unclad fibre cross section defects determ. *(French)* 79−89991
underground optical cable transmission meas. 78−50942
undersea cables, small, recent experiences 80−14488
undersea communications, use of low-loss fibre cables 78−59126
undersea fibre-optic cable link performance 78−46807
uniform asymptotic theory 80−28323
uniform theory of inhomogeneous waveguide modes near cut-off 80−28324
unit core cable structure design, fabrication and characterisation 79−37030
unordered fibre bundles, parallel image transmission, multicomponent hologram arranger 80−78957
US Navy fibre-optic technology and systems 77−39063
UV cured epoxy acrylate coated, zero stress ageing effect on strength 80−58753
UV radiation-induced losses during prepolymer coating crosslinking 80−87517
V-value measurement 77−7193
vacuum assisted Si chip multifibre chuck 77−72096
vacuum furnace, optical fibre-drawing 78−66960
VAD, OH-free 80−99887
VAD, ultimately low OH content achievement, by optimised dehydration 80−99845
VAD cables, charact. 80−43461
vapour deposition, plasma-augmented 79−50451
vapour phase axial deposited cable charact. *(Japanese)* 80−58691
vapour phase axial deposition, OH content reduction by flame hydrolysis control 80−48474
vapour-oxidation fabricated, refractive index modulation, pulse dispersion 80−58756
vapour-phase axial-deposition, OH-ion reduction 79−94376
variable attenuator 79−64328
variable optical alternator, calibrated, expt. 77−39047
vibration induced polarisation modulation 79−27385
vibration measurement using flexible coherent fibre probe 78−25975
vibration-induced intensity modulation of fibreguide transmission 77−23743
vibration-induced modulation in bent optical fibre waveguide 78−1405
video signal, fibre-optic transmission by laser diode analogue baseband modulation 80−58738
video transmission, using PFM noise performance, cable attenuation 77−65634
vitreous oxides, Raman cross sections, rel. to appl. in fibre Raman lasers 78−31176
voice transmission using unmodulated transmission of AF, telephone terminal sets *(German)* 80−28314
VSB-FDM system for video trunking, transmission performance, CATV design 77−62054
W-fibre, leaky mode struct. and attenuation 77−79928
W-fibre with square core, confined guided modes 79−59813
W-fibreguides with rectangular core, confined propag. of optical modes 79−98467
W-shaped fibre waveguide with rectangular core and two-layer shell, eigenmodes 80−28340
W-type fibre, parabolic core, cutoff frequencies 78−94436
W-type fibres, mode excitation by tilted and offset Gaussian beams 78−90498
wall thickness, effect on optical systems for data transmission *(Spanish)* 79−18543
water contamination, diffusion of OH in core and H_2O in cladding, transmission props. 78−42420
water diffusion, measured changes with time in OH absorpt. 79−46082
waveguide and cable parameter meas. techniques *(German)* 78−33860

optical fibres continued
waveguide for time-of-flight spectra 80−23767
waveguide tapers for optical coupling of optical fibres, appls. *(German)* 80−38107
waveguide theory, conf., Lannion, France (Sep. 1976) 77−23755
wavelength dispersion, difference method measurement 78−37974
wavelength dispersion directly measured by 'difference method' in 0.8-1.6 μm range 79−50395
wavelength division multiplexer using optical fibre pieces 80−91917
wavelength division multiplexing transmission technology 80−58727
wavelength division two-way fibre optic transmission expt. using micro-optic duplexers 78−22194
wavelength multiplexer, single-mode-fibre 80−102816
wavelength multiplexing for information transmission 79−22906
wavelength-division multiplexing transmission via single fibre, multiplexer design 80−33222
weak-guidance approximation, first-order correction 78−90519
weakly guiding, modal propagation for arbitrary cross sectional shape 80−10014
weakly guiding, modes calc. by integral representation technique 80−58758
weakly guiding fibres, Maxwell eqn. reformulation of EM propag. 80−78974
West German developments 1978 survey *(Swedish)* 79−55209
wideband subcarrier PFM analogue optical communications channel 77−27378
wideband transmission, short distance links, introduction 79−3773
wideband transmission systems, losses due to fibre joints *(German)* 79−64325
WKB approximation for step and parabolic index profiles, eigenvalues 77−34947
Y-branch, low-loss 80−10004
Y-branch for optical communication networks and measuring equipment *(German)* 78−66918
Y-shaped, signal splitter, constructed by fusion welding single clad fibre to 2 parallel unclad fibres 79−50432
zero dispersion wavelength, pulse delay meas. 78−30064
zero material dispersion wavelength determ. by pulse delay meas. 78−1322
zero total dispersion in graded-index single-mode fibres 79−76830
Ag halide optical fibres, extrusion, visible and IR transmission 80−58829
Ag halide polycrystalline fibre, 10.6 μm transmission loss obs. 80−64197
AgBr single-crystal IR optical fibres, growth from melt 80−53449
(Al,Ga)As LEDs, high-radiance double-heterostructure for optical fibre links 78−37991
Al coated, empirical formula for induced excess loss 79−46074
AlGaAs multimode laser, longitudinal modes intensity fluctuations effect on high bit-rate optical transmission 79−68415
AlGaAs-GaAs lasers for optical fibre transmission, defects and degradation 79−41382
As_2S_3 polyethersulphone sandwich ribbon fibre for coupling high refractive index integrated optics 79−32089
B_2O_3-SiO_2 fibres, exposed cladding technique, birefr. and polarization props. 79−14094
B_2O_3-SiO_2 low-loss single mode fibres, design, fabrication and transmission characts. 78−71199
$(B_2O_3)_x$-$(SiO_2)_{1-x}$, spontaneous Raman scattering *(French)* 79−78674
BaF_2, ultralow loss optical fibre material, loss mechanism 80−78920
BaO-GeO_2-Na_2O borosilicate core glasses for high numerical aperture fibres 80−69534
CsI, ultralow loss optical fibre material, loss mechanism 80−78920
GaAlAs DH laser coherent light, propagating in multimode optical fibre, speckle contrast 80−78978
(GaAl)As injection lasers operating with optical fibre external resonator, characts. 80−58544
(GaAl)As injection lasers operating with optical fibre resonators 80−91812
GaAlAs LED sources for fibre optic transmission, linearity improvement using phase-shift-modulation technique 77−19403
$Ga_{1-x}Al_xAs$ transparent LED, optical wavelength multiplex transmission system appl. 78−30063
GaAs DH laser/fibre transmission system modulation and injection 77−50764
GdF_3-BaF_2-ZrF_4 glass fibres, IR transmission, losses, fabrication 80−87516
Ge:SiO_2, zero total dispersion in step-index monomode fibres at 1.3 and 1.55 micron 79−68428
GeO_2 doped glass for optical fibres, wavelength dispersive props. 79−3774
GeO_2 doped gradient optical fibres, pulse dispersion *(German)* 80−74496
GeO_2 doped silica, low loss single mode fibre, CVD *(Japanese)* 78−37979
GeO_2-Al_2O_3-SiO_2 fibres, ageing effects of moisture on fatigue and tensile strength 80−66539
GeO_2-B_2O_3-SiO_2, glass fibre, pulse transmission meas. of zero material dispersion 77−88937
GeO_2-B_2O_3-SiO_2 fibres, optical transmission loss as function of drawing conditions 79−32038
GeO_2-Na_2O borosilicate glass fibre prod. by phase separation and leaching 80−69558
GeO_2-P_2O_5-SiO_2, optimum profile parameter on graded-index optical fibre at 1.27 μm wavelength 79−14096
GeO_2-P_2O_5-SiO_2 glass fibre, incorporation of OH in modified CVD process 80−50560
GeO_2-P_2O_5-SiO_2 graded-index fibres, effect of deposition rate on spectral loss 80−87485
GeO_2-P_2O_5-SiO_2 graded index optical fibres optimised for 1.3 μm wavelength region, fabrication techniques *(Japanese)* 80−99888
GeO_2-P_2O_5-SiO_2 long spliced graded-index fibre transmission characts. at 1.27 μm 79−81536
GeO_2.B_2O_3.SiO_2 glasses, material and mode dispersion 77−19415
$In_{0.53}Ga_{0.47}As$ p-i-n photodiodes, for long-wavelength fibre-optic systems 80−5826
KCl, ultralow loss optical fibre material, loss mechanism 80−78920
LiF, ultralow loss optical fibre material, loss mechanism 80−78920
$LiNdP_4O_{12}$ electroluminescent diode pumped miniaturized laser for optical transmission system, using graded index fibres 79−41395
Na_2O-B_2O_3-SiO_2 glass fibre, prep. with low loss 79−59850
optical fibres continued
Na_2O-B_2O_3-SiO_2 glass fibre, plastic coating influence on strength 80−58697
Na_2O-B_2O_3-SiO_2 glass fibre, plastic-coated, liq. N_2 strength 80−58707
Na_2O-B_2O_3-SiO_2 glass, low-loss GRIN fibres, double-crucible prod., loss and bandwidth meas. 80−69559
Na_2O-B_2O_3-SiO_2 low-loss optical fibre prep. by double crucible technique *(German)* 78−33929
Na_2O-B_2O_3-SiO_2:GeO_2 medium-loss graded-index preform fabrication by phase separation and leaching *(German)* 78−33930
Na_2O-CaO-SiO_2, for optical fibres, high purity glass production methods 78−87176
Na_2O-K_2O-GeO_2-SiO_2-As_2O_3 glass, water extraction for making graded index optical fibres 80−28361
Nd:glass fibre optical quantum image amplifier 78−1261
Nd:YAG fibre laser, self-contained LED-pumped single-crystal 78−1264
Nd^{3+}:quartz fibre, stimulated radiation generation and amplification 77−88729
Nd^{3+}:YAG, Raman laser with optical-fibre resonator, expt. investigation 79−31913
P_2O_5-SiO_2 clad low-loss monomode fibres for 1.2 to 1.6 μm, modified CVD prep. 80−48479
P_2O_5-SiO_2-GeO_2 graded-index optical fibre, UV induced losses 80−87518
$(P_2O_5)_x$-$(SiO_2)_{1-x}$, spontaneous Raman scattering *(French)* 79−78674
PbF_2-AlF_3 glass, optical props., crystn. and thermal expansion 80−48367
PbO-SiO_2 large-core, high-NA cable for short-distance communication systems 79−50427
Si, advances in fabrication using MCVD process 80−99875
Si alignment chips for optical fibre cable connector 78−1411
Si array connector with low splice loss 78−55441
Si, drawn at high temperatures, preform method *(Italian)* 77−3646
Si, mass production method using a plasma torch *(French)* 77−11026
Si-O fibres, parametric excitation of anti-Stokes coherent stimulated scatt. *(Russian)* 80−58637
$SiCl_4$-$GeCl_4$-BCl_4 particulate layers consolidation, in fabrication of optical fibre preforms 80−60787
$SiCl_4+O_2$ in modified CVD process for optical fibre prod., reaction IR spectra 78−80472
Si_3N_4 coated fibres for high-strength and improved fatigue 79−50470
SiO_2 *(German)* 78−33869
SiO_2 based glass systems, refr. index and comp. data 77−79950
SiO_2 based optical fibre waveguides, water impurity 77−68270
SiO_2 clad, elongation, force depend., deviations from linearity 80−45334
SiO_2, coated silica fibres, tensile strengths of 1 km lengths 78−1384
SiO_2, doped, waveguide, effect of ionising radiation on optical attenuation 78−63170
SiO_2, drawing, neck-down shape prediction from furnace temp. distrib. 78−5594
SiO_2, drawing using ZrO_2 induction furnace 78−1446
SiO_2, fibre, appl. to transmission of solar radiation 77−3663
SiO_2 fibre, CW tunable near IR Raman oscillator 78−1235
SiO_2 fibre lightguides, fused, zero stress strength reduction and transitions in static fatigue 80−87523
SiO_2 fibre near IR Raman laser, as universal fibre optic meas. system 79−23070
SiO_2, fibre waveguide, backward Raman amplification and pulse steepening 77−23740
SiO_2 fibres, fused, drawn from rods, oxy-H_2 flame, prep., strength, dia. var. 80−102868
SiO_2 fibres, reductions in static fatigue by hermetic jacketing with Al 79−43448
SiO_2, fused, for linking very large astronomical telescope array 78−32342
SiO_2, fused, polymer coated optical fibre, static and dynamic fatigue 79−29244
SiO_2, fused optical fibre, strength, appl. of Weibull type analysis 77−19418
SiO_2, fused silica fibres, high-strength epoxy-acrylate coated, dynamic and static fatigue 78−1385
SiO_2, fused silica fibre lightguide, static fatigue transitions 80−58744
SiO_2, GeO_2 doped single-mode fibre with low loss at material-dispersion-free wavelength of 1.27 μm 77−68266
SiO_2 glass, high rate MCVD of optical fibres 80−83671
SiO_2 glass, low loss optical fibre, radiation-induced IR absorpt. 80−87521
SiO_2 glass fibre, plastic-coated, liq. N_2 strength 80−58707
SiO_2 glass fibre drawing, caustic curves in solidified drawdown zones 77−39117
SiO_2 glass fibres, stimulated Raman scattering spectra 78−66869
SiO_2, intrinsic attenuation 78−30067
SiO_2, laser drawn fibers, tension rel. to drawing vel. and ultimate strength 78−74986
SiO_2, manufacture using modified CVD method *(Japanese)* 80−99864
SiO_2 multimode fibre stimulated Raman scatt. obs. 78−1396
SiO_2 optical fibres, self-phase modulation 78−66874
SiO_2, phys. behaviour of neck-down region during furnace drawing 78−83127
SiO_2, plastic-clad, short-term transient radiation effects 79−50420
SiO_2, scatt. cell for inverse Raman scatt. of liqs. 79−9249
SiO_2, silica, low-birefringence silicone-clad, for magneto-optic current measurements 79−50425
SiO_2, silica, plastic-clad, termination by stripping and recladding 79−41466
SiO_2, silica, synthetic, tubing and fibre fabrication using SiO_2-B_2O_3 79−50462
SiO_2, silica fibre, transmission of high power laser radiation, role of stimulated Raman scatt. 79−37011
SiO_2, silica fibres, silicone clad, in flat cable form, characts. 78−66930
SiO_2 silica glass fibre CVD manufacture and characteristics 80−28345
SiO_2, silica optical fibre preforms, OH-ion distribution 79−14121
SiO_2 silica preform, doped deposited, Cl drying simultaneous with consolidation 79−50466
SiO_2, single-mode, CW three-wave mixing 79−10352
SiO_2 single-mode optical fibre, wavelength dispersion characts. in low-loss region 80−53423
SiO_2, three-wave stimulated Raman scatt. obs. *(French)* 80−78902
SiO_2, ultralow loss optical fibre material, loss mechanism 80−78920
SiO_2:F, silica fibres, numerical aperture and attenuation, drawing from preforms 78−1449
SiO_2:F fibre preform plasma chemical deposition *(German)* 78−33926

optical fibres continued
SiO_2:F fibre preparation by plasma-activated CVD *(German)* 78−33927
SiO_2:F layers, deposition from $SiCl_4$-SiF_4-O_2 gas mixture by plasma CVD method 78−95699
SiO_2:Ge silica-core, effect of B, P and OH on radiation response 79−50419
SiO_2:Ge single mode fibre, low loss transmission of high speed pulse signals at 1.29 μm 78−42409
SiO_2:Ge single-mode fibres, dispersion meas., pulse synchronisation technique 80−48410
SiO_2:GeO_2, definitive profile-dispersion data over extended wavelength range 79−76828
SiO_2:GeO_2 graded-index fibres, without index dip, fabrication by CVD method 78−9431
SiO_2:GeO_2 intrinsic attenuation 78−30067
SiO_2:GeO_2 single-mode optical fabre fabrication 79−46050
SiO_2:GeO_2/SiO_2, SiO_2/SiO_2:B_2O_3, glass fibre waveguides, γ-radiation optical stability 80−23799
SiO_2:GeO_2-P_2O_5 graded-index fibre, spectral loss charact. in long wavelength band 79−59811
SiO_2:Ge(P) fibres, pulse delay meas. in zero-material-dispersion region 78−46769
SiO_2:P_2O_5, GeO_2 fibre, anomalous conc. profile of P_2O_5 and GeO_2 77−79943
SiO_2:P_2O_5, stimulated Raman scattering *(French)* 79−27324
SiO_2:P_2O_5 intrinsic attenuation 78−30067
SiO_2:P_2O_5-GeO_2 core graded index fibre with SiO_2:B_2O_3, P_2O_5 cladding, low loss at 1.3 μm 80−99874
SiO_2-B_2O_3(P_2O_5)(GeO_2), wavelength dispersive props. and composition in optical fibres 78−33793
SiO_2-based single-mode, dispersion minimisation over wide spectral range 80−9997
SiO_2-GeO_2, 21.2 km graded-index VAD fibre with low loss and wide bandwidth 80−53414
SiO_2-GeO_2, preform prep., particulate mass transfer mechanism in modified CVD, thermophoresis 80−2955
SiO_2-GeO_2 core single mode fibre with SiO_2:P_2O_5 cladding, 1.6 μm, low loss 80−99874
SiO_2-GeO_2 core with borosilicate cladding, low loss 77−62072
SiO_2-GeO_2 particles, deposition props. in flame hydrolysis reaction for optical fibre fabrication 80−48470
SiO_2-GeO_2/SiO_2 load bearing optical cable, geophys. appls. 80−91923
SiO_2-P_2O_5 binary glass, fibre fusion temp. rel. to composition 78−95131
SiO_2-P_2O_5 cladding vapour-phase axial deposition fibres at 1.3 μm and 1.6 μm 80−9996
SiO_2-P_2O_5 glass, refr. index behaviour, optical fibre appl. 77−46777
SiO_2-P_2O_5-GeO_2 optical fibres, CVD, losses, reactant impurity effects 80−87522
SiO_2(-GeO)$_2$(P_2O_5)(B_2O_3), optical attenuation in IR region 77−75665
$Si0_2$:Ge, B, P, radiation induced optical absorpt. spectra, 0.4 to 1.7 μm region 80−58761
TlBr, TlBr-TlI, polycryst. core waveguides, IR transmission charact. 77−88936
TlCl-TlBr, KRS-6, ultralow loss optical fibre material, loss mechanism 80−78920
W, fundamental mode microbending loss 77−23762
YAG:Nd, glass clad, 1.3 μm CW laser operation with LED end pumping 77−7120
$ZnCl_2$ glass, potential ultralow loss optical fibre material 78−74955

optical films
see also antireflection coatings
absorbing film on non-absorbing substrate, optical consts. calc. 77−11041
absorbing film-nonabsorbing substrate system optical parameters, FORTRAN code *(Rumanian)* 77−69923
absorbing films, optical parameters determ. by ellipsometry 80−254
absorbing multilayers, representation and appl. to refl. interf. filters 79−7207
absorption coefficients meas. by ATR spectroscopy 78−37073
absorption coefficients meas. by laser calorimetry 78−25905
absorption light filters, thin-film 80−19101
absorption measurement by 1.06 μm laser calorimeter 80−33066
absorption of weakly absorbing thin layer 79−11481
absorptive coatings, at normal incidence, program for TI-59 calculator 80−84793
absorptive laser damage analysis by Weibull distrib. 80−33061
achromatic low refl. and beamsplitting coating synthesis 79−98496
achromatic metal-dielectric mirror coating, computer synthesis 78−46750
adherent dielectric coatings of diamond-turned mirrors 78−33810
alkali halide thin films, photoacoustic determ. of optical absorptance of highly transparent solids 79−40632
alumina half-wave facet coatings, for (Al,Ga)As CW laser 77−23688
anisotropic waveguide for integrated optics, monomolecular layered film 78−66954
annular wedge-shaped layer coatings, apparatus for prod. 77−14817
anomalous resonances in anisotropic multilayer structures 79−45902
antireflection multiple wideband layers, expt. *(Hungarian)* 77−3645
application technology, review of problems 78−83069
aspherising layer prod., monitoring by interf. fringes in periscopic microscope 77−14820
automatic deposition of optically active layers, single and multicoated on industrial scale *(Hungarian)* 77−75718
baffle edge design using optical black coating 78−59154
beam splitter phase coatings, for producing phase quadrature interferometer outputs 78−77974
beam splitter using variable thickness film, for integrated optics 77−65626
black coatings on high-temp. alloys, for central-receiver, solar-thermal power systems 78−18071
blackened optical surfaces, IR absorpt. rel. to stray light reduction, spectral emittance meas. 79−61449
broadband dielectric mirror interference coatings, scatter losses 79−50365
buffer layer theory, effect of a single layer in stack of dielectric layers 78−33800
buried metal grating coated with polished dielec. layer and dielec. multilayer, phenomenological theory 79−50374
cermet film, as solar selective absorbers, production, struct. and optical props. 79−29485
characterisation, optical, struct. and mechanical properties 79−76772

optical films continued
chirp reversal, optical integration in degenerate four-wave mixing 78−46730
cholesteric liquid crystal coatings, superimposed left- and right-handed, peak refl. and colour gamut 80−74472
circular membrane reflector made by surface bending due to electrostatic tension 80−91876
coated metal mirrors, p-polarised light total absorpt. by surface plasma waves 78−88373
coated mirrors, large-spot DF laser damage obs. 79−14022
coating, low reflection, three layer, spectral charact. computed 77−759
coating, thin film surface irregularities rel. to optical props. *(Russian)* 77−11047
coating abrasion resistance characterisation test 79−14129
coating adhesion characterisation pull-off tests 79−14128
coating removal by Al_2O_3 powder and NH_4HF_2 soln. 80−74521
coating requirements in United States military specifications 80−48365
coating stabilities, refl. factor 77−83958
coating technique and refractive index meas. 80−43488
coating thickness measurement, optical monitoring 79−90041
coatings, basic developments 78−74964
cold light mirror multilayer coating deposition 80−87464
complex index of refraction determ. for highly absorbant film, appl. to Pb_xTe_{1-x} 78−54445
conference on optical coatings, Washington, USA (March 1978) 79−46028
constant measurement by light intensity ratios 77−2678
constant-thickness film formation on axially symmetrical substrate 79−27453
control of multidielectric stacks using chromatic maximeter, Fourier series anal. of signal *(French)* 78−83111
deformable mirror high-reflectance dielectric coatings 79−14085
deposition automated control system, design principles 80−64220
deposition by high freq. cathodic method, TiO_2, ZrO_2 and SiO_2 optical coatings 79−76900
deposition with periodically pulsed CO_2 laser, film charact. 79−28926
design of multi-layer systems, using equivalent films and graphical aids *(Czech)* 78−90486
dichroic multilayer mirror for 16 μm region, design and fabrication 80−5808
dielectric, fabrication, packing density, appls. 77−752
dielectric coating, highly dispersive artificial dielectric utilising metal spheres 80−5690
dielectric coating adhesion improvement of diamond turned mirrors, ion polishing surface prep. 79−23102
dielectric coatings, algorithms for determ. of reflectance and transmittance 79−98271
dielectric coatings, optical charact., effect of electric field during film condensation 80−69539
dielectric coatings on Be substrate based mirrors 77−62034
dielectric interference coatings, optical props. variation with time 79−99963
dielectric interference film, with equal optical thicknesses of layers, theoretical design *(Russian)* 80−43471
dielectric laser mirror production with variable transmissivity *(Russian)* 80−14362
dielectric multilayer coated optical surface, diffr. and diffuse scatt. 79−50220
dielectric multilayer coating, optical phase shift at boundary, reflection coeffs. 77−34926
dielectric multilayer interference devices, loss mechanisms 77−83943
dielectric multilayers, laser damage, elec. field strength role 77−61993
dielectric multilayers, optical and geometrical thickness monitoring using monochromatic maximeter, substrate effects *(French)* 80−38140
dielectric refractive index and thickness meas. by optical method 80−82806
dielectric thin film deposition by CW CO_2 laser, optical and struct. props. 80−7506
dielectric thin film multilayer systems, polarisation effects and use in laser physics *(German)* 78−33912
dielectric thin films, electron beam deposited, anomalous optical absorpt. 77−20947
directional coupler covered with high-index absorbing material, damped oscill. 80−91908
directional coupler phase tuning by chalcogenide glass film loading 78−1373
DOBAMBC, chiral smectic C-phase ferroelectric liq. crystal film, classical X-Y system, props. 80−44123
dye doped polyurethane film, photoinduced guided light stopping 77−23739
dye laser, thin film waveguide evanescent type, gain meas. 80−95908
dye molecule monolayer displaced from metal surface, light refl., coupling with metal surface modes 78−48246
electric field and absorption distributions 77−601
electron microscopy of cross sections 77−19387
ellipsometry, modulated light, for substrate and thin film meas. at 10.6 μm 78−54442
evaporated, optical thickness monitoring 78−5591
evaporator, tubular-type radiation-heated, ZnS film deposition 80−76191
exponentially varying refr. index layer, oblique incidence of light, interf. matrix 78−55296
far IR transmission spectral bandshape 77−32363
fibre coating structure for microbending loss minimisation 80−28346
film refractive index and thickness meas., error anal. of SYNCANG and SYNCWANG methods 78−8439
filter, narrowband reflection type, charact. calc. 77−766
fluorescent capping layers, powdered, solar cells wavelength shifting 80−85286
fluoride materials, refractive index, spectroreflectometry meas. 250 to 2000 nm 79−32006
Fresnel formula for dielectric multilayer mirrors 80−33118
Fresnel lens film prep. by electron beam irradiated mould polymerisation 79−98515
glass, 7059, film acousto-optical props. for integrated optical Bragg cell 79−55251
glass film compositions, electrochromism *(Russian)* 79−28721
graded index films appl. to solar absorbers 77−62042
graded-thickness, vacuum-deposited, filters for solar corona obs. appl. 80−76164
guided optics techniques for meas. of film props. 79−99958
hard overcoats in replicated optics 78−66968

optical films continued
heat-radiating coatings with variable degree of blackness, efficiency 77−28027
homogeneous and inhomogeneous films, produced by cosputtering, optical, mechanical and chemical props. 78−6849
hybrid metal-dielectric, reduces cube beamsplitters polarisation sensitivity 77−83981
immersed multilayers, optimum reflectance attainment for TM polarised flux 79−59627
inhomogeneous interface laser mirror coatings, durability improvement 80−1252
inhomogeneous layer synthesis with given spectral characts. 78−52588
inorganic thin layers, two-stage formation 79−27450
integrated optics, review 78−71234
integrated optics, waveguides, new wave phenomena, review 77−54817
interface total reflection and surface wave obs. 80−108292
interference coating, optical characts. topography var. 77−72102
interference coating, theoretical design, with two narrow spectral transmission bands *(Russian)* 79−72666
interference coating, with narrow reflection bands, design *(Russian)* 80−43472
interference coating deposition by Balzers BA-710 vac. system, photometric monitoring 78−46850
interference coating production, new ideas 79−32098
interference coatings, applied optics conf., Oakland, CA, USA (May-June 1980) 80−101661
interference coatings, design, specified characts. 79−3786
interference coatings, for Xe flashlamps, laser pumping efficiency improvement 79−10316
interference coatings for devices transmitting colour images 78−59108
interference coatings on projector reflectors, vac. deposition 77−75725
interference coatings perpared by electron beam evaporation, UV optical strength 79−59779
interference filters, multilayer, design method 80−48396
interference layers, absorpt. coeff. determ. 79−99961
interference polarizers on plane-parallel substrates 80−1336
intermetallic coatings, possible use in power optics elements 79−14084
intermodal dispersion props. for high silica fibres with B_2O_3-SiO_2 and GeO_2-$B_2O_3SiO_2$ graded index profiles 78−71204
ion polishing for diamond-turned mirror dielectric coating adhesion 80−1370
ion polishing of optical coatings, for multilayer interf. systems and integrated optics 80−33261
IR coating for high energy laser reflector and window 79−45951
IR energy-efficient interference coatings 79−23087
IR frustrated-total-reflection polarising beam splitter 79−46047
IR metallic film reflectivity rel. to thickness less than penetration depth 77−39018
IR multilayer optical medium produced by negative photoresist spin-coating 80−74451
IR multilayer partial mirrors effective from 1.3 to 16 μm, GeSe/KRS-6 and GeSe/NaF 80−9978
IR thin film plasma deposition processes 80−87466
laminates, with layers of unequal optical thickness, optical characts. *(Russian)* 77−34819
large optical components for high-power lasers, refl. and transmission meas. 79−44927
large-area uniform thickness evaporated thin films 78−76605
laser beam indicator/visualiser made from new thermochromic material 80−9976
laser coating, UV damage obs. 80−33056
laser coating materials, 100 ns pulsed laser damage at 2.7 and 3.8 μm 80−33057
laser components, conf., Boulder, Colo., USA (July 1976) 77−46729
laser cylindrical resonator thermal distortion due to surface absorbed energy *(Russian)* 78−13729
laser damage, photoacoustic study 80−80098
laser damage resist. for pulsed CO_2 laser 79−45989
laser damage thresholds of coatings for CO_2 laser components 79−14006
laser induced damage in optical materials, symposium, Boulder, USA (Sep. 1978) 80−31417
laser induced damage on coatings immersed in liquids 77−61994
laser optics, Shiva, system, thin film coatings technology 79−7135
laser pulse damage rel. to index and substrate OH^- content 79−14016
laser rate calorimetry analysis with coating absorption 80−33050
laser reflector with non-quarter-wave design, enhanced damage resist. 77−88819
laser window, mirror and reflector coatings, high power, materials selection 77−50735
laser-damage thresholds, meas. and identification 79−45988
laser-induced damage, conference, Boulder, USA (Oct. 1977) 79−14048
layered coating synthesis, optimisation formulae 78−25946
Luneburg thin film lenses, formation by sputtering through circular mask 78−87132
magneto-optical waveguide, semileaky thin film, for modulator appl. 77−62055
mechanical strength of optical components, film effects 78−1318
metal film mirror prep. by ultraclean DC sputtering, optical props. 77−50748
metal films on semicond. substrates transparency 77−16411
metal mirrors, dielec. enhanced, absorptance at 5.3 μm 77−50709
metal oxide layers, obtained by cathode and HF sputtering, light scatt. and refr. index reduction 80−29877
metal oxide/fluoride mirror coatings, light scatt. and optical strength in UV range 80−106595
metal-dielectric interference mirror coatings, high mech. strength 78−30043
metal-dielectric thin film coatings, designing, applications 78−30042
metal-insulator composite films, optical props., rel. to solar collector appls. 78−72622
metal-insulator layers on transparent substrates for making scales 77−798
metallic, structure-related optical characteristics in visible and UV 78−35217
metallic film, IR reflectivity, mirror appl. 78−5536
metallic mirror coatings, protected and unprotected specular reflectance 79−76792
metallic multilayer coatings, algorithms for determ. of reflectance and transmittance 79−98271
metallic reflecting coating for light filter, transmission coeff. zonal nonuniformity 79−32063
optical films continued
metallic thin film apodising and attenuating filters, phase shifts and aberrations 80−87552
microscopic interference obs. by reflection contrast 80−68248
mirror, asymmetric, with thin absorbing film, design 80−69493
mirror reflecting layer, appl. to instrument parts 79−37065
$Mn_{1-x}Cu_xSb$ films, $0 \leq X \leq 0.3$, magneto-optical props. 79−51981
monitoring of film deposition, error compensation 77−75721
monitoring of props. during deposition, wide band monitoring system 79−81582
monochromatic Maximeter control system for thin multidielectric films, stopping criterion *(French)* 80−60694
multi-layer optical system, reflection and transmission coeffs. calcs., computer program 80−66316
multicomponent thin film formation on K8 glass 79−72726
multidielectric film production monochromatic modulator controlled thickness *(French)* 78−75008
multifilm manufacturing, large scale, function stress testing 79−81576
multilayer, design. for non-polarizing beam splitters 78−83110
multilayer, electric field distrib. and laser damage reduction 80−87420
multilayer 532/1064 nm laser reflector damage resistance improvement by non-λ/4 design 79−14019
multilayer antireflection coatings 78−33797
multilayer beamsplitter coatings, accelerated fabrication method 80−102873
multilayer broadband dielectric mirror coatings for Fabry-Perot spectroscopy 77−18101
multilayer coating design achieving a broadband 90° phase shift 80−102801
multilayer coating design with reduced elec. field intensity 77−72046
multilayer coating preformance, thin-film volume or interface absorption effect calc. 80−33130
multilayer coating production with continuous thickness reoptimisation 79−76890
multilayer coatings, high-refl. or antirefl., vol., interface absorpt. and scatt. losses 80−63915
multilayer dielectric coating producing 90° phase change 79−76788
multilayer dielectric enhanced mirrors for 2 to 6 μm 79−14086
multilayer dielectric mirrors, reflectance under slight absorpt. conditions 80−83655
multilayer film, intrinsic and thermal stress modelling and interferometry 79−14059
multilayer film, optical scatt., matrix formulation 79−31804
multilayer highly reflective coating design for wideband 90° phase shift 80−74464
multilayer interference film, mass production by roll coating *(Japanese)* 79−81577
multilayer mirrors, high refl. at fundamental, second and third harmonic laser wavelengths 78−90490
multilayer nonabsorbent coating reflectivity computation program 80−28293
multilayer optical coatings, scatt. due to surface roughness, scalar theory 79−59637
multilayer optical film thickness analyser 78−32785
multilayer optical interference coatings via glow discharge polymerization techniques 78−87170
multilayer polariser, design, prep. and optical characterisation 79−76866
multilayer stack reflectance derivatives, fast computation method 78−46508
multilayer structure devices, nonideal, computation of optical props. 80−5684
multilayer synthesis computations, use of Fourier coeffs. 78−90509
multilayer synthesis program, Fourier transform model 79−7196
multilayers, oblique incidence, elec. fields 77−596
multilayers, polarisation avoidance or enhancement 80−43255
multilayers, ultrathin, optical characts. 80−104005
multiple beam spectral analyser with thin film waveguide feed, prism radiation tap 77−34944
multiple-plate glass systems, spectral directional radiation characts. prediction 78−74956
negative selection, for production of uniform intensity of light 77−2685
m-nitroaniline single crystal fibre waveguide core, melt growth and characts. 77−34965
non-homogeneous, oblique light incidence *(Russian)* 79−13905
nonpolarising glass cube 77−23736
opaque layered system, complete absorpt. of transverse mag. waves 78−39615
optical coatings, review 77−83946
optical consts., determ., matching methods 77−85682
optical inhomogeneity, rel. to struct. 79−83047
optical modulator crystal coatings 77−19431
organic thin film refractive index adjustment by absorbing dyes 80−43413
oscillating beam spectrometer for organic thin film transmission 80−18022
oxide materials, refractive index, spectroreflectometry meas. 250 to 2000 nm 79−32006
oxide single and multi-layer optical coatings, light scattering reduction and meas. 80−48381
paraffin oil coatings for high power laser system components 77−88730
photoacoustic spectroscopy study 80−64124
photochromic film waveguide, acousto-optical props., integrated optics appl. 80−33207
photoimaging system based on photopolymerisation in cryst. coatings 80−40716
photometric standards and coatings, retrofefl. meas. 78−25940
photothermal absorber stacks on Ag, stabilisation 77−32459
plasma polymerised ethane for laser window coatings 77−50737
polariser, thin film, design and fabrication 79−37010
polarising beam splitter, film coatings, cemented cube 77−19422
polymer films, plasma polymerisation, light propag. expt. *(Japanese)* 78−6846
polymer transparent film, protective ability for optical surfaces 77−31135
polymeric, preparation and optical properties meas., by integrated optical techniques 78−27342
polymers for optical waveguide and dye laser, prep. and characts. *(Japanese)* 78−5551
porcelain-on-aluminium, low-absorptance 80−76393
pulsed laser damage determ., optical techniques 80−33060

optical films continued
quarter wave multilayer monitoring, optical props. change rel. to error compensation 80−38139
quarter-wave dielectric reflector, spectral absorptance approximation 80−33131
quarter-wave mirrors, oblique incidence reflection coefficient, small absorption of layers effect 80−64140
quarterwave multilayers, secondary refl. maxima 79−64331
Raman spectrum of layer or thin slice at solid interface 77−48261
rare earth fluorides, CeF_3, PrF_3, LaF_3, coating materials for IR laser components 80−33105
rare earth oxide, transmission of refl. spectra, opt. consts. and parameters 79−95864
rare earth oxide films, optical absorpt., refractive index, band gap and zone struct. *(Russian)* 78−76544
rare earth oxides, electron beam evap., optical and mech. props. 77−79907
Rayleigh scattering, 441.6 nm, scatt. losses correl. with deposition parameters 79−78782
reflectance computation, Smith chart and charact. matrix 79−45904
reflection, transmission and scatt. of light, thin film influence *(French)* 77−34826
reflection coefficient for film with exponential refr. index distrib. *(Russian)* 79−56877
reflection coefficient partial derivatives, matrix calc. *(French)* 80−89080
reflection polarisers and analysers in vac. UV, design criteria 78−55424
reflection spectroscopy, single and multiple, of optical coatings 79−61448
reflective, refractive index, UV polariser mirror coating appl. *(Russian)* 77−34928
reflective multilayer coatings for far UV 77−758
refractive index and thickness, algorithm for determ. on basis of ellipsometric meas. 80−34881
refractive index calculation method for thin film coatings 77−5890
refractive index determ. by micromethod using liq. standards 79−67378
refractive index determ. using reflectance extrema 78−70178
refractive index dispersion meas. by optical waveguiding 79−85162
refractive index meas., modified Abeles method *(Italian)* 78−1427
refractive index meas. method 80−68242
refractive index variation for given reflectivity, analytic soln. to synthesis problem 80−34996
refractory oxide optical coatings, laser damage resist., spectral depend. 77−62022
refractory oxides, interference polarisers for lasers, development 78−83108
removal of coatings from precision optics, using Al_2O_3-HF mixture 78−75005
resonant amplification, total absorption in thin film *(Russian)* 77−7153
review of current problems 78−76540
rough surface light scatt., vector theory, surface plasmon effects 79−59638
scintillators for extended UV response Si detectors 80−86412
selective optical properties, for enhanced output and radiation spectrum correction, light sources appl. *(Russian)* 80−48372
semi-transparent, optical cond., complex index and thickness, photometric meas. *(French)* 77−52193
semileaky anisotropic film waveguide, wave propag. 77−65627
semileaky anisotropic thin-film optical waveguides and mode filters 78−13799
single layer gradient refr. index film, ang. refl. 78−5538
single mode, cut-off wavelength meas. 79−59802
single-layer film 2.8 μm, 3.8 μm absorpt. meas. 78−90463
single-mode exhibiting extremely low polarisation birefringence, fabrication 79−64318
solar collector coatings, for heating and cooling systems 78−30045
solar energy concentrators, optical coatings, accelerated tests, using reliability principle 79−96419
solar materials radiation properties study, wide temperature range 79−94307
space environment effect on coatings 78−85827
specular reflectance standards for visible and infrared region using thin Al film vacuum deposited on optical flats *(Japanese)* 80−102789
sputtered, production and props. *(Hungarian)* 80−53483
sputtered films, optical props. and appls. 78−72623
sputtering by plasma-enriched deposition 79−47629
stack, control by stationary ratio method, refractive index dispersion influence *(French)* 80−60693
stack of dielectric layers, Fourier description of analysis and synthesis operations 78−94449
stray light performance, surface and system scatt. characteristic specification 80−48389
stray light reduction from optical components 78−59114
stray light suppression in optical systems, optical design, computer analysis 78−59113
surface films and bulk material, optical props. meas. using ellipsometry, review 79−44926
system and component specifications, seminar, Washington, USA (Apr. 1979) 80−46731
thickness and optical consts., spectrophotometer meas., computer program evaluation *(French)* 77−13808
thickness limitations, one layer homogeneous coating, mech. strength and specularity 77−75646
thickness meas., Fizeau method and surface deform. of opt. flats 78−77970
thickness monitoring using quartz cryst. monitor 78−5592
thickness monitoring with optical time-domain reflectometer 79−55254
thin film and integrated optics review, theory, expt. techniques, waveguides 78−22220
thin-film lenslike light guide focusing properties 77−54786
thin-film waveguides fabrication, review *(Polish)* 79−3775
three-layer equivalent film design 78−66884
total absorbing optical coatings using black metallic mirrors 79−3767
transmittance standards in spectrophotometry, semi-transparent metallic thin films use 78−32852
transparent, thickness monitoring 79−97358
transparent conducting coatings, book contrib. 78−10587
transparent conducting film surface resistance obs. 77−77313
transparent film on absorbing substrate, optimum angle of incidence for monochromatic interference 80−43254
transparent film thickness and refr. index meas., polarisation-independ. reflectance matching 77−65052
optical films continued
transparent films, on absorbing substrate, refr. index, thickness, ellipsometric meas. 77−52194
transparent optical material surfaces and films, pulsed laser induced damage 79−89948
triethyl methacryloxystannane, protection from biological overgrowths 78−18034
TTF-chloranil visual pressure or temperature indicator 80−87443
two-layer chemical coating, laser radiation damage thresholds 79−76739
two-wave laser coatings for 0.63 and 3.39 μ line prod. *(Russian)* 77−83895
UV coating, damage resistance 80−33047
UV reflecting mirrors for space appls. *(French)* 77−67022
vacuum deposition, improved film quality, progress in vacuum generation and deposition technology 80−35101
vacuum deposition and sputtering, automation and programming of production plants *(Hungarian)* 77−4736
vacuum systems for optical coating prod., review 77−58493
vacuum UV coating technology 79−46030
vacuum UV optics, reflecting coatings and transmitting filters, review 79−46029
vacuum UV special application coatings, reflectance, transmission, technology 79−59788
waveguide fibre coating technology, overview 80−58828
waveshifter coatings for fluorescent radiation convertors 80−32574
weakly absorbing layers, interferometric determ. of optical parameters 79−17471
Ag chemically deposited layer, reflectivity rel. to heat treatment 79−27366
Ag, granular film, anomalous light absorpt., oblique incidence 79−6205
Ag halide thin-film optical recording medium 80−102786
Ag, high temp. stabilisation using SiO_2 78−1319
Ag, photodissolution in amorphous As_2S_3 78−26737
Ag, surface roughness determ. from light scatt. meas. 78−5541
Ag-SiO_2 composite film, optical props., appls. 77−754
$Ag_2S.HgI_2$ and $Ag_2Se.HgI_2$ thin films, transmission spectra and photochromism 79−52032
Al coating reflectivity in vacuum UV, heating effect 80−95981
Al reflective coating, reflectance in UV and visible 80−28307
Al-SiO_2 layered system, complete absorpt. of transverse mag. waves 78−39615
Al_2O_3 facet coating, effect on degradation behaviour of $Ga_{1-x}Al_xAs$ buried heterostruct. injection laser 79−50313
Al_2O_3 facet coating, self-pulsation stabilisation and initial degradation elimination in (Al,Ga)As laser 80−43347
Al_2O_3, film form. by reactive HF sputtering with voltage bias 78−3045
Al_2O_3, optical absorption and external photoeffect, 6-40 eV 77−55802
Al_2O_3, transparent films on Al refr. index, thickness, ellipsometric meas. 77−52195
Al_2O_3-Al, multiphase thin films, correlation between optical props. and chemical/metallurgical constitution 78−19588
Al_2O_3-Si, alternating layers, dielec. facet reflector for semiconductor lasers 78−66841
AnSe, strain induced anisotropy, ellipsometer and reflector meas. 79−33856
As-Ge-S(Se), glass films, photostruct. changes 77−85822
As-S, amorphous film, photoinduced RI changes, heterodyne interferometry 77−3639
As-S amorphous film, photo-induced optical changes, annealing effect 78−27345
As-S glassy film, photobrightening effect 80−11498
As-Se chalcogenide glass, semicond. film, laser stimulated refr. index change, writing/erase cycle 77−50677
As_2S_3 amorphous films, meas. of photoinduced transformations by optical waveguiding 79−43050
As_2S_3 film optical constants, wedged-film meas. 79−14066
As_2S_3, strain induced anisotropy, ellipsometer and reflector meas. 79−33856
$As_2S_3(Se_3)$, film on KCl, strain-induced refractivity anisotropy, 10.6 μ ellipsometric obs. 79−14064
As_2Se_3 film on CaF_2, interface and bulk absorption meas. 80−35001
As_2Se_3, strain induced anisotropy, ellipsometer and reflector meas. 79−33856
As_2Se_3-Cu (10-20%), glassy, darkening kinetics, and hologram diffr. efficiency 77−62027
Au black film, structural composition and its influence on optical props. 78−56530
Au black optical props. rel. to structural composition, appl. to solar absorption 79−83630
Au black solar absorbing film, particulate nature 77−39003
Au film on Al, reflectance and absorpt. obs. 80−7426
Au-MgO cermet, dielectric constant and selective solar absorption 78−2937
$BaTiO_3$, sputtered, refr. index, 0.3-1.0 μm, substrate temp. effects 77−55840
Bi, granular enhancement of laser machining and ageing charact., using $Mg_{0.25}In_{0.75}$ sensitising layer 77−62020
BiF_3 coating materials for IR laser components 80−33105
BiI_3 coating materials for IR laser components 80−33105
BiTm ferrite garnet coating on $LiNbO_3$:Ti optical waveguide *(Russian)* 77−42623
C, film, deposited on (AlGa)As DH laser facet to prevent deterioration 78−87049
CdO film, chromatic changes on heat treatment *(Russian)* 77−55843
CdO-SnO_2 film, DC sputtering prep., visible and near IR transmission, resist. 78−88049
CdS:In, high cond., high transmittance, growth by evaporation method, and characterisation 77−77386
CdS-ZnS(CdSe), film, light transmittance spectra, comparison with Schott GG 495 glass filter 78−33838
Cd_2SnO_4 heat mirror on plastic sheet for radiation insulation of visible windows 80−95985
Cd_2SnO_4 selective coatings, optical absorpt. edge 78−83046
CeO_2 coating of laser optical components, electron microscope obs. 80−43342
CeO_2, Rayleigh scatt., 441.6 nm, scatt. losses correl. with deposition parameters 79−78782
Cr film, evaporated, black selective solar absorbers, optical props. 77−34956
Cr, ultrafine particles, coatings for selective absorpt. of solar energy, efficiency 78−18060

optical films continued
Cr_2O_3-Cr, RF sputtered cermet film, selective black absorber 77−58399
Cr_2O_3-Cr black, on Ni, defects and their effect on props. 80−39474
Cr_2O_3-Cr film, optical props., rel. to chemical/metallurgical constitution, appl. as solar absorber 78−56531
Cu-Sn(Al)(Ga) reflecting surface absorpt. coeffs. at 10.6 μm 80−95984
Cu_2O, electroless deposition 78−27419
Dy_2O_3-TiO_3 sputtered film, optical waveguide with high refractive index 79−3797
$Er_3Al_{5-x}Ga_xO_{12}$, LPE, spectroscopic props. 80−93419
FeO ultrathin homogeneous absorbing films, ellipsometric nucl. microanalysis data analysis, opt. consts. *(French)* 78−11011
Ge-Al_2O_3 composite film, optical props., appls. 77−754
GeO, optical props., rel. to possible appl. in holography 80−29816
HFO_2, vacuum deposited film, use in multilayer reflector for near UV 77−34924
HfO_2, vac. deposited, near UV multilayer reflector 77−39014
In film, evaporated, resist., Hall effect and light transmittance, use as semitransparent electrode 77−39966
n-In_2O_3 film, RF sputter grown, substrate bias effect on elec. and optical props. 78−64150
In_2O_3 film reactive sputtering gas composition and film growth rate *(Russian)* 80−50554
In_2O_3, optically selective coating, for multiple-plate glass system design 78−74956
In_2O_3, thin film, sputter deposition form., optical and elec. props. 80−60123
In_2O_3 transparent conductive coating production 80−35092
In_2O_3, transparent heat mirror formation by ion plating on ambient temp. substrates and props. 80−25578
In_2O_3:Sn, electroreflectance effect, theory and expt. 78−6800
In_2O_3:Sn, sputtered films for selective transparent films, prep., elec. and opt. props. *(Japanese)* 77−68247
In_2O_3:Sn coated Si, temp. depend. of 10.6 μm refl., solar selective absorber appl. 77−58398
In_2O_3:Sn film, RF sputtered, effect of O_2 press. during deposition on props. 78−19664
In_2O_3:Sn films, elec. and optical props., solar energy conversion appl. 79−65945
In_2O_3-SnO_2 film, XPS expts., energy band model accounting for phys. props. 77−90241
In_2O_3-SnO_2 sputtered film, appls. in displays, vidicon tube windows, dielec. window surfaces 79−59778
$In_xSi_yO_z$, thin film, sputter deposition form., optical and elec. props. 80−60123
$(In_{1-x}Sn_x)_2O_{3-y}$, pyrolytic selective coating, Sn additions effect 78−43499
$In_{1.9}Sn_{0.1}O_3$ laser-damage-resistant transparent conductive coatings, appl. in Pockels cells 79−50333
$KGaF_4$ coating materials for IR laser components 80−33105
$K_xLi_{1-x}NbO$ films, epitaxial growth by melting on $K_{1.5}Bi_{1.0}Nb_5O_{15}$ substrate 79−33204
LiF film, refractive index as function of time, ATR meas. 79−65940
$LiNbO_3$, film lightguide, pulse signal convolution in acoustooptic interaction *(Russian)* 78−1345
$LiNbO_3$ film on Al_2O_3, optical guided wave mode conversion by Love waves 79−46055
$LiNbO_3$, LPE on $LiTaO_3$ substrate, using Li_2O-V_2O_5 flux 78−44031
$LiNbO_3$ optical waveguide, Bragg interaction of leaky and Rayleigh waves 77−23783
$LiNbO_3$ sputtered layers, on $LiTaO_3$, optical waveguide props. 77−11012
MgF_2, and ZnS-MgF_2 system, Rayleigh scatt., 441.6 nm, scatt. losses correl. with deposition parameters 79−78782
MgF_2 coated Al mirrors, AES, UV irrad. effect 77−72047
MgF_2 coated blazed Al grating, complete absorpt. of P-polarised specific wavelength light 78−25957
MgF_2, Fabry-Perot etalon plates for vac. UV 77−5895
MgF_2 layered Al, coating effects on diffraction grating efficiency 77−39064
MgF_2-Na_3AlF_6 thin film deposits, quenched ageing by chopping 80−97364
MgO-Au cermet film, selective black absorbers 77−1747
MgO-MgF_2 multilayer stack selective mirror with high reflectivity *(French)* 80−64131
Mo and oxide phase mixture CVD films, optical props., solar absorber appl. 77−55844
Mo, CVD films of high IR reflectance 79−52119
Na_3AlF_6, complete, struct., electron microscopy 77−59226
Na_3AlF_6, film on Si, fused quartz substrates, H_2O absorpt., IR anal. 80−75446
Na_3AlF_6, optical inhomogeneity, rel. to struct. 79−83047
NaF film on CaF_2, interface and bulk absorption meas. 80−35001
NaF film on ZnSe plate, absorption coeff. ATR spectroscopy 80−35000
Nd:glass films for integrated optics, RF sputtering and optical charact. 79−46087
Ni-Al_2O_3 composite film, selectively absorbing, optical props. 78−6798
Ni-P coating, electroless, ultra-black surface production by chemical treatment 80−76647
PbF_2-Na_3AlF_6, semitransparent wide band dielectric mirror synthesis using dispersive and absorbing materials 79−89986
PbF_2-TlI graded coatings on KCl laser windows, photoacoustic spectroscopy 80−33052
$Pb_xSn_{1-x}I_2$, thin films, photosensitivity, ageing and annealing effects *(Russian)* 78−6804
$Pb_{1-x}Sn_xSe$, thin film, opt. props. *(Japanese)* 77−1750
Pb_xTe_{1-x}, optical consts. calc. 77−11041
Pb(Zr,Ti)O_3, ferroelec. and optical props. 77−85674
Pt evaporated film, optical props. meas. in VUV, 220 to 150 Å 80−45159
Re-W/C multilayer films for X-ray mirrors 79−44992
Sb_2O_3-MgF_2, semitransparent wide band dielectric mirror synthesis using dispersive and absorbing materials 79−89986
Se, vacuum evaporated film, photoinduced amorphous-crystalline transition obs. *(German)* 79−82156
Si, polycrystalline, film thickness meas., visible spectral reflectance analysis 78−32786
Si:B ion implanted layers, light refl. and transmission coeffs., computer program 80−66316
Si-Ag-Si heat mirror on plastic sheet for radiation insulation of visible windows 80−95985

optical films continued
Si-CaF_2, dielectric constant and selective solar absorption 78−2937
Si-MgO, dielectric constant and selective solar absorption 78−2937
Si-Si_3N_4-SiO_2 non absorbing double layers, optical parameters reflectivity by liquid immersion method 80−71503
Si-SiC composite film, optical props., appls. 77−754
Si_3N_4, film, absorption, refr. index, freq. dispersion 78−48248
Si_3N_4 film acousto-optical props. for integrated optical Bragg cell 79−55251
Si_3N_4 on Si, optical waveguide, fabrication, propag. consts. 78−33826
SiO condensate distrib. from extended aspherising source 79−52118
SiO, prod. using large-capacity evaporator with filtering element 77−14819
SiO_2, and TiO_2-SiO_2 system, Rayleigh scatt., 441.6 nm, scatt. losses correl. with deposition parameters 79−78782
SiO_2, film form. by reactive HF sputtering with voltage bias 78−3045
SiO_2 film on Si substrate, reflectance and absorptance obs. 79−15542
SiO_2 films, vac. thermal evaporation, parameter stabilisation 80−87571
SiO_2, optical absorption an external photoeffect, 6-40 eV 77−55802
SiO_2, sputtered, facet protection of (AlGa)As lasers 79−81444
SiO_2, transparent film on Al, refr. index, thickness, ellipsometric meas. 77−52195
SiO_2-Si, film-substrate, single reflection retarders for different Hg spectral lines 78−79122
SiO_2-Si film-substrate refl. polariser, operation at Hg spectral lines 77−75655
SiO_2-Ta_2O_5, refr.-index-adjustable, for integrated optical ccts., prep. and props. 78−63203
SiO_2-Ta_2O_5 film channel optical waveguide, fabrication using CO_2 laser 79−27386
SiO_2-TiO_2 stack reflector and antireflection coating, 1064 nm 180 ps laser pulse damage 79−14017
SiO_x, amorphous, dispersion of refr. index and chem. comp. 80−7429
SiO_x, durable, ion plating onto plastics, optical and mech. props. 80−38141
SiO_x film, laser damage mechanisms 77−75592
SiO_x protected Al mirror, far UV refl., UV irrad. effect 79−7191
SnO_2 CVD film form. mechanism 78−38977
SnO_2, CVD using $SnCl_4$-H_2O and $SnCl_4$-H_2O_2 systems, elec. and optical props. 78−52686
SnO_2, optical and elec. props., rel. to stoichiometric deviation and struct. 77−47701
SnO_2 transparent electrodes, effect of Sb doping on elec. and optical props. *(Korean)* 77−1749
SnO_2, VUV transparent electrode formation by chemical deposition and vacuum sputtering 79−56929
SnO_2:F films, elec. and optical props., solar energy conversion appl. 79−65945
SnO_2:Sb transparent conductive coatings for Cu_2S-CdS solar cells 79−61992
$SrTiO_3$, sputtered, refr. index, 0.3-1.0 μm, substrate temp. effects 77−55840
Ta_2O_5 film acousto-optical props. for integrated optical Bragg cell 79−55251
Ta_2O_5, film form. by reactive HF sputtering with voltage bias 78−3045
Ta_2O_5, plane optical waveguide, fabrication by reactive sputtering 78−71221
Ta_2O_5 thin film protection of unstable OF-type glass components 79−14079
Ta_2O_5-SiO_2, plane optical waveguide, fabrication by reactive sputtering 78−71221
$Ta_2O_5N_x$, sputtered birefr. film, deposition conditions effect on refr. index 77−39118
Te facet coating, for side lobe suppression in far field of AlGaAs DH stripe laser 80−5744
Te film and trilayer antireflection structure for optical recording 79−94329
Te trilayer for high-performance optical recording 79−50382
TiN_x spectral reflectance, selective solar, absorber appl. 77−79954
TiO_2 and Dy_2O_3-TiO_3, high refractive index film growth by sputtering, waveguide appl. 77−48341
TiO_2, and TiO_2-SiO_2 system, Rayleigh scatt., 441.6 nm, scatt. losses correl. with deposition parameters 79−78782
TiO_2, deposition by electron beam evap., chem. comp., refr. index, struct. *(Japanese)* 77−62777
TiO_2 layers, activated reactive evaporation and absorpt. indices 80−97363
TiO_2 optical coatings, deposition, performance 77−88896
TiO_2, optical inhomogeneity, rel. to struct. 79−83047
TiO_2, reactive evap. of Ti-O phases, refr. index 77−19372
TiO_2, reactively sputtered optical coating for inertial confinement fusion laser components 80−23705
TiO_2, rutile, film, CVD in $TiCl_4$-H_2O system 77−12541
TiO_2 transparent film thickness and refractive index calc. 79−15547
TiO_2-Ag-TiO_2 heat mirror on plastic sheet for radiation insulation of visible windows 80−95985
TiO_2-SiO_2, multilayer dielec. mirrors, laser-induced damage resist. 79−10335
TiO_2-SiO_2 multilayered film striped optical filters, optical props. and fabrication of RF sputtering 80−10030
TiO_x durable, ion plating onto plastics, optical and mech. props. 80−38141
TiO_x, laser damage mechanisms 77−75592
TiO_x, reactive sputtering, film prep. conditions rel. to stoichiometry 77−40370
TlBr, and TlBr-TlI polycryst. fibre optical waveguides, for IR, fabrication and charact. 78−74974
TlI coatings on KCl laser windows, photoacoustic spectroscopy 80−33052
TlI films, polymorphic, double epitaxy and growth on KCl, X-ray and optical obs. 79−77944
TlI, on KCl, epitaxial growth habit rel. to optical scatt. 77−50738
UF_4 optical interference layers, electron-beam decomposition 78−34541
VO_2 film as holographic recording medium, diffr. efficiency 80−28180
VO_2 film sub-mm wave modulators and switchable polarisers 77−75664
VO_2 interference films, colour valencies as function of thickness and phase change *(German)* 78−56533
W, CVD, optical props., solar absorber appl. 77−55844
W-MgO cermet, dielectric constant and selective solar absorption 78−2937
WO_3 electrochromic films, bleaching by electric fields 79−99852

optical films continued
WO_3 film, evaporated, mech. of elec. cond. 80−44747
WO_3-BaO, electrochromic coloration and decoloration, BaO additive effects 78−72620
WO_3-MoO_3, amorphous, electrochromic optical absorpt., expt. results and model 78−27341
WO_3-H_x film, colouring, comp. depend. 78−15239
WS_2-oxide layer formation and props. 79−50359
WSe_2-oxide layer formation and props. 79−50359
YAG, optical films, high quality growth 79−46984
Y_2O_3 coated Ag mirror for the 0.5 to 14 μm region 80−87456
ZnO film acousto-optical props. for integrated optical Bragg cell 79−55251
ZnO, RF sputtered epitaxial film, appl. to integrated optics 77−14821
ZnO, surface acoustic-optic interaction, diffr. 77−3685
ZnS, and ZnS-MgF_2 system, Rayleigh scatt., 441.6 nm, scatt. losses correl. with deposition parameters 79−78782
ZnS, epitaxial growth on Si in ultrahigh vacuum, source nonstoichiometry effects 77−77387
ZnS evaporated film, refl. loss on UV irrad., ZnO form. 80−99813
ZnS, film on Si, fused quartz substrates, H_2O absorpt., IR anal. 80−75446
ZnS films prepared by thermal evaporation in vac., nature of defects 80−10835
ZnS interference layers on Fe whiskers, optimisation of magnification of magneto-optic Kerr effect 79−51808
ZnS, optical inhomogeneity, rel. to struct. 79−83047
ZnS, struct., electron microscopy 77−59226
ZnS:Mn on SnO_2/glass transparent conductive base, surface morphology effects on electroluminesc. *(Russian)* 78−48238
ZnS-Ag, broad band visible heat reflecting mirror 77−39017
ZnS-MgF_2 dielectric film, laser irrad. and microscopic inhomogeneities 78−2157
ZnS-MgF_2(SrF_2), dielec. films, transparent, microscopic inhomogeneities and optical breakdown 78−10844
ZnS-Mn sublimated phosphor films, annealing effects *(Russian)* 78−43949
ZnS-Na_3AlF_6 multilayer dielectric optical filter, irreversible thermal effect 77−7195
ZnS-SrF_2 dielectric film, laser irrad. and microscopic inhomogeneities 78−2157
ZnSe, IR laser window coating absorption rel. to deposition conditions 79−14061
ZnSe, RF bias-sputtered CVD films on CaF_2 79−14060
ZnSe sputtered laser window coatings, prep. and evaluation 77−50739
ZnTe MBE thin film growth, elec. and optical props. 78−47887
Zns film, dispersion characts. in vis. spectrum 77−59629
ZrN_x spectral reflectance, selective solar absorber appl. 77−79954
ZrO_2 film, electron beam deposition, refr. index and microporosity 78−90467
ZrO_2, optical layer form. from $ZrOCl_2$ in alcoholic soln. 77−88877
ZrO_2 thin film, optical props. rel. to cryst. struct. 80−97357
ZrO_2 transparent film thickness and refractive index calc. 79−15547
ZrO_2-$ZrTiO_4$, for high index layers, deposition 77−753

optical filters
see also light absorption; optical films; optical isolators; spatial filters
aberrated pupils, apodisation, anal. 79−98298
absorption light filters, thin-film 80−19101
absorption measurement, optical materials, real time holographic interferometry 80−83569
acousto-optic, tunable, theory and practice 77−58466
acousto-optic programmable filter characteristics and applications in optical computing 79−72716
acousto-optic tunable filter, programmable 80−74511
acousto-optical noncollinear UV tunable filter 80−102832
acousto-optical tunable filter, for optical coherent detect. 77−88932
acousto-optical tunable filter spectrometer development 80−101848
acoustooptic guided-wave tunable, using collinear TE-TM mode conversion 80−102852
acoustooptic tunable filter for staring IR sensor, performance 80−36407
active optical devices, seminar, San Diego, CA, USA (August 1979) 80−101664
anisotropic frustrated-total-internal-refl. filter, space limited 80−102821
aperture, partially apodised, diffracted field characts. 80−48139
apertures with Straudel Class of pupil functions, var. apodisation 80−23616
apodising filters, numerical exam., second moment of the point spread function 80−106611
apodizing filters for optimum Sparrow resolution in coherent systems with annular aperture 80−53435
aspectogram, spectral props., image multiplication appls. 79−55090
aspheric testing, in-line and carrier freq. holograms, comparison 80−87349
astronomical interference filters, nebulae observations, urban light pollution 79−88599
astronomical monochromatic imaging using filters, slitless (multislit) spectrograph, and interferometers 79−8840
atmospheric transmittance meter, absolute filter device 80−51584
atomic emission spectrometer, interference filter, stray light reduction 79−43645
band-pass filters for violet-blue region, glass characts. *(German)* 78−13802
band-pass interference filters, $D(2HL)^m2H$ struct., transmissivity 78−83096
bandpass, narrow, via nearly degenerate four-wave mixing 79−23013
bandpass filter glasses, 550-616 nm, transmission characts., CuO and NiO colorants 78−66919
bandpass filters for visible region, glass characts. 77−75659
bandpass interference filters for use in UV 79−46053
birefingent alternate partial polariser filter, design 77−7188
birefringent, tuning filters without secondary peaks 78−29994
birefringent chain light filters theory, fund. formulae *(Russian)* 77−50772
birefringent element, analogue, built from polarising wide field Michelson interferometer 80−91895
birefringent filter improvements, field of view effects 80−14428
birefringent filter mechanical tuning techniques 80−102834
birefringent filters, transmission expression derivation 79−18522
birefringent filters for tuning flashlamp-pumped dye lasers 78−74914
birefringent filters tunable from 4500 to 7000 Å 77−46806

optical filters continued
birefringent rotating plates as modulated optical filters, polarised light meas. appl. *(French)* 77−67490
birefringent single mode fibre filter 80−58713
birefringent tunable, theoretical anal. 77−88906
bleachable, appl. for lasers 78−50937
Bragg reflector, nonuniform, almost periodic, perturbation anal. 77−27356
Bragg reflectors, narrow band, in optical fibres 78−79130
brightening filter for solid laser, ultrashort light pulse optimum generation 79−36903
broad band grating filters for thin film waveguides 77−83962
buried metal grating coated with polished dielec. layer and dielec. multilayer, phenomenological theory 79−50374
camera, wide-field filter, for astronomical appl. 78−49335
certification of neutral light filters using spectrophotometers in UV, visible and near IR regions 80−273
chalcogenide glass films, kinoform optical elements and integrated optics elements prod. 77−75634
chalcogenide glass films, opt. inform. recording uses 77−75633
channel filter for fibre transmission systems, wavelength multiplexing 77−34950
character recognition, optimised filter 80−95837
chirped gratings in broad band filters, theory 78−25994
cholesteric liquid crystal coatings, superimposed left- and right-handed, peak refl. and colour gamut 80−74472
cinefilm copying equipment using interference light filters, additive printing appl. *(Russian)* 80−62774
coating, reflection coefficient partial derivatives, matrix calc. *(French)* 80−89080
coating stabilities, refl. factor 77−83958
coatings, problems of application technology 78−83069
codirectionally coupled waveguides with weighted coupling, filter characts. 79−23068
cold spectral filters for long-wave IR detectors, problems 79−3799
colour compensating filters with IR film, density shifts 78−62256
colour compensating filters with IR film 77−33210
colour-IR photographic filters 77−71396
coloured filter glasses, comparison of glasses made by different manufacturers 77−75630
component shape monitoring, tolerance field image production *(Russian)* 79−94154
component tolerance control, two-dimensional shadow image mapping filters *(Russian)* 79−94155
computer controlled optical plotter for filter generation *(French)* 78−90538
conference on optical coatings, Washington, USA (March 1978) 79−46028
continuously tunable filter for reson. Raman spectroscopy 77−22604
conversion filters for scientific photography 80−48394
corner reflector filter, fabrication 77−14809
correcting absorber selection for Si photodiodes, luminous meas. in flash photometry 79−72699
correction filter selection for Si photodiodes 77−50767
corrugated waveguide filters, mode conversion and filtering of obliquely incident waves 79−81571
corrugated-waveguide optical demultiplexer mode couplings 80−64194
CRT displays, viewability improvement, using optical absorptive filters 78−24820
cut-off type, for long wave range IR spectrum *(Russian)* 77−88957
cutoff filter for CO_2 lasers 77−88938
Dacron, multilayer, for CO_2 laser attenuation 80−58616
dark filter, integrated transmission coeff. meas., zonal method 77−34953
deconvolution techniques applied to astronomical images 80−46407
densitometry using pulsed dye laser and optical delay 77−61104
density monitoring by photometer *(Russian)* 78−86317
design, global optimisation methods appl. 79−59840
design and construction of unconventional interf. filter 79−46052
design using image admittances 79−76801
dichroic filter, vibrating, in astronomical IR photometer 77−26017
dichroic polarisers, spectral props. and appls. 77−46809
didymium glass filters for spectrophotometer wavelength scale calibration 80−43417
dielectric coatings, optical characts., effect of electric field during film condensation 80−69539
dielectric multilayer coating, optical phase shift at boundary, reflection coeffs. 77−34926
dielectric multilayer interference devices, loss mechanisms 77−83943
dielectric multilayer systems for optical appls., computer program synthesis *(German)* 78−46788
differentiation by spatial filtering 78−1171
diffracting gratings for colour filtering, zero diffr. order microimage system 79−18503
diffractive, prepared by reactive sputter etching, microfabrication and evaluation 79−90008
digital transmission using silica fibre waveguides for wavelengths beyond 1 μm 78−50907
diplexer reflection type periodic filter, elliptic response 80−43474
directional coupler for wave division multiplex system, dielectric multilayered filters appl. 79−94365
directional filter structure and characteristics for bidirectional transmission 80−58734
dispersive crystal-air, transmission depend. on scattering layer parameter *(Russian)* 77−84002
distributed Bragg reflector filter, polystyrene-collodion (polyvinyl alcohol) multilayers, fabrication 79−76838
distributed feedback structures, hybrid modes 79−27441
dye laser tuning by dielectric interference filter-coated prism 79−10322
edge detection filter, optimisation 77−27336
edge interference filters for WDM transmission over multimode opt. fibres 80−83677
electro-optic interference polarisation filter, Q-switching ruby laser with high-frequency control of lasing conditions 80−74363
electro-optic thin film periodic waveguide switch and amplitude modulators anal. 78−22215
electro-optical polarisation conversion and interference tunable filters 80−102829
electro-optical tunable filters, programmable 80−102830
electronographic photometry, narrow-band high spatial resolution, astron. appls. *(French)* 80−46408

optical filters continued
epoxy, for interference filter, γ-radiation effects on transmission 79−64297
evaporated thin film filter, durability and stability 77−75686
eye protection filter small dioptric powers local variation determ. *(German)* 78−27937
Fabry-Perot and Lyot filters, in Skylab Hα telescopes for solar obs. 77−60604
Fabry-Perot interference filter props. for oblique incidence illum. *(French)* 79−81545
Fabry-Perot interference filters, neutron irrad. effects 80−14437
Fabry-Perot interferometer as frequency selective filter external to CO laser 77−27292
far IR interference filters 77−22592
far IR narrow band-pass filter construction 77−39065
far IR narrow-bandpass interference filters, prod. and performance 78−5558
Faraday, for Fabry-Perot cavity, polarisation props. 77−46738
Faraday filter, freq. locking of CW dye laser to Na D-lines 78−5487
Faraday filter, freq. locking of CW dye laser to Ne absorpt. lines 79−22989
fibre, multimode, graded-index, low-pass filter characts. 77−23759
fibre and integr ed optical devices for signal processing 80−33233
fibre loss, dispersion and polarisation meas. by acousto-optical tunable filter 80−102855
fibre nonlinear equalisation by shaping filter *(German)* 78−33882
fibre transmission system filtering prism *(Japanese)* 78−9441
fibre waveguide photosensitivity, appl. to refr. filter fabrication 78−63171
fibre-optic band-pass attenuator 79−37003
filamentary spatial filter for use with interferometry in phase measurement 79−71518
first order waveguide grating filters, random fluctuations 79−94369
flame atomic absorption lines, appl. as background reduction method in plasma emission spectroscopy 79−16069
flat plate solar collector efficiency improvement by grating selective filters 79−62032
flaw detection using optical filters 78−53163
fluorescence angiography, colour and black and white, use of interference filters 78−48856
four-wave mixing, nearly degenerate, resonantly enhanced medium, narrow bandwidth optical filter appl. 79−31976
frequency-selective filters in ion-exchanged waveguides 79−50387
gas concentration meas. using Raman intensity depend. on giant pulse laser polarization 80−98986
general-purpose objective photometer, FOU 79−49268
geophysical image processing, apodisation for distortion reduction *(Russian)* 77−9564
glass:CuO, band-pass characts. improvement by doping 77−54797
glass, coloured, for short wavelength cutoff filters, fluoresc. data 79−61411
glass, for interference filter, γ-radiation effects on transmission 79−64297
glass fibre attenuation characts., light-wave propag. communication *(German)* 80−95997
glass filter, simulating CIE spectral tristimulus value $\bar{z}(\lambda)$ 78−30037
glass filters, SRM 930, spectrophotometric standards by NBS, clinical laboratory appl. 78−54331
glass filters for reproducing radiation of B and C sources 77−88947
glass UV filter, stray radiation level reduction in SF-26 spectrophotometer 80−101852
glasses with band-pass characts. for red spectral region 78−25936
glasses with band-pass characts. for yellow-orange region of visible spectrum 77−75683
glasses with band-reject characts., for visible spectral region 79−18525
grating filter, thin-film, characts. for oblique incidence 78−50949
height and flow velocity, optical pseudo-colour processing *(Japanese)* 80−9826
helically ruled optical filter, spherical refl. characts. 80−64171
high-throughput filter for altering spectrum of multiple-frequency lasers 80−58553
image-forming objectives and colour filters, application and mounting *(Hungarian)* 78−9424
industrial precision filter radiometer development and applications 79−21814
integral colour filter arrays for solid state imagers 77−79960
integrated branching filter using three-dimens. input waveguide, nonradiative condition 80−38130
integrated directional coupler switches, modulators and filters using $\Delta\beta$ reversal techniques, review 80−38132
integrated optical channel waveguide-CCD transversal filter 80−58797
integrated optical functional elements based on holographic gratings in As_2S_3 film waveguides 77−79972
integrated optics photoresist testing and phase filter synthesis 77−39116
integrated optics using periodic structures 77−39109
interference, commercial, defects in transmission profiles 78−25952
interference, optical consts. calc. of film 77−11041
interference, prod. of annular wedge-shaped layer coatings 77−14817
interference, single-graded, for monochromator 78−94444
interference coating, optical characts. topography var. 77−72102
interference coating deposition by Balzers BA-710 vac. system, photometric monitoring 78−46850
interference coating production, new ideas 79−32098
interference coating synthesis, computer calcs. 77−11042
interference coatings, design, specified characts. 79−3786
interference coatings, synthesis, nonlocal computer method 77−50761
interference coatings for devices transmitting colour images 78−59108
interference filter, transparency, effect of harmonic variation of layer thickness 80−28326
interference filter, V(λ), design appl. to visual system MTF evaluation 79−76843
interference filter for submillimetre astronomy 80−48393
interference filter polychromator and narrow band rejection filter 77−72061
interference filters, direct, quasi-telecentric and telecentric combinations with large astronomical Schmidt cameras 78−57441
interference filters, multilayer, design method 80−48396
interference filters, nonlinear, spectral characts. in strong fields *(Russian)* 77−54718
interference filters for field of view shaping of optical probe 77−58456
interference filters for improved solar radiation resistance 77−39015
interference multielement reciprocal grid filters, far IR transmission characts. 77−46789
interference polarisation filter steps, wide angle, made from various crystals 78−87156
interference polarization filters, crystal plate orientation depend. of spectral background 80−48426
interference spectrometer, spacing ratios of Fabry-Perot etalons and filter 77−79160
interfernece filter characteristics and specification 78−46773
interferometric, illum. with convergent beam, spectral response optimisation *(French)* 80−99868
intracavity Brewster-angle birefr. filter, line narrowing and tuning of Nd:glass 77−38916
inverse diffraction problems soln. using diffr. coeffs. 77−46698
inverse sampling spatial filtering for image multiplication 77−23627
IR dispersion crystal-crystal filters, effect of particle size, layer thickness and vol. conc. on transmission *(Russian)* 77−27369
IR dispersion filters, crystal-air, spectral characts. *(Russian)* 78−5581
IR dispersion filters crystal-air, spectral characts. *(Russian)* 77−54811
IR energy-efficient interference coatings 79−23087
IR filter, elmination of near from far IR, LiF Brewster angle plates *(French)* 79−3772
IR filter radiometer using selective interferometer 77−5880
IR frustrated-total-reflection polarising beam splitter 79−46047
IR multilayer interference filter manufacture, supposed longwave limit 80−9989
IR radiometer, passbands for clear-air-turbulence detect. 78−96318
IR windows, optical properties measurement 77−54788
isotropic medium, nonlinear refr. index, self-induced polarisation rot. 80−5802
Kaiser filters, window function, equivalent pass band, incoherent optical transfer function 80−1323
laser, saturated filter relax. time reduction, self-synchronising modes *(Russian)* 77−7145
laser beam indicator/visualiser made from new thermochromic material 80−9976
laser beam prod. by stochastic coherent optical filters *(Russian)* 79−982
laser detection using tunable acoustooptic filters 78 -29159
laser Doppler velocimeter with direct spectral anal., for instantaneous vel. meas. 80−99782
laser engineering and appls., conf., Washington, USA (May-June 1979) 80−1216
laser impulse shape regulation, electro-optic deflectors *(Russian)* 77−19354
laser pulse shaping with grating pair and filters 79−89940
laser pump, active medium and interference coating effect, temp. profile, electro-optical characts. 77−19275
laser safety eyewear, filter glasses 79−39525
laser ultrashort pulse form., filter clarification and amplification saturation coincidence 80−64085
lens-spectral filter combination, off-axis illum. distrib. determ. 79−26152
lenslike medium, with external higher-index surround, mode filter characteristic 77−62049
light flash envelope isolation from fluctuating background 77−37993
lined interference filter cementing technique 79−72729
liquid crystal electrically controlled colour filters 78−83113
long-wavelength IR optical filter development status 79−27423
low-pass light filter, using Polaroid film type H32 for GaAs beam 78−33853
low-temperature narrow-bandpass interference filter construction 79−32049
luminescence filters, efficiency for Nd:glass lasers 80−1213
Lyot depolarizer in quasimonochromatic light 79−62747
Lyot filter element for astronomical spectrogram calibration 78−36466
magneto-optical, for solar vel. fields meas. 79−25507
matched filter correlator memory techniques and storage capacity 80 -102643
matched filtering with multichannel US modulators *(Russian)* 77−58426
matched filters, performance 79−90012
metal film reflection filter for CO_2 laser line selection 78−55368
metal-clad optical strip waveguide lined with buffer layer, mode-filtering characts. 79−81559
metal-clad optical strip-line as cutoff mode filter 80−83680
metal-dielectric interference filter fabrication, phase correction method 77−72064
metal-dielectric interference filters in transmitted light 80−96013
metallic film, IR reflectivity, mirror appl. 78−5536
metallic film apodising and attenuating filters, phase shifts and aberrations 78−90514
metallic mesh interference filters, low temp. narrowbandpass 80−14430
metallic thin film apodising and attenuating filters, phase shifts and aberrations 80−87552
metallic thin film filters for long-wavelength IR, transmission curves 77−31136
metallized polyester film as a solar filter 80−51666
Michelson interferometer, use as selective filter for stratospheric trace gas concs. meas. 80−17408
micro-optic devices for coupling/branching in fibre optic communications 79−55211
microscope combined with TV equipment for teaching and quality control 80−82817
modal filters, effects on fibre loss meas. 79−50439
mode filter, for fibre single-mode propag. in 2-mode region 79−76825
moisture penetration patterns, rel. to filter drift 77−767
monitoring of film deposition, error compensation 77−75721
monitoring of props. during deposition, wide band monitoring system 79−81582
monochromatic light source with electronically variable wavelength 80−102791
motion picture printing using new colour attenuation system 79−2859
MTF evaluation with optical matched filters 77−27257
multi-element interference filter, far IR, generalised treatment 80−33174
multi-element interference filters using different grids, far IR characts. 78−90507
multicavity IR electro-optical tunable filter 80−102831
multicolour image storage on black and white film, using crossed grating 79−31813

optical filters continued
multidielectric spectral filters, synthesis and realisation *(French)* 78−74998
multidielectric stack control using chromatic maximeter, Fourier series anal. of signal *(French)* 78−83111
multilayer, thin films, automatic design method 77−58449
multilayer antireflection coatings, all-dielec. Fabry-Perot interf. filters, optimisation parameters 79−41432
multilayer coating production with continuous thickness reoptimisation 79−76890
multilayer coatings, algorithms for determ. of reflectance and transmittance 79−98271
multilayer filters, non normal incidence, optical monitoring, allowable tolerances *(French)* 80−87526
multilayer frustrated-total-internal-reflection filter, spatially limited 80−96014
multilayer interference film, mass production by roll coating *(Japanese)* 79−81577
multilayer interference filter, calcs. allowing for weak absorption *(Russian)* 78−13812
multilayer interference filter production for CO_2 ν_2 band 77−10998
multilayer interference filters with quarter-wave layers 79−64316
multilayer interference polarizer, Brewster angle determ. 79−64315
multilayer nonabsorptive coatings anal., gradient descent method *(Russian)* 77−50773
multilayer optical coatings, scatt. due to surface roughness, scalar theory 79−59637
multilayer polariser, design, prep. and optical characterisation 79−76866
multilayer synthesis computations, use of Fourier coeffs. 78−90509
multilayer synthesis program, Fourier transform model 79−7196
multilayer thin film, optical scatt., matrix formulation 79−31804
multilayers, polarisation avoidance or enhancement 80−43255
multimode optical fibre band widening 77−62048
multimode optical fibre wavelength-filtering effects 80−58731
multiphoton absorbers with intermediate reson., influence on light statistics 79−86208
multiple image formation by sampling Fraunhofer diffr. patterns 78−1334
multiplexer design for optical wavelength-division multiplexing transmission via single fibre 80−33222
multireflection interference-filter optical multiplexer/demultiplexer 80−58728
multireflection optical multi/demultiplexer using interference filters 79−76821
multistage interference-polarization filter for wavelength selection in dye lasers 80−64091
narrow band, computer controlled filters for solar astronomy *(Russian)* 78−16292
narrow band frequency freq. filter, light tunable 79−18490
narrow band interf., optical props. as function of incidence angle and polarisation 80−19102
narrow band interference, ZrO_2, TiO_2 and SiO_2 high-frequency sputtered optical coatings 79−76900
narrow band interference filter, spectral transmission curve meas. 78−297
narrow band interference filters in field of view shaper 77−74506
narrow band interference filters in system, energy anal. 78−16846
narrow bandpass, for far IR, using double half wave designs 80−33173
narrow-band interference filter with mica separating layer 77−7207
narrow-bandpass interference filters, appl. for Tokamak plasma spectroscopy 78−26326
narrowband optical wave filter with stacked directional coupler 79−7226
near IR metal-dielec. and dielec. filters of Fabry-Perot construction, fabrication 77−84016
nebular filters for visible astronomy 79−62746
negative selection, for production of uniform intensity of light 77−2685
neutral density, for solar corona obs. using vacuum deposited graded-thickness films 80−76164
neutral density filters, for UV-vis. spectrophotometry, calibration 78−45734
noise filter with two aperture stops, numerical analysis *(Japanese)* 77−14812
noise stability of receiver for pulsed signals with optimal filtering 77−31072
nonlinear distortion of laser beam transverse struct. by light filters 79−7170
nonpolarising glass cube 77−23736
nonquarterwave multilayer, optical monitoring with minicomputer allowing thickness error correction 80−23774
nonquarterwave multilayer, wideband optical monitoring during deposition 80−28309
nonquarterwave multilayer filter prod., optical monitoring of thickness 78−55476
OCR by spatial filtering with light beam deflection 78−1370
operating principles based on energy transfer between coupled orthogonally polarised EM waves *(French)* 78−33896
optical spatial filtering, of visualised results of flaw detection monitoring, rational regions of appl. 80−7751
parabolic filters for circular apertures, encircled energy in diffr. pattern 79−89845
patterned optical filters for solid-stage imager spectral encoding 78−66945
photodetector spectral response determ. using calibrated lamp and interference filters 79−71528
photographic amplitude filter for laser radiation uniform intensity distrib. *(Russian)* 77−54748
photographic colour printing, correcting light filter selection 80−62764
photographic light sources, characteristics and parameter definition using graphical method for correct choice of compensating filters *(German)* 80−52342
photoresist, negative, as phase profile material for near IR, IR spectrophotometric meas. 78−37953
plastic birefringent filters, design, construction and system appls. 78−50943
point spread function of systems with parabolic filters, effects of defocusing 78−13776
polarisation-conversion wavelength-selective fibre switches 80−58736
polarised beams selective interference in crysts. with isotropic pt. 79−72484
polarising, for high fidelity reproduction 79−44957
poly-4-methyl pentene-1, long wave IR filters 77−75695
optical filters continued
polyethylene mixtures as IR filters, transmission characts. 77−39020
quarter wave multilayer monitoring, optical props. change rel. to error compensation 80−38139
quarterwave multilayers, secondary refl. maxima 79−64331
quartz, pure, fused, optical consts. in far IR, 20 to 120 cm^{-1} 78−79080
radiation induced transmission loss in optical materials 79−94306
Raman spectroscopy, high local resolution, optical energy and spatial filter 79−35838
reflected-light fluorescence microscope, LABOVAL 2a.fl, for routine and research 80−56300
reflection filter, narrowband, characts. calc. 77−766
reflection interference filters, using props. of absorbing multilayers 79−7207
rhomb laser beam sampler, two-grating, inherent aberration correction, inverse filter description 80−37954
ring laser, solid state, with intracavity bleachable filter, conditions for CW stimulated emission 80−14368
rubeanic acid, in ethanol and water solns., UV transmission filter characts. 77−3679
safelight for Agfa 10E75 and 8E75 plates 78−74087
safelight for Agfa 10E75 and 8E75 plates 79−63318
saw-tooth wave target, modulation by optical system with triang. and assoc. filters 80−9817
schlieren optical filtering for sound-intensity measurements 80−87672
second- and higher-order waveguide grating filters, refl., transmission and loss coeffs. meas. 80−19110
second- and higher-order waveguide grating filters, spectral response calcs. 80−19109
sclective interferometer filter, beam splitter designs 78−30093
selective receivers for 0.2 to 0.3 μ spectral region 79−30560
semiconductor iso-index coupled-wave electrooptic filter 80−1324
semileaky anisotropic film waveguide, wave propag. 77−65627
semileaky anisotropic thin-film optical waveguides and mode filters 78−13799
semileaky thin-film optical waveguide mode filter radiation-coupling loss 77−88953
shearing interferometer as filter for scattered light reduction 77−25941
single mesh narrow bandpass filter, IR to submm. region 78−50911
slotted aperture for Moire photography 77−65053
solar receiver radiative loss and eye hazard evaluation by Net-Radiometer 80−89673
Solc birefringent filter, transmission spectrum calc. 79−55052
solid-state imaging devices, conference, San Diego (1977) 78−66944
space and time variables in optics and holography, expt. aspects 77−34830
spatial, pattern recognition by means of holography *(Japanese)* 80−5699
spatial filtering of incoherent imaging system *(Chinese)* 79−72500
spectral, optimisation for arbitrary criterion by method of basic extremals 80−96011
spectral adaptation for receivers and light sources *(German)* 80−77837
spectral intensity filtering for image recognition 78−46529
spectrally selective fibre filters 77−42600
spectralmasks for three-colour calorimeter, calibration 77−30196
spectrocolorimeter, SPEKOL, meas. of surface fluorescence 79−80664
spectrophotometer, cutoff system for filtering out higher spectral orders in 400 to 200 cm^{-1} region 80−28334
spectrophotometer IR rejection polariser system 79−63314
spectrophotometer transmittance transfer standards 78−45728
spectrophotometer-type filters of highest possible performance, 2.5-40 μm 80−14438
spectrophotometry, semi-transparent metallic thin films as transmittance standards 77−53991
spectropyrometer effective wavelength value, narrowband interference filter background transmission effect 79−72687
sputtered films production and props. *(Hungarian)* 80−53483
sputtered metal silicide solar selective absorbing surfaces 78−52671
stack of dielectric layers, Fourier description of analysis and synthesis operations 78−94449
stellar Balmer-index photometry, narrow-band filter profile calc. 78−96404
stellar spectra simulation, G- and F-type stars 77−37505
Straubel class of apodisation filters, diffr. field characts. 77−7198
striascopic imaging of profiles with laser light, surface tension measurement 79−2845
strip-guides, polarisation filtering 80−102861
sunglasses, commercial, UV and IR windows, transmission meas. 0.3 to 0.85 μm 77−36915
telescope, filter type, for viewing solar prominences 79−84670
tellurite glass, Cu^{2+} and Ni^{2+} doped, band-pass filters for 550 to 616 nm, transmission characts. 78−71166
TEM images of dislocation core, optical filtering for noise removal 80−107254
temporal frequency spectrum, optical filtering 78−33695
Therm-O-lux 85 film, reduction of thermal interference from photolamps 78−41302
thickness monitoring with optical time-domain reflectometer 79−55254
thin film technology, appls. in energy, optics, and electronics, review 80−78932
three colour channel hybrid system to synthesize complex point spread functions 79−41347
three-layer equivalent film design 78−66884
three-stage birefringent filter, tuning over visible region 80−58667
transmission band splitting elimination, oblique incidence 77−765
transmission bands of simultaneously fabricated filters, reduction of λ_{max} variation 77−14816
transmission coeff. zonal nonuniformity 79−32063
transmission measurement at low light levels 79−85158
transmission spectrophotometry, standardisation in UV and visible regions 78−32850
transmittance standards in spectrophotometry, semi-transparent metallic thin films use 78−32852
tunable acousto-optic filters, review 78−5570
tunable acoustooptic narrow band optical filters, appl. computer-controlled spectroscopy 77−75705
tunable coupler filter, composed of coupled nonidentical $LiNbO_3$ strip waveguides, description 78−38083
tunable narrow-band thin-film waveguide grating filters, performance 80−38124
tunable optical waveguide directional coupler filter 78−79144

optical filters continued
ultrahigh-Q isotropically sensitive optical filter employing atomic reson. transitions 79−55216
UV liquid filters, transmission characts. 77−3679
UV-visible range spectrophotometers, wavelength calibration by interference filters 77−33808
vacuum UV coating technology 79−46030
vacuum UV optics, reflecting coatings and transmitting filters, review 79−46029
vacuum UV special application coatings, reflectance, transmission, technology 79−59788
water continuously variable filter for I laser 78−55397
waveguide, laminar, 4-layer, dielectric, S-type, propag. characts., mode filtration *(Russian)* 78−30078
waveguide mode filter on anisotropic thin film, anal. of two coupled modes with losses 80−79000
waveguide mode filters using coupling between two nonidentical waveguides 78−46757
wavelength division multiplexing transmission technology 80−58727
wavelength multiplexing devices for multimode optical fibres 77−79926
wide aperture optical shutter with saturating filter at 1.06 μm 80−53457
zero-order noncoherent filtering methods 77−19423
Ag halide emulsion colouring, k-value and sensitivity relationship *(German)* 80−7815
Ag-SiO_2, coevaporated films, neutral density filters for near IR radiation 79−72673
Al filters, for use on Apollo Telescope Mount XUV spectrograph, fabrication 77−60602
As_2S_3 thin films, vacuum deposited on Ge and PbS, sealing props. and TEM 80−35097
Au ion plating process 79−66186
Be film, opt. filter in He discharge lamp for photoelectron spectroscopy 78−79115
C large unsupported film, prod., as UV filter 78−38092
CdS-ZnS(CdSe), film, light transmittance spectra, comparison with Schott GG 495 glass filter 78−33838
$CdS_{1-x}Se_x$, graded comp. semicond., tunable narrow-band filter, 5130 to 3700 Å 77−31128
$CdS_{1-x}Se_x$ gradient cryst., pseudointersection of dispersion curves n_o (λ) and n_e (λ) 79−15487
Ce-Ti containing glass for cut-on filters in visible region 78−13803
CeO_2-SiO_2(MgF_2), multilayer refractory oxide interf. coatings 79−7192
^{133}Cs, filter cells for hyperfine optical pumping, optical detect. of 0-0 transition *(French)* 77−443
Cu-PbI_2 photosystems, Fabry-Perot type interf. filter 78−46738
GaAs-polyethylene, for i.r. characts. rel. to powder band-pass filter design 78−90468
GaAs-polyethylene mixture, optical transmission spectra, IR filter prep. using computer appl. 80−2763
Ge-CsI, narrow band interference filters for 8-15 μm 77−34951
Ge-SiO multilayer edge filter design, 3.2 to 4.9 μm range 78−87131
HCl, isotopic transfer laser, intercavity cold gas isotope filter 78−46590
Hα, for solar photography 78−40833
I_2 filter, absorpt. lines removal from 514 nm excited Raman spectra 78−70200
I_2 filter structure, digital normalisation, in quasielastic light scatt. 77−13805
I_2 vapour cell as narrow band optical filter 78−74993
InAs IR filter properties, operational characts. of antireflection coatings 79−14107
In_2O_3:Sn, selective transparent film, for solar collector, efficiency 78−33836
$LiNbO_3$, acoustically tuned optical filter, electrostatic field effect 77−58443
$LiNbO_3$, acoustooptic mode convertor as tunable optical filter 77−19407
$LiNbO_3$ crystal acousto-optical tunable filter 77−19434
$LiNbO_3$ crystal acousto-optic tunable filter 79−55245
$LiNbO_3$ waveguide, thin-film optical filtering using acoustooptic interaction 79−81572
$LiNbO_3$:Ti optical waveguide electrooptic devices, polarisation independ. wavelength filters 80−58783
$LiNbO_3$:Ti phase-matched waveguide electro-optic TE⇄TM mode convertor 80−58749
$LiNbO_3$:Ti waveguide electro-optic TE⇄TM mode converter-wavelength filter 80−64210
$LiTaO_3$ platelet, electro-optical tunable filter, birefr. electro-optic cryst., light energy coupling 79−59804
MgF_2-PbF_2, multidielectric stacks as interf. filters, ageing characts. *(French)* 77−34939
Na_3AlF_6, effect of temp. var. on light transmission 78−79136
Nd:glass laser with continuously tunable ps output, polaris. filter 79−22985
Ne discharge Faraday filter, dye laser freq. locking to absorpt. lines 77−79870
NiO doped glass, improved band-pass characts. 78−42394
$NiSO_4$, aq. soln., UV transmission filter characts. 77−3679
Pb glass shower counters, optical filters to improve resolution 77−57818
PbF_2-Na_3AlF_6, interference filter prod. for near UV *(French)* 78−25974
Si detector-optical filter combination, packaging approaches, review 77−10108
Si guided-wave acousto-optical devices 80−102864
Si photodetector, preamplified, packaging approaches, review 77−10108
SiO_2, fused, filter in wide field-of-view SW radiometer for Earth radiation meas. 80−87473
TeO_2 acousto-optical tunable filter with microcomputer control 80−102833
TeO_2 noncollinear IR tunable acousto-optical filter 79−23086
TiO_2-SiO_2 interference filters, narrow band, 0.7 to 1.5 μm spectral region, from cathodic sputtering 79−7221
TiO_2-SiO_2 multilayered film striped optical filters, optical props. and fabrication of RF sputtering 80−10030
Tl_3AsSe noncollinear acousto-optic tunable filter, operation at 10 μm 79−41434
Tl_3AsSe_3 10.6 μm tunable acousto-optic filters 79−55248
$Zn_{1-x}Cd_xS$, graded comp. semicond., tunable narrow-band filter, 4272 to 4584 Å 77−31128
ZnO thin film opt. waveguide, collinear acousto-optic interaction and appl. to tunable opt. filter 80−74509
ZnS, effect of temp. var. on light transmission 78−79136
optical filters continued
ZnS evaporated film optical props. 160 to 2000 A, reflecting interf. filter appl. 79−15544
ZnS-Na_3AlF_6 Fabry-Perot interference filter, neutron irrad. effects on props. 79−76867
ZnS-Na_3AlF_6 multilayer dielectric optical filter, irreversible thermal effect 77−7195
ZnS-Na_3AlF_6 multilayer films, thermally evaporated, dispersion characts. 77−59629

optical free induction decay *see optical coherent transients*

optical frequency conversion
see also optical harmonic generation; optical parametric devices
acousto-optic diffraction degenerate regime, second harmonic, sum and difference freq. beams 80−74300
active media, possibilities of efficient freq. conversion 79−59764
alkali metal vapour, IR image upconversion using two-photon resonant optical four-wave mixing 80−58632
alkali metal vapour, two-photon reson. four-wave mixing process, phase matching 77−14772
anticorrelation effect in optical parametric processes, quantum statistical props. 79−7177
atmospheric turbulence, phase distortions, correction via nonlinear optical techniques 77−88855
atmospheric turbulence degradation compensation by nonlinear optical mixing 77−42558
atomic media, resonantly two-photon pumped, up-conversion schemes 77−23711
atomic system, transient four-wave mixing and real time holography 79−55171
atomic vapour, UV pulse prod., third order mixing of dye laser radiation 77−83892
atomic vapours, effects of magnetic fields on four-wave mixing processes 79−23024
autocorrelation of objects by four and three-freq. interactions 77−75432
beam vector combination, of differently polarised radiations, effective freq. shift *(Russian)* 78−71153
benzene vapour, four-wave sum mixing near 163 nm 77−10970
benzene-cyclohexane mixture, interference between Raman resonances in four-wave difference mixing 77−23712
benzenes, substituted, liq., optical nonlinearities and hyperpolarisabilities meas. 77−88857
coherence effect of generating radiation on parametric up conversion process 79−76756
coherence lengths and phase conjugation by degenerate four-wave mixing 80−64101
coherent optical pulse synthesis using phase-locked lasers and nonlinear optical processes 79−76724
coherent Raman scattering with three lasers 79−23016
degenerate 4-wave mixing in plasmas 80−24179
dielectrics, nonlinear phonon-photon interactions, physical basis 77−61998
difference frequency generation, Gaussian intensity profile effect 80−78906
difference frequency generation, superposed beams on nonlinear cryst., vector matching effects *(Russian)* 77−62014
difference frequency generation and 4-photon mixing of dye laser radiation *(German)* 77−7132
difference frequency generation by stimulated Raman scatt. using inhomogeneous electrostatic field 80−95954
difference frequency generation with intracavity absorption 77−42567
dye laser, difference frequency generation, degree of conversion depend. on linewidth 80−48347
dye laser, tunable, 545-680 nm radiation efficient conversion to 360-415 nm UV range 80−74439
dye laser radiation, tunable sources for vac. UV 77−68219
electro-optic crystal, single sideband generation at 10.6 μm 79−55179
EUV generation of coherent radiation 79−76758
far IR difference frequency generation of CO and CO_2 lasers, for isotope separation 77−19366
far IR generation, difference frequency mixing of CO_2 lasers, book contrib. 77−46763
far IR laser spectroscopic sources and applications 77−57415
far IR to visible conversion in ruby, for tunable quantum counter 77−5909
fibre, single-mode, large-freq.-shifted three-way mixing in low dispersion wavelength region 80−99792
fibre-optic parametric oscillator, sequence freq. generation 80−83636
fifth order atomic optical nonlinearities in multiphoton resonances 80−28275
four-wave mixing as real time holography 78−50853
four-wave mixing in optical fibre, image phase compensation and real-time holography 78−63039
frequency measurement and synthesis, near IR and visible ranges, up (down) conversion nonlinear crysts. 79−35808
frequency up-conversion to produce coherent vacuum UV radiation 77−7067
gas laser freq. synthesis and meas., using nonlinear device mixer *(French)* 79−31966
inert gases, XUV radiation generation by fifth, seventh order freq. conversion 78−83033
inhomogeneous media, efficiency of freq. conversion processes 78−30024
integrated coherent IR generator, difference freq. generation in nonlinear optical waveguide 80−33084
IR absorpt. spectra, broad, anal. by nonlinear conversion to optical freq. *(Russian)* 77−49793
IR and UV nonlinear processes 79−3738
IR broadband spectra upconversion 78−55406
IR generation, book 77−46761
IR generation, difference freq. mixing, parametric oscill. and stimulated Raman scatt., book contrib. 77−46762
IR generation, optical mixing, SHG and parametric oscills., book contrib. 77−46764
IR image nonlinear conversion allowing for turbulent atm. influence 80−23751
IR imaging, using nonlinear optical upconversion 78−79070
IR imaging using nonliner optical upconversion 78−59091
IR laser wavelength meas. by radiation conversion method, error anal. 79−7175
IR radiation, parametric up-conversion to visible range, review 80−64104

optical frequency conversion continued
IR radiation two-stage conversion, high sensitivity detector appl 79−59761
IR source, tunable, efficient 80−5789
IR tunable sources, operating characts. and limitations of nonlinear mixers 77−54713
IR upconversion to visible, detect. method for astronomy 78−45240
IR upconvertor for astronomical imaging 78−7883
IR-to-visible image conversion with a thick-layer hologram 80−87355
laser beam, spectral analysis, photomixing method 78−46698
laser beam possible freq. conversion by electron beam 79−68413
laser frequency measurement of I ion line, by harmonic mixing 77−83919
laser frequency synthesis 78−12675
laser system for optical wave mixing expts. 78−5521
laser-microwave mixing, tunable submm. source for isotope separation 77−38750
liquid, nonlinear, high intensity light diffr. by ultrasound 80−64270
liquid-liquid moving boundary, reflected freq. conversion *(Russian)* 77−7152
lithium formate, mixing of Nd laser radiation for coherent picosecond source, 350 to 680 nm 78−13762
lithium formiate, active spectroscopy under conditions of double-w-k-resonance *(Russian)* 78−33777
low noise mixing in far IR region, appl. of Schottky barrier diodes 78−68083
metal vapour, tunable IR generation by optical mixing, book contrib. 77−46766
metallic film, optical freq. mixing and detect. 77−75614
metals, surface EM wave enhancement of nonlinear optical effects 77−68240
MIM point-contact diodes for harmonic generation and mixing 78−88044
mixing, far-IR generation in noncentrosymmetric cryst. 77−58384
molecular gas, Stark-induced three-wave mixing, theory 77−14774
N two-level atoms, quantum theory of nonlinear optical phenomena 80−5790
narrow band gap semiconductor, optical nonlinearity due to free carriers 79−81491
(near) two-photon-resonant freq. up-convertors, limitations and optimisation 79−31985
nonlinear adaptive system, characteristic purposes 80−28273
nonlinear crystal, broad-band light conversion 80−64103
nonlinear crystals for frequency conversion of optical radiation, review *(Russian)* 80−38068
nonlinear optical phase conjugation for pulsed laser systems 78−59092
optical fibre, sum-freq. generation of visible light 80−43399
parametric, in readout systems without memory 78−1302
parametric frequency up-conversion with stochastic pumping, canonical model 80−53368
parametric image upconversion, thickness aberrations investigation rel. to multi-transverse mode pump 78−13765
parametric system, two-stage, up-conversion for IR image visualisation 77−83994
pentacene−p-terphenyl, optical dephasing, optical mixing-detected ps photon echoes obs. 78−71155
periodic stratified medium, birefr., phase matching, X-ray lasers 77−65566
phase distortion compensation by three-freq. parametric interaction 80−23750
phase matching condition for oscillator strengths determ. 77−10638
phase matching of 2-photon resonant 4-wave mixing processes 78−87104
phasematching of freq.-conversion processes induced by additional selective pump 80−28271
picosecond light continua generation by four-photon interactions 77−62007
picosecond luminescence detection using type II phase-matched freq. conversion 77−31024
picosecond nonlinear optics, book contrib. 77−65609
picosecond pulse freq. changing into UV, VUV and IR, book contrib. 77−61138
picosecond pulse generation possibility, frequenty-tunable visible and UV 79−23027
picosecond pulse sum frequency generation 80−91854
picosecond signal processing with nonlinear integrated optics 80−99882
polaritons, bulk and surface, nonlinear spectroscopy 77−50730
polarization convertors for 2-freq. optical interferometers 80−18005
polarization modulated light, freq. mixing detection using periodic analyzers 78−5433
proustite, CO_2 beam up-conversion, pulse temporal struct. determ. 77−3603
pyroelectric ionisation upconvertor for IR detection 80−77860
quadrupole transition moment meas. by interference of quadrupole and DC field-induced sum freq. generation 77−30830
Raman active media, nonlinear, third-order light mixing at polarition reson. frequencies 77−19364
real time linewidth meas. of tunable multiatom. CO_2 laser 78−9405
relativistic electron bunch, freq. conversion on refl., efficiency 78−1143
resonant parametric optical conversion in gases *(Russian)* 80−48351
ring laser, synchronisation region width calc. *(Russian)* 78−46681
ruby, CW backward wave generation by degenerate four-wave mixing 78−71147
semiconductor, magnetic, parametric down-conversion of laser beam 79−64287
semiconductor, non-linear optical props. of band charge carrier gas 78−33775
semiconductor film, optical freq. mixing and detect. 77−75614
semiconductors, nonlinear effects, induced by lasers 79−94300
SHG in crystals, two-photon radiation absorpt. effect 80−9950
signal detuning, effects on phase conjugation 80−23748
similitude theory 78−46710
spectroscopic studies in picosecond domain with synchronously mode-locked dye lasers 77−41697
spectroscopy, time-resolved, IR, using freq. upconversion, methyl isocyanide isomerisation obs. 80−57400
step tunable coherent radiation, generation in extreme UV region, fifth order freq. mixing 77−88837
stilbene derivatives, hyperpolarisabilities, four-wave mixing and SHG meas. 77−83925
stimulated EM shock radiation, freq. conversion and amplification 77−42475
optical frequency conversion continued
stimulated Raman scattering source with dye amplifier, development 78−87095
styrene derivatives, hyperpolarisabilities, four-wave mixing and SHG meas. 77−83925
submillimetre tunable HCN laser sideband generation, mixing with klystron radiation 78−46714
sum frequency wave, conversion coeff. depend. on exciting spectrum width 80−99800
ternary semiconductor crystals for nonlinear optical applics., review 78−33782
thermally induced index gratings Bragg refl., IR optical image conversion, thermal index changes 79−59753
three-level system, stimulated Raman scatt. and stimulated collision induced fluoresc. 78−87103
three-wave interactions in randomly inhomogeneous dispersive media *(Russian)* 80−53364
three-wave mixing, multiplicative stochastic processes in statistical physics appl. 80−22289
time evolution operators and Feynman diagrams appl. 78−18004
m-toluylenediamine, quadratic optical susceptibility dispersion 79−18477
transient nonlinear interactions of opposed waves, fluctuations 77−62011
transient two-photon resonant up-conversion, nonsynchronised excitation 77−10975
tunable coherent light sources, nonlinear freq. mixing, Raman, and semicond. lasers 77−7131
tunable high power lasers for isotope separation 77−34904
tunable IR lasers, principles and operating characts., review 79−98376
tunable laser resources development and appl., laser pulse width meas. 80−48262
tunable lasers, nonlinear device descriptions, characts. and potential 79−990
tunable picosecond UV pulse generator 79−36956
tunable UV and visible radiation prod., freq. conversion of dye, excimer lasers 78−59029
tunable UV generation by sum freq. mixing 78−74949
two-photon field nonlinear optical efficiency, sum freq. generation 80−9949
two-photon resonant Rayleigh-type optical mixing and relax. 78−42380
two-photon resonant up-conversion with ultrashort pulses, nonsynchronous generation 80−83637
ultrashort light pulse parametric freq. conversion 80−106570
undulated electron beams, for microwave to X-ray up-conversion 77−62006
uniaxial crystals, nonlinear optical props., review and summary of data 77−75615
up-conversion with stochastic pumping, exactly soluble model 80−23744
upconversion, three-freq. parametric, beam focusing effects 80−48340
upconversion with stochastic pumping, photon statistics 78−22168
urea, second and third order hyperpolarisabilities, SHG and four-wave mixing meas. 79−59759
urea crystal, efficient phase-matched SHG and sum freq. mixing 80−14391
UV pulse production, sum or SHG of dye laser radiation in nonlinear crysts. 77−83892
UV source, nonlinear cryst. with tunable 90° phase matching 77−14776
vapour, tunable, coherent radiation in the Lyman-α region, 1210 to 1290 Å 79−23023
vision, IR nonlinear perception in 800-1355 nm range 80−12123
whisker diodes sub-MM receivers, antenna characts. 78−12755
$AgAsS_3$, proustite, parametric upconvertor, temp. effects on tangential phase-matching condition 80−99804
Ag_3AsS_3, $CdGeAs_2$, freq. synthesis of 260 THz, 1.15 μm He-Ne laser 79−64263
Ag_3AsS_3, proustite, freq. conversion of CW chem. HF laser radiation 78−30023
Ag_3AsS_3, proustite, parametric conversion of single-pulse CO_2 laser for photographic recording 79−10357
Ag_3AsS_3, proustite, thin cryst., difference freq. power generation, 6.7-10.5 micron 77−83926
Ag_3AsS_3, proustite, upconversion linearity for short CO_2 laser pulse diagnostics 79−27304
Ag_3AsS_3, proustite upconvertor, effect of temp. on phase match angle characts. 80−5799
$AgGaS_2$, up-conversion of 10.6 μm radiation into visible 78−33783
$AgGaS_2$, α-HIO_3, thermal radiation recording by two-stage freq. conversion detects. 79−46002
$AgGaS_2$ crystal, IR radiation conversion for nonlinear spectrograph 79−10360
$AgGaS_2$, difference freq. generation for IR tunable radiation, 5.5 to 18.3 μm 77−10969
$AgGaS_2$, efficient up-conversion of 10.6 μm radiation into green spectral range 77−88838
$AgGaS_2$, IR signal detection by mixing with dye laser radiation 77−88846
$AgGaS_2$, parametric up-conversion of IR radiation 77−79901
$AgGaSe_2$, down-conversion of $LiNbO_3$ optical parametric oscillator output, 4 to 18 μm 79−86215
Be, 4-wave sum mixing around H Lyman-α 80−23747
Br_2 vapour, four-wave sum mixing near 177 nm 77−10970
CO, liq., IR four-wave mixing 78−18006
CO-O_2 liq. mixture, IR four wave sum and difference freq. generation 78−33771
CO_2 CW laser radiation, freq. conversion in Tl-Cs vapour mixture 80−74438
CS_2, amplified phase-conjugate refl. and optical parametric oscill., 4-wave mixing obs. 78−74946
$CaCO_3$, third order nonlinear optical difference frequency generation 78−22176
$CdGeAs_2$, Ag_3AsS_3, freq. synthesis of 260 THz, 1.15 μm He-Ne laser 79−64263
$CdGeAs_2$, develop. of tunable coherent radiation at 16 μm 78−90454
$CdGeAs_2$, freq. mixing for tunable IR sources 78−59030
CdS, biexciton, low intensity nonlinear coherent mixing study 80−49619
CdS, third order nonlinear optical difference frequency generation 78−22176
CdSe, down-conversion of picosecond IR source, 10 to 20 μm tuning range 80−5793
CdSe down-conversion of $LiNbO_3$ broadly tunable picosecond IR source 80−74435
CdSe, freq. tuning possibility by uniaxial press. 78−59084

optical frequency conversion continued
CdSe, temp. depend. phase-matched nonlinear optical devices 80−99794
CdTe crystal in square waveguide, single sideband generation at 10.6 μm 79−55179
Co:MgF_2, tunable transition-metal-doped solid state lasers 80−58549
Cs vapour, CO_2 laser freq. conversion by dye laser radiation mixing *(Russian)* 78−22175
Cs, vapour, IR image up-conversion two-photon reson. pumping by Nd:$La_2Be_2O_5$ laser 77−10968
Cs, vapour, optical frequency down conversion and stimulated electronic Raman scatt. 79−50350
Cs vapour, parametric conversion of 3.39 μm He-Ne laser radiation to visible 78−83036
Cs vapour, two-photon resonant parametric generation, 2 to 20 μm 77−42563
CuCl, light mixing induced by giant two-photon absorpt. of excitonic mols. 78−42383
CuCl, third-order nonlinear optical spectroscopy 77−23713
Er^{3+}, Yb^{3+}:glass, Nd laser radiation energy conversion *(Russian)* 77−62013
EuX, X=chalcogen, antiStokes luminesc. 77−63455
GaAs, insulating, generation of far IR radiation by freq. mixing 79−50347
GaAs, polaritons, surface nonlinear interactions, Green's function theory 78−42379
GaSe, 4 to 12 μm tunable down-conversion from $LiNbO_3$ parametric oscillator 78−66865
GaSe, down-conversion of $LiNbO_3$ optical parametric oscillator output, 4 to 18 μm 79−86215
GaSe, nonlinear cryst., IR parametric image conversion from 10 μm to near-IR 79−89970
Ge, 16 μm generation from phase-matched 4-wave mixing of CO_2, NH_3 lasers 79−3745
Ge, four photon mixing, intense tunable IR generation 77−68239
Ge, four wave mixing, intense tunable IR source for photochemistry 77−88852
Ge, four wave mixing, tunable IR generation 79−98444
Ge, four-photon mixing IR source, for isotope separation in UF_6 77−54760
Ge, non-collinear phase matched 4-wave mixing of CO_2 and NH_3 laser radiation 79−988
Ge, noncollinear phase matched four photon mixing, CO_2 laser radiation 77−14778
Ge, Sellmeier coeffs. temp. depend., nonlinear optics average power limit 79−50349
H, 97.2 nm generation by reson. freq. mixing *(Russian)* 78−46723
p-H_2 cooled gas, 16 μm source using four-wave mixing and stimulated Raman scatt. 78−1298
H_2 four-wave interactions for tunable IR generation 77−54759
H_2 gas, tunable coherent Raman mixing, 4.3-13 μm 77−88850
p-H_2, generation of 16 μm radiation by four-wave mixing 77−50720
H_2, tunable IR generation, by coherent Raman mixing 77−42561
α-HIO_3, $AgGaS_2$, thermal radiation recording by two-stage freq. conversion detects. 79−46002
$Hg_{0.77}Cd_{0.23}Te$ nonlinear optical IR generation 80−58642
$Hg_{0.77}Cd_{0.23}Te$, resonant four-photon and higher order mixing 79−41415
$Hg_{1-x}Cd_xTe$, nonlinear optical effects 80−14389
n-InSB, spin resonant four-wave mixing, CW meas. and transient effects 80−48344
InSb, difference freq. mixing via spin nonlinearities in far IR, book contrib. 77−46765
InSb, optical mixing by mobile carriers 78−25920
K vapour, tunable picosecond UV pulse generator 79−36956
K vapour, two-photon resonant parametric generation, 2 to 20 μm 77−42563
KB_5O_8, coherent CW radiation generation by mixing, tunable 211 to 216 nm 78−83029
KB_5O_8, sum freq. mixing, tunable coherent radiation source below 217 nm 77−19359
KB_5O_8, tunable coherent radiation generation, 201-212 nm 77−83921
KB_5O_8, tunable coherent vac. UV generation by sum freq. mixing 78−55404
$KB_5O_8.4D_2O$, SHG and sum freq. mixing 78−55407
$KB_5O_8.4H_2O$, efficient UV generation, 2073 to 2174 Å 77−62003
$KB_5O_8.4H_2O$, tunable UV generation at 1966 Å 77−68238
KH_2PO_4, high-power picosecond pulse generation 218 to 316 nm 80−64106
KH_2PO_4, servo tuning and stabilization of nonlinear optical crystals 79−55180
KH_2PO_4, sum freq. mixing, 212.8 nm pulse burst generation of Nd:YAG laser 78−74934
KH_2PO_4, third order nonlinear optical difference frequency generation 78−22176
KH_2PO_4, tunable CW UV radiation generation, 257 to 320 nm 77−88860
KH_2PO_4, tunable coherent radiation generation below 250 nm at MW power levels 78−59080
KH_2PO_4, types I and II optical mixing with ps laser pulses 77−72032
$LiIO_3$, 5.3 μm down-conversion, IR source appls. *(German)* 78−90452
$LiIO_3$ CW intracavity upconverter using Ar laser, noise props. 80−64099
$LiIO_3$ crystal, nonlinear optical freq. transform. of variously polarized laser radiation 79−55181
$LiIO_3$ crystals with optical freq. conversion, IR detect. characts. 77−87832
$LiIO_3$, difference freq. generation tunable under dispersive phase-matching conditions 78−46726
$LiIO_3$, freq. conversion of CW chem. HF laser radiation 78−30023
$LiIO_3$, freq. up-conversion, spontaneous parametric noise 77−75622
$LiIO_3$, generation of tunable CW IR radiation by difference freq. mixing 77−3623
$LiIO_3$, IR radiation parametric upconversion with pulsed ruby and CW Ar lasers 77−72026
$LiIO_3$, IR radiation generation, difference freq. mixing of N_2 and dye laser laser radiation 78−37942
$LiIO_3$, mixing of Nd laser radiation for coherent picosecond source, 350 to 680 nm 78−13762
$LiIO_3$, nonlinear cryst., difference freq. generation by superposed beams, vector matching effects *(Russian)* 77−62014
$LiIO_3$, parametric convertor of IR radiation, angular and spectral characts. 79−64282

optical frequency conversion continued
$LiIO_3$, simultaneous stimulated Ramam scatt. and optical freq. mixing 79−86210
$LiIO_3$, simultaneous stimulated Raman scatt. and optical freq. mixing using three-mirror config. 80−48342
$LiNbO_3$, 3.39 micron HeNe laser radiation, difference freq. mixing and SHG 77−83928
$LiNbO_3$, broadly tunable repetitive picosecond parametric oscillator, freq. conversion 78−66866
$LiNbO_3$ crystal and ruby lasers in difference freq. laser, tunable MM range emission 80−5764
$LiNbO_3$ crystals with optical freq. conversion, IR detect. characts. 77−87832
$LiNbO_3$, difference freq. generation of submm. waves *(Russian)* 77−10981
$LiNbO_3$, difference freq. radiation of IR radiation, high efficiency 77−19363
$LiNbO_3$, freq. conversion of CW chem. HF laser radiation 78−30023
$LiNbO_3$, freq. up-conversion, spontaneous parametric noise 77−75622
$LiNbO_3$ intracavity upconvertor for IR detect., limits to low noise equivalent power operation 80−74430
$LiNbO_3$, Nd laser radiation, difference frequency generation in rectangular mm waveguide 79−18479
$LiNbO_3$ optical waveguide, tuning characts. of parametric interactions 79−3779
$LiNbO_3$, SHG, two-photon radiation absorpt. effect 80−9950
$LiNbO_3$, third order nonlinear optical difference frequency generation 78−22176
$LiNbO_3$ three-dimens. optical waveguide, parametric difference freq. generation 80−48335
$LiNbO_3$, tunable IR sources, parametric oscillators and difference freq. generation 78−59030
$LiNbO_3$:Ti diffused channel waveguide, optical parametric amplification 80−106564
$LiNbO_3$/CdSe system, 16 μm tunable source 78−9414
$LiTaO_3$, quadratic optical susceptibility dispersion crystal struct. 79−18478
NH_3, resonantly enhanced 26 GHz parametric upconversion 79−23020
NH_3, Stark tuned 26 GHz parametric upconversion at 10.8 μm 77−88845
NH_2D, mixing of CO_2 laser radiation with 4 GHz microwaves, Stark-induced three-wave mixing, expt. 77−10974
NH_2D, mixing of CO_2 laser radiation with 4 GHz microwaves, Stark-induced three-wave mixing, calc. 77−14774
$NH_4H_2AsO_4$, freq. doubling of CW tunable dye laser 78−17965
$NH_4H_2PO_4$, blue tunable picosecond pulse generation by synchronous mixing of Nd:glass laser with sideband radiation 80−87431
$NH_4H_2PO_4$, efficient generation of tunable UV radiation down to 2400 Å 79−55182
$NH_4H_2PO_4$, harmonic and sum freq. generation, tunable CW UV radiation prod. 78−46712
$NH_4H_2PO_4$, N_2 and dye laser pulses mixing 0.68-1.1 μm output 77−27314
$NH_4H_2PO_4$, tunable coherent radiation generation below 250 nm at MW power levels 78−59080
NO, vapour, four-wave sum mixing, 130 to 180 nm, third harmonic generation 77−10970
Na, two-photon transition, distinction of competing processes in nonlinear resonant freq. mixing 80−33080
Na, vap., sum frequency generation, via reson. quadrupole transition, theory 78−42385
Na, vap., third harmonic generation, four wave parametric mixing 77−737
Na vapour, amplified refl. by degenerate four-wave mixing using Kerr nonlinearity 78−55413
Na vapour, conversion of He-Ne laser emission *(Russian)* 78−33776
Na vapour, effective freq. conversion of radiation 80−28278
Na vapour, quantum counter, IR detection 78−30016
Na vapour, reson. freq. conversion by two-photon reson. pumping 80−28277
Na vapour, two-photon reson. four-wave mixing process, phase matching 77−14772
Na vapour, two-photon reson. four-wave mixing 78−46716
Na vapour, two-photon resonantly pumped, upconversion of 3.39 μm He-Ne laser radiation 78−55409
Nd laser, emission freq. conversion by method of reson. pumping of active media 80−1206
Nd^{3+}:YAG laser, spontaneous mode locking necessary conditions, quadratic nonlinearity influence 79−64261
Ne, reson. four-photon parametric mixing conditioned by multipole relax. rates difference 79−89959
Ni:MgF_2, tunable transition-metal-doped solid state lasers 80−58549
Rb, vap., 1.06 micron conversion to 420 nm range 79−14040
Rb vapour, reson. four-photon difference freq. mixing of Nd:YAG and dye lasers 78−50854
Rb vapour, time-reversed optical wave front generation by degenerate four-wave mixing 79−14028
RbH_2PO_4, harmonic and sum freq. generation, tunable CW UV radiation prod. 78−46712
Si, degenerate four wave mixing of 1.06 μm laser radiation 80−5794
n-Si:P, Sb, reson. four wave mixing, valley orbit splitting 79−89960
SiO_2 optical fibre, single-mode, CW three-wave mixing 79−10352
Sr, CW VUV radiation generation by four-wave mixing 80−58640
Sr, vapour, effects of magnetic fields on four-wave mixing processes 79−23024
Sr vapour, enhanced production of coherent vacuum UV radiation by four-wave mixing 77−83923
Sr vapour, resonantly enhanced sum freq. mixing, coherence effect 77−88848
Sr vapour, vacuum UV coherent radiation generation by four-wave sum freq. mixing 79−10350
TeO_2, nonlinear optical susceptibility, antisymm. components 78−13755
TiO_2, third order nonlinear optical difference frequency generation 78−22176
Tl, ($6p^2P_{3/2}$), from selective photodissoc. of TlBr 78−90243
Tl, atomic vapour, optical difference freq. generation 77−27317
Tl vapour, He-Ne laser radiation freq. conversion 1.15 μm to 377.6 nm 80−95948
Tl vapour, Nd:glass laser output conversion from 1.06 micron to 388.1 nm 80−91850
W-Ni diode, He-Ne laser freq. meas. rel. to CO_2 laser 77−31113

optical frequency conversion continued
ZnGeP$_2$, IR radiation parametric conversion to visible range 79−94297
ZnGeP$_2$, temp. depend. phase-matched nonlinear optical devices 80−99794
ZnO, third order nonlinear optical difference frequency generation 78−22176
ZnSe crystal, difference freq. generation of 2 CO_2 lasers 79−10362

optical glass
absorption coeff. determ., refl. losses role 77−72100
absorption coeff. meas., calorimetric method, fibre glass assessment 77−58405
absorption coefficient measurement by calorimetric techniques *(Dutch)* 79−76774
absorption coefficient under laser radiation action, temp. depend. 79−89979
absorption coefficients at 632.8 nm, intracavity laser meas. 78−8454
absorption filters with bandpass characts. for green region *(German)* 77−34943
absorption waves in glass irradiated with quasi-CW laser pulse 79−89952
alkali and alkali earth metal metaphosphate glasses exam. of temp. dependence of thermooptical const. 78−88286
alkali boroaluminosilicate system, self-focusing fibres with aperture of 0.18 80−87548
alkali-PbSiO$_3$ optical fibres, high aperture, double-crucible preparation 78−1450
alkaline glass, ionic diffusion and exchange, integrated optics study *(French)* 77−88940
anisotropy due to laser-induced electrostriction *(Russian)* 79−99846
apochromat, four-lens three-colour, glass selection for design 78−13783
apochromat optical glass development status and prospects 79−27348
apochromatic glass pair dispersion coeff. selection 79−72657
apochromatic pancratic objective components, primary chromatic coeffs. 80−28298
apochromats from four types of glass, components for broad spectral region 79−32026
astronomical lightweight mirrors of glass, economical construction *(French)* 77−17370
athermal glasses, chemically stable 80−102783
athermal phosphate and silicate glasses, thermooptical characts. and stress coeffs. 77−31123
attenuation and optical density spectral curves 79−50361
band-pass filters for violet-blue region, glass characts. *(German)* 78−13802
bandpass filter glasses, 550-616 nm, transmission characts., CuO and NiO colorants 78−66919
bandpass filters for visible region, glass characts. 77−75659
birefringent element, analogue, built from polarising wide field Michelson interferometer 80−91895
blank for primary mirror for large azimuthal telescope, annealing 77−72101
blanks, stresses and birefr. changes with dimensions 78−30100
borosilicate optical waveguide glass, B content determ. using nuclear track counting 80−95969
borosilicate photochromic glasses, photosensitivity rel. to AgCl particle shape 78−31223
boundary with CS_2, optical bistability at nonlinear interface 80−33094
Brillouin scattering meas., sound vels., Pockels coeffs., phonon damping 79−95792
Brillouin scattering meas. of elastic, elasto-optic consts. and extinction coeffs., laser glasses 79−11429
bulk materials, low optical absorpt. coeffs. meas., adiabatic laser calorimetry with long rod samples 79−2804
capillary array, window for vac. UV 79−89990
caustic patterns for melt zones in solidified glass samples, asymmetric cases 79−22893
caustic patterns for melt zones in solidified glass samples, symmetric cases 79−22892
ceramic, (sital) surface operation parameters, selection using bending strength tests 79−32101
chalcogenide, as optical memory, density of recorded information 77−75433
chalcogenide, photoinduced struct. changes, interferometric meas. 77−49769
chalcogenide glass, O free, refr. index, temp. coeff. 77−58403
chalcogenide glass films, kinoform optical elements and integrated optics elements prod. 77−75634
chalcogenide glass films, opt. inform. recording uses 77−75633
chalcogenide glass optronic receiver with simultaneous direct and memory effect 77−75706
chalcogenide glass two-layer low-absorpt. antirefl. coating, for KCl laser window 78−37927
chalcogenide glass Z 79−14063
chalcogenide glass-metal light sensitive systems with barrier layer, new photographic materials 77−75635
chalcogenide glasses, O-free, cooling rate influence on optical consts. 80−88952
chalcogenides, prod. and acoustooptic props. *(Russian)* 78−63158
characteristics, electromagnetic, mechanical and thermal props. 80−106587
chemical durability, pragmatic view 80−78921
chemical incompatibility of core and cladding glasses 77−75694
chemically unstable glass components, protection from biological overgrowths 78−59107
chromatic aberration first-order theory, secondary spectrum correction with common glasses 78−90382
cleaning surface to micron level cleanliness 78−72921
coloured, for short wavelength cutoff filters, fluoresc. data 79−61411
coloured, type K8, laser damage threshold, optical absorpt. influence 80−91830
coloured filter glasses, comparison of glasses made by different manufacturers 77−75630
colouring by colloidal P 77−8961
communication fibre waveguide fabrication techniques 80−1322
components, for optical precision instruments 79−36968
compound glass fibres, mode-dependent effects, total loss decomposition, absorpt. and scatt. losses 80−53437
compound glass rod absorption coeff. calorimetry 80−106631
cracked layer thickness determ. by chemical method, K8 and TFl glasses 80−64226

optical glass continued
crown, corrosion by organic acid solns., exam. of corrosion depth by interferometry *(Japanese)* 79−20237
crown glass, triple-layer antirefl. coating in visible region 78−13777
crystallisation, reducing agent effect 78−46736
cuprous halide photochromic glasses, spectral props., shell model *(Russian)* 79−27354
CVD isotopic, of high silica content glass, for optical waveguide prod. 77−72093
cylinder refractive index variation by field-assisted ion exchange 80−14500
deflectors, beam quality, of acousto-optic frequency shifters 78−79127
development and manufacturing processes 80−53393
devitrification effect on striae coarseness 77−34972
diamond grinding of optical glass, kinetics 80−64224
didymium glass filters for spectrophotometer wavelength scale calibration 80−43417
diffused channel waveguides, direct index meas. 80−87562
diffusing glass, optically thick-layer transmission ang. distrib. 79−27179
diffusing glass catalogue and basic operational characteristics 79−46019
diffusion kinetics of glass used for optical fibres 79−90040
edge cladding glass-disc laser glass interface, reflection meas. 79−27300
electronic nonlinearity coeff. meas. 79−27341
ellipsometric study of zone of contact 80−4754
Faraday effect in transducer material, comparison with quartz 78−48149
fibre, epoxy-acrylate coated, strength and static fatigue 78−1386
fibre, high-temperature fatigue strength and OH^- stress-induced corrosion 78−1387
fibre, optical losses rel. to imperfections 77−88949
fibre, UV-cured, epoxy-acrylate coated, environmental effect on long-term strength 78−5582
fibre communication advances, materials and techniques 80−102853
fibre devices and materials for 4 μm-band communication 78−94441
fibre fabrication, low OH content, vapour phase axial deposition method 78−83125
fibre manufacture, double-crucible and plasma methods 77−50763
fibre optic components, radiation strength for ruby laser transmission 77−7108
fibre optic glass pair quality, effective aperture and light scatt. analysis 78−90522
fibre preform, high silica, continuous fabrication process *(Japanese)* 78−37978
fibre preparation methods and performance factors 80−69557
fibre production methods for optical communications, review *(German)* 80−23813
fibre technology and information transmission props. *(German)* 80−10010
fibre waveguide, γ-irrad., reversible optical bleaching of induced absorpt. 80−14462
fibre waveguide, glass core/polymer cladding, high numerical aperture 80−96024
filament waveguides for signal transmission in far IR region *(Czech)* 80−96017
film, RF sputtered, roughness parameters 77−69202
film, SiO_2 rich, prepared by modified CVD, refr. index behaviour 78−60526
film acousto-optical props. for integrated optical Bragg cell, 7059 glass 79−55251
film compositions, electrochromism *(Russian)* 79−28721
filter glass, simulating CIE spectral tristimulus value $\bar{z}(\lambda)$ 78−30037
filter glasses with band-pass characts. for red spectral region 78−25936
filter glasses with band-pass characts. for yellow-orange region of visible spectrum 77−75683
filter glasses with band-reject characts., for visible spectral region 79−18525
filters for reproducing radiation of B and C sources 77−88947
finishing with small-grained diamond grinding wheels *(German)* 80−38137
flash lamp shell transparency changes and dynamic colour *(Russian)* 79−10370
flat layered glass, ang. distrib. for various incidence angles 79−7079
flatness of test glass, reading errors of interf. fringes 79−32097
flint, dense and ultradense, acousto-optical props. and appl. *(Russian)* 80−2721
fluorescence standards in radiophotoluminesc. detector reading device 77−67944
fluorophate glasses, containing rare earth ions, magneto-opt. characts. 80−64126
fluorophosphate and fluoroberyllate glass laser damage thresholds and solid inclusions 80−33054
fluorophosphate glass produced in pyrocarbon coated melt vessels, increased light absorpt. 78−71167
fluorophosphate glasses with silicofluorides, optical props. 77−72040
fluorophosphate laser glass, highly homogeneous, production 80−14411
fluorophosphate laser glasses, low nonlinear refr. index, development 78−50870
fluorophosphate laser glasses, Nd doped, piezooptic coeffs. meas. 80−99815
fluorophosphate melt, disintegration of vitreous C 78−30101
fluorophosphate optical glass development 80−106588
four-colour thin apochromat design 79−27364
fused silica, GeO_2-, P_2O_5-, B_2O_3-doped fibres, IR characts. *(Japanese)* 78−37981
germanate glass, resistance to humidity and spotting agents 77−58404
glass:CuO, band-pass characts. improvement by doping 77−54797
glass:Nd laser materials, intensities of optical transitions 77−689
glass, high-transmission, least-squares method for extinction coeff. determ. 78−90470
glass polishing process acceleration with chem. reagents 78−90542
glass-Na vap. interface, dye laser frequency locking by selective refl. 78−29992
graded-index antireflection coatings, high laser damage threshold 80−83628
graded-index fibre material dispersion evaluation using nanosecond pulse radiator 79−81520
gradient index lens fabrication by molecular stuffing 80−14499
gradient index material models and exptl. verification 80−16002
gradient index optical elements and system design 80−106594
gradient index optical lenses, use, design, fabrication and refr. meas. 78−13780
gradient index SELFOC lens, aberration improvement 80−14425

optical glass continued
gravity glass, IR emissivity, 673-1673K 80−24623
greasy films on glass, due to everyday handling, effect on optical transmittance 80−27329
grinding process, variation of diamond tool working ability 77−7225
ground, surface height and correlation length from reflection scatt. of laser light *(French)* 80−54491
ground surface, fissured layer effect on scatt. of polarised light 79−64172
halogenide, transparent, prep. for IR spectroscopy 77−67514
high refractive index core glass for high NA optical fibres *(Japanese)* 79−59853
high volume low cost, as solar reflectors, compositions and weathering effects 80−106589
high-temperature transmission/wavelength characteristics *(French)* 79−7188
homogeneity deterination using holographic interferometer 78−90401
hyperchromatic lens, expressions for first order chromatic aberrations 80−91879
illuminating fibre bundles, improved characts. due to glasses type VS 1637 and VO 720 80−102844
index inhomogeneity, rapid interferometric determ. 79−93207
inhomogeneity, characterisation 79−86225
inhomogeneous glass sintering, self stresses producing bulk flow, optical wave guide appl. 80−14448
interferometer rod, inhomogeneity rel. to tempering 77−34919
IR glass, magneto-optic props. 77−73132
IR materials for measuring radiant flux, IKS glass *(Russian)* 80−48366
IR permeable materials *(German)* 80−38081
IR spectral emissivity and absorpt. coeff. at 600 to 1700K 80−16018
IR thermooptic coeff. of TI-20 glass, for laser window material 77−36208
IR transmitting, as optical material in passive systems, preparation and characterisation 79−23034
IR transmitting materials, appl. in 1 to 6 μm range, mech. props., review 79−4250
K8, bending strength, sample dimension effects 80−9975
K8, foam form. and suppression methods during polishing 80−28364
K8, TF5 and Na-7-B-23 glass, laser-induced damage, role of absorbing microinclusions, passive methods 79−31969
K-8 type, laser irradiated, transient thermal self-focusing and melting 77−50733
kinematic relationships in automatic glass grinding and polishing machines *(Czech)* 79−32096
Large Azimuthal Telescope primary mirror, glass blank quality 79−29991
large disc, optical homogeneity, high accuracy measurement *(Chinese)* 79−55195
large optical component antireflection and protective coatings 79−72660
laser, pulse-periodic, thermal lenses in glass active elements 79−89914
laser bulk damage, stimulated Brillouin scatt. influence 79−59762
laser damage threshold for 10 ms pulses, temp. depend. 77−75595
laser glass characts., review 79−27262
laser glass cladding composition and design criteria 79−18450
laser glass inversion density, direct meas. 79−13969
laser glasses, figures of merit and physical/optical property correlations 79−13970
laser glasses, gain coeffs. meas. and modelling 77−88726
laser heating, for multimode channel waveguide fabrication 77−7220
laser host material, production in outer space laboratory 77−21084
laser induced destruction threshold, types *(German)* 77−75631
laser induced pre-threshold changes, electron microscopy 78−29999
laser induced surface damage by wide beam 77−79885
laser irradiated glass surface catastrophic optical breakdown development dynamics *(Russian)* 78−2951
laser irradiation of K8 glass, advanced evaporation mechanism 77−79887
laser material, linear expansion coeff. and r.i., temp. depend. 77−733
laser pulse heating, softening and hardening points obs. 78−33794
laser radiation destruction, Brillouin-Mandelshtam scatt. influence *(Russian)* 77−72039
laser rod, glass mech. strength and heat resistance obs. 79−76776
laser rods, silicate and phosphate, pumped in pseudoelliptic cavities, thermal effects 79−76692
laser window, elec. fields and power dissipation at oblique incidence 77−46746
lens, double Gaussian objective, design *(German)* 80−64134
lens, Schott S-1005, static fracture resist. rel. to thickness 78−81063
light effects, history of development of photosensitive and polychromatic glasses 80−40080
light scatt. matrices of ground surfaces 79−72483
light scattering in optical glasses at microinhomogeneities *(German)* 78−46734
light sensitive, review of types 80−91870
light-sensitive, with intensive staining, props. *(German)* 79−27350
local structure exam. by EXAFS 80−108301
localised acoustic phonons, effects on thermal cond. and Raman spectra 77−81092
long range refractive index fluctuations, before and after annealing, light scattering exam. 78−13772
luminescence spectra of Fe^{3+} ion *(Polish)* 79−69886
magneto-optical properties of US light diffr. 78−76437
material dispersion meas. in lightguide glasses 78−55447
mechanical strength, antireflection or protective film effect 78−1318
mechanical strength values, symm. bending test 78−46737
medium-loss high-numerical-aperture fibre 77−39095
melting, fining, surface tension, diffusion, nucleation in microgravity 80−81016
melting in Pt crucibles, thyristor freq. convertor-fed power supply 77−50780
melting optical glass in Pt crucibles, power supply freq. convertors 79−72728
metallic and glass components compared 80−69473
meteorite impact on glass, surface erosion 77−90445
moulding, optimum rate rel. to degree of glass deformation 79−50456
multicomponent Schott, proton-induced colouring 80−9974
multicomponent thin film formation on K8 glass 79−72726
multilayer antisolar glazing heat throughput calc. 78−94415
multiple-plate glass systems, spectral directional radiation characts. prediction 78−74956

optical glass continued
Nd_2O_3-Y_2O_3-As_2O_5, spectroscopic props., rel. to possible appl. in lasers 78−84624
neutral absorbers of NS glass, meas. of transmission when irradiated with laser radiation 80−105692
nonlinear focal region formed in transient thermal self-focusing 78−50869
nonlinear refractive index coefficient at 1064 nm, meas. methods 79−3737
objectives, tolerancing of refr. index heterogeneity 80−78948
opal glasses, phosphate opacified, phase comp. and struct. 80−64919
opalescing, visible light scattering, angular depend. of intensity, correction for attenuation 79−4814
ophthalmic lenses, thin, chemtempered, strength meas. by drop-ball testing 80−5811
optical discharge, dynamics and props. for ZhS-12 type glass 79−61471
optical fibres, flexible, manufacture *(German)* 79−27393
optical glass containing PbO, effect of Al_2O_3/Na_2O ratio on rate of ion exchange 78−44377
optical tolerance, glass and plastics comparison 79−59780
packet specimens with antisolar filler 78−90469
phase separated, opt. props. of elongated phases 78−27179
phosphate, containing halogens glass formation 80−103254
phosphate, fluorophosphate large laser effect glasses 78−79021
phosphate, optical stress coeff., effect of alkali metal oxides 77−50740
phosphate glass for improved Nd:glass laser 77−88774
phosphate glasses, optical breakdown rel. to nicroscopic inhomogeneous struct. 80−102784
phosphate laser glass, Nd doped, piezooptic coeffs. meas. 80−99815
phosphate laser glasses, review 80−9888
phosphosilicate glass cored fibre CVD production 77−39120
photochromic, γ-ray effects on sensitivity *(Japanese)* 79−38583
photochromic, electron-hole separation, influence on recombination probability 80−11445
photochromic, holographic data recording optimisation, diffr. efficiency 78−25829
photochromic, spectral characts. control 80−16073
photochromic, thermo-optic transitions 80−50307
photochromic, thermochemical effects 80−87448
photochromic, types FkhS-3, S-4, S-4a and FkhPP, exam. of magnetooptical rotation 78−88284
photochromic glass, Ag halide type, photobrown, transmittance meas. at environmental extremes 79−46020
photochromic glass, coloration kinetics, isothermal relax., and spectral sensitivity using spectrosensitometer 80−27358
photochromic glass, with Ag halides:Cu formation and theoretical models, review 80−43418
photochromic glass darkening and bleaching kinetics, pulse photometry 79−46021
photochromic glasses, parameter standardisation 80−69476
photographic colour printing, correcting light filter selection 80−62764
photosensitive glass, full-colour polychromatic, subcolloidal Ag precipitation 79−47953
photosensitive glass, microstruct. rel. to props. *(German)* 80−38926
physical props., seminar, San Diego, CA, USA (Aug. 79) 80−105423
planar waveguide, fabricated by ion exchange in glass, refractive index profile 80−14460
plate with nonuniform temper, mottled pattern obs. 79−61750
polished, 1.064 μm laser damage threshold rel. to pulse duration and surface roughness 80−33055
polished glass surface, reflected light phase rotation 80−66147
polished surfaces of K8 glass, cryst. deposit form. with optical contacting 77−58492
polishing using diamond tool 77−72105
polishing with ZrO_2-SiO_2 powder mixture 80−28367
polychromatic, induced colour by optical/thermal treatment 80−34954
polychromatic thick lens glass selection *(German)* 80−23763
porous glass preform optical waveguide props. 79−94375
pressure vessels, testing of windows at high hydrostatic press. 79−90016
pressure-shaping components, glass bending monitoring 77−796
primary mirror of large azimuthal telescope, glass comp. selection 77−62025
production for high performance optical systems *(German)* 78−79084
production of optical glasses and single crysts. 79−94308
Pyrex, refr. index-matching soln. 78−12519
quartz, spectral absorptance in 0.25-1.25 μ wavelength, 293-1273K temp. ranges 77−36212
quartz glass, Ge and B dopants, OH impurities, preform material and fibre optic waveguide struct. 80−64173
quartz glass, hydroxyl-free, for low-loss fibre waveguides, γ-irrad. effects 78−13773
quartz glass, spectral absorpt., 3000-4000K 80−25401
quartz glass, spectral absorpt. coeff., 0.25 to 1.25 μ and 1300 to 1700K 80−20622
quartz glass, spectral absorption coeff. in 2.0 to 4.8 micron region, up to 800°C 77−43985
quartz glass fibre waveguides, material dispersion meas. 79−18545
quartz glass fibres, B and P radial doping profiles 77−50771
quenching, horizontal, technological parameters rel. to optical properties 80−45264
radiation coloration and bleaching of Schott optical glasses temp., time depend. 77−19981
radiation coloration due to fast electron irradiation 79−98452
radiation coloured K-8, msec laser pulse effects 77−16435
radiation effects on optical components, review 78−83054
radiation induced transmission loss in optical materials 79−94306
radiation protection by cage effect *(Russian)* 77−83938
rain erosion mechanisms 78−83049
Raman scattering and nonlinear refr. index 80−2749
recording refractometer for optical glasses, 300 to 2600 nm range 80−57363
reflective glass colour standards 80−90878
refraction coeff., photothermal effects *(Polish)* 78−52465
refractive index, effects of alkali oxide comp. changes *(Russian)* 78−22182
refractive index, Hartmann interpolation equation solves using TI-59 calculator 79−98451
refractive index freq. depend., dispersion eqn. calc. 80−40083
refractive index gradient, chromatic variation 80−74471
refractive index gradients, form. using ion exchange diffusion 80−64227
refractive index tables and calcs. for optical designer 80−83650

optical glass continued
refractive index under stress, polarisation charact. *(Japanese)* 79−4781
refractive index-density relationship changes assoc. with reannealing [illegible] 77−27155
refractometry, precision automatic vee block, for glass refr. index meas 80−68243
refractory materials for optical glass making, review 77−14818
relay, system design, secondary colour reduction 78−83067
RF sputtered glass optical waveguide, reduced SYNCANG method for refr. index 77−11046
sampling, of simplex variants and of multiplets *(German)* 78−90484
Schott BG20 and FG18, forced Rayleigh scatt. anomalies 79−82988
selection for lens design 79−81496
Selfoc lens, aberration improvement by glass composition and ion exchange process parameter choice 80−69486
silicate, containing subcolloidal Ag, full-colour photosensitive glass, processing and struct. 79−10369
silicate, optical stress coeff., effect of alkali metal oxides 77−50740
silicate, surface, nonlinearly-absorbing, laser-induced evap. 78−80438
silicate Fe activated glass, diffraction trating recording by UV laser 80−5842
silicate glass, Li_2O and Na_2O effect on thermo-optic props. 78−18029
silicate glass, single mode optical fibre, at zero dispersion wavelength, exam. 78−38043
silicate glass surface, photodichroic for laser recording 80−102785
silicate optical glass chemical stability, F effect 79−76777
silicate photochromic glass, CeO_2 activated, surface treatment effect on absorpt. 78−71168
silicone-glass hybrid Fresnel lens for solar energy concentration 80−61303
single-mode optical fibres with different B_2O_3-SiO_2 compositions 78−1392
SL100, commercial Nd laser glass, props. 78−74912
with small particles, opt. anomaly 77−48209
soda lime glass, Ag^+ ion exchanged, planar optical waveguide, manufacturing tolerances 78−71212
soda lime glass gradient index variation by ion exchange and migration 80−14412
soda-lime glass, effect of radiation heat transfer in thermal cond. meas. 77−23858
sodium-alumoborosilicate photochromic glasses, Weigert effect *(Russian)* 77−68250
solar energy absorbers, thermokinetics of glass and semi-transparent materials *(French)* 80−61410
solar glass components, specularity meas. using Fourier transform anal. 80−5804
space charged particle environment effect 80−69472
space glass technology *(German)* 80−40317
spherical lens generator, sphericity and fracture control 77−27394
spottability determ., reflectometric method 78−30102
stained glass, Ag- and Cu-, optical waveguide effect *(Japanese)* 80−14471
strength limit rel. to Knoop microhardness 79−72641
strength under linear tension, bending, torsion and compression of type K8 79−14062
stress optical coeff. 79−28713
superachromatic triplets, design method 80−64133
superachromatization, glass combination selection 78−1315
surface figuring by laser controlled chem. reactions 78−63209
surface height standard deviation on ground glass surface using interference microscopy 79−93098
surface layer structure after grinding and polishing, Kr sorption meas. 77−31122
surface light probability density function on ground glass surface from far-field coherent light scatt. 79−93099
surface radiation strength, grinding and polishing press. effect 77−72104
surface roughness effect on 1064 nm 150 ps laser pulse damage 79−14013
surface treatment by the low-energy ions of plasma accelerators 80−97608
surfaces joined by optical contact, spectral absorpt. of water layer 78−46852
surfacing, struct. of fine ground surface 77−27393
surfacing, using loose abrasives, impregnated diamonds and electro-plated diamonds 78−50956
technology and applications, review of advances 77−66618
tellurite glass, Cu^{2+} and Ni^{2+} doped, band-pass filters for 550 to 616 nm, transmission charact. 78−71166
tellurite glass film waveguide, Bragg electrostriction, power balance approach 77−75660
thermal diffusivity meas., calorimetric method 79−27349
thermal diffusivity of silicate glasses in range 0-600°C, influence of TiO_2 80−29233
thermal expansion, ultraprecise meas. 77−1247
thermal self-focusing of laser radiation, ZhS-12 glass *(Russian)* 77−31120
thermal-optical distortions of glass discs, rel. to solar obs. using 50 cm lens 79−72640
thermally induced index gratings Bragg refl., IR optical image conversion, thermal index changes 79−59753
thermally tempered, surface stress meas. by crit. ray method 80−106766
thermophysical props., temp. wave methods 80−24624
thin film glass lightguide boundary refraction expts. 80−106639
third order susceptibility meas. by degenerate four wave mixing *(Chinese)* 80−84708
three-lens cemented component calcs., reduced secondary spectrum 80−102800
TI-20, IR transmitting semicond., dn/dT, wavelength depend. 77−77163
torsional deform. above T_g under low stresses, temp. effect 80−21052
torsional deform. above Tg under low stresses of type K8 80−25804
toughening of coloured glass, spectral charact. 80−43416
transmission, reflection, absorption factors, solar radiation, calc. method 77−34918
transmission as a function of γ-irrad., for interf. filters 79−64297
transparent dielectric, laser induced plasma at surface 80−79531
Twyman effect in quartz and optical glasses, temp. effect 79−4784
Twyman effect plane-parallel glass preparation and interpretation *(German)* 77−58401
ultrapure glass preparation for optical waveguides, review 78−3086
unstable OF type glass components, Ta_2O_5 film protection 79−14079

optical glass continued
uranyl-doped glass, appl. in planar solar energy convertor and concentrator 78−71213
USSR-East German joint optical glass catalogue 79−76775
UV high-power laser material, refractive props. and optical constants 80−106555
waveguide, fabrication in glass by effusion 80−5850
waveguide, formed by thermal migration of Tl ions 79−46031
waveguide, graded-index surface or buried, realized by ion exchange in glass 80−69499
waveguide, in-plane scatt. and loss mechanisms 80−33216
waveguide, ion-exchanged, r.i. profile 77−772
waveguide, plane optical, form. by K^+ diffusion 79−90043
waveguide, trapezoidal cross-section ridge design, propag. charact. 78−55436
waveguide and material dispersion interdepend. 79−98470
waveguide fabrication, by elec. field controlled ion exchange 78−38094
waveguide fabrication by low-temperature diffusion process 80−102867
waveguides, diffused glass, graded refractive index, anisotropy 80−33210
weakly absorbing material calorimetric meas., theory 79−76773
wide-angle five-lens eyepiece 79−46027
X-ray screening glass antireflection surfaces 77−21601
Ag formation on Ag-halide surface, flash photolysis expts. on Ag halide photochromic glasses 79−94310
Ag halide, kinetics of photochromic processes 80−103930
Ag halide, photochromic glass, optically induced anisotropy 80−1282
Ag halide doped photochromic glass absorption spectra *(Russian)* 78−60490
Ag halide photochromic centres, isothermal relaxation kinetics 80−16072
Ag halide photochromic glass:Cu^{2+}, characterisation of Cu ions 78−5530
Ag halide photochromic glass, darkening mechanisms under pulsed laser excitation 78−25938
Ag halide photochromic glasses, props., effect of temp. 78−83057
Ag halide photochromic glasses, colour centres struct. 80−66254
Ag halide photochromic glass, darkening mech., temp. depend. 80−87449
Ag halide photochromic glasses, optical absorp. of Ag, optically induced dichroism 80−108177
Ag^+ migration for planar waveguide form. 77−27352
Ag-containing glasses, colour adaptation, photoinduced optical anisotropy 79−61331
AgCl photochromic glass, additional absorpt. spectrum, ellipsoidal model of colour centres 80−40142
$Al(PO_3)_3$-BaF_2-Al_3 glasses, opt. props., group I-III fluorides effect 80−66143
$Al(PO_3)_3$-NaF system, glasses, IR spectra and struct. 79−65882
As-Ge-Se and As-Ge-Se-Sb systems, acousto-optic props. 77−27327
As-S, glassy film optical props., photostimulated effects and hologram recording 79−27215
As-S chalcogenide glassy semiconductors, induced anisotropy 79−32013
As-S glassy film, photobrightening effect 80−11498
As-Se amorphous film, optical props. change under high-power light pulse action 79−47534
As-Se chalcogenide glass, optical const. photoinduced changes mechanism 80−7321
As-Se glass thin-film waveguide, for 10.6 μm range 77−50770
As-Se-S-Ge chalcogenide glass films, appls. to passive optical waveguide components 79−37048
As_2S_3 coating defects and impurities affecting damage threshold and absorptance 79−14065
As_2S_3 film optical constants, wedged-film meas. 79−14066
As_2S_5, amorphous, struct., vibr. and electronic spectra 80−64908
As_2S_5, thin film optical waveguide, for acoustooptic modulators 78−83051
$As_2S_3(Se_3)$ containing coatings, 10.6 μ laser damage obs. 79−14021
$As_2S_3(Se_3)$, film on KCl, strain-induced refractivity anisotropy, 10.6 μ ellipsometric obs. 79−14064
As_2Se_3 coating defects and impurities affecting damage threshold and absorptance 79−14065
$(B_2O_3)_x$-$(SiO_2)_{1-x}$, spontaneous Raman scattering *(French)* 79−78674
$Ba_{15}Ca_{27-x}Nd_xAl_{31}Be_{27}F_{231+x}$, $0 \leq x < 8$, optical props. and vitreous domain 79−65820
BaO crown and flint glasses, Ag and Cu diffusion for optical waveguide fabrication 78−59166
BaO-GeO_2-Na_2O borosilicate core glasses for high numerical aperture fibres, double crucible prep. 80−69534
$BaPO_3F$ charge component, prep. from $BaCO_3$, H_3PO_4 and NH_4HF_2, props. 79−52147
BeF_2 glass, IR and UV transmission spectra 80−89019
BeF_2 glass, nonlinear refr. index, meas. of electronic and nucl. contribs. 78−50866
Bi-Sb-O-I glasses, acousto-optic props. 77−31121
CaO-Al_2O_3 based glass development, water removal, use in IR to 5 μm 78−83052
CdO-GeO_2:Tl_2O photochromic glass for optical information retention media 80−33108
Ce-Ti containing glass for cut-on filters in visible region 78−13803
Cu halide based photochromic glasses, spectral props. 80−29708
Er_2O_3-TiO_2-WO_3-PbO, glass form., refr. indices and density meas. 77−90312
GdF_3-BaF_2-ZrF_4 glass fibres, IR transmission, losses, fabrication 80−87516
Ge-As-Se, appl. in 8 to 12 μm thermal imaging system 78−25935
Ge-As-Se, Se-As, and Se-Ge, for IR appl., prod. using H_2 distillation 77−32551
Ge-As-Se IR transmitting glass composition, prep. and props. 80−69474
Ge-As-Se-Te glasses for 8-12 μm IR optics 80−69475
Ge-Sb-Se glass, physical props., purification method for Sb, Se from surface oxides 78−46735
$Ge_{30}As_{17}Te_{30}Se_{23}$-$As_2S_3$, two-layer antirefl. coating, error considerations in design 80−74477
GeO_2 doped glass for optical fibres, wavelength dispersive props. 79−3774
GeO_2-B_2O_3-SiO_2, glass fibre, pulse transmission meas. of zero material dispersion 77−88937
GeO_2-P_2O_5-SiO_2 glass fibre, incorporation of OH in modified CVD process 80−50560
GeS_x, optical props., chem. struct. effects 77−63460
Hg-As-S modulating glasses, optical parameters and struct. *(Russian)* 78−63159

optical glass continued
Hg-As-S-I system, glasses, optical and acousto-optical props. 78−83053
K_2O-BaO-SiO_2:Nd^{3+} glasses, absorption and fluoresc. spectra, density 80−25417
K_2O-BaO-SiO_2-Ti(Ce)O_2 laser glasses, TiO_2 and CeO_2 antisolarisation additive effects 79−94309
K_2O-SrO-SiO_2 elastic constants 77−16630
Li aluminosilicate glasses, variation of refractive index during ion-exchange diffusion from molten salts *(Russian)* 77−28539
$LiTaO_3$ glass-ceramics, transparent fabrication by crystn. of aluminosilicate glasses 77−59734
Na vapour resistant, CaF_2 coating apparatus 80−90874
Na_2O-Al_2O_3-B_2O_3-SiO_2 photochromic glass, $AgCl_{1-x}Br_x$ activated, comp. optimisation by Box-Wilson method 77−50741
Na_2O-Al_2O_3-B_2O_3-SiO_2, CuCl crystal activated photochromic glasses, absorpt. spectra 79−27353
Na_2O-Al_2O_3-B_2O_3-SiO_2-AgCl(Br), photochromic glass, kinetics of thermal decolorisation 80−103931
Na_2O-B_2O_3-SiO_2, containing halogens glass formation 80−103254
Na_2O-B_2O_3-SiO_2 glass fibre, prep. with low loss 79−59850
Na_2O-BaO-SiO_2:Nd^{3+} glasses, absorption and fluoresc. spectra, density 80−25417
Na_2O-CaO-SiO_2, for optical fibres, high purity glass production methods 78−87176
Na_2O-CaO-SiO_2 glass, mm wavelength absorpt. 79−82978
Na_2O-SiO_2 glass containing halogens glass formation 80−103254
Na_2O-SiO_2:Ce photochromic glass absorption centres 79−27352
Na_2O-SiO_2:CeO_2, photochromic glass, form. and decay kinetics of absorpt. centres 78−13774
$Na_2O.3B_2O_3$, effect of Fe_2O_3 conc. and temp. on UV absorption 77−16340
Nd glasses, GLS-1 and GLS-22, luminesc. band, forced transition cross sections, laser meas. 80−40152
Nd:glass, comparative lasing characts. of silicate and phosphate laser glasses 80−74364
Nd:glass, laser bulk damage rel. to temp. and conc. 79−14023
Nd:glass, self-induced transparency on two-photon reson. line *(Russian)* 79−86221
Nd:glass films for integrated optics, RF sputtering and optical characts. 79−46087
Nd:glass surface struct., laser beam effects, IR spectra appl. 79−95250
NiO doped, improved band-pass characts. 78−42394
P_2O_5 glasses for laser amplifiers and optical isolators 78−25885
P_2O_5-SiO_2 glass, flow for integrated optical cct. fabrication 80−79005
$(P_2O_5)_x$-$(SiO_2)_{1-x}$, spontaneous Raman scattering *(French)* 79−78674
PbF_2-AlF_3 glass, optical props., crystn. and thermal expansion 80−48367
PbF_2-AlF_3 glass, prep. and props. 80−49120
PbO-Bi_2O_3-GeO_2, exam. of glass forming and liquid phase separation regions, and optical props. 78−88453
PbO-SiO_2 glass, use of $Na_2S_2O_3.5H_2O$ in polishing 80−33258
PbO-SiO_2 melts, resistivity rel. to viscosity 77−76589
$PbTiO_3$ glass-ceramics, transparent, fabrication method by crystn. 77−59733
phosphate glass, Li_2O and Na_2O effect on thermo-optic props. 78−18029
SbSI-GeS_2 system glasses with and without antireflection coatings, optical props. 77−8595
$SiCl_4+O_2$ in modified CVD process for optical fibre prod., reaction IR spectra 78−80472
SiO_2 based glass fibres, refr. index and comp. data 77−79950
SiO_2, coated silica fibres, tensile strengths of 1 km lengths 78−1384
SiO_2, doped and nondoped fused silica, IR characts. of optical fibres 79−18537
SiO_2, fused, absorption edge meas. 78−43887
SiO_2, fused, bubble gas comp. rel. to furnace atm. 77−58402
SiO_2, fused, laser damage threshold rel. to surface roughness 77−40306
SiO_2, fused, laser damage threshold rel. to subsurface struct. 77−40307
SiO_2, fused, optical elements, US cleaning, deleterious effects 77−42631
SiO_2, fused, shock compressed, refractive index, density, and polarisability behaviour 80−50295
SiO_2, fused, surface damage threshold rel. to prep. and OH^- conc. 77−62026
SiO_2, fused, US cleaning effect on laser damage threshold 77−62024
SiO_2, fused, ultraprecise thermal expansion meas. 77−71290
SiO_2, fused silica, KLR1, KLR2 and KU2, high-precision stability of end gauges 79−76778
SiO_2, fused silica fibres, high-strength epoxy-acrylate coated, dynamic and static fatigue 78−1385
SiO_2 glass, high rate MCVD of optical fibres 80−83671
SiO_2 glasses, opt. consts. in IR and vacuum UV 78−27238
SiO_2, vitreous, absorption edge, temp. depend. 77−20867
SiO_2, vitreous, electron irrad., vol., refr. index and stress changes 77−47482
$72SiO_2$ window glass, thermal cond., temp. depend. at low temps. 80−65322
SiO_2:F, silica fibres, numerical aperture and attenuation, drawing from preforms 78−1449
SiO_2:GeO_2/SiO_2, SiO_2/SiO_2:B_2O_3, glass fibre waveguides, γ-radiation optical stability 80−23799
SiO_2-Al_2O_3 glass, Raman spectra and refr. index meas. 77−24836
SiO_2-Al_2O_3-B_2O_3 glass mech. strength increased by etching 80−97609
SiO_2-Al_2O_3-B_2O_3-LiO_2 (LiO_2.Na_2O) (Na_2O) glass exam. of optical props. 78−88277
SiO_2-Al_2O_3-Li_2O:TiO_2(ZrO_2),Fe_2O_3, pyroceramic glass, coloration, absorpt. spectra obs. 77−8615
SiO_2-B_2O_3 used for fabrication of tubing and optical fibres 79−50462
SiO_2-B_2O_3(P_2O_5)(GeO_2), wavelength dispersive props. and composition in optical fibres 78−33793
SiO_2-GeO_2, refr. index and density, comp. depend. 78−23424
SiO_2-GeO_2 cored optical fibre, low loss 77−62072
SiO_2-GeO_2-B_2O_5-P_2O_5, optical waveguide glass, comp. determ., plasma emission spectra 80−87446
SiO_2-K_2O-Na_2O-BaO-SrO-ZnO system, props. optimisation 79−91611
SiO_2-P_2O_5, refr. index behaviour, optical fibre appl. 77−46777
SiO_2-P_2O_5 binary glass, fibre fusion temp. rel. to composition 78−95131
SiO_2-TiO_2-Na_2O glass, optical absorption coeff., 2.1-3.3 eV 77−77240
SiO_2(-GeO)$_2$(P_2O_5)(B_2O_3), optical attenuation in IR region 77−75665
WO_3(WO_3-UF)(WO_3-MoO_3) glass film compositions, electrochromism *(Russian)* 79−28721
Y_2O_3-SiO_2-Al_2O_3 system, composition depend. of refractive index in vitrification region 77−24812

optical glass continued
$ZnCl_2$ glass, potential ultralow loss optical fibre material 78−74955
ZnO-Al_2O_3-SiO2, transparent glass ceramics, heat treatment effect on microstruct. 78−56667
ZrF_4-BaF_2-NdF_3 glass, vitreous domain, prep. and optical props. 78−27304

optical harmonic generation
see also lasers
acousto-optic diffraction degenerate regime, second harmonic, sum and difference freq. beams 80−74300
active media, possibilities of efficient freq. conversion 79−59764
active periodic structure with quadratic nonlinearity, wave spatial harmonic spectra transformation 79−72630
akali metal vapour, seventh and ninth order nonlinear susceptibility meas. 79−55186
alkali metal vapours, fifth harmonic generation, saturation by picosecond pulses 78−33774
alkali vapour system, nonreson. third harmonic generation of I laser radiation 79−3746
AM of second harmonic 80−78908
ammonium malate, SHG, 492-640 nm, phase matching, refr. index and nonlinear susceptibility 77−72031
ammonium malate, single cryst., optical SHG, refr. index, susceptibility 78−63152
atomic fluid, SHG, microscopic theory 77−28535
atomic fluorescence detection, harmonic saturated spectroscopy method 80−104472
atomic media, resonantly two-photon pumped, up-conversion schemes 77−23711
barium formate, nonlinear optical susceptibility tensor, Maker fringes 78−13751
benzene, liquid, C-H stretch, seventh harmonic, absorption profile 79−56806
benzene, mol. hyperpolarisability meas. by optical SHG 79−22861
benzenes, para-disubstituted, liq., 2nd order hyperpolarisabilities, regularities, intramol. charge transfer 79−10353
benzenes, substituted, liq., optical nonlinearities and hyperpolarisabilities meas. 77−88857
biaxial crystal, phase matched directions in SHG 77−34909
biological structures, SHG study of non-centrosymmetric character 79−74599
biomolecule, non-centrosymmetry, optical second harmonic generation 80−72133
bistability and photon antibunching in sub-SHG 79−31991
bistable optical devices, overshoot and alternate switching, subharmonic generation 80−99790
bistable steady states in optical subharmonic generation, Wigner distrib. 80−53370
butadiene, mol. hyperpolarisability meas. by optical SHG 79−22861
cascade processes in focused beams, higher harmonics 77−72030
chalcopyrite crystals, temp. depend. Sellmeier coeffs. and coherence lengths 79−76752
chemical spectroscopy and dynamics, higher-order susceptibility effects, laser appls. 79−40625
cholesteric liquid crystal, phase-matched third harmonic generation efficiency 78−30021
cholesteric liquid crystals, third harmonic generation 77−50728
coherent optical pulse synthesis using phase-locked lasers and nonlinear optical processes 79−76724
coherent state technique, quantum statistical props. 77−46753
collagen, SHG in rat tail tendon 79−53046
conjugated molecules, large second-order polarisability, SHG 78−66683
crystal, third harmonic generation under reson. conditions *(Russian)* 79−31997
crystals, nonlinear susceptibility determ. using 4th and 5th harmonic generation 77−50717
dense optically transparent media, third-order optical susceptibilities 77−38981
dielectric breakdown with picosecond laser pulses, SHG sharp increase 80−102769
2,5-dimethoxy-4-nitrostilbene, hyperpolarisability meas. by DC induced second harmonic generation 78−87096
trans-4-dimethylamino-4′-nitrostilbene, mol. hyperpolarisability in soln., UV dispersion of charge transfer contrib. 79−31986
dipotassium tartrate single crystal, SHG 78−13757
discrete multilevel system, nonlinear polarisations and excitations, time depend. 77−27313
double-pass frequency doubler for Nd:glass laser, phase optimisation 80−9962
dye laser, flashlamp-pumped, two-stage amplification, for SHG 78−74922
dye laser, N_2 laser pumped, freq. doubling of output *(Japanese)* 79−68406
dye laser, second harmonic pulse structure and cavity length determ. 80−95935
dye laser, tunable, improved freq. doubling for 217-360 nm 78−33781
dye laser oscillator-amplifier system second harmonic generation using laser-flashlamp hybrid pumping 80−14359
dye lasers, mode-locked, exponential SHG autocorrelation function rel. to pulse to pulse var. 80−9920
dye ring laser, performance and appl., internal freq. doubling possibility *(German)* 79−36927
dye TEM_{00} tunable laser system high-power, with frequency-doubling crystal 79−50306
efficient generation, state of art 80−33090
ethylene, mol. hyperpolarisability meas. by optical SHG 79−22861
EUV generation of coherent radiation 79−76758
extreme UV coherent radiation generation by high order optical nonlinearities, book contrib. 79−31998
fast transform calcs., appl. to SHG with depletion and diffraction 80−53376
ferroelectric oxide crystals for electrooptics and nonlinear optics, optical inhomogeneities, review *(Japanese)* 77−65613
fixed intensity approximation *(Russian)* 78−9410
fluid, rarefied, symmetries of static elec. field induced opt. effects 78−55713
focused beam SHG in nonlinear crysts., temp., wavelength and angle bandwidths 79−50343
fourth harmonic generation of Nd:YAG laser radiation 78−17972

optical harmonic generation continued
fundamental-mode laser intracavity optical second-harmonic generation 77−10972
gas, harmonic generation by divergent radiation *(Russian)* 78−22170
gas, third harmonic generation near two-photon reson. 79−59760
gas, third harmonic resonant generation, exact theory *(Russian)* 79−76763
gas, unsteady quasiresonant third harmonic generation, spectral-temporal effects 79−14037
gas of two-level molecules, reson. interaction of standing freq. modulated wave 79−94295
gaseous system, 2-level, lowest order SHG 77−75611
gaseous system, SHG, photon statistics 77−54756
gaseous system, third harmonic generation, quantum theory 80−99795
gases, optical SHG, quadrupole moment pot. by mag. field 77−46760
glass microsphere heating, generation of $3/2\omega_0$ harmonic of Nd laser radiation *(Russian)* 77−43014
L(+) glutamic acid halogen acid salts, crystallographic, optical and calorimetric meas., halide effect 78−34505
L(+)-glutamic acid hydrochloride, deuterium isotope effect, cryst. struct., IR spectra and SHG 77−46755
glutamic acid hydrochloride, L(+), single cryst., soln. growth and characterisation, SHG 77−24943
hexatriene, mol. hyperpolarisability meas. by optical SHG 79−22861
hydrazonium tartrate enantiomers, and deuterates, struct. and opt. props. 77−68954
1,3-indandione derivatives, higher-order harmonic generation, laser-induced nonlinear optical effects *(Russian)* 78−55412
inert gas excimer and exciplex oscillators, VUV and XUV pulse generation 79−3688
inert gases, XUV radiation generation by fifth, seventh order freq. conversion 78−83033
inhomogeneous crystal optimal length for SHG, parametric amplifier and oscillator 80−106568
inhomogeneous media, efficiency of freq. conversion processes 78−30024
inhomogeneous nonlinear elements, coherent frequency doubling *(Russian)* 80−5795
inhomogeneous nonlinear materials, conversion coeff. of principal radiation into higher harmonics 79−81488
injection laser harmonic distortion analysis 80−58537
intense laser beam diffraction by long US wave in liquid column 78−60421
interference between SHG signals, accurate determ. of nonlinear optical coeffs. 77−31115
interference experiments, nonlinear, use of dispersive phase shifter 79−50348
intracavity SHG, phase effects 80−1276
intracavity SHG in CW dye laser 77−88842
intracavity SHG of Nd^{3+}:YAG laser, amplitude- and phase-freq. characts. 78−25884
ionic crystals, centrosymmetric, stimulated excitation of second harmonic, microscopic theory 80−91849
ionic grouping theory of electro-optical and nonlinear optical effects of crystals *(Chinese)* 78−27183
IR generation, book 77−46761
IR generation, optical mixing, SHG and parametric oscills., book contrib. 77−46764
IR source, tunable, efficient 80−5789
IR tunable laser for semiconductor multiphoton spectroscopy *(French)* 80−82836
$KNbO_3$, near IR noncritically phase-matched SHG 79−72620
laser, hysteresis effect in SHG 79−59766
laser beam characts. using DC induced SHG in gas 77−7093
laser beam optimal focusing conditions for freq. doubling 79−14036
laser beam spatial scanning by nonlinear freq. conversion *(Russian)* 79−50336
laser coupled output, importance on intracavity effects *(Chinese)* 79−64269
laser frequency doubling in isotropic dielectric waveguide *(Russian)* 79−94285
laser frequency measurement of I ion line, by harmonic mixing 77−83919
laser operation physical principles *(German)* 79−59664
laser plasma, convective parametric decay instability 80−64722
laser plasma, diagnostics in 1/4 crit. density region, harmonic generation expts. *(Russian)* 77−7578
laser plasma, SHG, review 80−53993
laser produced plasma, harmonic generation 77−84438
laser produced plasma, SHG *(Russian)* 79−86587
laser pulse duration measurement, 0.1 to 100 psec., nonlinear autocorrelation methods 78−46702
laser resonator fourth harmonic generation cascade process *(Russian)* 80−99797
laser with nonlinear active medium, transient intracavity SHG, giant pulse generation 80−9948
laser-target interaction expt., backscattered light and harmonic generation, spectral anal. 78−59676
layered compounds, SHG at 0.6943 and 1.06 μm, energy gap depend. 78−30019
liquid, laser radiation second harmonic intensity meas. 80−48338
liquid, nonlinear, high intensity light diffr. by ultrasound 80−64270
liquid crystal, nematic and smectic, potential of phase matched elec. field induced SHG 79−86214
liquid mixtures, associating, mol. hyperpolarisability, SHG 77−552
liquids, DC elec. field induced optical rectification and SHG 79−46005
lithium formate biaxial crystal, nonlinear conical refr. obs. in harmonic generation 80−23745
lithium formate cryst., 90° phase matching 80−58634
lithium formate monohydrate frequency-doubling system, automatic phase-matched, for 240-350 nm region 79−31979
lithium formiate, active spectroscopy under conditions of double-w-k-resonance *(Russian)* 78−33777
metal surface, optical SHG effects of electron band struct. 77−740
metal surface, SHG, hydrodynamic theory of electron gas 80−87437
metal surfaces, SHG, non-linear response to optical fields 80−83645
metal vapour coherent two photon reson. third and fifth harmonic VUV generation 79−72627
metal vapours, third harmonic generation, two-photon reson. 77−34907
metal-dielectric waveguide, third harmonic generation enhancement, comment 79−94283
metals, SHG by surface polaritons, theory 78−9416
optical harmonic generation continued
metals, surface EM wave enhancement of nonlinear optical effects 77−68240
methanes, halogenated, nonlinear optical polarisability, bond-bond interaction role 78−18010
2-methyl-4-nitroaniline, nonlinear cryst., large optical second-harmonic coeff. meas. 79−76750
methyl-(2,4-dinitrophenyl)-aminopropanoate, efficient cryst. 77−79890
methylene blue in methanol, concentrated solutions, intensity of third harmonic from Nd laser *(Russian)* 77−54753
microscope, harmonic, imaging props. and super-resolution 79−97430
microscope, scanning harmonic, using CW Nd:YAG laser 77−87821
MIM point-contact diode harmonic generators and mixers 80−60105
MIM point-contact diodes for harmonic generation and mixing 78−88044
mixed oxide crystals, SHG effects 79−99854
mode-locked frequency-doubled laser efficiency 77−19264
molecular fluid, optical props., intermol. forces effects, theory, appls. 77−28535
molecular gas vibrational nonlinearity rel. to CO_2 laser freq. tripling *(Russian)* 79−72618
molecular solids, Raman, fluoresc. and nonlinear props. 79−33702
multiple-pass second harmonic and reson. generation in cryst. *(French)* 79−46001
mutual mode quenching of SHG *(Russian)* 79−86218
n-order nonlinear phenomena, dispersion rels. 79−41410
naphthalene, hyperpolarisability meas. by DC induced second harmonic generation 78−87096
narrow band gap semiconductor, optical nonlinearity due to free carriers 79−81491
nematic liquid crystal, SHG, mol. symmetry and macroscopic nonlinearity *(Russian)* 78−90457
n-nitro-n′-methylbenzylidene-aniline, triclinic, struct., SHG due to monoclinic impurities 77−43205
p-nitroaniline, mol. hyperpolarisability in soln., UV dispersion of charge transfer contrib. 79−31986
nitroanilines, hyperpolarisability, second harmonic generation and four wave mixing, excited dipole moment 77−54624
1-nitronaphthalene, hyperpolarisability meas. by DC induced second harmonic generation 78−87096
noncentrally symmetric phase identification using SHG 78−74947
nonlinear active medium laser for both stimulated emission and SHG 79−64285
nonlinear adaptive system, characteristic purposes 80−28273
nonlinear crystals, interference of optical harmonics 80−64102
nonlinear crystals for frequency conversion of optical radiation, review *(Russian)* 80−38068
nonlinear second-order crystal processes, electro-optic, piezo-optic tuning 78−46718
nonresonant third harmonic generation, exam. of optimum conditions 78−55411
in optical fibres, bandwidth limitations due to harmonic distortion in single-mode optical fibers 79−64335
optimum focusing, for direct higher harmonics generation *(German)* 79−10349
optimum focusing conditions for twelfth optical harmonic generation *(German)* 80−64098
organic crystals for SHG, selection and characterisation 77−3626
organic materials, SHG efficiency 77−75619
organic molecules, conjugated, nonlinear props. of new class of cpds. 79−41413
parametric amplification processes, anticorrelation effect 77−88839
parametric amplification suppression for improved SHG efficiency 77−50725
parathymol, negative uniaxial cryst., linear and nonlinear optical and dielec. props. 77−75602
p-n-pentyl-p′-cyanobiphenyl, nematic ordering, electric field induced second harmonic generation 79−60263
periodic structure, synchronous radiation frequency conversion in conditions of Bragg diffraction *(Russian)* 79−31992
phase matching condition for oscillator strengths determ. 77−10638
phase matching longit. deviation in SHG of CW laser 78−59085
phase-matched SHG in four-layered optical waveguide struct. 78−74950
phosphate glass laser, statistical props. and stabilisation 80−48266
photon antibunching in parametric three-wave interaction 80−83638
picosecond nonlinear optics, book contrib. 77−65609
picosecond pulse freq. changing into UV, VUV and IR, book contrib. 77−61138
piezoelectric crystal, optical SHG with surface plasmons 78−18008
plasma, laser light absorption and harmonic generation 78−75359
plasma, laser-produced, intensity depend. of harmonic generation 79−55506
plasma, laser-produced, two-plasmon decay and generation of $3\omega_0/2$ harmonic *(Russian)* 77−89279
plasma, Nd:glass laser produced, 2nd to 5th harmonic lines obs. 78−30480
plasma diagnostics, laser, combination scattering method 80−79569
poly-γ-benzyl-glutamate, α-helix second-order hyperpolarisability meas. 77−14623
powder mixtures, doubling of freq. of laser radiation 77−62009
power breakthrough in nonlinear process, stabilisation by electro-, piezo-optical tuning 77−88856
prism coupling into optical waveguide second harmonic generation 80−102763
pulsed coherent radiation source, 118 nm, for use in plasma diagnostics 80−106572
pump fluctuations effect on SHG and parametric amplifications 79−55185
pyridine-I_2 charge transfer complex, hyperpolaris., SHG obs. 77−553
pyroelectric, uniaxial, spontaneous polarisation, calc. from results of optical meas. 78−27162
quadratic nonlinear medium, efficiency 77−23718
quantum fluctuations in SHG, anti-bunching effect 77−58382
quantum statistics of higher and sub-harmonic generation 77−58379
quartz, $\alpha \rightarrow \beta$ transition obs. from nonlinear optics and bond polarisability model 77−15336
quartz, periodic laminar struct. SHG *(Japanese)* 77−72029
quartz, struct. transitions, optical SHG and γ-ray diffr. results 78−14459
quartz slab, ruby laser interaction, SHG 77−7159
Raman scattering of light by polaritons, reviews 80−34928

optical harmonic generation continued
rare earth ditatantes, $R_2Ti_2O_7$, crystal synthesis and SHG, solid laser freq. manipulation 79−41421
rare earth iodates, crystallographic and nonlinear optic data 78−6044
rare earth titanates, pseudoperovskite struct., nonlinear spectral and luminesc. characts. 80−29771
rare-earth formates, second optical harmonic generation 80−43403
resonant media, two-photon interaction of light pulses, third harmonic generation 77−79900
ruby, phase modulated conjugate wave generation, hologram model 80−83643
scanning optical microscope, second harmonic imaging 78−82029
second harmonic and subharmonic generation, master eqn. approach 78−33773
second harmonic beam anal., laser pulses duration 80−1275
second-harmonic, in nonlinear crystals with longitudinally nonuniform refr. index, efficiency 80−43402
second-harmonic emission at resonance absorption 79−77391
second-harmonic interferometers 80−101833
self pulsing in SHG 79−14032
self-induced thermal effects on SHG 77−736
semiconductor, elec. field induced optical SHG theory, Brillouin zone integral 80−69457
semiconductor, laser monopulse energy meas., time-resolved spectroscopic method *(Russian)* 79−94272
semiconductor, non-linear optical props. of band charge carrier gas 78−33775
semiconductor, nonlinear optical props., non-stationary density matrix of electron-phonon system 78−71818
semiconductor with zero band gap, freq. tripling and self-interaction of strong EM wave 79−10355
semiconductors with direct band gaps, exciton-polariton interactions, Green's function approach 80−92831
semiconductors with superlattice, third harmonic generation *(Russian)* 77−27315
servo tuning and stabilization of nonlinear optical crystals 79−55180
SHG, computer controlled intracavity, in CW ring dye laser 80−91841
SHG, consecutively disposed crysts. optimisation *(Russian)* 77−7158
SHG, depend. on intermodal correlations 79−36958
SHG, effect of partial mode locking 80−9960
SHG, efficient intracavity, of unpolarised laser radiation 79−50352
SHG, heating effects, absorpt. coeffs. and temp. variation of refr. index difference 80−14390
SHG, Maker fringe method, effects of beam width and wedge angle 77−72028
SHG, parametric amplification and stimulated scatt. phenomena 77−38994
SHG, photon bunching and antibunching 78−63153
SHG, polarisation effects 80−48350
SHG as crystal class detection method *(Chinese)* 79−81490
SHG by guided radiation mode coupling in thin film optical waveguide 80−106567
SHG efficiency, limiting effects of nonlinear cryst. longit. optical inhomogeneity 79−89967
SHG in medium with Rayleigh-type nonlinearity *(Russian)* 77−72027
SHG intracavity generation, phase effects, harmonic feedback case 80−9945
SHG of flash-lamp pumped dye laser *(Japanese)* 78−90459
short wavelength sources, book 79−31921
single-mode optical fibres, bandwidths with AM and intensity modulation 79−81560
squaric acid, second harmonic generation 79−46000
stilbene derivatives, hyperpolarisabilities, four-wave mixing and SHG meas. 77−83925
stimulated Raman emission, mutual quenching of modes 79−36960
styrene derivatives, hyperpolarisabilities, four-wave mixing and SHG meas. 77−83925
sub-SHG, nonequilibrium transitions, semiclassical theory 80−83639
subharmonic generation, multiplicative stochastic processes in statistical physics appl. 80−22289
subMM radiation, monochromatic, simple tunable source 80−5788
surface plasmons, counterpropagating, for coherent SHG 80−33081
surface plasmons, theory of non phase-matched SHG 78−72101
synchronous nonlinear interaction between waves on Bragg diffr. in media with periodic struct. *(Russian)* 80−14399
temperature phase-matching curve hysteresis, SHG 80−91852
temperature tuned SHG, Dewar design 77−62002
tendon, rat-tail, coherent optical SHG 80−89796
ternary semiconductor crystals for nonlinear optical applics., review 78−33782
thin film external resonator for optimum SHG 79−18485
thin film waveguide, harmonic generation field anal. 79−98509
thin-film geometry, harmonic generation of surface-plasmon nature, off-synchronous treatment 79−18475
third harmonic generation, spatial modes effect 80−43400
third harmonic generation under 2-photon reson. conditions, ultrashort pulse propag. *(Russian)* 79−59768
third-harmonic generation in collisional plasma, self-focusing effect 77−7550
three-wave interactions in randomly inhomogeneous dispersive media *(Russian)* 80−53364
time-dependent perturbation calculations 79−68417
tunable UV and visible radiation prod., freq. conversion of dye, excimer lasers 78−59029
two photon reson. third harmonic generation, quantised field theory 80−43397
two-pass optical second-harmonic generation 80−74433
two-photon absorpt. coeffs., 355 and 266 nm for harmonic-generating crysts. 78−83037
two-photon interaction between coherent optical pulses and resonant media, third harmonic generation 80−91851
two-photon resonance, coherence effects on summation of optical frequencies *(Russian)* 77−62012
two-photon resonant THG process, coherent pulse propag. effect 79−31987
two-photon resonant third-harmonic generation, pump depletion and saturation 80−69454
uniaxial crystal, noncollinear SHG, temporal characts. anal. of short laser pulses 78−22171
uniaxial crystals, local field influence on electron contribution to linear electro-optical effect *(Russian)* 80−88968
optical harmonic generation continued
uniaxial crystals, nonlinear optical props., review and summary of data 77−75615
urea, efficient phase-matched SHG over wide spectral region 77−83929
urea, electro-optical coeffs. meas., rel. to nonlinear optics calcs. 80−34889
urea, fifth harmonic generation, high-efficiency high-power UV generation at 2128 Å 80−99793
urea, second and third order hyperpolarisabilities, SHG and four-wave mixing meas. 79−59759
urea, single cryst., optical SHG, refr. index, susceptibility 78−63152
urea crystal, efficient phase-matched SHG and sum freq. mixing 80−14391
UV coherent radiation generation using high order nonlinearities 77−88847
UV laser *(Japanese)* 79−3686
UV ps. pulse production for amplification in XeF discharge 77−88768
UV pulse production, sum or SHG of dye laser radiation in nonlinear crysts. 77−83892
UV radiation prod., freq. doubling of N_2 laser pumped dye laser output 77−743
UV tunable source using SHG of rhodamine 6G laser 77−42565
vector matching ang. width 80−9946
VUV radiation, narrowband tunable, at Lyman-α wavelength 80−78907
Ag_3AsS_3, proustite, freq. conversion of CW chem. HF laser radiation 78−30023
$AgGa(Se_{1-x}S_x)_2$, crystal growth, phase studies, optical props. 78−48305
AlN film, nonlinear optical susceptibility SHG expts. 78−30012
Ar, 57 nm third harmonic generation of Xe_2 excimer laser radiation 77−54738
Ar, third harmonic generation, bandwidth limitations in Lyman-α vicinity 79−81482
Ar, third-harmonic conversion of XeCl-laser radiation 79−89962
$BaBi_4Ti_4O_{15}$, SHG, temp. depend. ferroelec.-ferroelec. transition 78−15121
$Ba(NO_2)_2.H_2O$, nonlinear optical props. and polariton scatt. spectra 77−75616
$Ba_2Na(NbO_3)_5$, intracavity cryst., thermo-optical distortion, effect on freq. doubled Nd:YAG laser 77−71998
$Ba_2NaNb_5O_{15}$, absorption loss effects on frequency-doubled operation of Nd:YAG laser 79−36957
$BaTiO_3$, displacive type ferroelectric, SHG 79−36955
$Ba_2TiSi_2O_8$, fresnoite, unsuitability for phase matched SHG 78−46721
$BeSO_4.4H_2O$, SHG at 2660 angstroms 78−90451
$Bi_2Sn_2O_7$, polymorphic phase transition, X-ray, DSC, SHG, dielec. and optical obs. 80−44163
CO, gas, phase matched, IR third harmonic generation 77−38985
CO gas, third harmonic generation enhancement in metal-dielec. waveguides 79−50342
$CO-O_2$ liq. mixture, enhancement of nonlinear optical processes with double-pass tight-focusing geometry 79−18472
$CO-O_2$ liquid, IR third harmonic generation 77−88849
$CO-O_2-SF_6$, efficient CO_2 laser radiation 3rd harmonic generation, for fusion ignition 78−59087
$CO-O_2-SF_6$, liquid, phase matched IR third harmonic generation 78−42384
$CO-O_2(Ar)(N_2)$ dil. liq. solns., resonant IR third harmonic generation 77−31116
Ca, vap., optical SHG, quadrupole moment pot. by mag. field 77−46760
$CaCO_3$, calcite, quadrupole nonlinear coeff. dispersion meas. 78−37943
$Ca_2Mg(Co)(Zn)(Mn)(Cd)(Ca)TeO_6$, optical SHG study of acentricity, ferroelec. of low temp. phases 80−71324
$Ca_2Nb_2O_7$, crystal synthesis and SHG, solid laser freq. manipulation 79−41421
$Ca_2Nb_2O_7$, ferroelec., temp. depend. of SHG intensity 79−24267
$CdGeAs_2$, phase matched fourth harmonic generation, cascade process contrib. 79−76761
$CdGeAs_2$ tandem crystals, efficient freq. tripling of CO_2 laser radiation 79−45999
$CdGe(As_{1-x}P_x)_2$, crystal growth, phase studies, optical props. 78−48305
$Cd_{16}Ge_4S_{24}$, SHG obs. 78−46719
$Cd_2Mg(Co)(Zn)(Mn)(Cd)(Ca)TeO_6$, optical SHG study of acentricity, ferroelec. of low temp. phases 80−71324
$Cd_{14}P_4S_{24}$, SHG obs. 78−46719
$Cd_{13}P_4S_{22}I_2$, SHG obs. 78−46719
$Cd_{14-x}P_4S_{24-2x}I_{2x}$, icosahedral structs., synthesis and characts. 77−1107
CdS, excitonic region, nonlinear optical meas., 4.2K 78−68531
CdS, nonlinear optical suscept., resonant excitonic contrib. 77−3633
$Cd_{16}Si_4S_{24}$, SHG obs. 78−46719
CdTe, temp. depend. Sellmeier coeffs. SHG coherence length 77−69789
$Ce_2Ti_2O_7$, ferroelec., temp. depend. of SHG intensity 79−24267
$Cr_3B_7O_{13}Cl$, cubic, approx. nonlinear optical susceptibility 80−78904
Cs, vap., two-photon resonant third harmonic generation 77−738
Cs vapour, 3rd and 5th harmonic generation of Nd laser radiation quasi-reson. conditions *(Russian)* 78−25926
CsD_2AsO_4 crystals, SHG, temperature phase-matching curve hysteresis 80−91852
CsD_2AsO_4, high efficiency SHG of Nd:YAG laser radiation 78−59088
CsD_2AsO_4, high efficiency freq. doubling of Nd:YAG laser light 78−79071
CsD_2AsO_4, SHG, electro-optic and piezo-optic tuning 78−46718
CsD_2AsO_4, spectral phase-matching props. for SHG 77−83922
CsD_2AsO_4, temporal power variation of SHG of Q-switched YAG laser radiation 78−25922
$Cs(D_xH_{1-x})_2AsO_4$, soln. cryst. growth, optical absorpt. and SHG phase match data 78−11095
CsH_2AsO_4, CsD_2AsO_4, SHG, laser heating effect 77−79891
CsH_2AsO_4, laser accessory for freq. doubling 78−46725
$Cu_3B_7O_{13}Cl$, cubic, approx. nonlinear optical susceptibility 80−78904
DBr-N_2O mixture, third harmonic generation obs. 79−23018
DCl gas, tripling of CO_2 laser freq. 79−76751
DCl, two photon reson.-enhanced third harmonic generation 78−87094
$Fe_3B_7O_{13}I$, cubic, approx. nonlinear optical susceptibility 80−78904
GaAlAs DH lasers, nonlinearity, second and third harmonic distortion 79−31898
GaAlAs laser nonlinearities, harmonic distortion 80−74357
GaAs, isolated impurities, local mode sideband IR absorption and second harmonic intensity calc. 77−85707
GaAs periodic waveguide, phase-matched SHG obs. 77−19360
GaAs, polaritons, surface nonlinear interactions, Green's function theory 78−42379

optical harmonic generation continued
GaN, nonlinear susceptibility and coherence length, SHG meas. 78−25924
GaP ribbon waveguide, vapour-grown, phase-matched SHG 80−48339
$Gd_2Ti_2O_7$, ferroelec., temp. depend. of SHG intensity 79−24267
H detection by reson. fluoresc., coherent tunable VUV generation near Lv-δ transition 80−99798
H, optical harmonic coefficients, third order, at low freqs. 80−78905
H_2, two-photon enhanced third harmonic generation and Raman scatt. 77−88843
α-HIO_3, nonlinear conical refraction, second-harmonic cone 79−27329
α-HIO_3, second harmonic conical refraction 77−46758
He, comparison of 5th and 3rd harmonic conversion 79−18474
He, fifth harmonic conversion, 53.2 nm generation 77−10979
He, gas, fifth harmonic generation, coherent XUV light 79−46007
He, seventh harmonic conversion of mode-locked laser pulses to 38.0 nm 77−58378
Hg, vap., two photon reson. tripling of Nd laser fourth harmonic 78−30014
$HgGa_2S_4$, melt growth, optical props. and SHG, HgS-$HgGa_2S_4$ phase diagram 80−50548
I laser radiation, 2nd, 3rd and 4th harmonic generation 80−91844
I_2, doubly resonant third harmonic generation, spectrosc. 79−93984
n-InSb, optical SHG in rectang. waveguide 80−43401
InSe, SHG 79−81489
$KB_5O_8.4D_2O$, SHG and sum freq. mixing 78−55407
$KB_5O_8.4H_2O$, freq. doubling, angle tuning, mol. appl. 77−3632
$KB_5O_8.4H_2O$, phase matched 2314 Å generation 77−7155
$KB_5O_8.4H_2O$, phase matched 2120Å generation, Nd:YAG fifth harmonic 77−14777
$KD_{2x}H_{2(1-x)}PO_4$, 90° synchronism, second harmonic doubling of Nd laser *(Russian)* 77−58386
KD_2PO_4, high efficiency SHG of Nd:YAG laser radiation 78−59088
KD_2PO_4, Nd:YAG laser radiation freq. doubling 77−88776
KD_2PO_4, Nd:YAG laser radiation freq. doubling 78−46615
KD_2PO_4, SHG efficiency, 532 to 266 nm 77−23710
KH_2PO_4, 1.06 μm stable conversion into fourth harmonic, using composite medium master oscillator 78−46724
KH_2PO_4, and isomorphs, ruby SHG 78−50856
KH_2PO_4, cryst., cascade UV generation, by harmonic generation, temp. stabilisation calcs. 78−66868
KH_2PO_4 crystal, laser freq. conversion to produce UV coherent pulse, 45 GW, for laser fusion 80−69450
KH_2PO_4, efficient high-energy SHG of triaxial flashlamp-pumped dye laser 80−38061
KH_2PO_4, efficient SHG by YAG:Nd^{3+} laser pumping 79−18481
KH_2PO_4, improved automatically tunable SHG of dye laser 79−985
KH_2PO_4, laser accessory for freq. doubling 78−46725
KH_2PO_4, parametric amplification suppression for improved SHG efficiency 77−50725
KH_2PO_4, SHG of ps pulses, freq. tuning 77−50724
KH_2PO_4, servo tuning and stabilization of nonlinear optical crystals 79−55180
KH_2PO_4, spectral phase-matching props. for SHG 77−83922
KH_2PO_4, struct. transitions, optical SHG and γ-ray diffr. results 78−14459
$KNbO_3$, single domain crystal growth, SHG with Nd:YAG laser 78−74954
$KNbO_3$, high-efficiency SHG at 4250 to 4680 Å 79−81479
$KNbO_3$, SHG with $Ga_{1-x}Al_xAs$ lasers 80−5785
$KNbO_3$, SHG with $Ga_{1-x}Al_xAs$ laser 80−74431
K_2SeO_4, SHG, hexagonal phase centrosymmetry 79−37684
$KTaO_3$, SHG and quadratic electrooptic effect 78−76429
$KTaO_3$, second harmonic generation, bond charge theory 78−76395
$KTiOPO_4$, freq. doubling material for Nd lasers 78−71173
$KTiOPO_4$, nonlinear optical props., freq. doubling of 1.06 μm laser radiation 78−42386
Kr, 3rd harmonic generation for H conc. reson. fluoresc. plasma diagnostics *(Russian)* 77−79895
Kr compressed gas, 3371 to 1124 Å conversion by nonresonant freq. tripling of N_2 laser 79−64279
Kr gas, nonlinear susceptibility meas. via third harmonic generation, Lyman-α 1216 Å source 80−95947
Kr gas, tunable narrow-band coherent VUV source for Lyman-α region 80−38070
Kr, third harmonic generation, bandwidth limitations in Lyman-α vicinity 79−81482
Kr-Ar, phase matched, generation of Lyman-α radiation 80−91845
Kr-Xe, phase matched, generation of Lyman-α radiation 80−91845
KrF* laser, generation of high-spectral-brightness tunable XUV radiation at 83 nm 80−91846
$La_2Ti_2O_7$, ferroelecs., nonlinear optical props. 80−33086
Li, vap., two-photon coherent propag., third harmonic generation 78−30020
$LiCsSO_4$, thermal and dielec. props. 80−34860
LiH_2PO_3, P-H bond dipole direction, nonlinear optical coeffs. meas. 80−69253
$LiIO_3$ crystal, SHG, thermoelastic stresses and nonlinear refract. effect 80−74437
$LiIO_3$ crystal inside cavity of 1064 nm YAG:Nd^{3+} laser, optical SHG *(Russian)* 80−28272
$LiIO_3$, freely oscillating Nd:glass freq. doubling, phase matching 77−14780
$LiIO_3$, freq. conversion of CW chem. HF laser radiation 78−30023
$LiIO_3$, intracavity freq. doubling of Nd:YAG laser long pulse emission 80−102736
$LiIO_3$, laser accessory for freq. doubling 78−46725
$LiIO_3$, noncollinear SHG, background-free meas. of picosecond laser pulse time behaviour 79−59758
$LiIO_3$, noncollinearly phase matched SHG 77−46754
$LiIO_3$, SHG of ps pulses, freq. tuning 77−50724
$LiIO_3$, second harmonic optical coeffs. based on highly deformed oxygen-octahedra model of $(IO_3)^{-1}$ *(Chinese)* 77−75608
$LiIO_3$, simultaneous stimulated Ramam scatt. and optical freq. mixing 79−86210
$LiIO_3$, spectral phase-matching props. for SHG 77−83922
$LiKSO_4$, thermal and dielec. props. 80−34860
$LiN_2H_5BeF_4$, linear and nonlinear optical props. *(French)* 78−33778
$LiNH_4SO_4$ and $LiND_4SO_4$, dielec. pyroelec., and thermal props. 80−60509
$LiNH_4SO_4$, $LiNH_4SeO_4$, nonlinear opt. props. including SHG 78−76396

optical harmonic generation continued
$LiNH_4SO_4$, phase transitions, temp. depend. of NMR, spontaneous polarisation, birefringence and SHG 78−10191
$LiNH_4SO_4$, phase transitions and phys. props. 78−76399
$LiNH_4SO_4$, press.-temp. phase diagram, NMR and SHG meas. 78−23690
$LiNbO_3$, 3-D waveguide, efficient SHG, phase matching 77−7156
$LiNbO_3$, 3.39 micron HeNe laser radiation, difference freq. mixing and SHG 77−83928
$LiNbO_3$, broadly tunable repetitive picosecond parametric oscillator, freq. conversion 78−66866
$LiNbO_3$ crystals, SHG, temperature phase-matching curve hysteresis 80−91852
$LiNbO_3$ diffused waveguides, SHG *(Russian)* 79−59770
$LiNbO_3$, doubly resonant intracavity SHG of 1153 nm radiation with stabilization on HFS components of $^{127}I_2$ 80−33077
$LiNbO_3$, freq. conversion of CW chem. HF laser radiation 78−30023
$LiNbO_3$, heteroepitaxial growth on MgO by RF sputtering, SHG 79−27323
$LiNbO_3$, laser accessory for freq. doubling 78−46725
$LiNbO_3$ layers, Li out-diffused, SHG phase matching temp. variation 80−69455
$LiNbO_3$, optical consts. determ. by background stimulated Raman scatt. 80−48336
$LiNbO_3$, optical strength anisotropy, excitation of second harmonic 79−69923
$LiNbO_3$ optical waveguide, tuning characts. of parametric interactions 79−3779
$LiNbO_3$ periodic laminar struct. SHG *(Japanese)* 77−72029
$LiNbO_3$, planar optical waveguide, SHG in angle-matched conditions 79−41422
$LiNbO_3$, SHG, refr. index induced optical inhomogeneity effect 80−9951
$LiNbO_3$, SHG in external optical resonator, He-Ne laser radiation 79−27326
$LiNbO_3$, SHG of 260 THz ^{20}Ne laser, absolute freq. meas. in visible 79−93104
$LiNbO_3$, SHG of ps pulses, freq. tuning 77−50724
$LiNbO_3$, spectral phase-matching props. for SHG 77−83922
$LiNbO_3$ waveguide, diffused, 2nd harmonic generation 79−14041
$LiNbO_3$:Fe(Nb), SHG, phase-matching temp., impurity influence 80−69463
$LiNbO_3$:Ti optical waveguide, SHG with 25% conversion efficiency 78−94432
$LiNbO_3$:Ti optical waveguides, elec. field tuning of SHG, phase-matching condition 79−41412
$LiNbO_3$:Ti strip waveguide, SHG 80−102773
$MgBaF_4$, nonlinear optical susceptibility tensor, Maker fringes 78−13751
$(NH_4)_2BeF_4$, ferroelectric, incommensurate phase, nonlinear optical props., SHG study *(Russian)* 80−33089
$(NH_4)_2BeF_4$, linear and nonlinear optical props. in incommensurate phase 80−69452
$(NH_4)_2BeF_4$, unmatched phase, second optical harmonic generation *(Russian)* 78−79073
NH_4Cl, order parameter variation near multicritical pt., SHG 79−81484
NH_4Cl, order-disorder transition exam. by optical second harmonic generation 78−51671
$NH_4H_2AsO_4$, doubling crystal for ring dye laser 79−41392
$NH_4H_2AsO_4$, SHG, CW UV radiation prod. 78−46712
$NH_4H_2AsO_4$, tunable UV generation by freq. doubling 77−42571
$NH_2H_2PO_4$, temporal power variation of fourth harmonic generation of Q-switched YAG laser radiation 78−25922
$NH_4H_2PO_4$, 90° phase matching temp., refr. index freq. and temp. depend. 78−46720
$NH_4H_2PO_4$, cryst., cascade UV generation, by harmonic generation, temp. stabilisation calcs. 78−66868
$NH_4H_2PO_4$, focused beam SHG, temp., wavelength and angle bandwidths 79−50343
$NH_4H_2PO_4$, harmonic and sum freq. generation, tunable CW UV radiation prod. 78−46712
$NH_4H_2PO_4$, ruby SHG, comparison with RbH_2AsO_4 78−50856
$NH_4H_2PO_4$, SHG efficiency, 532 to 266 nm 77−23710
$NH_4H_2PO_4$, SHG method pulse width meas. of Nd:YAG laser *(Chinese)* 80−87432
$NH_4H_2PO_4$ thin crystal, intracavity SHG of synchronously mode-locked CW dye laser 80−95945
$NH_4H_2PO_4$, UV radiation prod., intracavity freq. doubling of rhodamine 6G laser 77−3628
NH_4LiSO_4, NH_4IO_3, phase transitions, SHG obs. 78−76398
$((NH_4)_{1-x}Rb_x)_2SO_4$, isomorphic impurity effect on dielec. and nonlinear optical props. 80−88911
$(NH_4)_2SO_4$, SHG expts. on microscopic origin of permanent dipoles 78−1299
NO nonlinear laser spectroscopy, VUV harmonic generation 80−74175
NO, vapour, four-wave sum mixing, 130 to 180 nm, third harmonic generation 77−10970
Na atomic vapour, optical sum-freq.-generation interference 77−42569
Na, magnetically induced SHG, intensity saturation 80−1273
Na, multiphoton ionisation in third harmonic generation by mode locked Nd:YAG laser 78−94413
Na, spontaneous field induced optical SHG, multiphoton ionisation 80−14395
Na, vap., fifth harmonic generation 77−65606
Na, vap., optical SHG, quadrupole moment pot. by mag. field 77−46760
Na, vap., third harmonic generation, four wave parametric mixing 77−737
Na vapour, direct ninth harmonic conversion of ps laser pulses 78−5526
Na vapour, saturation of transient reson. nonlinear processes 77−68243
Na vapour, seventh harmonic generation 78−18009
Na vapour, tunable resonant third harmonic generation of ps pulses 77−42566
Na vapour, two-photon resonant fifth harmonic generation 80−53374
Na-Ar, nonlinear optical 5th order susceptibility meas., VUV harmonic generation 78−42381
Na-Ar(Xe) phase-matched mixtures, seventh and ninth order nonlinear susceptibility meas. 79−55186
NaCl, additively coloured, SHG 80−1274
$NaNH_4SO_4.2H_2O$, $NaNH_4SeO_4.2H_2O$, nonlinear opt. props. including SHG 78−76396

optical harmonic generation continued
$NaNH_4SeO_4.2H_2O$ ferroelectric crystal optical SHG and pulse modulation *(Russian)* 77−14771
$NaNO_2$, optical harmonic generation near ferroelec. transition 80−91858
Nd:glass laser radiation, spatial coherence of fundamental and second harmonic 80−69442
Nd:glass laser system with parametric freq. conversion 80−1277
Nd:phosphate glass laser beam, single ps pulse props. 77−19273
Nd:YAG laser, CW mode-locked and intracavity freq. doubled, anal. 80−58548
Nd:YAG laser freq. doubled output for dye laser pumping 78−59090
Nd:YAG laser frequency tripling 79−14030
Nd:YAG laser with internal SHG in coupled resonators, CW coherent UV-source *(German)* 79−98438
Nd:YAG repetitively Q-switched laser, fifth harmonic generation for mW 213 nm source 79−55178
Nd:YAG solar pumped laser, freq. doubling 78−59045
Nd^{3+}:YAG electrooptically Q-switched laser pulse duration increase by intracavity SHG 79−94255
Nd^{3+}:YAG laser, spontaneous mode locking necessary conditions, quadratic nonlinearity influence 79−64261
$Nd_2Ti_2O_7$, ferroelec., temp. depend. of SHG intensity 79−24267
Ne, fifth harmonic conversion, 53.2 nm generation 77−10979
$Ni_3B_7O_{13}Br$, cubic, approx. nonlinear optical susceptibility 80−78904
PLZT ceramics, SHG, anomalous phase transition 79−45996
$PbGeO_3$, cryst. struct., dielec. and optical props. 77−1118
Pb_3GeO_5, cryst. struct. dielec. and optical props. 77−1118
$Pb_3(Ge_{1-x}Si_x)_2O_7$, optical SHG and pyroelectric effect 77−10982
$Pb_2Li_{1/2}Nb_{3/2}O_6$, antiferroelec. cryst. growth and props. 77−36189
$PbTiO_3$, tetragonal deform. of TiO_6 octahedron 77−55759
$Pr_2Ti_2O_7$, ferroelec., temp. depend. of SHG intensity 79−24267
Rb-Xe mixture, nonreson. third harmonic generation of I laser radiation 79−3746
Rb-Xe mixture, third harmonic generation with Nd:glass mode-locked laser 77−27318
RbH_2AsO_4, ruby SHG, comparison with other KH_2PO_4 isomorphs 78−50856
RbH_2PO_4, for tunable frequency-doubled CW dye laser 80−53372
RbH_2PO_4, harmonic and sum freq. generation, tunable CW UV radiation prod. 78−46712
$Rb_xK_{1-x}H_2PO_4$, 90° phase matching in freq. doubling, appl. to lasers 80−33088
SF_6 multiphoton absorpt. meas. by third harmonic generation 80−1036
$Sb_{1-x}Bi_xSI$, SHG at microwave freqs. 79−55188
$SbS_{1-x}Se_xI$, SHG at microwave freqs. 79−55188
Sf_6, third harmonic generation at 10.6μ 77−14775
$Sm_2Ti_2O_7$, ferroelec., temp. depend. of SHG intensity 79−24267
Sr-He, mixture, reson. third harmonic generation 79−27328
Sr-Xe, resonant third harmonic generation anal. 78−90460
$SrBi_2Ta_2O_9$, SHG, temp. depend. ferroelec.-ferroelec. transition 78−15121
$Sr_2Mg(Co)(Zn)(Mn)(Cd)(Ca)(Sr)TeO_6$, optical SHG study of acentricity, ferroelec. of low temp. phases 80−71324
$Sr_2Nb_2O_7$, crystal synthesis and SHG, solid laser freq. manipulation 79−41421
$Sr_2Nb_2O_7$, ferroelec., temp. depend. of SHG intensity 79−24267
$Sr_2Nb_2O_7$, ferroelecs., nonlinear optical props. 80−33086
$Sr_2Ta_2O_7$:Nd,Na, SHG, effect of dopants on Curie temp. 79−24267
$SrTiO_3$, optical SHG near phase transition 80−71348
$SrTiO_3$, SHG and quadratic electrooptic effect 78−76429
$SrTiO_3$, second harmonic generation, bond charge theory 78−76395
$SrTiO_3$, undispersive nonlinear dielectric, third harmonic generation *(Russian)* 80−95955
Te acousto-optically phase-matched noncollinear optical SHG obs. 79−50353
Te crystal, SHG, 60% efficiency, 12.8 μm NH_3 laser pumping 80−83640
Te, high efficiency SHF of 12.8 μm laser radiation 78−25923
Te, SHG, optical modulation 79−86212
Te, SHG in cryst., IR irrad. *(German)* 79−50345
Te, SHG of ps pulses 79−45995
Te, SHG under two-photon reson. conditions 80−99803
Te, self-defocusing of CO_2 laser radiation under phase matched SHG conditions 78−83043
Te, strained and unstrained, SHG and propag. of CO_2 laser radiation 80−58641
Tl, vapour, SHG 78−50855
Tl vapur, ruby laser third harmonic generation, flowing degree influence 80−48348
W-Ni diode, He-Ne laser freq. meas. rel. to CO_2 laser 77−31113
Xe, recently enhanced multiphoton ionisation and third harmonic generation 80−91526
Xe, third harmonic generation, bandwidth limitations in Lyman-α vicinity 79−81482
Xe-Ar, 3547 to 1182 Å conversion efficiency limited by Kerr-induced dispersion 78−37940
$Y_2Ti_2O_7$, ferroelec., temp. depend. of SHG intensity 79−24267
$Zn_xCd_{1-x}S$ monocrystal, optical and nonlinear optical characts. *(Russian)* 79−98442
$ZnGeP_2$, temp. depend. phase-matched nonlinear optical devices 80−99794
ZnP_2, birefringence dispersion *(Russian)* 77−85686
ZnS thin-film waveguide SHG phase-matching obs. with tunable parametric oscillator 77−58390
ZnSe single crystal, nonlinear optical coeff. and SHG coherence length 77−79893

optical images
see also aberrations
aberrational diffraction images, computation accuracy 80−87328
achromatic imaging, of distant objects, with plane, concave holographic gratings 78−94372
acoustic wave visualisation using Koster prism 80−5701
adaptive optics aberration coefficient estimation 77−19179
adaptive optics aberration coeffs. adaptive estimation 77−88659
adaptive optics for imaging, wideband real time atm. compensation 77−45320
additive colour viewing of LANDSAT imagery, for inexpensive remote sensing 79−29897
aerial landscape photography, haziness factor in image contrast *(Russian)* 77−37449

optical images continued
aerial lenses, for multispectral photographs from high altitudes 79−35868
amateur camera information capacity and image quality 79−49316
ambiguity function in diffraction and isoplanatic imaging by partially coherent beams 78−78925
analyser, semiautomatic, use in investigation of muscle biopsies 80−85466
analysis system, math. morphology and algorithms 80−82799
anamorphic system, image quality testing, resolving power determ. 77−7171
anisotropic material elements in optical systems, point and line image intensity distribs. *(German)* 79−55058
annular aperture, arbitrary point spread functions 80−87325
annular aperture, imaging performance, line spread functions 78−55304
annular apertures, imaging performance, apodization and MTF 80−23625
antenna array, T-type correlation, optical image forming system 79−27180
antireflection coatings on metal layers for photolithographic purposes 79−76837
aperiodic specious objects influence of AF sinusoidal phase deformations of wavefront *(Czech)* 80−14290
aperture, partially apodised, diffracted field characts. 80−48139
aperture ratio of optical devices *(Russian)* 80−1140
aperture synthesis by object rotation in coherent imaging 80−69336
apertures with Straudel Class of pupil functions, var. apodisation 80−23616
apertures with triangular and assoc. filters, variable apodisation 80−63914
apodisation and image contrast rel. to MTF 80−32920
apodisation for max. encircled energy with specified over-all transmittance 77−34835
apodisation for max. encircled-energy ratio, Sparrow limit of resolution 77−619
apodisation for max. Strehl criterion and specified Sparrow limit of resolution 77−68168
apodisation for max. Strehl ratio and specified Rayleigh limit of resolution 78−5425
apodisation for max. Strehl ratio and specified Rayleigh limit of resolution 80−28170
apodisation for minimising intensity distrib. second moment for Fraunhofer diffr. 77−31065
apodisation in coherent image form. 77−10844
apodised semicircular apertures, Fraunhofer diffr. pattern 79−901
apodiser, optimum, simulation by binary filters 78−5539
apodising filters, numerical exam., second moment of the point spread function 80−106611
apodization, optimal, by means of coupled calc. of pupil function and shape 80−95788
apodization and image contrast: author's reply to comment 80−58466
apodization and image contrast, MTF evaluation 79−59640
apodized optical systems, frequency response and point image irradiance distrib. 80−9819
apodizing filters for optimum Sparrow resolution in coherent systems with annular aperture 80−53435
aspherical deformations, rotationally symmetrical, representative model *(German)* 78−90375
astronomical image degradation, contrib. of lower atmospheric layers, use of photodiode array 79−21019
astronomical images, PDS microdensitometer processing for astrometry 78−16306
astronomical images iterative reconstruction, non-negativity constraint 79−101081
astronomical speckle patterns, image retrieval 77−22100
astrophysical applications of image restoration, conf., Bordeaux, France (Mar. 1979) 80−41935
atmosphere, phase correlation scale effects rel. to atmospheric imaging characts. 80−94604
atmospheric degradation due to refractive irregularities in clear turbulent atm. 77−42485
atmospheric dispersion effects on compensated imaging 77−42501
atmospheric imaging, conference, Reston, Va., USA (Mar. 1976) 77−42484
atmospheric isoplanation measurement using speckle interferometry 78−65385
atmospheric turbulence effect on imaging and optical communication, book contrib. 79−34960
atmospheric turbulence effects on optical and IR image form. *(French)* 80−46257
atmospherically degraded image restoration using complex spectral ratios 79−29854
atmospherically degraded images, linear invariant restoration 77−42503
autoidolon of quasi-periodic optical objects 78−50711
automated visual edge match system for image quality assessment 78−62218
automatic microimage analyser, MORPHOQUANT 78−37053
background limited system, defocused slit aperture, partial coherence 77−618
beam, image-bearing, nonuniformly polarized, generation of time-reversed replica 80−69459
biimidazole+leuco dye photochem. reaction, modulation by photopolymerisation 80−40714
bilinear transformations, general props. 79−98305
bilinearly distorted image linear restoration using Wiener filters 80−83557
binary filters simulating apodizers, expt. results 78−46780
binary image in noise, detection 79−36848
biological material, laser stereometry light-scatt. technique, cardiac images 80−56310
black hole, spherical, with thin accretion disc, image 79−67049
blurred image, sharpness improvement and multiplication 78−1173
broad-band coherent imaging 78−5424
C-CD imaging systems, large area, for deep space photography 77−57426
camera lens, 48 inch, image quality rel. to MTF 78−49938
catadioptric objective, development *(German)* 80−102796
centre of gravity coordinates, measurement accuracy analysis 79−36850
characteristic processing methods 77−625
circular aperture, non-uniform illumination, Straubel pupil function study 79−3623

optical images continued
circular pupil, diffraction pattern apodisation problem 77−612
coded aperture imaging: the modulation transfer function for uniformly redundant arrays 80−99019
coded aperture imaging, analogical deconvolution appl. to nucl. medicine *(French)* 78−35943
coded aperture imaging, predicted performance of uniformly redundant arrays 79−18351
coded aperture imaging, review 80−101914
coded aperture imaging with uniformly redundant arrays 78−37812
coded-aperture images, pre-folded Fourier filter reconstruction 80−53222
coherent and partially coherent light, image formation 77−88658
coherent apodisation problem, unified formulation 79−27187
coherent apodization problems, edge ringing effect 77−42495
coherent image deblurring using computer generated holographic filters 77−14669
coherent imagery of extended objects 80−106465
coherent imaging, speckle power spectrum, effect of moving diffuser 79−31811
coherent light observation, resolvable degrees of freedom 78−13666
coherent optical image spottiness reduction by liquid crystal screen 79−14109
coherent optical system, impulse response for image multiplication by spatial sampling filtration 80−33126
coherent optical systems evaluation, apodisation in beam propagation and image formation 77−88657
coherent optics fundamentals 78−78910
coherent synthesized aperture system, image form., resolution improved by diffr. grating 78−50715
coherently illuminated objects, image improvement *(Russian)* 80−28168
colour and black-and-white images, composition and decomposition 79−50233
colour coding of spatial freq. using incoherent optical processing 80−37956
colour distribution in polychromatic line spread function, aberration influence 77−7014
colour image evaluation from tristimulus values transfer functions measurements 80−87333
colour image interpretation, RADC's research 77−74534
colour photography, image stability and dye fading mechanisms 80−62754
colour reproduction, of images obtainable by two-primary colour projections 80−12125
coma, optimally balanced, influence on refractive images of annular object *(Czech)* 78−50710
compensated imaging system photon-limited performance 77−88960
compensation and restoration principles 79−58260
complex degree of coherence expansion, image intensity data, object reconstruction 80−32906
computer-generated polarisation holography system and reconstructed image quality 80−102677
computerized image reconstruction, computerized, fragment size choice 80−78785
concave holographic grating, imaging properties *(Japanese)* 78−37971
concave mirror, real image demonstration device 77−41447
concave mirrors, image light reflection, optical illusion teaching demonstration 78−49604
conference, Bad Harzburg, Germany (June 1979) 80−51951
confocal cavity imaging characts., mode decomposition method 79−31816
confocal scanning light microscopy, imaging modes 80−86401
confocal scanning light microscopy with high aperture optics 80−86400
confocal scanning microscope, image form. 80−68249
conjugate image appearance in volume reflection hologram 80−28181
conjugate wavefront generation and image reconstruction by four-wave mixing 78−13746
continuous tone picture reproduction, image quality and information capacity 79−59644
contrast loss in presence of chromatic magnification difference, numerical estimate 80−95823
contrast of time-averaged speckle patterns produced by small vibrations of diffuse objects 79−94169
cornea, photokeratoscopic technique 77−1993
coronograph, external occulting disc, scattered light reduction 78−36455
correction of optical systems, automatic, with large tolerances *(German)* 80−95977
correlation, real-time high-resolvance, by Bragg diffr. in saturable absorbers 80−48159
Correlation image formation with an axicon 80−48162
deblurring system using diffraction gratings 80−43274
deconvolution by noncoherent system 77−58271
defective periodic objects, self-restoration of autoidolon 78−29902
defocused optical system under partially coherent illumination, apodised aperture performance 77−10847
defocused picture restoration, image scanning method 77−14667
defocusing, partial coherence effect *(German)* 77−75430
degraded image restoration, periodic nonsinusoidal vibr. degradation, filter function 78−1169
depth imaging of pupil *(German)* 77−58270
detail sharpness and its quantitative expression *(Czech)* 80−1141
detection, phase-sensitive, representation of observable signals in Chebyshev polynomials 79−89857
diffraction and aberration effects, wave optical calc. 80−83549
diffraction at straight edge, partially coherent illum., aberrations *(Chinese)* 80−43267
diffraction image, intensity distrib., theory of eikonals 77−19185
diffraction image intensity fluctuations in turbulent atm. after refl., Huygens-Kirchhoff principle calcs. 80−63926
diffraction images of bar and edge objects, influence of optimum balanced coma 78−74850
diffraction limited image from obs. through irregular atmosphere *(Ukrainian)* 80−9814
diffraction patterns for optical systems with pupils of non-uniform transmittance 80−87470
diffraction theory of image form. 80−9822
diffuse object, optical system resolving power influence on laser image quality 79−31820
diffuse object imaging in randomly inhomogenous medium with amplitude distortions 80−63928
diffuser for Fourier transform hologram recording 80−43285
digital image restoration 77−23628
optical images continued
digital information optical recording in pictorial format 79−31831
direct picture transmission in single optical fibre, restoration with holographic filters 79−89871
discrete binary representation, halftone dot profile and aliasing 78−9335
discretisation using holographic filter, spectral analysis *(Russian)* 78−37809
dispersion relations, two dimens., phase problem appl. 80−102631
display, Fourier domain aliasing and quantization 79−81372
display system using computer generated integral photograph 78−87021
distortion elimination by eigenfunction method 79−7087
dither signals for binary display of images, computer-aided design 79−94161
double exposure interferometry through speckle photography *(French)* 80−83568
double-slit object illuminated with ultrasound-modulated laser light, resolution 80−37959
droplet, transparent, diameter meas. by side reflection 78−59518
dye-polymer system, diffusion based direct marking process, laser induced, spectral thermal characteristics 79−76779
dynamic laser speckle due to in-plane object motion, theory and appls. 77−50618
edge coding and detection using directional masks 78−42289
edge enhancement, real-time, using photorefr. effect 80−99642
edge enhancement with incoherent optics, using pupil plane mask 77−71921
edge filters for phase contrast imagery, theoretical design 79−86250
edge image anal., finite area sampling technique 79−22902
edge image analysis, Walsh functions used in Fourier transforms 79−72507
edge images, partial spatial coherence effect 79−89981
edge-ringing and edge-shifting, effects of coherence 79−36833
education, perspective distortion in photography, eye as simple lens 80−17734
electro-optical image sensors, performance evaluation of focal planes for aerial reconnaissance 79−31833
electrographic instrumentation for ultraviolet imaging and spectrography 80−46399
electrographic processes, increasing the effective sensitivity *(Russian)* 79−6211
electron micrograph, image processing systems, random noise removal 78−12791
electron microscope patterns, phase retrieval, algorithm 77−18140
electron microscopy, image reconstruction and holographic methods 77−65062
electronic focus, image contrast theory 79−13914
electrophotographic image information content and noise analysis 80−101861
evaluation criteria for optical systems *(German)* 80−43268
evaluation methods survey *(Czech)* 79−50235
exponential transformation using film nonlinearity for optical homomorphic filtering 80−58467
extended circular target, diffr. images in presence of coma 77−58250
extended objects, microscope imaging using apodised condenser and annular source 78−280
eye, aerial image modulation lowering, contribs. of retina and eye optical system 80−81584
eye, superposition images formed by refl. in some oceanic decapod crustacea 77−4997
eye movement measurement, IR technique *(French)* 77−36916
Fabry-Perot interferometer of large Fresnel no., image profile 79−54177
Fabry-Perot-interferometer imaging system for thermospheric temp. and wind meas. 80−101441
far-field diffraction, partial coherence, primary astigmatism 79−22899
fibre bundle, image transmission and resolving power *(Korean)* 79−14102
fibre tape for image and hologram transmission, using chromatic encoding *(French)* 79−3785
field wavefunction, analytic properties in optics 80−1138
film-grain noise degraded image estimation 78−54479
flat image focussing spherical lens, used for Si light detector 80−91880
fly's eye lens plates, superposed, image functions *(Japanese)* 77−34925
formation, propag. problems connected with special source structs. 80−87272
formation characteristics for partially coherent light at condenser exit pupil 77−10848
formation in photosensitive layers on highly conductive substrates 80−43419
Fourier image theory, self-imaging of plane periodic objects 79−81379
Fourier images theory, appl. of self imaging anal. *(German)* 79−89839
Fourier multiple-imaging system, compensation of distortion 79−76640
Fourier optics as approx. of Kirchoff integral, coherent imaging *(German)* 79−18357
Fourier spectrometry, optimal apodisation 80−99641
Fourier spectroscopy, apodising functions, use in spectral smoothing 79−35861
Fourier transform, significance in optical imaging *(German)* 78−50709
Fourier transform imaging, systems theory appl. *(German)* 78−74851
Fourier transform optical imaging, using SAW memory-correlator 78−83090
Fraunhofer diffraction pattern intensity distrib., apodization minimizing second moment 77−6997
Fresnel images, depth of focus 80−1145
Fresnel images, form. of 2-D transparencies with extended periodic struct., theory 78−82920
Fresnel images of periodic transparencies of finite dimensions 79−3627
Fresnel zone plates, image form. with short wavelength radiation 77−58437
fused xerographic images, optical density model 79−17550
Gaussian bundles optical imaging, mathematical description *(German)* 78−90376
Gaussian motion image degradation 79−10260
gradient index fibre array development and imaging props. 80−14483
gradient index imaging lens and system status 80−14420
gradient index imaging system theory 80−14294
gradient index optical imaging systems, topical meeting, Rochester, USA (May 1979) 80−12851
gradient-index imaging, theory 80−69331
gratings, embedded, optical imaging calc., Fourier optics methods appl. *(German)* 80−23805

optical images continued
gratings without contact, Moire fringe self images, partially coherent illum. *(French)* 77−83806
grazing incidence optics, total transverse aberration function 78−45765
grey-scale texture anal. and use of co-occurrence matrices 80−43276
half-symmetric image geometry 78−66773
halftone, information content of harmonics of spatial frequency spectra 78−50708
halftone images produced by random quasiperiodic process 77−622
halftone images with edge enhancement and Moire suppression 77−623
heterodyne optical correlation, photogrammetric appls. 77−42497
high-resolution astronomical imaging, results 80−82225
high-resolution film, facile image evaluation 77−74533
high-resolution imaging by degenerate four-wave mixing 80−69458
hologram, reflection, real image reconstruction, resolving power and diffr. efficiency 80−53237
hologram image reconstruction without using reference beam, brightness characts. *(Russian)* 80−69348
holograms, Fresnel amplitude and phase, reconstructed second-order image props. 80−63952
holograms of diffuse objects, autocorrel. of transmittance 78−1185
holographic grating, imaging props. 78−5563
holographic image contrast degradation with partially coherent light reconstruction 80−102678
holographic image formation, coherent transfer functions and resolution 80−43292
holographic image formation, role of organically accelerated bleaches 77−14672
holographic image formation modes, progress 79−50259
holographic image luminance, depend. on recording geometry 78−63042
holographic image luminance determ. 79−81394
holographic image magnification, new methodology 80−95851
holographic image quality, recording process statistics effect 77−50641
holographic lens element, s and t formulae 77−46785
holographic lens image quality, estimation criteria 78−25824
holographic lenses, coherent transfer functions anal. 77−68190
holographic lensless Fourier transform, spherical wave illum. 80−74312
holographic processing of mag. field distribs. of thin foils 79−89868
holographic recording, and reconstruction in spatially incoherent white light 78−78955
holography, filtering unwanted reference beams 79−89869
holography, image contrast changes during recording in nonlinear media with local response 80−69346
hyperbolic mirror virtual image, holography problem, for teachers 79−35476
iconics and image processing 79−94173
iconics and its basic goals 78−46527
ideal image-forming flux concentrator design 79−55201
illumination distribution calc. in image plane 77−31125
illumination with a moving light source 80−23632
image, dissector tubes, echelle spectrographs, design considerations 80−91918
image classification and tone reproduction determination, statistical method 77−74535
image evaluation by single bar and disc. anal. (aerial photographic system) 77−2704
image formation theory, work of D.S. Rozhdestvenskii 80−18999
image quality descriptor relationships using signal detect. theory 78−71050
imaging process efficiency and quality, electrophotographic process, electronographic cameras and image intensifiers 78−78932
imaging system assessment, conference, London, England (Nov. 1976) 78−50718
imaging system point spread function determ. by scatt. of two monochromatic beams 80−87316
imaging through randomly fluctuating media, stellar speckle interferometry appl. 77−13248
incoherent annulus, parabolic image motion effect 77−613
incoherent annulus object diffraction images in presence of primary astigmatism 79−22904
incoherent images, technique for addition and subtraction 79−98293
incoherent imaging system, diffr. images asymptotic behavior 80−1139
information content of image, physical limitations 78−33697
instrument image evaluation by multitarget array detection 80−1362
integral photography, transform of 3-D image produced by lens raster 78−82921
integral sampling, deterministic and statistic methods of investig. 77−10856
interference transfer function with quadratic detect., coherent illum. 80−78782
interferograms, image quality and wavefront profile determ. 79−85172
interferometric imaging through scatt. media with achromatic interferometer 79−58778
interferometric spectrometer, moving grating, analysis of spectral imaging capabilities 79−58799
interferometric two-dimens. imaging of rotating objects 78−1176
invariant Walsh spectrum definition and calc. *(Russian)* 79−94156
inverse source problems in optics, book 79−31821
inverse source problems in optics, book contrib. 79−31822
IR crystals, optical imaging of growth defects 80−64988
irradiance distribution parameters fast meas. by image chopping techniques 79−36839
irradiance moments optical calc., wave optical accuracy limitations 80−74302
isophotometric photorecording method for optical system image quality meas. 77−34967
isoplanatic degradation of tilt correction and short-term imaging systems 80−53219
isoplanatic imaging, complex degree of coherence determ. 77−2691
isoplanatic optical systems, partially coherent image form. through random absorbing media 80−14292
isoplanatism in optical systems, image form. 80−1144
isoplanatism varieties for imaging through turbulence 77−42499
in Kerr metric, appls. of geometrical optics, analytical results 77−29637
kinoform method, for filtering and image synthesis 77−58295
Kron electrographic camera, spurious image mistaken as nebula 78−8101
lake monsters, prod. by image distortion due to atmospheric refr. 80−46259
large-aperture optical system, energy distrib. calc. in diffr. image of point 80−74305

optical images continued
laser beam metal-coated apodising apertures 77−19439
laser beam propagation through turbulent atmosphere, interferometric evaluation of imaging characts. 77−88643
laser Doppler anemometry, image form., wall scatt. effect on S/N ratio 79−89953
laser fusion apodised apertures, Faraday rotators, and spatial filters 77−19290
laser pulse autocorrelation by optical processing of Fabry-Perot spectrograms 80−58465
latent image latensification, mathematical interpretation *(French)* 77−41707
least-squares wave front errors of minimum norm 80−48137
lens, gradient-index rod, aberrations in multimode optical fibre devices 80−69487
lens, gradient-index rod, evaluation by imaging 80−69485
lens array, for close-up imaging of documents and displays 79−36972
lens aspherical effect on image defects *(German)* 78−9332
lens guide, low-loss image transmission 80−91872
lens image forming by refraction, tutorial *(Hungarian)* 77−22359
lens imaging properties and OTF, Jones notation 78−25945
lens light-guide line, image transmission characts. 79−3789
lens-array photographic system, depth of sharp focusing, resolution 80−62763
lens-array photography, longitudinal distortion compensation, integral image reconstruction 80−52345
lenses and mirrors, graphical representation for teaching 77−49539
lenslet array with periodic sampling structure, for image form. 78−37964
level slicing performance using film nonlinearity *(Chinese)* 80−102628
light field reconstruction accuracy after stimulated scatt. 80−78911
light radiography application to measurement of density of hollow-charge jet in Cu *(French)* 78−44344
light-reflection microscope image flare factor rel. to illumination system aperture 79−14083
line image transmission through single fibre using spectral instrums. 80−102820
linear filtering operation, image forming process 78−22089
linear line screen for image reproduction, analysis 80−32925
linear systems, Fourier transforms and optics, book 79−41350
linearly degraded images, iterative image restoration 80−95807
linearly degraded images, iterative restoration, reblurring procedure 80−99640
liquid-crystal devices, variable-grating-mode, optical logic operations on binary images 80−106613
long-distance multimode waveguide image tranmission in coherent light 80−48435
low light and thermal imaging, conf. Nottingham, England, 1979, Apr. 79−36856
low light and thermal imaging systems, atmospheric effects 79−39860
Luneberg apodization problem 80−87302
magneto-optical imaging of domain struct. in thick cryst., multiple diffr. effects 77−8552
mammographic screen-film systems, comparison of laboratory and clinical evaluations 78−69187
Mars, Viking lander camera data, image processing 78−20649
mask, random amplitude, diffr. pattern intensity distrib., distant object imaging 77−58252
maximum entropy image restoration method, deterministic anal. 78−9336
maximum Strehl intensity ratio intensity ratio image plane determ., remarks *(German)* 78−71038
medical image formation by back-projection 79−83916
metal rough surface, speckle pattern statistics 77−75421
metal vapour pulsed lasers, quantum amplifiers, image distortion 79−18433
metal-photosemiconductor-insulator multilayered structure, charge pattern formation during recharging 80−47129
metal-photosemiconductor-insulator multilayered structure, optical image recording, As_2Se_3 photosensitive element 80−42286
metallic thin film apodising and attenuating filters, phase shifts and aberrations 80−87552
metaxial optics, centred refracting systems, undiaphragmed and without aberration *(French)* 78−94369
metaxial optics, light diffraction *(French)* 78−74844
microchannel plate system image contrast rel. to object size 79−27421
microscope, effect of magnification distrib. between objective and eyepiece on image quality 80−18013
microscope, focusing technique for digital image anal. system 80−68250
microscope, polarizing, with crossed polarizers, incoherent diffr. imagery 80−101838
microscope, scanning, multiple traversing of the object 80−90890
microscope, scanning and conventional, Fourier imaging of phase information 80−73444
microscope, wide-field objectives, image forming quality 79−35819
microscope photometer/semiautomatic image anal. instrument system for morphometric and photometric value meas. 80−82815
microscope with binocular tubes, image diagrams *(Russian)* 77−10102
microscopic image form., nonuniform source distrib. 77−14664
microscopic imaging analysis applied to phase, schlieren and interf. microscopy 78−45688
mirror imaging analysis, normal to grazing incidence 77−614
mirror scanning, 4th order matrix operator formulation *(Russian)* 78−18037
mirrors with circular coolant channels, imaging performance 77−68254
models of optical systems 80−9821
modulation contrast microscope, coherence theory 77−7010
modulation contrast microscope, image irrad. rel. to phase gradient, numerical aperture influence *(Spanish)* 79−55063
Moire patient topography imaging system, evaluation of 79−39464
moire technique for image alignment, focus and scaling 77−27362
moments of images aberrated by turbulences undersampling errors in meas. 80−1137
monochromatic aberrations in systems without symm., general and accidental identities 77−616
monochromator using concave holographic grating and plane mirror, imaging props. 80−99856
moving object imagery using large aperture telescope arrays 80−53225
moving object imaging, anticausal behaviour 79−81381
multi-image regeneration by white light processing 80−95814

optical images continued
multicolour image storage on black and white film, using crossed grating 79−31813
multicolour reflection holograms, improved image techniques 80−48184
multicoloured photothermoplasticity process, coding and decoding indices *(Russian)* 77−67523
multifibre image transmission, misalignment effect on MTF 79−14093
multigradation image, representation in Boolean algebra 77−31071
multiple image form. by addition of optical signals 78−66776
multiple image formation by sampling Fraunhofer diffr. patterns 78−1334
multiple imaging through nonredundant arrays 78−22095
multiplex image coding, astronomical IR speckle interferometry appl. *(French)* 80−67580
multislit spatial filtered pseudocolour holographic imaging 80−53236
near field speckle statistics 77−19182
noisy images, a priori information, degrees of freedom 77−38811
non-imaging optical design principals, appl. to solar energy concentrators 80−7928
noncentrally obscured circular pupil imaging systems 78−66774
nonisoplanatic spectral instruments, num. correction of images formed 80−249
nonlinear optical processing with Fabry-Perot interferometers containing phase recording media 80−48158
nonwhite noise, S/N ratio and detail detection 80−102648
obscured circular pupil imaging system, included power 78−46520
obscured pupil imaging system, OTF and point spread function 78−25809
one-dimensional coded apertures, applications 78−45746
optical transfer measure, system relations, appl. wide field microscopy and microelectronic photolithography *(German)* 80−9815
optimisation by apodisation filters in optical systems with residual aberrations 80−53223
optimum apodizers, performance, primary coma effects 79−98557
optimum colour rendering of holographic images *(Russian)* 77−7035
optoacoustic effect imaging 80−106473
optoacoustic material probing and imaging, far IR 80−83559
optoelectronic devices and optical imaging techniques, book 80−27059
optoelectronic instrument, image information content 77−39057
orientation angle calc. using image matrix transformation *(Russian)* 80−73314
OTF measurement, German standards on image assessment, review 78−50724
PAA, nematic liq. cryst., light transmission in high elec. field grad. 79−19150
parabolic gradient index lens, SELFOC, chromatic aberration in imaging system 80−14422
parabolic index glass rods and fibres, imaging props. 77−42599
parabolic off-axis mirrors, imaging props. 79−94316
parallel image transmission by single fibre 78−71216
parameter estimation potential accuracy anal. 77−88648
paraxial coherent, apodization by interposing masks in pupil plane *(French)* 80−23630
paraxial coherent light, image formation *(French)* 79−31815
partially coherent illumination, imaging of relatively strong objects, linear transfer theory 78−22091
partially coherent image form. in two dimens., computer simulation 80−106434
partially coherent image formation, bibliographic review 79−18356
partially coherent imagery, calc. method 78−90373
partially coherent imagery with spherical aberrations *(German)* 79−59641
partially coherent imaging, edge ringing, performance function 77−46699
partially coherent object, coherence props. in image 77−34833
$Pb_3M_gNb_2O_9$ crystals for optical radiation control 79−81554
perceptual coding in the cosing transform domain 80−102635
periodic complex object, defocused image under partially coherent illum. 77−611
periodic complex object, image irradiance for partially coherent illum. 77−610
periodic structure with coherent illum., resolution depend. on number of elements, wavelength and focal length 80−63941
phase distributions in images and Fraunhofer diffr. patterns prod. by non-aberrant lens 78−1172
phase estimates from slope-type wave-front sensors 78−66770
phase gratings, coherently illuminated, defocused diffr. images 78−46523
phase opto-electronic meas. system, with raster analysers, illumination distribution law effect on accuracy 77−79047
phase plate consisting of bleached holographic lens, for noise-free coherent imaging systems 79−31817
phase problem in image formation: the determination of coherent transfer functions 80−87329
phase reconstruction problem for wave amplitudes and coherence functions, book contrib. 79−31823
phase recording using sensitised photooxidation reactions 80−87350
phase retrieval from intensity meas., uniqueness question 79−13915
phase-inverting grating construction, use in deblurring filters 80−48398
photographic, random dot model theory incl. intragrain transmittance distrib. 77−45911
photographic emulsion, Callier effect, influence on image contrast 78−63017
photographic emulsion, latent image form. in Ag halide grains 77−5939
photographic film grain noise in partially coherent imaging 80−101860
photographic image quality, scattered light effect 78−16884
photographic image reproduction system, information losses 79−71558
photographic image sensitivity, improvement using Mn salts in developing soln. *(Russian)* 77−34050
photographic image threshold luminance detail value, effect of target and photographic parameters 78−56989
photographic imagery, transfer functions due to complex linear motions 79−18355
photographic images, information content 79−17548
photographic layer, homogeneous solid, diffusion, one-dimensional case *(German)* 80−73495
photographic lens, image quality improvement 80−47123
photographic lens system, serial testing, resolving power limits 79−35870
photographic papers, polarised light refl. 80−64127
photoimaging system based on photopolymerisation in cryst. coatings 80−40716
optical images continued
phthalocyanine-alkane interface, charge transfer, rel. to photoelectrophoretic image form. 80−65616
pictorial image transmission by single optical fibre by 1-D scanning 79−7229
point images resolution, decision theory 79−81375
point spread function, encircles light energy calc. 77−79766
point spread modification by polarisation masks 77−65615
polarisation features of image spectrum on FTIROS 77−75439
polarizer with spherical mirrors for VUV radiation 80−48375
positive image production on biazide-polymer based photoresist. films *(Russian)* 78−16887
power spectrum analysis, moment as image quality merit factor 77−7019
prawn's eye, optical model of cornea image form. by thin film metal mesh *(Japanese)* 77−25421
precision objectives, high resolution, image-forming quality *(German)* 78−87120
principles, w.r.t. electronics engineer appl. 77−83818
projection printing, partial coherence 79−31834
projector screen images, evaluation of colour distortions introduced by projector components *(Russian)* 79−32029
pseudo-colouring with coherent optical encoder 77−7020
pseudocolour density encoding, white-light, using contrast reversal 80−83560
pseudocolour encoding, of holographic imaging, new technique 78−78963
pseudoscopic image restored by a hologram, peculiarities of visual perception *(Russian)* 79−50255
quality criteria, OTF, modular transfer function, phase transfer function *(German)* 80−53221
quality criteria of photographs 77−79171
quality data derivation from edge sharpness, simple math. methods 78−50722
quality number rel. to wave aberration polynomial coeffs., best image plane position determ. *(Spanish)* 77−68180
quasars, image doubling assoc. with absorpt. systems 80−22112
quasicoherent light source image synthesis by phase measurable interferometry 77−58284
radiation correlation function, in linear system, symmetry props. 77−83824
radiographic decision making and phys. image props. 78−69189
radiographs optical and digital image processing 77−70241
Raman-Nath acousto-optical interaction, geometrical interpretation of image form. *(French)* 77−34836
random checkerboard process, two-dimens., generalisation 79−81374
random medium, image resolution limitation 78−37813
randomly aberrated wave imaging theory 79−76607
raster scanned images, matched filter processing 77−7018
ray tracing, generalised, caustic surfaces 79−23043
real time recorder and display for reconnaissance sensor data 79−32081
real-time optical image addition and subtraction using double-grating shearing interferometer 79−55069
real-time optical processing using the liquid crystal light valve 80−63936
real-time recognition of microscopic phase objects 79−7085
reconstruction, iterative computer method 80−102634
reconstruction from hologram, field diffracted by transparent object identity 78−37826
reconstruction from projections, filtering 77−68176
reconstruction in three-dimens. using stimulated Raman scatt. 78−83038
reconstruction of images distorted by smearing 79−76614
reconstruction of partially coherent objects from mutual intensity samples 78−9333
reconstruction using propag. law of mutual intensity 77−624
recording on magnetic film, banded domain structure, effect of recording field strength on energy charact. *(Russian)* 78−19297
reflectance map calc., rel. to image form. 79−75568
refractive index gradient tolerance in optical elements 78−71179
reimaging system, out-of-field radiation analysis 78−59117
remote sensing, evaluation of atmospheric effect on aerospace information 80−4101
representation using genetic geometrical functions 80−5702
restoration, pseudo-inverse, singular value matrix decomposition algorithm *(Russian)* 78−37810
restoration for invariant pointspread functions 80−69332
retinal image light distrib., cat 78−48790
retroreflective arrays as approximate phase conjugators 79−72508
rotation and magnification, optical system 80−48376
sampling expansion of bandlimited function 78−17863
satellite-generated radar images of the Earth 80−90249
SAW devices based on interaction of SAW with electrons in semicond. 77−80025
saw-tooth wave response of optical systems in presence of linear image motion 79−31810
scale transfer charact. *(Russian)* 78−37962
scanning and conventional imaging systems, basic equivalence 78−46534
scanning microscope, spherical aberration effect on imaging props. 79−58783
scanning microscope, types 1 and 2, image form. 77−79148
scanning microscope image formation 80−86399
scanning microscopes, partially coherent and confocal, imaging of periodic structs. 80−5700
scanning microscopes with partially coherent source and detector 78−58923
scanning of image-carrying light beams with acousto-optic deflection cell 80−14459
scanning optical microscope, second harmonic imaging 78−82029
scanning system, scanning aperture effect on image quality *(Japanese)* 77−42625
scanning type 2 microscope, bar-pattern image, effect of annular lenses 78−89535
scattered field data inversion for image form., expts. and computer simulation 79−89852
Schade detail S/N ratio derived from decision theory 78−63022
schlieren system, colour images of inhomogeneous transparent media 78−33905
schlieren system, phase object projection, imaging charact., recording conditions 78−25977
Scophony light valve, comparison with flying spot scanner 80−33147
secondary ion images observation, using channel plate *(French)* 79−58840

optical images continued
sector templets for determining the contrast transfer of imaging systems 80−32924
self-image resolution in multimode optical waveguides 78−63184
self-image techniques, optical computing 80−18998
self-imaging, light-optical experiments *(German)* 80−63938
self-imaging process, partially coherent light effects *(French)* 77−23621
Selfoc conically graded medium, aberration anal. 80−1142
Selfoc lens as imaging system, chromatic aberration 80−69480
shaded circular apertures, encircled energy in diffr. pattern, super-resolving and apodising props. 80−95787
shading effects and countermeasures 78−78922
shadowgraph apparatus, phase struct. visualisation by crossed statistical amplitude rasters *(Russian)* 80−5846
sharpness adjustment, teleobjective types characteristics *(Hungarian)* 78−12780
sharpness criterion, rel. to redundant spacing interferometry 78−5427
shift, Adamar transform appl. *(Russian)* 80−1134
short-exposure imaging through turbulence, wavefront distortion 79−41336
simple lens shape effect on image curvature 79−50368
simultaneous detection and intensity estimation 79−46040
single projector for abutting images of two light valves 80−87458
sinusoidal amplitude grating, with apodisation filter, coherent imagery 79−55067
sinusoidal complex object with a small phase modulation, Fresnel diffr. patterns, self-imaging 80−43256
slit image seen in total internal reflection *(French)* 80−95810
smectic A liquid crystals, thermooptical recording, echo images 80−91928
solar concentrator image characteristics, non-uniform intensity distrib. 80−55816
solar glass components, specularity meas. using Fourier transform anal. 80−5804
space and time variables in optics and holography, expt. aspects 77−34830
space filtering algorithm, influence on signal of optical system misalignment *(Russian)* 78−37815
space variant optical transfer with Fourier filter in extrapupilar position 77−10846
spatial filtering of incoherent imaging system *(Chinese)* 79−72500
spatial high pass filtering using photochem. adjacency effect 77−71929
speckle, properties and applications *(Japanese)* 78−22085
speckle averaging, imaging step, subchannel holography 79−22918
speckle coded image subtraction configs., optimal distrib. of exposures 79−55071
speckle contrast, depend. on object surface profiles 78−1168
speckle contrast measurement in and near image plane 78−42287
speckle elimination using random spatial phase modulation 77−71923
speckle image reconstruction of solar features 77−33354
speckle imaging, photon by photon, diffr. limited performance for large telescopes 79−53729
speckle interferometry, wideband, true imaging of astronomical objects 80−53226
speckle interferometry fundamentals and appl. *(Czech)* 78−29148
speckle interferometry in astronomical image reconstruction 77−37508
speckle noise, integration with finite aperture, logarithmic transform 77−19188
speckle noise and object contrast, detection thresholds eval. technique 78−5434
speckle pattern, point spread function effect on average contrast 77−46702
speckle pattern interferometry, electronic, using digital image processing techniques 80−87322
speckle patterns, contrast at defocused image plane 79−72491
speckle patterns, image plane, statistical props. 80−63940
speckle patterns, non-gaussian statistics, surface roughness meas. 78−66762
speckle patterns in white light images, average contrast meas. 80−9808
speckle patterns rel. to object surface profile, computer simulation 78−13660
speckle phenomenon fundamental image processing and evaluation *(Czech)* 78−29147
speckle reduction in coherent imaging, two-step process 78−37819
speckle statistics, gaussian approximation 77−46701
speckle structure, coherent optics, use of moving random mask 78−82922
speckled image subtraction setup, optimal distrib. of multiple exposures 77−34834
spectral image from point at spectrometer entrance slit, produced by toroidal diffr. grating *(Russian)* 78−57452
spectrogram imaging device, anamorphoses in spatio-temporal optics *(French)* 77−68179
spectroscopic system, OTF meas. and image correction 78−37083
spherical concave gratings, off-plane stigmatic imaging 77−38808
square law media, imaging characts. 77−7015
stabilisation, using liq. optical element 78−55462
star cluster high resolution imaging by speckle interferometry, simulation 78−77492
star image at telescope focus, quality, rel. to photoelectric obs. efficiency 80−62034
stars, imaging theory for extrasolar planets detect. 77−29882
statistical filter for image feature extraction 80−99636
statistical image anal., 3 parameter probability distrib. density function 80−43266
stellar images, improvement via real-time phase correction system, appl. to Sirius 77−22084
stellar interferometer, imaging using aperture synthesis 79−58244
stellar speckle interferometry data processing method 80−17498
stellar speckle pattern statistics, photon counting techniques 79−25324
STEM, Crewe's Z-contrast technique, study of Pt and Pd catalysts 79−46530
stereo image processing, control system 78−4728
stereo-pair images, correlation error prediction 80−102636
stigmatic imaging with pair of concave gratings 79−72670
storage, photoferroelectric image storage in antiferroelectric-phase PLZT ceramics 80−71353
storage and scanning using oppositely-directed surface acoustic waves 79−55238
straight edge coherent imagery, with Straubel apodisation filters 78−25808
optical images continued
strain measurement by speckle photography, hybrid optical and electronic image processing 80−99976
Straubel apodisation filter, rot. symmetric, circ. aperture diffr. pattern, pupil functions 79−81530
straubel apodisation filter systems, effects of defocusing on point spread function 78−25804
straubel apodisation filters in partially coherent light, sine-wave response 77−3545
Straubel class of apodisation filters, diffr. field characts. 77−7198
Strehl intensity applicability as image quality criterion *(German)* 80−28166
striascopic imaging of profiles with laser light, surface tension measurement 79−2845
structured image reproduction, quality, information rating 77−10851
subtraction through speckle modulated by Young fringes 80−95813
super-resolution derivation by analytical continuation methods 78−29915
surface orientation determ. from multiple images, photometric method 80−52163
surface profile from horizontal light source reflection, calc. from observed image 80−101777
surface profile from horizontal light source reflection, image calc. 80−101776
surface strain direct meas. using image-shearing camera 79−58773
system design, advances and problems 79−36975
systems performance quality evaluation *(German)* 80−95804
tapered gradient index rod, geometrical optics and imaging props. 80−14280
teaching, holographic experiments on optical imaging 80−12872
telescope, image vergence variation with object distance change, general case 80−63934
telescope, weak object image distorted by atm. effect, restoration possibility *(Russian)* 78−32349
telescope focal plane, freq. correl. by speckle interferometry 79−94153
telescope MTF curves, comparison of visual and photoelec. meas. imaging quality *(German)* 77−79763
TEM, appl. to organic solid-sate chemistry, review 79−60235
temporal coherence rel. to optical noise, partially coherent imaging 80−102611
texture pseudocolouring, single pass by spatial filtering 80−95809
thin film magnetic recorders of optical images, sensitometry using glass Nd laser *(Russian)* 77−79178
thin phase variation objects under partially coherent illum., effective transfer function *(Spanish)* 79−55064
three dimensional video images formed by parallax panoramagrams, real-time transmission 79−31807
three-beam interference images, sinusoidal complex object with phase modulation 80−53208
three-dimensional, no. of degrees of freedom 80−78794
three-dimensional image transmission by lens guides 79−76789
three-dimensional information 78−78973
tone reproduction analysis with square, circular and concentric-ring patterned screens 80−53229
transaxial tomography camera, photographic image reconstruction, analogue recording system 78−82085
transmission by variable refractive index, self-focusing waveguide 79−7208
triangular apodiation filter system, rectangular and triangular wave-response 79−59645
turbulence degraded image reconstruction, by spectral ratio meas. 78−9334
turbulence effects, imaging with telescope array 77−5458
twin hollow cathode interferometer-spectrometer, strongly cooled, imaging system *(German)* 77−61143
two dimensional image scanning of movies using surface acousto-optic interaction 79−94352
two-dimensional image transmission by wavelength multiplexing 79−27189
two-dimensional image transmission through randomly inhomogeneous medium, using Jamin interferometer 78−50706
two-dimensional object imaging by optical waveguides *(Japanese)* 78−87146
two-dimensional sampled imagery, aliasing and blurring effects 80−99635
two-mirror telescopes, image quality estimation and utilisation in cosmic astronomy *(Russian)* 79−96911
undersampled images, bounds on errors in reconstruction 79−89858
uneven interface of media with different refractive indices, statistical characts. of images 80−87331
unordered fibre bundles, parallel image transmission, multicomponent hologram arranger 80−78957
US imaging by acousto-optic interaction in Raman-Nath diffr. regime 79−55260
varifocal imaging in cardiology 79−70631
Viking 1975 Mars lander interactive computerized video stereophotogrammetry 78−20650
virtual image display using Fresnel lenses 80−1295
virtual image position determ., demonstration using TV camera 80−67992
vision, subjective effects of pictorial noise pattern 77−90799
visual, acuity experiments, image viewed through a rotating mirror 79−76790
visual analyser space-frequency filter harmonisation with statistics of images 80−30726
visual optical line spread width judgement, merits of Gaussian moment 80−16924
visual otpical line spread width judgement, merits of Gaussian moment 80−16923
visual simulation and image realism, seminar, San Diego, USA (Aug. 1978) 80−3639
visual task prediction from image quality data 78−53415
volume holograms, reconstruct. fidelity for finite width and variable index modulation 79−72533
volume holograms for image restoration 80−83566
volume-phase reflection hologram, recording medium thickness effect on image luminance 80−58479
Walsh functions in polar co-ords., appls. 77−23626
wavefront correction in real time for atm. distortion, Bragg diffr. by acoustic wave 77−42500
wavefront curvature meas. of small diam. laser beams using Fourier imaging 79−94273

optical images continued
wavefront distortion sensing for adaptive optics system control 77−19293
wavefront plot, aberrations, point spread function, three dimens. *(German)* 78−46521
wavefront reconstruction method, plane waveguide hologram coupled system 80−5708
wavefront reconstruction of light beams in stimulated Raman scatt. 79−41419
wavefront sensing using white light sources 80−1146
wavefunctions in image plane of system distorted by aberrations, integral eqn. inversion 79−98304
waveguide image transmission in coherent light, review 79−59831
waveguides with prescribed propag. consts., design 80−48419
Weigert effect for difference detect. between two images 79−81376
white light image speckle statistical props. 80−106461
white light image speckles, contrast depend. on surface roughness 79−13903
wide field imaging, significance of optical transfer measure *(German)* 78−90374
Wigner distribution function, optical production, speech signal analysis 80−48521
Wollaston prism type interferometer, diff. theory of image construction *(German)* 77−158
X-ray image quality, MTF anal. of influencing factors *(Japanese)* 77−73580
X-ray image reducing using crystal reflection, for sub-micrometre dimens. 79−58859
xerographic image, measurability of structure fluctuations 77−18119
xerographic images on paper, optical model 79−17549
Zernike moment invariants, image analysis via general theory of moments 80−102629
zone-plate coded imaging of laser-produced plasmas 77−55167
zone-plate coded imaging on microscopic scale 77−54673
zoom objective, displacement of individual lenses from ideal positions *(German)* 78−71186
AgCl emulsion, anisotropy induced by two incoherent and perpendicular light vibrs. 79−41428
AgCl emulsion, spatial differentiation, of intensity distrib., using Weigert effect 79−81377
Ge read out, by SAW, optical image memory in slow surface states 77−79942
$LiNbO_3$:Fe, white-light image processing 80−87321
$LiNbO_3$-gap coupled Schottky diode memory correlator, grating coupled optical imaging 80−64143
$LiNbO_3$-pn-diode airgap convolver struct. optical scanner using single SAW pulse 80−64144
V_2O_3, FTIROS thermochromic materials, colour and visual contrast 80−33100

optical information processing
see also spatial filters
2-D image processing applications of acoustooptical devices 80−53231
1978 and 1979 development trends 79−18354
A/C convertor using channel waveguide modulators, design and analysis 79−55249
A/D conversion, parallel real-time, using liq. cryst. light valve 80−53451
A/D conversion and page composition for holographic memory 78−5436
accurate fan-beam reconstruction 78−78931
achromatic coherent system, noise performance 79−98295
achromatic interferometers for white light optical processing and holography 80−53234
acoustic emission monitoring difficulties overcome by optical detectors 78−60968
acoustic Fourier transform, two-dimensional, high-speed 79−36844
acoustic image scanning, optical processing, photon integration technique *(French)* 79−32147
acoustic logging, optical filtering appl. in data processing *(Russian)* 79−39942
acoustic scanning, of optical images using SAW device 79−36845
acousto-optic correlators, spatial or time integrating, review 78−9341
acousto-optic processor, light diffr. by acoustic wave 79−76586
acousto-optic programmable filter characteristics and applications in optical computing 79−72716
acousto-optic signal correlators, review 77−58473
acousto-optical correlator, with two-dimensional reference transparency, testing 80−106485
acousto-optical devices for real- and near-real-time signal processing 80−10024
acousto-optical processors for wideband electronic signals 78−79137
acousto-optical signal processing system architectures and applications 80−102652
acousto-optical snapshot Pockels Readout Optical Modulator 77−19193
acousto-optical wideband programmable filter 80−102842
acoustooptic snapshot PROM, real-time optical, signal spectrum analyser 78−90494
active feedback optical processor, using coherent source and liq. cryst. light valves, design 78−22204
active optical devices, seminar, San Diego, CA, USA (August 1979) 80−101664
active optics imagery, postprocessing 77−29654
active phase compensation devices, post-processing of imagery 77−42502
active wavefront compensation device image degradation and post-processing 77−58283
adaptive binarisation using hybrid image processing system 78−87019
adaptive holographic matched spatial filter for pattern recognition 77−7011
adaptive laser beam control process, closed loop considerations 77−88660
adaptive optical system, performance with extended dynamic targets 77−46798
adaptive optics for imaging, wideband real time atm. compensation 77−45320
adaptive optics systems, bandwidth specification 77−46799
adaptive phase compensation, resolution through turbulent medium 77−46692
aerial photographic analysis and stereographic mapping with electro-optical pattern recognition 77−19186
aerial photography rapid screening by optical power spectrum analysis 78−63033
aerosol hologram, automatic assessment with new reconstruction config. 77−7031

optical information processing continued
air pollution, incoherent optical heterodyne detection 79−16679
airborne spectroradiometric data, and LANDSAT data, hydrothermal alteration mapping appl. 79−34973
algae sample analysis using coherent optical processing 80−98205
aliasing distortion in power spectra, digital processing of interferograms 77−45904
alkali halide photodichroic crystals use for coherent opt. data processing 77−68248
alkali halides, photodichroic, as optical processing elements 78−83056
ambiguity function display, improved coherent processor 77−42492
ambiguity function display using single 1-D input 79−94158
ambiguity processing by joint Fourier transform holography 80−58468
ambiguity-function generation using passive optical τ-shift technique 80−102647
analogue computer performance advantages 78−78949
analogue computing, past, present and future 78−46531
analogue data processing systems, polarised modulation of light *(Russian)* 80−91884
analogue image processing, Japanese achievements 77−50634
analogue processing systems, multichannel processing, spectral analyser, antenna system design appl. *(Spanish)* 80−95822
analogue-digital conversion, direct optical method, coherent or incoherent light 79−22908
analytic Fourier optics, information encoding by complex zeros 80−23628
annular aperture, arbitrary point spread functions 80−87325
annular coded-aperture images, decoding techniques 78−37818
antenna array, T-type correlation, optical image forming system 79−27180
aperture synthesis by object rotation in coherent imaging 80−69336
application examples 79−27183
applications and techniques, survey 79−59651
Arizona University optical signal processing activities 78−78946
aspectograms and composite holograms, Lippmann method anal. 77−10874
aspectrograms, produced with hexagonal lens raster, props. 78−46528
astigmatic coherent processor analysis 78−78927
astronomical active image restoration using flexible mirror telescope 77−45319
astronomical image coding in near IR, multiplex technique 77−53428
astronomical image restoration by regularisation method, appls. *(Italian)* 78−93124
astronomical images, coherent optical processing expts. *(Russian)* 80−12675
astronomical images, general anal. system 78−53834
astronomical images iterative reconstruction, non-negativity constraint 79−101081
astronomical negative information processing using thick-film holograms 79−48690
astronomical plates, meas. via automatic microdensitometer 79−80230
astronomical plates deconvolution by maximum entropy, appl. to M87 jet 80−62032
astronomical speckle imaging for diffr. limited image recovery 77−45318
astronomical speckle interferometry, image reconstruction by speckle masking 77−49308
astronomical speckle patterns, image retrieval 77−22100
astronomy, photon counting and analogue TV systems with digital real time image processing 78−96402
astronomy, thermal background subtraction in photodiode detectors 80−90342
atmospheric distorted wavefront compensation, optimal estimates 77−42487
atmospheric imaging, conference, Reston, Va., USA (Mar. 1976) 77−42484
atmospherically degraded image restoration using complex spectral ratios 79−29854
atmospherically degraded images, linear invariant restoration 77−42503
autocorrelation of objects by four and three-freq. interactions 77−75432
autocovariance functions and power spectra, statistical fluctuations anal. 78−63018
automated pattern recognition with hybrid optical/digital systems 78−63037
automatic microimage analyser, MORPHOQUANT 78−37053
automatic pattern processor for simple and complex interference patterns 80−13129
automatic target identification by hybrid pattern recognition 79−31829
autostereoscopic 3D image synthesis from binocular stereoscopic images 79−36842
band-limited function approx. realisation by low-pass filtering sequence of width-modulated pulses 80−95836
Bayesian deconvolution, appl. and algorithm implementation 78−70103
bilinearly distorted image linear restoration using Wiener filters 80−83557
binary discrete deflector with deflection angle degeneracy 79−55239
binary image correlator in absence of geometric distortion, statistical analysis 79−22907
biological shape pattern recognition, average similarities of Fourier spectra 80−104818
biological specimen pattern recognition, by real-time optical processor 78−40454
bipolar pointspread function synthesis by phase switching 77−38807
bipolar spatial filtering in incoherent optical systems, review of techniques 80−95821
bistable element array generation by liquid crystal light valve and optical feedback 80−48442
bistable optical device, transient response and applications 80−33214
bistable optical spatial device using direct optical feedback 79−18535
bistable TV-optical feedback system using optical flip-flops 80−53354
blind deconvolution, zero phase blurring function estimation 80−106482
blood cell smear pathology differentiation by optical transform method 78−69248
book, incoherent processing 78−42294
book, optics and information theory 78−5435
Bragg imaging in the reflection mode and designs for improved optics 80−17040
bubble chamber event recognition by optical correl. *(German)* 78−70704
C-CD transversal filter anal. in pattern recognition 78−71052
cancer prescreening, automated cell image analysing system *(German)* 79−83892

optical information processing continued
cell recognition and counting using adaptive coherent optical processor 78−77120
cervical cancer detection, comparison of coherent optical transform processing systems 78−48922
cervical smear screening with coherent optical processing 77−21653
charge-coupling photodetector for optical information processing 80−91753
chromosome metaphase spread, automatic finding, prep. and eval. of object spectra 80−98168
circularly symmetric positive filter function realisation by transparent rings 80−87343
clip-correlator, for fluorescence correlation experiments *(Russian)* 80−42270
coded and transmitted images, optimum restoration technique 77−58278
coded aperture imaging, analogical deconvolution appl. to nucl. medicine *(French)* 78−35943
coded aperture imaging, predicted performance of uniformly redundant arrays 79−18351
coded aperture imaging, review 80−101914
coded image obtained with nonredundant pinhole array, digital deconvolution 77−61919
coherence implications for laser appls. 77−75599
coherence properties modification of light beam, optical processing appls. 80−78769
coherent and incoherent optical spectrum analysis techniques in image evaluation 78−78928
coherent codes, iterative improvement algorithm 80−87330
coherent correlator operation in image segment identification, aerial photograph anal. 80−102654
coherent feedback, flexible filter operations 80−87337
coherent feedback systems using Fabry-Perot interferometer 77−71933
coherent image deblurring using computer generated holographic filters 77−14669
coherent information processing by a pair of lenses in spherical wave illumination 80−95816
coherent light source angular coordinates, meas. using received wave phase front 78−46526
coherent light valve optical processor for GHz bandwidth signals 78−78937
coherent light valve processor, two-dimens. optical modulator 80−102840
coherent optical A/D conversion using single halftone photograph 78−78919
coherent optical compensation of post-detection spatial distortion 79−98302
coherent optical computers, generalised linear processors 77−10859
coherent optical data processing fundamentals 78−78923
coherent optical feedback analogue computer for partial differential eqns. with inhomogeneous terms 79−76870
coherent optical feedback technique, multiplicative disturbance suppression 78−22094
coherent optical hybrid space- and time-integrating spectrum analysis 80−48177
coherent optical image amplification by injection locked dye amplifier 80−19041
coherent optical image processing, halftone screen techniques 77−75434
coherent optical implementation of generalized two-dimensional transforms 80−95835
coherent optical information processing systems, operations achievable 77−10861
coherent optical iterative extrapolation of 2-D band-limited signals 80−78780
coherent optical pattern recognition 79−64182
coherent optical power spectrum analysis for image evaluation, contrast effect 79−81367
coherent optical processing, basic principles 77−38820
coherent optical processing cervical cytological samples 78−36007
coherent optical processing equipment cervical cytological samples screening 78−36006
coherent optical processing for multisensor image processing 79−31830
coherent optical processing of biological cells, exam. of Fourier spectrum analyzer with optical transducer 78−36008
coherent optical processor for vehicle tracking and identification using laser diode light sources 80−37957
coherent optical signal processor for passive ambiguity function generation 79−72520
coherent processing system, modification to achieve some redundancy 80−106468
coherent space-variant processing, 2D, using temporal holography, theory 80−23624
coherent spatial frequency spectra of halftone images, information content of harmonics 78−50708
collimated laser beam propag. in turbulent atm., phase fluctuations spectrum 78−78914
colour coded equidensities production using nonlinear filtering 77−75426
colour edge detection, co-ords. selection 78−5432
colour encoded aperture masks used for incoherent filtering of images 79−41348
colour encoded image prod. by coherent-optical processor 77−88655
colour film archival storage, white light processing technique 80−99637
colour spatial filtering for image enhancement 80−87341
compensated imaging system photon-limited performance 77−88960
complex signal addition by matched spatial filtering 78−29905
complex surface shape inspection, coherent optical method evaluation 79−81578
complex-valued linear operations on complex valued data using incoherent light 78−5423
composite photographic-human visual system, spatial-freq. filtering effects in performance 78−4725
computation module, optical, for residue arithmetic 79−98296
computation using residue arithmetic 79−31808
computer constructed optical-rose diagrams 77−9505
computer generated holographic spatial filters for large objects 77−23753
computer holograms, space multiplexing 78−17874
computer-generated holograms, techniques and appls., book contrib. 79−76645
computerised scanning device, for 'Zenit' photogrammetric automaton *(Russian)* 78−21102
computerised tomography, analogue optical method of information processing *(French)* 80−94349
optical information processing continued
computers in optical systems conf. San Diego, CA, USA (Aug. 1978) 79−76356
computing, appls., review 77−10852
computing, conference, London (1978) 79−72511
conference, Bad Harzburg, Germany (June 1979) 80−51951
conference, Jerusalem, Israel (Aug. 1976) 78−33712
conference, San Diego, CA, USA (Aug 1976) 77−71932
confocal feedback system for partial differential eqn. analogue soln. 80−102630
constant variance enhancement, digital processing technique 77−61920
constrained least squares image restoration, improved computational scheme 78−82915
contactless thermal expansion meas. by double Michelson interferometer 80−73317
continuous tone picture reproduction, image quality and information capacity 79−59644
contrast improvement, noise-free, with LF polarising filter 77−75656
Controlled phase transparencies in coherent-optical systems performing Walsh and Hilbert transformations 78−50931
convolution of ps optical signals 80−58629
correlation, precision of detail recognition *(German)* 78−9340
correlation degradation sources 77−71924
correlation detection, optimization by prewhitening 80−95802
correlation filtering for increasing diffr. efficiency 80−96028
correlation function, real or complex, between two signals *(Spanish)* 79−76611
correlation reduction, spatial filtering and variation of resolution 80−102850
correlative data processing system using semiconductor injection laser 80−74307
correlator, estar base reconnaissance film, birefr. effects 77−74538
correlator, laser damage to photographic emulsions 79−27303
correlator, nonlinear t-E curve effects for matched spatial filter material 80−95812
correlator, spatially coherent white light 79−3642
correlator, using real time chromatic filtering and extended white light source *(French)* 79−3641
correlator, wavefront propagation error effects 79−50232
correlator length shortening using Fourier transform lens array 79−59646
correlator with shift invariant linear matched filter 80−37962
correlators, incoherent, analogue techniques 77−10863
correlators, real-time and memory devices using acousto-optic processing 78−46533
correlometer *(Russian)* 80−63935
covariance estimation, of stationary, ergodic processes, with non zero mean value *(French)* 79−80513
cross correlation by complex exponentiation of input data 77−71942
cross-correlation matrix processing 79−13910
cross-correlation of complex exponentiated input data 78−42290
cylindrical lens systems described by operator algebra 80−38086
cylindrical lenses, rotation of parallel fan of light, matrix representation 80−38089
cytofluorometer, imaging system for correlating fluoresc. cell meas. in flow 78−61240
cytological cell feature extraction using optical moments 80−98206
cytological preparation evaluation, optical preliminary data reduction *(German)* 79−5392
cytological preparation image processing, filter construction *(German)* 78−36026
cytological preparations, optical real-time filtering *(German)* 78−36025
data extraction and classification from film, conf., San Diego, USA (Aug. 1977) 78−63023
data extraction from film using optical and/or digital and/or electronic devices 78−63024
deblurring filter, space-bandwidth product 77−83959
deblurring of coherent optical image using digital computer 79−3646
decimal/residue/decimal optical converters 79−22905
decoders based on controlled transparencies *(Russian)* 80−28321
deconvolution by noncoherent system 77−58271
deconvolution techniques applied to astronomical images 80−46407
defocused grainy photographs, digital restoration by noise cheating and Fourier techniques 77−50626
defocused picture restoration, image scanning method 77−14667
deformable mirror adaptive optical system 77−46796
deformation invariant optical processors using co-ord. transforms. 77−79762
degraded picture restoration by scanning multiple-aperture *(Japanese)* 79−45908
density reconstruction using arbitrary ray-sampling schemes 78−80954
detector integration acouto-optic signal processing 79−72519
development trends *(Czech)* 80−14457
diatom recognition and counting, matched-filter and statistical method 80−101304
differential operation processor 77−52911
differential operator processor, filter fabrication feasibility studies 78−58925
differentiation by spatial filtering 78−1171
differentiation coherent spatial filtering, phase bias introduction 77−83821
diffraction correlators invariant to optical element shifts 80−106471
diffraction pattern sampling for optical power spectrum meas., error sources 78−63030
diffusing surface optical autocorrelation 80−99646
digital colour image processing within framework of human visual model 79−88077
digital correlator signal preprocessing 80−83556
digital fibre optical transmission timing recovery cct. 79−10397
digital image centring algorithm for astrometric positioning 78−69696
digital image coding techniques, performance analysis 77−58277
digital image processing, architectural breakthroughs 80−63939
digital image processing, book 79−910
digital image processing, conf., Bonas, France (June 1976) 78−58927
digital image processing, local filtering methods *(French)* 80−46406
digital image processing by smoothing spline functions 77−50628
digital image processing using parallel array processors 77−38816
digital image restoration 77−23628
digital processing aerial images, conf., Huntsville, Alabama, USA (May 1979) 80−48165
digital signal processing 78−33681

optical information processing continued
digital techniques for evaluation of optical fibres 79−94346
direct picture transmission in single optical fibre, restoration with holographic filters 79−89871
discrete binary representation, halftone dot profile and aliasing 78−9335
discrete image tone gradation scale transform. on grid coding basis 79−10266
discretisation using holographic filter, spectral analysis *(Russian)* 78−37809
dispersion correctors for compensated imaging, atm. dispersion minimisation 77−46695
display system using computer generated integral photograph 78−87021
distorted spectra, numerical image correction technique *(Russian)* 79−13921
distortion elimination by eigenfunction method 79−7087
dither signals for binary display of images, computer-aided design 79−94161
dynamic spatial filtration of coded optical image signals from noise 80−95826
edge coding and detection using directional masks 78−42289
edge detection filter, optimisation 77−27336
edge enhancement, real-time, using photorefr. effect 80−99642
edge enhancement of optical images, by Fourier transform optical system 78−33680
edge enhancement with incoherent optics, using pupil plane mask 77−71921
edge gradient preferential enhancement, median-window filter algorithm 77−50629
elastomer storage device evaluation for optical signal processing 80−48444
electro-optic crystal, holographically recorded data pages, digital processing 77−42511
electro-optic signal representation by implicit sampling 79−76620
electro-optical array processor for complex signals 78−94428
electro-optical focal planes, performance eval. for aerial reconnaissance 79−31833
electro-optical nonlinear Fabry-Perot resonator, for optical signal processing 78−42460
electro-optics/laser international conference, Brighton (1976) 77−38800
electron diffraction patterns, and optical transforms of atomic aggregates, symmetry aspects using computer simulation 79−7525
electron micrograph, optical vs. computerised 77−67541
electron micrograph optical and digital spatial freq. filtering 78−70231
electron micrograph optical and digital spatial freq. filtering, expt. results 78−82079
electron micrographs of layered silicates, optical filtering of faulted areas 80−84035
electron microscope patterns, phase retrieval, algorithm 77−18140
electron microscopy, optical Fourier transformation of two-dimens. image signals *(German)* 78−32932
electron microscopy, phase problems 78−70230
electron microscopy image restoration of weak phase objects 78−58098
electron microscopy of biomacromolecules, image analysis *(Czech)* 78−31983
electronic image data processing using incoherent light 80−78793
electronic speckle pattern interferometry, optimal signal processing 78−16837
electrooptical processor, iterative colour-multiplexed 80−23792
entropy expression for max. entropy image restoration 78−42283
equalizing and coherence measure correlators 79−13911
equidensitometry by coherent optical filtering 77−5936
experiment set for undergraduate students 78−28885
exponential transformation using film nonlinearity for optical homomorphic filtering 80−58467
extension to space-variant and nonlinear operations 78−78940
Fabry Perot resonator containing electrooptical element, light processing appls. 78−38001
Fabry-Perot spectrometer parameter evaluation, deconvolution methods 80−105705
Fabry-Perot-interferometer imaging system for thermospheric temp. and wind meas. 80−101441
feature enhancement using noncoherent optical processing 80−99651
feedback in incoherently illuminated systems 80−87336
feedback processing by TV-optical method 80−87335
feedback systems for analogue and digital optical image processing 80−102650
feedback techniques 79−55062
fibre and integrated optical devices 79−76887
fibre and integrated optical devices for signal processing 80−33233
fibre and integrated optics applications 77−27379
fibre laser plate for digital image processing, all-optical parallel logic operation 80−106463
fibre laser plate for optical parallel processing 79−76695
fibre optic rotation sensor, signal detection and processing, inertial reference device 79−54111
fibre optic signal processing devices 80−58768
fibre optics transmission characts. meas. by computerised signal processing system 79−76876
fibre transmission characteristic meas. by digital processing oscilloscope 79−12787
fibre-optic delay line signal processing devices 80−48443
film grain multiplicative noise anal. 78−58932
film-grain noise, low-contrast image detection 78−94370
film-grain noise degraded image estimation 78−54479
film-grain noise degraded images, nonlinear detection and estimation 77−50627
filter plane resolution requirements for coherent optical correlators 77−34828
filtering, background noise attenuation, spectrum anal., geological appl. *(French)* 78−9338
flexible band-pass filtering using coherent optical feedback 79−94166
fluorescence intensity correlation, photon counting using clip-correlator *(Russian)* 80−42271
focal plane design and optimal processing for scattered optical fields 78−78935
folded spectrum processor, signal demodulation and radar processing appls. 78−5429
four-component system design 78−42282
Fourier and Fresnel images, spatial freq. analysis *(German)* 77−79764
Fourier beam system, double, data recording and processing appl. *(Russian)* 80−28165
optical information processing continued
Fourier deconvolution of electronographic images 79−75112
Fourier processor phase accuracy, coherence effects 78−90377
Fourier spectroscopy and multichannel long integration time techniques 80−91751
Fourier transform imaging, systems theory appl. *(German)* 78−74851
Fourier transform of half-tone picture, spatial filtering using photographic replica 79−27184
Fourier transform program, two-dimensional *(Japanese)* 78−9330
Fourier transform signal processing in integrated optical format 78−50950
frequency variant optical signal analysis 77−19180
frequency variant optical signal processing 77−71934
frequency-variant signal waveform processing using 2-D optical processors 80−48178
Fresnel zone plate image optical decoding, for radioisotope imaging 77−86621
galaxy redshifts survey, data reduction techniques 80−22074
gas, Stark tunable, mirrorless optical bistability and optical limiting, obs. 80−38056
Gaussian field optical heterodyne detection, S/N ratio 79−13912
general multi-dimensional formulation of optical signal processing architectures 80−78789
generalised linear coherent optical processing system *(Chinese)* 79−89853
generalised matched filters for coherent optical pattern recognition 80−99654
generalised sampling theorem for Dirac Δ functions, appl. to computer-generated transparencies 78−42284
generalized sampling theorem with application to computer-generated transparencies 79−41343
geodesic lens design for integrated optics signal processing 80−33247
geomagnetic ground and airborne data, optical filtering 77−25797
geometrical distortion systems, bandlimiting considerations 77−71941
geophysical fields anal. in system with randomly misaligned parameters *(Russian)* 79−84524
geophysical image processing, apodisation for distortion reduction using optical filters *(Russian)* 77−9564
geophysical mapping and remote sensing by optical filtering 80−101458
geothermal research by IR scanning, image processing 77−64458
German standards on image assessment 78−58926
gratings optical imaging, embedded, for meas. by moire fringes *(German)* 80−23805
grey level on axis computer holograms for incoherent image processing 77−34848
grey-scale texture anal. and use of co-occurrence matrices 80−43276
guided wave acoustooptics, fundamental principles and wideband appls. 79−37038
guided wave opt. communication systems, appls. 79−36852
guided wave optics, appls. review 79−37054
guided-wave optical signal processing, diode laser sources and photodetectors 80−48465
guided-wave optical systems and devices, seminar, Washington, USA (April 1979) 80−31418
guided-wave signal transformers, synthesis 80−1358
Hadamard and M-sequence transforms are permutationally similar 80−32921
Hadamard techniques in optics and their relationship to other multiplexing schemes 79−80242
Hadamard transform image scanner, polarisation coding 77−14668
halftone image coding rel. to visual performance characteristics 77−58280
halftone images, histograms meas. 80−23631
halftone images, spatial resolution and tone reproduction 78−63016
halftone images produced by random quasiperiodic process 77−622
halftone images with edge enhancement and Moire suppression 77−623
halftone screen techniques for photographic film response shaping, medical X-ray image processing 79−83895
hazes, information provision on particle size distrib. of brightness and polarisation phase functions *(Russian)* 78−44998
height and flow velocity, optical pseudo-colour processing *(Japanese)* 80−9826
heterodyne array, joint signal probability distrib., clear air turbulent atm. 79−66804
heterodyne receiver array for light propag. through turbulent atm. 79−64183
heterodyne receiver arrays in turbulent atm., joint signal current probability distrib. 79−81368
heterodyne reception of information, on optical field distrib. 78−87024
heterodyne signal reception anal. *(Russian)* 78−46522
heterodyning, additive noise component reduction 79−50239
high energy physics, optical computing introduction 79−89581
high-speed image information preprocessor using channel plate image intensifier 80−78982
Hilbert transformation of phase object, optical simulation 78−1174
holocinematography, high speed, acousto-optic beam deflection for spatial freq. multiplexing 78−74860
hologram, 3-dimens., optical charact., acoustic field effects 77−10877
hologram filter for three dimens. object recognition *(French)* 79−18359
holograms, binary Fourier, wavefront coding by Lee method 77−75441
holograms, computer-generated, three-dimensional, image reconstruction using line printer 77−42506
holograms of acoustic field, moire processing 78−55539
holograms transmission over TV channel, image distortion anal. 77−54684
holographic applications 77−38837
holographic correlator, noise sources, accuracy improvement 77−23636
holographic correlators, expts. to improve accuracy 77−65583
holographic data storage and processing, photosensitive electro-optical materials *(French)* 77−31077
holographic Fourier transform lenses for matched-filter optical processor 79−45913
holographic image processing, resolution improvement and three-dimens. reconstruction 77−10862
holographic information, photoelec. recording, correl. methods 77−79784
holographic multiplexing by optical beam coding, applic. to interferometry *(French)* 77−159
holographic numerical optical processor configurations 80−48194
holographic optical sectioning for three-dimensional image information reduction 77−88679

optical information processing continued
holographic phase distributions, linear and nonlinear, determ. using electro-optical system 78−58954
holographic processing, space-frequency equivalence 79−76646
holographic recording, and reconstruction in spatially incoherent white light 78−78955
holographic reflective lenses for compact optical data processor 77−34829
holographic visualisation of information, theory 78−82930
holography, autocorrelation of diatoms as a function of depth of focus [holography in biology] 80−67324
holography and coherent optics, information theory, book 80−98764
holography with chromogen developed photography emulsions 78−55319
human visual system models for image enhancement and display design 77−58279
hybrid bistable optical devices, transient response 79−59803
hybrid field-effect liquid-crystal light valve, optical data processing performance 80−99860
hybrid image processing, potential of optical methods 79−27185
hybrid image processing 77−79767
hybrid image processing 78−25810
hybrid image processing based on coherent/incoherent lights 78−33689
hybrid image processing for feature extraction and constant variance enhancement 80−53224
hybrid image processing system, space and time picture oscillation, by active incoherent feedback 78−58924
hybrid image processing trends and prospects 80−32927
hybrid optical and electronic image processing 78−33690
hybrid optical and TV system with feedback 77−61922
hybrid optical corelator system for automated stereo compilation 78−63035
hybrid optical-digital image processing, appl. to handwriting and aerial photos 77−68178
hybrid optical-digital radiography system for lung disease detection 78−11753
hybrid optical/digital processing systems, assessment 77−10853
iconics and image processing 79−94173
iconics and its basic goals 78−46527
image analyser, semiautomatic, use in investigation of muscle biopsies 80−85466
image analyser and algorithm for pattern discrimination 79−18362
image analysis, structural methods, in diagnostic image systems 77−86564
image analysis system, math. morphology and algorithms 80−82799
image analysis via general theory of moments, Zernike polynomials 80−102629
image and signal processing, United States Air Force programmes 78−74854
image bandwidth compression, optical computing, analysis and simulation 78−94373
image charact. extraction methods 77−625
image coding with far-field holograms 78−90389
image correlation in white light by wavelength multiplexing 79−55072
image correlation with geometric distortion acquisition performance 78−71039
image correlation with geometric distortion effect on local accuracy 78−71040
image data processing system, Skylab X-ray solar obs. appl. 77−60619
image deblurring by convolution with impulse response operator 77−65580
image deblurring using diffraction gratings 80−43274
image deconvolution, complex spatial filters 77−10860
image degradation identification 78−58941
image detail enhancement system, for photographic recordings 78−58086
image detection in the presence of speckle 79−45909
image display, Fourier domain aliasing and quantization 79−81372
image emission GaAs platelet laser, for active coherent processing 77−58268
image encoding principle, optical spatial channel 77−71937
image enhancement and restoration concept 78−58931
image enhancement for objects embedded in scatt. media, mammary growth diagnosis appl. 78−40288
image enhancement with dynamic spatial filters 77−79769
image enlarging by composite holograms 77−10875
image intensifier tube for optical image processing 80−99825
image irradiance moments optical calc., wave optical accuracy limitations 80−74302
image matching using struct. information, edge vectôr correlation 78−63036
Image mensuration by maximum a posteriori probability estimation 78−63015
image parameter estimation potential accuracy anal. 77−88648
image plane correlator for ambiguity surface computation 79−76598
image processing applications at IBM Madrid Scientific Center 80−102657
image processing by spatial freq. spectrum phase modulation *(Korean)* 78−22090
image processing digital techniques 78−81555
image processing in incoherent light 80−87339
image reconstruction, from incomplete and noisy data 78−53837
image reconstruction, projection completion methods 78−42285
image reconstruction, projection completions methods, computational examples 78−46524
image reconstruction, turbulence degraded by spectral ratio meas. 78−9334
image reconstruction and partially coherent objects from mutual intensity samples 78−9333
image reconstruction by modified back projection methods, reconstruction error determ. 78−33682
image reconstruction from kinoforms and distorted holograms *(Russian)* 78−13664
image reconstruction from partial Fourier transform 78−33691
image reconstruction from projections, filtering 77−68176
image reconstruction performance of image-plane sharpness criteria 78−93123
image reconstruction problem ambiguity 79−98306
image reconstruction using polar sampling theorems 79−81366
image reconstruction using propag. law of mutual intensity 77−624
image registration limits, generalised model *(Russian)* 78−37811
image representation using genetic geometrical functions 80−5702

optical information processing continued
image resolution through atm. turbulence over ocean, optical transfer function 78−85695
image restoration, a posteriori method, OTF phase and magnitude estimation 79−72502
image restoration, algebraic methods comparison 78−58930
image restoration, following periodic nonsinusoidal vibr. degradation, filter function 78−1169
image restoration, pseudo-inverse, singular value matrix decomposition algorithm *(Russian)* 78−37810
image restoration, scanning multiple aperture coeffs. determ. 77−71930
image restoration, surface area or arc length constraints 77−38812
image restoration algorithm 77−14666
image restoration and synthesis, Japanese activities 77−58273
image restoration by far field correlation function meas. *(Russian)* 77−88652
image restoration by Gauss LU decomposition 79−76600
image restoration by Wiener filtering, signal dependent noise 77−88645
image restoration degraded by multiplicative noise, optimum spatial filter 77−10857
image restoration for invariant pointspread functions 80−69332
image restoration methods compared 79−13907
image restoration of space variant blurs by sectioned methods 78−66780
image restoration using volume diffraction gratings 78−94378
image restoration with signal-dependent noise, decomposed local algorithm 78−78951
image rotation and magnification, optical system 80−48376
image segmentation using prototype similarity 79−31832
image sensor, minicomputer controlled, fluctuating image time averaging and coherence function detect. 79−41341
image sharpening telescope, atm. distortion compensation 77−49294
image shifts, Adamar transform appl. *(Russian)* 80−1134
image spectrum in FTIROS, polarisation features 77−75439
image subtraction in real time, incoherent illumination 78−33677
image subtraction through speckle modulated by Young fringes 80−95813
image subtraction via processing simultaneously recorded holographic images 77−46700
image understanding systems, seminar, San Diego, CA, USA (Aug. 79) 80−94918
image-convertor camera, high-speed, computer treatment of images 78−42295
imagery, 2-D sampled, aliasing and blurring effects 80−99635
images degraded by spatially varying pointspread functions, 2D digital restoration 78−78920
imaging method for data processors, lens system design 77−27261
imaging of atoms, three dimensional molecular structure reconstruction, opto-digital computing 77−39510
imaging system fundamental limits and degrees of freedom 77−50630
imaging system using intensity triple correlator 78−74846
imaging through randomly fluctuating media, stellar speckle interferometry appl. 77−13248
implicit sampling for noncoherent optical data processing 80−99652
incoherent 78−46519
incoherent complex signal detection, spatial filtering technique 79−3639
incoherent complex spatial filtering 80−95834
incoherent diffraction correlator with a holographic filter 80−37955
incoherent extended source appl., Fourier holography in white light 80−37960
incoherent feedback optical system 78−66924
incoherent feedback using TV 80−87334
incoherent image optical matched filtering 80−14286
incoherent imagery system, introduction of partial coherence by holographic components 80−95853
incoherent images, technique for addition and subtraction 79−98293
incoherent method, fully parallel, high-speed, for performing discrete Fourier transforms 78−33684
incoherent optical correlation operations 80−99650
incoherent optical correlator using projected fringes patterns, for object shape and contour control 79−97357
incoherent optical discrete Fourier transform processing system 80−74303
incoherent optical processing via spatially offset pupil masks 78−82917
incoherent optical processor to make a 'spectrogram' of a 1-D function 80−87528
incoherent optical system, improving the accuracy of matrix calcs. 78−78924
incoherent processing of complex data, OTF synthesis 77−38806
incoherent processor for restoring images degraded by linear smear 78−78921
industrial X-ray film information processing methods *(German)* 78−15637
Infinite dimensional filtering problems in optical communication systems 78−66779
information retrieval in presence of speckle and quantum noise 79−76606
information storage, seminar, Washington, USA (Apr. 1979) 80−41942
integral equations soln. by optical spatial filtering 79−3643
integral photography, transform of 3-D image produced by lens raster 78−82921
integral sampling, deterministic and statistic methods of investig. 77−10856
integrated optic appls., future trends 79−37053
integrated optical circuit for Fourier transform 77−39111
integrated optical data processor, satellite data processing appls. 80−48458
integrated optical device for lightwave communications and data processing systems 79−37052
integrated optical devices and applications 79−14117
integrated optical multichannel data preprocessor, using holographic subtraction 79−3813
integrated optical prism-waveguide dual coupler theory and exptl. performance 80−33236
integrated optical RF spectrum analyzer, feasibility 78−5431
integrated optical signal processor, performance limits 79−36854
integrated optical spectrum analyzer dynamic range, waveguide scatt. effect 78−59163
integrated optical waveguide and CCD image array 77−34962
integrated optoelectronic Si devices, optical signal processing and communications, fibre-channel waveguide coupled 79−59847
integrated signal processor, using geodesic thin film lenses 78−42475

optical information processing continued
interactive image digital/optical processing system development problems 78−74855
interactive user-oriented digital image processing system 77−38813
interactive video image digitiser, appl. to interferogram anal. 78−58021
interferometer design, construction and interferogram processing, optical testing appl. 80−79020
interferomic wavelength meas. with post-detection signal processing 80−105699
International UV Explorer (IUE), image processing 79−80234
invariant processing using combined geometrical and optical transforms 77−71935
inverse problem uniqueness, scatt. object reconstruction, book contrib. 79−31824
inverse problems, source feature determination 80−14296
inverse radon transform, for image construction systems 78−42288
inverse radon transform by optical convolution 78−66777
inverse sampling spatial filtering for image multiplication 77−23627
inverse source problems in optics, book 79−31821
inverse source problems in optics, book contrib. 79−31822
IR heterodyne detect. of stars, atm. turbulence effects, corrections *(French)* 80−46409
IR phase conjugation adaptive array 77−46790
IR sensor noise reduction algorithms, Monte Carlo evaluation 80−95824
IR surveillance, continuous-time signal processors 80−78781
IR tracking receiver with holographic information processing 78−78970
joint Fourier transform processing with thermoplastic device 79−72512
joint measurements of angular coordinates and range on basis of phase front 78−78933
joint transform correlator performance rel. to wavefront modulator characteristics 80−102651
Kaiser filters, window function, equivalent pass band, incoherent optical transfer function 80−1323
kinoform method, for filtering and image synthesis 77−58295
Laboratoire d'Optique de Besancon, recent work 77−68177
Landsat imagery, planimetric restitution using Zeiss Stereotop 80−56648
Laplacian formation by holographic zone plate moire patterns 79−13917
laser and electro-optical systems, conf., San Diego, CA, USA (Feb. 1980) 80−62392
laser application 77−88832
laser applications to data handling and recording 77−38817
laser beam application *(Japanese)* 78−1170
laser digital communication system, 100 Mb/s, optical receiver and pulse generator *(Russian)* 79−94170
laser diode lensless MSF holographic optical element correlator, optical pattern recognition 80−102663
laser Doppler velocimeter signal analysis for pulsatile arterial flow meas. *(Japanese)* 79−2156
laser engineering and appls., conf., Washington, USA (May-June 1979) 80−1216
laser heterodyne signals from moving object, bandpass filtering by finite apertures 78−55306
laser line art optical processor, optimal enhancement filter 79−59648
laser line scanning sensor, spatial filtering design considerations 78−85752
laser pulse autocorrelation by optical processing of Fabry-Perot spectrograms 80−58465
laser self-focusing suppression through low-pass spatial filtering and relay imaging 78−74938
laser speckle reduction by US modulation 79−3638
lasers and applications, conference Erice, Italy (May-Jun. 1970) 77−38906
least squares image restoration 80−37961
least-mean-square spatial filter for IR sensors 80−38092
lens optimisation using Walsh functions, FEE-based criterion 78−79097
lenses, simple, as Fourier transform elements, performance meas. techniques 78−94374
lensless matched filter, operating principle, third order holographic aberration 77−7013
LF signal optical processing procedure 78−9343
lidar return signal geometrical compression, atm. remote sensing appl. 78−57329
light coherence reduction by amplitude-modulated US wave 79−3624
line image transmission through single fibre using spectral instrums. 80−102820
linear coherent processing by input scanning technique 79−76622
linear coherent systems, general theory, operational notation 77−38810
linear line screen for image reproduction, analysis 80−32925
linear motion blurred picture, motion estimate, spectrum anal. 77−3547
linear multiplane coherent optical processors, iterative Fourier transform description 79−94164
linear restoration of partially coherent images, minimum mean square error 79−3637
linear system characterization through response cataloging 79−50229
linear systems, Fourier transforms and optics, book 79−41350
linearly degraded images, iterative image restoration 80−95807
linearly degraded images, iterative restoration, reblurring procedure 80−99640
liquid crystal electro-optical modulators for two-dimensional data processing 78−79141
liquid crystal image transducer, input device for coherent optical processor, phase response 79−23051
liquid crystal image transducer, real-time, response time 78−74845
liquid crystal image transducer, spatial frequency spectrum temporal meas. 79−76810
liquid crystal light valve, appl. to real-time optical data processing 78−83102
liquid crystal light valve for coherent optical data processing 78−38041
liquid crystal light valve operation and appls. 78−46826
liquid crystal light valve-image tube hybrid device for data processing 77−72083
liquid crystals, as tunable spatial filters in optical signal convertors 78−50930
liquid-crystal devices, variable-grating-mode, optical logic operations on binary images 80−106613
liquid-crystal image transducer, normal incidence, on-state optical performance 80−99852
LMFBR fuel pins, reactor illuminated, coded aperture imaging 79−30989
local image restoration by a least-squares method 80−14289
logarithmic filtering using inherent film nonlinearity 77−88646

optical information processing continued
losslessness of optical systems in a vectorial treatment 80−83558
low-contrast optoelectronic primary information processing system, energy efficiency 79−76617
low-level imaging, optical signal detection and meas. 79−94350
Mach-Zehnder interferometric switch for integrated optical multivibrators 80−53479
magnetic diffraction gratings with alterable magnetic domains for optoelectronics 78−63197
magneto-optic bubble spatial light modulators, appl. in optical processing systems 78−79139
Mariner 10 images of Venus and Mercury, digital processing 77−78647
Mars, Viking orbiter images IPL processing 78−20679
matched filter, multicapacity, for correlator appl., using birefr. object film 80−74478
matched filter image correlator, for aerial reconnaissance film screening 78−94371
matched filter visibility effects on the correlation function 80−96031
matched filtering improvements for coherent optical pattern recognition 80−78786
matched filtering using binary digital hologram, Fourier domain quantization 77−3544
matched spatial filter synthesis, parameter optimisation 77−71925
materials for optical storage and reproduction 80−33109
matrix multiplication, two-dimens., using coherent optical astigmatic systems 79−59647
matrix multiplication using coherent astigmatic systems 77−71936
matrix transforming incoherent optical system, using extended lens-array 79−7086
maximum entropy image restoration method, deterministic anal. 78−9336
mechanical impulse testing techniques, computer evaluation, high-speed film recording 78−44343
medical, flashing tomosynthesis: three-dimensional X-ray imaging 80−26325
medical image processing, subjects and objectives 77−52898
Mellin transform, freq. plane and joint transform correlators 77−10849
Mellin transform using computer generated hologram 77−10850
Mellin transformation, one dimensional, performed by single element coherent optical processor 79−50231
Mellin transforms, 1-D, coherent optical technique 78−5422
membrane mirror performance as adaptive optical element 77−46782
membrane mirrors for image compensation system, performance and manufacture 77−42587
meteoradiolocator echo signals, optical spectral processing *(Russian)* 79−100968
micro-optoelectronic parallel processors *(Russian)* 78−46517
microchannel spatial light modulator, for real-time optical data processing 79−18534
microchannel spatial light modulator 80−91913
microchannel spatial light modulator as storage medium 80−43479
microchannel spatial light modulator development, for real-time optical data processing 79−72714
microdensitometer with minicomputer connecting facilities 78−21198
microobjects dimensions determining adaptive tracking algorithm appl. *(Russian)* 78−21094
micropattern array multiplication by sampling spatial filtering 77−65581
microprocessor-based interferometric data reduction system versatility 80−73439
microprocessor-based optical/digital processor 78−63027
microscope, focusing technique for digital image anal. system 80−68250
microscope photometer/semiautomatic image anal. instrument system for morphometric and photometric value meas. 80−82815
microscopical image analysis, problems and approaches 79−80725
mirror segment, parabolic, general Fourier transforming configuration 77−46687
mirrorless electrooptic device with feedback, optical multistable operations 79−32051
mixed integrator processors, comparison of continuous and discrete types 77−19190
modular arithmetic inner product processor optical implementation 80−48170
moire fringe electronic processing, comparison of moire topography and photogrammetry 79−40601
Moire photography, appls. of slotted apertures 77−65053
monochrome picture signal, digitally coded, level reassignment technique 78−55307
moonlit object real-time optical matched filtering 77−19192
motion paths display, speckle photography, holographic reconstruction 77−18084
multi-aperture system imaging props. 80−87332
multi-image regeneration by white light processing 80−95814
multichannel acoustooptic modulator for real-time recording and optical processing 79−10399
multichannel data processor using holography and integrated optics 79−36853
multichannel IR receiver performance 79−76596
multichannel signal processing using acoustooptic techniques 80−19160
multidither adaptive optical systems with zonal control of deformable mirrors 77−46795
multidither adaptive optics, estimation and control 77−50757
multidither adaptive optics system, speckle interactive effects 77−46797
multidither coherent optical adaptive techniques 77−46793
multiplane γ source image reconstruction using Fresnel zone plate aperture 77−52874
multiple imaging with thin phase filters, signal processing approach 78−66772
multiplex holographic representations of space-variant optical processors 80−48192
multiplexing, using phase modulation 80−95830
multisensor image pattern recognition, statistical and deterministic aspects 80−99647
N-loop ensemble reference phase control system, stability 77−46794
narrowband optical signal, spectral width estimation 80−102627
nematic liquid crystal elec. controlled transparency, optical data processing element 79−32074
NGC 5128 (Centaurus A) optical struct., picture processing anal. 79−53907
night vision system testing image scanner 77−39102
noise fluctuations and coherence 78−66771
noise problems in image processing by spatial filtering 78−37817

optical information processing continued
noise stability of receiver for pulsed signals with optimal filtering 77−31072
noisy blurred image restoration by smoothing spline filter 78−33679
noisy image restoration, eigenfunction expansion technique 78−63020
noisy images, a priori information, degrees of freedom 77−38811
noncoherent optical convolvers and correlators, generalised model 78−55303
noncoherent optical processing, temporal frequency carrier methods 79−76623
noncoherent optical processing, two-pupil hybrid systems 78−74858
nonlinear, input medium and precompensation effects 77−79761
nonlinear coded waveforms 79−72517
nonlinear coherent processing, synthesis algorithms, real time systems 77−71940
nonlinear halftone screen preprocessing, analysis and synthesis 77−58267
nonlinear image processing, binary pulse position encoding 78−29906
nonlinear image processing with optical feedback *(Russian)* 77−58258
nonlinear nonmonotonic function synthesis 77−50633
nonlinear optical processing, half-tone screen design methods 79−98294
nonlinear optical processing in real time 80−87338
nonlinear optical processing with Fabry-Perot interferometers containing phase recording media 80−48158
nonlinear optics methods in spatially modulated signal conversion, parametric image convertor 79−7179
nonlinear processing with halftones, techniques and appls. 77−71938
nonlinear systems, nonmonotonic halftone cells, phase halftones 77−75425
nonlinearity recorded matched filter, false alarm rate reduction 77−62037
nonstationary pattern reconstitution from 2-photon correls. and stellar interferometer *(Russian)* 77−82125
nonwhite noise, S/N ratio and detail detection 80−102648
numerical calculation using optics 80−95832
numerical holography application 78−33692
numerical image manipulation and display, Skylab EUV solar obs. appl. 77−60618
numerical optical data processor, representation and implementation 78−78947
numerical optical processor combining prime residue arithmetic representation and spatial light modulator 79−76871
object reconstruction from Fourier transform modulus 78−74852
object restoration beyond Rayleigh limit in presence of noise 80−102661
ocean surface wave imaging, synthetic aperture radar mechanism 79−5651
on-axis coherent optical feedback system 77−50631
one- to two-dimensional (and vice versa) mappings 78−78948
one-dimensional linear coherent processing by single optical element 79−94165
one-dimensional signal bilinear transformation by 2-D coherent optical processors 79−13909
online digital image restoration and manipulation using minicomputer 77−34831
operations achievable, real-time devices, systems and applications 80−9816
optical data processing, appls., book 78−90388
optical instruments, image evaluation using target detection 79−94378
optical multiple-invariant space-variant processors 78−42279
optical preprocessor, use in Earth-resources satellites 80−67430
optical reconstructions from projections via deconvolution 80−63962
optical spark chamber data automatic digitisation using CCD 79−89517
optical/digital pattern recognition automated system 80−48175
optics utilisation in radar systems, conference, Huntsville (1977) 78−78939
optimal estimation in signal-dependent noise 79−41344
optimisation of inversion of convolution products 79−76601
optimum filter for image restoration *(Ukrainian)* 78−55308
optimum processing of light fields, synthesis of algorithms for turbulent atmospheres 78−71047
optoacoustic effect imaging 80−106473
optoelectronic devices, digital data processing, review 80−19106
optoelectronic Si devices for optical signal processing and communications 79−37056
optoelectronic system, symmetrical input, direction-finding sensitivity control 79−50401
orthogonalization, Bernstein polynomials, and image restoration 79−36841
OTF, two pupil synthesis, incoherent spatial filtering 78−58919
OTF offset section utilisation for noncoherent processing 79−76625
OTF synthesis, pupil function replication 79−27182
parallel matched filtering, vol. effect minimisation 77−7012
partial spatial coherence blur correction by postdetection image processing 80−78792
particle population statistical inference from scattered light 80−37950
passive components for integrated-optics signal processing 80−48466
pattern processing and texture analysis by coherent optical computer 77−10855
pattern recognition, bipolar incoherent, by carrier encoding 79−50230
pattern recognition, deformation invariant, space variant, book contrib. 79−76619
pattern recognition, discriminant hypersurface prod. by average filters 80−99649
pattern recognition, hybrid method, suboptimal statistical transform *(French)* 77−46703
pattern recognition, hybrid optical-digital processor for invariant moment computation 80−102646
pattern recognition, hybrid parallel optical and serial digital processing systems 80−99657
pattern recognition, Mellin transform method 78−63021
pattern recognition, seminar, San Diego, CA, USA (Aug. 1979) 80−98759
pattern recognition by coordinate transform. in correlation 77−61921
pattern recognition by diffraction pattern sampling 80−99643
pattern recognition by thermoplastic complex filter 80−99656
pattern recognition using Mellin transform for nonvertical imagery 77−75427
perfect image correction by unsharp masking 78−33693
periodic structure defect detect. using optical processing 80−95829
petrographic characterization of coal using automatic image analysis 80−18002
phase coding with high quality computer holograms 77−628
optical information processing continued
phase compensation for multiple pulse thermal blooming 77−50732
phase computation from intensity meas. 78−66768
phase conjugate adaptive optical systems, convergence 77−46688
phase conjugate adaptive optics using perimeter phase meas. 77−46791
phase determination of amplitude modulated complex wavefront 78−55305
phase distributions in images and Fraunhofer diffr. patterns prod. by non-aberrant lens 78−1172
phase estimates from slope-type wave-front sensors 78−66770
phase mask fabrication and testing 79−27195
phase object differentiation by spatial filtering 77−65579
phase problems, image recovery from Fourier transform modulus 78−82918
phase profiles generation, recent advances, book contrib. 79−76644
phase reconstruction problem for wave amplitudes and coherence functions, book contrib. 79−31823
phase reconstruction problem in light and electron microscopy 78−25811
phase recovery from single intensity distrib., using spatial filter 77−83825
phase retrieval and polarisation identity 78−71042
phase retrieval from modulus data 77−3540
phase screen statistical features from scatt. data, book contrib. 79−36851
phase shift plate analysis and design *(Russian)* 80−5696
phase tracking, Fourier series and estimation appl. 78−25812
phase values reconstruction from phase differences, matrix formulation 79−59642
phase-conjugate backscatt., large-signal theory 79−86211
phase-inverting grating construction, use in deblurring filters 80−48398
phase-sensitive detection, representation of observable signals in Chebyshev polynomials 79−89857
phosphenes in the light of biohologhraphic models 79−74632
photochromic film, for real-time coherent optical processing 78−50876
photochromic tracer film, measurements using POLLY, film reading computer system 78−42696
photodetector matrices and scanistors for hologram information processing, switching transients 78−45703
photodichroic materials as coherent optical computing elements 77−71962
photodichroic spatial light modulator for joint Fourier transform correlation 80−106617
photodiode array integration with optical power spectral analysis 80−99645
photodiode sensor arrays, circuits and performance 77−39077
photoelectric convertors, one-coordinate, signal processing algorithm 80−33199
Photoelectric recording of optical fields by correlation processing 78−71048
photoelectric registration of Fourier transform of optical field distrib. 78−82925
photogrammetric automation 'Zenit' automatic processing of line images *(Russian)* 78−21106
photogrammetric automaton 'Zenit', program-control module for interference coordinate measuring system *(Russian)* 78−21103
photogrammetric automaton 'Zenit' positioning, electromechanical system *(Russian)* 78−21101
photogrammetric system 'Zenit', read-out procedures design, for images with convex boundaries *(Russian)* 78−21105
photogrammetric system 'Zenit', scanning spot intensity distribution *(Russian)* 78−21104
photogrammetry, automatic reseau meas. with simple optical correlator 78−69496
photograph, pseudo-colour encoding using halftone screens and coherent filtering 77−71939
photographic emulsion, Callier effect, influence on image contrast 78−63017
photographic grain in coherent optical system, signal dependence 79−30598
photographic image optical power spectra anal., S/N concepts 78−63028
photographic noise in holographh appls. *(Italian)* 78−22088
photometric signal processing unit based on hybrid fast instrumentation amplifier 78−41342
photon flare centre determ., online optoelectronic convertor *(Russian)* 79−75111
photostimulated processes in inorganic materials and optical information storage, review 78−82926
pick-up tube aperture distortion correction, optical method 80−95827
picosecond signal processing with nonlinear integrated optics 80−99882
pictorial image transmission by single optical fibre by 1-D scanning 79−7229
picture coding without point by point sampling 78−33678
picture processing, appl. to medical X-ray diagnostics 77−38814
picture scrambling holographically for confidential picture taking technology 77−19208
picture segmentation by preprocessing and averaging 77−58272
plasma, Thomson scatt. diagnostics using optical multichannel analyser 78−67432
Pockels effect relay applications 79−72513
Pockels readout optical modulator, current status and appls. 77−72085
pockels readout optical modulator, for optical/digital processing systems 78−79125
Pockels readout optical modulator, image and signal processing appls. 78−79123
Pockels readout optical modulator, optical processing appls. 78−83100
point images resolution, decision theory 79−81375
point spread function synthesis, geometrical optics approach, transaxial tomograph processing 79−94163
polarised light in holography and optical information processing 77−46708
positional coding optical correlator, tabular coordinate search method *(Russian)* 79−98292
post-detection compensation for atm. distortion of faint scene images 77−45322
post-detection digital image processing of noise degraded lunar images 77−45321
power spectrum analysis, moment as image quality merit factor 77−7019
power spectrum sampling and nonparametric pattern recognition algorithms 78−63032
precision optical evaluation by phase meas. interferometry 80−74533

optical information processing continued
principles and applications 79−81382
prism correlator, appl. to stereo photogrammetry 78−86368
profile digitised diffractographic data processing 77−58276
pseudo real-time coded aperture imaging system with intensified vidicon cameras 77−31133
pseudo-colouring with coherent optical encoder 77−7020
pseudocolour density encoding, white-light, using contrast reversal 80−83560
pseudocolour density encoding of photographic materials, white light processing system 79−18360
pseudocolour encoding, of holographic imaging, new technique 78−78963
pseudocolour encoding of holographic images using single wavelength 78−87025
pseudocolour encoding of spatial frequency information 78−87018
pseudocolouring through contrast reversal filtering 79−81378
pulse interval modulation for optical fibre communication system 78−50917
pulsed light source with thin-film modulator, fabrication and characts. 80−43467
pulsed optical radar system using photodetector with lag, characts. 79−13918
pulsed signals of variable length detection in correlated interference, S/N ratio 78−37816
quality enhancement, adaptive methods *(Russian)* 80−28163
quantitative image analysis, applic. to mineralogy *(French)* 79−5631
quantitative image analysis, appls. using sequential transforms. 80−23627
quantitative image analysis, theory and instrumentation 80−23626
quantum communication channels, statistical model, asymptotic relations 78−33687
quasi-staring IR sensor clutter rejection processor design 80−86417
quasicoherent light source image synthesis by phase measurable interferometry 77−58284
radar, synthetic aperture system, coherent optical simulation 77−27260
radar ambiguity function, optical processing techniques 78−78938
radar ambiguity function display and one-dimensional correlation/convolution by coherent optical processors 78−78950
radar and optical imaging, three-dimensional density function reconstruction, inverse problem 79−27197
radar and sonar coherent optical processing techniques 78−75018
radar signal processing, multichannel optical correlator 78−74847
radiation detectors, sensitivity, informational threshold, rel. to human vision 77−87838
radioastronomical aperture synthesis imagery data optical reconstruction 78−69702
radiographic image anal., computer aided, patient diagnosis appl. 78−61256
radiographic pictures, digital encoding, redundancy reduction 77−40850
radiography, flashing tomosynthesis 80−67243
radiography, holographic 3-D synthesis of X-ray pictures 80−67245
radiography, holographic methods of 3-D representation from no. of plane images 80−67244
radioisotope zone plate coded aperture imaging 77−40762
radiology and nuclear medicine image processing and synthesis *(German)* 78−40325
radionuclide tomographic image reconstruction, optical processing 77−73572
radiotelescope data, digital hologram reconstruction 77−64653
random checkerboard process, two-dimens., generalisation 79−81374
random digital scene generation with specified statistics 80−99666
random halftone contact screens, transmittance control of tone reproduction 78−66775
random pulse train processing by linear filter *(Russian)* 78−46518
random spatial phase modulation for speckle elimination 78−58920
raster scanned images, matched filter processing 77−7018
real 1D signal convolution and correlation by freq. plane filtering 80−32919
real time atmospheric compensation, active optical imaging 77−49307
real time grid coding and interlacing, for image subtraction 78−33694
real time image restoration through Walsh filtering 77−27264
real time light modulators for incoherent to coherent image conversion 77−72082
real time optical correlation of 3-D scenes 77−27262
real time optical signal processors with feedback control 77−23620
real-time coherent object edge reconstruction with $Bi_{12}SiO_{20}$ crystals 78−90372
real-time Fourier spectrum analysis, using acousto-optic devices 77−58285
real-time image contrast enhancement, local area histogram equalisation and gain control 77−50636
real-time image optical subtraction scheme 78−74856
real-time incoherent subtraction of irradiance 80−74301
real-time moving object tracking by optical correlation, using liq. cryst. image transducer 79−32035
real-time multichannel optical spectral analysis, by liq. cryst. display 78−38042
real-time nonlinear optical signal processing with liquid crystal light valves 79−76868
real-time one-step in incoherent level slicing of optical images 78−82919
real-time optical Fourier spectrum analysis using acousto-optic diffr. 78−5430
real-time optical image addition and subtraction using double-grating shearing interferometer 79−55069
real-time optical processing using the liquid crystal light valve 80−63936
real-time spatial modulators for optical/digital processing systems 78−63025
recent trends 78−33713
reciprocity relation derived from Helmholtz eqn. 78−1167
reconstruction, three-dimensional, from planar projections 80−99639
reconstruction from projections via circular harmonic expansion 78−42286
reconstruction from projections via deconvolution 79−55070
reconstruction of images distorted by smearing 79−76614
reconstruction spots for digital sampled images 78−63034
redundancy and parallel processing 80−95831
regularized object restoration, resolution beyond the diffr. limit 80−87324
remote sensing, image processing and information extraction 77−64438
remote sensing, thermal IR data conversion to equivalent blackbody temps. 77−56750
optical information processing continued
remote sensing imagery, optical and electronic enhancement 77−53253
remote sensing imagery, spatial filtering 78−90385
remote sensing multichannel data sets, integrated optical comparator 80−64213
residue arithmetic, correlation approach 79−31809
residue arithmetic computation, integrated-optical methods 79−76886
residue number optical processor design concepts 80−48168
residue-based optical processor 80−48169
restoration, of optical objects using regularisation 78−78929
restoring images with shift-varying degradations 77−58274
restoring with maximum entropy, Poisson sources and backgrounds 78−66769
retinal information processing, computer model 77−66814
Ruticon, image storage and optical processing appls. 77−72086
Ruticon optical processing capabilities 78−79140
sampled Fourier transform hologram, interpretation, simplification techniques 78−1181
sampled/raster displays, assessment of information visibility using signal detection model 80−19002
sampling imaging systems, linear gradient model for suppression of aliasing 78−33686
sampling theorem for space-variant systems 77−609
sampling theorems in polar coordinates 80−28169
satellite derived cloud imagery, optical Fourier transform anal. 78−85749
satellite image sensing and multiplexing system tradeoffs 77−60498
satellite IR pictures, automatic digital techniques for oceanic features enhancement and extraction 79−5682
SAW and optical signal processing techniques compared 80−48173
SAW delay line acousto-optic signal processing devices 79−94328
SAW device for optical image processing 78−71051
SAW oppositely propagating in optical waveguide, light diffr., signal processing appl. 79−41453
SAW spectrum analyser in photon-counting mode, statistical props. 80−105712
scale and rotation invariant optical pattern recognition and classification 80−99655
scanning image digitizer, playback corrections 77−83816
scanning optical sensor signal peak extraction and multiframe correlation methods 79−81380
scattered light spectroscopy, signal processing by add-subtract digital correlator 77−61053
scene content measurement from aerial images, appl. to building complex scene 80−78788
scene matching methods 80−48167
scene matching with feature detection 80−48166
segmentation method of detecting cellular images using colour information *(Japanese)* 78−11783
self-image techniques, optical computing 80−18998
SEM image enhancement and digital reproduction 77−38060
SEM image processing systems, summary of useful techniques and anal. 79−12901
sequential coherent optical reconstruction from projections using a ROACH filter 80−63961
side-entry surface acousto-optic interaction signal processor 80−48174
signal and image processing, conference, San Diego (1977) 78−74853
signal and image processing, US Air Force research programme 80−78791
signal detection methods, optical/digital components evaluation in hybrid processor 78−63026
signal processing activities of United States Army 80−48172
signal processing research programme of United States Air Force 80−48171
signal processor, using optical probing of SAW 77−59198
signal recording/processing, diffraction in anisotropic medium, anal. 78−90364
signal waveform optimisation 79−76618
single-threshold detection of random signal in noise, appl. to optical communications 79−18353
smeared photographic image restoration by white light processing 79−18352
software survey for digital image processing 77−75431
solar spectra, line profiles, rough reconstruction from series of narrow-band filtergrams *(Italian)* 80−98564
sonar Doppler phased array coherent imaging and processing by metaxial optics 79−72521
sound pattern recognition in foreign languages 77−68337
space and time variables in optics and holography, expt. aspects 77−34830
space filtering algorithm, influence on signal of optical system misalignment *(Russian)* 78−37815
space variant optical correlators, accuracy and space bandwidth 78−17864
space variant processors using coordinate transforms 77−88649
space-bandwidth product and accuracy of optical Mellin transform 77−71922
space-blur bandwidth product in correlator performance evaluation 80−43270
space-frequency conversions for image transmission and processing 78−71046
space-time optics, speckle phenomena and white light correlations 80−106460
space-time random speckle pattern optical analysis 80−102682
space-to-temporal freq. conversion for image processing 80−87340
space-variant coherent optical processing 80−102638
space-variant linear processing of 1D signals 77−42490
space-variant optical pattern recognition by coordinate transformations 78−78945
space-variant optical processors, use of coded waveforms 79−27191
space-variant processing of 1D signals, direct output and output spectrum displays 77−42491
space-variant processing of nonlinear coded waveforms, ambiguity function 79−76602
space-variant processing with polychromatic light 80−87342
spatial convolution and correlation of optical fields via degenerate four-wave mixing 78−71044
spatial filtering, detection of binary images buried in speckle 79−36849
spatial filtering for obtaining first and second order derivatives 77−27259
spatial filtering of 2-D periodic structures, inspection 77−38819

optical information processing continued
spatial filters, rotating circular involute reticle used in optical searching systems 79−98505
spatial filtration in coherent optics system, amplitude and phase spectra analysis *(Russian)* 80−28164
spatial frequency analysis with incoherent optical approach, using LED light panel 80−78779
spatial frequency determination, selected interference schemes 80−48146
spatial frequency filtering, appl. to microscopy 77−79760
spatial frequency plane filtering by dynamic coherent illumination 80−95825
spatial frequency sampling by phase modulation, multiple image generation 77−79759
spatial frequency spectrum in coherent optical processor, input object vibr. effects 77−46686
spatial high pass filtering using photochem. adjacency effect 77−71929
spatial light modulator, 1978 state of art and development trends 79−7201
spatial light modulator, using KD_2PO_4 and Se photoconductor, optical processing appl. 80−9988
spatial light modulator, using oil film deform. by surface tension var. 80−5831
spatial light modulators, input information approximation 77−83823
spatial light modulators, near real-time reusable for coherent optical processors 77−11035
spatial light modulators for coherent optical computing, performance evaluation 79−89989
spatial light modulators for optical data processing 78−78941
spatial multiplex tomography, coherent optical analysis 77−86684
spatial pattern recognition by spectral feature classification and coherent optical correlation 80−99644
spatial resolution of subwavelength sources from optical far-zone data, book contrib. 79−31825
spatially orthogonal optical information transfer system, design and anal. *(Chinese)* 80−43275
spatially-varying image degradation compensation 77−58275
speckle applications, review 77−83820
speckle applications 77−19189
speckle coded image subtraction configs., optimal distrib. of exposures 79−55071
speckle images quantised to two levels, recovery of fringe visibility 78−12104
speckle imaging, photon by photon, diffr. limited performance for large telescopes 79−53729
speckle interferometry, decorrel. effects, contouring and surface roughness meas. 77−45886
speckle interferometry, decorrel. effects, machine induced strain obs. 77−45887
speckle interferometry, image restoration by least squares method 79−25514
speckle interferometry, wideband, true imaging of astronomical objects 80−53226
speckle noise, integration with finite aperture, logarithmic transform 77−19188
speckle noise and object contrast, detection thresholds eval. technique 78−5434
speckle pattern interferometry, electronic, using digital image processing techniques 80−87322
speckle phenomenon fundamentals *(Czech)* 78−29147
speckle photography, flow velocity distrib. meas. 78−67288
speckle reduction, moving aperture method and incoherent spatial filtering 77−42489
speckled image subtraction setup, optimal distrib. of multiple exposures 77−34834
spectra, direct optical encoding using computer interfaced vidicon TV camera 77−10114
spectral analysis, log-freq. variable resolution system using holographic mapping 77−638
spectrogram, elimination of bright continuous spectral background *(Chinese)* 80−106464
spectrogram imaging device, anamorphoses in spatio-temporal optics *(French)* 77−68179
spectrum analyser, synchronous dual-channel processing 79−72499
spectrum analyser for radar signal processing 78−78942
spectrum analysis techniques, coherent and incoherent, in image evaluation 78−63031
spherically symmetric object reconstruct. from slit-imaged emission 80−23634
spherically symmetric objects, reconstruction from slit-imaged emission, appl. to spatially resolved spectroscopy 78−78930
spheroidal geodesic lenses for integrated optical processing, design 77−27385
spline functions for image restoration 78−42280
spread spectrum time- and space-integrating optical processor 80−78777
spread-spectrum signal optical processing 79−72518
statistical filter for image feature extraction 80−99636
statistical image anal., 3 parameter probability distrib. density function 80−43266
statistical reversal methods of linear transforms. *(Russian)* 78−1179
statistical thermogram classifiers using coherent and incoherent light 79−96644
stellar speckle interferometry data processing method 80−17498
stellar spectroscopy, appl. of linear filtering theory to line profiles *(Italian)* 80−90340
stereo electron micrographs restitution, approximate soln. 79−26189
stereology conference, Salzburg, Austria (Sep. 1979) 80−22134
stimulated Raman scattering, reconstruction of wavefront and real volume image 78−30018
stochastic image restoration procedure 77−10858
strain evaluation by specimen-grating photograph electro-optical processing 77−39266
strain meas. speckle photography with hybrid optical/electronic image processing 80−106768
strain measurement by speckle photography, hybrid optical and electronic image processing 80−99976
strip telescope, image synthesis, computer simulation 77−29660
Sun glitter on sea, correl. function appl. to sea surface slope distrib. function determ. *(Russian)* 80−94611
surface acousto-optic lens, Fourier and Mellin transform props. 78−78926
surface acoustooptic interaction for information processing 78−42461
surface displacement meas., coherent optical correlation technique 79−75499
surface modal deformation sensor for heterodyne interferometry 80−31859
surface orientation determ. from multiple images, photometric method 80−52163
surface-wave acousto-optic signal processors 80−102640
synthetic aperture radar, satellite-borne, optical decoding 78−90384
synthetic aperture radars, speckle reduction 77−19191
system design considerations in optical power spectrum analysis 78−63029
system parameters rel. to optical element characteristics 79−72510
system test interference pattern analysis program and error elimination method 79−76894
systems, seminar, Huntsville, USA (May 1979) 80−46732
T-E curve classification, appl. in spectrum analysis and holography 78−82916
target discrimination methodology in remote sensing 80−58470
telemetry, automation of information input and processing 77−78429
TEM images of dislocation core, optical filtering for noise removal 80−107254
temporal frequency spectrum, optical filtering 78−33695
textural pattern recognition, comparison of optical-digital and all-digital techniques 80−99638
texture analysis by hybrid optical/digital system 80−78787
texture pseudocolouring, single pass by spatial filtering 80−95809
thermoplastic optical phase recorder for data processing 77−72081
thermoplastic-photoconductor films for optical data processing 78−50875
thermoplastic-photoconductor image transducer, input to coherent optical processor 78−83098
thin film waveguide component interconnection and signal processing 78−5584
thin phase structure detection method spatial filtering props., under partially coherent illum. 80−95828
three colour channel hybrid system to synthesize complex point spread functions 79−41347
three dimensional video images formed by parallax panoramagrams, real-time transmission 79−31807
three-dimensional display limits 80−83561
time integrating acousto-optic signal processors 80−48176
time integrating optical signal processing, acousto-optic 80−102641
time-integrating acousto-optical correlator design and performance 80−106618
time-reversed optical wave front generation by degenerate four-wave mixing 79−14028
tomography, transaxial scanners for reconstructing objects from their X-ray projections, review 80−102632
tracking turbulence induced tilt errors with shared and adjacent apertures 77−46792
transaxial tomography, possibility of an optical treatment for expt. data *(French)* 79−22898
transaxial tomography, simple pupil function for OTF synthesis 79−41349
transaxial topography, optical method, optical fibre, refr. index meas. *(French)* 78−66778
transforms for pattern recognition, positional, rotational and scale invariant 77−10854
transparency optical thickness irregularity processing by laser heterodyne correlation 79−14119
truth-table look-up optical processing utilizing binary and residue arithmetic 80−69334
turbulent-degraded image reconstruction using nonredundant aperture arrays 78−93122
TV optical operational amplifier 79−94327
TV techniques in image processing, remote sensing imagery appl. 78−93005
TV-optical analogue computer soln. of partial differential eqns. 79−76869
two-beam interference pattern monitoring by phase modulation 80−77844
two-dimensional high accuracy signal processor 78−46532
two-dimensional linear transforms, generalized, in optical processing 80−9824
two-dimensional optical information correlation reduction in course of photoelectric registration 80−19000
two-photon laser communication system, optimum quantum noise suppression 78−71049
Two-stage holographic rejector filter *(Russian)* 77−75675
undersampled images, bounds on errors in reconstruction 79−89858
underwater camera data correl. and interpretation, systems approach 79−5688
uneven interface of media with different refractive indices, statistical charcts. of images 80−87331
unitary transformation and general linear transform. by optical method *(Chinese)* 79−10261
unordered fibre bundles, parallel image transmission, multicomponent hologram arranger 80−78957
US blood flow spectral anal. using coherent optics 78−53459
US blood flow spectrum, coherent optical anal. 77−40722
US-optical correlator for spatial freq. meas. 80−95995
Vander Lugt filter, effect of recording errors 77−23624
variable operator optical processor, design principles 79−13919
variable operator optical processor, realisation methods 79−13920
variable threshold zonal filtering 77−71926
vectorcardiography, 3-dimens. 80−94405
vectorial treatment of optical systems 79−10264
velocity distribution measuring system, 2D, using multiple line detectors and correlation analysis 80−14851
Venus, Mariner 10 UV images normalisation 77−56850
video disc information retrieval by optical readout 80−43284
video interferogram analysis by TV camera-microprocessor system 80−73440
visual processor, human colour-vision discrimination, statistical-communications approach 79−5288
visual system, review *(German)* 77−64034
visualisation of periodic amplitudes and phase structures *(Russian)* 80−1135
visualisation of wavefront shape, shadow instrument with subtraction, appl. *(Russian)* 78−37966
visually optimised image restoring filter 79−3644

optical information processing continued
volume hologram representation of space-variant systems 78−33696
volume holograms, functional properties and appls. 79−94187
volume holograms for image restoration 80−83566
volume holograms in far field zone 78−17867
Walsh functions in polar co-ords., appls. 77−23626
wavefront analyser using max. likelihood algorithm, phase aberration meas. 77−46694
wavefront compensation error due to finite corrector-element size 77−46693
wavefront distortion estimate, least-square fitting to phase difference meas. 77−46689
wavefront estimation from wavefront slope meas., least-squares curve fitting model 80−106467
wavefront optimal estimation for compensated imaging system 77−46691
wavefront reconstruction, linear filtering influence 80−99670
wavefront reconstruction for compensated imaging 77−46690
wavefront reconstruction method, plane waveguide hologram coupled system 80−5708
wavefront sensing by phase retrieval 80−106478
waveguide lens technologies for RF spectrum analyser 77−34961
wavelength multiplexing for information transmission 79−22906
white light, coherent method, wavelength compensation 77−83817
white light, information processing and transmission 80−95833
white light optical processor for edge enhancement and spectral filtering 79−76599
white light processing using diffr. grating method 80−106470
wide-band spectrum analysis with area modulation 79−36840
wideband acousto-optic radiometry 78−77983
wideband ambiguity function generator with Doppler compensation 78−78936
wideband integrated optic signal processors, review 79−89864
Wigner distribution function, optical production, speech signal analysis 80−48521
Wigner distribution function and its application to first-order optics 80−37958
Wigner distribution function display using coherent optical processor 80−48160
wind velocity estimation method 77−41107
X-ray imaging, coded aperture, flashing tomosynthesis 77−40848
X-ray imaging using holography or electronics, tomosynthesis 77−40847
X-ray pinhole camera, resolution improvement by image processing 77−30222
X-ray scanners, picture reconstruction 77−40849
X-ray tomogram reconstruction by holographic methods 80−67246
X-ray tomography, non-computed, using coherent light reconstruction 80−17116
zero-order noncoherent filtering methods 77−19423
$Bi_{12}GeO_{20}$, electron beam recording 79−32075
$Bi_{12}SiO_{20}$ electrooptic crystals, vol. phase holograms, light diffr. and nonlinear image processing 80−37972
$Bi_{12}SiO_{20}$, electrooptic photorefractive crysts. for optical information processing 80−74313
$Bi_{12}SiO_{20}$, image recording possibility 79−27432
$Bi_{12}SiO_{20}$, optical information recording, PROM device resolution 79−41443
$Bi_{12}SiO_{20}$ PROM device, image recording and erasure mechanism 80−74490
$Bi_{12}SiO_{20}$ photoelectret, in optical processing and X, γ ray imaging 80−23764
$Bi_{12}SiO_{20}$, photorefractive medium, real-time image processing via four-wave mixing 80−95944
CO_2 IR laser velocimetry, processing techniques and applications 80−87831
$CdO\text{-}GeO_2\text{:}Tl_2O$ photochromic glass for optical information retention media 80−33108
CsD_2AsO_4 Fourier transform plane superposition multiplier, for optical processing 79−7084
GaAs signal processing optical electronic devices 80−33242
$InAs/LiNbO_3$ structure, SAW generated transverse acoustoelectric voltage, image scanning and signal processing appl. 80−49826
$InSb/LiNbO_3$ acoustoelectric convolver, gap-coupled, for IR imaging device 78−94492
KD_2PO_4, electron beam addressed light valve, optical processing appl. 78−83099
KD_2PO_4 light valves for optical information processing 77−72080
KD_2PO_4 light valves 77−83992
KD_2PO_4, optically addressed light valve, optical processing appl. 78−83101
KD_2PO_4 photo-spatial light modulator, optical data processing 80−102839
$LiNbO_3$, electrooptic photorefractive crysts. for optical information processing 80−74313
$LiNbO_3$, $LiNbO_3$:Fe, dynamic holography and optical image processing 79−94194
$LiNbO_3$:Fe, two different phase holographic recording processes, expt. 77−19211
$LiNbO_3$:Fe, white-light image processing 80−87321
$LiNbO_3$:Ti waveguide, ps signal processing with planar, nonlinear integrated optics 80−64208
$LiNbO_3/CdS$ integrated optical half adder circuit 79−76877
PLZT ceramics, photoferroelectric effects, image storage device appl. 79−42924
PLZT real time 2 colour incoherent to coherent image convertor 79−3805
Si diode storage correlator optical imaging and memory characteristics 77−23772
$Sr_{0.61}Ba_{0.39}Nb_2D_6$, photoinduced birefr. 80−7325
TeO_2 time-integrating acousto-optical correlator for chirp spectrum analyses 80−106474
VO_2 thin film semiconductor-metal transition applications 80−49835

optical instrument testing
see also aberrations
aberration testing using speckle shearing interferometer *(French)* 77−65616
alignment sensing subsystem, using passive error compensating device 77−75726
anamorphic system, image quality testing, resolving power determ. 77−7171

optical instrument testing continued
aspherical systems manufacturing and testing techniques development, use of computer *(Italian)* 80−48467
astronomical camera lens, focal length determ. *(Spanish)* 77−64663
astronomical mirror reflection coefficient checking against control samples 79−75106
astronomical mirror testing, portable visible-IR reflectometer 77−62033
astronomical telescope, diffraction figure calc. by Fourier transform. *(French)* 79−48672
azimuth scan MTF techniques, for optical component and system evaluation 78−50900
collimating system alignment by shearing plate 78−79126
colour TV camera lens testing, meas. of spectral transmission and modulation transfer function 78−94456
control life test design 80−87572
double beam interferometer, meas. of background suppression and spectral detection 80−95130
ellipsometer with quarter-wave compensator, multireflection interference effects 79−12841
endoscopes, equipment for checking optical and illum. charcts. 80−56157
evaluation definition and test criteria 77−39119
Fabry-Perot, optically contacted, parallelism recording technique 77−18079
fibre-optic rotation sensor construction and laboratory test 79−98497
focusing testers, anal. of optical and construction parameters 78−83070
Fourier transform spectrometer performance, instrumentation for assessment 80−95165
goniometer verification prism manufacture and recertification 77−27392
Hartmann test for 105 cm Schmidt telescope *(Japanese)* 78−89073
Hartmann test for telescopes at Okayama *(Japanese)* 77−73956
hazemeter, NBS reference, development and testing 79−75565
high-pressure gas equation-of-state meas. interferometry 80−77810
image analyser comparative tests 79−14106
image evaluation by multitarget array detection 80−1362
image evaluation using target detection 79−94378
imaging system assessment, conference, London, England (Nov. 1976) 78−50718
interferometers, fringe signal generator for testing fringe shift measuring system 78−65962
interferometry, multiwavelength testing using modified Twyman-Green interferometer 78−59169
IR goniometric refractometer, construction and test results 79−71513
Large Azimuth Telescope penetrative power determ. 79−48681
Large Azimuthal Telescope, 6 m, test results using Hartmann method with stars 79−8838
large azimuthal telescope mirror, shop tests using modified Hartmann method 78−87173
laser double-beam interferometer for amplitude-phase transmission meas. in optical components 77−87815
laser gyro evaluation plan and test results 80−9934
linear coma, optimum balanced, influence on disc spread functions 78−37814
microscope, universal set of attachments design 77−5907
microscope binocular tube alignment method *(Russian)* 77−10102
microscope scanning stage, motion rectilinearity determ., method and device 80−10055
mirror flatness meas. using group of line light sources *(Japanese)* 80−1294
mirror of lunar laser ranging receiving telescope, polishing and Foucault test *(Japanese)* 78−89065
mirror surface of gyroscope rotor, reflectivity, statistical charcts. 77−10996
monochromator stray light transmission meas. and evaluation 77−38030
movie projector objective lenses, standardisation of optotechnical parameters and testing methods 80−28301
MTF equipment testing in IR using standard reference lens 78−50898
MTF measurement in France, ACOFAM and ACOMAT instruments 78−50727
optical device performance assessment, British standards 78−50729
OTF measuring equipment assessment using standard reference lenses 78−50897
OTF standardisation activities in Netherlands 78−50728
OTF standardisation in Japan 78−50726
OTF testing, USA standards 78−50725
pancratic binoculars with threefold magnification variation 79−72663
photographic lens system, serial testing, resolving power limits 79−35870
planimeter metrological characteristic test results 78−79148
polyhedral prisms checking instrument, unit of plane angle transmission 77−7221
projectors, multispectral, MSP-4 objectives, photoelectric distortion meas. *(German)* 80−95976
receiver, separation elements of radiation flux *(Rumanian)* 79−90027
reference mirror for alignment of optical instruments 80−10054
reflex cameras, lens-array focusing system tests 80−86479
refractometer, IRF-454, specification, testing method and facilities 80−73424
Rowland concave grating spectrometer, component alignment using optical bench *(French)* 79−98514
ruby ring laser with forced mode locking 80−95915
Schmidt-Cassegrain system, optical figuring 79−46025
single-particle-size spectrometer calibration and testing, monofilament fibres as substitute particles 80−58819
space testing and qualification, using NASA Long Duration Exposure Facility 79−5725
spatial and energy parameters of optical instrument, criteria for performance evaluation 80−33259
spectrophotometer, photometric scale calibration using fluorite 1200-800 cm^{-1} transmission 79−12837
spectrophotometer performance evaluation tests 79−67371
submarine periscope optical test equipment 80−78943
system with symmetry plane, fourth-order aberrations *(Russian)* 77−58417
UV optics, high intensity solar irrad. testing 77−5431
vibration insulation of equipment for optical system performance testing 78−90543
White Sands Missile Range, Optical Evaluation Facility 79−36981
zoom null lens design for optical component and system testing 80−23811

optical instruments
see also colorimeters; coronagraphs; ellipsometers; holographic instruments; light interferometers; optical microscopes; optical prisms; photometers; polarimeters; refractometers
aberroscope, using artificial astigmatism, Taylor polynomial representation of wave abberation surface, for eye aberrations 78−35837
acoustic emission measurement transducers, comparison of piezoelec. and optical sensors 79−14192
active optical systems, real-time control over optical wave fronts 78−71187
additive colour viewer, for inexpensive remote sensing 79−29897
aerosol dispersed comp. analyser, small-size instrument design 77−17257
amino acid chromatographic instrument analysis and synthesis *(Hungarian)* 79−92030
angular meas. instrum. in engineering 80−13119
apparatus for optical measurements under conditions of hydrostatic pressure up to 2 kbar at temperatures ≲25K 80−22379
aspheric optics developments and appl. 80−5813
aspheric optics production costs, instrumental and photographic applications 80−28308
automatic optical length meas., defocusing effects *(Japanese)* 80−68174
automtic optical plumbline requirements and design *(German)* 77−70877
Babinet compensator, modified, using interference-colour method, for small retardation meas. 78−16827
backscatter/absorption chamber optical device, for water backscatt. absorpt. coeffs. determ. 80−82074
Bausch and Lomb Autoplot tangent screen standardisation, for visual field meas. 78−64976
binocular eyepiece nonparallelism influence on visual perception 79−72665
binocular instrument collimation rel. to visual binocular summation 78−53417
binocular models, charact. and design features, review 80−74468
binocular summation, fusion and tolerances 80−104588
binoculars, 8×30, MTF, stray light and transmission characteristics 79−72655
binoculars, high magnification, optical charact. and aberration graphs 77−7170
binoculars, preferred dioptric settings for high and low light levels 77−21528
binoculars, systematic product related design procedures *(German)* 79−72649
biocular magnifier design for display system viewing 79−27361
boroscope, fibre optics instrument 78−50938
cell study, optical device for time lapse recording in vitro *(German)* 79−74813
cell suspension six-channel aggregometer 78−81001
circular rails, adjustable mountings 77−37957
coherence applications, seminar, San Diego, CA, USA (Aug. 1979) 80−77542
comparator, for fine sieves evaluation 80−37068
compensator with adjustable birefr. dispersion 78−82017
contrast enhancement viewer for film 78−16879
convolution square camera, for anal. scanning electron micrographs, review 79−21864
correlation instrument field-of-view, intensity distrib. selection 79−72688
cryostat with optical high-pressure chamber 80−31767
cryostats for optical studies 77−41619
cuvette attached to UR-20 spectrophotometer for recording refl. spectra of adsorbed mols. 78−298
dark adaptometer, normative and clinical data 80−41019
design, partial coherence effects 80−78767
design of instrument optics from basic elements 77−58418
diffractometer analogue of electron microscope 80−69494
dilatometer, for thermal expansion coeff. determ. of fibres, films and polymers 80−45454
directional spectral reflection on plane surfaces meas. device *(German)* 78−12745
discrete component Sagnac optical rate sensor, error sources 80−1342
dispersion analysis of aerosols, optoelectronic instrument adjustment 77−74476
dispersive phase shifter for use in nonlinear optical interference expts. 79−50348
economic potential of optical instrument developments 80−31841
electric dichroism measurement instrument with digital processing 80−82800
emissivity determination, metals and alloys, using low-inertia opt. dilatometry 80−59684
emissometers, refl. errors elimination by use of alternate instruments 77−10089
endoscope operational charact. *(Russian)* 79−32022
endoscopic contour technique for meas. dimensions of object detail *(German)* 80−31839
fibre optic probe for neonatal oximetry and dye curves 79−70603
fibre optic rotation sensor, signal detection and processing, inertial reference device 79−54111
fibre optic time domain reflectometer, high sensitivity fibre fault detection 79−54173
flexible fibre light-guides, viewing instrum. appls. 80−87545
flow cytometer, high-resolution, based on net flow configuration 80−8223
focal reducer using Fresnel lens, appl. to stellar photometry 80−67568
focometer, F-1, for lens focal length meas. 80−64138
focusing to take account of eye accommodation 80−101811
Fresnel condenser lens faces, nomogram for slope angle determ. 79−7193
gas high pressure cell for optical studies at low temp. and hydrostatic pressure 78−82016
gauging instrument for measuring hole misalignment in flat plates, control aspects 78−57895
geophysical distance-measuring instrument, using optical and microwave path lengths meas. 77−29484
glass thickness automatic measurement by laser beam 80−82744
goniometer accuracy effect of atm. turbulence 78−55461
grating detectability, aberration effect evaluation in visual instruments 79−55073
Hadamard transform optical instrument, systematic errors 78−94375
haploscope, automated miniaturised device for testing binocular visual function 77−2004
haploscopic apparatus for study of colour perception under different adaptation conditions 78−56997
hazemeter, NBS reference, development and testing 79−75565
hazemeter for window pollution assessment 80−67995
for high elec. current meas., using Faraday rotation effect 77−2669
high-power laser luminance contrast meas. 78−87055
human eye optical characteristics *(Hungarian)* 78−11641
ice particle counter, for ice particle/water droplet discrimination 79−100973
image analyser, semiautomatic, use in investigation of muscle biopsies 80−85466
image analysis system, math. morphology and algorithms 80−82799
influence on the polarisation of light 80−52290
innovative applications of optics, conf., San Diego, USA (Aug. 1977) 78−58899
instrument for checking autocollimators 80−77832
integrated semicond. transducer suitable for colour distinction 77−10086
interactive image scanner, high resolution 80−94423
Keplerian binoculars with erecting lens system 79−72662
Knollenberg light scattering counters, response to doublet latex aerosols 80−37152
laboratory experiments *(Spanish)* 79−21510
laser pupillometer, especially suitable for anesthetised cats 79−48317
laser retinoscope using He-Ne laser light source 80−41159
laser scanner, augmented resolution eqns. 78−55398
laser stereometry using range-dependent time delay in reflected light 77−10127
laser systems for on-line meas. of muscle sarcomere length 79−48383
LED luminous intensity ang. distrib. and total light flux meas. device *(Chinese)* 78−82018
lens centring devices, high accuracy, appls. *(French)* 78−33924
lens system, for polariton measurements 77−38018
light beam deflection indicator and beam stabiliser 79−6160
light scattering instruments, response function optimisation for aerosol particle size evaluation 79−50214
light shielding charact., mol. scatt. calc. 78−71189
line spread instrumentation for laser beam propag. 78−83013
line spread instrumentation for laser beam propag. 78−83015
linear dimensions meas. instrum. 80−13118
liquid crystals, high resolution birefr. meas. 79−2803
liquid-borne solids monitoring, general principles 79−37424
low light and thermal imaging, conf. Nottingham, England, 1979, Apr. 79−36856
magneto-optical effects meas., Kerr and Faraday, with accuracy up to 0.001° 80−47087
manometer, differential pressure meas., interference system 78−86323
manufacturing, cyclical growth characteristics and prediction 79−76862
manufacturing standardisation and unitisation 80−9016
manufacturing tolerances, by a deterministical statement *(German)* 78−90536
measurement equipment development tendencies 80−13117
measuring instrument standardisation 77−71357
measuring mark parameters rel. to stellar visibility 78−61736
medical and biological instruments 80−21517
micro contact imager, appl. to obs. of solid lubrication dynamics 78−85002
microcomputer appls. 79−54192
microprocessor-based optical multichannel analyser 80−33167
microscope, precision dove-tail guide slots improvement method *(Russian)* 79−222
microscope photometer/semiautomatic image anal. instrument system for morphometric and photometric value meas. 80−82815
microwave light-range finder, use of KH_2PO_4 modulator *(Russian)* 79−46041
monochromatic Maximeter control system for thin multidielectric films, stopping criterion *(French)* 80−60694
MTF measurement of low light level devices 80−33221
multiple-mirror telescope systems, astronomical appls. 80−94713
navigational sextant, hand-held SPT-2, construction features 79−32027
nodal slide, experimental and theoretical thick lens parameters comparison 80−67998
noise in optical instruments, stray light reduction, space appls. 78−59153
noncontact optical profilometer, fast, precise, automated measurement 79−54095
nondestructive thermal testing, scanning and printing head 78−44329
noninterferometric optical probe, target displacement meas. appl. 77−74362
nonisoplanatic spectral instruments, num. correction of images formed 80−249
Ophthalmetron, refractive error meas. cycloplegia effect 80−41002
ophthalmological instrument design and construction, for eye diagnosis 78−15918
ophthalmolscopic and vision function meas. instruments 79−96689
ophthalmoscope, for interior and refraction error of eye exams. 77−81606
ophthalmoscope, hand-type, supplementary unit for photoelectric measurements 78−48907
optical bed, referenceable and vibr. isolated 78−83129
optical fibre, measurement of attenuation and dispersion 80−33185
optical fibre, on-site defect location and transmission loss eval. 79−3801
optical fibre variable attenuator, calibrated, expt. 77−39047
opto-mechanical instruments developments *(Hungarian)* 78−50952
optomechanical device frictional elements, solid lubricant tests 79−52388
optometer, IR, highly sensitive, for accommodation microfluctuation dynamics study 80−81580
oximeter, for continuous noninvasive meas. of blood O_2 level 77−2068
passive ring cavity optical rotation sensor, drift performance 80−1343
patient-positioning laser alignment instrument 78−53471
periscope, rearview, using two concave cylindrical mirrors, design 78−71178
periscope, secondary colour correction 77−7169
phase contrast microscope with Ar laser and photon counting system, for cell ATP meas. 79−79695
photodetector relative spectral sensitivity meas. method using two tandem monochromators *(Japanese)* 80−101840
photokeratoscope for corneal curvature meas. 78−3624
photokeratoscopic technique for corneal image study 77−1993
photometric studies of low-absortion optical media, apparatus *(Russian)* 80−98965

optical instruments continued
phototachymeter, pulsed phase, distance meas. accuracy, semicond. laser temporal charact. effect 78−70097
physical object measurement characteristics, types *(German)* 77−75702
plexiglas plates, static and dynamic stress intensity factor meas. by method of optical transmitted caustics 77−66740
portable multipass cell, for aerosols scattering and extinction coeff. simultaneous meas. 79−62588
power meters for laser photometry 78−65953
precision, microcomputer-aided manufacture *(German)* 80−95116
precision instrum. production developments at Carl Zeiss Jena works *(German)* 80−57357
precisional requirements, on scientific instruments *(German)* 78−90535
preprocessor, use in Earth-resources satellites 80−67430
prism binoculars, wide-angle eight-fold magnification, aberrations 77−10997
production planning problems, system of indices 77−31145
production technology advances, seminar, London, England (April 1979) 80−67938
profilometer, fast versatile, for surface roughness of workpieces meas. 80−37069
pulsed light rangefinder, amplitude error in presence of signal fluctuations 80−28332
pupillometer, objective device using counter-rot. perspex blocks 78−81000
quantitative image analysis, theory and instrumentation 80−23626
radial scale and grating production using radial metrological pattern generating engine 80−57282
receiving optical antenna, sensitivity to scatt. aerosol particle, laser location of atm. aerosols 77−70847
reflection coupling device with LED, colour masters evaluation appl. *(German)* 80−95123
reflectometer, for laser mirrors, high accuracy 78−87118
reflectometer, time domain, reflected and backscatt. power meas. from fibre end 78−70177
reflectometer, versatile high-precision multiple-pass 78−93754
reflector surface design by numerical method, bivariate beamshaping in elliptic case 77−27225
refractometer for eye refr. error meas. 80−81583
refractor, for vision defect anal., remote subjective device using sphere-cylinder corrections 77−1992
resolving power optimisation, scatt. function 77−83822
retroreflectometer, NBS reference 80−73410
rheometer, analytical, optical sliding contact, for flow visualisation at articular surface 80−104847
rotating spiral scanner for frog muscle contraction meas. 78−96120
Royco aerosol particle counter 225, data processing system and modified system props. 80−37005
scale transfer charact. *(Russian)* 78−37962
scan system for encoding and tabulation of visually scored sleep data 80−8197
scanning device, two-coordinate, with single mirror 77−26275
scanning system for 3D objects identification and spatial position meas. *(German)* 79−71405
schlieren instrument large-aperture adapter for optical surface quality evaluation 79−14122
screen image divider for eye testing 78−57114
sensing systems, with automatic light-intensity control, stabilisation 77−54784
shadow device with photoelectric recording, for turbulence meas., resolving power 79−7210
shadow instrument with photoelec. recording, signal charact. rel. to turbulence spectrum charact. 77−35267
shadow optical method for turbulent flow microstruct. investig., stat. analysis problems 80−19534
shutter, electronic control system 77−3678
solar selective surfaces instrumentation for high temp. and hemispherical meas. 80−4756
space qualification of optical instruments, using long duration exposure facility 78−85826
spectral image analysis device, Chromotron 80−83683
spring actuated parallelogram as vibr. freq. converter 78−29150
stereo-ophthalmoscope 110, for viewing of fundus oculi 78−48905
stereo-ophthalmoscope 110, stereophotography of fundus 78−48906
stereoscope for viewing aerial photographs, interpretoskop optics, modifications 80−105081
submicron particulates size determ. by sideway light scattering method 80−98883
Superinvar alloy casting 79−81580
survey for Japan *(Japanese)* 80−73406
target position meas., statistical model 80−101778
theodolite, type 2T, highly unified instrum. 80−13120
thermal blooming cell design for use in evaluating adaptive optics 80−102780
tilt gauge, based on Hg pool 78−88931
tonometer, applanation, for intraocular pressure meas. 80−30833
transducer, for use with windvane 79−39889
transducer for machined surfaces testing 79−85124
transmissometers for atmospheric visual range monitors 80−13122
trichometer for hair growth rate assess. 79−92325
UV and IR instrument material mech. and thermal props. 80−106584
vacuum UV circular dichroism instrument improvement 77−49786
velocimeters, S/N ratio and scatt. power, detection angle effect 77−42936
vibration analyser, meas. principle 79−6119
visibility meter design, visibility concepts 77−87803
vision aids, training and practice effects on performance 78−11770
visual field expander for patients with retinitis pigmentosa 78−65148
visual fusional power and reserve determ. 79−88148
visual instruments, optical component contamination, effect on visibility of extended objects 80−64137
visual stimulator for flicker fusion expt. 78−96053
visual stimulus generator, electronically controlled 79−74817
vortex flow rotational speed meas. instrument 77−80247
wedge-sensitometer for photographic photometry *(Japanese)* 79−44373
Zeiss Stereotop, appl. to Landsat imagery planimetric restitution 80−56648

optical interferometers *see light interferometers*

optical isolators
0.8 μm band, for fibre-optic communication systems 79−50424
acousto-optic isolator for stabilisation of optically pumped submm. lasers 79−31918
acoustooptic modulator intensity servo, optical isolation and amplitude noise reduction 79−98472
Asterix III and German laser fusion programme 78−63136
chalcogenide spinels, Faraday effect optical isolators for CO_2 laser system 78−50816
1,1-difluoroethane, high intensity transmission charact., for possible appl. in CO_2 amplifier gain isolation 78−42387
1,2-difluoroethylene, high intensity transmission charact., for possible appl. in CO_2 amplifier gain isolation 78−42387
diode lasers, struct. simplification 80−1209
Faraday cell for fusion laser; mag. field calc. 78−13719
Faraday rotator isolator for laser systems, solid state switching 77−88734
fibre communication, elimination of polarisation in optical isolators 80−5844
fibre-optic communication applications, microoptic grating multiplexers, optical isolators 80−48408
fog, laser light nonlinear transmission 80−1256
gas isolator mixes for CO_2 laser system 78−46663
gas mixture, absorbing, for isolation between amplifiers in TEA CO_2 laser 80−95911
gas saturable absorber, formic acid and SF_6 cells, as isolator for 9 μm band CO_2 laser amplifier 79−76709
glass fibre long wavelength optical communication, materials and devices, review 80−99854
integrated isolator using Faraday and Cotton-Mouton effects 77−79966
large-aperture Pockels cell design 77−19438
laser driven subnanosecond blast shutter 77−79842
laser fusion apodised apertures, Faraday rotators, and spatial filters 77−19290
laser fusion systems, optical developments 77−19289
laser plasma isolator for retropulse in CO_2 laser amplifier chain 79−22959
mode convertor system using Faraday and Cotton-Mouton effects 77−88964
near IR Faraday rotation isolators 78−18042
nonreciprocal coupling principle appl., using magnetooptic crystal 79−76872
passive contrast enhancer for ultrashort pulses in high gain system 77−88873
passive nonresonant technique for pulse contrast enhancement and gain isolation 78−63142
pinhole plasma shutter for optical isolation in high-power glass lasers 80−23733
plasma pulse clipper and optical isolator for IR lasers 77−65601
plasma shutter, self-triggered, for laser beam switching 77−58367
polarising optical components for high power glass laser systems 77−46727
retropulse isolator for CO_2 laser light 78−9388
rotator, low loss, and appl. for isolator design 77−58447
saturable absorber gases, for CO_2 laser gain isolation 78−59095
saturable absorbers, large scale flowing gas, for CO_2 lasers 78−59096
saturable absorbers, laser multipass power amplifier stabilisation in CO_2 system 78−46664
saturable absorbers, stabilisation of CO_2 laser triple-pass power amplifier system 78−46619
semiconductor laser optical isolator in laser-to-fibre coupling module 80−48267
semileaky thin-film optical waveguides, guided-radiation mode coupling analysis 78−1372
Shiva, laser-target and laser isolation 78−59035
trigger system, optically isolated, for pulsed high voltage plasma expt. 77−41650
CO_2 laser amplifier isolation from target reflection 77−19288
$CdCr_2S_4$ Faraday effect isolator, laser damage tests 77−46750
$CdCr_2S_4$, hot-pressed, optical isolation appl. at 10.6 μm, intrinsic absorpt. props. 78−42368
CdTe, electron-beam-controlled transmission of 10 μm radiation 79−81466
$CoCr_2S_4$, Faraday effect, appl. to CO_2 laser systems, radiation damage resist. 78−95579
GaAs directional-coupler switch with stepped $\Delta\beta$ reversal 77−88962
GaAs-$Al_xGa_{1-x}As$ MOS rib waveguide polariser, modulator and isolator 80−64217
p-Ge broadband passive isolator for CO_2 laser system, pulse shaping 78−46662
Ge, electron-beam-controlled transmission of 10 μm radiation 79−81466
p-Ge, saturable absorption isolator for CO_2 laser systems 77−19284
p-Ge, saturation charact. over CO_2 laser spectrum 77−88869
p-Ge:Ga, saturation behaviour at CO_2 laser wavelengths 78−1307
$Hg_{1-x}Cd_xTe$, Faraday effect at CO_2 laser freq. 78−64348
InGaAsP/InP DH stabilised 1.3 μm laser diode-isolator module for hybrid optical integrated cct. 80−58583
InSb, 100 W average power 10.6 μm isolator based on interband Faraday effect 79−59706
$LiNbO_3$, Ti diffused, optical waveguide isolator using electrooptic branching waveguide 79−18532
P_2O_5 glasses for laser amplifiers and optical isolators 78−25885
SF_6 based broadband gas isolator, for high power CO_2 lasers, design and evaluation 78−42339
YIG, computer optical isolator for near IR region 78−83104
YIG Faraday rotation optical isolator, intensity fluctuation suppression in $LiNdP_4O_{12}$ laser 79−81437
YIG thin film gyromag. waveguide, on GGG substrate, optical propag. props. Faraday effect 80−74513
ZnSe, electron-beam-controlled transmission of 10 μm radiation 79−81466
ZnSe, Faraday effect visible optical isolator 77−75657

optical Kerr effect
alkyl-cyanobiphenyl homologues, isotropic-nematic phase, optical Kerr effect 80−91866
atomic resonant lines, ang. momentum depend. of laser-induced birefr. and dichroism 79−10367
binary liquids, coupled mol. reorientational relax. kinetics, Kerr effect 78−67636
cavity filled with Kerr dielectric, nonlinear effect of powerful laser radiation field 80−99787

optical Kerr effect continued
Cherenkov type parametric optical oscillator, optical saturation 80−102771
cone-type light beam structure in nonlinear medium 79−98437
4-cyano-4'(n-amyl)-diphenyl, isotropic phase, induced molecular orientation relaxation time, Kerr effect *(Russian)* 80−19699
cyanobiphenyls, isotropic phase, pretransitional behaviour, optical and elec. Kerr effects 79−10928
dense optically transparent media, third-order optical susceptibilities 77−38981
discrete multilevel system, nonlinear polarisations and excitations, time depend. 77−27313
Fabry-Perot interferometer, transient behaviour 78−33787
forward degenerate four-wave mixing, propag. anal. 80−69468
glass, optical anisotropy due to laser-induced electrostriction *(Russian)* 79−99846
intracavity absorbing gas Kerr nonlinearity rel. to dye laser emission spectral condensation 80−53286
IR and FIR tunable coherent sources utilising modulational instability 80−95967
IR to visible AC Kerr efficient switches using liquid O_2 and liquid CS_2 80−19078
laser passive mode-locking and Q-switching with optical Kerr effect modulator 78−9403
laser pulse shaping by nonlinear interferometers 78−59097
laser pulse shaping by nonlinear interferometers 78−79051
liquid, electronic and orientational contribs., obs. by coherent Raman techniques 77−88874
liquid crystal and solns. laser and pulsed electric field Kerr effect 77−40210
liquid crystals, pretransitional behaviour, nonlinear optical obs. 77−51483
liquid Kerr cell, pulse compression inside actively AM mode-locked Nd-YAG laser 79−22990
liquid laser and pulsed electric field Kerr effect 77−40210
liquids, nonstationary Raman-induced effect *(German)* 78−60427
liquids 80−23761
MBBA/n-hexane mixtures, isotropic-nematic transition, transient optical Kerr effect study 79−82323
p-methoxy-benzoate-p-n-pentylbenzene, isotropic phase nematogen optical Kerr const. 80−78919
molecular crystals, self-induced nonlinear optical rotation 78−1308
molecular polarizability, anisotropic, optical study *(Rumanian)* 80−74256
multiphoton absorption, Kerr nonlinearity, cone-type light beam struct. 78−33790
(near) two-photon-resonant freq. up-convertors, limitations and optimisation 79−31985
neat liquids, broadened and oscill. optically induced Kerr kinetics 80−78901
nematogen, isotropic phase, fast ps reorientation, optical Kerr signal 77−15313
nematogens, isotropic phase, direct obs. of picosecond mol. reorientation 78−1991
nitrobenzene, oscill. optically induced Kerr kinetics 80−1286
nitrobenzene, rot. relax. times of anisotropic mols., optical Kerr effect and viscosity expts. 77−79906
m-nitrotoluene, pure and in soln., rot. relax. times of anisotropic mols., optical Kerr effect and viscosity expts. 77−79906
nonlinear Fabry-Perot filled with Kerr liquids CS_2 and nitrobenzene 79−27316
nonlinear interferometer with Kerr cell, quantum effects 79−55193
octyl-cyanobiphenyl nematic cryst., optical and DC Kerr effects 79−7183
organic compounds, nonsaturated, Kerr effect kinetics induced by picosecond laser pulses 80−102779
passive contrast enhancer for ultrashort pulses in high gain system 77−88873
passive nonresonant technique for pulse contrast enhancement and gain isolation 78−63142
4-n-pentyl-4'-cyanobiphenyl, isotropic, optical and electrical Kerr effect 79−32886
pentyloxy-cyanobiphenyl, liq. cryst., laser and electrical Kerr effect 78−68477
4-phenyl n-pentyl ester, Nematel 105, nematogen, isotropic phase, Rayleigh scatt. and mol. reorientation 78−34429
piezocrystals, uniaxial, nonstationary Raman-induced effect *(German)* 78−60427
polarisation-sensitive nonlinear spectroscopy, improved geometry 80−1285
polydiacetylenes, cryst., picosec. pulse, nonlinear optics appls. 79−46017
Raman induced, background suppression, polarisation techniques 77−5924
Raman induced Kerr effect spectroscopy 77−87843
Raman-induced Kerr effect, in liq. line shape calc. *(German)* 79−50358
Raman-induced Kerr effect with nonmonochromatic waves 80−48359
resonant media, pulse steady propag. 79−72633
salol, liq., supercooled, relax. kinetics, optical Kerr effect obs. 77−84613
self-induced transparency in presence of Kerr nonlinearity 78−63155
semiconductor, high-freq. Kerr effect 79−64294
succinonitrile, plastic cryst. and liq., Kerr effect for relax. kinetics 78−59768
surface wave at a nonlinear interface 80−91867
ultrafast molecular processes, use of picosecond lasers 77−79709
ultrafast optical Kerr shutter, photography and signal sampling appls., book contrib. 77−31140
CS_2, coherent Brillouin spectrum, Raman induced Kerr effect, acoustic phonon excitation study 79−59754
CS_2, liq., struct. and equilib. optical props. 80−45026
CS_2-glass boundary, optical bistability at nonlinear interface 80−33094
Cs vapour, with dispersive delay line, optical pulse squaring effects 77−88808
H_2O, liq., pulsed elec. field applied to sharp point, prebreakdown field 80−6308
Kr-Ar, phase matched, generation of Lyman-α radiation 80−91845
Kr-Xe, phase matched, generation of Lyman-α radiation 80−91845
$LiIO_3$, Raman induced Kerr effect with elliptical polarisation 78−42392
$LiIO_3$, Raman-induced Kerr effect 77−40227
$LiIO_3$, single crystals, Raman induced Kerr effect 79−7185

optical Kerr effect continued
Na vapour, amplified refl. by degenerate four-wave mixing using Kerr nonlinearity 78−55413
Xe-Ar, 3547 to 1182 Å conversion efficiency limited by Kerr-induced dispersion 78−37940

optical links
see also optical communication equipment
1.5 Mb/s bipolar signal coding and decoding optical fibre link 77−27343
1.6 km half-duplex optical data link 80−14470
2.1 km optical cable link installation, TV and telephonic transmission expt. *(German)* 78−33890
2 Mb/s optical fibre transmission link for industry *(French)* 77−10843
5 km fibre-optic data transmission link 77−65622
8.448 Mb/s optical cable feasibility trial *(German)* 78−33888
9 km fibre-optic telephone transmission system 78−42435
10 Mb/s short-distance fibre-optic data bus 77−68276
16 and 32 Mb/s optical data links 77−68275
16 and 32 Mb/s short-haul high-performance optical data links 78−1421
32 km optical fibre transmission with data-rate-transparent repeaters 79−76875
32 Mb/s step-index optical fibre repeater equaliser *(German)* 78−33881
32Mb/s optical fibre transmission system planning and expt. 78−1418
35 Mb/s optical fibre cable transmission using IR LED optocouplers 80−33156
44.7 Mb/s fibre optic transmission system expts. 78−1420
140 Mb/s fibre-optic field demonstration system *(German)* 78−33889
140 Mb/s optical fibre transmission system 78−42436
400 Mb/s optical fibre communications, integrating and transimpedance front end performance comparison *(German)* 78−33879
400Mb/s SELFOC fibre transmission system expt. 78−1419
565 Mbit/s signal transmission on optical waveguides 80−43483
800 Mbit/s digital transmission expt. *(Japanese)* 80−33164
acoustooptic FM and freq. shifted heterodyne CO_2 laser system 78−5568
analogue and digital systems, charact., and state of development *(German)* 79−999
analogue fibre optic commandable communication system, 650 MHz 78−46819
analogue fibre optic data link, hardened, construction and analysis 78−30057
analogue fibre optical systems, linearised LED and laser transmitters 78−46818
atmospheric attenuation at 6328 Å statistical meas. 77−45144
atmospheric communication links 77−83980
atmospheric laser link confidence level, error probability deterioration causes 77−38977
atmospheric optical communication line operating under photon counting conditions, adaptation to turbulence 80−9930
atmospheric optical communication link, laser beam size 80−33064
atmospheric propagation of laser beams, turbulence effects 77−38975
attenuation and dispersion meas., faults location *(German)* 79−14097
avionic multiterminal data link, fibre-optic interconnection system 78−46805
bandwidth-limited operation of nonideal graded-index fibres 79−46037
bidirectional central couplers, for links with fibre bundles 78−46809
bidirectional optical-fibre transmission used for control appls. *(Japanese)* 78−66917
British Post Office optical-fibre field tests *(German)* 79−10395
Canadian 50 km fibre-optic trunking system 79−76818
cardiological data transmission to hybrid computer 77−86677
CERN Super Proton Synchrotron, beam observation via optical transmission system 80−38119
channel capacity of multilevel pulse phase modulation 78−78934
Chicago, Bell system eval. 78−46821
collimated laser beam propag. in turbulent atm., phase fluctuations spectrum 78−78914
colour multiplexing in fibre waveguide links 78−42444
commercial aspects of glass-fibre technology *(German)* 79−10396
communication technology, evaluation under normal telephone system conditions 78−30061
components selection for optical links in 1979 year of fibre optics *(French)* 79−37009
conference, optical fibres and integrated optics, London, England (May 1977) 78−38063
conference on optical fibre communication, Washington, DC, USA (Mar. 1979) 79−46058
controlled fusion expt. shielding and earth loop elimination using fibre optics 80−74007
convertors, O/E and E/O, connected to both ends of optical fibre giving low-loss, broad band, non-inductive line *(Japanese)* 80−87510
cost models for A-7 aircraft ALOFT project 78−59131
coupling of fibre optic data links 80−43450
crosstalk in bidirectional fibre, review 78−66901
crosstalk meas. for end-to-end cross coupled fibre link 78−90502
curved single-mode optical fibres, propag. charact. 78−66934
data transmission, using inexpensive fibre links 78−42413
data transmission systems, defence appl. 77−75670
development of basic units for PCM transmission *(Dutch)* 79−68365
development trends *(Czech)* 80−14457
digital data transmission, design criteria and experimental results *(Rumanian)* 78−46791
digital optical fibre communication link for 1 Gbit/s *(German)* 79−81565
digital optical fibre system, 4-level using LED, meas. at 68 Mbit/s 80−1313
diode-laser-fibre coupling, effects of fibre propagation loss 80−74484
dispersion-free single-mode fibre transmission experiments up to 1.6 Gbit/s 79−59812
distributed microcomputer control system for high-energy gas-laser facility 77−61975
Earth-space-Earth retroreflector link, scintillation statistics 78−11996
economic advantages of using optical links, compared with wire cable 79−10385
experimental, step-index multimode optical fibres characteristics *(Japanese)* 78−90503
experimental 140 Mbit/s optical fibre transmission system, preliminary test results 77−68261
experimental loop system field trial telephony, data, video appl. 79−72707

optical links continued
extended-line-of-sight optical communication approaches 77−19187
fail-safe fibre optics data bus using active electrooptic mirror terminals 79−23053
fibre, 137 Mb/s data link using LEDs, material dispersion limited operation 77−88908
fibre, 140 Mbit, experimental use of GaAs laser transmitter *(French)* 78−30088
fibre, broadband dual-mode, design considerations 78−94437
fibre, Canadian development w.r.t. economics 78−42408
fibre, characts. and technology for connector engineers 78−94440
fibre, communication link between computer units, using LED-photodiode pair 78−71224
fibre, for T1 PCM telephone carrier system 78−9458
fibre, graded index, baseband freq. response meas. 79−41439
fibre, graded-index, baseband bandwidth estimation for spliced system, empirical formula 80−53460
fibre, LED as semicond. junction transceiver 78−42410
fibre, LM Ericsson system *(Swedish)* 79−55210
fibre, transmission design analysis *(Spanish)* 79−94349
fibre, West German developments 1978 survey *(Swedish)* 79−55209
fibre 140 Mbit/s feasibility trial over 5.75 km for main telecommunication network use 78−30076
fibre cable, mechanical and optical properties *(Japanese)* 77−19395
fibre cable, underground, installation *(German)* 79−3783
fibre cable composed of 8 fibres made by vapour phase axial deposition, characts. *(Japanese)* 80−58691
fibre cable comprising 48 fibres, design and characts. *(Japanese)* 80−58688
fibre cable comprising 8 fibres, design and characts. *(Japanese)* 80−58689
fibre cable construction, installation, and testing 78−46797
fibre cable development, robust, installation and jointing development and experience 78−9460
fibre cable splice methods *(Japanese)* 80−58690
fibre cable transmission performance in operational ducts *(German)* 78−33864
fibre cables, 10-fibre filled, 6-fibre, connector for field installation 80−43470
fibre cables, historical development *(Japanese)* 80−87494
fibre cables, performance characts. 78−79121
fibre cables for use in ocean, design rel. to stresses 78−42439
fibre characts. and manufacture in France *(French)* 78−71201
fibre communication, cabling, light source and receiver technology, review 78−59125
fibre communication line with spectral multiplexing in 1.3 μm region 80−74504
fibre communication lines, optoelectric systems on injection lasers 78−42464
fibre communication lines, use of semicond. lasers and avalanche photodiodes 78−46793
fibre communication methods and field trial in Singapore 79−94361
fibre communication system, A-7 ALOFT economic analysis, EM interf. and pulse tests 78−42448
fibre communication system, connector for step-index multi-mode fibres 79−32060
fibre communication system, cost model 78−42447
fibre communication systems in Japan 78−46815
fibre communications and devices, present and future developments, review 80−69521
fibre communications system, installation in Chicago, USA *(German)* 78−38006
fibre communications systems, review of worldwide development 80−43468
fibre components, ccts. 78−30054
fibre connectors, hot forming versus epoxy bonding of bundles, single fibre techniques 78−42482
fibre connectors, single- and multi-fibre, basic construction *(Japanese)* 80−87509
fibre data and telemetry links 79−27390
fibre data link, high bit rate using InGaAsP 1.3 μm LED 78−46825
fibre data link, integrated industrial, circuit and system considerations 78−46817
fibre data transmission system, operational 18-channel 78−46823
fibre delay lines, for pulse coding 77−83970
fibre developments 80−53458
fibre digital transmission system, 2 km, for field use at 20 Mb/s 78−38064
fibre digital transmission system, expt. 78−66943
fibre fabrication study for long wavelength region *(Japanese)* 80−87499
fibre full-duplex single-strand multimode system, max. achievable crosstalk isolation 78−50923
fibre interconnection components 78−46812
fibre jointing techniques and connections to communication equipment *(Norwegian)* 80−64179
fibre leakage induced by non-destructive methods 78−42450
fibre light guide optimum parameter determ. 78−38023
fibre link systems, UK expts. 78−42462
fibre long distance link, injection laser transmitter appl. 78−42355
fibre manufacturing, cabling and splicing, developments in Japan 78−59124
fibre multiterminal data system for aircraft, based on time division multiplexing 78−46811
fibre optic, digital transmission appl., commercial components survey *(French)* 79−90007
fibre optic, graded-index, multimode, interconnection 79−90037
fibre optic 500 MHz link using injection laser diode 77−75704
fibre optic cable design 78−66916
fibre optic communication link, 500 MHz, injection laser diode 77−79964
fibre optic communication systems, world-wide, survey 79−46059
fibre optic connector system characteristics, aerospace user's viewpoint 78−46804
fibre optic connectors developments, cancellation of coupling mismatches 80−1332
fibre optic data distribution system using variable tap ratio couplers 77−83953
fibre optic interconnection, using compound-lens devices, telephone links appl. 80−74493
fibre optic long-haul transmission systems, bandwidth characts. of graded-index multimode fibres 80−64180

optical links continued
fibre optic sonar link, multichannel 78−42446
fibre optic systems and field trials, review 80−58700
fibre optic test gear, BPO, view of likely requirements 79−64349
fibre optic transmission system, radiation hardened, 400 MHz bandwidth, linear response 77−23750
fibre optic TV channels, evaluation of use of laser diodes and LEDs 79−68395
fibre optic undersea cables, small, recent experiences 80−14488
fibre optical route bandwidth prediction, statistical model 77−62046
fibre optical telecommunication line, long-distance, operating at 1.3 μm 79−64346
fibre optics, practical problems *(Swedish)* 78−25988
fibre optics, single mode, and integrated optics, for optical communication 78−42469
fibre optics applications 77−46819
fibre optics commercial developments, 1978 state of art 79−3776
fibre optics data link, radiation testing, degradation, transient outage time performance 77−19405
fibre optics for defence appls. in UK 78−42440
fibre optics for military appls., review and assessment 78−42438
fibre optics systems, technology and components *(Hungarian)* 78−66900
fibre optics tasks of NASA, review 78−42441
fibre optics telecommunication applications 78−42432
fibre optics use in telecommunications 80−87482
fibre PWM multilevel pulse transmission, theory and expt. 79−55078
fibre remote control system for 1.5 MeV heavy-ion fusion preaccelerator 80−73993
fibre ribbons and cables manufacture, mech. props. 78−90533
fibre short distance application in Italy, review 79−50369
fibre splicing tools for field applications *(Japanese)* 80−87503
fibre system with linear intensity modulation, bandwidth limitation 78−1339
fibre systems, Soviet studies *(German)* 78−25972
fibre systems for telecommunications 80−91906
fibre technology for military aeronautic appl. *(French)* 78−46813
fibre telecommunication developments 80−58678
fibre to fibre coupling loss due to displacement, separation, misalignment, automatic measuring technique 79−32036
fibre transmission, applications and cable techniques *(Japanese)* 80−87493
fibre transmission applications to military and industrial systems 78−38021
fibre transmission capability expansion 78−66914
fibre transmission experiment, 800 Mbit/sec at 1.05 μm 78−83075
fibre transmission lines, use of microoptical switches 78−38085
fibre transmission links 78−46772
fibre transmission system, component specifications 78−59157
fibre transmission system, for Command and Control System 280 78−42445
fibre transmission system, investigation of active and passive devices *(Japanese)* 80−58693
fibre transmission system components, baseband frequency response meas. system 78−42404
fibre transmission system field trial, investigation of MCVD and VAD processes 80−43462
fibre transmission system using graded-index fibres manufactured by MCVD and VAD *(Japanese)* 80−58692
fibre transmission systems, 1.2-1.5 μm, economic evaluations and forecasts 80−87533
fibre transmission systems, active and passive devices 80−43463
fibre transmission systems comparsion, 0.8 to 1.4 μm 78−46824
fibre transmission systems design 78−1352
fibre transmissions of 100 Mb/s and 400 Mb/s PCM signals 78−1323
fibre waveguide characts. 78−59156
fibre-optic area-ratio couplers for distributed data-processing equipment interconnection 79−50431
fibre-optic cable pulse dispersion and attenuation meas. *(German)* 78−33859
fibre-optic communication applications, microoptic grating multiplexers, optical isolators 80−48408
fibre-optic communication in industry, appls., glass fibre props., connectors 80−87550
fibre-optic communication link component selection considerations 77−72088
fibre-optic communication system appls., review of benefits 80−43480
fibre-optic communication systems, book 80−73117
fibre-optic communication systems, devices and ccts., book 80−38123
fibre-optic communications, optimum design of graded-index fibre struct. 79−46080
fibre-optic communications components and systems 77−50752
fibre-optic data bus design and circuit miniaturisation 79−90034
fibre-optic data transmission links *(Danish)* 80−10009
fibre-optic LED and laser source and Si photodetector development 78−42430
fibre-optic multiterminal data-distribution system, planar star and fused-tapered couplers 79−50428
fibre-optic repeater bypass DPDT switch 79−98484
fibre-optic systems, measurement techniques for passive optical components 80−1354
fibre-optic transmission expts. at 1.3 μm wavelength *(Japanese)* 80−28318
fibre-optic transmission system, UK Post Office feasibility trial 78−1417
fibre-optic transmission system components *(Spanish)* 79−94348
fibre-optic transmission systems, development progress 80−43482
fibres, design, mech. props. and performance tests and practical applications *(Japanese)* 80−99867
fibres, fabrication and construction of secondary coating for optimised design *(Japanese)* 80−87567
fibres, fabrication processes and transmission characts. *(Japanese)* 80−87496
fibres, high density, parallel transmission system for data transmission *(Japanese)* 80−87507
fibres, measurement techniques for transmission loss and refractive index distribution *(Japanese)* 80−87498
fibres, mechanical strength reinforcing and reliability improvement methods of fabrication *(Japanese)* 80−87568
fibres, multicore, high density, design and manufacture, characts. *(Japanese)* 80−87501
fibres, multimode, transmission props. and theory *(Japanese)* 80−87495

optical links continued
fibres, single- and multimode, fundamental mode signal transmission 78−42442
fibres, splicing, connecting and sheath jointing *(Japanese)* 80−87497
fibres differential delay time relationship with propagation mode number study by effecting selective mode excitation *(Japanese)* 80−87504
fibres microbend charact. and mech. prop. for design, applicational examples *(Japanese)* 80−87500
fibres system testing, optical time domain reflectometry by photon counting 80−95122
fibres with diff. wall thickness, data transmission appl. *(Spanish)* 79−18543
FM fibre optic transmission system, laser-diode noise 79−45968
FM optical fibre analogue signal transmission system *(German)* 80−58679
French PTT system comparative assessment of requirements and available systems *(French)* 78−42422
full duplex transmission link over single strand optical fibre 78−1341
glass fibre, 672 digital voice channels 77−14662
glass fibre communication: introductory review, status and development *(German)* 79−89997
glass fibre link, semiconductor junction lasers ageing and modulation *(German)* 79−32042
glass fibre performance specification *(Dutch)* 78−83112
glass fibres, types and props. *(German)* 79−10386
glass-fibres, Bell's field trial *(German)* 78−74990
graded index fibre, 0.95 Gbit/s PRS signals regeneration after transmission over 0.91 km of fibre, regeneration cct. 79−59807
graded index fibre cable links installed in operational ducts, transmission meas. 78−50928
graded-index fibres, transmission charact. 78−66938
graded-index multimode fibres, transmission charact., expt. 78−66937
half-duplex optical transmission link using LED source-detector scheme 78−71214
heterodyne systems, using GaAlAs laser diode, high frequency stability 80−99727
high capacity telephone cable, 140 Mbits/s Hitchin to Stevenage *(German)* 77−72079
High Density Connector Interface, fibre optic link 80−91901
high-speed pulse transmission at 1.29μm, using low-loss single mode fibres 79−23067
historical and technical features review, future prospects *(Japanese)* 80−99863
hollow dielec. optical waveguide light transmission props. anal. 78−83109
hybrid digital optical fibre transmission system, terminal equipment and reshaping/regenerative repeaters *(German)* 78−33880
hybrid digital transmission system, 2R repeater, step index multimode fibres appl. *(Japanese)* 78−90505
industrial appl., IR LED and optical cables improvements 78−59123
information transmission by laser, review *(German)* 77−54810
information transmission with laser beams, review 77−38821
integrated fibre-optic subsystems, progress in development and appls. 79−46068
interoffice trunk fibre-optic experimental transmission system 77−54795
Italian local digital network applicability of optical cables *(German)* 78−33886
Las Vegas telephone installation, 4.5 km fibre optic cable 78−46822
laser, 10.6 μm data relay link transmitter/receiver optical design 77−19442
laser, applications of Stark cells to CO_2 laser systems 77−19444
laser, intracavity CdTe electro-optical modulator for CO_2 laser 77−19443
laser 1 Gb/s satellite communication system 77−19440
laser 300 Mb/s communications terminal 77−19441
laser beam appl. at 0.63 micron wavelength, expt. 78−38022
laser diodes for fibre optic communication and data link systems 78−46637
laser propagation experiment in low visibility atm. 77−88829
laser propagation experiment in low visibility atmosphere 78−46703
lens, gradient-index rod, appl. in optical fibre communication systems 80−69488
light feedback suppression, from optical fibre into diode laser 79−1004
light guide cable links field trials *(German)* 79−7206
light mode stripping reservoir 79−76835
light transmission mechanism in optical fibres, communications appl. 80−43469
light velocity fibre optic wink-around expt. 80−90628
long distance communications, fibre optic developments *(Norwegian)* 80−1318
long-distance graded-index fibre bandwidth estimation 80−58742
long-haul communications optical fibre fault location method 80−64193
long-span single-mode fibre transmission charact. in long wavelength regions 80−99850
low loss optical conductors using doped deposited silica principle *(Dutch)* 78−66925
measuring equipment for experimental multimode fibre transmission system *(Japanese)* 78−90506
measuring equipment for optical fibre transmission system 79−32061
medium and long distance digital optical fibre communication systems 78−50941
microwave and satellite terminal fibre-optic links 77−27377
military, local distribution communication, use of plastic clad/fused silica fibre 78−9457
military fibre communication systems development 78−59158
military optical fibre communications 78−42433
mode-coupled multimode optical fibres, coupling length estimation 78−66933
modulated laser beam for gigabit communication 78−66860
modulated wave propag. in turbulent atm., correlation functions and freq. spectrum 79−34954
monomode optical fibre design and fabrication for submerged cable applications 80−91932
multichannel, GaAs laser source package 78−1266
multichannel data link, using AlGaAs DH LED *(German)* 78−38014
multichannel GaAs laser array output synchronisation 78−42417
multifibre splicing and butting developments *(Japanese)* 80−87502
multimode broadband fibre refractive index profile optimisation 78−66932
multimode electro-optic guiding for single fibre data links, system design 78−38065

optical links continued
multimode fibre couplers, structure anal. 78−63198
multimode fibre data link, freq. depend. of modal noise, speckle theory 80−102817
multimode fibre link, modal noise 80−87536
multimode fibre links, intermodal dispersion reduction by mode-delay equalising methods 80−48400
multimode optical fibre waveguides, army communication system appl. 78−55452
multimode optical fibres, effect of cladding 78−30050
multipath time dispersion theory of optical network 78−22207
multiterminal fibre systems 78−87147
multiwavelength monolithic integrated fibre-optic terminal development 80−33243
non-repeatered 50 km transmission experiment using low-loss optical fibres 78−79108
optical fibre, 5 Gbit/s multiplexer 78−18044
optical fibre analogue/digital communication system with 5 MHz bandwidth *(German)* 78−30062
optical fibre cable developments *(Japanese)* 79−27405
optical fibre cable structure, characteristics, telecommunications appl. 79−94366
optical fibre cables, longitudinal stress in fibres due to twisting in manufacture, anal. 78−30048
optical fibre nonlinear equalisation by shaping filter *(German)* 78−33882
optical fibre properties, signal to noise ratio, freq. response, dispersion effects, communication system design appl. 78−9435
optical fibre telephone carrier systems 78−42463
optical fibres, step-index, excess loss dependence on parameters, expt. 78−66936
over-the-horizon optical propagation in a maritime environment 80−41547
paper tape data transmission, wavelength multiplexing, optical fibres 80−43454
partial tracking optical heterodyne receiver arrays, operating in turbulent atm. 79−41345
passive telemetry, by modulated backscattered incident CW RF carrier beam, cattle temp. meas. appl. 77−90968
PCM 480 digital transmission system for Deutsche Bundespost 80−38120
PFM fibre-optic video transmission to and from undersea vehicles 80−46310
photoacoustic effect appl., optical links development *(Czech)* 78−77994
photodetector optimisation for radiation environments 78−29158
photoelectron counting distributions of laser light signal through turbulent atm. *(Japanese)* 77−50711
PO experimental link and fibre production outline 79−37015
polymer clad fibre appl. 80−69546
power station fibre-optic system installation 79−37028
pulse interval modulation optical fibre communication system field expt. 78−1424
random noise, statistical analysis *(Italian)* 77−50759
repeater design, high impedance input, equalisation cct. *(Italian)* 77−50758
repeater section lengths rel. to transmitter power and fibre dispersion *(German)* 78−38012
scintillator-fibre optic system, for high bandwidth radiation diagnostics 78−46820
Second European Conference on Optical Fibre Communication, September 1976, review *(Italian)* 78−5552
SELFOC fibre 400 Mb/s optical transmission system 78−1353
semiconductor light sources principle and appl. *(German)* 78−71108
Shiva laser fibre-optic digital links 79−85804
short distance communication systems *(Italian)* 77−42601
short-range fibre optics 78−46786
short-range optical fibre system applications *(German)* 78−33885
silicone and glass clad compound glass optical fibre comparison 80−69533
single laser diode CW output power limitation *(German)* 78−37886
single mode fibre, 800 Mbit/s transmission expt. 78−30058
single mode fibre network, coupling and integrated optical switches 78−59159
single mode fibres, optical communication techniques *(German)* 80−102811
single mode fibres, very low loss, 1.5 μm transmission expts. 79−50385
single-fibre connectors, demountable, loss meas. 78−94433
SiO_2, manufacture using modified CVD method *(Japanese)* 80−99864
space communications with Nd:YAG laser 78−66859
spliced graded-index fibres, 11.7 km link, measured and predicted transmission charact. 80−14454
star repeaters for fibre optic links 77−34934
step-index fibre transmission system variable equaliser 79−55243
stepping motor microprocessor controller for 100 kJ CO_2 laser beam alignment system 77−54035
surface wave acousto-optical device appl. 78−38040
T-coupler for multimode optical fibres 78−42457
Telecom Australia optical fibre communications, fibre research and measurement technique developments 80−43456
telecommunication network, role of fibre optics 80−43484
telephone, experimental system operating at 140 Mb/s 78−1321
telephone systems, fibre links in Europe 78−46781
telephone trunk systems, 4.5 km, viscous polyurethane filled cable 79−72708
terrestrial optical links at 10.6 μm, optimum design 79−84455
tetrachloroethylene filled optical fibre, transmission properties, compatible LED, optical link appl. 77−39060
transmission loss characteristics, low OH content optical fibres *(Japanese)* 79−64327
turbulent media, atm. beam propag., comments 77−41125
TV two-way transmission using single fibre and two light sources 79−27419
two-way transmission expts. over single fibre at same wavelength using micro-optic 3 dB couplers 78−55450
UK Post Office junction and trunk network applications for optical fibre systems *(German)* 78−38016
undersea communications, use of low-loss fibre cables 78−59126
undersea fibre-optic cable link performance 78−46807
UV communication based on molecular and aerosol scattering in atmosphere 79−3736
VAD fibre cables, charact. 80−43461

optical links continued
wave division multiplex system, bi-directional data link example 79−94365
waveguide, source and connector developments *(German)* 77−42613
waveguide, variable refractive index, self-focusing, for wideband and image transmission 79−7208
waveguide data bus system configurations 79−18544
waveguides appl., single-mode and gradient-index *(Czech)* 77−62065
waveguides technology, components and systems *(German)* 80−33168
wavelength division two-way fibre optic transmission expt. using micro-optic duplexers 78−22194
wideband fibre optic transmission, short distance links, introduction 79−3773
wideband subcarrier PFM analogue optical communications channel 77−27378
X-ray wavelength and optical transmission waveguides *(German)* 80−99847
AlGaAs multimode laser, longitudinal modes intensity fluctuations effect on high bit-rate optical transmission 79−68415
$Al_xGa_{1-x}As$-GaAs LED design and characterisation for fibre-optic communications 78−46796
CO_2 laser system, for Earth sensing satellite data transmission 77−19427
(GaAl)As lasers, low threshold proton isolated, spectral and transient response 78−87052
SiO_2:Ge single mode fibre, low loss transmission of high speed pulse signals at 1.29 μm 78−42409

optical mark reading *see mark scanning equipment*

optical masers *see lasers*

optical materials
see also glass; optical films; optical glass
absorption coeff. meas., photoacoustic technique 77−26402
absorption measurement, optical materials, real time holographic interferometry 80−83569
acrylamide, photopolymerisable, Fe^{3+} sensitised, holographic recording appl. 77−54677
acrylic, plastic optics, design patterns 79−32009
acrylic moulding formulations, optical and mech. props. 80−106582
active laser media, mats. search 78−63160
adverse environment effects conf., San Diego, USA (Aug. 1977) 78−82976
alkali halide, two-photon absorpt. coeffs., 355 and 266 nm 78−83037
alkali halide and other crystals, damage induced by $CaF_2:Er^{3+}$ laser radiation at 2.76 μm 79−91539
alkali halide crystals, activated, physical phenomena and optical data processing appl. *(Russian)* 80−80819
alkali halide crystals, optical components, melt growth conditions 78−50955
alkali halide pelleting technique for solid sampling in IR spectroscopy 78−87171
alkali halide photodichroic crystals use for coherent opt. data processing 77−68248
alkali halides, behaviour as materials for optical components, for high power lasers *(Rumanian)* 79−18462
alkali halides, finished optical components, forging 77−46824
alkali halides, laser induced breakdown, 10.6 μm, reproducibility 77−62023
alkali halides, polycrystalline, use as IR optical waveguide fibres 80−58750
alkaline earth fluorides, UV window and coating materials, two-photon absorpt. coeffs. 79−59734
trans-4-alkylcyclohexane carboxylic acids, visible and UV spectroscopy transparent matrix 80−45102
amorphous materials role as optical information media 77−54764
anthracene, selective epitaxy by vacuum evaporation on soln. grown anthracene substrate 77−63558
antireflection coatings for optical components, using materials with refr. index 1.7-2.0 79−72656
benzil cored fibres, void-free cryst. growth, X-ray diffr. and optical microscopy study 80−71586
birefringent plates, cracks, stress intensity factors, refl. caustics method 80−93718
bulk materials, low optical absorpt. coeffs. meas., adiabatic laser calorimetry with long rod samples 79−2804
cement requirements 78−50961
ceramic, gas-moulded, characteristics and application prospects 79−81495
ceramic, KO1, homogeneity in terms of refr. index 80−64125
ceramic, KO-1, IR scatt. and brightness indacatrices meas. 78−71164
ceramic crystalline materials, IR transmission, review 78−55417
ceramic KO-1 strain, yield limit, and stress relaxation obs. 79−46018
ceramics, dispersion, double refraction and storage effects, material appls. *(German)* 80−69471
ceramics, nephelometer for light scatt. meas. 77−10084
ceramics, Rochelle-type, controllable transparency *(Russian)* 77−630
ceramics, transparent ferroelectric, composition selection for appl. in light modulators *(Russian)* 80−91869
chalcogenide cubic compounds, melt grown, physical properties, application as lens or laser window materials 79−98450
chalcogenides, prod. and acoustooptic props. *(Russian)* 78−63158
chalcopyrite crystals, refractive index, temp. depend., appl. to nonlinear devices 80−60555
chemical laser window materials evaluation 77−46769
coherent inspection procedure using holographic filter technique *(German)* 77−31142
coherent-optical material testing, defect magnitude effect on vibration pattern *(German)* 77−77655
cold spectral filters for long-wave IR detectors, material optical props. 79−3799
composite materials, optical props., review 78−56496
compound optical polarisation materials for stress meas. *(Russian)* 78−87313
conference, basic optical props. of materials, Gaithersburg, MD, USA (May 1980) 80−101668
conference, optical production technology advances, London, England (Jan. 1977) 78−50954
corundum, growth of large crystals of high opt. quality 77−34916
corundum, optical, polished, surface layer obs. by IR reflection spectra *(Russian)* 78−19458
corundum, single crystal, dispersion medium for polishing 80−102870

optical materials continued
corundum optical crystal block structure 79−72637
crystalline material optical absorption meas. 80−105718
crystalline optical material props., symmetries and tensorial relationships 80−108174
damage-resistant components for 2-5 μm laser systems 77−19282
data storage material requirements and possibilities *(German)* 78−25937
detection thresholds at 10.6 μm 78−90471
dichromated gelatin as holographic storage medium 80−43303
dielectrics, highly transparent, refr. index dispersion 79−72635
diffracting periodic structure generation by coherent beam interference 80−69570
m-dinitrobenzene, electrooptic cryst., growth in monomode optical fibres 80−55288
m-dinitrobenzene cored fibres, void-free cryst. growth, X-ray diffr. and optical microscopy study 80−71586
elasto-optic coefficient determ. under static loading, by acousto-optic and Brillouin scatt. techniques 79−4787
electro-optic material cutting and polishing, book 79−81583
electro-optical and nonlinear-optical materials, review 80−74450
electro-optical beam deflector construction principles and efficiency characteristics *(Russian)* 79−94342
electroabsorptive devices, material requirements 79−3754
EM sensor window materials, particulate erosion 80−38080
epoxy, clear, refr. index and extinction coeff. meas. 79−18492
epoxy, for interference filter, γ-radiation effects on transmission 79−64297
epoxy replication of optics 77−27401
ferroelectric crystal., optically induced refr. index changes, holography appls. 77−50742
ferroelectric oxide crystals for electrooptics and nonlinear optics, optical inhomogeneities, review *(Japanese)* 77−65613
fibre devices and materials for 4 μm-band communication 78−94441
fibre material selection criteria for λ>1.8 μm 80−87554
fibre-optic communication and integrated-optics sources *(Italian)* 79−94371
fluorite crystal windows, transmission in vac. UV region, heat treatment effect 77−31137
fulgimide planar photochromic structures for optical waveguide components 80−64196
garnets development for laser cryst. matrices, spectral generation data survey 77−10928
Ge, refr. index, 95-298K, 2.5-12 μm 77−8535
graded index materials, optical props. meas. 79−9237
gradient index material profiles and chromatic props. 80−14409
gradient index optical imaging systems, topical meeting, Rochester, USA (May 1979) 80−12851
halides, melt grown, physical properties, application as lens or laser window materials 79−98450
halocarbon index matching fluids for long wavelength fibre-optic appl. 80−69470
harmonic-generating crysts., two-photon absorpt. coeffs., 355 and 266 nm 78−83037
holographic data storage and processing, photosensitive electro-optical materials *(French)* 77−31077
homogeneity, test methods and instrumentation 79−37063
index-matching fluids for long wavelength (1.2-1.6 micron) fibre-optic appls. 80−99841
information storage, seminar, Washington, USA (Apr. 1979) 80−41942
integrated and guided wave optics, materials and fabrication techniques 80−23809
interference measurement of continuous heterogeneities 78−93756
ion bombardment of materials containing alkali metals or alkaline earths, chem. sensitisation 80−3227
IR absorption measurement, interference calorimetric method, effect of crystal thermo-optic props. 80−47096
IR bidirectional refl. distrib. function meas. for baffle and mirror materials, recording instrument 78−58012
IR detector materials, irreversible laser damage 78−25914
IR elements, adsorbed water effect on laser breakdown threshold 77−79886
IR inhomogeneity scanner for transmitting material blanks 79−32099
IR laser window material extrinsic absorption 79−14049
IR laser window material refractive props., temp. depend. 79−14052
IR materials, high transparency, state of the art 77−27326
IR materials, laser residual absorpt. 2 to 10 μm, review 78−25906
IR materials, optical phenomena, conf., Annapolis, MD, USA (Dec. 1976) 78−25933
IR materials for measuring radiant flux *(Russian)* 80−48366
IR multilayer optical medium produced by negative photoresist spin-coating 80−74451
IR transmissive material guide 77−39004
IR transparent materials, bulk and surface absorpt., calorimetric meas. method 79−27347
IR transparent materials, forward and backward scatt. data 78−59099
IR transparent materials and components 77−19374
IR window materials, optical phenomena, book contrib. 78−9420
IR-optical material surface breakdown, adsorbed water evaporation model 80−35020
jelly-filled optical fibre cable fabrication and characteristics 80−53490
larch arabogalactan solns. as optical cement 77−75723
laser beam damage thresholds of CO_2 fusion laser optics 80−38050
laser components, high power, conf., Boulder, Colo., USA (July 1976) 77−46729
laser crystal evaluation, testing and meas. instrument 77−7226
laser damage in optical materials at 1.06 μm 80−28263
laser damage in transparent polymers of various atomic composition and viscoelastic props. 80−104017
laser damage threshold at 10.6 μm, up to 10^{10} W/cm^2 77−50707
laser damage thresholds for mirror and window materials, 10.6 μm 77−50708
laser heated IR windows, interferometric meas. 77−46748
laser induced breakdown, breakdown thresholds and multiphoton absorpt. coeffs. 79−3735
laser induced damage in optical materials, symposium, Boulder, USA (Sep. 1978) 80−31417
laser materials with inclusions, thermal stresses 77−729
laser measurement of optical, thermal and mech. props. of materials 77−74513
laser radiation resistivity *(German)* 77−58363

optical materials continued
laser radiation wavelength meas. using material spectral transmission curves 79−76738
laser shock production rel. to material damage 77−90221
laser window, mirror and reflector coatings, high power, materials selection 77−50735
laser window and rod critical orientations for stress-induced depolarisation elimination 79−14054
laser window construction, for type 300.1 TEM_{00} He-Ne laser *(Rumanian)* 80−9898
laser window materials, pulsed HF-DF laser damage 79−14011
laser window materials, surface and bulk absorpt., photoacoustic meas. 78−25912
laser window materials, temp. and stress effects on refr. index 77−46771
laser window materials stress birefr. elimination 77−58362
laser-induced damage, conference, Boulder, USA (Oct. 1977) 79−14048
lens array characts. on illuminated intensity distribution *(Russian)* 80−106591
leucosapphire, crystal growth by Kyropoulous method, temp. effect on structural and optical quality 80−20784
leucosapphire, large cryst., UV transmittance 77−88876
leucosapphire, spectral absorption coeff., 0.25-1.25 micron, up to 1800K, and 3.5-5.2, up to 1200K 78−27204
leucosapphire large crystals, anomalies in block struct. formation 80−9972
Lexan, optical and phys. parameters 79−32004
malachite green, Weigert effect, additional chroming effects 77−58406
matched filter correlator memory techniques and capacity 80−43280
metal IR window materials, diamond machinability 78−5586
metal mirrors for CO_2 laser fusion systems, material constraints and fabrication 78−5476
metal optics, reflective system specifications 80−48387
metal polishing and lapping 78−5587
metal surfaces for laser mirrors, ion polishing and vac. annealing 78−5588
metallic and glass components compared 80−69473
metals for mirror substrates, manufacturing processes, review 78−5542
mid IR laser window materials, absorption props. 77−46770
military optical system temperature effects and counter-measures 80−78938
multiple-plate glass systems, spectral directional radiation characts. prediction 78−74956
near IR transparent material, birefringence meas. polarimeter 79−44925
nonlinear materials for tunable coherent light sources in middle infrared, review 77−38991
nonlinear optical phenomena, principles *(French)* 78−71140
nonlinear optical uniaxial crystals, review and summary of data 77−75615
nonlinear refractive index coefficient at 1064 nm, meas. methods 79−3737
one-component optical cement 80−87445
optical breakdown threshold, illuminated spot dimension effects 78−68582
optical cements, IR refractometer meas. 79−6164
optical recording techniques appl. *(Japanese)* 80−105730
organic compounds, for possible electro-optic appl., cryst. growth in glass capillary 77−44150
organic electrooptical materials for light modulators and deflectors, characts. *(Japanese)* 77−73128
organic materials for volume phase holographic recording media and integrated optical devices 79−3755
organic molecules, conjugated, nonlinear props. of new class of cpds. 79−41413
organic nonlinear optical materials, SHG efficiency 77−75619
organic photochromic film, for real-time coherent optical processing 78−50876
paraffin oil coatings for high power laser system components 77−88730
Perspex for astronomical telescope lens and mirror manufacture 78−36458
phase changes in optical recording media, interferometric meas. 77−49769
phase profiles generation, recent advances, book contrib. 79−76644
photoacoustic spectroscopy study 80−64124
photochromic, temporal and spatial responses 77−34920
photochromic materials for holographic information storage 79−50265
photodichroic materials, writing vol. amplitude holograms 78−17871
photodichroic materials as coherent optical computing elements 77−71962
photoelastic investigation of freezing and defreezing of temperature stresses 77−66733
photopolymer for holographic recording, sensitised by redox system *(Japanese)* 77−7030
photopolymer laser recording materials development 77−54678
photopolymers, for holographic recording, using photopolymer material, redox sensitized 78−13674
photorefractive materials for optical data storage 78−79086
photorefractive materials for optical storage and display, phase hologram form. 77−75445
photorefractive materials for optical storage and display 77−71961
photoresist, negative, as phase profile material for near IR, IR spectrophotometric meas. 78−37953
photothermoplastic devices, performance and limitations 77−38832
photothermoplastic layers, optical transmission function, charge carrier drift effects *(Russian)* 79−3661
phototransport laser damage mechanism 77−63498
physical props., seminar, San Diego, CA, USA (Aug. 79) 80−105423
piezo-optic coefficients determ. under static loading, interferometric and polarimetric techniques 79−4787
plastic films, IR reflectance of aluminised thermal screens for energy conservation in greenhouses 80−64351
plastic materials in development of optical fibres *(French)* 79−55236
plastic mirror, large size lightweight, for airborne laser sensor system, fabrication 78−66891
plastic optical components, flexible rapid curing abrasion resistant coated film 78−66890
plastic optical components and systems 78−25967
plastic optics, components 79−32010
plastic optics for optoelectronics, moulding techniques for single, multi-element systems 78−63210
plastic recording media for holography at 10.6 μm 77−71952
plastics, moulded, design advantages and appl. 78−87119

optical materials continued
Plexiglas 55, optical and phys. parameters 79−32004
PMMA, glassy, optical absorpt., visible region, determ. by laser calorimetry 80−66218
PMMA, laser damage threshold, freq. and size depend. 80−104018
PMMA, transparent colourless cementing of milled surfaces 77−34970
polyamide-polyurethane, enamel lacquer, far IR transmission, encapsulation of optical devices 79−55194
polycarbonate, bisphenol A, birefringent plates, cracks, stress intensity factors, refl. caustics method 80−93718
polycarbonate ophthalmic-prescription lens series 79−81501
polymer structure and optical behaviour 80−106583
polypropylene, transparent film, strain anal. by scattered-light speckle photography 79−32399
polysiloxane urethane as optical cement, transmission 0.2 to 6.2 μm 77−7163
polystyrene, glassy, optical absorpt., visible region, determ. by laser calorimetry 80−66218
polystyrene, plastic optics, design patterns 79−32009
polyurethane optical solid cct., preferential doping of rhodamine 6G 77−62075
polyvinyl acoustal, enamel lacquer, far IR transmission, encapsulation of optical devices 79−55194
production of optical glasses and single crysts. 79−94308
production technology advances, seminar, London, England (April 1979) 80−67938
pulsed laser induced damage at DF laser wavelengths 77−46751
pyroceramic end gauge, high-precision stability 79−76778
quartz:Ti tube for I photodissoc. laser, C deposit elimination 77−10945
quartz, cultured cryst., vacuum UV transmittance before and after electron irrad. 78−83044
quartz, optical quality, culturing process 79−81494
quartz, pure, fused, optical consts. in far IR, 20 to 120 cm^{-1} 78−79080
quartz ground surface, structure features of dull layer 77−54763
quartz synthetic crystals, observation of growth defects by light scatt. tomography 78−71743
radiation strength, dissipative characteristic 79−27344
radioisotope methods and neutron activation anal. of waveguide materials 78−7286
rain erosion mechanisms 78−83049
rare earth ion containing inorg. materials, 3μm band stimulated radiation 80−97306
rare-earth formates, second optical harmonic generation 80−43403
recording media, review 78−71172
refractive index at laser wavelengths, calc. methods 77−58400
refractive index calcs. of optical materials, 0.365-2.6μm spectral region 80−87444
refractive index data interpretation, collection of program library 80−55056
refractive index variation from field-assisted ion exchange 80−74447
retroreflector photometric and goniometric accuracy 80−86375
retroreflectors and retroreflective materials, luminous intensity meas. by photometry, accuracy assessment *(Dutch)* 79−85159
reversible media for optical memories, 1978 state of art 79−18377
ruby, fabrication of optics 79−23099
ruby, spectral absorption coeff., 0.25-1.25 micron, up to 1800K, and 3.5-5.2, up to 1200K 78−27204
sailcloth, optical transmission characts., telescope dome slit cover appl. 77−83936
α_1-salicylideneaniline, photochromic props., appl. as holographic recording 77−68183
sapphire, fabrication of optics 79−23099
sapphire, shock compressed, refractive index, density, and polarisability behaviour 80−50295
scattering characteristics of optical materials containing irregularities 79−3753
selective absorber coatings for enhanced photothermal energy collection 80−12027
semiconducting plate, light absorption, temp. depend., threshold flux density 77−83937
semiconductors, laser window materials, residual lattice absorpt., freq. and temp. depend. 78−25910
silica based optical fibre dopants for 1 to 1.8 μm communications 80−91930
silica reflectors, ageing under flash lamp light pulses *(Russian)* 77−54737
silicone rubber, room temp. vulcanising, as optical element coupler 77−39002
silicone rubber, room temp. vulcanising, as variable focal length lens 78−66888
solar energy absorbers, thermokinetics of glass and semi-transparent materials *(French)* 80−61410
for solar energy appl. 77−19373
solar glazing hemispherical transmittance props. 79−52957
solar materials radiation properties study, wide temperature range 79−94307
solar mirror materials, reflected beam profile characterisation 78−33814
space charged particle environment effect 80−69472
specular reflection coefficient comparison, sample materials 79−71512
storage and reproduction materials 80−33109
storage materials and methods, conf., San Diego, USA (Aug. 1977) 78−71171
storage medium specification and performance trends, review 80−43415
stress birefringent materials, transition temp. and assoc. mechanical props. determ., simple test method 78−56454
styrene-acrylonitrile copolymer, synthesis and props. for optical use 78−90466
submillimetric reflectivity of common materials 77−39005
substrate heating in vac., heating method rel. to spectral characts. 77−7223
sucrose benzoate host for recording volume phase holograms 77−632
surface irregularity statistics for laser component materials 79−14057
surface meas. using FECO scanning interferometer 77−7219
system and component specifications, seminar, Washington, USA (Apr. 1979) 80−46731
Takiwax films for pulsed IR holography 79−18363
tellurites, acousto-optical criterion estimation 79−82945
thermal failures in long and short laser pulse regimes 77−19281
thermal strain of optically uniaxial and biaxial crysts. 78−46733
thermochromic material, vanadium oxides mixture, appl. to laser beam indicator/visualiser 80−9976

optical materials continued
thermochromic materials, IR hologram recording 79−86135
thermoplastic enamel lacquer, far IR transmission, encapsulation of optical devices 79−55194
thermoplastic films, quasistatic theory of frost deform. 79−56052
thermoplastic media for hologram recording *(Russian)* 78−58948
thermoplastic photoconductor tape performance for optical recording 80−43305
thermoplastic recording media, electrocapillary effect, tangential extension influence on 'frost' deform. *(Russian)* 77−68249
thermoplastics, wideband optical transmission meas. 79−76771
transmission and MTF in 8-13 μ band 79−36982
transparent dielectric, laser-induced damage by thermal explosion of absorbing inhomogeneities 79−10340
transparent dielectric destruction by laser radiation, review 77−50702
transparent dielectric with metallic inclusions, light pulse shape effect on optical breakdown threshold 80−20588
transparent materials, absorpt. coeffs. meas., interf. effects 78−46699
transparent materials, laser irradiated, in-depth and surface temp. meas. by Moire-Schlieren technique 80−53392
transparent materials, low-modulus, mech. props. determ. method 78−5704
transparent object, testing for bubbles and light scatt. inclusions 77−88973
transparent optical material surfaces and films, pulsed laser induced damage 79−89948
transparent optical materials, laser induced damage and lattice strain due to lattice defects 80−48315
transparent polymers for electronics *(German)* 77−62021
transparent solid, laser damage by electron avalanche ionisation 79−19952
transparent solid optical materials, laser damage statistics rel. to structural defect statistics 80−91829
transparent solids, absorpt. coeffs. by laser calorimetry, wavelength modulation spectroscopy 78−66876
tribromoethanol UV storage films, HBr prod. and sensitivity optimisation *(German)* 79−14068
triphenylmethane dyes, Weigert effect, additional chroming effects 77−58406
trivalent metal phosphates, condensed, synthesis in polyphosphoric acid melts, physicochem. equil. considerations 80−97419
Twyman effect theory based on Van der Waals interactions *(Russian)* 79−77890
ultra low loss materials *(Japanese)* 80−106581
US cleaning, deleterious effects 77−42631
UV and IR instrument material mech. and thermal props. 80−106584
UV high-power laser material, refractive props. and optical constants 80−106555
UV laser window material absorption obs. 79−14012
UV transparent material, multiphoton-induced cond. and free carrier lifetime 79−19629
UV transparent materials, 355 and 266 nm absolute two-photon absorption coeff. obs. 79−18493
vacuum UV special application coatings, reflectance, transmission, technology 79−59788
N-vinylcarbazole containing polymers, sensitization to Ar laser for single laser photothermoplastic devices 80−83651
viologens electrochromic solutions, for display appl., oxidant impurities elimination 80−78922
waveguide process and materials, review of progress 80−23768
window, composite vacuum-tight, for IR and visible observations, strength and IR transmission 80−48406
window materials for CO_2 lasers, optical suitability 77−58361
Ag, absorpt. coeff. temp. depend., IR, 3 to 30 μm 78−74953
Ag halide polycrystalline fibre, 10.6 μm transmission loss obs. 80−64197
Ag_3AsS_3, proustite, cryst., vibr. spectra 78−48172
$AgGaS_2$, optical quality, grown from melt, EPR characterisation 78−64260
$AgGaS_2(Se_2)$, IR nonlinear material, laser induced surface damage 77−19266
$AgGaSe_2$, growth by Bridgman method, optical characts. 77−69980
$AgGaSe_2$, seeded Bridgman growth of crack-free crysts., thermal expansion coeff. 78−11101
Ag_3SbS_3, IR refl. spectra, permittivity, lattice vibrs. 79−65862
Al, laser pulse damage at 10.6 μm, single cryst. target in vac. 77−50706
As_2S_3 evaporated film, optical props., depend. on light exposure and heat cycling 78−68572
As_2Se_3, IR window coating, prep. and optical props. 77−50736
Au, absorpt. coeff. temp. depend., IR, 3 to 30 μm 78−74953
$Ba_2AgNb_5O_{15}$, $Ba_2AgTa_5O_{15}$, ferroelec. and ferroelastic props. *(French)* 79−24266
BaF_2 and fluorite large crystal, block orientation determ. from light scatt. pattern 79−50964
BaF_2 crystal, refr. index temp. increments meas. 80−33098
BaF_2, illuminated over large area, optical strength 77−75593
BaF_2, large optical crystals, quality 80−33097
BaF_2, optical ceramic, hot pressing in vacuum, rel. to spectral transmission 78−52730
BaF_2, piezo-optical coeffs. meas. at 0.6328, 1.15 and 3.39 μm 80−34888
BaF_2 purification for laser components, selective ion filter design and construction 79−14051
BaF_2, refr. index, 20-85°C, temp. depend. 77−8536
BaF_2, single cryst. windows for high power lasers, stress-induced birefr. elimination 77−88818
$BaF_2:Y^{3+},Gd^{3+}$ production and mech. props. 79−72638
$Ba_2NaNb_5O_{15}$, birefr. material, thermal cond. determ. by optical method 78−18851
$Ba_2NaNb_5O_{15}$ crystal, high optical quality, and optical absorption coeff. meas. 78−30036
$Ba_2NaNb_5O_{15}$, Gd substitution, effect on linear thermal expansion, possible BSN replacement 78−43153
$BaSO_4$ white reflectance standard, Kubelka-Munk optical props. 78−4675
$Ba_xSr_{1-x}Nb_2O_6$ crystals, optical defects and edge dislocation distributions 80−19806
$Ba_xSr_{1-x}Nb_2O_6$, struct. and dielec. props., isomorphic substitution effect 78−27165
Be mirrors, props. and fabrication procedures 80−38138
Be substrate for lightweight mirror, surface quality and thermal props. 80−23762
BiF_3 thin films, optical props. 79−32005
optical materials continued
$Bi_{12}GeO_{20}$, electron beam recording 79−32075
$Bi_{12}GeO_{20}$, single crysts. optical homogeneity depend. on growth conditions 78−95007
$Bi_{12}SiO_{20}$ electrooptic crystals, vol. phase holograms, light diffr. and nonlinear image processing 80−37972
$Bi_{12}SiO_{20}$, for real-time double-exposure holographic interferometry 77−71951
$Bi_{12}SiO_{20}$, image recording possibility 79−27432
$Bi_{12}SiO_{20}$, laevorotatory, cryst. struct., absolute piezoelec. d_{14} coeff. 79−94974
$Bi_{12}SiO_{20}$, optical quality, Czochralski growth 78−31324
$Bi_{12}SiO_{20}$ photoconductive electrooptic crysts. for time average holographic interferometry 78−25813
$Bi_4Ti_3O_{12}$, thick single cryst. growth from Bi_2O_3-B_2O_3-TiO_2 77−8746
$Bi_4Ti_3O_{12}$-CdS optical storage plane 77−39006
$CaCO_3$ calcite linear polarizer, role in laser technology 80−64165
$CaCO_3$, Iceland spar, polarizing prism, struct. defects effect 78−18065
$CaCO_3$, Iceland spar natural crystals, optical characts. 77−10988
CaF_2, 0.36 μ absorptance/fluence dependence obs. 79−15506
CaF_2 ⟨111⟩ oriented windows, optical distortion coeffs. at chem. laser wavelengths 79−94269
CaF_2, adsorbed water film internal reflection spectroscopy 79−15549
CaF_2 antireflection coated, 3.8 μm CW laser damage threshold obs. 80−33053
CaF_2, fine-grained, forging and bulk optical props. 80−33103
CaF_2, hot forged, laser window material, fabrication, props. 77−46773
CaF_2, hot forged, refr. index, temp. coeff. 77−46772
CaF_2, illuminated over large area, optical strength 77−75593
CaF_2, large optical crystals, quality 80−33097
CaF_2, laser window material, absorpt. at CO wavelengths, calorimetric meas. 78−25911
CaF_2 laser window surface O_2 detection by X-ray photoelectron spectroscopy 79−14056
CaF_2, laser windows, intermediate temp. forging 77−46775
CaF_2, linear thermal expansion coeffs. meas., room temp. to 250°C 78−55416
CaF_2 low-loss laser window material, surface absorpt. meas. at 2.8 and 3.8 μm 79−94267
CaF_2, piezo-optical coeffs. meas. at 0.6328, 1.15 and 3.39 μm 80−34888
CaF_2, press forged, mech. and optical props. 80−38079
CaF_2, press-forged laser window, polishing, cleaning and grinding 79−59849
CaF_2, protection from biological overgrowths 78−18034
CaF_2, refr. index, 20-85°C, temp. depend. 77−8536
CaF_2, thermal expansion, 60-300K 78−33791
CaF_2, thermo-optic coeff., 95-175K 77−63403
CaFz crystals, grown from synthetic raw materials, quality, effect of impurities, composition 78−79083
$CaLa_4(SiO_4)_3O$:Nd, laser damage initiating inclusions 77−68246
$CdCr_2S_4$, hot pressed, Faraday effect isolation 10.6 μm, damage tests 77−46750
$CdCr_2S_4$, hot-pressed, optical isolation appl. at 10.6 μm, intrinsic absorpt. props. 78−42368
$CdGeAs_2$ crystals, Bridgman grown, optical props. rel. to O_2 content of starting materials 80−81213
$CdGeAs_2$, IR nonlinear material, laser induced surface damage 77−19266
$CdGeP_2$ synthesis and cryst. growth 79−87577
$Cd_{14-x}P_4S_{24-2x}I_{2x}$, icosahedral structs., synthesis and characts. 77−1107
CdS, temp. coeffs. meas. of refr. index and birefr. 77−55762
CdSe, two-photon absorption, laser calorimetric obs. 80−33076
CdTe, 10.6 μm absorption meas. using thermal emission 77−1649
CdTe, absorbing precipitates, catastrophic laser damage threshold estimate 78−25913
CdTe, cryogenic refractive indices and temp. coeffs. meas. 80−7319
CdTe, IR transmitting semicond., dn/dT, wavelength depend. 77−77163
CdTe, laser window material, absorbing Te inclusions, damage threshold 77−46749
CdTe, laser window material, vap. deposition, mech. props. 77−46776
CdTe, laser window material, vap. deposition 78−27391
CdTe optical applications, review 77−42580
CdTe, single cryst. IR laser window, low absorption at 10.6 μm 78−79081
CdTe single crystal IR window for CO_2 laser 77−75566
CdTe two-photon absorption, laser calorimetric obs. 80−33076
CdTe/HgTe superlattice, new IR material 79−72634
CsBr, cryogenic temp. IR refractive index obs. 80−7320
$CsCuCl_3$, optical props. rel. to IR electro-optical modulator appl. 78−42393
$Cs(D_xH_{1-x})_2AsO_4$, soln. cryst. growth, optical absorpt. and SHG phase match data 78−11095
CsI, cryogenic temp. IR refractive index obs. 80−7320
CsI, crysts., microplasticity mechanism 78−30696
α-$CsNd(PO_3)_4$, single cryst. struct. and spectral-luminescent props. 80−96490
Cu_2HgI_4, thermochromic material, IR hologram recording 79−86135
Eu_2O_3-Gd_2O_3-Ta_2O_5 system at 25, 50 and 75 mole.% Ta_2O_5, cross section investig. 77−12607
GaAs, 10.6 μm absorption meas. using thermal emission 77−1649
GaAs, aircraft IR window appl., development 77−72038
GaAs, and its alloys, as integrated optics materials, book contrib. 79−64362
$Gd_3Ga_5O_{12}$, opt. dispersion 78−64343
$Gd_2(MoO_4)_3$, and isotypes exam. of crystal growth, and defect generation 78−68617
$Gd_2(MoO_4)_3$, spontaneous birefringence, pulsed field switching, compression effect, domain movement 78−27187
Ge demand evaluation and supply comparison 80−33106
Ge, IR nonlinear material, laser induced surface damage 77−19266
Ge IR optical characteristics and performance requirements 80−48363
Ge, linear thermal expansion coeffs. meas., room temp. to 250°C 78−55416
Ge, monocryst., for IR optics, prod. techniques and characts. 78−50873
n-Ge, nonlinear absorption of CO_2 laser radiation by nonequilib. carriers 79−32000
Ge, polycrystalline thermal-imaging lens, optical requirements 80−69495
Ge, Sellmeier coeffs. temp. depend., nonlinear optics average power limit 79−50349
Ge single cryst. prism, refr. index meas., interlaboratory comparison 78−54443

optical materials continued
Ge, thermal expansion, 60-300K 78−33791
Ge transparent IR window design for uniform pressure loading 79−23088
HFO_2, vacuum deposited film, use in multilayer reflector for near UV 77−34924
α-HIO_3, near IR absorpt., influence of deuteration 78−27237
$Hg_{1-x}Cd_xTe$, Faraday effect at CO_2 laser freq. 78−64348
$Hg_{1-x}Cd_xTe$, homogeneous single cryst., growth by modified Bridgman technique 78−39682
Hg_2Cl_2, cryst., birefringence and dichroism, 200-500 nm and far IR 78−27257
$HgGa_2S_4$, melt growth, optical props. and SHG, HgS-$HgGa_2S_4$ phase diagram 80−50548
HgI_2, cryst. growth from soln., doping rel. to elec. cond., phase transitions 77−55880
KBr, additively coloured crystal, depend. of bleaching kinetics on F-light intensities, holographic storage *(Russian)* 79−27351
KBr crystal, cordlike defects and countermeasures 79−72636
KBr, plate, distortions due to 10.6 μm laser irrad., interferometric obs. 78−46697
KBr purification for laser components, selective ion filter design and construction 79−14051
KCl, absorpt. coeff. meas., using pulsed CO_2 laser, calorimetric method 78−18028
KCl, absorption coeff. determ. in 10.6 μm region, laser calorimetry method 79−7186
KCl, bulk and surface absorpt., 2 to 10 μm, calorimetric meas. 78−71160
KCl, bulk and surface absorption comparison, 9.2 to 10.85 μm 80−33051
KCl, cryst. laser irrad. effects, electron microscopic obs. 77−73192
KCl crystals with NaF surface absorpt. regions, photoacoustic detect. 79−87466
KCl diamond turned window surfaces, 10.6 μm pulsed laser damage 77−50704
KCl IR window material, polish layer effect, ellipsometric meas. 78−55419
KCl, internal damage threshold for CO_2 laser pulses rel. to absorption 77−75594
KCl, laser produced shocks rel. to material damage 78−31285
KCl laser window, thermal lensing, effective optical distortion parameter 77−83916
KCl, laser window material, absorpt. at CO wavelengths, calorimetric meas. 78−25911
KCl laser windows at 10.6 μm, optical distortion parameter 78−79036
KCl, linear thermal expansion coeffs. meas., room temp. to 250°C 78−55416
KCl low-loss laser window material, surface absorpt. meas. at 2.8 and 3.8 μm 79−94267
KCl, optical breakdown, γ-irrad. effects, rel. to appl. in high power lasers 77−8507
KCl, photoelastic consts. at 10.6 μm, interferometric and polarimetric meas. 78−25934
KCl plate, distortions due to 10.6 μm laser irrad., interferometric obs. 78−46697
KCl, surface radiative absorption meas., acoustic technique 77−3596
KCl surface texture and optical props. after forging between polished dies 80−33102
KCl, thermal expansion, 60-300K 78−33791
KCl, zone refined single crystal growth for high power CO_2 laser optics 78−22181
KCl:Ca, vol. holographic grating, modulation characts. 79−94197
KCl:Cu, additively-coloured crysts., for hologram recording plates *(Russian)* 78−29914
KCl:Eu IR laser window lattice equilibrium obs. 79−14055
KCl:K, F-centre coloured, for highly efficient holographic storage 78−37833
KCl:LiCl photodichroic crystals as adaptive spatial filters 79−72713
KCl:Na, photoinduced reorientation of A-centres near room temp. 78−64344
KCl:OH, absorpt. in high-transparency region 80−89037
KCl:RbCl, $SrCl_2$, IR window material, cryst. growth and props. 78−31333
KCl:RbCl, $SrCl_2$, laser window material, prep., grain boundary stability 77−46774
KCl-KBr mixed crystals, microhardness studies, nonlinear depend. on composition 78−83872
KCl(Br)(I), far IR complex refr. indices, dispersive Fourier transform 78−80322
$KD_{2x}H_{2(1-x)}PO_4$, deuteration effect on refr. index 77−59550
KF:LiF, photodichroic, real time recording medium, for optical spectrum analyzer 78−71174
KF:LiF, photodichroic real-time recording medium, for optical spectrum analyser 78−66878
KF:LiF photodichroic crystals as adaptive spatial filters 79−72713
KH_2PO_4, cryst. laser irrad. damage threshold, surface finish and defects effects *(German)* 78−59058
KH_2PO_4, near IR absorpt., influence of deuteration 78−27237
KH_2PO_4, optical props., plastic deform. effect 77−59552
KH_2PO_4, real structure influence on optical strength 79−7187
KH_2PO_4, thermal expansion, 60-300K 78−33791
KH_2PO_4, vac. UV transmission 77−73150
$KMgF_3$ residual IR absorption, freq. and temp. dependence obs. 79−15468
$KNbO_3$, single domain crystal growth, SHG with Nd:YAG laser 78−74954
$KNbO_3$, growth from soln. in melt and characterisation of optical quality cryst. 77−8741
$KNbO_3$:Fe, large single domain cryst., growth and prep. for optical storage 77−1799
$K_xRb_{1-x}TiOPO_4$, new nonlinear optical material 77−14784
$KTa_{0.65}Nb_{0.35}O_3$, ferroelectric devices for optical systems 78−90473
La_2O_3-P_2O_5-H_2O, solubility, regions of crystallisation, 100-500°C 77−16483
$LiBi(MoO_4)_2$, acoustooptic characteristics 79−8118
LiF ground surface, structure features of dull layer 77−54763
LiF mech. and optical props. rel. to forging conditions 80−33101
LiF, press forged, mech. and optical props. 80−38079
LiF_2, protection from biological overgrowths 78−18034
α-$LiIO_3$, cryst. growth of high piezoelec. and optical quality 78−31313

optical materials continued
α-$LiIO_3$, cryst. growth by conc. convection of soln. 78−72716
α-$LiIO_3$ single crystal, enantiomorphism 79−95725
$LiIO_3$, visible and UV refr. indices 78−19439
$LiNbO_3$, cryst., US vibrating laser beam diffr. *(Russian)* 78−31172
$LiNbO_3$ crystal, elec. cond., optical quality, impurity depend., space charge pyroelectric field compensation 79−64295
$LiNbO_3$, doped, photorefr. and photovoltaic effects 77−38835
$LiNbO_3$, ferroelectric devices for optical systems 78−90473
$LiNbO_3$, laser-induced optical damage, electrostatic obs. 78−18030
$LiNbO_3$, linear thermal expansion coeffs. meas., room temp. to 250°C 78−55416
$LiNbO_3$, optical stability to laser pulse, 1.54 μm 79−3734
$LiNbO_3$, optical strength, surface layer influence 78−50843
$LiNbO_3$ optical waveguides, elimination of Li_2O out-diffusion waveguide 77−65641
$LiNbO_3$, photorefractive medium, hologram form. theory 77−68185
$LiNbO_3$, thermal expansion, 60-300K 78−33791
$LiNbO_3$, vol. holograms, photorefr. recording dynamics, multiple storage 77−38834
$LiNbO_3$:$^{57}Fe^{2+}$ Mossbauer spectra, EFG axis 77−20760
$LiNbO_3$:Fe, calc. of photorefraction *(Russian)* 78−90474
$LiNbO_3$:Fe, characts. for holographic storage appls. 77−23630
$LiNbO_3$:Fe, thermally activated trapping caused by small polaron formation 77−20259
$LiNbO_3$:Fe spatial holograms, ageing mechanism and thermal fixing *(Russian)* 80−74311
$LiNbO_3$:Ti, dopant conc., refr. index profile rel. to integrated optics 78−5583
$LiNbO_3$:transition metal, photorefr. effect, 1.5-4.0 eV 77−28213
$LiNbO_3$ Li_2O diffusion for chemical control of laser induced optical damage 78−46693
$LiNb_{1-y}Ta_yO_3$, Czochralski growth and basic props. 77−63556
$LiNb_{1-y}Ta_yO_3$, Czochralski grown, refr. index, 5893-10600 Å, and zero birefr. 78−31166
Li_2O-Ta_2O_5 system phase diagram 79−47668
$LiRF_4$, R=rare earth, laser matrices prep. and characterisation 77−24945
$LiTaO_3$, refr. index distrib. after surface lapping, theory 78−72479
$LiYF_4$, prep. and crystal grwoth for laser appls. 77−55879
$LiYF_4$ UV reflectance, transmission and photoluminescence obs. 79−15488
$LiYF_4$, UV window and coating materials, two-photon absorpt. coeffs. 79−59734
$Lifa O_3$, optical waveguides, elimination of Li_2O out-diffusion waveguide 77−65641
$MgAl_2O_4$, spinel materials press forged, mech. props., IR appl. 78−39722
MgF_2, 0.36 μ absorptance/fluence dependence obs. 79−15506
MgF_2, Fabry-Perot etalon plates for vac. UV 77−5895
MgF_2, grinding, polishing, mech. props. anisotropy effect 77−797
MgF_2, hot pressing in vacuum, compaction kinetics, selective recryst. 77−16517
MgF_2, optical ceramic, synthesis 78−52729
MgF_2 optical window, VUV light source, low-current AR arc 79−35856
MgF_2 refractive index and extinction coefficient meas., 115 to 400 nm 79−78640
MgF_2, single cryst., tensile strength and yield point, temp. depend. 77−14785
MgF_2, thermal expansion, 60-300K 78−33791
MgF_2:Ni, growth by vertical gradient freeze method, in self-sealing graphite crucibles 78−31334
MgO:Cu, dopant conc., refr. index profile rel. to integrated optics 78−5583
Mo laser mirror, optical and metallurgical characterisation 80−33129
$NH_4H_2PO_4$, vac. UV transmission 77−73150
NaCl 46 cm window optical evaluation facility 80−74526
NaCl, bulk and surface absorpt., 2 to 10 μm, calorimetric meas. 78−71160
NaCl, bulk and surface absorption comparison, 9.2 to 10.85 μm 80−33051
NaCl Czochralski crystal growth for large CO_2 laser windows 80−74525
NaCl, damage induced by CaF_2:Er^{3+} laser radiation at 2.76 μm 79−91539
NaCl, illuminated over large area, optical strength 77−75593
NaCl, internal damage threshold for CO_2 laser pulses rel. to absorption 77−75594
NaCl large window continuous polishing 80−74527
NaCl, laser-induced damage threshold variations 80−14380
NaCl, plate, distortions due to 10.6 μm laser irrad., interferometric obs. 78−46697
NaCl Polytran laser windows, for CO_2 lasers, fusion appls. 78−59067
NaCl surface with adsorbed water layer, absorpt. and thickness meas. 80−16001
NaCl window production for Antares CO_2 laser system 80−74524
NaCl:Ca, light scattering coeff., effect of growing condition 78−55418
NaF coating defects and impurities affecting damage threshold and absorptance 79−14065
NaF crystal M-centre storage element, photosensitive characteristics 79−14067
NaF, IR window coating, prep. and optical props. 77−50736
NaF photodichroic crystals, hologram synthesis in in-line scheme 77−88670
NaF:Li, combined suppressive and extinction writing, using $M(M_A)$ centres 77−7164
NaF(Cl), far IR complex refr. indices, dispersive Fourier transform 78−80322
$Na_2Nd_2Pb_6(PO_4)_6Cl_2$, laser material, flux growth *(French)* 78−35288
NdP_5O_{14}, fluoresc. lifetime meas., IR and photoacoustic spectroscopy 80−60652
NdP_5O_{14}, laser site-selection time-resolved spectroscopy 78−76524
PLZT ceramic birefringence props., transverse electro-optical meas. 78−72487
PLZT ceramics, electro-optic characts., w.r.t. future instrument applics. *(German)* 78−33792
PLZT ceramics, optical recording *(French)* 77−31078
PLZT, ferroelectric devices for optical systems 78−90473
$Pb_2AgNb_5O_{15}$, $Pb_2AgTa_5O_{15}$, ferroelec. and ferroelastic props. *(French)* 79−24266
$(Pb_{1-y}Ba_y)_{1-x}La_xNb_{2-x/5}O_6$, transparent ferroelec. ceramic, optical transmittance, electrooptic props. and Curie temp. 77−32395

optical materials continued
$Pb_5Ge_3O_{11}$, Czochralski growth, secondary phase formation 78−3027
$PbHPO_4$, single cryst., growth, optical props., ferroelec. transition 78−35285
$Pb_{1-x}Hg_xS$ film, IR detector material, struct. and IR props. 78−26775
$PbMg_{1/3}Nb_{2/3}O_3$, photocond., 20-150°C, and photoelectret state 77−24590
$Pb_3MgNb_2O_9$, crystal growth procedure, meas. electro-optic and dielectric props. 78−88418
$Pb_3MgTa_2O_9$, crystal growth procedure, meas. electro-optic and dielectric props. 78−88418
PbTe, high mobility polycrystalline layer, mol. beam deposition 79−83138
$PbWO_4$, Czochralski growth method, optical props. 78−60566
$Pb(WO_4)_{1-x}(MoO_4)_x$ mixed crystal, growth by Czochralski method, props. 78−60566
$Pb(Zr,Ti)O_3$ photovoltaic ferroelectric as optical memory storage medium 78−50877
RbCl(Br)(I), far IR complex refr. indices, dispersive Fourier transform 78−80322
$RbD_{2x}H_{2(1-x)}PO_4$, deuteration effect on refr. index 77−59550
S powdered pressings proposed near IR reflectance standard 78−90464
Si amorphous films, laser beam annealing, optical information storage possibilities 79−87515
Si, beam extinguishment device, without scatter 78−87126
Si, refr. index, 95-298K, 2.5-12 μ 77−8535
Si single cryst., chem.-mech. polishing of low-scatt. optical surface 80−96040
Si:B(P)(Sb), single cryst., transmission characts. for IR optical components 77−27325
SiC, CVD, polished, total integrated vac. UV scatt. 77−62029
SiO_2, fused, high-temp. darkening and absorption spectra meas. 77−36258
SiO_2, fused, surface roughness rel. to prep. and treatment history 79−14058
SiO_2, fused silica, continuous inhomogeneities, refusing effect in H_2 77−50734
SiO_2:B_2O_3 doped, IR spectra 79−78664
SiO_2-TiO_2 antireflection coatings, 1064 nm 150 ps laser pulse damage rel. to barrier layering and smoothness 79−14018
SiO_2-TiO_2 stack reflector and antireflection coating, 1064 nm 180 ps laser pulse damage 79−14017
SmS film, laser beam threshold recording energy density meas. method 78−5520
SmS film for holographic storage, laser-induced semicond.-metal transition 77−88676
(Sr,Ba)Nb_2O_6:Ce, high sensitivity holographic storage 77−71953
$Sr_2AgNb_5O_{15}$, $Sr_2AgTa_5O_{15}$, ferroelec. and ferroelastic props. *(French)* 79−24266
$Sr_{0.75}Ba_{0.25}Nb_2O_6$, ferroelectric devices for optical systems 78−90473
$Sr_{0.75}Ba_{0.25}Nb_2O_6$, large cryst. growth, control of opt. defects 78−76595
$Sr_{1-x}Ba_xNb_2O_6$ crysts., defect-free growth 80−108346
SrF_2, 0.36 μ absorptance/fluence dependence obs. 79−15506
SrF_2 antireflection coated, 3.8 μm CW laser damage threshold obs. 80−33053
SrF_2 fusion-cast prism refractive index obs., 0.2138 to 11.475 μm 80−34882
SrF_2, IR window coating, prep. and optical props. 77−50736
SrF_2, laser window material, absorpt. at CO wavelengths, calorimetric meas. 78−25911
SrF_2 piezo-optical coeffs. meas. at 0.6328, 1.15 and 3.39 μm 80−34888
SrF_2, press-forged laser window, polishing, cleaning and grinding 79−59849
SrF_2 purification for laser components, selective ion filter design and construction 79−14051
SrF_2, refr. index, 20-85°C, temp. depend. 77−8536
$SrTiO_3$ electro-optic crystals, mechanical grinding and polishing 80−48471
$SrTiO_3$, fabrication damage characterisation by internal and external meas. 80−102782
$SrTiO_3$, flame fusion growth of optical quality crysts. 78−11099
Ta_2O_5, plane optical waveguide, fabrication by reactive sputtering 78−71221
TeO_2, single crystals, acousto-optic props., optical information processing *(Russian)* 77−55768
TeO_2, visible and UV refr. indices 78−19439
Tl halide single crystals, spectral transmission meas. 77−59581
Tl_3AsSe_3, IR nonlinear material, laser induced surface damage 77−19266
TlBr-TlI, TlBr-TlCl, KRS-5 and KRS-6 crystals, optical losses, laser calorimetric meas. 80−9973
TlBr-TlI, TlCl-TlBr, KRS-5 and KRS-6 crystals, refr. index temp. increments meas. 80−33098
TlBr-TlI KRS-5 single crystals, acousto-optical characts. 78−71165
TlBr-TlI(Cl) crystals, photoelastic moduli 80−97230
$TlBr_{0.42}I_{0.58}$, KRS-5 crystal, 10.6 μm absorption obs. by laser calorimetry 79−50360
TlCl-TlBr, internal damage threshold for CO_2 laser pulses rel. to absorption 77−75594
TlCl-TlBr, KRS-5, KRS-6 crystals, optical strength pulsed CO_2 laser radiation 79−27307
$TlCl_{0.7}Br_{0.3}$, KRS-6 crystal, 10.6 μm absorption obs. by laser calorimetry 79−50360
V oxides, FTIROS, polarisation of recorded image spectrum 77−75439
VO_2 film, dynamic hologram recording *(Russian)* 77−10873
V_2O_3, FTIROS thermochromic materials, colour and visual contrast 80−33100
$Y_3Al_5O_{12}$, laser cryst., struct. inhomogeneity obs. by vac. decoration 77−35701
Y_2O_3 sintered pieces, optical transmittance 80−40561
Y_2O_3:ThO_2, IR absorpt., 2-4 μm 77−55805
$ZnGeP_2$, synthesis, characts., applic. to laser windows *(French)* 78−80467
ZnO-$Al_2O_3SiO_2$, transparent glass-ceramic, microstruct., physical props., crystallisation ht. treatment depend. 78−80506
ZnS CVD IR material specifications 80−48364
ZnS CVD IR window, optical and physical characteristics 80−106620
ZnS, CVD sample, refractive index var. with temp., 22° and 34°C 79−14053
ZnS CVD window, IR lattice absorption, phonon assigments and image spoiling 80−33104

optical materials continued
ZnS CVD windows for forward looking IR radar systems 78−46816
ZnS hot pressed microcryst. compact, Irtran 2, refr. index meas. 78−66877
ZnS, linear thermal expansion coeffs. meas., room temp. to 250°C 78−55416
ZnS-MgF_2/MgF_2 double-layer antireflection coatings, transmittance meas. 79−36967
ZnS(Se), IR transmitting semicond., dn/dT, wavelength depend. 77−77163
ZnS(Se) multispectral aircraft window materials, production processes 77−73237
ZnS(Se), thermal expansion, 60-300K 78−33791
ZnSe, 10.6 μm absorption meas. using thermal emission 77−1649
ZnSe, CVD, laser window material, impurity absorpt. meas. 78−25909
ZnSe CVD IR material specifications 80−48364
ZnSe, coated/uncoated, effect of sand erosion on optical absorption 77−72037
ZnSe, commercial feasibility for optical ceramic manufacture 79−87598
ZnSe crystal, refr. index temp. increments meas. 80−33098
ZnSe, IR absorpt., temp. depend. 78−48155
ZnSe, IR laser window coating absorption rel. to deposition conditions 79−14061
ZnSe, laser window material, multiphonon absorpt. temp. depend., calorimetric meas. 78−25907
ZnSe, laser window material, absorpt. at CO wavelengths, calorimetric meas. 78−25911
ZnSe, linear thermal expansion coeffs. meas., room temp. to 250°C 78−55416
ZnSe, RF bias-sputtered CVD films on CaF_2 79−14060
ZnSe, refr. index meas. at 3.8 μm, 10.6 μm, 80 to 300K 79−82938
ZrO_2-$ZrTiO_4$, for high index layers, deposition 77−753
$ZrSiO_4$, single cryst. growth from soln. in melt, solvent system selection 80−55285

optical microscopes
see also optical microscopy
accommodation focusing control 80−82814
annular lenses in microscopes, imaging props., calcs. 80−22426
attachment for low temp. operation 80−47099
automatic focusing servo mechanisms, piezoelec. and electrodynamic, for microscope objective 80−73445
automatic microimage analyser, MORPHOQUANT 78−37053
autostigmatic, radius of curvature meas. of soft corneal lens 77−60198
bifocus element for microscope objectives 77−41680
binocular tube alignment method *(Russian)* 77−10102
birefringence detection system for polarisation opt. props. meas. 77−57385
blink microscope, exam. of new microscope at Lyon Observatory *(French)* 78−61742
boring attachment for isolating small specific areas from slide embedded monolayers in electron microscopy 78−53596
chromatic aberration-free projection system, CF 78−89534
chromatic-aberration-free microscope optics 80−86395
circumfusion chamber for microscopy of living single cells and other particles *(German)* 77−44865
cleaning of components, using solvents in US field *(Czech)* 79−40608
coherent optical processor with interference contrast microscope input 80−43281
cold stage for vacuum etching and freeze drying, comments and replies 78−54450
computerised focusing technique 77−22596
confocal scanning microscope, image form. 80−68249
confocal scanning microscope, imaging modes 80−42257
confocal scanning microscope with high-aperture immersion lenses, imaging characts. 80−42256
contact microscope for medical laboratory use 80−85540
contrast types generation, microscope adaptation 77−79146
cytogenetics microscope for automatic metaphase spread finding 77−56550
depth of field in scanning microscope 78−86328
design of instrument optics from basic elements 77−58418
dividing head adjustment test bench 77−30202
double-image system for measuring rotating objects 77−87822
electrophoretic measuring microscope, PARMOQUANT, biological appl. 79−79700
electrophoretic measuring microscope, test results with PARMOQUANT 79−79701
EPIQUANT automatic structure analyser for inclusion investigs. in free-cutting steel 80−55609
fluorescence microscope, FLUOVAL 2 79−49281
fluorescence polarisation microscope for cell membrane fluidity screening 77−44855
focusing screw mechanism improvement 77−30201
focusing system design for single mode laser 77−7109
focusing technique for digital image anal. system 80−68250
folding pocket microscope of 1920s 79−85176
Fourier transform microscope, with optical spatial filtering 78−58028
freeze drying microscope stages 78−45681
general-purpose meas. microscope with photoelectric readout 79−71524
grainless focusing screen for light scatter reduction 80−101836
hardness impression measurement, laboratory standard microscope 79−21808
harmonic, imaging props. and super-resolution 79−97430
high-temperature laser microscope, design details 80−90891
holographic, theory and appls., review 78−45690
holographic attachment for microscope 77−23631
holographic interferometric, for dynamic systems obs. 78−45685
holographic lens assisted system, resolution tests 78−46539
image detail enhancement system, for photographic recordings 78−58086
image formation, nonuniform source distrib. 77−14664
image formation in scanning microscopes with partially coherent source and detector 78−58923
image quality, effect of magnification distrib. between objective and eyepiece 80−18013
impressions in alloys, portable microscope for parameter meas. with 1 μ accuracy 77−53856
interference microscope, VELOMET interphako, for optical path difference measurement 78−37054
interference microscope with electronic image formation *(Slovak)* 80−31862

optical microscopes continued
interference microscope with freq. shift, for glass fibre refr. index profile meas. 80−64175
interference microscopes, calibration standards *(Slovak)* 79−71522
interferometric attachment 79−85179
inverted, differential interference contrast, appl. to study of in vitro perfused nephron 80−51303
inverted camera microscopes, IM 35 and ICM 405, for biology, medicine and metallography 79−30540
inverted incident light microscope, METAVAL, for metallographic examinations 79−49282
IR, interference and phase contrast microscopes 77−74496
IR laser and defectograph, semicond. flow detection 78−3299
IR microscope linked with TV display, for optical material control 79−17483
LAMMA mass analyser, laser microprobe *(German)* 79−29419
large field, for use in semiconductor manufacture 80−82812
laser Doppler, capillary blood flow of frog web study 77−36964
laser Doppler microscope, vel. measuring device 80−68251
laser Doppler microscope for blood velocity meas. 79−62329
laser Doppler microscope period meas. signal analyser *(Japanese)* 79−88998
laser Doppler microscopes for flow vel. meas. 78−37052
laser microbeam microscope, neuronal cell culture appl. *(German)* 78−3694
laser microscope *(Japanese)* 79−75589
laser projection microscope, transmitted light, Cu vapour laser as image amplifier 80−73446
laser projection microscope, with brightness amplifier for biology and medicine 80−76875
laser projection microscope with brightness amplifier *(Russian)* 79−98498
laser projection microscope with image-brightness amplifier using Pb and Mn vapour 80−106541
laser Raman spectrometer, 180° microscope sampling and viewing attachment 80−13150
laser-scanning, high resolution and depth of field 79−26118
Leitz Laborlux 11 and Leitz Laborlux 12, two new microscopes for the investigation of transparent objects 80−82813
lens objectives, visible and UV, for microscopes and microspectrophotometers 79−75591
light-reflection microscope image flare factor rel. to illumination system aperture 79−14083
line standard meas. using He-Ne laser photoelectric microscope 77−82599
manipulator for use with small crysts. on metallographic microscope 77−52567
measuring instrument standardisation 77−71357
medical microscopy, advent of intelligent microscopes 80−81678
membrane slide support for living cell obs. 79−74809
micro-objective, light transmitting, fogging field glare meas. 79−75590
micro-optics quality testing 79−27368
microdensitometer performance, effective incoherence and flare tradeoff 80−77851
microfluorimeter design for medical-biological research 79−57818
microscope-photometer for visible region absorpt. of single living cell *(German)* 79−66588
microscope-spectrophotometer, computer processed, for measurement of absorption spectra of rock-forming minerals 80−18010
modulation contrast, microphotography appl. 78−89533
modulation contrast microscope, coherence theory 77−7010
modulation contrast microscope, image irrad. rel. to phase gradient, numerical aperture influence *(Spanish)* 79−55063
modulation contrast microscope, principles and performance 78−62221
molecular microprobe, microscope system 78−45686
MORPHOQUANT automatic microscope image analyser, universal program system 80−56160
moving-condenser electrodynamic unit, for fast scanning microspectroscopy 77−5903
Nomarski reflection microscope, metallic mirror surface topography determ. 79−54185
nonachromatic objective design, for track obs. in nuclear emulsions 77−400
object table with articulated lever guides 77−74495
oculars, types and properties 79−71521
ophthalmological instruments and eye models in teaching, training and education 80−51993
optical instrument manufacturing, cyclical growth characteristics and prediction 79−76862
oral neoplasm geometry stomatoscopic apparatus 79−39539
paraboloid epimirror for microscope illuminator, design 80−28304
partially coherent imagery, calc. method 78−90373
particle size analysis using an ultramicroscope, laser illuminated 79−44902
PCB blind hole misalignment meas., dual microscope system 79−75586
phase contrast microscope attachment for weak phase object visibility 80−86396
phase contrast microscope with Ar laser and photon counting system, for cell ATP meas. 79−79695
phase-locked interference microscope, design and construction 78−49894
phase-locked interferometric, design and construction 78−45687
photoelectric, scale graduation reading method *(Russian)* 77−26395
photoelectric line locating chopper microscopes, classification *(German)* 77−74494
photoelectric microscope with oscillating slit 78−82030
photoelectric scanning, linearising methods comparison 77−5905
photoelectric setting microscopes, recent developments 77−41681
photomacrography, high resolution, zoom instrument with automatic exposure 80−62756
photometer/semiautomatic image anal. instrument system for morphometric and photometric value meas. 80−82815
photomicroscopes with automatic exposure control 80−86475
planetary lander camera, quasi-microscope for improved resolution 77−91426
polarisation adapter, for transparent material anisotropy and internal stresses meas. 80−31863
polarising microscope, resolving power in partially coherent light 77−87819
polarizing microscope, with crossed polarizers, incoherent diffr. imagery 80−101838
polarizing microscope components and applications 80−98973

optical microscopes continued
Polyvar, design of mech. tube length using infinity-corrected objectives 79−80678
production applic. for inspection 77−41679
programmed controlled temperature microscope stage 79−35821
projection, optical test equipment appls. in electronics industry *(German)* 80−77849
quality control and industrial production, new microscopes 80−82816
quantitative microscope for clinical appls. 77−60273
quasi-microscope concept for planetary missions, stereo pictures 78−81546
Raman effect optical microscope *(French)* 77−56290
reentrant Dewar, modified, for magneto-optical flux detection in superconductors 78−89486
reflected-light fluorescence microscope, LABOVAL 2a.fl, for routine and research 80−56300
reflected-light microscope, optical system effect on stray image light 78−45682
resolution of two pinholes by semitransparent and phase annular aperture, Gaussian illum. 77−53972
resolution power, influence on estimation of basic method spatial struct. parameters 79−52543
resonant scanning optical microscope, nonlinear interaction enhancement 78−93758
rotatable microscope stage, used for hybrid microcircuits inspection 80−90889
rotating mirror, Dimant, photomicrographic anal. of spray 77−36800
scanning, based on electron beam pumped CdS laser 80−31864
scanning, contrast and resolution, nonlinear effects 78−29154
scanning, imaging props. and appls. review 80−82811
scanning, increased depth of focus using slit aperture, MTF degradation 78−45689
scanning, multiple traversing of the object 80−90890
scanning, operation and appls. 80−47098
scanning, resolution, contrast and depth of focus improvements 78−29155
scanning, spherical aberration effect on imaging props. 79−58783
scanning, using semiconductor laser with longitudinal electron pumping 80−18012
scanning and conventional, Fourier imaging of phase information 80−73444
scanning and conventional imaging systems, basic equivalence 78−46534
scanning and reflection scanning types 79−21809
scanning for semicond. materials and devices 80−95136
scanning harmonic microscope, using CW Nd:YAG laser 77−87821
scanning IR microscope, photodetector field of view correction using additional mirror 80−52304
scanning laser microscope, electron beam excited 80−52303
scanning microscope image formation 80−86399
scanning microscope stage for microdensitometry, computer-controlled 79−26117
scanning microscopes, resolution criteria rel. to radiation detection technique 80−33388
scanning mirror, with optical sectioning characts., ophthalmology appls. 80−85461
scanning optical microscope, second harmonic imaging 78−82029
scanning optical microscope 79−9242
scanning optical microscope as new metallographic tool 80−71852
scanning stage, motion rectilinearity determ., method and device 80−10055
scanning type, description 77−87820
scanning type 2 microscope, bar-pattern image, effect of annular lenses 78−89535
scanning types 1 and 2, image form. 77−79148
selection criteria w.r.t. applications 80−13132
slit scanning photoelectric, image production of linear objects *(German)* 78−77978
small flow-through cryostat for polarization microscope 78−86327
stereo microscope construction and appls. 79−54184
stereophotography, using camera slit lamp, ophthalmic applications 78−48904
stereoscopic, MBS-9, design 77−57386
stereoscopic microscopes, domestic, review 80−27342
surface profile microscope, portable, design and performance 77−67495
surgical, model 310, photographic documentation in eye operations 80−56161
teaching microscope for investigation of transparent biological objects 80−82622
testing, universal set of attachments design 77−5907
three dimensional, tracking of bacterial dispersal 80−30965
three-coordinate workshop meas. machines 80−27280
tilt stage for stereoscopy 80−21587
tissue analysis by IR microinterferometer 79−79714
tracking microscope, design and operation 80−36214
transmission, object diffr. evaluation, object and field stop spectrum separation *(German)* 78−92685
TV microscopy system for teaching and quality control 80−82817
two point resolution, semitransparent π-phase annular aperture 77−82597
two-coordinate measuring microscope, supplementary unit 79−75588
two-coordinate measuring microscopes development 78−21213
two-coordinates measuring microscope, ZKM 02-250 79−75587
UIM-21 and UIM-23 (USSR), fitting of length meas. heads 80−57257
universal research and photomicroscope 77−57384
UV microscope for polarised light, determ. of birefringence, linear dichroism and optical rotary dispersion *(German)* 78−29152
VERTIVAL with interference contrast equipment after NOMARSKI for gonorrhoea types classification 80−56301
virometer, real time virus detect. and identification in biological fluids 78−7555
white light interferometric microscopes 79−223
wide-angle concentric dome and shell production, double-pass null test 80−79022
wide-field objectives, image forming quality 79−35819
Au vapour brightness amplifier at 627.8 nm, for projection microscope 80−83616
CuCl vapour laser, use for image amplification in projection microscope system 79−98407

optical microscopy
see also optical microscopes
F-actin, struct. changes in living muscle fibres, polarised UV fluoresc. microscopy 80−67037
n-alkane, long chain, syntactic coalescences between monoclinic and orthorhombic polymorphs 80−10520
p-alkoxy-phenyl-p-acryloyloxy benzoate polymers, mesomorphic struct. 80−38905
Allende meteorite, occurrence of Fe-Ni-Cr-S-O compounds *(French)* 78−32411
Amici's contribution 77−57138
anthracene crystals, growth in melts of cholesteryl-caproate-anthracene system 80−2943
asbestos fibre, identification techniques 77−60018
asbestos fibre counting by automatic image analysis 80−73538
asphcrising layer prod., monitoring by interf. fringes in periscopic microscope 77−14820
ATP measurement in single red blood cells using firefly biolum. reaction 78−48951
attachment for studying adhesion and stripping of metal coatings on transparent substrates 79−49280
automatic fluorescence microscope photometry data processing and display *(German)* 80−86369
automatic image analyser, performance, appls. *(German)* 78−4691
automatic image analysis, variables and errors, definition and quantitative description, nuclear carbons appl. *(German)* 78−25296
automatic image analyzer appls., densitometric and geometric studies 80−98974
automatic microstructure analyser, construction and operation, optical mechanical scanning advantages *(German, English)* 77−77697
automatic structure analyser, EPIQUANT, linear anal. of histologic preparations 78−40443
automatic structure analyser, EPIQUANT, quant. microscopic meas., of ceramic materials 79−83409
autoradiography, double radionuclide methods for tissue sections or cell smears, using light microscopy 77−5113
autoradiography, track density determ. in solid-state particle detector 79−85859
baryta crystal gas-liquid inclusion meas. with microscope heating stage 80−76967
benzil cored fibres, void-free cryst. growth, X-ray diffr. and optical microscopy study 80−71586
bidirectional illumination and viewing, living cells 80−51304
bimodal systems, particle size distrib. meas., forward scatt. techniques 79−21699
biological cell deposition system for deposition at predefined locations on microscopic slide 80−76876
biological image processing *(Japanese)* 80−81784
biological research, computer-assisted mapping with the light microscope 80−67308
biomedical low light level video fluorimetry and microscopy 77−44874
birefringence detection system for polarisation opt. props. meas. 77−57385
bis-(4′-n-heptyloxybenzylidene)-1,4-phenylenediamines, smectic phases, previously unclassified 79−77508
bituminous coal, identification of constituents for petrographic anal. 80−81888
book, advances in optical and electron microscopy, vol.7 80−31437
borided surface layers, Mossbauer and metallographic anal. 80−50769
brass (70:30), cold rolled, optical, X-ray and TEM exam. of deformation struct., and textures 78−88500
β_1 brass containing α-precipitates, reversible shape memory effect *(Japanese)* 78−60711
brass single crystal, intracrystalline slip bands in high temp. creep *(Czech)* 79−77604
brittle coating, ductility meas., four point bend test 78−48577
Brumberg, Y.E., biographical note 79−75309
bubble garnet, domain-wall dynamics in in-plane field 79−87296
caesium perfluorooctanate, thermodynamically independent nematic amphiphilic mesophase obs. 79−95126
camera system for automatic photomicrography 80−82841
camphor, rhombohedral, polycryst., compressive deform. and dynamic recrystn. 80−71698
carbonaceous mesophase, formation at lower temps. 79−90524
carbonaceous mesophase spherules, new mol. arrangement in mag. field, orientation behaviour 79−94869
carbonized bitumen, refractive index and absorpt. coeff. as measures of structural organization 79−35811
cartilage proteoglycan simultaneous localisation by light and electron microscopy 80−85571
cathodoluminescent microscopy of biological materials, improved resolution 77−56549
cell average size and shape meas. light scatt. photometry compared with microscopy 79−84030
cell element observations in same sections by light microscopy, TEM and/or SEM 80−85556
cellular identification of free cells by light microscopy and SEM 78−53589
cementite, in white pig Fe, deform. and fracture 77−4827
ceramic, brittle, specimen prep. for optical and SEM obs. *(German, English)* 80−35457
ceramic nuclear fuel, porosity characterization, optical and electron microscope exam. 78−44302
ceramics, crack propagation, microstructural aspects 79−15771
ceramics, porosity, exam. using image analyser and optical microscopy *(French)* 79−15880
ceramics specimen preparation, thin sections 79−52562
chamber for microscopical obs. of biophysical effects of US 77−13039
chemical, use of squaric acid as reagent 77−21450
chiral smectic C, distortion under shear, optical study 77−39536
cholesteryl acetate-cholesteryl octanoate system, phase transitions, thermoanalytical microscopy obs. 79−55871
chromosome analysis, automatic, specialised image treatment equipment *(French)* 77−37111
chromosome analysis by automatic image recognition *(French)* 77−37110
cinemicroscopic time-lapse unit circuit 79−67405
cinemicroscopy, beam deflection as alternative to light shuttering 78−21214
coke, metallurgical, microstruct., using refl. light microscopy and image anal. 80−66732

optical microscopy continued
coke, metallurgical, strength and struct. relationship 80−84997
colour schlieren technique 78−29151
compensator, Laves-Ernst, used to investigate regular intergrowths in incident light 79−96843
computer-controlled double-beam scanning microspectrophotometry for rapid microscopic image reconstructions 80−18008
conference, Reston, VA., USA (Apr. 1977) 78−45683
confocal scanning light microscopy, imaging modes 80−86401
confocal scanning light microscopy with high aperture optics 80−86400
contaminant particle microanalytical methods 80−86397
copoly(ethylene terephthalate)-p-oxybenzoate solns., polymer mesophases, optical microscopy obs. 79−99067
copper hexadecachlorophthalocyanine, radiation damage 77−19987
correlative light microscopy, SEM and TEM of argentaffin cells 80−85557
cover-slip and mounting-slide with graticule for light microscope and SEM exam. 78−29153
cracking metal surface deformation obs. by interference microscopy *(German)* 77−56210
crystal growth from high-temp. melt, reaction cell for microscopic obs. 78−64457
crystal optical orientation, large optical axis angles *(Chinese)* 80−68246
crystallography, optical, book 80−12862
crystals, interference fringes with projection hemisphere 79−94852
cubic single crystal, orientation determ. method using optical microscope 79−52482
culture device for cell growth, quantitative microscopy and autoradiography 78−65163
Cunial MNA13-3, Mn addition effect on props. 80−21035
cuvette, high-pressure, for investigating granule swelling of ion-exchange resins and cross-linked polymers 79−17482
cytofluorometric measurements by fluorescence extinction through a diaphragmed objective 80−67319
cytology, digital picture analysis 77−21650
cytophotometric and autoradiographic simultaneous anal. device 78−77172
defect visualisation in built-up soap multilayers 77−59186
desert varnish of Sonoran Desert, comp. from optical and electron probe microanal. 79−79834
detects in materials, direct observation and characterisation 78−88617
diamond, metastable overgrowths in dissoln. medium in Ni presence at atm. pressure 79−51030
diatom recognition and counting, matched-filter and statistical method 80−101304
p-dichlorobenzene, mol. cryst., martensitic phase transitions 77−19891
dielectric films, CW CO_2 laser-deposited, optical and struct. props. 80−7506
differential interference contrast microscopy, computer simulation 77−53973
diffraction analysis, in microscopy 80−32926
diffraction images of bar and edge objects, influence of optimum balanced coma 78−74850
digital image registration with automatic microscope, appl. to cell analysis 77−29239
digital photoelectric localisation of objects *(Slovak)* 77−18089
p-diiodobenzene, polymorphic transition hysteresis, optical path difference expt. 79−99312
m-dinitrobenzene cored fibres, void-free cryst. growth, X-ray diffr. and optical microscopy study 80−71586
dipropylammonium manganese chloride, layer perovskite, step bunching obs. by compound holographic microscopy 78−63682
dispersion staining technique for microscopical particle anal. 78−24855
double-shearing interference microscopy, appl. to optical fibres inhomogeneities *(French)* 77−54819
dust filtration, specimen prep. techniques for anal. of dust distrib. in fabrics 77−56191
electrocrystallisation, recent progress in electrochem. and physical methods *(French)* 80−7510
ellipsometric arrangement for microscopical obs. 80−17998
embedding with GMA and Quetol 523 for electron microscopic obs. on semi-thin sections for light microscopy 78−53588
enzyme reactions in tissue sections, quantitative microscopy using microdensitometry 77−86728
epidural neurostimulation, percutaneous, histological reaction, short and long term study results 80−67285
epoxy resin DGEBA, cured with TETA, crack propag. and fractography 79−70154
existence of β to α_m phase transformation 78−44123
eyepiece graticule, for quantitative microscopy 78−37055
failure analysis tools comparison and selection 80−71865
ferrography of polymer form. under lubricated nibbing contact 77−21292
fibre fracture stress and mirror size obs. 79−37020
fibre index profiling by video analysis of interference fringes 78−55460
fibre refractometry by interference microscopy, simplified method 79−18504
filler materials, scanning microscopy, plasticiser absorpt. obs. *(German)* 79−39082
filter dissolving for examination of material on filter 79−80676
fitted masses, dark field light microscope obs. *(Polish)* 77−77700
fluorescence microscopy, incident light, specimen prep. method 80−82755
fluorescence microscopy, simple preparation technique *(German)* 79−97429
fluorescence microscopy, water pollution abatement, self-cleaning capacity of epipelic bicenoses 79−79702
fluorescence microscopy of living cells, low level, appls. of image intensification 80−94432
fluorescent microscopical technique in diagnostic microbiology 78−20339
fluorite crystal gas-liquid inclusion meas. with microscope heating stage 80−76967
fractographic study of early stage fatigue cracks in vacuum *(Japanese)* 79−61781
fracture mechanism in various temperature and stress intervals *(Russian)* 79−24600
fretting expt. slip meas., high resolution optical method 79−61830
garnet bubble materials, low loss, mag. domain wall dynamics 78−10738
geometrically correct stereo-TV observation of micro-objects *(Russian)* 79−26116
glass, float, low-Fe, weathered, surface, characterisation 80−93666

optical microscopy continued
glass, impact damage, localised 77−44306
glass bead epoxy resin, direct obs. of debonding at crack tips 80−3167
glass fibre reinforced epoxy, short aligned fibres, mech. charact., SEM and optical obs. 78−72761
glass microbubbles, interference fringes, forbidden zone 77−18702
glass micropipettes, comparative calibration by optical microscopy and SEM *(German)* 80−98201
γ- globulin, single mol. fluoresc. tagging 77−21662
graphite fibre reinforced epoxy matrix laminates, microscopical anal. 78−3288
graphite nodule growth, kinetics and rate controlling process *(Japanese)* 80−35203
grid handling, of semi-thin sections of GMA-Quetol 523 embedded tissue, with reference to O_5O_4 78−92766
Hastelloy X, grain size effect. creep and creep-rupture *(Japanese)* 80−16382
Hasteloy B, equilibrium surface bombarded with high dose He^+ ions 78−95091
high-speed autoradiography, evaluation of effectiveness 80−47100
histological and cytological reflection contrast microscopy 80−72389
histological data quantitative anal. using optical-mark-recognition computer cards 77−81612
histological material, automatic image analysis, standard full area frame 77−52947
histopathological information obtained from US tissue signatures and microscopy of biopsy samples 80−51195
hole diameter meas. with universal microscope and electronic contact indicator 77−79055
holocamera, clinically useful, for 3-D microscopy of unanaesthetised eye 78−48863
holographic, image plane holograms of test target, blood cells and hair 78−58944
holographic attachment for microscope 77−23631
holographic interference microscope, MGI-1 80−5706
holographic interferometric microscopy methods, for dynamic systems obs. 78−45685
holographic real time microscopy using holographic illuminating system, rotary shearing interferometer 79−81388
holography, autocorrelation of diatoms as a function of depth of focus [holography in biology] 80−67324
holograqphic aberrations due to wavelength shift, elimination technique 78−74861
holomicroscopy for investigation of polymers 79−17474
hydroxypropyl cellulose in conc. aq. soln., mesophase struct., colour 77−19870
IC photomask and wafer linewidth meas. using optical spatial coherence 80−77850
ice crystals, vapour-grown, appearance of non-singular surfaces, microscope study 79−60297
illuminator, vertical, adaptation by laser microbeam system for cell irradiation 79−20727
image analysing computer, Quantimet, device for automatic scanning of irregular areas 77−5906
image analysis, problems and approaches 79−80725
image analysis by automated microphotometer *(French)* 77−10085
image formation, partially coherent, two dimens., computer simulation 80−106434
image formation, propag. problems connected with special source structs. 80−87272
image of periodic complex object under partially coherent illum. 77−610
image semi-automatic anal. device 79−79705
imaging analysis applied to phase, schlieren and interf. microscopy 78−45688
incident light microscope image enhancement device 79−85178
incoherent annulus object diffraction images in presence of primary astigmatism 79−22904
incoherent extended object imaging by polarising microscope with crossed polarisers 78−16841
Incoloy 800, creep and fatigue props. in high temp. gas cooled reactor He environment 79−47776
Incoloy 800, from KFA experimental duct at 700°C and 480 d in DRAGON reactor, mech. props. before and after contamination 79−47777
Incoloy 800, steam oxidised, oxide coating anal. 80−89399
Inconel, type 706, precipitation and creep rupture behaviour, optical and TEM study 79−74158
Inconel 600, equilibrium surface bombarded with high dose He^+ ions 78−95091
Inconel 718, blistering by 2 MeV He^+ ions, optical microscopy and SEM obs. 79−42119
incubator, improved air stream, for use in high resolution time lapse cinemicrography 80−98196
industrial, qualitative and quantitative surface testing 80−9033
inorganic fibre, diameter measurement by microscopy *(French)* 79−93095
instruments and appl. techniques for microscopy, Zeiss equipment 77−74497
interference microscopy, for colour development and phase separation 80−100976
interference microscopy, for plant cell wall and cytoplasm refr. index determ. 78−57151
interference microscopy, surface height standard deviation on ground glass surface 79−93098
interference microscopy for intercrystalline transport process obs. *(German)* 79−30538
interference obs. by reflection contrast 80−68248
interference reflection microscopy, image interpretation theory and appl. to cells 79−80677
interferometry with schlieren microscopy 77−34016
Interphako interference microscopy, refr. index profile determ. of light focusing rod 80−101832
IR microscopy coupled with scanning photoluminescence spectrophotometry 80−73447
IR radiometric microscope technique for melt growth kinetics determ. 78−34453
isoplanatic imaging, complex degree of coherence determ. 77−2691
Kevlar aramid fibre, regular fine bands obs. by polarization microscopy 80−107064
Kohler illumination 80−90887
optical microscopy continued
Kohler illumination using fibre optics and quartz-halogen lamp 78−58027
laser microprobe, modification for transmitted light illumination 77−5902
laser-Raman microprobe studies of mineralizing tissues 80−76884
lath martensite, habit plane and morphology 77−8823
layer thickness measurement, nondestructive method 78−77843
lecithin membranes, mag. susceptibility anisotropy, phase contrast microscope obs. 78−92601
lecithin vesicle shapes, rot. symmetric, opt. microscopy 77−64011
lecithin-water systems, bilayer connecting passages 78−96028
leucocytes, differential counts, comparison between light and electron microscopic results 79−5429
lighting arrangement, micro-irregularity inspection appl. 79−30539
linewidth measurement, operating conditions effect on image profile 77−79147
liquid crystal mixture phase equilibria and transition temperatures 78−63845
liquid crystals, defects, struct., optical, electron microscopy *(French)* 79−46567
LMFBR, Na test of bellows expansion joints, metallographic study *(Japanese)* 79−67850
low magnification phase contrast system, Olympus IMT microscope 80−68247
lymphocytes, living and dead, mag. props. and mag. sedimentation 80−35925
magnetic micro-rheometer evolution and theory 80−92099
martensite, shape memory, crystallographic similarities 79−66102
mask linewidth meas. effects of operating parameters 77−37977
mask linewidth meas. with coherent optical microscope 77−37978
matched spatial filter optimisation for diatom recognition 80−48180
materials science experiments, use of closed circuit TV as teaching aid 79−71209
MBBA, nematic liq. cryst., cylindrical domain struct. thermal excitation, optical obs. 79−73097
mesophase pitches, synthetic, mag. orientation study 79−94868
metal, microanalysis of migration processes 77−36706
metal oxides, high temperature interactions with Re 80−16665
metal sheets sliding on dies under plane strain drawing, sliding surface damage obs. *(Japanese)* 77−44369
metallisation corrosion, IR microscopy failure anal. 80−98976
metallographic, specimen preparation for edge profile microscopy 78−57921
metallographic sample preparation, procedures 80−57272
metallurgical problems, struct.-props. relation use of TEM and SEM and optical microscopy 77−56186
meteorite, Santa Barbara, mineralogy and petrology 79−25551
meteorite Zaisho, Japanese pallasite, mineralogical and petrographical study 80−46509
meteorites, identification of ordered FeNi 80−8604
microcirculation flow dynamics meas. using video microscope 77−78009
microelectrophoretic measurements using rotating prism in microscope 77−21389
microfluorometric measurements of DNA dye complex using cryostat 80−17949
microfractographic charcts., in determ. of failure stages in repeated loading 77−40490
microinterferometer, apochromat objective, with increased resolution, surface roughness testing 79−71519
microkymography, and related techniques 80−36215
microkymography, flow vel. meas. in microvascular bed after exdotoxin administration *(German)* 78−77173
micromanipulator using microscope focus, appl. to yeast asci single spare isolation 78−61292
micrometer slides, for linear meas. in range of 100 mm to 1 μm accuracy 77−5808
microneurology, appl. of colour TV as surgery teaching aid 78−40396
microphotography, exposure control, manual 80−98975
micropositioning stage, piezoelec. driven, 50 micron range, subnanometer resolution 79−17407
microscope photometry, appls. in materials science 80−21236
microscope photometry, on-line data collection and processing for solids, fossils and organic matter *(German)* 79−26101
microscope photometry in studies of molecular struct. of carbonized bitumens and pyrobitumens 80−18011
microscope stage, controlled temp., for high-resolution microscopy 79−17411
microslides for photomicrography 79−21833
microspectrofluorometry, low temp., design of cold chamber 78−57144
microstructures micrographs digital simulation 80−19679
mischmetal-cobalt alloy, $MMCo_5$, polished, domain wall grooving, optical microscopy and SEM obs. 77−8334
Mo, slip line study of pure single crystal compressively deformed at low temps. 79−43361
modulation contrast, principle and appl. 79−35818
molecule, fluoresc. pulse obs. 77−21662
muscle, frog, vacuolation and subcellular comp. in fatigue, cryo-ultramicrotomy 79−24963
myelinated nerve fibre simultaneous meas. and counting grid 79−39540
myosin, struct. changes in living muscle fibres, polarised UV fluoresc. microscopy 80−67037
'nematic' amphiphilic liquid crystalline mesophases, thermodynamic stability 79−95126
nematic liquid crystal, hexagonal arrays 77−11478
nematic liquid crystal with lateral substituents, mol. struct. effect 78−51411
nematic phases of rigid macromolecules, texture *(French)* 79−1394
nepheline concentrate, low Fe, phase composition 77−21110
neural histological section, computer-assisted mapping 80−30963
neural structure histological exam.; Epon block sectioning technique 79−74814
neuronal interconnection meas., semiautomatic system design 78−44742
neuronal population density estimation, robust distance method 79−70721
neurons, section embedding technique for sequential light and electron microscopic exam. 80−67317
neutron fluence meas. using fission foils of ^{235}U, ^{238}U, ^{237}Np used for neutron fluence meas. 78−13177
$NH_4H_2PO_4$, cryst. growth from aqueous solns., dislocation groups in (100) faces, kinetics 79−74072

optical microscopy continued
Nimonic PE-16, equilibrium surface bombarded with high dose He^+ ions 78−95091
Nimonic 80A, intergranular creep fracture under const. cavity density 78−60825
non-contact scanning system based on stereoscopic balancing *(German)* 77−82598
nuclear ceramics, quantitative image anal. using light and SEM obs. 79−12912
nuclear emulsion tracks, detection and meas. by inexpensive microscope television 79−3290
numerical density estimation, unbiased by edge effects 79−44928
Nylon 6, unidirectionally reinforced, mech. props. and fracture 77−21252
Nylon-6, injection moulded, struct. and morphology 80−38949
object delineation program 80−41338
oblique transmitted light techniques for photomacrography and photomicrography 78−58026
one dimensional imaging device *(French)* 77−68179
online difference image method, biological appl. *(German)* 78−92688
optical fibre index profiles, focusing method, nondestructive meas. 79−27375
optical glass containing PbO, effect of Al_2O_3/Na_2O ratio on rate of ion exchange 78−44377
optical transfer measure, system relations, appl. wide field microscopy and microelectronic photolithography *(German)* 80−9815
oxide systems, exam. of techniques used to determine phase diagrams and equilibria, and effects on equilibria 79−8415
PAA, isotropic-nematic phase transition, optical microscopic obs. 79−69230
PAN fibres, heat treatment, structural changes *(Polish)* 77−28835
particle size and velocity, simultaneous meas. on moving particles *(Japanese)* 78−95872
particle size distribution meas., online stroboscopic microscope apparatus 80−101783
pearlite spheroidization, quantitative meas. 77−44275
4-n-pentylphenyl-4′-n-octylthiobenzoate, smectic-C phase, undulation instabilities, microscopic obs. 77−68919
Permalloy, magnetic head wear resistance and surface charact. against magnetic tape *(Japanese)* 80−35335
petrographic anal. of bituminous coal, identification of constituents 80−81888
petrographic characterization of coal using automatic image analysis 80−18002
petrographic method of determ. of quantitative relation between phases in microcryst. structs. 78−35608
petroleum feedstocks and cokes, graphitisability 80−93580
phase contrast microscopic identification of cat neuron cytoplasmic laminar bodies 79−48385
phase differences meas. by phase modulation interferometry *(French)* 77−82593
phase microscopy techniques, review 78−45684
phase reconstruction problem 78−25811
phase-lock interference microscopy, real-time, design, appls. 79−17480
phospholipid membranes, artificial, lamellarity determ. by photometric phase-contrast microscopy 79−39368
phosphorescence microscopy of cells 78−3454
photomacrography and photomicrography, oblique transmitted light techniques 78−306
photometry of moving objects at resolution limit, theoretical considerations, exploitation in expt., stereometry 78−8441
photomicrographs, high quality image prod. 78−24881
photomicrography, exposure control 80−90888
photomicrography, instrumentation, vibr. problems, films, illum. and magnification 77−57417
photomicrography of submicrometer birefringent contaminants in C black dispersions in polymer particles 80−62757
photomicrography with colour films, colour reproduction *(German)* 78−20338
placental villi, human, average diameter estimation by stereologic method 80−67318
plastic surface coatings as alternative to standard thin section cover glass 78−73974
PMMA, craze shape and fracture, temp. depend. 77−52486
PMMA, thermochem. instability at Pt sphere inclusions caused by CW laser beam 80−29689
polarised light, evaluation of asbestos insulations 80−95134
polarising microscopy, college course 77−22360
polarizing microscope components and applications 80−98973
pollution control, polarisation and interference microscopy appls. 78−61544
poly(paraphenylene terephthalamide), nematic structure by optical and X-ray methods *(French)* 77−31584
poly-1-butene, sheared melts, nucleation and crystal growth meas. 79−69027
poly-ε-caprolactone-PVC blends, crystallisation kinetics 79−69020
polybutylene terephthalate, melt crystallised, solvent crystallised films and moulded bars, morpholigical obs. 80−84101
polycarbonate, crazes, statistical aspects optical microscopic obs. *(Japanese)* 79−29247
polycarbonate, deform. and failure modes, surface craze charact. 79−91753
polycarbonate, effect of mol. weight on craze shape and fracture toughness 80−25858
polycarbonate, fatigue crack propag., mol. wt. depend. 80−50700
polycrystals, deform. during cooling, revealed by deposited graphite layer *(Polish)* 80−25755
polydioxolan, crystn. kinetics, dilatometric analysis and microscopy obs. 80−79706
polyesters, thermotropic, quiescent crystn. 80−38937
polyethylene, crystn. under high pressure 80−38946
polyethylene, high density, film, melt growth, cryst. superstruct., small angle light scatt. 77−31602
polyethylene, oxidation rel. to spherulitic crystn. *(Russian)* 78−71689
polyethylene, supermolecular structure, polymerisation at low pressure *(Russian)* 79−64126
polyethylene melt, cryst. kinetics during cooling, nucleation density effect 80−100181
polyethyleneterephthalate, crystallised from thin layer melts, temp. depend. of morphology 80−54149
optical microscopy continued
polyethyleneterephthalate, foil, optical microscopy and low angle light scattering 80−55210
polyhexamethylene terephthalate/polyoxytetramethylene block copolymers, supramolecular texture 78−91261
polyisocyanates, rigid backbone, ternary phase relationships obs. 80−59371
polymer liquid-crystalline solns., struct. 80−103235
polymer particle pigment agglomerate display, optical microscopy method 79−85177
polymeric composites, sliding wear mechanisms at metal surfaces, microscope obs. 79−87742
polymeric mesophases, discotic phases, optical microscopy obs. 79−41951
polymers, high mol. wt., exam. techniques 77−32734
polymers, high mol. wt., polarisation-optical obs. methods 77−32733
polymers, multicomponent-multiphase, bulk struct. by rheo-optical techniques 78−91267
polyoxymethylene, nascent, morphology, optical and electron microscopic obs. 80−59403
polypropylene, impurities redistribution during crystn. 78−75577
polypropylene systems, elastomeric impact modifiers rel. to morphology 79−66154
polystyrene, angle of intersection of coarse shear bands, optical obs. 79−66110
polystyrene, shear bands, morphology and annealing behaviour 80−100873
polystyrene in tetrachloroxylene and tetrachlorobenzene, morphology of crystallized additives 79−99082
polystyrene latex, grain boundary struct. obs. and boundary diffusion 78−51552
polystyrene-co-divinylbenzene microgels in dimethylformamide, diffusion coeff., viscosity and mol. wt. meas. 80−30286
polythene sheets, crystalline formations study, light refl. from untreated surface 77−28945
porcelain, crack propag. data applicability to failure prediction 80−81154
pore size measurement, comparison of methods 80−62622
powders thermosetting, hot stage microscopic technique for examining curing 79−28979
projection microscope measurement gauge 77−5904
projection system with brightness amplifier, laser appl., for medicine and biology 80−36060
projection system with quantum amplifier 80−33116
PVC, crazes, statistical aspects optical microscopic obs. *(Japanese)* 79−29247
PVC, rigid, craze and yield zones in fracture 80−50701
PVC, slightly plasticised, fracture toughness tests, impact tests 79−5037
PVC powder, quinoline diffusion, microdiffusion technique 79−7713
PVC-chlorinated polyethylene blend, optical characterisation methods 79−8408
PVC-polyacrylonitrile blends, compatibility determ. 79−4416
quantitative image analysis, theory and instrumentation 80−23626
quartz, defects growth, study by X-ray diffr. topography *(French)* 80−39095
quartz, plate and fibre, internal stress and birefringence microanal. using optical phase microscope interference-polarisation 79−39109
quartz, subgrain boundaries, theoret. predictions and microscopic obs. methods 80−84187
quartzite, naturally deformed, textural and microstructural development, metallurgical approach 79−83228
rabbit ear chamber for continuous microscopy of implanted biomaterials 77−81755
rare earth fluorides, as antirefl. coatings, evaluation 77−61963
rare earth $Zr_{1-x}O_{2-x/2}$ growth from skull melting, directional solidification 78−60567
reflectance microscopy of coal, considerations involved in automation 80−18001
reflection microdensitometry, optical principles and practical solutions 80−4790
refractive index automatic profiling 78−46836
refractive index determ. of thin films by Nomarski differential interference contrast microscopy 78−24849
refractive index meas., heterodox method 79−30530
refractive index radial distrib. in light focusing rods, interf. microscopy meas. method 77−57381
refractive-index profile meas. of optical fibres, using scanning optical microscope 80−87535
Rene 95, as hot isostatically pressed (HIP) and HIP+forged, low cycle fatigue 80−25854
rocks, petrographic description, suggested method 78−81431
roughness meas. by reflected-light microscope *(German)* 80−31861
rubber, wear mechanisms, optical microscope obs. *(French)* 77−21285
S glass-Ni sphere composite, exam. of crack shape and fracture toughness 78−72886
sample preparation, IBMA equipment for ion bombardment *(Czech)* 77−61161
sapphire filament, grown by laser-heated floating zone method, microvoids obs. 77−32518
sapphire ribbon crystals, EFG growth and charact., voids, grain boundaries and dislocations 80−103283
scanning, CRTs with semiconductor laser screens 80−86398
scanning, use of lenses with annular aperture 77−65054
scanning attachment to dual-prism monochromator, appl. to cytospectrofluorometric installation 80−101837
scanning microscope photometric image analysis, appl. to chromatin packings *(German)* 79−5409
scanning microscopes, partially coherent and confocal, imaging of periodic structs. 80−5700
scanning photocurrent microscopy, recomb. centre distrib. in semicond. 79−35822
second order coherence meas. using microscope and grating 77−41672
semiconductor, ion-implanted, post annealing meas. using optical and electron microscopy 79−69121
semiconductor defect birefringence detection by polarisation IR microscopy 79−83405
semiconductor dislocation Burgers vector exam., birefringence method 78−30626
semiconductors, dislocation structure, optical microscopy obs. techniques 80−24458
Sendust alloy, magnetic head wear resistance and surface charact. against mag. tape *(Japanese)* 80−35335

optical microscopy continued
p-sexiphenyl, liq. cryst. phase transitions 79−82322
sharp-lip capillary nozzle production and meas. precision 77−80246
silica optical fibres, surface flaws obs., fracture strength 77−14793
sintered pellets, oxidation mechanism and kinetics, optical and SEM study 79−79137
slippage in crystals, photogrammetric obs. method 80−100975
small objects, detection using liq. cryst. method, expt. using graphite powder as model object 80−9034
small particle analysis, step-wise procedure 79−97369
small particle identification, review 78−48739
smectic liquid crystal, edge dislocations obs. by polaris. microscopy 79−7547
solar cells, polycryst., scanning optical microscopy examination of grain boundaries 78−79618
solid lubrications dynamics, obs. using Micro Contact Imager 78−85002
solid surface characterisation techniques, review 78−22945
spatial frequency filtering, biomedical appls. 77−79760
spatial frequency plane filtering by dynamic coherent illumination 80−95825
specimen preparation ion beam techniques 78−24778
spectral reflectance, developments in microscopic meas. of ore minerals *(French)* 79−5627
sphere population overall mean caliper diameter estimation 79−70719
spirals, growth and dissolution from liq. state 80−15027
stearic acid, microscopic obs. of cleaved surface 79−95248
stearic acid, single cryst. growth mechanism 78−30562
stearic acid crystals grown from solution, spatial correlation between growth spirals and inclusions 80−96527
steel, 0.2 to 0.8% C, ferrite-pearlite transformation, tensile strength, cooling rate effect 80−7549
steel, 0.7% C, welded zone, fatigue strength and microstruct. *(Japanese)* 80−89339
steel, 45G17Yu3, deformed, influence of hot rolling on struct. *(Russian)* 77−25073
steel, alloy structural, anomalous grain growth 80−20984
steel, and alloy, austenitic transformation, temp.-conc. range of product formation 79−100135
steel, austenitic, 16H2NMB, struct., texture and mech. props. of product of transform. 78−92273
steel, austenitic, Cr-Ni (25, 20 wt.%) recrystallisation and sigma phase formation 80−35211
steel, austenitic, metallography study of high temp. decomposition 79−61559
steel, austenitic, wire rod, austenite transform. kinetics accompanying interrupted cyclic cooling *(Russian)* 79−70064
steel, austenitic stainless, 18-8, effect of H on martensitic transformation *(Chinese)* 80−55394
steel, austenitic stainless, ferritic, single phase ferritic solidification in welds, exam. 80−7546
steel, austenitic stainless, intergranular corrosion evaluation 77−16741
steel, austenitic stainless, Ni-alloyed, Cr_2N precipitation, interface struct. and morphology 80−11644
steel, austenitic stainless, precipitates and grain orientation by non aqueous electrolyte potentiostatic etching method *(Japanese)* 80−15102
steel, austenitic stainless, structural inhomogeneity, electron and optical microscope exam. 78−72827
steel, ball bearing, martensitic decay during rolling contact fatigue 77−32682
steel, C1020, dual phase, mech. behaviours and structs. *(Korean)* 80−25779
steel, C, explosively fractured, struct. of white etching band 79−61722
steel, C, ferritic-pearlitic transform., struct. study by optical and electron microscopy *(French)* 78−68685
steel, C, second stage of tempering 79−61627
steel, C, spheroidised, fracture toughness, cementite particle effects, optic and electron obs. 78−60785
steel, C, transform. kinetics, heat cond. and elastic-plastic stresses during quenching *(Japanese)* 80−25688
steel, C (0.54 wt.%), torsional fatigue process, obs. by electron microscope *(Japanese)* 77−12690
steel, C and alloys, ion-softnitriding effects on metallurgical props. of nitrided layer *(Japanese)* 79−5079
steel, carbide cracking as source of acoustic emission 78−19872
steel, cavitation during superplastic flow, affecting factors 78−60728
steel, CC Cr-Mo-V, low alloy, creep fatigue interaction 78−64673
steel, chemical polishing for opt. microscopy 77−9021
steel, complex alloy, exam. of temper brittleness 78−44209
steel, Cr, ferritic, oxide scale etching 79−70204
steel, Cr and Ni-Cr, cyclic re-austenitizing 80−35222
steel, Cr-Mo(20, 1 wt.%), creep rupture tests, at 500°C loading times up to 300000 hours *(German)* 80−25828
steel, Cr-Mo(-V), ductility and heat resistant prop. prediction rel. to fine struct. and solid soln. state 79−15751
steel, Cr-Mo (2.25, 1 wt.%), small changes effect in impurity elements, creep life 80−25790
steel, Cr-Mo-V, press. vessel, fracture, effect of tempering 78−60799
steel, Cr-Ni (1.47, 1.48 wt.%), lath martensite microstruct. and props., cold rolling effect 80−55422
steel, Cr-Ni-Ti (18, 8, 0.7 wt.%), creep rupture tests, at 500°C loading times up to 300000 hours *(German)* 80−25828
steel, Cr-V (1.5, 0.5 wt.%), ferritic, effect of temp. and microstruct. on creep damage 79−5023
steel, CrMo(W)V, creep rupture tests, at 500°C loading times up to 300000 hours *(German)* 80−25828
steel, Fe-V-C (1, 0.2 wt.%), austenite formation 80−84927
steel, ferritic stainless, embrittlement 80−85041
steel, high Si dual-phase, mech. props and microstruct. anal. 80−40444
steel, hot deformed austenite, transition from discontinuous to continuous formation of pearlite *(German)* 80−35214
steel, inclusion, grain boundaries and H_2 attack, fracture analysis 77−32695
steel, low alloy, exam. of microstructure, in type PZhK-1000 soldered joint by metallography 79−52257
steel, low alloy structural, pre-treatments to enhance graphitisation, dilatometric and optical microscopy study *(Japanese)* 79−78992
steel, low C, kinetic aspects of diffusion zone and compound layer formed during ion-softnitriding *(Japanese)* 79−15866
steel, low-alloy, study of deformation and fracture processes by acoustic emission transient anal., SEM and optical microscopy study 79−43311
optical microscopy continued
steel, low-C-Si, LS1.2, LS1.5, phase transformation 80−45302
steel, maraging, hardening mechanism of quenched samples, tempering *(Czech)* 79−78989
steel, maraging, Ni (18 wt.%), fatigue crack initiation and propag. in earlier stage *(Japanese)* 77−8937
steel, martensitic, age hardening with Cu, Nb additions, exam. of hardness 80−7681
steel, mild, hot shortness mechanism, surface enrichment of residual elements and oxidation *(Chinese)* 79−74230
steel, mild, shear mode of ductile fracture 79−91785
steel, Mn-Cr-B (1.46, 1.03, 0.003 wt.%) 80−55422
steel, Ni-Co-Mo (17.55, 8.02, 4.92 wt.%) maraging, lath martensite microstruct. and props., cold rolling effect 80−55422
steel, NiCr, random load fatigue crack propag. 78−64692
steel, non metallic inclusion eval. using Quantinet systems 79−15923
steel, Pb and MnS inclusions 77−77685
steel, pearlitic or spheroidal plastic deform. and fracture *(French)* 78−35448
steel, plain C, creep rupture tests, at 500°C loading times up to 300000 hours *(German)* 80−25828
steel, plain C, quench ageing avoidance, critical cooling rate *(German)* 79−52244
steel, plain C having ferrite-martensite mixed structs., microstructural parameters effect on fatigue strength *(Japanese)* 80−71735
steel, reinforcing wires, high strength, microstruct. obs. *(Czech)* 79−43342
steel, rimmed, metallographic method of cleanliness eval. 77−52562
steel, rimming, continuously cast, nonmetallic inclusion distrib. *(Russian)* 78−80534
steel, rolled, anisotropic, fatigue fracture surface obs. *(Japanese)* 80−108546
steel, spheroidised, H_2 embrittlement, fracture surface study by SEM and optical microscopy 79−57109
steel, spheroidized, shear mode of ductile fracture 79−61714
steel, stainless, 12Kh13 and 15Kh11MF, austenite transform. kinetics 79−87612
steel, stainless, 304, fatigue crack growth at room temp., crack closure and cycle ratio effect 79−70139
steel, stainless, 316 and 304, equilibrium surface bombarded with high dose He^+ ions 78−95091
steel, stainless, Cr-Ni (18, 8 wt.%) average inclusion size and contents exam. measurements using optical microscopy and Br-Methanol methods *(Korean)* 79−66080
steel, stainless, fibre reinforced Al, CC strengthened by lattice transformations, mech. props. study *(Japanese)* 79−43332
steel, stainless, type 316, blistering by 2 MeV He^+ ions, optical microscopy and SEM obs. 79−42119
steel, stainless, type 316, microstruct. changes in creep ductility, SEM, TEM, optical microscopy and X-ray diffr. study 79−38927
steel, structural, supercooled austenite, structural characts. of decomposition 80−60870
steel, tool, blanking punch, chipping behaviour *(Japanese)* 79−100250
steel, tool, NC6, carbide lattice, kinetics of its destruction *(Polish)* 78−92280
steel, tool and high-speed, high freq. induction melting and centrifugal casting in instrumental anal. 80−84886
steel, type 35L, heat treated, exam. of surface defects using fluorescent liquids 79−15933
steel, types 45, 50, U8, U10, diffusion chromizing,, microscopic examination 79−43357
steel, white layers forming at high rates of friction, struct. props. *(Russian)* 79−15800
steel, X5CrNiTi26.6, ferrite-austenitic struct., optical and electron microscopy 78−84848
steel 12Kh1MF, fine struct., effect of isothermal transform. temp. 77−21137
steel ball bearing, fatigued, phase changes, nomenclature 80−89198
steel C60, machined, surface morphology, struct., SEM, topographic investigs. *(German)* 77−73372
steel hardness and ductility variations and micrographs rel. to heat treatment and phase diagram obs. 79−87609
steel wire, high C, fatigue and fracture 80−55531
steel-polymer wear mechanism during fretting corrosion 78−35522
steels, C, quenched and tempered, struct.-prop. relationships 80−7599
steels, low-C, aged after quenching, rel. between micro-cracks and coaxing effect *(Japanese)* 80−81159
steels, structural St 37-2, cleavage fracture, report 80−25868
step height measurement in μm range by two-ray interferometry with adjustable light wavelength *(German)* 77−82489
stereological microstruct. anal., two-phase matrix materials 77−61057
stereology, determ. of preferred orientations of cancellous bone 77−36987
stereology, quadrat choice for geometrical struct. determ. of two-phase specimen 78−12793
stereology of parallel straight circular cylinders, for appl. to intestinal crypts 77−13044
stereoscopic method of viewing internal structures in resin-embedded biological specimens 80−21586
submicron magnetic objects, mag. struct. study using magnetooptic micromagnetometer 80−57349
superconductor Faraday effect obs. in polarising microscope 80−70892
surface anal. tools review 80−103540
surface microdefects, instrument for measuring depth and dimensions 78−76812
surface roughness assessment, X-ray scattering and differential interference contrast microscopy 79−30410
surface topography quantitative determ. by Nomarski differential interference contrast microscopy 80−73318
synchrotron radiation appls., characts. and sources 78−74960
Teflon foils, cryst. struct. and texture changes due to polarisation process *(Polish)* 80−35209
test serums quality determ. by microscopic-fluorometric method 79−53290
texture anal. of sinter struct., appl. to Ca ferrites in sinters of rich Fe ores 80−18009
thermoplastic, partially crystalline, microscopic methods of struct. anal. *(German, English)* 80−30198
thread diam. meas. by three wire method, influence of shape deviation of taut measuring wires *(German)* 78−77845

optical microscopy continued
three-dimensional cellular tree structure meas. semiautomatic system 79−70720
tooth-profile error of cylindrical gear wheels 78−168
transition metal oxalate hydrates, powders, precipitation from aq. solns., cryst. numbers, sizes 77−44143
transparent films, independent determ. of thickness and refractive index by MIS-11 microscope 77−49770
transparent object, testing for bubbles and light scatt. inclusions 77−88973
travelling microscope meas. of Kirkendall shift in Ag-Cd alloys 78−87829
TV microscopy and cinephotomicrography with Zeiss Axiomat 80−27343
TV photomicrography using planimeter and trinocular microscope 79−71523
TV recording and display equipment 80−98972
type 35L, heat treated, exam. of surface defects using fluorescent liquids 79−5101
Udimet 700, microstruct. of resolidified zones formed by laser melting single crysts. 79−78953
ultramicroscopy in scanning microscopes 80−95137
ultramicrospectrophotometry techniques in intravital microcirculatory studies 80−21589
uses, differences from electron microscope 80−13186
vesicle visualisation in semi-thin sections by heat removal of epoxy resins 78−24194
video microscopy, review 79−58784
virus size measurement using optical microscope, Virometer design 78−61296
vital microscopy, electronic thermostatic system 80−85537
wear debris anal., quantitative methods 78−64912
Weissenberg Rheogoniometer, addition of polarizing microscope 79−68838
wetting, exam. of accompanying size effect *(Russian)* 80−6596
white blood cell automatic tracking using photodiode array 77−78064
zeolites, synthetic, effect of sintering on elec. cond., porosity and microstruct. 79−29009
Zircaloy, annealed, neutron irradiated, inhomogeneous deform. behaviour 80−85014
Zircaloy tubes, grain struct., texture, dislocation density effect on irradiation creep, X-ray diffr. and optical microscopy anal. 79−74208
Zircaloy-4, ^{51}Cr bulk diffusion 79−73347
Zircaloy-4, cyclic nature of corrosion in 633K water, optical and electron microscope study 79−66207
Zircaloy-4, resistance-welded, microstruct. of weld region 80−66549
Zircaloy-4, strain rate dependent mech. response 77−21254
Ag, (211)[$\bar{1}$11] single crysts., shear band effects on rolling deformation 80−50651
Ag-(100)InP contacts, interface struct. 79−60922
α-Ag-Cd, chemical interdiffusion and Kirkendall shifts 78−87829
β′-Ag-Cd (45 at.%), growth kinetics of bainite plates and Widmanstatten needles 77−36551
Ag-Cd (45 at.%), morphology and crystal struct. of stress-induced martensites 78−68693
Ag-Cd (47 at.%), crystal struct. and internal defects of thermoelastic martensite 77−48438
Ag-Zn (2 to 12 wt.%) containing several metals, internal oxidation *(Japanese)* 80−16570
AgCl, surface crystallisation, due to colloid adsorption 80−54544
Al alloy, type 2024-T3, fatigue deformation and crack growth, holographic study 80−25836
Al, cavitation erosion in water flow, initial stage 78−27648
Al, cold rolled, X-ray diffr. and optical microscope exam. of fatigue damage *(Japanese)* 78−84976
Al, fatigue crack propag., grain size effect *(Japanese)* 78−39889
Al, high purity, deformed at 573K, stress reductions effect on creep behaviour, subgrain size meas. 79−74216
Al-Ag, precipitation kinetics and coarsening, effect of interfacial props. 79−91651
Al-Al_2O_3, recrystallisation nucleation in drawn wires, optical and TEM obs. 79−47709
Al-Al_3Ni eutectic composite, structural response to shape variations 79−83190
Al-Bi-(Fe), directionally solidified monotectic, growth parameters for aligned microstructs. 79−43236
Al-Cr, rapidly solidified, crystalline and amorphous structures 77−44274
Al-Cr(Zr), simultaneous recrystallisation and precipitation *(French)* 80−16313
Al-Cu (4.5 wt.%) alloy, controlled electropotential corrosion in NaCl soln., microstruct. exam 78−39948
Al-Cu-Zn system, solid-phase reactions, phase diagram 80−50603
Al-Ge (2 wt.%), quenched and aged, deform. slip line obs. 78−51544
Al-Mg, homogenisation process, effect of solidification rate and alloying *(Polish)* 79−78949
Al-Mg (5 wt.%), recovered dislocation substruct. during plastic flow 79−83273
Al-Mg-Ag, age effect on age hardening *(Japanese)* 78−52831
Al-Mn-Si, recrystallisation and precipitation 78−52824
Al-Si eutectic alloy, banded struct., SEM and optical microscopy 80−104144
Al-Sn, (<0.28 wt.%) corrosion behaviour in 16% HCl 78−85054
Al-Ti, solid soln., unidirectionally solidified, segregation patterns revealed by etching 79−47693
Al-Ti alloys, growth crystallography and morphologies of Al_3Ti primary dendrites, metallography study 79−43230
Al-Zn, plastic deform. effect on struct. transform. at elev. temp. *(Czech)* 79−79044
Al-Zn-Mg, fractographic stage I fatigue facets 77−16680
Al-Zn-Mg alloy, microstruct. obs. by optical and electron microscopy *(German, English)* 77−52601
Al_4Ca, phase transformation, struct. and orientation relationships 79−78963
Al_2O_3 (96 wt.%), fractographic criteria for subcritical crack growth boundaries 80−81155
Al_2O_3 bicrystals, grain boundary obs. 80−39106
Al_2O_3, grinding and polishing, quantitative control and optimization *(German, English)* 80−35460
Al_2O_3, sintering temperature effect of titanate additions 80−60808
β-Al_2O_3:MgO, strength and delayed fracture behaviour 80−35290
Au, monodisperse sol, ordered struct. obs. 78−3384
optical microscopy continued
Au sol, grain boundary struct. obs. and boundary diffusion 78−51552
Au/Ti thin film, temp. and humidity effect on interdiffusion 79−51317
Au_3Zn, R_2-phase, long period domains, transmission, scanning and optical microscopy obs. 79−38801
B fibres, quality evaluation from morphological and fractographic characteristics *(Russian)* 79−70150
BN/BN composites, prep., mech. props. 77−21080
$BaAl_{12}O_{19}$, Czochralski cryst. growth, quality examination by polarisation microscopy, etching and X-ray topography 79−24428
BaFBr, single cryst. growth by flux method, dislocation etch pits on dissoln. 79−56925
$BaFe_{12}O_{19}$, effect of impurity concentrations, and sintering conditions on grain size *(German)* 79−23630
$BaMoO_4$ crystals, growth in SiO_2 gel under influence of elec. field 80−93469
BaO-SiO_2-Fe_2O_3 permanent mag. ceramics, exam. of phase diagram, using X-ray analysis, optical microscopy, electron probe anal., and thermal analysis *(German)* 79−29012
$BaO.6Fe_2O_3$, solubility of CaO 80−100333
$BaTiO_3$, single crysts., electron microscope study of domain and defect structs. 79−15425
Be, irradiated with He^+ at 20 keV, surface damage and gas trapping profile meas. *(French)* 80−84218
C materials, optical microscopy, reflection, interference colours, terminology 78−42871
$(CF_x)_n$ rubbed films applied to different finished surfaces, obs. 79−83332
$Ca_2Al_2SiO_7$, single cryst. growth by floating zone method, opt. microscopy charact. 79−47623
$CaCO_3$, calcite, gel grown crysts., spirals on rhombohedral faces 80−7486
$CaCO_3$ polydisperse particles, in $Ca(HCO_3)_2$ soln., growth, soln. in mag. field 78−53260
$CaHPO_4.2H_2O$, gel grown crysts., optical microscopy study 79−87572
$Ca_2MgSi_2O_7$, single cryst. growth by floating zone method, opt. microscopy charact. 79−47623
CaO-Al_2O_3-SiO_2 diffusion triangular diagram, diffusion between lime and sintered kaolinite *(French)* 79−69296
CaO-SiO_2-ZnO continuous unidirectional crystn. of fibrous metasilicates from melt 78−95739
$CaSO_4.2H_2O$, gypsum, cryst. growth rates and nucleation *(French)* 80−80959
$CaWO_4$, crystal growth from soln. in Na_2WO_4 melts, by continuous cooling, growth kinetics exam. 78−48303
$CaZrO_3$-$CaHfO_3$, solid soln. formation obs. 77−86003
Cd, deposition, on metal substrate, pot. sweep, potentiostatic and optical microscopic obs. 77−59967
CdI_2 polytypes, vapour growth mechanism 80−84124
Co, corrosion in Ar-SO_2 atmospheres, scale struct. obs. *(Japanese)* 80−55568
Co-B-Si ternary system, partial phase diagram, Co rich region 77−52293
Co-Cr(VC)((Ti,V)C)-(Al), eutectic alloy, unidirectional solidification, oxidation and tensile tests 78−52790
Co-Fe (2.92 to 30.05 wt.%), determination of phase equilibrium diagram *(Japanese)* 78−48374
Co-Ti-C, secondary precipitation and allotropic transform., TEM obs. 80−108453
Cr-Ni-Mo steel, low-cycle fatigue in sea water, mechanism *(Russian)* 77−59970
CrO_2, single mag. particle, remanent coercive force and remanent loop meas. 78−95480
Cr_2O_3-Al_2O_3-$ZrSiO_4$, exam. of microstructure by optical microscopy 79−29073
Cr_2O_3-WO_3, phase relations 78−92249
Cr_2S_3, single crystal, exam. of unit cell structures by interference contrast microscopy 78−67670
Cu alloy, superplastic, microscopic examination of internal void formation 80−16383
Cu alloys, cavitation during superplastic flow, affecting factors 78−60728
Cu, cold-rolled, microstruct. 79−83216
Cu complex, bis-(alkylammonium) (11) tetrachloride, perovskite, lattice perfection 78−87633
Cu, crack nucleation and stage I propag. in high strain fatigue, microscopic and interferometric obs. 78−52936
Cu, cracks in earlier stages of fatigue, fractography *(Japanese)* 77−8924
Cu, deposits on Cu (110) electrode, morphology and crystal growth 79−47644
Cu, irradiated with 20 keV He^+, surface damage and gas trapping profile meas. *(French)* 80−84219
Cu, polycrystalline, intracrystalline slip bands in high temp. creep, comparison with brass single crystal *(Czech)* 79−77604
Cu, polycrystn., strain localisation during hot deform. 80−104195
Cu, whiskers, Ar^+ ion implanted, X-ray study on lattice defects *(Japanese)* 79−99230
Cu-Al (10 wt.%), deformed and tempered transform. during heat treatment of β′ martensite *(Rumanian)* 79−34031
Cu-Al (13 wt.%), polycrystn. rod specimens effect of diameter on slip mode, optical microscopy obs. 79−79051
Cu-Al dil. alloys, dislocation etch pit obs. on {111} surfaces 79−10861
Cu-Al thin film multistructure, Xe^+ ion beam cratering 80−66708
Cu-Al-Fe-Mn (10,3,2 wt.%), phase comp. struct., continuous cooling from β-phase effect 79−24499
Cu-Al-Ni, mixed powder compacts, Ni content influence in sintering behaviour *(Japanese)* 80−35130
Cu-Al-Ni-Fe, (10, 5, 5 wt.%), cast microstruct. 78−80535
Cu-Al-Ni-Fe system, corrosion behaviour in sea water 80−45421
Cu-Ni diffusion couple, diffusion bonding process, fracture surface exam. *(German)* 77−35762
Cu-Ni-Al, ageing charact., optical TEM, X-ray, hardness obs. 79−29079
Cu-Ni-Al, grain boundary reaction under isothermal ageing at 623 to 973K *(Japanese)* 79−70090
Cu-Ni-Be-(Al) (30,0.5,(0.2-2) wt.%), Al addition effect on grain boundary reaction *(Japanese)* 80−54254
Cu-Ni-Fe (26,8 wt.%), microduplex struct. form., hardness meas., optical and electron microscopy *(Japanese)* 78−76659
Cu-Ni-Ti system, reactions with melt in Cu-rich region *(Japanese)* 80−89202

optical microscopy continued
Cu-Sn (16.5 wt.%) alloy, stress induced martensite from γ phase 79−70066
Cu-Ti (4 wt.%), isothermal transformation, electron and optical microscopy obs. of microstructure 80−16307
Cu-Zn-Al, β_1' martensite crystal crossing rel. to reversible shape memory effect *(Japanese)* 80−108499
Cu_3Au, disordered [001]-orientated single crysts., plastic deform., TEM and slip line studies 80−97541
Cu_2MnAl, Heusler alloy, single crystal, plastic deform. 77−44308
CuPt alloy, equiatomic, ordering processes, anisothermal annealing exam. *(Japanese)* 78−39765
Fe and alloys, brittle fracture, quantitative determ. of transcryst. and intercryst. portions by opt. and SEM fractography 77−52464
Fe, atomically clean, N_2 treatment, corrosion inhibition 78−19954
Fe, cast, abrasive wear rel. to lamellar or spheroidal graphite content *(German)* 78−85000
Fe, cast, heated in CO atm., obs. cracks around graphite flakes *(Japanese)* 78−84974
α-Fe, cold rolled, hydrostatic press. effect on microstructural changes during creep 78−39871
Fe, ductile, with different secondary struct., abrasive wear *(German)* 80−25871
Fe, effect of atm. corrosion on fatigue crack nucleation and fracture surface morphology, in air and vacuum *(Japanese)* 79−8387
α-Fe, exam. of structural defects due to shock waves, and induced hardness 78−48427
Fe, microhardness of single crysts. effect of temp. on dislocation structure *(German)* 79−52357
Fe one raw material, sintered, ionic etching as new method of struct. investigation 77−52588
α-Fe, plastic deform. in neck leading to fracture 78−64655
Fe, sintered, fatigue, metallographic obs. 78−64646
Fe whiskers, cryst. morphology and dislocation struct. study using optical and SEM, X-ray diffr. topography 79−23876
Fe zone refined crystals, cryst. orientation and distrib. of stray grains 80−70509
Fe-Al, single crystal, twinning and pseudoelasticity 79−15718
Fe-B, rapidly solidified, metastable phases *(German)* 79−29045
Fe-B_4C sintered material, mech. props. and struct. characts. 79−100084
Fe-C (0.64 wt.%), quasicleavage during fatigue crack propag., pearlitic microstruct. effect 79−11702
Fe-C(C-B)(C-Si), splat cooled, formation of metastable crystalline phases and glasses 78−88461
Fe-Co-V alloy, Remendur, heat treatment effects on mech. and struct. props. 77−8846
Fe-Cr, from ore reduction, metallographic investigation, optical miroscopy and SEM *(French)* 78−68648
Fe-Cr, high purity binary alloy, isothermal decomp. of austenite 78−64525
Fe-Cr, role of C in transform. by heating in ($\alpha+\gamma$) phase *(French)* 78−52798
Fe-Cr-Al (7, 5 wt.%), expt. stainless alloys, phys. and mech. props. 80−97637
Fe-Cu (30 wt.%) alloy, dendrite remelting during isothermal holding, microspin obs. *(Japanese)* 78−71836
Fe-Cu (4.54 wt.%) alloy, scaling behaviour, 700-1000°C, 1 atm. O_2 80−93679
Fe-Cu-Ni (2, 5 wt.%), interphase precipitation obs. in assoc. with Widmanstatten ferrite lateral growth 80−40365
Fe-Mn (15(24)(30)wt.%), high hydrostatic pressure influence on stress-strain curve 80−25805
Fe-Mn alloy, splat-quenched, martensite formation obs. 77−44247
Fe-Mn-C, austenitic, strain induced γ to ε transform., active slip systems 77−48427
Fe-Mn-C, $\gamma \rightarrow \varepsilon \rightarrow \alpha'$ martensitic transform. 79−24523
Fe-Mn-C, variation of martensite morphology with Mn and C composition 80−50635
Fe-Mn-Ni-C, age hardenable, struct. and strength 77−8844
Fe-Mn-Ti alloys, austenitic, precipitation strengthened 80−25714
Fe-N (0.022 wt.%), quenched, N precipitation during isothermal ageing 77−28820
Fe-Ni, $\alpha \rightarrow \gamma$ conversion, electron microscope and X-ray spectral microanal. 79−78966
Fe-Ni, interference microscopy, for colour development and phase separation 80−100976
Fe-Ni (31 wt.%), thermoelastic martensite obs. 80−3052
Fe-Ni (32.86, 30.65 wt.%), characts. of quenched struct. formed in textured sheets, TEM and optical microscopy study 79−34084
Fe-Ni alloys, graim growth texture 79−91687
Fe-Ni single crystals, stress induced martensite 77−8827
Fe-Ni-Al (10, 0.1 wt.%), clustering of Al_2O_3 inclusions 79−83205
Fe-Ni-C, internal friction anomaly with reheat transform. 79−100204
Fe-Ni-C (19 to 30, 0.04 to 0.8 wt.%) alloys, transformation of martensite in austenite, optical and electron microscopic exam. *(Russian)* 78−35382
Fe-Ni-C (19.5, 0.73 wt.%), banded struct. formed by deform., TEM and optical obs. 78−39869
Fe-Ni-C alloy, splat-quenched, martensite formation obs. 77−44247
Fe-Ni-Cr (40, 15.8 wt.%), precipitation and creep rupture behaviour, optical and TEM study 79−74158
Fe-Ni-Cr alloy, carbide form. by C diffusion, precip. distrib. and morphology 80−104164
Fe-Ni-Cr-Al-Y, oxidation mechanism, Y addition effect on kinetics and oxide adherence 80−97623
Fe-Ni-M alloys, (M=C, Ti,Mn), habit plane and morphology of lath martensites 77−8823
Fe-Ni-Ti (30, 6 wt.%), austenitic, discontinuous coarsening of lamellar cellular precipitates, morphology 79−78967
Fe-Ni-Ti (30, 6 wt.%), austenitic, discontinuous coarsening of lamellar cellular precipitates, growth kinetics 79−78968
Fe-Si (3.25 wt.%), single crystals and polycrystals, cutting surface texture 79−20291
Fe-V-C (0.3, 0.05 wt.%), interphase precipitation obs. in assoc. with Widmanstatten ferrite lateral growth 80−40365
Fe-WO_3 system, struct. phase exam. by optical microscopy and X-ray diffr. 78−31389
$Fe_{80}B_{20}$, amorphous, crystallization 78−42917
α-Fe_2O_3, interpretation of microcrysts. observed on faces (01.2) *(French)* 79−51038

optical microscopy continued
γ-Fe_2O_3, single mag. particle, remanent coercive force and remanent loop meas. 78−95480
Fe_2O_3-NiO-ZnO-CoO (15.1, 17.6, 0.6 wt.%) ferrite, effect of electron beam machining on surface layer 79−34178
Fe_2O_3-WO_3, phase relations 78−92249
$Ga_{1-x}Al_xAs$ based layer structures, optimum growth conditions, comp. and struct. perfection 80−104069
GaAs, alloying with Au and Au alloy ohmic contact metallisations, SEM and optical study 80−70820
GaAs, dislocation density, ⟨100⟩ cryst., quantitative light microscopy 77−31661
n-GaAs, dopant conc. determ. using laser IR microscopy 79−86811
GaAs, ellipsometer equipment used for microscopial arrangement 80−17998
GaAs, LPE layers, screw dislocations, optical microscope obs. 77−35561
GaAs layers, from gas phase, impurity influence on growth micromechanism 80−45237
GaAs, semi-insulating, optical and electron microscopy exam., line dislocation precipitates 80−70205
GaAs, surface chem. changes on annealing, optical and electron microscopy study 79−73383
GaAs, VPE growth, surface morphology study by optical microscopy 79−60651
GaAs, VPE layer on Ge, antiphase domain structures 77−69193
GaAs:Si(Cr), LPE, spiral growth patterns, dopants role 77−72800
GaAs-$Al_xGa_{1-x}As$ epitaxial layer heterointerface, toroidal defect obs. 79−77933
n-GaAs-n-GaN, diffusion growth kinetics, morphology and electrical properties 80−20294
GaN, epitaxial growth on sapphire substrate, surface feature exam. 79−4919
GaP, dislocation structure, optical microscopy obs. 80−24458
GaP, VPE layer on Si or Ge, antiphase domain structures 77−69193
GaSe, basal plane orientation determ. in vertical Bridgman grown single crysts. 78−19658
$\alpha(\beta)$-Ga_2Se_3, cryst. growth, optical, X-ray diffr. and SEM study 80−71587
Ge-Te, exam. of new compound, using light microscopy and X-ray diffr. exam. 78−48383
In-Cd, shape memory *(Japanese)* 79−43243
In-Tl, single crystal containing Li, X-ray study of FCC⇄FCT transform. *(Japanese)* 80−108435
InP/InGaAsP/InP double heterostructure, grown on InP(111)B substrate, threading dislocation multiplication 80−54237
InSb:Se, exam. of defects in crystal 80−6423
Ir-W (0.3 wt.%): Al(Fe)(Th)(Ni)(Rh), effect of additions on grain boundary composition 79−83309
$K_3Ba(NO_2)_4$, domain struct. obs. 79−55887
KCl(Br)(I), single cryst., quenched, microstruct. around indentations 80−7628
$K_2Cr_2O_7$, thermal props. thermal anal. and X-ray diffr. obs. 78−30752
KNO_3, orientations and twinning in the struct. transform. aragonite-type to calcite-type 77−24284
$KNbO_3$, layer growth, optical and electron microscopy 77−59021
K_2SnBr_6, transform. dynamics probed by Raman scatt. and microscopy 78−63832
LiF single crystals, exam. of void morphology effects on their disappearance kinetics 79−10843
LiF-AlF_3-Na_3AlF_6-Al_2O_3 system, phase equilibrium, X-ray diffr., DTA, quenching, optical microscopy study 80−50610
$Li_{0.5(1-x)}Mn_x\ Fe_{2.5-0.5}O_4$, rectangular hysteresis loop, microstruct. form. 77−12718
$LiNbO_3$ crystals, low temp. polarisation reversal, study of domains 79−61322
$LiNdP_4O_{12}$, grown by top seeded pulling technique, possible laser material 80−25542
LiO_2 pellets, sintered, exam. of microstructure 78−72749
Li_2O-SiO_2 glass, bulk crystn., SEM and optical microscope studies 80−44142
Li_2O-SiO_2 glass, water content effect on crystal nucleation and growth 79−55670
$Li_{x+2}P_xO_{3x+1}$, polyphosphate, melting and crystallisation 80−70376
Mg-Al-Zn (3, 1 wt.%), alloy AZ31, mech. props. of extruded and welded pipe and sheet, optical microscopy exam. 79−34065
Mg-Mn-Ce (1.5%, 0.3%) alloy, dislocation slip during superplastic deform. *(Russian)* 77−21214
Mg-Zr alloy, cavitation during diffusion creep 77−44296
MgO, spherical particle impact damage, effect of crystallographic orientation 79−79135
MgO:Ni, heavily doped, defect characterisation, rel. to use as laser material 80−65000
Mo cast alloy, shape, size, distrib. of carbides and oxides 79−24528
Mo, recrystallised sintered sheet, C addition effect on ductility 79−8319
Mo-Nb-TiN, dispersion hardened with strong interface, fracture mechanism 79−5058
Mo-Ti (up to 5.48 wt.%), internal nitriding, hardness, nitride type, precipitation *(Japanese)* 79−79157
Mo-W (30 wt.%), wrought, fracture, characteristic features 80−104278
Mo-Zr (0.15 wt.%), wrought, fracture, characteristic features 80−104278
Mo-Zr-C (0.63, 0.06 wt.%), quenched and deformed, structural changes during heating to ageing temp. *(Russian)* 79−1879
NH_4Cl, order-disorder transition, slip bands 78−22848
NaA and NaX zeolite crystals, crystn. study in presence of triethanolamine, Na_2O and SiO_2 content influence 79−65995
NaCl-$BaCl_2$ 1%, oriented growth of $BaCl_2$ phases, morphology 77−80627
$Na_2Mg_6Si_8O_{22}F_2$, fluoramphibole, fibrous, crystn. from gas phase, mechanism 78−34451
Na_2O-CaO-Al_2O_3-SiO_2 glass, crystn. for the purpose of obtaining vitroceramics *(French)* 80−75163
Na_2O-CaO-SiO_2, plates, exam. of Hertz crack branching 78−72887
Na_2O-CaO-SiO_2 glass, water content effect on crystal nucleation and growth 79−55670
Na_2O-NaF-CaO_xZnO_{1-x}-Al_2O_3-SiO_2, opal glasses, strength, surface composition 80−30066
$Na_5W_3O_9F_5$, single cryst., prep., optical and dielec. studies *(French)* 80−15994
Nb, deformation at 77-158K, slip and dislocation struct. 79−83277

optical microscopy continued
Nb, single crysts., plastic relaxation of internal stresses during mech. twinning at 4.2K, optical and SEM study *(Russian)* 79−66108
Nb-Zr-Al superconducting alloy, struct. determ. *(Russian)* 77−16628
NbH_x, supercond. T_c and low temp. resistivity, morphology 77−72940
Ni alloys, cast, interference microscopy, for colour development and phase separation 80−100976
Ni base alloys, hot corrosion in coal conversion system atmos. 79−96200
Ni, C precipitation 80−29958
Ni, fine particles, prep. by vacuum evaporation, crystal habits 78−88437
Ni, pure, anomalous grain growth 80−20984
Ni/Ni_3Al-Ni_3Nb, directionally solidified lamellar eutectic alloy, deform. anisotropy and fracture 77−36604
Ni-based alloys, binary, ternary, complex, TiC additions, effects 78−92305
Ni-Co-Cr superalloy, powder produced, necklace struct. development 80−40395
Ni-Cr, dispersion strengthening, prep. from powder, mech. props. 79−91658
Ni-Cr (2 wt.%), role of hydrostatic pressure on sintering of creep cavities 79−28980
Ni-Fe-Cr superalloy type 718, heat treatment effect on room temp. and elevated temp. fracture toughness response 80−100922
Ni-In, FCC, cellular precipitation kinetics 78−52823
Ni-Ta-Al system, phase equilibria and diagram, electron probe, X-ray diffr. anal. 80−29927
$Ni-ThO_2$ dispersion strengthened, high temp. strength, grain size and shape effects 77−48447
Ni-Ti (1.6, 7.64 wt.%), monophase high temp. scaling, metallography study 80−21159
Ni-Ti (49.7 at.%) alloy, deform. behaviour and shape memory effect 77−32638
β-Ni-Zn, eutectoid decomposition kinetics *(German)* 77−8819
Ni_3Al-Ni_3Nb, eutectic, temp. and thermal cycling influence on oxidation 80−45417
Ni_3Al-Ni_3Nb eutectic, directionally solidified, high-temp. oxidation mechanism 80−16544
$Ni_{2/3}Fe_{7/3}O_4$, precipitation of α-Fe_2O_3, optical microscopy, SEM and TEM studies *(French)* 80−11650
Ni_3GA single crystals, anomalous temp. depend. of strength, dislocation struct., optical and TEM 79−74228
Ni_3Ge single crystal, cleavage fracture 79−61694
NiO_2 single crystals, welding, optical and SEM study 79−65097
NiTi shape memory effects, substitution of Cu for Ni 79−61661
Pb, filament production, ejection of molten metal through nozzle, jet stability *(Japanese)* 78−52719
Pb-Sn eutectic, cavitation during superplastic flow, affecting factors 78−60728
$Pb_{1-y}Te$-$Pb_{1-x}Sn_xTe$ (x,y≤0.3), double heterostruct., LPE growth, heterointerface morphology 80−70550
$PbTiO_3$, single cryst., He^+ backscatt. shoulder spectra struct., domain struct. 80−35048
Pd-Cu-Si glass, cold drawn, serrated plastic flow, optical and SEM study 79−79052
$^{239}PuO_2$, hypostoichiometric, high temp. deformation rel. to cryst. microstruct. 79−79041
Sb-Ge, unidirectionally solidified, exam. of compressive props. and struct. 78−68730
Si (111) surface, heating effects on ellipsometric parameters 77−72764
Si, crystal, dislocation slip bands formation due to pores, nondestructive monitoring 79−55749
Si, Czochralski wafers, oxidation induced stacking fault sources 77−7737
Si, dislocation images, comparison of SEM and scanning optical obs. 79−51112
Si, ion-implanted, period surface struct. in laser annealing, new expt. evidence 80−29836
Si, near (111) slices, scratches made by diamond stylus 77−12726
Si, thermally induced microdefect form., C and O role 80−11439
Si wafer, oxidation induced stacking faults, surface vs. bulk nucleation 77−62545
Si-containing films, formed by reaction of Si with organic compounds of N, struct. investigation 79−87009
$Si-SiO_2$ interface struct., transient region 77−85115
SiC, CVD, microstruct. obs., optical and TEM 79−7560
SiC, high period polytype at interface of two interacting spirals 80−20041
SiC, impurity redistrib. and anomalous grain growth effects during polytypic transform. 80−15033
SiC, reaction bonded, microstruct. characterisation 78−48353
B SiC, sintered, effect of Al trace amounts on specimen props. 79−83289
SiC, uncommon mode of morphological development among coherent phases, optical and electron microscope exam. 78−80544
β-SiC whisker, failure and defects 79−96145
$SiC-B_4C$ (B+1 wt.% C), sintering 77−36432
SiC-ceramic, nondestructive evaluation, scanning photoacoustic microscopy 80−85115
Si_3N_4, reaction bonded, effect of Si powder grain size on microstructure, and mech. props. *(German)* 79−4998
Si_3N_4, reaction-bonded, microstructural analyses 77−8782
Si_3N_4, struct. of slow crack interface, light and electron microscope obs. 78−68770
$Si_3N_4-AlN-Al_2O_3-SiO_2-Y_2O_3$, phase equilibrium study by X-ray diffr. and optical microscopy 80−50614
$Si_3N_4-AlN-SiO_2-Al_2O_3$ solid-liquid equilibria 78−92247
Si_3N_4-ceramic, nondestructive evaluation, scanning photoacoustic microscopy 80−85115
$SiO_2-Al_2O_3-B_2O_3-MgO-CaO-Na_2O$, strengthened by ion exchange, exam. of internal stresses using polarising microscope 78−88549
$SiO_2-Al_2O_3-K_2O-Na_2O$, exam. of leucite crystal growth 79−19496
SiO_2-base cores, for superalloys, high temp. characterisation 80−10640
SiO_2-Na_2O (Li_2O), phase separation detection 77−1890
$SiO_2-Na_2O-CaO-MgO$ glasses, surface and near surface struct. 78−87850
$SiO_2-Na_2O-CaO-MgO$, glass, fibre and plate, internal stress and birefringence microanal. using optical phase microscope interference-polarisation 79−39109
$SmCo_5$, polished, domain wall grooving, optical microscopy and SEM obs. 77−8334
Sn droplets, on Bi, Zn and Al, heterogeneous nucleation 80−44294
Sn/graphite particulate composite, prep. using vacuum infiltration, microstruct., anal. 79−20005
$SrO-SiO_2-Fe_2O_3$, permanent mag. ceramics, exam. of phase diagram, using X-ray analysis, optical microscopy, electron probe anal., and thermal analysis *(German)* 79−29012
steel, Cr-Ni, ferrite precip. *(Japanese)* 80−35187
Ta-Nb-Ta sheet, interface topology, exam. method 77−72797
Tb-Sn-Se system, cross section $Tb_2Se_3-SnSe_2$ phase diagram, physicochem. anal. 79−87621
ThO_2, sintered, fracture props. studied by Hertzian indentation technique 80−50703
α-Ti, plastically deformed by rolling, optical and electron microscope obs. 79−91666
α-Ti, primary recrystallization study by three dimensional anal. of textures and annealing, HVEM obs. 79−91677
Ti-Al alloys, α_2 phase obs. using microscopy and X-ray diffr. 79−52497
Ti-Al-H, H effect on mech. props. and lattice constants 80−21036
Ti-Al-Sn (5, 2.5 wt.%), ductile fracture at low temps. 78−64659
Ti-Al-Sn-Zr (6.19, 1.92, 1.43 wt.%), fatigue cracking characteristics of β annealed microstruct. 79−5051
Ti-Al-Sn-Zr-Mo (6,2,4,6 wt.%), α-β type 6246, fusion zone fracture behaviour in weldments 80−30093
Ti-Al-V (6, 4 wt.%), hot isostatically pressed casting, fatigue crack initiation 79−79078
Ti-Al-V (6,4 wt.%), to H effect on fracture props. and microstruct. 80−40512
Ti-Al-V-Cr-Zr-Mo (3, 8, 6, 4, wt.%), phase transforms. 79−100113
Ti-Al-V-Sn (6,6,2 wt.%), α-β type 662, fusion zone fracture behaviour in weldments 80−30093
Ti-Al-Zr-Mo alloy 685, phase at α/β interface *(French)* 80−25661
Ti-Al(Mo), swaged and recrystallized, grain growth 80−3092
Ti-Mo, metastable β-phase, stress induced products formed by cold rolling *(Japanese)* 78−84843
Ti-Mo binary system, solid state phase transform. and miscibility gap, phase diagram 79−8298
Ti-Nb-V-Zr superconducting alloy, struct. determ. *(Russian)* 77−16628
Ti-Ni-Mo (1.5, 2 wt.%), Mo effect on microstructure 77−36536
Ti-V, metastable β-phase, stress induced products formed by cold rolling *(Japanese)* 78−84843
Ti-V (15.5 wt.%), {332} deformation twins, optical microscopy study 79−79047
TiC-Ni, particle growth quantitative anal. by metallography and stereology 77−77684
(U,Pu)C, sintering, role of Ni as sintering additive 80−84892
U core fuel elements, of A-1 reactor, volume growth *(Czech)* 80−27745
α-U, strain rate effect on flow and fracture 80−100887
U-Y-C FBR nuclear fuels, phase anal., 1400°C 80−66485
UAl_2-UNi_2, phase relationships, thermal, microscopic and X-ray exam. *(German)* 78−88447
UC, sintering, role of Ni as sintering additive 80−84892
UO_2, fine grained, low-stress creep study, metallographic obs. 79−43312
UO_2-zircaloy-4, reaction kinetics at high temps., O_2 diffusion 80−16667
$US-UC-UC_2$ system, potential nuclear fuels, phase solid soln. studies, prep. and props. exam. 79−40996
W cast alloy, shape, size, distrib. of carbides and oxides 79−24528
W, recrystallisation of commercially pure and doped wire drawn to high strain 79−100165
W, wire, doped, heavily drawn, recrystallisation 77−16609
W:Ni compacts, optimum conc. of Ni for activated sintering, optical microscopy obs. 79−38758
WC-Co, rupture of bending specimens, use of quantitative metallography and stereology *(French)* 77−28899
WC-Co (10%) alloy, high cycle fatigue, optical microscopy and SEM obs. 77−52494
YIG, single crysts. grown by floating zone method, quality eval. of etching and optical microscopy, ferromag. resonance linewidth meas. 79−19990
Y_2O_3 film in $Y-Y_2O_3$-Au junction, defect struct. and local conduction 78−26970
Zn, electrodeposition, on Ni surface, nondendritic granular deposit form. 77−59968
Zn film growth, HEED and projection microscope obs., surface orientation depend. on deposition parameters 77−32523
Zn-Al (22 at.%) eutectic, superplastic, microscopic examination of internal void formation 80−16383
Zn-Ge, eutectic, stereomorphology using SEM, TEM and optical microscopy *(Russian)* 79−52187
Zn_2GeO_4 single crystals, vapour growth 79−87571
ZnO, film for solar cell appl. structural, optical and elec. props. 80−2294
ZnS, crystal, layered struct. microscopic observations *(Japanese)* 78−38725
ZnS vapour grown crystals, morphology and structure 78−42937
$Zn_2SiO_4-SiO_2$ dielectric, struct. exam. by optical, photoemission electron and SEM 78−80706
Zr, blistering by 2 MeV He^+ ions, optical microscopy and SEM obs. 79−42119
Zr, creep, optical and electron metallographic anal., 473 to 873K 78−39986
Zr, deformed at 77K, effect of fast-neutron irradiation on deformation twinning, TEM and optical microscopy obs. 79−37741
α-Zr, H terminal solid solubility, optical metallographic study 80−34195
Zr-Cr (1.9 wt.%), β-quenched and tempered, optical and TEM study 79−66061
Zr-H formation, of $\delta \rightarrow \gamma$ transformation 80−84929
Zr-H formation, the $\delta \rightarrow \varepsilon$ transformation 80−84930
Zr-Nb-V-Si superconducting alloy, struct. determ. *(Russian)* 77−16628

optical model (nuclear) *see nuclear optical model*

optical modulation
2 Gbit/s electro-optic modulator for visible lasers 79−86262
4-bit digitally driven integrated optical amplitude modulator for data processing 80−53476
400 Mb/s optical transmission expts. 77−88954
A/C convertor using channel waveguide modulators, design and analysis 79−55249
acoustic sensor, fibre-optic, modulation processes 80−58771
acoustic sensor, single multimode fibre, using mode-mode interf. 79−50553
acoustic sensor, single optical fibre interferometric 78−38161

optical modulation continued
acoustically induced phase modulation in single-mode fibres, for acoustic detect. 79−50542
acoustico-optical and electro-optical modulators-areas of appl. 79−94359
acousto-optic, applications and device technology 77−58468
acousto-optic, laser beam transverse mode and polarisation effects on perform. 77−58469
acousto-optic bulk interactions in thin film waveguides, for GHz modulators 78−42471
acousto-optic modulator, improved contrast using spatial filtering 78−9448
acousto-optic modulator, wide bandwidth, design procedure 78−5569
acousto-optic modulator and driver for CW dye laser 77−61984
acousto-optic modulator efficiency optimisation, sound diffraction profile model and expt. 80−106615
acousto-optic modulator for CO_2 laser beams and detect. using W-Ni point contact diode 79−3730
acousto-optic modulator for CO_2 laser rangefinder using heterodyne detect. 80−102825
acousto-optic modulator temporal response, physical optics model in low scatt. efficiency limit 78−66897
acousto-optic modulators, nonreciprocal transmission phenomena 78−33898
acousto-optic planar guided-wave Bragg modulators, integrated optic communication appls. 80−38131
acousto-optic polarisation modulator, 200 to 2400 nm transmission band *(Russian)* 80−14472
acousto-optic programmable filter characteristics and applications in optical computing 79−72716
acousto-optical frequency and intensity control system for CW lasers 77−88804
acousto-optical laser beam intensity modulator *(Slovenian)* 80−43429
acousto-optical modulator, for intracavity laser intensity modulation, 0.01 Hz to 12. GHz 79−41400
acousto-optical modulator, freq. characts. 77−62069
acousto-optical modulator, geom. optics model in low scatt. efficiency limit 77−34935
acousto-optical modulator, metrological certification of photodetection devices 80−23727
acousto-optical modulator, standing wave, thermal detuning effects 78−71197
acousto-optical modulator for laser beam position sensor 78−46705
acousto-optical modulator for mode-locked CW Nd:YAG laser 80−87419
acousto-optical modulator using coupled plane waveguides 80−69527
acousto-optical modulator using TeO_2, appl. to laser Doppler anemometers 78−83082
acousto-optical modulator-deflector for light beam 79−55224
acousto-optical modulators for laser beams 77−19355
acousto-optical snapshot Pockels Readout Optical Modulator 77−19193
acousto-optical variable-ratio laser beam splitter 79−81538
acousto-optical wideband programmable filter 80−102842
acoustooptic hydrophone, coupled waveguide, using intensity modulation 80−14431
acoustooptic modulator, reduction of thermal distortion of diffracted light 80−5837
acoustooptic modulator intensity servo, optical isolation and amplitude noise reduction 79−98472
acoustooptic snapshot PROM, real-time optical, signal spectrum analyser 78−90494
acoustooptical modulation assoc. with periodic deform. of liquid crystal layer 78−52471
acoustooptical modulators, computer controlled laser interferometer 80−56294
active feedback optical processor, using coherent source and liq. cryst. light valves, design 78−22204
active optical devices, seminar, San Diego, CA, USA (August 1979) 80−101664
active pulse shaping in ps domain using fast Pockel cell and GaAs switch 80−28257
additive film copying machine, modulator mechanodigital design *(German)* 78−65987
aerial photographic analysis and stereographic mapping with electro-optical pattern recognition 77−19186
aerosol layer depth remote meas. by microwave-modulated laser *(Russian)* 78−57338
airborne laser scanner, modulation techniques- 80−5770
alkali halide, ReO_4^- doped, saturable absorber at 10.6 μm 80−53384
alkali halides, photodichroic, as optical processing elements 78−83056
AM, bandwidth of single-mode fibre 79−81560
amplitude-phase holograms, optical parameter dispersion 80−58481
analog modulation of light-emitting diodes for optical fiber *(Japanese)* 78−90516
analogue data processing systems, polarised modulation of light *(Russian)* 80−91884
angle modulated optical signals, parameter meas. *(Russian)* 78−37047
angular displacement meas. by photoelec. amplitude-phase modulation method 78−16774
anisotropic waveguide, guided-radiation mode interaction, appl. to direct-intensity modulators 79−76839
arbitrary profile beam, diffr. by periodically modulated layer 80−43252
astronomical application of resonant electromech. modulators 78−53831
AT-cut quartz plate vibration anal. using light modulated oscillator 78−71255
atmospheric propagation of modulated laser beam, acoustic pulse generation, thermal defocusing 79−92597
atmospheric scintillation effect on capacity of polarisation and amplitude modulated links 77−75428
atom, Stark effect, modulation light wave vibrs. *(Russian)* 79−98027
background suppression by selective modulation interferometric spectrometer 79−97443
bacterial cells, tethered, image-splitter-modulator for rot. rate and direction meas. 77−73620
balanced bridge modulator switch, using Ti-diffused $LiNbO_3$ strip waveguides 78−63201
binary input hologram recording with single acoust-optical modulator *(Russian)* 77−58287
biquartz modulator, light interf. effect on photoelec. polarimeter accuracy 80−62713
birefringence measurement using photoelastic modulator 80−31838
optical modulation continued
birefringence modulator devices for sensitive polarisation determ. 78−8437
birefringent rotating plates as modulated optical filters, polarised light meas. appl. *(French)* 77−67490
bistable optical devices, overshoot and alternate switching, subharmonic generation 80−99790
bistable optical devices 78−46763
bistable optical devices for integrated optics and fibre optics appls. 79−55175
bistable optical spatial device using direct optical feedback 79−18535
bistable optical systems based on Pockels cell 79−59827
branching waveguide stripe injection laser, beam scanning and wavelength modulation 79−7138
broadband optical modulator for laser range finder *(Russian)* 80−53424
bulk acousto-optic interactions in thin film waveguides, gigahertz modulators 79−32091
buried heterostructure laser, sinusoidal modulation characts. 78−87054
cavity optical tuning for optical modulation 79−64314
ceramics, transparent ferroelectric, composition selection for appl. in light modulators *(Russian)* 80−91869
chalcogenide glass films, kinoform optical elements and integrated optics elements prod. 77−75634
chalcogenide glass films, opt. inform. recording uses 77−75633
chalcopyrite crystal acousto-optical props. 79−46054
channel waveguide double-pole double-throw switch/coupler, using total internal refl. 78−71233
channel waveguide interferometric modulator for EM field detection 80−74498
chirp reversal, optical integration in degenerate four-wave mixing 78−46730
chopper wheel in photometer, third harmonic freq. suppression in modulated radiation 77−50754
chopper with digital control circuit *(Japanese)* 79−3784
closed-loop simple system for real-time optical phase meas. 79−63302
CO_2 laser R(18) line, wideband modulation with NH_3 Stark cell 77−23704
coherence modulation by US waves, partial coherence depend. on US parameters 80−58453
coherent, two component system producing by static phase modulation a directional light beam *(Russian)* 78−50940
coherent birefringent optical pulse compression 80−106437
coherent light valve optical modulator 79−72712
coherent light valve processor, two-dimens. optical modulator 80−102840
coherent OCR system using spatial light modulator *(Japanese)* 80−14291
coherent optical adaptive Modal Wavefront Control System 77−19295
coherent optical pulse synthesis using phase-locked lasers and nonlinear optical processes 79−76724
coherent pulse propagation, 0π pulse generation from zero-area pulse 80−48352
coherent signals, heterodyne detect. methods 78−82055
coherent transients by laser freq. switching 78−66873
coherent-radiation spectral power density unit reproduction, USSR standard 78−37957
complex spatial coherence meas. by sinusoidal phase modulation 80−106446
computing, conference, London (1978) 79−72511
continuum self-phase modulation and stimulated Raman scatt., combined effects 80−69460
convex beam integrator for laser beam shaping, heat treating appl. 80−53346
cooperative Raman scattering, effect of phase self-modulation of light 80−91855
coupled laser oscillators, injection modulation 80−99773
coupled waveguide modulator with pn-junction, strip loaded channel waveguide, design 78−46843
coupled-waveguide optical modulators *(Japanese)* 78−46789
coupled-waveguide optical modulators with Schottky contacts, embedded- and rib-waveguide configurations 79−23093
coupled-waveguide with pn junction, multilayer planar waveguide configuration 78−71235
coupler, directional, operation and manufacture *(German)* 77−75673
coupling coefficient modification by periodic modulation of propag. consts. 77−72092
cutoff modulator using Ti-diffused $LiNbO_3$ waveguide 80−9991
CW injection lasers and LEDs for optical communications 77−7210
cyanobiphenyl liquid crystal IR modulator expts. 80−102837
cylindrical waveguide optical modulator efficiency in thermal mode *(Russian)* 79−94345
cylindrical waveguide wideband modulator, parameter optimisation *(Russian)* 79−94344
decimal/residue/decimal optical converters 79−22905
decoders based on controlled transparencies *(Russian)* 80−28321
deflectors using electro-optically controlled interference 79−1007
delay line, OLZ-7 seven-frame, using multiple reflections in plane mirrors 79−23080
DFB dye lasers, dichromatic switching effect 79−10331
DH injection laser with coherent light injection, modulation behaviour 78−55352
differential electro-optic shutter with ns pulse operation 78−74994
differential optical spectra recorder using wavelength modulation method 79−2832
diffraction grating, refl. type elec. controllable, for intracavity laser modulation 77−58357
diffuser form. of simple known statistical props. 78−90539
digital light deflector with KD_2PO_4 polarisation switches 77−39049
diode laser, mode locking to external resonator, theory 80−106550
diode laser in external cavity, linearized theory 80−69391
direct modulation of light by sound 79−72715
directional coupler, phase tuning by photostructural effect of chalcogenide glass film 77−83963
directional coupler switch, electrooptic, used as amplitude modulator, exam. 78−42467
discrete PPM signal reception accuracy *(Russian)* 79−94171
dispersive delay line, optical pulse squaring effects 77−88808
dispersive medium, Stokes, anti-Stokes scatt. of ultrashort pulses, phase modulation effect 78−50857
dispersive modulator using Stark effect system, for optical pulse compression 77−54793

optical modulation continued
displacement meas. by interferometers with electro-optical modulators *(Russian)* 78−12667
distributed Bragg reflector laser, tunability by modulating refractive index in corrugated waveguide 77−79866
dithered-beam metrology 79−30408
Doppler frequency discriminator applic. in laser velocimeter 78−26220
dye, two-photon fluoresc. quenching, phase fluctuations and phase modulation effect 78−50570
dye CW laser, mode locking using externally modulated pumping laser 79−18456
dye CW lasers, RF tuning 80−1243
dye DFB laser, N_2 laser pumped, self Q-switched, tunable picosecond pulse generation 80−69432
dye doped polyurethane film, photoinduced guided light stopping 77−23739
dye laser, continuously pumped, actively mode locked, pulse props. 77−42546
dye laser, continuously pumped, pulse compression with slow saturable absorber 79−31959
dye laser, CW, synchronous pumping and passive mode-locking, for picosecond pulse generation 79−3727
dye laser, optogalvanic effect to freq. lock to discharge transition freqs. 77−19309
dye laser, self frequency locking, strong field effect on intracavity atoms 79−86198
dye laser, subnanosecond radiation pulse formation mechanism, axial period *(Russian)* 77−50700
dye laser, synchronously pumped mode-locked CW system, pulse characts., cavity detuning effect 79−3726
dye laser, tunable ultrashort pulse generation 80−95931
dye laser 5890 Å CW output, temporal compression using Na vapour delay line 78−46688
dye laser jet stream, thickness meas. in real time, by optical technique 78−82975
dye ring laser, flashlamp pumped, injection of N_2 laser excited oscillator beam 80−5754
efficient intensity modulator 78−22190
elasto-optical birefringence modulator construction method *(Japanese)* 77−54809
electro-optic A/D conversion using channel waveguide modulators 78−66898
electro-optic bistable devices, optical regenerative oscill. and monostable pulse generation 80−106612
electro-optic devices, guided wave, for logic and computation 78−66946
electro-optic guided-wave A/D convertor, high speed 80−33234
electro-optic light modulator, phase matched 78−83089
electro-optic microwave modulator, broadband electronically tunable, for CO_2 lasers 79−64256
electro-optic modular crystal length reduction by protruding electrodes 79−76860
electro-optic modulator, servo controlled, for CW laser power stabilisation and control 80−19060
electro-optic multimode waveguide modulator or switch 80−23783
electro-optic multimode waveguide switch 79−10383
electro-optic phase shifter pair with optical waveguide couplers 78−66952
electro-optic spatial phase modulators, resolution meas. techniques 77−79959
electro-optic thin film periodic waveguide switch and amplitude modulators anal. 78−22215
electro-optic waveguide modulators, capacitance of electrode system rel. to modulation efficiency *(Russian)* 80−1359
electro-optical active components for guided light 78−42470
electro-optical array processor for complex signals 78−94428
electro-optical Bragg deflection modulators in corrugated waveguides 79−59844
electro-optical broadband travelling wave modulator, expt. design principle 78−94438
electro-optical crystals, space-time light modulation 78−18056
electro-optical device with feedback, light modulation 79−41448
electro-optical device with feedback, multi-functional 79−32055
electro-optical devices for multimode optical switching 79−76882
electro-optical frequency modulator with rot. elec. field, appl. to laser Doppler velocimeters 77−42620
electro-optical gate for nonpolarised emission *(Russian)* 78−59132
electro-optical laser modulator for optical coherent transient generation 80−102776
electro-optical light modulator with small nonactive losses 80−78981
electro-optical linear interferometric modulator for electromagnetic field detection 80−58782
electro-optical modulator, asymmetrical, electric field config. anal. *(Russian)* 80−91885
electro-optical modulator, complex-internal-refl. config. 79−50384
electro-optical modulator large bandwidth, using mm-wave drivers 78−87164
electro-optical modulator use in or outside cavity for laser freq. shifting or stabilisation 78−5512
electro-optical modulator-based instrument, for polarisation dependent light scatt. meas. 78−58010
electro-optical modulators on flat waveguides, theory *(Russian)* 79−50411
electro-optical multivibrator operation, in optical bistable device 80−58674
electro-optical phase modulator, for dye laser freq. stabilisation 77−88802
electro-optical phase modulator in antiresonant ring laser, for cavity dumping 77−88792
electro-optical space-time light modulator 80−69526
electro-optical spatial light modulator resolution, stored point charge effects 80−106616
electrochromic ATR prism modulator 80−43440
electrochromic dye as modulator 77−7185
electromechanical beam choppers, review 77−27346
electromechanical modulator with synchronous motor 78−13806
electron beam spatial modulator using KH_2PO_4 77−72077
electrooptic analogue-digital conversion, using channel waveguide modulators 78−38051
electrooptic bistable devices, optical regenerative oscill., monostable pulse generation 80−96002
electrooptic diffraction modulator, large-aperature 80−33179

optical modulation continued
electrooptic distributed Bragg reflection modulators for integrated optics 77−27388
electrooptic four-modulator photopolarimeter, for Mueller matrix meas. 80−73417
electrooptic nonlinear devices with two feed signals, operation characts. 80−14441
electrooptic polarization modulated injection laser 80−58591
electrooptic prepulse suppression for fusion laser systems, using optically timed Pockels cells 80−102743
electrooptic radiation modulators utilizing semiconductor ridged waveguides 80−91925
electrooptical oscillator, integrated cutoff modulation 80−48424
electrooptical planar waveguide, phase modulation theory *(German)* 77−27367
electrostatic field distribution calc. *(Russian)* 80−87514
ellipsometer, modulated light, for substrate and thin film meas. at 10.6 μm 78−54442
ellipsometry, modulation error 80−255
ellipsometry, wavelength-scanning polarisation-modulation, practical considerations 78−41343
ellipsometry, wavelength-scanning polarisation-modulation, sample imperfection effect 78−24845
emission background corrections obtained with oscillating refractor plate, modulation waveform effect 77−90653
emissivity, measurement for low temp. sources, flux double modulation method 78−45634
energy expenditure minimum for light wave modulation 80−58611
excimer laser Raman pulse compression for appl. to laser fusion 79−59756
excimer laser Raman pulse compressor systems for laser fusion 79−59757
Fabry Perot wide-band electrooptic type modulator, modulation sensitivity 79−3724
Fabry-Perot bistable devices, as optical switch, limiter or memory element 77−88931
Fabry-Perot cavity, optical pulse tailoring and termination by self-sweeping 80−23760
Fabry-Perot cavity acoustooptic modulator for internal laser modulator *(Japanese)* 77−88814
Fabry-Perot cavity containing ruby, optical bistability and differential gain, 85 to 296K 77−39025
Fabry-Perot electro-optic type wide-band modulator sensitivity, surface error influence 79−50392
Fabry-Perot interferometer, effect of zero points in light modulation *(Russian)* 79−58781
Fabry-Perot non-linear optic media devices, instability and regenerative pulsation phenomena 78−46685
Fabry-Perot resonator, bistable, use as optical switch, limiter or memory element 77−39024
Fabry-Perot resonator, laser mode sweeping dynamics, optical length effects 78−83001
fact directional coupler switch/modulators, novel ps optical pulse sampling method 80−58784
far IR laser, modulational instability in piezoelec. semicond. 79−47117
far IR laser intracavity polarisation modulation by CdTe AC Faraday rotation 80−58613
far IR lasers, optically pumped, frequency modulated noise measurements 78−55392
far IR waveguide laser, Stark modulation 77−54744
Faraday rotator and modulator, IR, CaVG polycryst. appl. 78−10900
ferroelectric ceramic, optical modulation by electrostriction during electron beam charging, spatial characts. 79−7224
ferroelectric ceramic-photoconductor structure, as optically controlled transparency 80−28343
ferroelectric oxide crystals for electrooptics and nonlinear optics, optical inhomogeneities, review *(Japanese)* 77−65613
ferroelectrics, photoelectretic states in real time spatial light modulators, photorefractive effect 80−80676
ferromagnet, microwave modulation of light using magnetodynamic resonance 80−71393
ferromagnetic medium, magnetised, unattenuated refracted wave propag., optical modulation appl. *(Russian)* 78−25774
fibre, single mode, vibration induced polarisation modulation 79−27385
fibre communication technology, state of art *(Czech)* 78−5575
fibre data collection highway with piezoelectric phase modulators 77−39098
fibre dispersion investigation, scanning technique 79−76852
fibre laser plate for digital image processing, all-optical parallel logic operation 80−106463
fibre material dispersion meas. by baseband modulated envelope detection 78−1368
fibre optic rotation sensor, all-waveguide configuration, key element tests 80−58796
fibre optic system design and component selection 80−58767
fibre optical communication system with thin-film modulator 79−10407
fibre optical illuminator output speckle, smoothing methods 79−7209
fibre waveguide, transmission characts. of microwave-modulated radiation 78−25985
fibre-guided coherent light, phase modulation using HF sound 78−87142
fibre-optic communication and integrated-optics sources *(Italian)* 79−94371
fibre-optic data transmission, principle and methods 79−10393
fibre-optic delay line signal processing devices 80−48443
fibre-optic microphones and hydrophones compared with conventional devices 79−72717
fibre-optic transmission by laser diode analogue baseband modulation 80−58738
Fibredyne systems for passive or semipassive fibre-optic sensors 78−71206
fibreguide transmission, vibr. induced intensity modulation 77−23743
fibres as microphonic instrumentation transducers 77−17970
FIR lasers stabilizations, fast modulation technique 80−99777
fluoromethane far IR laser FM and stabilisation by Stark effect 78−59056
fluoromethane waveguide laser, tunable, for far IR freq. synthesis in 500-70 μm region 78−90439
FM optical communications, using electrooptically tuned semicond. lasers 80−14351
FM wide-band system using optical techniques 79−64308

optical modulation continued
four-photon processes stimulated by fluctuating pump in dispersive medium 79−23017
Franz-Keldysh, optically enhanced for n^+-p-n^+ phototransistor struct. 78−60423
Fraunhofer diffraction of apertures, analogy with SSB modulation 80−48138
frequency chirped optical pulse, compression by strongly dispersive grating pair 79−50373
frequency chirped pulse compression using phonon-polariton propag. modes 78−46689
frequency modulation by p-i-n structure, optical waveguide with moving walls 80−19099
frustrated total internal reflection switches and modulators 77−39066
gain-guiding stripe-geometry DH semiconductor laser small-signal modulation characteristics 79−45946
garnet film waveguides, magnetooptical effects 77−3650
garnets, skew cylindrical mag. domains, light modulator appl. anal. 79−38360
gas in applied elec. field, IR transmission modulation *(French)* 78−50912
gas laser, degree of excitation determ. 78−1285
gas laser, mode-locking operation using modulator with acoustic Fabry-Perot resonator 79−45976
gas laser, modulation method, for relative excitation level, cavity bandwidth and at. temp 80−5771
gas laser output characts., effect of spatial and temporal modulation of excitation 79−3681
gas laser radiation, internal modulation by acoustic surface waves 78−25901
gas multimode laser with excitation modulation, polaris. of active medium 78−82942
gas of two-level molecules, reson. interaction of standing freq. modulated wave 79−94295
gas-lasers, single-mode, fluctuations of laser beam diameter, lens effect 80−64090
gating, subps, by optical wavefront conjugation 79−46004
Gaussian laser beams, spatial modulation 79−7162
gel rods, elastic dilatational mode, light beam positional modulation 80−64167
gelatinous light modulating media, dynamic deform obs. by laser interferometry 79−32072
gyrotropic waveguide switching elements at optical wavelengths 79−37049
Hartmann modified wavefront sensor performance 80−74522
heterodyne interferometer with acoustooptical modulator 77−5896
heterostructure planar waveguides, guided-to-radiation mode conversion and appl. to light modulation 80−87557
heterostructures for integrated optics 77−39112
HF acousto-optic mode conversion and deflection 77−54776
HF laser nanosecond pulse generation using Ar gas breakdown 79−81465
HF self-modulation of laser with unstable resonator *(Russian)* 77−83911
hologram electronic heterodyne recording and processing using phase modulated reference waves 78−46537
hologram electronic heterodyne recording and self-interference term rejection 80−91756
holographic binary data recording with multichannel acousto-optical modulator *(Russian)* 79−94178
holographic data recording phase-random mask production by multichannel acousto-optical modulator *(Russian)* 79−94179
holographic interferometry, linearised subfringe, modulation errors effect 80−78803
holographiz correlometer with phase modulation, viscous, superviscous light scatt. media study 80−74321
holography of moving object, using Q-switched ruby laser freq. chirp 79−7093
HV pulse generator for modulation spectroscopy 78−77995
hybrid bistable optical devices, transient response 79−59803
hybrid field-effect liquid crystal light valve, sensitometry control 80−23788
hybrid field-effect liquid-crystal light valve, optical data processing performance 80−99860
hydrophone, moving fibre optic, based on intensity-modulation mech. 80−43455
II-VI semiconductor Franz-Keldysh effect modulators for laser radiation *(Russian)* 77−88813
III-V nitride semiconductors, physical properties and appls. in integrated optics *(Czech)* 80−28355
image and signal processing, United States Air Force programmes 78−74854
image detail enhancement system with PROM, for photographic recording 78−58086
image Fourier transform correlator using US light modulator *(Russian)* 77−58264
image processing by spatial freq. spectrum phase modulation *(Korean)* 78−22090
image subtraction through speckle modulated by Young fringes 80−95813
image weak modulation detection in film grain noise with partially coherent illumination 80−77897
inertial feedback laser, T-modulated giant pulses 77−19353
injection diode modulated laser pulse generator and digital control cct. *(Russian)* 80−14372
injection laser, bias quenching of relaxation oscillations 79−72570
injection laser, CW, optical feedback effects using external reflecting surface 78−79045
injection laser, output relax. oscill. suppression by elec. reson. cct. 77−88798
injection laser, reson.-like peak reduction in direct modulation due to carrier diffusion 78−74905
injection laser modulation using diode cct. 77−79935
injection laser radiation, 750 MHz modulation, for pulsed phase rangefinder 77−54804
injection lasers, directly modulated, suppression of reson. in light output 78−66853
injection lasers, harmonic distortion in direct modulation 79−68411
injection lasers, high-bit-rate pulse regeneration and modulation using planar Gunn device 79−59731

optical modulation continued
injection lasers, intraband electronic relaxation effect on relaxation oscillation 79−81433
injection lasers, optical ringing effects, internal loss modulation and direct modulation 78−87081
injection lasers operated with HF modulation, intensity fluctuations calc. 78−22123
integrated and guided-wave optics, conference, Incline Village, NV, USA, January 1980 80−58772
integrated directional coupler modulator, 1 Gbit/s 80−38125
integrated directional coupler switches, modulators and filters using $\Delta\beta$ reversal techniques, review 80−38132
integrated electro-optic modulators, review 79−37058
integrated electro-optical A/D convertor, using branching waveguide modulator channels 78−42474
integrated electro-optical two arm interferometer, optical bistability expts. 79−76883
integrated interferometric reflector 77−58490
integrated optical detector array, waveguide, and modulator, based on Si technology 77−11049
integrated optical elastomeric modulators 77−75715
integrated optical logic circuits, using electrooptic switches and modulators 78−38089
integrated optical switch for fibre data transmission system 77−27384
integrated optical switching system with input modulator 80−99884
integrated optics, modulator anal. using MIC formulas 77−39108
integrated optics and guided wave devices, review 78−42468
integrated optics for optical fibres, progress and components, review *(French)* 80−69524
integrated optics modulators and deflectors development, review 77 79973
integrated optics sub-ps gate 80−58809
intensity modulated sources, statistical props. of counting distribs. 79−72541
intensity modulation, bandwidth limitations due to harmonic distortion in single-mode optical fibers 79−64335
intensity modulation, bandwidth of single-mode fibre 79−81560
intensity modulation of transmitted light in curved optical fibres 77−75672
interference pattern electronic heterodyne recording 80−74316
interferometer, modulated fibre ring, laser appl. 80−74506
interferometer signal processing by acoustooptic correlation devices, radio astronomy applications 80−8543
interferometry, 10 μm, linear phase restitution *(French)* 78−12749
interferometry, phase modulation, combined with object scanning *(French)* 79−2814
interferometry, phase modulation, expt. process to restore phase sign and value 78−32869
interferometry, phase modulation, meas. of phase differences in microscopy *(French)* 77−82593
interferometry, phase-modulation, sine restoration of phase in object field *(French)* 77−79144
interlocked solid-state lasers, radiation intensity modulation for precision meas. 80−1250
interoffice trunk fibre-optic experimental transmission system 77−54795
intracavity absorber modulation, transients obs. in CO_2 or N_2O IR laser 78−74933
IR and FIR tunable coherent sources utilising modulational instability 80−95967
IR electrooptic waveguide for CO_2 laser modulation 77−27349
joint transform correlator performance rel. to wavefront modulator characteristics 80−102651
Josephson optical modulator with weak-link diffraction grating 79−98486
laser, acoustic DFB, EM and acoustic wave refl., freq. and amplitude modulation 77−54717
laser, acousto-optical at microwave frequencies 78−1282
laser, double heterostruct. junction type, US wave freq. modulation anal. 78−83009
laser, external self-modulation for double pulse prod. 77−83902
laser, passive mode locking, two laser amplifiers with slow saturable absorber 80−33041
laser absorption spectroscopy for point monitoring of gases ambient concs. using tunable lasers 78−61607
laser acousto-optical Q-switching, for interferometer light source 77−7489
laser alphanumeric character generator for line printer and COM 80−33067
laser amplifier, optooptic modulated based on gain saturation 79−22988
laser beam, electro-optical and acousto-optical devices comparison 80−43380
laser beam by microwaves, trapped-mode microwave resonator coupling and tuning 78−55389
laser beam expander for short cavity dye laser 80−87532
laser beam for stroboscopic holographic interferometry for vibration investigations *(Polish)* 79−3649
laser beam modulation by Fresnel acousto-optic conversion 77−27371
laser beam modulator using rotary diffraction grating 78−87080
laser beam refraction at spherical surface, distortion, geometrical optics calc. 80−95929
laser beam resonant chopper performance characteristics and limitations 80−64084
laser beam scanning by acousto-optic deflector array 80−10017
laser beam simple submicrosecond optical chopper 80−14373
laser beam spatial characts. meas. by modulation method 79−31967
laser beam wavelength, automatic reading by wavelength-modulation technique *(Japanese)* 78−1286
laser beat noise as multifreq. modulated source, for luminesc. lifetime meas. 77−57406
laser cavity dumping using antiresonant ring and electrooptic phase modulator 78−17980
laser communication system, using US light modulator, for teachers 79−40321
laser detection by coherence discrimination, angle-scanned interferometer as coherent energy modulator 79−58777
laser diode,, modulated, with short external cavity, single mode operation 80−5756
laser diode 1ns pseudo-random pulse modulation cct. 78−50836
laser diode modulator using current switching bipolar transistors 78−1288

optical modulation continued
laser engineering and appls., conf., Washington, USA (May-June 1979) 80 - 1216
laser extensometer with scanning beam modulation, improved gauging precision 78 - 57896
laser frequency modulation, single-mode 78 - 13737
laser frequency stabilisation, spectral profile modulation broadening 78 - 87083
laser heterodyne signals from moving object, bandpass filtering by finite apertures 78 - 55306
laser interferometer, principles and performance, distance meas. appl. 78 - 89442
laser interferometers, AM and FM operation and applications *(German)* 80 - 86389
laser interferometry by induced modulation of cavity field 78 - 49888
laser intracavity acousto-optical modulation 77 - 19356
laser intraresonator forced Raman radiation with polariton excitation *(Russian)* 79 - 94286
laser modulator for HF laser communication links 80 - 48311
laser output power stabilisation using acousto-optical method *(Polish)* 79 - 13994
laser passive mode-locking and Q-switching with optical Kerr effect modulator 78 - 9403
laser PCM, injection laser radiation, optimal conditions 79 - 59733
laser pulse generation and modulation devices 78 - 25899
laser pulse shaping on multiple rot. lines, using electro-optical cryst. modulator 80 - 78879
laser pulse shaping with grating pair and filters 79 - 89940
laser pulse timing by combined passive and active mode-locking, anal. 78 - 55391
laser radiation internal modulation, freq. limitation 79 - 72607
laser scanned acoustical imaging systems, demodulation scheme 79 - 59826
laser sensing system for elec. and mag. fields in power transmission 77 - 45870
laser signal, sinusoidally modulated, electron-optical recording with subpicosecond resolution *(Russian)* 77 - 7105
laser speckle reduction by US modulation 79 - 3638
laser speckle reduction in image plane by US modulation of spatial coherence 80 - 106459
laser subnanosecond pulse production, of variable length 78 - 94405
laser ultrashort pulse form., filter clarification and amplification saturation coincidence 80 - 64085
laser velocimetry using acousto-optical modulators 80 - 33715
laser wavefront correlation transformations *(Russian)* 80 - 99778
laser wideband modulator, 1 Gb/s 77 - 79965
laser wideband ring modulator, for CO_2 laser 77 - 88803
laser-Raman spectroscopy with AC differential analysis 77 - 38031
lens centring error tolerance study *(German)* 78 - 33806
LF modulator for use in vac., electrical drive circuitry 77 - 31138
light beams, optical phase modulation meas. using Michelson interferometer *(German)* 79 - 17473
light diffraction by real stationary US field in liquid 80 - 83551
light source coherence meas. and fibre modal noise simulation by Michelson interferometer 80 - 48324
light-controlled light modulator, fast resonantly enhanced, for laser beam modulation 78 - 5509
$LiNbO_3$ electro-optical total internal reflection diffraction industrial modulators and deflectors 77 - 19436
linear array acousto-optical modulator devices 77 - 39072
liquid crystal as IR modulator 78 - 25970
liquid crystal cells exhibiting dynamic scatt. for light flux attenuation 80 - 102845
liquid crystal device response time improvement 79 - 76806
liquid crystal electro-optic valve testing using laser light *(French)* 80 - 28311
liquid crystal electro-optical modulators for two-dimensional data processing 78 - 79141
liquid crystal light valve, appl. to real-time optical data processing 78 - 83102
liquid crystal light valve, light-modulated 79 - 14098
liquid crystal light valve operation and appls. 78 - 46826
liquid crystal waveguides for integrated optics 77 - 34960
liquid crystal-fibre optic modulator for display 79 - 72718
liquid crystals, piezoelectric effect use as light modulator 80 - 83679
liquid-crystal light modulator, time depend. of conductivity under dynamic scatt. conditions 80 - 64178
Mach-Zehnder interferometer, switch, integrated optical format 78 - 38084
Mach-Zehnder interferometric waveguide modulator, polarization-independent operation 79 - 18552
Mach-Zehnder type modulator, RF modulation characts. meas. method 80 - 74480
Mach-Zehnder waveguide modulators in Ti-diffused $LiNbO_3$ 80 - 33203
magnetic diffraction gratings with alterable magnetic domains for optoelectronics 78 - 63197
magneto-optic bubble spatial light modulators, appl. in optical processing systems 78 - 79139
magneto-optical waveguide, semileaky thin film, for modulator appl. 77 - 62055
magnetooptic bounce-cavity modulator, direct AM 80 - 5769
matched filtering with multichannel US modulators *(Russian)* 77 - 58426
matched holographic filters with Pockels readout optical modulators 80 - 53456
matrix-addressable controlled transparency, spatial modulation in holographic memory recording 79 - 10401
MBBA, light modulation by nematic liq. cryst., mech. excitation, response times 79 - 73094
MBBA, liq. crystal, morphological changes and electro-optical characts. appl. laser light modulation 77 - 20826
mechanical chopper, transmission sector effect on instrument threshold sensitivity 79 - 7222
mechanical light modulator, harmonic anal. of noise spectrum 78 - 1362
mechanical vibration meas. optical heterodyne systems 77 - 13746
methanol far-IR laser, optically pumped, intracavity polarization modulation 80 - 23726
methanol waveguide laser radiation modulation by Stark cell 77 - 38962
microcantilever electrostatic deflection system for transmission optical modulator array 80 - 87512
optical modulation continued
microchannel spatial light modulator, for real-time optical data processing 79 - 18534
microchannel spatial light modulator 80 - 91913
microchannel spatial light modulator as storage medium 80 - 43479
microchannel spatial light modulator development, for real-time optical data processing 79 - 72714
microfilm laser transfer printing 77 - 18121
micromechanical light modulator array fabricated on Si, laser display appls. 78 - 9433
micromechanical light modulator array fabricated on Si 78 - 1433
microoptical switch, Mach Zehnder interferometer, for use with optical fibre transmission lines, exam. 78 - 38085
microwave holographic imaging through aberrating media with phase-modulated ref. beam 78 - 42303
microwave light modulator *(Chinese)* 80 - 33169
microwave modulated laser velocimeter for meas. speed of diffusely refl. objects 78 - 4599
microwave optical radiation modulator using $LiNbO_3$ crystal resonator 77 - 27353
MIS photosensitive high resolution struct., spatial light modulation with liq. cryst. 80 - 96026
mm-wave Fabry-Perot tuning and freq. modulation by electrically variable external reactance 79 - 68409
mode locked lasers, effects of narrow-free-spectral-range etalons 80 - 38041
modulated-Mueller-matrix photopolarimetry [MMMP]: a technique for the study of elastic light scattering by depolarizing temporally modulated media and surfaces 80 - 90882
modulation bandwidth of superluminescent diodes for optical fibre transmission 79 - 36993
modulation contrast microscope, coherence theory 77 - 7010
modulation contrast microscope, principles and performance 78 - 62221
modulation photolysis as alternative method for photochromic soln. obs. 77 - 90613
modulator crystal coatings 77 - 19431
modulator freq. response calibration, signal level control appl. 78 - 33833
modulator in high scattering efficiency regime, temporal response, algorithm 79 - 50377
movie camera, laser based, operation and applications 80 - 57405
multi-gigahertz modulation concepts, for CO_2 laser communications 77 - 3681
multibeam acousto-optic modulator efficiency stabilisation 80 - 43439
multichannel acousto-optical modulator control system *(Russian)* 79 - 72525
multichannel acoustooptic modulator for real-time recording and optical processing 79 - 10399
multidielectric film production monochromatic modulator controlled thickness *(French)* 78 - 75008
multifrequency Bragg acousto-optic deflector, laser beam AM suppression 80 - 53426
multifunction integrated optic device with mag. alterable phase grating 77 - 11048
multilayer electro-optic space/time modulator resolution *(Russian)* 79 - 94343
multimode electro-optic guiding for single fibre data links, system design 78 - 38065
multimode fibre coupler-type acoustic sensor, optical intensity modulation 80 - 102945
multimode fibre lightguide, coherent light modulation 80 - 91926
multimode fibre optic switching devices, computational approach to predict optical behaviour 79 - 59845
multimode optical fibre incoherent chirp pulse transmission 78 - 1374
multimode optical fibre phase modulators and discriminators, theory 78 - 55446
multimode optical fibre phase modulators and discriminators, expts. 78 - 55449
multiple beam gratings produced by PWM and PPM, high efficiency, beam splitter appl. 79 - 81515
multiple-reflection-type light modulator using Kerr effect in mag. thin film 78 - 79110
multiplexing, using phase modulation 80 - 95830
multistep laser excitation, pulse modulation, Schrodinger eqn. anal. 78 - 63046
Nd laser, ns pulse length continuous control, appl. to Nd laser 78 - 1280
nematic liquid cryst., isotropic phase, pulse acoustic-optic modulator 80 - 95993
nematic liquid crystal light modulator, scanning mode of operation 80 - 33200
noise immunity of optical signal reception with unstable modulator characts. 78 - 46690
non-redundant scanning, high efficiency freq. modulation, of light beam in half space 78 - 78907
noncoherent optical signals coding, double-scanning monochromator appl. *(Russian)* 80 - 5697
nonlinear Fabry Perot devices, integrated optic format 78 - 38087
numerical calculation using optics 80 - 95832
numerical optical data processor, representation and implementation 78 - 78947
numerical optical processor combining prime residue arithmetic representation and spatial light modulator 79 - 76871
oil layer, deformable, spatial light modulator as incoherent to coherent image transformer 80 - 96008
one-dimensional Fourier hologram line data recording scheme *(Russian)* 79 - 22912
optical coherence modulation by two ultrasonic waves 80 - 1120
optical communication expt., graded index fibre, 1.12 Gbits/s PCM 77 - 83967
optical fibre, vapour-oxidation fabricated, refractive index modulation, pulse dispersion 80 - 58756
optical fibre guide, multimode, modulation transfer function 78 - 55442
optical fibres, acoustic modulation of light propagation 80 - 33209
optical video discs, pit spacing and length modulation 79 - 50338
optical wideband ambiguity function generator with Doppler compensation 78 - 78936
optoacoustic deflector planar, expt. 78 - 74995
optoacoustic detection using Stark modulation 79 - 94325
optoelectronic devices, lecture 78 - 25990
optoelectronic meas. system, comparison of pulsed and continuous modulation and pseudorandom coding 77 - 71374

optical modulation continued
organic electrooptical materials for light modulators and deflectors, characts. *(Japanese)* 77−73128
orthoferrites, skew cylindrical mag. domains, light modulator appl. anal. 79−38360
oscillating quartz crystal stress distribution meas. by laser probe 77−20803
p-*ν*-n Si diode, for CO_2 laser modulation, temp. and switching characts. 79−81467
p-n junction coupled-waveguide optical modulator, high freq. modulation 77−75678
parametric generation of picosecond light pulses with an energy conversion greater than 50% 80−53377
parametric interaction increment of modulated light beams *(Bulgarian)* 79−10351
partial coherence control, of light wave modulated by progressive US wave 79−76581
passive picosecond pulse shapers, throughput efficiency limitations 78−90436
passive pulse shaping by delayed superposition using grating 77−75580
$Pb_3M_8Nb_2O_9$ crystals for optical radiation control 79−81554
PCM with envelope modulation, pulse detection characteristics 77−11010
pendulum effect influence on optical modulation of diffr. electron beam in cryst. *(Russian)* 80−55219
periodic amplitude grating, diffr. of wave with spatial phase modulation 79−98274
periodic analysers for freq. mixing detect. of polarisation modulated light 77−45883
periodic nonstationary medium, refr. index dispersion 77−10832
phase contrast microscope attachment for weak phase object visibility 80−86396
phase determination of amplitude modulated complex wavefront 78−55305
phase fluctuation dispersion in turbulent atmosphere *(Russian)* 79−98277
phase fluctuation effect on deform. of caustic surfaces 79−94152
phase meas. receivers, closed loop direct detection 77−88661
phase nonuniformity over light beam cross-section, rel. to phase range-finder 79−50400
phase-locked interferometry 78−58022
phosphate glass oscillator, passively mode-locked, stabilised with acousto-optic modulator *(Japanese)* 79−13999
photo-optical polarising optical system as elec. signal generator 79−1000
photoconductor slab space-time light modulator sensitivity enhancement *(Russian)* 77−58427
photocounting distribution obs., dead-time-modified, for modulated laser radiation 79−12846
photodetector, heterodyne characts. meas. and modulation method 77−34029
photodichroic spatial light modulator for joint Fourier transform correlation 80−106617
photoelastic isodynes method, stress components meas. using scatt. light modulation 80−14638
photoelastic modulator for direct-reading linear dichroism apparatus 80−98962
photoelastic radiation polarisation modulators, review 80−102846
photoelectronic phase and frequency modulation 78−79131
photograhic film exposure, average transmission function synthesis 79−2843
photogrammetry, OTF/MTF standards 77−78471
photographic film characteristics control by modulating intensity and space 79−2844
photon counting distribution, modulation effect 80−43307
photoresist film, negative, index and surface simultaneous modulation 78−37951
photosensitive MIS structure in contact with nematic liq. cryst., light spatial modulation 80−48436
Phototitus spatial-temporal light modulators, image formation kinetics 79−50397
physical principles and Czechoslovak development *(Czech)* 80−19090
picosecond laser pulse stabilisation, attenuation and shaping by dye two-photon absorpt. 79−55165
picosecond light continua generation depending on various nonlinear processes 80−33095
picosecond optical sampling, cascade of waveguide interferometers driven by microwaves 80−99849
picosecond spectroscopy, methods and appls., laser mode-locking 80−42263
piezo-optical and photoelastic modulator/chopper for modulating polarization of light beam *(German)* 79−27395
piezoelastic modulator for 10.6 μm radiation using Au clad amorphous Se optical waveguide 78−66956
piezoelectric semiconductor, n-type, heavily doped, laser beam modulational instability 79−99570
planar waveguide, isotropic, polarisation conversion by Bragg deflection, expt. results 80−48462
planoconvex AT-cut quartz resonator vibration displacement meas. by laser interferometry 77−37976
PLZT ceramic modulator for 1064nm laser Q-switching 77−38964
PLZT electrooptic ceramic, electron beam surface charging, rel. to optical modulation 80−6952
Pockels cell drive pulser in multiarm laser 79−14001
Pockels cell modulator, max. depth of light modulation 80−102819
Pockels double shutter in ruby laser with active phasing of spectrum *(Russian)* 79−98419
Pockels readout optical modulator, current status and appls. 77−72085
pockels readout optical modulator, for optical/digital processing systems 78−79125
Pockels readout optical modulator, image and signal processing appls. 78−79123
Pockels readout optical modulator, optical processing appls. 78−83100
polarisation modulation, small ang., in diamag. glass, by Faraday rot. *(Korean)* 78−50918
polarisation scrambling using photoelastic modulator, appl. to linear dichroism meas. 78−4683
polarised light, elliptically, analysis using U-shaped glass modulator 79−63293
polariser + crystal plate + analyser system, passage of light 80−10023
polarization modulated light, freq. mixing detection using periodic analyzers 78−5433

optical modulation continued
PROM, diffr. efficiency 80−14467
pulse holography, appl. of active Q-modulators *(Russian)* 79−68371
pulse interval modulation for optical fibre communication system 78−50917
pulse interval modulation semiconductor laser communication system 78−9331
pulse shaping for inertial confinement fusion expts. 77−83905
pulsed acousto-optical modulator RF driver for laser mode locking 78−90438
pulsed light source with thin-film modulator, fabrication and characts. 80−43467
quantum optical field modulation concept rel. to degrees of coherence 77−83840
radiometer optical head thermostabilisation structure 78−86316
Raman spectroscopy, FM technique for luminescing sample 77−57412
Raman-Nath standing-wave mode-locking switch, modulation index 80−78980
random spatial phase modulation for speckle elimination 78−58920
randomly modulated pump, stimulated Raman scatt., method of successive approxs. 80−95951
randomly phase modulated laser beam, two-photon absorpt 78−55400
real time light modulators for incoherent to coherent image conversion 77−72082
real-time spatial modulators for optical/digital processing systems 78−63025
reflective object displacement and vibration meas. *(Russian)* 79−21695
resonant media, two-photon coherent interaction of light pulses, phase modulation 77−79905
RF target simulator using acousto-optical device 80−102843
ring gas laser under gain modulation conditions 77−72011
ring laser, CW oscillation in presence of passive medium, stability 78−37913
ring laser gyroscopes, multioscillator approach to locking problem 78−79042
rising-sun reticle, error signal rel. to target position 79−81548
ruby, optical free induction decay modulation and absorpt. line struct. due to superhyperfine interaction 80−33091
ruby laser, giant pulse self-modulation at 90K 77−38961
ruby laser, modulation by US surface waves on resonator mirror 77−50699
ruby laser, negative feedback, cavity Q insertion effect on parameters of modulated pulses 80−43376
ruby laser, Q-factor passive modulator unloading, in resonator with prism *(Russian)* 77−68234
ruby laser, radiation automodulation with passive switching of electro-optical shutter *(Russian)* 78−74936
ruby laser, radiation self-modulation with passive closing of electro-optic shutter 79−64258
ruby laser, ultrashort pulse generation by internal phase and amplitude modulation 80−106551
ruby laser with bisanthene phototropic Q-modulator *(Russian)* 77−83910
ruby lasers, freq. synchronisation and locking by passive modulator 80−1249
ruby negative feedback laser, external perturbations effect, intracavity modulation 77−83908
ruby ring laser with forced mode locking 80−95915
Ruticon optical processing capabilities 78−79140
SAW acousto-optic modulators for integrated optics 79−90032
SAW acousto-optical light diffraction grating, gas laser tuning *(Russian)* 78−33759
SAW acousto-optical total internal reflection modulator 77−19435
saw-tooth wave target, modulation by optical system with triang. and assoc. filters 80−9817
schlieren system, phase object projection, imaging characts., recording conditions 78−25977
Scophony light valve, comparison with flying spot scanner 80−33147
sector templets for determining the contrast transfer of imaging systems 80−32924
selective modulation interference spectrometer, operation and props. 77−74519
selective modulation interferometric spectrometer, simultaneous multiple monochromatic image obs. 79−75611
selective modulation radiometer for gaseous pollutant remote sensing *(French)* 78−20550
semiconductor, IR radiation ultra-fast switching by laser-produced carriers 79−98417
semiconductor etalon, optical bistability and ns modulation 80−64096
semiconductor Fabry-Perot interferometer retuning by optical excitation *(Russian)* 80−98970
semiconductor injection laser, direct modulation at high bit rates 77−7151
semiconductor injection laser, intensity pulsation enhancement by self focusing 80−48253
semiconductor injection laser, spectral modulation behaviour, theory 78−50775
semiconductor junction lasers in optical fibre links *(German)* 79−32042
semiconductor laser, direct modulation for optical fibre transmission *(Japanese)* 79−41402
semiconductor laser, fast pulse modulation with GaAs MESFETs 77−88797
semiconductor laser, HF AM, near-zone radiation field delay fluctuations 77−61987
semiconductor laser, pattern effect minimization at high-rate pulse modulation 80−19059
semiconductor laser, single mode criteria at high speed pulse modulation 79−10305
semiconductor laser, single-wavelength oscillation at high speed pulse modulation 79−7129
semiconductor laser diode, modulated optical output, relax. oscills., superradiation effects 77−7150
semiconductor laser direct PCM improvement by optical feedback 78−1287
semiconductor laser intensity modulation in GHz region, image tube streak camera obs. 80−87417
semiconductor laser modulation, non-linear distortion, communication systems appl. *(German)* 80−69395
semiconductor laser radiation, frequency self-modulation interpretation 80−64028
semiconductor lasers, high speed direct modulation methods 77−10965

optical modulation continued
semiconductor lasers, picosecond pulse generation using reson. oscill. 80−87391
semiconductor pulsed laser communications 79−22972
semiconductor sheet, free carrier confinement for IR modulation 78−25969
semiconductor stripe laser high-speed modulation, noise, and nearfield meas. *(German)* 78−37923
semiconductor thin film waveguides, radiation modulation by stationary phase gratings *(Russian)* 78−22209
semiconductor thin-film nonlinear Fabry-Perot interferometer for optical pulse shaping 79−89945
semiconductor waveguide switches, and modulators, review of development progress 78−38045
semileaky thin-film optical waveguides, guided-radiation mode coupling analysis 78−1372
sensitivity of optical metrology using time modulation, electronically generated limitation 78−16828
SHF light rangefinder, optical elements, orientation errors effects *(Russian)* 80−64158
short light pulse polarisation, analysis by quartz modulator 79−17465
side band spatial elimination associated with acoustooptical pulse-picking 79−59732
signal and image processing, US Air Force research programme 80−78791
single mode optical fibre, polarisation modulation 80−64176
single-mode optical fibre phase modulators, pressure sensitivity meas. 79−7205
sinusoidal complex object with a small phase modulation, Fresnel diffr. patterns, self-imaging 80−43256
sinusoidal radiation chopper for max. available light intensity modulation 77−58432
sinusoidally modulated laser, phase shift of light output 79−98365
slip-ring for transmission of transducer signals 78−13814
solid laser, multimode, with modulated resonator losses, radiation intensity fluctuations 80−74367
solid laser array spatially-coherent beam formation and mode locking 78−37898
sound generation by intensity-modulated laser beam in liquid half-space 79−91403
space-time light modulator for laser radiation control 80−48310
space-time modulators, based on $Bi_{12}GeO_{20}$ and $Bi_{12}SiO_{20}$ monocrystals *(Russian)* 77−1652
spatial frequency sampling by phase modulation, multiple image generation 77−79759
spatial light modulator, for optical data processing, 1978 state of art and development trends 79−7201
spatial light modulator, using KD_2PO_4 and Se photoconductor, optical processing appl. 80−9988
spatial light modulator, using oil film deform. by surface tension var. 80−5831
spatial light modulator using phase transition type liquid crystal *(Japanese)* 78−79119
spatial light modulator with CCD address 80−48445
spatial light modulators, input information approximation 77−83823
spatial light modulators, near real-time reusable for coherent optical processors 77−11035
spatial light modulators for coherent optical computing, performance evaluation 79−89989
spatial light modulators for optical data processing 78−78941
speckle elimination using random spatial phase modulation 77−71923
spectral modulator for optical inhomogeneities obs., using scanning image convertor 78−59144
spectrograph DFS-13 wavelength modulator 78−74069
spectrophotometer, combined double modulation of source, modulation functions 77−57400
spectroscopy, gas phase, narrow nonlinear reson. production by modulated optical radiation *(Russian)* 77−67507
spectroscopy, Rayleigh scatt., opt. freq. shifting of light and laser beams 78−79392
spectrum analyzer, time- and space-integrating 80−9983
star seeker using semidisc light-flux modulator, accuracy anal. 78−73648
Stark effect in high-frequency fields for resonant modulation 79−10274
stimulated scattering in extended media, pulse form., intensity modulation 77−50727
Stokes parameters, of light beam, polarisation modulation meas. 79−21803
strip-guides, polarisation filtering 80−102861
sub-mm-wave laser interferometer, use of low-inertia semiconductor structs. to modulate radiation 80−31848
sub-picosecond optical pulses, generation and meas. 80−23731
sub-SHG, nonequilibrium transitions, semiclassical theory 80−83639
submillimetre CW laser, amplitude stability improved by phase modulated pumping 79−22967
subnanosecond optical free-induction decay with novel laser freq. shifting 80−38075
subpicosecond gate, velocity-matched directional coupler 80−74512
superradiance, Doppler beat observation 78−66794
surface acoustooptic interaction for information processing 78−42461
surface wave acousto-optical modulator, for optical link 78−38040
switch/modulator, optically activated, using photoconductor and two channel waveguides 78−1437
systems aspects of optical-fibre communications 77−7016
temperature-compensated modulator, feedback control method 77−42611
temporal modulation, in thick-screen diffr. by ultrasound beam, plus amplitude grating 77−50755
temporal modulation by two antiparallel sound beams, thick-screen treatment 77−68256
thermoplastic light modulators, status and prospects 78−79138
thermoplastic optical phase recorder for data processing 77−72081
thermoplastic spatial light modulator 80−102841
thermoplastic-photoconductor image transducer, input to coherent optical processor 78−83098
thin film optical waveguide, attenuation due to roughness-induced mode coupling 79−10408
thin unbleached holograms, diffraction efficiency, relief phase modulation 78−66789
thin-film waveguide with liq. cryst. boundary modulation of refr. index, mode switching 80−23800
three dimensional image transmission, real-time, using vol. scanning spatial modulation 77−72060
optical modulation continued
three mirror HF laser modulator 79−3728
three-beam interference images, sinusoidal complex object with phase modulation, interferometric gratings 80−53208
three-level system, photon echo modulation 79−18486
total internal reflection modulator, small glancing angles 78−74987
transverse light modulator, improvement of permissible incident angle 80−5843
travelling wave optical modulator using a directional coupler $LiNbO_3$ waveguide 80−96035
trigonal crystal, optical heterodyne detection using collinear acousto-optic interaction 78−66927
tunable single-sideband generation in IR 80−78876
turbulent atmosphere, optical DPSK system performance 78−42293
turbulent atmosphere propag. of modulated waves, correlation functions and freq. spectrum 79−34954
TV picture, acousto-optically modulated laser beam 79−55237
two-dimensional image transmission by wavelength multiplexing 79−27189
ultralinear bistable electro-optic polarization modulator based on Pockels cell 78−83077
ultrashort pulse formation mechanism rel. to peak transition process *(Russian)* 77−54745
ultrashort pulse operations using flat lenses 78−66883
ultrasound modulated laser light, resolution of illuminated double-slit object 80−37959
unidirectional mode convertor, design considerations of nonreciprocal integrated optical devices 77−793
US lateral and range resolution improvement by optical computer 79−53203
US light modulators, multichannel optical processing and spectral anal. of radio signals 77−23763
US modulation of light, temporal, synthesis of formulae 79−76907
US modulator in interferometer arm, for photodetector amplitude-freq. charact. meas. 77−10112
US-optical, spatial freq. meas. 80−95995
variable attenuator for Gaussian laser beams 79−22987
vibration analyser, meas. principle 79−6119
vibration analysis by wavefront modulated holography 79−3652
vibration-induced modulation in bent optical fibre waveguide 78−1405
wavefront reversal and short pulse generation using steady-state stimulated Brillouin scatt. 80−53381
wavefront reversal of beam with incomplete spatial modulation, small-scale distortions 80−95953
waveguide light modulator, using Raman-Nath diffr. of vol. acoustic wave 80−48437
waveguide modulator, using electrooptic crystals, coupled mode analysis 77−42612
waveguide modulator for fibre transmission systems, temperature stabilized *(Japanese)* 79−27391
waveguide modulator for single-mode optical fibre transmission system, temp. stabilized 79−41450
waveguide structure, distributed capacitance of planar electrodes 77−27387
waveguide switches and modulators, performance limitations due to polarisation 77−7175
wedges as flux modulators 77−27355
wide-band spectrum analysis with area modulation 79−36840
wideband spectrum analysis with area modulation 79−94159
wideband spectrum analysis with area modulation 79−94160
wideband thin film modulators and switches, for optical communication 78−63206
wideband UHF standing-wave light modulators 79−72689
xerographic images on paper, optical model 79−17549
zone plate, frequency-modulated for coherent noise reduction 79−86134
Al-In multicomponent binding layers, acoustic light modulator 80−87546
Al_xGa_{1-x}-GaP structure, LPE, double heterostruct. light modulator appl. 79−28963
(AlGa)As DH CW laser diodes modulation charact. 77−38965
AlGaAs DH diode laser, ps optical pulse generation with RF modulated 80−9882
AlGaAs pulse modulate DH laser, oscillatory longitudinal mode competition 79−81427
$Al_{0.42}Ga_{0.58}As$-GaAs-$Al_{0.42}Ga_{0.58}As$, etalon, optical bistability and modulation 80−58628
$Al_xGa_{1-x}As$-$Al_yGa_{1-y}As$, electrooptic rib waveguide modulators and switches 78−38046
$Al_xGa_{1-x}As_{1-x}Sb_x/GaAs_{1-x'}Sb_{x'}$, buried heterojunction electroabsorption modulator, report of operation 78−38044
$Al_xGa_{1-x}As_{1-x}Sb_x$-$Ga_{1-z}Sb_z$ buried heterojunction electroabsorption modulation 78−55439
α-Al_2O_3, trigonal crystal, optical heterodyne detection using collinear acousto-optic interaction 78−66927
As_2S_3, film waveguide, acoustooptic deflection and modulation of light by stationary phase grating struct. 80−5841
As_2S_5, thin film optical waveguide, for acoustooptic modulators 78−83051
$(As_2Se_3)_{1-x}(As_2Te_3)_x$ amorphous films, changes in optical props. under elec. fields and optical excitation 79−61455
BCl_3 gaseous phototropic shutter control of CO_2 laser PRF 78−50833
$(Ba,Sr)Nb_2O_6$ monocrystal optical homogeneity requirement for light beam control 79−82952
$Ba_2NaNb_5O_{15}$ crystal domains, amplitude modulation of light by diffr. 79−59832
$Bi_{12}GeO_{20}$, electron beam recording 79−32075
$Bi_{12}GeO_{20}$, mechanism of creation of internal fields and photoelectret effect 80−25290
$Bi_{12}GeO_{20}$ monocrystal optical homogeneity requirement for light beam control 79−82952
$Bi_{12}GeO_{20}$, spatial-temporal electrooptic modulator, UV image conversion 77−3680
$Bi_{12}RO_{20}$, R=Ge, Si, photoinduced birefringence, dynamic transparency prod. 78−90472
$Bi_{12}SiO_2$ Pockels readout optical modulator, X-ray response 79−64313
$Bi_{12}SiO_{20}$ crystal, for programmable optical guided-wave device 79−23069
$Bi_{12}SiO_{20}$, mechanism of creation of internal fields and photoelectret effect 80−25290
$Bi_{12}SiO_{20}$ monocrystal optical homogeneity requirement for light beam control 79−82952

optical modulation continued
$Bi_{12}SiO_{20}$, optical information recording, PROM device resolution 79−41443
$Bi_{12}SiO_{20}$ PROM device, image recording and erasure mechanism 80−74490
$Bi_{22}SiO_{20}$, Pockels readout modulation struct., information registration *(Russian)* 77−10990
CO_2, atm. press. laser pulse duration reduction by stimulated emission quenching 79−18400
CO_2, fast flow discharge laser, amplitude modulation in stable, unstable resonators 77−75478
CO_2 laser, absorption of laser radiation in Stark tunable mol. gases *(Rumanian)* 79−86157
CO_2 laser, communications applications of Stark cells 77−19444
CO_2 laser, coupling modulation near intermode spacing freqs., freq. response 77−38956
CO_2 laser, detuning effects of FM mode-locking 80−69434
CO_2, laser, internal modulation 80−23728
CO_2 laser, possible freq. stabilisation using 1-1 difluoroethane in external Stark cell 79−94266
CO_2 laser, Stark effect modulation by iodomethane 78−17992
CO_2 laser, using p-ν-n diode 77−79873
CO_2 laser, vibr. energy transfer by current modulation 78−1204
CO_2 laser intracavity freq. modulation, transient behaviour 80−14374
CO_2 laser line, electro-optic frequency shift *(Chinese)* 80−43379
CO_2, laser lines, 12 GHz continuous tuning in integrated electro-optic modulator 77−83907
CO_2 laser modulation, plasma injection into cavity 80−83626
CO_2 laser modulation Si diode characteristics 78−42364
CO_2, laser pulse generation, cavity dumping by NH_2D Stark active mol. 77−88800
CO_2 laser pulse temporal shaping by controlled plasma switching 79−3725
CO_2 laser radiation, intracavity modulation of polarization direction 80−102744
CO_2 laser self-modulation by means of nonlinear absorbing filters, anal. 78−37925
CO_2 laser subnanosecond pulse generation by Pockels cell modulator 77−19357
CO_2 mode-locked hybrid TEA laser, variable width stable pulse prod. 79−76726
CO_2, short-pulse oscillator, variable pulse repetition freq., pulsewidth and wavelength control 77−88801
CO_2, single mode laser, internal freq. modulation up to 350 MHz 77−19308
CO_2 TEA laser, pulse shaping by independent excitation of coaxial discharge systems 79−7150
CO_2, TEA laser, pulse-forming and line-broadening in AM mode locking 77−54743
CO_2 TEA Laser pulse, PCM with CdTe crystal Pockels modulator 80−102742
CO_2 TEA oscillator, injection mode-locking using N_2 laser-controlled semicond. switching of 10-μm radiation 80−1247
CS_2 travelling wave Kerr cell, ultrafast pulse shaping and picosecond rise time elec. pulses 80−33152
$CaCO_3$, calcite, picosecond pulse stacking 79−61330
CaF_2 photoelastic modulator, for vibrational circular dichroism spectrometer 78−54476
CdS, charge in energy gap caused by acoustic domains 77−20822
CdS, epitaxial film, conductivity control by S vacancy form., light modulation appls. 77−4455
CdS, fast modulator for CO_2 laser, using two-photon magnetoabsorpt. 77−88805
CdS, fast optically controlled modulator using two-photon magnetoabsorpt., for CO_2 laser 78−13736
CdS, optical modulation caused by acoustic domains 77−85689
CdS spatial modulator, 16×18 bit, page composer 77−39050
$CdS_{0.75}Se_{0.25}$, linear electro-optic effect meas., light modulator appl. 78−76434
CdTe acousto-optic and electro-optic waveguide modulators 77−42624
CdTe, electro-optic IR phase modulator, phase and freq. characts. 77−54805
CdTe electro-optical modulator for CO_2 lasers 77−19443
CdTe, electron-beam-controlled transmission of 10 μm radiation 79−81466
CdTe, H^+ ion implanted, optical waveguiding and electrooptic modulation 77−75679
CdTe linear electro-optic translation of IR laser wavelengths 80−78878
CdTe optical applications, review 77−42580
CdTe:H^+, ion-implanted, optical waveguiding and electrooptic modulation 77−7197
Cs vapour, self-phase modulation complete compensation at 1.06 μm 77−58395
$CsCuCl_3$, optical props. rel. to IR electro-optical modulator appl. 78−42393
CsD_2AsO_4 Fourier transform plane superposition multiplier, for optical processing 79−7084
DF-CO_2 chemical laser, amplification of long and short pulses 80−95883
α-Fe_2C_3, anisotropic linear mag. birefr., light modulation 77−8548
GaAS-$Al_xGa_{1-x}As$, DH laser and modulation developments *(German)* 78−37903
$Ga_{1-x}Al_xAs$, metal-gap channel waveguides, intensity modulation 78−66899
GaAlAs DH laser diodes, small signal modulation, junction capacitance effect 80−83625
GaAlAs DHS laser, direct modulated from 260 Mbit/s to 1.4 Gbit/s, monomode operation 78−46601
GaAlAs injection DH laser and GaAs Schottky-gate FET, monolithic integration 80−58593
GaAlAs injection laser, monolithic integration with Schottky-gate FET 80−48275
GaAlAs LED sources for fibre optic transmission, linearity improvement using phase-shift-modulation technique 77−19403
GaAlAs laser, coherent pulse generation by active modelocking 79−89941
GaAlAs laser nonlinearities, harmonic distortion 80−74357
GaAlAs light intensity modulators using p-n junctions 80−99871
GaAlAs stripe laser, longit. and transverse mode dynamics on junction plane 77−38890
$Ga_{1-x}Al_xAs$ DH injection laser, FM at microwave freq. rates 80−58610

optical modulation continued
$Ga_xAl_{1-x}As$ diode laser, modulation characts. 77−83903
GaAs 400 MHz TW laser modulator 80−87541
GaAs, and its alloys, as integrated optics materials, book contrib. 79−64362
GaAs, CW laser, sinusoidal modulation 9 MHz to 1.1 GHz, appl. for fibre meas. 77−10966
GaAs DH injection laser, modulation behaviour, appl. in high bit-rate fibre optical communications 78−1281
GaAs DH laser, high speed direct modulation, multimode operation effects 78−13738
GaAs DH laser, self-induced modulation, noise, instability 80−48250
GaAs DH laser/fibre transmission system modulation and injection 77−50764
GaAs, Franz-Keldysh effect modulator parameters for integrated optics systems 80−106624
GaAs, high speed DH superluminescent diodes, modulation characts. 77−54783
GaAs homojunction rib waveguide directional coupler switch 80−69554
GaAs injection lasers, direct modulation enhancement effect of HF noise 80−83608
GaAs LED modulation bandwidth, influence of inhomogeneous current density distrib. 80−9993
GaAs laser, 100 ps risetime pulse drive circuit 77−7149
GaAs laser diode, for optical communication systems *(German)* 78−37919
GaAs laser with integrated interferometric reflectors 77−65642
GaAs lasers, at room temp., modulation at X-band frequencies 78−87079
GaAs MIS dynamic optically controlled transparencies 78−90523
n-GaAs, microwave biased, fast rise-time modulation of 337 μm radiation 77−54794
GaAs, optical modulation by optical tuning of cavity 79−64314
GaAs p^+-n-n^+ diode, ns modulation of 10.6 μm radiation by elec. injection 77−34937
n-GaAs X-band impact ionisation for 337 μm radiation modulation 77−39069
GaAs-(Ga,Al)As light modulators and distributed Bragg reflector laser, monolithic integration 78−50944
GaAs-$Al_xGa_{1-x}As$, single-mode rib waveguide switches electro-optical modulation 78−46839
GaAs-$Al_xGa_{1-x}As$ buried-heterostructure laser, wideband optical sources *(German)* 78−37904
GaAs-$Al_xGa_{1-x}As$ CW-diode laser, coupled to freq.-selective external cavity, self-pulsing 77−61982
GaAs-$Al_xGa_{1-x}As$ DH laser, modulation with coherent light injection *(German)* 78−37922
GaAs-$Al_xGa_{1-x}As$ electro-optic modulator, highly sensitive, with distributed Bragg-reflectors 77−75682
GaAs-$Al_xGa_{1-x}As$ electro-optic frequency- and polarisation-modulated injection laser 80−91810
GaAs-$Al_xGa_{1-x}As$ injection laser, direct modulation and spectral props. *(German)* 78−37921
GaAs-$Al_xGa_{1-x}As$ MOS rib waveguide polariser, modulator and isolator 80−64217
GaAs-GaAlAs injection lasers, narrow-stripe proton-implanted, high bit-rate modulation 80−91824
GaAs-GaAlAs laser, optical repeater using PFM at 1 GHz 79−98395
GaAs-on-sapphire spatially distributed thermal light modulator 79−59839
GaAsP epitaxial waveguide, electro-optic phase modulation of laser radiation 79−10417
GaAsP strip-waveguide modulator with GaAlAs embedded DH stripe laser 78−66957
GaInAsP/InP DH lasers, direct modulation charact. meas. by sharp pulse method 80−1245
GaInAsP-InP mesa substrate buried heterostruct. injection laser, fabrication and lasing props. 80−53319
GaP acoustooptic pulse modulator 78−46814
GaP-$Al_xGa_{1-x}P$, DH electrooptical strip modulator *(Russian)* 78−1344
GaP-AlGaP, stripe-geometry electrooptical modulator 80−23798
GaP-GaAsP planar heterostructure strip ridged waveguide under mech. load, polarisation modulation 80−96038
GaSb, piezoresistive vibrating circular membrane, reflectance light modulation 80−97232
$Gd_3Ga_5O_{12}$ monocrystal optical homogeneity requirement for light beam control 79−82952
p-Ge, broadband modulation of 3 μm light by 10 μm light 78−42389
Ge, electron-beam-controlled transmission of 10 μm radiation 79−81466
n-Ge, IR absorption by hot carrier 80−40087
p-Ge modulation of 3.39 μm abs. by CO_2 laser irrad. *(Japanese)* 80−74410
Ge optical switch, picosecond pulse generation at 10.6 μm 79−7159
Ge, p-n junction, IR radiation modulation, light absorption by injected current carriers *(Russian)* 80−10013
Ge, piezoresistive vibrating circular membrane, reflectance light modulation 80−97232
p-Ge sheet, free carrier confinement for IR modulation 78−25969
H_2 Raman laser, multiple-pass-cell, controllable pulse compression 80−91825
HF chemical laser beam, phase fluctuation meas. 80−48317
He-Cd laser, intracavity phase modulation, spectral and time characts. 77−61988
He-I_2 laser, sequential separate multicolour output operation *(Japanese)* 80−28205
He-Ne, 3.39 μm laser, actively mode-locked oscill., modulation freq. depend. 77−61983
He-Ne, laser, Ne absorber induced features in AC response 77−3613
He-Ne, lasing spectrum, modulation freq. of resonator losses 77−34902
He-Ne 3.39 μm laser mode-locking for ultrashort pulse generation 77−83909
He-Ne gas laser, behaviour in nonsynchronous frequency modulation regime *(Russian)* 79−7161
He-Ne IR laser, internal modulation of polarisation 77−19350
He-Ne laser, beat freq., high displacement sensitivity meas. 80−95926
He-Ne laser, internal pulse-code modulation, 0.6328 μm at 150 Mbits s^{-1} 79−76725
He-Ne laser, operating on 0.63, 3.39 μm coupled transitions, intensity modulation 80−69365
He-Ne laser, optical heterodyning of spontaneous emission 78−29995

optical modulation continued
He-Ne laser, unmodulated, stabilizing to $^{127}I_2$ hyperfine component, preliminary expt. 79−50328
He-Ne laser average output power, resonator losses, freq. modulation [illegible]34901
He-Ne laser pulsed internal modulation 77−61985
He-Ne ring laser beat frequency deviation rel. to dispersion and modulation 79−68410
Hg+Cd, quantum beats under transfer of orientation 79−98206
I photodissociation laser, stimulated emission pulse temporal characts. with active-medium gain control 80−28226
I switch, active modulation of transmission based on Zeeman effect 79−22994
InGaAsP buried stripe laser, modulation characts. 79−98418
InGaAsP-InP 1.27 μm CW DH injection lasers, 1.1 Gb/s pseudorandom PCM 78−55390
InGaAsP-InP DH laser emitting at 1.27 μm, fast pulse behaviour, high speed direct modulation 77−23676
InGaAsP-InP DH lasers, direct modulation 78−42363
InO_1:Sn transparent conducting films, homeotropic orientation of liquid crystals *(Russian)* 80−108181
In_2O_3:Sn film, electroreflectance effect, theory and expt. 78−6800
KCl:LiCl photodichroic crystals as adaptive spatial filters 79−72713
KCl:ReO_4 nonlinear absorption for CO_2 laser pulse compression and mode locking 80−74443
KD_2PO_4, cryst. high-freq. modulation in Pockels cell, acoustic phenomena 78−1336
KD_2PO_4 crystal electron-beam spatial light modulator, resolution 80−74503
KD_2PO_4, electron beam addressed light valve, optical processing appl. 78−83099
KD_2PO_4 electrooptic modulator, field of view extension 78−94429
KD_2PO_4 light valves for optical information processing 77−72080
KD_2PO_4 light valves 77−83992
KD_2PO_4, optically addressed light valve, optical processing appl. 78−83101
KD_2PO_4 photo-spatial light modulator, optical data processing 80−102839
KD_2PO_4 r_{63} laser modulator *(Chinese)* 80−28260
KD_2PO_4, ultrafast electro-optical modulator design and application 77−19432
KD_2PO4 transmission line Pockels cells, optical rise time meas. 78−46778
KF:LiF photodichroic crystals as adaptive spatial filters 79−72713
KH_2PO_4, cryst. high-freq. modulation in Pockels cell, acoustic phenomena 78−1336
KH_2PO_4, electro-optic modulators, transient acoustic waves 79−59809
KH_2PO_4 electro-optic modulator crysts., piezoelec. induced acoustic transients 80−70316
KH_2PO_4, KD_2PO_4 crystals used for laser control, acoustic vibr. suppression 78−1363
KH_2PO_4, light modulation in microwave light-range finder *(Russian)* 79−46041
$KNbO_3$ half-wave voltage, electro-optic and polarisation-optic coefficients 77−40211
KrF excimer laser, passive mode-locking using saturable absorber dyes 80−1244
$LaF_3:Pr^{3+}$, photon echo decay as modulation process 78−79078
$LaF_3:Pr^{3+}$, ultraslow opt. dephasing at 2K 80−91864
$LiNbO_3$ acousto-optical SAW interaction multicolour image scanner 77−58483
$LiNbO_3$, anisotropic multilayer waveguide for electro-optical modulator, propag. characts. *(Italian)* 78−50904
$LiNbO_3$ balanced bridge modulator/switch with ion-etched slot 79−89993
$LiNbO_3$ crystal, different interdigital electrode struct., electric field distrib. obs. 78−76433
$LiNbO_3$, diffused waveguide as Bragg electro-optic modulator 77−34955
$LiNbO_3$, electro-optical modulator/switch, switched directional coupler principle 77−7191
$LiNbO_3$ electro-optic phase modulator for unpolarised laser beam 79−50403
$LiNbO_3$ electrooptic light modulator 78−1349
$LiNbO_3$ electrooptic phase modulator, axial mode locking of CW Nd^{3+}:YAG ring laser 78−50835
$LiNbO_3$ electrooptic phase modulator, freq. shift device for optical range 78−59147
$LiNbO_3$ electrooptic device, interdigitally electroded, acoustic reson. 80−19097
$LiNbO_3$ fast-response broad-band electrooptic elements for laser beam control systems 79−89944
$LiNbO_3$, high freq. plane acousto-optical light modulators *(Russian)* 78−79106
$LiNbO_3$, light modulator with interdigital electrodes, operating characts. 78−90511
$LiNbO_3$ microwave laser beam electro-optic modulators using rectangular waveguides, 1.0 to 10 GHz 80−43381
$LiNbO_3$ optical waveguides, electrooptic modulation and switching, recent progress 78−50945
$LiNbO_3$, phase modulator, use in multimode integrated bistable switch 78−79145
$LiNbO_3$ planar HF acousto-optic modulator construction and expts. 79−76863
$LiNbO_3$ planar waveguide, light beam switching and modulation using built-in dielectric channel 77−88967
$LiNbO_3$ planar waveguide, light beam switching and modulation using built-in dielec. channel 78−46840
$LiNbO_3$ planar waveguide mode conversion and intensity modulation 79−10410
$LiNbO_3$ TE-TM mode convertor, using collinear acoustooptic interaction 77−19407
$LiNbO_3$, thin-film electrooptic modulator, optimal characts. 79−10405
$LiNbO_3$ total internal reflection modulator/deflector performance 77−42628
$LiNbO_3$ travelling wave optical waveguide modulator, 10 GHz bandwidth 78−59134
$LiNbO_3$, trigonal crystal, optical heterodyne detection using collinear acousto-optic interaction 78−66927
$LiNbO_3$ very high throughput damage resistant waveguide modulator 80−58788

optical modulation continued
$LiNbO_3$, waveguide, single-mode planar and rigid type electro-optic waveguide modulators, design 77−11029
$LiNbO_3$, waveguide and modulator form. by ion implantation 80−48469
$LiNbO_3$ waveguide modulators and switches, Ti-diffused, fabrication on directional coupler principle 80−83678
$LiNbO_3$, wedge shape cryst., diffr. by natural freq. US standing waves 77−75685
$LiNbO_3$:Cu, holographic grating, for electro-optical laser beam modulation 77−3672
$LiNbO_3$:Ti, broad-band travelling wave waveguide modulator 77−39036
$LiNbO_3$:Ti, electro-optic multichannel waveguide deflector 77−42607
$LiNbO_3$:Ti, electro-optic waveguide modulator, temp. stabilisation 78−50926
$LiNbO_3$:Ti, electrooptical modulator and switch *(French)* 78−30074
$LiNbO_3$:Ti active branching waveguide modulator 77−19392
$LiNbO_3$:Ti branched waveguide amplitude modulator 77−39037
$LiNbO_3$:Ti channel waveguide high-speed cutoff modulator 80−64195
$LiNbO_3$:Ti digitally driven integrated optics amplitude modulator 80−58808
$LiNbO_3$:Ti film structure, interdigital electro-optic modulator *(Russian)* 77−39115
$LiNbO_3$:Ti optical waveguide electrooptic devices, polarisation independ. directional coupler switch 80−58783
$LiNbO_3$:Ti optical waveguide, surface wave mode conversion, static strain-optic effect 80−87561
$LiNbO_3$:Ti single mode electrooptic waveguide modulator, high-speed operation 80−91915
$LiNbO_3$:Ti waveguide, integrated bistable Fabry-Perot resonator fabrication 79−41459
$LiNbO_3$:Ti waveguide directional coupler type modulator 78−66951
$LiNbO_3$:Ti waveguide thin film electrooptic Bragg modulator, bistable optical element 80−10034
$LiNbO_3$/CdS integrated optical half adder circuit 79−76877
$LiNbO_3$-Ge, acoustooptic modulator for CO_2 lasers 78−42365
$LiNbO_3$-Ge acousto-optic modulator for 10.6 μm CO_2 laser 80−99776
$LiNbO_3$-Ge acoustooptic modulator *(Japanese)* 80−69542
$LiNdP_4O_{12}$ laser, intensity fluctuations due to external perturbations 79−81437
$LiTaO_3$ electro-optical total internal reflection diffraction industrial modulators and deflectors 77−19436
$LiTaO_3$ fast electro-optic deflector, arbitrarily shaped optical pulsed generation 80−53421
$LiTaO_3$, Ti diffused, electrooptic diffraction modulation 79−10381
$LiTaO_3$ total internal reflection diffraction modulator/deflector performance 77−42628
$LiTaO_3$, waveguide, single-mode planar and rigid type electro-optic waveguide modulators design 77−11029
$LiTaO_3$ zig-zag reflection interferometric light modulator 78−90527
$LiTaO_3$:Cu waveguide, electro-optic control of radiation loss in off-axial propagation 80−23789
$LiTaO_3$:Ti waveguide modulator structs., high optical power capabilities 77−39023
N_2 laser, pulsed, interfacing with higher freq. electro-optic instrumentation 77−50698
NH_3, Stark effect modulation at 2.2 μm *(French)* 78−50912
$^{15}NH_3$, modulated coherent Raman beats 80−23464
$NH_4H_2PO_4$ total internal reflection intercavity laser switch 77−38955
$NH_4H_2PO_4$, total internal refl. diffr.-type modulator as laser cavity switch 78−5511
Na atomic vapour, Doppler-broadened system, degenerate four-wave mixing, line shape and strength angular depend. 80−43391
Na vapour doublet, dispersion free point, cooperative phased-array radiation 80−53352
NaCl, amplitude phase hologram recording on colloid type centres *(Russian)* 80−69347
$NaNH_4SeO_4.2H_2O$ ferroelectric crystal optical SHG and pulse modulation *(Russian)* 77−14771
Nd laser, stable passive switch using phthalocyanine dye, bleaching and relaxation 80−74368
Nd:glass laser, blue tunable picosecond pulse generation by synchronous mixing with sideband radiation in $NH_4H_2PO_4$ 80−87431
Nd:glass laser, mode-locked, ultrashort pulse duration meas., two-photon fluoresc. 79−27302
Nd:glass laser operation, self-focusing influence 79−13997
Nd:glass laser system, beam spatial profile optimization in amplifier channel 80−74407
Nd:glass laser with US modulated emission 80−48309
Nd:glass ring laser, actively mode-locked and Q-controlled, props. 79−18445
Nd:YAG, actively AM mode-locked Q-switched laser, pulse compression by liq. Kerr cell 79−22990
Nd:YAG, laser transition cross sections, modulation *(Chinese)* 78−90418
Nd:YAG acousto-optically mode-locked CW laser, optical spectra obs. by interferometer 79−7134
Nd:YAG actively mode-locked laser, short pulse generation for laser fusion 78−9404
Nd:YAG CW mode-locked laser, negative feedback power stabilization 80−69435
Nd:YAG FM laser, pulse compression in Nd:YAG laser dispersive delay line 77−88815
Nd:YAG laser, CW, with high output coupling modulation 80−9917
Nd:YAG laser, intracavity modulation, sum freq. mixing, 212.8 nm pulse burst generation 78−74934
Nd:YAG laser, subnanosecond pulse generation at 100K 80−74397
Nd:YAG laser as optical pulse generator, mode locking by acoustooptic loss modulation 79−64260
Nd:YAG negative feedback laser, external perturbations effect, intracavity modulation 77−83908
Nd^{3+}:YAG multimode laser radiation noise 80−74366
$Nd_{0.5}La_{0.5}P_5O_{14}$ laser, FM mode-locked 79−86184
Ne, high current discharge, short light pulse form. *(Russian)* 79−27846
Ni-Fe film, Kerr magnetooptic effect, appl. to waveguide type optical modulator, theory 77−11015
PLZT ceramic, modulator for optical communication 80−78964
PLZT ceramic, optical gate, dielec., optical props., electro-optical effect meas. 78−42418
PLZT ceramic, possible construction of matrix-addressable controlled transparency 78−71222

optical modulation continued
PLZT ceramics, optical information storage and spatial light modulation 78−83097
PLZT ceramics, photoferroelectric image storage in antiferroelectric phase 79−47404
PLZT spatial light modulator for a 1-D hologram memory 80−37963
PLZT, transparent, optical exam. of small signal behaviour, of 90° electric domain walls *(German)* 79−33645
PLZT transparent ceramic laser modulator *(German)* 78−5553
PZT paraelectric ceramic one-dimensional spatial light modulator 79−55240
$PbMoO_4$ acousto-optical modulator for wideband laser recording system 79−89942
$PbMoO_4$, diffr. modulator, two separate opposing US waves 77−3676
$Pb(Zr, Ti)O_3$ ceramic, appl. in electrically controllable diffr. grating for parallel polarised light refl. 77−39026
Rb vapour, Gaussian pulse propag. under two-photon near reson. conditions 80−87441
SF_6, relax. mechanism, narrow reson. obs. by amplitude-modulated wave method 79−10155
SbSI, photoelectric current, modulated due to light intensity 79−19626
Si rubber as electro-optic material for optical hydrophones 80−43412
Si, surface, optical modulation of low energy electron reflection and transmission 78−88388
Si_3N_4 waveguide layer, as electro-optic phase modulator 79−23081
SiO_2 optical fibres, self-phase modulation 78−66874
SiO_2 thin film grating for $LiNbO_3$:Ti waveguide mode convertor and reflector 80−64216
α-SiO_2, trigonal crystal, optical heterodyne detection using collinear acousto-optic interaction 78−66927
TbIG, anisotropic linear mag. birefr., light modulation 77−8548
Te acousto-optic modulator, props., for IR laser beam control *(Russian)* 77−72073
Te, acousto-optic props. at 10.6 μm 79−91401
Te, SHG, optical modulation 79−86212
TeO_2 acousto-optic laser beam deflector using shear wave propag. slightly off (110) crystal axis *(Japanese)* 80−102818
TeO_2 crystal multichannel acousto-optic modulator 77−39100
VO_2 film sub-mm wave modulators and switchable polarisers 77−75664
VO_2 thin films, light modulation appls., optical props. at metal-insulator transition 80−87547
Xe, laser light irrad. in mag. field, light modulation theory 78−82698
Xe, laser light irrad. in mag. field, light modulation expt. 78−82699
XeCl, high-energy subnanosecond pulse amplification 80−99770
XeF laser, output control by injection locking 80−74405
$Y_3Ga_xFe_{5-x}O_{12}$, HF Faraday light modulator, optical characts. crystal struct. depend. 77−39052
YIG, anisotropic linear mag. birefr., light modulation 77−8548
YIG, parametrically excited wave discrete structure obs., light diffr. and modulation *(Russian)* 79−95650
YIG thin film gyromag. waveguide, on GGG substrate, optical propag. props. Faraday effect 80−74513
YIG, YGaIG, Faraday effect and IR radiation modulation 79−10403
ZnO thin films, surface acoustic-optic interaction, diffr. 77−3685
ZnS film free carrier absorption for laser beam modulation *(Japanese)* 79−7164
ZnS leaky waveguide electro-optic modulator limitations 78−22218
ZnS, linear electrooptic coeff. dispersion 80−71380
ZnSe, absorpt. modulation of light, and its appl. to page composer 77−40258
ZnSe, absorpt. modulation of light, and its appl. to page composer *(Japanese)* 78−83083
ZnSe, electron-beam-controlled transmission of 10 μm radiation 79−81466

optical modulators *see modulators; optical modulation*

optical noise measurement
achromatic coherent system, noise performance 79−98295
amplifier, lock-in, with synchronous filter, construction *(Japanese)* 80−28362
avalanche photodiode receiver sensitivity, specification and testing *(German)* 78−38015
electrophotographic image information content and noise analysis 80−101861
fibre coupled diode lasers, LF noise meas. 80−58542
fibre modal noise anal. and meas. 80−10003
light flux fluctuations, limiting factors in photoelectric meas. 80−13136
light source coherence meas. and fibre modal noise simulation by Michelson interferometer 80−48324
long-pathlength interferometry accuracy and noise problems 80−31860
micro-objective, light transmitting, fogging field glare meas. 79−75590
nematic liquid crystal, orientational fluctuations causing light intensity fluctuations, spectral anal. 80−60618
nematic liquid crystal, viscoelastic properties, spectral noise intensity of scattered laser light obs. 79−23522
nonwhite noise, S/N ratio and detail detection 80−102648
pictorial noise pattern subjective effects 77−90799
radiography, fast Fourier digital quantum mottle anal. appl. to rare earth intensifiers 77−52868
semiconductor stripe laser high-speed modulation, noise, and nearfield meas. *(German)* 78−37923
signal-dependent film-grain noise, optimal image estimation 80−102659
GaAlAs lasers, return-beam-induced noise generation model 80−48244

optical parametric amplifiers
active media, possibilities of efficient freq. conversion 79−59764
anticorrelation effect in nondegenerate parametric amplification processes with quantum pumping 77−88841
anticorrelation effect in parametric amplification processes 77−88839
brightness standard, use of vac. fluctuations 78−13759
degenerate, photon-anticorrelation effect calc. 80−33079
degenerate amplification process, quantum statistics 77−58380
degenerate four-wave mixing, amplified refl., phase conjugation and oscill. 77−83927
fixed intensity approximation *(Russian)* 78−9410
four-photon processes stimulated by fluctuating pump in dispersive medium 79−23017
four-wave parametric processes in two-photon reson. 79−94296
four-wave resonant parametric processes, possibility of optical signal affective amplification 79−18483
generator based on nonlinear optical analogue of inverse Cherenkov effect *(Russian)* 77−75613

optical parametric amplifiers continued
generator-amplifier system, for ps pulse duration adjustment, spectroscopy appl. 79−46003
inhomogeneous crystal optimal length for SHG, parametric amplifier and oscillator 80−106568
inhomogeneous media, efficiency of freq. conversion processes 78−30024
interaction of travelling and pump accompanied waves, induced scattering by polaritons *(Russian)* 79−3739
inverse Cherenkov effect analogue for parametric oscillators and amplifiers 78−59082
IR grating tuned (1.9-2.4 μm) picosec. travelling wave generator 80−5793
IR tunable subpicosecond pulse efficient generation 79−31988
laser optical inhomogeneity cancellation using parametric convertor 80−33049
laser resonator, stationary amplification using stimulated Raman scatt. *(Russian)* 79−27333
light flux brightness meas., EM vacuum fluctuations, quantum noise 80−57361
lithium formate crystal, optical phase configuration 78−5524
N two-level atoms, quantum theory of nonlinear optical phenomena 80−5790
parametric interaction of two waves, scatt. radiation ang. struct., amplification *(Russian)* 77−58381
photon antibunching enhancement by interf., polarisation effects 79−31990
photon antibunching enhancement by interf., Young's interf. expt. 79−27313
photon parametric creation in model cosmological problems, nonlinear optics equivalence 80−73085
picosecond parametric light source, narrow output spectrum, high pulse rate 78−33780
picosecond spectroscopy of parametric superluminesc. 79−55187
picosecond spectroscopy using parametric amplification and generation 77−27320
picosecond three-photon parametric effects 78−71150
plasma laser pulse amplifier using induced Raman or Brillouin processes 80−1279
plasma-laser amplifier, 11-16 micron 10^{11} W cm^{-2} pump beam 77−88861
polydiacetylenes, cryst., picosec. pulse, nonlinear optics appls. 79−46017
ps light pulse length determ. by parametric amplification in nonlinear crysts. 78−1306
pump fluctuations effect on SHG and parametric amplifications 79−55185
pump statistics conversion by parametric amplification of picosecond light pulses 80−99802
quantum statistical properties, amplification and generation 78−46717
quantum statistical properties 77−46753
SHG, parametric amplification and stimulated scatt. phenomena 77−38994
theory and experimental results for KD_2PO_4, $LiNbO_3$ 79−81481
trilinear Hamiltonian governing parametric amplification, periodic oscills. 77−58385
two-photon resonant four-wave parametric amplification 80−48341
CdSe 16 μm parametric amplification with HF laser pumping 80−78910
I laser, high-power, beam quality, gain saturation effect, for fusion ignition 78−63149
KD_2PO_4, gain limitations 79−55177
KD_2PO_4, pumped at 354.7 nm, expt. meas. 79−81481
KD_2PO_4, rhodamine laser light shifting into blue-green 79−18471
$LiIO_3$, appl. to cancellation of optical inhomogeneities in Nd:glass laser 80−33049
$LiNbO_3$ continuously tunable parametric oscillator and amplifier, for remote SO_2 meas. 78−77365
$LiNbO_3$, double-pass config., parametric generation of single picosecond tunable pulses 80−19067
$LiNbO_3$ grating-tuned picosecond IR source with CdSe down-conversion 80−74435
$LiNbO_3$ parametric generator, producing high power tunable ps visible and IR pulses, spectroscopy appl. 79−46003
$LiNbO_3$ parametric oscillator-amplifier system, grating tuned 79−3747
$LiNbO_3$, picosecond IR-continuum generation by 3-photon parametric amplification 80−23746
$LiNbO_3$, pumped at 1064 nm, expt. meas. 79−81481
$LiNbO_3$, two properly aligned crysts., narrow-band tunable IR pulse prod. 78−42382
$LiNbO_3$:Ti diffused channel waveguide, optical parametric amplification 80−106564
$NH_4H_2PO_4$, gain limitations 79−55177
$NH_4H_2PO_4$, rhodamine laser light shifting into blue-green 79−18471

optical parametric devices
see also optical parametric amplifiers; optical parametric oscillators
anticorrelation effect in optical parametric processes, quantum statistical props. 79−7177
brightness determination of thermal source, use of optical parametric converter 80−98979
coherence effect of generating radiation on parametric up conversion process 79−76756
generation from quantum noise, depend. on intermodal correlations 79−36958
image convertor, nonlinear optics methods in spatially modulated signal conversion 79−7179
image convertor with freq. rise, phase aberrations *(Russian)* 78−9455
image upconvertors, matrix method for anal. 78−46727
incoherent four-photon parametric processes 80−48349
internal CW parametric upconversion using Ar laser and $LiNbO_3$ 78−42376
IR radiation, parametric up-conversion to visible range, review 80−64104
modulated light beam parametric interaction increment *(Bulgarian)* 79−10351
nonlinear adaptive system, characteristic purposes 80−28273
photon statistics of fields generated by correlated mode interf. 80−106500
picosecond light continua generation by four-photon interactions 77−62007
picosecond light pulse parametric generation with energy conversion greater than 50% 80−53377
picosecond nonlinear optics, book contrib. 77−65609

optical parametric devices continued
picosecond resonant spectroscopy, using nonlinear cryst. parametric excitation, stroboscopic method *(Russian)* 77−83930
ultrashort light pulse parametric freq. conversion 80−106570
upconversion, three-freq. parametric, beam focusing effects 80−48340
$AgAsS_3$, proustite, parametric upconvertor, temp. effects on tangential phase-matching condition 80−99804
Ag_3AsS_3, proustite upconvertor, effect of temp. on phase match angle characts. 80−5799
HgCdTe diode photomixer, wide bandwidth 77−3682
KH_2PO_3, tunable parametric single-pulse picosecond light source with 50% efficiency 79−59765
KH_2PO_4, type I and II phase matching, spectral backgrounds 77−27316
KH_2PO_3, ultrashort light pulse parametric transform. under optimum interaction conditions 80−99791
$LiIO_3$, parametric generation of nanosec. high-power pulse, tunable over 0.74-1.85 μm 79−18484
$LiIO_3$ CW intracavity upconverter using Ar laser, noise props. 80−64099
$LiIO_3$, IR radiation parametric upconversion with pulsed ruby and CW Ar lasers 77−72026
$LiIO_3$, parametric convertor of IR radiation, angular and spectral characts. 79−64282
$LiNbO_3$, double-pass config., parametric generation of single picosecond tunable pulses 80−19067
NH_3, resonantly enhanced 26 GHz parametric upconversion 79−23020

optical parametric oscillators
see also lasers
bistability and hysteresis phenomena 79−89963
Brillouin, mode-locked, optical fibre, bandwidth-limited operation 78−50851
Cherenkov type parametric optical oscillator, optical saturation 80−102771
degenerate four-wave mixing, amplified refl., phase conjugation and oscill. 77−83927
difference frequency generation with intracavity absorption 77−42567
distributed feedback in lasers due to parametric interaction 77−79898
doubly resonant 4-photon-oscillator, phasemismatching and double refr., threshold pump power *(German)* 78−22166
energy characts. with synchronous two-stage interaction 79−64281
fibre-optic parametric oscillator, sequence freq. generation 80−83636
four-photon parametric oscillator theory 79−86216
four-wave mixing, resonantly enhanced, pump intensity requirement 78−9412
four-wave parametric processes in two-photon reson. 79−94296
gas, reson. four-photon parametric processes, influence of collisions 77−79899
incoherent four-photon parametric processes 80−48349
inhomogeneous crystal optimal length for SHG, parametric amplifier and oscillator 80−106568
injection tuning, theoretical study 80−19069
interaction of travelling and pump accompanied waves, induced scattering by polaritons *(Russian)* 79−3739
intracavity absorption spectroscopy theory with singly resonant optical parametric oscillator 80−23742
intracavity polariton parametric oscill., stimulated Raman emission 78−30026
inverse Cherenkov effect analogue for parametric oscillators and amplifiers 78−59082
IR, Faraday effect obs. near mol. vibr. reson. 79−91413
IR generation, book 77−46761
IR generation, difference freq. mixing, parametric oscill. and stimulated Raman scatt., book contrib. 77−46762
IR generation, optical mixing, SHG and parametric oscills., book contrib. 77−46764
IR source, tunable, efficient 80−5789
IR tunable laser for semiconductor multiphoton spectroscopy *(French)* 80−82836
laser oscillator bandwidth, role of spontaneous emission, teaching 78−41114
multimode-pumped, double resonant, theory in CW and pulsed stimulated emission regimes 79−10359
nonequilibrium phase transition, dynamical features *(Chinese)* 78−83030
organic molecules in solution, selective two-stage excitation, ultrashort-pulse oscillator 79−64283
photosynthesis, primary, selectively excited by tunable ps parametric oscillator 79−48163
picosecond spectroscopy, broadly tunable repetitive laser system using parametric oscillator 79−46006
picosecond three-photon parametric effects 78−71150
review 77−75620
selective interaction appls., 0.3 to 20 μm 77−27319
signal and idler beam mixing device 79−14029
single cavity, energy characts. at strong absorpt. of nonresonant waves *(Russian)* 78−13754
single-resonator pulsed, with noncollinear interaction, angular and freq. spectra 77−23716
singly resonant, monochromatic and multi-mode pumping, theory 78−71148
singly resonant, optimal focusing of pump radiation 79−7176
spectroscopic light source for intracavity absorpt. spectra 77−10976
subnanosecond pumped, near to middle IR 80−19072
transient nonlinear interactions of opposed waves, fluctuations 77−62011
tunable, 1 to 1.1 μm, for SHG phase-matching obs. in thin-film waveguide 77−58390
tunable coherent light sources in middle infrared, materials 77−38991
tunable IR, for resonant nonlinear mol. susceptibilities meas. 79−10347
tunable IR solid-state laser characteristics and principles 80−87406
tunable lasers, nonlinear device descriptions, characts. and potential 79−990
tunable picosecond pulse generation 78−22169
ultrashort-pulse oscillator, tunable double-channel 79−64283
uniaxial crystals, nonlinear optical props., review and summary of data 77−75615
Ag_3AsS_3, proustite, multistage conversion of pump energy into low-freq. radiation 78−30022
Ag_3AsS_3, proustite, synchronous two-cascade interactions energy characts. *(Russian)* 78−83032

optical parametric oscillators continued
CS_2, amplified phase-conjugate refl. and optical parametric oscill., 4-wave mixing obs. 78−74946
CdSe, beam splitter coupled 77−88851
CdSe, freq. tuning possibility by uniaxial press. 78−59084
CdSe, grating-coupled, tunable 15.5 to 16.5 μm 77−58376
CdSe, laser damage resistant PbF_2 antirefl. coatings for 16 μm region 79−31963
CdSe, temp. depend. phase-matched nonlinear optical devices 80−99794
α-HIO_3, pumped by high stability phosphate glass laser second harmonic 80−48266
He-Ne laser IR applications 79−94275
KH_2PO_4, parametric excitation of continuously tunable visible picosecond pulses 79−18482
KH_2PO_4, parametric generation of picosecond light pulses with an energy conversion greater than 50% 80−53377
$LiIO_3$, freq. tunable single ultrashort light pulse generation 77−79896
$LiIO_3$, mode-locked, tunable IR ultrashort pulse prod. 77−3629
$LiIO_3$, multistage conversion of pump energy into low-freq. radiation 78−30022
$LiIO_3$, Nd laser pumping 77−744
$LiIO_3$, pulse-period parametric oscillator, tunable 0.63 to 3.4 μm, for nonlinear spectroscopy 78−59083
$LiIO_3$, stimulated Raman scatt. competition 78−18016
$LiNbO_3$, 4 to 12 μm tunable down-conversion in GaSe 78−66865
$LiNbO_3$, broadly tunable repetitive picosecond parametric oscillator, freq. conversion 78−66866
$LiNbO_3$ computer-controlled IR parametric oscillator source 77−19365
$LiNbO_3$ computer-controlled Nd:YAG-pumped parametric oscillator 77−54758
$LiNbO_3$ continuously tunable parametric oscillator and amplifier, for remote SO_2 meas. 78−77365
$LiNbO_3$, depend. on pump laser beam quality 79−23019
$LiNbO_3$, down-conversion using GaSe, $AgGaSe_2$, 4 to 18 μm 79−86215
$LiNbO_3$, for IR linear absorpt. spectroscopy 79−7180
$LiNbO_3$ grating-tuned picosecond IR source with CdSe down-conversion 80−74435
$LiNbO_3$, high energy tunable coherent source, remote air pollution detect. appl. 78−59089
$LiNbO_3$, IR parametric oscillator source for remote air pollution monitoring 77−21936
$LiNbO_3$, multistage conversion of pump energy into low-freq. radiation 78−30022
$LiNbO_3$, Nd:YAG laser pumped, as high energy tunable IR source 77−46767
$LiNbO_3$, Nd:YAG laser pumped, picosecond IR pulse generation 78−71151
$LiNbO_3$, nonstationary intracavity stimulated Raman scatt. by polaritons 79−18473
$LiNbO_3$ parametric oscillator-amplifier system, grating tuned 79−3747
$LiNbO_3$, synchronously pumped, design and operation 80−14388
$LiNbO_3$ three-dimens. optical waveguide, parametric difference freq. generation 80−48335
$LiNbO_3$, threshold parameters and linewidth control 79−81480
$LiNbO_3$, transient parametric generation of far IR radiation 79−94293
$LiNbO_3$, tunable IR sources, parametric oscillators and difference freq. generation 78−59030
$LiNbO_3$, tunable parametric Raman laser utilizing polaritons 79−41418
$LiNbO_3$:Ti optical waveguide, SHG with 25% conversion efficiency 78−94432
$LiNbO_3$/CdSe system, 16 μm tunable source 78−9414
NH_3 resonantly enhanced four-wave parametric generation of 823 cm^{-1} radiation 78−63151
$NH_4H_2PO_4$, parametric excitation of continuously tunable visible picosecond pulses 79−18482
Tl vapour, coherent anti-Stokes scatt. four-photon parametric oscill. 80−9959
$ZnGeP_2$, temp. depend. phase-matched nonlinear optical devices 80−99794

optical phase conjugation
adaptive optics technology status and prospects 80−33132
beam, image-bearing, nonuniformly polarized, generation of time-reversed replica 80−69459
benzaldehyde, wavefront reprod. obs. by stimulated Brillouin, Raman scatt. 80−53369
CARS, three-dimensional phase matching in four-wave mixing 80−83635
chlorophyll solution, degenerate four wave mixing, phase conjugated backward wave generation *(Chinese)* 80−87429
coherence lengths and phase conjugation by degenerate four-wave mixing 80−64101
compensation for channel dispersion 79−45993
compensation for phase distortions by three-freq. parametric interaction 80−23750
degenerate four-frequency interaction, compensation of phase distortions 80−53380
degenerate four-wave mixing, amplified refl., phase conjugation and oscill. 77−83927
degenerate four-wave mixing, hysteresis and optical bistability 80−69446
degenerate four-wave mixing, time-reversed phase-front generation theory 79−59751
degenerate four-wave mixing in absorbing media 78−71138
degenerate four-wave phase conjugation, signal-pump detuning effects 80−78895
DODCI, saturable absorber, picosecond phase-conjugate refl. 80−95960
Doppler-free spectroscopy and wave-front conjugation by four-wave mixing of monochromatic waves 80−28265
dye saturable absorbers, picosecond phase-conjugate refl. 80−95960
dye solution, laser illuminated, nonlinear interactions *(Russian)* 80−28266
dye solution amplifying dynamic holograms, wavefront reversal 80−48331
dye solutions, degenerate four-wave mixing and phase conjugation *(Chinese)* 80−102765
forward degenerate four-wave mixing, propag. anal. 80−69468
four counterpropagating wave interaction in medium with cubic nonlinearity, dynamic holography concepts 80−91839
four wave interaction, light induced crit. behaviour in nonlinear system 80−95941
four-wave mixing in waveguide, theory 79−31984

optical phase conjugation continued
four-wave mixing spectroscopy, coherent cancellation of background 80−91842
gain saturation of Nd:YAG laser for phase conjugation 79−64272
imaging, high-resolution by degenerate four-wave mixing 80−69458
impurity doped solid, electronic excitation spatial diffusion meas. by degenerate four-wave mixing 79−64274
irregular phase objects, dynamic interferometry, differential holography using phase conjugate refl. 80−37969
large-signal theory of phase-conjugate backscatterings 79−86211
laser amplifying medium, beam spatial struct. reproduction inaccuracy with reversing mirror 80−14379
laser engineering and appls., conf., Washington, USA (May-June 1979) 80−1216
laser resonator with phase conjugate mirrors, modes 80−14392
laser system with phase conjugation, stimulated Mandelstam-Brillouin scatt. 80−5786
lithium formate, optical distortion in nonlinear phase conjugation by 3 wave mixing 79−89956
MBBA, nematic liq. cryst. isotropic phase, phase-conjugate refl. by degenerate four-wave mixing 80−43389
mirror component for optical cavity, Gaussian transverse modes 80−58595
mirror forming optical cavity, Hermite-Gaussian higher-order reson. modes 80−58594
mirrors, phase-conjugate, for optical resonators, degenerate four-wave mixing 80−43393
nearly degenerate four-wave mixing, transient analysis 80−53359
nematic layers, optical phase difference and capacitance, elec. and mag. field depend. 80−28911
nonlinear molecular gases 79−31618
phase determination by conjugate wave-front generation, optical coherence theory 79−7174
phase distortion compensation 80−43392
photon echo and nonlinear mixing methods for phase conjugate wavefront generation 80−58650
plasma jet form. by focusing laser beam on plane target, investigation using wavefront method 80−75103
pulse time-reversal by four-wave mixing 80−91848
pump wave wavefront reversal in Brillouin mirror, influence of certain radiation parameters 80−9961
and real-time holography 78−83034
real-time holography and phase conjugate optics 79−81476
reflection, phase-conjugate, using TEM_{00} pump beams 80−48327
reflection, pulsed 10.6 μm, via intracavity degenerate four-wave mixing 78−87097
resonantly enhanced degenerate four-wave mixing, at. motion effects on wavefront conjugation 79−76746
retroreflective arrays as approximate phase conjugators 79−72508
rhodamine 6G solution in alcohol, degenerate four wave mixing, phase conjugation *(Chinese)* 80−102765
ruby, phase modulated conjugate wave generation, hologram model 80−83643
ruby laser, with stimulated Brillouin scatt. complex conjugate mirror 80−87438
signal detuning, effects on phase conjugation 80−23748
spatial polarisation wavefront reversal in four-photon interaction 80−9956
stimulated Brillouin and Raman scatt., phase conjugated wavefronts 80−5791
stimulated Brillouin scatt. in optical waveguides, method for small-signal wavefront reversal 79−94298
stimulated light scatt., wavefront reconstruction 80−64107
stimulated scattering, reprod. of light field weak components 80−5792
thermal defocusing of light beams, phase conjugation compensation method 80−64123
three-photon mixing wave conjugation, effect of strong wave front distrib. 80−5783
time-reserved replica obs. of monochromatic wave 78−33768
time-reversed wavefront generation by nonlinear refraction 77−34905
wavefront distortion compensation in thick inhomogeneous medium 80−102762
wavefront generation and image reconstruction by four-wave mixing 78−13746
wavefront reversal and short pulse generation using steady-state stimulated Brillouin scatt. 80−53381
wavefront reversal by stimulated Brillouin scatt., four-wave process 80−53382
wavefront reversal in four wave mixing with angular tilting of reversal wave 80−38057
wavefront reversal in four-photon process, two-quantum reson. conditions *(Russian)* 80−106574
wavefront reversal of fields using nonlinear optics methods 80−9958
wavefront reversal with freq. shift, based on anti-Stokes stimulated Raman scatt. 80−74440
wavefront sensing by phase retrieval 80−106478
weak beam wavefront inversion in stimulated light scatt. 80−5798
Al film, wave front reversal, holography applications *(Russian)* 80−58483
$BaTiO_3$, photorefractive effects and light-induced charge migration 80−69447
$Bi_{12}SiO_{20}$ crystals, phase-conjugate wavefront generation via real-time holography 79−27213
$Bi_{12}SiO_{20}$, phase-conjugate wavefront refl. depend. on dynamic hologram spatial freq. 80−53358
$Bi_{12}SiO_{20}$, photorefractive, vibr. struct. mode pattern visualisation, phase conjugation and dynamic holography 80−95938
CO_2, inverted, on-resonant phase-conjugate refl. and amplification at 10.6 μm 79−64275
CO_2, inverted, wavefront reversal, high efficiency 80−74436
CO_2 laser cavity and Ge phase-conjugate 10 μm reflection expts. 80−78894
CO_2 laser fusion system 80−74429
CS_2 filled waveguide, time-reversed wave generation by nonlinear refraction 78−90447
CS_2, wavefront reprod. obs. by stimulated Brillouin, Raman scatt. 80−53369
CdTe, backward degenerate four-wave mixing obs. 80−53361
Ge, high refl. phase conjugation at 10 μm, intracavity CO_2 laser techniques 80−78894
Ge in TEA CO_2 laser cavity, wavefront reversal, high efficiency 80−74436
Ge, phase conjugation of 4 μm for single line and multiline radiation 80−83641
$Hg_{0.77}Cd_{0.23}Te$ nonlinear optical IR generation 80−58642
$Hg_{1-x}Cd_xTe$, degenerate four-wave mixing of 10.6 μm radiation 80−95943
n-$Hg_{1-x}Cd_xTe$, optical phase conjugation 80−83644
InSb, degenerate four-wave mixing obs. at 5K 80−53355
$KCl:ReO_4$, resonantly enhanced phase conjugation through degenerate four-wave mixing 80−58635
$LiNbO_3$, complex conjugate wavefront generation via degenerate four-wave mixing 80−48329
$LiTaO_3$, complex conjugate wavefront generation via degenerate four-wave mixing 80−48329
$LiTaO_3$, time depend. phase inhomogeneity compensation via degenerate four-wave mixing 80−53353
NH_3, phase conjugation in an inhomogeneously broadened medium 80−83642
NH_3, phase conjugation via degenerate four-wave mixing 80−106566
Na atomic vapour, Doppler-broadened system, degenerate four-wave mixing, line shape and strength angular depend. 80−43391
Na vapour cell, physically thin, phase-conjugate wave generation in forward direction 79−89957
Na vapour doublet, dispersion free point, cooperative phased-array radiation 80−53352
Na vapour thin cell forward phase conjugation obs. 80−78917
Ni complex, BDN, saturable absorber, degenerate four-wave mixing, amplification and phase conjugation 80−43394
SF_6, multiwavelength phase conjugation using multiline CO_2 TEA laser 80−91847
SF_6, phase conjugation at 10.6 μm by resonantly enhanced degenerate four-wave mixing 79−64271
ZnSe crystals, degenerate four-wave interaction, nonlinear optics effects 80−91856

optical prisms
1×2 optical switch using new type of pentagonal prism switch, for optical fibres 80−64148
achromatism of optical wedge of holographic elements *(Russian)* 78−13787
achromatized wedge scanner design 77−88948
alignment testing in converging beams 78−30044
Amici roof prism polarisation characteristics 79−72647
amplitude interferometer, white light, 180 degree rot. shear astronomical appl. 78−77977
analysis of mirror-prism system, using biquaternions *(Russian)* 78−50882
anamorphotic, apochromatic connection *(Russian)* 80−87513
anisotropic, ray refr., appl. to atm. optics haloes 80−63916
astronomical spectra obtained with low-dispersion Fehrenbach prism, computer simulation 78−57468
ATR prism for IR laser absorpt. spectroscopy 79−98480
autocollimation instrument for checking angles and pyramidicity of AR-90° prisms during manufacturing process 80−87570
axicon, conical optical polar everter without field rot. 77−3658
axicon and related optical component diagnostic techniques 80−14417
axicon axial intensity distrib., influence of laser beam divergence 80−95934
axicon combined with mirrors and lenses, laser linear, annular and radial focusing 78−66856
azimuth scan MTF techniques, for optical component and system evaluation 78−50900
basing in convergent beam of rays 77−72054
beam expander, single prism, for tunable dye laser *(Chinese)* 80−74389
beam expander for dye laser, dispersion 78−17968
beam expander in N_2 laser pumped dye laser, prism material dispersion 79−27285
beam positioning and focusing system combination in optical memory system *(Russian)* 79−7194
beamsplitters, beam inherent parameters analysis 79−36999
binocular models, charact. and design features, review 80−74468
binoculars, 8×30, MTF, stray light and transmission characteristics 79−72655
binoculars, wide-angle eight-fold magnification, aberrations 77−10997
birefringence detection system for polarisation opt. props. meas. 77−57385
birefringent prism couplers, for thin film optical waveguides 78−55468
chalcogenide glass films, kinoform optical elements and integrated optics elements prod. 77−75634
chalcogenide glass semiconductor film kinoform production *(Russian)* 77−14670
channel filter for fibre transmission systems, wavelength multiplexing 77−34950
channel waveguides, single-mode, prism coupling efficiency meas. 80−99878
cholesteric prism, light refr. under applied mag. field *(French)* 78−80319
coherent image processing photodiode array 79−55076
conical elements in resonator, mode structure, polarisation effects 79−98411
corner cube, dihedral angle error determ. from Twyman-Green interferogram 77−65646
corner cube, Jones matrix *(German)* 77−19420
corner cube, polarisation props., Jones matrices *(German)* 77−19419
corner cube interferometer using extended sources 77−5894
correcting glass-angles 77−79975
correlator, appl. to stereo photogrammetry 78−86368
coupler fabrication technique 80−83685
coupler for Ti diffused $LiNbO_3$ waveguide 79−46089
coupling into clad uniform optical waveguides 80−96003
coupling into optical waveguide, second harmonic generation 80−102763
design methodology, dimensional, with and without computer *(Czech)* 80−53431
deviation prism interferometric testing 78−30095
diamond, light coupling prism, Raman spectra for thin film props. study 80−88978
diamond polishing method, technology and automated equipment 77−34968

optical prisms continued
dielectric film refractive index meas., synchronous angle integrated optical method 80−15976
diffused waveguide tunnel excitation and emission 78−59146
directional coupling device of two glass prisms, geometrical optics *(German)* 79−18524
double-prism, anamorphic system, for Gaussian beam expander 79−3716
double-tapered prism coupler for optical waveguides 78−94431
dye laser, longit. pumped, simultaneous two-wavelength operation using intracavity prism *(French)* 79−970
dye laser, narrow linewidth short pulse operation, using dual prism beam expander and grating 79−971
dye laser tuning by dielectric interference filter-coated prism 79−10322
electro-optic waveguide deflector performance characteristics 80−33213
electro-optical Bragg deflection modulators in corrugated waveguides 79−59844
electrochromic ATR prism modulator 80−43440
electrooptic beam deflectors as streak cameras, theory 79−58809
electrooptic surface prism laser deflector, for field destructive interference 80−87492
electrooptic waveguide array deflectors, performance criteria and limitations 80−5821
EM theory of prism couplers, tutorial approach *(French)* 77−37694
fabrication errors meas. by interference method 77−58494
far IR Fresnel prism as quarter-wave plate 77−39067
Fehrenback prism for stellar radial vel. meas. 79−84681
fibre mode analyser using refraction from oblique section 77−88952
fibre transmission system filtering prism *(Japanese)* 78−9441
figuring, optical path difference check by Hendrix interferometer 77−72094
film waveguide spectrum analyser with prism coupling 77−62071
filter, multilayer frustrated-total-internal-refl., spatially limited 80−96014
frequency shifts for light having traversed moving prism *(Spanish)* 77−88638
Fresnel rhomb design, TI 58/59 program 79−32040
gemstones, light coupling prism, Raman spectra for thin film props. study 80−88978
Glan-Taylor prisms and Faraday rotator, circulator for optical fibre transmission 80−23769
glass prism compact structure producing optical delay, laser pulse duration meas. 78−46702
glass reflecting angle testing in autocollimation modes 78−71194
goniometer verification prism manufacture and recertification 77−27392
grating-prism, prism-prism and grating-grating compounds for deflection angle compensation 80−95990
Iceland spar double refracting prism, rotated e-ray 77−769
ideal prism solar concentrators, features 79−43745
image filtering using prism and incoherent light *(French)* 80−14450
image processing in incoherent light 80−87339
inclined prism three-point meas. reliability *(German)* 80−28359
integrated optical prism-waveguide dual coupler theory and exptl. performance 80−33236
integrated optics, determ. of ray directions coupled out of waveguides through prisms and gratings 79−59841
interference coatings for devices transmitting colour images 78−59108
interference dividing prism 77−75676
interleaved glass layer prism for semiconductor mask testing 80−43425
Koster prism for progressive acoustic wavefront visualisation 80−5701
large high-precision prism grinding, use of 3G-71 lathe 80−102872
laser absorption spectroscopy with ATR plates for biomed. use *(German)* 78−36084
laser beam deflected by prismatic polygon mirror, focus path 77−19267
laser beam expander in N_2 laser pumped dye laser, dispersion 78−74924
laser slit beam prod. 77−72020
lens-axicon doublet illuminated by Gaussian beam, ring focal pattern 78−55421
matching of semiconductor sources to thin-film planar and stripe waveguides 80−64174
minimum angle of deviation, school corridor demonstration 78−81760
mirror-prism system transformations by biquaternions *(Russian)* 78−55426
monochromator, Littrow prism, wavelength calibration 78−25950
multifaceted prism test automation 79−72724
multilaser beam combination system 79−68402
multimode waveguide corner, rigorous soln. *(Ukrainian)* 79−76819
multiple beam spectral analyser with thin film waveguide feed, prism radiation tap 77−34944
multiple prism beam expander for short-cavity dye laser 78−1250
multiplexer design for optical wavelength-division multiplexing transmission via single fibre 80−33222
nonblocking 8×8 optical matrix switch using 64 pentagonal prisms 80−74485
object mutual orientation using active polarisers with tetrahedral reflectors 79−26109
pentagonal, roof, with constant functional angles at edges for convergent light beam, dimensional project *(Czech)* 79−37007
perspex, refr. index meas., crit. angle method, student expt. 80−12873
planar optical elements, dispersion props. 79−3811
planar prism mode separator for waveguide *(Russian)* 77−46803
plastic optical components and systems 78−25967
polarisation flipper for IR laser beams mirror and prism systems 77−75586
polarising beam splitter, film coatings, cemented cube 77−19422
polyhedral, unit of plane angle transmission 77−7221
prism-scanning panoramic camera for reconnaissance aircraft 77−79181
prismatic double monochromator 80−23796
Q-switched laser pumping lamp trigger circuit 79−68403
Raman laser, CW fibre, bandwidth reduction using prisms, gratings and etalons 80−53366
raster focusing device for laser radiation 77−19272
raster focusing-prism and light guide pump system for NH_3 laser 80−9905
reflection, deviating axial ray by ≠90° dimensional design minimisation *(Czech)* 77−19414
reflection prism, as variable-ratio beam splitter, use in holography *(Spanish)* 77−88945
refractive index gradient tolerance in optical elements 78−71179
refractive index meas. using critical angle method 78−30071
refractometer, PR2 Pulfrich, prism developments 78−24848
retroreflector, temp. stability testing under space conditions 77−62078
optical prisms continued
retroreflector and corner reflector terminology 77−11043
rhombic, dimensional design *(Czech)* 80−74494
rhombic, with wedge, construction and parameters calc. *(Czech)* 79−27411
ring laser, perturbed cavity calcs. 80−102739
roof and other prisms, MTF tests 80−69571
rotating prism camera lens, 100 mm focal length, White Sands Missile Range, testing methods 79−86249
rotating prism compensator, high speed filming techniques 77−75700
rotating prism display of multiple LED lines 79−93111
rotation shearing interferometer, with phase compensated roof-prisms 78−77971
rutile prism, high dispersion, for tuning dye lasers 77−7107
single mode fibre pickoff coupler 77−783
SISAM employing contracircular design, adjustment by prism system 80−31894
slit image seen in total internal reflection *(French)* 80−95810
solar collectors, rectangular glass prisms with total internal reflection, appl. 77−27372
solar energy collectors, flat-plate, optical valve design 79−81506
spectroscopic resolution increased with separated gratings and prisms 80−43271
spectroscopy, resonant internal-refl. prism, using surface, guided and Fabry-Perot EM waves 78−41358
spherical base prism, optical waveguide systems appl. 77−83985
stand for dynamic balancing 77−72052
surface EM wave coupling efficiency, prism gap height depend. 78−33914
surface waveguide electrooptical deflector, high-resolution, prism model 80−48454
symmetrical prism as input coupler for integrated optics 79−10412
tapered gap prism couplers for high index materials 77−72091
tapered gap prism coupling to diffused $LiNbO_3$ waveguides 80−78967
telescope triple-prism beam deflection compensation 79−75105
telescope with two magnifications, using Porro prism erector 77−14790
testing of prism optics for laser interferometer, interf. meas. 80−105698
thin film electrooptic deflector using induced grating with variable blaze angle 80−99862
threehedral reflecting prisms with two reflections, new design *(Czech)* 78−66913
transmission solar focusing collector 77−65617
triple frame camera, with beam-splitting prism 78−37097
two-coordinate acousto-optical prismatic deflector geometry *(Russian)* 77−58428
two-prism system, position and magnification chromatism calc. *(Russian)* 80−87515
two-wave interferometers for use with monochromatic source, prism components 79−35814
visual field testing, three-channel optical system *(Spanish)* 79−24993
waveguide, loss measurement, nondestructive, using three prisms 80−106596
waveguide input-output coupler, high efficiency, analysis 79−98468
waveguide-prism coupling efficiency for waveguides with arbitrary refr. index profile, WKB approx. 79−7231
waxicons for high-power chemical lasers, interferogram analysis 80−14418
wedge compensator, operating nonlinearity elimination 79−32065
wedge compensator for automatic control system 78−13808
wedge deflection angle calc., approx. formula 79−32068
wedge scanner, achromatisation 77−7205
wedge-sensitometer for photographic photometry *(Japanese)* 79−44373
Wollaston prism as convergent light beam splitter 79−14092
BaF_2, prism coupling efficiency optimisation for surface IR wave excitation 77−75708
$CaCO_3$, Iceland spar, polarizing prism, struct. defects effect 78−18065
GaAs laser array to channel groove waveguide coupling prism 78−38067
Ge single cryst. prism, refr. index meas., interlaboratory comparison 78−54443
$LiNbO_3$ waveguide, planar electro-optic prism array beam splitter 80−64209
NaCl prism IR spectrometer, calibration curve, non-min. deviation effect 77−13809
Nd:glass laser, short pulse mode-locked, using prisms 80−83617
SrF_2 fusion-cast prism refractive index obs., 0.2138 to 11.475 μm 80−34882
$SrTiO_3$ prism coupler for $LiNbO_3$ integrated optics very high throughput damage resistant waveguide modulator 80−58788
ZnS-Na_3AlF_6 layer achromatic interference polarizers, design, fabrication 79−55222

optical projectors
16 mm cine projection lens 79−72646
16 mm Perfectone Comitor for sound dubbing, fast synchronisation and foreign language recording 78−59103
16 mm projection installation, automatic, containing Ukraine-5 projector and ring bifilar magazine *(Russian)* 79−36980
adaptor device for horizontal to vertical stage conversion, cradle device 79−58500
anamorphic system, image quality testing, resolving power determ. 77−7171
audio-visual design and room acoustics for board rooms 79−37092
auto dissolve slide projector, Rollei P-3800 79−18499
automatic dioptometer with projection readout system 79−50455
autostereoscopic displays using stereo-pair of projected images 80−1296
centring projector 10, installation of halogen projection lamp 79−76782
cine, electronic ignition for Xe and metal halogen lamps *(Russian)* 77−41719
cinema, 35 mm, new projection lenses 80−87469
colour distortions in screen images introduced by projector components *(Russian)* 79−32029
colour transparency projector/scanner and printer 80−52343
commercial large-scale laser displays using path-controlled galvanometers 77−17963
component blank pressure shaping, semiautomatic apparatus 79−72731
deflection contour generation by white light projection speckle method 80−98881
diffraction grating, surface relief, for colour image storage and display 77−84004
double-image, for steel component contour meas. 77−88887
dual slide fader control cct., using a triac dimmer 80−69489

optical projectors continued
dubbing suite for Anglia TV using Comitor projector and Sepmag machines 78−59104
dynamic data display on large screen by brightness enhancing system 77−58462
enlarger analyser using Si-blue photoamplifier IC 80−42288
equipment and services, 1979 video yearbook 79−14197
glass industry, applications of gauges and optical projectors 80−21249
halogen projection lamps and light fittings *(German)* 77−58408
holographic, small formal hologram to large-screen projection appl. *(Russian)* 78−29918
holographic movie camera and projection system 80−78808
illumination control of cine projectors, foreign equipment *(Russian)* 80−105741
image digitiser system design 80−48441
lamp, incandescent, performance obs. *(Russian)* 77−10129
landform photograph three-dimensional projection system 77−74181
lantern slide projector remote control using IR-60 infrared system *(German)* 80−95169
large scale projector with separate movement and optical system for bubble chamber pictures *(Italian)* 79−75567
large-screen colour projection TV system, using electron-beam-scanned semicond. laser quantoscope 80−99783
laser application in brightness amplifier, for medicine and biology 80−36060
laser beam deflecting system, electro-optic, using Kerr cell and birefringent calcite prism 77−7103
laser projection microscope, transmitted light, Cu vapour laser as image amplifier 80−73446
lens-array photography, longitudinal distortion compensation, integral image reconstruction 80−52345
lenses for projection photolithography 77−58423
light valve projection systems classification 78−33812
liquid crystal light valve operation and appls. 78−46826
MagnaScope 35 mm half-frame projection system 79−40637
measuring, development and use of special mirror, examination of recording heads 80−83657
microfilm reader and projector 79−72648
microscopic image projection system with quantum amplifier 80−33116
mirror system use in light-valve projectors *(Russian)* 80−78930
motion picture, modern silent and sound 8 mm projectors and stereophonic models *(Russian)* 79−10372
motion picture projection equipment for 16 mm films, perspectives *(Russian)* 80−77903
motion picture switching projection lamp. transfer processes from thyristor rectifiers *(Russian)* 78−94421
movie, interference coatings on reflectors, vac. deposition 77−75725
movie projector objective lenses, standardisation of optotechnical parameters and testing methods 80−28301
multiple, microprocessor in slide projection control 78−55425
multispectral, MSP-4 objectives, photoelectric distortion meas. *(German)* 80−95976
multispectral photography appl. using MKF-6 camera and MSP-4 projector 80−56633
multispectral projector, colour synthesis instrument for evaluating multispectral photographs 78−40688
narrow-beam, beam-shape, intensity distribution curve prediction 78−59105
noncoherent optical projection system input holograms *(Russian)* 80−14297
operator's eye and projector having a thermoplastic target, characts. 80−96023
optical image immobiliser, Hollogon Skanner, cinematography appl. 78−37087
photoprojection method of image formation of submicron patterns 78−71180
polymer, composition coatings for rubbing mechanisms 78−29198
projection plotter system, for classroom demonstrations 79−33
raster-scanned laser display using TeO_2 acousto-optical deflector 77−10930
reflective light valve projector efficiency and image uniformity improvement 80−87459
review and appls. of new laboratory projectors 80−22459
rotating lens system for cine projection with continuous film transport 80−62766
SAW delay line fabrication by direct optical projection 79−81667
Schlieren, phase image reflection, coherent light source *(Russian)* 78−38025
schlieren 80−87544
schlieren system, phase object projection, imaging characts., recording conditions 78−25977
Schmidt corrector plate replication, testing and performance calc. 78−66967
Schmidt corrector plate replication 78−66966
single projector for abutting images of two light valves 80−87458
slide, 1978 state of art *(Czech)* 78−79095
slide changer, automatic, operated by signal level drop in commentary 77−65060
slide projector, dissolve control unit provides cross-fading and operational sequence recording 80−77833
slide projector, electronic control apparatus *(Dutch)* 80−105731
system quality determination methods *(Hungarian)* 79−89983
system transfer function definition and performance testing *(Hungarian)* 80−14413
tapered light guide condenser design approach 80−33218
telecine projection machines, Telekino-75, optical-mechanical systems *(Russian)* 79−76800
three-dimensional optical display unit 80−1297
TV projection systems for large screen pictures *(German)* 79−80660
uniform test picture for all projection equipment *(German)* 80−27328
unity-magnification projection system characteristics 79−27367
wavelength and coherence effects 80−64136
wide-aperture condenser design 78−55430
X-ray film viewing 78−59111
zoom projection lens, optical level system, paraxial characts. 80−53399

optical properties of substances
see also acousto-optical effects; birefringence; brightness; cathodochromism; colour; dichroism; dielectric function; electro-optical effects; electrochromism; magneto-optical effects; optical constants; optical Kerr effect; optical rotation; optical saturation; optical susceptibility; photochromism; piezo-optical effects; pleochroism; reflectivity; thermo-optical effects
acetylene smoke particles, agglomerated, optical extinction meas. at 0.5145 and 10.6 μm 80−48155
amber, natural, optical strength and laser induced rupturing 78−7039
amorphous and liquid semiconductors, conference, Cambridge, MA, USA (Aug. 1979) 80−41933
amorphous semicond., optical props. and densities of states *(French)* 77−72809
amorphous semiconductors, conference, Balatonfured, Hungary (Sept. 1976) 77−76802
benzene, soln., light deflection, near crit. point, due to gravitational effect 78−2818
benzenes, m-disubstituted, nonlinear optical props. 77−58373
carbonate mineral, (Si, Cl)-bearing, from limestone-granite contact zone, crystal struct. and optical props. *(French)* 78−69339
cholesteric liquid crystals optical properties, diffraction nature, review 80−70123
composite, metal spheres in dielec. medium, effective medium theory 77−24811
composite materials, phys. props. review 77−4720
composite media, dielec. and optical props. electrostatic polarisability calc. 79−51507
conference, basic optical props. of materials, Gaithersburg, MD, USA (May 1980) 80−101668
conference, condensed matter physics, Sarajevo, Yugoslavia (Oct. 1976) 77−51629
conference on elec. transport and optical props. of inhomogeneous media, Columbus, USA (Sep. 1977) 78−56114
constitutive relations in photomechanics 80−43251
crystal with spatial dispersion, exactly soluble model 77−43958
cylinders, perfectly conducting arrays, transport prop. investig. 80−13011
di-o-thymotide, cryst. chem. study and morphology *(French)* 79−46576
diamond, round brilliant cut, statistical assessment of brilliance and fire 78−90361
diamond, round brilliant cut style modifications, brilliance, sparkliness and fire 78−90362
diamond simulants, brilliance, sparkliness and fire 78−90363
dielectric molecular fluid, optical props., internal forces effects, theory 77−28534
dielectrics, electric, optical and acoustic interactions from Lagrangian representation, book 80−2715
discontinuous metallic film, struct., optical and electrophys. props. review 77−76698
DOBAMBC, ferroelec. liq. crysts., elec. and optical props., appls. *(Japanese)* 80−88943
ferroelectricity, conference, Leningrad, USSR (1977) 79−15406
filament waveguides for signal transmission in far IR region *(Czech)* 80−96017
gas, propag. of ultrashort light pulse in region of absorpt. line *(Russian)* 77−47141
gas mixtures, IR absorpt. theory using hard sphere model *(Russian)* 80−14879
glass, large disc, optical homogeneity, high accuracy measurement *(Chinese)* 79−55195
glass fibre reinforced plastic, fatigue fracture kinetics studied by diffusion scatt. of luminous fluxes 80−76446
insulating crystal, many-photon transitions 80−103932
kinetic effects in an optically excited gas 80−1721
layered compounds, book 77−39757
layered materials and intercalates, International Conference, Nijmegen, Netherlands (Aug. 1979) 80−36771
liquid crystal, lecture on optical props. 78−35118
magnetic semiconductors, conference, Montpellier, France (Sept. 79) 80−94916
Mars soil terrestrial analogues, optical props. compared with Mars disc IR spectra 78−85879
materials, electronic, optical, magnetic and thermal props., rel. to energy technology 78−88412
metal particle composite, physical and optical props. 78−56528
metal-NH_3 solutions, optical and microwave props. of microscopically inhomogeneous materials 77−77161
metallic granular films, optical and microwave props. of microscopically inhomogeneous materials 77−77161
metallic thin films *(French)* 80−60692
metallic ultrathin filaments, dielectric and superconducting fluctuations, Peierls transition *(Russian)* 80−65742
metals, solid and liq., optical props. by spectroscopic ellipsometry, review 80−103929
microwave radiation, kinetic theory of interaction with diatomic gas, j=0, j=1 transitions 78−9750
microwave radiation, kinetic theory of interaction with polyatomic gas 78−9749
molecular fluid, optical props., intermol. forces effects, theory, appls. 77−28535
optomechanical characts. determ., polarisation device application, by compensation method 80−40643
Perspex, clear, effect of storage temp. on dosimeter calibration 77−60256
phosphate system, containing halogens glass formation 80−103254
photon kinetic equation for Doppler line broadening, soln. 78−9751
polarisation propagator calculations of frequency-dependent polarisabilities, Verdet constants, and energy weighted sum rules 78−58647
polyethelene tubes and sheets, light resistance investigation under natural climatic conditions 80−21127
polymer materials, NDT, rigidity and hardness from acoustic, thermal, optical and dielectric props. *(Russian)* 77−48601
quartz:Ge, optical and piezoelectric props., ang. distrib. *(Russian)* 78−23404
rare earth glasses, R_2O_2S-Ga_2S_3, (R=La to Nd), exam. of preparation and props. *(French)* 78−80504
rough surfaces, discontinuous films, heterogeneous materials, review 80−103935
sea water, hydroptic struct. variability in S. Atlantic regions *(Russian)* 78−77262
seawater inherent optical props. rel. to Secchi depth 79−16472
semiconductors, book 80−77554
semiconductors, electrolytic cell for optical props. meas. 79−93199
spatial dispersion exponential model, boundary conditions *(Russian)* 80−75994

optical properties of substances continued
spectral selectivity of composite materials, optical props. and fabrication of composite solar absorbers, review 79−74520
spectrally selective surfaces and their impact on photothermal solar energy conversion, review 79−74519
swollen semirigid polymer, short-range orientational order *(Russian)* 77−84662
tensor operators, symm. props. 77−52033
textured surface, effects on optical props., applications in solar collectors 78−56443
TGSe, IR trichroism, epitaxial prop. process 77−63475
Twyman effect in quartz and optical glasses, temp. effect 79−4784
Ag, granular films, optical props., depend. on refractive index of surrounding medium 78−84672
Ag-Br-I emulsion, high illumination, departure from reciprocity, intermittence effects, charact. curves *(French)* 78−79085
Ag-Cl-Br emulsion, high illumination, departure from reciprocity, intermittence effects, charact. curves *(French)* 78−79085
AgCl, single cryst., optical, acoustic and acousto-optical props. *(Czech)* 78−76417
As-Ge-S(Se), glass films, photostruct. changes 77−85822
As-S amorphous film, photo-induced optical changes, annealing effect 78−27345
Au black optical props. rel. to structural composition, appl. to solar absorption 79−83630
Au-Ag-Cu, optical props. study using automatic nulling spectroellipsometer 80−55058
BN films, optical and electrophysical props. *(Russian)* 77−20941
Be, freq.-depend. polarisabilities and Verdet consts., calcs. 78−62781
CO, freq.-depend. polarisabilities and Verdet consts., calcs. 78−62781
$12CaO.7Al_2O_3$, single cryst. growth from melt, and some opt. and phys. props. 79−47614
Cd, band structure calc. by APW method, optical prop. prediction 77−20232
CdTe, physical props., review 77−39833
Co-Si, liquid alloy, optical charact. *(Russian)* 77−24810
$Cu_{2-x}Te$-CdSe heterojunction, elec. and opt. props. *(Korean)* 77−51811
FH, freq.-depend. polarisabilities and Verdet consts., calcs. 78−62781
Fe_3Al, order-disorder transform. effect on optical props. *(Russian)* 77−39820
γ-Fe_2O_3, small particle composite, preparation methods, superparamagnetism, optical transparency 78−60315
GaAs, optical cond. of free carriers 78−19436
Ge, amorphous, optical and microwave props. of microscopically inhomogeneous materials 77−77161
He, freq.-depend. polarisabilities and Verdet consts., calcs. 78−62781
Hg, optical props. by spectroscopic ellipsometry, review 80−103929
Li, optical props. by spectroscopic ellipsometry, review 80−103929
Na optical properties by spectroscopic ellipsometry, review 80−103929
Na vapour, induced optical anisotropy *(Russian)* 80−38526
Na vapour in inert gas, effect of oxidant on optical props. 80−1736
$NaAlSiO_4$, carnegieite, cathodochromic props., storage CRT applic. 77−8604
Na_2O-B_2O_3-SiO_2, containing halogens glass formation 80−103254
Na_2O-SiO_2 glass containing halogens glass formation 80−103254
Ni_xZrS_2, fundamental optical absorption edge 79−99904
$PbMoO_4$, optical purity determ., molecular light scattering obs. 78−72537
Si, amorphous, optical props. appl. as solar absorber, review 79−74519
Si-SiO_2 interface, optical props. 79−99908
Si_3N_4 reaction bonded, microstructure, formation, properties, phase composition 79−56947
Si_3N_4:Si amorphous film 77−76987
Sn, liq., optical props. by spectroscopic ellipsometry, review 80−103929
Zn, band structure calc. by APW method, optical prop. prediction 77−20232

optical pumping
see also lasers; multiphoton spectra
$3^2S_{1/2}$-$3^2P_{3/2}$, spectral distrib. and collisional depolarisation of laser light, D_2-fluorescence 80−58209
acetonitrile, far IR laser gas absorption obs. with and without DC field 79−31870
acetonitrile, sub mm laser, generation lines identification *(Russian)* 78−82952
acetonitrile, submillimeter rotational spectrum, laser generation line identification 79−64210
acetylene, multiphoton vacuum UV photodissoc. obs. and interpret. 80−11939
acetylene-d_2, 17 to 21 μm laser lines generated using CO_2 laser pump 80−69375
acridine, solvent depend. of radiationless relax., singlet lifetime, picosecond spectroscopy 78−66582
active mirror and disc amplifiers, laser glasses, physical props. 78−42337
active particles, Lorenz-Mie scatt. theory paradox 80−74324
aliphatic tertiary amines, laser action feasibility, emission spectra, two photon excitation 80−23683
alkali atom+alkali atom, laser-induced ionis. collisions 78−5333
alkali dimer laser, continuous, optically pumped 78−87046
alkali halides, F-centres, ESR in different states of relaxed configuration 80−108067
alkali halides, F-centres, optical pumping, spin-orbit and hyperfine coupling 77−16360
alkali metal atom, Bloch theory appl. to optical pumping and mag. reson. 79−59403
alkali metal atoms, in solid matrix, bistable state, optical trapping between levels 79−81187
alkali metal vapour, optically pumped, longit. relax. in hyperfine states 77−57908
alkali metal-He quantum magnetometer 80−17965
alkaline earth vapour, soft X-ray gain 77−23655
alkyliodides, UV photodissoc., time-resolved obs. of $I(^2P_{1/2})$ reactions 80−11940
anharmonic molecules, excitation, by steady-state and pulsed radiation 77−50476
anharmonic molecules, stochastic multiphoton absorpt. processes, classical model 79−45778
anharmonic molecules, vibr. relax. under strongly pumped conditions, anal. theory 78−5328
anthracene:tetracene, upper excited vibronic states optically pumped energy transfer matrix fluoresc. 78−76512

optical pumping continued
anthracene, cryst., exciton aggregate possible form. under intense optical pumping, fluoresc. spectra 80−84772
antiferromagnet, radiation problem of parallel pumping, magnon-photon interaction 79−51934
aromatic molecular crystals, optical nuclear polarization by optically excited triplet states 79−19804
atom, excitation by coherent pumping, induced Raman scatt. 78−66519
atom, gaseous, ground and excited states, review *(Japanese)* 78−25489
atom, induced coherent emission in spatially separated light fields *(Russian)* 79−50274
atom, many-photon excitation by multimode radiation 80−74154
atom, reson. interaction with laser field, nonperturbative theory 77−442
atom, resonance light scattering, intensity effects 80−91511
atom, resonance Raman scatt. modification in intense laser fields 77−27002
atom+molecule, IR induced vibr. transition, Schrodinger eqn. distorted wave calc. 77−23538
atomic and laser spectroscopy, book 77−79554
atomic beam tube with laser pump, interaction eqns. *(Russian)* 78−74801
atomic collisions, transverse relaxation in optically pumped vapours *(Polish)* 78−55229
atomic density matrix irreducible components, appl. to optical pumping 77−46546
atomic gas, laser irrad., field avoided crossings, new transition channels 78−33477
atomic lifetime meas., fast-beam-spectroscopy by combined gas cell-laser excitation 77−61714
atomic metastability exchange collisions, Pauli principle effects 80−99536
atomic polarisability, coherence between Zeeman sublevels, laser pumping 77−83549
atomic populations, coherent trapping 79−22670
atomic RF spectroscopy, nonlinear and parametric effects, review 80−18816
atomic spectra ionisation broadening under action of intense pumping wave *(Russian)* 77−42283
atomic spectroscopy, Doppler-free method with vel. selective pumping 79−81304
atomic states, laser induced distortion 77−3323
atomic three-level system, interaction with pump fields 78−33718
atomic transition probabilities meas. by time resolved optical pumping 77−46545
atoms, inversion to ground state by optical pumping 79−45681
atoms, laser excited, reactive collisions 80−66793
atoms, multiphoton rate equations, generalised 80−91525
atoms, optimum excitation *(Russian)* 78−13474
atoms, strongly driven by laser, emission spectra 78−42017
BBOT dye, vapour phase, optical props. *(Japanese)* 80−9879
binary solutions, pulsed excitation, energy transfer and laser action 77−75506
bird migration and homing, physicochem. mechanism for mag. field detect. 77−52811
bistability and spectrum of fluctuations, quantum anal. 78−71067
bromomethane, multiphoton vacuum UV photodissoc. obs. and interpret. 80−11939
bromotrifluoromethane, FIR laser action obs. at 823, 883 μm 80−14321
carbon tetrachloride, intense ps pulse excitation, multiple stimulated Raman spectra 78−66867
carbon tetrafluoride, laser parameters with optical pumping 79−72557
carbon tetrafluoride, lasing action, spectroscopy of features near 9 μm lines 79−22944
carbon tetrafluoride 16 μm laser, radiance enhancement 78−87045
carbon tetrafluoride $^{12}CF_4$ laser, Doppler-limited absorption spectroscopy 80−74347
carbon tetrafluoride $^{12}CF_4$ optically pumped laser efficiency 80−74348
carbon tetrafluoride laser, CF_4 molecule $\nu_3+\nu_4$ band optical pumping 80−74349
carbon tetrafluoride laser, frequencies of pump and laser transitions 79−94218
carbon tetrafluoride laser, high energy output in 16 μm region, CO_2 laser pump 79−89927
carbon tetrafluoride laser, optically pumped, freq. tuning 80−28208
carbon tetrafluoride laser, pulse-periodic operation, 0.2 W average output power 79−27247
carbon tetrafluoride laser, weakly forbidden vibr.-rot transitions 79−55121
carbon tetrafluoride laser oscillator amplifier meas., small signal gain and self-absorpt. 79−59683
carbon tetrafluoride laser with optical pumping, freq. tuning and stabilisation 80−99706
carbon tetrafluoride optically pumped laser, spectroscopic characts. 79−89896
carbon tetrafluoride optically pumped laser, stimulated emission stabilisation and tuning 80−9866
carbon tetrafluoride pulsed laser characts., optically pumped by CO_2 laser 80−91778
Cd+molecules collisions 80−58338
celestial masers physics, pumping processes 79−21455
cell for visible display of inhomogeneous mag. field or RF freq. spectrum 77−65027
chlorodifluoromethane subMM wave laser, optically pumped 80−87376
chloromethane-d_3, and isotopic forms, optically pumped mm laser transition assignments, 792 micron line 78−42328
chromium tri(bipyridyl)tri-perchlorate, aq. soln., Raman scatt. from electronically excited state 79−94001
coaxial cable pulse forming network as rare gas halide laser pump 80−69424
coaxial relay current pulse generator for laser pumping 78−59014
colliding atoms, optical excitation to state of quasibound motion *(Russian)* 78−58784
colour centre laser pumped by flashlamp-pumped dye laser 80−102737
commercial dye laser design and pumping configurations 78−25889
complex molecules in solns., picosecond generation, spectral polarisation characts. *(Russian)* 77−10918
complex organic vapor lasers, new active media, buffering gas influence 79−94213
coumarin derivatives in simple dye laser, pumping by N_2^+ ion laser 78−74903

optical pumping continued
coumarin dye laser, flashlamp-pumped, picosecond pulses at 520 nm *(French)* 78−42335
coumarin dye laser, mode-locked flashlamp pumped, tunable blue ps pulses 79−13974
coupled Doppler-broadened system, laser induced transients 77−3325
cumarine derivatives, stimulated emission by laser and lamp excitation 79−72563
cumulative resonance in atomic ground state induced by modulated light field 78−66518
CW far IR waveguide lasers, high power, scaling 77−54731
CW intracavity dye laser spectroscopy, enhancement, pumping power depend. 80−13155
CW optically pumped far IR laser performance, determinative molecular parameters 80−69377
CW optically pumped far IR waveguide lasers, high-power operation and scaling 77−38949
cyanine dye laser excitation by giant single pulses *(Russian)* 78−46596
3-cyano-4-methylumbelliferone in ethanol containing water, acid or alkali, laser emission 79−955
cycles of pumping, inclusion of spontaneous emission, semiclassical calcs. 79−35586
degenerate four-wave mixing, time-reversed phase-front generation theory 79−59751
degenerate four-wave phase conjugation, signal-pump detuning effects 80−78895
degenerate parametric generation from quantum noise, photon statistics 79−81398
depolarised radiation, stimulated scattering, wave front reversal effect 79−86217
1,4-di(2-benzoxazolyl)-benzene vapour lasers, generating capacity, stimulated emission *(Russian)* 77−679
diatomic molecule, ground state, opt. prod. and orientation, review *(Russian)* 79−27046
diatomic molecule, two identical 3-level atoms, excitation spectrum 80−23476
diatomic molecules, optical orientation under circularly polarised laser excitation 77−65443
dichloromethane, CD_2Cl_2, CW optically pumped, submm. laser action, 100 to 900 μm 79−929
dideuteroacetylene, optically pumped laser action, 17.4 to 20.5 μm 79−935
7-diethylamino-4-methylcoumarin acriflavine binary soln., stimulated emission 77−50670
diffraction-limited CW optically-pumped far IR lasers, beam characts. 77−38953
1,1-difluoroethane, unimol. decomposition, direct meas. via IR laser photolysis, collision effects 79−57254
1,2-difluoroethane in Ar matrix, IR hole burning and lineshape, vibr. transition 79−76425
cis-1,2-difluoroethene, CO_2 laser pumped, CW far IR laser lines 80−69372
1,1-difluoroethylene, complete freq. coverage for submm. laser spectroscopy 78−25860
1,1-difluoroethylene, optically pumped, far IR laser line assignment 79−31865
1,1-difluoroethylene, optically pumped mm laser transition assignments 78−42328
difluoroethylene, submm. wave amplification 78−29941
cis-1,2-difluoroethylene laser, far IR CW optically pumped 80−69368
1,1-difluoroethylene submillimetric wave emission assignments 80−102708
difluoromethane, optically pumped, CW far IR laser line frequencies 80−102706
difluoromethane, optically pumped, efficient CW far IR laser action obs. 79−928
difluoromethane, optically pumped by CO_2 laser, new CW FIR lines 79−94219
difluoromethane far IR laser gas, CW laser pumped, gain 80−69367
difluoromethane laser, optically pumped, FIR lines, performance efficiency 79−94220
dimethyl sulphoxide, high efficiency stimulated Raman scatt. source *(Chinese)* 80−87433
diphenyl with pyrene cryst., self induced transparency self stimulated excitation *(Russian)* 80−14403
2-4-diphenylyl-5-phenyloxazole vapour lasers, generating capacity, stimulated emission *(Russian)* 77−679
dipole transition, transient behaviour in intense laser field *(German)* 78−66520
dispersive medium, incoherent, coherent stimulated Raman scatt. with multimode pump *(Russian)* 80−38063
DODCI, lifetime of optically stimulated dyes, generation of time correlated picosecond laser pulses *(German)* 79−27045
Doppler-free Raman spectroscopy and suppression of laser-induced mol. Doppler broadened transitions 80−9638
doubly resonant 4-photon-oscillator, phasemismatching and double refr., threshold pump power *(German)* 78−22166
dressed atom system, energy levels and reson. phenomena, universal algorithm 80−69111
dressed atom system, phase represent. applic. to reson. fluoresc., universal algorithm 80−69112
dressed molecule, RF field, saturated absorpt. obs. 80−9648
dye, excited singlet-state absorpt. effect on lasing 78−17930
dye, lasing and amplified spontaneous emission on excitation by high-power N_2 laser *(Russian)* 78−25869
dye accessory invertor for LG-21 serial N_2 laser 77−68224
dye active solution, conical scatt. of laser beams 79−94294
dye amplifier, high average power, efficient, pumping by Cu vapour laser 77−88755
dye CW laser, mode locking using externally modulated pumping laser 79−18456
dye DFB laser, line narrowing and wavelength stabilisation technique 77−88783
dye DFB laser, N_2 laser pumped, external mirror effect on characts. 78−42352
dye DFB laser, N_2 laser pumped, self Q-switched, tunable picosecond pulse generation 80−69432
dye DFB laser, N_2 laser pumped, tunable single ps pulse generation 79−55147
dye gas laser, excitation by elec. discharge, electron beams, optical stimulation *(Czech)* 78−79016

optical pumping continued
dye in contact with Ag film, enhanced total refl. with surface plasmons 79−59694
dye IR laser, Nd:YAG laser pumped, continuously tunable 10810 to 12160 Å 78−22139
dye jet laser, pumping by Cu vap. laser 77−7128
dye laser, actively mode-locked, flashlamp pumped, streak camera obs. of pulses 78−22158
dye laser, by high power Ar^+ laser, CW 77−7130
dye laser, by hollow or coaxial pulse tubes, comparison *(Russian)* 77−83870
dye laser, by N_2 laser, spectral narrowing 78−25903
dye laser, by wall ablation lamps, high energy design 78−29961
dye laser, coaxial flashlamp pumped *(Chinese)* 79−55144
dye laser, CW, emission freq. shift due to pump intensity changes 77−79817
dye laser, CW, output power, effects of gaussian depend. of fields 79−952
dye laser, CW, pumped, stable multifreq. picosecond pulse emission, phase-locked radiation pumping 80−91789
dye laser, CW, synchronous pumping and passive mode-locking, for picosecond pulse generation 79−3727
dye laser, CW, technology developments and appl. 80−43383
dye laser, cylindrical active element with sheath, radiation intensity distrib. calc. 80−58531
dye laser, distrib. feedback formed by diverging pump laser beams, tuning curves 77−83893
dye laser, divergence of emitted radiation, excited transverse modes determ. 79−94228
dye laser, double mode-locked CW, pulse cross-correlation studies 80−69389
dye laser, double-wavelength, N_2 laser pumped 79−94241
dye laser, double-wavelength electro-optically tuned synchronously pumped mode-locked CW 79−89924
dye laser, efficient flashlamp pumped, driven by Marx-bank generator 77−19311
dye laser, efficient oscillator-amplifier, pumped by freq. doubled Nd:YAG laser 79−41389
dye laser, flash lamp pumped, tuning by grazing incidence grating technique 80−95914
dye laser, flashlamp pumped, freq. tunable ns duration pulses by pulsed Q-modulation 79−41403
dye laser, flashlamp pumped, injection locking without longit. mode matching 78−33760
dye laser, flashlamp pumped intense subnanosecond pulse generation, 0.58 to 0.80 μm 78−90422
dye laser, flashlamp pumping 78−29970
dye laser, flashlamp-pumped, two-stage amplification, for SHG 78−74922
dye laser, flashlamp-pumped high-energy, spectral narrowing by two-stage injection locking 79−81450
dye laser, four-fold symm. pumplight geometry 77−88756
dye laser, freq. shifting using stimulated Raman scatt. in H_2, tunable UV source 80−9963
dye laser, heating effect minimization 80−1198
dye laser, high average power, pumped by vortex stabilized flashlamp 77−14749
dye laser, high-power, longit. pumping by Nd:YAG and dye lasers 77−3612
dye laser, injection-locked pumped by Xe ion laser, 4-mirror ring-cavity 80−48280
dye laser, N_2 laser pumped, narrow linewidth short pulse operation 79−971
dye laser, N_2 laser pumped, single mode operation 78−87060
dye laser, N_2 laser pumped, tunable ultrashort light pulse generation *(German)* 79−27275
dye laser, N_2 laser pumped, two wavelength outputs with orthogonal polarisations 78−50792
dye laser, N_2 laser-pumped, subns. relax. oscills. 78−82959
dye laser, N_2-pumped subnanosecond pulse generation, design 80−87403
dye laser, narrow-band pulsed, for nonlinear spectroscopy, pumping by Nd:YAG laser 80−53318
dye laser, open dye stream, pumped by pulsed Xe ion laser 79−81448
dye laser, optically pumped, threshold singularities 79−3703
dye laser, PMMA modular matrix pulse width influence on power output 80−28247
dye laser, power scaling effects under high power laser excitation 78−46595
dye laser, production of tunable picosecond pulses 79−22976
dye laser, pulsed, high efficiency flash lamps as pumping sources 77−14710
dye laser, pulsed output, mode locking with synchronous-pumping 80−5760
dye laser, pumped by N_2 laser, short tunable pulses 77−7126
dye laser, pumped generation by UV N_2 laser in 420-470 nm range *(Russian)* 77−88719
dye laser, pumping by N_2 or Xe laser or flashlamp *(Japanese)* 77−58341
dye laser, radial distrib. of pumping in coaxial cell with external irrad. 80−53308
dye laser, reliable thyratron switched flashlamp pumped 79−31930
dye laser, rhodamine 6G in aq. and alcohol solns., thermooptical inhomogeneities, μ second pumping 77−75501
dye laser, self-injected laser-pumped, nanosecond pulse generation by cavity flipping 79−18457
dye laser, short resonantor, tunable, pumped by travelling wave N_2 laser 80−48291
dye laser, simmer-enhanced flashlamp-pumped, efficiency improvement 79−64240
dye laser, spark pumped compact modular design with high peak power 77−10950
dye laser, subpicosecond, directly pumped by mode-locked Ar laser, pulse train autocorrelation traces 79−22969
dye laser, synchronously pumped mode-locked CW system, pulse characts., cavity detuning effect 79−3726
dye laser, tunable, flashlamp excited, triplet quenching effect 79−31892
dye laser, tunable, flashlamp pumped, ultra-narrow bandwidth 80−9897
dye laser, tunable, N_2-laser pumped, using single prism beam expander *(Chinese)* 80−74389
dye laser, tunable emission by pumping with Nd:YAG laser 79−950

optical pumping continued
dye laser, tunable in 1.1 μm range, 13 MW peak power, Nd:YAG laser pump 79−86190
dye laser, tunable IR, IR N_2 laser as pump 77−61969
dye laser, tunable ultrashort pulse generation 80−95931
dye laser, unstable ring resonator, N_2 laser pumped 80−53326
dye laser, using lysozyme soln., threshold power for laser operation 79−68391
dye laser, UV, optically pumped by CO_2-laser-produced plasma 77−61947
dye laser, with high levels of coherent excitation, lasing characteristics 80−28229
dye laser, Xe ion laser pumped, tunable output in blue region 78−46621
dye laser design for nonlinear spectroscopy, cavity and ruby pumping laser 77−79852
dye laser development, gas phase 79−958
dye laser efficient emission charact., pumping at 248 nm with KrF* discharge laser 79−954
dye laser multiple system, flashlamp pumped, energy transfer 77−88720
dye laser oscillator-amplifier system second harmonic generation using laser-flashlamp hybrid pumping 80−14359
dye laser picosecond pulse generation, excitation by passively mode locked Ar laser 80−95930
dye laser pumping, charact. using KrF excimer laser at 248 nm 80−1199
dye laser pumping, inductive storage bank transfer to flash lamp discharge 80−5742
dye laser pumping by Nd:YAG laser freq. doubled output 78−59090
dye laser synchronisation, CW laser injection, spectral purity *(French)* 78−63118
dye laser system, flash lamp pumped, involute-related coupling reflector design 78−90425
dye laser tunable oscillator-amplifier system, N_2 laser pumped *(Japanese)* 79−68406
dye laser tuning range extension using electrochem. reaction products 79−31895
dye lasers, approx. analytic solns. 79−31890
dye lasers, flash lamp pumped, mode locking, picosecond, pulse generation 78−71131
dye lasers, flashlamp and laser pumping, review 77−38884
dye lasers, pumped by gas and solid-state lasers, review 77−10915
dye lasers, synchronous pumping, extension of spectral range 80−5731
dye lasers, tunable narrow bandwidth 2 MW, pumped by KrF* discharge laser 79−41378
dye lasers pumped by XeCl excimer laser 79−59691
dye lasers pumped by XeF, KrF excimer lasers *(Chinese)* 80−1234
dye lasers with tube pumping, spectral kinetics *(Russian)* 77−46719
dye oscillator-amplifier system, high power, pumped by Nd-YAG laser 79−18443
dye picosecond laser, tunable in 1.1 μm region, Nd:YAG laser pump 79−86191
dye ring laser, flashlamp pumped, injection of N_2 laser excited oscillator beam 80−5754
dye solution, excitation conditions effect on lasing, discharge source 77−3582
dye solution, laser illuminated, light field phase conjugation, nonlinear interactions *(Russian)* 80−28266
dye solution, nonlinear fluoresc. meas., two-photon pumping by low power laser 80−48037
dye solutions, amplified spontaneous emission with picosecond light pulses 78−82965
dye solutions, flashlamp-pumped, thermal effects 77−10917
dye solutions and their mixtures, excitation by Cu vapour laser, laser action 80−28230
dye synchronously pumped laser combined with external compressor, sub-ps pulse generation 79−55148
dye UV laser, tunable picosecond, pumped by Nd:YAG laser third harmonic 79−31927
dye UV lasers pumped by KrF, XeBr excimer lasers 79−10301
dye vapour pumped by N_2 laser, fluorescence and amplified spontaneous emission charact. 79−3694
dyes, 266 nm pumped, tuning ranges in near UV, 390 to 333 nm 80−48239
dyes, 355 nm pumped, tuning ranges from 410 to 715 nm 79−76683
dyes, optical pumping by gigawatt monopulse laser radiation 79−55133
dyes for tunable lasers, intersystem crossing rates and saturation parameters in triplet state 77−36280
electron scattering by Coulomb potential in Born approx., bremsstrahlung statistics 80−5665
electron spin polarised targets for polarised ion beam prod. 80−27851
emission kinetics of solutions of complex organic compounds for pumping with linearly polarised radiation *(Russian)* 77−83872
emulsion dye laser, pumped by N_2 laser 79−13962
energy level transitions, excitation by monochromatic laser radiation, Doppler-broadened transitions 80−78582
energy transfer dye lasers and laser induced intermol. and intramol. energy transfer processes 80−9647
energy trap, atomic device 77−88604
esculin in ethanol, coherent pumping, intracavity absorpt. anal. method sensitivity 79−57328
ethyl iodide submillimeter wave laser, optically pumped 80−87376
ethylene, excited with parametric oscillator, vibr. relax. obs. and interpret. 80−9702
ethylene, line selective excitation with CO_2 laser light and vibr. relax. 80−9705
ethylene, off-reson. IR laser action without population inversion, Raman type transition 77−10891
ethylene dimer, CO_2 laser induced photodissoc., pulsed mol. beam obs., van der Waals bond 80−9660
excimer lasers, optically pumped CW 80−14322
far IR CW lasers, optically pumped, review 78−46588
far IR CW optically pumped lasers, simple accurate method for wavelength meas. 80−106554
far IR CW waveguide laser, CO_2 laser pumped, efficiency high-power operation 77−10937
far IR gas laser pump line, optoacoustic determ. 79−31872
far IR gas lasers, common resonator with CO_2 pump laser 77−38950
far IR laser, electronic tuning and phase-locking 78−59055
far IR laser, pump radiation self-focusing and defocusing 78−79003
far IR laser design and performance, review 79−31917

optical pumping continued
far IR laser gases, CW laser pumped, saturated and small-signal gain calc. 80−58521
far IR laser lines, optically pumped, atm. transmission 77−19237
far IR lasers, optically pumped, frequency modulated noise measurements 78−55392
far IR oscillator, optically pumped, parametric study 80−95862
far IR pulsed lasers 78−46589
far IR receiver optical preamplifier 77−39068
far IR waveguide laser cavity design criteria 77−38951
fast atomic beam, optical reson. detect. by at. fluoresc. 80−102479
fast discharge-pumped visible and UV lasers *(Chinese)* 79−72559
feedback laser fusion using direct nucl. pumped laser 78−58445
FIR laser pump lasers, variable-frequency stabilisation 79−14005
flash lamp drive circuit discharge currents, Fourier anal. 80−23695
flash lamp high-power radiation for laser pumping, interaction with cooling fluid 78−13718
flash lamp pumping of lasers, optimal lamp filling, review *(Russian)* 78−63123
flash lamp pumping of rectangular cross section active elements, efficiency 77−695
flash lamp pumping source for lasers 77−50679
flash tube as laser pump source, discharge brightness radial profile 77−692
flashlamp drive circuit optimisation for lasers 77−75534
flashlamp-pumped dye lasers, 100 W 77−19334
flashlamps, coaxial and preionised linear, comparison as pumping sources for high power dye lasers 80−102730
fluorol 7GA dye laser, flashlamp pumped passive mode-locking 77−38922
fluoromethane, 496 μm high-power smooth-pulse laser systems 77−19332
fluoromethane, $^{12}CH_3F$, far IR CW laser emission by optical pumping 79−3687
fluoromethane, $^{12}CH_3F$, far IR Raman laser line obs., CO_2 laser pumping 80−69381
fluoromethane, and other optically pumped lasers, dynamic Stark effect 78−17911
fluoromethane, angular correlation between far IR emission and CO_2 pump radiation. Dicke superradiance theory 79−41370
fluoromethane, excited state rot. spectroscopy and kinetics, appl. of tunable sub-MM sources 80−14162
fluoromethane, laser excitation, energy storage and vibr. heating 77−58137
fluoromethane, laser pumped, overtone fluoresc., intermode energy flow 78−37673
fluoromethane, laser pumped, vibr. states collision dynamics fluoresc. obs. 80−53104
fluoromethane, laser pumping effects, translational and vibr. energy distribs. 79−844
fluoromethane, laser submillimetre with optical pumping energy yield, emission pulse delay time depend. on pumping pulse *(Russian)* 78−71088
fluoromethane, molecular pumping, thermal lens phenomena 80−9708
fluoromethane, near-MM-wave laser synchronous pumping, ultrashort pulse generation at 496, 193 μm 80−102705
fluoromethane, optical pumping of far-IR molecular lasers by CW CO_2 waveguide laser 80−83615
fluoromethane, single-mode optical pumping, superradiant far IR emission 78−42329
fluoromethane, two photon generated lasing, effect of pressure 77−88703
fluoromethane+O_2, laser induced translational-vibr. energy conversion obs. 79−72396
fluoromethane+SF_6(CS_2), fluoromethane laser, buffer gases collisional narrowing 80−99710
fluoromethane DFB gas laser, construction and operation 80−23715
fluoromethane high-power laser, tuning behaviour 80−63994
fluoromethane laser, optically pumped far-IR waveguide, output, temp. depend. 80−58512
fluoromethane laser, synchronously pumped, subnanosec. transients 79−89891
fluoromethane laser diagnostics using two CO_2 laser pump pulses 79−31869
fluoromethane optically pumped far IR lasers, 604 GHz, developments 77−83882
fluoromethane optically pumped molecular laser, relax. oscills. 80−95875
fluoromethane TEM_{00} far IR laser with integrated pump laser 80−43348
fluoromethane TEM_{00} far IR laser with integrated pump laser 80−58578
fluoromethane-^{13}C, pulsed far IR emission 80−69370
fluoromethane-^{13}C optically pumped molecular laser, relax. oscills. 80−95875
fluoromethane-d_3, vibr. energy transfer at low temps., inert gas and N_2 matrix obs. 80−9706
fluoromethane-SF_6 496-μm optically pumped laser, energy-transfer mechanisms 80−99712
formaldehyde, D_2CO, HDCO, CW optically pumped laser action 77−88700
formaldehyde, laser-induced fluorescence, rad. transition rates from two vibronic levels 77−3400
formaldehyde, multiphoton dissoc. by CO_2 laser, intensity/fluence depend. 80−11913
formaldehyde-d_2 733 μm line, Autler-Townes effect in laser interacting with RF field 80−53269
formaldehyde-d (d_2) submillimetre lasers, optically pumped, assignment of laser lines 80−58513
formic acid, far IR laser gas absorption obs. with and without DC field 79−31870
formic acid, laser transitions near 5.6 μm, HF laser optical pump 78−58995
formic acid, optically pumped by pulsed HF laser, emission obs. at 5.7μm 79−50283
formic acid laser, CW CO_2 laser pumped, far IR lines accurate meas. 77−88714
formic acid laser far IR pulse generation by Q-switched CO_2 laser pump source 80−69383
four-photon processes stimulated by fluctuating pump in dispersive medium 79−23017
Freon 14, optically pumped roto-vibr. mol. laser, low temp. operation and performance 79−50315

optical pumping continued
Freon 14, roto-vibr. mol. laser, low-temp. performance 80−9871
frequency up-conversion with stochastic pumping, exactly soluble model 80−23744
fused quartz flashlamps, correlation between static stress distrib. and explosion energy 77−10931
p-GaAs, spin relaxation of photoelectrons 77−85207
GaAs-$Ga_{1-x}Al_xAs$ DH crystals, <110> oriented dark line defects 77−80510
gain measurement in optically pumped materials, diffr. effect 77−19225
gas, resonance four-photon shift, optimal focusing of high-power pumping 80−95574
gas, third harmonic resonant generation, exact theory *(Russian)* 79−76763
gas cooling method, laser pumping followed by reradiation at higher freq. transitions 79−827
gas laser, atomic constants and collision cross sections determ. by level crossing 78−50763
gas laser, CW sub-mm, scaling 78−55341
gas laser, far-IR, optically pumped, operation, appl. of opto-acoustic effect 77−31105
gas laser, modulation method, for relative excitation level, cavity bandwidth and at. temp 80−5771
gas laser, synchronous mode-locked pumping, mode-locked far IR pulse generation 79−27271
gas laser, two-photon spatially periodic pumping, excitation threshold and output power *(Russian)* 78−13693
gas laser with wide-band optical pumping, review 79−31885
gas lasers, by CO_2 lasers, submillimetre wavelength tables 77−7095
gas lasers, mid IR output 79−22961
gas lasers, optically pumped IR, book contrib. 77−46718
glass disc amplifier output stages, energy characts. for silicate and phosphate glasses 79−64237
glass laser rods, silicate and phosphate, pumped in pseudoelliptic cavities, thermal effects 79−76692
ground state alkali molecules, mag. shielding and spin-rot. interaction 80−87186
Group VIA photolytic laser systems, for fusion research 78−59002
N-heterocyclics, radiationless transitions, vibronic coupling effect 78−33543
high gain amplifiers, gain meas. technique 80−1208
high-repetition-rate short-pulse gas discharge for discharge pumping gas lasers 80−1233
hole burning, photophysical and photochemical theories 80−58322
homonuclear molecules, vibrs. excitation by IR radiation 80−28068
incoherent resonance decay and coherent optical ringing from coherently prepared electronic states 77−10698
inert gas atom+diatomic molecule, collision in laser field, vibr. excitation 78−86937
interstellar H_2O maser sources, near IR pumping 77−78862
interstellar type I OH masers, radio and IR obs. rel. to pump models 79−25671
iodomethane, and deuterated, submm. wave amplification 78−29941
iodomethane, laser characts. with transverse optical pumping *(Russian)* 79−50286
iodomethane, laser submillimetre with optical pumping energy yield, emission pulse delay time depend. on pumping pulse *(Russian)* 78−71088
iodomethane, RF field dressed mol. saturated absorpt. obs. 80−9648
iodotrifluoromethane, high vibr. state excitation in high-power laser field, spectral characts. 80−91562
ion, electromagnetically confined, laser cooled, double resonance and optical pumping 80−87155
IR active molecules, homogeneous excitation by laser pulses 78−9202
IR Doppler free molecular spectroscopy, two photon coherence and pumping 80−48052
IR gas lasers 77−58348
IR laser, appl. of CO_2 laser amplifier pump 78−63133
isotope separation, by selective laser-induced mol. vibr. excitation effect on reaction kinetics 78−33627
jet stream dye laser, mode locked synchronous pumping, near IR ps pulses 78−17948
ketocyanine dye, lasing under lamp excitation 78−82964
laminated active laser element, thermal stresses produced by longit. nonuniform pumping *(Russian)* 78−5474
laser, double-current-confinement channelled-substrate struct., near-field and beam-waist position 80−106553
laser, far IR, injection phase locking 80−69431
laser, far IR optically pumped, monitoring by piezoelec. transducers 80−102729
laser, far IR optically pumped, output power, temp. depend. 79−59674
laser, pulsed broadly tunable IR, excited by N_2 pumped dye laser 79−76706
laser dye, saturable absorber props., stimulated propag. of pump flux 79−41377
laser dyes, inert gas halide laser pumped, photochem. stability 78−33733
laser far IR pulse generation by Q-switched CO_2 laser pump source 80−69383
laser far IR waveguide cavities, coherently pumped, geometrical design criteria 77−54739
laser generation energy changes, rel. to luminous intensity of pumping lamp *(Russian)* 77−68214
laser pulses, double, generation, gradual cutting-off resonator losses 80−69433
laser pump, active medium and interference coating effect, temp. profile, electro-optical characts. 77−19275
laser pump fluctuations, influence on resonance fluoresc. radiation intensity correlation 80−37981
laser pump sources, efficiency of Xe and Kr arc discharges 80−64812
laser pump system, analytical theory 80−106540
laser pumping by pulsed lamp *(Russian)* 78−22138
laser pumping system, thermodynamic calc. method 80−58551
laser specific and thermal reactions classifications 80−11919
laser spectroscopy of unstable isotopes, nucl. props. determ. from atomic spectra using fast beams 80−9720
laser three-photon transition theory 80−102690
laser utilizing self-terminating transitions, CW stimulated emission possibility 80−14329
laser-controlled unimolecular and bimolecular processes, field-depend. rate const. 80−11906
laser-excited atoms deflection by elec. field, isotope separation appl. 78−955

optical pumping continued
laser-induced chemical processes, optical selection of reagent orientation 80−11914
laser-induced processes in molecules, conf., Edinburgh, Scotland (Sept. 1978) 80−9577
light beam interaction with atomic system, description by irreducible tensorial sets 77−68195
magnetometer, optically pumped, design, characts. and development 79−93177
medium with varying energy level populations, evolution of coherent radn. probing pulse 79−76755
metal, self-limiting transitions, laser excitation, pulse freq. anal. *(Russian)* 78−66516
metal complexes containing methyleneiminobisacetic acid group 77−58324
methane, energy transfer obs. using excitation of fund., overtone and combination bands 80−9704
methane backward Raman amplifier, KrF laser driven, high-efficiency energy extraction 80−106533
methanol, CD_2HOH, CH_2DOH, CW optically pumped, submm. laser action, 100 to 900 μm 79−929
methanol, CH_3OH and CD_3OH, far IR laser lines, optically pumped by CO_2 laser 78−90415
methanol, CW far IR laser frequency characteristics 77−38873
methanol, far IR laser gas absorption obs. with and without DC field 79−31870
methanol, far IR laser line obs. and assignment 79−31867
methanol, far IR laser lines meas. and assignments 79−22939
methanol, far IR laser lines pumped by CO_2 laser sequence lines 78−9369
methanol, far IR laser transitions, small signal gain meas. 78−22114
methanol, optical pumping of far-IR molecular lasers by CW CO_2 waveguide laser 80−83615
methanol, optically pumped CW subMM emission lines 80−95876
methanol, pumping by narrow band CO_2 TEA laser 77−54729
methanol, submm. wave amplification 78−29941
methanol 70 and 118 μm laser line diagnostic expts. 80−69387
methanol assignment of weak FIR laser lines 80−14320
methanol CW optically pumped waveguide far IR laser, 10 to 100 mW, design and perform. 79−31934
methanol far IR laser, optically pumped, Stark effects 79−72552
methanol far IR laser, twin optically pumped, for plasma diagnostics 80−59306
methanol far IR laser gas, CW laser pumped, gain 80−69367
methanol far IR laser line Stark splitting obs. 80−58313
methanol far IR Stark spectroscopy and 9-P(34) CO_2 laser line 80−69145
methanol far-IR laser, optically pumped, intracavity polarization modulation 80−23726
methanol laser, CW, optically pumped, 170-μm emission, press. shift 80−106510
methanol laser, optically pumped, use of crystalline reflector in cavity 80−64080
methanol optically pumped 118.8 μm laser line, Stark splitting obs. 80−102710
methanol subMM laser line obs. 80−58523
methanol twin optically pumped far IR laser for plasma diagnostics 80−103189
methanol-d_1, CH_2DOH optically pumped CW far IR laser lines and frequencies 80−102707
methanol-d_1, CO_2 laser pumped, CW far IR laser lines 79−76672
methanol-d_3, CO_2 laser pumped, CW far IR laser lines obs., 34.5 to 287 μm 78−71082
methanol-d_3, CW far IR laser lines obs. 78−79005
methanol-d_x, optically pumped, new FIR laser lines 79−72553
methanol-d, CO_2 laser pumped, CW laser lines obs. 80−53272
methanol-d, optically pumped CW subMM emission lines 80−95876
methyl alcohol, and deuterated forms, complete freq. coverage for submm. laser spectroscopy 78−25860
methyl alcohol, optically pumped, far IR laser line assignment 77−38869
methyl alcohol, optically pumped, new CW FIR laser lines meas. and assignments 80−48224
methyl alcohol high-power optically-pumped CW laser line assignment 77−38868
methyl alcohol IR absorption, diode laser obs. 79−31518
methyl alcohol submm wave laser, optically pumped, intracavity double resonance obs. 80−58522
methyl alcohol-d, optically-pumped laser line freqs. 78−55345
methyl bromide, sub mm laser, generation lines identification *(Russian)* 78−82952
methyl bromide, submillimeter rotational spectrum, laser generation line identification 79−64210
methyl chloride, far IR laser lines, vibr. isotopic shift value 78−42055
methyl cyanide, far IR laser line assignments 80−69380
methyl cyanide, intracavity pumped submm wave laser, CW 77−88741
methyl cyanide submillimetric waveguide laser amplifier design and operation 77−38926
methyl fluoride, $^{13}CH_3F$, high-power pulsed laser 80−69386
methyl fluoride, deuterated, optically pumped near-MM laser 80−69379
methyl fluoride, Dicke superradiance obs. in far IR emission 77−38841
methyl fluoride, mirrorless laser at 496 μm 79−31871
methyl fluoride, stimulated emission at 9.75 μm following two-photon excitation 78−42323
methyl fluoride laser far IR pulse generation by Q-switched CO_2 laser pump source 80−69383
methyl fluoride Raman FIR laser, high-intensity CO_2 laser pumping, new emission lines 80−23675
methyl fluoride-d_3, optically pumped sub-MM wave laser 80−23676
methyl halides, candidate transition identification for optically pumped far IR lasers 79−931
methyl iodide, and deuterated, pulsed subMM lasers pumped by CO_2 laser 80−106511
methyl mercaptan, CW subMM emission lines, optical pumping 80−87381
methyl nitrile CW for IR mol. laser, optical pumping with $^{16}CO_2$ and $^{18}CO_2$ lasers 80−74343
methylfluoride, CW for IR mol. laser, optical pumping with $^{16}CO_2$ and $^{18}CO_2$ lasers 80−74343
Michelson output coupler with one-dimensional grid, for optically pumped near MM laser 80−58555

optical pumping continued
millimetric-wave high-power optically-pumped laser performance and applic. 78−5469
millimetric-wave optically-pumped laser CW performance 78−5468
molecular beam, laser-induced alignment 77−31025
molecular energy level transitions, excitation by monochromatic laser radiation, Doppler-broadened transitions 80−78582
molecular excitation, laser induced, effect of chem. reactions 78−21979
molecular excitation, quantum nonlinear oscillator model 78−50743
molecular gas, laser irrad., field avoided crossings, new transition channels 78−33477
molecular IR multilevel absorpt., field broadening and pump line selection effects 77−46599
molecular laser, optical pumping in damped photodissoc. wave propag. in dense gas 80−99714
molecular laser, optically pumped, review 80−58519
molecular laser development 78−13732
molecular lasers, 11-17 μm 78−46581
molecular lasers, IR-FIR transferred Lamb-dip, standing wave saturation effects 80−58520
molecular lasers, laser pumped, theory 79−36868
molecular lasers, laser pumping, dispersion 80−87375
molecular lasers, optically pumped, polarisation phenomena appl. 80−87384
molecular nonlinear vibrations, selective laser excitation 77−23522
molecular nonsteady-state luminesc. behaviour under narrowband laser excitation 80−87159
molecular species in defined quantum states, laser studies of relax. and reaction 80−11918
molecular system collision initiated by IR laser absorpt., vibr. inversion 77−10707
molecular vibration, coherent, parametric excitation 79−18241
molecular vibrations, coherent excitation dynamics, many-photon resonances 79−27050
molecule, collision-induced emission with laser irrad., cooperative chemical and optical pumping 78−22012
molecule, Doppler-free fluorescence induced by strong quasi-resonant laser field 79−41193
molecule, laser excitation of higher levels, weakly anharmonic oscillator model *(Russian)* 77−46603
molecule, reson. interaction with laser field, nonperturbative theory 77−442
molecule, spherical-top, rot.-vibr. transition moments in excited states 78−25639
molecules, inversion to ground state by optical pumping 79−45681
molecules, photoselection with intense laser pulses 78−66606
molecules excited by laser IR radiation, excited fraction determ. 80−78661
monochromatic laser radiation, excitation of atomic, mol. energy level transitions, inhomogeneous and mixed line broadening 78−55147
monochromatic laser radiation, excitation of atomic or mol. energy level transitions, strictly homogeneous line broadening 78−58629
multi-level excitation theory, analytic approximations 78−29922
multilevel atom, laser excitation, rot. wave approx. and calcs. 77−10708
multilevel molecular system, coherent pulse propag. effects 80−9968
multilevel molecules, laser excitation, rot. wave approx. and calcs. 77−10708
multilevel system, band type, excitation dynamics in laser field *(Russian)* 78−21980
multilevel system, laser excitation, Wilcox-Lamb rate eqn. approx. 79−27028
multilevel system, nontransient phase coherent light absorpt. effects 77−498
multiphoton cross-section determination by means of luminescence experiments 80−93377
multiphoton excitation in strong fields, rate eqns. 79−81185
multiphoton ionisation, simple model, transition rates 80−953
multistep laser excitation, pulse modulation, Schrodinger eqn. anal. 78−63046
N-level system in strong monochromatic field 78−29923
Na_2, laser-excited, emission bands obs. in visible and IR 80−48036
near MM wave laser synchronous pumping, ultrashort pulse generation 80−69385
nitromethane+H_2 reaction, CO_2 laser initiated, mechanism and yield 80−11912
non-equilibrium superconductors, formation of inhomogeneity 78−52150
nonequilibrium dissoc., Morse oscill. rigid rotator system, master eqn. soln. 80−40682
nonequilibrium semiconductor with electron-hole pairing, mag. moment quantum oscills. *(Russian)* 77−28131
nonequilibrium superconductor, optical pumping, transition point *(Russian)* 77−12064
nonequilibrium superconductor with optical and tunnel quasiparticle pumping, threshold instability and inhomogeneous states *(Russian)* 79−87209
nonequilibrium superconductors, crit. intensity of optical pumping, temp. depend. *(Russian)* 79−7933
nonlinear optical processes in atoms and mols. using inert gas halide lasers 79−59745
nonlinear quantum oscillator, stochastic instability 79−85007
nonlinear selection of optical radiation on refl. from stimulated Mandelstam-Brillouin scatt. mirror *(Russian)* 80−28280
nonresonant excitation, ensemble of two-level systems, rel. to multiphoton spectra, polyatomic mols. 80−5585
nuclear pumped laser, fusion reactor feedback 79−13516
nucleic acid-dye complexes, energy transfer obs. using laser-induced fluoresc. 80−12054
opaque region, asymptotic limit to optical pumping 79−70947
organic compound solution lasers, polarisation diagrams *(Russian)* 77−88721
organic compounds lasers, induced pump absorption, lasing threshold and efficiency 78−50773
organic molecules, polyatomic, stimulated emission, laser spectral kinetics 79−55132
organic solutions, lasing, excitation by excimer laser radiation 80−64007
Orion methanol masers, evidence for IR pumping from interferometric and multitransitional study 80−67891
over-pumping energy effect, two interfering beams in nonlinear medium *(Russian)* 77−7161
oxazine 1 and 9 laser dyes, absorpt. and gain with picosecond pumping 79−55134

optical pumping continued
parametric amplification, four-wave, two-photon reson. 80−48341
parametric frequency up-conversion with stochastic pumping, canonical model 80−53368
parametric interaction of travelling and pump accompanied waves, induced scattering by polaritons *(Russian)* 79−3739
pentacene, narrow band laser excitation, fluoresc. decay, optical free induction, dipole moment 78−21956
phase-conjugate reflection using TEM_{00} pump beam 80−48327
phasematching of freq.-conversion processes induced by additional selective pump 80−28271
phenyloxadiazole derivatives, dye laser, pumped by KrF laser, 3500 Å range 77−42532
phenyloxazolyl pyridinium salt dye lasers, flashlamp pumped, blue-greenlasing 80−95886
phosphate glasses, laser props. under pulse-periodic pumping conditions 79−64236
photochemistry in solid state, IR lasers appl. 80−11929
photofragment spectroscopy of mol. ions using fast ion beams 80−9755
photon antibunching in single atom fluoresc., rel. to wave packet reduction in detection process 80−52928
photon detector for subMM wavelengths using Rydberg atoms 80−77867
phthalimides, stimulated radn. with lamp pumping *(Russian)* 79−51987
polarisation beam splitters for F II-centre laser pumping 79−45960
polarisation spectroscopy and forward scatt., in Na gas 80−52336
polyatomic gas, laser-induced rate processes, intermol. and intramol. relax. formalism 79−27070
polyatomic mol. gas, laser-induced rate processes, collision-free dynamics 77−30934
polyatomic molecule, anharmonic model for mol. photoexcitation 80−9669
polyatomic molecule, collisionless multiphoton dissoc., threshold behaviour, nonthermal theory 80−11905
polyatomic molecule, high vibr. level excitation and dissoc. in laser field *(Russian)* 77−27132
polyatomic molecule, multiphoton absorpt. resons., dynamic Stark splitting 80−9670
polyatomic molecule, multiphoton collisionless dissociation via intramolecular amplification 77−30936
polyatomic molecule, multiphoton dissoc. dynamics, classical model 80−11904
polyatomic molecule, multiphoton excitation from many rot. states by IR laser pulse 78−21986
polyatomic molecule, multiple-photon IR laser pumping, collisional effects 80−9668
polyatomic molecule, ultrafast vibr. using laser light pulses 80−9699
polyatomic molecule, vibr. excitation in strong IR field, rot. level emptying *(Russian)* 77−75235
polyatomic molecules, IR laser sensitised chem. reactions 80−11910
polyatomic molecules, laser pumping effects, translational and vibr. energy distribs. 79−844
polyatomic molecules, multiphoton coherent excitation, two-photon vector model 77−61816
polyatomic molecules, multiphoton excitation, collisional deactivation, information theory anal. 78−90264
polyatomic molecules, multiple photon excitation, Bloch eqn. to rate eqn. transition 80−83437
polyatomic molecules excited by CO_2 laser pulses, stimulated emission *(Russian)* 79−94214
POPOP dye vapour laser excited by N_2 laser, temp. depend. 79−81423
POPOP dye vapour lasers, optical and electron beam pumping, review 80−48237
POPOP solution dye lasers, multiplate reflectors 80−83606
positive ions, RF spectroscopy, using optical pumping, review 78−1107
potassium halides, F-centres, optical pumping, spin-orbit and hyperfine coupling 77−16359
propynal, CW for IR mol. laser, optical pumping with $^{16}CO_2$ and $^{18}CO_2$ lasers 80−74343
propynal, IR photochem. in electronically excited state 80−11923
pulse forming network power source for electron-beam-controlled CO_2 laser 78−74928
pulse gas-discharge lamp appl. to optical pumping of YAG:Nd laser *(Bulgarian)* 78−33795
pulse time-reversal by four-wave mixing 80−91848
pulsed collinearly pumped far IR amplifier, rate analysis 79−81408
pulsed optically-pumped submillimetre-wave amplifier theory 79−31868
pump statistics conversion by parametric amplification of picosecond light pulses 80−99802
Q-switched laser pumping lamp trigger circuit 79−68403
quadraxial high repetition rate adapter for coaxial flashlamp pumping of laser dyes 79−45949
quantum magnetometer, alternating polarity modulating pulses, meas. errors *(Russian)* 80−90871
quantum nonlinear oscillator excitation by harmonic force, numerical computation 78−50743
p-quaterphenyl vapour laser, optically excited, laser action obs. at 350 nm 79−7123
quinoxaline, in p-dibromobenzene, triplet state NQR, nucl. spin polarisation effects 79−18208
Rabi oscillations, mag. sublevel degeneracy effects 78−63048
radiation problems, semiclassical theory 78−74684
Raman amplifier with broadband pumping, gain enhancement 80−43398
Raman effect, spontaneous, three-level system in intense laser fields 78−86802
Raman laser, external-resonator controlled, pumped by CW CO laser, mol. spectroscopy uses 80−9624
Raman spin-flip laser, multiply pumped, coherence effects 80−87398
randomly modulated pump, stimulated Raman scatt., method of successive approxs. 80−95951
rare earth:YAG crystal, laser freq. conversion by reson. pumping *(Russian)* 79−10314
resonance atom, spontaneous diffr. of light 80−91512
resonance light scattering, spectral props. and photon correls. 80−91510
resonance scattering methods in atomic spectroscopy 80−53167
resonant electronic-vibrational energy transfer and use in pumping IR mol. lasers 80−9700
resonant pumping, high-power, of molecular systems *(Russian)* 77−54690
rhodamine 6G, Cu vap. laser pumped, axial mode struct. 77−23671

optical pumping continued
rhodamine 6G, excited states prod. by direct and stepwise absorpt. of light 79−64055
rhodamine 6G, halo laser device 79−72597
rhodamine 6G, photoreaction mechanisms, effect of pumping spectral composition *(Russian)* 77−70323
rhodamine 6G dye in ethylene glycol, broadband optical diode, one directional traveling wave operation of ring laser 80−58606
rhodamine 6G laser, 33 W CW, multimode Ar laser pumped 77−61968
rhodamine 6G laser, pumping efficiency enhancement using luminesc. filters 77−38882
rhodamine 6G laser, radially nonuniform lamp pumping, lasing power 79−64220
rhodamine 6G laser, short-cavity, excited by electron beam pumped CdS laser 78−25887
rhodamine 6G laser amplifier pumped by N_2 laser, sub nsec pulse generation 80−1232
rhodamine 6G laser with lamp pumping, spatial coherence 77−50669
rhodamine 6G solns., acousto-optical distortions induced by pump lamp radn. 79−73898
rhodamine 6G solution laser, pulse tube pumping *(Russian)* 77−88785
rhodamine 6G water soln. laser with spatial lamp pumping, spatial coherent emission 78−82963
rhodamine 6G-isopropyl or ethyl alcohol solution, flashlamp pumped laser, photochem. effects 80−53287
rhodamine 6G-safranin-T mixed dye laser energy transfer, N_2 laser pumping source 80−58532
rhodamine 6Zh pulsed laser, simple transverse mode observation *(Russian)* 79−72565
rhodamine B activated waveguide, amplification of narrow-band signal 79−36930
rhodamine B dissolved in D_2O, electronic state two-stage excitation by light pulse 79−64056
rhodamine dye lasers, flashtube-pumped, calc. and expt. generated quantum power 78−50772
rhodamine G in ethanol, flash-lamp pumped, intracavity absorpt. anal. method sensitivity 79−57328
rhodamine G solutions, LiCl and $NaClO_4$ electrolyte influence on its lasing props. 80−91788
rhodamine GG tunable narrowband subnanosecond dye laser, optical pumped 79−81445
rhodamine laser, induced losses in active medium during incoherent excitation *(Bulgarian)* 79−10297
ring laser, far IR 79−7153
roto-vibrational molecular laser, optically pumped, rate eqn. model 78−37874
roto-vibrational molecular laser scaling, CO_2-TEA laser pumped 80−5728
ruby, bottlenecked 29 cm^{-1} phonon spectral width 77−12425
ruby, far IR lasing feasibility, pumping via ruby laser 79−81435
ruby, optically excited, diffusion of bottlenecked 29 cm^{-1} phonons 80−6472
ruby, optically induced two-phonon processes connecting ^2E states 80−25443
ruby, optically-pumped, excited-state Raman processes 79−4798
ruby, phonons, at 29 cm^{-1}, stimulated emission 80−45114
ruby, resonance interaction of electronic two-level states and short-wave phonon radiation 80−24551
ruby, spatial diffusion of weakly bottlenecked 29 cm^{-1} phonons, quasi-stationary techniques 79−73996
ruby, threshold pumping energy depend. on loss coeff. *(Russian)* 77−46723
ruby CW laser, pumping by Ar ion laser 78−1253
ruby far IR quantum counter 77−38001
ruby laser, continuously pumped, repetitive self-Q-switching 78−50781
ruby laser, generation, amplification of high power picosecond pulses depend. on superluminescence 80−53305
ruby laser, graphical method for pumping coeff. estimation 80−14343
ruby laser, two single-pulse generation *(Russian)* 77−46725
ruby laser total mode self-synchronisation 79−64259
Rydberg atom maser emission, heterodyne detection 80−78822
saturation spectroscopy including collisional effects, for three-level atomic system 80−37099
selective laser excitation of atoms and mols., photophys., photochem. processes, appls. 77−54630
semiconductor, electron-hole liquid, prod. and props. at low temp. 79−82527
semiconductor, saturated, dielectric response 78−10384
semiconductor, spin polarisation induced by optical pumping 79−95681
semiconductor DFB laser, operating in higher Bragg interaction orders, optical and electron pumping 79−89933
semiconductor junction lasers, transport phenomena, junction effects and devices, book 80−98766
semiconductor laser, electron beam pumping efficiency, coating effect 80−91795
semiconductor laser, III-V book contrib. 80−99732
semiconductor laser, mode broadening due to transient heating 77−75517
semiconductor shaper for pumping lamp ignition pulses 79−72585
semiconductors, free carrier optical props., book contrib. 80−80738
semiconductors, low carrier density, lasing action, exciton Bose condensate charact. function 79−64233
semiconductors, spin orientation by optical pumping, review 79−38410
signal parameters in optical pumping experiments *(German)* 79−59404
single-mode laser spectroscopy, optical ringing and incoherent resonance decay 77−24859
six-level model, triplet-triplet pumping 78−25870
small molecule, IR laser induced collisional pumping 78−25630
small molecule IR laser induced collisional pumping 78−25629
solid laser, active element thermal lens focal distance meas. by interf. method 80−48268
solid laser, flash lamp pumping, ballast vol. effect on efficiency 77−707
solid state CW lasers 77−38901
solid-state laser system performance and machine idealisation 77−19326
spectrometer, two-photon, based on flashlamp-pumped dye lasers 78−16860
spectroscopy of small molecules, recent developments 79−3426
spin oscillator action of transverse fields 78−49873
spin oscillators, optically pumped, orientation depend. of oscill. freq. 80−78896
optical pumping continued
spin wave parametric excitation, stochastic auto-oscills., Kolmogorov entropy *(Russian)* 80−75749
spin-flip Raman laser pumped by CO laser, SFRL multiline output 79−7132
Stark effects in optically pumped far IR lasers 77−38963
stilbene tunable narrowband subnanosecond dye laser, optical pumped 79−81445
stimulated Brillouin scatt. mirror, selective props. improvement using wide band pumping 77−88863
stimulated hyper-Raman scattering in a molecular gas via a three-photon process to obtain IR and far IR radiation 80−58633
stimulated Raman scatt. excitation by wideband pump in optical waveguide 80−64108
stimulated Raman scatt. of broad freq. spectrum pump radiation, antiStokes wave excitation and amplification *(Russian)* 79−50346
stimulated Raman scatt. of pump radiation, non-monochromatic, power transform. inversion *(Russian)* 79−3741
stimulated Raman scattering, spatial structure of first Stokes component 80−14398
stimulated Raman scattering excitations near resonance, action of broadband pumping *(Russian)* 77−34913
stimulated Raman scattering with spatially inhomogeneous pump, enhanced gain 80−28279
stimulated scattering, wavefront reversal of two-freq. pump radiation 79−41420
stimulated scattering radiation, pumping wave reproduction 79−64280
Stokes radiation spatial charact. in stimulated scattering, saturation conditions 80−53379
sub-Doppler laser spectroscopy of mol. ions in fast ion beams 80−9655
submillimetre, optically pumped lasers 78−46587
submillimetre CW laser, amplitude stability improved by phase modulated pumping 79−22967
submillimetre laser, two-photon transitions 78−22112
submillimetre laser molecules, Stark and ODR spectroscopy 79−31864
submillimetre laser output and efficiency, rel. to pump frequency displacement 79−31866
submillimetre laser stabilisation by acousto-optic isolator 79−31918
submillimetre lasers, design optimisation 77−14757
submillimetre lasers, theoretical operating charact. 77−54699
submillimetric laser models and rate eqns. 77−38871
submillimetric pulsed laser with optical pumping, charact. rel. to vapour pressure *(Russian)* 79−94215
superconducting film, nonequilibrium energy spectra of emitted phonons 77−27957
superconductivity destruction by optical pumping, theory 78−47905
superconductor, nonequilibrium, order parameter dependence on optical pumping intensity 78−91816
superconductor, nonequilibrium excitation of quasiparticles and phonons 77−43783
superluminescent laser theory for dye soln. *(Russian)* 79−951
superradiance in Raman light scatt., pump depletion effect 80−9957
superradiance waveguide laser, stimulated emission spectrum, leaky modes *(Russian)* 80−87400
temporal pump stochasticity in stimulated Raman scatt. in dispersionless media 79−98441
p-terphenyl:pentacene, optical coherence and resonance decay 77−24859
p-terphenyl, substituted, dye laser and spectral charact., output power, conversion efficiency 80−23681
p-terphenyl dye laser, tunable uv emission, KrF laser pumped 77−7117
tertiary amines, lasing action feasibility, excited state absorpt., two step photoionisation 80−23682
tetrafluoromethane laser, pulsed, high repetition rate, average power limitations at 10.6 and 16 μm 80−58503
tetrafluoromethane molecule, laser spectrosc. and optical pumping from CO_2 laser 80−74202
tetrafluoromethane optically pumped laser, tuning and stabilisation 79−13985
sym-tetrazine, isotope selective mol. spectroscopy and isotopically pure mols. prod. with dye laser 80−11926
thermal distortion of active element during pumping pulse *(Russian)* 77−50696
thermal lens phenomena in mol. pumping expts., time-resolved geom. optics approach 80−9708
three level system, coherently pumped, cooperative relax. 80−78816
three level system, nonlinear coherent effects, nonabsorpt. reson. 80−946
three two-level atoms system, continuously incoherently-pumped, radiation rate, spectrum 80−5716
three-level atom, multiphoton absorpt., finite bandwidth laser influence 78−25841
three-level molecular laser pumping and dispersion eqns. 80−69384
three-level molecular system, cooperative evolution, transient effects of dephasing and relax. 80−28184
three-level molecular system, populations, rate equations 80−37975
three-level molecules, cooperative behaviour, transient effects of coherent optical pumping 79−13938
three-level Mossbauer gamma-ray lasers, two-stage pumping 80−78857
three-level system, coherently driven, collisional contrib. to dynamic Stark effect 79−13765
three-level system, nonabsorbing atomic coherences, excited state populations 77−3332
three-level system, reson. interaction of opposite waves, relax. consts. of common level 78−50511
three-level system, strongly-excited, statistical broadening and population loss 79−41359
time-correlated picosecond laser pulses generation, rapid sampling of optical relax. phenomena 80−9969
TOPOT vapour dye lasers with multiplate reflectors 80−83606
transparency of optically thick medium induced by propagating optical-pumping wave fronts 79−89974
tricarbocyanine, laser dyes, flashlamp-pumped, photochemical stability 80−83604
trifluoroiodomethane, IR multiphoton dissoc. yields, new technique, nonlinear pumping effects 79−100406
trioxane, D_2CO, HDCO, CW optically pumped laser action CW optically pumped laser action 77−88700
triple optical reson. in crystal, weak absorpt. struct. in IR field 77−24808
tunable high power lasers for isotope separation 77−34904
two level system, wide band pump field, population inversion 77−644

optical pumping continued
two-atom resonance fluorescence, in strong EM field, excitation spectrum 78−82778
two-atom system, continuously pumped, radiation props., master eqn. 78−86828
two-level atom in multimode EM field anal., semiclassical anal. 77−10881
two-level molecular systems, increased inversion efficiency 80−23657
two-level spin system, mag. moment dynamics in mutually perpendicular mag. fields, of arbitrary freq. 79−3415
two-level system, adiabatic rapid passage, narrow IR saturation resons., book contrib. 78−9419
two-level system, fluctuations and mean value, intense nonmonochromatic rad. 77−68018
two-level system, in noise pumping field, absorpt. of probing rad. 77−68197
two-level system, nonmonochromatic radiation excitation, nonlinear optical phenomena *(Russian)* 78−87101
two-level systems, nonadiabatic population inversion by laser frequency switching 78−94381
two-photon resonant four-wave mixing with non-monochromatic waves 80−38066
unstable-resonator laser performance at near MM wavelengths 80−58607
upconversion with stochastic pumping, photon statistics 78−22168
UV laser possible pumping by synchrotron radiation, NaCl:I(Br) luminesc. 78−66835
vacuum UV laser possibility for crystals pumped by X-ray synchrotron radiation 79−41387
vibration relaxation time measurement, by coherent Raman-induced IR fluoresc. 79−7038
vinyl bromide maser, CO_2 laser pumped, stimulated emission at 45 freqs. 77−645
water, laser-induced ionisation, quantum yield, temp. and wavelength depend. 80−11924
wave front reversal, reproduction, during stimulated scatt. *(Russian)* 78−87100
wave front reversal accompanying VRMB of depolarised pumping *(Russian)* 78−90458
wavefront reversal, transverse enhancement of coherence of scatt. field 80−95952
wavefront reversal in stimulated light scatt., focused spatially inhomogeneous pump beam 79−27331
wavefront reversal of beam with incomplete spatial modulation, small-scale distortions 80−95953
waveguide gas lasers 78−5490
waveguide laser characteristics 77−38870
X-ray and VUV lasers, travelling wave source pumping 77−83864
X-ray lasers pumped with synchroton radiation and low-energy photons 79−41371
zinc porphin in n-octane, population hole-burning using triplet reservoir 79−87491
Ag_3AsS_3, proustite, ferroelectric phase transition under continuous illumination *(Russian)* 79−61315
^{107}Ag, hyperfine density splitting, density shifts meas. in inert gases 77−54540
$Al_xGa_{1-x}As$, indirect-gap, laser oscill. involving N isoelectronic impurities 77−10919
$Al_xGa_{1-x}As$, metalorganic-CVD, photopumped laser operation meas. GaAs quantum well 79−10303
$Al_xGa_{1-x}As$:N, indirect band-gap, visible laser oscill. at 77K 77−79820
$Al_xGa_{1-x}As$-GaAs, CW 300k quantum-well heterojunction laser, optical and injection pumping operation 80−5735
$Al_xGa_{1-x}As$-GaAs photopumped quantum-well heterostructure lasers grown by metalorganic CVD 79−98390
$Al_xGa_{1-x}As$-GaAs-$Al_xGa_{1-x}As$ photopumped quantum-well laser, room temp. CW operation 78−74908
α-$Al_2O_3:Cr^{3+}$, electronic Raman transition from optically pumped excited state 78−39531
$Al_2O_3:Cr^{3+}$, ruby, reson. scatt. and trapping of 29 cm^{-1} acoustic phonons 80−93403
$^{240}Am^m$, spontaneously fissioning isomer optical shift in pumped $^8S_{7/2}\rightarrow{}^{10}P_{7/2}$ transition, nuclear deformation 80−27971
$Ar^*(3p^54p)_1+Ar(^1S_0)$, collisional population transfer rate coeffs., 300K 79−10177
B, X-ray laser, inner-shell photoionis. pumped, practicability 77−58319
BCl_3, excitation by steady-state and pulsed laser radn. 77−50476
BCl_3+methane reaction, laser-induced, vibr. excitation influence on reactivity, isotope selectivity 80−11921
Ba atom, laser excited, ionisation studies 80−83330
Ba, diamagnetic Zeeman effect, 20-40 kG, induced config. mixing 78−17608
Ba, efficient ionis. by reson. laser pumping 80−32685
Ba I, laser-excited, absorpt. spectra, press. shifts 77−27007
Ba II resonance level lifetime meas. by pulsed laser excitation of ion beam 78−25480
Ba, laser saturation spectroscopy, atomic-resonance absorption transitions 80−47121
Ba, reson. transition, laser saturation spectroscopy with optical pumping 80−52334
Ba, saturation spectroscopy with laser optical pumping 80−83324
Ba vapour, level populations, laser pumping effects 80−91507
Ba^+, optical pumping and saturable absorpt. of fast ion beam superimposed on continuous laser beam *(French)* 78−5179
Ba-Tl laser optically pumped by pair-absorption transitions, 1.5 μm emission obs. 80−58517
$Ba+SO_2\rightarrow BaO+SO$ reaction, laser-induced fluoresc. obs., vibronic distrib. of BaO, collisional energy depend. 80−11917
Bi_2, optically pumped continuous laser oscill. 79−933
Bi_2, vap., optically pumped, laser action 78−71081
Br_2, optically pumped at 532 nm, lasing obs. in visible and near IR 78−63094
Br_2, optically pumped laser, operation 78−25858
Br_2, photolytic cage effect in high-press. gases, laser wavelength depend. 80−11925
C_2, interstellar, rot. fine-struct. levels radiative pumping rel. to obs. towards ζ Persei 80−67811
C_2, low lying $a^3\Pi_u$ state produced in intense IR field, fluoresc. and quenching obs. 80−11931
CF_4, molecular laser operating in 16 μm region 77−50656
optical pumping continued
CH_2, photoprod. from ketene, singlet-triplet energy separation and rovibronic level obs. 80−11936
CO, hole burning in single quantum power spectrum due to Autler-Townes splitting 80−9671
CO, istopically enriched, Ar matrix isolation, laser-included vibr. fluoresc. 80−9707
CO laser pumping with high-energy particles 79−64211
CO, nonequilib. dissoc. induced by electron-vibr. and IR laser pumping 79−86016
CO-Ar(-N_2), C_2 and CN form. by optical pumping, room temp. 80−16701
CO-NO mixtures, Ar matrix isolation, laser-included vibr. fluoresc. 80−9707
CO_2, 1 mJ line tunable optically pumped laser 78−66840
CO_2 16 μm laser, pumped optically in 4.3 μm, 9.6 μm bands, energy characts. 79−18398
CO_2, collisional laser-induced vib. excitation 77−27155
CO_2 high-power pump laser, direct narrow-line tuning 80−58579
CO_2 IR laser, line tunable and optically pumped 77−88747
CO_2 laser, pulsed, broadening of lasing spectrum 79−94205
CO_2 laser, transverse double-discharge, spectral characts. *(Russian)* 77−656
CO_2 laser freq. stabilization for far IR laser pumping 77−68223
CO_2 laser stabilization for use in far IR laser pumping 79−72551
CO_2 lasers, optically pumped, use of crystalline reflector in cavity 80−64080
CO_2 multiatmosphere laser tuning for methyl fluoride laser pumping 80−69421
CO_2, optical pumping in stimulated Raman scatt., tunable laser emitting at 14,16 μm, theory 78−46568
CO_2, optically pumped laser, simultaneous lasing in bands of sequence 80−5725
CO_2, pure and CO_2-He mixture, optically pumped continuously tunable lasers 78−13678
CO_2, seeded laser mixture, photoabsorption and ionisation cross sections 77−23645
CO_2 self-pumping on pulsed periodic energy input *(Russian)* 80−106506
CO_2 TEA far IR laser, optimum spectral matching 79−31857
CO_2, TEA laser pumping efficiency increased by longitudinal mode control 77−38924
CO_2, vibr.-rot. transitions power broadening by laser irrad. 77−3420
$^{13}C^{16}O_2$ laser, isotopically enriched, appl. in optically pumping far IR laser 80−58507
CO_2-Br_2-He mixture, possible gas lasers with solar excitation 80−99695
CO_2-DF-He CW optically reson. pumped transfer laser 77−75471
CO_2-N_2O, laser optical pumping in 4.3 μ band 77−7060
$CO_2{}^*+SO_2$, near-reson. energy transfer, fluoresc. obs. 80−106348
CS_2, fluorescence due to laser excitation, Hanle effect 78−25628
$^{13}CS_2$, laser emission at 6.9 μm, HF laser optical pump 78−58995
$^{13}CS_2$, optically pumped by pulsed HF laser, emission obs. at 6.9 μm 79−50283
Ca atom, laser excited, ionisation studies 80−83330
Ca, efficient ionis. by reson. laser pumping 80−32685
Ca laser, pumped via collision-induced absorpt. in Ca-inert gas mixture 79−7117
$Ca+CCl_4\rightarrow CaCl+CCl_3$ reaction, laser-induced fluoresc. obs. 80−11916
Ca+Sr, laser-induced inelastic collision, fluoresc. obs. 77−54603
CaF_2:Na, γ-irrad. cryst., spontaneous and induced colour centre emission 79−7131
Cd, electron impact, 6^2D_2 and 7^1P_1 level mixing 80−37889
Cd II, pulse excitation in discharge *(Russian)* 77−54704
CdHg, excimer kinetics and transmission meas. 80−37832
CdS crystals, one-photon pumping, active layer structure, light amplification 80−78858
CdS, exciton condensation effects on refr. index 77−20818
CdS, highly excited, stimulated emission process at 80K 80−97307
CdS laser radiation under excitation by pulsed bremsstrahlung X-rays 79−91467
CdS monocrystal petal lasers, single-photon excitation *(Russian)* 80−99736
CdS platelet lasers, optically pumped, spatial and spectral distribution of laser emission 80−64032
CdS, single crystal, subnanosecond light pulse generation by laser radiation pumping 79−64234
CdS, two-photon-excitation, tunable laser emission, luminesc. processes 80−55127
$CdS_{1-x}Se_x$ monocrystal petal lasers, single-photon excitation *(Russian)* 80−99736
$CdS_{1-x}Se_x$, spatial distribution and lasing modes under one photon optical excitation *(Russian)* 78−59012
CdSe 16 μm parametric amplification with HF laser pumping 80−78910
CdSe, fundamental absorpt. edge, influence of laser radiation intensity *(Russian)* 80−71445
CdSe, optically pumped, dynamic polarisation of nucl. moments 78−68411
Ce:LaF_3 286 nm laser, optically pumped 80−99738
Ce:$LiYF_4$, tunable UV laser at 325, 309 nm, KrF laser excitation 80−38022
Ce^{3+}:$LiYF_4$, UV laser at 325 nm, stimulated emission obs. 79−72574
Cl_2, resonance fluoresc. by Ar ion laser excitation 78−42122
ClF UV laser system 80−83597
ClF-H_2 chemical laser, HF rot. laser emission 79−98349
ClO_2, CW for IR mol. laser, optical pumping with $^{16}CO_2$ and $^{18}CO_2$ lasers 80−74343
Co:MgF_2, laser, broadly tunable CW operation, output powers, optical pumping 80−32995
Co:MgF_2, tunable transition-metal-doped solid state lasers 80−58549
Cr^{3+}:$BeAl_2O_4$, tunable laser performance, 701 to 794 nm, Xe flashlamp excitation 79−72573
Cs atomic beam, hyperfine, appl. 77−75108
Cs atomic beam, optical pumping and detection of 0-0 transition 79−18158
Cs atomic clock using laser optical pumping of Cs beam 80−101785
Cs atomic frequency standard, optically pumped, buffer gas mixture optimisation 77−37859
Cs cell, laser beam excitation, multipass, optical pumping and weak neutral current parity violation 80−58207
Cs, cooperative cascade emission transitions 80−14120

optical pumping continued
Cs, diffusion in Kr(Xe), determ. of diffusion coeffs. using π-pulse optical pumping method 79−68895
Cs gas, optically pumped, spatial distrib. of polaris. 79−76392
Cs isotopes, short-lived, determ. of nucl. spins by β radiation detected optical pumping 78−37262
Cs maser, optically pumped, cavity, buffer gas, press., temp., freq., characts. 77−10880
Cs, optical pumping with second resonance light 80−23376
Cs optically pumped frequency standard stability limitations 79−54104
Cs quantum current-frequency convertor, operation principles *(Russian)* 79−10275
Cs, spin relax., effect of optical pumping in high mag. field 77−88430
Cs vapour, optically pumped, transverse relax. times and diffusion coeff., spin echo meas. 79−10062
Cs vapour heat pipe discharge tube pumping for 823 cm^{-1} tunable IR laser 78−63069
Cs-Xe vapour mixture, possibility of solar direct energy conversion into laser radiation 79−59688
$Cs+Cs^{+}$, charge exchange cross-section, temp. depend. 78−9244
Cs+He(Ne)(Ar), optical pumping, spectral line shape *(Spanish)* 79−22662
Cs+insert gas, $5d^2D_{5/2}$ level excitation by laser photon absorpt. 77−3438
Cs_2+He(Ne)(Ar)(Kr)(N_2)(CH_4), collision-induced dissoc., atom-mol.-exchange optical pumping 78−22008
CsXe excimer, laser-excited fluoresc. in Cs-Xe mixture, pumping, level scheme 78−86909
^{133}Cs, filter cells for hyperfine optical pumping, optical detect. of 0-0 transition *(French)* 77−443
^{133}Cs, freq. standard, optimum conditions for population inversion for 0-0 transition 80−78824
$Cs^*(6D_{3/2})+Cs(6S_{1/2})$, preferential excitation transfer from laser populated state 78−37732
Cu halide laser, pumping efficiency 79−68385
D enrichment by CW vibr. photochem. of methane, economic aspects 80−11920
DF-HBr CW optical resonance transfer laser 80−64003
D_2O, angular correlation between far IR emission and CO_2 pump radiation, Dicke superradiance theory 79−41370
D_2O, candidate transition identification for optically pumped far IR lasers 79−931
D_2O, far IR CW laser emission by optical pumping 79−3687
D_2O, far IR laser, tunable single mode optical pumping 77−42526
D_2O, far IR laser system, high power optically pumped 77−54724
D_2O, far IR superradiant laser, 114, 66 μm emission, time-resolved pulse and wavelength meas. 77−88715
D_2O laser, superradiant line obs., 235, 280, 97 and 98 μm 78−1215
D_2O laser, synchronously pumped, subnanosec. transients 79−89891
D_2O laser, zigzag-pumped, oscillator and superradiance characteristics 79−31873
D_2O, laser submillimetre with optical pumping energy yield, emission pulse delay time depend. on pumping pulse *(Russian)* 78−71088
D_2O mirrorless laser at 385 μm 79−31871
D_2O, optical pumping using CO_2 CW capillary waveguide laser 80−48278
D_2O oscillator, zigzag pumped, superradiant 66 μ emission 78−33743
D_2O, pulsed laser-pumped submm amplifier, gain spectrum 78−79000
D_2O, single-mode optical pumping, superradiant far IR emission 78−42329
D_2O tunable vapour laser, optically pumped with single-mode CO_2 TEA laser 79−55145
D_2O vapour high-power 385 μm laser oscillator 80−69422
D_2O vapour high-power optically-pumped submillimetric laser system 77−38925
D_2O, near-MM-wave laser synchronous pumping, ultrashort pulse generation at 385, 66 μm 80−102705
Dy atom isotope separation, laser excitation, charge exchange with Cs^+ ions 80−83512
Eu chalcogenides, paramagnetic, optical orientation of 4f electrons 77−69799
Eu^{2+} in aqueous solution, multiphoton excitation and emission 78−94222
$EuCrO_3$, long term mag. ordering, antiferromagnetic resonance study *(Russian)* 80−54953
EuO, optical orientation of f-electrons, Curie temp. variation due to exchange interactions *(Russian)* 79−15431
F+$CH_3I(CF_3I)(ICl)$ reactions, product state analysis using laser-induced fluoresc. 80−11915
F_2 UV laser system 80−83597
^{19}F IX, high n states, laser induced resonances 77−83548
Fe laser, pumping using KrF laser, vap. form. by flash and discharge decomp. of $Fe(CO)_5$ 78−74890
$Fe(CO)_5$ photodissociation laser 78−74886
Fr, atom, evidence for optical transition *(French)* 78−86829
GaAs, DFB laser, with two-dimens. Bragg reflectors 78−1252
GaAs, density of states, spontaneous emission rate calcs., 120, 160, 200K 77−4292
p-GaAs, electron-nuclear spin coupling, low field, under optical pumping conditions 77−77126
GaAs, insulating, optically pumped electron-hole plasma, Raman scatt. 77−40236
GaAs laser, photopumping of quantum well heterostruct. $Al_xGa_{1-x}As$-GaAs-$Al_xGa_{1-x}As$ 79−22956
GaAs laser material, secondary dislocation climb during optical excitation 78−75672
GaAs, low-temp. absorption spectrum in presence of optical pumping 78−15188
GaAs, negative electron affinity, optically pumped, depolarization of emitted photoelectrons 79−8223
GaAs, optically pumped, absorption spectrum, band filling, hot electron effects 78−31199
GaAs, optically pumped laser with acoustic distributed feedback 78−82977
GaAs, point defect generation by electron-hole recombination at dislocations 79−37699
GaAs:Zn optically pumped ribbon-whisker laser, picosecond pulses 80−99771
GaAs/GaInP DH, MBE grown, optically pumped laser action at 77K 80−95890

optical pumping continued
GaAs-$Ga_{1-x}Al_xAs$, optically pumped ring laser fabricated by LPE over chemically etched channels 77−10958
GaAs-$Ga_{1-x}Al_xAs$ half-ring laser, fabrication by LPE over chemically etched channels 77−684
GaAs-$Ga_{1-x}Al_xAs$ laser, optically pumped, longit. mode broadening due to transient heating 77−61953
GaAs-GaAlAs DFB laser, wavelength tuning effect 78−82979
GaInPAs/InP heterostructure DFB laser under optical pumping, lasing characts. 80−87396
GaN, stimulated emission under high one and two quantum excitation 78−35171
p-GaSb, CESR, optically detected, giant Overhauser shift 79−4722
p-GaSb, interband optical pumping, optical detection of EPR 77−28483
Ge, electron-hole drops, in superfluid He, threshold phenomena *(Russian)* 79−42462
Ge, exciton condensate and electron-hole droplet, metastable state, effect of illumination and high-frequency heating 79−15097
Ge, immersed in liquid He, optical pumping to generate first and second sound 80−6581
H atom, many-photon excitation spectra, fine structure 79−59419
H, g-factor ratio, $g_J(^1H,1^2S_{1/2})/g_s(e)$, spin exchange optical pumping 77−79587
H, ionisation threshold for excited states in uniform elec. field 78−37607
H_2, interstellar, UV vibr. excitation model rel. to 8150 Å emission search 78−93346
H_2, reson. fluoresc. with Lyman α, astronomical appls. 79−8821
HCCF, CW for IR mol. laser, optical pumping with $^{16}CO_2$ and $^{18}CO_2$ lasers 80−74343
HCN (001)+HCN(Ar)(N_2)(CO_2)(CO), relax. rate consts., using Cs vap. IR source 80−9696
HF CW optically resonance-pumped laser 80−43356
HF, colliding system initiated by IR laser absorpt., vibr. inversion generation 77−10707
HF, IR laser induced collisional pumping 78−25629
HF, IR laser induced collisional pumping 78−25630
HF, rot. population transfer using IR-laser double-resonance expt. 79−55128
HF+HF(H_2)(D_2)(CO_2)(isobutene), vibr. relax. dye laser pumping effects 80−9703
H_2^+(HD^+), IR photodissoc. cross sections, calc. and simulation expt. 80−9659
HN_3 high energy density laser using unstable resonator CO_2 laser pump 80−53327
$H_2(a^3\Sigma_g^+ \rightarrow b^3\Sigma_u^+)$ continuum emission excited by low-energy Ar^+ collisions, UV laser appl. 79−41200
He, 2^3S_1 metastable state, interactions, optical pumping investig. 80−23377
He, 3^3P level, excitation and decay study up to high press. pumped by intense relativistic electron beam 80−74250
He, collisional radiative model, reson. optical pumping, plasma diagnostics appl. 79−37459
He, excitation in n=4 levels after laser pumping 77−3324
He, glow discharge, low press., excitation transfer and quenching of n=3 excited states 80−38743
He, high press., laser plasma optically pumped by focusing CO_2 laser beam with axicon 79−32792
He I glow discharge, low-press., quenching of singlet states by N_2 80−49030
He Mz magnetometer, improving accuracy by reducing intensity of optical pumping 80−62700
He, optical excitation function of 5876Å line near threshold 78−70797
He quantum magnetometer with optical pumping, sensitivity in 40-3000 Hz range *(Russian)* 80−90870
He^3-He^4 mixture, relax. of 2^3S_1 metastable atoms 80−102469
He+H_2^+, collision in laser field, vibr. excitation 78−86937
He+Na_2, optically pumped state to state differential cross sections for rot. transitions, rainbow phenomena 80−5609
He+water (cyanomethane), afterglow, excitation and quenching reactions, optical pumping 78−35690
He_2, laser-driven transitions to high Rydberg states 80−106360
^{3}He, opt. pumped maser, saturation polaris. intensity depend. *(Russian)* 77−7046
^{3}He, optical pumping signal, special features 78−82700
^{3}He, optically oriented nuclei, in two-chamber cell, NMR linewidth obs. 78−17591
^{3}He, optically oriented nuclei, maser excitation and characts., appls. 78−17891
^{3}He, optically oriented nuclei, in two-chamber cell, spin maser appls. 78−17892
^{3}He-^{4}He mixture, optical pumping, transients theory 80−91509
^{4}He magnetometer, pulsed optical pumping to reduce mag. reson. freq. error 79−67360
^{4}He magnetometer characteristics and operating principles *(Japanese)* 80−8434
$^4He^+$, g_j-factor determ., optical pumping method 80−87085
Hg II, pulse excitation in discharge *(Russian)* 77−54704
Hg ions, relaxation two constants meas. of optically pumped stored Hg ions 80−106287
Hg, nuclear magnetic moment ratio of odd isotopes *(French)* 77−75081
Hg, optically pumped positive column, E-I characts. 80−44035
Hg photodissociation laser, optically pumped 77−68206
Hg vapour, optically pumped positive columm, collisional processes 78−87499
Hg vapour laser, optically pumped, gain and output power 78−66843
Hg-N_2, optical pumping, vibr. excitation, laser theory 78−66517
Hg-N_2, optically pumped pulsed 546.1 nm laser emission 79−13952
Hg+He, laser excitation of Hg $6s6d^3D_1$ level, transition probabilities and collisional excitation transfer 78−55146
Hg_2 as energy storage medium, energy extraction from metastable excimers 79−59677
Hg_2, excimer fluorescence, electron beam and optically produced systems 77−27107
Hg_2 excimers, photoassoc., spectroscopy and kinetic processes of high-lying vibronic states, laser applics. 80−9649
Hg_2, optical pumping, continuous emission obs. 78−5296
HgBr, 502 nm stimulated emission, prolonged optical pumping of $HgBr_2$ 79−18414
$Hg_{1-x}Cd_xTe$, LPE-grown and optically pumped crystal, continuous lasing at 2.79 μm 79−68397
$Hg_{1-x}Cd_xTe$, photolum. and optical pumping 80−50424

optical pumping continued
HgCl(B→X) laser, photolytic pumping, HgCl(B) state radiative lifetime meas. 78−94390
HgI_2, cooperative fluoresc. by excitonic reson. pumping 79−33732
HgTl excimer laser, kinetics, optical excitation obs. 80−58527
HgTl optically excited excimers, upper state kinetics 80−37831
$^{199}Hg^+$ isolated ions, mag. hyperfine spectrum 78−29760
$^{199}Hg^+$ trapped ion frequency standard 78−57914
^{203}Hg nuclei, optically pumped, anharmonic mag. resonance phenomena 79−94015
Ho:$LiYF_4$, 750 nm laser oscill., flashlamp and dye laser pumping 78−9386
Ho^{3+}:$BaYb_2F_8$ 80−95902
Ho^{3+}:$ErVO_4$, CW and pulsed laser emission at 2.0416 μm 77−19254
Ho^{3+}:$LiYbF_4$, active medium for Nd laser freq. convertor, cascade stimulated emission 80−102727
Ho^{3+}:YAG, 2.09 μm stimulated emission, resonant pumping by Nd laser 78−17944
Ho^{3+}:YVO_4, CW and pulsed laser emission at 2.0412 μm 77−19254
I chemical laser, four-level model *(Korean)* 80−28224
I chemical laser, using high current plasmadynamic discharges 77−38923
I_2 dye laser pumped to dissoc. point of I_2, laser action 78−63064
I nanosecond single pulse laser, open electric discharge pumping 80−5763
I_2 produced in UV photodissoc. of alkyliodides, time-resolved obs. of $I(^2P_{1/2})$ reactions 80−11940
I_2, efficient laser action on 342 nm band, ArF laser pumping 80−99703
I_2, flashlamp excited photodissociation laser 79−72558
I_2, fluoresc. in 340 nm band, buffer gas press. depend. 79−13762
I_2 laser, CW optically pumped, laser oscill. 0.57 to 1.35 μm 79−943
I_2 laser, quasi-tunable IR emission, appl. to absorption meas. 77−42551
I_2 laser, three-level, pumped by CW dye laser 80−63993
I_2, lasing obs. on 342 nm band 78−79008
I_2 molecule B-X electron transition during Cu vapour laser optical pumping *(Russian)* 80−78845
I_2 molecule pumped by Cu vapour laser, pulsed stimulated emission due to electronic transitions 80−14330
I_2, optically pumped laser, I_2 transition moment from gain 79−54917
I_2, photolytic cage effect in high-press. gases, laser wavelength depend. 80−11925
I_2, UV laser, 1 μs pulse emission at 342 nm 77−79811
I_2 UV laser, quartz flashlamp pumped, pulse-periodic operation 80−53279
$I_2+O_2 \rightarrow 2IO$, flash photolysis, emission in 3400 Å band 77−3398
ICl selective photoaddition to acetylene, isotope enrichment, influence of press., buffer and wavelength 80−11927
$^{127}I_2$, two photon excitation, rot.-vibr. structure of E-state 79−41213
InGaAsP-InP DH laser, optical gain meas., low-intensity luminesc. and absorpt. spectra 79−98356
$In_{1-x}Ga_xP_{1-z}As_z$-$In_{1-X}Ga_XP_{1-Z}As_Z$ visible spectrum multiple-quantum-well heterostruct. lasers 80−106537
InSb laser with two photon pumping by CO_2 laser radiation 79−86182
InSb spin-flip Raman laser, pumped by TE CO_2 laser, fund. characts. *(Japanese)* 77−42542
K atomic Rydberg state tunable subMM laser 80−69378
K, emission and absorpt. spectra in inert gas matrix 79−54800
K, stimulated electronic Raman light scatt. by mag. sublevels 78−50492
$K+K^+$ collisions, charge exchange cross section 80−58374
K_2, absorpt. and relax. const. determ. by optical laser pumping method 80−102550
K_2, optically pumped, relax. in at. collisions 78−17765
KF, F_2+-centre excited-state absorption spectrum, rel. to H_2^+ model 80−16066
$K_5Nd(MoO_4)_4$, Ar^+ laser pumped, quasi-CW laser action 79−18421
$KNdP_4O_{12}$ epitaxially grown waveguide, laser operation at 1.051 μm 79−18423
KXe, dye laser induced emission, excimer bands and uses 80−9650
^{39}K, ground-state g-factor, rel. to ^{87}Rb, spin-exchange optical pumping meas. 77−34596
^{41}K vapour, optically pumped, RF shift for one quantum transitions 79−26930
Kr, g-factors meas. by optical pumping and mag. reson. 80−14246
Kr_2, kinetics of optically excited electronic states 78−63059
$LaBr_3$:Pr, continuous wave and pulsed laser pumped Pr IR quantum counters 79−93219
$LaCl_3$:Pr, continuous wave and pulsed laser pumped Pr IR quantum counters 79−93219
Li, $3d^2D$ level, lifetime meas., fast-beam spectroscopy 77−61714
Li atomic beam, spin-polarisation by dual-freq. optical pumping 80−43003
Li seeded in acetylene-air flame, optoacoustic pulses, energy transfer from laser excited atoms 78−25490
Li, vap., multiphoton absorption, space-charge ion detect. 79−54827
Li-$La_{1-x}Nd_x$ phosphate glasses, stimulated emission spectroscopy of $^4F_{3/2}$ to $^4I_{11/2}$ and $^4F_{3/2}$ to $^4I_{13/2}$ transitions 79−38573
Li_2, $A^1\Sigma_u^+$ state, radiative lifetime 77−27104
Li_2, circular polarisation of emission, influence of nucl. hyperfine interactions and elastic collisions 80−9635
Li_2, collisional depolarisation and rot. energy transfer, laser-induced fluoresc. obs. 80−9698
Li_2+inert gas, collision induced transition rate consts., two-laser spectrosc. 80−9629
LiF crystal with F_2^+ centres, periodic pulsed tunable laser, Nd laser second harmonic excited 80−38021
LiF, F_2^+ and F_2^- colour centre pumping *(Russian)* 77−48210
LiF, picosecond generation on F_2^+ colour centres, induced mode synchronisation *(Russian)* 80−64033
LiF with stable F_2 centres, F_2^+ colour centre generation accumulation, tunable laser production *(Russian)* 80−28238
$LiIO_3$, crystal inside Nd:$YA1O_3$ pumping laser, 0.9 W Raman oscillator operation 77−62004
$LiNbO_3$ waveguide, diffused, 2nd harmonic generation 79−14041
LiNd phosphate glass, spectral and generation props. 77−1700
$LiNdP_4O_{12}$ (LNP) laser, optical transmitter appl. 79−3712
$LiNdP_4O_{12}$ electroluminescent diode pumped miniaturized laser for optical transmission system 79−41395
$LiNdP_4O_{12}$ glass-clad rectangular waveguide, laser performance 80−32996
$LiNdP_4O_{12}$ laser, LED and semiconductor laser pumped 77−75552
$LiNdP_4O_{12}$ laser, relaxation oscillations and mode spectra, high density pumping effect 80−69396
$LiNdP_4O_{12}$, single-transverse-mode slab waveguide laser, characts. 79−55141
$LiNdP_4O_{12}$ stable miniature laser with compact resonator, single mode operation 79−50305
^7Li selective excitation, by intracavity nonlinear absorpt. in CW dye laser 79−866
N_2, high power UV lasers, travelling wave excitation via low-impedance high-voltage pulsers 77−3608
N_2, in CO_2 laser, electron beam-ionis. optical pumping characts. 77−75477
N_2 laser, TEA, pump for dye laser amplifier system 78−82984
N_2 laser pump for pulsed dye laser, optical resonator 79−94260
NH_2+H rot. energy transfer in vibronic levels, absolute transfer rates 80−9701
NH_3 81.5 μm subMM laser, optically pumped by N_2O laser, freq. meas. 80−74415
NH_3, CW efficient optically pumped far IR waveguide laser 77−72001
NH_3 CW far IR laser lines, CO_2 laser pumping and Stark tuning 80−69382
NH_3 CW far IR laser lines, CO_2 laser pumping and Stark tuning 80−106508
NH_3, efficient energy extraction by superradiant emission 80−53271
NH_3, far IR CW Raman lasing 80−83595
NH_3, far IR emissions by IR pumping using N_2O laser 80−74345
NH_3, far IR emissions from forbidden transitions, using Stark effect with CO_2 laser pumping 79−86168
NH_3 high power laser, improved optical pumping geometry in Littrow cavity config. 79−22973
NH_3 high power laser characts. 77−79806
NH_3, high power pulse laser pumped optically by CO_2 laser radiation 78−46631
NH_3, IR and far IR laser emissions, using TE CO_2 laser pump 79−934
NH_3 laser, 1 mJ output energy at 16 μm, optical excitation of mol. levels 77−88707
NH_3 laser, 12.08 μm, optically pumped, for appl. to UF_6 isotope separation 78−74923
NH_3 laser, 12.08 μm emission, CO_2 laser pumped, temp. depend. 78−46582
NH_3 laser, compact, high-efficiency optically pumped 78−5492
NH_3 laser, far IR cascade emission 77−38867
NH_3 laser, high energy output in 13 μm region, CO_2 laser pump 79−89927
NH_3 laser, high-power efficient optically pumped, tunable over 770 to 890 cm^{-1} range 80−91780
NH_3, laser, optically pumped, multi-line, 9.3-13.8 μm 77−14751
NH_3 laser, optically pumped by CO_2 laser, high power emission at 12.812 μm 77−38864
NH_3 laser, optically pumped, multiwatt, laser operation in 12-13 μm range 79−7141
NH_3 laser, optically pumped 12 μm, for UF_6 isotope separation, parametric study *(Japanese)* 79−81414
NH_3 laser, optically pumped, freq. tuning 80−28208
NH_3 laser, resonantly pumped, for spectroscopy 80−48277
NH_3 laser, sub mm, Michelson interferometric output coupling 77−14744
NH_3, laser submillimetre with optical pumping energy yield, emission pulse delay time depend. on pumping pulse *(Russian)* 78−71088
NH_3 laser transitions, CW, two-photon pumped 80−99702
NH_3 laser using a continuously tunable CO_2 laser, 11-13 μm region 80−83596
NH_3 laser with focusing-prism raster and light-guide pump system 80−9905
NH_3, near-MM-wave laser synchronous pumping, ultrashort pulse generation at 151 μm 80−102705
NH_3, off-reson. IR laser action without population inversion, Raman type transition 77−10891
NH_3 sensitiser, excitation in MW region using CO_2 laser, pumping models 80−11911
NH_3, stimulated hyper-Raman scatt. via 3-photon process to obtain IR and far IR radiation 80−58633
NH_3, two photon excited 16 μm laser 78−58986
NH_3, two photon generated lasing, effect of pressure 77−88703
$^{14}NH_3$, CW far IR lasing using CO_2 or N_2O pump lasers 79−81407
$^{14}NH_3$, Doppler free spectroscopy, 16 micron generation applications 79−94049
$^{14}NH_3$, far IR CW laser emission by optical pumping 79−3687
$^{15}NH_3$ far IR laser emission at 153, 375 μm, optically pumped by $^{13}C^{16}O_2$ laser 80−58507
$^{15}NH_3$, optically pumped by CW sequence band CO_2 laser, far IR laser emission 78−46578
NI:MgF_2, laser, broadly tunable CW operation, output powers, optical pumping 80−32995
NO, ($A^2\Sigma^+$) excitation using SHG from $KB_5O_8.4H_2O$ 77−3632
NO_2 excited, fluoresc. spectrum, IR multiphoton vibr. pumping, photon absorpt. probability distrib. study 80−18854
NO_2, laser-induced fluoresc. quenching rate const. and lifetimes 80−11930
N_2O isotopes, laser transitions near 4.6 μm, HF laser optical pump 78−58995
$^{15}N_2O$, $^{14}N^{15}NO$, $^{15}N^{14}NO$, optically pumped by pulsed HF laser, emission obs. at 4.6 μm 79−50283
N_2O-CO_2, optically pumped transfer lasers, continuously tunable 78−13678
NOCl, molecular laser operating in 16 μm region 77−50656
$^{14}NH_3$, four level system, two-photon jumping to obtain 12.16 μm radiation for isotope separation 78−90414
$^{14}NH_3$, high power vibr.-rot. emission, optically pumped off reson. 77−7068
$^{14}NH_3$, laser generation on two-photon excitation, 6 to 35 μm 77−10890
$^{15}NH_3$, far IR laser lines, optically pumped by CO_2 laser 78−90415
$^{15}NH_3$ far IR CW laser, optically pumped with $^{13}C^{16}O_2$ laser 80−78866
Na atom, cyclic interaction with circularly polarised laser radiation 80−78581
Na, atomic states highly excited by laser radiation, Stark effect 79−13669
Na atomic vapour, Doppler-broadened system, degenerate four-wave mixing, line shape and strength angular depend. 80−43391

optical pumping continued
Na beam, laser beam irrad., reson. fluoresc. intensity, Bloch model calcs. 80−58206
Na, excited state photon echo relax. 78−37606
Na free atom cooling in resonant laser field at scanning freq. *(Russian)* 79−72272
Na, ionisation and energy pooling in laser-excited vapour 79−795
Na, laser excited fluoresc., saturation power, calc. and obs. 77−42276
Na, laser orientated vapour, rotary power determ. 79−32737
Na, laser saturation spectroscopy, atomic-resonance absorption transitions 80−47121
Na, laser-excited, electron collision-induced alignment in 3P to nS transitions 77−19084
Na, Lorentzian power broadening by optical pumping 78−17613
Na, optical pumping, Hanle effect 78−33475
Na, population change induced by laser radiation, hook method 78−33476
Na, reson. transition, laser saturation spectroscopy with optical pumping 80−52334
Na, Rydberg states, optically pumped, electric field ionis. *(Russian)* 79−27095
Na, saturation spectra, crossover signals, effect of atomic alignment, optical pumping 80−58202
Na seeded in acetylene-air flame, optoacoustic pulses, energy transfer from laser excited atoms 78−25490
Na, spin polarisation in flames by optical pumping, mag. reson. transitions 78−29762
Na, two-photon absorpt. processes, polarisation selection rules 80−9574
Na vapour, reson. freq. conversion by two-photon reson. pumping 80−28277
Na-He-N_2 dense vapour system, optical pumping, RF spectrum analyser appl. 79−76393
Na_2, absorpt. and relax. const. determ. by optical laser pumping method 80−102550
Na_2, continuous laser oscill., optical pumping 77−88706
Na_2, excited state identification by two-step polarisation labelling 79−76472
Na_2, ground state, vibr.-rot. relax., optical pumping transients obs. 80−28067
Na_2, optical orientation under circularly polarised laser excitation 77−65443
Na_2 optically-pumped three-level dimer lasers, amplification profiles and dynamic Stark effect 79−41367
Na_2, rot. level repopulation rate by laser-induced depopulation 77−65528
Na_2, TOF spectra, molecular beam diagnostics with internal state selection 78−86968
Na_2+He(Ne), rot. transitions, state-resolved differential cross-sections 78−62887
Na_2+He(Ne)(Ar), collision induced dissoc. rate, vibr. distrib. depend. 79−22791
Na_2+Na, spin polarisation exchange via opt. pumping, NMR 77−14452
NaCl:I, UV laser generation by optical pumping 78−82973
NaF, F_2^+-like colour centre, room temp. stable, CW laser, 0.99-1.22 μm tunable 80−69399
NaK dimer formed in supersonic beam, laser-induced emission 80−9636
NaK+Na, spin polarisation exchange via opt. pumping, NMR 77−14452
^{23}Na, ground state g_J factor, meas. from weak-field Zeeman spectra 78−33469
Nd^{3+},Cr^{3+}:glass, nonradiative energy transfer from Cr to Nd, optical pumping efficiency improvement 80−33001
Nd compounds, diode pumped miniature laser 78−9392
Nd laser, emission freq. conversion by method of reson. pumping of active media 80−1206
Nd laser Mikron system, ultimate Xe pump lamp module operating conditions 80−91815
Nd laser pumping, Na plasma optical props. 79−4115
Nd, lasers, efficiency enhancement by pump radiation conversion in luminesc. liq. 80−48293
Nd pulsed garnet lasers, pulse repetition frequency, optimal operating regime 80−53303
Nd^{3+} miniature laser principles, materials and integrated optical design 80−33004
Nd:$CaY_1Mg_2Ge_3O_{12}$, CAMGAR low threshold CW room temp. laser operation at 0.941 μm 78−1234
Nd:glass, high efficiency short pulse laser, coaxial flashlamp pumping 77−75558
Nd:glass, laser material, luminesc., population inversion depend. on pump pulses 77−23679
Nd:glass, laser rod amplifier of 4 cm diam., design and performance 77−19339
Nd:glass, thermal distortion induced by optical pumping *(Chinese)* 78−50779
Nd:glass amplifier, pump radiation pulse shape influence on stored energy 79−64235
Nd:glass laser rod, pumped, thermal relaxation 80−69397
Nd:phosphate glass laser, CW oscillation 79−50311
Nd:YAG, LED end pumped laser, cavity loss, efficiency 77−14740
Nd:YAG, miniaturized laser, end-pumped by superlum. diode, CW operation 77−10938
Nd:YAG fibre laser, self-contained LED-pumped single-crystal 78−1264
Nd:YAG glass clad fibre laser, 1.3 μm operation with LED end pumping 77−7120
Nd:YAG laser, flash lamp discharge development effects on pumping efficiency 78−71114
Nd:YAG laser, Kr-pumped for space optical communications 77−19328
Nd:YAG laser, pumped by Kr arc lamp, conductive cooling, for space operation 77−88775
Nd:YAG laser, semicond. convertor in pump system 77−7129
Nd:YAG laser pumping system, heterostructure spectrum convertor, opaque and sapphire heat sink 79−27272
Nd:YAG oscillator, flashlamp pumped, const. gain Q-switching to improve stability 78−50837
Nd:YAG pumped tunable sources, appl. to spectroscopy 80−58576
Nd:YAG single crystal fibre laser, self-contained LED pumped 79−59711
Nd:YAG solar pumped laser for space communications 78−46645
Nd:YAG solar pumped laser, freq. doubling 78−59045
Nd:YAG space laser communication system, K-Rb arc lamp pump 78−46646

optical pumping continued
Nd:YaG laser reflection resonator with hole coupling 80−58597
Nd^{3+}:$Gd_3Ga_5O_{12}$ pulse-pumped laser action at 1.054 μm 80−64030
Nd^{3+}:YAG fibre laser pumped by single LED, optimum geometry *(German)* 78−55366
Nd^{3+}:YAG laser, high repetition rate electrooptic Q-switching, birefringence 80−69430
Nd^{3+}:YAG laser, improved efficiency with $Al_xGa_{1-x}As$-GaAs LED pump system 79−41396
Nd^{3+}:YAG laser, pumping by alkali metal vapour arc discharge 80−78924
Nd^{3+}:YAG laser, stable periodic-pulse, with CW pump 80−74400
Nd^{3+}:YAG multimode laser radiation noise 80−74366
Nd^{3+}:$YAlO_3$ laser double-pulse flashlamp trigger cct. 78−55378
$Nd(Al,Cr)_3(BO_3)_4$, CW laser action, CR^{3+} cross pumping, Nd^{3+} direct pumping 79−64231
$Nd(Al,Cr)_3(BO_3)_4$, efficient cross pumping of Nd^{3+} by Cr^{3+} 78−59010
$NdAl_3(BO_3)_4$ (NAB) laser, optical transmitter appl. 79−3712
$Nd_{0.75}La_{0.25}P_5O_{14}$, miniature laser system bonded mirrors, side pumped by LEDs 78−87058
$Nd_xLa_{1-x}P_5O_{14}$, laser properties 79−22957
NdP_5O_{14} (NPP) laser, optical transmitter appl. 79−3712
NdP_5O_{14} laser, flash-lamp-excited, operation 77−83883
NdP_5O_{14}, laser, flash-lamp excitation, room temp. operation 77−88779
NdP_5O_{14} laser, flashlamp excited, emission cross section at 1.32 μm 79−59701
NdP_5O_{14} microlaser pumped by second harmonic of Nd^{3+}:YAG laser 79−98377
NdP_5O_{14}, XeF excimer pumping 79−7130
$Nd_{1-x}Y_xP_5O_{14}$, laser emission at 1.32 μm, Ar laser pump source 79−31909
Ne, $1s_5$, depopulation effects, dye laser fluoresc. obs. *(French)* 78−41996
Ne, $2p^53p$ level, stepwise excitation, effective cross section 77−83550
Ne, $2p^53s^3P_0$ state, optical pumping, g-factor, metastability exchange cross section 80−947
Ne, metastable states, studied by Doppler-free spectrosc. with vel. selective pumping 79−81304
Ne, optical pumping of metastable ($2p^53s^3P_0$) state 78−25486
Ne, reson. interaction of opposite waves, relax. consts. of common level 78−50511
Ne, two and three level systems, laser induced dichroism and birefr. 78−79065
Ne+He, population transfer between Ne 2p levels *(French)* 77−30975
Ne*+Ne, metastability exchange by optical pumping *(French)* 77−61845
Ni:glass, amplifier module inversion investigation, active element with rectangular cross section 79−27264
Ni:MgF_2, efficient CW optically pumped laser, 1.63 to 1.75 μm operation 79−18425
Ni:MgF_2, tunable transition-metal-doped solid state lasers 80−58549
O, metastable ^{5}S-state, optical pumping 80−32678
O_2^+, predissociated $b^4\Sigma_g^-$ state, high resolution laser spectroscopy in fast ion beam 80−9656
O_3, multiphoton dissoc. dynamics, classical model 80−11904
OCS, optically pumped roto-vibr. mol. laser, low temp. operation and performance 79−50315
OCS, optically pumped CW subMM emission lines 80−95876
OCS, roto-vibr. mol. laser, low-temp. performance 80−9871
OCS, vibr. excitation and stimulated emission, CO_2 laser pulse pumping 77−23662
OH ($A^2\Sigma^+$)+$H_2(N_2)$(Ar), collisionally induced population change rates, laser-induced fluoresc. obs. 78−5326
OH in flames, laser excitation dynamics 80−74201
OH, interstellar, ground state Λ double maser emission as result of overlapping far IR transitions 77−45533
OH, NO, NO^+, inverted populations due to moving bodies and ejected gas, upper atm. 78−32265
OsO_4, multiphoton absorpt. under two CO_2 laser pulse excitation 78−86925
Pb, superconducting film, spatially inhomogeneous state appearance under laser pumping conditions 80−93053
PbI_2, cooperative fluoresc. by excitonic reson. pumping 79−33732
$Pb_{1-x}Sn_xSe_{1-y}Te_y$ optically pumped heterojunction laser with matched gratings, photolum. obs. 79−89909
$Pb_{1-x}Sn_xTe$ optically pumped lasers, power output and wavelength, 4 to 30K 78−79035
^{207}Pb, laser isotope separation using nuclear spin induced elec. dipole transitions 77−61877
Pr^{3+}:$LiYF_4$ laser, blue light emission, longit. pumping by dye laser 77−38899
Rb atomic frequency standard, optical pumping phenomenon and techniques, review 77−65022
Rb, induced mag. moment by laser excitaion *(Russian)* 79−68327
Rb isotopes, short-lived, determ. of nucl. spins by β radiation detected optical pumping 78−37262
Rb, optical pumped magnetometer *(Japanese)* 79−21790
Rb optical pumping light source 79−46023
Rb, optically pumped at. beam clock, theory 77−34866
Rb, radiative lifetimes up to n=12 excited states, pulsed dye laser and superradiance excitation 80−83322
Rb, vap. in mag. field, alignment due to π-polarised light 79−31476
Rb vapour, time-reversed optical wave front generation by degenerate four-wave mixing 79−14028
Rb+Xe, interatomic spectrum, theoret. and exptl. obs. 78−9112
^{85}Rb, ground state dipole HFS diamagnetic shift, high field optical pumping expt. 78−90129
^{85}Rb, hyperfine struct., diamag. shift obs. 77−61717
^{85}Rb unperturbed hyperfine transition frequency determ. 77−7047
^{87}Rb atomic beam 79−26941
^{87}Rb double resonance, signal intensity charact. due to pumping light 77−34603
^{87}Rb, ground state g-factor, rel. to ^{39}K, spin-exchange optical pumping meas. 77−34596
^{87}Rb resonant frequency change, due to spectral profile of pumping light 78−45590
S I emission lines in late-type stars EUV spectra, optical pumping by O I lines 80−82359
S_2 laser, optically pumped, lasing obs. 470 to 480 nm 78−63095
S_2 mol. $B^3\Sigma_u^- \rightarrow X^3\Sigma_g^-$ fluorescence induced by N_2 laser *(Japanese)* 80−14175

optical pumping continued
S_2, optically pumped superfluorescence molecular laser 80−63990
S_2, tunable visible and UV laser, $B^3\Sigma_u^- - X^1\Sigma_g^+$ transition 77−42522
SF_6 10.5 μm spectrum, high-J assignments, identification of levels pumped by CO_2 P(12) and P(22) 78−70837
SF_6 and S_2F_{10}, absorpt. of intense laser radiation, vibr. excitation 80−9667
SF_6 and S_2F_{10}, multiple-photon IR laser pumping, collisional effects 80−9668
SF_6, CO_2 laser excited, optoacoustic meas. of energy absorpt. 77−83667
SF_6, collisionless fluoresc., 16 μm, following laser pumping, vibr. quasicontinuum 78−42111
SF_6, collisionless multiple-photon laser excitation, anharmonic splitting effect 77−61815
SF_6, collisionless multiple-photon excitation, mol. rot. and vibr.-rot. interaction effects 78−74720
SF_6, comparison of multiple-photon excitation models 78−94297
SF_6, excited to dissoc. threshold, IR absorption 79−81245
SF_6, highly excited, time-resolved IR absorpt. obs. 80−9666
SF_6, inhibition of homogeneous condensation by vibr. excitation, isotope separation appl. 78−37688
SF_6, laser pumped, mol. vibr. amplitude changes, gas phase electron diffr. obs. 79−76513
SF_6, laser pumping in collisional region of nozzle beam, internal excitation, time-of-flight anal. 80−95719
SF_6, model system, coherent pulse propag. effects 80−9968
SF_6, multiphoton pathways, rot.-vibr. transition moments in excited states 78−25639
SF_6, multiphoton-excited in mol. beam, photoionsation probe of vibr. energy distrib. 79−76476
SF_6, multiphoton-excited, $\nu_2+\nu_6$ absorption and emission 80−63626
SF_6, multiple IR photon absorpt., collisional effects 78−86926
SF_6, multiple photon excitation, collisionless 80−53079
SF_6, multiple-photon two-freq. IR laser pumping, optoacoustic spectroscopy 79−36717
SF_6, photon-enhanced dissociative electron attachment 80−9749
SF_6, population of excited vibr. level, nonequilib. absorpt., 140K *(Russian)* 79−36708
SF_6, pumped by OC_6 laser, transition strengths 77−14416
SF_6, Q-branch pumping in ν_3 mode 78−90232
SF_6, resonant single-photon dissoc. route using prelim. electron excitation 80−9662
SF_6, time-resolved IR absorpt. meas. using injection-locked single mode TEA CO_2 laser 80−9665
SF_6, vibr.-translational relax. at high excitation rates 79−41201
SF_6, vibrational-translational relaxation, depend. on intensity of selective laser excitation *(Russian)* 78−9235
SF_6+H_2 chemical laser, electron beam pumping 80−91784
SF_6Ar, multiple photon excitation, saturation and linear absorpt., pulsed optoacoustic detect. 78−42148
SO_2-$^{18}O_2$ mixtures, IR laser pumped, intermol. vibr. energy transfer dynamics obs. 80−87207
Si, Overhauser effect in optically pumped compensated samples 79−73857
Si:Au donor and acceptor centre obs. using IR absorpt. and dynamic nucl. polarisation with optical pumping 80−54639
Si:S, electron-nuclear interactions during pumping, influence of mag. field 79−95378
Si-Al optically thick, plasma, use of multiple photoexcitation to obtain lasing at 44 Å 79−3684
Sr, associative ionisation of laser-excited Rydberg states, mass spectrometry obs. 78−94303
Sr, autoionising doubly excited Rydberg states 78−33479
Sr, efficient ionis. by reson. laser pumping 80−32685
Sr II, resonance level lifetime meas. by pulsed laser excitation of ion beam 78−25480
Sr, Rydberg series, absorpt. by selectively laser-excited atoms 79−3390
Sr^+, inversion and lasing on optically pumped reson. line 78−70798
Tb-Al-Cl vapour complex, fusion laser gain medium 78−63073
Te crystal, SHG, 60% efficiency, 12.8 μm NH_3 laser pumping 80−83640
Te_2, optically pumped continuous laser oscill., 550 to 660 nm 79−933
Tl, $6^2P_{3/2}$-$6^2P_{1/2}$ transition, population inversion 80−950
Tl, green line superradiance, selective optical excitation and inversions via excimer channel using Tl-Hg and Tl-Cd-Ar systems 79−50281
Tl, hyperfine struct. optical pumping, O-O transition perturbation 80−949
Tl I, photodissociative pumping effect 80−58182
Tl, in gas discharge, optical self pumping, hyperfine struct., microwave-optical spectroscopy 80−32680
Tl, optical excitation, Landau-Ziner nonlinearity, fluoresc. obs. *(Russian)* 80−52948
Tm^{3+}:YAG, 2.014 μm, stimulated emission, resonant pumping by Nd laser 78−17944
U I, laser spectroscopy, using stepwise excitation and fluoresc. detect. 79−54802
UF_6, laser chemistry 80−69198
UF_6, vibr. excitation kinetics, IR-UV reson. methods 79−45739
^{238}U I, transition probabilities meas. by time resolved optical pumping 77−46545
Xe flashlamps with interf. coatings, laser pumping efficiency improvement 79−10316
Xe, g-factors meas. by optical pumping and mag. reson. 80−14246
Xe, liq., ionising particle detector, signal amplification by optical pumping 79−54746
Xe, plasma-recombination laser, CO_2 laser prod. using periodic pumping 79−45927
XeCl excimer laser, electron-beam pumped, emission spectrum, saturation intensity, optical absorpt. 79−927
XeF laser, optically excited by incoherent Xe_2* radiation, B→X band emission 78−87044
XeF* and other rare gas excited complexes, optical excitation device 78−13629
XeO laser, pumping by discharge radiation 77−667
YVO_4:Nd, stimulated emission cross-sections at 1064 and 1342 nm 78−39575
Yb I, high Rydberg levels of $4f^{13}$ 6snd configs., very high resolution obs. 80−106300
Yb, Rydberg states, optically pumped, electric field ionis. *(Russian)* 79−27095
optical pumping continued
Yb, single atom detection by selective laser excitation and field ionisation from Rydberg states 79−18159
^{173}Yb, $6s6p\,^1P_1$ state, level crossing with additional pumping of ground state 77−34595
$Zn_xCd_{1-x}S$, lasing modes and spatial distrib. under one-photon excitation, cavity model 78−74913
$Zn_xCd_{1-x}S$ monocrystal petal lasers, single-photon excitation *(Russian)* 80−99736
$Zn_xCd_{1-x}S$, platelet single cryst. one-photon optical excitation, spatial distrib. and mode struct. of laser emission 79−31912
ZnHg excimer, optical pumping of Zn reson. line, optical and kinetic props. 78−58991
ZnO epitaxial film, UV luminesc. due to one-, two-photon excitation, laser possibility 79−11468
ZnO, two-photon-excitation, tunable laser emission, luminesc. processes 80−55127
ZnSe, optically pumped stimulated emission at 4580 Å, near band edge luminesc. 78−71105

optical quantum generators *see lasers*

optical radar
see also remote sensing by laser beam
acousto-optic modulator for CO_2 laser rangefinder using heterodyne detect. 80−102825
adaptive optical system, performance with extended dynamic targets 77−46798
adaptive optical systems, passive return-wave 77−88933
aerosol concentration deduction from 1.06 μm lidar meas. 79−25323
aerosol mass conc. meas. by Nd:glass lidar, ASSESS II Spacelab mission simulation *(German)* 78−69649
aerosol meas. by lidar, error analysis and simulation 80−26617
aerosol measurements with calibrated two- and three-freq. lidars 78−36334
aerosol pattern recognition *(Japanese)* 80−51028
air pollutants, laser spectroscopic detection 80−17366
air pollution above urban site, monitoring by Lidar meas. *(French)* 77−25780
air pollution detection, optical methods *(Czech)* 78−69444
air pollution detection appl. *(Czech)* 78−81359
air-truth lidar polarisation studies of orographic clouds 78−73454
airborne CO_2 heterodyning laser radar 77−88928
airborne laser sensor system, using large size lightweight plastic mirror 78−66891
airborne lidar, continuous long-distance system, flight tests *(German)* 78−36338
airborne lidar, multidisciplinary, planned operation 78−36335
airborne lidar, water pollution detect., FFT in evaluation of laser Raman and fluoresc. decay times 78−81444
airborne lidar system for geophysical and atmospheric expts. *(Italian)* 80−109277
airborne pulsed Doppler lidar system for wind meas. in severe storms 79−66812
analogue computing, past, present and future 78−46531
artificial satellite laser ranging, geodetic appls., San Andreas fault 77−64185
artificial satellite laser ranging, oceanographic appls. 77−64484
artificial satellite laser ranging for upper atmosphere wind determ. 77−64485
artificial satellite laser tracking, current status and future prospects of technology 79−66906
atmopsheric scattering of lidar pulses, four-component polarisation meas. 78−44996
atmosphere, propagation calcs., use of average complex refr. index 78−57314
atmosphere observations at Kingston, Jamaica, using lidar system 78−36284
atmospheric aerosol, use of lidars, laser rangefinders 80−51580
atmospheric aerosol conc. meas. by lidar 78−85693
atmospheric environmental research, appl. of lasers *(German)* 80−97849
atmospheric lidar scattering and relative humidity 80−77113
atmospheric measurement by lidar using Cassegrainian optics 77−37436
atmospheric measurements, laser radar system at University of West Indies 77−13134
atmospheric measuring equipment, steerable laser radar system 78−53746
atmospheric monitoring, laser systems appl. 78−69520
atmospheric multiple backscatt. and depolarisation obs. 78−36292
atmospheric parameters monitoring by laser radar, water droplet remote meas. 77−91299
atmospheric particulate concentration, rise of smoke plumes, application of lidar 80−51026
atmospheric pollution, cooling tower plumes, lidar meas. *(German)* 77−25781
atmospheric pollution monitoring by lidar systems 78−53765
atmospheric probing of fogs and clouds, double scatt. approx. 78−73512
atmospheric propagation of partially coherent radiation 78−65386
atmospheric properties meas., laser expts. on Spacelab missions 78−53793
atmospheric remote sensing by aerosol lidar backscatter *(Dutch)* 80−4110
atmospheric sounding, lidar characts., optical system parameters effect 80−33065
atmospheric transparency meas., laser radar meas. *(Italian)* 77−91333
atmospheric visibility meas. by modulated CW lidar, comment 77−64440
atmospheric visibility meas. by modulated CW lidar, reply to comment 77−64441
atmospheric visibility using lidar 80−31141
autoscreener with secondary screener for target screening 79−32082
avalanche photodiode, operating conditions in phase optical rangefinding 77−13799
background suppression by selective modulation interferometric spectrometer 79−97443
ceilometer measures cloud base height using laser beam 77−29441
ceilometer using low-power laser radar 78−24390
chemical laser lidar system, for air pollution remote meas. 77−21910
Chesapeake Bay, water surface laser radar refl. as function of wind speed 77−41034
circularly polarised laser light for improved visibility through mist 77−75596

optical radar continued
cirrus clouds backscatter and extinction coeffs. from laser radar obs. 77−60456
closed loop adaptive optics systems, target effects 77−88934
cloud altitude measurements 79−88444
cloud extinction coefficient, estimation from multiwavelength lidar backscatter meas. 80−98446
cloud rotational Raman and double scatt., lidar meas. 78−77318
cloud scattering at 347, 694 nm, polarisation props. 78−85689
coaxial and noncoaxial systems with central obstruction, lidar return signals 79−76744
coherent lidar target calibration, backscatter refl. for circularly polarised radiation 80−102750
coherent monopulse tracking with 10.6 μm radar 77−88929
conical scan tracking system, target angle estimate 77−27337
containerisation of heavy lidar system for environmental protection control 78−36336
correlator, Malvern, based on photon correlation and laser scattering spectroscopy, development and appl. 80−5741
deformable mirror adaptive optical system 77−46796
DFVLR mobile lidar system, for smoke stack emission meas. 77−53248
differential absorption CO_2 lidar, for ethylene remote meas. 78−49122
differential absorption lidar, complementarity of UV and IR systems for atmospheric species meas. 80−72634
differential absorption lidar, HCl detection using DF laser 77−27059
differential absorption lidar at 724 nm water vapour line 80−17384
differential absorption lidar from Space Shuttle, for atm. trace constituents meas. 78−45179
differential absorption lidar system sensitivity with heterodyne reception 79−27310
differential absorption lidar systems for atm. gases remote meas. 78−69525
differential absorption scattering lidar, detectivity estimation for NO_2 78−92991
differential lidar, SO_2 meas. in power station plumes 79−57556
differential lidar system, alternate-pulse wavelength switching of dye laser 78−25890
differential scatter lidar system, for atm. aerosols remote anal. 78−69524
differential-absorption lidar technique for remote meas. of atm. gases 78−61603
digital beam switch for 10.6 μm laser radar 80−102836
digital beam switch for agile beam laser radar 80−58620
discrimination, of quantum optical fields 77−10879
displays, speckle noise min. detectable contrast 77−19411
distinguishing close quantum signals 77−7044
doppler lidar processing for atmospheric turbulence measurements 78−73554
double scattering contribution to lidar returns from clouds 79−5615
dusty IR Test-1 lidar obs., transmission meas. 80−99625
dye laser, high energy pulsed, for atm. sounding 79−39868
dye laser differential absorpt. lidar, for atm. SO_2 detect. 77−88784
dye laser differential lidar for atm. SO_2 and NO_2 conc. meas. 78−32250
echo-signal calc. allowing for multiple scattering from cloud *(Russian)* 78−49137
excimer laser application to laser-radar obs. of stratospheric O_3 80−17410
fast-response photodetector for atm. sounding, photometric properties 80−51585
fluctuating pulsed signal detect., effect of unstable quantisation level 77−10113
fogs, radiational and advective, laser beam multiple scatt. 79−100950
forward looking IR radar system, effect of ZnS CVD windows 78−46816
gas absorption lines, half width and intensity, lidar remote probing technique *(Russian)* 80−21844
gas laser rangefinder and profilometer, high-resolution 80−102754
geometrical compression of lidar return signals, atm. remote sensing appl. 78−57329
geometrical form factor in laser radar eqn., experimental determ. 80−36391
geometrical form factors for lidar function, atm. backscatt. 78−37936
glint tracking by adaptive optical techniques 77−19458
Goddard laser systems and their accuracies 77−64482
gravitation theory testing by lunar laser ranging and planet radar ranging 77−53823
heterodyne detection receiver with TEA CO_2 laser transmitter 79−36948
heterodyne lidar systems, signal-to noise ratio in presence of atmospheric turbulence 79−100949
heterodyne optical radar S/N ratio in atmospheric turbulence 80−106558
high accuracy distance measurement by two-wavelength pulsed laser sources 80−192
hydrometeor backscattering cross sections, meas. at 6328 Å 78−49135
image centroid, size and orientation estimation 77−88901
imaging system, fast frame rate, 10.6 μm radar 77−88930
incoherent backscatter heterodyne lidar, antenna parameters 79−72613
inhomogeneous atmosphere, double-scatt. approx. of lidar eqn. 79−29855
integrated optical devices and applications 79−14117
intensity fluctuation meas. by remote Doppler technique 77−791
IR continuously tunable lidar, remote meas. of SO_2 and methane 79−21025
IR Doppler wind-sensing system, spaceborne, atmospheric effects 79−96828
IR extinction meas. using lidar, with CO_2 laser radiation 78−40655
IR phase conjugation adaptive array 77−46790
IR tracking receiver with holographic information processing 78−78970
joint measurements of angular coordinates and range on basis of phase front 78−78933
JROE II LIDAR, meteorological instrument, atmospheric gas component measurements *(Italian)* 78−3957
Lageos, Earth's rotation and Earth's crust movement meas. by employing laser tracking technique 77−41206
laser, focused apertured Gaussian beam, focal length and target range estimation 77−19299
laser and electro-optical systems, conf., San Diego, CA, USA (Feb. 1980) 80−62392
laser cloud location, microstructure of scatt. particles *(Russian)* 77−73850
laser engineering and appls., conf., Washington, USA (May-June 1979) 80−1216

optical radar continued
laser heterodyne system, dual Bragg cell local oscillator 77−19279
laser pointing and tracking, adaptive optimal filtering appl. 77−88959
laser pulse tracking position-sensitive photodetector characteristics 77−18098
laser rangefinder, with improved accuracy 79−17384
laser rangefinder and 3D object recognition algorithm 80−96016
laser rangefinder operating frequency selection 79−72691
laser rangefinder using pulsed CO_2 TEA laser 77−88926
laser ranging, time-of-flight, at very low signal levels, accuracy analysis 77−111
laser ranging system, effects of random path fluctuations 77−7094
laser ranging systems, ground based and space based 77−88925
laser ranging systems, NASA applications 78−81527
laser ranging systems, space appl. 79−40081
laser requirements for strategic and tactical appls. 77−38978
laser satellite-tracking, Ondrejov station site evaluation 78−36418
laser sounding method and equipment for water absorpt. and attenuation coeffs. meas. *(Russian)* 79−34998
laser system for rocket attitude measurement 79−12763
laser tracking system testing by 1 m unobscured IR collimator 80−78991
lidar, appl. to bathymetry and near-shore charting, preliminary field test results 79−5679
lidar, cirrostratus clouds remote sounding and IR emissivity 80−82061
lidar, continuous wave, atmospheric visibility meas. 78−40651
lidar, laser detect. of air pollution 77−9569
lidar, meas. of effective stack height of smoke plumes *(German)* 77−9490
lidar, multiple scatt. effects on light pulses refl. by turbid atm. 77−29442
lidar, multiple scatt. from turbid atm., Monte Carlo anal. 77−25779
lidar, wave-like struct. obs. in atmospheric Na layer 78−88955
lidar and anemometer meas. of wind vel., comparison 79−39885
lidar assembly, appl. to plume struct. and trajectories meas. 79−58016
lidar atmospheric sounding, nondispersive gas analyser appl. *(Russian)* 77−60477
lidar backscatter from horizontal ice crystal plates 78−92984
lidar investigation of inhomogeneous atmosphere optical parameters *(Dutch)* 79−80026
lidar measurement of Na conc. and neutral temp. at mesopause level 78−61613
lidar measurement problems in hazy visibility conditions 77−9572
lidar measurements of high ice clouds, visible and IR optical props. calc. 80−82060
lidar measurements of post-Fuego stratospheric aerosol layer 77−56679
lidar obs. of atmospheric aerosols 79−66841
lidar obs. of atmospheric particulate matter props. 78−61501
lidar obs. of stratospheric aerosols long term vars. after Fuego volcano eruption 79−16597
lidar observation of ice clouds, microphys. props. 79−39811
lidar observation of plume dispersion in northern Alberta 79−83679
lidar observation of smoke and dust clouds, at 0.7 μm, 10.6 μm 78−49181
lidar observations of altostratus mixed-phase cloud 77−91220
lidar observations of high plains thunderstorm precipitation 78−32167
lidar observations of Labadie Power Plant plume, particulate density and behaviour obs. 80−55956
LIDAR observations of plume diffusion at Rancho Seco Generating Station 78−11991
lidar polarisation meas. for cloud phase discrimination 78−96269
lidar Raman spectroscopy of atmosphere *(Russian)* 78−24387
lidar return, simulated, from one-dimensional stratospheric aerosol model 79−44247
Lidar return from fogs, effect of non-uniform extinction coeff. on double scatt. contrib. 79−100952
lidar returns, interpretation problems with single-wavelength transmissometers 79−21054
lidar returns depolarization, scatt. from virga and source cloud 77−49169
lidar returns from fog, doubly scatt. radiation contrib. 78−77326
lidar returns from homogeneous fogs, doubly scattered radiation effects 79−53516
lidar system, two-freq. downward looking, for atm. monitoring 78−69523
lidar techniques for atm. pollution remote meas. *(Italian)* 79−70889
lidar techniques for atm. struct. and comp. obs., proposed Spacelab program 78−61602
LIDAR teledetection and measurement of minority atmospheric constituents for pollution control *(French)* 80−7992
lidar temperature profiling of planetary atmsopheres 77−33352
Lidar visibility measurements, using Raman/aerosol ratio method 79−100953
long range injection laser radar 78−5549
lower atmosphere dynamics study, optical and acoustic techniques *(Italian)* 77−91327
lunar and satellite laser ranging, future developments 77−64483
lunar laser ranging, introductory review of ephemerides 77−64617
lunar laser ranging, limits of theories of lunar libration 77−64677
lunar laser ranging, McDonald Observatory results 77−64678
lunar laser ranging, reference frame for positional astronomy 77−64618
lunar laser ranging ephemerides and reduction of observations 77−56815
lunar laser ranging rel. to orbital theory 77−64676
Mason method for lidar temp. profiling, computer simulation 80−21827
meteorological phenomena observation, mobile computerised laser radar system 80−56644
microprocessor controlled lidar for tropospheric O_3 meas. 79−58137
microprocessor-controlled 64-cell pulsed optical receiver for crosswind sensing 77−18096
mirror, large size lightweight scanning, for airborne laser sensor system 79−23045
mixed integrator processors, comparison of continuous and discrete types 77−19190
mobile lidar system for atmospheric gaseous pollutant meas. 80−35814
modulation phase nonuniformity over light beam cross-section, rel. to phase rangefinder 79−50400
multidither adaptive optical systems with zonal control of deformable mirrors 77−46795
multidither adaptive optics system, speckle interactive effects 77−46797
multidither coherent optical adaptive techniques 77−46793
multifrequency lidar, appl. to stratosphere aerosol microstruct. sounding *(Russian)* 77−64374

optical radar continued
multifrequency lidar, sounding of lower-stratospheric aerosol microstruct 80−56645
multiple atmospheric parameter meas. laser radar system 78−4009
oceanographic laser bathymetry, airborne, environmental subtraction technique 78−57372
oceanographic lidar system,; airborne, near-shore charting laser bathymetry 78−57371
oceanographic lidar system, airborne, bathymetric and fluorescing modes 78−57370
oceanology, lidar techniques *(Russian)* 79−39975
oil pollution on sea, remote sensing using laser radar 78−77373
oil spill remote detection by laser radar 79−25332
oil spills remote detection using laser-excited Raman backscatt. and backscatt. fluoresc. 78−32242
oil spills remote monitoring, computer controlled laser radar system *(Japanese)* 78−92994
oil water pollution detect. using scanning lidar system *(Russian)* 78−32123
optoelectronic system for detect. and tracking, optimisation in search operation mode 77−50765
partial tracking optical heterodyne receiver arrays, operating in turbulent atm. 79−41345
passive and active environmental remote sensing techniques 77−21935
petroleum oil pollution at sea, detection by CO_2 laser radar 77−91324
phase conjugate adaptive optics using perimeter phase meas. 77−46791
phase distortion correction using nonlinear optics 77−88855
photocounting radar analysis, optimum photon detect. 78−27956
photoelectronic position sensor, light sensitive head and elec. circuit 77−54806
pollution plume transport and diffusion studies using fluorescence lidar 80−101139
portable LIDAR for antipollution problems *(German)* 79−74583
power detected by receiver, narrowly collimated beam backscattered by reflector in turbulent atm. 80−32918
pulsed and Doppler CO_2 laser radar, for simultaneous velocity and range determ. 77−19320
pulsed laser radar, max. ang. accuracy in photocounting limit 77−75662
pulsed laser rangefinder using CO_2 TEA laser 78−46760
pulsed phase light rangefinder, 750 MHz modulation of injection laser radiation 77−54804
pulsed ranging, meas. accuracy improvement 77−23737
pulsed ranging, meas. accuracy improvement 78−25951
pulsed systems using photodetectors with lag, signal detection anal. 79−13918
radiation effect on laser system performance 80−38054
Raman lidar for industrial atmospheric pollutant remote analysis 80−12047
Raman lidar for quantitative pollutant meas. from stationary source 78−36291
Raman lidar humidity sounding of atmospheric boundary layer 79−66809
Raman lidar meas. of atm. temp. profiles 79−100974
Raman spectroscopy, remote spontaneous, new trends in recording of signals 80−73485
randomly rough target, laser radar cross section statistics 77−19169
rangefinder, AN/GVS-5 hand-held laser, production engineering techniques 78−59018
rangefinder principle, construction and test results 79−27427
ranging laser atmospheric transmissometer with retroreflector 77−21905
ranging system using non-Gaussian laser pulse shapes 77−10929
reference range for differential absorption lidars 80−89700
refractive effects of atmosphere on 10.6 μm lidar 80−36392
remote measurement of gases using discretely tunable IR lasers 77−87118
remote sensing, operational meteorological satellite system LEOS 79−5727
remote sensing of SO_2 molecules in air, methods assessment *(Japanese)* 78−96288
ruby lidar and stimulated Raman scatt. for differential absorpt. lidar meas. in O_2 A-band 79−39904
ruby lidar meas. of stratospheric dust from St. Augustine Volcano 77−29431
S/N ratio statistics, signals with specific energy and var. duration 78−17866
satellite laser ranging, corrections for atm. refractivity 77−75663
satellite laser ranging, effect of horizontal refractivity gradients 77−25910
satellite laser ranging, scintillation statistics 77−88900
satellite laser ranging system, 2cm accuracy, for geodetic research 77−21932
satellite laser ranging system 79−39994
satellite laser tracking data, horizontal refractivity gradient correction 77−91276
satellite ranging, compact ruby oscillator-amplifier system 79−966
satellite ranging, picosec. pulse freq. doubled Nd:YAG laser system 77−21933
satellite-borne lidar for global wind meas., computer simulation 79−58231
scattering and fluorescent targets, lidar eqn. analysis 77−58370
scattering from large dielec. spheres, lidar signal analysis from rainfall 78−66754
sea surface oil pollution detect. by lidar *(Russian)* 77−45019
SHF light rangefinder, optical elements, orientation errors effects *(Russian)* 80−64158
short-pulse photodiode receiver quasioptimal filtering 79−26132
signal processing, multichannel optical correlator 78−74847
simulator for low scatter charact., three-mirror design 78−59118
Smithsonian Astrophysical Observatory laser tracking systems 77−64481
smoke plume concentration meas. *(Chinese)* 78−58006
space autonomous rendezvous and docking with 10.6 μm ladar 78−57428
Space Shuttle lidar, OH radical in upper atmosphere, meas. 80−51590
spaceborne laser ranging systems for Earth crustal motions detect. 78−92995
Spacelab lidar, atm. expts. and methods 77−21948
Spacelab lidar, for atm. props. meas. 77−21943
Spacelab lidar for atmospheric topside sounding 77−21942
Spacelab lidar system for tropospheric aerosol monitoring 77−21876
stack plume obs. by laser radar *(Japanese)* 78−11990
optical radar continued
stratosphere, O_3 vertical profile determ. by lidar sounding from ground 78−11972
stratosphere aerosol meas. using two-colour lidar 77−25752
stratosphere aerosol size distrib., lidar obs. at 0.6943 μm and 1.06 μm 77−41120
stratospheric O_3 density meas., feasibility 77−60493
submarine periscope optical design for laser rangefinding compatibility 80−78987
submillimetric laser wave propagation, range and resolution 77−41242
submillimetric wavelength bad-weather vehicle recognition system 77−19450
surface oscillations meas. by 1.06 μm laser heterodyne method 79−50339
surveillance radar, range meas. potential accuracy 77−7202
target designator, 10.6 μm 77−88927
tetrahedral reflectors with metallised reflecting surfaces, polarisation state changes, effect *(Russian)* 77−27354
theory and methods for atmospheric composition meas. *(Japanese)* 78−16206
toronado clouds, expected lidar returns 77−21901
tracking system, laser designated target, simulation of low-level laser pulses 78−59074
tracking turbulence induced tilt errors with shared and adjacent apertures 77−46792
transit-time lidar velocimeter, detect. of atm. aerosol flow 77−13127
transmitter-receiver system, nearly coaxial, limiting detect. range through water 77−78461
troposphere, pressure and temp. meas. by lidar differential absorpt., influence of laser emission spectral width *(French)* 80−41554
tunable dye lasers for pollution monitoring 80−3562
turbulence compensating tracking system, lead angle effects 78−33763
turbulence-induced wavefront tilt error tracking with shared apertures 77−19459
two-photon lidar technique for atm. O remote sensing 79−39869
two-wavelength double-pulse tunable dye laser for differential absorption lidar 77−21939
University of Hawaii lunar ranging expt., geodetic-geophysics support programme 77−56569
visibility measurements, atmosphere extinction coeff. extraction accuracy 78−24369
water depth measurement using airborne pulsed Ne laser system 80−61908
water vapour, Raman lidear meas., daytime atmosphere 80−85718
wind meas. from orbit using lidar system 80−4114
wind remote measurements, individual particle scatt. and single-burst digital correl. 79−100980
wind velocity lidar meas. by spatial filtering 79−29901
Zeiss Eldi 2 electro-optical rangefinder, accuracy and range *(German)* 77−68274
CO_2 laser radar used to measure average atmospheric temp. 80−90225
(Hg,Cd)Te IR detector array, 72-element, 8-12 micron, performance, FLIR system appl. 79−2829
Na, K, mesospheric abundances, simultaneous nighttime lidar meas. 78−36239
Nd:glass laser/parabolic mirror lidar for airborne aerosol mass conc. meas. 77−21937
Nd:YAG laser as source for airborne lidar system for atmospheric expts. *(Italian)* 80−109278
O_3, conc. meas. by differential absorpt. CO_2 laser radar 79−96829
OH fluorescence lidar instrument for stratospheric temp. and press. determ. 79−80033
SO_2 air pollution detect. by differential lidar 78−96298
SO_2 remote meas. at 4 μm with continuously tunable source 78−77365
XeCl excimer laser radar, stratospheric O_3 layer meas. 79−16681

optical resolving power
see also optical instrument testing
140 keV γ position-sensitive multiwire proportional chamber characteristics 79−54749
acousto-optic deflector, resolution criteria 80−43265
acousto-optic deflector for TV and oscillograph displays 77−39099
acousto-optical scanner design, resolution 77−39045
active mirror characterisation by heterodyne interferometry 79−59799
aerosol particle sizing by optical scattering counters 77−21896
air at Ti surface, optical breakdown, interferometric investigation 80−100064
alkali metal vapour, IR image upconversion using two-photon resonant optical four-wave mixing 80−58632
amplitude filtering for superresolution, maximum central irradiance under energy constraint 80−91914
anamorphic system, image quality testing, resolving power determ. 77−7171
annular aperture, two point resolution limit with partially coherent light 77−88654
annular strips, point spread functions, super-resolution 79−907
apertures, multiple circular, located on circle, resolution 80−102615
apodisation for max. encircled-energy ratio, Sparrow limit of resolution 77−619
apodisation for max. Strehl ratio and specified Rayleigh limit of resolution 78−5425
apodisation for max. Strehl ratio and specified Rayleigh limit of resolution 80−28170
apodizing filters for optimum Sparrow resolution in coherent systems with annular aperture 80−53435
astronomical doublet system resolution, random speckle structure model and expt. *(Russian)* 79−7082
astronomical speckle patterns, interference, point spread function 77−22101
astronomical telescope resolution explanation *(Spanish)* 79−40075
axially symmetric filters, two-point resolution evaluation method 77−46697
birefringence in optical systems, brightness definition *(German)* 77−75429
butt-joined fibre component combination, resolution 78−30079
C-CD imagers, evaluation techniques 77−83990
calligraphic projection display resolution and contrast photometer and X-Y plotter 80−86373
camera, remote sensing, film and solid-state-array types comparison w.r.t. imagery 78−4723

optical resolving power continued
camera, resolving power type, sinusoidal targets design and construction 77−53999
centrally obstructed objective, resolution limit *(German)* 80−95811
channel waveguide array coupled to integrated C-CD, appl. 80−102860
circular apertures with parabolic filters, encircled energy in diffr. pattern 79−89845
COCHISE: laboratory spectroscopic studies of atmospheric phenomena with high sensitivity cryogenic instrumentation 80−95166
coded aperture imaging: the modulation transfer function for uniformly redundant arrays 80−99019
coherent light observation, resolvable degrees of freedom 78−13666
coherent light valve optical modulator 79−72712
coherent optical system, resolving power enhancement by aperture synthesis 78−25987
coherent synthesized aperture system, image form., resolution improved by diffr. grating 78−50715
coherent-optics image recognition using contour transparencies *(Russian)* 77−58260
computerised tomography scanners, survey of noise, dose and contrast detectability and resolution 80−104750
confocal scanning microscope, image form. 80−68249
contact-copying process resolution improvement 79−12876
contactless photoelectric fibre-optic vibration transducers 77−57319
correlation reduction, spatial filtering and variation of resolution 80−102850
degenerate four-frequency interaction, compensation of phase distortions 80−53380
diagnostic radiological high-resolution low light level video systems 77−40759
diffuse object, optical system resolving power influence on laser image quality 79−31820
diode laser, mear and far field characterization 80−48242
double beam interferometer, meas. of background suppression and spectral detection 80−95130
double-slit object illuminated with ultrasound-modulated laser light, resolution 80−37959
dye laser fast light deflection, ultrahigh resolution 78−63178
electro-optical spatial light modulator resolution, stored point charge effects 80−106616
electron micrograph, image processing systems, random noise removal 78−12791
electrophotographic KC film digital recording performance 78−78024
endoscopic miniature camera with fibre-optic faceplate 80−77896
etalon-spectrograph system, improved resolution over wide spectral range 80−101843
exponential transformation using film nonlinearity for optical homomorphic filtering 80−58467
eye, photoreceptor diameter and spacing for highest resolving power 77−70452
Fabry-Perot scanning interferometer, far IR performance 80−86388
far IR interferometric spectrometer, sampling comb generation and precision 80−47122
far IR modular Fourier interferometer construction, very high resolution 80−57401
fibre bundle, image transmission and resolving power *(Korean)* 79−14102
fibre near-field scanning technique resolution limit *(German)* 78−33856
field meas. Fourier transform spectrometer 80−86470
film waveguide spectrum analyser with prism coupling 77−62071
flexible high-resolution film recorder system 80−102827
Fourier holography, two-point resolution *(German)* 78−82933
Fourier spectrometer, 0.010 cm^{-1} working resolution, 20 to 1200 cm^{-1} 79−75603
Fourier spectrometer resolution determ. using solid-state Fabry-Perot etalon 78−89569
Fourier transform hologram, resolving power characts. *(Korean)* 77−50638
Fourier transform hologram spectrograph, parameters 78−37858
Fourier transform spectrometer, high resolution ruggedized 80−95152
Fourier transform spectroscopy, resolution limits 77−2701
Fresnel zone plates, image form. with short wavelength radiation 77−58437
Gaussian aperture operating in partially coherent light, two-point resolution 78−78918
graded-index optical waveguide characteristics meas. 79−14108
grating monochromator, real instrumental function 80−43452
grazing incidence spectrograph-monochromator with focusing toroidal mirror 79−75617
high resolution scanning resonant Raman spectrometer 79−6185
high-resolution AES in diffusion-pumped SEM 77−40515
high-resolution holographic aplanatic objective *(French)* 77−83837
high-resolution laser spectroscopy, techniques and applications 77−57403
high-resolution spectroscopy using tunable lasers 80−101849
hologram, multiple-beam type, resolution 79−13927
hologram, reflection, real image reconstruction, resolving power and diffr. efficiency 80−53237
holographic image and plate substrate quality relationship 80−48193
holographic image formation, coherent transfer functions and resolution 80−43292
holographic image magnification, new methodology 80−95851
holographic laser beam deflector performance characteristics 77−19287
holographic microscopy, lens assisted system, resolution tests 78−46539
holographic particle sizing high-resolution system 79−81392
holographic recorders, high resolution, using transparent electrophotographic film 80−102671
holographic reflective lenses for compact optical data processor 77−34829
holographic scanner imaging systems, active and passive, 8 to 13 μm, characts. 80−91755
holography, super resolution technique in Fresnel transform holography 80−9840
holography, white light refl., developer compositions compared 80−102669
holography advantages for physical structure meas. and recording 80−95843
IC nondestructive evaluation by improved reflective scanning acoustic microscope 79−50551
image anal., subjective and objective criteria 79−31828
image convertors, time resolution, contrast-time characts., calcs. 77−7208
image correlation, real-time high-resolvance, by Bragg diffr. in saturable absorbers 80−48159
image evaluation methods, project SENTINEL SIGMA for Air Force, resolution meas. 79−31826
image evaluation methods survey *(Czech)* 79−50235
image formation, super-resolution derivation by analytical continuation methods 78−29915
image reconstruction, computerized, fragment size choice 80−78785
imaging, high-resolution by degenerate four-wave mixing 80−69458
incoherent optical correlator using projected fringes patterns, for object shape and contour control 79−97357
instrument resolution power, influence on estimation of basic method spatial struct. parameters 79−52543
integrated focal plane arrays for thermal imaging 77−19448
intensified CCD photon counting array photometer 77−37964
interferometer, polarising, ultimate resolution, laser beam phase front radius of curvature meas. 79−88997
interferometer, rot. shearing, for imaging through turbulent atm., spatial freq. resolution 78−69450
interferometer spectrometers, field-widened 80−95146
interferometry, real-time heterodyne, high spatial and temporal resolutions 79−75574
i.r. imaging, airborne system resolution, object contrast depend. 77−2285
IR interferometric spectrometer, slow scan, resolution and performance 80−42274
IR sky survey telescope, wide field photography 80−105167
IR spectrum deconvolution beyond the Doppler limit 80−86467
Keplerian binoculars with erecting lens system 79−72662
land use classification by thermal IR scanning imagery 77−26422
Large Infrared Telescope on Spacelab 78−12070
laser diffraction-limited system, resolution, intensity, and power distribution 77−58425
laser Doppler velocimeter, spatial resolution and accuracy 77−24043
laser recording and information handling, seminar, San Diego, CA, USA (Aug. 1979) 80−101663
laser scanner, augmented resolution eqns. 78−55398
lens film system resolution computation from numerical MTF data 79−44960
lens light-guide line, image transmission characts. 79−3789
lens-array photographic system, depth of sharp focusing, resolution 80−62763
light divider phase distortion compensation improvement 78−58073
line image transmission through single fibre using spectral instrums. 80−102820
linear isoplanatic instrument, optimisation 77−83822
lithographic coated polyester panchromatic plate system 80−13172
long-wave imaging with super-resolution by wavelength diversity 80−102675
machine part, rotating, surface finish, laser method for determ. 80−89454
mammographic screen-film systems, comparison of laboratory and clinical evaluations 78−69187
mammographic X-ray screen sensitivity and resolution 78−7449
matrix multiplying optical system resolution calc. *(Russian)* 79−98456
Michelson inclined mirror interferometer, high spectral resolution, gaseous D_2O-H_2O-HDO mixture, absorpt. meas. 80−9023
microchannel image intensifier quality evaluation *(Spanish)* 79−72681
microdensitometer precision focus control 79−58769
microinterferometer, apochromat objective, with increased resolution, surface roughness testing 79−71519
microscope, harmonic, imaging props. and super-resolution 79−97430
microscope, two point resolution, semitransparent π-phase annular aperture 77−82597
microscope with semitransparent and π-phase annular aperture under Gaussian illum. 77−53972
microscopic image form., nonuniform source distrib. 77−14664
MIS photosensitive high resolution struct., spatial light modulation with liq. cryst. 80−96026
moderate-resolution spectrometer with interf. selective amplitude modulation, construction of prototype 79−30588
monochromator interdependent parameters and performance tradeoffs 79−90006
monochromator using concave holographic grating and plane mirror, imaging props. 80−99856
monolithic acoustic retina resolution improvement 79−55305
multilayer electro-optic space/time modulator resolution *(Russian)* 79−94343
multiple graybody resolution from spectrally sampled optical systems 79−76615
nonlinear image processing with optical feedback *(Russian)* 77−58258
object restoration beyond Rayleigh limit in presence of noise 80−102661
objects of unequal intensity, resolution in partially coherent light 77−88647
oligourethaneacrylate photopolymerised layers, production of holograms *(Russian)* 79−7102
one-dimensional system, two-point resolution with antiphase coherent illumination 79−72505
optical fibre, multimode, graded index, mode conversion coeff. meas. method 80−99820
partially coherent illumination, resolution of small double-bar targets in bright background *(Japanese)* 77−71928
periodic structure with coherent illum., resolution depend. on number of elements, wavelength and focal length 80−63941
phase angle effect on resolution of two coherently illuminated points 78−33683
phase contrast objective, point spread functions of annular phase filters 78−25805
photographic lens system, serial testing, resolving power limits 79−35870
photographic materials *(Russian)* 80−42292
photographic system, field and aperture quantitative determ. *(Spanish)* 78−49921
plastic focusing fibre for imaging appls., fabrication and characts. 77−62040
point images resolution, decision theory 79−81375
point source pair, resolution, S/N ratio and meas. precision, revised numerical results 80−95806
point source pair, resolution, S/N ratio and meas. precision 79−59643
polarimeter, precision, systematic errors, instrumental errors *(German)* 78−272

optical resolving power continued
polarising microscope, resolving power in partially coherent light 77−87819
precision objectives, high resolution, image-forming quality *(German)* 78−87120
predisperser for large plane-grating spectrograph 80−73477
prism-scanning panoramic camera for reconnaissance aircraft 77−79181
pseudocolour density encoding, white-light, using contrast reversal 80−83560
pupil filters for moderate superresolution 77−19181
radiography, resolution and contrast reduction 79−20663
random medium, image resolution limitation 78−37813
raster electron microscope test object 78−86393
reflection holograms, reduction of resolving power requirements of photographic. materials *(Russian)* 79−59658
regularized object restoration, resolution beyond the diffr. limit 80−87324
resonator, Gardner-Fresnel-Kirchhoff propag. algorithm 80−83621
reticle and scale fabrication, cyclohexadiene-1,3 pleinomer photoresist 79−27452
ruled steel grating system for length meas. 80−13039
satellite image sensing and multiplexing system tradeoffs 77−60498
scanning Fabry-Perot interferometer for balloon-borne astrophysical obs. 79−35092
scanning microscope, contrast and resolution 78−29154
scanning microscope, imaging props. and appls., super-resolution, review 80−82811
scanning microscopes, resolution criteria rel. to radiation detection technique 80−33388
scanning optical microscope for semicond. materials and devices 80−95136
schlieren photography, aberration and diffr. effects on resolution 77−34040
selective modulation interference spectrometer, operation and props. 77−74519
self-image resolution in multimode optical waveguides 78−63184
shaded circular apertures, encircled energy in diffr. pattern, super-resolving and apodising props. 80−95787
shadow device with photoelectric recording, for turbulence meas., resolving power 79−7210
slow scan SEC vidicon system coupled to telescope 77−25945
solid-state image sensor resolution evaluation by aperture sampling response 78−50939
Space Telescope optical design and performance control 79−80224
spatial resolution enhancement in coaxial light scatt. geometries 77−57393
spatial resolution of subwavelength sources from optical far-zone data, book contrib. 79−31825
speckle effects 77−19183
spectral instrument choice in plasma and flame emission spectrometry of traces 80−35613
spectrophotometer for measuring small sharp absorption bands in solids at low temps. 80−86456
spectroscopic resolution increased with separated gratings and prisms 80−43271
submillimetric laser wave propagation, range and resolution 77−41242
subwavelength spaced scatterer resolution, by superdirective data processing simulating evanescent wave illum. 79−36847
super resolution and cost of entropy 79−89862
superresolution of space-limited source fields by nonuniform plane waves 79−18358
surface waveguide electrooptical deflector, high-resolution, prism model 80−48454
system design, advances and problems 79−36975
telescope, weak object image distorted by atm. effect, restoration possibility *(Russian)* 78−32349
telescope with severe aberration, MTF for speckle interferometry 78−12103
telescope-spectrometer combination, optical props. 80−87455
tetrafluoromethane molecule, laser spectrosc. and optical pumping from CO_2 laser 80−74202
thermal imaging system resolution and S/N ratio, optical aberration effect 79−81552
thin-film waveguide, with plane diffr. grating, radiation fields and spectrosc. characts. 79−3790
tomography, computerized, NDT appls. *(German)* 80−76439
toroidal diffraction grating, monochromatic image of entrance slit, form., theory *(Russian)* 78−12770
turbulent medium, optical resolution with adaptive phase compensation 77−46692
twin hollow cathode interferometer-spectrometer, strongly cooled, imaging system *(German)* 77−61143
two dimensional image scanning of movies using surface acousto-optic interaction 79−94352
two-dimensional object imaging *(Japanese)* 78−87146
two-frequency microwave holographic imaging with axial resolution 78−1184
US lateral and range resolution improvement by optical computer 79−53203
UV high-resolution optical telescope design 80−90335
very-small-angle light scatt. apparatus design and performance 77−10082
vidicon varizonal target, resolution, internal elec. field effects *(Russian)* 77−7201
X-ray pinhole camera, resolution improvement by image processing 77−30222
zone plate with circular sensor, spectral resolution 77−42591
Ag-O-Cs photocathodes, time resolution, contrast-time characts., calcs. 77−7208
As_2S_3-Ag, light sensitivity for high exposure densities *(Russian)* 79−6212
EuO film for thermomagnetic recording, anisotropy of resolving power 80−20404
KD_2PO_4 crystal electron-beam spatial light modulator, resolution 80−74503
$LiNbO_3$ photorefractive reversible optical memory *(Russian)* 78−58943
Si array/$LiNbO_3$ gap-coupled imaging devices 79−46057
Si photodiode imaging array design factors 77−39085

optical rotation
see also Faraday effect; Kerr magneto-optical effect; rotational isomerism
absorbing anisotropic and gyrotropic slab between crossed polarisers, transmitted intensity patterns 80−78762
absorbing crystal, appearance of optical activity and circular dichroism, theory 77−63390
absorbing optically active crystal, singular directions 79−78646
absorption bands, optical activity, scatt. formalism treatment 78−72481
absorptive uniaxial optically active crystal, between crossed polarizers, light transmitted calcs. 79−61329
alkali halide:Tl^+, magneto-optical rot. dispersion anomaly near absorpt. bands 77−63400
alkali metal vapour, induced optical anisotropy in laser radiation field *(Russian)* 80−38525
4-n-alkoxybenzylidene-4′-methylalkylanilines, chiral nematic cryst., mesorphic behaviour and binary systems 78−2000
alkyl-cyano-biphenyls (and p-terphenyls) and related cmpds., chiral, synthesis and liq. cryst. props. 77−27820
para-alkylanilines having optically active modes, vibr. relax. studied by absorpt. and fluoresc. spectra 80−83340
amino acid photoresolution, rel. to origin of optical activity in life 77−40634
amino acid racemization, appl. to geochronology and geothermometry 78−20341
amino acids, high energy radiation effects and chemical evolution 77−63937
anisotropic acoustooptic deflector, using otically active uniaxial crysts. 78−66928
anisotropy in magnetic multidomain mats. 77−16279
aspartic acid racemisation and ^{14}C dating of Lake Ontario sediments 78−73415
atomic spectra, search for optical rot. induced by weak neutral currents 78−82710
atoms, and ions, parity nonconservation effects 79−10086
autorotation of polarisation ellipse in nonlinear medium *(Russian)* 77−58374
bacteria, E. Coli, optical activity, spectropolarimetric meas. *(Russian)* 79−26110
benzene, magneto-optic rotatory dispersion curves 80−45040
benzil, optical activity and circular dichroism 79−61328
1,1′-bianthryl derivatives, dimer optical activity, vibronic circ. dichroism, theoretical anal. 78−62821
1,1′-bianthryl derivatives, theoretical analysis of UV, circular dichroism and optical rotating dispersion vibronic spectra 77−34652
biaryls, dimer optical activity, vibronic circ. dichroism, theoretical anal. 78−62821
binuclear complex, M_2X_7YZ, optical activity calcs. *(Russian)* 79−95726
biomolecules, rel. to polarised bremsstrahlung 77−63938
biomolecules asymmetry correl. with parity violating weak interaction 78−69000
biopolymers, circular dichroism, optical rotatory dispersion, conformational anal., review 77−3497
biopolymers, studied by circular dichroism and optical rot., review 78−44457
bromochlorofluoromethane, and d_1, Raman optical activity atom dipole interaction model 79−82033
bromochlorofluoromethane, Raman optical activity parameters, circular intensity differentials comput. 79−85950
caesium tartrate, optical rot. dispersion, dichroism and spectra, in soln. and cryst. *(Russian)* 77−90124
camphor, d- and dl-solns. in carbon tetrachloride, electro-optical Kerr effect 79−91406
d-camphor, optical rot. dispersion spectra, solvent effects 77−10684
d-10-camphorsulphonic acid ammonium salts, characts. rel. to spectropolarimetry 77−24816
l-carvone, optical rot. dispersion spectra, solvent effects 77−10684
chemical reactions, prochiral, gravitational field effects 80−71899
chiral molecule, optical activity as mixed parity phenomenon 79−86011
chiral molecules, averaged discriminatory interactions, chem. effects 78−13562
chiral molecules, photodissoc. fragments, ang. distrib. theory 77−10713
chiral molecules containing ^{57}Fe, Mossbauer expts., optical activity analogy 78−27124
chiral substances, electro-optical responses, Jones matrix, meas. sytem for rot. anisotropy 80−84723
1-chloro-2-methylbutane, conformer depend. C-Cl stretching vibrs., Raman optical activity spectrum simulation 80−14146
cholesteric liq. cryst., pitch, temp. depend. and relation to optical activity, mol. model 79−86706
cholesteric liquid cryst., opt. activity, polaris. azimuthal depend., helical chain model 77−11479
cholesteric liquid crystal, chirality determ. by circularly polarised light obs. *(Japanese)* 77−1078
cholesteric liquid crystal, gyrotropy, depend. on thickness of layer 77−40204
cholesteric liquid crystal, imperfect, optical props. *(Russian)* 77−80420
cholesteric liquid crystal, influence of orientational order 78−42900
cholesteric liquid crystal, microstruct. rel. to optical props. 78−47240
cholesteric liquid crystal, normal incidence, boundaries effect 77−32345
cholesteric liquid crystal, optical activity, light scatt., theory 77−36195
cholesteric liquid crystal, optical rotatory power using multiple scaling 78−27176
cholesteric liquid crystal, screw sense determ. by droplet method 79−90544
cholesteric liquid crystal, spatial dispersion effect on optical props. 79−99844
cholesteric liquid crystal film, optical rotating power near cholesteric to smectic A transition 78−10865
cholesteric liquid crystal mixture, optical activity *(Russian)* 78−71677
cholesteric liquid crystal transforms. with temp. hysteresis 77−84902
cholesteric liquid crystals, apparent rotatory power *(French)* 80−50294
cholesteric liquid crystals, gyrotropy, region of electron absorption bands 78−10866
cholesteric liquid crysts., asymmetric synthesis failure using bimolecular reactions 80−44115
cholesteric mixtures, binary, IR rotatory dispersion 77−36194
cholesterol benzoates, intermolecular interaction, influence on optical props. *(Russian)* 79−77516

optical rotation continued
cholesterol cinnamates, intermolecular interaction, influence on optical props. *(Russian)* 79−77516
cholesteryl chloride-cholesteryl nonanoate mixture, pitch, temp. and comp. depends. 77−39535
cholesteryl decanoate, optical activity in blue phase 80−100641
cholesteryl esters, blue phase, model 80−88030
cholesteryl esters, isotropic mesophase, optical props. 79−65891
cholesteryl nonanoate, polymorphism of blue phase, optical rot. and refl. 79−37820
chromophone, natural optical activity, symmetry rules for dynamic excitation 77−18990
chromophores, semiempirical rules in circular dichroism, Cotton effect sign correl. with stereochem. 80−1006
circularly polarised laser radiation frequency shifting via rotating half-wave retardation plate 80−9800
classical crystal optics, lattice dynamical background, review 80−97221
classical scattering theory of optical activity of large molecules 77−31060
closed shell chiral molecule, polarised neutron beam interaction, optical activity 79−64111
cobalt(III) complex, octahedrally-coordinated with monodentate ligands, optical activity 79−50090
collagen, enzyme- and alkaline-soluble, optical rot. dispersion and circular dichroism 77−70411
collagen, optical activity rel. to ordered aggregation 79−11899
coupled oscillator model for opt. activity in Occupation Number Representation 79−31619
crystal, anisotropic, circ. dichroism, modulated polaris. spectra 78−23429
crystal gyrotropy, meas. in IR region 80−88957
crystal optical activity meas. method, appl. to KH_2PO_4 78−52466
crystallography, optical, book 80−12862
crystals, optical activity meas. technique *(Japanese)* 79−65832
cubic crystal, absorpt. saturation and radiation polarisation rot. by local vibrs. *(Russian)* 77−69797
cubic crystals, electro-optical effect rel. to spatial dispersion of permittivity 80−66151
cubic crystals, paramagnetic nonlinear Faraday effect, EM wave propagation *(Russian)* 80−80761
cyanine dyes, J-aggregates, swirl-induced optical activity 78−72482
demonstrations with polarised light 77−45657
1,6diazaspiro[4,4]nonane-2,7-dione, optical rot. strength calcs. 80−95793
dicalcium strontium propionate, ferroelasticity and opt. activity rel. to transition 78−76420
dicalcium strontium propionate, ferroelasticity and optical activity rel. to transition 77−76547
dicalcium strontium propionate, ferroelec. domains, direct optical visibility 80−84704
dielectric tensor field determ. in weakly inhomogeneous anisotropic media 79−72492
L-β-3,4-dihydroxyphenyl-α-alanine with L-glutamic acid, polymers and copolymers, synthesis and conform. 79−33996
direction dependent, photoselection, fluoresc. detected circular dichroism, circular polarisation of luminesc. 77−36279
dispersion-induced, new theory of olfaction 77−56393
DOBAMBC, smectic A to C transform., birefringence and optical rotary power 78−75812
doped cubic crystals, resonance absorption region, self-induced rot. of polarisation 80−2805
dye soln. tensor susceptance, reson. linearly polarised radiation, optical dye maser polarisation rot. *(Russian)* 77−58325
dynamic isomers and spontaneous generation of optical activity, phase rule prediction 79−34421
electrogyration in ferroelec. crystals, appls. 78−76394
electrogyration rel. to birefr. 78−27190
elliptic retarder, expt. method for optical parameters determ. 77−88941
elliptically polarized Gaussian beams, nonlinear precession 80−28269
ellipticity, azimuth and system parameters linking eqns., 3-dimens. model propag. 78−50695
enantiomeric compounds, optical purity, prod. by β-decay 78−40459
enantiomers, discrimination using liq. crystalline solns., IR rot. dispersion meas. 79−16064
ethylene, electronic states, optical rot. dispersion, oscill. strength calcs. 78−9095
ethylenediamine sulfate, cryst., induced gyrotropy of CrO_4^{2-} ion 80−108175
Faraday nonreciprocal effect for moving optically active material *(Russian)* 78−55298
ferrocytochrome c, mag. reson. Raman opt. activity at different laser wavelengths 77−38681
ferromagnetic fluid, magneto-optical activity in polarised reflected light *(Russian)* 78−76438
fibre waveguide, Brillouin and Rayleigh scatt. meas. 78−30085
formaldehyde-d_2, $\tilde{A}^1A_2$-$\tilde{X}^1A_1$ system, mag. rot. spectra 79−98127
free particle on helix, light circular dichroism and optical rotation, theoretical anal. 80−66146
gas, nonlinearly absorbing medium, light-induced optical activity 79−72615
gas, reson. optical activity induced by right-left nonsymm. mol. collisions 78−75254
gaseous medium, one- and two-photon resons., polarisation ellipse rot. 77−3621
L(+) glutamic acid halogen acid salts, crystallographic, optical and calorimetric meas., halide effect 78−34505
gyroanisotropic crystal light polarisation states, Cauchy problem 80−20609
gyrotropic absorbing crystals, nonorthogonal eigenwave refl. 80−99624
gyrotropic crystal, EM wave polarisation 77−4615
gyrotropic crystals, behavior of Poynting vector of EM waves in optically active crysts. 79−56758
gyrotropic layer, 4×4 interference matrix 79−55054
gyrotropic medium, Green's function and field of moving charges 80−58445
gyrotropic phase transitions 78−71852
gyrotropy, an implicity form of ferroicity 79−73286
HOAB-cholesteryl benzoate mixture, twisted smectic-C and twisted nematic phases, optical and X-ray investig. 77−84634
HOAB-DOBAMBC nonchiral-chiral smectic C mixture, spontaneous polarization and induced circular dichroism 79−27910
homogeneous wave energy flux under conical refraction and induced gyrotropy 78−17861
optical rotation continued
hydrazonium tartrate enantiomers, and deuterates, struct. and opt. props. 77−68954
hydroxypropyl cellulose in conc. aq. soln., mesophase struct., colour 77−19870
induced elliptic double refraction, separation into linear and circular components *(German)* 77−24817
inhomogeneous birefringent optically active medium, polarisation evolution 78−9328
inhomogeneously magnetised media, Faraday effect, polarisation plane rotation *(Russian)* 80−66154
isotropic medium, moments of optical rotary power and circular dichroism 80−88956
isotropic medium, nonlinear refr. index, self-induced polarisation rot. 80−5802
ketones, rigid, optical rot. dispersion spectra, solvent effects 77−10684
lactams, optical rot. strength, sector rules 78−17737
lactones, optical rot. strength, sector rules 78−17737
laser polarisation rotator, broad band, using successive refls. from 4 mirrors 79−981
laser-induced optical activity, QED theory of multiphoton processes 79−31794
lattice dynamical background of optical activity 80−93267
lattice dynamical theory of optical activity in crystals 80−34883
lens-mirror reflector system, optical rotation multiplier *(Russian)* 78−46745
linear anisotropic crystals, acousto-optic interactions, general theory 79−99850
linear gyrotropic media, E2, M1 moment contribs. to linear polarisation *(Russian)* 77−8540
linearly polarised light, optical rot. by linearly polarised light in active medium 77−27248
liquid, dynamic and static orientational pair correls., depolarised light scatt. 77−16321
liquid crystal polarization rotator for intermodulation spatial-bandwidth reduction holography 80−53439
liquid crystal thermometry, optically active binary mixture 79−42952
liquid crystal thin layer, polarised light ellipticity after passage 80−88036
low value rotation angles, detection and measurement *(Rumanian)* 80−22418
low-temp. cryst. modification, gyrotropy *(Russian)* 77−85684
lysozyme protein solution, threshold power for laser operation 79−68391
macromolecular conformation under press., optical rotatory dispersion meas. method 77−48984
magnetic crystals with natural optical activity optical props. 78−60415
magnetic gyrotropic absorbing crystals, refr. index tensors 77−8539
magnetoelectric susceptibilities, phenomenological rules for computation 80−55068
MBBA, cholesteric struct. induced by chiral sulphoxides 79−86683
mesogens, chiral, liq. cryst. phase transition temp. 78−2241
methyl ethyl ether, charact. vibrs., isomer and isotope effects, rel. to reverse spectral problem 80−63613
methyl torsion modes, vibrational optical activity, inertial contrib. 80−5524
1-methylindan, circular dichroism, rot. strengths, CNDO/S calc. 79−3452
mirror image molecules, parity non-conserving energy difference 79−76366
molecular crystal, optical rotation induced by ultrasonic wave *(Russian)* 80−93270
molecular crystal symmetry props. from optical activity and gyrotropic birefringence calc. *(French)* 78−42941
molecular crystals, self-induced nonlinear optical rotation 78−1308
molecular isomers, quantum beats in optical activity and weak interactions 78−94293
molecular negative ion, photoelectron ejection ang. distrib. theory 77−491
molecular optical activity, hyperpolarisability contrib. 78−70890
molecule, chiral, Rayleigh and Raman circ. intensity differential 77−34639
molecule, optical rotatory strength, CI role in CNDO/S calc. 77−83561
molecule, optically active, photoelectron ejection ang. distrib. theory 77−491
molecules, electronic transitions, g-factor determ. by polarisation plane mag. reson. rot. *(Russian)* 78−70954
molecules, latent optical activity *(Russian)* 77−83670
molecules, optically active, coherent Raman scatt., quantum theory 80−69150
molecules, optically active, differential Raman scatt. of right and left circularly polarized light *(Japanese)* 78−17675
molecules, optically active and inactive, electric and mag. dispersion forces interaction 80−99533
molecules, optically active mirror systems, parity-violating effects of weak interactions 80−52455
molecules, Rayleigh and Raman optical activity, scatt. angle anal. 80−69151
molecules, rot. optical activity 79−72298
nematic liquid crystals, induced cholesteric order by chiral 2,2′-spirobiindane derivatives *(German)* 80−64884
nematic liquid crystals, mixtures with optically active substances, stable inhomogeneities and diffr. gratings 78−1988
neodymium oxydiacetate, magneto-optical rotatory dispersion and oxid absorption spectra 79−91409
nonlinear optical susceptibility meas. by polarimetry *(Russian)* 77−61112
nonlinear polarisation resonances in a continuum, optical activity, spin-orbit interactions *(Russian)* 80−53391
nonracemic mixtures, theory of chirality functions, concept of qualitative completeness 80−69255
nonrigid molecules, optical activity criterion reformulation 79−86010
organic compound soln., relax. of rot. rel. to laser emission polarisation *(French)* 78−58738
oscillating electric dipole contrib. to light scatt. and interpret. in terms of polarisability and hyperpolarizability 80−53212
parity non-conservation effect in atoms and molecules 80−68395
peptides, optical rot. strength, sector rules 78−17737
phase IV, cholesteric struct. induced by chiral sulphoxides 79−86683
(+)-(S)-2-phenyl-3,3-dimethylbutane, optical activity, circular dichroism, polarisability model 80−43082
polarimeter for reflected or transmitted light 77−74487

optical rotation continued
polarimetry, noise suppression by polarization-plane rotation-angle amplification 80−68241
polarisation-optical mechanical-stress meter 77−45879
polished glass surface, reflected light phase rotation 80−66147
poly(γ-benzyl-L-glutamate), in benzene soln., cholesteric liq. cryst. props. 79−94889
poly L-lysine, temp. induced conformation transition in solns., optical rotary meas. 78−46474
poly O-carbobenzoxyl-L-tyrosine, in soln., conformation, helix-coil transition, circular dichroism, NMR spectra 77−31037
poly-9-vinyl carbazole, fluoresc. props. 78−84647
poly-γ-benzyl-L(D)-glutamate, soln., liq. cryst. and pretransitional regions, optical rot. 80−66145
poly-thio-1-N,N-diethylaminomethylethylene, optically active samples, ^{13}C NMR spectra 80−28127
polyamide, aromatic, persistence length, rel. to optical anisotropy of worm-like chain 77−50577
polydisperse system, rotatory diffusion const., electro- optic decay curve, size distrib. 78−20079
polymer, infinite helical, classical theory of circ. dichroism 77−65550
polymer, optically active stereoregular, conform. props., rel. to config. 78−33644
polymers, helical, optical activity, decorrel. approx. theory 77−63389
polymers, synthetic, chiral, with aromatic side chains, conform. from circ. dichroism 79−55014
polymers containing carbazole units, optically active, fluoresc. props. 78−84647
polynucleotide, double-stranded, conform. inhomogeneity of sugar-phosphate chain rel. to compact particle optical activity 80−35839
polypeptides, poly-L-lysine based, comb-like, struct., physicochem. props. *(Russian)* 79−55644
poly[trityl methacrylate-co-(S)-α-methylbenzyl methacrylate], abnormal optical rot. 79−31749
praseodymium oxydiacetate crystal, opt. rot. dispersion 77−36193
pressure jump method for fast kinetics using optical rotation and circular dichroism 78−77175
propyleneimine, circular dichroism, optically active Rydberg transitions 77−18952
pseudoisocyanine bound by sulphated polysaccharides, dil. aq. soln., visible and circular dichroism spectra 80−45107
PT asymmetry and four-fold EM degeneracy lifting, appl. to ring laser mode splitting, optical prop. effects 80−23606
Q-switched pulse stretching by intracavity nonlinear ellipse rot. 78−17991
QED theory of differential scatt., Rayleigh scatt. of circularly polarised light, two chromophores model 78−9157
quartz, birefr. and opt. rot. near structural phase transition points 78−75823
quartz, electrogyration effect, electric field depend. of optical activity 77−32352
quartz, electron irradiation effects on optical, dielec., elastic props. 80−59521
quartz, induced elliptic double refraction, separation into linear and circular components *(German)* 77−24817
quartz, nonlinear polarisation plane rotation due to ruby laser irrad. *(Russian)* 80−53390
quartz, X-ray optical props. determ. using novel X-ray polarimeter 79−6251
Raman and Rayleigh scatt. by optically active mol., elliptical polaris. production 77−58089
Raman optical activity parameters, circular intensity differentials comput. by atom-dipole interaction model 79−76407
Raman spectroscopy, recent advances, reivew 78−41359
Raman spectroscopy of chiral molecules in mag. fields 80−102532
resonance medium, high power radiation polarisation ellipse, mag. rot. *(Russian)* 78−70794
resonance medium, induced dichroism and gyrotropy 80−9971
resonant degenerate four-wave mixing, polarisation rotation and thermal motion 80−5779
reverse spectral problem, charact. vibrs. effects calcs. 80−63613
rhodopsin, bovine, conform. in situ and solubilised with detergent 77−44587
ring interferometers, optically active samples, polarisation props. *(German)* 80−77846
ring laser, unidirectional system efficiency comparison *(French)* 79−76717
Rochelle salt, electrogyration during phase transitions 79−19859
rotatory strength, gradient matrix eqn. of motion calcs. 80−95793
rubidium tartrate, optical rot. dispersion, dichroism and spectra, in soln. and cryst. *(Russian)* 77−90124
scattering objects, optical activity, spectropolarimetric meas. *(Russian)* 79−26110
semiclassical theory, appls. to pure rot. spectroscopy 77−75132
semiclassical theory, near reson. absorpt. 77−75131
semiconductor with wurtzite structure, natural optical activity *(Russian)* 79−78647
semiconductors, role of excitons in dispersion effects, band gap determ. 79−65393
semiconductors polarised light nonlinear rotation 80−93268
simulation of mech. rot., appl. to Fourier photopolarimeter 78−65958
single-mode fibre birefringence and optical activity obs. 78−1394
sinusoidal, for hybrid null-photometric ellipsometer 77−61110
Sodium ammonium tartrate, L- and D-mol. energy difference, parity violation 78−25744
2,2′-spirobiindane derivatives, chiral, cholesteric order induction in nematic systems *(German)* 80−64884
Stokes relations in optically active media, macroscopic reversibility principle appl. 80−53207
sugar, optical rotatory power, polarisation modulation meas. 79−21803
sugars, detect. in HPLC systems using polarimetry, refractometry and optical rot. 78−48734
sum rules in optical activity 77−26993
tangential isotropic polarisable atomic unit model, optical rotation calc. *(French)* 79−54989
TGS, electrogyration during phase transitions 79−19859
thermal optical rotation, temp. depend. 79−8111
three-mirror system as IR broadband polarisation rotator 77−58413
time-dependent birefringence, linear dichroism, and optical rotation resulting from rigid-body rotational diffusion 79−47411
optical rotation continued
transition metal complexes, octahedral, optical rot. dispersion theory 77−77164
tryptophan, stereoselective energy transfer induced by circularly polarised light 80−1010
tunnel centres, resonant optical orientation, kinetic eqn. *(Russian)* 78−43911
twisted IR metal waveguide, low-loss propag. and polarisation rotation 79−41435
twisted single-mode fibres, polarisation optics 79−81524
two-level atom gas, optically induced optical activity 79−18490
two-level system, optical rotary saturation 78−13770
uniaxial crystal with scalar permittivity, optical activity 77−4614
UV microscope for polarised light, determ. of birefringence, linear dichroism and optical rotary dispersion *(German)* 78−29152
vibrational Raman optical activity spectra, perpendicular polarisation recording method 79−21821
visual excitation, mol. mechanism for initial process, optical activity in rhodopsin and bathorhodopsin 77−52783
β-AgI, exciton refl. spectra, optical activity *(Russian)* 78−64380
As_2S_3 glass, natural optical activity and related phenomena 79−73895
As_2S_3 glass, natural optical activity and related phenomena 79−95727
$Ba_2Fe[Ge_2O_7]$, hydrothermal growth, struct. and opt. props. 77−65971
Bi, neutral current-induced parity nonconserving optical rot., Dirac-HF calcs. 80−47948
Bi, outer electron shielding, parity non-conserving optical rot. 79−18153
Bi parity non-conserving optical rotation search 77−10642
Bi, parity non-conserving optical rot., Weinberg-Salam relativistic central field theory vs. obs. 78−953
Bi, parity nonconserving optical rot. upper limit, obs. vs. Weinberg-Salam theory 78−952
Bi, parity-nonconserving optical rotation 79−63968
Bi, vapour, optical activity and HFS, neutral weak currents *(Russian)* 79−13660
Bi, vapour, optical rot., parity nonconservation 80−23353
Bi, vapour, optical rot., parity nonconservation expts. 80−23354
Bi, vapour, parity violation in optical activity 79−26938
$Bi_{12}GeO_{20}$, cryst. chirality and optical rotation sense 79−61327
$Bi_{12}GeO_{20}$, light polarisation, elec. field effect *(Russian)* 77−66480
$Bi_{12}SiO_{20}$, cryst. chirality and optical rotation sense 79−61327
$Bi_{12}SiO_{20}$, laevorotatory, cryst. struct., absolute piezoelec. d_{14} coeff. 79−94974
$Bi_{12}SiO_{20}$, light polarisation, elec. field effect *(Russian)* 77−66480
$Bi_{12}SiO_{20}$, optically active photorefractive cryst., light diffr. by vol. holograms 79−64185
$Bi_{12}SiO_{20}$, use in incoherent-to-coherent optical image convertor of transmission type 79−94340
$Bi_{12}SiO_{20}$, volume hologram polarisation props. and appls. 78−74859
^{209}Bi, P violating eN pot., determ. of effects by optical rotation meas. 79−26277
$CaS_2O_6.4H_2O$, isomorphic substitution effect on optical activity 77−32347
$CaWO_4$, centrosymmetric cryst., linear electrogyration study 80−60540
$Cd_2(NH_4)_2(SO_4)_3$, X-ray and optical studies of ferroelec. phase transition 79−38495
CdP_2, 442 class gyrotropic crysts., self-induced rot. of light polarisation plane 80−99810
CdP_2, birefringence and optical activity 78−15143
p-CdP_2, Faraday rot., inherent optical activity dispersion *(Russian)* 78−35119
CdP_2, light polarisation, self-induced rotation 79−19860
CdS, optical activity in exciton spectra region, reflectance spectra 79−28707
CdS, optical axis inversion *(Russian)* 79−24284
CdS, spontaneous optical activity in exciton spectrum *(Russian)* 78−35167
CdS, strain- and electro-gyration, polarised light dispersion curve pseudocrossing 77−36196
CdS, wurtzite structure, natural optical activity *(Russian)* 79−78647
$CdSiP_2$, optical activity near isotropic point, absorpt. spectra 79−69804
Co complex, C0(l-spartein)Cl_2, IR circular dichroism spectra, vibr.-electronic interaction 80−55074
Co complex, $\Lambda(+)[Co(en)_3]^{3+}$, quadrupole transition circ. dichroism, production mechanism 79−3428
Cs, $7P_{3/2}$-$6S_{1/2}$ transition, photon-echo quantum beats obs. 80−23373
$CsCuCl_3$, cryst., gyrotropy, anomalous dispersion curves 80−2719
$CsCuCl_3$, optical props. rel. to IR electro-optical modulator appl. 78−42393
$CsCuCl_3$, phys. props. 77−62511
EuO, optical orientation of f-electrons, Curie temp. variation due to exchange interactions *(Russian)* 79−15431
$FeBr_2$, Faraday rotation in pulsed mag. field, linear absorpt. const. 80−45041
$FeCl_2$, magnetic phase diagram, optical studies 78−88121
GaAs-$Al_xGa_{1-x}As$ electro-optic frequency- and polarisation-modulated injection laser 80−91810
GaSe, optical orientation and free exciton alignment on reson. excitation *(Russian)* 77−69812
$Gd_2(MoO_4)_3$, optical activity, gyration tensor determ. near Curie point 79−33660
$Gd_2(MoO_4)_3$, optical activity *(Japanese)* 79−65832
$Gd_2(MoO_4)_3$, spontaneous rot. of plane of polarisation of light in external field 80−93282
α-HIO_3, electrogyration coeff. meas. 79−19859
α-HIO_3, optically active biaxial crystal, conical diffr. intensity patterns 79−4785
H_2O_2, electronic states, optical rot. dispersion, oscill. strength calcs. 78−9095
H_2O_2, twisted mol., optical rot. strength calcs. 80−95793
α-HgS, synthetic cinnabar, morphological, optical and X-ray studies *(French)* 77−43223
KCl:Li, self-induced resonant optical rotation 79−65831
KD_2PO_4, optical activity in paraelec. phase 80−60539
$KD_3(SeO_3)_2$, optical and dielec. props. near ferroelastic phase transition 79−38518
KH_2PO_4 crystal, optical activity 80−71373
KH_2PO_4, electrogyration near transition pt. in nonenantiomorphic cryst. 79−61339
KH_2PO_4, optical activity meas. 78−52466
KH_2PO_4, optical activity, gyration tensor determ. near Curie point 79−33660

optical rotation continued
KH_2PO_4, optical activity *(Japanese)* 79−65832
$KH_3(SeO_3)_2$, optical and dielec. props. near ferroelastic phase transition 79−38518
$KLiSO_4$:(Cr), uniaxial crysts., circular dichroism and optical activity 80−45029
$KLiSO_4$:Cr; optical activity characts. cryst.-chem. exam. 78−95569
$KMnF_3$, $CsCuCl_3$, NH_4Br, birefr. and opt. rot. near structural phase transition points 78−75823
$(La,Nd)P_5O_{14}$, optical props., ferroelastic phase transition induced 79−95731
$LiIO_3$, circular dichroism and UV absorpt. spectra, optical activity 77−20879
$LiIO_3$, electrogyration coeff. meas. 79−19859
$LiIO_3$, nonlinear optical activity *(Russian)* 79−45994
α-$LiIO_3$ single crystal, enantiomorphism 79−95725
$LiNbO_3$, hologram, light diffr. with electro-optical rot. *(Russian)* 78−1190
$LiNbO_3$:Fe, induced optical inhomogeneity, refr. index and short-circuit photocurrent meas. 79−69806
MBBA+optically active substance, pretransition optical rotation in isotropic phase *(Russian)* 80−92657
n-GaAs semiconductor, inhomogeneities visualisation by CRT displays *(Russian)* 77−90123
NO_2, g-factors of electronic transitions determ., use of resonance optical rot. 79−54876
Na, laser orientated vapour, rotary power determ. 79−32737
Na laser oriented atoms, refl. by non-disorienting surfaces, optical activity detect. 80−55252
Na vapour, diffusion coeff. of oriented atoms in buffer gases 80−53908
$NaBi(MoO_4)_2$, electrically induced optical activity 79−82942
$NaBrO_3$, cryst. chirality and optical rotation sense 78−10026
$NaBrO_3$, light polarisation, elec. field effect *(Russian)* 77−66480
$NaBrO_3$, optically active, crystal atomic struct. remeas. 78−10009
$NaClO_3$, cryst. chirality and optical rotation sense 78−10026
$NaClO_3$, electrogyration and piezogyration meas. 79−28716
$NaClO_3$, optically active, crystal atomic struct. remeas. 78−10009
$Na_2O.SiO_2$-Tb_2O_3 glass magnetooptical study 80−88976
Ni complex, Ni(l-spartein)Cl_2, IR circular dichroism spectra, vibr.-electronic interaction 80−55074
NiO, multidomain mat., opt. anisotropy meas. at T_N 77−16279
$NiSO_4.6H_2O$, uniaxial crysts., circular dichroism and optical activity 80−45029
Pb, parity nonconservation, weak electron-electron interaction, light polarisation, vapour optical activity *(Russian)* 78−55132
$(Pb_{1-x}Ba_x)_5Ge_3O_{11}$, ferroelec. transition blurring, US relax., dielec. and opt. props. 78−95559
$(Pb_xBa_{1-x})_5Ge_3O_{11}$, electrogyration, and dielectric props. 78−19444
$(Pb_{1-x}Bi_x)_5Ge_3O_{11}$, spontaneous and induced electrogyration 79−42946
$Pb_5Ge_3O_{11}$, electrogyration during phase transitions 79−19859
$Pb_5Ge_3O_{11}$, ferroelec., induced and spontaneous optical activity, permittivity 79−33661
$Pb_5Ge_3O_{11}$, multidomain mat., opt. anisotropy meas. at mag. crit. temps. 77−16279
$Pb_5Ge_3O_{11}$, uniaxial ferroelectric, optical activity dispersion 78−48141
$xPb_5GeO_4(VO_4)_2$, $(1-x)Pb_5SiO_4(VO_4)_2$, solid solution of centrosymmetric crystals, electrically induced optical activity 80−108180
$Pb_5GeO_4(VO_4)_2$, centrosymmetric crysts., induced linear electrogyration 80−45039
$Pb_5(Ge_{1-x}Si_x)_3O_{11}$, electrogyration, phase transition and dielectric props. 80−93269
$PbHPO_4$, optical props. near ferroelec. transition 79−33663
$PbMoO_4$, centrosymmetric cryst., linear electrogyration study 80−60540
$PbMoO_4$, electrogyration coeff. meas. 79−19859
$PbS_2O_6.4H_2O$, isomorphic substitution effect on optical activity 77−32347
$Pb_5SiO_4(VO_4)_2$, centrosymmetric crysts., induced linear electrogyration 80−45039
$RbNO_3$, low-temp. cryst. modification, gyrotropy *(Russian)* 77−85684
SF_6, polarization-rotation and thermal-motion studies via resonant degenerate four-wave mixing 80−5779
Si, X-ray rot. polarisation, absorpt. crystal orientation effects 78−47206
$Sm_xTb_{1-x}FeO_3$, rotation of polarisation plane, ang. depend. 77−43961
$SrMoO_4$, centrosymmetric cryst., linear electrogyration study 80−60540
$SrS_2O_6.4H_2O$, isomorphic substitution effect on optical activity 77−32347
TE, current induced optical activity, polarisation plane rotation rate *(Russian)* 79−65830
Te, natural optical activity and features of struct. of electronic energy spectrum 79−8110
Te, optical activity, de Haas-van Alphen oscillations and cond. band parameters 80−54605
Te, optical activity rel. to band struct., 4 to 300K 77−77165
Te, optically active crystals, circular photogalvanic effect 80−54739
Te, synthetic, optical props. in visible spectrum and microhardness meas. *(French)* 77−28590
Tl, parity nonconservation, weak electron-electron interaction, light polarisation, vapour optical activity *(Russian)* 78−55132
YIG, forced magneto-optical rot. 79−61347
YIG:Tb garnet, Faraday effect in strong mag. field *(Russian)* 80−100651
Zn complex, Zn(l-spartein)Cl_2, IR circular dichroism spectra, vibr.-electronic interaction 80−55074
ZnP_2, 442 class gyrotropic crysts., self-induced rot. of light polarisation plane 80−99810
ZnP_2, birefringence, circ. dichroism, temp. depend. *(Russian)* 79−1748
ZnP_2, birefringence and optical activity, dispersion 78−2821
ZnP_2, light polarisation, self induced rotation 79−19860
ZnP_2, rotation of plane of polarisation of light 79−15432
ZnP_2, tetragonal bright red crysts., natural optical activity 77−16276

optical saturable absorption
$^1\Sigma$ state, anomalous Zeeman effect, Doppler-free standing wave saturated resonance, book contrib. 78−9279
acetylene flame, Na and MgO concs. meas. by laser saturation spectroscopy 79−29425
aerosol medium bleached zone, probe radiation propag., intensity and phase fluctuations 80−67411
alkali halide, ReO_4^- doped, saturable absorber at 10.6 μm 80−53384
aqueous polydisperse aerosol, bleaching by high intensity beam 77−58394

optical saturable absorption continued
atmospheric laser beam transmission at 10.6 μm, analytic model of bleaching 78−85688
atom, Doppler-free multiphoton excitation, light shift and saturation 79−76399
atom, resonant two-photon ionisation, saturation and Rabi oscills. 77−79589
atom, three-level, saturation spectroscopy including collisional effects 80−37099
atom, two transitions sharing common level, simultaneous saturation 77−75114
atomic collisions, vel. changing, saturation spectroscopy, internal coherences 78−42245
benzene derivatives, monohalogenated, saturable absorpt. of CO_2 laser 80−69465
bistability, dispersive, beyond mean-field theory 80−43408
bistability, in lasers containing saturable absorbers, semiclassical and quantum theory 79−3674
bistability through nonlinear dispersion and absorpt. 79−76653
bistable absorber system, in ring cavity, photon statistics 79−31847
bleaching-wave front, stability 77−42574
cone-type light beam structure in nonlinear medium 79−98437
CW laser, homogeneously broadened gain, longit. mode selection 78−63143
difference frequency generation by stimulated Raman scatt. using inhomogeneous electrostatic field 80−95954
1,1-difluoroethane, high intensity transmission characts., for possible appl. in CO_2 amplifier gain isolation 78−42387
1,2-difluoroethylene, high intensity transmission characts., for possible appl. in CO_2 amplifier gain isolation 78−42387
diphenyl butadiene, absorption recovery lifetime, use in UV mode-locked lasers 80−19075
DODCI, saturable absorber, picosecond phase-conjugate refl. 80−95960
DODCI dye dissolved in glycerine, time delayed picosecond pulse transmission obs. 80−48355
Doppler line profile, saturation, influence of atomic collisions 78−70792
Doppler-free intracavity polarization spectroscopy using elliptically polarized light 80−5537
Doppler-free two photon and saturation spectroscopy, using thermionic detector 78−46465
DQOCI saturable absorber, passive mode-locking of fluorol 7GA dye laser 77−38922
dressed molecule, RF field, saturated absorpt. obs. 80−9648
dye, bleachable no.3955, relax. time meas., laser passive shutter appl. 80−23759
dye, bleaching, coherence time meas. of laser radiation 80−23739
dye, saturable, regerative compression of mode-locked laser pulses 80−95925
dye bleaching, no. 3955 in soln., relaxation and correlation times meas. 80−28281
dye bleaching, picosecond light pulse shape and duration determ. 79−86220
dye cell, contacted mode-locking, for use with Nd^{3+}:glass laser 79−18454
dye cell saturable absorber, for intense laser beam apodizing 79−31965
dye compositions bleachable by I laser, for passive Q-switching 80−91826
dye laser, continuously pumped, pulse compression with slow saturable absorber 79−31959
dye laser, CW, synchronous pumping and passive mode-locking, for picosecond pulse generation 79−3727
dye laser, mode-locked CW, subpicosecond pulse generation with slow saturable absorber 80−9915
dye laser, synchronous mode locking, composite gain and absorber medium, sub ps pulses 78−79046
dye laser with saturable absorber, stationary pulse parameters, approximate theory 79−3690
dye lasers, flash lamp pumped, mode locking, picosecond, pulse generation 78−71131
dye passive switch for Nd laser pulses, transmission coeff. depend. on power density 77−23686
dye saturable absorber, double mode locking of ruby laser 80−99763
dye saturable absorbers, picosecond phase-conjugate refl. 80−95960
dye saturable absorbers for Nd laser, bleaching spectra 77−42573
dye solutions, high power UV irrad., bleaching and diffusion 77−42533
dye solutions for laser beam modulation, population relaxation lifetime meas. *(Russian)* 80−95964
dye synchronously pumped laser combined with external compressor, sub-ps pulse generation 79−55148
dye ultrafast saturable absorbers for Nd lasers 80−53386
enhanced photon bunching, from saturable absorber, exptl. verification 79−50356
enhanced photon bunching from saturable absorber 78−37948
Fabry-Perot cavity, absorptive bistability, mean-field approx., truncated Bloch hierarchy 80−83631
Fabry-Perot cavity, instabilities for coherently driven absorber 80−53387
fast absorber model, periodic pulse solns. and stability 78−59054
fluoremethane, saturable absorpt. of CO_2 laser radiation, theory 78−37946
fluorescence excitation, transition probabilities and particle density determ. 78−58871
fluoromethane, IR absorpt., CW saturation, theory 77−83933
frequency stabilisation of He-Ne lasers by ref. to I and methane absorption transitions 77−83913
gas isolator mixes for CO_2 laser system 78−46663
gas mixtures, nonlinear absorpt. spectroscopy 79−63315
gas saturable absorber, formic acid and SF_6 cells, as isolator for 9 μm band CO_2 laser amplifier 79−76709
glass fibre waveguide, γ-irrad., reversible optical bleaching of induced absorpt. 80−14462
grating dip obs., tunable-laser-induced 79−3751
high-pressure saturable absorber gases, for CO_2 laser gain isolation 78−59095
high-sensitivity, high-resolution spectroscopy techniques 79−40626
hole burning, photophysical and photochemical theories 80−58322
homogeneously broadened medium, dispersive bistability 79−50355
homogeneously broadened transition, shape of absorpt. line *(Russian)* 78−46729
hydroxyquinones, H-bonded, zero-phonon photochem., hole burning obs. 79−11802

optical saturable absorption continued
image correlation, real-time high-resolvance, by Bragg diffr. in saturable absorbers 80−48159
inhomogeneously broadened spectra, dip contour saturation *(Russian)* 78−76503
instability of pulse front transversing reson. saturable absorber 79−72631
intense picosec. pulse photodynamics 77−34887
interference spectroscopy, saturated, improved S/N ratio 78−70193
interferometric spectroscopy using Jamin interferometer 78−74079
intracavity absorber modulation, transients obs. in CO_2 or N_2O IR laser 78−74933
intracavity inverted Lamb dip, of laser with nonlinear absorpt. cell 77−14765
intracavity laser spectroscopy sensitivity, saturation absorpt. influence 79−63312
iodomethane, dressed mol., ν_6 band, saturated absorption spectrosc. 79−54844
iodomethane, RF field dressed mol. saturated absorpt. obs. 80−9648
iodomethane-d_3, ν_2 band, laser Stark saturation spectra 78−42125
IR saturable mol. absorbers, five-level rate eqn. anal. 77−27321
laser, containing saturable absorber, bistability, semiclassical and quantum theories 78−82943
laser, multimode, containing saturable absorbers, bistable operation 80−91862
laser, passive mode locking, two laser amplifiers with slow saturable absorber 80−33041
laser, photon distrib. with 1st-order phase-transition analogy 80−23659
laser amplifier pair mode locked by fast saturable absorber, periodic pulse soln. 80−83623
laser beam, saturation parameter from gain meas. 78−66797
laser beam nonlinear propag. through fog, thermal blooming 77−91268
laser dye, saturable absorber props., stimulated propag. of pump flux 79−41377
laser instability below threshold, laser-saturable absorber system 78−94385
laser intracavity absorber, reson. obs. in output, freq. stabilisation 77−83854
laser mode locking with slow saturable absorber in transverse resonator 79−22993
laser mode selection using spatially inhomogeneous saturable absorpt. *(German)* 78−83011
laser multipass power amplifier stabilisation in CO_2 system 78−46664
laser nonlinear spectroscopy polaris. selective optical heterodyne detection 79−58798
laser power amplifier stabilisation by saturable absorbers, eight-beam CO_2 system 78−46619
laser pulse propagation in two-photon absorbents 78−50862
laser pulse shaping by nonlinear interferometers 78−59097
laser pulse shaping by nonlinear interferometers 78−79051
laser pulse timing by combined passive and active mode-locking, anal. 78−55391
laser saturable absorber cells for CO_2 fusion, parasitic oscills. suppression 78−87066
laser saturation molecular spectroscopy in time-delayed mode, appl. to NH_3 78−86976
laser saturation spectroscopy, main features 79−35846
laser spectroscopy, effects of truncated Gaussian beam variations 77−31119
laser spectroscopy, review of progress 78−82867
laser with extracavity absorpt. cell, inverted Bennett hole 79−64292
laser with saturable absorber, analogy with convective instability in two-component liquid layer heated from below 80−79319
laser with saturable absorber, correlation function, near threshold 79−27266
laser with saturable absorber, first-order phase transition 79−18394
laser with saturable absorber, metastable states in phase transitions 79−922
laser with saturable absorber, near threshold, correlation functions, renormalised Fokker-Planck eqn. 80−48208
laser with saturable absorber, stability of semiclassical solns. 80−78828
laser with saturable absorber, stationary state, nondiffusive approx. 80−19076
laser with saturable absorber, tricritical phenomena 78−78989
laser with saturable absorber and dye laser, comparison of time depend. density matrix eqns. 79−86176
laser with saturable absorber driven by coherent field 79−50304
laser with unstable saturable absorber, fluctuations influence 80−83587
laser-induced amplitude and phase gratings, theory 79−94302
laser-induced line shifts and double-quantum Lamb dips 78−86825
laser-radiofrequency double quantum saturation spectroscopy 80−48105
loss modulation for active mode locking of dye laser 77−72002
membrane, molecular motion determ. using periodic pattern photobleaching 79−34719
methane, $^{13}CH_4$ line hyperfine splitting at 3.39 μm, laser saturated absorpt. obs. 79−76470
methane, freq. stabilisation of He-Ne laser *(French)* 79−31935
methane, frequency stabilisation of 0.633μm line with 3.39μm line locked to saturated absorpt. line 80−28258
methane, saturated absorpt. meas. at 3.39 μm using multipath cell 80−74442
methane, saturated absorpt. of 3.39 μm line in external cell 79−50354
methane, saturated absorpt. profile using methane-stabilised laser spectrometer 79−98446
methane 3.39 μm transition in ring laser field, freq. shift 79−27298
methane absorber for He-Ne laser, reson. obs. in output freq. stabilisation 77−83854
methane absorption cell for He-Ne laser, hyperfine struct. influence on freq. reproducibility 78−50864
methane absorption cell for He-Ne ring laser, power resonances 80−28255
methane cell for ring laser, backscatt. influence on operation 79−10329
methane E-component saturated absorpt. for stabilising He-Ne laser, quantum freq. standard 80−9901
methane E-component stabilisation of He-Ne laser, freq. reproducibility 80−106507
methane external cell, for freq. stabilised 3.39 μm He-Ne laser 79−76700
methane locked freq. stabilisation of 3.39 μm He-Ne laser in dual feedback control 80−99772

optical saturable absorption continued
methane saturable absorption stabilised He-Ne lasers *(Chinese)* 79−59718
methanol, excited by CO_2 laser, sub-Doppler optoacoustic spectrum 80−5545
methyl fluoride, passive Q-switching of CO_2 laser 78−9402
methyl iodide FIR laser gas, passive Q-switching of CO_2 laser 80−1246
3-methylpentane-d_{14}, glass, trapped electron optical spectra, wavelength selective bleaching 79−83480
2-methyltetrahydrofuran, glass, trapped electron optical spectra, wavelength selective bleaching 79−83480
molecular beam Ramsey reson. obs. by linear laser spectroscopy 80−99514
molecular gas, IR saturation characts. versus oscill. strength 78−78751
molecular gases, saturation of light absorption 80−14401
molecular laser, optical excitation by photodissoc. wave propag. in dense gas 80−74352
molecular rotation spectroscopy, radiospectroscopes operation *(Russian)* 77−75335
molecular transition identification, coherence resonances for hyperfine struct. interpretation 79−54920
molecule, optical transient signals, saturation dips 78−18020
molecule, rot. relax. under vibr.-rot. transition saturation conditions 79−64083
multicomponent gaseous saturable absorber for CO_2 laser Helios system, optimisation 80−74393
multipath optical cavities in saturated absorpt. expts. 77−65610
multiphoton ionisation spectra, symmetry assignment of two-photon states from polaris. characts. 78−74718
multiple-frequency excitation to increase signal strength in saturation spectroscopy 80−102774
Na-coloured intracavity flame, in dye laser, mode competition 78−46594
nonlinear spectroscopy, recoil effects on Doppler-free lineshapes 80−82829
optical feedback effects on saturated absorpt. signals, suppression by phase modulation of refl. light 78−21225
optical fibres, reversible photobleaching of radiation-induced losses 79−94356
organic compounds usable as solvents in laser saturable absorber, nonlinear refr. index meas. 80−102758
organic laser dyes, nonlinear transmission including stimulated emission influence 80−99720
organic molecules, photophysics, data anal. method 79−59735
passive mode locking, transient evolution 77−34900
passive Q-switch, relax. time effect on Nd:YAG laser pulse length 77−38960
passively mode locked pulse stability in fast absorber limit 78−59052
phosphate glass laser, statistical props. and stabilisation 80−48266
photoresist, Shipley AZ-1375, sensitivity and nonlinearity at 441.6 and 457.9 nm 78−90475
phthalocyanines, controlled flashlamp illuminated phototropic switch 77−88735
picosecond pulse selection, from pulse train, by saturable absorbers *(German)* 77−68241
pinacyanol as mode locking saturable absorber for rhodamine dye lasers 77−42554
polarisation spectroscopy, Doppler free intracavity 80−52335
polarisation spectroscopy, high resolution, in strong saturation regime 79−55189
polymethine dye solutions, brightening depend. on laser pulse length 79−41425
polymethine dye solutions, photochem. transformations and short-wavelength luminesc. 80−100686
polymethine pyrylium dye, IR saturable-absorbing, transient visible absorption 78−33784
polymethine saturable absorbing dyes, dual component fluoresc. lifetime meas. 80−106359
POPOP laser, bleaching of vapour 80−19027
porphyrin-pyridine complex, 4.2K, visible absorption spectrum gap burning-out 78−53232
pulse shaping in saturable amplifiers and absorbers, of I laser 77−23691
pulsed laser intensity evaluation using saturation, organic mol. photophysical parameters 79−59735
radiative-decay-induced four-level crossover signals, saturation spectroscopy 78−77997
Raman effect, spontaneous, three-level system in intense laser fields 78−86802
Ramsey fringes in saturation spectroscopy 78−82868
rare earth phthalocyanine solutions, bleaching by ruby laser beam 78−30030
repeater, multistage, consisting of nonlinear amplifiers and saturable absorbers 79−59772
resonantly excited laser media, possible use in wavefront reversal 79−94281
resonator with distributed Bragg refl. 77−3684
resonator with distributed Bragg reflectors, transient behaviour 79−23029
rhodamine 6G in soln., photochem. stability 78−37878
rhodamine (6G-DTDC and 6G-CV) in alchohol solns., energy transfer by means of photobleaching 79−23031
ring cavity, dispersive bistability in homogeneously broadened systems 80−14306
ring cavity system, multiple-valued stationary state, instability of transmitted light 79−94301
ring laser, resonance phenomena with saturated absorpt. *(Russian)* 78−59048
ring laser, solid state, with intracavity bleachable filter, conditions for CW stimulated emission 80−14368
ruby, optical free induction decay modulation and absorpt. line struct. due to superhyperfine interaction 80−33091
ruby, optical hole burning, Stark and pump-probe studies 80−48356
ruby laser, continuously pumped, repetitive self-Q-switching 78−50781
ruby lasers, freq. synchronisation and locking by passive modulator 80−1249
ruby passively mode-locked laser, subnanosecond pulse generation using saturable absorber 79−86197
saturated absorption optical Ramsey fringes 79−54204
semiconductor, high-power light pulse propag. under interband interaction conditions 79−10366
semiconductor, high-power radiation propagation, rel. to interband absorption or amplification 79−76727

optical saturable absorption continued
semiconductor, strong EM wave interband absorption, saturation dynamics 79−992
semiconductor CW lasers, intensity self-pulsation simulation 79−94232
semiconductor in quantising mag. field, Stark effect *(Russian)* 77−73126
semiconductor laser, self-sustained pulsations 80−106522
semiconductors, light absorption, amplification and luminescence, saturation effects *(Russian)* 78−13771
SF_6, buffered, 10.6 μm transmission props. for nanosecond pulses 80−58644
single mode laser, photon statistics, intracavity two-photon absorption effect *(German)* 77−10933
solid laser, passively mode-locked, statistical props. of ultra-short pulses 79−36941
solvated electrons in alcohols, spectral broadening, laser saturation 78−31750
spectroscopic techniques based on Lamb's laser theory 79−35847
spectroscopy, high-resolution polarisation, in 10 μm region 79−6196
spectroscopy, recoil component intensity, level degeneracy *(French)* 78−12762
spectroscopy, relax. processes using Lamb's laser theory 78−70194
spectroscopy, superhigh resolution, using coherent phenomena 80−22445
sub-Doppler line shapes, saturation and two-photon spectra, elastic collisions, review 78−82697
submillimetre laser, as saturable absorber 77−83885
three-level atom, optically dressed, in spectroscopy 78−962
three-level coupled Doppler-broadened system, optical time-delayed laser saturation spectroscopy 78−54472
three-level system, narrow nonlinear resonances *(Russian)* 80−78898
three-state atom, saturated two-photon absorpt. in perturber gas 80−106310
time averaging for spectroscopy sensitivity improvement, using dye laser spectrometer 80−101850
time-correlated picosecond laser pulses generation, rapid sampling of optical relax. phenomena 80−9969
TOPOT, 1,4-bi[2-(5-p-tolyloxazolyl)]benzene laser, bleaching of vapour 80−19027
transient in absorptive optical bistability, analytical treatment 80−19077
transient optical phenomena, picosecond time scale monitoring 79−46012
tricarbocyanine dye passive Q-switch for Nd^{3+} lasers 79−10333
two level system, homogeneously broadened, saturable absorpt., coherence effects 80−95958
two-level atomic system, weak probe field absorption spectra in coherent laser field 80−23758
two-level atoms, saturation in chaotic field 80−37982
two-level Doppler-broadened medium in Fabry-Perot, optical bistability 80−102759
two-level molecular gas, nonlinear absorption near gas-medium reson. 79−41409
two-level molecules in low press. gas, nonlinear power reson., field broadening and shifts 79−45768
two-level system, adiabatic rapid passage, narrow IR saturation resons., book contrib. 78−9419
ultranarrow resonance, use in spectroscopy and for gas laser freq. stabilisation 79−59775
ultrashort light pulse form. dynamics, relax. time induced reduction influence 78−59093
ultrashort light pulses, shaping and shortening in excited level by optical controlled absorber *(German)* 78−87106
ultrashort-pulse generation by lasers with saturable absorbers 78−46687
velocity-changing collisions, study by time resolved saturated absorption 80−82832
wave beam distortion by thermal self-interaction in droplet medium 80−19082
waveguide, laser, pump efficiency, saturation effects 78−17981
wide aperture optical shutter with saturating filter at 1.06 μm 80−53457
window photobleaching of H_2 lamp, radiation coloration removal 79−72698
Zeeman coherence in saturated absorpt., velocity changing collisions study 77−46527
Ag halide, photochromic glass, optically induced anisotropy 80−1282
AgCl photochromic glass, additional absorpt. spectrum, ellipsoidal model of colour centres 80−40142
(Al,Ga)As DH laser, pulsations produced by saturable absorber Q-switching, possible model 79−81426
(Al,Ga)As DH lasers, superlinear emission charact., negative resist. obs. 80−95895
p-AlAs, saturation charact. over CO_2 laser spectrum 80−83646
(AlGa)As self-pulsing junction laser, saturable absorpt. effects 79−72568
AlGaAs semiconductor lasers, single-mode stabilisation by traps 80−95893
$Al_{0.4}Ga_{0.6}As$:Te, saturable optical absorpt. of deep Te-complex centre 79−99917
Al_2O_3, thermoluminescence, optical bleaching/stimulation effects following irrad. 78−43940
Al_2O_3, X-irrad., electron and hole traps, TSC and optical bleaching meas. 79−28356
p-AlSb, saturation charact. over CO_2 laser spectrum 80−83646
Ar laser emission under passive mode-locking conditions, temporal structure 80−9923
Ar^+ laser 582 THz stabilisation by I_2 cell, improvements 80−102741
As_2S_3, amorphous semicond., photo-induced optical and structural changes *(Japanese)* 78−47244
Ba, reson. absorpt. transitions, laser saturation spectroscopy with optical pumping 80−47121
Ba, time-resolved saturated absorption expt., collisions effects 78−29758
Ba^+, optical pumping and saturable absorpt. of fast ion beam superimposed on continuous laser beam *(French)* 78−5179
C_2, concentration in oxy-acetylene flame, $^3\pi_u$ state, saturation spectroscopy 77−77832
CO_2, anomalous Zeeman effect, nonlinear optical techniques, book contrib. 78−9279
CO_2, excited by CO_2 laser, sub-Doppler optoacoustic spectrum 80−5545
CO_2, heated, for passive Q-switching of CO_2 laser 78−25900
CO_2, intense sub ns CO_2 laser pulse attenuation and reshaping 77−88870
CO_2 laser, optical isolation by flowing gaseous saturable absorbers 78−59096
optical saturable absorption continued
CO_2 laser, SF_6 intracavity hysteresis, bistability, critical behaviour onset and extinction of lasing 79−98336
CO_2 laser Antares fusion system power amplifier optics 80−74394
CO_2 laser pulse, nonlinear propagation, computer simulation *(Japanese)* 80−95963
CO_2, saturable absorpt. and rot. relax., (00°0) vibr. level 77−19367
Ca, 6573Å line photon recoil struct. 79−85925
Ca 657.3 nm line saturated absorption spectroscopy, photon-recoil component resolution 80−86457
Ca, intercombination line, at. beam saturation and reson. fluoresc. spectroscopy 79−36580
CaF_2, additively coloured, photothermal bleaching of Ca colloids 79−15500
$CaF_2:Sm^{2+}$, coherent population oscills. and hole burning observed using polarization spectroscopy 80−71457
CdSe, saturation of optical absorpt. and photocond. 79−18487
Cs_2, 6250 Å band recorded using thermionic detector 78−46465
Cu, Doppler-free laser spectroscopy in hollow cathode discharge 80−9537
Fe complex, tris (1,10-phenanthroline) iron(II), transient bleaching, excitation wavelength absorpt. 78−73060
GaAlAs DH lasers, self-sustained pulsation suppression, effect of SiO_2 facet coating films 80−95894
p-GaSb, saturation charact. over CO_2 laser spectrum 80−83646
p-Ge, bleaching, optical heating and cooling of electrons involving intraband transitions 79−10365
p-Ge, bleaching assoc. with intraband transitions in CO_2 laser radiation absorpt. 77−68244
p-Ge, broadband modulation of 3 μm light by 10 μm light 78−42389
p-Ge broadband passive isolator for CO_2 laser system, pulse shaping 78−46662
p-Ge, hot hole relax., IR saturated absorption, LO phonon emission 77−28569
p-Ge, passive mode locking of TE CO_2 lasers 78−71127
Ge, positive, CO_2 TEA laser mode locking 78−46694
Ge, pressure tuning of picosecond pulse transmission, enhanced transparency 77−88871
p-Ge, saturable absorption isolator for CO_2 laser systems 77−19284
p-Ge, saturable absorption of picosecond CO_2 laser pulses 80−95956
p-Ge, saturation charact. over CO_2 laser spectrum 77−88869
Ge, saturation of transmitted intensity of CO_2 laser pulses 80−64111
p-Ge, tunable laser induced grating dip for sub-picosecond relax. meas. 77−75623
p-Ge:Ga, saturation behaviour at CO_2 laser wavelengths 78−1307
Ge:Ga, simultaneous multiline saturation at 10.6 μm 77−88868
Ge:Ga surface, antireflection coated, laser pulse damage resistance obs. 79−14020
$Ge_{30}S_{70}$ glass film, Ag photodoping sensitivity 80−39121
H_2CO stabilised He-Xe laser, freq. stabilisation using inverted Lamb dip 79−22991
H_2O absorption lines at ruby laser wavelengths, saturation effect 80−4098
$H_2{}^{17}O$, $H_2{}^{18}O$, Stark spectra with CO laser, Lamb dip spectra of ν_2 band 78−62840
He, 3^3D_1-2^3P_0 line, press. broadening studies by saturated absorpt. techniques 80−52939
He-Ne laser, unmodulated, stabilizing to $^{127}I_2$ hyperfine component, preliminary expt. 79−50328
He-Ne laser stabilisation, I_2 absorption cell power densities 80−99767
He-Ne laser stabilisation by I_2 612 nm saturated absorption 80−99765
He-Ne laser stabilisation by I_2 611.8 nm saturated absorption 80−99766
He-Ne laser with methane nonlinearly absorbing cell, freq. self-stabilisation effect 79−98420
$Hg_{1-x}Cd_xTe$, nonlinear absorption and saturation, 10.6 μm 77−746
I hot wall cell, freq. stabilisation of He-Ne laser 77−65598
I passive switch for 1.315 μm radiation 77−23685
I saturable absorber, transmission tests using AO coupled Ar-ion laser 78−30031
I, thermally dissociated, saturable absorpt. cell for I 1.315 μm laser wavelength 77−10985
I_2 absorption cell for He-Ne laser 77−79867
I_2 absorption cell for He-Ne laser, narrow nonlinear resonances at 0.63 μm *(Russian)* 79−59672
I_2 cell, freq. stabilisation of Ar^+ laser 79−22965
I_2, dynamic friction coeff. meas. by saturation spectroscopy, radiative lifetimes 78−18368
I_2, freq. stabilisation of He-Ne laser *(French)* 79−31935
I_2 freq. stabilised He-Ne laser with hot wall I_2 cell 78−87073
I_2 frequency stabilised He-Ne laser 78−90429
I_2, high-resolution saturated absorpt. spectroscopy with short light pulse coherent trains 80−64110
I_2, hyperfine component classification, suitability for laser wavelength stabilisation 78−86965
I_2, hyperfine predissoc., Doppler-free spectrosc. obs. 78−89558
I_2, hyperfine struct., saturated absorpt. at 612 nm, stabilisation of He-Ne laser 79−59730
I_2, hyperfine structure, 612 nm and 640 nm, saturated absorpt. expt. 78−66871
I_2, hyperfine transition saturation intensities, saturated absorpt. technique 80−43208
I_2, molecular vapour, saturable absorpt., self-focusing and nonlinear susceptibility 80−83647
I_2, multiwavelength stabilisation of an Ar-Kr ion laser 80−28282
I_2, RF optically heterodyned saturation spectroscopy, reson. degenerate four-wave mixing 80−74211
I_2, saturated absorpt. lines press. and power broadening 79−76765
I_2, saturated absorpt. obs. using interferometric spectroscopy 78−74079
I_2, saturated absorption, He-Ne laser stabilisation 77−46740
I_2, saturated absorption, He-Ne laser stabilisation, freq. shifts 77−50697
I_2 saturated absorption stabilised He-Ne lasers, performance charact. *(Chinese)* 79−59717
I_2, stabilisation of He-Ne laser 78−1270
I_2, stabilisation of He-Ne laser, wavelength meas. 80−28264
I_2 stabilised He-Ne lasers, conf., Germany (Feb. 1977) 78−87069
I_2, stabilised He-Ne laser design, freq. reproducibility 78−87070
I_2 stabilised He-Ne laser research 78−87071
I_2 stabilised He-Ne laser status 78−87072
I_2, stabilised He-Ne lasers, length metrology *(French)* 78−87074
I_2, stabilised He-Ne lasers, technological principles *(French)* 78−87075

optical saturable absorption continued
I_2 stabilised He-Ne laser, spectral profile modulation broadening 78−87083
I_2, stabilised He-Ne laser, instrumental freq. offsets 78−87084
I_2, stabilised He-Ne lasers, hyperfine struct. spacings, international intercomparison meas. 78−87088
I_2 stabilised He-Ne lasers, beat freq., international comparison *(French)* 78−87090
I_2 stabilised He-Ne laser 79−22964
I_2 stabilised He-Ne laser, practical approach to design and construction 80−19051
I_2 stabilized He-Ne laser, saturated absorption signal 77−75481
I_2 vapour passive Q-switch for ruby laser 77−79872
I_2 warm walled cell, freq. stabilisation of He-Ne laser freq. standard *(French)* 78−42343
$^{127}I_2$, saturation resons., recoil shift meas. 79−93985
I_2 hot wall cell for He-Ne laser freq. stabilisation 77−83914
^{127}I saturated absorpt. for He-Ne laser stabilisation, wavelength standard development *(German)* 78−79034
$^{127}I_2$, absolute frequencies of ten hyperfine components, freq. meas. in visible 79−93104
$^{127}I_2$, hyperfine struct. in electronic spectrum, saturated absorption spectroscopy 78−37645
$^{127}I_2$, laser stabilisation, gas cell 78−17971
$^{127}I_2$, saturated absorption, in laser cavity 77−58393
$^{127}I_2$, single saturated-absorption feature obs. using optically pumped Hg laser 77−83932
$^{127}I_2$, weakly saturable absorber for He-Ne laser, high contrast power reson. 78−29976
$^{127}I_2$ absorption lines at 582 THz, Ar^+ laser freq. stabilisation 78−90430
$^{127}I_2$ hyperfine structure components, stabilization of doubly resonant intracavity SHG of 1153 nm radiation 80−33077
$^{127}I_2$ rovibronic absorpt. lines, hyperfine struct. 80−78596
$^{127}I_2$ saturated absorption for Ar laser freq. stabilisation at 582.49 THz 77−79850
$^{127}I_2$ saturated absorption stabilised He-Ne laser, wavelength meas. *(Russian)* 79−22996
$^{127}I_2$ saturated absorption for He-Ne laser stabilisation, wavelength international comparisons 80−95872
$^{127}I_2$ stabilised ion laser, beat freq. intercomparisons at 514.5 nm 80−74338
$^{129}I_2$, $^{129}I^{127}I$, $^{127}I_2$ high resolution saturated absorption spectra at 633 nm using He-Ne laser 80−95637
$^{129}I_2$ absorption cell, freq. stabilisation of He-Ne 0.63 μm laser 80−53333
$^{129}I_2$ rovibronic absorpt. lines, hyperfine struct. 80−78596
p-InAs, saturation characts. over CO_2 laser spectrum 80−83646
InSb, absorpt. saturation by nonequilib. electron-hole plasma, luminesc. 78−9418
InSb, intensity depend. interband Faraday rot. obs., saturation and reson. enhancement effects 80−108186
KBr, dynamic equilib. between F and F_2 centres at room temp. 79−51103
KBr:Na(Rb)(Cs), microcrystalline powders, isothermal decay of colour centres 80−2804
KCl, doped, saturable absorber for CO_2 laser 79−10363
KCl, gamma-irradiated crystal, interrelation between V_2 and V_3 centres *(Russian)* 79−69862
KCl:Na, thermoluminescence peaks cleaning using optical bleaching 77−81162
KCl:ReO_4^- nonlinear absorption for CO_2 laser pulse compression and mode locking 80−74443
KI, optical bleaching of V_2 and V_3 bands 79−33739
Kr I, (A=78 to 86), isotope shift, saturated absorpt. technique 77−75102
KrF excimer laser, passive mode-locking using saturable absorber dyes 80−1244
Kr*+He(Ar), vel. changing collisions studied by saturated absorpt. 78−62892
$LaCl_3:Pr^{3+}$, hyperfine struct. of 6011 Å line, laser-induced absorpt. line narrowing 78−15196
LiCl aqueous glass, X-irradiated, localised electron optical, IR and photoconductivity spectra 78−73064
$LiNbO_3$:Fe, photoinduced scatt. and bleaching effect 80−95959
$MnSb_{1-x}Sn_x$ films, Faraday rotation, optical absorpt. coeffs. 80−97242
NH_3, saturated absorpt. at 888 cm^{-1} using tunable diode laser 78−94239
NO, laser mag. reson. and IR-RF double-reson. near 5.3 μm 78−5258
N_2O, anomalous Zeeman effect, nonlinear optical techniques, book contrib. 78−9279
Na, at. vap., CW optical wave-front conjugation 78−71154
Na, D-line saturation, under high power laser illumination 80−32653
Na, flame absorption and fluorescence, laser saturation broadening 78−88661
Na, population change induced by laser radiation, hook method 78−33476
Na, reson. absorpt. transitions, laser saturation spectroscopy with optical pumping 80−47121
Na vapour, quantum counter, IR detection 78−30016
Na vapour, saturation of transient reson. nonlinear processes 77−68243
$Na_6Al_6Si_6O_{24}.NaX_{(2-n)}$, (X=Cl, Br, I), X-ray irrad., thermal-erase cathodochromism and dihalide mol. centres *(Russian)* 80−66236
Na_2O-B_2O_3 glass, γ- or UV-irrad., laser and thermal bleaching of colour centre, absorpt. spectra 79−33744
Nd laser, stable passive switch using phthalocyanine dye, bleaching and relaxation 80−74368
Nd:glass laser picosecond pulses, background energy content meas. with saturable absorbers 78−59062
Nd:glass ring laser, actively mode-locked and Q-controlled, props. 79−18445
Nd:glass saturated amplifier, direct meas. of gain recovery 78−71104
Ne, $3s_2$-$2p_4$ transition relax. consts. using cross saturation of travelling waves in ring laser 79−76374
Ne discharge Faraday filter, dye laser freq. locking to absorpt. lines 77−79870
Ne intracavity saturable absorber for He-Ne laser, response enhancement 77−65602
Ne, reson. obs. in saturated absorpt. spectroscopy 79−89972
Ne* 5882 Å line, Doppler free spectra, press. broadening and shifts, saturation spectroscopy 80−78565

optical saturable absorption continued
Ni complex, BDN, degenerate four-wave mixing, amplification and phase conjugation 80−43394
Ni complex, BDN II in tetrahydrothiophene-1,1-dioxide, saturation behaviour, Q-switching appl. 80−48354
Ni complex soln., BDN II, saturable absorber for 1.315 I laser 79−27297
OsO_4 absorber for freq. stabilised CO_2 laser, output freq. reproducibility 78−50800
Rb, laser saturation spectra, collision broadened line struct. *(Russian)* 79−45678
RbCl, undoped and Sn doped, γ-irrad. crysts., thermolum. and emission, 300 to 560K 79−15539
ReO_4^- molecules in alkali halide matrices, CO_2 laser saturation of internal vibr. modes 78−86922
SF_6 based broadband gas isolator, for high power CO_2 lasers, design and evaluation 78−42339
SF_6, collisionless intramolecular vibr. relax. obs. 79−45706
SF_6, collisions, laser spectroscopy investig. 80−9697
SF_6, gas, heating effect on optical props., transmittance meas., CO_2 laser IR irradiation 79−27737
SF_6, gas, intensity depend. transmission at 936.8 cm^{-1}, pulsed and CW laser beams 77−88867
SF_6 gaseous saturable absorber effects on eight-beam CO_2 laser fusion system performance 80−106577
SF_6, IR saturation, five-level rate eqn. anal. 77−27321
SF_6, IR saturation spectrum, mag. hyperfine struct. 79−13714
SF_6, in cryogenic liqs., vibr. kinetics, IR spectrosc. obs. 79−18182
SF_6, intense sub ns CO_2 laser pulse attenuation and reshaping 77−88870
SF_6, nonlinear absorpt. spectrum using Doppler-free polarisation spectroscopy 79−3440
SF_6, nonlinear absorpt. of CO_2 laser pulse, computer simulation 80−106575
SF_6, partial saturation of ν_3 ladder in IR absorpt., rate process model 80−58645
SF_6, phase conjugation at 10.6 μm by resonantly enhanced degenerate four-wave mixing 79−64271
SF_6, population of excited vibr. level, nonequilib. absorpt., 140K *(Russian)* 79−36708
SF_6, refl., absorpt. and transmittance depend. on irradiance at normal incidence 78−13769
SF_6, saturable absorpt. of high IR intensity CO_2 laser band 77−58391
SF_6 saturated absorption for CO_2 laser freq. stabilisation 77−75556
SF_6, saturation characts. at 10.4 μm 77−54761
SF_6-He extracavity saturable absorber, nsec. pulse selection in CO_2 oscillator 79−98382
SF_6Ar, multiple photon excitation, saturation and linear absorpt., pulsed optoacoustic detect. 78−42148
Se-As-Ge, glass alloy system, light irradiated, annealed, photoinduced absorption change, random network model predictions 79−59773
Se-based chalcogenide glasses, band gap variation 78−90461
Sf_6, simultaneous multiline saturation at 10.6 μm 77−88868
Si, brightening and darkening wave generation by Nd:glass laser 78−18023
SiF_4 molecule, saturated absorpt. of CO_2 laser radiation 80−37811
SiF_6, evidence of tumbling multiplets 79−36637
SrF_2, saturated absorption of colour centres, ruby laser Q-switching appl. 78−71157
$SrSO_4$, celestite, colouring mechanisms 79−82998
Te, optical bleaching near fundamental absorpt. edge at 80K 80−28287
Xe, 3.51 μm broadening due to velocity-changing collisions 78−37597
Xe three-level system, collisional effects on optical coherence 79−93954
Xe+He, saturated absorpt. of 3.51 μm line, vel. changing collisions by line width 78−86819
$ZnIn_2S_4$ single cryst., intense radiation effect on optical transmission, absorpt. saturation 80−53385
ZnTe: group I element, absorption saturation *(Russian)* 78−35183
ZnTe:Li, bleaching by green laser radiation 77−62015

optical saturation
see also optical saturable absorption
alkali metal vapours, fifth harmonic generation, saturation by picosecond pulses 78−33774
atom in laser field, reson. light press. forces, cooling and trapping appls. 79−98045
atomic fluorescence detection, harmonic saturated spectroscopy method 80−104472
atomic fluorescence spectrometry, laser excited, saturation expt. verification 79−79330
atomic fluorescence spectroscopy, saturation of energy levels 78−65980
atomic transition cross section meas. by saturation flux with laser oscill. 79−27114
atomic transition in stochastic field, saturation and Stark splitting 80−9546
atomic vapours, stimulated electronic Raman scatt., saturation of tunable IR lasers 78−37941
bidirectional laser amplifiers, amplified spontaneous emission intensity fluctuations 80−37988
Cherenkov type parametric optical oscillator, optical saturation 80−102771
cresyl violet, rot. diffusion, picosec. saturation spectrosc. obs. 80−5634
degenerate four-wave phase conjugation, signal-pump detuning effects 80−78895
diffracted stimulated emission induced by coherent crossed laser beams for conc. meas. 80−35585
dimethyl ether, optical saturation characts., using CO_2 laser radiation 78−30027
dye lasers, gain and saturation considerations 78−94393
fluctuating signal, detector threshold and saturation effects on statistics 79−31803
fluorescence, laser-induced, rot. redistrib. effect 79−81259
fluoromethane, gas, optical rotary saturation 79−27338
fluoromethane, optically pumped laser, IR-FIR transferred Lamb dip spectra 80−1193
fluorotrichloromethane, optical saturation characts., using CO_2 laser radiation 78−30027
free electron laser, classical theory 80−23655
free electron laser, saturation behaviour from barrier reflection 80−9846
free electron laser, saturation effects, classical theory 80−95864
free electron lasers, classical theory, saturation, perturbation calcs. 80−83580

optical saturation continued
free electron lasers, nonlinear saturation, thermal effects using EM pump 80−87364
gain saturation of Nd:YAG laser for phase conjugation 79−64272
gas, resonance four-photon shift, optimal focusing of high-power pumping 80−95574
gas, Stark tunable, mirrorless optical bistability and optical limiting, obs. 80−38056
Goldstone mode in stationary state of non-equilibrium dissipative system *(Chinese)* 80−87365
hexafluorobutadiene, electronic ground state photochem., isotope separation by IR multiphoton isomerisation 79−79264
hexafluorocyclobutene, electronic ground state photochem., isotope separation by IR multiphoton isomerisation 79−79264
high-resolution spectroscopy using tunable lasers 80−101849
homogeneously broadened three level atoms, intense standing wave saturated, spatial inhomogeneity, mode competition 80−23646
hyper-Raman scattering, saturation effects, resonant three photon processes 80−38069
inhomogeneously broadened spectrum, saturation kinetics *(Russian)* 79−86222
intrinsic waveguide, in medium with saturated nonlinearity, theory 80−14405
IR laser Stark spectroscopy, RF elec. field modulation effects 80−52989
laser, high-intensity, multimode, dynamics theory 79−41363
laser, solid-state, two-standing mode operation with stationary ats., saturation effects and stimulated scatt. 79−68398
laser amplifier, optooptic modulated based on gain saturation 79−22988
laser fields, stochastically fluctuating, saturation and Stark splitting of resonant transitions 80−53245
laser induced fluorescence spectroscopy, saturation effects 77−44526
laser resonator gain saturation, interf. effects 80−37987
laser saturation spectroscopy, time-resolved, free induction decay of two-level resonances 80−102775
laser ultrashort pulse form., filter clarification and amplification saturation coincidence 80−64085
laser-induced atom-atom collision line shape 80−9691
laser-induced quantum beats, external static fields effects on sequential laser excitation 79−14044
laser-induced quantum beats, saturation effects of single laser excitation 79−14043
lasing system, three-level one-dimens., saturation effects 80−53253
metal vapour pulsed lasers, quantum amplifiers, image distortion 79−18433
methane, backward Raman amplifier, large-signal gain and intensity enhancement 78−90450
methanol, optically pumped laser, IR-FIR transferred Lamb dip spectra 80−1193
microwave modulated saturation spectroscopy 79−68245
molecular gas, optical nutation in standing wave, Rabi oscillations *(French)* 79−31999
molecular lasers, IR-FIR transferred Lamb-dip, standing wave saturation effects 80−58520
molecular nonsteady-state luminesc. behaviour under narrowband laser excitation 80−87159
molecule, ordinary Raman scatt., two-photon saturation effect 78−82738
molecule, saturation spectroscopy using tunable spin flip Raman laser, review 80−55762
multilevel systems, nonlinear reson. freq. shifts and saturation effects 78−78675
nonlinear optical amplifier, coherent radiation statistical props. 80−99691
nonlinear spectroscopy, coherent background noise elimination from saturation spectrosc. signals using freq. offset pump 80−62733
phase-polarisation nonlinear high-resolution spectroscopy in longit. mag. field 79−41423
plasma, laser energy coupling based on resonance saturation 79−77408
polarised light absorpt. spectra, forbidden transitions and discrete saturation 80−71464
pulse shaping in saturable amplifiers and absorbers, of I laser 77−23691
Raman spin-flip laser, higher modes and saturation effects, theory 78−71106
reflection spectroscopy, interference phase shift 77−2696
resonance Raman scattering and resonance fluoresc., time and freq. resolved 77−75624
resonant transitions in strong chaotic fields, saturation and Stark splitting 79−72542
rhodamine 6G, lasing, reson. CARS spectra in methanol, ethanol, acetonitrile, H_2O 78−74948
ring laser, saturating opposite waves interaction 77−50695
ring laser, two-mode, intensity fluctuations 80−33038
rotary saturation 78−13770
ruby, optically-pumped, excited-state Raman processes 79−4798
saturable optical amplifier, quantum theory 80−78916
self-synchronising modes, saturated filter relax. time reduction *(Russian)* 77−7145
semiconductor, saturated, dielectric response 78−10384
semiconductor injection laser switching, effect of gain saturation 79−86180
semiconductor lasers, single mode, spontaneous emission spectrum dip observation, generation saturation *(Russian)* 79−76691
semiconductors, nonlinear effects, induced by lasers 79−94300
semiconductors, optical saturation for high carrier recomb. freq. *(Russian)* 80−88585
single atom detection by saturated optical nonresonant emission spectroscopy 78−31741
slab, steady state theory 77−68242
spectroscopy, developments and applics. *(Japanese)* 80−4777
spectroscopy, lineshape, vel. changing collisions *(French)* 78−12765
steady-state theory, new laws of optics 77−68242
stimulated Raman scattering with saturation, transient regime theory *(Russian)* 78−22174
Stokes radiation spatial characts. in stimulated scattering, saturation conditions 80−53379
three-photon vector model, resonant coherent interaction *(Chinese)* 80−43306
time-resolved laser saturation spectroscopy and coherent transients survey 80−9965
transient stimulated Raman scatt., saturation effects 79−23021
two-level atom, phase transition induced by laser field *(Russian)* 78−29924
optical saturation continued
two-level system in two RF fields, saturation effects 79−59660
two-mode oscill. gas laser, saturation-induced polaris. preferences 79−22929
two-photon light shift and two-photon Lamb dips, cross-saturation method appl. 79−36591
two-photon resonant third-harmonic generation, pump depletion and saturation 80−69454
two-photon saturation effect on ordinary Raman scatt. 80−9967
wavefront reversal in stimulated light scatt., focused spatially inhomogeneous pump beam 79−27331
BO_2, intermodulated fluoresc. spectra using stabilised dye laser 79−27020
Ba, reson. transition, laser saturation spectroscopy with optical pumping 80−52334
Ba^+, electrodynamically trapped, saturation dip in fluoresc. 77−65437
CO CW electric discharge laser, saturation parameter expt. determ. 78−50762
CO laser with selective resonator, gain saturation law, lasing transition efficiency 80−48227
CO_2, electric discharge convection laser, saturation charcts. *(Chinese)* 78−90408
CO_2 high-power pulsed laser, wave-optical resonator modelling, gain saturation law 80−99693
CO_2, inverted, wavefront reversal, high efficiency 80−74436
CO_2 laser Antares fusion system optical diffraction computation 80−74424
CO_2 waveguide laser, saturation intensity, effect of wall deexcitation 79−924
CO_2 waveguide laser, saturation parameter 79−94209
CO_2 waveguide laser, saturation parameter 80−9856
CO_2 waveguide laser, saturation parameter meas. method 80−87372
CO_2-N_2, CW mixing gasdynamic laser, saturation parameter and small signal gain 79−45923
Ca, stable and radioisotopes, hfs, isotope shifts, dye laser saturation spectroscopy, beam expt. 80−58169
Ca, weak intercombination line, Lamb-dips obs. by resonance fluorescence monitoring 79−3392
CaCl, free radical, $A^2\Pi$-$X^2\Sigma^+$ system obs. by saturation spectroscopy 78−46353
Cd II ($4d^95s^2\ ^2D_{5/2}$), high order mode-crossing signals, g-factors 79−796
Cs, multiphoton ionis. cross sections, absolute meas. evaluation 80−14122
Cu vapour pulsed laser, spectral comp. of superradiance, stimulated and spontaneous radiation 80−102713
DF-CO_2 chemical laser, amplification of long and short pulses 80−95883
(Ga,Al)As transverse mode stabilised laser, direct obs. of saturation behaviour of spontaneous emission 78−46600
p-Ge, hot-hole relax. rates by saturation spectroscopy 77−65611
H Balmer-α fine struct. lines, anomalous shifts, in He-H_2 DC discharge 79−45677
He, gas, fifth harmonic generation, coherent XUV light 79−46007
He-Ne travelling wave laser, spontaneous emission spectra, 3.39 μm region 80−37995
I laser, high-power, beam quality, gain saturation effect, for fusion ignition 78−63149
$^{127}I_2$, hyperfine structure obs. in saturated fluoresc. 78−50569
$^{127}I_2$, weak rot. R(98), 58−1 line, HFS struct., saturated intermodulation fluoresc. 79−94024
$^{129}I_2$, hyperfine struct., saturated fluoresc. obs. 79−31591
InGaAsP-InP DH lasers, spatial hole burning, spontaneous emission saturation, direct obs. 80−95892
KrF electron-beam-excited amplifier, master-oscillator power-amplifier expt. for gain coeff. and saturation intensity determ. 80−48222
Li, saturated three-step resonance ionisation spectroscopy 79−81189
N_2^+ ion laser, gain and saturation 78−79001
NH_2, microwave modulated saturation spectroscopy, hyperfine energy levels 79−68245
NH_3, decay of saturation reson., IR ν_2 as Q(8,7) transition 78−25609
NH_3, mol. alignment relax. rate, laser saturation reson. technique 78−25755
N_2O-N_2, CW mixing gasdynamic laser, saturation parameter and small signal gain 79−45923
Na, fluoresc., CW laser excitation, appl. to flame diagnostics 77−79571
Na, fluoresc. in flame, saturation curves with pulsed tunable dye laser 79−36579
Na, magnetically induced SHG, intensity saturation 80−1273
Na, reson. transition, laser saturation spectroscopy with optical pumping 80−52334
Na vapour, electron and ion beam transportation channel form., reson. saturation based laser ionis. 79−77410
Na vapour, saturation holes meas. using FM spectrosc. 80−42262
Ne 6328 Å laser transition, homogeneous saturation due to collisions, weak collision model 78−78995
SF_6, refl., absorpt. and transmittance depend. on irradiance at normal incidence 78−13769
Tl vapour, coherent anti-Stokes scatt. four-photon parametric oscill. 80−9959
Xe 3.51 μm laser amplifiers, spectral narrowing and saturation induced rebroadening optical heterodyne obs. 80−63976
Xe-He, 3.51 μm laser amplifiers, spectral narrowing and saturation induced rebroadening optical heterodyne obs. 80−63976
Xe-He source, intensity fluctuations of amplified spontaneous emission at 3.51 μm 80−32957
XeF, superradiant laser, gain saturation effects 78−66808

optical self-focusing
see also electrostriction; Kerr electro-optical effect; self-trapping
active medium, EM field self-focusing, laser transverse struct. form. 80−87442
air, nonlinear susceptibility and self-focusing *(Russian)* 79−86224
air, whole beam, profile distortion, temp. depend. 77−88875
alkali boroaluminosilicate system, self-focusing fibres with aperture of 0.18 80−87548
alkali halide, rel. to optical breakdown, damage threshold calcs. 79−95708
Argus two beam system, 5 TW performance 78−46656
atmospheric propagation of modulated laser beam, acoustic pulse generation, thermal defocusing 79−92597
beam reflection and refraction from nonlinear medium 79−86206

optical self-focusing continued
beam splitting into filaments, numerical simulation 77−62019
beams of elliptic cross-section, crit. modes 80−19081
cloud medium evaporation by CO_2 laser radiation, self-focusing possibility 79−27306
coaxial atomic and light beams, simultaneous self-focusing and self channelling *(Russian)* 80−28292
coherent light pulses in absorbing media, resonance detuning effect *(Russian)* 79−27343
confined beam small-scale self-focusing 79−89977
contemporary optics, book 79−81353
convex analysis and variational inequalities *(Japanese)* 80−77606
convex dielectric thin film fibre optical modes, conformal mapping 77−83996
cubic media, four photon interaction, collective self-focusing, integrals of motion 77−83935
cubic media self-focusing, field struct. near produced singularity *(Russian)* 79−18491
cubic medium, asymptotic of the solution 79−76769
degenerate magnetoactive solid state plasma, enhancement of self focusing of laser beams 77−83934
dense optically transparent media, third-order optical susceptibilities 77−38981
dielectric, thermal focusing of elliptically shaped optical beams 79−18489
diffraction instability of light 2π pulses, numerical anal. 79−89975
distortions, nonlinear, of scanning light beams 80−14407
dynamic holograms for light stimulated scatt. 79−89964
EBBA, self-focusing, stimulated Brillouin scatt. 77−75625
elliptically polarised beams in cubic media *(Russian)* 78−63156
empirical relationship for a nonlinear index coefficient 80−74445
extraparaxial region, laser beam self-focusing/defocusing, geom. optics approx. 78−5529
far IR laser, pump radiation self-focusing and defocusing 78−79003
ferroelectric, with anomalously high dielec. const., self-focusing of EM wave 80−14408
fibre, self-focusing, matching elements calc. 80−28339
filament of light form., self-focusing and trapping of intense laser beams 77−39001
fluorophosphate laser glasses, low nonlinear refr. index, development 78−50870
fog clearing by laser beam, thermal self-defocusing effect 77−64432
gas-laser beam intensity fluctuations, spatial distrib. 79−18458
gaseous medium with solid microfilling, theoretical analysis *(Russian)* 78−25797
Gaussian beam, equal phase, self-focusing effect calcs. 77−23722
gaussian beam formalism applied to nonlinear propag. problem 79−14046
Gaussian beam profile, critical power, self focusing length, intensity profile, analytical soln. 79−993
Gaussian beam self-focusing in supersonic gas flow, thermal self-action effect 79−76768
Gaussian laser beam, transverse self-focusing and self-trapping investig., moment method 80−58652
Gaussian laser beams, Gaussian instability growth 80−69469
glass, optical and laser, electronic nonlinearity coeff. meas. 79−27341
glass, optical anisotropy due to laser-induced electrostriction *(Russian)* 79−99846
glass, ZhS-12, nonstationary self-focusing *(Russian)* 77−31120
glass rod amplifier, circularly polarised light to reduce self-focusing 77−58396
II-VI semiconductor, self-interaction dynamics of Nd laser radiation 79−27342
injection laser, mode deformation due to self-focusing, rel. to output charcts. nonlinearity 79−13966
intrinsic waveguide, in medium with saturated nonlinearity, theory 80−14405
isotropic, solid, due to electrostriction by laser beam 77−75626
isotropic solid, electrostrictive birefr. induced by high-intensity laser radiation 79−27340
Kerr medium, laser beam compression *(Russian)* 79−46016
laser amplifier output enhancement by self-focusing suppression 79−13986
laser amplifier system, small-scale self-focusing 80−106580
laser amplifier with spatial filters, optimal length and operating conditions 80−48323
laser beam, high-power, self-focusing in fully ionised plasma 78−87451
laser beam, ps, spatial struct. in a non-linear medium 79−94287
laser beam contraction dynamics due to thermal transient self-focusing 79−10368
laser beam self-focused in turbulent plasma, average field 80−79505
laser beams, elliptically shaped Gaussian, nonlinear propagation 80−43409
laser beams, self-focusing in nonlinear media 80−48360
laser fusion, critical surface bubbles and corrugations 77−11376
laser self-focusing suppression through low-pass spatial filtering and relay imaging 78−74938
laser single picosecond pulse, freq. sweeping and self focusing, direct streak meas. 78−25915
lattice vibration nonlinear interaction with powerful light beam 78−46711
lens coupling DH laser to fibre 77−79931
liquid crystal, isotropic phase, self-focusing stability of laser beam 80−99812
liquid crystal laser self-focusing, effect of spatially dispersed nonlinearity 80−38908
liquid crystals, pretransitional behaviour, nonlinear optical obs. 77−51483
local wave perturbations development, anal. *(Russian)* 77−27322
magnetoplasma, axially inhomogeneous, laser beam self-focusing and filamentation 79−19042
magnetoplasma, collisional, self-focusing effect on filamentation instability 78−51305
magnetoplasma, laser beam self-focusing 80−102778
magnetoplasma, overdense, anomalous penetration of laser radiation, upper hybrid and whistler modes 79−77386
magnetoplasma, self-focusing of EM beams on short-time-scale 79−55512
magnetoplasma, transverse filamentation and self-focusing of laser beam 78−67358
optical self-focusing continued
magnetoplasma EM wave propagation, conversion from ordinary to extraordinary beam 79−64872
molecular lasers, laser pumping, dispersion 80−87375
moving media, thermal self-focusing of laser beams 80−64122
moving medium, light beam instability and its decomposition with thermal self-stress 79−94305
multimode self-focusing fibre, mode excitation and impulse response *(Japanese)* 78−83107
nematic liquid crystal, gigantic optical nonlinearity, self focusing in oriented mesophase *(Russian)* 80−64120
nonaxisymmetric beam self focusing 77−75627
nonlinear pressure forces for laser radiation in plasma, experimental confirmation 80−28682
on-resonance self-focusing, optical pulses in thick absorbers 77−14783
on-resonance self-focusing of coherent optical pulses in absorbers 79−7184
optical fibre, impulse response 77−42593
optical glass, K-8 type, laser irradiated, transient thermal self-focusing and melting 77−50733
optical glass, nonlinear focal region formed in transient thermal self-focusing 78−50869
optical waveguides with var. refr. index 78−46837
optimisation of light beam focusing, in moving nonlinear media, using gradient method 80−106578
organic molecule solns., stimulated Raman scatt., self-focusing, rel. to Kerr const. *(German)* 79−61355
parametric excitation temporal grwoth by self-focused beam 78−50868
paraxial self focusing theory, EM wave propagation in plasma 79−94304
periodic system, suppression of filamentation of intense light beam 79−59777
phosphate glasses, optical breakdown rel. to nicroscopic inhomogeneous struct. 80−102784
picosecond light continua generation depending on various nonlinear processes 80−33095
picosecond nonlinear optics, book contrib. 77−65609
plasma, collisional, mixed mode operation, cross-focusing 80−83945
plasma, current generation due to light pressure *(Russian)* 78−63571
plasma, elliptically shaped Gaussian laser beam, self focusing and self defocusing 79−32777
plasma, enhanced Brillouin scatt. of Gaussian laser beam 79−94799
plasma, laser beam self-focusing, nonlinear absorption effect 78−79436
plasma, multiply ionised absorbing, laser beam self-focusing 79−32776
plasma, self-focusing generation of high laser flux densities in laser prod. plasma 78−18413
plasma, short-range self-focussing due to relativistic effects on refr. index 79−10673
plasma laser beam relativistic self-focusing, short-range shrinking and dielec. swelling 77−42985
plasma pulse clipper and optical isolator for IR lasers 77−65601
polarisation state evolution near self-focusing or stimulated Raman threshold 78−50867
propagation in active media, Maxwell-Bloch eqns., coherent self-focusing 78−87109
quartz, fused and cryst. laser pulse breakdown freq. depend., self-focusing elimination 77−55855
Raman or Brillouin dispersion mechanism 77−23721
randomly inhomogeneous medium, incoherent beam *(Russian)* 78−18025
ray propagation and self-focusing, variational principle derived theories 79−27339
relativistic self focusing from laser irrad. target, MeV and GeV ion prod. 78−51323
resonant media, coherent optical pulse propag., transverse effects 77−65612
resonant orientation of tunnelling centres, self-induced anisotropy 78−79075
resonantly absorbing media, instability of coherent pulse propag. *(Russian)* 77−62017
sapphire, damage by UV laser radiation, self-focusing mechanisms 80−76110
self-focusing media, filament form 80−28291
SELFOC fibre, non-Gaussian laser beam propag. 78−1335
semiconductor laser, stripe geometry, self-focusing obs., comprehensive model 77−79826
semiconductor lasers, stripe geometry 78−29954
semiconductors, mixed and binary, nonlinear polarisability, self-action effects 80−99786
short pulse propagation, thermal and hydrodynamic effects 79−41426
sideband amplification, in self-focused laser beam in atomic vapour 79−76767
simulation of self focusing of beams 77−75628
six-level atomic medium, self-focusing of two intense monochromatic waves *(Russian)* 78−25932
solid laser, nonlinear limitation for fine-scale self-focusing 79−23032
solid laser for fusion, imaging props. of spatial filter to reduce self-focusing 77−58360
soliton solutions, light beam self-action in nonlinear media 80−14404
solitons, laser physics appls. 80−48333
steady-state self-focusing and filamentation in presence of longit. inhomogeneity 80−19079
stimulated Brillouin scatt., three dimensional, for focused Gaussian beam 80−69456
stimulated Raman scatt. in substances with different Raman cross section, self-focusing of light *(Russian)* 77−10984
stimulated Raman scatt. thresholds for ultra-short excitation 80−33078
stimulated Raman scattering, wavefront reconstruction and self-focusing 80−23752
strictional self-focusing, induced anisotropy 77−75629
thermal self-focusing of pulses, unsteady-state case, theory 79−68421
thermally induced self-focusing, laser beam with spatial and temporal inhomogeneity 79−32002
transient to quasi-steady state, quantitative meas. 77−19371
transparent solid target, self-focusing effect on plasma generation 78−30460
vector theory 79−14045
very high-intensity laser beam, autofocusing propag. effects *(Italian)* 79−68420
wave mutual focusing in media with quadratic nonlinearity 78−30033
wave packet, dispersion and relaxation effects 77−72036

optical self-focusing continued
wave packet self focusing in medium with striction nonlinearity, numerical simulation 78−83042
waveguide, variable refractive index, self-focusing 79−7208
weakly nonlinear media, spatial and temporal self-focusing, ray theoretic anal. 78−18026
Ba, vapour, laser excited, anomalous conical emission and self focusing 80−43411
CO_2 laser, self-focusing parallel-plate waveguide, transverse excitation 77−7139
CdS, nonlinear self-action effect and absolute two-photon absorption coeff. 80−83649
CdS_xSe_{1-x}, laser damage, self-focusing influence 78−50844
D_2O, single 1.06 μm picosecond pulse superbroadening, concurrence with dielec. breakdown 79−86223
D_2O, superbroadening, by self-focused picosec. laser pulses 77−75612
(GaAl)As-heterostruct. stripe lasers, light/current characts. and near field shifts, waveguide self focusing effects 78−29952
n-GaAs, laser beam self-focusing in mag. field, carrier mechanism 78−33788
GaAs-AlGaAs CW laser coupled to external cavity, multimode operation, output intensity low freq. pulsations 79−68394
GaAs-AlGaAs DH injection laser with stripe contacts, radiation pulse stepped shape 80−91799
H_2O, single 1.06 μm picosecond pulse superbroadening, concurrence with dielec. breakdown 79−86223
H_2O, superbroadening, by self-focused picosec. laser pulses 77−75612
I atomic vapour, self-induced transparency and reson. self focusing 80−64114
I laser, short pulse amplification, multilevel paraxial Maxwell-Bloch eqn. 79−36889
I_2, molecular vapour, saturable absorpt., self-focusing and nonlinear susceptibility 80−83647
InSb, laser beam self-focusing, effect of quantising mag. field 77−42578
InSb, low-power nonlinear refraction effect on laser beam propagation 80−5801
InSb, nonlinear optical effects obs. using CW CO laser 79−3752
KCl laser window, thermal lensing, effective optical distortion parameter 77−83916
$KNiF_3$, antiferromag., pulse freq. broadening and self-focusing, spin wave contrib. 77−10987
$LiNbO_3$, optical stability to laser pulse, 1.54 μm 79−3734
NaCl cryst., laser pulse breakdown freq. depend., self-focusing elimination 77−55855
Nd laser, with mirror plasma-optical Q-switch *(Russian)* 80−33028
Nd:glass, mode locked laser, self-focusing effect on output power 77−751
Nd:glass, Nd:YAG, ps pulse amplification, self-focusing brightness limitation 77−14725
Nd:glass laser amplifier, small scale self-focusing effects, exam. 78−55415
Nd:glass laser amplifiers, self-focusing and suppression by spatial filtering 80−14406
Nd:glass laser fusion systems, optical developments 77−19289
Nd:glass laser operation, self-focusing influence 79−13997
Nd:glass laser system, beam spatial profile optimization in amplifier channel 80−74407
Nd^{3+}:phosphate glass laser, brightness enhancement by spatial filtering in amplifying channel 80−48321
Ne glow discharge plasma, coherent on-resonance self-focusing of optical pulses 79−41427
SF_6, self-focusing and self-defocusing using IR laser 79−89978
SiC, self-focusing of ruby laser radiation, free carrier conc. depend. *(Russian)* 77−42579
SiF_4, self-focusing and self-defocusing using IR laser 79−89978
SiO_2 optical fibres, self-phase modulation 78−66874
Te, self-defocusing of CO_2 laser radiation under phase matched SHG conditions 78−83043
$Zn_xCd_{1-x}S$, laser damage, self-focusing influence 78−50844

optical storage devices
see also holographic storage
buffer store, liquid crystal image convertor appl. 80−33166
correlators, real-time and memory devices using acousto-optic processing 78−46533
crystal resonances, requirements and attainable bandwidths *(Russian)* 77−10841
disc, data recording using diode laser 80−19001
disc, large capacity (ten billion bits), using diode laser, Philips development 79−81369
disc, optical recording with capacity of 10^6 bytes *(French)* 79−55207
elastomer storage device evaluation for optical signal processing 80−48444
electron beam laser technology and applications 77−19262
Fabry-Perot resonator, bistable, use as optical switch, limiter or memory element 77−39024
ferroelectric devices for optical systems 78−90473
holographic colour video memories, recording and playback technique 80−9833
holographic memory devices, optoelectronic ROM memory, injection laser appls. in construction *(Polish)* 80−19007
laser application 77−88673
lenslet-array optical device for paginal information reproduction 79−27194
magneto-optical photoconductor sandwich 77−40213
MBBA-PCB (41 wt.%)+pleochroic dye, electrothermo-optic effect, optical storage device appl. 78−87611
memory disc development and capacity *(German)* 79−68364
memory readout by superluminescent diode with integrated photodetector 80−32922
microchannel spatial light modulator as storage medium 80−43479
$Mn_{1-x}Cu_xSb$ films, $0 \leq X \leq 0.3$, magneto-optical props. 79−51981
MNOS structure photoelectric writing operation 78−95382
MOS structure, with ion implanted oxide layer, optically induced charge storage 77−35994
optical video discs, laser read-out system, diffraction theory 79−50338
photo-thermoplastics for fast optical recording *(German)* 79−72530
photoconductor thermoplastic devices for high density storage, expt. 77−3546
piezoelectric semiconductor, multilayer struct., storage and scanning using surface acoustic waves 79−55238

optical storage devices continued
Pockels readout optical modulator, current status and appls. 77−72085
polyvinylacetate film, dissolved polyester yellow, ablative optical recording 80−83555
prismatic storage device with anisotropic optical waveguide, theory *(Russian)* 78−87144
RAM with data record in bits, information capacity anal. 79−41342
Ruticon, image storage and optical processing appls. 77−72086
thermoplastic photoconductor tape performance 80−43305
three- and four-dimensional photoacoustic store readout 80−48413
tunable dye lasers for future optical storage, patent 79−98301
very-small-angle light scatt. apparatus design and performance 77−10082
As-Ge-S(Se), glass films, photostruct. changes 77−85822
$Bi_{12}RO_{20}$, R=Ge, Si, photoinduced birefringence, dynamic transparency prod. 78−90472
Cu-PbI_2, thin sprayed layer, glass substrate, hologram recording *(Russian)* 77−71956
GaAs MIS dynamic optically controlled transparencies 78−90523
$LiNbO_3$ acoustophotorefractive memory correlator enhancement 79−55080
$LiNbO_3$, optical damage in doped and undoped ferroelectric, mechanism 78−95570
$LiTaO_3$:M, optical damage of transition-metal-doped ferroelectric 78−95571
MnBi film for recording optical information, analogue characts. *(Russian)* 78−50716
NaF, reversible optical storage element using M-centre polarisation 78−94416
PLZT ceramics, optical recording *(French)* 77−31078
PLZT, deposition of transparent electrodes, opt. storage device applic. 78−74848
$PbMg_{1/3}Nb_{2/3}O_3$, electro-opt., elasto-opt., opt. and photo-induced props. 78−95560
$PbZn_{1/3}Nb_{2/3}O_3$, electro-opt., elasto-opt., opt. and photo-induced props. 78−95560
VO_2, laser induced metal-insulator transition, thermal switching dynamics 77−76885

optical stores
see also holographic storage
ablative optical recording, computer modelling 80−91752
alkali halide crystals, appl., activated *(Russian)* 80−80819
alkali halide photodichroic crystals use for coherent opt. data processing 77−68248
alkali halides, photodichroic, as optical processing elements 78−83056
amorphous semiconductors 77−10989
beam positioning and focusing system combination *(Russian)* 79−7194
bistable TV-optical feedback system using optical flip-flops 80−53354
colour film archival storage, white light processing technique 80−99637
computer-controlled liquid-crystal transparency array *(Russian)* 77−58430
conference, Bad Harzburg, Germany (June 1979) 80−51951
content-addressable optical memory systems *(Russian)* 77−58257
density of recorded information, influence of information carrier nonlinearity 77−75433
direct read after write recording on Bi, high density 77−38818
disc data recorder, laser machining for recording 78−71136
electro-optical beam deflector using KD_2PO_4 polarisation switches 77−39049
electrophotographic KC film digital recording performance 78−78024
ferroelectric semiconductors appl. *(Russian)* 80−80749
focus error detection, skew beam and Foucault knife-edge techniques 80−102649
frequency-domain nonvolatile optical storage scheme 80−43282
information retrieval in presence of speckle and quantum noise 79−76606
information storage, seminar, Washington, USA (Apr. 1979) 80−41942
laser and electro-optical systems, conf., San Diego, CA, USA (Feb. 1980) 80−62392
laser applications to data handling and recording 77−38817
laser image storage mass memory 80−102752
laser recording and information handling, seminar, San Diego, CA, USA (Aug. 1979) 80−101663
laser recording systems development *(Russian)* 77−54751
laser scanning read/write device, distortion correction using parabolic mirror 79−7171
laser storage, recording and retrieval systems 78−33688
magnetic film, banded domain structure, effect of recording field strength on energy characts. *(Russian)* 78−19297
magneto-optic, laser beam deflecting system appl. 77−7103
magneto-optic memories, state of the art 77−42494
mass storage systems, digital optical data storage and retrieval 80−78790
matched filter correlator memory techniques and capacity 80−43280
material requirements and possibilities *(German)* 78−25937
materials and methods, conf., San Diego, USA (Aug. 1977) 78−71171
materials for optical storage and reproduction 80−33109
medium specification and performance trends, review 80−43415
memory system principles and descriptions *(German)* 78−29910
metal film, laser hole melting for real-time, high density digital data storage 78−71135
metal thin film, preheating as aid to laser recording 80−102753
microscopically rough substrate local smoothing for optical storage 80−14288
multielement objectives synthesis, for focusing monochromatic laser beam *(German)* 77−68231
noncoherent optical memory multichannel data searching *(Russian)* 77−58261
optical modulator, space-time, based on $Bi_{12}GeO_{20}$ and $Bi_{12}SiO_{20}$ monocrystals *(Russian)* 77−1652
optoelectronic memories, data storage density enhancement 77−58298
optoelectronic memory, bit-organised, method for information capacity increase 80−102656
organic charge transfer salt process for high-density video storage 80−43269
page composer using 16×18 bit CdS spatial modulator 77−39050
PCM encoding and decoding for optical memories 80−102658
photochemical hole-burning memory magnetic and electric field addressing 79−81371
photodiode storage matrix control system *(Russian)* 77−58263

optical stores continued
photoinduced surface storage of SAW patterns in $LiNbO_3$ 80−74309
photorefractive materials for optical data storage 78−79086
photostimulated processes in inorganic materials and optical information storage, review 78−82926
recording of optical data in absorbing materials, effective depth determ. *(Russian)* 78−29908
recording system for burning perforations in metal, optics 77−58459
review of recording media 78−71172
surface polariton use 80−48414
thermoplastic information recording, frost deformations 77−50624
thermoplastic optical phase recorder for data processing 77−72081
V_2O, semicond.-metal transition, hysteresis effects, appl. in optical information storage 78−88006
wideband archival optical storage technology assessment 80−43283
wideband optical disc data recorder systems 80−102751
As-Se, relation between glass-transition temp. and optical memory-eraser temp. 80−10650
As-Se chalcogenide glass, semicond. film, laser stimulated refr. index change, writing/erase cycle 77−50677
As_2S_3 film, effect of light exposure and heat cycling 78−94417
As_2S_3, relation between glass-transition temp. and optical memory-eraser temp. 80−10650
AsSe, chalcogenide glass, efficiency of optical recording and erasing, temp. depend. *(Russian)* 77−79908
$Bi_{12}SiO_{20}$, Pockels readout modulation struct., information registration *(Russian)* 77−10990
$Bi_4Ti_3O_{12}$-CdS optical storage plane 77−39006
CdS:Cu, Cl, data storage, optical and photoelec. reading 78−1193
Cr_7Te_8 film, optical and magneto-optical props., appl. as storage medium 78−23545
EuO film threshold characteristics in holographic and bit recording *(Russian)* 80−63944
GaAs based MIS structures as possible optical memory elements 79−65556
Ge slow surface states, optical image storage for $LiNbO_3$ SAW readout 77−23773
$Ge_{13.3}Te_{61.7}As_{19}$ film, amorphous, characts. of optical switching 78−18031
$Ge_{15}Te_{81}As_4$ film, amorphous, characts. of optical switching 78−18031
$Ge_{15}Te_{81}Sb_2S_2$ film, amorphous, characts. of optical switching 78−18031
$LiNbO_3$ crystals, non-alloyed, spatial and transient characts. *(Russian)* 77−636
$LiNbO_3$:$^{57}Fe^{2+}$, Mossbauer spectroscopy 77−20782
$MnCu_{1-x}Dy_xBi_{0.86}$ film, mag. and magneto-optic props., appl. as storage medium 77−8550
$Mn_{0.75}Ti_{0.25}Bi$ films as magnetooptic storage medium, mag. interferogram recording 78−19288
NaF, photodichroic, direct-writing M-centre, Hurter-Driffield curves 77−4662
PLZT ceramic, transverse electro-optical effect, matrix-addressable transparency 79−27431
PLZT ceramic photoferroelectric image storage and display systems 77−72084
PLZT ceramics, optical information storage and spatial light modulation 78−83097
PLZT ceramics photosensitivity enhancement by H- and He-ion implantation 80−96934
$Pb(Zr,Ti)O_3$ photovoltaic ferroelectric as optical memory storage medium 78−50877
Te film, stability in moist air, rel. to information storage capability, atmospheric corrosion model 80−71774
Te film and trilayer antireflection structure for optical recording 79−94329
Te trilayer for high-performance optical recording 79−50382

optical susceptibility
see also nonlinear optical susceptibility
anharmonically coupled oscills., time depend. Hartree theory, susceptibility, absorpt. and Raman spectrum 80−58241
benzene, derivatives, calc. of second-order susceptibility, using electronic spectra data 80−29756
bromomethane, dielectric susceptibility at radio frequencies 78−14123
canted magnetic structured materials, exciton spectra, optical props. 80−70622
cerium ethylsulphate, elec. susceptibility evidence for electronically driven lattice dilation 77−76781
chalcogenide, charge transfer, influence of cryst. field 79−99516
chloromethane, dielectric susceptibility at radio frequencies 78−14123
condensed matter, low frequency responses *(Chinese)* 80−80669
conjugated hydrocarbon chains, linear and nonlinear elec. susceptibilities calcs. 78−19437
cyanomethane, dielectric susceptibility at radio frequencies 78−14123
p-decyloxbenzylidene p′-amino 2-methyl butyl cinnamate, smectic A to C transition, Landau theory 77−84906
dielectric behaviour of materials undergoing dipole alignment transitions 80−88922
dielectric susceptibility, mol. cryst. with extended defects, exciton contrib. 77−55486
dielectrics, fluctuation theorem 79−47381
dimerized interrupted strand model, optical absorption 77−16271
dipolar hindered rotators, dielec. response calcs. 77−24781
dye soln. tensor susceptance, reson. linearly polarised radiation, optical dye maser polarisation rot. *(Russian)* 77−58325
elemental semiconductor, electric susceptibility from chemical-bond approach 78−51922
excitons in semi-infinite crystals, microscopic calc. of optical refl. 79−69430
ferroelectric, susceptibility, Raman line shape of overdamped mode 79−91426
ferroelectric, uniaxial, dipolar crossover effects from Ising crit. behaviour 77−89961
ferroelectric and other structural phase transitions at low temps. 80−75990
ferroelectric crystals, polariton light scatt. freq.-angle spectra, nonlinear susceptibility interference *(Russian)* 80−92834
ferroelectric in paraelectric state, Curie-Weiss law, anharmonic oscillator anal. 79−8087
ferroelectric liquid crystals, temp. depend. of elec. susceptibility and spontaneous polarisation *(Japanese)* 78−68467
ferrofluid, dielec. behaviour in uniform mag. field 80−60390

optical susceptibility continued
fluoromethane, dielectric susceptibility at radio frequencies 78−14123
gas in two opposite EM waves, rel. to ring laser 77−50695
glass, dielectric instabilities in high permittivity glass 78−52433
glass, third order susceptibility meas. by degenerate four wave mixing *(Chinese)* 80−84708
hydrocarbon, conjugated, nonlinear susceptibility, extended basis set calcs. 79−27107
III-V semiconductors, ionic tetrahedral, electrical susceptibility, chemical bond approach 78−87931
iodomethane, dielectric susceptibility at radio frequencies 78−14123
Jahn-Teller crysts., ferroelec. transitions, elastic and dielec. anomalies, microscopic model 80−71332
LF fluctuation, dissipation and relaxation properties, universality 80−84687
liquids, anisotropic, light propag., intermol. correlation technique for mol. susceptibility tensor 77−58251
liquids, third-order elec. polarisation, appl. of theory of nonlinear rot. relax. 77−90097
lithium ammonium tartrate, piezoelec., proper ferroelastic transition 78−2812
Lorentz-Lorenz formula, microscopical derivation 78−92014
lower bounds for the electric susceptibility 79−87380
metallic ultrathin filaments, dielectric and superconducting fluctuations, Peierls transition *(Russian)* 80−65742
methylene blue in methanol, Nd laser radiation *(Russian)* 77−54753
modulation spectroscopy, anal. of Kramers-Kronig relations 78−23423
molecular crystal, Brillouin scatt. intensity 79−73958
molecular crystals, dielectric susceptibility tensor of composite lattice 77−12355
molecular fluid, optical scatt. dielec. screening and susceptibility fluctuations 77−90162
nonoptically active media, susceptibilities, elec. and mag. polarisation fluctuation 77−77140
one-dimensional conductor, CDW in random pot., large dielec. susceptibility *(Russian)* 77−69264
one-dimensional electron system, generalised susceptibilities in mag. field, fluctuations *(Russian)* 77−80750
one-dimensional systems, optical props. 77−43472
orthovanadates, centrosymmetric exhibiting cooperative Jahn-Teller effect, dielec. props. 79−28694
perovskite and tungsten bronze cryst. struct. types, ionic grouping theory, electrooptical, nonlinear optical effects *(Chinese)* 78−52472
pnictides, charge transfer, influence of cryst. field 79−99516
polymers, helical, optical activity, decorrel. approx. theory 77−63389
polypeptide lyotropic liq. crystals, van der Waals-Lifshitz forces 77−84624
praseodymium ethyl sulphate, specific heat, electric suscept. and thermal cone., one-dimens. electric dipolar XY system 77−32148
pyroelectric detector materials, thermal noise and dielec. response 80−75952
random uniaxial systems with dipolar interactions, crit. dynamics 77−73034
semiconductor, disordered, photodielectric effect 78−6413
semiconductor, resonant Raman scatt., book contrib. 77−36251
semiconductor thin films, ferroelectric properties, quantum size effect 80−97201
small particles, optical absorpt., sum rule for polarisability 77−28532
smectic liquid crystal, A-C* transition in chiral smectic 79−28088
smectic liquid crystal, A-C* transition in chiral smectic 79−28089
spatially dispersive media, optics, energy theorem and boundary conditions 79−47408
spatially dispersive medium, transient optical response 77−69792
structural phase transition induced refractive index changes in crysts. 80−16000
structural phase transitions, Landau theory 80−92639
ternary chalcopyrite, bond orbital theories 77−55761
TGS, L-α-alanine disordered regions, dielec. prop. changes in transition region 80−108159
thin island films, statistical theory for dielectric props. 80−80699
three-level system, interacting with two strong EM fields, steady-state population distrib. and complex susceptibility 80−37978
three-level system in strong nonmonochromatic radiation field, linear susceptibility 78−70877
triglycine fluoroberyllate, thermodynamic props. 78−15123
two-level atom, EM radiation interaction, elec.- and mag.-dipole contribs., reaction field 78−94215
β-Al_2O_3-Ag_2O, low temp. dielec. susceptibility meas. 79−82911
β-Al_2O_3-K_2O, low temp. dielec. susceptibility meas. 79−82911
β-Al_2O_3-Li_2O, low temp. dielec. susceptibility meas. 79−82911
β-Al_2O_3-Na_2O, low temp. dielec. susceptibility meas. 79−82911
$BaTiO_3$, Clausius-Mossotti formula and irreducible susceptibility *(Japanese)* 79−65802
$BaTiO_3$, dielec. and optical props. using shell model 79−33654
$BaTiO_3$, ferroelec., susceptibility of eight site order-disorder model calcs. 77−8523
CaF_2:Er, near-Debye dielectric responses 80−71291
Co, HCP, low energy interband absorption, electronic struct. exam. 79−73930
$CoCO_3$, birefringence of light *(Russian)* 78−56456
CsH_2PO_4, ferroelec., X-ray and dielec. studies on phase transition 79−38477
$DyAsO_4$, first-order cooperative Jahn-Teller phase transition, dielec. suscept. studies 80−19940
$DyVO_4$ Jahn-Teller crystal, deform. induced transitions, elastic and dielectric characts. *(Russian)* 80−80726
Fe, BCC, low energy interband absorption, electronic struct. exam. 79−73930
Fe_3O_4, magnetite, magnetoelec. effect at 77K and cryst. symm. 80−29593
GaAs:Be, ion-implanted, IR refl. and transmission meas. 80−34908
$Gd_2(MoO_4)_3$, ferroic, linear and nonlinear optical susceptibility 78−22164
Ge, electron-hole droplet decay kinetics, microwave expts. 77−43517
H_2, molecule, dynamical optical susceptibility, third-order 79−31724
^3He, superfluid A-phase, anisotropy of electric suscept. 77−80670
$Ho_{2x}Gd_{2(1-x)}(MoO_4)_3$, ferroic, linear and nonlinear optical susceptibility 78−22164
KCl coloured crystal, susceptibility variation calculations 80−55055
KDP-type cryst., Raman scattering and phase transitions, deuteration effects 78−76400

optical susceptibility continued
KD_2PO_4, Rayleigh scatt. and narrow central component, depend. on scatt. wave vector direction 80−29747
$K(H_{1-x}D_x)_2PO_4$, ferroelec., dielec. susceptibility, pseudo-spin model 77−52024
$KH_{2(1-x)}D_{2x}PO_4$, Raman spectra of overdamped mode 79−91427
KH_2PO_4, central peak susceptibility and US propag. near T_c 78−15125
KH_2PO_4, critical and tricritical phenomena, susceptibility, exponents 80−75976
KH_2PO_4 type crystals, transverse elec. susceptibilities 80−50273
$K_{1.6}Mg_{0.8}Ti_{7.2}O_{16}$, solid electrolyte, dielec. response, 5.2-77K 79−56709
$K_2Mn_2(SO_4)_3$, optical and dielectric props. 79−11403
$K_{1-x}Na_xTaO_3$ quantum ferroelectric, dielec. susceptibility 80−103922
$KNbO_3$, dielec. and optical props. using shell model 79−33654
$KTa_{1-x}Nb_xO_3$ quantum ferroelectric, dielec. susceptibility 80−103922
$KTaO_3$:Li, susceptibility extrinsic peak, dielectric const. meas. 79−11394
$LiNbO_3$, polydomain, nonstoichiometric crysts., elastic, piezoelec., dielec. constants. 77−8513
$LiNbO_3$, single crystal, dielectric const., dispersion, loss tangent and susceptibility 77−16245
ND_4Cl, ordered phase, Raman spectrum, dipole and polarisability derivatives 77−52072
NH_4Cl, ordered phase Raman spectrum, dipole and polarisability derivatives 77−52072
$(NH_4)_2SO_4$, ferrielec., dielec. behaviour and nature of phase transition 78−88262
$Nd_{2x}Gd_{2(1-x)}(MoO_4)_3$, ferroic, linear and nonlinear optical susceptibility 78−22164
P-As-Se glasses, mag. susceptibility, dielec. const., opt. props. 78−64184
$Pb_{1-x}Cd_xS$ epitaxial layer, metastable, optical props. and electronic struct. 79−15543
PbI_2, ionic layer cpd., electronic susceptibility 79−28057
PbTe epitaxial film, many valley semicond., band population effects, intraband magneto-optical props. 79−78007
$xPbTiO_3+(1-x)PbCd_{1/3}Nb_{2/3}O_3$, phase transition spread, polarisation relaxation, dielectric susceptibility *(Russian)* 80−75922
$PbZrO_3$, Clausius-Mossotti formula and irreducible susceptibility *(Japanese)* 79−65802
$Pr_2Mg_3(NO_3)_{12}$, sp. ht. and elec. susceptibility 77−85642
RbH_2PO_4, critical and tricritical phenomena, susceptibility, exponents 80−75976
SF_6, liq., near crit. point, optical props. meas. 77−72673
Si, diamag. and dielec. susceptibility, temp. depend. 78−10646
Si:P, dielec. susceptibility meas., polarisation catastrophe at metal-insulator transition 80−59873
SiO_2, vitreous, effect of neutron irrad. on low temp. dielec. susceptibility 79−73878
$Sm_{2x}Gd_{2(1-x)}(MoO_4)_3$, ferroic, linear and nonlinear optical susceptibility 78−22164
$Sn_{1-x}Mn_xTe$, IR reflectivity, elec. susceptibility mag. order effects 79−47433
$Tb_{2x}Gd_{2(1-x)}(MoO_4)_3$, ferroic, linear and nonlinear optical susceptibility 78−22164
W (001), surface phase transition, electronic contribs., surface susceptibility, ab initio self-consistent thin-film energy band calc. 80−29255
$Yb_{2x}Gd_{2(1-x)}(MoO_4)_3$, ferroic, linear and nonlinear optical susceptibility 78−22164

optical systems
see also adaptive optics
aberration approximation using wave, transverse and longit. values *(Russian)* 80−28167
aberrations, automatic correction routine 80−58464
aberrations, refractive index nonlinearity influence *(Russian)* 78−58921
acceptance testing with interferometer 80−95987
achromatic triplet using holographic elements 77−58415
acoustic emission optical interfereometer and auxiliary direct viewing system 79−79217
acousto-optical modulator for laser beam position sensor 78−46705
active feedback optical processor, using coherent source and liq. cryst. light valves, design 78−22204
adaptive, bandwidth specification for phase corrector and servo control 77−46799
adaptive optical components, seminar, Washington (1978) 79−59792
adaptive optical components, seminar, Washington USA (Apr. 1979) 80−31421
adaptive optical system, performance with extended-dynamic targets 77−46798
adaptive optical systems, passive return-wave 77−88933
airborne multispectral scanner design 80−74458
alignment mechanism, testing by interferometric method 80−53454
alignment testing in converging beams 78−30044
amplitude filtering for superresolution, maximum central irradiance under energy constraint 80−91914
angular tracking, annular apertures 77−83957
annular pupil system, use of orthogonal polynomials, appl. to Fraunhofer diffr. 78−50714
aperiodic spacious objects imaging, influence of AF sinusoidal phase deformations of wavefront *(Czech)* 80−14290
aplanatic optical system containing two aspheric surfaces, design 79−81500
apodisation for minimising intensity diffr. pattern second moment in systems with aberrations 79−81358
apodiser, optimum, simulation by binary filters 78−5539
apodization, optimal, by means of coupled calc. of pupil function and shape 80−95788
apodized optical systems with third-order spherical aberrations, MTF 80−9823
aspheric reflecting systems, geometrical design 80−38083
aspherical, manufacturing and testing techniques development, use of computer *(Italian)* 80−48467
aspherical surface measurement *(Hungarian)* 80−38087
astigmatism due to surface cylindricity, vectorial representation *(Russian)* 78−87121
astronomical instruments, optical anal. 78−32629
atmospheric baffling system, high rejection, terrestrial meas. of performance 78−7802
audio-visual design and room acoustics for board rooms 79−37092
automatic Abel inversion of emission from cylindrical vol. radiator 77−39040

optical systems continued
automatic correction of optical systems by accurate ray tracing *(Spanish)* 80−53401
automatic correction of optical systems by accurate ray tracing *(Spanish)* 80−53402
average square deformation of wave surface for system evaluation *(German)* 77−88882
axially mobile mirror components design *(Russian)* 77−54769
beam pointing control system, visible to IR wavelengths 79−98426
beam-guide lines, elec. length instability 78−46748
bidirectional fibre, Rayleigh scattering freq. depend. meas. 79−64317
bilinear transformations, general props. 79−98305
bipolar spatial filtering, incoherent, review 80−102822
birefringence elements, generalisation of pupil function 78−55310
Bragg cell laser Doppler velocimeter, increase in optical power by using multiwavelength lasers 78−34211
brightness meter optical system, viewfinder operation 77−10090
camera system for automatic photomicrography 80−82841
Cassegrainian 40 cm reflector, qualitative and quantitative examination *(Japanese)* 79−44366
catadioptric lenses, two-component, small zonal spherical aberration *(German)* 79−50366
centering, mirror compensator of image surface curvature 77−72053
channel transmission calc., matrix method 78−18033
chromatic aberrations of real rays, role of each lens in optical system 80−102655
circular symmetrical reflector with laterally defocused light source, axial ray trace equations *(Russian)* 78−90365
clinical endoscopic system advances 78−57096
closed loop adaptive optics systems, target effects 77−88934
closed loop control system for light industry *(French)* 77−83941
coherent, impulse response for image multiplication by spatial sampling filtration 80−33126
coherent, system evaluation, apodisation is beam propagation and image formation 77−88657
coherent, two component system producing by static phase modulation a directional light beam *(Russian)* 78−50940
coherent illumination of nonselfluminous object *(Russian)* 77−72067
coherent optical image processing system, expts. and astronomical appls. *(Russian)* 80−12675
coherent optical system, resolving power enhancement by aperture synthesis 78−25987
coherent speckle interferometry system, for stars cold satellites searching *(Russian)* 80−12672
coherent synthesized aperture system, image form., resolution improved by diffr. grating 78−50715
colour scanner imager for colour picture reproduction 78−42415
compact Gaussian relations for n-component optical systems 79−14082
compensated levels, high-precision, geodetic appl. 80−101813
complex optical system design, factor analysis methods 79−81509
compound elliptical concentrator, geometrical vector flux field 80−33119
compound parabolic concentrator, derivation of 79−72651
computer optimisation program 77−54766
concentrator, compound parabolic, phase space conservation for incoherent propag. 80−69491
condenser, refracting beam, for very high press. IR spectroscopy with diamond anvil cell 77−71389
condenser synthesis, astigmatism-free, using spherical mirrors 78−50887
conference, Bad Harzburg, Germany (June 1979) 80−51951
correction, automatic, with large tolerances *(German)* 80−95977
correlation filtering for increasing diffr. efficiency 80−96028
correlator, wavefront propagation error effects 79−50232
correlators, incoherent, analogue techniques 77−10863
coupling methods, optical fibre waveguides *(German)* 77−19416
cryogenic and contamination effects 80−38113
cylindrical lens systems described by operator algebra 80−38086
data acquisition of Auger and line optical information 78−63019
deflecting system, 3-slit, for isotopic spectral anal. 79−37005
deflection mapping technique for convective diffusion study in falling drops 78−42690
deflection system, X-Y beam, accuracy and repeatability improvement 77−58480
defocused, under partially coherent illumination, apodised aperture performance 77−10847
defocused system with shaded apertures, performance 78−5535
deformable mirror adaptive optical system 77−46796
design, advances and problems 79−36975
design, geometrical method 79−36974
design, w.r.t primary aberrations *(Italian)* 80−69490
design using cylindrical retractive index distribution *(Russian)* 78−74962
diffraction analysis, in microscopy 80−32926
diffraction and aberration effects, wave optical calc. 80−83549
diffraction dispersing systems with scarcely altering spectral line curvature *(Russian)* 80−1292
diffraction in dispersive media, system theoretical approach 79−98272
diffraction patterns for optical systems with pupils of non-uniform transmittance 80−87470
diffraction patterns of off-axis gaussian beams in optical system with astigmatism and coma 78−55309
diffuse reflectors, light collection and dissemination 80−83658
diffuse system design, optimum conditions, appl. to optical system 78−50886
distortion elimination by eigenfunction method 79−7087
double exposure interferometry through speckle photography *(French)* 80−83568
double focon, concentration factor 78−1316
double-image system for measuring rotating objects 77−87822
doublet-type eyepiece equations *(German)* 77−54767
driven member rotation uniformity test installation 80−92094
dye laser demonstration system, educational appl. *(German)* 80−51994
dye laser fast light deflection, ultrahigh resolution 78−63178
eccentric system, paraxial approx. 79−98459
edge image anal., finite area sampling technique 79−22902
electro-optical system manufacture, test and process control changes 80−96044
electro-optics, systems aspects, seminar, Huntsville, AL, USA (May 1979) 80−94921
electromagnetic fields, near wide angular lens and mirror systems 77−72051

optical systems continued
electromechanical deflector with quasi-time-optimal scanning control *(Russian)* 77−58431
electromechanical mirror scanning devices 77−58477
electron-optical system, object field conversion *(Russian)* 79−68425
engineering, seminar, San Diego, CA, USA (Aug. 1979) 80−77541
error compensators, calc. procedure 80−28296
evacuated chamber with specimen cooling via a mechanical switch [for optical measurements] 79−35765
evaluation criteria and problems, review *(German)* 80−43268
eye autorefractor, optical subsystems 79−25127
eyepieces, imaginary front focal planes, negative collection lens, design considerations 80−64139
factor analysis methods for designing complicated optical systems 80−28303
farfield method for temp. depend. study of US induced birefringence in liquids 78−16826
fast Fourier transform, two dimens., for optical systems analysis 80−78986
fibre, gradient-index light-focusing, image enhancement 80−69501
fibre array, gradient-index, appl. in copying machine 80−69500
fibre array, gradient-index, unevenness of illuminance 80−69482
fibre optic system design and component selection 80−58767
fibre optic systems and field trials, review 80−58700
fibre second generation systems, 1300 to 1600 nm 80−64163
field correctors, for astronomical telescopes at better observing sites 80−4257
film thickness monitor for vac. deposition 77−36401
first surface simplified aspherising procedure *(Russian)* 78−63013
fixtures for mounting on optical bench 78−13822
flow visualisation by foreign particle or energy optical tracing 80−96329
flux concentrators, approach to ideality 78−66885
focal-reducer system, for slitless fieldspectroscopy 80−36504
focused beam approach for SF_6 dissoc. by multiphoton IR absorption 78−42369
four-component system design for optical data processing 78−42282
Fourier hologram recording in optical system with synthetic aperture 80−95852
with Fresnel surfaces, third order aberration formulae *(Russian)* 78−63014
fundamental chromatism coefficients 78−1317
fusion reactor visible monochromator scanning drive 78−54940
geometrical optics field of general optical systems 79−81503
gradient index fibre array for photocopying machine 80−14482
gradient index imaging lens and system status 80−14420
gradient index imaging system theory 80−14294
gradient index optical elements and system design 80−106594
gradient index optical imaging systems, topical meeting, Rochester, USA (May 1979) 80−12851
heliostat mirrors array, in Solar Thermal Test Facility, Albuquerque 78−66887
Herschel's condition as wave optics theorem 80−87301
high performance system development and design at Carl Zeiss Jena works *(German)* 80−58660
high speed, nanosecond, resolution of elec. discharge using light delay technique 78−87584
high-speed non-impact printer, optical character generation requirements 78−21246
hologram achromatic lens system, design using ray tautochronism principle 79−3759
hologram lens system, astigmatism and coma reduction 80−53238
holographic memory, optical arrangements, generalised design method 79−7098
holography, twin-image, chromatic lens system, astron. appls. 80−87346
hyperbolic cone-channel condenser system 78−33811
illumination system, optical design 80−64135
illuminator using laser light source, geometrical optical anal. *(Russian)* 78−79094
image contrast loss in presence of chromatic magnification difference, numerical estimate 80−95823
image formation characteristics for partially coherent light at condenser exit pupil 77−10848
image optimisation by apodisation filters in optical systems with residual aberrations 80−53223
image overlay with single projection lens, colour display appl. 79−36973
image quality criteria, modular transfer function, phase transfer function *(German)* 80−53221
image quality evaluation *(German)* 80−95804
image quality number rel. to wave aberration polynomial coeffs., best image plane position determ. *(Spanish)* 77−68180
image rotation and magnification, optical system 80−48376
image scanning system, scanning aperture effect on image quality *(Japanese)* 77−42625
image speckle pattern, point spread function effect on average contrast 77−46702
image-forming reflection system testing by grazing-incidence Linnik interferometry 79−76891
imaging performance of mirrors with circular coolant channels 77−68254
imaging system, real time Doppler, colour TV display of particle size or density 77−62038
imaging system, speckle statistics, gaussian approximation 77−46701
imaging system fundamental limits and degrees of freedom 77−50630
imaging system point spread function determ. by scatt. of two monochromatic beams 80−87316
imaging system requirements interacting with copier architecture 80−77895
imaging system using intensity triple correlator 78−74846
imaging systems, equivalence between scanning and conventional types 78−17862
immersion optics in multichannel photoelectric systems 80−53405
impact machines, pendulum, energy meas. using optical system 80−69746
incoherent electro-optical meas. systems with arbitrary stops and misfocusing *(German)* 78−1366
incoherent feedback optical system 78−66924
incoherent optical system, improving the accuracy of matrix calcs. 78−78924
infinitely-thin-component optical system design principle 79−76794
information processing system parameters rel. to optical element characteristics 79−72510
optical systems continued
innovative applications of optics, conf., San Diego, USA (Aug. 1977) 78−58899
integrated optical systems, EM surface-wave modes ray theory 79−64360
integrated optics long-term role in optical and electronic systems 80−33232
interference filters, nonlinear, spectral characts. in strong fields *(Russian)* 77−54718
IR, image scanning systems, tilting plane mirrors 77−83944
IR, input diffr. effects and use of spatial apodisation 78−79113
IR optical scanning system, narcissus effect suppression, computer results 78−59151
IR optical train handling high pulse powers, thermal distortion thresholds 77−46745
IR phase conjugation adaptive array 77−46790
isophotometric photorecording method for optical system image quality meas. 77−34967
isoplanatism, image form. 80−1144
Kalliroscope effect based improved light diffuser, fabrication 78−59121
large F-number optical system, focal spot shift 78−1175
large-aperture optical system, energy distrib. calc. in diffr. image of point 80−74305
large-variation phase object visualisation method 77−50637
laser and electro-optical systems, conf., San Diego, USA (May 1976) 77−19278
laser beam deflection, scanner complementary control 77−83982
laser beam expander for short cavity dye laser 80−87532
laser chemical analysis systems, modular component optics system 79−1974
laser Doppler velocimeter receiving system, optimisation for sampling volume reduction 77−72379
laser galvanometer scanning system, CAD 77−58475
laser integration into optical systems, Nd:YAG laser 80−78887
for laser light transformation, parameter calc. *(Russian)* 77−65614
laser machining of thin films, projection system 77−26276
laser optical system, influence of imperfections on signal in space filtering scheme *(Russian)* 78−37815
laser optical-mechanical scanning system, phase relations, grating screen quality *(Russian)* 78−94451
laser pump system, analytical theory 80−106540
laser scanning components and techniques, conference, San Diego (1976) 77−58474
laser scanning system design, stable fixed freq. 77−58478
laser system, high energy, thermally induced optical distortion 80−38051
laser system, interferometric optical anal. 80−87401
laser velocimeter optical scanning system 77−58481
lateral motion analyser sensitivity stabilisation along ranging line 79−72694
lens, gradient-index spherical, design for optical pickup systems 80−69483
lens array, for close-up imaging of documents and displays 79−36972
lens array for extended coherent light source *(Russian)* 78−30040
lens aspherical effect on image defects *(German)* 78−9332
lens light-guide line, image transmission characts. 79−3789
lens system, distortion by means of numerical transformation *(German)* 80−64132
lens-hologram optical system, monochromatic aberrations 79−3760
lens-mirror combinations with max. conc. 78−9422
light scattering experiments using optical system 79−76786
line image transmission through single fibre using spectral instrums. 80−102820
line scanning sensor, spatial filtering design 79−53527
linear, distrib. theory as basis of postulational foundation 77−34927
lobster-eye optical configuration, appl. in X-ray telescopes 80−17491
long focal length aerial reconnaissance system response to thermal shock 80−78939
longitudinal aberration calc. by stereo-self-collimation method *(Russian)* 80−91878
losslessness of optical systems in a vectorial treatment 80−83558
low light and thermal imaging, conf. Nottingham, England, 1979, Apr. 79−36856
low light and thermal imaging, optical systems design 79−37041
low light and thermal imaging systems, atmospheric effects 79−39860
low spatial frequency enhancement with triangular and associated filters, incoherent transfer functions, equiv. passband 79−94168
low-temperature chamber with fixed pressure, use of liquefied gases 80−57358
low-temperature chamber with fixed pressure up to 16 kbar, single-window, 1.5-300K 79−35770
luminance determination by critical flicker fusion apparatus *(Japanese)* 77−75645
machine shop operations 80−96045
manufacturing tolerances, by a deterministical statement *(German)* 78−90536
matrix transforming incoherent optical system, using extended lens-array 79−7086
measuring chamber for high-temp. investigations of opt. characts. of materials 79−21798
memory, bit-organised, method for information capacity increase 80−102656
merit function, diffr. based, for automatic lens design *(Chinese)* 80−5809
micro-optic system, for reflectance meas. at press. to 70 kilobar 77−61133
micropositioner specification, static, dynamic alignment problems 77−37958
microscope photometer/semiautomatic image anal. instrument system for morphometric and photometric value meas. 80−82815
military optical system temperature effects and counter-measures 80−78938
mirror-prism, analysis using biquaternions *(Russian)* 78−50882
moire gratings strain meas., long time high temperature appl. 80−38361
moire system, for counting winding turns 80−73428
MTF, two-dimensional, meas. by second order speckle statistics calc. 80−63937
MTF measurement using positive photoresists, cross sectional features 78−9337
MTF of system with magnification chromatism 79−31818
multichannel detection system, for modulation spectroscopy 77−41693
multichannel time analyzers for luminescence spectroscopy 79−85185

optical systems continued
multidither adaptive optical systems with zonal control of deformable mirrors 77−46795
multidither adaptive optics, estimation and control 77−50757
multidither adaptive optics system, speckle interactive effects 77−46797
multidither coherent optical adaptive techniques 77−46793
multidither hillclimbing adaptive optical system, secondary intensity maxima correction 80−106593
multielement objectives synthesis, for focusing monochromatic laser beam *(German)* 77−68231
multielement optical assembly for omnidirectional coherent illumination *(Russian)* 78−87122
multilaser beam combination system 79−68402
multilayer mask and lens for neural structure bioholographic model investigation *(Russian)* 77−52769
multimode fibre link, modal noise 80−87536
multiple image form. by addition of optical signals 78−66776
multiple imaging through nonredundant arrays 78−22095
multiple-lens, astigmatism zonal error correction *(Russian)* 79−32021
N-loop ensemble reference phase control system, stability 77−46794
narrow-field receiver system, spherical aberration effect on radiation power losses 80−28299
negative system astigmatism and coma anal., third order aberration theory appl. *(Russian)* 78−30039
night vision system with refractive optics, glare characts., surface defect influence 79−32024
noisy image restoration, optical system with feedback 78−63020
non-coaxial aspherical IR optical system, automatic design *(Chinese)* 80−5810
nonaligned systems, off-centre aberrations 79−10263
nonconfocal, for single-mode laser beam formation study *(Russian)* 78−71132
nonimaging concentrators and geometrical vector flux 79−72650
nonsymmetrical optical system, matrix representation 80−64130
objectives corrected to infinity, k-stage, CAD *(Hungarian)* 79−81502
oceanography, integrating optics and sonar for deeply towed vehicle 78−45045
oculars of optical sights, for target and hunting guns 77−58419
off-axis imaging system, polarisation dependent MTF defects 77−34837
withone symmetry plane, third order aberration analytic expression obtention *(Russian)* 77−34832
optical bench accessory for distance meas. and positioning 78−21111
optical transfer measure, system relations, appl. wide field microscopy and microelectronic photolithography *(German)* 80−9815
optimisation of parameters, using damped least-squares method *(German)* 77−68255
optoelectronic Kvant classifier for aerosol dispersion anal. 78−12739
optoelectronic memories, data storage density enhancement 77−58298
optomechanical scanner, noise analysis 80−47090
optometer, refractive error correction optical system with continuously variable spherocylindrical power 79−62385
OTF measurement using autocorrelation method 80−58469
OTF synthesis, pupil function replication 79−27182
pancratic sights for sporting and hunting guns, design 78−71192
pancratic system with mechanical compensation, design *(Russian)* 78−37961
pancratic systems with linear and nonlinear relations between component motion, comparison 78−13782
paraxial air angles between cemented surfaces, calc. 79−76799
paraxial optical systems, nomographic diagrams for design and anal. 80−48377
partially coherent illumination, resolution of small double-bar targets in bright background *(Japanese)* 77−71928
passive error compensating device for optical alignment sensing subsystem 77−75726
periodic-pattern-defects omnidirectional-spatial-filter optical detection system 80−69333
phase compensation for multiple pulse thermal blooming 77−50732
phase conjugate adaptive optical systems, convergence 77−46688
phase conjugate adaptive optics using perimeter phase meas. 77−46791
phase imaging systems, chromaticity, luminous efficiency 78−33824
phaseoptical record visualisation, description *(Russian)* 77−58416
photographic materials, MTF automatic evaluation 80−95170
photographic recording system for three-dimensional trajectory of luminous pointlike object 78−12671
photometer conversion to scanning microphotometer 80−86374
piezoelectric bimorph optical beam scanners, analysis and construction 79−36992
Pioneer-Venus large probe infrared radiometer optical system 78−81543
plasma temperature field determ., asymmetrical, spectral method *(Czech)* 80−38704
plastic optical components and systems 78−25967
plastics appls. in optical systems 79−32008
plate impact experiments, optical alignment of impact faces 77−45876
point spread function of systems with parabolic filters, effects of defocusing 78−13776
point spread modification by polarisation masks 77−65615
polariser + crystal plate + analyser system, passage of light 80−10023
positioning equipment, hardware tradeoffs 78−62187
practical IR optics, conference, Los Angeles, USA (Jan. 1978) 79−23085
precisional requirements, on scientific instruments *(German)* 78−90535
processor, incoherent, for making 'spectrogram' of 1-D function 80−87528
production quality trends and limits 80−69566
production technology advances, seminar, London, England (April 1979) 80−67938
pseudo real-time coded aperture imaging system with intensified vidicon cameras 77−31133
radiation polarisation state calc. method *(Russian)* 79−98458
ray differentials calc. algorithm *(Russian)* 80−87462
ray tracing, generalised, caustic surfaces 79−23043
ray tracing through tilted and decentred optical surfaces, computer program 80−33120
real time atmospheric compensation, active optical imaging 77−49307
recording system for burning perforations in metal, optics 77−58459
reflection system, diffraction image intensity in turbulent atm., Huygens-Kirchhoff principle calcs. 80−63926
reflector illumination estimation using electronic calculator *(Croatian)* 78−16835
refracting sphere system, skew ray tracing *(German)* 78−9322
optical systems continued
refractive systems for IR apparatus, design *(Japanese)* 78−55428
reimaging system, out-of-field radiation analysis 78−59117
relay optical system, derivation and appl. of Gaussian design relationships 78−94424
remote sensing system specification using computer image simulation 80−48439
remote sensing techniques, book 80−101675
reversed Cassegrain, seventh-order design of a reflecting optical system 80−48378
rotating table eccentricity error compensation 79−71415
rotationally symmetric, of plane and spherical refractive surfaces, ray tracing *(German)* 77−61913
scanner, high-speed, using guided acoustic travelling wave lens 79−36991
scanning and conventional imaging systems, basic equivalence 78−46534
scanning device, two-coordinate, amplitude and freq. characts. 77−58457
scanning system with multifaceted mirror, tracking sweep 80−33123
scanning system with reflecting elements, angular distortions 78−37965
schlieren system using doubly refracting crysts. optical assembly 77−11040
secondary colour aberration limited system performance estimation 79−23041
secondary spectrum correction with normal glass 77−62032
sensor system simulation and evaluation 80−96030
shaded circular apertures, encircled energy in diffr. pattern, superresolving and apodising props. 80−95787
shadow device, characts., scattering medium effects, Monte Carlo calcs. 80−99630
shadow instrument with subtraction, wavefront shape visualisation *(Russian)* 78−37966
shadowgraph apparatus, phase struct. visualisation by crossed statistical amplitude rasters *(Russian)* 80−5846
sharpness index autofocus system, depth of convergence 77−79913
Shiva alignment systems 78−59033
Shiva optical system 78−59039
sighting devices for colour images of transparent inhomogeneous medium 78−22199
simple Gaussian lens equations, content expansion and expansion of usefulness 77−42586
simulation for luminescence spectroscopy 77−34036
simulator for UHF antennas 80−26742
sine-wave response, straubel apodisation filters in partially coherent light 77−3545
solar power plant, direct tracking using two-mirror unit with plane and hyperboloidal counter-reflectors 80−91875
space optics, conference Huntsville, Alabama (1979 May 22 to 24) 80−62385
space optics, imaging X-ray optics workshop, Huntsville, Alabama (1979 May 22 to 24) 80−62384
space telescopes, optical systems review *(Russian)* 77−17367
speckle noise and object contrast, detection thresholds eval. technique 78−5434
spectral analysis incoherent optical system, smoothness parameters meas. of polished surfaces 80−86261
spectrophotometer measurement system for Hewlett-Packard 8450A model 80−68269
spherical and nonspherical diopters, in three-dimens. space, calc. method *(Rumanian)* 79−13898
spherical irradiation of target by high power laser beams 77−15219
spherical-cylindrical lens combination, combined 1-D image-orthogonal Fourier transform processing 80−58658
star pointing with coelostat, Meudon solar tower 80−90338
steady temperature field determination 77−50747
step-stare spaceborne optical system image motion compensation 80−90322
step-stare spaceborne optical system smear compensation by focal plane manipulation 80−82172
stigmats using two curved Fresnel surfaces 80−38084
strain and centering sensitivity computation in paraxial region *(German)* 79−55202
straubel apodisation filter systems, effects of defocusing on point spread function 78−25804
stray light obs., spectrophotometers 79−30569
stray light performance, surface and system scatt. characteristic specification 80−48389
stray light phenomena, GUERAP III Monte Carlo simulation 78−58907
stray light problems in optical systems, conf., Reston, VA., USA (Apr. 1977) 78−59112
stray light simulation with advanced Monte Carlo techniques 78−58906
stray light suppression, optical design, computer analysis 78−59113
stray radiation analysis using first-order deterministic APART program 78−59116
stray radiation rejection capabilities, GUERAP II program analysis 78−59115
Strehl intensity applicability as image quality criterion *(German)* 80−28166
striascopic imaging of profiles with laser light, surface tension measurement 79−2845
Subjective Refraction System, American Optical SR III, phoropter comparison 79−83953
subwavelength focused light beam, knife edge scanning meas. 77−75641
superachromatic triplets, design method 80−64133
supermarket checkout system, laser/photomultiplier optical and scanning system 78−83021
surface damage from fusion experimental lasers, high fluence and contamination effects 80−38049
surfaces CAD *(Russian)* 78−74963
synthetic aperture objectives, use of toroidal elements 77−75650
system and component specifications, seminar, Washington, USA (Apr. 1979) 80−46731
systems engineering approach to optical design, fabrication and operation 80−95986
target and hunting gun optical sights 79−72664
telecentric imaging system focus detector 80−53397
telecentric system condenser alignment 80−33115
test interference pattern analysis program and error elimination method 79−76894
thermal band imaging, glare in optical systems 79−32025
thermal imaging systems, optical components testing 78−33911

optical systems continued
thin three-lens optical systems, secondary spectrum investigation *(Russian)* 78−57456
three plane mirrors, transform. of vectors 77−75654
Tokamak, far IR laser collective scatt. system 80−59300
tolerancing, encircled energy performance prediction 80−78935
tolerancing plan activities and documents 80−48382
topogram sensitivity, wavefront correl. effect 80−69345
tracking system properties and advantages 79−14080
tracking turbulence induced tilt errors with shared and adjacent apertures 77−46792
transducer, noncontacting, for machined surface profile meas. 79−58765
transmitter-receiver system, nearly coaxial, limiting detect. range through water 77−78461
triangular apodiation filter system, rectangular and triangular wave-response 79−59645
triangulation system for real-time noncontacting distance meas. 77−5801
trihedron optical system, for linear displacement meas., accuracy estimation 80−101780
truncated sinusoidal test and exptl. MTF meas. 78−25806
two-component pancratic systems containing mirrors, paraxial calc. 79−72661
two-dimensional optical system MTF meas. by second-order speckle statistics computation 80−74304
two-lens standard phase inhomogeneity 79−14111
two-mirror pancratic system, extraneous image plane highlights elimination 80−87467
uncentred surface system, field aberrations of object meridional points 78−82923
unit magnification system, improved field coverage 77−88881
US Stoneley wave meas. 78−75919
vacuum monochromator low-temp. attachment construction and optics 80−31764
variable magnification three component system, fabrication errors 77−88895
variable-scale single-lens optical transform systems 80−58656
vectorial treatment of optical systems 79−10264
velocity sensor, for liquid flow *(Russian)* 78−1759
vibration electronic damping in optical structures, using piezoelec. transducers 79−50372
visual field testing, three-channel optical system *(Spanish)* 79−24993
visual optical system specification and test procedures 80−48385
visual system quantitative tolerance specification and standard development 80−48384
wave aberrations caused by misalignments of aspherics, and their elimination 80−33127
wave propagation in large aperture optical systems 78−66746
wavefront meas. control, and conjugation, adaptive optical system aspects 79−59796
wavefront sensing systems compared 79−58766
wedge compensator for automatic control system 78−13808
well-baffled axially symmetric system design program GOSBOP 80−78940
wide angle system with corrected distortion 77−75653
wide aperture, irradiance field formation, models, comparative analysis 78−90479
X-ray optical systems, construction and appls. 79−17582
zonal spherical aberrations in optical systems, correction, use of aplanatic lens 79−27360
zoom lens focusing system *(Japanese)* 80−31922
zoom projection lens, optical level system, paraxial characts. 80−53399
CO_2 laser Antares fusion system power amplifier optics 80−74394
CO_2 laser fusion system, optical design considerations 80−78868
Nd:glass laser system, beam spatial profile optimization in amplifier channel 80−74407
Nd:glass laser system, multichannel, for fusion experiments, model 80−58557

optical telescopes *see telescopes*

optical television recording *see telerecording*

optical testing
see also optical instrument testing; optical workshop techniques
3 m parabolic dish heliostat system design, fabrication and testing 79−62111
8.448 Mb/s optical cable feasibility trial *(German)* 78−33888
active mirror characterisation by heterodyne interferometry 79−59799
adiabatic laser calorimeter design for window and mirror evaluation 79−13971
advances in optical metrology, conf., San Diego, USA, Aug. 1978 79−80565
alignment chuck for optical fibres, light transmission characteristic determination appl. 78−30090
alignment mechanism, testing by interferometric method 80−53454
alignment monitoring by diffr. from superimposed dual gratings 79−41447
alignment of mirrors and prisms in converging beams 78−30044
Amici roof prism polarisation characteristics 79−72647
antireflection coating evaluation by attenuated total refl. 77−50783
aplanatic two mirror telescope from near-normal to grazing incidence, comparative performance anal. 80−58654
applied optics, fabrication and testing, conf., Oakland, CA, USA (May-June 1980) 80−101661
aspheric, testing in reflected light using blazed synthetic holograms 80−91881
aspheric profile gauging using bootstrap data interpretation technique 79−59786
aspheric surface contour meas. machine and computer system 80−14494
aspheric surface quality assurance 78−50962
aspheric testing, in-line and carrier freq. holograms, comparison 80−87349
aspherical lenses, side band Ronchi test, hologram appl. 78−33798
aspherical surface interferometric testing using dual computer-generated holograms 80−9830
aspherical surface profile testing by goniometer 79−76895
aspherical surface testing, interferometer optical system modification 79−7236
aspherical surfaces, holographic methods of testing, review 80−33257
aspherical wavefront testing by shearing interferometer 77−31144
astronomical optical surface shaping process automation 80−105169
astronomical optics testing by Hartmann method, estimation of reliability of results 80−67564

optical testing continued
astronomical telescope concave mirrors, design of lens compensators for testing 80−28305
attenuator metrological certification methods 80−91941
autocollimation apparatus to test manufacturing quality of aspherical mirror profile 80−10053
autocollimation instrument for checking angles and pyramidicity of AR-90° prisms during manufacturing process 80−87570
automatic correction of optical systems with large tolerances *(German)* 80−95977
automatic dioptometer with projection readout system 79−50455
automatic pattern processor for simple and complex interference patterns 80−13129
average square deformation of wave surface for system evaluation *(German)* 77−88882
axicon and related optical component diagnostic techniques 80−14417
azimuth scan MTF techniques, for optical component and system evaluation 78−50900
Babinet compensator, appl. in optical testing 80−33251
beam splitters, multilayer polarised light, laboratory and factory testing 79−27428
beam-guide lines, elec. length instability 78−46748
birefringent plates, cracks, stress intensity factors, refl. caustics method 80−93718
camera lens, 48 inch, image quality rel. to MTF 78−49938
camera window for aerial photography large interferometer for testing 78−13821
characterisation for IR diamond-turned aspherical elements 80−1373
circular surface trueness testing, simple holographic method 79−50245
circular surface trueness testing by laser speckle photography 79−86266
clad optical fibres, nondestructive interferometric meas. of α and Δ 77−84013
coating abrasion resistance characterisation test 79−14129
coating adhesion characterisation pull-off tests 79−14128
coating surfaces of optical components, reflection coeff. meas. 80−28366
coating thickness measurement, optical monitoring 79−90041
coherent fibre optics testing techniques 80−78992
coherent optical materials inspection procedure using holographic filter technique *(German)* 77−31142
coherent quadratic detect. systems, quality evaluation 79−72504
coherent-optical materials testing for vibration pattern and defect discrimination *(German)* 80−30181
colour image evaluation from tristimulus values transfer functions measurements 80−87333
communication lightguide cable design and manufacture 79−37027
compact four-mirror optical system design and testing 79−23049
complex aspheric mirror testing by phase meas. interferometry 80−74467
complex surface shape inspection, coherent optical method evaluation 79−81578
component manufacture and evaluation, seminar, Los Angeles, USA (Jan. 1979) 80−12850
compound glass optical fibres, total and scatt. loss coefficient meas. 80−69536
computer-controlled interferometry, in-process production tool 80−74531
concave aspheric surfaces, quantitative test using Babinet compensator 79−98512
concave paraboloidal mirror, prod. method, interferogram tests 80−58823
conference, optical production technology advances, London, England (Jan. 1977) 78−50954
conic mirrors, caustic coordinates in Platzeck-Gaviola test 78−33799
contact lens, soft, in-office meas. 78−7339
contactless laser interferometer sweep gauge for diamond-turned surfaces 80−73441
corner cube, dihedral angle error determ. from Twyman-Green interferogram 77−65646
coronagraph objective component surface scatt. angular distrib. obs. 80−74463
CVD optical fibre, long length strength 80−58752
cylindrical mirror and lens optical figure characterisation with conventional interferometer 80−78944
dark-field surface inspection using total internal reflection 80−74519
deformable metal mirror characterisation techniques 79−59798
deviation prism interferometric testing 78−30095
diamond turned surface production, interferometric test repeatability 80−74538
dielectric multilayers, optical and geometrical thickness monitoring using monochromatic maximeter, substrate effects *(French)* 80−38140
diffraction gratings, fabrication and performance testing 77−27361
double-shearing interference microscopy, appl. to optical fibres inhomogeneities *(French)* 77−54819
electro-optic material cutting and polishing, book 79−81583
electro-optical gauging system, microcomputer-controlled 79−86271
electro-optical system manufacture, test and process control changes 80−96044
electron optical demountable system for studying image tube designs 79−81575
electronic phase meas. techniques 80−106643
fabrication and testing, removal of test optics errors 79−86270
far IR optics testing and specification for night vision thermal imaging 80−48440
fast aspheric mirror figure control by profile monitor, wire tester and null lens 80−14419
fiber-optic measurements, using standards and instruments 80−74488
fibre, furnace drawn, tensile strength 80−58751
fibre, optical time domain reflectometry 77−84014
fibre attenuation meas. techniques *(Italian)* 78−50903
fibre attenuation measurement comparison among USA manufacturers 80−58747
fibre break testing by interferometry, comparison of breaking methods 77−58491
fibre cable construction, installation, and testing 78−46797
fibre cable testing, for lightwave communications systems 80−102865
fibre cable testing 80−64230
fibre characterisation techniques compared 80−64202
fibre characteristics testing, differential interferometry 80−48397
fibre diameter checking, laser interference method 78−18080
fibre diameter meas. using microprocessor based system 78−1443
fibre end face quality check 80−64164
fibre fault detection using optimal time domain reflectometer 79−54173

optical testing continued
fibre fractographic anal. of fracture surface, after proof stressing, SEM exam. 78−38093
fibre frequency response meas., combined time/frequency domain technique 79−76809
fibre impulse response meas., refined deconvolution technique 79−55242
fibre inhomogeneous dispersion, direct meas. method 78−1400
fibre long length for communications cable, proof testing 77−54818
fibre measurements using optical-bench equipment 80−58695
fibre preform core diameter and Ge doping profile meas., X-ray nondestructive method 80−64231
fibre preform index profiling, automatic nondestructive focusing method 79−50448
fibre preforms, index profile determ. using focusing technique 79−50464
fibre radius meas. method, geom. perturbation detect. 77−42592
fibre refractive index profile meas., nondestructive transverse interference method 78−38024
fibre splice insertion loss meas., backscattering method 80−58720
fibre strength tests, pulling machine construction 78−33931
fibre tensile strength testing 78−42481
fibre with polymer cladding, Raman spectrum 78−30073
fibre-optic cable design, testing and installation 79−37026
fibre-optic cable manufacture, testing, and installation *(German)* 78−33863
fibres, compound glass, nylon-covered, reliability and verification tests and results *(Japanese)* 80−99866
fibres and cables, tensile testing machine 77−3687
field plotting of optical fields using single-mode optical fibre 78−30097
film pulsed laser damage determ., optical techniques 80−33060
filter, densitometry using pulsed dye laser and optical delay 77−61104
Fizeau interferometer, spherical-wave, direct phase meas. 80−95126
flat mirrors, flatness meas. theory, Foucault method 78−33802
flatness of test glass, reading errors of interf. fringes 79−32097
focometer, F-1, for lens focal length meas. 80−64138
forward-looking IR system improvement by aspheric elements 79−23048
Foucault, phase edge and wire optical test 80−96046
Fourier transform lens, spatial invariance test 80−69492
Fourier transform spectrometer based on Michelson interferometer, problems in optical measurements 79−85187
glass, absorption coeff. determ., refl. losses role 77−72100
glass, index inhomogeneity, rapid interferometric determ. 79−93207
glass, large disc, optical homogeneity, high accuracy measurement *(Chinese)* 79−55195
glass, spottability determ., reflectometric method 78−30102
glass, surfaces joined by optical contact, spectral absorpt. of water layer 78−46852
glass assessment, low absorption coeff. meas., calorimetric method 77−58405
glass blanks, devitrification effect on striae coarseness 77−34972
glass fibres complex transfer function determ. *(German)* 77−27366
graded-index fibre differential mode attenuation meas. 78−1403
Hartmann modified wavefront sensor performance 80−74522
heliostat facets, optical characterisation 80−53485
high-energy, IR laser component optical characterisation techniques 80−14347
high-energy laser diffraction grating evaluation approach 80−14474
high-energy laser mirror thermal distortion test facility 80−14348
high-performance telescope aspheric mirror test error budget 80−48386
holographic lateral shear interferometer, appl. to testing 77−7023
holographic store automated test using BASIC M-400 interpreter *(Russian)* 79−94180
Huygens eyepieces, simple testing method 77−50746
hybrid fibre optic/electrical connector, environmentally sealed, multispin, cylindrical 79−41457
illuminator for testing coordinate-sensitive photodetectors 79−72643
image assessment, review of German standards 78−50724
image convertor dynamic range meas. device 79−68431
image quality data derivation from edge sharpness, simple math. methods 78−50722
image quality evaluation from aspheric replica master data, using ACCOS V SPLINE program 78−66964
image-forming reflection system testing by grazing-incidence Linnik interferometry 79−76891
imaging system assessment, conference, London, England (Nov. 1976) 78−50718
inclined prism three-point meas. reliability *(German)* 80−28359
information storage and processing phase mask fabrication and testing 79−27195
interference pattern analysis program and error elimination method 79−76894
interference surface testing with quarter-wavelength sensitivity 78−32870
interferogram aberration evaluation program 80−13130
interferogram analysis, point spread function and OTF determ. 79−76616
interferogram fringe pattern reduction, automated system 80−47097
interferometer, description of new interferometer for optical surface control *(French)* 78−58017
interferometer, large aperture AC, for optical testing 79−27446
interferometer, lateral shear, using twin three-beam holograms, lens tests appl. 80−99673
interferometer, real-time shearing, quality factors testing appl. 80−37081
interferometer, unequal path interferometer alignment and use as optical test tool 79−85169
interferometer design, construction and interferogram processing, optical testing appl. 80−79020
interferometer with computer generated holograms 77−42632
interferometers, IR lateral shearing, as optical testing tools 80−68244
interferometric examination of lenses, mirrors and optical systems, 3D display 80−69497
interferometric examination techniques for lenses and other components 80−69498
interferometric flatness testing by self-levelling reference plane 78−63207
interferometric instrumentation as a cost-effective production tool 80−74535
interferometric MTF meas. technique 77−3688
interferometric optical testing status and prospects 80−74529
interferometric testing method with computer-generated holograms, aberration balancing 78−46845
interferometry seminar, San Diego, CA, USA (Aug. 1979) 80−73096
IR aspherical lens and surface evaluation 77−39019
optical testing continued
IR inhomogeneity scanner for transmitting material blanks 79−32099
IR laser interferometer operation and testing 80−73433
IR lens production tests 78−50890
IR material and lens evaluation interferometer 77−39121
IR optical components and aspherics, 10.6 μm interferometric testing 80−74523
IR scanning system modular design, assembly and alignment 80−78989
IR test facilities for sensors 77−65647
IR window, large aperture, interferometric meas. 79−85170
isophotometric photorecording method for optical system image quality meas. 77−34967
kinoform lens production and optical testing *(Russian)* 79−98310
Large Azimuth Telescope primary mirror blank testing 79−50367
large azimuthal telescope, primary mirror testing in observatory 78−20642
large azimuthal telescope primary mirror, Hartmann test 77−91430
laser alignment accuracy on target, Hartmann test, direct meas. 79−23004
laser damage threshold meas., statistical methods 79−18464
laser diode fabrication reproducibility *(French)* 78−42357
laser equipment, pulsed, multichannel device structure and testing *(German)* 80−95933
laser fusion Optical Evaluation Laboratory, Antares CO_2 laser system 80−14346
laser interferometer for routine aspheric surface testing 80−14495
laser measurement of optical, thermal and mech. props. of materials 77−74513
laser system, interferometric optical anal. 80−87401
laser tracking system testing by 1 m unobscured IR collimator 80−78991
laser unequal path interferometer with electro-optical camera and minicomputer, fabrication/test appl. 80−77847
lateral shearing interferometry for stochastic inputs, data reduction 77−26386
lens, high aperture, for laser plasma compression expt. 79−14076
lens, large-size, simplified MTF meas. *(Japanese)* 80−33121
lens assessment techniques, polychromatic and monochromatic, in far IR 78−50899
lens design and testing for laser systems, assets and liabilities 78−46753
lens evaluation for 35 mm cameras, MTF based test method 78−41363
lens MTF measurement, accuracy of spectral response matching 78−50721
lens quality measurement using lateral shearing interferometer *(German)* 80−22425
lens sphericity non-contact testing method *(German)* 78−5534
lens surface quality testing at Zeiss factory *(German)* 80−33113
lens system evaluation, use of OTF for image anal. 80−53481
lens testing, MTF-based optical sensitivity and tolerancing computer programs 80−83686
lens testing at 1.06 μm, using laser unequal path interferometer 78−49893
lenses, OTF test criterion, development and implementation of instrums. 77−19383
lenses, simplified Talbot interferometers 77−757
lenses for 35 mm camera, MTF based simplified test method 78−49937
liquid crystal electro-optic valve testing using laser light *(French)* 80−28311
liquid crystal image transducer, spatial frequency spectrum temporal meas. 79−76810
long-haul communications optical fibre fault location method 80−64193
long-radius concave optical surface curvature meas., differential technique 80−74534
matched filter visibility effects on the correlation function 80−96031
material homogeneity, test methods and instrumentation 79−37063
metal mirror, diamond turned, optical figure inspection by interferometry 78−5545
metal surface, diamond turned, finish meas. by differential light scatt. 78−5544
metallic mirror surface topography determ. by Nomarski reflection microscopy, theory 79−54185
micro-optics quality testing 79−27368
micro-optics testing, width meas. of slit test objects 80−64223
microinterferometer, apochromat objective, with increased resolution, surface roughness testing 79−71519
microscope polarisation adapter, for transparent material anisotropy and internal stresses meas. 80−31863
microscopic imperfection detect. on high quality surfaces using interf. patterns 77−74493
mirror, plane lattice point light source appl. *(Japanese)* 78−9463
mirror, point spread function energy distrib. rel. to surface deform. 77−58422
mirror, primary, of large azimuthal telescope, testing by Hartmann method 78−20641
mirror, single-point diamond-turned, performance before and after polishing 80−74466
mirror fiducial system compatible with computer-controlled polishing facility 80−74539
mirror optical scatter meas. specification proposal 80−48390
mirror production and testing, low-scatter, low-loss mirrors for laser gyros 80−1272
mirror reflectance meas. using multiple wave interferometer *(French)* 77−42585
mirror reflection coefficient meas. instrument 78−18036
mirror surface contamination assessment by bidirectional refl. distrib. function meas. 79−59790
mirror surface curvature and local distortion meas. by holographic interferometry 79−76796
mirror surface testing of 6m LAT mirror, Hartmann method under shop conditions 78−90540
mirror surfaces for solar power stations, specular reflectance obs. 78−13786
mirror testing using autocollimation method with multiple pendulum mirrors 80−102792
mirrors, coated and uncoated, using coaxial reference interferometer with low mapping distortion 79−85175
mirrors, Ronchi interferometry appl. to large aperture flat mirrors 79−85171
moire methods for contouring displacement, deflection, slope and curvature 79−80674

optical testing continued
monomode fibre selective excitation for differential group delay meas. 80−99876
MTF measurement for lens test, light source polar intensity distrib. influence 78−50723
MTF measurement in France, ACOFAM and ACOMAT instruments 78−50727
MTF measurement of standard lenses in Japan, interlaboratory comparison 78−50720
MTF measurement via diffraction shearing with optically superimposed gratings 79−64366
multiactuator deformable mirror evaluations 80−14416
multifaceted prism test automation 79−72724
multimode optical fibre dispersion rel. to wavelength, frequency-domain meas. 78−1401
near IR transparent material, birefringence meas. polarimeter 79−44925
night vision system testing image scanner 77−39102
null Ronchi grating from spot diagrams 78−5548
null testing in modified scatterplate interferometer, test of 20 cm diam. f/3 parabola 80−79015
objective lens manufacturing, present status and future prospects 79−94323
objective lens of amateur camera, production quality, MYF test freq. selection 79−81581
objective lenses, two-channel device for meas. transmission coeff. 80−106642
objective time-varying lateral aberration meas. 79−76797
objectives, commercially manufactured, probability analysis of centring accuracy 78−90491
objectives, quality testing by semiautomatic modulation transfer coeff. meas. 79−14124
objectives' two-dimensional transfer functions, holographic meas. test 79−50253
objectives in large scale production 78−18035
ocular design, new type, experiences from common ocular testing 79−18501
off-axis parabolic mirror fabrication for laser function expt. 80−1374
opaque optical components' parallelism meas. 79−81549
opaque polished surface roughness determ., diffuse reflection method 79−49274
ophthalmic lens distortion display 78−7338
ophthalmic lenses, basic principles of fracture testing 79−96233
ophthalmic lenses, thin, chemtempered, static load strength testing 80−5812
ophthalmic lenses, thin, chemtempered, strength meas. by drop-ball testing 80−5811
optical communication testbed 78−33925
optical fibre, rapid Δ meas. by refr. index tuning 78−13792
optical fibre, single layer, dimensions and refractive index meas. 77−79952
optical fibre, transmission meas. without disturbing integrity 77−72076
optical fibre coating concentricity meas. and anal. 77−88898
optical fibre transmission meas. technique using time dispersion of Cerenkov radiation 78−5557
optical fibres, backscattering method, compact optical test unit *(German)* 78−30098
optical fibres, breaking strain estimation for long lengths of fibres 78−30060
optical surface, scratch classifier for inspection of scratch severity 77−75722
optomechanical element system, for laboratory meas., Hungarian development *(Hungarian)* 79−81574
OTF standardisation activities in Netherlands 78−50728
OTF standardisation in Japan 78−50726
OTF test standard, afocal system 79−36978
OTF testing, USA standards 78−50725
pancratic objectives, aberration stabilisation during focusing 80−102799
parabolic cylinder testing with asphérometer 77−31146
parabolic mirror testing by vibration-insensitive laser unequal path interferometer 80−74537
parabolic mirror testing during fabrication by long-wavelength interferometer 80−74536
parabolic reflectors, medium size, surface shape quantitative evaluation 79−72654
phase grating testing and meas., visual demonstration of non-uniformities 77−34966
phase relief in photographic layers, determ. using optical methods *(Russian)* 79−98518
photo-optic measuring systems using bifurcated fibre-optic probe 79−81569
photoelastic coating method of meas. stress and strain 78−1614
photoelectric photometer for point spread function energy conc. meas. 78−30099
photographic image quality, MTF meas., for lens testing 77−45912
photographic objective lens, use of m.t.f. 77−181
plane mirrors, planarity deviations detection method 77−27329
point spread function of systems with parabolic filters, effects of defocusing 78−13776
point-diffraction interferometer principles and applications 80−74530
polycarbonate, bisphenol A, birefringent plates, cracks, stress intensity factors, refl. caustics method 80−93718
polychromatic MTF measurement reproducibility 78−50719
precision optical element testing by phase meas. interferometry 80−74520
precision optical evaluation by phase meas. interferometry 80−74533
precision testing techniques, using laser interferometers, microprocessors and computers 80−69563
primary mirror of large azimuthal telescope, interference testing method 77−73952
primary mirror of large azimuthal telescope, isophotometric recording 77−73953
prism fabrication errors meas. by interference method 77−58494
prism figuring, optical path difference check by Hendrix interferometer 77−72094
prism glass reflecting angle testing in autocollimation modes 78−71194
prism optics testing for laser interferometer, interf. meas. 80−105698
production technology advances, seminar, London, England (April 1979) 80−67938
projection system quality determination methods *(Hungarian)* 79−89983

optical testing continued
projection system transfer function definition and performance testing *(Hungarian)* 80−14413
proof glass superposition method for testing convex spherical surfaces, errors 77−75649
pulse dispersion test bench for optical fibre characterisation 77−50778
pulsed laser damage to optical surfaces, multithreshold analysis 79−18465
pyroceramic plate surface quality obs. after mechanical polishing 79−72732
quarter wave multilayer monitoring, optical props. change rel. to error compensation 80−38139
quasi-Ronchigrams for interpreting wave-front and glass-error slopes 80−37078
quick Hartmann method for studying astronomical optics 79−8837
random digital scene generation with specified statistics 80−99666
ray-tracing techniques for infrared scanners 79−36984
real time wavefront anal. automatic method for interferograms 79−75585
real-time interferometer for optical system testing 79−85168
refractive null corrector design for testing aspheric surfaces 77−19377
retroreflector, temp. stability testing under space conditions 77−62078
Ronchi test, fringe sharpening 80−53480
Ronchi test, practical formulae and experimental verification 80−43490
Ronchi test formulae, theory 80−23817
roof and other prisms, MTF tests 80−69571
rotating prism camera lens, 100 mm focal length, White Sands Missile Range, testing methods 79−86249
rotational symmetric aspheric in compensated interferometers, computer-generated-holography testing 80−33128
ruby rods, quality control, EPR method 79−14047
Sayce test chart, modified design 78−16877
scanning gauge for surface form meas., spherical and aspherical 79−32100
scatterplate interferometer principles, limitations and tolerances 80−73436
schlieren instrument large-aperture adapter for optical surface quality evaluation 79−14122
Schmidt camera, simple null test for aspheric corrector plate 80−91940
Schmidt correction plates, aspherical surfaces 78−20643
Schmidt corrector plate replication, testing and performance calc. 78−66967
semiconductor radiation sources testing, coherence analysis, meas. system with Michelson interferometer *(Polish)* 78−33762
Shack interferometer for optical shop use 80−73434
shearing interferogram evaluation improvement *(German)* 80−27339
SHIVA laser optical component manufacture and testing 79−22980
single mode fibre coupling to semiconductor laser, fibre strength tests 78−33900
single mode fibre homogeneous CVD fabrication and characterisation 80−69562
solar concentrator facet quality evaluation for deformational forming 78−90483
solar concentrators, luminescent, operation theory and performance evaluation techniques 80−7913
solar energy concentrators, reflecting, performance evaluation 80−87457
solar radiation concentrator accuracy assessment, using laser radiator and sectioned photoreceiver 79−23038
solar reflecting concentrators, optical evaluation techniques 78−50893
solar simulator design for testing solar collectors 80−50996
Solar Thermal Test Facility, 5 MW, heliostat focus and alignment system 78−50894
spatial filtering, appl. to bubble materials characterisation 77−12175
spectacle lens inspection apparatus *(French)* 79−7235
spectacle lens test facility complex 79−39603
spherical aberration measurement of photographic lenses, using solid-state image sensor 80−23812
spherical surface error absolute definition technique, use in interferogram analysis 79−86268
spherical surfaces shape deviation determ., using sphero-interferometer *(Czech)* 80−58821
sphericity standards, interferometric meas. *(German)* 80−87569
standard test method development by ASTM 80−74528
standards in Britain for optical device performance assessment 78−50729
star simulator lightguide test instrument and method 79−27422
steep aspheric surface measurement, holographic comparison test 78−42402
stroboscopic interferometer, dynamic optical component evaluation, remote-site operation 79−85164
stroboscopic interferometry, active mirror testing appl. 79−58782
subwavelength focused light beam, knife edge scanning meas. 77−75641
superposition fringes as measuring tool in optical testing 79−86267
surface contaminant generation and bidirectional reflectance distrib. function meas. 80−14493
surface contour and inhomogeneity testing, interf. fringe distortion with imprecise focusing 78−89531
surface contract interaction zone, thickness calc. and distance meas. methodology *(Russian)* 80−99889
surface errors rel. to optical performance, effect of mid- and high-spatial freqs. 79−59789
surface evaluation techniques for optical components 79−46094
surface mapping with quarter wavelength fringes 78−46846
surface measurement technique, 3-D, using computerised electro-optical instrument 79−86272
surface measurement using real-time digital heterodyne broad-beam interferometry 79−85173
surface microstructure, on optical element production line 77−27397
surface profile meas. and angular deflection monitoring using scanning laser beam 79−85125
surface profile testing with set of spherometers, math. analysis 78−13823
surface quality standards based on total integrated scatt. 80−48391
surface testing by caustic method using phase stripe as spatial filter 79−72722
surface testing using microcomputer-based heterodyne interferometer 79−85174
surface topography quantitative determ. by Nomarski differential interference contrast microscopy 80−73318
synthesized hologram accuracy testing 77−31079
system acceptance testing with interferometer 80−95987

optical testing continued
system and component specifications, seminar, Washington, USA (Apr. 1979) 80−46731
systems engineering, seminar, San Diego, CA, USA (Aug. 1979) 80−77541
telescope PPS 12, meas. of surfaces up to 30 m in extent 78−94423
tensile tester, for long optical fibres 78−83123
testplate testing interferometry in precision optical shop 80−74532
thermal blooming cell design for adaptive optics evaluation 80−33096
thermal imaging systems, optical components testing 78−33911
transmission holographic bench, for qualitative and quantitative analysis *(Rumanian)* 78−46545
transparency, large area, distortion measurements using shearing interferometer with scanned photodiode array and microcomputer 79−80675
transparency optical thickness irregularity processing by laser heterodyne correlation 79−14119
transparent object, testing for bubbles and light scatt. inclusions 77−88973
turbine blade vibration meas., optical methods *(French)* 78−71300
two-wave interferometers for use with monochromatic source, optical testing appl. 79−35814
unequal path interferometer, alignment and use as optical test tool 80−9031
UV objectives, for submicron photolithography 79−32032
vacuum chamber for cryogenic optical meas., upgrading design 79−23098
vibration insulation of equipment for optical system performance testing 78−90543
visual optical system specification and test procedures 80−48385
wave aberrations caused by misalignments of aspherics, and their elimination 80−33127
wavefront analysis, automatic real-time meas. of interferograms, technique 80−9029
wavefront determ. using Ronchi and Hartmann tests 77−50777
wavefront interpretation with Zernike polynomials 80−78776
waveguide performance before and after storage 79−27392
waxicons for high-power chemical lasers, interferogram analysis 80−14418
wide-angle concentric dome and shell production, double-pass null test 80−79022
window interferogram evaluation method 77−84011
Wolter lens component replication 80−95972
X-ray mirror profile meas. machine 80−69496
Zernike polynomials computation 77−50776
Zernike test, analytical aspects 77−23785
Zernike test, experimental aspects 77−23786
zonal Foucault test, diffr. effects 77−72099
zoom null lens design for optical component and system testing 80−23811
Zygo interferometer system 80−73437
NaCl 46 cm window optical evaluation facility 80−74526
Si, diffraction grating, rectangular profile, fabricated from single cryst. 80−38093
Si photodiode as position sensing detectors for precision measurement and control 79−86273
SiO_2 lightweight 370 mm mirror fabrication and testing 78−57447
TeO_2 monocrystal acousto-optical deflector design and testing *(Russian)* 79−98460

optical transfer function
acoustic microscope modulation transfer function 79−64454
acousto-optic heterodyning image processor 80−5833
aerosol atmosphere, MTF and PSF calcs. rel. to space-meteorological photography, multiple scatt. effect 79−66792
amateur camera information capacity and image quality 79−49316
ambiguity function in diffraction and isoplanatic imaging by partially coherent beams 78−78925
analytic recurrence procedure for computing cross-multiplication coeffs. 78−13667
angiographic information visualisation correl. with measured system MTFs 78−73230
angiography, effects of asymm. focal spots 77−21617
annular aperture, arbitrary point spread functions 80−87325
annular aperture, imaging performance, line spread functions 78−55304
annular apertures, imaging performance, apodization and MTF 80−23625
annular lenses in microscopes, imaging props., calcs. 80−22426
annular strips, point spread functions, super-resolution 79−907
aperiodic spacious objects imaging, influence of AF sinusoidal phase deformations of wavefront *(Czech)* 80−14290
aperture shaping, diffracted energy spatial distrib. control, computer analysis 78−59152
apochromatic collimator design for MTF evaluation 77−79946
apodisation and image contrast rel. to MTF 80−32920
apodising filters, numerical exam., second moment of the point spread function 80−106611
apodization and image contrast: author's reply to comment 80−58466
apodization and image contrast, MTF evaluation 79−59640
apodized optical systems with third-order spherical aberrations, MTF 80−9823
astronomical speckle interferometry, defocusing effects 78−40834
astronomical speckle patterns, interference, point spread function 77−22101
atmosphere, contrast reduction of broadband optical signals 78−69455
atmosphere, image resolution through turbulence over ocean 78−85695
atmosphere modulation transfer function, estimation via coherence interferometer *(Russian)* 79−16715
atmosphere modulation transfer function, vel. to IR speckle interferometry 80−31216
atmospheric correlation scale meas., spatial freq. modulation of stellar images 78−40661
atmospheric degradation of electro-optical system performance 79−66805
atmospheric degradation of electrooptical system performance 79−34940
atmospheric horizontal imaging, spectra characts. of image quality 77−91265
atmospheric lens MTF changes, solar speckle interferometry calibration 79−2370
atmospheric MTF meas. along vertical path 79−84478
atmospheric OTF degradation meas. by TV system 79−92590
optical transfer function continued
atmospheric turbulence degraded beam quality, tilt-corrected MTF 77−42481
atmospheric turbulence effect on vertical optical path, phase coherence function meas. 77−45155
atmospheric turbulence effects on optical imaging 79−66806
atmospheric turbulence effects on optical imaging systems performance 79−66799
atmospheric turbulence phase distortion, modal compensation 78−69451
atmospherically degraded image restoration using complex spectral ratios 79−29854
autocorrelation method for measuring the transfer function of optical systems 80−58469
average square deformation of wave surface for system evaluation *(German)* 77−88882
azimuth scan MTF techniques, for optical component and system evaluation 78−50900
binoculars, 8×30, MTF, stray light and transmission characteristics 79−72655
biomedical gamma camera systems, methods for MTF meas. 80−94324
birefringence elements in optical systems, generalisation of pupil function 78−55310
blind deconvolution, zero phase blurring function estimation 80−106482
C-CD, charge transfer inefficiency effect on MTF, compensation techniques 80−10026
C-CD imagers, evaluation techniques 77−83990
camera lens, 48 inch, image quality rel. to MTF 78−49938
camera objectives, quality testing by semiautomatic modulation transfer coeff. meas. 79−14124
channel plate in image tube, MTF 80−19108
charge injection devices for astronomy 77−41317
charge transfer inefficiency affecting modulation transfer function of CCD 79−94175
chromatism transverse, effect on transfer characts. of optical systems 79−908
cine objectives quality evaluation, measuring scheme *(Russian)* 77−41718
coded aperture imaging: the modulation transfer function for uniformly redundant arrays 80−99019
coherent and incoherent optical spectrum analysis techniques in image evaluation 78−78928
coherent apodization problems, edge ringing effect 77−42495
coherent feedback, flexible filter operations 80−87337
coherent fibre optics testing techniques 80−78992
coherent optical feedback technique, multiplicative disturbance suppression 78−22094
coherent optical system, impulse response for image multiplication by spatial sampling filtration 80−33126
coherent optics fundamentals 78−78910
coherent quadratic detect. systems, quality evaluation 79−72504
collimator monochromatic MTF computation program 80−14451
colour distribution in polychromatic line spread function, aberration influence 77−7014
colour encoded aperture masks used for incoherent filtering of images 79−41348
colour image evaluation from tristimulus values transfer functions measurements 80−87333
colour image form., optical transfer functions for tristimulus values 78−33685
component shape monitoring, tolerance field image production *(Russian)* 79−94154
computed tomography scanner geometry optimisation 80−46037
computer programs for optical design 79−36977
computerised tomography, computer assisted determ. of OTF 80−46030
computerised tomography scanner resolution, geometrical limitations 78−73237
confocal scanning microscope, image form. 80−68249
contemporary optics, book 79−81353
contrast enhancement viewer for film 78−16879
deblurring filter, space-bandwidth product 77−83959
defocus spread and illumination aperture effect, in brightfield electron microscopy 79−231
diffraction analysis, in microscopy 80−32926
diffraction images of bar and edge objects, influence of optimum balanced coma 78−74850
diffraction patterns for optical systems with pupils of non-uniform transmittance 80−87470
diffraction point spread function, second moment as image quality criterion 80−9818
display, perceived image sharpness thresholds 78−65019
display design, visual psychophysics appl. 78−65017
double beam interferometer, meas. of background suppression and spectral detection 80−95130
double beam interferometer for background suppression and spectral detection 80−95129
double grating diffraction shearing, for MTF meas. 79−64366
double-beam interferometry with optical background suppression 79−75576
edge enhancement with incoherent optics, using pupil plane mask 77−71921
edge image anal., finite area sampling technique 79−22902
edge image analysis, Walsh functions used in Fourier transforms 79−72507
edge-ringing and edge-shifting, effects of coherence 79−36833
electron image formation, partial coherence and inelastic scatt. 78−58897
electron micrograph optical and digital spatial freq. filtering 78−70231
electron microscope, coherence in bright field microscopy of weak objects 78−32955
electron microscope, contrast transfer for tilted and conical bright field illumination 78−37115
electron optical convertor, pulsed, dynamic spatial MTF estimate 80−74502
electron phase microscopy using spherically corrected foil lens, contrast transfer function *(German)* 80−83546
electron-optical convertor stroboscopic interpolation of spread function 77−7204
Electrotitus, detective quantum efficiency 80−42307
endoscope with rigid to flexible imaging multifibre coupling, MTF 79−23052

optical transfer function continued
eye, accommodation microfluctuations, IR optometer recorder *(French)* 78−7463
eye, aerial image modulation lowering, contribs. of retina and eye optical system 80−81584
eye, contrast sensitivity function 77−25442
eye, human, MTF of defocused optical system for incoherent monochromatic light 80−67072
eye, kitten, optical quality development 78−64982
eye, of horseshoe crab, anal. of adapting bump model 78−73160
eye, subjective meas. of monochromatic aberrations 78−35837
Fabry-Perot interferometer instrumental function for short light pulses 80−105704
Fabry-Perot interferometer of large Fresnel no., image profile 79−54177
feedback systems for analogue and digital optical image processing 80−102650
fibre, multimode, graded-index, low-pass filter characts. 77−23759
fibre bandwidth determination in time domain, OTF meas., laser diode source evaluation 80−79002
fibre baseband transfer function, indirect tests, simplified procedure 79−50386
fibre OTF meas. method *(French)* 78−42458
fibre transfer function meas., swept-frequency technique 78−1375
fibre-optic communication cables, measurement of baseband transfer function 80−1355
fibres, graded index, with mode scramblers, spliced, OTF 78−33832
filter, single mode fibre birefringent 80−58713
finite-width line axial optical density prediction 79−27193
first and second generation image intensifiers compared 77−39105
flexible band-pass filtering using coherent optical feedback 79−94166
flexible high-resolution film recorder system 80−102827
FORTRAN program for MTF calc. 78−25807
Fourier optical evaluation techniques, user oriented 79−86131
Fourier transform imaging, systems theory appl. *(German)* 78−74851
Fresnel diffraction pattern, spatial freqs., spectral analysis *(French)* 77−58269
gamma camera, line spread function meas., practical considerations 79−17585
gamma camera data, evaluation in moving organ exam. 80−30845
gamma camera transfer function, statistical study 77−70541
gamma camera visual outcome units comparison, use of MTF 80−94323
Gaussian motion image degradation 79−10260
gaussian quadrature for OTF calc., rel. to lens system design 78−90383
German standards on image assessment 78−58926
glass fibres, determ., test *(German)* 77−27366
graded-index optical waveguide characteristics meas. 79−14108
grating detectability, aberration effect evaluation in visual instruments 79−55073
high-resolution film, facile image evaluation 77−74533
hologram forming process, using multiple grating interferometers, MTF first order theory 79−76632
hologram recording medium, photochromic, heuristic exponential model appl. 80−78796
holographic image formation, coherent transfer functions and resolution 80−43292
holographic interferometry method, Francon's, meas. of MTF, wavefront aberration 79−3647
holographic lenses, coherent transfer functions anal. 77−68190
holographic optical elements for incoherent polychromatic imaging 80−69349
holographic recording media comparative indices, optimal linear transfer function 79−89870
holographic recording medium, optimal linear transfer function determ. 80−23635
human visual system, MTF *(Japanese)* 77−73526
image assessment, review of German standards 78−50724
image contrast loss in presence of chromatic magnification difference, numerical estimate 80−95823
image eval., post-flight eval. of sensor performance 79−31827
image evaluation, coherent and incoherent optical spectrum analysis 78−63031
image evaluation methods, project SENTINEL SIGMA for Air Force, resolution meas. 79−31826
image evaluation methods survey *(Czech)* 79−50235
image facsimile synthesized with Gaussian spot, fine structure 79−76604
image formation by inversion of scatt. field data, expts. and computer simulation 79−89852
image formation in scanning microscopes with partially coherent source and detector 78−58923
image optimisation by apodisation filters in optical systems with residual aberrations 80−53223
image parameter estimation potential accuracy anal. 77−88648
image processing, analogue and digital, feedback, review 80−102639
image processing nonlinear nonmonotonic function synthesis 77−50633
image quality criteria, modular transfer function, phase transfer function *(German)* 80−53221
image quality data derivation from edge sharpness, simple math. methods 78−50722
image restoration, a posteriori method, OTF phase and magnitude estimation 79−72502
image speckle pattern, point spread function effect on average contrast 77−46702
images degraded by spatially varying pointspread functions, 2D digital restoration 78−78920
imaging device testing, USA standards 78−50725
imaging in the presence of random wave aberrations 79−76607
imaging of relatively strong objects in partially coherent illum., linear transfer theory 78−22091
imaging system, incoherent, diffr. images asymptotic behavior 80−1139
imaging system assessment, conference, London, England (Nov. 1976) 78−50718
imaging system with obscured pupils, OTF and point spread function 78−25809
imaging systems in water, point and beam spread functions 78−5426
incoherent annulus object diffraction images in presence of primary astigmatism 79−22904
incoherent optical processing via spatially offset pupil masks 78−82917
incoherent processing of complex data, OTF synthesis 77−38806
industrial X-ray film information processing methods *(German)* 78−15637
optical transfer function continued
information processing system parameters rel. to optical element characteristics 79−72510
integral equations soln. by optical spatial filtering 79−3643
interference filter, V(λ), design appl. to visual system MTF evaluation 79−76843
interference transfer function with quadratic detect., coherent illum. 80−78782
interferogram analysis, point spread function and OTF determ. for optical system testing 79−76616
interferogram fringe pattern reduction, automated system 80−47097
interferometer, Martin-Puplett, for OTF of component meas. in output beam 78−70179
interferometer, real-time shearing, quality factors testing appl. 80−37081
interferometric meas., variable shear interferometer using correlated diffusers 79−97419
interferometric MTF meas. technique 77−3688
interferometry, multiwavelength testing using modified Twyman-Green interferometer 78−59169
introduction to OTF *(Chinese)* 79−98308
inverse diffraction problems soln. using diffr. coeffs. 77−46698
IR lens production tests 78−50890
IR segmented composite window design 80−106621
IR stellar speckle interferometry, modulation transfer function and evidence for log-normal statistic 79−101079
isophotometric photorecording method for optical system image quality meas. 77−34967
isoplanatic degradation of tilt correction and short-term imaging systems 80−53219
isoplanatic optical systems, partially coherent image form. through random absorbing media 80−14292
isoplanatism varieties for imaging through turbulence 77−42499
laser beam, phase compensated, propag. through atm. turbulence 78−83012
laser beam line spread instrumentation for propag. meas. 78−83013
laser beam line spread instrumentation for propag. meas. 78−83015
laser beam propagation through turbulent atmosphere, interferometric evaluation of imaging characts. 77−88643
lens, large-size, simplified MTF meas. *(Japanese)* 80−33121
lens, standard reference, for MTF equipment testing in IR 78−50898
lens assessment techniques, polychromatic and monochromatic, in far IR 78−50899
lens design data, OTF numerical calc. *(Korean)* 80−19085
lens design with simultaneous image spot, optical path difference, diffraction MTF and Seidel abberation minimisation 80−74459
lens evaluation for 35 mm cameras, MTF based test method 78−41363
lens film system resolution computation from numerical MTF data 79−44960
lens imaging properties and OTF, Jones notation 78−25945
lens light-guide line, image transmission characts. 79−3789
lens MTF measurement, accuracy of spectral response matching 78−50721
lens optimisation using Walsh functions, FEE-based criterion 78−79097
lens system design with extended depth of focus, Version 14 optimisation program 78−90489
lens system evaluation, use of OTF for image anal. 80−53481
lens testing, MTF meas., light source polar intensity distrib. influence 78−50723
lens testing, MTF-based optical sensitivity and tolerancing computer programs 80−83686
lens testing criterion, development and implementation of instrums. 77−19383
lens wavefront aberration, interferometric examination techniques, OTF meas. standards 80−69498
lenses, standard reference, for assessment of OTF meas. equipment 78−50897
lenses, ultrashort pulse propagation, temporal spreading at focus 77−58414
lenses and optical materials, transmission and MTF in 8-13 μ band 79−36982
lenses for 35 mm camera, MTF based simplified test method 78−49937
lenses for projection photolithography 77−58423
lensless scanning telescope, MTF 80−58655
Limb Infrared Monitor of Stratosphere, radiometer spatial frequency response 79−101048
line spread function, notation 77−620
linear system characterization through response cataloging 79−50229
linear transfer, three-dimensional, by holographic depth selection 77−10867
lithography, optical and electron-beam, MTF evaluation 80−4801
logarithmic Hilbert transform, use in solving phase problem 77−88653
low spatial frequency enhancement with triangular and associated filters, incoherent transfer functions, equiv. passband 79−94168
mammographic screen-film systems, comparison of laboratory and clinical evaluations 78−69187
mammography, detective quantum efficiency anal. of electrostatic imaging and screen-film imaging 80−41232
mammography, optimum radiographic image conditions 77−90879
mass-produced camera objectives, effects of cosmetic defects 80−47135
matched filter visibility effects on the correlation function 80−96031
medical imaging systems, information capacity considerations 80−98090
merit function, diffr. based, for automatic lens design *(Chinese)* 80−5809
metaxial optics, centred refracting systems, undiaphragmed and without aberration *(French)* 78−94369
micro-optics testing, width meas. of slit test objects 80−64223
microchannel image intensifier quality evaluation *(Spanish)* 79−72681
microchannel plate X-ray image intensifier, image resolution 78−35937
microdensitometer flare, methodology for quantifying 80−52293
microdensitometer temporal reponse, MTF determ. 78−32904
microscopic image form., nonuniform source distrib. 77−14664
minicomputer optical design and analysis program 79−14075
modal wavefront compensative system performance, finite bandwidth effect 79−81361
mode-coupled multimode fibre 79−10409
modulation contrast microscope, image irrad. rel. to phase gradient, numerical aperture influence *(Spanish)* 79−55063
monochromator, total spread function description of props. 80−19100
mountain and desert atmospheric MTF comparison 80−82063
MTF, two-dimensional, meas. by second order speckle statistics calc. 80−63937

optical transfer function continued
MTF determination from edge response function, single step calc., appl. to computerised tomography 78−35938
MTF evaluation by photoresist 79−3636
MTF evaluation with optical matched filters 77−27257
MTF in radiography, screen sharpness quantum noise depend. 78−20261
MTF measurement in France, ACOFAM and ACOMAT instruments 78−50727
MTF measurement of low light level devices 80−33221
MTF measurement using positive photoresists, cross sectional features 78−9337
MTF tolerancing computer program 80−78934
Muehllehner's tomographic camera, quantitative evaluation of depth effect 77−86609
multi-aperture system imaging props. 80−87332
multiactuator mirrors, wavefront error compensation capabilities 79−59797
multifibre image transmission, misalignment effect on MTF 79−14093
multimode fibres, basic transmission characteristics 79−18538
multimode optical fibre guides, MTF 79−7199
multimode step-index fibre, OTF, geometrical optics calc. 77−65637
near field speckle statistics 77−19182
noisy images, a priori information, degrees of freedom 77−38811
noncentrally obscured circular pupil imaging systems 78−66774
nonlinear halftone screen preprocessing, analysis and synthesis 77−58267
objective lens of amateur camera, production quality, MYF test freq. selection 79−81581
objectives' two-dimensional transfer functions, holographic meas. test 79−50253
objectives in large scale production, testing 78−18035
obscured circular pupil imaging system, included power 78−46520
off-axis gaussian beam, third order spherical aberration, diffr. pattern 77−14665
off-axis imaging system, polarisation dependent MTF defects 77−34837
offset section utilisation for noncoherent processing 79−76625
on-axis system, OTF rapid calc. using Tchebycheff polynomial orthogonal props. 78−90386
one-dimensional coded apertures, applications 78−45746
optical background suppression technique in double-beam interferometry 79−97428
optical fibre guide, multimode, modulation transfer function 78−55442
optical transfer measure, system relations, appl. wide field microscopy and microelectronic photolithography *(German)* 80−9815
optoelectronic device transfer function meas. and digital data processing apparatus 79−50399
optoelectronic instrument, image information content 77−39057
partial tracking optical heterodyne receiver arrays, operating in turbulent atm. 79−41345
partially coherent imaging, edge ringing, performance function 77−46699
perfect lens with polarisation masks, OTF 78−90380
phase contrast objective, point spread functions of annular phase filters 78−25805
phase problem in image formation: the determination of coherent transfer functions 80−87329
phase retrieval from intensity meas., uniqueness question 79−13915
photogrammetry, OTF/MTF standards 77−78471
photographic emulsion layers, image restitution quality and effective MTF concept *(Russian)* 77−38044
photographic film, undeveloped, MTF meas., target base dimension influence 80−102653
photographic image quality, MTF meas., for lens testing 77−45912
photographic image quality, scattered light effect 78−16884
photographic image threshold luminance detail value, effect of target and photographic parameters 78−56989
photographic imagery, transfer functions due to complex linear motions 79−18355
photographic layer, homogeneous solid, diffusion, one-dimensional case *(German)* 80−73495
photographic lenses for low cost high production, design example 79−85193
photographic materials, modulation transfer function, interference-diffraction method 79−21844
photographic materials, MTF automatic evaluation 80−95170
photographic shutters, efficiency rel. to picture quality 77−74531
photolithographic technology, optical MTF *(Japanese)* 78−90387
photoprinting on electric copier, low contrast negative, time modulation of exposure, contrast enhancement *(Russian)* 77−67526
photosensor array aliasing and MTF effects 77−39086
pinhole camera graphic design 79−35863
plane-mirror two-beam interferometer analysis 79−2812
point spread function, encircles light energy calc. 77−79766
point spread function of systems with parabolic filters, effects of defocusing 78−13776
point spread function synthesis, geometrical optics approach, transaxial tomograph processing 79−94163
polarisation and interference in optics, matrix theory 77−23625
polychromatic line apread function colour meas., colorimetric MTF 78−50712
polychromatic MTF measurement reproducibility 78−50719
precision optical element testing by phase meas. interferometry 80−74520
projection system, wavelength and coherence effects 80−64136
projection system transfer function definition and performance testing *(Hungarian)* 80−14413
projector having a thermoplastic target and operator's eye, characts. 80−96023
proximity focused image tubes, image transfer props. 77−83950
pupil function replication 79−27182
pupil-mounted opaque band effect on SISAM spread function 79−12871
quasi-monochromatic incoherent optical image processing 79−76626
radiographic imaging system OTF 80−17085
radiographic intensifying screen equivalent blur 78−69197
radiographic screen-film systems, modulation transfer function 79−100712
radiographic system, OTF as means of evaluation of image characts. *(German)* 80−35450
radiography, field characts. of geometric unsharpness due to X-ray tube focal spot 77−21616
radiography, metal screen-film detector MTF at megavoltage X-ray energies 80−30868
radiography, rare-earth screens, effect of P X-rays 80−30867
radiography, Siemens star X-ray image artifacts computer simulation 77−21615
radiography, star test pattern image interpretation 77−21614
radiography, straight-line tomography, linearising mechanisms 78−35934
radiography, tomographic image quality evaluation 77−86607
radiography, use and abuse of MTF concept 77−86623
radiological imaging system line spread function and MTF determ., effect of finite slit 78−24118
radiological imaging systems, unified view using Schade aperture theory, noisy images 77−73563
random medium, image resolution limitation 78−37813
random small-angle scattering theory, dispersion coeff., MTF and contrast loss 77−68174
real-time interferometer for optical system testing 79−85168
reconstruction spots for digital sampled images 78−63034
reflection microdensitometry, optical principles and practical solutions 80−4790
relay, system design, secondary colour reduction 78−83067
resolution, S/N ratio and meas. precision 79−59643
retina, Limulus, temp. dependence of dynamic response 79−43866
retinal diffusion and eye optics quality, OTF and light scatt. characterisation 80−41004
retinal image light distrib., cat 78−48790
roof and other prisms, MTF tests 80−69571
satellite retroreflector arrays 80−5778
SAW disc delay line beamguide 'optical' transfer function 77−31183
saw-tooth wave response of optical systems in presence of linear image motion 79−31810
saw-tooth wave target, modulation by optical system with triang. and assoc. filters 80−9817
scanning microscope, increased depth of focus using slit aperture, MTF degradation 78−45689
scanning microscope, spherical aberration effect on imaging props. 79−58783
scanning microscope, types 1 and 2, image form. 77−79148
scanning telephotometer, spatial transfer characts. 80−73415
Schade detail S/N ratio derived from decision theory 78−63022
schlieren instrument, amplitude transfer charact., Monte Carlo method 80−28336
schlieren techniques represented by phase contrast function 80−9813
scintillation camera collimator image form. 80−89844
scintillation detector MTF calc. on programmable pocket calculator 77−66844
sector templets for determining the contrast transfer of imaging systems 80−32924
Seya-Namioka monochromators, automatic design of holographic gratings 79−10390
space variant optical transfer with Fourier filter in extrapupilar position 77−10846
space variant systems, holography using phase coded reference beams 78−33698
space-variant holographic systems using phase-coded reference beams 78−74868
spatial and energy parameters of optical instrument, criteria for performance evaluation 80−33259
spatial filter OTF, for noise degraded image restoration 77−10857
spatial filters, rotating circular involute reticle used in optical searching systems 79−98505
speckle interferometry, bandwidths, exposure times, effects on MTF 78−69701
speckle interferometry, image reconstruction of single stars 78−32350
speckle photoelasticimetry technique, time impulse response and spectral transfer function 77−58523
spectral-temporal effects, white-light interferometry and phase-locked pulse anal. 77−88656
spectrophotometer, combined double modulation of source, modulation functions 77−57400
spectroscopic system, direct meas. 78−74849
spectroscopic system, OTF meas. and image correction 78−37083
spiral tomography, optimum blurring 78−69181
square law media, imaging characts., OTF in incoherent case 77−7015
standard lens MTF measurements in Japan, interlaboratory comparison 78−50720
standardisation activities in Netherlands 78−50728
standardisation in Japan 78−50726
standards in Britain for optical device performance assessment 78−50729
statistics, correl. random amplitude and random phase effects 79−72503
stellar speckle interferometry, lens-atmosphere modulation transfer function meas. 79−101078
stellar speckle interferometry lens-atm. MTF meas. 77−22103
STEM, imaging of phase objects *(German)* 78−32931
step-index fibre baseband equalisation 78−1371
straubel apodisation filter systems, effects of defocusing on point spread function 78−25804
Straubel apodisation filters, equivalent passband of optical system 78−50880
surface errors rel. to optical performance, effect of mid- and high-spatial freqs. 79−59789
surface scattering rel. to microroughness, surface transfer function 78−58917
system with magnification chromatism, MTF 79−31818
systems with small residual aberrations, schlieren effects *(German)* 80−32923
telescope MTF curves, comparison of visual and photoelec. meas. imaging quality *(German)* 77−79763
telescope with severe aberration, MTF for speckle interferometry 78−12103
Terskol Peak telescope and electrophotometer, apparatus function and atmosphere monochromatic extinction coeffs. *(Russian)* 79−44246
test standard, afocal system 79−36978
thermal imaging systems, optical components testing 78−33911
thermoplastic spatial light modulator 80−102841
thermoplastic-photoconductor films for optical data processing 78−50875
thin phase structure detection method spatial filtering props., under partially coherent illum. 80−95828
thin phase variation objects under partially coherent illum., effective transfer function *(Spanish)* 79−55064

optical transfer function continued
three colour channel hybrid system to synthesize complex point spread functions 79−41347
tolerancing procedure based on MTF, lens appl. 79−86237
tomodensitometry, image quality 78−44589
tomography, linear, optimum spread functions 77−66846
transaxial tomography, simple pupil function for OTF synthesis 79−41349
transparent electrophotographic films, information recording 78−70210
triangular apodiation filter system, rectangular and triangular wave-response 79−59645
truncated sinusoidal test and exptl. MTF meas. 78−25806
turbulent medium, optical resolution with adaptive phase compensation 77−46692
turbulent medium, OTF separation 77−42498
TV optical operational amplifier 79−94327
TV zoom lenses, MTF meas., distortion influence, normal and inverse conjugate techniques 78−78008
two dimensional image scanning of movies using surface acousto-optic interaction 79−94352
two pupil synthesis, incoherent spatial filtering 78−58919
two-dimensional optical system MTF meas. by second-order speckle statistics computation 80−74304
undeveloped emulsion layer, MTF calc. 79−21840
uneven interface of media with different refractive indices, statistical charcts. of images 80−87331
UV objectives, for submicron photolithography 79−32032
visibility, definition, confirmation using marine optics data 80−23633
vision, line spread function meas., implications for channel bandwidths 78−65030
vision, matched filter model of brightness change detect. 78−65001
vision model relating image quality and MTF 77−86487
visual processing, Fourier transform models, adaptation to spatial impulse 77−9191
visual stimulus device for characterizing temporal MTFs in man 80−51204
wavefront aberration difference function, variance 77−3543
wavefront plot, aberrations, point spread function, three dimens. *(German)* 78−46521
wavefront sensing by phase retrieval 80−106478
wavelength selection for transhorizon optical communication 79−7088
wide field imaging, significance of optical transfer measure *(German)* 78−90374
Wiener image filtering, object fast restoration after PSF degradation 78−90379
X-ray film screen combinations, modulation transfer data 78−66016
X-ray film/intensifying screen system, contrast detail from Wiener spectrum *(German)* 80−73559
X-ray film/intensifying screen system, MTF and Wiener spectrum, film and screen quality effect *(German)* 80−73560
X-ray focal spot, MTF, modified meas. method 80−37149
X-ray image quality, MTF anal. of influencing factors *(Japanese)* 77−73580
X-ray images, electronic recording 80−62815
X-ray imaging system, MTF 77−38815
X-ray intensifying screen, relationship between resolution and speed 78−65124
X-ray intensifying screen MTF, empirical eqn. 78−65123
X-ray pinhole camera, resolution improvement by image processing 77−30222
X-ray screen-film detectors, megavoltage OTF meas. technique 79−80736
X-ray systems for 3-D imaging, MTF 77−40851
X-ray tube focal spots, effective size of transverse dimension 77−71414
X-ray tube focus, MTF rel. to current *(Japanese)* 77−70545
X-ray TV chain MTF and image quality determ. factors 80−36126
xerographic development, transfer function model 78−65991
xeroradiographic imaging linearity and MTF applicability 80−4825
$As2S_3$ amorphous chalcogenide film inorganic photoresists, holographic resolution evaluation 79−76629
$Bi_{12}SiO_{20}$ PROM device, image recording and erasure mechanism 80−74490
KD_2PO_4 photo-spatial light modulator, optical data processing 80−102839
KF:LiF, photodichroic real-time recording medium, for optical spectrum analyser 78−66878
Nd^{3+}:YAG multimode laser radiation noise 80−74366
Si photodiode imaging array design factors 77−39085
ZnS CVD IR window, optical and physical characteristics 80−106620

optical variables control
acousto-optic programmable filter characteristics and applications in optical computing 79−72716
active optical systems, real-time control over optical wave fronts 78−71187
adaptive laser beam control process, closed loop considerations 77−88660
adaptive laser resonator, intracavity phase variations 77−88793
adaptive optical systems, passive return-wave 77−88933
adaptive optics aberration coeffs. adaptive estimation 77−88659
closed loop adaptive optics systems, target effects 77−88934
closed loop control system for light industry *(French)* 77−83941
colour film printer, rapid-acting light-setting mechanism *(Russian)* 79−35878
compensation densitometer servosystem using integrated operational amplifiers 78−89525
CW dye laser control techniques 77−58347
darkroom exposure control circuit *(German)* 79−6198
fibre-optic band-pass attenuator 79−37003
film, optical thickness monitoring 78−5591
film, optical thickness monitoring using quartz cryst. monitor 78−5592
injection laser output regulation by NTC resistor cct. 80−14353
laser automated alignment, CO_2 10 kJ laser for fusion research 79−76703
laser beam, single-pulse, spatial characts. control 78−79058
laser beam intensity control circuit 78−9394
laser beams, adaptive control 77−88833
laser beams, high energy, adaptive phase and amplitude control, book contrib. 79−31971
laser pointing and tracking, adaptive optimal filtering appl. 77−88959
light and water exposure apparatus 79−15914

optical variables control continued
luminous flux, controllable regulator for KIM-9-75 source 77−39010
motion picture film, automatic system for estimation of exposure conditions *(Russian)* 79−35877
multiple exposure hologram generation from controlled transparencies *(Russian)* 79−94177
photographic recording, using centrifugal density regulator, streaks in mine shafts meas. appl. 77−79173
pretilted liquid crystal structure formation and props. 77−76306
refractive index profile of graded index optical fibres 79−59856
sensing systems, with automatic light-intensity control, stabilisation 77−54784
simultaneous feedback control of bias and modulation currents for injection lasers 80−43332
spectral filter thickness optical monitoring 78−55476
spectrophotometric measurement, dual wavelength, precision optimisation 79−92019
thermal-blooming compensation, using closed-loop adaptive single parameter system 78−94407
tide-recording equipment, phototransducers emission source light output ratio stabilisation *(Russian)* 78−88949
tunable laser linear scan control by Fabry-Perot interferometer 79−76693
wedge compensator for automatic control system 78−13808
$Al_{0.42}Ga_{0.58}As$-GaAs-$Al_{0.42}Ga_{0.58}As$, etalon, optical bistability and modulation 80−58628

optical variables measurement
see also colorimetry; densitometry; light velocity measurement; optical noise measurement; photometry; polarimetry; Q-factor measurement; refractive index measurement; streak photography; turbidimetry
aberration sensor for high-energy laser system, interference problems 79−98422
absolute luminous intensity meas., apparatus *(Danish)* 78−62217
absorption coefficient, precise meas. of small change *(Japanese)* 80−4749
absorption coefficients, meas. by photoacoustic spectroscopy 78−24864
absorption coefficients, small values, automated calorimeter and scanning Doppler interferometer 78−45680
absorption coefficients at 632.8 nm, intracavity laser meas. 78−8454
absorption coefficients meas. by transmission emittance and calorimetry 78−24839
absorption coefficients meas. of transparent materials, interf. effects 78−46699
absorption coefficients of film coatings, laser calorimetric meas. 78−25905
absorption of laser materials, static profile calorimetry meas. 78−25908
absorption of laser window materials, calorimetric meas. of CO wavelengths 78−25911
amplitude correlation mehtod for optical polarisation meas. 80−53206
amplitude-phase distributions of light fields, Rayleigh interferometer meas. 77−30200
angular reflectance variations of rough surfaces, near IR, correction method 77−75424
anomalous dispersion measurements with Michelson-type interferometers *(Russian)* 79−93211
apparatus for optical measurements under conditions of hydrostatic pressure up to 2 kbar at temperatures ≲25K 80−22379
atmospheric turbulence, corner-cube reflector and plane mirror comparison in folded-path and direct transmission 78−85697
attenuated total reflection, optical consts. determ. *(Spanish)* 77−69788
automatic concentric shaft reflectometer for use in vacuum UV 77−2684
automatic power-spectrum density meter for pulsed laser beam 78−45698
backscatter in optical fibres, theory *(German)* 80−91921
baseband frequency response meas. system, for fibre transmission system components 78−42404
bench equipment for optical fibre characteristics measurement 80−58695
bidirectional reflectance distribution function meas., mirror surface contamination assessment 79−59790
birefringence, new method for nematic liquid crystals 78−79526
birefringence detection system for polarisation opt. props. meas. 77−57385
birefringence dispersion in glass, meas. with Babinet compensator using white light 78−27177
birefringence measurement using photoelastic modulator 80−31838
birefringence small area change real-time detection *(Japanese)* 78−15938
birefringent crystal faces, meas. method of growth and dissoln. rates 80−79719
Brewster's angle measurement using ordinary lab. apparatus, for high-school students 78−86097
cable, attenuation and dispersion meas. and faults location *(German)* 79−14097
camera lens performance, routine checking system 80−277
chemical CW laser, optical diagnostics 79−36916
chiral substances, electro-optical responses, Jones matrix, meas. sytem for rot. anisotropy 80−84723
circular dichroism in presence of birefr. and linear dichroism, meas. method 78−27178
circular dichroism meas. in vacuum UV 78−49913
closed-loop simple system for real-time optical phase meas. 79−63302
coherence length measurement of laser radiation *(German)* 78−79052
colour of displays, using colorimeters and spectroradiometers 79−40605
compound glass optical fibres, total and scatt. loss coefficient meas. 80−69536
conductive liquid Kerr constant meas. 78−88279
constants at two incidence angle values 80−101831
crystal scattering, meas. installation 78−4673
cuvette for studying optical nonuniformities in aggressive liquids 79−2810
dental material transparency meas. device 78−31975
depolarisation ratio of light scattered by compressed gases, meas. apparatus 80−38527
differential mode attenuation meas. in graded index fibres, automated apparatus 78−71198
diffuse reflectance meas. for buildings 80−27334
diode laser wavelength monitoring using fibre interferometer 80−74413
disperse systems, electro-optical phenomena, induced dichroism rel. to elec. field calc. 78−50699

optical variables measurement continued
dispersion in single-mode optical fibres pulse synchronisation meas. technique 80−48410
dual-mode optical fibre, spatial technique for modal delay difference meas. 80−78950
electric dichroism measurement instrument with digital processing 80−82800
electro-optical apparatus, conformation of change in polypeptides 80−85336
electrogyration and piezogyration in polar crysts., meas. method 79−28716
electrolytic cell for meas. optical props. of semiconds. 79−93199
extinction coefficient of high-transmission glasses, least-squares method 78−90470
far IR reflection measurements, He cryostat modification for asymm. Michelson interferometer 78−74053
Faraday effect and susceptibility of garnet films, meas. using magnetooptical apparatus 80−105680
fiber-optic measurements, using standards and instruments 80−74488
fibre, multimode, freq. response meas., wavelength depend. 77−27341
fibre, zero material dispersion wavelength determ. by pulse delay meas. 78−1322
fibre amplitude and group delay distortion, using link analyser 78−66940
fibre and measurement technique *(Japanese)* 78−22200
fibre attenuation, continuous meas. during manuf. 77−19400
fibre attenuation and dispersion meas. techniques and interpretation pitfalls 78−1399
fibre attenuation meas. by backscattering method, effect of noise 80−102824
fibre attenuation measurement comparison among USA manufacturers 80−58747
fibre attenuation measurements performed by backscattering technique 80−64152
fibre backscatter attenuation measurements, optimised technique 80−53447
fibre cut-off wavelength meas. for single mode fibres 79−59802
fibre cutoff wavelength meas. method for HE_{21}-, TE_{01}-, TM_{01}-modes 79−76820
fibre inhomogeneous dispersion, direct meas. method 78−1400
fibre link, end-to-end cross coupled, crosstalk meas. 78−90502
fibre loss measurement using enhanced sensitivity nondestructive method 78−66895
fibre material dispersion meas. 78−63174
fibre material dispersion meas. by baseband modulated envelope detection 78−1368
fibre parameter characterisation techniques, comparison 80−64147
fibre transfer function meas., swept-frequency technique 78−1375
fibre transmission characteristic meas. by digital processing oscilloscope 79−12787
fibre transmission system, meas. equipment 79−32061
fibre waveguides characteristics 78−59143
fibre wavelength dispersion, difference method measurement 78−37974
fibre Y-branch, low-loss, attenuation and far-field meas. 80−10004
fibres, measurement techniques for transmission loss and refractive index distribution *(Japanese)* 80−87498
fibres optical, measurement of main parameters 79−46076
field plotting of optical fields using single-mode optical fibre 78−30097
film, 10^{-1} to 10^{3} nm, using laser microellipsometer *(Czech)* 77−61109
film, optical absorption meas. at air-film interface, within film and at film-substrate interface 79−80659
film, optical consts., thickness and surface roughness determ., technique and appl. to AlN *(German)* 77−41670
film optical consts. meas., Shamir-Graff method evaluation 80−11489
film optical parameters meas. method, reevaluation 80−104004
films, by light intensity ratios 77−2678
fluorescence, apparatus for meas. electrically induced polarization changes 77−46662
fluorescence, polarisation anisotropy meas. via single-photon counting 77−18072
fluorescence de-excitation function recording, one-quantum method, error anal. *(Russian)* 77−65925
focus-position sensing using laser speckle 79−59785
formic acid laser 311 μm line, freq. meas. by mixing with HCN laser 79−76728
four-point field coherence function meas. in laser random focusing region *(Russian)* 78−58910
frequency, direct method for visible light 80−47041
frequency measurement and synthesis, near IR and visible ranges 79−35808
gain measurement technique for high gain amplifiers 80−1208
gas phase fluorescence spectra, temp. controlled X-cell 78−66692
Gaussian laser beam focus, intensity distrib. determ. 79−14002
glass, large disc, optical homogeneity, high accuracy measurement *(Chinese)* 79−55195
glass assessment, low absorption coeff. meas., calorimetric method 77−58405
glossiness of curved surface, physical and psychological, meas. method 80−37074
graded index fibre optical loss meas. using dummy fibre 80−5819
graded-index fibre, optical loss meas. in the field 80−102851
graded-index fibre differential mode attenuation meas. 78−1403
graded-index fibre material dispersion evaluation using nanosecond pulse radiator 79−81520
graded-index fibre modal power distrib. determ. from near-field patterns 79−81518
graded-index optical fibre intermodal dispersion, frequency-domain meas. 80−58729
graded-index optical waveguide mode-dependent attenuation meas. 78−46774
grating absolute efficiency meas. device 80−87540
guided optics techniques for meas. of film props. 79−99958
high power continuous laser emission meas. appls., pyroelectric ceramic appl. *(Russian)* 78−16845
high-power laser luminance contrast meas. 78−87055
integrating cavity for small optical absorption meas. 79−12838
interferomic wavelength meas. with post-detection signal processing 80−105699
interlocked solid-state lasers, radiation intensity modulation for precision meas. 80−1250

optical variables measurement continued
interstellar grains, interaction of light with small-particle system 77−74111
intracavity method for optical densities meas., dynamic range extension 79−9231
IR bidirectional refl. distrib. function meas. for baffle and mirror materials, recording instrument 78−58012
IR emissivity meas. method and equipment 79−35812
IR laser wavelength meas. by radiation conversion method, error anal. 79−7175
IR pulse laser intensity profiles meas. *(Japanese)* 80−22413
IR transparent materials, bulk and surface absorpt., calorimetric meas. method 79−27347
Kerr effect, meas. apparatus for water and conducting liquids 79−12832
lambdameter, improved design based on moving mirror Michelson interferometer, accuracy tests 79−63194
laser, pulse width, meas. by two-photon absorpt. fluoresc., contrast ratio variation 79−76737
laser beam, CW, radiated power meas. *(German)* 78−79053
laser beam diameter fluctuations meas. 78−87086
laser beam diameter meas. methods survey, safety aspects 80−53348
laser beam interferometric wavelength measurements through post-detection signal processing 80−42254
laser beam phase front radius of curvature meas., polarising interferometer ultimate resolution 79−88997
laser beam profile measurement using spatial sampling, Fourier optics and holography 79−86201
laser beam radiation intensity distrib. meas., high-speed unit 77−38969
laser beam spatial charact. meas. by modulation method 79−31967
laser beam spot size meas. by scanning with opaque ribbon 77−38972
laser calorimetric data analysis for surface and bulk absorpt. determ. 78−25904
laser cavity resonator, photon lifetime and reflectance meas., phase-shift method 80−38039
laser coherence length, for holographic appl. 77−7100
laser CW digital wavemeter, moving cube-corner interferometer system 78−50840
laser freq. and vel. of light meas., interference methods, accuracy 78−17997
laser frequency instability, short duration, interferometric meas. 79−3733
laser gaussian beam divergence, lensless meas. method 79−18459
laser heterodyne apparatus for measuring small angle scattering from particles 80−1261
laser light pulse parameter meas., integral method 77−72018
laser mirror reflectivity meas. technique, precision 78−17947
laser mirrors, high precision reflectivity meas. technique 77−23698
laser power, using miniature calorimetric convertor 79−22998
laser power meas., radiometric and calorimetric scales' equivalence 77−7115
laser pulse bandwidth limitation, fringe resolved autocorrelation meas. method 79−45979
laser pulse duration measurement, 0.1 to 100 psec., nonlinear autocorrelation methods 78−46702
laser pulse energy meas., liquid calorimeter *(Russian)* 78−22163
laser pulse power meter 79−86202
laser quasi-Gaussian beam geometric parameters, interf. determ. methods 79−64265
laser radiation, pulsed and steady-state, metrological provision for parameter meas. 79−14007
laser radiation fluctuation-spectrum recording for USSR state standard 78−45696
laser radiation in liquid second harmonic intensity meas. 80−48338
laser radiation intensity distrib. meas. using Bragg diffraction of light 80−64092
laser radiation pulse, based on semiconductor radiators 80−23710
laser radiation pulse length meas., discussion 80−1259
laser radiation pulse width, from solid-state meas. lasers 80−23736
laser radiation pulse width meas., integral method with direct reading 77−72019
laser radiation pulse-length monitor testing, precision test system 78−45697
laser radiation spatial distribution determ., mode parameters 80−95055
laser radiation transmission meas. at 10.6 μm 78−92977
laser radiation wavelength meas., 3.39 μm and 0.63 μm 79−30555
laser radiation wavelength meas. using material spectral transmission curves 79−76738
laser signal, sinusoidally modulated, electron-optical recording with subpicosecond resolution *(Russian)* 77−7105
laser single pulse spectral distrib. meas., using Fabry-Perot interferometer and CCTV system 79−3732
laser sounding method and equipment for water absorpt. and attenuation coeffs. meas. *(Russian)* 79−34998
laser sources coherence, meas. system with Michelson interferometer *(Polish)* 78−33762
laser spherical beam curvature radius mem. using Talbot effect *(Polish)* 79−86200
laser transition gain coeff. maximal meas. method for cascade laser 77−31104
laser wavefront analyser for diagnosing high-energy lasers 79−59740
laser wavefront analyzer for diagnosing high-energy lasers 79−59738
laser wavelength calibration using optogalvanic effect, atlas 80−62727
laser wavelength comparison by two-beam interferometer, I_2 stabilised He-Ne laser 78−86326
laser wavelength determ., random/systematic errors statistical estimation 78−17996
laser wavelength measurement, review 78−50841
laser wavelength measurements, review of recent developments 80−48320
laser wavelength meter for pulsed or CW lasers, Fizeau interferometer system 78−46701
laser-fusion expts., calorimeters for meas. of ions, X-rays and scatt. radiation 78−16800
layer surfaces, reflectivity at 3.39 μm, meas. method, relevance to pipelines 80−52340
light absorption, quantitative high press. cell, variable thickness *(German)* 78−12769
light beam diffusion, in absorbing-scatt. layered medium, obs. method 78−62215
light flux charact., multichannel recording system 79−35809

optical variables measurement continued
light intensity variations, metal-halide discharge lamps appl. to film lighting 80−4796
light polarisation measurement, modelling 77−87804
light scattering by solns. containing dust particles, meas. technique 77−37959
light scattering in aqueous polyiner solutions meas., apparatus 78−74058
light scattering technique, comparison of optico-optical scattering and birefringence, of Wyoming Na bentonite suspensions 80−85226
light source displacement vel. meas. for improving telescope photoguide system *(Russian)* 77−41306
light transmission characteristics of optical fibres, alignment chuck design 78−30090
light transmission loss measurement by hazemeter 80−67995
linear birefringence meas. turning birefr. method *(French)* 79−8112
linear dichroism apparatus for extended wavelength ranges, direct-reading 80−98962
liquid absorption cell, for pulse energy meas., digital readout *(Russian)* 78−18000
liquid crystal displays, optical characterisation apparatus 77−7222
liquid He cryostat for optical meas. 79−88962
long-path light absorption cell meas., automation, optical alignment 79−17491
loss of multi-mode fibres, non-destructive method 80−69550
low optical absorpt. coeffs. meas., adiabatic laser calorimetry with long rod samples 79−2804
luminance of optical system determ. by flicker value apparatus *(Japanese)* 77−75645
luminescent screens, resolution determ. with thermal quenching 78−21131
luminous fields, integral charact. meas. *(Czech)* 79−40604
luminous intensity of retroreflectors and retroreflective materials, photometry accuracy assessment *(Dutch)* 79−85159
magnifying power of Keplerian telescopes 79−18497
maximum spectral luminous efficacy determ. *(Chinese)* 78−16831
measuring chamber for high-temp. investigations of opt. characts. of materials 79−21798
measuring equipment for fibre optic communications *(German)* 79−32043
metallic thin film, optical absorpt. meas. by multiple attenuated total reflections *(Japanese)* 79−40603
metals, far IR studies using multireflection cell 77−18075
microwave to visible frequency synthesis 80−48319
minerals optical constants, derivation from measured reflectances, errors in two-media method 79−58100
mirror optical scatter meas. specification proposal 80−48390
mirror reflectance meas. using multipath optical cavity *(French)* 77−13797
mirror reflection coefficient meas. instrument 78−18036
modal wave-front estimation from phase derivative meas. 79−89856
mode power distribution meas. method for multimode parabolic-index fibres 80−14439
MTF measurement of low light level devices 80−33221
multimode optical fibre, group delay meas., swept frequency tech. *(Japanese)* 78−37984
multimode optical fibre dispersion rel. to wavelength, frequency-domain meas. 78−1401
multimode optical fibres, mode conversion coeffs. meas. 80−53433
multimode optical waveguide propag. meas. problems 78−71231
nanosecond laser pulse stretch meas. in underwater propagation 80−87426
objectives' two-dimensional transfer functions, holographic meas. test 79−50253
opacity measurement of smoke and suspensions under ambient lighting conditions 77−26382
opal glass, spectral reflection coeff. and luminanance factor absolute meas. *(German)* 77−87802
optical cell for high- and low-temp. reflectivity, transmission and scattering experiments 79−80668
optical constants meas. method using polarised light refl. coeffs., accuracy 80−73423
optical fibre, graded index, differential mode attenuation meas. 78−13797
optical fibre, measurement of attenuation, numerical aperture and input-output radiation profile 80−33186
optical fibre, measurement of attenuation and dispersion 80−33185
optical fibre, on-site defect location and transmission loss eval. 79−3801
optical fibre, transmission meas. without disturbing integrity 77−72076
optical fibre, V-value measurement 77−7193
optical fibre attenuation charact. meas. by backscatter technique *(Italian)* 80−106600
optical fibre characterisation, measurement techniques 80−95998
optical fibre impulse response measurement system time domain technique 77−19406
optical fibre parameter measurement using optical time domain reflectometer 80−58755
optical fibre variable attenuator, calibrated, expt. 77−39047
optical fibres, baseband freq. response meas. by modulated InGaAsP laser beam, dispersion characts. 80−1308
optical fibres, numerical aperture depend. spectral loss meas. 78−66942
optical glass and fibres, absorption coefficient measuremnt by calorimetric techniques *(Dutch)* 79−76774
optical power meter for fibre-optic appls. 78−93746
optoacoustic power monitors for laser radiation 79−41404
optoelectronic device transfer function meas. and digital data processing apparatus 79−50399
particulates, frustrated total reflectance meas., interface model 77−71362
path difference measurement in birefringent plates, Senarmont compensation method, photoelectric polarimeter *(German)* 77−10091
phase changes in optical recording media, interferometric meas. 77−49769
phase delay measurement using Fourier optical synthesis of Zernike's three-slit interferometer 78−65960
phase difference and axis of birefr. medium, point by point determ. *(French)* 77−762
phase difference variations in transparent object, using Fabry-Perot etalon with overlap bands *(Russian)* 77−26394
phase fluorometer for measurement of picosecond processes 78−66691
phase meas. receivers, closed loop direct detection 77−88661
optical variables measurement continued
phase measurement in real time using photodetector array, Fourier transform computation 80−9013
phasemeter, IR compensation-type based on Mach-Zehnder interferometer 77−39039
photodetector, conversion factor meas., kinetics of laser radiation appl. 79−2820
photodetector relative spectral sensitivity meas. method using two tandem monochromators *(Japanese)* 80−101840
photoelastic constants meas., precision interferometer 77−26384
photoelectric digital energy meter for laser pulse meas. 77−71375
photoelectric distortion on MSP-4 objectives *(German)* 80−95976
photographic recording device based on oscillographic delayed-coincidence method 77−38025
photometric meas., digital meter, cct. and operation *(Polish)* 78−65943
photomultipliers, linearity meas. in pulsed mode using GaAs injection laser 77−37961
photon correlation in nanosecond range using programmable digital counter, photomultiplier evaluation 78−54464
picosecond light pulse, meas. techniques *(Japanese)* 80−52291
picosecond light pulse shape and duration determ. by bleaching of dyes 79−86220
plastics, filled and reinforced, optical const. determ. 78−19472
polarisation of short light pulses 79−17465
polymer film, automated light-scattering apparatus 77−53969
polymer film, stretched, interpretation of polarised absorption and emission spectra of molecules 78−1012
polymeric thin film, by integrated optical techniques 78−27342
power and energy units reproduction for optical, elec. and mech. quantities 77−71287
power of CO_2 laser beam, meas. by new thermoelec. detector *(French)* 77−58365
power of light beam, high-sensitivity optical power meter with tuning fork optical chopper 79−80661
precision loss measurement of photoelectric pulse signals using microcomputer 80−13142
pulse dispersion in conventional Selfoc fibres 79−64305
pulse picosecond waveform meas. 78−57923
pulsed injection light sources, installation for meas. their characteristics 77−75640
quantum fluctuations in light beam meas. using nonlinear interferometer 79−80672
quantum radiation from a point source, angular coords. determ. 77−65050
radiation measurement at Bureau of Radiological Health, rel. to Federal standards 77−38012
radiometer, portable, with Cu_2S-CdS photo-cell, solar radiation meas. appl. 78−53763
reflectance and transmittance, arrangement for accurate meas. *(German)* 80−31844
reflectance measurement attachment for spectrophotometer 77−174
reflectance of diffuse surfaces, in situ laser meas. 78−82022
reflection coeff. of laser mirrors, of Fabry-Perot interferometer *(Russian)* 78−1237
reflection coefficient meas., effect of light beam collimation 80−18003
reflection index determination, IR region, by interferometric meas. of phase shift *(French)* 77−87812
reflectivity, mirror arrangement for meas. by changing incident angle 80−18000
reflectivity, total, using specular-reflectance and diffuse reflectance references 80−73421
reflectivity measurement of highly reflective mirrors 78−54444
reflectivity of steel at 10.6 μm, calorimeter meas. 78−55393
resolution, image eval. methods, Air Force project SENTINEL SIGMA 79−31826
resolution, S/N ratio and meas. precision, revised numerical results 80−95806
rotation angles in polarised light, detection and measurement *(Rumanian)* 80−22418
scattered light measurement for lenses and spectacle lenses *(German)* 78−46746
scattering and depolarisation meas. in liquids 79−93198
scattering from single particle, photodiode array meas., appl. to biological cell anal. 78−28146
semiconductor, optical absorpt. coeff. and minority-carrier diffusion length, differential photocurrent method of meas. 80−96896
semiconductor and dielectric optical nonuniformity, spatial distrib. determ. 80−13116
sensitivity of metrology using time modulation, electronically generated limitation 78−16828
shadow device with photoelectric recording, for turbulence meas., resolving power 79−7210
simultaneous meas. of optical parameters of crystals under electron beam irradiation *(French)* 77−26378
single mode fibres for optical field mapping, interf. technique 78−74966
single-fibre connectors, demountable, loss meas. 78−94433
single-mode fibre, suitable parameter determ. 79−27387
spectral response, pulsed measurement, test set-up and apparatus, shortcomings and planned improvements 80−45695
specular reflectance standards for visible and infrared region using thin Al film vacuum deposited on optical flats *(Japanese)* 80−102789
specular reflection coeff. meas. on SF-4A spectrophotometer, 0.5% accuracy 77−13804
specular reflection coefficient comparison, sample materials 79−71512
spherical specimen glossiness meas. 79−54175
step index multimode fibre, baseband frequency measurement, mode scrambler technique *(Japanese)* 78−37983
step-index multimode optical fibre fundamental mode meas. 79−46051
Stokes parameters of light meas. using Fourier photopolarimeter 79−21805
streak camera dynamic range measurements, picosecond time resolution 80−73490
sub-picosecond optical pulses, generation and meas. 80−23731
surface brightness, newly developed reflectometer appl. *(German)* 80−42253
surface modal deformation sensor for heterodyne interferometry 80−31859
surface quality standards based on total integrated scatt. 80−48391
surfaces, concave and convex, radii of curvature meas. 80−83654
suspension of absorbing particles, simultaneous meas. of dichroism and birefringence in elec. field., photocurrent signal obs. 80−82801

optical variables measurement continued
tapered fibre coupler for optical pulse backscatter meas. 77−7212
terrestrial solar spectral irradiance distrib. variations, sensitivity of solar transmittance, reflectance and absorptance 80−82739
Thermophysical method for optical characts. determ. of scatt. medium 80−9014
thin films, vac. deposited, mass change, optical transmittance, and reflectance, simultaneous meas. apparatus 79−75501
thin films condensed onto cold substrate, prism-film coupler for in vacuo investigation 78−24873
thin sandwich film photovoltaic analyzer for wavelength meas. in 2000-7000 Å range *(French)* 79−95441
transmission, meas. by UR-20 spectrophotometer, attachment for computer handling of data 77−26409
transmission characts. of fibre optical equipment, Tektronix digital radiometer/photometer appl. *(French)* 79−89000
transmission coeff. of objective lenses, meas. using two-channel device 80−106642
transmittance and reflectance, double-beam single-detector wavelength-modulating spectrometer, AGC 80−86447
transmittance and reflectance of scatt. material, specular hemisphere method 78−58004
transparent fibre, optical parameter meas., laser method 77−18062
UV microscope for polarised light, determ. of birefringence, linear dichroism and optical rotary dispersion *(German)* 78−29152
UV radiation. accurate measurement techniques 78−37954
visual telescope light scatt. factor meas. apparatus 79−27365
water transparency, in situ meas. 79−25355
wavefront curvature meas. of small diam. laser beams using Fourier imaging 79−94273
waveguide attenuation and bandwidth meas. techniques 79−94367
waveguide properties, components and systems for optical links *(German)* 80−33168
waveguides meas. procedure quality, standards 80−1351
wavelength dispersion of optical fibres directly measured by 'difference method' in 0.8-1.6 μm range 79−50395
wavelength measurement with self-calibrating grating spectrograph 78−24869
wavelength meter, compact static, based on Fizeau interferometer, for pulsed and CW lasers 79−36947
wavelengths of CW far IR optically pumped lasers, simple accurate meas. method 80−106554
wavemeter for CW lasers 79−26112
weak light flow, analysis of measurement methods *(Russian)* 78−45694
XUV spectrographs in Apollo Telescope Mount, scatt. light meas. for optical contamination assessment 77−60603
CO_2 laser transition absolute freqs. by multiplication of difference freqs. 80−37992
CdS plane parallel slab, optical const. determ. methods 80−60531
He-Ne laser, radiation field spatial distrib. distortions due to multilayer dielectric mirrors 77−38970
He-Ne laser freq. determ., interferometric comparison with upconverted CO_2 laser radiation 78−55395
NH_3 laser, two-photon-excited, 16μm emission, wavelength meas. technique 78−71085
Nd:YAG mode-locked laser picosecond pulse profile and power meas. 77−7112
Si epitaxial layers using IR laser ellipsometer expt. 78−62219

optical waveguide components
see also optical couplers; optical isolators
1×2 optical switch using new type of pentagonal prism switch, for optical fibres 80−64148
acousto-optical devices, critical assessment and development trends *(Czech)* 80−23777
acousto-optical planar deflector, with colinear propagation of optical and surface acoustic waves *(Russian)* 77−62053
active and passive devices for fibre transmission systems 80−43463
anisotropic or gyrotropic materials, theory and appl. 77−54789
attenuator, variable, for use in single-mode fibre transmission systems 80−99821
bistable optical fibre switch, construction and performance 80−95994
Bragg reflectors, narrow band, in optical fibres 78−79130
branching waveguide mode order convertor 78−1379
broad band grating filters for thin film waveguides 77−83962
chalcogenide glass films, kinoform optical elements and integrated optics elements prod. 77−75634
chalcogenide glass films, opt. inform. recording uses 77−75633
channel waveguide double-pole double-throw switch/coupler, using total internal refl. 78−71233
chirped gratings in broad band filters, theory 78−25994
circulator, polarisation independ., for optical fibre transmission systems 80−23779
circulator, polarization-independent, configuration method 80−38095
circulator for optical fibre transmission, using Faraday rotator and Glan-Taylor prisms 80−23769
colinear interaction between acoustic and optical waves in planar waveguide, radiation into substrate 80−53452
collimator, waveguide optical system, Luneberg lenses with plane connecting waveguides 79−68446
communication systems, demountable connector, fibre switch, and fanout couplers 78−74989
compact optical circulator for near-infrared region 79−23063
coupled-waveguide TE/TM mode sputter 80−99855
crosstalk in bidirectional fibre, review 78−66901
cutoff mode filter with structure of metal-clad optical strip-line 80−83680
deflector using chalcogenide amorphous film on graded index $LiNbO_3$ waveguide 80−48463
diplexer reflection type periodic filter, elliptic response 80−43474
directional coupler as waveguide tap with infinitesimal insertion loss 80−99883
directional couplers and phase shifters for guided-wave signal transformers, synthesis 80−1358
disk, variable effective refractive index, in thin film *(French)* 79−98476
electro-optic multimode waveguide modulator or switch 80−23783
electro-optic thin film periodic waveguide switch and amplitude modulators anal. 78−22215
electro-optic waveguide deflector performance characteristics 80−33213
electro-optic waveguide modulators, capacitance of electrode system rel. to modulation efficiency *(Russian)* 80−1359

optical waveguide components continued
electro-optical active components for guided light 78−42470
electro-optical Bragg deflection modulators in corrugated waveguides 79−59844
electro-optical modulators on flat waveguides, theory *(Russian)* 79−50411
electron-beam and photolithographic fabrication of guided-wave optical components 78−13818
electrooptic waveguide array deflectors, performance criteria and limitations 80−5821
fact directional coupler switch/modulators, novel ps optical pulse sampling method 80−58784
fibre Faraday rotators in fibre Raman lasers 80−58775
fibre optic rotation sensor, all-waveguide configuration, key element tests 80−58796
fibre optic Y-shaped, signal splitter, constructed by fusion welding single clad fibre to 2 parallel unclad fibres 79−50432
fibre optics components and integrated optics 80−1356
fibre switches for fault terminal isolation 78−46833
fibre tapers for optical coupling of optical fibres, appls. *(German)* 80−38107
fibre transmission systems 79−10384
fibre-optic communication systems, devices and ccts., book 80−38123
fibre-optic power divider, single-mode, fabrication using encapsulated etching technique 79−50433
fibre-optic variable attenuator 79−64328
frequency-selective filters in ion-exchanged waveguides 79−50387
fulgimide planar photochromic structures 80−64196
garnet film, double heteroepitaxy, magneto-optical devices for phase matching *(French)* 77−3675
geodesic aspherical perfect lens, general sol. for integrated optics 80−10049
geodesic lens, diffraction-limited, in polyurethane waveguide struct. 78−94453
geodesic lenses, aberration-corrected rounded edge, profile calcs. 80−10048
geodesic lenses, anal. by beam propag. method 80−58686
geodesic optical lens prod. by anisotropic etching 80−10047
geodesic optical waveguide lens analysis: comment 79−76879
guided-wave signal transformers, synthesis 80−1358
gyrotropic waveguide switching elements at optical wavelengths 79−37049
integrated fibre-optic subsystems, progress in development and appls. 79−46068
integrated optical circuits, thin film technology appls. 78−38068
integrated optics, electrooptical channel waveguide matrix switch using total internal reflection 80−58810
integrated optics and guided wave devices, review 78−42468
integrated optics and optical waveguide devices, review 78−66948
integrated optics Bragg-effect polarizer/analyzers and lens-less waveguide beam expanders 80−58807
integrated optics sub-ps gate 80−58809
integrated programmable planar waveguide components formed by optically writing Bragg diffraction gratings into photochromic structs. 80−79011
isolator, for fibre-optic communication systems, 0.8 μm 79−50424
lenses, Bragg and Luneburg type 80−10050
lenses, review *(Japanese)* 80−10019
lenses for integrated optics, progress 78−66950
light deflection using electro-optically controlled interference 79−1007
Luneberg geodesic lenses 79−76880
Mach-Zehnder interferometric waveguide modulator, polarization-independent operation 79−18552
Mach-Zehnder waveguide modulators in Ti-diffused $LiNbO_3$ 80−33203
microfabrication for guided-wave optical devices 80−58812
microlenses to improve LED-to-fibre optical coupling and alignment tolerance 80−19088
mode filter on anisotropic thin film, anal. of two coupled modes with losses 80−79000
mode scrambler for step-index multimode fibres, curvature distrib. and mode conversion *(Japanese)* 79−98500
modular element as coupler, mode convertor and beam splitter 77−771
modulator, coupled waveguide *(Japanese)* 78−46789
modulator, coupled-waveguide with pn junction, multilayer planar waveguide configuration 78−71235
modulator, using electrooptic crystals coupled mode analysis 77−42612
modulator for fibre transmission systems, temperature stabilized *(Japanese)* 79−27391
modulator for singe-mode optical fibre transmission system, temp. stabilized 79−41450
modulator using electro-optic phase shifter pair with optical waveguide couplers 78−66952
modulators, switches and deflectors, physical principles and Czechoslovak developments *(Czech)* 80−19090
multimode fibres, tapping element 77−3670
multiplexers, micro-optic grating, for fibre-optic communication systems 79−50423
multiposition optical-fibre switch 79−41438
planar waveguide blazed dielectric diffraction gratings, anal. and design 80−58779
polariser, using anisotropic cladding *(Japanese)* 78−18047
polariser using dichroic absorpt. of M centres in NaF 79−995
polariser with synchronous absorption 79−90002
polarizer, using anisotropic crystal 77−88950
polarizer development using anisotropic crystal, 18 dB extinction ratio 79−18542
prism in multimode waveguide corner, rigorous soln. *(Ukrainian)* 79−76819
prism tunnel coupler for multiple-layer optical waveguide, storage device 79−76885
prism tunnel coupler for multiple-layer optical waveguide, theory 79−76884
second- and higher-order waveguide grating filters, refl., transmission and loss coeffs. meas. 80−19110
second- and higher-order waveguide grating filters, spectral response calcs. 80−19109
SEM written diffraction gratings for integrated optics, characts. 79−68450
semiconductor waveguide switches, and modulators, review of development progress 78−38045

optical waveguide components continued
semileaky thin-film optical waveguide mode filter radiation-coupling loss 88953
separator of TE_0 and TM_0 modes, planar prism, characts. obs. *(Russian)* 77−46803
switch, 3×3, using single-mode waveguides in electrooptical material 78−55470
switch with high reproducibility for optical fibre transmission 79−64329
switches and modulators, performance limitations due to polarisation 77−7175
tapping elements with thin-film beam splitters directly applied to optical fibre endfaces, fabrication 79−37016
TE-TM mode splitter for optical waveguides, glass comp., r.f. sputtered fabrication 78−46841
thin film waveguide component interconnection and signal processing 78−5584
thin-film spectrograph for guided waves 80−58778
tunable narrow-band thin-film waveguide grating filters, performance 80−38124
tunable open resonator with cylindrical mirrors 79−90024
wideband thin film modulators and switches, for optical communication 78−63206
Y-branch for optical communication networks and measuring equipment *(German)* 78−66918
$Al_yGa_{1-y}As$-$Al_xGa_{1-x}As$, electrooptic rib waveguide modulators and switches 78−38046
As-Se-S-Ge chalcogenide glass films, appls. to passive optical waveguide components 79−37048
$Bi_{12}SiO_{20}$, optically controlled multimode planar switch 78−42476
CdS semiconducting thin-film optical waveguide polariser 80−33180
CdTe acousto-optic and electro-optic waveguide modulators 77−42624
GaAs waveguide cladding, exam. as cutoff polariser for integrated optics 78−55474
GaAs-$Al_xGa_{1-x}As$, single-mode rib waveguide switches electro-optical modulation 78−46839
$LiNbO_3$, electrooptic modulation and switching, recent progress 78−50945
$LiNbO_3$ lenses, diamond-turned aspheric geodesic waveguide lenses 80−58804
$LiNbO_3$, optical filter, for integrated optical waveguide structures 77−58443
$LiNbO_3$ TE-TEM light mode convertor using acousto-optic interaction, expt. 78−46794
$LiNbO_3$ travelling wave optical waveguide modulator, 10 GHz bandwidth 78−59134
$LiNbO_3$ very high throughput damage resistant waveguide modulator 80−58788
$LiNbO_3$ waveguide, form. of geodesic lenses 77−88966
$LiNbO_3$ waveguide modulators and switches, Ti-diffused, fabrication on directional coupler principle 80−83678
$LiNbO_3$:Ti, diffused, branched waveguide efficient intensity modulator 78−22190
$LiNbO_3$:Ti, electro-optic multichannel waveguide deflector 77−42607
$LiNbO_3$:Ti, electro-optic waveguide modulator, temp. stabilisation 78−50926
$LiNbO_3$:Ti, electrooptical modulator and switch *(French)* 78−30074
$LiNbO_3$:Ti 3-dB optical waveguide mode convertor using chirped gratings, power transfer 80−79014
$LiNbO_3$:Ti digitally driven integrated optics amplitude modulator 80−58808
$LiNbO_3$:Ti electro-optic branching waveguide, characts. 80−83681
$LiNbO_3$:Ti optical waveguide electrooptic devices polarisation independ. directional coupler switch and wavelength filters 80−58783
$LiNbO_3$:Ti optical waveguide channel branches 80−58811
$LiNbO_3$:Ti waveguide geodesic lens 77−84005
$LiNbO_3$:Ti waveguide directional coupler type modulator 78−66951

optical waveguide theory
see also guided light propagation
active waveguide analysis, general approach 78−74991
active waveguide with refr. index quadratic distrib., parameters selection 78−50933
active waveguides modes with inhomogeneous gain profiles as applied to injection lasers 78−79017
alkaline glass, ionic diffusion and exchange, integrated optics study *(French)* 77−88940
alpha-power graded-core fibre dispersion, closed-form approximation 80−1320
analogue transmission of one-dimens. spatial images 78−55458
anisotropic, waveguide, guided-radiation mode interaction in off-axis propag. 79−76839
anisotropic channel waveguides, modal fields 77−65625
anisotropic graded index waveguide, acoustooptic interaction efficiency freq. depend. 80−23776
anisotropic graded-index waveguide, optical mode propag. consts. calc. 80−69540
anisotropic inhomogeneous medium with axial symm., mode struct. 78−18069
anisotropic metal-diffused guide, leaky surface wave propagation 78−55454
anisotropic optical waveguides of $LiNbO_3$ type, guided and semileaky modes 79−18530
anisotropic or gyrotropic materials, appl. 77−54789
anisotropic symmetric slab waveguide with optical axis not in slab plane, modes 79−996
arbitrary-index profile fibres, bending loss of propag. modes 78−66896
asymmetric dielectric-slab waveguide, beam mode scatt. characts. 80−38114
asymmetric gas-dielectric optical waveguide with wall resonances 79−7216
asymmetric slab waveguide, mode conversion and radiation loss 77−34936
asymmetric three-layer optical waveguide, radiation losses due to discontinuities 80−53446
asymmetric three-layered slab waveguide, leaky TE modes 80−43447
asymmetric-slab optical waveguide losses due to refractive index inhomogeneities 78−1381
asymmetrical, 2-dimensional, application of the equivalent-index method to DH diode lasers 80−23772
bandwidth of distorted multimode waveguides excited by laser sources 80−43436

optical waveguide theory continued
bandwidth spectrum of multimode fibres, depend. on refr. index profile 80−9985
beam capacity influenced by mode conversion, in lens waveguides, spatial crosstalk 77−54785
bending losses of dielectric rectangular waveguides for integrated optics 78−63205
bent multimode guide, loss calcs., geometric optics method 79−37013
bent step index fibre, optical power flow 78−30092
birefringence in optical fibres with elliptical cross-section 79−59816
blazed waveguide corrugations, loss coeffs. 77−34948
Bloch waves in periodic planar optical waveguides 80−58777
Bragg cylindrical fibres, confined lossless optical propag. 78−38062
Bragg effect waveguide coupler analysis 78−33827
Bragg electrostriction, power balance approach 77−75660
Bragg fibres, theory 79−10389
Bragg interactions, asymmetric first order, in active dielectric waveguide 79−3807
Bragg mirror reflectance, dielectric waveguide inhomogeneity effect 80−28356
Bragg reflection waveguides, lossless propag. 77−14804
Bragg reflector, nonuniform, almost periodic, perturbation anal. 77−27356
branching optical waveguide, mode coupling 80−69518
buried 2D waveguide with asymm. graded refr. index profile, modal solns. 79−41431
cable design considering structural imperfection 80−64184
channel waveguides and directional couplers with graded-index profile, analysis 79−81542
chirp pulse transmission characts. in a dielectric waveguide 78−9438
circularly curved graded index fibre, optical beam propag. 78−25973
clad parabolic-index square-law dielectric waveguide, perturbation anal. 80−33190
cladded fibres, inhomogeneous wave propag. 79−81531
cladded optical fibre, parabolic-index core and homogeneous cladding, guided waves anal. 77−11013
cladded parabolic index profile waveguide, model for stripe-geometry laser 78−22205
coherence of EM field in plane dielec. waveguide 78−59145
colinear interaction between acoustic and optical waves in planar waveguide, radiation into substrate 80−53452
colour image transmission through multimode waveguide 77−58461
complete EM field of dielectric lossy fibre excited by dipole source, numerical calc. 80−43427
condensing light pipes and reflecting baffles, skew rays 77−3648
conference, Lannion, France (Sep. 1976) 77−23755
conic and quasi-conic profile, calc. and construction *(Rumanian)* 80−28331
conical light guide, theory, divergence reducing props. *(German)* 79−14090
contemporary optics, book 79−81353
corrugated dielectric waveguide, radiation loss calcs. for TM polarisation 80−43445
corrugated dielectric waveguide, second order stop band numerical study 80−23807
corrugated disc dielec. waveguide radiation mode anal. 78−63199
corrugated optical disc waveguides 80−58701
corrugated waveguide, guided mode diffr., coupled-wave eqns. 80−48434
corrugated waveguide leaky modes, anomalies of dielec. coated gratings *(French)* 77−79969
corrugated waveguides, effective index approach to distrib. feedback, TE polarisation 80−102859
coupled resonator model for resonant polarization conversion and anomalous beam shift *(Japanese)* 78−87133
coupled thin-film dielectric waveguides with tapered edges, EM surface waves 79−3792
couplers, linearly tapered directional, analytic solns. 77−779
coupling characteristics of parallel slab waveguides with index profile 78−75000
coupling coeffs. in strongly coupled dielectric waveguides 78−1356
coupling efficiency between two multimode optical fibres analysis 78−46766
coupling length due to random bending in multimode optical fibres 78−63195
coupling problems, scattering matrix theory for open waveguides 77−27331
cross-talk noise analysis, optical multichannel waveguides 80−91922
crosstalk between light pipes, mode theory 77−785
curved dielectric waveguide loss and appl. to rectangular dielectric channel 78−1354
curved fibre, single mode, radiation of discrete beams 78−18041
curved graded-index fibres as image relays, aberrations 79−55219
curved hollow metallic waveguide, IR TE mode propag. 77−79923
curved multimode waveguide, geometrical optics shape of nonmeridional rays *(German)* 78−5566
curved single-mode fibre, field deformation 78−37972
curved single-mode fibres, discrete beams of radiation, anal. 77−75671
curved single-mode fibres radiation loss 78−74984
curved single-mode optical fibres, propag. characts. 78−66934
curved slab waveguide, excitation 80−14445
curved step index fibre, integrals 78−1340
curvilinear multimode optical waveguide statistical tolerance calc. 78−1361
cylindrical, two-layer, light depolarisation, theory and expt. *(Russian)* 78−9454
cylindrical dielectric optical waveguides, hybrid mode classification 78−1358
cylindrical inhomogeneity in homogeneous medium of infinite extent, guided EM field numerical computation 80−14274
cylindrical lightpipe, steady and transient radiation transport, exact soln. 77−27365
cylindrical optical fibre transmission and guided mode behaviour 80−28348
deflection and focusing of radiation by stepwise inhomogeneities 78−83093
DFB resonators, dielectric waveguide with periodic surface inhomogeneity 77−7146
DFB waveguide laser theory, Green's function approach 78−5504
dielectric fibres of arbitrary cross-section, fundamental mode propag. 80−43443
dielectric rib waveguide, propag. and radiation characts. 77−79933

optical waveguide theory continued
dielectric slab and fibre waveguides, dispersion props. approximate formula 79−55217
dielectric slab optical waveguide, scattering characteristics 78−87163
dielectric slab waveguide, propagation loss due to scatt. centres *(Japanese)* 77−68267
dielectric slab waveguide, radiation pattern determ. due to refractive index fluctuations 78−22216
dielectric slab waveguide, scatt. characts. of beam mode 79−55230
dielectric tube waveguide, cutoff freqs. derivation under weak guidance 78−18059
dielectric waveguide, corrugated, light emission 80−96027
dielectric waveguide hybrid and transverse mode dispersion calc. *(Russian)* 80−99857
dielectric waveguide modal props., one-dimens. wave eqn. analysis 79−81537
differential mode delay rel. to refr. index profile, geometrical optics treatment 80−69529
diffraction at locally deformed flat boundary, numerical soln. 77−42480
diffraction at waveguide corner with mirror *(Russian)* 77−19396
diffraction optical coupling, heteroepitaxial GaAs-AlAs film waveguide 77−11045
diffraction problem at locally deformed plane waveguide, numerical calcs. 77−79947
diffused channel waveguides, dispersion characts. 77−778
diffused channel waveguides, mode dispersion by effective index method 77−27334
diffused corrugated waveguide, diffr. emission and excitation of E and H-waves 78−25984
diffused optical waveguide mode analysis, variational method 77−88956
diffused optical waveguide numerical analysis and applications 78−1377
diffused rectangular anisotropic waveguide, modal characts. rel. to integrated optics devices 79−27443
diffused strip-loaded waveguide, modal analysis by variational method 78−46776
diffused waveguide, acoustooptic interaction efficiency of TE modes, freq. depend. 80−53455
diffused waveguide, attenuation characteristics of TE modes and surface scatt. 80−5822
diffused waveguide, characts. determ. by profile approx. with parabola and exponential function 79−64341
diffused waveguide, corrugated section, H and E wave refl. and emission 77−34954
diffused waveguide, E and H wave emission from corrugated section 77−50769
diffused waveguide, gaussian index profile, modes, perturbation anal. 77−3671
diffused waveguide, generalised parameters describing acoustooptic interaction 80−91924
diffused waveguide, refractive index profile determ. by inverse scatt. theory 80−5838
diffused waveguide energy distribution determ. by rigorous solution 78−63200
diffused waveguide tunnel excitation and emission 78−59146
disc waveguide, coupled power theorem and orthogonality relations 78−38003
discontinuities analysis using least squares boundary residual method 79−59823
discrete radiation from curved single-mode fibres, comparison of theories 78−33847
dispersion, waveguide and material, interdepend. 79−98470
dispersion properties, approx. formulas 80−14444
dispersion relation for waveguide mode with arbitrary anisotropy 80−5840
distributed feedback waveguide structure, refl., emission and transmission calcs. 78−13819
distributed-feedback waveguide structure, dispersion characts. 78−66949
divergence and aperture angle of conical guides 77−46802
electrooptical, planar, thick, phase modulation theory *(German)* 77−27367
elliptical dielectric waveguides, higher-mode cutoff 80−43432
elliptical fibres, selectively excited, near-field distrib. 80−48401
elliptical multimode fibres, leaky ray correction factors 80−87487
elliptical multimode fibres, whispering and bouncing mode evaluation 80−10015
elliptical square-law medium, astigmatic Gaussian beams 78−94427
envelope wave stability 80−43410
excess loss increase mechanism of jacketed fibers at low temperature 80−83682
fibre, arbitrary index profile, formula for TE_{01} cutoff freq. 80−48418
fibre, arbitrary refr. index profile, light backscatt., uniform approx. approach 79−14100
fibre, broadband signal response 78−33818
fibre, dispersive, multimode, optimum index profile 77−23757
fibre, doubly clad W-type, range of monomode operation 79−7212
fibre, elliptical step-index multimode fibre, rays and modes 80−14442
fibre, graded index and W, fundamental mode microbending loss 77−23762
fibre, graded-core, numerical description of propag. characts. 77−23758
fibre, graded-index, exact field expressions for guided modes 78−74977
fibre, graded-index, geometric optics approach to light acceptance and propag. 77−23756
fibre, GRIN, leaky modes, WKB method 77−7180
fibre, immersed in high-index surrounding medium, attenuation 77−42614
fibre, M-like refractive index distrib., light pulse dispersion 78−71225
fibre, modal noise, dependence on source coherence and fibre length 80−48402
fibre, mode coupling in small-core diameter circ. dielec. fibre *(Korean)* 79−23072
fibre, multimode, finite cladding radius effects 78−66893
fibre, multimode, graded-index, low-pass filter characts. 77−23759
fibre, multimode, propag. modelling, effects of mode conversion due to microbends *(French)* 77−23760
fibre, multimode irregular focusing with random ellipticity, light propag. 80−74501
fibre, near square law, propag. characts., perturbation analysis 78−22202
fibre, near square law type, propag. consts. perturbation anal. 78−33891
fibre, power-law graded-index, core/cladding power distrib., propag. const. and group delay 80−48420

optical waveguide theory continued
fibre, power-law refractive index profile, scalar modal eigenvalues and group delays 80−28322
fibre, pulse broadening, inter- and intramodal dispersion 78−5547
fibre, quantitative mode anal. and excitation condition meas. 79−18517
fibre, quasiparabolic index profile, propag. characts., perturbation anal. *(French)* 80−33189
fibre, random gradient, partially coherent optical wave excitation 77−23761
fibre, rectangular cored multilayer fibre 80−83667
fibre, refractive index profile, Marcatili condition derivation and interpretation 78−22193
fibre, refractive profile distortion and dispersion, group delay calc. 78−55433
fibre, self focusing, rectangular and Gaussian pulse propag. 78−33831
fibre, single-mode systems, instability due to interference and polarization effects 80−58774
fibre, step or graded index, refr. index dip effect on propag. 78−18053
fibre, step-index, curved, field distribs. of natural modes 77−79936
fibre, tube waveguide with outer higher-index cladding, far-field radiation pattern 79−90033
fibre, two-mode, temporal spreading of pulse 80−33183
fibre, unclad, backscattered light, approx. ray theory 77−7177
fibre and film waveguides, local normal modes, superlocal modes, ideal modes 80−14466
fibre bend radiation calc., WKB method 78−59130
fibre cables, single-mode and parabolic-index multimode, random-bend loss 80−78951
fibre excitation by lenses 79−32057
fibre excitation by partially coherent sources, geometric optics theory 77−79948
fibre excitation by polychromatic partially coherent sources 77−31131
fibre intensity profile distortion, due to index profile determ., near field method 78−37977
fibre laser-amplifier, coupled-mode theory 78−66848
fibre light propagation, review of analytic methods of study *(French)* 79−90001
fibre lightguide transmittance, approx. calc. 79−55228
fibre loss increase due to stranding in optical cables 80−38117
fibre microbending theory, principal mode numbers use 78−94434
fibre minimal dispersion refractive index profiles 79−98469
fibre modal delay calc. method for fibres with arbitrary refractive index 79−46038
fibre mode coupling coeffs. determ. using fibre resonator 78−5560
fibre mode excitation, using extended two-dimensional theory *(French)* 78−5546
fibre mode excitation by Lambertian and totally incoherent sources 78−63182
fibre mode excitation by laser diode *(German)* 78−50921
fibre mode properties, computation by propagating beam method 80−69502
fibre optics, uniform asymptotic theory 80−28323
fibre optics theory, first-order correction to weak-guidance approx. 78−90519
fibre refractive index profile, effect on fibre bandwidth 80−23773
fibre refractive index profile models 80−14453
fibre refractive index profile optimisation for broadband multimode fibres 78−66932
fibre scattering, ray theory 80−69528
fibre splice loss, Gaussian power model 78−46828
fibre tapered sections, ray trajectories 79−18508
fibre tapers for optical coupling of optical fibres, appls. *(German)* 80−38107
fibre theory, review 78−1351
fibre waveguide, chromatic signal distortion depend. on optical carrier coherence 80−1317
fibre waveguide, rays, modes and beams 77−34945
fibre with arbitrary cross section, charact. mode at HF, asymptotic theory 79−1006
fibre with arbitrary refr. index profile, mode cutoff freqs. formula 79−55244
fibre with modified hyperbolic secant index distrib., modal treatment 79−90010
fibres, backscatter meas. theory *(German)* 80−91921
fibres, basic properties of multimode, single-mode, graded-index fibres *(Czech)* 79−81551
fibres, characteristic modes of arbitrary profile 79−72684
fibres, curved, intensity modulation of transmitted light, coupled-mode theory 77−75672
fibres, dispersion minimisation in single-mode fibres between 1.3 μm and 1.7 μm 79−76832
fibres, dispersion-free single-mode fibre in 1.5 μm wavelength region 79−76831
fibres, graded-index with polynomial profiles, propag. characts. 80−38118
fibres, gradient index, pulse dispersion calc. *(German)* 78−50920
fibres, gradient-index, numerical analysis *(German)* 78−5550
fibres, lossy, coupled power eqns. 79−10376
fibres, min. dispersion at 1.55 micron for single-mode step-index fibres 80−10006
fibres, modal dispersion with composite α-profile graded-index core 80−9998
fibres, mode dispersion, material dispersion and profile dispersion in graded-index single-mode fibres 80−14443
fibres, mode-coupled multimode, baseband transmission theory based on scattering matrix 80−14468
fibres, multimodal double-layer with random axial bends, losses 79−90025
fibres, pulse distortion at wavelength of dispersion min. 78−22187
fibres, radially inhomogeneous, vectorial wave anal. using finite elements method 78−37999
fibres, randomly bent, ray theory 78−66921
fibres, scalar approximation technique, accuracy 80−58703
fibres, scalar Helmholtz eqn. *(German)* 78−50919
fibres, single-mode, exit-end reflection and transmission module, theory *(Japanese)* 79−98474
fibres, single-mode limit with arbitrary refractive-index profile, formula 78−46771
fibres, single-polarisation, slab model, strain birefr. 79−50381
fibres, truncated index with minimum mode dispersion, anal. 78−38000

optical waveguide theory continued
fibres, weakly guiding and slightly elliptical, birefringence expression using perturbation theory 80−1309
fibres, zero total dispersion in graded-index single-mode fibres 79−76830
fibres with arbitrary index profile, pulse propag. and dispersion 80−78984
fibres with parabolic index core and homogeneous cladding, guided modes 79−76853
fibres with power-law core profile, perturbation theory 79−7211
field distribution of a point source inside a lossy optical fibre 80−10044
finite element anal. 80−87558
flat dielectric optical waveguide synthesis, inverse Sturm-Liouville problem soln. 79−7215
flexible hollow waveguide, IR light propag., optical losses 77−19389
flexible IR waveguides, high-power transmission 80−48409
four layer waveguide, with metal buffer, guided modes 78−87136
Fraunhofer diffraction by bundled fiber-optical waveguides 78−25978
frequency modulation by p-i-n structure, optical waveguide with moving walls 80−19099
gas waveguide laser, mode comp. of radiation 80−28192
gas-dielectric fibre, wave conversion in irregular portion 80−74500
gas-dielectric optical waveguide, general azimuthal asymmetry, loss evaluation 80−53453
Gaussian beam propagation in thin film waveguides 78−79102
Gaussian beams, waveguided, coupled by misaligned or curved grating effect 80−33228
Gaussian light beam propagation in thin films 78−33817
Gaussian profile diffused waveguides, perturbation analysis for modes 79−18529
Gaussian pulse transmission through monomode fibres, source linewidth effect 78−83073
geodesic waveguide lens anal., ray tracing 78−13778
geometrical optics relations for lightguides with oblique input endface 77−68271
glass fibre transmission props. *(Swedish)* 78−90525
glass optical waveguide fibres, propagation theory, review 79−90015
graded core W-type fibre and its propagation characteristics 80−1334
graded fibres, mode propag. time calc. using multimode theory *(German)* 80−58710
graded fibres with non-circular index contours, core fields 80−14455
graded glass fibre, effect of shape of refractive index profile, on distortion 80−33197
graded index fibre, error estimates fo first order WKB calc. method 80−87488
graded index fibre, guided modes, asymptotic theory 78−9447
graded index fibre, light pulse propag. *(Czech)* 79−98501
graded index fibre, new form of characteristic eqn. *(Italian)* 78−50901
graded index fibre, random bends, variational soln. of power flow equation 79−18549
graded index fibre, wave eqn. for propag. fields 80−58757
graded index fibre propag., impulse response, expt. and theory 78−90496
graded index fibres, excitation of bound and tunnelling rays 79−55218
graded index fibres, for matching injection lasers to optical fibres 79−32069
graded index fibres, Gaussian approx. of fundamental modes 78−66907
graded index fibres, mode conversion caused by splices 80−1340
graded index fibres, propag. consts. and group delays 80−23770
graded index fibres, soln. of wave eqns. using modal approach 79−36995
graded index fibres guided propag., asymptotic theory of inhomogeneous waves 78−66941
graded index multimode fibres, cladding loss effect 78−50927
graded index planar lightguide, electrooptical diffraction 80−78995
graded index slab waveguides, exact solns. for TM modes 79−27397
graded index waveguide, pulse broadening, cladding effect 77−79924
graded index waveguide problem soln., comparison of wave and ray techniques 78−59140
graded monomode fibres and planar waveguides 80−43435
graded noncircular multimode fibres, leaky modes, analytical ray theory 80−33192
graded single-mode fibres, dispersion 79−59810
graded weakly guiding fibres, fundamental HE_{11} modes 80−43444
graded-index anisotropic waveguides, WKB analysis of guided and semileaky modes 79−27416
graded-index curved media, generalised Fresnel power transmission coefficients 80−102815
graded-index fibre, minimum impulse response 77−68258
graded-index fibre, spatial degree of coherence 80−53441
graded-index fibre propag., ray optics approach 79−76849
graded-index fibre transmission characteristic computation 80−1321
graded-index fibre with polynomial-profile core, propag. constants of guided modes 80−10005
graded-index fibres, analytical relations between model power distrib. and near-field intensity 80−9995
graded-index fibres, light propag., Helmholtz eqn. soln. 79−27372
graded-index fibres, mode analysis using scalar wave eqn. and direct numerical integration 80−78971
graded-index fibres, near-optimum, pulse broadening 79−7213
graded-index fibres, propag. consts. and group delays of guided modes 79−98464
graded-index fibres, refracting leaky rays 78−79103
graded-index fibres, tunnelling rays in pulse propag. 78−18057
graded-index fibres with lossy outer layer, transmission characts. 78−55437
graded-index fibres with non-power-law refractive profiles, group delay calc. 77−14796
graded-index glass fibres for optical communication, light propag. props. 78−83106
graded-index monomode fibres with elliptical cross-section, birefringence 80−53416
graded-index multimode fibres, bandwidth characts., appl. on long-haul transmission systems 80−64180
graded-index multimode fibres, dispersion calc. by propag. beam method 79−98465
graded-index non-circular fibres, ray theory 79−55229
graded-index noncircular fibres, geometric optics analysis 79−55231
graded-index optical fibres, mode eigenfunction computation propagating beam method 80−95988
graded-index optical fibres, ray optical paths and relative delays, calcs. 79−89987
graded-index slab, with metal cladding, propag. losses of guided modes 77−83972
optical waveguide theory continued
graded-index slab and fibre waveguides, bent, power attenuation 78−87134
graded-index slab waveguide TE mode analysis 77−72087
graded-index slab waveguide TE modes, exact soln. 79−81568
gradient refractive index fibres, optical characts. 77−787
grating, diffraction efficiency, Brewster's law 80−91935
group delay differences in waveguides with graded index profiles *(German)* 78−50906
helically deformed optical fibre, radiation loss calcs. 77−786
higher order mode filtering 79−41451
hollow dielec. optical waveguide light transmission props. anal. 78−83109
hollow rectangular anisotropic dielec. guide, wave propag. 78−83084
hollow rectangular dielec. waveguide, discontinuity for grazing angles near Brewster angle 77−770
holography with guided optical waves, diffr. efficiencies, theory 80−83563
homogeneous optical fibres with deformed boundaries, modal anal. 79−59824
impulse response of nearly parabolic fibres, evaluation 77−39055
incoherent lightguide transmission, radiance diminution, Hamiltonian ray optics analysis 78−46787
inhomogeneous, phase and group vels., numerical computation 77−42605
inhomogeneous circular waveguide, asymptotic eigenvalues of vector waves 80−96010
inhomogeneous dielectric filled uniform waveguides, EM wave propag. 80−83666
inhomogeneous dielectric waveguides, generalized WKB approach 78−1359
inhomogeneous dielectric-slab waveguide, synthesis 79−94337
inhomogeneous medium, two-dimens., light propag. problems rel. to thermogasdynamic waveguide development 80−32914
inhomogeneous mutlimode dielectric fibre waveguide analysis 79−59833
inhomogeneous planar dielec. waveguides for integrated optics structs., synthesis *(Russian)* 80−38135
inhomogeneous slab, propag., rigorous soln. 78−18055
inhomogeneous waveguide, nonlinear pulse (soliton) propag. theory 79−72617
inhomogeneous waveguide lens anal. 78−5561
injection laser harmonic distortion analysis 80−58537
integrated optical multimode waveguides, Fourier domain propagation calc. 80−64219
integrated optical waveguide analysis methods and improvements 77−79974
integrated optics and optical waveguide devices, review 78−66948
integrated optics multilayer anisotropic structures, impedance matching effects 79−7233
integrated twin guide laser, coupled wave theory 77−27307
intrinsic waveguide, in medium with saturated nonlinearity, theory 80−14405
irregular thermodynamic guide mean energy density of light beam 77−83976
junction between infinitely conducting metallic guides, transmission and refl. of modes, total refl. *(French)* 78−9451
laser diode-to-diffused waveguide coupling efficiency, waveguide mode asymm. effects 80−9990
launching and propagation of light in optical fibres 80−69504
leaky dielectric waveguide, planar hollow structure, eigenmode analysis 80−78973
leaky mode correction, near square law fibres 77−79934
lens-like media with off-axis complex permittivity, light beam propag. 79−81562
lenslike fibres, density-matrix method applied to mode coupling 80−78970
light distribution, irradiance patterns, over endface or cross section 78−63181
light propagation in fibres *(Czech)* 78−74997
locally deformed slab waveguide propagation and diffraction patterns 80−106630
long fibre, mirror and hollow dielec. lightguides, photometric characts. 80−33201
long fibre lightguide limiting aperture angle and props. 79−72692
long fibres with random inhomogeneities, output pulse shape 79−3791
long step-index fibres, propagation model 77−19390
long-distance multimode waveguide image tranmission in coherent light 80−48435
losses at corner bends, mode conversion for integrated optics 77−42594
lossless fibres, mode power fluctuation smoothing, source bandwidth 77−3667
lossy fibre propagation, leaky-mode radiation field computation *(German)* 78−33867
lossy planar waveguide, radiating normal modes 79−55220
lossy waveguide, Brewster phenomena, cut-off thickness 80−87524
low-loss dielectric tube leaky waveguide, transmission characts. 80−95999
low-V optical fibre with dip in refractive index, perturbation theory 79−37012
Luneburg lens index profile for planar waveguide 78−5562
matching optical dielectric waveguides 78−1357
material absorption, multilayered waveguides, effect on ray power attenuation 78−83103
Maxwell's eqn., numerical soln., refractive indices 80−87520
mechanical stress effect on transmission characts. of clad fibre 78−5579
metal clad dielectric slab waveguide, longit. plasma wave 77−777
metal clad diffused optical waveguides, characts. of propag. modes, WKB anal. 79−3768
metal cladding with positive permittivity, effect on modes 77−7184
metal shielded optical fibre transmission characteristics 78−1369
metal-diffused, laser beam/acoustic surface wave interaction, TE-TM mode conversion 78−42411
microcapillary gas-dielectric filled waveguide with azimuthally asymmetrical cross-section, attenuation calcs. 78−83105
modal characts. determ. for integrated optics 78−1439
modal dispersion in optical fibres with any numerical aperture and doping profile 78−1391
modal power distribution determination 78−87162
modal propagation for arbitrary cross sectional shape 80−10014
modal properties of dielec. waveguide, one dimens. wave eqn. analysis 79−27398

optical waveguide theory continued
mode attenuation, phase const. permittivity (real part) variation, eqns. derivation 77−50768
mode coupling between two connected multimode parabolic-index optical waveguides 79−94353
mode coupling in multimode fibres, techniques and formulation 78−66902
mode coupling to metal films and metal-barrier-metal devices 79−81567
mode derivation 78−63180
mode-coupled multimode fibre transfer function 79−10409
mode-coupled multimode fibres, coupling length estimation 78−66933
mode-coupling mechanisms in optical fibre, quantitative estimations 79−27380
mode-mixing in optical fibres 79−46034
modes, exact analytical soln. for rectangular waveguide 79−98490
modes coupling, in three dielectric slab waveguides 77−42610
modes in Ag-Na ion exchanged planar waveguides 78−59133
modulator, waveguide type, using Kerr magnetooptic effect in Ni-Fe film 77−11015
monomode dielectric waveguide, gaussian pulse transmission 77−23738
monomode fibre, step discontinuity radiation characts., anal. 77−62047
monomode fibre total dispersion and loss minima 80−91929
monomode fibres, baseband response function 79−50434
multi-dielectric slab, W type structure, optical transmission props. 77−42615
multifibre image transmission, misalignment effect on MTF 79−14093
multilayer circular waveguide, negative dispersion and strong higher order filtering 78−13809
multilayer dielectric waveguide, effective index nonlinearity 78−9446
multilayer gyrotropic structures, light propag. anal. *(Polish)* 79−3809
multilayer gyrotropic structures for nonreciprocal light propagation 78−90529
multilayer multimode optical fibre, ray theory, optimal distrib. of refractive index 80−87489
multilayer waveguides, higher dielec. losses in central layer 78−71223
multilayered structures containing anisotropy, EM wave anomalies 79−41460
multilayered waveguide, attenuation and tunnelling coeffs. for leaky rays 78−38002
multimode, resolution of self-images 78−63184
multimode, variable dia., light propag. 78−33894
multimode and single-mode optical fibre guides with rectangular cores 80−33220
multimode coupling structure of two parallel parabolic index waveguides, exact analysis 79−90013
multimode fibre, beam evolution 78−42443
multimode fibre, finite-bandwidth propag. 78−42456
multimode fibre, impulse response calc. 80−74486
multimode fibre, optimum index profile w.r.t. mode coupling 78−18054
multimode fibre, pass band depend. on excitation conditions 80−48433
multimode fibre, ring shaped and graded index with central dip, dispersion evaluation 78−42455
multimode fibre, splice loss and mode conversion 80−99830
multimode fibre, transmission characts., two-mode waveguide model 78−83085
multimode fibre, truncated Gaussian beam propag. 78−90510
multimode fibre, wavelength depend. propag. 78−38018
multimode fibre couplers, structure anal. 78−63198
multimode fibre with z-depend. α-value, impulse response 79−81521
multimode fibres, arbitrary index profile, propag. mode anal. using ray optics adiabatic approx. 80−53418
multimode fibres, comparison of impulse response calc. and meas. 79−81517
multimode fibres, freq. depend. of modal noise, speckle theory 80−102817
multimode fibres, loss mechanisms of leaky skew rays 77−39054
multimode fibres, loss mechanisms of leaky skew rays 78−46768
multimode fibres, mode dispersion characts. with polynomial refractive index profile 78−74999
multimode fibres, numerical evaluation of impulse response 78−59127
multimode fibres, parallel-beam impulse response, numerical results 77−39056
multimode fibres, universal tunnelling coeff. 78−66922
multimode fibres of arbitrary refr. index profile, pulse dispersion 80−74475
multimode fibres with index profiles varying along length, pulse propag. 80−87534
multimode fibres with mode mixing, pulse broadening 79−81516
multimode fibres with polynomial refr. index profile, mode dispersion and minimisation *(Japanese)* 79−50408
multimode focusing fibre with random bends, optical power loss 79−7214
multimode graded fibre, near and far field power distribs. 78−1337
multimode graded index fibres, group delay times of skew rays 77−34949
multimode graded index lightguide, mode coupling 80−78999
multimode graded-index fibre, near field intensity and modal power distrib. 80−102810
multimode GRIN fibre, power launching theory 77−7179
multimode irregular fibre, with fluctuation focusing ray calcs. of power loss 80−33195
multimode lightguide, time dependent propag. 78−13801
multimode localised index gradient fibre, parallel beam analysis 77−46801
multimode optical fibre bandwidth computation from refractive index profiles 79−76815
multimode optical fibres, group delay derivation 77−75688
multimode optical fibres, optimum refr. index distrib., vector wave anal. 78−63183
multimode optical fibres, power attenuation, pulse distortion, electromagnetic wave propagation eqns. *(Italian)* 77−79930
multimode optical fibres, transmission characts. *(German)* 78−30069
multimode optical waveguide propagation and interference effects *(Japanese)* 78−46764
multimode randomly bent fibres, ray theory of impulse response 78−22208
multimode self-focusing fibre, mode excitation and impulse response *(Japanese)* 78−83107
multimode square-law fibres, microbending loss, ray theory 77−42604
multimode step index fibre, excess loss due to outer layer 78−9430
multimode step-index fibre, OTF, geometrical optics calc. 77−65637
optical waveguide theory continued
multimode step-index waveguides, leaky modes and rays 78−74979
multimode three-layer fibre waveguides, mode attenuation 79−59835
multimode W-type fibres, power flow numerical soln. 80−78955
multimode W-type fibres, steady-state characts. 80−5818
multimode waveguide core-cladding interface, macroscopic roughness effect 79−18523
multimode waveguide with elliptical cross-section, geometrical optics analysis *(German)* 79−76844
multimode waveguides, step index limit of power law refr. index profiles 79−10387
multimodel fibres, energy description of propagation of monochromatic radiation 80−38116
multiple integrals in waveguide scatt. problems 79−3796
multiple-α index profile analysis 79−50371
multiply reflected Gaussian beams in circular cross section 79−18343
non-circular graded index fibres, leaky modes 79−1003
noncircular cross section fibres, perturbation approx. for propag. characts. 78−71195
nonlinear dielectric slab, surface wave propagation characts. 77−42609
nonlinear pulse propagation in fibres 79−18536
nonmeridional rays in multimode optical waveguides, transmission characts., multimode propag. *(German)* 77−54799
nonparabolic graded-index medium, wave propagation 79−18516
normal mode propagation in multilayer waveguide, energy characts. 77−23765
normalised cut off frequency, asymptotic evaluation, with quadratic index variation 78−9443
oblique input end-face lightguides 77−75684
optical fibre, bend radiation calculation 77−46817
optical fibre, multimode, mode-coupling phenomena anal. using matrix method, accuracy 80−23803
optical fibres, bandwidth limitations due to harmonic distortion in single-mode optical fibers 79−64335
optical fibres, broadband dual-mode, design considerations 78−94437
optical fibres, total dispersion in step-index monomode fibres 79−68427
optimisation of props. of $\Delta\alpha$ waveguide 79−32076
optimum parameter determ. 78−38023
parabolic fibre cutoffs 78−13800
parabolic index fibres, light propag. along helical bends 77−7183
parabolic index fibres, $LP_{\mu\mu}$-mode excitation by Gaussian TEM_{00}-beams, power coupling coeff. 80−78958
parabolic index with random dielectric constant gradient, Gaussian beam propag. 80−58698
parabolic-index fibre modes, propag. characts., linearly polarised approx. 80−78972
parabolic-index fibres, single mode, step-mode and multimode, microbending losses 77−3654
parabolic-index slabs and fibres with bent axes, radiation losses 78−46758
parabolic-index waveguides with distorted optical axis, beam propag. 79−46035
parabolic-profile splices with unequal core diameters, transmission vs. transverse offset 77−3652
paraxial approximation to scalar Helmholtz eqn., discrete eikonal and ray eqns. 78−90360
particle motion in potential channel, waveguide-optical analogy 80−12942
periodic fibre waveguide, mode coupling, appl. to DFB laser 77−27348
periodic optical waveguides of lenslike media with complex permittivity 77−83997
permittivity profile of inhomogeneous planar waveguide, determ. from mode spectrum *(Czech)* 80−28312
perturbed, propagation constants calc., leaky waves along W-type slab waveguide *(Japanese)* 78−42423
phase mismatched, high efficiency coupling 79−94339
planar anisotropic structures, waveguiding properties *(Czech)* 80−28313
planar dielectric branching waveguide, coupled mode analysis 79−997
planar graded-index waveguide, TE and TM modes, WKB analysis accuracy 78−50925
planar ion exchange waveguides, TE and TM mode analysis, using WKB calculations 78−9444
planar optical elements, dispersion props. 79−3811
planar waveguide, isotropic, polarisation conversion by Bragg deflection coupled mode theory 80−48461
planar waveguide with interacting step discontinuities, field and network anal. 79−55214
planar waveguides and fibres, book 78−42426
plastic rectilinear waveguide, geometric optics and illustration of meridional rays *(German)* 77−34941
plastic waveguide, characts. exam. *(German)* 78−38007
polarisation preservation in optical fibre waveguides with elliptical cores 79−64324
polygonally bounded waveguides, hybrid finite element analysis 77−27358
polymer lightguide, light propag., nonlinearity, quasi-optical approx. 80−99837
power attenuation calc., in bent multimode step index slab and fibre waveguides 78−25961
power launching analysis in multimode opt. waveguide with graded refractive index, appl. 78−46767
power-law profiles of arbitrary exponent, power series solns. of scalar wave equation 79−94355
prism accumulator with anisotropic optical waveguide, theory 79−64336
prism coupling into clad uniform optical waveguides 80−96003
propagation characteristic analysis, for slab and fibre waveguides 78−87160
propagation of optical mode in guided interlayer struct. with variable thickness *(French)* 79−23089
propagation theories, results from International workshop Lannion, Sept. 1976 *(French)* 77−11018
pulse dispersion in a clad lens-like medium 80−53445
pulse propag., nonlinear, homogeneous and inhomogeneous waveguides 80−83669
quasilinearly tapered couplers, weighted coupling strength 80−83674
radiation from bends, volume-current method 79−94336
radiation from optical waveguides: leaky-mode interpretation 79−32039
radiation loss caused by discontinuities in dielectric slab waveguide 79−7227
radiation modes, coupled mode theory and vol. current method comparison 77−72058

optical waveguide theory continued
radiation modes of arbitrary waveguides 79−27379
random mode coupling in fibre waveguide, ray theory 77−788
random mode coupling in fibre waveguide, ray theory for graded fibres [illegible]
randomly bent multimode fibres, ray theory 78−79129
randomly bent singly and doubly clad waveguides, mode conversion losses [illegible]
randomly gradient fibres with irregular bends, optical mode propagation and scattering 78−1325
ray statistics of multimodal optical fibres 78−94450
ray tracing in general nonhomogenous cylindrical medium 79−94335
rectangular core fibre optic waveguide, dispersive props. 80−64172
rectangular core optical fibres, guided wave propag. anal. 79−81556
refractive index smoothly graded, near and far fields 79−72705
refractive-index profiles, in diffused optical waveguides 79−7204
rib waveguide with trapezoidal cross section, numerical analysis 80−96009
ring index fibres, dispersion equalisation 79−32046
ring resonator, high-Q, asymmetric three-layered dielectrics, design 78−83118
S-shaped dielectric waveguide, guided leaky waves 80−28341
sandwich-ribbon optical fibre, near-field intensity patterns of mixed modes 77−62073
SAW resonator optical waveguide model 77−39146
scalar approximation accuracy 79−81561
scattering from arbitrarily located inhomogeneity 78−87161
scattering from core region of dielec. slab waveguide, radiation pattern 78−22197
scattering matrix and radiation charac.ts. of junction between monomode waveguides 77−34946
scattering of light in optical waveguides 79−10375
self-filtering multilayer S-waveguides with absorption and radiation losses 80−38102
self-filtering ring waveguide analysis 79−10402
self-imaging along homogeneous tapered waveguide *(German)* 77−79764
SELFOC dielectric waveguide, signal distortions 77−75699
SELFOC fibre, non-Gaussian laser beam propag. 78−1335
semiconductor injection lasers and integrated optics 77−14807
semiconductor junction lasers, narrow stripe geometry, non-Gaussian fundamental mode patterns, waveguide model 78−94394
semiconductor laser, stripe geometry, self-focusing obs., comprehensive model 77−79826
semileaky anisotropic film waveguide, wave propag. 77−65627
semileaky thin-film optical waveguides, guided-radiation mode coupling analysis 78−1372
semitransparent thin cylinder, radiation-conduction heat transfer, light-guide approx. 80−96179
sensitivity analysis of waveguides dimensional tolerances 79−76833
SHG by guided radiation mode coupling in thin film optical waveguide 80−106567
short fibre, leaky modes effect on response 78−9449
signal distortion, intensity distrib., single and coupled waveguides 80−33202
signal polarisation, effect of dielectric lightguide layer *(Russian)* 78−55466
single material fibre, with two support slabs of different thickness, modal anal. 79−23084
single mode fibers, microbending loss evaluation, core index profile effects 80−48412
single mode fibre near- and far-field characteristics, profile-independent representation 80−58739
single mode fibres, arbitrary-index, microbending loss evaluation 80−48411
single mode fibres, curvature and microbending losses 79−27418
single mode inhomogeneous fibre problems, scalar wave approach 79−64312
single-mode, simplified parameter based anal. 80−69507
single-mode fibre, pulse distortion due to microbending calc. 77−14798
single-mode fibre, pulse spreading due to third-order dispersion 79−50370
single-mode fibre pulse spreading due to third-order dispersion, optical source bandwidth effect 79−81523
single-mode fibre with refr. index dip 78−63194
single-mode fibres, pulse distortion, Gaussian pulse propag. theory 80−78956
single-mode fibres, simplified bending loss formula 79−59800
single-mode fibres, simulation of near field using microwave model 79−59825
single-mode optical fibre microbending loss and pulse distortion analysis 78−1395
single-mode optical waveguides with inhomogeneous index variations 79−76804
single-mode radially inhomogeneous fibre, propag. modes 78−22206
single-mode step-index fibre, minimum dispersion 79−89992
single-mode step-index fibres, practical microbending loss formula 79−81534
sinusoidal microbending loss of HE_{11}-mode in step-index fibres 78−79109
slab waveguide, inhomogeneous step-index and WKB anal. 78−66923
slab waveguide, modified zigzag ray model 77−39035
slab waveguide, TE Mode dispersion rel. to DH semiconductor lasers 80−91886
slab waveguide with refractive index irregularities, three dimens. scatt. patterns 78−87158
spatially periodic media, modal theory 77−7218
step index fibre, Lambertian source, impulse response 78−33819
step index fibre, pulse widths, Goos-Hanchen shift effects 77−83952
step index fibres, mode conversion due to scattering from off-axis inhomogeneity, Green's function analysis 80−10045
step index waveguide, effective index calc. method 78−50916
step-index fibre, scattering from arbitarily located off-axis inhomogeneity 80−58702
step-index fibres, pulse responses investig. using WKB approx. 80−91898
step-index fibres with microbending, bandwidth 80−23775
step-index monomode fibre, mode dispersion anal. of approx. for propag. const. 80−1307
step-index multimode guide, optical diffusion coefficients 77−11031
step-index optical fibre, scatt. from off-axis inhomogeneity, radiation loss 80−43446

optical waveguide theory continued
step-index optical fibre, scattering and guided mode conversion due to spherical object, theoretical anal. 80−64153
step-index optimal fibre, scatt. and mode conversion of guided modes by spherical object 79−81558
step-index single-mode fibres, zero-mode dispersion 78−87141
step-index waveguide, Goos-Hanchen shift for leaky waves 78−63176
stratification method in numerical anal. of transmission parameters 78−1324
strip line, optical, theory and numerical anal. 77−79956
strip waveguide analysis, reflection-transmission of obliquely incident wave on strip side 79−50378
strip waveguides, leakage and reson. effects, anal. 78−66953
stripe geometry diode laser, gain induced waveguiding 78−59007
stripline, modal charact.s. 77−3661
superluminal radiator theory *(Russian)* 80−64156
surface wave effective parameters in diffused waveguide 77−75696
surface wave line, dielec. obstacle on impedance jump 78−18063
surface wave propag., in optical fibre, influence of bulk losses and bulk dispersion 78−33892
surface waveguide electrooptical deflector, high-resolution, prism model 80−48454
surface waveguiding structures, radiation from circular bend between discontinuities 78−1355
surface-diffused and buried waveguides, scatt. losses caused by surface imperfections 79−64332
surface-wave modes in integrated optical systems, ray theory 79−64360
symmetric slab waveguide in birefr. media, coplanar optical axis slab, modes 79−32053
symmetrical rib optical waveguide fundamental modes 77−23744
synthesis using inverse differential operator 78−55465
tapered coupler, coupled-mode eqns., parabolic cylinder functions 77−46821
tapered cylindrical optical fibre, radiation charact.s. 79−10388
tapered optical slab waveguides with hypothetical boundaries 80−64185
tapered optical waveguide structs., mode coupling in terms of local modes 80−38126
tapered parabolic-index fibre waveguide 79−76803
TE-wave scatt. from blazed dielectric gratings 77−11005
temporal frequency dependence of modal noise in fibres [optical] 80−58687
thin film, using Maxwell EM theory *(Czech)* 80−33229
thin film lasers and waveguides with arbitrary refr. index distribs., optical processes 77−79971
thin film rib waveguide, numerical anal. by mode-matching method 80−48421
thin film waveguide, anisotropic, field excited by sources 79−7198
thin-film periodic structures, optoelectronic devices appls. *(Polish)* 78−50947
thin-film strip waveguide on dielectric substrate, optical dispersion 80−53478
thin-film two parallel waveguides, numerical anal. 80−106626
thin-film waveguides, propag. modes 78−71218
thin-film waveguides with refractive index fluctuation anal. using coupled power eqns. 79−72710
three-layer quasisingle-mode fibre waveguides, data transmission 79−94360
three-layer waveguides for wideband optical communication lines 80−28310
three-waveguide system, interference effects on couplings 80−78969
TM mode in Eckart-Epstein optical strip guides, exact solution 80−10046
toroidal metallic guide, optical surface waves, theoretical anal. and expt. 79−7197
transmission characteristics of mode-coupled graded-index multimode optical fibers 78−90526
transmission charact.s. of optical waveguides with periodic external force 80−99873
transversally nonhomogeneous waveguide EM wave propagation, using variational methods *(Czech)* 80−33155
trapezoidal cross-section dielectric waveguides, mode dispersion by effective-index method 80−9999
tunnelling ray attenuation in fibres, generalised parameters 78−66908
two-dimensional fibres, microbending theory, role of nonadjacent mode coupling 79−27415
two-dimensional waveguide analysis with misaligned or curved gratings 79−23092
two-layer elliptical fibre waveguides, first higher-mode cutoff 80−58684
two-mode fibre with near optimum index-profile, transmission charact.s. 80−96000
underground optical waveguide beam distortion by air convection 77−62063
uniaxial graded-index waveguides, mode propag. and conversion 79−55204
uniform theory of inhomogeneous waveguide modes near cut-off 80−28324
unstable resonator, effects of medium and gain inhomogeneities, waveguide model 77−58349
unstable strip resonators with misaligned circular mirrors, waveguide approach 78−82991
W-fibre with square core, confined guided modes 79−59813
W-fibreguides with rectangular core, confined propag. of optical modes 79−98467
W-type fibre, parabolic core, cutoff frequencies 78−94436
W-type fibres, mode excitation by tilted and offset Gaussian beams 78−90498
wavelength dispersion 80−91887
waves in asymmetrical gas dielectric waveguide, with resonances in walls 77−65639
weakly anisotropic rectangular dielec. optical waveguides, wave propag. anal. using coupled modes 80−64154
weakly anisotropic waveguide, propag. 77−79929
weakly guiding fibre, modes calc. by integral representation technique 80−58758
weakly guiding fibres, Maxwell eqn. reformulation of EM propag. 80−78974
weakly guiding three layer slab, attenuation coeff. 78−5567
whispering-gallery waves, polarisation and losses along twisted trajectories 80−9798
WKB approximation for step and parabolic index profiles, eigenvalues 77−34947

optical waveguide theory continued
zero total dispersion in step-index monomode fibres at 1.3 and 1.55 micron 79−68428
$Al_xGa_{1-x}As$ CSP laser, analytical waveguide study 79−10302
GaAs, electron beam pumped laser, far-field radiation pattern, optical confinement effects 79−86181
GaInAs, electron-pumped laser, far-field radiation pattern, optical confinement effects 79−86181
GeO_2 doped gradient optical fibres, pulse dispersion *(German)* 80−74496
$LiNbO_3$, Ti diffused waveguide, leaky mode loss coeffs., calc. 80−19094
$LiNbO_3$ waveguide, diffusion fabricated, angular variation calcs. using mode propag. consts. 80−69540
$LiNbO_3$:Ti optical waveguide channel branches 80−58811
$LiNbO_3$:Ti single-mode waveguides, losses due directional changes 80−58789
$Si-SiO_2-Si_xO_yN_z$ waveguide model *(Russian)* 79−10374

optical waveguides
see also optical fibres; optical waveguide components; optical waveguide theory
absorption spectroscopic technique using waveguide loss meas. 78−45729
acousto-optic light modulator, using Raman-Nath diffr. of vol. acoustic wave 80−48437
acousto-optic tunable TE-TM mode convertor on diffused waveguide 80−53477
acousto-optical beam deflector design, fabrication, and applications 77−19433
acousto-optical modulator using coupled plane waveguides 80−69527
acoustooptic guided wave Bragg diffr., optical pulse compression, light beam scanning 78−38053
acoustooptic TE⇌TM mode convertor utilizing doubly confined optical and acoustic waveguide struct. 78−83087
acoustooptic tunable filter, using collinear TE-TM mode conversion 80−102852
active dielectric, symmetric first-order Bragg interactions 78−46765
additional film in thin film slab waveguide, effect on waveguide propag. 79−81543
amplification of narrow-band signal in active waveguide 79−36930
amplifier based on resonant tunnelling between passive and active optical waveguides 79−59838
anisotropic diffraction by bulk acoustic waves 77−23784
anisotropic optical waveguides based on Langmuir organic films 80−64177
anisotropic or gyrotropic materials, theory and appl. 77−54789
anisotropic waveguide for integrated optics, monomolecular layered film 78−66954
aperture-type light conductor, photometric charact., computerised calc. by Monte Carlo method *(Russian)* 80−1339
arbitrary index profiles, loss due to radial offsets 77−11003
arc motion in narrow chamber, photography with optical waveguides and rotating mirror *(German)* 77−74542
asymmetric slab, mode conversion analysis, Green's function method 77−27344
asymmetric slab, thick dielectric grating, scattering losses approximate theory 77−68257
asymmetric waveguide structure semicond. laser, anomalous stimulated emission, theory 79−64228
asymmetric waveguide structure semicond. laser using external resonator, anomalous stimulated emission 79−64227
balanced-bridge switch modified config. with two straight waveguides 79−98506
beam dividers for quasi-optical transmission line *(Russian)* 79−3777
bent Guide structure semiconductor lasers, optimal ICs, appl. 79−41462
bent hollow metal waveguides, low-loss optical transmission 77−88904
benzene liquid-filled waveguide, genera'ion of enhanced CARS signals 79−89961
blanks, thermal and elastic stresses in a cylinder 80−14447
Bragg deflection of guided optical wave by surface acoustic waves in $LiNbO_3$ Ti-diffused waveguides 79−14118
Bragg deflector, using photorefract. effect in $As_{40}Se_{15}S_{35}Ge_{10}$ film loaded on $LiNbO_3$ waveguide 80−58673
Bragg electrostrictive mixing, acoustic surface wave generation, theory 77−19424
Bragg reflection in planar dielectric waveguides with periodic thickness modulation 77−79970
branching waveguide stripe injection laser, beam scanning and wavelength modulation 79−7138
Brillouin scattering in thin film waveguide 78−35153
bulk acousto-optic interactions in thin film waveguides, for GHz modulators 78−42471
bulk acousto-optic interactions in thin film waveguides, gigahertz modulators 79−32091
bypass dielectric waveguide mode order convertor 79−81570
cell type optical circuitry fabrication using photopolymer 77−42633
chalcogenide glass film, optical waveguide form. by laser and electron beam irrad. 77−79978
channel waveguide array, coupled to integrated CCD, fabrication and operation 78−38077
channel waveguide array coupled to integrated C-CD, appl. 80−102860
channel waveguide array in fan-out pattern for high resolution optical imaging 80−38129
channel waveguide arrays coupled to integrated CCD 80−33244
channel waveguide coupling with fibres on Si substrate 78−46761
channel waveguide interferometric modulator for EM field detection 80−74498
channel waveguides, single-mode, prism coupling efficiency meas. 80−99878
characteristics determination, far-field radiation patterns, semiconductor laser structure appl. 80−48407
chemical laser, electronic phototransition, with thermal initiation by shock wave 80−53283
chirped-grating multiplexers in dielectric waveguides 77−58445
chirped-grating output couplers in dielec. waveguides 77−39021
circular dielectric screened three-layer waveguide, cut-off characteristics and modal inversion 80−1303
circular strip type, fabrication by Ag ion migration 80−96042
coherent and nonlinear optics, conf., Leningrad, USSR (Jun. 1978) 80−98753
collimator, waveguide optical system, Luneberg lenses with plane connecting waveguides 79−68446

optical waveguides continued
communication, errors in determ. of output signal parameters 78−1365
communication links appl. *(Czech)* 77−62065
communication systems review 79−41455
composite light-controlled waveguide struct., polystyrene film with methyl red dye as active medium 80−14464
composite waveguide laser with end-fire excitation, output charact. 80−23738
concave metallic waveguide, beam modes 79−81533
concentrated solar radiation transmission appl., optical props. 77−50751
cone receptor, inhomogeneous waveguide model and Stiles-Crawford effect 77−90797
conference, Bad Harzburg, Germany (June 1979) 80−51951
conference, basic optical props. of materials, Gaithersburg, MD, USA (May 1980) 80−101668
conference on integrated and guided wave optics, Salt Lake City, UT, USA (Jan. 1977) 78−38072
confined propagation obs. in Bragg waveguides 77−58444
conic and quasi-conic profile, calc. and construction *(Rumanian)* 80−28331
conical light pipes with smooth and mosaic ends for photomultiplier 78−1328
corrugated, resonant wave conversion 80−74505
corrugated planar waveguides in the mid-IR region 79−98494
corrugated surface, E-wave emission 77−781
corrugated waveguide boundary, TM-polarized light diffraction, zero diffraction effect 79−64339
corrugated waveguide filters, mode conversion and filtering of obliquely incident waves 79−81571
corrugated waveguide filters, sidelobe suppression 77−84008
corrugated waveguides and lasers, improved coupled mode analysis 78−46842
corrugated-waveguide optical demultiplexer mode couplings 80−64194
coupling characteristics of parallel slab waveguides with index profile 78−75000
coupling techniques, laser to fibre and fibre to fibre *(German)* 77−42613
coupling to fibres 77−88915
coupling to heterojunction laser, transition struct. fabrication 78−38029
coupling to waveguides with linearly tapered horns, theory 78−33917
curved chemically strengthened glass *(Japanese)* 79−32077
curved waveguide, with parabolic refr. index profile over cross section, light propag. 80−19104
curved waveguide, with refr. index varying over cross section, light propag. 80−19103
CW optically pumped far IR waveguide lasers, high-power operation and scaling 77−38949
cylindrical, two-layer, light depolarisation, theory and expt. *(Russian)* 78−9454
cylindrical light pipe coupling, design 77−7187
cylindrical waveguide optical modulator efficiency in thermal mode *(Russian)* 79−94345
cylindrical waveguide wideband modulator, parameter optimisation *(Russian)* 79−94344
data bus system configurations 79−18544
deflection and focusing of radiation by stepwise inhomogeneities 78−83093
demultiplexer, using coupling between nonidentical waveguides 79−10380
design of waveguides with prescribed propag. consts. 80−48419
detection of light in dielec. waveguide by photodiode through direct evanescent field coupling 78−30094
deveopment strategy, Poland *(Polish)* 80−48438
DH junction laser, stripe-geometry below threshold waveguiding 77−46720
DH lasers, phase and group indices 80−64016
DH lasers, symmetric waveguide, near and far-field analytical approx. for fundamental mode 79−50296
DH stripe geometry lasers, three-dimensional anal. of mode props. 80−64020
dielectric strip waveguide, losses due to radiation of E_{11}^x and E_{11}^y waves from imperfect joint calc. 80−102847
diffraction, at corrugated surface, Brewster affect analogues 79−13901
diffraction grating form. on optical waveguide surface, ion-beam etching through photoresist mask 80−14492
diffraction optical coupling, heteroepitaxial GaAs-AlAs film waveguide 77−11045
diffractive logic elements for optical computers 80−78993
diffused, mode perturbation by thin film cladding 77−19398
diffused, refr. index profile determ., quick method 77−31130
diffused channel waveguides, direct index meas. 80−87562
diffused microwaveguide, refr. index profile determ. 77−23764
diffused waveguide, effective thickness meas. 79−32070
distributed, Bragg-reflector laser amplifiers, analysis 77−19348
distributed Bragg reflector for saturable resonator, bistability using Kerr effect 77−46737
distributed Bragg reflector laser, tunability by modulating refractive index in corrugated waveguide 77−79866
distributed Bragg reflector laser design, waveguide struct. 77−27306
distributed feedback structures, hybrid modes 79−27441
dye DFB laser with integrated Si and polyurethane channel waveguide 80−74373
dye doped polyurethane film, photoinduced guided light stopping 77−23739
dye high gain mm. bore laser, transverse mode control in waveguide resonator 78−1268
dye laser, thin film waveguide evanescent type, gain meas. 80−95908
elastic rubber waveguide, multimode thinfilm optical component fabrication 80−102857
electric field and refractive index distribs., electro-optic structures 77−72068
electro-optic A/D conversion using channel waveguide modulators 78−66898
electro-optic multimode waveguide switch 79−10383
electrooptic analogue-digital conversion, using channel waveguide modulators 78−38051
electrooptic phased array light beam deflector, application to analogue-digital conversion 78−38052
electrooptic radiation modulators utilizing semiconductor ridged waveguides 80−91925

optical waveguides continued
electrooptic surface prism laser deflector, for field destructive interference 80−87492
electrooptical, planar, thick, phase modulation theory *(German)* 77−27367
endoscopic laser photocoagulation, comparison of optical waveguides *(German)* 77−78037
energy diffraction input induced power depend. on impact parameter 80−64170
energy flux distrib. in plane anisotropic waveguide *(Russian)* 77−84003
Epitaxial waveguide laser with distributed second-order feedback by electron excitation *(Russian)* 78−29973
equiangular, spiral, for beta-ray detector 77−3212
evanescent fields, use in obs. of laser radiation effects on mammalian cells 80−12183
evanescent fields used for exposing mammalian cells to intense laser radiation 78−73298
fabrication, electric field controlled ion exchange in glass 78−38094
fabrication in glass by effusion 80−5850
far IR CW waveguide laser, CO_2 laser pumped, efficiency high-power operation 77−10937
far IR IC, antennas and waveguides for integration, review 80−69553
far IR laser mode losses 77−38954
far IR waveguide laser, Stark modulation 77−54744
far IR waveguide laser cavity design criteria 77−38951
far IR waveguide laser Stark effect obs. 77−38875
ferrite film lightguides for nonreciprocal optical systems 80−99880
ferrite-dielectric optical waveguide, azimuthally magnetised, theoretical characteristics *(Russian)* 78−22211
ferrite-dielectric optical waveguides, longitudinally magnetised, theoretical characteristics *(Russian)* 78−18061
ferrite-garnet film, waveguide light propag. charact., integrated optics appl. *(Russian)* 78−1346
ferroelectric materials, use in guided wave devices, review 78−38048
fibre optic sheets fabricated by selective photopolymerization 79−55235
fibre structure, characteristics, telecommunications appl. 79−94366
fibre transmission system in low-loss 1.0 to 1.4 μm wavelength region 77−11030
fibre-optical interferometer two-beam, and beam splitter 77−87811
fibres, evaluation of normalised cutoff frequencies in radially inhomogeneous fibres, perturbation theory 80−43434
film, SAW signal convolution 77−27428
film refractive index and thickness meas., error anal. of SYNCANG and SYNCWANG methods 78−8439
film refractive index dispersion meas. by optical waveguiding 79−85162
film thickness and refractive index, accurate meas. by symmetric prism wave couplers *(Chinese)* 80−2885
film waveguide spectrum analyser with prism coupling 77−62071
filter, multilayer frustrated-total-internal-refl., spatially limited 80−96014
five-layer planar dielectric waveguides 77−75697
flexible fibre light-guides, viewing instrum. appls. 80−87545
flexible IR waveguides, high-power transmission 80−48409
fluoromethane DFB gas laser, construction and operation 80−23715
fluoromethane laser, optically pumped far-IR waveguide, output, temp. depend. 80−58512
focon raster lightguide for transmission onto photomultiplier photocathode, optimisation 78−13805
four-layer isotropic waveguides, TE and TM modes 77−58433
four-layer waveguide diffractive injection efficiency optimisation *(Russian)* 80−64206
free electron laser, amplification in spatially periodic optical waveguide 78−37865
Fresnel lens in thin film waveguides 78−38075
Fresnel lenses in BaO optical waveguides 80−96034
GaAs epitaxial layer photoelastic channel optical waveguides 80−48457
garnet double layer prod. for magneto-optical devices, LPE 77−21043
garnet film waveguide, magnetooptical effects 77−3650
garnet film with high Faraday rotation, mode degeneracy 78−94454
garnet thin film waveguide, magneto-optical effects 77−54802
gas DFB laser waveguide precision calc. and pulse energy obs. 80−58577
gas laser, miniaturised, communication appl. 79−31936
gas waveguide lasers, props. and current-voltage charact. of discharges 78−1208
geodesic lens formation in diffusion fabricated optical waveguides 80−91937
glass, control of refractive index profile for integrated optics 79−27442
glass, fabrication by low-temperature diffusion process 80−102867
glass, high GeO_2, zero material dispersion wavelength and waveguide props. 80−58733
glass, high silica content, isotopic CVD for low-loss optical waveguide prod. 77−72093
glass, ion-exchanged, r.i. profile 77−772
glass, plane, form. by K^+ diffusion 79−90043
glass, Tl ion thermal migration formed optical waveguides, props. 79−46031
glass diffused and thin-film waveguides, light interf. 79−14115
glass fibres as optical waveguides 78−1332
glass waveguide, in-plane scatt. and loss mechanisms 80−33216
glass waveguides, diffused channel, multimode and single mode, direct index meas. 80−87562
graded index planar waveguide formed by Ag^+ migration in glass 77−27352
graded refractive index, diffused glass waveguide, anisotropy 80−33210
graded-index optical waveguide characteristics meas. 79−14108
graded-index optical waveguide mode-dependent attenuation meas. 78−46774
graded-index slab, with metal cladding, propag. losses of guided modes 77−83972
graded-index surface or buried, realized by ion exchange in glass 80−69499
grating coupled radiation, oscillatory function of waveguide thickness 77−19408
grating formation, asymm. line profile, on glass waveguide surface, ion etching method 79−10418
guided wave acoustooptics, fundamental principles and wideband appls. 79−37038
guided wave optics, appls. review 79−37054
guided-beam splitter, refl. meas., fabrication method 80−74473
optical waveguides continued
guided-wave optical systems and devices, seminar, Washington, USA (April 1979) 80−31418
guided-wave optics, design of devices, laser beams in thin transparent films 79−64337
gyrator, thin-film waveguide, theoretical analysis 78−25993
harmonic generation in thin-film integrated optics, field analysis 79−98509
heterostructure planar, guided-to-radiation mode conversion and appl. to light modulation 80−87557
heterostructures for integrated optics 77−39112
high quantum efficiency waveguide coupled photodetectors for integrated optics 80−58805
high-bandwidth, freq. response meas. 78−50924
high-silica, OH-ion distrib. profiles in rod preforms 77−54781
hollow cylindrical anisotropic dielectric guide, propagation 79−32047
hollow dielectric lightguide fabrication defects 79−27425
hollow dielectric waveguides, 10 micron propagation losses 77−50756
hollow light guides, dielectric-type, light transmission characteristics, minimum losses *(Russian)* 79−98503
hollow lightguides for H lamp, optical and operational charact. 80−53395
hollow rectangular dielectric waveguide laser resonator and external spherical mirrors, coupling radiation 78−37914
hologram recording with guided reference and readout waves 80−106492
hologram using optical thin films high-efficiency relief-type hologram 78−66958
holograms, recording and reconstruction, integration 77−14674
holography with guided optical waves, expt. techniques and results 80−28173
holography with guided reference and/or reconstructing wave 78−1198
III-V nitride semiconductors, physical properties and appls. in integrated optics *(Czech)* 80−28355
image transmission, lens light-guide line 79−3789
index profile determ. methods 80−1337
index profiles with low pulse dispersion over extended spectral range 78−55448
indiffused waveguides with thin metal buffer, TE_0-TM_0 mode splitting device 80−106638
information processing using guided wave opt. communication systems 79−36852
infrared microwaveguides with a mode-guiding layer of chalcogenide glass 80−28329
inhomogeneous glass sintering, self stresses producing bulk flow 80−14448
injection laser, high-power coupled-multiple-stripe phase-locked, beam charact. 79−50307
injection laser, transverse mode control by strip loaded waveguide 77−75543
injection laser/optical waveguide connection module 78−59023
integrated acousto-optical spectral analyser waveguide geodesic lens correction 79−50241
integrated coherent IR generator, difference freq. generation in nonlinear optical waveguide 80−33084
integrated electro-optical A/D convertor, using branching waveguide modulator channels 78−42474
integrated grating circuit for guided-beam multiple division fabricated by electron-beam direct writing 80−91934
integrated interferometric reflector with elec. control for laser reflector 77−58490
integrated optic Bragg spectrum analyser design 80−33237
integrated optical channel waveguide array for CCD parallel signal injection 78−37996
integrated optical channel waveguide-CCD transversal filter 80−58797
integrated optical circuits, selective LPE 78−6868
integrated optical detector array, waveguide, and modulator, based on Si technology 77−11049
integrated optical device for Hadamard transformation 78−22221
integrated optical functional elements based on holographic gratings in As_2S_3 film waveguides 77−79972
integrated optical spectral analyser design and fabrication 79−50445
integrated optical waveguide and CCD image array 77−34962
integrated optics, high density multichannel waveguides with integrated couplers 77−794
integrated optics, mode anal., prism coupling method 78−66947
integrated optics, waveguides, new wave phenomena, review 77−54817
integrated optics and guided wave devices, review 78−42468
integrated optics and optical waveguide devices, review 78−66948
integrated optics and thin-film technology 77−54815
integrated optics laboratory for teaching and research in optical waveguides 77−39034
integrated optics review 78−1429
integrated optoelectronic Si devices, optical signal processing and communications, fibre-channel waveguide coupled 79−59847
integrated waveguide-hologram memory design approach 80−32940
interaction between optical and acoustic surface waves, expt. 77−19428
interferometer using modular holographic elements 77−61116
inverted-ridge-waveguide DH injection laser with current and lateral optical confinement 77−75540
ion exchanged, fabrication from dilute $AgNO_3$ melts 79−23097
ion exchanged, thin film overlay effect on mode props. 80−33191
ion implanted integrated optic devices, attenuation *(German)* 78−83119
ion-exchanged, influence on step-index profile, double alkali effect 80−5824
ion-exchanged optical waveguide repeatability improved by melt dilution 80−53493
IR electrooptic waveguide for CO_2 laser modulation 77−27349
IR flexible hollow metallic rectangular pipes, beamshaping and polarisation control props. 79−76856
IR laser power transmission waveguides 77−19430
IR planar waveguide with chalcogenide glass-BaF_2 emitting grating, mech. fabrication 79−50443
IR surface wave propag. along metal surface *(Russian)* 79−68441
IR transmissive, flexible, meas. of propagation 77−88924
IR waveguides, development for fibre and integrated optics 79−98491
laminar, 4-layer, dielectric, S-type, propag. charact., mode filtration *(Russian)* 78−30078
Langmuir film, integrated optics applications 77−75711
Langmuir-Blodgett films, lightguiding 80−79006
laser, construction and operation characteristics *(Rumanian)* 78−59049
laser, coupled waveguide, as optical oscillator 78−9399

optical waveguides continued
laser, far i.r., with metal-dielectric waveguide, for Stark effect obs. 77−700
laser, pump efficiency, saturation effects 78−17981
laser, waveguide TEA, operation in IR 77−88752
laser beam intensity fluctuations, waveguide channel with large-scale random inhomogeneities 80−33194
laser far IR waveguide cavities, coherently pumped, geometrical design criteria 77−54739
laser frequency doubling in isotropic dielectric waveguide *(Russian)* 79−94285
laser gyro applications 80−1345
laser interferometer, 500-m base, Earth surface deform. detect. 80−105087
laser-induced damage in diffused waveguide 80−9925
lasers, operation under multimode conditions, relative efficiency of cavities, comparison 79−55158
leaky-mode propagation in Ti-diffused $LiNbO_3$ and $LiTaO_3$ waveguides 78−87149
lens guide, low-loss image transmission 80−91872
lens technologies for RF spectrum analyser 77−34961
lenslike medium, with external higher-index surround, mode filter characteristic 77−62049
light diffraction by oppositely propagating surface acoustic waves in an optical waveguide 79−41453
light pipes, timing errors evaluation 80−5445
light polarisation in twisted tape lightguides and braided cylindrical liquid-filled lightguides *(Russian)* 80−19107
$LiNbO_3$:Ti, suppression of LiO_2 out-diffusion 77−50749
$LiNbO_3$ single-mode planar waveguides for integrated optics, fabrication *(Korean)* 80−43448
linear low loss structures of ferroelec. materials, fabrication, heat treatment effect 77−23769
liquid crystal waveguides for integrated optics 77−34960
long-term stress failure probability estimation 80−58745
loss compensation using distributed gain amplifier 77−14811
loss measurement, nondestructive, using three prisms 80−106596
low loss optical conductors using doped deposited silica principle *(Dutch)* 78−66925
low loss waveguides, transient radiation effects, Cherenkov radiation, absorpt., in fibres 78−30055
Luneburg thin film lenses, formation by sputtering through circular mask 78−87132
magneto-optical, semileaky thin film, for modulator appl. 77−62055
magneto-optical TE-TM mode convertor, coupling and phase matching coeffs. 77−54816
manufacture, CAD, doped deposited SiO_2, optical fibres *(Italian)* 77−19385
materials and fabrication techniques for integrated and guided wave optics 80−23809
MBE, device appls. 80−25570
measurement techniques, attenuation, bandwidth 79−94367
metal, hollow, multimode IR laser losses 79−23076
metal clad, positive permittivity, attenuation, mode props. 77−27351
metal clad waveguide as cutoff polariser for integrated optics 77−27386
metal film optical absorption meas. application *(Japanese)* 79−40603
metal overlays, effect on 3-D optical waveguides 78−94425
metal-clad diffused optical waveguide propagation losses 77−84000
metal-clad optical strip waveguide lined with buffer layer, mode-filtering characts. 79−81559
metal-dielectric waveguide, third harmonic generation enhancement in CO gas 79−50342
metal-dielectric waveguide, third harmonic generation enhancement, comment 79−94283
metallic, helical-circular, invariant props. 79−23056
methyl cyanide submillimetric waveguide laser amplifier design and operation 77−38926
microcapillary gas-dielectric filled with azimuthally asymmetrical cross-section, attenuation calcs. 78−83105
mode selection using organic Langmuir films 79−98495
modes of propagating light waves in thin film waveguides for integrated optics *(Japanese)* 79−98510
modified mode propag. due to perturbing overlayer 77−65624
modulator switch, balanced bridge, using Ti-diffused $LiNbO_3$ strip waveguides 78−63201
monolithic integration for new devices 77−75714
monolithic integration of laser and amplifier/detector by twin-guide struct. 78−42466
multilayer gyrotropic structures, light propag. anal. *(Polish)* 79−3809
multimode, image transmission in coherent light, review 79−59831
multimode, propag. meas. problems 78−71231
multimode capillary light guide, effect on light polaris. *(Russian)* 79−37017
multimode channel fabrication in glass by laser heating 77−7220
multimode optical fibre coupling to single-mode waveguide 79−98485
multimode strip-waveguides made by thick film technology, loss meas. 79−59846
multiple beam spectral analyser with thin film waveguide feed, prism radiation tap 77−34944
multiple fibre end fire coupling with single-mode channel waveguides 79−7230
nitrobenzene, boundary phase in 5-layered light guide, birefr.. and equilib. thickness determ. 79−28711
nonreciprocal optical IC mode convertor analysis 77−84010
nonreciprocal using anisotropic lightguide and gyrotropic coating *(Russian)* 77−42623
offset straight integrated optical waveguides, length optimisation of S-shaped transition 78−46838
optical communication testbed 78−33925
optical fibre communication, conference, Paris, France, Sept. (1976) 77−11016
optically pumped CW far IR waveguide lasers, high power, scaling 77−54731
optically pumped waveguide gas lasers 78−5490
optics for electronic engineers *(Japanese)* 80−38106
optoacoustic deflector planar, expt. 78−74995
optoacoustic device, planar, SAW loss meas. using light beam diffraction 78−74996
organsilicon films for waveguide structure, optical props. *(Russian)* 79−98481

optical waveguides continued
p-n junction coupled-waveguide optical modulator, high freq. modulation 77−75678
passive components for integrated-optics signal processing 80−48466
performance before and after storage 79−27392
periodic dielectric rod array optical delay equalisation characteristics 78−5578
periodic thin films, integrated optics appls. 77−39109
phase conjugation by four-wave mixing in waveguide, theory 79−31984
phase conjugation by stimulated scatt. in waveguide, theory 79−3742
phase distribution controlled correction, thin-film optical waveguide with diffr. grating 79−76850
phase profiles, waveguides and gratings by optical methods 78−38071
photochromic film waveguide, acousto-optical props., integrated optics appl. 80−33207
photoconductive detector with integrated waveguide struct. 80−48456
photorecombination laser, shock wave triggered, waveguide mode optical gain 80−5730
picosecond optical sampling, cascade of waveguide interferometers driven by microwaves 80−99849
planar, constructed by diffusion methods *(Czech)* 79−41452
planar, fabricated by ion exchange in glass, refractive index profile 80−14460
planar, index profiles determ. from angular depend. of refl. 78−71210
planar, method for efficient interconnection 77−19393
planar, optoacoustic interaction, Raman-Nath type diffr. 78−87153
planar, refractive index distrib., fabrication methods 79−27429
planar, with exponential variation of refractive index, pulse dispersion 77−11027
planar anisotropic structures, waveguiding properties *(Czech)* 80−28313
planar coupler in data bus system with single multimode fibres 77−11024
planar diffused waveguide, WKB approx. for refr. index profile determ. 78−30086
planar diffused waveguides, refr. index distrib. function 79−55227
planar electrodes, distributed capacitance, optic and SAW device appls. 77−27387
planar ion exchange waveguides, TE and TM mode analysis, using WKB calculations 78−9444
planar ion-exchanged, fabrication technique 80−79003
planar multilayered structure, resonant polarization conversion and beam shift 78−1438
planar optical waveguide interconnection method 80−58671
planar optics, goals, methods, potential appl., principles and trends 80−33231
planar waveguide, isotropic, polarisation conversion by Bragg deflection, expt. results 80−48462
planar waveguide structure for integrated optics, props. *(Czech)* 80−96018
planar waveguides and fibres, book 78−42426
planar waveguides prepared by solid-state diffusion, refr. index distrib. function 79−10404
plane four-layer waveguide with diffr. grating, surface light waves 79−55250
plane waveguide laser, with semitransparent wall, kinetics 77−54740
plasma column waveguide, time varying, laser beam propagation 78−94916
plastic light guides development for high optical power transmission *(German)* 78−33913
plastic optical components and systems 78−25967
plastic scintillation counter with air light guide 78−29713
polyethylene, O-type, loss characts. at 337 μm 80−33175
polymer, optical waveguide and appl. *(Japanese)* 78−90518
polymer films, plasma polymerisation, light propag. expt. *(Japanese)* 78−6846
polymer films, prep. and characts. *(Japanese)* 78−5551
polymeric medium, guided light diffr. by holographic grating 77−7215
polymeric thin films appl., preparation and optical properties meas. 78−27342
polyurethane optical solid cct., preferential doping of rhodamine 6G 77−62075
porous glass preform optical waveguide props. 79−94375
power coupling efficiency, generalised scatt. matrices theory 77−27350
power decay evaluation, backscatter technique 80−106599
prism coupler fabrication technique 80−83685
prism coupling into optical waveguide second harmonic generation 80−102763
prismatic storage device with anisotropic optical waveguide, theory *(Russian)* 78−87144
probe for Langmuir film props. meas. 77−40294
progress in optical waveguide process and materials, review 80−23768
pure and doped silica, intrinisc attenuation 77−65633
quartz, anisotropic waveguide, for IR propag., coupling 77−34938
quartz, bombardment by B^+ ions, waveguide layer form. 79−27454
quartz, fused, waveguide struct. form. by H_3^+ ion irrad. 78−18072
quartz lightguide resonator for Nd^{3+}:YAG laser, Raman generation 80−99735
radiation modes of arbitrary waveguides 79−27379
radioisotope methods and neutron activation anal. of waveguide materials 78−7286
raster focusing-prism and light guide pump system for NH_3 laser 80−9905
rectangular, coupling to semiconductor laser, efficiency anal. 77−23767
rectangular, propagation losses at 10.6 μm for distributed feedback appl. 80−38101
rectangular light pipes of different dimens., coupling efficiency 77−7186
rectilinear optical resonators for curved metallic waveguides 80−69425
reduced depth polariser for integrated optics 77−84006
reflective coating for optical waveguides with abrupt turns 78−30059
refractive index, profile determ. of light focusing rod, Interphako interf. microscopy method 80−101832
refractive index measurement, methods and results 77−83965
refractive index profile calc. from measured coupling angles 80−78954
refractive index profile determ. in diffused waveguide 77−23745
refractive index radial distrib. in light focusing rods, interf. microscopy meas. method 77−57381
refractive index smoothly graded, near and far fields 79−72705
resonant tunnelling in film optical waveguides 79−27430
resonant tunnelling systems, review 77−780
RF sputtered glass optical waveguide, reduced SYNCANG method for refr. index 77−11046

optical waveguides continued
ridge waveguide, multilayer side cladded light propag. 78−33835
saturable optical resonator with distributed Bragg reflectors, transient behaviour 79−23029
saturable resonator with distrib. Bragg reflectors, bistability, bleaching and loss effects 77−27309
SAW acousto-optic modulators for integrated optics 79−90032
SAW electrostrictive mixing analysis 77−27390
scattering, out-of-plane, in sputtered optical waveguides 80−38127
scattering problem, comparison of two perturbation theories 80−83662
self-filtering S-type strip waveguides 80−33219
semiconductor clad, attenuation and propagation coeffs. 80−79004
semiconductor DH injection laser with gain-induced waveguiding, spontaneous emission factor calc. 79−81429
semiconductor laser, optical systems using caustic region or antiwaveguide struct. 77−61972
semiconductor laser with composite waveguide, emission characteristics 79−72592
semiconductor lasers, stripe geometry, waveguide props. 78−29954
semiconductor sheet, free carrier confinement for IR modulation 78−25969
semiconductor stripe geometry junction laser, waveguiding mechanism 77−75521
semiconductor thin film waveguides, radiation modulation by stationary phase gratings *(Russian)* 78−22209
semiconductor-waveguide lasers in bent-guide structs., charact. *(Japanese)* 78−87062
semiconductor-waveguide-laser amplifier, with anisotropic gain by drift carriers 77−79818
semileaky anisotropic thin-film optical waveguides and mode filters 78−13799
SHG, phase-matched, in four-layered optical waveguide struct. 78−74950
shock-wave-initiated photorecombination kinetics and lower mode waveguide amplification *(Russian)* 79−96313
signal polarisation, effect of dielectric lightguide layer *(Russian)* 78−55466
single mode coupling of fibre to indiffused waveguide 77−34959
single-mode ring-type, EM propag. charact. *(Russian)* 80−38104
slab waveguide with refractive index irregularities, three dimens. scatt. patterns anal. 78−87158
slab-type, mode coupling via dichroic absorpt. of M centres 80−33178
slab-type directional coupler with activated rhodamine 6G top layer, amplified oscill. 80−99718
soda lime glass, Ag^+ ion exchanged, planar optical waveguide, manufacturing tolerances 78−71212
stained glass, Ag- and Cu-, optical waveguide effect *(Japanese)* 80−14471
step discontinuity, radiation loss 77−42588
step-index waveguide, Goos-Hanchen shift for leaky waves 78−63176
stimulated Brillouin scatt. in optical waveguides, method for small-signal wavefront reversal 79−94298
stimulated Raman scatt. excitation by wideband pump 80−64108
stimulated Raman scattering, freq. scanning *(Russian)* 77−10983
Stokes radiation spatial charact. in stimulated scattering, saturation conditions 80−53379
stress induced (embossed), refractive index profile obs. 77−14799
strip guides, Eckart-Epstein type, exact soln. for TM mode propagation 80−10046
strip-guides, polarisation filtering 80−102861
stripe, Ag^+/Na ion exchanged, propag. charact. 80−83664
stripe lasers, twin-transverse junction, dielec. const. of inbuilt waveguide, injection current effect 79−50294
stripe optical waveguide, formed by ion exchange, diffusion profile 78−87137
stripline waveguides, dispersion charact. and radiation fields 80−64155
submarine communication lightguide cable design and manufacture 79−37027
submerged diffused waveguide prep., refr. index distrib. determ. 78−18068
submillimetre wave laser waveguides 78−5505
submillimetric-wave laser waveguides 77−38952
superconducting weak links induced by optical guided waves 78−14886
for superconductor junction devices 78−66955
superradiance waveguide laser, stimulated emission spectrum, leaky modes *(Russian)* 80−87400
surface acoustic wave scattering of guided optical beams 79−98508
switch/modulator, optically activated, using photoconductor and two channel waveguides 78−1437
tapered horn shaped channel waveguide coupling 77−42619
tapered light guide condenser design approach 80−33218
TE channel waveguide, CO_2 optical gain, discharge-related limitations 78−17951
technology, components and communication systems *(German)* 80−33168
tensile strength, dependence on sample length, Weibull distribution figures 78−30084
terminated crossbar matrix 77−19386
thick, highly multimode, fast fabrication method 78−18043
thick film optical waveguide integration with fibre-optic connectors 80−33246
thick planar films, transmission method for index meas., modal effects 80−102862
thin dielectric film optical waveguides, ideal fabrication technology, comparison of four techniques 80−79025
thin film, theory, technology and appl. *(Czech)* 80−33229
thin film and integrated optics review, theory, expt. techniques, waveguides 78−22220
thin film dielectric waveguide with emitting diffr. grating, inhomogeneity in thickness 80−48425
thin film glass lightguide boundary refraction expts. 80−106639
thin film optical waveguides for passive planar optical element construction 79−27440
thin film waveguide, mode conversion by two-stage coupling process 79−32034
thin film waveguide, phase distrib. along emitting aperture 79−55226
thin film waveguides, attenuation due to roughness-induced mode coupling 79−10408
thin film waveguides, optical damage thresholds 79−46033
thin-film, coupling of semiconductor laser radn. 77−19426
thin-film, on Si substrated, optical power losses calc. and obs. 80−106640
thin-film, propag. modes 78−71218
thin-film, TE and TM modes phase-matching dielectric constant relations *(Japanese)* 80−58677
thin-film laser with a two-dimensional diffraction grating 80−9906
thin-film laser with spatially separated multiple-frequency outputs 80−43368
thin-film lenslike light guide focusing properties 77−54786
thin-film multimode waveguides, higher order mode amplification 80−96012
thin-film periodic structures, optoelectronic devices appls. *(Polish)* 78−50947
thin-film waveguide, Fresnel lens 78−94452
thin-film waveguide, refr. index meas. using diffr. method 79−30532
thin-film waveguide, with plane diffr. grating, radiation fields and spectrosc. charact. 79−3790
thin-film waveguide laser amplifier with lossy cladding 80−64074
thin-film waveguide with liq. cryst. boundary modulation of refr. index, mode switching 80−23800
thin-film waveguides fabrication, review *(Polish)* 79−3775
thin-film waveguides of dense crown glass, HF sputtering prep. 79−10415
three layer optical waveguide for photolithographic fabrication of film lenses 77−39113
three-dimensional image transmission by lens guides 79−76789
three-layer heteroepitaxial struct., strip waveguide optimum width *(Russian)* 77−7200
toroidal metallic guide, optical surface waves, theoretical anal. and expt. 79−7197
transparent magnetic material, wave props. of domain wall 78−48011
trapezoidal cross-section dielectric waveguides, mode dispersion by effective-index method 80−9999
trapezoidal cross-section ridge design, propag. charact. 78−55436
trapezoidal-cross-section ridge, dispersion charact. 77−88909
travelling wave optical modulator using a directional coupler $LiNbO_3$ waveguide 80−96035
tube waveguide with outer higher index cladding, fundamental mode excitation by Gaussian beams 79−50410
twin-guide lasers theory, oscillation conditions and efficiency calc. 77−62076
twisted IR metal waveguide, low-loss propag. and polarisation rotation 79−41435
two-dimensional object imaging *(Japanese)* 78−87146
two-layer low mode dielectric waveguide, field config., temp. depend. 78−25983
ultrapure glass preparation, review 78−3086
underground, for Earth crust deform. determ. 77−53230
underground beam-guide lines with periodic light beam corrections 80−33196
underground optical waveguide air refractive index thermal fluctuation obs. 78−9452
variable refractive index, self-focusing 79−7208
variable refractive index waveguides 78−46837
wavefront reconstruction method, plane waveguide hologram coupled system 80−5708
X-ray wavelength and optical transmission waveguides *(German)* 80−99847
Ag doped glass fabricated by solid-state electro-thermal diffusion, low-loss charact. 80−58792
(Al,Ga)As:Zn planar stripe lasers with deep Zn diffusion, guiding mechanisms controlled by impurity concs. 80−78853
Al anodised waveguide for CW CO_2 laser 78−55376
Al-Ga-As heterostruct. with confined current flow, fabrication 78−68081
(AlGa)As CW narrow stripe injection laser with induced waveguide, expt. props. 80−32988
(AlGa)As DH narrow stripe injection laser with rigid waveguide, expt. props. 80−32987
AlGaAs, heteroepitaxial waveguides for image transmission *(Russian)* 77−11037
AlGaAs, heteroepitaxial waveguides, far radiation field charact. *(Russian)* 77−11038
AlGaAs heterostructures in integrated optics 77−75713
AlGaAs junction laser, with optical waveguiding 77−42540
AlGaAs rib waveguides, charact. 80−33177
AlGaAs twin guide struct., monolithic integration of laser and laser amplifier or detector 78−38082
AlGaAs-GaAs, DH laser, with bent guide of planar struct. 78−1256
AlGaAs-GaAs DH laser, bent-guide struct. 77−75544
AlGaAs-GaAs transverse mode stabilised plano-convex waveguide laser made by single step LPE 80−48274
$Al_xGa_{1-x}As$ buried heterostruct. laser, fabrication, optical props. and reliability 80−53322
$Al_xGa_{1-x}As$, fabrication of mesa-type waveguides by laser irrad. 80−5849
$Al_xGa_{1-x}As$, waveguide heterostruct. epitaxial growth with gradual composition change 79−42416
Al_2O_3 optical waveguide, fabrication by reactive Al sputtering in O_2-Ar atm. 80−33262
As-S film, guided light reversible control by electron beam irrad. 78−1331
As-Se glass thin-film waveguide, for 10.6 μm range 77−50770
As_2S_3 amorphous film waveguide and grating coupler 80−53448
As_2S_3 amorphous films, meas. of photoinduced transformations by optical waveguiding 79−43050
As_2S_3, film waveguide, acoustooptic deflection and modulation of light by stationary phase grating struct. 80−5841
As_2S_5, thin film, for acoustooptic modulators 78−83051
BN fabricated CO_2 CW capillary waveguide laser for optically pumping D_2O 80−48278
BaO crown and flint glasses, Ag and Cu diffusion for optical waveguide fabrication 78−59166
$Bi_{12}SiO_{20}$ crystal, for programmable optical guided-wave device 79−23069
$Bi_{12}TiO_{20}$, RF sputtered epitaxial film on $Bi_{12}GeO_{20}$, for optical waveguiding 78−9462
CO waveguide CW laser, 280-290K *(Russian)* 77−71975
CO_2, CW waveguide laser, nearly atm. press., using plasma injection technique 78−74925

optical waveguides continued
CO_2 compact sealed waveguide laser, design, construction and performance data 77−10947
CO_2, forced air convection cooled waveguide laser 77−38921
CO_2 high stability CW waveguide laser, for high resolution saturation spectroscopy 78−71112
CO_2 hollow dielectric waveguide, high press. laser, line selection 78−59026
CO_2 laser, saturation parameter 80−9856
CO_2 laser, self-focusing parallel-plate waveguide, transverse excitation 77−7139
CO_2 laser waveguide, photoionisation stabilisation using Blumlein-type pulser 77−54734
CO_2, simple preionised waveguide TE laser with continuous discharge electrodes 77−54721
CO_2 TE laser, waveguide, role of elec. field to press. ratio 78−17901
CO_2 TEA waveguide laser, high power 80−91814
CO_2, transversely excited waveguide laser, high field preionisation, design considerations 77−88751
CO_2 waveguide amplifiers, temp. depend. of small signal gain and saturation power 78−46569
CO_2 waveguide laser, design and performance characts. 80−9909
CO_2 waveguide laser, electrooptically Q-switched 79−98416
CO_2 waveguide laser, for space link transceiver 77−19322
CO_2, waveguide laser, gain calcs. 78−25849
CO_2 waveguide laser, gain and saturation *(Rumanian)* 80−23667
CO_2, waveguide laser, low prime power, gain and discharge power meas. 77−88749
CO_2 waveguide laser, multibeam, excited by AC discharge 80−99754
CO_2 waveguide laser, parameters meas. 79−31859
CO_2 waveguide laser, performance characts. *(Japanese)* 77−19318
CO_2 waveguide laser, pulsed operation 78−42353
CO_2 waveguide laser, saturation intensity, effect of wall deexcitation 79−924
CO_2 waveguide laser, saturation parameter 79−94209
CO_2 waveguide laser, saturation parameter meas. method 80−87372
CO_2 waveguide laser, transversely excited multiatmosphere, construction and characts. 77−79845
CO_2 waveguide laser, transversely RF excited 78−63127
CO_2 waveguide laser, tunability calc. *(Rumanian)* 80−87371
CO_2 waveguide laser 79−98380
CO_2 waveguide laser amplifier, using short BeO ceramic discharge tube, gain meas. 80−33027
CO_2 waveguide laser amplifier with strong discharge tube 80−74398
CO_2 waveguide laser and appls. 77−75568
CO_2, waveguide laser structures, design, construction and performance 77−88750
CO_2 waveguide laser with BN channel 77−14743
CO_2 waveguide laser with plane parallel mirror resonator 79−3715
CO_2 waveguide laser with pulsed high-freq. discharge 80−99755
CO_2 waveguide lasers, engineering aspects 79−31941
CO_2 waveguide lasers, high stability 77−3615
CO_2 waveguide lasers, high-power, high-press., photoionisation-stabilised 78−46641
CO_2, waveguide TE laser, modes of operation 79−81451
CS_2 filled waveguide, time-reversed wave generation by nonlinear refraction 78−90447
CdS_xSe_{1-x}, photosemiconductor, optically controlled deflector based on thin-film waveguide 80−33206
CdTe crystal in square waveguide, single sideband generation at 10.6 μm 79−55179
CdTe, fabrication by LPE using boat-slide technique 77−63570
CdTe, H^+ ion implanted, optical waveguiding and electrooptic modulation 77−75679
CdTe:H^+, ion-implanted, optical waveguiding and electrooptic modulation 77−7197
Cu light pipe, submm. wave transmission, and refl. of surfaces 50-10 cm^{-1} 78−18050
DCN, 250 mW continuous discharge laser at 195 μm 79−31949
DCN, CW submm. waveguide laser, high volumetric efficiency 78−42351
DCN waveguide lasers, optimised 190/195 μm, amplifying medium characts. 80−99709
Dy_2O_3-TiO_3 sputtered film, optical waveguide with high refractive index 79−3797
$Ga_{1-x}Al_x$ As, metal-gap channel waveguides, intensity modulation 78−66899
(GaAl)As buried-heterostructure laser with buried optical guide, highly efficient operation 80−1219
GaAlAs mode stabilised separated multiclad layer stripe geometry DH laser, optical waveguide 80−64051
GaAlAs-GaAs heterostructure, waveguide characteristics, mode spectrum, universal dispersion curves 79−72706
(GaAl)As-heterostruct. stripe lasers, light/current characts. and near field shifts, waveguide self focusing effects 78−29952
$Ga_{1-x}Al_xAs$ buried heterostructure lasers for analogue communication 80−48297
$Ga_{1-x}Al_xAs$ integrated optical waveguide LPE 77−75703
$Ga_{1-x}Al_xAs$ stripe laser with stable transverse mode structure 80−48298
$Ga_{1-x}Al_xAs$ symmetrised epitaxial variable-gap waveguide, coherent radiation generation 80−38018
$Ga_{1-x}Al_xAs$ transverse mode DH laser with inbuilt plano-convex waveguide 80−48296
$Ga_xAl_{1-x}As$ embedded stripe DH laser monolithically integrated with strip waveguide 78−59025
$Ga_xAl_{1-x}As$ layer, optical guiding in Bragg configuration 78−1431
GaAs and GaAlAs embedded heterostruct.-channel waveguide struct. 77−75712
GaAs, and its alloys, as integrated optics materials, book contrib. 79−64362
GaAs double cavity laser, with branching output waveguides, exam. 78−37918
GaAs double-cavity laser with branching output waveguides 78−63128
GaAs, electroabsorpt. avalanche photodiode, waveguide detector for 1.06 μm 78−16842
GaAs, electroabsorpt. avalanche photodiode waveguide detectors 78−65965
GaAs, electron-beam excited, efficient generation of electron-hole plasma 80−76051
GaAs epitaxial layer, strain induced optical waveguiding 79−27388
GaAs laser with integrated interferometric reflectors 77−65642

optical waveguides continued
GaAs oxide confined optical waveguides formed by lateral epitaxial growth 80−58815
GaAs periodic waveguide, phase-matched SHG obs. 77−19360
GaAs waisted-rib optical waveguides 80−74487
GaAs:Zn waveguide, light coupling at fundamental absorption edge 79−23082
GaAs-(GaAl)As channelled substrate buried heterostruct. injection laser, fabrication 77−7087
p-GaAs-$Al_{0.3}Ga_{0.7}As$, cladded dielec. waveguide, loss meas. using Raman scatt. 79−81539
GaAs-$Al_xGa_{1-x}As$, integrated twin-guide laser with distrib. Bragg reflectors 77−19310
GaAs-$Al_xGa_{1-x}As$, single mode optical rib waveguides, MOS control of switches 78−1432
GaAs-$Al_xGa_{1-x}As$, film waveguide, heterojunction lasers with Bragg mirrors, threshold characts. 79−23095
GaAs-$Al_xGa_{1-x}As$ integrated injection lasers and detectors with etched reflectors 77−62074
GaAs-$Al_xGa_{1-x}As$ MOS rib waveguide polarizers 80−64207
GaAs-$Al_xGa_{1-x}As$ MOS rib waveguide polariser, modulator and isolator 80−64217
GaAs-$Al_xGa_{1-x}As$ single mode rib waveguide COBRA switches, MOS control 77−88970
GaAs-AlAs, alternate monolayer single cryst., prop., losses 77−72065
GaAs-$Ga_{0.8}Al_{0.2}As$ layered struct., LPE, optical surface waves 78−48244
GaAs-$Ga_{1-x}Al_xAs$ DH laser, curved stripe, operation and appl. 78−42341
GaAs-$Ga_{1-x}Al_xAs$ stripe geometry lasers 79−94245
GaAs-GaAlAs heterostructure injection lasers, room temp. operation with curved stripe waveguides 78−37909
GaAs-GaAlAs monolithically integrated DFB lasers as freq. multiplexing source 77−34958
GaAsP epitaxial waveguide, electro-optic phase modulation of laser radiation 79−10417
GaAsP strip-waveguide modulator with GaAlAs embedded DH stripe laser 78−66957
$Ga_xIn_{1-x}As_{1-y}P_y$-InP, room temp. electron-beam-pumped laser with dielec. waveguide, output characts. 80−5761
$Ga_xIn_{1-x}As_yP_{1-y}$-InP, rib-waveguide injection lasers made by one-step LPE 79−59710
GaN epitaxial films, planar waveguides for integrated optics appls. 79−10416
GaP ribbon waveguide, vapour-grown, phase-matched SHG 80−48339
GaP-GaAsP planar heterostructure strip ridged waveguide under mech. load, polarisation modulation 80−96038
p-Ge sheet, free carrier confinement for IR modulation 78−25969
H_2, Raman laser, use of waveguide for improved conversion efficiency 77−658
HCN, CW 337 μm waveguide laser, scaling laws 77−19300
He-Ne laser with waveguide resonator, oscill. modes 77−27311
He-Ne optical waveguide amplifier, operation 80−43363
He-Ne waveguide lasers, props. and current-voltage characts. of discharges 78−1208
$In_xGa_{1-x}As$ epitaxial layer, waveguiding at 1.06 μm, losses 78−18052
InGaAsP/InP, DH laser, 1.5 μm, with optical waveguide structure, fabrication 79−72587
InGaAsP-InP DH laser with self-aligned struct., oscillation characts. 80−38017
InP-$In_{1-x}Ga_xAs_yP_{1-y}$-InP 1.53 μm single-mode CW ridge-waveguide laser 80−64072
$K_3Li_2Nb_5O_{15}$ films for optical waveguides epitaxial growth and characterisation 80−79016
$K_3Li_2Nb_5O_{15}$ optical waveguides fabricated on sapphire by RF sputtering 79−98488
$KNdP_4O_{12}$ epitaxially grown waveguide, laser operation at 1.051 μm 79−18423
$KNdP_4O_{12}$, laser waveguide, fabrication by LPE 79−36925
$KNdP_4O_{12}$ laser waveguide, epitaxial growth 79−91597
KrF*, waveguide laser excited by capacitively coupled discharge 78−94391
$LiBi_xNd_{1-x}P_4O_{12}$ waveguide laser layer epitaxially grown on $LiNdP_4O_{12}$ substrate 80−23709
Li(Nb,Ta)O_3 solid solution, LPE growth of thin film waveguides on $LiTaO_3$ substrates 79−41467
Li(Nb,Ta)O_3/$LiTaO_3$, multi-layer optical waveguide fabrication by LPE 80−71605
$LiNbO_3$, 3-D waveguide, efficient SHG, phase matching 77−7156
$LiNbO_3$, Ag-Li and Tl-Li ion exchange effects 80−58791
$LiNbO_3$, anisotropic, metal-diffused, leaky surface wave obs. 78−55454
$LiNbO_3$, anisotropic diffused optical waveguides, polarisation and spectral characts. 79−32073
$LiNbO_3$, anisotropic multilayer waveguide for electro-optical modulator, propag. characts. *(Italian)* 78−50904
$LiNbO_3$, anisotropic planar waveguide, TE to TM mode conversion *(Russian)* 77−11039
$LiNbO_3$, anisotropic planar waveguide, acoustooptic interaction 77−68273
$LiNbO_3$ balanced bridge modulator/switch with ion-etched slot 79−89993
$LiNbO_3$, beam-to-waveguide coupler 79−90003
$LiNbO_3$ branching waveguide, optical TE-TM mode splitter 80−96033
$LiNbO_3$, channel waveguide to single-mode fibre high-efficiency flip-chip coupling 80−99833
$LiNbO_3$, chemical control of optical damage, due to laser beams 78−38056
$LiNbO_3$, cleaved, crystallographic and electrooptic props. 80−59575
$LiNbO_3$ corrugated optical waveguide, electrooptic scanning of coupled light 78−38050
$LiNbO_3$, diffused waveguide as Bragg electro-optic modulator 77−34955
$LiNbO_3$ diffused waveguides, optical insertion loss meas. 78−38054
$LiNbO_3$ diffused waveguide, with exponential profile, metal-clad and dielec. overlay effects 78−46755
$LiNbO_3$ diffused waveguides, SHG *(Russian)* 79−59770
$LiNbO_3$, diffused waveguide for acoustooptical signal processing 79−90029
$LiNbO_3$ diffused waveguide, induced diffr. grating, integrated optics applications 79−98511
$LiNbO_3$, diffusion waveguide, acousto-optic mode conversion at surface wave freqs. *(Russian)* 78−1348

optical waveguides continued
$LiNbO_3$, Fi diffused, single-mode waveguide, comparison of bending losses in integrated optical circuits 80−83684
$LiNbO_3$, film lightguide, pulse signal convolution in acoustooptic interaction *(Russian)* 78−1345
$LiNbO_3$ graded index loaded with chalcogenide amorphous film, light deflector 80−48463
$LiNbO_3$ graded-index planar waveguide, $As_{40}Se_{50-x}S_xGe_{10}$ film strip-loaded 78−74965
$LiNbO_3$, heteroepitaxial growth on MgO by RF sputtering, SHG 79−27323
$LiNbO_3$, laser induced optical damage, pyroelec. contrib., electrostatic obs. 78−37935
$LiNbO_3$ layers, Li out-diffused, SHG phase matching temp. variation 80−69455
$LiNbO_3$ microwave laser beam electro-optic modulators using rectangular waveguides, 1.0 to 10 GHz 80−43381
$LiNbO_3$ optical branch and switch fabrication, by diffusion layer of Ti 78−33834
$LiNbO_3$, optical diffusive waveguide, profile determ. *(Russian)* 77−42622
$LiNbO_3$ optical waveguide, Bragg interaction of leaky and Rayleigh waves 77−23783
$LiNbO_3$ optical waveguides, elimination of Li_2O out-diffusion waveguide 77−65641
$LiNbO_3$, optical waveguide fabrication, closed tube control of out-diffusion 79−10419
$LiNbO_3$ optical waveguide, diffused with mag. garnet film top layer, non-reciprocal props. 79−41444
$LiNbO_3$ optical waveguide surface, acoustooptical interaction for TE modes, metallisation effect 80−69541
$LiNbO_3$, optical waveguides by ion implantation 80−106622
$LiNbO_3$, phase modulator, use in multimode integrated bistable switch 78−79145
$LiNbO_3$ planar HF acousto-optic modulator construction and expts. 79−76863
$LiNbO_3$, planar lightguide, optical mode interaction with standing elastic surface waves 80−99836
$LiNbO_3$, planar optical waveguide, SHG in angle-matched conditions 79−41422
$LiNbO_3$ planar waveguide, light beam switching and modulation using built-in dielectric channel 77−88967
$LiNbO_3$ planar waveguide, light beam switching and modulation using built-in dielec. channel 78−46840
$LiNbO_3$ planar waveguide, refractive index rel. to Ti diffusion *(Russian)* 78−59120
$LiNbO_3$ planar waveguide mode conversion and intensity modulation 79−10410
$LiNbO_3$, ridge struct. fabrication by CF_4 plasma etching 80−28357
$LiNbO_3$ sputtered layers, on $LiTaO_3$, optical waveguide props. 77−11012
$LiNbO_3$ TE-TM mode convertor, using collinear acoustooptic interaction 77−19407
$LiNbO_3$ three-dimens. optical waveguide, parametric difference freq. generation 80−48335
$LiNbO_3$, Ti diffused, mode control by doping 77−88903
$LiNbO_3$, Ti diffused, tuning charact. of parametric interactions 79−3779
$LiNbO_3$, Ti diffused, ferroelectric domain inversion 79−94338
$LiNbO_3$, Ti diffused optical waveguides, efficient prism-coupling 79−46089
$LiNbO_3$, Ti diffused planar waveguide, WKB approx. for refr. index profile determ. 78−30086
$LiNbO_3$ Ti diffused single-mode waveguide coupling to single-mode fibre 79−81547
$LiNbO_3$, Ti diffused waveguide, refr. index and thickness precise determ. 79−41446
$LiNbO_3$, Ti diffusion and charact. of graded-index lightguide 79−27433
$LiNbO_3$ Ti-diffused C-plate waveguide with metal cladding, buffer layer effects 78−25956
$LiNbO_3$ Ti-diffused optical waveguide coupled to GaAlAs DH laser, anal. 80−58706
$LiNbO_3$ Ti-diffused waveguide for cutoff modulator 80−9991
$LiNbO_3$ waveguide, corrugated, electro-optic scanning of light diffr. from grating output coupler 78−63172
$LiNbO_3$ waveguide, diffusion of Ti, exam. by electron probe anal. and X-ray diffr. 78−47588
$LiNbO_3$ waveguide, diffused, 2nd harmonic generation 79−14041
$LiNbO_3$ waveguide, holographic writing technique based on multiphoton photorefractive processes 77−38824
$LiNbO_3$ waveguide, horn struct. and thin film optical switch 77−88968
$LiNbO_3$ waveguide, planar electro-optic prism array beam splitter 80−64209
$LiNbO_3$, waveguide, single-mode planar and rigid type electro-optic waveguide modulators, design 77−11029
$LiNbO_3$ waveguide, thin-film optical filtering using acoustooptic interaction 79−81572
$LiNbO_3$ waveguide absorption losses, laser calorimetric meas. 79−64311
$LiNbO_3$, waveguide and modulator form. by ion implantation 80−48469
$LiNbO_3$, waveguide form. technique, using organometallic soln. diffusion sources 78−38099
$LiNbO_3$, waveguide formation using organometallic solns. as diffusion sources 80−23810
$LiNbO_3$ waveguides, diffused channel, multimode and single mode, direct index meas. 80−87562
$LiNbO_3$ waveguides, optical scattering phenomena 80−58786
$LiNbO_3$, Y-cut, waveguide form. by Ti diffusion, refr. index and electrooptic coeffs. 79−14114
$LiNbO_3$:He, ion implantation, optical waveguide form., refr. index changes 78−46762
$LiNbO_3$:Ti, BiTm ferrite garnet coated, nonreciprocal optical waveguide system *(Russian)* 77−42623
$LiNbO_3$:Ti, broad-band travelling wave waveguide modulator 77−39036
$LiNbO_3$:Ti, coupled waveguided TE/TM mode splitter 80−64142
$LiNbO_3$:Ti, diffused, Mg diffusion effects on charact. 78−66905
$LiNbO_3$:Ti, diffused, optical channel waveguides, Bragg switch 78−75002
$LiNbO_3$:Ti, diffused waveguide, +4 valence state, XPS 77−11014
$LiNbO_3$:Ti, diffused strip waveguide, refractive index changes, two-dimensional distrib. 79−86254

optical waveguides continued
$LiNbO_3$:Ti, dopant conc., refr. index profile rel. to integrated optics 78−5583
$LiNbO_3$:Ti, elec. field tuning of SHG, phase-matching condition 79−41412
$LiNbO_3$:Ti, fabrication and waveguiding props. 78−30091
$LiNbO_3$:Ti, graded-index optical waveguides, mode dispersion charact. 79−3770
$LiNbO_3$:Ti, in-diffused waveguide, integrated bistable optical device development 78−75001
$LiNbO_3$:Ti, in-diffused waveguide, acousto-optical meas. of optical field profiles 79−23054
$LiNbO_3$:Ti, in-diffused waveguides, optical damage thresholds 79−46033
$LiNbO_3$:Ti, integrated bistable optical device using Mach-Zehnder interferometric optical waveguide 79−59843
$LiNbO_3$:Ti, nondegenerate four-wave mixing in integrated optics 79−46088
$LiNbO_3$:Ti, planar and channel optical waveguides, anisotropic diffusion expts. 80−64200
$LiNbO_3$:Ti, planar optical waveguides, processing and props. 80−78965
$LiNbO_3$:Ti, SHG with 25% conversion efficiency 78−94432
$LiNbO_3$:Ti, Ti diffusion process and control, waveguide charact. 80−58790
$LiNbO_3$:Ti, Y-cut thin film waveguide, acousto-optical deflector, electro-optical modulator *(Russian)* 77−39115
$LiNbO_3$:Ti active branching waveguide modulator 77−19392
$LiNbO_3$:Ti branched waveguide amplitude modulator 77−39037
$LiNbO_3$:Ti branching optical waveguide, mode coupling 80−69518
$LiNbO_3$:Ti channel waveguide high-speed cutoff modulator 80−64195
$LiNbO_3$:Ti cleaved, waveguide, attenuation coefficient and coupling loss 78−74975
$LiNbO_3$:Ti diffused, fabrication problems *(Japanese)* 80−33256
$LiNbO_3$:Ti diffused channel waveguide, optical parametric amplification 80−106564
$LiNbO_3$:Ti diffused optical waveguide, guided light scatt. sources 80−78966
$LiNbO_3$:Ti diffused optical waveguide, efficient tapered gap prism coupling 80−78967
$LiNbO_3$:Ti diffused strip waveguide, optical insertion losses 78−74985
$LiNbO_3$:Ti diffused strip waveguide, optical propag. losses and coupling losses 80−58664
$LiNbO_3$:Ti electro-optic TE-TM mode convertor structure 80−64215
$LiNbO_3$:Ti guides, pyroelectric loss meas. 79−46046
$LiNbO_3$:Ti in-diffused optical waveguide fabrication 79−76892
$LiNbO_3$:Ti in-diffused waveguide, refractive index profile calc. from measured coupling angles 80−78954
$LiNbO_3$:Ti narrow ridge optical waveguides and electro-optical, ion-bombardment-enhanced etching 80−38133
$LiNbO_3$:Ti optical waveguide, technique for suppressing Li_2O out-diffusion 78−18040
$LiNbO_3$:Ti optical waveguide diffusion profile, AES obs. *(German)* 78−33876
$LiNbO_3$:Ti optical waveguide, surface wave mode conversion, static strain-optic effect 80−87561
$LiNbO_3$:Ti phase-matched waveguide electro-optic TE⇄TM mode convertor 80−58749
$LiNbO_3$:Ti planar and channel waveguides, appl. of Li_2O compensation technique 78−74976
$LiNbO_3$:Ti planar and channel optical waveguides, Ti diffusion coeff. meas. 80−19096
$LiNbO_3$:Ti planar waveguide, edge coupling to GaAlAs DH laser diode 80−87559
$LiNbO_3$:Ti single mode electrooptic waveguide modulator, high-speed operation 80−91915
$LiNbO_3$:Ti single-mode waveguide, fabrication by sequential combination of Ti diffusion and masked ion-implantation 80−58785
$LiNbO_3$:Ti single-mode waveguides, losses due directional changes 80−58789
$LiNbO_3$:Ti strip waveguide, SHG 80−102773
$LiNbO_3$:Ti thin film acousto-optic deflector 77−75698
$LiNbO_3$:Ti waveguide, precise determ. of refr. index 78−94442
$LiNbO_3$:Ti waveguide, integrated bistable Fabry-Perot resonator fabrication 79−41459
$LiNbO_3$:Ti waveguide, in-plane scatt. obs. and countermeasures 80−33215
$LiNbO_3$:Ti waveguide, operation of geodesic lens, anisotropic and curvature losses 80−48453
$LiNbO_3$:Ti waveguide, ps signal processing with planar, nonlinear integrated optics 80−64208
$LiNbO_3$:Ti waveguide laser diode end-fire coupling 79−94368
$LiNbO_3$:Ti waveguide thin film electrooptic Bragg modulator, bistable optical element 80−10034
$LiNbO_3$:Ti waveguide and cryst., absorpt. loss and photorefractive index changes 80−48368
$LiNbO_3$:Ti waveguide directional coupler switches, optically-induced cross-talk 80−48417
$LiNbO_3$:Ti waveguide electro-optic TE⇄TM mode converter-wavelength filter 80−64210
$LiNbO_3$:Ti waveguides, convolution of ps optical signals 80−58629
$LiNbO_3$:Ti waveguides, absorption loss and photorefractive index changes 80−58787
$LiNbO_3$, Li_2O diffusion for chemical control of laser induced optical damage 78−46693
$LiNb_xTa_{1-x}O_3$ stripe waveguides, fabrication, physical and optical props. 78−38055
$LiNdP_4O_{12}$, glass clad, slab waveguide laser 78−46625
$LiNdP_4O_{12}$ glass-clad rectangular waveguide, laser performance 80−32996
$LiNdP_4O_{12}$, single-transverse-mode slab waveguide laser, charact. 79−55141
Li_2O out-diffusion waveguide elimination in $LiNbO_3$ and $LiTaO_3$ 77−65641
$LiTaO_3$, Ag-Li and Tl-Li ion exchange effects 80−58791
$LiTaO_3$, Czochralski growth technique, light guide prod. by Nb diffusion *(German)* 80−20783
$LiTaO_3$ optical waveguide, Ag-Li ion exchange 80−91888
$LiTaO_3$, Ti diffused, electrooptic diffraction modulation 79−10381
$LiTaO_3$, waveguide, single-mode planar and rigid type electro-optic waveguide modulators design 77−11029
$LiTaO_3$:Cu, waveguide with periodic electrodes, mode conversion 78−33840

optical waveguides continued
$LiTaO_3$:Cu waveguide, electro-optic control of radiation loss in off-axial propagation 80−23789
$LiTaO_3$:Ti, diffused waveguide prep., parameters determ. 80−14465
$LiTaO_3$:Ti waveguide modulator structs., high optical power capabilities 77−39023
$LifaO_3$, optical waveguides, elimination of Li_2O out-diffusion waveguide 77−65641
MgO:Cu, dopant conc., refr. index profile rel. to integrated optics 78−5583
NH_3 laser, waveguide cavity, efficient CW far IR output 77−72001
Na_2O-B_2O_3-SiO_2, optical waveguide glass, molar absorptivity of water 80−80066
Na_2O-SiO_2 glass waveguides, low loss, new fabrication method, exam. 78−55481
Nb_2O_5, passive components, electron-beam and photolithographic fabrication 78−13818
Nb_2O_5 waveguide, in-plane scatt. and loss mechanisms 80−33216
Nd:glass films for integrated optics, RF sputtering and optical characts. 79−46087
Nd:YAG, single freq. laser with waveguide resonator 78−1277
Nd:YAG waveguide resonator laser, time characts. 77−58345
PbO-SiO_2 interdiffusion layer optical waveguide, prep. and props. 80−43489
Se amorphous Au clad waveguides piezoeleastic modulator for 10.6 μm radiation 78−66956
Si guided-wave acousto-optical devices 80−102864
Si monolithic optical integrated circuits for laser system applications 78−1436
Si, optical waveguides along both sides of groove 80−96006
Si photodiode for optical channel waveguides 80−102805
Si waveguide photodetector matrix, appl. in integrated-optics demultiplexer 79−32095
Si_3N_4 on Si, fabrication, propag. consts. 78−33826
Si_3N_4, RF-sputtered thin-film optical waveguide, effect of deposition parameters on optical loss 79−76881
Si_3N_4 waveguide layer, as electro-optic phase modulator 79−23081
SiO_2 film, bombardment by B^+ ions, waveguide layer form. 79−27454
SiO_2, fused silica, isotopic CVD for low-loss optical waveguide prod. 77−72093
SiO_2, glass, form. by low energy electron irrad. 77−7189
SiO_2, ion implanted, fused, refr. index profiles 80−54272
SiO_2 ion implanted, radiation defects and optical props. 80−107293
SiO_2 optical fibres, appl. to transmission of solar radiation 77−3663
SiO_2 thin film grating for $LiNbO_3$:Ti waveguide mode convertor and reflector 80−64216
SiO_2-Ta_2O_5 film channel optical waveguide, fabrication using CO_2 laser 79−27386
Ta_2O_5, colinear interaction between acoustic and optical waves in planar waveguide, radiation into substrate 80−53452
Ta_2O_5 film with protective coating, optical waveguide prod. 79−72682
Ta_2O_5, plane optical waveguide, fabrication by reactive sputtering 78−71221
Ta_2O_5, RF-sputtered thin-film optical waveguide, effect of deposition parameters on optical loss 79−76881
Ta_2O_5-SiO_2, plane optical waveguide, fabrication by reactive sputtering 78−71221
$Ta_2O_5N_x$, sputtered birefr. film, deposition conditions effect on refr. index 77−39118
TiO_2 and Dy_2O_3-TiO_2, high refractive index film growth by sputtering, waveguide appl. 77−48341
TiO_2 planar optical waveguide preparation and props. 78−90524
XeF waveguide laser operation on 351, 353 nm transitions 79−22942
XeF*, waveguide laser excited by capacitively coupled discharge 78−94391
$(Y,Gd)_3(Fe,Ga)_5O_{12}$, thin film lightguide, noninteracting mode conversion *(Russian)* 78−1347
YIG LPE film, optical waveguide in mag. strip domains *(French)* 77−83979
YIG substituted film waveguides, TE→TM mode conversions 78−66904
YIG thin film gyromag. waveguide, on GGG substrate, optical propag. props. Faraday effect 80−74513
ZnO, CVD films on sapphire substrates, use as optical waveguide 78−90500
ZnO epitaxial film with smooth surface from CVD onto a sputtered ZnO film on sapphire, waveguide appl. 78−56588
ZnO film, optical waveguide fabrication, CVD on sputtered ZnO film on sapphire 79−86269
ZnO film on ozidised Si, optical measure of acoustic quality 80−80893
ZnO, high rate epitaxy on sapphire by planar magnetron RF sputtering 79−28916
ZnO low-loss optical waveguides on amorphous substrates 80−58793
ZnO piezoelectric films, RF planar-magnetron sputtered, characterisation 80−96751
ZnO thin film, collinear acousto-optic interaction and appl. to tunable opt. filter 80−74509
ZnO thin films, surface acoustic-optic interaction, diffr. 77−3685
ZnS film free carrier absorption for laser beam modulation *(Japanese)* 79−7164
ZnS leaky waveguide electro-optic modulator limitations 78−22218
ZnS thin-film waveguide SHG phase-matching obs. with tunable parametric oscillator 77−58390
ZnSe-ZnS semiconductor waveguide laser, electron beam excited, blue emission 79−18447
ZnTe ion implanted planar waveguides, refr. index profiles 77−62039

optical workshop techniques
accelerated preparation for optical production 78−83131
acrylic coating, surface tension effects 80−53487
active abrasive conc. determ. by static method based on etch figure stars count 80−74544
air bearing and diamond machine design 80−1365
alkali germanoscilicate glasses, water extraction for making graded index optical fibres 80−28361
alkali halide crystals, optical components, melt growth conditions 78−50955
alkali halide pelleting technique for solid sampling in IR spectroscopy 78−87171
alkali lime germanosilicate GRIN fibre prep., losses and geometrical props. 80−69560
annular lapping of precision flatware 77−27396

optical workshop techniques continued
annular wedge-shaped layer coatings, apparatus for prod. 77−14817
antireflection coating deposition from hydrolyzable soln. 77−58495
antireflection coatings, thickness monitoring during deposition 80−19114
antireflection coatings applied from metal-organic derived liquid precursors 80−5847
applied optics, fabrication and testing, conf., Oakland, CA, USA (May-June 1980) 80−101661
arc fusion splicing of low-loss single-mode fibres 80−53489
aspheric axisymmetric lens figuring, wear pattern prediction 77−27398
aspheric element generation by sputtering techniques 78−59168
aspheric figuring, single-spindle, with flexible pads 77−84017
aspheric lens, steep, fabrication of concave and convex faces 77−65645
aspheric optics low scatter finishing, polishing of f/2 paraboloids 79−59855
aspheric rotationally symm. surface generation, computer control 77−27395
aspherical lens, polishing technique with equal polishing rate distrib. 80−58818
aspherical optical surface low-scatter finishing 79−14125
aspherical surface diamond turning machine development 80−1372
aspherical surface polishing with ring polisher 79−41465
aspherical surface prod., review 77−7224
aspherical surface production by mechanical means 78−50964
aspherical systems manufacturing and testing techniques development, use of computer *(Italian)* 80−48467
aspherics precision manufacture with programmed microelectronic control 80−1368
aspherising layer prod., monitoring by interf. fringes in periscopic microscope 77−14820
astronomical optical surface shaping automation methods 79−84675
astronomical optical surface shaping process automation 80−105169
autocollimation apparatus to test manufacturing quality of aspherical mirror profile 80−10053
autocollimation instrument for checking angles and pyramidicity of AR-90° prisms during manufacturing process 80−87570
automated apparatus for grinding large optical components 80−102869
automatic deposition of optically active layers, single and multicoated on industrial scale *(Hungarian)* 77−75718
bench, automated scanning, optical coupling loss investigations 78−83124
bench base selection, accuracy/cost tradeoffs 79−27447
blank fabrication for large azimuthal telescope primary mirror, work program 78−16302
blank grinding and polishing, for LAT primary mirror 78−90541
blank shaping by free grinding method, system of allowances 78−46849
blazed ion-etched holographic grating, prod. methods, optical props. *(Japanese)* 80−10021
blazed ion-etched holographic grating prod., high spectroscopic qualities 79−76847
camera objective matching with film channel in serial prod., tolerances 78−16885
camera optical component fine diamond grinding on modernised equipment 79−46092
cell type optical circuitry fabrication using photopolymer 77−42633
cement requirements 78−50961
ceramic mould accelerated shell heat treatment models 79−76896
cermet grinders with fillers, performance 77−72103
chalcogenide glass film, optical waveguide form. by laser and electron beam irrad. 77−79978
chemical purity in glass fibres for communication appl. 79−41437
chemical spray silvering of optical components 78−25995
circular ruling machines, test results of the TKF 1000/1 and TKF 1000 S high precision instrums. 79−7237
cleaning method for low scatter mirrors after silicone oil exposure 78−59167
cleaning techniques for optical surfaces 79−46093
coating deposition of ZrO_2, TiO_2 and SiO_2, high freq. cathodic method 79−76900
coating removal by Al_2O_3 powder and NH_4HF_2 soln. 80−74521
coating technique and refractive index meas. 80−43488
coatings, problems of application technology 78−83069
cold light production by high vacuum deposition of multilayer interference coatings *(German)* 80−53486
communication fibre waveguide fabrication techniques 80−1322
complete ellipse of rotation fabrication 79−37060
component blank pressure shaping, semiautomatic apparatus 79−72731
component manufacture and evaluation, seminar, Los Angeles, USA (Jan. 1979) 80−12850
component polishing process modelling *(German)* 80−87565
computationally directed axisymmetric aspheric figuring 79−23105
computer controlled optical plotter for filter generation *(French)* 78−90538
computer controlled polisher using small grinding-polishing tool assembly 78−75006
computer-controlled interferometry, in-process production tool 80−74531
computer-controlled machine tool for diamond-turned surface accuracy improvement 80−1367
computer-controlled polisher for small-tool fabrication of mirrors 80−14496
concave paraboloidal mirror, prod. method, interferogram tests 80−58823
concave spherical mirror fabrication using flexure 77−42583
concave stigmatic grating mech. prod. on spherical surface 80−38109
concrete optical table 79−50449
conference, optical production technology advances, London, England (Jan. 1977) 78−50954
constant-thickness film formation on axially symmetrical substrate 79−27453
contact lens fabrication, spincasting using polyhydroxyethyl methacrylate 77−795
contact lens fabrication and fitting, state of art and science 80−12311
contact problem soln. in optical surface shaping 80−33260
contact problems in optical surface shaping 80−74540
contacting of K8 glass polished surfaces, cryst. deposit form. 77−58492
corundum large optical crystal production with zero orientation 79−50457
cost reduction in manufacturing 80−1361
crystal component blank production 79−72725
crystal surface finishing using diamond cup grinding wheels *(German)* 80−19112

optical workshop techniques continued
cutting traces of single diamond, friction force 77−50781
cylindrical lens surface generation, grinding and polishing machinery design 80−79023
cylindrical parts, centreless smoothing 77−90507
diallyl isophthalate-methyl methacrylate copolymer, light focusing rod prep. by copolymerisation, refractive index distrib. const. *(Japanese)* 79−46042
diamond grinding of optical glass, kinetics 80−64224
diamond machined optical surface specification 80−48472
diamond machining of IR window materials 78−5586
diamond smoothing techniques 78−50957
diamond tool bit machining, comparison with conventional optical process 80−69569
diamond turned metal optics, book contrib. 79−32104
diamond turned optics facility 77−50782
diamond turning, Honeywell Corporation facilities 80−5852
diamond turning, optics and TWT components manufacture 79−81584
diamond turning, state of the art update 78−46853
diamond turning, technology developments, appls. 77−27400
diamond turning air-bearing spindle and eddy-current motor 80−5851
diamond turning and precision engineering 80−1364
diamond turning at large optical manufacturer, aspheric surface generation 79−23101
diamond turning fabrication of IR optical components 78−5590
diamond turning for optical component fabrication 79−76899
diamond turning machine characteristics and turned surface microtopography 80−33263
diamond turning of F-111 windscreens, feasibility 79−23106
diamond turning of optics, past, present and future 79−23100
diamond turning optical surfaces on electroless Ni 80−1375
diamond turning precision machine tool system 80−69568
dielectric coating adhesion improvement of diamond turned mirrors, ion polishing surface prep. 79−23102
diffracting periodic structure generation by coherent beam interference 80−69570
diffraction grating form. on optical waveguide surface, ion-beam etching through photoresist mask 80−14492
diffraction grating generation for integrated optics, interference method 80−48460
diffraction grating production, review of Japanese research 80−10018
diffraction grating production, three-dimens. for integrated optics 78−42480
diffraction grating residual ruling errors, magnetostrictive correction method 79−50454
diffraction grating ruling engine with piezoelec. control 78−83128
diffraction gratings, fabrication and performance testing 77−27361
diffraction gratings, photoresist and GaAs, exposure and etching time optimalisation 80−23816
diffuser form. of simple known statistical props. 78−90539
dispersion medium for polishing single cryst. corundum 80−102870
distributed Bragg reflector filter, polystyrene-collodion (polyvinyl alcohol) multilayers, fabrication 79−76838
dividing head adjustment test bench 77−30202
double-layer antireflection coatings for plastic lenses, evaporation coating process 80−14491
double-layer coating with double cone nozzle in-line with optical fibre drawing 80−53488
drawing facility for lightguide fibres 80−64229
elastic tools for finishing optical components with noncircular cylindrical surfaces 80−28368
elasticity method for telescope mirror aspherisation 77−29649
electro-optic material cutting and polishing, book 79−81583
electro-optical film production, highly-oriented, m-nitroaniline type 77−19463
electro-optical system manufacture, test and process control changes 80−96044
electron beam evaporator, UELI-1, for optical industry 78−46847
electron optical demountable system for studying image tube designs 79−81575
electron-beam and photolithographic fabrication of guided-wave optical components 78−13818
element fabrication and assembly, centration errors 80−9980
element polishing simulation calc. and results *(German)* 80−87566
end preparation and fusion splicing of fibre array with CO_2 laser 80−10051
epoxy replication, materials, techniques and appls. 77−27401
evaporator, large-capacity, with filtering element, for SiO film prod. 77−14819
evaporator, tubular-type radiation-heated, ZnS film deposition 80−76191
eyeglass lens blanks mode from molten glass, defects elimination 77−34971
fabrication of synthetic silica tubing and fibres using SiO_2-B_2O_3 79−50462
far IR narrow band-pass filter construction 77−39065
far IR narrow-bandpass interference filters, prod. and performance 78−5558
fibre, 7-core, construction and transmission props. 79−46077
fibre, coating with Ni film, on line magnetron sputtering, mechanical properties improvement 79−72723
fibre, end preparation using CO_2 laser 78−55478
fibre, fusion splices by discharge heating 78−75007
fibre, low-loss graded index, produced by double crucible technique 80−48449
fibre, single-mode, ultra-low-loss, optimised structure for fabrication 80−99843
fibre, step-index, nearly elliptical, with high eccentricity, fabrication for studying modes 80−95989
fibre alignment tool 80−23814
fibre and cable splicing and sheath jointing expts. 80−23806
fibre arc splicing unit *(German)* 80−19115
fibre breaking tool 78−5585
fibre bundle drawing from double crucible 78−33920
fibre butt-joining to Ti-diffused $LiNbO_3$ waveguide 79−76812
fibre cable formats and construction techniques *(German)* 79−55206
fibre coating concentricity improvement by tapered nozzles *(German)* 78−38095
fibre coating technique improvement 78−5593
fibre coating technology, overview 80−58828
fibre coating with cylindrical bore dies 79−46095
fibre communication advances, materials and techniques 80−102853

optical workshop techniques continued
fibre connectors, hot forming versus epoxy bonding of bundles, single fibre techniques 78−42482
fibre coupling, simple permanent connection method for single-mode fibres 77−72097
fibre crystals floating zone growth, far IR optical waveguides 80−79019
fibre cutting machine for rectangular and circular fibres 78−33932
fibre cutting tool 80−1360
fibre cutting tool 80−33255
fibre cutting tool and automatic splicing machine 80−87575
fibre cutting with hot metal wire 77−19462
fibre devices and materials for 4 μm-band communication 78−94441
fibre doped deposited silica preform, Cl drying simultaneous with consolidation 79−50466
fibre drawing, CO_2 laser system limitations 78−1447
fibre drawing, diameter control improvements 78−1445
fibre drawing, influence on fibre loss 78−68667
fibre drawing, neck-down shape prediction from furnace temp. distrib. 78−5594
fibre drawing, semi-automatic machine development 79−27449
fibre drawing, split beam CO_2 laser heat source 77−19465
fibre drawing conditions 79−18557
fibre drawing from compound glasses, using double-crucible and glass-plastic methods 79−3815
fibre drawing process, control of diameter 79−50468
fibre drawing process control, optimisation theory appl. 79−90039
fibre drawing technique for bundle of 19 fibres drawn from double crucible 78−55480
fibre drawing techniques for plastic-clad and doped-deposited silica fibres 79−37066
fibre drawing using laser, galvanometer beam-scanning rotating lens system 79−41463
fibre drawing using ZrO_2 induction furnace 78−1446
fibre end face quality check 80−64164
fibre endface preparation by AC discharge heating and stretching 80−64232
fibre fabrication, computer-aided MCVD system *(Japanese)* 79−59852
fibre fabrication, GeO_2 doped silica core single mode fibres, telecommun. appl. 79−18556
fibre fabrication, low OH content, vapour phase axial deposition method 78−83125
fibre fabrication, MCVD system design 79−55255
fibre fabrication, OH-free VAD 80−99887
fibre fabrication, substrate tube diameter control during MCVD preform preparation 79−50463
fibre fabrication by CVD 78−33922
fibre fabrication by improved CVD method 77−79976
fibre fabrication by improved CVD method 78−1448
fibre fabrication by isothermal plasma-activated CVD *(German)* 78−33928
fibre fabrication by vapour phase axial deposition, 1.3 μm, low-loss and wide bandwidth 80−38136
fibre fabrication method *(Japanese)* 79−27448
fibre fabrication techniques using MCVD and refr. index profile control 79−59856
fibre fabrication with MCVD method, graded index fibres *(Japanese)* 79−59851
fibre geometry specifications rel. to measured fibre statistics 79−27371
fibre high speed coating, forced convective cooling 80−23815
fibre high-speed drawing, effect on losses 79−14095
fibre holder, electrostatic 77−72095
fibre joining by arc welding, practical machine for splicing in field 79−50450
fibre lens, plastic focusing, change of ref. index profile during heat treatment process in fabricating 78−83091
fibre manufacture by double-crucible method 80−83688
fibre manufacturing, cabling and splicing, developments in Japan 78−59124
fibre manufacturing processes, parameter specifications 80−96041
fibre manufacturing processes *(Japanese)* 79−27403
fibre modified CVD prep., optical and mechanical props. reproducibility 80−69535
fibre optic element end forming of optical precision surfaces 77−50779
fibre optic elements, damaged layer struct. after diamond grinding and polishing 79−7220
fibre optic sheet form. by selective photopolymerisation, appl. in image guiding equipment 78−42477
fibre plasma activated CVD, influence of substrate temp. 80−48475
fibre plasma augmented vapour deposition 80−69561
fibre preform, high-silica, fabricated by CVD, OH-ion distribution 79−14121
fibre preform index profiling, automatic nondestructive focusing method 79−50448
fibre preform manufacture using modified CVD process 80−64228
fibre preform preparation using RF plasma deposition 78−55479
fibre preforms produced at high rates by particulate-deposition methods 79−50461
fibre preparation, long lengths of ultra-low-loss single mode fibres 79−76893
fibre preparation, single-mode low birefr., polarisation characts. 79−7195
fibre preparation by Ar plasma augmented vapour deposition 80−48478
fibre preparation for high tensile strength, pulling and coating techniques 78−63211
fibre preparation methods and performance factors 80−69557
fibre processing techniques, review 79−50460
fibre refractive index dip removal by etching method 79−14120
fibre ribbon splicing with vacuum-assisted injection mould 80−53491
fibre ribbons and cables manufacture, mech. props. 78−90533
fibre splicing and connecting 79−41436
fibre splicing techniques 78−79147
fibre splicing techniques for compound glass and silica optical fibres *(Japanese)* 80−99890
fibre splicing using arc fusion method, protection and reliability 80−69565
fibre splicing using CO_2 laser, thermal conditions 78−13820
fibre splicing using low MP glass solder 79−55252
fibre splicing using self-aligning ceramic capillary 79−76829
fibre splicing with low-power CO_2 laser 77−72098
fibre strengthening by molecular stuffing 80−58830
fibre tip lens fabrication and smoothing 78−33923
fibre waveguide processes and materials, progress review 79−50459

optical workshop techniques continued
fibre waveguides with large-diameter core and low optical losses, prod. technology 80−14463
fibre-optic cable manufacture, testing, and installation *(German)* 78−33863
fibre-optic polariser, in-line, formation and props. 80−106603
fibre-optic sintered plates, micropore sealing, vac. tightness improvement 80−28333
fibre-optic waveguide, flat-surface ends preparation, using handheld tool 79−37062
fibreguide to metal hermetic seal, using Cu tube component 78−83120
fibres, compound glass, manufacturing process and fundamental charact. *(Japanese)* 80−99865
fibres, fabrication processes and transmission charact. *(Japanese)* 80−87496
fibres, graded-index advances in production using phase-separable glasses 79−50465
fibres, low-loss, manufacture, modified rod-in-tube method *(Japanese)* 80−33253
fibres, low-loss step-index, fabrication using modified rod-in-tube method 79−50467
fibres, multimode, splicing method using elec. arc 77−27391
fibres, optical, production of fibre optics, exam. *(Polish)* 78−83130
fibres, single-mode, fabrication by VAD 80−83687
fibres, structural characteristics, CVD fabrication 79−59806
fibres, VAD, ultimately low OH content achievement, by optimised dehydration 80−99845
fibres drawn by laser heating, heat transfer 79−94377
fibres prepared by modified CVD, reproducibility 78−90531
fibres prepared by plasma-augmented vapour deposition 79−50451
fibres pulled in graphite furnace, effect of drawing conditions on tensile strength 79−50469
fibres termination, silica, plastic-clad, by stripping and recladding with fluorine based copolymer 79−41466
fibres with high tensile strength, furnace drawing method 78−68666
fibrescopes using leached fibre image bundles, manufacture 80−83670
film deposition on fibre end, thickness monitoring with optical time-domain reflectometer 79−55254
film transport rollers, fabrication accuracy improvement 78−18077
filter, nonquarterwave multilayer, optical monitoring with minicomputer allowing thickness error correction 80−23774
filter, nonquarterwave multilayer, wideband optical monitoring during deposition 80−28309
filter fabrication, reducing variation in transmission band location 77−14816
filter fabrication technology for near IR Fabry-Perot filters 77−84016
filter fabrication using Ge and CsI 77−34951
filters, diffractive, prepared by reactive sputter etching, microfabrication and evaluation 79−90008
fine wire free standing grid fabrication 78−5559
fluorophosphate glass produced in pyrocarbon coated melt vessels, increased light absorpt. 78−71167
foam-film solar energy reflector fabrication, physical and chemical processors 78−90530
Fresnel lens film prep. by electron beam irradiated mould polymerisation 79−98515
Fresnel lenses in BaO optical waveguides 80−96034
furnace drawn silica fibres, contamination reduction 78−33918
fusion splices for single-mode optical fibres 78−83126
fusion splicing machine for optical fibres 80−74516
geodesic lens formation in diffusion fabricated optical waveguides 80−91937
geodesic lenses, spherical aberration correction and fabrication tolerances 79−27435
glass, blanks, stresses and birefr. changes with dimensions 78−30100
glass, IR transmitting, as optical material in passive systems, preparation and characterisation 79−23034
glass, kinematic relationships in automatic glass grinding and polishing machines *(Czech)* 79−32096
glass, polishing with ZrO_2-SiO_2 powder mixture 80−28367
glass, refractive index gradients, form. using ion exchange diffusion 80−64227
glass and single crystal production 79−94308
glass blank for primary mirror for large azimuthal telescope 77−72101
glass ceramic, (sital) surface operation parameters, selection using bending strength tests 79−32101
glass cylinder refractive index variation by field-assisted ion exchange 80−14500
glass deformation degree rel. to optimum moulding prod. rate 79−50456
glass development and manufacturing processes 80−53393
glass disc amplifier assembly, necessity for dust-free environment 77−83879
glass fibre, continuous coating applicator 77−3659
glass fibre, forming process, charact., anal. techniques 80−58827
glass fibre cutting device *(Italian)* 78−50951
glass fibre development, large-core, for military appls. 80−48451
glass fibre drawing process, characterization and control 80−58826
glass fibre manufacture, double-crucible and plasma methods 77−50763
glass fibre manufacture, smooth fracture faces, using incandescent wire 78−38098
glass fibre manufacture using CVD *(German)* 78−33933
glass fibre optical waveguides, materials systems, fabrication and charact. 77−19394
glass fibre preparation, low loss multicomponent *(Japanese)* 79−3814
glass fibre production methods for optical communications, review *(German)* 80−23813
glass fibre thickness meas. and control system in production *(German)* 80−10052
glass fibre vapour phase axial deposition, OH content reduction by flame hydrolysis control 80−48474
glass fibre waveguide drawing using CO_2 lasers 79−59857
glass fibre waveguides fabrication, mech. props. 77−23766
glass fibres, low-loss, fabrication technologies state of art 79−10420
glass fibres for optical communications, colloquium, London, England (Jan. 1979) 80−67930
glass finishing with small-grained diamond grinding wheels *(German)* 80−38137
glass grinding, variation of diamond tool working ability 77−7225
glass melting in Pt crucibles, thyristor freq. convertor-fed power supply 77−50780

optical workshop techniques continued
glass optical fibre, vapour phase materials and processes, review 80−58825
glass optical fibre drawing, fluid-dynamic stability analysis 77−11053
glass polishing process acceleration with chem. reagents 78−90542
glass production, wetting of graphite vat liners 77−1831
glass surfaces, cracked layer thickness determ., chemical method 80−64226
glass surfacing, using loose abrasives, impregnated diamonds and electroplated diamonds 78−50956
glass tubing dia. and wall thickness meas., P-329M instrum. 80−86262
graded index fibres made by vapour phase axial deposition, refr. index profile 80−48477
graded-index fibre vapour-phase axial deposition method, fibre characteristics 80−58824
gradient index lens fabrication by molecular stuffing 80−14499
gradient index optical lenses, use, design, fabrication and refr. meas. 78−13780
gradient-index optics: a review 80−69478
grating direct writing using SEM 78−83121
grating formation, asymm. line profile, on glass waveguide surface, ion etching method 79−10418
grating lens fabrication for integrated optics 78−75004
grating writing, interferometric piecewise generation 77−42590
grinding and polishing machines, semiautomatic, kinematic relationships *(Czech)* 78−50953
grinding and polishing of low stiffness plates 78−71236
grinding and polishing semiautomatic machines, kinematic relations *(Czech)* 78−63208
grinding of large spherical surfaces with annular tool 78−18074
grinding tool surface contact area determination 80−64221
guided-beam splitter, refl. meas., fabrication method 80−74473
hard overcoats in replicated optics 78−66968
hermetic seal, optical fibre-to-metal, construction 78−83078
high speed production line design 77−27397
hollow tube fabrication of microchannel plates from reducible glasses 77−50766
holographic grating blazing techniques comparison 80−53438
holographic grating production by laser irradiation of photoresist *(German)* 80−33254
holographic grating ruling with stepped profile 79−76898
holographic optical element fabrication using dye-sensitised dichromated gelatin 78−63043
honeycomb optical tables development 78−18073
hyperboloid lens manufacturing technique 80−96039
image quality evaluation from aspheric replica master data, using ACCOS V SPLINE program 78−66964
inorganic lithography using metallo-organic photoresists 80−79024
inorganic thin layers, two-stage formation 79−27450
instrumentation production planning problems, system of indices 77−31145
integrated grating circuit for guided-beam multiple division fabricated by electron-beam direct writing 80−91934
integrated optical grating circuit fabrication by electron beam direct writing 80−64214
integrated optics, functional components, fabrication of microstructs. in micrometre/submicrometre range, microlithographic techniques *(German)* 80−106637
integrated polariser, reduced cladding-medium, fabricated in ion-exchanged guides 80−14489
interference coating, optical charact. topography var. 77−72102
interference coating deposition by Balzers BA-710 vac. system, photometric monitoring 78−46850
interference coating production, new ideas 79−32098
interference coatings on projector reflectors, vac. deposition 77−75725
interference polarizer with large entrance aperture, charact. 80−43453
interferometric fabrication of diffraction grating and optical waveguide coupler 78−1440
interferometric instrumentation as a cost-effective production tool 80−74535
interferometry seminar, San Diego, CA, USA (Aug. 1979) 80−73096
ion beam erosion, grating profile evolution 79−94374
ion commercial laser systems, design and manufacture 78−59046
ion exchange, field assisted, for production of graded-index optical materials 80−74447
ion implantation in colour centre research, appl. to optical waveguide form 79−19272
ion polishing for diamond-turned mirror dielectric coating adhesion 80−1370
ion polishing of fused silica surface, rel. to laser damage thresholds 77−75717
ion polishing of optical coatings, for multilayer interf. systems and integrated optics 80−33261
ion-exchanged optical waveguide repeatability improved by melt dilution 80−53493
IR component fabrication 77−27402
IR multilayer interference filter manufacture, supposed longwave limit 80−9989
IR multilayer optical medium produced by negative photoresist spin-coating 80−74451
IR planar waveguide with chalcogenide glass-BaF_2 emitting grating, mech. fabrication 79−50443
IR polariser grid prod. process *(Russian)* 78−46795
jelly-filled optical fibre cable fabrication and characteristics 80−53490
joining of optical fibres *(Norwegian)* 79−1008
Large Azimuthal Telescope mirror blank fabrication facilities 79−14123
large high-precision prism grinding, use of 3G-71 lathe 80−102872
large optical component antireflection and protective coatings 79−72660
Large optical component grinding and polishing condition selection 79−81579
large-diameter radius surface generation with small cutters 79−94373
laser diode fabrication reproducibility *(French)* 78−42357
laser fibre drawing, tension rel. to drawing vel. and ultimate strength 78−74986
laser mirror and window charact. rel. to fabrication method 79−14014
laser mirror manufacture, ion beam/plasma chemical etching mixed batch process *(French, English)* 77−83880
laser mirrors, optical fabrication techniques 77−65600
laser rangefinder, AN/GVS-5 hand-held, production engineering techniques 78−59018
lens, high performance, manufacturing methods *(German)* 80−53482

optical workshop techniques continued
lens, individual meniscus-type, coarse grinding errors 79−50458
lens, water soluble cryst., protective coating to aid polishing 80−33250
lens blank fabrication with reduced finishing allowances 80−74541
lens centring devices, high accuracy, appls. *(French)* 78−33924
lens grinding, as student lab. project 77−5614
lens manufacture automation *(Russian)* 78−50884
lens mass production yield estimation by centering tolerance simulation 80−78941
lens mounting 77−27399
lens mounting systems, construction *(Hungarian)* 77−72050
lens polishing and shaping techniques *(German)* 80−33114
lens surface geometry model, high-speed generating, smoothing and polishing 78−50889
lenses surface grinding and polishing, spectacle type, using automatic and semi-automatic machines *(French)* 80−58822
leucosapphire, unique polishing features of hard crystals 80−64225
light diffuser fabrication, Kalliroscope effect based diffuser 78−59121
light focusing plastic rod prep. by photocopolymerisation 77−11000
light guide manufacture, heavy ion beams application 77−55310
$LiNbO_3$ single-mode planar waveguides for integrated optics, fabrication *(Korean)* 80−43448
linear Fresnel lens, fabrication process, solar radiation concentration 80−106592
linear motor slide drive system for optical machining 80−1366
lined interference filter cementing technique 79−72729
lithographic focused laser system, integrated optical device fabrication appl. 78−55477
low-loss graded-index fibre, 3 km and 10 km preform design and modified CVD method 80−58746
low-loss optical fibre fabrication for long wavelength region 80−99874
low-loss optical fibre production with high numerical aperture 80−48450
Luneburg guided-wave optical thin-film lens, fabrication technique and props. 80−33223
machine, semiautomatic, for ruling circular scales 78−46851
machine shop operations 80−96045
machine tool computerised control for diamond-turned surface finish 79−98517
manufacturing tolerances, by a deterministical statement *(German)* 78−90536
mask synthesis, for diffr. limited waveguide Luneburg lenses 78−38076
masked MBE, GaAs-$Al_xGa_{1-x}As$ film prod. 78−38100
materials and fabrication techniques for integrated and guided wave optics 80−23809
MBE, device appls. 80−25570
MBE of injection lasers, integrated optics device fabrication 79−90042
measuring instrument standardisation 77−71357
melting optical glass in Pt crucibles, power supply freq. convertors 79−72728
metal coated optical fibres, high-strength advances in reduction in microbending loss 79−46066
metal coating of optical fibres, for strengthening and surface protection 78−30103
metal mirrors, diamond turned, evaporated and sputtered, surface and optical studies 78−79098
metal polishing and lapping 78−5587
metal reflective optics, single-point diamond-turned, polishing 79−23104
metal sheet for manufacture of scales and grids, one-sided etching 79−32102
metal surface ion polishing for laser mirrors 78−5588
metal-dielectric interference filter fabrication, phase correction method 77−72064
metal-insulator layers on transparent substrates for making scales 77−798
metals for mirror substrates, manufacturing processes, review 78−5542
mica phase retardation plate, cleaving and optical meas. method 79−64364
micro-slit production method by elec. discharge machining *(Japanese)* 77−84015
microchannel plate surface finishing using liquid 78−90544
microfabrication for guided-wave optical devices 80−58812
microfabrication techniques for integrated optics, review 78−38091
microgratings for guided-beam deflection, electron-beam direct-writing fabrication 80−102856
microscopic optics cleaning, using solvents in US field *(Czech)* 79−40608
milling spherical surfaces 80−64222
mirror, nonaxisymmetric, fabrication by stressed mirror polishing 80−99885
mirror, off-axis parabolic, for laser fusion expt., fabrication process 79−23103
mirror, paraboloid, off-axis section, fabrication by stressed mirror polishing 80−99886
mirror, single point diamond-turned, polishing technique 79−14126
mirror, single-point diamond-turned, performance before and after polishing 80−74466
mirror basing in convergent beam of rays 77−72054
mirror coatings, selective reflectors, and antireflection coatings for nonlinear optics, chemical method 80−28300
mirror fabrication, metal and dielec. coatings on Be 77−62034
mirror fabrication for projecting target surface in solar furnace *(Japanese)* 78−90534
mirror fiducial system compatible with computer-controlled polishing facility 80−74539
mirror machining of nonconventional shapes, for laser systems 78−5589
mirror production and testing, low-scatter, low-loss mirrors for laser gyros 80−1272
mirror reflecting layer, appl. to instrument parts 79−37065
mirror reflectors, large, facet surface approx. methods *(Russian)* 80−69564
mirror surface manufacture on pyroceramic blanks 77−62079
mirrors diamond turning, process control 79−37061
modern production methods in manufacturing optical components 78−50960
monitoring of film deposition, error compensation 77−75721
monolithic component glasses and rigid sintered fibre-optic elements, microcrack form. during grinding 78−87175
multicomponent thin film formation on K8 glass 79−72726
multidielectric film production monochromatic modulator controlled thickness *(French)* 78−75008
multifibre chuck, vacuum assisted Si chip 77−72096
optical workshop techniques continued
multifilm manufacturing, large scale, function stress testing 79−81576
multilayer beamsplitter coatings, accelerated fabrication method 80−102873
multilayer coating production with continuous thickness reoptimisation 79−76890
multilayer cotaings, reactive evaporation technique for TiO_2 and SiO_2 films 77−10994
multilayer interference film, mass production by roll coating *(Japanese)* 79−81577
multilayer interference filter production for CO_2 ν_2 band 77−10998
multilayer optical interference coatings via glow discharge polymerization techniques 78−87170
multimode fibre branch fabrication 77−88955
multimode fibres, recent advances in production 78−30096
multimode optical fibres, fusion splicing using gas flame heat source, development of splicing machine 80−102866
multimode strip-waveguides made by thick film technology, loss meas. 79−59846
Nanjing Astronomical Instruments Factory, lightweight 4 m telescope design 80−105162
NC diamond turning system evolution 80−1369
near perfect optical square fabrication 79−72721
nonquarterwave multilayer filter prod., optical monitoring of thickness 78−55476
objective lens manufacturing, present status and future prospects 79−94323
off-axis mirrors made using conventional milling machine 79−59848
off-axis parabolic mirror fabrication for laser function expt. 80−1374
one-component optical cement 80−87445
operational control optimisation in element prod. start up 78−18078
optical bed, referenceable and vibr. isolated 78−83129
optical cements, commercial, trials and meas. *(French)* 79−50452
optical coating removal using Al_2O_3-HF mixture 78−75005
optical fibre, grinding and polishing productivity, diameter depend. 77−62067
optical fibre coating with conical shape applicator 80−58820
optical fibre connections end to end, instructions *(Swedish)* 79−68430
optical fibre faceting 77−84012
optical fibre formation of microcapillary by pulling from billet, azimuthal asymmetry effects, theory 78−87172
optical fibre multimode access coupler, fabrication method 80−87478
optical fibre packaging in loose fitting tubes of orientated polymer 78−1338
optical fibres, flexible, glass and polymer types *(German)* 79−27393
optical tolerance, glass and plastics comparison 79−59780
optomechanical element system, for laboratory meas., Hungarian development *(Hungarian)* 79−81574
parabolic mirror made by rotation method, fabrication and defects 79−76889
parabolic mirror testing during fabrication by long-wavelength interferometer 80−74536
parabolic mirrors, fast off-axis, design and fabrication 78−46741
pellet precision grinding and high-speed polishing using synthetic material 78−50958
penta mirror assembly, fabrication and performance description 79−81505
periodic surface corrugation generation by holography 78−55469
phosphate glass optical fibres, transparent in UV region, manufacturing 78−87113
photoresist microlens production for semiconductor lasers 78−9398
pitch polisher profiling 79−7234
pitch-polymer polisher layer, durability 77−34969
planar multimode coupling structure fabrication by ion exchange 80−64233
plasma-enriched deposition for thin film appls. 79−47629
plastic accurate convex hyperbola prod. using pantograph and rotating abrasive drum 79−98513
plastic birefringent filters, design, construction and system appls. 78−50943
plastic fibre fabrication for imaging 77−62040
plastic gradient index lens fabrication and image evaluation 80−14426
plastic lens manufacture, mould punch surface radii calc. 77−799
plastic light focusing fibre, heat drawing process prep. 77−14815
plastic mirror, large size lightweight, for airborne laser sensor system, fabrication 78−66891
plastic optical components, flexible rapid curing abrasion resistant coated film 78−66890
plastic optics for optoelectronics, moulding techniques for single, multielement systems 78−63210
plastic rods, light focusing, prep. by two step copolymerisation of diallyl phthalate with methyl methacrylate *(Japanese)* 79−37064
PMMA, optical waveguide, direct writing of gratings by electron beam 79−46091
Polirit, commercially produced, for optical surface polishing, phys., chem. and tech. props. 78−46848
Polirit, optical polisher powder, particle size distrib., dispersion analysis 77−9141
Polirit granules for polishing, evaluation of disintegration degree 77−11057
Polirit polishing ability and physicochemical props. 79−72730
Polirit suspension, factors reducing polishing ability 80−74543
Polirit suspension for optical component polishing, chem. antifoaming agents 80−74542
polisher, computer controlled, efficiency 80−91938
polishing, cleaning and grinding of press-forged CaF_2, SrF_2 IR laser windows 79−59849
polishing, computer controlled, optimisation 77−23787
polishing and grinding machines, semiautomatic, kinematic ratios calc. *(Czech)* 78−79146
polishing efficiency obtained on standard machines, quantitative analysis 78−50959
polishing process, two-step, of KH_2PO_4 and other soft water-soluble crystals 79−64363
polishing using diamond tool 77−72105
polygon production, twelve-sided, of hardened steel 79−81573
polymer powdered coatings, guide element fabrication of cine cameras 78−78021
Polytron polishing pad, method and applications 80−69567
porous glass preform optical waveguide props. 79−94375
precision machining, seminar, San Diego, USA (Aug. 1978) 80−1363

optical workshop techniques continued
precision machining commercialisation for military economy 80−1371
precision machining in optics, conf., San Diego, California (1976) 77−42637
precisional requirements, on scientific instruments *(German)* 78−90535
pressure-shaping components, glass bending monitoring 77−796
prism, correcting glass-angles 77−79975
prism, diamond polishing method, technology and automated equipment 77−34968
prism basing in convergent beam of rays 77−72054
prism coupler fabrication technique 80−83685
production quality trends and limits 80−69566
production technology advances, seminar, London, England (April 1979) 80−67938
purification of KBr, SrF_2 and BaF_2 for laser components, selective ion filter design 79−14051
pyroceramic lightweight mirror blank fabrication using standard metal-working equip. 80−102871
pyroceramic plate surface quality obs. after mechanical polishing 79−72732
quartz, optical quality, culturing process 79−81494
quartz, waveguide layer form. on bombardment by B^+ ions 79−27454
rare earth polisher powders, comparative analysis 79−50453
raster manufacture and copying, for strain anal. by Moire method *(German)* 77−121
Reciprocating motion for fine diamond grinding 78−71237
refractory materials for optical glass making, review 77−14818
replica optics 78−66889
replicated and plastic optics, conf., San Diego, USA (Aug. 1977) 78−66961
replication for laser components 79−55253
replication of large lightweight mirrors 78−66963
replication of light-weight components, mirrors for space use 78−66965
replication of refracting optics 78−50963
replication process 78−66962
resin polishers, holders, and tools 80−33248
reticle and scale fabrication, cyclohexadiene-1,3 pleinomer photoresist 79−27452
rod-in-tube fabricated optical fibre characteristics 80−87574
rotary press operation stabilisation during optical component blank prod. 78−59165
rotating optical components in vac. system, using linear asynchronous motor drive 80−102874
ruby, fabrication of optics 79−23099
ruby, unique polishing features of hard crystals 80−64225
ruling tool for diffr. grating, effects on efficiency and scattered light 77−39044
sapphire, fabrication of optics 79−23099
Schmidt corrector plate replication, testing and performance calc. 78−66967
Schmidt corrector plate replication 78−66966
self-centring technique for mounting microsphere coupling lens on fibre 80−74517
Selfoc lens, aberration improvement by glass composition and ion exchange process parameter choice 80−69486
SEM written gratings in chalcogenide films, for optical integrated circuits 79−32087
semi-automatic machine for hot splicing glass fibres for optical communication 80−23818
servosystem, opto-electronic, correction of nonrectilinearity of ruling engine 78−87174
silica fibre, plastic coated, furnace drawing technique *(Italian)* 78−55475
silica fibres, epoxy acrylate coated, tensile strength >500 ksi, km length prod. 77−11052
silica-plastic fibres, propag. characts. and fabrication for short-medium distance appls. 78−66892
silicate photochromic glass, CeO_2 activated, surface treatment effect on absorpt. 78−71168
silicone and glass clad compound glass optical fibre comparison 80−69533
single mode fibre homogeneous CVD fabrication and characterisation 80−69562
single-mode fibre optical power divider, encapsulated etching technique 79−27420
single-mode low-loss silica fibre prep., 10 km long 80−48476
single-mode optical fibre coupling techniques using microscopic lenses 80−53462
small grinding and polishing tool control by computer 79−98516
small nonsymmetrical aspheric surface fabrication, using grinding or polishing minipad 79−64365
soda lime glass, Ag^+ ion exchanged, planar optical waveguide, manufacturing tolerances 78−71212
solar concentrator facet quality evaluation for deformational forming 78−90483
solar energy concentrator reflecting surface formation, deform. method evaluation 78−90481
spatial frequency filtering appl. in instrum. production *(German)* 78−71208
spectacle lenses, astigmatic, technological construction *(Russian)* 80−99817
spherical cementing fixtures for holding lenses by rigid method 80−96043
spherical diamond tool, durability 78−18075
spherical end faced coupling fibre fabrication by selective etching/melting 80−53492
spherical lens generator, sphericity and fracture control 77−27394
spherical optical component, cutting process for coarse grinding, optimisation 79−32103
splice machine, semi-automatic, for multimode fibres *(Japanese)* 79−59854
splicing of single mode fibres 78−1442
splicing technique for multifibre cables using slippery fibre holder 79−50471
spring-loaded partial kinematic mount for alignment of components in giant pulse laser 80−74518
sputtered films production and props. *(Hungarian)* 80−53483
square wave grating with μm dimensions, reactive sputter etching 78−33921
stand for dynamic balancing 77−72052
optical workshop techniques continued
styrene-acrylonitrile copolymer, synthesis and props. for optical use 78−90466
submicron structures, National Research and Resource Facility at Cornell 78−38101
substrate heating by special lamp 78−59164
substrate heating in vac., heating method rel. to spectral characts. 77−7223
Superinvar alloy casting for optical instruments 79−81580
surface errors rel. to optical performance, effect of mid- and high-spatial freqs. 79−59789
surface figuring by laser controlled chem. reactions 78−63209
surface grinding and polishing, appl. to MgF_2 77−797
surface plastic deformation treatment, tool design for 78−13824
surface programmed aspherisation accuracy rel. to tool size 79−72727
surface shaping by successively corrected mask method 78−18076
surfacing, struct. of fine ground surface 77−27393
synthetic diamond drills, improved durability 80−87573
system aspects of electro-optics, seminar, Huntsville, AL, USA (May 1979) 80−94921
taper couplers utilizing SiO_2, photolithographic fabrication processing sequence 79−41464
telescope primary mirror manufacture, monitored null corrector 80−78946
telescopic finder, PPS-11, alignment method 79−14081
testplate testing interferometry in precision optical shop 80−74532
thin and polished section preparation status and trends *(German)* 80−28360
thin dielectric film optical waveguides, ideal fabrication technology, comparison of four techniques 80−79025
thin film coating manufacture, automated deposition control system, design principles 80−64220
thin film optical circuit fabrication using CO_2 laser 80−99881
thin-film waveguides of dense crown glass, HF sputtering prep. 79−10415
three layer optical waveguide for photolithographic fabrication of film lenses 77−39113
tiO_2 antireflection coatings by a low temperature spray process 78−90537
tolerancing tradeoffs for mass production economies 80−48473
toroidal mirror optical polisher 80−5848
transition fibre production for coupling DH lasers to single mode fibre 77−39062
transmission grating fabrication, photochemical replication for space astronomy 80−14490
transparent colourless cementing of milled PMMA surfaces 77−34970
trifluoroethyl methacrylate vinyl chlorobenzoate copolymer light focusing rod, photocopolymerisation temp. effect *(Japanese)* 79−46043
ultrapure glass preparation for optical waveguides, review 78−3086
uniformly thick film sputtering optimisation 79−27451
US cleaning of optical fibres, deleterious effect 78−33821
US cleaning of optical materials, deleterious effects 77−42631
vacuum deposition, improved film quality, progress in vacuum generation and deposition technology 80−35101
vacuum sealing LiF window to thin-walled Au or Cu cylinder using PbF_2 77−54820
vacuum seals for $MgFl_2$ windows 78−94457
vacuum systems for optical coating prod., review 77−58493
variable magnification three component system, fabrication errors 77−88895
waveguide, circular strip type, fabrication by Ag ion migration 80−96042
waveguide, fabrication in glass by effusion 80−5850
waveguide, graded-index surface or buried, realized by ion exchange in glass 80−69499
waveguide fabrication, by elec. field controlled ion exchange in glass 78−38094
waveguide fabrication, ion exchanged, from dilute $AgNO_3$ melts 79−23097
waveguide fabrication, laser heating technique for glass multimode channel guides 77−7220
waveguide fabrication by CW Ar laser irrad. of $Al_xGa_{1-x}As$ 80−5849
waveguide fabrication by thermal migration of Tl ions in glass 79−46031
waveguide fabrication in glass, optical, by low-temperature diffusion process 80−102867
waveguide holography, expt. techniques and results 80−28173
waveguide process and materials, review of progress 80−23768
waxicon design and fabrication 78−5543
wide band monitoring system for film props. meas. during deposition 79−81582
wideband dielectric mirror production of TiO_2 and SiO_2 79−76897
Wolter lens component replication 80−95972
X-ray lithography for fabrication of submicrometer period gratings with precisely defined profiles for integrated optics applications 80−58814
zone plate production by laser irradiation of photoresist. *(German)* 80−23782
Ag halide optical fibres, extrusion, visible and IR transmission 80−58829
Ag mirror formation by photolysis of high mol. wt. compounds 77−75720
AgBr single-crystal IR optical fibres, growth from melt 80−53449
Al, polygon construction via diamond cutting 78−33919
Al spherical mirror generation with single point diamond cutting tool 80−33249
$Al_xGa_{1-x}As$ buried heterostruct. laser, fabrication, optical props. and reliability 80−53322
$Al_xGa_{1-x}As$-GaAs, DH integrated optics development 80−33240
As_2S_3 thin film, diffr. grating production, using laser photolithographic process, image evaluation 78−42479
B_2O_3-SiO_2 low-loss single mode fibres, design, fabrication and transmission characts. 78−71199
B_2O_3-SiO_2 optical fibres, exposed cladding technique, birefr. and polarization props. 79−14094
BaF_2 and fluorite large crystal, block orientation determ. from light scatt. pattern 79−50964
BaO crown and flint glasses, Ag and Cu diffusion for optical waveguide fabrication 78−59166
BaO-GeO_2-Na_2O borosilicate core glasses for high numerical aperture fibres, double crucible prep. 80−69534
Be lightweight optical substrate fabrication 79−23107

optical workshop techniques continued
Be mirrors, props. and fabrication procedures 80−38138
$Bi_{12}TiO_{20}$, RF sputtered epitaxial film on $Bi_{12}GeO_{20}$, for optical waveguiding 78−9462
C large unsupported film, prod., as UV filter 78−38092
CaF_2 vapour deposition apparatus for Na-resistant glass cell 80−90874
CaFz crystals, grown from synthetic raw materials, quality, effect of impurities, composition 78−79083
$CaO-Al_2O_3$ based glass development, water removal, use in IR to 5 μm 78−83052
Cr particulate layer on Cr_2O_3, high solar absorpt. characts., selective surface electroplating 78−87111
Cu film self-generation on Cu doped glass ceramics, for low-expansion IR laser mirrors 79−14127
Cu mirror, single-point diamond-turned, evaluation for 8-beam CO_2 laser, Helios 79−23044
GaAs film optical components, prep. by MBE using Si shadow masking technique 80−28358
GaAs integrated optical circuits by wet chemical etching 79−32092
GaAs, ion etching, effects on optical props. and lattice disorder 78−83122
GaAs:Zn, diffusion of Zn by two-temp. method, LED fabrication 80−49416
$GaAs-Al_xGa_{1-x}As$ integrated optics structs., dry processing 77−27383
GaInAsP-InP DH lasers made by melt-back method, operating characteristics 80−48287
GaP ribbon waveguide, vapour-grown, phase-matched SHG 80−48339
$GdF_3-BaF_2-ZrF_4$ glass fibres, IR transmission, losses, fabrication 80−87516
Ge, monocryst., for IR optics, prod. techniques and characts. 78−50873
Ge-As-Se IR transmitting glass composition, prep. and props. 80−69474
$GeO_2-B_2O_3-SiO_2$ optical fibres, optical transmission loss as function of drawing conditions 79−32038
GeO_2-Na_2O borosilicate glass fibre prod. by phase separation and leaching 80−69558
$GeO_2-P_2O_5-SiO_2$ graded index optical fibres optimised for 1.3 μm wavelength region, fabrication techniques *(Japanese)* 80−99888
He-Ne laser, manufacturing problems with low noise specification 78−59047
$Li(Nb,Ta)O_3$, LPE growth of thin film waveguides on $LiTaO_3$ substrates 79−41467
$LiNbO_3$ geodesic lens fabrication by single-point diamond turning 80−33239
$LiNbO_3$, microfabrication by ion-bombardment enhanced etching 78−76779
$LiNbO_3$, optical waveguide fabrication, closed tube control of out-diffusion 79−10419
$LiNbO_3$, ridge struct. fabrication by CF_4 plasma etching 80−28357
$LiNbO_3$, waveguide form. technique, using organometallic soln. diffusion sources 78−38099
$LiNbO_3$, waveguide formation using organometallic solns. as diffusion sources 80−23810
$LiNbO_3$:Ti diffused, optical waveguide, fabrication problems *(Japanese)* 80−33256
$LiNbO_3$:Ti in-diffused optical waveguide fabrication 79−76892
$LiNbO_3$:Ti optical waveguides, fabrication and waveguiding props. 78−30091
$LiNbO_3$:Ti Z-cut crystals, Ti diffusion process parameters 80−102849
$LiTaO_3$, refr. index distrib. after surface lapping, theory 78−72479
Mo sputtering for laser mirror refurbishment 80−14498
NaCl 46 cm window optical evaluation facility 80−74526
NaCl Czochralski crystal growth for large CO_2 laser windows 80−74525
NaCl large window continuous polishing 80−74527
NaCl window production for Antares CO_2 laser system 80−74524
$Na_2O-B_2O_3-SiO_2$ glass fibre, prep. with low loss 79−59850
$Na_2O-B_2O_3-SiO_2$ glass fibre, plastic coating influence on strength 80−58697
$Na_2O-B_2O_3-SiO_2$ glass, low-loss GRIN fibres, double-crucible prod., loss and bandwidth meas. 80−69559
$Na_2O-B_2O_3-SiO_2$ low-loss optical fibre prep. by double crucible technique *(German)* 78−33929
$Na_2O-B_2O_3-SiO_2:GeO_2$ medium-loss graded-index preform fabrication by phase separation and leaching *(German)* 78−33930
$Na_2O-CaO-SiO_2$, for optical fibres, high purity glass production methods 78−87176
Na_2O-SiO_2 glass waveguides, low loss, new fabrication method, exam. 78−55481
Ni plated aspheric metal mirror fabrication for IR optical systems 80−14497
$P_2O_5-SiO_2$ clad low-loss monomode fibres for 1.2 to 1.6 μm, modified CVD prep. 80−48479
PbF_2, antireflection coating deposition technique, 2.87 μm laser damage threshold 80−33264
$PbO-SiO_2$ glass, use of $Na_2S_2O_3.5H_2O$ in polishing 80−33258
$PbO-SiO_2$ interdiffusion layer optical waveguide, prep. and props. 80−43489
Si, diffraction grating, rectangular profile, fabricated from single cryst. 80−38093
Si, optical waveguides along both sides of groove 80−96006
Si single cryst., chem.-mech. polishing of low-scatt. optical surface 80−96040
Si substrate package for integrated GaAs laser arrays, fabrication 79−18555
SiC diffraction grating for vac. UV, fabrication 77−79920
SiO condensate distrib. from extended aspherising source 79−52118
SiO_2 fibres, fused, drawn from rods, oxy-H_2 flame, prep., strength, dia. var. 80−102868
SiO_2 films, vac. thermal evaporation, parameter stabilisation 80−87571
SiO_2 glass fibre drawing, caustic curves in solidified drawdown zones 77−39117
SiO_2 lightweight 370 mm mirror fabrication and testing 78−57447
SiO_2, optical fibre, phys. behaviour of neck-down region during furnace drawing 78−83127
SiO_2, silica, optical fibre-drawing, vac. furnace 78−66960
SiO_2:F, silica fibres, numerical aperture and attenuation, drawing from preforms 78−1449
SiO_2:F fibre preform plasma chemical deposition *(German)* 78−33926
SiO_2:F fibre preparation by plasma-activated CVD *(German)* 78−33927
SiO_2:F layers, deposition from $SiCl_4-SiF_4-O_2$ gas mixture by plasma CVD method 78−95699
$SiO_2:GeO_2$ single-mode optical fabre fabrication 79−46050
optical workshop techniques continued
$SiO_2-B_2O_3-Na_2O-K_2O$ system glass, phase separated, loss of oxides during acid leaching, atomic absorpt. anal. 79−11716
SiO_2film, waveguide layer form. on bombardment by B^+ ions 79−27454
$SrTiO_3$ electro-optic crystals, mechanical grinding and polishing 80−48471
$SrTiO_3$, fabrication damage characterisation by internal and external meas. 80−102782
Ta_2O_5 thin film protection of unstable OF-type glass components 79−14079
TiO_2, film deposition, reactive evap. of Ti-O phases, refr. index 77−19372
TiO_2 planar optical waveguide preparation and props. 78−90524
TlBr, and TlBr-TlI polycryst. fibre optical waveguides, for IR, fabrication and characts. 78−74974
TlI/KCl/TlI low absorpt. antireflection coatings for KCl surfaces 80−38078
$TlI-PbF_2$ graded-index film coating technique and results 80−33265
ZnS/ZnSe composite window, erosion-resistant, fabriction and evaluation 78−71211
ZrO_2 film, electron beam deposition, refr. index and microporosity 78−90467

optical zone plates
axially symmetric filters, Fresnel diffr. field, series representation 77−46696
axially symmetric filters, two-point resolution evaluation method 77−46697
binary Fresnel zone plate construction, computer-generated holography 80−78809
curved zone plates and Fresnel lenses, third-order aberrations 77−72043
dielectric mirrors, reflection and wavefront shaping, limits of coexistence 78−46747
diffraction patterns, white light, of amplitude and phase zone plates 80−14449
dispersive device linear in wave-numbers, space-time optics appls. 77−72071
elliptical and hyperbolic zone plates produced by wavefront coherent superposition 80−78953
elliptically polarised light, quantitative anal., $^1/_4$-wave plate, student expt. 78−49608
Fabry-Perot interference rings, focusing props. 77−58454
Fabry-Perot interferometer, wavefront form. by multilayered dielec. mirror 78−54449
Fourier transformation, noncoherent methods 79−76624
Fourier transformation, qualitative and semiquantitative, using noncoherent system 80−5698
frequency-modulated, for coherent noise reduction, fabrication by holographic techniques 79−86134
Fresnel, for optical image form. with short wavelength radiation 77−58437
Fresnel, ultrashort pulse propag. through lenses 77−58414
Fresnel zone plate, appl. to neutrons imaging and focusing 80−106433
Fresnel zone plate support UV window as lens and monochromator 80−1326
Fresnel zone plate synthesis inside Vander Lugt matched filter 77−7013
Fresnel zone plate used as aperture for shadow holograms prod., min. acceptable no. of zones determ. 77−68193
grating equation, Hilbert's independence integral 79−899
hologram scanner, interferometric zone plate, for point-of-sale systems, aberration corrections 79−81383
holographic grating scanner with aberration corrections 77−61924
holographic optical element design using analogous lens model 78−58955
holographic simulation of non-circular zone plates 79−50252
holographically made zone plates and gratings, for X-ray microscope 78−37855
image rotation and magnification, optical system 80−48376
Laplacian formation by holographic zone plate moire patterns 79−13917
linear zone plates, optically produced 80−1299
moire pattern calculations, geometrical approach 77−19164
multiplane γ source image reconstruction using Fresnel zone plate aperture 77−52874
one-dimensional coded apertures, applications 78−45746
phase and amplitude zone plate theory and realisation *(Spanish)* 79−23073
production by laser irradiation of photoresist. *(German)* 80−23782
profiled, chromatic props. 80−43451
profiled, chromatic props. calc. 80−28328
spectral resolution with circular sensor 77−42591
ultrashort pulse operations using flat lenses 78−66883
varifocal moire zone plates for straightness meas. 77−88902
waveplate design for two or more specific wavelengths 77−22593
x-ray zone plates fabricated using electron-beam and X-ray lithography 80−68335

optics
see also aberrations; adaptive optics; atmospheric optics; fibre optics; Fourier transform optics; geometrical optics; holography; integrated optics; nonlinear optics; optical elements; physical optics; quantum optics
applied optics rel. to electronics and digital data 77−38814
book, optics and lasers 78−22079
book, progress in optics 77−31059
book, progress in optics XVI 79−76577
Bremmer, H., contrib. to optics 79−62984
business side of optics industry, conf., San Diego, USA (Aug. 1978) 79−81354
conference, Bad Harzburg, Germany (June 1979) 80−51951
conference, Los Alamos, NM, USA (May 79) 80−73095
conference, Madrid, Spain (Sept. 1978) 80−77547
conference, trends in physics, York, England (Sep. 1978) 80−31416
education, Age of Newton workshops in optics, mechanics and mathematics 77−87586
education, graduate, at Air Force Inst. of Technology, programme 80−62417
education at Georgia Tech, development and current status overview 80−62420
education at Texas Tech. University, programme methods 80−62424
education programmes in US, development 80−62410
educational course in modern optics and lasers at San Diego State University 80−62423
educational programmes and opportunities in US 80−62412

optics continued
educational programmes in US, attacks and recommendations 80−62409
experiments using He-Ne laser beams, book 77−27246
glorified optics, appl. to seismic wave propag. in nonplanar struct. 79−66629
graduate degree programme, on-site, case study 80−62416
graduate education at Carnegie-Mellon University, programmes review 80−62419
graduate training at Optical Sciences Centre, programmes 80−62418
Hartmann method for studying astronomical optics 77−25949
history, contributions of Isaac Newton and Carl Friedrich Gauss *(German)* 78−4453
Institute of Optics, Univ. or Rochester, 1929-79, brief commemorative 80−4501
irradiance distribution function in turbulent media, theoretical review 79−64155
Laboratoire d'Optique de Besancon, recent work 77−68177
Liechtenstein, development of Balzers AG 77−19162
liquid crystal and solns. laser and pulsed electric field Kerr effect 77−40210
medical and biological applics. of optics, conf., San Diego, California (1977) 77−44876
medicine, optical instrumentation in, conf., San Diego, California (1976) 77−44829
Modern Optics Project Laboratory course at MIT, programme 80−62421
ocean optics, conf. proceedings (San Diego, 30-31 August 1978) 80−8325
Optical Society of America meeting, Rochester, USA (Oct. 1979) 80−12841
optical systems, entropy and neguentropy *(French)* 80−102608
Raman effect, combinational scatt. of light, discovery and history 80−27101
review of recent advances 80−28155
ripple tank, wave form. and interactions using modified elec. toothbrush 77−33756
teaching by Inst. of Optics, profile 80−62422
undergraduate laboratory in American universities, status 80−62411
utilisation in radar systems, conference, Huntsville (1977) 78−78939
visual perception, failure of classical optics, to account for observed phenomena 79−5289
X-ray optics, diffr. from wedged shaped solid, from solid wedge, ghost source theory 79−2900
Zernike circle polynomials, appl. in optics 77−67182
Ar, glow discharge, imprisonment of reson. rad. in cold cathode region 78−59703

optimal control
see also dynamic programming; game theory; maximum principle; predictive control
above-knee prosthesis, myoelectric control system development 78−53575
absorption chillers, solar-fired, capacity modulation 80−66952
adaptive laser beam control process, closed loop considerations 77−88660
aeroelastic vibr. elimination, appl. of Pontriagin max. principle 78−55584
air pollution control, prediction of pollutant concentration 79−52992
anaesthesia administration, use of dynamic programming model 77−5107
arterial system least energy regulation 78−53434
attitude control of space vehicle descent to surface of atmosphere-less planet 78−16265
beam nonlinear elastic optimal design for minimum compliance 79−1108
bilinear systems, unconstrained, nuclear reactor shut-down control applic. 77−10464
biological system modelling appl. 77−40628
boiling water reactor optimal control, regulator problem, feedback control laws 77−54315
BWR control rod programming, heuristic and mathematical approaches 79−9779
BWR load following plant, low sensitivity design fo controller 78−78473
BWR nuclear plant nonlinear digital simulator, optimal digital control methods appl. 79−9826
BWR power plant, direct cycle, low sensitivity controller study 78−8947
BWR turbine, simulation 78−737
cantilever beam axial vibration, min. mass structures determ. 78−63278
cell growth appl. of time-optimal control theory 77−40638
classical filtering model, optimal impulse control, separation theorem *(French)* 80−90659
counterflow heat exchanger, optimal control synthesis *(Polish)* 79−97384
coupled inverted pendulums, stabilising control *(Japanese)* 79−35545
coupled-core reactor, optimal control by two level scheme based on decomposition principle *(Japanese)* 79−17961
differential eqn., canonical, functional relation expressed by Volterra series *(French)* 80−73159
discrete periodic systems, optimisation by analytic construction of control 79−21543
distributed parameter nuclear reactor system pointwise control and observation problems 78−54859
distributed parameter reactor core, optimal control by function space method, numerical experiences 77−54317
distributed parameter system control, conference, Coventry (1977) 79−3897
drying, heat and mass transfer, optimal control 78−67006
dynamic systems, equations of motion canonical transform 80−36843
Earth-Mars-Venus orbital transfer minimal flight time calc. 78−4090
electromechanical deflector with quasi-time-optimal scanning control *(Russian)* 77−58431
end-temperature in semi-infinite rod, distributed parameter optimal control problem 78−13886
estuary water quality management for P treatment 77−21823
evolution equations, impulse and distributed control *(French)* 80−68049
evolution equations, unknown control dates, periods and type, optimal control, existence theorem *(French)* 80−62478
extremal problems, theory, book 79−63001
fission reactor suboptimal control param. inbedding method appl. 77−34421
gyrostat motion time-optimal damping under random perturbations 77−68379
heart disease, haemodynamical parameters optimal control 79−53182

optimal control continued
heart ejection process, model, stroke volume calc. appl. *(German)* 78−3631
heat conductivity theory *(Russian)* 79−50567
heat diffusion process, parabolic boundary-value control problem, numerical treatment 77−847
heat exchange on porous surface, optimal control 79−32661
heat storage device, off-peak, ambient temp. observer/predictor control system 80−66950
heat transmission between bodies in contact 80−19223
heating of body with thermoelastic stress restrictions *(Ukrainian)* 78−83245
heating of solid body with max. temp. stress constraint *(Russian)* 79−14205
initial state transformation, using gradient restoration algorithms, hypersonic flow with axisymmetric body appl. 78−4474
interstellar travel, optimum transfer in uniform motion 78−20614
intracavity tip/tilt adaptive control system 79−59728
Kustaanheimo-Stiefel two-point boundary-value problems 77−25927
laminar boundary layer, optimal control, group theoretic approach 79−32452
laminar boundary layer, optimal control by wall suction or blowing 79−1242
Large Space Telescope, optimal manoeuvring and fine pointing control with annular momentum storage device 77−22078
Large Space Telescope optimal fine pointing control using Annular Momentum Control Device 77−73934
lungs long-term forced ventilation control excitation 77−60296
LWR plant control, linear quadratic theory appls. 77−88265
mammalian neuromuscular system energy-optimal controls 77−73522
Mars entry vehicle, lifting spacecraft control and ballistics 78−16264
Mars probe, optimal atmospheric entry trajectories with two-dimensional control 77−91400
MHD generator, Faraday type, current profile optimisation, electrode cond. profile 78−94939
minimum mass design of continuous structural members 77−80063
minimum weight disk design 78−36821
molecular structure models, discrete optimal control 77−61694
motion stabilisation *(Russian)* 78−86145
motoneuron optimal control model 77−86486
moving bodies, use of Bulgakov normal coords. method *(Russian)* 79−9104
multicore fission reactor, optimal control determ. from energy release profile *(Russian)* 80−73974
multicriteria simplex method, 1-D linear distributed parameter systems 78−59257
neuron modelling with extremum control of parameters *(Russian)* 77−29133
nonlinear noisy sine wave oscillator 80−27218
nuclear fuel reprocessing plant, material diversion, probability of detection, optimisation of safeguards 77−14258
nuclear plant mix with minimum natural fuel requirement, optimum theory 79−26469
nuclear reactor, 1-D slab, program for optimal control of Xe oscills. *(German)* 77−61529
nuclear reactor, digital control using linear quadratic Gaussian regulator 80−37554
nuclear reactor, point-model, heuristic approach to reinforcement learning control 78−46144
nuclear reactor, Xe spatial oscillation, time optimal control 80−32320
nuclear reactor control by neutron flux, expt. investigation of optimal processes 77−3139
nuclear reactor core 78−54860
nuclear reactor distributed parameter optimal control methods 78−54858
nuclear reactor flux control system design, optimal control theory 77−3138
nuclear reactor optimal control using Walsh function variational synthesis technique 77−38347
nuclear reactor optimal shutdown control, quasilinearisation and numerical soln. *(Korean)* 79−89395
nuclear reactor suboptimal control using functional anal. 77−71636
nuclear reactor system fixed end-point problem suboptimal control, perturbation theory appl. *(Japanese)* 78−33259
nuclear reactors, development of maneuvering strategies using optimal control theory 79−30959
nulcear reactors, PWR core control, multistage mathematical programming 80−91227
optical fibre drawing process control, optimisation theory appl. 79−90039
optical multilayer coating production with continuous thickness reoptimisation 79−76890
optimal control of dynamically controllable motions, appl. to hollow cylinder deform. 78−79214
optimal feedback control of plasma parameters in Tokamak 79−64891
oscillating systems, optimal and free motions 77−72229
oscillators, nonlinear stochastic, triangular wave, optimally controlled, Weiner process and Poisson process, numerical studies 80−52128
packed bed, heat and mass transfer *(Ukrainian)* 79−32655
parabolic boundary value problem optimal control, heating process 78−67021
pendulum, optimal starting with velocity limit and integral quality criterion *(Russian)* 79−23198
physiology system models, breathing control example 80−41058
plate heating, optimal fast response control under temp. field gradient constraints 80−38232
point controlled distributed parameter system multiple shooting and sweep algorithm 77−25728
pollution, air, optimal timings and number of observations determ., w.r.t. cost 79−88026
polychromatic wave, refl. from absorbing layer, coeff. minimisation 77−82396
power reactor Xe oxcillations control problem *(German)* 78−46153
problems with constraints, transformation methods of an exponential function type 78−12541
prosthetic arm decentralised control hierarchical approach 77−40924
proton synchrotron, CERN, online function generation optimisation 78−834
pulsed MHD convertor, threshold energy characts. for elec. power production with resistive load 78−1908
PWR, core control optimisation for scheduled load changes 79−71911
PWR manoeuvring strategy optimisation 79−629

optimal control continued
PWR steam supply control system optimisation 78−50251
reactor dynamics optimal control, exact closed-form soln. for terminal cost problem 79−54472
relativistic wave mechanics 79−40660
reload core design optimisation 79−604
respiration model analytical soln. 79−48282
river aeration system subject to random disturbances, feedback structure 78−16078
river network artificial aeration methods 78−36203
robots and manipulators, symposium, Warsaw (Sept., 1976) 78−53574
satellite, gravitational stabilization system, optimum parameters 77−41280
satellite, optimal trajectory-meas. program and meas. error effects 77−53409
satellite, spinning notion, optimal nutation damping by flywheel 77−53396
satellite orientation, optimal parameters of passive systems 77−41279
satellite stabilizer system, rate-optimal parameters 78−69641
satellite-gyrostat reorientation, optimal attitude control 80−61980
segmented mirror control system optimality criterion choice *(Russian)* 77−34010
seismic inverse problem appl. of control theory 79−2402
seismic reflection recordings, control theory appl. to inverse problem *(French)* 77−87081
shallow arches, natural structural shapes 77−80064
Shiva laser beam diagnostics 78−59037
shuttle reentry trajectory, perturbation method 77−67021
soft landing guidance algorithms based on terminal control principles 78−73602
solar energy systems, modern control theory appl. reviews 80−66949
solar heating system for large buildings 79−87995
space vehicle orbit determination optimization 79−8808
space vehicle orbiting oblate planet, optimal low-thrust takeoff 77−60580
space vehicles, optimal thrust of cruise engines in interorbit flights 78−4069
space vehicles in close near-circular orbits, optimal multimomentum transfers 77−41290
spacecraft, optimal aerodynamic attitude control 80−77250
spacecraft optimal accel. with electroreactive engine with bound on thrust vector 77−53393
spacecraft trajectory optimisation using closed soln. of constant thrust-accel. motion 77−25926
spaceflight dynamics problems, gradient method for optimal control 78−69638
spaceship, fission-engined series-staged, overall payload-optimal control 77−2320
spatial reactor control methods 77−83056
spatial Xe oscillation time-optimal control in PWR 79−628
speed-optimal control synthesis in near spherical symmetry problems *(Russian)* 79−9095
starship, single-stage constant-power, optimal exhaust vel. programming 78−20613
Stefan problem simulation and control, associated variational inequality 78−67009
stochastic control, regularity of weak solns. of variational irregularities *(French)* 79−54053
stochastic integro-differential operator, optimal non-anticipative policy *(French)* 77−17786
stochastic object, suboptimal adaptive control 79−30371
stochastic systems, partially observable, measurer containing unknown variable parameters *(Russian)* 80−86218
stream pollution dissolved O concentration optimisation using instream aeration 77−17153
suboptimal control of reactors with distributed parameters, computer model, singular perturbation theory 77−6530
telemetry device, chronically implanted, controlled transcutaneous powering 80−98152
TFTR, plasma position control, linear feedback optimal method 78−50365
thermodynamic systems 78−29071
thermoelement cooling control by variation of geometric shape 78−62195
three-impulse min.-time orbital transfer generation, numerical method 78−73607
Tokamak plasma equilibrium, feedback control 78−55738
transonic flow, num. simulation by finite element method using optimal control theory 77−55025
transonic flow simulation by finite element method via optimal control, book contrib. 79−32557
transonic potential flow finite element method program stability 80−24045
transport process adaptive criterion study 77−17931
unilateral thin plates 77−60935
variable speed wind power generator, control strategy for 3-phase output *(French)* 80−76591
ventricle dynamic model, for systolic elastance optimisation 77−16951
vibrating beam min. wt. design 77−80059
vibrating struct. design, singular optimal control problems 77−89058
vibration-absorbing coatings, optimal control method 77−823
CO_2 laser, vibrational control in stabilisation of ionisation-thermal instability 77−19302
P control in estuaries, parallel shooting models, Corpus Christi Bay (Texas) and Jamaica Bay (New York) appls. 79−57521
SO_2 gas pollution of Osaka city, optimal discharge control 79−52993

optimal systems
600 MW pulsed energy convertors for toroidal field coil, design philosophy 78−58496
circuit breaking air blast arc, near current zero, local elec. props., optimisation 78−87516
composite sheets, fixed upper bound on number of layers 78−30177
condenser tube fin geometry optimisation, surface forces-enhanced film condensation 78−75039
diffuse system design, optimum conditions, appl. to optical system 78−50886
filter, Kalman, digital, synthesis with a priori uncertainty of data 80−98934
flow rate convertor, EM, optimal mag. system design 79−77313
flowmeter, EM type, optimal mag. system design *(Russian)* 79−1275

optimal systems continued
grillage with free edge, optimal beam layout 78−63332
gyros appl. to angular velocity meas., precision increase using structural redundancy *(Russian)* 78−49804
heat engine, irreversible, optimal config., dynamical treatment 79−54086
heat engine, irreversible, optimal config. 79−54085
heat storage, periodic, heat-carrying fluid and storage material transport kinetics 79−3901
holographic memory readin system parameter optimisation *(Russian)* 78−13670
initial temp. distrib. determ. by optimal dynamic filtering 80−19208
inverse filter which is optimum in error-distrib. sense, stability charact. 78−81424
laser interferometer for shock wave diagnostics 79−64814
maser dissociator, H beam production performance charact. 78−87034
MHD channel, frame type, optimal selection of frame and transverse cross section form 78−91164
NDT system, choice 79−11752
nuclear plant mix with minimum natural fuel requirement, optimum theory 79−26469
parametric linear systems, time delays, optimality, control coordination and entropy *(French)* 77−9161
plasma accelerator, three-rail type, one cluster regime, optimum length 80−6288
power plant cooling system design, optimal system synthesis, tower, pond 77−14260
reinforced concrete deep beams, optimal force transmission 78−34009
restoration filter for Poisson noise impaired and linearly blurred images 80−106481
rotary mixer, two-phase flow over working surfaces, optimal dimensions 78−63485
scanning optoelectronic systems, optical and electrical filter simultaneous optimisation 79−72696
SHG, optimum, in thin-film external resonator 79−18485
superconducting magnet cooling, optimal cryogenic gas flow 79−93149
symmetric structures, optimal design against postbuckling collapse 78−51100
thermophysical process ambiguous data gathering and processing optimisation *(Russian)* 80−73335
toroidal field coils, bending-free, for Tokamak reactor 78−55012
N_2 laser, high-power, TE, UV, using Blumlein transmission line, construction charact. *(Korean)* 79−22971

optimisation
see also mathematical programming; minimax techniques; minimisation
aberrations, in electron optical systems 80−87290
abrupt transformation, data partitioning, cluster anal. optimisation 78−36956
absorption spectrometry, standard addition method, evaluation and optimisation 79−16058
acoustic energy optimisation using secondary sources *(French)* 80−53518
acoustic logging in cased wells, simulation rel. to excited wave freq. optimisation *(Russian)* 78−40707
activation analysis, optimisation, computer-selected conditions 78−15740
active damping of vibrations in elastic systems with distributed parameters, active stabilisation *(Russian)* 79−27577
aeration system optimal design for polluted streams 77−37251
aerial prospecting magnetometer cable length optimisation *(Russian)* 77−73881
aerospace, optimum low-thrust multiple rendezvous between inclined orbits 78−4086
aerospace solar panels with concentrating reflectors 79−96472
air-core Tokamak, optimisation of ohmic heating coil configurations 80−14914
aircraft landing trajectories of minimum noise *(Spanish)* 80−53546
aircraft wing weight optimisation with static aeroelasticity constraints *(Russian)* 79−23240
airport wind reports, optimum averaging time for along-runway and across-runway components 77−17177
alloys, continuously cast, numerical study of optimal solidification conditions 79−83188
alloys, multicomponent, optimal composition determ., mathematical-statistical methods *(Czech)* 79−15624
analytic radial orbitals, optimisation on variational parameters 80−42941
analytical chemistry, time sharing computers, data processing and optimisation appls. *(German)* 78−35750
anodic stripping voltammetry, standard addition method, evaluation and optimisation 79−16058
antagonistic muscles, functional elec. stimulation optimisation, math. modelling, joint motion 80−61730
antitumor drug dosage schedule, cell cycle kinetics approach 77−86700
apodiser, simulation by binary filters 78−5539
apodization, optimal, by means of coupled calc. of pupil function and shape 80−95788
aqueous soln. liquid scintillation counting optimisation 79−76269
aquifer mineralisation field dynamics simulation, porosity estimate optimisation 77−56664
Archibald rubber band heat engine, optimisation 79−5936
artificial satellite with gravitational attitude control, dynamics 77−25905
astronomical images optimal classification into stars or galaxies, Bayesian approach 80−21920
astronomical information transfer, appl. of multiple-mirror telescope systems 80−94713
astronomical observations errors, optimum linear estimation of mathematical expectation and standard deviation *(Russian)* 80−12673
atomic fluorescence spectrometry, hollow cathode lamp, pulsing conditions optimisation 78−65972
bar optimal design by dynamic programming *(Polish)* 79−64542
bar undergoing bending oscillations, shape optimisation *(Russian)* 79−37210
basic metrological operations, validation and optimisation 78−41264
beam mode function series approximating beam field *(Japanese)* 77−22427
beam resting on elastic foundation, optimum shape design with normal stress restrictions *(Polish)* 78−22267
beams, elastic structures, optimal rigidity *(French)* 78−59305
beams, optimal layouts, allowance for cost of shear and bending 79−68566
biological system, sequential actions model 78−44441

optimisation continued
biological two compartment model parameter estimation, computer expt. study 77−70402
Bitter solenoid, optimum dimensions 79−21787
body joints, centres and angles of rotation meas., errors and optimisation study 80−61604
bolometer, ^{3}He-cooled, low heat capacity, differentiated-structure, performance 79−30544
Brayton-Rankine binary cycles in HTGRs 80−22904
breathing control hierarchical goal-seeking model description 78−80899
Brunswick plant post-startup optimization 80−23048
building insulation, w.r.t. internal and solar gains 79−62147
BWR, feasibility study of core management system by data communication 78−13254
BWR, optimal fuel pin enrichment distribs. 77−83008
BWR, optimal in-core fuel management using OPTLWR computer code 78−17363
BWR, quasioptimum fuel assembly loading, hierarchical level scheme 78−29609
BWR power plant turbine building, radiation protection, calc. and obs. 78−74461
capacitor banks, optimum design rules, neutral beam power supply 78−74487
cardiac assistance, performance criteria 79−74782
catchment model design, parameter estimation method 79−5536
CECG waveform, statistical algorithm and struct. anal. 80−72341
character recognition, optimised filter 80−95837
chemical activation analysis, multielement 79−16089
chemical analysis, simplex optimisation calcs., high speed algorithms 80−40767
chemical first order kinetic data anal., optimisation method 78−12500
chemical kinetics meas. computational processing iterative optimisation techniques 77−32765
chemical processes, using computer 79−52628
chemical reaction kinetics optimisation method, simultaneous reactions anal. *(French)* 78−19994
chromatography, multicomponent sorbents, composition, computer optimisation 78−27842
circular ring, inner boundary shapes, optimised, diametral compression 80−38369
circular ring transverse axial positron camera system efficiency optimisation 77−12994
coded mask X-ray telescope for rocket appls., optimum design 77−13239
column design, optimisation of support conditions and segmentation 78−51062
complex spectrum, computer separation, optimisation *(Russian)* 78−82051
composite, slab, spatially reinforced, optimisation in stability problem 80−102978
composite materials, hybrid, 3-layered plates, optimisation 80−20996
composite rib stiffened constructions, design criteria 80−102977
composite ribbed multilayer cylindrical shells, stability and optimal design 80−58949
compound column, shape optimisation for largest critical buckling load 77−46948
computational techniques for many-beam struct. images in electron microscopy 80−95203
computer-aided optical design, optimisation and interactive graphics improvements 80−78933
continuous bodies under gravity load, centrifugal force, optimum strength shape 79−98665
convective annular/circular fin of minimum mass 80−79109
conversion function of meas. facility, optimal value determ. 78−73958
cooled epoxy resin vacuum mould computational simulation of design *(German)* 80−81020
CORAVEL, Cassegrain spectrophotometer, mask optimisation 80−82210
cracking problem in timber 77−39261
cryogenic power plants current lead, indefinite Lagrange multipliers appl. 77−87768
cryogenic refrigeration system, computer design and optimisation 79−71457
cryogenic refrigeration system, computer design and optimization 79−58750
curved electron beam electron-optics with strong deceleration at collector 78−74106
cylinders, elastic doubly connected hollow, min. weight design for given torsional, flexural rigidities 78−18172
cylinders working with compressible fluid, optimum stepped piston 77−42860
cylindrical shell stresses by local heating, optimisation *(Russian)* 77−39225
D-optimal design for quadratic regression on a hypercube 79−92921
DC plasmatron with axially-blown arc, optimisation *(Russian)* 77−39476
delayed coincidence techniques with accelerator beams, anal., optimisation rules 78−78598
design of freely vibr. elastic bodies *(German)* 78−65775
design optimisation of solar energy district, systems anal. of external energy supply 80−30398
design problems with singularities, soln. 77−72151
diatomic molecule production, using matrix isolation spectroscopy, optimisation 78−46462
diffusion nonlinear equation, perturbation, iterative and optimal techniques for arbitrary diffusivity 77−66943
digital computer applications to process control, conference, The Hague (1977) 78−49808
digital holograms, optimum quantisation 78−33699
discrete Kalman filter, rel. to inverse thermal conductivity problem 78−5628
diseases, communicable, anal./control, novel model 80−30634
district heating systems, optimal conditions of combining fossil fired and nuclear power plants 78−37457
double Gauss basic lenses, design *(German)* 80−53398
earthquakes, records, optimal digitisation 77−91044
ECG, fixing locations of multiple dipole heart generators 77−44809
effective hamiltonian matrix parameter optimisation, least squares method 79−26874
elastic continuum dynamic response determ. using modal anal. 78−8242
elastic medium, extremum problem for distributed parameter, and determ. of optimum props. 79−88811

optimisation continued
elastic plate, arbitrary shape, weight optimality condition *(Russian)* 77−23879
elastic ribbed plate, optimal design 80−14578
elastic solid, beam of minimum weight, optimal design, quasioptimal soln. *(Russian)* 77−72158
elastic structures, computer automated synthesis for minimum struct. weight 78−34015
elastohydrodynamic contact optimisation 78−79288
electrodynamic drivers, monotone performance optimisation using tubular couplers 77−7279
electron optics optimisation using dynamic programming 77−61907
electron probe analysis, precision and optimisation of thin specimens *(French)* 77−77849
electronic structure, multiconfigurational HF calculations, quadratically convergent reference state optimisation procedure 79−97966
electrostatic electron oscillator design optimisation, ion source and vacuum gauge 78−74107
elliptic problems, representations of first variations, appl. to optimisation and sensitivity anal. 78−77674
EM transducer dynamic range optimisation 77−19506
emergency protection drive, optimum ratio between operational component times 78−82474
energy storage systems, compressed air, w.r.t. economics 80−26167
energy system modelling, New Zealand appl. 80−76590
enrichment zoning and control rod programming for reactivity and power shape control 79−18003
equilibria prediction, vapour-liquid, Wilson and NRTL equations assessment 79−86883
ESCA spectrometer retarding lens system, computer optimisation 77−13827
evoked potential analysis, on-line signal optimisation using minicomputer 77−5112
experiment planning, appl. to calibration of X-ray radiometric analyser 80−61186
experiment planning, optimum plans calc. on convex polyhedrals 80−57084
extremal problems, theory, book 79−63001
FAPMAN-5, a computer code for optimum operation of LWR power stations 79−22450
fast power reactor, material distrib. optimisation by nonlinear programming method 77−14210
fatigue-critical structure, optimal periodic proof test based on cost-effective and reliability criteria 77−63838
ferromagnetic materials, magnetisation curved optimal analytical representation, automatic choice method *(Italian)* 78−47998
fins, circular, with heat generation, using variational technique 77−65658
first-order kinetic model, optimal design of experiments to estimate parameters 78−15650
fission reactor, optimisation of spatial flux distrib. and Xe fluctuations by differential dynamic programming 79−45358
fission reactor core, optimisation of energy distrib. 79−59186
fission reactor core energy distribution, algorithm for extremal control 80−83209
fission reactor fuel, U enrichment, optimal blending 78−13309
fission reactor fuel cycle back-end services, utility optimization model 79−30906
fission reactor fuel management optimization, influence of poison management 79−26585
fission reactor shutdown for known period, optimal conditions 78−86642
fission research reactor, Missouri University, fuel cycle optimisation 79−67930
flat-plate photovoltiac array design optimisation 80−94037
flexible coupling flange geometry stress distribution, moire holography appl. *(Italian)* 77−42508
flood control planning 78−81245
flood flows routeing in rivers, parameter optimisation 77−37263
flow in lung and vascular tree structs., optimisation of diameters and bifurcation angles 78−11683
fluoroscopic spot film system image quality evaluation and optimisation 78−69205
forced vibration prevention by damped dynamic absorber 78−63355
four-layer waveguide diffractive injection efficiency optimisation *(Russian)* 80−64206
fusion reactor, FTR, equilib. field coils, electrical supply system, optimisation and computer aided performance anal. 80−91288
fusion reactor, Tokamak constant tension D-shaped coils, lateral support struct. 78−55013
gasdynamic laser, CO, energy characts. 80−23665
geometric discontinuities, in stress fields, optimization 79−37150
geometrically imperfect stiffened cylindrical shells, optimisation under axial comparison 79−3916
geometry optimisation, Newton-Raphson method algorithm 77−10612
geophysical inverse problems soln. by method of dynamic models *(Russian)* 78−85714
geothermal energy resources for electricity generation, discounted cash flow anal. 80−85263
geothermal plant design, Geysers Unit 16, Northern California (USA) 79−52877
geothermal power plants flash cycle optimisation, analytical expression in terms of temp. only 80−40894
GFRP sheet moulding compound, influence of cure time restrictions, on minimum weight design of double layer panels 80−11623
global, appl. of methods to technological problems 79−59840
gradient-type methods convergence, singular parameter optimisation problems 77−82375
gradiometer, ferromagnetic probe, fault detection optimisation 78−53096
grating profile optimization, inverse scattering methods 80−48142
gravitational-wave resonant antennas, optimum filtering and sensitivity 80−8545
gravity networks, optimisation *(German)* 78−15950
groundwater, computer assisted management *(German)* 79−57989
hard magnetic materials, demagnetisation curve, single function approx. using computer *(Hungarian)* 78−60307
heart, minimal O_2 consumption and optimal contractility, theoretical approach 79−74694
heat conduction, interior algorithm for optimisation of forms *(French)* 77−72130
heat exchanger design, w.r.t. heat transfer efficiency *(Russian)* 78−16789

optimisation continued
heat flow inequalities, appl. optimisation problem involving free boundaries 78−13889
heat pumps, compression, w.r.t. heat utilisation *(German)* 79−96483
heat treatment by simplex method 78−84869
heat treatment regimes anal. and optimisation using simplex proportional designs 80−25734
heavy chain rotating, duality principle for non-convex optimisation, calculus of variations 79−71237
Helmholtz coils, optimisation, critical current rel. to mag. induction 79−67353
hemispherical electrostatic 180° deflector, optimisation *(French)* 78−21269
hepatic scintiphotography, clinical value optimisation 79−88169
high resolution spectrometers, online polynomial optimisation 79−89563
hologram recording conditions optimisation 79−72536
holographic memory, parameter optimisation allowing for aberration 79−55085
holographic recording medium, optimal linear transfer function determ. 80−23635
holographic spatial filter, CAD *(Russian)* 80−28171
hot-film anemometers, freq. optimisation theory 78−26218
hydrologic design, choice of distrib. functions 79−53392
hydrology, Cobb-Douglas functions in multiobjective optimization 79−53397
hydrometeorological information, optimum conversion to digital form 79−29903
hypersonic body shape optimisation, principal approx. methods 78−5765
hypersonic three-dimensional shapes, optimal surfaces and total drag coeffs. 80−59068
ICRF heating in PLT 80−28742
image restoring with constrained optimisation filtering 79−39494
impact absorbers, optimum damping ratio 77−72225
induction MHD pumps, with transverse mag. flux, active element optimisation *(Russian)* 78−94840
Infinite dimensional filtering problems in optical communication systems 78−66779
intervertebral joint, systems identification for material props. 78−69125
ionography, optimisation of design parameters 78−31888
IR detector-preamplifier for cryogenic spectrometer, optimization 80−95164
Ir dryers, spectral composition of radn., optimisation 78−90676
IR photodiode optimisation for higher temp. operation by excess volume reduction 79−2824
IR spectroscopy, Fourier transform, emission optimisation for nearly transparent gases 77−5931
IRT reactor, optimisation of operation regime *(Russian)* 80−37473
isotopic microgenerator design and construction optimisation due to min. power 80−108813
Kalman filter technique, neutron flux distrib., optimal allocation of in-core detectors 78−54839
lake hydrographic surveys optimization 79−53378
laminates, fibre-reinforced, optimum design under natural frequency restraints 80−53688
laser, double heterostruct. junction type, US wave freq. modulation anal. 78−83009
laser Doppler velocimeter receiving system, optimisation for sampling volume reduction 77−72379
laser heating of metals, in oxidising medium 80−69445
laser U enrichment plant, optimum operating conditions 79−54578
laser ultra-short light pulse formation 80−64085
layered thin composites, optimum design and strength 80−10210
leg muscle forces, normal human walking, optimisation methods 79−16240
lens, three-element, optimisation by damped minimum method *(German)* 77−23726
lens optimisation using Walsh functions, FEE-based criterion 78−79097
light beam focusing, in moving nonlinear media, using gradient method 80−106578
light beams propagation algorithms, thermal self-action problems and their compensation 80−106579
limit analysis in continuum mechanics, nonlinear optimisation problems, numerical methods 79−2628
liquid metal MHD induction pump, transversely closing mag. flux, optimisation of parts 79−77278
LMFBR, 1500 MW, breeding perfomrance optimisation of He-bonded carbide fuel 78−17325
LMFBR, development and Pu allocation, optimal policies 80−725
LMFBR, enrichment and control optimization for reactivity losses during burnup 78−21692
LMFBR, fuel cycle cost optimisation anal. of core design modifications 80−22900
LMFBR, high power, optimisation by nonconvex programming mathematical model 78−41810
LMFBR, pin diam. optimisation in heterogeneous vs. homogeneous core 78−8892
LMFBR design, risk-based approach 77−88198
LMFBR power reactor, objective function optimisation *(Russian)* 78−70590
LMFBR refuelling scheme optimisation by man machine interactive method 77−67826
lubrication, hydrodynamic, free boundary problem including surface tension 80−19542
lunar surface gravimetric surveying process optimization 79−8846
LWR, optimal power profile fuel management 78−37411
LWR, optimum fuel loading and coastdown operation 79−30970
machine design problems, optimum, interactive method of soln. 79−17204
machine element of shape, finite, element technique 77−62152
magnetic bubble generator modelling and optimisation 78−6547
magnetic bubble propagation circuits, optimum design 79−78481
magnetic fields, boundary-value problems, finite element and finite difference anal. 78−94353
magnetic problems, grid and metric optimisation, finite difference and finite element methods 78−94352
magnetic spectrograph for very heavy ions 79−31315
magnetometer freq. optimisation, computer anal. and expt. 77−18057
magnetometers, induction-coil, optimisation theory at audio and higher freqs. 79−85156
mammography, optimum radiographic image conditions 77−90879
Markov decision process monotone optimal policies 77−53757

optimisation continued
Markovian biological system modelling via optimisation operators 79−1994
mass produced parts, appl. of statistical algorithms for optimisation of mech. props. 77−68550
mass separator, plasma-optical model, optical props. optimisation 78−16894
matched spatial filter synthesis, parameter optimisation 77−71925
maximum-likelihood method, measuring baseline coordinate vectors of multielement radio interferometer 80−26753
MC-SCF theory, orthonormality-constrained orbital optimisations 78−86766
measurement of medium loss with time, optimal planning *(Polish)* 78−93642
mesh generation-optimisation, for partitioning of intricate biological struct. for 3-D finite element anal. 77−40630
metal-composite shell, three-layer, stochastic formulation of optimisation using heuristic methods 80−38268
meteorology, optimum difference schemes, synthesis on sphere 78−93011
MHD combustion, operating mode aspects 78−18388
MHD conduction channel, optimal operating charact. calcs. *(Russian)* 78−47190
MHD convertor, diagonal channel, conversion efficiency optimisation by sliding descent method, turbulence *(Russian)* 78−75226
MHD generator, diagonal-type, nonequilib. plasma, steam plant appl. 78−67443
MHD steam power plant, coal-fired, w.r.t. economics, using computer-based model 79−52942
microcalorimeters, conductive, limiting potentialities, anal. 80−17942
microtron electromagnet optimum shape, computer numerical anal. 77−18718
Mirror Fusion Test Facility, neutral beam injection, optimisation by computer graphics 78−66376
molecular geometry optimisation, Newton-Raphson method algorithm 77−10612
molecular geometry optimisation with explicit inclusion of electron correl. 80−37748
molecule, multiconfiguration wave functions, optimisation 77−23406
molecule with d-orbitals, automatic geometry optimisation, Slater orbital derivatives 79−6831
Monte Carlo biased transport calcs. optimisation, prediction of statistical error 79−58654
multicomponent spectra, numerical anal., least squares, optimisation methods 77−56264
multiconfiguration wave functions, optimisation 78−33411
multielement flame spectrometry, flame condition optimisation 78−31723
multilayer plates, optimum design for cylindrical bending 79−87698
multiple dipole heart generator location optimisation in simple torso model 80−41277
muscle activity prediction, optimisation method adaptation 79−92273
muscle force prediction, use of optimisation techniques 79−16242
myocardial electrical activity modelling, dialogue mode *(Russian)* 79−2021
myoelectric signal processing, expt. demonstration of optimal myoprocessor performance 80−89882
myoelectric signal processing, optimal myoprocessor derivation 80−89881
n^+-p-p^+ bifacial back surface field solar cells, optimisation of p^+ doping level by ion implantation 80−97784
nerve signal optimal filtering 77−73616
neutron activation analysis of rare earth elements in rocks, optimum method 79−88491
neutron diffusion modelisation, optimal design and eigenvalue problems 78−66329
neutron inelastic scattering, optimisation of struct. studying conditions *(Russian)* 80−79641
NMR, automated spin-lattice relax. time meas., pulse optimisation 77−21437
NMR linear field correction, optimum size of rectangular current shim off mag. pole face 78−86314
non-linear optimized fibre reinforced plates in bending 79−27550
nondeliverable fabrication plant fuel material with various enrichment, determ. of optimal comp. 78−13312
nondestrictive inspection parameters, as operations research problem 77−90548
nonlinear image restoration with signal-dependent noise, decomposed local algorithm 78−78951
nonlinear transfer processes, optimisation *(Russian)* 80−8934
nonstationary heat conduction process, optimisation, soln. 79−81686
nuclear energy for combined electricity and district heating prod. 78−37459
nuclear fuel cycle, core design optimisation 78−82420
nuclear fuel cycle management, w.r.t. economics 77−14241
nuclear fuel reprocessing plant, optimal installation program 77−46370
nuclear plant operating margin optimization 79−85592
nuclear plant size and optimum mixes, optimisation techniques appl. to energy planning 79−24886
nuclear power, system criterion appl. to problems 77−23313
nuclear power plant, optimal operating conditions 78−37427
nuclear power plants, mathematical modelling methods 77−23315
nuclear power reactors in elec. utility system, short range system analysis method 77−50252
nuclear power station with desalination plant, steam-cycle and optimisation calc. 79−26724
nuclear power station with GCFR and N_2O_4 dissociating working substance *(Russian)* 79−59159
nuclear power station with VVER, for semi-peak load generation, mathematical model 80−68936
nuclear power stations, optimisation of the cyclical operating regime using maximum principle 79−71916
nuclear reactor, fast reactor design, desirable accuracy eval. for nucl. data using optimisation method 77−57704
nuclear reactor, LMFBR, refuelling scheme optimisation using heuristic enumeration method 77−46301
nuclear reactor, multigoal fuel cycle optimization including nonproliferation objectives 80−52764
nuclear reactor, multizone, reactivity and power shape control, optimisation method 77−6529
nuclear reactor, PWR core, finite cylindrical, synthesis program soln. of flattest power density 77−50202
nuclear reactor fuel replacement, optimal strategy *(Czech)* 77−42112

optimisation continued
nuclear reactor power distrib. flattening, burn up optimisation *(Japanese)* 78−17397
nuclear reactor protective system, optimum supervision intervals and order of supervision 78−37419
nuclear steam turbines for power prod., district heating, desalination 78−37438
ocean remote sounding instruments, quasi-optimum operating functions *(Russian)* 78−77362
ocean thermal energy conversion, OTEC power modules optimisation, w.r.t. economics 79−83615
ocean thermal energy conversion plant, 100 MW, systems aspects 78−96235
ocean wave energy extraction, system optimization by diffraction theory 79−20867
one-electron density matrix 77−79532
optical constants, ATR meas., 2-polarisation method, accuracy, optimisation 78−45673
optical correlation detection, optimization by prewhitening 80−95802
optical fibre refractive index profile optimisation for broadband multimode fibres 78−66932
optical film, layered coating synthesis, optimisation formulae 78−25946
optical optimisation of inversion of convolution products 79−76601
optical signal waveform optimisation 79−76618
optical system, computer optimisation program 77−54766
optical system, with aid of computer, k-stage objectives corrected to infinity *(Hungarian)* 79−81502
optical system parameters, using damped least-squares method *(German)* 77−68255
optimal design of dynamically loaded continuous structs. 78−38185
optimal nodal point distribution for improved accuracy in computational fluid dynamics 80−48670
optimality criteria methods in elastic struct. design 78−83253
optimization of practical stability problems 80−5966
optimum re-entry configuration via the method of steepest decent 79−37339
optoelectronic device S/N ratio optimisation 79−26133
orbit transfer, three burn, optimal, nonlinear programming trajectory simulation 77−84133
orbital transfer, optimal, low-thrust, limited power, elliptical orbits 78−4087
orthotropic materials design for stress optimisation 78−63291
oxide-semiconductor/base-semiconductor solar cells 80−81440
panel structural optimisation under supersonic flutter conditions *(Italian)* 79−41600
Paris regional air pollution monitoring network optimisation *(French)* 77−37387
PCM optical fibre communication system numerical aperture optimisation *(German)* 78−38017
periodic systems, optimisation by analytic construction of control 79−21543
phase diagrams, optimization by least squares method 79−10915
phase diagrams optimisation by least squares method using simultaneously different types of data 78−6143
photodetector optimisation for radiation environments 78−29158
photodetector parameters in interference measuring devices 78−16844
photon counting spectrometer, computer controlled, rapid scanning of low light level spectra 78−86338
photovoltaic receiver for parabolic trough concentrator, optimisation 80−93983
photovoltaic systems, all component optimisation, theory and appls. 79−29475
physiological systems, optimisation concepts in models 79−74591
piezoelectric transducers, optimum size determ. *(Russian)* 79−88943
pipe-and-fin solar water heating plate material economy 79−62050
planar explosion mag. generator with resistive load, work performance optimisation 79−6156
plasma cross section reconstruction, Farey dissection optimization, computer anal. 77−84523
plasmotron, capacitative, optimisation 79−55568
plastic design of circular plates, variational formulation 77−68440
plasticity theory, variational inequalities and multilevel optimisation techniques 78−79224
plate bending theory, optimal thickness distrib. *(Russian)* 78−63295
Poisson eqn. soln. by successive overrelaxation technique, optimisation hazard 78−81813
polarography, double tone, optimisation, measuring, dropping freq. synchronisation 77−25340
positron emission computerised tomography, optimisation of system design parameters 80−26347
potential energy surfaces, analytical expressions from constrained optimisation 77−6698
power plant cooling system design, optimal system synthesis, tower, pond 77−14260
pressure component manufacture, new materials, technologies and equipment development 78−74436
pressure vessel and nozzle junction, optimum shape design 78−89941
proportional counters in X-ray fluorescence spectrometer, optimisation of energy response 78−40792
pulse counting measurement systems, optimum parameters determ. 79−89523
pulsed multipole mag. field with zero skin depth, anal. method, nonstandard electrode optimization 79−13863
PWR, development and Pu allocation, optimal policies 80−725
PWR fuel assembly design 80−821
PWR power plants, condensate treatment in secondary cct. *(Hungarian)* 77−30654
quadratic, for image reconstruction 77−16981
quantum systems control, pure states and mean values 80−22210
quartz filter resonators with energy trapping, optimum design 78−32663
radiation therapy treatment 77−86593
radio astronomy, arc meas. procedure optimisation using radiointerferometer *(Russian)* 79−101082
radioisotope scintigraphy, zero summation filter optimisation 77−16963
radioisotope thermoelec. generators, design optimisation program 80−40880
radioisotope thickness meter, increasing speed of response by optimising detector parameters 79−75494
radionuclides, short-lived, meas., counting statistics 80−58098
radiopharmacy optimisation by redesign 77−90899

optimisation continued
radiotelescope sensitivity optimisation, deterioration coeff. *(Italian)* 78−85845
radiotherapy, external beam, optimisation using computer 77−86632
radiotherapy treatment planning, FORTRAN program for optimisation using complication probability factor 80−81686
Ramsauer chamber, positron scatt., optimisation study using Monte Carlo method 78−70706
reactor fuel assemblies, optimum location 79−17968
reactor optimal shutdown problem algorithm by branch and bound method *(Japanese)* 79−36341
reconstruction angles in CT 80−8178
rectilinearity measurement, laser transit prototype parameter optimisation 79−76745
reflection seismograms, simultaneous spherical divergence correction and optimal deconvolution 80−98258
refrigerators for superconducting power transmission lines, He, w.r.t. cost and reliability 78−24802
regional water quality management, optimisation model 77−66945
regional water quality management, pilot study 79−57515
reinforced cylindrical shell, nonuniform thickness, optimisation 77−68465
reinforced plastic cylindrical shells, optimal design under dynamic constraints 80−102996
remote sensing, multispectral information volume optimisation in natural formations studies 80−4118
remote sensors, signal correction optimisation considering internal noises *(Russian)* 78−16191
reoentgenokymographic unit, physical and operational charact., plate thickness optimisation 79−57747
reservoir, information value 78−49060
resonance Raman spectra, optimum sample concs. 78−66555
respirator, narcosis, ergonometric design *(German)* 79−2163
RF size effects meas., optimisation of marginal oscillator for 77−26377
satellite imagery, optimum linear filtering to remove cloud cover 77−56744
satellite orbit determ. by astromeas. optimisation 78−16279
satellite-borne IR scanning radiometer obs. of stratosphere, optimum field view and spacing 78−16201
satellites integration and test phase *(French)* 80−17464
SAW filter design using optimisation technique 80−74671
scattering, multichannel, optimised anomaly-free and restricted anomaly-free variational methods 79−3515
scatterometer, satellite- and aircraft-borne, optimization of charact. for investigating underlying surfaces 80−67436
seasonal reservoir, optimal releases, deterministic case 80−8362
seismic surveys, optimum multichannel filters theory *(Russian)* 79−39921
self-reproducing macromolecules, selection, controlled energy fluxes constraint 80−67027
shell, axially stiffened, mode interaction in postbuckling behaviour 77−89046
shell, cylindrical, composite with viscoelastic filler, optimisation w.r.t. long-term stability 79−18760
shell, reinforced plastic, optimisation with allowance for geometrically nonlinear factors 80−38270
shell, shallow, limit analysis and optimal design *(Russian)* 77−42752
shell of rotation exposed to vibrs., optimum shape and reinforcing struct. 79−18792
SIMS, recording, optimisation 79−43683
single-photon fluorimetry, time-correlated, data acquisition rate optimisation 79−20494
solar cell array optimisation for use with concentrators 79−62001
solar cell collection grid structure, optimisation of area, shape and spacing 80−72042
solar cell device modelling 79−39297
solar central receiver 77−27330
solar collector, compound parabolic type, optical and thermal design 77−23735
solar collector energy collection area and carrier fluid flow rate optimisation 79−62080
solar collector horizontal coaxial cylinder design optimisation 79−62110
solar collector optimum tube pitch expt. 79−62083
solar collector with flat specular mirror, optimal tilt angles with seasonal variations 80−72081
solar collectors orientation 77−81965
solar energy concentrators, optimisation for tubular evacuated receivers aligned north-south 80−72015
solar energy systems, modern control theory appl. reviews 80−66949
solar flat plate collector design and optimisation for Indian conditions 79−62087
solar flat plate collector tilt optimisation 79−62090
solar heating and air conditioning system; CAD w.r.t. maximum solar heat gain 79−57466
solar heating and cooling systems, using continuous flow control 79−62127
solar heating system components, optimal insulation anal. 80−35745
solar heating system economic evaluation and optimisation 80−35644
solar heating systems, optimisation formulation of collector area based on TRNSYS computer code 80−61414
solar hot water systems, with various storage systems 79−57461
solar photovoltaic arrays, optimisation of total annual energy output from constant/adjustable tilt systems 80−94059
solar planar reflector-collector array optimisation 79−62071
solar plant composite heliostat, computer anal. and optimisation 79−39283
solar power system, mathematical model, operating regimes optimisation 79−83562
solar thermal collector, fixed, design optimisation 80−40905
solar turbopack, using organic Rankine cycle and flat-plate collectors, irrigation pump drive appl., 79−62019
sound and vibration fields suppression, synthesis of systems 78−9494
source biasing optimisation technique using Monte Carlo calc. 79−26005
space tug, ion-propelled, optimisation 78−53798
spacecraft four-impulse planetary landing and return under time constraints 79−62711
spacecraft payload optimisation using parametric modelling 77−5410
spacecraft solar arrays, in-orbit performance, review 80−94054
spectral filter, optimisation for arbitrary criterion by method of basic extremals 80−96011

optimisation continued
spectrophotometric measurement, dual wavelength, precision optimisation 79−92019
spectroscopic two-parameter information processing on small computer, optimum method 79−76322
spherical mirror solar collector, geometrical concentration determ. *(French)* 78−33808
spiral tomography, optimum blurring 78−69181
spring-mass system, optimum design of untuned viscous dynamic vibration absorber 79−86370
square-field scanned image construction time optimisation *(Russian)* 80−63933
SQUID gradiometer, DC, thin-film, design optimisation 80−98951
starship flight optimisation, time plus energy minimisation criterion 79−44330
statistical system unknowns optimal evaluation *(French)* 79−9194
steel ingot, state of viscoelasticoplastic stress deformation, in process of solidification *(Russian)* 80−45295
stiffened cylinders under torsion with axial compression 78−26065
Stirling cycle machines, free piston design 79−48172
Stirling free piston engine technology and appls., design optimisation 80−35723
stochastic constraints on iterative maximisation of system of differential eqns. 78−57757
stochastic gradient problems, error of estimation of direction 80−22282
storage reservoir analysis, mass-curve techniques, systems and perspective 80−8457
string, stretched, appl. of optimisation methods to vibr. control 78−83305
structural elements having 1- and 2-section; freedom, vibr. charact., optimum design 77−72207
structural optimisation, homogeneous functionals 79−98619
structural optimisation problems, optimal archgrids 79−67160
structural wt. optimisation, optimality criteria and mathematical programming 78−26029
superconducting magnet for magnetic flux compression, compression generator, PULSAR, design optimisation 80−68957
superconducting solenoid with variable current density 79−17450
superheavy elements, prod. method optimisation 78−46103
supersonic wave drag of planar singularity distributions 78−83430
surface heat exchanger, using generalised geometric characteristic and mean vel. *(Russian)* 80−82760
telex-communication system, subcarrier recovery ccts. *(Rumanian)* 77−27427
TEM crystal atomic structure imaging technique and applications 80−105752
thermal conductivity detector, with a narrow packed column 80−22355
thermal imaging scanners, mirror rotation axis optimisation 80−86426
thermal power reactor, operations research 79−13396
thermionic converter, ideal, output power optimisation 79−27841
thermionic converter, Knudsen Cs-Ba type, performance optimisation 79−27840
thermionic convertor, elec. power density on optimisation 79−10723
thermoelectric heat pumps, single-stage, simplified method for optimization 80−108811
thermoelectric thermometer cold junction thermo-EMF compensation, parameter optimisation *(Russian)* 78−86270
thermoelement with deliberately induced anisotropy, optimisation of figure of merit 79−95433
thin-film laser logic elements, charact. and limiting capability optimisation *(Russian)* 79−18431
Tokamak, optimum conceptual scaling 78−54908
Tokamak fusion reactor, dynamic model for energy optimisation of cycled reactor 78−13318
toroidal pinch equil. config., nonlinear operator eqn., optimisation soln. 78−59649
torsion of elastic bars, 2-D optimisation problem *(Russian)* 77−23877
torsional vibrators, design by computer optimisation *(Japanese)* 80−33405
transducers, magnetically anisotropic force, optimisation of mechanical and electric operating conditions 79−17412
transient aquifers, modified optimisation method for parameters estimation 78−61462
transition state determination by the X-method 77−90580
transport and diffusion theory, optimal iteration strategies, geometric interpretation 79−22358
transport processes optimization method for exponential biasing in Monte Carlo calculations 79−54080
trunk pipeline systems, oil and gas, investigation and optimisation of thermal regimes 80−107579
two-stream plasmatron flow structure obs. and optimisation 78−71556
undersea acoustic transponders, locations optimal estimation 79−5684
underwater sound, cancellation of turbulent boundary-layer press. fluctuations 77−88978
uniformly thick film sputtering optimisation 79−27451
Universal Products Code supermarket scanners, pattern optimisation 78−42297
US transducer lumped wideband equaliser design optimisation 79−46159
vapour absorption refrigeration flat plate solar collector tube pitch optimisation 79−62084
variable pressure-drop flowmeter parameter optimisation 77−58826
Venezuelan research reactor reload fuel optimisation 79−9737
vertical evaporating circuit, heat exchange calc. and optimisation *(Russian)* 77−71321
vibrating beam, distrib. of additive damping 80−38310
vibrating beams, uniform non-homogeneous, design 79−14315
vibration isolation forces for system with random excitations 77−39240
vibration simulating system 80−53729
vibration-simulating systems, rel. to efficiency and cost 80−53728
vibrations simulator design, random, wide-band 80−53731
viscoelasticity, linear, scalar and vector-valued optimisation 78−5665
walking apparatus, parametric optimisation *(Russian)* 77−50871
water-water reactor parameters mathematical model 77−74912
wave energy system, economic assessment 79−43732
wave mechanics, optimisation theory approach *(French)* 77−13598
weak optical signal meas. in strong interference *(German)* 77−65623
Wheatstone bridge sensitivity 77−26330
Wheatstone bridge using thermistors for temp. meas. in calorimeter *(German)* 78−86275
WPDC, systems analysis appl. 80−26182
optimisation continued
X-ray diffraction topographic patterns, spectral sensitivity of TV system for visualisation *(Russian)* 80−62814
X-ray scattering curves, optimisation of smoothing procedures, polynomial fitting and modified frequency filtering 79−60215
X-ray sources, point-like, positions determ., lunar occultations optimisation 79−92652
X-ray spectrometer for energy-dispersive XFA using X-ray tubes in combination with secondary targets 80−30316
xerographic toner, charge optimisation 77−182
Al-Si-Cu casting alloy, optimum selection of chem. contents for optimum strength *(Czech)* 79−15625
AlGaAs DH laser epilayer struct. optimization for integrated optical circuits 80−99879
CO-^{3}He nuclear pumped laser, optimisation with 2 MeV protons 80−64000
CO_2 gasdynamic laser, gain supersonic flow heating effect, condition optimisation 78−82947
CO_2, gasdynamic laser, optimisation of gain coeff. in nozzle stream *(Russian)* 77−27272
CO_2 laser, long and short pulse formation, optimum conditions 78−87037
CO_2 TEA laser, optimum operational conditions with double discharge at atm. pressure *(Bulgarian)* 78−33720
Co permanent magnet material savings *(German)* 80−103851
Cs atomic frequency standard, optically pumped, buffer gas mixture optimisation 77−37859
Cu ingots, solidification, quality and optimal modes of solidification, prediction from temp. fields 79−83187
Cu tube and plate solar collector geometry optimisation 79−62040
Cu-Fe-Mn-Ni-Pb-Zn copper based alloys optimisation of atomic absorption analysis 77−56274
Fe-Cr-Mo, white cast, optimising fracture toughness and abrasion resist. 80−85042
GaAs-$Al_xGa_{1-x}As$ proton-isolated DH laser, threshold current optimisation *(German)* 78−37905
HCN compact CW laser optimisation 78−59022
Li/$SOCl_2$ D cells, optimisation with respect to energy density, storability and safety 80−97775
LiAl-$NaAlCl_4$-$MoCl_5$ thermal battery evaluation and optimisation 79−29458
NH_3 continuous absorption cooling flat plate collector design and optimisation 79−62081
Nd:glass laser system, beam spatial profile optimization in amplifier channel 80−74407
Nd:glass lasers, optimisation for 1-10 ns pulses operation 78−46651
Pu fuel cycle back end services, utility optimisation model 78−41845
Si epitaxial film growth on sapphire in SiH_4-H_2 system, optimum deposition 77−77397
Xe transient processes optimisation, interrelation of various problems 78−17295
Zn electroplating process, optimisation 79−43452
Zn spectral line breadth from pulsed supply hollow cathode discharge 78−33471
Zn-AgO cell, Zn electrode slurry-paste fabrication optimisation 79−96430

optimum control *see optimal control*

opto-isolators
displacement transducer 78−24783
electrical diagnostic stimulator with insulated sources of power *(German)* 79−16324
light versus current characteristic simulation of injection laser 79−22960
liquid level monitor with optical coupler isolation *(German)* 78−73963
operational amplifier, for current meas. in 10^{-11} to 10^{-6} A range 77−67473
optoelectronic devices development 80−91902

optoacoustic spectroscopy *see photoacoustic spectroscopy*

optoelectronic devices
see also opto-isolators; photoelectric devices
A^{III}-B^V, optoelectronic devices, conf., Berlin, DDR 78−91755
aerial colour photograph interpretation *(Russian)* 80−61920
aerosol classification pulse amplitude analyser 78−61587
analyzer for seismic data processing *(Russian)* 77−29516
angular meas. devices, error anal. method *(Russian)* 80−95066
arc plasma temp. meas., electro-optical device *(Polish)* 79−82121
astronaut aid, for observing Earth and atmosphere photometric charact. *(Russian)* 77−5412
biomedical target tracker for limb movement meas. and anal. 80−56166
circuits, using multicolour semicond. detectors *(Czech)* 79−26126
coincidence detection fo optical pulse streams, high resolution heterodyne system 77−690
colour imaging multispectral optoelectronic system effectiveness evaluation 79−81553
colour sensing optoelectronic device, neural mechanism modelling 80−12128
conference, Munich, Germany (June 1975) 77−7111
couplers, advantages of design and appl. trends *(Rumanian)* 80−33165
detection and tracking system, optimisation in search operation mode 77−50765
diamond turning, optics and TWT components manufacture 79−81584
digital data processing, review 80−19106
displacement sensor, breath amplitude meas. appl. 77−66868
dynamic investigations using modulated light source *(German)* 79−55197
electric signal pulse shaping using laser-excited solid-state plasmas in Si, expt. 77−19397
electrically controlled diffr. grating and optical modulator using Pb(Zr, Ti)O_3 77−39026
electrolyte concentration meas. by portable optoelectronic convertor 78−80820
electrolyte concentration meas. instrum. using laser diode, optimisation of parameters 79−20488
electron gun, with point cathode, electron-optical props. *(German)* 78−82901
extended part diameter meas. contactless instrument *(Russian)* 80−27270
fibre optic, sound reading systems for cine projectors *(Russian)* 78−312
free damped mech. vibration logarithmic decrement, optoelectronic meas. 80−92095
gas discharge phenomena meas. 80−107007

optoelectronic devices continued
goniometer, linearity and sensitivity ranges increase 80−23786
holographic memories, interfaces between optics and electronics 77−7042
holographic memory, data readout reliability by optoelectronic channel 79−27216
holographic memory devices, optoelectronic ROM memory, injection laser appls. in construction *(Polish)* 80−19007
human motion 3-dimens. monitoring by optoelectronic means, calibration and meas. 78−31913
HV electrical meas. by optical methods 78−24822
hybrid optoelectronic modules for OEM fibre-optic data systems 79−86259
II-VI semiconductors appl. *(German)* 77−7745
III-V semiconductor appls. 79−74088
III-V semiconductor materials preparation technology *(Czech)* 78−3037
III-V semiconductors, radiative recomb. and related phenomena, conference, Prague, Czechoslovakia (Sept. 1979) 80−51940
III-V semiconductors for optoelectronic appls., review 78−30975
image detectors, for mol. fluoresc. spectrometry 79−21815
incremental transducer description and design problems *(French)* 78−21121
instantaneous linear velocity meas. by scanistor 79−67261
IR technology, radiator and detector designs *(German)* 80−22430
IV-VI optoelectronic devices, MBE techniques 79−95942
lecture 78−25990
light beam deviation from straight line meas. instrum. *(German)* 78−77850
light curtain for measuring speed trajectory, of object *(German)* 78−12738
lightning stroke current meas. using optical fibre cable and optoelectronic conversion, rocket launched 78−92930
liquid optical element for image stabilisation 78−55462
long-term role in optical and electronic systems 80−33232
low-contrast optoelectronic primary information processing system, energy efficiency 79−76617
magnetic diffraction gratings with alterable magnetic domains for optoelectronics 78−63197
MBE process and problem areas, review 80−10815
measurement errors 79−6073
mechanical laws, optoelectronic apparatus for classroom demonstrations 80−46773
memories, data storage density enhancement 77−58298
memory, bit-organised, method for information capacity increase 80−102656
metal-semiconductor structure, variable-gap, differential optospectrometric effect 77−62994
metrological provisions for opticophysical measuring instrums. 80−8953
micron scaled cathodoluminescence with SEM, review 78−23537
narrow band gap semiconductors, characts. and appls. *(German)* 77−20356
nematic liquid crystal in contact with photoconductor EHD instability, nematic liquid crystal in contact with photoconductor 80−79695
noncontact optoelectronic position transducers 79−50406
optical image information content 77−39057
opticoelectronic phase goniometers compared to opticoelectronic amplitude goniometers 79−71412
optomechanical/electronic unit, for measuring photodetector parameters 78−284
oximeter, red/IR, catheter tip mounted, for blood oxygen saturation 77−40836
particle counting and vol. determ. in suspensions 78−57894
pattern tracer for laser plate cutting 79−55170
photogram meas. system using optoelectronic convertor of linear coordinates 80−17917
photon flare centre determ., online optoelectronic convertor *(Russian)* 79−75111
physical fundamentals *(German)* 77−37981
pressure meas. and phase equilib. study of coloured or turbid liquids, optoelectronic method 78−70152
ps switch using pulsed lasers and photoresistive semiconductor *(German)* 77−72066
reference mirror for alignment of optical instruments 80−10054
refractometers, design, construction and quantitative characteristics *(Russian)* 80−62716
retinal hue signal generation, optoelectronic robot model 80−3647
revolution counter for X-ray tube anodes *(German)* 78−12678
S/N ratio, scanning rate effect in optoelectronic devices with matching filter 79−7223
S/N ratio optimisation 79−26133
scanning device accuracy, raster distortion and instability effects 79−72697
scanning optoelectronic systems, optical and electrical filter simultaneous optimisation 79−72696
semiconductor thin films, MBE, device appls. *(German)* 78−68630
single-channel optoelectronic raster-type displacement transducer 77−74384
solid-state device conference, Tokyo, Japan (Sept. 1976) 77−76901
surface diffuse reflection optoelectronic meters 77−79135
symmetrical-input optoelectronic system, direction-finding sensitivity control 79−50401
tachometer, with contamination prevention 80−73344
thin-film optical waveguide periodic structures, appls. *(Polish)* 78−50947
three dimensional computerised monitoring of human motion 77−48886
threshold sensitivity calc., background spatial charact. determ. errors 79−26134
tonometer, non-contact, for intra-ocular press. meas., status report 77−2063
transfer function meas. and digital data processing apparatus 79−50399
two-component spirit-level for whole-arm prostheses *(German)* 79−8572
vibration transducer based on coordinate photodetector 79−75495
visual pyrometric systems, optoelectronic convertor characteristics *(Russian)* 78−77919
Al-Ga-As heterostruct. with confined current flow, fabrication 78−68081
GaAlAsSb/GaSb alloys, prep. and optoelectronic device appl. 80−25587
GaAs and related cpds., conference, St. Louis, MO, USA (Sept. 1978) 80−8737
GaAs, picosecond optoelectronic switching 77−23742
GaAs semi-insulating substrates, monolithic integration of optical and electronic devices, review 80−58543
GaAs thin film growth by MBE process, military appl. 79−52129

optoelectronic devices continued
GaP-anodic oxide devices, optoelectronic device, processing appl. 78−84304
In_2O_3:Sn films, doping profiles and elec. props., appl. to optoelectronic devices 79−38203
$LiTaO_3$ monocrystal lapping and precision machining characteristics *(Japanese)* 79−80593
Si devices for optical signal processing and communications 79−37056

optrons *see opto-isolators*

OPW calculations
alkali metal binary intermetallic cpds., OPW calc. of struct., bonding and stability 77−43169
anisotropic normal metal, thermopower calc. 80−24879
band structure calculations, criticism of OPW method 78−56064
binary alloys, and intermetallic cpds., struct. and stability, ab initio pseudopot. calcs. 78−34460
binary alloys, form factors of pseudopot., OPW calc. *(Russian)* 79−19498
bound states, orthogonalised plane wave set construction method 79−25894
completely orthogonalised plane wave method, model pseudopotentials *(Russian)* 78−34740
diamond, valence electrons XPS spectrum, OPW calc. 77−4715
diborides of light metals, X-ray emission spectra and transition probability calcs. *(Russian)* 77−52203
electron gas, uniform, electronic props. of H and He impurities 80−96807
graphite, band theory, Fermi surface constructed, ab initio energy band calc. 77−11841
graphite, band theory, press. effects on Fermi surface 77−85131
halide anions, in gas, photodetachment cross-sections, OPW and APW calcs. 77−38607
Hartree-Fock energy bands using OPW method 80−10856
instability rel. to error in core eigenvalues 78−63963
metal, pseudopotential theory, completely OPW method and orthogonalised hole conception *(Russian)* 77−62792
nontransition metals, zone struct., fully OPW calc. *(Russian)* 79−46994
phonon spectra, exact normalization of single conduction electron states in pseudopot. calcs. 77−7803
photodetachment cross-sections, OPW and APW calcs. comparison 77−38607
α-quartz, valence electron states and X-ray emission spectra, pseudopot. and OPW calcs. 77−35866
α-quartz, valence electron states calc. by pseudopotential method 77−20239
simple metals, electronic charge density, OPW-based pseudopot. calc. 78−87896
solid, orthogonalised augmented plane wave method, appl. to ZnS 77−66105
transition metals, OPW and MOPW calcs. 79−90942
X-ray photoelectron spectra struct. *(Russian)* 77−63544
X-ray photoionisation cross section calcs., at. and mol. levels, HF rel. to OPW method 77−42353
Ag (111) surface, photoemission, final states 78−11080
Ag, electronic contribution to thermal cond. at low temps. 79−95384
Al alloy, dil., Hall coeff., calc. by 4-OPW approx. 78−76052
Al dilute alloys, elec. resist., impurity and temp. depend. 80−65526
Al, Fermi surface under homogeneous strain, local pseudopot. model 80−29308
Al, impurity low-field galvanomag. coeffs., 4 OPW calcs. 77−69304
Al, magnetoresistance size effect, effect of cyclotron orbit nature 78−47767
Al-Ag(Mg)(Zn)(Ga)(Ge), dil., deviations from Matthiessens's rule, 4-OPW approx. calc. 79−19574
Al-Ga(Ag), dil, Hall coeff. by OPW Fermi surface model 80−6816
Al-Ga(Ge)(Mg)(Si)(Zn)(Ag), dil., Dingle temp. calc. 78−39005
Al-Ge(Mg)(Zn)(Ga), dil., electronic transport coeffs. for point defect scatt., 4-OPW calc. 79−42531
AlB_2, band struct. and density of states, metallic behaviour 77−59249
BeB_2, band struct. and density states, metallic behaviour 77−59249
C, amorphous, inelastic electron scatt., valence electron contrib. 80−55240
CaF_2, electronic band struct. determ., combined OPW and tight binding calc. 77−85145
CdS, band structure calcs. by modified orthogonalised plane wave (MOPW) method 80−54609
Cu, electronic contribution to thermal cond. at low temps. 79−95384
Cu, electronic transport properties, OPW calcs. 77−43553
CuCl, band struct., OPW calc. and X-ray spectra meas. 80−75506
Ge, valence electrons, XPS, LCAO and OPW calc. 77−12496
InSb, at Γ-point, spin depend. wave functions and band parameters 77−72818
KCl, band struct. calc. by mixed LCAO and OPW method 77−8019
Li, electronic structure and lattice const. determ. using orthogonalised modulated plane wave method *(Ukrainian)* 79−42436
LiCL, band struct. calc. by mixed LCAO and OPW method 77−8019
LiH, solid. Hartree-Fock energy band calc. using OPW method 80−10856
Mg, electric field gradient and Knight shift, temp. depend., OPW calcs. 78−56387
Mg, thermopower calc., 1-OPW model 79−38053
MgB_2, band struct. and density of states, metallic behaviour 77−59249
NaCl, band struct. calc. by mixed LCAO and OPW method 77−8019
Pb and Pb-Mg, dil., resistivity, multiple plane wave calc., Fermi surface, vel. and band struct. 77−51723
Pb, Fermi surface, uniaxial stress depend. 79−65362
Rb, lattice dynamical props., conduction-core exchange, Lindgren approx. 79−1481
$(SN)_x$, electronic struct., X-ray and UV photoemission obs., OPW and pseudopot. calcs. 78−6832
$(SN)_x$, electronic struct. and opt. props. 78−6256
Se, charge density, self-constent OPW and pseudopot. calcs. 80−92813
Se, Compton profile, charge density and momentum density determ. 77−63480
Se, trigonal, behaviour of optical gap under press. 80−80171
Se, valence electron Compton profile, self-consistent OPW calcs. 77−36307
Si, valence electrons XPS spectrum, OPW calc. 77−4715
SiAs, monoclinic , band struct calc. 77−59255

OPW calculations continued
Sn, white, band masses and deformation pots., OPW pseudopotential model 80−100430
Sn, white, Fermi surface, dilational strain depend., OPW calcs. 80−84418
Fe, trigonal, self-consistent ground state, X_α calcs. 80−54604
TiS_2 layer compound, electronic ground state, band struct. calcs. 77−51651
TiS_2, valence density of states 80−44465
$TiS_2(Se_2)$, charge densities, X-ray form factors, and bonding props. 79−94950
$TiS_2(Se_2)$, core states, energy bands, and valence densities of states 79−95322
$TiS_2(Se_2)$, valence density of states, Gilat-Raubenheimer method 80−88465
$TiSe_2$ layer compound, electronic ground state, band struct. calcs. 77−51651
ZnS, band structure calcs. by modified orthogonalised plane wave (MOPW) method 80−54609
ZrS_2 layer compound, electronic ground state, band struct. calcs. 77−51651
ZrS_2, valence density of states 80−44465
$ZrS_2(Se_2)$, charge densities, X-ray form factors, and bonding props. 79−94950
$ZrS_2(Se_2)$, core states, energy bands, and valence densities of states 79−95322
$ZrS_2(Se_2)$, valence density of states, Gilat-Raubenheimer method 80−88465

OR *see operations research*

OR gates *see logic gates*

orbital calculation methods
see also APW calculations; atomic orbitals calculations; EHT calculations; GO calculations; GTO calculations; HMO calculations; KKR calculations; LCAO calculations; molecular orbitals calculations; NDO calculations; OPW calculations; PNO calculations; PPP calculations; STO calculations
$\langle J^2 \rangle$ quantum number calcs. 78−90059
ab initio effective core pot. method appl. to F_2, Cl_2 and LiCl 80−32625
ab initio molecular fragment calculations with pseudopotentials 79−93905
addition theorems of spatial functions, multicentre integrals of arbitrary atomic functions, symmetry and analytical struct. *(German)* 80−37729
additive-orbital scheme for calculating atomic and molecular polarizabilities 77−3273
atom, orbital rel. to total SCF energies, HF SCF approx. formula 78−21837
atom, valence electrons local-density theory of exchange and correlation energies 80−52854
atomic correlation energies calc., Wilson's scaling parameter evaluation 80−5486
atomic system, two-electron, Schrodinger local energies 79−41090
atomic two-parameter exponential-type basis functions 80−52847
basis sets, completeness and linear independence 78−62691
basis sets completeness, Lowdin's criterion 77−23411
bond orbital model, model pot. approach, appl. to Li_2 and LiH 79−49923
bond order, max. principle rel. to choice of basis orbitals and wavefunctions 79−36498
Brillouin theorem, proof 80−91415
chemical bonding, possible new interpretation *(French)* 79−9989
CI, high-order replacements inclusion, appl. to H_3O^+ inversion barrier 80−63504
CI SCF calc., improved virtual orbital constuction 79−93928
Combination of Atomic Boxes MO model, development and testing 80−32592
comparison of classical analytic theories for the motion of artificial satellites 80−8515
configuration interaction method formulation for triplet states 78−37536
contracted Gaussian basis set for correl. wave functions, appl. struct. and energies 80−52881
Coulomb interaction integrals bounds 80−52856
coupled cluster many electron theory, unitary group formulation 80−52859
coupled oscillator natural orbitals 77−57853
D_{4h} symmetry, even and odd parity orbital combination Clebsch-Gordan coefficients 78−45514
density functional theory, quantum mech. system, accurate pot. and energy functionals 80−52849
density functionals in unrestricted Hartree-Fock theory 79−89583
diagram approach to character formulas for finite and compact groups 80−36888
diatomic orbitals, shielded, two-centre integral evaluation methods *(French)* 79−49931
dipole absorption oscillator strengths, simple approx. method for computing radial wave functions 78−62111
effective convergence to complete orbital bases and at HF limit through systematic Gaussian primitive sequences 80−14065
electron correlation calculations, scaling and Pade approximants rel. to perturbation series 80−5487
electron density calc., approx. differential eqn. 80−47864
equation of motion-Green's function and CI methods comparison, appls. 80−47841
equations of motion Green's function methods, higher order terms, ionisation pots. 80−52891
equations of motion Green's function methods, higher order terms, ionisation pots., CI comparison 80−52892
equivalent spherical harmonics 78−41911
excitation energy, eqn. of motion method calcs., approxs. and error anal. 79−36501
excited states, generalised Brillouin theorem multiconfig. method 77−67993
excited states, wavefunction calcs., symmetry-adapted cluster expansion method 79−9994
extension of Gauss' method for the solution of Kepler's equation 80−8524
finite electron no. system, approx. Green's-functions algebraic formulations 80−47849
floating orbital geometry optimisation with floating outer-shell basis functions 80−95517
function expansion about displaced centre 78−17556

orbital calculation methods continued
Gaussian basis sets, uniform quality 77−34555
generalised HF natural orbital CI approach, appl. to trimethylene diradical 77−75062
generalised perturbation theory, quality of first order wave function 77−67963
gravity gradiometers mounted on satellites used to improve orbit estimation 80−8523
group theory, space and point group factorization, appl. to crystallography and spectroscopy 79−60295
HAM/3, semiempirical MO calc. method 79−89587
Hamiltonians, effective, appl. to atomic pot. transferability in hydrocarbons 80−42933
Hartree-Fock energies, scaled 1/Z expansion, integral eqns. 80−47886
hybrid orbitals and Runge-Lenz vector, matrix elements 77−38606
hydrocarbons, double-zeta quality ab initio mol. fragment calcs. with pseudopots. 79−85879
improved uncoupled Hartree-Fock perturbation methods, 2nd-order energy bounds in UCHF perturbation theory 79−85884
incomplete basis set problem, perturbative corrections to coupled Hartree-Fock theory 79−18100
incomplete basis set problem, virtual orbitals and CIBS expansion of HF energies 80−52844
independent-particle Hamiltonian, group struct. 79−22580
inner charge defect method, appl. to bound and free excited atomic states 80−78511
lagrangian multipliers in frozen core Dirac-Fock calculations 78−73881
limited MC SCF theory 79−36537
LMO population calc. method from given SCF eigenvector matrix, appls. 80−14063
local multigaussian FSGO one-determinant wave functions, energy gradient expression 80−23282
localisability in spatial and energetic methods, measured by absolute overlap and 2nd moment dispersions 78−74557
localised and pseudo orbitals, steepest descent method 79−18102
many-body system, effect of increasing N *(French)* 78−37539
many-electron problems, density equation approach, limitations 79−76328
many-valence-electron pseudo-wavefunction, ats. and mols., exact theory 77−79534
matrix element formulas, off-diagonal hypervirial and off-diagonal Hellman-Feynman methods 78−33409
maximum overlap and shape instabilities 79−40401
MC-SCF theory, orthonormality-constrained orbital optimisations 78−86766
method of moments, pair functions, biorthonormal orbitals 77−26965
MNDO method, approx. and parameters 78−910
MNDO results for H-, C-, N-, and O-containing mols. 78−911
MNDO semiempirical calcs. accuracy rel. to current MO methods 80−47893
model potential method, for atoms 79−36513
molecular, geometry optimisation in ab initio SCF calcs., appl. of Hellmann-Feynman force 79−49927
molecular electronic structure, multiple scattered wave method, incl. interatomic forces 79−59325
molecular open shells, RHF treatment without Lagrange multipliers 80−32589
molecular spinors from the quasi-relativistic pseudopotential approach 79−97963
molecule, incomplete basis set correction, HF approx., differential eqn. formulation 79−63890
molecule, modified Sharma formula for STO Lowdin alpha functions, coeff. matrix recurrence relations 79−31364
molecule, one-particle Green's function with multiconfiguration reference states 79−31363
molecule, orbital rel. to total SCF energies, HF SCF approx. formula 78−21837
molecule, orbtial and total SCF energies, Ruedenberg's formula evaluation 78−37537
molecules, multiconfigurational wave functions, optimization scheme 77−57889
multiconfigurational complex MO method simplification 79−85878
multiconfigurational reference states, orbitals optimisation 79−10002
multiple scattering technique space partitioning effects, appl. to H_2 and H_2^+ 79−85883
multipole expansion of diatomic overlap method, 2-electron integral evaluation 78−908
NDO schemes, calc. of largest mol. integrals over orthogonal hybrid orbitals 78−41956
Newton-Raphson scheme, comparison with super-C I, for complete active space SCF method 80−47904
nonbonded interactions, density response theory, appl. to rot. barriers 78−41913
nonperturbative open-shell many body formalism, core-valence separation and nonorthogonal basis sets 78−896
numerical differentiator for atom orbital calcs. 79−81147
one-electron density matrix, optimisation 77−79532
one-electron wavefunctions, optimisaton method, effectiveness 77−34538
open shell orbital theory with electron correl., wavefunction cluster expansion 79−13647
open shell SCF theory 78−94179
open shell systems, orbital energies 78−78613
optimised one-electron wave functions, determ. ionisation energies of atoms 77−38599
optimised one-electron wave functions, general procedure of optimisation 77−38597
optimized one-electron wave functions, appl. to isoelectronic series Li, Be, B, and C 77−38598
organic semiconductor, electron energy states, alternate mol. orbital method 79−65353
orthogonality, radial orbitals, energy invariance 78−84
orthonormality constrained orbital optimisation technique 80−5465
orthonormality-constrained variation method, appl. to max. and min. overlap, localised and hybrid orbitals 79−6830
orthonormally constrained variation method, basis vector sets, pair orthogonality 77−75050
partitioning method, appl. to polyglycine conformation 78−94189
PCILO method, modified, second-order energy using CNDO/2 and INDO Hamiltonian approxs. 79−36533
perturbation theory, variable basis sets, numerical finite perturbation vs. analytic approach 79−59330

orbital calculation methods continued
perturbed Hartree-Fock calculations, with reduced Green's functions, theory 77−14338
polar molecule, excited state MCSCF wave functions, BeO appl. 80−47916
positive orbital energies and the instabilities of orbital-optimized wave functions 80−58109
positronium negative ion, autoionisation states, complex rotation method 79−81307
quantum chemistry, spin-free, alternacy, quantum no. assignment 79−9988
quaternionic molecular orbital approach to electron correlation 79−59327
Rayleigh-Ritz method, convergence of Slater, Gauss and two-electron functions 77−65419
Rayleigh-Ritz method, criteria for convergence 77−67959
reduced Bessel functions, as at. orbitals, appls. 79−31361
reduced density matrices, permutational symmetry 78−41912
relativistic HF calculations, appl. of effective pots., appl. to PbO mol. props. 78−74559
relativistic pseudopotential theories and corrections to Hartree-Fock method 80−63523
revised IOC-ω technique 79−18099
SCF open shell orbitals, iterative process 78−90066
SCF orbital equations, closed-shell, open-shell, and multiconfig., orthogonal gradient soln. method 79−36503
self consistent electron pair theory, perfect pairing valence bond generalisation 80−63532
semiempirical methods, two-centre Coulomb integrals 79−10005
Singer polymal tempering methods 80−52845
Slater-transform-Preuss functions, appls. 78−37547
spectral props. of many electron atomic Hamiltonians, appl. to 2-electron atoms 79−63922
spin optimised SCF general spin orbitals, theoretical formulation 78−5125
spin-coupled particle-hole excitation, general matrix element formulas 80−69086
spin-free CI procedure using 1-parmaeter alternant MOs, appl. to butadiene 79−85887
spin-free quantum chemistry, Hartree-Fock theory, unitary group-formulation 79−85885
stochastic transition, determination method 79−71366
symmetry-adapted-cluster expansion, variational determ., open-shell orbital theory applic. 78−54213
ternary chalcopyrite, optical and diamag. susceptibility, bond orbital theories 77−55761
thermochemical parameters, orbital model, quantum mech. theory 78−31675
three-centre one-electron integral calc. in Slater orbitals with different exponents 79−26876
Titius Bode Rule for solar planets and planetary satellites, c.f. Bohr atomic orbitals 79−101057
trial wave functions, by off-diagonal hypervirial theorem 79−22578
two-determinant numerical self-consistant at. orbitals, appl. to ^{11}B 79−93937
two-electron atom, exchange and correlation pots., density functional theory 80−52848
universal basis set, for atoms and mols. 79−36502
valence electron methods, effective core pot. valence electron UHF method 77−30786
variational method, metric-constrained, for atoms and mols. 79−22579
variationally optimised local central pot. model, single-term at. state props. calc., $2<Z<55$ 79−41123
virtual orbitals modification, computational implementation 79−85880
Waller-Hartree spin-free method, many-electron theory 77−38600
wave function structure, complex coord. method 78−94190
^3He, superfluid, orbital dynamics of ABM state, microscopic approach near absolute zero 77−39716
Li chain, disordered system, ab initio cryst. orbital calcs. 77−47715

orbitals, atomic *see atomic structure*

orbitals, molecular *see molecular energy levels*

order, long-range *see long-range order*

order, short-range *see short-range order*

order-disorder changes *see order-disorder transformations*

order-disorder transformations
see also polymorphic transformations
A_3B alloys, order-disorder phase transition at (100) surface 78−95747
Abelian and non-Abelian models, dual transforms., phase transition points *(Russian)* 79−2735
adamantane, plastic-phase transition, cell model 77−11665
adlayer-induced LEED beams near order-disorder transitions, Monte Carlo study 79−82438
adsorbed film, on BCC cryst., modelling of order-disorder transition, Monte-Carlo method 78−60033
adsorbed layers, order-disorder transition, effect on work function 80−59791
adsorbed monolayer, classification of continuous order-disorder transitions 79−7743
adsorbed monolayer, classification of continuous order-disorder transitions 80−19910
adsorbed monolayers, order-disorder transitions, classification and characterisation, review 80−52149
adsorbed overlayer, order-disorder transition, Ising model, LEED superlattice beam intensity distrib. 80−65371
adsorbed system, order-disorder transition classification, realisation of four-state Potts model 77−51605
alkali halide, electric-dipole ordering of tunnelling impurity centres 80−2215
n-alkane, order-disorder phase transition bits. calc. 77−72684
n-alkane binary mixtures, melting and solid-state transition 77−72685
alkylammonium compounds with perovskite-type layer struct., symmetry of lattice vibrs. 78−22797
alkylammonium metal tetrachlorides, struct. phase transitions 80−75348
alkylammonium zinc tetrachloride cpds., high temp. phase transitions 80−54372
alkylenediammonium metal tetrachlorides, struct. phase transitions 80−75348
alloy, AB type, equilib. props. by Markovian simulation 78−91302
alloy, BCC, order-disorder transform. in surface layers, theory *(Russian)* 78−19739

order-disorder transformations continued
alloy, binary, order-disorder transition kinetics, computer simulation 80−92643
alloy, binary, simultaneous mag. and spatial long-range order 77−69491
alloy, binary, with arbitrary mole fraction, order disorder transition in case of FCC lattice 80−88295
alloy, CuAu type struct., interstitials distrib. *(Russian)* 77−47542
alloy, FCC closed packed, ordering-type transitions 80−2140
alloy, HCP, variations in Brillouin zone due to order-disorder phase transform. *(Russian)* 79−51100
alloy, $L1_2$ ordered, yield stress 77−52392
alloy, statistical theory of atomic ordering 77−15542
alloy, ternary, ordered, Green's function treatment, disorder transition 77−15540
alloy, theory of ordering, crystal lattice parameters rel. to composition and order *(Russian)* 79−77543
alloy, variation in interatomic interaction and lattice parameters during ordering *(Russian)* 77−81255
alloys, A_3B type, surface effects on order-disorder phase transition 77−76556
alloys, AB stoichiometry, mean field theory of ordering 78−2233
alloys, binary, BCC, order-disorder transform., three-body interaction effects 80−39257
alloys, binary, ferromagnetism and spatial long-range order 80−60159
alloys, concentrated, local atomic arrangements, associated with ordering, review 80−50632
alloys, disordered binary, crit. US attenuation 79−99272
alloys, DO_{22} and $L1_0$ superstructures, atomic ordering, multicluster approx., order-disorder transition 80−38990
alloys, ferromagnetic exam. of atomic ordering mech., when in mag. field *(Russian)* 79−11609
alloys, interstitial solid solns., HCP, ordering type transitions within thermodynamics theory framework 80−49162
alloys, $L1_2$ and $L1_0$ superstructure atomic ordering phase diagrams, order-disorder transition 80−38989
alloys, ordered, cryst. struct. and phase transforms. *(Russian)* 79−29047
alloys, substitutional disorder description within supercell model 78−26479
alloys, transformation kinetics 80−2138
alloys ternary and binary, phase diagrams and transition temp., correl. function approach 79−95164
ammonium halides, cryst., H bonding, order-disorder phenomena 80−6379
ammonium hydrogen chloracetate, order disorder type transition 79−47399
amorphisation due to ion bombardment, SRO struct. 80−79844
aniline hydrobromide, ferroelastic, acoustic softening near transition temp. 80−96617
anthracene:tetracyanobenzene charge transfer complex, cryst. struct., temp. effects 80−96508
anthracene-TCNB, 1:1 charge transfer complex, phase transition at 206K, NMR meas. 79−7690
antiferroelectric model dynamics, order-disorder transition, correl. functions and polarisation waves *(Russian)* 80−50282
antiferroelectric transition, phenomenological theory 79−4771
antiferromagnets, order parameter of dimens. 6 and 3 79−42762
antimonates, $M_4^{II}M^{III}Sb^VO_8$ spinels, struct. determ., IR and Mossbauer spectra 79−91431
aqueous suspensions of spherical colloid particles, phase transitions 77−4938
argyrodites, new family of tetrahedrally close-packed structs. 79−60300
aspartate-transaminase, phys. state in cryst., heating curves 77−70409
BEC binary alloys, order-disorder transformation kinetics 79−20040
binary alloy, atomic ordering and ferromagnetism 79−87278
binary alloy, elec. resist. due to crit. fluctuations near order-disorder temp., theory 77−40071
binary alloy, ordered BCC to disordered FCC transition 77−43327
binary alloy with BCC type lattice, order-disorder transition 79−78957
binary alloys, acoustic modes in random and correlated alloys, order-disorder transform. 80−65189
binary alloys, crit. dynamics of order-disorder transition 78−87788
binary alloys, meas. of ordering instability 79−38818
binary alloys, nonstoichiometric, mean field theory, improved approx. 80−79910
binary BCC lattice model, Monte Carlo calc. of transition temp. 77−62614
binary ordering alloy, gas absorption, correl. effects *(Russian)* 78−47525
binary ordering alloy, theory of surface effects 79−19434
binary oxides fluorite related struct., order-disorder phenomena, Raman spectra 77−65960
bitransitions, two-level disordered systems 78−43102
β-brass, disordering under γ-irrad., elec. resist. meas. *(Russian)* 77−48429
α-brass, electron irradiated, defect production and interdiffusion 78−67739
β-brass, quenched single crystal, deform. and slip 79−79026
β-brass, vacancy form., ordering effect, positron annihilation obs. 80−93427
brass, vacancy formation enthalpy, composition depend., position annihilation obs. in Cu rich phase 79−95872
β-brass order-disorder transition, crit. temps. and exponents rel. to composition 77−8818
Brightray S, lattice contraction during ageing 80−3030
catalase, phys. state in cryst., heating curves 77−70409
ceramics, local atomic arrangements, associated with ordering, review 80−50632
chain conductors, CDW ordering 78−79731
chalcopyrite compounds, ternary, review 79−70048
chemisorbed layer, depend. of work function in order-disorder phase transition 79−19460
chiral order in helimagnets 79−42715
2-chloronaphthalene, order disorder transition, 253 to 309K, X-ray diffr., calorimetry study 78−75829
chromocene, heat capacity meas., phase transitions 78−38853
classification of struct. transforms., using coupled double-well model 78−14443
cluster approach 79−94943
cluster phenomena, displacive to order disorder crossover 80−10629
cluster walls and phonons in structural phase transitions 79−77720

order-disorder transformations continued
colloidal systems, ordering, statistical mech., theory 78−23968
commensurate-incommensurate transition, coupling between phase solitons and strain 79−28073
cond. electron wave function, lattice symm. depend. 77−85844
conference, phase transformations in metallurgy, York, England (Apr. 1979) 80−2994
continuous transformations 77−8817
coupled oscillator system, stochastic transition, Toda criterion reliability 77−74308
critical dynamics below T_c 80−27256
critical dynamics far from equilibrium 80−27258
critical phenomena, use of renormalisation group, review 77−20625
critical scattering of neutrons and X-rays, meas. techniques 79−55609
crystal classification by transition mechanisms *(Russian)* 78−60401
crystal layer order-disorder structures 80−38981
crystals with dislocations, phase transitions of the second kind, dislocation superparamagnetism *(Russian)* 80−1957
de Gennes pseudospin model, lattice phonons tunnelling effects 79−73290
n-decylammonium cadmium chloride, perovskite-type layer cmpd. n-decylammonium chain dynamics 79−99313
degenerate semiconductors, heterogeneous state, first-order phase transition, Ginzberg-Landau method analogue 80−70372
1,2-di(1-naphthyl)-ethylene, cis-trans photoisomerization in condensed phase, polycryst. phase transition 79−10139
dialkylammonium cupric chloride, calorimetric study of phase transitions 78−75804
dialkylammonium manganese chloride, order-disorder transition mechanism 78−79772
dialkylammonium metal chlorides, soft modes, phase transitions 78−79723
dialkylammonium zinc dichlorobromides, long chain cpds., phase transitions, calorimetric study 80−70390
diamantane, structural changes within plastic phase 79−14929
dicalcium strontium propionate, Raman scatt., order-disorder type transform. 77−12373
dichlorodurene, order-disorder phase transition, struct. from neutron diffr. at 70K 78−55825
diethylammonium cadmium chloride, X-ray study of structural phase transition 78−2055
diethylammonium cadmium tetrachloride, first order phase transition, optical phonon line broadening, spin-phonon coupling model 80−7335
dimethylammonium cadmium chloride, soft modes, order-disorder transition model 78−22817
dimethylammonium cadmium chloride type crysts., struct. transitions model 78−71834
dimethylammonium manganese chloride, neutron diffr., 188K, cryst. struct. 77−47434
dimethylammonium manganese tetrachloride, H-bonding, struct. transition, neutron diffr. study 79−42004
disorder parameter, phase transition theory, rel. to entropy 80−52146
distortive phase transitions, order-disorder and displacive regimes, mol. dynamics study 80−75324
education, renormalisation group theory, second order phase transitions, undergraduate statistical physics 78−62012
electron irradiation effects on kinetics of order-disorder transformations 80−34056
electrostatic energy of disordered distribs. of vacancies or altervalent ions 78−9995
ethane submonolayer on graphite, struct. and melting, elastic neutron scatt. 80−29266
ethylammonium cadmium tetrachloride, order-disorder transition, far IR reflectivity obs. 79−65870
fcc alloy, A_3B ordering process time evolution, Monte Carlo simulation 79−86869
FCC alloys, atomic ordering and antiferromagnetism 78−72330
FCC lattices, ordered superstruct., phase diagrams, cluster variation calc. 80−39256
ferrocene, model, established from NMR expts. 77−15328
ferrocene, ordered, disordered phases, structs. *(French)* 78−63749
ferroelastic transitions, order parameter symm., free energy expansions 80−49164
ferroelectric, crit. dynamics, NMR data compared with dielec. data 78−76415
ferroelectric, mixed order-disorder displacive transition, model 77−59540
ferroelectric, order-disorder model, thermodynamic props. 78−10856
ferroelectric, unified theory for order-disorder and displacive types 77−12329
ferroelectric transition unified theory 77−20808
ferroelectric with orientational transition, coupled elastic, EM and polarisation oscill. spectrum 79−8103
ferroelectrics, exactly solvable model 77−32337
ferroelectrics, order-disorder, displacive transformations, tunnelling, phonons 80−75975
flexible polymer chain in nematic solvent, phase diagram *(French)* 80−39253
fluctuations of order-parameter with two time scales, critical growth and saturation effects 77−9975
fluorite crystals, disorder at high temp., Brillouin scatt. 78−2866
fluorite crystals, Raman scatt., anharmonicity and high temp. disorder effects 78−35132
free energy, order-parameter expansion appl. to some phase transition model 78−43099
gauge systems and two-dimens. spin systems 78−70072
glass-fibre reinforced PET, order-disorder transitions during extrusion 80−50633
graphite, Cs-intercalated, melting and staging, X-ray scatt. obs. 79−19180
graphite, intercalation compounds with alkali metals and halogens, intralayer crystal struct. and order-disorder transform., electron diffr. 78−26540
graphite intercalation compound $C_{24}K$, order-disorder transition, X-ray study 80−33922
graphite intercalation compounds with K, Rb, Cs, resistivity anomalies and phase transform. 78−26839
graphite intercalation cpds., struct. and order-disorder transforms. 78−71710
graphite intercalation cpds. with K, Rb, or Cs, phase transitions, resistive anomalies, electronic props. 79−95405
graphite-halogen intercalation compound, calorimetric study of order disorder transform. 79−52206
graphite-HNO_3 intercalation compounds, differential scanning calorimetry investigation 79−42234
graphite-ICl intercalation compounds, anomalous sp. ht. due to order-disorder transform. 79−42235
graphite-K intercalation compounds, electronic props., resistivity, Hall effect and magnetoresistance 80−75585
group theory end of ordering type phase transforms *(Russian)* 80−103287
hard core trigonal mols. on triangular lattice, phase transition, eqns. of state 77−59089
Heusler alloys, order-disorder transitions, intermediate model 80−54341
Heusler alloys, ternary, Bragg-Williams approx. 79−90755
Heusler alloys, ternary Bragg-Williams approx. 79−90756
HMTTF-TCNQ chain, three dimensional ordering 78−95152
ice, phase transition from disordered VII phase to ordered VIII phase 80−19911
ice, VII to VIII transition, lattice model 78−10187
ice IV, thermal expansion anomaly rel. to order/disorder transition at 115K, 10.54 kbar 79−46819
ice VII-ice VIII phase transition, second-order, Haus-Tanaka model 80−70385
illite, vacancy ordering, transition state cluster model, electron diffr. 77−47547
α-In_2Te_3. I phase, order-disorder transform. for DO_{22} struct., thermodynamic study 80−70155
incommensurate systems, transitions, solitons 79−77714
intrinsic and extrinsic central peak properties, review 80−34168
ionic crystal, sublattice disorder, phenomenological models 77−35663
irradiation induced crystalline to amorphous transition, Gibbs energy 80−70371
Ising model percolation and phase transitions 77−13704
Ising model with nearest neighbour ferromagnetic interactions, phase transition theorems 77−22501
kinetic Ising model with quenched relaxing impurities, crit. dynamics 78−10167
kinetic theory, master equations *(Russian)* 78−47498
Landau crit. point, mean-field theory, scaling theory and crit. exponents to second order in ϵ^2 79−4395
Landau theory of structural phase transitions 80−92639
laser instability, example from synergenetics 80−9848
latex, monodisperse, mechanical props. 78−48701
latex, monodisperse, order-disorder phase transitions, short-range order 77−29056
latex, monodisperse, phase transition pressure determ. from sedimentation equil., Alder transition model 77−70344
latex, monodisperse, reflectivity obs. of phase separation into ordered and disordered phases 77−70345
lattice gases of hard core molecules having two orientations, phase transitions 78−29059
layer systems, intercalates, phase transforms., CDW and mass density waves 80−39281
lipid membrane order, mol. theory 79−66452
lipid membranes, orientational phase transitions with mol. config. change 78−14444
lyotropic liquid crystal, struct. rel. to amphiphilic structure 78−51416
metal, HCP structure, interstitial ordering *(Russian)* 78−79610
metal, thermopower near magnetic and order-disorder critical points 79−65454
metal-H, phase transitions 80−50631
metallic system, heterogeneous state form. due to long range interaction *(Russian)* 77−7842
methane, solid, probing phase transition with Mossbauer effect in ^{57}Fe impurities 79−4751
methane-d_4, critical behaviour at orientational order-disorder transitions, neutron scatt. 77−43308
methane-d_4, solid, US attenuation, phase transitions 79−51204
model for crystal with several orderly sublattices 77−59098
molecular crystal, conditions of existence as mesogenous system 79−60488
molecular crystal, unidimensional struct. instability charge under torsional force, liquid cryst. transition *(Russian)* 78−87776
molecular crystal spin model for orientational phase transition 78−30735
molecular crystals, crit. dynamics of orientational phase transitions 77−7838
molecular solids, melting curves, Lennard-Jones Devonshire theory 80−65201
multirhythm system, transition in causal dynamics 78−4580
multistate order-disorder model 80−70366
naphthalene-TCNB (PMDA), Raman spectra orientational disorder, charge transfer cryst. 78−19459
naphthalene-tetracyanobenzene, order-disorder transition, heat capacity and thermodynamic props., 5 to 300K 79−33100
Nimonic 80A, lattice contraction during ageing 80−3030
noncritical fluctuations and temp. depend. of order parameter 77−1204
nonlinear cooperative system, kinetic Ising model in Bethe approx. 77−13709
nonstoichiometric solid solutions, ordering 78−87794
omphacite, P2/n to C2/c transform. study 79−65183
one-dimensional diatomic chain, order-disorder transition, simple model 79−4394
ordered alloys, effect on mechanical strength *(Czech)* 77−1854
ordering alloys, effect of press. on phase diagrams and order-disorder transforms. 78−52797
organic molecular crystal, phase transforms. obs. using TEM, electron beam damage 78−34621
organic solids under pressure, IR spectra and phase transitions 79−95743
PAC method appl. *(German)* 80−2679
n-paraffin, rotator phase transformation, lattice dynamics Helmholtz free energy 78−34585
Permalloy, magnetic props. and struct. obs. by neutron diffraction method *(Slovak)* 79−4963
perovskite crystal, ABX_3, transition involving BX_6 octahedra rot., distorted phase symm. 77−4197
perovskite structure, phase transitions due to octachedra rots. 80−70151
perovskite structure, phase transitions due to octahedra rot., model 79−99103

order-disorder transformations continued
phase ordering, in quasi-one-dimensional system, review *(Japanese)* 80−2352
phase transition in BCC hard sphere lattice gas with second neighbour exclusions 80−160
physics of transitions, introduction 78−26660
plastic crystal, critical behaviour at orientational order-disorder transitions 77−43308
plastic flow, order-disorder transform. effect on creep, traction and relaxation *(French)* 80−35180
polyethylene, hydrostatically compensated, SRO in precrystallisation phase 79−69033
polyethylene oxide ionic complexes 78−47251
polystyrene, monodisperse latex, shear US meas. 78−31711
polystyrene monodisperse latex, anomalous viscosity in disordered state 80−74822
polyvinylcarbazole, fast hole transport 79−51628
Potts model, first order phase transitions, Monte Carlo renormalisation group method 80−34645
Potts model, three state, order-disorder structural transform. exam. 78−83918
Potts model, three-state, first order phase transitions 80−60333
propyl-1,3-diamino manganese chloride, structural phase transitions at 336 and 305K, NQR meas., DTA 78−63855
pyridinium iodide, order-disorder phase transition and reorientation fluctuations studied by Raman spectra 80−80764
pyrimidine bases, water vapour effect on struct. and amorphous-cryst. transition 77−70408
quantum crystals, discontinuous orientational phase transitions, thermodynamics, isotope effects 80−6590
quantum optics, transition phenomena, review 80−32944
quaternary alloy, order-disorder transition using classical fluctuation theory and correl. functions 79−73288
refractive index changes induced by struct. transitions 80−16000
relaxation processes in order-disorder transitions under short range correl. conditions 79−73889
rigorous bounds, quantum anharmonic phonon model 77−15541
Rochelle salt, phase transition mechanisms by optical spectroscopy 79−15411
self organisation mechanisms, synergetics, laser theory, chem. reactions and heat transfer analogies 77−34867
semi-infinite system, Landau-Ginzburg theory 78−47500
simple liquid intermolecular interaction, extremal values 78−87602
solid, phase transition, Raman study 78−80345
solid solution, interstitial and substitutional, ordering 78−79744
solid solutions, interstitial phase struct., reconstructive transition struct. symm. relationships 79−69246
solid solutions, ordering and disordering under irradiation 79−87626
solid solutions binary, order-disorder transitions, long range order parameter and chemical potential 80−6487
sp. hts., librational and reorientational 77−84946
spin system, isotropic, critical behaviour with long-range interaction 77−89966
spinel compounds, 1:3 octahedral order, review 80−88079
squaric acid, antiferrodistortive phase transition, proton chemical shift tensor determ. 77−63300
static critical behaviour, structural phase transitions 80−92640
static precursor nuclei, anomalies in high temp. superconductors, ferroelectrics, organic conductors 78−10165
steel, Si, commercial, ordering after heat treatment, Mossbauer meas. 80−7556
structurally incommensurate system, theory 78−79729
substitutionally disordered system in transition state, cluster model, electron diffr. patterns 77−20046
substitutionally disordered system in transition state, cluster model, electron diffr. patterns 77−47547
superionic conductor, phase transitions induced by elec. field 78−63856
superionic crystal, domain formation, thermodynamic theory 77−84963
superionic fluorites, structure and transport 80−84318
surface polariton scatt. at order parameter fluctuations, phase transition investig. *(Russian)* 77−20179
surface polariton scatt. by order parameter fluctuations near phase transition 77−35981
symmetry, of order-disorder structures 80−38982
system with nonconserved order parameter, influence of heat cond. on relax. of unstable states 80−10637
TCNB-pyrene 1:1 charge transfer complex, heat capacity, 10-300K, and entropy of transition 77−11702
TCNQ salt., $NMeQn(TCNQ)_2$, role of solvent in phase transition, thermal anal. and transport props. 79−33312
TCNQ salt, TSeF-TCNQ, short-range ordering investigated by XDE 80−59652
ternary alloy ordering, correlation effects, Kirkwood method calcs. *(Russian)* 79−66038
ternary alloys, AB-AC quasi-binary sections of order-disorder phase diagram 78−88463
ternary oxides, short-range order and superstructures 80−49159
p-terphenyl, crit. slowing down at struct. phase transition, high resolution neutron spectroscopy 79−82329
p-terphenyl, Raman scatt., order-disorder phase transition 78−43841
tetramethylammonium chlorate, order-disorder transitions, DTA and NQR meas. 77−66022
tetramethylammonium hexachloroplatinate, due to weak CH-Cl hydrogen bonds 78−92060
TGS:Cr^{3+}, EPR obs. of fluctuations near phase transition 78−43820
TGS, proton and deutron NMR anal. of temp. depend. 80−33919
TGS(Se), optical phonons near T_c, IR refl. and Raman spectra 77−48136
thermal expansion tensor for crysts. showing order-disorder transition, temp. depend. *(French)* 78−34636
thermodynamics of quenched random spin systems, phase transitions in spin glasses 77−73024
thiophenechromium tricarbonyl, sp. ht. and thermal expansion tensor meas., order-disorder phase transform. obs. *(French)* 78−79788
thiourea, phase transitions accompanied by noncommensurate superstruct. form. 77−32336
thiourea, phonon modes near order-disorder transforms., hard-core modes due to pseudospin-phonon coupling 80−44285
thiourea, phonon modes near phase transitions, IR and Raman spectra 80−45084
thiourea, Raman spectra of external frequencies 77−24840
order-disorder transformations continued
thiourea, soft modes 78−80361
TMCC chain compounds, Raman spectra and struct. phase transitions 79−56794
TMMC(-d) chain compounds, Raman spectra and struct. phase transitions 79−56794
transition metal alloys, ferromag., effects of order on electronic struct. 79−90938
transition metal hydrides, H ordering, review 80−60850
triamantane, phase transistions, X-ray diffr. meas. 79−14930
triangular and honeycomb lattice gases, order-disorder transitions to 2×2 struct. 80−4674
trimethylammonium cadmium trichloride, struct. phase transitions, low-freq. Raman scatt. obs. 80−80783
$(TTF)Cl_x$, disorder transition, cond. decrease and commensurate charge density waves 80−70153
TTF-TCNQ, Landau free energy function, CDW-libron interaction, sp. ht. near phase transitions 80−19963
TTF-TCNQ, phason and metal-insulator microdomain model, Young's modulus temp. depend. anal. 77−31964
TTF-TCNQ, short-range and long-range order of phason clusters 77−35874
tunnelling effects, self-consistent pseudospin-phonon formalism 79−55858
two dimensional periodic lattice, electron ordering, CDW-disordered state transition, Hubbard model *(Russian)* 80−6754
two dimensional system, ordering 80−107407
two order parameter model, thermodynamics in mean field approx. 79−33633
two-dimensional order-disorder phenomena, Monte Carlo simulation 78−67904
uniaxial dipole system, order-disorder transition, computer expt. and high temp. expansion 79−38494
urea-n-paraffin adducts, order-disorder transition, thermal anal., X-ray diffr., and NMR 79−33084
vanadocene, order-disorder phase transition, sp. ht. and crystallographic study *(French)* 80−84131
vibronic theory of ferroelectricity 79−19854
virial series divergence for hard discs and spheres at closest packing 79−94859
X-ray powder patterns of order-disorder structs. 80−38864
Ag Zn system, β-β' order-disorder phase transition 79−47678
Ag-Au, order-disorder transforms., s-band model 79−60502
Ag-Cd (approx. 50 at.%), disordered hcp to ordered bcc transition, meas. of activation energy 78−72773
Ag-Mg (18.5 wt.%), rheological study of crystallographic order on creep *(French)* 80−97548
AgAu, quenched, short range order effects on specific heat 80−29181
$AgBiS(Se)_2$, polymorphism and defects, electron microscopy 78−2254
$AgCrS_2$, mixed conductor props., near order-disorder transition temp. 80−44675
Ag_2HgI_4, 51°C, sound vels. and dielec. losses 78−10129
Ag_2HgI_4, superionic cond., cation disordering 77−84692
AgI, phase transition, statics and local dynamics, mean field and Mori theory 80−39347
AgI solid electrolyte plastic deformation and thixotropy obs. 78−79660
α-AgI, superionic, continuous order-disorder transition, Raman spectroscopic evidence 80−45070
Ag_2MI_4 (M=Cd, Zn), fast ionic cond. and order-disorder transition 79−99363
$AgNa(NO_2)_2$, ferroelec., Raman scatt. and phase transitions 80−71349
$AgNa(NO_2)_2$, single cryst., specific heat anomaly, −90-55°C, ferroelec. transition entropy 77−77157
$AgNa(NO_2)_2$, ultraslow crit. dynamics of order parameter, ^{23}Na spin relax. times obs. 78−76410
βAg_3SI, anharmonic thermal vibr. of cations 80−65214
Ag_3SI, superionic conductor, ordered phase struct. 78−83792
Ag_3SI, superionic cond., phase transition and cryst. structs., sp. ht., neutron and X-ray diffr. obs. 80−10662
Ag_2SbS_3, order-disorder phase transition, NQR and spin-lattice relax. expts. 78−47523
Ag_3SbS_3, NQR elec. field effect, temp. depend. near ferroelec. transition 77−77121
Ag_3SbS_3, pyrargyrite, order-disorder phase transition and elec. polarisation 79−38468
Al-Cu, anal. of electron diffr. micrographs using Patterson function *(French)* 79−20044
Al-Mn, metastable Ll_0 phase, transformations, mag. struct., TEM study 80−3029
τ-Al-Mn-C, permanent magnetism and microstruct. 80−75811
$Al_{45}Mn_{55}$, pure and C doped, phase transforms. 79−96022
α-Al_2O_3, atomic disorder, dominant type 78−63757
β-Al_2O_3 compounds, stoichiometry, phase transition and conductivity 79−23773
β-Al_2O_3, stoichiometric, Raman and IR spectra, Frenkel defects, order-disorder transition and cation cond. 80−55086
β-Al_2O_3-Ag_2O, stoichiometric and nonstoichiometric, structure comparison, phase transitions in stoichiometric compound *(French)* 80−60856
β-$11Al_2O_3$-Ag_2O, sublattice phase transition, stoichiometric 79−42241
Al_2O_3-SiO_2 system, andalusite and kyanite powders, shock induced transformations 80−45301
$AlPO_4$, twinning and phase transform., X-ray diffr. obs. 77−47466
As, condensed layers, low temp. allotropic phase transition *(Russian)* 80−54553
Au-Ag-Cd pseudobinary alloys, thermodynamic study of order-disorder and martensitic transform. 78−48399
Au-Mg (18 at.%) alloy, superstruct. determ., electron microscope obs. 78−75630
Au_3Cd, order-disorder phase transform., X-ray diffr. anal. *(Russian)* 80−45297
Au_3Cd, sputtered epitaxial films, order-disorder reaction obs. 78−84092
$AuCu_3$, quantum theory of order-disorder transition energy 77−62640
Au_3Cu, ht. of order-disorder transform., differential microcalorimetry *(French)* 78−57950
$Au_{11}Mn_4$, ordering, electron diffr. and high resolution TEM obs. 78−71707
Au_4Mn, electron irrad. in electron microscope, radn. ordering 79−86818
Au_4V, effect of structural changes on phys. props. 78−31400
B-transition metal thin films, amorphous to cryst. transformation 80−7563
$BaMnF_4$, dielec. anomaly, mechanism, spin canting 78−10744

order-disorder transformations continued
$BaTiO_3$, $A_1(TO)$ phonon spectrum, ferroelectric phase transition, Raman scatt. meas. 78−56478
Bi_2O_3, elec. props. of α, β, γ and δ phases 79−23771
C, structure change, during thermal ordering, radiation disordering 80−54283
$C_{24}Cs$ and $C_{36}Cs$, graphite intercalated, ordering of intercalant layers, X-ray diffuse scatt. 80−44182
C_8Cs, intercalation cpd., theory of order-disorder phase transitions 80−19908
$(C_5H_5NH)Ag_5I_6$, solid electrolyte, low-temp. phase transitions 77−72686
$C_{12n}K$, graphite intercalated, two-dimens. structurally disordered phases, X-ray diffr. profiles 80−44181
C_6Li, intercalate ordering in first stage graphite-Li 80−6380
C_8Li, theory of order-disorder phase transitions 80−19908
$(CO(NO)_2CL)_2$, order-disorder struct., X-ray data 80−39037
C_8Rb, intercalation cpd., theory of order-disorder phase transitions 80−19908
$CaBSi_2O_6$, B=Mg, Fe^{3+}, Al, pyroxenes, order-disorder interpretation 80−38987
CaF_2-rare earth trifluoride, characts. of ordering of solid solns., superstructure form. 79−14725
CaF_2-YF_3, fluorite- and tysonite-related ordered phases *(German)* 79−23725
$CaHPO_4$, monetite, low-temp. ordering of H atoms, X-ray and neutron diffr. study at 145K 80−39022
$CaWO_4$, solid-phase synthesis, disordering and vacancy defect form. 77−8774
$CdGa_2Se_4$-$CdIn_2Se_4$ solid solutions, order-disorder transition 79−19181
$CdGa_2Te_4$ film, effect of thermal annealing on struct., optical absorpt. and photocond. 79−65342
CdHg alloy, ω phase, mag. susceptibility anisotropy w.r.t. uniform compression *(Russian)* 80−71143
$Cd_{65}Hg_{35}$ and $Cd_{55}Hg_{45}$, X-ray study of cryst. struct. and thermal expansion 80−24405
$Cd(NH_3)_6Cl_2(Br_2)(I_2)$, crit. behaviour of light scatt. intensity at phase transitions 77−90141
Co-Pt, mag. annealing, form. of ordered phase, study using X-ray scatt. *(Russian)* 80−81052
Co-Pt, struct. and mag. props. rel. to degree of order 78−72368
$Co_{50}Mn_xGa_{50-x}$, ordering and disordering phenomena, mag. study 80−70154
$CoPt_3$, meas. of ordering instability 79−38818
Cr-Al, disordered alloy, effect of high press. on resistivity 78−95286
$CrNi_2$ type alloys, ordering, influence of static stresses *(Russian)* 78−56631
$CsHSeO_3$, and deuterated analog, vibr. spectra 79−24311
$Cs_3MoO_3F_3$, ferroelec. and order-disorder phase transitions 78−92037
$Cs_2PbCu(NO_2)_6$, one-dimensional stacking order 80−28941
Cs_2TiF_6, Raman spectra, internal and lattice vibrs. 77−8569
$Cs_3WO_3F_3$, ferroelec. and order-disorder phase transitions 78−92037
Cu, cluster and bulk, struct. and electronic props. 78−95592
Cu complex, $Cu(ONC_5H_5)_6X_2$, X=ClO_4, BF_4, cooperative Jahn-Teller ordering and mag. struct., EPR meas. 79−60505
Cu-Ag, order-disorder transforms., s-band model 79−60502
Cu-Al (21 at.%) transition state, tempered and quenched alloy *(French)* 80−55392
Cu-Al (9 wt.%) deformed, dispersed, ordered, microcalorimetry of plastic zones during fatigue crack propag. 79−47769
Cu-Au, influence of strain energy 78−84796
Cu-Ga alloys, massive phase ζ tempering, kinetics, order-disorder transform. *(French)* 78−44118
Cu-Mn, positrons as probe of phase transforms. 78−31401
Cu-Pd alloy, pressure effect on β-phase transition by elec. resist. meas. 79−15660
Cu-Pd alloy, singularities of physical props. and ordering *(Russian)* 78−76643
Cu-Pt, influence of strain energy 78−84796
Cu-Zn, rheological study of crystallographic order on creep *(French)* 80−97548
Cu-Zn strain energy 78−84796
β-Cu-Zn-Al, ordering, TEM obs. 78−39768
β-Cu-Zn-Al, ordering 78−68687
β-Cu-Zn(-Ni)(-Mn), order-disorder transformation temperature effect on quench hardening 78−95745
CuAu, order-disorder transform., band theory for internal energy 79−19539
Cu_3Au alloy, dynamics of ordering clusters in thermal non-equilib. state 79−51257
Cu_3Au and $CuAu_3$, band theory of order-disorder transforms. 79−60501
Cu_3Au, dynamics on transitional ordering process from disordered to ordered state 79−4267
Cu_3Au, heterophase fluctuations near order-disorder transform., X-ray and neutron diffr. 77−73272
Cu_3Au, meas. of ordering instability 79−38818
Cu_3Au, metastable states domain existence, phase transition ordering energy, press. effect *(Russian)* 80−45303
Cu_3Au, ordering process, cluster size evolution 78−39766
Cu_3Au, radiation disorder model of phase stability 80−16297
Cu_3Au thin films, fine-grained and disordered, low temp. ordering 80−97433
Cu_3Au, X-ray and inelastic neutron scatt. investig. of spinodal ordering 77−77473
Cu_3Au-$Cu_3Pd(Pt)$, quasibinary system, order-disorder transform., superlattice form. 80−2159
$Cu_{81.5}Au_{18.5}$, meas. of ordering instability 79−38818
CuAuI superlattice, (101) lattice twinning mode assoc. with ordering transition 77−15431
Cu_3Ga, transition state between long range order and short range order, model, computer simulation *(French)* 80−49371
Cu_2HgI_4, fast ionic cond. and order-disorder transition 79−99363
Cu_2HgI_4, superionic cond., cation disordering 77−84692
CuI, ionic motions nature, mol. dynamics calcs., sp. ht. anomaly due to order-disorder transform. 80−107533
CuI, superionic, NMR relax. evidence for sublattice melting 77−15623
$CuIn_5S_8$, sulphospinel electron diffr. and electron microscopy study, order-disorder transform obs. 80−88080
$Cu_{0.5}In_{2.5}Se_4$, transition state and domain struct. by electron microscopy and diffr. studies 80−15095
$Cu_{3-x}Mn_xAl$, and $Cu_2Mn_{2-y}Al_y$, Heusler alloys, order-disorder transitions 80−59619

order-disorder transformations continued
$Cu_{0.5}NbS_2$ and $Cu_{0.5}TaS_2$, order-disorder and displacive transforms., domain-type microstruct. 77−4195
Cu_xNbS_2, $0.8<x<1$, order-disorder transitions and incommensurate superstruct. 77−15587
Cu_xNbS_2 and Cu_xTaS_2, electron diffuse scatt., microstruct., of transition state 77−31771
Cu_2NiZn, atomistic approach to ordering 79−94944
Cu_2NiZn, characterisation of superlattice dislocations by TEM 79−55748
Cu_3Pd, electron irrad. in electron microscope, radn. ordering 79−86818
CuPt alloy, equiatomic, ordering processes, anisothermal annealing exam. *(Japanese)* 78−39765
CuPt equiatomic alloy, effects of quenching temp. on ordering, study by elec. resistivity meas. *(Japanese)* 79−43285
CuPt type alloys, static stress influence on ordering, theory *(Russian)* 77−59775
Cu_3VS_4, out of equil. mixed cond., off-centre positions and order-disorder transition, ultrafast nucl. relax. obs. 80−108103
CuZnAl, martensitic, ordering effect on yield stress 79−100133
p-D_2, order-disorder phase transition 78−79726
DBr(DCl), solid, ferroelec. and paraelec. phases, transitions, Raman scatt. 77−43980
Dy, domain effects near order-disorder and order-order ferromagnetic transitions 80−65886
electrical resistivity, relax. time near order-disorder transition 78−87788
ErO, vac. deposited films, struct. changes due to annealing 79−77741
Fe, cast, ferritic grey, exam. of ordering kinetics by elastic modulus meas. 79−100136
Fe-Al, equilibria of Fe, Al ordered phase *(Japanese)* 79−70042
Fe-Al, high temp. Mossbauer study of order-disorder transform. 79−100137
Fe-Al, Mossbauer study of ordering *(Japanese)* 79−19822
Fe-Al, optical props., comp. and order-disorder transform. depend. *(Russian)* 79−28852
Fe-Al, optical props. rel. to order-disorder transformations 80−29736
Fe-Al α phase solid solution, interdiffusion coeff. depend. on ordering *(Russian)* 79−99373
Fe-C-Mn-Si (4, 2, 1.5 wt.%), cast wire, influence of B addition on struct. and elec. cond. *(Russian)* 80−55391
Fe-Co, equiatomic, atomic order, Mossbauer study *(French)* 78−27135
Fe-Co, long range order, neutron powder diffr. meas. 79−42243
Fe-Co, Mossbauer investig. of order-disorder and α-γ transitions 77−48110
Fe-Co, order-disorder transformation, metallography, ordering kinetics 80−3026
Fe-Co (25-35%), ordering, Cr addition effects, Mossbauer expts. *(Russian)* 78−19741
Fe-Co (30-70 at.%), comp. depend., neutron diffr. expts. 78−15393
Fe-Co alloy, atomic ordering phenomena, neutron diffr. obs. *(Russian)* 77−81254
Fe-Co films, optical props. order-disorder transformation influence, absorpt. band existence *(Russian)* 79−65942
Fe-Co films, ordered and disordered, Mossbauer study 79−24241
Fe-Co-Cr, magnetic, phase transform. obs. *(French)* 79−47676
Fe-Co-Cr (50, 0.4 wt.%), ordering and recrystallisation 79−34029
Fe-Co-Si, BCC solid soln. interchange energies, high temp. neutron diffr. 80−29166
Fe-Co-Ta for semipermanent magnets *(French)* 79−47675
Fe-Co-Ti(V)(Cr)(Mn), sp. ht. in ordered and disordered phases 80−71061
Fe-Co-V, ordered and disordered, dynamic ageing *(French)* 80−16355
Fe-Cr-C solid solns., ordering and γ to α transforms, effect of heat treatment *(Russian)* 79−24520
Fe-Ga, solid soln., order-disorder transform. *(French)* 78−3121
Fe-Mn, dilute, short-range ordering and segregation ascending diffusion *(Russian)* 77−24406
Fe-N (10 at.%), structural transforms., expt. investig. *(Russian)* 77−12613
Fe-Ni alloys, qualitative analysis of order-disorder structure by secondary ion-ion emission *(Ukrainian)* 77−69950
Fe-Ni-Al alloys, ordering X-ray and neutron diffr. obs. *(Russian)* 79−20038
Fe-Pd (50 at.%), ordering under load, nuclear gamma reson. obs. *(Russian)* 78−92258
Fe-Pd (50 at.%) alloy, structural changes during ordering *(Russian)* 77−77471
Fe-Pt, plastic deform. effect on struct. singularities and mag. props. *(Russian)* 80−44892
Fe-Si, 6.3-25 at.% Si, single crysts., adiabatic elastic consts., room temp. US pulse echo meas. 77−48467
Fe-V, order-disorder transition and σ-phase form. 80−7555
Fe-Zn, stable and metastable alloys, order-disorder, mag. interactions and corrosion behaviour 78−68422
Fe_3-Al, solid soln., rheological study of crystallographic order on creep *(French)* 80−97548
Fe_3Al, effect on optical and elec. props. *(Russian)* 77−39820
Fe_3Al, exam. of hyperfine field variations with order state 80−6800
Fe_3Al, order-disorder transition, elec. resistance meas. 79−42518
Fe_3Al, order-disorder transition effect on low energy spin waves 79−47271
Fe_3Al, phase separation 77−63664
$Fe_{70.8}Al_{29.2}$, meas. of ordering instability 79−38818
$Fe^{2+}BSi_2O_6$, B=Mg, Fe^{3+}, Al, pyroxenes, order-disorder interpretation 80−38987
FeCo, electronic structures, order effect 79−90938
FeCo, ordered alloy, 550°C change, study through elec. cond. and specific heat meas. 78−56633
$Fe_{2(1-y)}Mg_{1+y}Ti_yO_4$ spinel, incomplete mag. ordering, static magnetisation and Mossbauer meas. 77−16056
Fe_xNbS_2, ordering of Fe atoms 78−38650
$(Fe_yNi_{1-y})_{80}B_{20}$, mag. anneal anisotropy in amorphous alloys 77−16069
Fe_3O_4, multistage phonon softening in Verwey transition region, Mossbauer spectra 77−72670
$Fe_{50}Pd_{50}$, order-disorder transition, Mossbauer study 80−71268
$Fe_{25}Pd_{50}Au_{25}$, atomic ordering influence on mag. props. and elec. resistance *(Russian)* 80−7551
FePt lattice, symmetry, state of order, vibration, temp. effects *(German)* 77−4067
Fe_3Pt austenite, long range order parameter, temp. depend. discussion 80−97481

order-disorder transformations continued
Fe_3Pt austenites, ordering kinetics 80−104155
Fe_xTaS_2, vacancy ordering, transition state cluster model, electron diffr. 77−47547
FeTi alloy, elec. and mag. props. near order-disorder transition 79−82576
Fe_xVS_2 ($0.20<x<1.00$), phase diagram and order-disorder transition of vacancies 80−81039
$Fe_2[As^{III}(As^{V}O_4)_3]$, order-disorder transformation by thermal treatment *(French)* 79−90600
Ga-Se system, phase diagram and cryst. struct. of phases *(French)* 80−93544
GaAs (110) surface, O_2 interaction, order-disorder effects, LEED, UPS anal. 80−6634
Gd, domain effects near order-disorder and order-order ferromagnetic transitions 80−65886
$Gd_xZr_{1-x}O_{2-x/2}$, elec. cond. of ceramic solid solutions 80−107554
H, adsorbed on Ni(111), proposed struct. 79−60628
H, chemisorbed on Ni (111), order-disorder transition, cluster-variation method 80−15372
H_2 adsorbed on W (011) face, bidimensional lattice *(Russian)* 79−7744
H_2 monolayer, on triangular lattice, orientational phases 78−75934
o-H_2, order-disorder phase transition 78−79726
H_2 overlayer on Ni(111), geometry, order and disorder 79−65311
p-H_2, solid, NMR spectra, motional-narrowing model interpretation, order-disorder transition below 0.18K 78−79855
p-H_2, solid, very low O-H_2 conc., order-disorder transition, NMR 78−56384
HBr(HCl), solid, ferroelec. and paraelec. phases, transitions, Raman scatt. 77−43980
HCl, solid, ferroelec., comparative calcs. 77−8529
HF, solid, ferroelec., comparative calcs. 77−8529
H_2SeO_3, and deuterated analog, vibr. spectra 79−24311
He monolayer, phase diagram, order-disorder transition 80−107604
He monolayer films, on graphite, ordering 79−65287
^{4}He, monolayer adsorbed on Kr-plated graphite, possible Ising transition 80−34298
HfO_2, Y_2O_3-stabilised, solid soln., Raman scatt. anal. of struct. transform. 78−88312
HfO_2-Gd_2O_3, phase relations 78−72769
HfV_2D_4, disordered solid solution, order-disorder transition 80−88321
$Hg_{3-\delta}AsF_6$, one dimens. fluctuations and chain ordering transform 80−24593
$Hg_{3-\delta}AsF_6$, one-dimens. phonons and phase-ordering phase transition, neutron scatt. expts. 78−26644
$Hg_{3-\delta}AsF_6$, one-dimens. fluctuations and chain ordering transform., neutron scatt. calc. 78−59923
$Hg_{3-\delta}AsF_6$, one-dimens. liq., fluctuations and freezing in order-disorder transitions 79−82301
$Hg_{3-\delta}AsF_6$, space group symmetry and phase ordering 80−6396
$Hg_{3-x}AsF_6$, phase-ordering phase transition, elastic neutron scatt. obs. 79−33087
$Hg_{1-x}Mn_xTe(S)(Se)$, EPR of Mn^{2+}, order-disorder transitions 80−50176
In_4CdI_6, fast ionic cond. and order-disorder transition 79−99363
In_4CdI_6, ionic conductivity, Raman spectra 77−69113
InSb, morphological and structural changes due to ion bombardment 80−79843
In_2Te_3, low temp. ordered phase and transition state, TEM obs. 79−28095
In_2ZnI_4, fast ionic cond. and order-disorder transition 79−99363
In_2ZnI_4, ionic conductivity, Raman spectra 77−69113
KAg_4I_5, ionic conductivity and heat capacity near T_c 78−47584
KAg_4I_5, superionic phase transition, dynamical and crit. pt. props. 80−107535
KC_{24}, intercalated graphite cpd., anisotropic mag. susceptibility and phase transitions 79−19370
KC_{24}, intercalated graphite, struct. phase transitions, X-ray diffr. 79−65189
KCN, cryst., struct., phase transition, 6-300K, neutron diffr. obs. 77−76347
KCN, lattice dynamics and order-disorder transitions, neutron scatt. expts. 78−14434
KCN, order-disorder transition, light scatt., Raman obs. 77−1672
KCN, order-disorder transition, high-press. Brillouin scatt. exam. 77−44009
KCN, order-disorder transition, press. and temp. depend. of soft elastic const. 78−79769
KCN, polymorphism, high pressure, Raman spectra 78−88302
KCN, single cryst., orientationally disordered, Brillouin scatt., elastic consts. 77−85732
KCN-KCl mixed system, dielec. props. meas. 78−15112
KCN-KCl mixed system, Raman spectra obs. 78−15113
KCNS, librational modes in phase transition, Raman spectra obs. 79−55885
KD_2PO_4, coexistence states during first order transition, optical obs. 80−75350
KD_2PO_4, ferroelec. transition, ^{31}P chemical shift tensor meas. 77−28527
KD_2PO_4, ferroelec. transition, ^{31}P chem. shift obs. 78−76414
KD_2PO_4-type crysts., relax. processes in order-disorder transitions under short range correl. conditions 79−73889
$K_3Fe(CN)_6$, Raman scatt. and electronically-induced phase transition at 130K 77−90142
$KHSeO_3$, and deuterated analog, vibr. spectra 79−24311
$KH_3(SeO_3)_2$ and $KD_3(SeO_3)_2$, ferroelastic phase transition, mech. stress effect 80−70394
$K_3MoO_3F_3$, ferroelec. and order-disorder phase transitions 78−92037
KNO_2, polymorphism, calorimetric investigation 78−75827
KNO_3(II), Raman spectral study of struct. props., disordered groups 77−66486
$KNbO_3$, ferroelectric soft modes and order-disorder transition 77−47534
$KNiCl_3$, disorder as observed by electron diffr. 80−75213
K_2OsCl_6, ferrorotative transition, neutron scatt. expt., consistency with displacive and order-disorder models 78−51673
$K_2PbCu(NO_2)_6$, Jahn-Teller phase transitions, order-disorder model 78−79762
$K_2PbCu(NO_2)_6$, phase transitions induced by Jahn-Teller effect, uniaxial stress effects 80−6512
$KSbO_3$, cubic, K^+ ion ordering, electron microscopy 78−79550
$K_3WO_3F_3$, ferroelec. and order-disorder phase transitions 78−92037
La-D, phase transition, NMR meas. 80−66508

order-disorder transformations continued
La-H, ordered struct. near $LaH_{2.65}$ at 250K, NMR 80−66508
Li-Zn ferrite, mag. and microstruct. props., effect of V_2O_5 addition *(Japanese)* 77−28415
LiAl, pseudopotential method and ordering problem 77−35500
$LiAlSiO_4$, β-eucryptite one-dimens. fast ion cond., temp. depend. of cryst. struct. 80−107191
β-$LiAlSiO_4$, superionic cond., NMR relax. 77−12220
$LiAlSi0_4$, β-eucryptite, superionic conductor, order-disorder transition, microwave impedance obs. 79−14966
$LiFeO_2$, ion ordering, transition state cluster model, electron diffr. 77−47547
$LiFe_5O_8$, microstruct. and magnetic props., electron microscope obs. 79−87290
$Li_{0.5}Fe_{2.5}O_4$, ht. treatment conditions effect on superlattice formation 77−84922
$Li_{0.5}Fe_{2.5}O_4$-$CuFe_2O_4$-$ZnFe_2O_4$, order-disorder transition, quadratic transformation *(French)* 78−76447
$Li_{0.5}Ga_{2.5}O_4$-$CuCr_2O_4$ system, phase diagrams, IR spectra, Cu^{2+} electronic spectra *(French)* 78−51461
$LiHSeO_3$, and deuterated analog, vibr. spectra 79−24311
$LiRbSO_4$, order-disorder phase transitions with many-minimum potential, thermodynamic props. 80−96623
Li_2SO_4 solid electrolyte plastic deformation and thixotropy obs. 78−79660
$Li_2SO_4.H_2O$, far IR spectra, H_2O flipping motion, lattice modes 80−84258
Li_2TiO_3-MgO (20 to 40 at.%), order-disorder transitions, DTA and X-ray anal. 79−29050
LiTl, pseudopotential method and ordering problem 77−35500
Mg-Cd, thermodynamic props., order-disorder transitions based on Helmholtz free energy 79−37853
$MgBSi_2O_6$, B=Mg, Fe^{3+}, Al, pyroxenes, order-disorder interpretation 80−38987
MgCd wire, elongation during disorder-order transform. *(Russian)* 80−104148
Mg_3Cd, lattice imaging of B19 ordering transform. and interfacial struct. 77−36495
Mg_3Cd, order-disorder transformation kinetics 80−2138
$MgFe_2O_4$, sintered, cation ordering, grain size effects 78−39763
Mn-Pt (<29 at.%), eutectoid transform., antiferromag. struct. transform. *(French)* 78−92259
Mn_5Ge_3-Mn_5Si_3, electrical resistivity meas., order-disorder transition 80−10945
$Mn_{0.25}NbS_2$, mag. anomaly rel. to struct. disordering 78−43557
Mo-Tc system, supercond. behaviour, quick-quench production technique 78−56251
β-ND_4Br, ND_4^+ orientational fluctuations, neutron scatt. obs. 79−7557
ND_4Cl, order-disorder transformation, elasticity and heat capacity temp. depend., US obs. 78−71851
ND_4Cl, sp. ht. at high press. meas., near order-disorder transition 77−84944
ND_4Cl, ultrasonic exam. near order-disorder transition, elastic consts. 79−46799
ND_4Cl:Cu^{2+}, high-press. EPR, order-disorder transitions 78−19310
$(ND_4)_2Cu(OD_2)_2Cl_4$, Raman spectra, order-disorder transition *(French)* 79−91436
ND_4NO_3, Raman spectra meas., rel. to first order phase transitions, 250-420K 77−20845
NH_3 halides, acoustic anomalies above critical temps., volume magnetostriction type terms 80−2123
NH_4, halides, sound attenuation near lambda point 77−66002
$NH_4Ag_4I_5$, ionic conductivity and heat capacity near T_c 78−47584
$NH_4Ag_4I_5$, superionic phase transition, dynamical and crit. pt. props. 80−107535
NH_4Br, ^{14}N NMR obs., rel. to structural transforms. 79−15368
NH_4Br, heat capacity meas. near order-disorder transition 80−88332
NH_4Br, λ-type phase transition, Brillouin scattering 78−79725
NH_4Br, order-disorder phenomena, high press. US investigation 79−37835
NH_4Br, partially disordered, librational modes below 235K, Raman scatt. obs. 78−72500
NH_4Br, partially disordered, librational modes below disorder-order phase transition temp. 78−79680
NH_4Br, proton spin-lattice relax. time up to 2200 bar, phase transitions 77−63307
NH_4Br, self-polarisation at order-disorder transition 78−52432
NH_4Br:Cu^+, luminesc., orientation phase transition 80−100687
$NH_4Br(Cl)$, dynamic crit. phenomena 79−77690
$NH_4Br_xCl_{1-x}$, cryst., order-disorder phase transitions, US investig. 80−6378
$NH_4Br_xCl_{1-x}$, heat capacity meas. near order-disorder transition 80−88332
NH_4Cl, coexistence states during first order transition, optical obs. 80−75350
NH_4Cl, crit. behaviour near tricritical point, phenomenological interpretation 80−70389
NH_4Cl, doped and undoped, spontaneous polarisation at order-disorder phase transition 80−25281
NH_4Cl, electro-optical props. near order-disorder transition 78−31173
NH_4Cl, λ-type phase transition, hypersonic study using Brillouin scatt. 80−34165
NH_4Cl, NH_4^+ ion rotation, near order-disorder transition, quasielastic neutron scatt. obs. *(German)* 77−84679
NH_4Cl, order parameter, electro-optic measurement 78−88280
NH_4Cl, order parameter variation near multicritical pt., SHG 79−81484
NH_4Cl, order-disorder transition, slip bands 78−22848
NH_4Cl, order-disorder transition exam. by optical second harmonic generation 78−51671
NH_4Cl, order-disorder phase transition, type of multicritical point, nonlinear quadratic susceptibility 78−83947
NH_4Cl, order-disorder phase transform., effect of plastic deform. and electrooptic effect 79−33672
NH_4Cl, proton spin resonance relaxation time near ordering transition 79−61251
NH_4Cl, Raman scatt. of light on limiting and nonlimiting dipole vibr. 80−11402
NH_4Cl Raman spectra, pressure effects 80−97268
NH_4Cl, self-polarisation at order-disorder transition 78−52432
NH_4Cl single crystals, quasielastic neutron scattering expts. near order-disorder phase transition 79−4410

order-disorder transformations continued
NH_4Cl, sp. ht. at high press. meas., near order-disorder transition 77−84944
$NH_4Cl(Br)$, effect of NH_4^+ internal motion on elec. and optical props. 80−100454
$NH_4Cl_{1-x}Br_x$ mixed cryst., phase diagram and charact. of phase transitions 77−62637
$(NH_4)_2CuCl_4.2H_2O$, HDO and NH_3D^+ species, IR spectrum, low-temp., phase transitions 77−77182
$(NH_4)_2CuCl_4.2H_2O$, Raman sepctra, dynamics, struct., phase transition 79−47434
$(NH_4)_2CuCl_4.2H_2O$, order-disorder transition, Raman spectra obs. 79−61357
$(NH_4)_2H_3IO_6$, Raman spectra and phase transition 77−77196
NH_4HSO_4-type crystal, ferroelectric phase transform. model, SO_4 group ordering 77−77156
α-NH_4HgCl_3, Raman study of phase transition *(French)* 80−11378
NH_4I, ^{14}N NMR obs., rel. to structural transformations 79−15368
NH_4I, coexisting phases and NH_4^+ dynamics, neutron scatt. exam. 79−42158
NH_4NO_3, Raman spectra meas., rel. to first order phase transitions, 250-420K 77−20845
$(NH_4)_2SO_4$, e.s.r., of NH_3^+ and SeO_3^- radicals, ferroelec. transition obs. 77−16180
$(NH_4)_2SO_4(BeF_4)$, order-disorder phase transitions with many-minimum potential, thermodynamic props. 80−96623
$(NH_4)_2SiF_6$, trigonal, proton and ^{19}F relax, 30 to 200K 77−76549
$(NH_4)_2SnBr_6$, structural phase transitions study by Raman scatt. 80−93318
$(NH_4)_2TiF_6$, Raman spectra, internal and lattice vibrs. 77−8569
$NH_4UO_2(NO_3)_3$, Raman spectra 6-293K, phase transition 78−27220
NI_3Al, structural order and homogeneity, X-ray, mag. susceptibility and Mossbauer meas. 77−63663
Na, adsorbed on W(110) plane, ordering, theoretical anal. 78−18892
$NaBD_4$, ^{11}B spin-lattice relax., struct. phase transition 78−84492
$NaBH_4$, ^{11}B spin-lattice relax., struct. phase transition 78−84492
$NaBH_4$, $NaBD_4$, first order struct. transition, NMR meas. 78−80240
$NaBSi_2O_6$, B=Mg, Fe^{3+}, Al, pyroxenes, order-disorder interpretation 80−38987
NaCN, Brillouin backscatter spectra of (100) LA phonons, elastic consts. determ. 79−65886
NaCN, cryst., struct., phase transition, 6-300K, neutron diffr. obs. 77−76347
NaCN, lattice dynamics and order-disorder transitions, neutron scatt. expts. 78−14434
NaCN, order-disorder transition, press. and temp. depend. of soft elastic const. 78−79769
NaCN, Raman spectrum, hydrostatic press. effects 78−6663
NaCN, single cryst., orientationally disordered, Brillouin scatt., elastic consts. 77−85732
$NaClO_3$, lattice vibrations and sp. ht., neutron spectroscopic study 80−107388
$NaClO_4$, Raman spectra temp. depend. near 581K phase transition 78−56477
$NaD_3(SeO_3)_2$, polarised Raman spectra, lattice vibrs., ferroelec. transition 77−24851
$NaHSeO_3$, and deuterated analog, vibr. spectra 79−24311
$NaH_3(SeO_3)_2$, $NaD_3(SeO_3)_2$, IR and Raman spectral interpretation of ferroelectric phases 79−24312
NaN_3, orientational motion and elastic anomaly 79−46803
NaN_3, phase transitions and N_3^- librational motion 77−4178
NaN_3, struct. phase transform., microscopic model 79−65022
$NaNO_2$, 163°C phase transition, thermal history effects on range of modulated struct. 78−95563
$NaNO_2$, adiabatic and isothermal elastic compliances, critical behaviour 78−92031
$NaNO_2$, mechanism of ordering type ferroelec. transition, vibr. spectroscopy 78−76402
$NaNO_2$, mechanism of order-disorder transition, opt. spectra 78−76403
$NaNO_2$, NQR of ^{14}N at ferroelec. transition, order-disorder fluctuations 77−63311
$NaNO_2$, phase transitions accompanied by noncommensurate superstruct. form. 77−32336
$NaNO_3$, disordered, temp. depend. of Raman spectra, Rayleigh wing scatt. 78−31209
$NaNO_3$, lattice vibration neutron diffusion study *(French)* 80−103429
$NaNO_3$, lattice vibrs., order-disorder transform., IR spectra study 80−65176
$NaNO_3$, order-disorder transition point, hyper-Rayleigh scatt. due to rotation of NO_3^- 78−52520
$NaNO_3$, Raman scatt. band lineshape, orientational disorder of NO_3^- ion in pre-transition region 77−8589
NaO_2, elastic interaction, role in disordered-pyrite to ordered-pyrite phase transition 80−19739
NaO_2, physical mechanisms of phase transitions 80−6381
Na_3PO_4-$M_3(PO_4)_2$, M=Ca, Sr, system *(French)* 77−44235
$Na_3Pr(C_4H_4O_5)_3.2NaClO_4.6H_2O$, absorpt., circular dichroism, and mag. circular dichroism spectra 80−97243
α-$NaSbS_2$, cryst. struct. and $\beta \rightarrow \alpha$ phase transform. features 80−33961
NaTl, pseudopotential method and ordering problem 77−35500
$Na_xV_2O_5$ β-phase single cryst., phase transitions EPR meas. 78−95514
$Na_6[Ti(Ti_{0.9}Nb_{0.1})_4(Si_6O_{17})_2(O,OH)_5].11H_2O$, zorite, X-ray cryst. struct. determ. 80−92513
Nb-H, modulated ordering, elastic free energy theory 79−94945
Nb-H(D), H ordering, review 80−60850
$NbD_{0.85}$, localised D vibrs., temp. depend., neutron inelastic scatt. study 80−107395
Nb_3Ge, metallic glass, internal friction peak obs. 78−79666
$NbH_{0.82}$, localised H vibrs., temp. depend., neutron inelastic scatt. study 80−107395
NbH_x, structural transform. rel. to order-disorder transform. 80−60858
$NbH_x(D_x)$, cryst. struct., phase diagrams, order-disorder transition 78−55836
NbS_2, intercalation compounds, octahedral, microstructural study 77−84729
Nd-H, phase transform. induced by H ordering in octahedral sites 79−52174
$Nd_xZr_{1-x}O_{2-x/2}$, elec. cond. of ceramic solid solutions 80−107554
Ni, H chemisorption, order-disorder transitions on (111) surface, LEED observation 78−47668
order-disorder transformations continued
Ni-Al, rheological study of crystallographic order on creep *(French)* 80−97548
Ni-Al, spinodal decomposition, atom probe field ion microscopy study 80−3028
Ni-Al film, high-temp. condensed, electron diffr. and elec. resist. *(Russian)* 79−4485
Ni-Al-Fe system, order-disorder phase transform., Gorskii-Bragg-Williams approx. *(Russian)* 79−29048
Ni-Co (25 at.%), polycrystalline, mech. damping 77−28850
Ni-Cr, ordering in the vicinity of Ni_2Cr 79−38819
Ni-Cr alloys, low temp. transform. mechanism, electrophys. props. obs. *(Russian)* 77−59777
Ni-Cr-type alloys, theory of ordering, superstruct. form. *(Russian)* 77−81256
Ni-Fe alloy, atomic and mag. ordering, cluster variation calc. *(Russian)* 78−15391
Ni-Mn, ordered and disordered, press. effect on Curie temp. 80−71148
Ni-Mo (10.7 wt.%) alloy, ordering energy calc. 80−10522
Ni-NiAl solid soln., high temp. transforms *(Russian)* 79−56973
Ni-S, defect control by heat-treatment in S atmos. 79−43293
β-Ni-Ti, struct. changes during annealing, TEM and selected area diffr. 79−34081
$Ni_{1-x}Al$ solid solution, vacancy ordering exam. by electron diffr. after annealing 78−3123
Ni_3Al, Mossbauer experiments on homogeneity 78−48395
Ni_3Fe, change of H_2 diffusivity with order-disorder transformation 80−59729
Ni_3Fe, electronic structures, order effect 79−90938
Ni_3Fe, Mossbauer effect 78−10811
Ni_3Fe, order-disorder transition phase diagram, Mossbauer meas. 80−39995
Ni_3Fe, ordered and disordered states, strain hardening charact., temp. depend., multiple slip case *(Russian)* 78−15421
Ni_3Fe, X-ray diffraction investig. of order-disorder transform. *(Russian)* 77−70043
$Ni_{73}Fe_{27}$, order-disorder transition, Mossbauer study 79−95163
$Ni_3(Mn, Al)$, ordering process mechanism by neutron diffr. *(Russian)* 77−55961
Ni_3Mn, at. ordering during annealing, mag. field effect 78−15394
Ni_3Mn, change of H_2 diffusivity with order-disorder transformation 80−59729
Ni_3Mn, elec. resist., relax. time near order-disorder transition 78−87788
Ni_3Mn, nonstoichiometric, order-disorder transition, A1 to $L1_2$ *(French)* 79−1861
Ni_3Mn, partially ordered, spin-wave dispersion relation, inelastic neutron scatt. meas. 80−20394
Ni_3Mn, quenching temp. effects on long-range order *(Russian)* 77−59776
Ni_3Mn thin films, transmission spectra, structural order depend. 80−66318
Ni_2MnIn, Heusler alloy, order-disorder phase transitions, X-ray diffr. meas. 77−66640
$Ni_3(Mo,Ta)$, quenched alloys, DO_{22} type ordered phase form. 78−95768
Ni_4Mo, electron irrad. in electron microscope, radn. ordering 79−86818
Ni_4Mo, order-disorder phase transform., X-ray diffr. *(Russian)* 79−1855
Ni_4Mo, ordered, electrical resistivity and thermal EMF, temp. depend. *(Russian)* 77−55513
Ni_4Mo, ordering near Kurnakov point, form. of coherent phase in stress concentrators 79−7691
Ni_4Mo, statistically homogeneous ordering, computer-simulated field ion images 78−9991
Ni_4Mo, stoichiometric and quenched, short range order and order-disorder transform. 79−78955
Ni_xNbS_2 vacancy ordering, transition state cluster model, electron diffr. 77−47547
NiPt, quenched, ordering kinetics and domain struct. form. during isothermal tempering *(Russian)* 80−66502
Ni_3Pt, change of H_2 diffusivity with order-disorder transformation 80−59729
NiSe film, vac. deposited, phase transformation, electron microscope studies 80−2302
Ni_4W, order-disorder phase transition, X-ray struct. exam. *(Russian)* 78−64532
O adsorbed on Ni (111), order-disorder transition 79−82447
O adsorbed on W, order-disorder transition, theory 78−38811
O chemisorbed layer, on W(110) surface, phase transitions, coverage effects 78−79879
O, chemisorbed on W (110), theory compared with LEED data 79−7748
O_2, adsorbed on polycryst. W, electron stimulated desorpt. study, 300K, kinetics, order-disorder transition 78−71985
$PbHPO_4$, protonic order-disorder transition 78−26478
$PbZr_{1-x}Ti_xO_3$, paraelec. phase, first-order phase transition 77−89540
Pd, H(D) interstitial interactions rel. to diffusion and ordering transition 80−34249
Pd-D, crystallite size effects, simultaneous sorption and X-ray study 80−65237
Pd-H, nature of the 50K anomaly, residual resist. 79−7818
Pd-H alloys, X-ray diffr. study, β-phase anomaly near 50K 78−26496
Pd-H_x, model possibilities for the 50K transition 79−8299
Pd-Si, amorphous thin films, laser irrad., metastable phases 80−96622
$PdD_{0.64}$, neutron scatt. exam. of 50K transition 78−55942
PdD_{1-x}, deuteron density modulation of D atoms 79−99101
Pd_3Fe, hyperfine interactions during atomic ordering, Mossbauer obs. *(Russian)* 78−56630
$(Pd_{0.67}Fe_{0.33})_{1-x}Au_x$, ordering effects on mag. props. *(Russian)* 78−47942
$PdFe_{1-x}Cr_x$ ordering alloys, elec. resist., temp. depend. *(Russian)* 80−24866
PdH_x, PdD_x, ordering, resistivity, annealing and neutron diffr. obs. 79−34030
phase transition in transverse field with deform. depend., phonon anomaly separation KH_2PO_4 80−39258
Pt-Cr, disordered, atomic order-disorder transform. effect on resist. min. 80−65911
Pt-Cu (49.37 at.%), coexistent phases in homogeneous ordering 79−29052
Pt-Ir, structural phase transform., ion field emission microscopy obs. *(Russian)* 80−50628

order-disorder transformations continued
Pt-Si, amorphous thin films, laser irrad., metastable phases 80−96622
Pt(111), adsorption of Br, irreversible order-disorder transition, LEED AES, thermal description and work function meas. 79−69361
$RbAg_4I_5$, 208K phase transition, Jahn-Teller-like model 77−35694
$RbAg_4I_5$, critical dynamics, role of acoustic phonons, and Z-branch 77−84887
$RbAg_5I_5$, ionic cond. near order-disorder transition 77−11728
$RbAg_4I_5$, ionic conductivity and heat capacity near T_c 78−47584
$RbAg_4I_5$, phase transition, statics and local dynamics, mean field and Mori theory 80−39347
$RbAg_4I_5$, superionic phase transition, dynamical and crit. pt. props. 80−107535
RbCN, molecular motion and ordering from dielec. and Raman techniques 79−73932
$RbCaF_3$, struct., phase transitions, neutron diffr. study 80−33918
$Rb_3MoO_3F_3$, ferroelec. and order-disorder phase transitions 78−92037
$RbNO_3$, single cryst., DC cond., dielec. and thermophys. props., temp. depend., transitions interpret. 78−26682
$Rb_3WO_3F_3$, ferroelec. and order-disorder phase transitions 78−92037
Rh (111), chemisorption of acetylene and ethylene, EELS, LEED and thermal desorption mass spectrometry 80−80057
S, monoclinic, order-disorder transition, X-ray struct. determ. 78−30750
$Sc_{0.8}S$, order-disorder transition, ionic model appl. 80−107096
Si ion implanted, amorphous to crystalline transition due to laser irrad. 80−103451
Si_3N_4 films, struct. 80−54545
SiO_2-Li_2O-K_2O-ZnO glass ceramic, prep., phase transformations and physical props. 80−45299
$SnCl_2.2D_2O$, order-disorder transition, neutron diffr. study, lattice statistical model 80−24558
$SnCl_2.2H_2O$, effect of hydrostatic press. on isomorphous phase transition, complex dielec. const. meas. 77−76551
$SnCl_2.2H_2O$, ferroelec., Cl NQR study 79−38467
$SnCl_2.2H_2O$ layered single cryst., protonic cond. and crit. behaviour 79−28136
$SnCl_2.2H_2O$, protonic order-disorder transition, H-bond vibr. Raman spectra temp. depend. 78−23437
$SnCl_2.2H_2O$, protonic order-disorder transition, inelastic light scatt. obs. 78−68497
$SnCl_2.2H_2O$, protonic cond. in layered single cryst. 80−19983
$SnCl_2.2H_2O$, quasi two-dimensional, DC protonic cond., crit. contrib. near order-disorder transition temp. 80−44362
$SnCl_2.2H_2O$-type layer cpds., two dimens. ferroelec. ordering sp. ht. obs. 78−92034
$SrCl_2$, high temp. powder neutron diffr., transition to highly conducting phase 78−47586
$SrCl_2$, specific heat anomaly and sublattice disorder, neutron diffr. meas. 79−42238
$Sr_2Fe_2O_5$, order-disorder transition from brownmillerite to perovskite under heat treatment in N_2 stream 79−11612
$SrTiO_3$ ceramic, electrocaloric effects for refrigeration at cryogenic temp. 80−77789
$SrTiO_3$:Fe^{3+}, displacive struct. transition, order-disorder behaviour, phonon softening, EPR obs. 79−23695
Ta, interstitial ordering, O effect, $Ta_{64}C$ artifact 79−99185
Ta-H, physical properties, plastic deformation, H ordering *(Ukrainian)* 80−71689
Ta-H(D), H ordering, review 80−60850
Ta-N (4 at.%), TEM obs. of ordering 79−96021
Ta_2D, neutron diffr. meas. of disorder-order phase transitions 80−29947
$TaH_{0.75}$, calorimetric study of phase transform. 77−48426
Ta_2H, ordered, distortion-induced superstruct. modulation, from X-ray scatt. 80−49186
$TaH_x(D_x)$, cryst. struct., phase diagrams, order-disorder transition 78−55836
TaS_2, intercalation compounds, octahedral, microstructural study 77−84729
$TaSe_2$ (2H), softening of CDW excitation, at superstructure transition 78−79728
$TbAl_3$, polytypism occurrence 80−44164
Ti_3Al-(Nb), ordering transform. and mech. props. 78−31402
TiO, ordered phase, vacancy-strain coupling 78−79549
$TiO_{0.42}$, diffuse X-ray and neutron scatt. due to out-of-step configurations of O atoms 77−62518
$Ti_{1+x}S_2$, vacancy ordering, transition state cluster model, electron diffr. 77−47547
$Ti_{1+x}Se_2$, superlattice form. and phase transition, IR reflectivity meas. 79−24322
$(Ti_{1-c}V_c)_4O_7$ order-disorder and metal-insulator transition theory 80−24802
$(Ti_{1-x}V_x)_4O_7$, order-disorder and metal-insulator transitions 80−39504
Tl-Bi system, phase transitions near Tl_3Bi, elec. props. meas. 80−35181
Tl_4CdI_6, ionic conductivity, Raman spectra 77−69113
$Tl_2ZnBr_4(I_4)$, fast ionic cond. and order-disorder transition 79−99363
Tl_2ZnI_4, ionic conductivity, Raman spectra 77−69113
UI_3 sublattice magnetisation, mechanism 77−55671
U_3O_8, λ-type heat capacity anomalies 77−20080
V-C system, ordering and phase equilibrium processes 79−99311
V-H, NMR of anomalous diffusion of H and phase transition 77−16571
V-H(D), hydrogen ordering, review 80−60850
V-H(D), metallographic and thermal differential anal., potential for H energy storage appls. 80−45281
V-Mn, equiatomic, ordering kinetics and antiphase domain coarsening 80−7559
V-N system, ordering and phase equilibrium processes 79−99311
V-Pt, sp. ht. and mag. meas. in ordered and disordered phases 80−70422
V-S system, order-disorder transition of metal vacancies, statistical thermodynamics 78−43012
V-S system, quenched, order-disorder transition of metal vacancies, DTA and X-ray analysis 78−30576
V-Se system, quenched, order-disorder transition of metal vacancies, DTA and X-ray analysis 78−30576
VC_x, VN_x, vacancy ordering, transition state cluster model, electron diffr. 77−47547
$VD_{0.8}$, antiphase domains during ordering, neutron diffr. 77−90348
V_2D, elec. resistivity studies of order-disorder phenomena 79−78961
V_2D, ordered, distortion-induced superstruct. modulation, from X-ray scatt. 80−49186
order-disorder transformations continued
V_2D, short-range interstitial order above crit. temp., diffuse X-ray scatt. obs. 79−95159
V_4D_3, multistage ordering process, neutron diffr. obs. 77−59114
V_2H, elec. resistivity studies of order-disorder phenomena 79−78961
V_2H, long-range order and β to β' transition, X-ray scatt. obs. 79−95160
δ-VMn, ordering and disordering behaviours 77−48428
VN_{1-x}, vacancy ordered structure in cubic mononitride phase, transition entropy determ. 78−43011
$VO_{1.30}$, ordered phase, X-ray anal. of defect struct. 79−99177
VO_2, metal-insulator transition and electronic struct., ion bombard. effects 80−92948
V_3O_5, increase of X-ray refl. intensities and profile widths at phase transition temp. 79−69052
Va_2D, neutron diffr. meas. of disorder-order phase transitions 80−29947
$VaH_x(D_x)$, cryst. struct., phase diagrams, order-disorder transition 78−55836
Zn-Li silicates, cryst. struct. and phase transform. 79−65036
Zr-Al (8.6 wt.%), effect of fast neutron irradiation on irradiation growth of Zr_3Al 78−55896
$Zr(Ca)O_{2-x}$, internal, external distortion mechanisms, neutron diffr. study 78−83946
$ZrH_{1.5}$ and $ZrH_{1.75}$, low temp. phase transitions in H sublattice 77−24405
ZrO_2, R_2O_3-stabilised (R=La, Gd, Y or Yb), solid soln., Raman scatt. anal. of struct. transform. 78−88312
ZrO_2-Sc_2O_3-Yb_2O_3 system, order-disorder phenomena, Raman spectra study 80−97254
ZrO_2-Y_2O_3, phase equilibria and ordering 78−48385
$Zr(Y)O_{2-x}$, internal, external distortion mechanisms, neutron diffr. study 78−83946

ores *see minerals*

organic acids *see organic compounds*

organic compounds
see also DNA; free radicals; macromolecules; organic semiconductors; organometallic compounds; plastics; polymers; proteins; Rochelle salt; waxes
2,4-D herbicide, long-distance transport and damaging levels in Washington vineyards 77−17213
abietic acid, transverse US wave propag., glass and liquid transition region 80−79883
abietic acid glass, corona-charged, TSC curves 77−55744
abietic acid in polymer matrix, photosensitised oxidation, singlet O_2 diffusion *(Russian)* 79−52655
acenaphthalene, mol. and cryst., vibr. anal., normal coord. calcs. 79−47428
acenaphthene, liq. scintillator system, energy transfer, fluoresc. intensity-max. solvent depend. 78−21966
acenaphthene, vibr. spectra, mol. crystal dynamics, librational modes 78−64356
acenaphthene, vibronic spectra, electronic-vibr. interactions 78−1021
acenaphthene in n-alkane matrices, Shpolskii spectra fluorescence 78−9190
acenaphthene single crystals, radicals produced by γ irrad., room temp. EPR study 78−84483
acenaphthene-α-nitronaphthalene, binary mol. system, phase diagram 77−39664
acenaphthenequinone, solid phase NMR spectra, 77-430K 79−15360
acenaphthylene, anisotropic mesophase during refluxing carbonization 78−14274
acenaphthylene, orientational disorder, spectroscopic exam. 78−14670
acenaphthylene pyrolysis, carbonaceous mesophase and disc-like liquid crystals 80−79687
acetaldehyde, adsorbed on Al_2O_3, inelastic electron tunnelling spectra, surface vibr. struct. determ. 80−35572
acetaldehyde, anodic oxidation, voltammetric meas. 79−57247
acetaldehyde, carbonyl addition, model transition states, vibr. anal. 80−71898
acetaldehyde, chemisorption and decomp. on Pd 77−63953
acetaldehyde, Coriolis resonance bands in IR spectrum 80−47995
acetaldehyde, dichroic effects, computational expts. 80−83424
acetaldehyde, first triplet state geometry, fragmentation into free radicals 80−47915
acetaldehyde, force consts., vibr. freqs., CNDO/2 and MINDO calcs. 77−14607
acetaldehyde, gas, stopping cross section for 0.3 to 2.0 MeV He^+ ions 78−63537
acetaldehyde, internal rotation barriers, exchange energy and orbital orthogonality effects 77−75049
acetaldehyde, lowest Rydberg state, multiphoton ionisation spectra 80−83435
acetaldehyde, matrix isolation spectra using tunable diode laser 78−45739
acetaldehyde, mm emission lines obs. in Orion A 77−2477
acetaldehyde, multiphoton ionisation mass spectra 80−83436
acetaldehyde, multiphoton ionisation meas., two-photon polarisation ratio of n→3s transition 80−91610
acetaldehyde, optimum geometry, force fields, CNDO/force method 77−46498
acetaldehyde, photodissoc., HCO form., wavelength depend. 79−83490
acetaldehyde, primary and secondary photoionis. processes, ion-mol. reactions 79−36709
acetaldehyde, proton affinity, geom. and basis set depend., MO calcs. 78−50461
acetaldehyde, single vibronic level fluoresc., radiative lifetimes 78−82769
acetaldehyde, soln., C-O stretching band intensity calcs., intermol. interaction effects 77−68081
acetaldehyde, T_2-relax. meas. press. depend. for rot. transitions, pulse spectrometer 80−78612
acetaldehyde, torsional fundamental and combination bands, K-struct. anal. 78−78696
acetaldehyde, UV photolysis, transient species IR spectra 80−86464
acetaldehyde+CO_2, (00^01) mode deactivation, laser induced fluoresc. obs. 80−83453
acetaldehyde+CO_2, vibr. relax., search for unquenchable species, room temp., 5-2200 torr 78−9229
acetaldehyde+F, HF IR chemiluminesc., vibr. and rot. energy disposal 77−86318

organic compounds continued
acetaldehyde + $H_2(N_2)(CO_2)$, rot. line broadening, mol. quadrupole moments calc. 80−28065
acetaldehyde + H, absolute reaction rate consts., 298-500K 77−16788
acetaldehyde + OH, rate consts., 299-426K, UV flash photolysis, reson. fluoresc. obs. 78−68873
acetaldehyde ($A,^1A_2$), laser induced fluoresc. 79−50075
acetaldehyde formation on radiolysis of ethanol formaldehyde systems *(Russian)* 80−55684
acetaldehyde photolysis, HCO product microwave spectra 79−5163
acetaldehyde photolysis products, time resolved Fourier transform spectrum 78−58071
acetaldehyde radical cation, fragmentation, MO calc. 79−18109
acetaldehyde-d_1(-d_3), fragmentation processes, H scrambling, photoionis. mass spectra 78−42139
acetaldehyde-propane binary mixtures flowing through activated C, adsorpt. interference 80−107635
acetaldoxime, photoelectron and far UV absorpt. spectra 78−17712
acetalehyde decomposition reaction, intracavity laser spectroscopy obs. 79−61858
acetamide, aqueous solution, ultrasonic velocity measurement 80−19878
acetamide, effect of small additions of water struct., from permittivity obs. 78−9937
acetamide, geometry from ab initio calcs., rel. to formamide, N-methylformamide, and N-methyl acetamide 80−23338
acetamide, IR spectra, amino group inversion transitions and pot. functions 80−43041
acetamide-d_x, ^2H quadrupole resonance, double transitions 79−3465
acetanilide, bromination, fast reaction kinetics, rot. Pt. electrode meas. 77−16821
acetanilide, cryst., low-freq. polarised Raman spectra 78−84574
acetanilides, Hammett freq. factors, effects of non-monotonic ν(XH) function variations *(French)* 79−22690
acetate, deuterated, dimeric, single crysts., inelastic neutron scatt. 80−92867
acetate, OH abstraction, H^- formation, CIDEP in pulse radiolysis 77−48656
acetate, photo-oxidation at n-TiO_2 electrode 80−81331
acetate crystal hydrates, bonding determ. from IR spectra 77−42321
acetate ion radicals, solns., pulse radiolysis, CIDEP, viscosity depend. 77−75189
acetate ions adsorbed on Ag particles in aqueous soln. Raman spectra 80−69148
acetate radical CIDEP, appl. of ns time-resolved EPR in pulse radiolysis 80−43075
acetate trihydrate:Mn^{2+}, ESR, elec. cond. 80−93165
acetate-ferrileghemoglobin, X-ray struct. anal., 3D refinement at resoln. of 2.0 Å 80−104554
acetic, acid, ideal gas thermodynamic props. 78−51275
acetic acid, ^{13}C enriched 2D heteronucl. NMR spectrum 77−90068
acetic acid, ^{18}F-labelled, carrier-free, production via a recoil labelling method 80−104756
acetic acid, $-d_1(=d_4)$ liquid, molecular motion, proton spin echo study *(Russian)* 80−32745
acetic acid, active medium of optically pumped submm laser, double reson. 79−18215
acetic acid, adsorbed on Al_2O_3, inelastic electron tunnelling spectra, surface vibr. struct. determ. 80−35572
acetic acid, adsorbed on Cu (100), interaction with formic acid, EELS study 80−76120
acetic acid, adsorption on Ag (111) and Pt (111), LEED obs. 80−80073
acetic acid, adsorption on Fe and Ni, XPS study 80−76132
acetic acid, and derivatives, vibr. spectra in soln. 80−63633
acetic acid, cavitation erosion of stainless steel *(German)* 79−39050
acetic acid, chemisorbed on CU(100), acetate species struct. obs. 79−98232
acetic acid, chemisorbed on MgO, decomposition mechanism 78−92502
acetic acid, chemisorption on goethite, IR spectra 80−7855
acetic acid, Cl_2 absorpt. kinetics in presence of homogeneous catalysts 80−11876
acetic acid, correlation between chem. shift and charge for OH 77−18946
acetic acid, cryst., and isotopic species, H-bond, ν_s-ν_o coupling and ν_s anharmonicity, IR spectra at 10K 79−15450
acetic acid, cryst. binding, ab initio MO SCF calc. 79−37657
acetic acid, deuterated, neutron powder diffr. anal. at 4.2 and 12.5K 78−75649
acetic acid, dielectric meas. at microwave freqs. 79−19827
acetic acid, dil. soln., dielectric polaris., linear correlation factor 78−6624
acetic acid, dimer, config and energy, ab initio MO SCF calc. 79−37657
acetic acid, effect of impurities on US relaxation 78−10130
acetic acid, electrochemical behaviour obs., in molten alkali acetates, fuel cells technology appl. 79−57244
acetic acid, electrochemical behaviour obs. in molten alkali acetates, fuel cells technology appl. 79−57244
acetic acid, hypothetical dimer-based cryst. struct. calc. 77−19940
acetic acid, in cyclohexane soln., Raman scatt. near crit. stratification, temp. depend. *(Russian)* 79−11420
acetic acid, ionised, pot. energy profiles for unimol. reactions 80−43210
acetic acid, liq., diamagnetism, mass mag. suscept. meas., temp. depend. 80−97054
acetic acid, liq., sp. ht. of 2nd relax. step *(German)* 79−37766
acetic acid, methyl group dynamics, NMR 78−29802
acetic acid, monomer and dimer, photoelectron spectrosc. 80−87172
acetic acid, permeation of large unilamellar vesicle membranes, ^1H NMR obs. 80−8031
acetic acid, photocatalytic oxidation, photoacoustic spectroscopic obs. 79−16010
acetic acid, protonated complexes, IR and Raman spectra *(French)* 78−78691
acetic acid, PVT props., 448.15-603.15K, press. up to 10 MPa 78−14455
acetic acid, Rayleigh-Brillouin scatt., 20-115°C, viscoelastic theory anal. 79−28774
acetic acid, relative Raman scatt. cross section 80−100061
acetic acid, self association, IR spectra, book contrib. 78−21931
acetic acid, solid, structural features during melting process 79−7596
acetic acid, sound vel. meas. at 5 to 20 kHz in small-volume cells 78−9516
acetic acid, thermal cond. meas. using Peltier effect 78−45615

organic compounds continued
acetic acid, vapour, chem. reaction effect on speed of sound 80−103100
acetic acid, viscosity of dissociating vapour 78−5840
acetic acid + $CH_3^+(CD_3)^+$ reactions, products mass spectra obs. 77−63901
acetic acid + CO_2, (00^01) mode deactivation, laser induced fluoresc. obs. 80−83453
acetic acid + formic acid, liqs., mixing enthalpy 79−60515
acetic acid + $K_4(MoCl_4)_2$, reaction kinetics and mechanism 77−86305
acetic acid amides, polarisabilities and π-π^* transitions, dipole interaction calcs. 80−23411
acetic acid and isomeric methyl formate, Compton profiles 77−30928
acetic acid dimer, gas phase, H-bonded complex struct. from elec. dipole moment obs. 78−74791
acetic acid dimer, soln., vibr., IR spectra 80−63633
acetic acid dimer, vibr. spectra at low temp., Witkowski-Marechal theory 78−46314
acetic acid double resonance Fourier transform spectra, isotope effects 78−86897
acetic acid odorant, nose stimulation, olfactory evoked brain pot., correl. anal. of recorded waveforms from human scalp *(Japanese)* 80−97946
acetic acid vapour, homogeneous nucleation, assoc. clusters, crit. supersaturation temp. depend. 77−31762
acetic acid vapours, clustering, effect of supersonic mol. beam sampling, mass spectrometric study 80−104481
acetic acid-$^{13}C_1$, in nematic phase soln., dipole-dipole couplings, selective spin population transfer investig. 80−60427
acetic acid-acetone mixture, physical parameters 80−2716
acetic acid-aliphatic amide intermol. H-bonded systems, charge transfer bands 77−58041
acetic acid-aniline (pyridine) complex, in CCl_4, dielec. polarisation 80−29675
acetic acid-benzenes (carbon tetrachloride) dilute solns., dielec. consts., dipole moments, H bonding investig. 77−48673
acetic acid-carbon tetrachloride, US absorption, coupled dimerisation cyclisation reaction *(French)* 79−42148
acetic acid-d_0, -d_1, -d_4, cryst., IR spectra, H bonding 77−40217
acetic acid-d_0, -d_1, -d_4, H bonding in solid, IR spectra, vibr. and librational modes 78−43843
acetic acid-d_0(-d_1,-d_3,-d_4), cryst., H bonds, stretching, temp., isotope effects 79−51938
acetic acid-d_0(-d_1), Fermi reson., IR spectra band profiles 80−60569
acetic acid-d_1(-d_2), equilib. config. from microwave spectrum 79−59442
acetic acid-d_4, adsorbed on TiO_2 (rutile) IR obs. 78−30827
acetic acid-formic acid, 'dimer', tritium β^--decay causing H^+ transfer, ab initio MO calc. 80−3391
acetic acid-H_2O, assoc. liq., struct. props., static and dynamic phys. props. meas. 79−70316
acetic acid-H_2O, liq. mixture, thermodynamic excess functions, calorimetric meas. 77−52666
acetic acid-H_2O-silver acetate, ternary liq., elec. cond. and density 78−91464
acetic acid-methanol-tetrahydrofuran-d_8, superimposed intermolecular spin exchange reactions, NMR lineshape theory 80−32740
acetic acid-pyridine, H-bonding, proton transfer, isolated system, solvent effect, MO calc. 80−55629
acetic acid-water, liq., Verdet const., pulsed mag. field meas. 80−16012
acetic acid-water, PMR relax. obs., mol. assoc. 79−33553
acetic anhydride, multiphoton dissoc., CH_2 and C_2 prod., fluence depend. meas. 80−5586
acetic anhydride mixtures, elec. resist. near crit. soln. temp. 78−71874
acetic anhydride-CS_2 binary liq. mixture, crit. behaviour of elec. resist. 78−6422
acetic anhydride-cyclohexane, crit. resistivity, H_2O impurity effect 79−51565
acetic anhydride-cyclohexane binary liq. mixture, crit. behaviour of elec. resist. 78−6422
acetone, ^{17}O chemical shift and NMR linewidth meas., self-association equilib. const. determ., mol. reorientations obs. 80−87148
acetone, γ-irrad., isothermal luminesc. decay, temp. depend. 79−66322
acetone, ab initio CI valence and Rydberg states, spectral assignments 77−14346
acetone, absorption bands, vibronic intensification obs., floating-orbital method 80−63619
acetone, activation energy for viscosity, rel. to charge distrib. 79−37865
acetone, adsorbed on ZnO, decomp., IR and kinetic obs. 80−59780
acetone, adsorption on water-preadsorbed alkali halide *(Japanese)* 78−18897
acetone, AES, chem. state effects, for water and simple organic cpds. 78−72687
acetone, boiling, under increased gravitation, heat exchange mechanism, review 77−46895
acetone, chemisorpt. on ZnO, UPS, mol. orbitals effect on bonding 78−72699
acetone, chemisorption and decomp. on Pd 77−63953
acetone, condensation in presence of instabilities, photographic study 78−10180
acetone, electrification during laminar flow in metal pipe 80−6954
acetone, gas, electron-ion recombination, at 292K, three-body interaction 79−46418
acetone, heat emission in crit. region, press. and heating surface temp. effects *(Russian)* 80−69634
acetone, in soln., IR spectral, band halfwidths determ., rot. Brownian motion investig. 77−36248
acetone, isothermal Joule-Thomson coeff. 80−43828
acetone, liq., C-C stretching mode relax., Fermi reson. influence 80−25352
acetone, liq., diamagnetism, mass mag. suscept. meas., temp. depend. 80−97054
acetone, liq., rot. motion, nucl. mag. relax. obs. 78−88209
acetone, macroscopic model for solvated ion dynamics, cation conductance calcs. 80−65261
acetone, mol., radiative lifetime of phosphoresc. state, influence of high lying triplet states 79−86006
acetone, photochem. and photophysics, 330-250 nm, 0-1000 torr 78−17706
acetone, Raman scatt., intermol. vibr. coupling effects 77−58026
acetone, refr. index. temp. depend., deviation from Lorentz-Lorenz formula 77−40200
acetone, relative Raman scatt. cross section 80−100061

organic compounds continued
acetone, solid, effects of tunnelling on spin-lattice relax. of methyl protons 77−12216
acetone, soln. in EBBA, nematic liq. cryst., NMR, orientation 77−1605
acetone, solvent effects on oscillator integrated strength, IR absorpt. bands 78−84575
acetone, stimulated Brillouin scatt. wave front reversal for depolarised light 79−3743
acetone, stimulated Raman scatt. excited by picosecond light pulses 79−14034
acetone, thermal energy charge transfer reactions 79−87828
acetone, Townsend coeffs. of avalanche counter gases 78−78582
acetone, transient heat transfer during natural convection *(Russian)* 77−68367
acetone, transient pressure-drop fluctuations in electroviscous effect 80−15286
acetone, unsteady critical heat flux during boiling 77−23946
acetone, vibr. dephasing theories, test using selective coherent ps. Stokes scatt. 80−59609
acetone+H(2S), collisional quenching, mass spectral obs. 78−25685
acetone + p-difluorobenzene, reson. electronic energy transfer, generalised oscill. strength 78−66668
acetone $A^{1}\Delta$-$X^{1}\Pi$, dissociative excitation, form. environment and parent mol. effects 80−78682
acetone and acetone-d_6, molecular beam photoionisation 79−3504
acetone cation+ketene, proton transfer, CH_3CO^+ heat of form. 77−90592
acetone complex with Br_2, electronic absorpt. spectral calc. *(Russian)* 78−37628
acetone decomposition, near IR laser action 78−63055
acetone in mixed protic-aprotic solns., C=O stretching, IR spectra 80−45056
acetone ions, fragmentation, kinetic energy release, mass spectra 77−79192
acetone oxime, photoelectron and far UV absorpt. spectra 78−17712
acetone vapour, mol. assoc., monomer-dimer equilib., thermal cond. meas., MO calcs. 79−52647
acetone-Ar, conc. profile and interdiffusion coeffs. meas. 79−94763
acetone-benzene(cyclohexane), vap.-liq. equilibria 78−30745
acetone-chloroform (-iodomethane) (-CS_2), liq. mixture, excess Gruneisen parameter, intermol. interaction 78−67635
acetone-chloroform solution, Monte Carlo calcs. for interface struct. with directed intermol. forces *(Russian)* 78−1975
acetone-chloroform-methanol system, multicomponent vapour-liquid equilibrium, direct integration of Gibbs-Duhem eqn. 79−23714
acetone-chloroform-methyl isobutyl ketone, ternary phase diagrams, interactive computer program 80−71629
acetone-d_0, d_6, Raman spectral study of aq. soln. struct., H-bond effects 77−88454
acetone-d_6, deuteron NMR spin echo, time domain spectrum 78−88223
acetone-d_6, multiphoton dissoc., recomb. to ethane 80−3371
acetone-methanol, acetone-CCl_4, methanol-CCl_4 and acetone-methanol-CCl_4 mixtures, acoustic and physicochem. obs. 79−96347
acetone-methanol, vapour-liquid equilibrium data, determ. and correlation 78−87781
acetone-methyl iodide liquid mixture, excess energy of vaporisation, US study 80−65209
acetone-toluene-tetrachloromethane, mol. interaction and thermodynamic props. 80−71935
acetone-water system, electro-optical Kerr constant meas. at 632.8 nm 79−4788
acetones, fluorinated, absorpt., fluoresc. spectra, quantum yields, decay times meas., mechanism 77−3410
acetones, halogen substituted, photoelectron spectra 77−14490
acetonitride-d_1, ^2H NMR spectra, vibr. and asymmetry corrections to quadrupole coupling consts. 80−74184
acetonitrile, ^{13}C chem. shift calcs. using approx. SCF perturbation theory 77−18945
acetonitrile, ^{13}C mag. shielding from beam maser meas. of spin-rot. interaction 79−45707
acetonitrile, ^{13}C relaxation times anal. using J-diffusion model of mol. reorientation 80−87149
acetonitrile, ν_2, ν_3 and $2\nu_3$ bands, vibr. relax., Raman spectra of liq. and dil. soln. 78−9154
acetonitrile, adsorbed on ZnO, IR spectrum species identification *(French)* 79−82967
acetonitrile, adsorpt. on Ag colloids, surface enhanced Raman spectra obs. 80−97251
acetonitrile, adsorption on MgO, IR and TPD study 80−70528
3d-acetonitrile, cryst. struct., ^{14}N NQR free induction decay times meas. 80−54985
acetonitrile, dissolved in liq. cryst., NMR, ^{13}C, ^{14}N relax. times, temp. depend. 79−94016
acetonitrile, dissolved in nematic EBBA, oriented CH_3 group relax., multiple quantum NMR 80−66057
acetonitrile, electrolyte solns., IR and Raman spectra interpretation, CN-stretching region 79−73941
acetonitrile, far IR laser gas absorption obs. with and without DC field 79−31870
acetonitrile, in dilute CCl_4 soln., far IR spectra and mol. dynamics models 79−99876
acetonitrile, in liq. phase, Ramon band profiles, calc. using IR intensities 80−2741
acetonitrile, in soln., IR spectral, band halfwidths determ., rot. Brownian motion investig. 77−36248
acetonitrile, intermolecular interaction, band contour exam. *(Russian)* 79−808
acetonitrile, interstellar, emission obs. in Sagittarius B2 77−64835
acetonitrile, IR and Raman spectra, vibr. and reorientational and energy transfer width separation, rot. const. determ. 80−87131
acetonitrile, liq., Brownian reorientation barriers *(Russian)* 79−27901
acetonitrile, liq., $CD_3C^{15}N$, neutron diffr. 77−11460
acetonitrile, liq., mol. pair-correl. function, X-ray and neutron diffr. 78−26420
acetonitrile, liq., rotational motions, diffusion coeffs., quasi-elastic neutron scatt. study 79−50979
acetonitrile, liq. and solns., IR absorpt. band intensity, temp. depend., CC and CN bonds 77−75157
acetonitrile, liq. struct., RISM equation calc. 78−71665
acetonitrile, low press. IR multiple photon photolysis 79−16022

organic compounds continued
acetonitrile, macroscopic model for solvated ion dynamics, cation conductance calcs. 80−65261
acetonitrile, mol. pair correl. functions, scatt. intensities, statistical mechs. calcs. 79−1382
acetonitrile, mol.excitation by electron impact, 500 and 25-70 eV, expt. and HAM/3 79−72434
acetonitrile, possible source of amino acids on primitive Earth 80−4112
acetonitrile, quadratic force fields, MOCIC pot. functions calcs. 80−5475
acetonitrile, Raman spectral study of aq. soln. struct., H-bond effects 77−88454
acetonitrile, Rayleigh linewidth, in crit. region 79−24329
acetonitrile, soln., high press., mol. reorientation, correl. times, depolarised Rayleigh scatt. obs. 80−29748
acetonitrile, soln., IR perpendicular bands, profiles, rot. models 78−58695
acetonitrile, soln., vibr. relax., isotropic Raman spectrosc. obs. 79−50025
acetonitrile, sub mm laser, generation lines identification *(Russian)* 78−82952
acetonitrile, submillimeter rotational spectrum, laser generation line identification 79−64210
acetonitrile+CS_2 liquid mixture, elec. cond. crit. phenomena 77−4212
acetonitrile binary liq. mixtures, excess thermodynamic functions, complex formation 79−52736
acetonitrile in liq. cryst., ^{13}C and ^{14}N relax. times 79−19793
acetonitrile molecule dissociation in IR field, laser-induced fluoresc. obs. 80−53075
acetonitrile soln., photoelectrochem. behaviour of n- and p-GaAs and InP electrodes 79−4600
acetonitrile solvent for poly[(R)-oxypropylene], effect on opt. rot. dispersion and vac. UV circular dichroism 80−40084
acetonitrile-Ar mixture, anomalous thermal cond. in const. elec. field 77−7505
acetonitrile-carbon tetrachloride solns., rot. and vibr. relax., Rayleigh and Raman scatt. 77−66513
acetonitrile-carbon tetrachloride-n-butanol, mixtures, compressibility, free length, molar and available vol., US meas. 78−2200
acetonitrile-CS_2 binary liq. mixture, crit. behaviour of elec. resist. 78−6422
acetonitrile-d_2, liq., intermol. ^1H spin-lattice relax. and pair-diffusion 79−99781
acetonitrile-HCl complex in liq. Xe, IR spectral study 80−95626
acetonitrile-methanol, excess vol. and isentropic compressibility, from density and US vel. meas. 78−79776
acetonitrile-phenol(-d_1), in CCl_4 ($CDCl_4$) solns., H-bonds vibr. relax. bands anal. 78−84560
acetonitrile-toluene-benzene, mol. interaction and thermodynamic props. 80−71935
acetonitrile-toluene-n-butanol, mixtures, compressibility, free length, molar and available vol., US meas. 78−2200
acetonitrile-water mixture, electrolyte transfer, thermodynamic props. 80−3395
acetophenone, enolate anion, electron photodetachment cross-section resons. 78−5298
acetophenone, highly purified, luminesc. props. 80−32764
acetophenone, in soln., IR spectral, band halfwidths determ., rot. Brownian motion investig. 77−36248
acetophenone, liquid, far IR absorpt., mol. vibrs., internal rot., dipoles *(French)* 77−24827
acetophenone, PPP limited CT calcs. 79−31406
acetophenone, T_1-S_0 intersystem crossing, nonradiative decay rate, excitation energy depend. 80−63609
acetophenone, triplet-triplet energy transfer naphthalene-d_8, in EPA rigid soln., donor phosphoresc. decay 78−10971
acetophenone dispersed in benzene polycryst. host, active N_2 induced chemilum. 80−60691
acetophenone enolate anion radicals, substituted, electron photodetachment cross sections, reson. states 80−1030
acetophenone in toluene glass, quasi-line phosphoresc. spectra 77−69883
acetophenones, di- and trisubstituted, π^*-π systems, UV electronic absorpt. spectra 80−74132
acetophenones, mono substituted, semi empirical Π-electron calcs. 80−74131
acetophenones, spectrosc. characts. using PPP SCF CI calcs. 80−102448
acetophenones, substituted, IR absorpt. spectra, vibr. anal. 77−10672
o,m-acetotoluidide, bromination, fast reaction kinetics, rot. Pt electrode meas. 77−16821
p-acetotoluidide, cryst., low-freq. polarised Raman spectra 78−84574
N-acetoxy-2-fluorenylacetamine effect on in vitro development of mouse embryos 77−12967
N-acetoxy-fluorenyl-acetamide, effect on cell morphologic transform. induced by UV irrad. 77−1981
acetycholine null potential, in mouse pancreatic acinar cells 77−4988
acetyl, vibration and electronic excitation results obtained with magnetically collimated electron impact spectrometer 79−49334
acetyl chloride, liq., proton spin-lattice relax., temp. depend. 78−39435
acetyl chloride, thermal ion-mol. reactions, long-lived intermediate ion form. 79−20360
acetyl cyanide, (^{15}N), microwave spectrum, rot. consts., internal rot. barrier 77−75141
acetyl cyanide, IR and Raman spectra, vibr. spectrum and vibr. anal. 77−10676
acetyl cyanide, rot. spectrum, rot.-torsion-vibr. interaction, A-E rot. splittings 77−10667
acetyl cyanide-d_1, microwave spectra, r_s, r_0-struct. 78−13491
acetyl fluoride, triplet state, trapped electron ICR spectrosc. 79−59373
acetyl halide-titanium tetrahalide adducts, coordination, IR and Raman spectra 78−42050
acetyl iodide, photodissoc., secondary product decomposition 78−25636
acetyl radical, absorpt. spectrum obtained by flash photolysis and kinetic spectroscopy 79−13731
acetyl radical, photofragment spectroscopy, collision dynamics 78−25636
4-acetyl-4′-n-alkanoyloxy-azobenzenes, type A, B smectic, nematic phase, solid state polymorphism, preparation, melting behaviour 78−59745
5-acetyl-5H-benzo[b]carbazole-5H-benzp[b]carbazole, singlet-singlet energy transfer *(German)* 80−93402
acetyl-acetone-carbon tetrachloride, mixtures, excess volume of mixing, mol. interactions 79−57281
N-acetyl-DL-valine, monocrystal, γ-induced free radicals at 77K 79−24774

organic compounds continued
N-acetyl-DL-valine, single cryst., paramag. centre form. by UV photolysis, room temp. 77−21480
N-acetyl-L-cysteine, X-irrad., ^{33}S nucl. coupling and nature of free radicals 77−52743
N-acetyl-l-phenylalanine methyl ester, model for amino acid side chains internal motions in peptides and proteins 80−48017
N-acetyl-N′-methylamide dipeptides, bends and conformational space, statistical mech. anal. 77−68146
N-acetyl-valine, NMR of solid, ^{14}N-^{1}H dipolar spectra, NH bond length 78−48055
acetylacetonate, in nematic liq. cryst., EPR singularities in partially ordered matrix 77−77103
acetylacetone, adsorption on Ge (111) surface, surface recomb. centre neutralization 79−38147
acetylacetone, H bonding, dielec. dispersion obs. 77−63356
3- and 4-acetylamino-N-methylphthalimide, in alcoholic solns., phosphoresc. decay laws 78−17709
2-acetylanthracene, soln., excitation spectra rel. to recording wave length *(Russian)* 77−12438
2-acetylanthracene solutions, excitation spectra rel. to absorption spectra, 77-300K 79−85970
9-acetylanthracene subpicosecond laser photolysis and time resolved absorpt. spectra *(Japanese)* 79−79272
acetylcholine, detect. by liq. chromatography with ion-exchange membrane detector 79−16055
acetylcholine, dielectric transient response following UV-irradiation 80−51166
acetylcholine, diffusion in synaptic cleft of normal and myasthenia gravis human endplates 80−94198
acetylcholine, nonenzymatic hydrolysis, Raman obs. 79−29505
acetylcholine, quantal event at nicotine synapses, numerical reconstruction 79−83748
acetylcholine asynchronous release by motor nerve impulse, mediated by conventional Ca^{2+} channel 78−11638
acetylcholine induced current fluctuations in tissue-cultured muscle cells 77−29119
acetylcholine neurotransmitter, PCILO-INDO calcs. 80−58153
acetylcholine receptor molecules heterogeneity of clonal muscle cells surfaces 80−16910
N-acetyle DL-methionine, γ-irradiated, radical cation EPR, ^{33}S hyperfine coupling 77−40559
acetylene, ν_2 band, Q-branch, high resolution CW CARS 77−42329
acetylene, $A^2\Delta$-$X^2\Pi$, dissociative excitation, form. environment and parent mol. effects 80−78682
acetylene, absorpt. coeffs. meas. in Nd laser emission band 80−78620
acetylene, absorpt. spectrum, 9240-9520 cm^{-1}, rot. anal. and consts. 79−54855
acetylene, absorption spectrum, LiF F_2^+-centre laser intracavity spectroscopy appl. 80−32999
acetylene, abundance in Jupiter atmosphere 78−16337
acetylene, adsorbed on Ni(111), benzene form., vibr. spectra 78−95952
acetylene, adsorbed on Ni (111), vibr. spectra from electron energy loss *(French)* 78−34696
acetylene, adsorbed on type 13X zeolites, inelastic neutron scatt. 78−14584
acetylene, adsorbed on W (111), vibr. states, EELS 77−66090
acetylene, adsorption, surface dissoc. and desorption on Pt (110) 77−62749
acetylene, adsorption and decomp. on Ni (111), high resolution EELS study 80−40739
acetylene, adsorption of Pt (100), intermolecular forces and kinetics of adsorption 78−75930
acetylene, adsorption on Ni (111), identification of CH species by electron energy loss spectra 79−15022
acetylene, adsorption on Ni (111), surface structs., LEED and AES obs. 79−60636
acetylene, adsorption on polycryst. and (0001) single cryst. Re surfaces 78−38947
acetylene, adsorption on Pt(111) surface, UPS meas. 77−52223
acetylene, adsorption on Pt (100) surface 77−59216
acetylene, adsorption on Pt (111), cooxidation, AES *(German)* 78−14619
acetylene, adsorption on Pt (111) surface, LEED intensity obs. 77−51592
acetylene, adsorption on Si (111), low-energy electron loss spectroscopy obs. 77−1303
acetylene, adsorption on W (100), room temp. electron spectroscopy obs. 79−7749
acetylene, AES, chem. state effects, for water and simple organic cpds. 78−72687
acetylene, ambient concs. and ratios to other hydrocarbons in atmosphere 79−12182
acetylene, and -d_1, 1.1 μm band, rot. struct. 77−27069
acetylene, and -d_2, integrated IR intensities, effective charges 77−18921
acetylene, and -d_2, integrated IR intensity, meas. and interpretation 78−66551
acetylene, and $C_2H_2^+$, ionis. pots., photoelectron spectra, ab initio VB calcs. 77−88396
acetylene, and cation, SCF MOGO calc. of electronic struct. 77−34556
acetylene, and deuterated derivative, adsorbed on Ag exchanged zeolite, inelastic neutron scatt. 78−6229
acetylene, angular dependent photoelectron spectral meas. 80−28060
acetylene, as origin of 3.9 micron absorpt. band in C stars 78−93231
acetylene, average mol. polarisability, Frost model wavefunctions calcs. using p-type Gaussians 78−41924
acetylene, C K-shell excitation by electron impact, electron energy loss spectra 77−31014
acetylene, catalytic decomposition, STEM of catalyst particles 80−24328
acetylene, chemical state effects in AES 78−92566
acetylene, chemisorbed Ni and Pd films, IR refl. study 79−69343
acetylene, chemisorbed on metal surfaces, geometric and electronic struct., UPS obs. and HF LCAO calc. 79−86988
acetylene, chemisorbed on Pt (111), self-consistent EHT studies 79−61896
acetylene, chemisorbed on Pt and Pd (111), surface complex form., UPS spectra 77−12826
acetylene, chemisorbed on W, IR vibration spectroscopy using refl. inelastic electron scatt. 78−14603
acetylene, chemisorbed on W(100), geometry distortion 77−30919
acetylene, chemisorbed on W(110), rehybridization 78−31289

organic compounds continued
acetylene, chemisorpt. on Pd (100) and Ru (0001), electronic spectrum, substrate effects on bonding 78−63933
acetylene, chemisorption and reaction on Ir(100), geometric and electronic effects 77−21421
acetylene, chemisorption on α-Fe, struct., bonding, dissoc., UPS obs., MO calcs. 78−84050
acetylene, chemisorption on clean Fe (100) and (111) surfaces, LEED and thermal desorption 78−71996
acetylene, chemisorption on Ir (100), geometric and electronic effects 77−55457
acetylene, chemisorption on Ir surface, LEED, AES and thermal desorption meas. 77−1297
acetylene, chemisorption on Ni(100), LEED and AES obs. 77−31904
acetylene, chemisorption on Ni (001), final state relax. 77−62752
acetylene, chemisorption on Ni (100), angular resolved UPS exam. 78−72685
acetylene, chemisorption on Pt, characteristic loss spectrum and AES 77−55458
acetylene, chemisorption on Pt(111), reaction at room temp., form. of vinyl-like species 79−46939
acetylene, chemisorption on Pt (100), LEED, AES, HPS and temp. programmed dehydrogenation exam. 77−55456
acetylene, chemisorption on Pt (111), ethylidyne form. 79−57291
acetylene, chemisorption on Pt (111), ethylidyne group form., LEED and ELS obs. 78−73075
acetylene, chemisorption on Pt (111) surface, EHT calcs. 77−62733
acetylene, chemisorption on Rh (111) and (100) surfaces, LEED, AES and thermal desorption meas. 78−38951
acetylene, chemisorption on Rh (755), (331), desorpt. temp. and decomp. characts. 79−65318
acetylene, circumstellar, in IRC+10°216 IR spectrum 77−5591
acetylene, CO-C_2H_2 energy transfer laser 77−27277
acetylene, computer controlled CARS spectra of Q branches 78−62241
acetylene, condensed, electron energy loss spectra meas. 77−59652
acetylene, core ionised, core-excited and shake-up states, ab initio MRD-CI methods 80−42950
acetylene, Coulombic energy calcs. 79−99104
acetylene, cryst., semiempirical atom-atom pots. appls. 80−100200
acetylene, dehydrogenation on stepped Ni surface 79−52752
acetylene, dissoc. chemisorption on Pt (111) surface, EHT calcs. 79−39190
acetylene, effective core potential calcs. 79−31437
acetylene, effects on soils N_2O emission 79−83672
acetylene, electron energy loss spectra, C K-shell excitation, vibr. struct. 79−22851
acetylene, electron impact, dissoc. excitation cross-sections, fragment obs. 78−62936
acetylene, electron impact ionis., valence electron momentum distribs. 78−33617
acetylene, electron impact ionisation, valence orbitals, momentum distrib. and correl. effects 78−5361
acetylene, electron ionisation efficiency curves, fragment ion appearance pot. 78−86959
acetylene, electron momentum distribs. in π orbitals from (e,2e) expts. 80−14239
acetylene, electron propagator theory for mol. electron binding energies and photoionis. intensities 80−47848
acetylene, electronic struct. and physicochem. props., modified partial neglect of differential overlap 78−82645
acetylene, electronic structure, SCEP theory calcs. 77−10579
acetylene, electrostatic terms in lattice energy calcs. 79−51040
acetylene, excited state, photochem. and spectrosc. investig. 80−95553
acetylene, force consts. of symmetric stretch motions, accurate ab initio calcs. 77−83567
acetylene, form. on Jupiter, by photolysis or thunderstorms 79−66957
acetylene, geometry optimisation, using bond function augmented basis sets 78−905
acetylene, ground and triplet states, electronic and geom. struct. 78−94184
acetylene, harmonic and anharmonic stretching force consts., ab initio calcs. 78−58587
acetylene, He-Ne laser line, high temp. absorpt., anal. by high resolution IR spectra 80−91554
acetylene, higher excited states, electron energy loss spectra 80−91664
acetylene, in Ar matrix, irrad., C_2^- form. 77−75172
acetylene, inner shell electron energy loss obs. 79−45853
acetylene, ionis. by mol. orbital method, many-body calc. 79−36512
acetylene, ionis. efficiency curves by electron impact, CH_2^+(C_2H^+) form., ~10 eV 78−62935
acetylene, ionis. spectral intensity, valence electron binding energy depend. 78−90234
acetylene, ionisation meas. and $\bar{W}_n$ derivation for neutron irradiation 79−36430
acetylene, ionisation pot. Koopman's theorem, corrections using energy shifted perturbation theory 79−6845
acetylene, IR spectra, rot. and vibr. struct. 78−21922
acetylene, line search in photographic IR spectrum of C stars 77−78786
acetylene, LMO population calc. method appl., from given SCF eigenvector matrix 80−14063
acetylene, magnetic susceptibility, frost model wavefunctions with p-type Gaussians 80−5477
acetylene, mean polarisability derivatives, variational calc. procedure 79−27108
acetylene, mol. and cluster Auger spectrum calc., SCF core-valence-valence spectra 80−48045
acetylene, mol. beam apparatus, appl. as target for storage ring 77−6586
acetylene, mol. geometry basis set depend., geometry optimisation ab initio method 79−31382
acetylene, molecular charge density contours for cryst. struct. 78−38645
acetylene, molecule floating spherical GO calcs. of electron momentum distrib. and Compton profile 77−30933
acetylene, multiphoton i.r. absorption, optoacoustic detection 77−507
acetylene, multiphoton UV photodissoc. 78−50602
acetylene, multiphoton vacuum UV photodissoc. obs. and interpret. 80−11939
acetylene, multipole moments and polarisabilties, SCF calcs. 80−5471
acetylene, near HF dipole polarizability, using EFV GTOs 79−31395
acetylene, on Pt surface, electron energy loss spectra, surface vibrs. 78−15701

organic compounds continued
acetylene, orientation depend. intermol. force, solid struct. 77−50487
acetylene, photoelectron spectrum, satellite line intensity, photon energy depend. 80−53042
acetylene, photoionisation cross section at distance from threshold, chemical bond influence 80−69196
acetylene, prod. by coal gasification process, development and economics 80−30338
acetylene, pure rot. Raman spectra of ground and vibr. Π states, intensity distrib. 77−65476
acetylene, Q-branch of CARS, form and width alteration due to press. *(Russian)* 78−29795
acetylene, Q-branches, diode laser IR spectra, rot. consts. and struct. 79−45723
acetylene, Q-branches, high resolution pulsed CARS 78−17676
acetylene, quartic anharmonic pot. energy function 78−58662
acetylene, Raman spectra, high resolution using laser source 78−42072
acetylene, reaction with Ni (100) and (110), room temp., UPS expts. 80−61151
acetylene, reaction with Si (111) surface, 1225 to 1380°C 79−100441
acetylene, relationships between higher-transition frequencies 80−69119
acetylene, rot. vibr. anal., Raman spectra obs. 80−69146
acetylene, scavenger mol. in UV photolysis of PH_3 in Jovian atmosphere 78−81582
acetylene, selective photoaddition of ICl, isotope enrichment, influence of press., buffer and wavelength 80−11927
acetylene, sign of rot. g-factor, mol. beam expt. 79−59600
acetylene, spherical cryst. grown in situ for low-temp. X-ray work 78−68612
acetylene, surface interaction with transition metal atoms, MO calc. 80−6623
acetylene, surface reaction on Pt (111), EELS of radical vibrs. 78−71947
acetylene, synthesis in HF plasma torch 80−61099
cis-acetylene, triplet state, near IR electronic absorption spectrum, and form. 79−63997
acetylene, triplet state quenching by foreign gases 80−91596
acetylene, triplet states, electron impact energy-loss spectra 77−68128
acetylene, tropospheric and lower stratospheric vertical profiles 80−4073
acetylene, valence excitation energy and UV spectra, HAM/3 calc. 78−25453
acetylene, valence level photoelectron spectra, excitation sources effects 78−78749
acetylene, variationally deorthogonalised localised molecular orbitals, electronic struct. 79−97968
acetylene, Verdet consts., ab initio calcs. 77−3390
acetylene, vertical ionisation pots., CI calcs. 79−13645
acetylene, vibr. fine struct. accompanying core ionis., STO calcs. 78−62844
acetylene, vibr. freqs., MINDO/3 calcs. 78−13429
acetylene, vibr. intensities, G sum rule appls. 80−32776
acetylene, vibr. relax. study using laser-induced fluoresc. 80−74219
acetylene, vibr.-rot. IR spectra, mol. force field determ. ^{14}C effects 77−61748
acetylene, VUV multiphoton dissoc., electronically excited fragment emission 78−90238
acetylene+acetylene-d_2(D_2O), H-D exchange, equilib. consts. 77−86299
acetylene+Ar^{12+}, C K-shell Auger effect 77−6908
acetylene+Ar^{2+}, reactions in flow-drift tube, rate consts. 78−15664
acetylene+Bi($6^4S_{3/2}$), absolute rate consts., time-resolved reson. fluoresc. meas. 78−27731
acetylene+Br_2, laser-induced photochemistry 80−45498
acetylene+C_2, C_2 Swan band transition probabilities, collisional energy transfer effects 80−87214
acetylene+$C_2(a^3\Pi_u)$, reaction rate consts. and quenching, multiphoton UV photolysis, fluoresc. obs. 79−74355
acetylene+Cl, reaction kinetics, stratospheric implication 78−31618
acetylene+HCN, cyanodiacetylene form. in RF discharge 79−5156
acetylene+I_2, laser-induced 1,2-diiodoethylene form., isomerisation 80−85157
acetylene+ICl, isotopically selective photoaddition, ^{37}Cl enrichment 77−60084
acetylene+inert gas, vibr. relax. study using laser-induced fluoresc. 80−74219
acetylene+methyl radical, reaction pot. surfaces, MINDO/3 calcs. 79−22601
acetylene+Mg($^3P_1$) metastable atom, afterglow quenching rate consts. 77−6720
acetylene+N, CN quartet state production, fluoresc. anal. 78−68888
acetylene+N, reaction rate consts., pulse radiolysis obs. 80−35508
acetylene+Na, total cross sections 79−27064
acetylene+O_2 detonation products, enhancement of CO laser gain measurements 78−33729
acetylene+OH radical, reaction rate consts. meas. 78−35663
acetylene+Si*, collisional quenching, reson. line absorpt. expt. 78−46297
acetylene+SO_2, photochem. reactions, rate consts. 78−23956
acetylene+XH^+(X^-), proton transfer reactions, rate consts. meas., Average Quadrupole Orientation Theory 77−63887
acetylene(-d_1,d_2), integrated IR intensities 80−23457
acetylene(-d_2) solns., IR absorpt. band profile *(French)* 77−83597
acetylene(-d), Raman and vibr. spectra and force const. calcs. 80−108747
acetylene (-d_1,d_2), and isotopic forms high resolution absorption spectra, Renner-Teller interactions 79−72332
acetylene (-d_2), fluoresc., in matrix-isolated acetylene and ethylene photolysis 79−59505
acetylene adsorbed on Fe containing segregated C, hydrogenation, C-1s XPS spectra obs. 80−84366
acetylene adsorption on Ni(111), chemisorbed O_2 effects, CH formation 78−18902
acetylene cation, UPS by threshold photoelectron spectrosc. by electron attachment method 79−89708
acetylene cation+methane, reaction, vibr. and translational energy depend., mass spectrosc. obs. 79−47908
acetylene chemisorbed on Ni (111), ind. vibrs., high resolution electron energy-loss meas. 79−90877
acetylene chemisorption on Cu, Ni, Pd and Pt surfaces, molecular geometries determ., using SCF-LCAO calc. 79−19454
acetylene chemisorption on Rh (111), EELS, LEED and thermal desorption mass spectrometry 80−80057

organic compounds continued
acetylene cryst., lattice energy, spheroidal multipolar expsn. for intermol. energy 79−14726
acetylene dimer, ab initio HF calc. for 64 conforms. 80−23333
acetylene flame, Na and MgO concs. meas. by laser saturation spectroscopy 79−29425
acetylene gas, reaction with Ta foil, periodic chemical var. effect on mech. props. 79−91590
acetylene in Saturn atmosphere, detect. using IUE satellite 79−48731
acetylene ketones, absorpt. and phosphoresc. spectra 79−54865
acetylene on Pt (111), nature of adsorption state, surface vibrs. meas. 77−76657
acetylene overlayers on Pt (111), surface, surface struct. and bonding, LEED analysis 77−85067
acetylene photoelectron spectroscopy, review 78−50578
acetylene photopolymers, presence in Jupiter stratosphere 80−31244
acetylene polymerisation in RF discharge, discharge power effect 79−43581
acetylene pyrolysis, nucleation of C black particles *(French)* 79−52648
acetylene smoke, optoacoustic meas. of absorpt. at 0.5145, 10.6 μm 80−43060
acetylene smoke aerosols, optical absorption to extinction ratio, photoacoustic determ. 80−58459
acetylene smoke particles, agglomerated, optical extinction meas. at 0.5145 and 10.6 μm 80−48155
acetylene smoke particles, optoacoustic meas. 80−50895
acetylene submonolayer-covered Ni (111), surface phonons obs. by EELS 80−39403
acetylene type acid corrosion inhibitors, elongation effect on Fe polarised wire 80−55590
acetylene-air flame, eddy entrainment and combustion in depth process, three-region model 79−100384
acetylene-air flame, energy transfer from laser excited Na, Li, optoacoustic pulses 78−25490
acetylene-air flame, Li(Na)(K)(Mg)(Ca) damping consts., Lorentz collisions, mag. field effect 80−66805
acetylene-air flame, multichannel apparatus detect. limits using atomic absorpt. spectra 80−76586
acetylene-air flames, local temp. profiles and at. fluoresc. intensity profiles meas. 77−52680
acetylene-Ar van der Walls molecule, radiofreq. spectroscopy and Stark effect meas., equilib. struct. and props. 80−91543
acetylene-cumulene dehydro annulenes, anomalous polarisation in resonance Raman spectra 80−60574
acetylene-d_0, (−d_2), IR intensities, relative error anal. 78−58686
acetylene-d_0(-d_1)(-d_2) metastable state, mol. beam elec. deflection obs. 80−74137
acetylene-d_0(-d_2), CH^+(CD^+), A-X luminesc., in near-thermal charge exchange 78−50632
acetylene-d_1, vibr. bands, IR spectrum in region of bending fundamental ν_4 80−23418
acetylene-d_2, 17 to 21 μm laser lines generated using CO_2 laser pump 80−69375
acetylene-d_2, $\nu_4+\nu_5$ band, diode laser meas. 78−78664
acetylene-d_2, IR spectra of ν_5 bending fundamental, and $^{12}C^{13}CD_2$ isotope 79−50020
acetylene-d_2, microwave spectrum, P-branch transitions, Stark shifts 77−27057
acetylene-d_2+NH(ND), ($b^1\Sigma^+$) states quenching, kinetic isotope effects 77−63891
acetylene-d_2(d_1), rot.-vibr. Raman spectra 80−83372
acetylene-d, IR absorpt. spectra around 700 cm^{-1} 79−50021
acetylene-ethane, binary mixtures flowing through activated C, adsorpt. interference 80−107635
acetylene-LiH, struct. and props., SCF ab initio calcs. 80−106250
acetylene-N_2O flame, chem. equilib. rel. to AAS 77−4957
acetylene-N_2O flame, spectral source profiling using Reticon photodiode array 77−63999
acetylene-NO-O_2, combustion products, 1400-2600K, minimisation of NO, computer model 78−85161
acetylene/H_2 mixing ratio in Neptune stratosphere 80−51692
acetylenes, substituted, CH wag group freqs., CNDO/2 calcs. 77−6745
acetylenic compound, 1,5-hexadiyne, hydrogen bonding effects on Raman line ν(≡C-H) *(French)* 77−75167
acetylenic compounds, 1- and 4-octyne, hydrogen bonding effects on Raman line ν(≡C-H), solvents effects *(French)* 77−71805
acetylenic compounds, linear mol., Compton profile bond additivity, HF calc. 79−68268
acetylenic hydrocarbons, cyclohexane soln., structureless fluoresc. 80−5575
acetylenic iron carbonyls, mass spectra *(Italian)* 79−18313
acetylenic material, solid, on Pd-$CaCO_3$ catalyst, H getter, hydrogenation rates 77−44510
2-acetylfuran, IR spectra, cis/trans equilib. 77−469
N-acetylglucosamide, substrate-inhibitor of lysozyme, localisation of unpaired electrons 78−68992
N-acetylglycine, X-irrad., stable radical electronic and mol. struct., ENDOR and ESR 80−80637
acetylperoxy radicals, absorpt. spectrum and reaction kinetics 80−91571
acetylpyridines, vibr., IR and Raman spectra 78−74653
acid oxalate ion in aq. soln., vibr. studies, IR and Raman spectra 80−95589
acid phthalate crystals, diffr. props., 0.1-2 nm 77−41740
acid phthalate curved crystal spectrograph, diffraction efficiency calc. method 80−79630
acid-base indicators, ionisation consts. determ., spectrochem. anal. method 77−56264
acid-labile amino acid precursors in Murchison meteorite, chromatographic fractionation 77−64707
acid-labile amino acid precursors in Murchison meteorite, peptides and amino acylamides 77−64708
acoustic spectroscopy, H bonds investigation, N-butyl acetamide association in solns. 80−5891
acridene yellow, glycerol soln., luminesc. intensity and polaris., temp. and viscosity effects 79−56833
acridene-toluene-phenol, luminescence of complexes with hydrogen bonding at 4.2-77K 79−87486
acridine, aqueous soln., laser induced two-photon ionisation investig. 80−32780
acridine, Ar matrix-isolated, lowest triplet state IR and visible absorption spectra 79−68228

organic compounds continued
acridine, dye solns., luminesc. spectra, conc. depend. effects 79−54885
acridine, electronic relax., internal conversion, intersystem crossing, psec. spectra 77−65499
acridine, excited single state kinetics on a subnanosecond time-scale 79−36677
acridine, excited singlet state, fluoresc. quenching by metal ions, rate meas., mechanism 77−38685
acridine, excited state proton transfer reactions, ns fluorometry obs. 79−5132
acridine, methanol soln., edge excitation red shift, excited state proton association 79−18228
acridine, nonradiative electronic relax., picosecond absorption spectrosc. obs. 78−82053
acridine, single cryst., X-irrad., ENDOR obs. 79−87330
acridine, singlet state absorption profile, time resolved spectra 79−45769
acridine, solvent depend. of radiationless relax., singlet lifetime, picosecond spectroscopy 78−66582
acridine, T-T absorpt. build-up, following picosec. pulse singlet excitation, in gas phase 78−9161
acridine, temp. depend. of fluoresc. decay meas. using picosecond techniques 80−99518
acridine C-radical, polarised absorpt. and ESR spectra, dichroism and HF-CI calc. 78−50563
acridine dyes, resonance multiplex CARS spectra 79−13722
acridine dyes in methanol-water glasses, EPR spectra of triplet state 79−18212
acridine in fluorene matrix, RF induced mag, reson. transitions, triplet state, optical nucl. polarisation 79−31561
acridine orange, fluoresc. decay meas. by high repetition rate gated photon counting 80−86402
acridine orange, solvent effect on fluoresc. polaris. 79−41191
acridine orange dye soln., dimerisation equilib., absorpt. spectra least squares anal. 79−50007
acridine orange in ethanol, soln., excited single state lifetimes, aggregates, visible luminesc. spectra, conc. depend. 80−55172
Acridine Orange rot. diffusion from absorpt. relax. 80−1008
acridine-PMTA complex, cryst. struct. determ. 77−11535
acridine-xanthene dye laser mixture, tuning props. 77−3579
acridizinium ion, fluoresc. quenching by external heavy atom, via charge-transfer complex 78−42112
acridone, excited singlet state fluoresc. quenching by metal ions, rate meas., mechanism 77−38685
acriflavine, fluoresc. polaris., solvent effect 77−50468
acriflavine solution, fluoresc. polarisation, effect of aggregation of molecules 79−91485
acrolein, detect. in subway air 78−36273
acrolein, excitation, ionisation and electron affinity, expts., HAM/3 calcs. 80−18790
acrolein, He I and He II photoelectron spectra, CNDO/S calcs. 78−55201
acrolein, mol., conformational anal., inapplicability of MINDO/3 79−94105
acrolein, s-trans and s-cis, trapping from thermal mol. beams and UV-induced isomerisation in Ar matrices, enthalpy determ. 80−97688
acrolein, triplet state vertical and adiabatic excitation energies, CI calcs. 78−9083
acrolein, vap., visible luminesc. excited by pulsed CO_2 laser 79−54894
acrylamide, He I and He II photoelectron spectra, CNDO/S calcs. 78−55201
acrylamide, laser-initiated polymerisation kinetics, holographic obs. 79−29383
acrylamide+urea, γ-irradiated reactions under high pressure *(Japanese)* 79−52707
acrylamide aqueous solution, ultrasonic investigation *(Chinese)* 80−107371
acrylic, ductile-brittle transition conditions 77−66001
acrylic, Raman spectra using pulsed laser and gated detection 77−74529
acrylic acid, He I and He II photoelectron spectra, CNDO/S calcs. 78−55201
acrylic acid+urea, γ-irradiated reactions under high pressure *(Japanese)* 79−52707
acrylic acid doped polystyrene film, elec. cond. and activation energy conc. depend. 80−15631
acrylonitrile, ^{13}C chem. shift calcs. using approx. SCF perturbation theory 77−18945
acrylonitrile, dielectric constant effect on nuclear spin-spin coupling constants 79−72240
acrylonitrile, in soln., IR spectral, band halfwidths determ., rot. Brownian motion investig. 77−36248
acrylonitrile, IR multiphoton dissoc., C_2 prod. and quenching obs. 80−11931
acrylonitrile, IR multiphoton dissoc., prod. of $CN(X^2\Sigma^+)$ and $C_2(a^3\Pi_u)$ radicals 80−63723
acrylonitrile, multiple photon dissoc., photofragment spectroscopy by laser-induced fluoresc. 80−11937
acrylonitrile, NMR and relax. props., liq.-liq. transition rel. to mol. motion 80−70382
acrylonitrile, semiempirical CNDO calcs. of electronic struct. and absorpt. spectra 78−995
acrylonitrile, trace gas detection, using IR laser 79−43653
acrylonitrile-carbon tetrachloride, mixtures, excess volume of mixing, mol. interactions 79−57281
acrylonitrile-dimethylaminoethyl methacrylate membrane, as burn wound covering 78−44676
actinium (III) axalate decahydrate, lattice consts. 78−2102
actinomycin D, response of X-ray resist. hybrid cell line, rel. to X- and UV irrad. 77−86541
actinomycin-DNA bindings, first-neighbour specificities, circular dichroism 78−3442
actomyosin, X-irradiated ENDOR and ELDOR obs. 80−63689
acyl-alkyl photolytic biradicals, scavenging rate const. from mag. field depend. S-T_0 CIDNP 79−3461
acyloxy radical ion, in irrad. Rochelle salt, decarboxylation, pulse radiolysis and EPR obs. 78−70854
adamantane, ^{13}C NMR using high-speed magic angle spinner 78−89516
adamantane, γ-irrad., free radicals EPR and ENDOR 80−69170
adamantane, γ-irrad., positron lifetime rel. to free radical conc. 78−72635
adamantane, cryst., vacancy formation energy, positron annihilation study 80−60706
organic compounds continued
adamantane, crystalline, lattice and sub-grain boundary self-diffusion coeffs. meas. 78−6179
adamantane, cubic, cohesive energy and Gruneisen parameter calcs. 79−19183
adamantane, derivatives in solution, mol. motion and methyl group rot. barriers from ^{13}C NMR relax. times 80−74179
adamantane, deuterated single plastic cryst. high-symmetry dispersion curves, coherent inelastic neutron scatt. meas. *(French)* 79−14905
adamantane, elastic props., press. depend. rel. to intermol. forces 80−54297
adamantane, growth rate from vapour, variability under const. conditions 78−34452
adamantane, heteronuclear spin coupling and decoupling dynamics 77−48066
adamantane, Ising, diffuse scatt., hard-core correl., weak-graph method 80−49137
adamantane, lattice dynamics in disordered phase 78−55923
adamantane, Lennard-Jones (6-12) interaction pot., Debye temp. calc. 78−63828
adamantane, mol. cryst., thermal expansion coeff. and Gruneisen coeff. 77−84952
adamantane, mol. reorientation activation parameters, determ. by NMR method under press. 77−89393
adamantane, NMR, spin-lattice relax., plastic-brittle phase transform. 79−95665
adamantane, nucl. spin echoes ^{13}C magnetisation and intermol. dipolar coupling 78−35062
adamantane, order cubic $F\bar{4}3m$ phase, X-ray diffuse scatt. 78−38684
adamantane, orientation and deform. in nematic liq. cryst., PMR obs. 77−71815
adamantane, plastic and solid-solid transitions, Raman study 80−60590
adamantane, plastic cryst., radio- and photothermoluminesc. *(Russian)* 79−11477
adamantane, plastic cryst., Rayleigh scatt. of Mossbauer radiation 78−27125
adamantane, plastic cryst., rotational motion, elastic incoherent struct. factor determ. 77−4056
adamantane, plastic cryst., thermolum. curves 80−2876
adamantane, plastic cryst. lattice vibr. study of phase transition 80−7355
adamantane, plastic cryst. rotational motion, quasielastic neutron scatt. study 79−41991
adamantane, plastic phase, C_4 rot. jumps, existence and uniqueness 80−88067
adamantane, plastic phase, librations, phonon branches, neutron scatt. study *(French)* 79−51222
adamantane, plastic-phase transition, cell model 77−11665
adamantane, proton enhanced ^{13}C NMR, T_1 value method 78−91972
adamantane, proton-enhanced NMR, magic-angle spinning, polarisation transfer 78−19349
adamantane, radiation chem. alkylation 77−48663
adamantane, thermal cond. and heat capacity under press. 80−80008
adamantane crystals, vapour grown, temp. depend. of morphology of initial growth forms 79−47608
adamantane powder, dipolar relaxation, short time behaviour, pulse method meas. 80−84667
adamantane-adamantane interactions, expansion of intermol. energy in set of symmetry-adapted functions 80−106371
adamantane-d_{16}, collective librational modes and orientational correlations 79−73266
adamantane-d_{16}, in soln., deuteron spin-lattice relax. time, mol. rotational correl. time 78−84491
2-adamantanone, absorption and fluoresc., high-press. 77−52113
2-adamantanone, cryst. struct. in plastic phase 80−88065
adenine, hydroxy and methoxy derivatives, absorption UV spectroscopy and electronic struct. of ionic and tautomeric forms 80−74177
adenine, nucleic acid component, selective action by ps light pulses 80−72213
adenine, restraining effect on photographic emulsion *(German)* 79−39175
adenine, tautomeric equilibria with cytosine in aq. solns., electrostatic model of solvation, SCF MO calc. 79−96305
adenine, tautomers, polarisation, barriers and tunneling times calcs. 79−41114
adenine, UV photoelectron spectra, valence electronic struct. 77−16905
adenine film, polycryst., energy conversion processes, quantum yields, 4 to 10 eV 80−88589
adenine hemisulphate hydrate, single cryst. growth from soln., props., cryst. parameters, X-ray anal. 79−32929
adenine nucleotide content of human blood platelets after γ-irrad. 78−28021
adenine sulphate, single cryst. growth from soln., props., cryst. parameters, X-ray anal. 79−32929
adenine tautomers, relative stabilities, nonempirical MO calcs. 80−21442
adenine-uracil polynucleotides, alternating, premelting, melting, postmelting transitions 79−57574
adenosine, association, spin label appl. 78−81086
adenosine 5′-monophosphate, UV resonant Raman spectra 78−48756
adensoine 5′-diphosphate, interactions with kyosin, intermolecular spin diffusion study 80−18951
adenylate kinase, photokinetic microassay using the firefly luciferase reaction 80−56306
adenylyl 3′-5′ adenosine, conform. equilib., Raman temp. jump obs. 78−8450
adipic acid, monoclinic crystals, IR absorption and dichroism 78−88293
adipic acid crystals, H bonds, harmonic couplings, IR vibr. modes, isotope effect origin 80−34902
adipic acid crystals, IR spectra, O-H(O-D) stretching bands 79−91422
ADP, association, spin label appl. 78−81086
ADP, Na:K rel. to Na:Na exchange by Na pump of skeletal muscle 77−66807
ADP, role of respiratory chain in oxidative phosphorylation 78−15795
ADP induced mitochondrial absorbance changes rel. to ATP synthesis 78−27908
adrenaline, acid aq. solns., pulse radiolysis, H., OH. react. kinetics, UV spectra 77−16841
adrenocorticotropic hormone polypeptide chain left helical conform., aqueous soln. 77−70414
adsorbed dyes, ionization energies rel. to spectral sensitization 79−19553
adsorbent mesopores, capillary evaporation and struct. 80−107614
adsorption on Bi 80−20038

organic compounds continued
aerosol OT-n-heptane-water, reversed micellar solution; addition of electrolyte, neutron small angle scattering 80−104468
aerosol samples, organic material 78−73463
aerosols, atmospheric, total organic constituents estimate 77−37289
agarose gels, bubble prod., stabilisation by nonionic surfactants 80−76562
agarose gels, $H_2{}^{17}O$ enriched, ^{17}O NMR, hydration anal. 77−81426
agarose-water gels, stability, conc. and isotope effects, photometric obs. 79−66362
agarose-water systems, gel-sol transition, thermal hysteresis and reversibility 79−66361
aggregate organic photoconductor, composition prep., struct. and optical props. 79−24006
aggregate organic photoconductor, photoconduction props. 79−24007
air pollution, evaluation of Co_3O_4 catalysts for oxidation 77−37353
air pollution, extraction from airborne particulate matter 77−33181
air pollution control, evaluation of catalysts for vapour phase oxidation of odorous organic compounds 79−70482
air-acetylene flame, atom form., theory 78−7208
airborne particulate matter, size distrib. of organic pollutants 79−57553
2-(4-n-aklylphenyl)-5(4-nalkoxyphenyl)-pyrimidines, smectic polymorphism, miscibility meas. 79−86678
L-alanine:Cr^{3+}, X-irrad., thermoluminesc., ESR, UV photobleaching 77−9104
L-alanine:Cu(II), EPR and ligand-ENDOR measurements 80−44907
L-alanine, ^{17}O NMR chemical shifts and linewidths, pH dependence 80−80625
α-alanine, adsorbed on Ag, XPS and SIMS study 79−86986
β-alanine, aq. soln., dielectric relax. spectrum, Debye domains 77−8498
β-alanine, aqueous solution, ultrasonic velocity measurement 80−19878
L-α-alanine, cryst., cationic radicals, EPR 78−11537
DL-alanine, cryst., Raman spectra and lattice dynamics 79−28741
β-alanine, cryst., X-irrad. producting radicals, ESR and ENDOR 79−56612
L-alanine, nucl. spin-lattice relax. of CH_3 and NH_3 groups 77−8440
alanine, oligomer, vibr. spectra rel. to polymeric form 79−83695
L-alanine, solid, H bonding, wide line NMR obs. 78−52362
alanine, unionised, ab initio equilib. structs. calcs. 79−68181
L-alanine and DL-alanine, cryst., Raman band intensities of local group modes 80−93298
L-α-alanine disordered regions in TGS crystals, dielec. props. 80−108159
l-alanine incorporation in TGS crysts., orientation depend. 78−42938
l-alanine powder, short dipolar relaxation time meas. by saturation method 80−60441
^{14}C-alanine transport, photo-depend., into H.halobium cells 77−70439
DL-alanine-α,β-d_4, Raman spectra, intermol. pot. 79−91432
alanine-d_3, vibr. circ. dichroism, mechanism 78−33505
alaninium copper tetrahalides, exchange, mag. anisotropy, and spin diffusion contribs. to EPR linewidth 80−80597
β- alaninium tetrachloroferrate (III), X-ray cryst. struct. determs. 79−90635
alarm pheronomes, activity rel. to mol. similarity, electron density function meas. 80−91413
albumin reticulated with rhodopsin, membrane permeabilities, dynamic, meas. under non-equilib. conditions 80−46107
4-alcanoyloxybenzoyloxy-4′-cyanoazobenzene series, influence of substituent on reentrant mesophases 80−88027
4-alcanoyloxybenzoyloxy-4′-cyanobiphenyl series, influence of substituent on reentrant mesophases 80−88027
4-alcanoyloxybenzoyloxy-4′-cyanostilbene series, influence of substituent on reentrant mesophases 80−88027
alchohols, glassy, spectra shift of trapped electrons, after γ-irrad. 79−78709
alcohol, alternate liquid fuel development, for diesel engines and gas turbines 80−55782
alcohol, dielec. const., hindered mol. rot. influence 78−43767
alcohol, thermal electret, persistency of surface change *(Japanese)* 77−81048
alcohol+$H_x{}^+$, methanol to butanol, x=1-3, charge exchange ionisation *(German)* 77−83700
alcohol+$H_x{}^+$, methanol to octanol, x=1-3, charge exchange and ionisation *(German)* 77−83699
alcohol binary mixtures, nonlinear dielec. effects, shift in assoc. equilib. 77−73108
alcohol fuel production from biomass 80−55773
alcohol fuel production from wood, Brazil, ethanol and methanol 80−30328
alcohol galsses, tunnelling reactions of trapped electrons with electron acceptors 78−76887
alcohol glasses, X-irradiated, electron scavenging mechanism 77−56235
alcohol H-complexes interactions, H-bond vibr. freq., anharmonic calcs. 80−99453
alcohol homologous series, $^1HT_1$-relax. time, paramagnetic, diamagnetic shift reagent effects *(German)* 78−43673
alcohol modification of silica gel skeletal struct., thermal analysis obs. 78−88659
alcohol monolayer on water, eqn. of state 78−6195
alcohol solutions, fluoresc. damping curves in reson. quenching by one-photon counting method 78−10978
alcohol solutions of pyrene, polar fluid electrons optical absorption coeffs., ns laser ionis. obs. 78−84600
alcohol-active soln., assoc. soln. thermodynamics, H^E, V^E curves 78−31671
alcohol-aliphatic hydrocarbon mixture, critical soln. temp. 79−37844
alcohol-alkane dilute system, electron solvation, picosecond spectral obs. 77−44573
alcohol-benzene, liq. mixtures, excess free vol., US vel. meas. 77−51294
alcohol-H_2O, microemulsion, elec. cond. and struct. 79−20471
alcohol-H_2O solutions, structure, luminesc. probe obs. 78−84636
alcohol-inert compounds mixtures, thermodynamic props. *(German)* 79−52748
alcohol-inert soln., assoc. soln. thermodynamics, enthalpy, Gibbs free energy 78−31670
n-alcohol-Lewis base mixtures, glass transition temp. composition depend. 77−66015
alcohol-nonassociating active component mixtures, thermodynamic props. 78−64878
alcohol-solvent, associated, excess free energy and enthalpy of mixing 78−31680
organic compounds continued
alcohol-unassociated active component liquid mixtures, associated soln. theory, thermodynamic parameters 80−7836
alcohol-water mixtures, US attenuation meas., method of streaming 80−88272
alcohol-water solutions, containing radioisotopes, radiochemical purification *(Russian)* 77−86432
alcohol/water mixtures, NMR and IR obs., low temp., shifts, interpretation 77−52065
alcohols, α-particle impact, 0.3-2.0 MeV, O stopping cross-sections 78−17753
alcohols, adsorption on Si surface *(Russian)* 78−91537
alcohols, aliphatic, permitt., dielec. relax., time-domain multiple refl. meas. 77−57350
alcohols, assoc. liq., viscous props. 80−2186
alcohols, chemical ionisation mass spectra 77−75273
alcohols, chiral, circular dichroism, RPA calc. 79−36672
alcohols, dil. aqueous solns., isentropic compressibility behaviour from sound vel. meas., dissolution mechanism 80−30269
alcohols, dil. solns., dielec. loss and relax., microwave and sub-mm. wave absorpt. obs. *(German)* 78−23396
alcohols, electrochem. oxidation, kinetic isotope effect *(German)* 78−15681
alcohols, electron solvation dynamics, rel. to interaction pots. 77−9052
alcohols, glass, electron trapping, pulse radiolysis obs. 80−30264
alcohols, H-bond system, liq., high-press. effect 80−49080
alcohols, liq., picosec. mol. dynamics and electron localisation 79−46548
alcohols, liq. mol. rot., deuteron relax. obs. 77−8432
alcohols, long chain conformations, ^{13}C pseudocontact shifts 79−13743
alcohols, modified CNDO calcs., conformations, binding energies 77−6682
alcohols, monohydric, dielec. polarisation 79−99818
alcohols, monohydric saturated, vibrational bandshapes 78−90226
alcohols, normal, semiempirical theory of surface tensions 79−51391
alcohols, OH-stretching vibr. band in overtone region, IR-Fourier spectral investig. *(German)* 80−976
alcohols, opt. consts. in IR, stretch band obs. 79−91421
alcohols, optical spectra of solvated electrons, band resolution 79−78698
alcohols, saturated, bonded and nonbonded, quantum chem. calcs. 80−9514
alcohols, saturated, list of OH stretching frequencies, using averages and least squares approx. methods 79−53966
alcohols, self-association in binary mixtures, 2-const. model, vap. press. meas. *(German)* 78−18532
alcohols, self-diffusion, flow meas., 25-65°C 78−2278
l-alcohols, stopping power meas. for Li projectiles 79−4345
alcohols, temp. coeff. of refr. index *(Japanese)* 77−28537
alcohols, trapped electron spectral relax., random-walk model 78−60493
alcohols, US effects on shear viscosity 78−59184
alcohols, vapour and liq. IR spectra, bandwidth, directional mol. rot., H-bonding 79−78661
alcohols, vapour-liq. equilib. and heats of mixing, simplified group method anal. 80−96637
alcohols+Sc(La)(Y), O atom abstraction, product internal state distrib., fluoresc. study 78−48643
alcohols and solutions in $SnCl_4$, spin echo obs. of self-diffusion *(Russian)* 79−95197
alcohols in organic solvents, H_2O absorption 80−66788
alcohols in solution, dielectric relax. depend. on conc. 77−1636
p-alcoxybenzilidene butylaniline, liq. cryst., mag. anisotropy and polymorphism *(French)* 77−76532
aldehydes, conjugated, ethylenic, UV photoelectron spectra *(French)* 78−90215
aldehydes, formation by photochemical reactions *(Japanese)* 78−88648
aldehydes, molecular stopping cross section of He^+ ions and atomic stopping cross section of O 78−67746
aldehydes in air, gas chromatography 79−12284
aldosterone action mechanism and phospholipase A 78−24053
aldosterone monohydrate, appl. of three phase struct. invariant, in $P2_1$, probabilistic theory 79−51033
alene, -d_2, -d_4, harmonic force field, ground state average struct. 77−61732
alicyclic compounds, nucl. spin-spin coupling via nonbonded interactions, γ-substituent effects 80−69078
alicyclic ketones, triplet state behaviour, non-RRKM photochemical decay, vibr. relax. 78−61030
alicyclic ring compounds, vibrational spectra and structure, book 78−78700
alicyclic ring cpds., vibr. spectra, conformational props., book contrib. 78−78702
aliphatic, in dil. solns., dielectric relax. dipole reorientation, rot., microwave obs. 77−28516
aliphatic acids, interaction with phosphine 3R hydrochloride, IR and electron spectra *(Russian)* 78−21930
aliphatic alcohol, in nonpolar solvent, dil. associated soln., lattice model, chem. equilib. laws 79−82139
aliphatic alcohol, thermodynamics of adsorption at air/aqueous soln. interface 80−10752
aliphatic alcohols, conform., rot. isomerism calcs. *(German)* 78−50541
aliphatic alcohols, glass transitions 80−54357
aliphatic alcohols, interaction with phosphine 3R hydrochloride, IR and electron spectra *(Russian)* 78−21930
aliphatic alcohols in carbon tetrachloride, association processes, NMR spectroscopy 77−16792
aliphatic amine mixtures, ionis. consts. determ. by gas-chromatographic anal. *(Russian)* 79−61921
aliphatic amines, tertiary, fluoresc. decay 80−91590
aliphatic amino acids, N-acetyl substituted, photolytic production of methyl radicals 79−96622
aliphatic anhydrides, photoelectron spectra, orbital energies 79−10151
aliphatic chains, mol. orientation correls. with squalane in soln., depolarised Rayleigh scatt. *(French)* 79−65885
aliphatic chlorocarbons, electron impact dissoc., $\lesssim$10 eV, negative ion prod. 78−5359
aliphatic compounds, alkyl substitution effects on photoionisation, photoelectron spectrosc. obs. 79−31604
aliphatic compounds, nucl. spin-spin coupling via nonbonded interactions, γ-substituent effects 80−69078
aliphatic diallyl esters, radical polymerisation, rel. between vol. contraction and chem. changes *(German)* 78−61009
aliphatic esters, mol. dielec. relax. in soln. 79−82918

organic compounds continued
aliphatic ethers, dil. solns., dielec. loss meas. for dielec. relax. 78−68451
aliphatic ethers, thermal conductivity, hot-wire meas. 78−63885
aliphatic ethers-HF, H bonded complex, gas phase, first overtone reconstruction 80−43040
aliphatic ketones, freq.-topology-milieu relation, IR study, struct. and solvent effect *(French)* 80−95623
aliphatic liquid crysts., trans, trans-cyclohexyl cyclohexanoates, synthesis, mesomorphic phases 80−44121
aliphatic nitroxyl radicals, quenching of triplet state aromatic hydrocarbons, energy transfer 78−35651
aliphatic perfluorocarbons, electron attachment, fragmentation 0-12 eV 80−5618
aliphatic short chain compounds, oxidation and degradation by hyperazeotropic nitric acid 78−37431
aliphatic surface monolayer, on water, phase transition model 79−56041
aliphatic tertiary amines, laser action feasibility, emission spectra, two photon excitation 80−23683
aliphatic unsaturated normal hydrocarbons, positron annihilation time spectra, polarisability depend. 78−6806
alkali alkanoates, phase relationships and thermal behaviour branching effects 78−43111
alkali alkanoates, solid-state transitions, diffractometric and conductometric meas. 79−60507
alkali atom+alkyl oxide cross-sections, hard-sphere model 78−7176
alkali metal acid oscalates, neutron inelastic scatt. spectra in 2200-200 cm^{-1} range 80−70327
alkali metal carboxylates, ionic melts, novel class of liquids 77−35463
alkali metal cation-electron pair in ethers, optical spectra, coordination effects 77−66788
alkali metal dicarboxylates, H bonding and motion, incoherent inelastic neutron scatt. spectroscopy 80−48095
alkali metal salts with aromatic hydrocarbons, photoelectron emission and optical absorption *(Russian)* 78−80456
alkali n.-alkanoates, long-chain, ethanolic solns., solubility temp. depend. 78−15724
alkali-anthracene ion-pairs and triple-ions in solution, far IR spectra 79−78663
alkaline earth citrate electrolyte, Ni electrodeposition, cathodic process rate *(Russian)* 79−8440
alkaline phosphatase, slow reaction, vidicon-based spectrometer obs. 79−21817
alkane:toluene, radiolysis at 77K, luminesc., excited singlet toluene form., energy transfer mechanism 77−16846
n-alkane, adsorption energy of mols. on long-chain even n-alkane crysts., rel. to cryst. growth kinetics 78−42933
n-alkane, long chain, syntactic coalescences between monoclinic and orthorhombic polymorphs 80−10520
n-alkane, long-chain even, adsorpt. energies of n-alkane mols., rel. to cryst. growth kinetics 78−42933
n-alkane, OCS solute, rot. relax., solvent hydrodynamic props., Raman and IR spectra 80−45055
n-alkane, order-disorder phase transition bits. calc. 77−72684
n-alkane, polymer, liq., mol. arrangement, computer model 80−92446
n-alkane+Ar mixtures, intermol. pot. using Kihara model with spherical cores 77−54591
alkane+He, scattering at high velocities, short-range pot. determ. 77−27143
alkane+He, scattering at high velocities, short-range pots. determ. 77−27142
alkane+SO_2, $^3B_1$-state lifetime saturation, chem. and phys. quenching channels 79−814
n-alkane binary mixtures, infinite dilution activity coeffs. 78−15695
n-alkane binary mixtures, melting and solid-state transition 77−72685
alkane chain internal rot. correlation times, from ^{13}C T_1 data 78−17688
n-alkane chains, pure liq. and solns., small angle neutron scatt., ang. depend. 79−1384
alkane chains in liquids, rot. and torsional dynamics, Riemann tensor theory 80−54084
n-alkane crystal test for porphin, phototautomerism IR spectral obs. 80−34963
alkane dimer, PCILO calc. of geom. struct. and energy 79−63930
n-alkane gases, depolarised light scatt., internal field effects 79−76471
alkane glass, γ-irradiated, charge trapping, isotope and mol. struct. effects 79−5164
alkane hydrocarbon+Cd, $^3P_{0,1,2}$ state distrib., E to V,R transfer 80−28088
n-alkane liquids, molecular orientational correlations 79−19131
n-alkane mol. config. in melt and cyclohexane soln., small-angle neutron diffr. 78−55800
n-alkane pollutants, N.Atlantic gas and particle concs. in troposphere 80−7969
alkane systems, hot H replacement reactions 78−68906
n-alkane-benzene, liq. mixtures, excess free vol., US vel. meas. 77−51294
n-alkane-benzene mixtures, mol. orientation correls., depolarised Rayleigh scatt. 79−22714
n-alkane-cyclohexane, liq. mixtures, density meas. for excess volume *(German)* 79−73324
n-alkane-dimethylsiloxane mixtures, shear viscosity press. depend. 78−30775
alkane-H_2O-SO_2 gaseous mixture, photoinduced nucleation and quantum yields 79−96348
alkane-N_2O, mech. of thermal electron attachment, microwave cond. meas. 78−59536
alkane-silicone oil mixtures, thermal cond. 79−42323
alkanediol-eicosane, interface tension, sessile bubble method *(Japanese)* 78−79857
alkanediols, surface tension, sessile bubble method *(Japanese)* 78−79857
alkanes, ν(CH_2) and (CH_3) Raman bands, global integrated intensity, dilution effects *(French)* 77−61755
n-alkanes, adhesion to muscovite mica, model high surface energy solid 77−55435
n-alkanes, adsorption into bimolecular lipid layers 80−88435
n-alkanes, adsorption on chlorosilane covered quartz crystal surface 79−4466
alkanes, and cycloalkanes, saturated hydrocarbon chains PMR characterisation *(Portuguese)* 80−5562
n-alkanes, anisotropic London dispersion forces, surface effects 80−74214
organic compounds continued
alkanes, band struct. evolution and electronic relax. in photoemission *(French)* 77−36358
n-alkanes, Bender eqns. of state 78−26656
alkanes, bonding, optical anisotropy and polarisability 79−22713
alkanes, collisional dissoc., time of flight mass spectrometric obs. 77−74545
n-alkanes, conduction band struct., LEED, secondary electron emission and UPS study 80−70601
n-alkanes, depolarised Rayleigh spectroscopy 79−4808
alkanes, diamag. susceptibility, graph theoretical anal. 78−33449
alkanes, diamagnetic properties, susceptibility contributing terms 79−47228
n-alkanes, dielec. permittivity and pvT data 80−44996
n-alkanes, diffusion anomaly in NaMgA zeolites *(German)* 79−77817
alkanes, diffusive Langevin dynamics of model systems 79−86671
alkanes, electron density, bond order, hydrogen suppressed graphs, extended Huckel theory 78−90088
alkanes, electron impact, threshold excitation by monoenergetic electrons 78−58854
alkanes, electron impact dissoc. excitation, H sublevels populations meas. 77−75073
alkanes, electron localisation and solvation, radical ion theory 78−87936
alkanes, electron mobilities through liq. and critical regions 78−2536
alkanes, ethane-, hexane-polar component binary mixtures up to 1000 bar, phase separation, critical phenomena 77−35695
n-alkanes, even, long-chain, layer interaction energies for different twin and polytypic positions 77−65985
alkanes, fourth order nonlinearity acoustic parameter 78−51612
alkanes, glassy, radiation chem., D isotope effects 77−36767
alkanes, H^+ chemical shifts, extended Huckel calcs. with gauge in variant atomic orbitals 80−102449
n-alkanes, hydrophobic effect, dil. soln. struct. and thermodynamic props., semi-empirical model 78−20060
alkanes, IR spectral intensity for electro-optical parameter 79−54835
alkanes, latent heat of vaporisation calc. at normal boiling pt. by group contrib. method 79−77737
alkanes, light, solubility in liq. N_2, IR spectroscopy obs. 80−59654
alkanes, linear, elec. struct., evolution of electronic level towards band struct. *(French)* 78−5282
alkanes, linear, electronic struct., electronic relax. during photoemission *(French)* 78−5283
alkanes, linear, K-shell ion relax. energy chain length depend. 79−72252
alkanes, liq., energy transfer rate parameters, emission intensity, lifetime meas. 79−86031
alkanes, liq., mol. struct., selective deuteration and IR vibr. spectra 80−96432
In-alkanes, liq., radiolysis mechanisms rel. to hot H atom reactions 77−36771
n-alkanes, liq., Raman spectra, longit. acoustic modes and gauche-trans energy difference 80−93295
alkanes, liq. and glassy, semicontinuum model with structured first solvation shell for excess electrons 77−90711
n-alkanes, liq. mixtures, thermodynamics 80−55700
alkanes, liq. state rot. dynamics for nonrigid 4-, 5-, and 6-bond chains 79−99054
alkanes, liquid, chain reorientation, Brownian dynamics simulation, comparison of models 80−49067
alkanes, liquid, press. induced changes in mol. conform. 78−9269
alkanes, liquid, relation between density and refractive index *(Japanese)* 79−24279
n-alkanes, longitudinal acoustic modes, Raman intensities 80−32718
alkanes, low press. triboelectric discharge, decomposition products *(French)* 77−48622
alkanes, mag. susceptibility simple additive approx. calcs. 78−86775
n-alkanes, methane to n-tridecane, ESCA of core electron relax. and valance bands 77−18978
alkanes, mixtures, order, enthalpy of mixing, calorimetric obs. *(German)* 78−18773
alkanes, mol. electro-optical props. 79−50162
n-alkanes, mol. Rydberg S←S and S←T transitions, semi-empirical SCF MO calc. 80−91453
alkanes, molecular topology, branching, distance matrix, information theoretic calcs. 78−25405
n-alkanes, monoclinic, polygonized spiral growth patterns on {001} faces *(Italian)* 79−23559
alkanes, normal, semiempirical theory of surface tensions 79−51391
alkanes, nucl. spin-spin coupling via nonbonded interactions, conformational and substituent effects 80−69077
n-alkanes, numerical method for mol. dynamics 77−27804
n-alkanes, obs. and anal. of depolarised Rayleigh doublet 78−35154
alkanes, OH radical photooxidation, 305K, absolute and rel. rate consts. 77−16782
n-alkanes, orientational phase transitions with mol. config. change 78−14444
alkanes, overtone spectra, local mode anal., discrete excitation of nonequivalent CH oscills. 78−78688
alkanes, polycryst., radiation chem., D isotope effects 77−36767
alkanes, polycyclic, three-photon ionisation spectra, 3s Rydberg orbital 79−68282
n-alkanes, purification and single cryst. growth 80−71589
alkanes, saturated, ab initio LCAO MO SCF calcs., core ionis., electronic relax. 77−71745
n-alkanes, single cryst., γ-irrad., ESR, energy deposition rel. to alkyl radical form. 77−16844
n-alkanes, solid, core electron relax. energies and valence band form., XPS exam. 77−36372
alkanes, solubility in liquid O_2, estimation by Preston-Prausnitz method 80−39285
l-alkanes, stopping power meas. for Li projectiles 79−4345
alkanes, temp. coeff. of refr. index *(Japanese)* 77−28537
alkanes, thermal accommodation coeffs., on Al(Fe), translational (internal) gas-solid energy exchange 78−92506
alkanes, thin plate microcrystals, transmission electron diffraction intensities 78−83821
n-alkanes, translational diffusion coeff. calc. 77−14626
alkanes, tritiated, fragmentation by β-decay, dissoc. of daughter species 78−31669
alkanes, van der Waals dimers, PCILO calcs. 79−36542
alkanes, vap., fluoresc. lifetimes meas. 79−50064
n-alkanes, vap. press. eqn. appls. 77−69091

organic compounds continued
alkanes, vapour-liq. equilib. and heats of mixing, simplified group method anal. 80−96637
n-alkanes, vibr. calcs. and nonrigid mol. symmetry groups 77−6756
n-alkanes, vibr. data and force field consts., review 79−31750
alkanoate, Li, Na, K and Rb salt mixtures, DSC anal. 78−10192
n-alkanols, complex. permitt. meas. by time-domain spectroscopy 77−49741
1-alkanols, liq., H-bond order temp. depend. from Hildebrand rule 80−7838
n-alkanols, nerve Na channel potentiation, squid giant axons 79−83744
p-alkanoyl-benzylidene-p'-aminoazobenzenes, liq. cryst., proton mag. relax., self-diffusion 77−84632
alkene+N, reaction rate consts., pulse radiolysis obs. 80−35508
alkene+O(^{3}P), absolute reaction rate consts., 298-439K, photolysis-chemiluminesc. determ. 77−77747
alkene-halogen, matrix isolation vibr. spectroscopy, complex form. studies 78−62952
alkene-halogen compounds, assoc., matrix isolation vibrational spectra, appls. 78−46416
alkenes, 1,1-, 1,2-disubstituted, fragmentation modes in perturbational MO anal. 80−58138
alkenes, π bond dissoc. energies, derivation from isomerisation kinetics, for teaching 79−58498
alkenes, bonding, optical anisotropy and polarisability 79−22713
alkenes, diamag. susceptibility, graph theoretical anal. 78−33449
alkenes, electron impact, threshold excitation by monoenergetic electrons 78−58854
alkenes, ethene-, 1-hexene-polar component binary mixtures up to 1000 bar, phase separation, critical phenomena 77−35695
alkenes, halogen substituted, chemisorption on Pt (100), Pt (111) substrates, photoelec. spectroscopy, dissociation model 77−43429
alkenes, IR absorpt. curves calc. using standard fragments computer library 80−982
alkenes, IR multiphoton dissoc., IR detection of H atoms 80−83356
n-alkenes, n even, interaction energy at twin boundary, dihedral reentrant, salient angle effect on growth morphology 78−55876
alkenes, OH radical photooxidation, 305K, absolute and rel. rate consts. 77−16782
n-alkenes, photoelectron spectra, MINDO/1, MINDO/3 and Fenske-Hall calcs. 78−5285
alkenes, solubility in liquid O_2, estimation by Preston-Prausnitz method 80−39285
n-alkenes, stopping power meas. for Li projectiles 79−4345
alkenes, substituted, core electron binding energy shifts, σ- and π-relax. energies 78−29750
1-alkenyl-2-pyridones, photocyclisation rel. to energy storage 80−89680
alklylammonium ions, adsorpt. potential determ., at soln.-solid interface 79−56068
4-n-alkoxy benzoyloxybenzylidene 4'-cyanoaniline series, nematic reentrant mesophases, phase diagrams 80−103467
alkoxy free radicals, produced by X-irrad. of hydroxy containing cpds., characterisation by ESR and ENDOR 78−95938
alkoxy radical, trapped in nucleosides or nucleotides, EPR, INDO calcs. 77−90623
4-alkoxy-4'-cyanobiphenyls, smectic A phases 78−94968
4-n-alkoxy-4'-cyanodiphenyldiacetylenes, synthesis and mesomorphic props. 79−82148
4-n-alkoxy-4'-cyanostilbenes, synthesis and mesomorphic props. 79−82148
4-n-alkoxy-4'-cyanotoluenes, synthesis and mesomorphic props. 79−82148
trans-p-n-alkoxy-α-methyl cyanophenyl cinnamates, elastic consts. and orientational order parameters 80−44244
n-alkoxy-α-methyl-p'-cyanophenyl cinnamate, orientational order, tricrit. behaviour 79−27907
trans-p-n-alkoxy-α-methyl-p'-cyanophenyl cinnamates, nematic liq. cryst., static dielec. props. 78−60376
alkoxy-benzoic-acids, temp. depend. of Raman spectra of homologous series 77−81098
1-(4-alkoxy-benzoyloxy-phenyl)-2-(4'-pentylphenyl)-ethanes, synthesis and mesomorphic props. 79−90536
alkoxy-cyanobiphenyls, isotropic phase, Cotton-Mouton effect 80−16013
p,p'-n-alkoxyazoxybenzene homologous compounds, nematic, DC Kerr constants 78−27185
alkoxyazoxybenzenes, isotropic-nematic transitions, RI, orientational relax. times 77−24390
p-n-alkoxybenzoates of p-n-alkoxyphenyl, smectic A phases mol. struct. and elastic behaviour 80−59382
p-n-alkoxybenzoic acic series, nematic liq. crysts., electrooptical props. 79−15438
p-n-alkoxybenzoic acid, elec. cond. anisotropy of nematic structs. 80−1928
p-n-alkoxybenzoic acid, homologs, principal mol. polarisabilities calc., refr. indices of nematic mesophase meas. 78−2004
alkoxybenzoic acids, liq. crystal, solid phase, methyl group C_3 reorientation, proton spin relax. 77−1071
p-n-alkoxybenzoic acids, mol. arrangement in cryst., nematic, and smectic C phases 79−32889
p-alkoxybenzoic acids, nematic liq. cryst., proton spin lattice relax., mol. dynamics 78−34425
4(4'-n-alkoxybenzoyloxy)benzylidene-4''-aminophenols, synthesis and mesomorphic props. 79−90546
4-alkoxybenzoyloxy-4'-cyanotolanes, stable nematic reentrant phase 79−77506
alkoxybenzylidenaminobenzonitriles, elec. field and press. induced transitions, transparency and texture 77−43317
N-(4-n-alkoxybenzylidene)-4'-alkylanilines, smectic-B to H transition, B-phase struct. 79−94896
N,N'-bis(p-alkoxybenzylidene)-α,α'-bi-p-toluidines, nematic phase, synthesis, thermodynamic props., gas-liq. chromatographic anal. 79−90763
L-p-alkoxybenzylidene p'-amino 2 methylbutyl cinnamate chiral smectic liq. cryst., dielec. and ferroelec. props. 79−91394
L-p- alkoxybenzylidene p'-amino 2 methylbutyl-cinnamate, dielec. props. in ferroelec. smectic phase *(Japanese)* 79−82154
4-n-alkoxybenzylidene-4'-methylalkylanilines, chiral nematic cryst., mesorphic behaviour and binary systems 78−2000
N-4-n-alkoxybenzylidene-4'-n-alkylanilines, classification of polymorphic smectic phases 79−55661
N-4-alkoxybenzylidene-4'-n-alkylanilines, smectic F phases 79−94891

organic compounds continued
N-4-n-alkoxybenzylidene-4'-n-butylanilines, elec. cond. in nematic and smectic phases *(German)* 77−15860
p-alkoxybenzylidene-alkylanilines, solid state, nucl. spin-lattice relax. 78−64294
p-alkoxybenzylidene-p,n-butylanilines, IR absorpt. spectra, elec. field effects, orientational order parameter determ. by IR dichroism 80−80778
p-alkoxybenzylidene-p-alkylaniline, liq. crysts., ^{2}H NMR, aliphatic and chain conformation 79−14670
p-alkoxybenzylidene-p-aminocyanoanilines, IR absorpt. spectra, elec. field effect, orientational order parameter determ. by IR dichroism 80−80777
p-alkoxybenzylidene-p-n-alkylanilines, solid state, nuclear spin relax. 78−76337
p-alkoxybenzylidene-p-n-alkylanilines, thermotropic mesophases, proton spin-lattice relax. 78−91968
p-alkoxybenzylidene-p-n-butylanilines, optical and mag. anisotropies in liq. cryst. phase, thermal variations of order parameter *(French)* 79−82149
4-4'-n-alkoxybenzylideneamino-biphenyls, central Schiff's base linkage reversal effect on liq. cryst. props. 80−79683
4'-n-alkoxybiphenyl-4-carboxylic acids, 4-(2'-methylbutyl)phenyl esters, smectic phases 79−86684
alkoxylbenzoic acids, orientation in their nematic state 78−42903
6-alkoxynicotinic acid, liq. cryst., prep. and transition temp. 77−27811
4-n-alkoxyphenyl 4-n-alkylcyclohexanecarboxylates, smectic polymorphism, miscibility meas. 79−86678
4''-n-alkoxyphenyl biphenyl-4-carboxylates, liq. cryst. props. 79−82150
4-alkoxyphenyl-4'-alkylbenzoates, mesomorphic props., terminal alkyl chain length effect 80−88024
p-alkoxyphenylazo-p-phenylesters, polymorphism, calorimetry *(French)* 78−51650
p-alkoxyphenylazody-p'-phenylesters, mesomorphis, synthesis and transition temps. *(French)* 77−27815
alkoxysilanes, mol. alignment of nematic liq. crysts., rel. to surface energy 80−100164
alkoxysilyl groups, cross linking with polythene, effects internal stress parameter 79−57035
n-alkyl 4'-n-alkoxybiphenyl-4-carboxylates, smectic C and tilted smectic B phases 79−32888
n-alkyl 4'-n-alkoxybiphenyl-4-carboxylates, smectic polymorphism, X-ray diffr. and miscibility meas. 79−27912
alkyl β-hydroxy quinoline-Cu, (KELEX 100-Cu), distribution coeffs. model 78−53244
alkyl β-ketoacetals, cyclic, diamag. susceptibility, O at. contribution rel. to ring closure 77−14606
N-alkyl amides in H_2O, dioxan solns., Kerr consts. 80−2727
n-alkyl amines, long chain conformations, ^{13}C pseudocontact shifts 79−13743
alkyl amines, plasma chromatography, reduced mobilities 79−74436
alkyl ammonium copper chloride, two-dimensional ferromag., low temp. lattice cond., phonon spectrum 77−4227
alkyl ammonium halide:Tl phosphors, exciton absorpt. spectra 79−28782
alkyl ammonium manganese chloride, birefringence, two-dimens. mag. behaviour, magneto-optical meas. 78−31175
alkyl aryl ketones, in homogeneous n-heptane solns., quasi-isoenergetic triplet energy migration, photolysis obs. 79−61878
alkyl benzenes, jet-cooled, intramol. vibr. relax., reson. fluoresc. and excitation obs. 80−14152
alkyl benzenes, jet-cooled, vibr. relax., nanosecond time evolution 80−95584
alkyl benzoates, phosphoresc. and fluoresc. spectra in organic matrices 80−32756
alkyl bromides, and perfluorinated mols., Br branching ratios, broadband flash photolysis 78−27787
alkyl cadmium, valence and core electron energies, photoelectron spectra, ab initio calc. 78−25613
n-alkyl carboxylic acids, vibr. spectra, C-H stretching mode assignments 79−47429
alkyl chains, ^{13}C longitudinal relax. times and nuclear Overhauser enhancement anal. 80−83390
alkyl chlorides, mol. electro-optical props. 79−50162
alkyl chlorides, proton affinity correl., ab initio SCF calc., MINDO/3, STO and G basis sets 78−33421
alkyl cyanobiphenyls, pretransitional behaviour, alkal chain length depend., light scatt. in isotropic phase 80−44301
alkyl cyclobutane hydrocarbons, multiple initial vibr. state selection by chem. activation, relax. rate 77−40538
alkyl fluorides, geometries, props. and protonation, ab initio mol. orbital study 79−22588
N-alkyl free radicals, ESR study, conformational anal. of N-alkyl group 78−62831
alkyl halide, amorphous, depolarisation thermocurrents and dielectric relaxation time distrib. *(French)* 80−60490
alkyl halide, chem. struct. determ. using electron capture response 77−21428
alkyl halide+K potentially reactive collisions, electronic excitation 80−74239
alkyl halide and σ^* anion radicals, stability 80−89468
alkyl halide photolysis by pulsed CO_2 TEA laser, mechanism 77−12807
alkyl halides, conform. energy calcs., polar bonds and polarisability, polaris. model appl. 80−58188
alkyl halides, depolarisation thermocurrent obs. of main relax. around glass transition 78−27158
alkyl iodide+K, collisional electronic excitation, time-of-flight obs. 79−86049
alkyl iodide molecules, photodissoc. by 254 nm radiation 78−3354
alkyl iodide photodissoc. laser, radn. field in plane cavity 77−19245
alkyl iodide-I$_{(atom)}$ complex, multiple charge-transfer bands in liquid-phase 77−32776
alkyl iodides, two-photon reson . ionis. spectra 80−28071
alkyl metal carbonyls, phosphine monosubstituted, LF vibrs., IR and Raman spectra 80−95585
alkyl nitrates, NO_2^+ transfer to tolyl cation 77−52619
2-alkyl pyridine N-oxides, effects on photosynthesizing membranes, near photosystem II, hydrophobic pocket 80−55999
alkyl silanes, far UV and He I photoelectron spectra 79−18204
alkyl styrenes, fluoresc., ns time resolved emission spectra 77−6822
alkyl substituted diacetylene radical cations, optical emission and photoelectron spectra, fragmentation decay 80−53004
alkyl sulphides, C-S stretching vibrs. 78−25533

organic compounds continued
alkyl trichloroacetates, solns., intramol. rot., permittivity and dielectric loss, microwave meas. 78−31145
5-alkyl-2-(4′-cyanophenyl)-1,3-dioxanes, nematic liq. cryst., synthesis and electro-optical characts. 80−88029
4-alkyl-3-phenyl-3 4-dihydrocoumarins cis- and trans-, ^{13}C NMR spectra 80−43067
4-n-alkyl-4′-cyanobiphenyls, deuteriated, improved synthesis 79−32893
4-n-alkyl-4′-cyanobiphenyls, Raman spectra in solid state, polymorphism of mesogenics 79−82964
4-alkyl-4′-cyanobiphenyls, smectic A phases 78−94968
4-n-alkyl-4′-cyanobiphenyls, synthesis method from biphenyl 80−79684
4-alkyl-4′-cyanostilbenes, liq. cryst., prep. and transition temps. 77−27823
4,n-alkyl-4′-cyanotolanes, and related compds., homologous series, mesomorphic transition temps. 77−27991
4′-n-alkyl-4-cyanobiphenyls, dielec. dispersion 78−2798
4′-n-alkyl-4-cyanobiphenyls, elasticity, orientational order, and nematic-isotropic transition 77−84643
4-n-alkyl-4-cyanobiphenyls, liq. cryst. of strong positive dielec. anisotropy, static dielec. consts. meas. 78−2790
4′-n-alkyl-4-cyanobiphenyls, nematic, elastic and optical props. 77−11613
4′-n-alkyl-4-cyanobiphenyls, press. effect on liq. cryst. phase transitions 79−95138
3-nalkyl-6-(4-n-alkyloxy-phenyl)-1,2,4,5-tetrazines, stable dyestuffs with liq. cryst. props. 80−19693
alkyl-cyano-biphenyls, nematic to isotropic phase transition, volumetric studies 79−86878
alkyl-cyano-biphenyls (and p-terphenyls) and related cmpds., chiral, synthesis and liq. cryst. props. 77−27820
alkyl-cyanobiphenyl homologues, isotropic-nematic phase, optical Kerr effect 80−91866
alkyl-cyanobiphenyls, isotropic phase, Cotton-Mouton effect 80−16013
S-alkyl-isothiouronium iodides in methanol-water mixtures, conductance at 25°C, solute-solvent interaction 79−95194
p-alkyl-p′-cyanocyclohexylcyclohexanes, thermotropic nematics with positive dielectric and negative diamag. anisotropy 78−34435
p-n-alkyl-p′-n-alkoxytolanes, hydrostatic pressure effects, phase transitions *(French)* 78−14448
alkylamines coordinated to Ni(II) acetylacetonate, ^1H and ^{13}C NMR, hyperfine coupling const. 79−41187
alkylammonium cadmium tetrachloride, struct. phase transition, PMR, spin-lattice relax. time 77−35688
alkylammonium compounds, $(C_nH_{2n+1}NH_3)_2CuCl_4$ and $(C_6H_5C_mH_{2m}NH_3)_2CuCl_4$, interlayer exchange field 77−20714
alkylammonium compounds, synthesis, exchange ion props. 80−64985
alkylammonium compounds with perovskite-type layer struct., symmetry of lattice vibrs. 78−22797
alkylammonium copper chlorides, high-temp. susceptibility obs., 80-300K, ferromag. interactions 77−66274
alkylammonium copper halides, mag. sp. ht., two-dimens. S1/2 Heisenberg ferromag. behaviour 77−32206
di-alkylammonium copper tetrachloride, weakly discontinuous phase transition, linear birefringence obs. 80−11362
alkylammonium iodides, solns., MCD spectra of iodide ions 78−94268
alkylammonium iodides, UV spectra 79−36663
alkylammonium metal tetrachlorides, struct. phase transitions 80−75348
alkylammonium tetrachloromanganate (II) IR and Raman spectroscopic exam. 78−31189
alkylammonium zinc tetrachloride cpds., high temp. phase transitions 80−54372
para-alkylanilines having optically active modes, vibr. relax. studied by absorpt. and fluoresc. spectra 80−83340
alkylbenzenes, electronic struct., photoelectron spectra rel. to semiempirical CNDO/S CI calcs. 79−54770
alkylbenzenes, intramol. hydrophobic interactions, direct meas. 79−45648
alkylbenzenes, jet-cooled, vibr. relax., absorpt. spectra 80−74236
alkylbenzenes, jet-cooled, vibr. relax., fluoresc. spectra 80−78694
alkylbenzenes, liquid, relation between density and refractive index *(Japanese)* 79−24279
alkylbenzenes, temp. coeff. of refr. index *(Japanese)* 77−28537
p-alkylbenzenesulphonate mixed micelles, dimens. determ., small angle X-ray scatt. *(French)* 77−29053
4-alkylbenzoyl chlorides, liq. cryst. intermediates, syntheses 79−90540
1-4-n-alkylbenzoyloxyphenyl 2-(4′-cyanophenyl) ethane series, nematic reentrant mesophases, phase diagrams 80−103467
4′-n-alkylbiphenyl-4-carboxylic acids, 4-(2′-methylbutyl)phenyl esters, smectic phases 79−86684
alkylcyano-cyclohexyl-cyclohexanoates, nematic and smectic mesophases 80−19692
alkylcyanobiphenyls, far IR absorpt. in nematic and isotropic phases, order parameter determ. *(French)* 80−50330
trans-4-alkylcyclohexane carboxylic acids, visible and UV spectroscopy transparent matrix 80−45102
alkylcyclohexyl-cyclohexyl-cyclohexanoates, nematic and smectic mesophases 80−19692
trans-4-n-alkylcyclohexylbenzylamines, synthesis and mesomorphic props. 80−44116
alkylene di-ammonium cadmium tetrachlorides, sp. ht. anomalies at phase transitions 80−70421
alkylene diammonium cadmium tetrachloride, struct. phase transformation, PMR, spin-lattice relax. time 77−35688
alkylene-di-ammonium cadmium chloride, influence of C atoms and metal ions on structural phase transitions 78−2256
alkylenediammonium metal tetrachlorides, struct. phase transitions 80−75348
alkylenedimethacrylic acid esters, study of methacrylates, cross-linked, structure-transformation relations properties *(German)* 79−55677
trans-bis(N-1alkyliminodiacetato)-chromate(III) complexes, luminesc. spectra 80−1020
alkyliodides, UV photodissoc., time-resolved obs. of $I(^2P_{1/2})$ reactions 80−11940
4-alkyloxy-4′-cyanobiphenyls (nematic, smectic)-tetrabutylammonium picrate, elec. cond., temp. (conc.) depends. *(German)* 78−55966
4-4-n-alkyloxybenzoyloxy-benzylidene-4′-cyanoanilines, reentrant nematic and smectic phases 80−88308
n-(4-n-alkyloxybenzylidene)-4-n-alkylanilines, smectic polymorphism, miscibility meas. 79−86678
N-4-n-alkyloxybenzylidene-4-n-alkylanilines, smectic polymorphism, calorimetric study 80−88307
organic compounds continued
4-n-alkylphenyl 2′-chloro-4′-(6-n-alkyl-2-naphthoyloxy)benzoates, synthesis and liq. cryst. props. 78−34433
(+)-4-n-alkylphenyl-4′-(4″-methylalkylbenzoyloxy)benzoates, optically active, synthesis and effect on liq. cryst. display props. 78−1997
2-4-n-alkylphenyl-5-(4-n-alkyloxyphenyl)-pyrimidines, smectic polymorphism, calorimetric study 80−88307
2-[4-n-]alkylphenyl-5-[4-n-alkyloxyphenyl]-pyrimidines, X-ray study of smectic modifications 79−32882
alkylphosphonium iodides, UV spectra 79−36663
N-alkylpyridinium salts, electrochem. reduction, radical form., INDO calcs., EPR obs. 77−71821
N-alkylpyridium halides, molten, and mixtures with $AlCl_3$, density, elec. cond. and viscosity meas. 80−24630
alkylsilanes, vibr. spectra, normal vibrs. and rot. isomerism 79−31524
alkylsilanes, vibr. spectra, normal vibrs. and rot. isomerism 79−31523
alkynes, $\nu(CH_2)$ and (CH_3) Raman bands, global integrated intensity, dilution effects *(French)* 77−61755
alkynes, electron impact, threshold excitation by monoenergetic electrons 78−58854
alkynes, normal coord. calc. and valence force field 79−72294
1-alkynes+$O(^3P)$, CO prod., vibr. population distrib., rate consts., laser reson. absorpt. technique 80−40676
alkynoyl cations, struct., charge distrib., ab initio population anal. calcs. 80−58407
allene, C-C double bond rot. barrier, ab initio open-shell restricted SCF calc. 78−1099
allene, gas and soln., UV absorpt. and MCD spectra 79−50056
allene, internal rot. in ground electronic state 77−67975
allene, ionis. pots., Green's function method 77−14608
allene, ionis. spectral intensity, valence electron binding energy depend. 78−90234
allene, IR multiphoton photolytic C_3 prod., C_3 vibr. relax., chem. kinetics 80−66820
allene, laser induced reaction, energy distrib. 80−16710
allene, liq., orientational dynamics, Raman obs. *(French)* 79−28746
allene, non-degenerate vibr. mode induced Jahn-Teller effect, photoelectron spectra calc. 79−817
allene, photoionis., vibr.-excited ions form. in Franck-Condon gaps, threshold photoelectron spectra obs. 79−68262
allene, photoionisation and threshold photoelectron photoion coincidence obs. 78−21981
allene, rot. diffusion in CS_2 soln., IR spectral profiles 79−87426
allene, transition state for internal rot., HF/STO-3G calcs. with correlation energy corrections 78−25430
allene, vertical valence ionis. pots., ab initio UB calcs. 79−85917
allene+methyl radical, reaction pot. surfaces, MINDO/3 calcs. 79−22601
allene+$O(^3P)$, absolute rate consts. meas., 297-439K 78−7196
allene($-d_4$), IR absorption intensities 80−1026
allene-1,1-d_2, rot.-vibr. Raman spectra 77−65477
allene-d_4, high resolution IR spectra 80−83365
allene-d_4, Raman and IR spectra, rot.-vibr. bands, ground state constants 78−25545
1H-alloxazine, and derivatives electronic struct., photoelectron spectrosc. and ab initio study 80−106261
alloxazine, photoconduction *(German)* 79−78129
allyl cation and radical, ab initio non-paired spatial orbital wavefunctions 77−26968
allyl free radical decay, in irrad. polyethylene, const. diffusion controlled rate const. 78−15651
allyl isocyanide, state-selected, visible absorption spectra and photoisomerisation kinetics 80−11879
allyl radical, ab initio SCF solns., doublet stability 78−33423
allyl radical, doublet state, open shell RPA unitary group formulation, Hartree Fock stability eqns. 80−52860
allyl radical, ionisation potential, ab initio valence bond calcs. 79−31407
allyl radical, restricted ab initio SCF LCAO solns., doublet stability 77−79539
allyl radical, restricted SCF and MC SCF calc. of C_{2v} and C_s structs. 80−83289
allyl radicals, in irrad. polyethylene, distrib., trapping regions 78−91957
allylamine, anomalous Stark effect for torsional splitting 79−64040
allylamine, laser-microwave double and triple reson. 80−83397
allylamine, N-cis lone electron pair trans isomer, total dipole moment, rel. orientation 80−69259
allylamine, N-cis lone-pair gauche rotamer ground state microwave spectrum anal. 78−82720
allylamine, NGLT, rot. and centrifugal distortion consts., microwave spectrum 78−74644
allylmethylether, thermal and IR laser induced unimol. decompositions 78−20012
π-allyls, LF vibr. modes of hydrogeneous ligands, incoherent inelastic neutron scatt. 78−6229
alternant hydrocarbons, approx. calc. by spin-extended HF method 79−26889
alternant hydrocarbons, HOMO-LUMO separation, approx. topological formula 79−49928
alternant hydrocarbons, polarisabilities rel. to bond orders using Huckel's method *(French)* 79−31405
alternant molecules with conjugated bonds, ground state multiplicity, ferromag. 79−774
aluminium acetylacetonate, pyrolysis rel. to Al_2O_3 film prod. 77−85943
aluminium and boron hydrides of titanium(III) bis-cyclopentadienyl, exam. of catalytic props. 80−30278
aluminium methylammonium selenate alum, effect of hydrostatic pressure on dielec. props., near transition pt. 79−56712
amantadine, neuromuscular blockade by suppression of acetylcholine receptor ionic cond. 78−64975
amaranth, reson. Raman spectra, sample conc. optimisation 78−66555
amaranth, trace amount determ., by reson. Raman spectroscopy *(Japanese)* 79−48017
amide+Li^+ pair pots., ab initio LCAO SCF MO calcs. 80−58184
amide+Na^+ interaction, pair pots., ab initio SCF LCAO MO calc. 79−36721
amide C-N bond character, metal ion bonding effects 77−6801
amide group in soln., interactions, IR, Raman spectral investigs., peptide, protein struct., review 78−90330
amide group molecules empirical pot. model EPEN/2, development, parameter testing 79−54935

organic compounds continued
amides, in carbon tetrachloride, dielec. relax., time-domain reflectometric obs. 79−4762
amides, substituted, aqueous solns., UV-irradiated, EPR and spin-trapping study of free radicals 79−16154
amidinium salts, ^{14}N NQR spectra, H^+ relax. times 80−60448
amidofluorosulphuric acid, and Hg salt, IR spectra *(French)* 80−18858
amiloride effect on rabbit colon Na transport blocked and reversed by p-chloromercuribenzene sulphonate 78−44479
amine, chemisorbed on metal or oxidised metal, surface ionisation, mass spectra expts. 78−2360
amine additives in CO_2 TEA lasers, cyanide deposits prod. 77−71991
amine solutions, US analysis method 78−7277
amines, adsorbed on oxidised metal surfaces, identification by surface ionis. 77−21456
amines, aliphatic and aromatic, H-bonding, strong, stochastic model and IR spectra temp. effects 78−62805
amines, aromatic, photochem. reactions with carbon tetrachloride, initiation mechanism 79−61888
amines, caged, multiphoton ionisation, two-photon transition resons. 78−33558
amines, detection by chemiluminescence analyser 78−40094
amines, liq. cryst., low transition temp., incorporating biphenyl ring system 79−94892
amines, modified CNDO calcs., conformations, binding energies 77−6682
amines, Raman bands and H bonding in liq. phase *(French)* 77−65479
amines, saturated, bonded and nonbonded, quantum chem. calcs. 80−9514
amines, self-association in binary mixtures, 2-const. model, vap. press. meas. *(German)* 78−18532
amines+$O(^3P)$, rate consts. temp. depend., 298-440K 78−48616
amines intercalated with FeOCl, cryst. struct. 78−51512
amino acid, cryst., mol. dielec. function 79−7043
amino acid, monolayer on solid, SIMS anal. 79−89038
amino acid anal. by ion exchange chromatography 80−11986
amino acid formation by ^{60}Co γ-ray irradiation of HCN solns. 77−37410
amino acid formation by reactor irrad. of ethanol and aqueous ammonia 79−66305
amino acid formation in ultrasound in water masses of primordial Earth 77−37409
amino acid methyl esters, photoelectron spectrosc. 79−24954
amino acid overlayers, static SIMS exam. 79−83074
amino acid percutaneous electrophoresis 78−61237
amino acid photodegradation in presence of TiO_2 78−11531
amino acid photoresolution, rel. to origin of optical activity in life 77−40634
amino acid protonation ab initio Hartree-Fock-Roothaan SCF calcs. 80−9503
amino acid racemization, appl. to geochronology and geothermometry 78−20341
amino acid radioracemisation, geochem. and cosmochem. implications 80−45975
amino acid residues, contacting, ligand binding rate dependence on specific microdynamics 80−51031
amino acid residues, form. of mixed micelles and relative compatibility at interface 80−71951
amino acid side chains, internal motions in peptides and proteins, N-acetyl-l-phenylalanine methyl ester model 80−48017
amino acid stimulatable transport system in rat liver after hole-body γ-irrad. 78−65098
amino acid transport hormonal control in liver of rats exposed to whole-body γ-irrad. 78−65099
amino acid transport in lymphoid cell lines, differences in ionising irrad. effects 80−72264
amino acid transport in rat liver after whole-body gamma irrad. 77−9232
amino acid utilisation in cultured insect cells, X-irrad. effects 77−5043
amino acid valine, heavy ion induced desorption, time-of-flight mass spectra anal. 80−54509
amino acid-quinone complexes, surface bubble form. during SEM obs. 77−15450
amino acids, ^{15}N-labelled, nanomole isotopic assay by collision induced dissoc. MS 78−20095
amino acids, γ-irrad., radiation damage studies using aqueous LiCl glass as neutral matrix 79−96632
α-amino acids, γ-irradiated, primary oxidation products, ESR and ENDOR 77−48754
amino acids, aq. solns. EPR of spin-trapped radicals, hydrated electron reactions 78−27796
amino acids, dissolved, in seawater, rel. to organic pollution 78−44883
amino acids, He(I) photoelectron spectra 79−34499
amino acids, high energy radiation effects and chemical evolution 77−63937
amino acids, isotopic enrichment determ. by chem. ionis. mass spectra 79−79694
α-amino acids, mass spectrometers study of evaporation 77−86402
amino acids, naturally occurring, helix-coil stability consts., random copolymer method determ. 78−94333
amino acids, permeability through membrane in E. coli K12 78−77029
amino acids, polycryst., proton mag. relax. and mol. motion 78−20139
amino acids, positron annihilation in D and L isomers 77−12887
amino acids, surface bubble form. during SEM obs. 77−15450
amino acids, technique for study of radiation in induced free radicals using lyoluminesc. 77−29230
amino acids, X-irradiated, EPR determ. of radical yields 79−34491
amino acids and their complexes, corrected G-values 79−20516
amino acids in C2 Antarctic carbonaceous chondrite, meteoric origin 80−67674
amino acids in carbonaceous chondrites 79−88632
amino acids in meteorite, carbonaceous chondrite 80−26822
p-amino benzoic acid, solid, H bonding, wide line NMR obs. 78−52362
amino radical adsorbed on zeolite, extra coupling with ^{23}Na 77−7963
5-amino-1-hydrogen-1,2,4-triazole, cryst. and mol. struct., X-ray study 79−55735
4-amino-2,2,6,6-tetramethylpiperidine-N-oxyl and deuterated derivatives, mag. resonance study 80−63686
1-amino-2-phenyl benzocycloheptanol-hydrobromide monohydrate, cryst. struct., heavy atom method 78−79601

organic compounds continued
4-amino-4′-nitrostilbene, fluoresc. emission anisotropy, solvent effects 79−3489
4-amino-4′-nitrostilbene, thermal motion of prolate luminescent molecules in solvents with different viscosities 79−83029
2-amino-4-chlorophenol in solutions, IR absorpt. spectra 80−69135
7-amino-4-methylcoumarin, fluoresc., solvent depend., shift of max. wavenumber 79−85997
2-amino-5-chloropyridine, IR absorption, vibr. assignments 80−979
2-amino-5-chloropyridine, rot. modes, ^{35}Cl NQR 78−74677
6-amino-7-hydroxy-4-methylcoumarin solutions, additions effect on fluoresc. 80−2833
2-amino-7-nitrofluorene, in binary solvent soln., time-resolved fluoresc. spectroscopy 79−36680
3-amino- and 4-amino-N-methylphthalimide, effect of orientational-relax. processes in fluoresc. kinetics 80−18886
3-amino-N-methylphthalimide, in polar-nonpolar solvent mixture fluorescence band struct. 78−15213
3,4-amino-N-methylphthalimide, intermolecular orientational relax. 'upwards', fluorescence spectra displacement *(Russian)* 79−78748
4-amino-N-methylphthalimide, reversible induced absorpt. spectra in binary solvents 79−98117
4-amino-N-methylphthalimide in n-propanol, nanosecond laser fluorometry 80−102721
4-amino-N-methylphthalimide-decalin-n-propanol, translational relax. kinetics, luminesc. obs. 79−8180
2-amino-p-cresol in solutions, IR absorpt. spectra 80−69135
4(6)-amino-uracil, IR absorpt. spectra, vibr. anal. 78−61143
aminoacetaldehyde, conformation calcs. rel. to protein struct. and bonding 80−74273
aminoacetonitrile, microwave rot. spectrum, quadrupole hyperfine struct. 78−17658
m-aminoacetophenone+t-amyl alcohol, in soln., fluoresc. and absorpt. spectra, excimer form. 78−78737
α-aminoacids, stereoselective catalysed hydrolysis of esters *(French)* 79−66438
aminoacridines, pulse radiolysis study of interactions with nucleic acids 78−85186
aminoarsines containing As-NH group, IR spectrometry, configuration isomers and hybridization state of N *(French)* 77−23495
aminobenzoic acid, aqueous and dioxane solns. with nonfluoresc. impurity, fluoresc. and pH *(Russian)* 77−83635
p-aminobenzoic acid hydrochloride, X-ray cryst. struct. determ. 80−39063
aminobenzonitrile, para- and meta-, NQR linewidth, Zeeman effect, mol. config., H bonding, cryst. struct. 77−51986
4-aminobenzophenone, fluoresc. quenching of p-terphenyl solvent dielec. const. depend. *(German)* 79−83030
aminobenzotrifluoride, benzene soln., permittivity and dielec. loss 78−64320
aminoborylpolyynes, intermolecular interaction through triple bonds, internal rot. 80−106370
aminobromotoluenes, NQR freqs., temp. depend. 78−70850
γ-aminobutyric acid, aq. soln., low freq. vibrs. Raman spectra obs. 80−987
γ-aminobutyric acid, cryst., film, matrix IR spectra, low temp., neutral and zwitterion forms. 77−18920
γ-aminobutyric acid-induced conductance fluctuations in cultured spinal neurones 78−80867
aminochlorotoluenes, UV aborpt. spectra 79−36660
7-aminocoumarins fluorescence efficiency of laser dyes 77−42531
^{11}C-1-aminocyclopentane carboxylic acid, tumour location, clinical trials with single photon detect. 78−31895
2-aminoethanol-$(d_2)(-d_3)$, microwave spectra, hydrogen bonding, rot. const. 77−6765
N(2-aminoethylcarbonyl)-5(6)-aminofluorescein, fluorescent labelling of polyaspartamides 80−58426
β-1′-aminofuranoside, mol. geometry, computer retrieval and anal. 78−83645
aminohydroquinone as photographic developer 77−5947
α-aminoisobutyric acid, cryst., γ-irrad., cation radicals, ESR obs., SCF-MO-INDO calcs. 78−11537
4-aminomethyl-7-hydroxycoumarine, fluorescent labelling of polyaspartamides 80−58426
4-aminomethylphthalimide-decalin-n-propanol, electronic spectra of 3-component solns., temp. depend. 79−4822
p-aminophenol, gas phase, near UV absorpt. spectra 79−22725
m-aminophenol, nonlinear optical susceptibility, second order, calc. from mol. spectra *(Russian)* 79−27318
p-aminophenol, oxidation in aq. soln., chem. equilib. of free radicals, review 79−43573
aminophenols, photographic development, comparison with 1-phenyl-3-pyrazolidone 78−64825
aminophenols, photographic development, rate/conc. relationship 78−21244
3-aminophthalimide, continuous spectra, electronic transition freq. determ. 77−50425
4-aminophthalimide, soln. in n-propanol, fluoresc., orient. relax. of solvent 79−24357
4-aminophthalimide soln., fluoresc. nanosec. kinetics, dielec. relax. 79−78737
3-aminophthalimide-ethanol soln., luminesc. quantum yield, photoacoustic method 77−86335
aminophthalimides, dynamic dipole induced interactions in absorption spectra 78−13553
aminopolyynes, intermolecular interaction through triple bonds, internal rot. 80−106370
3-aminopropanol, and deuterated forms microwave spectrum, dipole moment, struct. 79−59441
2-aminopurine, in viscous soln., fluoresc. quenching, emission, intensity and reson. transfer *(German)* 80−91599
2-aminopurine, triplet state, electric dipole moments 79−22742
aminopyrazine, far IR spectra, barrier to planarity, pot. function and energy levels 80−69137
1-aminopyrene, protonated, excited state proton dissoc., time-resolved spectrosc. obs. 79−50164
4-aminopyridine hemiperchlorate, neutron diffr. and IR spectral obs. of strong asymmetric N-H-N hydrogen bond 80−92515
14-aminopyridine-I_2, charge-transfer complexes, hyperpolarisability 77−34568

organic compounds continued
aminopyridines, in 1,4-dioxane soln., dielec. consts., losses and relax. 78−64319
2-aminopyrimidine(-d_1), amino inversion vibr., planarity, far IR obs. 79−31515
5-aminopyrimidine triplet state, electric dipole moments 79−22742
aminoquinoline derivatives, solvent effect on absorpt. and fluoresc. spectra 79−59494
aminosilane stationary phase, for HPLC separation of polynuclear aromatic compounds 78−35747
ammonia Rochelle salt, temp. depend. of optical axis angle, phase transitions *(Russian)* 80−97216
ammonium acetate, irrad. crysts., freq. swept ELDOR obs. at 77K, resolution of spin packets 79−95686
ammonium acetate, methyl groups, spin symmetry species, neutron scatt. transitions 80−92470
ammonium benzoate, IR spectrum, cryst. struct. 78−19455
ammonium bioxalate monohydrate, refractive indices in IR region 78−52512
ammonium bioxalate monohydrate spontaneous parametric scatt. spectra, polariton wave vector and Stokes lines analysis 78−43885
ammonium hydrogen bisbenzoate, IR spectrum, cryst. struct. 78−19455
ammonium hydrogen chloracetate, order disorder type transition 79−47399
ammonium hydrogen glutarate, H bonding, vibr. spectra 78−43860
ammonium hydrogen oxalate hemihydrate, low temp. dielec. and thermal props. 77−28510
ammonium hydrogen oxalate hemihydrate, single cryst., DNMR obs., elec. field gradients, reorientation 77−85618
ammonium hydrogen oxalate hemihydrate, X-ray TDS effects on at. parameters and electron density distribs. 77−19819
ammonium hydrogen tartrate, struct. refinement using X-ray diffractometer equipped with Si(Li) detector 79−58855
ammonium malate, SHG, 492-640 nm, phase matching, refr. index and nonlinear susceptibility 77−72031
ammonium malate, single cryst., optical SHG, refr. index, susceptibility 78−63152
ammonium methyl sulphite, IR spectra of NH_3D^+ ion, mol. motion 77−36232
ammonium oxalate monohydrate: Mn^{2+}, ESR, 77-345K 79−19768
ammonium oxalate monohydrate:Mn^{2+}, model for defect formation, EPR 80−103880
ammonium oxalate monohydrate, IR refl. and Raman spectra, internal and external modes *(French)* 77−36231
ammonium oxalate monohydrate, Raman spectrum, internal and external vibrs. 79−73924
ammonium Rochelle salt, cryst. with modulated struct., neutron scatt. obs. 79−95713
ammonium Rochelle salt, dipole interaction symm. aspect 77−20805
ammonium Rochelle salt, first order phase transition 78−43818
ammonium Rochelle salt, incommensurate phase transitions under existence of Lifshitz invariant 79−15416
ammonium salts, reorientation of NH_4^+, PMR relax. and inelastic neutron scatt. 79−82167
ammonium tartrate, oxidation of anodic Al films, anonization rate and augmentation factor 79−79152
ammonium tartrate, triboluminescence and cryst. fracture dynamics 80−50437
ammonium tetraphenylboride, IR spectra of NH_3D^+ ion, mol. motion 77−36232
ammonium thiocyanate, testing aspherical atom refinements 79−7516
ammonium uranyl formate, struct. determ. from X-ray diffr. and IR spectrum *(French)* 78−75653
amobarbital, radiation-prod. free radicals in pyrimidines, EPR 77−25374
amonium alginate, aq. solns., laminar flow heat transfer in helical coils 80−59030
AMP, association, spin label appl. 78−81086
AMP, cyclic, postsynaptic modulation of excitatory process in sympathetic ganglia 78−27931
AMP, cyclic, role in synaptic facilitation and behavioural sensitisation in Aplysia 77−36913
cAMP−induced struct. changes in erythrocyte membrane, spin-probe study 78−31779
cAMP-induced structural changes in membranes, rel. to acetylcholinesterase activity 80−30674
AMP-PNP induced cross-bridge slippage in glycerol extracted fibrillar muscle fibres 78−77075
dAMP.dTMP costacking complexes, γ-irrad., charge migration, computer-assisted EPR 77−86446
amphetamine, Gaussian wavefunctions, transcorrelated method 77−61678
amphetamine derivatives, detect. by GC/MS selected ion monitoring 79−43643
amphotericin B action on lipid planar bilayers, spin label study 77−29108
amphotericin B in H_2O and hydroalcoholic solns., circular dichroism, Rayleigh scatt., absorpt. spectra, temp. depend. *(French)* 78−62807
3-amyl alcohol, sound vel. and absorpt. meas. at hypersonic freqs. 78−18708
t-amyl alcohol+m-aminoacetophenone, in soln., fluoresc. and absorpt. spectra, excimer form. 78−78737
amyl-acetate odorant, nose stimulation, olfactory evoked brain pot., correl. anal. of recorded waveforms from human scalp *(Japanese)* 80−97946
α-amylase isoenzymes, formation in germinating wheat, γ-irrad. effect 80−56143
amylopectin, glycerin impregnated, dynamic viscoelasticity *(Japanese)* 80−104203
amylose, glycerin impregnated, dynamic viscoelasticity *(Japanese)* 80−104203
amylose V, bonding characts. of powders mixed with Mg stearate, SEM 78−84731
p-n-amyloxybenzoic acid, refr. index and orientational order parameter, temp. depend. 79−90537
anaesthetic drugs, inhibition of Ca^{2+}-induced luminesc. of aequorin 78−76985
analgesic group commercial tablet samples, IR spectra 78−74652
analysis, by gas chromatography/photoionisation mass spectrometry 78−92531
Δ^5-androster-3-ol-17-one, polycryst., NMR, selection of nonprotonated C resonances 80−50201
organic compounds continued
anilides of 1-piperidine carboxylic acids, $CDCl_3$,$CHCl_3$ solns., intramol. easily polarisable H-bonds, IR spectra 78−25523
aniline, $^1B_2$ state, single vibronic level fluoresc. 79−54903
aniline, amino group inversion and torsion, far IR spectra 77−10670
aniline, far IR absorpt. spectra, 20 to 60 cm^{-1}, temp. depend. 79−59450
aniline, gas phase electrochromism studies in vacuum UV 77−50562
aniline, in benzene, polar dielectric system, RF cond. and dipole moment 78−2788
aniline, in p-xylene host cryst., phosphoresc. triplet state, ESR and MIDP obs. 80−66077
aniline, inhibition of acid dissolution of iron and steel 79−79181
aniline, IR absorpt. and MCD spectra, Rydberg transitions 77−27068
aniline, laser two-photon ionisation in mol. beam and bulk gas phase 80−18891
aniline, liq., depolarised light scatt. from shear waves 80−97288
aniline, liq., far IR absorpt. spectra, electric field effects 80−95625
aniline, liq., viscosity parameters, RF cond. meas. 80−96677
aniline, nonlinear second-order optical susceptibility 80−9947
aniline, photoemission for mol., polarised photoelectrons 78−66607
aniline, prereson. Raman effects, intensity enhancement mechanism 78−42069
aniline, singlet-singlet electron transitions, modified CNDO-CI method exam. 78−25552
aniline, US velocity under press., determ. of thermodynamic props. *(Japanese)* 77−59068
aniline, vibronic perturbations of UV spectrum 78−37654
aniline+AR, $^1B_2$-state collision induced intramol. vibr. energy transfer, SVL fluoresc. obs. 79−54904
aniline+carbon tetrachloride, binary liquid mixtures, excess free vol. calcs. 80−34202
aniline+cyclohexane critical mixture, gravity-induced concentration gradients 77−28004
aniline black, superconductivity at room temp. 78−80089
aniline having optically active modes, vibr. relax. studied by absorpt. and fluoresc. spectra 80−83340
aniline hydrobromide, ferroelastic, acoustic softening near transition temp. 80−96617
aniline hydrobromide, ferroelastic phase transition, Raman scatt. study 80−108195
aniline intercalated with PbI_2 NQR meas. *(Russian)* 79−91311
aniline surfactants effectiveness, H absorpt. of steel, HCl conc. effect 80−108638
aniline yellow, dye soln., photothermal spectroscopy 78−32808
aniline-chlorophenol complexes, ^{35}Cl NQR, inter- and intramol. interactions 80−63666
aniline-cyclohexane, crit. mixture with shear flow, light scatt. obs. 80−6521
aniline-cyclohexane, hypersound velocity, absorption temp. depend *(Russian)* 80−75303
aniline-cyclohexane, viscosity conc. and temp. depend. in crit. mixing region 77−35686
aniline-cyclohexane solution, depolarised mol. light scatt. near critical exfoliation temp. *(Russian)* 80−108222
aniline-HBr, ferroelasticity, orthorhombic to monoclinic phase transition, X-ray scatt. 80−39276
aniline-ND_2(-NHD), far-IR vap. phase spectra, assignments pot. function calcs. 77−75144
aniline-PbI_2, intercalation cpd., heat capacity of low temp., intercalation effect *(Russian)* 80−92682
aniline-phenol, liq., US vel., adiabatic compressibility, H-bonded complex form. 77−35635
8-anilinenaphthalene-1-sulphonic acid, edge excitation red shift, temp. depend. 77−6849
anilines, conc. depend. of influence on steel hydrogenation *(Russian)* 79−15854
anilines, free and H-bonded, Hammett freq. factors, effects of non-monotonic ν(XH) function variations *(French)* 79−22690
anilines, substituted, in benzene, dielectric relax. and mutual viscosity, obs. 79−38449
anilines, substituted, in benzene soln., dielectric relax. time, dipole moment 80−50259
anilines, substituted, in nonpolar solvent, dielec. relax. obs. 80−55022
anilinium chloride, NH_3^+ intraionic C_3 reorientation, NMR and rot. frame expt. 79−28630
anilinium halides, and anilinium sulphate, proton mag. relax. obs. 80−34800
anilinium ion, $C_6H_5NH_3^+$, fluoresc. and phosphoresc., pKa values 79−13755
8-anilino-1-naphthalenesulfonic acid, fluoresc. probe mol. in mixed solvent 79−45746
1-anilino-8-naphthalene sulphonate, bound to chloroplast membrane, fluoresc. study of proton and cation effects 78−24034
2-anilinonaphthalene, excited state solvation dynamics in polar solvent 77−44572
1,8-anilinonaphthalene sulphonate, aq. and ethanolic solns., excited singlet state decay pathway 78−17703
1,8-anilinonaphthalene sulphonate in bacterial suspension, fluoresc. spectra 79−88052
anilinonaphthalenesulphonate, room temp. phosphoresc., isomer effects 79−61429
anils, cryst., high-press. optical effects 78−31170
anils, polystyrene soln., high-press. optical effects 78−31171
p-anisalaminoazobenzene, acoustic relax. in nematic phase 77−1184
anisaldazine, colloidal particles in water, elec. polarisability anisotropy 79−39208
anisaldazine, nematic liq. cryst., mol. statistical interpretation of viscosity *(Portuguese)* 77−47351
p-anisidine, crystal structure determination with DAR-UM+BESM-6 automatic system 77−76386
p-anisidine, polycryst., intramol. reorientations, PMR 78−64279
p-anisidine, single cryst. growth from cyclohexane-water immiscible system 80−40244
p-anisidine soln., dielectric const., loss and relax., dipole moment 78−43782
anisole and -d_3, Raman spectra, low freq. vibrs., torsional barrier 78−25543
anisole-carbon tetrachloride, mixtures, excess volume of mixing, mol. interactions 79−57281
1-(N-p-anisyl-N-methyl)-amino-3-anthryl-(9)-propane, intramol. exciplex formation 77−58059

organic compounds continued
anisylidene-p-aminophenyl acetate, nematic liq. cryst., refractive index, density, orientational order 78−76419
anisylidene-p-aminophenyl butyrate, nematic liq. cryst., refractive index, density, orientational order 78−76419
anisylidenebenzidine, particle size distrib. function, electrooptical diffusion method for determ. 80−8956
18-annulene, geometrical parameters, STO-3G ab initio calc. 80−52867
annulene, graph theory for axial symmetry molecules *(Chinese)* 79−36792
annulenes, graph theoretical polynomials 80−69048
[4N+2]annulenes, MCD spectra, B terms, semiempirical models 77−6814
annulenes, MINDO calcs., electron correlations 79−45636
anodic oxide films on Al, photoluminesc. obs. 77−1729
anthanthrene, mol. cryst. images in electron diffr. patterns 80−103315
anthanthrene, mol. imaging by high resolution electron microscopy 78−79600
anthracence, photocond. model, exciton-charge transfer state mixing near charged defect 77−51663
anthracene:2-aminoanthracene, polarised guest absorpt. spectra, transition dipole moment direction, cryst. packing 77−8610
anthracene:2-hydroxyanthracene, site-selective photochem., fluoresc. spectra at 3K 78−80756
anthracene:2-hydroxyanthracene cryst., site selective photochem. change, fluoresc. obs. 77−40273
anthracene:9-vinylanthracene, electroluminesc. at room temp. 79−15532
anthracene: phenazine, optical nuclear polarisation, 1.4 to 300K *(German)* 77−63321
anthracene: tetracene, singlet exciton trapping mechanism, fluoresc. mag. field modulation obs. 77−77267
anthracene: tetracene cryst., triplet-state EPR for isolated mol. orientation 78−26583
anthracene:acridine, electroluminesc. exam. 77−63463
anthracene:acridine(carbazole), fluoresc., structural traps for singlet excitons 78−19542
anthracene:chloranil, charge transfer spectra line shape 79−78700
anthracene:cyclohexadienyl type radicals, charge transfer reactions 78−52535
anthracene:naphthalene, guest mol. orientation 79−19161
anthracene:tetracene, absorpt. spectra, energy transfer over highest vibronic levels 79−65904
anthracene:tetracene, crysts., triplet kinetics model *(German)* 79−4518
anthracene:tetracene, delayed fluorescence excitation spectra 78−39594
anthracene:tetracene, electronic absorpt. spectrum, host-cryst. field effect 80−100669
anthracene:tetracene, guest mol. orientation 79−19161
anthracene:tetracene, nonlinear quenching of fluoresc. 79−65924
anthracene:tetracene, singlet exciton fission, fluoresc. in mag. field 79−69877
anthracene:tetracene, upper excited vibronic states optically pumped energy transfer matrix fluoresc. 78−76512
anthracene:tetracene crysts., mag. field modulation of scintillation under α-irrad. 77−48256
anthracene:tetracyanobenzene charge transfer complex, cryst. struct., temp. effects 80−96508
anthracene, 340-310 nm absorption spectrum dichroism, masked ^1L_b-$^1A_1$ transition 78−17685
anthracene, α-particle tracks, excited states, creation and evolution 78−43934
anthracene, γ-irrad., radical pairs EPR detection 78−31664
anthracene, γ-irradiated, temp. depend. of photolum. *(Russian)* 78−56511
anthracene, γ-irradiation influence on defects, luminesc. study *(Russian)* 80−55185
anthracene, (100) and (110), scintillation response of α-particles in planar channelling and blocking expts. *(German)* 79−14869
anthracene, anharmonic props., temp. (press.) depend., rel. to TTF-TCNQ 80−15200
anthracene, aromatic solvents, two-photon absorption cross section meas. by energy migration 77−58204
anthracene, attachment energy as habit controlling factor 80−59421
anthracene, birefr. changes due to thermal expansion 78−52468
anthracene, carbonyl derivatives, triplet state population, picosec. laser obs. 78−13544
anthracene, charge carrier photoexcitation quantum yield 79−99581
anthracene, charge storage and trapping levels, TSC studies 80−6875
anthracene, chemical thermodynamic props. 80−21312
anthracene, chemisorbed on Al_2O_3, radiative and nonradiative processes 79−36686
anthracene, coherent exciton scatt. and recomb. 80−39510
anthracene, coherent pairing of excitons in reson. EM field, biexciton spectra 77−47736
anthracene, cryst., exciton aggregate possible form. under intense optical pumping, fluoresc. spectra 80−84772
anthracene, cryst., fluoresc. spectra, press. tuning 77−28612
anthracene, cryst., heat pulse propag., exciton condensation, time-resolved fluoresc. spectra 80−84771
anthracene, cryst., photocurrent induced by detrapping of charge carriers trapped by radicals 79−82643
anthracene, cryst., polariton luminesc. 80−84775
anthracene, cryst., radiation induced radicals, optical absorpt. bands, SCF-CI MO calc. 79−91463
anthracene, cryst., triplet exciton pair kinematics, diffusion model 78−79931
anthracene, cryst., with electrolytic contacts, photocurrent anomalous behaviour, current-volt. characts. 77−39933
anthracene, crystal-electrolyte interface, ionis. energy of uppermost cryst. mols. 78−27764
anthracene, Davydov splitting of lowest singlet exciton under high press. 77−72823
anthracene, diacetyl-sensitised delayed fluoresc. 79−54888
anthracene, dipolar exciton band struct., optical model 77−15770
anthracene, dispersed in stretched PVC, dichroic meas. of orientation 77−30867
anthracene, dissolved in toluene and cyclohexane, scintillation from α-particles, time depend. *(Spanish)* 79−99950
anthracene, dynamic electron densities, anharmonic contribs. from large molecular librations 79−97971
anthracene, electron and hole generation under electron bombardment 79−73524
organic compounds continued
anthracene, electron diffr. of topochem. conversion and phase transition 78−83680
anthracene, electronic vibr. spectra, stochastic description, numerical modeling, comparison with expt. 80−63620
anthracene, EPR linewidth of triplet excitons 78−15011
anthracene, EPR of triplet excitons, source of residual linewidth 79−15338
anthracene, evaporated films, fluoresc. 77−85777
anthracene, excimer fluoresc. lifetime and quantum yield in soln. 77−6834
anthracene, excimer form. in soln. and cryst., fluoresc. study 79−45759
anthracene, excitation and propagation of phonons, luminesc. meas. *(Russian)* 78−35202
anthracene, excitation spectra of exciton fission 78−92116
anthracene, excited states calc., unrestricted HF theory in PPP approx. 77−50377
anthracene, exciton bands, dipolar lattice sums *(Japanese)* 77−43167
anthracene, exciton sounding of α-particle induced radiation defects 77−12423
anthracene, Faraday spectrum, sign rel. to mag. field strength *(German)* 77−36204
anthracene, field depend. of photocond. 79−99578
anthracene, film substruct., vacuum deposited, low temp. luminesc. *(Russian)* 78−15226
anthracene, fluoresc., site selection spectroscopy, 2-300K 77−1731
anthracene, fluoresc. and photoreactivity 77−48668
anthracene, fluoresc. by electron beam excitation 79−94031
anthracene, fluoresc. from (001) surface and sub-surface excitons 79−33763
anthracene, fluoresc. quenching by inorganic anions 78−74694
anthracene, fluoresc. quenching by triethylamine 79−50057
anthracene, fluoresc. spectra and decay curves, 4-300K, reabsorpt. in cryst. *(German)* 78−68561
anthracene, fluorescence spectra in aq. and surfactant solns. 77−83639
anthracene, Frenkel exciton, coupled coherent and incoherent motion 77−35870
anthracene, harmonic force fields, bond orders, normal coord. anal. 78−25418
anthracene, high exciton conc., low temp. fluoresc. *(Russian)* 77−28623
anthracene, hot luminesc. in solid matrix at 4.2K, intramol. thermal bath 79−85999
anthracene, impurity effects on elec. cond. *(Russian)* 77−62930
anthracene, in acethylcellulose, fluorescence, time dependent emission anisotropy *(German)* 78−94279
anthracene, in atmosphere, photooxidation on particulate matter 80−61487
anthracene, in cyclohexane soln., triplet state decay consts. by sampling flash apparatus 79−51998
anthracene, in n-hexane, Shpolskii absorpt. spectra at 77K, vibronic struct. *(German)* 79−59507
anthracene, in n-paraffin matrices, luminesc. spectra, depend. of inhomogeneous broadening *(Russian)* 79−10145
anthracene, in stretched polyethylene film, UV-visible and fluoresc. spectral shifts 78−62852
anthracene, in stretched polythene films, molecular distribution determ. 78−27298
anthracene, inelastic-electron tunnelling spectroscopy, exptl. test of symmetry selection rules 77−83671
anthracene, intermol. relax. energies, UPS 78−31304
anthracene, IR absorpt., intermol. reson. interaction, temp. depend. 78−72506
anthracene, IR spectra, strong anharmonicity effects *(Russian)* 77−66511
anthracene, isotopically mixed cryst., exciton dynamics 80−29329
anthracene, laser excited single crystal, numerical anal. for TSC results *(Japanese)* 80−34464
anthracene, lattice parameters press. depend., elastic consts. 78−38686
anthracene, lifetimes of exciton-polariton luminesc. 79−33761
anthracene, light polarisation depend. on energy transfer from excited to emitting mols. *(German)* 78−37677
anthracene, liq., EHD transit flow 78−75895
anthracene, liq., elec. current decrease due to electrode coverage form. 77−8108
anthracene, liq. chromatography, sublimation, zone refining, exciton fluoresc., mobility meas., melt grown crystal 79−38736
anthracene, mag. susceptibility anisotropies, high field ^{2}H NMR quadrupolar effects obs. 80−25225
anthracene, matrix isolated, vibr. relax., hot luminesc. obs. 79−85986
anthracene, melt and dil. soln., UV spectra, line broadening and shift vibr. struct. 78−17684
anthracene, mesophase formation during carbonisation under pressure 77−44182
anthracene, metastable triclinic phase 80−59452
anthracene, mol. cryst., elec. field independent electron drift mobility 79−51645
anthracene, mol. cryst., polariton fusion, two-photon excitation spectra 77−90139
anthracene, mol. crystal, meas. of US attenuation coeff. by optoacoustical methods *(French)* 80−70317
anthracene, molecular crystal, exciton-phonon coupling, absoprt. band profile in first singlet system 78−83888
anthracene, noncryst. solid, excimers, time resolved fluoresc. obs. 79−52006
anthracene, nonequilibrium phonon propag. with freq. down-conversion 80−84260
anthracene, nonlinear fluorescence quenching 78−52562
anthracene, normal coord. calcs., simplified valence force field models 78−94229
anthracene, off-diagonal electron mobility and lateral space charge drift 78−72192
anthracene, optical determ. of vapour conc., vap. press. and heat of sublimation 78−22840
anthracene, orientated in nematic liq. cryst., UV-visible dichroism meas. *(German)* 77−34668
anthracene, orientation in polyethylene film, linear dichroism 78−29864
anthracene, orientationally disordered cryst., lattice relax. effect 80−107278
anthracene, oxidation to anthraquinone, in fixed bed catalytic reactor with KS-14 catalyst *(Russian)* 79−66268

organic compounds continued
anthracene, photocond. spectrum induced by excitons *(Japanese)* 80−29440
anthracene, photoconduction *(German)* 79−78129
anthracene, photogeneration of charge carriers through two photon excitation 80−11033
anthracene, photon-emitting singlet excitons spatial distrib. 79−83009
anthracene, polarisation energy of localised charge 80−15034
anthracene, polarised refl., surface excitons, Davydov splitting 77−16327
anthracene, polariton effects in transmission and absorpt. spectra in thin crysts. 77−20886
anthracene, polycrystalline, optical props., 3.2-9.3 eV 80−76097
anthracene, polymorphic forms, generation by repeated slip 78−34457
anthracene, protection against radiation damage, exciton effects 80−29055
anthracene, pulsed electron excitation, triplet excitons, spectral and electrical investigations 80−92828
anthracene, pure and d_n, PMMA soln., triplet lifetimes, 77-300K 78−25594
anthracene, radiation-induced radicals, EPR and optical absorpt. obs. 77−12816
anthracene, radiation-induced topotactic conversion from di-para-anthracene, low temp. TEM obs. 78−35710
anthracene, radical cation, EPR, acidic surface anisotropic rot. diffusion 78−27095
anthracene, radiolysis, ion-pair clusters and excited-state yields 77−29024
anthracene, Raman intensities rel. to vibronic coupling and excited electron state geometries 77−27075
anthracene, Raman spectrum, in-plane vibr. force fields, five-parameter approx. calcs. 79−59436
anthracene, rarefied vap., fluoresc. spectrum shape distortion in presence of intense radiation 79−3487
anthracene, reflectivity and fluoresc. of (001) surfaces, sub-surface exciton states 79−15508
anthracene, reson. Raman emission and hot luminesc. *(Russian)* 79−61377
anthracene, resonance Raman effect in pre-resonance region 77−77201
anthracene, scintillation decay time determ. using low energy spectra 79−9964
anthracene, scintillation response to deuteron bombardment, energy, temp., and deuteron direction depend. *(German)* 78−6779
anthracene, selective epitaxy by vacuum evaporation on soln. grown anthracene substrate 77−63558
anthracene, shape of vibronic absorpt. and luminesc. spectra 79−76469
anthracene, Shpolskii spectra, vibronic struct., fluoresc. *(German)* 79−22754
anthracene, single cryst., CARS and CSRS, two-photon reson. effect 80−95946
anthracene, single cryst., fluoresc. decay, Monte-Carlo simulation *(German)* 79−61440
anthracene, single cryst., photocond. threshold, excitation spectrum 80−44639
anthracene, single cryst., piezomodulated reflection spectra 79−61392
anthracene, single cryst., X-radiation damage recovery, using triplet state exciton probe 78−75694
anthracene, single cryst. growth using zone melting furnace 79−52110
anthracene, single cryst. triplet excitation form. 79−69437
anthracene, single cryst. with discrete shallow traps, computer simulation of TSC 79−99819
anthracene, single cryst. with photoinduced local centres, luminesc. 79−61433
anthracene, single crystal, disperse photocurrent transients rel. to multiple trapping 79−99564
anthracene, single crystal, photoconductivity quantum yield, experimental validation of fund. theory 80−6909
anthracene, singlet and triplet excitons as probes for photochem. reactivity 79−74406
anthracene, singlet exciton fission, fluoresc. in mag. field 79−69877
anthracene, singlet exciton fission, prompt and delayed fluoresc. mag. field depend., temp. effects 78−52540
anthracene, singlet exciton transitions, energies and oscillator strengths, boson theory with PPP wavefunctions 80−92820
anthracene, singlet-triplet absorpt. spectra, 2-300K, photoexcitation spectra 78−43890
anthracene, slip planes, atom-atom pot. method 77−35569
anthracene, slip systems in deformed crysts. 79−42138
anthracene, solid, electronic struct., comparative ESCA study of polyacenes 78−52631
anthracene, soln. and melt, second vibronic transition, spectroscopic charcts., effective field dispersion calcs. 80−55102
anthracene, space-charged-limited photo-enhanced currents 79−82599
anthracene, spectra, PPP approx., CI clacs. *(German)* 79−36602
anthracene, spectral evidence for green incipient dimers after photo-oxidation and photodimerisation 78−15687
anthracene, stable monoclinic phase, (001) planar faults 79−69115
anthracene, structural defect, photolum., γ-irrad. and temp. depend. *(Russian)* 79−28797
anthracene, substrate for epitaxial crystn. of polyesters 79−61521
anthracene, surface polaritons, attenuated total refl. 77−63423
anthracene, temp. depend. of mol. motion in lattice 79−33045
anthracene, temp.-independent mobilities, phonon-induced electron hopping 79−28347
anthracene, temperature independent intersystem crossing 78−39030
anthracene, theory of fission of singlet Frenkel exciton into two localised triplet excitons 79−23901
anthracene, thermal cond. and heat capacity, meas. under press. 79−90796
anthracene, thermally stimulated currents from shallow trapping centres *(Japanese)* 78−92015
anthracene, thermodynamic function calc. using cell model 77−7879
anthracene, thick crystals, excitation spectrum of fluorescence 80−76068
anthracene, thin film vacuum deposited, exciton reflection spectra *(Russian)* 78−15194
anthracene, thin surface layer, delayed fluoresc. obs., surface trap influence 77−77291
anthracene, time-resolved transient photocond. obs. 80−6892
anthracene, total reflection spectra, site shift surface exciton dispersion 77−77233
anthracene, transient photocurrent, appl. of Scher-Montroll method 79−7851

organic compounds continued
anthracene, trapping effects on emission-limited current flow 80−29413
anthracene, triplet energy migration in polystyrene matrix, rate meas. 78−35185
anthracene, triplet exciton absorpt. lines 79−47475
anthracene, triplet exciton trapping by dislocations 78−30871
anthracene, triplet excitons, phosphoresc. and delayed fluoresc. excitation spectra 78−63986
anthracene, triplet-exciton fine struct., high resolution optical meas. 80−45099
anthracene, TSC and carrier retrapping 80−39599
anthracene, ultrathin films on fused quartz and sapphire 80−59812
anthracene, UV irrad. effects on fluoresc. emission at room temp. 79−83019
anthracene, vap., laser-excited long-lifetime luminesc. 79−54887
anthracene, vap., line fluoresc. response to IR laser 79−54893
anthracene, vap. phase dye laser media, photophysical parameters 80−95884
anthracene, vapour, fluoresc. spectra, mol. vibr. freq. reson. laser IR irradiation, quenching 80−18883
anthracene, vibronic absorpt. spectra in soln. and cryst., universal mol. interactions effects 77−68031
anthracene, with pentracene and tetracene impurities, laser-pulse-excited luminesc. 80−7408
anthracene 9,10 epiperoxide, fluoresc. and photoreactivity 77−48668
anthracene and dianthracene, phase equilib. in photocondensation *(Russian)* 79−7561
anthracene anion+dimethylaniline cation, recombination reaction in soln., time-resolved mag. field effect 80−3308
anthracene anion radicals, enthalpy of disproportionation, calorimetric determ. technique 79−96296
anthracene crystal, dynamical matrix eigenvectors from Raman scatt. 80−100315
anthracene crystal, stimulated emission and Raman scatt. 78−1303
anthracene crystal, triplet exciton absorpt., high resolution photoconductivity spectroscopy 78−10504
anthracene crystal film, nonequilibrium phonon distribution, at low temp. *(Russian)* 77−47520
anthracene crystal scintillators, meas. of light pulse shapes 78−74534
anthracene crystals, α-particle induced scintillation, mag. field effects 80−40161
anthracene crystals, and thin films, electroabsorption in disordered solids 78−95590
anthracene crystals, basal dislocations, fluoresc. spectra and etching obs. 77−84755
anthracene crystals, carrier trapping in deformed surface region 78−47806
anthracene crystals, growth in melts of cholesteryl-caproate-anthracene system 80−2943
anthracene crystals, local biexciton formation, luminesc. spectra *(Russian)* 78−2428
anthracene crystals, pre-reson. Raman scatt., 4.2-30K 80−60571
anthracene crysts., mol. orientational disorder calc. vacancies, dislocations, photodimerisation 77−4915
anthracene crysts., nonlinear fluorescence quenching, recomb. of free excitons 80−7397
anthracene derivative, Langmuir-Blodgett multilayer film, semiconducting props., optical and elec. meas. 80−11122
anthracene derivative films, Langmuir-Blodgett built-up multilayer, prep. and characterisation 79−95293
anthracene derivatives in soln., fluoresc. and laser parameters 79−27251
anthracene derivatives in solution, polarisability and dipole moments, emission and absorpt. spectra obs. 80−69256
anthracene dianions in dimethyl ether, rotational diffusion meas. 80−65262
anthracene dimer anion, charge reson. transition anal. 80−42931
anthracene doped naphthalene cryst., decay times and diffusion coeffs. of singlet excitons, under press. 77−20911
anthracene film, effect of struct. on luminesc. quenching *(Russian)* 80−7411
anthracene films, optical props., comparison between free and optical contact mounting 80−89079
anthracene glass, excess electron optical absorption spectrum model, band shape 78−33500
anthracene in 2 methyl-THF glass, low temp. fluoresc. bandshape, excess energy effects 78−76509
anthracene in glassy matrix, triplet state spin relax. time, anisotropy *(French)* 77−65492
anthracene in naphthalene crystal, second-order Stark shifts in optical spectrum 80−88966
anthracene in polychlorinated alkanes photochemical study by rapid scanning fluoresc. spectroscopy 80−86440
anthracene in PVC film, photodichroism at 257 and 383 nm 79−31539
anthracene in Shpolskii systems, key and hole rule test, fluoresc. 77−42347
anthracene intramolecular excimer in 1,3-dianthrylpropane, direct obs. 80−48029
anthracene ion in liqs., photoelectron emission and photocond. 80−75600
anthracene isotopic mixed crystals, exciton spectra 79−38602
anthracene Langmuir film, lightly substituted, electrolum., photolum. and electroabsorption 80−20726
anthracene Langmuir films, lightly substituted, AC and DC cond. 80−80425
anthracene like crysts., charge-transfer electron-exciton bound states, theory 78−10365
anthracene microcrystals suspended in vapour-gas stream, naphthalene crystal nucleation 80−76165
anthracene mol. cryst., exciton-lattice interaction and exciton absorption line shape 78−18968
anthracene plate, ballistic propagation of phonons *(Russian)* 78−34582
anthracene radical cation EPR spectra, ion-pair effects 79−13742
anthracene scintillator, response to low energy electrons 77−54391
anthracene single cryst., Frenkel exciton spectra at dielectric and conducting layer interfaces 80−44510
anthracene single cryst., injection of holes, current-voltage characts. *(Russian)* 77−1433
anthracene single crystals, effect of γ-irrad. on photolum. *(Russian)* 80−2852
anthracene single crystals, hole trapping by photo-oxidation products, injection currents *(Russian)* 80−92904

organic compounds continued
anthracene solution, singlet-triplet-transitions influence on two photon absorpt. cross section meas. *(German)* 77−38703
anthracene sulphonate sensitized photooxidation of I^- in aq. soln. 77−32812
anthracene surface, Ar impact, Penning ionisation electron spectra and photoelectron spectra 80−66352
anthracene surface UV light irrad. effect on organic layer nucleation during crystallisation 80−75478
anthracene thin films, high field effects and switching, local centres importance 79−73548
anthracene thin films, struct. rel. to substrate temp., thickness, condensation rate 78−30845
anthracene vapour, conc. depend. of diffuse component of fluoresc. spectrum *(Russian)* 77−46601
anthracene vapour, optically induced dynamic gratings 80−28289
anthracene vapours, shape of absorpt. bands, temp. depend. 78−82743
anthracene with adsorbed rhodamine B, electron-hole pair in external elec. field 79−73558
anthracene with powdered graphite electrodes, electrolum., ambient gas effects 77−69917
anthracene-β-sulphonic acid, 340-310 nm absorption spectrum dichroism, masked ^1L_b-$^1A_1$ transition 78−17685
9-anthracene-$(CH_2)_n$-N,N-dimethylaniline, electrogenerated chemiluminesc., intramol. exciplex form. 78−11503
anthracene-acridine, order parameters and lattice energy, mean field approx. 78−22688
anthracene-aliphatic amine, photochemically induced H isotope exchange 79−11771
anthracene-amine cation radicals, electron transfer with heterocyclic and carbonyl anion radicals, triplet state electrogeneration 80−63803
anthracene-Au interface, energy transfer 77−85775
anthracene-Au interface exciton luminescence Frenkel exciton metallic quenching *(Russian)* 80−50421
anthracene-d_{10}-s-tetracyanobenzene, rotational mode coupling in phase transition 78−71827
anthracene-dimethylpyromellite-imide, CT complex, reaction yield detect. double reson., delayed fluoresc. quenching *(Russian)* 78−88230
anthracene-dimethylpyromellitimide, CCT crystals, mag. field effect on fluorescence 78−19543
anthracene-dimethylpyromellitimide, cryst., triplet exciton pairs, EPR spectra 77−43906
anthracene-dimethylpyromellitimide charge-transfer complex, photoconductivity mechanism 77−47860
anthracene-doped naphthalene, singlet exciton energy transfer dyanmics, time-resolved spectra 79−83032
anthracene-He-Xe, gaseous mixture with one low conc. component, thermal diffusion calcs. 77−19661
anthracene-N,N-diethylaniline exciplex, intersystem crossing 77−30905
anthracene-PDMA, weak donor-acceptor complexes, electron mobility model 80−15511
anthracene-perylene energy transfer dye laser, gain meas. 79−59695
anthracene-phenanthrene-tetracyanobenzene, CT-cryst., mini-excitons and lattice dynamics, ESR, optical and Raman spectra 80−60406
anthracene-PMDA, charge transfer cryst., 2K, zero-phonon lines, singlet spectra 78−23484
anthracene-PMDA crysts., phosphorescence blue shift of charge transfer config. 77−36278
anthracene-pyromellitic dianhydride, cryst., charge transfer exciton transitions, refl. spectra obs. 78−72540
anthracene-pyromellitic dianhydride, mol. charge transfer cryst., Raman scatt. meas. 80−29743
anthracene-pyromellitic dianhydride complex, optical and photoelectric props. *(Russian)* 80−15570
anthracene-pyrometallitic dianhydride cryst., refl. and absorpt. spectra of singlet charge transfer excitons 80−71442
anthracene-quartz interface exciton luminescence, Frenkel exciton metallic quenching *(Russian)* 80−50421
anthracene-TCNB, 1:1 charge transfer complex, phase transition at 206K, NMR meas. 79−7690
anthracene-TCNB, charge transfer cryst., Raman study of phase transition 79−19885
anthracene-TCNB charge transfer cryst., phosphoresc. and delayed fluoresc. detected mag. reson. 79−33565
anthracene-TCNB charge transfer crystal, orientational phase transition, EPR, Raman spectroscopy exam. 78−26817
anthracene-tetracene amorphous films, host-guest energy transfer 78−60505
anthracene-tetracenebenzene, triplet excitons annihilation, mag. reson. sign reversal 79−65769
anthracene-tetracyanobenzene, charge transfer complex, phase transitions, deuteration effect, mag. reson., spectral and thermal meas. 79−4412
anthracene-tetracyanobenzene, triplet exciton annihilation, mag. double reson. *(Russian)* 78−19380
anthracene-tetracyanobenzene 1:1 charge transfer complex, low temp. phase, cryst. struct. 80−6397
anthracene-tetracyanobenzene charge-transfer complex, EPR of triplet excitons, phase transitions 77−28425
anthracene-tetracyanobenzene charge-transfer complex, RYDMR of triplet excitons annihilation 78−39448
anthracene-tetracyanobenzene cryst., triplet exciton annihilation, time correlated delay fluoresc., ODMR 80−39895
anthracene-tetracyanobenzene cryst., triplet excitons, zero-field EPR splitting temp. depend. 78−10748
anthracene-tetracyanobenzene crysts., deuteration effect on phase transition, triplet state EPR study 80−50163
anthracene-trinitrobenzene complex, neat and mixed cryst. and glass opt. spectra 77−40274
anthracene/aq. electrolyte contact, illuminated, space charge behaviour 78−84290
anthracene/TCNB, charge-transfer cryst., fluoresc., 1.2-300K, mobile triplet excitons 78−43913
anthracene/trans, trans-2,4-hexadiene-exciplex, fluoresc. rel. to photodimerization 77−3401
anthracenes, anthronyl substituted, solvent-assisted form. of luminesc. intramol. exciplexes 78−25589
anthracenes, bridged, photochemistry and spectra 77−77793
anthracenes, exciplex form. with amines, form. kinetics and luminesc. props. 80−66792
anthracenes, in soln., triplet-triplet fluoresc. 79−59501
anthracenes, long-lived luminesc. in solid state *(German)* 78−23528

organic compounds continued
anthracenes, meso-substituted, thermally assisted and heavy atom assisted intersystem crossing 79−31573
anthracenes, nonradiative relax. of higher excited triplet states, double excitation obs. 78−29805
anthracenes, substituted, disordered crysts., optical transforms 80−78783
anthracenophanes, fluoresc. and photoisomerisation 79−33781
9-anthraldehyde, struct. by TEM 80−79771
anthranilic acid, solid, amino group reorientation, PMR second moment obs. 78−35046
anthraquinoide, electrochromism, display devices, multiplexing 80−45037
9,10-anthraquinone, electronic-vibr. interaction between close excited electronic states 79−63980
anthraquinone, fluoresc. and photoreactivity 77−48668
anthraquinone, in Shpolskii matrices, triplet state spin-lattice relax. rates 78−21952
β-F-9,10-anthraquinone, internal heavy atom effect, vibronic phosphoresc. spectrum, intermol. spin-orbit coupling 78−82774
9,10anthraquinone, lower triplet states, interactions and position, matrix isolation spectra 80−63634
9,10-anthraquinone, phosphorescence, external heavy atom in mol., 4.2 to 77K, quasiline spectra 78−82773
9,10-anthraquinone, Shpolskii quasi-line phosphoresc. spectra, electronic-vibrational interactions 78−55196
anthraquinone, site selective sublevel phosphoresc. spectra in octane or hectane soln. 79−69878
anthraquinone, UV light effect on nucleation during crystallisation on anthracene surface 80−75478
anthraquinone dyes, phototropic transformations, fibre-forming polymer substrates effects *(Russian)* 77−66762
anthraquinone in pentane solvent, sublevel phosphorescence spectra, molecular distortion 80−74190
anthraquinone pleochroic dyes in liq. cryst. soln., photostability, appl. to liq. cryst. displays 80−88961
anthraquinone-xanthone liq. soln., upper excited singlet state, delayed fluoresc. 80−106345
9,10-anthraquinones, Π-Π^* electronic transitions, substituent effects calcs. 80−28006
9-anthroic acid, excimer-type transition polaris. 79−50062
anthrone, 533 nm excited state absorpt. kinetic, triplet quenching solvent, internal conversion, vibr. relax. 78−21935
anthrone, fluoresc. and photoreactivity 77−48668
anthrone, intersystem crossing rates, ps time-resolved spectra 77−6821
anthrone, UV light effect on nucleation during crystallisation on anthracene surface 80−75478
anthrone-biphenyl derivative, donor-acceptor solns., triplet-triplet energy transfer under Shpolskii effect conditions 79−64031
9-anthronitrile, struct. by TEM 80−79771
anthronyl radicals, ESR, temp. depend. phenyl twist angles 79−18210
4-(9-anthryl)-N,N-dimethylaniline, fluoresc., dipole moments and polarisabilities 80−1019
p-(9-anthryl)-N,N-dimethylaniline derivatives, excited emitting states in polar solvents, fluoresc. 78−5263
anthryl-$(CH_2)_3$-N,N-dimethylaniline, excited charge-transfer ps. kinetics 77−30986
antimalarial drugs, lifetime meas. via reiterative convolution using fluorescence decay curves 80−57380
antimalarials, interaction with coenzyme-Q_{10}, theory 78−27885
antipyrine, radioiodinated, prep. and stability for use in local blood flow determs. 80−94366
antrhacene crystals, thermal expansion meas. by quartz diatometer 80−34212
apomyoglobin-arylaminonapththalenesulfonate system, fluorescent behaviour 79−39359
aqueous binary mixture, pseudophase transition, heat capacity evidence 78−83937
L(+)arabinose, irradiated single crystals, electron trapping, ESR obs. 78−88646
arabinose, X-irradiated single crystal, intermol. electron trapping, hyperfine ESR pattern 79−39166
arachidate monolayers, optical props. integrated optics meas. 78−35214
arachidate-Cd, multilayer struct., hopping rate, direct evaluation 78−88045
arene, photophysics, functionalised micellar assembly, phosphoresc. and triplet Ag^+ enhancement 78−95598
arenediazonium salts, photolysis, quantum efficiencies, reactive intermediaries, EPR 78−64860
arginine, polycryst., proton mag. relax. and mol. motion 78−20139
L-arginine L-ascorbate, X-ray cryst. struct. determ. 80−35826
aromatic, absolute fluorescence quantum yield, calorimetric determ. 80−43092
aromatic acids, mixtures, quantitative anal. by ^{13}C NMR 78−31716
aromatic aldehyde, phosphorescence spectra of mol., intensity and vibronic coupling 79−76461
aromatic aldehyde, triplet state dipole moments, vibronic coupling effects 79−31493
aromatic aldehydes, and deuterated forms, $n\pi^*$ and $\pi\pi^*$ assignments in 0-0 band, pot. surface method 78−9197
aromatic aldehydes, in polystyrene matrix, group relax., weight factor effects determ. 78−68446
aromatic amides, intersystem crossing, mol. geom. effects 77−6828
aromatic butadienes, dipole moment and dielectric relax. meas. 80−83516
aromatic compound-carbon tetrachloride, liq. mixture, sound vel. theories 78−2199
aromatic compounds, diamag. susceptibility 78−80123
aromatic compounds, electrophilic substitution sites, perturbation theory calcs. 77−30800
aromatic compounds, in n-paraffin cryst., luminesc. characts. 79−3480
aromatic compounds, intersystem crossing theory, El-Sayed rule extension, anomalous rate consts. 77−30911
aromatic compounds, isothermal recomb. fluoresc., decay kinetics 78−29809
aromatic compounds, mol. rearrangement in excited electronic state, fluoresc. with anomalously large Stokes shift 79−85983
aromatic compounds, oriented in stretched polyethylene film, phosphoresc. polarisation 79−6961
aromatic compounds, out-of-plane mol. vibrs., force field approx. calcs. 80−91538
aromatic compounds, oxidative bromination, chem. oscills. 80−3335

organic compounds continued
aromatic compounds, reduction by KC_{24} intercalation compound 80−3306
aromatic compounds, subpicosecond states, fluoresc. spectroscopy in liquids 79−45758
aromatic compounds, two-stage photoionisation in solns., UV laser irrad. effects *(Russian)* 78−13556
aromatic compounds, with nonbonding electrons, proximity effect and radiationless transitions 78−58736
aromatic compounds in benzene polycrystalline host, active N_2 induced chemilum., 77K 80−60691
aromatic compounds luminesc. polarisation, quasilines and bands in Shpolskii spectra *(Russian)* 79−31592
aromatic compounds mixture, charge transfer equilib. consts., adiabatic ionis. energies, entropy changes 78−37738
aromatic dimethacrylates, study of methacrylates, cross-linked, structure-transformation relations, properties *(German)* 79−55677
aromatic esters, phosphoresc. and fluoresc. spectra in organic matrices 80−32756
aromatic esters derived from naphthalene, liqs. cryst. props. 78−47235
aromatic ethers, comparative study of X-ray and γ-induced photolysis and radiolysis *(German)* 78−64854
aromatic ethylenes, dipole moment and dielectric relax. meas. 80−83516
aromatic heterocycles, MC-SCF and CI calcs. in PPP framework 79−26892
aromatic heterocyclics, (N- and S-), electron attachment, mass spectroscopic obs. *(German)* 77−64001
aromatic higher perfluoro compounds, He(Iα) photoelectron spectra 79−31610
aromatic hydrocarbon, centrosymmetric, two photon excited upper state fluoresc. spectra, reson. fluoresc. and vibr. mode selectivity 80−18878
aromatic hydrocarbon, quenched with Ag^+ in ethanol, triplet state form. 79−11801
aromatic hydrocarbon acceptor, energy-deficient, and tetrathiafulvalene donor systems, electrogenerated chemiluminesc. 79−20372
aromatic hydrocarbon crysts., effective mol. polarisability 77−88590
aromatic hydrocarbon derivatives, low-temp. singlet-triplet conversion probability rel. to optical parameters 79−54898
aromatic hydrocarbon in soln., excited electronic state vibr. relax., time resolved fluoresc. 80−48024
aromatic hydrocarbon soln., delayed fluoresc., mag. field effect, excimer form. 77−14479
aromatic hydrocarbon-dicyanobenzene, aq. micellar soln., fluoresc. quenching mechanism 79−50063
aromatic hydrocarbon-N,N-dimethylaniline, aq. micellar soln., fluoresc. quenching mechanism 79−50063
aromatic hydrocarbons, π-ionisation energies correl. with free electron MO energies 80−14073
aromatic hydrocarbons, absorpt. spectra, electronic-vibr. sequence band broadening 77−65453
aromatic hydrocarbons, adsorption on Ag, heat of adsorption, coating and fine struct. *(German)* 79−23844
aromatic hydrocarbons, aqueous micellar soln., triplet state room temp. phosphoresc., hydrophillic quenchers 78−9181
aromatic hydrocarbons, carbonisation, microscopic features of carbons obtained using catalysts 77−66597
aromatic hydrocarbons, carbonisation of heterocyclic cpds. catalysed by $AlCl_3$ 77−63572
aromatic hydrocarbons, catacondensed, photoelectron spectra, correlations with UV absorpt. spectra 77−34690
aromatic hydrocarbons, doped mol. crysts., singlet host exciton nonradiative heterofission 77−28122
aromatic hydrocarbons, electron attachment, mass spectroscopic obs. *(German)* 77−64001
aromatic hydrocarbons, ethanol-KI solns., fluoresc. affected by I^- 79−13749
aromatic hydrocarbons, excimer decay dynamics, rate const. rel. to solvent 78−58729
aromatic hydrocarbons, excited state vibr. freqs. 79−85947
aromatic hydrocarbons, fluorescence quenching rate constant, undergraduate expt. using Spectronic 20 77−57119
aromatic hydrocarbons, heat transfer to ascending (descending) streams, near-crit. press. 77−65742
aromatic hydrocarbons, in airborne particulates, gas chromatography/mass spectrometric, NMR analyses 77−13116
aromatic hydrocarbons, in organic glasses, nonphotochemical burning, impurity site relaxation 78−25548
aromatic hydrocarbons, intersystem crossing mechanism, rate consts. 77−65497
aromatic hydrocarbons, IR spectra and high-pressure phase transitions 80−10659
aromatic hydrocarbons, kata-annellated, para band energy-topology empirical correlations *(German)* 79−13657
aromatic hydrocarbons, liq. solns., delayed fluoresc., mag. field induced polarisation inversion 77−88485
aromatic hydrocarbons, melting behavior and role of free radicals and molecular site in producing mesophase pitch 79−90523
aromatic hydrocarbons, mol. polarisability, INDO calc. 80−52886
aromatic hydrocarbons, mol. struct. determ. from electronic spectra, oscill. strengths *(French)* 77−71888
aromatic hydrocarbons, molar mag. susceptibility, localised π-bond model 79−22862
aromatic hydrocarbons, molecular crystals, intermolecular interactions, spectroscopic studies, review 80−103958
aromatic hydrocarbons, Morse oscill., transition probabilities for mol. bond modes 79−18172
aromatic hydrocarbons, oxygen quenching of triplet states, charge-transfer interactions 77−23516
aromatic hydrocarbons, penetration into graphite intercalation cpds. of alkali metals *(French)* 78−27433
aromatic hydrocarbons, proton chem. shifts with ring currents, π-bond model 79−81215
aromatic hydrocarbons, proton chemical shifts, localised π-bond model calcs. 80−43070
aromatic hydrocarbons, rot. anisotropy and solvent-fluorophase bonds, differential polarised phase fluorimetric investig. 77−61779
aromatic hydrocarbons, $S_0 \rightarrow T_1$ phosphoresc. under Shpolskii effect conditions 77−83643
aromatic hydrocarbons, sequential coupling 80−58297
aromatic hydrocarbons, Shpolskii systems, key and hole rule test, fluoresc. 77−42347

organic compounds continued
aromatic hydrocarbons, singlet energies, correlation with anion radical protonation 78−40064
aromatic hydrocarbons, singlet-triplet conversion at low temp. 80−43094
aromatic hydrocarbons, solubility in liquid O_2, estimation by Preston-Prausnitz method 80−39285
aromatic hydrocarbons, struct., UV absorption band calc. *(French)* 77−18989
aromatic hydrocarbons, thermal cond. at high press. and temp. 79−18988
aromatic hydrocarbons, thermophysical properties rel. to compressibility 78−83964
aromatic hydrocarbons, triplet state quenching by nitroxyl radicals, energy transfer 78−35651
aromatic hydrocarbons, UV photoelectron spectra 77−88498
aromatic hydrocarbons, vibronic calcs. 80−58238
aromatic hydrocarbons, vibronic coupling model, nontotally symm. harmonic mode 77−3337
aromatic hydrocarbons in Antarctic marine sediments 79−92096
aromatic hydrocarbons in Shpolskii matrices, $S_0 \rightarrow T_1$ absorpt. spectra 79−85995
aromatic hydrocarbons in soln., low quantum-yield mol. fluoresc. 77−58063
aromatic hydrocarbons in soln., mag. field effects on delayed fluoresc., perturbation theory applic. 77−30913
aromatic hydrocarbons with condensed nuclei, ring current calcs. *(Chinese)* 79−93916
aromatic hydrocarbons-amine, π-axciplexes, intermolecular interactions 80−43134
aromatic impurity molecule, internal conversion processes 78−82776
aromatic isolated mol. nonradiative conversion, internal and S-T conversion, vibr. excitation and fluoresc. quantum yield 80−43095
aromatic isomers, analysis by IR spectroscopy, preconcentration, separation and computer techniques 78−31730
aromatic media, electron excitation, delayed fluoresc. 79−52024
aromatic molecular crystal, electron-intramol. vibr. coupling, rel. to carrier mobility 77−15854
aromatic molecular crystals, optical nuclear polarization by optically excited triplet states 79−19804
aromatic molecule, electronic excitation energy degradation, electronic-vibr. spectrum 77−488
aromatic molecule, orientation and linear dichroism in stretched polyethylene 77−88480
aromatic molecule luminescence, heavy atom substituents at different bonding sites *(German)* 79−81236
aromatic molecule with nonbonding electrons, $T_1(\pi\pi^*) \rightarrow S_0$ radiationless transition, vibr. coupling 77−18957
aromatic molecules, and derivatives, radiationless conversion processes, regularities 80−14171
aromatic molecules, effects of vapour phase application to stretched polyethylene films 77−90276
aromatic molecules, phosphoresc. triplet spins phase coherence, ESR 79−31559
aromatic molecules, UV photoelectron spectroscopy, basic concepts, spectra 78−17715
aromatic molecules in clathrates, Raman and phosphoresc. spectra 79−36647
aromatic molecules in O_2 matrices, singlet-triplet absorpt. spectra 78−17683
aromatic nitrocompounds, electrolytic reduction, using $Ti(SO_4)_2$ addition 79−57248
aromatic nitroso compounds, fluoresc. from upper singlet 79−6958
aromatic organic macromolecules, energy-gain satellite in C(1s) XPS 79−1813
aromatic polycrystals, γ-irrad., radical pair form., EPR meas. 78−80757
aromatic radical ion recomb., mag. field modulation, Liouville eqn. soln. 77−28995
aromatic rigid soln. phosphoresc. promotion by I^- 80−50387
aromatic ring compounds, single, nitro-substituted, inelastic electron tunnelling spectroscopy 77−42367
aromatic ring ompounds adsorbed on Al-AlO_x-Pb and Mg-MgO-Pb, inelastic electron tunnelling 79−59521
aromatic rings, substituted electronic energy effects 79−49957
aromatic scintillators radioluminesc. yield *(French)* 78−52574
aromatic solutions, triplet-triplet absorption, anomalous broadening 79−54842
aromatic substitution mechanisms 77−9056
aromatic systems, alternant, sign-alternation rule for triplet state 80−102420
aromatic-hydrocarbon crystals, model for fission of singlet excitons into triplet-exciton pairs 78−14672
aromatic-molecules, conformeric fluoresc. and phosphoresc., rotation of chromophoric fragments around single chemical bonds 77−68068
aromatics, biphotonic reactions at 77K, quantum efficiency 78−80763
aromatics, condensed, new force field, appl. to pyrene inplane vibrs. 79−81201
aromatics, electronic absorpt. spectra absolute intensities estimation 77−34702
aromatics, fluoresc. polarisation red edge effect, rot. anomaly 79−3472
aromatics, halogen substituted, as positronium inhibitor 80−93783
aromatics in stretched PVA films, ESR of phosphorescent triplet state 77−30908
aryl ammonium hydrogen difluorides, IR vibr. spectra and NMR reson. obs. 80−34788
aryl cations, triplet state, multiple site splitting, ESR obs. 80−97126
aryl esters, cyano-substituted, liq. cryst. props. 77−27822
aryl halides, mol. beam photodissoc., fragment translational energy distrib. 77−50481
aryl p-fluoroalkoxybenzoates, synthesis and mesomorphism 78−91243
aryl p-fluoroalkylbenzoates, synthesis and mesomorphism 78−91243
2-aryl-3-benzylidenamino-4-thiazolidones, IR and NMR spectra, solvent effects and isomer conform. *(Italian)* 79−3596
arylbenzoxazols, lasing, excitation by excimer laser radiation 80−64007
1-arylbutadienes, lowest excited singlet states, photochemical implications 77−30795
3-arylcholest-2-enes and 3-arylcholest-3,5-dienes, synthesis and liq. cryst. props. 80−79689
N-aryliminophosphorane, XPS spectra, satellite lines obs. 78−37680
aryloxazols, lasing, excitation by excimer laser radiation 80−64007
N-arylsulphilimines, XPS spectra, satellite lines obs. 78−37680

organic compounds continued
ascorbic acid, action with perhydroxyl radicals, radiolytic study 80−35523
L-ascorbic acid, cryst. isolated OH iscillators, IR absorption, temp. and H-bond effects 80−7351
ascorbic acid adduct model systems, SCF calc., rel. to protein internal charge transfer 80−69072
ascorbic acid developer, lith development mechanism 80−77889
asparagine, polycryst., proton mag. relax. and mol. motion 78−20139
L-asparagine.H_2O, X-irrad. at room temp., ESR and ENDOR 77−40131
aspartic acid, complexation with Zn, free metal, ligand conc. determ. 79−87892
aspartic acid chelation with Zn(II), Cd(II) and Hg(II), US study 77−44464
aspartic acid racemisation and ^{14}C dating of Lake Ontario sediments 78−73415
asphalt, glass transition temp. and viscosity 79−77045
asphaltenes, from coal liquefaction, IR characterisation 77−52683
associated liquids, dielec. props. calc. 77−81045
astatotyronine and astato-iodotyronine, prep. and stability 80−55687
astaxanthin, aq. soln., aggregate, reson. Raman spectra, and IR spectra, exciton interactions 78−31770
astrochemistry, organic mols. prod. rel. to origin of life 78−73660
atactic polypropylene waste, pyrolytic conversion to fuel oil 80−35627
atebrin fluorescence photo-induced quenching and photosynthetic electron transport, pea chloroplast 77−56351
atmosphere organic compounds photooxidation, rates, reactivity and mechanism for reaction with OH radicals 80−72104
atmospheric aerosols, role of organic material 78−73464
atmospheric micropollutants in precipitation in Norway 78−36262
atom-pair interactions in molecules, semi-empirical MO calc. 80−915
ATP, association, spin label appl. 78−81086
ATP, chemiosmotic theory of manufacture in cells 78−61151
ATP, effect on Na-Ca and Ca-Ca exchange in squid axons 77−90745
ATP, phys. aspects of intracellular energy transform. 77−86462
ATP as energy source for Ca pump in squid giant axons 78−77043
ATP content meas. in single red blood cell, using firefly bioluminescent reaction with optical instrument 79−79695
ATP determination, extracellular, in native platelet-rich plasma 77−25615
ATP disodium salt, hydrated, vibr. assignments, force consts., coincidence method appl. 78−62953
ATP effect on Na pump activation by external cations in squid axon 78−35818
ATP hydrolysis by chloroplast ATPase, proton transfer from water to octane 77−36876
ATP measurement in single red blood cells using firefly biolum. reaction 78−48951
ATP synthesis, participation of free radicals 79−92183
ATP synthesis rel. to ADP induced mitochondrial absorbance changes 78−27908
ATP-actomyosin system kinetics, energy transform. anal. 77−81476
auramine O, fluoresc. efficiency, solvent viscosity effects at high press. 78−9188
auramine single crystal, lifetime and mobility of photogenerated charge carriers 78−2516
autonitrile, photolysis in solid Ar, CCN radical spectra 78−70868
autonitryl, electronic struct. and geometry, open-shell SCF calcs. 79−18106
aza-6-uracile, synthesis, computer simulation *(French)* 79−52653
aza-aromatic molecules, intersystem crossing, quantum interference effects 80−53037
aza-aromatic systems, luminescence, $AgNO_3$ heavy atom effect, donor-acceptor interaction *(German)* 78−84651
9-aza-bicyclo (3,3,1)nonan-3-one-9-oxyl, dimerisation, ESR, NO radical pair exchange 78−19330
2-azaanthracene and methyl derivatives, electron-vibr. props., UV spectra *(Russian)* 77−75177
2-azaanthracene in heptane, benzene and ethanol, max. intensity of fluoresc. on axis of cylindrical cell *(Russian)* 77−55814
azaarenes, presence in marine sediments 77−37181
azaaromatics, neutral and protonated, excited singlet and triplet states, charge densities, INDO calcs. 80−58152
azabenzene dimers, C, N, H atom-atom pot. parameters, dispersion energy calcs. 80−23489
azabenzenes, multipole moments, polarisabilities and long-range interaction coeffs. calcs. 79−89599
1-azacarbazole, IR spectra, Fermi reson., H-bonding *(German)* 77−12392
azacyclobutadienes, conjugated mols. electronic struct. and geometry, Hartree-Fock instability 80−69055
azaheterocyclic molecules, radiationless conversion processes, regularities 80−14171
7-azaindole, IR spectra, Fermi reson., H-bonding *(German)* 77−12392
7-azaindole dimers, photoautomerisation by double proton transfer, fluoresc. kinetics 80−11880
2-azanoradamantane N-oxyl, crystal-plastic transition, plastic crystal struct. exam. 78−2100
1-azaphenanthrene, aq. soln., proton transfer photoreaction kinetics, in singlet excited state 78−48671
1-azaphenanthrene H-bonded complex formation, enthalpy change due to electronic excitation, spectroscopic determ. 78−92496
azaphenanthrenes, lowest triplet state zero field splitting parameters calcs. 80−83391
azastilbenes, fluoresc., excitation energy anomaly, pot. energy model. 77−50466
azastilbenes, trans-cis photoisomerisation, theory 77−50466
azide salts, univalent, lattice energy, direct minimisation eqns. 77−62501
azides, in polymer matrices, photooxidation, rel. to crosslinking 80−66832
4-azido-2-nitrobenzyltriethylammonium fluoborate labelling of axon TEA binding sites 77−64026
aziridine, ab initio calcs., appl. of convergent SCF procedure 80−47875
aziridine, anhydrous and hydrated, inversion calc. 78−9272
1-aziridineethanol, mol. spectrum and hydrogen bonding 78−70820
aziridines, substituted, ^{14}N NQR, electron distribs. 77−3385
1-(2-N-aziridinoethyl)-4-vinylbenzene, polymerisation 79−39146
azo dye, photo-isomerising, voltage transients in lipid bilayer membranes 79−92166

organic compounds continued
azo dye sulphonates and analogs., aqueous solns., surface tensions 78−47641
azo dyes, cis-trans photochem. isomerisation 78−27785
azo dyes, photoanisotropy, effect on holographic reconstruction *(Russian)* 80−42290
azo dyes, tautomerisation, structs., laser Raman spectra 77−38672
azo dyes, UV-visible spectrophotometric 80−61207
cis-azo group, ionisation and excitation energies depend. on bond angle, ab initio MO calc. 79−72236
azo pigments, dispersions in flow system, nucleation and growth kinetics meas. 77−63967
1-azo-bicyclo-2,2,2-octane, multiphoton ionis. spectra polaris. characts., two-photon symmetry assignment 78−74718
azoalkanes, cyclic, quenching of 1,5-dimethylnaphthalene fluoresc., micelle system probe 80−35578
azoalkanes, fluoresc., solvent isotope effect 78−25591
azobenzene, derivatives, photoelectron spectra, ionisation pot., electronic struct. determ. 80−1024
azobenzene, emission from $^1(n,\pi^*)$ state, spectrum and ultrashort decay time 77−30895
azobenzene, foreign particle behaviour during growth 78−47264
azobenzene, parasubstituted derivatives, reson. Raman spectra *(French)* 79−59472
azobenzene, polarisability optical anisotropy 79−72441
trans-azobenzene, $S_2 \rightarrow S_0$ fluoresc. 80−28044
azobenzene, stoichiometric and catalytic reactions with Mo cpds. 77−86370
azobenzene, vapour press. meas, using torsion-weighing effusion apparatus 77−89530
azobenzenes, p-acryloyl- and p-methacryloyl-oxy-p′-substituted, monomers and polymers, liq. cryst. props. 79−99065
azobenzenes, substituted, isotropic, nucl. spin-lattice relax. 79−23519
azobilirubin, form., fast reaction vidicon-based spectrometer obs. 79−21817
azoethane, in hydrocarbon glass, 77K, photoisomerisation, matrix memory effect, quantum yield 78−7213
azoethane, pyrolysis, master eqn. for rate coeff. 78−48612
azomethane, steric strain relief accompanying isomerisation 79−10230
azomethane, trans-cis isomerisation, INDO-SCF and CI calc. 78−25440
azomethane+OH, rate const. meas. 80−7771
azomethine compounds, nonaromatic, photoelectron and far UV absorpt. spectra 77−58079
azomethines, photochromic, intramol. proton phototransfer sensitisation, organic cation energy transfer 78−53230
p-azotoluene-azulene, order parameters and lattice energy, mean field approx. 78−22688
p-p′-azoxy di-n-undecyl α-methylcinnamate, smectic C layer thickness meas. by X-ray scatt. 78−94986
azoxy-4,4′(di-undecyl α-methyl cinnamate), refr. index at 2nd order smectic A to C phase transition 79−19357
azoxy-4,4′-(di-undecyl α-methylcinnamate), smectic A to smectic C phase transition, optical tilt angle meas. 78−95141
p-azoxyanisole, depend. of phase transition temp. on thickness 78−26669
p-azoxyanisole, directed crystn. in elec. and mag. fields 80−107052
p-azoxyanisole, nematic eqn. of state, incorporating short-range orient. order. 77−55237
p-azoxyanisole, orientated in nematic liq. crysts., UV-visible dichroism meas. *(German)* 77−34668
4,4′-azoxyanisole, temp. depend. of refractive indices in nematic phase 79−47410
azoxybenzene, nematic liq. crystal, elastic consts., varying mag. field and temp. 78−18540
azoxybenzenes, nematic, mag. susceptibility, orientational order parameter 78−34426
azoxybenzenes, nematic, refr. index, birefringence, internal field 78−34427
azoxybenzenes, p-acryloyl- and p-methacryloyl-oxy-p′-substituted, monomers and polymers, liq. cryst. props. 79−99065
azoxybenzenes, substituted, isotropic, nucl. spin-lattice relax. 79−23519
azoxyphenetole, deuterated, cryst. and mol. struct. 79−86782
p-azoxyphenetole, single cryst., deuterated, phonon dispersion curves, inelastic neutron scatt. obs. 80−84261
azulene, electron excitation, electron resonance, triplet states 79−54976
azulene, induced circular dichroism of π-π^* bands in presence of (+)-nopinone 80−53058
azulene, multiphoton ionisation, mass spectra 80−63717
azulene, nonradiative relax. lifetime of first excited singlet state, subpicosecond optical technique 78−78741
azulene, picosecond dynamics 77−30896
azulene, resonance Raman spectrum 77−10677
azulene, ring currents hypersusceptibilities calcs. 80−102588
azulene, Shpol'skii matrix, $S_2 \rightarrow S_1$ fluoresc., spectral anal. 77−18956
azulene, soln., laser-excited $S_2 \rightarrow S_1$, $S_1 \rightarrow S_0$ emission and $S_2 \rightarrow S_n$ absorption 79−10131
azulene($-d_8$), ultrafast $S_2 \rightarrow S_0$ internal conversion 79−3474
azulene in cyclohexane, relax. time of first excited electronic singlet state 77−6825
azulene in naphthalene, reson. Raman and reson. fluoresc. spectra, 30K 78−80323
azulene in naphthalene mixed cryst., $S_2 \rightarrow S_1$ fluoresc., vibr. anal. 78−66586
azulene vapour, IR and CO_2-laser absorpt. spectra 80−87120
azulene-fluoranthene, soln., triplet energy transfer, delayed fluoresc. study of $S_2 \rightarrow S_0$ 80−23331
azulenes, substituted, internal conversion, energy gap correl. 79−54901
(2,2) (2,6) azulenophanes, mag. circular dichroism and anomalous fluoresc. spectra 80−83398
azuleno[5,6,7-cd]phenalene, slow internal conversion between close lying singlet state 77−30907
B-group vitamins in aqueous systems, radiation protection 79−2006
bacteriochlorophyll, photochem. oxidised, kinetics of dark reduction, R. rubrum chromatophores 77−25390
bacteriochlorophyll, R. rubrum reaction centres, selective ps laser excitation in condensed phases 79−48217
bacteriochlorophyll a, bacterial photosynthesis primary electron transfer processes, psec. dynamics 78−80841
bacteriochlorophyll a, stimulated fluoresc. and fluoresc. quenching, pump photon density 78−27895
bacteriochlorophyll cation in soln., N atom ENDOR and proton triple resonance 78−96018

organic compounds continued
bacteriochlorophyll monolayer quantum yield and image contrast in photoelectron microscopy 78−44453
bacteriochlorophyll P870, photo-oxidised, dark reduction kinetics, temp. depend. 77−36888
bacteriopheophytin, bacterial photosynthesis primary electron transfer processes, psec. dynamics 78−80841
bacteriorhodopsin, Debye rot. relax. times, modulation excitation spectrophotometric obs. 79−3532
bacteriorhodopsin, selective ps laser excitation in condensed phases 79−48217
bacteriorhodopsin emission lifetime, using picosec. meas. method 77−17009
bacterioviridin, photochem. oxidation mechanism 77−25370
bacterioviridine photo-oxidation in monomer and aggregated states, free radical form, EPR 78−76994
barbiturates, ^{14}N NQR freq. at 77K 77−43900
barium acid oxalate, lacunary phase, thermodynamic and crystallographic characts. 79−55731
barium beauvuricin complex, appl. of cryst. struct. refinement technique based on fast Fourier transform algorithm 78−91197
barium formate, γ-irrad., ESR of free radicals 79−65737
barium formate, cryst., Raman scatt. 79−4804
barium formate, nonlinear optical susceptibility tensor, Maker fringes 78−13751
barium margarate film, thickness influence on dielec. loss meas. 77−81051
barium methylsulphonate, X-ray powder cryst. data 80−59451
barium oxalate, lacunary phase form., morphological and kinetic characts. 79−60299
barium palmitate film, thickness influence on dielec. loss meas. 77−81051
barium stearate, in MIM struct., internal voltage work function meas. 79−82684
barium stearate, in MIM struct., thickness depend. of internal voltage 77−72920
barium stearate, in MIM symmetric junction, internal voltage due to Al_2O_3 film on electrodes 79−78202
barium stearate film, between Al electrodes, intrinsic voltage 78−72277
barium stearate film, in Al/(Al_2O_3)-BaSt/Sn struct., internal voltage temp. variation 80−20326
barium stearate film, low energy electron range meas. using radioisotope Auger electrons 80−70257
barium stearate film, thickness measurement using Talbot effect 78−9321
barium stearate in MIM struct., diode characts. obs. 77−4449
barium stearate multilayer films on EDF glass, interference colours, thin film thickness step gauge 77−5900
barium stearate single-layer Langmuir films, elastic and inelastic tunnelling 80−80403
barium titanyl oxalate exam. of chemical production and thermal dissocation *(German)* 79−4935
bases, biologically important, and derivatives, optical crystallographic props. 78−3449
basketene, electron diffr. determ. of struct. 78−37764
BBOA:Sn-BBA, liquid crystal glass, unresolved Mossbauer quadrupole doublet, orientation depend. 77−84645
BBOA, polymorphism, radiothermoluminescence and differential scanning calorimetric study 80−24570
BBOA, pretransitional shear viscosity divergence near smectic A-smectic B transition 79−33077
BBOA, smectic B phase, containing 4 ferrocene derivatives, ^{57}Fe Mossbauer study 78−27136
BBOA, smectic B phase, fluidlike mol. dynamics, Raman scatt. study 80−20630
BBOA, smectic liq. cryst. glass-supercooled transition and Debye temp., ^{57}Fe Mossbauer effect 80−54999
BBOA, thermal diffusivity meas. by forced Rayleigh scatt. 78−76483
BBOA, uniaxial, polarized Raman scatt., orientational order 77−76296
BBOT, time-depend. fluoresc. depolarisation, mol.-rot., slip boundary conditions in soln. 78−9179
BBOT dye, vapour phase, optical props. *(Japanese)* 80−9879
BCNU-modification of in vitro X-ray response of rat brain tumour cells 77−70498
benezene, vapour press. meas, using torsion-weighing effusion apparatus 77−89530
Bengal pink-anthracene, mixed annihilation delayed fluoresc. 80−74193
bent molecular organic crystals, electron diffr. intensities 80−100132
benz-1,2, anthracene, nonlinear third-order electric susceptibility 78−74944
benzalaniline, polarisability optical anisotropy 79−72441
benzalazine, thermal expansion, lattice consts. meas. 78−47539
benzaldehyde, and deuterated forms, in p-xylene, 4.2K, $n\pi^*$ phosphoresc. assignments 78−9197
benzaldehyde, and isomeric phthalaldehydes, dipole moments meas., config., ab initio MO calc. 80−58410
benzaldehyde, and substitution products, spectral props. 79−27007
benzaldehyde, electronic spectra, Cl and F substitution effects 80−23456
benzaldehyde, in polymer matrix, dielec. absorption, Eyring parameters 79−4761
benzaldehyde, $n\pi^*$ and pi pi* triplet states, props., SCF calcs. 77−6695
benzaldehyde, photoionisation mass spectra formation by UV laser radiation *(Russian)* 80−93781
benzaldehyde, photomag. positronium quenching, spin conversion 77−31030
benzaldehyde, PPP limited CI calcs. 79−31406
benzaldehyde, prereson. Raman effects, intensity enhancement mechanism 78−42069
benzaldehyde, proton affinity, MINDO/3 results compared to ICR obs. 78−1103
benzaldehyde, Stark effect on electron spin transition in zero-field 77−27099
benzaldehyde, transition energies, oscill. strength, time-depend. Hartree-Fock model *(Spanish)* 77−6684
benzaldehyde, wavefront reprod. obs. by stimulated Brillouin, Raman scatt. 80−53369
$^3\pi\pi^*$benzaldehyde, zero field splitting and sublevel decay rates, deuteration and host effect 80−37750
benzaldehyde+F, HF IR chemiluminesc., vibr. and rot. energy disposal 77−86318
organic compounds continued
benzaldehyde derivatives, Raman intensities obs., phenyl ring-carbonyl group conjugation 78−29792
benzaldehyde gas, nonradiative electronic transition 80−83413
benzaldehyde in methylcyclohexane, $n^3\pi^*$ spectra 80−63627
benzaldehyde in toluene glass, quasi-line phosphoresc. spectra 77−69883
benzaldehyde molecules, photoionisation mass-spectrometry with excimer KrF laser 80−95691
benzaldehyde-biacetyl system, self-quenching and electronic energy transfer obs. 80−5571
benzaldehydes, in mixed cryst., T_1/T_2 interstate interactions, modulation polaris. phosphoresc. spectra, 4.2K 78−9185
benzaldehydes, o- and m-substituted fluoro- and chloro- forms, rot. isomerism, $n\pi^*$ spectra obs. 80−5631
benzaldehydes, para-halogenated, IR and Ramam spectra, vibr. assignments, thermodynamic functions 80−14139
benzaldehydes in EBBA liq. cryst., NMR, mol. struct., reorientation and order matrix 78−5251
benzamide, single cryst., far i.r. absorpt. spectrum *(French)* 77−4637
1,2-benzanthracene, monomer and excimer fluoresc. in soln., triplet-triplet annihilation and mag. field depend. 78−78738
1,2-benzanthracene, secondary reson. radiation and hot energy transfer, soln. luminesc. 80−87167
1,2-benzanthracene in polystyrene films, delayed luminesc. decay kinetics 80−43088
1,2-benzanthracene in soln., luminesc. and vibr. relax. 79−52007
benzazoles, liq. cryst., prep. and transition temp. 77−27811
benzene:I_2, charge transfer spectra line shape 79−78700
benzene:tetra-n-butylammonium bromide, electroviscous effect, AC characts. 79−99341
benzene, 1036 cm^{-1} band, optical consts. correction 77−61145
benzene, 260 nm absorpt. spectrum, band contours, vibr. ang. mom. components 79−13736
benzene, 260 nm absorpt. spectrum, band maxima positions and intensities 79−13735
benzene, 260 nm absorpt. spectrum, vibronic anal. 79−13737
benzene, 50000 cm^{-1} band, electron impact study 79−86075
benzene, 607-μm line absorption curve 78−95581
benzene, ^{13}C substituted, mass selective two-photon ionis., mass spectroscopy obs. 80−9651
benzene, $^1A_{1g}\rightarrow{}^1B_{2u}$ absorption band, Franck-Condon factors calc. 79−36701
benzene, $^1B_{1u}$ state, vibronic mag. rot. strengths and oscill. strengths, CNDO/S calcs. 77−34670
benzene, $^1B_{2u}(\pi\pi^*)$-$^1A_{1g}(6_0^1)$ band, in supersonic jet, rot. anal. 79−31578
benzene, $^1B_{2u}$ and $^3B_{1u}$ states nonradiative decay, collisional deactivation 77−6819
benzene, $^1B_{2u}$-$^1A_{1g}$ transition, vibronic coupling, Duschinsky effect 77−88439
benzene, ^1H chem. shift tensor, proton mag. shielding anisotropy 78−19348
benzene, $-d_0-d_8$ vapour at low press., intersytem crossing and internal conversion, press. depend. of triplet form. 77−30918
benzene, γ-irrad., radical pairs EPR detection 78−31664
benzene, γ-radiolysis, phenyl radical intermediate, spin trapping, EPR 78−7218
benzene, $\pi\pi^*$ and Rydberg bands, cryogenic solvent effects 78−55182
benzene, π electron system, excitation energy, appl. of MBPT 80−52876
benzene, π face bonding of cyclobutadiene 79−98180
benzene, ab initio model calc., variational 77−46492
benzene, ab initio non-paired spatial orbital wavefunction, π-electron correl. energy 77−54509
benzene, absolute Raman intensities determ. 77−68046
benzene, absolute Raman scatt. cross-sections for totally symm. modes 80−102510
benzene, adsorbed at metal surface, obs. of vibrational modes 80−6649
benzene, adsorbed layer on graphite, spreading press. 77−15692
benzene, adsorbed on γ-alumina, high-temp. IR spectra *(German)* 79−28757
benzene, adsorbed on Al_2O_3, Raman spectroscopy study 80−65358
benzene, adsorbed on Ni and Pd surfaces ang. distrib. of photoemitted electrons 77−69968
benzene, adsorbed on porous vycor glass, adsorpt. spectrum 80−9615
benzene, adsorbed on Pt(111), electronic energy losses 79−46931
benzene, adsorbed on Pt (111) surface, Auger spectra 79−52077
benzene, adsorbed on silica, laser Raman spectra 77−3367
benzene, adsorpt. on H-mordenite *(German)* 79−90892
benzene, adsorption on $Co(OH)_2$, $Ni(OH)_2$, $Cd(OH)_2$ and $Cr(OH)_3$ 79−66343
benzene, adsorption on exfoliated graphite, −70 to −5°C *(French)* 79−33177
benzene, adsorption on graphitized C black, exptl. determ. of models 78−6216
benzene, adsorption on Ir (110) surface 78−38961
benzene, adsorption on Ir (111), electronic transitions sensitivity to molecule-surface orientation, energy loss spectra 80−45184
benzene, adsorption on Pt (100) surface 77−59216
benzene, adsorption on W, isothermal ramped field desorption technique 79−82450
benzene, and -d_6, $^1B_{2u}$ excited state, force field, normal coords. 78−5193
benzene, and aza-substituted derivatives, out-of-plane vibrs. force field 77−83572
benzene, and derivatives, Jahn-Teller instability 79−47062
benzene, and deuterated analogues, electronic relax. process, energy depend., book contrib. 77−34688
benzene, and deuterated forms local mode oscill. strengths 79−27039
benzene, and methyl derivatives, $^1E_{1u}$ N-V state mag. moments, MCD obs. 80−23575
benzene, and methyl derivatives, chemisorpt. on Fe, MO LCAO calcs. 77−52674
benzene, and substituted forms, thermodynamic ionis. energy, rel. photoionis. energy 77−16858
benzene, appl. of new force field for condensed aromatics, mean amplitudes and freqs. 79−81201
benzene, Ar and Kr matrix isolated, IR spectra, vibr. freqs. and intensities 78−50548
benzene, benzene-d_6, thermal cond., 300-600K 78−63528
benzene, benzene-d_6, vibrational anharmonicity, condensation effect, vap. press. isotope effect 78−58657
benzene, benzene-d_6 soln. excess thermodynamic props. 78−53245

organic compounds continued
benzene, binary mixture with cyclohexane and tetrachloromethane, ultrasonic velocity, compressibility, heat capacity, at 298.15K 79−10898
benzene, Brillouin scatt., cryst. at 0°C, elastic consts. 78−43882
benzene, bromination on zeolite adsorption complex, Raman spectroscopic anal. 80−16670
benzene, C K-shell excitation by electron impact, electron energy loss spectra 77−31014
benzene, C-H stretching overtones, thermal lensing spectrosc. obs. 79−35851
benzene, cation radical, charge exchange reagent appls. 78−70929
benzene, charge and current densities, valence bond technique 77−3261
benzene, chem. shielding tensor obs. using proton-enhanced ^{13}C reson. in He-cooled probe 80−17978
benzene, chemisorbed on Ni catalyst, Raman and vibr. spectra 80−108747
benzene, chemisorbed on Pd (100), angle-resolved photoemission symm. anal., polarisation depend. and lateral interactions 79−91568
benzene, chemisorbed on W(100), decomp., UPS and thermal desorpt. obs. 80−59782
benzene, chemisorpt. on Ni(100) and (111), LEED and high resoln. electron energy loss spectra 78−6224
benzene, chemisorption and reaction on Ir(100), geometric and electronic effects 77−21421
benzene, chemisorption on (111) surface of Pt, LEED and Auger spectroscopy obs. 78−30823
benzene, chemisorption on Ir (100), geometric and electronic effects 77−55457
benzene, chemisorption on Ir surface, LEED, AES and thermal desorption meas. 77−1297
benzene, chemisorption on Ni (111) and (100), vibr. EELS study 80−39436
benzene, chemisorption on Pt (100), LEED, AES, UPS and temp. programmed dehydrogenation exam. 77−55456
benzene, coherent anti-Stokes Raman spectra in UV 77−46567
benzene, coherent polarisation spectroscopy of Raman scatt. 78−13758
benzene, complex refractive index meas. at mm and sub-mm wavelength 77−82595
benzene, corrected valence force field, force constants calc. 80−63868
benzene, correl. problem, open-shell coupled-cluster approach, PPP calc. 79−81157
benzene, Coulombic energy calcs. 79−99104
benzene, critical heat flux of saturated natural convection boiling with heating from below 80−10114
benzene, cryst., IR and Raman intensity of lattice vibrs., theory 80−11381
benzene, cryst., IR spectrum assignments rel. to benzene Br_2 complex 77−36217
benzene, cryst., molecular exciton cluster states and spectra 77−66123
benzene, cryst., orthorhombic, lattice energy and cell dimensions, spheroidal approx. 79−51041
benzene, cryst., press. depend. of nuclear spin-lattice relax. time 79−28635
benzene, cryst., vibronic spectra using 2-photon fluoresc. excitation 79−47493
benzene, crystal, inelastic coherent neutron scatt., phonon spectra 78−51629
benzene, crystalline, press.-vol.-temp. relations 78−22819
benzene, crysts., Raman and two-photon reson. in three wave mixing 79−38538
benzene, d_3, -d_6, vibr. freqs., force consts., CNDO/2 calcs. 77−65449
benzene, deep oxidation on Al-Pt catalyst, kineti model depend. of reaction rate 77−90583
benzene, density meas. using flexible capillary 80−98886
benzene, depolaris. Rayleigh scatt., optical anisotropy 78−27245
benzene, depolarisation ratios 77−32387
benzene, derivatives, calc. of second-order susceptibility, using electronic spectra data 80−29756
benzene, deuterated, neutron diffraction by electron LINAC 79−50974
benzene, deuterated and chemisorbed on glass, vibr. bands, Raman scatt. study 80−84737
benzene, deuterated mixed crysts., phonon assisted trap-trap triplet energy migration, 0K limit, phosphoresc. obs. 77−48218
benzene, dielec. const. meas. using 3-terminal meas. cell 78−21170
benzene, dielectrophoretic heat transfer in liquids 78−94874
benzene, diffusion coeff. meas., Fourier transform NMR, pulsed field gradient system 80−57353
benzene, diffusive motion on graphite basal planes, neutron scatt. study 79−42385
benzene, dipole polarisability, finite-field SCF MO calcs. 80−83255
benzene, doubly charged ion fragmentation, ion kinetic energy spectrum peaks, collision gas sensitive 80−40679
benzene, doubly degenerate high-resolution rot.-vibr. Raman bands 79−6941
benzene, droplet vaporisation in moderately-high temp. stationary media, Chang model 78−34609
benzene, dynamic polarisabilities, calcs., superposition method of excited config., nonstationary perturbation theory eqns. 80−69257
benzene, elec. breakdown mechanism, high speed photography expts. 79−91367
benzene, elec. dipole forbidden states, high resolution electron impact obs. 80−43195
benzene, electrification during laminar flow in metal pipe 80−6954
benzene, electron diffraction cross-section, finite scatt. geom. in mol. beam expt. 78−74803
benzene, electron energy loss, Monte Carlo anal. 77−31703
benzene, electron impact, electronic energy levels, (below 7 eV) obs. 78−17807
benzene, electron impact dissoc. excitation, H_α and H_β Balmer line intensities 77−10778
benzene, electron impact-induced generalised oscill. strength, 400 eV, 500 eV, momentum change depend. 78−1088
benzene, electronic struct., mag. susceptibilities, ab initio calcs. 78−74571
benzene, electronic struct. calc. using free-electron orbitals basis set 77−79537
benzene, epitaxial film, on metal (111) substrates, surface struct., LEED obs. 79−86969
benzene, equation of state studied using statistical theory results 80−84276

organic compounds continued
benzene, ethylene, and fluorinated derivatives, photoelectron ang. distribs. of C-C π electrons 79−10146
benzene, excitation spectra, cluster configuration method appl. 80−78546
benzene, excited electronic states, variable angle electron impact spectroscopy 78−13612
benzene, excited state props., by electrochromism in polymer matrix 79−22737
benzene, extinction coeff. in 4.6-36 eV range 78−86877
benzene, Faraday spectrum, sign rel. to mag. field strength *(German)* 77−36204
benzene, film boiling from cylindrical surfaces 79−23194
benzene, film condensation inside pipes, heat transfer, general correlation 79−46312
benzene, first-ionisation Rydberg spectrum assignment via John-Teller splitting 80−69155
benzene, fluoresc., triplet state and isomerisation yields, photochem. 77−1942
benzene, fluoresc. quantum yield in soln., dipole-dipole interaction 78−25598
benzene, fluoresc. quenching by pulsed proton irrad. of cyclohexane soln. 78−5270
benzene, fluoresc. triplet state and isomerisation yields, low vibr. levels 79−64035
benzene, force const. calc., resonance integral distance depend. 77−88443
benzene, force constants, local mode approx. 77−71791
benzene, free convection heat transfer in tube at supercrit. press. 78−42518
benzene, frozen liquids, high-resolution ^{13}C NMR using magic angle spinning 79−33544
benzene, FSGO calcs. of orbital energies locations, dipole moments, charge distribs. 77−67976
benzene, gas, liq. and crit., cation mobility 80−48842
benzene, gaseous, critical and liquid, electron transport 80−64673
benzene, graph theory for axial symmetry molecules *(Chinese)* 79−36792
benzene, ground, singlet and triplet states, ab initio VB STO, GTO calcs. 77−75060
benzene, ground state props., coupled cluster and MBPT methods appl. 80−47881
benzene, H^+ chemical shifts, extended Huckel calcs. with gauge in variant atomic orbitals 80−102449
benzene, He ion stopping cross sections, ring struct., bond strain and Bragg rule deviations 79−98188
benzene, heat transfer to ascending (descending) streams, near-crit. press. 77−65742
benzene, high order stimulated Raman scatt. *(Chinese)* 79−81206
benzene, high press. Brillouin scatt., hypersonic speed 77−48182
benzene, high resolution AC coupled Raman spectra 79−40619
benzene, high-order stimulated Raman scatt. obs. *(Chinese)* 80−45053
benzene, hypersound propagation temp. depend., Mandelshtam-Brillouin spectra meas. 78−31210
benzene, in benzene-d_6 soln., IR and Raman spectra, line breadths, rot. diffusion consts. 79−56772
benzene, in Br_2-carbon tetrachloride soln., complex form., IR spectra 78−70828
benzene, in inorganic frozen solns., structured phosphoresc. spectra 77−65504
benzene, in liquid binary mixtures of optically anisotropic molecules, depolarized Rayleigh scatt. 80−40122
benzene, in polar solvent, excess thermodynamic props., Rayleigh scatt. meas. 78−52523
benzene, in rigid hydrocarbon soln., laser-induced refractive index transients 79−87411
benzene, intersystem crossing mechanism, rate consts. 77−65497
benzene, intramol. nonradiative transitions, Franck-Condon principle at high energies 77−14478
benzene, intramolecular vibr.-electronic conversion, relative rate calcs. method 77−65496
benzene, ionis. spectral intensity, valence electron binding energy depend. 78−90234
benzene, ionisation by electron bombard., empirical and semi-empirical calcs. 79−36784
benzene, ionised, H atom scrambling, SCF calcs. 77−9062
benzene, IR spectra, fine struct. of rot.-vibr. bands 80−102504
benzene, IR spectra, vibr. exciton cluster states, percolation and pairwise interactions 78−43844
benzene, IR spectrum deconvolution beyond the Doppler limit 80−86467
benzene, isothermal compressibility 78−47461
benzene, isothermal ramped field desorption on W surface 79−90870
benzene, isotope-mass effects in self-diffusion 80−92695
benzene, isotopic mixed crysts., triplet excitation energy transfer theory 77−28611
benzene, isotropically mixed crysts., singlet and triplet exciton percolation theory 78−26818
benzene, Jahn-Teller active states, vibronic struct., vibr. perturbation, spectral obs. 78−13440
benzene, Kerr const., elec. field distrib. *(Russian)* 77−63395
benzene, laser breakdown, photoacoustic and photohydrodynamic parameters 78−52597
benzene, laser wavefront reconstruction by stimulated scatts. in picosecond range 79−986
benzene, LCAO-MO-SCF calcs., MODPOT, VRDDO and MODPOT/VRDDO procedures 77−71742
benzene, liq., Brownian reorientation barriers *(Russian)* 79−27901
benzene, liq., C-H stretch vibr. overtones, optoacoustic spectrosc. obs. 79−93982
benzene, liq., elec. current decrease due to electrode coverage form. 77−8108
benzene, liq., ion injection obs. 78−63870
benzene, liq., laser pulsation kinetics, optical damage effects 80−58614
benzene, liq., light scatt. coeff. determ., absolute method 78−2868
benzene, liq., mol. motion at high press. 80−103509
benzene, liq., nonlinear third order optical susceptibility *(German)* 79−50358
benzene, liq., sound velocity between 283 and 463K, up to 62 MPa 79−55827
benzene, liq., spectral broadening of mol. transitions, librational broadening 79−51939
benzene, liq., stimulated Raman scatt. 78−29172

organic compounds continued
benzene, liq., two-photon spectra, $^1E_{2g}$ state 79−11431
benzene, liq., vibr. excitons, reson. energy transfer and local struct., IR spectra 77−75145
benzene, liq., visible region absorpt. spectra, overtones meas. 80−78625
benzene, liq. and adsorbed mol., Raman spectra using pulsed laser and gated detection 77−74529
benzene, liquid, C-H stretch, seventh harmonic, absorption profile 79−56806
benzene, liquid, high-speed schlieren studies of elec. breakdown 77−89332
benzene, liquid, numerical exam. of neutron quasielastic scattering 78−9938
benzene, liquid, polarised light two photon thermal blooming near UV spectra 80−66216
benzene, liquid, under high press., refr. index vs. density 79−28712
benzene, liquid, visible absorpt. expt. using wavelength-modulation spectroscopy 78−24868
benzene, liquid and gaseous, total cross section meas. for cold neutron interactions 79−99055
benzene, LMO population calc. method appl., from given SCF eigenvector matrix 80−14063
benzene, local mode combination bands and local mode mixing 80−27999
benzene, location of $^1B_{2u}$, $^1B_{1u}$, $^1E_{2g}$ states, from two-photon spectra 77−30940
benzene, low concs. in air, determ. by gas chromatographic method *(German)* 80−21429
benzene, low lying $^1A_{2u}(\sigma,\pi^*)$ and $^1E_{2g}(\pi,\pi^*)$ states, Raman line intensities 78−78709
benzene, Lowdin orthogonalisation procedure, rel. to orbital localisation procedures 79−6848
benzene, lowest triplet state, pulse radiolysis obs. 79−39168
benzene, luminesc. yield spectra in VUV 79−36685
benzene, magneto-optic rotatory dispersion curves 80−45040
benzene, mass spectra following reson. enhanced multiphoton ionisation 80−106362
benzene, matrix fluoresc. spectra, rel. intensities of multiplet components 79−54882
benzene, mean amplitude of mol. vibration, approx. calc. method 79−13697
benzene, mean free path meas., US relax. 80−59585
benzene, melting temp. and latent heat 79−55869
benzene, microwave line width and quadrupole moments, perturbation theory 80−69190
benzene, mixed deuterated crysts., triplet energy transfer mechanism 77−16365
benzene, mol., directional Compton profile, ab initio SCF LCAO MO calc. 78−62857
benzene, mol., spectral line shape, vibr. overtone lineshape 79−27040
benzene, mol. beam, fragmentation by reson. enhanced multiphoton ionisation 79−54213
benzene, mol. cryst., quadrupole contribs. to lattice vibr. freqs. 79−82290
benzene, mol. cryst., reson. four-wave mixing, third order susceptibilities 80−100654
benzene, mol. cryst., US absorption, rel. to lattice vibrs. 77−24358
benzene, mol. cryst. $S_0 \rightleftharpoons S_1$ transition, non-Born-Oppenheimer phonon coupling 77−15523
benzene, mol. hyperpolarisability meas. by optical SHG 79−22861
benzene, mol. reorientationally disordered phases, thermodynamics 79−46782
benzene, mol. semiempirical RPA calc. using PPP Hamiltonian, triplet instability 79−26893
benzene, mol. transilicon consignment, two-photon gas-phase spectra 77−54582
benzene, molecule translational mobility in depolarised Raman spectra 80−14150
benzene, mono-substituted, MCD, CNDO/S calcs. using capable ang. momentum operator 77−46587
benzene, monohalogenated, orientation in lyotropic surfactant soln., NMR 77−28456
benzene, monosubstituted, dipole moments, isomerisation and H bonding, INDO calcs. 77−54515
benzene, monosubstituted, ring protonation and C_{1s} binding energies, STO-3G calc. 79−29336
benzene, multiphoton ionis. spectra polaris. characts., two-photon symmetry assignment 78−74718
benzene, multiphoton ionisation fragmentation patterns, statistical theory 80−95693
benzene, multiphoton ionisation mass spectra 80−57420
benzene, nanosecond laser photolysis 80−66825
benzene, negative ion states and π-electron affinity 79−10206
benzene, noncrossing and degeneracy in Hubbard models 80−14096
benzene, nonlinear acoustic coeff. determ. *(French)* 77−1175
benzene, nonplanar vibr., force field calcs. 79−41148
benzene, normal coord. calcs., simplified valence force field models 78−94229
benzene, normal vibr. anal. 78−13487
benzene, ns time-resolved emission spectra, collisional processes 77−3490
benzene, nucleate boiling heat transfer, press. factor 77−69080
benzene, optical consts. determ. from IR absorpt. spectra *(Spanish)* 77−69787
benzene, optical Kerr const., electronic and orientational contribs., obs. by coherent Raman techniques 77−88874
benzene, optoacoustic spectroscopy, weak visible absorpt. spectra, pollution monitoring in liquid phase 79−58797
benzene, optoacoustic spectroscopy using cell with ultimate corrosion resistance 80−42269
benzene, out-of-plane mol. vibrs., force field approx. calcs. 80−91538
benzene, overtone spectrum, intramol. lineshape narrowing 79−45705
benzene, p-disubstituted, MCD and absorpt. spectra, PPP calcs. 78−66574
benzene, P-V-T relations, 5-300 MPa and 323-683K range 77−69069
benzene, partially ordered solid, NMR line shape, orientational distrib. 78−35048
benzene, Penning electron and photoelectron spectra, relative intensities comparison 79−81237
benzene, phase transform. process, energy-dispersive X-ray diffractometry 80−96631
organic compounds continued
benzene, phosphoresc., radiative and non-radiative decay routes, spin sublevel origin 77−58064
benzene, photoelectron and optical spectra, occupied virtual orbital energies and eigenvalue ordering, CNDO/S calc. 77−61796
benzene, photoelectron ang. distrib. with linearly polarised HeI radiation 78−50580
benzene, photoelectron spectra, HAM/3 MO calcs. 78−13414
benzene, photoelectron spectra ang. distrib., π- and σ-orbital assignments 79−818
benzene, photoexcitation, triplet factor group states assignment 77−85741
benzene, photoionis., vibr.-excited ions form. in Franck-Condon gaps, threshold photoelectron spectra obs. 79−68262
benzene, photoionisation, appl. of valence electron spectroscopy using polarized He I radiation 77−492
benzene, photoionisation mass spectra formation by UV laser radiation *(Russian)* 80−93781
benzene, photoluminesc. at 5K, N_2 and inert gas matrices 77−6838
benzene, plasma polymerisation in glow discharge, thin film IR and free radical EPR obs. 80−2964
benzene, polarisability, CNDO calcs. including polarisation functions in the basis set 79−6891
benzene, polycrystalline heteronuclear dipolar modulated chemical shift spectra, geometrical and orientational obs. 77−20750
benzene, prereson. Raman scatt. of overtones in μV 79−59471
benzene, proton chem. shift, chem. substitution influence, LCAO perturbation method 77−68064
benzene, protonated, electronic struct., SCF MO LCAO calcs. 78−82638
benzene, quadrupole moments, elec. field-gradient birefringence method 80−95746
benzene, Raman and IR intensity anal. 78−70829
benzene, Raman and IR spectra at high press. 78−35127
benzene, Raman laser as efficient excitation source for stimulated Raman scatt. 79−18480
benzene, Raman nonlinearity characterisation by two-beam interferometry 77−38986
benzene, Raman scatt. cross sections 79−6945
benzene, refr. index temp. depend., deviation from Lorentz-Lorenz formula 77−40200
benzene, reson. Raman cross sections, forbidden electronic transitions, depolaris. ratios 78−42075
benzene, reson. Raman effect in gas, liq., and solid phases 79−31531
benzene, resonance-enhanced multiphoton ionis. and fragmentation of mol. beam 79−100411
benzene, ring currents hypersusceptibilities calcs. 80−102588
benzene, rot. motions and cryst. growth, Monte Carlo calcs. 79−46577
benzene, Rydberg series, second ionis. process assignment, vibronic coupling 77−42333
benzene, S_0-S_1 transitions, two-photon absorpt. spectra by nozzle beam-multiphoton ionisation method 80−63728
benzene, S_1 state, mode to mode vibr. energy flow, low pressure fluorescence spectra exam. 78−25664
benzene, saturable absorpt. of CO_2 laser 80−69465
benzene, SCF-EHT polarisability calc. 80−47895
benzene, schlieren method for the determination of electric field distributions in dielectrics 80−31720
benzene, second order CARS, dispersion curves 78−58707
benzene, secondary ion reactions, branching ratios 78−40035
benzene, self-diffusion coefficients determ. by gel sectioning technique 80−92694
benzene, self-diffusivity data 78−6169
benzene, semiempirical CNDO calcs. of electronic struct. and absorpt. spectra 78−995
benzene, single crystals, Brillouin spectra, elastic consts. and intermol. pot. 79−42977
benzene, single vibronic level decay rate, analytical representation 77−79645
benzene, single vibronic level fluoresc. after two-photon excitation 77−6818
benzene, solid, double-quantum cross-polarization in solids 80−100623
benzene, solid, electron transmission, 0 to 15 eV, reson. structs. 79−87536
benzene, solid, electronic struct., comparative ESCA study of polyacenes 78−52631
benzene, solid, electronic struct., XPS 77−73213
benzene, solid, fluoresc. decay times and quantum yields, rel. to vap. phase 80−55154
benzene, solid, ion implantation, chem. effects 80−55635
benzene, solid and isolated in rare-gas matrices, spectroscopic study 79−3455
benzene, soln., fluoresc., quenching in pulsed proton and alpha particle irrad., radiation quality effects 80−66259
benzene, soln., light deflection, near crit. point, due to gravitational effect 78−2818
benzene, sorption on hydrated Ce_2O_3 rel. to dehydration conditions 79−66345
benzene, static polarisability, ab initio SCF wave functions 80−74106
benzene, stimulated diffusion induced by two photon absorption *(French)* 78−90455
benzene, stimulated Raman scatt., anti-Stokes components, class II radiation cones 80−28276
benzene, substituted benzenes, liq., Kerr effect in UV region, mol. optical anisotropy dispersion 78−72488
benzene, substituted cations, spectroscopy, substituent effects 78−58709
benzene, substituted cations, spectroscopy, substituent effects 78−58710
benzene, superheated liquid, growth of spherical bubbles, anal., numerical calcs. 77−24399
benzene, SVL fluoresc. band intensities, Franck-Condon factors, Fermi reson. 77−10700
benzene, symmetry forbidden transitions in MCD and electronic spectra 77−65494
benzene, T_1-S_0 intersystem crossing vibronic interactions IR absorpt. spectrum obs. 80−28042
benzene, tables of thermodynamic props. 77−24419
benzene, thermal cond., heat capacity, 105-375K, up to 2.4 GPa 79−90839
benzene, thermal cond. and heat capacity, meas. under press. 79−90796
benzene, thermal expansion at high press., near melting 79−77777
benzene, thermal lensing effect, absorptivity meas. at 607 nm 80−34900

organic compounds continued
benzene, third channel decay mechanism, radiationless transitions 77−50463
benzene, third-order nonlinear electric susceptibility, from CNDO wavefunction 78−37558
benzene, topological resonance energy, rel. to cyclobutadiene 80−5462
benzene, torsion, one-electron props. variation, electronic and nuclear components partitioning 77−83491
benzene, total neutron cross sections for subthermal energies 78−74779
benzene, totally symm. bands, high resolution rot.-vibr. Raman spectra 78−70838
benzene, totally symmetric rot.-vibr. Raman bands 79−59474
benzene, trifluoromethyl derivatives, first ionis. pots., CF_3 group nature 79−27110
benzene, two photon absorptivity, ion cyclotron reson. photodissoc. spectra, CNDO/S-CI-perturbation theory 80−74123
benzene, two-photon ionis. of mol. beam, mass spectrometer ion source 79−27118
benzene, two-photon molecular spectra using two synchronised tunable dye lasers 77−34783
benzene, unlabelled and ^{13}C labelled PMR, oriented in liq. crysts., r_α struct., solvent effects 79−94017
benzene, unoccupied orbitals, excitation energy, electron affinity, HAM/3 MO calcs. 78−13415
benzene, UV fluoresc. quantum yield, photoacoustic technique 77−88595
benzene, UV laser photolysis, electronic 3-wave mixing spectra of transient fragments 79−68223
benzene, UV photoelectron spectra, valence electron shake up approx. methods 80−18788
benzene, UV two-photon absorpt. relative to known Raman cross section 79−81487
benzene, valence electron spectra, vibr. band struct. 77−23520
benzene, van der Waals interaction energy calc., perturbation theory, MO LCAO method 77−42373
benzene, vapour, flow calorimeter, meas. of isothermal Joule-Thomson coeff. 79−58688
benzene, vapour, solubility in polystyrene *(Japanese)* 80−59667
benzene, vapour, thermal conductivity, 300-700K 78−38444
benzene, vapour, transport coeffs., theoretical study 77−3904
benzene, vapour press., 5-80°C, isotope effects 78−59939
benzene, vapour-flow calorimetry 78−91058
benzene, vapour-phase, absolute fluoresc. quantum yields, nonradiative processes 77−6829
benzene, variable angle electron impact energy loss spectra 79−68321
benzene, VB calc. with CI, basis sets orthogonality problem 77−23435
benzene, vib. relax. and Raman line widths 77−32359
benzene, vibr. freqs., MINDO/3 calcs. 78−13429
benzene, vibr. relax. in soln., ν_1 C-H stretching band Raman spectra 78−25540
benzene, vibronic coupling and IR intensities, CNDO/S semiempirical calc. 79−36596
benzene, visible absorpt. spectra, local mode overtone intensity of C-H stretching mode 79−81207
benzene, visible and UV photoionisation and fragmentation 80−69195
benzene, X-ray photoelectron spectra, C 1s shake-up struct., PPP CI calc. 78−42126
benzene, zero- and four-photon NMR coherence, selective excitation 80−23439
benzene+acetone, energy transfer cross-sections, generalised oscill. strength calcs. 79−10173
benzene+benzene, potential well depth estimation method 79−86034
benzene+benzene-d_6, electronic energy transfer between vibronic levels, fluoresc. obs. 77−38712
benzene+bromomethane, microwave line width and quadrupole moments, perturbation theory 80−69190
benzene+CO, vibr. energy transfer, quenching efficiency 79−3539
benzene+cyclohexane, excess enthalpy, calorimetric cell 79−58689
benzene+Hg, electronically excited, mol. fluoresc., vibr. relax. cross sections and equilibration rates determ. 80−87205
benzene+$Li^+(Mg^+)$, relative level excitation, orbital ang. momentum quantum number depend. 78−25688
benzene+molecular ion, fragmentation and electron transfer collisions 79−79229
benzene+$O_2(^1\Sigma_u^-)$, photo-oxidation mechanism, optoacoustic determ. 77−12808
benzene+$O(^3P)$, absolute reaction rate consts., 299-440K 79−70304
benzene+$O(^3P)$, phenol radical prod., crossed mol. beam investig. 80−71902
benzene+$O(^3P)$, reaction product identification by mass spectrometer 78−7185
benzene+OCS (methyl bromide), spectral line broadening, quadrupole moment meas. 77−6848
benzene+OH, cross mol. expt., product anal., 300K 78−44353
benzene+$Si^+(SiH^+)(SiH_3^+)(SiD_3^+)$, energy-rich collision complex form. 77−9068
benzene(−d_6), prereson. Raman effects, intensity enhancement mechanism 78−42069
benzene(−d_6) vapour, SVL fluoresc. lifetimes and quantum yields 77−10701
benzene(-cyclohexane), second virial coeff. meas. using new apparatus 80−44289
benzene(-d_1,d_2,d_4), two-photon $^1B_{2u}\leftarrow{}^1A_{1g}$ spectrum, deuterium effect 80−32788
benzene(-d_6), in Ar-Kr matrices, phosphorescence decay, external heavy atom effect 79−10132
benzene(-d_6)-tetracyanoethylene, excited charge transfer state nonrad. decay, vibrs. role 78−82765
benzene(substituted)-n-alkane mixtures, mol. orientation correls., depolarised Rayleigh scatt. 79−22714
benzene ($^1B_{2u}(S_1)$)+Ar(benzene), rot. relax. to Boltzmann distrib. 78−86936
benzene (deuterobenzene), adsorpt. on Ag colloids, surface enhanced Raman spectra obs. 80−97251
benzene (S_1)+OCS, V-V reson. energy transfer, microscopic reversibility, level degeneracies role 79−86045
benzene adsorbed on graphite, melting and orientation, NMR study 80−100403
benzene adsorbed on Pt(111) and Ni(111) surfaces, vibr. loss spectra 79−23838
benzene and deuterates, highly vibr. excited intramolecular V-V transfer, visible and photoacoustic spectra 80−32729
organic compounds continued
benzene and its monohalogen derivatives, intermolecular nucl. relax. by translational and rot. diffusion, effect of pair correl. functions *(French)* 79−19794
benzene and monosubstitutes, hyperpolarisabilities, perturbed INDO calc. 79−68189
benzene aqueous hetero-azeotrope mixture, condensation heat transfer coeff. *(German)* 80−33425
benzene binary liquid mixtures, US study of mol. interaction 77−15494
benzene cation, internal energy selected, dissoc. dynamics 79−66274
benzene cation+benzene, trapped ion mass spectra 80−89470
benzene chemisorbed on Raney Ni, struct., neutron inelastic spectroscopy study 80−101038
benzene chromophore orientation in micellar, liposome solns., liq. cryst. phases, dichroism, NMR 79−53059
benzene complex with $AgClO_4$, heat capacity 78−75843
benzene cryst., electron irrad., phenylcyclohexadienyl radical form., absorpt. and fluoresc. spectra study 80−89035
benzene derivatives, atomic localisation of electronic excitation 77−18806
benzene derivatives, carbon tetrachloride dil. soln., electrooptical quantities, ellipsoidal cavity model *(French)* 78−35114
benzene derivatives, mol. electrostatic pot., approx. evaluation 80−58337
benzene derivatives, solid, phase transition under press., IR spectra 79−38531
benzene derivatives, symmetrically substituted, IR spectra, high press. solid-state phase transform. 77−43984
benzene dimer, mol. beam elec. deflection obs. 79−72336
benzene excimer, nanosecond laser photolysis 80−66825
benzene filled capillary fibres, stimulated Raman scattering spectra 78−66869
benzene film, on metal substrate, surface struct. using LEED 79−77879
benzene film, vacuum UV absorpt. spectrum, 1100-2500 Å, effect of deposition temp. 78−23542
benzene free and coordinated mols., X-ray and X-ray electron spectra 77−27087
benzene glow discharge, junction barrier, inelastic electron tunnelling 77−72916
benzene in 3-methylpentane glass, phosphoresc. polarisation and intensity, 77K 77−46588
benzene in CCl_4, weak 607nm absorpt. band obs. by optoacoustic spectroscopy 79−35855
benzene in dilute cyclohexane solution, fluoresc. quenching on pulsed proton irrad., temp. depend. 80−21307
benzene in PMA and PEA, penetrant diffusion, statistical mech. model 80−44352
benzene in rare gas matrices, photoelectron energy distrib. 79−10147
benzene in solid rare gas matrix, effect of surface on phosphorescent state 77−88489
benzene in solution, CW coherent Raman gain spectrum 78−58057
benzene in solution, rotational motion, Raman study 80−44104
benzene in Xe-doped solid Ne, luminesc. 77−32416
benzene liqs., refractive index, pressure effect 80−71375
benzene liquid, two-photon absorption spectra and cross-section meas. 79−82993
benzene liquid core in hollow quartz fibre, stimulated Raman scatt. 78−30087
benzene liquid multiphoton ionisation polarisation experiments, molecular symmetry 79−98162
benzene liquid-filled waveguide, generation of enhanced CARS signals 79−89961
benzene molecule, slow electron scattering, resonances to 1.1 and 1.7 eV 77−58181
benzene molecules, bound positrons, time spectrum of positron annihilation 78−42248
benzene molecules, photoionisation mass-spectrometry with excimer KrF laser 80−95691
benzene monosubstituted derivs., light scatt. obs. of orientational pair correls. in anisometric molec. liq. 77−36252
benzene monosubstitutes, hyperpolarisabilities, perturbed INDO calc., substituent effects, σ-π contributions 79−68190
benzene p-dihalides, IR absorpt., intermol. reson. interaction, temp. depend. 78−72506
benzene p-dihalogen derivatives, electron-vibr. spectra *(Russian)* 79−89686
benzene peroxide+dibenzylsulphide in atactic polymeric medium, reaction kinetics *(Russian)* 77−21362
benzene phenol crystal, asymmetry of phonon side bands, absorption, luminesc. and specular spectra 77−1730
benzene radical anion, ab initio MO calcs., struct. 79−18113
benzene radical cation in solid Ar, fluorescence spectra obs. 80−83382
benzene refractive index temp. depend., differential photoelectro-optical refractometer 77−40202
benzene soln., stimulated Raman scatt., self-focusing, rel. to Kerr const. *(German)* 79−61355
benzene soln., UV Raman scatt., forbidden states 78−9155
benzene solutions, liq. and solid, positron and positronium annihilation 77−1152
benzene submonolayer on silica gel, PMR and DMR dynamics and surface heterogeneity 79−69735
benzene sulphonyl hydrazine, in nonpolar solvent, thermodynamics of dipolar relax. 79−91347
benzene triplet state, self quenching, effect on naphthalene internal conversion rate estimate 78−25586
1,3,5-benzene triyltris (1,5-diphenyl-3-verdazyl), rot. diffusion in nematic phase, EPR spectra 77−36135
benzene vapour, four-wave sum mixing near 163 nm 77−10970
benzene vapour, slow neutron scatt., effect of pressure total interaction cross section 78−17273
benzene with 2,2-diethoxypropane, excess enthalpy *(French)* 78−11542
benzene X-ray diffr. pattern and liq. models using C-H group scatt. factors 78−6004
benzene-^{13}C, liq., vibr. spectra, band assignments 78−13500
benzene-acetone donor-acceptor pair, energy transfer cross sections rel. to generalised oscill. strengths 78−46452
benzene-acetone-chloroform ternary liq. mixture, US vels. rel. to interactions 77−69044
benzene-acridine orange, Raman spectra using pulsed laser and gated detection 77−74529
benzene-air combustion products for CW gasdynamic laser, gain values 77−75494

organic compounds continued
benzene-alcohol (n-alkane), liquid mixtures, excess free vol. US vel. meas. 77−51294
benzene-aniline gas mixture, fluoresc. spectra, lifetimes, yields, electronic energy transfer 77−14477
benzene-Ar, conc. profile and interdiffusion coeffs. meas. 79−94763
benzene-benzene (anthracene) diiners, ground and excited states, EHT calc. 79−36553
benzene-$Br_2(Cl_2)$ π-σ complexes, low freq. spectra 78−78713
benzene-Br_2 charge transfer complex, Raman spectra, bending modes, electronic excited states 78−56485
benzene-Br_2 complex, cryst., IR spectrum assignments, site symmetry, rel. to benzene 77−36217
benzene-carbon tetrachloride, mixture, mol. and Raman scatt., profile shape, conc. depend. 77−58025
benzene-carbon tetrachloride-cyclohexane system at atmospheric pressure, isobaric-liquid equilib. data 79−46793
benzene-carboxylic acid derivatives bound to Tb^{3+}, emission intensity 79−18230
benzene-chlorobenzene, benzene-toluene, perfect binary liquid mixtures on silica gel, adsorption thermodynamics 80−44428
benzene-chlorobenzene, liquid system, rough hard spheres treatment of tracer diffusion 78−87798
benzene-chloroform mixture, reorientational motion and intermolecular interaction by Raman spectroscopy 77−24839
benzene-CS_2 mixture, third-order nonlinear susceptibility ratio by CARS 78−46713
benzene-cyclohexane, adsorbed onto silica gel from soln. 79−23826
benzene-cyclohexane, liquid system, rough hard spheres treatment of tracer diffusion 78−87798
benzene-cyclohexane, solution, self-diffusion, capillary cell meas. 78−34637
benzene-cyclohexane, vap.-liq. equilibria 78−30745
benzene-cyclohexane(carbon tetrachloride), binary liq. mixtures, molar heat capacity isothermal compressibility 79−66328
benzene-cyclohexane (methane) vapour mixture, excess enthalpy meas. appl. of differential-flow mixing calorimeter 78−12700
benzene-cyclohexane mixing enthalpy, using isothermal dilution calorimeter 77−41615
benzene-cyclohexane mixture, excess vol., indirect meas. 77−29032
benzene-cyclohexane mixture, interference between Raman resonances in four-wave difference mixing 77−23712
benzene-cyclohexane system, vap. press., excess free energies, isotope effects 78−59939
benzene-cyclohexane system, vap. press., isotope effects, theory 78−59940
benzene-cyclohexane-butanol, evaluation of US vel. 80−38201
benzene-cyclohexane-ethanol, evaluation of US vel. 80−38201
benzene-cyclohexane-methanol, evaluation of US vel. 80−38201
benzene-d_0, -d_6, electronic relax., absorpt. spectra 77−75129
benzene-d_0, -d_6, in glass matrix, phosphoresc. lifetime and polarisation, rot. relax. time meas. 77−79648
benzene-d_0, -d_6, intramol. vibr. energy relax. calcs. 78−33574
benzene-d_0, -d_6, vapour absorpt. spectrum, band intensities meas. 79−81212
benzene-d_0,-d_6, $^1B_{2u}$ excited states, high resolution two-photon spectra 77−506
benzene-d_0,-d_6, phosphoresc., Boltzmann population and spin-lattice relax., decay processes 78−31230
benzene-d_0(-d_3)(-d_6), vibronic coupling, hot band absorpt. spectra 78−58708
benzene-d_0(-d_6), radiationless triplet decay, non-Condon effects 80−83405
benzene-d_0(-d_6)+$I(^5P_{1/2})$, fluoresc. quenching, spin-orbit interaction, isotope effect obs. 78−62763
benzene-d_0 (-d_6), polar tensors and at. effective charge, calculated from IR intensity 78−74703
benzene-d_0-d_6, pre-reson. Raman effect and vibronic coupling 77−83604
benzene-d_1, ^{2}H NMR spectra, vibr. and asymmetry corrections to quadrupole coupling consts. 80−74184
benzene-d_1, (-d_2)(-d_3), oriented, order, D nucl. quadrupole coupling, mag. reson. spectra 78−74683
benzene-d_3, gas phase Raman spectrum, E′ and E″ species, Coriolis consts. *(French)* 78−5235
benzene-d_5, C-H vibr. states, thermal lensing spectra, local mode model test 77−71812
benzene-d_6: (benzene, pyrazine), disordered, exciton migration, dynamical approach 79−65916
benzene-d_6:benzene-d_0, phonon side bands of specular optical transitions 78−26649
benzene-d_6, deuteron NMR spin echo, time domain spectrum 78−88223
benzene-d_6, high resolution rot.-vibr. Raman spectra 79−64006
benzene-d_6, intermol. dynamics, neutron scatt. obs. 79−863
benzene-d_6, liq., Raman spectra vibr. relax. and band widths 78−23440
benzene-d_6, liq., reorientational motion, Raman obs. 78−70841
benzene-d_6, NMR double-quantum spin decoupling 78−88227
benzene-d_6, solubilization in hexadecyltrimethylammonium bromide aq. soln., D NMR 78−24015
benzene-d_6, splitting of vibrationless level in Jahn-Teller active state of D_{2h} symmetry 77−58080
benzene-d_6+CO, vibr. energy transfer, quenching efficiency 79−3539
benzene-d_6+N_2+CO_2, electronically excited, mol. fluoresc., vibr. relax. cross sections and equilibration rates determ. 80−87205
benzene-d+$O(^3P)$, phenol radical prod., crossed mol. beam investig. 80−71902
benzene-deuterate benzene cryst., triplet migration, cluster method 79−73510
benzene-Dewar benzene, lower excited states pot. energy surfaces for isomerisation 80−104429
benzene-diazonium salts, absorption band *(Ukrainian)* 79−78001
benzene-doped inert gas crystal, luminescence excitation investig. 77−77276
benzene-doped inert gas solid, excitons and energy transfer processes 77−69886
benzene-doped rare gas crystal, photoelectron emission, exciton states 77−44116
benzene-ethanol, excess vol. and isentropic compressibility, from density and US vel. meas. 78−79776
benzene-ethanol-$(NH_4)_2SO_4$-H_2O, tricritical mixture, light scatt. 79−15473
benzene-ethanol-water, shear viscosity at plait points 77−35685
organic compounds continued
benzene-ethanol-water-$(NH_4)_2SO_4$, liq. mixture, near tricrit. pt., thermodynamic model and sum rules 80−34196
benzene-ethylacetate triethylamine mixture, US absorption, 7.56 MHz 77−39630
benzene-ethylene dichloride (-CCl_4), liq. mixture, excess Gruneisen parameter, intermol. interaction 78−67635
benzene-ethylene glycol-sodium dioctylsulphosuccinate emulsion, effect of added water on stability 78−40082
benzene-fluorobenzene system, phase transitions, Raman spectra 79−91449
benzene-H_2N_2 gas ternary diffusion coefficient obs. *(Japanese)* 79−10626
benzene-hexa-n-alkanoates, disc like mols., highly ordered lamellar liquid crysts. 78−14279
benzene-hexa-n-alkanoates and benzene mixture, disc-like mesogens, thermotropic mesophases 79−86699
benzene-hexa-n-alkylanoates, disc-like molecules, miscibility studies of mesophases 80−19696
benzene-hexa-n-hexanoate, phase transitions and mesophase form., sp. ht. and IR spectra, 13 to 393K 80−79955
benzene-hexafluorobenzene, liq., mol. interactions 80−28907
benzene-hexafluorobenzene, mixtures, dielectric relax. and US absorpt. 77−12307
benzene-hexafluorobenzene, mol. beam elec. deflection obs. 79−72336
benzene-hexafluorobenzene mixture, percolation model of electron and hole mobility 80−29452
benzene-I_2, π-σ charge-transfer complex, frozen soln., Mossbauer spectra obs. 80−91655
benzene-I_2, binary soln., charge transfer spectrum 78−90183
benzene-I_2 mixture, N_2 and Ar matrix isolated magnetic circular dichroism spectrum 80−5567
benzene-methyl carbonate, binary liq. soln., surface cluster functions 78−67631
benzene-n-alkane mixtures, mol. orientation correls., depolarised Rayleigh scatt. 79−22714
benzene-n-decane-n-tetradecane, molar enthalpies of mixing *(German)* 79−42253
benzene-n-dodecane mixtures, excess surface tension calc. and theories of solns. 78−91508
benzene-n-heptane, excess vol. and isentropic compressibility, from density and US vel. meas. 78−79776
benzene-n-heptane, liquid system, rough hard spheres treatment of tracer diffusion 78−87798
benzene-n-heptane-n-tetradecane, molar enthalpies of mixing *(German)* 79−42253
benzene-n-hexane, liquid system, rough hard spheres treatment of tracer diffusion 78−87798
benzene-n-hexane mixtures, excess surface tension calc. and theories of solns. 78−91508
benzene-nitrobenzene, liq., stimulated Raman scatt., intensity changes, selective excitation 78−13753
benzene-p-dioxan, mixtures, mol. reorientation and assoc., depolarised Raman scatt. obs. 80−7341
benzene-p-xylene, excess vol., enthalpies, Gibbs free energies 80−44335
benzene-p-xylene (p-dioxan) liq. mixture, excess energy of vaporisation, US study 80−65209
benzene-polystyrene, semidilute solns., viscosity and reptation time 79−99345
benzene-S systems, liq.-liq. phase separation 80−96658
benzene-similar liquids, US attenuation in 10 to 1300 MHz range 80−39229
benzene-sodium tetraethylaluminate-donor two-phase system, Na^+ ion solvation number 78−95987
benzene-TCNE, charge transfer theory, Mulliken population, ab initio calc., multiconfiguration scheme 80−106392
benzene-tetrachloroethylene binary mixtures, dielec. polarisations 79−56713
benzene-tetrahydrofuran, soln., excess thermodynamic props. and interactions, US vel. and density meas. 80−39288
benzene-toluene, perfect binary liquid mixtures on silica gel, adsorption thermodynamics 80−44428
benzene-toluene, solution, self-diffusion, capillary cell meas. 78−34637
benzene-toluene and benzene-o-xylene mixtures, US vels., compressibility, expsn. coeff. 79−33038
benzene-toluene system, vapour-liquid equilib. meas., automatic gas chromatographic anal. *(German)* 78−88667
benzene-toluene-n-tetradecane, molar enthalpies of mixing *(German)* 79−42253
benzene-triethylamine mixture, US absorption, 7.56 MHz 77−39630
benzene-water-ethanol-$(NH_4)_2SO_4$, liq. mixture, near tricrit. pt., light scatt. and sum rules 80−34933
benzene/benzene-d_6, cryst., X-trap phosphoresc., ODMR, 1.3K, triplet state struct. 77−20902
benzene/cyclohexane reversible chemical reaction systems for thermal energy transport 80−67009
benzened$_0$:phenol, phonon side bands of specular optical transitions 78−26649
benzenediazonium compounds, structure-property relationships, quantum chemical calcs. 79−22605
benzenes, 1,4-disubstituted, ^{13}C NMR spectra, chem. shift, substituent effects 77−14456
benzenes, adsorbed, IR multiple refl. spectra recording via cuvette attached to spectrophotometer 78−298
benzenes, di- and mono-substituted, NMR spectral data, aromatic proton chemical shifts 77−79632
benzenes, disubstituted, monosubstituted, effect of bonding electrons on molecular dimensions as determ. by X-rays 79−7595
benzenes, IR spectral intensity for electro-optical parameter 79−54835
benzenes, isomeric substituted, viscosity near freezing pt. 79−51292
benzenes, lowest triplet states, instability rel. to environmental effects 77−57893
benzenes, m-disubstituted, nonlinear optical props. 77−58373
benzenes, monosubstituted, ^{13}C NMR chem. shifts 79−42850
benzenes, monosubstituted, high resoln. ^{1}H coupled ^{13}C NMR, INDO calcs. 77−50457
benzenes, monosubstituted, NMR, high resolution, automated anal. by computer program DAVINS appl. 80−63669
benzenes, monosubstituted and related cpds., He(I) photoelectron ang. distrib. 79−18236

organic compounds continued
benzenes, nitrohalide substituted, microwave absorpt., mol. struct. 78−75522
benzenes, para-disubstituted, liq., 2nd order hyperpolarisabilities, regularities, intramol. charge transfer 79−10353
benzenes, substituted, average mol. polarisability, δ-function calcs. 77−551
benzenes, substituted, C-C coupling consts., coupled Hartree-Fock calcs. 77−27091
benzenes, substituted, CH wag group freqs., CNDO/2 calcs. 77−6745
benzenes, substituted, cryst., reorientation motion, site models with non-equivalent sites, dielec. relax. 79−11382
benzenes, substituted, dense liq., mol. reorientation and shear viscosity 77−4213
benzenes, substituted, dielectric absorpt. and NMR 78−88251
benzenes, substituted, dihydroxy, electronic structure, photoelectron spectra and ab initio MO calculations 79−49937
benzenes, substituted, electronic struct., ab initio calcs., photoelectron spectra 80−58314
benzenes, substituted, electronic structure, photoelectron spectra and ab initio MO calculations 79−49937
benzenes, substituted, fluoroderivatives, electronic structure, photoelectron spectra and ab initio MO calculations 79−49937
benzenes, substituted, gaseous, negative ion states, electron transmission spectra 77−31007
benzenes, substituted, liq., optical nonlinearities and hyperpolarisabilities meas. 77−88857
benzenes, substituted, methyl-derivatives, electronic structure, photoelectron spectra and ab initio MO calculations 79−49937
benzenes, substituted, optical bond anisotropies, by depolarised Rayleigh scatt. 78−90171
benzenes, trisubstituted, dil. solns., relax. mech., Debye relax. times 78−80744
benzenes, trisubstituted, UV aborpt. spectra 79−36660
benzenes, trisubstituted, valence force fields, normal modes of planar vibrations *(French)* 78−37626
benzenes-1-octanol (5-methylheptanol-3)(acetic acid) dilute solns., dielec. consts., dipole moments, H bonding investig. 77−48673
benzenesenol, CCl_4 soln., PMR, barrier to internal rot. 78−1006
benzenoid aromatics, triplet zero field splitting parameters, ODMR obs., struct. effects 80−78636
benzenoid hydrocarbons, atom numerical code scheme for classification of chemical shifts 78−94205
benzenoid hydrocarbons, normal coord. calcs., simplified valence force field models 78−94229
benzenoid hydrocarbons, reson. energy calcs. 78−70762
benzenoid hydrocarbons, triplet state decay, kinetic spectroscopy, 220-250 nm 78−62820
benzenoid system intercalation with AsF_5, EPR, NMR and X-ray diffr. obs. 80−19775
benzenoid-o-quinoidal systems, valence isomerisation, EHT calcs. 77−77757
benzidine, cryst. struct. and lattice energy 79−37694
benzil, cryst., excited triplet state spin-lattice relax. probabilities, temp. depend. *(Russian)* 80−88860
benzil, cryst., phosphoresc. kinetics rel. to spin-lattice relax. 79−87485
benzil, crystallographic study of solid-solid phase transition *(French)* 78−55939
benzil, ENDOR study of geom. struct. of lowest triplet state 79−89696
benzil, ENDOR study of phase transition 79−73855
benzil, excited electronic states; conformational relax., time resolved matrix isolation spectral obs. 80−32701
benzil, free radical adducts, organometallic group dynamic migration, EPR 77−58049
benzil, heat capacity near phase transition 78−2250
benzil, high temp. ODMR obs. of cryst. phases 79−38407
benzil, in PMMA glass, luminesc. temp. depend. matrix controlled photorotamerism 79−22743
benzil, NMR of cryst., 77-367K 79−38387
benzil, optical activity and circular dichroism 79−61328
benzil, phase transition, far IR spectroscopy meas. 80−71407
benzil, phase transition study be simultaneous Raman-scatt. and domain-struct. investigations 79−60504
benzil, structural transition model, cryst. symm. spontaneous strain components 80−2161
benzil cored fibres, void-free cryst. growth, X-ray diffr. and optical microscopy study 80−71586
benzil crystals, mol. triboluminesc. meas. 80−40172
benzil crystals, triplet state spin-lattice relaxation, zero field magnetic resonance spectrometer analysis 79−97409
benzil triplet-anisole, reversible exciplex form., phosphorescence, photostationary and transient obs., simulation 78−9182
benzil X-trap, ODMR, near planarity in triplet state 77−32295
benzil-benzene, dil. soln., thermodynamic equilib., ebulliometric investig. 78−18752
benzilnitrile intermolecular interaction, band contour exam. *(Russian)* 79−808
benzimidazole, electronic struct., photoelectron spectra and MO calcs. *(French)* 79−31598
benzimidazole, excited states, solvent interactions, fluoresc. obs., rel. to chromophore 78−37670
benzo(a)-pyrene, separation and struct. resolution by thin layer chromatography-mass spectrometric meas. 78−7270
benzo(a)phenazine diaza derivatives, excited singlet and triplet states, charge density, INDO calcs. 80−58152
benzo(a)pyrene, determ. in water using spectrofluorimetry 80−7997
benzo(a)pyrene, distrib. with respect to particle size in submicron atm. aerosols 79−74563
benzo(a)pyrene, effect on cell morphologic transform. induced by UV irrad. 77−1981
benzo(a)pyrene, pollution of lake sediment, western USA 80−61476
benzo(a)pyrene and C black combined aerosol form., rel. to air pollution and health hazards 78−80796
3,4-benzo-1,6-methano(10)-annulene, mol. geom. and gas phase thermodynamic props., minimisation scheme 78−78829
benzoate derivatives, m-cyano or m-halogeno synthesis and mesomorphic props. 78−1990
benzoate/benzotriazole mixture, for corrosion inhibition of Fe in ethanediol/water soln., synergistic effect 80−45425
n-benzoates, MP and rot. mobility of struct. groups *(Russian)* 77−69074
organic compounds continued
benzocondensed five-membered heterocycles continuing S and O, optical anisotropy, depolarised Rayleigh scatt. obs. *(French)* 79−31533
1,2-benzocoronene, phosphoresc. and ODMR meas. 79−18220
benzodiazepine, autoradiographic localisation of receptors in brains of humans and animals 79−83752
1,3-benzodioxole, far IR spectrum anal., pot. function 79−76427
1,3-benzodioxole, geometry electronic absorpt. spectra 80−971
benzoic acid, adsorption on Al_2O_3, benzoate ion binding energy 79−60629
benzoic acid, and p-deuterobenzoic acid, sensitivity of inelastic electron tunnelling spectroscopy 77−88605
benzoic acid, chemisorbed layers, electron beam damage, tunnelling spectra obs. 77−76672
benzoic acid, diffusivities in water 79−73328
benzoic acid, dimer, cryst., IR and Raman spectra, vibr. assignments 78−31191
benzoic acid, dissolution, mass transfer at vibr. spheres 80−57220
benzoic acid, ENSH method of oriented thin film growth 79−99443
benzoic acid, in acidic solns., room temp. fluoresc. 78−50568
benzoic acid, IR absorpt. spectra, fundamental assignments 80−5542
benzoic acid, single cryst. growth from nitrobenzene-water immiscible system 80−40244
benzoic acid, single cryst. growth using zone melting furnace 79−52110
benzoic acid, spectral shift due to electron-repelling substituents 79−72362
benzoic acid, struct. refinement at room temp. 80−96502
benzoic acid, transition energies, oscill. strengths, time-depend. Hartree-Fock method *(Spanish)* 77−6684
benzoic acid, used to test adiabatic heat capacity small sample low temp. calorimeter with automatic data acquisition system 78−12697
benzoic acid inhibitor film on Fe, passivation and inhibitor props., X-ray photoemission spectroscopy exam. 78−88561
benzoic acid-dioxan solns., compressibility, internal press., US vol., H-bonding 79−82272
benzoic acid-water, liquid fluidised bed, mass transfer at low Reynolds number 78−9698
benzoin containing system, photosensitized free radical polymerisation 80−7825
benzol, liq., dark conductivity obs. *(Russian)* 77−55560
benzol, liq., thermal cond. coeffs. at high-press., 298-573K 79−73350
benzol, monohalide-substituted, electrical model of conductivity *(Russian)* 77−8101
benzol surface tension, AC field influence calc. comparison with exptl. data *(Russian)* 77−55417
benzol-paraffin, solid-liq. mixtures, phase equilib., Wilson eqn. *(German)* 79−42245
benzonitrile, 198K, cryst. struct. *(French)* 78−51524
benzonitrile, anodic polymer growths during electrical breakdown conditions, TEM study *(French)* 78−75960
benzonitrile, depolarised Rayleigh scatt. 78−68522
benzonitrile, excited single state B_1, electron-vibr. spectra and electronic struct. 79−26904
benzonitrile, field depend. ^{13}C NMR spin-lattice relax. and anisotropic mag. shielding 79−76450
benzonitrile, HCN elimination, ion kinetic energy spectrum peaks, collision gas sensitive 80−40679
benzonitrile, hexane and CCL_4 solns., nonlinear dielec. effect 79−78602
benzonitrile, intermolecular interaction, band contour exam. *(Russian)* 79−808
benzonitrile, IR absorpt. and Raman bands, half-band width conc.-depend. 80−74171
benzonitrile, LCAO-MO-SCF calcs., MODPOT, VRDDO and MODPOT/VRDDO procedures 77−71742
benzonitrile, transverse sound wave and mol. motion, light scatt. obs. 77−79621
benzonitrile, vibronic spectrum, semiempirical method 80−43031
benzonitrile-isooctane mixture, dielec. const. near consolute point, temp. and freq. depend. meas. 80−71292
1,12-benzoperylene, in heptane, Stokes and anti-Stokes fluoresc., transition moment 77−61781
1,12-benzoperylene, in n-paraffin solns., quasiline spectra, press. effects *(Russian)* 77−68053
1,12-benzoperylene, phosphoresc. in solid matrix, electronic transition multiplets 77−3413
1,12-benzoperylene in n-alkane, zero-phonon lines in luminesc. spectra 78−56512
3,4-benzophenanthrene, dual fluoresc. (S_1, S_2), collision-free conditions 79−45741
benzophenone: diphenylmethylene, mixed cryst., emission and absorpt. spectra, 2-30K_2 exciton-phonon coupling 79−99900
benzophenone, $^3(n\pi^*)$, carbonyl ^{13}C hyperfine coupling tensor, ENDOR obs. 79−13744
benzophenone, and d_{10}, ODMR and phosphorescence spectra in organic matrix 79−36671
benzophenone, aqueous system, LET depend. of transient yields in deuteron and alpha pulse radiolysis 77−63940
benzophenone, charge carrier generation and mobility 78−84231
benzophenone, cryst., charge carrier generation by exciton-exciton collisions 80−88568
benzophenone, cryst., phosphoresc. spectra and decay time, temp. depend. 79−87479
benzophenone, fluoresc. quenching and intermol. intersystem crossing, nonlinear press. depend. 78−25603
benzophenone, high resolution ODMR and optically detected ENDOR 79−19811
benzophenone, in DDE at 2K, vibr. overtone characterisation and local modes by emission spectroscopy 79−89682
benzophenone, in o-terphenyl soln., dielectric absorp. studies, molecular relax. 78−95544
benzophenone, laser spectroscopy by cascade photoionisation method in mass spectrometer 80−99496
benzophenone, lowest triplet state, ODMR spectra, D- and g-tensors 77−75191
benzophenone, melt growth kinetics, determ. using IR radiometric microscope 78−34453
benzophenone, metastable triplet state, SCF CI calcs. 79−54776
benzophenone, migration of triplet excitons, EPR profiles and phosphoresc. decay data 80−84641
benzophenone, mol. fluoresc., intensity of decay rel. to laser irrad. intensity 78−82772

organic compounds continued
benzophenone, molecular nonsteady-state luminesc. behaviour under narrowband laser excitation 80−87159
benzophenone, propag. of longit. and shear hypersonic waves, light scatt. meas. 77−51442
benzophenone, sensitised crosslinking, polymerisation, UV curing, IR investig. 78−35709
benzophenone, triplet, optically detected EPR, ENDOR and ODMR, HFS, isotope and spin-orbit effects 78−86898
benzophenone, triplet exciton absorpt. lines 79−38563
benzophenone, triplet state in organic cryst., ENDOR spectra for spin density 79−64021
benzophenone, triplet state zero-field ODMR, ^{17}O HFS 79−18216
benzophenone, vap., laser-excited long-lifetime luminesc. 79−54887
benzophenone, vapour press. meas, using torsion-weighing effusion apparatus 77−89530
benzophenone $^3(n,\pi^*)$, and isotopic forms, in 4,4′-dibromodiphenylether, level anticrossings, ODMR obs. 78−2772
benzophenone betyl radical, photochem. yield mag. field effect on spin rephasing, double-pulse technique 77−90615
benzophenone containing system, photosensitized free radical polymerisation 80−7825
benzophenone in cyclohexane dilute soln., far IR absorption obs. 77−40250
benzophenone in isopropanol, submicrosecond time resolved EPR, lser photolysis, CIDEP polarisation mech. 78−80764
benzophenone in toluene glass, quasi-line phosphoresc. spectra 77−69883
benzophenone ketyl radical, in micelle, decay rate in mag. field, photolysis meas. 80−85154
benzophenone L in dibromodiphenylether, benzophenone triplet state, nanosecond resolved ODMR, freq.-agile techniques appl. 80−34825
benzophenone soln., stimulated Raman scatt., self-focusing, rel. to Kerr const. *(German)* 79−61355
benzophenone vapour, fluoresc. and phosphoresc., nonradiative transitions between triplet and singlet state obs. 80−99516
benzophenone-d_{10}, $^3(n,\pi^*)$ state, containing ^{13}C, in 4,4′-dibromodiphenylether, hyperfine ENDOR spectrum 78−42102
benzophenone-Eu complex, triplet-triplet energy transfer, viscosity and temp. depend. 79−87847
benzophenone-N,N-dimethylaniline, intramolecular exciplex systems, laser photolysis obs. 80−35550
benzophenones, in host crysts., triplet state PMDR, phosphoresc. spectra, transitions mechanisms 77−46585
Benzophenones, substituted solvent independence of radiative rate constant 77−30904
benzophenones, triplet state fine struct. parameters and phosphoresc. spectra 79−50065
$^3(n,\pi^*)$benzophenones in 4,4-dibromodiphenylether, oriented triplet state, LAC and cross relax., phosphoresc. 77−81143
benzoquino-dimethanes, nonlinear third-order electric susceptibility 78−74944
5,6- and 7,8-benzoquinoline trapped in n-paraffins at 77K, quasilinear absorption spectra 78−90179
p-benzoquinone, electronic struct., CNDO/S calcs. 78−70754
p-benzoquinone, hydroxy substitutions effect on $^1B_{1g}$←^1A_g transition 79−18200
p-benzoquinone, mixed crysts., PMDR and thermal modulation spectroscopy, electron-phonon interaction 77−32297
p-benzoquinone, photo-oxidation of chlorophyll a, nature of electron-excited state 78−76991
p-benzoquinone, second order Stark shift of zero-field transitions, isotope effects 77−24860
p-benzoquinone(-d_4), n-π^* excited states, distant intramol. interaction between identical chromophores 78−90203
benzoquinone-naphthoquinone, equilib. electron-transfer reactions in gas phase involving long-lived neg. ion radicals 78−58807
p-benzoquinones, chlorinated, transferable force field for in-plane vibrs. 80−964
benzoselenazole, electronic struct., photoelectron spectra and MO calcs. *(French)* 79−31598
1,4-benzosemiquinone, monoprotonated radical, spin distrib., INDO calcs. 77−14357
p-benzosemiquinone monoprotonated radical, submicrosecond time resolved EPR, lser photolysis, CIDEP polarisation mech. 78−80764
2,1,3-benzothiadiazole, EPR of phosphorescent state 77−8405
benzothiazole, and homologues electronic struct., photoelectron spectra and MO calcs. *(French)* 79−31598
benzothiazole, dielec. loss, relax. and const. in liq. and soln. 79−91346
benzothiazoline products, bicondensed, for thermographic recording 79−24767
benzotriazole, corrosive protection coating of Cu against SO_2 attack 78−11385
benzotriazole developer additives, effect on photographic development mechanism 80−77891
benzotrifluoride, and mono-substituted derivatives, vibr. spectra, internal rot. 77−83598
benzoxazole, aromatic derivatives, spectral luminesc. and lasing props. rel. to electronic struct. 80−99519
benzoxazole, electronic struct., photoelectron spectra and MO calcs. *(French)* 79−31598
benzoxazole, laser action at 330 nm 78−29949
benzoxazole, polarisation of 274 nm absorpt. system, band contour analysis 79−27043
benzoyl chloride, HeI/He photoelectron spectra, band intensity anal. 79−31601
benzoyl ions, collisional activation mass spectra, energy depend. 80−104482
benzoyl peroxide, photodecomp. low temp., isotope effects 77−42365
benzoyl peroxide thermolysis, CIDNP obs. in low mag. fields 77−30885
2-benzoyl-1,3,4-triphenyl-1-cyclopentanol, cryst., thermal vibr. of mols., rigid body anal. 78−38787
benzoylacetone, dil. soln. in benzene, dielectric behaviour 79−42886
benzoylacetone, H bonding, dielec. dispersion obs. 77−63356
benzoylacetones, p-substituted, dil. soln. in benzene, dielectric behaviour 79−42886
9-benzoylanthracene, subpicosecond laser photolysis and time resolved absorpt. spectra *(Japanese)* 79−79272
2-benzoylpyridine, mol. cryst. triplet state selective photoexcitation, phosphoresc. spectra and microwave-optical double reson. 79−15507
2-benzoylpyridine, triplet states, phosphoresc. and ODMR 79−38603

organic compounds continued
2-benzoylpyridine crystals, lowest triplet state, optically detected EPR 80−15827
2-benzoylpyridine crystals, optical spectra of lowest triplet state 80−16081
benzo[α]pyrene-DNA complex, triplet state props., optically detected zero-field mag. reson. obs. 77−79636
benzo[α]pyrene-DNA complex, triplet state props., optically detected zero-field mag. reson. obs. 79−18222
benzo[g,h,i]perylene high density excitation effects on fluoresc. 79−1782
1, 12-benzperylene, in alkane matrices, zero-phonon lines, press. shifts *(Russian)* 78−76502
1,12-benzperylene, in benzene, 77K, quasi-line luminesc. spectra obs., Shpolskii's method 77−69894
1,12-benzperylene, in n-paraffin cryst., luminesc. characts. 79−3480
1,12-benzperylene exciplexes, radiative and radiationless decay 77−6817
3,4-benzphenanthrene cation radical, in boric acid glass, spectrum 200-1400 nm, MO calcs., assignments 77−75174
1,2-benzpyrene, butyl bromide solid soln., phosphoresc. line struct. obs., vibr. assignments 77−58075
1,2-benzpyrene, in cyclohexane, 77K, quasi-line luminesc. obs., Shpolskii's method 77−69894
3,4-benzpyrene, in n-paraffin cryst., luminesc. characts. 79−3480
3,4-benzpyrene, monomer and excimer fluoresc. in soln., triplet-triplet annihilation and mag. field depend. 78−78738
3,4-benzpyrene, relative S_1^* emission yield vibronic states density 77−486
benzyl, 1^2B_2→2^2B_2 electronic excitation, natural orbital occupation numbers calcs. 79−45638
benzyl, circular dichroism 78−27178
benzyl acetate, phosphoresc. and fluoresc. spectra in organic matrices 80−32756
benzyl alcohol, C-C spin coupling, two-dimens. Fourier transformation 78−90194
benzyl alcohol, dielectric time-domain spectrosc., short and refl. method 80−101805
benzyl alcohol, liq., viscosity parameters, RF cond. meas. 80−96677
benzyl alcohol-n-butanol, excess vol. and isentropic compressibility, from density and US vel. meas. 78−79776
benzyl anion, IR multiphoton electron detachment 79−94043
benzyl benzoate, supercooled, depolarised lines in quasielastic light scatt. 80−45095
benzyl bromide, photolysis, free radical form., investig. 80−102523
benzyl bromide and chloride, bond orders estimation, bond polarisability derivative 80−32594
benzyl carbonium ion, internal rot. barrier, MINDO/2(3) forces method 78−9078
benzyl chloride, liq., viscosity parameters, RF cond. meas. 80−96677
benzyl chloride, mol. polarisability, bond polarisability derivatives 78−74793
benzyl chloride, photolysis, free radical form., investig. 80−102523
benzyl chloride+Cs^+, beam reactions for 5.8 eV collision energy, mechanism 80−66777
benzyl chloride+SbF_5, chemi-ionis. reaction, temp. depend., flow tube investig. 80−108701
benzyl crystal, determ. of linear birefringence in absorpt. band 79−56761
benzyl cyanides, α-substituted, in dil. soln., dielec. absorpt. obs., enthalpy of activation 80−55019
benzyl fluoride, mol. struct., NMR and gas electron diffraction obs., ab initio and mol. mechanics calcs. 80−23574
benzyl mercury chloride, cryst. struct. and absorpt. calcs. 80−84166
benzyl propionate, phosphoresc. and fluoresc. spectra in organic matrices 80−32756
benzyl radical, 1^2B_2-3^2B_2 transition in absorpt. spectrum, extinction coeffs. 80−102523
benzyl radical, in solid Ar, absorption and photodissociation spectra 80−69156
benzyl radical, IR absorpt. spectra, matrix isolated at 77K 79−22706
benzyl radical, MINDO/3-FORCES, geom. of heat of formation 78−66472
benzyl radical trapped in X-irrad. potassium hydrogen bisphenylacetate, ENDOR 77−10695
benzyl radical-halide ions, form. by dissoc. electron attachment in matrix, charge transfer band 77−16854
benzyl radicals, monomtheyl- and dimethyl-substituted, electronic spectra and electron affinity 80−63618
benzyl viologen, mechanism of electrochromism *(Japanese)* 80−34893
2-benzyl-5-benzylidenecyclopentanone, and substituted form, topochem. single-cryst.-to-single-cryst. photodimerisation 80−66819
benzyl-phosphonium radical, EPR spectra temp. depend., H-P coupling consts., conformation and rot. *(German)* 77−18950
benzylalcohol, gas chromatography peak identification by ^{13}C and ^1H Fourier transform NMR 77−77836
benzylethylamine+glycerol, coexistence curve, exactly solvable decorated lattice model predictions 78−95158
benzylic alcohols, Hammett freq. factors, effects of non-monotonic ν(XH) function variations *(French)* 79−22690
benzylidene aniline series, nematic liq. crysts., depolarised scatt. strength, free-energy, coherence length anisotropy 77−62470
benzylidene anilines, nematic phase, dipole coupled ^{13}C NMR technique 79−99073
benzylidene t-butylamine N-oxide, amphiphilic liq. cryst. solvent effect on hydrolysis 79−100355
benzylideneanilines, ordered smectic phases, X-ray diffr. meas. 77−89375
benzylideneanilines, thermal parameters for cryst.-mesophase and cryst.-cryst. transitions 77−11679
benzyne, struct. and IR spectrum, MNDO calc. 79−31403
benzynes, geometry optimisation by generalised Hartree-Fock 78−25427
BEPC, nematic liq. cryst., EPR of VO^{2+} spin probes 79−50985
berzonitrile, in soln., IR spectral, band halfwidths determ., rot. Brownian motion investig. 77−36248
betamethylnaphthalene in $C_{10}D_8$, exciton percolation and coherence 77−59258
(2,2′-bi-2-thiazoline) iron thiocyanate, high spin to low spin transition, X-ray diffr. and Mossbauer obs. 79−38418
biacetyl, aq. solns., fluoresc., phosphoresc. 77−3395
biacetyl, cryst., low temp. absorpt. spectra, thermal detection 77−74522
biacetyl, IR/UV double resonance, fluoresc. and phosphoresc. obs. 77−6810

organic compounds continued
biacetyl, lower excited electronic states, ab initio SCF and CI calcs., absorption band assignment 78−74589
biacetyl, multiphoton excitation of triplet state, fluoresc. decay 79−31632
biacetyl, quencher for triplet excitons in poly-N-vinylcarbazole 80−66267
biacetyl, single rovibronic state fluoresc., quantum beats 79−31570
biacetyl, SO_2 photosensitised phosphoresc., triplet energy transfer 78−25608
biacetyl, thermal energy charge transfer reactions 79−87828
biacetyl, triplet kinetics, EPR fine struct., ODMR 77−71824
biacetyl, triplet $n\rightarrow\pi^*$ and $\pi\rightarrow\pi^*$ transitions studied by low-energy electron diffr. 80−83502
biacetyl+pyrene, physical and chem. kinetics competition, fluoresc. quenching obs. 79−43567
biacetyl in supersonic jet, emission spectra, energy-resolved decay times 79−81224
9,9′-bianthryl, excited, proton-induced radiationless processes 77−88486
1,1′-bianthryl derivatives, dimer optical activity, vibronic circ. dichroism, theoretical anal. 78−62821
1,1′-bianthryl derivatives, theoretical analysis of UV, circular dichroism and optical rotating dispersion vibronic spectra 77−34652
bianthryls, vibronic anal. of circular dichroism and absorption spectra 77−38683
biaryls, dimer optical activity, vibronic circ. dichroism, theoretical anal. 78−62821
biaryls, model, mol. vibronic circular dichroism 78−37665
biaryls, nonplanar, spin-orbit coupling effects, luminesc. quantum yields *(German)* 77−42349
biazide-polymer based photoresist. films, positive image production *(Russian)* 78−16887
bicyclic ring compounds, Raman circular intensity differential spectra obs., mol. struct. 80−87130
bicyclo(3.2.0)hept-6-ene, LF vib. spectra, conformations 78−58685
Δ^6-bicyclo(3,2,0)heptane, conformational mobility 80−99587
bicyclo(4,2,0)octane, cis and trans isomers, struct. mol. mechanics and electron diffr. 77−54608
bicyclo [222] octane, Lennard-Jones (6-12) interaction pot., Debye temp. calc. 78−63828
bicyclo [2,2,2] octane, cohesive energy and Gruneisen parameter calcs. 79−19183
bicyclo [4.4.0] dicane, cis and trans forms, mol. struct., electron diffr., mol. mechanics 78−50658
bicyclobutyl+methylene, products decomposition, competitive channels and vibr. relax. 80−83336
bicyclohexanes, nematic liq. crysts. with negative diamag. anisotropy, high resolution NMR spectrometry 79−40596
bicyclopropyl, Raman study of rotational isomers 79−18194
bicyclo[2.2.2]octane, thermal expansion coeff., Gruneisen parameter 77−76581
bicyclo[3.1.0]hex-2-ene, microwave spectra, rot. consts., ring struct. and config. 78−42041
bicyclo[3.1.0]hexane, zero-point average struct., microwave spectra and electron diffraction 78−25738
Δ^6-bicyclo[3.2.0]heptene, microwave spectrum and dipole moment 80−9591
bie-solicylato-diaquo calcium (II), cryst. struct. 80−100222
biimidazole+leuco dye photochem. reaction, modulation by photopolymerisation 80−40714
bile acid hepatobilary kinetics, compartmental model validity 80−30971
bile acids absorption, effect of pelvic irrad. in gynaecological malignancy 80−67160
bilirubin, anomalous solvent shift effect and phosphoresc. 77−30899
bilirubin, aq. soln., pulse radiolysis 78−48761
bilirubin, soln. luminesc. 79−31572
1,1′-binaphthyl, conformational changes, picosec. dynamics 78−25625
1,1′binaphthyl, electronic struct., fluoresc. CNDO/S CI calcs. 78−90084
1,1′-binaphthyl, $T_n\leftarrow T_1$ absorption spectrum in rigid and fluid media, CNDO/A study 79−76355
binaphthyl anion radicals, photoisomerisation, local heating effects 78−85179
1,1′-binaphthyl mononegative ion conformation 77−30774
binary complex, quinone-phenol radical pair EPR, geometry calc. 78−90101
binary liq. mixture, relax. times and dipole moments, RF and microwave obs. 77−12308
binary liquid mixtures, excess free vol. calcs. 80−34202
binary liquid mixtures, excess free vol. US vel. meas. 77−51294
binary liquid mixtures, excess Gruneisen parameter and intermolecular interactions 77−20082
binary liquid mixtures, US vel. rel. to non-ideal behaviour 78−95109
binary mixtures, vapour-liquid critical volume estimation 77−39662
binary system forming simple association complexes, liq. diffusivities prediction 80−34216
bio-organic materials, bioelectrochemical sensor using immobilised enzyme electrodes *(Japanese)* 80−109071
bio-organic molecules, polar, nonvolatile, anal. by laser desorpt.-mass spectrometry 78−92534
biocyclo[2.2.2]octane, mol. cryst., thermal expansion coeff. and Gruneisen coeff. 77−84952
biological molecules, ab initio calcs., small Gaussian basis sets 79−59341
biologically active molecules, photoelectron spectrosc. 79−24954
biomotrifluoromethane, multiphoton dissoc., isotopically selective 80−28113
biophysical substances, chemical and structural anal. by fluorescence and phosphorescence spectroscopy *(Norwegian)* 78−92596
biotin, NMR of ^{13}C, spectrum assignment 80−26204
$(biphenol)^+/(biphenol)^-$ ion-radical pair, ODMR, hyperfine struct. *(Russian)* 80−15829
biphenyl:fluoranthene(pyrene)(chrysene), triplet and singlet transport rate ratio 79−56832
biphenyl:tetracene, electronic absorpt. spectrum, host-cryst. field effect 80−100669
biphenyl, carbonyl derivatives, absorpt. and luminesc. spectra, solvent effects and triplet lifetimes 77−24889
biphenyl, cryst., electronic absorpt. and refl. spectra 78−64377
biphenyl, crysts., Raman and two-photon reson. in three wave mixing 79−38538
biphenyl, diamagnetism and thermal motion 80−25076

organic compounds continued
biphenyl, electron mobility and photogeneration temp. depend., polaron hopping 78−19033
biphenyl, fluoresc. quenching by inorganic anions 78−74694
biphenyl, growth rate from melt *(Japanese)* 78−23605
1,1′-biphenyl, heat capacity anomalies due to successive phase transitions 80−96664
biphenyl, heat capacity near phase transition regions 80−44330
biphenyl, in propylene glycol, mol. fluoresc., effect of mol. conformation 78−78736
biphenyl, incoherent inelastic neutron scatt. time of flight spectra, vibr. spectra model calc. 78−63816
biphenyl, incommensurable phases, obs. of excitations, inelastic neutron scatt. 80−49334
biphenyl, incommensurate phases, elastic neutron scatt. study 79−86887
biphenyl, INDO geometry optimisation 78−74575
biphenyl, lowest excited singlet states, polyexcited CI calc. 79−772
biphenyl, luminesc. yield spectra in VUV 79−36685
biphenyl, luminescence spectrum intensity distribution 79−3476
biphenyl, melting temp. and latent heat 79−55869
biphenyl, mol. cryst., reson. four-wave mixing, third order susceptibilities 80−100654
biphenyl, phase transitions at 40 and 16K, transmitted light intensity meas. 78−51663
biphenyl, photoelectron spectroscopy obs. of heterocycles 78−94286
biphenyl, proton chem. shift, chem. substitution influence, LCAO perturbation method 77−68064
biphenyl, radiolysis, ion-pair clusters and excited-state yields 77−29024
biphenyl, second order phase transition at 40K, Raman spectral obs. 77−32361
biphenyl, semi-empirical lattice energy calcs. 79−73126
biphenyl, solid/melt interfacial tension and contact angles of small particles, determ. from crit. vel. of engulfing 80−79915
biphenyl, substrate for epitaxial crystn. of polyesters 79−61521
biphenyl, three-dimensional cryst. struct. data and refinement, 203K 77−47439
biphenyl, two photon absorptivities, CNDO/S-CI calc. with second order time depend. perturbation eqns. 80−74122
biphenyl, vibr. level classification by Longuet-Higgins group 80−43030
biphenyl cryst., nonbonded atom-atom interact. model, low freq. vibr. modes 77−1188
biphenyl crystals, electronic and vib. states, cryst. field mixing, two-photon spectra 77−59603
biphenyl doped molecular crystals, stimulated emission at 4.2K 79−28790
biphenyl gluterate diacetylene, monomer, single cryst., stable and metastable UV photoexcited states, EPR obs. 79−78522
biphenyl in Ar matrix, mol. struct., IR spectra 77−30875
biphenyl in Ne or Ar matrix, biphenyl ring torsion by vibronically resolved spectra 79−81228
biphenyl mixtures with cholesteryl chloride, static and dynamic electro-optical props., cholesteric-nematic transition 80−100646
biphenyl polyenes, vibronic states, quasi-linear spectra *(Russian)* 80−95598
biphenyl single crysts., γ-ray induced radicals, EPR and optical absorpt. studies 80−44921
biphenyl soln., stimulated Raman scatt., self-focusing, rel. to Kerr const. *(German)* 79−61355
biphenyl-4-p-n-alkoxybenzoates, nematic liq. cryst., static dielec. props. 78−60376
biphenyl-d_{10}, Brillouin scatt. at room temp. 80−71433
biphenyl-d_{10}, phase transitions at 38 and 24K, transmitted light intensity meas. 78−51663
biphenyl-p-ethylbenzoate, high press. mesomorphic and polymesomorphic transitions 78−18750
biphenylbenzoates, synthesis, mesomorphic, and thermodynamic props. 80−44117
biphenylene, fluoresc. from higher singlet levels 79−83473
biphenylene, harmonic force fields, bond orders, normal coord. anal. 78−25418
biphenylic bridged systems, appl. of Faraday rot. data to conform anal. 77−65495
2,4-biphenylpentane, depolaris. Rayleigh scatt., optical anisotropy 78−27245
biphenyls, cholesteric blue phases, struct. and props. 80−103243
biphenyls, polychlorinated, gas chromatographic anal. using electron capture detector *(Japanese)* 80−55764
2-(4-biphenylyl)-5-phenyloxazol, vapour, electron beam excited luminesc. *(Russian)* 78−82780
4-biphenylyl 4″-n-alkoxybenzoates, smectic liq. crysts., transition temps., DTA 78−75815
2-[4-biphenyl]-5-phenyloxazole, fluoresc. by electron beam excitation 79−94031
2,2′-bipyridine, photoelectron spectra, SCF LCAO calcs. 78−33551
bipyridines, torsional isomerisation of biologically active bicyclic molecules 80−27996
2,2′-bipyridyl, two photon absorptivities, CNDO/S-CI calc. with second order time depend. perturbation eqns. 80−74122
2,2′-bipyrimidine, in nematic solvent, conformation, ab initio and PMR determ. 80−47869
biradical metal chelates, rot. motion in polar solvents, rel. to ESR line-shape 80−27994
1,6-bis(2,4-dinitrophenoxy)-2,4-hexadiyne, obs. of apparent ferroelec. transition 80−66121
bis(4-maleic acidimidphenyl)methane, enthalpies and related thermodynamic functions 79−42276
bis(benzonitrile)trichloromonooxovanadium(V), cryst., stacking faults *(French)* 80−49238
bis(diethylamino)dithiaboretane, cryst. struct., bond lengths and angs. X-ray diffr. obs. 78−18628
bis(diethylammonium) copper tetrachloride, mag. susceptibility, EPR spectra 78−68193
β-bis(ethylammonium)tetrachloromanganate, cryst. struct. refinement, neutron diffr. 78−55858
bis(fluoroxy)difluoromethane, ab initio MO calcs. of geometry, torsional barriers 78−90313
4,4′-bis(heptyloxy)azoxybenzene, nematic liq. cryst., refractive index, density, orientational order 78−76419
4,4′-bis(hexyloxy)azoxybenzene, nematic liq. cryst., refractive index, density, orientational order 78−76419

organic compounds continued
bis(n-butylammonium) tetrachloromanganate(II), X-ray cryst. struct. determ. at 294K 79−60346
α-bis(N-methylsalicylaldiminato) copper II, dynamic behaviour of antiferro- to ferromagnetic transition 79−73715
bis(N-methylsalicylaldimine) copper (II), Jahn-Teller effect in EPR 77−80994
bis(p-cyanophenyl) terephthalamide, thermotropic liq. cryst. behaviour, optical microscopy obs. 79−32895
bis(p-toluene sulphonate) diacetylene, partially polymerised, defect-induced absorpt. and fluoresc. 77−44030
bis(p-toluene sulphonate)diacetylene, monomer and polymer, solid state phase transformation, far IR transmission spectra obs. 80−55077
1,2-bis(p-tolysulphonyloxymethylen)-1-buten-3-inylen, ESR of X-irrad. cryst., 77K 79−11806
4,4′-bis(pentyloxy)azoxybenzene, cryst. data 79−60347
bis(propylammonium)tetrachlorocadmate, first-order phase transition, X-ray diffr. meas. 78−55826
bis(tetrathiotetracene) triiodide, 1-D organic metal, cryst. struct. 77−59000
bis(tetrathiotetracene)triiodide, low temp. metallic cond. 77−24550
bis(tetrathiotetracene)triiodide, struct., reson. Raman spectra 78−66556
bis(triethylbenzylammonium)tetrachlorocuprate(II), mag. anisotropy, susceptibility, EPR of Cu^{2+} 78−52344
bis(trifluoromethyl)disulphide, chemisorpt. on clean Ni surface 78−14595
bis(trifluoromethyl)peroxide, gas and solid, Raman, IR spectra, internal rot. barrier of CF_3 78−29789
bis(trimethylbenzylammonium)tetrachlorocuprate(II), mag. anisotropy, susceptibility, EPR of Cu^{2+} 78−52344
bis (methylammonium) tetrachlorometallates (II), IR spectra and phase transitions of 10-25 kbar at 25°C 80−10658
α-bis (N-methylsalicylaldiminato) copper II, one-dimens. spin-$^1/_2$ Heisenberg antiferromag., high-field spin dynamics 80−71224
bis-4-n-alkylphenyl tetrafluoroterephtalates, synthesis and mesomorphic props. *(French)* 79−86679
bis-4-nalkyltetrafluorophenyl tetrafluoroterephtalates, synthesis and mesomorphic props. *(French)* 79−86679
bis-(2-fluoro-2,2-dinitroethyl)nitramine, mol. density, depend. on ratio of intramolecular and intermolecular contacts 79−86781
bis-(4,4′-n-alkoxybenzylidene)-1,4-phenylenediamines, smectic polymorphism up to 3 kbars, differential thermal anal. 79−55873
bis-(4′-n-alkoxybenzal)-2-chloro-1,4-phenylenediamines, liq. cryst., improved preparation technique 78−75541
bis-(4′-n-heptyloxybenzylidene)-1,4-phenylenediamines, smectic phases, previously unclassified 79−77508
bis-(4-aminophenyl)methane, enthalpies and related thermodynamic functions 79−42276
bis-(p-toluene-sulphonate) of 2,4 hexadiyne 1,6 diol, X-ray scattering obs. of polymerisation mechanism and phase transition *(French)* 80−70399
bis-heptyloxy-azoxybenzene, tilt angle in C-phase, dielectric measurements 78−63673
bis-merocyanine dye, intramol. dimer soln., Stark effect, optical absorption and density 78−50573
bis-methyldigermyl chalcogenide, ^1H and ^{13}C NMR study, chemical shifts 80−71201
bis-methyldisilyl chalcogenide, ^1H and ^{13}C NMR study, chemical shifts 80−71201
p-bis-octyloxyazoxybenzene, liq. cryst., thermal diffusivity, Rayleigh scatt. obs. 78−94977
bis-p-toluene sulphonate of 2,4-hexadiyne-1,6-diol, X-ray scatt., incommensurable modulated struct. obs. 80−70185
bis-styryle dyes, lasing characts. 78−42333
bis-styryles, sulphonated, laser dyes, CW operation in blue and violet spectral region 78−42334
bis-tetraethylammonium tetrachloronickelate, heat capacity, structural transitions 79−65209
bis-tetraethylammonium tetrachlorozincate, heat capacity, structural transitions 79−65209
bisanthenes, phototropic Q-modulators for ruby lasers *(Russian)* 77−83910
4,4″-bisbutyloctyloxy quaterphenyl, dye laser pumping characts. using KrF excimer laser at 248 nm 80−1199
1,3-bisdiphenylene-2-(p-chlorophenyl)-allyl, antiferromag. resonance, antiferromag. phase transition 78−6579
1,3-bisdiphenylene-2-phenyl allyl benzene complex, free radical, EPR, antiferromag. long range ordering 79−47335
bisgalvinoxyl biradical, cryst., spin-spin dipolar and exchange interactions 78−52356
bisphenol-A-polycarbonate, hole transport meas. in solid soln. 78−43438
bispyrrol-indigo, π-electronic struct., PPP-type calc. and config. anal. 78−21855
bistilbenes used as mixers of luminesc. spectra of plastic scintillators 77−23373
1,4-bis[2-(5-phenyloxazolyl)]benzene, saturated vap. press., absorpt. and fluoresc. spectra 79−76442
1,1′-Bis[phenylglyoxyloyl]-ferrocen, mol. and cryst. struct. *(German)* 80−10538
Black Sea sediment cores, organic geochemistry 78−49040
bleomycin radioimmunoassay 77−37050
bleomycin-^{64}Cu complex, lethal effects on Ehrlich ascites tumour cells 79−57709
BMAOB-cholesteryl caprinate mixture, spiral pitch temp. depend. 78−79529
borazine, triplet instability, RPA calculations 80−27938
borneol, methyl groups internal rotation, ^{13}C spin lattice relaxation times and force field calcs. 80−74255
boroxines, trioxadiborolanes, evidence for aromaticity from mass spectral and NMR meas. 78−9172
BPBAC, smectic B phase, neutron diffr. and X-ray obs. 78−94973
brass corrosion in HCl, HNO_3 and NaOH, p-thiocresol inhibitor effectiveness 79−57147
brilliant green dye, dielec. const. and loss meas., 10^2 to 10^5 Hz 78−6622
Brillouin scatt. and refr. index measurements 80−76035
brom phenol blue aqueous soln., irradiation induced discolouring as dose meas. 78−41866
bromal, in benzene soln., dielec. relax., loss, and dipole moment 80−2692
bromanil, electron affinity, bound and excited negative ion states, lifetimes, electron and alkali metal collisions 79−869
bromanil and radical anion, Raman and IR freq. shifts 78−33516

organic compounds continued
m-bromaniline delayed depolarisation obs. *(Russian)* 79−95703
1-bromo-1-chloro-1-fluoroethane(-2-d_1), IR and Raman spectra, vibr. assignments, normal coord. anal. 78−42053
1-bromo-1-chloroethylene, vibr. assignment, IR and Raman spectra 77−18925
1-bromo-2,2-dimethylpropane, Raman and IR spectra, vibr. anal. 78−90173
1-bromo-2,3 dimethylbenzene, IR vibr. spectrum, internal modes, overtones, combination freqs. 78−9146
1-bromo-2,4 dimethylbenzene, IR vibr. spectrum, internal modes, overtones, combination freqs. 78−9146
1-bromo-2,4-dimethylbenzene, liq., IR and Raman spectra 78−42049
1-bromo-2,5 dimethylbenzene, IR vibr. spectrum, internal modes, overtones, combination freqs. 78−9146
1-bromo-2,6 dimethylbenzene, IR vibr. spectrum, internal modes, overtones, combination freqs. 78−9146
1-bromo-2,6-dimethyl benzene, IR and Raman spectra, vibr. anal. 77−57997
1-bromo-2, 4-dinitrobenzene, cryst., ^{79}Br NQR Zeeman effect 78−2765
2-bromo-2-methylpropane, vapour deposition, no glass transition detected by DTA 77−24388
2-bromo-4-nitroaniline, for possible electro-optic appl., cryst. growth in glass capillary 77−44150
2-bromo-4-nitroaniline, nonlinear optical susceptibility, second order, calc. from mol. spectra *(Russian)* 79−27318
2-bromo-4-nitrotoluene, IR absorpt. spectra, vibr. assignments 78−42048
2-bromo-5-nitrotoluene, IR absorpt. spectra, vibr. assignments 78−42048
4-bromo-m-thiocresol, liq., dielectric relax. mechanisms 79−42891
9-bromo-meta-carborane, mol. reorientation, ^1H and ^{11}B NMR 77−16185
5-bromo-uracil, IR absorpt. spectra, vibr. anal. 78−61143
bromoacetic acid, cryst., films, polarised IR spectra, struct. 78−72502
bromoacetic acid, microwave spectrum, rot. consts., nucl. quadrupole coupling, conform. 79−13702
bromoacetonitrile, ground state microwave spectrum assignments, mol. struct., rot. consts., quadrupole coupling 77−6763
bromoacetylene, microwave spectrum, dipole moment 78−17660
bromoacetylene, microwave spectrum, r_s-struct., dipole moment, quadrupole coupling consts., vibr. excited states 77−79606
1-bromoadamantane, orientationally disordered, γ-irrad. free radical defects, positron probe obs. 79−23647
bromoallene, microwave spectra in vibr. ground state, rotational consts., nuclear quad. coupling consts. *(French)* 77−10664
bromoamiloride, photosensitive amiloride analogue, irreversible inhibition of Na entry sites in frog skin 78−69030
9-bromoanthracene, fluoresc. and phosphoresc. spectra 77−14480
o-bromobenzene, electronic absorpt. spectra, vibr. anal. 77−3379
bromobenzene, in EBBA, ^1H NMR and NQR of D, geometric struct. 78−17689
bromobenzene, in potassium laurate mesophase, NMR, proton distance ratios and order tensor elements calcs. 80−63672
bromobenzene, liq., third order optical susceptibility *(German)* 79−50358
bromobenzene, liquid, vibr. relaxation, Brillouin spectra 80−108219
bromobenzene, mol. polarisability, bond polarisability derivatives 78−74793
bromobenzene, nonlinear dielectric effect temp. depend. 79−82908
bromobenzene, optoacoustic spectroscopy using cell with ultimate corrosion resistance 80−42269
bromobenzene, photoelectron spectra ang. distrib., π- and σ-orbital assignments 79−818
bromobenzene, saturable absorpt. of CO_2 laser 80−69465
bromobenzene+m-xylene, US vel. and adiabatic compressibility 78−51614
bromobenzene -d_0(-d_5) radical cation, electron impact dissoc., secondary isotope effect 80−63836
bromobenzene ion fragmentation, photoelectron-photoion coincidence spectra 80−95682
bromobenzene molecular ion+neutral atom, collisional relax., 2-photon photodissoc. 79−18258
bromobenzene solutions, influence of strong elec. field on dielec. permeability 77−90086
bromobenzene-chlorobenzene solid soln., NQR investig. of impurity distrib. 77−12222
bromobenzene-d_0, -d_1, -d_4, vibr. spectra and force fields 77−65463
bromobenzenes, intermol. forces in cryst. 77−76349
bromobenzenes ^{13}CBr bond, spin-spin coupling consts., correl. with C hybridisation s-character 80−34806
4-bromobenzoyloxymethyl-trifluorosilane, cryst. struct., X-ray study 80−70187
4-bromobiphenyl, dielectric const., mol. reorientation in solid 78−72448
p-bromochlorobenzene, T_1 states, zero-field ODMR, MIDP and phosphorescence excitation spectra 80−74191
p-bromochlorobenzene, vibr. relax., Raman active phonons temp. depend. 80−29139
bromochlorodifluoromethane+Ar excited, IR spectra, matrix isolation study, C-F stretching fundamentals 78−37632
1,2-bromochloroethane, photoelectron spectra, trans- and gauche-conformers 79−27034
bromochlorofluoromethane, and d_1, Raman optical activity atom dipole interaction model 79−82033
bromochlorofluoromethane, gas, IR band contours and intensities anal. 78−82788
bromochlorofluoromethane, narrow saturated reson. absorpt., weak current detection 77−14433
bromochlorofluoromethane, Raman optical activity parameters, circular intensity differentials comput. 79−85950
bromochlorofluoromethane, struct., vibr. amplitudes, gas phase electron diffr. obs. 79−31690
bromochlorofluoromethane-d_0, -d_1, Urey-Bradley force field calcs. 77−57968
bromochloromethane, rotational-vibrational energy transfer, US absorpt. obs. 79−98537
bromocyanoacetylene, cryst., IR, far-IR and Raman spectra, vibr., struct. 77−63407
bromocyclotriphosphazatrienes, ^{81}Br NQR, conformation investig. 80−63665
5-bromodeoxyuridine pulse labelling of cells, near UV light sensitivity in cell cycle 79−83854

organic compounds continued
bromodifluoromethyl radical, IR matrix isolation spectrum, stretching fundamentals 78−27788
bromoethane, and -d_5, first s-Rydberg transitions 78−42094
bromoethane, liq., relative mol. orientation appl. of nucl. mag. relax. data 79−41933
bromoethane, mol. parameters, vibr., pot. barrier height etc., data tables 79−76409
bromoethylene, and perfluoro analogue, VUV spectra, perfluoro effect on Rydberg states 77−61764
bromoethylene, vac. UV spectra 77−23507
α-bromofluoro alkyl pi-radical, signs of hyperfine and quadrupole couplings, ESR determ. 80−97141
p-bromofluorobenzene, UV electronic absorption spectrum, band shape and molecular geometry 80−87147
bromofluorobenzens, He(Iα) and He(IIα) photoelectron spectra, assignments, ionis. energies 80−78651
bromofluoromethane cations in solid Ar, absorpt. spectra and photochem. 79−96339
bromofluoromethylene radical, laser-induced fluoresc., $^1A''$-$^1A'$ transition 80−91589
bromoform, highly excited vibr. states, thermal lensing spectrosc. and local mode model 80−87140
bromoform, liq., orientational motion, Raman spectra 77−50443
bromoform, polycryst., cryst. struct., IR spectrum 77−44000
bromoform, Raman spectra, intermol. interactions 79−76436
bromoform, refr. index, temp. depend., deviation from Lorentz-Lorenz formula 77−40200
bromoform, solid, phase transform., dielec. dispersion and differential scanning calorimetric obs. 80−24582
bromoform and Cl substitutes, VUV photoionis. during condensation with Ar, IR spectra of $(CHX_2^+)X$ and X^--HCX_2 ions 79−13773
bromoform delayed depolarisation obs. *(Russian)* 79−95703
bromoform liquid, NMR spin-lattice relax. time 80−25232
bromogermane radical anion, ESR spectra and struct. 80−87153
bromohaemin, ferric porphyrins with fifth ligands, ^{57}Fe and ^{14}N hyperfine consts. 78−50475
bromohippuric acid preparation, ^{80}Br labelled 79−88187
4-bromoisoquinoline, UV and IR spectra, f-values and ground state vibr. freqs. 78−58714
bromomethane, ^{79}Br, ^{81}Br quadrupole bond magnitude ratio *(Russian)* 79−76452
bromomethane, ab initio SCF MO calcs., ionis. pots., dipole moment, config., electronic props. 78−1104
bromomethane, and isotopic forms, self-broadening and self-shifting of rot. spectra 78−13551
bromomethane, dielectric susceptibility at radio frequencies 78−14123
bromomethane, IR multiphotonic excitation, depend. on cell geometry, mol. fluoresc. and decomp. obs. 80−83430
bromomethane, IR spectra, $2\nu_2$, $2\nu_5$ and $\nu_2+\nu_5$ 78−42059
bromomethane, microwave spectra, isotope substitution, Br quadrupole coupling, J=0←1 transitions 79−45709
bromomethane, microwave spectrum obs., B rot. and centrifugal distortion consts. 77−75135
bromomethane, mol. dipole moment derivative, sign of 79−86082
bromomethane, mol. Rydberg transitions mag. circular dichroism 80−43081
bromomethane, multiphoton vacuum UV photodissoc. obs. and interpret. 80−11939
bromomethane, rotational spectrum in ground state of vibr., 18 to 350 Hz *(French)* 77−57980
bromomethane, second dielectric virial coeff. of polar gas, temp. depend. *(German)* 78−26234
bromomethane, vibr., rot. and translational energy exchange, semiclassical theory 80−48067
bromomethane, VUV laser multiphoton dissoc., CH excited state branching ratio, chemiluminesc. 78−70884
bromomethane+$OCS(SO_2)$, (cyanomethane), microwave spectral line width, dipole-dipole interaction calc. 78−74648
bromomethane+Rb(K), product translational energy calcs., energy depend. 79−70314
bromomethane+Xe, high Rydberg state, ionis. 78−50620
bromomethane(-d_1,d_2,d_3), F and G sum rules as vibr. intensity data error indicators 79−3494
bromomethane (-d_1, d_2, d_3), exptl. vibr. intensity data error indication by F and G sum rules 79−72364
bromomethane derivatives, NQR frequency of Br, substituent group effects 80−95648
bromomethane-$d_{0,1,2,3}$, IR spectra intensities, dipole moment, bond charge, force consts. 77−83588
bromomethane-d_3, IR spectra of ν_3 band, $^{79/81}$Br substitution 79−64000
bromomethanes, ^{13}C-Br spin-spin coupling consts., isotope effects 78−13522
bromomethyl methyl ether, microwave spectra, quadrupole computing effect 80−18848
bromomethyl methyl ether, microwave spectra, quadrupole coupling effect 80−14135
bromomethyl oxirane, conformation, microwave spectrum in ranges 12.5-18 and 26.6-40 GHz 79−98076
bromomethyl radical+alkane, rate constants 77−25248
bromomethylsilane, microwave spectra, quadrupole computing effect 80−18848
bromomethylsilane, microwave spectra, quadrupole coupling effect 80−14135
bromomethyne radical+paraffins (olefins)(O_2)(NO), absolute reaction rate parameters 77−1909
bromonaphthalene, bond and mol. polarisability, semi-empirical delta-function 79−31441
β-bromonaphthalene, IR absorption spectra, forbidden character 77−58002
α-bromonaphthalene, soln., dielec. relax. and permittivity 78−64318
α,βbromonaphthalenes, thermodynamic functions calcs. 298-1500K 77−31418
1-bromopentane, low freq. mol. vibrs., neutron inelastic scatt. study 79−46760
2-bromophenoxaycetyl-4-propylbenzene, cryst. and mol. struct., X-ray anal. 79−60349
4-bromophenoxyacetyl-4-ethylbenzene, single crystal, X-ray struct. determ. 79−1426
m-bromophenylbenzoyloxybenzoate, nematic phase, freq. depend. of dielec. props. *(French)* 79−91337

organic compounds continued
1-bromopropane, photoionisation mass spectrometry 80−40779
3-bromopropene, ^{79,81}Br, microwave spectrum, mol. struct., nucl. quadrupole coupling consts., rot. consts. 77−6767
2-bromopropene, barriers to internal rotation 78−9273
bromopropyne, mol., He(I) photoelectron spectra 79−27033
2-bromostearic acid, photoelectron escape depths determ. from X-ray photoelectron spectra 78−27368
N-bromosuccinimide, X-irrad., ESR study of Br and σ* radical 80−66037
N-bromosuccinimide lone-pair struct., photodetection spectra 78−37684
α-bromotoluene, liq., IR absorpt. spectrum 78−979
bromotrichloromethane, ^{13}C isotope selectivity press. depend., multiphoton IR photolysis 80−45523
bromotrichloromethane, vac. UV absorpt. cross section 80−91574
bromotrifluoromethane ^{79}Br (^{81}Br), vibrational spectra and force constants of symmetric tops, rotational analysis 79−98090
bromotrifluoromethane, CW optically pumped, FIR laser action obs. at 823, 883 μm 80−14321
bromotrifluoromethane, E-species force consts., using L-F approx. method, HLFS applicability 80−962
bromotrifluoromethane, IR multiphoton dissoc. 79−18243
bromotrifluoromethane, IR multiphoton selective dissoc., effect of acceptor radicals 80−66854
bromotrifluoromethane, mol. struct., electron diffr., microwave spectra, CNDO/2 calcs. 78−37766
bromotrifluoromethane, multiphoton decomp., ^{13}C enrichment 79−830
bromotrifluoromethane, photoelectron spectra, spin-orbit splitting, vibr. fine struct. 78−21974
bromotrifluoromethane, vac. UV absorpt. cross section 80−91574
bromotrifluoromethane 823 laser line, simple accurate method for wavelength meas. 80−106554
bromotrifluoromethane cation, photodissoc. by quasi-continuum single IR photon absorption 80−61124
bromotrifluoromethane-^{12}C, -^{13}C, matrix IR spectra and harmonic force fields *(German)* 79−76431
bromotrifluoromethyl cation, IR photodissoc. 80−87188
bromoxylenes, near UV absorpt. spectra 79−31542
bromoxylenes, near UV absorption spectra, assignments 79−81209
bromtrinitromethane, electron diffr. study of gas phase mol. struct., rot. isomerism 78−1080
bumetanide-^{14}C, whole body autoradiography in dogs by round saw method 80−72399
α-bungarotoxin effect on transmitter release at neuromuscular junction 78−44496
1-1-d_2-but-1-ene skew form, microwave spectra, rot. const. and centrifugal distortion coefficients determ. 80−83351
but-3-yn-2-ol, mol., He(I) photoelectron spectra 79−27033
trans-butadiene, $^1B_{1u}$-state dynamics in cooled supersonic expansion, electronic absorpt. spectra obs. 80−78629
1,3,-butadiene, π-electron struct., generator coord. method 79−26880
1,3-butadiene, absolute rate consts. meas., 297-439K 78−7196
trans-butadiene, all-valence-electron CI calcs. of electronic spectrum 77−10654
butadiene, cis- and trans-, appl. of spin-free CI procedure using alternant MOs 79−85887
1,3-butadiene, condensed, electron energy loss spectra meas. 77−59652
trans-butadiene, correl. problem, open-shell coupled-cluster approach, PPP calc. 79−81157
trans-1,3-butadiene, electron impact energy loss spectra, energy levels 79−68323
butadiene, electron momentum distribs. in π orbitals from (e,2e) expts. 80−14239
trans-1,3-butadiene, electronic spectra vibr. struct. calc. 79−63981
trans-butadiene, excitation energies, effective Hamiltonian convergence props. 79−3346
butadiene, excitation spectra, cluster configuration method appl. 80−78546
1,3-butadiene, excited singlet states, vibronic struct., electron impact energy loss spectra, 35-90 eV 78−62932
1,3-butadiene, FSGO calcs. of orbital energies, locations, dipole moments, charge distribs. 77−67976
butadiene, $J_{C\text{-}H}$ spin-spin coupling const., bond length depend. 78−37660
butadiene, LMO population calc. method appl., from given SCF eigenvector matrix 80−14063
1,3-butadiene, matrix isolation, trapping from thermal mol. beam, IR spectra 78−46330
butadiene, mol., conformational anal., inapplicability of MINDO/3 79−94105
butadiene, mol. hyperpolarisability meas. by optical SHG 79−22861
trans-butadiene, mol. semiempirical RPA calc. using PPP Hamiltonian, triplet instability 79−26893
1,3-butadiene, molecular vibration, mean. square amplitude, extreme value determ. 78−25507
trans-1,3-butadiene, multiphoton ionis. spectra polaris. characts., two-photon symmetry assignment 78−74718
trans-butadiene, multiphoton transitions, multiphoton ionisation, thermal lensing spectroscopy 78−33559
s-cis-butadiene, natural orbitals, photochem. cyclisation 79−85900
butadiene, oscillator and rotatory strengths, RPA in ab initio calc. 78−25617
1,3-butadiene, Penning electron and photoelectron spectra, relative intensities comparison 79−81237
butadiene, photoelectron spectra, HAM/3 MO calcs. 78−13414
trans-butadiene, polarisability, nonlinear elec. susceptibility, SCF calcs. 80−95547
butadiene, resonance-enhanced multiphoton ionis. and fragmentation of mol. beam 79−100411
butadiene, singlet and triplet state, open shell RPA unitary group formulation, Hartree Fock stability eqns. 80−52860
butadiene, thermal isomerisation rate theory 79−34291
butadiene, twisted zwitterionic excited states, SCF calcs. 80−58179
trans-butadiene, two-photon spectra, press. effects, transient lensing spectrosc. 78−58756
butadiene, unoccupied orbitals, excitation energy, electron affinity, HAM/3 MO calcs. 78−13415
butadiene, UV and photoelectron spectra, first Rydberg states, vibr. components 77−46573
1,3-butadiene, UV spectra, polarisation of strongest Rydberg transitions 78−46360

organic compounds continued
trans-1,3-butadiene, valence electronic excited states, SCF ab initio GVB and CI calcs. 79−31423
trans-butadiene, weak low-energy band, S and T levels by fragment method 78−82625
1,3-butadiene+N, reaction rate consts., pulse radiolysis obs. 80−35508
1,3-butadiene+OH, absolute rate consts. 78−23927
butadiene chromophores, cis- and trans- (α- and β-phellandrene) absorpt. and CD spectra 78−62834
butadiene coatings, on steel, delamination by corrosion 78−64765
butadiene iron tricarbonyl, adsorbed on graphite, diffusion and melting, Mossbauer meas. 79−61270
1,3-butadiene-1-one, spectroscopic consts., IR and microwave spectra, prep. 80−18859
butadiene-styrene, polymer reaction, below a glass transition, limiting conversions 78−88632
butadiene-sytrene; polymer reaction, below glass transition, limiting conversions 78−88632
butadienes, cis- and trans-, ionisation potential, ab initio valence bond calcs. 79−31407
1,3-butadienes, methyl substituted, singlet-triplet transitions, energies, relative cross-sections, $He^+(H_2^+)$ impact spectra 78−86942
butadienes, optical activation energy and dipole moment, electron repelling and attracting groups 78−46341
butadiynyl in IRC+10216, N=12→11 doublet study 80−51829
butadiynyl radical, interstellar, detect. towards (IRC+10216) 78−93374
butan-2-ol, catalytic dehydrogenation and dehydration, MgO catalyst selectivity obs. 79−24820
butane, α-particles stopping cross-section determ. 79−49917
butane, adsorbed on graphite, struct. and dynamics, empirical interatomic pots. 79−99417
butane, adsorbed on graphite, struct. and dynamics, neutron scatt. study 78−87870
n-butane, adsorption on water, 0-50°C, press. effects on surface tension 78−56024
n-butane, and +octafluorocyclobutane mixtures, surface tension meas. 79−19371
butane, condensation in porous bulk media 78−47510
n-butane, condensed, electron energy loss spectra meas. 77−59652
n-butane, conformational hypersurface, anal. 79−41252
n-butane, decomposition in RF discharges, 10-40 torr 78−3318
butane, diffusion coeff. in linear polyethylene, nucl. spin echo obs. 79−38404
butane, dissociative excitation, form., environment and parent mol. effects 80−78682
butane, flexible chain molecules, momentum space diffusion eqns. 80−75142
n-butane, freejet flow, vibr. relax. time 79−98760
butane, gas, absolute viscosity 77−35299
butane, gas, electron drift vel., Ramsauer-Townsend minima in electron scatt. 78−87427
n-butane, impurity in liq. and solid neopentane, effect on electron mobility and electron-ion recomb. 80−24984
n-butane, in solid neopentane, electron mobility and electron-ion recombination rate const. 79−73557
n-butane, intermol. pair correls., RISM integral eqn. 78−63656
butane, ionisation by electron bombard., empirical and semi-empirical calcs. 79−36784
n-butane, LF vibr. spectrum, methyl torsional pot. function, internal rot. 79−89670
butane, liq., enthalpy difference between rot. isomers, IR spectrosc. obs. 80−106404
n-butane, liq., temp.-depend. free vol. 79−99052
2-butane, proximity and conform. effects, ^{13}C chem. shifts at γ position INDO computations 77−50451
n-butane, skeletal alkane fluid simulation, vibr., rot., torsional gauche/trans relax., diffusion const. 79−1378
n-butane, solid, mol. reorientation, PMR 77−8431
butane, total emissivity, press. depend. 78−90673
n-butane, trans or gauche, solute mol., solvent mol. distrib. 80−96433
n-butane, vertical electronic spectra, limited CI calcs. 79−13693
n-butane, vibr. shrinkages, mol. struct., electron diffr. obs. 77−50535
n-butane, viscosity meas. at atm. press. and 25-195°C 79−86550
n-butane+$O(^3P)$, reaction rate constants using flash photolysis-NO_2 chemiluminesc. method 77−44458
butane adsorbed on graphite, intramol. and surface vibr. modes, inelastic neutron scatt. obs. 77−72780
butane adsorbed on small graphite particles, struct. and dynamics, appl. of neutron scatt. 79−4481
butane diol, asymm. dielectric dispersion, 1-25000 MHz 78−15092
butane drops, nucleation in flowing water 79−1099
n-butane formation by fission fragment radiolysis in ethane-ammonia system 77−56236
n-butane in CCl_4 soln., intermol. struct., superposition approx. and two-cavity model 78−71656
n-butane in liq. solvents, conformational structure 80−28115
n-butane in tetrachloromethane, gauch-trans equilib. const., mol. dynamics and Monte Carlo anal. 79−70308
butane RF plasma, initial etching prior to deposition of C 79−66224
n-butane solvent effects, quantum mech., macroscopic electrostatic contribs. 77−30801
butane-1,4-diol, high press. expansivity, piezo-thermal anal., phase transformations 77−72705
n-butane-CO_2, freejet flow, vibr. relax. time 79−98760
n-butane-CO_2 mixture, oxidation under RF discharge conditions 78−15670
n-butane-decane-methane, heterogeneous flows of multi-component mixtures in porous media−review 78−59471
n-butane-isobutane mixtures, viscosity meas. at atm. press. and 25-100°C 79−86550
t-butane-KOH-O_2-N_2O pulse radiolysis, kinetics of transient O compound form. meas. from Cherenkov emission 77−70321
n-butane-$N_2(CO_2)$ mixtures, viscosity, diffusion coeffs. 80−1722
n-butane-n-hexane-ethane, vap.-liq. equilib. behaviour, visual cell, for 48.3-143.5°C, up to 7619 kPa 79−46790
1,4-butanediol, dielectric behaviour, LF dispersion 77−48126
2,3-butanediol, dielectric dispersion 78−72455
1,4-butanediol, low freq. dielectric dispersion, charge carrier hopping anal. 78−43772
2,3-butanediol, meso, l, d forms, separation using circulation chromatography in steam 79−16074

organic compounds continued
butanediol 1, 3, associated liq., correl. between acoustic and dielectric relaxation times 78−9925
2,3-butanediol doped with Cr(V)-complex, materials with adjacent hydroxyl groups, dynamic proton polarisation 77−79492
butanediol-1,3, viscoelastic props., digital correlation Brillouin scatt. 78−2865
2,3-butanedione, mol., conformational anal., inapplicability of MINDO/3 79−94105
1-butanethiol, simulated ab initio MO method calcs. 80−47867
butanethiol, volume change on melting and reduced Lindemann's relation 80−29151
butanol, adsorbed layer on graphite, spreading press. 77−15692
2-butanol, adsorpt. on Al_2O_3, PMR spectra 79−19457
n-butanol, adsorpt. on PAN-based C fibres, surface characts. 78−48694
t-butanol, aq. soln., excess heat capacity, H bonding 78−3362
t-butanol, aqueous system, LET depend. of transient yields in deuteron and alpha pulse radiolysis 77−63940
n-butanol, at Hg/solution interface, diffusion layer theory, exptl. test 78−35701
t-butanol, correlation between chem. shift and charge for OH 77−18946
n-butanol, dielectric response function, by lumped capacitance method 78−95539
t-butanol, dilute aqueous solns., excess partial molal heat capacities 79−57280
butanol, effect on conductivity and time of adhesion of lipid membranes 79−53070
n-butanol, glassy and crystalline forms, trapped electrons, conc. of mol. vacancies determ. 77−65948
t-butanol, influence on ferric yield of Fricke dosimeter 78−11736
1-butanol, IR and Raman spectra, vibr., conformers 78−25532
butanol, mean sojourn time of molecules on surfaces, meas. in practical vacuum system *(Japanese)* 80−57315
t-butanol, melting point, structure function, H-bonded hydroxyl groups 79−99053
n-butanol, microemulsion, dynamical and structural props., by chem. physics method 79−79308
tert-butanol, mol. dynamics, liq. and cryst. states, neutron inelastic scatt. obs. 78−75599
n- butanol, natural convection from temp. fields in spherical partially filled vessel 80−1561
1-butanol, permitt., dielec. time domain spectroscopy, total transmission method study 80−27323
1-butanol, permitt. meas. by transmission time domain spectroscopy 77−67462
n-butanol, phonon MFP formula, H bond collisions, low temp. 77−35655
2-butanol, sound vel. and absorpt. meas. at hypersonic freqs. 78−18708
1-butanol, time domain spectroscopy, superposition integral approximation 77−1630
2-butanol, vapour, adsorption in In-Sn liq. alloy 79−14981
n-butanol, vapour, effect of adsorpt. on surface oxidised activated C, paramag. props. 77−32238
t-butanol and -d_1, deuteration effect on self-assoc., dielectric polaris meas. 79−28672
n-butanol and methanol, effect on fatigue lifetime of polystyrene 79−43455
t-butanol aq. soln., heat capacity anomaly, struct. phase transformation 79−10959
t-butanol aqueous soln., sound absorpt. coeff. meas., acoustic relax. 78−83883
n-,t-butanol in alkanes, molecular relaxation processes studied by ^{13}C NMR 80−63654
n-butanol in ethyl methyl ketone, measurements of US vel. and density for determination of excess props. 80−37910
Butanol recycling from irradiated proton target material 79−63852
n-butanol-1,1,2,2-tetrachloroethane, isobaric vapour-liquid equilibria at atmospheric pressure 79−51246
t-butanol-acetone-cyclohexane, complexation, thermodynamic parameters *(Russian)* 78−76905
n-butanol-benzyl alcohol, excess vol. and isentropic compressibility, from density and US vel. meas. 78−79776
t-butanol-CCl_4, excess thermodynamic functions, 15, 30 and 45°C, composition depend. *(Russian)* 78−31677
butanol-methylethyl ketone, soln., excess thermodynamic props. and interactions, US vel. and density meas. 80−39288
t-butanol-water, X-ray scatt. intensity composition depend., soln. struct. 78−6005
n-butanol-water-Ca $(SCN)_2$ system with hypercrit. point, US absorpt. 80−49306
butatriene, ionis. pots., Green's function method 77−14608
butatriene, ionis. spectral intensity, valence electron binding energy depend. 78−90234
butatriene, vertical valence ionis. pots., ab initio UB calcs. 79−85917
1-butene, adsorbed on δ-Al_2O_3, isomerisation, IR study 80−76554
trans-2-butene, Ar matrix, TEA CO_2 laser irrad. photoisomerisation study 80−21303
butene, cations, photodissoc., branching ratio meas., unimolecular decay theory 77−6873
cis-2-butene, charge transfer mass spectra and photoelectron spectra 80−40778
cis-2-butene, cis-2-butenenitrile, isomerisation, SCF perturbation theory 79−91918
cis- and trans-2-butene, Compton profiles, theory and expt. 78−50597
butene, isomers, ion-mol. reactions, photoionisation mass spectra 80−81298
cis-butene, ozonolysis, radical form., matrix ESR spectrosc. 80−16653
cis- and trans-2-butene, proton-proton coupling consts., valence angle depend. 77−23508
cis-2-butene, Raman and IR spectra, torsional mode pot. function 79−89676
trans-2-butene, twisted, oscillator and rotary strengths, ab initio calculations 77−65510
1-butene+OH, absolute rate consts., 297K 79−100353
trans-2-butene+OH, reaction products, O_2 and NO_2 effects obs. 80−85156
1-butene adsorption on delta alumina, microgravimetric-IR study 80−75432
2-butene ion, fragmentation, angular momentum in ion-mol. reacts., RRKM calc. 80−66773

organic compounds continued
butene isomers, gaseous, density and temp. effects on electron mobilities 80−33725
1-butene oxide, gas, microwave spectrum 79−13703
cis-butene-1, microwave rot. spectrum, centrifugal distortion effects, rot. consts. 78−9137
butene-1, solubility in liq. N_2 80−39286
butene-1, Townsend primary and secondary ioniz. coeffs. and sparking voltages 78−51372
cis-butene-2, high density vapour thermal electron attachment density depend. 79−90369
butene-N_2O, mech. of thermal electron attachment, microwave cond. meas. 78−59536
butenes, electron energy loss spectra, 0-90°, 20-150 eV impact 79−68322
n-butoxy radicals, intramol. isomerisation, following n-butyl nitrite pyrolysis 79−20355
p-n-butoxybenzoic acid, refr. index and orientational order parameter, temp. depend. 79−90537
N-(p-butoxybenzylidene)-p-pentylaniline, refr. index and density in nematic and isotropic phases 79−90538
4-butoxybenzylidene-4′-alkylaniline, EHD instabilities in nematic and smectic A phases 79−90530
butoxybenzylidene-aminobenzonitrile, crystalline and liq. cryst. states, low freq. spectra 78−34437
N-n-butoxybenzylidene-n-butylaniline, US propag. near nematic-smectic A transition, mag. field effect 80−39266
N-p-butoxybenzylidene-p-n-octylaniline, smectic A-B transition, birefringence pretransitional behaviour 80−15226
N-(p′-butoxybenzylidine)-p-n-octylaniline, order parameters in nematic and smectic phases, X-ray diffr. meas. 79−94874
4-n-butoxybenzylidine-4′-n-octylaniline, liquid cryst., smectic B phase lattice vibr. anisotropy, Mossbauer anal. 77−7666
2-butoxyethanol, aq. binary mixture, pseudophase transition, heat capacity evidence 78−83937
n-butyl acetate, alkaline hydrolysis in water-alcohol mixture, solvent polarity effects 77−48639
n-butyl acetate, electroviscous effect, AC charact$_3$ 79−99341
tert-butyl acetate, frozen liquids, high-resolution ^{13}C NMR using magic angle spinning 79−33544
t-butyl acetate, rot. isomerism, dielect. and Raman spectra 80−106328
sec-butyl acetate+OH, reaction rate const., in irrad. NO_x mixture 78−7171
t-butyl alcohol, and deuterates, gaseous and matrix IR spectra, liq. Raman spectra, vibr. assignment 79−10113
t-butyl alcohol, aq. soln. 80−88237
t-butyl alcohol, aq. solns., US relax. freqs., clathrate-hydrate model 78−30704
n-butyl alcohol, dil. aq. soln., US vel., 4.04 MHz 78−67770
tert-butyl alcohol, interaction of muonium with radiolysis products in pure water, OH. scavenging action 79−24806
t-butyl alcohol, mixtures, assoc., thermodynamic study using 2-constant model 80−66789
butyl alcohol, pumping down curve, P(t), rel. to adsorption isotherm *(Japanese)* 80−52249
t-butyl alcohol, self-assoc., linear and nonlinear dielec. effects obs. 80−60484
t-butyl alcohol, simultaneous meas. of NOE and T_1 79−42854
t-butyl alcohol, struct. determ. from vibr. spectra, H-bonding and heat of mixing *(Russian)* 78−3368
tert-butyl alcohol in nonpolar solvents, liq. struct. from dielectric studies 80−38894
butyl alcohol surface tension, AC field influence calc., comparison with exptl. data *(Russian)* 77−55417
butyl alcohols, H bonding to 2,6-lutidine, PMR obs. 79−27008
butyl boron halides, equilib. reacts., redistribution of −F, −Cl monofunctional groups *(French)* 78−64816
t-butyl bromide, bond lengths, nucl. quadrupole coupling, microwave spectrum 79−31512
t-butyl bromide, elec cond., temp. depend. in liq. and plastic phases 80−1944
t-butyl bromide, vibr. relax. in pure liq. and soln., Raman spectra 80−66167
t-butyl bromide+Na, anisotropic interactions from double rainbow struct., interaction pot. meas. 80−99540
n-butyl bromide conformers, IR and Raman spectra, vibr. anal. *(German)* 77−88451
butyl cation, H-elimination, energy partitioning, transition state geometry calc. using MINDO/3 80−104430
t-butyl chloride, dipolar liquid, far IR absorpt. rel. to Mori continued fraction for autocorrel. function 78−2875
t-butyl chloride, elec cond., temp. depend. in liq. and plastic phases 80−1944
n-butyl chloride, glass transition rel. to press. depend. of viscosity 80−34171
t-butyl chloride, rotational motions, cold neutron scatt.study 79−51023
t-butyl chloride, solid phases, mol. motion, cold neutron scatt obs. 78−26460
t-butyl chloride, vibr. relax. in pure liq. and soln., Raman spectra 80−66167
t-butyl chloride+Na, anisotropic interactions from double rainbow struct., interaction pot. meas. 80−99540
t-butyl chloride $+Cs^+$, reactive scatt., stripping model, ang. and energy distrib. 80−35510
t-butyl chloride-d_0 and -d_9, polymorphism, Raman spectra 80−20617
t-butyl cyanide, adsorbed on silica, laser Raman spectra 77−3367
t-butyl cyanide-HF, hydrogen bonded heterodimer, spectroscopic consts. from IR and microwave spectra 80−43039
t-butyl derivatives, liq., reorientational correlation times, Hubbard model 79−61353
t-butyl formate, IR and Raman spectra, liquid, solid and gaseous states 79−50016
t-butyl formate, rot. isomerism, dielect. and Raman spectra 80−106328
tert-butyl formate-d_1, Fermi reson. parameters meas. attempt 80−48103
butyl iodide, two-photon reson . ionis. spectra 80−28071
t-butyl iodide+Na 80−99540
n-butyl nitrite, pyrolysis at low-press., 590-750K, n-butoxy radical isomerisation 79−20355
tri-n-butyl phosphate, quantitative IR absorpt. meas. 80−87106
t-butyl radical, VUV photoelectron spectrum, geometry, vibr. struct. and ionisation pots. 78−50577
organic compounds continued
butyl radical+O_2, reaction rate consts. meas. 80−45490
t-butyl radicals, ab initio geometry calc., ^{13}C hyperfine coupling 77−10580
tert-butyl sulphide, UV spectra, assignments 78−46359
n-butyl-4-(4′-phenylbenzylideneamino)cinnamate-d_9, smectic E, B and A phases, quasielastic neutron scatt. obs. 78−75539
2-butyl-7-(1-oxopentyl)-9,10-dihydrophenanthrene, mesomorphous, cryst. struct. determ. *(French)* 77−4095
n′-n-butyl-n-methoxyazoxybenzole, specific heat anomaly and isotropic liquid to nematic liquid cryst. transition *(Russian)* 77−62624
n-butyl-p,p′-hexyloxyphenyloxycarbonyl-phenyl carbonate, nematic liq. cryst., order paremeter determ. by fluoresc. 79−4240
p-n-butyl-p′-heptanoyloxyazoxybenzene oriented on NaCl MgF_2 coated NaCl, surface phenomena and IR spectra 80−79678
p-n− butyl-p′-methylhydroxyazobenzene/p-n-butylheptanoylazoxybenzene mixture, temp. depend of elec. cond. 80−1925
butyl-PBD laser, tunable narrow-band coherent VUV source for Lyman-α region 80−38070
n-butylamine, adsorpt. on PAN-based C fibres, surface characts. 78−48694
n-butylamine, second virial coeff. meas. using new apparatus, 40°C 80−44289
n-butylamine-n-propanol, isothermal vapour-liquid equilib. 80−59639
p-n-butylaniline having optically active modes, vibr. relax. studied by absorpt. and fluoresc. spectra 80−83340
butylated hydroxyanisole, diffusion in liq. polyethylene, gas chromatography determ. 78−2277
butylated hydroxytoluene, diffusion in liq. polyethylene, gas chromatography determ. 78−2277
t-butylbenzene, α-substitution effect and radiative lifetime, solvent effects, rel. to ethylbenzene 79−98154
t-butylbenzene, depolaris. Rayleigh scatt., optical anisotropy 78−27245
t-butylbenzene, two photon absorptivity, ion cyclotron reson. photodissoc. spectra, CNDO/S-CI-perturbation theory 80−74123
butylbenzene-nitrobenzene binary mixtures, with weak charge transfer interactions, thermodynamic props. 80−54360
1,3-butyleneglycol, density rel. to temp. and pressure *(Russian)* 79−10890
N-t-butylformamide, in carbon tetrachloride, dielec. relax., time-domain reflectometric obs. 79−4762
t-butyllithium, dissoc. photoionis. 79−6976
butyloxybenzylidene octylaniline, liq. cryst., phase transitions, calorimetric obs. 80−103466
butyloxybenzylidene octylaniline, liq. cryst. film, smectic B-A transition, mech. meas. 80−79918
butyloxybenzylidene octylaniline, two- and three-dimensional smectic B liq. cryst. film, long range order 80−96442
butyloxybenzylidene octylaniline film, freely suspended, smectic A layer spacing, optical determ. 80−64883
p-butyloxybenzylidene-p′-octylaniline, liq. cryst., thermal diffusivity, Rayleigh scatt. obs. 78−94977
4-n-butyloxyphenyl-4′-nonyloxybenzoate, edge dislocations in smectic C mesophase 78−91231
butyloxyphenylnonyl oxybenzoate, smectic C layer thickness meas. by X-ray scatt. 78−94986
t-butylphosphine, microwave spectrum, meas., determ. 78−58675
di-butylphthalate, critical nuclei, meas. of number of mols. and surface tension from rate of nucleation 79−65293
butylsilane-d_0,(−d_n), vibr. spectra, normal vibrs. and rot. isomerism 79−31523
4-butylthiophenol, synthesis 78−51408
p-t-butyltoluene, selective deuteration, proton spin-lattice relax. 79−1721
3-butyn-1-ol, vibr. spectra, assignments, rot. isomerism 80−58257
1-butyne, and propyne, electron impact spectra, comparison with acetylene 79−3585
n-butyraldoxime, photoelectron and far UV absorpt. spectra 78−17712
n-butyric acid, adsorpt. on PAN-based C fibres, surface characts. 78−48694
butyric acid, viscosity of dissociating vapour 78−5840
n-butyric acid-water, PMR relax. obs., mol. assoc. 79−33553
cadmium acetate trihydrate, hyperfine forbidden ESR lines of Mn^{2+}, spin Hamiltonian calc. *(French)* 77−28431
cadmium arachidate, monolayer, electron mean free path length, XPS obs. 79−74051
cadmium arachidate mixed with cyanine dyes, mol. layers, photoelec. props. 80−80401
cadmium arachidate monolayer, Ag(Au) substrate, reson. surface plasmon reflection 78−56536
cadmium arachidate monolayer, surface plasmon spectra, refractive index dispersion 78−64424
cadmium arachidate monolayer on Au, surface plasma reson., optical consts. 77−90210
cadmium arachidate monolayer transfer from air-water interface to solid, contact angles 77−55424
cadmium arachidate monolayers, bonding on oxidised In, Rh, Si, Sn, surfaces, XPS 79−15011
cadmium behenate in Langmuir multilayer assembly system, single layer conductance 79−51701
cadmium formate, γ-irrad., ESR of free radicals 79−65737
cadmium formate, anhydrous, cryst. struct. 80−107195
cadmium glutarate complexes in aqueous soln., enthalpy and entropy meas. *(Italian)* 79−19378
cadmium histidine, unique phase determination, two-wavelength Bijvoet pair method, reson. neutron scatt. 78−91201
cadmium maleate dihydrate:Cu^{2+}, EPR at 77 and 303K 79−33530
cadmium oxydiacetate trihydrate, monoclinic, cryst. struct. determ. and refined 77−47438
cadmium salts of fatty acids, multilayer assembly Langmuir film structure 77−39740
cadmium stearate, multilayer Langmuir films, DC cond., $T^{-1/2}$ law 77−12022
cadmium stearate based Langmuir films, deposition on p-CdTe, characts. and MIS struct. 80−92998
cadoxen solvents, acoustic relax. mechanisms *(Russian)* 79−90733
caesium acetate, molten, elec. cond. and density 77−15613
caesium alkanoates, phase transitions, differential scanning calorimetry 77−43315
caesium hydrogen tartrate, anomalous dispersion of Cs, refined struct. from modified least squares program 78−51522

organic compounds continued
caesium hydrogen tartrate, Cs L_{III}-edge anomalous X-ray scatt., meas. by synchrotron radiation 79−24389
caesium perfluorooctanate, thermodynamically independent nematic amphiphilic mesophase obs. 79−95126
caesium propanoate, solid state transitions and melting process, diffr. and conductometric meas. 80−10670
caesium tartrate, optical rot. dispersion, dichroism and spectra, in soln. and cryst. *(Russian)* 77−90124
caesium trichloroacetate, temp. depend. of ^{31}Cl NQR spectra 80−20495
caffeine, electronic struct., UV photoelectron spectra, CNDO calc. 79−24949
caffeine, inhibition of anodic dissolution of Cu (100) in acidic $CuSO_4$ soln. 78−27672
caffeine, UV PES, constitutive subunits, methylatron effects 78−29798
caffeine effect on RNA synthesis in slime-mould after electron and neutron irrad. 77−12962
caffeine in aq. electrolyte, adsorpt. isotherm and solute activities from spreading pressure-surface charge data 78−14576
caffeine in New York City air 77−91191
calcination methods, for spectrochem. anal. *(Russian)* 78−23997
calcium adenosine triphosphate, X-ray Ca K-edge meas. 79−6950
calcium alginate gels, Raleigh scatt., spectral broadening, density fluctuations 79−1776
calcium behenate monolayers, mol. orientation determ. by IR absorpt. 79−11423
calcium behenate monomolecular layers between Al electrodes, nonlinear dielec. props. 80−80405
calcium bromide hexamethanol solvates, cryst. struct. *(French)* 78−34500
calcium cadmium acetate hexahydrate, Mn^{2+} doped, EPR 79−65715
calcium copper acetate hexahydrate, $CaCu(CH_3COO)_4.6H_2O$ and $CaCu(CD_3COO)_4.6H_2O$, antiferromag. transition obs. 78−2680
calcium copper acetate hexahydrate, mag. susceptibility behaviour at low temp. 77−24679
calcium copper acetate hexahydrate, mag. susceptibility field depend. 79−87241
calcium copper acetate hexahydrate, PMR at low temp., atomic position determ. 77−20728
calcium copper acetate hexahydrate($-d_{12}$), tunnelling reson. effects in non-reson. spin-lattice relax. 79−86726
calcium di-DL-glycerate dihydrate, Ca binding, X-ray cryst. struct. determ. 79−46642
calcium dipicolinate trihydrate, IR and Raman spectra, isotopic frequency shift, mol. vibr. obs., point groups determ. 80−89001
calcium formate, intermolecular shielding contributions, proton mag. shielding 80−34783
α-calcium formate, neutron diffr., cryst. struct., 100 and 296K 77−59004
calcium formate, polycrystalline, heteronuclear dipolar modulated chemical shift spectra, geometrical and orientational obs. 77−20750
calcium formate, selective high resolution ^1H NMR 79−61245
calcium hydrogen dihomophthalate pentahydrate, cryst. struct. 77−15395
calcium malonate dihydrate, cryst. struct. 77−59003
calcium oxalate, biological mineralisation mechanism 78−31764
calcium oxalate hydrates, crystn. kinetics, comparison for mono-, di-, and trihydrates 80−81528
calcium oxalate monohydrate, IR and Raman spectra, vibrational studes 80−69139
calcium oxalate trihydrate and monohydrate, dissolution kinetics charact. by SEM 79−42250
calcium phthalate monohydrate, single cryst., X-ray cryst. struct. refinement 79−14790
calcium propionate monohydrate, cryst. struct. 77−76385
calcium stearate, Van der Waals forces, direct meas. 78−43461
calcium strontium propionate, compressed powder, dielectric props., particle size effects 77−59503
calcium tartrate tetrahydrate:Cr^{3+}, optical absorpt. spectrum, cryst. field parameters 80−16067
calcium tartrate tetrahydrate:Cu^{2+}, spin-orbit coupling, optical absorpt. spectra 80−45120
calcium tartrate tetrahydrate:Ni^{2+} optical absorpt. spectrum 78−84610
calcium tartrate tetrahydrate:VO^{2+}, optical absorption spectrum 78−6713
calcium tartrate tetrahydrate, X-ray irrad. single cryst., free radical EPR 77−63936
dl-2,3-camphanedione, elec. cond., brittle-to-plastic region, cond. jump 78−39169
camphene, plastic cryst., ^{13}C NMR obs. 79−95667
dl-camphene, self-diffusion, effect of impurities, radiotracer and plastic deform. study 78−43177
camphene, simulation of grain boundary groove migration at solid-liquid interface 78−52789
camphene-coated surface, convective local mass-transfer coeffs., holographic interferometry method 78−75234
(X)-D-camphor, circularly dichroic band at 3000 Å, RPA calc. 78−94267
camphor, d- and dl-solns. in carbon tetrachloride, electro-optical Kerr effect 79−91406
d-camphor, high resolution ^{13}C NMR spectra, 275 to 343K 79−56621
d-camphor, NO diffusion, ELDOR, self-diffusion 77−1618
d-camphor, optical rot. dispersion spectra, solvent effects 77−10684
camphor, orientational disordering, thermodynamic props., stat. mech. model 80−96453
d-camphor, plastic crysts., impurity size effect on self-diffusion 77−11727
camphor, rhombohedral, polycryst., compressive deform. and dynamic recrystn. 80−71698
camphor crystals, investigation of structural formation and growth kinetics 79−47610
Camphor Fourier transform IR vibrational circular dichroism 79−99845
camphor methyl groups internal rotation, ^{13}C spin lattice relaxation times and force field calcs. 80−74255
camphor odorant, nose stimulation, olfactory evoked brain pot., correl. anal. of recorded waveforms from human scalp *(Japanese)* 80−97946
dl-camphor oxime, elec. cond., brittle-to-plastic region, cond. jump 78−39169
camphor separated optical isomers, inverted IR Lamb dips, IR-RF double reson. obs. 78−21951
d-camphor systems, mol. reorientation dynamics, Raman spectra 78−31178

organic compounds continued
dl-camphoric anhydride, elec. cond., brittle-to-plastic region, cond. jump 78−39169
camphorquinone, cryst., PMDR and fluoresc., S_2 state, intersystem crossing 77−32296
camphorquinone, vapour, nonradiative electronic relax. rate, excess energy depend. 77−38687
d-10-camphorsulphonic acid ammonium salts, charact. rel. to spectropolarimetry 77−24816
n-caproic acid, colloidal dissolution in water 79−66358
caproic acid, dielectric meas. at microwave freqs. 79−19827
caprolactam oligomers, low-mol. wt., crystallisation kinetics from melt, solid structs. *(Russian)* 79−69034
capronate, proton spin-lattice relaxation in various phases *(Russian)* 80−97163
capsular polysaccharide antigen, structure investig. by ^{13}C NMR 80−35828
carbamide phosphate, neutron diffr. 77−31652
carbamides, electronic absorpt. spectra, expt. and CNDO calcs. *(Russian)* 78−37647
carbamylmethylenephosphonate solvent extraction processes for nuclear wastes 77−26861
carbazine 720, single freq. CW dye laser operation in 690-700 nm gap 80−99719
carbazole:tetracene, electronic absorpt. spectrum, host-cryst. field effect 80−100669
carbazole, birefr. meas., 20 to 190°C, crystal-to-crystal phase transform. 80−45031
carbazole, CNDO/S and CI calcs., photoelectron spectrum assignment 77−67982
carbazole, crystalline, room temp. afterglow 78−27314
carbazole, excited state, dissociation rate, normal isotope effect 77−32767
carbazole, in presence of KI, decay functions of triplet state of fluoresc. and phosphoresc. 78−66590
carbazole, mol. orbital study, spin-unrestricted, donor and acceptor states 78−9077
carbazole, multiexponential fluorescence decay, systems theory approach to anal. 79−59495
carbazole, photoelectron spectroscopy obs. of heterocycles 78−94286
carbazole, triplet state of X-traps, ODMR 79−24231
carbazole, two photon absorptivities, CNDO/S-CI calc. with second order time depend. perturbation eqns. 80−74122
carbazole cation radical, optical absorpt. spectra 77−40564
carbazole dispersed in benzene polycryst. host, active N_2 induced chemilum. 80−60691
carbazole H-bonded complex formation, enthalpy change due to electronic excitation, spectroscopic determ. 78−92496
carbazoles, luminescence, $AgNO_3$ heavy atom effect, donor-acceptor interaction *(German)* 78−84651
carbazolyl substituted diacetylene monomer cryst., ODMR and triplet state kinetics 78−76355
N-carbazolyl-$(CH_2)_n$-tetrachlorophthalimide, (n=2,3,4,7) intramol. electron donor-acceptor system, photophys. 78−82763
carbene in polydiacetylene, zero field splitting parameter 78−27075
carbenes, bond angles, inversion barriers, singlet-triplet energy differences, struct. fragments method 77−10782
carbenes, core ionised states, singlet and triplet state binding energy, struct. changes, LCAO-SCF calc. 79−97982
carbenes, heterosubstituted, singlet-triplet splitting depend. on heteroatom electronegativity and conform. 80−63553
carbenes, triplet state g-tensors and hyperfine coupling tensors 80−52895
carbenes, unrestricted HF calcs. of electronic structure 77−6683
2-carbethoxy-4-aminoindole, liquid scintillator, γ-irrad., energy transfer and quenching 77−8622
2-carbethoxy-4-aminoindole, soln., liq. scintillator, UV excitation, energy transfer and quenching 78−64395
2-carbethoxy-5-chloro-7-aminoindole, liquid scintillator, γ-irrad., energy transfer and quenching 77−8622
2-carbethoxy-5-chloro-7-aminoindole, soln., liq. scintillator, UV excitation, energy transfer and quenching 78−64395
carbocations, degenerate $(CH)_N^+$ type, permutation description *(German)* 79−45658
carbocyanin dye, amplification and absorpt. from excited state *(Russian)* 77−54707
carbocyanine dye CW laser emission, spectral range extension up to 1020 nm 78−74901
carbocyanine dye lasers, synchronous pumping, extension of spectral range 80−5731
carbocyanine dye orientation in erythrocyte membrane, microscopic fluorescence polarisation obs. 79−83694
carbocyanine dye solns., photoisomerisation and internal conversion rates, time-resolved spectra 77−75201
carbocyanine dyes, fluoresc. probes, effect on Ca-depend. K efflux 77−12896
carbocyanine dyes, sterically hindered short-lived isomers, laser photolysis study 78−40063
carbocyanine dyes, triplet state quenching by nitroxyl radical, charge transfer complexing 78−25585
carbocyanines, dye laser appls., soln. chem. 77−40568
carbohydrate compounds, X-irrad., trapped electrons, ESR and ENDOR obs. 80−93161
carbohydrate membrane, potassium p-nitrophenoxide transport, ionic equilibria perturbation by cyclodextrin 79−96523
carbohydrate on intradiscal surface of retinal rod discs 77−4998
carbohydrate soln., γ-irradiated, fluoresc. spectra obs. *(Russian)* 77−83644
carbohydrate solutions, irradiated, lyoluminesc. and carbohydrate peroxy radical reactions 77−48665
carbohydrates, reactions with hydrated electrons and hydroxyl radicals, rate constants obs. 80−50825
carbon disulphide, refr. index, temp. depend., deviation from Lorentz-Lorenz. formula 77−40200
carbon phenolic, pulsed/CW laser beam-surface impact, transient momentum transfer 77−89013
carbon tetrabromide, ^{13}C NMR in liq., FCC plastic cryst. and monoclinic cryst. 79−78549
carbon tetrabromide, Brillouin scatt., plastic-liquid transition 77−32389
carbon tetrabromide, cryst. growth from melt, dissolution morphology *(German)* 77−24283
carbon tetrabromide, disordered phase, neutron, diffuse scatt. 80−79717

organic compounds continued
carbon tetrabromide, disordered phase, neutron diffuse scattering 80−79716
carbon tetrabromide, inherent moisture as purity probe *(German)* 77−85933
carbon tetrabromide, ordered, polymorphism 78−22700
carbon tetrabromide, ordered phases, polymorphism obs. 80−54217
carbon tetrabromide, phase I cryst. struct. 78−18626
carbon tetrabromide, phase II cryst. struct. 78−18623
carbon tetrabromide, plastic phase, orientational disorder 79−73115
carbon tetrabromide, solid, Raman spectrum, temp. depend. 78−52488
carbon tetrabromide, valence-shell MO calc. with pseudopot. 78−907
carbon tetrabromide, vapour deposition for optical studies, Raman spectra 78−64451
carbon tetrachloride, adsorbed on silica, laser Raman spectrum 77−3367
carbon tetrachloride, adsorption on Fe (100), AES, LEED, work function, and thermal desorption study 80−15376
carbon tetrachloride, atm. conc. meas. in southern hemisphere 79−5602
carbon tetrachloride, Auger electron spectra and chem. shift 78−90231
carbon tetrachloride, binary liquid mixtures, excess free vol. calcs. 80−34202
carbon tetrachloride, charge exchange mass spectra 80−43177
carbon tetrachloride, chemisorption on Si, SiO_2 and Si_3N_4, role in plasma etching 79−11714
carbon tetrachloride, Cl isotopes thermodifusion 79−90810
carbon tetrachloride, clusters, collision induced polarisability, mol. frame distortion 80−32798
carbon tetrachloride, complex refractive index meas. at mm and sub-mm wavelength 77−82595
carbon tetrachloride, cryst. cond mol. struct. determ. 79−77559
carbon tetrachloride, cryst. phase transformations at atm. pressure *(French)* 77−84920
carbon tetrachloride, detect. in ambient air by gas chromatography 78−85739
carbon tetrachloride, drops, on brass surface, Leidenfrost pt., press. effect 78−87784
carbon tetrachloride, dual melting curves and metastability 80−92647
carbon tetrachloride, elec. breakdown mechanism, high speed photography expts. 79−91367
carbon tetrachloride, emulsion dispersed, metastable phases at high press. *(French)* 77−56253
carbon tetrachloride, equation of state studied using statistical theory results 80−84276
carbon tetrachloride, freezing and melting of stable and metastable phases 77−27984
carbon tetrachloride, generalised transport coeffs., hydrodynamic eqn. 78−87803
carbon tetrachloride, in porous medium, allotropic and liq.-solid-solid transformations *(French)* 78−83944
carbon tetrachloride, inner-shell excitation and EXAFS-type phenomena 79−13828
carbon tetrachloride, intense ps pulse excitation, multiple stimulated Raman spectra 78−66867
carbon tetrachloride, internucl. parameters meas. using total scatt. of fast electrons 80−32857
carbon tetrachloride, isotopically selective dissociation by NH_3 laser radiation 79−41206
carbon tetrachloride, isotropically selective dissoc. by NH_3 laser radiation 78−17815
carbon tetrachloride, isotropy, mol. interactions, effects, Raman scatt. obs. 78−58697
carbon tetrachloride, laser generated acoustic wave press. saturation, absorptivity at higher laser power 79−60435
carbon tetrachloride, liq., Brillouin scatt. for vibr. relax. time 79−4806
carbon tetrachloride, liq., diamagnetism, mass mag. suscept. meas., temp. depend. 80−97054
carbon tetrachloride, liq., diffusion, free vol. theory, Macedo-Litovitz eqn. 77−51530
carbon tetrachloride, liq., luminesc. on giant ps. pulse irrad., spectral and time characts. *(French)* 78−88348
carbon tetrachloride, liq., self-diffusion coeff., temp. and density depend. 78−91461
carbon tetrachloride, liq. and plastic cryst. phases, thermodynamic props., light scatt., US propag. 78−2863
carbon tetrachloride, liq. struct. by neutron diffr. 79−73089
carbon tetrachloride, liq. struct. by pulsed neutron diffr. 79−69004
carbon tetrachloride, liquid, under high press., refr. index vs. density 79−28712
carbon tetrachloride, low-energy X-ray emission spectra, MO anal., ionis. pot., rel. to CH_4 and $CHCl_3$ 79−85975
carbon tetrachloride, M-X bond flexibility, by compliance scheme 80−37805
carbon tetrachloride, mol. characts. from fast low-angle scatt. 77−50537
carbon tetrachloride, mol. cryst., US absorption, rel. to lattice vibrs. 77−24358
carbon tetrachloride, mol. struct. factors, X-ray diffr. 77−76291
carbon tetrachloride, mol. vibr. excitation, photodissoc., in strong IR field *(Russian)* 79−89721
carbon tetrachloride, neat and cyclohexane mixture, nonlinear susceptibility, $\chi^{(3)}$, reson. and non-reson. contribs. 79−987
carbon tetrachloride, non-polar liq., microwave induced Kerr effect meas. 78−76435
carbon tetrachloride, optical props. under press., molecular polarisability depend. on thermodynamical state 78−80312
carbon tetrachloride, ordered phases, polymorphism obs. 80−54217
carbon tetrachloride, phase transform. process, energy-dispersive X-ray diffractometry 80−96631
carbon tetrachloride, photochem. reactions with aromatic amines, initiation mechanism 79−61888
carbon tetrachloride, polarized light scatt., relaxation processes 80−60615
carbon tetrachloride, polymorphism, solid-solid phase transformations 77−62499
carbon tetrachloride, prep. of glassy state, DTA 77−24388
carbon tetrachloride, quantitation using GC peaks 79−20479
carbon tetrachloride, quenching effects on scintillation yield of dioxane liq. scintillators *(French)* 77−3217
carbon tetrachloride, Rayleigh scatt. from liq. near solidification temp. 79−4807
carbon tetrachloride, Rayleigh scattering, depolarisation ratios 77−32387

organic compounds continued
carbon tetrachloride, refr. index temp. depend., deviation from Lorentz-Lorenz formula 77−40200
carbon tetrachloride, solid, phase transition, Raman study 78−80345
carbon tetrachloride, solid, Raman and far IR spectra 79−33680
carbon tetrachloride, solid, Raman study of phase transition and dynamic struct. 80−34916
carbon tetrachloride, Stokes wave phase fluctuations in stimulated light scatt. *(Russian)* 80−87436
carbon tetrachloride, struct., oscill. amp., neutron diffr. study 79−46544
carbon tetrachloride, superheated liquid, growth of spherical bubbles, anal., numerical calcs. 77−24399
carbon tetrachloride, supersaturated vapour, photonucleation 79−7682
carbon tetrachloride, surface study, ellipticity coeff., ellipsometric method 80−84343
carbon tetrachloride, thermal cond. and phase diagram under pressure 78−75893
carbon tetrachloride, thermal cond. meas. by transient hot wire method 77−30144
carbon tetrachloride, transport coefficients for a fluid of square-well rough spheres 79−55634
carbon tetrachloride, US vel., 265-435K 80−6464
carbon tetrachloride, vac. UV absorpt. cross section 80−91574
carbon tetrachloride, vac. UV absorpt. spectra, 250-115 nm 77−79628
carbon tetrachloride, volume effect in metastability of crystalline phases on cooling 79−77716
carbon tetrachloride+$Ba \rightarrow BaCl_2+CCl_2(\tilde{A})$, chemiluminesc. spectrum and ang. distrib. obs. 79−15962
carbon tetrachloride+$Ba(^1S,^3D)$, $Sr(^1S,^3P)$, chem. reaction products, laser-induced fluoresc. obs. 79−66270
carbon tetrachloride+Ca reaction, laser-induced fluoresc. obs. 80−11916
carbon tetrachloride+Kr, differential elastic scatt. cross-section 79−45784
carbon tetrachloride+$Xe(6s,^3P_2)$, vibr. energy disposal from XCl* spectrum 79−100345
carbon tetrachloride aqueous hetero-azeotrope mixture, condensation heat transfer coeff. *(German)* 80−33425
carbon tetrachloride dil. solns., ellipsoidal cavity model, electro-optical quantities *(French)* 78−35114
carbon tetrachloride drops falling through H_2O, surfactants rel. to deform., oscill. *(French)* 80−66880
carbon tetrachloride in benzene, positronium inhibition by Cl 77−8678
carbon tetrachloride liq. struct., TOF pulsed neutron diffraction using electron linac 78−18504
carbon tetrachloride soln. of Br, adsorpt. of Br on C 78−10273
carbon tetrachloride with 2,2-diethoxypropane, excess enthalpy *(French)* 78−11542
carbon tetrachloride with aromatic amines mixture, theoretical evaluation of US vel. 80−39224
carbon tetrachloride-1-octanol (5-methylheptanol-3)(acetic acid) dilute solns., dielec. consts., dipole moments, H bonding investig. 77−48673
carbon tetrachloride-acetic acid, US absorption, coupled dimerisation cyclisation reaction *(French)* 79−42148
carbon tetrachloride-acetone (chloroform) mixtures, film boiling on elec. heated horizontal wire, atm. press. 77−20061
carbon tetrachloride-$AsCl_3$ mixture, purification by selective photodissociation 77−79708
carbon tetrachloride-benzene, liq. mixture, excess Gruneisen parameter, intermol. interaction 78−67635
carbon tetrachloride-benzene(cyclohexane), binary liq. mixtures, molar heat capacity isothermal compressibility 79−66328
carbon tetrachloride-benzene-cyclohexane system, quaternary diffusion, capillary-cell method using ^{14}C labelling 78−87800
carbon tetrachloride-chloroform (methyl cyanide) solutions, anisotropic light scatt., interactions between solvent and solute mols. 78−27239
carbon tetrachloride-cyclohexane mixture, Dufour effect, Onsager heat-mass reciprocal relation 78−34638
carbon tetrachloride-EBBA, binary liq. cryst. system, two-phase premelting, NMR obs. *(Russian)* 78−30743
carbon tetrachloride-ethanol (methanol), binary soln. with mol. assoc., interdiffusion anal. 79−55912
carbon tetrachloride-$GaCl_3$-Nd^{3+} nontoxic liquid phosphor system, synthesis 80−55157
carbon tetrachloride-heptane, SF_6 electron scavenging in positron spur in nonpolar liqs. 79−100421
carbon tetrachloride-I_2 soln., ps dye laser excitation, fluoresc. and resonance Raman emission 80−28021
carbon tetrachloride-I_2-water system, mass transfer in pulsed perforated plate column 78−71385
carbon tetrachloride-methanol, soln., Raman spectra in OH(OD) stretching region *(French)* 79−26986
carbon tetrachloride-n-octanol-water miscible liq. systems, isopiestic vapour press. meas., activity coeffs. determ. 77−48679
carbon tetrachloride-o-cresol-acetophenone (ethylmethylketone) (ethylacetate) mixtures, intermolecular interaction, US vel. meas. 80−79879
carbon tetrachloride-perfluoroethylcyclohexane, crit. mixture, brilliant total refl. from liq.-liq. interface 79−90786
carbon tetrachloride-pyridine(anisole)(acrylontrile)(acetyl-acetone) mixtures, excess volume of mixing, mol. interactions 79−57281
carbon tetrachloride-tetrachloroethylene binary mixtures, dielec. polarisations 79−56713
carbon tetrachloride-water soln., fundamental H_2O IR spectrum, liq. struct. 80−23419
carbon tetrachloride-xylene, liquid mixtures, excess free vol. US vel. meas. 77−51294
carbon tetrafluoride, atmospheric content, sources and residence time 80−61879
carbon tetrafluoride, atmospheric content meas. 79−34927
carbon tetrafluoride, clusters, collision induced polarisability, mol. frame distortion 80−32798
carbon tetrafluoride, compressed gas, ν_1 vibr. Raman line 78−32884
carbon tetrafluoride, intensities of binary overtones and combinations in IR spectrum 78−55172
carbon tetrafluoride, laser parameters with optical pumping 79−72557
carbon tetrafluoride, lasing action, spectroscopy of features near 9 μm lines 79−22944
carbon tetrafluoride, liq. and plastic crystn., Raman spectra 77−59565
carbon tetrafluoride, liquid, comparison on interaction induced light scatt. and IR absorption 80−60561
carbon tetrafluoride, molecular effects in F K-shell ionisation by 0.5 to 1.5 MeV protons 77−50515

organic compounds continued
carbon tetrafluoride, valence-shell MO calc. with pseudopot. 78−907
carbon tetrafluoride, vib. anharmonicity 78−55160
carbon tetrafluoride, weak absorpt. spectra of $\nu_2+\nu_4$ vibr. using CO_2 laser 80−5762
carbon tetrafluoride+4% O_2 plasma, Si etch rate uniformity 80−40568
carbon tetrafluoride+H scattering, obs. of resonance maximum 77−58126
carbon tetrafluoride+methyl trichlorosilane, reaction, metastable C phase prod. 79−29341
carbon tetrafluoride+SiC(Si), reaction, metastable C phase prod. 79−29393
carbon tetrafluoride 16 μm laser, radiance enhancement 78−87045
carbon tetrafluoride $^{12}CF_4$ laser, Doppler-limited absorption spectroscopy 80−74347
carbon tetrafluoride $^{12}CF_4$ optically pumped laser efficiency 80−74348
carbon tetrafluoride laser, CF_4 molecule $\nu_3+\nu_4$ band optical pumping 80−74349
carbon tetrafluoride laser, emission spectrum in 16 micron range, CO_2 laser stimulation 80−9870
carbon tetrafluoride laser, frequencies of pump and laser transitions 79−94218
carbon tetrafluoride laser, high energy output in 16 μm region, CO_2 laser pump 79−89927
carbon tetrafluoride laser, optically pumped, freq. tuning 80−28208
carbon tetrafluoride laser, weakly forbidden vibr.-rot transitions 79−55121
carbon tetrafluoride laser oscillator amplifier meas., small signal gain and self-absorpt. 79−59683
carbon tetrafluoride laser with optical pumping, freq. tuning and stabilisation 80−99706
carbon tetrafluoride mols., electron scavenging studied by electron cyclotron reson. 79−50143
carbon tetrafluoride optically pumped laser, pulse-periodic operation, 0.2 W average output power 79−27247
carbon tetrafluoride optically pumped laser, spectroscopic characts. 79−89896
carbon tetrafluoride optically pumped laser, stimulated emission stabilisation and tuning 80−9866
carbon tetrafluoride plasma, loading effect and temp. depend. of etch rate of Si, SiO_2 and Si_3N_4 79−34167
carbon tetrafluoride pulsed laser characts., optically pumped by CO_2 laser 80−91778
carbon tetrahalides, matrix photodissoc. and photoionisation by inert gas reson. radiation 77−83587
carbon tetraiodide, ordered phases, polymorphism obs. 80−54217
carbonaceous chondrites, organic polymer anal. rel. to organic matter origin in early solar system 78−20767
carbonaceous insulating films, RF diode sputtering growth, IR absorpt. and Rutherford backscatt. meas. 79−99458
carbonaceous material, electron-optical image contrast, comparison of theory and expt. 77−10142
carbonaceous mesophase, formation at lower temps. 79−90524
carbonaceous mesophase spherules, new mol. arrangement in mag. field, orientation behaviour 79−94869
carbonaceous surface contamination growth on ion bombard. 77−90229
carbonic acids and solutions in $SnCl_4$, spin echo obs. of self-diffusion *(Russian)* 79−95197
carbonic anhydrase, active site substrate binding, environmental effects, CNDO and SCF LCAO calcs. 80−8002
carbonium ions, adsorption on porous Vycor glass, reson. Raman spectra 78−84571
carbonized bitumen, refractive index and absorpt. coeff. as measures of structural organization 79−35811
carbonized bitumens and pyrobitumens, studies of molecular struct. using microscope photometry 80−18011
carbontetrachloride+N, CN quartet state production, fluoresc. anal. 78−68888
carbonyl anion radicals, electron transfer with anthracene-amine cation radicals, triplet state electrogeneration 80−63803
carbonyl chlorofluoride, rot. Zeeman effect, g-factors and mag. suscept. anisotropies, microwave meas. *(German)* 77−57993
carbonyl compounds, ^{13}C chem. shifts, approximate SCF perturbation theory 77−6804
carbonyl compounds, core electron binding energy shifts, σ- and π-relax. energies 78−29750
carbonyl compounds, empirical pot. model EPEN/2, development, parameter testing 79−54934
carbonyl compounds, interpretation of Raman spectra 79−18193
carbonyl compounds, localisation of $n\pi^*$ excitation, config. interaction method 78−50482
carbonyl compounds O X-ray emission spectra, Kα line 77−28653
carbonyl fluoride, IR laser driven reverse internal conversion 79−81230
carbonyl fluoride, laser excited IR fluoresc. C=O and C-F stretching modes 78−21960
carbonyl fluoride, transformation and compliance matrices determ. 77−18898
carbonyl fluoride, triplet state, trapped electron ICR spectrosc. 79−59373
carbonyl fluoride, vertical electronic states, ab initio SCF CI calc. 79−49942
carbonyl fluoride, vibr. transition moments and force fields, gaussian basis set calcs. 79−81152
carbonyl frequency correlation of aromatic derivatives with nonaromatic analogues 79−22709
carbonyl group, mag. rot. strength of spin-forbidden transitions 77−14468
carbonyl group stretching freq. force consts., CNDO/2 and localised orbitals calc. 77−30784
carbonyl groups, intermol. interactions in H_2CO-H_2CO system, quantum chem., classical calcs. 78−86932
carbonyl groups, spin-lattice relax. mechanism, mathematical relaxation model *(German)* 80−80633
carbonyl halogen substituted cpds., geometric and electronic struct., LCAO-SCF calc. 79−89603
carbonyl oxide, config. interaction calc., using DODS natural orbit approach 78−66476
carbonyl sulphide, roto-vibrational molecular laser scaling, CO_2-TEA laser pumped 80−5728
carbonyl to oxacarbene rearrangement, conformation, ab initio SCF MO calcs. 77−32780

organic compounds continued
carbonyl-containing biological molecules, UV photoelectron spectra 77−88498
carbonyls, all-reactive-electrons closed-shell SCF-CI MO calcs. 79−36541
o-carborane, dielectric permittivity meas. *(French)* 79−71480
carborane, ortho- and para-, phase transition and mol. reorientation, isomer effects, PMR obs. 80−80628
carborane anion, ^{11}B NMR 78−90190
carboranes, ab initio 6-3G and 3G/MODPOT LCAO-MO-SCF calcs. 79−10026
carboranes, small cage, antipodal H-H coupling 80−1003
3-carboxy-2,2,5,5-tetramethylpyrrolidinyl 1-oxyl system, enantiomer solid soln., cryst. struct. and phase diagram 79−86778
carboxyl groups, $-COO^-$, $-COOH$, $-COOCH_3$, bond lengths and angles relations 80−53158
carboxyl groups, H_2 bonded, C-O vs. O-H length correlation using neutron diffr. data 79−54987
n-carboxylic acid, IR-spectra and dimeric molecules normal vibr. *(Russian)* 77−77218
carboxylic acid dimer, Fermi reson. 79−31501
carboxylic acid film, on Al, heat treatment effect on photoluminesc. props. 77−28610
carboxylic acid metallic salts, laminated cpds., nature of cond. *(Russian)* 79−42512
carboxylic acid systems, H(D) complexes and dimers, ν_{CO} IR band intensities 80−63715
carboxylic acid-ethanol systems, proton exchange process kinetics, effect of H bond strength in intermediate state *(Russian)* 79−96306
carboxylic acid-fluoride system, H---F bond, ab initio MO study 79−76528
carboxylic acids, diamag. susceptibility of carbonyl group 77−75329
n-carboxylic acids, IR spectra, normal vibrs. forms and freqs. *(Russian)* 79−91450
carboxylic acids+urea, γ-irradiated reactions under high pressure *(Japanese)* 79−52707
carboxylic acids in aqueous soln., complex form. with metal ions, thermodynamic parameters *(Italian)* 77−48669
carboxylic esters, γ-irrad. glass, trapped radical photolysis, ESR 78−85178
carboxymethylcellulose, aq. soln., hydrodynamics of falling liquid film *(Russian)* 79−64715
carboxymethylcellulose, aq. soln., real flow curve determ., with wall effects, in rotation viscosimeters *(Russian)* 79−64714
carboxymethylcellulose soln., flow in profile channel of extrusion head 79−98780
carbyne, π-electronic struct., alternant MO method 78−62708
carbyne and interstellar grains 78−69859
d-3-carene, differential Raman scatt. of right and left circularly polarized light *(Japanese)* 78−17675
carnauba wax, and rosin mixtures, hetero- to homocharge transition, temp. depend. *(Japanese)* 78−35082
carnauba wax, orientation prod., by mech. press. or US waves 78−64314
carnauba wax, thermal electret, persistency of surface charge *(Japanese)* 77−81048
carnauba wax, thermoelectret, lattice parameter changes at elevated temps. 80−29674
carnauba wax thermoelectret, mag. anisotropy evidence for dipolar orientation 77−16240
β-carotene, ν_1 line shape, CARS and CSRS 78−82727
trans-β-carotene, coherent anti-Stokes Raman spectra 77−79169
β-carotene, coherent anti-Stokes reson. Raman spectrum excitation profiles 77−56342
β-carotene, elec. cond. depend. on chemisorbed O_2, use as vacuum gauge *(Czech)* 77−139
β-carotene, excitation profile of ν_2 line in resonance Raman spectrum, solvent effects 80−74173
β-carotene, Franck-Condon effects in resonance Raman spectra and excitation profiles 80−14129
β-carotene, in CS_2, reson. Raman spectra, room temp. 78−35803
β-carotene, optical absorpt., theory 79−62189
β-carotene, orientated in nematic liq. crysts., UV-visible dichroism meas. *(German)* 77−34668
β-carotene, quenching of chlorophyll-a fluoresc. in phosphatidyl choline bilayers 79−20506
trans-β-carotene, Raman excitation profile spectra, prereson. region 78−33514
β-carotene, resonance CARS results 79−6189
β- carotene, valence bands, XPS obs. 78−24030
β-carotene, very dilute benzene soln., picosecond reson. Raman spectroscopy 79−98102
β-carotene in PVC matrix, photo-oxidation *(French)* 79−34327
β-carotene quenching of chlorophyll fluoresc. 77−52735
carotenoid pigments, in geochem. systems, HPLC determ. 78−61078
carotenoid pigments, radical ions, radiolysis generation, absorpt. spectra, MO calcs. 77−65488
carotenoids related to visual chromophore, electronic struct., band shape model 78−20142
β-carotin, resonance Raman effect *(Hungarian)* 78−74666
l-carvone, optical rot. dispersion spectra, solvent effects 77−10684
dl-carvoxim, order parameters and lattice energy, mean field approx. 78−22688
castor oil, viscosity and solidification press., 0-10^4 Pa, 20-180°C 77−43266
castor oil, viscosity meas. under nonisothermal conditions with rotary viscosimeter 79−68664
catalase, electron microscope exam. of new cryst. form, Fourier transform. method 77−11447
catalase+H_2O_2, effect of mag. field on decomposition rate 79−52631
catechol, solid, H bonding, wide line NMR obs. 78−52362
catechol borane, geometry, electronic absorpt. spectra 80−971
catecholamines, role in cardiac pacemaking 77−70437
catecholamines in kitten brain, ocular dominance shift failure after monocular occlusion 77−1998
cations, extraction from acid soln. by elec. field, mass spectrometric anal. 79−66390
CBNA, nematic-isotropic transition at high press., turbidity meas. 80−92655
CBOOA:nitroxide, liq. cryst. phase transition study by electron spin relax. *(French)* 79−55874

organic compounds continued
CBOOA, acoustic emission at liq. cryst. transitions prod. by thermo-optically excited defects 79−95137
CBOOA, isotropic, nematic, smectic-A phases, Brillouin scatt. 80−11421
CBOOA, liq. cryst., mag. aligned, smectic A-nematic transition, US absorpt meas. 78−95137
CBOOA, liq. cryst., nematic to smectic A transition, high resolution X-ray scatt. exam. 78−94984
CBOOA, liq. cryst., smectic A to nematic phase transition, crit. neutron scatt. 78−95135
CBOOA, liq. cryst., twist viscosity and mech. props. near smectic A-nematic transition 78−95136
CBOOA, liq. cryst. of strong positive dielec. anisotropy, static dielec. consts. meas. 78−2790
CBOOA, liq. cryst.-isotropic transition at high press., P-V-T eqn. of state 79−95135
CBOOA, nematic and smectic, anisotropic shear viscosity meas. 77−15310
CBOOA, nematic phase laser light scatt., mag. field depend., crit. deform. *(Japanese)* 78−2826
CBOOA, nematic-smectic transition, singularities, elastic const. var. 77−39537
CBOOA, smectic A, nematic and isotropic phases, surface tension 77−39539
CBOOA, smectic A order parameter meas. and crit. scatt. near smectic A⇄nematic phase transition 77−84649
CBOOA, smectic A phase, specific volume and layer spacing, X-ray diffr. and dilatometry meas. 79−55659
CBOOA, smectic A-nematic transition, X-ray and light scatt. obs. 79−95129
CBOOA, smectic-A reentrant nematic transition under press., X-ray obs. 80−59637
CBOOA, smectic-A-nematic and nematic-isotropic transitions, vol. behaviour 77−39666
CBOOA, smectogenic, cryst. and mol. struct. determ. 78−2103
CBOOA, temp. depend. of apparent viscosity and density 78−18542
CBOOA, US absorpt. and dispersion at nematic-smectic-A transition 79−82287
CBOOA, US attenuation near nematic-smectic A transition 78−87773
CBOOA, with cholesterol decanoate, short range smectic A order in nematic phase, NMR meas. 77−28475
CBOOA film, freely suspended, smectic A layer spacing, optical determ. 80−64883
CBOOA/4-cyanobenzylidene-4′-n-octyloxybiphenyl mixture, reentrant nematic phases 79−41953
celenious acid, rel. determ. of protons coordinates using moments of NMR spectra 79−60239
cellobiose, vibr. spectrum, freq. calcs. *(Russian)* 78−21909
cellophane, props. for membranes in disposable haemodialysers 77−78049
cellophane film condenser transducer, operation in air, 0-100 kHz 78−42509
cellulose, from N.American trees, D/H ratios rel. to palaeoclimatology (9500-22000 BP) 77−60462
cellulose, proton and photon induced X-ray emission anal., depth sensitivity 78−23988
cellulose, with adsorbed water, NMR relaxation times 79−78552
cellulose acetate, solid state track detector, sensitisation technique *(Chinese)* 79−22558
cellulose acetate membrane water permeab. at low press., nature of flow 77−73467
cellulose acetate membrane water permeab. at low press., temp. var. 77−73466
cellulose complexes with pyredene and its derivatives, photosensitivity *(Russian)* 80−73506
cellulose membranes bearing ATPase, permeabilities, dynamic, meas. under non-equilib. conditions 80−46107
cellulose nitrate, detect. of ion beam in HV electron microscope 78−45755
cellulose nitrate, nonlinear viscoelastic deform., hydrostatic press. and third invariant of deviatoric stress tensor 80−93587
cellulose nitrate (CN) detectors, effect of pre-irrad. thermal treatment on track revealing props. 78−94168
cellulose nitrate film, ion track density, quantitative assessment using Fourier transform techniques 79−86610
cellulose nitrate film ion data, dark-field illum. image recording photographic method 80−70031
cellulose nitrate foils, personnel neutron dosimetry meas. by induced molecular wt. changes 79−59269
cellulose nitrate thin foil manufacture for α particle track detector *(Spanish)* 80−74091
cellulose triacetate, for electrochem. etching of fast neutron induced recoil tracks 80−91406
cellulose triacetate, vibr. spectra, theory 79−54836
central rigid cores, mesogenic power, depolarised Rayleigh scatt. study 80−89012
cephalosporins, radiation-sterilisation by γ-irrad. 80−66822
cerebron, thermotropic and lyotropic mesomorphism 80−76703
ceresin wax magnetoelectret, X-ray diffr. pattern 78−6014
cerium ethylsulphate, elec. susceptibility evidence for electronically driven lattice dilation 77−76781
cetane, Aerosil suspension, thermal cond. rel. to elec. field, struct. form. 77−9138
cetyl orange monolayers on water surface, reson. Raman spectra 79−91434
cetyl pyridinium bromide, adsorpt. on Aerosil, pH depend., mechanism 79−20466
cetyliodide, cryst. phase transitions, mol. dynamics, spectroscopic and dielectric meas *(Russian)* 79−51965
4-n-cetyloxy-N-4′-cyanophenyl benzamide, thermotropic liq. cryst. behaviour, optical microscopy obs. 79−32895
cetyltrimethylammonium bromide, aq. soln., mol. conform., laser Raman spectra 78−21934
cetyltrimethylammonium bromide, micellar soln., internal elec. fields, linear dichroism obs. 77−86325
cetyltrimethylammonium bromide, micelles, solubilised nitroxide spin probes, ESR 78−21950
cetyltrimethylammonium bromide and chloride aqueous micelle, fluoresc. showing coexistence of rod-like and globular struct. 79−61910
cetyltrimethylammonium bromide-1-butanol system, micellar conc. meas. using fluoresc. probe study 80−85217

organic compounds continued
CF_3X^+ cations, (X=Cl, Br, I, H), IR spectra in Ar matrix 78−74710
CH-OH, rotationally inelastic collisions, maser action 79−94068
chain mols., conformational transition kinetics 80−83339
charge transfer complex, mixed-stack crystalline, phonon bands 78−75767
charge transfer complexes, doped, excited cryst., fine and hyperfine struct., ESR 77−12188
charge transfer complexes, refl. spectra, excitons 79−47477
charge transfer complexes, solid, positron annihilation and ang. correl. meas. 79−87521
charge transfer salt process for high-density video storage 80−43269
charge transfer salts, valence bond theory 79−73473
charge-transfer salts, comparison of ESR spectra 80−50164
charge-transfer salts, neutral-ionic interface, energy states and mag. props., VB anal. 79−4537
charge-transfer salts, strongly correlated, interband absorpt., long-range Coulomb interaction 79−4525
charged excitonic complexes, coupled states, exciton interaction with charge carriers study 80−20090
chemistry courses, unified approach to teaching of struct. and bonding 80−17732
Chichibabin's hydrocarbon, ESR spectra, electron exchange integral 78−50562
chiral smectic C, ferroelec. props., dielec. meas. 78−52463
chiral substituted dibenzo[b,f][1,4-diazocines in nematic MBBA, helical twisting power 78−34431
chitin, in lobster shell and apodeme, piezoelec. rel. to remodelling 78−64929
chloral, dielec. consts. and dielec. losses meas. 77−20795
chloral, in benzene, permittivity, dielectric loss, 36 GHz 77−32323
chloral, liq., permittivity, dielec. loss, up to 60 GHz 78−60384
chloral hydrate, phase transform. rate, ^{35}Cl NQR rate 80−54983
chloramine, HOCl, isoelectronic mols., vap. phase UV photoelectron spectra, struct. 78−66600
chloramine T, adsorption on bentonite 79−92001
o-chloranil, adsorbed on phthalocyanine films, effect on surface photovoltage 80−34485
chloranil, electron affinity, bound and excited negative ion states, lifetimes, electron and alkali metal collisions 79−869
chloranil, mol. cryst., soft mode and central peak neutron scatt., struct. transition 79−42209
chloranil, neutron superlattice reflection, soft phonon and central peak scatt., phase transition 78−18732
chloranil, NQR press. depend. 77−12225
chloranil, phase transition, Zeeman effect of ^{35}Cl NQR 78−59944
chloranil, use in free radical form., obs. in stretched vinylidene chloride copolymer 79−61923
p-chloranil+tetrachlorohydroquinone, H atom abstraction by p-chloranil triplet 78−80720
chloranil and radical anion, Raman and IR freq. shifts 78−33516
p-chloranil crystal/cyanine dye monolayer, charge carrier injection rate const. determ., energy transfer vs. charge transfer method 79−83031
chloranil pellets, thermally stimulated discharge current and dielectric studies 80−93236
p-chloranil-N,N,N′,N′-tetramethyl-p-phenylenediamine, optical spectra, temp. and environment effects 79−54861
p- chloraniline cryst., lattice vibr., IR and Raman spectra, lattice energy 78−56481
chlordane, in soils of Everglades National Park and adjacent agricultural areas 79−92098
chlorides, NQR, crystal splitting, bonding effects 77−12221
chlorin, ab initio CI calcs. on ground, singlet and excited states, visible spectrum 79−16139
chlorin, electronic struct. props. and photosynthesis 80−16902
chlorin, UV absorption and photoelectron spectra, CNDO/S3 calcs. 77−75210
chlorin in n-alkane host, photoautomerisation and hole-burning 79−47954
chlorinated hydrocarbons, background levels in air over S.Norway 79−12239
chlorinated hydrocarbons in ambient air, washout effect and diurnal var. 78−28305
chlorinated naphthalene, Kerr electro-optic coeff. 77−4625
chlorinated organics, conc. meas. in urban runoff 79−24923
4-chloro, 3-nitrotoluene, partially aligned in elec. field, ^{13}C NMR, dipole moment determ. 80−78633
chloro(2,4-dithiobiuret)copper(I)-N,N-dimethylformamide, cryst. and mol. struct. 79−99170
chloro(ethyl)silanes and its C derivatives, Raman spectra, mol. vibr. and rot. isomerism 80−87134
6-chloro 2,4-dimethoxypyrimidine, ^{35}Cl NQR, Zeeman effect 80−18874
α-chloro radical in X-irradiated 5-chlorodeoxyuridine single crysts., ESR, ENDOR 77−4916
2- chloro-1,3,2-dioxa-arsolane, temp. depend. of NQR spectra parameters of ^{75}As and ^{35}Cl 80−20494
2- chloro-1,3,2-X, Y-arsolanes, temp. depend. of NQR spectra parameters of ^{75}As and ^{35}Cl 80−20494
3-chloro-1,3,4-triphenylazetidin-2-one, phase refinement, random approach to struct. determ. 79−10747
3-chloro-1-butene, rot. isomerism, vibr. spectra assignments 78−58702
chloro-1-propanol, ^{38}Cl for Cl substitution, optical enantiomers use 78−73031
1-chloro-2,2-dimethylpropane, IR and Raman spectra, vibr. assignment 80−74169
1-chloro-2-methylbutane, conformer depend. C-Cl stretching vibrs., Raman optical activity spectrum simulation 80−14146
3-chloro-2-methylpentane, IR spectra of film, rot. isomerism 79−59595
1-chloro-2-methylpropane, IR and Raman spectra, vibr. assignment 80−74169
4-chloro-2-nitrobenzoic acid, ^{35}Cl NQR 79−50044
2-chloro-2-nitropropane, far IR-microwave estimation of binary collision approx. 80−55095
2-chloro-3-fluoro-1-propene, struct. and conformers, force field and vibr. amplitudes 78−25747
4-chloro-3-nitrobenzotrifluoride-benzene (carbon tetrachloride) dilute soln., dielec. relax. time, dipole moment, microwave obs. 78−35084
4-chloro-3-nitrotoluene, IR absorpt. spectra, vibr. assignments 78−42048
4-chloro-3-nitrotoluene-benzene (carbon tetrachloride) dilute soln., dielec. relax. time, dipole moment, microwave obs. 78−35084

organic compounds continued
trans-3-endo-chloro-4-(phenylthio)-9,10-cis-endo-bis(methoxycarbonyl)tricyclo[4,2,2,$0^{2,5}$]dec-7-ene, cryst. and mol. struct. 79−90639
2-chloro-4-methylpentane, IR spectra of film, rot. isomerism 79−59595
2-chloro-4-nitroaniline, nonlinear optical susceptibility, second order, calc. from mol. spectra *(Russian)* 79−27318
2-chloro-6-methyl benzonitrile, vibr. spectra 79−89665
1-chloro-9,10-anthraquinone crystal, electronic structure of lowest triplet state *(Japanese)* 79−8158
6-chloro-α-pyridine anthraquinone, cryst. and mol. struct., X-ray diffr. meas. 77−43206
4-chloro-α-toluothiol, liq., dielectric relax. mechanisms 79−42891
3-chloro-diphenyl-dimethylsulphoxide, diagonalized tensor of rot. diffusion, main components *(German)* 78−31121
chloro-hydrocarbons, interaction between atmospheric pollutants *(French)* 80−7976
2-chloro-p-nitroaniline, in benzene soln., dipole moment from solute relax. time-solvent viscosity relation 80−37905
z-chloro-p-nitroaniline, soln., dielectric const., loss and relax., dipole moment 78−43782
chloroacetaldehyde, s-trans conformation barrier height 77−61872
α-chloroacetamide, alkoxy radical form., effect, of α-hydroxyacetamide, ESR study 80−80610
chloroacetamide, X-irrad., ESR of $CH_2ClCO^{\cdot}$ radical 78−76882
m-chloroacetanilide, cryst., ^{35}Cl NQR, Zeeman effect 77−8443
chloroacetanilides, NQR freqs., torsional vibr., temp. var. 78−2766
α-chloroacetic acid, ^{35}Cl and ^{37}Cl pure NQR, H bonding, isotope effects 78−27111
chloroacetic acid, acid salts, NQR obs. of H-bond pot. energy curves 77−18941
chloroacetic acid, NQR press. depend. 77−12225
chloroacetic acid, soln., vibr., IR spectra 80−63633
chloroacetoacetanilides, NQR freqs., torsional vibr., temp. var. 78−2766
chloroacetylene, harmonic and anharmonic stretching force consts., ab initio calcs. 78−58587
chloroacetylene decomposition, unimolecular lifetime and relative translational energy distribs. 80−25994
chloroacetylene dissoc. and predissoc., state selected unimolecular reaction dynamics 77−36744
chloroalkanes, modified Urey-Bradley force field calcs. 78−25500
chloroalkanes, vapour-liq. equilib. and heats of mixing, simplified group method anal. 80−96637
chloroaluminium phthalocyanine, sublimed layer, IR absorption, vibr. assignments 78−55174
p-chloroaniline, IR spectra of cryst. at low temp. 79−38533
o-chloroaniline-iso-octane, crit. system, comp. depend. of absorpt., US obs. *(German)* 80−19879
o-chloroaniline-iso-octane critical system, US absorpt. meas. 77−51440
o-chloroaniline-n-heptane, crit. system, comp. depend. of absorpt., US obs. *(German)* 80−19879
chloroanilines, corrosion inhibitors for the Al alloy in trichloroacetic acid 79−83389
2-chloroanisole, and sulphur analogue, benzene dipole moment anal. 78−25748
chloroanisoles, ^{35}Cl NQR, inter- and intramol. interactions 80−63666
2-chloroanthracene:acridine, electrolum. at 300K 79−15531
chloroaromatics, mol. crysts. Cl atom pot. energy calcs. 78−42948
chlorobenzaldehyde, $a^3A'' \rightarrow X^1A'$ phosphoresc., conformations and ground state fundamentals 80−78642
p-chlorobenzaldehyde, p-dibromobenzene and p-dimethoxybenzene hosts, dipole moments, lowest electronic states 77−18954
p-chlorobenzaldehyde, Stark effect on electron spin transition in zero-field 77−27099
p-chlorobenzaldehyde and deuterated derivs., vibrational spectra 79−3441
p-chlorobenzaldehyde in methylcyclohexane, matrix perdeuteration effects on $^3\pi\pi^* \rightarrow S_0$ phosphoresc. 77−20903
p-chlorobenzene, and deuterated forms, in p-dibromobenzene and p-dimethoxybenzene, 4.2K, $\pi\pi^*$ phosphoresc. assignments 78−9197
chlorobenzene, dielectric time-domain spectrosc., short and refl. method 80−101805
chlorobenzene, gas phase electron diffr. struct. determ. 80−69251
chlorobenzene, HF dielec. relax. test for extended Nee Zwanzig formula 79−33602
chlorobenzene, in CCl_4 soln., quadratic changes in elec. permittivity, intermol. interactions 77−73107
chlorobenzene, in organic soln., soln., positronium formation inhibited by chlorobenzene 79−50170
chlorobenzene, in potassium laurate mesophase, NMR, proton distance ratios and order tensor elements calcs. 80−63672
chlorobenzene, liq., spin lattice relax. time, elec. field induced charges 80−44945
chlorobenzene, liq., vibr. relax., Brillouin scatt. and US vel. meas. 79−77692
chlorobenzene, liquid, submillimetre wave dispersive Fourier transform spectroscopy obs. 77−37915
chlorobenzene, liquid, under high press., refr. index vs. density 79−28712
chlorobenzene, liquid, vibr. relaxation, Brillouin spectra 80−108219
chlorobenzene, nonlinear dielectric effect temp. depend. 79−87372
p-chlorobenzene, NQR press. depend. 77−12225
chlorobenzene, optical Kerr const., electronic and orientational contribs., obs. by coherent Raman techniques 77−88874
chlorobenzene, optoacoustic spectroscopy using cell with ultimate corrosion resistance 80−42269
chlorobenzene, permitt. meas. by transmission time domain spectroscopy 77−67462
chlorobenzene, photoelectron spectra ang. distrib., π- and σ-orbital assignments 79−818
chlorobenzene, S_0-S_1 transitions, two-photon absorpt. spectra by nozzle beam-multiphoton ionisation method 80−63728
chlorobenzene, saturable absorpt. of CO_2 laser 80−69465
chlorobenzene, self-diffusivity data 78−6169
chlorobenzene drops falling freely through water, breakup 80−69899
chlorobenzene in cyclohexane dilute soln., far IR absorption obs. 77−40250
chlorobenzene in EBBA, ^1H, D NMR and NQR, geometric struct. 78−17689
chlorobenzene ion fragmentation, kinetic shift and phenyl ion heat at formation, photoelectron-photoion coincidence meas. 80−25998

organic compounds continued
chlorobenzene submillimetric permittivity obs. and Debye eqn. extrapolation 77−40173
chlorobenzene-bromobenzene, perfect binary liquid mixtures on silica gel, adsorption thermodynamics 80−44428
chlorobenzene-cis-decalin, mixtures, dielec. const. and loss tangent in liq. and solid phases 80−100628
chlorobenzene-cis-decalin mixtures, phase transitions and dielec. behaviour study in 77-330K 80−29680
chlorobenzene-d_0, -d_1, mol. reorientation and D nucl. relax. time, temp. depend. 78−39424
chlorobenzene-d_5, and isotopic forms, microwave spectrum, rot. consts. 78−58667
chlorobenzenes, substituted, NQR freqs. 80−20504
chlorobenzenes determination by gas chromatography with photoionis. detection, air and biological samples 80−35809
chlorobenzenes in benzene, positronium inhibition by Cl 77−8678
o-chlorobenzoic acid: Nd^{3+} (Pr^{3+}) solid, vibrational spectra 80−84758
o-chlorobenzoic acid, solid, H bonding, wide line NMR obs. 78−52362
chlorobenzotrifluoride, benzene soln., permittivity and dielec. loss 78−64320
p-(N-chlorobenzylidene)-p-chloraniline, cryst., polymorphism, cryst. struct. rel. to mol. conform. 78−75611
p-chlorobenzylidene-p-n-pentylaniline, metastable phases formed by rapid cooling of mesophase, IR and Raman spectra and DSC obs. 80−34919
o-chlorobromobenzene, phase transition evidence from far IR absorption and Raman spectra 79−33693
p-chlorobromobenzene, single cryst., polarised Raman and IR spectra, assignments 78−60431
p-chlorobromobenzene, spectral meas. of static interaction changes in molecular crystals *(Ukrainian)* 78−6708
p-chlorobromobenzene in p-dichlorobenzene cryst., absorpt. spectra, mol. clusters static interaction 78−15198
trans-1,4-chlorobromocyclohexane, liquid, crystalline and amorphous state, conformation and vibr. spectra, IR obs. 80−60568
2-chlorobuta-1,3-diene, far IR and Raman spectra, internal rot. 79−89668
4-chlorobutyrylchloride, Raman and vibr. IR spectra of solid and liq., rot. isomerism 78−62810
chlorocarbon industry impact on atmospheric O_3 layer 78−40648
chlorocyanoacetylene, cryst., IR, far-IR and Raman spectra, vibr., struct. 77−63407
chlorocyclohexane, US relaxation 80−24540
chlorocyclohexanes, o-Ps yield in nonpolar solvents, rel. to chlorinated ethenes and ethanes 79−70357
5-chlorodeoxyuridine, X-irrad., α-chloro radical ESR and ENDOR 77−4916
chlorodifluoroethane, CW laser induced reactions, activation energies, temps. and rate consts 80−40710
chlorodifluoroethane, CW laser-induced reaction, vibr. rate enhancement obs. 80−11922
chlorodifluoromethane, heat absorbed when laser irrad., laser calorimetry 79−16012
chlorodifluoromethane, IR multiphoton dissoc., CF_2 form., time-resolved optical absorption obs. 80−16702
chlorodifluoromethane, IR multiphoton dissoc., mag. field effect 80−93772
chlorodifluoromethane, IR multiphoton dissociation, laser intensity effects, fluoresc. obs. 79−98168
chlorodifluoromethane, laser induced decomp., nonthermal reaction 79−20387
chlorodifluoromethane, laser-induced decomp. rate, laser fluoresc. investig. 79−68257
chlorodifluoromethane, photoacoustic spectra meas. at CO_2 laser wavelengths 80−18849
chlorodifluoromethane, unimol. reaction by IR radiation, rate consts. and prod. yield, fluence and intensity depend. 80−97713
chlorodifluoromethane subMM wave laser, optically pumped 80−87376
chlorodifluoromethyl cation, transient species, matrix isolation spectra 78−48635
3-chlorodiphenyl, in dipolar aprotic solvent, internal rot. barrier, ^{13}C T_1, obs. 78−29860
chloroethane, reson. multiphoton dissoc. 80−53077
chloroethane+T, recoil reaction, 5×10^{-2} torr 78−44389
chloroethane diradical, MINDO/3 for optimised geometry and heat of form. 78−78830
chloroethane molecular ion, laser induced photodissoc. in gas phase 79−94048
chloroethane-d_1, laser multiphoton dissoc., intramolecular isotope effect 78−17733
chloroethanes, electro-optical parameters, Raman spectra absolute intensities and depolaris. 77−10678
chloroethanes, o-Ps yield in nonpolar solvents, rel. to chlorinated ethenes and cylcohexanes 79−70357
2-chloroethanol, IR and Raman spectra, normal coord. anal., isomerism 78−74661
chloroethenes, o-Ps yield in nonpolar solvents, rel. to chlorinated ethanes and cyclohexanes 79−70357
2-chloroethyl radical, struct., ab initio calcs. 80−83252
chloroethylene, adsorbed on silica, laser Raman spectra 77−3367
chloroethylene, CO_2 laser absorption, Stark modulation 78−17671
chlorofluorobenzene cations in gaseous phase, emission spectra and lifetimes in B(0°) states 80−63711
chlorofluorobenzenes, He(Iα) and He(IIα) photoelectron spectra, assignments, ionis. energies 80−78651
chlorofluorocarbene, ($^1A''$) state, radiative lifetime, quenching rate, press. depend., laser-induced fluoresc. obs. 78−5259
chlorofluorocarbons, photodecomposition under simulated tropospheric conditions *(German)* 79−53408
chlorofluorocarbons, stratospheric photodissoc., residence times 78−53703
chlorofluorocarbons 11 and 12, in atmosphere, observability of possible removal processes 77−25773
chlorofluorocarbons and ozone depletion in the lower atmosphere 79−53498
chlorofluorocarbons in stratosphere, NO photolysis rel. to effects on O_3 layer 77−29399
chlorofluorocarbons in stratosphere, O_3 layer depletion calc. using two-dimensional model 80−109221
chlorofluoroethane, multiphoton dissoc. under CO_2 laser irrad., decomposing mol. energy distrib. 80−30251

organic compounds continued
chlorofluoroethanes, gas, photoabsorption cross-sections, 46-100 Å 78−42095
chlorofluoromethane, computer based policy analysis to reduce human health impacts 80−89698
chlorofluoromethane, mol. centrifugal distortion and Urey-Bradley force field 79−89807
chlorofluoromethane cations in solid Ar, absorpt. spectra and photochem. 79−96339
chlorofluoromethane depth profiles in Norwegian Sea 78−73405
chlorofluoromethane effects on stratospheric O_3 *(German)* 79−20959
chlorofluoromethane induced IR cooling of atm., effect on general circulation model 80−90122
chlorofluoromethane IR radiation, effect on zonal atmospheric temp. 79−80019
chlorofluoromethane photolysis in stratosphere, effect on O_3 conc. 80−109197
chlorofluoromethanes, ^{18}F recoil labelling 79−52732
chlorofluoromethanes, atm. O_3 depletion, two-dimens. time-depend. model 78−24341
chlorofluoromethanes, $CHFCl_2$ and CHF_2Cl, diffusion and chem. reaction 77−70804
chlorofluoromethanes, collision-free multiphoton dissoc., X CF_2 translational energy meas. 78−92491
chlorofluoromethanes, contradiction of stratospheric O_3 depletion prediction 78−49099
chlorofluoromethanes, electron attachment, electron swarm method 80−69245
chlorofluoromethanes, electron energy loss spectra, oscill. strengths 78−58846
chlorofluoromethanes, electron impact excitation, resons. and dissoc. attachment 79−7020
chlorofluoromethanes, gas, photoabsorption cross-sections, 46-100 Å 78−42095
chlorofluoromethanes, ideal gas thermodynamic props., mol. struct. 77−3912
chlorofluoromethanes, laser photolysis, product vibr. relax. rates and diffusion coeffs. 80−55680
chlorofluoromethanes, liq., NMR spin-lattice and dielec. relax. 79−33604
chlorofluoromethanes, MS Xα calcs., ionis. pots., electron affinities 77−79540
chlorofluoromethanes, negative ion form. by 0.10 eV near-monoenergetic electron impact 79−41245
chlorofluoromethanes, valence photoelectron spectra, electronic and vibr. bands 78−50582
chlorofluoromethanes CCl_2F_2 and CCl_3F in Wuppertal-Dusseldorf region, ground level meas. 78−73478
chlorofluoromethanes effect on atm. surface temp. 79−70832
chlorofluoromethanes in lower stratosphere, latitudinal profiles 78−44989
chlorofluoromethanes in stratosphere, vertical distrib. 78−73476
chlorofluoromethanes in upper troposphere and lower stratosphere, vertical distrib. 78−73477
chlorofluoromethylene, radical, laser-induced fluoresc. excitation spectra 79−98131
chlorofluoromethylene radical, gas phase laser-induced floresc. spectroscopy 80−14173
chlorofluromethane + $O(^1D)$, stratospheric chem. reactions 79−53499
chloroform, absolute Raman intensities determ. 77−68046
chloroform, adsorbed on silica, laser Raman spectrum 77−3367
chloroform, adsorption by activated and impregnated carbons 77−70333
chloroform, and d, polar soln., Raman line shape of ν, band 78−74705
chloroform, Auger electron spectra and chem. shift 78−90231
chloroform, charge exchange mass spectra 80−43177
chloroform, dense liq., mol. reorientation and shear viscosity 77−4213
chloroform, detect. in ambient air by gas chromatography 78−85739
chloroform, dielectric constant effect on nuclear spin-spin coupling constants 79−72240
chloroform, drops, on brass surface, Leidenfrost pt., press. effect 78−87784
chloroform, effect on conductivity and time of adhesion of lipid membranes 79−53070
chloroform, electroviscous effect, AC characts. 79−99341
chloroform, electroviscous effect, AC characts. 79−99342
chloroform, highly excited vibr. states, thermal lensing spectrosc. and local mode model 80−87140
chloroform, in isotropic MBBA, nucl. spin-lattice relax., reorientation 79−4735
chloroform, inner-shell excitation and EXAFS-type phenomena 79−13828
chloroform, internal field factor, rot. correlation calc. 77−449
chloroform, isothermal Joule-Thomson coeff. 80−43828
chloroform, laser, energy transfer from D_2, 4-5 μm 77−88701
chloroform, liq., crit. fluctuations, proton spin relax. obs. 78−19358
chloroform, liq., diamagnetism, mass mag. suscept. meas., temp. depend. 80−97054
chloroform, liq., light scatt. coeff. determ., absolute method 78−2868
chloroform., liq., two-photon absorpt. meas., using nonlinear light mixing spectroscopy 77−79620
chloroform, liq., X-ray diffr., struct. of mol. in liq. 78−26421
chloroform, liq. vibr.-translational energy exchange, temp. depend., Brillouin scatt. obs. 79−73959
chloroform, liq.-gas transition, crit. dynamics nuclear relax. 78−75805
chloroform, optical constants and dispersion eqns. 80−30762
chloroform, production from polyelectrolytes 77−78252
chloroform, quenching effects on scintillation yield of dioxane liq. scintillators *(French)* 77−3217
chloroform, refr. index, temp. depend., deviation from Lorentz-Lorenz formula 77−40200
chloroform, rot. rough sphere friction, hydrodynamic boundary conditions 78−9926
chloroform, second virial coeff. meas. using new apparatus 80−44289
D-chloroform, soln., Raman scattering tensor components 80−99508
chloroform, solns., vibr. dephasing and reorientational relax., solvent depend., Raman spectra 79−85968
chloroform, variable energy blast wave, shock trajectories, flow field densities 77−68620
chloroform, volume effect in metastability of crystalline phases on cooling 79−77716
chloroform $-d_0$, $-d_1$, absolute Raman intensities and force fields 77−71808

organic compounds continued
chloroform and -d, Raman spectra study of mol. reorientation 79−24303
chloroform delayed depolarisation obs. *(Russian)* 79−95703
chloroform diluted in CS_2, proton transverse relax. time and reorientation of chloroform *(French)* 77−32280
chloroform HV polarisation and space charge obs. *(Russian)* 80−25277
chloroform. liq., reson. nonlinear susceptibilities using IR optical parametric oscillator 79−10347
chloroform. liquid, RIMS calc. of struct. 79−37610
chloroform molecule, liq. phase, Faraday rot. dispersion near vibr. reson. 79−91413
chloroform sorption effect on cross-linked polyester film struct. *(Russian)* 80−59405
chloroform-acetone, liq. mixture, excess Gruneisen parameter, intermol. interaction 78−67635
chloroform-carbon tetrachloride mixture, Lennard-Jones pots., mol. dynamics calcs. 78−34418
chloroform-carbon tetrachloride solutions, anisotropic light scatt., interactions between solvent and solute mols. 78−27239
chloroform-chlorobenzene, isobaric vap.-liq. equilib. 79−73299
chloroform-d_0(-d_1), Raman and IR intensity anal. 80−18857
chloroform-d_1, and isotopic forms, liq., neutron diffr. obs. 79−32878
chloroform-d_1, D NMR relax., in nematic liq. cryst., motion spectral densities determ. 77−63304
chloroform-d_1, isotropy, mol. interactions, effects, Raman scatt. obs. 78−58697
chloroform-d_1, Raman scatt., intermol. vibr. coupling effects 77−58026
chloroform-d_1 + $H^* \rightarrow HD + CCl_3$, hot atom reaction, threshold energy meas. 78−44356
chloroform-d, liq., neutron diffr., struct. of mol. in liq. 78−26422
chloroform-d and di-n-butyl ether, complex formation, IR spectra, book contrib. 78−21931
chloroform-d in soln., vibr. and reorientational relax., Raman study 80−63636
chloroform-d-acetonitrile-d_3, IR spectra liq. and solid at −180°C. *(French)* 78−15154
D-chloroform-dimethylsulphoxide, soln., Raman scattering tensor components 80−99508
chloroform-ethanol solns., light scatt. spectra, conc. fluctuations, assoc. complex form. 77−40254
chloroform-He(Ar)(N_2) gaseous compressed mixture, mol. reorientation, Raman spectra 80−23422
chloroform-hexamethylphosphoramide complex, mol. motion and assoc., PMR obs. *(French)* 78−72429
chloroform-methanol mixtures, thermodynamic props. 79−87865
chloroform-n-hexane, liq. mixture, radiolysis, mechanism, rate consts. 78−20039
chloroform-p-dioxan and chloroform-benzene mixtures, mol. reorientation and assoc., depolarised Raman scatt. obs. 80−7341
chloroform-paraffin system chem. changes after ^{60}Co γ-irradiation, dosimetry appl. 80−30258
chloroform-tetrahydrofuran system, excess free energies and vols. 79−82357
chloroform-triethylamine mixture, US absorption, 7.56 MHz 77−39630
chloroform-water-ethanol mixture, light scatt. near plait point 78−72532
chlorohaemin, ferric porphyrins with fifth ligands, ^{57}Fe and ^{14}N hyperfine consts. 78−50475
trans-1,4-chloroiodocyclohexane, liquid, crystalline and amorphous state, conformation and vibr. spectra, IR obs. 80−60568
p-chloromercuribenzene sulphonate blocking and reversal of amiloride effect on rabbit colon Na transport 78−44479
chloromethane, and isotopes, $\nu_2+\nu_3$ band, Coriolis reson. with $\nu_3+\nu_5$ band *(French)* 78−5229
chloromethane, charge exchange mass spectra 80−43177
chloromethane, collisional rot.-line widths and shifts, microwave region 78−25619
chloromethane, dielectric susceptibility at radio frequencies 78−14123
chloromethane, IR spectrum, evidence for $2\nu_3$ overtone 79−68226
chloromethane, liq., transient stimulated vibr. Raman scatt. 78−71144
chloromethane, low density gas, proton spin-lattice relax., mol. reorientation 79−3462
chloromethane, microwave rot. absorpt. lines, press. broadened width and shift 77−61807
chloromethane, microwave spectrum, width and shift parameters 77−18985
chloromethane, mol., valence and core ionis. energy, RHF-SCF and PNO-CEPA calc. 79−85890
chloromethane, mol. dipole moment derivative, sign of 79−86082
chloromethane, mol. vibr., radial distrib. function of vibr. excited mol. 79−85951
chloromethane, rot. dynamics, far IR spectra 77−19864
chloromethane, second dielectric virial coeff. of polar gas, temp. depend. *(German)* 78−26234
chloromethane, vibr., rot. and translational energy exchange, semiclassical theory 80−48067
chloromethane+Cl^+, reactions at room temp. 80−93749
chloromethane+Cl^-, S_N2 reaction, local orbital description, ab initio FSGO method 78−76842
chloromethane+Ne^+, thermal energy, reaction rate coeffs. and product distrib. 79−29333
chloromethane+OH, mean collision cross sections from microwave spectroscopy 80−1046
chloromethane+OH, rot. inelastic collision, microwave spectra 79−45806
chloromethane gas, linear electro-optical effect 80−87843
chloromethane in atmosphere, biomass burning as source 80−26586
chloromethane-d_2, microwave spectrum, rot. consts. 78−9140
chloromethane-d_3, A_0 determ. from ν_4 Raman band obs. 78−82737
chloromethane-d_3, and isotopic forms, optically pumped mm laser transition assignments, 792 micron line 78−42328
chloromethane-d_3, multiphoton IR C-Cl dissoc. classical trajectory calc. 78−11532
chloromethanes, Auger electron spectra and chem. shift 78−90231
chloromethanes, elec. bond moments calcs. *(French)* 79−36562
chloromethanes, fluorescence quenching of indole due to electron transfer 79−94027
chloromethanes, inner-shell excitation and EXAFS-type phenomena 79−13828
chloromethanes, vapour phase, Kerr effect temp. depend., polarisability and hyperpolarisability 79−31568
chloromethanes, VUV fluoresc., UV multiphoton dissoc. 80−28076

organic compounds continued
chloromethoxyyaniline, NQR freqs., torsional vibr., temp. var. 78−2766
chloromethyl cyclopropane, microwave spectra and struct. 79−36625
chloromethyl formate, conformation potential energy surfaces, ab initio calcs. 80−69065
chloromethyl formate(-d_1,d_2,d_3), gas, solid. and liq., IR spectra assignments and struct. 80−32715
chloromethyl methyl ether, on-column reaction GC determ. in ambient air 78−20093
chloromethyl oxirane, microwave spectra and conformations of cis and gauche-2 forms 80−5534
chloromethylene radical, MINDO/3 for optimised geometry and heat of form. 78−78830
chloromethylethyl ether, GT isomer, microwave spectra and geom. config. 79−59444
chloronaphtalene, stimulated diffusion induced by two photon absorption *(French)* 78−90455
α-chloronaphthalene, -Z 78−64318
1-chloronaphthalene, A^1A'-X^1A' electronic transition, rot. band contour 79−6935
chloronaphthalene, bond and mol. polarisability, semi-empirical delta-function 79−31441
2-chloronaphthalene, elastic props. exam. by Brillouin scatt., rel. to polymorphism 79−77669
α-chloronaphthalene, IR absorption spectra, forbidden character 77−58002
2-chloronaphthalene, order disorder transition, 253 to 309K, X-ray diffr., calorimetry study 78−75829
β-chloronaphthalene, thermodynamic functions calcs. 298-1500K 77−31418
2-chloronaphthalene, vibr. and calorimetric investigation of polymorphism 78−87641
m-chloronitrobenzene, cryst., low freq. vibrs., polarised Raman and IR spectra study *(French)* 80−16029
m-chloronitrobenzene, crystal growth from soln., obs. of surface steps using cine camera 77−76341
chloronitrobenzene, IR spectral intensity, N-O group in aromatic ring 79−41199
m-chloronitrobenzene, molecular crystals, translational and orientational vibr. determ. 80−55103
p-chloronitrobenzene, struct. determ. by electron diffr., influence of NO_2 group on C-Cl bond 80−69251
o-chloronitrobenzene-benzene (carbon tetrachloride) dilute soln., dielec. relax. time, dipole moment, microwave obs. 78−35084
p-chloronitrobenzene-p-bromonitrobenzene system, growth rate depend. of solid soln. supersaturation 77−1804
chloronitrotoluenes, ^{35}Cl NQR temp. depend. 80−106334
chloroparaffins, lubrication of Ti alloys, friction and wear *(Russian)* 80−93657
chloropentafluoroethane, isotopically selective multiphoton dissoc., CO_2-laser wavelength, pressure and additives effects 80−78666
chloropentafluoroethane, multiphoton dissoc., crossed laser and mol. beam obs. 80−11908
chloropentafluoroethane-(He)(Xe)$(O_2)(H_2)$(NO), multiphoton dissoc., ^{13}C enrichment factor, CO_2 laser wavelength and fluence depend. 80−58331
β-chlorophenetole, UV and IR electronic and vibr. spectra, model assignments 77−10673
o-chlorophenol+base, binary liquid mixture, excess vol., viscosity 77−21408
4-chlorophenol+N,N-dimethylmethanesulphonamide, assoc., PMR 78−23941
o-chlorophenol+o(m)-toluidine, H-bonded mol. complex, microwave absorpt., dipole moment and relax. times 80−14134
2-chlorophenol and sulphur analogue, benzene dipole moment anal. 78−25748
o-chlorophenol-acetone (ethyl methyl ketone), thermodynamic and transport props. 80−92686
chlorophenols, ^{35}Cl NQR, inter- and intramol. interactions 80−63666
chlorophenols in surface waters, 1976-7 obs. in Netherlands 80−16858
4-chlorophenoxy aluminium dibromide, intramolecular configs., nucl. quadrupole double reson. obs. 80−34821
4-chlorophenoxyacetyl-4-propenyl benzene, cryst. struct. 78−63750
chlorophyl-pheophytin pigment associations, conc. effects, luminesc., absorpt. spectra and dichroism obs. 80−1007
chlorophyll, -a and -b, fluoresc. fading curve of lowest triplet state 79−36691
chlorophyll, -a and -b in cyclohexane soln., far IR and reson. Raman spectra 77−48753
chlorophyll, and related mols., in solid solns., fine-structured vibronic spectra under tunable dye laser excitation *(Russian)* 80−74164
chlorophyll, charge transfer across oil-water interface, effect of dielec. const. 77−70419
chlorophyll, colloidal solns., elec. charge of particles 80−94438
chlorophyll, distrib. in Lake Tahoe, California-Nevada, effects of coastal front 79−2301
chlorophyll, electron transfer across octane-water interface 77−81474
chlorophyll, energy migration between native forms at −196°C using sensitised fluoresc. 77−70429
chlorophyll, energy trapping dynamics in photosynthetic unit model 78−88697
chlorophyll, enhancement of fluorescent mag. resonance detection, under intense laser excitation *(Russian)* 78−91995
chlorophyll, fluoresc. decay time depend. on luminesc. and excitation wavelengths 79−66447
chlorophyll, fluoresc. detection of triplet state kinetics 77−30903
chlorophyll, fluoresc. in bilayer lipid vesicles and liposomes, conc. quenching 77−4985
chlorophyll, fluorescence line obs. in passive remote sensing of phytoplankton 77−86938
chlorophyll, in maple leaf, −196-18°C, red shift explanation 78−61144
chlorophyll, in ocean, airborne remote sensing under cloudy sky 79−25359
chlorophyll, mol. electronic excitation interactions, transition monopole theory 78−22016
chlorophyll, native forms., var. fluoresc. at −196°C 77−70417
chlorophyll, photooxidation, triplet state mechanism 78−27791
chlorophyll, photosynthesis mechanism, upconversion, EPR and O_2 evolution data anal. 78−35811
chlorophyll, photosynthetic unit of H_2 evolution 77−77875
chlorophyll, singlet-triplet optical resonance in solid soln. 77−52741

organic compounds continued
chlorophyll, transfer of electronic excitation energy from monomer to dimer *(Russian)* 78−27289
chlorophyll *a*-lecithin mixed monolayer coated electrodes, highly efficient quantum conversion, solar energy appl. 79−39314
chlorophyll a: Cu^{2+}, in pyridine fluoresc. quenching mechanism 79−56837
chlorophyll a, absorpt. and fluoresc. spectra, observance of Stepanov relation 80−81554
chlorophyll a, bimol. quenching of excitons and fluoresc. in photosynthetic unit 77−16908
chlorophyll a, cation radical formation by pulse radiolysis, oxidation and demetalation rate consts. 80−61505
chlorophyll a, electronic struct. props. and photosynthesis 80−16902
chlorophyll a, fluoresc. at 685 nm, rel. to diffuse reflectance of ocean 79−66700
chlorophyll a, fluoresc. decay rate obs., inhomogeneous struct. and relax. time effects 79−86007
chlorophyll a, Langmuir-Blodgett films, deposition onto SnO_2 optically transparent electrode 80−80093
chlorophyll a, stimulated fluoresc. and fluoresc. quenching, pump photon density 78−27895
chlorophyll a and analogues, triplet state, phosphoresc. polaris. 79−39358
chlorophyll a and b, assoc. solns., excited state deactivation, flash photolysis obs. 79−54895
chlorophyll a and b, triplet state level positions 79−89706
chlorophyll a and protochlorophyll a, optical transitions anisotropy 79−43825
chlorophyll a delayed fluoresc. in absence of electron transport on acceptor side of photosystem 2 77−70428
chlorophyll a dihydrate photoelectrochemical cell 80−61387
chlorophyll a film, charge injection and storage 78−53317
chlorophyll a fluorescence duration in chloroplasts rel. to ferricyanide and vitamin K_3 conc. 77−25393
chlorophyll a in benzene solns. and monolayers, chem. stability 79−47912
chlorophyll a in photosynthetic material, luminesc. 79−34498
chlorophyll A low-intensity two-step absorpt. in vivo 78−35801
chlorophyll a of photosystem II, fluoresc. when electron transport on acceptor side is blocked 78−7324
chlorophyll a phosphorescence in cellulose triacetate polymer matrix 77−36867
chlorophyll a-containing phospholipid bilayer, photo-oxidation of water 77−16917
chlorophyll a-water interaction, NMR obs. in CCl_4 and trichloromethane 79−34501
chlorophyll adsorption films, electrochem. behaviour 78−31778
chlorophyll and analogues, role of O_2 in regeneration of photoreduced pigments in soln. 78−68980
chlorophyll and Mg-free derivatives, lasing and stimulated emission 77−52742
chlorophyll b derivatives, metal substitution effect on triplet state, intersystem crossing 77−88476
chlorophyll black lipid membranes in dil. electrolyte solns., bifacial tension meas. 79−16162
chlorophyll black lipid membranes photoelectric response, appl. to solar energy conversion 80−81482
chlorophyll concentration in sea, estimation from outgoing radiation spectrum meas. from helicopter 80−36333
chlorophyll excited stated, redox pots. 77−25372
chlorophyll fluorescence changes in isolated broken chloroplasts and involvement of elec. double layer 78−44464
chlorophyll fluorescence quenching by β-carotene 77−52735
chlorophyll in aqueous solns., electrochem. behaviour, cathodic reduction 79−29373
chlorophyll in marine dinoflagellates, photosynthetic characts. and organisation 79−5260
chlorophyll in Pacific and Atlantic oceans, gradient maps from U-2 aircraft platform 80−101385
chlorophyll in vesicles, energy transfer and fluorescence quenching 79−39349
chlorophyll in vitro, fluorescence quenching, exciton annihilation excited state absorption and stimulated emission 79−98137
chlorophyll mixed associates, intermol. interaction, energy transfer, luminesc. and absorpt. spectra 78−64924
chlorophyll monolayer electrodes, light energy conversion, photosynthesis electrochem. simulation 79−43833
chlorophyll photo-oxidation, role of singlet-excited and triplet states 80−51156
chlorophyll photo-oxidation, spectral detect. of exciplex in triplet state 77−25368
chlorophyll photo-oxidation by quinones, cation-radical yield 77−86442
chlorophyll photo-oxidation mechanism, effect of spectral composition of light 77−25369
chlorophyll photochemical activity, rel. to microviscosity of detergent micelles 77−21478
chlorophyll photoexcited aggregates, pigment-pigment electron transfer and charge separation 77−81468
chlorophyll pigments, aggregated forms in soln., spectral-luminesc. characts. *(Russian)* 78−23529
chlorophyll pigments of photosynthetising organisms redox pots. rel. to evolutionary development 77−56337
chlorophyll radical cations, NMR, hyperfine coupling 79−8482
chlorophyll solution, degenerate four wave mixing, phase conjugated backward wave generation *(Chinese)* 80−87429
chlorophyll solutions, photolum. of singlet O_2 78−80831
chlorophyll solutions, triplet state props., ODMR meas. 79−20517
chlorophyll special pair models, reaction centres 80−3574
chlorophyll spectral forms, Chlamydomonas mutants with inactive photosynthesis 80−51054
chlorophyll-a, conc. quenching rel. to functional charge transfer 80−30666
chlorophyll-a, crystalline film, energy levels and carrier generation by photocond. and fluoresc. 77−16909
chlorophyll-a, fluoresc. at low concs., noise reduction by low pass filter for DC signal 80−87249
chlorophyll-a, hydration, field desorpt. mass spectral obs. 80−71936
chlorophyll-a, interaction with β-carotene in phosphatidyl choline bilayers, fluoresc. quenching 79−20506
chlorophyll-a, laser action and excited singlet state absorpt. 77−27288

organic compounds continued
chlorophyll-a, microcryst., trapped-electron doping in photovoltaic sandwich cells 78−53334
chlorophyll-a, mol. interaction in monolayers and multilayers, IR obs. 77−71799
chlorophyll-a, mols. and complexes in PMMA and MTHF matrices, optical spectra 79−3433
chlorophyll-a, nonlinear absorpt. spectra 78−25522
chlorophyll-a, photoinduced electron transfer to duroquinone in micellar soln., charge separation 78−23955
chlorophyll-a, soln., luminesc. spectrum, impurity bands *(Russian)* 77−88493
chlorophyll-a, solns., vis. absorpt. spectra of monomer, dimer and oligomers 77−29101
chlorophyll-a, triplet and excited singlet optical absorpt. spectra 79−59477
chlorophyll-a (b), dimerisation, fluoresc. and ODMR study 80−18876
chlorophyll-a arrays, exciton transition calculations 78−35802
chlorophyll-a in metal-metal sandwich cell, photovoltaic, rectifying and tunnelling effects 79−1628
chlorophyll-a radical cation lifetime in water-acetonitrile soln. 80−72136
chlorophyll-a radical cations, in disordered systems, electron spin echo envelope modulation, isotope effects 78−61141
chlorophyll-b, mols. and complexes in PMMA and MTHF matrices, optical spectra 79−3433
chlorophyll-duroquinone photochemical interaction, photopot. 77−16903
chlorophyll-like molecules, fluoresc. and phosphoresc. polarisation spectra 79−85980
chlorophyllide fluorescence quantum yield during photochlorophyllide reduction in etiolated leaves 80−81542
chlorophylls, luminesc. analysis of triplet states *(Russian)* 78−27288
chlorophylls, mag. reson., site selected fluoresc. detection 80−69164
chlorophylls, triplet state ESR, fine struct. and rate consts. determ. 78−25574
chlorophylls, triplet state ESR, fine structs. and rate consts. determ. 78−25575
chlorophylls, zero field triplet spin sublevel ordering, magnetophotoselection obs. 77−42342
chlorophylls a and b and pheophytins, fluoresc. and phosphoresc. 80−12057
chloroplast discs, photoelectric response, appl. to solar energy conversion 80−81482
2-chloropropane, and deuterated derivatives, modified Urey-Bradley force field 77−27048
2-chloropropane, conformation, vibr. spectrum, from simple harmonic force field 78−33494
1-chloropropane, formation of chlorohexanes by ion-mol. reactions in radiolysis 78−27802
2-chloropropane, photoionisation mass spectrometry 80−40779
2-chloropropane, separation of collision-induced from intrinsic mol. depolaris. Rayleigh scatt., C-Cl bond optical anisotropy 78−27244
1-chloropropane 80−40779
chloropropyne, mol., He(I) photoelectron spectra 79−27033
1-chloropropyne cation, internal energy decay studied by photoelectron-photoion coincidence spectroscopy 80−69185
2-chloropyrimidine, CS_2 soln., mol. reorientation, ^1H, ^{13}C nucl. mag. relax. 78−27105
chloroquine-biopolymer binding interactions, PMR effects 80−55982
chloroquinolines, photophys. behaviour, substituent and solvent effects 80−106342
N-5-chlorosalicylideneaniline, H^+-^{14}N double reson. NQR spectra temp. depend. thermochromism and tautomeric mech. 78−70849
N-5′-chlorosalicylideneaniline, photochromism and thermochromism, NQR spectra, temp. and UV irrad. depend. 80−54968
N-chlorosuccinimide, lone-pair struct., photodetection spectra 78−37684
chlorotetracycline, fluoresc. probe detect. of cell Ca redistrib. during stimulus-secretion coupling 77−77872
2- chlorothiophene, σ^* anion radical, prod., ESR spectrum assignment 78−11539
o-chlorotoluene(-benzene), liq. and dilute soln., microwave absorption and relax. processes 79−82920
chlorotriflouromethane, UV photoelectron spectra, vibr. fine struct. 78−9196
chlorotrifluoremethane, IR rovibr. spectrum *(German)* 80−47998
chlorotrifluoroethylene, multiphoton dissoc., fragment energy partitioning 80−55681
chlorotrifluoroethylene radical anions, EPR spectra and struct. 79−31558
chlorotrifluoroethylenes, electronic transitions, electron impact spectra 77−10775
chlorotrifluoromethane, 11.8 μm band, statistical model anal., integrated intensity 77−460
chlorotrifluoromethane, compressibility, 298 to 348K, Burnett expansion obs. 79−27733
chlorotrifluoromethane, E-species force consts., using L-F approx. method, HLFS applicability 80−962
chlorotrifluoromethane, electron impact dissoc., light emission from fragments 79−13826
chlorotrifluoromethane, IR absorption spectrum, binary overtone and combination bands 78−46342
chlorotrifluoromethane, matrix IR spectra and harmonic force fields *(German)* 79−76431
chlorotrifluoromethane, matrix radiolysis, photoionis., IR spectra of CF_2Cl^+ and parent cations 78−80767
chlorotrifluoromethane, mol. struct., electron diffr., microwave spectra, CNDO/2 calcs. 78−37766
chlorotrifluoromethane, multiphoton dissoc., ^{13}C enrichment *(French)* 80−91615
chlorotrifluoromethane, photoabsorpt. cross-section, 175-770 Å 77−88462
chlorotrifluoromethane, photolysis, transient species, matrix isolation spectra 78−48635
chlorotrifluoromethane, self-diffusion coeff. near crit. temp., density depend. obs. 78−95530
chlorotrifluoromethyl cation, IR photodissoc. 80−87188
chlorotrinitromethane, electron diffr. study of gas phase mol. struct., rot. isomerism 78−1080
chloroxylenes, UV absorpt. spectra 78−86879
chloroxylenes, UV absorpt. spectra 79−22727
chlorpheniramine, liq., new ionis. method appl., using Penning effect and chem. ionis. *(Japanese)* 79−93255
organic compounds continued
chlorpromazine, automated synthesis of ^{11}C-labelled radiopharmaceuticals 80−17133
chlorpromazine effect on glucose transport in human red cell ghosts 78−77026
cholecalciferol, UV dependent synthesis in a green plant 80−35860
cholesta-4,6,8(14)-triene, fluoresc. and absorpt. spectra in UV, lifetimes 79−27017
cholesta-5,7,9(11)-triene-3β-01, fluoresc. and absorpt. spectra in UV, lifetimes 79−27017
5α-cholestanes, molecular geometry polarisation factors and mesomorphic phases *(French)* 77−84647
cholestanyl benzoate, liq. cryst., orientational order, EPR study 78−75540
cholesteric esters, effect of nature of organic solvent on gamma radiolysis 80−7835
cholesteric liquid crystal soln., γ-irrad. induced colour transition, dosimetry appls. 77−48877
cholesteric liquid crystal with anisotropic dielec. permeab., transient electrodynamic instability *(Russian)* 78−51418
cholesteric liquid crystals, viscosity coeff. at smectic-cholesteric transition 79−77791
cholesteric nonanoate, US attenuation near cholesteric to smectic A transition 79−28091
cholesteric products, gamma irradiation, effect of presence of organic solvents 79−24777
cholesteric systems, with nonmesogenic additives, Keating-Bottcher theory 80−84057
cholesterilcinamate, low press. phase transition temp. change, relative transparency *(Russian)* 78−2242
cholesterin, liq. cryst., synthesis and light refl. props *(German)* 80−10497
cholesterin ethers, dielec. absorption, heating/cooling and oxidation depth effects *(Russian)* 79−50984
cholesterol, adsorbed monolayer on aerosil, IR spectra 78−15753
cholesterol, dielectric props. under UV excitation 80−6912
cholesterol, dielectric transient response following UV-irradiation 80−51166
cholesterol, in carbon tetrachloride, self-assoc., IR absorbance 79−47920
cholesterol, optical constants and dispersion eqns. 80−30762
cholesterol, proton-coupled ^{13}C NMR spectrum, double Fourier transform 78−78725
cholesterol, solid-solid phase transitions, positron annihilation study 80−84289
cholesterol, T-labelled, prod. by catalysed exchange with T_2 *(German)* 77−90599
cholesterol+water, interaction in organic media, dielec. and NMR spectroscopy 78−76979
cholesterol benzoates, intermolecular interaction, influence on optical props. *(Russian)* 79−77516
cholesterol cinnamates, intermolecular interaction, influence on optical props. *(Russian)* 79−77516
cholesterol crystal, polymorphic transition 77−1229
cholesterol derivatives, mol. packing coeffs. and thermal stabilities 80−100201
cholesterol derivatives, piezoelec. rel. to atherosclerosis 77−78076
cholesterol esters, molecular-optical, and structural anisotropy 80−84056
cholesterol in membranes, interaction of lucensomycin, spectral parameters 77−9177
cholesterol interactions with Na pump in red blood cells 77−12898
cholesterol modulation of Aplysia neurone elec. activity 78−7329
cholesterol pelargonate, liq. cryst., crystallisation rate const. and Avrami index 78−94994
cholesterol transmembrane movement in human erythrocytes, radioactive tracer expt. 78−3459
cholesterol-lecithin interaction, effect of lecithin struct. 78−64922
cholesteryl 2-(2-ethoxy-ethoxy) ethyl carbonate, dynamics of isotropic-cholesteric transition, normal and blue phases 79−95134
cholesteryl acetate:cetyl alcohol, optical behaviour of spherulite texture 77−51314
cholesteryl acetate, cryst. struct. at 123K 79−46643
cholesteryl acetate, long period obs. 77−62515
cholesteryl acetate-cholesteryl ethyl carbonate mixtures, spherulite textures, optical effects and mol. ordering 79−1746
cholesteryl acetate-cholesteryl octanoate system, phase transitions, thermoanalytical microscopy obs. 79−55871
cholesteryl alkanoates, mol. packing coeffs. 79−82195
cholesteryl alkanoates, orientational order, spectral depend. of circular dichroism 78−26437
cholesteryl alkanoyl esters, effect on red-green transition temp. of cholesteryl nonanoate (decanoate) 80−19924
cholesteryl azo dyes, liq. cryst., prep. and struct. props. 78−51412
cholesteryl benzoate, crystallographic data, rel. to mesogenic state 79−77590
cholesteryl benzoate, elec. drift mobility, 140 to 185°C *(Korean)* 79−65481
cholesteryl benzoate liq. cryst., orientational order, EPR study 78−75540
cholesteryl bromide, cryst. and mol. struct. 79−82194
cholesteryl caprilate, conduction mechanism 78−64046
cholesteryl caprinate, liq. cryst. mesophase electron emission 79−55664
cholesteryl caproate, isothermal crystn., spherulites growth rate, optical microscopy obs. 79−32892
cholesteryl caprylate solns. in decane, crystn., electrogravitational effect 77−62496
cholesteryl caprynate, liq. cryst., DTA *(Russian)* 79−77496
cholesteryl capsylate and laurate, and their mixtures, elec. cond. *(Rumanian)* 79−64988
cholesteryl chloride, binary mixtures with cholesteryl benzoate and β-halogeno cholesteryl alkanoates, reciprocal helical pitch 79−90528
cholesteryl chloride, cryst. and mol. struct. 79−82194
cholesteryl chloride, depolarised light transmission, microstructural changes 78−22647
cholesteryl chloride, optical rotatory power using multiple scaling 78−27176
cholesteryl chloride-cholesteryl crotonate, polarised light transmission, DC elec. field effect 77−77173
cholesteryl chloride-cholesteryl crotonate (75:25% wt.) mixture, cholesteric-nematic transition field effect temp. depend. 78−75813
cholesteryl chloride-cholesteryl nonanoate mixture, pitch, temp. and comp. depends. 77−39535

organic compounds continued
cholesteryl chloride-cholesteryl pelargonate mixture, cholesteric-nematic transition 78−91244
cholesteryl chloride-MBBA mixture, mol. orientation during mag. field induced cholesteric-nematic transition 79−28086
cholesteryl chloride-myristate, liq. cryst., mag. aligned, mag. aligned, anisotropic US propag. 78−42895
cholesteryl chloroformate, crystal structure 78−91331
cholesteryl cimmanate, photoreaction in solid, mesomorphic, and isotropic phases 79−87863
cholesteryl crotonate, depolarised light transmission, microstructural changes 78−22647
cholesteryl decanoate, effect of cholesteryl alkanoyl esters on red-green transition temp. 80−19924
cholesteryl decanoate, NMR spectroscopy of blue phase 79−4236
cholesteryl decanoate, optical activity in blue phase 80−100641
cholesteryl decanoate organic solns., γ radiolysis, colour transition temp. 79−57266
cholesteryl esters, blue phase, model 80−88030
cholesteryl esters, isotropic mesophase, optical props. 79−65891
cholesteryl esters, kinetics of cholesteric/blue phase transform. 79−95140
cholesteryl ethyl carbonate, long periods in sol. state, X-ray diffr. study 80−96503
cholesteryl ethyl carbonate, unit-cell dimensions and space group 80−84165
cholesteryl laurate, conduction mechanism 78−64046
cholesteryl laurate, crystallisation kinetics and phase transitions, differential scanning dilatometric obs. 79−69230
cholesteryl laurate, liq. cryst., DTA *(Russian)* 79−77496
cholesteryl laurate, X-ray cryst. struct. determ. at 298K 79−37692
cholesteryl laurate-cholesteryl caprilate mixture, elec. cond. mechanism 79−10796
cholesteryl laurate-cholesteryl caprylate (75 wt.%), polymorphic behaviour, optical, elec. and dielec. meas. 80−65208
cholesteryl linoleate, dielec. props., phase transitions rel. to temp. 79−33592
cholesteryl m-fluorobenzoate, NMR spectroscopy of blue phase 79−4236
cholesteryl methacrylate, mono- and polymer, liq. cryst. order 78−9942
cholesteryl methyl carbonate, liq. cryst., low-ang. X-ray diffr. obs., solid and liq. 80−49093
cholesteryl myristate, cholesterogenic, blue phase, D NMR obs. 80−97151
cholesteryl myristate, density of smectic, cholesteric, blue, isotropic phases 78−42897
cholesteryl myristate, high press. mesomorphic and polymesomorphic transitions 78−18750
cholesteryl myristate, press. depend. of cholesteric pitch near cholesteric-smectic A phase transition 77−68918
cholesteryl myristate, smectic A-cholesteric transition, tricritical behaviour, DTA and DSC study 80−65206
cholesteryl nonanoate, cholesterogenic, blue phase, D NMR obs. 80−97151
cholesteryl nonanoate, cyclohexanone admixture effect on mesophase order parameter, refr. index meas. 80−100165
cholesteryl nonanoate, effect of cholesteryl alkanoyl esters on red-green transition temp. 80−19924
cholesteryl nonanoate, high press. mesomorphic and polymesomorphic transitions 78−18750
cholesteryl nonanoate, liq. cryst.-isotropic transition at high press. 79−95135
cholesteryl nonanoate organic solns., γ radiolysis, colour transition temp. 79−57266
cholesteryl nonanoate-MBBA, liq. cryst. mixture, two colour display device 80−70116
cholesteryl oleate, isotropic liq. cryst., shear viscosity 78−26668
cholesteryl oleate, solid-solid phase transitions, positron annihilation study 80−84289
cholesteryl oleate (linoleate), solid-solid transition, glass transition, cryst. nucleation temps., DSC obs. 78−34604
cholesteryl oleyl carbonate, high-purity, prep. for thermal radiography 77−15311
cholesteryl oleyl carbonate, isotropic liq. cryst., shear viscosity 78−26668
cholesteryl oleyl carbonate, isotropic phase, polarisation of scattered light 79−78691
cholesteryl oleyl carbonate, optical rotatory power using multiple scaling 78−27176
cholesteryl oleyl carbonate, press. depend. of cholesteric pitch near cholesteric-smectic A phase transition 77−68918
cholesteryl p-acryloyloxybenzoate, mono- and polymer, liq. cryst. order 78−9942
cholesteryl pelargonate, liq. cryst. phase transitions *(Russian)* 79−37818
cholesteryl pelargonate, optical dispersion 79−64990
cholesteryl propionate, liq. cryst., DTA *(Russian)* 79−77496
cholesteryl propionate, struct. in characteristic phase, X-ray diffr. obs. 79−32891
cholesteryl propionate-acetate mixture, light refl., twisting power 77−84641
cholesteryl vinyl succinate (fumarate), polymer+monomer systems, liq. cryst. phase states 79−1494
cholesteryl-m-fluorobenzoate, cholesteric liq. cryst., NMR, orientational order parameter 77−8429
cholesterylalkanoates, liq. cryst., optical anisotropy and struct. ordering *(Russian)* 78−87616
cholesterylbenzoate, substituent effects on mesomorphic props. 77−11465
cholesterylcinnamate, substituent effects on mesomorphic props. 77−11465
cholestryl nonanoate-MBBA mixture, anomalous behaviour of electrical dissipative power 79−4237
cholic acid, dielectric props. under UV excitation 80−6912
cholic acid, dielectric transient response following UV-irradiation 80−51166
choline bromide, radiation sensitivity, cryst. struct. depend., calorimetric investig. 78−88647
choline bromide, solid, mol. dynamics, NMR obs. 78−56390
choline chloride, radiation sensitivity, cryst. struct. depend., calorimetric investig. 78−88647
choline chloride, solid, mol. dynamics, NMR obs. 78−56390
β-choline chloride, X-ray diffr. 78−55861
choline detect. by liq. chromatography with ion-exchange membrane detector 79−16055
choline iodide, radiation sensitivity, cryst. struct. depend., calorimetric investig. 78−88647
choline phosphate calcium chloride tetrahydrate, struct., conformation, metal coordination, model for membrane surface interactions 80−15085
choline salts, hydration, NMR spin-lattice relax. obs. 79−87830
choline salts, mol. motion, proton spin-lattice relax. 77−59474
choline transport across synaptic terminal 79−70544
cholinesterase-acetylcholine soln., anion-cation site interactions, solvent effects on aggregate stability 80−61070
cis-1-cholobutadiene-1,3, microwave spectrum, struct., nuclear quadrupole coupling, distortion const., thermodynamic functions calc. 80−99500
chromatin, factors affecting the heat-induced increase in protein content 80−97882
chromatin, low-angle X-ray and neutron diffr., interparticle effects 80−72134
chromatography and mass spectrometry, conference, Carlsbad, Czechoslovakia (April 79) 80−73097
chromium acetylacetonate, Mrad range dosimeter appls. 77−16997
chromium dithiocarbamate complexes, IR, electronic and mass spectra, mag. susceptibility, cond. meas. 80−97270
chromium formate, mol., Hartree-Fock instability of SCF wavefunctions 80−9492
chromium tetraphenylporphyrin, reson. Raman spectra, excitation profiles, nucl. distortion and Jahn-Teller effects 77−58018
chromium tri(bipyridyl)tri-perchlorate, aq. soln., Raman scatt. from electronically excited state 79−94001
chromone, solns., pH dependent fluorescence spectra, pK_a and tautomerism 79−59506
chromophone, natural optical activity, symmetry rules for dynamic excitation 77−18990
chromophore, excited state, solvent interactions, fluoresc. obs. 78−37670
chromophore emission spectra, exciting wavelength depend., hydroxylated solvent reorientation 78−76514
chromophore phospholipid Langmuir films, photoeffects 80−80409
chromophores, $^1O_2$, annihilation luminesc., in polymer matrices 77−88488
chromophores, biochemical, in cosmic dust, contrib. to interstellar UV extinction 80−26945
chromophores, circular polarisation of luminescence, book contrib. 79−5250
chromophores, model for simulation of EPR spectra, in partially oriented membrane multilayers 78−86894
chromophores, semiempirical rules in circular dichroism, Cotton effect sign correl. with stereochem. 80−1006
chrysene, butyl bromide solid soln., phosphoresc. line struct. obs., vibr. assignments 77−58075
chrysene, crystal-electrolyte interface, ionis. energy of uppermost cryst. mols. 78−27764
chrysene, dual fluoresc. (S_1, S_2), collision-free conditions 79−45741
chrysene, excited electronic state, CARS obs. 79−31514
chrysene, excited singlet and triplet state, CARS obs. 80−83374
chrysene, mag. susceptibility anisotropies, high field ^2H NMR quadrupolar effects obs. 80−25225
chrysene, nonlinear third-order electric susceptibility 78−74944
chrysene high density excitation effects on fluoresc. 79−1782
cinnamaldehydes, electronic spectra, CNDO CI calcs. 78−29774
cinnamic alcohol, in DMF, electrochem. reduction, automatic pH control appl. 77−63928
cinnamyldehyde, rotational isomerism study by US absorpt. and vel. meas. 77−27196
cinnoline, excited state absorpt. spectra and intersystem crossing kinetics 80−74176
cinnoline, prereson. Raman spectra, vibr. band intensities obs. 80−102515
cis-3,5-dibromo-4-oxo-2,2,6,6-tetramethylpiperidin-1-yloxy, cryst. struct., secondary and multi-centre bonding 78−63751
cis-trans-difluoroethylene 79−59514
citric acid, single cryst., X-irrad., EPR and ENDOR, 4.2K radical identification 79−65764
citric acid monohydrate, crystallisation and cryst. growth rate 78−87638
citric acid monohydrate, triboluminescence and cryst. fracture dynamics 80−50437
citrinin distribution in tissues and serum protein, radioactive chem. anal. 79−53292
classification from voltammetric data, computerised pattern recognition 79−16057
clathrate deuterohydrates, ^1H NMR lineshape of tunnelling methyl group, <5K 78−46370
clathrate hydrates, identification from NMR line shapes 78−27861
clathrate hydrates, longitudinal acoustic vel. 80−88275
coal tar and petroleum pitches, pyrolysis, press. effects on coke yield and microstruct. form. 77−70289
coal tar pitch, containing mesophase, thixotropic changes occurring on reheating 79−90205
coatings, development *(French)* 80−30127
cobalt, phthalocyanine, sublimed film, absorption spectra and association 78−48174
cobalt(II) metalloporphyrin, Z-ray photoelectron spectra satellites 80−5582
cobalt(III) complex, octahedrally-coordinated with monodentate ligands, optical activity 79−50090
cobalt(III) complexes, mixed glycylglycinate, synthesis and config. *(French)* 80−2005
cobalt (III) diacetylmonoxime, Schiff base cryst. and mol. struct. 79−94998
cobalt (III) diacetylmonoxime thiosemicarbazone, X-ray cryst. and mol. struct. 79−90641
cobalt (III) methylhydrazinedithiocarboxylate, cryst. and mol. struct. 79−94998
cobalt complex, $Co_{1-x}Zn_x$hexa(pyridine-N-oxide)$(ClO_4)_2$, dilute cubic S=1/2 XY antiferromag., sp. ht. data 77−66358
cobalt dimethyl glyoximate, molecular struct., cryst. structure 80−79769
cobalt formate dihydrate, mag. relax. phenomena near T_N 79−65656
cobalt formate dihydrate, mag. struct., antiferromag. mode 79−99678
cobalt formate dihydrate, ordered state, paramag. cross relax. *(Japanese)* 77−43873
cobalt naphthalate electret, thermally stimulated discharge, 55-75°C 80−25279
cobalt oxalate, crystal growth in silicate gel, X-ray diffr. and i.r. spectrum 77−4724

organic compounds continued
cobalt phthalocyanine film, sorption of O_2 and water, AES obs. 78−91531
cobalt platino-oxalate, one-dimens. conductors, prep., struct. and elec. cond. 80−24900
cobalt stearate, monomolecular layer, electron escape depth, XPS *(Japanese)* 80−11532
cobalt stearate, monomolecular multilayers, XPS escape length depend. on emission angle, elastic scatt. role *(Japanese)* 80−84833
cobalt sulphate hexacarbamide, cryst. struct. 78−34507
cobaltous acetate tetrahydrate, weak ferromag. obs. below 85 mK 79−73695
COC, cholesteric liq. cryst., positron lifetimes and phase transitions 80−59383
COC, cholesteric liq. cryst., shear flow, helix distortion, optical meas. 78−94982
COC, dynamics of isotropic-cholesteric transition, normal and blue phases 79−95134
COC, prep., cryst. state, and mesophases 79−95143
COC test of tricriticality 80−10648
coccine, new, trace amount determ. by reson. Raman spectroscopy *(Japanese)* 79−48017
coenzyme-Q_{10}, interaction with antimalarials, theory 78−27885
cofacial diporphyrins, electron transfer reactions following picosecond excitation, CT state lifetimes, optical difference spectra 80−25995
colchicine, cryst. struct., multiple soln. direct methods 78−34384
colchicine interaction with phosphatidylcholine membranes, spin-label study 77−86455
collodion, film, IR spectrum, vibr. assignments, chain config. 77−34789
collodion coating on Fe, corrosion protection, qualitative ellipsometric-electrochem. approach 80−104344
combustion products, seeded oxy-liq. petroleum gas system, elec. cond. meas. 77−58835
combustion products plasma with mixed alkali impurities, elec. cond. calc. 79−86621
cometary nuclei, simulation of UV effects *(Russian)* 78−32406
complex, laser active substances, props. *(Russian)* 78−74904
complex, nuclear relaxation influence on stimulated emission 80−48019
complex formate, spray-dried, thermal treatment to produce $Li_{0.5}Fe_{2.5}O_4$ spinel ferrite 79−24482
complex heteroorganic molecule, semi empirical SCF-CI MO method 79−63917
complex mixtures in solid-state matrices, dip shape saturation effects on nonuniformly broadened spectra 79−95799
complex molecule solutions, stimulated emission, light quenching *(Russian)* 78−33735
complex molecules, fluoresc. decay in nonhomogeneous level broadening conditions *(Russian)* 79−50073
complex molecules, triplet state, photoinstability and quenching effects on lasing kinetics *(Russian)* 79−13778
complex organic vapor lasers, new active media, buffering gas influence 79−94213
complexes wiht rare earth ions, energy transfer in strong donor solvents 79−54930
concanavalin A binding to cell membrane of Herpetomonas samuelpessoai, UV effect 78−48835
condensation, two-dimensional, with adsorbed mol. reorient. 78−61051
condensed aromatics, in-plane vibr. force fields, five-parameter approx. calcs. 79−59436
conductors, narrow band, valence bond theory 80−24777
conjugate heterosystems, UV spectra, substituent effects 79−27006
conjugate systems, atomic localisation of electronic excitation 77−18806
conjugated compounds, mol. polarisability additive scheme, CNDO approximation calcs. 77−50363
conjugated compounds, ring currents static octopole hyperpolarisabilities calcs. 80−102588
conjugated cpds., aromaticity determ. by topological reson. energy method 80−42915
conjugated heterocycles with single heteroatom, stability, graph theoret. approach 77−38604
conjugated hydrocarbon, graph theoretical formulation of London diamag. 80−27919
conjugated hydrocarbon chains, linear and nonlinear elec. susceptibilities calcs. 78−19437
conjugated hydrocarbon chains, nonlinear elec. susceptibilities calcs. 78−66484
conjugated hydrocarbons, conformational analysis and heats of form. by force field method 77−60105
conjugated hydrocarbons, dipole polarisabilities, tensor components 79−36795
conjugated molecule, H_3C-NC_5H_4-CH-CH-C_6H_4-O, large second-order polarisability, resonance struct. 78−66683
conjugated molecule diamagnetic anisotropy, graphical anal. 79−76360
conjugated molecules, alternant, with one heteroatom, stability, graph theory calcs. 77−3253
conjugated molecules, excited state, self-consistent HMO theory *(Japanese)* 77−42253
conjugated molecules, nonlinear props. of new class of cpds. 79−41413
conjugated molecules, resonance Raman spectra calc. 78−984
conjugated molecules, triplet-triplet excitation, atomic localisation calcs. 79−54830
conjugated molecules and ions, diamag. susceptibility, quinonoid character 78−62945
conjugated system, N-electron CNDO Hamiltonian, approach to exact soln. 77−26979
conjugated systems, nonparametric resonance energies, graph theory and MO 77−61681
contact charge transfer complexes of organic molecules with O_2, CNDO/S calcs., absorpt. spectra obs. 80−69076
contact charge transfer interactions at 10K between oxygen and aromatic mols. 77−46637
COOB, acoustic emission at liq. cryst. transitions prod. by thermo-optically excited defects 79−95137
COOB, sheared liq. crystal, near T_{A-N}, optical response 79−94895
COOB, smectic A-nematic transition, X-ray and light scatt. obs. 79−95129
COOB, solid state dimorphism and cryst.-smectic transition, Raman study 80−45063
COOB film, freely suspended, smectic A layer spacing, optical determ. 80−64883
organic compounds continued
COOB-cholesteric liq. cryst. mixtures, helix pitch, temp. depend. 80−64895
copper, benzoate, one-dimens. antiferromag., heat capacity, field-induced crossover of spin-dimensionality 80−97099
copper(II) metalloporphyrin, Z-ray photoelectron spectra satellites 80−5582
copper(II) methylphosphonate monohydrate, cryst. struct. *(French)* 79−99172
copper 1,4-butanedisulphonate tetrahydrate, struct. 78−18630
copper (I)-butyrate, dimorphism, X-ray diffr. and fluoresc. *(German)* 79−51090
copper (II) carboxylates, magnetic and spectroscopic props. 79−91204
copper (II) complex, bis(dithiocarbamate), HF-Slater-LCAO calcs., mag. coupling parameters and optical spectrum 80−99447
copper acetate, lasant for Cu vapour laser 79−31875
copper acetate, use as lasant for Cu vapour laser 78−25854
copper acetate mono-α-picoline, binuclear, cryst. and mol. struct. 79−99174
copper acetate monohydrate, ESR in resonant cavity, meas. of Cotton-Mouton-Voigt effect *(French)* 78−89514
copper acetate monohydrate, pure quadrupole reson., covalency 77−16205
copper acetates, antiferromag. exchange coupling, superexchange mech. 78−39310
copper benzoate, antiferromag., spin dynamics at low temp. 77−32278
copper benzoate, antiferromag. reson. below 1K, Neel temp. determ. 78−39407
copper benzoate, EPR sidebands 79−78508
copper benzoate, low-dimensional Heisenberg antiferromag., high field magnetisation 80−80558
copper benzoate, mag. heat capacity and Neel temp. in mag. field 79−61147
copper benzoate, spin 1/2 system, one-dimensional nucl. relax. 78−39427
copper benzoate di-(γ-picoline)hydrate, structural study using heavy atom method *(French)* 79−69098
copper benzoate trihydrate, half-field EPR, 1.5-300K 78−60333
copper complex $CuBr_2$ (pyrimidine)$_2$, mag. susceptibility and magnetisation curve, 1.2-4.2K 80−11177
copper di-isopropyldiselenophosphate, soln. anisotropic g and hyperfine tensors, ESR linewidth meas. 79−85978
copper dichloride dipyridine, ground state wave function and superexchange interaction 79−42752
copper diethyldithiocarbamate single crystal, EPR exchange coupled pairs, low temp. hyperfine anomaly 77−90021
copper dipyridine dichloride, antiferromag. reson. below 1K 79−28619
copper dipyridine dichloride, dynamic shift of the ESR field 80−2630
copper formate.4D_2O, field-induced antiferromag. order above T_N 78−84389
copper formate tetradeuterate, deuterated, paraelec. and antiferroelec. phases, neutron diffr. obs. of struct. 79−87404
copper formate tetradeuterate, paramag., induced staggered magnetisation, NMR 77−12212
copper formate tetrahydrate, antiferroelec., dielec. anisotropy 78−43768
copper formate tetrahydrate, antiferromag. phase, neutron diffr. study 80−93085
copper formate tetrahydrate, dielec. anisotropy and dimer theory 79−38427
copper formate tetrahydrate, dielec. props. under hydrostatic press. 77−20789
copper formate tetrahydrate, ferrielectricity 80−2706
copper formate tetrahydrate, ice rule ferroelectric, polarisation correlations 80−97190
copper formate tetrahydrate, model two-dimensional ferroelec., short-range order, neutron scatt. 78−68458
copper formate tetrahydrate, short-range order, diffuse neutron scatt. 78−15124
copper formate tetrahydrate, stress effect on antiferroelec. phase transition, dielec. meas. 79−38498
copper formate tetrahydrate, two-dimens. spin 1/2 Heisenberg antiferromag., phase transition characts. 77−66352
copper formate urea hydrate, two dimens. antiferromagnet, EPR, temp. depend. 80−54937
copper glutarate complexes in aqueous soln., enthalpy and entropy meas. *(Italian)* 79−19378
copper hexadecachlorophthalocyanine, radiation damage 77−19987
copper iminodiacetate dihydrate, X-ray cryst. struct. and molecular struct. determ. 79−19237
copper oxalate, crystal growth in silicate gel, X-ray diffr. and i.r. spectrum 77−4724
copper oxalate, two dimens. antiferromag., proton reson. exam. 77−28453
copper oxalate complex with aliphatic amines, X-band ESR line width 77−20687
copper oxalate hemihydrate, photographic props. eval. for use as high-speed photographic materials 77−44497
copper phthalocyanide, cryst. struct. sensitivity of band struct. 79−42444
copper phthalocyanin, thin film, thermal behaviour *(Japanese)* 80−24753
copper phthalocyanine, autoionisation in electron energy loss spectra 78−35232
copper phthalocyanine, chlorinated, radiation damage mechanism 80−88000
copper phthalocyanine, chlorinated, stacking disorder 78−34622
copper phthalocyanine, cryst. growth from vapour, hollow cryst. form, mechanism *(German)* 77−55252
β-copper phthalocyanine, dislocation detection *(German)* 78−63773
β-copper phthalocyanine, dislocation etching kinetics *(German)* 78−67719
β-copper phthalocyanine, large single crystal growth from vapour *(German)* 77−32513
copper phthalocyanine, on graphite, epitaxial growth of new polymorph 77−80712
copper phthalocyanine, polycryst. film, charge transfer state and optical spectra *(Russian)* 78−84607
copper phthalocyanine, polycrystalline, forbidden ESR transition 79−95638
copper phthalocyanine, simulated mol. images, point models and kinematical struct. amplitudes 80−103223

organic compounds continued
β-copper phthalocyanine, single cryst., equilib. shape, growth shape, vapour phase growth *(German)* 77−43163
copper phthalocyanine, size distribs., transient elec. birefr. 80−85223
α′-copper phthalocyanine, struct. and susceptibility to radiation damage 79−32986
copper phthalocyanine, sublimed film, absorption spectra and association 78−48174
copper phthalocyanine α-β phase transform., heat of transform., DTA investig. *(German)* 78−30754
α′ copper phthalocyanine and chlorinated derivative mol. crysts., radiation damage in electron microscope 80−107328
copper phthalocyanine dye on Si, optical modulation of low energy transmission electrons 79−69939
copper phthalocyanine film, electron acceptor surface states due to O_2 adsorption 80−88586
copper phthalocyanine film, photocelectrochem. behaviour on SnO_2 electrodes 80−15626
copper phthalocyanine thin film electrodes, near IR photoelectrochemical responses 80−93766
copper platino-oxalate, one-dimens. conductors, prep., struct. and elec. cond. 80−24900
copper porphin, IR spectra and vibr. anal., and deutero-derivatives 79−22705
copper porphin, Zeeman expt. on phosphoresc. triplet and quartet states 79−33786
copper porphine, Xα multiple scatt. calcs., EPR and electronic spectra 78−13426
copper porphins, vibr. spectra, planar vibrs., normal coord. anal. 77−65474
copper porphyrins, mag. susceptibility and EPR, sample grinding effects 80−60420
copper salicylaldoxime, vitrified solution, additional absorpt., in axially symmetric ESR spectra 77−16151
copper sulphate tricarbamide, $CuSO_4.3CO(NH_2)_2$, cryst. struct. determ. 78−34506
copper tetra-4-dimethylaminophthalocyanine intercalated with TaS_2, layered cpd., struct. and supercond. 78−84342
copper tetraamine sulphate, two-dimensional Heisenberg antiferromag., high field magnetisation 80−80558
copper tetrammine sulphate monohydrate, evidence for exchange coupled quadratic nets 77−24705
copper tetraphenyl porphyrins, mag. diluted, EPR meas. 78−39391
copper tetraphenylporphyrin, reson. Raman spectra, vibronic coupling 79−26985
copper-porphin-d_4, reson. Raman and IR spectra 77−75164
copperporphin, metastable quartet state radiative decay 80−23453
cordycepin, response of X-ray resist. hybrid cell line, rel. to X- and UV irrad. 77−86541
cordycepin, X-ray cryst. struct. determ. 80−107198
core electron binding energy, prediction with four-parameter equation 77−30745
core ionisation and electronic redrganisations, LCAO MO SCF calcs. 79−18115
coronene, an ordered struct. 80−19786
coronene, butyl bromide solid soln., phosphoresc. line struct. obs., vibr. assignments 77−58075
coronene, distrib. with respect to particle size in submicron atm. aerosols 79−74563
coronene, electron escape depths and absorpt. coeffs. 78−23580
coronene, excited state Faraday values mag. circular dichroism spectra and MO CI calcs. 80−18877
coronene, fluorescence spectra, zero field line splitting *(Russian)* 78−17604
coronene, graph theory for axial symmetry molecules *(Chinese)* 79−36792
coronene, in alkane matrices, zero-phonon lines, press. shifts *(Russian)* 78−76502
coronene, in cyclohexane, 77K, quasi-line luminesc. spectra obs., Shpol'skii's method 77−69894
coronene, in ethanol soln., external heavy atom effect on triplet state, phosphorescence meas. 79−18231
coronene, in n-heptane, Shpol'skii effect multiplets, struct. obs. by ESR and X-ray diffr. 77−62513
coronene, in n-paraffin cryst., luminesc. characts. 79−3480
coronene, in n-paraffin solns., quasiline spectra, press. effects *(Russian)* 77−68053
coronene, in-plane vibr. force fields, five-parameter approx. calcs. 79−59436
coronene, luminesc., spin-orbit coupling perturbation by metal chlorides *(German)* 80−1021
coronene, mag. susceptibility anisotropies, high field ^2H NMR quadrupolar effects obs. 80−25225
coronene, metastable inert gas atom impact, surface electron emission energy distrib. 78−43970
coronene, minimal exposure high resolution electron microscopy 80−79653
coronene, mol. vibr. amplitude of condensed phase, five-parameter approx. 79−82295
coronene, mono- and dianions, reson. spontaneous Raman spectra, vibronic interactions 79−3451
coronene, multiplet struct., insertion modes, Shpol'skii spectra 79−13752
coronene, n-alkane matrix, up to 1.8 kbar emission multiplet struct. shift 77−34677
coronene, n-alkane solvent effect on low temp. fluorescence spectra 77−36274
coronene, polycrystal, photoemission 78−27367
coronene, protection against radiation damage, exciton effects 80−29055
coronene, solution in bromobutane, Zeeman effect in phosphoresc. at laser $T_1 \leftarrow S_0$ excitation 78−37679
coronene, sub psec radiationless relax. in soln. 77−18955
coronene, triplet mol. in n-heptane Shpol'skii sites, distortion and orientation meas. by MIDP 78−37668
coronene, triplet state, photomagnetism 80−97125
coronene in n-heptane cryst., MIDP, distortion and orientation of mols. 79−31581
coronene polycrystals, electron scatt. 77−32478
coronene thin films, elec. cond. mechanism 77−28189
coronene trimer radical cation, spin densities in CH_3Cl_2-CH_3NO_2 solvent mixture, −100°C 80−5565

organic compounds continued
coronene-rhodamine 6G, energy transfer in PMMA matrix, fluoresc., temp. depend. 78−13539
coronene-TCNQ, solid complexes, spectra, stoichiometry 78−23435
corrins, field-desorption mass spectrosc. 78−80821
corrosion inhibitor efficiency for Zn 80−40589
corrosion inhibitors, diammonium salt-based, protective props. for steel 20 *(Russian)* 78−56808
cortisol, gas phase fragmentation, high voltage scanning field desorption obs. 78−3320
coryol, crystal structure determ. using NQEST(x) function 80−64986
coumaran, geometry, electronic absorpt. spectra 80−971
coumarin, aq. soln., response to high LET radiation from $^{10}B(n,\alpha)^7Li$ reaction 78−24149
coumarin, aqueous solution, fast neutron irrad., dosimetry appl. 78−44613
coumarin, dye in ethanol, laser stability, photodegradation parameters 78−71098
coumarin 102, excited state interaction dynamics, picosec. time-resolved spectral shift obs. 80−78624
coumarin 102, excited state protonation kinetics, laser pH jump and picosecond spectroscopy 80−25992
coumarin 1, multiphoton cross-section determination by means of luminescence experiments 80−93377
coumarin 481, dye laser, mixed solvent systems for optimising output 79−13981
coumarin 6, ultrashort vib. population lifetime of ground state in vapour phase 77−30929
coumarin 6 dye mols. in liq. cryst., fluoresc. intensity, orientation control 78−82759
coumarin 6-diethylamine, soln. fluoresc. induced by laser, vibr. relax. 79−26984
coumarin aqueous system as low-range chemical dosimeter 79−79659
coumarin deriv. solns., mol. struct. effects on luminesc. and lasing characts. *(Russian)* 77−83873
coumarin derivatives in simple dye laser, pumping by N_2^+ ion laser 78−74903
coumarin dye in ethanol, laser dye stability, photodegradation relationships 78−55349
coumarin dye laser, flashlamp-pumped, picosecond pulses at 520 nm *(French)* 78−42335
coumarin dye laser, mode-locked flashlamp pumped, tunable blue ps pulses 79−13974
coumarin dye molecules, CH stretching modes, population lifetime meas. 80−58185
coumarin dye-doped polymer film laser, optical gain 77−61948
coumarin in aqueous soln., fluorescent prod. form. on γ-irrad. 77−60094
coumarin in water and heavy water, fast neutron response 80−845
coumarin laser dyes, in methanol, ethanol, and water, fluoresc. lifetimes meas. 79−27252
coumarin laser dyes, solvent effects on photophysical parameters 80−91598
coumarin laser dyes, stability, lasing characts. obs. 78−1223
coumarin-6, tunable-pulse dynamic picosec. spectrosc. 79−44941
coumarine 1-rhodamine 6G-water-Triton X100, micellar dye soln., energy transfer 80−45581
coumarine dye laser, N_2 laser-pumped, pulse time behaviour 79−31894
coumarins (C-30, C-102, C-7), synchronous pumping and mode locking 79−45966
covalently-bound dyes on semiconductor surfaces in new type of photocell 77−69414
CPB, nematic temp. range broadening by nonmesogenic solute 77−47559
CPHB, nematogenic liq. cryst., above T_c, Kerr effect response time, temp. depend. 78−34434
creatine monohydrate, single cryst., radiation damage, ENDOR obs. 78−96016
o-cresol, binary liquid mixtures, excess free vol. calcs. 80−34202
m-cresol, vibr. spectrum determ. using Al-insulator-Pb tunnel junction 77−6782
0-cresol+OH^-, gas phase reaction, 299-435K, kinetics and mechanism 78−11515
cresols, ideal gas thermodynamic props. 78−75250
cresyl violet, excited singlet-singlet absorpt. *(Russian)* 79−42985
cresyl violet, luminesc. quantum yield standard for red, calorimetric obs. 80−190
cresyl violet, rot. diffusion, picosec. saturation spectrosc. obs. 80−5634
cresyl violet 620, injection locked dye amplifier, coherent optical image amplification 80−19041
cresyl violet in ethanol soln., and dye mixtures, excitation by Cu vapour laser 80−28230
Creutz-Taube complex, mixed valence, reson. Raman calcs. using vibronic coupling model 80−97249
croconate ion, Jahn-Teller coupled vibrs., reson. Raman profiles 77−83602
croconate ion, reson. Raman scatt., Jahn-Teller effect 79−18190
trans-crotonaldehyde, rot. Zeeman effect, microwave spectra, mol. parameters 79−3491
crotonaldehyde, rotational isomerism study by US absorpt. and vel. meas. 77−27196
crown ethers, use in freezing out intramol. cation migration in radical ion pairs 77−58047
18-crown-6 complexed sodium-2, 6-di-+-butyl-p-benzosemiquinone ion pairs, soln. ESR spectra, temp. and conc. depend. 80−63675
18-crown-6 complexed sodium-duroquinone ion pairs, soln. ESR spectra, temp. and conc. depend. 80−63675
crude oils, fluoresc. spectra, using 3-dimens. contour plotter 78−58046
crude oils, heavy, Ni determ. by at. absorpt. spectroscopy 77−52681
cryptand-containing alkali metal-ammonia solns., metal anion and trapped electrons form. by evap. 79−100340
cryptocyanine, soln., $S_2 \rightarrow S_0$ fluoresc. 78−13541
cryptocyanine, solns., fluoresc. lifetime, viscosity depend. 79−59497
cryptocyanine-methanol, soln., nonlinear optical absorpt., 310-815 nm 79−85973
cryptopleurine derivatives, absorpt. and fluoresc. obs. of photodecomp. processes, dye laser relevance 80−55686
cryst., IR spectra in polarised light, cryst. struct. 78−27223
β-succinic acid, cryst., slip system and dislocation detect. by etching 77−59015
crystal, molecular rearrangements, intermol. cooperation and dipole-dipole interactions 77−1087

organic compounds continued
crystal, struct. and habit correspondence, mol. centre of gravity determ. *(German)* 79−32934
crystal growth from soln., computer simulation 78−30558
crystal violet, fluoresc. efficiency, solvent viscosity effects at high press. 78−9188
crystal violet, prereson. Raman spectra 80−32721
crystal violet, soln., picosec. relax., wavelength depend. 79−99921
crystallographic pedigree 78−91287
crystals, quantitative validity domains of single scattering approximations 80−28888
CT complex, equilib. distances and stabilisation energy, PCILO calc. 78−41963
CTA-DNA crystal growth and morphology 80−26198
CTIP, exciton surface polaritons at room temp. 79−47476
cumarine derivatives, stimulated emission by laser and lamp excitation 79−72563
cumene, depolaris. Rayleigh scatt., optical anisotropy 78−27245
cumene, droplet vaporisation in moderately-high temp. stationary media, Chang model 78−34609
cumene, films, thin, wetting, rheological characts. determ., capillary method 78−51788
cuminaldehyde, dil. soln., dielectric relax., solid rotator phase 79−42890
cummulene type infinite chain cryst., energy bands, ab initio Hartree-Fock orbital calc. 78−60066
cupferron and complexes, amorphous, hopping cond., 0 to 150°C 79−60828
cupric formate tetrahydrate, dielec. props. under hydrostatic press. 77−12343
cupric formate tetrahydrate, pressure effect on dielectric props. *(Japanese)* 79−65787
cupric formate tetrahydrate, uniaxial stress effect on dielec. props. 78−48125
cupric formate urea, atom assignment problems, alternative to Hamilton's R-factor ratio test 79−7506
cupric mixed ligand complexes, mechanism of spin transfer to next neighbours ^{13}C and ^{31}P 78−86892
cupric oxalate cathodes for seawater cells 79−92067
cuprophane, props. for membranes in disposable haemodialysers 77−78049
cyan pigment photoconducting, electric field-induced fluoresc. quenching 80−34967
4-cyan-phenyl esters of 4′-N-alkoxycinnamic acids, liq. cryst., refr. indices, optical anisotropy 79−28704
cyanamide, ab initio VB wave functions, π-electrons 78−70748
cyanine adsorption on AgBr, pH depend. 78−62254
cyanine dye, crysts., extraordinary exciton polaritons in refl. spectra, macroscopic dielec. theory 77−89715
cyanine dye, spectral sensitisation of CdS:Cu 78−64064
cyanine dye in lipid bilayer, photosensitization of semicond. electrode 80−75639
cyanine dye laser excitation by giant single pulses *(Russian)* 78−46596
cyanine dye monolayer assemblies with Al and Ba electrodes, photovolt., dark cond. and photocond. 80−80400
cyanine dye monolayer/p-chloranil crystal, charge carrier injection rate const. determ., energy transfer vs. charge transfer method 79−83031
cyanine dye sensitisers, J-aggregate formation, spectral changes of UV bands 77−70318
cyanine dye sensitisers, J-aggregates, circular dichroism and induced Cotton effect 77−70319
cyanine dye sensitisers, J-aggregates, meso substituents effect on mol. assoc. 77−70320
cyanine dyes, all-reactive-electrons closed-shell SCF-CI MO calcs. 79−36541
cyanine dyes, excited electronic states, CNDO/S CI calc., visual pigment spectra appl. 80−85333
cyanine dyes, influence of (100) and (111) faces of AgBr on aggregation 79−39202
cyanine dyes, solns., excited states, duration meas. 77−65503
cyanine dyes, substituted symmetric, optical nonlinearities, free-electron like model 79−41407
cyanine dyes, trans-cis isomerisation, ps kinetics 79−87853
cyanine dyes for spectral sensitization of evaporated AgBr layers 80−26035
cyanine dyes in methanol-water glasses, EPR spectra of triplet state 79−18212
cyanine fluorescent dye membrane probe effects on cell props., rel. to bacterial chemotaxis 78−35815
9-cyano anthracene-dimethyl aniline, exciplex, fluoresc. of vap., 185-231°C 78−74693
9-cyano anthracene-tributyl amine, exciplex, fluoresc. of vap., 185-231°C 78−74693
9-cyano anthracene-triethyl amine, exciplex, fluoresc. of vap., 185-231°C 78−74693
cyano biphenyl-substituted benzoates, exhibiting reentrant nematic behaviour, polymorphism and X-ray diffr. 79−94890
cyano compounds, liq. cryst. phases, incommensurate coexistent density fluctuations 80−79691
cyano derivatives, smectic layer spacings 79−46561
cyano Schiff bases, high press. reentrant nematic bilayer smectic-*A* transition 79−28087
1-cyano-1,3-cyclopentadiene, microwave spectrum, rot. consts., dipole moment 78−42043
1-cyano-2,4-pentadiyne, symm. top, microwave spectra 78−58676
1-cyano-2-methyl-3-(cis-propenyl) cyclopropanes, rotational propensities and bond rupture identity 80−104437
4-cyano-4′-alkyltolans, liq. cryst., prep. and transition temp. 77−31588
4-cyano-4′-d_{17}-n-octylbiphenyl, D spin-lattice relax. time, partially averaged quadrupole tensors 77−1076
4-cyano-4′-n-pentyl-d_{11}-2′,3′,5′,6′-tetradeuteriobiphenyl, improved synthesis 79−32893
4-cyano-4′-n-pentylbiphenyl, refr. index meas. and isotropic-nematic phase transition study, surface plasmon technique 80−84282
4-cyano-4′-octylbiphenyl, dielec. props., 1 Hz-1 GHz, in smectic, nematic and liq. phases *(French)* 77−40168
4-cyano-4′-octylbiphenyl, dielectric relax. anal. in nematic and smectic phases 80−108153
4-cyano-4′-octylbiphenyl, smectic A phase, defect patterns induced by ultrasounds 79−86695
4-cyano-4′-octylbiphenyl, smectic A phase, ENDOR study of galvinoxyl radical 79−78567

organic compounds continued
4-cyano-4′n-heptyl biphenyl, nematic phase, torsional absorptions 77−48161
4-cyano-4′(n-amyl)-diphenyl, isotropic phase, induced molecular orientation relaxation time, Kerr effect *(Russian)* 80−19699
4-cyano-4′-octyloxybiphenyl, nematic-smetic-A transition, optical birefr. temp. coeff. 78−47505
3-cyano-4-methylumbelliferone in ethanol containing water, acid or alkali, laser emission 79−955
4-cyano-4-n-cyanobiphenyl, smectic A mesophase, plasticity anal., defects motion, Grandjean wall form. 78−91227
4-cyano-4-n-octylbiphenyl, smectic A phase, focal conics motion and plasticity, stroboscope obs. 79−86692
5-cyano-biphenyl, nematic phase, effect of elec. field on flow alignment angle 79−10792
cyano-biphenyl cpds., nematic, mag. susceptibility and order parameters 79−86709
cyano-biphenyl eutectic mixtures, tilt angle meas. of nematic phases 77−80417
cyano-biphenyl LC alignment on obliquely evaporated SiO_2 films 80−79677
cyano-biphenyl series, nematogens and smectogens, props. characterised by even-odd effect 80−107046
cyano-biphenyls, 7-CB and 8-CB, nematic liq. crysts. director fluctuation quenching by mag. field *(French)* 78−87613
p-cyano-dialkylanilines, twisted intramol. charge transfer states, dual fluoresc. 79−36683
p-cyano-N,N-dimethylaniline in polar solvents, double fluorescence, theoretical model 80−58296
4-4′-cyano-octyl-biphenyl, smectic A liq. cryst., elec. field effects, capacitance meas. 78−91237
4-4′-cyano-octyloxy-biphenyl, smectic A liq. cryst., elec. field effects, capacitance meas. 78−91237
p-cyano-p′-pentylbiphenyl/p-pentylbenzoic acid, mixture, induced smectic phase, dielec. props. 80−6498
cyanoacetylene, ^{13}C and ^{15}N isotopic species, rot. transitions, 8-220 GHz 77−61740
cyanoacetylene, ν_3 vibr.-rot. band, diode laser spectrum 80−91563
cyanoacetylene, and ^{13}C substituted species, in Sagittarius B2 and Orion A, relative isotope fractionation 79−21374
cyanoacetylene, and deuterate, microwave spectrum, ground and excited vibr. states 78−90157
cyanoacetylene, and isotopic forms, $^{13}C/^{12}C$ effects on partition function 79−29352
cyanoacetylene, and-d_1, cryst., IR, far-IR and Raman spectra, vibr., struct. 77−63407
cyanoacetylene, collisional excitation of interstellar molecule 78−81664
cyanoacetylene, cyanodiacetylene in interstellar clouds, obs. 80−46634
cyanoacetylene, in Sagittarius B2 mol. cloud, chemical fractionation of ^{13}C isotopes 77−29900
cyanoacetylene, IR absorpt. bands, integrated intensities, ab initio and LMO calcs. 79−72234
cyanoacetylene, lab. study of ion-molecule reactions, rel. to interstellar synthesis 79−1940
cyanoacetylene, liquid, N and ^1H relax. rates using pulsed NMR *(French)* 79−38394
cyanoacetylene, microwave spectrum, mol. consts. 78−74647
cyanoacetylene, photodissoc., CN radicals fluoresc. 79−52725
cyanoacetylene, photoelectron spectra, electronic states of radical cations 79−22756
cyanoacetylene, rate coeffs. for reactions with ions of interstellar significance 79−57221
cyanoacetylene, vibrational excitation in Orion molecular cloud 80−22067
cyanoacetylene ^{13}C distribution at thermodynamic equilib. 79−59590
cyanoacetylene (HC_3N), interstellar, in $^1\Sigma$ state, collisional excitation by H_2 80−109508
cyanoacetylene in L 183 (L 134 N) dust cloud high density core, SHF obs. 80−105307
cyanoacetylene-d_1, (DC_3N) in IRC+10216, detect. possibility 78−69901
cyanoacetylenes form. in atm. of C stars and W Hydrae 80−67708
α-cyanoacrylate adhesive in first monolayer on bulk Al surface, IR spectra, H-bond form., stretching vibr. 80−87119
cyanoacrylate adhesive Kanokonlit-E, metal surface pretreatment effect on joint bond strength *(German)* 79−57202
9-cyanoanthracene:perylene, exciplex emission 78−60513
9-cyanoanthracene, cryst., excimer emission, spectra, photochem. and multiphonon processes 78−10914
9-cyanoanthracene, cryst., polarised refl. spectra at 2K, 360-460 nm, dielec. function 79−91461
9-cyanoanthracene, luminesc., excimeric species 78−84637
9-cyanoanthracene, metastable crystal, red excimer emission 78−6757
9-cyanoanthracene, quenching of solid state photodimerisation reaction by cryst. doping 78−68547
9-cyanoanthracene excimer emission, in glassy and cryst. matrices 79−11445
9-cyanoanthracenes-N,N-dimethylaniline, fluoresc. exciplex emission in gas phase 79−68250
2-cyanoaziridine, microwave rot. spectrum, assignments 80−91546
cyanobenzenes, weak triplet-triplet absorpt. spectra 77−58027
p-cyanobenzilidene p-octyl oxyaniline, nematic, new type of hydrodynamic instability 77−43142
4-cyanobenzoyloxy-4′-pentylstilbene, nematic, smectic A, and orthogonal smectic B phases 80−64890
6-cyanobenzquinuclidine, intramol. electron-transfer excited state 80−58295
cyanobenzylidene octyloxyaniline, director bend mode behaviour near nematic to smectic-A phase transition 78−1985
cyanobenzylidene octyloxyaniline, smectic A phase, parabolic focal conic 77−89374
n-pcyanobenzylidene-p-n-octyloxyaniline, liq. cryst., proton FFT of aromatic and alkyl motions 77−15302
N-p-cyanobenzylidene-p-n-octyloxyaniline, smectic-A liq. cryst., nematic pretransitional mech. effects 77−11481
N-p-cyanobenzylidene-p-octyloxyanilene, second order nematic-smectic-A phase transition 77−72681
cyanobiphenyl, meas. near nematic-isotropic transition temp. 78−43219
cyanobiphenyl, nematic liq. cryst., refr. index, crit. angle meas. 78−60413
4-cyanobiphenyl and 4′-alkyl- or 4′-alkoxy-substituted liq. cryst. derivatives, soln., absorpt. and fluoresc. spectra 80−87164

organic compounds continued
4-cyanobiphenyl derivatives, deuterated, transition temp. meas. 78−14449
cyanobiphenyl eutectic mixture, liq. cryst., glassy transition, DTA obs. 79−4405
cyanobiphenyl liq. cryst. mixtures, mol. mechanism producing dielec. relax. 78−84521
cyanobiphenyl liquid crystal IR modulator expts. 80−102837
cyanobiphenyl nematic homologous series, Kerr consts., relax. times, refr. index, dielectric const. 79−19863
4-cyanobiphenyl/4-cyano-p-terphenyl liq. cryst. mixture, order parameters of dissolved dyes 80−100167
cyanobiphenyls, 8OCB and its mixtures with 7CB, orientational order and elastic consts. 78−91245
cyanobiphenyls, high press. reentrant nematic bilayer smectic-*A* transition 79−28087
cyanobiphenyls, isotropic phase, pretransitional behaviour, optical and elec. Kerr effects 79−10928
cyanobiphenyls, liq. cryst., thermal diffusivity, Rayleigh scatt. obs. 78−94977
cyanobiphenyls, liq. crysts. flow alignment 79−50988
cyanobiphenyls, nematic, diaelec. consots. and diamag. anisotropies 80−7253
cyanobiphenyls, physical props., appl. to Kerr cells 79−19142
cyanobiphenyls molecular conformational mobility study by optical probing method *(Russian)* 80−92459
cyanobutadiyne, interstellar, in Heiles 2 dust cloud, emission distrib. rel. to NH_3 emission 80−17641
cyanobutadiyne (HC_5N), interstellar, obs. in Taurus 80−26957
cyanobutadiyne-d_0,d_1, microwave spectrum, substitution struct., dipole moment 77−3348
t-cyanobutane, dielectric relaxation study, complex permittivity 80−80688
t-cyanobutane, solid, uniaxial molecular reorientation, quasielastic neutron scatt. 78−42927
cyanocobalamin-^{58}Co, whole-body retention in rats, age effect 77−70559
cyanocyclohexylcyclohexanes, nematic, diaelec. consots. and diamag. anisotropies 80−7253
cyanocyclopentane, microwave spectral study of axial and equatorial conformers 80−95604
cyanodiacetylene, 2663 MHz transition obs. in Sagittarius B2 77−33669
cyanodiacetylene, cyanotriacetylene, detect. in C star (IRC+10216) 79−17126
cyanodiacetylene, discovery in variable star W Hydrae 77−82238
cyanodiacetylene, form. in RF discharge 79−5156
cyanodiacetylene, interstellar, detect. of J=9 to 8 transition 77−91603
cyanodiacetylene, lab. study of ion-molecule reactions, rel. to interstellar synthesis 79−1940
cyanodiacetylene (HC_5N), interstellar, obs. in (Heiles's cloud 2) 80−22054
cyanodiacetylene cation, gas phase, UV emission spectra of $\tilde{A}(\pi^{-1})\rightarrow\tilde{X}(\pi^{-1})$ band system 80−95636
cyanodiacetylene emission at 24 GHz assoc. with Heiles 2 cloud collision 78−65675
cyanodiacetylene in mol. clouds Sagittarius B2 and Cloud 2, SHF obs. 80−101627
cyanodiacetylene in Sagittarius B2, 5 and 7 GHz obs. 79−92817
cyanoethylene, photofragment recoil, state selective time of flight- fluoresc. method 79−11809
N-cyanoformimine, stability, identification by microwave spectroscopy 79−10095
N-cyanoformimine-d_2, struct., microwave transitions 80−973
2-cyanofurane, rot. consts., dipole moments, nuclear quadrupole coupling, spectral obs. 77−34620
cyanogen adsorbed on (100) surface, electron energy loss spectrum 78−14592
cyanogen azide, electron-density maps of bent bonds 80−1084
cyanogen fluoride, fund., hot bands, laser microwave two photon and double reson. spectroscopy 80−32752
2-cyanoguanidine, electron-density maps of bent bonds 80−1084
cyanohaemin, ferric porphyrins with fifth ligands, ^{57}Fe and ^{14}N hyperfine consts. 78−50475
cyanohexatriyne, detect. at 14.7 GHz in Heiles Cloud 2 and Sagittarius B2 78−73745
cyanohexatriyne, in mol. clouds Sagittarius B2 and Cloud 2, SHF obs. 80−101627
cyanohexatriyne detection in Heile's Cloud 2 at SHF 78−41018
cyanomethane$^-$, ab initio calcs., electron affinity, stability 77−42239
cyanomethane, collisional rot.-line widths and shifts, microwave region 78−25619
cyanomethane, dielectric susceptibility at radio frequencies 78−14123
cyanomethane, heavy nucleus isotope shift calcs. 78−86917
cyanomethane, IR laser photofragmentation CN($X^2\Sigma^+$) radical energy partitioning, rovibronic distrib. 77−61813
cyanomethane, IR photolysis, CN radical photoluminesc. 77−73452
cyanomethane, matrix-isolated, VUV photolysis, CNC radical vibr. and electronic spectra 78−85180
cyanomethane, multiple quantum coherence in dipolar relaxation measurements 79−73845
cyanomethane+bromomethane, microwave spectral line width, dipole-dipole interaction calc. 78−74648
cyanomethane+He, afterglow, excitation and quenching reactions, optical pumping 78−35690
cyanomethane-d_0, -d_3, vacuum UV photodissociation spectroscopy 79−834
cyanomethane-d_0,-d_3, soln., for IR spectra, band shape and moment anal. 80−58252
cyanomethane-d_1, ^{13}C-D quadrupole coupling const., ^{2}H-NMR spectra 77−481
cyanomethane-d_3, deuteron NMR spin echo, time domain spectrum 78−88223
cyanomethane-EBBA, binary liq. cryst. system, two-phase premelting, NMR obs. *(Russian)* 78−30743
cyanomethane-HF, hydrogen bonded heterodimer, spectroscopic consts. from microwave spectrum 80−43038
cyanomethane-HF, microwave spectroscopic investigations of hydrogen-bonded complexes 78−62794
cyanomethyl radical, electronic struct. and props. 79−49938
cyanonaphthalene, fluoresc. quenching by inorganic anions 78−74694
cyanooctatetrayne, detect. in interstellar space 78−93370
cyanooctylbiphenyl, smectic A phase, X-ray diffr. study 80−79690

organic compounds continued
cyanopentyl-d_{11}-biphenyl-d_4, ordering matrix, proton dipolar coupling obs. 78−63671
p-cyanophenol, cryst. struct. determ. 77−24312
p-cyanophenol mixtures, p-alkylbenzoates twisted nematic effect 79−82947
4-cyanophenyl 4-heptyloxybenzoate, nematic and smectic modifications, dielec. relax. meas. 77−69769
4-cyanophenyl 4-n-pentyloxybenzoate, electrical Kerr effect studies 80−25339
4-cyanophenyl esters, of 4′-n-alkylcinnamic acids, birefringence 79−64991
p-cyanophenyl p-n-alkylobenzoates, nematic, birefringence, polarisability and order parameter 80−100642
4-cyanophenyl-3-methyl-4-(4-n-alkylbenzoyloxy) benzoates, mesomorphic props. 79−94888
p-cyanophenyl-p'-caproyloxybenzoate, charge carrier behaviour, thermal depolarisation current study 80−7283
2-p-cyanophenylazo-S-akloxypyridines, synthesis, phase transition temps., and dielec. props. 79−86876
m-cyanophenylbenzoyloxybenzoates, nematic phase, freq. depend. of dielec. props. *(French)* 79−91337
cyanophenylcyclohexanes, nematic, diaelec. consots. and diamag. anisotropies 80−7253
cyanopolyynes, form. in gas discharges 79−5156
cyanopolyynes, interstellar, and related molecules, synthesis 80−12793
cyanopyridine, isomeric forms, adsorbed of Ag electrodes, Raman scatt., orientational specificity 79−69822
3-cyanopyridine, NQR Zeeman obs., crystal packing 80−54978
4-cyanotetrafluorophenyl 4-n-alkylbenzoates, synthesis and mesomorphic props. *(French)* 79−86679
2-cyanothiophene, rot. consts., dipole moments, nuclear quadrupole coupling, microwave spectra 77−34620
3-cyanothiophene, rot. spectrum and consts., elec. dipole moment, quadrupole coupling, r_0-struct. 77−79607
3-cyanothiophene-^{34}S(-^{15}N), partial r_0-struct., microwave spectra 80−91552
4-cyanothiophenol, synthesis 78−51408
cyanotriacetylene, interstellar, discovery, implications for theories of interstellar molecule formation 78−41029
cyanotrifluoromethane, vacuum UV photodissociation spectroscopy 79−834
4-cyanphenylene-4'-n-alkoxybenzoates, pulsed NMR Fourier spectroscopy 77−24266
cyanuric acid, electron-density matrix extraction from X-ray diffraction data 77−65930
cyanuric acid, molecular charge distrib. refinement 79−55730
cyanuric acid, X-N and X-X($1s^2$ core) maps 79−50922
cyanuryl chloride, quadrupole spin echo envelope EFG tensor axisymmetry in mag. field 80−20497
9-cycanoanthracene, subpicosecond laser photolysis and time resolved absorpt. spectra *(Japanese)* 79−79272
cycasin, cryst. growth and struct. 78−18631
cyclic carbonates, supercooled liqs., dielec., acoustic, NMR, viscoelastic relax. props. 77−1609
cyclic ethers-HF H-bonded complexes, calorimetry, IR spectra and MO calcs. 79−52738
cyclic hydrocarbons, chemisorpt. on W(100) surface, decomp., UPS and thermal desorpt. obs. 80−59782
cyclic ketones, electrochromism and electric dichroism for studying transitions to second excited singlet 80−63692
cyclic mol. struct., topological characterisation 80−74254
cyclic molecules, calc. of orbital mag. moment of π-electronic terms, collective motion model *(Russian)* 77−14335
cyclic molecules, localised electronic vacancies lifetimes 80−106264
cyclic monocarboxylic acid radicals, ring inversion barriers, EPR 80−53025
cyclic nucleotides, permeability across black lipid membranes 79−39376
cyclic olefin, ($C_{20}H_{19}ClN_2O_8S$), stressed, cryst. and mol. struct. X-ray anal. 79−86784
cyclo-(glycine-tyrosine-glycine)$_2$, crystal struct. from packing anal. 77−2070
cyclo-hexyl-ammonium-copper-trichloride, specific heat, ferromagnetic chain system 80−103491
cycloalkane, mol. ion struct., photodissoc., charge transfer, ICR obs. 79−45774
cycloalkanes, stopping power meas. for Li projectiles 79−4345
cycloalkanones, carbonyl charact. freqs., kinematic and pot. energy effects 80−95578
cyclobutadiene, π face bonding with CO, HCN, benzene 79−98180
cyclobutadiene, noncrossing and degeneracy in Hubbard models 80−14096
cyclobutadiene, topological resonance energy, rel. to benzene 80−5462
cyclobutadiene(-d_1), singlet and triplet ground states, vibr. freqs., MINDO/3 and ab initio SCF calcs. 78−13429
cyclobutadiene iron tricarbonyl, LF vibr. modes of hydrogeneous ligands, incoherent inelastic neutron scatt. 78−6229
cyclobutane, dissoc., frontier orbitals and activation energy, HAM/3 method 78−92452
cyclobutane, molecule, floating spherical GO calcs. of electron momentum distrib. and Compton profile 77−30933
cyclobutane, MS-Xα-MT study 80−52906
cyclobutane, thermal decomp., unimol. reaction theory 78−80712
cyclobutane+diazomethane (ketene) photolysis, methylcyclobutane form., decomp., CH_2 vibr. energy distrib. 78−61032
cyclobutane+T, recoil reaction, 5×10^{-2} torr 78−44389
cyclobutane(-d_8), centrifugal distortion const. calc., rel. to struct. and mol. wt. 80−95580
cyclobutane decomposition, vibr. excitation transients using variable encounter method 80−61072
cyclobutane derivatives, heterocyclic, elec. dipole moment in benzene soln. 79−36796
cyclobutane derivs., nucleophilic substitution, mechanism 77−9057
1,1-cyclobutane dicarboxylic acids and K salts, IR and Raman vibr. spectra *(French)* 80−2758
cyclobutane-d_0(d_8), cryst. modifications, low. freq. Raman and IR spectra 80−7342
cyclobutane-t_1, recoil hot reaction product, unimol. behaviour 79−16024
cyclobutane-t, chem. activated by nucl. recoil reaction, energy transfer interpret. 80−25985

organic compounds continued
cyclobutane-t, chemically activated by nuclear recoil, vibr. energy transfer 77−66763
1,1-cyclobutanedicarboxylic acid, X- and γ-irrad. cryst., EI-EPR overlapping spectra resolution 77−16179
cyclobutanol-d_0-d_1, conformation, microwave spectrum 78−86852
cyclobutanone, ^{1}H NMR anal., deconvolution technique 80−58289
cyclobutanone, absorpt. of pulsed IR radiation and decomp., joulemeter and opto-acoustic obs. 80−58328
cyclobutanone, clathrate hydrate, struct. II, for IR spectra, 4-100K 79−13707
cyclobutanone, electrochromism and electric dichroism for studying transitions to second excited singlet 80−63692
cyclobutanone, IR laser photolysis sensitised by NH_3, and reaction temp. 79−47944
cyclobutanone, ring puckering in $^1B_2(n,3s)$ Rydberg state, VUV spectrum 78−74675
cyclobutene, strong collision and thermal decomp. on surface, variable encounter method calcs. 80−50885
cyclobutenedione derivatives, photoelectron spectra, 2p lone pair delocalisation 78−46392
cyclobutylmethylether, IR and Raman spectra, config. 79−31525
cyclodextrin, α and β, positronium decay, test of freq. vol. model 78−19592
α-cyclodextrin, positron annihilation, effects of adsorbed gases 79−65952
cyclodextrin, trapped electrons in cryst. matrices, ESR, optical absorption spectra 78−80768
α-cyclodextrin and α,β-D-xylose, absorption mode spin-echo spectra appl. 80−78634
β-cyclodextrin dimeric complexes as models for lipid bilayer diffusion transport 78−80838
cyclodextrin induced perturbation of ionic equilibria during potassium p-nitrophenoxide biomembrane transport 79−96523
β-cyclodextrin-azulene complex, circular dichroism spectra 78−58713
cyclodextrins, diffusion in aq. polymer solns., complex form. 78−91460
β-cyclodextrinylbisimidazole, ribonuclease model, catalysis of cyclic phosphate substrate 78−85287
cyclododecane, force field, PMR of deuterated isotopomers 79−45695
cyclododecanone, photolytic biradical anomalous CIDNP enhancement, pulse spin echo NMR obs. 78−46369
cyclododecatrienetriyne, model for exciton theory of excited states in poly-1,4-hexadiyn-1,6-diol bis(p-toluene sulphonate) 77−80733
1,3-cycloheptadiene, electron impact, electronic spectra 79−45855
1,3-cycloheptadiene, microwave spectrum, conform. 79−98074
1,3-cycloheptadiene, Raman and IR spectra, normal coord. analysis, conform. 77−77203
cycloheptane, conformation maps 77−57900
cycloheptane, geom. struct. by electron diffr. 79−31682
cycloheptane, high resoln. rot. Raman spectra 77−75163
cycloheptane, loss angle, temp. depend., 9 and 36 GHz 78−48114
cycloheptanone, electrochromism and electric dichroism for studying transitions to second excited singlet 80−63692
cycloheptanone, photolysis, CIDNP effects 80−18869
cycloheptanone, vibr. spectra, pot. functions and conformers 77−83569
cycloheptatriene, and substituted forms, vibr. highly excited, steady-state photoisomerisation 80−16704
cycloheptatriene, field ionis. to excited states 77−19002
1,3,5-cycloheptatriene, singlet→singlet (triplet) excitation, electron impact energy loss spectra 78−46451
cycloheptatrienes, highly vibr.-excited thermal isomerisation in shock waves 79−79236
cycloheptatrienes, substituted, photoisomerisation, rate consts. 78−35708
2-cycloheptene-1-one, microwave spectrum, dipole moment and mol. conform. 79−72303
cyclohexadepsipeptide, refinements of mol. and cryst. struct. 77−39576
1,3-cyclohexadiene, electron impact, electronic spectra 79−45855
1,4-cyclohexadiene, excited electronic states, electron impact spectrosc. 79−45842
1,3-cyclohexadiene, He ion stopping cross sections, ring struct., bond strain and Bragg rule deviations 79−98188
cyclohexadiene, shock compression, dynamic high press. eqns. of state 80−6450
cyclohexadienes, chemisorbed on W(100), decomp., UPS and thermal desorpt. obs. 80−59782
cyclohexahydroxyisovaleryl, $C_{30}H_{48}O_{12}$, cryst. and mol. structs. 77−31653
cyclohexanal, liq., viscoelastic and structural relax., US rel. and absorption meas. 78−26634
cyclohexane$_{(c)}$ solns., positive ion-solute mol. reaction rate consts. in radiolysis 77−9091
cyclohexane, adsorbed on silica, laser Raman spectra 77−3367
cyclohexane, adsorpt. on Ru(001), LEED, ESD study 78−87872
cyclohexane, adsorption, on activated wood charcoal 79−28973
cyclohexane, adsorption and decomp. on Ni (111), high resolution EELS study 80−40739
cyclohexane, adsorption on exfoliated graphite, −70 to −25°C *(French)* 79−33178
cyclohexane, adsorption on graphitized C black, exptl. determ. of models 78−6216
cyclohexane, cation-electron pair distrib. irrad. and elec. field effects 77−81419
cyclohexane, chemisorbed on W(100), decomp., UPS and thermal desorpt. obs. 80−59782
cyclohexane, chemisorption on Ir surface, LEED, AES and thermal desorption meas. 77−1297
cyclohexane, conform. equilib., CNDO/2 calcs. on six-membered rings 80−23336
cyclohexane, conformation, distance geometry calcs. 77−50553
cyclohexane, conformation maps 77−57900
cyclohexane, cyclohexane-d_{12}, thermal cond., 300-600K 78−63528
cyclohexane, dielec. const. meas. using 3-terminal meas. cell 78−21170
cyclohexane, differential thermal anal. under high press. 78−51669
cyclohexane, dynamic props. investig. by Rayleigh scatt. of Mossbauer radiation *(Russian)* 77−69760
cyclohexane, excited electronic states, electron impact spectrosc. 79−45842
cyclohexane, FCC plastic phase, self-diffusion coefficient, 6 to −40°C, nucl. spin-lattice (spin) relax. 77−36144
cyclohexane, gaseous, crit. and liq., density and temp. effects on electron mobilities 79−27739
cyclohexane, gaseous, crit. and liq., positive ion mobility 79−37439

organic compounds continued
cyclohexane, He ion stopping cross sections, ring struct., bond strain and Bragg rule deviations 79−98188
cyclohexane, in benzene soln., mol. motion, correl. functions 80−96431
cyclohexane, IR absorption in Ar matrices and perdeutero-cyclohexane, vibrational anal. *(French)* 77−6769
cyclohexane, isomerisation, proton spin-echo NMR 77−9053
cyclohexane, isotope-mass effects in self-diffusion 80−92695
cyclohexane, laser wavefront reconstruction by stimulated scatts. in picosecond range 79−986
cyclohexane, liq., absolute Raman intensities determ. 77−68046
cyclohexane, liq., ion injection by metallic electrodes *(French)* 79−51289
cyclohexane, liq., ps time-resolved energy transfer, ultra-fast process, ps single pulse radiolysis 79−79267
cyclohexane, liq., two-photon absorpt. meas., using nonlinear light-mixing spectroscopy 77−79620
cyclohexane, liq., vibr. relax. at high press., Raman obs. 79−50026
cyclohexane, liq. and solid, mobility of excess charge carriers 78−2489
cyclohexane, liq. and soln., Raman scatt. for vibr. and rot. relax. 79−82969
cyclohexane, liquid, density effect on transport properties 80−65264
cyclohexane, loss angle, temp. depend., 9 and 36 GHz 78−48114
cyclohexane, mean amplitude of mol. vibration, approx. calc. method 79−13697
cyclohexane, mol. cryst., US absorption, rel. to lattice vibrs. 77−24358
cyclohexane, mol. motion, press. and temp. depend., PMR relax. obs. 78−64289
cyclohexane, monolayers and thin crystals grown on Pt (111), LEED obs. 77−59230
cyclohexane, neat and CCl_4-C_6H_{12} mixture, nonlinear susceptibility, $\chi^{(3)}$, reson. and non-reson. contribs. 79−987
cyclohexane, neutron irradiation, radical distribution, ESR study *(Japanese)* 80−44920
cyclohexane, NMR spin-lattice relax., periodically-irrad. system, master eqn. predictions 78−43664
cyclohexane, NO diffusion, ELDOR, self-diffusion 77−1618
cyclohexane, non-polar liq., microwave induced Kerr effect meas. 78−76435
cyclohexane, on Ni and Pt, C-H stretch vibration, broadened and softened, dehydrogenation 78−47666
cyclohexane, optical Kerr const., electronic and orientational contribs., obs. by coherent Raman techniques 77−88874
cyclohexane, plastic and liquid crystal phase, rot. correl. func. by Raman spectroscopy 80−23403
cyclohexane, plastic cryst., NMR determ. of phase diagram 77−12210
cyclohexane, plastic phase, Brillouin scatt., elastic consts. determ. 79−24324
cyclohexane, plastic-phase, NO-doped, heterogeneous solid soln., mag. reson. evidence 78−34449
cyclohexane, polystyrene solution, acoustic absorption and dynamic compressibility 77−55321
cyclohexane, Raman spectra intensity analysis, electrooptical parameters transferability 78−29820
cyclohexane, rapid anal. by mass spectrometry/mass spectrometry 80−61173
cyclohexane, Rayleigh scattering, depolarisation ratios 77−32387
cyclohexane, reactions catalysed by Pt surfaces with variable kink concs., surface O_2 effects 80−35576
cyclohexane, refr. index, temp. depend., deviation from Lorentz-Lorenz formula 77−40200
cyclohexane, rot. correl., Raman scatt. 77−83603
cyclohexane, rotational reorientation anisotropy near phase transition *(Russian)* 79−4261
cyclohexane, self-diffusion coefficients determ. by gel sectioning technique 80−92694
cyclohexane, shock compression, dynamic high press. eqns. of state 80−6450
cyclohexane, solid, neutron scatt. spectra using inverted geometry, white beam, t. of f. spectrometer 78−34395
cyclohexane, solid, NMR second moment calc. 77−8420
cyclohexane, solid, Raman spectra near 186K phase transition 78−56480
cyclohexane, thermal cond. and sp. ht. under press. 78−22906
cyclohexane, thin crysts. and monolayers on Ag(111) surface, LEED 79−11014
cyclohexane, Townsend coeffs. of avalanche counter gases 78−78582
cyclohexane, two-photon spectra; fluoresc. spectra, decay times, intensities obs. 77−75245
cyclohexane, US absorption and vel. meas. 77−51450
cyclohexane, US velocity under press., determ. of thermodynamic props. *(Japanese)* 77−59068
cyclohexane, vap., adsorption, on montmorillonite, specific surface area 79−29406
cyclohexane, vap. press. from 451K to crit. temp. and press. 78−47512
cyclohexane, vapour, effect of adsorpt. on surface oxidised activated C, paramag. props. 77−32238
cyclohexane, vapour press., 5-80°C, isotope effects 78−59939
cyclohexane, visible absorpt. spectra, local mode overtone intensity of C-H stretching mode 79−81207
cyclohexane, volume effect in metastability of crystalline phases on cooling 79−77716
cyclohexane+acetic anhydride, elec. resist. near crit. soln. temp. 78−71874
cyclohexane+benzene, excess volume 78−47527
cyclohexane+benzene, isotropic light scattering, excess Gibbs function 79−8150
cyclohexane+n-heptyl alcohol, measurements of US vel. and related parameters 80−38200
cyclohexane+n-hexane, effect of pressure on excess enthalpies at 298.15K 78−48689
cyclohexane+NH*, rate const., time resolved chemiluminesc. 78−60982
cyclohexane+toluene, binary liq., viscosity and excess free energy of mixing 78−51680
cyclohexane+toluene, energy transfer, pulse radiolysis obs. 80−16714
cyclohexane adsorption on graphite, conformers *(Italian)* 77−55439
cyclohexane aqueous hetero-azeotrope mixture, condensation heat transfer coeff. *(German)* 80−33425
cyclohexane crystals, luminesc. emitted at 55 cm^{-1} near phase transition point 77−52180
cyclohexane dehydrogenation, limitations of kinetic studies of catalysis on single-cryst. surface in UHV system 77−9126

organic compounds continued
cyclohexane derivatives, low melting nematic cpds., characterisation 79−10798
cyclohexane derivatives, mesophases obs. *(French)* 78−59747
cyclohexane flow in capillaries, Washburn eqn. 79−64767
cyclohexane fluorinated derivatives, $C_6F_9H_3$, C_6H_{12}, mol. rot. in plastic phases 77−35495
cyclohexane in ethyl methyl ketone, measurements of US vel. and density for determination of excess props. 80−37910
cyclohexane loss meas. at 35, 72 and 144 GHz 77−82560
cyclohexane menisci, exptl. verification of Kelvin eqn. for capillary condensation 79−33159
cyclohexane solvent for poly[(R)-oxypropylene], effect on opt. rot. dispersion and vac. UV circular dichroism 80−40084
cyclohexane vapour, flow calorimeter, meas. of isothermal Joule-Thomson coeff. 79−58688
cyclohexane- nitrobenzene, binary liq. soln., surface cluster functions 78−67631
cyclohexane-acetic anhydride, crit. resistivity, H_2O impurity effect 79−51565
cyclohexane-acetic anhydride binary liq. mixture, crit. behaviour of elec. resist. 78−6422
cyclohexane-acetic anhydride mixture, impurity effects on crit. behaviour of elec. resist. 79−65527
cyclohexane-acetone-butanol ternary liq. mixture, US vels. rel. to interactions 77−69044
cyclohexane-acetone-ethanol ternary liq. mixture, US vels. rel. to interactions 77−69044
cyclohexane-aniline, crit. mixture with shear flow, light scatt. obs. 80−6521
cyclohexane-aniline, viscosity conc. and temp. depend. in crit. mixing region 77−35686
cyclohexane-aniline critical mixture, shear and critical fluctuations, instantaneous mapping of velocity gradients 80−79420
cyclohexane-aniline mixture, shear induced transition to mean-field crit. behaviour 80−7364
cyclohexane-benzene, adsorbed onto silica gel from soln. 79−23826
cyclohexane-benzene, second virial coeff. meas. using new apparatus 80−44289
cyclohexane-benzene(carbon tetrachloride), binary liq. mixtures, molar heat capacity isothermal compressibility 79−66328
cyclohexane-benzene (methane) vapour mixture, excess enthalpy meas., appl. of differential-flow mixing calorimeter 78−12700
cyclohexane-benzene liquid mixing, volume changes 79−90782
cyclohexane-benzene mixing enthalpy, using isothermal dilution calorimeter 77−41615
cyclohexane-benzene-carbon tetrachloride ternary liq. mixture, US vels. rel. to interactions 77−69044
cyclohexane-chlorobenzene, soln., positronium formation inhibited by chlorobenzene 79−50170
cyclohexane-d_0, -d_{11} ^{13}C-^1H coupling constant 78−13519
cyclohexane-d_0(d_6), plastic crystal phase transition, mol. reorientation, Raman scatt. phonon spectra 80−20631
cyclohexane-d_{12}, Raman linewidth and molecular diameter meas. 80−69153
cyclohexane-d_6, solubilization in hexadecyltrimethylammonium bromide aq. soln., D NMR 78−24015
trans-1,4-cyclohexane-di-4′-n-alkoxybenzenes, synthesis and mesomorphic props. 79−94887
trans-1,4-cyclohexane-di-n-octyloxybenzoate, struct. of smectic phases, X-ray diffr. meas. 79−86702
cyclohexane-I_2 soln., ps dye laser excitation, fluoresc. and resonance Raman emission 80−28021
cyclohexane-methanol, crit. opalescence, AC elec. field effect 78−35159
cyclohexane-methanol, crit. opalescence, elec. field effect 79−28775
cyclohexane-methanol, mixture, thermal expansion near crit. soln. point 78−71871
cyclohexane-methanol soln., crit. exponents *(Russian)* 79−77766
cyclohexane-n-hexane, liquid system, rough hard spheres treatment of tracer diffusion 78−87798
cyclohexane-NO_2-air mixtures, photochem. particulate form. 78−11529
cyclohexane-octamethylcyclotetrasiloxane liq. mixtures, u.p. and excess Gibbs free energy determ. 77−30225
cyclohexane-polybutadiene-benzene system, vapour-liq. equilibrium 79−95147
cyclohexane-polystyrene mixture, Rayleigh and Brillouin scatt. and struct. relaxation 80−63640
cyclohexane-polysytrene, polymer solns., coexistence curve 79−28101
cyclohexane-sodium dodecyl sulphate-pentanol I-water microemulsion, light scatt. *(French)* 79−1968
cyclohexane-sodium tetraethylaluminate-donor two-phase system, Na^+ ion solvation number 78−95987
cyclohexane-tetrachloromethane, heteromolecular vibr. relax. time, Rayleigh-Brillouin spectra 78−59731
cyclohexane-transdecaline mixture, percolation model of electron and hole mobility 80−29452
cyclohexane-triethylamine mixture, US absorption, 7.56 MHz 77−39630
cyclohexane-water microemulsions, struct., use of variable-contrast method appl. to neutron scatt. 79−16043
cyclohexanecarbonitrile, rot. consts., conformers, struct., microwave spectrum 77−42314
cyclohexanol, dehydrogenation on Cu-Mg catalyst, kinetic model depend. of reaction rate 77−90583
cyclohexanol, glassy cryst., diffuse X-ray scatt. study 80−100171
cyclohexanol, low temp. solid phases, far IR absorpt. spectra, 93 to 303K 79−56785
cyclohexanol, orientationally disordered phase, Brillouin scatt. study 80−93351
cyclohexanol, polymorphism, Raman spectroscopy 77−73138
cyclohexanol, struct. information from OH-stretching freqs., axial/equatorial hydroxyl ratio 79−72438
cyclohexanol, US relaxation at 0.5 to 45 MHz 78−59868
cyclohexanol binary liquid mixtures, US absorpt. meas. 77−27948
cyclohexanol in soln., coop. mol. orient. rel. to OH proton chem. shift 78−1974
cyclohexanone, electrochromism and electric dichroism for studying transitions to second excited singlet 80−63692
cyclohexanone, He ion stopping cross sections, ring struct., bond strain and Bragg rule deviations 79−98188
cyclohexanone, solid, phase behaviour, at press. up to 3 kbar, DTA 78−43108
organic compounds continued
cyclohexanone, wetting of polyfluoroethylene resin, angle meas., porosimetry method 77−1278
cyclohexanone(-polystyrene), thermal cond., appl. of spherically symmetric apparatus for liqs. and solns. *(French)* 79−94477
cyclohexene, chemisorbed on W(100), decomp., UPS and thermal desorpt. obs. 80−59782
cyclohexene, He ion stopping cross sections, ring struct., bond strain and Bragg rule deviations 79−98188
cyclohexene, reactions catalysed by Pt surfaces with variable kink concs., surface O_2 effects 80−35576
cyclohexene, shock compression, dynamic high press. eqns. of state 80−6450
cyclohexene vapour, IR spectra anal. 80−63628
2-cyclohexene-1-one, planarity barrier, from LF Raman spectrum 79−54859
cyclohexene-Br_2 (Cl_2) π-σ complexes, low freq. spectra 78−78713
2-cyclohexenone, reduction by hydride ions, delocalised model, CNDO/2 calc. 79−79231
cyclohexone, graph theory for axial symmetry molecules *(Chinese)* 79−36792
cyclohexyl ammonium copper chloride, one dimensional spin $^1/_2$ ferromag., mag. props. 80−71000
cyclohexyl halide-thiourea clathrate, conform., Raman spectra 77−77200
cyclohexylcyclohexanes, substituted, anisotropic liq. cryst. solvent for optical absorption spectroscopy 78−45724
1,2,6-cyclononatriene, mol. struct. and conformation, gas phase electron diffr. 80−106400
1,2-cyclooctadiene, conformational energy surface, Boyd's iterative force field investig. 80−95737
1,5-cyclooctadiene, gas, high resolution Raman spectroscopy with laser sources, rot. spectra 79−27000
cyclooctane, adsorpt. on Ru(001), LEED, ESD study 78−87872
cyclooctane, He ion stopping cross sections, ring struct., bond strain and Bragg rule deviations 79−98188
cyclooctane, high resoln. rot. Raman spectra 77−75163
cyclooctane, solid, NMR lineshape and spin-lattice relax. 77−24757
cyclooctane+toluene, binary liq., viscosity and excess free energy of mixing 78−51680
cyclooctane-d_{14}, in oriented solvent, conformation, NMR determ. 77−61770
cyclooctanone, vibr., rot. spectra and conformations, pot. function 78−78707
1,3,5,7-cyclooctateraene, gas, high resolution Raman spectroscopy with laser sources, rot. spectra 79−27000
cyclooctatetraene, anions, in condensed media, electronic spectra 79−22723
cyclooctatetraene, effect on lasing props. of rhodamine 6G 78−13698
1,3,5,7-cyclooctatetraene, electron impact energy loss spectrum 79−10214
cyclooctatetraene, negative effect on small coaxial flashlamp-pumped dye lasers 77−14708
1,3,5,7-cyclooctatetraene, photoelectron ang. distrib. meas. 79−50082
1,3-cyclopentadiene, electron impact, electronic spectra 79−45855
cyclopentadiene, HAM/3 calc. of ionis. and excitation energy and electron affinity 79−26894
cyclopentadiene, LCAO-MO-SCF calcs., MODPOT, VRDDO and MODPOT/VRDDO procedures 77−71742
cyclopentadienone, photoelectron spectra, ionisation pot., PERTCI method and obs. *(German)* 78−42130
π-cyclopentadienyl (carvone) iridium (I), synthesis and protonation 77−60062
cyclopentadienyl cation, geometry optimisation by generalised Hartree-Fock 78−25427
cyclopentadienyl ion, electron affinity and Jahn-Teller effect, laser photoelectron spectra 77−88499
cyclopentadienyl radical, pot. surface and vibronic states, ab initio CI calcs. 80−47897
cyclopentadienyl radical, vibronic valence isomerisation, Jahn-Teller effect, D_{5h} symmetry 79−97986
cyclopentane, electron mobilities through liq. and critical regions 78−2536
cyclopentane, extreme case of dispirated diamond, Volterra-Weingarten dislocations 77−84747
cyclopentane, film boiling from cylindrical surfaces 79−23194
cyclopentane, gaseous, crit. and liq., density and temp. effects on electron mobilities 79−27739
cyclopentane, gaseous, crit. and liq., positive ion mobility 79−37439
cyclopentane, He ion stopping cross sections, ring struct., bond strain and Bragg rule deviations 79−98188
cyclopentane, plastic cryst. and liq. phases, thermal cond. and sp.ht., 100-300K, 0-2.1 GPa 78−34663
cyclopentane, pseudorot., effect of 10 fold barrier 78−74792
cyclopentane, solid, neutron scatt. spectra using inverted geometry, white beam, t. of f. spectrometer 78−34395
cyclopentane+isomeric octanes, excess volume 78−47527
cyclopentanol, solid, phase behaviour, at press. up to 3 kbar, DTA 78−43108
cyclopentanone, centrifugal perturbation consts., determ. from forbidden rot. transitions 79−6931
cyclopentanone, electrochromism and electric dichroism for studying transitions to second excited singlet 80−63692
cyclopentanone, excited triplet state, intramolecular tunnelling, optically detected electron spin coherence 77−61774
cyclopentanone, n−π^* transition, vibr. band intensities 80−74116
cyclopentanone, solid, phase behaviour, at press. up to 3 kbar, DTA 78−43108
cyclopenta[h]cycl[4.2.2]azine, photoelectron and visible, and UV spectra 78−5286
cyclopentene, He ion stopping cross sections, ring struct., bond strain and Bragg rule deviations 79−98188
cyclopentene, mol., pot. functions of bending modes 80−9753
cyclopentene, ring puckering, semi-empirical and ab initio calcs. 78−9065
cyclopentene-3,5-dione(-d_1) microwave spectrum assignments, rot. consts., dipole moment, config. 78−55168
cyclopentyl chloride, microwave spectrum, conformation, quadrupole coupling consts. 79−3434
cyclopentylamine, vibr. spectra and struct. 80−102516
cyclophanes, double and triple-layered, triplet state zero field splitting parameters, HMO calc. 77−50366

organic compounds continued
cyclophosphazene-DNa complex, spectrofluorometric and spectrophotometrics investig. 80−95643
cyclopopane, conformations, rot. consts., microwave spectrum 79−98075
cyclopropane, 3e′-orbital, electron momentum distribs., mol. distortions effects 80−18773
cyclopropane, γ-ray Compton profile meas., MO calcs., rel. to propene 77−10706
cyclopropane, adsoprtion on Pt NMR and PMR obs., chem. shift 77−51591
cyclopropane, adsorpt. on Ru(001), LEED, ESD study 78−87872
cyclopropane, clathrate hydrate, struct. II, for IR spectra, 4-100K 79−13707
cyclopropane, electron correlation, double SCF method 78−17575
cyclopropane, electron momentum distribs. in π orbitals from (e,2e) expts. 80−14239
cyclopropane, ionis. pot., many-body Green's function method 77−67972
cyclopropane, ionis. spectral intensity, valence electron binding energy depend. 78−90234
cyclopropane, IR band intensities using press. broadening technique 79−41172
cyclopropane, IR laser photolysis, decomposition, flame reaction 77−66760
cyclopropane, IR spectra studied by tunable laser, $\nu_{10}+\nu_{11}$ band anal. 80−95615
cyclopropane, $J_{C\text{-}H}$ spin-spin coupling const., bond length depend. 78−37660
cyclopropane, laser induced reaction, energy distrib. 80−16710
cyclopropane, lattice vibrs., IR and Raman spectra, 4 to 78K 78−27209
cyclopropane, liq., mol. dynamics, Raman and NMR studies of orientational motion 80−93296
cyclopropane, liq., mol. dynamics, self-diffusion, quasielastic neutron scatt. and NMR spin-echo meas. 78−10201
cyclopropane, liq., molecular motion, incoherent neutron scatt. study 79−50978
cyclopropane, localisation of MOs using density matrix formalism *(Russian)* 79−93911
cyclopropane, molecule, floating spherical GO calcs. of electron momentum distrib. and Compton profile 77−30933
cyclopropane, multiphoton IR laser-induced reactions 79−66312
cyclopropane, partial vibr. energy transfer map 80−32760
cyclopropane, rot. Raman spectrum 78−86873
cyclopropane, surface isomerisation to propylene, role of vibr. energy 79−74376
cyclopropane, thermal decomp., unimol. reaction theory 78−80712
cyclopropane, thermal unimol. isomerisation, vibr. energy transfer, diffusion cloud method 80−26001
cyclopropane, triplet states, electron impact and photosensitised dissoc., chem. effects 77−14592
cyclopropane, unoccupied orbitals, excitation energy, electron affinity, HAM/3 MO calcs. 78−13415
cyclopropane, vibr. energy transfer processes, laser induced fluorescence exam. 78−25663
cyclopropane, vibr. intensities, G sum rule appls. 80−32776
cyclopropane+inert gas, reactant decomp., rot.-vibr. energy transfer, relax. analytic soln. 80−55650
cyclopropane+NH*, rate const., time resolved chemiluminesc. 78−60982
1,1-cyclopropane($-d_2$), isomerisation in He bath, vibr. transfer, temp. depend. 79−24723
cyclopropane($-d_6$), centrifugal distortion const. and thermodynamic functions calc. 80−95582
cyclopropane-d_0, $-d_6$, force fields, Raman spectra 77−71806
cyclopropane-d_0, $-d_6$, multiphoton ionisation spectra, electronic struct. 78−82803
cyclopropane-d_0, d_6, absolute IR intensities, dipole moment derivatives and polar tensors 78−90165
1,1-cyclopropane-d_2, isomerisation transient vibr. energy distrib., collisional relax., variable encounters method 80−50836
1,1-cyclopropane-d_2, rearrangement, collisional vibr. energy transfer, temp. depend. 78−15668
1,1-cyclopropane-d_2, struct. isomerisation, vibr. distrib. collisional relax. dynamics, surface collisions 79−91926
cyclopropane-d_6, high resolution IR spectra, vibr. rot. band anal. 80−95621
cyclopropanone, electronic struct., UV photoelectron spectrum 78−33428
cyclopropene, dipole moment, reversed sign, theory 79−59440
cyclopropene, photoionisation and threshold photoelectron-photoion coincidence study 80−53062
cyclopropene fragment ions, from photoionisation, efficiency curves, isomerisation 80−53062
cyclopropenyl radical and anion, planar, E state pot. surfaces, CI and SCF calcs. 78−5155
cyclopropyl bromide, IR absorption, Raman scatt., assignments, thermodynamic functions 80−984
cyclopropyl carbinyl cation, internal rot. barrier, MINDO/2(3) forces method 78−9078
cyclopropyl chloride, ab initio SCF-MO calc., electronic and mol. struct. 78−25425
cyclopropyl cyanide, high-resolution microwave spectra, quadrupole hyperfine struct. of rot. transitions anal. 80−95601
cyclopropyl ketones, photoelectron spectra, MO calcs. 77−27115
cyclopropyl silane, rotational spectrum (9.0-35 GHz), transitions of ground vibrational state 79−98077
γ-cyclopropyl-bis (1,3,3-trimethylindolenine-2-yl)pentamethinium fluoroborate, exciton surface polaritons, reflecting faces obs. 80−65645
cyclopropylamine, intercalated in $SnSe_2$, photoelectron spectra study of electronic struct. 78−84698
cyclopropylamine struct., microwave spectrum 79−10096
cyclotrimethylene trinitramine, high explosive, fracture surface energy determ. 77−44337
cyclotrimethylene trinitramine, high explosive, surface energy from contact angle meas. 79−51393
cylcohexane, liq., energy transfer rate parameters, emission intensity, lifetime meas. 79−86031
DL-cysteine, phase transition obs. at 10°C *(French)* 80−49355
cysteine, polycryst., proton mag. relax. and mol. motion 78−20139
L-cysteine HCl, free radical formation by two photon absorpt. at 3371 Å 77−32815
cytidine, cryst. powder, absorption spectrum, unusual narrow line FIR modes, cryogenic temps. 79−69824
organic compounds continued
cytidine, pulse Fourier transform proton mag. resonance, equivalent to CW INDOR 77−32293
cytidine monophosphate, aq. soln., spectra, 300-450 nm, polarisation study 78−96015
cytidine-5′-monophosphate, γ-irrad. aq. soln., spin-trapped radicals, liq. chromatography and EPR spectroscopy 78−53340
3′-cytidylic acid, electron adduct, spin density distrib., INDO calcs. 77−71754
3′-cytidylic acid, X-irrad., stable radical in ribose moiety, compared with cytidine 77−25375
cytidylyl-3′,5′-cytidine, aq. soln., spectra, 300-450 nm, polarisation study 78−96015
cytochrome c, ferric- and ferro-, reson. Raman excitation profile, Soret excited 79−92147
cytochrome c, very dilute benzene soln., picosecond reson. Raman spectroscopy 79−98102
cytochrome C, vibronic theory of reson. Raman scatt. 79−94004
cytochrome c complexes, reduction by Mo cysteine complexes 77−86371
cytochrome-c, CARS near one-photon reson. 77−65466
cytochrome-c, coherent reson. Raman scatt. and incoherently broadened reson. fluoresc., condensed phase 78−60429
cytosine, cryst., electron damage, electron microscope study 78−22762
cytosine, hydroxy and methoxy derivatives, absorption UV spectroscopy and electronic struct. of ionic and tautomeric forms 80−74177
cytosine, tautomeric equilibria with adenine, in aq. solns., electrostatic model of solvation, SCF MO calc. 79−96305
cytosine derivatives, photosensitised induction by H-addition radicals in frozen aqueous soln. 78−20146
cytosine hydrochloride, cryst. growth, crystallographical parameters 78−14332
cytosine molecules, vertical interactions evaluation methods 79−54772
cytosine monohydrate, cryst. growth from aq. soln., elec. props. 78−3007
cytosine monohydrate, deuterated, neutron diffr. cryst. struct. determ. 80−54215
cytosine monohydrate, single cryst., γ-irrad., ion radical recomb., EPR 78−15776
cytosine monohydrate single cryst., X-irrad., OH addition radical and decay product 77−86447
cytosine monohydrate single crystal growth, effect of pH 79−34473
cytosine.H_2O crystals, radical form. by X-irrad. at 77 and 300K 77−12886
cytosol aspartate-transaminase, of chicken heart, prep. of orthorhombic crysts., X-ray determ. of unit cell 79−57577
Czochralski growth, assessment of perfection 78−64460
D-leucine, exchange diffusion in mouse Ehrlich ascites tumour cells, temp. reduction effect 80−67053
Davydov splitting theory, excitonic parameters, split absorption bands, organic molecular aggregates *(Spanish)* 79−59437
DBS micelle solution, hydrophobe molecule solubility, NMR 79−83517
$DBTTF(BF_4)_{0.8}$, new conducting compound, synthesis, elec. and mag. props. 79−28341
$(DBTTF)_{2.67}.SnCl_6$, Peierls transition, fluctuations effect *(Russian)* 79−60809
DBTTF halogen complexes, IR, UV spectra, EPR study 80−108215
DCM laser dye, spectral props., synthesis, broad tuning range, comparison with other dyes 79−76684
deca-2,4,6,8-tetraene, fluoresc. and absorpt. spectra, forbidden transition 78−82764
decacyclene, MCD and absorpt. spectra 79−54875
decacyclene, mono- and dianions, reson. spontaneous Raman spectra, vibronic interactions 79−3451
decacyclene anion, photoexcited quartet state, transient EPR 80−78635
decahydronaphthalene-H_2O, liq.-liq. phase equilib., crit. phenomena 78−18764
trans-decahydronaphthalene-polystyrene system, press. and mol. wt. depend. of polymer solubility 79−23734
decalin, cis- and trans-, diffusion in liq. polyethylene, gas chromatography determ. 78−2277
decalin, liq., energy transfer rate parameters, emission intensity, lifetime meas. 79−86031
trans-decalin, liq., irrad., positive charge mobility meas. by microwave absorpt. 77−20100
decalin, liq. and glass mol. motion, kinematic and electrodynamic solns. 80−25293
cis-decalin, shift difference between chem. exchange sites using ^{13}C T_1 meas. 80−18945
decalin, two-photon spectra; fluoresc. spectra, decay times, intensities obs. 77−75245
decalin-dichloromethane glass, mol. dynamics, from dielec. loss meas., 107-148K, 293K 78−76379
trans-decaline-cyclohexane liq. mixtures, hole mobility, percolation model 80−65551
decane: pyrene (coronene), quasiline spectra, multiplet struct., freezing conditions and solvent effects 79−1786
n-decane, emulsion drop, efficiency of capture by bubble in noninertial flotation 80−11956
decane, film flow calc., effect of temp. and press. gradients in conical capillaries 79−55416
n-decane, films, thin, wetting, rheological charact. determ., capillary method 78−51788
n-decane, liq., thermal cond., meas. by transient hot-wire technique 80−103522
decane on Teflon FEP, effect of drop size on contact angle 80−2245
decane-air mixture, spontaneous ignition temp. limits determ. 77−52641
decane-n-butane-methane, heterogeneous flows of multi-component mixtures in porous media−review 78−59471
n-decane-n-decane-d_{22}, γ-irrad., H_2/D_2 product ratio mass spectra, mechanism 77−40558
n-decane-nitrobenzene critical system, US absorpt. meas. 78−6126
decane-water-Na p-octylbenzene sulphonate-1-pentanol-NaCl, microemulsion system, existence of bicontinuous zone 80−104466
decanoic acid, associated vapours, homogeneous nucleation 80−96638
decanoic acid, mol. config. change in cryst., IR spectra, normal coord. anal. 78−33506
decanol, dynamic mol. struct. in cyclohexane-d_{12}, ^{13}C NMR 78−33519
decanol, sound vel. and absorpt. meas. at hypersonic freqs. 78−18708
n-decanol-CCl_4, excess thermodynamic functions, 15, 30 and 45°C, composition depend. *(Russian)* 78−31677
n-decylammonium cadmium chloride, perovskite-type layer cmpd. n-decylammonium chain dynamics 79−99313

organic compounds continued
decylammonium chloride micelles, ^{13}C longitudinal relax. times and nuclear Overhauser enhancement anal. 80−83390
decylammoniumchloride and bromide, lyotropic nematic struct. 78−51410
p-decyloxbenzylidene p′-amino 2-methyl butyl cinnamate, smectic A to C transition, Landau theory 77−84906
p-n-decyloxybenzoic acid p-n-hexyloxyphenyl ester, dielec. permittivity in nematic and smectic phases 79−32899
L-p-decyloxybenzylidene-p′-amino-2-methylbutyl-cinnamate, ferroelec. smectic liq. cryst., electro-optical effect 78−39527
l-p-decyloxybenzylidene-p′-amino-2-methylbutylcinnamate, (l-DBC), liq. cryst., pyroelec. const. stationary value over ferroelec. temp. range 79−65801
l-p-decyloxybenzylidene-p′-amino-2-methylbutylcinnamate, ferroelec. liq. cryst., pulsed pyroelec. effect 79−15405
cis-dekalin, dynamic props. investig. by Rayleigh scatt. of Mossbauer radiation *(Russian)* 77−69760
DEM(TCNQ)$_2$, ESR study 80−97127
2-deoxy-D-erythro-pentonic acid solution from alkali-labile site in γ-irrad DNA 78−20144
2′-deoxyadenosine in aq. deaerated soln., new radiolysis mechanism 80−81350
deoxycholic acid, lyotropic and thermotropic phase transitions, clathrate form. 80−49341
deoxycytidene 5′-phosphate-H_2O, cryst., X-irrad., ESR and ENDOR obs. 79−34330
deoxycytidine 5′-phosphate, H_2O, X-irrad., 3αH radial. form., ENDOR, ESR 77−73453
deoxycytidylyl-(3′,5′)-deoxyguanosine, DNA double helical fragment intercalator complex, molecular struct. 79−16140
deoxyhaemoglobin, porphin-Fe-imidazole system, SCF-LCAO-ASMO and CI calcs. of low-lying multiplets and excited states 80−94155
deoxyribonuclease I in aq. soln., inactivation by thermal neutrons 80−104664
2′-deoxyuridine, γ-irrad., positron lifetime rel. to free radical conc. 78−72635
desferrioxamine B, chelation therapy for transuranic elements, rats 77−44758
detergent micelles, mol. shape, form dichroism of cryst. 78−60417
detergents, effect on bleaching and laser props. of solns. of rhodamine dyes 79−59697
deuteriochloroform, Raman spectra, mol. orientational relax. 79−65865
deuterochloroform, solns., vibr. dephasing and reorientational relax., solvent depend., Raman spectra 79−85968
deuteromethane, crystalline, X-ray powder diff. study 80−96500
deuteromethane, solid, thermal expansion *(Russian)* 78−26698
deuteronaphthalene:β-deuteromethylnaphthalene crystal, asymmetry of phonon side bands, absorption, luminesc. and specular spectra 77−1730
dextran T-10 and α-cyclodextrin, absorption mode spin-echo spectra appl. 80−78634
dextrans, surface adsorpt. on human red cell membrane 78−15799
DHAB, nematic, ordering change due to external DC elec. field, permittivity obs. 78−94990
1,2-di(1-naphthyl)-ethylene, cis-trans photoisomerization in condensed phase, polycryst. phase transition 79−10139
di(1-pyrenylmethyleneoxycarbonyl) alkanes, intramol. excimer emission 78−70862
1,4-di(2-(5-phenyloxazolyl))-benzene, vap., lasing kinetics calcs. *(Russian)* 79−13778
1,4-di(2-(5-phenyloxazolyl))benzol, vapour, electron beam excited luminesc. *(Russian)* 78−82780
1,4-di(2-benzoxazolyl)-benzene vapour lasers, generating capacity, stimulated emission *(Russian)* 77−679
4,4′-di(2-butoctoxy-1)p-quaterphenyl, emulsfied, dye laser, pumped by N_2 laser 79−13962
di(2-ethylhexyl) phosphoric acid, organic extractant in liquid radwaste, gamma radiolysis 79−67879
2,5-di(4-biphenylyl)oxazole, fluoresc. emission anisotropy, solvent effects 79−3489
di(alkyl ammonium)copper tetrachloride, two-dimens. magnon and phonon thermal cond. in high mag. fields 77−69123
di(alkylammonium)$CdCl_2Br_2$, solid-solid phase transitions 80−84290
di(alkylbenzylthio)ethane, oil additive, thermal stability determ. by chromatography, colorimetry 79−15969
di(ethylene diamine H_2)$_2$ zince hexachloride, single crystals, EPR parameters for Mn^{2+} 79−56607
di(ethyleneammonium) manganese tetrachloride, 2-dimens., EPR linewidth and spin-dimens. crossover 77−69670
di(methylamino) zinc tetrachloride, single crystals, EPR parameters for Mn^{2+} 79−56607
di(methylammonium) cadmium tetrachloride, LF Raman spectra and phase transitions 77−63414
di(methylammonium) manganese tetrachloride, LF Raman spectra and phase transitions 77−63414
N,N′-di(methyloctadecyl) squarylium monolayers on Ag surface, attenuated total refl. 79−11480
1,2-di(N-piperidyl)ethane-bis-N-oxide tetrahydrate, synthesis, cryst. and mol. struct. obs. 79−32985
4,4′-di(p,n-alcoxybenzylideneamino) biphenyls, smectic polymorphism, dilatometric exam. *(French)* 77−51480
4,4′-di(p,n-alcoxybenzylideneamino)biphenyl series, smectic polymorphism, molecular area and tilt angle *(French)* 77−43139
4,4′-di(p,n-alcoxybenzylideneamino)diphenyls, X-ray diffr. study of smectic polymorphism *(French)* 77−76299
di(propylammonium) copper tetrachloride, mag. suscept. meas. 77−63131
di(tert. butylperoxy)triphenylantimony, X-ray cryst. struct. determ. 80−92517
di(thiomethyl)methane, vapour, far ultraviolet spectra, valence-shell and Rydberg transition interpretation 79−50037
1,4-di(triphenyl lead)diacetylene, phosphoresc. spectra, triplet state 79−47490
1,4-di(triphenyl tin)diacetylene, phosphoresc. spectra, triplet state 79−47490
di thioformic acid, cis and trans isomers, rot. microwave spectra and config. 79−63989
di-1′,4″-octyloxybenzylidene-1,4-diaminochlorobenzene, nematic with some smectic ordering, EHD instabilities 77−84640
1,4-di-2-5-p-tolyloxazolylbenzene, vapour, rot. fluoresc. depolaris. 79−54889

organic compounds continued
di-2-pyridyl sulphide, mol. struct. gas phase electron diffr. obs. 79−81296
trans-1,2-di-(1-napthyl)-ethylene, conformeric fluoresc., chromophoric fragments rot. 77−485
di-(2,2,6,6-tetramethyl-4-piperidinyl-1-oxyl) suberate, nitroxide radical polarised neutron study in paramag. phase 79−47231
di-(2,2,6,6-tetramethyl-4-piperidinyl-1-oxyl)-suberate, spin densities, polarised neutron diffr. meas. 80−50037
di-(2-ethylhexyl)phthalate, ^{13}C and ^{1}H relax., reorientational correlation times 79−51869
1,4-di-(2-naphthyl)-benzene, conformic fluoresc., chromophoric fragments rot. 77−485
di-(4-n-alkyloxy) benzoic esters, of hydroquinone series, effect of polar substituents on electro optical props. 79−46569
1,6-di-(N-carbazolyl)-2,4 hexadiin, cryst. struct., luminesc., γ-ray polymerisation 78−18629
di-butyl-sebacate, HV evaporation, mass transfer in evaporating space *(Japanese)* 80−50558
di-isobutyl kitone, γ-irrad., isothermal luminesc. decay, temp. depend. 79−66322
4,4′-di-n-acyloxydiphenyldiacetylenes, synthesis and mesomorphic props. 79−82148
p,p′-di-n-alkoxy-azoxybenzenes, homologous cpds., nematic, refr. indices and opt. anisotropy, temp. depend., order parameters 77−16278
p,p′-di-n-alkoxyazoxybenzene series, C_1-C_7, submillimetre wave absorpt. investig. 80−34910
di-n-butyl phthalate, complex. permitt. meas. by time-domain spectrosopy 77−49741
p,p′-di-n-butylazobenzene, high press. mesomorphic and polymesomorphic transitions 78−18750
di-n-decyl azoxy methyl cinnamate, smectic-A liq. cryst., anisotropic US propag. 79−55829
di-o-thymotide, cryst. chem. study and morphology *(French)* 79−46576
di-p-anthracene, electron beam induced monomerisation 77−12789
di-p-anthracene, fluoresc. and photoreactivity 77−48668
2,4-di-p-bromophenyl pentane, polystyrene model mol., US relax., mol. dynamics 79−73258
1,6-di-p-methoxybenzene sulphonyloxy-2,4-hexadiyne, thermal polymerization, Raman spectra 80−103952
di-potassium 2-amino-6, 8-naphthalene disulphonic acid, wavelength shifter in water Cherenkov detector 79−26834
di-t-butyl nitroxide, in benzene, solvent-solute interactions, ESR, DNP 78−17698
di-t-butyl nitroxide radical, in soln., proton relax., meas. of H-bonding 78−27103
di-t-butylnitroxide radical, solid, nucl. and electron spin relax. times meas. 78−60350
di-tert-butyl nitroxide, N hyperfine coupling const., solvent effect, model 79−54870
di-tert-butyl radical, ^{1}H NMR in organic solvents, press. depend. 79−31546
3,5-di-tert-butyl-4-hydroxybenzylidenemalononitrile, excited-state proton transfer, cryst. and mol. struct. 78−84630
di-tert-butylazodicarboxylate, photochem. generated alkali cationic triple ions, ESR 78−80758
1,4-di-[2-(5-n-tolyloxazolyl)] benzene, absorption spectra and stimulated emission dependence on pressure of extraneous gas *(Russian)* 77−50660
diacetyl, triplet-singlet conversion, by laser spectrosc. technique 79−86002
diacetyl, vap., laser-excited long-lifetime luminesc. 79−54887
diacetyl vapour, fluoresc. and phosphoresc., nonradiative transitions between triplet and singlet state obs. 80−99516
N,N′-diacetyl-1,2,1′,1′-tetrahydro-1,1′-diisoquinoline, cryst. and mol. struct. 78−2106
3,6-diacetylamino-N-methylphthalimide, in alcoholic solns., phosphoresc. decay laws 78−17709
diacetylene, luminesc. and ODMR spectra 79−38604
diacetylene, near UV band system, rot. and vibr. anal., rot. fine struct. 77−61761
diacetylene, obs. of ν_4 band near 3 microns 80−47977
diacetylene, single cryst., EPR of low-temp. photoproducts, photopolymerisation 78−85175
diacetylene, single cryst., photopolymerisation, intermediate states, struct. changes 80−30235
diacetylene, UV spectra of mol. excited states 79−31540
diacetylene (TSHD), low temp. photopolymerisation, short chain intermediates obs. 80−93754
diacetylene chains in partially polymerised diacetylene cryst., temp. depend. optical absorpt. 78−64376
diacetylene derivatives, solid-state polymerisation, isotope effects 80−66799
diacetylene mixed crystals, co-crystallisation, influence of crystal composition on struct., reactivity in solid state 80−81324
diacetylene monocarboxylic acids, multilayers, struct. phase transitions and polymerisability 80−80129
diacetylene radical cation, and deuterated forms, electronic spectrum in solid inert gases 79−94026
diacetylene single crystals, photopolymerisation, optical transmission spectroscopic exam. 78−27757
diacetylene-d_2, excited quintet states during photopolymerisation, ESR obs. 80−84635
diacetylenes, photopolymerisation, solid-state reaction, photoacoustic photocalorimetric obs. 80−61089
diacetylenes, solid state photopolymerisation, reaction products, electron spin resonance anal. 80−81338
diacetylhydrazine, ^{14}N NQR echo envelope slow beats 80−29643
diacetylhydrazine, ^{14}N NQR lines fine structure 80−63667
diacrylate fissure sealants, film charact., dentistry appl. 80−12306
diacyl peroxides, photochem. decomp. for matrix isolation study of IR spectra of alkyl radicals 78−33510
diakyl-cyclohexyl-cyclohexanoates, nematic and smectic mesophases 80−19692
4,4′-dialkoxydiphenyldiacetylenes, synthesis and mesomorphic props. 79−32890
2,3-dialkoxynaphthalene, H_2O and D_2O solns., solubility and ht. of soln. 79−66333
dialkyl ammonium cadmium chloride, influence of C ions and metal ions on structural phase transition 78−2256

organic compounds continued
dialkyl ammonium copper chloride, Cu-Cu exchange interactions 77−69529
dialkyl ammonium manganese chloride, influence of C ions and metal ions on structural phase transition 78−2256
dialkyl ammonium manganese chloride, phases and structural phase transitions, DSC and X-ray diffr. meas. 77−47574
dialkyl carbonates, liq., US, microwave dielect. relaxation 79−56717
N,N′-dialkyl dipyridinium cation radicals, struct., INDO calcs., EPR obs. 77−71821
dialkyl phthalates, plasticizers, surface tension, contact angle, surface energy, entropy determ. *(Japanese)* 77−31843
dialkyl tartrates, Raman circular intensity differential spectra obs., mol. struct. 80−87130
dialkylammonium compounds, $(C_nH_{2n+1}NH_3)_2MX_4$, cryst. growth solubility, and props. 78−43999
dialkylammonium copper chloride, nearly 2-D ferromag., low temp. NMR 77−28455
dialkylammonium copper chloride, two-dimens. ferromag., energy transport by paramag. magnons 77−80909
dialkylammonium copper chlorides, mag. and struct. transitions, IR absorption 77−52097
dialkylammonium copper chlorides nearly two dimens. Heisenberg ferromagnet, NMR study of magnetisation 77−85586
dialkylammonium copper tetrachloride, ferromagnetic layer compound, magnetostatic mode excitation 80−29538
dialkylammonium copper tetracholorides, quasi 2-dimens., lattice- and spin-dimens. crossovers 77−59416
dialkylammonium cupric chloride, calorimetric study of phase transitions 78−75804
dialkylammonium iron tetrachloride, antiferromag., mag. susceptibility meas. 80−60220
dialkylammonium manganese chloride, order-disorder transition mechanism 78−79772
dialkylammonium manganese tetrachloride, lattice consts. and phase transition temps. 79−86779
dialkylammonium manganese tetrachloride, quasi two-dimensional antiferromag., temp. depend. of absorption spectra 78−43894
dialkylammonium metal chlorides, soft modes, phase transitions 78−79723
dialkylammonium zinc dichlorobromides, long chain cpds., phase transitions, calorimetric study 80−70390
dialkylaniline derivatives, twisted intramol. charge transfer states, dual fluoresc. obs. and form., dipole moments 80−18881
dialkylanilines, p-substituted, twisted internal charge transfer excited state form. 79−22683
1,4-dialkylbenzene, H_2O and D_2O solns., solubility and ht. of soln. 79−66333
4,4′-dialkyldiphenyldiacetylenes, synthesis and mesomorphic props. 79−32890
dialkyloxyazoxybenzenes, synthesis of ferroelec. smectic B, smectic C, and nematic phases 78−94969
s-cis, s-trans-diallyl, twisted, low-lying singlet states, sudden polarisation effect 78−86792
diallyl phthalate methyl methacrylate, copolymerisation, two-step, prep. of light focusing plastic rods *(Japanese)* 79−37064
diamagnetic susceptibility calcs., extended London theory 79−47228
diamantane, LF light scattering temp. depend., 40 to 340K 79−24307
diamantane, low temp. soft librational mode, Raman spectra exam. 78−30730
diamantane, molecular motions below plastic phase transition 77−24278
diamantane, NMR meas. of mol. motion 79−42858
diamantane, plastic and solid-solid transitions, Raman study 80−60590
diamantane, Raman study of three solid-state phase transition 79−51946
diamantane, sp. ht., thermodynamics of transition and fusion 79−55899
diamantane, structural changes within plastic phase 79−14929
4′,6-diamidino-2-phenylindole, use for fluorescent microscopical technique in diagnostic microbiology 78−20339
3,5-diamino-1,2,4-dithiazolium salts as development accelerators, evaluation 79−34336
2,5- diamino-1,4-benzoquinones, long distance bonds between sp^2 hybridised C atoms, polymethine coupling effect 79−13836
diamino-quinone, π-electronic struct., PPP-type calc. and config. anal. 78−21855
diaminoazobenzene, photodecomp., low temp., isotope effects 77−42365
4,4′-diaminodiphenyl ether, enthalpies and related thermodynamic functions 79−42276
3,6-diaminophthalimide vapour, mol. electronic excitation energy degradation path depend. on pentane 80−74195
3,4-diaminopyridine, new axonal K channel blocking agent 78−69028
diammonium layer compound, $(CH_2)_2(ND_3)_2MnCl_4$, mag. and optical props. 79−51760
diammonium layer compound, $(CH_2)_n(NH_3)_2CuCl_4$, mag. and optical props. 79−51760
diammonium layer compound, $Mn(NH_3)_2(CN)_42C_{12}H_{10}$, mag. susceptibility and sp. ht. meas. down to antiferromagnetic state 79−7999
diammonium layer compound, ND_3-$(CH_2)_2$-ND_3CuCl_4, antiferromag., magneto-optical meas. birefringence 78−68483
diammonium layer compounds $(CH_2)_n(NH_3)_2MnCl_4$, quasi-two-dimens. antiferromag., magnetis., spin-flop and crit. exponents 77−66311
diammonium oxalate monohydrate, NMR spectra, ^{13}C-^{13}C interaction, chemical shift effects 78−29800
diamond formation from hydrocarbon dissociation, Hugoniot data, high temp. and press. 79−47927
dianthracene, photodissoc., electronically excited products 78−27790
dianthronylidene ethane, luminescent excimer geometries, intermol. shift 78−27294
9,9′-dianthryldisulphide, UV/visible absorption spectrum *(German)* 79−59487
diarylalkane, in isooctane soln. triplet excimer form., phosphoresc., delayed fluoresc., triplet-triplet absorption 78−25597
diarylethanes, bromo- or cyano-substituted, mesomorphic props. 79−90535
diarylethylene, luminesc. spectra and rot. isomerism 79−85991
α,ω-diarylperfluorpolienes, X-ray spectra, phase transition temp. depend., struct. and mesomorphic props. *(Russian)* 78−38621
diastereomeric compounds, nonrigid mols., in soln., conform. determ., NMR, lanthanide shift reagents 77−30887
1,3-diazaazulene, vibronic coupling, Duschinsky effect, mixed cryst. spectra 77−79622
1,3-diazaazulene-azulene, Stark spectra, vibronic perturbations in mixed cryst. 77−79623
diazabicyclooctane, photoreduction of fluorenone, ion-radical yield enhanced by mag. field, cage recomb. region 79−79268
4,10-diazachrysene, absorpt. spectra and luminesc. in cryst. and glassy matrices, 77K 78−37650
2,7-diazanaphthalene, cryst. and mol. struct. 77−59002
diazanaphthalenes, excited state absorpt. spectra and intersystem crossing kinetics 80−74176
1,4-diazaphenanthrene, zero-field splitting, basic triplet states, H bond effects 78−5366
diazaphenanthrenes, lowest triplet state zero field splitting parameters calcs. 80−83391
1,6diazaspiro[4,4]nonane-2,7-dione, optical rot. strength calcs. 80−95793
1,4-diazatriphenylene, zero field splitting, basic triplet states, H bond effects 78−5366
diazines, LCAO-MO-SCF calcs., MODPOT, VRDDO and MODPOT/VRDDO procedures 77−71742
p-diazines, polycyclic, $T_1(\pi\pi^*)\rightarrow S_0$ intersystem crossing, isotope effects, ODMR and phosphoresc. obs. 80−91586
diazo compounds, continuous tone diazotype imaging films, model 78−32911
1,5-diazo-3,7-dithiabicyclo (3,3,1) nonane, molecular and cryst. struct. 78−51528
diazoles, LCAO-MO-SCF calcs. MODPOT VRDDO and MODPOT/VRDDO procedures 77−71742
diazomethane, appl. to struct. determ. of acidic surface oxides on carbon black and graphite 79−52404
diazomethane, electronic struct., least energy dissoc. path to CH_2 and N_2 products 78−5131
diazomethane, isomers, electronic and isomerization energies calc. 79−50161
diazomethane+cyclobutane photolysis, methylcyclobutane form., decomp., CH_2 vibr. energy distrib. 78−61032
diazomethane+triplet methylene$\rightarrow CH_3$, reaction rate const. determ. 77−36727
o-diazonaphthoquinones, thermal decomposition of light sensitive materials *(Russian)* 80−73504
diazonium, amplifying material, kinetic and sensitometric props. *(German)* 79−43607
diazonium salts in aqueous solns. and polymer matrices, IR absorpt. spectra 80−76030
p-diazoquinone, photodecomp. 80−7827
diazoxycinnamates, synthesis of ferroelec. smectic C and smectic A phases 78−94969
dibarium cobalt formate tetrahydrate Cu^{2+} doped, EPR of Cu-Co interactions 78−60334
dibenz-1,2,3,4-anthracene, nonlinear third-order electric susceptibility 78−74944
dibenzene-naphthalene, relax. time of vibr. levels of ground state *(Russian)* 77−44054
dibenzoate-TBBA, polar smectic A to non-polar smectic A transition line 79−82324
1,2,5,6-dibenzocoronene, phosphoresc. and ODMR meas. 79−18220
dibenzofuran:anthracene, cryst., prompt fluoresc., temp. depend., trap effects *(German)* 80−93400
dibenzofuran, cryst., phosphoresc. spectra and ODMR meas. 80−11470
dibenzofuran, cryst., prompt and delayed spectra, purity *(German)* 77−28622
dibenzofuran, photoelectron spectroscopy obs. of heterocycles 78−94286
dibenzofuran, single cryst. 2-photon excitation spectrum, 4.2K 79−56807
dibenzofuran, triplet state of X-traps, ODMR 79−24231
dibenzofuran-fluorene, mixed cryst., phosphoresc. spectra and ODMR meas. 80−11470
dibenzoquinoxaline, $T_1(\pi\pi^*)\rightarrow S_0$ intersystem crossing, isotope effects, ODMR and phosphoresc. obs. 80−91586
dibenzotetrathiafulvalene cation radical salts, cryst. struct. by X-ray anal., rel. to elec. props. 80−24436
dibenzothiophene, photoelectron spectroscopy obs. of heterocycles 78−94286
dibenzothiophene, triplet state of X-traps, ODMR 79−24231
dibenzoyl, X-ray TDS effects on at. parameters and electron density distrib. 77−19819
dibenzoyl methane, H bonding, dielec. dispersion obs. 77−63356
dibenzoyl peroxide, UV irrad., radical pairs EPR 79−73813
1,5-dibenzoylnaphthalene, cryst., ODMR, discrimination between homogeneous and inhomogeneous lines 79−44923
dibenzoylperoxide, triplet sensitized photolysis, mag. isotope effect 77−60081
dibenzo[a,d]cycloheptene, chem. shift, ring-current and excess-charge effects, semi-empirical calc. 78−33523
3,4,9,10-dibenzpyrene, hexane soln., UV fluoresc. line-narrowing two-photon site selective excitation 77−88484
dibenztetrathiafulvalene, absorbed on Au, Al, ionisation and polarisation energies of mol., UPS meas. 78−79886
dibenzyl: naphthacene, cryst., ground electron state, vibr. levels, relax. time determ. *(Russian)* 78−15195
dibenzyl, US velocity and absorption near melting point 78−6127
dibenzyl doped molecular crystals, stimulated emission at 4.2K 79−28790
2,2-dibenzyl-1,3-dibromopropane, crystal structure and thermal motion 79−99173
dibenzyl-tolan system, phase diag. 77−63642
dibenzyl-tolane, single cryst. growth from melt, influence of supercooling and impurity conc. on growth rate of faces 79−14714
dibenzylketone, photolysis in micellar soln., quantum yield and ^{13}C enrichment 80−97711
dibenzylmercury, cryst. struct. and conformation determ. 79−42045
dibenz[b,f]azepine, chem. shift, ring-current and excess-charge effects, semi-empirical calc. 78−33523
dibernzofuran, two photon absorptivities, CNDO/S-CI calc. with second order time depend. perturbation eqns. 80−74122
1,3-dibiphenylpropane, intramol. excimer form., kinetic and thermodynamic obs. 79−13750
diborane, density distribution of bonding electrons, simple refinement 78−18574
meso-2,3-dibromo-1,4-dichlorobutane, rot. isomerism, IR and Raman spectra 80−981
2,4-dibromo-1,5-diphenylpenta-3-one, cryst. struct., secondary and multicentre bonding 78−63751

organic compounds continued
p-dibromo-tetrafluorobenzene mol. cryst., in commensurate phase, quasielastic neutron scatt. 80−107386
dibromoalkanes, energy partitioning in mass spectrometric displacement reactions 80−89471
9,10-dibromoanthracene, fluoresc. and phosphoresc. spectra 77−14480
p-dibromobenzene, cryst. electronic and vibr. energy transfer and relax. 78−31229
p-dibromobenzene, crystal nucl. spin polarisation cross relax. study 80−29647
p-dibromobenzene, in p-dichlorobenzene cryst., absorpt. spectra, mol. clusters static interaction 78−15198
o-dibromobenzene, r_α-struct. determ. from PMR with ^{13}C satellites, bond lengths and angles 78−25560
p-dibromobenzene, static interaction changes in molecular crystals *(Ukrainian)* 78−6708
p-dibromobenzene, T_1 states, zero-field ODMR, MIDP and phosphorescence excitation spectra 80−74191
4,4′-dibromobenzophenone, ODMR and phosphorescence spectra in organic matrix 79−36671
4,4′-dibromobiphenyl, dielectric const., mol. reorientation in solid 78−72448
1,3-dibromobutane, IR and Raman spectra, normal coord. anal., C-halogen stretch bands and conformers 79−31522
dibromodifluoromethane, excimer laser photolysis, luminesc. from Br_2, Br, C_2, and CF_2 79−39184
dibromodifluoromethane, isotopically specific TE laser induced chem. reactions 77−90622
dibromodifluoromethane, laser-induced dissoc., CF_2 vibr. distrib. 77−88511
dibromodifluoromethane, UV laser fluoresc. and photochem., CF_2, CF and Br_2 fluoresc. obs. 80−16703
dibromodifluoromethane, vac. ultraviolet photodissociation, CF_2 emission 79−47955
dibromodifluoromethane+Ar excited, IR spectra, matrix isolation study, C-F stretching fundamentals 78−37632
4,4′-dibromodiphenylether:benzophenone-d_{10}, optical decay constants, photoexcited triplet state near level anticrossing field 78−80250
p-dibromodiphenylether surface, normal and ultra-Brewster refl. spectra 80−25400
1,2-dibromoethane, gauche and trans conformers, photoelectron spectra 78−50574
1,2-dibromoethane, volume change on melting and reduced Lindemann's relation 80−29151
1,2-dibromoethane in various solvents, dipole moments, concs. of anti and gauche forms 79−27106
cis-dibromoethylene, vac. UV spectrum, Rydberg transitions, ionisation limits 78−78718
trans-dibromoethylene, VUV and photoelectron spectra, Rydberg series, vibr. fine struct. 77−6799
dibromoethylenes, vac. UV spectra 77−23507
dibromofluorobenzene, IR absorpt. spectra, vibr. assignments 78−17665
dibromofluoromethane, photolysis, IR matrix isolation spectra of CF_2Br free radical 78−27788
dibromomaleic acid thioanhydride, mol. and cryst. structs., X-ray obs. *(German)* 80−44199
dibromomethane, highly excited vibr. states, thermal lensing spectrosc. and local mode model 80−87140
dibromomethane, IR spectra, local mode description for overtone spectra 78−42047
dibromomethane, photoionis., vibr.-excited ions form. in Franck-Condon gaps, threshold photoelectron spectra obs. 79−68262
dibromomethane, rotational-vibrational energy transfer, US absorpt. obs. 79−98537
dibromomethane, US relax., 60-700 MHz, high resolution Bragg refl. method 77−84853
1,4-dibromonaphthalene:octafluoronaphthalene, absorpt. and phosphoresc. spectra, intermol. reson. 79−33764
1,4- dibromonaphthalene, highly disordered quasi-one-dimens., excitation transport 80−34961
1,4-dibromonaphthalene, k-k scatt., exciton dephasing time-resolved phosphoresc. obs. 80−11458
1,4-dibromonaphthalene, mol. cryst. 77−1371
1,4-dibromonaphthalene, optical props., struct. disorder effects 78−52525
1,4-dibromonaphthalene, proton spin relaxation by optically excited triplet states 79−19810
dibromonaphthalene, quasilinear chain excitons, Stark effects 80−97239
1,4-dibromonaphthalene, S_0 to T_1 exciton transition, optical dephasing time and lineshape function 78−15183
1,4-dibromonaphthalene, space group C_{2h}^5, triplet excitons energy band struct. 78−6276
(1,4)-dibromonaphthalene, triplet exciton scatt., absorpt. spectra 78−6696
1,4-dibromonaphthalene, triplet-triplet exciton annihilation in quasi-1-dimens. cryst. 78−27297
1,4-dibromonapthaline, isotopic mixture, Anderson localisation of mol. excitons 77−89733
x-dibromononaphthalene, mol. aggregates, ESR line shape in solid matrix, fine and HFS 78−58878
1,5-dibromopentane, low freq. mol. vibrs., neutron inelastic scatt. study 79−46760
2,3-dibromopropionic acid, Fourier transform double resonance NMR 78−80249
p-dibromotetrafluorobenzene, neutron diffr. determ. of struct., constrained refinement 77−19839
1,3- and 1,4dibromotetrafluorobenzene cations in gaseous state, emission spectra 80−63648
dibromotetrafluoroethane, plasma quench reactions, electron attachment 77−90586
2,3-dibromothiophene, Fourier transform double resonance NMR 78−80249
dibutyl phthalate, absolute evaporation rate meas. 78−2244
dibutyl phthalate, liq., new ionis. method appl., using Penning effect and chem. ionis. *(Japanese)* 79−93255
dibutyl phthalate, plasticiser for PVC, effect on secondary relax. 79−4995
dibutyl phthalate, vapour press. determ. by submicron droplet evaporation 79−88993
dibutyl sebacate, vap. press., diffusivity, Lennard-Jones parameters, from droplet evap. obs. 79−43639

organic compounds continued
dibutyl sebacate, vapour press. determ. by submicron droplet evaporation 79−88993
p-p′-dibutyl-azoxybenzene, DIBAB, light scatt. studies *(Dutch)* 80−33885
p-p′-dibutyl-azoxybenzene, nematic liq. cryst., elasticities and viscosities, light scatt. meas. 79−4245
dibutyl-phenyl-benzoyloxy-benzoate, nematic liq. cryst., rot. barrier, PCILO and CNDO/2 calcs. 80−33874
dibutylammonium copper chloride, parallel pumping of two-dimens. spin waves, spin wave bandwidth 77−66425
dibutylammonium copper chloride, two-dimens. spin wave spectrum, parallel pumping meas. 77−20715
dibutylphthalate, supersaturated vapour, aerosol form. by mixing of flows 79−39212
dicadmium dimethylammonium pentachloride dihydrate, X-ray cryst. struct. 79−77588
dicalcium barium propionate, ferroelec. in press. induced phase VI 79−91393
dicalcium barium propionate, press. induced ferroelectricity, dielectric meas. 79−51920
dicalcium lead propionate, effect of particle size on dielec. behaviour 79−38429
dicalcium lead propionate, ferroelec., annealed, crit. exponents, dielec. const. temp. depend. 80−55050
dicalcium lead propionate, ferroelec., piezoelec. and elastic props. 78−84528
dicalcium lead propionate, improper ferroelectric, dielectric props., IR radiation pyroelectric detection 80−80711
dicalcium lead propionate, Raman scatt., order-disorder type transform. 77−12373
dicalcium lead strontium propionate, mixed cryst., phase diagram, dielec. and dilatometric anomalies 77−11689
dicalcium strontium propionate, anomalous US attenuation near ferroelec. phase transition 79−91383
dicalcium strontium propionate, cryst. symmetry in low temp. phase 79−37693
dicalcium strontium propionate, effect of particle size on dielec. behaviour 79−38429
dicalcium strontium propionate, elastic stiffness consts., determ. in US freq. region 79−37752
dicalcium strontium propionate, ferroelasticity and opt. activity rel. to transition 78−76420
dicalcium strontium propionate, ferroelasticity and optical activity rel. to transition 77−76547
dicalcium strontium propionate, ferroelec. domains, direct optical visibility 80−84704
dicalcium strontium propionate, improper ferroelectric, electro-opt. props. 78−76426
dicalcium strontium propionate, Landau theory breakdown in ferroelec. transition 77−12344
dicalcium strontium propionate, Raman scatt., order-disorder type transform 77−12373
dicalcium strontium propionate, temp. depend. of elastic const. c_{16} 79−28029
1-10-dicarba-closo-decarborane (10), mol. struct., vibr. and shrinkage corrections calc. from force field 80−95739
1,12-dicarbaclosododecaborane, plastic solid, phase transitions, 10-320K, Raman and IR obs. 79−28744
dicarbaclosododecaboranes, icosahedral, electron transfer phenomena in isolated borane units 80−18871
dicarbocyanine solns., photoisomerisation, fluoresc. and absorpt. spectra of photoisomer 78−85181
dicarbonitrile-anthracene solutions, absorpt. and emission spectra, solvent influence 80−43083
dicarbonyl compounds in soln., internal motion, dielectric relax., ^{13}C NMR relax., far IR spectra 77−28517
dicarboxylic acid, solid, binary mixtures of long chain mol. systems, diamag. susceptibility 77−32154
dicarboxylic acids, D quadrupole coupling constants, ENDOR study 78−90195
dicarboxylic acids, IR spectra Davydov splitting, methylene chain pendular vibrs. *(Russian)* 80−89008
dicarboxylic acids, low-energy electron irrad., ESR obs. 79−95646
dichelated protohaeme, model haemoglobin cpd., Mossbauer spectra 80−16904
β′-dichlordiethyl ether n-hexadecane-β exfoliating mixture, light scatt. and hypersound vel. 77−28586
β,β′-dichlorediethyl ether-n-dodecane crit. mixture, Rayleigh line wing 77−20864
dichloride 2.4′-bis (trimethylammonium-acetamide)-benzal-fluorene, thin layers, behaviour in electric field *(Rumanian)* 80−35108
dichloro(dimethyl)germane, mol. struct. determ. by vap. phase electron diffr. 77−54621
1,5-dichloro anthracene, cryst. struct. calc., use of at.-at. pots. 79−46646
dichloro bis-cyclopentadienyl titanium+dialkoxy bis chelated titanium compounds reaction, IR spectra 79−79239
2,2-dichloro-1,1,1-trifluoroethane, CO_2 laser multiphoton dissociation, D separation with single step enrichment 79−64112
5,5′-dichloro-1,1′-dianthraquinonyl synthesis by Ullman reaction *(Japanese)* 79−96304
2,5-dichloro-1,4-benzoquinone, mol. cryst., transition moment directions 78−64351
2,3-dichloro-1,4-napthoquinone in EBBA, PMR obs., mol. struct., orientation and solute-solvent interactions 77−27806
1,1-dichloro-1-nitroethane, dil. soln. in benzene, dielec. relax. study 80−29679
1,8-dichloro-9-methylanthracene, structural changes, photodimerisation and stacking fault energy 77−62548
dichloro-benzofuran in PCN, anal. by MS-GC *(Japanese)* 78−35767
2,5-dichloro-p-benzoquinone, adsorption on metal oxide surface, strength and distrib. of electron donor sites 78−84055
2,6-dichloroacetanilide, NQR, cryst. struct., band character 78−6596
dichloroacetic acid, soln., vibr., IR spectra 80−63633
dichloroacetic acid-d_0, -d_1, ^{35}Cl, ^{37}Cl NQR, isotope effects 77−46578
3,6-dichloroaniline, soln., dielectric const., loss and relax., dipole moment 78−43782
2,4-dichloroaniline, UV aborpt. spectra 79−36660
dichloroaniline (2,3- and 3,5-) IR absorpt. spectra 250 to 4000 cm^{-1}, vibr. anal. 79−13717

organic compounds continued
dichloroanilines, vibr. assignments, Raman spectra obs., thermodynamic functions 80−52992
2,6-dichloroanisole, anisotropic reorientation, nucl. relax. in coupled spin systems 77−40145
2,4-dichloroanisole and sulphur analogue, benzene dipole moment anal. 78−25748
9,10-dichloroanthracence, monoclinic, photocond. carrier mobility 80−39630
9,10-dichloroanthracene, cryst., singlet-triplet absorpt. spectra, delayed fluoresc. 77−8619
1,5-dichloroanthracene, photodimerisation, orientational defects, lattice energy 78−80724
9,10-dichloroanthracene, quasi 1D α-cryst., exciton transitions, optical refl. spectra obs. 77−81116
9,10-dichloroanthracene with iso-amyl acetate or esters as solvents, dye laser material 80−74354
1,5-dichloroanthraquinone, solid state transformation, X-ray powder anal. 79−51251
2,6-dichlorobenzamide, IR spectrum, vibr. assignment 80−95608
p-dichlorobenzene, ^{35}Cl NQR line narrowing by nonreson. RF photon dressing 80−63662
p-dichlorobenzene, ^{35}Cl NQR spectrum using digital freq. modulation 78−21189
p-dichlorobenzene, ^{35}Cl powder Zeeman NQR, injection and phase locked NQR spectrometer 80−54979
p-dichlorobenzene, ^{35}Cl spin-lattice relaxation under press. 79−4738
p-dichlorobenzene, α, β and γ forms, cryst. struct. and pot. energy 78−38685
p-dichlorobenzene, bicentric expansion of potential function of mol. interaction 79−94056
p-dichlorobenzene, charge transfer complexes, NQR shifts 78−55186
p-dichlorobenzene, Cl-Cl interactions at 100K, isotropic pot. functions calcs. 78−18578
p-dichlorobenzene, collision induced photodecomposition with ethane, CO_2 and SF_6, quantum yields 79−79270
p-dichlorobenzene, contact nucleation 77−52661
p-dichlorobenzene, cryst., Raman spectra , intensity of low freq. line 78−2846
o-dichlorobenzene, dil. soln. in CS_2, nucl. relax. and anisotropic mol. reorientation 79−95669
p-dichlorobenzene, expansivity, determ. by calorimetric compression from 0 to 400 MPa 80−44339
p-dichlorobenzene, in p-dibromobenzene, optical detection of Cl NQR in mag. field 80−50228
p-dichlorobenzene, lattice dynamics, thermodynamic functions and phase transitions 78−67777
o-dichlorobenzene, liq. mixtures, excess vols. and eqns. of state 77−29036
p-dichlorobenzene, mol. cryst., martensitic phase transitions 77−19891
p-dichlorobenzene, mol. cryst., US absorption, rel to lattice vibrs. 77−24358
p-dichlorobenzene, mol. dynamics, allotropy, solid-state phase transitions effects, Raman spectra *(French)* 77−42372
p-dichlorobenzene, NQR study of zone melting purification 79−91583
m-dichlorobenzene, nucl. quadrupole coupling consts., hyperfine struct., bonding 77−14422
p-dichlorobenzene, nuclear dipole absorpt. signal, under quadrupole reson. saturation conditions 78−48082
p-dichlorobenzene, optically detected X-band ENDOR of excited triplet state 79−18221
p-dichlorobenzene, orientation and deform. in nematic liq. cryst., PMR obs. 77−71815
o-dichlorobenzene, phase transition evidence from far IR absorption and Raman spectra 79−33693
1,2-dichlorobenzene, PVC soln. mol. wt. meas. by gel-permeation chromatography 135°C 79−7045
o-dichlorobenzene, r_α-struct. determ. from PMR with ^{13}C satellites, bond lengths and angles 78−25560
p-dichlorobenzene, Raman spectra, P-T diagram for α, β and γ-phases 78−68515
p-dichlorobenzene, spectral meas. of static interaction changes in molecular crystals *(Ukrainian)* 78−6708
p-dichlorobenzene, triplet state symmetry, geometry, ODMR, ENDOR obs. 79−18214
p-dichlorobenzene, vibr. relax., Raman active phonons temp. depend. 80−29139
1,2-dichlorobenzene, volume effect in metastability of crystalline phases on cooling 79−77716
p-dichlorobenzene+CO, vibr. energy transfer, quenching efficiency 79−3539
dichlorobenzene+metastable inert gas atom, mol. ionis., collisional energy depend. 79−54950
p-dichlorobenzene($-d_4$), mixed cryst. phases, mol. reorientations and intermol. interactions, Raman obs. 79−28751
o-dichlorobenzene(-benzene), liq. and dilute soln., microwave absorption and relax. processes 79−82920
1,3- and 1,4-dichlorobenzene radical cation, emission and photoelectron spectra, lifetimes meas. 78−86905
p-dichlorobenzene-naphthalene alloys, solid solns., NQR study 80−66063
p-dichlorobenzene-p-dibromobenzene, mol. cryst., intermol. mixing of electronic states 77−85768
p-dichlorobenzene-p-dibromobenzene, solid soln., local struct. and triplet energy migration 78−60489
p-dichlorobenzene-p-dibromobenzene mixed crysts., triplet exciton migration, time resolved emission spectroscopy 80−89052
2,5dichlorobenzenesulphonic acid trihydrate, neutron diffr. obs. of $H_3O^+.2H_2O$ 78−58855
4,4′-dichlorobenzophenone, cryst., $T_1 \leftarrow S_0$ singlet-triplet absorption profiles, temp. depend., phonon-exciton anal. 78−60436
4,4′-dichlorobenzophenone, cryst., X-traps, rel. populations, elec. field effect 77−12414
4,4′-dichlorobenzophenone, phase changes, Raman spectra *(French)* 80−2756
4, 4′-dichlorobenzophenone, triplet exciton absorpt. band, zero phonon line *(French)* 79−33726
4-4′ dichlorobenzophenone, triplet exciton absorpt. lines 79−38563
4,4′-dichlorobenzophenone single crysts., mutual annihilation of triplet excitons, 1.5 and 4.2K, phosphoresc. obs. 80−80850
3,5-dichlorobenzyl mercaptan, PMR, barrier to rot. about C-C bond 78−17696
organic compounds continued
cis-dichlorobis (cyclopentylamine) platinum II, potentiation of radiation effect 78−85345
3,4-dichlorobromobenzene, liq., laser Raman spectrum, LF band assignments 80−48002
2,4-dichlorobromobenzene, UV absorpt. spectra of vap. phase, vibr. anal. 79−81211
2,4-dichlorobromobenzene, vap. phase UV absorpt. spectra 79−22726
dichlorobromobenzenes, IR absorpt. spectra, vibr. assignments 78−17665
1,3-dichlorobutane, IR and Raman spectra, normal coord. anal., C-halogen stretch bands and conformers 79−31522
2,2-dichlorobutane, liquid and solid., vibr. spectra, IR and Raman obs. 80−60567
dichlorocarbene, $^1B_1$ state, radiative lifetime, quenching rate, press. depend., laser-induced fluoresc. obs. 78−5259
dichlorocarbene, electronic spectrum, ab initio CI calcs. 79−85948
dichlorocarbene, new value for proton affinity 79−18312
1,1-dichlorocyclopropane, ab initio SCF-MO calc., electronic and mol. struct. 78−25425
1,1-dibromo-2,2-dichlorocyclopropane, IR and Raman spectra 79−41170
dichlorodiethyl ether, propag. of longit. and shear hypersonic waves, light scatt. meas. 77−51442
dichlorodifluoromethane, absorpt. meas., laser power density depend. 80−92251
dichlorodifluoromethane, CO_2 laser induced photochem. enrichment of C isotopes 79−50151
dichlorodifluoromethane, conc. and pressure dependence of diffusion in poly(dimethyl siloxane) 77−55392
dichlorodifluoromethane, conc. meas. in air over Europe 77−37351
dichlorodifluoromethane, conc. meas. in stratosphere 78−32171
dichlorodifluoromethane, diode laser spectra near 10.8 μm, air-broadening effects 78−61555
dichlorodifluoromethane, dissociation by CO_2 laser radiation into trifluorochloromethane 78−40062
dichlorodifluoromethane, electron impact dissoc., light emission from fragments 79−13826
dichlorodifluoromethane, in atmosphere, interhemispheric gradients meas. 78−81289
dichlorodifluoromethane, infrared multiphoton processes, apparent step cross-sections, pulse spatial structure, irradiation techniques 80−32792
dichlorodifluoromethane, IR multiple-photon laser-induced decomposition, Cl and Cl_2 form. 78−40066
dichlorodifluoromethane, IR photolysis, isotopic selectivity factors 79−47946
dichlorodifluoromethane, IR spectrum and mol. force field 79−72309
dichlorodifluoromethane, isotopically selective photodissoc. 79−86013
dichlorodifluoromethane, isotopically specific TE laser induced chem. reactions 77−90622
dichlorodifluoromethane, laser photolysis for Cl isotope enrichment 78−58859
dichlorodifluoromethane, laser-induced dissoc., CF_2 vibr. distrib. 77−88511
dichlorodifluoromethane, liq. Refrigerant 12 sonic velocity meas. at 26.7°C 77−89497
dichlorodifluoromethane, matrix radiolysis, photoionis., IR spectra of CF_2Cl^+ and parent cations 78−80767
dichlorodifluoromethane, microwave rot. absorpt. spectra, nuclear quadrupole coupling, hyperfine splitting 77−30861
dichlorodifluoromethane, Rayleigh scatt. props., nephelometer meas. 79−29865
dichlorodifluoromethane, stratospheric conc. meas., mixing ratio 78−81281
dichlorodifluoromethane, study of ν_6 fundamental 79−31526
dichlorodifluoromethane, threshold multiphoton dissoc. Cl_2 elimination 80−9653
dichlorodifluoromethane, total ionis. and electron attachment cross sections by electron impact 79−59586
dichlorodifluoromethane, US vels. and absorption coeffs., determ. of relaxation times 78−63530
dichlorodifluoromethane, UV absorpt. cross sections temp. depend., stratospheric appls. 77−64423
dichlorodifluoromethane, UV photodissoc. cross-section, 223 and 296K 79−52729
dichlorodifluoromethane, UV photoelectron spectra, vibr. fine struct. 78−9196
dichlorodifluoromethane, UV photolysis, free radical emission 80−30263
dichlorodifluoromethane, vertical profile meas. in seawater *(German)* 78−3814
dichlorodifluoromethane+Ar excited, IR spectra, matrix isolation study, C-F stretching fundamentals 78−37632
dichlorodifluoromethane energy threshold effects in collisionless dissociation by IR laser radiation 77−58096
dichlorodifluoromethane in stratosphere, height profile meas. at several latits. 80−72601
dichlorodifluoromethane mols., electron scavenging studied by electron cyclotron reson. 79−50143
dichlorodifluromethane, dissoc. into metastable fragments following electron impact excitation 78−37757
dichlorodinitromethane, mol. struct., electron diffr. investig. 78−86950
4,4′-dichlorodiphenylsulphide, NQR line, Zeeman effect 77−59481
dichlorodurene, order-disorder phase transition, struct. from neutron diffr. at 70K 78−55825
dichlorodyfluoromethane, concentration in stratosphere, simultaneous inference using inversion algorithm 80−82000
1,2-dichloroethane, conformer equilibrium by effusive beam-matrix IR spectroscopy 80−48100
1,2-dichloroethane, enclathrated, conform., reorientation, PMR line shape anal. 79−91300
1,2-dichloroethane, orientationally disordered crystal., mol. orientation 78−34448
trans-1,2-dichloroethane, solid, NQR at high press., hindered rot. 79−95672
1,1-dichloroethane, tilt-effect and interference with rel. sign determination in weak irrad. expts. 80−32742
1,2-dichloroethane, vapour deposition, no glass transition detected by DTA 77−24388
1,2-dichloroethane, volume change on melting and reduced Lindemann's relation 80−29151
1,2-dichloroethane+benzene(toluene)(p-xylene), liq., molar heat capacities 78−18787
dichloroethane drops falling freely through water, breakup 80−69899

organic compounds continued
1,2-dichloroethane-$AsCl_3$ mixture, purification by selective photodissociation 77−79708
dichloroethane-EBBA, binary liq. cryst. system, two-phase premelting, NMR obs. *(Russian)* 78−30743
2,2-dichloroethanol, vibr. spectra, normal coordinate anal. 79−22694
β,β′-dichloroethyl ether-iso-octane, critical indices, allowance for light double scatt. *(Russian)* 80−60624
trans-1,2-dichloroethylene, Ar matrix, TEA CO_2 laser irrad. photoisomerisation study 80−21303
trans-dichloroethylene, isomerisation by laser multiphoton vibr. and electron excitation radiation *(Russian)* 78−73041
1,2-dichloroethylene, photodissoc., photoisomerisation, sensitised laser-induced reactions 78−7179
1,2-dichloroethylene, recoil tritium reactions 78−3360
dichloroethylene+metastable inert gas atom, mol. ionis., collisional energy depend. 79−54950
dichlorofluorobenzene, IR absorpt. spectra., vibr. assignments 78−17665
dichlorofluoromethane, ^{1}H and ^{19}F dynamic polarisation, Cl scalar coupling enhancement 78−66568
dichlorofluoromethane, chemiluminescence spectra, excited Li *(German)* 78−92485
dichlorofluoromethane, evidence for presence in atmosphere 79−62565
dichlorofluoromethane, IR absorpt. spectra, 1155-1163 cm^{-1} 80−37807
dichlorofluoromethane, photoacoustic spectra meas. at CO_2 laser wavelengths 80−18849
dichlorofluoromethane pollution, conc. obs. in background troposphere air 80−97843
dichlorofluoromethyl peroxynitrate, UV absorpt., spectra, photodissoc. lifetime meas. 80−83386
dichloromethane, ($-d_2$), liq. and vap., IR spectra, intensity anal. 79−64003
1,2-dichloromethane, adsorption on Ag, surface-plasmon modulated reson. 79−83045
dichloromethane, adsorption on dropping Hg electrode 77−32798
dichloromethane, Auger electron spectra and chem. shift 78−90231
dichloromethane, CD_2Cl_2, CW optically pumped, submm. laser action, 100 to 900 μm 79−929
dichloromethane, charge exchange mass spectra 80−43177
dichloromethane, $d_{0\text{-}3}$, Raman intensity, force consts. and electro-optical parameters 79−36651
dichloromethane, dielectric constant effect on nuclear spin-spin coupling constants 79−72240
dichloromethane, high press. and temp. IR absorpt. spectra, stretching fundamentals *(German)* 80−47999
dichloromethane, highly excited vibr. states, thermal lensing spectrosc. and local mode model 80−87140
dichloromethane, in liq. hexane, radiolysis 78−80769
dichloromethane, inner-shell excitation and EXAFS-type phenomena 79−13828
dichloromethane, IR spectra, local mode description for overtone spectra 78−42047
dichloromethane, liq. and dil. CCl_4 soln., far IR spectra and Rayleigh scatt. for planar itinerant oscillator 78−47229
dichloromethane, liq. dynamics, neutron inelastic scatt. 78−71664
dichloromethane, liq. state dynamics, models 79−73087
dichloromethane, mean free path meas., US relax. 80−59585
dichloromethane, mol. struct. factors, X-ray diffr. 77−76291
dichloromethane, Raman line intensities, modified CNDO/2/INDO calc. 78−25621
dichloromethane, solidified, solubility in liq. N_2 at 77.4K 80−10673
dichloromethane, US relax., 60-700 MHz, high resolution Bragg refl. method 77−84853
dichloromethane, vibr. population lifetimes in liqs. anti-Stokes Raman scatt. 78−74665
dichloromethane+F reaction products, modulated mol. beam mass spectrosc. obs. 80−97742
dichloromethane+N, CN quartet state production, fluoresc. anal. 78−68888
dichloromethane in nematic liq. crystal , $A_2(^{12}CH_2Cl_2)$ nuclear relax., dipole-dipole interaction 77−54567
dichloromethane-cyclohexane, liq. mixture, intermol. vibrational energy transfer, US study 80−70313
dichloromethane-d_0,-d_2, soln., far IR spectra, band shapes and moment anal. 80−58252
dichloromethane-d_0($-d_2$), rotational-vibrational energy transfer, US absorpt. obs. 79−98537
dichloromethane-d_2, spectral densities determ. from spin-lattice relax. and spin-echo decay rates 80−75877
dichloromethane-d_2, vibr.-vibr. energy transfer, laser-induced fluoresc. obs. 80−78689
dichloromethane-decalin glass, mol. dynamics, from dielec. loss meas., 107-148K, 293K 78−76379
dichloromethane-EBBA, binary liq. cryst. system, two-phase premelting, NMR obs. *(Russian)* 78−30743
dichloromethylene, radical, emission and excitation spectra, in Ar matrix 77−34657
dichloromethylene, radical, laser-induced fluoresc. excitation spectra 79−98131
dichloromethylene radical, MINDO/3 for optimised geometry and heat of form. 78−78830
dichloronaphthalenes, heavy atom effects on subrates of lowest triplet states, MIDP obs. 80−91594
3,5-dichloronitrobenzene, NQR line, Zeeman effect 80−28034
1,8-dichlorooctane, quadrupolar relax. centres, limited spin diffusion 80−100649
9,10-dichlorophenanthrene, intramol. heavy atom effect, PMDR obs. 79−13745
2,6- dichlorophenol, soln., anisotropic reorientation, H-bonding effect, NMR obs. 79−99782
3,5-dichlorophenol, torsional-vibr. freq., ^{35}Cl NQR 78−70851
2,4-dichlorophenol and sulphur analogue, benzene dipole moment anal. 78−25748
dichlorophenol isomers, elec. dipole moments determ. *(Spanish)* 77−69762
2,6-dichlorophenol-O-d_1, anisotropic reorientation, nucl. relax. in coupled spin systems 77−40145
3,5-dichlorophenoxy aluminiumdibromide, intramolecular configs., nucl. quadrupole double reson. obs. 80−34821
2,4-dichlorophenoxyacetic acid, ion transport modification in lipid bilayer membranes 79−83710

organic compounds continued
2,4-dichlorophenoxyacetic acid, modification of K^+ transport in lipid bilayer membranes 79−83709
2,4-dichlorophenoxyacetic acid, NQR of ^{35}Cl, 77-300K 78−50560
2,2-dichloropropane, normal coordinate calcs. 80−60567
2,2-dichloropropane, thermodynamic and structural studies of polymorphism 78−18571
1,3-dichloropropyne and -d_1, vibr. spectra, normal coord. anal. and centrifugal distortion constants 78−70832
3,6-dichloropyrazine, orientation and deform. in nematic liq. cryst. 77−71815
3,6-dichloropyridazine, liq. and solid soln. spectra, fundamental freqs. and assignments 80−5541
4,6-dichloropyrimidine, ^{35}Cl NQR, Zeeman effect 80−18874
dichloropyrimidines, UV-vis. absorpt. spectra, anal. 77−50445
2,3-dichloroquinoxaline, in tetramethylbenzene cryst., sublevel phosphoresc. spectra 78−70863
1,1-dichroethane and d, IR and Raman spectra, βCH stretching interaction force consts. 77−79616
dichroic dye guest, depend. of absorption and optical contrast on pitch of chiral nematic host 77−90164
dichroic dye in chiral nematic host, visible absorpt., pitch relationship 78−48193
dichroic dyes, guest-host interactions in liquid cryst. devices, colour switching 77−51312
dicumyl peroxide, crosslinking of natural rubber rel. to modulus, swelling 80−59551
dicyano compounds, liq. crysts., synthesis and dielec. props. 79−86685
dicyanoacetylene, solns., NMR and mol. reorientation 79−73840
dicyanoacetylene radical cation, $\tilde{A}^2\Sigma_g^+ \rightarrow \tilde{X}^2\Pi_u$ emission band system 79−22721
dicyanoalkanes, in benzene soln., microwave absorption, internal rot. 78−60385
9,10-dicyanoanthracene, exciplexes, electronic struct. by electro-optical expts. 78−25581
dicyanoanthryl-naphthyl, intramol. exciplex, fluoresc. quenching by pyridine (γ-picoline), triple exciplex form. 79−50061
dicyanobenzene, deuterated isomers, vibr. spectra 79−31521
1,2-dicyanocyclopropane, stereomutations, isomerizations, reaction rate consts., extended Huckel calcs. *(Italian)* 79−20348
dicyanodiacetylene radical cation, photoelectron and emission spectra 80−5558
1,1′-dicyanoethene($-d_2$), microwave spectrum, Coriolis interaction, rot. assignments 78−82721
dicyanoethylenes, substituted, vibr. spectra, intramol. effects 79−31528
dicyanoketene, and isomeric forms, heat of form., ab initio STO-3G calcs. 80−58190
dicyanomethane, multiple scatt. Xα calc. of electronic struct. 78−78626
$\Delta^{1,1'}$-dicyclohexenyl ketone, molecular motion anal. with allowance for intramolecular torsion 79−7656
dicyclohexyl phthalate, plasticiser for PVC, effect on secondary relax. 79−4995
dicyclopentadiene, liq., CO_2 laser pulse induced chem. reactions 80−66821
dideuteroacetylene, optically pumped laser action, 17.4 to 20.5 μm 79−935
α,α-dideuterotetrabutylammonium iodide, in soln., deuteron spin-lattice relax. time, mol. rotational correl. time 78−84491
α,α-dideuterotetraethylammonium iodide, in soln., deuteron spin-lattice relax. time, mol. rotational correl. time 78−84491
didodecyldimethylammonium bromide-benzene inverted micelles, solubilisation of pyrene-3-sodium sulphonate 80−3417
dielectric liquid, ionic mobility estimation from charge relax. 77−11719
dielectric liquid, polarity effect on breakdown voltage in inhomogeneous field 77−52018
dielectric liquids, high-field electron transport *(Japanese)* 78−2495
diemthyl sulphoxide-H_2O-NaCl system, DTA exam. of primary ice phase field 78−48382
diene-iron tricarbonyl complexes, π-orbital perturbation energies, ionisation energies; UV photoelectron spectra 80−32775
diesel fuel surface tension, AC field influence calc., comparison with expt. data *(Russian)* 77−55417
6,6′-diethoxy-thioindigo, cis⇌trans isomerisation, nanosecond flash photolysis and steady state methods, triplet state 78−35648
p-diethoxybenzene, ^{13}C shielding tensors determ. by NMR from powder patterns 78−25556
2,2-diethoxypropane with heptane, benzene and carbontetrachloride, excess enthalpy *(French)* 78−11542
p,p- diethoxythiocarbonylthiomethylaniline, cryst. and mol. struct. 79−94990
1,1′-diethyl 2,2′-dicarbocyanine iodide, high power DFB laser, tunable 7420-10500 Å 77−88782
diethyl ether, adsorption on water-preadsorbed alkali halide *(Japanese)* 78−18897
diethyl ether, field ionisation, thermal energy distribution and energy deposition 80−95732
diethyl ether, liq., spin lattice relax. time, elec. field induced charges 80−44945
diethyl ether, refr. index, temp. depend., deviation from Lorentz-Lorenz formula 77−40200
diethyl ether, tensile strength determ. using Brigg's method 77−62574
diethyl ether, weakly polar, electric field effects obs., heat emission during vapours condensation *(Russian)* 79−1055
diethyl ether vapour, effect on SiO_2 amorphous films 79−55667
diethyl ether vapour effect on SiO_2 layers, room temp. transforms. 79−99456
diethyl ether-ethanol-water, shear viscosity at plait points 77−35685
N,N-diethyl formamide, dipole moment, dielectric relax., internal rot., microwave absorpt. 79−56716
diethyl malonate-polystyrene, strongly opalescent critical isochore, scattered light intensity 80−71436
diethyl malonate-polystyrene system, osmotic compressibility and correlation range near crit. point 78−6694
diethyl phthalate, enhanced arcing as function of organic exposure and arc current 80−38778
3,3-diethyl thiadicarbocyanine iodide dye, stimulated fluoresc. and stimulated reson. Raman scatt. relationship 80−91853
1,1′-diethyl-2,2′-cyanine iodide, neat and mixed crysts., visible absorption and emission spectra assignments 77−1692
1,1′-diethyl-2,2′-cyanine iodide, sensitising dye 77−72602
1,3′-diethyl-2,2′-quinolylthiacarbocyanide iodide, soln., 78−68530

organic compounds continued
3,3′-diethyl-2,2′-selenacyanine-[TCNQ]$_2$, elec. cond., and quasi-two-dimensional mag. props. 78−6564
3,3′-diethyl-2,2′-thiatricarbocyanine iodide, solns., photoisomerisation and internal conversion rates, time-resolved spectra 77−75201
1,1'-diethyl-2,2'-cyanine chloride, J-aggregates, swirl-induced optical activity 78−72482
1,1-diethyl-2,2'-dicarbocyanine iodide, solns., fluoresc. lifetime, viscosity depend. 79−59497
1,1′-diethyl-4,4′-quinocyanine iodide, S_0-S_1 transition, relax. time meas. by reson. Rayleigh technique 78−42374
N,N-diethyl-4-phenyl-butylamine, fluoresc. spectra intramol. exciplex formation, fluoresc. spectra 79−59499
^{99m}Tc-diethyl-acetanilido-iminodiacetate, evaluation as hepatobiliary reagent 77−90874
3,3′-diethyl-oxadicarbocyanine iodide, model-locking of picosecond transverse-flow flashlamp-pumped dye laser 80−38025
N,N′-diethyl-p-nitroso aniline, dil. benzene soln., dielec. props., microwave region, mechanisms 78−35085
diethylamine, liq., Raman scatt. following optical excitation, vibr. relax. 79−26984
diethylamine melanin, sound wave anomalous absorption and dispersion 79−77688
diethylamine-coumarin 6, soln., fluoresc. induced by laser vibr. relax. 79−26984
diethylamine-ethylformate-ethanol-diethylformamide system, liq.-vapour equilib. *(Russian)* 77−63947
4-diethylamino-4′-nitrostilbene, luminesc. impurity in nematic liq. cryst., fluoresc. and absorpt. meas. 79−4240
7-diethylamino-4-methylcoumarin acriflavine binary soln., stimulated emission 77−50670
7-diethylamino-4-trifluoromethyl coumarin, dye laser pumping characts. using KrF excimer laser at 248 nm 80−1199
diethylammonium cadmium chloride, X-ray study of structural phase transition 78−2055
diethylammonium cadmium tetrachloride, dielec. props., phase transition 80−80675
diethylammonium cadmium tetrachloride, first order phase transition, optical phonon line broadening, spin-phonon coupling model 80−7335
diethylammonium copper chloride, Heisenberg ferromag., spin wave theory 77−89922
diethylammonium copper chloride, non-Lorentzian EPR lineshape and magnetostatic modes 77−43862
diethylammonium copper tetrabromide, mag. struct., NMR meas. 80−71192
diethylammonium copper tetrachloride, ^{63}Cu NMR, hyperfine interactions 80−54956
diethylammonium copper tetrachloride, antiferromag. mode excitation in EPR spectra 78−56373
diethylammonium copper tetrachloride, ferromag., static and dynamic mag. props. 80−50074
diethylammonium manganese chloride, 20 spin diffusion, EPR linewidth meas. 79−47289
diethylammonium manganese chloride, antiferromag., low temp. luminesc. spectra, magnetoelastic effect 80−2810
diethylammonium manganese chloride, antiferromag., magnon sideband exam. by absorpt. spectra 77−12108
diethylammonium manganese chloride, Heisenberg magnet, spin diffusion, EPR study 80−66019
diethylammonium manganese chloride, planar Heisenberg magnet, spin diffusion, EPR study 80−15793
diethylammonium manganese chloride, T_1 and T_2 meas. by LODESR 78−15064
diethylammonium manganese tetrachloride, IR active modes, interlayer and intralayer forces 77−59575
diethylammonium manganese tetrachloride, quasi two-dimensional antiferromag., magnon sideband in absorption spectra 78−43895
diethylammonium-manganese chloride, spin diffusion, quasi-two-dimensional Heisenberg paramagnet 78−88129
N,N-diethylaniline, IR absorpt. and MCD spectra, Rydberg transitions 77−27068
N,N-diethylaniline-pyrene, photochem. polarisation transfer, scalar paramagnetic exchange mechanism 78−25557
5,5′-diethylbarbituric acid, EPR and INDO-MO study of radical formation after irrad. 80−93774
diethylcarbonate, liq., alkoxy group internal torsion, extended microwave/far IR anal. 78−19457
diethylcyanine, reson. Raman spectra *(French)* 77−65484
diethylcyanine, vibrational Raman bands, excitation profiles *(French)* 80−83380
diethyldithiophosphoric acid, group separation procedure for superheavy elements 77−26953
diethylene, critical nuclei, meas. of number of mols. and surface tension from rate of nucleation 79−65293
diethylene glycol, absolute evaporation rate meas. 78−2244
diethylene glycol, associated liq., US absorpt. and hole theory 78−10124
diethylene glycol, asymm. dielectric. dispersion, 1-25000 MHz 78−15092
diethylene glycol diethyl ether, aq. mixtures, miscibility, enthalpy of mixing, solvation *(German)* 78−18779
diethylhydroxylamine, atmos. additive to control photochem. smog 79−52982
N,N′-diethylhydroxylamine enhancement of photochem. smog in polluted ambient air 77−91262
diethylimidacarbocyanines, relation between photographic desensitising action and alkalinity *(Russian)* 79−67418
3,3'-diethyloxadicarbocyanine iodide, kinetic model and expt. results of picosecond photobleaching 78−53226
3,3′-diethyloxadicarbocyanine iodide, lasing and photoisomerisation, conc. and temp. effects 77−7081
diethylsilane-d_0($-d_n$), vibr. spectra, normal vibrs. and rot. isomerism 79−31524
3,3′diethylthiacarbocyanine iodide-rhodamine 6G, mixed dye laser system, laser and fluorescence behaviour 78−25876
3,3'-diethylthiacarbocyanine iodide-rhodamine-6G-sodium lauryl sulphate, soln., premicellar region, energy transfer 80−20685
3,3′-diethylthiacarbocyanine iodine-rhodamine 6G, energy transfer with increased local conc., Forster mechanism 80−69220
3,3′-diethylthiatricarbocyanine iodide, cryst. and molecular struct. 78−26554
diethynylbenzene, radiative and nonradiative processes, triple bond effects 79−3481
organic compounds continued
O-, p-, m-diethynylbenzene, vibrational spectra, deuterated isomers 78−58705
diffusion of radical-ion pairs, spatial distrib., electron spin echo obs. 80−29622
difluoramine, centrifugal distortion anal., microwave rot. spectrum 78−58650
1,1-difluorethane, optically pumped, use of optoacoustic effect to discover CW far IR laser lines 77−79803
1,4-difluoro-2-butyne, sum of states, isometric group, symmetry no., thermodynamic functions 80−58186
difluoroacetaldehyde, optimum geometry, force fields, CNDO/force methods 77−46498
difluoroacetic acid, soln., polarisable H bonds, IR spectrosc. obs. 80−58408
p-difluorobenzene, $^1B_{2u}$, fluoresc. quantum yield, radiative and nonradiative lifetimes, vibronic level depend. 77−75204
p-difluorobenzene, $^1B_{2u}$, quenching by cyclobutanone, fluoresc. lifetime meas. 77−75205
p-difluorobenzene, $^1B_{2u}$-^1A_g transition, two-photon spectra 78−46408
p-difluorobenzene, electron impact singlet-singlet transition generalised oscill. strength 78−66668
p-difluorobenzene, electronic struct., many-body calc., photoelectron spectrum assignment 77−23421
1,3difluorobenzene, rot. Zeeman effect, g-tensor, mag. susceptibility 77−497
S_1p-difluorobenzene, time resolved fluoresc. spectra, direct view of intramolecular vibr. redistribution 80−83341
p-difluorobenzene+acetone, generalised oscill. strength, for reson. electronic energy transfer 78−66668
p-difluorobenzene+ketone reson. energy transfer cross section, 1st Born approx. appraisal 77−65519
1,3- difluorobenzene radical cation, and deuterated forms, laser-induced fluoresc. matrix. study 79−98138
1,2-difluorobenzene-d_0, -d_4, IR spectra, vibr. anal., force field 77−27063
difluorobenzenes, X-ray and UV photoelectron spectra, ionis. pots., ab initio GO calcs. 77−61795
2,2′-difluorobiphenyl, two photon absorptivities, CNDO/S-CI calc. with second order time depend. perturbation eqns. 80−74122
difluorocarbene, $\tilde{A}^1B_1$-$\tilde{X}^1A_1$ system spectrosc. and photophysics 80−5577
difluorodiacetylene radical cation, $\tilde{A}$-$\tilde{X}$ band emission spectra, $\tilde{A}$ state lifetime 79−72327
difluorodiazine, cis-trans isomerisation, mechanism and kinetics, CNDO/2 study 77−90589
difluorodichloromethane, high-resolution polarisation spectroscopy in 10 μm region 79−6196
difluorodichloromethane, spectral data evaluation for atm. sensing 79−62582
difluorodichloromethane+^{38}Cl, reactions due to ^{37}Cl(n,γ)^{38}Cl 77−86342
1,2-difluoroethane, gauche-trans conformers, IR and Raman spectra, vibr. 78−17667
1,1-difluoroethane, high intensity transmission characts., for possible appl. in CO_2 amplifier gain isolation 78−42387
1,2-difluoroethane, in Ar matrix film, interference enhanced IR ATR spectra 79−9248
1,2-difluoroethane, internal rotation temp. frozen in supersonic jet, matrix IR spectroscopy 80−9594
1,1-difluoroethane, IR multiphoton dissoc., inert gas collision effects 79−16021
1,2-difluoroethane, matrix isolation, trapping from thermal mol. beam, IR spectra 78−46330
1,1-difluoroethane, mol. struct., gas phase electron diffr. obs. 80−58385
1,1-difluoroethane, nucl. recoil ^{18}F chemistry at high press. 80−89510
1,1-difluoroethane, rot. relax., anharmonic shifts and excited state absorpt. 80−43154
difluoroethane, Stark effect, appl. to CO_2 laser modulation and stabilisation 79−59667
1,1-difluoroethane, unimol. decomposition, direct meas. via IR laser photolysis, collision effects 79−57254
1,2-difluoroethane in Ar matrix, IR hole burning and lineshape, vibr. transition 79−76425
1-1 difluoroethane in external Stark cell, CO_2 laser possible freq. stabilisation 79−94266
2,2-difluoroethanol, vibr. spectra, normal coordinate anal. 79−22694
difluoroethene, cis- and trans-, photoelectron-photoion coincidence study, fluoresc. obs. 80−95678
cis-1,2-difluoroethene, CO_2 laser pumped, CW far IR laser lines 80−69372
1,1 difluoroethylene, -d_1, -d_2, mol. struct., rot. consts., gas phase electron diffr., microwave data 77−65542
difluoroethylene, absorption coeff. at 10.6 μm 77−23654
difluoroethylene, cis-, trans- and perdeuterated isomers, absorpt. spectra, 120 to 165 nm 78−94256
1,1-difluoroethylene, CO_2 laser Stark spectra of ν_4 and ν_9 bands 79−36694
1,1-difluoroethylene, diode-laser heterodyne spectrosc. meas. 80−43051
cis- and trans-difluoroethylene, force consts., mean vibr. amplitudes 77−6748
1,2-difluoroethylene, high intensity transmission characts., for possible appl. in CO_2 amplifier gain isolation 78−42387
1,1-difluoroethylene, IR multiphoton dissoc., inert gas collision effects 79−16021
1,1-difluoroethylene, laser Stark saturation spectroscopy, assignments 79−31864
1,1-difluoroethylene, optically pumped, complete freq. coverage for submm. laser spectroscopy 78−25860
1,1-difluoroethylene, optically pumped, far IR laser line assignment 79−31865
1,1-difluoroethylene, optically pumped mm laser transition assignments 78−42328
difluoroethylene, optically pumped sub mm laser design 77−14757
difluoroethylene, optically pumped submm. wave amplification 78−29941
1,1-difluoroethylene, rot. dynamics, far IR spectra 77−19864
cis-1,2-difluoroethylene laser, far IR CW optically pumped 80−69368
1,1-difluoroethylene near-MM-wave emission assignments 80−58260
cis-1,2-difluoroethylene oxide, substituent and isotope effects, microwave assignments 78−78682
1,1-difluoroethylene submillimetric wave emission assignments 80−102708
1,2-difluoroethylenes, ab initio HF comparison of cis and trans energies 77−18786

organic compounds continued
difluoroethylenes, plasma polymerisation, ESCA characterisation of polymers 80−21283
difluoroformaldehyde, IR intensities, vibronic calcs. 79−10108
difluoroiodomethane, vacuum UV photolysis, IF in solid Ar visible spectra 80−87137
difluoromethane, binding energy, ionisation pots., overlapping sphere MS Xα 77−83499
difluoromethane, dielectric constant effect on nuclear spin-spin coupling constants 79−72240
difluoromethane, ionisation energies, SCF Xα calcs. 77−14360
difluoromethane, IR laser-induced reactions 77−77792
difluoromethane, IR spectra, local mode description for overtone spectra 78−42047
difluoromethane, microwave spectral line widths 78−70816
difluoromethane, microwave spectral lines, line-width parameters 77−68077
difluoromethane, optically pumped, CW far IR laser line frequencies 80−102706
difluoromethane, optically pumped, efficient CW far IR laser action obs. 79−928
difluoromethane, optically pumped by CO_2 laser, new CW FIR lines 79−94219
difluoromethane, photoionis. cross section calc., for YMζ line, HF vs OPW methods 77−42353
difluoromethane, triplet state emission spectra, phosphoresc. and energy transfer 78−53196
difluoromethane cation, in solid Ar, IR spectra, vibr. modes 79−68231
difluoromethane far IR laser gas, CW laser pumped, gain 80−69367
difluoromethane laser, optically pumped, FIR lines, performance efficiency 79−94220
difluoromethyl cation, in solid Ar, IR spectra, vibr. modes 79−68231
difluoromethylborane, microwave spectra and struct. obs. 80−43036
difluoromethylborane, nonrigid, symmetry group calcs. 80−106254
difluoromonochloromethane, parameters of Lennard-Jones 12-6, Stockmayer 12-6-3, 6-Exp, Kihary intermol. pots. 77−34711
1,5-difluoronaphthalene, IR and Raman study of crystal dynamics 78−80346
1,1-difluorotetrachloroethane, in nematic liq-cryst., transient nutation, modulation effects 77−8424
1,2-difluorotetrachloroethane, mol. motions and Zeeman-quadrupole cross relax., NMR obs. 79−65751
1,2-difluorotetrachloroethane, orientationally disordered, mol. reorientation, depolarised Rayleigh scatt. obs. 78−88316
difluorotetrachloroethane, quadrupole-Zeeman cross-relax. between two nucl. spin species 79−65766
diformamide, excited singlet and triplet states, CNDO-CI calcs. 77−26990
diformamide, torsional pot. barriers, ab initio and partition of energy methods 77−88588
diformylhydrazine, ^{14}N NQR echo envelope slow beats 80−29643
diformylhydrazine, ^{14}N NQR lines fine structure 80−63667
digalactosyl diglyceride multipole internal rot., ^{13}C-{^1H} nuclear Overhauser enhancement, ^{13}C spin lattice relax. 77−479
diglycine, cyclic, solid phase laser Raman spectrum 77−85695
diglycine barium chloride monohydrate:Cu^{2+}, optical absorpt. and EPR, lattice sites, hybridisation 77−43872
diglycine nitrate, cryst. growth, dielec. and electromech. props. 80−2701
diglycine nitrate, dielec. relax. in paraelec. and ferroelec. regions 78−31149
dihaleothanes, CNDO/2-type calc., FORCE method, relative stability, intramolecular atomic interaction energies 78−41957
p-dihalobenzene, mixed cryst., Raman spectra, phonons and vibr. excitons, criteria for solid solns. 78−43840
p-dihalobenzene alloys, successive perturbation of phonon bands 77−35653
p-dihalobenzene series, cryst., chem. perturbation and lattice instability, X-ray and Raman scatt. 77−39654
p-dihalobenzenes, apparent NQR spin-spin relax. times obs. 80−54991
dihalobenzenes, IR and Raman spectra, phase transitions *(French)* 78−84557
4,4'-dihalobenzophenone, lowest triplet state, ODMR spectra, D- and g-tensors 77−75191
trans-1,4-dihalocyclohexanes, far IR spectra of high press., using diamond anvil cell 79−12874
dihalodiacetylene radical cations, $A^2\Pi_u$-$X^2\Pi_y$ system, emission spectra and state lifetime 79−10121
dihaloethylene, CNDO/2-type calc., FORCE method, relative stability, intramolecular atomic interaction energies 78−41957
dihalogenated benzene derivatives, 77K, gamma radialysis radical pair formation, EPR 79−29334
dihalogenoacetylene radical cations, $C_2X_2^+$, emission spectra, $A^2\Pi \rightarrow X^2\Pi$ band systems 78−17679
2,2-dihalohexafluoropropane, IR and Raman spectra, gas, liq. and solid, normal coord. anal. 79−72314
dihalomethanes, mol. vibr. spectra internal coord. model, and d_2 substitution 79−63974
1,4-dihalonaphthalene: octafluoronaphthalene, Raman spectra, phonon band mass coeff. tuning 79−8131
1,4-dihalonaphthalenes, binary solid solns. lattice stability, mol. motions 78−31182
1,3-dihalopropane, dielectric permittivity and loss, dipole moment 78−60383
p,p'-diheptylazobenzene, nematic, physical props. 78−79524
dihexadecylphosphate, surfactant vesicles, low-ang. light scatt. and photon correlation spectroscopy 79−79484
dihexyl-N,N-diethylcarbamylmethylenephosphonate for actinide partitioning from nuclear waste 79−26583
4,4-dihexylazoxybenzene, nematic liq. cryst., alignment on surfactant treated obliquely evaporated surfaces 80−49092
p,p'-dihexyloxyazoxybenzene-fluorobenzene, solute orientational order, NMR obs. 77−84627
p,p'-dihexyloxytolan, flexoelec. coeff. in nematic phase, thermal depend. 80−79685
5,10-dihydro-5,10-diethylphenozinium-iodide, average struct. 79−90636
dihydro-6-methyl uracil single cryst., electron and UV irrad., free radicals, EPR 77−29100
5,6-dihydro-6-methyluracil, X-ray irrad., free radical form; ESR spectra obs. 80−50189
9,10-dihydroanthracene, chem. shift, ring-current and excess-charge effects, semi-empirical calc. 78−33523

organic compounds continued
2-5-dihydrofuran, liq. phase far IR spectra, ring puckering *(French)* 78−92068
2,5-dihydrofuran, mol., pot. functions of bending modes 80−9753
dihydromuconic acid, C=C bond, ^{13}C shielding tensor, NMR meas. 78−1005
dihydroporphin, single crystal Shpolskii matrix, fluoresc. anisotropy 79−85994
dihydroporphin free base, in n-octane cryst., zero-field optically detected mag. reson., triplet state kinetics 78−42103
2,3-dihydropyran vapour, IR spectra anal. 80−63628
dihydropyrimidine bases in aq. soln., spin-trapped OH radical reactions, EPR obs. 79−88053
dihydroquinoxalinediones, conjugated mols. electronic struct. and geometry, Hartree-Fock instability 80−69055
dihydroxy benzenes in ethyl alcohol, dielec. dispersion charact. 80−75932
2,4-dihydroxy benzoic acid, PMR obs., proton second moment, 77 to 383K effect of OH group rot. 78−10784
dihydroxy toluene in ethyl alcohol, dielec. dispersion charact. 80−75932
2,5-dihydroxy-1,4-benzoquinones, long distance bonds between sp^2 hybridised C atoms, polymethine coupling effect 79−13836
dihydroxyanthraquinone, light-induced proton transfer, photochem. hole-burning obs. 80−76535
1,5-dihydroxyanthraquinone-d_0,-d_2, mol. vibr., IR spectra 77−467
dihydroxycarbene, singlet and triplet state rot. pot. surfaces 80−32627
1,5-dihydroxynaphthalene, monodispersed airborne particles, ice nucleation 79−20947
4,6-dihydroxypyrimidine, aq. soln., reaction with OH, short-lived radicals, ESR 80−101031
1,2-diidobenzene, vibr. spectra, packing calcs. and crystal structure investig. 80−28938
diimide, electron-density maps of bent bonds 80−1084
diimide, trans-cis conversion in lowest excited states, SCF calcs. 78−46284
p-diiodobenzene, far IR single cryst. transmission spectrum, temp. and polaris. depends., assignments 78−72498
p-diiodobenzene, polymorphic phase transformation 79−46591
p-diiodobenzene, polymorphic transition hysteresis, optical path difference expt. 79−99312
o-diiodobenzene, r_α-struct. determ. from PMR with ^{13}C satellites, bond lengths and angles 78−25560
1,2-diiodoethylene, form. from I_2+acetylene, isomerisation 80−85157
diiodomaleic acid thioanhydride, mol. and cryst. structs., X-ray obs. *(German)* 80−44199
diiodomethane, IR spectra, local mode description for overtone spectra 78−42047
p-diiodotetrafluorobenzene, neutron diffr. determ. of struct., constrained refinement 77−19839
1,2-diiodotetrafluoroethane, Raman and far IR spectra, conformation 78−78715
diisopropylammonium copper chloride, mag. interactions, susceptibility, 2-230K 80−60237
diketomorpholine, cyclodepsipeptide, cryst. and mol. struct. 78−2104
α-diketone radical anions, spin-lattice relax. in soln. 79−22735
diketones, adsorbed on SiO_2, under carbon tetrachloride immersion, IR obs. 79−24821
diketopiperazine, cryst. and molecular struct. determ. 77−11534
1,1-dilithiocyclopropane, planar struct. stability, RHF/STO-3G calcs. 77−6671
3,3-dilithiocyclopropene, planar struct. stability, RHF/STO-3G calcs. 77−6671
dilute spin species in crystals, separated local field ^{13}C NMR 77−90044
2,6-dimenthylnaphthalene, liq. scintillator system, energy transfer, fluoresc. intensity-max. solvent depend. 78−21966
dimer, PCILO calc. of geom. struct. and energy 79−63930
dimercaptosuccinic acid:^{99m}Tc, renal differential function in dogs 79−79639
$^{99}Tc^m$-dimercaptosuccinic acid evaluation as static renal imaging agent 78−77102
dimesitylboranes, phenyl substituted, absorption and emission 78−27311
1,4-dimethoxy-2,6-dimethylbenzene, methyl reorientations, NMR relax. and inelastic neutron scatt. obs. 79−61253
2,5-dimethoxy-4-nitrostilbene, hyperpolarisability meas. by DC induced second harmonic generation 78−87096
4-4'-dimethoxyazoxybenzene-d_{14}, orientational order and internal rot., D NMR obs. 79−50987
dimethoxybenzaldehyde, IR absorpt. spectra, 400-4000 cm^{-1} 79−41163
p-dimethoxybenzene, ^{13}C shielding tensors determ., by NMR from powder patterns 78−25556
dimethoxyethane and propylene carbonate mixed electrolyte solns., for high energy density batteries 80−76627
5,7-dimethoxyindane-1-one, cryst. and mol. struct. 80−100223
dimethoxymethane, vibr. spectra and rot. isomerism 80−106325
dimethoxyphenyl-1,1-dicyanomethylene, donor-acceptor systems, fluoresc., through-band interaction 79−13751
2,2-dimethoxypropane, enthalpy of hydrolysis meas., microprocessor-controlled system 80−22361
N,N-dimethyl acrylamide (−d_3,d_6,d_9), force field, IR and Raman spectra obs. 80−47979
dimethyl ammonium cadmium tetrachloride, dynamics of structural phase transitions 79−73309
dimethyl ammonium copper chloride, nearly two-dimensional ferromag., nucl. transverse relax. rates meas. 77−81024
dimethyl ammonium copper chloride, spin dynamics near crit. pt. 80−7112
dimethyl ammonium copper manganese tetrachloride, EPR study *(German)* 80−54941
dimethyl ammonium manganese chloride, quasi one-dimensional mag. systems, impurity effects 80−71015
dimethyl ammonium manganese chloride, sp. ht., quasi-one dimens. behaviour 78−52293
dimethyl ammonium manganese trichloride, NMR for mag. ordered state at 3.6K 79−47340
dimethyl aniline, IR spectra, 250-4000 cm^{-1}, vibr. anal. 78−62797
dimethyl aniline, photoionisation by vac. UV laser *(Russian)* 78−9205
9,10-dimethyl anthracene, excited singlet state quenching by nitroxyl radical, triplet form. 77−88487
9,10-dimethyl anthracene, vap. phase dye laser media, photophysical parameters 80−95884
dimethyl disulphide, chemisorpt. on clean Ni surface 78−14595

organic compounds continued
dimethyl disulphide+O(^{3}P), absolute reaction rate const. determ. 80−89472
dimethyl ether, chemisorption and decomp. on Pd 77−63953
dimethyl ether, condensed multilayers, electron bombard. effects, AES line-shape anal., XPS, and desorption meas. 80−7450
dimethyl ether, internal rot., struct. relax., ab initio SCF calcs. 78−90077
dimethyl ether, interstellar, detect. in Sagittarius B2 and Orion Nebula 79−53862
dimethyl ether, low-lying excited states, improved virtual orbitals calcs. 77−14372
dimethyl ether, multiphoton selective dissoc. induced by pulsed CO_2 laser 79−20381
dimethyl ether, nonlinear optical polarisability meas. 79−54991
dimethyl ether, O donor capacity *(Russian)* 77−71741
dimethyl ether, optical saturation characts., using CO_2 laser radiation 78−30027
dimethyl ether, review of microwave spectrum, tabulated data 80−51965
dimethyl ether, spin-orbital interaction *(Russian)* 78−66461
dimethyl ether+CH_3^+(CD_3^+) reactions, products mass spectra obs. 77−63901
dimethyl ether+Cl, absolute rate consts., 200-500K, stratospheric chem. appl. 79−66271
dimethyl ether+F, HF IR chemiluminesc., vibr. and rot. energy disposal 77−86318
dimethyl ether -d_0, -d_3, -d_6, internal rot., far IR and Raman spectra 77−79612
dimethyl ether-d_0,(-d_6), solid solns., vibr. Raman spectra and intermol. pot. function 78−68494
dimethyl ether-d_0,d_3,-d_6, microwave spectra, torsional splittings 77−3347
dimethyl ether-HF H-bonded complex, cubic force consts. calcs. 80−47868
dimethyl ether-trioxane mixtures, condensation-elimination ion-mol. reactions obs. 78−23939
dimethyl ether-water complex, $(H_2O)_2$ analogue, Ar matrix i.r. spectra, struct. 77−3365
dimethyl ether.HCl, gas-phase Raman spectra, profile of stretching vibr. 79−45728
dimethyl ethyl amine, mol. struct. determ. by gas phase electron diffr. 80−95743
dimethyl mercury, indirect coupling constants, vibr. corrections 79−50050
dimethyl oxalate, oriented cryst. film, polarised IR spectrum 80−29730
dimethyl oxide, geometric struct. 79−13835
dimethyl phosphate, potentials of internal rot. 77−16901
dimethyl POPOP, multiphoton cross-section determination by means of luminescence experiments 80−93377
2,2-dimethyl propane+Na, rainbow scatt. at thermal energy, anisotropic pot. 78−29837
dimethyl propane diol, dioxane soln., asymm. dielec. dispersion, 1-25000 MHz 78−15092
dimethyl selenide, r_s-struct., methyl top axis tilt 77−46554
dimethyl selenide-d_6, microwave spectrum in ground and excited torsional states *(German)* 77−57992
dimethyl silicone oil, laser-induced breakdown mechanism *(Japanese)* 77−43935
dimethyl sulfone, X-irrad. cryst., ESR spectrum 78−3351
dimethyl sulphide, biologically prod., contrib. to global S cycle 77−70786
dimethyl sulphide, S donor capacity *(Russian)* 77−71741
dimethyl sulphide, spin-orbital interaction *(Russian)* 78−66461
dimethyl sulphide, sulphoxide and sulphone, electronic struct. and spectra *(Russian)* 78−66460
dimethyl sulphide+O(^{3}P), fast flow reson. fluoresc. obs. of absolute rate consts. 80−61077
dimethyl sulphide+OH, flash photolysis reson. fluoresc. rate consts. determ., pollution aspects 78−95913
dimethyl sulphide dimerisation, S lone pair nonbonded contacts, EH, MINDO/3, CNDO/2 calcs. 79−773
dimethyl sulphide in seawater rel. to S budget 78−96237
dimethyl sulphoxide, 1:1 and 1:2 complexes with H_2O and D_2O, H-bonding, IR and Raman vibr. spectra 77−34633
dimethyl sulphoxide, chemisorpt. on ZnO, UPS, mol. orbitals effect on bonding 78−72699
dimethyl sulphoxide, form. of $(CH_3SOCH_3)_2H^+$ and $CH_3.CH_3SOCH_3^+$ in ICR mass spectrometry, proton affinity 78−3319
dimethyl sulphoxide, high efficiency stimulated Raman scatt. source *(Chinese)* 80−87433
dimethyl sulphoxide, UO_2^{2+} γ-irrad. frozen solns., radiothermolum. and temp. deactivation *(Russian)* 79−33854
dimethyl sulphoxide radioprotection of mammalian cells, exposed to X-rays, heavy charged-particle beams 79−79609
dimethyl sulphoxide-d_6, intensities in inelastic electron tunnelling, IR, and Raman spectroscopy *(French)* 79−822
dimethyl tartrate, chirality detection with chem. ionis. mass spectroscopy, meso ion obs. 77−68139
dimethyl tellurium diiodide, ^{129}I Mossbauer spectra, coupling consts. 78−62833
dimethyl thioether+OH, reaction rate consts., 299-430K 78−35653
dimethyl tin difluoride, solid, methyl group motion, neutron scatt. study 80−10607
dimethyl urea, aqueous solution, ultrasonic velocity measurement 80−19878
3,3′-dimethyl-1′-phenyl-6-nitro-spiro [(3H-7,8-benzochromen)-3,2′-indoline] (II), photochromic transform., temp. depend. 80−104456
3,3′-dimethyl-1′-phenylspiro [(3H-7,8-benzochromen)-3,2′-indoline] (I), photochromic transform., temp. depend. 80−104456
1,1-dimethyl-1-silacyclopentane, IR and Raman spectra 80−60577
1,5-dimethyl-2,4-hexadiene-Cu,$^{2+}$ fluoresc. quenching method for determ. binding const. 80−89530
3,8-dimethyl-2-azaanthracene in heptane, benzene and ethanol, max. intensity of fluoresc. on axis of cylindrical cell *(Russian)* 77−55814
2,5-dimethyl-2-hexyn-2, 5-diol, deuterated, profile analysis, influence on struct. parameters and deformation density distribs. 79−73064
2,5-dimethyl-3-hexyn-2,5-diol-d_{12}, cryst. struct. and electron density distrib., 90K 77−51362
4-dimethyl-amino-4′-nitrostilbene, fluoresc. emission anisotropy, solvent effects 79−3489
4-dimethyl-amino-4′-nitrostilbene, in EBBA, nematic ordering influence on fluoresc., temp. depend. *(German)* 79−81235

organic compounds continued
dimethyl-diacetylene, radical cation, fluoresc. spectra, matrix isolated 79−45752
S,S-dimethyl-N-4-nitrophenylsulphilimine, XPS spectra, satellite lines obs. 78−37680
dimethyl-N-nitrosamine, assessment is urban air 78−81378
N,N′-dimethyl-p-methyl aniline, dil. benzene soln., dielec. props., microwave region, mechanisms 78−35085
N,N-dimethyl-p-nitrosoaniline, coherent anti-Stokes Raman spectra, negative peak intensities 77−75161
N,N′-dimethyl-p-toluidene, UV photoelectron spectra, up to 21.2 eV 77−71831
dimethyl-POPOP, soln., and vap., fluorescence rise time, intramolecular vibrational relaxation 79−98134
dimethyl-s-tetrazine, s-tetrazine, photodissoc., in hexane soln., Ar matrix, and mol. cryst. 78−73059
dimethyl-s-tetrazine, vapour, mol. fluoresc., photodissoc. product 80−81352
N,N-dimethylacetamide, amide band rot., ^{13}C NMR using modified DEFT pulse sequence 79−93191
N,N-dimethylacetamide, two-site exchange kinetics, NMR spectral line-shape analysis 77−26118
N,N-dimethylacetamide in tetrachloromethane, dielectric relax. and complex permittivity 80−108149
dimethylacetylene, laser Raman spectra, pure rot. anal. 79−59468
dimethylacetylene, librational motion, inelastic neutron scatt. obs. 78−75742
dimethylacetylene, solid-solid phase transition, NMR meas. 78−6583
dimethylacetylene, tunnel splitting, rot. pot., μeV neutron scatt. study 79−41993
dimethylallene, excited states, microwave spectrum and strong Coriolis coupling 78−9141
dimethylamine+O, reactive routes, identification 79−39129
dimethylamine+OH, rate const., 298-426K, Arrhenius expressions and activation energy 78−48619
dimethylamine iron tetrachloride, antiferromag., mag. susceptibility meas. 80−60220
dimethylamine proton-bound dimers, form. in ion-mol. assoc. reactions, rates analysis 77−60054
dimethylamine-HCl systems, H-bonded complexes studied by ab initio MO method, dipole moments determ. 80−83253
1,5-bis dimethylamino pentamethinium perchlorate, refl. spectra calcs. 77−85154
dimethylamino radical+O_2(NO)(NO_2), reaction rate constants, FTIR obs. 80−16652
trans-4-dimethylamino-4′-nitrostilbene, mol. hyperpolarisability in soln., UV dispersion of charge transfer contrib. 79−31986
4-dimethylamino-4′-nitrostilbene, thermal motion of prolate luminescent molecules in solvents with different viscosities 79−83029
4-dimethylamino-4′-nitrostilbene in solvent fluorescence lifetime meas. by picosecond optical amplification 79−81227
7-N-dimethylamino-4-methylcoumarin, fluoresc., solvent depend., shift of max. wavenumber 79−85997
1-dimethylamino-4-phenylbicyclo-[2,2,2]octane, intramolecular energy transfer, fluoresc. spectra 79−59499
p-dimethylaminoacetophenone, ps reversible isomerisation kinetics, O_2 quenching obs. 79−5133
p-N,N-dimethylaminobenzonitrile, multiple fluoresc., mechanism 79−45742
p-dimethylaminobenzonitrile, picosecond relax., fluoresc. spectroscopy, solvent effects 78−58737
2-p-dimethylaminobenzylidene-1,3-indandione, X-ray cryst. struct. determ. 79−14793
4- dimethylaminochalcone fluorescence, distrib. of hydrophobic mols. in artificial lipid membrane 77−16912
2-dimethylaminoethanol(-d_1), microwave spectrum, hydrogen bonding, rot. consts., struct., dipole moment 77−6764
dimethylaminophenyl-(methylene)$_n$-(1-pyrenyl), intramolecular charge transfer, heteroexcimer formation processes 78−27783
dimethylammonium cadmium chloride, proton-^{14}N double reson. exam. of struct. phase transitions 77−4583
dimethylammonium cadmium chloride, soft modes, order-disorder transition model 78−22817
dimethylammonium cadmium chloride type crysts., struct. transitions model 78−71834
dimethylammonium cadmium tetrabromide, room temp. struct. 80−29000
dimethylammonium cadmium tetrachloride, far IR refractive index, extinction coeff. and dichroism obs. 80−66144
dimethylammonium cadmium tetrachloride type compounds, structural phase transition model 79−37829
dimethylammonium cadmium tetrachloride-type compounds, theory struct. phase transitions 80−10668
dimethylammonium copper chloride, magneto-optical props., 0.03-13.5 eV 77−52132
dimethylammonium copper chloride bromide, mag. props., pulsed NMR expts. 80−11292
dimethylammonium copper manganese chloride, two-dimens. mixed magnet, EPR 80−66030
dimethylammonium copper tetra(chlorobromide), mag. susceptibility, 1 to 30K, mag. phase transition 79−4675
dimethylammonium copper tetrabromide, quasi two-dimensional antiferromag., mag. behaviour 80−97098
dimethylammonium copper tetrachloride, crit. slowing down and anomalous relax. near Curie temp. 80−71053
dimethylammonium copper tetrachloride, ferromag., quasi two-dimensional, ordering temp., press. depend. 80−84601
dimethylammonium copper tetrachloride, ferromag., static and dynamic mag. props. 80−50074
dimethylammonium copper tetrachloride, two-dimens. ferromag., saturation of parallel-pumped magnons 80−97147
dimethylammonium copper tetrachloride-tetrabromide mixed cryst., mag. transition 80−65874
dimethylammonium copper tetrahalide, layer compound $(CH_3NH_3)_2Cu(Cl_xBr_{1-x})_4$, antiferro- to ferromag. transition 80−108005
dimethylammonium ferric dichloride dibromide, two-dimensional antiferromag., field depend. of susceptibility meas. 77−63130
dimethylammonium halides, UV exciton absorpt. bands 78−72547
dimethylammonium iron bromotrichloride, canted spin system, mag. susceptibility meas. 78−39303

organic compounds continued
dimethylammonium iron chloride, two-dimens. antiferromag., ^{57}Fe Mossbauer obs., sublattice magnetis. 77−66443
dimethylammonium iron tetrachloride, Mossbauer study of struct. phase transition 80−39278
dimethylammonium manganese chloride, antiferromag., low temp. luminesc. spectra, magnetoelastic effect 80−2810
dimethylammonium manganese chloride, neutron diffr., 188K, cryst. struct. 77−47434
dimethylammonium manganese chloride, neutron diffr., 404K, cryst. struct. 77−47435
dimethylammonium manganese chloride, perovskite type layer struct., lattice dynamics 79−33053
dimethylammonium manganese chloride, perovskite-type layer structure submillimetric-wave spectroscopy 79−33540
dimethylammonium manganese tetrachloride, 2D Heisenberg antiferromag., spin wave anal. 80−54879
dimethylammonium manganese tetrachloride, antiferromag. and spin-flop resonance obs., 70 to 100 GHz 80−71190
dimethylammonium manganese tetrachloride, elastic props. 79−60418
dimethylammonium manganese tetrachloride, H-bonding, struct. transition, neutron diffr. study 79−42004
dimethylammonium manganese tetrachloride, Heisenberg ferromag., spin wave anal. 79−61237
dimethylammonium manganese tetrachloride, IR active modes, interlayer and intralayer forces 77−59575
dimethylammonium manganese tetrachloride, phonon density of states, expt. and calc. 80−54323
dimethylammonium manganese tetrachloride-d_6, structural and mag. phase transitions, neutron scatt. and AC susceptibility meas. 80−44825
dimethylammonium manganese trichloride:Cd(Cu), impurities in quasi-one-dimens. Heisenberg systems, anisotropy effect 80−80502
dimethylammonium manganese trichloride, antiferromag. props. 79−73694
dimethylammonium manganese trichloride, pseudo one-dimens. Heisenberg antiferromag., phase diagrams 79−61148
dimethylaniline, exciplex with anthracene, form. kinetics and luminesc. props. 80−66792
N,N-dimethylaniline, laser seed cpds., photoionisation and photoabsorpt. characts. 78−13688
N,N-dimethylaniline+carbon tetrachloride, binary liquid mixtures, excess free vol. calcs. 80−34202
dimethylaniline cation+anthracene anion, recombination reaction in soln., time-resolved mag. field effect 80−3308
dimethylanilines, photoemission for mol., polarised photoelectrons 78−66607
9,10-dimethylanthracene, conc. solns., fluoresc. quenching by anthracene and derivatives 78−17711
9,10-dimethylanthracene, in n-hexane, Shpolskii absorpt. spectra at 77K, vibronic struct. *(German)* 79−59507
9,10-dimethylanthracene, Shpolskii spectra, vibronic struct., fluoresc. *(German)* 79−22754
9,10-dimethylanthracene derivative, intramol. fluoresc. quenching, attached CBr_3 groups 78−42113
9,10-dimethylanthracene radical cation EPR spectra, ion-pair effects 79−13742
dimethylbenzaldehydes, in durene single cryst., zero-field splitting, guest and host isotope effects 80−107752
dimethylbenzaldehydes in durene matrix, phosphoresc., $^3n\pi^*$ and $^3\pi\pi^*$ states vibronic coupling 79−22746
dimethylbenzaldehydes in durene single crysts., ZFS D-parameters 77−55731
N,N-dimethylbenzamide+$POCl_3$ reaction products, Raman spectra 78−7199
2,6-dimethylbenzoic acid, ^{1}H chem. shift recovery from combined multiple pulse NMR and sample spinning 80−32738
4-4′ dimethylbenzophenone, ^{1}H spectrum using multiple pulse decoupling-magic angle spinning NMR probe 78−12735
dimethylboric anhydride, IR and Raman spectra, vibr. and struct. 78−25531
2,3-dimethylbuta-1,3-diene, IR, Raman spectra, torsional pot. function, thermodynamic function 80−43046
2,3-dimethylbutane, CH stretching local mode anharmonicity, intramol. perturbation overtone spectra 79−18171
2,2′-dimethylbutane, differential thermal anal. under high press. 78−51669
2,2-dimethylbutane, electron mobilities through liq. and critical regions 78−2536
2,2-dimethylbutane, fluid phases, electron mobility, density effects meas. 77−7619
dimethylcadmium, effective core potentials calcs. rel. to bond lengths and energies 78−66464
N,N-dimethylcarbomoylchloride, chem. exchange rate by NMR method, temp. depend. 79−79243
dimethylcarbonate, liq., alkoxy group internal torsion, extended microwave/far IR anal. 78−19457
cis-3,4-dimethylcyclopentanone, conformational analysis, vib. spectra 77−75325
1,1-dimethylcyclopropane-d_0,-d_6, internal rot., Raman spectra 78−985
3,3-dimethylcyclopropene, microwave spectrum, dipole and quadrupole moments calcs. 79−59440
dimethyldiacetylene, laser Raman spectra, pure rot. anal. 79−59468
trans-dimethyldiazene-1, 1, 1-d_3, IR and Raman spectra, vibr. assignments and pot. functions 78−33507
trans-dimethyldiazene-d_0,d_6, IR and Raman spectra, vibr. assignments and pot. functions 78−33507
1,2-dimethyldiborane, IR and Raman spectra of cis and trans isomers 78−86868
dimethyldichlorosilane, microwave spectrum, rot., centrifugal distortion and quadrupole coupling consts. 80−91547
dimethyldihalostannanes, cryst., IR spectra bandwidth, CH_3 group internal rot. 78−52490
dimethyldithiocarbamate, in lyotropic liq. cryst., EPR singularities in partially ordered matrix 77−77103
S,S′-dimethyldithiocarbonate, pot. for rot. about C(sp^2)-S bonds, electron diffr. obs. 80−23572
dimethylether, ab initio SCF calcs., force field, IR and Raman intensities 77−79601
dimethylether, and d_6, microwave spectra of torsionally excited states 79−26974
dimethylether, equilib. struct., SCF ab initio calcs. 77−3265
organic compounds continued
dimethylether-HCl(I)(Br) mixture in N_2 matrix, IR induced proton transfer isotope effects, bond strengths 79−29335
dimethylether-HCl complex, gaseous, H-bond IR spectra, temp. depend. theory 78−62804
N,N-dimethylformamide, enthalpies and related thermodynamic functions 79−42276
N,N-dimethylformamide, in nematic solvent, PMR spectrum 77−90049
dimethylformamide, intramolecular exchange rate determ. from ^{13}C spin-lattice relax. times 80−69169
dimethylformamide, triple NMR technique for N-containing molecules, ^{13}C-{^{1}H,^{14}N} triple reson. 79−81219
N,N-dimethylformamide+$POCl_3$ reaction products, Raman spectra 78−7199
N, N-dimethylformamide based electrolytes, for Al foil electrolyte capacitors *(Slovene)* 78−31641
dimethylformamide binary systems, critical mixing temp. *(German)* 79−77762
dimethylglyoxime, O X-ray emission spectra 77−28653
2,5-dimethylhex-3-yn-2,5-diol, mol., He(I) photoelectron spectra 79−27033
dimethylhydrazine-oxyhaemoglobin interaction, γ-reson. spectroscopy 80−81525
dimethylketene, thermal dimerisation mechanism, CNDO/2-INDO calcs. *(German)* 79−54771
dimethylketone, streaming current and cross-coeff. meas. in electrokinetic processes 80−76531
dimethylmercury, effective core potentials calcs. rel. to bond lengths and energies 78−66464
N,N-dimethylmethanesulphonamide+phenol (chlorophenol), assoc., PMR 78−23941
1,5-dimethylnaphthalene, fluoresc. quenching by cyclic azoalkanes, micelle system probe 80−35578
dimethylnaphthalene, growth rate from melt *(Japanese)* 78−23605
2:3dimethylnaphthalene, in polystyrene matrix, singlet O_2 induced excimer fluoresc. 77−6832
dimethylnitrosamine, in aq. soln., detect. and meas. by laser Raman spectroscopy 78−15725
dimethyloropane+H_2, (oriented), total collision cross-sections, anisotropic pot. parameters calcs. 78−13568
N,N-dimethyloxamide, conform. anal., CNDO/2 energy optimisation, mol. props. 77−75328
3,3-dimethyloxetan, far IR spectra, ring puckering vibration 78−42058
6,6′-dimethyloxyindigo, picosec. kinetics, and photostability, spectrosc. obs. 79−45748
2,2-dimethylpentane, gas, Kerr effect, virial coeffs. 79−50843
2,4-dimethylpentane, glasses, γ-irrad., trapped electron yields, mol. struct. and temp. effects 77−40561
5,10-dimethylphenazine, in 3-methylpentane (ethanol) (PMMA), radiationless processes, temp. depend. 80−43087
3,5- dimethylphenol formaldehyde resin carbon, catalytic graphitisation from various metals 80−11871
dimethylphosphine, microwave spectra, internal rot. barrier 78−5205
dimethylphosphines, IR spectra, coupling between methyl rocking, PH bending, and PC stretching, force field interpretation 80−69141
dimethylphthalate-cellulose acetate gel, mech. props., substitution effect *(Russian)* 79−23291
2,2-dimethylpropane, electron mobilities through liq. and critical regions 78−2536
2,2-dimethylpropane, liq., O_2^- electron laser-photodetachment 79−64057
2,2-dimethylpropane, liq., self-diffusion coeff., temp. and density depend. 78−91461
2,2-dimethylpropane-CO_2,, liq.vapour equil., 220 to 300K and 6.7 MPs 80−62821
2,6,dimethylpyrazine, PMMA soln., fluoresc. and phosphoresc. quantum yield and lifetime, 20-120 kbar 79−54902
N,N-dimethylselenourea, deuterated forms and methyl derivatives, fundamental IR vibr. assignments 80−961
dimethylsolphoxide, effects on water struct., Raman and IR spectral study 80−14143
1,4-bis(2,5-dimethylstyryl)benzene, lasing characts. on UV N_2 laser excitation 80−32979
dimethylsulphate, cryst., liq., and oriented film, vibr. spectra, internal rot. 79−91444
dimethylsulphide, liq., solvated electrons, optical absorpt. spectrum obs. 80−97250
dimethylsulphide, Raman spectra, torsional pot. consts. and kinetic coeffs. 78−5233
dimethylsulphide-d_3, two interacting C_{3v} rotor system, mol. coupling parameters, Raman spectra 78−42074
dimethylsulphite(-d_6), cryst., liq., and oriented film, vibr. spectra, force fields 79−91443
dimethylsulphoxide, aqueous solns., IR spectra *(Italian)* 79−63994
dimethylsulphoxide, density up to 257°C, vap. press. up to 189°C, crit. density 79−90768
dimethylsulphoxide, $Eu^{3+}\rightarrow Pr^{3+}$ and $Eu^{3+}\rightarrow Er^{3+}$ non-radiative energy transfer 79−47510
dimethylsulphoxide, r_3-struct. calcs. 78−70770
dimethylsulphoxide as labelling aid in radioiodine labelling of insulin *(Korean)* 78−88746
dimethylsulphoxide-d_6, Jeener-Broekaert three-pulse sequence, inhomogeneous lineshapes second rank spin interactions 80−39891
dimethylsulphoxide-d_6, NMR double-quantum spin decoupling 78−88227
dimethylsulphoxide-water-0.9 m $NaClO_4$, salt effect on vap.-liq. equilib. 79−51245
dimethyltetraphenylmethylphenylsiloxanes, density, viscosity, surface tension and crit. temps. 79−86830
N,N-dimethylthiourea, deuterated forms and methyl derivatives, fundamental IR vibr. assignments 80−961
dimethyltin difluoride, neutron scatt. exam. methyl group motion 78−59769
N,N-dimethyltrichloroacetamide, two-site exchange system, total line shape anal. 80−35519
9,10-cis-endo-dimethyltricyclo[4,2,2,$0^{2,5}$]dec-7-ene, substituted, crystal and molecular struct. 79−86785
2,12-dimethyltridecahexaene, optical spectra, vibr. anal., rel. to visual chromophore 77−29102
2,10-dimethylundecapentaene, optical spectra, vibr. anal., rel. to visual chromophore 77−29102
1,3-dimethyluracil, non-hydrogen bonding crystal, radical formation 80−35552

organic compounds continued
dimyristoyl lecithin lipid vesicles, sonicated, ^{13}C relax. times model for gauche-trans isomerisation 78−33520
dinaphtho-(2′.3′:1.2);(2″3″:6.7)-pyrene, triplet state, phosphoresc. and ODMR obs. 79−27013
α,α-dinaphthylalkane in isooctane soln., excimer phosphoresc., delayed fluoresc., triplet-triplet absorption 78−25597
α,α-dinaphthylalkanes, absorpt. spectra and phosphoresc. in soln., triplet excimers 78−62816
dinaphthylalkanes, triplet-triplet annihilation of excimers in soln. 78−86904
dinaphthylamine, fluoresc. in soln., intramol. excimer and exciplex form. 78−62836
m-dinitobenzene, adsorption on metal oxide surface, strength and distrib. of electron donor sites 78−84055
dinitrato[N,N′-propane-1,3-diylbis(salicylideneimine)]calcium(II), cryst. struct. anal. 79−99171
p-dinitrobenzene, adsorption on metal oxide surface, strength and distrib. of electron donor sites 78−84055
m-dinitrobenzene, cryst., low-freq. polarised Raman spectra 78−84574
m-dinitrobenzene, electrooptic cryst., growth in monomode optical fibres 80−55288
m-dinitrobenzene, for possible electro-optic appl., cryst. growth in glass capillary 77−44150
m-dinitrobenzene, nonlinear optical susceptibility, second order, calc. from mol. spectra *(Russian)* 79−27318
m-dinitrobenzene, nonlinear optical susceptibility tensor, calc. 79−23011
m-dinitrobenzene, oriented film, intermol. vibr. coupling, polarised IR spectra 80−97264
m-dinitrobenzene cored fibres, void-free cryst. growth, X-ray diffr. and optical microscopy study 80−71586
4-(2′,4′-dinitrobenzyl)-pyridine, photochromism, nanosec. laser absorpt. spectrosc. obs. 80−85193
2-(2′,4′-dinitrobenzyl)-pyridine, photochromism, ns laser absorption spectra 78−48138
2-(2,4-dinitrobenzyl)pyridine, powdered sample, kinetic photochromic characts. 78−23957
4,4′-dinitrobiphenyl complexes, intermol. interacts. and geometry of nonrigid mols., vibr. spectra 78−88294
4,4′-dinitrodiphenyl ether, enthalpies and related thermodynamic functions 79−42276
2,2′-dinitrodiphenylmethane, nanosecond laser flash photolysis and absorpt. spectra, photochromism, solvent polarity 78−61029
1,5-dinitronaphthalene, diamag. cryst., mag. axis, struct. interpretation 80−50039
1,8-dinitronaphthalene, orthorhombic, cryst. struct., X-ray determ., 22 and 97°C 78−6048
2,4-dinitrophenol, cryst. and mol. struct. 77−15394
2,2-dinitropropane, specific heat meas., adiabatic calorimetric method 78−71854
2,2-dinitropropane-d_0(-d_6), phase polymorphism, vibrational assignments, IR and Raman study 80−16031
2,4-dinitrotoluene, laser optoacoustic absorpt. spectra of explosive vapours 78−76941
dinitrotoluene isomers, occurrence and determ. in seawater 80−7966
dinucleoside monophosphates, conformational anal. by nuclear Overhauser effects 79−20509
dinucleoside monophosphates, struct. and conform. in aq. soln., Raman spectra 78−78847
dinucleoside phosphates, polaris. spectra, excimer phosphoresc. and fluoresc. 79−34497
dioctadecyl hydrogen maleate crystals, X-ray spectroscopic true $2d_{cr}$ value, 'effective' 2d value concept of Bragg spectrometer crystals 80−70081
dioctadecyldimethylammonium chloride, surfactant vesicles, low-ang. light scatt. and photon correlation spectroscopy 79−79484
dioctyl adiapte, antiplasticisation of PVC, viscoelasticity transitions 79−5015
dioctyl phthalate, antiplasticisation of PVC, viscoelasticity, transitions 79−5015
dioctyl phthalate, vapour press., determ. by submicron droplet evaporation 79−88993
dioctyl phthalate plasticised pentaplast, thermal treatment effect on props. 80−40324
dioctyl phthalate polydisperse, aerosol number and mass conc. meas. by elect. aerosol anal. 80−108753
dioctylphthalate, monodisperse aerosol, automatic method of determ. Stokes size of particles 79−93096
diolefins, substituted, topochemically controlled solid-state polymerization 80−35532
dioleoyl-phosphatidylcholine/dipalmitoyl-phosphatidylcholine bilayer membranes, phase transitions 79−39367
9,10-dioxa-anti-bimanes, fast intersystem crossing, picosecond spectrosc. obs. 79−85998
2,6-dioxaadamantane, plastic phase, transition and fusion thermodynamics, DSC meas. 78−75603
1,4-dioxadiene, mol., pot. functions of bending modes 80−9753
dioxan, aq. mixtures, miscibility, enthalpy of mixing, solvation *(German)* 78−18779
dioxan(-oxalic acid)(-benzoic acid), solns., compressibility, internal press., US vol., H-bonding 79−82272
dioxan-acetone mixtures, US props., molecular interaction between components 78−63657
p-dioxan-benzene liq. mixture, excess energy of vaporisation, US study 80−65209
dioxan-chloroform mixtures, US props., molecular interaction between components 78−63657
dioxan-cyclohexane-chloroform, mixtures, compressibility, free length, molar and available vol., US meas. 78−2200
dioxan-$H_2{}^{16}O(H_2{}^{18}O)(D_2{}^{16}O)$, solns., FP determ., equilib. method 77−20048
dioxan-methanol system, US vel., compressibility, complex form. 79−82283
dioxan-phenol(-d_1), in CCl_4 solns., H-bonds vibr. relax. bands anal. 78−84560
dioxane, 1:1 and 1:2 complexes with H_2O and D_2O, H-bonding, IR and Raman vibr. spectra 77−34633
p-dioxane, aq. soln., excess molar heat capacities, 298.15K, US vel. obs. 80−6523
1,4-dioxane, conform. equilib., CNDO/2 calcs. on six-membered rings 80−23336
p-,(m-)dioxane, conformation maps 77−57900
organic compounds continued
p-dioxane, He ion stopping cross sections, ring struct., bond strain and Bragg rule deviations 79−98188
dioxane, isomerisation, proton spin-echo NMR 77−9053
1,4-dioxane, liq., reorientational correl. times from light scatt. 77−32385
dioxane, liq., spin lattice relax. time, elec. field induced charges 80−44945
dioxane, Raman spectral study of aq. soln. struct., H-bond effects 77−88454
1,4-dioxane, refr. index, temp. depend., deviation from Lorentz-Lorenz formula 77−40200
dioxane based gel, scintillation yield and mechanisms involved study *(French)* 80−52816
dioxane liquid scintillators, scintillation yield, chloroform and carbon tetrachloride quenching effects *(French)* 77−3217
dioxane solutions, radioluminescence quenching in mixtures of solvents *(Russian)* 80−55192
1,4-dioxane-1,1,2,2-tetrachloroethane, isobaric vapour-liquid equilibria at atmospheric pressure 79−51246
dioxane-D_2O mixture, nuclear Overhauser effect factors determ. using dynamic Overhauser enhancement with least square procedure 79−4746
p-dioxane-H_2O at 11 and 25°C, US absorption 80−65171
dioxane-$HgCl_2$ complexes, IR and Raman vibr. spectra, inter- and intramol. forces 77−66489
p-dioxane-water mixtures, adiabatic compressibilities and sound vels., temp. depend. 79−28044
dioxane-water mixtures, compressiblity, density, US vel. rel. to temp., conc., struct. *(German)* 77−43263
dioxane-water system, electro-optical Kerr constant meas. at 632.8 nm 79−4788
4,7-dioxaoctanal, equilib. anionic polymerisation, −90 to −68°C, polar substituent effects 78−88631
dioxirane, decomposition products, mass spectrometric obs. 78−11504
dioxirane, form. in O_3+ethylene reaction, identification by microwave spectra 78−15659
dioxodiazacycloalkanes, electronic struct., mol. orbital theory 77−14359
1,8(6′,7′-dioxododecamethylene) phenanthrene, intramol. electronic energy transfer, emission obs. 79−31571
2,3-dioxogulonic acid, reversible transformation to enol, kinetics, pH effects 79−5152
1,3-dioxolane, clathrate hydrate, struct. II, for IR spectra, 4-100K 79−13707
2,2′-dioxy-3,3′-di(α-methylcyclohexyl)-5,5′-dimethyldiphenylmethane *(Russian)* 79−33092
dioxymethane, singlet-triplet splitting, appl. of direct CI method generalisation 79−81144
dipalmitoyl lecithin bilayer, ^2H NMR in liq. cryst. and gel phases 79−92173
dipalmitoyl lecithin bilayer, mol. tilt, X-ray diffraction obs. in gel phase 80−84059
dipalmitoyl lecithin dihydrate, phase transforms., 20 to 70°C, X-ray diffr. obs. *(French)* 78−91436
dipalmitoyl lecithin elastic monolayer, dynamic surface potentials 80−3603
dipalmitoyl lecithin-water system, lyotropic liq. cryst., pretransitional effects, PMR second moment meas. 78−91234
dipalmitoyl phosphatidyl choline, deuterated gel phase lipid bilayer, neutron scatt. sudy 79−43829
L-α-dipalmitoyl phosphatidyl choline, monolayers, laser-ripplon scatt. at air-water interface 79−99894
dipalmitoyl phosphatidyl choline vesicle damage by picosecond laser pulses 79−79599
dipalmitoyl phosphatidylcholine, gel and liquid crystalline phases, deuterium mag. resonance obs. 79−91308
dipalmitoyl phosphatidylcholine(-cholesterol) aligned multilamella lipids, elastic props., Brillouin spectra 79−5255
dipalmitoyl phosphatidylcholine containing $CaCl_2$, monodomain sample phase behaviour birefr. obs. 79−83712
dipalmitoyl phosphatidylcholine monodomain samples with varying concs. of water and other ingredients, prep. 78−15780
dipalmitoyl phosphatidylcholine vesicles, appl. of depolarised light scatt. theory from hollow spherical particles 80−45946
dipalmitoyl-lecithin, lipid bilayer, NMR dispersion of layers dispersed in D_2O 79−48223
dipalmitoyl-phosphatidylcholine bilayer membrane, melting point rel. to electrostatic field 78−92602
1,2-dipalmitoylglyceride, DTA and X-ray diffr., polymorphism *(French)* 78−43008
dipalmitoylphosphatidylcholine, changes in vol. mag. susceptibility at the phase transition 80−76770
dipeptides, aliphatic, EPR studies of direct photolysis 78−48678
dipeptides, bend form., conformational space, statistical mech. anal. 77−68146
dipeptides, reactions with hydrated electrons, EPR and spin-trapping studies 79−16124
diphenanthra[4,5,6-abcd, 4,5,6-jklm]perylene, high photoresponse, O_2, N_2 and SF_6 effects 77−32036
1,6-diphenly-1,3,5-hextriene, mol. derivatives, absorpt. and fluoresc. spectral props. 79−72344
diphenyl.2$SbCl_3$, Raman spectra 77−16291
diphenyl:(benzophenone, naphthalene), triplet exciton diffusion, phosphoresc. obs. 78−10964
diphenyl:naphthacene, relax. times of ground electronic state vibrational levels 79−19907
diphenyl:naphthalene, benzophenone, phosphoresc., triplet diffusion excitons 78−63985
diphenyl:pyrene, self induced transparency under nonreson. excitation, luminesc. and stimulated emission 80−11436
diphenyl:pyrene, stimulated emission at 0-0 transition, 4.2K 80−11437
diphenyl, cold neutron interaction cross-sections, 353-653K 79−93682
diphenyl, double mols. with weak reson. bonds, quasilinear spectra 79−94030
diphenyl, IR absorpt., intermol. reson. interaction, temp. depend. 78−72506
diphenyl, solid and liquid, total neutron cross sections for subthermal energies 78−74779
diphenyl, US velocity and absorption near melting point 78−6127
1,6diphenyl 1,3,5, hexatriene cholesteryl chlorided cholesteryl laurate mixture, nematic, polarisation fluoresc. meas. 79−78723
diphenyl anion salts, sublimed layer, electronic and IR absorpt. spectra 80−66189

organic compounds continued
9,10-diphenyl anthracene, cyclohexane soln., solute excited state form. kinetics in pulse radiolysis 79−79263
9,10-diphenyl anthracene, excited singlet state quenching by nitroxyl radical, triplet form. 77−88487
diphenyl anthracene, inelastic-elastic scatt. ratio of 80 keV electrons 77−4127
9,10-diphenyl anthracene, vap. phase dye laser media, photophysical parameters 80−95884
diphenyl butadiene, absorption recovery lifetime, use in UV mode-locked lasers 80−19075
1,4-diphenyl butadiene, additive to dye solns., lasing efficiency 77−19249
diphenyl crystallites, changes in face growth rate from vapour phase 79−55686
diphenyl disulphide, sensitiser in γ-ray induced cis-trans isomerisation of polybutadiene 79−74374
diphenyl ether, dielec. relax. pseudorot. diffusion 79−33600
diphenyl ether, dil. solns., dielec. loss and relax., microwave and sub-mm. wave absorpt. obs. *(German)* 78−23396
diphenyl ether, preparation, purification and use in triple-point cell 79−21750
diphenyl halonium compounds, X-ray struct. anal. and NQR, chem. bonding 77−12232
diphenyl hexachloride, liq., imaginary compressional modulus (compressional viscosity) 77−76480
diphenyl methane, critical nuclei, meas. of number of mols. and surface tension from rate of nucleation 79−65293
diphenyl mixture, superheated cap. and liq., enthalpy, press. depend. 78−42702
2,4-diphenyl pentane, polystyrene model molecule, US relax. 77−6965
diphenyl polyenes, effects on lasing characts. of rhodamine dye solns. 77−3581
diphenyl selenium halides, correlation between NQR spectra and cryst. struct. 77−12233
diphenyl styryl pyrazoline-active electrolyte system, electrochemiluminesc. spectral shift 77−20929
diphenyl tellurium halides, correlation between NQR spectra and cryst. struct. 77−12233
diphenyl with pyrene cryst., self induced transparency self stimulated excitation *(Russian)* 80−14403
3,5-diphenyl-1,2,4-oxadiazole, saturated vap. press., absorpt. and fluoresc. spectra 79−76442
2,5-diphenyl-1,3,4-oxadiazole, fluoresc. quantum efficiency, one-photon dissociation, temp. depends. 80−69180
2,5-diphenyl-1,3,4-oxadiazole, vapour, spectral, fluoresc., photochem. and laser props. 80−106344
1,8diphenyl-1,3,5,7-octatetraene, high press. fluoresc. studies of radiative and nonradiative processes 80−1011
1,6-diphenyl-1,3,5-h-hexatriene and derivatives in n-paraffins, electronic spectra and fluoresc. 78−13509
1,6-diphenyl-1,3,5-hexatriene, high press. fluoresc. studies of radiative and nonradiative processes 80−1011
2,5-diphenyl-1,3-oxazole vapour, spectral, fluoresc., photochem. and laser props. 80−106344
2,6-diphenyl-1,4-benzoquinone+aromatic amine, triplet exciplex quenching, H-transfer mechanism 79−79228
1,3-diphenyl-5-(p-chlorophenyl)-2-pyrazoline, singlet excitation energy migration in cryst. and glassy states 79−95831
diphenyl-benzene, dil. soln., thermodynamic equilib., ebulliometric investig. 78−18752
diphenyl-d_{10}: diphenyl, triplet state EPR and ENDOR, 1.9K, mol. struct. implications 79−94021
diphenyl-diphenyl ether mixture, Dowtherm vapour, speed of sound meas. 79−18989
N,N′-diphenyl-m-phenylenediamine, crystal and mol. struct., X-ray diffr. 78−47312
N,N′-diphenyl-p-phenylenediamine, cryst. and mol. struct. 77−7706
N,N′-diphenyl-p-phenylenediamine, current carrier traps, space-charge-limited currents 78−47799
3,6-diphenyl-pyridazine, valence electronic structure 79−72360
3,6-diphenyl-s-tetrazine, valence electronic structure 79−72360
diphenyl-stilbene dye, sulphonated, CW laser emission, tunable down to 390.4 nm 79−41379
diphenylamine, in nitrobenzene soln., dry hole capture in pulse radiolysis expt. 79−79266
diphenylamine, spherol crystals, morphology and growth 78−18567
diphenylamine+2,6-diphenyl-1,4-benzoquinone, triplet exciplex quenching 79−79228
diphenylamines, Hammett freq. factors, effects of non-monotonic ν(XH) function variations *(French)* 79−22690
N-(4-diphenylamino) phthalimide, X-ray cryst. struct. determ. 79−42048
9,10-diphenylanthracene, electrogenerated chemiluminescence, T_2 state emission 78−60524
diphenylanthracene, fluoresc., site selection spectroscopy 2-300K 77−1731
9,10-diphenylanthracene, luminesc. quantum yield, fluoresc. spectra polarisation effect, solvent viscosity depend. 78−27303
9,10-diphenylanthracene, refr. index meas. of frozen gas matrices, fluoresc. method 80−90884
9,10-diphenylanthracene, soln. grown, cryst. struct. by computational and X-ray study 79−37690
diphenylanthracene in 2,2,4-trimethylpentane, light scatt. and fluoresc. standard by monochromator 80−57247
diphenylanthracene in benzene soln., extrinsic photocond. kinetics 80−92691
9,10-diphenylanthracene-toluene, soln., electron beam pulse radiolysis, energy transfer 80−7808
1,4-diphenylbutadiene, quenching of triplet dye mols., in intercombination conversion rate consts. determ. 79−956
1,4-diphenylbutadiene, UV lasers pumped by KrF, XeBr excimer lasers 79−10301
E,E-1,4-diphenylbutadiene-(1,3), isomerisation, reaction quantum yields, exciting light bandwidth influence study *(German)* 80−21310
diphenylene, n-paraffin soln., quasiline sensitised phosphoresc. spectra at 4.2K 77−68071
diphenylene sulphide, phosphoresc. vibronic struct., solvent heavy at. effect 78−17710
diphenylethers, 1st ionisation energy, substituent effects, photoelectron spectra 77−42354
1,1-diphenylethylene, adsorbed on porous Vycor glass, reson. Raman spectrum, surface species identification 78−42066

organic compounds continued
diphenylethylene, UV spectra, quantum-mechanical investigation of isomerisation pathways 80−43065
2,5-diphenylfuran vapour, spectral, fluoresc., photochem. and laser props. 80−106344
diphenylhaloselenium radical trapped in single crysts., FSR, struct. 80−44919
diphenylhexatriene, low-energy ^1A_g state obs., by two-photon matrix spectroscopy 78−74715
1,6-diphenylhexatriene, lower excited states fluoresc. quenching 80−1016
diphenylhexatriene, quantitation of hindered rotations in lipid bilayers 79−16128
1,6-diphenylhexatriene, radiationless transitions and natural lifetimes, solvent effects 80−63622
diphenylhexatriene, two-photon excitation of low-energy excited states 77−14507
1,6-diphenylhexatrienes, electronic and fluoresc. spectra, solvent effects, 77K 78−21959
1,3-diphenylisobenzofuran, oxidation, dissoc. oxciplex relax., solute reencounter probabilities 79−34285
1,3-diphenylisobenzofuran, rubrene sensitised photooxidation, efficiency meas. 78−27792
diphenylketyl radical, fluoresc. lifetime and quantum yield, organic matrix, 77-130K 78−42110
diphenylmethylene, triplet state, ENDOR in $P2_1$ benzophenone, conformation and spin distrib. 77−483
diphenylmethylene-d_0,-d_{10}, in benzophenone, ground triplet state, electron spin echo expts. 77−16144
diphenyloctatetraene, two photon excitation of low-energy excited states 77−14507
diphenyloctatetraene, two-photon spectra, ^1A_g state confirmation 78−17736
2,5-diphenyloxazole, liq. scintillator system, energy transfer, fluoresc. intensity-max. solvent depend. 78−21966
2,5-diphenyloxazole, multiexponential fluorescence decay, systems theory approach to anal. 79−59495
2,5-diphenyloxazole, phosphoresc., 77K, solvent effect 78−42118
5,10-diphenylphenazine, in 3-methylpentane (ethanol) (PMMA), radiationless processes, temp. depend. 80−43087
5,10-diphenylphenazine, photoconduction *(German)* 79−78129
4-diphenylphosphenylstilbenes, fluoresc., photodimerisation 80−1015
diphenylpolyene, oriented in polymer film, polaris. reson. Raman spectra 79−59466
diphenylpolyene molecules, excited electronic states, vibronic mixing, wave functions, method of fragments anal. 80−63615
diphenylpolyenes, photoisomerisation, 'phantom' photochem. singlet state, PPP SCF CI calcs. 78−73058
diphenylpolyenes, two-photon absorptivities via three wave mixing 79−68416
1,3-diphenylpropane, in isooctane soln., monomer phosphoresc., low binding energy triplet excimer not obs. 78−25597
diphenylselenone crystals, gamma irradiation, ESR study of trapped phenylselenonyl radical 80−44917
diphenylsilanediol, recrystallized, cell const. refinement precision powder data 79−10841
diphenylsulphides, 1st ionisation energy, substituent effects, photoelectron spectra 77−42354
p,p′-diphenylsulphines, (He I) photoelectron spectra, assigned by perturbational mol. orbital and CNDO/2 calcs. 78−46396
all-trans-diphenyltetradecaheptaene, oriented, photochem. reaction production and monitoring, reson. Raman spectroscopy 77−29020
diphenyltriafulvenes, absorpt. and fluoresc. spectra, dipole moments, solvent effects 77−75169
2-4-diphenylyl-5-phenyloxazole vapour lasers, generating capacity, stimulated emission *(Russian)* 77−679
dipicolinic acid, IR and Raman spectra, isotopic frequency shift, mol. vibr. obs., point groups determ. 80−89001
diplosporin derived from (1,2-^{13}C)acetate, ^{13}C-^{13}C coupling assignment using DANTE excitation 80−80617
dipolmitoyl phosphatidylcholine lamellar phases and bilayer phase transitions, structural parameters 78−64948
dipotassium glucose-1-phosphate, X-irrad., ESR-ENDOR obs 80−60419
dipotassium malonate, aq. soln., IR and Raman vibr. spectra *(French)* 79−26989
dipotassium tartrate single crystal, SHG 78−13757
dipotassium uridine 5′-diphosphate trihydrate, X-ray cryst. struct. determ. 79−57569
dipropionyl peroxide, photochemical production of ethyl radical 80−3373
dipropylammonium copper chloride, ferromag., low temp. magnetism *(Japanese)* 77−20748
dipropylammonium copper chloride, nearly 2D ferromag., spin wave theory 77−85436
dipropylammonium coppertetrabromide, Faraday effect obs. of mag. struct., and domains 77−63399
dipropylammonium manganese chloride, layer perovskite, step bunching obs. by compound holographic microscopy 78−63682
dipropylammonium manganese tetrachloride, and tetrabromide, two-dimens. antiferromagnet, spin canting and exchange 80−34620
dipropylammonium manganese tetrachloride, two-dimens. weak ferromagnet, AC susceptibility 80−65823
dipyridinium copper bromide, $Py_2Cu_5Br_7$, Cu^+ ion conductor, cryst. struct. 78−51527
dipyridylethylenes, photoelectron spectra, conformation, SCF LCAO calcs. 77−79651
diquinolyl cyanomethane, fluoresc. quantum yields, viscosity effects 80−60646
1,4-disilabutane, rot. isomerism, Raman and IR spectra 80−74168
1,3-disilacyclobutane, ring-puckering combination band spectra in SiH_2 stretching region 78−70836
disilylmethane, microwave spectrum, struct., dipole moment and internal rot. 79−13699
dispiro compound I, pyrolysis, CIDNP, S-T mixing, nuclear Overhauser effect 77−6803
dissolved organic matter in seawater, fluoresc. spectra *(Russian)* 77−13083
distamycin A, analog cryst. and molecular struct. 79−88051
2,5-distyrylpyrazine, absorpt., Raman and fluoresc. spectrosc. 80−28049
distyrylpyrazine, topochemically controlled solid-state polymerization 80−35532
1,2-disubstituted imidazole compounds, IR and Raman spectra, vibr. anal. *(French)* 79−45713

organic compounds continued
p,p'-disubstituted phenyl thiolbenzoates, nematic liq. cryst., synthesis and props. 77−15308
p-disubstituted phenylcyclohexane, liq. cryst., investigation of elec. field induced deform. by capacity measurements 79−4234
N,N'-disubstituted piperazinium diiodide-AgI, binary salts, ionic cond. study *(French)* 78−2293
p-ditertiarybutylbenzol electron absorption spectra and struct. *(Russian)* 77−16338
ditetraethylammonium manganese bromide $^4T_1$ excited state, absorpt., MCD, Jahn-Teller model 78−43907
1,4-dithiane-1-oxide, cryst., IR and Raman spectra 79−69839
dithiobismorpholine, cryst. data 77−35544
dithiocarbamate complexes of Cr, Mn, Sn and Pb IR, electronic and mass spectra, mag. susceptibility, cond. meas. 80−97270
dithioformic acid, pot. for rot. about C(sp^2)-S bonds, ab initio calc. 80−23572
dithioformic acid, prod. and microwave spectra 78−58671
dithiolato nickel complexes with aliphatic substituents, synthesis and mesomorphic props. 77−84646
dithiosuccinimide-d_0,-d_1, normal coord. anal. calcs. 77−30844
ditolylmethane, boiling in circuit system, effect of intense electric field *(Russian)* 78−46887
divinyl benzene, topochemically controlled solid-state polymerization 80−35532
divinyl benzene suspension, dielectrophoresis 80−3362
divinyl ether, microwave spectrum, doublet splitting, vinyl group internal rot. 78−86849
diynes, acyclic, non-conjugated, UPS comparison, obs. and calc. 80−32772
1,4-di[2-(5-phenyloxazoyl)] benzene, fluoresc. by electron beam excitation 79−94031
DMBCA, nematogen, incoherent neutron quasielastic scatt. 79−32887
DMSO:Cr^{3+}, Nd^{3+}, energy transfer and migration, donor-acceptor interaction, phosphoresc. quenching conc. depend. 78−64403
DMSO, centrifugal distortion analysis including P^6-terms 77−14413
DMSO solutions of alkali halides, modelling of interactions 79−77469
DMSO-$PdCl_2$ complex semi-empirical INDO calc. of bonding 80−32611
DMSO-Tl^+, spin-lattice relax., chem. shift anisotropy 79−51870
DNA-acridine dye complex, fluorescence studies 80−37921
DNA-cetavlate crystal growth and morphology 77−66583
DOBAMBC, and DOBAMBCC, chiral smectic C liq. cryst., dielec. consts., electroclinic effect 78−94980
DOBAMBC, chiral smectic, ferroelec., press. and solute effects 80−103920
DOBAMBC, chiral smectic, flexoelectric effect and polarisation props. *(Russian)* 80−15002
DOBAMBC, chiral smectic C-phase ferroelectric liq. crystal film, classical X-Y system, props. 80−44123
DOBAMBC, chiral smectic phases, pyroelectric and dielec. props. 79−91380
DOBAMBC, dielec. dispersion at ferroelec. smectic A-smectic C transition 79−91385
DOBAMBC, dielec. props. near ferroelec. smectic A to C transition 80−45015
DOBAMBC, ferroelec. liq. cryst., helical struct., elec. field depend. *(Japanese)* 80−38910
DOBAMBC, ferroelec. liq. crysts., elec. and optical props., appls. *(Japanese)* 80−88943
DOBAMBC, ferroelectric liquid crystal film, freely suspended, polarisation, elastic consts. and viscosity meas. 79−55663
DOBAMBC, polarized Raman scatt. and elec. field effects in aligned smectic phases 79−94873
DOBAMBC, smectic, ferroelec. transition mechanism obs. by X-ray scatt. 79−77515
DOBAMBC, smectic A and ferroelec. smectic phases, ^{13}C NMR study 80−75153
DOBAMBC, smectic A to C transform., birefringence and optical rotary power 78−75812
L-DOBAMBC, smectic liq. cryst., ferroelec. behaviour 77−43949
DOBAMBC, smectic liquid crystal, ferroelectric, colour switching in elec. field 80−29719
DOBAMBC, specific heat determ., temp. depend. 78−91250
DOBPC, smectic C liq. cryst., elasticity and defects 78−91233
n-docosane, depolarised Rayleigh spectroscopy 79−4808
n-docosane, liq., hypersonic attenuation, temp. depend. of Brillouin spectra 79−11426
docosane, purification and single cryst. growth 80−71589
DODCI, lifetime of optically stimulated dyes, generation of time correlated picosecond laser pulses *(German)* 79−27045
DODCI, ps absorption relax. lifetime, isomers, pulse excitation 77−9098
DODCI, rot. diffusion time, time depend. fluoresc. depolarisation meas., photoisomer effects 77−71825
DODCI, saturable absorber, picosecond phase-conjugate refl. 80−95960
DODCI+malachite green (DQOCI), electronic energy transfer obs. 80−5633
DODCI dye dissolved in glycerine, time delayed picosecond pulse transmission obs. 80−48355
DODCI in ethanol, DQOCI added, electronic energy transfer, real-time ps meas. 80−58311
DODCI in ethanol, malachite green added, electronic energy transfer, real-time ps meas. 80−58311
dodecahexenes, sudden polarisation effect, ab initio and CI calcs. 80−58160
dodecan-1-ol+n-hexane, vap. press. and thermodynamic props., 298.230 to 342.824K 78−47528
dodecanate/decyltrimethylammonium micelles, type II mesophase, bilayer struct., NMR spectra study 80−75149
n-dodecane, depolarised Rayleigh spectroscopy 79−4808
n-dodecane, diffusion in liq. polyethylene, gas chromatography determ. 78−2277
n-dodecane, tertiary alkylamines as sensitisers for charge injection from Se, and as charge carriers 79−91116
n-dodecane liqs., refractive index, pressure effect 80−71375
n-dodecane-β,β'-dichlorediethyl ether crit. mixture, Rayleigh line wing 77−20864
n-dodecane-dichlordiethyl ether, stratified solns., depolarisation of scatt. light 78−10910
n-dodecane-n-hexane, 'ideal' mixture, viscosity, theory *(German)* 78−22882

organic compounds continued
dodecane-sodium octylbenzene sulphonate phase diagram *(French)* 79−82339
dodecane-tributyl phosphate solns., radiolysis, liquid products 80−40723
dodecane-tributylphosphate solns. radiolysis 78−74459
dodecane-water microemulsions, dielec. study of phase transition 79−28668
dodecane-water microemulsions, struct. transitions in liq. cryst. phase, dielec. props. 79−28669
dodecanol, additive to $Na_2SO_4.12H_2O$ aq. soln., near critical micelle conc. 77−73472
p-dodecanoylbenzylidene-p'-aminoazobenzene, smectic A mesophase, self- and impurity diffusion, NMR spin echo obs. 78−94975
dodecylamine ($-NH_2$)/H_2O_2 and deuterated cpd., liquid crystal, phase relationships, isotope effects 79−19358
dodecylcyanobiphenyl, pretransitional behaviour of isotropic to smectic A phase transition 79−60487
p-n-dodecyloxy benzoic acid, liq. cryst. phase transition, thermal studies 78−71843
p-ndodocyloxy benzylidene p-azophenyl aniline, smectic phases, mol. order, EPR study 80−79693
dopamine derivatives, detect. by GC/MS selected ion monitoring 79−43643
DOTC, dye laser, emission at 810 nm, 0.1 J in 1 μs *(French)* 77−42549
doublet radicals in nematic and smectic liq. crysts., ENDOR obs. 80−91585
doubly charged negative ions, electron impact 77−31006
DPPH, dil., saturated spin system, spin decoupling effect and variation of dipolar energy reservoir temp. 80−88877
DPPH, exchange integral determ. by ESR in weak Zeeman fields 78−2740
DPPH, mag. susceptibility of solvent-free and DPPH-benzene complex 78−70963
DPPH, polycryst., forbidden EPR transition 78−48044
DPPH, solid, mag. susceptibility meas. 300 to 2.2K, pair model 77−66245
DPPH-benzene, organic radical, pressure induced mag. ordering *(Russian)* 78−88120
DPPH-benzene complex, ht. capacity, 0.55-20K, mag. susceptibility, 0.4-300K 78−56317
DQOCI+DODCI, electronic energy transfer obs. 80−5633
drugs, analysis by IR spectroscopy, preconcentration, separation and computer techniques 78−31730
DTGS:VO^{2+}, ENDOR 79−99791
DTIC, effect on human malignant melanomas in athymic nude mice 77−48839
DTPA effect on biological availability of transuranics 78−73264
DTPA for U(VI) removal from rat body, decontamination efficiency 78−44617
DTPA therapy, Pu body burden estimation from urine data 78−73259
DTPA-induced radionuclide excretion in faeces for estimation of skeletal Pu levels 78−85390
DTPP for U(VI) removal from rat body, decontamination efficiency 78−44617
DTTC, subpicosecond laser photolysis and time resolved absorpt. spectra *(Japanese)* 79−79272
dulcitol, X-irrad., 4.2K, electron traps, alkoxy hyperfine coupling, ENDOR obs. 80−50863
dulcitol, X-irradiated single crystal, intermol. electron trapping, hyperfine ESR pattern 79−39166
duraldehyde, S_1-T_1 nonradiative transition mechanism, double reson. obs. 77−30893
duraldehyde, Stark effect on electron spin transition in zero-field 77−27099
durene:fluoranthene(pyrene)(chrysene), triplet and singlet transport rate ratio 79−56832
durene:naphthalene, spin-lattice relax. in photo-excited triplet states, spin axes rot. on thermal excitation 78−76294
durene:quinoline-d_0,(-d_n), phosphorescent triplet spins, phase coherence, spectral diffusion effects 79−87334
durene, aldehyde doped cryst., photolysis 10 to 20K, physical and chem. defects 79−52721
durene, ENSH method of oriented thin film growth 79−99443
durene, mol. cryst., Stark effect origins, point dipole approx. soln. 77−77252
durene, transient photocond. and charge carrier mobility anisotropy, temp. depend. 77−80805
durene crystalline complexes with octafluoronaphthalene, triplet exciton emissions 80−84760
durene-naphthalene melt, exciton diffusion, percolation approach 80−2390
durene-p-dibromobenzene system, phase diagram and X-ray diffr. expts. 78−79774
durene-para-dibromobenzene, binary mol. system, X-ray struct. anal. 79−55734
duro-semiquinone monoprotonated radical, submicrosecond time resolved EPR, laser photolysis, CIDEP polarisation mech. 78−80764
duroquinone, EPR time profiles, CIDEP, electron spin-echo method 79−6953
duroquinone, photochem. interaction with chlorophyll, photopot. 77−16903
duroquinone, soln., electrochem. props. obs. *(French)* 79−66301
duryal radical in durene matrix, optical coherent transient spectra 79−76764
dye, adsorbed on ZnO electrode, sensitisation mechanism, from reson. Raman spectrum 78−42066
dye, bleachable no.3955, relax. time meas., laser passive shutter appl. 80−23759
dye, bleaching, coherence time meas. of laser radiation 80−23739
dye, excited mol. decay near metal surface, energy transfer to plasmon surface polaritons 80−50440
dye, fluoresc. lifetime meas. using synchronised ultrashort laser pulses and streak photography 79−44951
dye, sensitisation using modified TiO_2 electrode, rel. to water photoelectrochem. oxidation 79−91964
dye accessory invertor for LG-21 serial N_2 laser 77−68224
dye bleaching, no. 3955 in soln., relaxation and correlation times meas. 80−28281
dye bleaching, picosecond light pulse shape and duration determ. 79−86220

organic compounds continued
dye crystal, CTIP, exciton surface polaritons detect. by ATR spectra at 295K 79−4818
dye in nematic liquid crystals, order parameter 77−83614
dye in polymer matrices, electrochromic props. and use as probe of matrix softening around T_g 80−84724
dye indicators of membrane pot., review 80−21594
dye laser materials, PPP calcs., ground and excited states, triplet yields and efficiency 80−37743
dye layer, adsorbed on ZnO cryst., charge transfer 80−49815
dye molecule, excited, thermal rotations and relaxation of vibr. energy 79−81231
dye molecule monolayer displaced from metal surface, light refl., coupling with metal surface modes 78−48246
dye molecules, dissolved, influence of environment on luminesc., intense laser excitation 78−84622
dye molecules, excited state lifetimes and lasing conditions, time-resolved spectroscopy 77−71983
dye molecules, long wavelength conc. shift in luminesc. 79−64032
dye molecules, two-photon absorpt. in laser fields with arbitrary statistical characts. *(Russian)* 80−37842
dye molecules adsorbed on Ag, Au and Cu films, absorpt. and luminesc. study 80−103981
dye molecules excited by surface plasmon waves in Ag film, fluoresc. angular emission profiles 79−89703
dye monolayers, on Ag film, effect on surface plasmons, ART obs. 79−87001
dye monomolecular layers, energy transfer between sensitizers and acceptors 80−80861
dye pair, chromophorically degenerate, adsorbed on AgBr, supersensitised photoconductance 79−61887
dye proflavine bound to synthetic polynucleotides, selective laser photodamage 80−99525
dye soln., fluoresc. amplitude anisotropy, polarised light excited 79−85990
dye solns., alcoholic, stimulated emission in blue and violet regions *(Russian)* 78−25874
dye solns., lasing efficiency with 1,4-diphenyl butadiene additive 77−19249
dye solns., single and two-photon spectroscopy, using pulsed acousto-optical effect 77−68087
dye solns., two-component, before-relax. energy transfer and absorpt. spectra overlap 78−27285
dye solution, fluoresc. yield, photoacoustic determ. method 78−42117
dye solution, fluorescent, contact with metal electrodes, photovoltage generation, comprehensive model 80−40871
dye solution, laser illuminated, light field phase conjugation, nonlinear interactions *(Russian)* 80−28266
dye solution, luminesc. quenching, pulsed photoacoustic detection technique 77−85780
dye solution, nonlinear fluoresc. meas., two-photon pumping by low power laser 80−48037
dye solution, polarisation of stimulated emission *(Russian)* 78−25872
dye solution amplifying dynamic holograms, wavefront reversal 80−48331
dye solutions, dil., fluoresc. decay time determ. 78−68540
dye solutions, excited fluorescence film thickness meas., report 78−81945
dye solutions, in micellar media, rot. diffusion, transient absorpt. meas. 79−92005
dye solutions, light-induced quenching of spontaneous and stimulated emission *(Russian)* 78−27290
dye solutions, liq. scintillation counting, rel. to colour quenching ability 79−1790
dye solutions, mixed, energy transfer and conc. depolarisation of fluoresc. 78−25583
dye solutions, mixed, fluoresc. conc. quenching, sensibilisation 79−24347
dye solutions, picosecond flash photolysis and very fast processes 80−30249
dye solutions, vibronic struct. in two-photon absorpt. spectra *(Russian)* 79−64004
dye solutions for laser beam modulation, population relaxation lifetime meas. *(Russian)* 80−95964
dye two-photon absorption, for picosecond laser pulse stabilisation, attenuation and shaping 79−55165
dye ultrafast saturable absorbers for Nd lasers 80−53386
dye vapour, fluoresc. meas., buffer gases effect 77−75503
dye-detergent model systems, degree of fluoresc. polarisation 78−27287
dye-nematic liquid cryst. soln., generation of induced radiation *(Russian)* 77−3583
dye-polymer system, diffusion based direct marking process, laser induced, spectral thermal characteristics 79−76779
dye-releasing compounds, colour imaging technology, instant photography 78−62247
dyes, absolute fluorescence quantum yield, calorimetric determ. 80−43092
dyes, absorbing, for organic thin film refractive index adjustment 80−43413
dyes, absorption edge struct. in stimulated fluorescence spectra, Raman scatt. 78−55350
dyes, accel. of photographic bleaches, role in holographic image form. 77−14672
dyes, adsorbed, for student phosphorescence expts. 77−26114
dyes, electronic transitions obs. by inelastic electron tunnelling spectroscopy 79−3511
dyes, fluoresc. conc. depolarisation, during intense excitation *(Russian)* 77−65507
dyes, fluoresc. spectra calcs., β-variation method *(German)* 80−69182
dyes, laser, electrochemiluminescence, electrochem. oxidation, reduction 77−70304
dyes, methyl orange, red and yellow corrosion inhibition of Al alloys 78−44255
dyes, photographic emulsion spectral sensitisation, latent image form., subcond. band events 78−32905
dyes, rot. diffusion time, fluoresc. depolaris. meas. 79−24846
dyes, S_2-S_0 luminesc. for picosec. excitation 79−87506
dyes, secondary fluoresc. under very powerful pumping, fine struct. spectra 77−58383
dyes, solns., polarisation spectroscopy 78−89559
dyes, spectral sensitization and electronic struct. 79−19551
dyes, stimulated fluoresc., four-photon parametric interaction 79−13748

organic compounds continued
dyes, stimulated fluorescence, energy level scheme, photoisomerisation effect 77−70310
dyes, stimulated reson. Raman scatt. at transverse pumping, mol. vibrs. 77−88453
dyes, substituted methane, press. effs. on viscosity-depend. fluoresc. 77 34672
dyes, two-band stimulated fluorescence, laser action and bleaching effect 79−41190
dyes for tunable lasers, intersystem crossing rates and saturation parameters in triplet state 77−36280
dyes in organic solvents of high viscosity, diffusion coeffs. 78−10203
dyes in polymer matrices, intramol. charge transfer, electrochromism 79−73901
dyes in rigid matrices, solvent reorientation relax. effect on luminesc. 79−43009
dysprosium ethyl sulphate 77−24703
dysprosium ethylsulphate, pure dipolar Ising ferromag., critical thermodynamics 77−16095
E. coli, light scatt., ribosomal subunit diffusion coeffs. 80−21438
E. coli cells, anaerobic metabolism, ^1H correlation NMR spectra 79−43978
EABAC, liq. cryst., smectic and nematic, distrib. functions by X-ray diffr. 79−99072
EABAC, smectic A, nematic, and isotropic phases, NMR and quasielastic neutron scatt. obs. 80−88022
EBBA: nitroxide, mol. reorientation in nematic and isotropic phases, EPR study *(French)* 79−91297
EBBA, binary systems with non-nematic solutes, phase transition behaviour and ^1H NMR anal. 80−34174
EBBA, containing $FeSnO_3$ particles, Mossbauer study of Brownian motion 79−95691
EBBA, crystallisation and melting of metastable solid crystalline phases 78−2240
EBBA, fusion of metastable solid cryst. forms 79−14678
EBBA, in benzene soln., dielec. relax. meas., 4.0, 9.4 and 30.4 GHz 77−40176
EBBA, IR absorpt. spectra, elec. field effects, orientational order parameter determ. by IR dichroism, bend elastic consts. 80−80778
EBBA, isotropic phase, order fluctuations, self-diffusion, and rot. motion, proton spin relax. meas. 79−87328
EBBA, liq. cryst., IR and far IR spectra, vibr. assignments 77−16298
EBBA, liq. cryst., isotropic phase, NMR pulsed field grad. study of self-diffusion 79−90814
EBBA, liq. cryst., phase transitions up to 3 kbar, transition enthalpy, entropy 77−20051
EBBA, liq. cryst., Raman and calorimetric evidences for existence of three solid modifications 77−77207
EBBA, liq. cryst., rapid cooling and mag. field effects on NMR relax. and thermal behaviour 79−82321
EBBA, liq. crysts., thin layers, addition of iminoxyl radicals, effect on elec. cond. *(Russian)* 78−67641
EBBA, mematic, orientational order, effect of hexa-n-alkoxy-triphenylene disc-like solutes 80−79682
EBBA, metastable phases formed by rapid cooling of mesophase, IR and Raman spectra and DSC obs. 80−34919
EBBA, mol. and cryst. struct., X-ray diffr. study 80−88134
EBBA, mol. order study by means of C^{13}-H^1 double resonance 79−60275
EBBA, nematic, dielec. permittivity and transmitted light intensity, in DC field 77−12296
EBBA, nematic, linear and nonlinear relaxations of fluid dynamical motion 77−31585
EBBA, nematic, mol. alignment, elec. and mag. field effects, dielec. const. obs. 77−11472
EBBA, nematic, ordering parameter temp. depend. 79−23517
EBBA, nematic and isotropic phases, dielec. props. 79−87383
EBBA, nematic liq. cryst., refr. indices, densities, polarisabilities and mol. order 77−28536
EBBA, nematic liq. cryst., RF dielec. props. 79−4238
EBBA, nematic-isotropic transition, birefringence anomaly at clearing pt. 79−46788
EBBA, nematic-isotropic transition at high press., turbidity meas. 80−92655
EBBA, NMR and Raman scatt. studies in nematic phase 80−100619
EBBA, orientational order in glassy and nematic phases, IR dichroism meas. 80−64891
EBBA, phase transition enthalpies, 1 bar to 2.5 kbar 78−75814
EBBA, polymorphism, radiothermoluminescence and differential scanning calorimetric study 80−24570
EBBA, pVT data and viscosity-press. behaviour 78−94989
EBBA, self-focusing, stimulated Brillouin scatt. 77−75625
EBBA, stable and metastable solid phases, dielec. dispersion meas. 78−60390
EBBA, Tsvetkov parameter, temp. depend. 80−88035
EBBA elec. props solid and liquid states, temp. and freq. depend. *(Russian)* 78−72450
EBBA liq. cryst., anisotropic light scatt. 79−78692
EBBA liq. cryst., dynamic light scatt., effect of paramag. iminoxyl radical addition *(Russian)* 77−43131
EBBA liq. cryst., orient. of dissolved acetone investig., NMR 77−1605
EBBA-aromatic hydrocarbon systems, solute size and shape effect on nematic-isotropic equilib. 79−23710
EBBA-dimethylaminonitrostilbene mixture, nematic, polarisation fluoresc. meas. 79−78723
EBBA-MBBA mixture, differential IR spectroscopy determ. of orientation of molecules 77−7670
EBBA-non-mesogenic binary liq. cryst. system, two-phase premelting, NMR obs. *(Russian)* 78−30743
EBBA-polymer systems, phase diagrams 79−23709
EBBA/EBCA mixed cryst., mol. alignment, field, temp. freq. depend. 78−75542
EBRA, nematic, EPR investig. 80−108077
echtblau saltz dye, dielec. const. and loss meas., 10^2 to 10^5 Hz 78−6622
EDDIP for U(VI) removal from rat body, decontamination efficiency 78−44617
EDTA-methylene blue photogalvanic cell, solar energy conversion and storage appl. 80−21406
EEBAC-TBBA, mixed liq. cryst., layer thickness of smectic-B phases 78−38822
n-eicosane, freezing, control by natural convection 80−39262

organic compounds continued
eicosane, purification and single cryst. growth 80−71589
n-eicosane, single cryst., electron irrad., free radical pair form., ESR 77−4913
n-eicosane, triclinic phase, self-diffusion, 295 to 309K 80−88359
eicosane-alkanediol, interface tension, sessile bubble method *(Japanese)* 78−79857
n-eicosane-n-docosane binary mixture, solid-solid phase transform. rate, positron annihilation meas. 77−20066
n-eicosane-n-docosane mixtures, positron lifetime spectra as function of temp. for various solid mixtures 78−18768
eicosane-poly(alkylene glycol), interface tension, sessile bubble method *(Japanese)* 78−79857
electrochemiluminescence as possible source of coherent radiation, and role in biological processes *(Russian)* 80−76093
electrochemiluminescent organic dyes and new type of laser 77−678
electrochemistry, organic, progress, 1952-77, review 77−60078
electron delocalisation, ground and excited states, fluoresc. *(German)* 77−34567
electron donating, PMR spectra, paramag. shifts induced by N_2O_4 *(Russian)* 78−21946
electron microscope imaging with superconducting lenses 80−73553
electronic theory, electronegativity *(Chinese)* 77−26958
electronic transitions polaris. determ. by dichroism in nematic solvents 77−42344
electrophotographic system, organic double-layer, photoconduction mechanism 79−26161
elemental analysis, by ICP optical emission spectrometry 78−76936
empirical potential model EPEN/2 for conform., intermol., solvation studies 79−50102
emulsion, hexadecane-H_2O-butanol-Brij 96, drop dia., comp. depend. light scatt. obs. 80−45573
emulsion, hexadecane-H_2O-pentanol-Tween 60, drop dia., comp. depend. light scatt. obs. 80−45573
enneaaquo rare-earth ethyl sulphates, cryst. field parameters, angular overlap model 79−56171
enniatin B, DLLLLL-stereoisomer, molecular and cryst. struct. 78−25745
enniatin B, Rb^+ complex of LDLLDL analog, struct. and conformation anal. 79−60348
enolate anion from acetone, gas phase, negative ion chemistry 80−87060
environmental air sample testing using capillary GC/MS/computer techniques 78−80799
EOBC, liquid crystal phase transforms., Raman obs. 78−87774
eosin, activator in aquoluminescence spectra from γ-irradiated NaCl 77−69913
eosin, fluoresc. polarisation, solvent effects 79−36678
eosin, in glycerine-water mixture, excitation and emission peaks, concentration shifts 78−33540
eosin, photoacoustic spectra in soln. 80−9606
eosin-erythrosin, soln., qualitative anal. using fluoresc. polarisation 79−24849
eosin-sensitised photochemiluminescence of human serum albumin solns. 78−68991
eosin-Y, in n-alcohols (ethylene glycol)(glycerol), rot. relax., time-resolved fluoresc. depolaris. obs. 80−58300
eosine^{2-}, in dimethylsulphoxide, transition metal ionic associations, fluoresc. quenching 77−73163
epichlorohydrin, microwave spectra and struct. 79−36626
epifluorohydrin, IR and Raman spectra and conformations 80−60576
1,2 epoxy propane, adsorpt. on PAN-based C fibres, surface characts. 78−48694
epoxy resin, electroluminesc. 78−56522
epoxy system, inelastic electron tunnelling spectroscopy appl. 79−15952
epoxysilicon organic tar DFM-135 cement composition, internal friction meas. by composite oscill. method *(Russian)* 80−54312
epoxytitanisilicon organic tar TK-75 cement composition internal friction meas. by composite oscill. method *(Russian)* 80−54312
EPR, rat liver and hepatoma mitochondrial lipids, stochastic anal. 78−76984
erbium ethylsulphate, cryst. laser-excited fluoresc. intensity 79−33751
erbium triethyl sulphate, single cryst., H^+ coords., NMR 80−97152
ergocalciferol, phase refinement using magic determinants 79−7512
eriochrome cyanine R, spectophotometric agent for Be, Al, Ga determ. in aq. organic medium 77−36829
erythrosin, aq. soln., polarisation of fluoresc. spectra, aggregation of mols. 78−31227
erythrosin B, photosensitising dye, effect on charge transfer in ZnO 78−72193
erythrosin B photosensitising dye effect on charge transfer in ZnO surfaces 78−68049
erythrosin in water-acetone, subnanosecond fluoresc. lifetime meas., environmental effects 78−5268
erythrosine B, dye soln., transient dichroism, rot. diffusion anomalies 79−87414
Erythrosine B, rot. diffusion from absorpt. relax. 80−1008
erythrosine dye, vibrational decay and fluoresc. in S_1 excited state 78−25605
esculin in ethanol, coherent pumping, intracavity absorpt. anal. method sensitivity 79−57328
ester, smectic C phase liq. cryst., ferroelectricity and spontaneous polarisation *(Russian)* 79−8102
ester+amine, consecutive reactions, reaction rate constants, absorbance meas. using isosbectic points 77−73433
ester vapours, reactions with OH radicals, reaction rate consts. determ. at 292K 78−27729
esters, diamag. susceptibility of carbonyl group 77−75329
esters, incidence of smectic liq. cryst. phases, effects of mol. framework changes 77−27819
esters, liquid crystals, smectic C and H phases 78−94968
esters, long-chain, X- and Y-type multilayers, form. conditions and struct. characterisation 80−80127
esters, SLC, ferroelectric behaviour, specific heat, spontaneous polarisation 80−75958
esters, thermal electret, persistency of surface charge *(Japanese)* 77−81048
estradiol, ^{125}I labelled a γ-emitting estradiol analogue that binds to the estrogen receptor 80−61697
estriol antigen, immunoassay using differential pulse polarography method 79−79709

organic compounds continued
ethane, ^{13}C NMR, density depend. mag. shielding in gas phase 77−75187
ethane, $^{13}CH_3{}^{12}CD_3$, $^{12}CH_3{}^{13}CD_3$, microwave spectra, Stark effect, C-C bond length and mol. consts. 77−50428
ethane, (e,2e) spectroscopic obs., valence electron momentum distribs. and separation energies 77−3480
ethane, ab initio calcs. using FSGO, internal rot. 78−82639
ethane, ab initio MRD-CI calc., 14-25 eV PES region, Rydberg states 78−41962
ethane, adsorbed on graphite, struct. and dynamics, empirical interatomic pots. 79−99417
ethane, adsorpt. on Ru(001), LEED, ESD study 78−87872
ethane, adsorption on water, 0-50°C, press. effects on surface tension 78−56024
ethane, barrier and one electron charge transfer states in strong orthogonal group function theory 78−13421
ethane, boiling heat exchange, surface roughness influence, press. depend. *(Russian)* 79−68562
ethane, C K-shell excitation by electron impact, electron energy loss spectra 77−31014
ethane, CH bond orbitals, internal rot. barriers, antisymmetrization effects 80−63529
ethane, chem. shift, paramagnetic term, Pople formalism calcs. 78−21945
ethane, chemisorption on Rh surface, sticking coefficient per landing site 79−46941
ethane, clusters, excess electron localisation 79−68341
ethane, coexistence curve diameter singularity, phase boundary position *(Russian)* 79−65179
ethane, conc. meas. in nonurban troposphere 78−32184
ethane, condensation in porous bulk media 78−47510
ethane, condensed, electron energy loss spectra meas. 77−59652
ethane, d_2, microwave spectra for internal rot. barrier 79−93986
ethane, decomposition in RF discharges, 10-40 torr 78−3318
ethane, dense fluid, cond. band energy determ. 79−87136
ethane, dense gas and liquid, meas. of C_σ and C_v 77−69093
ethane, diode laser spectra, baseline variations, elimination by ultra-low freq. filtering 80−90901
ethane, dipole moment derivatives, MINDO/3 semiempirical calcs. 77−75055
ethane, doubly degenerate torsional states, pure rot. transitions, theory 79−72299
ethane, effective core potential calcs. 79−31437
ethane, electron impact dissoc., absolute total cross section, 10-600 eV 79−36781
ethane, electron impact dissoc., high Rydberg fragments 77−83749
ethane, electron impact excitation, 30-250 eV, 0-90° 79−54949
ethane, electron ionisation efficiency curves, fragment ion appearance pot. 78−86959
ethane, electronic struct. and physicochem. props., modified partial neglect of differential overlap 78−82645
ethane, emission detect. on Neptune but not on Uranus 78−16344
ethane, excess electron localisation, density effects 77−31970
ethane, flow continuity in arterial capillary systems in cryogenic heat pipes 80−64536
ethane, fluid, saturated, compressed, sound velocity meas., compressibility, sp. ht. determ. 77−76488
ethane, force consts., model potential function vs. mol. orbitals calcs. 78−29829
ethane, force consts., vibr. stress and isotope effects 78−21897
ethane, free molecule flow and interdiffusion, through porous glass 79−32658
ethane, gas, absolute viscosity 77−35299
ethane, gas, electron drift vel., Ramsauer-Townsend minima in electron scatt. 78−87427
ethane, gas, liq., and crit., electron mobility, density and temp. effects 80−92246
ethane, gas, second virial coeffs., intermol. pot. at low temp. 79−46416
ethane, gas, up to 50 atm, refr. index, 328, 3103 MHz *(French)* 78−14129
ethane, gas-liquid crit. pt. region, depolarised light scatt. 78−34612
ethane, gas-phase radiolysis, inhibition of free radical prod. by H_2O, ethylene and SF_6 79−39178
ethane, geometry optimisation, using bond function augmented basis sets 78−905
ethane, ground state parameters and IR absorpt. spectra 80−47986
ethane, H^+, H_2^+, and H_3^+ kinetic energy distribs., electron impact dissoc. ionisation, time of flight mass spectra 80−32843
ethane, heat transfer during boiling in tube *(Russian)* 77−68589
ethane, high resolution IR spectrum using $Pb_{0.93}Sn_{0.07}Te$ laser 78−33511
ethane, in air, IR spectra, optical-acoustic investig. *(Russian)* 78−74663
ethane, inclusion of nonbonded interactions in vibr. freq. calcs. 80−95590
ethane, intensity of $^RQ_0$ branch in ν_9 fundamental 77−6856
ethane, internal rot. barrier, energy decomposition anal. 77−75327
ethane, internal rot. splittings, vibr.-rot.-torsion energy levels perturbations 80−91531
ethane, internal rotation barriers, exchange energy and orbital orthogonality effects 77−75049
ethane, ionis. efficiency curves by electron impact, fragment appearance pots. 77−61863
ethane, ionis. spectral intensity, valence electron binding energy depend. 78−90234
ethane, ionisation by electron bombard., empirical and semi-empirical calcs. 79−36784
ethane, IR obs. spectra meas. using $Pb_{1-x}Sn_xTe$ diode laser *(Japanese)* 79−49306
ethane, Kerr consts., depolarisation ratios and hyperpolarisabilities meas. 78−25624
ethane, liq., correl. function modelling, third order memory function method 80−7339
ethane, liq., excess electron mobility, elec. field depend. 78−72218
ethane, liq., excess electron mobility, field and temp. depend., −50 to +26°C 79−91115
ethane, liq., IR torsion band, 98-173K mechanism, Coriolis coupling 77−38662
ethane, liq., photoelectric determ. of conduction state energies and electron ranges 77−89487
ethane, liq., viscosity, density depend., theory 77−20105
ethane, liq.-vap. coexistence curve, interferometric meas. 79−99303

organic compounds continued
ethane, liquid-vapour coexistence curve, neutron transmission exam. *(Russian)* 78−79758
ethane, localised molecular orbitals, orthogonal transformations calcs. 80−47892
ethane, long path photoelec. absorpt. spectra 4200-10600 Å, appl. to Uranus 77−83592
ethane, mag. suscept., vector pot. variational calc. 77−68137
ethane, mass spectrometric ionis., dissociation 77−3488
ethane, mean amplitude of mol. vibration, approx. calc. method 79−13697
ethane, mean polarisability derivatives, variational calc. procedure 79−27108
ethane, molecule, floating spherical GO calcs. of electron momentum distrib. and Compton profile 77−30933
ethane, multipole moments and polarisabilties, SCF calcs. 80−5471
ethane, nonlinear IR absorpt. spectra 78−13492
ethane, nucl. spin-spin coupling, scanning MO HF LCAO calc. 79−50045
ethane, nuclear spin-spin coupling consts., vicinal proton-proton coupling calcs. 80−32737
ethane, one-electron props. in terms of localised mol. orbital components 79−6840
ethane, ordered cryst., Raman spectra, 74K 79−73942
ethane, perturbed-hard-sphere eqn. of state applicable to sub- and supercritical temps. 79−19350
ethane, photoabsorption cross sections, 1380 to 1600 Å, at 295 and 200K 78−90181
ethane, photoelectron spectrum below 14 eV, ab initio calc. 77−54575
ethane, photoionisation cross section at distance from threshold, chemical bond influence 80−69196
ethane, photoionisation spectra, cond. hole model 80−58326
ethane, photolytic decomp. to ethylene via triplet ethylidene, MINDO/2 calcs. 78−64869
ethane, pool boiling heat transfer 79−1058
ethane, positive-ion drift vels., Townsend primary ionis. coeffs. 79−55592
ethane, proximity and conform. effects, ^{13}C chem. shifts at γ position INDO computations 77−50451
ethane, pure gas, enthalpy, Carlson-Thodos van der Waals eqn. calcs. 80−83878
ethane, pyrolysis, thermodynamics and kinetics 79−43577
ethane, quadrupole moment from $K^+(Ar)(Kr)(Xe)$ scatt. total cross section 77−50495
ethane, Ramsauer-Townsend minimum in electron scatt. cross section 77−89821
ethane, rot. anal., perturbational MO analysis of ab initio SCF-MO wave functions 77−57867
ethane, rot. barriers, MS-SCF-X_α calcs. 80−106267
ethane, shift of electronic spectrum during dissoc., CNDO calc. 80−37759
ethane, single cryst. X-ray struct. determ., plastic and monoclinic forms 78−63744
ethane, solid, mol. reorientational motions, incoherent neutron scatt. studies 80−107070
ethane, solid, PMR line shape, band width and second moment, phase transition 77−85584
ethane, solid, thermodynamic props. between double solid-to-solid transition and triple point temp. 78−75828
ethane, spectral parameters, Lamb dip method investig. 78−89560
ethane, spherical cryst. grown in situ for low-temp. X-ray work 78−68612
ethane, supercritical, electron mobility as function of density and temp. 80−59163
ethane, thermal electron mobility at high density, electron quasilocalisation 79−27740
ethane, thermodynamic props., use of high press. recycle-flow calorimeter 80−42228
ethane, thermophysical props. from 90 to 600K at press. up to 700 bar 77−84940
ethane, tropospheric and lower stratospheric vertical profiles 80−4073
ethane, two-channel dissoc., dynamical effects, classical trajectory study 78−40042
ethane, two-stage diagonalisation of Hamiltonian in CNDO/2 method 80−42946
ethane, unimol. decomp., energy transfer processes, Monte Carlo simulation 80−99555
ethane, unimol. decomp., mode localised excitation, trajectory studies 78−64815
ethane, valence electronic struct., model pot. in floating spherical GO formalism 78−74563
ethane, variationally deorthogonalised localised molecular orbitals, electronic struct. 79−97968
ethane, vertical electronic spectra, limited CI calcs. 79−13693
ethane, vibr. anal. using torsional coords. 79−93977
ethane, vibr. freqs., MINDO/3 calcs. 78−13429
ethane, vibr. intensities, G sum rule appls. 80−32776
ethane, viscosity and thermal cond. of liquid and gas, correl. eqns. 78−26715
ethane, X-irradiated, 4.2K, pairwise radical trapping mechanism, EPR obs. 79−100412
ethane+$C_2(a^3\Pi_u)$, reaction rate consts. and quenching, multiphoton UV photolysis, fluoresc. obs. 79−74355
ethane+Cl, rate consts., stratospheric temps., radiotracer meas. 77−48632
ethane+CO_2 system, isothermal vapour-liq. equilibrium data, 10 to 25°C, and high press., critical points 78−79754
ethane+CsF, rot. inelastic collisions, mol. beam meas. 80−1049
ethane+H_2, hydrogenolysis mechanism and kinetics on evap. Ir film 79−100436
ethane+H, chemical reaction, 357-544K 78−7198
ethane+He^+, 0.7-2 MeV, charge-changing collisions, electron capture 80−58372
ethane+N_2, system, vapour-liq. equilib. data 78−83929
ethane+thermal energy reaction, mass spectra 77−9067
ethane(-d_6,d_3,d_1), electro-optical parameters from IR intensities, least-squares calc. 80−9584
ethane(-methane), heat transfer in nucleate boiling of liquified gases and binary mixtures *(German)* 79−18687
ethane (-d_1), reduced partition function ratio, generalised finite polynomial approx. 78−66529
ethane cation, relative stability of $^2A_{1g}$, ^2E_g states 80−58140

organic compounds continued
ethane chemisorption on W(111), AES and LEED pattern exam. 79−15005
ethane derivatives, diastereoselective form. and symm. props., semirigid mol. model 80−48099
ethane gas, electron-mol. collision freqs. from breakdown data in crossed mag. field 80−43835
ethane gas, local mode overtone bands 80−83444
ethane solvent effects, quantum mech., macroscopic electrostatic contribs. 77−30801
ethane submonolayer on graphite, struct. and melting, elastic neutron scatt. 80−29266
ethane-1,1,1-d_3, gas-phase IR spectra, rot. fine struct. obs. 80−83359
ethane-Ar(N_2) binary and ternary mixtures, dielec. const., excess vol. 80−7254
ethane-C mol. sieve system, adsorptive pot. distrib., entropy, enthalpy 77−72778
ethane-CO_2(N_2)(SF_6)(tetrafluoromethane) mixtures, viscosity, diffusion coeffs. 80−1722
ethane-d_0-d_6, normal coord. and IR intensity anal. 79−36604
ethane-d_n, IR spectra, r_0, r_z and r_e structs. 79−59453
ethane-hydrocarbon mixture, phase equilibria and critical phenomena at high press. 78−51648
ethane-N_2O, gas phase N_2O electron attachment, temp. depend. 79−36757
ethane-n-butane-n-hexane, vap.-liq. equilib. behaviour, visual cell, for 48.3-143.5°C, up to 7619 kPa 79−46790
ethane-propane, binary mixture near crit. point, conc. fluctuation decay rate, spectrosc. obs. 77−81108
ethane/H_2 mixing ratio in Neptune stratosphere 80−51692
1,2-ethanediol, aq. soln., proton NMR study of H-bonding 79−78545
ethanediol, dielec. props., 10 MHz-70 GHz, 10-40°C 78−43769
ethanedithiol, mol. vibr., conformational anal., Raman spectra 79−31534
10,10′-ethanediylidenedianthrone, fluoresc. efficiency, mol. geom. effects in two cryst. structs. 77−18953
ethanes, diastereotopic nuclei, magnetic nonequivalence, chiral shielding in NMR 77−3383
ethanes, substituted, dielec. relax. by intramol. motion 78−23391
ethaneselenol, IR, Raman and microwave spectra, barriers to internal rot. 77−38666
ethanethiol, rare gas sensitised radiolysis and charge exchange mass spectra 77−48664
ethanoic, acid, ideal gas thermodynamic props. 78−51275
ethanol$_{(l)}$, hydroxyl proton chem. shift, density and temp. effects 77−1607
ethanol, adsorbed on Al_2O_3, inelastic electron tunnelling spectra, surface vibr. struct. determ. 80−35572
ethanol, adsorption on Ag islands on Al_2O_3 substrate, inelastic electron tunnelling spectra and TEM obs. 79−90884
ethanol, alcoholic electrolytic solutions, Dielectric constants 79−99813
ethanol, aq. soln., conc. fluctuations, shear and longit. relax., Brillouin scatt. and pulse techniques 78−71792
ethanol, aq. solns., contact angs. with metals, 20-70°C 78−56025
ethanol, aq. subcooled soln., acoustic phenomena during nucleate boiling 78−10181
ethanol, assoc. in dil. soln., dielec. obs., dipole moment meas. 78−83714
ethanol, Benedict-Webb-Rubin parameters 77−39660
ethanol, boiling, crit. heat flux in low press. region 78−90663
ethanol, boiling, under increased gravitation, heat exchange mechanism, review 77−46895
ethanol, boiling at subatmospheric press., heat transfer rate, heating surface effects 80−69630
ethanol, boiling heat transfer coefficients, heater plate thickness effects 78−34124
ethanol, boiling in large enclosure, critical heat flux 79−18685
ethanol, chemical state effects in AES 78−92566
ethanol, chemisorbed on MgO, decomposition mechanism 78−92502
ethanol, chemisorpt. and oxidation on Cu(110) and Ag(110) catalysts 78−61044
ethanol, collisionless production of $C_2(a^3\pi_u)$ in intense IR laser field 78−55206
ethanol, config. and vibr. heat capacities, H-bonds 79−99331
ethanol, cooling fluid for flash lamp, interaction with high-power lamp radiation 78−13718
ethanol, critical heat flux of saturated natural convection boiling with heating from below 80−10114
ethanol, dielectric const. in mag. field 79−78606
ethanol, dissoc. adsorption on porous glass, IR obs. 79−23830
ethanol, effect of small additions of water struct., from permittivity obs. 78−9937
ethanol, electron solvation, ps laser study 80−101032
ethanol, evap. rate var. with vap. press. 78−18758
ethanol, evaporating meniscus profile, evaporative heat flux 79−77868
ethanol, film condensation inside pipes, heat transfer, general correlation 79−46312
ethanol, glassy, electron trap relaxation model 80−15470
ethanol, glassy matrix, absorpt. spectra after X-irrad., solvated electrons 79−65903
ethanol, H^+, H_2^+, and H_3^+ kinetic energy distribs., electron impact dissoc. ionisation, time of flight mass spectra 80−32843
ethanol, H-bonding investigated with supersonic mol. beam using photoionisation quadrupole mass spectrometer 80−102543
ethanol, industrial, production from municipal cellulosic waste 80−61502
ethanol, ion internal energy selection by angle-resolved mass spectrometry 80−53164
ethanol, liq., Compton profile at 60 keV 79−47535
ethanol, mean sojourn time of molecules on surfaces, meas. in practical vacuum system *(Japanese)* 80−57315
ethanol, multiphoton absorpt. and dissoc. 80−99530
ethanol, multiphoton UV photodissoc. 78−50602
ethanol, nucleate boiling heat transfer, press. factor 77−69080
ethanol, phonon MFP formula, H bond collisions, low temp. 77−35655
ethanol, picosecond stimulated Raman effect, time-resolved spectra 77−3369
ethanol, plural glass-transitions, thermodynamic functions 78−38820
ethanol, polymorphic forms, mol. motion, NMR obs. 80−88885
ethanol, positronium form., unsolvated electron effects 78−17826
ethanol, pulse radiolysis, solvated electrons decay kinetics 79−66319
ethanol, pulsed adsorption on Ge heteroepitaxial films, effect on elec. cond. 80−93014

organic compounds continued
ethanol, Raman generated pulses amplified by dye amplifer, for laser-matter interaction diagnostics 79−41414
ethanol, semiquantitative model for electron conc.-dose depend. in glassy matrix 78−20034
ethanol, soln., excess electron optical absorption spectrum model, band shape 78−33500
ethanol, solns., local struct. equilib., light scatt. and IR spectra obs. 78−84564
ethanol, stimulated Raman scatt. of tunable Raman freq. generation 78−33772
ethanol, surface reaction with Cu (100), EELS study 80−16728
ethanol, thermodynamical Gruneisen parameter, press. depend. 78−14479
ethanol, US studies of mol. relax. 78−22790
ethanol, vap., decomposition by HF pulses IR laser irrad., press. depend. 78−85176
ethanol, vibr. population lifetimes in liqs. anti-Stokes Raman scatt. 78−74665
ethanol+Al_2O_3, surface reaction, 295-575K, surface specieis study 79−100435
ethanol+muonium in aq. soln., rate const. 77−38752
ethanol+Na, reaction rate determ., rel. to cleaning from LMFBP components 78−21689
ethanol + NH_3, reactor, irrad., amino acid production 79−66305
ethanol aqueous soln., sound absorpt. coeff. meas., acoustic relax. 78−83883
ethanol as energy source, large-scale prod. from biomass review 79−52864
ethanol effects on biomembranes, spin label study of drug tolerance 77−66799
ethanol evaporating meniscus, capillary flow heat transfer model anal. 79−82416
ethanol fuel, octane booster for inferior regular unleaded gasoline 80−55783
ethanol fuel, substitution of large proportion of diesel fuel in diesel engines 80−61230
ethanol fuel for vehicles, gas turbines, and boilers, Brazil 80−61229
ethanol fuel production from municipal cellulosic wastes using enzymatic hydrolysis 80−55779
ethanol glass, 4.2K, trapped electron photocond. and optical spectra following radiolysis 79−29378
ethanol glass, 4K γ-irradiated, presolvated electron photoconductivity 78−47827
ethanol glass, trapped and solvated electrons produced in presence of applied electric field 80−7379
ethanol glass containing triphenylamine, γ-radiolysis, IR spectra, trapped electron 77−16842
ethanol glasses containing anion radicals of fluorene and isologs, γ-irrad., optical absorpt. and EPR obs. after photobleaching 77−44491
ethanol in CCl_4, vibr. energy redistrib. after ultrashort IR excitation 77−6894
ethanol mols. reorientation in ethanol-water mixtures, Raman and Rayleigh spectra 78−76449
ethanol solution in benzene, dielec. relax. time by RF cond. meas. 80−71302
ethanol vapour, isothermal Joule-Thomson coefficient, equation of state 80−24119
ethanol-Ar, conc. profile and interdiffusion coeffs. meas. 79−94763
ethanol-benzene, excess vol. and isentropic compressibility, from density and US vel. meas. 78−79776
ethanol-benzene(diethyl ether)-water, shear viscosity at plait points 77−35685
ethanol-benzene-$(NH_4)_2SO_4$-water, liq. mixture, near tricrit. pt., light scatt. and sum rules 80−34933
ethanol-benzene-water-$(NH_4)_2SO_4$, liq. mixture, near tricrit. pt., thermodynamic model and sum rules 80−34196
ethanol-carbon tetrachloride, binary soln. with mol. assoc., interdiffusion anal. 79−55912
ethanol-chloroform solns., light scatt. spectra, conc. fluctuations, assoc. complex form. 77−40254
ethanol-covered LiF(001), atomic H scatt. 77−31905
ethanol-CS_2 mixture, in external transverse resonator, stimulated Rayleigh wing scatt. line, anomalous shift 78−13763
ethanol-CS_2 mixture, Rayleigh and depolarised Raman scatt. lines near crit. temp. 77−20863
ethanol-CS_2 mixture, thermal diffusion ratio determ. by forced Rayleigh scatt. 78−75858
ethanol-d_0, -d_1, -d_5, γ-irrad., trapped electron spin-lattice relax. 77−60089
ethanol-d_0-d_1, solvated electrons reacting with scavengers, inverse isotope effects 78−31751
ethanol-$d_1(d_2)(d_3)$, glassy state, solvated electron geometry, electron spin echo modulation obs. 80−66009
ethanol-H_2O, liq., Compton profile at 60 keV 79−47535
ethanol-H_2O mixture, liq. and solid, US vel., −80 to 20°C, 1-5 MHz 78−59933
ethanol-normal hexane mixture, percolation model of electron and hole mobility 80−29452
ethanol-t, charge spectrometer studies of chem. effects of nucl. transforms. *(Japanese)* 77−57420
ethanol-water, inversion of Kirkwood-Buff thery 78−27807
ethanol-water, liq., Verdet const., pulsed mag. field meas. 80−16012
ethanol-water mixture, nonlinear acoustic coeff. meas., 0-50°C *(French)* 80−34142
ethanol-water mixture, saturated, min. film boiling temp. on horiz. stainless steel and Cu surfaces 78−90692
ethanol-water mixture, Soret coeff. determ. 79−19386
ethanol-water mixtures, hydrophobic interaction, scaled particle theory 78−22625
ethanol-water mixtures, specific volume, compressibility, viscosity, up to 3200 bar, 15, 25°C 78−10113
ethanol-water system, complex dielec. permitt. in UHF region and NMR spectra *(Japanese)* 80−100620
ethanol-water system, metastable states, hydrates existence and props., low temp. 78−71835
ethanol-water-chloroform mixture, light scatt. near plait point 78−72532
ethanolic dye solution laser, cylindrical active element with sheath, radiation intensity distrib. calc. 80−58531
ethene, chem. shift, paramagnetic term, Pople formalism calcs. 78−21945

organic compounds continued
ethene, dipole polarisability, finite-field SCF MO calcs. 80−83255
ethene, general valence force field, ab initio calcs., IR and Raman intensities 77−71746
ethene, optical synchrotron-Cherenkov radiation threshold effects 80−28154
ethene+Kr liq. mixture, thermodynamic excess functions 78−48690
ethene+N_2 system, vapour-liq. equilib. data 78−83929
ethene-hydrocarbon mixture, phase equilibria and critical phenomena at high press. 78−51648
ethenediol, σ conjugative interactions role in rot. isomerism 79−31443
ethenethiol, σ conjugative interactions role in rot. isomerism 79−31443
ethenoadenosine, influence of pH and metal complexion on fluorescence parameter 79−34483
ethenol, σ conjugative interactions role in rot. isomerism 79−31443
ethenoxy, config. interaction calc., using DODS natural orbit approach 78−66476
ether, thermodynamical Gruneisen parameter, press. depend. 78−14479
ether+HF, mol. electrostatic pot., H-bonds, CNDO/2 calc. 77−61822
ether+Li^+, pair pots., ab initio LCAO SCF MO calcs. 80−58184
ether+Na^+ interaction, pair pots., ab initio SCF LCAO MO calc. 79−36721
ether-Ar, conc. profile and interdiffusion coeffs. meas. 79−94763
ether-water mixtures, miscibilities, enthalpy of mixing, solvation *(German)* 78−18779
ethers, α-particle impact, 0.3-2.0 MeV, O stopping cross-sections 78−17753
ethers, and alkane solid solns., dielec. props. and IR spectra *(French)* 79−4378
ethers, and solid alkane solns., far IR spectra *(French)* 79−4793
ethers, modified CNDO calcs., conformations, binding energies 77−6682
ethers, Raman spectra, interpretation 77−65483
ethers, saturated, bonded and nonbonded, quantum chem. calcs. 80−9514
ethers and solutions in $SnCl_4$, spin echo obs. of self-diffusion *(Russian)* 79−95197
ethidium bromide derivatives, binding to DNA *(German)* 79−79446
ethidium bromide E-DNA, intercalated birefringent fibres, microspectrophotometric investig. *(German)* 80−57392
ethinyltetrafluorophosphorane, mol. struct., electron diffr. obs. 79−50133
trans-4-ethoxy-4′-alkanoyloxyazobenzenes, nematogenic liquid crysts., birefr., order parameters, vol. changes during nematic-isotropic transitions 78−59742
ethoxy-hexyltolane, orientation-statistical props. studies by optical methods *(Russian)* 79−77518
ethoxy-octyltolane, orientation-statistical props. studies by optical methods *(Russian)* 79−77518
p-(p'-ethoxybenzylidene)amino-benzonitrile, cryst. struct. rel. to liq. crystallinity 80−100225
N-p-ethoxybenzylidene-p′-cyanoaniline, nematic, mol. reorientation in DC elec. field, IR ATR spectra study 80−45064
ethoxyhexyltolan, Raman spectra, molecular conformational instability, internal field effects 80−54127
ethoxyoctyltolan, Raman spectra, molecular conformational instability, internal field effects 80−54127
p(p-ethoxyphenyazo)phenyl undecylenate, nematic liq. cryst., refractive index, density, orientational order 78−76419
p(p-ethoxyphenylazo)phenyl heptanoate, nematic liq. cryst., refractive index, density, orientational order 78−76419
p(p-ethoxyphenylazo)phenyl hexanoate, nematic liq. cryst., refractive index, density, orientational order 78−76419
p(p-ethoxyphenylazo)phenyl valerate, nematic liq. cryst., refractive index, density, orientational order 78−76419
p-p-ethoxyphenylazo phenyl heptanoate, mesogenic compounds, thermal stabilities, packing coeffs. and mol. packings 79−46558
p-p-ethoxyphenylazophenyl hexanoate, dielec. relax. in stable and metastable solid phases 80−34851
ethoxysilanes, adsorpt. on Fe, XPS 77−89639
ethoxysilanes, adsorption on BK 7 glass, IR spectra *(German)* 78−30834
ethyl 4-(4′-methoxybenzylideneamino)cinnamate, mesomorphic compound, cryst. struct. and binding energy 77−80494
ethyl acetate, heat absorbed when laser irrad., laser calorimetry 79−16012
ethyl acetate, multiphoton dissoc. by CO_2 laser beam 80−7811
ethyl acetate, photoacoustic spectra meas. at CO_2 laser wavelengths 80−18849
ethyl acetate-isopropyl bromide, IR laser induced decomposition 79−16011
ethyl alcohol, angular distrib. of scatt. press. to carrier press. ratio 77−27942
ethyl alcohol, anodic oxidation, voltammetric meas. 79−57247
ethyl alcohol, dil. aq. soln., US vel., 4.04 MHz 78−67770
ethyl alcohol, electrification during laminar flow in metal pipe 80−6954
ethyl alcohol, free convection on turbulent horizontal layer, effect of thermocapillary forces 79−98722
ethyl alcohol, free fluid surface, thermo-capillary forces on transport process, turbulent gravitational heat convection 77−75920
ethyl alcohol, influence on human DC registered electroretinogram 79−2052
ethyl alcohol, liq., viscosity parameters, RF cond. meas. 80−96677
ethyl alcohol, micropolar effects in liquids, characts. evaluation under rotating electric field *(Polish)* 79−55638
ethyl alcohol, solution, struct. determ. from vibr. spectra, H-bonding and heat of mixing *(Russian)* 78−3368
ethyl alcohol, stimulated Raman scattering of psec. pulse train, dynamics 79−64286
ethyl alcohol, superheated liquid, growth of spherical bubbles, anal., numerical calcs. 77−24399
ethyl alcohol, turbulent absorbing liq. medium, laser radiation thermal self-interaction 80−91868
ethyl alcohol, unsteady critical heat flux during boiling 77−23946
ethyl alcohol, US attenuated temp. depend. in association liq. 77−51441
ethyl alcohol, US attenuation, for vol. viscosity, 0-60°C 78−63871
ethyl alcohol-d_0(-d_1)(-d_1)(-d_2), internal rot. and microwave rot. spectra 80−69128
N-ethyl carbazole, CNDO/S spectrum calc. rel. to poly-n-vinylcarbazole solid state spectrum 79−89815
ethyl carbazole, in nitrobenzene soln., dry hole capture in pulse radiolysis expt. 79−79266

organic compounds continued
ethyl cation, rearrangement pseudorotation modes, reaction mechanisms, permutation theoretic anal. 78−44369
ethyl cation+alkane reaction, temp. and kinetic energy relative rate consts. determ. 80−81299
ethyl cellosolve acetate on wafer surface, trace analysis 78−3433
ethyl cellulose membrane, sorption and transport of hydrocarbon gas 78−76913
ethyl chloride, inner-shell excitation and EXAFS-type phenomena 79−13828
ethyl chloride, reson. multiphoton dissoc., excitation mechanism 79−100414
ethyl chloride, second dielec. virial coeffs. *(German)* 79−32729
ethyl chloride, thermal cond. meas. using thermal lens 79−12795
ethyl chloride, thermal decomp., unimol. reaction theory 78−80712
ethyl chloride-NH_3, positive ion molecule reactions 79−24729
ethyl chlorophyllide a, electronic struct. props. and photosynthesis 80−16902
ethyl cyanide, collisionless production of $C_2(a^3\pi_u)$ in intense IR laser field 78−55206
ethyl cyanide, isotopic species, rot.-torsion-vibr. interaction in rot. spectra 77−458
ethyl cyanide, pyrolysis kinetics and mechanism 79−24728
ethyl cyanoformate, conformers, dipole moments, rel. energies, microwave spectra 78−55164
ethyl ether, nucleation press. for bubble form., dissolved N_2 effect 77−51486
ethyl ether-N_2, bubble homogeneous nucleation in gas-liq. soln., press., expt. and theory 78−91430
ethyl fluoroformate, microwave spectra of rot. isomers 79−10097
ethyl formate, microwave rot. spectrum, centrifugal distortion effects 80−52979
ethyl formate, US absorpt. and relax. intervals 77−1183
ethyl hyoochloride, microwave spectrum, dipole moment, quadrupole coupling consts. 78−58673
ethyl iodide, microwave spectra and internal rot. anal. 80−69130
ethyl iodide, two-photon reson . ionis. spectra 80−28071
ethyl iodide submillimeter wave laser, optically pumped 80−87376
ethyl isocyanide, N isotope enrichment, IR laser isomerisation 79−27096
ethyl isocyanide, thermal decomp., unimol. reaction theory 78−80712
ethyl isocyanide, thermal isomerisation in presence of at. gases, vibr.-translational energy transfer 78−23924
ethyl lactate, sound vel. and absorpt. meas. at hypersonic freqs. 78−18708
ethyl methyl ketone+cyclohexane, measurements of US vel. and density for determination of excess props. 80−37910
ethyl methyl sulphide, low freq. vibr. spectra, methyl torsional pot. functions and internal rot. 80−5543
ethyl methylketone+n-butanol, measurements of US vel. and density for determination of excess props. 80−37910
ethyl n-dodecoate, photocapillary effect, temp. depend. *(Russian)* 78−34682
ethyl nitrite, microwave spectra, rot. isomerism and dipole moments 79−93990
ethyl p-methoxybenzilidene aminocinnamate, dimer, mesogenic, intermol. interactions 79−46564
ethyl phenyl acetate, phosphoresc. and fluoresc. spectra in organic matrices 80−32756
ethyl radical, $^{13}C_\alpha$ and H^+ hyperfine interactions, EPR spectra, vibr. anal. 80−23443
ethyl radical, C-C bond barrier rot., IR spectra 80−76536
ethyl radical, geom. struct., Hartree-Fock calcs. 78−62722
ethyl radical, photoelectron spectra, first ionis. pot. 77−58078
ethyl radical decomposition, mol. dynamics, trajectory studies 80−7780
ethyl substituted ammonium halides, exciton absorpt. spectra 79−28782
ethyl trichloroacetate, in benzene, permittivity, dielectric loss, 36 GHz 77−32323
ethyl trichloroacetate, in non-polar solvents, dielectric const., dielec. loss meas. 78−2796
ethyl trichloroacetate, soln., dielectric props. and relax. mechanisms at microwave freqs. 78−15089
ethyl vinyl ether, IR multiphoton dissoc., branching ratio and laser pulse duration 78−80772
ethyl vinyl ether, laser induced reaction, energy distrib. 80−16710
ethyl-3-chloropropionate, liq., microwave absorption and relax. 78−60386
1-ethyl-4-isopropylcyclohexane, cis-, trans isomers, 79−16074
ethyl-(methoxybenzylidene-amino)cinnamate, low freq. dielec. constant meas. in cryst. and liq. cryst. phase 78−91226
ethyl-furan-2-carboxylate, skeletal vibr. of IR spectra, conformational props., solvent polarity effect 80−87118
(N-ethyl-o-phenanthrolinium)(TCNQ), cryst. and mol. struct. *(French)* 77−15396
ethyl-p-azoxybenzoate, far IR and Raman spectra, smectic polymorphism 80−76022
ethyl-trimethyl phosphines, $(C_2H_5)_{3-n}P\{E^{IVB}(CH_3)_3\}_n$, ($E^{IVB}$=C;Si;Sn; n=0,1,2,3), ($^1H$, ^{13}C, ^{29}Si, ^{31}P, ^{119}Sn) NMR 80−32744
N-ethylacetamide, in carbon tetrachloride, dielec. relax., time-domain reflectometric obs. 79−4762
ethylacetate, CW laser induced reactions, activation energies, temps. and rate consts. 80−40710
ethylacetate, thermal and IR laser induced unimol. decompositions 78−20012
ethylacetate-methanol system, vapour-liquid equilib. meas., automatic gas chromotographic anal. *(German)* 78−88667
N-ethylacridone, cryst. and mol. struct. 80−33988
ethylamine, ^{13}C chem. shift calcs. using approx. SCF perturbation theory 77−18945
ethylamine, collisionless production of $C_2(a^3\pi_u)$ in intense IR laser field 78−55206
ethylamine+OH, rate const., 298-426K, Arrhenius expressions and activation energy 78−48619
ethylamines, torsional Raman spectra 77−77195
4-ethylaminobenzil, dil. soln. in benzene, cyclohexane and dioxane, dielectric behaviour 78−52421
ethylammonium cadmium tetrachloride, order-disorder transition, far IR reflectivity obs. 79−65870
ethylammonium tetrachloromanganate, dielec. props. in phase transition region 80−55011
ethylammoniumtetrachlorochromate, optical absorption intensity, short-range spin correlation 80−108185
organic compounds continued
ethylbenzene, α-substitution effect and radiative lifetime, solvent effects, rel. to t-butylbenzene 79−98154
ethylbenzene, oxidation, complex network calcs. 78−11497
ethylbenzene, vapour, conform. and struct. obs. 80−69247
ethylbenzene+toluene, binary liq., viscosity and excess free energy of mixing 78−51680
ethylbenzene-nitrobenzene binary mixtures, with weak charge transfer interactions, thermodynamic props. 80−54360
ethylbenzocarbazole, soln., luminesc., effect of electronic excitation energy vibr. 80−55174
ethylbenzol, liq., thermal cond. coeffs. at high-press., 298-573K 79−73350
ethylbenzole, thermal cond., 30-400°C, 1-10^3 kg cm^{-2} 78−26739
N-ethylcarbazole, soln., laser induced ionic photodissoc., transient polyelectrolyte form. 80−53068
ethylcellosol, aq. soln., light scatt. rel. to conc. fluctuations *(Russian)* 78−3450
ethylchloride, d_0-d_5, microwave spectra, elec. field gradient tensor at Cl nucleus *(German)* 78−46325
ethylcyanodiacetylene cation, gas phase, UV emission spectra of $\tilde{A}(\pi^{-1})\rightarrow\tilde{X}(\pi^{-1})$ band system 80−95636
ethylcyclopropane, solid, liquid, vapour phase, IR and Raman vibr. spectra 80−84740
ethyldifluoroborane, microwave, Raman, IR spectra, conform., dipole moments, vibr. assignment 78−90155
ethylebenzene, chem. thermodynamic props. 78−40074
ethylendiaminetetraacetate in the scala media, effect on cochlear pots. 80−16952
ethylene, 10 μm absorption line profile, high resolution meas. 77−42359
ethylene, ^{13}C NMR, density depend. mag. shielding in gas phase 77−75187
ethylene, ^{13}C substituted, isotope analysis by CO_2 laser absorpt. spectroscopy 77−44529
ethylene, $^2B_{3u}+e^-\leftarrow{}^1A_g$ transition, appl. of photoelectron spectroscopy using supersonic mol. beam source 79−68264
ethylene, μ, ρ and T-surfaces, global behaviour, rel. to catastrophe theory 78−26226
ethylene, $\pi\pi^*$ singlet state, using general CI method 79−36539
ethylene, $\pi\rightarrow\pi^*$, electron energy loss spectroscopy 79−72432
ethylene, π-electron system, self-consistent many-body theory 78−25432
ethylene, π-electron system photoionisation cross-section, 2nd Born approx. calcs. 77−3424
ethylene, (e,2e), correlation effects, electron momentum distributions in valence orbitals 79−862
ethylene, -$d_{0\text{-}4}$, UPS using 584Å line, adiabatic ionis. pot. of excited states 79−76467
ethylene, ab initio GO calc. 78−94187
ethylene, absorpt. cross sections at CO_2 laser wavelengths, temp. and press. depend. 80−78613
ethylene, adsorbed monolayer on Cu surface, UV-visible polarised modulation spectra obs. 78−72619
ethylene, adsorbed on Na zeolite, uniaxial rot., translational dynamics 78−91538
ethylene, adsorbed on Ni (111), vibr. spectra from electron energy loss *(French)* 78−34696
ethylene, adsorbed on Pt(111), electronic energy losses 79−46931
ethylene, adsorbed on Pt (111) surface, Auger spectra 79−52077
ethylene, adsorption, on ZnO, adsorption rate spectra, freq. response method 78−51817
ethylene, adsorption and decomp. on Ni(110) 77−85071
ethylene, adsorption and decomp. on Ni (111), high resolution EELS study 80−40739
ethylene, adsorption and decomp. on Pt, 90 to 500K 79−46933
ethylene, adsorption and decomposition on Ni films, coverage depend. meas. 80−96743
ethylene, adsorption on Ag (111) surface, XPS and UPS investigation 80−103573
ethylene, adsorption on Fe (110), UPS and LEEO/Auger meas. 77−72773
ethylene, adsorption on Ir (110) surface 78−38961
ethylene, adsorption on Ni, Pd and Pt films, reactivity with adsorbed H, surface pot. meas. 79−86995
ethylene, adsorption on Ni (111), surface structs., LEED and AES obs. 79−60636
ethylene, adsorption on polycryst. and (0001) single cryst. Re surfaces 78−38947
ethylene, adsorption on polycryst. Re, work function *(French)* 77−28075
ethylene, adsorption on Pt(100) 78−18905
ethylene, adsorption on Pt(111) surface, UPS meas. 77−52223
ethylene, adsorption on Pt (100), intermolecular forces and kinetics of adsorption 78−75930
ethylene, adsorption on Pt (111) surface, LEED intensity obs. 77−51592
ethylene, adsorption on stepped Pt (111) surface 78−71992
ethylene, adsorption on W (100) and decomposition to acetylene, AES obs. 79−66353
ethylene, adsorption on water, 0-50°C, press. effects on surface tension 78−56024
ethylene, AES, chem. state effects, for water and simple organic cpds. 78−72687
ethylene, air pollution monitoring, by CO_2 laser system 78−49182
ethylene, air pollution monitoring, computer controlled CO_2 laser absorpt. system 80−89699
ethylene, and ^2H, ^{13}C, ^{15}N, ^{18}O isotopic derivatives, vibr. freqs. using MINDO/3 force consts. 77−71793
ethylene, and ethylene-d_4, thermal conductivity in gaseous phase, 300-650K 77−11301
ethylene, and perfluoro derivatives, negative ion states, electron affinities, ionisation pots., overlapping spheres Xα calc. 79−26885
ethylene, and radical ion, SCF-MO calc., bonding and electronic struct. 77−38610
ethylene, autoionisation and photoemitted electron ang. distrib., cylindrical mirror analyser study 80−18049
ethylene, average mol. polarisability, Frost model wavefunctions calcs. using p-type Gaussians 78−41924
ethylene, boiling heat exchange, surface roughness influence, press. depend. *(Russian)* 79−68562
ethylene, C atom pyramidalisation rel. to bonding, ab initio SCF calcs. 79−93936

organic compounds continued
ethylene, C K-shell excitation by electron impact, electron energy loss spectra 77−31014
ethylene, C-C double bond rot. barrier, ab initio open-shell restricted SCF calc. 78−1099
ethylene, chemical state effects in AES 78−92566
ethylene, chemisorbed on Ag or Pt, IR refl. obs. 77−31903
ethylene, chemisorbed on metal surfaces, geometric and electronic struct., UPS obs. and HF LCAO calc. 79−86988
ethylene, chemisorbed on Ni and Pd films, IR refl. study 79−69343
ethylene, chemisorbed on W(100), geometry distortion 77−30919
ethylene, chemisorption and reaction on Ir(100), geometric and electronic effects 77−21421
ethylene, chemisorption of Pt, vibr. anal. of C_2H_3 species 80−61150
ethylene, chemisorption on α-Fe, struct., bonding, dissoc., UPS obs., MO calcs. 78−84050
ethylene, chemisorption on clean Fe (100) and (111) surfaces, LEED and thermal desorption 78−71996
ethylene, chemisorption on Ir (100), geometric and electron effects 77−55457
ethylene, chemisorption on Ir surface, LEED, AES and thermal desorption meas. 77−1297
ethylene, chemisorption on Ni(100), LEED and AES obs. 77−31904
ethylene, chemisorption on Ni (100), angular resolved UPS exam. 78−72685
ethylene, chemisorption on Ni (110), adsorption and decomposition exam. 77−55459
ethylene, chemisorption on Pt(111), reaction at room temp., form. of vinyl-like species 79−46939
ethylene, chemisorption on Pt (111), ethylidyne form. 79−57291
ethylene, chemisorption on Pt (111), ethylidyne group form., LEED and ELS obs. 78−73075
ethylene, chemisorption on Rh (111) and (100) surfaces, LEED, AES and thermal desorption meas. 78−38951
ethylene, chemisorption on Rh (755), (331), desorpt. temp. and decomp. characts. 79−65318
ethylene, chemistry in RF discharge, mass spectrometric obs. 77−9084
ethylene, chiroptical props., appl. of RPA-CI method using hypervirial relations as constraints 79−76413
ethylene, coadsorption with O_2 on Re *(French)* 78−85194
ethylene, comparison of dielectric and refractive virial coefficients and collision induced absorption bands 79−86547
ethylene, compressed gas, far IR dipolar absorpt., meas. and theory 77−14425
ethylene, computer generated phase diagrams 78−83928
ethylene, condensation, zero point energy shift, isotope effects 78−95147
ethylene, config. interaction calcs. for SCF basis sets 78−58593
ethylene, core ionised, core-excited and shake-up states, ab initio MRD-CI methods 80−42950
ethylene, CW CO_2-laser irrad., low-press., chem. relax. 79−74404
ethylene, decomposition in RF discharges, 10-40 torr 78−3318
ethylene, dehydrogenated adsorption on Ni (111), thermal desorption and AES study 80−29274
ethylene, diatomics-in-mols., semiempirical valence bond π-electron theory 80−99461
ethylene, dimer and trimer, dissoc. following photoionis. of mol. beam 79−57212
ethylene, dimer interaction, lattice energy, multipole expsn., at.-at. pots. 78−9218
ethylene, dipole moment derivatives, IR vibr. intensities, STO-3G, 4-31G, calcs. 77−6750
ethylene, dipole moment derivatives, MINDO/3 79−59599
ethylene, dipole moment derivatives, MINDO/3 semiempirical calcs. 77−75055
ethylene, dye laser probing of C_2 radicals, IR intense field photolysis 77−16851
ethylene, effective core potential calcs. 79−31437
ethylene, electron affinities, pi* anion, bond lengths, electron transmission spectroscopy study 80−18925
ethylene, electron energy loss spectra, 0-90°, 20-150 eV impact 79−68322
ethylene, electron energy loss spectra, C K-shell excitation, vibr. struct. 79−22851
ethylene, electron energy loss spectrum, intensity distrib. 79−64110
ethylene, electron impact dissoc., high Rydberg fragments 77−83749
ethylene, electron impact dissoc., optical emission from fragments 77−83750
ethylene, electron impact ionis., valence electron momentum distrib. 79−18297
ethylene, electron ionisation efficiency curves, fragment ion appearance pot. 78−86959
ethylene, electron momentum distribs. in π orbitals from (e,2e) expts. 80−14239
ethylene, electronic states, optical rot. dispersion, oscill. strength calcs. 78−9095
ethylene, electronic struct., CNDO/S2 calc., photoelectron and UV absorpt. spectra 77−30783
ethylene, electronic struct. and physicochem. props., modified partial neglect of differential overlap 78−82645
ethylene, eqn. of state, nonanalytic, modification for low density limit 79−46779
ethylene, excited states, continuum embedded, SCF-stabilisation approach 78−928
ethylene, excited states, spectral assignments 79−85915
ethylene, excited states, V←N spectrum 77−50446
ethylene, excited with parametric oscillator, vibr. relax. obs. and interpret. 80−9702
ethylene, gas, absolute viscosity 77−35299
ethylene, gas, second virial coeffs., intermol. pot. at low temp. 79−46416
ethylene, gas, virial coeffs., from theory of system of nonpolar mols. of arbitrary symmetry 78−9743
ethylene, gas-liquid crit. pt. region, depolarised light scatt. 78−34612
ethylene, geometry optimisation, using bond function augmented basis sets 78−905
ethylene, glow discharge, junction barrier, inelastic electron tunnelling 77−72916
ethylene, Green's function electronic struct. calc., improving Σ perturbation approach 79−13642
ethylene, Hartree-Fock energy and Moller-Plesset perturbation energy, harmonic vibr. freq. 80−52852
organic compounds continued
ethylene, He-Ne laser line, high temp. absorpt., anal. by high resolution IR spectra 80−91554
ethylene, heat transfer during boiling in tube *(Russian)* 77−68589
ethylene, high density behaviour, extrapolated $P\rho T$ surfaces and critical density 80−87834
ethylene, high pressure polymerisation investig. using near IR spectroscopy *(German)* 77−21384
ethylene, high resolution heterodyne absorption spectra 78−267
ethylene, high resolution spectroscopy with diode laser heterodyne system 77−91300
ethylene, imperfect gas contrib. to refractive index and quadrupole moment 78−55253
ethylene, in air, IR spectra, optical-acoustic investig. *(Russian)* 78−74663
ethylene, inhibition of free radical prod. in gas-phase radiolysis of ethane 79−39178
ethylene, intense IR field multiphoton dissoc., primary products, fluoresc. obs. 79−36715
ethylene, interaction with O_2 on Ag (110), LEED and AES obs. 80−89520
ethylene, intracavity IR absorpt. in CO_2 laser, enhanced sensitivity 78−78835
ethylene, ion ejection mass resolution test of wideband freq.-swept marginal oscillator detector for ion cyclotron reson. spectrometer 80−9069
ethylene, ionis. pot., Green's function method and CI calcs. 79−13839
ethylene, ionis. pots., Green's function method 77−14608
ethylene, ionis. spectral intensity, valence electron binding energy depend. 78−90234
ethylene, ionisation energy, LCAO Xα calcs. 77−50353
ethylene, ionisation potential, ab initio valence bond calcs. 79−31407
ethylene, ionisation pots. and excitation energies, correl. calcs. 77−26986
ethylene, IR absorpt. spectra of ν_1, ν_{10} and ν_4 interacting band 80−83369
ethylene, IR and near IR spectra, high press. cell meas. *(German)* 78−12769
ethylene, IR and Raman intensities calc., efficient ab initio computation method 79−45698
ethylene, IR double reson. obs., external-resonator controlled Raman laser pumped by CW CO laser 80−9624
ethylene, IR multiphoton excitation, optoacoustic meas. 80−1038
ethylene, IR spectra, solid and matrix isolated, dimer config. 79−36638
ethylene, isotopically mixed, crystal, dilute guest probe orientational energy, IR, Raman spectra 78−68496
ethylene, laser spectroscopy with CO_2 and N_2O lasers 79−59455
ethylene, laser-induced IR photolysis mechanism 78−56909
ethylene, lattice dynamics of cryst., ab initio interaction pot. 79−33043
ethylene, line selective excitation with CO_2 laser light and vibr. relax. 80−9705
ethylene, liq., far IR absorption spectrum, quadrupole induced dipole interaction 78−86857
ethylene, liq., orthobaric density, 105 to 200K 79−35679
ethylene, magnetic susceptibility, frost model wavefunctions with p-type Gaussians 80−5477
ethylene, matrix isolated, shielding tensor anisotropy, ^{13}C NMR meas. 79−59491
ethylene, mean amplitude of mol. vibration, approx. calc. method 79−13697
ethylene, mol. and cluster Auger spectrum calc., SCF core-valence-valence spectra 80−48045
ethylene, mol. geometry, ab initio calcs., basis set depend. 78−82636
ethylene, mol. hyperpolarisability meas. by optical SHG 79−22861
ethylene, mol. ion, mass spectra ion intensity internal energy depend., quasi equilibrium theory calcs. 80−53163
ethylene, mol. semiempirical RPA calc. using PPP Hamiltonian, triplet instability 79−26893
ethylene, molecular charge density contours for cryst. struct. 78−38645
ethylene, molecular geometry optimisation, variable metric method, internal geometry 80−95744
ethylene, molecule, floating spherical GO calcs. of electron momentum distrib. and Compton profile 77−30933
ethylene, multiphoton absorption, luminesc. and dissoc. in laser pulse field 78−1040
ethylene, multiphoton dissoc., CH_2 and C_2 prod., fluence depend. meas. 80−5586
ethylene, multiphoton excitation from many rot. states by IR laser pulse 78−21986
ethylene, multiphoton UV photodissoc. 78−50602
ethylene, multipole moments and polarisabilties, SCF calcs. 80−5471
ethylene, narrow resonances of multiple-photon IR absorpt. 80−99529
ethylene, near HF dipole polarizability, using EFV GTOs 79−31395
ethylene, near IR absorption at high press. and temps. 77−14435
ethylene, near vac. UV MCD obs., assignments, new transition 77−38684
ethylene, nucl. spin-spin coupling, scanning MO HF LCAO calc. 79−50045
ethylene, obtained from gas cylinder, particle size distrib. 80−55723
ethylene, off-reson. IR laser action without population inversion, Raman type transition 77−10891
ethylene, on Ni, C-H stretch vibration, broadened and softened, dehydrogenation 78−47666
ethylene, on Pt surface, electron energy loss spectra, surface vibrs. 78−15701
ethylene, optoacoustic trace gas analyser with CO_2 laser 79−5245
ethylene, ozonolysis, intermediate struct., multiconfig. SCF CI calcs. 80−18803
ethylene, ozonolysis, radical form., matrix ESR spectrosc. 80−16653
ethylene, P ρ T surfaces, butterfly catastrophe 79−86546
ethylene, Penning electron and photoelectron spectra, relative intensities comparison 78−81237
ethylene, phase transition, IR spectra, 15-85K 79−36638
ethylene, photoassisted decomposition at room temp. over Pt/TiO_2 80−55703
ethylene, photoelectron spectra, HAM/3 MO calcs. 78−13414
ethylene, photoelectron spectrosc., ang. depend. 80−9641
ethylene, photoelectron spectrum, vibronic coupling effects 79−10090
ethylene, photoionis. cross section calc., for YMζ line, HF vs OPW method 77−42353
ethylene, photoionisation cross section at distance from threshold, chemical bond influence 80−69196

organic compounds continued
ethylene, planar, V-N vertical transition, SCF and correlation energies 77−68032
ethylene, planar $^1(\pi,\pi^*)$ state, CI calcs. 77−57887
ethylene, planar dissociation, electronic rearrangement, states, bonds, ab initio multiconfigurational SCF calcs. 80−27937
ethylene, polarisability, nonlinear elec. susceptibility, SCF calcs. 80−95547
ethylene, polymerisation kinetics, heterogeneous Ziegler-Natta catalysts, polyethylene struct. and morphology 79−96307
ethylene, polymerisation plant, high-press. equipment design 79−24746
ethylene, pool boiling heat transfer 79−1058
ethylene, pot. energy and dipole moment surfaces, polarisation effect, ab initio CI calcs. 80−106272
ethylene, press. broadened linewidths 79−6971
ethylene, proton-proton coupling consts., valence angle depend. 77−23508
ethylene, pure, IR absorption obs. of C-H stretching fundamentals up to 2 kbar and 200°C 79−22701
ethylene, quadrupole moment from K^+(Ar)(Kr)(Xe) scatt. total cross sections 77−50495
ethylene, quadrupole moment tensor determ. by collision-induced absorpt. spectrum 80−91555
ethylene, quasidegeneracy and effective Hamiltonians, canonical transformation cluster expansion formalism 80−52888
ethylene, Raman intensities, CNDO approximation, polarization functions 79−93925
ethylene, Raman line intensities, modified CNDO/2/INDO calc. 78−25621
ethylene, Raman spectra, ν_1, ν_3 and ν_5 bands, polarisability 77−58021
ethylene, Raman spectra, ν_3 and ν_5 band centres 78−74669
ethylene, Raman spectra of ν_3 band, rot. consts. 79−26988
ethylene, reaction heat, HF limit energies, correlation energy 79−8447
ethylene, reaction with Si(111) and (100) at high temp., crit. conditions for SiC growth 79−47981
ethylene, rot. around double bond, four orbital-four-electron model 80−95592
ethylene, RPA hypervirial relation, ab initio minimal basis calcs. 77−18779
ethylene, S_0,S_1-states, twisting vibrs., pot. curve calcs., absorpt. spectra 77−83576
ethylene, scavenger mol. in UV photolysis of PH_3 in Jovian atmosphere 78−81582
ethylene, single cryst. X-ray struct. determ. at 85K 77−47440
ethylene, singlet Rydberg states, CI calcs. 78−33437
ethylene, solid, phase diagram and NMR at high press. 80−11279
ethylene, solid, self-consistent phonon calcs. 78−75745
ethylene, solubility in liq. N_2 80−39286
ethylene, solubility in molten polyethylene, statistical thermodynamical method, sorption data 78−71859
ethylene, static polarisability, ab initio SCF wave functions 80−74106
ethylene, stopping cross-sections using alpha particles in energy range 1.5 to 4.2 MeV 78−53510
ethylene, supercritical, mass-flow meter inaccuracy 79−68842
ethylene, surface interaction with transition metal atoms, MO calc. 80−6623
ethylene, surface reaction on Pt (111), EELS of radical vibrs. 78−71947
ethylene, TEA laser induced multiphoton dissoc., model and expt. 79−16016
ethylene, thermal cond., high temp. high press. meas. 79−68898
ethylene, thermal cond. meas. using thermal lens 79−12795
ethylene, Townsend primary and secondary ioniz. coeffs. and sparking voltages 78−51372
ethylene, transition moment closure tests of basis sets 79−6968
ethylene, twisted, intervalence charge transfer and reson., sudden polarisation effect 80−69230
ethylene, twisted, oscillator and rotary strengths, ab initio calculations 77−65510
ethylene, unoccupied orbitals, excitation energy, electron affinity, HAM/3 MO calcs. 78−13415
ethylene, UV photoelectron spectra, valence electron shake up approx. methods 80−18788
ethylene, V←N transition origin determ. 78−13510
ethylene, V-state config. selection methods 79−10041
ethylene, vacuum ultraviolet absorption spectra 80−63653
ethylene, valence states, effective Hamiltonian from canonical transformation 80−74130
ethylene, valence XPS spectrum satellite struct., C(2s) region, correlation states 78−5278
ethylene, van der Waals dimer, PCILO calcs. 79−36542
ethylene, variationally deorthogonalised localised molecular orbitals, electronic struct. 79−97968
ethylene, vertical, N(^1A_g), T($^3B_{1u}$), V($^1B_{1u}$) states, large scale CI calc. 78−70752
ethylene, vertical $^1(\pi$-$\pi^*)$ V-N transition, MRD-CI calc. 79−27004
ethylene, vibr. energy transfer, fluoresc. detect. 79−64026
ethylene, vibr. freqs., MINDO/3 calcs. 78−13429
ethylene, vibr. intensities, G sum rule appls. 80−32776
ethylene+Ar^+(Kr^+)(Ne^+)(Xe^+), 2-stage ion beam mass spectrometric obs. 77−9061
ethylene+Bi($6^4S_{3/2}$), absolute rate consts., time-resolved reson. fluoresc. meas. 78−27731
ethylene+$C_2(a^3\Pi_u)$, reaction rate consts. and quenching, multiphoton UV photolysis, fluoresc. obs. 79−74355
ethylene+C^+, branching ratios 78−44354
ethylene+$C(2^1S_0)$ 80−74241
ethylene+cis-N_2H_2, chem. reaction, intermediate geom. calcs. 78−35655
ethylene+Cl_2(Br_2) complex, intermolecular interaction and struct. SCF-MO-LCAO CNDO/2 calc. 78−58763
ethylene+Cl^+, reactions at room temp. 80−93749
ethylene+Cl, nuclear recoil, addition and abstraction reactions, kinetics 77−86340
ethylene+CO_2^+, rate coeffs. and product distribution determ. 80−97693
ethylene+$CO.CO_2^+$, rate coeffs. and product distribution determ., dissoc. energy and heat of form. 80−97693
ethylene+diimide, reduction, reaction tree algorithm, using pot. surfaces 77−70286
ethylene+F(CH_3), transition state, ab initio calc. 78−48640
ethylene+F, dynamics, stochastic reduction for reactions with complex form. 78−3315
organic compounds continued
ethylene+H_2O^+, rate constants determ. as function of relative kinetic energy 80−81292
ethylene+H→C_2H_5*, rate const., 198-320K, high press. 78−48618
ethylene+H=ethyl radical, pot. energy surface, analytic function 79−11779
ethylene+HBr, low temp. chain hydrobromination, kinetics and mechanism 80−93735
ethylene+HF*, vibr. deactivation rate constant 78−50615
ethylene+Hg($^3P_1$), quenching rate consts. determ. with nanosecond light pulser with Hg vapour 80−100111
ethylene+inert gas, vibr. energy transfer, fluoresc. detect. 79−64026
ethylene+methyl radical, reaction pot. surfaces, MINDO/3 calcs. 79−22601
ethylene+N_2H_2 reaction, H transfer, ab initio SCF GO calcs. 77−44469
ethylene+Na*(3^2P), electronic to vibr.-rot. energy transfer, differential cross sections 77−38715
ethylene+Ne^+, thermal energy, reaction rate coeffs. and product distrib. 79−29333
ethylene+NH*, rate const., time resolved chemiluminesc. 78−60982
ethylene+NO, HNO excitation by $O_2(^1\Delta_g)$ 79−52674
ethylene+NO, laser-generated radical kinetics 79−100352
ethylene+O, OH chemiluminesc., mechanism, rate const., mathematical model calcs. 78−48655
ethylene+O, reaction dynamics, IR laser excitation, vibr. effects 77−12788
ethylene+O, reaction dynamics, IR laser excitation effects 79−66288
ethylene+Si*, collisional quenching, reson. line absorpt. expt. 78−46297
ethylene+thermal energy reaction, mass spectra 77−9067
ethylene(−d_4), matrix-isolated, photolysis, acetylene fluoresc. 79−59505
ethylene(−d_4), Rydberg states assignments, electron energy loss specta 80−53153
ethylene(-d_1,d_2), high-resolution UPS, mol. ion vibr. assignments, symmetry 79−27032
ethylene(-d_1), reduced partition function ratio, generalised finite polynomial approx. 78−66529
ethylene(-d_4) clusters, IR photodissoc. 80−89506
ethylene(-d), chemisorbed on Ni catalyst, Raman and vibr. spectra 80−108747
(ethylene)$_x$, mol. crystals, quantum theory, mol. tight binding method calcs. 80−49572
ethylene + N_2, gaseous, excess enthalpy, determ. by flow calorimetry 78−91057
ethylene (and halogen substituted forms)+OH, reaction rate consts., room temp. 0.7-7 torr 77−21356
ethylene adsorbed on Ag, photon-induced field ionisation mass spectroscopy 80−6639
ethylene adsorbed on Ag exchanged zeolite, inelastic neutron scatt. 78−6229
ethylene adsorption on Ni (111) at room temp., surface complex vibr. from electron energy loss spectroscopy 79−73404
ethylene and propylene adsorbed on Ag, enhanced Raman spectra obs. 80−95607
ethylene as singlet methylene dimer, nonempirical double zeta calculations, zwitterionic singlet excited states 80−83258
ethylene bromide, liq., proton spin-lattice relax., temp. depend. 78−39435
ethylene carbonate, Fermi reson., isotopic substitution meas. 78−86870
ethylene cation, state geometries, electronic vibr. coupling consts., HF calcs., comparison with Xalpha calcs. 80−27946
ethylene cation+ethylene, collision complex stability, photodissoc. expts. on dimer and trimer 79−57212
ethylene chemisorbed on W, reaction with atomic H 77−36789
ethylene chemisorption on α-Fe(111) single cryst. surface, photoelectron spectroscopy study 77−62740
ethylene chemisorption on Cu, Ni, Pd and Pt surfaces, molecular geometries determ., using SCF-LCAO calc. 79−19454
ethylene chemisorption on Pt (100), Pt (111) substrates, photoelec. spectroscopy, dissociation model 77−43429
ethylene chemisorption on Rh (111), EELS, LEED and thermal desorption mass spectrometry 80−80057
ethylene condensed, electron energy loss spectra meas. 77−59652
ethylene deuterates, VP isotope effect in liq. and solid, chromatographic purification 77−43337
ethylene dibromide, photoabsorption and photodissociation, 190-300 nm 79−50038
ethylene dibromide in urban air 79−70481
ethylene dichloride-benzene, liq. mixture, excess Gruneisen parameter, intermol. interaction 78−67635
ethylene dimer, CO_2 laser induced photodissoc., pulsed mol. beam obs., van der Waals bond 80−9660
ethylene dimer, exchange forces, Hellmann-Feynman theorem calc. 77−54589
ethylene dimer, intermot. pot., dissoc, energy, CNDO/2 calcs. 79−31641
ethylene episulfide+H→HS+ethylene, absolute rate parameters, flash photolysis reson. fluoresc. 78−3312
ethylene episulphide, form. at S surface by laser irrad. in presence of ethylene 79−57258
ethylene free and coordinated mols., X-ray and X-ray electron spectra 77−27087
ethylene glycol; used in construction of polarised proton filter for polarisation of slow neutrons 79−63238
ethylene glycol, aq. soln., excess heat capacity, H bonding 78−3362
ethylene glycol, associated liq., US absorpt. and hole theory 78−10124
ethylene glycol, Brillouin scatt. and segmented motion 79−37609
ethylene glycol, conformational anal., photoelectron spect. 80−43107
ethylene glycol, critical nuclei, meas. of number of mols. and surface tension from rate of nucleation 79−65293
ethylene glycol, dilute aqueous solns., excess partial molal heat capacities 79−57280
ethylene glycol, heat transfer and power expenditure in agitated vessels with bare (finned) tube baffles 79−1052
ethylene glycol, IR spectra, ab initio calcs., vibr. anal., conformations of isotopic modifications 78−5210
ethylene glycol, NMR meas., microprocessor-controlled target polarization monitor 79−88990
ethylene glycol, polarised proton filter for slow neutron polarisation 78−90046
ethylene glycol, solution structure, adiabatic compressibility studies 78−87605

organic compounds continued
ethylene glycol, spin-lattice proton relaxation time, mol. rot. motion, kinetics 77−51984
ethylene glycol, UV photoelectron spectra, up to 21.2 eV 77−71831
ethylene glycol, vibrational dephasing time of subgroup, transient stimulated Raman scatt. 78−37718
ethylene glycol adsorption on Al_2O_3, inelastic electron tunnelling spectroscopic study rel. to lubrication 80−70302
ethylene glycol dinitrate, laser optoacoustic absorpt. spectra of explosive vapours 78−76941
ethylene glycol on Teflon FEP, effect of drop size on contact angle 80−2245
ethylene glycol solution, flow boiling and pool boiling critical heat flux, effect of flow passage geometry 77−62250
ethylene glycol-H_2O-lauryl alcohol-nitromethane-nitroethane, liq., multicrit. pts., 37-42°C 79−86868
ethylene glycol-water, glass, 4.2K, trapped electron photocond. and optical spectra following radiolysis 79−29378
ethylene glycol-water, uninhibited soln., corrosion of Al 79−70222
ethylene glycol-water glass, γ-irrad., temp. depend. photobleaching of trapped electrons 79−66320
ethylene imine, ionis. pot., many-body Green's function method 77−67972
ethylene in exhaust gas, optoacoustic detect. using line-selectable CO_2 laser 78−56947
ethylene in gas mixtures, optoacoustic detect. in urban areas and fruit storage chambers 79−87886
ethylene isomerisation, SCF perturbation theory anal. 79−91918
ethylene mean polarisability derivatives, variational calc. procedure 79−27108
ethylene mol. Green's function Σ perturbation method for mol. calcs. 78−55123
ethylene molecules, long range forces in multipole expsn., ab initio calcs. 78−9219
ethylene oxide, ^{13}C and D variants, T_2-relax., 2_{20}-2_{11} rot. transition by microwave pulse spectrometer 80−47976
ethylene oxide, cryst. symmetry, X-ray diffr., far IR and Raman spectra 78−35123
ethylene oxide, gas, EPR rot. transitions, T_1 and T_2 relax. 80−9622
ethylene oxide, in clathrate hydrates, mol. rot., inelastic neutron scatt. 78−91275
ethylene oxide, in clathrate hydrates, mol. rot. motion, quasielastic neutron scatt. 78−91274
ethylene oxide, ionis. pot., many-body Green's function method 77−67972
ethylene oxide, rot. relax., double reson. and Stark switching obs. 80−106340
ethylene oxide, stopping cross section for 0.3 to 2.0 MeV He^+ ions 78−63537
ethylene oxide+CH_3^+(CD_3^+) reactions, products mass spectra obs. 77−63901
ethylene oxide+CO_2, (00^01) mode deactivation, laser induced fluoresc. obs. 80−83453
ethylene oxide cation, existence of open isomer, ab initio calcs. 79−22593
ethylene oxide clathrate, reorientation, residence times, Debye-Waller factors, activation energy, neutron scatt. study 79−41989
ethylene oxide clathrate deuterate, rotational motion, quasi-elastic neutron scatt. study 79−51022
ethylene oxide derivatives, substituents effect on electronic state of epoxide ring, CNDO/2 calcs. 79−26891
ethylene oxide deuterohydrate, cryst. struct. at 80K 77−72607
ethylene oxide-d_0, -d_4, centrifugal distortion const., thermodynamic functions 79−41149
ethylene oxide-d_0, -d_4, ion chemistry, photoionisation and ion cyclotron reson. obs. 77−21373
ethylene ozonide, ab initio gradient and MC SCF calc., conformational anal. 80−83290
ethylene ozonide-d_4, isotopic species, microwave rot. spectrum assignments, struct. 77−57982
ethylene plasma polymerisation by magnetron discharge 79−33995
ethylene polymerisation and dissociation in high-freq. discharge 77−70299
ethylene radical cation, electronic states assignments, ab initio SCF CI calcs. 77−10584
ethylene remote meas. using CO_2 differential absorpt. lidar 78−49122
ethylene spherical cryst. grown in situ for low-temp. X-ray work 78−68612
ethylene sulphide, centrifugal distortion const., thermodynamic functions 79−41149
ethylene to acetylene conversion on Ni (111), UPS 78−88657
ethylene V state, ab initio study of spatial extension 80−27952
ethylene-^{14}C, adsorb. on Ni sheet, determ. by autoradiography 77−63989
ethylene-Ar mixtures for drift chamber appl. 78−25391
ethylene-Br_2(Cl_2) π-σ complexes, low freq. spectra 78−78713
ethylene-butane matrix, D atom bombardment, ethyl radical proton exchange reaction, indirect ESR obs. 80−16700
ethylene-CO_2 gaseous mixture, thermoosmotic conc. difference across membranes 79−83508
ethylene-d_0, -d_4, electron impact, vibr. excitation cross-sections, 1 MeV 79−22850
ethylene-d_0,-d_2, Raman spectra, vibr.-rot. selection rules and general band contours 77−58020
ethylene-d_0,-d_4, IR band intensity and Coriolis interactions 79−54851
ethylene-d_1, ν_9 B-type band analysis, ground state rot. parameters 77−42316
ethylene-d_1, IR absorpt., ν_{12} and $\nu_2+\nu_9$ bands, rot. consts., Fermi and Coriolis coupling consts. 77−27070
ethylene-d_4, phases I and II, struct. determ. by neutron diffr. 77−27870
ethylene-d_4, Raman spectrum, fundamental bands 79−59473
ethylene-d_4+NH(ND), ($b^1\Sigma^+$) states quenching, kinetic isotope effects 77−63891
ethylene-ethane mixtures, boiling heat transfer 78−9535
ethylene-H_2O, nonbonded interaction, pot. energy curves, MO calcs. 77−27140
ethylene-Li, mol. complex, electronic struct. calcs. 78−66465
ethylene-LiF complex, molecular orbital calcs., Li bonding exam. 78−29745
ethylene-LiH, struct. and props., SCF ab initio calcs. 80−106250
organic compounds continued
ethylene-N_2, liq. Zwanzig perturbation expansion convergence, free energy 77−76274
ethylene-NH_3 mixtures, crit. curves at high-press. 79−23715
ethylene-O_2, thermal electron attachment meas., microwave cond., pulse radiolysis 80−28592
ethylene-O_2 complex, CI calcs., singlet-triplet transitions 79−63923
ethylene-O_2 mixture, thermo-osmosis, heat of transport 79−43628
ethylene-O_2-N_2-Al particle mixture, two-phase detonation and combustion *(French)* 80−61097
ethylene-polyethylene mixtures, phase behaviour under high-press., polymer mean mol. wt. influence 79−24745
ethylene-propylene fluorinated mixtures, mol. ion reactions, cyclotron reson. spectrometer 77−21367
ethylene-vinyl acetate emulsion, morphology 77−48692
ethylenediamine, adsorption on Fe and Ni, XPS study 80−76132
ethylenediamine, solvated electrons, optical spectra and model potentials 80−30318
ethylenediamine sulfate, cryst., induced gyrotropy of CrO_4^{2-} ion 80−108175
ethylenediamine-H_2O mixtures, inhibition of Ps form. by NO_3^- ions 78−95988
ethylenediamine-water, liq.-solid equilibrium *(French)* 79−51236
ethylenediaminetetraacetic acid, complexing agent migration of ^{60}Co radioactive waste 79−20687
ethylenediammonium metal chlorides, $(NH_3CH_2CH_2NH_3)MCl_4$, M=Ni,Pd,Cu,Cd,Mn, struct. and mag. props., vibr. spectra 79−10842
ethyleneglycol dye laser, conversion efficiency and tuning, solvent effect 79−55131
ethyleneoxide, elec. dipole moment, g-values, mag. susceptibility, moments and charge distrib. 77−58077
ethylenes, optical activation energy and dipole moment, electron repelling and attracting groups 78−46341
ethylenes, substituted, He I and He II photoelectron spectra, CNDO/S calcs. 78−55201
ethylenes, substituted, unstable twisted forms, excited states, DODS-NO CI calcs. 79−13643
ethylenic compounds, H^+ chemical shifts, extended Huckel calcs. with gauge in variant atomic orbitals 80−102449
ethylenimine, gas phase photolysis and γ radiolysis, mass spectra of fragments 77−29022
ethylenimine, multiphoton ionisation spectra, electronic struct. 78−82803
ethylidene, rearrangement to ethylene, barriers, ab initio MO calcs. 80−104424
ethylidene-N,N′-diacetamide, interpretation of X-ray diffr. patterns, applic. of dynamic symmetry 78−47265
ethylidenimine, pyrolysis product, microwave spectra, rot. distortion and electric quadrupole const. and rot. barriers determ. 80−78608
ethylidyne group formation, in Pt (111) chemisorption of acetylene (ethylene) LEED and ELS obs. 78−73075
ethyliodide-d_2, NMR, spin-torsional spectra 79−15363
ethylmethylamine, low freq., vibr. spectra, methyl torsional pot. functions, mol. struct. 80−43045
ethylmethylether(-d_3), low freq. vibr. spectra, methyl torsional pot. functions, internal rot. 79−26978
ethylmethylsilane-d_0(−d_n), vibr. spectra, normal vibrs. and rot. isomerism 79−31524
ethyloxirane, solid, liquid, vapour phase, IR and Raman vibr. spectra 80−84740
ethylperoxy radical+NO_2, reaction rate const. meas. 80−21262
ethylperoxy radicals+NO reaction, flash photolysis and kinetic spectroscopy obs. of rate consts. 79−83470
N-ethylphthalimide+olefins, photochemical reaction, absorpt., fluoresc., phosphoresc. and triplet-triplet absorpt. spectra 80−85197
ethylsilane, redundancy coeffs. for vibrs. involving atoms with four bonds 77−27049
ethyltoluenes, fluoresc. and triplet state quantum yields, biacetyl method 78−37671
ethyltrichloroacetate, dielec. consts. and dielec. losses meas. 77−20795
ethyltrichloroacetate, liq., permittivity, dielec. loss, up to 60 GHz 78−60384
ethyne, chem. shift, paramagnetic term, Pople formalism calcs. 78−21945
ethyne, electron energy loss spectra, excited states investig., electron impact spectrometer 78−25756
ethynol, ab initio calc., energy levels and geom. struct. of C_2H_2O isomers 78−62716
ethynol, struct., isomerisation, ab initio SCF MO calcs. 78−41941
ethynyl cation, dissociative recomb. cross section determ., merged beam obs. 80−78715
ethynyl compounds, vibr. dephasing of C-H stretching vibrs. 79−6927
ethynyl radical, emission spectra and pot. energy surface, ab initio MRD CI calc. 79−41099
ethynyl radical, interstellar abundance and distrib. 78−65664
ethynyl radical, mm wave emission obs. of interstellar clouds 80−90503
ethynyl radical, vertical electronic spectrum, CI calcs. 77−34656
ethynylbenzene, radiative and nonradiative processes, triple bond effects 79−3481
ethynylradical, photodetachment, parturbation theory calcs., ICR spectroscopy obs 79−98166
ethythioxanthate, amperometric titration appl., Ag, Hg (II) and Pb determ. 79−57326
europium acetate, X-ray L-absorption spectra, 'white line' absorpt. maximum, chem. shifts 77−58042
europium B-diketone chelate solns., fluoresc. quenching by appl. voltage, display devices appl. 79−87497
europium ethylsulphate nonahydrate, MCD due to mag. dipole transitions 77−24825
europium oxalate, X-ray L-absorption spectra, 'white line' absorpt. maximum, chem. shifts 77−58042
eutectics, surface nucleation parameters 79−19163
excimer laser organic material forming quasi-one-dimensional crystals 80−23673
exciplexes, electronic struct. by electro-optical expts. 78−25581
exciplexes and excited aromatic molecules, donor-acceptor props., comparison of fluorescence quenching 80−69174
excitation energies, CNDO/S-CI method calc. appls. *(German)* 80−106275
2-exo-acetoxy-7-anti-dinitrophenylthionorbornane, mol. and cryst. struct. 80−2007

organic compounds continued
explosives, secondary, thermal decomp., solid-state kinetics, differential scanning calorimetry 78−92449
fatty acid derivatives, spin-labelled, interaction with biomembrane lipid and protein components 77−70421
fatty acid film, ($CH_3(CH_2)_nCOOH$), etching in glow discharge 77−16506
fatty acid Langmuir films, AC and DC cond. 78−56239
fatty acid monolayers, capillary waves, photon correlation spectroscopy, viscoelastic props. 79−75608
fatty acid monolayers, electron tunnelling 77−69428
fatty acid systems, Langmuir multilayer film, structure-dependent carrier transport obs. *(Japanese)* 80−20339
fatty acid-albumin complexing rel. to struct. lability of biomembranes, using fluoresc. probes 77−25381
fatty acid-cyanine dye mixed monolayer, on metal electrodes, photocond. 78−68050
fatty acid-serum albumin molecule binding kinetics, fluoresc. probe method 77−25365
fatty acids, anisotropic layers, multipole emission, energy transfer, classical theory 77−8625
fatty acids, dielectric meas. at microwave freqs. 79−19827
fatty acids, LF Raman spectra, accordion vibrs. *(French)* 77−27074
fatty acids, long chain, spread monolayers, rheological behaviour 79−95245
fatty acids, thermal electret, persistency of surface charge *(Japanese)* 77−81048
fatty acids, unsaturated, containing peroxide oxidation products, free radicals formed on UV irrad. 80−51165
fatty acids in anhydrous solvents, partial molar volume from density meas. 79−43616
fatty alcohol, oil-water interface adsorption, high-press. effect on phase transition 79−99395
fatty alcohol solid monolayers in H_2O, interface struct., model 80−54505
fatty carboxylic acids, C_{15} to C_{19}, solid phase, ^1H and ^{13}C NMR spectra 79−95653
fatty-acid monolayer, on water, eqn. of state, liq.-gas crit. region 77−76520
ferric myoglobin compounds, single crysts., Mossbauer spectrum in small mag. field 79−100571
ferrichrome A, selective excitation double Mossbauer meas. 80−8015
ferrocene, neutron diffr. study of cryst. struct. 79−55728
ferrocene, new interpretation of disordered cryst. struct., X-ray anal. 79−65063
ferrocene derivatives, exhibiting mesomorphic props., synthesis, appl. in Mossbauer spectroscopy 77−31589
ferrocenecarbaldehyde, plastic cryst. state, Mossbauer spectroscopy and microscopic obs. 77−76333
1,1′-ferrocenedicarboxylic acid, triclinic, X-ray and neutron cryst. and mol. struct. determ. at 78 and 298K 80−29008
ferrocytochrome c, horse, transient proton-proton Overhauser effects 79−43822
ferrocytochrome c, mag. reson. Raman opt. activity at different laser wavelengths 77−38681
ferrocytochrome c, picosec. and subpicosec. relax. and dephasing, reson. light scatt. obs. 79−45876
ferroelec. crystal, Barkhausen effect study 79−38507
ferrous formate dihydrate, mag. sp. ht. 79−91235
ferrous formate dihydrate, paramagnetic specific heat, decoration iteration transformation anal. 80−70938
ferrous formate dihydrate, sp. ht. 78−22865
ferrous oxalate dihydrate, Mossbauer spectrum, hyperfine fields 78−39483
ferrous oxalate dihydrate, reaction with sodium disilicate glass 78−11191
ferrous porphyrin, intermediate (S=1) spin state, PMR characterisation 80−48014
ferrous porphyrin, intermediate spin, reson. Raman spectra 79−69820
ferrous porphyrins, 4-coordinated, PMR 77−58044
ferrous sulphamate radiolytic instability in nuclear process solns. 77−70314
ferrous tetraphenylporphyrin, Mossbauer effect, mag. hyperfine interaction 79−24236
ferrous-formate dihydrate, mag. system model, mag. sp. ht. *(Japanese)* 78−31091
field ionisation mass spectrometry, review 78−35763
film, synthesis and characterisation, review 79−91584
film, thin, prep. methods in ultrahigh vacuum *(Japanese)* 80−84851
films, possible exptl. production in space 78−35304
flavanthrene molecules, stationary stochastic adparticle flip-flop as a precursor to surface diffusion 80−15371
flavin adenine dinucleotide, resonance CARS line shapes, excited state parameters 79−3448
flavin aqueous solns., fluorescence quenching by iodide ions, temp. and viscosity effects 77−34673
flavins, meas. of sub ns fluoresc. decay by time-correl. photon counting and Ar laser 80−94429
flavins, phosphoresc. props., solvent effects 77−12885
flavins, photochemical ionisation reactions in soln., automatic conductimetric instrument for kinetic studies 77−4971
flavins, photoemission of electrons in polar media 79−29507
flavocytochrome b_2, rotation function study using X-ray data 79−51035
fluid charge carrier generation, role of molecular electroinduction effects *(Russian)* 79−96321
fluoradene, absorpt. and fluoresc. in solvents, excimer form., aggregation 77−79625
p-fluoranil, ^{19}F NMR and spin-lattice relax. meas., pot. profile calc., mole. reorientation 80−29634
fluoranil, electron affinity, bound and excited negative ion states, lifetimes, electron and alkali metal collisions 79−869
fluoranil-macrocyclic polyether mol. complexes, configs., IR and NMR obs. 78−33529
fluoranthene, in rigid glass, S_1 and S_2 fluoresc. 77−3403
fluoranthene, single cryst. and in fluorene matrix, polarised absorption spectra, assignments 80−55122
fluoranthene, vapour, laser excited fluorescence 78−29807
fluoranthene high density excitation effects on fluoresc. 79−1782
fluoranthene-Rose Bengal, singlet-singlet energy transfer in Manoxol OT-cyclohexane-water 80−9531
fluoremethane, saturable absorpt. of CO_2 laser radiation, theory 78−37946

organic compounds continued
fluorene: acridene, radical pair form. from excited states, optical nucl. polarisation obs. 80−14155
fluorene: pyrene-d_{10}, triplet state energy transfer, EPR 79−15354
fluorene:acridine, EPR of excited triplet state complex 79−19767
fluorene:acridine (phenazine)(anthracene), optical nuclear polarisation, non-crossing rule, guest-host complex 77−42339
fluorene:benz(f)indan(anthracene), single cryst., γ-irrad. rel. to luminesc. decay 77−12417
fluorene:dibenzofuran, mixed cryst., dipole-forbidden guest-host energy transfer 79−38585
fluorene:phenazine, excimer form. transient EPR phenomena, wide-band detect. 77−13793
fluorene:pyrene-d_{10}, exciton-guest, triplet-triplet annihilation, impurity traps effects 80−25433
fluorene:pyrene-d_{10}, single cryst., host-guest triplet pairs, mag. field effect 80−60649
fluorene:pyrene-d_{10} cryst., magnetic resonance absorpt. of host-guest triplet paired centres 80−34750
fluorene, ^{13}C-{^1H} off-resonance spin decoupling, variable decoupler field strength 77−67485
fluorene, γ-irrad., void form. 80−2068
fluorene, cryst., low-freq. polarised Raman spectra 78−84574
fluorene, cryst., phosphoresc. spectra and ODMR meas. 80−11470
fluorene, electroluminesc. *(Russian)* 78−92129
fluorene, exciton band struct., two-photon fluoresc. excitation 78−64402
fluorene, hole mobility temp. depend., transit time meas. *(German)* 77−66169
fluorene, in ethanol soln., external heavy atom effect on triplet state, phosphorescence meas. 79−18231
fluorene, in polystyrene matrix, singlet O_2 induced excimer fluoresc. 77−6832
fluorene, lowest singlet state, exciton band struct. calc. 78−63983
fluorene, mol. polarisabilities and opt. props. of cryst. 79−24285
fluorene, molecular nonsteady-state luminesc. behaviour under narrowband laser excitation 80−87159
fluorene, n-paraffin soln., quasiline sensitised phosphoresc. spectra at 4.2K 77−68071
fluorene, near 6K, two-photon excitation spectrum, g-exciton states location 78−64393
fluorene, optical birefr., temp. depend., 25 to 90°C 79−82944
fluorene, optical polarisation of H nuclei, 4.2K *(Russian)* 77−12255
fluorene, photoconductive props., sample purity depend. 78−10508
fluorene, photoelectron spectroscopy obs. of heterocycles 78−94286
fluorene, single cryst., dielec. matrix suspension, electroluminesc. 80−2862
9H-fluorene, soln., correl. times from ^{13}C relax. 80−23438
fluorene, triplet state of X-traps, ODMR 79−24231
fluorene, two photon absorptivities, CNDO/S-CI calc. with second order time depend. perturbation eqns. 80−74122
fluorene+o-terphenyl, supercoded, liquid systems, dielectric and dynamic Kerr-effect studies 80−60496
fluorene and 9-allyl derivations, electronic struct. and reactivity 79−36523
fluorene conjugate bases, chem. shift, ring-current and excess-charge effects, semi-empirical calc. 78−33523
fluorene crystal, doped, photochemical hydrogen abstraction, proton hyperfine structure via optical nuclear polarisation 80−63659
fluorene doped molecular crystals, stimulated emission at 4.2K 79−28790
fluorene ketone polycryst., radical pair formation, 77K, EPR study 79−56610
9-fluorenone, excited single state kinetics on a subnanosecond time-scale 79−36677
fluorenone, in DMF, galvanostatic reduction, chronopotentiometry convolution procedures 77−25278
9-fluorenone, in o-terphenyl soln., dielectric absorp. studies, molecular relax. 78−95544
fluorenone, intersystem crossing rates, ps time-resolved spectra 77−6821
fluorenone, O X-ray emission spectra 77−28653
fluorenone fluoresc. in plastic, high press. effects., quantum yield 78−25601
fluorenone photoreduction by DABCO, ion-radical yield enhanced by mag. field, cage recomb. region 79−79268
fluoresc. decay time and emission spectra obs. *(Spanish)* 77−69873
fluorescein, activator in aquoluminescence spectra from γ-irradiated NaCl 77−69913
fluorescein, excitation and emission polarisation spectra, cell cycle changes 78−96013
fluorescein, fluoresc. quenching by rose bengal 79−78726
fluorescein, in n-alcohols (ethylene glycol)(glycerol), rot. relax., time-resolved fluoresc. depolaris. obs. 80−58300
fluorescein, photosensitising dye, effect on charge transfer in ZnO 78−72193
fluorescein, photosensitising dye effect on charge transfer in ZnO surfaces 78−68049
fluorescein 27, rot. diffusion and level kinetics separation in transient absorpt. spectroscopy 77−30877
fluorescein dye, halogen substituted, in dimethyl sulphoxide, spectral evidence for anion-counterion association 80−71909
fluorescein dye(-Yb^{3+}), triplet state energy transfer, fluoresc. quenching obs. 79−54897
fluorescein dye laser, solvation effects on tunability 80−53285
fluorescein in mammalian cells, appl. of fluoresc. polarisation meas. by flow cytometry 77−52942
fluorescein-rose bengale, soln., qualitative anal. using fluoresc. polarisation 79−24849
fluoresceindiacetate conversion to fluorescein, in living cells and in vitro, kinetics 77−56332
fluoresceindiacetate hydrolysis and transport in mammalian cells after UV and gamma irrad. 77−56333
fluorescence quantum yield, light quenching meas. 79−98147
fluorescent dyes, evaluation for water tracing 77−64493
fluorescent molecules, stimulated spectra, excited state intramol. vibrs. 80−32717
fluorinated alkyl iodides, stimulated emission, laser appls. 77−27285
fluorinated ethylenes, valence bond polar parameters, IR intensities, MO calc. 80−28013
fluorinated hydrocarbons, mol. recognition and self-organisation, information storage appls. 78−82806

organic compounds continued
fluorinated organic iodides, absorpt. spectra and primary photolysis processes, near and vac. UV 79−20393
fluorine, fluoresc. quenching by inorganic anions 78−74694
1-fluoro, 2,4-dinitrobenzene, partially aligned in elec. field, ^{13}C NMR, dipole moment determ. 80−78633
1-fluoro 2:4-dinitrobenzene, laser Raman and infrared spectra 79−22711
2-fluoro ethanol, Ar matrix, induced conformational isomerisation by IR irrad. 80−101010
fluoro sulphuric acid methyl ester, rot. isomerism 78−86964
1-fluoro-2-propanol, conformational energies and rot. barrier, ab initio calc. 79−31390
3-fluoro-4-chloroaniline, Raman and IR spectra, vibr. anal. 79−81198
3-fluoro-4-methyl aniline, near UV electronic absorpt. spectra, line shift, vibr. anal. 77−10682
2-fluoro-5-bromotoluene, IR and Raman spectra 78−70830
2-fluoro-5-chloro-toluene, IR vibr. spectra 79−68232
2-fluoro-5-methyl aniline, near UV electronic absorpt. spectra, line shift, vibr. anal. 77−10682
3-fluoro-6-chloro-toluene, IR vibr. spectra 79−68232
fluoroacetylene, and -d_1, vibr. Zeeman effect, g-factors 78−46391
fluoroacetylene, fund. and hot bands, laser microwave two-photon and double reson. spectroscopy 80−32752
fluoroacetylene, harmonic and anharmonic stretching force consts., ab initio calcs. 78−58587
fluoroacetylene, He(II) photoelectron spectra 80−91601
fluoroacetylene, IR absorpt. spectra, ν_4 C-H bending fundamental near 17 μm 77−75151
fluoroacetylene, laser Stark and IR-microwave double resonance, E1 moment, vibr. states 77−6813
fluoroacetylene, laser-microwave two-photon spectroscopy, appl. of tunable source 79−30579
fluoroacetylene-d_0,-d_1, microwave spectrum, laser enhancement effects 79−41161
fluoroacetylene-d_1, bending vibr.-rot. band ν_4, IR spectrum 77−75149
fluoroacetylene-d, Stark and microwave double reson. laser spectra 80−63690
4-fluoroaniline, amino group inversion and torsion, far IR spectra 77−10670
o-fluoroaniline, conformation by microwave spectroscopy, rot. consts. 78−9144
4-fluoroaniline, far IR spectrum, efficiency of heatable long path gas cell 79−58807
m-fluoroaniline, vap. (liq)., Raman and IR spectra, vibr. assignments 78−58699
fluoroanilines, isomers, thermodynamic functions and fundamental vibr. freqs. 80−9581
fluoroanthene, cryst. struct., X-ray and neutron diffr. meas. 77−47437
fluoroanthene in micelles soln., fluoresc., halide ion induced quenching and enhancement 80−95672
fluoroaromatics, CH stretching, vibr. force fields, substitution pattern effects 77−54550
p-fluorobenzaldehyde, vap., high-resolution electronic emission spectrum assignments 78−78742
pfluorobenzaldehyde(-d_1), in smectic mesophase, mol. struct. and reorientation, NMR 77−27093
fluorobenze, optoacoustic spectroscopy using cell with ultimate corrosion resistance 80−42269
fluorobenzene, 2644 Å band system, rovibronic anal., isotope effects 79−6949
fluorobenzene, adsorption on CuO-Cr_2O_3 based oxide catalysts, binding energy of F 1s electrons *(French)* 79−69346
fluorobenzene, cryst., absorpt. spectrum, vibronic states 77−59588
fluorobenzene, IR vibr. spectra 79−13713
fluorobenzene, lattice vibs. *(French)* 77−32366
fluorobenzene, liq., vibr. relax., Brillouin scatt. obs. 79−51206
fluorobenzene, liquid, vibr. relaxation, Brillouin spectra 80−108219
fluorobenzene, mol., UV prereson. Raman scatt., interference effects 79−64008
fluorobenzene, mol., UV prereson. Raman scatt. intensity 79−64007
fluorobenzene, mol. reorientation and weak mol. interaction influence, ^2D spin-lattice relax. obs. 80−106333
fluorobenzene, multiphoton ionisation spectrum in one-photon wavelength region 80−63727
fluorobenzene, multiphoton reson, ionis. spectrum, 51000 cm^{-1} assignment 79−86021
fluorobenzene, nonlinear dielectric effect temp. depend. 79−87372
fluorobenzene, photoelectron spectra ang. distrib., π- and σ-orbital assignments 79−818
fluorobenzene, S_0-S_1 transitions, two-photon absorpt. spectra by nozzle beam-multiphoton ionisation method 80−63728
fluorobenzene, singlet-singlet electron transitions, modified CNDO-CI method exam. 78−25552
fluorobenzene, two-photon contours comparison with band contours of toluene 79−41212
fluorobenzene, vap., two-photon excitation spectrum assignments 79−59519
fluorobenzene, variable angle electron impact energy loss spectra 79−68321
fluorobenzene(-benzene), liq. and dilute soln., microwave absorption and relax. processes 79−82920
fluorobenzene cations, emission spectra, Jahn-Teller effects and vibronic coupling 79−10120
fluorobenzene cations, fluoresc. quantum yields and lifetimes, electronic state relax. processes 80−48027
fluorobenzene crystal, localised excitons 77−31963
fluorobenzene in liq. NH_3, solvated electrons reaction kinetics 77−73434
fluorobenzene ions, fluoresc. quantum yields and lifetimes, meas. method ion form. 77−6815
fluorobenzene radical anion, ab initio MO calcs., struct. 79−18113
fluorobenzene radical cations, in gas phase, laser-induced fluoresc. 79−27022
fluorobenzene radical cations, matrix laser fluoresc. spectra 80−1009
fluorobenzene radical cations in solid Ne, laser-induced fluoresc. spectra, vibr. struct. of excited and ground states 80−95671
fluorobenzene solutions, influence of strong elec. field on dielec. permeability 77−90086
fluorobenzenes, electronic struct., CNDO/S2 calc., photoelectron and UV absorpt. spectra 77−30783
fluorobenzenes, excited electronic states, variable angle electron impact spectroscopy 78−13612
fluorobenzenes, negative ion states, comments and reply 80−32599
fluorobenzenes, partially oriented in lyotropic liq. cryst., NMR spectra 77−68059
fluorobenzenes, radical cations, B(π^{-1}) excited states, radiative relax. 78−13546
fluorobenzenes, substituted, cryst., ^{19}F NMR, chem. shift tensor meas. 78−10789
fluorobenzenes, UV photoelectron spectroscopy, basic concepts, spectra 78−17715
fluorobenzenes, UV spectra calc., oscill. strengths 79−18203
fluorobenzenes, vibr. relax. in first electronically excited singlet state 79−3535
fluorobenzenes in Ne matrices, molecular cation electronic absorption spectra, new photolytic technique 80−58415
fluorobromomethanes, matrix photoionisation and radiolysis, IR spectra of free radicals 79−24765
fluorocarbon, atm., detect. using computer simulated IR solar spectra 77−53217
fluorocarbon 11, detect. in ambient air by gas chromatography 78−85739
fluorocarbon detection by gas chromatography *(German)* 78−96117
fluorocarbon emulsions, colloidal props. 78−48703
fluorocarbon foil, Ftoroplast, homogeneity study *(Polish)* 80−35278
fluorocarbon glow discharges, plasma polymerising and etching, mass spectrometric obs. 77−32790
fluorocarbon liquid, breakdown characts., comparison with hydrocarbon liqs. 79−91361
fluorocarbon measurements, interlaboratory comparison 79−70483
fluorocarbon mixing and photolysis, tropospheric mixing ratios 79−12181
fluorocarbon monomers, plasma polymerisation 78−35304
fluorocarbon refrigerant, film boiling heat transfer from heated plate 79−55380
fluorocarbon solutions, dye-sensitized, spectroscopic obs. of 1.27 μm and 1.58 μm emission of single ($^1\Delta_g$) mol. O_2 80−85178
fluorocarbon-11, estimated future atmos. concs. for various tropospheric removal rates 77−21892
fluorocarbon-hydrocarbon mixtures press. second virial coeff., graph theory prediction 80−43823
fluorocarbon-ozone theory, atm. modelling, diurnal steady state calc. 79−88390
fluorocarbon-water mixture, phase equilibria and critical phenomena at high press. 78−51648
fluorocarbons, atm. conc. meas., model validation 77−45138
fluorocarbons, atm. lifetime determ. methods 79−20920
fluorocarbons, destruction of stratospheric O_3 77−9459
fluorocarbons, in Earth's atmosphere, global distrib. 79−53407
fluorocarbons, press. second virial coeff., graph theory prediction 80−43823
fluorocarbons, press. second virial coeffs., walks on graphs method 80−7841
fluorocarbons, world production and release, 1975, rel. to stratospheric O_3 78−3919
fluorocarbons 11 and 12, contamination effects of stratospheric HNO_3 channel spectral meas. 77−87054
fluorocarbonyl compounds, triplet state, trapped electron ICR spectrosc. 79−59373
5-fluorocytosine, electron beam damage assessed by EELS 80−89809
fluorodiacetylene, He(II) photoelectron spectra 80−91601
fluorodiiodomethane, vacuum UV photolysis, IF in solid Ar visible spectra 80−87137
fluoroethanes, IR multiphoton dissoc., HF vib. energy distribs. 80−53073
fluoroethanes, IR photodissoc. by multiphoton absorpt., collisional effects 79−36713
fluoroethanes, mol. liqs., dielectric solvent effects, quantum chem. calcs. 77−14375
2-fluoroethanol-d_0,-d_1, IR spectra in Ar, N_2 and Ar-N_2 matrices, normal coordinate anal. 78−25538
fluoroethyl radical, unimol. dissoc., pot. energy characts. and energy partitioning calcs. 80−45488
2-fluoroethyl to ethylene fluoronium ion interconversion, pot. energy surface, MNDO calc. 79−34296
fluoroethylene, chemisorption on Ni(100), LEED and AES obs. 77−31904
fluoroethylene+HF*, vibr. deactivation rate constant 78−50615
fluoroethylenes, electron affinities, pi* anions, bond lengths, electron transmission spectroscopy study 80−18925
fluoroethylenes, electronic transitions, electron impact spectra 77−10775
fluoroethylenes, IR multiphoton dissoc., HF vib. energy distribs. 80−53073
fluoroethylenes, IR photodissoc. by multiphoton absorpt., collisional effects 79−36713
fluoroethylenes, variable angle photoelectron spectra, ionisation pot. asymmetry parameter 80−28064
fluoroform., ^{13}C vap. press. isotope effect 78−59938
fluoroform, ν_3, ν_6 and hot bands, high resolution IR spectrum 79−81204
fluoroform, absolute IR intensities of fundamental vibrs. 77−79655
fluoroform, quadratic force fields, MOCIC pot. functions calcs. 80−5475
fluoroform, vib. relax., 183-295K, US absorpt. meas. 77−34722
fluoroform, Zeeman effect, mag. moments and susceptibility, nuclear shielding 79−13764
fluoroform+T, 4.5 to 6.0 eV, substitution reactions 78−85146
fluoroform(-d_1)-trimethylamine-Ar(Kr), cryospectroscopic IR study of association 77−468
fluoroform-d, laser isotope separation of D multiphoton dissoc. 79−94096
fluoroformaldehyde, pot. energy surface characts., substitution effect 80−89505
fluorohaemin, ferric porphyrins with fifth ligands, ^{57}Fe and ^{14}N hyperfine consts. 78−50475
fluoroiodomethane, vibr. excited, dissociation, trajectory calcs. using pot. energy surface parameters 80−76508
fluorol 7GA dye laser, flashlamp pumped passive mode-locking 77−38922
fluoromethanal, visible spectrum, rot., vibr. and vibronic anal., double min. pot. 79−41182
fluoromethane, 496 μm high-power smooth-pulse laser systems 77−19332
fluoromethane, 496 μm transition, laser pumped mol. laser theory 79−36868

organic compounds continued
fluoromethane, $^{12}CH_3F$, far IR CW laser emission by optical pumping 79−3687
fluoromethane, $^{12}CH_3F$, far IR Raman laser line obs., CO_2 laser pumping 80−69381
fluoromethane, $^{13}CH_3F$ and $^{12}CH_3F$, vibr. energy transfer between ortho- and para-mols. *(Russian)* 78−29845
fluoromethane, ν_3 band Lamb dips, effects of RF elec. field modulation on Stark spectra 80−52989
fluoromethane, ν_3 mode, laser induced fluoresc. of V→T/R transfer 77−6899
fluoromethane, -^{12}C (-^{13}C), Doppler-free optical double reson. spectroscopy using single-freq. laser and modulation sidebands 80−68274
fluoromethane, and other optically pumped lasers, dynamic Stark effect 78−17911
fluoromethane, angular correlation between far IR emission and CO_2 pump radiation, Dicke superradiance theory 79−41370
fluoromethane, binding energy, ionisation pots., overlapping sphere MS Xα 77−83499
fluoromethane, chem. shielding. mol. rot. and anharmonic vibr. 78−94258
fluoromethane, core energy levels, pseudopot. calcs. *(French)* 79−49935
fluoromethane, deuterium separation at high press. by ns CO_2 laser multiple-photon dissoc. 80−91616
fluoromethane, dielec. props. in far IR range 77−85639
fluoromethane, dielectric susceptibility at radio frequencies 78−14123
fluoromethane, dipole moment derivatives, MINDO/3 79−59599
fluoromethane, dipole moment derivatives, MINDO/3 semiempirical calcs. 77−75055
fluoromethane, Doppler-free optical double reson. Stark spectra 77−58051
fluoromethane, excited state rot. spectroscopy and kinetics, appl. of tunable sub-MM sources 80−14162
fluoromethane, far IR laser, electronic tuning and phase-locking 78−59055
fluoromethane, far IR laser, pump radiation self-focusing and defocusing 78−79003
fluoromethane, fluid, second dielec. virial coeff. calc. 78−22449
fluoromethane, gas, 2nd and 3rd virial coeffs. calc., including nonadditive interactions 77−76013
fluoromethane, gas, electron-ion recombination, at 292K, three-body interaction 79−46418
fluoromethane, gas, optical rotary saturation 79−27338
fluoromethane, geometry optimisation, using bond function augmented basis sets 78−905
fluoromethane, in interstellar mol. clouds, search for $J_K=1_0$-0_0 transition 77−60808
fluoromethane, in Kr matrix, vibr. relax., IR double reson. 77−79635
fluoromethane, in liq. O_2(Ar), vibr. energy relax. obs. 78−5208
fluoromethane, IR absorpt., CW saturation, theory 77−83933
fluoromethane, laser excitation, energy storage and vibr. heating 77−58137
fluoromethane, laser pumped, overtone fluoresc., intermode energy flow 78−37673
fluoromethane, laser pumped, vibr. states collision dynamics fluoresc. obs. 80−53104
fluoromethane, laser pumped molecular lasers, sub MM laser expts. 80−1192
fluoromethane, laser pumping effects, translational and vibr. energy distribs. 79−844
fluoromethane, laser submillimetre with optical pumping energy yield, emission pulse delay time depend. on pumping pulse *(Russian)* 78−71088
fluoromethane, LCAO-Xα-SCF, atoms in mols. theory and appl. 77−57869
fluoromethane, liq., transient stimulated vibr. Raman scatt. 78−71144
fluoromethane, microwave spectrum, and 2nd order Coriolis reson., mol. consts. 77−18915
fluoromethane, mol. dipole moment derivative, sign of 79−86082
fluoromethane, mol. rot.-vibr. consts. of ν_3 band of $^{12}CH_3F$ 79−64118
fluoromethane, molecular pumping, thermal lens phenomena 80−9708
fluoromethane, multiphoton excitation from many rot. states by IR laser pulse 78−21986
fluoromethane, near-MM-wave laser synchronous pumping, ultrashort pulse generation at 496, 193 μm 80−102705
fluoromethane, optical pumping of far-IR molecular lasers by CW CO_2 waveguide laser 80−83615
fluoromethane, optically pumped laser, IR-FIR transferred Lamb dip spectra 80−1193
fluoromethane, photoionis. cross section calc. for YMζ line, HF vs OPW methods 77−42353
fluoromethane, pulsed optically-pumped submillimetre-wave amplifier theory 79−31868
fluoromethane, pulsed submm. laser, high intensity, narrow bandwidth, for plasma diagnostics 77−19307
fluoromethane, rot. mag. moment spectra, mol. beam mag. reson. obs. 77−14509
fluoromethane, rotary photon echoes 78−25929
fluoromethane, second dielectric virial coeff. of polar gas, temp. depend. *(German)* 78−26234
fluoromethane, single-mode optical pumping, superradiant far IR emission 78−42329
fluoromethane, submillimetre laser Thomson scatt. system for plasma diagnostics 77−84526
fluoromethane, total energy, MOs nonempirical minimum STO-4LGF calcs. 78−9074
fluoromethane, two photon generated lasing, effect of pressure 77−88703
fluoromethane, vel.-tuned multiphoton processes in laser cavity 77−27134
fluoromethane, very high resolution IR spectrum anal. 77−34630
fluoromethane, vibrational-translational transfer rate, optoacoustic meas. using short pulse CO_2 laser 80−74258
fluoromethane+Ar, vibr. time depend. on equilib. and vibr. temps. *(Russian)* 79−27071
fluoromethane+Br, isotope selective photobromination, using c.w. CO_2 laser irrad. in excess inert gas 78−76843
fluoromethane+Br($^2P_{3/2}$)($^2P_{1/2}$), photobromination 78−11535
fluoromethane+Cl$^-$(Br$^-$)(I$^-$), excitation functions, reactive scatt., eV region *(German)* 78−35677
fluoromethane+Cl($^2P_{3/2,\ 1/2}$), photochlorination electron and oscill. energy 80−81320

organic compounds continued
fluoromethane+CO_2, rot. transfer collisions, momentum transfer distributions 77−523
fluoromethane+D(H)(O), reactions, selective vibr. excitation effects 78−35643
fluoromethane+fluoromethane, collision induced mode selective energy transfer, fluoresc. obs. 80−69177
fluoromethane+fluoromethane, collisionally induced relax. processes and vibr. energy transfer 80−53107
fluoromethane+HCl, IR spectra, intermol. interactions 80−9605
fluoromethane+HCN, HCN excited vibr. state, T_2 meas. 80−102498
fluoromethane+O_2, laser induced translational-vibr. energy conversion obs. 79−72396
fluoromethane+O_2, vibr. energy equilibration, IR laser fluoresc. 79−846
fluoromethane+OCS, rot. relax. parameters, microwave spectra linewidth parameters 80−28009
fluoromethane+SF_6(CS_2), fluoromethane laser, buffer gases collisional narrowing 80−99710
fluoromethane+SO_2, collisionally induced relax. processes and vibr. energy transfer 80−53107
fluoromethane 496-μm laser, CO_2 laser pumping dispersion 80−87375
fluoromethane +F$^-$, S_N2 reaction, ab initio LCAO SCF calcs. 77−81402
fluoromethane ν_2, ν_5 rot.-vibr. Raman bands, anisotropic components, ^{13}C shifts 78−74667
fluoromethane DFB gas laser, construction and operation 80−23715
fluoromethane far IR CW laser, Stark effect, large freq. tuning and resolved structures 79−45931
fluoromethane far IR laser FM and stabilisation by Stark effect 78−59056
fluoromethane far IR Stark laser using rectangular metal-dielec. waveguide 79−27245
fluoromethane for IR laser, evidence for Stark induced freq. shift 77−58358
fluoromethane laser, optically pumped far-IR waveguide, output, temp. depend. 80−58512
fluoromethane laser, synchronously pumped, subnanosec. transients 79−89891
fluoromethane laser diagnostics using two CO_2 laser pump pulses 79−31869
fluoromethane laser emission from unstable resonator 79−22983
fluoromethane optically pumped far IR lasers, 604 GHz, developments 77−83882
fluoromethane optically pumped molecular laser, relax. oscills. 80−95875
fluoromethane TEM_{00} far IR laser with integrated pump laser 80−43348
fluoromethane TEM_{00} far IR laser with integrated pump laser 80−58578
fluoromethane waveguide laser, tunable, for far IR freq. synthesis in 500-70 μm region 78−90439
fluoromethane-^{12}C+fluoromethane-^{13}C, vibr. energy transfer, IR double resonance monitor 77−61833
fluoromethane-^{13}C, IR spectra, pulse Fourier transform technique 77−26405
fluoromethane-^{13}C, pulsed far IR emission 80−69370
fluoromethane-^{13}C optically pumped molecular laser, relax. oscills. 80−95875
fluoromethane-d_0, -d_1, vibr. relax. in matrix, rot. effects, double reson. obs. 78−46375
fluoromethane-d_2, matrix isolated, vibr. energy transfer at low temps. 80−37860
fluoromethane-d_3, deuteron quadrupole coupling const. 78−33522
fluoromethane-d_3, laser Stark spectra, ν_6 band, vibr.-rot. consts., dipole moment 78−5277
fluoromethane-d_3, vibr. energy transfer at low temps., inert gas and N_2 matrix obs. 80−9706
fluoromethane-SF_6 496-μm optically pumped laser, energy-transfer mechanisms 80−99712
fluoromethane-SF_6-SO_2 mixture, laser irrad., IR fluoresc. meas. of equilib. and vibr. temps. 78−82766
fluoromethanes, ^{19}F shielding anisotropies, NMR of smectic mesophase solns. 77−34662
fluoromethanes, ab initio calcs. of K-shell ionisation potentials 77−18784
fluoromethanes, and perfluoroethane, NMR gas-to-liquid shifts, 2nd-virial coeff. of chem. shielding validity 79−85976
fluoromethanes, condensation, zero point energy shift, isotope effects 78−95147
fluoromethanes, diffusion in air 77−15154
fluoromethanes, dipole moment derivatives and infrared intensities, transferable polar tensors 78−17668
fluoromethanes, GVFF from SCF ab initio energies 78−74635
fluoromethanes, ionisation pots., SCF-multiple scatt.-Xα calcs. 78−5141
fluoromethanes, optimum geometries, force fields, CNDO/force method 77−46498
fluoromethanes, soft X-ray absorpt. spectra, fine struct. above K-edge of C 78−42096
fluoromethanes, vibr. spectra, force consts. and geom., SCF ab initio calcs. 78−62785
fluoromethanes, Xα calcs. using ΔSCF formalism 79−6861
fluoromethanes and CO_2 in stratosphere, simultaneous effects on O_3 column density 79−74940
fluoromethanols (mono and tri), decomposition activation of HF, non-statistical energy partitioning, laser emission 79−945
fluorometh.HF, H-bonded complex, ab initio calcs. *(French)* 80−52866
fluoromethyl formate, conformation potential energy surfaces, ab initio calcs. 80−69065
fluoromethylene+NO→HF+CNO, vibr. energy distrib., lasing action in dichlorofluoromethane-O_2 78−48644
fluoromethylene+O_2→HF+CO_2, vibr. energy distrib., lasing action in dichlorofluoromethane-O_2 78−48644
fluoromethylene cation, in solid Ar, IR spectra, vibr. modes 79−68231
fluoronaphthalene, bond and mol. polarisability, semi-empirical delta-function 79−31441
2-fluoronaphthalene, disordered form, thermal expansion, neutron and X-ray diffr. study 80−24621
α-fluoronaphthalene, IR singlet-singlet absorption and emission spectra, forbidden character 77−58002
2-fluoronaphthalene, vibr. and calorimetric investigation of polymorphism 78−87641
2-fluoronaphthalene-2-naphthol system, phase relations, X-ray diffr. and DTA study 80−45287

organic compounds continued
fluoronitrobenzene, equilib. config. and barriers, microwave spectra 80−95606
fluoroparaffin+He, binary gas mixture, mutual diffusion press depend. 77−24047
fluorophenol cations, emission and photoelectron spectra in gaseous phase 80−58316
2-fluoropyridine, IR and Raman spectra, vibr. assignments 78−25534
2-fluoropyridine, natural abundance ^{1}H coupled ^{15}N NMR spectra, selective population transfer method 79−95682
fluorosilanes, far UV and He I photoelectron spectra 79−18204
p-fluorostyrene, 288 nm electronic absorpt. spectra, vibr. assignment 79−13738
fluorostyrene, UV Raman spectra, reson. effect in photoreactive states 80−106326
fluorotrichloromethane, optical saturation characts., using CO_2 laser radiation 78−30027
fluorotrichloromethane, spectral data evaluation for atm. sensing 79−62582
fluorotrichloromethane in N.American troposphere and stratosphere 79−79430
^{18}F-5-fluorouracil, synthesis and purfication by fractional sublimation 80−17134
fluoroxyperoxytrifluoromethane, ab initio MO calcs. of geometry, torsional barriers 78−90313
fluroesceinisothiocyanate, fluorescent labelling of polyaspartamides 80−58426
fly ash and trace organic compounds anal., from municipal incinerators 80−45584
formadehyde, interstellar 5 GHz survey of southern dark clouds 80−73028
formadelhyde(-d_2), S_1 rot. levels, collisionless nonradiative decay rates 79−72346
formaldazine, mol., conformational anal., inapplicability of MINDO/3 79−94105
formaldehyde^{+}, excited state dissoc., nonadiabatic interactions, conical and Jahn-Teller intersections, classical trajectory method 80−25997
formaldehyde, 17(2,15)→17(2,14) line press. broadening relationship 79−98093
formaldehyde, 3.5 μ region spectrum, ground state consts. 79−13712
formaldehyde, 4.8 GHz line, preferred freq. for interstellar communications 79−16845
formaldehyde, 4_0^1 band anal., isotope effects 78−86878
formaldehyde, ^{18}O isotope, 4389 MHz obs. 79−44591
formaldehyde, $^{1}A_2$-state, radiative and nonradiative decay calcs., rel. to photochem. decomp. 78−37669
formaldehyde, $^{1}A_2$-state, SVL fluoresc.-spectra, absolute radiative lifetime, ab initio CI calcs. 79−63919
formaldehyde, $^{3}A_1$ and $^{1}A_1$ states, electrostatic mol. pot., basis set and wave function calcs. 79−10020
formaldehyde, $^{3}A''$ state, zero-field splitting param., ab initio CI calcs. 80−99454
formaldehyde, $-d_0$, $-d_1$, $-d_2$, multiple-photon dissociation, intensity and press. depend. 77−88515
formaldehyde, α-cleavage, feasible forbidden photochem. reaction 77−9092
formaldehyde, $a^{3}A_2$-$X^{1}A_1$ system, rot. anal. 78−62818
formaldehyde, ab initio calcs., appl. of convergent SCF procedure 80−47875
formaldehyde, absorpt. coeff. meas. using optothermal detector 79−40634
formaldehyde, abundance in ρ Ophiuchi dark cloud 79−71100
formaldehyde, adiabatic CI pot. surface LCAO calc., gradient determ., mol. dynamics 80−48056
formaldehyde, adsorbed on Ru(110), UPS study, 80K 78−73080
formaldehyde, adsorbed on W(100) single cryst., XPS obs. of decomp. 77−4927
formaldehyde, and -d_2, lifetime of ($^{1}A_2$) rovibronic levels 79−3495
formaldehyde, and cation, vertical proton affinity in singlet and triplet states 78−90079
formaldehyde, anharmonic pot. function, vibr. freqs., vibr.-rot. interaction, centrifugal distortion 77−38651
formaldehyde, atmos. composition, air over N.Germany coast, obs. 80−26584
formaldehyde, atomisation and bond energies, LMO calc., conjugation contrib. 80−9496
formaldehyde, bond polarity effect on other bonds and lone pairs, LMO calc. 80−9495
formaldehyde, chemisorbed on Rh, catalytic decomposition, transmission IR spectra 79−39199
formaldehyde, chemisorption and decomp. on Pd 77−63953
formaldehyde, CO laser Stark and IR absorpt. spectra, dipole moment and rot. consts. 77−75150
formaldehyde, concs. in rain water and on atmospheric aerosol 78−57243
formaldehyde, config. interaction calcs. for SCF basis sets 78−58593
formaldehyde, core ionisation, valence orbital relax. calcs. 78−5135
formaldehyde, D_2CO, HDCO, CW optically pumped laser action 77−88700
formaldehyde, decomp. and absorpt. on hot W filament 77−90641
formaldehyde, detect. of new interstellar transition 77−60808
formaldehyde, dipole moment derivatives, MINDO/3 semiempirical calcs. 77−75055
formaldehyde, Doppler-limited spectra of C-H stretching fundamentals 78−70831
formaldehyde, electrochromism of 1749 Å band, electric dipole moment and polarisability 78−66572
formaldehyde, electronic excited states, GO calcs., $\pi\rightarrow\pi^*$ transition 79−22616
formaldehyde, electronic states, oscill. strengths calcs. 78−9095
formaldehyde, electronic struct., dipole moments, mol. polarisability, force fields, ab initio calcs. 80−78531
formaldehyde, electronic structure, SCEP theory calcs. 77−10579
formaldehyde, emission spectrum, forbidden n-π^* transition, electronic-vibr. struct., CNDO/2 calcs. 77−58035
formaldehyde, excited state photodecomp., rotationally resolved spectra 77−60088
formaldehyde, excited state vibr. freq. calcs. by method based on scaled ab initio force fields 80−87092
formaldehyde, excited states, generalised Brillouin theorem multiconfig. method 77−67993
organic compounds continued
formaldehyde, first hyperpolarisability, Hartree-Fock-Slater calc. *(French)* 78−78625
formaldehyde, force consts., ab initio CI calcs. *(French)* 78−90093
formaldehyde, force consts., vibr. freqs., CNDO/2 and MINDO calcs. 77−14607
formaldehyde, force field calcs., damped least-squares method 80−91533
formaldehyde, four-level system, time-resolved microwave double reson. 79−59493
formaldehyde, geometry optimisation, using bond function augmented basis sets 78−905
formaldehyde, ground and low lying excited states, CNDO/V^{N-1} method *(Russian)* 78−74576
formaldehyde, ground state, potential energy surface 80−42967
formaldehyde, ground state rot. consts. 79−45701
formaldehyde, hyperfine interactions, mol. beam elec. reson. spectra 77−88445
formaldehyde, in ρ Ophiuchi dark cloud complex, lifetime rel. to anisotropic light scatt. 78−8080
formaldehyde, in Ar, 0.17-1.4 gm cm^{-3}, VUV absorpt. spectra, Rydberg excitations 77−79627
formaldehyde, in Ar, medium perturbations of extravalence excitations, VUV absorpt. 78−1002
formaldehyde, in interstellar clouds, abundance rel. to cloud chemical evolution 77−13421
formaldehyde, in marine air and rainwater, wet season obs. 80−85703
formaldehyde, in troposphere and stratosphere, meas. by high resolution IR absorpt. spectroscopy 79−84371
formaldehyde, intermolecular interaction energies calcs. using minimal basis sets 80−78681
formaldehyde, interstellar, 5 GHz absorpt. spectra obs. in directions towards galactic centre regions 79−84855
formaldehyde, interstellar, 6.8 cm obs., mol. isotopic abundance ratio $H_2{}^{13}CO/H_2C^{18}O$ determ. 79−35347
formaldehyde, interstellar, absorpt. in Cassiopeia A direction 78−45381
formaldehyde, interstellar, absorpt. line meas. towards galactic H II region (G48.6+0.0) 78−85996
formaldehyde, interstellar, collisional excitation 78−89237
formaldehyde, interstellar, detailed struct. in NGC 6334 mol. cloud complex 78−4324
formaldehyde, interstellar, detect. at 1.3 mm in mol. clouds 79−25683
formaldehyde, interstellar, detect. in M31 79−48929
formaldehyde, interstellar, excitation, effects of microwave background radiation observed spectrum 80−36681
formaldehyde, interstellar, excitation temp. in dust cloud L134 77−5552
formaldehyde, interstellar, form, rel. to interstellar dust new model 80−26934
formaldehyde, interstellar, kinematics and distrib. near Cone nebula and NGC 2264 IR source 80−4418
formaldehyde, interstellar, obs. in southern dark dust clouds 77−13434
formaldehyde, interstellar, obs. in southern radio sources rel. to $^{12}C/^{13}C$ ratio 79−84838
formaldehyde, interstellar, obs. towards bright rims in diffuse nebulae 77−87510
formaldehyde, interstellar, prod. in diffuse clouds 79−40246
formaldehyde, interstellar absorption line in galactic radio sources, SHF obs. 80−77472
formaldehyde, interstellar mol. clouds rel. to variable extinction at galactic centre 79−48909
formaldehyde, intramol. energy transfer, photodecomp., radiationless decay 77−29027
formaldehyde, ion laser induced photopredissociation, ^{17}O, ^{18}O, ^{13}C isotope separation 77−61871
formaldehyde, IR Doppler-limited spectrum, wavenumbers, line strengths and assignments 79−72310
formaldehyde, IR intensities by electron impact spectroscopy 77−6851
formaldehyde, IR spectra, Coriolis-coupled ν_4, ν_6 and ν_3 fundamental bands 78−5227
formaldehyde, IR spectrum, rot. anal., P-and Q-branch assignments 77−18923
formaldehyde, isolated Voigt line. off-peak spectral absorpt. coeff. 80−106355
formaldehyde, laser-excited reson. fluoresc., rot. struct., rot. and vibr. consts. 79−54993
formaldehyde, laser-induced fluorescence, rad. transition rates from two vibronic levels 77−3400
formaldehyde, laser-induced photodecomposition from single vibronic levels, H atom quantum yield determ. 79−96344
formaldehyde, low-temp. matrix photolysis, hydroxymethylene intermediacy, IR obs. 78−76877
formaldehyde, mag. rot. spectrum, $A^{1}A_2$ state, singlet-triplet perturbations 79−98126
formaldehyde, mag. rot. spectrum, singlet-triplet perturbations 78−25580
formaldehyde, MC SCF method in full and pseudopot. versions 77−83487
formaldehyde, meas. in atm. by ground based IR absorpt. obs. *(French)* 79−66764
formaldehyde, microwave absorpt. coeff. 77−64378
formaldehyde, microwave spectra, low-freq. 79−81305
formaldehyde, microwave-microwave double resonance 80−53029
formaldehyde, MO, electron density calcs., computer programs 78−70742
formaldehyde, mol., UV absorpt. cross-section, and stratosphere chem. 80−109209
formaldehyde, mol. beam, vel. meas. by Doppler effect on RF spectrum splitting *(French)* 78−13627
formaldehyde, mol. orbital calcs., new set of generalised hybrid atomic orbitals 77−67962
formaldehyde, mol. Rydberg S←S and S←T transitions, semi-empirical SCF MO calc. 80−91453
formaldehyde, molecular beam rotation temp. meas. *(French)* 80−78724
formaldehyde, molecular correlation energies, estimation from semi-transferable orbital correlation energies 78−82650
formaldehyde, multiphoton dissoc. by CO_2 laser, intensity/fluence depend. 80−11913
formaldehyde, multiphoton dissoc. intensity depend. 80−28073
formaldehyde, multiphoton dissoc. using focused DF laser, H-isotope separation 79−94094
formaldehyde, multipole expansion of diatomic overlap, MEDO calcs. 78−46264

organic compounds continued
formaldehyde, near UV predissoc., appl. to heavy water production by laser isotope separation 77−83106
formaldehyde, nonradiative transition rates and predissociation process 77−54574
formaldehyde, normal and deuterated solid films, UV dissociation at 77K 77−29021
formaldehyde, O and C 1s ionis. pots., shakeup XPS spectra electron spin coupling depend. 77−30925
formaldehyde, orbital contribs. to relax. energies accompanying core ionis., ΔSCF HF calcs. 78−82642
formaldehyde, oxidation, appl. of sensitivity analysis, numerical Green's function procedure 79−100334
formaldehyde, oxidation on Cu (110), temp. programmed desorption obs. 79−87878
formaldehyde, photoabsorpt. and ionis., intensities, assignments, ST, IVO calc. 79−31614
formaldehyde, photochem., ab initio calcs. rel. to hydroxycarbene intermediate 79−61880
formaldehyde, photochemistry, past and present 79−52711
formaldehyde, photodecomposition in tropospheric clean air *(German)* 79−53405
formaldehyde, photodissoc., H_2 and CO relative quantum yields, 270-360 nm 78−44384
formaldehyde, photodissoc., pot. energy surface features 79−79271
formaldehyde, photodissoc. dynamics, isolated mol. behaviour and collision induced effects 79−11807
formaldehyde, photoionisation by vac. UV laser *(Russian)* 78−9205
formaldehyde, photolysis, HCO prod., vibr. relax., chem. kinetics and spectra 79−11808
formaldehyde, photolysis in Ar matrix, role of cage dimer 79−91973
formaldehyde, photooxidation products, HO_2CH_2OH observed in IR spectra 79−93994
formaldehyde, polymer formation in interstellar space 77−78858
formaldehyde, predissociation, reson. multiphoton dissoc. 80−53077
formaldehyde, pressure-broadened linewidths in microwave region, temp. depend. 77−34694
formaldehyde, proton affinity, geom. and basis set depend., MO calcs. 78−50461
formaldehyde, relative Raman scatt. cross section 80−100061
formaldehyde, relativistic Dirac-Fock multiconfig. SCF calcs. 80−99456
formaldehyde, rot. struct. of 3500 Å transition, large amplitude vibr. effect 79−93976
formaldehyde, Rydberg states, excitation energies, oscillator strengths ab initio GVB-CI calcs. 77−54518
formaldehyde, selective laser photolysis for ^{14}C enrichment 80−108720
formaldehyde, sequential coupling 80−58297
formaldehyde, solid soln. in Xe, precipitation, IR spectra obs. 80−45059
formaldehyde, spectral linewidth press. broadening, Anderson-Tsao-Curnutte calcs. 77−75220
formaldehyde, survey in Orion dust cloud L1641 79−71099
formaldehyde, T_2-relax., rot. transitions, time resolved spectra, microwave pulsed spectrometer study 80−18846
C_{2v}-formaldehyde, Tamm-Dancoff approx., relativistic correction, vertical excitation energy, radiative lifetimes 78−9090
formaldehyde, transformation and compliance matrices determ. 77−18898
formaldehyde, triplet instability, RPA calculations triplet instability, RPA calculations 80−27938
formaldehyde, triplet state g-tensors and hyperfine coupling tensors 80−52895
formaldehyde, two-step photoionisation, $^1A_2$ state lifetime 77−10711
formaldehyde, unique force field, parametric representation method 77−18897
formaldehyde, UV photolytic separation of D from H in cryogenic solns. 78−95937
formaldehyde, UV photopredissociation, H-laser isotope separation 79−94095
formaldehyde, vertical photoexcitation and photoionisation spectra, CI calc. 78−918
formaldehyde, vibr. and electronic energy transfers, from single vibronic level 78−82820
formaldehyde, vibr. excited states, RF spectrum *(French)* 77−30863
formaldehyde, vibrational band intensities of $^1A_2$-$^1A_1$ transition, ab initio calc. 80−43028
formaldehyde, vibronic and spin-orbit coupling, radiative and non-radiative transitions 77−3414
formaldehyde, width of inverted Lamb dip, meas. using low-noise He-Xe lasers 79−54915
formaldehyde, X^1A_1, a^3A'' and A^1A'' states, SCF and CI ab initio calcs. 79−36545
formaldehyde+Ar* thermal collisions, $CH(A^2\Delta$-$X^2\Pi)$ emission 77−86304
formaldehyde+Ar(N_2O), mol. isolated Voigt line, off-peak spectral absorpt. coeff. 80−106355
formaldehyde+Br(F) reactions, rate consts. by EPR 80−93736
formaldehyde+CH_n^+, (n=Q-4), reactions at 300K 78−44357
formaldehyde+Cl, photolysis, Fourier transform IR studies, metastable species detection 80−81293
formaldehyde+Cl, rate const., 200-500K 79−39133
formaldehyde+Cl, rate const. 78−85136
formaldehyde+Cl→HCl+HCO, stratospheric O_3 decreased sensitivity to Cl perturbations 79−12190
formaldehyde+ClO radical, expt. showing no reactivity, stratospheric implications 80−90119
formaldehyde+$CO_2(NH_3)$, cross sections meas. *(French)* 79−76487
formaldehyde+F, HF IR chemiluminesc., vibr. and rot. energy disposal 77−86318
formaldehyde+F, microscopic reaction dynamics, branching ratio, IR chemiluminesc. 78−73021
formaldehyde+formaldehyde, medium distance interaction, SCF LCAO MO, supermol., perturbation and MCF calc. 79−837
formaldehyde+$H_3O^+(H_3S^+)(HCNH^+)(HCHO.H^+)$, proton transfer, rate and equilib. consts. 78−48636
formaldehyde+He, rot. excitation, coupled-channel calcs., microwave doublets cooling 77−3436
formaldehyde+He, rot. excitation, IOS approx. calcs. 79−45801
o-formaldehyde+He, rot. excitation at interstellar temps., coupled states cross sections 77−54593
formaldehyde+He, rot.-translational energy transfer, nonlinear vs. linear rotors, surprisal anal. 79−76492

organic compounds continued
formaldehyde+He(H_2), collisional relax. times and lineshape distortion, Stark absorpt. linewidth obs. 78−74744
formaldehyde+O, absolute rate consts., discharge flow and flash photolysis reson. fluoresc. meas. 80−55648
formaldehyde+O(H), reaction, absolute rate coeffs., 250-500K 79−100349
formaldehyde+OH, rate consts., 299-426K, UV flash photolysis, reson. fluoresc. obs. 78−68873
formaldehyde($-d_1$, d_2), and isotopic forms, microwave spectrum, ν_4-ν_6 vibr. states Coriolis reson. 78−82719
formaldehyde($-d_1$), reduced partition function ratio, generalised finite polynomial approx. 78−66529
formaldehyde($-d_2$), photolysis quantum yields, radical production, NO reactions, freq. depend. 78−44387
formaldehyde($-d_2$), S_1 state, collisionless decay, vibr. relax., quenching 79−27019
formaldehyde ($-d_1$,d_2), isotopic forms. vac. UV Rydberg spectra, vibr. assignments origin isotope effect 77−61763
formaldehyde (A^1A_2) single vibronic level photolysis, H atom prod., HNO chemiluminescence 77−9108
formaldehyde absorption in Lynds 134 dust cloud, turbulence determ., 6 cm obs. 80−94845
formaldehyde and $-d_1$, MODR and collision-induced transitions in laser cavity 78−74686
formaldehyde and its isotopic species, rot. spectra of ground vibr. state, rot. const. determ. 80−83350
formaldehyde anion radical, hyperfine coupling consts., vibr. depend., ab initio calcs. 80−87150
formaldehyde as probe to investigate dark cloud struct. EHF and SHF obs. 80−105317
formaldehyde decomposing to H_2+CO, reaction path Hamiltonian 80−45486
formaldehyde dimers, matrix isolated, struct., IR spectra 80−99504
formaldehyde in air, photodecomposition, CO and H_2 quantum yields 79−66311
formaldehyde in galactic centre region 80−94852
formaldehyde in giant molecular clouds, H_2 densities and $^{12}C/^{13}C$ ratio 80−51837
formaldehyde in HD 97048 circumstellar shell, visible and IR obs. 80−85943
formaldehyde in M82 nucleus, λ6 cm absorpt. detect. 79−17088
formaldehyde in New Jersey air, statistical anal. 77−73833
formaldehyde in NGC 5128 (Centaurus A), 14 GHz absorpt. obs. 80−17657
o-formaldehyde in rho Ophiuchi dark cloud, excitation temp. and optical depths 80−51846
formaldehyde in stratosphere, positive ion chemistry 78−57251
formaldehyde maser in IRS 1 in NGC 7358, SHF band obs. 80−67822
formaldehyde photopredissociation, laser isotope separation of D 78−55040
formaldehyde polymer formation mechanism in interstellar space 78−54032
formaldehyde S_1 levels, collisionless single rot. level lifetimes, elec. field depend. 80−63566
formaldehyde substituted with ^{17}O and ^{18}O, microwave spectra of ground vibr. states, rot. and distortion const. determ. 80−83349
formaldehyde UV spectrum, selective laser photolysis for ^{14}C enrichment 79−10220
formaldehyde-^{13}C, A^1A_2-X^1A_1 system, UV absorpt. spectra, rot. anal. 80−9614
formaldehyde-d_0, $-d_1$, $-d_2$, single vibronic level photochem., radiative and nonradiative processes 78−66583
formaldehyde-d_0, $-d_2$, $^1(n\pi^*)$ radiationless transition, ab initio CI calc. 79−767
formaldehyde-d_0, $-d_2$, $^1(n\pi^*)$ transition, vibr. struct., ab initio CI calc. 79−766
formaldehyde-d_0, $-d_2$, fluoresc. quantum yields, rot. depend., single rovibronic level values 79−22748
formaldehyde-d_0,$-d_2$, higher Rydberg states, vac. UV transitions assignments 77−42334
formaldehyde-$d_0(-d_2)$, S_1 single rot. level lifetimes, isotope, elec. field and vibr. state depend. 80−78655
formaldehyde-$d_0(-d_1)(-d_2)$, matrix isolated, IR spectra, monomer absorpt. 80−99503
formaldehyde-d_1, ν_3 fundamental band, IR absorpt. and laser Stark spectra 77−34629
formaldehyde-d_1, ν_5 and ν_6 vibr. excited states, microwave spectrum obs. 79−72304
formaldehyde-d_1, absorpt. spectra, 9-11 μm, ν_5 and ν_6 fundamental bands 78−70827
formaldehyde-d_1, detect. in interstellar clouds 80−8670
formaldehyde-d_1, rot. transitions, millimetre wave spectrum 77−34617
formaldehyde-d_1, rotational transitions, IR-RF double reson. meas. 77−61775
formaldehyde-d_1, unsuccessful search in dark interstellar clouds 79−12500
formaldehyde-d_1 ($-d_2$), single vibronic levels, fluoresc. emission, radiative lefetimes and vibr. relax 80−23521
formaldehyde-d_2, $\tilde{A}^1A_2$-$\tilde{X}^1A_1$ system, mag. rot. spectra 79−98127
formaldehyde-d_2, fluoresc. quenching *(Russian)* 79−50074
formaldehyde-d_2, inert gas and N_2 matrix fluoresc. spectra, radiationless transitions and lifetimes 79−3469
formaldehyde-d_2, laser Stark spectra, Coriolis coupled ν_4 and ν_6 fundamentals 77−27065
formaldehyde-d_2, reson. multiphoton dissoc. 80−53077
formaldehyde-d_2 733 μm line, Autler-Townes effect in laser interacting with RF field 80−53269
formaldehyde-d_2 vapour, far IR laser emissions 78−63072
formaldehyde-d_2 vapour, IR-UV double resonance 80−43078
formaldehyde-d (d_2) submillimetre lasers, optically pumped, assignment of laser lines 80−58513
formaldehyde-gelatin crosslinking, ^{13}C NMR obs. 79−5187
formaldehyde-H_2O complex, IR spectrum in solid Ar, N_2 matrix 80−43042
formaldehyde-water, heuristic intermol. pot. function, ab initio MO calcs. 78−33566
formaldehyde.$H_2S(H_2O)$ complexes, ab initio SCF MO calcs., binding energy dispersion contrib. 80−27967
formaldehydes, (deuterated), A^1A_2 state, photoluminesc. in low temp. matrices, vibr. relaxation 79−50070

organic compounds continued
formaldoxime, centrifugal distortion effects, microwave rotational spectrum 79−22699
formaldoxime, photoelectron and far UV absorpt. spectra 78−17712
formamide, $^1\pi\pi^*$ state, perturbation theory calcs. 78−62705
formamide, ab initio calcs. on ground and excited states 77−83494
formamide, and related cpds., INDO-CI calc., transition moments 79−45637
formamide, CI calc. of vertical ionisation and excitation energy 78−78836
formamide, comparison of theoretical and experimentally determined electron density distrib. 78−82634
formamide, dielec. props., 10 MHz-70 GHz, 10-40°C 78−43769
formamide, far IR spectrum, efficiency of heatable long path gas cell 79−58807
formamide, force consts. and dipole moment derivatives, ab initio MO calcs. 80−95521
formamide, geometry from ab initio calcs., rel. to N-methylformamide, acetamide, and N-methylacetamide 80−23338
formamide, hydration by H_2O mol., point charge model 77−34569
formamide, intermol. H bonding, vibr. spectrosc. obs. 79−50018
formamide, IR spectra, amino group inversion transitions and pot. functions 80−43041
formamide, liq., vac. UV optical and dielec. meas. 80−25329
formamide, low temp. electron density distrib. 78−34502
formamide, low-lying triplet states, relative energies and conformational preferences 77−3266
formamide, mol. geom., self-consistent MINDO calcs., torsion and relax. effects 77−42243
formamide, near-IR spectra, anharmonic pot. 77−14430
formamide, partial at. charges calc. from ab initio mol. electrostatic pots. 78−70739
formamide, partly deuterated, in electrolytic soln., IR spectra, anion-solvent H-bonding 78−84558
formamide, photoelectron spectrum, Green's function calcs., satellite lines 80−28061
formamide, UV photoelectron spectra, up to 21.2 eV 77−71831
formamide, valence ionisation energy and electron affinity, HAM/3 calc. and photoelectron, UV spectra 79−50081
formamide+formamide, medium distance interaction, SCF LCAO MO, supermol., perturbation and MCF calc. 79−837
formamide+malic acid, γ-irradiated reactions under high pressure *(Japanese)* 79−52707
formamide(-d_2), vibr. spectra NH_2 stretching modes assignment 79−89675
(formamide)$_x$, mol. crystals, quantum theory, mol. tight binding method calcs. 80−49572
formamide dimer, hydrogen bond, ab initio MO calcs. 78−58588
formamide dimer, tritium β^--decay causing H^+ transfer, ab initio MO calc. 80−3391
formamide oxidation at Pt alloy catalytic electrodes 79−57245
formamide-d_x, ^2H quadrupole resonance, double transitions 79−3465
formamide-glyoxal, charge transfer theory, Mulliken population, ab initio calc., multiconfiguration scheme 80−106392
formamide-water soln. permeability of cellulose membrane 78−11557
formate bisurea dihydrate, magnetisation curves 78−23298
formate esters-d_1, Fermi reson. parameters 80−48103
formate ion, hydration, ab initio LCMO calcs. 79−59342
formate ions adsorbed on Ag particles in aqueous soln. Raman spectra 80−69148
formation by fission fragment radiolysis in ethane-ammonia system 77−56236
formazan dye, physical development, high gain amplification process 79−39170
formiate, proton spin-lattice relaxation in various phases *(Russian)* 80−97163
formic acid, ^{13}C, NMR spectra, transition intensities, off-resonance proton spin decoupling influence 80−74183
formic acid, ^{13}C NMR spectra and relax. under intermediate decoupling power conditions 80−20515
formic acid, ^{16}C, ^{18}O, microwave spectra and centrifugal distortion consts. 80−83352
formic acid, adsorbed on Cu (100), interaction with acetic acid, EELS study 80−76120
formic acid, adsorpt. and decomp. over Ni surface, obs. using combined SIMS-FDS-AES system 78−40076
formic acid, adsorption and surface reaction on metals 80−40741
formic acid, and dimer, ab initio MO calcs., ground and excited states 77−83492
formic acid, catalytic decomposition on Pt, appl. of modulated mol. beam mass spectrometry anal. 78−56944
formic acid, chemisorbed on Al_2O_3, effect of formate ion conc. on conductance of MIM struct. 79−15233
formic acid, chemisorpt. on Al(Al_2O_3), electron tunnelling spectra study 78−84049
formic acid, chemisorption and decomp. on Cu (100), EELS study 80−16729
formic acid, conform. hypersurface determ. and analysis 80−1078
formic acid, cryst., electrostatic energy, multipole moments and point-charge lattice sums 77−76350
formic acid, cryst., H bonded, IR spectrum computer simulation 80−97253
formic acid, cryst. binding, ab initio MO SCF calc. 79−37657
formic acid, cryst. struct. at 98K 78−26555
formic acid, CW submm. laser assignment 79−27244
formic acid, decomp. on W (100), flash desorption obs. 79−29402
formic acid, decomposition, using Ni (110) catalyst, reaction kinetics and mechanism, mol. beam relax. spectroscopy 77−70340
formic acid, deuterated, neutron powder diffr. exam. at 4.5K 78−75650
formic acid, diffr. limited CW optically pumped laser 77−54727
formic acid, dimer, config. and energy, ab initio MO SCF calc. 79−37657
formic acid, dimer, UPS, expt. and MO theory 79−86005
formic acid, dimerisation energy, ab initio calcs., distortion energy effects 79−10022
formic acid, dimerisation energy, non-empirical MO SCF calc. 79−37656
formic acid, electron-density maps of bent bonds 80−1084
formic acid, far IR laser gas absorption obs. with and without DC field 79−31870

organic compounds continued
formic acid, form. by photofixation of CO_2 in vitro, photosynthesis mimicking 78−88650
formic acid, fragmentation, fragment structs. and energies calcs. 80−74124
formic acid, H bonding, electronic struct., geometries, moments, dimerisation energies, charge distrib., pseudopotential calcs. 80−27942
formic acid, harmonic force consts., ab initio calcs. and uniqueness problem 79−6834
formic acid, heteronuclear double reson., spin echo modulations 78−1009
formic acid, ideal gas thermodynamic props. 78−51275
formic acid, ionis. and photoelectron spectra, inner valence electrons 78−82784
formic acid, laser transitions near 5.6 μm, HF laser optical pump 78−58995
formic acid, lattice dynamics model to explain neutron scatt. data 79−86856
formic acid, lattice energy, non-empirical MO SCF calc. 79−37656
formic acid, lattice vibr., pot.-function calcs., comp. to neutron scatt. data 79−42168
formic acid, liq., microdynamic behaviour, struct., nucl. spin-lattice relax. 77−76270
formic acid, microwave spectrum, 10-200 GHz, vibrational excited states, ν_6, ν_8 79−93987
formic acid, molecular correlation energies, estimation from semi-transferable orbital correlation energies 78−82650
formic acid, monomer, cyclic dimer, charge transfer through H bonds, Hartree-Fock calcs. 77−58157
formic acid, normal and deuterated, dynamic modes, neutron inelastic scatt. study 79−51214
formic acid, normal vibr. pot. energy distrib. 77−451
formic acid, on Ni surface, decomp., dipole interactions effects 80−61143
formic acid, optically pumped by pulsed HF laser, emission obs. at 5.7μm 79−50283
formic acid, optically pumped sub mm laser design 77−14757
formic acid, partial at. charges calc. from ab initio mol. electrostatic pots. 78−70739
formic acid, proton affinity, geom. and basis set depend., MO calcs. 78−50461
formic acid, reactivity with metal surfaces, electron spectra 77−62748
formic acid, saturable gas absorber isolator for 9 μm band CO_2 laser amplifier 79−76709
formic acid, soln., polarisable H bonds, IR spectrosc. obs. 80−58408
formic acid, valence and Rydberg state empirically adjusted ab initio calcs. 77−10609
formic acid, vap., laser lines identification 78−1222
formic acid, vibr. states, rot. and Coriolis parameters 1R Fourier transform spectra 80−32709
formic acid, viscosity of dissociating vapour 78−5840
formic acid+acetic acid, liqs., mixing enthalpy 79−60515
formic acid+Ar($^3P_{2,0}$) crossed mol. beams, ionisation and dissociative fluorescence, energy depend. 79−52669
formic acid+CO_2, (00^01) mode deactivation, laser induced fluoresc. obs. 80−83453
formic acid(−d_1), dilute deuterated mixture, high-sensitivity NQR, double quadrupole reson. 78−68412
cis-formic acid (-d_2,d_2), and isotopic forms, bond lengths and angs., microwave spectrum obs. 78−55169
formic acid (-d), microwave spectra and rot. consts., astrophysical appl. 80−91550
formic acid -d_1, chemisorption and dissoc. on Ni (100) 79−34361
formic acid amides, polarisabilities and π-π^* transitions, dipole interaction calcs. 80−23411
formic acid and isotopic species, microwave spectra, Coriolis reson. between vibr. excited states 79−13700
formic acid anhydrides, valence force consts., IR spectra, isotope effects 79−93997
formic acid corrosion of ferritic steel, electrochem. pot. and Mo additions effect *(French)* 80−45439
formic acid crystals, low temp. IR spectra 77−48153
formic acid crystals $\nu_{O\text{-}H\ldots O}$ and $\nu_{O\text{-}D\ldots O}$ vib. anharmonicities 77−48154
formic acid decomposition by IR laser radn., photochem. isotope enrichment 79−52712
formic acid dimer, gas phase, H-bonded complex struct. from elec. dipole moment obs. 78−74791
formic acid dimer, hydrogen bond, ab initio MO calcs. 78−58588
formic acid dimer, tritium β^--decay causing H^+ transfer, ab initio MO calc. 80−3391
formic acid dimer, vibr. spectra, CNDO/2 interpretation *(French)* 80−58155
formic acid dimer-t_1, H bonding, β^--decay effects, ab initio calcs. 79−54763
formic acid external doping in MIM tunnel junctions, inelastic tunnelling spectroscopy obs. 79−3510
cis-formic acid geometry, force fields and fundamental vibr. freq., ab initio study 80−87040
formic acid ions, fragmentation, energy selected, photoelectron-photoion spectra 80−95676
formic acid laser, CW CO_2 laser pumped, far IR lines accurate meas. 77−88714
formic acid laser 311 μm line, freq. meas. by mixing with HCN laser 79−76728
formic acid laser far IR pulse generation by Q-switched CO_2 laser pump source 80−69383
formic acid monomer, vib. spectra and normal coordinate analysis 77−58003
formic acid on Ni (100)-p(2×2)C, decomp. 79−91995
formic acid on Ni (110) surface, adsorption and decomp., modulated mol. beam scatt. anal. 79−89032
formic acid on Ru ($10\bar{1}$), decomp. into H_2, CO_2, H_2O and CO 79−79245
formic acid solvent system, behaviour of electrolytes 79−57239
formic acid submillimetre laser CW lines *(French)* 77−725
formic acid-acetic acid, gas phase, H-bonded complex struct. from elec. dipole moment obs. 78−74791
formic acid-d_0, -d_2, OH(OD) stretching, vibr. band struct. 77−6751
formic acid-d_0,-d_1,-d_1,-d_2, submillimetre laser appls. 77−27282
formic acid-d_0(-d_1)+F, microscopic reaction dynamics, branching ratio, IR chemiluminesc. 78−73021

organic compounds continued
formic acid-d_0(-d_1)(-d_1)(-d_2), vibr. spectra, CNDO/2 interpretation *(French)* 80−58155
formic acid-d_1, NQR sensitive detection by double resonance with spin mixing by continuous coupling 77−77128
formic acid-d, decomposition on partially oxidised Ni (110) surface 77−85066
formic acid-water, PMR relax. obs., mol. assoc. 79−33553
formic acid-water polymers, gas phase, H-bonded complex struct. from elec. dipole moment obs. 78−74791
formic anhydride, He(I) and He(II) photoelectron spectra 79−54910
1-formyl 2(4-nitrophenyl) hydrazine, preparation, optical and electro-optical props. 77−36201
formyl cation-d_1, interstellar strongly deuterated mol. obs. and implications for interstellar chemistry 79−5891
formyl chloride, equilib. geometries and one-electron props., ab initio calcs. 80−47878
formyl chloride, photoelectron spectrum, vibr. struct., ionis. pots., assignments 78−9195
formyl chloride, rot. Zeeman effect of low-J transitions 78−25519
formyl fluoride, and isotopic forms, mol. struct., from electron diffr. and microwave data 80−23570
formyl fluoride, equilib. geometries and one-electron props., ab initio calcs. 80−47878
formyl fluoride+HF, multiple site reactivity, ab initio GO supermol. calc. 78−11498
formyl fluoride (-d_1), IR absorption intensity anal. 78−70813
formyl fluorides, gas phase ion-mol. reactions, comparison with H_2CO+F_2CO, H_2CO+Cl_2CO 77−63900
formyl ion, electron impact rot. excitation, Glauber approx. with Coulomb effect 80−63840
formyl ion, interstellar, detect. in Sagittarius B2 79−35346
formyl ion, interstellar, in Orion Molecular Cloud, J=3-2 line detect. 79−25669
formyl ion (HCO^+), interstellar, shock enhancement of abundance in supernova remnant (IC 443) 80−82464
formyl radical, -d_0, (-d_1), first ionis. pot., photoelectron spectrosc. determ. 80−48039
formyl radical, atmospheric oxidation, IR Fourier transform spectroscopic obs. 79−66785
formyl radical, electronic struct., dissoc. energy and pot. energy surface many body perturbation theory and couple cluster doubles calc. 80−23296
formyl radical, form., vibr. relax., spectrosc. 79−36746
formyl radical, laser mag. reson. spectrum at 5.3 micron 80−47981
formyl radical, lower electronic states, ab initio calc. of pot. energy surface, hydrocarbon flame band 79−68287
formyl radical ion, mm wave emission obs. of interstellar clouds 80−90503
formyl radical-d_0,-d_1, microwave spectroscopy, high field Zeeman effect 78−37631
(formyl-H-F)$^-$, strong H-bond, using recent difinition 79−98240
formyl-nitrophenyl hydrazine, for possible electro-optic appl., cryst. growth in glass capillary 77−44150
formyl-triglycyl amide-H_2O, analytical pot., ab initio calc. 79−48206
free radicals, solid, selective pulse NMR expts. 80−60452
free-base porphin, S_2-S_0 transition vibronic bands, photochem. hole-burning 79−36631
free-base porphin, Zeeman shift meas. by photochem. hole-burning 80−83416
Freon, F-13V1 and F-23, thermal cond., −168 to 160°C, up to 6.10^7 Pa 77−47628
Freon, matrix radiolysis, photoionis., IR spectra of CF_2Cl^+ and parent cations 78−80767
Freon, photochemical ^{13}C and ^{37}Cl isotope enrichment using CO_2 laser pulses 79−36787
freon, plasma etching characts., effect of dark space in RF glow discharge 79−15830
Freon(-11, -12, 113), boiling, under increased gravitation, heat exchange mechanism, bubble form., review 77−46895
freon 113, 114 and 115, thermal cond., rot. relax., investigation *(Russian)* 77−89226
Freon 113, film boiling from cylindrical surfaces 79−23194
Freon 123, deuterium separation at high press. by ns CO_2 laser multiple-photon dissoc. 80−91616
Freon 123-d and natural 123, selective absorpt. cross section at 10.2 and 10.6 μm 80−5546
freon 12, gas, up to 50 atm, refr. index, 328, 3103 MHz *(French)* 78−14129
Freon 12, P-V-T relation determ., student lab. apparatus 79−62970
Freon 13-B1 and mixtures with Xe and Kr, saturation curve 1 to 8 atm., for ionography ionisation chambers 77−12997
Freon 14, optically pumped roto-vibr. mol. laser, low temp. operation and performance 79−50315
Freon 14, roto-vibr. mol. laser, low-temp. performance 80−9871
freon 22, gas, up to 50 atm, refr. index, 328, 3103 MHz *(French)* 78−14129
freon (freon-N_2), gas, sparking pots., ionisation and electron attachment coeffs. 78−42705
Freon electrohydrodynamic flow, jet dynamic pressure obs. *(Russian)* 80−59117
Freon F-113, boiling on porous Cu coating *(Russian)* 79−72788
freon F-13V1, specific heat standards choice and certification, for liquids and vapours in 90 to 273.15K range 80−23877
freon gas flow around blunt object, bow shock instability 80−10266
Freon IR mass absorption coefficients, 3 to 15 μm 79−76422
Freon plasma, Si plasma etching, microelectronics appls. 80−3080
Freon-113, boiling and heat transfer on horizontal pipes with annular fins 80−74855
Freon-113, correlation properties near phase-separation boundary, gravitational field effect 80−107410
Freon-113, correlative and optical props. near critical pt. 79−65822
Freon-113, Freon-11, sustained and transient boiling flow instabilities, inlet subcooling effect 78−94809
freon-113, non-polar, electric field effects obs., heat emission during vapours condensation *(Russian)* 79−1055
Freon-113, pure and mixed with methanol, EHD coupled minimum film boiling, surface wave model 78−87240
Freon-114, Leidenfrost phenomena, crit. press. obs. 78−90667
freon-114 boundary layer, stability, press. gradient and heating effects 79−18891

organic compounds continued
Freon-11, forced convection boiling heat transfer in vertical annular passage 79−32509
Freon-11, liq., elec. birefringence *(French)* 78−88278
Freon-11, pool-boiling, heat transfer from inclined plate 78−51046
Freon-11, reactor coolant, steady-state and transient CHF meas. 79−49732
Freon-11(-113)(-12), heat pipe working fluid, crit. heat/mass transfer 78−42517
Freon-12, absorpt. coeffs. for CO_2 laser radiation, press. and temp. depend. 78−55170
Freon-12, annular mist flow in tube, wall film mass flow rate 80−69905
freon-CO_2, under pressure, breakdown voltage data *(Rumanian)* 77−19782
freon-isopropanol, mixture, Raman spectra in OH(OD) stretching region *(French)* 79−26986
freon-N_2 low-pressure mixture prebreakdown current obs. 79−18995
Freons, C51-12, 113, drops, on brass surface, Leidenfrost pt., press. effect 78−87784
Freons, film condensation inside pipes, heat transfer, general correlation 79−46312
Freons, IR absorpt. band intensities meas. in atm. window region 77−30871
freons, tropospheric photodissoc. rates from solar 1950-2150 Å radiation ground level meas. 79−2345
Freons 21, 22 and 23, thermal cond. 78−83513
Freons and their mixtures with N_2 and SF_6, breakdown voltage in uniform electric field *(German)* 78−71423
Freons of ethane series, thermal cond. meas. 78−63884
freons of methane series, pulsed US investigation of vibr. relaxtion 77−39397
frozen liquids, high-resolution ^{13}C NMR using magic angle spinning 79−33544
frozen solution spectra, inhomogeneous broadening and phonon effects 79−33725
β-D-fructose, film, electron irrad., struct. changes, tunnelling spectra 77−10781
fructose, stereoviews and morphological data on microcrystals 78−18510
FTF-TCNQ, libron freqs., temp. and press. effect 79−86860
fucose, optical constants and dispersion eqns. 80−30762
fulminic acid, semirigid bender Hamiltonian, rot.-vibr. level separations, config., bending pot. 79−41152
fulminic acid-d_0, -d_1, rot. Zeeman effect and nucl. quadrupole coupling 78−78683
fulvalene, electronic structs., semi-empirical MIEHM calcs. 77−75057
fulvene, correl. problem, open-shell coupled-cluster approach, PPP calc. 79−81157
fulvene, electronic struct., spectra, ionisation pot., INDO-CI LACO-MO-SCF calcs. 79−54834
fulvene, ground and excited states, electronic correl. and struct. 79−26898
fulvene, ring currents hypersusceptibilities calcs. 80−102588
β-fumaric acid, empirical interatomic potential functions 79−7567
fumaric acid, vapour press. meas, using torsion-weighing effusion apparatus 77−89530
fumaronitrile exciplexes, photoisomeris. and photoionis, dissolved O_2 effect 78−27789
fungicides, in water, detect. by laser excited reson. Raman spectroscopy 78−31732
furan, adsorbed on NaCl, evidence of new condensed phase, IR spectra *(French)* 80−16028
furan, electronic struct. calc., σ^-pi consistency method 77−67957
furan, FSGO calcs. of orbital energies, locations, dipole moments, charge distribs. 77−67976
furan, gas, X-ray photoelectron spectra, satellite struct. 78−5281
furan, HAM/3 calc. of ionis. and excitation energy and electron affinity 79−26894
furan, ionisation pots., transition operator calcs. 77−30771
furan, liq., US phase vel. decay in space and time 80−99891
furan, liq., US relax., light scatt. meas. 77−77231
furan, mean free path meas., US relax. 80−59585
furan, mol. reorientationally disordered phases, thermodynamics 79−46782
furan, P-V-T relations, 210 to 260K, up to 1000 MPz 79−95122
furan, Penning election spectra and photoelection spectra, rel. intensities 80−95725
furan, photoacoustic spectra meas. at CO_2 laser wavelengths 80−18849
furan, photoelectron ang. distrib. from mol. 79−31596
furan, resonantly enhanced multiphoton ionisation 80−106362
furan, trifluoromethyl derivatives, first ionis. pots., CF_3 group nature 79−27110
furan-cyclohexane, liq. mixture, intermol. vibrational energy transfer, US study 80−70313
furane, cryst., low freq. vibr. spectrum, temp. depend., 12 to 253K 80−84743
furane, crystalline, lattice vibr. 78−79694
furane, lattice dynamics calc. for low-temp. phase 77−55329
2-furanmethanethiol, mol. struct., electron diffr. and IR spectroscopic examination 79−10106
[2,2](2,5)furanophane, through bond and through space interactions, UPS obs. 78−82786
furfural-water interface, anomalous mass transfer, coupling of heat and mass transfer 77−80626
furfuraldehyde liquid, US relaxation meas. 77−20016
furil, photochem. generated alkali cationic triple ions, ESR 78−80758
furil, photochem. reduction by pentachlorophenol, zero-field CIDNP study 77−90625
furil + pentachlorophenol, photochem. reduction, cross-relax. and CIDNP, PMR relax. obs. 79−52694
furoyl chloride, mol. vibr., normal in plane coord. calc. *(French)* 79−68218
GABA uptake or exchange by synaptosomal fractions 77−12907
gadolinium acetate, L_3 X-ray absorpt. discontinuity 77−85840
gadolinium oxalate, L_3 X-ray absorpt. discontinuity 77−85840
gallic acid+BrO_3^-+H_2SO_4 system, uncatalysed oscillatory chemical reactions 78−61004
gallium transferrin, formation constant, nuclear medicine appls. 79−96285
galvinoxyl, radical in a smectic liq. cryst., ENDOR study 79−78567
galvinoxyl radical in phenol matrix, ESR spectra 80−54950
ganglioside synthesis, chick retina, light stimulation 77−9189

organic compounds continued
gas chromatography, modified geophitised C black obsorbent 79−96358
gaseous hydrocarbons, removal from atmosphere with allophane adsorber *(Japanese)* 77−78412
gases, IR fluoresc. by CO_2 laser 80−78619
gasoline, Mn determ. by AAS using N_2O-H_2 flame 78−15729
gasoline, sample preparation for P determ. by at. absorpt. 78−31729
gasoline additives, analysis by IR spectroscopy, preconcentration, separation and computer techniques 78−31730
gasoline-air flame, laser induced fluorescence spectra obs. 80−91587
gelatin-Pd II complex formation, circular dichroism and absorpt. spectra meas. 79−61881
gelatine, absorption on AgBr *(Russian)* 79−100420
gelatine, effect on lifetime and formation of latent image in photographic layers *(Russian)* 80−3389
gelatine films containing AgBr, effect of AgBr comp., aging, UV exposure *(Russian)* 79−67408
gelatine-polyvinyl alcohol films, effect of pH on transparency *(Russian)* 79−58830
gentamycine, radioimmunological assay *(French)* 79−96652
geochemical indicators of palaeoenvironmental conditions of sedimentation 78−40539
geometry optimisation, Newton-Raphson method algorithm 77−10612
germanium phthalocyanine, elec. cond. temp. depend. 80−80271
germanyl acetylenes, fine structure due to internal rotation in IR-active perpendicular bands 79−98096
germyl radicals, benzil adducts, organometallic group dynamic migration, EPR 77−58049
germylacetylene-d_0($-d_3$), centrifugal distortion const. and thermodynamic functions calc. 80−95581
glass, creep under shear with superposition of hydrostatic press. 78−31482
glass, photochem. of trapped electrons 79−52722
glasses, low temp. mol. mobility, NMR T_1 meas. 80−60439
glasses and glassy crystals, organic, entropy of struct. disorder, rel. to mol. struct. 79−65219
glassy matrices, electron spin-lattice relax. of radiation-produced Ag atoms, temp. depend., tunnelling relax. 79−34331
globular hydrocarbons, cohesive energy and Gruneisen parameter calcs. 79−19183
glucagon, helical folding, Zimm-Bragg anal. 78−76356
α-D-glucose, further struct. refinement based on neutron diffr. data 79−42043
glucose, glucose oxidase determ., continuous flow anal. 80−61736
glucose, meas. of utilisation in brain by emission tomography 78−69183
glucose in pancreatic islet cells, effect on K^+ permeability 79−74615
glucose powder and aqueous soln., photoacoustic spectra in middle IR 77−81101
glucose sensitive Ca pools in pancreatic islets, rel. to secretion 77−32883
glucose transport system from pig small intestine, reconstitution in phospholipid vesicles 77−29111
glutamate as transmitter of hippocampal perforant path 78−11635
glutamate induced ionic channels, pot.-depend. transition temp., locust muscle 77−77882
glutamate Na-stimulated uptake in membrane vesicles of E. coli, role of ion gradients 78−48776
L-glutamic acid, solid, amino group reorientation, PMR second moment obs. 78−35046
L(+) glutamic acid halogen acid salts, crystallographic, optical and calorimetric meas., halide effect 78−34505
L(+)-glutamic acid hydrochloride, deuterium isotope effect, cryst. struct., IR spectra and SHG 77−46755
glutamic acid hydrochloride, L(+), single cryst., soln. growth and characterisation, SHG 77−24943
glutamic acid hydrochloride, L(+), solution growth of large single crystals, using cylindrical seeds 78−60556
glutamine, polycryst., proton mag. relax. and mol. motion 78−20139
glutamine synthetase reconstruction from electron micrographs using computer averaging 79−92452
glutaric acid, γ-irrad. single crysts., free radical EPR obs. at 77K 80−81340
glutaric acid-polyoxyethylene eutectic, melting and crystn. 80−28924
glyceraldehyde 3-phosphate dehydrogenase, EPR, saturation transfer EPR 79−98124
glycerides, high mol. wt. species prod. after contact with lunar grains 78−3333
glycerin, aq. soln., heat transfer in oscillating liquid-filled cylinders 80−10117
glycerin, laser breakdown, photoacoustic and photohydrodynamic parameters 78−52597
glycerin, propag. of longit. and shear hypersonic waves, light scatt. meas. 77−51442
glycerin nonadecane, critical nuclei, meas. of number of mols. and surface tension from rate of nucleation 79−65293
glycerin-water solns., visualization of standing vortices behind cylinder 80−59151
glycerine, absolute evaporation rate meas. 78−2244
glycerine, aq. solns., contact angs. with metals, 20-70°C 78−56025
glycerine, refractive index at X-ray wavelengths *(Russian)* 79−47409
glycerine, sound vel. meas. at 5 to 20 kHz in small-volume cells 78−9516
glycerine, thermal diffusivity, constant-rate heating method *(Japanese)* 80−6570
glycerine solutions, fluoresc. damping curves in reson. quenching by one-photon counting method 78−10978
glycerine-water drops, collision dynamics, ang. of incidence influence *(Russian)* 78−83461
glycerine-water mixture, boundary surface velocity of rising air bubbles *(German)* 79−32631
glycerol, aq. soln., excess heat capacity, H bonding 78−3362
glycerol, aq. soln., proton NMR study of H-bonding 79−78545
glycerol, associated liq., correl. between acoustic and dielectric relaxation times 78−9925
glycerol, cryst. and glassy states, sp.ht. 80−2176
glycerol, dilute aqueous solns., excess partial molal heat capacities 79−57280
glycerol, effect on fatigue lifetime of polystyrene 79−43455
glycerol, high press. heat capacity and thermal cond. meas. 77−41613
glycerol, highly viscous state, static and dynamic Kerr effect obs. 80−60545
organic compounds continued
glycerol, liq., effective Debye temp., temp. depend., quasi-cryst. model 77−4209
glycerol, liq., reflectivity, in VUV region, for optical and dielec. functions 79−15475
glycerol, liq. and glass, thermal diffusivity meas. 79−82394
glycerol, Mossbauer and neutron scatt. 80−20559
glycerol, natural convection from temp. fields in spherical partially filled vessel 80−1561
glycerol, natural convection in inclined box, three-dimensional photography 77−19600
glycerol, NMR, nucl. mag. spin relax. and high freq. motion 79−51874
glycerol, relaxing fluid, thermally induced light scatt. 77−32388
glycerol, reorientation in associated liqs. 79−77481
glycerol, shear relaxation, KCl or NaBr additive effects 79−60537
glycerol, solution structure, adiabatic compressibility studies 78−87605
glycerol, supercooled, Mossbauer effect and model of mol. motion 78−64301
glycerol, supercooled liq., dynamical struct. factor, Mossbauer spectroscopy 78−27126
glycerol, supercooled liq., mol. motion, Mossbauer effect, Rayleigh scatt. obs. 77−73099
glycerol+guaiacol (m-toluidine) (benzylethylamine), coexistence curve, exactly solvable decorated lattice model predictions 78−95158
glycerol($-d_3$), single cryst., glassy, and supercooled, polarised Raman spectra, anharmonic multiphonon interactions 79−91419
glycerol concentration effect on temp. depend. of survival of slowly frozen human erythrocytes 78−77019
glycerol monooleate bilayers, photoinitiated mediated transport of OH^- and H_3O^+ 79−88059
glycerol protection of slowly frozen human erythrocytes, phys.-chem. basis 78−77020
glycerol-D_2O:Tb^{3+}, Nd^{3+} soln. and frozen glass, energy transfer 78−60509
glycerol-d_3($-d_4$), compressed viscous liq., reorientational motion, NMR obs. 80−7183
1-glyceryl 1-octanoate-water-CsCl, Cs^+H_2O interaction in lamellar phase, NMR quadrupole splitting and chemical shift 80−50209
glyceryl dibenzoate, external plasticiser, for styrene-acrylic terpolymer, compatibility, surface tension meas. 79−15834
glyceryl tristearate, soln. growth, surface entropy factor calc. 78−42934
glycine, ^{13}C-enriched, spin-lattice relax. times in frog muscle and free soln. 77−44605
glycine, ^{17}O NMR chemical shifts and linewidths, pH dependence 80−80625
glycine, cryst., cationic radicals, EPR 78−11537
X-glycine, cryst., Raman band intensities of local group modes 80−93298
γ-glycine, cryst. struct. by neutron diffr. at 83K and 298K 80−35825
α-glycine, deuterated, low freq. intermol. modes, neutron diffr. obs. 80−15086
glycine, electron-irrad. polycrysts., stable products obs. by ^{13}C NMR 78−15775
glycine, interstellar, 22-83 GHz search in mol. clouds 79−30115
α-glycine, irradiated, oxidation prod. N-centred π radical ERR 77−14459
glycine, mm wave spectrum 79−3435
α-glycine, natural and ^{15}N-substituted, solid, Raman spectra, normal vibrs. 77−63408
glycine, neutral and zwitterion interaction with water, Monte Carlo simulation 79−53026
glycine, nucl. spin-lattice relax. of CH_3 and NH_3 groups 77−8440
glycine, oligomer, vibr. spectra rel. to polymeric form 79−83695
α-, β-, γ- glycine, thermal expansion tensor 79−95187
glycine, uptake by renal brushborder membrane vesicles 77−44614
α-glycine crystal, Cu(II) impurity complex, ligand ENDOR spectra 79−65765
glycine overlayers, adsorbed on Ag, XPS and SIMS study 79−86986
glycine silver nitrate, and deuterated analogue, ferroelec. transition, hydrostatic press. effects 77−36185
glycine silver nitrate, dielec. relax. in paraelec. and ferroelec. phases 80−29678
glycine sulphate:L-alanine, unirradiated, optical spectroscopy of scintillations 80−80863
glycine zwitterion+water, interaction pot., ab initio SCF LCAO calc. 78−48747
glycine-$AgNO_3$, single cryst., X-irrad., oxidation product form. 77−48660
α-glycine-C-d_2, Raman spectra, intermol. pot. 79−91432
glycine-d_2 crystal, X-irrad., H-D exchange reactions 77−16837
glycine-d_3, pulse radiolysis, primary reaction product optical and EPR spectra 79−79265
glycogen, ^3H distribution in glycogen, haemoglobin and chromatin of mice drinking tritiated water 78−31910
glycogen and metabolising enzymes following radiation-induced atrophy in rat testes 78−15869
glycol, aq., in swelling equilib. with polyvinyl alcohol, interactions 80−104201
glycol methacrylate embedded chick embryonic tissue, histologic investigation 79−84038
glycol solutions, diffusion coeffs., viscosity 78−51711
glycol-alkane systems, interfacial tensions, regular soln. theory and Antonow's rule 79−14983
glycyl anion radical, in α-glycine cryst., struct., ESR obs. 78−33530
α-glycylglycine, cryst. struct. and deform. electron density, X-ray and neutron diffr. 79−86777
glyoxal, 4550Å bond system, rot. anal. mol. consts. and geometry 77−42330
glyoxal, ^1A_u state energy transfer, D effects 77−58066
glyoxal, $^3n\pi^*$ states, ab initio STO-3G CI calcs., ΔE_{SCF} transition energies 78−94194
glyoxal, electron affinity at centrosymm. trans geometry 80−87225
glyoxal, gas phase emission spectra, mag. quenching 77−18968
glyoxal, internal conversion, energy redistrib. 80−53036
glyoxal, intersystem crossing in weak mag. field 78−78743
glyoxal, lowest triplet state, excitation energies, electron correl. effects 78−5147
glyoxal, mag. quenching of fluoresc. 79−31582
glyoxal, magnetic quenching, enhancement of radiationless decay, direct and indirect mechanisms 77−42345

organic compounds continued
glyoxal, mol., conformational anal., inapplicability of MINDO/3 79−94105
glyoxal, radiationless transitions in weak mag. field, fluoresc. quenching 77−58062
glyoxal, relax. processes, single vibronic level fluoresc. spectroscopy 78−58789
glyoxal, $S_0 \rightarrow S_1$ band, opto-acoustic phase angle meas. 80−68256
glyoxal, S_1-S_0 fluorescence after narrow band excitation, deconvolution 78−58734
glyoxal, selected state photodissoc., vibronic effects, CO quantum yield, 1-10 torr 78−37691
glyoxal, singlet-triplet coupling, double reson. and level-anticrossing spectroscopy 80−48053
glyoxal, singlet-triplet radiationless processes in mag. field 80−106347
glyoxal, sum of states, isometric group, symmetry no., thermodynamic functions 80−58186
glyoxal, triplet $n \rightarrow \pi^*$ and $\pi \rightarrow \pi^*$ transitions studied by low-energy electron diffr. 80−83502
glyoxal, triplet state excitation energy calc., modified CI method 78−37536
glyoxal, vapour, predissoc. in S_1 zero-point level states 80−102544
glyoxal, vibr. energy redistrib. following internal conversion 80−23452
glyoxal, vibr. relax. of ^1A_u state in gaseous environments 79−45800
glyoxal+glyoxal, potential well depth estimation method 79−86034
glyoxal (^1A_u), fluoresc. quantum yields, radiative and nonradiative lifetimes 80−32759
glyoxal in supersonic jet, fluoresc. excitation, collision-induced intersystem crossing, van der Waals complex 79−81223
glyoxal-d_0, -d_2, triplet kinetics, microwave-saturation recovery and MIDP obs. 77−71823
glyoxal-formamide, charge transfer theory, Mulliken population, ab initio calc., multiconfiguration scheme 80−106392
glyoxal-photoreduction-product-radicals, kinetics and intramol. dynamics 77−32808
GMP, cyclic, in giant barnacle muscle fibres, conc. associated with contraction 77−56369
GMP, cyclic, possible mediation of slow excitatory postsynaptic pot. in sympathetic ganglia 78−27930
GMP, cyclic, proposed role in visual cell function 78−64997
GMP, cyclic, rel. to negative isotropic effect of acetylcholine in atrial muscle 77−48781
dGMP γ-irrad. in frozen soln., free radical form., computer EPR spectra anal. 78−31774
gold complex, AuI (triphenylphosphine)$_n$ chlorates (n=2,3,4,), Mossbauer spectra 79−54874
gramicidin, succinyl derivatives, channel structs. in artificial lipid bilayers 79−8484
graphite, trifluoromethanesulphonate intercalate, prep. by anodic oxidation 78−27439
graphite-alkali metal-benzene ternary intercalation compounds thermal and X-ray anal. *(French)* 78−27434
guadinium aluminium sulphate hexahydrate, high resolution multipulse NMR appls. 78−60345
guaiacol+glycerol, coexistence curve, exactly solvable decorated lattice model predictions 78−95158
guanadinium zinc sulphate:Cu^{2+}, EPR of Cu^{2+} at tetrahedrally coordinated Zn^{2+} sites 78−39388
guanidine aluminium sulphate, lattice charge contribution to coordination polyhedron cryst. potential 80−103651
guanidine aluminium sulphate hexahydrate:Cr^{3+}, ESR spectra fine struct. 80−93169
guanidine aluminium sulphate hexahydrate, ferroelec. cryst., growth, domain struct., dielec., switching props. 77−43950
guanidine aluminium sulphate hexahydrate, SEM obs. of ferroelec. domain struct. in single crysts. 80−97219
guanidine aluminium sulphate hexahydrate type ferroelectrics, ESR of Fe^{3+} exchange pairs 77−90022
guanidinium aluminium sulphate, domain wall energies and domain structures 78−92039
guanidinium aluminium sulphate hexahydrate:Cr^{3+}, EPR, 295.5, 78.45, 1.61K, zero field splitting 78−68359
guanidinium aluminium sulphate hexahydrate:Cr^{3+}, isotope effect, zero field splitting, vibr. coupling 78−6570
guanidinium aluminium sulphate hexahydrate:Cr^{3+} pressure meas. from ESR 79−38375
guanidinium aluminium sulphate hexahydrate:Cr, temp. depend. of zero field splitting parameter in EPR spectra 77−69679
guanidinium aluminium sulphate hexahydrate:Fe^{3+}, EPR spectra, angular var. calc. 80−54940
guanidinium aluminium sulphate hexahydrate:Mn^{2+}, NMR 78−91939
guanidinium aluminium sulphate hexahydrate, ESR of V^{3+}, 21.5 GHz, 4.2K 78−91942
guanidinium aluminium sulphate hexahydrate, pyroelectric coeff., 1.8-300K, dynamic method *(French)* 79−19844
guanidinium aluminium sulphate hexahydrate, surface obs., SEM and AES expts. 80−71362
guanidinium aluminium sulphate hexahydrate, temp. depend. quadrupole coupling const. for $^{27}Al^{3+}$ and $^{71}Ga^{3+}$ 78−19368
guanidinium aluminium sulphate hydrate, ferroelec., decoration patterns on cleavage surface, domain obs. 80−97218
guanidinium chromium sulphate hexahydrate, multilevel system, spin-lattice relax. from AC susceptibility 77−55702
guanidinium gallium sulphate hexahydrate:Cr^{3+} pressure meas. from ESR 79−38375
guanidinium ion, rot. barriers, ab initio calcs. 78−41923
guanidinium uranyl sulphate hydrate, ferroelec., decoration patterns on cleavage surface, domain obs. 80−97218
guanidinium uranyl sulphate trihydrate, new ferroelec., dielec. props. 78−43824
guanidinium uranyl sulphate trihydrate, X-ray diffr., crystal struct. 78−14331
guanidinium vanadium sulphate hexahydrate, low temp. mag. props., mag. sp. ht. *(Japanese)* 78−19268
guanidinium vanadium sulphate hexahydrate, mag. behaviour in applied fields below 1K 77−66376
guanidinium vanadium sulphate hexahydrate, singlet ground state system, low temp. mag. props. 80−44843
guanidinium vanadium sulphate hexahydrate, susceptibility meas. spin-lattice relax. effects 77−66279

organic compounds continued
guanidium salt, $(C(NH_2)_3)_2Pt(CN)_4Br_{0.23}.H_2O$, pseudo-one-dimens., solitary wave excitation 78−6307
guanido iodate, cryst. struct. 78−83807
guanine, ^{15}N and D substituted, in acid and base solutions, vibr. anal. 79−26994
guanine nucleotides, purinic 8-CH exchange kinetic isotope effect, Raman spectral study 80−83381
guanine nucleotides, role in protein biosynthesis 78−68982
guanine tautomers, relative stabilities, nonempirical MO calcs. 80−21442
guanine-cytosine system rearrangement, reaction tree algorithm, using pot. surfaces 77−70286
guanosine, γ-irrad., positron lifetime rel. to free radical conc. 78−72635
gummosine, cryst. and mol. structs., and absolute config., X-ray expts. 78−79602
HAB, dielectric and calorimetric investig. in solid, liq. cryst. and liq. phases 77−84639
haematoporphyrin-derivative in fluoresc. bronchoscopic lung tumour localisation 77−86580
haematoporphyrine, complexed with chloranil and tryptophane, energy spectra, transition moments and intermolecular distances 80−72127
haematoxylin, reagent for spectrophotometric determ. of As (V) 78−20104
haeme proteins and metalloporphytins, redox chem. and oxygen binding 80−3573
haemoglobin, dielectric transient response following UV-irradiation 80−51166
haemoglobin hydroxide, Fe Mossbauer quadrupole splitting 78−55192
haemoproteins, fluoresc., reson. Raman and radiationless decay 77−30916
halides, aryl and aryl-alkyl 193 nm photodissoc., fragment translational energy distrib. 80−48048
halides, NQR shift in external elec. field, rel. to bonding 77−12237
1-halo-1-n-propylcyclohexanes, conform. equilib., and pot. barriers, IR spectra *(Russian)* 78−21928
halo-alkanes, IR-microwave double resonance, book contrib. 80−54997
haloacenaphthenes in n-heptane, quasi-line phosphoresc. spectra, vibronic spin-orbit interaction 80−43096
haloacetaldehydes, rot. isomerism, semi-empirical model calcs. 78−50659
haloacetylene cations, electron impact excitation $A \rightarrow X$ band system assignment 80−32766
haloacetylenes, photoelectron spectra, electronic states of radical cations 79−22756
haloacylhalides, rot. isomerism, semi-empirical model calcs. 78−50659
haloalkane-aromatic complexes, ground and excited states, CNDO calcs. 80−69082
haloalkanes, ^{19}F chem. shielding, temp. depend., FT NMR obs. 78−86888
haloalkanes, liq., transport through barrier plastic 78−76921
haloalkanes, max. overlap approx., heat of form. and dipole moment 78−94198
1-haloalkanes, microwave spectra, conformation 78−21913
haloalkanes, mol. second hyperpolarisability, atom-dipole interaction model 77−34543
haloalkanes, rot. isomerism, semi-empirical model calcs. 78−50659
haloalkanes+$O(^1D)$, deactivation reactions, absolute rate consts. determ. 79−11783
haloalkyl peroxy radical+NO_2, haloalkyl peroxynitrate form., FT IR obs. 79−34283
haloalkyl peroxynitrate, form., FTIR obs., rel. to stratospheric chem. 79−34283
haloanilines, far IR spectra, vibr. assignments 78−82726
haloanilines, T_1-states, EPR and zero-field ODMR obs. 78−58725
haloanilines+thionine triplets, electron transfer reaction, radical yield meas. 80−3330
haloanisoles, T_1-states, EPR and zero-field ODMR obs. 78−58725
haloazulenes, S_2-state deactivation, intersystem crossing and heavy atom effects 78−13545
halobenzene cations, in solid Ne matrix, slow vibr. relax., fluoresc. obs. 80−74194
halobenzene type ions, high resolution spectrosc. with new emission source *(French)* 80−57383
halobenzenes, aqueous molar solubilities and partitioning, 25°C obs., rel. to melting pts. 80−40803
halobenzenes, benzene solns., positronium form., additive effects 79−43610
halobenzenes, singlet excited states decay, substituent effects 77−75175
halobenzonitriles, T_1-states, EPR and zero-field ODMR obs. 78−58725
halocarbon destruction by siliceous land surfaces, possible tropospheric sink 79−12168
halocarbon index matching fluids for long wavelength fibre-optic appl. 80−69470
halocarbon lifetimes and conc. distrib. using two-dimens. tropospheric model 79−12180
halocarbon meas. in Alaska troposphere and lower stratosphere 77−70719
halocarbons, atm. conc., rel. to tropospheric OH conc. 77−45069
halocarbons, atm. conc. meas. in southern hemisphere 79−5602
halocarbons, atmospheric global distrib., sources and sinks, rel. to 0_3 depletion 80−4088
halocarbons, benzene solns., positronium form., additive effects 79−43610
halocarbons, decomp. by natural tropospheric ions 77−21889
halocarbons, global budget analysis 79−34881
halocarbons, identification and meas. in troposphere and lower stratosphere 78−32186
halocarbons, in Adrigole, Ireland atmosphere 77−70809
halocarbons, in British Isles atmosphere, aircraft sampling 77−73832
halocarbons, meas. in air and water, W. Europe 78−36272
halocarbons, multiphoton dissociation, product identification 78−37694
halocarbons, tropospheric, decomp. by natural ionisation 77−33139
halocarbons+OH rate consts., appl. to tropospheric degradation 79−52622
halocarbons in air, determ. via gas chromatography after cryogenic sampling 78−81468
halocarbons in atmosphere, global monitoring stations 79−57555
haloethane+OH, reaction rate consts., reson. fluoresc. meas. in discharge-flow system 79−72350
2-haloethanols, gauche conformer stability, exchange interaction 79−18311

organic compounds continued
2-haloethanols, Raman spectra, rot. isomerism and conform. energies 79−10117
2-haloethanols, torsional interaction, IR spectra, ab initio calcs., 2-dimens. model 80−74160
2-haloethyl ethers, relative conformational energies, Raman obs. 79−27002
haloethylenes+$Ar^+(Kr^+)(Ne^+)(Xe^+)$, 2-stage ion beam mass spectrometric obs. 77−9061
halofluorescein dyes, fluoresc. internal conversion, intersystem crossing 77−3405
halofluorocarbons, in ambient air, background levels in situ quantification 78−69530
halogen compounds, NQR spectra correl. anal. 77−12239
halogenated compounds, CH and C_2 flame emission *(German)* 79−52668
halogenated hydrocarbon HCl elimination, three and four centre, IR multiphoton dissoc. 79−5137
halogenated propanes, IR and Raman spectra, LF vibrs. 79−10105
halogenoacetylene radical cations, C_2HX^+, emission spectra, $A^2\Pi\rightarrow X^2\Pi$ band systems 78−17678
halogenobenzenes, dipolar liquid, far IR absorpt. rel. to Mori continued fraction for autocorrel. function 78−2875
halogermane radical anions, ESR spectra and struct. 80−87153
halomethane+Hg, $^3P_1$-state total quenching 80−52927
halomethane+$O(^1D)$, direct reaction in flow system 80−3333
halomethane+OH, reaction rate consts., reson. fluoresc. meas. in discharge-flow system 79−72350
halomethanes, 2.5 keV electron impact energy loss spectra, inner shell excitation 78−42232
halomethanes, ^{13}C chem. shifts, trigonal additivity procedure 80−1002
halomethanes, ^{13}C chemical shifts, diamag. susceptibility, effect of nonbonded interactions 78−78726
halomethanes, -d_0 and -d_3, IR intensity anal. 77−58082
halomethanes, absorpt. coeffs. meas. in Nd laser emission band 80−78620
halomethanes, C K-shell electron energy loss spectra, assignments 79−89797
halomethanes, collision induced vibr.-rot. transitions, semiclassical theory 78−78785
halomethanes, dipole moment derivatives, unique sign set selection 78−66682
halomethanes, electron impact dissoc., tropospheric lifetimes *(German)* 79−50141
halomethanes, ideal gas thermodynamics props. 79−32733
halomethanes, Kerr consts., depolarisation ratios and hyperpolarisabilities meas. 78−25624
halomethanes, liquid densities, data tables 78−75703
halomethanes, multiphoton dissoc., energy deposition 78−82800
halomethanes, Raman spectra, totally symmetric vibr. bands depolaris. ratios 79−89677
halomethanes, second dielectric virial coeff. of polar gas, temp. depend. *(German)* 78−26234
halomethanes, surface tension temp. dependence from triple point to critical point *(German)* 80−100376
halomethanes, synchrotron radiation photoabsorption cross sections, Rydberg states 80−28033
halomethanes, UV multiphoton dissoc., photofragment fluoresc. 80−14165
halomethanes, UV photoelectron spectroscopy, basic concepts, spectra 78−17715
halomethanes, valence photoelectron spectra, vibr. and vibronic struct. 78−50581
halomethanes, vap. press. and boiling point data tables 79−77736
halomethanes, vibronic struct. in electron spectra, Jahn-Teller and spin-orbit coupling 78−50537
halomethanes+Ba(^1S,^3D), Sr(^1S,^3P), chem. reaction products laser-induced fluoresc. obs. 79−66270
halomethanes in troposphere and stratosphere, O_3 depletion 80−16866
halonaphthalenes, heavy atom effect on radiative and nonradiative decays 79−31584
halonaphthalenes, intersystem crossing-singlet excited state to triplet state spin sublevel 80−53035
1-halonaphthalenes, lowest triplet state, spin sublevels decay, internal heavy atom effects 79−95819
2-halopropionates, liq., dielec. relax. and permittivity 80−15948
halothane, effect on conductivity and time of adhesion of lipid membranes 79−53070
halotoluenes, singlet excited states decay, substituent effects 77−75175
5-halouracils, solid, radiation damage, free radicals in 5-fluorouracil single crysts. 80−71926
s-halouracils, solid, radiation damage obs., deoxyribose ring opening in single crysts. 80−71929
HBAB, temp. depend. of apparent viscosity and density 78−18542
HBAB soln. in CBOOA, re-entrant nematic phase 79−14674
HBBOP and HBH-HBBOP nematic mixtures, relax. freqs. and dielec. anisotropy, binary system behaviour *(German)* 79−33606
HBCA liq. cryst., anisotropic light scatt. 79−78692
HBHA, liq. cryst. cpds. synthesis and smectic B-smectic B transition 77−15562
HBPA, smectic liq. cryst. glass-supercooled transition and Debye temp., ^{57}Fe Mossbauer effect 80−54999
HBT, liq. cryst., phase transitions, quenching effects obs. 78−22833
HBT liquid crystal, mag. susceptibility and anisotropy, smectic, nematic, isotropic phases 78−18748
heart cytosol, aspartate transaminase, electron density map interpretation 80−55990
heat of formation, dissociation energy from dynamic electronegativity *(Chinese)* 79−96351
heavy hydrocarbons, surface transient deformation by laser-induced thermocapillarity 79−33157
heavy-ion induced desorption of organic cpds. from solid surfaces 80−100739
heaxadecane solvents of different mol. shapes, effect on DCl vib.-rot. spectra 77−34623
helicenes, fluoresc., intersystem crossing, rate parameters 77−3392
hepanoate, Li, Na, K and Rb alkanoate mixture, DSC anal. 78−10192
heparin assay in animal model of Pseudomonas sepsis, rheological approach 77−52953
n-heptacosane, differential thermal anal. under high press. 78−51669

organic compounds continued
α,β-heptacyclene, double mols. with weak reson. bonds, quasilinear spectra 79−94030
α-heptacyclene, in solid matrix, photodissoc. quantum yields, fluoresc. temp. depend., phosphoresc. IR spectra 77−25292
α-(β-)heptacyclene, vibronic spectra, electronic-vibr. interactions 78−1021
n-heptadecane, short-chain mol. liq., statistical thermodynamics 79−73084
heptafluoroiodopropane, photodissoc., appl. in I ring laser 80−48236
heptafluoroiodopropane, Raman spectum, cross-sections, implications for large-scale atomic I laser 79−23022
heptafluoroiodopropane light amplifier, wave-front distortion due to photolysis-gas dynamic effects 79−18412
heptafulvene, microwave spectrum and dipole moment 77−14421
n-heptane, boiling heat transfer coefficients, heater plate thickness effects 78−34124
n-heptane, Clausius eqn. of state, thermodynamic props. calc. 78−83909
n-heptane, electrification during laminar flow in metal pipe 80−6954
heptane, liq., Raman scatt. at high-press., chain kinking 79−87429
n-heptane, loss angle, temp. depend., 9 and 36 GHz 78−48114
n-heptane, mass spectra, using QUISTOR, phase-synchronised ion ejection from quadrupole ion storage mass spectrometer 79−44975
n-heptane, organic impurity molecular fluoresc., effect of heat pulses 78−88360
n-heptane, pseudoboiling mechanism, improved heat transfer 78−6152
n-heptane, refractive index at X-ray wavelengths *(Russian)* 79−47409
n-heptane, self-excited thermoacoustic oscills. in heat transfer 78−79186
n-heptane, solvent crazing of polystyrene, micromechanics 77−12680
n-heptane, solvent crazing of polystyrene, structure 77−12681
n-heptane, Townsend primary and secondary ionisation coeffs. and sparking voltages 80−1732
n-heptane+acetic anhydride, elec. resist. near crit. soln. temp. 78−71874
heptane(-carbon tetrachloride), SF_6 electron scavenging in positron spur in nonpolar liqs. 79−100421
n-heptane liqs., refractive index, pressure effect 80−71375
heptane with 2,2-diethoxypropane, excess enthalpy *(French)* 78−11542
n-heptane-benzene, excess vol. and isentropic compressibility, from density and US vel. meas. 78−79776
n-heptane-methanol, elec. resistance, crit. phenomena, freq. depends. 79−60884
n-heptane-methyl alcohol, crit. resist. of binary liq., 10 Hz-100 kHz 78−76123
n-heptane-nitrobenzene, critical fluid, ratio of sound dispersion to attenuation 79−55826
n-heptane-nitrobenzene, US study of crit. mixing 78−75732
n-heptane-toluene, vapour-liquid equilibrium, T-x meas. by semi-micro method 78−87782
n-heptane/3-pentanone mixture, vap. press. meas., thermodynamic functions calcs. 80−75345
heptanoic acid, associated vapours, homogeneous nucleation 80−96638
heptanoic acid, soln., US relax. *(German)* 78−22792
heptanol isomers, static permittivity and density, press. and temp. depend. 78−35078
1,3,5-heptatriyne, symm. top, microwave spectra 78−58676
1-heptene, field ionisation mass spectra, surface processes 79−11503
n-heptene, Townsend coeffs. of avalanche counter gases 78−78582
p,n-hepthyloxybenzoic acid, smectic C liq. cryst., coherent light diffr. 78−1999
heptyl alcohol, associated liq., US absorpt. and hole theory 78−10124
n-heptyl alcohol in tetrachloromethane, cyclohexane, measurements of US vel. and related parameters 80−38200
n-heptyl cyanobiphenyl, near IR dichroic spectrum, using unpolarised radiation 78−27201
4-n-heptyl-4′-β-cyanovinylbiphenyl, liq. cryst., isotropic mechanism of mol. rot., dielec. permitt. meas. 80−10491
4-n-heptyl-4′-cyanobiphenyl, linear dichroism spectra in nematic and isotropic phases 80−25336
4-heptyl-4′-cyanobiphenyl, liq. cryst., dielec. props. *(French)* 78−10820
4-heptyl-4′-cyanobiphenyl, nematic liq. cryst., alignment on surfactant treated obliquely evaporated surfaces 80−49092
4'-n-heptyl-4-cyanobiphenyl, nematic, mag. field depend. of birefringence and order parameter 77−76534
n-heptyl-4-cyanobiphenyl, nematic phase, dielec. loss, diffusion equations 80−71305
4′-n-heptyl-4-cyanobiphenyl, nematogenic liq. cryst., above T_c, Kerr effect response time, temp. depend. 78−34434
n-heptyl-cyanobiphenyl, dielec. relax. in nematic and isotropic phases 79−82151
p-p′-n-heptyl-cyanobiphenyl-isotropic solute systems, nematic-isotopic phase transformation, volumetric study 80−92653
4-n-heptyl-d_{15}-oxybenzoic acid-d_1, nematic and smectic phases, mol. and relative segmental order 80−96439
p-heptyl-p'-cyanobiphenyl, refractive index, dielec. const., mag. susceptibility, orientational ordering *(Dutch)* 80−33884
heptylazoxybenzene, smectic liquid crystal, A phase, dielec. permittivity 78−71673
heptylcyanobiphenyl, nematic, surface and bulk order parameters, refr. index anisotropy 79−90522
p-n-heptylhydroxybenzylidene-p'-n-butylaniline, phase transition study from 22 to 80°C 79−14679
4′-n-heptyloxy-4-cyanobiphenyl, 70CB, anomalous mag. field induced birefr. in isotropic phase 78−56461
n-heptyloxy-cyanobiphenyl, dielec. relax. in nematic and isotropic phases 79−82151
heptyloxyaminofluorenone-octyloxycyanobiphenyl, liq. cryst. mixtures, nematic-smectic A-smectic C Lifshitz point 77−69077
4,4′-di-heptyloxyazoxybenzene, diffuse X-ray scatt. near smectic C-nematic transition 79−95139
heptyloxyazoxybenzene, filamentary structures 80−107051
heptyloxyazoxybenzene, liq. cryst., pretransition behaviour, volumetric study 77−69076
4-4′-di-heptyloxyazoxybenzene, liq. cryst.-isotropic transition at high press. 79−95135
p-p′-heptyloxyazoxybenzene, smectic-C phase, mag. aligned, anisotropic US propag. 77−84630
p-heptyloxybenzylidene p'-heptylaniline, smectic C layer thickness meas. by X-ray scatt. 78−94986
4-n-heptyloxybenzylidene-4′-n-hexylaniline, nematic and smectic phases, long mol. axis reorientation, LF dielec. dispersion 80−70124

organic compounds continued
p-n-heptyloxybenzylidene-aminofluorenone/COOB mixtures, dynamic twist viscosity near polycrit. points 79−95133
N-p-n-heptyloxybenzylidene-p'-n-pentylaniline, X-ray diffr. of smectic phases 77−51318
p-n-heptyloxybenzylidene-p-aminobenzoic acid, smectic C to nematic transition 79−33076
4-n-heptyloxybenzylideneamino-4'-cyanobiphenyl, reentrant nematic phase and low temp. smectic phases 80−88031
N-p-heptyloxylbenzylidene-p-heptylaniline, liq. cryst., dislocations obs. in smectic A and C mesophases 78−91230
4-n- heptyloxyphenyl 4-n-hexydexybenzoate, liquid crystal, freezing polarisation, electret effect *(Polish)* 80−10496
n-heptylviologen radical cation films, cathodic, growth, for alphanumeric display appl. 79−69999
n-heptylviologen salt soln., electrochemical props. 77−77788
N-heteroarenium cations B, resonant, nonradiative energy transfer *(German)* 78−25659
heteroaromatic compounds, two-stage photoionisation in solns., UV laser irrad. effects *(Russian)* 78−13556
heteroaromatic mol. radiationless transition decay rate freq. shift depend., quantum statistical mechanics anal. 78−74691
heteroaromatic molecules, planar, orientation and phosphoresc. polarisation in stretched film 80−14169
heteroaromatic molecules, radiationless conversion processes, regularities 80−14171
heterobenzenes, electronic struct., π electron mag. susceptibility anisotropy 79−59353
heterocycles, five membered ring, MCD spectra dnd π-electron approx. calcs. 79−812
heterocyclic anion radicals, electron transfer with anthracene-amine cation radicals, triplet state electrogeneration 80−63803
heterocyclic aromatic molecules, Penning election spectra and photoelection spectra, rel. intensities 80−95725
heterocyclic compounds, bond lengths, fifth overtone of C-H stretching vibrs. obs. 80−91528
heterocyclic compounds in dilute solutions, dielectric relax., microwave technique 78−84520
heterocyclic five membered mols., methyl top barrier to internal rot. 78−78833
heterocyclic liquids, US attenuation in 10 to 1300 MHz range 80−39229
heterocyclic N compounds, radiationless transitions, isotope effects 80−48033
heterocyclic N-containing compounds, crysts., intermol. pots. calcs. 80−49169
heterocyclics, in polystyrene matrices, energy barriers, dielec. absorpt. meas. 78−70958
N-heterocyclics, radiationless transitions, vibronic coupling effect 78−33543
heteroexcimers, intramolecular, picosecond time-resolved fluorescence studies 80−83401
heteroorganic group III compounds, NQR expts., review 78−25565
heteroorganic molecules, all-reactive-electrons closed-shell SCF-CI MO calcs. 79−36541
hexa(trifluoromethyl) germanium, gas and liq., IR and Raman spectra, normal coord. anal. *(German)* 79−72315
hexa-antipyrene iodide of Ce or CIP, heat transfer with dil. ^{3}He below 50 mK 79−51413
hexa-deutero dimethyl selenide, microwave spectrum, first excited torsional states, top-top interaction 77−10668
hexa-n-alkoxy-triphenylene disc-like solute effect on orientational order of nematic EBBA 80−79682
hexa-phenylthiobenzene, cryst. and mol. struct. of carbontetrachloride adduct 77−42436
hexa-urea aluminium complex: VO^{2+}, cryst., one-dimens. interactions, EPR 77−73074
hexabenzocoronene, MCD and absorpt. spectra 79−54875
hexabromobenzene, cryst., IR and Raman spectra, vibr. normal coordinate anal. 77−79602
hexabromobenzene, cryst. struct., constrained refinement of neutron powder diffr. data 79−27970
hexachlorobenzene, γ-irrad., ESR spectrum 79−65735
hexachlorobenzene, mol. cryst., effective mol. polarisability calcs. 77−12298
hexachlorobenzene, quadrupole spin echo envelope EFG tensor axisymmetry in mag. field 80−20497
hexachlorobenzene, Raman intensities, polarised scatt. from lattice rot. modes. 78−43845
hexachlorodisiloxane, normal vibr. and force field calc. 79−54994
hexachloroethane, orthorhombic, neutron struct. refinement 80−29009
hexachloroethane, phase II-III polymorphic transformation kinetics 79−42240
hexachloroethane, phase II-phase III polymorphic transformation rate 79−23728
hexachloroethane, surface roughening transition in vapour phase growth 78−2044
hexachloroparaxylene, crystn. from heptane, optimising purification 80−100774
hexacyanobenzene-naphthalene, charge transfer triplet states, electron distrib., ESR 77−3388
hexadecachlorophthalocyanato-copper discrimination of individual atoms in mol. images 80−100226
hexadecane, boundary viscosity, meas. by blowoff method 79−11006
n-hexadecane, depolarised Rayleigh spectroscopy 79−4808
n-hexadecane, high press. expansivity, piezo-thermal anal., phase transformations 77−72705
hexadecane, liq., Raman scatt. at high-press., chain kinking 79−87429
hexadecane, liq. film, boundary viscosity using blow-off method 79−23383
n-hexadecane, pure liq. and solns., small angle neutron scatt., ang. depend. 79−1384
n-hexadecane-β,β'-dichlordiethyl ether exfoliating mixture, light scatt. and hypersound vel. 77−28586
n-hexadecane-acetone, noncritical interface near crit. end point, surface tension meas. 79−69322
hexadecane-water microemulsion, dielectric behaviour, Cole-Cole type relax., temp. depend. 78−56426
1,2 hexadecanediol, inelastic electron tunnelling spectroscopic study of lubrication props. 80−70302
organic compounds continued
hexadecanoic acid, inelastic electron tunnelling spectroscopic study of lubrication props. 80−70302
hexadecanol, inelastic electron tunnelling spectroscopic study of lubrication props. 80−70302
^{123}I-hexadecenoic acid, exptl. basis for myocardial imaging 77−16970
hexadecyltrimethyl-ammonium bromide, micelle form. in aq. soln., laser light scatt. 78−27825
hexadecyltrimethylammonium bromide, micelle shape and aggregation, conc. depend. 79−24833
n-hexadecyltrimethylammonium bromide micelles, ^{13}C relax. times model, for gauche-trans isomerisation 78−33520
hexadecyltrimethylammonium bromide-hexan-1-ol-water system, liq. cryst., rheological props. 79−23289
cis-2,trans-4-hexadiene, addition kinetics of HCl, Raman spectra meas. *(French)* 79−91940
1,5-hexadiene, D-labelled, IR laser induced isomerization via electronic ground state 77−25289
2,4-hexadienoic, chemisorbed layers, electron beam damage, tunnelling spectra obs. 77−76672
2,4-hexadiine-1,6-diol-bis(p-toluene sulphonate), cryst., polymerisation, elastic consts., Brillouin scatt. 79−1950
2,4-hexadiyne, solid, methyl group tunnelling and torsion, neutron scatt. 78−18560
1,5-hexadiyne, time-depend. mass spectra, ionisation efficiency and breakdown curves 80−95747
1-5hexadiyne ion+neutral 1,5-hexadiyne, trapped-ion mass spectrometry 80−97694
2,4-hexadiyne-1,6 diol bis(p-toluene sulphonate) ester, demonstration of high mobility 80−20212
2,4-hexadiynyl-1,6-bis(p-toluenesulphonate), programmed temp. and DSC obs., cryst. forms and polymerisation kinetics 79−43583
2,4-hexadyne-1,6-diol-bis-p-toluene sulphonate, fluoresc. of localized states in single crystal 78−6756
hexafluoro ethyl cation fragmentation, mass spectrometry 80−53070
hexafluoroacetone, 147 nm photolysis, quantum yield press. depend. 78−68903
hexafluoroacetone, IR multiphoton decomposition, press., fluence, wavelength, temp. depend. 80−7809
hexafluoroacetone, IR multiphoton dissociation, isotopic selectivity and yield, temp. effect 80−53069
hexafluoroacetone, multiphoton absorption and dissociation in strong IR CO_2 laser field 79−98172
hexafluoroacetone, multiphoton dissoc., mechanisms 79−6978
hexafluoroacetone, natural isotopic abundance, selective multiphoton decomposition at threshold 79−89723
hexafluoroacetone, triplet state, trapped electron ICR spectrosc. 79−59373
hexafluorobenzene, γ-radiolysis, matrix isolation spectra of radical anions 79−52704
hexafluorobenzene, cation, visible emission spectra of gas, Jahn-Teller effect 79−50034
hexafluorobenzene, cryst., press. depend. of nuclear spin-lattice relax. time 79−28635
hexafluorobenzene, in liquid binary mixtures of optically anisotropic molecules, depolarized Rayleigh scatt. 80−40122
hexafluorobenzene, IR multiphoton excitation, vibr. energy redistrib. and hot band spectrum 80−95656
hexafluorobenzene, liq., self-diffusion and denisty as functions of press. and temp. 80−92696
hexafluorobenzene, liquid sample freezing with quartz wool for neutron diffr. exam. 78−18502
hexafluorobenzene, polar tensors and at. effective charge, calculated from IR intensity 78−74703
hexafluorobenzene, slow electron attachment obs., π-orbital calcs. 77−6948
hexafluorobenzene+bisdiphenylenephenylallyl radical, solvent effects on collisions, dynamic nucl. polaris., spin-lattice relax. 77−63303
hexafluorobenzene+Xe, high Rydberg state, ionis. 78−50620
hexafluorobenzene anion-radicals in squalane, ESR spectrum optical detection 80−95655
hexafluorobenzene cation, laser fluoresc. in solid Ar 79−18229
hexafluorobenzene dimer, mol. beam elec. deflection obs. 79−72336
hexafluorobenzene liq., electron mobility, percolation model 80−65551
hexafluorobenzene radical anion, ^{13}C hyperfine interaction, EPR obs. 80−83392
hexafluorobenzene-benzene, liq., mol. interactions, IR and Raman lineshape obs. 80−28907
hexafluorobenzene-benzene liq. mixture, electron mobility, percolation model 80−65551
hexafluorobenzene-benzene mixture, percolation model of electron and hole mobility 80−29452
hexafluorobenzene-benzene soln., dynamic and static orientational pair correls., depolarised light scatt. 77−16321
hexafluorobenzene-n-paraffins, binary liquid solns., self diffusion, spin echo meas. 80−65263
hexafluorobenzene-O_2, soln., NMR for translational O_2 diffusion 79−65749
hexafluorobutadiene, electronic ground state photochem., isotope separation by IR multiphoton isomerisation 79−79264
hexafluorobutene, vibrational broadening, dense fluid region, Raman and NMR study 80−43056
hexafluorocyclobutene, electronic ground state photochem., isotope separation by IR multiphoton isomerisation 79−79264
hexafluorocyclobutene, ground state, electrocyclic isomerisation of ground state induced by IR laser multiphoton absorpt. 77−32811
hexafluorocyclopropane, centrifugal distortion const. and thermodynamic functions calc. 80−95582
hexafluoroethane, ^{19}F chem. shielding, temp. depend., FT NMR obs. 78−86888
hexafluoroethane, chemical conversion and uniformity of etching SiO_2 in radial flow plasma reactor 80−76391
hexafluoroethane, far IR multipole induced absorpt. 78−37639
hexafluoroethane, molecular effects in F K-shell ionisation by 0.5 to 1.5 MeV protons 77−50515
hexafluoroethane, photoabsorpt. cross-section, 175-770 Å 77−88462
hexafluoroethane, photochem. prod., ^{13}C enrichment *(French)* 80−91615
hexafluoroethane, RF discharge chem., added acetylene effect, mechanistic model for fluorocarbon plasmas 80−84017
hexafluoroethane, RF discharge chemistry, added H_2 effect 80−33832

organic compounds continued
hexafluoroethane, rot. barriers, MS-SCF-X_α calcs. 80−106267
hexafluoroethane+H_2(hexane), multiphoton induced chemistry 79−20382
hexafluoroethane+S_2, fluoresc. quenching and lifetimes of S_2 78−46386
hexafluorohalopropanes, gas and solid, IR and Raman spectra, normal coord. anal. *(German)* 79−72317
hexafluoroisopropanol, third order optical susceptibility obs. 77−34906
bis(1,1,1,5,5,5-hexafluoropentane-2,4-dionato)dioxouranium (VI), isotope selective IR laser induced unimol. dissoc. 80−69197
hexafluoropropane, isolated CH stretching freqs. and bond props. 79−94104
hexafluoropropane(-d_2), IR and Raman spectra, gas and liq., normal coord. anal. 79−68235
hexafluoropropene, mol. struct. by electron diffr. of gas phase 79−59572
hexafluoropropene, struct. and vibr. spectra, IR, Raman polarisation study 80−18845
hexafluoropropyl cation, laser multiphoton dissoc. probabilities, collisional enhancement 79−68277
hexafluoropropylene, radiation chem. alkylation with adamantane in liq. phase 77−48663
hexafluoropropylene+^{18}F nonequilibrium effects in moderated nuclear recoil experiments 80−89509
hexahydrohexahelicene, in Shpolskii matrix, absorpt., fluoresc., phosphoresc. spectra 79−76463
hexaidobenzene, cryst., IR and Raman spectra, vibr. normal coordinate anal. 77−79602
hexamethyl benzene, high press., variable temp. Raman spectra 78−56488
hexamethyl benzene-d, NMR, 4π and 2π rot. symmetry in spin-1 system 78−62830
hexamethyl indatricarbocyanine iodide-ethanol soln., luminesc. quantum yield, photoacoustic method 77−86335
hexamethyl-2,2′-indotricarbocyanine iodide, solns., photoisomerisation and internal conversion rate, time-resolved spectra 77−75201
hexamethylbenzene, cryst., Raman spectra, intensity of low freq. line 78−2846
hexamethylbenzene, exciton band struct. for first singlet state 77−55483
hexamethylbenzene, high press. expansivity, piezo-thermal anal., phase transformations 77−72705
hexamethylbenzene, IR polarised spectra 79−28758
hexamethylbenzene, mol. dynamics, allotropy, solid-state phase transitions effects, Raman spectra *(French)* 77−42372
hexamethylbenzene, perdeuterated, D nucleus, spin-1, spinor behaviour of double quantum transition 79−47355
hexamethylbenzene charge-transfer complexes, heavy atom effect on radiative and radiationless transitions 78−25607
hexamethylbenzene in tetrachloromethane soln., local mode overtone bands 80−83444
P-hexamethylcyclotriborophosphanes, substituted, struct., vibr. spectra 77−65460
hexamethyldisilane, mol. motion, press. and temp. depend., PMR relax. obs. 78−64289
hexamethyldisilane, plastic cryst., NMR determ. of phase diagram 77−12210
hexamethyldisilane, plastic deform., and diffusion of hexamethylethane-^{14}C 78−14510
hexamethyldisiloxane plasma polymerised thin film, charge trapping characts. 80−96895
hexamethyldisiloxane-Ar, glow discharge positive column ion mass spectra identification 80−38834
hexamethylene tetramine, appl. in calibration of diamond anvil press. cell, 0-15 kbar 77−41635
hexamethylene tetramine, cryst. growth kinetics from soln., role of solvent-solute interactions 77−24282
hexamethylene tetramine, cryst. growth mechanisms from soln., role of solvent-solute interactions 77−24281
hexamethylene tetramine, polycryst. ^{14}N NMR elec. field gradient effects 77−77112
hexamethylene tetramine crystals, growth from aqueous and ethanolic solns., (110) surface struct. 77−76338
hexamethylene tetramine in water-acetone soln., crystal growth kinetics 78−30554
hexamethylenetetramine, mol. ultraslow rot. obs. using D probe spin alignment tech. 80−88890
hexamethylenetetramine, orientation and deform. in nematic liq. cryst., PMR obs. 77−71815
hexamethylenetetramine, thermal cond. and heat capacity under press. 80−80008
hexamethylenetetramine, ultraslow tetrahedral jumps, deuteron NMR spin alignment obs. 80−66046
hexamethylenetetramine in oriented mesophases, mol. distortion, PMR 77−6802
hexamethylenetetramine-phenol mol. complexes, cryst. data 77−27871
hexamethylethane, ^{13}C-^{13}C dipolar interaction, NMR longit. cross relax. 80−93196
hexamethylethane, crystal structures and phase transitions, X-ray diffr. study 79−73158
hexamethylethane, mol. motion, press. and temp. depend., PMR relax. obs. 78−64289
1,3,3,1′,3′,3′-hexamethylindotricarbocyanine iodide, laser dye, ultra-fast excited state absorpt. spectroscopy 77−30876
hexamethylolmelamine, doped, phosphoresc., crystallinity, cross-linking and H-bonding effects 79−73984
hexamethylphosphoramide:Li glass, metallic condensation of Wannier-Mott impurity states 78−2420
hexamethylphosphoramide-chloroform complex, mol. motion and assoc., PMR obs. *(French)* 78−72429
hexamethylphosphoramide-K(Cs)(Rb), low temp. glass, EPR of solvated ats. 78−91927
hexamethylphosphortriamide, effect of small additions of water struct., from permittivity obs. 78−9937
hexamine, BCC, dislocation slip initiation 77−43222
hexan-1-ol+n-hexane, vap. press. and thermodynamic props. 298.230 to 342.824K 78−43129
hexane:pyrene (coronene), quasiline spectra, multiplet struct., freezing conditions and solvent effects 79−1786
hexane, adsorption on $Co(OH)_2$, $Ni(OH)_2$, $Cd(OH)_2$ and $Cr(OH)_3$ 79−66343
n-hexane, avalanche breakdown 79−55449
n-hexane, colloidal dissolution in water 79−66358
organic compounds continued
n-hexane, elec. breakdown mechanism, high speed photography expts. 79−91367
hexane, electric breakdown strength of vapour and liq., behaviour in critical region 77−47285
n-hexane, field emission into liq., 275-334K 78−88406
hexane, film flow calc., effect of temp. and press. gradients in conical capillaries 79−55416
n-hexane, gaseous, crit. and liq., density and temp. effects on electron mobilities 79−27739
n-hexane, gaseous, crit. and liq., positive ion mobility 79−37439
n-hexane, geminate ion scavenging yield, external elec. field effect 79−47909
n-hexane, heat transfer from horizontal wire, AC and DC electric field effect 77−31202
n-hexane, high press. expansivity, piezo-thermal anal., phase transformations 77−72705
n-hexane, impurity particle behaviour and cond. pulses 79−91059
n-hexane, impurity particle motion, under DC and AC conditions, expt. results and computer simulation 78−88642
n-hexane, ionisation by electron bombard., empirical and semi-empirical calcs. 79−36784
n-hexane, isomerisation over Mo-containing catalyst 77−86361
hexane, liq., burning rate in small vessel, convection effect 78−35680
hexane, liq., Raman scatt. at high-press., chain kinking 79−87429
n-hexane, liq. trapped electron photoionis., photocond. 80−2418
hexane, liquid, chain reorientation, Brownian dynamics simulation, comparison of models 80−49067
n-hexane, liquid, ground state energy of excess electrons 78−68976
hexane, liquid, high-speed schlieren studies of elec. breakdown 77−89332
n-hexane, loss angle, temp. depend., 9 and 36 GHz 78−48114
n-hexane, mass selective storage mass spectra by quadrupole ion storage mass spectrometer 80−52351
n-hexane, non-polar liq., microwave induced Kerr effect meas. 78−76435
n-hexane, optical props. under press., molecular polarisability depend. on thermodynamical state 78−80312
n-hexane, prebreakdown events, divergent field study 79−91371
n-hexane, refr. index meas. to 14 kilobars by optical interferometry 77−49764
n-hexane, refractive index at X-ray wavelengths *(Russian)* 79−47409
n-hexane, shock compression, dynamic high press. eqns. of state 80−6450
n-hexane, subjected to charge injection, low stress mobility, induced motion effects 79−91063
n-hexane, superheated, thermodynamic props. from ultrasound speed 80−92036
n-hexane, superheated liq., US wave vel., adiabatic compressibility, heat capacity 78−2198
n-hexane, tank flame, turbulence, holographic interferometric synchronous photography *(German)* 78−51255
n-hexane, Townsend primary and secondary ionisation coeffs. and sparking voltages 80−1732
n-hexane, trigatron spark gap, time-lag characts. 77−1030
n-hexane, viscosity meas. at 353 to 436K, and corresponding vapour press. 77−69107
n-hexane, visible absorpt. spectra, local mode overtone intensity of C-H stretching mode 79−81207
n-hexane+cyclohexone, excess enthalpy, calorimetric cell 79−58689
hexane+hexafluoroethane, multiphoton induced chemistry 79−20382
n-hexane and mixtures with n-pentane, nucleate boiling from tube arrays 78−22251
n-hexane droplets, coalescence in n-alcohol aqueous solns. 79−87882
n-hexane droplets coalescence in aq. electrolyte solns. 79−64742
n-hexane induced changes in visual evoked pots. and ERG of industrial workers 80−45886
n-hexane liqs., refractive index, pressure effect 80−71375
n-hexane-cyclohexane mixture, viscosity and density, 25 to 100 C, up to 500 MPa 80−103510
hexane-cyclohexane mixtures, quantitative IR spectrosc. anal. 79−96377
n-hexane-ethanol liq. mixtures, electron mobility, percolation model 80−65551
hexane-ethanol mixture, percolation model of electron and hole mobility 80−29452
n-hexane-n-butane-ethane, vap.-liq. equilib. behaviour, visual cell, for 48.3-143.5°C, up to 7619 kPa 79−46790
n-hexane-n-dodecane 'ideal' mixture, viscosity, theory *(German)* 78−22882
n-hexane-n-pentadecane mixtures, solns., mech. of US absorption and viscosity *(Russian)* 79−90732
n-hexane-nitrobenzene, crit. mixture, depolarised Rayleigh linewidth meas. 77−81112
n-hexane-nitrobenzene crit. mixture, in ultracentrifuge, dynamic phenomena 80−44310
n-hexane-nitrobenzene crit. mixture, Rayleigh line and depolarised scatt. 77−20864
n-hexane-nitrobenzene mixture, Raman line scatt. near crit. temp. 77−20863
hexane-nitrobenzene soln., dielec. permitt. in two-phase region 80−2682
hexane-nitrobenzene solution, double-scatt. light intensity near critical point of mixing *(Russian)* 80−55117
hexane-nitroethane soln., crit. exponents *(Russian)* 79−77766
n-hexane-perfluoro-n-hexane mixtures, US vel. and absorpt. mixtures 80−88281
n-hexane/3-pentanone(acetone) mixtures, vap. press. meas., thermodynamic functions calcs. 80−75345
n-hexane/acetone mixtures, electroviscous effect, AC and DC meas. 79−14949
hexanes, isomeric, 80−95732
hexanes, isomeric, unimol. decomp. processes following field ionisation, temp. depend. 80−95733
hexanetriol 1,2,6, liq., light scatt. study of struct. relax., viscosity and dielec. relax. 79−86672
hexanetriol 1, 2, 6, associated liq., correl. between acoustic and dielectric relaxation times 78−9925
hexanoate, Li, Na, K and Rb alkanoate mixture, DSC anal. 78−10192
hexanoic acid, chemisorbed layers, electron beam damage, tunnelling spectra obs. 77−76672
p-hexanoylbenzylidene-p′-aminoazobenzene, smectic A mesophase, self- and impurity diffusion, NMR spin echo obs. 78−94975
hexaphenylcarbodiphosphorane, cryst. struct., triboluminesc., polymorphism effects 79−61447

organic compounds continued
hexatriacontane, contact angle data with many liquids, interaction parameter calc. 77−55423
n-hexatriacontane, cryst., orthorhombic modification, vibr. spectra 80−50314
n-hexatriacontane, cryst. struct., γ-ray effects obs. 78−43048
n-hexatriacontane, depolarised Rayleigh spectroscopy 79−4808
hexatriacontane, polycryst., UPS, 11.4-21.2 eV, polyethylene model compound 77−66570
n-hexatriacontane, pure liq. and solns., small angle neutron scatt., ang. depend. 79−1384
hexatriacontane, single crystal, elec. props. *(Japanese)* 79−51592
n-hexatriacontane, suitability as model cpd. for cond. band struct. of polyethylene 80−16131
hexatriacontane single cryst., elec. cond. and dielec. breakdown 80−6849
hexatriacontane single cryst., temp. depend. of dielec. breakdown 79−51905
hexatricontane, growth kinetics of (001) faces from soln. 79−52098
1,3,5,-hexatriene, π-electron struct., generator coord. method 79−26880
trans-hexatriene, correl. problem, open-shell coupled-cluster approach, PPP calc. 79−81157
1,3,5-hexatriene, electron scatt. at low-energy, vibronic struct. of triplet state 79−3574
trans-1,3,5-hexatriene, electronic spectra vibr. struct. calc. 79−63981
hexatriene, excitation spectra, cluster configuration method appl. 80−78546
all-trans-1,3,5-hexatriene, excited electronic states calcs., spectra assignments 79−22606
1,3,5-hexatriene, low energy, variable angle electron-impact excitation 77−27187
trans-1,3,5-hexatriene, low-lying ππ* excited states, ab initio STO method 77−3284
hexatriene, mol. hyperpolarisability meas. by optical SHG 79−22861
hexatriene, mol. semiempirical RPA calc. using PPP Hamiltonian, triplet instability 79−26893
trans-hexatriene, multiphoton ionization spectrum in 6.2 eV region 77−27133
hexatriene, polarisability, nonlinear elec. susceptibility, SCF calcs. 80−95547
1, 3, 5-hexatriene, radical cations, emission spectra of cis and trans isomers 77−6793
1,3,5-hexatriene, two-photon spectra, failure to find low-lying excited ^1A state 77−79665
trans,trans-1,3,5-hexatriene, valence electronic excited states, SCF ab initio GVB and CI calcs. 79−31423
trans-hexatriene, weak low-energy band, S and T levels by fragment method 78−82625
1,3,5-hexatriene radical cation, in Ne matrix, laser induced fluoresc. and emission spectra 80−87163
hexaurea aluminium perchlorate:VO^{2+}, single cryst. ESR 77−16158
1-hexene-water(-D_2O), field-induced surface reactions, field ionis. mass spectra obs. 78−95949
HEXOAB/7CBP, mixed crystals, induced smectic A phases, elec. cond. 78−76068
hexomethylenetetramine complexes, ^{14}N NQR pulsed apparatus 77−10075
hexose monophosphate, effects of X-irrad. on shunt pathway in human lymphocytes 80−76798
n-hexyl 4′-n-decyloxybiphenyl-4-carboxylate, smectic C phase, tilt angle using electron reson. spectroscopy 80−33886
hexyl alcohol, associated liq., US absorpt. and hole theory 78−10124
n-hexyl alcohol colloidal dissolution in water 79−66358
n-hexyl chain bound to macromol., ^{13}C spin-lattice relax. 77−23510
4-n-hexyl-4-cyanobiphenyl, liq. cryst., isotropic mechanism of mol. rot., dielec. permitt. meas. 80−10491
hexyl-azoxybenzene, liq. cryst., twist viscosity and mech. props. near smectic A-nematic transition 78−95136
p-hexyl-oxy-benzylidene-p′-amino-2-chloro-propyle-cinnamate, ferroelec. smectic C liq. cryst., permanent polarisation meas. 77−32331
n-hexylamine-nickel di-acetylacetonate, ^{13}C nucl. spin relax., electron spin delocalisation 78−5248
n-hexylamine.Gd$(FOD)_3$, flexible chain dynamics, NMR, steric effects calcs. 77−6800
p-n hexyloxy benzylidine-p-toludine, liquid crystal, elec. cond. and dielectric constant, in solid phase 79−61293
hexyloxy-cyano-biphenyl, nematic liq. cryst. pretilt angle, temp. depend. 78−26432
4-n-hexyloxybenzilidene-4′-n-propylaniline, liq. cryst. phases, thermal and structural studies 78−1989
N-(p-hexyloxybenzylidene)-p-toluidine, dil. soln. in benzene, dielectric behaviour 79−42893
4-n-hexyloxybenzylidene-4′-n-hexylaniline, liquid crystal, exam. of orientation order of dissolved molecules 80−44112
4-n-hexyloxybenzylidene-4′-n-propylanilene, smectic S_H and S_m phase structs. 79−14673
4-n-hexyloxybenzylidene-4-n′-hexylaniline, nematic and smectic phases, long mol. axis reorientation, LF dielec. dispersion 80−70124
N-p-hexyloxybenzylidene-p′-toluidene, positron lifetime meas. in solid and liq. cryst. phases 79−61460
p-n-hexyloxybenzylidene-p-aminobenzoic acid, liq. cryst. phase transitions, X-ray diffr. and DSC meas. 79−86877
N-p-hexyloxybenzylidene-p-toluidine, optical props., density, and order parameter in liq. cryst. phases 79−55657
p,n-hexyloxybenzylideneamino-p′-chlorobenzene, liq. cryst., sp. ht. meas. 78−22831
p-hexyloxyphenyl-p-pentoxybenzoate, nematic liq. cryst., elec. discharge meas. of persistent internal polarisation 80−10488
highly fluorescent compounds coherent antiStokes reson. Raman spectra 79−36655
hippuric acid, solid, second moment meas. by wide-line NMR 80−108081
hippuric acid, X-irrad. single cryst., ^{14}N and ^1H ENDOR study; 80−71240
histamine monocation, FSGO calcs. of orbital energies locations, dipole moments, charge distribs. 77−67976
histidine, quenching of pH-dependent fluoresc. in tryptophan and indole *(Russian)* 78−90209
histidine decarboxylase quarternary struct. 79−92129
L-histidine HCl, X-irrad., $=C\text{-}^+NH_3$ radical form., exchangeable H^+ hyperfine coupling 79−36669
organic compounds continued
histidine quenching of fluoresc. of tryptophan, indole solns. rel. to pH 80−2826
L-histidine.HCl.H_2O, photographic neutron diffr. by modified Laue method 77−66791
histones, H2A and H4, effect of molecular interactions on fluorescence intensity 80−51032
HMPA:alkali metal, density of states in band gap, EPR and optical correlations 79−61201
HMTSF-TCNQ, metallic state at He temps., elec. props. and band struct. 79−65462
HMTSF-TCNQ, obs. of the de Haas-Shubnikov oscills. 78−84201
HMTSF-TNAP, elec. cond. under press. 78−84200
HMTSF-TNAP, microwave cond. at 35 GHz 80−24963
HMTSF-TNAP, one-dimens. conductor, transport props. 80−20165
HMTSF-TNAP, organic low temp. cond. 78−43368
HMTTF-TCNQ, quasi-one dimensional conductor, sp, ht. 79−55897
HMTTF-TCNQ chain, three dimensional ordering 78−95152
HNBP, nematic, statistical mechanics, particle pots. and distrib. functions calcs. 78−2001
HNS, role in grain modification of TNT 79−100129
HOAB, chain ordering model 80−24357
HOAB, cryst. and mol. struct. rel. to smectic C phase struct. 79−55732
HOAB, effect of smectic C struct., on dielectric relax. 79−19140
HOAB, liq. cryst., smectic and nematic, distrib. functions by X-ray diffr. 79−99072
HOAB, liq. cryst. phase transitions, specific ht. meas. 79−33075
HOAB, liquid crystal, mol. orientational order in uniaxial and biaxial phases by NMR 77−84629
HOAB, smectic, C-phase, magnetic instabilities studied by electron spin resonance spectroscopy 79−82147
HOAB, smectic C-phase pyroelectric effect 78−79522
HOAB, thermotropic mesophase, DMR chain segments assignment 80−24356
HOAB-cholesteryl benzoate mixture, twisted smectic-C and twisted nematic phases, optical and X-ray investig. 77−84634
HOAB-d_{30}, biaxial liq. cryst., NMR of spinning sample 79−64987
HOAB-DOBAMBC nonchiral-chiral smectic C mixture, spontaneous polarization and induced circular dichroism 79−27910
HOAOB, isotropic-nematic transition, supercooling and nucleation, interface dendrites 78−42896
HOBA, isotropic phase, Brillouin scatt. spectra, hypersound data determ. 79−91453
HOBA, smectic C liq. cryst., EHD instabilities 78−91238
HOBACPC, chiral smectic C liq. cryst., dielec. consts., electroclinic effect 78−94980
HOBHA, smectic A to C transition, crit. biaxiality *(French)* 77−4039
holmium ethylsulphate, pseudomagnetic moment of ^{165}Ho and spin-lattice relax. times 77−63306
homogeneous linewidths in ODMR and optical transitions, connection 79−91316
homologous linearity rule for energies of mol. orbitals and related props. 78−58569
homologous series, mol. orientational interaction, Maxwell effect 79−65833
homotetrahedryl cation, rearrangement pseudorotation modes, reaction mechanisms, permutation theoretic anal. 78−44369
horseradish peroxidase, transport in γ-irrad. brain tissue 80−41119
humic acid sorption of actinide cations, effect on radioactive waste storage 80−13715
humic acids, dissolved, in rivers, removal during estuarine mixing 79−34830
HxBPA, liq. cryst., transitions, DSC and X-ray diffr., 170-380K 77−15314
HxBPA smectic phases, X-ray diffr. and Raman spectra 78−6012
hyaluronic acid, Raman spectrum, primary and secondary structs. 79−59467
hydraxine-oxyhaemoglobin interaction, γ-reson. spectroscopy 80−81525
hydrazine, decomp. on Ir(111) surface, N_2 emission, ang. depend. 80−97731
hydrazine, interaction with Fe(111) surface 79−46956
hydrazine, intercalation in $NbSe_2$(2H), kinetic studies by transmittance meas. at 1600 nm 78−71981
hydrazine, rocket fuel in ambient air, CO_2 laser absorption spectra and photoacoustic detection 80−104540
hydrazine adsorbed on Al, decomp., XPS obs. 80−92783
hydrazine derivatives, adsorption on Al surface, inhibiting dissoln. in HCl soln. 80−50759
hydrazine monohydrate, ^{14}N NQR, echo envelope modulation obs. 80−50218
hydrazine-1,2-d_2, microwave spectra, mol. structural parameters 77−27056
hydrazines, adsorbed on oxidised metal surfaces, identification by surface ionis. 77−21456
hydrazinium hydrogen oxalate, electron and proton distrib. in the short O-H-O bond 79−14789
hydrazinium iron tri(hydrazoformate) monohydrate single cryst., effective EFG tensor, Mossbauer spectra obs. 79−56628
hydrazoic acid, electron-density maps of bent bonds 80−1084
hydrazones, protonation energy and basic strength 80−37719
L(+) hydrazonium tartrate, soln. growth and cryst. morphology 79−33914
hydrazonium tartrate enantiomers, and deuterates, struct. and opt. props. 77−68954
N-hydro-N′-methylphenaziniumyl cation in HMP-ClO_4, mol. config. 78−62938
hydrocarbon, ^{13}C NMR shielding constants and tensors, finite perturbation calcs. 77−27092
hydrocarbon, (C_nH_{2n+2}, n=1-4)+H^+, electron capture and loss cross-sections 1-20 keV *(French)* 77−38728
hydrocarbon, (e,2e), angular correlations *(Russian)* 77−46648
hydrocarbon, conjugated, electrophilic substitution, graph theory 77−9076
hydrocarbon, conjugated, nonlinear susceptibility, extended basis set calcs. 79−27107
hydrocarbon, contamination in vacuum systems, determ. by field emission microscope 77−18002
hydrocarbon, dielectric liquid, drift mobility and conduction band energy of excess electrons 77−4348
hydrocarbon, internal degrees of freedom, Eucken factor, effect on transfer props. 78−22445

organic compounds continued
hydrocarbon, pyrolysis in gas phase, pyrocarbon form. 77−40459
hydrocarbon, unsaturated, +hydrogen halide, vibr. stimulated addition reaction 79−91928
hydrocarbon+CO_2, in mixtures, vibr. energy transfer, laser induced fluoresc. obs. 78−58731
hydrocarbon+CO_2(H_2S) mixtures, vapour-liq. equilibrium, crit. locus curve, Soave eqn. 78−83913
hydrocarbon+N oxide mixtures in air, photochemistry 79−53427
hydrocarbon bearing anticlines, pattern space of seismic anomalies, location tool and theory 80−17234
hydrocarbon carcinogenesis, fluoresc. meas. in cells 79−39343
hydrocarbon catalysis 78−11550
hydrocarbon chain, gauche-trans isomerisation, ^{13}C relax. times and nucl. Overhauser enhancement model 78−33520
hydrocarbon chain ordering in model membrane, D quadrupole splitting 78−64947
hydrocarbon chains, stability of lyotropic phases 80−24359
hydrocarbon contamination, of vacuum dependent scientific instruments 79−63259
hydrocarbon cracking in glow discharge C stripper foil irradiation lifetime 79−76249
hydrocarbon crystal, calc. of internal friction resulting from molecular defects 78−31448
hydrocarbon crystal structure calc. by molecular packing analysis 78−14303
hydrocarbon diffusional combustion in air, finite activation energy anal. 78−95930
hydrocarbon drops levitated in water, acoustically forced shape oscill. 79−47987
hydrocarbon emissions from vegetation, oxidation as atmospheric CO and H_2 source 78−88881
hydrocarbon formation on interstellar graphite grain surfaces 80−82458
hydrocarbon fuel flame, electron density determ. by Michelson interferometry 78−1890
hydrocarbon fuels, universal formula for elec. cond. of combustion-products plasma 79−19004
hydrocarbon fuels combustion prod. plasma with alkali impurity, elec. cond. 79−55466
hydrocarbon gas, sorption and transport in ethyl cellulose membrane 78−76913
hydrocarbon gases, additivity of stopping cross-sections for 50 to 150 keV protons 77−66853
hydrocarbon gases, energy loss distributions of transversing protons, 51, 102, 153 keV 77−6649
hydrocarbon ions, mass spectra, H atom scrambling, delocalisation 80−58135
hydrocarbon ions+H_2(methane), rate coeffs., ionised product. distribs. 77−44471
hydrocarbon liq., effect of mol. struct., temp. and elec. field on electron mobility 78−2535
hydrocarbon liquid, breakdown characts., comparison with fluorocarbon liqs. 79−91361
hydrocarbon liquid, model for thermalisation of quasifree electrons rel. to electron mobility 77−40316
hydrocarbon liquid, residual energy and entropy, rel. to liq. and mol. structs. 78−71869
hydrocarbon liquids, elec. cond. at fields up to breakdown strength, crit. review 77−80787
hydrocarbon liquids, electrostatically charged, incendivity of sparks from surface 80−6303
hydrocarbon liquids, streamer breakdown in divergent field 80−25308
hydrocarbon mixture, vapour-liquid equilibria, generalised method for calc. and prediction at high press. 78−87780
hydrocarbon mixtures, estimation of surface and interfacial tension 78−67887
hydrocarbon mixtures, photochemical reactivities 78−61533
hydrocarbon molecules, mutual polarisability of two atoms *(French)* 78−78834
hydrocarbon molecules, strongly adsorbed, contamination rate reduction 79−1550
hydrocarbon molecules adsorbed on specimen surface, contamination by surface diffusion 80−99013
hydrocarbon monolayer effects on wetting of Au, macroscopic continuum model 77−85018
hydrocarbon permeation through polyethylene membrane 80−30281
hydrocarbon prod. from H_2 and CO, C_8FeCl_3 behaviour, effect of activation 79−43623
hydrocarbon radicals, ab initio calc. of spin densities 79−93938
hydrocarbon radicals, planar and nonplanar, g-factors, π-σ delocalisation 78−58580
hydrocarbon reductions, potential effects on NO_2 nighttime concs., outdoor smog chamber expts. 77−70720
hydrocarbon turbulent diffusion flame, flame-zone model anal. 80−16684
hydrocarbon vapour, spontaneous condensation in submerged turbulent jet 79−64721
hydrocarbon working fluid selection, for conventional geothermal binary cycle 79−48091
hydrocarbon-Ar mixtures, electron drift velocity meas. 79−41079
hydrocarbon-CO_2(H_2S)(N_2)(CO) mixtures, phase equilib. calcs., modified Soave eqn. of state 79−19353
hydrocarbon-CO_2 mixture, phase equilibria and critical phenomena at high press. 78−51648
hydrocarbon-SF_6 mixtures, IR laser induced ionis., mechanism 77−81415
hydrocarbon-simple fluid gas streams, second virial coeffs. calcs. 78−1777
hydrocarbon-water, emulsions, superheated, bubble nucleation 78−61056
hydrocarbon/O_2 flames, resonance fluoresc. investig. technique for C_2 real-time meas. 77−30894
hydrocarbons, 30.4 nm He(II) photoelectron spectra 80−82589
hydrocarbons, 6-π electron conjugated, orbital pair correlation energy calc. method 77−88374
hydrocarbons, ^{13}C chem. shifts, simplex optimised INDO calcs. 80−83284
hydrocarbons, α-substituent effects in ^{13}C NMR, quantum chem. calcs. 78−74680
hydrocarbons, γ-radiolysis in glassy and polycryst. states, EPR spectra 77−52658
hydrocarbons, π SC bond orders 77−50349

organic compounds continued
hydrocarbons, (C_2-C_9), determ. in rock samples by capillary gas chromatograph 79−39226
hydrocarbons, adsorbed on Ru(001), characterisation by electron-stimulated desorpt. 78−71958
hydrocarbons, adsorption on Ni, C 2s levels, initial state shift 78−34703
hydrocarbons, aerosol growth rates in photochem. smog, gas-to-particle conversion 77−73826
hydrocarbons, air pollution sources in 1974, Los Angeles-Palm Springs 77−78408
hydrocarbons, alternant, perturbational MO calcs., appls. 78−74565
hydrocarbons, alternate conjugated, topological props. of HOMO-LUMO separations 80−69049
hydrocarbons, appl. of ab initio molecular fragment calculations with pseudopotentials 79−93905
hydrocarbons, aromatic, ultrasensitive detection by two-photon photoionisation 80−104473
hydrocarbons, aromatic and aliphatic, gas chromatographic determ. in airborne matter 79−79434
hydrocarbons, assoc. with airborne particles, dispersion and transport 79−20990
hydrocarbons, associated, Electric dipole polarizability of molecules in excited electronic states 78−70966
hydrocarbons, atmospheric, potential contrib. to photochemical air pollution form. in United Kingdom 80−76682
hydrocarbons, atmospheric global distrib., sources and sinks, rel. to 0_3 depletion 80−4088
hydrocarbons, average elec. polarisabilities and mag. susceptibilities, ab initio valence electron calcs. 80−87033
hydrocarbons, binary solns., critical points calc. using Soave eqn. of state 77−1209
hydrocarbons, boiling heat transfer 78−9535
hydrocarbons, bond functions, for ab initio calcs. 80−5469
hydrocarbons, bond order, max. principle rel. to choice of basis orbitals and wavefunctions 79−36498
hydrocarbons, bond polarisation characts. 77−3487
hydrocarbons, C_1, C_2 and C_3, heats of reaction, inner and outer shell electron energies contribs. 79−66331
hydrocarbons, C_1 to C_3, cryoscopic system for purity assessment in range 0 to −190°C 78−3418
hydrocarbons, CH, bond moments, sense and magnitude 79−45861
hydrocarbons, chemisorbed on SiO_2-supported Ni, chemical composition *(German)* 79−92002
hydrocarbons, coating nuclear fuel particles for HTR *(German)* 80−18585
hydrocarbons, Compton profiles, deviations from bond additivity, rel. to strain energy 79−81240
hydrocarbons, concs. over Pacific 78−73468
hydrocarbons, conformational anal., modified Urey-Bradley force field, gauche-H_2 interactions 77−6749
hydrocarbons, conjugated, ^1H chem. shifts calc. 79−98121
hydrocarbons, conjugated, dynamic polarisability and eigenfreqs. in one-electron approx. 79−64117
hydrocarbons, conjugated, effect of semi-empirical parameters on simple RPA calcs. 79−10037
hydrocarbons, conjugated, heat of formation and reson. energies 80−7839
hydrocarbons, Coulombic nonbonded interatomic pot. functions from vibr. freqs. 77−80587
hydrocarbons, cyclic, ionis. pot., electron affinity, semiempirical MO theory 77−50365
hydrocarbons, cyclic, non alternant, nonsingle instabilities of HF solns. 80−58164
hydrocarbons, detect. in water and sediment of wilderness lake, Canada 79−12155
hydrocarbons, deuterated, mol. polarisability and intermol. dispersion energy, 1-D delta pot. function 78−29862
hydrocarbons, diffusion, sorption, solubility, permeation in polyvinyltrimethylsilane *(Russian)* 80−6564
hydrocarbons, dipole moments, NDDO calcs. 80−47894
hydrocarbons, double-zeta quality ab initio mol. fragment calcs. with pseudopots. 79−85879
hydrocarbons, effective Hamiltonians for atomic pot. transferability 80−42933
hydrocarbons, electric polarisability, in excited singlet and triplet states *(Bulgarian)* 80−52897
hydrocarbons, electron energy influence on yields under electron impact 79−43602
hydrocarbons, electron impact cross section for H_α and CH($A^2\Delta \rightarrow X^2\Pi$) emission 77−27189
hydrocarbons, existence of positronium in mol. solids 77−59638
hydrocarbons, floating spherical Gaussian orbital calculation, ab initio pseudopotential 77−83496
hydrocarbons, fluoresc. quenching by TMPD cations, diffusion effects 77−6823
hydrocarbons, force constants, CNDO-2 calcs. *(French)* 77−14381
hydrocarbons, formation on metal surfaces in fusion reactors 80−21322
hydrocarbons, gas chromatographic quantitative anal., unrecognised systematic errors 78−92537
hydrocarbons, gas phase, thermal electron interactions, drift vel. meas. 78−62919
hydrocarbons, gas phase oxidations and pyrolysis, wall-less reactor technique 80−45500
hydrocarbons, gaseous, pyrocarbon deposition, kinetic model *(German)* 78−23851
hydrocarbons, glass transitions, cellulose blotter/torsion pendulum technique, for relax. determ. 80−54357
hydrocarbons, glasses, γ-irrad., trapped electron yields, mol. struct. and temp. effects 77−40561
hydrocarbons, heavy, self-holograms of laser-induced surface depressions 78−82927
hydrocarbons, heavy liq., vapour press. and enthalpies of vaporisation by group-contrib. method 80−40726
hydrocarbons, high speed laser schlieren techniques 78−15093
hydrocarbons, high-temp. absorptivity of 3.39 μm laser line 78−86856
hydrocarbons, ht. of formation calc. by MINDO method *(German)* 78−82646
hydrocarbons, ignition by small sparks 79−55587
hydrocarbons, in Gulf of Mexico, concs. in seawater at proposed deep-water port sites 78−44880

organic compounds continued
hydrocarbons, in Mars atm. and implications for channel form. 78−65543
hydrocarbons, in residual gas, polymerisation by electron bombard. *(German)* 77−40315
hydrocarbons, ion injection, low field elec. cond. 79−91064
hydrocarbons, ionisation pots. calc., PPP method 78−58592
hydrocarbons, IR intensities, C-H bond moments and bending modes 77−10703
hydrocarbons, IR intensities, polar tensors, atomic population densities 77−23497
hydrocarbons, light, in Recent Texas continental shelf and slope sediments, origin 79−2213
hydrocarbons, liq., competitive reactions in radiolysis 79−39179
hydrocarbons, liq., Compton profiles, bond additivity 80−93423
hydrocarbons, liq., dynamics of elec. breakdown 78−88253
hydrocarbons, liq., mobility of localised and quasi-free excess electrons 79−4589
hydrocarbons, liq., positronium form., mechanism rel. to electron solvation 78−70980
hydrocarbons, liq. mixtures, thermodynamics *(German)* 78−20047
hydrocarbons, liquid, high-field carrier transport at pre-breakdown and breakdown regions 80−25305
hydrocarbons, localised and quasifree excess electron mobility, cond. state energy and temp. depend. 79−4588
hydrocarbons, long chain, interstellar formation mechanism expt. 80−46653
hydrocarbons, mag. susceptibility and anisotropy *(French)* 78−37559
hydrocarbons, meas. in urban and industrial air pollution, Houston, Texas 77−78406
hydrocarbons, mol. geometry, CNDO/BW and MINDO/2 calcs. 79−41109
hydrocarbons, mol. graphs, eigenvalues 77−26996
hydrocarbons, mol. Raman intensities calcs. 80−52993
hydrocarbons, mol. thermodynamics, information-theoretic aspects 78−13409
hydrocarbons, molecular packing anal. of alkyne structs., lattice energy minima 78−95011
hydrocarbons, Ni-catalysed decomp., morphologies and growth mechanisms of carbons 78−35679
hydrocarbons, NMR parameters, chem. shielding, ^{13}C chem. shifts 80−23435
hydrocarbons, non-alternant, reson. energies 80−106278
hydrocarbons, non-methane, in atmosphere, monitoring via photoionisation 78−73549
hydrocarbons, nonlinear absorpt. spectroscopy 79−63315
hydrocarbons, normal, mass-spectrometric fragmentation processes, quantum field theory 80−40782
hydrocarbons, occupied mol. orbital energy levels, rel. to chemisorption activity 79−19449
hydrocarbons, phase equilib. calcs., modified Soave eqn. of state 79−19352
hydrocarbons, photochem. in atm. of Titan 79−53766
hydrocarbons, plasma polymerisation 78−88634
hydrocarbons, pollutants, comp. and sources in Severn Estuary 79−12148
hydrocarbons, pool boiling, heat transfer, surface roughness effect 80−48705
hydrocarbons, press. second virial coeff., graph theory prediction 80−43823
hydrocarbons, press. second virial coeffs., walks on graphs method 80−7841
hydrocarbons, proton NMR chem. shifts, mag. shielding effect of neighbouring C atoms 77−27094
hydrocarbons, pulsed irrad. electron mobilities and reaction rate consts. for electron-solute reactions 79−91112
hydrocarbons, reactions, rate consts., temp. depend., photolysis, high temp. fast flow reactor technique 80−42231
hydrocarbons, reduced vap. press. eqn. 79−37823
hydrocarbons, refrigerated liquids, density meas. by capacitance method 77−26273
hydrocarbons, San Francisco air basin, biogenic emission related to high ozone levels 79−83676
hydrocarbons, saturated, bonded and nonbonded, quantum chem. calcs. 80−9514
hydrocarbons, saturated, modified CNDO calcs., conformations, binding energies 77−6682
hydrocarbons, saturated, thermal cond., rad. effect interferometry method 77−11745
hydrocarbons, saturated, topological orbitals, graph theory and ionis. pots. 78−82615
hydrocarbons, saturated and unsaturated, ionisation spectral intensities, correlation effects 78−90234
hydrocarbons, saturated open-chain, transport behaviour of excess electrons and props. 80−39643
hydrocarbons, second virial coeff., empirical eqn. 77−58831
hydrocarbons, shock compression, dynamic high press. eqns. of state 80−6450
hydrocarbons, simple ions, reaction with simple mols. at thermal energies 77−40532
hydrocarbons, soln. radiolysis, electron scavenging, Warman-Asmus-Schuler parameter 79−70354
hydrocarbons, sorption, diffusion, solubility in polyvinyltrimethylsilane rel. to temp. *(Russian)* 80−6565
hydrocarbons, substituted, monolayers on Pt (100) surface, AES quantitative anal., calibration 78−31724
hydrocarbons, thermal conductivity, corresponding states model 80−69964
hydrocarbons, thermodynamic props., multiparameter conformal solution theory 78−18796
hydrocarbons, thermodynamic props., optimum incremental diagram calc. method *(German)* 78−51702
hydrocarbons, thermodynamic props. correls., third parameters 79−95184
hydrocarbons, unsaturated, ang. distrib. He I, Ne I and Au I photoelectron spectra 79−31605
hydrocarbons, unsaturated, empirical potential model EPEN/2 parameterisation, testing 79−50103
hydrocarbons, vehicle generated, in atmosphere, correl. study 79−21012
hydrocarbons, vibr. intensities, G sum rule appls. 80−32776
hydrocarbons, volatile, contrib. to organic C budget of estuary 79−70473

organic compounds continued
hydrocarbons, volatile, detection and meas. in atm. review 77−64492
hydrocarbons+N^+, chemiluminescence, total reaction cross sections dependence on collision energy 79−47530
hydrocarbons+N^+, rotational vibrational product excitation 79−47901
hydrocarbons+O^+, chemiluminescent reactions 79−96299
hydrocarbons and halogen-hydrocarbons, solidified, solubility in liq. N_2, calc. by Preston-Prausnitz method 78−26686
hydrocarbons and mixtures, second virial coeffs. calcs. incl. angular coordinates 77−19659
hydrocarbons and organic halides, fragment ion kinetic energy determ. by mass spectra 77−6958
hydrocarbons at Argo Merchant wreck site, gas chromatography 79−83645
hydrocarbons decomposition reaction, with Ta and α-Hf, surface segregation influence of O_2 or N_2 80−55654
hydrocarbons emissions inventory in United Kingdom 79−62158
hydrocarbons flowing through circular pipe, streaming currents developed in laminar and turbulent flows 78−87413
hydrocarbons in air, determ. via gas chromatography after cryogenic sampling 78−81468
hydrocarbons in Jupiter atmosphere, photochemistry rel. to Lyman alpha albedo 80−105194
hydrocarbons in surface sediments on Scotian Shelf 78−49008
hydrocarbons liq., geminate pair of charges, neutralisation escape with field depend. electron mobility 78−26865
hydrocarbons meas. in seawater, risk of contamination from Niskin sampling bottles 78−45039
hydrocyanic acid laser, 0.337 mm, for interferometric plasma density meas. 78−5922
hydrofluorocarbon monitoring using telluric absorption line *(German)* 78−49133
hydrogen chloride/dimethyl ether complex, temp. depend. of IR spectra of H bond in gaseous state 77−34624
hydrogen maleate ion, electronic spectra, CNDO/S CI calcs. 77−75128
hydrolysis in water, rate consts. 78−76856
1-hydronaphthyl radical, 4.2K absorpt. spectrum *(French)* 80−80809
1-hydronaphthyl radical, in naphthalene single cryst., anisotropic oscill. strength 78−50591
hydronaphthyl radicals embedded in naphthalene cryst., optical transition energies and ionisation energies 80−78595
hydroocarbon chain synthesis in interstellar clouds, ion-molecule scheme 80−12786
hydroperoxy-hydroxy-methane, metastable mol., IR spectra of formaldehyde photooxidation products 79−93994
hydrophobic compounds, effect on luminesc. of spectrally sensitised AgBr microcrysts. 80−97331
hydrophobic pollutants, sorption on natural sediments 79−83651
hydroquinone, oxidation of centre of photographic development, electrochem. kinetics *(Russian)* 80−3367
hydroquinone+ammoniated electrons, reaction rate consts. 77−9043
hydroquinone developer, lith development mechanism 80−77889
8-hydroxy, 1,3,6-pyrene trisulphonate, picosec. proton ejection, ultrafast pH jump 79−83475
β-hydroxy acrolein, lower excited states, electronic struct. and H-bonding, ab initio SCF and CI calcs., photochemical mechanism 80−83278
β-hydroxy benzophenone oxime-Cu, distribution coeffs., model 78−53244
hydroxy compound dilute solutions, dielec. relax. at 20 to 40°C *(German)* 79−33605
15-hydroxy prostaglandin dehydrogenase activity in tissues of mice, X-irrad. effects 80−51169
8-hydroxy quinoline, single cryst. growth from cyclohexane-water immiscible system 80−40244
4-hydroxy-2,2,6,6-tetramethylpiperidine, radiation-induced oxidation to paramag. nitroxide free radicals 80−81341
5-hydroxy-2,3-dihydro-1,4-phthalazindione, electron beam excited chemiluminesc., chem. and light yields 78−53209
3-hydroxy-2-methyl-1,4-naphthaquinone, pH indicator *(Rumanian)* 78−23947
7-hydroxy-2-methylchromone, solns., pH dependent fluorescence spectra, pK_a and tautomerism 79−59506
2-hydroxy-3-(2-undecyl, pentadecyl or heptadecyl amidoethylamine) propane-1-triethyl ammonium hydroxides, acid-corrosion inhibitors, effect on corrosion of low C steel in HCl 80−50761
2-hydroxy-3-crotonyloxypropyl methacrylate, synthesis, copolymerisation with maleic anhydride, photocrosslinking *(Japanese)* 78−31376
3-hydroxy-4-formylpyridine, glutamic acid, ^{99m}Tc labelled, possible cholescintigraphic agent 79−79653
hydroxy-carboxylic acid film, on Al, heat treatment effect on photoluminesc. props. 77−28610
N-hydroxy-N-p-tolyl-N'-(3-chloro-4-methylphenyl)-p-toluamidine, as reagent for V, synergic extraction and photometric determ. 79−79345
hydroxy-tetraazaindenes, sensitisation of photographic emulsions 77−54006
hydroxy-tetraazaindenes for photographic emulsion supersensitization 80−3384
p- hydroxy-trans-cinnamic acid, cryst. struct. basis for absence of thermal mesomorphism 80−96509
β-hydroxyacrolein, intramol. H bonds, orbital and transition energies, ab initio SCF and SCF CI calcs. 77−14345
para-hydroxyaniline, mol. complex., electronic struct., basis set and correlation effects 80−91436
hydroxyanthraquinones, lightfastness and flash photolysis 79−96341
hydroxyapatite, automated scan of X-ray powder diffraction pattern 80−22492
p-hydroxyazobenzene, acidic soln., reson. Raman spectra, ring deuterated derivatives 79−26987
p-hydroxybenzoic acid, lattice rigidity, mol. motions, wide-line NMR at room temp. 77−51967
2-hydroxybenzophenone, excitation singlet, internal H^+ transfer, visible spectra 80−32728
ortho-hydroxybenzophenone, soln., intramol. proton transfer and energy relax. photostability, transient absorption obs. 80−28032
hydroxycarbene, intermediate formaldehyde photochem., ab initio calc. methods 79−61880
α-hydroxycarboxylic acids, discovery in Murchison meteorite 78−45294
7-hydroxycoumarin, absorpt. and emission spectra, ionic forms 78−21955
hydroxycoumarin dyes, laser emission 78−82962
7-hydroxycoumarine, one- and two-photon absorption, fluoresc. obs. 78−46407

organic compounds continued
7-hydroxycoumarine, two-photon visible absorpt. spectra, fluoresc. obs. 78−42147
3-hydroxyflavone, excited state proton transfer, luminesc. 80−35818
hydroxygallium phthalocyanine, exciton electroabsorpt., optical density spectra 77−85746
hydroxyhaemin, ferric porphyrins with fifth ligands, ^{57}Fe and ^{14}N hyperfine consts. 78−50475
5-hydroxyindole, near ab initio and pseudopotential calcs. 77−71749
hydroxyl protons, temp. depend. of chem. shift, in R-OH cpds. 78−35054
7-hydroxylepidone, solns., multiple fluoresc. emission 78−33547
tris(hydroxymethyl)aminomethane, enthalpy of reaction meas. microprocessor-controlled system 80−22361
hydroxymethyl cation, geom. and electronic struct., ab initio SCF calc. 79−76331
hydroxymethyl radical, isotropic hyperfine coupling consts., temp. depend., nuclear vibrs. 78−35039
hydroxymethyl radical+solvated electron, reaction in methanol, dose and base effects 78−20043
hydroxymethyl radical $+0_2$, rate coefficient meas. by laser magnetic resonance flow tube method 80−66767
hydroxymethyl radicals, adsorption on A-type zeolites, electron spin echo obs. 78−21947
3-hydroxymethyl-2,2,5,5-tetramethylpyrrolidinyl 1-oxyl system, enantiomer solid soln., cryst. struct. and phase diagram 79−86778
hydroxymethylene radical cation stability, $CH_2O^{+\cdot}$ isomers, ab initio MO study 80−42965
hydroxyproline HCl, X-irrad., free radical products, ENDOR meas. 78−76883
hydroxypropyl cellulose in conc. aq. soln., mesophase struct., colour 77−19870
2- and 4- hydroxypyridine tautomers, ab initio SCF LCAO MO calcs. 79−81154
hydroxypyridines, phosphoresc. emission, polarisation and lifetimes 78−31232
hydroxypyrimidines, ^{14}N NQR, tautomerism 77−83620
8-hydroxyquinoline+phthalic anhydride, solid-state reaction kinetics 77−36746
8-hydroxyquinoline+Tl_2CO_3, solid state reaction 80−108708
hydroxyquinones, H-bonded, zero-phonon photochem., hole burning obs. 79−11802
N-(2-hydroxythiobenzoyl)morphiline, ^1H NMR, spin decoupling by torsional transitions 78−62832
2-hydroxytropone, in β-cyclodextrin complex, UV circ. dichroism spectrum assignments, complex struct. 78−46358
hydroxytryptamines, near ab initio and pseudopotential calcs. 77−71749
hydroxyurea, combined effect of US and cytotoxics on Zea mays root growth 77−5025
hydroxyurea effect on Chinese hamster ovary cell X-ray induced division delay 78−31865
3-hydroxyxanthine, monocrystals, UV-induced nitroxide radical and pair species 79−24775
hypohalites, electron structure, stability and reactivity 80−14086
hypotaurine oxidation to taurine by UV irradiation 79−96617
hypsorhodopsin, squid, form., picosec. spectrosc. obs. 79−39183
hyrocarbons, on activated C, rel. between adsorption and polarizabilities 80−76558
IBPBAC, cryst. struct. and struct. of ordered smectic phases, X-ray diffr. obs. 79−86780
IBPBAC, dynamics of smectic phases, quasi-elastic neutron scatt. meas. 79−86700
IBPBAC, order parameters in nematic and smectic phases, X-ray diffr. meas. 79−94874
IBPBAC, smectic B phase, neutron diffr. and X-ray obs. 78−94973
IBPBAC, smectic phases, self-diffusion coeffs., radiotracer meas. 80−49394
ice nucleation on surfaces, importance of OH groups 79−48530
idolalkylamines, conformational varieties in cryst. 78−10030
imidazole, cryst. struct. at 103K by neutron diffr. 79−37691
imidazole, photoelectron spectra and electronic struct. 79−22758
imidazole, quadrupole coupling consts. interpretation, ab initio field gradient calcs. 80−58282
imidazole, single cryst. Raman spectrum, ν(NH) region temp. depend. 77−8561
imidazole, solid, H bonding, wide line NMR obs. 78−52362
imidazole, vibr. spectra, mol. crystal dynamics, librational modes 78−64356
imidazole, Z-irrad., EPR study of H exchange 80−40718
imidazole-Cu^{2+} complex, electron spin echo, nuclear modulation effects 79−18211
imidazoles, reaction with photochemically generated α-hydroxyalkyl radicals, EPR study 80−35558
imidazoline nitroxide radical, H-bonding with H donors, NMR, DNP and spin lattice meas. 79−15971
imidazolium cation, near ab initio and pseudopotential calcs. 77−71749
4,5-iminophenanthrene, polymorphism, X-ray diffr. and photoluminesc. obs., 77 to 300K 77−63449
iminoxyl radicals, influence on elec. cond. of MBBA, EBBA liq. crysts. *(Russian)* 78−67641
imipramine, automated synthesis of ^{11}C-labelled radiopharmaceuticals 80−17133
impact on fog and cloud processes 78−73467
impurity crystals, press. effect on shift of zero-phonon lines 79−95824
in cyclohexane-ethanol mixtures, UV spectra, solvent effect 79−22770
in front of χ Ophiuchi, optical obs. 79−25673
1,3-indandione derivatives, higher-order harmonic generation, laser-induced nonlinear optical effects *(Russian)* 78−55412
indandione-1,3 derivative, layer, electrooptical effect *(Russian)* 79−73900
indane, 271 nm spectrum, rot. band contour anal., puckering vibr. 78−1001
2-indanone, single cryst., ODMR and phosphoresc. of $^3n\pi^*$ state 79−78570
1-indanone, T_1-S_0 intersystem crossing, nonradiative decay rate, excitation energy depend. 80−63609
n-indecyl-p-azoxy-α-methyl cinnamate, dislocations obs. in smectic A and C mesophases 78−91230
indene, fluoresc., ns time resolved emission spectra 77−6822
indene, microwave spectrum, assignments, rot. consts. and config. 79−31510
organic compounds continued
indeno[2,1-a]indene, in glassy media, phosphoresc., heavy atom effects 80−55153
indenyl-Li ion pair in dimethoxyethane, ^{13}C NMR, temp. and counterion depend. 78−48062
indenyl-Na ion pair in dimethoxyethane, ^{13}C NMR, temp. and counterion depend. 78−48062
indigo, picosec. kinetics, and photostability, spectrosc. obs. 79−45748
indigo derivatives, fluorescence decay times, meas. by synchroscan streak camera 80−84759
indigo dye, excited state lifetime, influence of inter- and intramol. H bonding 77−79659
indigo dye, S_1-lifetime determ. by two-photon fluoresc. 77−18966
indigo dyes, triplet state config., laser flash absorpt. spectrosc. obs. 80−5557
indigoid dyes, Raman, IR and Shpolskii spectra 79−65866
indium oxine (^{111}In), cell damage resulting from labelling rat lymphocytes and HeLa S3 cells 80−56145
indium transferrin, formation constant, nuclear medicine appls. 79−96285
indocyanine green fluoresc. spectrum in blood and other solvents, rel. to angiography 78−28057
indole, and derivatives, temp. fluoresc. quenching, rel. to H_2O solvent struct. 78−5265
indole, aq. alkaline soln., charge transfer, luminesc. obs., 77 and 300K 79−69876
indole, aq. solns., flash photolysis, transient absorpts., 600 to 800 nm 78−53228
indole, fluoresc. polaris., solvent effects 78−33542
indole, fluorescence quenching by chloromethanes due to electron transfer 79−94027
indole, in PMMA matrix, high press. luminesc. 78−84629
indole, in water-ethanol soln., radiolysis *(Russian)* 77−86338
indole, oriented in polyethylene film, dichroism spectrum 79−54864
indole, pH dependent fluoresc., quenching by histidine *(Russian)* 78−90209
indole, UV absorpt, spectra, low-lying Rydberg band 77−58037
indole decapeptide luteinising hormone, high-press. liq. chromatography, fluorometric detect. 78−20096
indole soln. containing histidine, fluoresc. rel. to soln. pH 80−2826
indoles, excited states, solvent interactions, fluoresc. obs., rel. to chromophore 78−37670
indoles, fluoresc. anomalies, mixed valence-Rydberg states 78−17707
indoles, in glassy hydrocarbons, complexation vs. aggregation, absorption and fluoresc. obs. 79−98132
indoles, laser flash spectroscopy in presence of nitroxide radicals, protein-membrane interaction probing 79−87855
indoles, temp. effects on electronic transition moments in n-heptane and water 78−58744
indolic compounds in pigmentary retinal epithelium of trout, chromatography detect. *(French)* 79−53115
indoline spiropyrane, photocolouring process, spectral depend. 79−66315
indoline spiropyrans, methoxysubstituted, activated solns., photochromism, laser nanosecond spectroscopy 77−70317
indomethacin, liq., new ionis. method appl., using Penning effect and chem. ionis. *(Japanese)* 79−93255
inductive-resonance energy transfer, heterogeneous electron level broadening *(Russian)* 78−23530
industrial gaseous environment characterisation, Brinkley method 80−93817
industrial organic chemicals production, electrical power applications development *(French)* 79−96327
inelastic electron tunnelling, vibr. spectra, review 77−54632
inelastic electron tunnelling spectroscopy meas. in MIM junction 77−14510
inositol, X-irrad., deuteration effects, ENDROR and ESR meas. 78−73067
inositol, X-irrad., radical form. detection by ESR and ENDOR, oxidation process 78−27797
inositol isomers, occurrence in marine sediments 77−5240
insecticide, DDT and DDE in New York rain following Pacific N.W. spraying 77−29425
intercalation compounds, metal guests in chalcogenide hosts, struct., review 79−46627
intercalation inorganic-organic layered complexes, effects of intercalation on elec. and mag. props. *(Japanese)* 79−8255
interstellar, synthesis of complex molecules 79−92826
interstellar and prebiotic organic chemistry 77−37641
interstellar C-H chemical system, mols. form. in diffuse cloud 77−26033
interstellar cyanodiacetylene (HC_5N), J=2-1 transition detect. 79−25692
interstellar formamide, ^{13}C isotope detect. in galactic centre 79−25680
interstellar grains, organic compositon, IR obs. 80−77460
interstellar grains comprised of organic cpds., 3.4 microns absorpt. obs. 80−109514
interstellar HC_5N, HC_7N, obs. in dark dust clouds 78−54023
interstellar medium, organic grains existence questioned 79−21397
interstellar molecules, mm emission lines obs. in Orion A 77−2477
interstellar molecules in cosmic dust, possible spectral signature at 2200 Å 77−57074
interstellar obs. using uncooled millimeter wave receiver *(Swedish)* 78−24461
interstellar organic compounds, gas phase chemistry model in diffuse and dense clouds 80−105298
interstellar organic compounds, origin and nature 78−24543
interstellar polysaccharides and related hydrocarbons, identification from IR spectra 78−28763
interstellar prebiotic molecules, assoc. with grain clumps 77−26042
intersteller CH, radio obs. 78−28751
inversion geometry, ab initio SCF calcs., basis set effects 80−78532
5-iodo-2′-deoxyuridine, γ-irrad., positron lifetime rel. to free radical conc. 78−72635
2-iodoacetamide, mol. struct., electron diffr. obs. 80−63819
3-iodoaniline, photoemission for mol., polarised photoelectrons 78−66607
^{11}C-α-p-iodoanilinophenylacetonitrile, conc. of activity in brain 80−3776
iodobenzene, liquid, vibr. relaxation, Brillouin spectra 80−108219
iodobenzene, nonlinear dielectric effect temp. depend. 79−82908
m-iodobenzene, nonlinear optical susceptibility, second order, calc. from mol. spectra *(Russian)* 79−27318
iodobenzene, photoelectron spectra ang. distrib., π- and σ-orbital assignments 79−818

organic compounds continued
iodobenzene, soln., non-linear dielec. effect, comparison with fluoro, chloro and bromobenzene 80−60478
iodobenzene bis(dichloroacetate), cryst. struct., secondary and multi-centre bonding 78−63751
iodobenzene diacetate 78−63751
iodobenzenes, in potassium laurate mesophase, NMR, proton distance ratios and order tensor elements calcs. 80−63672
iodobenzoic acid, NQR of ^{127}I and Mossbauer spectra of ^{125}I, bonding 77−12241
iodocyanoacetylene, cryst., IR, far-IR and Raman spectra, vibr., struct. 77−63407
^{125}I-iododeoxyuridine, effect of ^{125}I-decay, mol. consequences of Auger effect 77−4982
N-iododimethylamine, polymeric, mol. struct. exam. *(French)* 78−2101
iodoethane, mol. parameters, vibr., pot. barrier height etc., data tables 79−76409
iodoethane, UV photolysis, metastable I radiative lifetime, reson. fluoresc. obs. 79−11799
iodoethylene, and perfluoro analogue, VUV spectra, perfluoro effect on Rydberg states 77−61764
iodofluoropropane-fluorohexane, photodissoc. I laser *(Russian)* 77−38877
iodoform, soln., MCD spectra, assignments 79−31567
iodoform in cyclohexane soln., γ-radiolysis, G-values 79−52705
iodogermane radical anion, ESR spectra and struct. 80−87153
iodoheptafluoropropane, photolysis, reaction rate consts. meas., photodissociation I laser charcts. 79−52671
o-iodohippurate, ^{131}I labelled, in vitro stability 80−16668
iodohippuric acid, NQR of ^{127}I and Mossbauer spectra of ^{125}I, bonding 77−12241
iodomethane, ^{13}C enriched 2D heternucl. NMR spectrum 77−90068
iodomethane, and deuterated, optically pumped submm. wave amplification 78−29941
iodomethane, and isotopic forms, self-broadening and self-shifting of rot. spectra 78−13551
iodomethane, collisional rot.-line widths and shifts, microwave region 78−25619
iodomethane, dielectric susceptibility at radio frequencies 78−14123
iodomethane, dressed mol., ν_6 band, saturated absorption spectrosc. 79−54844
iodomethane, first s-Rydberg transitions 78−42094
iodomethane, IR-RF double reson., NQR of spin-rot. coupling consts. 78−66569
iodomethane, laser charcts. with transverse optical pumping *(Russian)* 79−50286
iodomethane, laser submillimetre with optical pumping energy yield, emission pulse delay time depend. on pumping pulse *(Russian)* 78−71088
iodomethane, liq. (liq. mixtures), vibr. relax. and reorientation, symmetric C-H bending mode 1st overtone 78−62884
iodomethane, mol. dipole moment derivative, sign of 79−86082
iodomethane, oriented in nematic liq. crystal, longit. NMR, relax. mech. 77−63302
iodomethane, P-line and ν_6 band spectra using CO_2 laser absorpt. 80−69142
iodomethane, photofragmentation in vap. phase, photoacoustic meas. 78−95943
iodomethane, photoionis., vibr.-excited ions form. in Franck-Condon gaps, threshold photoelectron spectra obs. 79−68262
iodomethane, Raman band shapes, mol. oscill. bands *(German)* 80−69154
iodomethane, RF field dressed mol. saturated absorpt. obs. 80−9648
iodomethane, Stark effect modulation of CO_2 laser 78−17992
iodomethane, thin single cryst., IR spectra anal., Fermi-Davydov intensity distrib. 77−59577
iodomethane, vibr., rot. and translational energy exchange, semiclassical theory 80−48067
iodomethane, vibr. population lifetimes in liqs. anti-Stokes Raman scatt. 78−74665
iodomethane, vibr. relax., Raman overtone band obs. 77−14436
iodomethane+F, IF product internal rot.-vibr. distribs., fluoresc. obs. 80−48078
iodomethane+F reactions, product state analysis using laser-induced fluoresc. 80−11915
iodomethane+K, mol. rearrangement, optical pot. calcs. 77−81399
iodomethane+K(Ba)→K(Ba)I+CH_3, products translational distrib., crossed beam reaction 78−31629
iodomethane+Rb(K), product translational energy calcs., energy depend. 79−70314
iodomethane+Rb reaction cross section, translational energy depend. min. 77−66753
iodomethane+Sn, crossed beam kinetics, SnI recoil vel. spectra 79−1947
iodomethane+Xe, high Rydberg state, ionis. 78−50620
iodomethane(-d_3)$^+$→CH_3^+(CD_3^+)+I, kinetic energy release distrib. meas. 77−1922
iodomethane cation, photodissoc., mass spectrometric obs., isotope effects 77−75241
iodomethane laser, photolysis wavelength, repetitive operation 79−3689
iodomethane-acetone, liq. mixture, excess Gruneisen parameter, intermol. interaction 78−67635
iodomethane-d_0, (−d_3)+I($5^2P_{1/2}$), temperature dependence for quenching 79−45755
iodomethane-d_1, ^{13}C enriched, NMR, oriented, symmetry related isotope effects 77−61772
iodomethane-d_1, in nematic soln., D NQR coupling const., isotope effect 79−27009
iodomethane-d_3, ν_2 band, laser Stark and laser-microwave double resonance spectra 77−27067
iodomethane-d_3, ν_2 band, laser Stark saturation spectra 78−42125
iodomethane-d_3, Stark tuned level crossings and saturated absorpt., RF elec. field modulation effects 80−52989
iodomethane-d_3($^{13}CD_3I$), 690 and 806 micron laser transitions 78−42328
iodomethyl radical, vibr. excited, photofragmentation IR emission obs. 80−87162
iodomethyl-norcholesterol: ^{131}I, adrenal imaging in primary aldosteronism 79−79634
iodomethylnorcholesterol: ^{131}I, human adrenals absorbed dose 79−79660
iodonaphthalene, bond and mol. polarisability, semi-empirical delta-function 79−31441
α-iodonaphthalene, IR absorption spectra, forbidden character 77−58002
organic compounds continued
1-iodonaphthalene-perfluorated naphthalene solid soln., sensitised phosphoresc., site selection method, Dexter's theory 79−4836
iodonium cyclic compound, ESR signal *(Chinese)* 78−15025
β-iodophenylacetylene radical, PhC_2I^-, from γ-irrad. morpholine β-iodophenylacetylene complex, EPR obs. 77−52652
^{125}I-iodoproflavine binding with DNA, double strand break induction 78−20145
1-iodopropane, photoionisation mass spectrometry 80−40779
1-iodopropane, pyrolysis, intermol. energy transfer in two-channel unimol. reaction 79−11769
n-iodopropane+Sn, crossed beam kinetics, SnI recoil vel. spectra 79−1947
2-iodopropene, barriers to internal rotation 78−9273
3-iodopropene, microwave spectra, rot. consts. and HFS 78−975
3-iodopropene, microwave spectra, torsionally excited, rot. consts. 79−63986
2-iodopropene, microwave spectrum, quadrupole coupling consts., internal rot. barrier 79−45710
3-iodopropene, rot. spectra, quadrupole hyperfine struct. 80−91545
2- and 3-iodopyridine, IR and Raman spectra, vibr. assignments 78−25534
iodoseptofluoropropane photodissoc. laser, refr. index distrib. fields, double exposure holography 80−9873
iodotrifluoromethane, continuous absorpt. band contour, temp. depend. 78−70876
iodotrifluoromethane, E-species force consts., using L-F approx. method, HLFS applicability 80−962
iodotrifluoromethane, high vibr. state excitation in high-power laser field, spectral charcts. 80−91562
iodotrifluoromethane, IR multiphoton dissoc., source of trifluoromethyl radicals 80−26036
iodotrifluoromethane, IR multiphoton selective dissoc., effect of acceptor radicals 80−66854
iodotrifluoromethane, isotope selective photodissoc. by multiphoton vibr. and electronic excitation *(Russian)* 79−59517
iodotrifluoromethane, mol. struct., electron diffr., microwave spectra, CNDO/2 calcs. 78−37766
iodotrifluoromethane, multiphoton dissociation for C isotope separation 79−3592
iodotrifluoromethane, photoelectron spectra, spin-orbit splitting, vibr. fine struct. 78−21974
iodotrifluoromethane, photolysis, reaction rate consts. meas., photodissociation I laser charcts. 79−52671
3-iodotyrosine, intramolecular effects of ^{131}I decay 77−36870
iodoxybenzene, cryst. struct., secondary and multi-centre bonding 78−63751
ion-radical compounds, microscopic parameters 79−78025
ionic melts, novel class of liquids 77−35463
ionic surfactants, conductance stopped flow study of micellar equilibria 79−43642
ionisation of non-volatile compounds by heavy-ions, separation by mass spectrom. 77−27170
ionisation potential, heat of formation, improved IOC-ω technique 77−14336
ionisation potential and electron affinites of molecule containing C, N, O, and H atoms, semiempirical calcs. 80−78535
ionone, dipole moment determ. 78−27882
ions, pot. energy profiles for unimol. reactions 80−43210
IR absorpt. bands halfwidths transferability in related mols. series 79−54921
IR intensities anal., hybrid orbital rehybridisation model, mol. charge distrib. 78−74630
IR photoacoustic spectroscopy of solids and surface species 80−90909
(iron, chromium) carboxylates, heteronuclear trimer exchange clusters, ESR spectra 80−80603
iron (4,7-dimethyl-di-1,10-phenanthroline)$(NCS)_2$, spin state transition, X-ray and Mossbauer obs. 80−7195
iron (II) formate dihydrate, mag. sp. ht., S_z^4-term 79−61127
iron formate dihydrate, higher order term of uniaxial anisotropy *(Japanese)* 80−2571
iron formate dihydrate, mag. sp. ht., S_z^4-term 80−60289
iron oxalate, γ-ray and neutron irrad. effects, Mossbauer spectra obs. 79−65778
iron oxalate, quadrupole splitting, Mossbauer spectroscopy 79−11365
iron phthalate, reduction, prep. of Fe powder 77−40090
iron phthalocyanine, annealed, elec. cond., daylight exposure and thickness effect *(French)* 80−84484
iron phthalocyanine cathode, performance in fuel cells with H_2SO_4 electrolyte 80−21293
iron poprhin, A_{2u} out of plane vibration, pseudo-Jahn-Teller effect 78−82712
iron porphin in triphenylene, ESR 78−60329
iron porphyrin chlorides, X-ray, EPR and mag. susceptibility obs., intermol. exchange interaction 78−10765
iron tetraphenylporphyrin chloride, electron spin pairs, low and ultralow temps. 77−77092
irradiated single crystals, electron trapping, ESR obs. 78−88646
iso-butene, flash photolysis, β-methallyl radical extinction coeffs. 77−1938
iso-octane, refr. index, temp. depend., deviation from Lorentz-Lorenz formula 77−40200
iso-octane-methanol-nitrobenzene, US vel. and absorpt., along line of plait points in ternary liq. 78−79669
iso-octane-nitroethane soln., crit. exponents *(Russian)* 79−77766
10H-isoalloxazine, and derivatives electronic struct., photoelectron spectrosc. and ab initio study 80−106261
isobacteriochlorins, π cation radicals, implications for NO_2^-, SO_2^- reductases 80−63684
isobutane, adsorption on water, 0-50°C, press effects on surface tension 78−56024
isobutane, condensation in porous bulk media 78−47510
isobutane, viscosity meas. at atm. press. and 25-195°C 79−86550
isobutane+Cl ions, energy straggling 78−58785
isobutane+HO→H_2O+iso(or t-)C_4H_9, 700 and 100 torr, 25°C, FT-IR anal. 77−25247
isobutane+methylal+Ar, drift properties of tubular drift chambers in high magnetic fields 80−53917
isobutane hydrogenolysis, limitations of kinetic studies of catalysis on single-cryst. surface in UHV system 77−9126

organic compounds continued
isobutane-air, in packed bed, heat and mass transfer, axial mass dispersion 78−75200
isobutene, droplet nucleation from crit. gas-phase+positive ions 79−39222
isobutene+C_2O, absolute reaction rate consts. meas. by laser induced fluoresc. 80−93738
isobutene+HF, vibr. relax. dye laser pumping effects 80−9703
isobutene-d_0, -d_6, torsional pot. functions, spectra anal. 78−25528
isobutyl alcohol, absorpt. on η-, γ-Al_2O_3, gravimetry, IR investigs. 79−1546
isobutylene, liq., vibr. phase relax. and freq. shifts, density and temp. effects 80−74235
isobutylene, photoelectron spectrosc., ang. depend. 80−9641
isobutyric acid+water, thermal expansion near upper crit. soln. temp. 77−29031
isobutyric acid and water, shear viscosity of critical mixture, amplitude ratios 80−2188
isobutyric acid-d_{10}-D_2O, coexistence curve, liq. densities 78−18780
isobutyric acid-H_2O, crit. mixture, partial molar vol., temp. depend. 78−18800
isobutyric acid-H_2O, liquid-vapour surface tension near liquid-liquid consolute point 80−107613
isobutyric acid-water, crit. mixture, conc. fluctuation mean relax. time, US absorpt. and vel. meas 80−29163
isobutyric acid-water, crit. mixture 80−24601
isobutyric acid-water, mixture, heat of transport, crit. exponent 80−15277
isobutyric acid-water binary fluid system, crit. props. 77−76563
isobutyric acid-water critical mixtures, shear viscosity, pseudospinodal curves and scaling 78−22844
isobutyric acid-water critical mixtures, US and hypersonic study 80−88268
isobutyric acid-water mixture, electrical conductivity near crit. pt. 77−15612
isobutyric acid-water mixture critically quenched, phase separation and coalescence 80−24581
isobutyric acid-water mixtures, phase separation, light scatt. 78−84592
isobutyric acid-water mixtures, spinodal decomposition, light scatt. 77−72688
isobutyric acid-water near-critical liquid mixture, nucleation 80−92664
isobutyric acid-water system, liq.-liq. critical pts., Ising exponents, extended scaling 77−20072
isobutyric-acid-H_2O, crit. fluid, refr. index, α and Δ components 79−82940
isocitrate dehydrogenase from Azotobacter vinelandii, essential amino-acid residues identification 80−76538
4-isocyanate-trans-stilbenes, donor substituted, anisotropic fluoresc. in low viscosity solvents *(German)* 80−93401
isocyanates, nonbonding and π-orbital interactions, photoelectron spectra 80−32774
isocyanic acid, molecular structure and centrifugal distortion constants 80−47974
isocyanoacetylene theoretical study and rot. const. 78−33633
isocyanoethynyl radical, theoretical study and rot. const. 78−33633
isocyanomethane, charge exchange mass spectrometry, HNC^+ ion recombination and ionisation pot. 78−76838
isocyanomethyl radical, electronic struct. and props. 79−49938
isoeugenole, liq. scintillator system, energy transfer, fluoresc. intensity-max. solvent depend. 78−21966
isooctane, liquid, high-speed schlieren studies of elec. breakdown 77−89332
isooctane, SF_6 electron scavenging in positron spur in nonpolar liqs. 79−100421
isooctane-benzonitrile mixture, dielec. const. near consolute point, temp. and freq. depend. meas. 80−71292
isooctane-nitroethane, crit. fluid, refr. index, α and Δ components 79−82940
isooctane-nitromethane, liq. mixture, coexistence curve, refr. index meas. 80−10655
Isopar-M, pressure-volume isotherms determ., use in deep-sea instrument float 77−25786
isopentane, thermodynamical Gruneisen parameter, press. depend. 78−14479
isopinocampheol, methyl groups internal rot. ^{31}C spin lattice relaxation times and force field calcs. 80−74255
isopropanol, ^{13}C T_1 value temp-depend. field-depend. 79−61247
isopropanol, anodic oxidation *(Rumanian)* 78−19907
isopropanol, boiling, under increased gravitation, heat exchange mechanism, review 77−46895
isopropanol, decomp. on α- and β-V_2O_5 bronzes, 186-300°C, kinetics and mechanism 78−11553
isopropanol, nucleate pool boiling, bubble freq. model, surface effects 78−90651
isopropanol, US studies of mol. relax. 78−22790
isopropanol aqueous soln, sound absorpt. coeff. meas., acoustic relax. 78−83883
isopropanol on RuO_2 and CdO_2 catalysts, surface active sites during dehydrogenation 79−43621
isopropanol-freon, mixture, Raman spectra in OH(OD) stretching region *(French)* 79−26986
isopropanol-n-propanol aq. mixtures, US relax., US absorpt. and vel. meas. *(French)* 80−103426
isoproplyiodide, microwave spectrum, quadrupole coupling 78−86848
2-isopropoxyphenyl-N-methyl carbamate, fluoresc. and phospheresc. in solns. 79−61426
isopropyl alcohol, adsorbed on ZnO, decomp., IR and kinetic obs. 80−59780
isopropyl alcohol, glass transition rel. to press. depend. of viscosity 80−34171
isopropyl alcohol, wetting of polyfluoroethylene resin, angle meas., porosimetry method 77−1278
isopropyl alcohol decomposition using MoO_3:Li catalyst 78−60122
isopropyl ammonium chloroplatinate and chlorostannate, ferroelastic transition, thermal, optical, and elastic meas. 79−28096
isopropyl benzene, mol. solid, temp. depend. UPS linewidths 80−89115
isopropyl fluoroformate, microwave spectrum and conformation 79−10098
isopropyl radical, Ar matrix isolated, IR spectra and UV photolysis 80−66827
isopropyl radical, pot. energy surfaces, ab initio UHF calcs. 80−106258
organic compounds continued
isopropyl vinyl ether, chem. initiated soln. polymerisation and radiation-initiated bulk polymerisation 79−91952
isopropylamine-d_0,-d_1,-d_2, microwave spectra, struct., dipole moments and quadrupole coupling consts. 77−34613
isopropylaniline having optically active modes, vibr. relax. studied by absorpt. and fluoresc. spectra 80−83340
isopropylbenzene, IR spectra of oxidation products *(Rumanian)* 78−23838
isopropylbromide, thermal and IR laser induced unimol. decompositions 78−20012
isopropylcyclopropane, solid, liquid, vapour phase, IR and Raman vibr. spectra 80−84740
isopropylphosphine, gauche form, microwave spectrum, identification 78−58674
isoquinoline, adsorbed on Ag, surface enhanced Raman spectrum 80−100400
isoquinoline, dil. soln., dielec. absorpt., relax. and thermodynamic parameters meas. 80−50258
isoquinoline, fluoresc., phosphoresc. and H bonding 77−79647
isoquinoline, polycyclic monoazines, temperature dependence, triplet formation 79−54900
isoquinoline, quasilinear absorpt. spectrum, in Shpolskii system 77−46571
isoquinoline, radiationless transitions, internal conversion, energy depend. 78−94272
isoquinoline, solns., dielec. polarisation, π-electron system effects 77−90096
isoquinoline, solns. and mixtures, dielectric relax., const. and loss factor 77−55747
isoquinoline luminesc. in polymeric media at high press. 79−13756
isoquinoline semiperchlorate, H-bonding, strong, stochastic model and IR spectra temp. effects 78−62805
isorhodopsin chromophore conform. and orientation in frog disc membrane 78−64980
isothiazole, ^{14}N NQR of mol., expt. and MO calc. 79−36667
isothiazole, rot. Zeeman effect, localised susceptibilities 80−91600
isothiocyanic acid, $H^{13}NCS$, $HN^{13}CS$ and $HNC^{34}S$, ground state spect. constants and molecular struct. 80−47973
isothiocyanic acid, interstellar detect. in Sagittarius B2, mm wave spectrum 80−41878
isothiothiocyanates, nonbonding and π-orbital interactions, photoelectron spectra 80−32774
isotopically mixed organic solid, electronic energy transfer, Anderson transition 80−44545
isotopically mixed solid, electronic energy transfer, Anderson localisation model 79−19557
isotopically mixed solid, electronically excited states localisation model 79−47044
isotopically modified compounds, nomenclature 80−3294
isovaline radioracemization, cosmochemical implications 80−62087
isoxazole, ^{14}N NQR of mol., expt. and MO calc. 79−36667
isoxazole-4D, microwave spectrum, ^{14}N nucl. quadrupole coupling tensor 78−90154
isoxazolines, thermodynamics charact. of phase diagrams 78−23673
jasmone and intermediate compound synthesis *(Japanese)* 79−8436
in Jilin meteorite 80−17557
K-vitamins, IR absorpt. spectra, vibr. anal., quinonoid struct. 78−61139
KEL-F, ^{19}F, spectrum using multiple pulse decoupling-magic angle spinning NMR probe 78−12735
kerogen-like compounds, possible presence in Trojan asteroids 80−56751
kerosene, combustion in air rel. to press. 3-15 kgf.cm^{-2} 79−66297
kerosene, fuel drops, liq., blast wave initiated detonation waves 79−64691
kerosene+Fe_3O_4, ferrofluid, thermal and electrical cond. in mag. field *(Russian)* 78−6188
kerosene combustion products, porous evaporative cooling of construction elements 79−55372
kerosene drops, direct contact cooling of crystallising brine 79−1053
kerosene-air flame laser induced fluorescence spectra obs. 80−91587
kerosene-base mag. fluid, sound vel. meas. 77−63969
kerosine-brine system, horizontal layer, convective stability 77−7392
ketene, ab initio calc., energy levels and geom. struct. of C_2H_2O isomers 78−62716
ketene, CH_2 photoprod., wavelength depend. 80−11936
ketene, electron correlation problem, graphical unitary group approach 79−76324
ketene, hyperfine interactions, mol. beam elec. reson. spectra 77−88445
ketene, interstellar, microwave detect. in Sagittarius B2 77−37638
ketene, IR spectra, rot.-vibr. anal. of Coriolis coupled bands 78−86859
ketene, multiphoton dissoc., CH_2 and C_2 prod., fluence depend. meas. 80−5586
ketene, multiphoton laser-induced decomp. chemilum. and collision-assisted dissoc., rephotolysis 79−83491
ketene, near UV photolysis, bimol. mechanism, products quantum yield, press. depend. 77−77799
ketene, photodissoc., in near UV, bimolecular mechanism 78−64870
ketene, photoionis., ion fragmentation kinetic energy 78−9206
ketene, photolysis, methylene singlet-triplet splitting investig. 79−100407
ketene, UHF-INDO perturbation calc., localised spin orbitals, spin anomaly and second order substituent effect 79−68191
ketene, vertical ionis. pot., Koopmans' theorem perturbation corrections 79−76336
ketene+H, reaction rate consts., lab. meas., rel. to interstellar cloud processes 79−74359
ketene→CH_2+CO, photodissoc. at 337 nm, visible fluoresc. of CH_2 78−42121
ketene(-d_2), radical cations, doublet electronic states, photoelectron spectra 77−88496
ketene-cyclobutane photolysis, methylcyclobutane form., decomp., CH_2 vibr. energy distrib. 78−61032
ketene-cyclobutane-O_2, UV photolysis producing chem. activated methylcyclobutane, S/D ratio 79−87856
ketene-d_0, -d_2, Coriolis coupling, centrifugal distortion and force consts., mean vibr. amplitudes calcs. 79−36607
ketene-d_0,-d_2, mol. ion reactivity, vibr. energy effects, mass spectrometric obs. 77−44470
ketene-d_1(d_2), microwave and millimetre spectra, rot. transition, centrifugal distortion anal. 77−57991
ketocarbene-ketene rearrangement, reaction path, ab initio calc. 78−20008

organic compounds continued
ketocyanine dye, lasing under lamp excitation 78−82964
ketocyanine-rhodamine 6G mixed solns., wideband lasing 79−957
ketocyanines alcohol solns., spectral-luminesc. props. 80−2835
ketone, H abstraction, feasible forbidden photochem. reaction 77−9092
ketone chemiluminescence during disproportionation, nonradiative transition processes 79−87846
ketone-paraffin solid soln., dielec. relax., temp. and lattice const. depend. *(German)* 78−76383
ketones, bonding, optical anisotropy and polarisability 79−22713
ketones, conjugated, ethylenic, UV photoelectron spectra *(French)* 78−90215
ketones, cyclic, photolytic biradicals, mag. field depend. ^{13}C and ^{1}H CIDNP, hyperfine coupling 79−3460
ketones, dispersion-induced optical activity rel. to olfaction 77−56393
ketones, effect of polyethylene, environmental stress relax. study 80−45336
ketones, mol. cryst., interband transitions, triplet-triplet absorptions 79−11452
ketones, molecular stopping cross section of He^{+} ions and atomic stopping cross section of O 78−67746
ketones, rigid, optical rot. dispersion spectra, solvent effects 77−10684
ketones, saturated, MCD spectra, forbidden transitions generated by struct.-vibr. perturbations 77−50460
ketones, solns., IR absorpt. band parameters rel. to temp. 80−2762
ketones, triplet-triplet absorption carbonyl group role 77−83641
ketyl radical+benzophenone, triplet-doublet energy transfer, viscosity and mag. field effects 77−71850
kiton red S, mol. fluoresc. decay time, self-absorption 79−68255
β-lactam antibiotics, ab initio SCF-MO-LCAO calcs., amidic bond breaking, methoxy substitution effect 80−78533
lactam-lactim tautomeric equilibria, quantum chem. calcs. 80−50833
lactams, N-methylated, cis-trans isomerism, ^{1}H and ^{13}C NMR obs. 80−106335
lactams, optical rot. strength, sector rules 78−17737
l-lactic acid, ^{11}C-labelled, enzymatic synthesis 80−61695
lactones, optical rot. strength, sector rules 78−17737
lactose powder coated with fatty acids, tensile strength 77−21304
lanthanide complex, struct. and equilib. by time resolved Eu(III) spectrosc. 80−78736
lanthanide ion bound to macromol., struct. and equilib. by time resolved Eu(III) spectrosc. 80−78736
lanthanide shift reagents, pseudocontact shift, temp. depend. 79−95659
lanthanide-porphyrin complexes, upper $\pi\pi^{*}$ electronic states, fluoresc. 80−83410
lanthanum bicarbamide acetate, cryst. struct. 79−19240
lanthanum ethyl sulphate.$9D_2O$:$^{160}Gd^{3+}$, EPR transition energies at low mag. fields 77−12198
lanthanum ethyl sulphate:Gd^{3+}, X-band EPR, near room temp., spin Hamiltonian parameters 77−63275
lanthanum ethyl sulphate:Pr, phase transition under pressure, absorpt. spectra *(Russian)* 80−92667
lanthanum ethyl sulphate=Gd^{3+}, proton position determ. by ENDOR 77−51992
lanthanum ethyl sulphate nonahydrate: Tb^{3+}, ESR spectrum, spin lattice relax., effect of hydrostatic compression 78−88185
lanthanum ethyl sulphate nonahydrate:Pr^{3+}, absorpt. spectrum, 400-700 nm, 78K, 22 kbar press. effects 77−81133
lanthanum ethylsulphate:Gd^{3+}, zero-field splitting, contributory mechanism 80−80231
lanthanum nicotinate dihydrate:Nd^{3+} cryst., H coords., EPR and ENDOR determ. 77−59005
lanthanum nicotinate dihydrate, cryst., nucl. quadrupole interactions, D atom coords., ENDOR obs. 80−97161
laser, limiting length, stimulated radiation reabsorpt. by unexcited and excited singlet mols. 80−48240
laser dyes, fluoresc. efficiency and standards 78−35205
laser dyes, fluorescence decay, aggregation effects 78−25879
laser dyes, for transverse pumping by frequency-doubled Nd:YAG laser, lasing characts. 79−72561
laser dyes, inert gas halide laser pumped, photochem. stability 78−33733
laser far IR pulse generation by Q-switched CO_2 laser pump source 80−69383
lasers, organic cpds. as active media *(Russian)* 80−38015
lasing, excitation by excimer laser radiation 80−64007
lasing ability, substitution effects 78−82941
lasing ability *(French)* 79−31893
latex, sol, diffusion coeff. meas. by photon correl. spectroscopy 77−10117
lauryl alcohol, aq. subcooled soln., acoustic phenomena during nucleate boiling 78−10181
LC-440, flexoelec. charact. of longitudinal domains 79−46570
lead dithiocarbamate complexes, IR, electronic and mass spectra, mag. susceptibility, cond. meas. 80−97270
lead formate, intermolecular shielding contributions, proton mag. shielding 80−34783
lead myristate, multilayer analyser for X-ray spectroscopy 78−49944
lead phthalocyanine:O_2, photocond., impurity-induced 79−47120
lead phthalocyanine:O_2(I), Schottky barrier effect on AC current response 80−75623
lead phthalocyanine, photoemission, outer core levels, cross-section depend. 79−50079
lead phthalocyanine film, switching effects 79−28384
lead stearate, Langmuir-Blodgett multilayers, comp. and transfer mechanism 80−80125
lead stearate in MIM structure, transient and alternating electric currents 78−84311
lead tartrate, single cryst. growth in gel, dendrite form. and self-regulation 77−77352
lead-containing stabilisers in PVC, degradation obs. using X-ray diffr. *(German)* 79−34297
lecithin-cholesterol interaction, effect of lecithin struct. 78−64922
lecithin, adsorbed monolayer on aerosil, IR spectra 78−15753
lecithin, optical constants and dispersion eqns. 80−30762
lecithin, rheology and structure in conc. solns. and liquid crystalline state 77−64007
lecithin+cholesterol interaction, equilib., stoichiometry of complexes in bulk systems 78−68985
lecithin+cholesterol interaction, equilib., surface film phase relations and cholesterol condensing effect 78−68986
lecithin bilayers, spontaneous form. at air-water surface 79−74603

organic compounds continued
lecithin cryst. growth rel. to mol. bilayer props. 78−31780
lecithin liposomes, negatively charged, rate of interaction with ferricytochrome c 77−16914
lecithin membranes, mag. susceptibility anisotropy, phase contrast microscope obs. 78−92601
L_α-lecithin multilayers, shear-induced biaxiality near solid surfaces 78−24035
lecithin surface films, equilib. and metastable states rel. to use as biological model 77−60188
lecithin translational diffusion, pulsed NMR 77−9176
lecithin-cholesterol interaction, hydrocarbon chain length and unsaturation effects, Raman spectra 77−64012
lecithin/ethylene glycol and lecithin/water systems, lyotropic liq. crysts., X-ray diffr. and microscopic obs. 79−60266
lecithins, L_α phase, shear-induced biaxiality 78−95997
leghemoglobin, X-ray structural determ. at a resolution of 2.8 Å, electron density synthesis 79−42049
lepidopterene exciplex, luminesc. intramolecular anthracene-ethylene exciplex, mol. geometry-fluoresc. relationship 78−58728
D-leucine, preferential removal by polarised beta-rays rel. to origin of biological chirality 77−86445
leucine aminopeptidase, 3D reconstruction by photosummation of projected functions 79−62183
DL-leucine degradation with longitudinally polarised electrons 79−79474
leuco dye+biimidazole photochem. reaction, modulation by photopolymerisation 80−40714
lidocaine, quaternary, interactions with Na channel gates and tetrodotoxin in squid axons 79−83745
light elements, X-ray fluoresc. determ., matrix composition effects on line intensity 78−7257
d-limonene, differential Raman scatt. of right and left circularly polarized light *(Japanese)* 78−17675
d-limonene-1,2-epoxide, isomerisation *(Japanese)* 79−8435
lindane, organic water pollutant, influence of detergents on hydrosolubility and suspension *(French)* 80−7961
linear chain cpds., diffuse $4k_F$ refls., small intramolecular Coulomb interaction 80−34376
linear hydrocarbon or deuterocarbon molecules, diffusion through bulk polyethylene 79−23784
linear hydrocarbons, cryst. nucleation and cryst.-melt interfacial tension 79−69024
linoleic acid, adsorbed on Al_2O_3, under carbon tetrachloride immersion, IR obs. 79−24822
linoleic acid, lipid membrane model, dose-rate and O_2 effects 77−48841
linuron, herbicide, interaction with soil, Fourier transform IR spectra 77−9142
lipid, monolayer, backfolding, self-consistent field theory 79−8451
lipid bilayer phase transition, semiphenomenological model 77−35670
lipid composition of marine aerosols, sea surface microlayer and subsurface water 80−17297
lipid contamination, removal from freeze fracture replicas using chloroform 79−5426
lipid free radical oxidation kinetics rel. to lipid composition, photoreceptor membrane 78−80872
lipid function in excitable membranes 80−12095
lipid hydrocarbon chain, biomembrane, rot. motion and fluidity 80−76714
lipid molecules, asymm. struct. of purple membrane, X-ray diffr. data anal. 77−73512
lipid monolayer phase transitions, model 78−2338
lipid organisation in Acholeplasma laidlawii membranes, ^{2}H NMR 77−86456
lipid peroxide formation in irrad. synthetic diets, storage effects 80−101025
lipid-protein interactions, review 77−90719
lipid-rhodopsin interactions in photoreceptor membranes 80−12094
lipids, liq. crysts. in living and dying systems, review 77−44602
lipids, modified iodometric method for peroxide conc. determ. in small samples *(German)* 79−52799
lipids, struct. order in membranes, fluoresc. anisotropy data eval. 80−97873
lipids in aquatic sediments, Recent and ancient 80−51583
lipids in marine environment from aeolian transport 77−64327
lipids of cell organelles, anti-radical activity change due to deep freezing 77−70426
liquefaction shock waves in org. fluids 77−51484
liquefied, petroleum gas, combustion products, seeded, elec. cond. meas. 77−58835
liquefied natural gas, 2Z 79−1503
liquefied petroleum gas, burning velocity, gas comp. and air/fuel ratio effects 80−66804
liquid, branched-chain, surface tension temp. coeff. *(Japanese)* 78−75913
liquid, cohesive energy density, surface and interfacial tension and heat of mixing 77−55431
liquid, elec. field effect on BP 77−15566
liquid, layer, thermal cond. from IR absorption 77−89598
liquid, Moelwyn-Hughes parameter calc. from US data 80−59375
liquid, optical anisotropy, determ. from refr. index, Rayleigh's const. and depolarisation *(French)* 77−59548
liquid, orthopositronium pick-off annihilation lifetime calc. 78−56541
liquid, Rayleigh factor absolute meas. 79−99896
liquid, simple, struct. exam. and scatt. data interpret. 80−54096
liquid, thermal cond., comparison of predicted values with experimental results at different temps. 80−103523
liquid, under high press., refr. index vs. press. and strain 79−33668
liquid binary mixtures, evaluation of excess internal pressure, Van der Waals' constant and ultrasonic velocity from flory's theory 80−70310
liquid chromatography effluents on line anal., micro liq. chromatograph-interfaced Fourier transform IR spectrophotometer 80−73483
liquid crystal cpds. incorporating trans-1,4-substituted cyclohexane ring system, synthesis and phys. props. 79−90543
liquid mixture, thermal cond. calc. 77−20135
liquid mixtures, positronium form., spur process 78−1113
liquid organic compound ionisation under atm. press. 80−86488
liquid phase elution chromatography for determining solubilities of organic liqs. in H_2O 80−71958
liquid scintillator, γ-irrad., energy transfer and quenching 77−8622
liquid scintillators, theory of fluorescence, appl. *(Rumanian)* 79−81135
liquid surface, charged drop formation from bubble bursting 77−14634

organic compounds continued
liquid-liquid equilibrium data, retrieval 79−46797
liquids, Brownian reorientation barriers *(Russian)* 79−27901
liquids, diamagnetism, mass mag. suscept. meas., temp. depend. 80−97054
liquids, electrohydrodynamic ionisation, solvated ion mass spectroscopy, anal. appl. 78−73102
liquids, interdependence of specific acoustic impedance and surface tension *(Polish)* 80−39223
liquids, laser beam pyrolysis of organic liqs. *(Russian)* 77−56226
liquids, laser-induced breakdown, threshold fields 79−91363
liquids, low-to-medium loss, complex permittivity meas. at 285 GHz 78−15023
liquids, polar and nonpolar, entropies of vaporisation 78−26676
liquids, thermal conductivity meas., radiant heat exchange effect 80−19996
liquids, US resonance absorption 78−95110
liquids with branched chain, dielectric const. temp. coefficient *(Japanese)* 78−35079
lithium acetate, methyl group dynamics, NMR 78−29802
lithium acetate, methyl groups, spin symmetry species, neutron scatt. transitions 80−92470
lithium acetate, proton relax. study of nearly free methyl rotors 78−39428
lithium acetate dihydrate, γ-irrad., methyl radical, ENDOR, line-shape model appl. 79−73853
lithium acetate dihydrate, γ-irradiated single crystal, $CH_3...CO_2$ pairs, e.s.r. 77−9100
lithium acetate dihydrate, nearly free methyl rotors, rot. energy states, nucl. reson. props. 80−34784
lithium ammonium tartrate, ferroelectric and ferroelastic transitions, Brillouin scatt. meas. 79−33716
lithium ammonium tartrate, piezoelec., proper ferroelastic transition 78−2812
lithium ammonium tartrate dihydrate, ferroelectric-elastic phase transition, theoretical model and expt. *(Russian)* 80−75961
lithium ammonium tartrate monohydrate, dielec., EPR *(Japanese)* 77−85550
lithium ammonium tartrate monohydrate, in paraelec. phase, Brillouin scatt. 78−64373
lithium ammonium tartrate monohydrate, isostructure with lithium potassium tartrate monohydrate: Mn^{2+}, EPR obs. 80−29607
lithium ammonium tartrate monohydrate, Raman spectra, anomalous low-lying response 80−2746
lithium ammonium tartrate monohydrate, spontaneous shear strain, X-ray obs. 78−56433
lithium ammonium tartrate monohydrate elastic props., piezoelec. reson. method meas. 77−63370
lithium benzoate-DMSO, cryst., nitrobenzene anion radical impurity, EPR 77−1597
lithium formate, and deuterated, polaritons, spontaneous parametric light scatt. 77−90150
lithium formate, Fermi reson. of optical phonons with two particle state zone, interference effects *(Russian)* 77−90149
lithium formate, mixing of Nd laser radiation for coherent picosecond source, 350 to 680 nm 78−13762
lithium formate, optical distortion in nonlinear phase conjugation by 3 wave mixing 79−89956
lithium formate, optical phonons, small oscillator strength meas. from frequency-angular polariton spectra 80−92629
lithium formate, UV radiation prod. by freq. doubling 77−743
lithium formate biaxial crystal, nonlinear conical refr. obs. in harmonic generation 80−23745
lithium formate cryst., 90° phase matching 80−58634
lithium formate crystal, dehydration, influence of hydrostatic press., ^7Li NMR 78−2758
lithium formate crystal, optical phase configuration 78−5524
lithium formate monohydrate, dehydration, kinetic parameters from thermogravimetric data 79−61859
lithium formate monohydrate, elec. props. 79−87371
lithium formate monohydrate, non-centrosymmetric struct., X-N and multiple deform. electron density maps 78−91328
lithium formate monohydrate, temp. depend. Raman spectra, H bonds 78−6673
lithium formate monohydrate, thermal dehydration, dislocation effects 80−3331
lithium formate monohydrate, X-N difference density and structural parameters from different expts. 78−18627
lithium formate monohydrate frequency-doubling system, automatic phase-matched, for 240-350 nm region 79−31979
lithium formiate, active spectroscopy under conditions of double-w-k-resonance *(Russian)* 78−33777
lithium hydrogen phthalate monohydrate, X-ray cryst. struct. determ. 79−14791
lithium n-alkanoates, long-chain, thermal and phase props. 77−62619
lithium oligopentadienyl and complexes, IR spectra *(Russian)* 80−71424
lithium oscalate, neutron inelastic scatt. spectra in 2200-200 cm^{-1} range 80−70327
lithium oxalate hydrate, proton spin-lattice relax., 180° flips and diffusion of water mol. 77−15327
lithium perfluoro-octanoate-water, liquid crystal, ^{19}F multipulse NMR obs. 80−34795
lithium perfluoro-octanoate-water system, liq. cryst. struct., self-diffusion, NMR 78−15036
lithium potassium tartrate monohydrate: Mn^{2+}, isomorphism with lithium ammonium tartrate monohydrate, EPR obs. 80−29607
lithium propanoate, solid-state transitions, diffractometric and conductometric meas. 79−60507
lithium thallium tartrate, single cryst., thermal cond. at low temps. 79−33125
lithium thallium tartrate, sp. ht., 0.3 to 25K, second-order ferroelec. transition 80−59674
lithium thallium tartrate monohydrate, paraelectric phase structure by neutron diffraction data 79−19238
long chain paraffins, thermodynamic functions, Monte Carlo method appl. *(German)* 80−19962
long-chain organic molecules diffusion through polymer matrix, hydrostatic press. effect on diffusion coeff. 80−92697
low freq. dielec. dispersion near Curie point 79−38432

organic compounds continued
low frequency anharmonic vibrations, pot. function determ., Raman and IR spectra obs. 80−52997
low-temperature materials, IR spectra rel. to heat shield prod. for changing mag. fields 77−74408
lucensomycin interacting with phosphatidylcholine-cholesterol vesicles, PMR obs. 80−40954
lucensomycin interaction with cholesterol in membranes, spectral parameters 77−9177
lumichrome, photoconduction *(German)* 79−78129
luminol, chemiluminesc., quantum and excited state yields, pulse radiolysis 79−47930
luminol, electron beam excited chemiluminesc., chem. and light yields 78−53209
luminol interaction with human serum albumin, chemilum. and fluoresc. 77−21471
lutein, aq. soln., aggregate, reson. Raman spectra, and IR spectra, exciton interactions 78−31770
lutetium diphthalocyanine, solid-state anion migration in anodic oxidation 80−60994
2,6-lutidine, fluoresc. of vap. phase, nonradiative electronic relax. 79−86000
2,6-lutidine, H bonding to iso- and tert-butyl alcohols, PMR obs. 79−27008
2,6-lutidine-H_2O, phase separation, hydrodynamic effects 78−83960
2-6-lutidine-water, anomalous supercooling near critical point 80−70384
2,6-lutidine-water, fluid film, crit. phenomena, scaling, law of corresponding states 79−90787
2,6-lutidine-water, fluid film, crit. temp. shift, crossover temp., coexistence curve amplitude, fluid-boundary interaction 79−90788
2,6-lutidine-water, spinodal decomposition, light scatt. obs. 78−34625
2,6-lutidine-water critical mixture, spinodal decomposition, Rayleigh scatt. 80−70416
2,6-lutidine-water mixture, critically quenched, phase separation and coalescence 80−24581
2, 6-lutidine-water mixture, phase separation near crit. point, spatial and temporal fluctuations 79−82346
2,6-lutidine-water thick films, interferometric obs. of crit. behaviour 80−93266
lycopene, soln., depolarised Rayleigh light scatt. in absorpt. bands 79−87451
lyotropic nematic liquid crystals, mag. susceptibility, mol. aggregation meas. 80−19690
lysine, aq. solns., $H^+(D^+)$ exchange rates, ^{17}O NMR linewidths, pH depend. 80−91661
lysine vasopressin, amide H exchange rates in aq. soln., ^1H NMR effects 79−83692
lysozyme, aq. solns., H_2O ordering, NMR relax. investig. 79−62171
lysozyme, mag. suscept. 77−43807
macrocyclic hexaketone, polymer-bound, appl. to U extraction from seawater 79−92052
magenta pigment, photoconducting, electric field-induced fluoresc. quenching 80−34967
magnesium acetate, aq., glass forming soln., I^- charge transfer to solvent spectra 77−50447
magnesium bromide hexamethanol solvates, cryst. struct. *(French)* 78−34500
magnesium chlorin, ab initio CI calcs. on ground, singlet and excited states, visible spectrum 79−16139
magnesium formate, γ-irrad., ESR of free radicals 79−65737
magnesium hexahydrate $H_2EDTA:VO^{2+}$, single cryst., ESR spectra and spin Hamiltonian parameters 80−75845
magnesium platino-oxalate, one-dimens. conductors, prep., struct. and elec. cond. 80−24900
magnesium platinum oxalate, X-ray diffuse scatt., 1-D Peierls-Kohn anomaly and struct. transforms. 78−14680
magnesium porphin, ESR study of metastable triplet state, in n-octane matrix, 1.3K 79−72340
magnesium porphin, lowest triplet state, zero-field ODMR 79−31562
magnesium porphin soln., mag. circular dichroism spectra, Jahn-Teller coupling 77−3391
magnesium porphine, ab initio CI calcs., electronic absorpt. spectra 78−78639
magnesium porphin.ethanol, in n-octane cryst., triplet state splitting, fluoresc. intensity microwave-induced changes 77−6820
magnesium stearate, bonding characts. of powders mixed with Mg stearate, SEM 78−84731
magnesium tetraphenylchlorin, lowest triplet state, zero-field ODMR 79−31562
malachite green, luminesc. decay kinetics on ps time scale 79−19916
malachite green, soln. picosec. relax. polarisation spectrosc. meas. 78−68530
malachite green, Weigert effect, additional chroming effects 77−58406
malachite green+DODCI, electronic energy transfer obs. 80−5633
malachite green+rhodamine 6G, in low viscosity solvent, ps time resolved energy transfer 78−70910
malachite green in glycerol, subnanosecond fluoresc. lifetime meas., environmental effects 78−5268
malachite green leucocyanide, photoionization in polar solvents, mechanism 77−25295
malachite green soln., photoacoustic spectra, spectrometer sample cell design investig. 77−74520
maleic acid, acid slats, melts, H_2 bonding, IR, NMR investigs. 79−65859
maleic acid, behaviour during anodisation of Al 78−44262
maleic acid, permeation coeffs. determs. for phospholipid vesicles, NMR obs. 79−83711
maleic acid+muonium in aq. soln., rate const. 77−38752
maleic anhydride, and its photochem. transform. products, IR spectra *(Russian)* 77−66761
maleic anhydride, struct., DRM microwave spectra, isotope shifts 78−21918
maleimide, monomer, valence force field in Ar matrix at 20K, self-assoc. *(French)* 79−81165
malic acid+formamide, γ-irradiated reactions under high pressure *(Japanese)* 79−52707
malondialdehyde, UV electronic absorpt. spectra, G_4 mol. symmetry group 77−6798
malonic acid, and α-alkyl derivatives, photoelectron spectra, lone-pair interactions 80−58315
malonic acid, aq. soln., IR and Raman vibr. spectra *(French)* 79−26989

organic compounds continued
malonic acid, electron spin echo exam. of mutual flip flop electron spin reversals involving forbidden transitions 79−24216
malonic acid, in oscill. Belousov-Zhabotinskii system, detection of BrO_2 *(German)* 79−29351
malonic acid, phase transition at 360K, IR study 80−44311
malonic acid-$Ce(Br_3)_3$, multiple stationary states in oregonator 78−20061
malononitrile, ^{14}N PNQR obs. of phase transition press. depend., line splitting 77−77120
malononitrile, cryst., phase transitions, Raman and IR obs. 80−88980
malononitrile, displacive phase transition, 294.7K, Raman and Brillouin-Rayleigh scatt. obs. 80−16047
malononitrile, solid phases I-IV, vib. spectra 77−20840
malononitrile+VO^{2+}, reaction, CN stretching freqs., bonding effects 77−16820
malononitrile ion+VO^{2+}, reaction, CN stretching freqs., bonding effects 77−16820
manganese(II) propionate dihydrate, cryst. struct. determ. 77−80495
manganese (II) oxalate hydrates, prep. and cryst. props. 77−76377
manganese acetate, crit. slowing down, 180-350 MHz 77−16083
manganese acetate tetrahydrate, crit. relax. studied by HF mag. susceptibility 78−39299
manganese acetate tetrahydrate, Heisenberg ferrimag. magnetisation 79−47304
manganese acetate tetrahydrate, neutron diffr., cryst. struct. 77−47436
manganese acetate tetrahydrate, paramag. susceptibility, spin trimer model 80−97055
manganese acetate tetrahydrate, single cryst., ESR spectra, temp. depend. 77−43877
manganese acetate tetrahydrate, susceptibility and magnetis. meas., crit. exponents and crossover behaviour 77−66309
manganese adipate dihydrate, cryst. struct., H-bonding and O atom coordination 80−96506
manganese carboxylate, dodecanuclear mixed-valence, prep., struct., and mag. props. 80−107196
manganese copper formate dihydrate, conc. depend. of EPR linewidth 79−38376
manganese dithiocarbamate complexes, IR, electronic and mass spectra, mag. susceptibility, cond. meas. 80−97270
manganese formate dihydrate, 2-D Heisenberg antiferromag., sp. ht. 78−14965
manganese formate dihydrate, IR absorption spectra 79−19893
manganese formate dihydrate, Zn- and Mg-substituted, anomalous crit. phenomena 80−60316
manganese oleate, in benzene soln., liq. and solid, positron annihilation 77−1152
manganese oxalate, crystal growth in silicate gel, X-ray diffr. and i.r. spectrum 77−4724
manganese stearate: cadmium stearate, dil. quasi two-dimensional, ESR line width 80−71155
manganese stearate, Langmuir-Blodgett layers, high resolution X-ray diffr. 80−80126
manganese stearate, literally two-dimensional magnet, mag. ordering, EPR 79−28597
manganese stearate, mag. two-dimensional system, mag. susceptibility 78−10669
manganese stearate, two-dimensional mag. struct. 80−108040
manganese stearate Langmuir-Blodgett layers on Ag, IR surface EM wave prism spectroscopy 78−52587
manganese stearate Langmuir-Blodgett type multilayers, periodic and near-periodic, small-angle interferences of reflected X-rays 79−94846
manganese stearate monolayer, two-dimensional mag., prep. and characterisation 78−31097
manganese zinc formate dihydrate, two-dimens. antiferromag., anomalous crit. phenomena, neutron scatt. and PMR obs. 80−50104
mannitol, aq. solns., stirred, transient diffusion through glass membranes, thermodynamics 78−92507
mannose, γ-irrad., EPR spectra 79−73814
mannose, increased lyoluminescence response on storage 79−25112
mannose lyoluminescence dosimetry in photon and fast neutron beams 78−15902
Manoxol OT-cyclohexane-water reversed micellar system, singlet-singlet energy transfer 80−9531
margaric acid, evaporated film, X-ray diffr. anal. and mass-spectrography 77−15718
margaric acid film, HF dielectric const. 77−36175
marine aerosols, organic and inorganic Cl gas concs. and particulate Cl size distrib. 78−32187
marine atmosphere particulate matter, organic C conc. and particle size distrib. 78−32139
marine environment, stable C isotope comp. of dissolved and particulate organic C 79−20862
marine plankton, C isotope ratio rel. to surface water masses 79−29783
marine sediments, nature and reactions of dissolved organic matter in interstitial waters 78−49039
mass spectra, mol. wt. from 186-273, EPA/NIH mass spectral data base vol. 79−68329
mass spectra, mol. wt. from 273-381, EPA/NIH mass spectral data base vol. 79−64120
mass spectra, mol. wt. from 30 to 186, EPA/NIH mass spectral data base, vol.I 79−64119
mass spectra, mol. wt. from 381-1674, EPA/NIH mass spectral data base, vol.IV 79−64121
matrine, X-ray cryst. and mol. struct. determ 79−94993
matrine N-oxide, X-ray mol. and cryst. struct. 79−94997
MBAB:cholesteryl chloride, thickness depend. of threshold elec. field for instabilities 79−32896
MBAB, liq. cryst., Brillouin-Mandelshtam light scatt. and refr. index 80−55119
MBAB, twist viscosity, temp. depend. 77−35472
MBAB-chiral cpd. mixture, cholesteric, helical screw sense and pitch determ., Grandjean-Cano method *(German)* 77−80609
MBBA: 4-methoxybenzaldehyde, pure and doped, nematic-isotropic transition temps., appl. to purity control 79−55872
MBBA:trichlorobenzene, solute orientation in nematic soln., temp. and conc. depends., NMR obs. 79−46556
MBBA, acoustic emission rate at nematic-isotropic transition 78−91232
MBBA, and MBBA-EBBA mixtures, determ. of viscosity coefficients by torsional vibrs. 79−14953
organic compounds continued
MBBA, anisotropic interactions with surface-treated substrates, wall effects on Freedericksz transition 79−99070
MBBA, anisotropic refr. indices from optical interference meas. 77−8538
MBBA, annihilation of disclinations with Frank index m=+2 77−58955
MBBA, anomalous behaviour of electrical dissipative power 79−4237
MBBA, Brillouin scatt. in isotropic phase 78−2867
MBBA, calc. of order parameter from X-ray diffraction data 79−69009
MBBA, cholesteric struct. induced by chiral sulphoxides 79−86683
MBBA, dielec. permittivity and loss meas., −196 to 0°C 77−59511
MBBA, dielec. relax. in metastable modification of solid phase 80−84689
MBBA, dielec. relax. in nematic phase 79−82153
MBBA, dielectric and calorimetric investig. in solid, liq. cryst. and liq. phases 77−84639
MBBA, dielectric permitt. rel. to molecular props., effect of anisotropy of medium and local field 80−25270
MBBA, doping effect on cond. anisotropy and dynamic scatt. 77−40208
MBBA, dye activated, isotropic phase, induced Raman emission *(Russian)* 78−13766
MBBA, dynamic critical behaviour in NLC above nematic-isotropic transition 80−49096
MBBA, elec. field effect on optical indicatrix orientation 77−36202
MBBA, electrohydrodynamic instabilities, flow patterns and phase diagrams 77−68915
MBBA, electrohydrodynamic instabilities, power spectra and autocorrel. in flow transitions 77−68914
MBBA, electronic spectra 78−52530
MBBA, electroviscous effect 79−69010
MBBA, film, nematic-isotropic crit. thickness, Landau-de Gennes theory 77−4189
MBBA, flexoelec. charact. of longitudinal domains 79−46570
MBBA, flexoelec. coeff. in nematic phase, thermal depend. 80−79685
MBBA, fluorinated analogues, mesomorphic props. 80−70118
MBBA, Frank elastic const. ratio determ. by Rayleigh scatt. 79−99059
MBBA, frozen nematic glass, EPR spectra of copper and cobalt triazene-1-oxide complexes 80−88871
MBBA, HF electrohydrodynamic instability in NLC *(Russian)* 80−54130
MBBA, homeotropic nematic layer, torsional shear flow in normal elec. field 79−82155
MBBA, homotropic liq. cryst. growth 78−26439
MBBA, hypersonic props., Mandel'shtam-Brillouin spectra obs. 79−4813
MBBA, IR absorpt. spectra, elec. field effects, orientational order parameter determ. by IR dichroism, bend elastic consts. 80−80778
MBBA, isotropic, depolarised Rayleigh doublet, de Gennes viscosity coeffs. 78−31207
MBBA, isotropic, obs. and anal. of depolarised Rayleigh doublet 78−35154
MBBA, isotropic, surface-induced ordering 80−108176
MBBA, isotropic phase, Brillouin scatt. spectra, hypersound data determ. 79−91453
MBBA, isotropic phase, order fluctuations, self-diffusion, and rot. motion, proton spin relax. meas. 79−87328
MBBA, laser radiation transmitted near isotropic transition, spatial coherence 78−18003
MBBA, light modulation by nematic liq. cryst., mech. excitation, response times 79−73094
MBBA, light scatt. by disclinations, spatial coherence props. 77−8544
MBBA, liq. cryst., electrohydrodynamic instability, fluctuation of light transmission meas. 77−11468
MBBA, liq. cryst., flexoelectricity and surface polarisation 77−89376
MBBA, liq. cryst., IR and far IR spectra, vibr. assignments 77−16298
MBBA, liq. cryst., isotropic phase, NMR pulsed field grad. study of self-diffusion 79−90814
MBBA, liq. cryst., light scatt. and birefr. 78−22646
MBBA, liq. cryst., mass diffusion meas., tracer dye-laser method 78−59738
MBBA, liq. cryst., phase transitions up to 3 kbar, transition enthalpy, entropy 77−20051
MBBA, liq. cryst.-isotropic transition at high press., P-V-T eqn. of state 79−95135
MBBA, liq. crystal, hydrodynamic instabilities and elastic deformation created by US 77−19873
MBBA, liq. crystal, morphological changes and electro-optical characts. appl. laser light modulation 77−20826
MBBA, liq. crysts., thin layers, addition of iminoxyl radicals, effect on elec. cond. *(Russian)* 78−67641
MBBA, liquid crystal, spin thermometric anal. of spin-lattice relax. by order director fluctuation 77−47346
MBBA, magnetically aligned liq. cryst., highly damped waves studied 79−1277
MBBA, meas. of nonlinear optical susceptibilities in isotropic and nematic phases *(Russian)* 78−74945
MBBA, metastable phases formed by rapid cooling of mesophase, IR and Raman spectra and DSC obs. 80−34919
MBBA, mol. alignment, comparison of exptl. data at high press. with mean field theory predictions 79−99075
MBBA, mol. alignment in elec. and mag. fields 77−58956
MBBA, mol. dynamics near nematic-isotropic liq. cryst. transition *(Russian)* 78−84495
MBBA, nematic, aligning props. for Si film surface tension 79−90846
MBBA, nematic, anomalous spectra of current induced noise under high DC field 78−38617
MBBA, nematic, birefringence determ. by new simple method 78−79526
MBBA, nematic, dielec. permittivity and transmitted light intensity, in DC field 77−12296
MBBA, nematic, diffusion coeff. determ. *(German)* 79−51291
MBBA, nematic, EHD flow patterns, analogy of instabilities with classical fluid behaviour 77−84335
MBBA, nematic, EHD instabilities, director-fluctuation autocorrelation and power spectrum 79−41944
MBBA, nematic, EHD instabilities, director-fluctuation second moment 79−41943
MBBA, nematic, EHD transitions, white noise effects 80−6159
MBBA, nematic, flexibility gradient of fatty acid spin labels, EPR study 80−71181
MBBA, nematic, freq. depend. of proton T_1, rot. diffusional mechanism interpret. 77−12219

organic compounds continued
MBBA, nematic, in alternating elec. field, two-dimens. lattice form. *(French)* 77−11473
MBBA, nematic, mag. susceptibility and order parameters 79−86709
MBBA, nematic, mol. alignment on SiO film, film thickness effects 80−59384
MBBA, nematic, order parameters meas. by Raman scatt. 78−6011
MBBA, nematic, ordering parameter temp. depend. 79−23517
MBBA, nematic, statistical mechanics, particle pots. and distrib. functions calcs. 78−2001
MBBA, nematic, transient elec. current obs. 77−20324
MBBA, nematic, US attenuation anisotropy, temp. depend. 78−43071
MBBA, nematic, viscosity coeffs., Onsager-Parodi relation validity 79−19147
MBBA, nematic and isotropic phases, dielec. props. 79−87383
MBBA, nematic film, with two free surfaces, EHD flow 79−98817
MBBA, nematic liq. crys., refractive index distrib. and mol. alignment in electro-optical effect *(Japanese)* 80−20613
MBBA, nematic liq. cryst., ^{2}H NMR, mol. order and reorientation 79−27906
MBBA, nematic liq. cryst., acoustohydrodynamic instability 77−4036
MBBA, nematic liq. cryst., anisotropy of US attenuation 78−43070
MBBA, nematic liq. cryst., charge carrier drift mobility 78−87801
MBBA, nematic liq. cryst., circumferential surface orientation, in capillary, optical studies 77−47349
MBBA, nematic liq. cryst., cylindrical domain struct. thermal excitation, optical obs. 79−73097
MBBA, nematic liq. cryst., deflector based on frustrated total internal light refl. 78−50934
MBBA, nematic liq. cryst., dielec. relax. under shear 79−10794
MBBA, nematic liq. cryst., dynamic scatt. mode due to electrohydrodynamic instability *(Japanese)* 77−43133
MBBA, nematic liq. cryst., dynamically excited, transversal EHD instabilities and umbilics 78−94983
MBBA, nematic liq. cryst., elastic consts. determ. 77−27824
MBBA, nematic liq. cryst., electroviscous effect, electrohydrodynamic investigation 78−87804
MBBA, nematic liq. cryst., flexoelectric and dielec. relax. behaviour 78−94979
MBBA, nematic liq. cryst., flow patterns and mol. alignment due to elec. fields 77−27825
MBBA, nematic liq. cryst., homeotropic cylindrical boundary, in capillary, cols. and noeuds 77−47350
MBBA, nematic liq. cryst., mol. order and motion, EPR study 77−76298
MBBA, nematic liq. cryst., nonlinear optical amplification above Frederiks transition 80−95937
MBBA, nematic liq. cryst., nonlinear optical processes near Freedericks transitions 79−69011
MBBA, nematic liq. cryst., nonlinear optical suscept. using light combination scatt. *(Russian)* 80−38064
MBBA, nematic liq. cryst., parallel and cross-like domains due to DC and LF electric fields 79−46557
MBBA, nematic liq. cryst., quasihomeotropic orientation induced by PTFE deposited on SiO surface 79−90525
MBBA, nematic liq. cryst., relaxation times for formation and break-up of Williams domains 78−34423
MBBA, nematic liq. cryst., secondary dynamic scatt. mode, light transmission and microscopic obs. 79−4246
MBBA, nematic liq. cryst., spin-lattice relax., orientational depend. 77−84625
MBBA, nematic liq. cryst., surface alignment using lecithin monolayers, contact angle meas. 79−4247
MBBA, nematic liq. cryst., temp. depend. of EHD instability 78−1998
MBBA, nematic liq. cryst., thermal diffusivity, Rayleigh scatt. obs. 78−94977
MBBA, nematic liq. cryst., transverse electrooptic effect 79−94897
MBBA, nematic liq. cryst., ultrasound produced rolls, spatial coherence props. of scatt. light 78−75534
MBBA, nematic liq. cryst. isotropic phase, phase-conjugate refl. by degenerate four-wave mixing 80−43389
MBBA, nematic liq. crysts., AC excited, dynamic light scatt., orient. fluctuations 79−1769
MBBA, nematic liquid cryst., omeotropically aligned thin slice, dielectric permeability *(Italian)* 80−6354
MBBA, nematic liquid crystals, refr. index 77−51313
MBBA, nematic liquid crystals, wave number spectrum of dissipative structures 80−38904
MBBA, nematic mesophase, struct. of flow in cylindrical capillary 77−7671
MBBA, nematic phase, elec. field induced biaxiality, PMR study 79−90532
MBBA, nematic phase, high freq. EHD instabilities, temp. depend. 79−94879
MBBA, nematic phase, quasielastic and elastic 10 Å neutron scatt. 78−42904
MBBA, nematic twist cells, bi-dimensional struct. in cond. region 79−90542
MBBA, nematic-isotropic pretransition regions, ±15K, volumetric obs. 77−76535
MBBA, nematic-isotropic transition, birefringence anomaly at clearing pt. 79−46788
MBBA, nematic-isotropic transition, compressibility-press. relations obs. 77−51481
MBBA, nematic-isotropic transition, intermolecular forces, IR N_2O mol. probe obs. 80−29155
MBBA, nematic-isotropic transition, isothermal compressibility and thermal expansion coeff. meas. 79−99301
MBBA, nematic-isotropic transition at high press., turbidity meas. 80−92655
MBBA, NMR and Raman scatt. studies in nematic phase 80−100619
MBBA, one dimens. dielectric-flexoelectric deformations 78−38616
MBBA, orientational order in glassy and nematic phases, IR dichroism meas. 80−64891
MBBA, partially deuterated, D spin-lattice relax. 78−48070
MBBA, polymorphism, positron annihilation obs. 78−72632
MBBA, pretransitional effects above phase transition temp., nonlinear dielectric meas. 79−15390
MBBA, proton spin-lattice relax. in crit. regime 80−80631
MBBA, pure and mixed with bezene (chlorobenzene), nematic-isotropic transition, US absorpt., visual hysteresis 80−54355
organic compounds continued
MBBA, pVT data and viscosity-press. behaviour 78−94989
MBBA, quasi-elastic light scatt. near instability point, conduction regime 77−15306
MBBA, Raman spectra in cryst., frozen glassy, and liq. cryst. states 80−60601
MBBA, refr. index, high press. meas. 78−26428
MBBA, refr. index anisotropy, meas. using different methods *(French)* 77−16274
MBBA, refractive index, dielec. const., mag. susceptibility, orientational ordering *(Dutch)* 80−33884
MBBA, ring deuterated, dipolar spin system exam. 77−39533
MBBA, secondary light scatt. in low frequency field, in dielectric state 78−48147
MBBA, shear modulus and viscosity relax. near isotropic-nematic phase transition *(Russian)* 77−39543
MBBA, solid, metastable, wide-line NMR 77−51966
MBBA, solid, NMR and thermal behaviour, cooling and mag. field effects 78−76336
MBBA, solid, proton spin-lattice relaxation in metastable and stable phase 78−64286
MBBA, solid phase polymorphism, IR and Raman spectra study *(French)* 79−87438
MBBA, solid phase polymorphism and phase transforms., IR spectra obs. 79−8128
MBBA, specific heat anomaly and isotropic liquid to nematic liquid cryst. transition *(Russian)* 77−62624
MBBA, temp. depend. of apparent viscosity and density 78−18542
MBBA, thermal diffusivity meas. by forced Rayleigh scatt. 78−76483
MBBA, tilted alignment induced by short chain surfactants 77−4037
MBBA, Tsvetkov parameter, temp. depend. 80−88035
MBBA, uniaxial liq. crystalline phase, orientational order, polarised Raman scatt. 77−76296
MBBA, US propag., nonlinear effects 77−59069
MBBA, viewed in transverse elec. field, voltage-freq. thresholds 77−7661
MBBA, volume meas. and phase transitions at high press. 79−90764
MBBA, Williams mode in EHD, applied voltage depend. 79−37620
MBBA, Williams patterns, transverse obs. 77−19869
MBBA, with chiral impurities, cholesteric struct. shear flow normal to helical axis 79−86689
MBBA+optically active substance, pretransition optical rotation in isotropic phase *(Russian)* 80−92657
MBBA(:TEAI), elec. drift mobility, carrier identification *(Korean)* 78−51998
MBBA binary mixtures with a nematogenic or nonmesogenic cpd., dielec. relax. 78−72457
MBBA domains, in presence of iminoxyl free radicals, elec. field influence 79−64992
MBBA film, homeotropic nematic cell, subjected to ultrasound, impedance variations 79−41948
MBBA film, nematic liq. cryst., visible interaction of low-intensity US waves 78−10126
MBBA film, optical study of second dynamic scatt. regime *(Italian)* 78−15146
MBBA liq. cryst., anisotropic light scatt. 79−78692
MBBA liq. cryst., dynamic light scatt., effect of paramag. iminoxyl radical addition *(Russian)* 77−43131
MBBA liq. cryst., free iminoxyl radical addition, domain struct. parameter depend. *(Russian)* 77−58948
MBBA liquid crystal, premelting detected by spin probes, effect of spin probe size 79−46563
MBBA matrix, polarised fluoresc. of organic mols. 78−90207
MBBA nematic crystal, EHD instability, damped oscill. of current and flow patterns 79−46562
MBBA nematic liq. cryst. systems, orientational order rel. to solute size, shape 77−4565
MBBA nematic liquid crystals excited by 20 MHz US surface waves, acousto-hydrodynamic effects 80−76003
MBBA-based binary nematic mixtures, dielec. L-relax. 77−40178
MBBA-BBCA mixture, field-induced distortion of mol. orientation 79−99060
MBBA-BBCA-cholesteryl chloride, field induced nematic-cholesteric relax. processes, transient helical pitch 80−38906
MBBA-cholesteryl chloride mixture, liq. cryst., bubble domain texture, obs. of interference fringes 79−23520
MBBA-cholesteryl chloride mixture, mol. orientation during mag. field induced cholesteric-nematic transition 79−28086
MBBA-cholesteryl nonanoate, liq. cryst. mixture, two colour display device 80−70116
MBBA-cholesteryl oleate mixture, memory effect charact., crit. freq. rel. to erase voltage 78−94993
MBBA-CN mixed liquid crystal, dissipative structs. caused by EHD instability 77−80416
MBBA-CPB nematic complex, dielec., elastic and electro-optical props. 77−32350
MBBA-d_{13}, ^{1}H spin-lattice relaxation, intermol. and intramol. contribs. 80−75873
MBBA-d_{13}, nematic phase, mol. order and director fluctuations, ^{2}D NMR meas. 79−90529
MBBA-d_{13}, nematic phase, rot. frame spin-lattice relax. 80−84668
MBBA-d_8, H and D spin-lattice relax. 77−59475
MBBA-EBBA, controllable liq. cryst. transparency, electrooptical charcts. 80−78996
MBBA-EBBA, homotropic liq. cryst. growth 78−26439
MBBA-EBBA eutectic mixture, vitrified orientation of Cr(III) acetyl acetonate in liquid cryst. 77−16152
MBBA-EBBA mixture, behaviour in alternating elec. field 78−26440
MBBA-EBBA mixture, nematic layers with homogeneous orientation, acousto-optical props. 77−20824
MBBA-EBBA mixture, transverse electro-optic effect 77−59556
MBBA-EBBA mixtures, quinone and hydroquinone doped, dynamic scatt., elec., electro-optical props. 79−37616
MBBA-EBBA mixtures, thin and mol. films, between Hg electrodes, I-V charcts. 79−11253
MBBA-n-heptane, nematic soln., lattice model, thermodynamic functions *(Russian)* 80−64896
MBBA-n-heptane system, thermodynamic functions in lattice model *(Russian)* 80−33887
MBBA-PCB (41 wt.%)+pleochroic dye, electrothermo-optic effect, optical storage device appl. 78−87611

organic compounds continued
MBBA/CC mixtures, cholesteric phase, torsional shear flow in elec. and mag. fields 79−86697
MBBA/EBBA, nematic, mol. interaction energy 80−33881
MBBA/EBBA binary liquid crystal mixture, US absorpt. and vel. dispersion, phase transition and alignment effects *(Korean)* 80−29121
MBBA/n-hexane mixtures, isotropic-nematic transition, transient optical Kerr effect study 79−82323
MBBA/non-mesogenic cpd., binary nematic mixtures, dielec. relax. and intermolecular interaction 79−91350
MBPAA, nematogen, cryst. and mol. struct. 77−72604
melamine, electron density, exponent refinement 78−38579
melanin, electron spin-lattice relax. times, saturation recovery meas. 78−96017
melanostatin, correl. between X-ray struct. and conform. in soln. 77−48752
Menshutkin complexes, Raman spectra 77−16291
menthane ring compounds, Raman circular intensity differential spectra obs., mol. struct. 80−87130
l-menthol, vap., homogeneous nucleation, high-temp. Becker-Doering theory predictions 78−67820
menthol, vap. phase nucleation and growth on C, glass and fused quartz 77−7992
mercaptans+$O(^3P)$, reaction rate consts., O_2 effect 79−52630
2-mercaptobenzimidazole, corrosion inhibition on Cu, XPS and X-ray induced Auger spectra obs. 80−40600
2-mercaptobenzothiazole, corrosion inhibition on Cu, XPS and X-ray induced Auger spectra obs. 80−40600
β-mercaptoethylamine, protective effect in rat small intestine, crypt survival after X-irradiation 79−11979
2-mercaptopropionylglycine, protection of mouse intestine against gamma irrad. 77−90863
6-mercaptopurine, electron beam irrad., free radical formation at 77K 79−5165
8-mercaptoquinoline, synthesis, physiochem. props., review *(Russian)* 79−39140
Merck nematic phases, ZLI 1052 and ZLI 389, mag. susceptibility anisotropy and order parameter 79−86704
mercuric trifluoroacetate, staining of polymer blends for TEM obs. of morphology 80−84103
mercury acetate, direct observation of Hg atoms in make-up of heteroorganic compound 79−35898
mercury carboxylates, phase transitions, DTA 79−90759
merocyanine dye, adsorption on ZnO cryst., spectral sensitisation of photocond. 77−47854
merocyanine dye, solvent-depend. hyperpolarisability, polar (nonpolar) solvents 78−70962
merocyanine dye monolayer on p-chloranil cryst. in sandwich cell, electrochromic detection of internal charges 78−11549
merocyanine dyes, non-photochromic, for autoprocessor reprography system 80−35555
merocyanine organic solar cells, photovoltaic props. in terms of exciton transport 79−43763
merocyanine-oxazolone dye optical probe for simultaneous recording from several neurones 77−66880
mesitylene:tetracyanoethylene, charge transfer spectra line shape 79−78700
mesitylene, luminesc. excitation spectra in rare gas matrices 78−66575
mesitylene-d_{12}, extended diffusion with internal rot., NMR test 79−31549
mesogens, chiral, phase transition temp. 78−2241
meta-toluylene-diamine, refr. index, equal-deflection method, UV laser rad. 78−29145
metachlorobenzoic acid, kinetics of epoxidation reaction with poly(trans-1,4-butadiene) 79−61861
metal ethoxide ethanol system, thermodynamic anal. of ion-ion association, conductance meas. 79−29386
metal phthalocyanine, vap., photoelectron spectra 79−64043
metal phthalocyanines, IR spectra, vibr. transitions during intermol. interactions 79−54857
metal porphyrins, Jahn-Teller instability 79−47062
metal-containing, appl. to glass and ceramic prep., state-of-the-art 77−55922
metaldehyde, cloud seeding expts., Fujian province, China *(Chinese)* 80−46235
metaldehyde particles, fluid-breaking, ice nucleation *(Chinese)* 80−12468
metallic state at He temps. 79−65462
metallo-octaethyl porphyrins, I oxidation products, metallic cond., EPR and reson. Raman spectra 80−29610
metallocenes, photochemistry with applications to imaging systems 77−4914
metallooctaethylporphyrin, ^{15}N-enriched, reson. Raman spectra, haemoprotein oxidation state marker bands 77−58008
metallophthalocyanines, α-phase solid, absorpt. and MCD spectra 79−73964
metalloporphins, deuterated, resonance Raman spectra, vibr. and vibronic levels 78−62812
metalloporphyrin, cation radical formation by pulse radiolysis, oxidation and demetalation rate consts. 80−61505
metalloporphyrin, low symmetry environment, Raman excitation spectra and absorpt. spectrum 80−74172
metalloporphyrin, vibronic coupling, Raman scatt. 78−21933
metalloporphyrin triplet state quenching by Fe II- and Fe III-porphyrins 78−76992
metalloporphyrins, Jahn-Teller effects 78−58599
metalloporphyrins, mol. origin of anomalous polarisation in reson. Raman spectra 77−3368
metalloporphyrins, photoelectrochemical props. 80−50991
metalloporphyrins, reson. Raman specta, intra- and inter-manifold couplings interference 80−28020
metalloporphyrins, Soret excited, reson. Raman excitation profiles, Jahn-Teller distortion and vibronic anal. 78−58698
metalloporphyrins, two quantum fluoresc. excitation from higher excited electronic states 80−106350
metarhodopsin II, effect of light on photoreceptor membrane fragment modified artificial lipid membranes 77−77898
metastable isomers as new class of interstellar molecules 79−48872
meteorites, primitive grain clumps and organic compounds in carbonaceous chondrites 77−2374

organic compounds continued
methacryloyloxyethyleneoxycarbonyloxypropylene, NMR relaxation mechanism *(German)* 78−33527
β-methallyl radical, formed in photolysis, extinction coeffs. 77−1938
methane:O_2, crystal field, O_2 catalysis of spin-species conversion 77−51706
methane, $1B_1(1T_2)$ state, photodissoc., extended basis calcs. 78−9093
methane, 20K, cold neutron pulse emission, time dependence 77−67928
methane, 25 to 40 eV electron dissoc. ionisation, proton formation 80−91690
methane, $2\nu_3$ band, R_1 line, spectrum reconstruction using test response 80−77884
methane, $2\nu_4$ band, IR spectral assignments *(French)* 77−42319
methane, $2\nu_4$ band anal. *(French)* 79−41168
methane, $3\nu_3$ band in Saturn's atm., seasonal phenomena detect. 80−26803
methane, 4350-10600 Å bands, intensity profile, vibr. assignments, rel. to major planets spectra 78−42084
methane, 6190 Å spectral line, press. broadening detected by photoacoustic 79−94033
methane, 6825 Å band obs. in Uranus and Neptune 77−78715
methane, 7300 Å band obs. of Uranus disk structure 80−17544
methane, ^{129}Xe chem. shift, chem. shielding 77−6707
methane, ^{12}C and ^{14}C, line parameters for ν_2 and ν_4 bands, isotope shifts, appln. to planetary atmospheres 80−95622
methane, ^{13}C and ^{12}C, line strength ratios of $2\nu_3$ singlet 80−78616
methane, ^{13}C and proton medium shifts in gas phase and in soln. 77−88467
methane, ^{13}C enriched, IR spectrum, ν_3-band forbidden lines, ground state consts. 77−18922
methane, ^{13}C NMR, density depend. mag. shielding in gas phase 77−75187
methane, $^{13}CH_4$, spin conversion time constants, NMR meas. 78−64281
methane, $^{13}CH_4$ line hyperfine splitting at 3.39 μm, laser saturated absorpt. obs. 79−76470
methane, ^1H and ^{13}C mag. shielding, He and methane intermol. effects 78−37571
methane, α-particles stopping cross-section determ. 79−49917
methane, γ-ray Compton profile meas. 78−25623
methane, μ, ρ and T-surfaces, global behaviour, rel. to catastrophe theory 78−26226
methane, $\nu_1+\nu_4$ vibration-rotation spectrum, spectroscopic constants *(French)* 79−13709
methane, $\nu_1(a_1)$ vibrational state rotational structure, CARS obs. 79−98109
^{13}C-methane, ν_1 fund., quasi-CW inverse Raman spectra 80−48004
methane, ν_1 fundamental, CW stimulated Raman gain spectroscopy 79−6943
methane, ν_1 line contour anomalous behaviour on pressure changes *(Russian)* 80−43052
methane, ν_2 and ν_4 bands Coriolis interaction, using a general Hamiltonian formalism *(French)* 78−5192
methane, $\nu_3=1$ state, dipole moment and IR-radiofrequency double reson. spectra 80−14161
methane, ν_3 band, IR spectrosc. meas. and anal. 79−98098
methane, ν_3 P(6) transition, Doppler-free intracavity polarisation spectroscopy 80−5537
methane, ν_4 band, high resolution spectrosc. 80−5529
methane, ν_4 band Q-branch spectrum 80−5530
methane, ν_4 fundamental, Q and R branch absolute line intensities 80−5539
methane, ν_4 fundamental band strength, line-intensity meas. 79−22700
methane, (methane-Xe)(methane-NH_3), mol. relax., optoacoustic reson. meas. 80−27351
methane, ab initio calcs., appl. of convergent SCF procedure 80−47875
methane, ab initio calcs. using FSGO, internal rot. 78−82639
methane, absolute line strengths meas. using dual-beam diode laser spectrometer 80−101853
methane, absorpt. bands in Uranus spectrum 78−45275
methane, absorpt. in Jupiger atm. 77−29707
methane, absorpt. line profile, press. and temp. effects 77−495
methane, absorpt. meas. in 3.3 μm band, temp. depend. 78−90159
methane, absorpt. of 3.39 μm He-Ne laser line, 300-2400K 78−90166
methane, absorption and press. coeffs., 4500-10500 Å, band model calcs., astronomy appls. 77−83593
methane, absorption spectra, 3.5-4.1 μm, appl. of pulsed source spectrophone 77−23494
methane, absorption spectra, 6000-6500 Å, intracavity laser detection 79−89684
methane, absorption spectrum, LiF F_2^+-centre laser intracavity spectroscopy appl. 80−32999
methane, adsorbed monolayer on graphite, two-dimens. diffusion by mol. dynamics method 79−90873
methane, adsorbed on α-cyclodextrin, positron annihilation, effects of adsorbed gases 79−65952
methane, adsorbed on γ-Al_2O_3, γ-radiolysis, reaction kinetics 78−95940
methane, adsorbed on graphite, NMR pulsed field gradient method, diffusion coeff. meas. 80−15362
methane, adsorbed on graphite, orientational phases, Monte Carlo calc. 80−2263
methane, adsorbed on graphite, struct. and dynamics, neutron diffr. and inelastic scatt. 78−87869
methane, adsorbed on W, electron beam induced C deposition AES obs. 77−89651
methane, adsorbed submonolayer on graphite, two-dimens. fluid 79−37920
methane, adsorption, on graphitised carbon black, surface excess isotherms, gravimetric determ. 78−51816
methane, adsorption on BN and graphite in first monolayer domain, thermodynamic props. *(French)* 80−29275
methane, adsorption on graphite, phase transitions and orientational order, mol. field theory 79−95257
methane, adsorption on graphite, substrate deform. meas. 80−54520
methane, adsorption on graphitised C black, rot. tunnelling, neutron scatt. obs. 79−15000
methane, adsorption on W (100) and (111), work function meas. 78−38963
methane, adsorption on water, 0-50°C, press. effects on surface tension 78−56024
methane, adsorption potential on NaCl cryst. surface 80−24739

organic compounds continued
methane, AES, chem. state effects, for water and simple organic cpds. 78−72687
methane, air pollutant, remote meas. using chem. laser lidar system 77−21910
methane, and $-d_4$, solid-phase transitions, hysteresis effects 79−99316
methane, and -d_4, electron impact K-shell excitation spectra, isotope effects 77−71879
methane, and -d_4, electron ionis., excited states between 18 and 22 eV 79−3588
methane, and -d_4, soft X-ray absorpt. spectra, fine struct. above K-edge of C 78−42096
methane, and -t_1, β-decay, ab initio SCF MO calcs. 77−71842
methane, and d_{1-4}, intensity sum rules, dipole moment derative 79−13695
methane, and d_1-d_4, absolute Raman intensities of fundamental, overtone and combination bands 77−65468
methane, and d_4, Raman scatt. activity and IR intensity, finite field method 79−59462
methane, and deuterates, absolute Raman intensities, depolaris. ratios, bond polaris. theory 77−10705
methane, and fluoro derivatives, correl. energy rel. to valence electron no., modified PCILO method 79−36533
methane, and isotopic forms, ν_4 band, line parameters, Jovian atmosphere transmission, 7.7 micron 78−85894
methane, and isotopic forms, anharmonic force field, equilib. struct. 79−76365
methane, and methane-d_4, thermal conductivity in gaseous phase, 300-650K 77−11301
methane, angular correl. for (e, 2e) reaction 77−6950
methane, anharmonic molecular vibrations, coherent spectroscopy 79−18187
methane, appl. of band-model parameters to Uranus visible and near IR spectrum 80−98609
methane, aq. soln., Monte Carlo simulation of isothermal-isobaric ensemble 78−30531
methane, atm. absorption line parameters, AFGL, compilation update 79−21013
methane, atm. conc. over ocean, var. with latit. 78−81372
methane, atmospheric circulation, destruction through photochemical oxidation *(German)* 79−84424
methane, atmospheric content meas. in N and S hemispheres *(Russian)* 77−13103
methane, backward Raman amplifier, large-signal gain and intensity enhancement 78−90450
methane, backward Raman gain meas. for KrF laser radiation 78−66863
methane, Balmer radiation production by electron impact 0-2000 eV 79−76521
methane, boiling heat exchange, surface roughness influence, press. depend. *(Russian)* 79−68562
methane, boiling on water, initial water temp. effect 77−19606
methane, bond bending, bond orbitals rel. to nucl. motion 80−95513
methane, bond dissociation, MCSCF LMO calcs. 77−57886
methane, bonding, electron pairs, size and shape parameters, Gaussian basis set MO calcs. 80−27935
methane, C X-ray spectrum meas. by soft X-ray spectrometer 78−24911
methane, chemisorption on Rh, vibr. excitation and surface reactivity 79−73393
methane, clusters, collision induced polarisability, mol. frame distortion 80−32798
methane, cohesive energy and Gruneisen parameter calcs. 79−19183
methane, collision induced rot. Raman scatt., polarisability effects 78−86874
methane, collision-induced light scatt., spectral features 78−13493
methane, collision-induced Rayleigh scatt. intensity calcs. 77−46569
methane, combustible gas production from organic wastes using bacteria 80−7898
methane, combustion, appl. of sensitivity analysis, numerical Green's function procedure 79−100334
methane, combustion, free turbulent jet form. 78−30329
methane, comparison of dielectric and refractive virial coefficients and collision induced absorption bands 79−86547
methane, compressed, drift velocity of excess electrons 79−91113
methane, compressed gas, apparatus for depolarisation ratio meas. of scatt. light 80−38527
methane, compressibility isotherms, thermodynamic props., 0 to 150°C 80−6196
methane, Compton profiles, high energy electrons impact spectroscopy 77−27188
methane, conc. in atmospheric surface layer from IR absorpt. meas. *(Russian)* 77−29366
methane, conc. meas. in nonurban troposphere 78−32184
methane, concentration along line in jet, spatially resolved coherent anti-Stokes Raman spectra 79−74476
methane, concentration meas. in troposphere, geographical and altitude distrib. *(Russian)* 77−60449
methane, condensation, zero point energy shift, isotope effects 78−95147
methane, continuous coherent radiation in spatially separated fields 78−30007
methane, continuous coherent radiation obs. in spatially spaced fields *(Russian)* 78−9372
methane, conversion in H_2 plasma flow, Monte Carlo study 78−61010
methane, coord. bond calcs. 80−58129
methane, core 1s shakeup study, XPS and Xalpha calcs. 80−69064
methane, core ionis., single orbital relax., LCAO MO SCF calcs. 78−29739
methane, crystalline, deform. under hydrostatic press. 77−70136
methane, crystalline, struct. and compression at high press., room temp. 80−107199
methane, CW coherent antiStokes Raman spectrum, ν_1 band, press. depend. 78−42377
methane, CW vibr. photchem. for D enrichment, economic aspects 80−11920
methane, D enrichment by CW CO_2 laser induced reaction 79−18300
methane, decomposition in RF discharges, 10-40 torr 78−3318
methane, dense gas, electron drift velocity 78−1785
methane, dense gaseous and liq., thermal cond.-viscosity correlation, up to 500 atm., 95-500 K 77−80657
methane, desorption, from Cu surface, production and meas. of atomically clean surface environment 80−52250
organic compounds continued
methane, detect. in Orion A molecular cloud 79−17060
methane, diffusion in Kr, isotope effects at various densities 77−68732
methane, dil. aqueous soln., Monte Carlo calcs. on struct. 79−32874
methane, dilute gas, transport props., simple pair pot. model 80−87835
methane, dipole moment derivatives, MINDO/3 semiempirical calcs. 77−75055
methane, dissoc. by adsorption-desorption process on W 78−92511
methane, dissoc. chemisorption on Rh (111) surface, vibr. activation 79−57292
methane, dissociation mechanism in singlet states and superexcited states, ionised states deduced 79−43602
methane, distrib. in near-surface waters of western subtropical N.Atlantic Ocean 77−60423
methane, effective core potential calcs. 79−31437
methane, effects of impurities and annealing on triple point 78−83919
methane, elastic and inelastic electron scatt. differential cross section, obs. and calc., struct., binding energy 80−28110
methane, elastic scattering of electrons, differential cross-sections 79−89780
methane, elec. dipole polaris., near Hartree-Fock value, using EFV GTOs 77−88591
methane, elec. dipole polarisability, coupled and uncoupled Hartree-Fock calcs. 77−34539
methane, electron energy loss spectra, C K-shell excitation, vibr. struct. 79−22851
methane, electron impact, Balmer-α emission Doppler profile energy depend. 77−42423
methane, electron impact, H,D(2s,2p) prod. 78−42230
methane, electron impact dissoc., excitation of H Lyman β and Balmer α radiation 78−46450
methane, electron impact dissoc., H atom sublevel excitation 77−14593
methane, electron impact dissoc., high Rydberg fragments 77−83749
methane, electron impact dissoc. excitation cross sections 77−61861
methane, electron impact excitation, 30-250 eV, 0-90° 79−54949
methane, electron impact spectra, C atom inner shell excitation 77−10776
methane, electron irrad., $CH_2(b^1B_1)$ prod. and rad. lifetime from $b^1B_1 \rightarrow a^1A_1$ emission 77−3476
methane, electron pair interactions calcs. 80−23298
methane, electron radial diff. coeff. to mobility ratio 77−19666
methane, electron transmission function and mean energy per ion pair, obs. 80−23566
methane, electron transport coeff. calc. in counting gas mixtures 79−32727
methane, electronic density, multiple scatt. method, muffin-tin approx. 80−27924
methane, emission at 76 GHz obs. from Jupiter correl. with decameter activity 78−4140
methane, emission detect. on Neptune 78−16344
methane, energy quantities from localised charge densities, dependence on geometry and basis set 80−63525
methane, energy transfer obs. using excitation of fund., overtone and combination bands 80−9704
methane, enrichment of D using vibrationally sensitized reaction 80−76532
methane, entropy and sp. ht., 0.4 to 28K, spin-species conversion 77−28015
methane, equations of state, molecules interacting via Kihara pot. with spherical core *(Spanish)* 77−31749
methane, excess electrons, zero-field mobility in dense gas 78−22452
methane, excimer laser Raman pulse compression for appl. to laser fusion 79−59756
methane, excited states, photochem., ab initio calcs. 77−14371
methane, $F_2^{(2)}$ doublet Zeeman effect obs., nonlinear reson. *(Russian)* 77−38027
methane, first detection in interstellar medium 78−16503
methane, first hyperpolarisability, Hartree-Fock-Slater calc. *(French)* 78−78625
methane, fluid, collision-induced light scatt. 78−68509
methane, fluid, electron mobility, density and temp. effects 80−10351
methane, force consts., ab initio CI calcs. *(French)* 78−90093
methane, force consts., equilib. geom., Hartree-Fock and CEPA calcs. 78−70753
methane, force consts., vibr. freqs., CNDO/2 and MINDO calcs. 77−14607
methane, force consts. by modified Redington and Aljibury method 80−69261
methane, form., 10 keV H^+-graphite sputtering *(Russian)* 77−4707
methane, form. by deuteron bombardment of pyrolytic C energy depend. 78−95939
methane, formation by D^+ interaction with C surface, exam. of temp. depend. 78−79645
methane, freq. depend. polarizability, LCAO SCF perturbation theory 79−31387
methane, freq.-depend. shear viscosity 79−77798
methane, frequency stabilisation of 0.633μm line with 3.39μm line locked to saturated absorpt. line 80−28258
methane, frequency stabilisation of He-Ne lasers by ref. to absorption transitions 77−83913
methane, FSGO calculations using pseudopotentials 77−26971
methane, gas, absolute viscosity 77−35299
methane, gas, electron drift vel., Ramsauer-Townsend minima in electron scatt. 78−87427
methane, gas, electron transport, kinetic theory 77−84391
methane, gas, Kerr effect, virial coeffs. 79−50843
methane, gas, liq., collision-induced microwave absorpt. 77−42312
methane, gas, rarefied flow, visco-magnetic heat flux 79−98844
methane, gas, Rayleigh-Brillouin scatt., hydrodynamic effects calcs. 77−470
methane, gas, second virial coeffs., intermol. pot. at low temp. 79−46416
methane, gas, total ionization created by completely stopped H^+ ions 79−46419
methane, gas, up to 50 atm, refr. index, 328, 3103 MHz *(French)* 78−14129
methane, gas density fluctuations, orthopositronium annihilation rate depend. 78−37773
methane, Gaussian basis sets, quality studies 79−59345
methane, geometry optimisation, using bond function augmented basis sets 78−905
methane, global anthropogenic emission into atm. *(Russian)* 79−100547

organic compounds continued
methane, ground state, dipole oscill. strength distrib., rel. to molar refractivity and dispersion energy 77−71835
methane, group theory, space and point group factorization, appl. to crystallography and spectroscopy 79−60295
methane, H_2 production by steam reforming of natural gas, chemical kinetics 80−97815
methane, H^+, H_2^+, and H_3^+ kinetic energy distribs., electron impact dissoc. ionisation, time of flight mass spectra 80−32843
methane, H abstraction by thermal H, 10-30K, ESR evidence 78−76839
methane, H-X bond position, correlation with electronegativity 78−9069
methane, halogenated+K, negative ion form., electron affinities, bond dissoc. energies 78−82827
methane, harmonic and anharmonic matrix elements comparison, appl. to vibrational energy transfer 80−63760
methane, Hartree-Fock perturbation theory, first-order, symmetry calcs. 79−6854
methane, heavy, cryst., temp. depend. of Debye-Waller factor, Monte Carlo calc. 78−47492
methane, heavy nucleus isotope shift calcs. 78−86917
methane, high density fluid, LF Raman spectra, dimer formation 77−46566
methane, high resolution coherent anti-Stokes Raman scatt. *(Russian)* 77−75168
methane, high resolution photoelectron spectra, vibr. progression 78−74700
methane, high-purity, triple point temp. and press. meas. 77−31753
methane, high-resolution CARS, press. depend. of intensity 80−9964
methane, high-resolution coherent Stokes Raman scattering, of ν_1 and ν_3 bands 79−31981
methane, hyperfine struct., Racah finite group algebra appls. 78−78617
methane, hyperfine struct. of $F_2^{(2)}$ line, appl. of laser spectrometer 77−58201
methane, identificiation in atmosphere of Triton from IR spectrum 80−21945
methane, in air, IR spectra, optical-acoustic investig. *(Russian)* 78−74663
methane, in alkane soln., ^{13}C nucl. spin-spin relax., for mol. correl. times 79−95661
methane, in liq. SF_6, ν_3 band IR profile, temp. depend. 78−58696
methane, in SF_6, CCl_4 soln. and Ar, IR band profile *(French)* 79−54913
methane, in water, cavitation, gas supersaturation thresholds under high press. 77−16861
methane, inner-shell excitation and EXAFS-type phenomena 79−13828
methane, integrated CARS power, press. depend. 78−59081
methane, intensity pertubations due to ν_3/ν_4 coriolis interaction 79−98087
methane, interaction kinetics with Ni (110), AES-LEED-ellipsometry 77−62756
methane, interaction with Ni (100), diffusion of deposited C, AES-LEED study 79−99418
methane, intermol. pair pot. energy function 77−10721
methane, intermolecular interaction energies calcs. using minimal basis sets 80−78681
methane, intradoppler CARS saturation spectroscopy 80−43057
methane, ion internal energy selection by angle-resolved mass spectrometry 80−53164
methane, ion-molecule reactions in glow discharge, mass spectrometric obs. 78−63627
methane, ionis. by mol. orbital method, many-body calc. 79−36512
methane, ionis. spectral intensity, valence electron binding energy depend. 78−90234
methane, ionisation, energy dependence of $\bar{W}$ for alpha particles 79−6999
methane, ionisation by electron bombard., empirical and semi-empirical calcs. 79−36784
methane, ionisation pot., quasidegenerate many-body perturbation theory calcs. 77−50346
methane, IR anal. of ν_2 and ν_4 bands *(French)* 80−87113
methane, IR intensities, C and H atomic polar tensors 78−50592
methane, IR line intensities 78−58687
methane, IR radiation flux in Earth atmosphere 78−71268
methane, IR spectra, 2862-3000 cm^{-1}, line positions and strengths 78−5217
methane, IR spectra of ^{13}C mol. isotope, ν_4 band line strengths 79−94036
methane, IR spectral atlas for 1120-1800 cm^{-1} region 80−23415
methane, isotopic variants, IR intensity anal. 77−58081
methane, J-multiplet intensity meas., ν_4 fundamental at 300K 77−68080
methane, jet, free turbulent flow, diffusion coeff. variation, mixing processs velocity 77−7480
methane, Jovian line profiles near 1.1 μ as probe of cloud struct. and C/H ratio 80−62067
methane, Kerr effect in gas, statistical theory 79−50842
methane, Kuiper bands detect. in Titan spectrum 78−85898
methane, lack of C isotope exchange, methane and C oxides, high temp. 79−84263
methane, large angle elastic and inelastic electron scatt. differential cross section, exchange corrections 80−28111
methane, Lennard-Jones 12:6 parameters calc. from viscosity data 77−46612
methane, line profile of coherent radiation in separated fields due to $F_2^{(2)}$ transition 80−37835
methane, liq., compressed, self-diffusion coeff. temp. and density depend. calcs. 78−38864
methane, liq., drift vel. of excess electrons 80−54744
methane, liq., estimation of solubility of solidified substances, by Preston-Prausnitz method 79−37842
methane, liq., medium cluster model, vapour press. isotope effects 77−65943
methane, liq., medium cluster model, vapour press. isotope effects, mol. orientation effect 77−72542
methane, liq., mol. dynamics calcs. 77−19857
methane, liq., mol. dynamics simulation using singularity-free algorithm 80−54116
methane, liq., optical consts. meas. in IR, possible planetary cloud cover component 78−64341
methane, liq., pure vibr. Raman spectra 80−97262
methane, liq., surface tension and density profile from expression for excess free energy 77−80681

organic compounds continued
methane, liq., temp.-depend. free vol. 79−99052
methane, liq., thermodynamic perturbation theory, equilib. props. 79−64976
methane, liq., viscosity, density depend., theory 77−20105
methane, liq. and gas, mol. dynamics simulation, thermodynamic props., struct. factors, etc. 79−50976
methane, liq. and solns., Raman spectra, vibr. anal. 79−27001
methane, liquid, Brillouin scatt. obs., US vel. and absorpt. 80−45085
methane, liquid, comparison on interaction induced light scatt. and IR absorption 80−60561
methane, liquid, compressed, excess electron mobility, density depend. 77−11924
methane, liquid, compressibility, long wavelength limit of liquid struct. factor 78−67633
methane, liquid, opto-acoustic study of weak optical absorpt. 80−93278
methane, liquid, photoelectric determ. of conduction state energies and electron ranges 77−89487
methane, liquid, Ramsauer-Townsend minimum in electron scatt. cross section 77−89821
methane, liquid, vibrational overtone spectrum, planetary appls. 79−2497
methane, liquid ionisation chamber media, review of physical props. 79−41071
methane, localisability in MO calcs., measured by absolute overlap and 2nd moment dispersions 78−74557
methane, localised molecular orbitals, HF theory 79−97980
methane, localised orbital construction for calcs. using multiconfigurational SCF methods *(Russian)* 78−922
methane, longitudinal variability in Jupiter atm. visible spectra 80−82270
methane, low-energy electron scatt., total 0.16 eV cross sections, vibr. excitation 79−86076
methane, low-energy X-ray emission spectra, MO anal., ionis. pot., rel. to CCl_4 and $CHCl_3$ 79−85975
methane, machine treatment of chromatographic curves using statistical moments method 77−63981
methane, mag. hyperfine struct., laser spectroscopy 77−88757
methane, mag. shielding consts., coupled HF perturbation theory 79−6863
methane, mag. struct. of vibr.-rotational transition, review of laser appl. to precision meas. 78−42246
methane, mag. suscept., vector pot. variational calc. 77−68137
methane, mag. susceptibility, HF perturbation method 77−79702
methane, mantle related thermodynamic props. and reactions at high press. and temp. 80−81874
methane, matrix isolation spectra using tunable diode laser 78−45739
methane, mean polarisability derivatives, variational calc. procedure 79−27108
methane, meas. and predictions for stratosphere 79−84432
methane, melting curve investig. by blocked capillary method 77−35672
methane, melting transitions, thermodynamic props., positional disordering energies 80−96452
methane, microwave Q branch distortion moment Stark spectrum, rot. transitions, C isotope shifts 77−455
methane, mol. and cluster Auger spectrum calc., SCF core-valence-valence spectra 80−48045
methane, mol. cations, struct., Jahn-Teller effect, MINDO/3 calcs. 80−74135
methane, mol. collisions, energy transfer, multi-dimens. harmonic oscillator model 78−42174
methane, mol. force consts., parametric representation method 78−25503
methane, mol. multipole polarisabilities, extended variational method calcs. 79−36558
methane, mol. nuclear spin-spin coupling, ab initio SCF perturbation theory 78−33525
methane, mol. rot.-vibr. consts., calc. using ν_1 band data 79−76529
methane, mol. transition freqs. in resonant optical field, Stark shift 77−14487
methane, molecular charge density contours for cryst. struct. 78−38645
methane, molecule, floating spherical GO calcs. of electron momentum distribs. and Compton profiles 77−30933
methane, mud volcanoes, Copper River Basin, Alaska, composition of emitted gases 79−84308
methane, multipole expansion of diatomic overlap, MEDO calcs. 78−46264
methane, multipole moments, far IR spectrum determ., pot. function effects 77−50435
methane, multipole moments and polarisabilities 79−85910
methane, narrow reson., elastic scatt., spectroscopic studies 80−53094
methane, NMR chem. shift., temp. depend., virial coeffs. 78−58722
methane, nonlinear laser spectroscopy, inside Doppler line *(Russian)* 78−21231
methane, nonlinear optical reson. shift in mag. field, vibr.-rot. transition 78−13549
methane, nucl. elec. shielding tensor calcs. 80−83296
methane, nuclear spin conversion at triple point 79−77723
methane, nuclear spin-spin coupling consts., finite perturbation-CI calcs. 80−5563
methane, nuclear steam reforming for coal gasification 80−55775
methane, obs. in IR spectra of Uranus, Neptune and Titan (0.8 to 2.5 microns) 80−21946
methane, optical Ramsey resonance, in three separated fields produced by corner reflector, theory 80−74166
methane, orbital relax. energy for single and double ionis. from valence shells 80−106253
methane, orbital valency force field 77−34779
methane, orbitals calcs. using modified Adams-Gilbert eqn. 77−34542
methane, outgassing from Earth interior 78−92809
methane, outgassing from Ti sublimation pump 80−77796
methane, oxidation, complex network calcs. 78−11497
methane, oxidation in nonurban troposphere 78−32183
methane, permeability of coal *(Russian)* 79−66695
methane, perturbed-hard-sphere eqn. of state applicable to sub- and supercritical temps. 79−19350
methane, phase II, IR and Raman spectra of ν_3 and ν_4 modes 78−2834
methane, phase II, nuclear spin-lattice relax. and site symm. 80−97155
methane, photoabsorpt. cross section, 10 to 50 nm 77−61797
methane, photoabsorpt. cross sections, 1400-1850 Å spectral region 77−46572
methane, photoabsorpt. cross-section, 175-770 Å 77−88462

organic compounds continued
methane, photoabsorption cross sections, 1380 to 1600 Å, at 295 and 200K 78−90181
methane, photoacoustic Raman spectroscopy under pulsed laser excitation 80−82825
methane, photoacoustic Raman spectroscopy using CW laser sources 79−44947
methane, photodissoc. ionis., 16-41 eV 77−18995
methane, photoelectron ang. distrib., near threshold to 30 eV, photon energy depend. 80−53045
methane, photoelectron spectra, 21.2-151.4 eV and soft X-ray, ionis. cross-section 78−37683
methane, photoionis., ion fragmentation kinetic energy 78−9206
methane, photoionis. cross section calc. for YMζ and ZrMζ lines, HF vs OPW methods 77−42353
methane, positive corona discharge, current oscills. 77−11431
methane, positron annihilation rates in applied electric field 77−27179
methane, possible microwave interstellar maser lines 78−41020
methane, pot. energy curves, Monte Carlo and SCF LCAO MO calcs. 80−63526
methane, pot. energy surface of excited singlet state, appl. to photodissoc. 79−83440
methane, prod. from H_2O+CO_2, by photoassisted reaction on $SrTiO_3$ surface 78−76878
methane, prod. in Walvis Bay waters 78−28246
methane, proportional counter gas, primary ion pairs distrib. prod. by C-K_α source 78−29704
methane, proton mag. shielding const., HF perturbation theory 78−46258
methane, proximity and conform. effects., ^{13}C chem. shifts at γ position INDO computations 77−50451
methane, pseudospectral dipole oscillator strength distribs. 78−50503
methane, pulsed photoacoustic Raman spectrosc., gaseous trace anal. 80−40769
methane, pure and O_2 doped solid, neutron scatt. and proton spin conversion 77−89391
methane, pure rot. Raman scatt. 78−86875
methane, pyrolysis, spiral growth of pyrolytic C *(German)* 78−42931
methane, $Q(\nu_1)$ Raman line, CW high-resoln. CAR spectra 77−27076
methane, quantum mech. rot. partition function 80−102501
methane, Raman intensity from electro-optical parameters 79−36645
methane, Raman spectra, 2850-3100 cm^{-1}, ν_3 band anal. 77−75162
methane, Raman spectra intensity analysis, electrooptical parameters transferability 78−29820
methane, recoil effect, optical resolution by saturated absorpt. spectroscopy 77−18937
methane, relativistically parameterized extended Huckel theory 79−49924
methane, remote conc. meas. using tunable IR laser 77−87118
methane, rot. mag. moment spectra, mol. beam mag. reson. obs. 77−14509
methane, rot. states, coherent neutron scatt. 77−84678
methane, rotational anal. of $(\nu_3+\nu_4)$ combination bands *(French)* 78−21900
methane, rotational partition function, isotope effects 80−14130
methane, rotational state, avoided-crossing molecular beam spectroscopy 80−63730
methane, rotational transition in condensed Xe, 6K, optical excitation 78−60494
methane, saturated absorpt., freq. stabilisation of He-Ne laser *(French)* 79−31935
methane, saturated absorpt. for freq. stabilised 3.39 μm He-Ne laser 79−76700
methane, saturated absorpt. meas. at 3.39 μm using multipath cell 80−74442
methane, saturated absorpt. of 3.39 μm line in external cell 79−50354
methane, saturated absorpt. profile using methane-stabilised laser spectrometer 79−98446
methane, saturated absorpt. reson. shape, geometry and field intensity effects *(Russian)* 80−32778
methane, scaled Raman pulse compression experiments at 248 nm, KrF pump laser 80−38071
methane, SCF calcs. including polaris. functions 80−87034
methane, second refractivity virial coeff. direct determ. 77−15158
methane, self-diffusion coeffs. evaluation from expt. data 77−42953
methane, semiempirical electron impact ionis. cross-sections 78−1089
methane, shock-tube oxidation, equilibrium and nonequilibrium radiation emission 78−27760
methane, simultaneous analysis of ν_2 and ν_4 bands 77−10662
methane, single mode 3.39 μm laser obs. of absorpt. lineshape 77−46600
methane, slow electron scatt., rigid mol. model with exchange and polarisation 80−43194
methane, solid, discontinuous orientational phase transitions, thermodynamics, isotope effects 80−6590
methane, solid, far IR spectra, and lattice vibr., 4.2K, 0.4-4.5 kbar 79−19868
methane, solid, high press. NMR obs. 80−50214
methane, solid, high press. PMR, second moment 79−8059
methane, solid, lattice distortions and phase transitions 77−19882
methane, solid, melting curves, Lennard-Jones Devonshire theory 80−65201
methane, solid, nucl. longit. relax. near rot. ordering transition 77−43896
methane, solid, orientational order of molecules in phase III 79−51042
methane, solid, phase II, Raman spectrum, vol. and temp. depend. 80−97260
methane, solid, phase II, theory of phase transitions 77−51494
methane, solid, phase II and in Kr, Ar matrices, IR spectra, quantum rot. 77−28562
methane, solid, phase III, Raman spectra 79−65849
methane, solid, plastic phase, mol. dynamics simulation 80−79715
methane, solid, probing phase transition with Mossbauer effect in ^{57}Fe impurities 79−4751
methane, solid, Raman spectra and II-III phase transition 80−2745
beta-methane, solid, Raman spectrum in intramol. and lattice region 79−33697
methane, solid, rot. ordering and proton spin-lattice relax. 78−91967
methane, solid, theory of nucl. spin conversion in β phase 77−31608
methane, solid, thermal cond. calc. 78−51753
methane, solid, thermal expansion and conversion processes *(Russian)* 78−95163
organic compounds continued
methane, solid, thermal expansion coefficient and Gruneisen parameter 78−47540
methane, solid, thermodynamic props. from US velocity obs. 79−46753
methane, solid, with O_2 and N_2 impurities, thermal expansion, 2 to 14K, conversion processes 79−65228
methane, solid phase II Raman spectrum, lattice vibr. and ν bands 78−19456
methane, solid-state phase transitions, 5-80K, PMR spin-lattice relax. up to 3 kbar 77−40137
methane, solubility parameters, calc. from eqn. of state 77−11660
methane, solvent effects, quantum mech., macroscopic electrostatic contribs. 77−30801
methane, spontaneous thermal fluctuations, Rayleigh scatt. obs. 78−88317
methane, steam reforming for H production, kinetic anal. 80−35788
methane, stimulated Raman scatt. obs. 80−53003
methane, stimulated Raman scatt. of excimer laser wavelengths for new lines in UV 79−59755
methane, Stokes collision-induced Rayleigh scatt. 78−25546
methane, stored energy needed to ignite by discharger from charged person 80−54063
methane, supersaturation in Neptune's stratosphere 79−40137
methane, thermal cond. meas. at room temp., and pressures up to 5 MPa 79−86551
methane, thermal diffusivity in critical region, Rayleigh scatt. obs. 78−34607
methane, thermal electron mobility at high density, electron quasilocalisation 79−27740
methane, thermodynamic perturbation theory 80−14985
methane, torsional ground state splitting in cryst. field 80−15019
methane, total scatt. cross sections for intermediate-energy positrons 80−91692
methane, transport coeffs., statistical mech. calcs. 77−7494
methane, triboelectric discharge of Hg rolling on glass, chem. effect *(French)* 79−77438
methane, triple-dipole energy calc. using pseudo spectral theory 78−46418
methane, troposphere vertical profile, eastern USA in winter 80−77035
methane, tropospheric abundance and flux from Earth surface *(Russian)* 78−36223
methane, V-V energy transfer 80−83469
methane, valence bond calc. convergence 78−9081
methane, VB calc. using minimal Slater basis set, $^1A_1$ ground state 78−62729
methane, vertical electronic spectra, limited CI calcs. 79−13693
methane, vibr. induced rot. spectrum in $(u_4=1)$ state 79−18184
methane, vibr. relax. time, spectrophone meas. 77−38669
methane, vibration-rotation ν_3-ν_4 band, theoretical spectra 78−42037
methane, vibration-rotation energies, $2\nu_2$ and $\nu_2+\nu_4$ bands 80−47963
methane, vibration-rotation energies of harmonic and combination levels 80−47962
methane, viscomagnetic heat flux, in a Burnett regime 78−71400
methane, volcanic hydrothermal vents from E.Pacific rise, H_2 and CH_4 content 80−41422
methane, W-value determ. for α-particles 79−39518
methane, wetting of flat smooth aolid, calc. using Lennard-Jones pot. 77−89618
methane, X-irradiated, 4.2K, pairwise radical trapping mechanism, EPR obs. 79−100412
methane+^{125}I, γ irrad. effects on organic iodide form. and decomp. *(Japanese)* 77−81418
methane+$^{12}C(^{13}C)$, thermal energy reaction, mass spectra 77−9067
methane+^{18}F, nonequilibrium effects in moderated nuclear recoil experiments 80−89509
methane+acetylene cation, reaction, vibr. and translational energy depend., mass spectrosc. obs. 79−47908
methane+Ar^{12+}, C K-shell Auger effect 77−6908
methane+Ar, CH chemiluminesc. in flowing afterglow 78−64839
methane+Ar, enthalpy of mixing, 123 to 145K and 2.03 to 9.12 MPa 77−70330
methane+Ar, low energy collision, close coupling and coupled states, rot. transitions 78−78784
methane+Ar, rot. compound state resons. 80−28090
methane+B(Be)(C), target atom K-shell binding energy by Auger spectra 78−50525
methane+BCl_3 reaction, laser-induced, vibr. excitation influence on reactivity, isotope selectivity 80−11921
methane+Be^+ collisions, autoionising core-excited Be II states, alignment prod. 80−14204
methane+$Be(2^3P)$, reaction, ab initio MO calcs. 79−8431
methane+Br^-, total electron detachment cross sections for energies around threshold 80−99550
methane+$C_2(a^3\Pi_u)$, reaction rate consts. and quenching, multiphoton UV photolysis, fluoresc. obs. 79−74355
methane+$Cd(5^3P_{0,1})$, absolute quenching cross sections 80−5604
methane+CH_3^+, condensation reactions mechanism 80−25996
methane+Cl^+, reactions at room temp. 80−93749
methane+Cl^-, total electron detachment cross sections for energies around threshold 80−99550
methane+$Cl^-(Br^-)(I^-)$, excitation functions, reactive scatt., eV region *(German)* 78−35677
methane+Cl, rate const., discharge flow-reson. fluoresc. meas. 78−7178
methane+Cl, rate consts., stratospheric temps., radiotracer meas. 77−48632
methane+Cl, reaction rate const., stratospheric modelling appl. 79−20345
methane+Cl→HCl+CH_3, absolute reaction rate, flash photolysis-reson. fluoresc. obs. 77−56222
methane+$Cl(^2P_{3/2})$, reaction kinetics, temp. depend., reson. fluoresc. obs. 77−4903
methane+$Cl(^2P)$→CH_3+HCl, reaction rate const., laser flash photolysis-resonance fluoresc. kinetic study 80−45485
methane+CO, vibr. relax. rates, energy transfer 80−37862
methane+Cs_2, collision-induced dissoc., atom-mol.-exchange optical pumping 78−22008
methane+d_2, Ar vibr.-vibr. energy transfer process diagnostics 80−32807
methane+F^-, MINDO/3-FORCES study, reactant energy, products and paths 78−95926
methane+F, reaction in Ar matrix, IR spectra obs. 79−96293

organic compounds continued
methane+F, reaction rate consts. rel. to stimulated emission 78−3317
methane+H_2^+, bimol. and thermol. charge transfer reactions, rate coeffs. 77−1910
methane+H_2, (oriented), total collision cross-sections, anisotropic pot. parameters calcs. 78−13568
methane+H_2, rot. line width of vibr. bands 78−33552
methane+H_2O^+, rate constants determ. as function of relative kinetic energy 80−81292
methane+H_2O, interaction energy calc. using minimal basis sets 80−9678
methane+H^+→H_2^++methyl radical, quantum calcs. 80−71911
methane+H^+(He^{2+})(Li^{3+}), inner shell electron capture cross-sections 79−76510
methane+H^-→H^-+methane, force decomposition anal. along reaction coord. 78−27741
methane+H^-→H^-+methane, nucleophilic substitution, ab initio pot. energy classical trajectory anal. 78−68886
methane+H, abstraction and exchange reaction, barrier height calc. using POL-CI wave functions 80−81304
methane+H, abstraction and exchange reactions, energy barriers, UHF-CI calcs. 78−11512
methane+H(D), differential collision cross sections, diffraction oscills., data anal. 79−22783
methane+H(HO)(O)(O_2), H abstraction, rate consts. calcs. 78−95921
methane+HCl, pure rot. line broadening obs., transition cross sections 77−75134
methane+He^+, 0.7-2 MeV, charge-changing collisions, electron capture 80−58372
methane+He, differential scatt. cross-section, intermol. pot. 79−36728
methane+hydrocarbon ions, rate coeffs., ionised product. distribs. 77−44471
methane+I, excited atoms, quenching time resolved reson. fluoresc., isotope effects 80−32656
methane+I($5^2P_{1/2}$), collisional deactivation, rate consts. meas. 77−86300
methane+inert gas, vibr. relax. time, spectrophone meas. 77−38669
methane+inert gas (H_2)(HD)(methane), vibr. energy transfer, fluoresc. 77−519
methane+inert gas ion, thermal energy charge transfer 78−37739
methane+Kr^{2+}, charge transfer reactions, rate coeffs. and product-ion distributions meas. 80−104431
methane+Kr(Xe), ^{13}C-mag. shielding density depend. 78−9173
methane+Kr liquid mixtures, intermol. forces effect on phase diagram and excess props., perturbation theory 80−39287
methane+Li^+, vibrational excitation, time of flight measurements 79−45826
methane+Li^+(Be^+)(B^+), single collision, time delayed autoionisation spectra 78−1067
methane+Li(Be)(B)(C), collisional excitation, prompt decay line energy, projectile Auger spectrosc. 79−85941
methane+linear molecule (one-electron atom) collisional energy transfer by octupole coupling 78−62881
methane+methane, intermol. pot., electron gas approx. calc. 78−9214
methane+methane, rot. line width of vibr. bands 78−33552
methane+methane, vibr. energy transfer, Morse pot. 79−31653
methane+methane (He)(Ne)(Ar), dispersion forces 78−13565
methane+methane and methane+monatomic collisions, photoacoustic study of vibr. relaxation *(French)* 77−30969
methane+methyl fluoride, intermol. vibr. energy transfer, double reson. investig. *(Russian)* 77−61839
methane+N_2^+(CO^+), charge transfer cross-section, low energy 78−58791
methane+N_2, ionis. at low energy 78−58791
methane+N_2, liq., press. effect on excess thermodynamic functions 78−47494
methane+N_2, liquid, high resolution CW CARS spectra 80−63635
methane+N_2, N_2 fixation, catalytic processes in non-equilibrium plasma chemical reactors *(French)* 80−89483
methane+N_2, rot. line width of vibr. bands 78−33552
methane+N_2*, deactivation, from laser-induced CO_2 fluoresc. obs. 80−63776
methane+N_2(Ar), compressed-liquid dielectric const., derived excess vol. 79−11377
methane+N^+, charge transfer reaction, dissoc., isotope effects, mass spectra 77−21382
methane+N^+, product distribs., rate consts., ion cyclotron reson. obs. 77−52618
methane+N, CN quartet state production, fluoresc. anal. 78−68888
methane+Na, total cross sections 79−27064
methane+Ne^{2+}, charge transfer reactions, rate coeffs. and product-ion distributions meas. 80−104431
methane+Ne^+, thermal energy, reaction rate coeffs. and product distrib. 79−29333
methane+Ne^{m+}(N^{n+}), K-shell vacancy prod. cross-section, charge state depend. 78−17751
methane+NH^*, rate const., time resolved chemiluminesc. 78−60982
methane+NO^+, reaction rate consts. meas. 80−7782
methane+NO, NO γ(0,0) band, oscillator strength and line broadening 80−106356
methane+O_2^+, reaction rate const. kinetic energy depend., 300K, 0.125-0.450 torr 78−76850
methane+O^+_4(O_2^+), products, rate consts., rel. to stratosphere 77−9040
methane+O, photochem. reaction, high temp., rate coeff. meas. 80−16699
methane+O→methyl radical+OH reaction, photolytically initiated, high temp. kinetics meas. technique 80−61085
methane+O(2^1D_2), collisional deactivation meas., 295K, rel. to atmospheric processes 80−16663
methane+O(^1D), direct reaction in flow system 80−3333
methane+O(^1D), rate consts., temp. depend. 78−27747
methane+O(^3P), barrier height and transition state geometry, POL-CI calc., H abstraction reaction 80−66782
methane+pentyl ion, energy transfer, modified statistical theory 79−50107
methane+Rb, $5^2P_{1/2}$⇄$5^2P_{3/2}$ excitation transfer cross section temp. depend. 80−91630
methane+S, electronically excited atom, reson. fluoresc. 80−99476
methane+SF_6, vibr.-vibr. relax 80−99537
methane+SiH_4, vibr. energy transfer 77−524
methane+tritium reaction, reaction ergodography 77−21371

organic compounds continued
methane+X^{n+}, (X=Ar,Kr,Xe,U), Auger emission line shape after dissoc. 78−86838
methane+Xe liquid mixtures, intermol. forces effect on phase diagram and excess props., perturbation theory 80−39287
methane(-^{13}C), absorpt. spectra. optoacoustic laser meas. 78−37635
methane(-d_1,d_2,d_3), electro-optical parameters from IR intensities, least-squares calc. 80−9584
methane(-d_4), force field representation, equilib. struct. 78−42238
methane(-d_4), vibrationally-hot, bond lengths, simple treatment 79−68202
methane(-d_4)+HF, collision relaxation rate constants and rot. equilibration time meas. 80−69213
methane(-ethane)(-N_2), heat transfer in nucleate boiling of liquified gases and binary mixtures *(German)* 79−18687
methane(-H_2), long path photoelec. absorpt. spectra 4200-10600 Å, appl. to Uranus 77−83592
methane $2\nu_4$-ν_4 and ν_2+ν_4-ν_2 hot bands, difference bands 80−63632
methane 3.39 μm transition in ring laser field, freq. shift 79−27298
methane 6819 Å line interpretation rel. to inhomogeneous scattering models for Uranus and Neptune 78−53871
methane 7300 Å band in Neptune atm., limb brightening, photometry obs. 80−82297
methane 7300 Å band of Uranus, limb brightening obs. 78−85902
methane +H_2O, pairwise interaction pot. function, ab initio SCF MO calc. 79−22786
methane + O_2^+($a^4\Pi_u$), 0.04-1.2 eV, reaction rate consts. 79−47911
methane (-d_1,d_2,d_3,d_4) Raman electro-optical parameters, overlay least squares calcs. 78−42105
methane (-d_1), reduced partition function ratio, generalised finite polynomial approx. 78−66529
methane (methane-^{13}C) band strength, spectral line breadth in ν_3 bands 79−98069
methane absorber for He-Ne laser, reson. obs. in output, freq. stabilisation 77−83854
methane absorber in He-Fe ring laser, narrow nonlinear resonances at low press. *(Russian)* 79−76722
methane absorbing cell for two-mode He-Ne laser, freq. stability and reproducibility 79−89934
methane absorption cell for He-Ne laser, hyperfine struct. influence on freq. reproducibility 78−50864
methane absorption cell for He-Ne laser, reson. freq. shift with methane press. 77−50687
methane absorption cell for He-Ne ring laser, power resonances 80−28255
methane absorption on Jupiter, rel. to polar regions limb darkening and atmosphere props. 79−62790
methane adsorbed on γ-Al_2O_3, γ-radiolysis 80−3375
methane adsorbed on graphite basal plane, first order melting transition, triple point 80−2269
methane adsorbed submonolayer on graphite, structural transitions between epitaxially ordered phases 80−96740
methane adsorption on Ti, W evaporated films, mutual replacement of CH_4, CO and NO *(Japanese)* 78−22949
methane aerosol, possible presence in Uranus clouds 80−31253
methane and halogen derivatives Raman scatt. parameters at.-dipole interaction model calcs. 77−65465
methane and methane-d_4, Lennard-Jones (6-12) interaction pot., Debye temp. calc. 78−63828
methane and methane-d_4, low energy electron impact dissoc. autoionisation 80−9744
methane and N_2 counter diffusion through porous solids 77−80649
methane as fuel, solid state storage device study using physisorption data *(German)* 79−96414
methane atmospheric sources and sinks 78−73472
methane backward Raman amplifier, KrF laser driven, high-efficiency energy extraction 80−106533
methane cation, photodissoc., ab initio RHF and MRD CI calcs. 80−95695
methane cell for freq., stabilised He-Ne ring laser, operating characts. 80−14366
methane cell for ring laser, backscatt. influence on operation 79−10329
methane chemical state effects in AES 78−92566
methane combustion, flame propagation through stratified charge combustion channel, model 79−64795
methane compounds, halogen-substituted, formation of excited fragments on dissociation by electron impact *(Russian)* 77−79698
methane content of atmospheric surface layer and vertical air column, synchronised meas. *(Russian)* 79−88407
methane derivatives, stabilisation of planar tetracoordinate C, substituent effects, RHF/STO-3G calcs. 77−6671
methane diffusion in He, coeff. determ., gas chromatography method 77−11298
methane E-component saturated absorpt. for stabilising He-Ne laser, quantum freq. standard 80−9901
methane E-component stabilisation of He-Ne laser, freq. reproducibility 80−106507
methane electron impact dissoc., optical emission from fragments 77−83750
methane flux from wetlands areas rel. to mean air temp. 77−78382
methane formation, CO hydrogenation kinetics, using polycryst. Ni ribbon catalyst 78−40078
methane formation in pyrocarbon during p and d irrads. and thermal release of H 77−36788
methane frost, presence of Pluto from 1.5 to 2.5 μm spectrum obs. 80−56765
methane frost on surface of Pluto, IR photometry obs. 77−22136
methane gas→C(dissolved)+$2H_2$ (gas), kinetics on Fe and Fe-Ni surface 80−55712
methane gas interferometer for coal mine safety 78−44423
methane gas plumes, in atmosphere, tracking via acoustic sounder 80−55968
methane growth in T gas exposed to stainless steel, CTR research 77−50296
methane He-Ne FM eliminated laser, freq. stability meas. 80−87423
methane in condensed inert gas matrices, optical excitation of rotational transition, far IR absorption spectra 80−37808
methane in inner absorptive cell of He-Ne laser, wavelength switching using var. pressure 77−19312
methane in IR spectrum of IRC+10°216, cool C-rich object 78−57694

organic compounds continued
methane in Jupiter atmosphere, abundance deduced from absorpt. bands in refl. sunlight 80−56758
methane in marine sediments, profiles 80−12373
methane in outer atmosphere of Saturn, obs. and model *(Russian)* 77−33406
methane in solid rare gas matrices, rotational states, inelastic neutron scatt. study 79−51020
methane in stratosphere at several latitudes in 0-35 km altitudes 79−34894
methane in stratospheric ion chemistry, reactions with $O_2^+.O_2$ and $O_2^+.O_3$ 79−2343
methane in Titan atmosphere, visible and near IR spectrum 80−46471
methane ions, fragmentation, kinetic energy release, mass spectra 77−79192
methane jet, turbulent conc. field meas. by Raman spectrum, data interpretation 79−32609
methane jet flow, average conc. meas. by Raman scatt. 79−98827
methane locked freq. stabilisation of 3.39 μm He-Ne laser in dual feedback control 80−99772
methane locked He-Ne laser, freq. stability meas. 80−87422
methane molecular pair, polarisability tensor anisotropy 79−31725
methane nonlinearly absorbing cell for He-Ne laser, self-stabilisation effect 79−98420
methane prod. on electrodes of electrical arcs in ultra high vacuum 77−60065
methane production from cellulose by sewage bacteria 80−72005
methane pulsed injection into DIVA Tokamak, transport props. 78−79411
methane pyrolysis, AC arc discharge plasma temp., electron density meas. 79−87843
methane reforming by nuclear steam for coal hydrogasification 80−30325
methane release from graphite, desorption study 79−51420
methane remote meas. by continuously tunable IR lidar 79−21025
methane saturable absorption stabilised He-Ne lasers *(Chinese)* 79−59718
methane saturated absorpt. resonances, shift and broadening due to curvature of laser wavefronts 77−18981
methane solid, spin model for orientational phase transition 78−30735
methane solid film, contaminant on cryocooled Ge optical window, IR transmission 79−32007
methane stabilised He-Ne ring laser, nonlinear resonance freq. shift due to back scatt. *(Russian)* 80−78874
methane triple point sealed cells using stainless steel envelope 80−95099
methane two-dimens. hypercrit. fluid, mobility, on graphite, neutron scatt. obs. 77−20193
methane-2,2-dimethylbutane-2,3-dimethylbutane, tricritical point obs., opalescence 77−76562
methane-air combustion product, electron-neutral energy exchange in AC field 77−42519
methane-air flame, OH conc., temp. and rot. temp., laser absorption spectroscopy 78−76862
methane-air flame, Raman scattering diagnostics of turbulent flow field 78−18328
methane-air flame, reactions, radical overshoot 79−34308
methane-air flame, stimulated Raman scatt. obs. 80−53003
methane-air flames, meas. of temp. and OH conc. 80−16687
methane-air flames, OH conc. profile 80−35534
methane-air mixtures, ignition energy by capacitive discharge *(French)* 80−10446
methane-Ar, cryogenic fluid mixture, transport phenomena, shear viscosity *(Russian)* 80−29198
methane-Ar, gas diffusion of Cs atoms, by reson. ionis. spectrosc. 79−18984
methane-Ar, liq., drift vel. of excess electrons 80−54744
methane-Ar, liq. mixture, self-diffusion and nuclear mag. relaxation *(Russian)* 78−87799
methane-Ar(N_2) binary and ternary mixtures, dielec. const., excess vol. 80−7254
methane-Ar liquid mixture, viscoelastic props., acoustic relax. *(Russian)* 78−75736
methane-Ar liquid mixtures, excess electrons drift vel. 77−59288
methane-Ar proportional counter, light emission obs. 80−78488
methane-BCl_3, single-photon absorption reaction chemistry in solid state 77−73454
methane-benzene (cyclohexane) vapour mixture, excess enthalpy meas. appl. of differential-flow mixing calorimeter 78−12700
methane-CO_2, shock wave refr. at slow-fast gas interface 79−32573
methane-CO_2 mixture, oxidation under RF discharge conditions 78−15670
methane-CO_2 reforming-methanation cycle for Solchem thermochemical solar energy transport 80−94096
methane-d_0, -d_4+OH^+(H_2O^+), reaction, ICR obs. 79−8429
methane-d_0,-d_1,-d_2,-d_3,-d_4, ^{13}C NMR chem. shifts, coupling consts. 78−37657
methane-d_0(-d_4), binary collision-induced light scatt., rot. Raman scatt. 80−78660
methane-d_0(-d_4), binary collisions induced light scatt. 80−83428
methane-d_0(-d_4), electron drift and diffusion, elec. field effects 78−63531
methane-d_0(-d_4), unimol. decomp., energy transfer processes, Monte Carlo simulation 80−99555
methane-d_0(-d_4) vibrational state rotational struct., CARS spectra *(Russian)* 80−99513
^{13}C-methane-d_1:O, annealed, spin conversion and proton 2nd moment time-depends. 80−11283
methane-d_{1-4}+CO_2(N_2O), time resolved fluoresc. for vibr. relax 79−31659
methane-d_1, 9613 Å band rot. anal. 78−86861
methane-d_1, ν_3 band anal., 7.6 micron 80−47980
methane-d_1, ν_6 band at 8.6 μm, vibr.-rot. band 78−21923
methane-d_1, A_0 determ. from ν_4 Raman band 77−83608
methane-d_1, and -d_3, reorientation in simple fluids, IR band profiles 77−36237
methane-d_1, dipole moment, rot. depend., IR-IR double reson. obs. 79−81298
methane-d_1, high resolution spectra, line intensities, ground-state rot. const. determ. 80−83517
methane-d_1, in Jupiter, D/H and C/H ratios determ. 78−28572
organic compounds continued
methane-d_1, laboratory rotational spectrum and upper limits on abundance in (OMC-1) 80−56705
methane-d_1, obs. on Saturn 79−25543
methane-d_1, solid, ^{13}C and ^1H NMR, spin conversion obs. 77−20731
methane-d_1, tunnelling states and nuclear spin conversion 79−10944
methane-d_1(-d_2,-d_3), solid, struct. of phase III from thermodynamic meas. 79−82193
methane-d_1 absorpt. spectrum in 6000-12000 Å region 77−42318
methane-d_2, IR spectrum, ν_2 and ν_8 bands, rot. struct. and consts. 77−27066
methane-d_2, orientational ordering and tunnelling states meas. 79−10963
methane-d_2, rotation-vibration constants, C−H bond length 79−94055
methane-d_2, vibr. energy transfer, laser-induced fluoresc. 79−13753
methane-d_3, activation, dissoc., internal energy distrib., trajectory calcs. 77−4899
methane-d_3, vibr. energy flow, fluoresc. 78−82770
methane-d_3 + inert gas, vibr. deactivation, laser-induced fluoresc. obs. 77−42377
methane-d_3-polyatomic gas mixture, vibr. energy flow, fluoresc. 78−82770
methane-d_4, ν_2 and ν_4 IR bands meas. and anal. 80−18851
methane-d_4, ν_2 Raman band anal. 79−31536
methane-d_4, adsorbed on graphon, neutron scatt. study 79−60640
methane-d_4, B_0 determ., from ν_3 Raman band and IR spectrum 77−88455
methane-d_4, critical behaviour at orientational order-disorder transitions, neutron scatt. 77−43308
α-methane-d_4, crystalline, X-ray powder diff. study 80−96500
methane-d_4, IR laser sideband obs., ro-vibr. struct., isotope shifts, line widths 79−72306
methane-d_4, isotope effect on rot. and vibr. consts. 79−22688
methane-d_4, laser sideband spectroscopy *(German)* 79−26975
methane-d_4, low temp. phase, X-ray study *(Russian)* 80−33985
methane-d_4, quantum crystal, growth from melt at low temps. 78−31319
methane-d_4, rotational transition in condensed Xe, 6K, optical excitation 78−60494
methane-d_4, selectively excited, cooling, vibr.-vibr., vibr.-translational relax. 80−33723
methane-d_4, solid, lattice parameters and thermal expansion for different phases 78−51526
methane-d_4, solid, phase I, II, acoustic phonon dispersion curve meas. by neutron inelastic scatt. 78−2212
methane-d_4, solid, rot. tunnelling, neutron scatt. obs., isotope effect 80−92468
methane-d_4, solid, sound velocity meas., 4-77K 78−75734
methane-d_4, solid, thermal cond. calc. 78−51753
methane-d_4, solid, thermodynamic props. calc. using significant structures method, 6 to 87K 80−24616
methane-d_4, solid, tunnel splittings, heat capacity meas. 80−96451
methane-d_4, solid, US attenuation, phase transitions 79−51204
methane-d_4, Stark effect, rot. transitions in vibr. ground state, isotope shift 79−27029
methane-d_4, vibr.-translational relax. 80−99537
methane-d_4+Ar, vibr.-translational relax. 80−99537
methane-d_4+methane, vibr. relaxation 80−99537
methane-d_4+NH(ND), ($b^1\Sigma^+$) states quenching, kinetic isotope effects 77−63891
methane-d_4 *(Russian)* 80−91540
methane-d_4 monolayer films on graphite, neutron diffr. studies of phases 80−96739
methane-d, 4.5 μm absorpt., $2\nu_6$ overtone band anal. 80−91557
methane-d, Doppler-free optical double reson. spectroscopy using single-freq. laser and modulation sidebands 80−68274
methane-d+methane-d_4 (inert gas), vibr. relax. time meas. by photoacoustic effect 77−88541
methane-ethane liq. mixture, phase equilib., heat of mixing, vol. change, data evaluation 80−15233
methane-ethane liquid mixture, field-depend. excess electron mobility 77−89822
methane-ethane-propane-butane, binary and multicomponent mixtures, viscosity, diffusion coeffs. 78−94883
methane-H_2, in packed bed, heat and mass transfer, axial mass dispersion 78−75200
methane-H_2 mixture, D isotope enrichment by flow discharge exposure 78−13343
methane-H_2 mixture properties for hydrogen supplementation of natural gas 80−45781
methane-H_2 system in plasma reactor, exptl. and thermodynamic investig. *(French)* 78−15698
methane-He-Ne stabilised ring laser, freq. stability calcs. *(Russian)* 78−9401
methane-hydrogen mixture, flow through glass bead bed, axial dispersion coefficients 79−46378
methane-I plastic crystal, surface modes 78−71926
methane-Kr, liq., Soret coeff. at low temp. 77−89565
methane-Kr, mixture self-diffusion of Kr, density depend. 77−76587
methane-Kr mixtures, rot. self-diffusion and spin-lattice relax. *(Russian)* 79−69745
methane-methane interactions, expansion of intermol. energy in set of symmetry-adapted functions 80−106371
methane-methane-d_2+cl, free radical chain reaction, D isotope photochem. enrichment 79−36790
methane-N_2, gas, vibr. relax. time by US meas. 79−98852
methane-N_2, liq., N_2 Raman scatt. parameters, high resolution coherent active spectroscopy 80−66207
methane-N_2, rapidly developing discharge, streak camera records interpretation 80−59280
methane-N_2 mixture, US propag. vel. up to 40 kbar, additivity deviation 77−42959
methane-N_2-H_2 gas mixtures, RF discharge, vibr. and rot. anal. of CN, N_2 and C_2 78−5241
methane-N_2-isobutane gas mixture composition by Raman spectra 80−87124
methane-n-butane mixtures, triple-values dew-point curve, Redlich-Kwong eqn. of state 77−39659
methane-n-butane-decane, heterogeneous flows of multi-component mixtures in porous media−review 78−59471
methane-n-pentane-2,3-dimethylbutane, tricritical point obs., opalescence 77−76562
methane-Na_2*(AΣ) 79−98204

organic compounds continued
methane-Ne mixture breakdown obs. 78−67553
methane-O_2, solid mixture, electron diffraction study *(Russian)* 78−83953
methane-O_2 aquamechanical foam, propag. characts. of detonation waves 78−31713
methane-O_2 mixture, laser initiated combustion 80−55661
methane-O_2-N_2 mixtures, prediction of propagating laminar flames 79−52663
methane-O_2-N_2 premixed flat flame, ruby laser-induced gas breakdown thresholds 79−1951
methane-O_2-N_2Cl_2 mixture for CO_2 gasdynamic laser 77−50649
methane-propane(pentane)(n-heptane)(n-decane)(H_2S) mixtures, densities calc., van der Waals model 78−79740
methane-SF_6, single-photon absorption reaction chemistry in solid state 77−73454
methane-SF_6 mixture, CO_2 laser induced multiphoton dissociation and chemilum., laser fluence depend. 79−57233
methane-stabilized He-Ne laser, low n noise laser tube characts. *(Japanese)* 78−25891
methane-trifluoromethane, liq.-liq. phase equilib., crit. phenomena 78−18764
methane/H_2 mixing ratio in Neptune stratosphere 80−51692
methanediol, bond length distortions and torsion pots., ab initio calcs. 79−6836
methanes, $^{12}CH_4$ and $^{13}CH_4$, IR spectra obs., anal of v_2+v_3 band 80−95614
methanes, halogenated, interacting segment model for elec. tensor props. 78−5111
methanes, halogenated, nonlinear optical polarisability, bond-bond interaction role 78−18010
methanes, solid, heat capacity, possible dimens. effect 78−75844
methanes, substituted, +F HF IR chemiluminesc., H abstraction rel. rate consts. 77−86319
methanes, substituted, calculation of proton chemical shifts by INDO approximation method 79−45657
methanes, substituted, internal torsion modes, inelastic neutron scatt. 77−19104
methanes, substituted, Kerr consts., depolarisation ratios and hyperpolarisabilities meas. 78−25624
methanes+CsF, rot. inelastic collisions, mol. beam meas. 80−1049
methanesulphonyl chloride, geom. struct., CNDO/2 calc., comparison with CF_3SO_2Cl 79−81295
methanethiol, ab initio force consts., anharmonic vibr. 78−21898
methanethiol+Cl_2, laser-initiated chain reactions, rates, mechanisms, chemiluminesc. obs. 80−55651
methanethiol+OH radical, reaction rate const., 299-426K 77−40525
methanetrithiol, pyrolysis, dithioformic acid prod. and microwave spectra 78−58671
1,6-methano(10)-annulene, mol. geom. and gas phase thermodynamic props., minimisation scheme 78−78829
1,6-methano-[10]annulene, electron excitation, electron resonance, triplet states 79−54976
methanoic, acid, ideal gas thermodynamic props. 78−51275
methanol:chromium acetylacetonate, NMR, degenerate transitions, selective excitation transfer and separated relax. meas. 78−80235
methanol, ^{13}C spin-lattice relax., cross correlation of rot. motion 79−42855
methanol, β-irrad., radical truck struct., electron spin-echo obs. 80−93776
methanol, ab initio calcs. of K-shell ionisation potentials 77−18784
methanol, ab initio force consts., anharmonic vibr. 78−21898
methanol, absorption spectrum, LiF F_2^+-centre laser intracavity spectroscopy appl. 80−32999
methanol, adsorbed on CsCl(Br)(I), IR spectrometric obs. *(French)* 78−46343
methanol, adsorbed on graphite, proton mag. relax. times obs. 77−51590
methanol, adsorpt. on lunar soil 15081,2, microcrystallinity determ. 77−87292
methanol, adsorption, on activated wood charcoal 79−28973
methanol, adsorption and decomp. on Al, UPS, XPS and thermal desorption obs. 79−82441
methanol, adsorption and decomp. on Ni (100) 80−66876
methanol, adsorption and decomposition on W 77−31887
methanol, adsorption in GaAs(110) surface, UPS study 80−6632
methanol, adsorption on water-adsorbed alkali halide *(Japanese)* 78−18897
methanol, adsorption on ZnO powder, electron spectrosc. obs. 79−52076
methanol, AES, chem. state effects, for water and simple organic cpds. 78−72687
methanol, alcoholic electrolytic solutions, Dielectric constants 79−99813
methanol, and $-d_{1,3,4}$, thermodynamic props. struct. and spectroscopic data 77−39396
methanol, and -d_1, -d_4, photoelectron spectra, internal rot. in ground ionic state 77−65509
methanol, and deuterates, dissoc. ionisation mechanisms, photoionisation mass spectra, ionic struct., interstellar formation 79−3503
methanol, and dimer, CNDO/2 calcs. of O-H stretching vib. freqs. and intensities 77−18927
methanol, aq., radiolysis, CIDNP, methoxy radical involvement 78−53223
methanol, aqueous, damped coupled oscillator model used to study Fermi resonance 80−69152
methanol, as energy source, large-scale prod. from biomass 79−52864
methanol, boiling, on Cu surface, rel. to H_2O 78−90654
methanol, C-O-H bending mode in α- and β-forms at 85K 77−8588
methanol, catalytic decomp. on NiO, mol. beam relax. spectrometry using surface temp. modulation 79−29401
methanol, CD_2HOH, CH_2DOH, CW optically pumped, submm. laser action, 100 to 900 μm 79−929
methanol, CH_3OH and CD_3OH, far IR laser lines, optically pumped by CO_2 laser 78−90415
methanol, charged fragments, structure and stability 78−90085
methanol, chemical state effects in AES 78−92566
methanol, chemisorption and decomp. on Pd 77−63953
methanol, chemisorption on Ni(111), methoxy species, electron energy-loss spectra 79−29391
methanol, chemisorption on Ni (111), decomposition, UPS and flash-desorption exam. 77−55455
methanol, coherent anti-Stokes Raman spectra in UV 77−46567

organic compounds continued
methanol, collision-induced rot. energy transfer, M-resolved microwave double reson. 79−6955
methanol, Compton profile meas., non-additivity of elastic and inelastic X-ray scatt. 78−43953
methanol, condensed multilayers, electron bombard. effects, AES lineshape anal., XPS, and desorption meas. 80−7450
methanol, coord. bond calcs. 80−58129
methanol, correlation between chem. shift and charge for OH 77−18946
methanol, dielec. props., 10 MHz-70 GHz, 10-40°C 78−43769
methanol, dielectric const. in mag. field 79−78606
methanol, diffr. limited CW optically pumped laser 77−54727
methanol, dissoc. ionisation mechanism, correlation diagram approach, mass spectra obs., metastable processes 80−95728
methanol, double resonance Stark spectrosc., Doppler-free, using acousto-optic modulator 79−44935
methanol, droplet evaporation, modelled by wet porous sphere, heat-transfer meas. 78−59268
methanol, droplet vaporisation in moderately-high temp. stationary media, Chang model 78−34609
methanol, dry-electron localisation, impurity trapping, solvated electron rate consts. 79−1990
methanol, effect of hydrogen bonding on Raman spectrum 79−18197
methanol, effect of small additions of water struct., from permittivity obs. 78−9937
methanol, electron impact dissoc., optical emission from fragments 77−83750
methanol, electron solvation, ps laser study 80−101032
methanol, emission from Orion A, ang. size lower limit 77−13429
methanol, enantiomers, racemic mixture nucleation 78−26677
methanol, equilib. struct., general valence force field, SCF ab initio calcs. 77−3265
methanol, evaporating droplets in vert. hot air tunnel, radiative transfer effect 79−46400
methanol, excitation of acoustic radiation by pulsed proton beam *(Russian)* 77−80580
methanol, excited by CO_2 laser, sub-Doppler optoacoustic spectrum 80−5545
methanol, far IR laser, intracavity pumped by TE CO_2 laser 80−87382
methanol, far IR laser gas absorption obs. with and without DC field 79−31870
methanol, far IR laser line obs. and assignment 79−31867
methanol, far IR laser lines pumped by CO_2 laser sequence lines 78−9369
methanol, far IR laser resonator for TEM_{00} mode operation 78−66847
methanol, far IR laser transitions, small signal gain meas. 78−22114
methanol, field ionisation, geometry changes, INDO-SCF-MO calc. 77−38614
methanol, film condensation inside pipes, heat transfer, general correlation 79−46312
methanol, free O-H overtone absorpt. in vis. region, thermal lensing spectra 77−34644
methanol, gas thermal conductivity, H-bonds, tetramer form. 77−34776
methanol, gaseous and dil. soln. in nonpolar solvent, lattice models, association consts. 79−82141
methanol, glassy matrix, absorpt. spectra after X-irrad., solvated electrons 79−65903
methanol, H bonding, electronic struct., geometries, moments, dimerisation energies, charge distrib., pseudopotential calcs. 80−27942
methanol, H diffusion, neutron radiography study, results review 78−59961
methanol, H-bonded struct., IR spectra, assignments 78−62800
methanol, heat pipe working fluid, crit. heat/mass transfer 78−42517
methanol, high power optically pumped CW laser, line assignments 77−54701
methanol, high temp. n, γ-radiolysis *(Russian)* 79−61890
methanol, in carbon tetrachloride, permitt. meas. by time-domain spectroscopy 77−43926
methanol, in PMMA sheets, case II swelling and transport kinetics 78−76922
methanol, incipient boiling characteristics at atmospheric and subatmospheric pressures 78−90688
methanol, influence on ferric yield of Fricke dosimeter 78−11736
methanol, intermolecular interaction energies calcs. using minimal basis sets 80−78681
methanol, internal rotation barriers, exchange energy and orbital orthogonality effects 77−75049
methanol, interstellar, 84.5 GHz and 96.7 GHz lines obs. in Sagittarius B2 and Orion A 80−62245
methanol, interstellar, two new transitions obs. in Orion A 79−25667
methanol, interstellar masers, search for microwave emission 78−32543
methanol, ion internal energy selection by angle-resolved mass spectrometry 80−53164
methanol, ionic dissoc., photoelectron-photoion coincidence spectroscopy 80−66774
methanol, ionic solvation, spectroscopic study *(French)* 79−70363
methanol, IR absorption using opto-acoustic rapid scan Fourier spectroscopy 79−30585
methanol, IR complex refr. index spectra, FT interferometry, errors in liquid-cell expts. 77−87814
methanol, IR multiphoton photolysis, OH and CH form., rovibronic relax. 78−68902
methanol, IR spectra in soln., OH group fundamental and first overtone bands *(French)* 77−27071
methanol, laser-induced decomp., comparative obs. using pulsed HF and CO_2 lasers 80−11888
methanol, liq., compressed, self-diffusion, NMR spin-echo meas. 77−77122
methanol, liq., Compton profile at 60 keV 79−47535
methanol, liq., diamagnetism, mass mag. suscept. meas., temp. depend. 80−97054
methanol, low-lying excited states, improved virtual orbital calcs. 77−14372
methanol, methyl group, ^2H quadrupole coupling const. by high-resolution NMR spectroscopy 78−25563
methanol, minimal basis set localised orbitals, conjugate gradients method calcs. 79−6849
methanol, mm emission lines obs. in Orion A 77−2477
methanol, mol., nucl. spin-spin coupling const., Hartree-Fock calc. 80−9618

organic compounds continued
methanol, mol. and cluster Auger spectrum calc., SCF core-valence-valence spectra 80−48045
methanol, molecular correlation energies, estimation from semi-transferable orbital correlation energies 78−82650
methanol, molecular geometry optimisation, variable metric method, internal geometry 80−95744
methanol, molecular laser, optically pumped, development 78−13732
methanol, multiphoton absorpt. and dissoc. 80−99530
methanol, multiphoton absorpt. of intense HF laser radiation 80−23475
methanol, multiphoton decomposition with laser, isotope separation 79−66306
methanol, multiphoton UV photodissoc. 78−50602
methanol, nonlinear optical polarisability meas. 79−54991
methanol, optical pumping of far-IR molecular lasers by CW CO_2 waveguide laser 80−83615
methanol, optical-optical double reson., CO stretching band origin, assignments 79−31864
methanol, optically pumped, assignment of weak FIR laser lines 80−14320
methanol, optically pumped, far IR laser lines meas. and assignments 79−22939
methanol, optically pumped, laser line assignment 77−54698
methanol, optically pumped CW far IR laser frequency characteristics 77−38873
methanol, optically pumped CW for IR laser lines, freq. meas. 80−58514
methanol, optically pumped CW subMM emission lines 80−95876
methanol, optically pumped laser, IR-FIR transferred Lamb dip spectra 80−1193
methanol, optically pumped sub mm laser design 77−14757
methanol, optically pumped submm. wave amplification 78−29941
methanol, oxidation to formaldehyde, effect of Al_2O_3 additives on catalytic activity of Cr_2O_3-Mo_2O_3 catalysts *(Russian)* 79−66346
methanol, oxidation to formaldehyde in fluidized bed, Fe-Mo/SiO_2 oxide catalyst 79−100440
methanol, partial at. charges calc. from ab initio mol. electrostatic pots. 78−70739
methanol, phonon MFP formula, H bond collisions, low temp. 77−35655
methanol, photolysis, IR multiphoton decomposition processes 78−3358
methanol, photolysis of vap. using IR laser 79−39160
methanol, polymers, structs., binding energies, LCAO SCF MO calcs. 77−83498
methanol, positronium form., unsolvated electron effects 78−17826
methanol, processes of photoionisation studied using ion-electron coincidence method 80−74204
methanol, pure liq. and soln., Raman and IR intensity, polymerisation degree *(French)* 79−28740
methanol, Rayleigh linewidth, in crit. region 79−24329
methanol, refr. index, temp. depend., deviation from Lorentz-Lorenz formula 77−40200
methanol, second virial coeff. meas. using new apparatus 80−44289
methanol, solar thermal energy storage utilising $CaCl_2$-methanol thermochem. cycle 80−30587
methanol, solid, phase behaviour up to 3 kbar by DTA 77−76528
methanol, solubility in liquid O_2, estimation by Preston-Prausnitz method 80−39285
methanol, solvated electron lifetime and reaction with hydroxymethyl radical, dose and base effects 78−20043
methanol, solvated electron yield and spur decay following electron irrad. 78−20042
methanol, solvated electrons, optical spectra and model potentials 80−30318
methanol, solvation in water, discrete, continuum and discrete-continuum models 78−73130
methanol, solvent crazing of polystyrene, micromechanics 77−12680
methanol, solvent crazing of polystyrene, structure 77−12681
methanol, surface reaction with Cu (100), EELS study 80−16728
methanol, thermal cond. meas. by transient hot wire method 77−30144
methanol, thermodynamical Gruneisen parameter, press. depend. 78−14479
methanol, total energy, MOs nonempirical minimum STO-4LGF calcs. 78−9074
methanol, trace detection using phase fluctuation optical heterodyne spectroscopy 80−68266
methanol, trace gas detection, using IR laser 79−43653
methanol, US studies of mol. relax. 78−22790
methanol, UV multiphoton dissoc., photofragment fluoresc. 80−14165
methanol, valence photoelectron spectra, vibr. and vibronic struct. 78−50581
methanol, vap., rot. spectrum, 8-50 cm^{-1}, 293K 79−72305
methanol, vapour, effect of adsorpt. on surface oxidised activated C, paramag. props. 77−32238
methanol, vibr. dephasing theories, test using selective coherent ps. Stokes scatt. 80−59609
methanol, vibrational dephasing time of subgroup, transient stimulated Raman scatt. 78−37718
methanol, viscosity meas. at 353 to 463K and corresponding vapour press. 77−69107
methanol+Ar(Kr), methoxy radical prod., UV emission spectra 80−91572
methanol+CH_n^+, (n=Q-4), reactions at 300K 78−44357
methanol+Cl, absolute rate consts., 200-500K, stratospheric chem. appl. 79−66271
methanol+H_2^+, dissoc. charge transfer reaction studied at rel. translational energies from 600 eV to 5000 eV 80−104432
methanol+H(2S), collisional quenching, mass spectral obs. 78−25685
methanol+He^+, dissoc. charge transfer reaction studied at rel. translational energies from 600 eV to 5000 eV 80−104432
methanol+HF, mol. electrostatic pot., H-bonds, CNDO/2 calc. 77−61822
methanol+methanol, potential well depth estimation method 79−86034
methanol+OCS, rot. energy collisional transfer, M-depend., microwave double reson. 78−46435
methanol+OCS, rot. energy transfer, microwave-microwave double resonance 77−19016
methanol+water mixtures, solubility of AgCl 77−47579
methanol 118 μm laser line, simple accurate method for wavelength meas. 80−106554
methanol (-d), H-bonding investigated with supersonic mol. beam using photoionisation quadrupole mass spectrometer 80−102543
organic compounds continued
methanol (d_3), OH stretch fund., torsion-rot. levels, IR spectra obs. 80−32711
methanol adsorbed on Ag (110) catalyst, oxidation 78−88556
methanol adsorbed on Si/SiO_2 surface, light scatt. from clusters 79−33721
methanol adsorbed on ZnO powder, appl. of XPS method for surface anal. 78−40104
methanol adsorption on CrVO, IR spectra *(Russian)* 79−51435
methanol adsorption on Cu(110), XPS, UPS and thermal desorpt. study 80−84388
methanol and deuterated methanols, vibr. energy transfer probabilities, breathing-space theory 79−86039
methanol and deuterates, H^+, H_2^+, and H_3^+ kinetic energy distribs., electron impact dissoc. ionisation, time of flight mass spectra 80−32843
methanol aqueous soln., temp. depend. of dielec. relax. time *(French)* 77−59509
methanol CW optically pumped waveguide far IR laser, 10 to 100 mW, design and perform. 79−31934
methanol dehydrogenase, spin echo powder ENDOR, line shape aspects 79−34485
methanol derivation from lignite, fuel appl. 80−61223
methanol dimer, intermol. function from ab initio calcs. 80−32629
methanol far IR CW laser, Stark effect, large freq. tuning and resolved structures 79−45931
methanol far IR laser, CW laser pumped, saturated and small signal gain calc. 80−58521
methanol far IR laser, optically pumped, Stark effects 79−72552
methanol far IR laser, twin optically pumped, for plasma diagnostics 80−59306
methanol far IR laser emission spectroscopy 80−58524
methanol far IR laser gas, CW laser pumped, gain 80−69367
methanol far IR laser line Stark splitting obs. 80−58313
methanol far IR Stark spectroscopy and 9-P(34) CO_2 laser line 80−69145
methanol far-IR laser, optically pumped, intracavity polarization modulation 80−23726
methanol fuel, substitution of large proportion of diesel fuel in diesel engines 80−61230
methanol fuel for vehicles, gas turbines, and boilers, Brazil 80−61229
methanol glass, H atom abstraction by methyl radicals, 15-100K, limiting rate const. rel. to tunnelling 77−60037
methanol glass solvated electrons, EPR, ^1H spin flip satellites, geometrical model 80−7146
methanol in stratosphere, positive ion chemistry 78−57251
methanol laser, 118 μm, diagnostic experiments and modelling 80−58515
methanol laser, CW, optically pumped, 170-μm emission, press. shift 80−106510
methanol laser, CW far IR optically pumped, anisotropic gain 77−61944
methanol laser, optically pumped, use of crystalline reflector in cavity 80−64080
methanol laser, twin optically pumped far IR, use in plasma diagnostics 80−54049
methanol masers in Orion, interferometric and multitransitional study 80−67891
methanol mol., microwave linewidth parameter 79−31508
methanol molecule enxlosed in β-quinol clathrate, mol. reorientation, diele meas. 78−2026
methanol motor fuel, technico-economic study 79−74512
methanol optically pumped 118.8 μm laser line, Stark splitting obs. 80−102710
methanol optically pumped laser, frequency instability meas. at 70.5 and 118 μm 80−1254
methanol reaction with Ru (110) surface, thermal desorpt. meas. 78−31685
methanol solns., IR spectroscopic detection of free lone-pair groups or terminal methanol mols., PMR 79−19869
methanol solution in benzene, dielec. relax. time by RF cond. meas. 80−71302
methanol solvation of Ag, geometrical model, electron spin-echo modulation obs. 80−63682
methanol sorption effect on cross-linked polyester film struct. *(Russian)* 80−59405
methanol subMM laser line obs. 80−58523
methanol vapour, HF laser irrad., visible luminesc. 77−46593
methanol vapour, isothermal Joule-Thomson coefficient, equation of state 80−24119
methanol waveguide laser radiation modulation by Stark cell 77−38962
methanol-2-methyltetrahydrofuran glasses, electron solvation conversion, pulse radiolysis obs. 77−77795
methanol-2-methyltetrahydrofuran mixed glasses, annealed, γ-ray produced electrons transfer from IR to bisible traps 80−11440
methanol-^{13}C, torsion-rotation transitions, C-O stretch fundamental, FIR spectra obs. 79−93998
methanol-β-quinol clathrate, orientation and reorientation dynamics, dielec. and NMR obs. 79−99783
methanol-acetonitrile, excess vol. and isentropic compressibility, from density and US vel. meas. 78−79776
methanol-acetonitrile, solns., H bonding, IR and Raman band profiles 77−42320
methanol-benzene mixtures, adsorption on organophilic montmorillonites, effect of surface modification 78−84056
methanol-benzene solutions, adsorption on carbon 78−14568
methanol-Br_2 solution, InP substrate etching and polishing appl. *(Slovak)* 78−56576
methanol-carbon tetrachloride, binary soln. with mol. assoc., interdiffusion anal. 79−55912
methanol-carbon tetrachloride, soln., Raman spectra in OH(OD) stretching region *(French)* 79−26986
methanol-chlorobenzene, isobaric vap.-liq. equilib. 79−73299
methanol-chloroform mixtures, thermodynamic props. 79−87865
methanol-CO-H_2O-NH_3 solid mixture vibr. modes, IR spectra 80−90504
methanol-cyclohexane, crit. mixture, single and multiple light scatt., autocorrel. spectroscopy 77−85734
methanol-cyclohexane, mixture, thermal expansion near crit. soln. point 78−71871
methanol-cyclohexane film, crit. temp. and coexistence-curve determ., optical meas. 77−7952
methanol-cyclohexane soln., crit. exponents *(Russian)* 79−77766
methanol-d_0($-d_1$)($-d_4$)+H_2O(D_2O), D exchange reaction, thermodynamics 78−94328

organic compounds continued
methanol-d_1, ^{13}C-D quadrupole coupling const., ^{2}H-NMR spectra 77−481
methanol-d_1, (CH_2DOH), microwave torsional-rot. spectrum, rel. to interstellar search 80−99498
methanol-d_1, CH_2DOH optically pumped CW far IR laser lines and frequencies 80−102707
methanol-d_1, CO_2 laser pumped, CW far IR laser lines 79−76672
methanol-d_1, H-bonded in soln., ν_s(OD) band 79−18183
methanol-d_1, laboratory freqs. of J=2-1, a-type transitions 80−63624
methanol-d_1(-d_4), far-IR internal rotation spectrum 80−47989
methanol-d_3, CO_2 laser pumped, CW far IR laser lines obs., 34.5 to 287 μm 78−71082
methanol-d_3, multiphoton absorpt. and dissoc. 80−99530
methanol-d_3, optically pumped, CW far IR laser lines obs. 78−79005
methanol-d_3(d_1) in freon 11, self-associated, OH frequency temp. depend. 80−37809
methanol-d_4, 869 micron laser transition 78−42328
methanol-d_4, dissoc. following photoionis., using coincidence spectrometer 79−54998
methanol-d_x, optically pumped, new FIR laser lines 79−72553
methanol-d, CO_2 laser pumped, CW laser lines obs. 80−53272
methanol-d, optically pumped CW subMM emission lines 80−95876
methanol-dioxan system, US vel., compressibility, complex form. 79−82283
4:1methanol-ethanol, glass transition rel. to press. depend. of viscosity 80−34171
methanol-ethanol, vapour-liquid equilibrium, transpiration method meas. 79−99305
methanol-ethanol (n-propanol)(n-butanol) binary systems, excess vol. of mixing, dilatomitric meas. 80−59656
methanol-ethanol mixture, dielectric const. composition depend. rel. to struct. effects 79−11378
methanol-ethylacetate system, vapour-liquid equilib. meas., automatic gas chromatographic anal. *(German)* 78−88667
methanol-H_2O, liq., Compton profile at 60 keV 79−47535
methanol-H_2O, liq., zero-angle X-ray scatt., conc. depend. 79−27897
methanol-H_2O matrix, 77K, electron solvation and presolvation, electron spin-lattice relax. 79−57260
methanol-H_2O mixture, evaporating droplets in air, temp. modelling *(German)* 80−2243
methanol-methyltetrahydrofuran glass:β-naphtholate, electron solvation, laser flash photoionis. compared with pulse radiolysis 79−74405
methanol-n-heptane, elec. resistance, crit. phenomena, freq. depends. 79−60884
methanol-nitrobenzene-iso-octane, US vel. and absorpt., along line of plait points in ternary liq. 78−79669
methanol-O_2 flame, combustion and ionisation 79−20357
methanol-proton acceptor binary systems, hydrogen bonded, anharmonicity of OH stretching vibr. 77−6772
methanol-pyridine base systems, excess enthalpies of mixing 79−42255
methanol-water, assoc. mixture, rot. barrier solvent effect, CNDO/2 calc. 78−29861
methanol-water, binary mixtures, nucleation 80−44305
methanol-water, heat of mixing, high-press. calorimetric obs. *(German)* 78−16797
methanol-water, liq., Verdet const., pulsed mag. field meas. 80−16012
methanol-water, nucleate boiling heat transfer, conc. depend. 78−87249
methanol-water (propylene glycol), proton medium effects, ferrocene redox couple reference obs. 77−77786
methanol-water mixture, Compton profile meas., non-additivity of elastic and inelastic X-ray scatt. 78−43953
methanol-water mixture, nonlinear acoustic coeff. meas., 0-50°C *(French)* 80−34142
methanol-water soln. permeability of cellulose membrane 78−11557
methanol-water vapour, condensation in presence of inert gas 77−80051
methanol-water-air mixing, in perforated disc type stirring cascade, power dissipation, mechanism and correlation 79−1238
methanols, labelled, proton T_1 in presence of intramol. rots., intermol. relax. rate 80−2656
methine dyes, spectral props., solvent effects 80−69181
methiodides of nitrogen heteroaromatics, frequencies of multiple charge transfer bands 79−94009
methionine, automated synthesis of ^{11}C-labelled radiopharmaceuticals 80−17133
methionine sulfoxide in protein, ^{13}C NMR anal., method and expt. obs. 80−56305
methotrexate-dihydrofolate reductase complex form., conform., laser Raman obs. 80−104553
2-methoxacyclobutane, mol. struct., electron diffr. obs. 80−1065
methoxide surface complexes on Li, He(I) photoelectron spectra, MO calcs. 80−83417
methoxide-d_0(−d_3) anion, electron affinity, vibr. struct., photodetachment electron spectra 78−94282
methoxy, Jahn-Teller induced rovibronic effect, nuclear spin-electron spin hyperfine Hamiltonian 80−83298
methoxy+NO, reaction rate upper limit, laser induced fluoresc. 80−85200
p-methoxy benzonitrile, IR absorpt. spectra, vibr. assignments 80−95609
methoxy free radical, laser mag. reson. submillimetre spectrum, linear Zeeman effect 77−46579
methoxy prod. from methyl nitrite photolysis 80−85200
methoxy radical, LMR spectra anal. 80−63677
methoxy radical+NO, reaction rate meas. 80−76534
methoxy radical and deuterate, vibronic level fluoresc. spectrum 80−58305
methoxy radical fluoresc. spectra induced by laser, UV region 79−59498
methoxy radical prod. from 266 nm photolysis of methyl nitrite 80−76534
methoxy species on Ni (111), photoelectron spectra, electronic struct. and orientation 80−83420
methoxy thiomethyl methane 79−50037
4-methoxy-4′-azoxybenzene, nematic liq. cryst., elasticities and viscosities, light scatt. meas. 79−4245
p-methoxy-β-methylstyrene, triplet lifetime meas. by electron transfer interception 79−79269
methoxy-amyltolane, orientation-statistical props. studies by optical methods *(Russian)* 79−77518
p-methoxy-benzoate-p-n-pentylbenzene, isotropic phase nematogen optical Kerr const. 80−78919

organic compounds continued
methoxy-benzylidene-alkyl-cinnamates, smectic mesophase, ESR of spin probes, nonunique ordering 77−47344
p-methoxy-p′-alkyl tolanes, Raman scatt. in isotropic, nematic, and solid phases *(French)* 77−15309
p-methoxy-p′-alkyltolanes, molecular arrangement in solid state *(French)* 77−51364
p-methoxy-XY-p′-alkyl tolanes, mol. struct., packing coeffs., and thermal stability 78−95046
methoxyamyltolane, nematic phase orientation mol. ordering determ. by Raman scatt. *(Russian)* 79−19153
3-methoxybenzanthrone in ethanol, photoprotolytic reactions, spectra, rate consts. and lasing thresholds 80−43327
methoxybenzene+OH^-, gas phase reaction, 299-435K kinetics and mechanism 78−11515
p-methoxybenzilidenebutylaniline, nematic, domain pattern changes in electric field 77−1079
p-methoxybenzoate-p′-n-pentyl benzene, slow non-critical mol. reorientation in isotropic phase 80−84062
p-(p′-methoxybenzylidene)amino-phenyl acetate, cryst. struct. rel. to liq. crystallinity 80−100225
p-methoxybenzylidene-cyanoaniline, mol. and cryst. struct., X-ray diffr. study 80−88134
p-methoxybenzylidene-p′-alkyl anilines, Raman scatt. in isotropic, nematic and solid phases *(French)* 77−15309
methoxydifluorophosphines-d_0 and -d_3, IR and Raman spectra, mol. vibr. and struct. obs. 80−87103
2-methoxyethanol, methyl torsional barriers to internal rotation calc. 80−95603
2-methoxyethanol-1,1,2,2-tetrachloroethane binary system, isobaric vapour-liquid equilib. data 79−46792
2-methoxyethanol-chlorobenzene binary system, isobaric vapour-liquid equilib. data 79−46792
2-methoxyethylomine, microwave spectra, H-bond, torsional motion and mol. vibr. obs., rot. isomerism, mol. moments determ. 80−95603
methoxyfluorane, effect on conductivity and time of adhesion of lipid membranes 79−53070
methoxynaphthalene, fluoresc. quenching by inorganic anions 78−74694
3-methoxynaphthalide, cryst. and mol. structure. 77−31654
3-methoxypropionitrile, microwave spectrum, rot. conformer, rot. consts., vibr. state 77−14419
8-methoxypsoralen detection in ocular lens, rel. to psoriasis treatment with photosensitising agent 78−15937
12-methoxypyridine, phosphoresc. emission, polarisation and lifetimes 78−31232
methoxytrifluorosilane and -d_3, IR and Raman spectra, vibr. anal., barrier to internal rot. 79−18185
methoxytrimethylsilane-$d_{0,9}$(−d_3) 78−86853
methy propionate-H_2O(Ba^{2+}) mixtures, in DMSO, acetonitrile solns. IR, assoc., solvent, catalytic effects *(French)* 79−87827
methyl(-d_3) ions, association reactions, isotopic exchanges, SIFT study, review 80−58435
methyl(-d) radical recombination rate const. calcs. in low press. limit 77−4891
methyl 2,3:4,5-di-O-isopropylidene-α-D-glucoseptanoside, struct. determ., X-ray and neutron diffr. study 79−42050
4-methyl 2,6 di-tertiary butyl phenol, gamma-irradiated, electron-methyl group dynamical interactions 77−43161
4-methyl 2,6-di-tertiary butyl phenol, change in barrier to methyl group rotation near cryst. surface 78−38634
methyl 2-bromopropionate, IR and Raman liq. phase spectra, rot. isomerism 78−58680
methyl 2-chloropropionate, IR and Raman liq. phase spectra, rot. isomerism 78−58680
methyl 4(l-pyrenyl)butyrate, decreased stabilisation energy of excimers and exciplexes in polymer matrices 80−25431
methyl (CH_3D) group tunnelling in solids, quantum model rel. to two T_1 temp. depend. minima 78−2028
N-methyl acetamide, geometry from ab initio calcs., rel. to formamide, N-methylformamide and acetamide 80−23338
methyl acetate, liq., proton spin-lattice relax., temp. depend. 78−39435
methyl acetate, microwave spectra and internal rot. 80−87100
methyl acetate+CH_3^+(CD_3^+) reactions, products mass spectra obs. 77−63901
methyl acetylene, IR absorpt. intensities 79−10103
methyl acetylene, Kerr consts., depolarisation ratios and hyperpolarisabilities meas. 78−25624
methyl acetylene, mm emission lines obs. in Orion A 77−2477
methyl acrylate, He I and He II photoelectron spectra, CNDO/S calcs. 78−55201
methyl acrylate, poly(vinyl alcohol)-based membranes for haemodialysis *(Japanese)* 78−96115
methyl alcohol, adsorbed on silica, low temp. thermally stimulated depolarisation spectra fine struct. 79−78611
methyl alcohol, and -d_3, far IR spectra of internal rot. 78−5222
methyl alcohol, and deuterated forms, complete freq. coverage for submm. laser spectroscopy 78−25860
methyl alcohol, angular distrib. of scatt. press. to carrier press. ratio 77−27942
methyl alcohol, assignment of submillimetre laser transitions 79−22943
methyl alcohol, detect. of new interstellar transitions 77−60808
methyl alcohol, dielec. relaxation spectroscopy in microwave region, double-beam interferometry *(German)* 80−71309
methyl alcohol, dil. aq. soln., US vel., 4.04 MHz 78−67770
methyl alcohol, intermol. interaction, thermodynamic parameters determ. from chem. shifts of functional groups 79−64068
methyl alcohol, internal rot. barrier, energy decomposition anal. 77−75327
methyl alcohol, interstellar, obs. 79−25666
methyl alcohol, IR-microwave double reson., CO_2 laser pumped 79−64024
methyl alcohol, IR-microwave double reson. of mol. 79−64023
methyl alcohol, liq., ratio of Brillouin to total light scatt. intensity 78−52515
methyl alcohol, liq., viscosity parameters, RF cond. meas. 80−96677
methyl alcohol, liquid, under high press., refr. index vs. density 79−28712
methyl alcohol, molecular FIR laser design, freq. tunable by Stark effect 80−5750
methyl alcohol, optically pumped, far IR laser line assignment 77−38869

organic compounds continued
methyl alcohol, optically pumped, new CW FIR laser lines meas. and assignments 80−48224
methyl alcohol, optically pumped far IR laser, spectroscopy appl. 77−5932
methyl alcohol, photoacoustic spectra meas. at CO_2 laser wavelengths 80−18849
methyl alcohol, sound vel. meas. at 5 to 20 kHz in small-volume cells 78−9516
methyl alcohol, superheated liquid, growth of spherical bubbles, anal., numerical calcs. 77−24399
methyl alcohol, Townsend coeffs. of avalanche counter gases 78−78582
methyl alcohol, US attenuation, for vol. viscosity, 0-60°C 78−63871
methyl alcohol, US attenuation temp. depend. in associated liq. 77−51441
methyl alcohol, US attenuation temp. dpeend. in associated liq. 77−51441
methyl alcohol gaseous, diode laser spectra of C-O stretch band 79−59449
methyl alcohol high-power optically-pumped CW laser line assignment 77−38868
methyl alcohol IR transitions, saturated absorption spectroscopy 77−38874
methyl alcohol laser, freq. meas. at 4.25 THz using Josephson harmonic mixer and phase lock techniques 80−95078
methyl alcohol submm wave laser, optically pumped, intracavity double resonance obs. 80−58522
methyl alcohol-CO_2 far i.r. laser with metal-dielectric waveguide, Stark effect obs. 77−700
methyl alcohol-d_3, Fermi resonance due to large amplitude vibrs. 80−83519
methyl alcohol-d, optically-pumped laser line freqs. 78−55345
methyl alcohol-n-heptane, crit. resist. of binary liq., 10 Hz-100 kHz 78−76123
methyl allenyl sulphide, UV absorpt. spectra, role of 3d valence-shell and 4s Rydberg-type atomic orbitals 80−83384
methyl amine, photodissoc. products, Doppler spectroscopy 80−53124
methyl ammonium aluminium sulphate, ferroelec., proton spin-lattice relax. time anomaly 80−60440
methyl ammonium alums, dielec. behaviour and ferroelectricity 79−38431
methyl ammonium chloride, Raman spectra, 70 to 300K, H stretching vibrs. 80−20628
methyl ammonium compounds with $Nb_{10}O_{28}^{6-}$, mol. config. 77−71886
methyl aniline, photoionisation by vac. UV laser *(Russian)* 78−9205
methyl anilines, IR spectra, 250-4000 cm^{-1}, vibr. anal. 78−62797
methyl anion, geometric struct., electron correlation effects, self-consistent electron pairs 78−22050
methyl azidoformate, microwave rot. spectrum, satellite transitions 80−69127
methyl bromide, ^{13}C relaxation times anal. using J-diffusion model of mol. reorientation 80−87149
methyl bromide, ν_6 band, CO_2 and N_2O laser Stark spectroscopy 78−78698
methyl bromide, and isotopic modifications, rotational spectrum in vibr. ground state 79−54853
methyl bromide, far IR laser lines, rot. anal. of ν_6 perpendicular band 77−3359
methyl bromide, l-reson. perturbations in overtone and combination vibr. systems 80−52962
methyl bromide, liq., NMR relax., anisotropic mol. reorientation 78−2764
methyl bromide, mol. force field at SCF ab initio levels, quantum-mechanical calc., LCAO-MO method 80−106319
methyl bromide, NQR and A_1-A_2 splitting, RF spectrosc. inside laser cavity 80−91579
methyl bromide, optically pumped submillimetre laser characts. *(Russian)* 79−68384
methyl bromide, photoabsorption and photodissociation, 190-300 nm 79−50038
methyl bromide, pressure-broadened linewidths in microwave region, temp. depend. 77−34694
methyl bromide, pure rot. spectrum, fundamental and $\nu_3=1$ levels *(French)* 77−18919
methyl bromide, rot. absorption spectrum of ν_3 and $2\nu_3$ excited vibr. states, mol. consts. determ. 78−82732
methyl bromide, rot. spectrum, microwave region *(Russian)* 78−70823
methyl bromide, rot. Zeeman effect 79−54909
methyl bromide, sub mm laser, generation lines identification *(Russian)* 78−82952
methyl bromide, submillimeter rotational spectrum, laser generation line identification 79−64210
methyl bromide+Cl→HCl+CH_2Br, IR laser isotope separation appls. 79−64113
methyl bromide+K→KBr+CH_3, yields, crossed mol. beam study 79−34293
methyl bromide+Rb→RbBr+CH_3, yields, crossed mol. beam study 79−34293
methyl bromide delayed depolarisation obs. *(Russian)* 79−95703
methyl bromide-^{81}Br+nonpolar perturber, JK0,0-1,0 line broadening 77−6848
methyl bromide-methyl iodide solid soln., NQR investig. of impurity distrib. 77−12222
methyl carbonate-benzene, binary liq. soln., surface cluster functions 78−67631
methyl cation, force consts., ab initio calcs. with differentiated estimation of integrals 77−67974
methyl cation+$H_2(N_2)(O_2)(CO)(CO_2)$, ternary assoc. reaction, rate coeffs., 100-300K 79−61845
methyl cation+NH_3, reaction kinetics, 0.04-1 eV *(French)* 80−66768
methyl cation-He interaction energy, nonempirical calc. 78−86799
methyl chloride, ν_1 band absorpt. strengths 77−75226
methyl chloride, ab initio force consts., anharmonic vibr. 78−21899
methyl chloride, ab initio SCF-MO calc., electronic and mol. struct. 78−25425
methyl chloride, absorption strength of perturbed ν_4 band 78−70833
methyl chloride, Auger electron spectra and chem. shift 78−90231
methyl chloride, charge distrib., substituents effect 80−905
methyl chloride, cryst., Raman band anomalous splitting, isotope effects 77−8562
methyl chloride, far IR laser lines, vibr. isotopic shift value 78−42055
organic compounds continued
methyl chloride, inner-shell excitation and EXAFS-type phenomena 79−13828
methyl chloride, liq., NMR spin-lattice and dielec. relax. 79−33604
methyl chloride, microwave spectrum of excited vibr. states, Coriolis coupling, rot. consts. 77−14420
methyl chloride, mode-matching model of collisional-induced vibr. transitions 77−10735
methyl chloride, mol. force field at SCF ab initio levels, quantum-mechanical calc., LCAO-MO method 80−106319
methyl chloride, pressure-induced shift of the J=0→1 transition, 193 to 366K 77−14497
methyl chloride, rot. anal. of IR absorpt. spectra, mol. vibr., rot. const. determ. 80−99505
methyl chloride, vacuum UV absorpt. spectrosc., Rydberg transitions obs. 80−5561
methyl chloride, Zeeman effect, mag. moments and susceptibility, nuclear shielding 79−13764
methyl chloride+T* reaction, methyl abstraction to substitution ratio 78−85187
methyl chloride in stratosphere, conc. profile up to 32 km. altitude 80−36368
methyl chloride optically pumped submillimetre laser characts. *(Russian)* 79−68384
methyl chloride-d_3, 9.4 μm region laser Stark spectrum, ν_2 and ν_5 bands 77−27112
methyl chloride-d_3, activation, dissoc., internal energy distrib., trajectory calcs. 77−4899
methyl chloride-NH_3, positive ion molecule reactions 79−24729
methyl chloroform, atmospheric residence times rel. to HO tropospheric concs. 78−32140
methyl chloroform, impact on stratospheric O_3 78−53722
methyl chloroform, vap., multiphoton dissoc. by CO_2 laser beam 80−61123
methyl chloroformate, struct., microwave, Raman, far IR and NMR spectra 77−34614
methyl compounds, rotational tunnelling, temp. dependence 80−38970
methyl compounds with hindered rot. ^{13}C spin-rot. relax. times 79−50049
methyl cpds., MeP, MeS, isolated CH stretching freq., bond strength, bond length 78−90167
methyl cyanide, anomalous Senftleben effect *(Russian)* 78−71415
methyl cyanide, CH_3CN and CH_3NC, ^{14}N quadrupole coupling consts., ab initio calcs. 80−58283
methyl cyanide, far IR laser line assignments 80−69380
methyl cyanide, intracavity pumped submm wave laser, CW 77−88741
methyl cyanide, IR rot.-vibr. spectrum, ν_2 and ν_3 and ν_4 bands anal. 77−75159
methyl cyanide, isotopically substituted species, IR spectra, vibr. freq. displacements, harmonic pot. function 78−42057
methyl cyanide, Kerr consts., depolarisation ratios and hyperpolarisabilities meas. 78−25624
methyl cyanide, linewidth parameters in rot. spectrum, multiple differentiation calcs. 79−98070
methyl cyanide, liq., NMR spin-lattice and dielec. relax. 79−33604
methyl cyanide, microwave rot. spectra, mol. consts. 77−34615
methyl cyanide, mm emission lines obs. in Orion A 77−2477
methyl cyanide, molecular FIR laser design, freq. tunable by Stark effect 80−5750
methyl cyanide, submm. rot. spectra in ground vibr. state *(Russian)* 77−34636
methyl cyanide, vibr. relax., Raman overtone band obs. 77−14436
methyl cyanide+Cs(K), collisional ionisation obs. 80−95716
methyl cyanide (-d_3), vib. dephasing, Raman obs. 77−59566
methyl cyanide and isocyanide, microwave spectra, harmonic force field and r_z struct. 79−36627
methyl cyanide submillimetric waveguide laser amplifier design and operation 77−38926
methyl cyanide-Ar mixture, thermal cond. in mag. field 80−100058
methyl cyanide-carbon tetrachloride solutions, anisotropic light scatt., interactions between solvent and solute mols. 78−27239
methyl cyanide-CO_2 far i.r. laser with metal-dielectric waveguide, Stark effect obs. 77−700
methyl cyanide-water (methanol), Ag^+ ion solvation, γ-irrad., ESR obs. 80−97726
methyl cyanides and isocyanides, isomerisation, ab initio (STO-3G) geometry optimised calc. 78−46265
1-methyl cyclohexanol, struct. information from OH-stretching freqs., axial/equatorial hydroxyl ratio 79−72438
1-methyl cytosine: 5-fluorouracil X-irrad. at 300K, EPR 78−64941
N-methyl diformamide, excited singlet and triplet states, CNDO-CI calcs. 77−26990
methyl ethyl ether, charact. vibrs., isomer and isotope effects, rel. to reverse spectral problem 80−63613
methyl ethyl ketone, processes of photoionisation studied using ion-electron coincidence method 80−74204
methyl ethyl ketone-n-heptane-toluene ternary system, bubble pt. equilib. compositions determ. from dew pt. meas. 79−77733
methyl fluoride, $^{13}CH_3F$, high-power pulsed laser 80−69386
methyl fluoride, ab initio force consts., anharmonic vibr. 78−21899
methyl fluoride, charge distrib., substituents effect 80−905
methyl fluoride, coord. bond calcs. 80−58129
methyl fluoride, CW optically pumped far IR laser with variable output Michelson coupler 78−55372
methyl fluoride, deuterated, optically pumped near-MM laser 80−69379
methyl fluoride, Dicke superradiance obs. in far IR emission 77−38841
methyl fluoride, diffr. limited CW optically pumped far IR laser 77−54727
methyl fluoride, double-ended unstable resonator submillimetre laser characts. 79−81461
methyl fluoride, harmonic force field calcs. and exptl. configs. 80−63865
methyl fluoride, high-power narrow-linewidth linearly pumped oscillator-amplifier system 77−54726
methyl fluoride, IR spectra deconvolution in real time 77−38034
methyl fluoride, laser, 496 μm line, freq. meas. 77−42557
methyl fluoride, laser collision-induced energy absorpt. and vibr. excitation 80−74233
methyl fluoride, mol. force field at SCF ab initio levels, quantum-mechanical calc., LCAO-MO method 80−106319
methyl fluoride, molecular FIR laser design, freq. tunable by Stark effect 80−5750

organic compounds continued
methyl fluoride, optically pumped mirrorless laser at 496 μm 79−31871
methyl fluoride, passive Q-switching of CO_2 laser 78−9402
methyl fluoride, rot. absorpt., Stark modulation expt. 79−59396
methyl fluoride, second-order Coriolis resonance between ν_2 and ν_5 states, microwave spectra 78−74646
methyl fluoride, solid, IR and Raman spectra, cryst. struct., and deutero deriv. 77−36218
methyl fluoride, stimulated emission at 9.75 μm following two-photon excitation 78−42323
methyl fluoride, tunable diode laser spectroscopy, 9-10 μm 77−54558
methyl fluoride, vibr. transition moments and force fields, gaussian basis set calcs. 79−81152
methyl fluoride+methane, intermol. vibr. energy transfer, double reson. investig. *(Russian)* 77−61839
methyl fluoride laser far IR pulse generation by Q-switched CO_2 laser pump source 80−69383
methyl fluoride laser pumped with continuously tunable multiatm. CO_2 laser 80−69421
methyl fluoride pulsed high-power laser development 77−38872
methyl fluoride Raman FIR laser, high-intensity CO_2 laser pumping, new emission lines 80−23675
methyl fluoride-d_3, optically pumped sub-MM wave laser 80−23676
methyl fluoroformate, isomer conformation, CNDO and ab initio STO calcs. 80−58151
N-methyl formamide, isotopically enriched, isotropic and nematic phases, NMR spectra 77−32270
methyl formate, microwave spectra, rot. consts., moments and struct., radio astronomy appl., review 80−17637
methyl formate(-d_1,d_3,d_4), mol. vibr. spectrum, struct., beginning with PCILO calc. *(French)* 80−23401
methyl formate and isomeric acetic acid, Compton profiles 77−30928
methyl furan-2-carboxylate, skeletal vibr. of IR spectra, conformational props., solvent polarity effect 80−87118
methyl furan-2-thiolcarboxylate, skeletal vibr. of IR spectra, conformational props., solvent polarity effect 80−87118
methyl glyoxal, $^3n\pi^*$ states, ab initio STO-3G CI calcs., ΔE_{SCF} transition energies 78−94194
methyl glyoxal, electron affinity at centrosymm. trans geometry 80−87225
methyl green-DNA binding, linear dichroism anal. 77−88479
methyl group, ^{13}C chemical shifts, H/H, H/Me and Me/Me interactions 80−95652
methyl group, ^2H quadrupole coupling const. by high-resolution NMR spectroscopy 78−25563
methyl group, calc. of optimal orientation in crystals 77−89392
methyl group, conform. problems, correlation effects 79−97999
methyl group, NMR relax., spin rot. and chem. shift anisotropy effects 78−31117
methyl group, NMR relax. due to dipolar interactions 77−14455
methyl group, proton spin relax. due to intermol. proton coupling, reorientation 78−25564
methyl group, proton tunneling reson. at low temp. 80−108087
methyl group dynamics, NMR 78−29802
methyl group hinderance barrier, spin-rot. relax. times 80−53011
methyl group internal rot., pot. barrier and activation energy, absolute rate theory 79−79220
methyl group nuclear spin symmetry species, torsional relax. 79−60287
methyl groups, adsorption on Li, complex form., STO calcs. 77−9124
methyl groups, detection of proton NMR at arbitrary temps. of tunnelling system 78−39432
methyl groups, electric dipole moment, perpendicular component, orbital calcs. 77−68138
methyl groups, reorientation in solids, nonexponential Zeeman relax. 78−6589
methyl groups, tunnelling, proton second moment, signal-to-noise ratio effects 78−70766
methyl groups correlated quantum rotation effects on ESR spectra 77−18948
methyl groups in solids, proton spin-lattice relax. mechanisms at low temp. 77−51982
methyl groups in solids, reorienting and tunnelling, spin-lattice relax. 80−50217
methyl groups in solids, tunnelling freq. for internal rotation in pot. function 80−49134
methyl halide+inert gas, vibr. relax. transition rates, anharmonicity effects 79−89747
methyl halide+K, ion pair form., vibr. energy depend. 79−34287
methyl halide ions, unimol. dissoc. and internal conversions, coincidence meas. 77−6869
methyl halides, candidate transition identification for optically pumped far IR lasers 79−931
methyl halides, force consts. evaluation using gp. vibrs. and centrifugal distortion consts. 80−9580
methyl halides, harmonic force fields, high-low freq. separation calcs. 78−90067
methyl halides, liq., orientational dynamics, local coherence 77−27805
methyl halides, low energy mol. Rydberg states from Feshbach reson. spectra 77−34768
methyl halides, mol. force field at SCF ab initio levels, quantum-mechanical calc., LCAO-MO method 80−106319
methyl halides, mol. force fields, IR intensities, and vibr. props. 80−47879
methyl halides, photodecomp., primary products and secondary reactions 77−90624
methyl halides, Raman spectra and lattice motions 77−77197
methyl halides, second dielec. virial coeffs. *(German)* 79−32729
methyl halides, semiclassical theory for collision induced vibr.-rot. transitions 80−63767
methyl halides, vibr. energy relax., opto-acoustic obs. 80−95711
methyl hypochlorite-d_0, -d_3, microwave Zeeman spectra, dipole moment, nuclear quadrupole tensor 77−459
1-methyl indole, UV absorpt. spectra, low-lying Rydberg band 77−58037
methyl indoles, UV and IR absorpt. spectra, f-values and ground state vibr. freqs. 78−58716
methyl iodide, ^{13}C, NMR spectra, transition intensities, off-resonance proton spin decoupling influence 80−74183
methyl iodide, ^{13}C NMR with coherent proton decoupling, peak-height distortions within spin multiplets 79−31547
methyl iodide, ^{13}C relaxation times anal. using J-diffusion model of mol. reorientation 80−87149
organic compounds continued
methyl iodide, and -d_1, dissolved in nematic phase, C-H bond orientation, ^{13}C NMR 78−46371
methyl iodide, and deuterated, pulsed subMM lasers pumped by CO_2 laser 80−106511
methyl iodide, biexciton states, IR absorpt. exam. 77−89714
methyl iodide, $CH_3{}^{131}I$, radioactive, airborne, diffusion coeffs. 79−2142
methyl iodide, dense liq., mol. reorientation and shear viscosity 77−4213
methyl iodide, diffr. limited CW optically pumped far IR laser 77−54727
methyl iodide, dissolution into aqueous NaOH solns., fission reactor accident conditions 77−88236
methyl iodide, in 3-methyl pentane glassy matrix, γ-radiolysis and effects caused by aggregation 78−64864
methyl iodide, in Ar, 0.25-1.38 gm cm^{-3}, VUV absorpt. spectra, Rydberg excitations 77−79627
methyl iodide, in Ar and Kr, medium perturbations of extravalence excitations, VUV absorpt. 78−1002
methyl iodide, liq., A_1 modes, vibr. relax., temp. depend. Raman spectra obs. 80−32806
methyl iodide, liq., expt. comparison with rough sphere rot. diffusion model 78−30532
methyl iodide, liq., mol. reorientation, dielec. and viscosity meas. 80−100157
methyl iodide, liq., Raman meas. of transversal angular velocity correlation function 79−87422
methyl iodide, liq., vib. relax., A_1 Raman bands 77−40220
methyl iodide, liquefied gas solns. bound exciton model for Rydberg bands 78−31214
methyl iodide, liquid, rough sphere rot.-diff. model, relax. times 77−15294
methyl iodide, mag. circular dichroism, mol. Rydberg transitions 78−66573
methyl iodide, mag. hyperfine struct. of quadrupole spectra *(Russian)* 77−34622
methyl iodide, mol. force field at SCF ab initio levels, quantum-mechanical calc., LCAO-MO method 80−106319
methyl iodide, molecular FIR laser design, freq. tunable by Stark effect 80−5750
methyl iodide, optically pumped sub mm laser design 77−14757
methyl iodide, pulsed photodissociation laser, transverse current, characts. 78−50767
methyl iodide, rot. microwave spectra, nucl. quadrupole, spin-rot. and nucl. shielding tensors 78−42040
methyl iodide, Rydberg states, quantum defect theory applic. 80−32700
methyl iodide, solns. with liq. Ar, Kr, Xe, CH_4 and CF_4, Rydberg band positions, temp. depends. 78−17686
methyl iodide, UV absorpt. spectra, ionis. limit region, assignment 78−21940
methyl iodide, van der Waals mol., electron self-scavenging 80−95727
methyl iodide, vib. relax. and Raman line widths 77−32359
methyl iodide+alkali metal reaction cross section energy depend. 77−28991
methyl iodide+K(Rb), reaction cross sections 78−40043
methyl iodide+Na, anisotropic interactions from double rainbow struct., interaction pot. meas. 80−99540
methyl iodide delayed depolarisation obs. *(Russian)* 79−95703
methyl iodide FIR laser gas, passive Q-switching of CO_2 laser 80−1246
methyl iodide in CCl_4, vibr. energy redistrib. after ultrashort IR excitation 77−6894
methyl iodide ion, dissociation, induced by collision with Kr atom, mass spectra *(Russian)* 77−88549
methyl iodide mol. nonlinear resonant interaction with pulsed subMM radiation *(Russian)* 80−99523
methyl iodide photodissoc. laser, kinetic model, cross-section calcs. 80−58530
methyl iodide removal by Ag impregnated Al and zeolite 78−53719
methyl iodide-acetone liq. mixture, excess energy of vaporisation, US study 80−65209
methyl iodide-d_0, (−d_3), two-photon reson . ionis. spectra 80−28071
methyl ion, electrostatic force theory appl. to mol. geometry ab initio verification 79−98002
methyl ion+H_2O(He) ternary association reaction in energy range 0.04-0.1 eV 80−71896
methyl ion+HD(D_2), isotopic exchange, interstellar implications 80−61087
methyl isocyanate, isomerisation RRKM theory using effective strong collision freq. 78−44365
methyl isocyanide, and ^{15}N derivative, microwave spectra in $4\nu_8$ state 77−83582
methyl isocyanide, CO_2 laser induced isomerisation 78−35644
methyl isocyanide, intracavity CW dye laser state-selective activation of isomerisation 78−11533
methyl isocyanide, Kerr consts., depolarisation ratios and hyperpolarisabilities meas. 78−25624
methyl isocyanide, laser induced thermal isomerisation, obs. by new time resolved IR photographic technique 80−57400
methyl isocyanide, laser initiated thermal isomerisation, thermal explosion 78−80725
methyl isocyanide, laser initiated thermal isomerisation, time behaviour of CN radicals 80−11887
methyl isocyanide, microwave spectrum, anal., N isotope effects 77−50430
methyl isocyanide, N isotope enrichment, IR laser isomerisation 79−27096
methyl isocyanide, thermal decomp., unimol. reaction theory 78−80712
methyl isocyanide, thermal explosion, scaling laws 78−15676
methyl isocyanide, thermal isomerisation in presence of at. gases, vibr.-translational energy transfer 78−23924
methyl isocyanide, unimol. isomerisation to methyl cyanide 79−24725
methyl isocyanide, vacuum UV photodissociation spectroscopy 79−834
methyl isocyanide photodissoc., cyanide radical energy partitioning chemical laser determ. 78−73063
methyl isocyanide photoisomerisation, laser isotope separation, C-isotope enrichment by one-photon vibr. photochemistry 80−81336
methyl isocyanide-d_2, IR spectrum, rovibr., ground state struct. 78−25537
methyl isonitrile, chemisorption on Fe (110), UV photoelectron obs. 78−19629
methyl isothiocyanate, in benzene (tetrachloromethane), nonlinear dielectric solvent effect 79−28702

organic compounds continued
5-methyl isoxazole, microwave spectrum internal rot. barrier 78−58665
3-methyl l-butanethiol, Raman and vibr. IR spectra of solid and liq., rot. isomerism 78−62810
3-methyl lumiflavin, in soln., absorpt. spectrum 80−58277
3-methyl lumiflavin in soln., optical absorption, theory 78−74569
N-methyl m-fluoroaniline, conformational anal., microwave spectra obs. 80−58247
methyl mercaptan, CW subMM emission lines, optical pumping 80−87381
methyl mercaptan, hot-atom synthesis on Jupiter 79−101109
methyl mercaptan, interstellar detect. in Sagittarius B2, mm wave spectrum 80−41877
methyl mercaptans, atmospheric, determ. using automatic odour analyser *(Japanese)* 80−50924
methyl mercapto acetate, Raman and vibr. IR spectra of solid and liq., rot. isomerism 78−62810
methyl mercury, in isolated estuarine sediments, growth and decay during storage 77−66937
^{203}Hg-methyl mercury chloride retention in man after inhalation 77−9277
methyl meristotropate, mol. and cryst. struct. 78−95047
methyl methacrylate, free radical polymerisation, viscosity effects 77−81404
methyl methacrylate, oligomers, dielectric relax., end-group effects 78−92019
methyl methacrylate, poly(vinyl alcohol)-based membranes for haemodialysis *(Japanese)* 78−96115
methyl methacrylate, polymerisation in toluene in presence of s-PMMA 78−76321
methyl methacrylate+diallyl phthalate, two-step copolymerisation, light focusing plastic rod prep. *(Japanese)* 79−37064
methyl nitrile CW for IR mol. laser, optical pumping with $^{16}CO_2$ and $^{18}CO_2$ lasers 80−74343
methyl nitrite, internal rotation temp. frozen in supersonic jet, matrix IR spectroscopy 80−9594
methyl nitrite, IR multiphoton dissoc., time resolved IR emission from prods. 78−29822
s-methyl nitrite, methyl group rot. barriers in cis and trans forms, ab initio calcs. 80−74111
methyl nitrite, N-isotope separation by multiphoton dissoc. in intense IR field 77−68086
methyl orange, aq. soln., reson. Raman spectra of D and ^{14}N isotopes 80−91566
methyl orange, trace amount determ. by reson. Raman spectroscopy *(Japanese)* 79−48017
methyl oxirane, centrifugal distortion consts. and struct. parameters calcs. 77−34616
2-methyl pentanediol 2, 4, associated liq., correl. between acoustic and dielectric relaxation times 78−9925
methyl peroxy radical+NO, rate const., flash photolysis and kinetic spectroscopy 79−70305
methyl peroxynitrate, UV absorpt., spectra, photodissoc. lifetime meas. 80−83386
methyl piperidines, PMR spin-lattice relax. times and lineshapes, 100-300K 77−81027
methyl protons, NMR relax. in presence of chem. exchange 78−13515
N-methyl pyrrole, resonantly enhanced multiphoton ionisation 80−106362
methyl radical, ab initio projected unrestricted Hartree-Fock calcs. 78−58582
methyl radical, HeI photoelectron spectrum, Franck-Condon factors 77−34692
methyl radical, hyperfine coupling, in ground and excited states, Green's function calcs. 77−6692
methyl radical, hyperfine coupling consts., vibr. depend., ab initio calcs. 80−87150
methyl radical, isotropic hyperfine coupling consts., temp. depend., nuclear vibrs. 78−35039
methyl radical, vibr. excited, photofragmentation IR emission obs. 80−87162
methyl radical+ethylene(acetylene)(propene)(allene), reaction pot. surfaces, MINDO/3 calcs. 79−22601
methyl radical+O_2 (NO), mass spectra, absence of reaction in combustion system 78−53195
methyl radical+O(F), infrared chemiluminescence obs. 80−61080
methyl radical and anion, electron affinity determ., ab initio SCF and CI calcs. 78−5149
methyl radical decay in methanol glass, accumulation and dark decay kinetics 79−74352
methyl radical in glassy organic matrices, electron spin-lattice relax. 78−76312
methyl radical in sodium acetate, EPR spectra, anisotropic hyperfine interaction, rot. tunnelling 80−34775
methyl radicals, reactions behind shock waves, UV absorpt. obs. 78−46362
methyl rotator in isotropic fluid, motional asymm. determ. from ^{13}C spin dynamics 77−69718
methyl salicylate, vapour phase, absorption and fluorescence spectra 79−81232
methyl selenocyanate, and isotopic forms, microwave spectrum 79−13705
methyl substituted antimony chlorides, $(CH_3)_xSbCl_{3-x}$, lone pair electrons, ^{121}Sb Mossbauer spectroscopy study 80−39984
methyl sulphoxide, photoacoustic spectra meas. at CO_2 laser wavelengths 80−18849
methyl symmetric stretching vibr. bandwidths, vibr. and reorientational effects, IR and Raman spectra 78−78686
2-methyl tetrahydrofuran radical formation on liq. phase γ-radiolysis 77−60080
methyl thionine chloride, intramol. vibr. spectra 80−977
N-methyl thiopropionamide-N-d_3, normal coord. calcs. 79−36598
N-methyl thiopropionamides, normal coord. calcs. 79−36598
methyl thiyl radical, emission spectrum, collisional quenching 78−13543
methyl toluates, o-, m-, and p-, NMR spin energy transfer using zero mag. field, spin echoes 79−95675
methyl torsion modes, vibrational optical activity, inertial contrib. 80−5524
methyl transfer reactions, Marcus theory 80−21279
methyl trichloroacetate, soln., dielectric props. and relax. mechanisms at microwave freqs. 78−15089

organic compounds continued
γ-methyl valerophenone, photolysis, biradical form., lifetime, interaction with O 77−60086
methyl vinyl ether, and -d_3, IR and Raman spectra, vibr., torsion and internal rot. 78−94250
methyl vinyl ether, microwave spectrum, quartic centrifugal distortion and rot. consts. 79−10099
methyl vinyl ether, rot. Zeeman effect, g-values, mag. susceptibility, quadrupole moments 77−490
methyl vinyl sulphide, rotational isomerism, variable temp. photoelectron spectroscopy appl. 77−6846
methyl vinyl sulphide, syn-gauche equilib., force field and ab initio calcs., microwave and Raman spectra 80−23573
methyl viologen, chlorophyll a sensitised reduction in non-ionic micelles 79−1962
5-methyl-10-phenylphenazine, in 3-methylpentane (ethanol) (PMMA), radiationless processes, temp. depend. 80−43087
cis-3-methyl-1,3-pentadiene-1,2-d_2, nonrandom isomerisation, internal energy relax. 79−70313
3-methyl-1-butene+OH, absolute rate consts. 78−23927
2-methyl-1-propanol, liq. struct. at 20°C 79−32873
5-methyl-1-thia-5-azacyclooctane-1-oxide perchlorate, single cryst. transform., evidence for intermediate state 80−88078
4-methyl-2,6-di-tert-butylphenol, γ-irrad. cryst., ENDOR transitions, ELDOR detect. 78−95531
4-methyl-2,6-di-tert-butylphenol, methyl group rot. mechanisms, Raman effect 78−71691
4-methyl-2,6-di-tertiary butylphenol, gamma-irradiated, effect of radiation damage on hindered methyl group rotation 77−35494
4-methyl-2,6-ditert-butylphenol, temp. depend. of methyl tunnelling spectrum by inelastic neutron scatt. 79−51015
4-methyl-2,6-ditertiarybutyl phenol, proton spin relax., 80-340K methyl rot. 79−78553
4-methyl-2,6-ditertiarybutylphenol, flip-flop motion and spin symmetry conversion of methyl groups 77−15326
4-methyl-2,6-ditertiarybutylphenol, methyl group reorientation, classical dynamics, NMR relax. and inelastic neutron scatt. 80−88066
4-methyl-2,6-ditertiarybutylphenol, proton spin-lattice relax. and activation energies of tunnelling CH_3 groups 77−48071
4-methyl-2,6-ditertiarybutylphenol, tunnelling methyl groups, EPR 79−4723
4-methyl-2,6-t-butylphenol, γ-irrad., electron-methyl group spin-spin interaction 77−85572
4-methyl-2, 6-ditertiarybutylphenol, tunnelling methyl group, inelastic neutron scatt. study 79−46580
2-1methyl-2-butene+O, (OH), reaction rate consts. meas. 78−61001
N-methyl-2-N-phenylamino-6-naphthalene sulphonates, triplet excitation, multiple fluoresc. 77−71826
2-methyl-2-propanethiol, proton abstraction by biradical scavenging, rate const. from mag. field depend. CIDNP 79−3461
1-methyl-2-pyrolidone, enthalpies and related thermodynamic functions 79−42276
1-methyl-2-thiomethyl imidazole, IR and Raman spectra, vibr. anal. *(French)* 79−45713
methyl-3-bromopropionate, liq., microwave absorption and relax. 78−60386
methyl-4-chlorobutyrate, liq., microwave absorption and relax. 78−60386
2-methyl-4-nitroaniline, nonlinear cryst., large optical second-harmonic coeff. meas. 79−76750
methyl-(2,4-dinitrophenyl)-aminopropanoate, for nonlinear optics 77−79890
1-and 2-methyl-anthrasemiquinone radicals, EPR 'reduced' spectra 80−23444
2-methyl-but-3-yn-2-ol, mol., He(I) photoelectron spectra 79−27033
β-methyl-butyl-methoxybenzylidene amino cinnamate, smectic-B liq. cryst., US attenuation anisotropy 79−55828
4-2′-methyl-butylphenyl-4′-n-octyloxybiphenyl-4-carboxylate, smectic F phase, characterisation and struct. 79−86707
methyl-containing mol. solids, proton NMR line shape, methyl group tunnelling 78−6588
methyl-d_3 ion+HD(H_2), isotopic exchange, interstellar implications 80−61087
methyl-d groups, reorienting or tunnelling spin-lattice relax. 80−97156
α-methyl-D-glucopyranoside, X-irrad., ESR and ENDOR study of free radicals 80−45526
α-methyl-D-glucopyranoside, X-irrad. cryst., radical form., EPR-ENDOR study 79−56613
6-methyl-mercaptopurine, cryst., light sensitive free radical EPR after electron irrad. 80−7167
N′-methyl-N-β-D-xylosylurea 79−94995
N-methyl-N-nitrosourea, electronic interactions with DNA, ESR obs. and INDO calcs. 80−94154
m-methyl-p-cyanodimethylaniline, ps reversible isomerisation kinetics, O_2 quenching obs. 79−5133
N-methyl-p-fluoroaniline, struct. of $HNCH_3$ group 80−95741
3-methyl-pentane glass, trapped electrons, model 77−48661
N-methyl-piperidinium-acet-meta-chloro-anilide-iodide, crystallisation from water, X-ray exam. of cryst. struct., mol. config. *(German)* 79−51095
3-methyl-pyridine, rot. pot., proton spin-lattice relax., inelastic neutron scatt. study 79−47351
2-methyl-pyrimidine, microwave spectrum, V_6 barrier, dipole moment, rot. consts. 77−3345
5-methyl-uracil, IR absorpt. spectra, vibr. anal. 78−61143
N-methylacetamide, solid, Fermi resons. 80−97266
N-methylacetamide, structure, Raman spectroscopy and neutron diffr. obs. *(French)* 80−7343
N-methylacetamide, vertical excitation energies, ab initio SCF CI calcs. 79−45647
N-methylacetamide, vibr. spectra and normal coord. calcs. 79−36632
N-methylacetamide in organic solns., dielec. const., dipole moments, monomer-dimer equilib. 80−40031
N-methylacetamide-Li^+(K^+) assoc. in aq. soln., potentiometric obs. 77−29005
N-methylacetamide-N-d_3, vibr. spectra and normal coord. calcs. 79−36632
o-methylacetophenone, laser flash photolysis, temp. depend. 80−93770
methylacetylene, ν_5 band, microwave and IR laser Stark spectrosc. 80−91558
methylacetylene, quadratic force fields, MOCIC pot. functions calcs. 80−5475

organic compounds continued
9-methyladenine monohydrochloride hydrated salts, cryst. data 77−15398
9-methyladenine single crysts., protonic cond. 77−55388
methylalkanes, CH stretching local mode anharmonicity, intramol. perturbation overtone spectra 79−18171
methylamine, ab initio force consts., anharmonic vibr. 78−21898
methylamine, affinities for $H^+(Li^+)(K^+)(CH_3^+)$, ab initio SCF calculations 80−102443
methylamine, and ^2H, ^{13}C, ^{15}N, ^{18}O isotopic derivatives, vibr. freqs. using MINDO/3 force consts. 77−71793
methylamine, aq., effect on polyethylene terephthalate, chem. stress cracking 79−57131
methylamine, C-N and N-H bond nucl. mag. isoscreening line diagrams 80−78555
methylamine, $CH(X^2\Pi)$ and $OH(A^2\Sigma^+)$, production by multiphoton dissociation, rate constant, laser induced fluorescence and chemiluminescence study 79−98135
methylamine, charge exchange mass spectrometry, HNC^+ ion recombination and ionisation pot. 78−76838
methylamine, coord. bond. calcs. 80−58129
methylamine, internal rot. barrier, energy decomposition anal. 77−75327
methylamine, IR multiphoton dissoc., NH_2 prod. fluence depend. 79−68275
methylamine, methyl group, ^2H quadrupole coupling const. by high-resolution NMR spectroscopy 78−25563
methylamine, multiphoton discoc., N isotope separation 80−35553
methylamine, multiple photon dissoc., NH_2 fragments, laser-excited fluoresc. obs. 80−11938
methylamine, multiple-photon dissociation, laser induced fluoresc. photofragment detect. 80−37840
methylamine, perturbational molecular orbital analysis 79−89608
methylamine, photochemical conversion to HCN with ArF laser, mol. fluoresc. obs. 80−97710
methylamine, total energy, MOs nonempirical minimum STO-4LGF calcs. 78−9074
methylamine, vibr.-inversion-internal rot.-rot. Hamiltonian 78−86840
methylamine+CH_n^+, (n=Q-4), reactions at 300K 78−44357
methylamine+OH radical, reaction rate const. 299-426K 77−40525
methylamine in Jupiter atmosphere, prod. and distrib. 77−64693
methylamine intercalated with 2H-TaS_2, supercond. layer cpd., crit. field enhancement and reduced dimensionality 80−60152
methylamine liquid, 293K, solvated electron decay kinetics obs., IR spectra 80−71928
methylamine proton-bound dimers, form. in ion-mol. assoc. reactions, rates analysis 77−60054
methylamine-d_1, interstellar, probable detect. 77−33610
methylamine-d_1, unconfirmed from interstellar 10 GHz obs. 79−92822
methylamine-HCl systems, H-bonded complexes studied by ab initio MO method, dipole moments determ. 80−83253
methylamine-Li solution, NMR investig. of metal-nonmetal transition 77−40142
methylamine-t_1-NH_3, β^-decay effect on H-bond, ab initio LCAO SCF MO calc. 78−76894
methylamino cation+Ca, proton transfer reaction cross sections, 1-6 eV 78−20003
2-methylamino-1-(spiro[cyclopentane-1,1′-inden]-3′-yl)ethanol hydrochloride, triclinic cell parameters from Weissenberg photographs 79−7518
methylammonium aluminium selenate dodecahydrate, dielec. dispersion and relax. 77−28515
methylammonium aluminium sulphate, third order elastic consts. from stress shifted reson. freqs. 78−55905
methylammonium aluminium sulphate dodecahydrate, ferro to paraelectric transition, low freq. dielectric behaviour 79−4770
methylammonium aluminium sulphate dodecahydrate, single crysts., high-order EPR transitions of Cr^{3+} 80−108052
methylammonium aluminiumselenate:Cr^{3+}, EPR and linewidth anomaly 77−12191
methylammonium alums, dielec. relax. near transition point 80−71301
methylammonium bromide, solid, phase transitions, PMR, DTA study 80−107421
α-methylammonium chloride, disordered, lattice vibrs. Raman spectra 77−85699
methylammonium chloride, torsional motion, harmonic oscillator and free rotor bases calcs. 79−72232
methylammonium chromium alum, single cryst., Cr^{3+} EPR, g-factor, hyperfine splitting 78−2729
methylammonium chromium selenate, lattice consts. and ferroelec. props. 79−33641
methylammonium chromium selenate dodecahydrate crystals, dielectric relaxation 80−40043
methylammonium gallium selenate, lattice consts. and ferroelec. props. 79−33641
methylammonium gallium sulphate dodecahydrate, dielec. relax. meas. 79−28677
methylammonium halides, UV exciton absorpt. bands 78−72547
methylammonium hexahalometallates (IV), halogen NQR obs. of struct. phase transition 79−95673
methylammonium ion, deuterated, NMR in lyotropic systems 79−22732
methylammonium manganese trichloride dihydrate, cryst. struct. 77−51363
methylammonium-Ga$(SO_4)_2.12H_2O$, ferroelec. alum single crysts., dielec. dispersion and characts. 79−15408
methylammoniumgallium sulphate:Cr^{3+}, EPR and linewidth anomaly 77−12191
methylammoniumtetrachlorochromate, optical absorption intensity, short-range spin correlation 80−108185
2-methylaniline, photoemission for mol., polarised photoelectrons 78−66607
N-methylaniline, UV photoelectron spectra, up to 21.2 eV 77−71831
methylanilines, far IR spectra, pot. energy barriers 80−43043
N-methylanilines, substituent effects on geometry, IR spectra obs. 79−10107
9-methylanthracene, in acetylcellulose foil, time-depend. fluoresc. anisotropy, crit. transfer distance *(German)* 78−21964
9-methylanthracene, in n-hexane, Shpolskii absorpt. spectra at 77K, vibronic struct. *(German)* 79−59507
9-methylanthracene, Shpolskii spectra, vibronic struct., fluoresc. *(German)* 79−22754
9-methylanthracene, solubilisation in water by hypercoiled polymethacrylic acid 80−91591

organic compounds continued
methylated benzene+tetracyanobenzene, fluorescent exciplex form., electronic relax. 80−5573
methylated benzene-I_2, π-σ charge transfer complex, frozen soln., Mossbauer spectra obs. 80−91655
p-methylbenzaldehyde, p-dimethoxybenzene host, dipole moments, lowest electronic states 77−18954
1, 3,5-methylbenzene, coherent polarisation spectroscopy of Raman scatt. 78−13758
methylbenzene, solid, pulsed cold neutron source, moderation props., radiation decomp. 77−83407
methylbenzene cations, photodissoc. spectra, substituent effects 78−58710
methylbenzene cations, spectroscopy, substituent effects 78−58709
methylbenzene sulphinate, vapour and soln. UV spectra, solid IR spectrum, assignments 77−50444
methylbenzenes, 3p Rydberg transitions, multiphoton ionis. spectrosc. obs. 80−95644
methylbicyclobutyl decomposition intramolecular vibr. relax., competitive channels 80−83336
7-methylbicyclo[2.2.1]-hept-2-ene-5-one, config., microwave spectrosc. obs. 80−9593
methylbixin, low-lying forbidden π-electronic state, spectral evidence 77−58029
methylborodichloride-d_0(-d_3), vibr. spectra and force constants *(German)* 79−26982
2-methylbut-1-ene, flash photolysis, β-methallyl radical extinction coeffs. 77−1938
S-(+)-4-2′-methylbutyl phenol, cholesteric derivatives, appl. in display devices 79−19145
N-methylcarbamoyl chloride(-d_1), vibr. spectra, normal coord. anal. 78−33497
methylchloramines, CH_3NHCl, CH_3NCl_2, $(CH_3)_2NCl$, UV photoelectron spectra, assignments 78−86911
methylchloride, CH_3Cl^{+}, photofragmentation at 366 nm 78−58752
methylchloride, high resoln. rot spectrum, spin-rotation and nucl. mag. shielding tensors 77−27054
methylchloroform, polymorphism, solid-solid phase transformations 77−62499
methylchloroform, vapour phase, UV absorpt. spectrum, photodissoc., stratospheric appls. 79−81208
2-methylchromone, solns., pH dependent fluorescence spectra, pK_a and tautomerism 79−59506
methylcyanide, photodissoc., CN radicals fluoresc. 79−52725
methylcyanodiacetylene cation, gas phase, UV emission spectra of $\tilde{A}(\pi^{-1})\rightarrow\tilde{X}(\pi^{-1})$ band system 80−95636
methylcyclobutane, form. by ketene (diazomethane)+cyclobutane photolyses, decomp., CH_2 vibr. energy distrib. 78−61032
methylcyclohexane:styrene-d_0, -d_3, -d_5, d_8, fluorescence meas., 77K 78−25606
methylcyclohexane, γ-irrad., isothermal luminesc. decay, temp. depend. 79−66322
methylcyclohexane, and d_{14}, evidence for two crystalline phases, low-temp. Raman spectra 79−56771
methylcyclohexane, dense liq., self-diffusion and viscosity 80−15278
methylcyclohexane, differential thermal anal. under high press. 78−51669
methylcyclohexane, trapped electron charge distribs., optical transitions 77−28139
methylcyclohexane glass, γ-radiolysis, electron tunnelling from matrix trapped biphenyl ions 79−29379
methylcyclohexane glass, trapped electrons, model 77−48661
methylcyclohexane-1,1,2,2 tetrachloroethane binary system, isobaric vapour-liquid equilib. data 79−46792
methylcyclohexane-chlorobenzene binary system, isobaric vapour-liquid equilib. data 79−46792
methylcyclohexane-polystyrene, coexistence curve, comparison obs. and free energy calc. 80−88323
methylcyclohexane-polystyrene, coexistence curves, range of simple scaling and critical exponents 80−88322
methylcyclohexane-tetramethyl-p-phenylenediamine, γ- and UV-irrad. solvent matrices at 77K, H^- fluoresc. 78−70779
(+)-(3R)-methylcyclohexanone, vibr. optical activity, Raman obs. 80−102499
trans-methyldiazene, pot. function 78−33507
methyldiborane, microwave spectra, bond lengths, dipole moments, rot. consts. 77−83579
methyldichlorosilane, Stark effect and microwave-microwave double reson., struct. *(German)* 80−47975
methyldisilylamine, and -d_3, vibr. assignment and barriers to internal rot., IR and Raman spectra 78−13496
methylene, 2^1A_1 state, CI and multiconfiguration SCF calc. 79−10052
methylene, $^1B_1$-$^1A_1$ separation, ab initio 80−106251
methylene, electron affinity, $^1A_1$-$^3B_1$ T_0-value, ab initio MRD-CI method calcs. 78−50478
methylene, electronic structure, SCEP theory calcs. 77−10579
methylene, force consts., ab initio calcs. with differentiated estimation of integrals 77−67974
methylene, geometry, SCF and CI calcs., basis set effects 78−62715
methylene, optimised geometry, CI calcs. using partitioning theory 77−38616
methylene, photoelectron spectra, singlet and triplet state calcs. 78−42127
methylene, quadruple energy, self-consistent electron pairs with higher order effects 78−46276
methylene, singlet a^1A_1 state, laser-induced fluoresc. spectrum 79−18225
methylene, singlet-triplet excitation energy, relativistic correction 80−69059
methylene, singlet-triplet separation, ab initio calcs. 78−74582
methylene, singlet-triplet separation, configuration interaction study 78−13438
methylene, singlet-triplet separation, relativistic corrections 80−32618
methylene, singlet-triplet splitting, ab initio calc. 78−5128
methylene, singlet-triplet splitting 79−100407
methylene, triplet ground state, var. and perturbational calcs. 77−61680
methylene, vibronic anal., ab initio CI pot. curves calcs. 78−50479
methylene, zero-field splitting, absolute sign, EPR determ. 77−10692
methylene+$H_2\rightarrow CH_3+H$, triplet methylene abstraction, partial open shell FSGO calc. 78−80719
methylene+$H_2\rightarrow$methane, ab initio CI calc. on SCF level, insertion reaction min. energy path 80−7774

organic compounds continued
methylene* + $H_2 \rightarrow CH_3$ + H, barrier height, CI with double zeta polarisation basis 78−64812
methylene (triplet) + CO_2, reaction rate constant determ. 77−36727
methylene (triplet) + diazomethane → CH_3, reaction rate const. determ. 77−36727
methylene anion, electron affinity, $^1A_1$-$^3B_1$ T_0-value, ab initio MRD-CI method calcs. 78−50478
methylene anion, vibronic anal., ab initio CI pot. curves calcs. 78−50479
methylene blue, due soln., photothermal spectroscopy 78−32808
methylene blue, effect on colour attenuation in Cherenkov radiation *(Spanish)* 80−7432
methylene blue, sensitiser and electron carrier for photoinduced electron transport across phospholipid wall of liposome 79−74614
methylene blue dye, dielec. const. and loss meas., 10^2 to 10^5 Hz 78−6622
methylene blue in methanol, concentrated solutions, third harmonic generation and optical characteristics by Nd laser radiation *(Russian)* 77−54753
methylene bromide, ^{13}C, NMR spectra, transition intensities, off-resonance proton spin decoupling influence 80−74183
methylene bromide-d_0-d_2, liq., nucl. spin-lattice relax., rot. correl. times 77−59476
methylene chloride, in EBBA-d_{23}, intermol. dipolar random field cross-relax. term obs. 80−60438
methylene chloride, liq., NMR spin-lattice and dielec. relax. 79−33604
methylene chloride, liq., proton spin-lattice relax., temp. depend. 78−39435
methylene chloride, microwave spectra, rot. consts. and geometric struct. 79−63990
methylene chloride, partially deuterated, NMR, T_1 meas. and anal., −96 to 40°C 78−80237
methylene chloride, sorption and diffusion in drawn low-density polyethylene 79−74210
methylene chloride HV polarisation and space charge obs. *(Russian)* 80−25277
methylene chloride-cyclohexanol system, acoustic props. 77−51450
methylene dichloride, vapour deposition, no glass transition detected by DTA 77−24388
methylene diiodide, in 3-methyl pentane, γ-radiolysis 79−24776
methylene fluoride, ν_9 fundamental band, 9.4-μm CO_2 laser Stark spectroscopy 78−9191
methylene fluoride, anharmonic pot. function and equilib. struct. 78−78774
methylene fluoride, excited vibr. state, microwave spectrum 78−58672
methylene glycol(-d_A) ⇌ formaldeyhyde(-d_2) + $H_2O(D_2O)$ Raman spectra and normal vibr. 80−58271
methylene iodide, benzene soln., spin-lattice relax., struct., dynamics 77−1610
methylene iodide, soln., MCD spectra, assignments 79−31567
methylene ion, pot. energy surfaces of excited states, ab initio GTO SCF CI calcs. 78−58602
methylene ion + $HD(D_2)$, isotopic exchange, interstellar implications 80−61087
methylene isolectronic radical, separation of two lowest states, comparison with NH_2^+ 80−53047
methylene ketene, microwave spectrum, rot. and centrifugal distortion consts., dipole moment 78−17659
methylene peroxide, multiconfig. SCF CI calcs. 80−18803
methylene peroxide, struct., energy levels, ab. initio UHF and MRUHF NO CI calcs. 80−83287
methylene phenanthrene cryst., delayed fluoresc., mag. field effect, sense depend. 77−73160
methylene radical, classical stretching dynamics 80−23400
methylene radical, vibronic bands obs. in pulsed supersonic jet 80−28024
methylene radical anion and dimer, semiempirical CNDO/2 and nonempirical SCF calcs. 77−79535
methylene radicals, rotational transitions, laser mag. resonance spectra 80−5538
methylene-bridged liquid crystals, homologous series, mol. struct. effects on mesomorphism 77−47347
4-methylene-cyclohexadiene-2,6-one-1, proton affinity, MINDO/3 results compared to ICR obs. 78−1103
methylene-d_0, -d_2, in Xe matrix, EPR, temp. depend. 78−5255
methylene-d_2 ion + $HD(H_2)$, isotopic exchange, interstellar implications 80−61087
4,4′-methylenebis(1,3,5-trimethyl-4-imidazolin-2-one), cryst. and mol. struct. 80−107201
4,4′-methylenebis(2-chloroaniline), air sampling and anal. method 79−79420
3-methyleneoxetane, electron structure, orbital-O interaction, MO calcs., UV photoelectron spectra 80−28058
methylenes, substituted, INDO calcs. 77−30782
methylenimine, ν_4 fundamental band, laser Stark spectroscopic obs. 79−64039
methylenimine, lowest excited state, singly excited config. interaction calcs. 79−59361
methylenimine, mol. struct., microwave spectra, isotope effects 77−61738
methylenimine, n→π* transition, ab initio SCF MO CI calc. 78−58584
methylenimine, photoisomerisation, SCF MO pot. surfaces 79−11772
methylethyl ketone-butanol, soln., excess thermodynamic props. and interactions, US vel. and density meas. 80−39288
methylethylketone, in soln., IR spectral, band halfwidths determ., rot. Brownian motion investig. 77−36248
methylethylketone-butanol-water-isobutadiene quaternary system, isobars of liq.-vapour and liq.-liq. equil. *(German)* 79−33079
methylethylketone-water interfacial instability, mass transfer under high press. 79−94601
methylfluoride, anomalous behaviour of proton chemical shift in gas-liquid crit. region 78−39419
methylfluoride, CW for IR mol. laser, optical pumping with $^{16}CO_2$ and $^{18}CO_2$ lasers 80−74343
methylfluoride, rot. IR spectra, line width study 79−76426
methylfluoride laser, CW, 496 microns, rate equation model, review 78−55343
N-methylformamide, cis-isomer rot. struct., IR absorpt. spectrosc. obs. 80−14138
N-methylformamide, geometry from ab initio calcs., rel. to formamide, acetamide, and N-methyl acetamide 80−23338
N-methylformamide, in carbon tetrachloride, dielec. relax., time-domain reflectometric obs. 79−4762

organic compounds continued
N-methylformamide intercalate, cryst. struct. determ. using film-scanned data 79−55729
3-methylfurane, rot. Zeeman effect, g-tensor, mag. susceptibility 77−497
methylglyoxal, fluoresc. mag. field effect 80−102535
methylglyoxal-protein complexes, hopping conduction, theory 79−24935
methylhalosilanes + $CCl(X^2\Pi)$, reaction rate const. determ. by kinetic absorpt. spectroscopy 80−97683
5-methylheptanol-3-benzenes (carbon tetrachloride), dilute solns., dielec. consts., dipole moments, H bonding investig. 77−48673
N-methylhexamethylenetetramine bromide-CuBr, solid electrolyte galvanic cell applic. 77−77775
3- methylhexane, glass, γ-irradiated, trapped electron-radical mag. energy transfer, ELDOR, cross relax. 77−16209
methylhydrazine, electrochem. oxidation on Au, appl. to gas monitoring 79−39248
methylhydroperoxide, UV absorpt. spectra of vap. 80−69159
N-methylhydroxylamine, double excitation wavefunctions, multiconfigurational SCF method 77−10604
o-methylhydroxylamine, ionisation energies, He I photoelectron spectra, orbital calcs. 77−88497
methylidyne, interstellar, obs. in AFGL IR sources 80−51856
methylidyne, interstellar obs. of 3.3 GHz ground state transitions 78−77592
methylidyne, obs. in Sagittarius B2 direction 78−65671
methylidyne (CH), interstellar, abundance and column density in post-shock gas 80−56911
methylidyne A-X, B-X and C-X systems, rotational dependence of Franck-Condon factors 78−74701
methylidyne in diffuse interstellar medium, optical and radio obs. 78−93356
1-methylimidazole complexes, with ferriporphyrins, PMR obs. 77−12214
methylimidazoles, photoelectron spectra and electronic struct. 79−22758
methylimine, double resonance Stark spectrosc., Doppler-free, using acousto-optic modulator 79−44935
1-methylindan, circular dichroism, rot. strengths, CNDO/S calc. 79−3452
5-methylindole, in PMMA matrix, high press. luminesc. 78−84629
1-methylindole-n-butanol (ethyl acetate), soln., ground state complex form., fluoresc. spectra, Stoke's shift origin 80−58299
methylisoeugenole, liq. scintillator system, energy transfer, fluoresc. intensity-max. solvent depend. 78−21966
methylisonitrile, mol.excitation by electron impact, 500 and 25-70 eV, expt. and HAM/3 79−72434
3-methylisoquinoline, quasilinear absorpt. spectrum, in Shpolskii system 77−46571
3-methylisoquinoline, semiperchlorate, H-bonding, strong, stochastic model and IR spectra temp. effects 78−62805
6-methylmercaptopurine riboside, S-substituted nucleoside, ESR and ENDOR obs. 77−36766
methylmercury, equilib. concs. in Ottawa River sediments 78−11923
β-methylnaphthalene, IR absorpt., intermol. reson. interaction, temp. depend. 78−72506
β-methylnaphthalene, kinetics and morphology of lamellar-spiral growth hillocks 78−18566
α-methylnaphthalene, scintillators activated by 1,3,5-triarylpyrazolins containing difluoromethylsulphonyl group *(Russian)* 77−52187
α- methylnaphthalene, soln., dielec. relax. and permittivity 78−64318
1-methylnaphthalene, two photon absorptivity, ion cyclotron reson. photodissoc. spectra, CNDO/S-CI-perturbation theory 80−74123
methylnitrene, symmetry restricted multiconfiguration annihilation of single excitations calcs. 78−62695
methylnitrite VUV photodissoc., NO electronically excited photofragment identification and quantum yield 80−99527
3-methylpent-4-yn-3-ol, mol., He(I) photoelectron spectra 79−27033
12-methylpentane, γ-irrad. glass, trapped electron yield, elec. field effects 77−16848
3-methylpentane, γ-irradiated, isothermal luminescence in presence of aromatic solutes at 77K 78−76519
3-methylpentane, C-H stretching diagonal local mode anharmonicity, intermol. perturbation 78−25524
3-methylpentane, glassy insulator, γ-irrad., IR enhancement of carrier radiation yield 77−76870
3-methylpentane, glassy soln., Hg sensitised UV photolysis, radical production 79−52720
3-methylpentane, refr. index, temp. depend. deviation from Lorentz-Lorenz formula 77−40200
3-methylpentane, trapped electron charge distribs., optical transitions 77−28139
3-methylpentane glass, γ-radiolysis, electron tunnelling from matrix trapped biphenyl ions 79−29379
3-methylpentane glass, electron-ion pair polarisation, γ-irrad. induced current and IR photocurrent 77−69768
3-methylpentane glass containing triphenylamine, γ-radiolysis, IR spectra, trapped electron 77−16842
3-methylpentane glassy matrix, localised electrons, cavity model 80−107743
4-methylpentane-1, liq., density, 302.55-450.80K and 0.098-68.6 MN/m^2 77−7780
13-methylpentane-d_{14}, glass, γ-irrad., solvated electron struct. obs. 77−9101
3-methylpentane-d_{14}, glass, trapped electron optical spectra, wavelength selective bleaching 79−83480
3-methylpentane-nitroethane, binary fluid, Rayleigh linewidth meas. near crit. point 78−48190
3-methylpentane-nitroethane, binary liq. mixture, crit. correlation function, universality 77−7840
3-methylpentane-nitroethane, correl. function near crit. mixing point 79−55893
3-methylpentane-nitroethane, crit. conc. fluctuations, nonexponential decay 80−44309
3-methylpentane-nitroethane, dynamical scaling and crit. point universality 80−88297
3-methylpentane-nitroethane crit. mixture, dynamical scaling for sound propag. 80−49305
3-methylpentane-nitroethane critical binary liquid mixture, US absorpt. 80−107376
methylpentanes, electron mobilities and penetration ranges in liq. and crit. regions 78−72220
methylphenylsiloxanes, density, viscosity, surface tension and crit. temps. 79−86830

organic compounds continued
methylphosphinosilane, IR and Raman spectra, vibr. assignment and asymmetric potential function 79−85962
methylphosphorous pentafluoride, CH_3PF_4, pseudorotation, quantum dynamics 77−34570
N-methylphthalimide in ethanol soln., gain and induced absorpt., struct. props. 77−24890
N-methylphthalimides, laser, lamp-pumped, solvent and temp. depend. 79−3692
2-methylPOPOP, soln., anisotropic fluoresc. of prolate mol. *(German)* 80−1018
methylpropylether, trans-trans isomer, microwave spectra, struct., dipole moment and rot. barriers calcs. 80−83348
methylpropylketone, P-v-T data, 270-670K, 1-800 bar *(Russian)* 77−39661
methylpropylsilane, vibr. spectra, normal vibrs. and rot. isomerism 79−31524
N-methylpyrazole, microwave spectrum, internal rot. barrier 78−58666
1-methylpyrene, fluoresc. quenching by Cu^{2+} in micellar system, general kinetic model 80−32753
2-methylpyridine+D_2O, p-T-X miscibility dome critical point, US vel. meas. 77−27979
methylpyridine adsorbed on Ag, surface enhanced Raman spectra 80−83376
3-methylpyridine-D_2O soln., consolute points, crit. soln. temps., light scatt. obs. 77−77230
methylpyridines, rot. tunnelling, NMR relax. and inelastic neutron scatt. 79−4733
methylpyridines, US wave propag. vel. and attenuation coeff. as functions of temp. 79−14886
5-methylpyrimidine, singlet-triplet intersystem crossing, ODMR and MIDP in matrix at 1.6K 79−50055
methylpyrimidines, fluoresc. quantum yield, methyl substitution effects 79−13757
α-bis(N-methylsalicylaldiminato)-copper (II), ^{1}H NMR spin-lattice relax. time, spin dynamics 79−99786
methylsilylene, isomerisation, lowest triplet state reaction surface studies 79−15963
α-methylstyrene, photoinduced ionic polymerisation 80−7828
1,4-Bis(2-methylstyryl)benzene, laser dye, picosec. laser obs. 79−36891
1,4-bis(2-methylstyryl)benzene, picosec. gain kinetics 79−45940
12-methylsulphonyl-1-phenylethanol, S-O interactions, conform. anal. 79−31418
2-methyltetrahydrofuran, glass, γ-irradiated, trapped electron-radical mag. energy transfer, ELDOR, cross relax. 77−16209
2-methyltetrahydrofuran, glass, trapped electron optical spectra, wavelength selective bleaching 79−83480
2-methyltetrahydrofuran glass, 77K matrix ENDOR line shape model and expt. 78−6600
2-methyltetrahydrofuran glass, solvated electrons by electron spin echo modulation spectra 79−88991
methyltetrahydrofuran glass, three-pulse echo modulation, phase reversal 77−1584
methyltetrahydrofuran-methanol glass:β-naphtholate, electron solvation, laser flash photoionis. compared with pulse radiolysis 79−74405
2-methyltetrahydrofuran-methanol mixed glasses, annealed, γ-ray produced electrons transfer from IR to bisible traps 80−11440
N-methylthioacetamide(-d_1), reson. Raman spectra obs. and mechanism 78−17672
3-methylthiomethylpropionate, liq., dielec. relax. and permittivity 80−15948
2-methylthiophene, action on Pd/Al_2O_3 catalyst, neutron effects *(Russian)* 79−20467
1-methylthymine single cryst., cond. determ. using proton-injecting solution electrodes 78−18825
methyltrifluorosilane-d_3, extended diffusion with internal rot., NMR test 79−31549
β-methylumbelliferone, amplification spectra, triplet-triplet absorpt. 77−31101
4-methylumbelliferone, excited state reaction rate, fluoresc. and decay time 77−63919
β-methylumbelliferone in ethanol solns., spontaneous luminesc. kinetics 80−74192
methylviologen, photoreduction to H_2, adsorbed on cellulose, hydrogen economy 80−81491
methylviologen reduction, photosensitised electron transport across phospholipid vesicle walls 78−80787
methylzinc methoxide, tetrameric, X-ray cryst. struct. determ. 80−107197
methyoxy radical, electronic absorpt. spectra, visible, vibr. freqs., vibronic intensities and oscill. strengths 80−28025
1-methythymine cryst., theory of IR spectra of H-bond 77−40223
micellar systems, aqueous, thermochemistry 80−61133
microbial degradation of organic molecules in lake sediment 79−84331
microemulsion, H_2O-toluol-sodium dodecylsulphate-alcohol, diffusion coeff., light scatt. data 78−15722
micropollutants, adsorpt. on chrysotile and crocidolite, XPS and gas solid elution chromatography exam. 78−80790
microwave spectra, 2-bromo-2,3-dimethylbutane, low resolution 79−54846
microwave spectra, 2-iodo-2,3-dimethylbutane, low resolution 79−54846
mineral oil-polystyrene mixture, viscosity and normal stress coeff. 80−44349
mirex in lake Ontario sediments, circulation simulation 80−26556
mixed crystals, energy transfer 78−76515
mixed crystals, transverse relax. and freq. shifts of optical transitions 78−84599
mixed organic solids, Anderson transition, electronic energy transfer in impurity bands 79−99502
mixture analysis by high-resolution mass spectrometry/mass spectrometry 80−104476
molecular conformational props., internal rot. barriers, PCILO-CNDO calcs. 77−75056
molecular crystal, band structure, excitonic processes, trap distrib. 80−6720
molecular crystal, charge transfer biexciton spectra, theory 77−51664
molecular crystal, delayed fluoresc., anisotropic spin relax. effects 79−61416
molecular crystal, doped, two-particle electronic excitation, optical cooperative excitation 80−93368
organic compounds continued
molecular crystal, exciton scatt. by lattice defects, absorpt. line shape 79−38576
molecular crystal, p-$Cl_3P{=}NSO_2C_6H_4Cl$, quadrupole nature of spin-lattice relax. 77−59480
molecular crystal, phase transforms. obs. using TEM, electron beam damage 78−34621
molecular crystals, exciton annihilation at high exciton densities, Suna equation calcs. 79−78016
molecular crystals, IR absorpt. spectra, intermol. reson. interaction, temp. depend. 78−72506
molecular crystals, optical spin alignment, phosphoresc. *(Russian)* 78−84652
molecular crystals, phosphoresc., optical spin alignment 79−95827
molecular crystals, struct. disorder effect on optical props. 77−90165
molecular crystals of solid replacement solns., NQR investig. of impurity distrib. 77−12222
molecular liquids and their binary solns., glass transition temps. 79−51239
molecular organic crystals, triexcitons, theory 79−33787
molecular polarisability, semi-empirical delta-function method 79−31442
molecular reactivities rel. to struct., Taft and Kirkwood-Westheimer eqns. 78−62738
molecular solid, dynamic struct., NMR 79−73829
molecular solid, film, 0-15 eV electron transmission spectra 80−35023
molecular solid, space group C_{2h}^5, triplet excitons energy band struct. 78−6276
molecular spectroscopy book 80−27051
molecular structure, computer-assisted interpretation, using fluoresc. spectra 77−36805
molecular systems, polarisabilities, susceptibilities, electron impact ionis. cross-sections calcs. 80−63835
molecules, incorporation in electrodeposited films, stereomicroscopic method for obs. 80−2288
molecules, information content, thermodynamic props., electropy (bondtropy) theory 77−54500
molecules, small, harmonic force consts., vibr. freqs., integrated intensities, MINDO/3 method 80−58411
molecules in monolayers, reactivity 80−81367
molecules in Shpolskii matrices, phosphoresc. site selection spectrosc., ODMR 79−36687
molecules involving B and C atoms, self-consistent charge calcs. of core-electron binding energy shifts 80−69084
di-molybdenum cyclopentadienyl tri-carbonyl, dual luminesc., ps pulse excitation 80−32754
molybdenum formate, mol., Hartree-Fock instability of SCF wavefunctions 80−9492
dimolybdenum tetraformate, metal-metal bond energy, SCF-Xα-SW calcs. 80−78538
12-molybdophosphoric acid, determ. of Mo content by NAA and AAS 80−15148
monoadipate-tetraquo-cobalt (II), cryst. struct., H-bonding scheme 80−96504
monoalkylbenzenides, anion radicals, EPR, temp. depend., vibronic interaction, proton HFS 77−34666
monoalkylcyclohexanes, heats of vaporisation by gas chromatography-calorimetry method 79−34344
monobromomethane+CO_2 mixture, Raman laser optical excitation, electron phototransition theory *(Russian)* 80−99711
monocarboxylic acids, chemisorbed on Al_2O_3, tunnelling spectroscopy 78−91545
monocarboxylic acids in meteorite, Murchison carbonaceous chondrite isomer struct. 80−26823
α-monochloroacetic acid, hydrogen-bond motifs 77−11529
β-monochloroacetic acid, hydrogen-bond motifs 77−15397
monochloroacetic acid, isolated molecules, internal rotation, CNDO/2 calcs., IR spectra 80−69254
monochloroacetic acid single crystal, Zeeman and ^{35}Cl NQR investig. 80−66066
monochlorobenzene, electroviscous effect, AC characts. 79−99341
monochlorobenzene, in KOH-2-propanol soln., chain dechlorination by γ-rays 78−56904
monochlorobenzene, overlapping Raman lines resolution by coherent ellipsometry 79−98110
monochlorobenzene, partially oriented, r_α-struct., ^{13}C satellite PMR obs. 79−50048
monochlorobenzene, prereson. Raman effects, intensity enhancement mechanism 78−42069
monochlorodifluoromethane, US vels. and absorption coeffs., determ. of relaxation times 78−63530
monochlorodifluoromethane-Ar mixture, US vels. and absorption coeffs., determ. of relaxation times 78−63530
monocrotaline sulphite hydrochloride, struct., space groups from X-ray crystallography *(Chinese)* 80−49210
monofluoromethane, ν_6 band, Q-branches, diode laser IR spectra, mol. consts. 79−45722
monofluoromethane, force consts. and IR intensities, ab initio SCF finite difference method 78−86783
monofluoromethane, X-ray photoelectron spectral linewidth of F core, ab initio HF calc. 78−62841
monofluoromethane+Ar, vibr.-vibr. energy transfer process diagnostics 80−32807
monohalobenzenes, circularly polaris. Raman spectra, vibr. symmetries assignment 78−29787
monohalobenzenes, inner shell excitation and ionis., electron energy loss spectra, XPS, assignments 78−62934
monohalonaphthalenes, electronic transition spectra forbidden charact., symmetric vibr. interaction 78−58663
monolayers, bidimens., hydrocarbon chains on aq. substrate, phase transition model 78−51795
monomethylamine, dilute mixtures, decomposition, shock tube studies, IR emission obs. 79−96301
3-monomethylamino-N-methylphthalimide solns., fluoresc. and excitation spectra 79−61425
mononucleotides, conformational anal. by nuclear Overhauser effects 79−20509
2(4)-monooxopyrimidines, gaseous, matrix, soln., tautomeric equilib., IR and UV absorpt. spectra 80−58256
monophenyl phosphate in aq. soln., pulse radiolysis obs. 80−30261
monopyrazine zinc sulphate trihydrate:Cu^{2+}, ESR meas. 78−84478
monostearine crystals, spiral growth from organic soln. 80−93467

organic compounds continued
monoterpene hydrocarbons in rural atmospheres, gas chromatography/mass spectrometric anal. 80−17336
monothioformate anion, protonation site, ab initio SCF calc. 79−47894
monothioformic acid, cis-, trans-rotamers, rot. spectrum, force consts. and isotopically substituted struct. 78−9145
monothioformic acid, pot. for rot. about $C(sp^2)$-S bonds, ab initio calc. 80−23572
morphine, spin-labelled, EPR study of synaptosome opiate receptor 77−9215
morpholine, centrifugal distortion consts., microwave spectrum 80−5531
MTHF, localised excess electrons, semicontinuum models 78−73129
MTPA$(TCNQ)_2$ radical salt, triplet exciton system, motional correlation effects, model 78−75997
mucobromic acid, vibr. spectra, struct. 78−46326
mucochloric acid-d_0, -d_1, vibr. spectra, struct. 78−46326
trans,trans-mucodinitrile solid, NMR relax., mol. motions between unequal pot. wells 78−19353
trans,trans-muconodinitrile, mol. reorientation, unequal well pot. energy calcs. 78−26461
multicomponent liquid mixtures, empirical excess volume model, for estimating densities 79−1503
muonium-substituted transient radicals observed by muon spin rotation 78−74678
in Murchison carbonaceous chondrite, spectroscopic evidence for interstellar grain clumps 77−25987
Murchison meteorite, evidence for alcohols and carbonyl compounds 77−33433
myoglobin, atomic vibr. mean square displacement, Rayleigh scatt. of Mossbauer radiation meas. *(Russian)* 80−100665
myoglobin, electronic and mag. struct., semiempirical MO cluster calcs. 78−62733
myoglobin+CO, recombination, kinetics meas. using minicomputer 78−7200
myosin, X-irradiated ENDOR and ELDOR obs. 80−63689
myosin-auramine O system, conform. changes and excitation energy transfer 79−96512
myristic acid, associated vapours, homogeneous nucleation 80−96638
myristyltrimethylammonium bromide, micelle size, press. dependence, photon correlation spectrosc. 80−11953
N_1-aryl-N_2-alkyl thioureas herbicides, structure-activity relationships 79−62176
N,N′-dioxy-2, 6-diazoadamantane, exchange interaction, spin density delocalisation 78−9056
N-(4-alkoxybenzylidene)-4′-n-alkylanilines, Raman spectra in solid state, polymorphism of mesogenics 79−82964
N-(p-chlorophenyl) maleamic acid, cryst. struct. 79−65065
N-(p-tolyl)-maleamic acid, cryst. struct. 79−65064
N-acetyl-L-leucine, single crysts., X-ray induced free radicals 80−45525
n-alcohol short chain molecules, optical investig. of mol. motions 80−40123
n-alkane short chain molecules, optical investig. of mol. motions 80−40123
N-alkylated phenazine type radicals, mag. props. 79−73671
N-hetrocyclic biomolecules, IR absorpt. spectra, vibr. assignment 77−10671
11-cis-N-methyl PRSB-benzene complexes, spectral props., CNDO/S calcs., bathochromic shift 78−31767
N-methylhydroxylamine, microwave spectra, struct., moments, internal rot., HFS and rot. consts. 79−45708
N-methylpropionamide, in carbon tetrachloride, dielec. relax., time-domain reflectometric obs. 79−4762
N-nitroso compounds, estimation in environmental samples at parts-per-billion level 79−74448
n-propyl alcohol, angular distrib. of scatt. press. to carrier press. ratio 77−27942
N-substituted amides, liquid, acoustic spectroscopy method for H-bond studies 79−96303
[n-]alkanes, cryst., vibr. correl. splitting and chain packing 80−7338
NAD.H, oxidative phosphorylation, role of respiratory chain 78−15795
NAD.H oxidation by atm.O, coupled with peroxide oxidation of lipids in bilayers 77−36875
naphtene hydrocarbons, solubility in liquid O_2, estimation by Preston-Prausnitz method 80−39285
naphtha tar pitch, mesophase formation during carbonisation under pressure 77−44182
naphthacene, electron escape depths and absorpt. coeffs. 78−23580
naphthacene, excited states calc., unrestricted HF theory in PPP approx. 77−50377
naphthacene, in Shpolskii systems, key and hole rule test, fluoresc. 77−42347
naphthacene, metastable inert gas atom impact, surface electron emission energy distrib. 78−43970
naphthacene, nonlinear third-order electric susceptibility 78−74944
naphthacene, thermoluminesc., exam. at liquid N_2 temp. 77−4692
naphthacene film, electron escape depth, energy depend. 79−38709
1,2-naphthacoronene, phosphoresc. and ODMR meas. 79−18220
α-naphthaldehyde, soln., dielec. relax. and permittivity 78−64318
naphthalene.$2SbCl_3$, Raman spectra 77−16291
naphthalene:2-fluoronaphthalene, photoexcited triplet state X-traps, ENDOR meas. 78−39444
naphthalene:2-fluoronaphthalene(2-chloronaphthalene), triplet state X-traps, ENDOR obs. 79−33561
naphthalene:ββ′-dinaphthylethylene, stimulated emission, phonons role 77−8606
naphthalene:ββ′-dinaphthylethylene, stimulated emission suppression in phonon wing 78−2881
naphthalene:β-chloronaphthalene, reaction rate constants of triplet excitons 78−80407
naphthalene:β-methylnaphthalene, impurity phosphoresc. centres *(Russian)* 77−81151
naphthalene:β-naphthyl-n-biphenyl-ethylene, relax. time of vibr. levels of ground state *(Russian)* 77−44054
naphthalene:β-naphthyl-n-biphenyl-n-biphenylyl ethylene, relax. times of ground electronic state vibrational levels 79−19907
naphthalene:β-naphthyl-n-biphenylylethylene, cryst., ground electron state, vibr. levels, relax. time determ. *(Russian)* 78−15195
naphthalene: anthracene, cryst., triplet-state EPR for isolated mol. orientation 78−26583
naphthalene: pentacene, intermol. interaction dynamics and optical dephasing 80−64112

organic compounds continued
naphthalene: quinoxaline, anisotropic spin lattice relax. of triplet mols. in high mag. field 77−81141
naphthalene: quinoxaline, isolated triplet mol. direct spin-lattice relax., librational model 79−11444
naphthalene:anthmacene, singlet exciton energy transfer dynamics, time resolved spectra 79−83032
naphthalene:anthracene, cryst. energy transport and luminesc. at room temp. and 4.2K 79−56828
naphthalene:anthracene, guest mol. orientation 79−19161
naphthalene:anthracene, pure and doped, delayed fluoresc. *(French)* 80−80846
naphthalene:anthracene, two-photon picosec. excitation, sensitised fluoresc. kinetics 79−47516
naphthalene:azulene, reson. fluoresc., Raman spectra, single vibronic level relax. 79−38588
naphthalene:benzofuran, luminescence spectra and intensity, 1.6-77K 79−87477
naphthalene:indole, luminescence spectra and intensity, 1.6-77K 79−87477
naphthalene:octafluoronaphthalene, cryst., interactions, Raman spectra 77−43982
naphthalene:pentacene, mol. mixed cryst., picosec. coherent transients obs. 79−46013
naphthalene:pentacene, picosec. optical coherence obs. 80−14400
naphthalene:quinoxaline, spin-lattice relax. of triplet states of high mag. fields 79−19933
naphthalene:tetracene, electronic absorpt. spectrum, host-cryst. field effect 80−100669
naphthalene:thionaphthalene, luminescence spectra and intensity, 1.6-77K 79−87477
naphthalene, 2-methylnaphthalene and anthracene doped, single cryst., sensitised fluoresc. 78−68548
naphthalene, $^1B_{2u}$ supertransfer, exciton percolation, fluoresc. spectra obs. 77−55482
naphthalene, $^1B_{3u}$-state lifetime, temp. depend. under Boltzmann conditions 79−86008
naphthalene, β-naphthol impurity mol. distrib., spectral obs. *(Russian)* 79−82253
naphthalene, γ-irrad., radical pairs EPR detection 78−31664
naphthalene, (001) and (100) surface struct. models 79−86966
naphthalene, a-exciton lineshape, exciton-photon coupling 79−33243
naphthalene, a-exciton temp. depend. scatt., optical absorpt. profile 78−72088
naphthalene, absolute quantum yields, high resolution laser excitation, low press. gas 77−3404
naphthalene, absorption spectrum in rare-gas matrices 79−3454
naphthalene, adsorbed on silica gel surface, biphasic photochemistry, time-resolved spectra 80−30252
naphthalene, and aza-substituted derivatives, out-of-plane vibrs. force field 77−83572
naphthalene, and d_4 and d_8, vibr. anal. using best struct. and spectroscopic data 79−76410
naphthalene, and deutero derivatives, fluoresc., absorpt. spectra under Shpolskii conditions 80−2825
naphthalene, anharmonic props., temp. (press.) depend., rel. to TTF-TCNQ 80−15200
naphthalene, anion, cation and triplet, GO LCAO MO calcs. of electronic struct. 78−25416
naphthalene, atomic localisation of electronic excitation 77−18806
naphthalene, $C_{10}H_8$ and $C_{10}D_8$, optical absorpt. spectra of hydronaphthyl radicals, isotope effects 78−60487
naphthalene, charge carrier drift mobility, semi empirical anal. 80−65553
naphthalene, charge separation during cryst. growth, Costa Ribeiro effect 80−7316
naphthalene, chemisorbed on Al_2O_3, radiative and nonradiative processes 79−36686
naphthalene, conc. profile for mass transfer in gas-fluidised beds 77−11256
naphthalene, Coulombic energy calcs. 79−99104
naphthalene, cryst., fluoresc. spectra, press. tuning 77−28612
naphthalene, cryst., laser reson. Raman effect, near 3200 Å, B_{3g} vibr. enhancement 77−52067
naphthalene, cryst., low freq. Raman spectra, defects and lattice vibr., 80-320K 78−31194
naphthalene, cryst., luminesc., excitons, phase aspects 79−56838
naphthalene, cryst., photocurrent induced by detrapping of charge carriers trapped by radicals 79−82643
naphthalene, cryst., radiation induced radicals, optical absorpt. bands, SCF-CI MO calc. 79−91463
naphthalene, cryst., singlet exciton interactions, prompt fluoresc. decay 78−60500
naphthalene, cryst., singlet exciton interactions fluoresc. decay 79−47027
naphthalene, cryst., three-particle complex as impurity-exciton-phonon bound state *(Russian)* 77−62842
naphthalene, cryst., vibronic absorpt. spectrum with totally symm. phonons 79−4817
naphthalene, cryst. plasticizing by surface active organic media, creep rate meas. 79−55813
naphthalene, crystal optics and Raman intensities 79−4795
naphthalene, crystal-electrolyte interface, ionis. energy of uppermost cryst. mols. 78−27764
naphthalene, crysts., Raman and two-photon reson. in three wave mixing 79−38538
naphthalene, deformation potential consts. of exciton-phonon interactions *(Russian)* 78−56498
naphthalene, diaza derivatives, excited singlet and triplet states, charge densities, INDO calcs. 80−58152
naphthalene, dimer triplet state line shape, small excitons 80−48041
naphthalene, dipole polarisability, finite-field SCF MO calcs. 80−83255
naphthalene, doped, fluoresc., impurity centre struct. depend. *(Russian)* 77−48231
naphthalene, doped, role of nonequilibrium phonons in stimulated radiation emission 80−103971
naphthalene, doped, zero-phonon lines and absorpt. spectra, temp. depend. of shift and broadening 79−69866
naphthalene, doped crysts., fine struct. strengths in vibronic spectra 77−44004
naphthalene, dye vapour, intense multistep photoionisation 79−10298

organic compounds continued
naphthalene, electron and hole off-diagonal mobility component determ. 80−65552
naphthalene, electron band hopping transition 78−39155
naphthalene, electron excitation, electron resonance, triplet states 79−54976
naphthalene, electron excitation energy transfer efficiency, temp. depend. *(Russian)* 77−52182
naphthalene, electron trapping, one-carrier TSC and SCL currents 80−70715
naphthalene, embedded heater in solid, melting and natural convection 78−90646
naphthalene, energy transfer from upper triplet states to toluene and hexene-1 79−10142
naphthalene, ENSH method of oriented thin film growth 79−99443
naphthalene, epitaxial film, on metal (111) substrates, surface struct., LEED obs. 79−86969
naphthalene, excited states calc., unrestricted HF theory in PPP approx. 77−50377
naphthalene, exciton migration, variable range cluster model 79−33762
naphthalene, external mode one-density states, low freq. Raman scatt. spectra *(French)* 80−76012
naphthalene, far IR spectrum, efficiency of heatable long path gas cell 79−58807
naphthalene, Faraday spectrum, sign rel. to mag. field strength *(German)* 77−36204
naphthalene, films, on metal substrate, surface struct. using LEED 79−77879
naphthalene, fluoresc. and phosphoresc., singlet/triplet excimers conform. difference 77−14469
naphthalene, fluoresc. lifetimes of single vibronic levels 79−27016
naphthalene, fluoresc. of isolated mol. in supersonic beam 79−45750
naphthalene, fluoresc. probe of micellar systems 78−95599
naphthalene, fluoresc. quenching by inorganic anions 78−74694
naphthalene, fluorescence and absorpt. spectra, deviations from Condon approx. 80−28004
naphthalene, fluorescence decay induced by electron pulse, exciton interactions 77−16403
naphthalene, fluorescence quenching by biacetyl, effect of viscosity 78−29810
naphthalene, harmonic force fields, bond orders, normal coord. anal. 78−25418
naphthalene, hole mobility, anomalous current transients 78−76091
naphthalene, hyperpolarisability meas. by DC induced second harmonic generation 78−87096
naphthalene, i n Shpolskii systems, key and hole rule test, fluoresc. 77−42347
naphthalene, in benzene, two-photon spectra 78−16860
naphthalene, in durene, photoexcited triplet state spin-lattice relax., local phonons effects 78−6605
naphthalene, in durene and perdeutero-naphthalene mixed crystals, photon-echo decay 78−42388
naphthalene, in naphthalene-d_8, Anderson-Mott transition model for excitation transport 80−96812
naphthalene, in naphthalene-d_8, energy trapping from localised states 80−100440
naphthalene, in nonpolar solvents, IR absorpt. bands 79−6939
naphthalene, in stretched polythene films, molecular distribution determ. 78−27298
naphthalene, in-plane vibr. force fields, five-parameter approx. calcs. 79−59436
naphthalene, inclined dimers, transition energies and moments, excitation energy, four-electron MO-CI treatment 77−42237
naphthalene, internal conversion rate, effect of benzene triplet state self-quenching 78−25586
naphthalene, IR absorpt., intermol. reson. interaction, temp. depend. 78−72506
naphthalene, isotopic mixed cryst., phospheresc., photoselection of pure initial triplet states 78−35189
naphthalene, isotopically mixed crystals, electronic energy transfer, crit. conc. 77−76771
naphthalene, lattice dynamics, inelastic neutron scattering 78−79690
naphthalene, lattice parameters, elastic consts., press. depend., neutron diffr. obs. 78−26558
naphthalene, LCAO SCF MO CI calcs., integral approx. scheme using semiorthogonalised orbitals 79−6873
naphthalene, liq., EHD transit flow 78−75895
naphthalene, long range exciton percolation, superexchange, energy denominator 77−28609
naphthalene, mag. effects on delayed fluoresc. at high and low triplet exciton density 77−8634
naphthalene, mag. polarised electret, X-ray diffr. obs. 78−43775
naphthalene, matrix fluoresc. spectra, rel. intensities of multiplet components 79−54882
naphthalene, melting of rotational degrees of freedom near cryst.-liq. transition 80−54352
naphthalene, microcryst. and evaporated film, excimer emission 80−2823
naphthalene, mol. cryst., effective mol. polarisability calcs. 77−12298
naphthalene, mol. cryst., elec. field independent electron drift mobility 79−51645
naphthalene, mol. cryst., impurity reson. interaction effects 77−1396
naphthalene, mol. cryst., polariton fusion, two-photon excitation spectra 77−90139
naphthalene, mol. cryst., quadrupole contribs. to lattice vibr. freqs. 79−82290
naphthalene, mol. cryst., reson. four-wave mixing, third order susceptibilities 80−100654
naphthalene, mol. cryst., Stark effect origins, point dipole approx. soln. 77−77252
naphthalene, mol. crystal, meas. of US attenuation coeff. by optoacoustical methods *(French)* 80−70317
naphthalene, mol. vibr., high-energy C-H vibr. overtones, intensity 79−76404
naphthalene, molecular cryst., phonon scatt. and exciton linewidths 78−15185
naphthalene, multiphoton excitation 79−61414
naphthalene, multiphoton ionisation, mass spectra 80−63717
naphthalene, nonlinear fluorescence quenching 78−52562
naphthalene, nonlinear third-order electric susceptibility 78−74944
naphthalene, nonplanar vibr., force field calcs. 79−41148
naphthalene, nonradiative transition rates, rot. struct. 78−42119

organic compounds continued
naphthalene, nontotally symmetric Raman lines, destructive interference effects 77−6789
naphthalene, normal coord. calcs., simplified valence force field models 78−94229
naphthalene, out-of-plane mol. vibrs., force field approx. calcs. 80−91538
naphthalene, phonon eigenvectors, neutron scatt. intensities determ. 80−44271
naphthalene, phosphorescence spectra in rare gas matrices, multiplet struct. and pot. energy functions 80−106341
naphthalene, photoconductivity elec. field depend. 77−32035
naphthalene, photoionis., negative ions role in photoionis. plasma 79−27048
naphthalene, polarisation energy of localised charge 80−15034
naphthalene, prereson. Raman spectra, vibr. band intensities obs. 80−102515
naphthalene, proton chem. shift, chem. substitution influence, LCAO perturbation method 77−68064
naphthalene, pure and deuterated, band-hopping mobility transition 80−6833
naphthalene, pure and doped, exciton-phonon luminesc. 80−84773
naphthalene, quantitative structural studies by means of the energy-dispersive method with X-rays from a storage ring 80−24314
naphthalene, radiationless transitions, sharp Doppler-free resons. *(German)* 77−58076
naphthalene, Raman active phonon freqs., linewidths and line shapes, temp. depend. 79−47432
naphthalene, Raman intensities, polarised scatt. from lattice rot. modes. 78−43845
naphthalene, Raman intensities rel. to vibronic coupling and excited electron state geometries 77−27075
naphthalene, reson. Raman scatt. from non-totally symm. mode 78−37641
naphthalene, ring currents hypersusceptibilities calcs. 80−102588
naphthalene, Rydberg spectra, antireson. lineshapes 77−50424
naphthalene, single crystal, anomaly in permittivity due to thermodielectric space charge 80−7258
naphthalene, singlet and triplet excimer interactions, exciton resons. 80−95535
naphthalene, singlet and triplet exciton percolation, tunnelling and thermalisation 80−84432
naphthalene, singlet exciton transitions, energies and oscillator strengths, boson theory with PPP wavefunctions 80−92820
naphthalene, singlet-singlet transition, Born-Oppenheimer approx., CNDO/S calcs. 77−27045
naphthalene, solid, electronic struct., comparative ESCA study of polyacenes 78−52631
naphthalene, solid, high-energy vibr. overtone spectra, local modes, intramol. relax. 79−28052
naphthalene, solid/melt interfacial tension and contact angles of small particles, determ. from crit. vel. of engulfing 80−79915
naphthalene, soln. and melt, second vibronic transition, spectroscopic charcts., effective field dispersion calcs. 80−55102
naphthalene, solns., two-photon absorpt. meas., using nonlinear light-mixing spectroscopy 77−79620
naphthalene, solution, structured UV spectrum obtained by ultrafast two-pulse excitation 80−78630
naphthalene, space charge transport 80−20209
naphthalene, spectra, PPP approx., CI clacs. *(German)* 79−36602
naphthalene, spectra of directionally deformed crystals and phonon-exciton interaction constants 79−78703
naphthalene, stepwise photoionisation process 78−82791
naphthalene, sublimation, mass transfer at vibr. spheres 80−57220
naphthalene, substrate for epitaxial crystn. of polyesters 79−61521
naphthalene, surface dynamics, calc. 80−92772
naphthalene, surface pot. decay, trap modulated mobility 78−72164
naphthalene, temp. depend. of mol. motion in lattice 79−33045
naphthalene, temp.-independent mobilities, phonon-induced electron hopping 79−28347
naphthalene, theory of fission of singlet Frenkel exciton into two localised triplet excitons 79−23901
naphthalene, thermal cond. and heat capacity, meas. under press. 79−90796
naphthalene, thermal diffuse scattering, errors in X-ray diffr. intensities and atomic parameters 79−73155
naphthalene, thermodynamic function calc. using cell model 77−7879
naphthalene, trifluoromethyl derivatives, first ionis. pots., CF_3 group nature 79−27110
naphthalene, triplet excimer conformation, σ-π interaction transitions 77−6701
naphthalene, triplet exciton annihilation and triplet spin relax. 80−29792
naphthalene, triplet exciton annihilation at high triplet densities 79−37996
naphthalene, triplet exciton tunnelling, crit. concs. 79−15086
naphthalene, triplet excitons, phosphoresc. and delayed fluoresc. excitation spectra 78−63986
naphthalene, triplet pairs in naphthalene-d_8, ESR, nonreson. 78−64257
naphthalene, triplet state time evolution after radiationless transition, initial vibronic distrib. effects 80−23450
naphthalene, two-photon and mutiphoton excitation, UV fluoresc. spectra 77−88517
naphthalene, UV spectra and extinction coeffs. for $S_n \leftarrow S_1$ absorption 80−18866
naphthalene, vap., Doppler free two-photon absorption spectra 78−5307
naphthalene, vapour press. meas, using torsion-weighing effusion apparatus 77−89530
naphthalene, vapour-phase, absolute fluoresc. quantum yields, nonradiative processes 77−6829
naphthalene, vibr. dephasing and Raman active localised internal mode temp. depend. 80−45060
naphthalene, vibr. relax. studied by four wave mixing (CARS), spectral lineshapes obs. 80−80762
naphthalene, vibronic fluorescence spectrum, intensity distribution 79−3477
naphthalene, X-ray diffr. anal. of cryst. and mol. struct. at −150°C 77−7707
naphthalene+CO, vibr. energy transfer, quenching efficiency 79−3539
$(naphthalene)^-(naphthalene)^+$ radical pairs, ESR absorption, optical detection 80−7166

organic compounds continued
naphthalene β-chloronaphthalene, optically induced detrapping of triplet excitons 79−28828
naphthalene (-d_8), gamma irradiated soln., fluoresc. mag. field depend., spin correls. 77−44492
naphthalene and −d_8, vibronic spectra 79−51956
naphthalene and fluoro derivations, CNDO calcs., σ core effect 79−41107
naphthalene anion radical+H_2O, react., H_2 prod. 78−92460
naphthalene anions, electron affinities, transition energy, comparison for gaseous liquid and solid 80−29731
naphthalene anthracene, crystal second-order Stark shifts in optical spectrum of anthracene 80−88966
naphthalene anthracene doped, decay times and diffusion coeffs. of singlet excitons, under press. 77−20911
naphthalene charge transfer complexes, cryst., vibr., factor group splittings 79−7658
naphthalene charge transfer complexes, orientational disorder, spt. ht. meas. 79−46813
naphthalene cryst., anthracene doped, fluoresc., two-photon excited 78−68560
naphthalene crystal, dynamical matrix eigenvectors from Raman scatt. 80−100315
naphthalene crystal, external phonon modes, inelastic incoherent neutron scatt. spectra and computer calc. 78−34577
naphthalene crystal, multiphonon i.r. absorption 77−1686
naphthalene crystal, vibronic spectra at 1.6K, two-photon fluoresc. excitation 77−59604
naphthalene crystal nucleation on anthracene microcrystals suspended in vapour-gas stream 80−76165
naphthalene crystalline complexes with octafluoronaphthalene, triplet exciton emissions 80−84760
naphthalene crystals, investigation of structural formation and growth kinetics 79−47610
naphthalene crysts., nonlinear fluorescence quenching, recomb. of free excitons 80−7397
naphthalene derivatives, film struct., electron microscope and diffr. obs. 79−11029
naphthalene dispersed in benzene polycryst. host, active N_2 induced chemilum. 80−60691
naphthalene doped molecular crystals, stimulated emission at 4.2K 79−28790
naphthalene in Ar matrix, geometry changes and multiplet struct., mol. fluoresc. and phosphoresc. obs. 80−95663
naphthalene in $C_{10}D_8$, exciton percolation and coherence 77−59258
naphthalene in durene matrix, spin-lattice relax. of phosphoresc. triplet state, PMDR study 79−27012
naphthalene in EBBA, PMR obs., mol. struct., orientation and solute-solvent interactions 77−27806
naphthalene in nonpolar solvent, vibr. and reorientational relax., correl. function 80−45065
naphthalene in various crystals, luminesc. and stimulated emission on laser irrad. *(Russian)* 77−48236
naphthalene mesophase pitch, thermotropic transformations 79−95127
naphthalene mixed crystal, Nh_8/Nd_8, phosphoresc., energy transfer model 79−38600
naphthalene mixed crystal, time resolved excitation migration, triplet and singlet critical concs. 79−78010
naphthalene mixed crysts., dimer reson. self-energy 80−99459
naphthalene molecular ion, two and four photon absorpt., dissoc. 80−74210
naphthalene molecule in durene and xylene crystals, vibronic interactions 80−84755
naphthalene molecules in frozen n-butanol, mol. motion, ESR spectra 77−90014
naphthalene pair ($C_{10}H_8$) in $C_{10}D_8$ host, mini-exciton obs., electron spin echo and ODMR 77−4559
naphthalene radical anion, ethereal soln., far IR spectra 78−62796
naphthalene radical anion+TCNQ, electron transfer reactions, theory 78−15661
naphthalene radical cation, in organic glass, 77K, reson. Raman spectra 78−78704
naphthalene radical cation EPR spectra, ion-pair effects 79−13742
naphthalene single crystal, 4.50 MeV α bombardment, scintillation response, planar channelling, blocking *(German)* 78−6780
naphthalene single crysts., steady creep obs. 80−75296
naphthalene single crysts., surface active substances effect on plastic flow 80−44248
naphthalene sublimation, radial diffusion rate, mothball lifetime, for teaching 78−54124
naphthalene vapour, fast obs. of primary triplets with tandem laser pulse absorption 77−58056
naphthalene vapour, resonant scatt. of slow electrons 77−58182
naphthalene-α-naphthol eutectic, heat of fusion and excess thermodynamic functions 78−3104
naphthalene-β-naphthol, concentration effects in exciton absorption region 80−108241
naphthalene-β-naphthol mixed mol. cryst., multiplet struct. of electron absorption spectra 77−1706
naphthalene-β-naphthol mixture, exciton absorpt. depolarisation 80−103972
naphthalene-adipic acid system, crystal growth from melt, V-ΔT and V-λ relations 80−19734
naphthalene-betamethylnaphthalene, mixed cryst. ($C_{10}H_8/C_{10}D_8$), luminesc., test of excitation transport model 79−65914
naphthalene-catechol eutectic, heat of fusion and excess thermodynamic functions 78−3104
naphthalene-catechol eutectic struct., crystallisation behaviour 79−55868
naphthalene-coumarin solid solution, struct. parameters and phase diagram 77−11532
naphthalene-d_0, (-d_4), (-d_8), inequivalent local C-H modes, subpicosec. dephasing, high energy overtones 79−86850
naphthalene-d_0, in naphthalene-d_8 cryst., mol. pair mini-exciton form., electron spin echo and ODMR 77−72822
naphthalene-d_0(−d_8), fluoresc. spectra, vibronic intensities 77−50464
naphthalene-d_3:(naphthalene, beta-methylnaphthalene), disordered, exciton migration, dynamical approach 79−65916
naphthalene-d_4(d_8) crystal, with isotopic impurities, Rashba effect, luminescence spectra, impurity states 80−29768
naphthalene-d_8:β-methylnaphthalene -d_{10}, phonon side bands of specular optical transitions 78−26649
organic compounds continued
naphthalene-d_8:naphthalene, betamethylnaphthalene, $^1B_{2u}$ naphthalene exciton percolation kinetics, exciton coherency 79−33750
naphthalene-d_8:naphthalene, symmetry reduction obs. of deformed crysts. by absorbt. spectrum method 79−15504
naphthalene-d_8:naphthalene-h_8 cryst., triplet excitons in A-B pairs, origin of inhomogen. broadened ESR lines 78−91623
naphthalene-d_8, cryst., phonon dispersion curves calcs., low temp. 80−96599
naphthalene-d_8, in diethylether soln., ^2H NMR, mag. field induced alignment effects 79−13740
naphthalene-d_8, metastable triplet states, spin-lattice relax. at high mag. fields, phosphoresc. meas. 78−15063
naphthalene-d_8, phonon dispersion meas. and calc. 78−2211
naphthalene-d_8, Raman spectra at 70 and 293K, polarisation spectra of melt 77−32358
naphthalene-d_8, struct. facators, time of flight neutron diffr. 78−47212
naphthalene-d_8 and -h_8, Davydov splitting of Raman-active vibr. levels 77−36210
naphthalene-d_8 crystal, dispersion of LF phonons 77−69058
naphthalene-d_8 triplet-triplet energy transfer from acetophenone, in EPA rigid soln., donor phosphoresc. decay 78−10971
naphthalene-d, press. depend. of lattice freqs. at 100K 79−46768
naphthalene-h_8, and -d_8 mixed crystals, phosphoresc. excitation spectra of clusters 78−43914
naphthalene-h_8, gas phase two-photon spectra calcs. 78−94298
naphthalene-h_8 (-d_8), two-photon excitation spectra, vibronic coupling 77−75246
naphthalene-h_8 and -d_8, gas phase far IR 78−37638
naphthalene-h_8 and d_8, isotopic mixed crystals, exciton spectra in IR region 80−71400
naphthalene-h_8-naphthalene-d_8 mixed crystal, monomer cluster states 79−15089
naphthalene-h_8-naphthalene-d_8-β-methylnaphthalene, mixed cryst., dynamic exciton percolation, photosynthesis simulation 77−28124
naphthalene-He photoionis. plasma, CO_2 additive effect 80−10359
naphthalene-I_2 soln., elec. cond., thermoelec. power, conc. depend., 120°C 77−39845
naphthalene-naphthol solid soln. system, excess thermodynamic functions 80−107445
naphthalene-O_2 in polystyrene fluff, oxciplex emission 77−23515
naphthalene-octafluoronaphthalene complex, Raman spectrum, intermol. vibrs. 77−66004
naphthalene-p. chloronitrobenzene system, eutectic, solidification 78−64530
naphthalene-p-chloronitrobenzene eutectic system, phase diagrams and crystn. 77−47551
naphthalene-$SbCl_3$ system, phonon bands in π-electron charge transfer complex 77−39644
naphthalene-TCNB, charge-transfer cryst., donor mol. orient. and dynamics 79−32926
naphthalene-TCNB (PMDA), Raman spectra orientational disorder, charge transfer cryst. 78−19459
naphthalene-TCNE π-π three mol. complexes, absorpt. spectra, assoc. const., extinction coeffs. *(German)* 77−35465
naphthalene-TCNE π-π three mol. complexes, UV-visible spectra, assoc. const., extinction coeff. determ. *(German)* 77−35464
naphthalene-TCPA charge transfer triplet states, electron-phonon coupling 79−38601
naphthalene-tetrabromophthalic anhydride, complex cryst., visible spectra, singlet-triplet absorpt. 79−19897
naphthalene-tetrachlorophthalic anhydride, complex cryst., visible spectra, singlet-triplet absorpt. 79−19897
naphthalene-tetrachlorophthalic anhydride charge-transfer cryst., electronic states 77−32415
naphthalene-tetracyanobenzene, charge transfer complex, phase transitions, deuteration effect, mag. reson., spectral and thermal meas. 79−4412
naphthalene-tetracyanobenzene, doped cryst., EPR of triplet state for mol. reorientation 79−38368
naphthalene-tetracyanobenzene, order-disorder transition, heat capacity and thermodynamic props., 5 to 300K 79−33100
naphthalene-tetracyanobenzene, Raman spectra, phase transition and isotopic substitution 78−80364
naphthalene-triethylamine exciplex, effect of dipolar molecules on quenching curves 78−52551
naphthalenes, heavy atom effects on phosphorescent triplet states 78−70858
naphthalenes, methyl substituted radical cations, UHF spin densities, additivity model calcs. 80−58139
naphthalenes, phonon satellite narrowing in local exciton luminesc. *(Russian)* 79−47507
naphthalenes, substituted, CH wag group freqs., CNDO/2 calcs. 77−6745
naphthalenes, substituted, dielec. relax. and permittivity in pure liqs. 78−64318
naphthalenes, substituted, dielectric relax. in solns. 78−2795
naphthalenes, substituted, electronic singlet-singlet spectra 77−3378
2-naphthalensulphonate, fluoresc. and phosphoresc., external heavy atom effect 78−29812
naphthalimide derivatives, solutions, lasing characts. in green spectral region, photostability 80−32978
naphthaline, sublimation rates in axisymmetric turbulent impinging jets 77−42887
1,2-naphthalocyanine-rare earth ion complexes, electronic excitation deactivation mechanism 79−85988
2-naphthamide, excited singlet state, fluoresc. quenching by metal ions, rate meas., mechanism 77−38685
1,8-naphthoilene-1′,2′-benzimidazole-phenylimide of 4-aminonaphthalic acid luminophor mixture *(Russian)* 79−47514
α-naphthol, ν(O-H) k=0 phonon band, width and splitting 77−52066
β-naphthol, aq., solvated electron prod. using laser excitation 77−60087
1-naphthol, aq. ethanolic soln., proton transfer photoreaction kinetics, in singlet excited state 78−48671
2-naphthol, aq. soln., proton transfer photoreaction kinetics, in singlet excited state 78−48671
2-naphthol, diffusivities in water 79−73328
1- and 2-naphthol, ideal gas thermodynamic props., vibr. fundamentals, rot. isomerism 79−24813
β-naphthol, IR absorpt., intermol. reson. interaction, temp. depend. 78−72506

organic compounds continued
β-naphthol, IR dichroic ratio, oriented gas and effective charge models calcs. 78−60437
β-naphthol, preresonance enhancement in CARS 78−29786
α-naphthol, solid, H bonding, wide line NMR obs. 78−52362
naphthol complexes, H-bonded, form. of ion pairs in presence of crown ethers, proton-transfer photoreactions 80−85199
β-naphthol in naphthalene, spectral study of distrib. of noncentral symmetric impurity mols. *(Russian)* 79−82253
2-naphthol-3,6-disulphonate, picosec. proton ejection, ultrafast pH jump 79−83475
α-naphthol-β-naphthol eutectic, heat of fusion and excess thermodynamic functions 78−3104
2-naphthol-toluene-phenol, luminescence of complexes with hydrogen bonding at 4.2-77K 79−87486
β-naphtholate in methanol-methyltetrahydrofuran glasses, electron solvation, laser flash photoionis. compared with pulse radiolysis 79−74405
naphthols, IR spectra, assignments 78−58681
naphthoquino-dimethanes, nonlinear third-order electric susceptibility 78−74944
1,4-naphthoquinone, and derivatives, singlet electronic transitions, SCF MO CI calcs. 79−49948
1,4-naphthoquinone, $T_1 \leftarrow S_0$ transition, elec. and mag. field spectra 78−88322
1,4-naphthoquinone in EBBA, PMR obs., mol. struct., orientation and solute-solvent interactions 77−27806
naphthoquinone series charge transfer complexes, cryst. and electronic structs. 79−73474
naphtho[1,8-cd:4,5-c′d′]bis[1,2,6]thiadiazine, mol., electronic, cryst. struct. 80−64984
naphthyl, excited electronic states; conformational relax., time resolved matrix isolation spectral obs. 80−32701
2-(1-naphthyl)-5-phenyloxazole, vap. phase dye laser media, photophysical parameters 80−95884
naphthyl 1,3,4 oxadiazole derivatives, lasing ability rel. to struct., appl. as UV dye laser 77−7080
β, β,-naphthyl ethylene, nonlinear third-order electric susceptibility 78−74944
naphthyl group, excited singlet state, intramol. fluoresc. quenching by halogeno substituents 80−102537
1-β-naphthyl-2-N-piperidinoethane, intramol. exciplex form., ground state conform. control 80−102547
naphthylalanine polypeptides, fluoresc. quenching and energy transfer 79−34332
1-naphthylamine, anisotropic rot., red edge transition moment, fluoresc. 77−10699
β-naphthylamine, cryst., amino group reorientation, PMR obs., 77-373K 79−82881
β-naphthylamine, fluoresc. quenching and spectra, excited state reaction, red edge effect obs. 80−83400
β-naphthylamine, fluoresc. quenching by strong radiation due to linear Stark effect 77−58074
β-naphthylamine, soln., fluoresc., photochem. quenching, excitation wavelength depend. 77−50470
β-naphthylamine-cyclohexane soln., luminesc. quantum yield, photoacoustic method 77−86335
naphthylamines, abnormal fluorimetric titration behaviour, kinetic anal., fluoresc. quantum yields and lifetime meas. 80−89560
naphthylamines, excited state pK_a^* values, proton-induced fluorescence quenching 78−21958
β-naphthylmethyl amine, solvent-induced intramol. exciplex fluoresc. 78−25592
napthalene:pentacene, zero-phonon transition bottlenecks, photon echo detect. 80−33092
napthalene-$d_{0\text{-}8}$, fluoresc. and absorpt. Shpolskii spectra *(Russian)* 78−90208
napthalene-m nitroaniline eutectic, excess thermodynamic functions 80−107445
β-naptholate ion, preresonance enhancement in CARS 78−29786
naphthalene-benzophenone mixed crysts., phosphoresc., emitting centres 79−61427
natural gas, liq., thermodynamic props. for mixed fluid densities 78−18775
natural gas mixtures, simulated, enthalpy and phase equil., correl. with modified Starling eqn. 80−61127
natural gas-related saturated liquid mixtures, molar vols. 79−1505
natural waters, heavy metal-organic matter interactions 77−60439
nematic liq. cryst., PMR line breadth temp. depend. 77−8419
nematic liquid cryst. mixture, ZLI-207, nonideally oriented layers, Freedericksz transition dynamics 80−100163
nematic liquid crystal, Merck 389, polymorphism, radiothermoluminescence and differential scanning calorimetric study 80−24570
nematic mixtures, Merck 5 and 7a, EHD, ion mobility 79−33104
nematogens, enthalpy of fusion 78−22645
neodymium ethyl sulphate, cryst. c-axis demag. from 25000G, magnetohydrodynamic props. to 0.01K 77−20599
neodymium ethyl sulphate, magnetothermodynamics, absolute temp. scale, mag. moment and magnetization , below 0.5K 78−34984
neodymium ethyl sulphate enneahydrate, mag. susceptibility, 2-27K, appl. as mag. thermometer 79−63224
neodymium ethyl sulphate hydrate, spherical single crystal, magnetothermodynamic props. 77−55365
neodymium oxalate, X-ray fluoresc. spectrometric anal. of trace rare earth impurities 79−24853
neodymium oxydiacetate, magneto-optical rotatory dispersion and oxid absorption spectra 79−91409
neopentane:n-butane, electron mobility and electron-ion recombination rate const. 79−73557
neopentane:tetramethyl tin, Mossbauer exam. of plastic phase transition 77−20778
neopentane:tetramethyltin, Mossbauer exam. of plastic phase transition 77−69759
neopentane, adsorbed on graphite (TiO_2), NMR pulsed field gradient method, diffusion coeff. meas. 80−15362
neopentane, Brillouin scatt. near liq.-plastic cryst. transition 78−19495
neopentane, critical, electron mobility, gravity effect 78−91738
neopentane, diamond force const., rel. to crystal elastic consts., Raman freq., bulk compressibility and freq. assignments 80−65183
neopentane, electron impact excitation, 30-250 eV, 0-90° 79−54949
neopentane, gas, electron drift vel., Ramsauer-Townsend minima in electron scatt. 78−87427
organic compounds continued
neopentane, Kerr effect in gas, statistical theory 79−50842
neopentane, Lennard-Jones (6-12) interaction pot., Debye temp. calc. 78−63828
neopentane, liq., excess electron mobility, elec. field depend., parity and differentiability restrictions 79−38141
neopentane, liq., field depend. electron mobility, probability of escaping neutralization 77−8105
neopentane, liq. struct. by X-ray diffr., −17-150°C 79−27898
neopentane, mol. motion in cryst., liq. and plastic phases, neutron scatt. obs. 78−6021
neopentane, molecular dynamics simulation of rough spheres 79−82137
neopentane, neutron scatt., comparison with computer simulations of rough sphere fluid 79−99041
neopentane, photoinjected electrons, escape probability, field depend. mobility effect 78−72219
neopentane, plastic crysts., rot. correlation functions, neutron scatt. obs. 79−46578
neopentane, rotational motions, cold neutron scatt.study 79−51023
neopentane, SF_6 electron scavenging in positron spur in nonpolar liqs. 79−100421
neopentane, solid and liq., effect of n-butane impurity on electron mobility and electron-ion recomb. 80−24984
neopentane, soln., positronium form. inhibition by organic iodide addition, momentum distrib. 77−90631
neopentane, spherical Compton profile, rel. to diamond C-C bond, SCF calcs. 77−75232
neopentane, steady state in flow pyrolysis, determ. individual rate consts. 78−35650
neopentane, unimolecular ion dissociation branching ratios and kinetic energies 77−502
neopentane, virial coefficient, meas. at various temps. using differential Burnett apparatus 80−22373
neopentane+Cs, atom line shape broadening, satellite data inversion, interaction pot. 78−74608
neopentane adsorbed on graphite, quasi two-dimens. fluid, NMR 80−102525
neopentane liq., local mode overtone bands 80−83444
neopentane-d_{12}, ^{13}C and ^2H spin-lattice relax. times, orientational and ang. momentum correl. times 79−33551
neopentane-d_{12}, adsorbed on TiO_2, neutron scatt. study 79−60640
neopentane-N_2O, gas phase N_2O electron attachment, temp. depend. 79−36757
neopentane-O_2, thermal electron attachment meas., microwave cond., pulse radiolysis 80−28592
neopentylcyclobutane, $^1CH_2$-activated, decomposition rate const., press. depend., internal vibr. relax. 78−64819
neostigmine, determ. using enzymatic sensor *(French)* 78−73099
niacin, biologically active forms, radiometric microbiologic assay 80−17208
nickel(II) metalloporphyrin, Z-ray photoelectron spectra satellites 80−5582
nickel acetate tetrahydrate:Mn^{2+}, EPR spectra, angular var. calc. 80−54940
nickel etioporphyrin, reson. Raman spectra, excitation profiles, nucl. distortion and Jahn-Teller effects 77−58018
nickel glutarate complexes in aqueous soln., enthalpy and entropy meas. *(Italian)* 79−19378
nickel hexapyridol perchlorate, $Ni(C_5H_5NO)_6(ClO_4)_2$, sp. ht., mag. ordering transition 77−48004
nickel octaethylporphyrin, vibronic coupling, Raman scatt. 78−21933
nickel octaethyltetrachloroporphyrin, vibronic coupling, Raman scatt. 78−21933
nickel oxalate, electronic struct. from Huckel calcs., optical props. and reactivity 77−89741
nickel oxalate dihydrate, photographic props. eval. for use as high-speed photographic materials 77−44497
nickel phthalocyanide, cryst. struct. sensitivity of band struct. 79−42444
nickel phthalocyanine, resonant photoemission at 3p-core threshold from quasiatomic Ni 79−78847
nickel phthalocyanine film, electron acceptor surface states due to O_2 adsorption 80−88586
nickel phthalocyanine iodide, single-cryst. elec. cond., low-dimens. mol. metals 78−76057
nickel-octaethylporphyrin, in benzene soln., reson. CARS and CSRS line shapes 80−74432
nickel-porphin, reson. Raman spectra 77−75164
nicotinamide, and related compounds, dipole moments, electronic transitions, chemical and biological activity, MO calcs. 78−90086
nicotine, automated synthesis of ^{11}C-labelled radiopharmaceuticals 80−17133
nicotine, determ. using enzymatic sensor *(French)* 78−73099
nicotinic acid, and related compounds, dipole moments, electronic transitions, chemical and biological activity, MO calcs. 78−90086
nicotinic acid soln. in HCl, standard for UV spectrophotometry 77−77819
nigericin action, on bilayer lipid membranes, dimer mechanism 78−24048
nigrosin black dye-Teflon spheres-water dispersion, turbid, laser backscatt. 80−1129
Nile blue, excited singlet-singlet absorpt. *(Russian)* 79−42985
Nile Blue, subpicosecond spectroscopy, tunable probe, spectral dynamics 80−23429
Nile blue-A-oxazone, tunable-pulse dynamic picosec. spectrosc. 79−44941
nitrile reaction mechanisms and kinetics, obs. of $O(^3P)+CH_3CN(CF_3CN)$ 77−36728
nitriles, nonlinear 3rd-order elec. susceptibility calcs. 79−54786
nitriles, solns., IR absorpt. band parameters rel. to temp. 80−2762
nitriles, spin-lattice relax. times obs. *(German)* 79−47350
nitrilotri (methylenephosphonic acid), adsorption on $BaSO_4$ crystals, effect on crystal growth 78−88417
nitro compounds in cyclohexane, electron attachment reaction rates from pulse radiolysis 78−31663
4-nitro-1-chlorobenzene, enthalpies and related thermodynamic functions 79−42276
n-nitro-n′-methylbenzylidene-aniline, triclinic, cryst. and mol. struct. 77−43205
3-nitro-o-anisidine, in benzene soln., dipole moment from solute relax. time-solvent viscosity relation 80−37905

organic compounds continued
3-nitro-o-anisidine-o-nitroaniline, soln., dielectric const., loss and relax., dipole moment 78−43782
p-nitro-p'-methylbenzylidene aniline, polymorphism 78−18633
p-nitroacetophenone, effect on size of DNA mol. under electron irradiation 80−89807
p-nitroaniline, adsorbed layer, core ionisation, negative shake-up energy 79−56913
p-nitroaniline, binding energy, XPS obs. 80−37833
p-nitroaniline, core ionisation negative shake up energy, ab initio SCF CI calc. 79−64041
p-nitroaniline, cryst., electronic excited states, config. interaction calcs., UV spectrum 78−10913
m-nitroaniline, cryst., low-freq. polarised Raman spectra 78−84574
m-nitroaniline, cryst., nonlinear optical susceptibility and spontaneous polarisation 77−58372
p-nitroaniline, exciton level directional dispersion, absorpt. band profiles 78−48192
n-nitroaniline, IR and Raman spectra, internal modes 79−61366
nitroaniline, IR spectral intensity, N-O group in aromatic ring 79−41199
p-nitroaniline, mol., second-order hyperpolarisability CNDO/S calc. 79−76358
p-nitroaniline, mol. hyperpolarisability in soln., UV dispersion of charge transfer contrib. 79−31986
m-nitroaniline, nonlinear optical susceptibility, second order, calc. from mol. spectra *(Russian)* 79−27318
m-nitroaniline, nonlinear optical susceptibility tensor, calc. 79−23011
p-nitroaniline, nonlinear second-order optical susceptibility 80−9947
nitroaniline, pulse radiolysis in aq. soln., intermediates form. and decay 77−60096
p-nitroaniline, Raman spectra, mol. struct. in molten state 79−91435
n-nitroaniline, UV light effect on nucleation during crystallisation on anthracene surface 80−75478
p-nitroaniline, valence and core photoionisation, spectral lines, many body effects 80−47853
nitroaniline admixture in TGS crystals, effect on thermal parameters 80−107580
m-nitroaniline single crystal fibre waveguide core, melt growth and characts. 77−34965
m-nitroaniline type, electro-optical film production 77−19463
nitroaniline-admixtured TGS, longit. US wave propag. domain struct. effects 77−55322
nitroanilines, hyperpolarisability, second harmonic generation and four wave mixing, excited dipole moment 77−54624
p-nitroanilines, intramol. charge transfer satellites, XPS 80−78650
nitroanilines electronic states, CNDO/s-CI correlative calcs. 78−58604
9-nitroanthracene, semiconductive props., gas adsorpt. effect 79−65471
9-nitroanthracene, subpicosecond laser photolysis and time resolved absorpt. spectra *(Japanese)* 79−79272
nitroaromatic compound+anion radical, photo-CIDNP, acid-base equilib. effects 77−75185
nitrobenzene:n-hexane, depolarised Rayleigh scatt., crit. anomalies 78−68524
nitrobenzene$^-$, positive ion formation energetics by negative ion charge stripping 80−78700
nitrobenzene, absolute Raman cross section determ. from inverse Raman effect 79−3447
nitrobenzene, activation energy for viscosity, rel. to charge distrib. 79−37865
nitrobenzene, adsorbed radicals, oxide surface chem., ESR 77−21417
nitrobenzene, anion radical, in benzoate crysts., EPR and X-ray diffr. obs. 77−1597
nitrobenzene, anisotropic mol. reorient., ^{13}C, ^{14}N and ^{2}H mag. relax. 77−48070
nitrobenzene, boundary phase in 5-layered light guide, birefr.. and equilib. thickness determ. 79−28711
nitrobenzene, collision-induced dissoc., ionisation characts. in corona discharge 77−60156
nitrobenzene, contact angle on pretreated polyethylene, H_2O environment *(Japanese)* 78−79858
nitrobenzene, DC elec. field induced optical rectification 77−38980
nitrobenzene, dielectric const. in mag. field 79−78606
nitrobenzene, dynamic and static orientational pair correls., depolarised light scatt. 77−16321
nitrobenzene, electric dichroism spectroscopy 78−1013
nitrobenzene, energy based integral repulsion method calcs. 78−82606
nitrobenzene, fluoresc. quenching of alternant and nonalternant polycyclic aromatic hydrocarbons *(German)* 78−21967
nitrobenzene, hyperpolarisability, mol. interaction effects in associating liquid mixtures 77−552
nitrobenzene, in acetone-isopropanol soln., Rayleigh scatt. and viscosity 80−5550
nitrobenzene, in benzene soln., liq. and solid, positron annihilation 77−1152
nitrobenzene, intensities in inelastic electron tunnelling, IR, and Raman spectroscopy *(French)* 79−822
nitrobenzene, IR absorpt. and Raman bands, half-band width conc.-depend. 80−74171
nitrobenzene, linear electrooptic effect 77−16283
nitrobenzene, liq., ^{14}N and D NMR, ^{14}N quadrupole coupling const., environmental effects 78−48052
nitrobenzene, liq., induced Raman scatt., anomalous line broadening 78−56490
nitrobenzene, liq., spin lattice relax. time, elec. field induced charges 80−44945
nitrobenzene, liquid, electrohydrodynamic convection, laser light scatt. exam. 78−14094
nitrobenzene, liquid and CCl_4 soln. shear waves and translation-rotation coupling obs. by depolarised Rayleigh scattering 80−71432
nitrobenzene, micropolar effects in liquids, characts. evaluation under rotating electric field *(Polish)* 79−55638
nitrobenzene, nonlinear second-order optical susceptibility 80−9947
nitrobenzene, oscill. optically induced Kerr kinetics 80−1286
nitrobenzene, polarised, simultaneous variation of dielec. const. and discharge current, room temp. to beyond melting point 80−11314
nitrobenzene, pulse radiolysis in aq. soln., intermediates form. and decay 77−60096
nitrobenzene, quenching and inhibition of orthopositronium 80−35002
nitrobenzene, Raman laser as efficient excitation source for stimulated Raman scatt. 79−18480

organic compounds continued
nitrobenzene, reduction, radical generation in tube electrode, laminar flow, convective diffusion, EPR 77−24746
nitrobenzene, refr. index, temp. depend., deviation from Lorentz-Lorenz. formula 77−40200
nitrobenzene, rot. relax. times of anisotropic mols., optical Kerr effect and viscosity expts. 77−79906
nitrobenzene, solns., elec. permittivity near crit. point 78−76372
nitrobenzene, spectral splitting of stimulated Raman scatt. 78−50860
nitrobenzene, steady state electroconvection, self beating laser spectroscopy 78−87408
nitrobenzene, substituted, IR spectra, vibr. modes 77−68039
nitrobenzene, temp. depend. of electro-optic Kerr coeff. 80−2725
nitrobenzene Aliquat nitrate liquid membrane ion-selective electrodes, free and supported, ion transport 79−83534
nitrobenzene Aliquat nitrate liquid membrane ion-selective electrodes, free and supported, ion transport 79−83535
nitrobenzene Kerr liquid filled nonlinear Fabry-Perot 79−27316
nitrobenzene molecules, bound positrons, time spectrum of positron annihilation 78−42248
nitrobenzene-aniline, US vel., sp. ht. and compressibility 79−33037
nitrobenzene-cyclohexane, binary liq. soln., surface cluster functions 78−67631
nitrobenzene-cyclohexane system, viscosity and activation energy 78−26615
nitrobenzene-d_0(p-d)(d_5), vibr. spectra 79−26966
nitrobenzene-d_5, vibr. spectra 79−22695
nitrobenzene-hexane, soln., dielec. permitt. in two phase region 80−2682
nitrobenzene-hexane critical solutions, crit. exponent determ. by nonlinear dielec. method 79−87373
nitrobenzene-hexane mixture, critical conc. determ. from dielectric const. meas. 77−20788
nitrobenzene-hexane mixtures, nonlinear dielec. effect beyond critical pt. 79−99816
nitrobenzene-hexane solution, double-scatt. light intensity near critical point of mixing *(Russian)* 80−55117
nitrobenzene-i-ioctane, soln., with critical point, US dispersion 77−1179
nitrobenzene-in-benzene optical fibre amplifier performance estimation 79−7217
nitrobenzene-methanol-iso-octane, US vel. and absorpt., along line of plait points in ternary liq. 78−79669
nitrobenzene-n-heptane, crit. mixture, conc. fluctuation mean relax. time, US absorpt. and vel. meas 80−29163
nitrobenzene-n-hexane, crit. mixture, multiply scatt. light, LF spectrum 77−52125
nitrobenzene-n-hexane, crit. mixtures, reorientation spectra, linewidths and intensities 79−28777
nitrobenzene-n-hexane, liq. mixture, static and dynamic viscosities near crit. point 77−69108
nitrobenzene-n-hexane, rapid evaluation of crit. multiple scatt. 78−84594
nitrobenzene-n-hexane, shear viscosity, critical conc. fluctuation rate, verification of renormalisation prediction 78−47514
nitrobenzene-n-hexane crit. mixture, depolarised Rayleigh linewidth meas. 77−81112
nitrobenzene-n-hexane crit. mixture, in ultracentrifuge, dynamic phenomena 80−44310
nitrobenzene-n-hexane crit. mixture, Rayleigh line and depolarised scatt. 77−20864
nitrobenzene-n-hexane critical mixture, shear viscosity meas. 77−72689
nitrobenzene-n-hexane critical mixture, ultrasound absorpt. 77−1178
nitrobenzene-water interface, mechanoelectrical energy conversion using interfacial tension changes 79−14982
nitrobenzene/n-hexane (n-heptane), critical exponent β, phase coexistence curve anal., viscosity coeff. meas. 80−100327
nitrobenzenes, substituted ^{14}N-NQR, elec. field gradient of NO_2 78−21944
5-nitrobenzimidazole in photographic processing solns., AC polarography determ. 79−24861
p-nitrobenzoic acid:rare earth laser materials, vibr. spectra, wavelength 125 to 500 mm 80−2769
nitrobenzoic acid, IR spectral intensity, N-O group in aromatic ring 79−41199
nitrobenzoic acid, lattice rigidity, mol. motions, wide-line NMR at room temp. 77−51967
nitrobenzol-n-hexane, hypersound velocity, absorption temp. depend *(Russian)* 80−75303
nitrobenzotrifluoride, benzene soln., permittivity and dielec. loss 78−64320
t-nitrobutane, phase, II, quasielastic neutron scatt. 78−26458
t-nitrobutane, plastic cryst., proton spin-lattice relax. time meas. 77−90058
nitrocellulose fibres, polarised light study 80−80736
nitrocyclopropane, vibr. spectra struct. and bonding 80−102520
N-nitrodimethylamine-do,(-d_6), structural phase transition, Raman study 80−34911
nitroethane, crit. soln. in cyclohexane, nonlinear dielectric effect 78−27152
nitroethane, cyclohexane and benzene solns., nonlinear dielec. effect 79−78602
nitroethane, dispersing agent for Na salt crystals in aq. slurries 79−61918
nitroethane, refr. index, temp. depend., deviation from Lorentz-Lorenz formula 77−40200
nitroethane+O, H atom abstraction in discharge flow system 78−35671
nitroethane-3-methylpentane, binary liq., depolarised light scatt. at crit. point 78−39558
nitroethane-3-methylpentane, crit. conc. fluctuations, nonexponential decay 80−44309
nitroethane-3-methylpentane, liquid-vapour surface tension near liquid-liquid consolute point 80−107613
nitroethane-3-methylpentane mixture, crit. temp. press. variation 80−15235
nitroethane-cyclohexane, pretransitional effects above phase transition temp., nonlinear dielectric meas. 79−15390
nitroethane-iso-octane(Hexane) solns., crit. exponents *(Russian)* 79−77766
nitroethane-isoctane, crit. mixture, conc. fluctuation mean relax. time, US absorpt. and vel. meas 80−29163
nitroethane-isooctane, crit. fluid, refr. index, α and Δ components 79−82940
nitroethane-isooctane mixture, crit. temp. press. variation 80−15235

organic compounds continued
nitroethane-isooctane mixture, depolarised Rayleigh scatt. near crit. point 80−45089
nitroethane/iso-octane, crit. mixture, refractive index 79−87413
2-nitrofluorene, $^1A \rightarrow {}^1L_a$ transition, electronic absorpt. spectra, solvent effects 77−58028
p-nitrofluorobenzene, nematic phase NMR, ^{19}F shielding anisotropy 78−62824
nitrofuranes, substituted, electron affinity, HAM/3 calc. 79−27109
nitrofurantoin, inhibition of X-ray induced UV resistance in E. coli K-12 cells 78−85342
nitrogen compound, reactivity with Si, rel. to polishing *(Russian)* 79−70192
nitrogenase, structure and function, role of Mo 77−86367
nitrogenated bicycle compounds, as source of interstellar 2200 Å absorpt. feature 78−12346
nitroglycerine, in waste water, monitoring continuous electrochem. analyser 77−60147
nitroglycerine, laser optoacoustic absorpt. spectra of explosive vapours 78−76941
nitroimidazoles, substituted, electron affinity, HAM/3 calc. 79−27109
nitromethane, 1-dimens. reorientation and tunnel splitting in solid 79−99086
nitromethane, ab initio SCF MO calcs. of geom. and bond energies 79−31381
nitromethane, DETA sensitized, steady state detonation vel., chemical inhomogeneity effect 80−89493
nitromethane, detonation reaction time 77−4904
nitromethane, dipolar plasmon, appl. calc. of solvated electron props. 77−89720
nitromethane, far IR reflection meas. and plasmon model relevance 79−33687
nitromethane, fluoresc. quenching of alternant and nonalternant polycyclic aromatic hydrocarbons *(German)* 78−21967
nitromethane, IR laser mutliple photon ionis. 79−74403
nitromethane, Kerr consts., depolarisation ratios and hyperpolarisabilities meas. 78−25624
nitromethane, liq., NMR relax. obs. of internal mol. rot. 79−95668
nitromethane, liq., proton spin-lattice relax., temp. depend. 78−39435
nitromethane, low lying electronic states, electron energy loss spectra, singlet→triplet excitation 79−27093
nitromethane, multiquantum absorption in intense IR field, isotope shift 77−19000
nitromethane, neat, external scale for ^{14}N NMR chem. shifts 78−24834
nitromethane, photodissoc., vibr. excited NO_2 form., fluoresc. obs. 78−37693
nitromethane, proton spin-lattice relax. time, methyl group rot., 1 to 10K 77−48080
nitromethane, Raman laser as efficient excitation source for stimulated Raman scatt. 79−18480
nitromethane, shock-induced elec. polarisation *(French)* 79−11381
nitromethane, shocked, utilisation of thermal ignition-time data for vol. of activation determ. 80−16683
nitromethane, solid, tunnel states investig. 80−103274
nitromethane, torsional barriers, electronic spectrum 79−59424
nitromethane, variable angle electron-impact excitation, transitions in 7-12 eV energy-loss range 80−69244
nitromethane, vibr. relax., Raman overtone band obs. 77−14436
nitromethane+alkali atom, collisional ionisation, electron affinity 78−66639
nitromethane+CS_2 liquid mixture, elec. resist. crit. phenomena 77−4212
nitromethane+H_2 reaction, CO_2 laser initiated, mechanism and yield 80−11912
nitromethane+O, H atom abstraction in discharge flow system 78−35671
nitromethane($-d_3$), CC ^{15}N NMR chem. shift references evaluation 78−24835
nitromethane in carbon tetrachloride, polarised line widths (intensities) in Raman scatt., conc. depend. 78−70879
nitromethane molecule dissociation in IR field, laser-induced fluoresc. obs. 80−53075
nitromethane-CS_2, crit. resist. of binary liq., 10 Hz-100 kHz 78−76123
nitromethane-CS_2, elec. resistance, crit. phenomena, freq. depends. 79−60884
nitromethane-CS_2 binary liq. mixture, crit. behaviour of elec. resist. 78−6422
nitromethane-d_0,-d_3, polycryst., methyl torsion, Raman spectra 79−82970
nitromethane-EBBA, binary liq. cryst. system, two-phase premelting, NMR obs. *(Russian)* 78−30743
nitromethane-isooctane, liq. mixture, coexistence curve, refr. index meas. 80−10655
nitromethyl anion, ab initio SCF ab initio MO calcs. of geom. and bond energies 79−31381
nitromethyluracil, radiation-induced oxidation and reduction 77−32816
1-nitronaphthalene, hyperpolarisability meas. by DC induced second harmonic generation 78−87096
nitronaphthylamines, ESCA and UV photoelectron spectra, assignments 78−50588
nitrone, config. interaction calc., using DODS natural orbit approach 78−66476
o-nitrophenol, cryst. and mol. struct., H bond distance 78−51523
n-nitrophenol, H-bonded complexes, IR absorpt. band struct., freqs. and intensities *(Russian)* 77−18928
nitrophenol, IR spectral intensity, N-O group in aromatic ring 79−41199
nitrophenol, pulse radiolysis in aq. soln., intermediates form. and decay 77−60096
o-nitrophenol, solvent effects on oscillator integrated strength, IR absorpt. bands 78−84575
4-nitrophenyl 4′-decyloxybenzoate, mol. struct. rel. to mesomorphic props. 77−89372
4-nitrophenyl 4-n-octyloxybenzoate, electrical Kerr effect studies 80−25339
4-nitrophenyl 4-n-octyloxybenzonate, space group unit-cell and crystallographic props. 80−6399
4-nitrophenyl 4-n-pentyloxybenzoate, electrical Kerr effect studies 80−25339
4-nitrophenyl 4-octyloxybenzoate, smectic-A and nematic phases, dielectric meas. 79−23516
p-nitrophenyl p-n octyloxy benzoate, liquid crystal, elec. cond. and dielectric constant, in solid phase 79−61293
organic compounds continued
4-nitrophenyl-4′-alkoxybenzoates, incommensurate smectic A phase 80−10647
4-nitrophenyl-4-octyloxybenzoate, nematic and smectic-A phase, dielec. meas. 78−60392
4-nitrophenyl-4-octyloxybenzoate/cholesteric liq. cryst. mixtures, helix pitch, temp. depend. 80−64895
1-nitropropane, electroviscous effect, AC characts. 79−99341
1-nitropropane, gaseous, photolysis, primary processes, study at 22°C and 100°C 80−89507
3-nitropyrene, triplet state, absorption spectra in soln. 78−33440
p-nitropyridine N-oxide, dynamic electron densities, anharmonic contribs. from large molecular librations 79−97971
nitrosamine, air sampling sorbents testing 80−77026
nitroso and nitrosyl cpds., ^{14}N chem. shifts correl. with nuclear quadrupole coupling consts. 77−30888
2-nitroso-2-bromo-3,3-dimethyl-butane, cryst. data 78−67703
N-nitroso-dimethylamine-d_0, -d_3, -d_6, struct., microwave spectra 79−59446
nitrosobenzene, fluoresc. quantum yields, determ. from Raman scatt. 80−58294
N-nitrosodimethylamine, trapping for GC/MS analysis 78−20094
p-nitrosodimethylaniline, solid and CCl_4, H_2O solns., Raman and IR absorpt. spectra 77−79615
nitrosodisulphonate ion salt dimerisation, ESR of dimers in triplet state *(French)* 77−12791
nitrosofluorene-lipid adducts, mutagenicity, ESR spectra investig. 80−91583
nitrosomethane, ground state and nonvertical n-π^* excitation energy calcs. 80−18804
nitrosomethane, microwave spectrum, structure, dipole moment and centrifugal distortion 78−66540
nitrosomethane, mol., spectra 600-720 nm, and geom. change on excitation 79−72329
nitrosomethane-d_3, electronic excitation, conformational changes obs. 79−98233
nitrosourea compounds, 2, anal. of interaction with X-radiation in rat brain tumour cells 80−72230
nitrosourea-^{13}N prep., chemical considerations in accelerator prod. of ^{13}N 79−53242
3-nitrothiophene, rot. transitions, torsion, microwave spectra 77−42313
p-nitrotoluene, in nematic mixture of octyl cyanobiphenyl, octyloxy cyanobiphenyl, dichroic exam. 78−27201
nitrotoluene, IR spectral intensity, N-O group in aromatic ring 79−41199
p-nitrotoluene, low-freq. vibr. spectrum, Raman and IR spectra 78−56484
m-nitrotoluene, pure and in soln., rot. relax. times of anisotropic mols., optical Kerr effect and viscosity expts. 77−79906
p-nitrotoluene, vibr. spectra, normal mode calcs. 77−65482
p-nitrotoluene crystal film, exciton spectrum, IR absorpt. and Raman scatt. 80−80771
nitrotoluene-pentane, pretransitional effects above phase transition temp., nonlinear dielectric meas. 79−15390
o-nitrotoluene-saturated hydrocarbon soln., critical exponent, permittivity meas. 78−22858
nitroxide free radical mag. interaction with lanthanides or Cu^{2+} in liqs., ESR 78−68380
nitroxide free radicals in liquids, electron spin-echo obs. 80−63685
nitroxide groups in crystals, H bonds and short intermolecular contacts 80−63855
nitroxide radical, long range Y-P hyperfine coupling, ESR spectra obs. 80−75858
nitroxide radicals, q- and A-tensor components, rot. mobility 2 mm EPR spectrosc. determ. 80−102530
nitroxide spin probes, solubilised, ESR obs. in cetyltrimethylammonium bromide micelles 78−21950
nitroxide spin probes, unresolved hyperfine broadening convection in EPR, linewidth and Heisenberg spin exchange freq. determ. 80−71180
nitroxyl radical, aromatic hydrocarbon singlet state quenching, triplet form. 77−88487
nitroxyl radical, cationic surfactant, intramicellar fluorescence quenching of $[1\text{-pyrenyl-}(CH_2)_n\text{-}N(CH_3)_3]^+Cl^-$ 80−9627
nitroxyl radical ($C_{13}H_{17}N_2O_2$), paramagnetic, deformation electron density *(Russian)* 79−90637
nitroxyl radical rotation in liquids, ESR, dielec. relax. 77−28447
nitroxyl radicals, cyclic, conform. flexibility, EPR obs. 80−91581
nitroxyl radicals, UHF saturation effects use for slow jumplike rot. obs. in ESR 79−28617
NMBA, monoclinic, cryst. struct. and nonlinear optical props. 78−26560
NMP-TCNQ, low temp. specific heat 78−52297
NMP-TCNQ, magnetic susceptibility and chem. pot. of two-site Hubbard Hamiltonian 77−47963
NMP-TCNQ, one-dimensional conductor with disorder, singularities in density of electronic states 77−8006
NMP-TCNQ, partial charge transfer effect, one dimensional disordered Hubbard model study 80−70687
NMP-TCNQ, Peierls insulator and antiferromagnetic mixed phase, mean field approx. 77−20626
NMP-TCNQ, X-ray diffuse scatt., and cond. study 80−49701
NMP-TCNQ epitaxial film, oriented, prep. by vacuum evaporation and properties obs. 79−15040
NMR investigations, reference list of solids 79−19786
NMR spectra, mag. field induced mol. alignment effects 79−18207
NMR spin-spin coupling consts., Fermi contact contrib., mol. orbital calcs. 77−68060
NOBAMBC, chiral smectic phases, pyroelectric and dielec. props. 79−91380
nonadecane, mol. motion in solid, ^1H spin relax. 78−15048
n-nonadecane, plastic phase, neutron quasielastic scatt. 79−51013
nonadecane, purification and single cryst. growth 80−71589
nonafluoro-iso-butane, isolated CH stretching freqs. and bond props. 79−94104
nonafluorobutane($-d_1$), and halo-substituted forms, gas and liq., IR and Raman spectra, normal coord. anal. *(German)* 79−72318
nonafluoroisobutane, IR spectra, spectral bandshape and intensity of C-H chromophore 80−83355
nonalternant hydrocarbons, charge distrib. rule 78−90060
n-nonane:H_2-tetra-4-tert-butylphthalocyanine, thermal broadening of zero phonon lines, hole burning 78−71803

organic compounds continued
nonane, liquid, chain reorientation, Brownian dynamics simulation, comparison of models 80−49067
n-nonane, short chain mol. liquid, statistical thermodynamics 79−64974
nonane dimer, intermolecular interaction energy, PCILO calc. 77−34572
nonane-NO_2, supersaturated gas, photoinduced nucleation 78−80760
nonanoic acid, soln., US relax. *(German)* 78−22792
nonanol, sound vel. and absorpt. meas. at hypersonic freqs. 78−18708
nonbenzenoid aromatic hydrocarbons, ionisation pot. and electron affinities, semiempirical MO theory 79−6843
nonbenzoid hydrocarbons, ionisation pot. and heat of form., IOC-ω method 79−31733
nondecane, plastic cryst., Rayleigh scatt. of Mossbauer radiation 78−27125
nonelectrolyte aqueous solutions, temp. of max. density rel. to partial compressibility, struct. strengthening 80−30270
nonlinear optical materials, SHG efficiency 77−75619
nonmethane hydrocarbons, photochemical effects in atmosphere 78−49090
nonpolar binary mixture, partial molar vol. prediction from Lee-Kesler eqn. of state 80−10632
nonpolar liquids, far infrared absorption 80−50331
nonylammonium bromide, micellar aggregation number, ^{13}C NMR chemical shift conc. depend. 80−48016
p′-nonylhydroxybenzoic acid, struct. characts., cylindrically symmetrical interatomic-distance function 77−11482
p-nonyloxy benzoate p-butyloxyphenol, smectic A to smectic C transition, crit. ang. fluctuations, Rayleigh scatt. obs. 79−95131
p-nonyloxybenzoate p-butyloxyphenol, smectic A to smectic C transition, crit. fluctuations, Rayleigh scatt. obs. 78−95140
p-n-nonyloxybenzoic acid, nematic, cond. anisotropy, dopant effect 77−7667
p-n-nonyloxybenzoic acid, smectic C phase, electro-optical effect *(Russian)* 80−92458
nonyloxybenzoic acid/cholesteric liq. cryst. mixtures, helix pitch, temp. depend. 80−64895
p-n-nonyloxybenzylidene-p-aminobenzoic acid, liq. cryst. phase transitions, X-ray diffr. and DSC meas. 79−86877
nonylphenol diethylene glycol ether-water-p-xylene system, liquid crystal stabilization of multiple emulsions 79−16046
(+)-nopinone induced circular dichroism of azulene π-π^* bands 80−53058
noradrenaline local perfusion maintains visual cortical plasticity 78−35847
norbornadiene, excited electronic states, electron impact spectrosc. 79−45842
norbornadiene-quadricyclene photoisomeric interconversion for solar energy chemical conversion and storage 80−89664
norbornadienes, LF vibr. modes of hydrogeneous ligands, incoherent inelastic neutron scatt. 78−6229
norbornane, derivatives in solution, mol. motion and methyl group rot. barriers from ^{13}C NMR relax. times 80−74179
norbornane, microwave spectrum and dipole moments 80−78606
norbornene, excited electronic states, electron impact spectrosc. 79−45842
norbornylene and norbornane, HCP plastic cryst. phases, radiotracer self-diffusion obs., monovacancy mechanism 79−33111
α-NPO, fluoresc. spectrum light quenching factor wavelength depend. 80−18882
α-NPO in polystyrene, 77K phosphorescence *(Russian)* 78−27286
α-NPO-Ar mixture, vapour phase laser, electron beam pumping 78−63097
α-NPO-inert gas vap. mixture, electron beam pumping 77−42535
nuclear magnetic shielding constant, calc. by extended Huckel method with expansion by Gaussian functions 77−79634
nuclei acid phosphate group, analytical atom-pair pot., SCF-LCAO calc. 79−70516
nucleic acid, multiphoton photoreactions of aq. soln., picosec. UV pulse 79−34487
nucleic acid bases, ^{14}N relax. and N-proton spin coupling, NH-proton spin-lattice relax. 80−26202
nucleic acid bases, charge carrier photoexcitation quantum yield 79−99581
nucleic acid bases, excited state geometry distortion, normal modes reson. Raman intensity anal. 79−68236
nucleic acid bases, excited states formation, EHT calc. 79−13651
nucleic acid bases, proton mag. relax., methyl group reorientation 77−64009
nucleic acid bases, Zn^{2+} binding, ab initio SCF (pseudopot.) calcs. 80−12052
nucleic acid constituents, reson. Raman spectra using synchronously pumped dye laser 79−12869
nucleic acid determination by multiparametric pulse cytophotometry *(German)* 77−78060
nucleic acid molecules, preprocessing of electron micrographs for automatic computer anal. 79−70711
nucleic acid optical measurements in presence of phenol and protein impurities 77−56546
nucleic acid purine, pyrimidine bases, base pairs, hydration scheme 79−92127
nucleic acid solutions, dye-tagged, electrically induced fluorescence polarised component change meas. 80−32863
nucleic acid-TCNQ complex, charge transfer interaction 80−3576
nucleic acids, bases and base pairs, water struct. in soln., Monte Carlo simultion 80−76709
nucleic acids, double-helical, conformations 77−12880
nucleic acids, electronic absorpt. and emission spectra 80−55989
nucleic acids, H_2 exchange kinetics and internal motions 80−21440
nucleic acids, pulse radiolysis study of interactions with amino acridines 78−85186
nucleic acids, Raman spectroscopy obs. *(German)* 79−27119
nucleic acids and related compounds, photoemission rel. to absorpt. and luminesc., 120 to 250 nm 77−81466
nucleic acids and their aggregates, optical activity, review, book contrib. 80−108847
nucleic acids bases, excited state dipole moments and geometries 80−95738
nucleic bases, interactions and self-organisation, ionisation and solvent salt comp. effects 80−55985
nucleoside anion + hydrocarbon cation, electrochemiluminescent electron transfer reaction 79−88046
organic compounds continued
nucleoside cyclic monophosphates, phosphodiester stretching vibrs., IR and Raman spectra 77−65461
nucleoside phosphates, adsorption on volcanic rocks rel. to origin of life 77−91273
nucleosides, X-irrad., alkoxy radical form., ESR, INDO calcs. 77−90623
3′-nucleotide, calcs. to assess rigidity 80−61506
nucleotide anion + hydrocarbon cation, electrochemiluminescent electron transfer reaction 79−88046
nucleotide base stacking interactions in vacuum, field mass spectrometry 80−81526
nucleotide bases, electronic absorpt. and emission spectra 80−55989
nucleotide sugar-phosphate region, γ-irradiated, deoxycytidine 5′-phosphate alkoxy radical EPR 79−5249
nucleotide threadlike crystal form. 78−95994
nucleotides, cyclic, prejunctional role in neuromuscular transmission 77−1987
nucleotides, interactions and self-organisation, ionisation and solvent salt comp. effects 80−55985
nucleotides, X-irrad., alkoxy radical form., ESR, INDO calcs. 77−90623
nylon 6-Li halide mixtures, viscoelastic behaviour, stress relaxation 80−58995
nystatin action on lipid planar bilayers, spin label study 77−29108
o-phosphorylethanolamine, ESR of phosphite radicals in X-irradiated single crystals 79−51857
OBPA, liq. cryst., proton spin-lattice relax., freq. cut-off effect 77−20738
8OCB, nematic-smectic A transition, impurity effects 78−47507
7-8-OCB mixture, nematic-smectic A transition, impurity effects 78−47507
octachlorofulvalene, electronic structs., semi-empirical MIEHM calcs. and photoelectron spectra 77−75057
n-octacosane, depolarised Rayleigh spectroscopy 79−4808
octacosane crystals, complex growth polytypism and periodic polysynthetic twins 77−47360
n-octadecane, surface charge decay 78−43463
n-octadecane, thermal energy storage material heat transfer during melting of cylinders 79−3894
n-octadecanol, growth of high temp. α-phase crystals in γ phase single crystals 78−71700
octadecanol, normal, single cryst., lattice defects, X-ray topographic obs. 78−18650
octadecyl hydrogen maleate, spectrometer cryst., 2d value determ. method 77−65933
octadecyl-trichlorosilane in MIM junction, elec. cond. mech. 78−95386
octadecylacrylamide films, oriented ultrathin, radiation-induced solid state polymerisation 80−80128
octadecylamine, adsorption on NaCl, effects on dislocation motion *(Russian)* 77−51372
p-n-octadecyloxybenzoic acid, thermal props. 77−47345
octaethylchlorin, metal complexes, polaris. fluoresc. and phosphoresc. spectra 79−54906
octaethylchlorin, phosphoresc. polarisation spectra obs. 77−18963
octaethylisobacteriochlorin metal complexes, polaris. fluoresc. and phosphoresc. spectra 79−54906
octaethylporphin, phosphoresc. polarisation spectra obs. 77−18963
octaethylporphin, radiationless transitions, fluoresc. and phosphoresc., isotope effects 77−65502
octaethylporphin in Al-Ag sandwich cell, electroluminesc. 77−59615
octafluorocyclobutane, and +n-butane mixtures, surface tension meas. 79−19371
octafluorocyclobutane, laser induced unimolecular decomposition 77−32775
octafluoronaphthalene, high press. struct., neutron powder diffr. 78−63743
octafluoronaphthalene, phase transitions at elevated press., Raman and mid-IR spectroscopy obs. 80−45062
octafluoronaphthalene, struct. phase transition exam. 77−47572
octafluoronaphthalene crystalline complexes with naphthalene and durene, triplet exciton emissions 80−84760
octafluoronaphthalene crystals, phase transition, Raman spectra 77−24829
octafluorotoluene, γ-radiolysis, matrix isolation spectra of radical anions 79−52704
octamethylcyclotetrasilazane, gas, liq., cryst., CCl_4 soln. IR and Raman spectra, assignments, struct. *(French)* 78−29790
octamethylcyclotetrasiloxane-cyclohexane liq. mixtures, u.p. and excess Gibbs free energy determ. 77−30225
n-octanal, equilib. anionic polymerisation, −90 to −68°C, polar substituent effects 78−88631
octane: pyrene(coronene), quasiline spectra, multiplet struct., freezing conditions and solvent effects 79−1786
octane, first-order props. of simulated ab initio molecular orbital wave functions comparison with SCF wavefunctions 79−41094
octane, fragmental and molecular orbitals, CNDO/2 approx. calcs. 80−42947
octane, liq., Raman scatt. at high-press., chain kinking 79−87429
n-octane, liq., thermal cond., meas. by transient hot-wire technique 80−103522
n-octane, liquid, under high press., refr. index vs. density 79−28712
octane, loss angle, temp. depend., 9 and 36 GHz 78−48114
n-octane, low-press. boiling on Cu surface, accel. heat transfer due to porous Ni layer 77−85056
octane, melting surface, ablation in impingement region of water jet 80−14766
n-octane, organic impurity molecular fluoresc., effect of heat pulses 78−88360
octane, pore filling of wetproofed electrode 80−40702
n-octane, refractive index at X-ray wavelengths *(Russian)* 79−47409
n-octane, relax. about porphyrin defects and vacancies, Monte Carlo calcs. 79−46577
n-octane fluid, gauche-trans. relax. 79−69002
n-octane fluid, spontaneous cavitation 80−69886
n-octane liqs., refractive index, pressure effect 80−71375
octane radical cations in γ-irrad. pentane matrices, ESR 77−36765
octane-water interface, electron transfer in presence of chlorophyll 77−81474
octane-water interface, water photo-oxidation in presence of adsorbed porphyrins 78−64933
1-octanol, dielec. consts., solvent struct., effect of H bonding solutes, chain length 77−48674

organic compounds continued
octanol, sound vel. and absorpt. meas. at hypersonic freqs. 78−18708
1-octanol-benzenes (carbon tetrachloride) dilute solns., dielec. consts., dipole moments, H bonding investig. 77−48673
n-octanol-carbon tetrachloride-water miscible liq. systems, isopiestic vapour press. meas., activity coeffs. determ. 77−48679
1-octanol-H-bonding solute system, chain assoc., dipole correl. theory, dielec. const. anal 77−48675
1-octanol-nonhydroxylic solvent complexes, H bonding, assoc. consts., elec. dipole moments, dielec. consts. 77−48672
octaphenylcyclotetrasiloxane, mesophase form., neutron diffr. obs. 78−91224
octaphenylcyclotetrasiloxane, phase behaviour and nucleation kinetics 80−29168
1,3,5,7-octatetraene, π-electron struct., generator coord. method 79−26880
trans, trans-1,3,5,7-octatetraene, high-resolution one and two photon excitation spectra 80−78669
trans, trans-1,3,5,7-octatetraene, low freq. normal modes, CFF-π calcs. 79−68217
1,3,5,7-octatetraene, lowest excited singlet state, dipole forbidden character 79−27024
1,3,5,7-octatetraene, UV, visible, and fluoresc. spectra and assignments, evidence for ^1A_g state 78−33518
trans-octatetraene, weak low-energy band, S and T levels by fragment method 78−82625
n-octatriacontane 78−51669
1-n-octene-n-octane, vapour-liquid equilibrium, T-x meas. by semi-micro method 78−87782
cis-9-octodecenoic acid+cyclohexane excess enthalpy, calorimetric cell 79−58689
p-octoxybenzoic acid:cholesteric nonanoate, mag. field induced cholesteric→nematic transition Raman spectra 77−27988
4n-octyl-4′-cyano-biphenyl, liq. cryst., density, and rel. change at phase transitions determ. 77−80605
4-n-octyl-4′-cyano-diphenyl, appl. in detection of graphite powder particles by optical microscopy 80−9034
4-octyl-4′-cyanobiphenyl, liq. cryst. phases, dielec. relax. meas., short range interactions 78−94976
4-n-octyl-4′-cyanobiphenyl, smectic A and nematic liq. cryst., refr. indices and order parameters 78−22644
4-n-octyl-4′-cyanobiphenyl, smectic A liq. cryst., shear-induced textures and rheology 78−91228
4-n-octyl-4′-cyanobiphenyl, smectic A phase, stimulation of EHD instability 79−78656
4-n-octyl-4′cyanobiphenyl/4-n-decyl-4′cyanobiphenyl mixture, dynamic characts. of electrooptical effect with memory 80−108183
4-octyl-4-cyano-biphenyl, nematic to smectic A phase transition texture changes, thermoelectrooptic effect 80−49098
4′-n-octyl-4-cyanobiphenyl, chain ordering model 80−24357
4′-n-octyl-4-cyanobiphenyl, interlayer elastic const. meas. close to smectic-A to nematic transitions 77−80606
4′-n-octyl-4-cyanobiphenyl, thermotropic mesophase, DMR chain segments assignment 80−24356
octyl-cyano-biphenyl, elastic props. near smectic-A nematic transition 79−23704
octyl-cyano-biphenyl, influence of laser light wave field on nematic phase *(Russian)* 80−92456
octyl-cyano-biphenyl, nematic and smectic-A phase, dielec. meas. 78−60392
octyl-cyano-biphenyl, smectic-A and nematic phases, dielectric meas. 79−23516
octyl-cyanobiphenyl, elastic props. near nematic-smectic A transition 78−59756
octyl-cyanobiphenyl, smectic A-nematic transition, X-ray and light scatt. obs. 79−95129
octyl-cyanobiphenyl nematic cryst., optical and DC Kerr effects 79−7183
4-n-octyl-d_{17}-oxybenzoic acid-d_1, nematic and smectic phases, mol. and relative segmental order 80−96439
p-n-octyl-p′-cyanobiphenyl, thermally addressed liq. cryst. display, light scatt. and contrast 80−34892
octylcyanobiphenyl, crit. heat. capacity near nematic-smectic A transition 80−100323
octylcyanobiphenyl, second sound propag. and smectic response function, forced Rayleigh scatt. obs. 79−86693
octylcyanobiphenyl, smectic liq. cryst., orientation between different interface and induced struct. *(French)* 77−51310
octylcyanobiphenyl thin film, asymmetrical and symmetrical structure of smectic liquid crystal *(French)* 77−35473
p-n-octyloxy benzylidene-p-toluidine, mol. order, EPR VAAC probe 80−70114
p-n octyloxy benzylidine-p-toludine, liquid crystal, elec. cond. and dielectric constant, in solid phase 79−61293
4-octyloxy-4′-cyanobiphenyl, CN stretching in liq. cryst. phases, vibr. spectra 78−80325
4-n-octyloxy-4′-cyanobiphenyl, smectic A liq. cryst., elastic modulus determ., stress/strain relationships 78−91229
4-octyloxy-4′-heptyl-α-cyanstilbene liquid cryst., mag. props. 78−87615
4-n-octyloxy-4'-cyanobiphenyl, liquid cryst., dielect. polarisation and its dispersion 79−1397
trans-p-n-octyloxy-α-methyl-p′-cyanophenyl cinnamate, mag. and elec. birefr. in isotropic phase 80−80744
4-n-octyloxybenzoyloxy-4′-cyanostilbene, re-entrant polymorphism, nematic-smectic A-nematic-smectic A, X-ray study 80−34172
4-octyloxybenzoyloxy-4'-cyanostilbene, enantiotropic reentrant nematic behaviour at atmos. press. 79−60490
octyloxybenzylidene-β-methyl-butyl-aniline, freely suspended ferroelec. smectic-C liq. cryst. film, light scatt. meas. 78−47236
n-p-octyloxybenzylidene-p-toluidine, dielectric behaviour in nematic mesophase at RF 80−34842
N-p-octyloxybenzylidene-p-toluidine, optical props., density, and order parameter in liq. cryst. phases 79−55657
octyloxycyanobenzylidene, smectic A, anomalous ordering, Landau-Peierls system 78−30538
octyloxycyanobenzylidene, smectic A liq. cryst., high resolution X-ray scatt. exam. 78−94984
p,p′-octyloxycyanobiphenyl, flexoelec. coeff. in nematic phase, thermal depend. 80−79685
octyloxycyanobiphenyl, liq. cryst., twist viscosity and mech. props. near smectic A-nematic transition 78−95136
organic compounds continued
octyloxycyanobiphenyl, nematic-smectic A transition, heat capacity study 80−88033
octyloxycyanobiphenyl, nematic-smectic-A transition sp. ht. 79−42225
octyloxycyanobiphenyl, smectic-A phase, dislocation effects on viscoelastic props. 77−84633
octyloxycyanobiphenyl-heptyloxyaminofluorenone, liq. cryst. mixtures, nematic-smectic A-smectic C Lifshitz point 77−69077
4-n-octyloxyphenyl 4-n-pentyloxybenzoate, permittivity, microwave dielectric relaxation 80−80671
p-octyloxyphenyl-p′-pentyloxybenzoate, charge carrier mobility and cond. in nematic and isotropic phases 80−44347
p-octyloxyphenyl-p-pentoxybenzoate, nematic liq. cryst., elec. discharge meas. of persistent internal polarisation 80−10488
4″-n-octylphenyl-4′-n-octylbiphenyl-4-carboxylate, orthogonal smectic B to tilted smectic B (smectic H) transition 79−94881
OEBBA, polarised luminesc. 77−24897
OHMBBA, nematic, dielectric behaviour at RF 79−7548
OHMBBA, solid phase dielectric relax. times and strength, mol. rot. 78−72456
oil, lubricating, radn. effects and radn. dosimetry appl. 80−2069
oil, spreading on water, rel. to surface contamination 79−43795
oil, US flow measurement in laminar-turbulent transition region 79−68850
oil layer, deformable, spatial light modulator as incoherent to coherent image transformer 80−96008
oil-polymer mixture, acoustic attenuation CW meas., tissue simulation appl. 80−35961
olefin+NH_3, gas mixtures, γ-radiolysis over whole composition range *(Japanese)* 79−5172
olefin+O reactions, relative rate consts., N_2O photolysis obs. 79−83472
olefin+thiirane+O_3+SO_2, excited neutral metastable SO_2 form. mass spectrometric study 80−83300
olefin hydrocarbon vapour, thermal cond., 160 to 400°C 78−1783
olefin triplet lifetime measurement by electron transfer interception 79−79269
olefines, radiation chem. alkylation with adamantane in gas phase 77−48663
olefins, chemiluminesc. reaction with ozone, use in stratospheric ozonometer *(French)* 79−48574
olefins, minimum energy goemetry, torsion of double bond 77−71755
olefins, zwitterionic states, polaris. and vibronic interactions 80−32620
olefins+N-ethylphthalimide, photochemical reaction, absorpt., fluoresc., phosphoresc. and triplet-triplet absorpt. spectra 80−85197
oleic acid, absolute evaporation rate meas. 78−2244
oligo methines, thermotropic nematic phase formation, role of molecular mass *(French)* 78−75547
oligobutenes, anomalous behaviour of viscoelastic props. 77−63704
oligocarbonatemethacrylates, and their cross-linked polymers, thermophysical characts., temp. depend. anal. 80−19721
oligoesters, effect of mol. architecture on dispersion props of TiO_2 in non-aqueous liquids 80−40751
oligoethylene glycols, ref. index meas. 79−34375
oligomers, polymer-derived, mass spectral charact. 80−37916
oligopeptides, conformational studies, kinetic energy problems 79−13848
olive oil, melting surface, ablation in impingement region of water jet 80−14766
one-dimensional and two-dimensional conductors, optical props. of small organic metal particles 80−45106
one-dimensional conductors, electron-electron scatt. 80−107776
OOAB, liq. cryst., smectic and nematic, distrib. functions by X-ray diffr. 79−99072
OOAB, nematic thermotropic mesophases, end-chain ordering and even-odd effects, deuterium mag. reson. 79−82890
OOBPD, smectic, DTA obs. of phase transitions to 3 kbar 79−23708
optical Kerr effect kinetics induced by picosecond laser pulses 80−102779
optical purity origin in living beings, effects of β-decay 78−40459
optically active molecules and polarised bremsstrahlung 77−63938
optically detected mag. reson. study of lowest excited triplet state xanthione, optically detected mag. reson. study of lowest excited triplet state of aromatic thioketones 78−86901
organic carbon analysis, automation 80−45592
organic dielectric layered structures quasi two dimensional conductors *(Russian)* 80−33989
organic heat carriers, charact. *(German)* 78−79198
organic molecules, multiphoton ionisation mass spectra by ArF excimer laser 80−81381
organic tensio-active compounds, mol. orientation correlations in hydrophobic groups *(French)* 79−73957
organic water pollutant, DDT, influence of detergents on hydrosolubility and suspension *(French)* 80−7961
organo-arsenic compounds, $(CF_3)_2AsSCH_3$ and $(CF_3)_2AsSeCH_3$, gas phase IR and liq. Raman spectra, normal coord. anal. *(German)* 80−32725
organoarsinoboranes, ^{11}B NMR 78−90190
organochlorine, pesticide residual levels, pollution in Sathiar reservoir water, mud and organisms 80−45828
organochlorine residues in rainwater 78−73495
organolead compounds adsorbed on atmospheric particulates in urban air 77−73831
organometallics, photochemistry with applications to imaging systems 77−4914
organonitrogen derivatives of Si, Ge and Sn, prep. and props. 78−60456
organonitrogen molecules, synthesis in interstellar clouds, ion-molecule scheme 80−12786
organophosphorus compounds, $(CF_3)_2PSCH_3$ and $(CF_3)_2PSeCH_3$, gas phase IR and liq. Raman spectra, normal coord. anal. *(German)* 80−32725
organophosphorus pesticide residual levels, pollution in Sathiar reservoir water, mud and organisms 80−45828
organophosphorus pesticides, trace analysis by mass spectroscopy, ionisation methods 78−76939
organosilane coupling agent interphase of glass-fibre reinforeced plastics, molecular organisation 80−44195
organosilicon binder, for prod. of spalling-resistant quartz glass based ceramic 80−40313
organotellurium compounds, thermally developable light sensitive systems 79−2850
orientational correlation parameter for liquid 79−73090

organic compounds continued
orthocarboranes, IR spectra, CH intra-, intermol. perturbations, hydrogen bonds *(French)* 77−68044
orthocyanobenzyl bromide, lattice consts., space group, density, X-ray obs. 78−51525
orthorhombic crystals, triboluminescence and piezoelectric behaviour 79−95861
ouabain, binding sites on $(Na^+ + K^+)$ATPase rel. to subunit comp. 79−83704
ovalene, isolated ultra cold mol., intermediate level structure of S_2 state 80−28048
ovalene, minimal exposure high resolution electron microscopy 80−79653
ovalene, vibrational quasicontinuum threshold, spectrosc. criterion 80−52972
2-oxa-6-thiaadamantane, plastic phase, transition and fusion thermodynamics, DSC meas. 78−75603
oxa-bis(t-butylperoxytriphenyl-antimony); X-ray cryst. and mol. struct. determ. 79−60350
2-oxaadamantane, plastic phase, transition and fusion thermodynamics, DSC meas. 78−75603
7-oxabicyclo (4.1.0) hept-3-ene, conformation, dipole moment, microwave spectrum 78−66539
7-oxabicyclo-[4,1,0]-hept-3-ene, far IR spectrum, Q-branch transitions calcs. 77−6770
1,3,4-oxadiazole derivatives, in soln., IR absorpt. and fluoresc. spectra, vibr. anal. 78−66597
oxadiazoles, ^{14}N NQR of mol., expt. and MO calc. 79−36667
2′-oxaindan (dihydroisobenzofuran) spiropyrans, photochromic transforms, spectrokinetic study 80−30259
oxalacetic acid-Mn^{2+}-H_2SO_4-$KBrO_3$, chaos type reactions anal. 80−85165
oxalate decomposition kinetics, in polymeric medium, thermogravimetry and DTA 78−52749
oxalate esters, low intensity long duration chemilum., disposable lighting device appl. 80−11488
oxalate ion, vibr. assignments, force consts., coincidence method appl. 78−62953
oxalate ion in aq. soln., vibr. study and Raman bands 80−95588
α-oxalic acid.$2H_2O$, proton mag. shielding, rel. to deuterium shielding 77−77106
oxalic acid, cryst. binding, ab initio MO SCF calc. 79−37657
oxalic acid, monomeric, IR matrix-isolation spectra, vibr. anal. 78−66550
oxalic acid, theoretical deformation density, ab initio Hartree-Fock calcs. 79−32982
oxalic acid diamide, mol., PMR and IR spectra, easy polarisable H-bonds 79−31516
α-oxalic acid dihydrate, H_2O proton shielding tensor, multiple pulse proton NMR obs. 80−63655
α-oxalic acid dihydrate, low-lying excited states, ODMR and optical obs. 79−41188
oxalic acid dihydrate, NMR spectra, ^{13}C-^{13}C interaction, chemical shift effects 78−29800
oxalic acid dihydrate, PMR, water mols., reorientation 79−42856
oxalic acid dihydrate, proton spin-lattice relax., 180° flips and diffusion of water mol. 77−15327
oxalic acid dihydrate, pulsed excitation of luminesc. 78−27326
oxalic acid film, on Al, heat treatment effect on photoluminesc. props. 77−28610
oxalic acid films on Al, photoluminesc. obs. 77−1729
oxalic acid in aq. soln., vibr. studies, IR and Raman spectra 80−95589
oxalic acid-dioxan solns., compressibility, internal press., US vol., H-bonding 79−82272
oxalic and dihydrate, monocrystals, high resolution PMR 78−64283
oxalyl bromide, normal vibr. freqs., force fields 79−41155
oxalyl chloride, normal vibr. freqs., force fields 79−41155
oxalyl chloride, rot. isomerism, CNDO and EHT-type methods 78−58591
oxalyl chloride (fluoride), centrifugal distortion consts. and thermodynamic functions, pot. energy calc. 79−22619
oxalyl fluoride, $^1A_u(n\pi)$-^1A_g fluoresc. excitation spectrum in pulsed supersonic jet 79−31577
oxalyl fluoride, radiative and nonradiative transitions, self-quenching, unimol. dissoc. 78−17708
oxamide, thermal expansion tensor, calc. from lattice constant changes with temp. 77−76582
oxanilide, IR and Raman spectra, cryst. struct. and vibr. 79−42954
oxaxine-1, laser dye, electrochem. reduction, EPR spectra 77−70304
oxazine 1 and 9 laser dyes, absorpt. and gain with picosecond pumping 79−55134
oxazine 720, single freq. CW dye laser operation in 690-700 nm gap 80−99719
oxazine dyes, comparative photostability 80−3376
oxazine dyes, orientation of $S_1 \rightarrow S_n$ transition moments, continuous ps photometry 79−10152
oxazine dyes fluorescence efficiency of laser dyes 77−42531
oxazine-1-perchlorate mode-locked CW dye lasers, tunable near IR ps and subps pulse generation 79−45972
oxazole(-d_1), dipole moment, quadrupole coupling tensor, from microwave spectrum 78−55166
oxazole scintillator solns., two- and three-component, laser emission spectra 80−32980
oxetane, clathrate hydrate, struct. II, for IR spectra, 4-100K 79−13707
3- oxetanone, electron structure, orbital-O interaction, MO calcs., UV photoelectron spectra 80−28058
oxidation, catalytic effects on electrode reactions, review 80−61110
1,6-oxido-[10]annulene, electron excitation, electron resonance, triplet states 79−54976
oximes, reaction with bis(cyclopentadienyl)titanium(IV) chloride, IR spectra 78−92471
oxiphenol, radical transform. in aqueous solns., chem. equilib. *(Russian)* 79−39138
oxirane, triplet state, torsional motion relax. 79−49959
oxirane cation, struct. rearrangement following vertical ionisation, ab initio CI calc. 80−58191
oxiranecarboxaldehyde, microwave spectrum, torsional excitation energy, partial struct., dipole moment 77−38655
oxiranylidene, struct., isomerisation, ab initio SCF MO calcs. 78−41941
oxirene, ab initio calc., energy levels and geom. struct. of C_2H_2O isomers 78−62716
oxocarbon ions, reson. Raman scatt., Jahn-Teller effect 79−18190

organic compounds continued
oxoniomethylene cation, rearrangement to hydroxymethyl cation, barriers, ab initio MO calcs. 80−104424
oxovanadium carboxylates, near one-dimensional antiferromagnetism, thermal and mag. props. calc. 77−20602
oxtyloxycyanobiphenyl, nematic-smectic-A transition, high-resolution 80−10649
β-oxy butyric acid ethyl ester, scaled spectra using three joined pulse sequences 80−73405
oxy-acetylene combustion products, seeded, elec. cond. rel. to MHD power generation 77−3922
oxyacetylene, critically-initiated detonation waves, quasi-steady regime 78−90930
2-oxybicyclo(3.2.0)hept-6-ene, LF vib. spectra, conformations 78−58685
oxyhaemoglobin, spin labelled, rot. correl. times, saturation transfer EPR 77−8387
2-oxyphenylbenzoxazol, proton intramolecular transfer, light absorpt. and emission, dichroism, polarised fluoresc. 80−87166
oxypyrenetrisulphonate anion, aq. soln., ps time depend. fluoresc. depolaris. obs. rot. diffusion determ. 77−81139
oxytocin, amide H exchange rates in aq. soln., ^1H NMR effects 79−83692
p-(p-ethoxybenzylidene) amino benzonitrile, positron annihilation exam. 79−19149
p-alkoxybenzylidene-p′-amino-2-chloropropyl-cinnamate, chiral smectic, dielec. props. 80−96441
p-azoxyanisole, nematic phase Couette flow mag. field and boundary condition effects 77−3887
p-terphenyl, positronium and thermal defects 80−24496
[p-]quinquaphenyl film between metal electrodes, memory switching 80−2484
PAA, cryst. phase transitions, intermolecular motion, Raman and inelastic neutron scatt. spectra 80−2164
PAA, deuterated, mol. reorientation, quasielastic neutron scatt. study 79−86705
PAA, effect of mol. struct. on nematic liq. cryst., phase 78−42901
PAA, flexoelec. charact. of longitudinal domains 79−46570
PAA, fluctuations near Rayleigh-Benard instability, real time obs. by neutron scatt. 80−59390
PAA, homologous series, isotropic phase, mol. self diffusion by spin echo method 80−44109
PAA, isotropic, nucl. spin-lattice relax. 79−23519
PAA, isotropic phase, Brillouin scatt. spectra, hypersound data determ. 79−91453
PAA, isotropic-nematic phase transition, optical microscopic obs. 79−69230
PAA, isotropic-nematic transition, appl. of integral eqn. for ang. distrib. function *(Russian)* 78−6147
PAA, isotropic-nematic transition, mean-field theory, thermodynamic props. 77−24391
PAA, isotropic-nematic transition, supercooling and nucleation, interface dendrites 78−42896
PAA, light scatt. near cryst. to nematic transition 80−16046
PAA, liq. cryst., empirical form for orientation-ordering intermolecular pot. 77−27809
PAA, liq. cryst., phase transitions up to 3 kbar, transition enthalpy, entropy 77−20051
PAA, liq. cryst., solid-state polymorphism obs. 77−4200
PAA, methoxy deuterated, reorientational correl. times, comparison of neutron scatt. and dielec. relax. data 79−7545
PAA, methyl deuterated, dipolar spin system exam. 77−39533
PAA, methyl deuterated, nematic liq. cryst., soft-mode dynamics, proton NMR 78−79749
PAA, methyl group rotation in solid and nematic phases, NMR obs. 78−6595
PAA, nematic, adjustable domain struct. in inhomogeneous elec. field, electro-optic props. obs. 80−10494
PAA, nematic, freq. depend. of proton T_1, rot. diffusional mechanism interpret. 77−12219
PAA, nematic, NMR study of ordering, intramol. mobility 80−100162
PAA, nematic, orientation in thick layers, continuum theory validation 77−15312
PAA, nematic, temp. depend. of sp. vol. 77−7665
PAA, nematic and crystalline phases, NMR and relax. 79−4740
PAA, nematic liq. cryst., collective excitation dispersion, neutron inelastic scatt. data 77−35475
PAA, nematic liq. cryst., elastic consts. determ. 77−27824
PAA, nematic liq. cryst., elec. field effects, neutron diffr. study 80−28912
PAA, nematic liq. cryst., eqn. of state 77−47560
PAA, nematic liq. cryst., light transmission in high elec. field grad. 79−19150
PAA, nematic liq. cryst., mol. statistical interpretation of viscosity *(Portuguese)* 77−47351
PAA, nematic liq. cryst., orientation ordering, mol. dynamics obs. 78−91239
PAA, nematic liq. cryst., propagating collective modes, neutron scatt. data 77−35476
PAA, nematic liq. cryst., rot. barrier, PCILO and CNDO/2 calcs. 80−33874
PAA, nematic liq. cryst., thermomagnetic behaviour *(French)* 78−87612
PAA, nematic molecular theory, orientation-averaged pair correlations 78−42905
PAA, nematic to isotropic liquid cryst. transform. at high press. *(Russian)* 77−4191
PAA, nematic-isotropic phase transition, US meas. 79−90761
PAA, nematic-isotropic pretransition regions, ±15K, volumetric obs. 77−76535
PAA, neutron scatt. by collective excitations 77−84651
PAA, quasielastic neutron scatt., isotope effects 78−83719
PAA, refractive index, dielec. const., mag. susceptibility, orientational ordering *(Dutch)* 80−33884
PAA, selectively deuterated, proton spin-lattice relax. temp. freq. depend., diffusion 77−43132
PAA, solid state polymorphism 78−42945
PAA, Tsvetkov parameter, temp. depend. 80−88035
PAA with deuterated methyls, nematic phase, quasieleastic neutron scatt. study of fast reorientations 78−14280
PAA-d_6, -d_8, H and D spin-lattice relax. 77−59475
PAA-di, nematic liquid crystal, NMR data, appl. of Landau-de Gennes theory 80−64893

organic compounds continued
PAA-PAP, nematic orientational order parameter calc. 77−24259
paeonol and urinary metabolites labelled with ^{13}C and D, synthesis and physicochem. props. 80−67250
palladium bis-β-diketonates, IR and Raman spectra 78−46327
palladium porphin, in n-alkane crystal, Zeeman and crystal field effects, absorpt. vibr. anal. 80−7372
palladium porphin, IR spectra and vibr. anal., and deutero-derivatives 79−22705
palladium porphin, triplet state, optically detected EPR and Zeeman meas. 79−19809
palladium porphin, Zeeman expt. on phosphoresc. triplet and quartet states 79−33786
palladium tetrabenzotetra-azacyclohexadecine, I_2 oxidation product, synthesis and characterization 79−47900
palladium-octaethylporphyrin, gas phase delayed fluoresc. and phosphoresc., triplet excimer formation 80−18884
palladiumporphin, in n-alkane, $S_1 \leftarrow S_0$ absorpt. spectrum, vibronic coupling and avoided crossing, field splitting 78−84613
palmitate-Cd, multilayer struct., hopping rate, direct evaluation 78−88045
palmitic acid, evaporated film, X-ray diffr. anal. and mass-spectrography 77−15718
palmitic acid film, HF dielectric const. 77−36175
palmitic acid monolayer on water, characterisation by multiple wavelength ellipsometry 78−92136
palmitic acid-choleic acid complex, cryst. struct. and van der Waals energy 80−64983
pancuronium inactivation of alamethicin-induced conductance in lipid bilayer membranes 79−39189
PAP, cryst. phase transitions, intermolecular motion, Raman and inelastic neutron scatt. spectra 80−2164
PAP, liq. cryst., phase transitions, up to 3 kbar, DTA obs. 77−20051
PAP, nematic liq. cryst., thermomagnetic behaviour *(French)* 78−87612
PAP, Tsvetkov parameter, temp. depend. 80−88035
paraaminophenol and paraphenylenediamine analogue molecular complex, free radicals of developers, EPR obs. *(Russian)* 80−7814
parabanic acid, charge density and cryst. struct. redeterm. by X-ray and neutron diffr. 79−46644
parabenzoquinone, and perfluoro derivatives, negative ion states, electron affinities, ionisation pots., overlapping spheres Xα calc. 79−26885
parabromophenol, supercooled liq., LF region of scatt. line wing 79−65888
paracetamol, radiosensitisation of E. coli B/r, mechanisms 77−86544
[2.2]paracyclophane, delayed luminesc. in cryst. and rigid glass solns. 79−15510
2,2 paracyclophane, dimer vibration influence on emission spectrum 80−69133
paradibromo benzene crystals, investigation of structural formation and growth kinetics 79−47610
paradibromobenzene-paradichlorobenzene solid solutions, mol. cryst., NQR study 80−25242
paradichlorobenzene, ^{35}Cl nucl. quadrupole spin-lattice relax. meas. 77−28469
paradichlorobenzene, electronic struct., X-ray emission obs. 78−5246
paradichlorobenzene, NQR freq., intermol. force effect 80−66065
paradichlorobenzene, NQR study of the lattice dynamics *(Russian)* 80−97160
paradichlorobenzene-paradibromobenzene solid solutions, mol. cryst., NQR study 80−25242
paradiheptyloxyazoxybenzene, mol. cryst., charact. of mesomorphic transition to smectic phase 79−14920
paradiheptyloxyazoxybenzol-d, dynamics of smectic-nematic liq. cryst. phase transiton *(Russian)* 78−55938
paradiheptyoxyazoxybenzol, low press. phase transition temp. change, relative transparency *(Russian)* 78−2242
n-paraffin, cryst., first-order phase transition 77−80615
n-paraffin, crystals, phase transitions, statistical theory 80−44290
paraffin, electron microscopy using electrostatic field *(German)* 78−82081
paraffin, evaporation neutron propag. Monte Carlo calcs. 79−89346
paraffin, liq., electron mobility, mol. struct. depend. 77−4350
paraffin, liquid, interface with photoconductor, carrier injection 80−24970
n-paraffin, longitudinal acoustic mode, perturbing forces 80−70348
paraffin, polymer modelling, mol. motion, thermal expansion and phase transitions 78−51436
n-paraffin, rotator phase transformation, lattice dynamics Helmholtz free energy 78−34585
paraffin, shock compressed, vel. of sound meas. 78−10123
paraffin, single crystal, STEM versus CTEM beam damage 80−103393
paraffin, solid-liq. interface motion during melting, convection effects, photographic obs. 79−18890
paraffin+He, binary gas mixture, mutual diffusion press. depend. 77−24047
n-paraffin crystal matrices, organic impurity molecular fluoresc., effect of heat pulses 78−88360
paraffin crystals, molecular motion, thermal expansion and phase transitions *(German)* 78−67837
paraffin microcrystals, electron diffr. intensities 80−100132
paraffin model experiment of plate tectonics 77−13073
paraffin oil, aq. emulsion, polyelectrolyte stabilised, mech. props. 79−39223
paraffin oil, thermal cond., appl. of spherically symmetric apparatus for liqs. and solns. *(French)* 79−94477
paraffin oil coatings for high power laser system components 77−88730
paraffin plate heat storage element, fusion, periodic solidification, heat transfer kinetics *(French)* 80−40913
paraffin thermal storage by sensitive, latent heat, *(French)* 80−40917
paraffin wax, elec. cond., 33-55°C and 1-2 kV cm^{-1} 79−99555
paraffin wax, solar energy thermal storage *(French)* 79−24916
paraffin wax, two-phase Stefan problem solns. 80−43594
paraffin waxes, melting point determ., automatic analyser, based on dilatometry 79−14223
paraffinic multilayer crystal, slightly bent, electron diffraction intensities, Patterson function 78−5993
paraffins, γ-ray irradiated samples, thermoluminescence 77−69922
paraffins, appl. of longitudinal acoustic mode 79−73277
n-paraffins, cryst. struct., rel. to polyethylene, surface effects on core 79−23593
n-paraffins, generalised eqn. of state from acoustical meas. 78−51642

organic compounds continued
n-paraffins, IR spectra, −180°C, two-phonon absorpt. bands 78−72495
n-paraffins, monolayers and thin crystals grown on Pt (111), LEED obs. 77−59230
n-paraffins, Raman spectra obs. of longitudinal acoustic modes intensities 78−84584
paraffins, solid, binary mixtures of long chain mol. systems, diamag. susceptibility 77−32154
n-paraffins, solid and liq., Raman spectra, longitudinal acoustic vibr. mode 78−31183
paraffins, solid and liquid, diamagnetic susceptibility 78−14923
pararosaniline cyanide dye dosimetry for continuous and pulsed fields over wide range 77−60255
parasubstituted alkyloxybenzoic acids, molecular motion in solid phase 79−61239
paraterphenyl, dye laser pumping charact. using KrF excimer laser at 248 nm 80−1199
paraterphenyl, fluoresc. quantum efficiency, one-photon dissociation, temp. depends. 80−69180
paraterphenyl, laser, efficiency, 323-364 nm tuning 77−14752
paraterphenyl pumped by pulsed laser radiation, photodissociation 79−98353
parathymol, negative uniaxial cryst., linear and nonlinear optical and dielec. props. 77−75602
partial molar heat capacities, in aq. solns., additivity schemes calcs. 78−22861
partly charged organic solids, mol. energies calcs. 79−55694
parylene, solid, 1.06 μm laser radiation interaction 78−91132
parylene disc, 1.06 μm laser beam irrad., beam and plasma diagnostics, 2D simulation 77−43010
parylene disc, high-power glass laser interaction 78−9804
parylene disc, irrad. by 1.06 μm laser beam Brillouin scatter 78−18430
parylene discs, plasma prod processes 1.06 μm laser irrad. 78−18431
pattern recognition anal. of IR and Raman spectra for cpd. classification 77−75158
PBABA, skewed cybotactic nematic phase, X-ray diffr. obs. 79−77504
PBBA, liq. cryst., phase transitions up to 3 kbar, transition enthalpy, entropy 77−20051
PBD, and p-terphenyl mixtures, tunable narrow bandwidth 2 MW lasers 79−41378
PBD, dissolved in toluene and cyclohexane, scintillation from α-particles, time depend. *(Spanish)* 79−99950
PBLG, cholesteric, Rayleigh scatt. caused by orientational fluctuations, low. freq. light scatt. modes 78−19496
PCB, nematic, smectic phases, dielec. and optical props. 78−60377
PCB, nematic liq. cryst., US imaging, convertor, acousto-optical effect 78−59218
PCB and DDT residues, atmos. dry aerial deposition rate, meas. techniques 80−81506
PCB liquid crystal, conductivity depend. on thickness and electrode molecular orientation 78−91248
PEBAB, liq. cryst., phase transitions up to 3 kbar, transition enthalpy, entropy 77−20051
PEBAB, nematic, EPR investig. 80−108077
PEBAB/HEXOAB, mixed crystals, induced smectic A phases, elec. cond. 78−76068
PEBAP, nematic liq. cryst., PMR line breadth temp. depend. 77−8419
pelagic tar, ocean distribution and surface circulation 80−16856
penicillins, semi-synthetic, radiation sterilisation 80−17064
pentacene, ATIR spectra, Davydov splitting 77−24865
pentacene, disordered solid layer, absorpt. spectra 80−93417
pentacene, electron escape depths and absorpt. coeffs. 78−23580
pentacene, evaporated on quartz, optical absorption, substrate temp. depend. 78−2932
pentacene, excited states calc., unrestricted HF theory in PPP approx. 77−50377
pentacene, first excited singlet state, butterfly motion studied by fluoresc. spectra 80−78615
pentacene, in naphthalene (p-terphenyl), picosec. coherent transients obs. 79−46013
pentacene, in p-terphenyl, electronic excitation transport, acousto-optical effects 78−72079
pentacene, in p-terphenyl, polarisability calcs., from Stark meas., anisotropic Lorentz approx. breakdown 78−5276
pentacene, in p-terphenyl mixed cryst., low temp. optical phase relax. obs., mechanism 77−52112
pentacene, intersystem crossing and internal conversion rates, fluoresc. transient and optical FID spectrosc. 79−81229
pentacene, laser fluoresc. of mol., excitation bandwidth and optical dephasing 79−36679
pentacene, mol. dephasing, radiationless decay meas. by laser-acoustic diffr. spectroscopy 78−37667
pentacene, narrow band laser excitation, fluoresc. decay, optical free induction, dipole moment 78−21956
pentacene, polycrystal, photoemission 78−27367
pentacene, singlet exciton transitions, energies and oscillator strengths, boson theory with PPP wavefunctions 80−92820
pentacene, vibrational quasicontinuum threshold, spectrosc. criterion 80−52972
pentacene dianions in dimethyl ether, rotational diffusion meas. 80−65262
pentacene doped p-terphenyl mol. cryst., laser induced photoacoustic grating effects 79−55215
pentacene films, luminesc., struct. 80−11461
pentacene in naphthalene, intersystem crossing rates following single-mode laser excitation 80−43085
pentacene in naphthalene, triplet state, EPR study by electron spin-echo and laser flash excitation 80−58172
pentacene in naphthalene (p-terphenyl), mol. mixed crysts., optical dephasing and vibronic relax. 80−95957
pentacene in naphthalene crystal, relax. of vibronic states, photon-echo and ab absorpt. relax. expts. 79−95807
pentacene in p-terphenyl, free induction decay by extracavity laser freq. switching 78−79076
pentacene in p-terphenyl, intermolecular interactions, laser induced phonon probe 80−79891
pentacene in p-terphenyl, laser excitation of stationary molecular states 77−68084
pentacene polycrystals, electron scatt. 77−32478
pentacene-d_0, -d_{14}, in p-terphenyl-d_0, mixed cryst., photon-echo relax. 77−72034

organic compounds continued
pentachloro aniline, far IR spectra, mol. crystal orientational dynamics 78−60428
pentachlorobenzene, in KOH-2-propanol soln., chain dechlorination by γ-rays 78−56904
pentachloronitro benzene, far IR spectra, mol. crystal orientational dynamics 78−60428
pentachloronitrobenzene, single cryst., far IR absorption 79−73940
pentachloronitrobenzene crystal, anomalous microwave permittivity, IR absorption and Raman spectra *(Japanese)* 78−15169
pentachlorophenol + furil, photochem. reduction, cross-relax. and CIDNP, PMR relax. obs. 79−52694
pentachlorotoluenes, positional isomers, ^{13}C Fourier transform NMR spectrometry, struct. and compositional anal. 80−91576
pentacoordinated ferrous porphyrins, ^{1}H and ^{19}F NMR, hyperfine shift, π electron binding 78−78719
n-pentadecane, two-photon spectra; fluoresc. spectra; decay times, intensities obs. 77−75245
pentadecanoic acid, insoluble monolayer, phase transition, simple lattice model 80−70527
pentadecanoic acid, monolayer on water, surface pot. meas. in coexistence region 77−28236
s-trans-1,3-pentadiene, photoisomerisation, excited state pot. energy curves, CIPSI calc. CNDO/2 parametrisation 78−11505
pentaerythritol, aq. solns., stirred, transient diffusion through glass membranes, thermodynamics 78−92507
pentaerythritol, Bragg reflection, thermal diffuse scatt. meas. *(German)* 78−75509
pentaerythritol, calibration of Bragg analyser crystal polarimeters for X-ray astronomy 77−64664
pentaerythritol tetranitrate, high explosive, fracture surface energy determ. 77−44337
pentaerythritol tetranitrate, high explosive, surface energy from contact angle meas. 79−51393
pentafluoroacetone, IR laser induced decomp., free radical mechanism 80−71924
pentafluorobenzene, C-H vibr. states, thermal lensing spectra, local mode model test 77−71812
pentafluorobenzene, cation, visible emission spectra of gas, Jahn-Teller effect 79−50034
pentafluoroethyl iodide, electron impact, time of flight mass spectrometry 77−42424
pentafluoromethyl iodide, ion-molecule reactions, amongst radiolysis products, reaction rates, mechanisms, mass spectra 79−5136
pentafluorophenol, liq. IR absorpt. spectrum, fundamental freqs. and combinations 79−36633
pentamethinemerocyanine dye, electronic spectrum and struct., solvatochromism, microstructural model 77−61817
pentamethinium cyanine dye, single cryst., photocond. meas. 79−51626
pentamethylbenzene-TCNB, charge transfer triplet states, electron distrib., ESR 77−3388
pentan-3-one, adsorbed on SiO_2, under carbon tetrachloride immersion, IR obs. 79−24821
pentane:octane, γ-irrad., octane radical cations ESR 77−36765
pentane, combustion, form. and destruction of pentenes 79−1953
pentane, effect on 3,6-diaminopthalimide vapour molecule electronic excitation energy degradation path 80−74195
n-pentane, electron mobilities through liq. and critical regions 78−2536
n-pentane, film boiling from cylindrical surfaces 79−23194
neo-pentane, gas, electron-ion recombination, at 292K, three-body interaction 79−46418
n-pentane, ionisation by electron bombard., empirical and semi-empirical calcs. 79−36784
pentane, isomers, gas and liq. phases, electron transport, density and temp. depend. 79−91114
pentane, liq., enthalpy difference between rot. isomers, IR spectrosc. obs. 80−106404
pentane, liquid, chain reorientation, Brownian dynamics simulation, comparison of models 80−49067
n-pentane, liquid, containing suspended particles, superheating expt. 78−90642
n-pentane, optical props. under press., molecular polarisability depend. on thermodynamical state 78−80312
n-pentane, proximity and conform. effects, ^{13}C chem. shifts at γ position INDO computations 77−50451
n-pentane, refr. index meas. to 14 kbar by optical interferometry 77−49764
n-pentane, refractive index at X-ray wavelengths *(Russian)* 79−47409
pentane, thermodynamical Gruneisen parameter, press. depend. 78−14479
n-pentane, Townsend primary and secondary ionisation coeffs. and sparking voltages 80−1732
n-pentane and mixtures with n-hexane, nucleate boiling from tube arrays 78−22251
pentane drops, Leidenfrost boiling on hot silicone oil surface neutral stability line 78−94588
pentane isomeric vapours, electon transport mechanisms, density induced transition 80−24122
pentane isomers, free molecule flow and interdiffusion through porous glass 79−32658
pentane isomers, vapour and liq., electron mobility 79−72984
n-pentane-benzene, light scatt. of liq. near crit. vaporisation state, correl. radius 79−24328
pentane-benzene solution, vapour-liquid equilibrium study, vaporisation critical state *(Russian)* 80−79931
pentane-o-nitrotoluene critical solution, nonlinear dielectric effect 78−55952
n-pentane-water interface, nucleate boiling 78−2342
pentane/chloroform mixture, liquid, containing suspended particles, superheating expt. 78−90642
2,4-pentanediol, meso, l, d forms, separation using circulation chromatography in steam 79−16074
pentanoate, Li, Na, K and Rb alkanoate mixture, DSC anal. 78−10192
pentanol activity in bulk phases, distribution and surface activity *(French)* 80−24712
N-pentanol-Na-N-octanoate-water system, partial molar enthalpies 78−75543
pentaphenyl group V compounds, $(C_6H_5)_5M.^1/_2C_6H_{12}$, M=P, As, Sb, cryst. packing 78−9994
pentaphthalidene dye, ^{210}Po contamination of surfaces, removal coeff. determ. 79−26769
organic compounds continued
pentatetraene, non-degenerate vibr. mode induced Jahn-Teller effect, photoelectron spectra calc. 79−817
1-pentene+OH, absolute rate consts., 297K 79−100353
pentenes, form. and destruction during pentane combustion 79−1953
pentenes, in combustion of pentane, further reactions, isotopic tracer obs. 79−8438
pentofuranosyl nucleosides, isomeric, ^{1}H NMR coupling consts., SCF FPT INDO approx. calc. 80−14156
p-pentoxy-benzylidene-alkylaniline series, smectic phases, dielec. anisotropy 80−55010
p-pentoxybenzilidene alkylaniline, liq. cryst., mag. anisotropy and polymorphism *(French)* 77−76532
n-pentyl 4-(4-n-dodecyloxybenzylidene-amino)-cinnamate, X-ray studies in smectic I phase 80−70119
pentyl cyanobiphenyl, laser and electric field induced Kerr effect 80−84061
pentyl cyanobiphenyl nematogen, depolarised light scatt. 79−95790
pentyl ion+methane, energy transfer, modified statistical theory 79−50107
p-n-pentyl p′-cyanobiphenyl, anisotropic viscosity, US meas. 77−31581
p-n-pentyl p′-cyanobiphenyl, isotropic phase, viscosity coeffs. 77−31582
p-n-pentyl p-cyanobiphenyl, resolution of acoustic image detector 78−46871
4-n-pentyl phenyl-4(4-pentyl benzoyloxy)3-chlorobenzoate, liq. cryst., flexoelectric and dielec. relax. behaviour 78−94979
4-n-pentyl-4′-cyanobiphenyl, isotropic, optical and electrical Kerr effect 79−32886
4-n-pentyl-4′-cyanobiphenyl, mol. alignment, comparison of exptl. data at high press. with mean field theory predictions 79−99075
4-n-pentyl-4′-cyanobiphenyl, nematic liq. cryst., refr. indices and order parameters 78−22644
4-n-pentyl-4′-cyanobiphenyl, nematogen, incoherent neutron quasielastic scatt. 79−32887
4-n-pentyl-4′-cyanobiphenyl, refr. index, high press. meas. 78−26428
4′-n-pentyl-4-cyanobiphenyl, nematogenic liq. cryst., above T_c, Kerr effect response time, temp. depend. 78−34434
4-n-pentyl-(4-cyanophenyl)-cyclohexane, surface alignment using lecithin monolayers, contact angle meas. 79−4247
pentyl-cyano-biphenyl, nematic, hydrodynamic parameters meas. with and without applied elec. field 80−100297
pentyl-cyano-biphenyl, nematic liq. cryst., pretilt angle, temp. depend. 78−26432
pentyl-cyano-biphenyl, nematic phase, transport props. of dissolved ionic species, electrochem. meas. *(French)* 79−90811
p-n-pentyl-p′-cyanobiphenyl, nematic liq. cryst., Raman depolaris. ratios, order parameters 79−28733
p-n-pentyl-p′-cyanobiphenyl, nematic ordering, electric field induced second harmonic generation 79−60263
p-n-pentyl-p′-cyanobiphenyl, nematic phase, mapping of acoustical fields 79−91402
4-n- pentyl-phenylthiol-4′-alkoxybenzoate, homologous series, specific heat meas., nematic-smectic-A tricritical point 80−15227
4-n-pentyl-phenylthiol-4′-n-octyloxybenzoate, smectic A-smectic C phase transition, high-resolution X-ray study 80−79921
4-n-pentylbenzenethio-4′-n-alkoxybenzoates, birefr., crit. behaviour near smectic A-C transition 80−80745
4-n-pentylbenzenethio-4′-n-octyloxybenzoate, liq. cryst. phase transitions, press. and temp. depend. 79−77730
pentylcyanobiphenyl, liquid crystal, isotropic phase, surface induced ordering, birefringence obs. 80−14998
pentylcyanobiphenyl, nematic, elastic and dielec. props. from capacitance-voltage curve 79−32894
pentylenetetrazole, synaptic action, selectivity for Cl cond. 78−7336
pentyloxy-cyanobiphenyl, liq. cryst., laser and electrical Kerr effect 78−68477
4-n-pentyloxy-phenyl-4′-n-octyloxybenzoate, nematic, dielec. relax. and freq. depend. of threshold voltage 80−60497
4,4′-di-n-pentyloxyazoxybenzene, anomalous smectic mesomorphism, calorimetric and optical texture obs. 79−77505
N-4-n-pentyloxybenzylidene-4-n-hexylaniline (50.6), unclassified smectic phase 80−75157
4-n-pentylphenyl 2'-chloro-4'-(6-n-hexyl-2-naphthoyloxy) benzoate, smectic A phase, positive and negative dielec. anisotropy 79−10793
4,n-pentylphenyl (pentylbenzoyloxy)-3-chlorobenzoate, flexoelec. coeff. in nematic phase, thermal depend. 80−79685
4-pentylphenyl-4′-benzoyloxybenzoate/TBBA system, smectic A_1-smectic A_2 transition, X-ray diffr. obs. 80−44303
4-n-pentylphenyl-4′-n-octylthiobenzoate, smectic-C phase, undulation instabilities, microscopic obs. 77−68919
4-n-pentylphenylthiol-4′-n-octyloxybenzoate, sp. ht. and crit. behaviour of liq. cryst. phases 78−67816
peptide, HCO-(L-Ala-L-Ala-Gly)$_5$-OMe, synthetic voltage-dependent cation-selective transmembrane channel characterisation 78−77009
peptide analysis by field desorption mass spectrometry using pretreated Si emitter 80−55751
peptide aqueous solution, EPR of spin-trapped radicals, OH radical reactions 78−68993
peptide architectural units, ab initio SCF MO calcs. 78−96004
peptide formation in prebiotic era with clay catalysts 77−64435
peptide sequencing by DADI mass spectra 79−57573
peptide-Cu II interaction, EPR and optical absorpt. 78−27881
peptides, ^{13}C NMR, review 78−24023
peptides, α-aminoisobutyric acid containing, ^{1}H NMR conform. obs. 79−81311
peptides, bradykinin-potentiating, spatial structs. 80−95736
peptides, cyclic associated-induced circular dichroism, dipole approx. 77−71795
peptides, NMR spectroscopy study 78−88694
peptides, optical rot. strength, sector rules 78−17737
perchloro-3cyclopentenone, ^{35}Cl NQR Zeeman obs. 80−54981
perchloro-[4]-radialene, IR and Raman spectra 77−77198
perchlorohydrocarbons, crystn., intermol. potential-function models 80−49168
perdeuterio-N-1-oxyl-2,2,6,6-tetramethyl-4-piperidinyl maleimide, spin label, biological EPR 80−32746
perdeuterobenzene, liquid, reorientation and spin-rotation interaction 78−39423
perdeuterobenzophenone, in 4,4'-dibromodiphenylether, cross-relax., microwave pulse obs. 80−53031

organic compounds continued
perdeuteronaphtthalene, use of neutron time-of-flight technique for cryst. structs. investigation 79−19126
perfluorinated mixtures, hydrostatic liquids for obs. of NMR 79−2801
perfluoro fatty acid in MIM junction, elec. cond. mech. 78−95386
perfluoro polyethers, props. and use in vacuum appls. 78−70136
perfluoro-1,2-dimethylcyclobutane, electron attachment, elec. field and energy depends. 79−36759
perfluoro-1,3-butadiene, electron attachment, press.-reduced elec. field and energy depends. 79−36758
perfluoro-1,3-butadiene, vibr. spectra, struct. and barrier to planarity 78−9147
perfluoro-1,3-dimethylcyclohexane, electron attachment, elec. field and energy depends. 79−36759
perfluoro-1-heptene, electron attachment, ≲3 eV, rel. to perfluoromethylcyclohexane 79−36755
perfluoro-2-butene, electron attachment, press.-reduced elec. field and energy depends. 79−36758
perfluoro-2-butyne, electron attachment, press.-reduced elec. field and energy depends. 79−36758
perfluoro-trans-4-methyl 2 pentene, liq. breakdown characts. *(Japanese)* 79−82925
perfluoroalkyl bromide+CO_2(CO), collisional relax. rate consts., laser induced fluoresc. obs. 79−13799
perfluoroalkyl halides, at. I form., quantum yields 78−3355
perfluoroalkyl iodide+CO_2(CO), collisional relax. rate consts., laser induced fluoresc. obs. 79−13799
perfluoroalkyl iodides, laser photolysis, quantum yields 79−29382
perfluoroalkyliodide, pyrolysis of vapour due UV irrad. 78−73070
perfluoroalkyliodide photodissoc. laser, optical inhomogeneities of active medium 79−55129
perfluorobenzene, electron attachment, radiative and dissoc., negative ion lifetimes, ion cyclotron reson. spectra 80−74251
perfluorobenzene, orientational correlation parameter for liquid 79−73090
perfluorocarbon compounds, electron attachment obs., dielectric strength 79−36759
perfluorocarbon-SF_6 mixtures, sparking C inhibition, decomp. product investig. 80−89478
perfluorocarbons, γ-irrad. solns., mag. field effect on fluoresc. 80−55677
perfluorocarbons, plasma polymerisation 78−88634
perfluorocyclobutane, dense fluid, self-diffusion, shear viscosity, density, and temp. depend., NMR 77−36152
perfluorocyclobutane, electron attachment, press.-reduced elec. field and energy depends. 79−36758
perfluorocyclobutane, electron attachment, radiative and dissoc., negative ion lifetimes, ion cyclotron reson. spectra 80−74251
perfluorocyclobutane, matrix isolation Raman and IR spectra, pot. function 77−3352
perfluorocyclobutanone, IR and Raman spectra, vibr. anal. 77−38661
perfluorocyclobutene, electron attachment, press.-reduced elec. field and energy depends. 79−36758
perfluorocyclohexane, spin-lattice relax. during pulsed spin locking 78−39425
perfluorocyclohexene, electron attachment, elec. field and energy depends. 79−36759
perfluorocyclopentane, electron attachment, elec. field and energy depends. 79−36759
perfluorodimethylcyclohexane, retrograde vapour, shock wave induced condensation 80−34177
perfluoroethane, and fluoromethane, NMR gas-to-liquid shifts, 2nd-virial coeff. of chem. shielding validity 79−85976
perfluoroethane+ClF, thermal and photochem. reactions investig. 80−61117
perfluoroethylcyclohexane-carbon tetrachloride, crit. mixture, brilliant total refl. from liq.-liq. interface 79−90786
perfluorohexadiyne radical cation, $\tilde{A}$-$\tilde{X}$ band emission spectra, $\tilde{A}$ state lifetime 79−72327
perfluoroiodoethyl perfluoromethanoate, photolysis, absolute quantum yields of $I(^2P_{1/2})$ and $I(^2P_{3/2})$ 79−34339
perfluoromethyl bromide+alkali atom, collisional ionisation, electron affinity 78−66639
perfluoromethyl iodide+alkali atom, collisional ionisation, electron affinity 78−66639
perfluoromethylcyclohexane, 'inert' solvent, fluoresc. quenching of trimethylamine 78−46438
perfluoromethylcyclohexane, electron attachment, ≲3 eV, rel. to perfluoro-1-heptene 79−36755
perfluoromethylcyclohexane, electron attachment, radiative and dissoc., negative ion lifetimes, ion cyclotron reson. spectra 80−74251
perfluoromethylcyclohexane-methylcyclohexane, near-critical liquid mixture, nucleation 80−92664
perfluoromethylcyclohexane-tetrachloromethane, specific heat temp. depend., critical composition mixture near critical temp. 78−26689
perfluoroneopentane, geom. struct. of mol., gas phase electron diffr. 78−78810
perfluoropentadiyne radical cation, $\tilde{A}$-$\tilde{X}$ band emission spectra, $\tilde{A}$ state lifetime 79−72327
perfluoropropyl iodides, photolysis, absolute quantum yields of $I(^2P_{1/2})$ and $I(^2P_{3/2})$ 79−34339
perfluorotertiarybutanol, IR spectra in soln., OH group fundamental and first overtone bands *(French)* 77−27071
perfluorotoluene, electron attachment, elec. field and energy depends. 79−36759
perfluorotoluene, electron attachment, radiative and dissoc., negative ion lifetimes, ion cyclotron reson. spectra 80−74251
perhalo-compounds, labelled, high yields from ^{18}F and ^{38}Cl reactions with CCl_xF_{4-x} and C_3F_6 80−109025
perhalonitrosomethanes, gas phase IR spectra, assignments, isomerism 80−28017
peroxidase, photo-induced reduction, reaction with indole acetic acid 79−79452
peroxyacetic acid, and isotopic forms, matrix IR spectra, force spectrum, force const., thermodynamic props. calc. 77−14427
peroxyacetyl nitrate, atmospheric, absorpt. by natural surfaces 77−45139
peroxyacetyl nitrate+OH, reaction rate const., in irrad. NO_x mixture 78−7171
peroxyacetyl nitrate (PAN), dosage in photochemical smog, depend. on latit. 77−2227
peroxyacetyl nitrate in polluted ambient air, enhancement of photochem. smog by N,N′-diethylhydroxylamine 77−91262

organic compounds continued
peroxylamine disulphonate, EPR lineshape, dispersion vs. absorpt. plots, modulation broadening and instrumental distortion 80−58290
peroxymethyl radical+NO, reaction rate const. 79−61848
peroxymethyl radical+peroxymethyl radical, reaction kinetics, H_2O vap. depend 79−61844
perylene, α- and β-crysts. and soln., polarised reflection and absorption spectra 77−8598
perylene, anthracene, radical cation, EPR, acidic surface anisotropic rot. diffusion 78−27095
perylene, cryst., fluoresc. at low temp. 78−27299
perylene, cryst., fluoresc. spectra, time-resolved, excimer and excitons 79−78724
perylene, crystal-electrolyte interface, ionis. energy of uppermost cryst. mols. 78−27764
perylene, disc, laser-irrad., plasma electron energy profile steepening, polarimetry obs. 78−34349
perylene, electron escape depths and absorpt. coeffs. 78−23580
perylene, energy structure, photocond., photoemission and absorpt. spectra meas. 77−39895
perylene, excimer form. process, ps laser fluoresc. obs. 79−11448
perylene, excitation spectra of exciton fission 78−92116
perylene, excited singlet state quenching by nitroxyl radical, triplet form. 77−88487
perylene, exciton fission in excimer forming cryst., fluoresc. 79−15511
perylene, fluoresc., exciton fission in excimer forming cryst. dynamics 79−61423
perylene, harmonic force fields, bond orders, normal coord. anal., mean amplitudes calcs. 78−25418
perylene, hot luminesc. in solid matrix at 4.2K, intramol. thermal bath 79−85999
perylene, intermolecular interactions, laser induced phonon probe 80−79891
perylene, metastable inert gas atom impact, surface electron emission energy distrib. 78−43970
perylene, radiolysis, ion-pair clusters and excited-state yields 77−29024
perylene, solid soln. in ethanol, fine struct. in absorpt. spectra, laser technique 77−90178
perylene, vapour phase dye laser, quantum efficiency and thermal stability 78−50771
perylene, vapour phase excitation energy transfer from pyrene 77−12802
(perylene)$_3$TCNQ, prep. and spectra, electron-mol. vib. coupling 77−16290
α-perylene crystal, emission spectra, temp. variation and pair states 78−27300
perylene crystal, molecular exciton system, resonance Raman and fluorescence studies, dynamical effects 80−66169
perylene doped pyrene cryst., decay times and diffusion coeffs. of singlet excitons, under press. 77−20911
perylene film, electron escape depth, energy depend. 79−38709
perylene fluorescence polarisation in erythrocyte membranes, rel. to fluidity 77−36885
perylene in EBBA, nematic ordering influence on fluoresc., temp. depend. *(German)* 79−81235
perylene in n-alkane, zero-phonon lines in luminesc. spectra 78−56512
perylene in n-heptane cryst., polarised fluoresc. 80−1017
perylene in n-paraffin crystal matrices, effect of heat pulses on fluoresc. 78−88360
perylene in paraffin, anisotropic rot. and libration 77−32417
perylene polycrystal, photoelectron spectroscopy 77−59670
perylene radical cation EPR spectra, ion-pair effects 79−13742
perylene-N,N-dimethylaniline exciplex, effect of dipolar molecules on quenching curves 78−52551
perylene-TCNQ complexes, Raman spectra intensities, freq. depend. 79−61362
perylene-tetracene in liquid crystals, temp. depend. of absorption and fluoresc. *(German)* 80−18887
perylenetetracarboxylic dianhydride pyrolysis for synthesis of C films with high conductivity 80−80983
pesticide, DDT analysis in biological extracts, mass fragmentography with glass capillary columns 77−9312
pesticide, DDT translocation by resuspension over Pacific N.W. forests 77−29422
pesticide pollution in Soviet rivers concs. 80−81495
pesticide residues, gas chromatogram quantitation, using algorithms for microprocessor based integrator 78−27839
pesticides, chlorinated, gas chromatographic anal. using electron capture detector *(Japanese)* 80−55764
pesticides, in water, detect. by laser excited reson. Raman spectroscopy 78−31732
pesticides, sampling in ambient air, using polyurethane foam 78−20080
pesticides and heavy metals in Bavarian snow 80−61488
petroleum, study of colloidal nature using automated Bonse-Hart X-ray small-angle scatt. unit 79−16044
petroleum, two phase flow in underground reservoirs, soln. of nonlinear eqn. by random choice method 79−50773
petroleum, weathered, source identification using IR spectra and correl. coeffs. 78−15153
petroleum fractions from USSR fields, isobaric integral heats of condensation *(Russian)* 79−65181
petroleum gas, liq., thermodynamic props. for mixed fluid densities 78−18775
petroleum hydrocarbons in water, fish and sediments of North Sea following Ekofisk Bravo blow-out 79−74559
petroleum products, X-ray fluoresc. anal. with solid and aqueous standards 77−60145
petroleum samples, extinction coeff., refractive index meas., 0.25-25 microns 79−65818
petroleum spills on water, control using gellants 80−61496
petroleum-acetylene-O_2 combustion products, seeded, elec. cond., for MHD power plant 78−34256
petroleum-water-gas mixture, in inclined stratum, nonstationary filtration, including gravity 78−1729
petrols, optical consts. in 0.25 to 25 micron region, sea pollution detection appl. *(Russian)* 78−76976
[2.2]phanes in glass matrices, transanular π-electron interaction, emission spectra 79−36682
phase IV, cholesteric struct. induced by chiral sulphoxides 79−86683
phase transitions at high pressure, IR spectra of 11 compounds 79−95743

organic compounds continued
Phase V, nematic, transient response to redirected mag. field, EPR study 80−33879
$(phenacetin)_2.HI_5$, cryst. struct. determ. using Patterson methods 79−46647
phenacyl halides, IR spectra, $\delta(CH_2)$ vibrs. correlation with structs. *(French)* 80−23417
phenanthrene.$2SbCl_3$, Raman spectra 77−16291
phenanthrene:anthracene, cryst., triplet-triplet annihilation, shallow traps effect, 77-293K 79−11446
phenanthrene:anthracene, delayed fluores. of cryst. in mag. field 79−52023
phenanthrene, and dideuteroisomers, vapour phase fluoresc. lifetimes, position dependent D effects 77−30901
phenanthrene, chemical thermodynamic props. 80−21312
phenanthrene, chemisorbed on Al_2O_3, radiative and nonradiative processes 79−36686
phenanthrene, cryst., Raman spectra, intensity of low freq. line 78−2846
phenanthrene, cryst., refl. spectra of first singlet transition 78−88323
phenanthrene, crystal-electrolyte interface, ionis. energy of uppermost cryst. mols. 78−27764
phenanthrene, crystalline, Raman band intensity temp. depend. 77−59564
phenanthrene, diaza derivatives, excited singlet and triplet states, charge density, INDO calcs. 80−58152
phenanthrene, fluoresc. quenching by inorganic anions 78−74694
phenanthrene, growth rate from melt *(Japanese)* 78−23605
phenanthrene, IR and Raman spectra, lattice and internal mode coupling 77−20843
phenanthrene, low freq. Raman spectra intensity temp. depend., phase transition, conformation change 77−36211
phenanthrene, lowest triplet state zero field splitting parameters calcs. 80−83391
phenanthrene, mesophase formation during carbonisation under pressure 77−44182
phenanthrene, mol. cryst., thermolum. build-up 78−27334
phenanthrene, molecular cryst., phonon scatt. and exciton linewidths 78−15185
phenanthrene, nonlinear third-order electric susceptibility 78−74944
phenanthrene, phase transition, Raman spectral obs. 77−59112
phenanthrene, photoelectron spectroscopy obs. of heterocycles 78−94286
phenanthrene, planar normal vibrs. calcs. 80−5525
phenanthrene, proton chem. shift, chem. substitution influence, LCAO perturbation method 77−68064
phenanthrene, subpicosecond laser photolysis and time resolved absorpt. spectra *(Japanese)* 79−79272
phenanthrene, triplet state conc. quenching in propan-1,2-diol 77−75196
phenanthrene, two photon absorptivities, CNDO/S-CI calc. with second order time depend. perturbation eqns. 80−74122
phenanthrene, two-photon excitation spectra, exciton-phonon and intramol. vibronic coupling 80−84774
phenanthrene, vibr. spectra, mol. crystal dynamics, librational modes 78−64356
phenanthrene+solvated electrons, diffusion controlled reactions in polar solvents, reaction parameters 80−97687
phenanthrene birefr. changes due to thermal expansion 78−52468
phenanthrene in glass, non-photochem. hole burning appl. to two-photon spectrosc. 79−18246
phenanthrene-d_{10}, oriented in biphenyl, triplet zero-field splittings, conc. depend. 78−2773
phenanthrene-dimethylnaphthalene mixture, growth rate from melt *(Japanese)* 78−23605
phenanthrene-PMDA, cryst., triplet charge transfer state symmetry 77−72836
phenanthrene-PMDA, spin polarization of charge-transfer excitons, EPR meas. 79−19766
phenanthrene-pyromellitic acid dianhydride, single cryst., EPR, delocalised and localised charge transfer excitons 77−85545
phenanthrene-pyromellitic dianhydride, single cryst., charge-transfer triplet excitons, spin polaris. 79−11069
phenanthrenequinone, in n-paraffin matrix, electronic-vibr. interaction in phosphoresc. 79−27027
phenanthrenequinone, NMR of cryst., 77-480K 79−38387
phenanthrenoid compounds, abnormal bond lengths, MO calculations 77−31020
phenanthridinic spiropyran photocoloration mechanism 79−83487
phenanthrolines, in Shpolskii matrices, phosphoresc. spectra 78−94276
phenazine: azulene, EPR, azulene triplet state 78−35024
phenazine, charge carrier transport rel. to cryst. and band struct. 79−95403
phenazine, dimer triplet state line shape, small excitons 80−48041
phenazine, excited single state kinetics on a subnanosecond time-scale 79−36677
phenazine, first excited state ^{14}N quadrupole tensor by ODNQR 78−50561
phenazine, isotopic mixture Anderson localisation of mol. excitons 77−89733
α-phenazine, multiple scattering, secondary reflections and their interference 80−33856
phenazine, prereson. Raman spectra, vibr. band intensities obs. 80−102515
phenazine, T-T absorpt. build-up, following picosec. pulse singlet excitation, in gas phase 78−9161
phenazine, triplet formation kinetics temp. depend., analogue computer anlaysis 77−58058
phenazine, triplet state, ^{14}N quadrupole tensor, optical detection of NQR 79−18218
phenazine, triplet state intersystem crossing, picosec. singlet excitation 77−6824
phenazine, zero field studies of spin lattice relaxation in excited triplet states 79−18219
phenazine-d_3:(phenazine, $(phenazine)_2$), disordered, exciton migration, dynamical approach 79−65916
phenetole, in cyclohexane-ethanol mixtures, UV spectra, solvent effect 79−22770
p-phenitidine, in benzene soln., dipole moment from solute relax. time-solvent viscosity relation 80−37905
p-phenitidine, soln., dielectric const., loss and relax., dipole moment 78−43782
phenol, adsorbed layer, inelastic electron tunnelling spectral lineshapes below 100 mK 78−31000
organic compounds continued
phenol, aq. soln., electron ejection, picosec. obs. 80−87187
phenol, cryst., mol. vibrs., factor group splittings 80−16021
phenol, field ionis. to excited states 77−19002
phenol, H bonds to proton acceptors, PCILO calcs. 79−26895
phenol, H-bonded complexes, IR absorpt. band struct., freqs. and intensities *(Russian)* 77−18928
phenol, ideal gas thermodynamic props. 78−75250
phenol, leaches from gasworks site, Kingskettle, Scotland 79−88020
phenol, PMR in absence of intermol. proton exchange, long-range coupling and conformations 77−34660
phenol, polluted-water, ^{60}Co and ^{137}Cs fixation on natural sorbents 79−57506
phenol, self association, IR spectra, book contrib. 78−21931
phenol, singlet-singlet electron transitions, modified CNDO-CI method exam. 78−25552
phenol, transition energies, oscill. strength, time-depend. Hartree-Fock model *(Spanish)* 77−6684
phenol, vapour, viscosity coeff. and second virial coeff., conformity with Lennard-Jones pot. *(German)* 79−32732
phenol+ammoniated electrons, reaction rate consts. 77−9043
phenol+N,N-dimethylmethanesulphonamide, assoc., PMR 78−23941
phenol(-d_1)-dioxan(-acetonitrile), in carbon tetrachloride ($CDCl_3$) solns., H-bonds vibr. relax. bands anal. 78−84560
phenol (-d_1, d_5, d_6), excited A state, normal vibr. freqs, force consts., compliance coeffs. 78−50534
phenol (oestrogen) compounds, high-press. liq. chromatography, fluorometric detect. 78−20096
phenol derivatives, neutral aq. solns., flash photolysis, N_2O and alcohol effects 78−40065
phenol formaldehyde resin carbon, catalytic graphitisation from various metals 80−11871
phenol I and II, permittivity and molar polarisation at pressures between 140-2000 bar 77−77136
phenol NH_3, intermolecular H-bond, semi-empirical CNDO/2 78−13427
phenol-aniline (quinoline) (pyridine), liq., US vel., adiabatic compressibility, H-bonded complex form. 77−35635
phenol-chloromethane, US absorpt., phenol cyclic assoc. 77−15501
phenol-cyclohexane (-ether), UV spectra, solvent effects, matrix rank anal., species determ. 79−22768
phenol-formamide, intermol. H-bond, semiempirical CNDO/2, substituted derivatives 78−13427
phenol-methanol, dimers CNDO/2 calcs.. H-bond energy 78−13428
phenol-organic solvent mixtures, UV spectra, solvent effects 79−22769
phenol-phenyl complex, electrostatic mol. pot. contour maps, MODPOT and VRDDO calcs. 80−102463
phenol-water mixture, pure and KCl-doped, electrical conductivity near crit. pt. 77−15612
phenolate, aq. soln., electron ejection, picosec. obs. 80−87187
phenolic compounds, electrooxidation, polymeric surface film form. on Pt electrodes 80−104450
phenolic Mannich bases, dielec. relax. study 80−97196
phenolic resin carbon catalytic graphitisation by Al powder 77−28734
phenols, ^{13}C and D substituted, microwave spectra, substitution struct. and absolute dipole moment 79−31511
phenols, chemisorbed on Al-Al_2O_3-Pb oxide layer, electron tunnelling spectra, 2K 77−62736
phenols, dil. solns., dielec. loss and relax., microwave and sub-mm. wave absorpt. obs. *(German)* 78−23396
phenols, halogenated, internal rot. barriers, torsional vibr. freqs. 77−68041
phenols, orthosubstituted, proton acceptor soln., PMR of H-bonding 78−13517
phenols, substituted, in cyclohexane-ethanol mixtures, UV spectra, solvent effect 79−22770
phenols, substituted, proton NMR chem. shift in aprotic solvents 79−47342
phenoselenazine, cryst. struct. from X-ray automatic diffractometer data 77−4093
phenothiazine derivatives, semicond. elec. props., optical spectra, and EPR 80−103693
phenoxy radical dimer, reversible diffusion controlled dissoc., detailed equilib. principle 80−7770
phenoxy radicals, electronically excited states, photochem., flash photolysis obs. 77−77797
6-phenoxy-5,11-napthacenequinones, photochromism, molar extinction coeffs. meas. 80−66220
phenoxyacetic acid, photoinduced selective isomerisation in comparison with X-ray induced decomp., aq. soln., 25°C *(German)* 77−63931
phenoxyl type radical, ^1H and ^{13}C ENDOR studies in soln. 78−94266
phenyl 4(4-alkylphenyl)cyclohexanecarboxylates, mesomorphism and dielec. props. 77−27810
phenyl 4-alkylbiphenyl-4′-carboxylates, mesomorphism and dielec. props. 77−27810
phenyl 4-benzoyloxybenzoates, influence of lateral substitution on liq. cryst. props. 79−4242
phenyl 5-alkoxypicolinates, synthesis, phase transition temps., and dielec. props. 79−86876
phenyl 6-alkoxynicotinates, synthesis, phase transition temps., and dielec. props. 79−86876
phenyl acetylene, liq., phase relax., vibr. dephasing, Raman spectra obs. 80−91567
phenyl alkyl ammonium copper chloride, quasi-two-dimens. Heisenberg ferromag., mag. props. 77−66273
phenyl benzoate, liq. cryst., DC dynamic scatt. and dopant electrochem. props. 77−90130
phenyl benzoate and thiobenzoate, 4,4′-disubstituted, mag. susceptibility anisotropy and order parameter 79−86704
phenyl benzoate liq. cryst., doping effect on cond. anisotropy and dynamic scatt. 77−40208
phenyl benzoate nematic liq. cryst., dynamic scatt., alignment effects 77−40207
2,2′-p-phenyl bis (5-phenyloxazole), vap. phase dye laser media, photophysical parameters 80−95884
1-phenyl butadiene, nonlinear third-order electric susceptibility 78−74944
phenyl cation, singlet, triplet state mol. geometries, energies, ab initio UHF STO calcs. 77−6672
phenyl cation, struct., ion-molecule reactions studied by trapped ion mass spectroscopy 80−102586

organic compounds continued
phenyl isocyanate, electronic absorpt. spectrum, vibr. struct., f-values, spectroscopic moment and config. 78−58715
phenyl isocyanate, microwave spectrum, rot. consts., dipole moment 77−61739
phenyl isothiocyanate, in benzene (tetrachloromethane), nonlinear dielectric solvent effect 79−28702
4-phenyl n-pentyl ester, Nematel 105, nematogen, isotropic phase, Rayleigh scatt. and mol. reorientation 78−34429
phenyl propargyl ether, dimerised, with $CaCO_3$-Pd catalyst, as H getter 77−18001
1-phenyl-2-(4-pyridyl) cyclopropanes, UPS of cis- and trans-forms 79−36699
N-phenyi-2-naphthylamine, liq. scintillator system, energy transfer, fluoresc. intensity-max. solvent depend. 78−21966
(+)-(S)-2-phenyl-3,3-dimethylbutane, optical activity, circular dichroism, polarisability model 80−43082
4-phenyl-3-thiosemicarbazide, single cryst., X-irrad., EPR, ENDOR, radical identification 79−31560
1-phenyl-3-thiosemicarbazide, X-irrad., radical prod., ESR, ENDOR 77−36770
2-phenyl-5(4-difluoromethyl-sulfonylphenyl)oxazole, stimulated emission, laser pumped 77−75504
p-phenyl-benzylidene-p'-alkylaniline, ordered smectic B phase, mol. length, influence on charact. *(French)* 79−14671
phenyl-trimethine-merocyanine, X-ray diffr. exam. of cryst. and mol. struct. 80−6398
phenylacetylene, excited single state B_1, electron-vibr. spectra and electronic struct. 79−26904
phenylacetylene, He ion stopping cross sections, ring struct., bond strain and Bragg rule deviations 79−98188
phenylacetylene, phosphorescence polarisation, intramolecular heavy atom effect 78−52550
phenylalanine, and derivatives, circ. dichroism and mag. circ. dichroism 79−87418
phenylalanine, hydrated electron impact dissoc., laser flash photolytic investig. 80−58396
phenylalanine, polycryst., proton mag. relax. and mol. motion 78−20139
phenylalkylamines, effect on frog muscle fibre end-plate current pot. depend. 78−31799
phenylamine difluoride, and derivs., ^{19}F NMR 78−2754
9-phenylanthracene, fluoresc. lifetime and quantum yield in solns. 77−6834
9-phenylanthronyl radical, ESR, temp. depend. phenyl twist angle 79−18210
4-phenylbenzylidene-4'-n-alkoxyanilines, central Schiff's base linkage reversal effect on liq. cryst. props. 80−79683
phenylcarbene, singlet and triplet ground states, rearrangement to cycloheptatrienacarbene, MINDO/3 calc. 78−13430
2-phenylcycloalkane, photolysis products studied by ^{13}C CIDNP and intersystem crossing 79−79275
phenylcyclohexadienyl radical form in electron irrad. benzene cryst., absorpt. and fluoresc. spectra study 80−89035
phenylcyclohexanes, alkylamino substituted, synthesis and mesomorphic props. 80−44120
phenylcyclohexanes, nematic, low melting liq. crysts. with positive dielec. anisotropy, phys. props. 77−43148
phenylcyclohexanes, p-disubstituted, elastic consts. and diamag. anisotropy 79−65639
phenylcyclohexanes, substituted, anisotropic liq. cryst. solvent for optical absorption spectroscopy 78−45724
p-phenylene bis (p-substituted benzoates), cryst.-nematic transition, mol. struct. effects, DTA 78−47504
phenylene compounds in n-paraffins, electronic spectra and fluoresc. 78−13509
phenylene derivatives, effect of substitution on liq. crystalline props. 80−70113
m-phenylene diacrylic acid, four-centre-type photopolymerisation in cryst. state, holographic appl. 78−37832
phenylene sulphides, NMR relaxation for mol. motions *(German)* 80−11288
p-phenylenebis(galvinoxyl)biradical, molar mag. susceptibility, 4-300K 78−47939
p-phenylenediacrylic acid dimethyl ester, photopolymerisable cryst., struct. determ. 78−63747
p-phenylenediacrylic acid diphenyl ester, photopolymerisable cryst., struct. determ. 78−63748
p-phenylenediamine, reson. Raman spectra 77−58009
phenylenediamine-dihydroxybenzene mixtures, solid-liquid equilibria, phase diagrams 77−27986
phenylenediamines, transition energies, oscill. strengths, time-depend. Hartree-Fock method *(Spanish)* 77−6684
phenylethanolamine, putative neurotransmitter in Aplysia 77−48783
d,l-α-phenylethylamine, differential Raman scatt. of right and left circularly polarized light *(Japanese)* 78−17675
phenylethylamine, Gaussian wavefunctions, transcorrelated method 77−61678
2-phenylindole, in viscous soln., fluoresc. quenching, emission, intensity and reson. transfer *(German)* 80−91599
2-phenylindole, liq. scintillator system, energy transfer, fluoresc. intensity-max. solvent depend. 78−21966
phenylnaphthalenes isomers, fluoresc. lifetime difference and mol. geometry 80−69176
phenyloxadiazole derivatives, dye laser, pumped by KrF laser, 3500 Å range 77−42532
phenyloxazolyl pyridinium salt dye lasers, flashlamp pumped, blue-greenlasing 80−95886
p-phenylphenol in stretched polyvinyl alcohol film, phosphorescent triplet states, ESR spectra obs. 80−83393
p-phenylphenolate ion in stretched polyvinyl alcohol film, phosphorescent triplet states, ESR spectra obs. 80−83393
phenylphosphines, and derivatives, ^{1}H, ^{13}C and ^{31}P NMR studies 80−87152
phenylpolyenes, donor-acceptor disubstituted, INDO calc. of hyperpolarisability 79−93924
3-phenylpropanol-hexane, nonlinear dielectric effect, critical exponent 80−93227
3-phenylpropanol-n-hexane, Kerr effect near crit. pt. 79−61336
1-phenylpyrazolidin-3-one adsorption on metal electrodes, obs. 79−100391
phenylpyrimidines, liq. crysts., synthesis and phys. props. 78−1995
organic compounds continued
phenylsilanetriol-d_0,(-d_3), cryst. and liq. vibr., IR and Raman spectra 78−86855
phenylthiobenzoate derivatives, thermodynamic and mesomorphic props. 77−11678
pheophytin a and b, assoc. solns., excited state deactivation, flash photolysis obs. 79−54895
pheophytin containing monolayers, phase separation and domain interaction, surface press. and fluoresc. meas. 79−100580
pheophytin reduction obs. in higher plant photosystem II 79−43817
pheophytin solutions, photolum. of singlet O_2 78−80831
pheophytin-a, fluoresc. fading curve of lowest triplet state 79−36691
pheophytin-a, photochem. generation of cation-radical, spectral-kinetic charact. 78−96008
pheophytin-a (b), dimerisation, fluoresc. and ODMR study 80−18876
pheophytin-chlorophyl, pigment associations, conc. effects, luminesc., absorpt. spectra and dichroism obs. 80−1007
pheophytins, lowest triplet state, zero field splitting consts., decay rate consts., EPR determ. 78−27896
phlorin, UV adsorption and photoelectron spectra, CNDO/S3 calcs. 77−75210
phloroglucinol, monodispersed airborne particles, ice nucleation 79−20947
phloroglucinol dihydrate crystals, growth charact., X-ray diffr. and optical microscopic study 79−19986
phosgene, adsorption by activated and impregnated carbons 77−70333
phosgene, spectrophone meas. at selected CO, CO_2 laser wavelengths 78−57310
phosgene, transformation and compliance matrices determ. 77−18898
phosphamides, carcinostatic, ^{14}N NQR, electron distrib. and bonding configs. 80−48018
1-phosphapropyne, microwave spectrum, vibration-rotation analysis, dipole moment, structural parameters 79−93989
phosphate ester, electrical prop. rel. to lubrication 79−38150
phosphate esters, scuffing resistance 79−38990
phosphates, cellular, heteronucl. two-dimens. NMR as conform. probe 80−3590
phosphatidyl choline, oxidised, free radical formation on UV irrad. 80−76790
phosphatidyl choline vesicle phase transition probed by positron annihilation lifetime technique 79−88061
phosphatidylcholine bilayers, fluidity changes and phase transitions, intramol. excimer fluoresc. obs. 80−85342
phosphatidylcholine membranes, interaction of colchicine, spin-label study 77−86455
phosphatidylcholine monolayer vesicles, US irradiation formation, quasielastic laser light scatt., dynamics 77−48764
phosphatidylcholine-cholesterol vesicles interacting with lucensomycin, PMR obs. 80−40954
phosphine, IR spectrum, ν_1 and ν_3 band analysis 80−83366
phosphine 3R hydrochloride, interaction with aliphatic acids and alcohols, IR and electron spectra *(Russian)* 78−21930
phosphodiesterase, control in rod disc membranes 79−79527
phosphoglycerate kinase, sequence, struct. and activity, hingee-bending enzyme 79−74595
phospholipid bilayer, Gramicidin antibiotics effect on Raman spectra 77−66798
phospholipid bilayer melting transition, thermodynamic fluctuations, ion permeability, statistical mechanics model 78−73140
phospholipid bilayer membrane modified by valinomycin, volt. fluctuations 78−31777
phospholipid bilayers, carbonyl groups dynamics, ^{13}C chem. shift anisotropy obs. 80−85326
phospholipid bilayers, van der Waals interactions, total potential curves 78−77006
phospholipid inter-and intra-molecular interactions, PCILOCC and pot. function calc. 80−3570
phospholipid membrane, polar head motion, NMR and EPR linewidth study using $TCNQ^-$ ion-radical *(French)* 80−45865
phospholipid membrane solubilisation by human plasma high density lipoprotein 77−16916
phospholipid monolayers, polymorphism 78−40120
phospholipids, ^{31}p NMR, slow-motional lineshapes for very anisotropic rot. diffusion 80−5644
phosphonates, influence on precipitation of $CaCO_3$ 79−43119
phosphonium cations, quaternary, produced by field desorption, collisional activation spectra 78−56946
phosphoranyl radicals obs. in ESR spectra of triphenylphosphine sulphide in deuterated methanol 80−84651
phosphors, surface impregnation of Al_2O_3 anodised film, fluoresc. spectrum *(Japanese)* 80−55170
phosphorus containing compounds, analysis by spectrophotometry 79−34379
phosphorus-containing compounds, liq., ^{31}P nucl. spin-lattice relax. and Overhauser effect 79−36666
photo-electron-microscope pictures of organic samples on metal supports 80−26431
photocatalytic oxidation on Mars 78−85883
photochemically produced, abundance in outer planets atmospheres, lab. simulation 79−75142
photoelectron angular distribution, for band assignment rule 79−13768
photoelectron spectroscopy, ionis. pots., MO models 78−17716
photoemission and photoionisation in three stage model 80−100744
photographic dye, colour coupling in soln., kinetic anal., appl. of flashlight photolysis *(German)* 79−39173
photophysics, data anal. method 79−59735
photoproduction, in simulated Jovian atmosphere, mol. anal. 78−69740
photosynthetic pigment, intersystem crossing 77−58057
photosynthetic pigments, fluoresc. spectra, using 3-dimens. contour plotter 78−58046
photosynthetic systems, reaction centre struct., triplet state ODMR 77−29093
photosynthetic systems, temperature dependence of excitation transfer 78−92598
photosystem I, of green plants and algae, CIDEP obs. 80−63679
phthalamide derivative with aromatic amine, exciplex formation and fluoresc. quenching 79−87848
phthalamide derivatives, solutions, excitation spectra rel. to absorption spectra, 77-300K 79−85970
phthalan, geometry, electronic absorpt. spectra 80−971

organic compounds continued
phthalazine, excited state absorpt. spectra and intersystem crossing kinetics 80−74176
phthalazine, excited states, protonation influence, semiempirical CNDO/S CI calc. 79−76353
phthalazine, fluoresc. and phosphoresc., expt. and CNDO/S CI calcs. 79−31585
phthalazine, prereson. Raman spectra, vibr. band intensities 80−102514
phthalic acid, IR absorpt. spectra, fundamental assignments 80−5542
phthalic acid derivatives, excitation energies, CNDO/S-CI method calc. appls. *(German)* 80−106275
phthalic acid diamide, mol., PMR and IR spectra, easy polarisable H-bonds 79−31516
phthalic anhydride, dendritic growth 78−18936
phthalic anhydride, single crystals growth and perfection 79−78869
phthalic anhydride, vibr. excitons reson. interaction in IR and Raman spectra *(Russian)* 79−61386
phthalic anhydride, whisker crystals, vapour growth and morphology 77−35841
phthalic anhydride, whisker growth in closed cryst.-vapour system 78−34734
phthalic anhydride+8-hydroxyquinoline, solid-state reaction kinetics 77−36746
phthalic anhydride and halogen derivatives, phosphorescence spectra *(Japanese)* 78−48217
phthalic anhydride crystal, Raman spectra, overlapping spectral bonds separation by computer *(Russian)* 79−51968
phthalic anhydride derivative, quartet invariants in space group P1, least-squares analysis 77−84570
phthalic anhydride spherulites, cryst. growth from melt 79−32930
phthalimide, soln., excitation spectra rel. to recording wave length *(Russian)* 77−12438
phthalimide, soln., triplet state accumulation and deactivation depend. on solvent polarity 79−85982
phthalimide acetyl derivatives in polar solvents, luminesc. kinetics and phosphoresc. quenching 80−18885
phthalimide derivative-tetramethyldiaminodiphenylmethane exciplexes, luminesc. props. 77−68070
phthalimide derivatives, hidden vibr. band determ. method, fluorescence and excitation spectra meas. 80−40158
phthalimide derivatives, in hexane and isopentane, vap., inversion freq. determ., from fluoresc. quantum yield obs. 79−54892
phthalimide derivatives, solns., ultrafast mol. relax. 79−85984
phthalimide derivatives, solutions, lasing characts. in green spectral region, photostability 80−32978
phthalimide P derivatives 79−56836
phthalimide solutions, fluoresc. optical quenching by ruby laser rad. *(Russian)* 77−12437
phthalimides, solns., solvent effects on absorpt. spectra and fluoresc. 77−34650
phthalimides, spectrum luminesc. props., laser generating capacity and generation features *(Russian)* 79−31897
phthalimides, stimulated radn. with lamp pumping *(Russian)* 79−51987
2-phthalimido-4-ethoxy-γ-butyrolactone, statistical treatment of unobs. reflexions 79−50937
2-phthalimido-4-methylthio-γ-butyrolactone, statistical treatment of unobs. reflexions 79−50937
phthalocyanides, thermal stability, DTA *(German)* 80−11945
phthalocyanine, dye photosensitiser for SiO_2 film MIM struct. 78−6408
phthalocyanine, fluoresc. spectra in supersonic expansion 79−3475
phthalocyanine, free base, fluoresc. excitation spectrum, cooling in supersonic free jet 80−95670
phthalocyanine, in n-alcanes and polyethylene, absorpt. and fluoresc. spectra, 4.2 and 77K 78−976
phthalocyanine, metal-free, molecular imaging and phase transformations using electric microscopy 79−33198
phthalocyanine, metal-free, photovoltaic props. in Al/H_2Pc Schottky barrier solar cells 79−100527
phthalocyanine, metal-free, singlet-triplet fusion rel. to carrier photogeneration 77−36276
phthalocyanine, metal-free, solid, fluoresc., lifetimes temp. depend., polymorphic modification 78−80388
phthalocyanine, optical density spectra, charge transfer states 79−95800
phthalocyanine, polycryst. film, charge transfer state and optical spectra *(Russian)* 78−84607
phthalocyanine, quasiline emission spectra using low temp. laser luminesc. spectrosc. *(Czech)* 80−86445
phthalocyanine, sublimed film, absorption spectra and association 78−48174
phthalocyanine, supersonic free jet-cooled, fluoresc. obs. 79−45753
phthalocyanine, surface, luminesc. accompanied by ion implantation 80−60683
phthalocyanine, vap., photoelectron spectra 79−64043
phthalocyanine, x-metal-free, photogeneration and fluoresc. quenching theory 79−65513
phthalocyanine, X-metal-free in polyvinylacetate, elec. field induced fluoresc. quenching, carrier photogeneration 78−48207
phthalocyanine compounds, valence band studies, UPS meas. 77−52221
phthalocyanine compounds, XPS and change transfer 80−95681
phthalocyanine dye for stable passive Nd laser switch, bleaching and relaxation 80−74368
phthalocyanine films, electronic transitions, 0.5 to 2.5 eV, inelastic electron tunnelling spectra 79−41214
phthalocyanine films, metal-free, adsorbed o-chloranil effect on surface photovoltage 80−34485
phthalocyanine films, metal-ligand and π singlet-triplet transitions, IETS obs. 78−90252
phthalocyanine layers, metal-free, between Ag and Al electrodes, switching effects 80−65706
phthalocyanine metal free films, TSC, ferroelectric-semiconductor transition 80−66105
phthalocyanine metal-free, photoconducting, electric field-induced fluoresc. quenching 80−34967
phthalocyanine monolayers and vapour-grown films, surface struct., LEED 77−35830
phthalocyanine sensitization of Se photoreceptors, charge decay characts. 80−15630
α-phthalocyanine target, reactor-irrad., extraction rate and mechanism of ^{64}Cu 80−35563
phthalocyanine thin layers, metal-free, mobility and thermally stimulated polarisation meas. 79−73527

organic compounds continued
phthalocyanine-alkane interface, charge transfer, rel. to photoelectrophoretic image form. 80−65616
phthalocyanine-Cu, photoemission multielectron effects from quasi-atomic Cu 80−93458
phthalocyanine-dodecane interface, photostimulated charge transfer flash expt., trapping model 77−66182
phthalocyanine-halogen complex, influence of halogen on elec. and optical props. *(Japanese)* 79−51586
phthalocyanine-halogen complexes, elec. props. 80−29424
phthalocyanine-metal interfaces, surface photovoltage 80−20308
phthalocyanines, controlled flashlamp illuminated phototropic switch 77−88735
phthalocyanines, dye laser appls., soln. chem. 77−40568
phthalocyanines, elec. cond., compensation effect 80−100455
phthalocyanines, lasing props. obs. 78−17931
phthalocyanines, metal free, mol. cryst. images in electron diffr. patterns 80−103315
phthalocyanines, partially oxidised, highly conductive molecular solids 77−47800
phthalocyanines, photovoltaic effects, dark elec. props. of rectifying cells 79−4604
phthalocyanines, photovoltaic effects, illuminated thin-film cell props. 79−4605
phthalocyanines, UV photoemission, valence band struct. 77−85884
phthalocynanine, doped photovoltaic cell, photoconductivity, elec. field induced flouresc. quenching, charge carrier photogeneration 80−84485
phthalozine, oriented in lyotropic mesophase, proton NMR spectra 79−82886
phthoralocyanin porous films, Becquerel photovoltaic effect 77−16907
physostigmine, determ. using enzymatic sensor *(French)* 78−73099
phytanic acid, in phospholipid bilayers, struct., order parameters, liq. cryst. transition, entropy 79−83713
phytochrome chromophore, models, absorption wavelengths and oscillator strengths calc. 77−81469
phytol in phospholipid bilayers, struct., order parameters, liq. cryst. transition, entropy 79−83713
picene, EPR in p-terphenyl cryst., triplet state 79−36668
picene, nonlinear third-order electric susceptibility 78−74944
β-picoline, fluoresc. of vap. phase, nonradiative electronic relax. 79−86000
γ-picoline, fluoresc. quenching of dicyanoanthryl-naphthyl intramol. exciplex, triple exciplex form. 79−50061
γ-picoline, proton Zeeman relax., CH_2D groups effect 79−8067
picoline compounds, proton spin-lattice relax. time, methyl group rot., 1 to 10K 77−48080
β-picoline-water solution, light scatt. spectra, ultra- and hypersonic absorpt. *(Russian)* 80−93353
picolines, freq. assignment, vibr. spectra interpretation *(Russian)* 79−22684
picosecond transient spectroscopy of molecules in solution 79−36621
picric acid-o-bromoaniline binary system, phase diagram and DC elec. resist. 77−15546
pigment associations, conc. effects, luminesc., absorpt. spectra and dichroism obs. 80−1007
pigment crystalline soln., electrically induced fluorescence polarised component change meas. 80−32863
pigment soln., luminesc. of singlet state O_2 in energy transfer 79−54886
pinacyanol, adsorbed cationic dyes, ionisation energy, local environment effects 79−34337
pinacyanol, picosecond photobleaching and absorpt. recovery, solvent effects 77−44493
pinacyanol, solns., fluoresc. lifetime, viscosity depend. 79−59497
pinacyanol as mode locking saturable absorber for rhodamine dye lasers 77−42554
pinacyanol dye, adsorbed on CdS substrate, aggregation effect on mol. electronic states 80−37757
pinacyanol in ethanol, electronic relax., analysing light ps spectroscopy 80−99517
pinacyanol sensitizer adsorbed on CdS, spectral sensitization at low surface density 79−47973
pinacyanole, dye photosensitiser for SiO_2 film in MIM struct. 78−6408
pinakryptol yellow, photographic dye desensitization mechanism *(French)* 79−9250
d,l-α-pinene, differential Raman scatt. of right and left circularly polarized light *(Japanese)* 78−17675
α-pinene, methyl groups internal rot. ^{31}C spin lattice relaxation times and force field calcs. 80−74255
1,4-piperazine, conform. equilib., CNDO/2 calcs. on six-membered rings 80−23336
piperazine-2,5-diones, and N-chloro derivatives, UV photoelectron spectra and geom. struct. 79−18235
2,5-piperazinedione, X-ray damaged, ENDOR, δ proton hyperfine interaction 77−9103
piperazines, PMR spin-lattice relax. times and lineshapes, 100-300K 77−81027
piperazinium $Ag_{10}I_{12}$.4-dimethylformamide, exam. of electrical cond. and crystal structure 78−75871
piperazinium-AgI binary salts, ionic cond. study *(French)* 78−2293
piperdinyloxy 2,2,6,6-tetramethyl radical, recrystallised samples, EPR study 80−100615
1-piperidine carboxylic acids, intramol. H bonds, struct., IR spectra 77−14426
piperidine intercalation with PbI_2, rel. to NQR, spin-lattice relax. temp. depend. *(Russian)* 78−27108
piperidine solution of PbI_2, crystn. of intercalation cryst. 80−16170
piperidine-$MnBr_2$ complexes, substituted, excitation spectra, ligand field theory 77−27103
piperidine-PbI_2, intercalation cpd., heat capacity of low temp., intercalation effect *(Russian)* 80−92682
piretanide inhibition of active Cl^- transport in teleost intenstine cell 78−64967
pitch, coal-derived low-volatile residues, glass transition, rheological props., DSC anal. 80−39331
pitch, mesophase, solubility 78−67831
pitch and coke-pitch disperse system, viscoelastic props. 80−1500
pitch weathering processes, IR multiple internal refl. obs. 79−74461
pivalic acid, liq. and plastic crysts., ^{13}C NMR chem. shift, temp. depend. 80−2652
pivalic acid, long ultra-pure single crysts. grown by modified Bridgman technique 77−55883

organic compounds continued
pivalic acid, orientationally disordered crystal., mol. orientation 78−34448
pivalic acid, plastic cryst., self-diffusion 79−46832
pivalic acid($-d_1$, d_9), liq. and soln., Raman assignments, CH_3 rot. barrier, dimerisation 79−26991
pivalophenone, organic soln., triplet reactivity solvent depend., flash photolysis study 80−11902
planar aromatic hydrocarbons in polymer films, polarisation data interpretation, photoselection spectroscopy appl. 80−58302
planar cyclic radicals, C-H proton isotropic hyperfine consts., C hybridisation 80−95646
plasma chromatography and electron capture detector, comparison between two techniques 80−61176
plastic scintillator, degree of fluorescence light polarisation, energy depend. *(German)* 78−37677
plasticizer effect on electric strength of polystyrene 80−29688
γ-platinum phthalocyanine, energy band structs., carrier mobilities 77−72817
platinum phthalocyanine, photoemission, outer core levels, cross-section depend. 79−50079
platinum phthalocyanine single cryst., triplet state Zeeman effect, phosphoresc. 78−6747
pleochroic dyes, dissolved in nematic liq. crysts., guest-host interactions, appl. to electrooptic displays 80−44113
PMDA, ab initio SCF MO wavefunctions for ground and excited states 79−10028
PMMA, circular plates, thermoviscoelastic anal. of a thermorheologically simple material 80−10161
PMMA, effect of light on adhesion to metallic substrates *(Russian)* 79−97464
PMMA, resonance size effect in space charge relaxation 80−75937
PMMA-spirobenzopyran mixed monolayers, photoresponsive effects 79−66316
PMMI-carbazole, 1:1 complex, X-ray cryst. struct. determ. 79−94991
PMTA-dibenzthiophene, 1:1 complex, X-ray cryst. struct. determ. 79−94991
PNAOBA, type C smectic liq. crysts., electrohydrodynamic instability 80−1927
polar and H-bonding compounds, vap. press. behaviour, generalised treatment 78−2227
polar liquids, activation energy for viscosity, rel. to charge distrib. 79−37865
polar liquids, binary mixtures, Sarma and Rao's rel. for dielectric relax. time 80−88914
polar liquids, US sound vel. meas. 78−87742
polar liquids in double layer capacitors, RF conduction, ion diffusion effect 80−107883
polar molecules, in nonpolar solvent, dipole moments and relax. times 78−43782
polar organic molecules, external doping in MIM tunnel junctions, inelastic tunnelling spectroscopy obs. 79−3510
polar solutes, in o-terphenyl soln., dielec. relax. 79−33598
polar solvents, fast electron transfer processes, investigation by magnetic fields 79−8479
polarisability of conjugated hydrocarbons and aromatics, linear and dynamic polarisability 79−98242
polarographic maximum suppression by substituted vinyl quinolones 79−57325
pollutants in airborne particulate matter and gas phase 79−12238
poly(γ-benzyl-D-glutamate), liq. cryst., tactoidal shell defects 78−22642
poly(γ-benzyl-L-glutamate), in benzene soln., cholesteric liq. cryst. props. 79−94889
poly(γ-benzyl-L-glutamate) solns., osmotic press. in isotropic and anisotropic phases 79−94886
poly(ethylene oxide) aq. soln., adsorpt. on mica, force meas. between mica surfaces 79−23833
bis-catena-poly(methylarsenic), one-dimensional homonuclear molecular systems, nature of energy gap 79−11063
poly(n-dodecyl L-glutamate), thermotropic polymorphism, low-angle X-ray diffr. *(French)* 78−34601
poly(N-vinylcarbazole), space charge effects on triboelec. charge exchange 80−54763
poly(p-phenylene terephthalamide) fibres, optical anisotropy determ. 79−4786
poly(paraphenylene terephthalamide), nematic structure by optical and X-ray methods *(French)* 77−31584
poly (γ-benzyl-l-glutamate)-dioxane system, periodic struct. under elec. field 78−47234
poly chlorinated biphenyls, in soils of Everglades National Park and adjacent agricultural areas 79−92098
poly-l-glutamic acid, soln., u.s. absorpt., linear Ising chain kinetics 77−4980
poly-2,4-hexadiyne-1,6-diol bis (p-toluene sulfonate), exciton surface polaritons, reflecting faces obs. 80−65645
poly-γ-benzyl-L-glutamate, mag. oriented liq. cryst. solns., order parameter 77−15305
poly-γ-benzyl-L-glutamate, sidechain order parameters, ^2H NMR meas. 80−1923
poly-γ-benzyl-L-glutamate helices, optical activity 80−48113
poly-γ-benzyl-L-glutamate-dioxane liq. cryst., orientational order temp. depend., diamag. susceptibility 77−47966
poly-L-lysine, membrane phase, transport processes, helix-coil transition 78−77031
poly-N-benzamide, lyotropic liq. crystals, viscosity anisotropy 80−10693
poly-N-vinylcarbazole and N-isopropylcarbazole with p-dicyanobenzene in dimethylformide soln., laser photolysis 79−100360
poly-ynes, struct., vibr. freqs., ionis. energies, MNDO calc. 77−88390
polyacenes, alternant, internal conversion, energy gap correl. 79−54901
polyacenes, atomic localisation of electronic excitation 77−18806
polyacenes, electronic transition bands, Franck-Condon factors, PPP SCF MO/CI calc. 78−33430
polyacenes, linear, open-shell ground state wave functions 79−762
polyacenes, MCD, CNDO/S calcs. 77−79637
polyacenes, planar vibrs. classification using potential energy distrib. anal. 79−98065
polyacenes, S_1-T_1 interconversion, excitaiton indices calcs. 79−54830
polyacenes, spectra, correlation effects 79−81199
polyacetylene, doped and neutral, resonance Raman scatt. 80−55107
polyacetylene, electronic struct., spectra interpretation, CNDO/S2 calcs. 79−6870
organic compounds continued
polyacetylene, metallic, mixed Peierls phase, Hartree-Fock calcs. 80−70689
polyacetylene, pristine and acceptor doped isomers, EPR, DC cond., evidence against solitons 80−15782
polyacetylene compounds, rot. consts. 78−86841
polyacetylene type infinite chain cryst., energy bands, ab initio Hartree-Fock orbital calc. 78−60066
polyacrylamide gel, automated scanning of ^{14}C 80−17221
polyacrylamide gel containing metal hydroxides, U(VI) extraction from seawater 78−54861
polyamine, ligand interference preventive buffer appls., for Cu II ion selective electrode 78−20099
polyamine iodide-AgI solid electrolytes, elec. cond. and cryst. struct. 80−107537
polyamine iodide/AgI solid electrolytes, conc. depend. of elec. cond. 80−24647
polyamino acids, macromolecules, relax., modified Glauber theory 77−12879
polyaromatic hydrocarbons, n-alkane solvent effect on low temp. fluorescence spectra 77−36274
polyaromatic hydrocarbons, quasi-linear fluoresc. spectra, temp. effect 79−22745
polyaromatic molecule, high resolution dark-field images 78−26398
polyatomic chain molecules, vibr. freqs. 79−31731
polyatomic molecules, IR photodecomp. mechanism 79−52716
polyatomic organic molecules, electronic excitation transport in inhomogeneity broadened 79−54884
polybutadiene, adsorption behaviour, surface tension exam. *(Japanese)* 78−31690
cis-1,4-polybutadiene, vulcanised composite system, viscoelasticity 77−75823
polybutadiene-n-hexane-n-heptane soln., Rayleigh scatt., diffusion coeff., viscosity 78−15179
polybutadienes, epoxidised, epoxide content, ^{13}C NMR determ. 79−51872
polychlorinated biphenyls, Kerr electro-optic coeff. 77−4625
polychlorinated biphenyls, pollutants, radiation degradation in organic solvents, H_2O 80−30262
polychlorinated biphenyls, sampling in ambient air, using polyurethane foam 78−20080
polychlorinated biphenyls waste disposal by pyrolysis, plasma torch appl. 80−76487
polychlorinated naphthalenes, sampling in ambient air, using polyurethane foam 78−20080
polycrystalline, charge carrier drift mobility 78−34835
polycrystalline dipeptides, X-irradiated ENDOR and ELDOR obs. 80−63689
polycyclic aromatic hydrocarbon impurity luminescence spectral anal. in calcite 80−71483
polycyclic aromatic hydrocarbons, air pollution from combustion processes, health hazards 78−81394
polycyclic aromatic hydrocarbons, air pollution long-range transport 79−83653
polycyclic aromatic hydrocarbons, alternant and nonalternant, fluoresc. quenching by nitro cpds. *(German)* 78−21967
polycyclic aromatic hydrocarbons, appl. of matrix isolation microsampling procedure, quantitative anal. 79−100460
polycyclic aromatic hydrocarbons, benzenoid system PO-MO character and PMO localisation energy 79−54767
polycyclic aromatic hydrocarbons, detect. using laser-induced mol. fluoresc. 77−81431
polycyclic aromatic hydrocarbons, diamagnetic susceptibility NCHF (SCF-PPP) calcs. 77−6686
polycyclic aromatic hydrocarbons, electrophilic superdelocalisability rel. to carcinogenesis, Pullman theory 79−63897
polycyclic aromatic hydrocarbons, in particles from coke oven, size distrib., health hazards 78−36268
polycyclic aromatic hydrocarbons, matrix isolated, quasilinear Shpol'skii fluoresc. spectra 78−9189
polycyclic aromatic hydrocarbons, trace analysis using automated HPLC 79−96384
polycyclic aromatic hydrocarbons in Gulf of Maine sediments and Nova Scotia soils 79−74555
polycyclic aromatic hydrocarbons in long-range transported air pollutants 77−78410
polycyclic aromatic hydrocarbons in recent sediments, global distrib. 78−57192
polycyclic aromatic hydrocarbons sorbed on fly ash, recovery for quantitative determ. 80−61177
polycyclic aromatic quinone, epitaxy on alkali halides, adsorbed water effect 79−28239
polycyclic aromatic ring systems, localised MOs and wave functions 79−31398
polycyclic compounds, ^{13}C NMR, spin-lattice relaxation meas., rot. barriers in hindered methyl groups 77−10689
polycyclic conjugated compounds, isomeric, Kruszewski's rule for stability 80−106249
polycyclic conjugated molecules, π-electron energy contrib. of ring, rel. to linear analogue 77−30787
polycyclic hydrocarbons, alternant and nonalternant, fluoresc. quenching by electron transfer 79−6959
polycyclic hydrocarbons, fluoresc. spectra, using 3-dimens. contour plotter 78−58046
polycytosine, ab initio energy band struct. 77−70415
polydiacetylene, cryst., one-dimens. conjugated semicond., vibronic coupling, Fano interference effects 80−34939
polydiacetylene, single cryst., polymerisation under hydrostatic press. 79−20367
polydiacetylene fibre resonance Raman spectrum meas. 79−17507
polydiacetylenes, cryst., picosec. pulse, nonlinear optics appls. 79−46017
polyenals related to visual chromophores, absorpt. spectra rel. to chain length 79−34494
polyenals related to visual chromophores, emission spectra 79−34495
polyene, deformed excited state, bond length rel. to bond order 77−75071
polyene, energy bands, ab initio Hartree-Fock cryst. orbital calcs. 77−89717
polyene, linear, band gap calcs. 77−31969
polyene band struct. calc., excitons in polyene chain 78−26816

organic compounds continued
polyene chromophones, band broadening in electronic-vibr. absorpt. spectra 80−28003
polyene chromophores, electronic absorpt. spectra, charact. spectral band criteria 80−63651
polyene derivatives, horizontal radiationless transitions, singlet-pot. and rot. angle, semi-empirical model 78−42109
polyenes, 2^1A_g-1^1B_u energy gap, extended CI study 79−81159
polyenes, π-electron correlations, canonical and localised orbitals calcs. 79−36547
polyenes, absorpt. spectra, electronic-vibr. sequence band broadening 77−65453
polyenes, conjugated, homologous linearity rule for electronic spectra 79−6933
polyenes, DODS methods with HF variations 77−23425
polyenes, electronic absorpt. spectra, charact. spectral band criteria 80−63651
polyenes, electronic absorpt. spectra, intensity distrib. anal. 77−58034
polyenes, electronic absorpt. spectra absolute intensities estimation 77−34702
polyenes, energy spectrum, electron correlation effects 78−46279
polyenes, linear, π-electron system, appl. of extended RPA excitation operators 79−97993
polyenes, linear, radiative rate consts., environmental effects 79−72348
polyenes, linear, two-photon absorptivities, SCF-PPP-CI calcs. 79−31631
polyenes, localised representation, correlation contrib. to energy 79−59370
polyenes, model results for π electrons 78−55128
polyenes, photoiosomerisation, triplet pot. energy surfaces and normal mode anal. 80−108700
polyenes, radiative rate consts., solvent depend. 78−66587
polyenes, substituted, spectra, four-level state scheme 79−54840
polyenes, symmetric, combinatorial enumeration of chemical isomers 80−28114
polyenes, twisting force consts., CNDO theory potential energy surface 78−50474
polyenic aldehydes, energy spectrum, electron correlation effects 78−46279
polyenones related to visual chromophores, absorpt. spectra rel. to chain length 79−34494
polyenones related to visual chromophores, emission spectra 79−34495
polyester fibres, thiuram and dithiocarbamate rubber accelerator degradation 79−78986
polyethersulphone, thin film TLD, skin dosimetry appl. 80−52790
polyethlene crosslinking by electron beam radiation *(Japanese)* 79−70353
polyethylene: octadecanol, contact charging and donor impurity conc. relationship 80−20286
polyethylene, cross-linked, appl. as freeze-tolerant material for solar water heaters 80−66944
polyethylene, deuterated, diagnostic neutron spectra from deuterons 2.5, 3.0, 3.5 MeV 79−40933
polyethylene, diagnostic neutron spectra from deuterons 2.5, 3.0, 3.5 MeV 79−40933
polyethylene, high β-plasma in spindle-cusp mag. container, laser produced 78−59650
polyethylene, in toluene, pressure crystallised, swelling behaviour, rel. to densities 80−2167
polyethylene glycol, effect on photographic film during fast development *(Russian)* 80−45533
polyethylene pellets, plasma heating using CO_2 laser 79−1331
polyethylene plate, interaction of laser with laser produced plasma 77−19734
polyethylene terephthalate film, interaction of laser with laser produced plasma 77−19734
polyethylene-paraffin mixtures, crystallisation kinetics 79−41985
polyethylsiloxane, PES-S-2, PES-5, viscosity and solidification press., 0-10^4 Pa, 20-180°C 77−43266
polyferrocene, in MIM sandwich, I-V and I-d charcts. 78−80064
polyfluorinated polyethers, appl. lubrication and cooling of turbomolecular pump rotor bearing 77−87776
polyglutamic acid, helix-random coil transition observed by gamma-ray ang. correlation 78−80828
polyglycine, total energy, conformational calc. using quantum mech. partitioning method 78−94189
polyglycine chain, electronic struct. and transport props., ab initio Hartree-Fock crystal orbital calc. 79−42448
polyhydroxy compounds, X-irrad., trapped electrons, ESR and ENDOR obs. 80−93161
polyhydroxyl alcohols, H-bonded solns., microwave dielec. relax. 79−33599
polyisobutylene, circular plates, thermoviscoelastic anal. of a thermorheologically simple material 80−10161
polyisobutylene-tetralin, binary liq. soln., surface cluster functions 78−67631
polyisoprenes, epoxidised, epoxide content, ^{13}C NMR determ. 79−51872
polymer additives, analysis by IR spectroscopy, preconcentration, separation and computer techniques 78−31730
polymer-bisazide system, light sensitivity of photoresisting films *(Russian)* 79−6214
polymeric conjugated hydrocarbons, energy gap estimation, graph-theoretical approach 80−24789
polymers, renormalized CI for electron correlation in excited states 78−55130
polymers formed in Fischer-Tropsch and Miller-Urey reactions, N isotope fractionation 80−46496
polymethin cyanine dyes, vibronic energy relax., picosec. spectrosc. obs. 80−5526
polymethine, IR-140 laser dye, photoisomerisation processes 78−27800
polymethine cyanine dyes, viscosity depend. fluoresc. lifetime using synchronously operated ps streak camera 80−28041
polymethine dye behaviour in lasers, efficiency and photoisomer generation 80−14335
polymethine dye laser, near IR, optimal molecular struct. and lasing characteristics 80−19026
polymethine dye lasers, mode-self-synchronisation, broadband, picosecond pulses *(Russian)* 78−29946
polymethine dye lasers, optical absorpt. 80−64009
polymethine dye layer, vibr. spectrum anal., inelastic electron tunnelling spectroscopy 79−13716

organic compounds continued
polymethine dye nonequilib. protolytic forms, lasing, fluoresc. and nonradiative transitions 80−102722
polymethine dye solns., phonon-free electron-vibration transitions, stimulated emission *(Russian)* 77−79660
polymethine dye solutions, brightening depend. on laser pulse length 79−41425
polymethine dye solutions, photochem. transformations and short-wavelength luminesc. 80−100686
polymethine dye unstable photoisomers, superluminesc. and stimulated emission 79−31896
polymethine dyes, excited mols., photoisomeric transformations 79−87854
polymethine dyes, highly excited states, absorption and fluoresc. *(Russian)* 77−19248
polymethine dyes, laser action and photoisomeric transforms. 79−89905
polymethine dyes, mol. struct., lasing props. 79−3693
polymethine dyes, relax. mechanisms in picosecond range *(German)* 78−33737
polymethine dyes, secondary luminesc. 79−99934
polymethine dyes, ultrafast absorpt. spectra 77−18934
polymethine dyes development for CW infrared output 78−1224
polymethine pyrylium dye, IR saturable-absorbing, transient visible absorption 78−33784
polymethine saturable absorbing dyes, dual component fluoresc. lifetime meas. 80−106359
polymethinecyanines, symm. solvent effects on electronic struct., ^1H, ^{13}C NMR 78−13516
polymethines, total π-electron energy bounds 77−88609
polymethinium dye, cryst. metallic refl., damping theory 77−16294
polymethinium dye, excitonic fluoresc., absorpt. trapping spectra 78−27302
polymethyl methacrylate, joint determ. of thermophysical charcts., quasi-linear method 77−41601
polymethylene, extended chain, C-H stretching band struct., Fermi reson., Raman spectrum 80−5552
polymethylene chains, conformations, mag. field dependent biradical CIDNP 77−27097
α,ω-polymethylene diammonium metal (II) tetrahalides, cryst. growth, solubility and props. 78−43999
polymethylphenylsiloxane, PMFS-4, viscosity and solidification press., 0-10^4 Pa, 20-180°C 77−43266
polymethylsiloxane-toluene gels, light scatt., compression moduli, cooperative diffusion 78−23970
polymethyltrifluoropropylsiloxane, FS-169, viscosity and solidification press., 0-10^4 Pa, 20-180°C 77−43266
polynaphthoquinone-SO_2-I_2 system for H_2O decomposition for H_2 production 80−16825
polynitramines, solid cyclic, luminesc. meas. 77−32424
polynuclear aromatic compounds, HPLC separation using aminosilane stationary phase 78−35747
polynuclear aromatic compounds, second derivative UV absorption spectrosc. anal. 79−83526
polynuclear aromatic hydrocarbons, analysis by X-ray excited optical luminescence technique 80−66891
polynuclear aromatic hydrocarbons, atom. distrib. 78−3934
polynuclear aromatic hydrocarbons, effluent toxicity from nuclear fuel reprocessing, rel. to carcinogenecity 78−5005
polynuclear aromatic hydrocarbons, synchronous excitation spectrofluorometry *(Japanese)* 80−86452
polynucleotide hydration charcts. in H_2O/D_2O frozen solns., γ irrad. effects, PMR 78−31772
polynucleotide solution, elec. birefringence, stabilised induced dipole behaviour 80−85349
polynucleotide solution, elec. field induced orientation and effects 80−85348
polynucleotides, bihelical, conform. anal. 77−36862
polynucleotides, double helical, conformation, pairwise pot. function calcs. 80−53173
polynucleotides, double helix, high resolution NMR, review 77−86450
polynucleotides, double-helical, conform anal. 79−96513
polynucleotides, gamma-ray effects on hydration, PMR of frozen and liq. solns. 78−27900
polynucleotides, interactions and self-organisation, ionisation and solvent salt comp. effects 80−55985
polynucleotides, polaris. spectra, excimer phosphoresc. and fluoresc. 79−34497
polynucleotides, potentials of internal rot. 77−16901
polynucleotides, single-stranded, reaction of O_2 with radiation-induced free radicals 78−48759
polynucleotides and components, temp. depend. of UV absorpt. spectra 77−21475
polynucleotides poly(A+U), double-stranded, radiolysis in presence of O_2 78−48760
polyolefins, elec. cond., review 78−26867
polyoxymethylene co-polymers on interstellar grains 77−87500
polypeptide chain, helix-coil transition and isotope exchange reaction 79−3602
polypeptide hormone, microelectrolytic radioiodination using Pt microcell 79−48340
polypeptide hormones, folding, ODMR and phosphoresc. 79−20518
polypeptide hormones, liquid chromatographic separation 79−74450
polypeptide hormones fragmentation anal. by chromatography 79−92448
polypeptide monolayers, circ. dichroism 79−74598
polypeptides, α-helical, π-π^* absorpt. and circular dichroism spectra 80−23398
polypeptides, β-form, vibronic exciton approach to NV_1 absorption band 77−79626
polypeptides, conformational analysis, empirical pot. energy algorithm 79−50174
polypeptides, cyclic, cryst. state conformations 79−24942
polypeptides, helix-random coil transition rates, mean relaxation rate, internal friction 77−38763
polypeptides, in aq. poly(L-glutamic acid) soln., helix-coil transition, US relax. times 80−45849
polypeptides, ionic and non-ionic, electro-optical studies of conformation 80−71379
polypeptides, mean field Ising-type model for helix-coil transition 77−70416
polypeptides, poly-L-lysine based, comb-like, struct., physicochem. props. *(Russian)* 79−55644

organic compounds continued
polypeptides, total energy, conformational calc. using quantum mech. partitioning method 78−94189
polypeptides, unordered, circular dichroism, Green operator method 77−14467
p-polyphenyl, thin polycryst. layer, TSC 79−60946
polyphenyl 1 laser dye for pulsed and CW operation in UV 80−78850
polyphenyl melts, viscosity near freezing pt., association 79−51292
polyphenylenes, lasing, excitation by excimer laser radiation 80−64007
polyphenyls, fluoresc. and sensitization props. 79−38599
polyphenyls, inelastic neutron scatt. study of structural phase transitions 79−51255
polyphenyls, S_1-T_1 interconversion, excitaiton indices calcs. 79−54830
polypropylene, isostatic, uniaxially oriented, Raman spectra *(French)* 80−60557
polypyridines, photoelectron spectra, SCF LCAO calcs. 78−33551
polyriboadenylic acid, soln., Raman spectra, struct. and conformation 77−71899
polyribonucleotides, dye tagged, aqueous solns., elec. induced fluoresc. changes 80−85346
polysaccharide components dissolved into chlorite liquor according to the variation of treating conditions *(Japanese)* 80−3291
polysaccharide grain model for IR spectrum of interstellar maser OH 26.5+0.6 78−12342
polysaccharide interstellar grains, rel. to IR fluxes from galactic IR sources 78−54008
polystyrene, amorphous, failure in methanol and ambient air 80−3165
polystyrene, effect of light on adhesion to metallic substrates *(Russian)* 79−97464
polystyrene-chloranil molecular complex, glass-rubber and liquid-liquid transitions 80−45002
polystyrene-PMMA-benzene, soln., polystyrene diffusion, photon correl. spectroscopy 80−34220
polysubstituted peri-condensed compounds, combinatorial enumeration of chemical isomers 80−28114
polythionic acid, stainless steel stress corrosion cracking protection, 18-8 Ti and 18-8 Nb 78−56824
polyvinyl alcohol, effect on lifetime and formation of latent image in photographic layers *(Russian)* 80−3389
polyvinyl alcohol-gelatine films, effect of pH on transparency *(Russian)* 79−58830
polyvinyl formate, far IR molecular vibrational spectroscopy by inelastic electron tunnelling 78−50546
polyvinylalcohol, gel macromol. gel layer formed on ultrafiltration tubular membrane, charact. 80−14260
polyvinylcarbazole overlayer on electrophotographic plate with CdS-resin layer 77−61146
polyvinylcarbazole-trinitrofluorenone, organic photoconductor, photoinduced paramag. centres 80−25188
polyvinylidenefluoride film as diaphragm material for electroacoustic transducer 80−10100
^{125}I-polyvinylpyrrolidone, pluridisperse soln., permeab. of artificial membranes 77−12890
polyynes, intermolecular interaction through triple bonds, internal rot. 80−106370
POPOP, dissolved in toluene and cyclohexane, scintillation from α-particles, time depend. *(Spanish)* 79−99950
POPOP, fluoresc. quantum efficiency, one-photon dissociation, temp. depends. 80−69180
POPOP, fluoresc. spectrum light quenching factor wavelength depend. 80−18882
POPOP, polarisation of spontaneous and stimulated radiation 79−31583
POPOP, pumped by pulsed laser radiation, photodissociation 79−98353
POPOP, soln., anisotropic fluoresc. of prolate mol. *(German)* 80−1018
POPOP, vap., electron energy loss spectra rel. to lasing 78−29947
POPOP, vapour phase dye laser, quantum efficiency and thermal stability 78−50771
POPOP+Ar+N_2, electron beam excited, energy transfer mechanisms 80−23497
POPOP+Cd(5^3P_1), vap., electronic energy transfer, laser appl. 77−30980
POPOP+tribromomethane, physical and chem. kinetics competition, fluoresc. quenching obs. 79−43567
POPOP dye vapour laser excited by N_2 laser, temp. depend. 79−81423
POPOP dye vapour lasers, optical and electron beam pumping, review 80−48237
POPOP laser, bleaching of vapour 80−19027
POPOP solution dye lasers, multiplate reflectors 80−83606
POPOP vapour, electron beam excited superradiance 78−66820
POPOP vapour, fluoresc. meas. buffer gases effect 77−75503
POPOP vapour, optically induced dynamic gratings 80−28289
POPOP vapour, picosecond generation of radiation 80−48238
POPOP vapour, spectral, fluoresc., photochem. and laser props. 80−106344
POPOP vapour laser, induced losses mechanism 77−75505
POPOP vapour lasing, buffer gases influence, theory 80−91790
POPOP-Ar-N_2, electron beam pumped, intense laser emission at 381 nm 78−74898
POPOP-inert gas vap. mixture, electron beam pumping 77−42535
porphin, electron spectra, PPDP/S approx. calc. *(Russian)* 78−13435
porphin, free base, in n-octane crystal, S_1 from S_0 transition, freq. shift and dephasing temp. depend. 78−25584
porphin, free-base, in n-octane cryst., photochem. hole-burning, vibronic relax. 79−31587
porphin, ground-state energies, force consts. and vibr. freqs., CNDO/2 calc. 79−18118
porphin, hypersurface of adiabatic pot. calc. by CNDO/2 method, vibr. freqs., absorpt. spectra calc. 80−95543
porphin, MCD, LCAO MO SCR π-electron calcs., PPP approx. 78−9178
porphin, single crystal Shpolskii matrix, fluoresc. anisotropy 79−85994
porphin, spin-spin coupling const., MO LCAO CNDO/2 calc. 79−41108
porphin ($-d_2$,d_4,d_6,d_8,d_{10},d_{12},d_{14}), nonradiative transition probabilities, deuteration effects 79−3485
porphin free base, triplet state electron spin echoes, fluoresc. detection 78−70856
porphin free base, vibr. and normal mode anal. 80−69122
porphin free base in cryst. anthracene, site selective optical spectra, vibronic freqs. 79−13730
porphin in host n-alkane crystals, phototautomerism, IR spectral obs. 80−34963
organic compounds continued
porphin in n-alkane host, photoautomerisation and hole-burning 79−47954
porphin-d_n, (n=2-14) electronic-vibr. interaction, quasi-line absorption (fluoresc.), mirror symmetry 78−55197
porphine, ab initio CI calcs., electronic absorpt. spectra 78−78639
porphine, electronic struct. props. and photosynthesis 80−16902
porphine, semiempirical Xα calcs. 79−26886
porphine-d_4, vibronic transitions, polaris. determ. 80−63614
porphins, UV absorption and photoelectron spectra, CNDO/S3 calcs. 77−75210
porphins orientation in n-alkane Shpolskii hosts, spectra 80−48035
porphyrexide solutions, EPR meas., isotropic hyperfine coupling constants and g-factor determ. 77−81009
porphyrin, dication and dianion, spectra, quantum chem. calcs. 79−36597
porphyrin a, MCD, LCAO MO SCR π-electron calcs., PPP approx. 78−9178
porphyrin films, methine bridge substituted, surface photovolt. depend. on fabrication method 80−60119
porphyrin free base, spin-dependent D isotope effect in triplet state decay, N-H vibrs. 77−30909
porphyrin free base in n-octane, S_1←S_0 transition homogeneous linewidth, photochemical hole burning 78−7217
porphyrin free base in n-octane crystal at 4.2K, laser-induced photochem. isomerisation 77−12815
porphyrin free lasers, radiationless decay of triplet state, position dependent D effect 77−30902
porphyrin in n-octane Shpolskii matrix, defect props., Monte Carlo obs. 80−63533
porphyrin light-activated reduction, rapid spot test for stannous Sn levels in ^{99}m Tc kits 77−86630
porphyrin metallation, in monolayer films and assemblies 79−11817
porphyrin pigments, in geochem. systems, HPLC determ. 78−61078
porphyrin solns., quenching of excited states by nitro-cpds., donor-acceptor interactions 78−2899
porphyrin-pyridine complex, 4.2K, visible absorption spectrum gap burning-out 78−53232
porphyrin-water interface, photoinduced charge separation 77−81408
porphyrins, complex Raman tensors, irreducible tensor method, antisymmetric scatt. 78−37623
porphyrins, determ. in blood by phosphoresc. of porphinatocopper(II) 78−11574
porphyrins, isomers, enumeration by combinatorics, Polya's theorem 78−93501
porphyrins, metal-free, EPR, sample grinding effects 80−60420
porphyrins, non-radiative deactivation of lower excited states, effect of mol. struct. 78−68987
porphyrins, photochemical ionisation reactions in soln., automatic conductimetric instrument for kinetic studies 77−4971
porphyrins, reson. Raman scatt. by degenerate mode, Renner-Teller coupling 79−59461
porphyrins, solid solns., phosphoresc. rel. to solvent heavy ats. *(Russian)* 77−40286
porphyrins adsorbed on octane-water interface, photo-oxidation of water 78−64933
porphyrins in liquid crystal, oriented photoexcited triplets, EPR study 80−84636
porphyropsin responses to prolactin in trout, effect of thiourea 78−69065
potassium acetate, thermal expansion 79−51280
potassium acetylacetonate, polycryst., elec. cond., pyroelectricity, phase transition, UV spectrum 78−76392
potassium acid phthalate, crystal as Bragg mode analyser, Bragg refl. integral obs. 80−95204
potassium acid phthalate, Raman spectra and lattice vibr., 77, 300K 78−27219
potassium alkanoates, phase transitions, differential scanning calorimetry 77−43319
potassium antimonyl tartrate, neutral aq. soln., gamma radiolysis 80−101030
potassium bis(oxalato)beryllate, cryst. struct. *(French)* 78−34499
potassium butyl xanthate, X-ray cryst. struct. determ. 80−33987
potassium chloranil, IR spectra, mag. and optical props., phase transition and solvation 77−43983
potassium formate, IR absorpt. spectra, sampling effects, Davydov splitting and struct. 78−52508
potassium formate, X-ray cryst. struct. determ. 80−107194
potassium hydrogen bisphenylacetate, X-irrad., ENDOR of trapped benzyl radical 77−10695
potassium hydrogen glutarate, H bonding, vibr. spectra 78−43860
potassium hydrogen malonate, γ-irrad. cryst., ESR and ENDOR of trapped radical 79−78524
potassium hydrogen malonate, aq. soln., IR and Raman vibr. spectra *(French)* 79−26989
potassium hydrogen malonate, carboxylic proton chem. shift tensor 80−58280
potassium hydrogen malonate, deuterate, NQR data (I=1) from ENDOR expts. 80−54994
potassium hydrogen malonate, room-temperature ENDOR spectra obs. 80−106339
potassium hydrogen malonate single cryst., IR and Raman spectra 78−60444
potassium hydrogen oxalate, oriented single cryst., Raman spectra with very strong H-bonding 80−25359
potassium hydroxymethanesulphonate, X-ray cryst. and mol. struct. determ. 79−32983
potassium iron tri(hydrazoformate), Debye-Waller factor, Mossbauer spectra obs. 79−56627
potassium laurate-1-decanol-water mixtures, biaxial nematic phase obs. 80−107409
potassium n-alkanoates, thermal behaviour, differential scanning calorimetry obs. 80−92650
potassium oscalate, neutron inelastic scatt. spectra in 2200-200 cm^{-1} range 80−70327
potassium oxalate, anhydrous, phase II, vibr. spectra and cryst. struct. 80−34901
potassium oxalate, D_2O, D quadrupole coupling, temp. depend. 79−31551
potassium oxalate, EPR of Mn^{2+} and VO^{2+} 80−39858
potassium oxalate monohydrate:Cu^{2+}, ESR and isomorphism of Cu^{2+} 77−32252

organic compounds continued
potassium oxalate monohydrate:VO^{2+}, cryst., IR absorpt. 80−55134
potassium oxalate monohydrate, cryst., O-H bond lengths, H-O-H angles, corrections 79−32945
potassium oxalate monohydrate, force fields and normal coords. of H_2O mols. 79−31500
potassium p-chloranil, solvated with acetone, X-ray cryst. struct. determ. 80−39062
potassium p-nitrophenoxide transport across carbohydrate membrane, cyclodextrin induced ionic equilibria perturbation 79−96523
potassium palmitate-d_{31}, spin-lattice relax., chain position and temp. depends. 78−68405
potassium palmitate-water solution, deuterated, NMR asymmetry parameter 80−88882
potassium propanoate, solid-state transitions, diffractometric and conductometric meas. 79−60507
potassium soaps, heterogeneity of chain lengths, factor in lyotropic polymorphism 78−59746
potassium tetrachlorophthalimide, IR and Raman spectra 79−50015
potassium zirconium oxalate, X-ray K-absorpt. spectra 78−76558
PPD pumped by pulsed laser radiation, photodissociation 79−98353
PPO, dissolved in toluene and cyclohexane, scintillation from α-particles, time depend. *(Spanish)* 79−99950
PPT liq. cryst., anisotropic light scatt. 79−78692
praseodymium β-ketoesters, Pr^{3+}, visible spectrum, interaction, intensity and bonding parameters 80−993
praseodymium ethyl sulphate, appl. of thermal props. of X-Y model on linear chain in random fields 79−65679
praseodymium ethyl sulphate, cooperative Jahn-Teller antiferroelec. ordering 77−66144
praseodymium ethyl sulphate, one-dimensional X-Y model, hyperfine contrib. to specific heat 79−1678
praseodymium ethyl sulphate, phase transition under pressure, absorpt. spectra *(Russian)* 80−92667
praseodymium ethyl sulphate, specific heat, electric suscept. and thermal cone., one-dimens. electric dipolar XY system 77−32148
praseodymium ethylsulphate:Sm, one-dimens. X-Y system, spin dynamics, electron spin echo meas. 80−66031
praseodymium ethylsulphate:Sm, XY system, mag. relax. and spin dynamics 79−61211
praseodymium oxydiacetate crystal, opt. rot. dispersion 77−36193
praseodymium tricarbamide acetate hydrate, cryst. struct., Patterson function anal. 80−79770
pre-biotic compounds, chemistry rel. to origin of life 78−69460
prealbumin, human plasma, secondary struct. refinement from circular dichroism data 78−27888
prebiological compounds, form. in volcanic processes 78−40667
prebiotic molecules in Martian dust clouds 77−64688
prebiotic oceans, soluble organic matter scavenging 77−64436
prebiotic terrestrial atmosphere, organic compounds prod. by far UV irradiation 78−40668
primitive Earth, volcanic processes role in organic compounds evolution 78−32230
progesterone in crude serum extracts, radioimmunoassay using ^3H and ^{125}I labelled tracers 80−56185
prolactin responses of visual pigments in trout, effect of thiourea 78−69065
l-proline, aqueous soln. US absorpt. 78−87743
proline, oligomer, vibr. spectra rel. to polymeric form 79−83695
proline, polycryst., proton mag. relax. and mol. motion 78−20139
L-proline, structure amplitude phases, statistical-thermodynamic determ. 80−84028
L-proline, uptake by renal brushborder membrane vesicles 77−44614
l-proline monohydrate single cryst., X-irrad., ESR and ENDOR study of radicals 80−45528
promethazine picrate, cryst. data and molecular packing 79−94988
prop-1, 2-dienyl radical, ab initio SCF HF MO calc., electronic struct. and one electron props. 77−42231
prop-2-yn-1-ol, mol., He(I) photoelectron spectra 79−27033
propan-1,3-dioic acid, H_2O_2, KIO_3, $MnSO_4$, $HClO_4$, I_2, periodic chem. reactions, bi- and tristability, rel. to biological mech. *(French)* 78−80726
propan-1-ol, ion internal energy selection by angle-resolved mass spectrometry 80−53164
propanal, methyl torsional pot. functions, LF Raman and IR vibr. spectra 80−95612
propane, α-particles stopping cross-section determ. 79−49917
propane, ab initio calcs. using FSGO, internal rot. 78−82639
propane, adsorbed on graphite, struct. and dynamics, empirical interatomic pots. 79−99417
propane, adsorpt. on ice surface, gas capture by crystallising aq. aerosols investig. 79−39191
propane, adsorption of Al, SIMS and EID obs. 77−69167
propane, and propane-N_2 gas mixture, CO_2 laser radiation absorpt. coeff. 77−58366
propane, best calcs. of MO-modelling of mass spectrometric fragmentation 77−417
propane, compressibility, virial coeffs., Burnett method 78−47083
propane, condensation in porous bulk media 78−47510
propane, diffusion flame, coherent spectral interference from C_2, CARS spectra 80−43404
propane, excess electron localisation, density effects 77−31970
propane, force const. selection, backward elimination regression-refinement procedure 79−31497
propane, freejet flow, vibr. relax. time 79−98760
propane, gas, absolute viscosity 77−35299
propane, gas, electron drift vel., Ramsauer-Townsend minima in electron scatt. 78−87427
propane, gaseous, dielectric losses, absorpt. of 8 and 12 mm radiation under pressure *(French)* 79−93991
propane, graphite hollow cathode glow discharge C conc. determ. 80−44032
propane, ignition by small sparks 79−55587
propane, ion internal energy selection by angle-resolved mass spectrometry 80−53164
n-propane, ionisation by electron bombard., empirical and semi-empirical calcs. 79−36784
propane, ionisation chamber dosimetry, Ar/propane, mixed X-ray/neutron fields 79−20682
propane, liq., temp.-depend. free vol. 79−99052

organic compounds continued
propane, mol. ion, mass spectra ion intensity internal energy depend., quasi equilibrium theory calcs. 80−53163
propane, oxidation, Pt catalysts surface morphology and faceting obs. 77−52669
propane, perturbed-hard-sphere eqn. of state applicable to sub- and supercritical temps. 79−19350
propane, radiative thermal cracking on porous glass *(Russian)* 79−39205
propane, Ramsauer-Townsend minimum in electron scatt. cross section 77−89821
propane, refr. index and Lorentz-Lorenz functions, 944 cm^{-1} and 15803 to 22002 cm^{-1} 78−59543
propane, saturated and compressed liq., sp. ht. 79−86898
propane, solubility in high-press. polyethylene *(German)* 79−33093
propane, thermal cond., high temp. high press. meas. 79−68898
propane, total emissivity, press. depend. 78−90673
propane, triboelectric discharge of Hg rolling on glass, chem. effect *(French)* 79−77438
propane, unimolecular ion dissociation branching ratios and kinetic energies 77−502
propane, vapour-liquid and vapour-solid equilib. data, mass spectroscopic tracer pulse chromatography 80−37115
propane, vertical electronic spectra, limited CI calcs. 79−13693
propane, vertical electronic spectrum, ab initio MRD-CI calcs. 78−70810
propane, vibr. combustion, modulation in injection-vibr. apparatus *(Russian)* 77−9083
propane, vibr. intensities, G sum rule appls. 80−32776
propane, viscosity and thermal cond. correl., liq. and gas 140-500K 79−77332
propane+He^+, 0.7-2 MeV, charge-changing collisions, electron capture 80−58372
propane+$I(5^2P_{1/2})$, collisional deactivation, rate consts. meas. 77−86300
propane+N_2 system, vapour-liq. equilib. data 78−83929
propane and deuteropropane, fragmentation, threshold photoelectron photoion coincidence mass spectra 77−14505
1,2-propane diol-dipropylene glycol, dielec. dispersion charact. 80−75932
propane flame, wake stabilized, response to sudden accel. or deceleration of free stream 80−61096
propane flame plasma, Langmuir probe teaching expt. 78−12456
propane gas detector using SnO_2 doped with Nb, V, Ti, or Mo 79−29426
propane mol. ion, competing slow metastable processes, tunnelling mechanism, tandem-ICR obs. 77−28976
propane pyrolysis, model, kinetics *(French)* 79−52649
propane solvent effects, quantum mech., macroscopic electrostatic contribs. 77−30801
propane-(1,2)diol:$^{57}Fe^{2+}$, dil. solution, Mossbauer exam. of struct. relax. at glass transition 77−66016
propane-air flame, chem. anal. of reaction zone by Raman spectra 78−64837
propane-air flame, eddy entrainment and combustion in depth process, three-region model 79−100384
propane-air flame, premixed turbulent, three region model 79−100383
propane-air flame premixed turbulent, three region model 79−100382
propane-air flame-generated turbulence, approach stream turbulence effects 79−64793
propane-air flat flame, high resolution spectroscopy on CO 77−81434
propane-air mixture, turbulent combustion, model 79−64792
propane-air mixture, turbulent combustion zone, initial temp. fluctuations influence on reaction evolution *(French)* 79−15998
propane-air mixtures, combustion limits in large vols. 79−100368
propane-Ar, reson. absorpt. of 10.6 μm light, shock wave in Ar mixture 79−64002
propane-CO_2, freejet flow, vibr. relax. time 79−98760
propane-d_0(-d_6)+thermal energy reaction, mass spectra 77−9067
propane-d_0 and -d_3, Raman spectra, torsional pot. function 77−58015
propane-d_8, liq., solvated electron optical absorpt. band 78−72544
propane-inert gas liquid systems, ground state energy of excess electrons 79−57346
propane-N_2(CO_2), mixtures, viscosity, diffusion coeffs. 80−1722
propane-N_2 mixture, total emissivity, press. depend. 78−90673
propane-O_2 aquamechanical foam, propag. characts. of detonation waves 78−31713
propane-O_2 flame, microwave-emission plasma diagnostics 80−45503
propane-O_2 mixture, combustion to detonation transition, stochastic aspects 79−100381
propane-O_2 system with Ar, N_2 diluents, detonation wave instabilities 78−5762
propane-O_2-air flame, temp. meas. by laser Raman spectroscopy 77−5833
propane-propene mixtures, compressibility, virial coeffs., Burnett method 78−47083
1,3-propanediammonium $MnCl_4$, 2-dimens. antiferromagnet, with dipolar broadening, spin diffusion, EPR obs. 79−38371
1,3-propanediammonium tetrachloromanganate(II) mag. props. 4.2-220K 77−20567
1-3-propanediammonium-$CuCl_4$, ferromag., antisymmetric and anisotropic exchange, EPR linewidth 78−10761
1,2-propanediol, aq. soln., proton NMR study of H-bonding 79−78545
propanediol, behaviour of nucl. spins near highly polarised paramag. centres 77−77127
propanes, substituted, dielec. relax. in liquid state 77−8500
propanes, substituted, liq., microwave absorpt., dielectric relax., loss, permittivity, moments and reorientation 77−63362
propanes, substituted, rot. isomerism, semi-empirical model calcs. 78−50659
propanoic acid, adsorption on Ag (111) and Pt (111), LEED obs. 80−80073
propanol, adsorbed layer on graphite, spreading press. 77−15692
n-propanol, aq. soln., excess heat capacity, H bonding 78−3362
n-propanol, centrifugal distortion constants, OH-trans-trans and OH-trans-gauche conformers *(Russian)* 79−10089
propanol, chemisorbed on MgO, decomposition mechanism 78−92502
2-propanol, dielec. time domain spectroscopy, total transmission method study 80−27323
n-propanol, dilute aqueous solns., excess partial molal heat capacities 79−57280
1-propanol, dry-electron localisation, impurity trapping, solvated electron rate consts. 79−1990

organic compounds continued
1-propanol, electron traps, prestabilised electron relax. model 78−27803
1-propanol, glassy, electron trap relaxation model 80−15470
1propanol, glassy, electron trapping, pulse radiolysis obs. 80−30264
n-propanol, glassy and crystalline forms, trapped electrons, conc. of mol vacancies determ. 77−65948
1-propanol, low temp. pulse radiolysis, solvated electrons, absorpt. spectral changes 77−12813
n-propanol, positronium form., unsolvated electron effects 78−17826
n-propanol, preferred conformers, PCILO study 80−95542
n-propanol, solution structure, adiabatic compressibility studies 78−87605
n-propanol, sparking pot. and ionis. coeffs. 80−1864
1-propanol, time domain spectroscopy, superposition integral approximations 77−1630
n-propanol, US studies of mol. relax. 78−22790
1-propanol, X-ray diffr. study of struct. at −25°C 77−55227
n-propanol aqueous soln., sound absorpt. coeff. meas., acoustic relax. 78−83883
n-propanol mixtures, US vel. depend. on association compounds 79−60436
n-propanol-3-methylpentane mixtures, pulse radiolysis, solvated electrons 79−66321
n-propanol-isopropanol aq. mixtures, US relax., US absorpt. and vel. meas. *(French)* 80−103426
n-propanol-water, binary mixtures, nucleation 80−44305
n-propanol-water, nucleate boiling heat transfer, conc. depend. 78−87249
propanolol, (adrenergic blocking agent), high-press. liq. chromatography, fluorometric detect. 78−20096
propargyl alcohol, film growth on steel surface, ellipsometric obs. of corrosion inhibition *(Rumanian)* 80−60996
propargyl mercaptan ($-d_1$), microwave spectra, struct., rot. anal. 77−18916
propene, γ-ray Compton profile meas., MO calcs., rel. to cyclopropane 77−10706
propene, adsorption on and interaction with V_2O_5, IR emission spectra obs. 79−90881
propene, adsorption on WO_n, struct., rel. to catalysis 78−51826
propene, catalytic oxidation, modification of $V_2O_5(001)$ surface *(French)* 80−45557
propene, compressibility, virial coeffs., Burnett method 78−47083
propene, force constants, SCF ab initio calcs. 77−34780
propene, P ρ T surfaces, butterfly catastrophe 79−86546
propene, solubility in high-press. polyethylene *(German)* 79−33093
propene, triplet states, electron impact and photosensitised dissoc., chem. effects 77−14592
propene+$^{38}Cl \rightarrow CH_3CHCH_2{}^{38}Cl(CH_3CH^{38}ClCH_2)$, thermal, terminal and central addition 77−86341
propene+methyl radical, reaction pot. surfaces, MINDO/3 calcs. 79−22601
propene+N_2 system, vapour-liq. equilib. data 78−83929
propene+OH, absolute rate consts., 297K 79−100353
propene soft oxidation, gas-solid catalytic reaction, kinetics, automatic meas. *(French)* 77−1912
2-propene-1-imine, rot. isomers, microwave spectra 78−58670
propenoyl chloride, far IR and Raman spectra, internal rot. 79−89668
propenoyl chloride, IR bands, torsional struct. 80−28018
propenoyl fluoride, far IR and Raman spectra, internal rot. 79−89668
β-propiolactone, electron structure, orbital-O interaction, MO calcs., UV photoelectron spectra 80−28058
propiolamide($-d_2$, d_3), microwave spectrum, struct., dipole moment 78−78685
propiolic acid, adsorbed in thin film tunnel junctions, hydrogenation and deuteration, IETS obs. 80−45547
propiolyl chloride(-d), 357-333 nm absorpt. system 80−69161
propiolyl fluoride(-d), 290 nm absorpt. system 80−87142
propion-aldehyde ion, fragment/mol. ion current ratio, field ionis. mass spectrum, CNDO/BW calc. 77−65544
propionamide+ammoniated electrons, reaction rate consts. 77−9043
propionic acid, dielectric meas. at microwave freqs. 79−19827
propionic acid, homogeneous nucleation in associated vapour 79−10933
propionic acid, viscosity of dissociating vapour 78−5840
propionic acid-water, PMR relax. obs., mol. assoc. 79−33553
propionitrile, intermolecular interaction band contour exam. *(Russian)* 79−808
propionitrile, quartic and sextic centrifugal distortion consts., microwave spectrum 78−94236
propionitrile-hydrocarbon systems, critical solns., Kerr electrooptical Kerr effect meas. 80−100645
propionitriles (-O, NH, S), conformational investig., NMR, IR and semiempirical MO methods 80−95650
proplybenzene-nitrobenzene, binary mixtures, with weak charge transfer interactions, thermodynamic props. 80−54360
proplyene oxide+C^+, branching ratios 78−44354
trans-p-n-propoxy-α-methyl-p′-cyanophenyl cinnamate, high press. mesomorphic and polymesomorphic transitions 78−18750
N-(p-propoxybenzylidene)-p-pentylaniline, refr. index and density in nematic and isotropic phases 79−90538
p-propoxybenzylidene-p-butylaniline, nematic and isotropic phases, dielec. props. 79−87383
N-p-propoxybenzylidene-p-pentylaniline, orientational order in glassy and nematic phases, IR dichroism meas. 80−64891
N-p-propoxybenzylidene-p-pentylaniline, Williams domains, interference study 80−44114
p-propoxysalicylidene-p′-butylaniline cryst. and mol. struct., intramolecular bonding 80−44197
n-propyl acetate+OH, reaction rate const., in irrad. NO_x mixture 78−7171
propyl acetate-propyl alcohol, dielec. dispersion charact. 80−75932
propyl alcohol, activation energy for viscosity, rel. to charge distrib. 79−37865
n-propyl alcohol, dil. aq. soln., US vel., 4.04 MHz 78−67770
n-propyl alcohol-α-picoline, donor-acceptor complex form., solvent effects, IR spectra 77−38660
isopropyl chloride, torsional pot. function, far IR and Raman obs. 80−28022
propyl compounds, photolysis, photofragment free radicals, mass spectra *(Japanese)* 78−7220
propyl formate, US absorpt. and relax. intervals 77−1183
propyl iodide, two-photon reson . ionis. spectra 80−28071

organic compounds continued
di-n-propyl p-terphenyl-4,4″-dicarboxylate, biaxiality of smectic E mesophase 79−41949
propyl stearate monolayers, elasticity and viscosity determ. by laser light scatt. 77−72749
n-propyl trichloroacetate, soln., dielectric props. and relax. mechanisms at microwave freqs. 78−15089
propyl-1,3-diamino manganese chloride, structural phase transitions at 336 and 305K, NQR meas., DTA 78−63855
n-propylammonium chloride, NMR, spin-lattice relax., cation dynamics 79−11353
n-propylbenzene, broad band far IR absorpt., temp. depend. 78−2835
n-propylboranes, ^{11}B NMR 78−90190
propylene, μ, ρ and T-surfaces, global behaviour, rel. to catastrophe theory 78−26226
propylene, adsorption on MgO:Mo catalyst, oxidation reactions, surface structs., IR absorpt. spectra obs. 80−66868
propylene, chemisorbed on η-Al_2O_3, desorption and D exchange obs. 78−51827
propylene, computer generated phase diagrams 78−83928
propylene, condensed, electron energy loss spectra meas. 77−59652
propylene, electron energy loss spectra, 0-90°, 20-150 eV impact 79−68322
propylene, electron impact ionisation and dissoc. 80−37894
propylene, equation of state for gas-liq. transition, catastrophe theory 77−59092
propylene, equations of state, search procedure, based on step-wise least-squares technique 80−19900
propylene, He-Ne laser line, high temp. absorpt., anal. by high resolution IR spectra 80−91554
propylene, high density behaviour, extrapolated PρT surfaces and critical density 80−87834
propylene, intracavity IR absorpt. in CO_2 laser, enhanced sensitivity 78−78835
propylene, liquid, effect of libration transitions on sound absorpt. 78−2203
propylene, mol. dissoc. on bombardment by low energy electrons 80−43845
propylene, proton-proton coupling consts., valence angle depend. 77−23508
propylene, rot. anal., perturbational MO analysis of ab initio SCF-MO wave functions 77−57867
propylene, solubility in liq. N_2 80−39286
propylene, Townsend primary and secondary ioniz. coeffs. and sparking voltages 78−51372
propylene, viscosity meas. at 298 to 473K *(German)* 77−42954
propylene+thermal energy reaction, mass spectra 77−9067
propylene 1.3-diamine-water, liq.-solid equilibrium *(French)* 79−51236
propylene and ethylene adsorbed on Ag, enhanced Raman spectra obs. 80−95607
propylene carbonate, SEM study of electrochem. behaviour of Li *(French)* 78−56899
propylene carbonate and dimethoxyethane mixed electrolyte solns., for high energy density batteries 80−76627
propylene carbonate-$LiClO_4$ solution, composition of passivation layers on Li electrode *(French)* 80−11899
propylene glycol-isobutene (dimethyl siloxane), oligomeric liquid mixtures, transition to, polymer systems, thermodynamics 78−20048
propylene glycol-water (methanol), proton medium effects, ferrocene redox couple reference obs. 77−77786
propylene glycols, dielec. props., chain length effect 80−44995
propylene oxide, stopping cross section for 0.3 to 2.0 MeV He^+ ions 78−63537
propylene ozonide formation mechanism, Fourier IR spectra 77−33132
1,2-propylene sulphide-S_8, copolymer preparation method, anionic copolymerisation 78−64836
propylene-NH_3 mixtures, crit. curves at high-press. 79−23715
1,3-propylenediammonium manganese tetrachloride, vibr. study of phase transitions, IR and Raman spectra 80−40103
propyleneimine, circular dichroism, optically active Rydberg transitions 77−18952
n-propylhalides, gauche conformer stability, exchange interactions effects 79−13817
propylsilane-d_0($-d_n$), vibr. spectra, normal vibrs. and rot. isomerism 79−31523
propynal, ν_2 vibr. state, IR-microwave triple resonance 79−13746
propynal, CW for IR mol. laser, optical pumping with $^{16}CO_2$ and $^{18}CO_2$ lasers 80−74343
propynal, energy dispersion and relax., laser IR-visible double reson. 80−48023
propynal, energy dispersion and relax., laser IR/visible double reson. obs. 80−53028
propynal, internal energy distrib., collisional effects, IR-vis. double reson. obs. 80−14159
propynal, IR photochem. in electronically excited state 80−11923
propynal, IR-microwave double reson., rot.-vibr. transitions, microwave assignment, mol. consts. 78−86902
propynal, IR-microwave double reson. and two-photon expts. 80−83396
propynal, rovibronic populations, collisionless IR multiphoton spectra, energy deposition, photoacoustic determ. 80−83354
propynal+propynal, potential well depth estimation method 79−86034
propynal-d, in ground vibrational state, IR microwave double resonance spectra, rot. and centrifugal distortion const. determ. 80−83358
propynal-d, IR microwave double reson. spectroscopy 80−69172
propyne, ^{13}C isotopic species, microwave spectra, rot. consts. 78−86850
propyne, and 1-butyne, electron impact spectra, comparison with acetylene 79−3585
propyne, microwave rot. absorpt. lines press. broadened width and shift 77−61807
propyne, microwave spectra and mol. consts., rot. anal. 79−76411
propyne, mol.excitation by electron impact, 500 and 25-70 eV, expt. and HAM/3 79−72434
propyne-d_0($-d_3$), absolute and integrated IR intensities of fundamental modes 80−87179
propynyl cation+propyne, reactant structure effects 80−89469
prostaglandins, ^{125}I labelled *(Hungarian)* 80−94368
prostatic acid phosphatase, human, development of determ. by radioimmunoassay *(Japanese)* 80−98110
prostratin derivative, cryst. struct., overlapping Patterson peaks and direct methods 78−55779

organic compounds continued
proteoglycans, swelling pressures at the concs. found in cartilaginous tissues 80−67327
protocatechualdehyde, PMR, 77-427K, OH group rot., struct. 77−30886
protocatechuate 3,4-dioxygenase, reduced, Mossbauer effect zero field splitting 79−24955
protochlorophyl, mag. reson., site selected fluoresc. detection 80−69164
protochlorophyll, fluoresc. fading curve of lowest triplet state 79−36691
protohaeme-CO binding dynamics, flash photolysis, activation energy, entropy 77−21472
proton chemical shifts, combined pulse NMR and magic-angle spinning 80−44934
protoporphyrin: Cu^{2+}, in pyridine fluoresc. quenching mechanism 79−56837
protoporphyrin, MCD, LCAO MO SCR π-electron calcs., PPP approx. 78−9178
protoporphyrin IX, triplet states, flash photolysis, obs. 80−95555
protoporphyrin IX dimethyl ester, triplet states, flash photolysis, obs. 80−95555
Prussian blue analogues, Mossbauer spectra 80−15898
pryazine, fluoresc. $^1B_{3u}\rightarrow{}^1A_{1g}$ band, vibr. struct. and intensities 79−64033
pryromellitic and dianhydride, intermolecular shielding contributions, proton mag. shielding intermolecular shielding contributions, proton mag. shielding 80−34783
pseudoazulenes, anomalous fluoresc., radiationless transitions 80−91593
pseudocyanine, I aggregates, fluoresc. decay time 77−27105
psoralen and near UV light as probe for study of protein synthesis control 77−66881
PTS, pyroelectric effect 78−95554
PTZ:PMDA, purification, growth, struct., optical and elec. props. 80−54216
purine, γ-irrad. investig. by diffuse refl. spectrophotometry 77−48756
purine, powder, γ-irrad., dose-response curves 78−7215
purine, single cryst., Raman spectra and lattice vibr. 77−66498
purines, biological, UV photoelectron spectra, valence electronic struct. 77−16905
purines, pyrimidines, orientation and transition moment directions of small planar molecules, in stretched polymer films 78−1015
purines in Murchison meteorite, search 78−7948
PVC, ^{210}Po contamination of surfaces, removal coeff. determ. 79−26769
PVC, electroluminescence, influence of cell electrodes 79−74005
PVC-chlorinated, piping for secondary criticality control of fissable solns. 80−13607
PVC/coal blends, fluidized bed combustion of plastic waste with coal, removal of HCl 80−30347
PVK/PVK-TNF/TNF.PMG system, electrophotographic characts. 80−62759
pyraozine, vibronic coupling via C-H bending mode 79−76403
pyrazine, ^{14}N quadrupole coupling consts., ab initio calcs. 80−58283
pyrazine, cavity radius and mean polarisability 79−45862
pyrazine, cryst., 3300 Å reson. Raman band, vibr. assignments 77−1684
pyrazine, cryst., mol. reorientation, NMR meas., pot. energy calc. 78−76335
pyrazine, cryst. phases, entropy changes and struct. implications 80−54397
pyrazine, dimer interaction, lattice energy, multipole expsn., at.-at. pots. 78−9218
pyrazine, dispersion induced circular dichroism, determ, of mag. dipole allowed transitions 80−14163
pyrazine, electronic energy transfer to metal surface, classical image dipole theory 80−97318
pyrazine, excited and N_{1s} ionised states, ab initio calcs. broken orbital symm. 80−27931
pyrazine, in pyrazine-d_4, p-dioxane, X-trap, p-xylene, benzene(-d_6), cryst., MIDP, PMDR, low temp., assignments 77−36154
pyrazine, intensity of intercombination transitions, influence of n-σ-type complex form. *(Russian)* 77−26980
pyrazine, lowest triplet state, phosphoresc., intersystem crossing 78−5269
pyrazine, mol., radiative lifetime of phosphoresc. state, influence of high lying triplet states 79−86006
pyrazine, mol. struct. determ. from gas phase electron diffr., r_α struct. 78−25739
pyrazine, multiphoton ionisation spectra, circular to linear polarisation ratios, lowest ionisation pot. 78−74716
pyrazine, multiphoton ionisation spectra, of three-photon ionisation region 78−37689
pyrazine, nπ^* transitions, vibronic coupling 78−25501
pyrazine, on Ag, time-resolved molecular electronic energy transfer 80−92957
pyrazine, phase transitions, sp. ht., X-ray diffr., LF vibr. spectra 78−43122
pyrazine, physisorbed on Ni (111), UV spectroscopic ellipsometry obs. 79−86997
pyrazine, PMDR due to single defect species, vibronic structs. 78−19535
pyrazine, PMMA soln., fluoresc. and phosphoresc. quantum yield and lifetime, 20-120 kbar 79−54902
pyrazine, prereson. Raman spectra, vibr. band intensities obs. 80−102515
pyrazine, pyrazine-Kr, ground and n-π^* excited state struct. 79−68241
pyrazine, Raman spectrum, correlation with vibronic coupling and adiabatic potential 77−71804
pyrazine, reson. Raman and absorpt. spectra to $S_2(\pi,\pi^*)$ state, excited state geometry 79−76433
pyrazine, reson. Raman spectra, vibronic theory of Raman intensity 78−37643
pyrazine, reson. to the $S_2(\pi,\pi^*)$ state, Raman spectra calcs. 80−69147
pyrazine, single vibronic level fluoresc., non-exponential decay 77−27108
pyrazine, thermal diffuse scattering corrections, choice of elastic constants in evaluation 79−32849
pyrazine, thermal expansion tensor determ. 77−15600
pyrazine, triplet-triplet absorpt. related to state splitting 80−47917
pyrazine, two-photon spectra of gas phase 79−89724
pyrazine, vap., single vibronic level fluoresc., dye laser excitation 79−18224
pyrazine, vapour, fluoresc. quantum yields, rot. effects 80−95661
pyrazine, vibr. struct. and nonlinear vibronic coupling, pseudo Jahn-Teller effect 78−94234
pyrazine, vibronic and spin-orbit coupling interaction 80−14126
pyrazine, vibronic bands, MIDP and polarised phosphoresc. in benzene matrix 77−6833

organic compounds continued
pyrazine, vibronic coupling by out-of-plane modes 77−6747
pyrazine, zero field studies of spin lattice relaxation in excited triplet states 79−18219
pyrazine.$(H_2O)_n$, n=1,2, ground and n-π^* excited state struct. 79−68241
pyrazine (-d_4), single vibronic level fluoresc. spectra, rel. to vibronic coupling 80−28043
pyrazine (-d_4) vapour, single vibraonic level fluoresc. from n, π^* 80−37827
pyrazine absorbed on electrode, surface enhanced Raman spectra, symmetry and polarisability changes 80−50310
pyrazine complexes with H_2O, Br_2 and I_2, electronic absorpt. spectra calc. *(Russian)* 78−37628
pyrazine H-bonded complex formation, enthalpy change due to electronic excitation, spectroscopic determ. 78−92496
pyrazine triplet state, mol. distortion, MIDP using polarised light 79−10137
pyrazine-d_4, in p-dioxane, p-xylene, benzene, cryst., MIDP, PMDR, low temp., assignments 77−36154
pyrazole and deuterated species, CH stretching vibrs., anharmonicity, pseudo-symm. 78−78710
pyrene:rubicen(coronen), exciton migration and energy transfer, temp. depend., model 78−79932
pyrene, absorbed on albumin, pulsed laser study of excited states 77−86448
pyrene, adsorbed on silica gel surface, biphasic photochemistry, time-resolved spectra 80−30252
pyrene, appl. of new force field for condensed aromatics, inplane vibrs. 79−81201
pyrene, band structure, excitonic processes, trap distrib. 80−6720
pyrene, cryst. struct., atom-atom pot. calcs., micro electron diffr. obs. 78−43007
pyrene, cryst. struct. calc., use of at.-at. pots. 79−46646
pyrene, crystal-electrolyte interface, ionis. energy of uppermost cryst. mols. 78−27764
pyrene, crystalline, EPR spectrum of triplet excitons 78−27076
pyrene, distinction of delayed fluorescences $S_1\rightarrow S_0$ and $S_2\rightarrow S_0$ by selective quenching of $S_1\rightarrow S_0$ 80−69175
pyrene, emission from triplet state in electrochemical at low temps. 77−77307
pyrene, excimer fluoresc., struct. depend. in cryst. 77−75200
pyrene, far i.r. spectra, phase transition effects 77−1685
pyrene, fluoresc. quenching by 1,4-diazabicyclo[2-2-2]octane in cyclohexane soln. 79−31575
pyrene, fluoresc. quenching by inorganic anions 78−74694
pyrene, fluorescence produced by low energy electrons *(German)* 77−18967
pyrene, fluorescence spectra in aq. and surfactant solns. 77−83639
pyrene, in alcohol solns., polar fluid electrons optical absorption coeffs., ns laser ionis. obs. 78−84600
pyrene, in aq. micelle system, fluoresc. quenching by inorganic ion 77−10697
pyrene, in cyclohexane soln., triplet state decay consts. by sampling flash apparatus 79−51998
pyrene, in micellar environments, fluoresc. quenching by nitroxyl radical 79−13754
pyrene, in polystyrene, excimer fluorescence 79−68249
pyrene, in polystyrene matrix, singlet O_2 induced excimer fluoresc. 77−6832
pyrene, laser-induced two-photon photoionisation, simulation, double pulse investig. 78−37690
pyrene, low temp. phase transform., TEM obs. 78−22851
pyrene, luminescence of free and self-trapped excitons 80−108250
pyrene, micellar solns., fluoresc. quenching 78−25588
pyrene, micellar system, fluoresc., solubilisate distrib. statistics, kinetic model 79−34366
pyrene, migration between lipid vesicles in aq. soln., fluoresc. stopped-flow obs. 80−85360
pyrene, mol. ionisation pot., two photon ionisation, micellar interface effects on ionisation threshold 80−91609
pyrene, monomer and excimer fluoresc. in soln., triplet-triplet annihilation and mag. field depend. 78−78738
pyrene, multiexponential fluorescence decay, systems theory approach to anal. 79−59495
pyrene, nonlinear third-order electric susceptibility 78−74944
pyrene, orientated in nematic liq. crysts., UV-visible dichroism meas. *(German)* 77−34668
pyrene, perylene doped, decay times and diffusion coeffs. of singlet excitons, under press. 77−20911
pyrene, photoionisation in alkane liqs., laser induced fluoresc. 78−61038
pyrene, positronium and thermal defects 80−24496
pyrene, S_1, fluoresc. decay in micellar and homogeneous liq. dispersions 77−75199
pyrene, single cryst., γ-irradiated, EPR and optical absorption meas. 78−72412
pyrene, space group C_{2h}^5, triplet excitons energy band struct. 78−6276
pyrene, triplet exciton absorpt. lines 79−47475
pyrene, triplet state, excitonic energy transfer, phosphoresc. and delayed fluoresc., 2 to 300K 80−84776
pyrene, use in fluoresc. probe study of cetyltrimethylammonium bromide-1-butanol system 80−85217
pyrene, UV spectra and extinction coeffs. for $S_n\leftarrow S_1$ absorption 80−18866
pyrene, vapour phase dye laser, quantum efficiency and thermal stability 78−50771
pyrene+biacetyl, physical and chem. kinetics competition, fluoresc. quenching obs. 79−43567
pyrene+N,N-dimethylaniline (deuterate)(3,5 dimethoxy-N,N-dimethylaniline), geminate recomb., solvent, isotope, mag. field effects 78−56888
pyrene central core, discotic mesophase potentiality, isobaric phase diagram method 79−86680
pyrene cryst., delayed fluoresc., mag. field effect, sense depend. 77−73160
pyrene crystal, mechanism of structural phase transition 78−30757
pyrene crystals, anomalous emission excited near absorption edge 80−100682
pyrene dodecanoic acid, lateral diffusion at air-water interface, monomer excimer dynamics 80−92693

organic compounds continued
pyrene excimer fluorescence, erythrocyte membrane fluidity changes after X-irrad. obs. 80−72262
pyrene excimer formation in micellar surfactant solns., distributional effects 78−64855
pyrene excimer formation in micelle, time-resolved spectra 79−79298
pyrene high density excitation effects on fluoresc. 79−1782
pyrene in diphenyl cryst., luminesc. polaris. to induce radn. at O-O transition freq. *(Russian)* 79−38663
pyrene in glassy matrix, triplet state spin relax. time, anisotropy *(French)* 77−65492
pyrene in n-heptane solution, laser two-photon ionisation spectroscopy, photoionisation threshold determ. 80−78668
pyrene picrate, charge transfer complex, thermally stimulated discharge current 79−78610
pyrene picrate, crystal struct. oscill. and Weissenberg photographs 80−107200
pyrene single crystals, γ-irradiated, free radical form. ESR spectra 78−72410
pyrene solutions, emission spectra 77−30910
pyrene solutions, radical ion pairs, pulse radiolysis, time resolved EPR spectra meas. by ODMR of fluoresc. 80−83395
pyrene vapour, laser excited fluorescence 78−29807
pyrene-3-sodium sulphonate solubilised in didodecyldimethylammonium bromide-benzene inverted micelles 80−3417
pyrene-d_{10}, EPR line shape of photo-excited triplet state, in cryst. and glass 79−24210
pyrene-d_{10}, in diethylether soln., ^2H NMR, mag. field induced alignment effects 79−13740
pyrene-d_{10} high density excitation effects on fluoresc. 79−1782
pyrene-diethyl aniline in acetonitrile-toluene, triplet exciplex state in pulsed laser photolysis 77−16836
pyrene-DMA-methanol solution, photoinduced radical ion pair geminate recombination, triplet yield 78−76879
pyrene-guest mixed mol. cryst., positronium formation 78−91647
pyrene-h_{10}, -d_{10}, dual fluoresc. quenching by O_2 and NO 78−5266
pyrene-I_2 soln., elec. cond., thermoelec. power, 155°C, conc. depend. 77−39845
pyrene-N,N-diethylaniline exciplex, visible spectra obs., picosec. laser photolysis, solvent polarity depend. 77−38677
pyrene-N,N-dimethylaniline heteroexcimer systems, micellar solns., fluoresc., photoinduced electron transfer 78−25590
pyrene-N,N-dimethylaniline system, radical ion pair geminate recomb., mag. field modulated, Liouville eqn. 77−86302
pyrene-naphthalene complex radical cation, in γ-irrad. glass, visible spectrum obs. 78−44385
pyrene-PMDA complex, electron-phonon interaction, phosphoresc. 78−48208
pyrene-sodium 5-[1-pyrenyl]pentanoate intramicellar excimer formation in CTAC and SDS micelles, fluoresc. probe 80−16733
1-pyrene-sodium sulphonate, excimer form. in inverse micelles, fluoresc. probe 77−88491
pyrene-TCNE, vapour-grown cryst., transit-time meas. of photocarriers 78−39149
pyrene-tetracyanobenzene, charge transfer complex, phase transitions, deuteration effect, mag. reson., spectral and thermal meas. 79−4412
pyrene-triethylamine exciplex, effect of dipolar molecules on quenching curves 78−52551
[2.2](2,7)pyrenophane, emission spectra, transannular interaction 77−489
pyrenophanes, excimer fluoresc., struct. depend. in cryst. 77−75200
(1-pyrenyl-$(CH_2)_n$-$N(CH_3)_3)^+Cl^-$, intramicellar fluorescence quenching 80−9627
pyridazine, π bond order calc. using U(3) basis algebra 80−18810
pyridazine, cavity radius and mean polarisability 79−45862
pyridazine, elec. field induced spectrum, 0_0^0 band near 3752Å 78−17700
pyridazine, liq., nucl. relax. and mol. reorientation, nucl. Overhauser enhancement 78−60351
pyridazine, prereson. Raman spectra, vibr. band intensities 80−102514
pyridenes ^{15}N NMR chem. shifts, paramag. relax. reagent effect 78−15042
pyridil-benzo-X-azoles, NMR spectra, chemical shift and coupling const. data *(Italian)* 77−54566
pyridine, ^{13}C-^1H spin-spin coupling consts. 78−25562
pyridine, ^{14}N quadrupole coupling consts., ab initio calcs. 80−58283
pyridine, $\pi \rightarrow \pi^*$ transition, 1800 Å, electronic absorpt. spectrum 77−71813
pyridine, π-electronic structs., ab initio VB calcs. 78−70749
pyridine, adsorbed on Ag, 210-243 cm^{-1} mode in surface enhanced Raman scatt. 80−89003
pyridine, adsorbed on Ag, giant Raman scatt. 79−95768
pyridine, adsorbed on Ag, Raman active librational modes 80−65359
pyridine, adsorbed on Ag, Raman intensity enhancement using surface plasmons 80−7334
pyridine, adsorbed on Ag electrode with graphic C overlayer, Raman spectra obs. 80−103954
pyridine, adsorbed on Ag electrodes, ang. resolved Raman spectra 80−16017
pyridine, adsorbed on Al_2O_3, surface acidity meas. 80−35611
pyridine, adsorbed on Cu(Au) electrode, angle-resolved Raman spectroscopy 80−52991
pyridine, adsorbed on gold substrate with Ag monolayer, giant Raman effect 80−63637
pyridine, adsorpt. on Ag colloids, surface enhanced Raman spectra obs. 80−97251
pyridine, adsorpt. on Pt/Al_2O_3, electron accepting sites 80−71947
pyridine, adsorption on Ag, UPS, AES and flash desorption meas. 80−92776
pyridine, adsorption on Cu (110), angle-resolved photoemission, selection rules 80−40231
pyridine, adsorption on CuO and MgO powders for surface area determ. 80−107636
pyridine, adsorption on Ir (111), electronic transitions sensitivity to molecule-surface orientation, energy loss spectra 80−45184
pyridine, and -d_1, microwave spectra, mol. struct., rot. consts. 78−25517
pyridine, chemisorpt. on ZnO, UPS, mol. orbitals effect on bonding 78−72699
pyridine, chemisorption on goethite, IR spectra 80−7855
pyridine, compressed liq., self-diffusion coeffs., viscosity, density, temp. press. depend., NMR spin-echo 79−37862
pyridine, cyclohexane soln., depolarised Rayleigh scatt. 79−47467

organic compounds continued
pyridine, deuterium substituted, Raman and IR vibr. spectra 80−84739
pyridine, dispersion induced circular dichroism, determ, of mag. dipole allowed transitions 80−14163
pyridine, electronic struct. calc., σ^-pi consistency method 77−67957
pyridine, ethyl pyridine, heat of adsorpt. on sponge Fe, Fe_2O_3, CuO, adhesive wear, flow calorimetry 78−85193
pyridine, fluoresc. of vap. phase, nonradiative electronic relax. 79−86000
pyridine, fluoresc. quenching of dicyanoanthryl-naphthyl intramol. exciplex, triple exciplex form. 79−50061
pyridine, FSGO calcs. of orbital energies, locations, dipole moments, charge distribs. 77−67976
pyridine, in benzene single cryst., electronic spectrum Stark modulation, dipole moment 78−29814
pyridine, in carboxylic acid soln., stimulated Raman scatt., H-bonded complex effects *(Russian)* 77−3625
pyridine, intercalation cpd. with TaS_2, NbS_2, nucl. spin-lattice relax. meas. 80−54962
pyridine, IR spectra, adsorpt. on $Zr(HPO_4)_2$, acidity 78−92377
pyridine, i.r. spectra and electronic struct. 77−3363
pyridine, liq. and in CCl_4 soln., depolarised Rayleigh scatt. 79−51973
pyridine, liquid, vibrational double relaxation 79−42154
pyridine, macroscopic model for solvated ion dynamics, cation conductance calcs. 80−65261
pyridine, mean free path meas., US relax. 80−59585
pyridine, multiphoton ionisation spectra, circular to linear polarisation ratios, lowest ionisation pot. 78−74716
pyridine, multiphoton ionisation spectra, of three-photon ionisation region 78−37689
pyridine, on Ag surface, enhanced Raman scatt., ultrahigh vac. study 80−88993
pyridine, on hot W filament, mass spectrometric obs. 79−81302
pyridine, optical Kerr const., electronic and orientational contribs., obs. by coherent Raman techniques 77−88874
pyridine, Penning election spectra and photoelection spectra, rel. intensities 80−95725
pyridine, photoelectron spectra, HAM/3 MO calcs. 78−13414
pyridine, proton-coupled ^{13}C J NMR, strong coupling 78−17691
pyridine, proton-coupled ^{13}C J spectra, strong coupling 77−68063
pyridine, solid, electron transmission, 0 to 15 eV, reson. structs. 79−87536
pyridine, solns., dielec. polarisation, π-electron system effects 77−90096
pyridine, solns. and mixtures, dielectric relax., const. and loss factor 77−55747
pyridine, solution structure, adiabatic compressibility studies 78−87605
pyridine, sorption on Ag, surface enhanced Raman scatt., mol.-surface separation depend. 80−92775
pyridine, unoccupied orbitals, excitation energy, electron affinity, HAM/3 MO calcs. 78−13415
pyridine, vapour, $S_1(n,\pi^*)$ state fluoresc. 78−5267
pyridine, vibronic coupling by out-of-plane modes 77−6747
pyridine+carbon tetrachloride (o-cresol), binary liquid mixtures, excess free vol. calcs. 80−34202
pyridine+HCl, proton transfer interactions, NMR obs. 78−20007
pyridine(-d), force consts. and vibr. spectra by CNDO/2 force method 80−95540
$(pyridine)_{1/2}.NbS_2$ intercalation complex, superlattice struct., NMR meas. 80−70180
pyridine (gas)+TaS_2(2H) react., intercalation, X-ray diffr. investig. 77−12828
pyridine adsorbed on Ag, reson. Raman scatt. 80−25380
pyridine adsorbed on Ag (100), (111), and polycryst. electrode surfaces, intense Raman spectra 78−72492
pyridine adsorbed on Cu (110) surface, photoemission selection rules 80−100751
pyridine adsorbed onto roughened Ag electrode, Raman band intensity 78−48160
pyridine and derivatives, CNDO/2 approx., unshared pairs of electrons 78−25443
pyridine and methyl derivatives, fluoresc. and nonradiative processes 79−36684
pyridine and salts, deuterium NQR, double reson. method, ring charge distrib. 80−53015
4-pyridine carbaldehyde, microwave spectrum, rot. assignments, quadrupole coupling consts. 80−91548
4-pyridine carboxaldehyde-doped Al-Al_2O_3-Ag tunnel junction, surface enhanced Raman spectra, surface plasmons 79−98111
pyridine cation radical in trichlorofluoromethane matrix, gamma irrad., EPR and optical obs. 80−23442
pyridine cobalt chloride, $CoCl_2.2NC_5H_5$, 1D Ising ferromag., charact ESR modes 79−91287
pyridine cobalt chloride, $CoCl_2.2NC_5H_5$, quasione dimens. Ising system, thermodynamic props. 78−27042
pyridine copper chloride, antiferromag., spin dynamics at low temp. 77−32278
pyridine electronic struct., spectra, ionisation pot., INDO-CI LACO-MO-SCF calcs. 79−54834
pyridine in aliphatic alcohol solns., relationship between stimulated Raman scatt. and complex formation *(Russian)* 77−48174
pyridine in rare gas matrices, absorpt. spectra, 1700-2900 Å, progressions 77−3376
pyridine intercalation with FeOCl, mechanism, nucleation and diffusion 80−49420
pyridine iodine complexes, charge transfer complexes, vibr. spectra, laser Raman obs. 80−52990
pyridine isotopes, mol. g-values, mag. susceptibility anisotropies, mol. quad. moments, electron charge distrib. second moments 77−58077
pyridine molecules, adsorbed on rough Ag surface, Raman scatt. 79−15448
pyridine N-oxide, 341 nm band system, out-of-plane modes assignment 77−34646
pyridine N-oxide, in benzene, dipolar assoc. investig. 80−107035
pyridine N-oxide, monomethyl-substituted, frequency assignment and interpretation of vibratory spectra *(Russian)* 79−22684
pyridine on Ag electrode, appl. of pot. modulation Raman spectroscopy 79−63310
pyridine on Ni-Co-Cr/Al_2O_3 catalyst, IR spectra of adsorption and interaction 80−71946
pyridine solutions, degree of depolaris. in stimulated Raman scatt. 79−55184
pyridine-2,3,5,6-d_4, vibr. spectra, IR and Raman, assignment 80−102519

organic compounds continued
pyridine-3,4,5-d_3, vibr. spectra, IR and Raman, H exchange rates meas. 80−102518
pyridine-3,5-d_2, vibr. spectra, IR and Raman, H exchange rates meas. 80−102518
pyridine-3-aldehyde, partially oriented in nematic solvent, rot. isomerism and conformation, NMR obs. 77−71820
pyridine-acetic acid, H-bonding, proton transfer, isolated system, solvent effect, MO calc. 80−55629
pyridine-Ag_5I_6, superionic conductor, dynamical aspects 78−79695
pyridine-Br_2, charge transfer complexes, $\nu_{Br\text{-}Br}$ vibr., Raman intensity obs. 79−36644
pyridine-bromine charge transfer complexes, Raman spectra 77−6788
pyridine-carbon tetrachloride, mixtures, excess volume of mixing, mol. interactions 79−57281
pyridine-d_0, -d_5, vap. fluoresc. spectra 78−82771
pyridine-d_0-d_5, $n\pi^*$ excited state vibronic coupling, vis. and Raman spectra 77−14438
pyridine-d_5, intercalation with 2H-TaS_2 79−90612
pyridine-d_5, physisorbed thin film on Ag surface, enhanced Raman scatt. study 80−20620
pyridine-d_5, vibr. spectra, IR and Raman, assignment 80−102519
pyridine-H_2O, bonding, double quadrupole reson. obs. 80−32749
pyridine-H-bond donors, D spin-lattice relax. meas., mol. interactions anal. *(French)* 80−87151
pyridine-HCl complex, self assoc., intermolecular interactions, matrix isolation vibr. spectra obs. Raman and IR spectra 80−52995
pyridine-I_2, n-σ charge-transfer complex, frozen soln., Mossbauer spectra obs. 80−91655
pyridine-$I_2(Br_2)$ charge transfer complexes, vibr. spectra, vibronic contrib., intensity enhancement 80−53048
pyridine-I_2(ICl), charge-transfer complexes, hyperpolarisability 77−34568
pyridine-I_2 charge transfer complex, hyperpolaris., SHG obs. 77−553
pyridine-I_2 complexes, stability const. determ. by spectrophotometric methods 80−87056
pyridine-methylbenzene cyclic ring compound, $C_{13}H_{13}N_2I$, crystal struct. 77−35545
pyridine-$MnBr_2$ complexes, substituted, excitation spectra, ligand field theory 77−27103
pyridine-N-oxide, electronic struct. assignment, He I/He II intensities *(German)* 80−83423
pyridine-N-oxides, substituted, absolute energy levels in gas and condensed media, ionis. energy, electron affinity 77−67995
pyridine-PbI_2, intercalation cpd., heat capacity of low temp., intercalation effect *(Russian)* 80−92682
pyridine-water soln., reorientational relax. and activation energy of pyridine, depolarised Rayleigh scattering 80−76037
s-trans-3-pyridinecarbaldehyde, microwave spectrum, assignments 78−21912
4-pyridinecarboxaldehyde monolayer in inelastic electron tunnelling spectroscopy junctions, Raman scatt. 80−93344
pyridines, monosubst., H_2O complexes, n-π^* transitions, H bonding, MO theory 80−95550
pyridines, substituted and N-oxides, dielectric relax. in solns. 78−6627
pyridines and water complex, Raman spectra, Fermi reson. in ν_8 region 79−89679
pyridines in n-heptane soln., heat of adsorpt. on outgassed η-Al_2O_3 80−61154
pyridinium(-d_5) ion, triplet state obs. by ODMR, rel. to CNDO/2 STO calcs. 77−18951
(pyridinium)Ag_5I_6, low-temp. phase transitions 77−72686
pyridinium cuprous bromide, solid electrolyte, crystal growth from melt 78−64462
pyridinium iodide, order-disorder phase transition and reorientation fluctuations studied by Raman spectra 80−80764
pyridinium manganese (II) chloride monohydrate, crystal struct. and mag. susceptibility 79−19239
pyridinium manganese chloride, anhydrous, quasi one-dimensional mag. behaviour, heat capacity meas. 80−80549
pyridinium manganese trichloride, pseudo one-dimens. Heisenberg antiferromag., phase diagrams 79−61148
pyridinium molten salts, ^{1}HNMR rel. to transport props. 77−73087
pyridinium nickel chloride, anhydrous, quasi one-dimensional mag. behaviour, heat capacity meas. 80−80549
pyridinium pentasilver hexaiodide, solid, far IR refl. spectra, incoherent neutron scatt., low freq. optical modes 78−2291
pyridinium pentasilver hexaiodide, solid electrolyte, contrib. of non-Brownian motion to transport props. 80−70453
pyridinium pentasilver hexaiodide, sp. ht. and cond., gradual solid electrolyte transition 77−76604
pyridinium salt solns., electrochromism in visible absorpt. spectra 77−77244
pyridinium salts, hydrogen-bonded systems, deuteron quadrupole coupling 79−78563
pyridinium silver iodide, fast ion conductor, phase transitions, thermoelec. power meas. 80−107540
pyridinium tetrachloromanganate II, luminesc. spectra, expt. and calcs. *(French)* 78−10967
pyridinyl radicals, hyperfine splitting consts., vibronic effects 77−57890
pyridizine, 0-0 bands in n-π^* absorption, rot. contour anal. 78−55184
2-pyridone, dimer, vibr. Hamiltonian for IR spectra of H bonding 78−37620
^{99m}Tc-pyridoxal-phenylalanine evaluation as hepatobiliary imaging agent 78−31893
^{99m}Tc-pyridoxal-phenylalanine evaluation as hepatobiliary imaging agent 78−31894
di-α-pyridyl hydroperchlorates, intramol. H bonds, steric conditions and polarisability obs. 80−53160
pyridyl imidazoline-1-oxyl radical, trifluoroacetic acid solns., ^{1}H scalar dynamic polaris. 78−23371
2-pyridyl phenyl sulphide, dipole moments, absorpt. spectra, meas. and calcs. 77−46574
2-pyridyl phenyl sulphone, dipole moments, absorpt. spectra, meas. and calcs. 77−46574
pyrimidene, cavity radius and mean polarisability 79−45862
pyrimidine, $^1B_1$ state zero level fluoresc. decay, press. effects 78−13540
pyrimidine, γ-irrad. investig. by diffuse refl. spectrophotometry 77−48756
pyrimidine, and derivatives, intersystem crossing rates, triplet sublevel decay, vibronic coupling 78−5271
organic compounds continued
pyrimidine, bi-exponential decay, methylation and vibr. excitation, proximity effects 80−78641
pyrimidine, fluoresc. quantum yield 79−13757
pyrimidine, liq., nucl. relax. and mol. reorientation, nucl. Overhauser enhancement 78−60351
pyrimidine, singlet-triplet intersystem crossing, ODMR and MIDP in matrix at 1.6K 79−50055
pyrimidine, vapour, fluoresc. quantum yields, rot. effects 80−95661
pyrimidine, vapour, phosphoresc. 80−83408
pyrimidine, zero field studies of spin lattice relaxation in excited triplet states 79−18219
pyrimidine bases, electron adducts, spin density distribs., INDO calcs. 77−71754
pyrimidine derivatives, absorpt., luminesc. and polarisation spectra, electronic struct. 79−85993
pyrimidine H-addition radicals in single crystals, long range proton hyperfine coupling, EPR and INDO 77−54568
pyrimidine in cyclohexane at 77K, absorption and phosphorescence spectra 78−61138
pyrimidine N_2O aq. solns., dimer formation in γ-radiolysis, chromatographic obs. 80−7785
pyrimidine nucleotides, UV reson. Raman excitation profiles 80−58265
pyrimidine powder, γ-irrad., dose-response curves 78−7215
pyrimidines, substituted, UV irrad. in aq. solns., EPR of free radicals 78−40115
pyrimidines, substituted analogues, absorption UV spectroscopy and electronic struct. of ionic and tautomeric forms 80−74177
pyrimidines in Murchison meteorite, search 78−7948
pyrocalciferol, struct. determ. using Karle-Hauptman determinants 79−7513
pyrocatechol, oxidation pots., correl. of V-I characts. and photographic developing power *(Russian)* 80−45534
pyrocatechol derivatives, developing ability and structural data, correlation analysis 79−20448
pyrocatechol-phenylenediamine mixtures, solid-liquid equilibria, phase diagrams 77−27986
pyrogallol, PMR, OH group rot., H-bonds 79−47339
pyromellitic acid dianhydride, cryst. struct., anisotropic proton mag. shielding 79−87326
pyromellitic acid diimide, cryst. struct. determ. 77−11533
pyromellitic dianhydride-anthracene, cryst., charge transfer exciton transitions, refl. spectra obs. 78−72540
pyromellitic N,N′-dimethyldiimide-anthracene, cryst. struct. determ. 78−2107
pyrometallic dianhydride radical anion, MTHF glass, 77K, reson. Raman spectra 78−78704
pyronin dye, use as fluorescent indicator of energetic state of mitochondria 77−66790
pyronine, reson. Raman scatt., normal and excited mol. struct. determ. 77−58024
Pyronine G rot. diffusion from absorpt. relax. 80−1008
pyrrole, 6-electron 5-centre bonding units, increased valence theory calcs. 77−46500
pyrrole, electronic struct., spectra, ionisation pot., INDO-CI LACO-MO-SCF calcs. 79−54834
pyrrole, electronic struct. calc., σ^-pi consistency method 77−67957
pyrrole, excited state electronic struct., ab initio SCF and CI calcs. 78−78644
pyrrole, free radicals produced by X-irrad. and decay of tritium atom, EPR study 78−48676
pyrrole, FSGO calcs. of orbital energies, locations, dipole moments, charge distribs. 77−67976
pyrrole, gas, X-ray photoelectron spectra, satellite struct. 78−5281
pyrrole, ground state, (π-π^*) state, ab initio SCF CI calcs. 78−33438
pyrrole, HAM/3 calc. of ionis. and excitation energy and electron affinity 79−26894
pyrrole, liq. and nonaq. solns., ^{14}N NQR, ^{1}H line shape anal. 78−6598
pyrrole, multiphoton ionisation, photoionisation threshold meas. 79−27047
pyrrole, natural abundance ^{1}H coupled ^{15}N NMR spectra, selective population transfer method 79−95682
pyrrole, Penning election spectra and photoelection spectra, rel. intensities 80−95725
pyrrole, photoelectron ang. distrib. from mol. 79−31596
pyrrole, resonantly enhanced multiphoton ionisation 80−106362
pyrrole-acetonitrile, H-bonded complex, ab initio MO calcs. 80−102440
pyrrolidino-methyl tetracycline, labelled with ^{99m}Tc, prep. and control 79−29623
pyruvic acid, ^{11}C-labelled, enzymatic synthesis 80−61695
pyruvic acid, cryst. struct., X-ray diffr. 77−19942
pyrylium, substituted, electronic struct., CNDO/S calcs. 78−29749
pyrylium dye J-aggregate species, circular dichroism spectropolarimetric characts. 79−3456
pyrylium salt solns., electrochromism in visible absorpt. spectra 77−77244
quanidinium aluminium sulphate hexahydrate:Fe^{3+}, EPR, zero-field splitting 77−8395
quasi one dimensional charge transfer salts, soliton model for dielectric permeability 80−40036
quasi one dimensional organic materials, microwave cond., dielectric const. *(Hungarian)* 78−26850
quasi-one-dimensional organic metals, electron spin relax., temp. depend., Peierls fluctuations, EPR meas. 79−73802
quaternary ammonium ions, detect. by liq. chromatography with ion-exchange membrane detector 79−16055
quaternary pyridine salts as inhibitors of corrosion fatigue in $MnCl_2$ soln. of steel *(Russian)* 77−59973
p-quaterphenyl, melting temp. and latent heat 79−55869
p-quaterphenyl, polarisation of spontaneous and stimulated radiation 79−31583
p-quaterphenyl, polycryst. thin layer-metal sandwich, elec. cond. 80−34526
p-quaterphenyl, Raman spectra, struct. transitions 79−19870
quaterphenyl, vapour, rot. fluoresc. depolaris. 79−54889
p-quaterphenyl oriented layers, charge carrier transport, hopping model 80−2506
p-quaterphenyl oriented layers, field depend. mobility 79−91169
p-quaterphenyl vapour laser, optically excited, laser action obs. at 350 nm 79−7123

organic compounds continued
quaterrylene, minimal exposure high resolution electron microscopy 80−79653
quercetin, excited state proton transfer, luminesc. 80−35818
trans-quinacridones, absorpt. and emission spectra, struct. and solvent effects 77−478
quinacrine, fluoresc. probe interaction with acetylcholine-activated synaptic membrane 77−90762
quinacrine mustard, 2-step laser-induced photodamage 80−85198
Quinacrine Mustard, time-resolved fluoresc. spectrum 80−87165
quinazoline, excited state absorpt. spectra and intersystem crossing kinetics 80−74176
quinazoline, in n-pentane (isooctane) Shpolskii matrices, luminesc. props., vibr. struct. 79−22739
quinazoline, prereson. Raman spectra, vibr. band intensities obs. 80−102515
quinazolines, enzyme inhibitory, structure-activity quantitative study 80−78540
quinine bisulphate, aq. soln., abs. fluoresc. quantum efficiency, optoacoustic determ. 78−16849
quinine sulphate, acid soln., edge excitation red shift and proton migration 78−1028
quinine sulphate, excited singlet state, fluoresc. quenching by metal ions, rate meas., mechanism 77−38685
quinine sulphate, fluorescence polarisation meas. at high press. 78−66576
o-quinoidal-benzenoid system, valence isomerisation EHT calcs. 77−77757
β-quinol, low frequency mode investig. by IR absorpt. and neutron scatt. *(French)* 77−36220
β-quinol clathrate, CH_3OH mol. reorientation investig. by IR and dielec. meas. 77−12369
β-quinol clathrate, quest host interaction with N_2 or O_2, NQR 78−76346
β-quinol clathrate, single cryst., double NMR obs. of mol. motion of trapped methanol 79−87332
quinolene, dye in ethanol, laser stability, photodegradation parameters 78−71098
quinoline, dil. soln., dielec. absorpt., relax. and thermodynamic parameters meas. 80−50258
quinoline, fluoresc., phosphoresc. and H bonding 77−79647
quinoline, in binary solvents, phosphorescent and fluorescence 80−7409
quinoline, liq., depolarised light scatt., 1-1800 bar 79−24327
quinoline, liq., depolarised light scatt. from shear waves 80−97288
quinoline, photooxidation on rutile, ESR and effects of surface states 79−66352
quinoline, polycyclic monoazines, temperature dependence, triplet formation 79−54900
quinoline, radiationless transitions, internal conversion, energy depend. 78−94272
quinoline, solns., dielec. polarisation, π-electron system effects 77−90096
quinoline, solns. and mixtures, dielectric relax., const. and loss factor 77−55747
quinoline+carbon tetrachloride, (o-cresol) binary liquid mixtures, excess free vol. calcs. 80−34202
quinoline complexes with proton donors in triplet state, phosphorescence spectra 77−48230
quinoline derivative, interaction with coenzyme Q_{10} 79−91948
quinoline diffusion in PVC powder, microdiffusion technique 79−7713
quinoline in alcoholic glasses, induced fluoresc. 79−33775
quinoline-I_2 complexes, stability const. determ. by spectrophotometric methods 80−87056
quinoline-isoquinoline, dil. soln., dielec. absorpt., relax. and thermodynamic parameters meas. 80−50258
quinolines, heavy atom effects on phosphorescent triplet states 78−70858
quinolinium $(TCNQ)_2$, charge transport, proton spin-lattice relaxation 80−88545
quinolinium $(TCNQ)_2$, random exchange Neisenberg antiferromag. chain, intermediate field magnetisation meas. 80−103857
quinolinium manganese (II) chloride monohydrate, crystal struct. and mag. susceptibility 79−19239
quinolone dye in ethanol, laser dye stability, photodegradation relationships 78−55349
quinolone laser dyes, stability, lasing characts. obs. 78−1223
quinone adsorption on electron-donor and electron-acceptor centres of oxiphenol radical *(Russian)* 79−39138
quinone anions, ELDOR study of nucl. spin exchange due to cation migration 79−68244
quinone electrochemical reduction at packed, fluidised bed electrodes, kinetic behaviour 79−57235
1:1quinone-hydroquinone complexes, struct. 79−73159
quinones, spectral solvent shifts, electrostatic model and semi-empirical PPP calcs. 77−83507
quinones, triplet quenching by organometal cpds., time resolved CIDEP and ESR obs. 80−95654
quinones-Zn porphyrin, quinones sensitised reduction in vesicle systems 80−71897
quinoxaline$^+$, (singly protonated), struct. and kinetics of fluoresc. and phosphoresc. states 77−30906
quinoxaline, excited single state kinetics on a subnanosecond time-scale 79−36677
quinoxaline, excited state absorpt. spectra and intersystem crossing kinetics 80−74176
quinoxaline, excited states, protonation influence, semiempirical CNDO/S CI calc. 79−76353
quinoxaline, fluoresc. quenching and intermol. intersystem crossing, nonlinear press. depend. 78−25603
quinoxaline, in naphthalene-d_8, sublevel phosphorescence spectra, radiative mechanisms 77−75203
quinoxaline, in organic solvent, excited state absorpt. spectra, 422 and 533 nm, picosec. relax. 79−89683
quinoxaline, in p-dibromobenzene, ^{81}Br, elec. field grad. distortion near defect sites, optically NQR 79−38409
quinoxaline, in p-dibromobenzene, triplet state NQR, nucl. spin polarisation effects 79−18208
quinoxaline, optically detected X-band ENDOR of excited triplet state 79−18221
quinoxaline, oriented in lyotropic mesophase, proton NMR spectra 79−82886
quinoxaline, prereson. Raman spectra, vibr. band intensities 80−102514
quinoxaline, solns., excited state absorpt. kinetics 79−45734

organic compounds continued
quinoxaline, $T_1(\pi\pi^*)\rightarrow S_0$ intersystem crossing, isotope effects, ODMR and phosphoresc. obs. 80−91586
quinoxaline, triplet state symmetry, geometry, ODMR, ENDOR obs. 79−18214
quinoxaline, vibronic coupling by out-of-plane modes 77−6747
quinoxaline, zero field studies of spin lattice relaxation in excited triplet states 79−18219
quinoxaline, zero-field splitting, basic triplet states, H bond effects 78−5366
quinoxaline guest molecule in p-dibromobenzene crystal nucl. spin polarisation cross relax. study 80−29647
quinoxaline in durene (naphthalene) crystal, Stark effect, space charge, local field tensor and dipole moment 77−28601
quinoxaline in perdeuterated naphthalene, triplet spin-lattice relax. anisotropy 79−42822
quinoxaline in Shpolskii-type hydrocarbon matrices, vib. struct. of electronic spectra 77−85773
quinoxalinones, new class of high-efficiency laser dyes 78−46597
p-quinquephenyl, melting data and liq. cryst. transitions 79−55869
p-quinquephenyl, nematic, mag. susceptibility and order parameters 79−86709
quinuclidine, cubic phase disorderd struct., X-ray diffr. study 79−69037
quinuclidine, plastic phase, mol. reorientations, ^1H and ^{14}N NMR relax. 79−69039
quinuclidine, plastic phase, rot. motion, quasielastic neutron scatt. 79−69038
quinuclidine struct. determ. by gas phase electron diffr. 80−95742
quinzarin in alcohol glasses, electron-phonon coupling, photochemical hole burning 80−97265
R-113, refrigerant, critical heat flux of saturated natural convection boiling with heating from below 80−10114
racemic [1-^{11}C]-alanine and partially resolved [3-^{11}C]-alanine synthesis 79−88186
radialene, graph theory for axial symmetry molecules *(Chinese)* 79−36792
radialenes, graph theoretical polynomials 80−69048
radiation damage by electron diffraction 79−65119
radicals, EPR spectra, line intensity ratios, saturation 78−90192
radicals, HFS coupling const. calcs., RHF+CI method in INDO approx. 79−770
Π-radicals, open shell systems, spin density calc., program for semiempirical calc. *(Rumanian)* 79−72241
radioactive methyl iodide, removal using Ag-alumina 79−85638
radioactive waste, microbial prod. of tritiated and ^{14}C methane 80−45868
Raman spectra intensities, electronic polarisabilities, quantum mech. calc. 79−27041
randomised X-ray powder diffraction patterns, adjustable sample holder 80−6317
rare earth ethyl sulphate:Gd^{3+}, host lattice effects on EPR spectra 77−69684
rare earth ethyl sulphate nonahydrate:Gd^{3+}, high-precision EPR of cryst. 79−69717
rare earth ethyl sulphate nonahydrates:Gd^{3+}, $g_\parallel$, EPR obs. 78−35031
rare earth ethyl sulphates:Ce^{3+}, Kramers ions, virtual phonon exchange, field theoretic formalism 80−20137
rare earth ethyl sulphates, sp. ht., susceptibility 79−24129
rare earth formate, IR spectra and phase transitions, under pressure 78−31179
rare earth oxydiacetate, spectra, energy level patterns 79−38561
rare earth phthalocyanine solutions, bleaching by ruby laser beam 78−30030
rare-earth ethylenediaminetetracetates, formation constants *(French)* 80−104458
rare-earth formates, second optical harmonic generation 80−43403
recrystallisation, solvent selection, student experiment 79−84917
refractive indices, and optical anisotropies of some monoclinic and orthorhombic crysts. 80−50287
refrigerant R-113, incipient boiling characteristics at atmospheric and subatmospheric pressures 78−90688
refrigerant R-113 upflow in heated tube, liq. film dryout 78−90989
refrigerants, nucleate boiling, oil impurity effects 78−90657
relaxation phenomena, following core ionis., LCAO MO SCF calc. 79−10030
residual carbonaceous material, in urban airborne particulates, Raman microprobe obs. 78−69441
resorcin, Raman line intensity as function of mol. orientation 80−11383
resorcinol, cryst., nonlinear optical susceptibility and spontaneous polarisation 77−58372
α-resorcinol, nonlinear optical susceptibility, second order, calc. from mol. spectra *(Russian)* 79−27318
α-resorcinol, nonlinear optical susceptibility tensor, calc. 79−23011
resorcinol-phenylenediamine mixtures, solid-liquid equilibria, phase diagrams 77−27986
resorufin, in PMMA, site selection spectra, hole burning and Stark effect 78−9159
retinal, dipole moment determ. 78−27882
11-cis-retinal, donor energy effects on triplet-sensitized isomerization 78−3353
trans-retinal, ground and excited state dipole moments, permittivity, solvent effects, spectrophotometry 78−27883
retinal, in ethanol soln., methyl groups effect optical absorpt. 79−53047
retinal, isomeric triplets, low temp. spectrosc. and kinetic flash photolysis obs. 79−85972
retinal, isomers, intersystem crossing quantum efficiencies, solvent effects 79−22751
trans-retinal, picosecond photophysics 77−9169
all-transretinal, two-photon spectrum, rel. to photophysics of vision 79−41159
9-cis retinal, visual pigment chromophore, twisting mechanism 80−58333
retinal analogue, initial photochem. process, evidence against proton transfer 77−1999
retinal isomers, dark equilib. and photochem. 78−15771
retinal photoisomerisation mechanism for light-driven proton pump in H. halobium 78−35820
11-cis-retinal prep. by irrad. of all-trans-retinal and high press. liq. chromatography 78−40453
retinal Schiff bases, Raman spectra modelling of rhodopsin and bacteriorhodopsin chromophores 79−62190

organic compounds continued
11-cis retinal visual pigment chromophore, twisting mechanism 80−58333
retinals, catalysed cis-trans isomerisation by crude tissue extracts 78−64925
retinals, emission spectra, state ordering 77−25373
retinals, polarised fluoresc. at room temp. 78−96014
retinals, visual pigment model systems, spectroscopy and photochem. 77−32871
retinol, fluoresc., polarised emission study 79−29504
retinols, visual pigment model systems, spectroscopy and photochem. 77−32871
retinyl acetate, fluoresc., polarised emission study 79−29504
retinyl acetate, high press. fluoresc. studies of radiative and nonradiative processes 80−1011
trans-retylidene-n-butylamine, ground and excited state dipole moments, permittivity, solvent effects, spectrophotometry 78−27883
rhamnose, single cryst., X-irrad. at 4.2K, trapped electrons and electron traps characts. 79−78037
rhodamine, 6G, laser, lamp-pumped, solvent and temp. depend. 79−3692
rhodamine, 6G and B, low quantum yield mol. fluoresc., polarisation, excitation energy depend. 77−50462
rhodamine, activated 6G top layer in slab-type directional coupler, amplified oscill. 80−99718
rhodamine, anal. by fluoresc. spectrophotometry, optics 77−34030
rhodamine, CARS spectroscopy, vibr. spectra of electronic states 80−27964
rhodamine, dye soln., photoinduced dichroism and vibronic relax. 77−14465
rhodamine, soln., triplet state accumulation and deactivation depend. on solvent polarity 79−85982
rhodamine, solns., lasing characts., diphenyl polyene addition effects 77−3581
rhodamine 101, quenching of emission in methanol and latex particle suspensions 80−3374
rhodamine 3B solutions in polyvinyl alcohol matrix, spectrum-luminesc. characts. 79−13761
rhodamine 4C, in ethanol soln., rot. relax. time using ps. spectroscopy technique 80−1013
rhodamine 590 picosecond transverse-flow flashlamp-pumped dye laser 80−38025
rhodamine 640, subpicosecond spectroscopy, tunable probe, spectral dynamics 80−23429
rhodamine 69, soln., bleaching and laser props., detergent effects 79−59697
rhodamine 6 Zh solution, radiant transport effect on luminesc. duration 80−103995
rhodamine $6G_2$ molecules in solution, photoluminescence study, fluorescence decay time 80−80832
rhodamine 6G, aggregation, modulation Stark spectrosc. obs. 79−27030
rhodamine 6G, aqueous soln., absorpt. spectra, ground and triplet state photoprotonation pH depend. 80−42961
rhodamine 6G, associated, in polyvinyl alcohol film and soln., emission, room temp. 79−54896
rhodamine 6G, B, subpicosecond relax. time meas. using pulsed lasers *(Czech)* 78−78838
rhodamine 6G, B in ethanol soln., and dye mixtures, excitation by Cu vapour laser 80−28230
rhodamine 6G, blue and UV luminesc., obs. and mechanism 79−3486
rhodamine 6G, Cu vap. laser pumped, axial mode struct. 77−23671
rhodamine 6G, CW jet stream laser, high output power in visible and near UV 78−1249
rhodamine 6G, CW laser, passive-active mode locking 78−29993
rhodamine 6G, delayed fluoresc. of simple associates in polar and nonpolar solvent mixtures *(Russian)* 78−48185
rhodamine 6G, dye laser pumping characts. using KrF excimer laser at 248 nm 80−1199
rhodamine 6G, dye soln., laser flash photolysis 77−21402
rhodamine 6G, effect of cyclooctatetraene on laser props. 78−13698
rhodamine 6G, electronic energy transfer from S_2 state to BBOT in soln. 78−88346
rhodamine 6G, emission kinetics in ps. range 78−13699
rhodamine 6G, excited states prod. by direct and stepwise absorpt. of light 79−64055
rhodamine 6G, fluoresc. polaris. spectra in glycerol soln. 79−76458
rhodamine 6G, fluoresc. polarisation, solvent effects 80−32755
rhodamine 6G, halo laser device 79−72597
rhodamine 6G, in binary compensated cholesteric mixture, electro-optical colour effect 80−71378
rhodamine 6G, in ethanol, time-depend. fluoresc. spectrum, using synchrotron radiation 80−62736
rhodamine 6G, in glycerine-water solns., anti-Stokes fluoresc., conc. quenching 79−24349
rhodamine 6G, in methanol, fluoresc. lifetime meas. 78−29811
rhodamine 6G, in n-alcohols (ethylene glycol)(glycerol), rot. relax., time-resolved fluoresc. depolaris. obs. 80−58300
rhodamine 6G, in organic solvent, hot luminesc. 79−4842
rhodamine 6G, in rigid matrix, conc. effects in spectra 80−83347
rhodamine 6G, in Triton X-100 water soln., energy migration and laser performance 77−71982
rhodamine 6G, lasing, reson. CARS spectra in methanol, ethanol, acetonitrile, H_2O 78−74948
rhodamine 6G, micellar soln., aq., fluoresc. decay for rot. diffusion const. 79−11826
rhodamine 6G, mol. fluoresc. decay time, self-absorption 79−68255
rhodamine 6G, molecular nonsteady-state luminesc. behaviour under narrowband laser excitation 80−87159
rhodamine 6G, on surface of stilbene cryst., sensitised luminesc., energy migration 79−56831
rhodamine 6G, orientated relax. times, streak camera meas. 80−14168
rhodamine 6G, photoacoustic spectra in soln. 80−9606
rhodamine 6G, photoreaction mechanisms, effect of pumping spectral composition *(Russian)* 77−70323
rhodamine 6G, preferential doping in polyurethane optical solid cct. 77−62075
rhodamine 6G, quantum efficiency of intercombination conversion to triplet state by sensitised phosphoresc. *(Russian)* 77−85798
rhodamine 6G, resonant interference of nonlinear optical suscept. *(Russian)* 77−7160
rhodamine 6G, ring struct. laser emission, resonator exit mirror effect 77−38941
organic compounds continued
rhodamine 6G, rot. diffusion, fluoresc. spectra, solvent effects 77−75198
rhodamine 6G, rot. diffusion from absorpt. relax. 80−1008
rhodamine 6G, soln., triplet state lifetime determ., solvent effect 78−1225
rhodamine 6G, solns., delayed fluoresc. of simple associates 79−56847
rhodamine 6G, solns., electronic absorpt. spectra, mol. assoc. effects *(Russian)* 77−88460
rhodamine 6G, sub ns dye laser with optical pumping, spectral width, efficiency, tuning *(Russian)* 78−29974
rhodamine 6G, superluminesc. band structureless spectra 79−7124
rhodamine 6G, tunable freq. doubled CW laser using ADA 78−17965
rhodamine 6G, tunable lasing molecule *(Chinese)* 80−74389
rhodamine 6G, two-photon fluoresc., phase fluctuations and phase modulation effect 78−50570
rhodamine 6G, ultrashort pulse generation in resonator *(Russian)* 79−50289
rhodamine 6G+BBOT donor-acceptor system, intermol. electronic energy transfer 78−17702
rhodamine 6G+malachite green, in low viscosity solvent, ps time resolved energy transfer 78−70910
rhodamine 6G activated polymer (liq.) films adjoining amplifying media, stimulated emission 78−17932
rhodamine 6G alcohol soln., two-photon absorpt. efficiency 78−13749
rhodamine 6G and 3B, excited singlet-singlet absorpt. *(Russian)* 79−42985
rhodamine 6G and 4B, amplification spectra, triplet-triplet absorpt. 77−31101
rhodamine 6G and rhodamine B adsorbed on AlH_3, luminesc. spectra during AlH_3 photolysis 80−55171
rhodamine 6G aqueous solution, surfactant effect on fluoresc. intensity *(Japanese)* 77−42536
rhodamine 6G associates, spectroscopic evidence of luminesc. *(Russian)* 77−48233
rhodamine 6G dissolved in liq. cryst. hosts, laser emission obs. 79−41376
rhodamine 6G doped polyurethane film, fluoresc., photoinduced effects 77−1727
Rhodamine 6G doped polyurethane film coated with CF_3 coumarin-doped PMMA film, dye laser characts. 77−83868
rhodamine 6G dye in ethylene glycol, broadband optical diode, one directional traveling wave operation of ring laser 80−58606
rhodamine 6G dye in quartz glass microcomp. matrix, as tunable solid laser 80−99734
rhodamine 6G dye laser, amplifier system pumped by TEA N_2 laser 78−82984
rhodamine 6G dye laser, CW 33 W output power 77−61968
rhodamine 6G dye laser, CW synchronously mode-locked, subpicosecond pulse generation 78−71128
rhodamine 6G dye laser, degree of polaris., solvent effect 79−41375
rhodamine 6G dye laser, induced radiation spectral characts., effect of vibr. relax. 80−64008
rhodamine 6G dye laser, long pulse, high average power 77−58342
rhodamine 6G dye laser, N_2 laser-pumped, pulse time behaviour 79−31894
Rhodamine 6G dye solutions, flashlamp-pumped, thermal effects 77−10917
rhodamine 6G ethanol soln., absorpt. and luminesc. spectra using picosecond excitation 80−106351
rhodamine 6G in dimethylsulphoxide, concentratational red shift and luminesc. spectra 80−83426
rhodamine 6G in ethanol, injection locked ring amplifier 77−88788
rhodamine 6G in ethanol, photobleaching mechanism *(Russian)* 78−48680
rhodamine 6G in ethanol dye soln., lasing props. recovery after photolysis 77−34888
rhodamine 6G in PMMA, luminesc. greenhouse solar collector 78−13789
rhodamine 6G in polyurethane film, laser, etched cavity 77−7140
rhodamine 6G in soln., photochem. stability 78−37878
rhodamine 6G jet stream CW laser, tuning range, mode competition effects 78−50791
rhodamine 6G laser, intracavity freq. doubling in $NH_4H_2PO_4$ 77−3628
rhodamine 6G laser, pumping efficiency enhancement using luminesc. filters 77−38882
rhodamine 6G laser, radially nonuniform lamp pumping, lasing power 79−64220
rhodamine 6G laser, short-cavity, excited by electron beam pumped CdS laser 78−25887
rhodamine 6G laser amplifier pumped by N_2 laser, sub nsec pulse generation 80−1232
rhodamine 6G laser soln., freq. shift due to RI changes 77−7078
rhodamine 6G laser with lamp excitation, cavity thermooptical distortions effect 79−55135
rhodamine 6G laser with lamp pumping, spatial coherence 77−50669
rhodamine 6G lasers, synchronized CW psec. pulse train generation at 2 independently tunable wavelengths 78−33758
rhodamine 6G polar solution, conc., temp effect on spectral props. 79−87505
rhodamine 6G pulsed dye laser, locking by anomalous dispersion in vapour cell 79−7163
rhodamine 6G soln., cyclooctatetraene effects on laser props. *(Russian)* 78−25875
rhodamine 6G soln., delayed annihilation fluoresc., external heavy at. effect 79−99931
rhodamine 6G soln., hot luminesc. and vibr. relax. 79−22752
rhodamine 6G soln., stimulated reson. Raman scatt., first excited and ground electronic states contrib. 79−89968
rhodamine 6G soln. in ethanol, luminesc. liq., pump radiation conversions to enhance laser efficiency 80−48293
rhodamine 6G solns., acousto-optical distortions induced by pump lamp radn. 79−73898
rhodamine 6G solns., picosec. kinetics of emission 79−76685
rhodamine 6G solution, absolute fluoresc. quantum yield determ. by calorimetric method 80−78851
rhodamine 6G solution, stimulated emission under internal refl. conditions 77−58327
rhodamine 6G solution in alcohol, degenerate four wave mixing, phase conjugation *(Chinese)* 80−102765
rhodamine 6G solution laser, pulse tube pumping *(Russian)* 77−88785
rhodamine 6G synchronously mode locked CW laser, pulse width depend. on intracavity bandwidth 78−66821

organic compounds continued
rhodamine 6G thin film ring laser, emission features 79−64221
Rhodamine 6G-3,3′-diethylthiacarbocyanine iodine, energy transfer with increased local conc., Forster mechanism 80−69220
rhodamine 6G-alcohol, two-photon luminesc. intensity, appl. to picosecond pulse meas. 78−71134
rhodamine 6G-coumarine 1-water-Triton X100, micellar dye soln., energy transfer 80−45581
rhodamine 6G-isopropyl or ethyl alcohol solution, flashlamp pumped laser, photochem. effects 80−53287
rhodamine 6G-ketocyanine mixed solns., wideband lasing 79−957
rhodamine 6G-safranin-T mixed dye laser energy transfer, 31 nm tuning range 80−58532
rhodamine 6GDN, synchronous tunable ps laser 77−75560
rhodamine 6Zh, electronic spectra, intermol. interactions effect *(Russian)* 77−48237
rhodamine 6Zh pulsed laser, simple transverse mode observation *(Russian)* 79−72565
rhodamine (6G-DTDC and 6G-CV) in alchohol solns., energy transfer by means of photobleaching 79−23031
rhodamine B, 6G, resonance CARS line shape, scatt. processes in ground or excited states 80−48043
rhodamine B, 6G, spectra of lowest excited singlet states 79−81424
rhodamine B, absorption on Ag electrode, anisotropy of optical props. 80−60534
rhodamine B, acid-base equilib., photophys., fluoresc. lifetime meas. 78−82762
rhodamine B, adsorption on ZnO single crystal, photooxidation, electrochem. meas. 78−31645
rhodamine B, doping density dependent attachment on TiO_2 electrodes 80−54777
rhodamine B, double Davydov's splitting of visible absorpt. band 78−82746
rhodamine B, in glycerine-water mixtures mol. agglomeration effect on fluoresc. polaris. spectrum 78−25595
rhodamine B, injection locked dye amplifier, coherent optical image amplification 80−19041
rhodamine B, laser, lamp-pumped, solvent and temp. depend. 79−3692
rhodamine B, mol. fluoresc. decay time, self-absorption 79−68255
rhodamine B, photosensitisation of Lexan:triphenylamine 78−34856
rhodamine B, soln., bleaching and laser props., detergent effects 79−59697
rhodamine B, tunable freq. doubled CW laser using RbH_2PO_4 cryst. 80−53372
rhodamine B+heteroarenium cations, resonant, nonradiative energy transfer *(German)* 78−25659
rhodamine B activated waveguide, amplification of narrow-band signal 79−36930
rhodamine B adsorbed on anthracene, electron-hole pair in external elec. field 79−73558
rhodamine B adsorbed on NaCl, photoelectric meas. and contact charging 79−19643
rhodamine B and 6G, fluoresc. decay time meas. in different solns. 80−9637
rhodamine B dissolved in D_2O, electronic state two-stage excitation by light pulse 79−64056
rhodamine B dye, adsorbed on PbO powder layers, charge storage and photocond. 78−64056
rhodamine B dye laser, N_2 laser-pumped, pulse time behaviour 79−31894
rhodamine B in aq. LiCl soln., absorpt., pH, electric conductance 77−27079
rhodamine B in ethylene glycol, fluoresc. decay meas. via modulated gain spectroscopy 80−63699
rhodamine B lactone, dual fluoresc., solvent polarity depend. 77−3394
rhodamine B surface state hole traps, surface photovoltage meas. 80−39654
rhodamine B-ethanol soln., luminesc. quantum yield, photoacoustic method 77−86335
rhodamine C and 6G, strong base solns., electronic spectra, temp. depend. 79−85987
rhodamine dye, coherent ellipsometry determ. of third order polarisability 79−71511
rhodamine dye, intercombination conversion rate consts. from triple quenching by 1,4-diphenylbutadiene 79−956
rhodamine dye, photodecomposition of laser dyes *(Russian)* 77−29017
rhodamine dye laser, synchronously pumped, electronically tunable pulse prod. 79−76698
rhodamine dye lasers, flashtube-pumped, calc. and expt. generated quantum power 78−50772
rhodamine dye mixtures, qualitative anal. by fluoresc. polarisation spectroscopy 79−34396
rhodamine dye polar frozen solns., luminesc. broadening 80−2834
rhodamine dye solns., amplified spontaneous emission 79−45941
rhodamine dye solutions, additional heavy atom effects on triplet state transitions *(Russian)* 77−85800
rhodamine dye solutions, vibr. relax. in S_1-state 77−6826
rhodamine dyes, amplified spontaneous emission, picosecond pulse generation 79−3691
rhodamine dyes, methanol-water solns., triplet state EPR spectra, aggregation, mol. orientation 77−48031
rhodamine dyes, phosphoresc. quantum yields determs. 79−8179
rhodamine dyes, soln. induced singlet-singlet absorption spectra 78−46363
rhodamine dyes, triplet state, role in intermediate prod. 77−29018
rhodamine dyes in methanol-water glasses, EPR spectra of triplet state 79−18212
rhodamine dyes in soln., bleaching, electronic and vibr. absorpt. spectra, fluoresc. 80−42960
rhodamine G, in glycerine-H_2O mixture, fluoresc. polarisation spectra, 350 and 540 nm excitation 79−98139
rhodamine G in ethanol, flash-lamp pumped, intracavity absorpt. anal. method sensitivity 79−57328
rhodamine G solutions, LiCl and $NaClO_4$ electrolyte influence on its lasing props. 80−91788
rhodamine GG tunable narrowband subnanosecond dye laser, optical pumped 79−81445
rhodamine laser, induced losses in active medium during incoherent excitation *(Bulgarian)* 79−10297
rhodamine laser light shifting into blue-green, using parametric amplifiers 79−18471

organic compounds continued
rhodamine R derivatives, water (heavy water) detergent solns., luminesc., lasing 79−56836
rhodamine solns., short-wavelength luminesc. 79−78738
rhodamine solution, picosec. spectroscopy with antiStokes excitation, orientational rearrangement *(Russian)* 79−42984
rhodamine solutions, quenching of two-photon fluoresc. and stimulated anti-Stokes emission 79−72619
rhodamine Zh, isomer separation, identification and emission efficiencies *(Russian)* 77−83871
rhodamine-6G mode locked dye laser pulse width monitoring by rapid scan autocorrelator 80−87421
rhodamine-6G-3,3'-diethylthiacarbocyanine iodide-sodium lauryl sulphate, soln., premicellar region, energy transfer 80−20685
rhodamine-B, fluorescence decay meas. via modulated gain spectroscopy 79−64025
rhodamine-B and -6G, sub psec radiationless relax. in soln. 77−18955
rhodamine-B fluoresc. polarisation, solvent effects 77−54569
rhodamine-B solutions, thermochromic and hyperchromic effects 79−91977
Rhodamine-dye double-pulse method stimulated emission 77−90172
rhodamine-methanol soln. energy transfer to Ag film surface plasmons 79−91119
rhodamines, 5G, 6G, B, 3B in ethanol soln., luminesc. quenching by photoirradiation 80−87168
rhodamines, reson. Raman scatt., normal and excited mol. struct. determ. 77−58024
rhodamines, solns., amplification and induced absorpt., cross-sections, spectra 77−68208
rhodamines, solutions, electronic absorption spectra and dimeric props. 77−88458
rhodamines in ethanol soln., gain and induced absorpt., struct. props. 77−24890
NH-rhodanine-merocyanine films, electronic transitions, 0.5 to 2.5 eV, inelastic electron tunnelling spectra 79−41214
rhodanines, tautomeric, electronic struct. and spectra, MO calcs. 79−13629
rhodizonate ion, reson. Raman scatt., Jahn-Teller effect 79−18190
rhodophorphyrin XV metal complexes, phosphoresc. polarisation 77−23517
rhodopsin, bathorhodopsin and isorhodopsin, mech. of photoconversion 78−53336
rhodopsin, bullfrog, thermosensitive prop. 77−25431
rhodopsin, thermal isomerisation rel. to visual transduction mechanism in retinal obs. 79−74651
rhodopsin regeneration in frog, effect of MS-222 anaesthetic 77−36925
riboflavin, light-induced lysozyme binding 78−27899
riboflavin, transition moments in 300 nm region 79−53042
riboflavin in various solvents, absorpt. spectra, relative quantum yields, electronic transitions 77−52149
rigid molecules solns. and mixtures, dielectric relax., const. and loss factor, microwave region 77−55747
rigid polar molecules in dil. solns., dielectric loss in far IR region *(German)* 77−16248
ring compounds, dopants in Al-AlO_x-Pb junctions, tunnelling asymmetries 79−95549
ring compounds, three-membered, vibr. spectra and struct., book control 78−78701
ring current theory 80−87240
RNA, conformational fluctuations, internal motion correl. times, ^{31}P NMR obs. 80−72135
RNA, form. of covalent linkages with proteins in gamma-irrad. E. coli ribosomes *(French)* 77−56340
RNA, heterogeneous nucl., effects of UV irrad. and postirrad. incubation on size in murine cells 78−69139
RNA, laser Raman spectra, cloverleaf secondary struct. 79−100569
RNA, messenger, synthesis in rat livers, ionising radiation and partial hepatectomy effects 79−92144
RNA, nuclear Overhauser effect and solvent exchange rate, NMR expts. using supercond. magnet 79−74811
t-RNA, rot. relax. time, 10^{-9}s range Fabry-Perot and photoelectron time of arrival method 80−21437
RNA, solid hydrated samples, hysteresis loops, nonlinear dielectric properties 80−71294
RNA in frog retinal cell, indicator of sensitivity to movement of stimuli and flickers 77−86490
RNA nucleotide sequence, determ using computer 79−29500
RNA of Novikoff Hepatoma ascites cells, effects of sparsely-ionising radiation after in vivo labelling 78−7389
RNA synthesis in slime-mould, effects of electrons and neutrons, caffeine modification 77−12962
RNA synthesis kinetics, infolding and unambiguity of soln. of inverse problems 78−64921
RNA synthetic, duplexes in soln., struct., dynamics 79−57574
Rochelle salt, ferroelec. phase transition, Raman scatt. study 80−97211
Rochelle salt, irrad. cryst., acyloxy radical ion decarboxylation, pulse radiolysis and EPR obs. 78−70854
rose bengal, adsorbed on ZnO electrode, reson. Raman spectra 78−76446
Rose Bengal, appl. of nsec. time resolved photoacoustic spectroscopy 77−74511
rose bengal, dye soln., photothermal spectroscopy 78−32808
rose bengal, electron transfer to TiO_2 electrodes, photoelectrochem. meas. 77−66758
rose bengal, excited state orientational relax., in protic and aprotic solvents 78−46383
rose bengal, photosensitising dye, effect on charge transfer in ZnO 78−72193
rose bengal photosensitising dye effect on charge transfer in ZnO surfaces 78−68049
rose bengal soln., photoacoustic spectra, spectrometer sample cell design investig. 77−74520
Rose Bengal-fluoranthene, singlet-singlet energy transfer in Manoxol OT-cyclohexane-water 80−9531
rose bengale, fluoresc. polaris., solvent dipole moment effect 78−25596
rubeanic acid, in ethanol and water solns., UV transmission filter charcts. 77−3679
rubidium acetate, molten, elec. cond. and density 77−15613
rubidium acid phthalate, solution growth of large single crystals, using cylindrical seeds 78−60556
rubidium hydrogen glutarate, H bonding, vibr. spectra 78−43860

organic compounds continued
rubidium n. alkanoates, long-chain, phase transformations, in melt, DTA obs. 77−76536
rubidium platino-oxalate, one-dimens. conductors, prep., struct. and elec. cond. 80−24900
rubidium propanoate, solid state transitions and melting process, diffr. and conductometric meas. 80−10670
rubidium tartrate, optical rot. dispersion, dichroism and spectra, in soln. and cryst. *(Russian)* 77−90124
rubidium tetramethylborate, vibr. spectra and force constants *(German)* 79−26981
rubrene, electrochemilum. by DC, highly organised EHD convection obs. 80−71499
rubrene, electrogenerated chemilum., production of excited states by direct heterogeneous electron transfer 79−20371
rubrene, excited singlets, O quenching, singlet O formation 78−27792
rubrene, in benzene soln., extrinsic photocond. kinetics 80−92691
rubrene, orthorhombic cryst. photogenerated carriers, transit time meas. 80−49811
rubrene, photooxidation, photoacoustic spectroscopic obs. 79−16010
rubrene, sensitised photooxidation of 1,3-diphenylisobenzofuran solns., S_1 excited state O_2 quenching 80−45529
rubrene, soln. in benzonitrite, electrochem. luminesc. 77−77776
rubrene film, excited complex with charge transfer, fluoresc. obs. of mag. reson. *(Russian)* 77−8454
rubrene film, photooxidation in solid, UPS obs. 79−52693
rubrene radical cation reduction at n-ZnO electrode, triplet state formation, luminesc. 77−16825
rubrene thin layer and flow cells, steady DC electrogenerated chemilum. 80−55205
rubrene-in-benzene, excited state migration and charge transfer 77−55559
RX^-, radical anion stability conditions, pot. energy diagrams 80−85161
s- and pi-electron contribs. to contact proton spin-spin coupling, INDO perturbation calc. 77−50361
saccharides, lyoluminescence dosimetry 77−52881
saccharose, far IR absorpt. spectra, pyroelec. coeff. temp. depend. *(French)* 78−72503
saccharose, far IR absorption, low temp. pyroelectricity 78−80348
saccharose, single cryst. low-temp. pyroelectricity 79−42906
saccharose crystal, low temp. pyroelectricity 79−42909
salicelidenanilines, SLC, ferroelectric behaviour, specific heat, spontaneous polarisation 80−75958
salicyclic acid, luminesc. probe for alcohol-H_2O soln. struct. investig. 78−84636
salicylamide, excited state proton transfer, kinetics, picosec. fluoresc. 79−59502
salicylic acid, diffusivities in water 79−73328
salicylic acid, IR absorpt. spectra, fundamental assignments 80−5542
salicylic acid, Raman active external modes *(French)* 78−23458
salicylic acid, vapour press. meas, using torsion-weighing effusion apparatus 77−89530
salicylidene-2-chloroaniline, photochromism and thermochromism, NQR spectra, temp. and UV irrad. depend. 80−54968
salicylideneaniline, photochromic, optically induced changes in refr. index 79−81497
α_1-salicylideneaniline, photochromic props., appl. as holographic recording 77−68183
salicylideneaniline hologram, image reconstruction, reading beam not satisfying Bragg condition 78−37828
N-salicylideneanilines, photo- and thermo-chromic, ^{14}N quadrupole resonance temp. depend. 78−48077
N-salicylideneanilines, thermochromic and photochromic, ^{14}N quadrupole coupling, NQR meas. 77−28480
salol, liq., supercooled, relax. kinetics, optical Kerr effect obs. 77−84613
salol, liq. and supercooled, VH light scatt. spectra *(French)* 77−1755
salol, propag. of longit. and shear hypersonic waves, light scatt. meas. 77−51442
salol, solid/melt interfacial tension and contact angles of small particles, determ. from crit. vel. of engulfing 80−79915
salol, solidification, stability of spherical particle growing from stirred melt 77−47365
salol crystals, investigation of structural formation and growth kinetics 79−47610
samarium oxalate, IR and Raman spectra exam. *(French)* 78−48159
sandwich compounds, prep. from free atoms of metals *(French)* 80−21281
tris-sarcosine calcium chloride, elastic props., US damping 80−84229
saturated fatty acid in MIM junction, elec. cond. mech. 78−95386
saturated hydrocarbon, and diamond cluster, ab-initio HF and PCILO calc., bond length 78−42951
saturated hydrocarbon+$O(^3P)$, reaction dynamics, model pot. surfaces, quasiclassical trajectory calcs. 80−97696
saturated hydrocarbon+$O(^3P)\rightarrow$OH+alkyl radical 80−97695
saturated hydrocarbon +$O(^1D_2)$, chem. reaction dynamics. OH prod. investig. 80−101016
saturated hydrocarbon photoelectron spectra correl. effective hamiltonian matrix parameter optimisation, least squares method 79−26874
saturated hydrocarbons, adsorption on alumina 80−26053
saturated molecules, empirical potential model EPEN/2, parameterisation testing 79−54933
saturated monatomic alcohols and water mixtures, effects of chlorides on struct. from US vel. meas. 79−86840
saturated organic molecule, photolysis, primary step prediction using Rydberg and valence-shell transitions 77−21404
scandium nitrate tetracarbamide, cryst. struct. determ. 79−23588
scandium octaethylporphyrin, μ-oxo bridged dimer, triplet states and geometrys, ODMR obs. 80−9625
scandium octaethylporphyrin, triplet states and geometrys, ODMR obs. 80−9625
scandium oxalate, IR and Raman spectra exam. *(French)* 78−48159
Schiff's base, thin layer samples, mechanism of change carrier photogeneration *(Russian)* 77−32045
Schiff's base compounds, double axis, Siamese Twin type liq. crysts., thermal and X-ray obs. 80−39312
Schiff's bases, deuterated, transition temp. meas., comparison with normal compounds 78−14449
Schiff's bases, mesomorphic, two-component system, tricritical nematic-smectic A point 77−51482
Schiff's bases, nematic phase, relation between elasticity and mol. struct. 79−90711

organic compounds continued
Schiff's bases, nematic phys. props. 79−99057
Schiff base azo dyes in nematic liq. cryst. hosts, order parameters, optical density meas. 80−84055
Schiff base compounds, cholesteryl esters, mesomorphic behaviour 78−1994
Schiff base esters, mesomorphic behaviour 78−1993
Schiff base eutectic mixture, liq. cryst., glassy transition, DTA obs. 79−4405
Schiff base liq. crysts., multicomponent, phase diagrams and metathetic reactions 79−56965
Schiff base-retinal, visual pigment model systems, spectroscopy and photochem. 77−32871
scintillators, captured γ quanta yield, fast neutron irrad. 77−46457
scirpene toxins, in animal feeds, chem. anal. 78−48707
in seawater, dissolved and particulate, meas. using automatic sampling buoy 78−49149
seawater off Ireland west coast, dissolved organic matter conc. rel. to surface waters colour 78−85603
sebacate ester, viscosity and density determ. up to 150°C and 150000 psig 77−59940
sec-butyl radicals, intermol. potential well depth estimation method 79−86034
secondary light scatt. in low frequency field, in dielectric state 78−48147
sedimentary organic matter, subaerial weathering effects 78−57206
seignette salt, refractive index temp. depend., differential photoelectro-optical refractometer 77−40202
1,2,5-selenadiazole, partially oriented in mesophase, r_z struct. PMR obs. 78−58719
selenoacetaldehyde, microwave spectrum, struct. internal rot. barrier 78−74645
selenoacetamide (-d_n), IR spectra, vibr. assignments, normal coord. anal. 79−22708
selenocyclopentane, interconversion barrier, spectra and struct. 79−10115
selenoketene, formation, microwave spectrum, struct. determ. 78−25515
selenoketene, microwave spectra, 26.5-40 GHz, mol. config., bond angle and length 78−46322
selenophene, flash photolysis, transient absorpt. spectra 80−14153
semicarbazide hydrochloride, phase transition, IR spectra and thermal study 79−37833
semicarbazide hydrochloride, vibr. spectra, normal coord. anal. 80−58255
semicarbazide-d_0, -d_6, vibr. spectra, normal coord. anal. 80−58255
o-semiquinone, form. by photolysis, isomerisation, ESR 77−16840
o-semiquinone, radicals, intra- and intermolecular H^+ transfer, ESR 77−16840
semiquinone Q_{10}, EPR signal with unusual relax. parameters 77−56338
semiquinones in protic solvents, saturation behaviour, ESR 77−6808
semitetrafluoroborates, H-bonding, strong, stochastic model and IR spectra temp. effects 78−62805
serine, adsorbed on Ag, XPS and SIMS study 79−86986
DL-serine, X-irrad., $\equiv C\text{-}^+NH_3$ radical form., exchangeable H^+ hyperfine coupling 79−36669
L-serine hydrate, D_2O of crystn., ^2H quadrupole resonance, double transitions 79−3465
serine zwitterion+water, interaction pot., ab initio SCF LCAO calc. 78−48747
L-serine-L-ascorbic acid, X-ray cryst. struct. determ. 80−35827
L-serines-d_0 and -d_4, IR and Raman spectra, rot. isomers *(French)* 79−45714
serotonin, role in synaptic facilitation and behavioural sensitisation in Aplysia 77−36913
serotonin effect on cytochrome c soln. optical props. after UV irrad. 80−30663
serum thyroxine, radioimmunoassay by the antibody-coated test tube method *(Japanese)* 80−67237
p-sexiphenyl, liq. cryst. phase transitions 79−82322
SHG materials, selection and characterisation 77−3626
Shpolskii spectra, identification and struct. anal. of unknown compounds in organic mixture 79−87891
1-silabicyclo 2,2,2 octane, double-min. skeletal torsion, microwave spectroscopy 80−47972
silacyclopentane, Raman spectra, pot. energy surface, barrier to interconversion 78−25541
silaethylene, isomerisation, lowest triplet state reaction surface studies 79−15963
silaethylene, singlet-triplet energy separation 78−58594
silaethylene, singlet-triplet energy separations 77−57866
silaethylene, triplet carbenoid isomers, thermodynamic stability 78−90076
silanes, diamagnetic susceptibility, semiempirical calcs. 78−17820
silicon oil, thermal diffusivity, constant-rate heating method *(Japanese)* 80−6570
silicon phthalocyanine, elec. cond. temp. depend. 80−80271
silicon tetramethoxide, prep. from metal alkoxide, props. as precursor of oxide glass 78−48700
silicone oil, ionic behaviour, carrier mobility and viscosity 80−107453
silicone oil, Newtonian, vel. meas. in die entry region of capillary rheometer 80−99988
siloxanes, bridging bond angle variation, mol. orbital calc. 78−55125
silver acetate-H_2O-acetic acid, ternary liq., elec. cond. and density 78−91464
silver iodide-N,N,N,N′,N′,N′-hexamethyl-1,3-propylenediomine diiodide, solid electrolyte, cryst. struct. determ. 77−7705
silver methanedisulphonate, cryst. struct. and information determ. 79−90633
silver salts of organic acids, photolysis investig. for use as photosensitive material for PC forming 77−44496
silver thioamides, precip., electron microscope and potentiometric studies, growth of photosensitive crysts. 80−33107
silyl acetylene, microwave spectra in ground and ν_{10} vibr. state 80−78610
silyl acetylenes, fine structure due to internal rotation in IR-active perpendicular bands 79−98096
silyl radicals, benzil adducts, organometallic group dynamic migration, EPR 77−58049
silylacetylene, centrifugal distortion consts., thermodynamic functions 80−47959
silylcarbene, isomerisation, lowest triplet state reaction surface studies 79−15963
silylene, decomp. kinetics under shock tube conditions 79−34292

organic compounds continued
simple molecules, conformation, electronic spectra, NDDO calcs. 79−85901
sisal wax, electronic conduction and persistent internal polarisation 78−80277
sisal wax, space-charge-limited currents, thermoelectret state 79−51901
sitosteryl esters, mesomorphic props. 79−90539
soap system, C_{18} mono-cis-unsaturated, lyotropic liq. cryst., X-ray diffr. and EPR meas., Monte Carlo simulation 78−94981
sodium 10-undecanoate, γ-ray induced polymerisation in aq. micelle solns. 80−61093
sodium 4-biphenylcarboxylate, room temp. phosphoresc., student demonstration 77−29
sodium acetate, methyl group, ^2H quadrupole coupling const. by high-resolution NMR spectroscopy 78−25563
sodium acetate trihydrate, cryst. struct. and bonding 77−24309
sodium acetate trihydrate, press. depend. of methyl tunnelling motion 80−10603
sodium acetate trihydrate, whisker growth on membrane in aq. soln. 78−30854
sodium acetylacetonate, anomalous dielec. behaviour, evidence for ferroelectricity 79−91390
sodium aluminium tartrate, β-particle effects on crystallisation from aq. solns. 77−36387
sodium ammonium tartrate, crysts., temp. depend. of elastic compliances at phase transition 79−15409
sodium ammonium tartrate, ferroelec., thermodynamic theory of phase transitions 77−90112
sodium ammonium tartrate, improper ferroelec. transition anomalies 78−19430
Sodium ammonium tartrate, L- and D-mol. energy difference, parity violation 78−25744
sodium ammonium tartrate, polarisation, improper ferroelec. transition 78−72477
sodium benzoylacetonate, dielec. props. and cryst. struct. 79−8099
sodium benzoylacetonate, piezoelectricity, transition of 70°C 79−8092
sodium benzoylacetonate, pyroelectric effect, peak near Curie temp. 79−8096
sodium benzoylacetonate, unit cell dimensions, X-ray determ. 79−69097
sodium biphthalate, cryst. struct., X-ray diffr. meas. 77−39577
sodium biphthalate, water of crystn. detection, PMR 77−35546
sodium carboxymethyl cellulose solns., rheodynamics of immersed rotating disc 77−15067
sodium cholate-decanol, soln., aggregate form., comp. and dynamics 80−45575
sodium decanoate-n-decanol-water system, lamellar G-phase, orientational-order, EPR investigation 80−24355
sodium decyl sulphate/water/decanol/Na_2SO_4, lyotropic mesophase, mag.-oriented, X-ray diffr. obs. 80−1921
sodium decylsulphate-Li_2SO_4-decanol-H_2O system, lyotropic liq. cryst., high resolution NMR 79−4243
sodium di-2-ethylhexyl suphosuccinate in H_2O-n-heptane micellar soln., neutron small-angle scatt. *(French)* 80−26059
sodium diethyldithiocarbamate, for improved removal of ^{60}Co from radioactive waste water 78−37415
sodium dodecyl sulfate, micelle form. in aq. soln., laser light scatt. 78−27825
sodium dodecyl sulphate: Gd^{3+}, micellar system, chain folding, ^{13}C NMR obs. 80−61158
sodium dodecyl sulphate, micelle shape and aggregation, conc. depend. 79−24833
sodium dodecyl sulphate, microemulsion, dynamical and structural props., by chem. physics method 79−79308
sodium dodecyl sulphate, solution, micellar, quasielastic light scattering, at low conc. limit 79−79307
sodium dodecyl sulphate micelles, diarylalkane intramolecular excimer formation, microfluidity and fluoresc. meas. 78−80791
sodium dodecyl sulphate micelles-ω-(α-naphthyl) dodecanoic acid soln. fluoresc. decay obs. 80−61158
sodium dodecyl sulphate NaCl aq. soln., micellar props., laser light scatt. exam. 78−92513
sodium dodecylsulfate, micellar solution, critical micelle concentraion for thermalized positronium formation 79−96345
sodium dodecylsulphate, micellar system, 1-methylpyrene quenching by Cu^{2+}, general kinetic model 80−32753
sodium dodecylsulphate micelle, intramicellar fluorescence quenching of $[1\text{-pyrenyl-}(CH_2)_n\text{-}N(CH_3)_3]^+Cl^-$ by cationic surfactant nitroxyl radical 80−9627
sodium ethanoate, solid, low energy photoelectron spectra 78−95656
sodium fluorescein dil. soln., luminesc. absolute quantum yields, thermal blooming method 78−72582
sodium fluorescein-rhodamine B, energy transfer in luminescent mixed solutions 80−103976
sodium formate, ^{13}C-enriched in D_2O, two-spin system, NMR relax. rate parameters 77−69720
sodium formate, vibr. spectrum, lattice modes 79−28759
sodium formate($-d_1$), far IR and IR absorpt. spectra, lattice mode assignment 77−85717
sodium hexanoate, micellar aggregation number, ^{13}C NMR chemical shift conc. depend. 80−48016
sodium hydrogen oxalate, crystal growth in silicate gel, X-ray diffr. and i.r. spectrum 77−4724
sodium hydrogen oxalate monohydrate, crystal struct. neutron diffr., deform. electron density analysis 78−10032
sodium hydrogen oxalate monohydrate, oriented single cryst., Raman spectra with very strong H-bonding 80−25359
sodium lauryl sulphate, aq. subcooled soln., acoustic phenomena during nucleate boiling 78−10181
sodium lauryl sulphate micelles, chlorophyll-a, soln., dilution expts., solubilisation anal. 80−35587
sodium lauryl sulphate-3,3'-diethylthiacarbocyanine iodide-rhodamine-6G, soln., premicellar region, energy transfer 80−20685
sodium magnesium aluminium oxdate, elastic consts., Debye temp. 79−82275
sodium n-alkanoates, long-chain, thermal and phase props. 77−62619
sodium naphthalate, room temp. phosphoresc., student demonstration 77−29
sodium octanoate, micellar aggregation number, ^{13}C NMR chemical shift conc. depend. 80−48016
sodium octanoate-decanol-water system, liq. cryst. C phase, struct. determ. using electron microscopy 77−47341

organic compounds continued
sodium octyl benzene sulphonate, micellar aq. soln., Cotton-Mouton effect in mag. field 79−16047
sodium oleate, frozen soln., NMR study of phase transitions 79−56617
sodium oscalate, neutron inelastic scatt. spectra in 2200-200 cm^{-1} range 80−70327
sodium oxalate:Cu^{2+}, anhydrous spin Hamiltonian and bonding parameters and orbital-reduction factors 80−60408
sodium oxalate, cryst. struct. rel. to those of SnC_2O_4, $Na_2Sn(C_2O_4)_2$ *(French)* 80−2004
sodium p-nitrophenoxide, enthalpies and related thermodynamic functions 79−42276
sodium p-octylbenzenesulphonate ionic micellar solns., neutron diffr. meas. *(French)* 78−44409
sodium pentadecyl sulphonate, lyotropic liquid crysts., X-ray study of domain structure *(Russian)* 77−62469
sodium propanoate, solid-state transitions, diffractometric and conductometric meas. 79−60507
sodium propionate, methyl group, ^2H quadrupole coupling const. by high-resolution NMR spectroscopy 78−25563
sodium salicylate, UV convertor layer, fluoresc. props. *(French)* 77−4676
sodium salicylate, vac. UV scintillators, characteristic props. at 253.7 nm 79−71525
sodium salicylate-toluene, singlet-singlet energy transfer in Manoxol OT-cyclohexane-water 80−9531
sodium stearate, Langmuir-Blodgett multilayers, comp. and transfer mechanism 80−80125
sodium tartrate tetrahydrate, gel-grown single crysts., charact. 77−90261
sodium tin oxalate, cryst. struct. rel. to those of $Na_2C_2O_4$, SnC_2O_4 *(French)* 80−2004
sodium undecanoate/water system, lyotropic liq. cryst. struct. change due to polymerisation of amphiphilic component 80−59386
sodium uranyl acetate, absorpt. spectra, MCD and natural dichroism, UV and visible 79−69853
sodium uranyl acetate, fluoresc., circ. dichroism 79−38598
sodium uranyl acetate-d_0,-d_q, cubic crysts., low temp. optical spectra *(Russian)* 78−92083
sodium valerate, mesophase, self-diffusion and spin-lattice relax. 79−69008
sodium-caesium acetate, molten mixture, elec. cond. and density 77−15613
sodium-napththalene, catalyst for polymerisation of methacrylamide by H transfer *(Japanese)* 78−95726
sodium-rubidium acetate, molten mixture, elec. cond. and density 77−15613
solar energy conversion, photoelectrochemical cells, chlorophyll sensitised reactions 80−7948
solid solutions, cell parameters calc. *(Russian)* 77−72687
solids, cryst. and amorphous, optical spectra, Urbach rule, struct. disorder effect 78−23479
solids, electron microscopic approach to struct. and reactivities 79−73077
solids, neat and Ar-diluted, secondary ion mass spectrometry 79−74441
solids, Raman phonon spectra, mol. motions 79−73921
solubility, correl. with mol. polarities *(Chinese)* 79−37847
solute rejection by reverse osmosis, regular soln. theory appl. *(Japanese)* 80−101041
solutes in liquids, conc. determ. by (n,α) and (n,γ) reacts., scintallation counting 80−35602
solutions, line struct. of broad absorption bands 79−54841
solutions, picosecond generation, spectral, polarisation characts. *(Russian)* 77−10918
solvents, trace H_2O determ., IR spectrophotometric method 78−31731
solvents in laser saturable absorber, nonlinear refr. index meas. at 1.32 μm 80−102758
somatostatin as excitatory transmitter in hippocampus 78−64973
sorbitol, crystallisation, thermal investig. 78−47257
sorbitol, relax. processes, optical probe obs. 79−47430
sorbitol, X-irrad., 4.2K, electron traps, alkoxy hyperfine coupling, ENDOR obs. 80−50863
soyabean oil, heat transfer from horizontal wire, AC and DC electric field effect 77−31202
spectra of diffuse reflection and photoluminesc. *(Russian)* 79−11447
spectral line narrowing of triplet state, in laser excited experiments 80−63703
spectroscopic identification, computer methods 78−88679
sphingomyelin-cholesterol interaction in oriented bilayers, X-ray diffr. exam. 77−44603
2,2'-spirobiindane derivatives, chiral, cholesteric order induction in nematic systems *(German)* 80−64884
spirohydrocarbons, strained, bond angles, interatomic distances, semiempirical and ab initio calcs. 80−95533
spiropyran, membrane, lipid effect on photoinduced potential change *(Japanese)* 78−31703
spiropyrane, triplet-triplet absorpt. by laser photoexcitation 77−10685
spiropyrans, photochromic, thermophotodegradation for autoprocessor reprography system 80−35555
spiropyrans, photochromic transform., dipolar cryst. form. 79−20386
spiropyrans, photochromic transformation by electro-optical chronography 79−57264
spiropyrans, polymer matrix effect on photochromism, thermal decolouration kinetics 80−76537
spiropyron solutions, nitro-substituted, electronic state participation in photochromy 80−81347
squalane, mol. orientation correls. with aliphatic chains, depolarised Rayleigh scatt. *(French)* 79−65885
squarate ion, reson. Raman scatt., Jahn-Teller effect 79−18190
squaric acid, 2-dimens., phase transition studied by Raman scatt. 79−82330
squaric acid, ^{13}C chemical shift tensor study of antiferroelec. second order phase transition 78−52462
squaric acid, antiferrodistortive phase transition, proton chemical shift tensor determ. 77−63300
squaric acid, antiferroelec., struct. phase transition mechanism 80−75969
squaric acid, $C_4H_2O_4$ and $C_4D_2O_4$, struct. transitions, theory 77−15585
squaric acid, critical slowing down of fluctuations at phase transition, ^{13}C spin-lattice relax. 80−44948
squaric acid, cryst., neutron diffr., bond lengths and angles, vibr. modes 77−76384

organic compounds continued
squaric acid, dielec. const. and PMR near struct. phase transition 79−10946
squaric acid, dielec. props., press. and temp. depend. 79−99815
squaric acid, ferroelasticity, elastic hysteresis loop and domain struct. 79−55814
squaric acid, H-bonded antiferroelec., cluster form., NMR obs. 79−28628
squaric acid, hydrostatic press. effect on phase transition, dielec. and dilatometric meas. 78−55941
squaric acid, layered, antiferroelec., phase transition mechanism 80−97210
squaric acid, neutron diffr. mol. and crystal struct. determ. 78−26557
squaric acid, second harmonic generation 79−46000
squaric acid, sp. ht. near phase transition 79−91389
squaric acid, struct. and Raman spectra 78−47311
squaric acid, struct. transition, US vel. meas. 78−79770
squaric acid, structural phase transition, US vel. meas. as function of temp. below and above T_c 79−14927
squaric acid, two dimensional antiferroelec., Brillouin scatt. at structural phase transition 80−71430
squaric acid, two-dimens., phase transition, elastic neutron scatt. 78−6155
squaric acid, two-dimens. antiferroelec., temp. depend. of order parameter, birefr. obs. 80−11351
squaric acid, two-dimens. phase transition, Raman scatt. study 80−71401
squaric acid, use as reagent in chem. microscopy 77−21450
squaric acid, vibr. props., 2D model 79−90735
squaric acid and deuterated derivative, vibrational study, IR and Raman spectra 78−92076
squaric acid-d_0,-d_2, 2-dimens. antiferroelec., dielec. props. and phase transitions, press. effects 79−95700
squarylium and cyanine-TCNQ dye Schottky-barrier sandwich cells 79−29468
squarylium dye films, surface photovolt. 80−75594
stanol/stenol ratio control process in Black Sea water and sediments 79−92549
starch, energy absorption distrib., spatially varying optical props. 77−75419
starch, glycerin impregnated, dynamic viscoelasticity *(Japanese)* 80−104203
starch, H_2O mol. transverse PMR, temp. effects *(German)* 77−60186
starch, hydrocarbon suspension, temp. depend. of electroviscous effect and dielectric parameters 79−79299
steam-gas system, joint use of nucl. and organic fuels 80−40807
stearate, proton spin-lattice relaxation in various phases *(Russian)* 80−97163
stearic acid, adsorption on CuO and MgO powders for surface area determ. 80−107636
stearic acid, aerosols, collection on micro-porous plates 79−64760
stearic acid, Au nucleation, ion bombard. effects 78−75965
stearic acid, etching on large single crysts. 77−89442
stearic acid, evaporating cryst. surfaces in vacuum 79−77740
stearic acid, heat of adsorpt. on sponge Fe, Fe_2O_3, CuO, adhesive wear 78−85193
stearic acid, insulator in MIM struct., electric dipole moment internal voltage meas. 79−76532
stearic acid, large single cryst. growth from organic soln. 78−31314
stearic acid, microscopic obs. of cleaved surface 79−95248
stearic acid, photoelectron escape depths determ. from X-ray photoelectron spectra 78−27368
stearic acid, single cryst., characterisation *(Japanese)* 79−46587
stearic acid, single cryst. growth mechanism 78−30562
stearic acid, submicronic aerosol, laser spectrometer for photoelectric determ. of conc. and dispersity 79−54244
stearic acid, vacuum evaporated film, for low-loss capacitors 80−71317
stearic acid cryst., etch pit obs. of dislocations 78−87676
stearic acid crystals grown from solution, spatial correlation between growth spirals and inclusions 80−96527
stearic acid film, DC cond. using unconventional electrode geometry, Poole-Frenkel effect 77−55631
stearic acid film, in MIM struct., AC cond. and dielec. props., freq. depend. 80−55030
stearic acid film, permittivity meas. using varying gap immersion method 78−6620
stearic acid films, evaporated, vac. effects 80−97435
stearic acid homogeneous vapour phase nucleation, diffusion cloud chamber obs. 80−79923
stearic acid layers, charge transport processes 78−84316
stearic acid monolayer, detection by harmonic generation of SAW 77−80688
stearic acid monolayers on HCl subsoln., surface diffusion by ^{14}C-tracer 78−34679
stearic acid multilayer films, dark and photo-generated dielec. response 77−72882
stearic acid multilayer films, lattice and carrier contribs. to dielec. polarisation 77−69775
stearic acid multilayers, dielec. props. 80−80404
stearic acid on Fe_2O_3 powder, heat of adsorpt., surface area meas., flow microcalorimetry 78−81974
stearic acid salts, pseudocryst. integral X-ray reflectance coeff., cation depend. 77−11437
stearic acid substrate, effect of glow discharge on nucleation characts. of Au 79−77963
stearic acid-based, layer periodic structure, prep. and optical props. 77−69199
stearic acid-calcium stearate monomolecular films, multilayer deposition 80−54550
stearyl alcohol, H bonding effects on skeletal optical and longitudinal acoustical modes 80−34914
steroids, ^{13}C chemical shifts, β-, γ- and δ-substituent effects 77−23509
steroids, mass spectra, computer-aided interpretation by pattern recognition methods 78−64898
steroids, maximum overlap. mol. orbitals versus ab initio HF-SCF-MO calc., dipole energy 78−9070
Δ^5-steroids, methyl group rot. barriers from ^{13}C relax. data, geometry effect 78−13626
steroids, mixtures, quantitative anal. by ^{13}C NMR 78−31716
sterol geochemistry of sediments from NW.Atlantic Ocean 79−74885
organic compounds continued
stibabenzene, struct., microwave spectrum and nucl. quadrupole coupling consts. 78−70817
stilben crystal scintillators, meas. of light pulse shapes 78−74534
stilbene:rhodamine-6Zh, luminesc. of adsorbed mols., excitonic energy transfer to surface 78−31255
stilbene, adsorbed rhodamine 6Zh, mol. cryst., role of excitonic and radiative mechs. of energy transport 80−108276
stilbene, cis→trans photoisomerisation rate const., direct meas. 80−30250
stilbene, cis and trans, transient spectra, radiative lifetimes and quantum yields 80−78640
stilbene, cis- and trans-, picosecond flash photolysis, intramol. charge-reson. transition obs. 80−7810
stilbene, cryst., rhodamine 6G luminesc. at surface 79−56831
trans-stilbene, cryst., triplet excitons, $S_0 \rightarrow T_1$ transition 78−76518
stilbene, depend. of phase transition temp. on thickness 78−26669
stilbene, diphenylpolyenes, photoisomerisation, 'phantom' photochem. singlet state, PPP SCF CI calcs. 78−73058
stilbene, direct photoisomerisation theory, from fluoresc. and absorption spectra 79−79262
trans-stilbene, disorder and degree of misorientation 78−38683
trans-stilbene, excited state orientational relax., sub-picosec. pulse obs. 79−50006
trans-stilbene, fluoresc. decay, picosecond anal. 79−31569
stilbene, horizontal radiationless transitions, singlet-pot. and rot. angle, semi-empirical model 78−42109
trans-stilbene, in glassy media, phosphoresc., heavy atom effects 80−55153
stilbene, monoanions, reson. spontaneous Raman spectra, vibronic interactions 79−3451
stilbene, photo excitation kinetics 77−23525
stilbene, polarisability optical anisotropy 79−72441
stilbene, ps photoisomerisation, time-resolved spectra obs. 79−57252
stilbene, pulsed electron excitation, triplet excitons, spectral and electrical investigations 80−92828
stilbene, radiolysis, electron transfer and protonation, vis. spectra, isomer effects 77−60085
trans-stilbene, scintillator used for pulse shape discrimination for alpha-gamma separation with trans-stilbene 78−13386
stilbene, single cryst. under pulsed electron excitation, elec. and spectral characts. 79−7838
trans-stilbene, soln., lifetime and anisotropic fluoresc., viscosity effects *(German)* 80−106352
stilbene, thin single cryst., IR spectra anal. Fermi-Davydov intensity distrib. 77−59577
trans-stilbene, time resolved fluoresc. in ps. regime 80−14164
stilbene, trans-, cis-forms, singlet excited state, picosecond dynamics 78−17677
trans-stilbene, two-photon absorpt. near maximum, three wave mixing expt. 77−58106
stilbene, two-photon absorptivities via three wave mixing 79−68416
trans-stilbene, two-photon excitation, phantom photochemical singlet, assignment 77−75247
stilbene anion radicals, photoinduced isomerisation, 77K 80−66818
stilbene aza-analogues, lowest excited states, INDO/S calcs. 80−95545
stilbene derivatives, electronic struct., frontier electron density, chem. reactivity *(Rumanian)* 79−72242
stilbene derivatives, fluoresc. props. 79−85992
stilbene derivatives, hyperpolarisabilities, four-wave mixing and SHG meas. 77−83925
stilbene derivatives containing 2-pyrazoline and 1,3,4-oxadiazole groups, spectral-luminescent props. 80−7394
trans-stilbene dianion, photolysis, intermediate struct., time-resolved reson. Raman spectra obs. 79−52695
trans-stilbene photoisomerisation, ps dynamics under collision-free conditions 79−91975
cis-stilbene radical anion, ESR, proton coupling const. 78−21948
stilbene soln., stimulated Raman scatt., self-focusing, rel. to Kerr const. *(German)* 79−61355
stilbene tunable narrowband subnanosecond dye laser, optical pumped 79−81445
stilbenes, prolate molecules in solvents, anisotropic fluoresc. *(German)* 80−69183
stilbenes, substituted, dipole moment calcs., in excited singlet state *(German)* 77−50367
stilbenes, substituted, donor-acceptor interaction effects on excited singlet state polarity *(German)* 80−91470
trans-stilbenes, triplet energy, substituents effect, singlet-triplet absorpt. and electrochemilum. obs. 79−81225
2-(stilbenyl-4)-5-phenyloxazole derivatives, electrolytic effects of substs. on electrochemiluminesc. intensity *(Russian)* 77−55834
stramonin-B, X-ray cryst. struct. anal. 79−77589
streptomycin oxime selenate tetrahydrate, antibiotic, cryst. and mol. struct. 78−24028
strontium acetate hemihydrate:Cu^{2+}, EPR of cryst. 78−19312
strontium acetate hemihydrate:Mn^{2+}(Cu^{2+}), EPR, spin Hamiltonian anal. and unit cell symmetry 80−29603
strontium calcium tartrate mixed crystal, growth in silica gel 77−48325
strontium calcium tartrate tetrahydrate, crystals grown by ion diffusion through silica gels, exam. of preps. 79−52102
strontium calcium tartrate tetrahydrate, gel grown mixed single crystals, defect characterisation 80−2027
strontium formate:Mn^{2+}, cryst., e.p.r., spin Hamiltonians 77−4552
strontium formate dihydrate:Cr^{3+}, optical absorption spectrum 80−50380
strontium formate dihydrate, H bonds, deuteron mag. reson. meas. 77−85593
strontium maleate tetrahydrate, cryst. struct., H-bonding scheme 80−96505
strontium malonate, cryst. struct. 77−59003
strontium propionate monohydrate, cryst. struct. 77−76385
strontium tartrate tetrahydrate Co^{2+} electronic absorpt. spectrum 78−92098
strontium uranyl tetraformate hydrate, struct. determ., orthorhombic unit cell, UR spectrum *(French)* 78−22705
structural changes induced by UV irradiation *(German)* 79−42100
structure elucidation algorithm (ASSEMBLE), computer construction 79−18104
structures, topological code, modified Morgan algorithm 80−58122

organic compounds continued
strychnine, quaternary, poisoned squid giant axons, block of Na conductance and gating current 79−83746
styrene, and isotopic forms, IR and Raman spectra, normal vibr. assignments 77−18930
styrene, anions, in condensed media, electronic spectra 79−22723
styrene, cationic polymerisation by $SnCl_4$ in presence of C black 78−68891
styrene, fluoresc., ns time resolved emission spectra 77−6822
styrene, Penning electron and photoelectron spectra, relative intensities comparison 79−81237
styrene, plasma polymerisation, polymer struct., NMR 77−25264
styrene, plasma polymerisation in glow discharge, thin film IR and free radical EPR obs. 80−2964
styrene, polymerisation, photoinitiation by aliphatic azo cpds., EPR obs. 78−80746
styrene, styrene-β-d_2, 288 nm electronic absorpt. spectra, vibr. assignment 79−13738
styrene, thermal polymerization, PMR obs. 80−3342
styrene, two photon absorptivity, ion cyclotron reson. photodissoc. spectra, CNDO/S-CI-perturbation theory 80−74123
styrene, UV Raman spectra, reson. effect in photoreactive states 80−106326
styrene(-butadiene), polymer reactions, below glass transition, limting conversions 78−88632
styrene (-d_3, d_5, d_8), fluoresc. quantum yields and lifetimes, 298 and 77K 79−59500
styrene anions, electron affinities, transition energy, comparison for gaseous liquid and solid 80−29731
styrene derivatives, ^{13}C NMR spectra, Hammett eqn. appl., undergraduate experiment 79−84913
styrene derivatives, hyperpolarisabilities, four-wave mixing and SHG meas. 77−83925
styrene divinylbenzene, viscosity meas. during radical copolymerisation 80−3344
styrene monomer, polymerisation by glow discharge method, formation mech. *(Japanese)* 80−61094
styrene polymerisation in RF discharge, discharge power effect 79−43581
styrene-β-d_2, IR and Raman spectra, vibr. assignments 79−13711
styrene-ethylbenzne system, separation by liq. membrane permeation, operating parameters influence on selectivity 79−87871
styrene-ethylene glycol, oligomeric liquid mixtures, transition to, polymer systems, thermodynamics 78−20048
styrenes, 4-substituted, NMR substituent parameters, pattern recognition interpretation 80−58284
styrolene, nonlinear third-order electric susceptibility 78−74944
substituent π-conjugative effects, ab initio calcs. 79−45633
substituted benzoic acids, PMR study 80−39881
substituted phenolic compounds, effect on dark charge exchange process in photoactive pigment electrophotographic imaging system 80−62758
subtilisin charge-relay system, electrostatic pot. map, STO transferable bond calc. 80−3571
succinamic acid, X-irrad., primitive radn. damage, ESR, ENDOR 78−3352
succinic acid, partially deuterated, ^1H and ^2H distant ENDOR obs. of mol. struct. parameters 80−23445
succinic acid and its alkaline salts in aqueous soln., Raman and IR spectra *(French)* 80−32723
succinic acid diamide, mol., PMR and IR spectra, easy polarisable H-bonds 79−31516
succinonitrile, crystn. kinetics and shapes 77−31617
succinonitrile, defects in plastic phase, positron annihilation obs. 80−11504
succinonitrile, dendritic growth rates, evidence for a universal law 79−4496
succinonitrile, orientationally disordered crystal., mol. orientation 78−34448
succinonitrile, phase transition, Raman spectrosc. obs. using low-temp. sample holder 78−86342
succinonitrile, plastic, diffuse scatt., hard-core correl., weak-graph method 80−49137
succinonitrile, plastic and liq., NMR, ^{13}C spin-lattice relax. and ^{14}N linewidth 79−24227
succinonitrile, plastic cryst., orientational order, depolarised Rayleigh scatt. method 78−75612
succinonitrile, plastic cryst. and liq., Kerr effect for relax. kinetics 78−59768
succinonitrile, plastic cryst. with steric hindrance, dielectric const. 77−24779
succinonitrile, plastic crystal, HF electro-optical Kerr effect, orientation depend. 77−24822
succinonitrile, plastic phase, mol. motions correlation times, incoherent neutron scatt. 80−49138
succinonitrile, plastic phase, mol. reorientation and rotational isomerization, anal. of elastic incoherent struct. factor 78−22674
succinonitrile, plastic phase, molecular reorientation, rotational isomerism, incoherent neutron scatt. study 79−51021
succinonitrile, undercooled, analysis of dendritic growth 78−75970
succinonitrile+VO^{2+}, reaction, CN stretching freqs., bonding effects 77−16820
sucrose, aq. solns., stirred, transient diffusion through glass membranes, thermodynamics 78−92507
sucrose, crystn. rate in impure solns., influence of non-sugar and colouring substance quantity 80−100767
sucrose, mathematical model of crystn. rate in pure solns. 80−49151
sucrose, polycryst., NMR, selection of nonprotonated C resonances 80−50201
sucrose, single cryst., absorption spectrum of electron traps, pulse radiolysis obs. 80−93369
sucrose, single cryst., X-irrad. at 4.2K, trapped electrons and electron traps characts. 79−78037
sucrose benzoate host for recording volume phase holograms 77−632
sucrose crystal formation, and growth, effect of same metallic impurities 80−100768
sucrose loading into plant sieve tubes, role of pH gradient and membrane ATPase 77−52757
sucrose polydisperse aerosol number and mass conc. meas. by elect. aerosol anal. 80−108753
sucrose solution, holographic interferometric meas. of liq. diffusion 79−37861
organic compounds continued
sucrose-NaCl-H_2O, phase diagram determ., appls. in cryobiology 78−15777
sucrose-water system, supersaturation evaluation, in cryst. growth from soln. 79−46584
sugar, cryst., triboluminesc. kinetics 77−8669
sugar, mechanical relax. time, determ. from tribolum. 77−1173
sugar, mechanoluminesc., cryst. size depend. 79−38685
sugar, optical rotatory power, polarisation modulation meas. 79−21803
sugar, triboluminesc. kinetics 77−77306
sugar, triboluminescence and cryst. fracture dynamics 80−50437
sugar, triboluminescent intensity, fracture in air and liq. anhydrous diethylether 78−19582
sugar char, EPR in transition range 80−34751
sugar chars, heat treatment, EPR rel. to temp., A-centers 78−43639
sugar chars, heat treatment, EPR rel. to temp., spin centres 78−48036
sugar crystal, triboluminesc. kinetics and mech. relax. 77−73178
sugar crystals under stress, fracture-initiation time from triboluminesc. 77−59065
sugar solution, boiling, natural convection mechanisms on horizontal tube 77−24396
sugars, detect. in HPLC systems using polarimetry, refractometry and optical rot. 78−48734
sulphate cellulose prod. waste water, radiation treatment *(Russian)* 80−55688
sulphides, d-orbital participating in bonding, positron ang. correlation 79−97979
sulphides, interacting mechanisms with Fe and Cu surfaces rel. to friction and lubrication behaviour 80−45546
N-sulphinylaniline, microwave rot. spectra, torsional freq., dipole moment and internal rot. barrier 78−973
sulpholan, molecular solid, laboratory frame and rotating frame spin-lattice relax., pulsed NMR meas., phase transitions obs. 80−93197
sulphones, d-orbital participitation in bonding, positron ang. correlation 79−97979
sulphones, group electronegativities, empirically estimated from geometrical and vibr. data 79−81300
sulphonic acids, adsorption and orientation on Al_2O_3, tunnelling spectroscopy obs. 78−34707
sulphonium cations, tertiary, produced by field desorption, collisional activation spectra 78−56946
sulphononaphthols, rapid pH and $\Delta\mu H^+$ jump by short laser pulse 80−16709
sulphonyl compounds, H-bonding by methyl groups, Raman spectra obs. 79−24320
sulphophthalein dyes in aq. soln., reson. Raman spectra 79−89678
sulphorhodamine $G+I^-$, physical and chem. kinetics competition, fluoresc. quenching obs. 79−43567
5-sulphosalicylic acid, dideuterate, $D_5O_2^+$ obs., neutron 77−35543
sulphur compounds, antiwear additives in oils, wear testing of steel surfaces, XPS obs. 77−36668
sultams, characteristic band in IR region, Raman obs. 78−29784
supercrit. hydrocarbons radiolysis, electron reaction rate const./diffusion coeff. ratio 80−101033
supersaturated solns. of ethanol and water, bubble nucleation, contact angle effects 79−94702
surface active agent effects on fracture toughness and dynamic strength of steel *(Russian)* 78−56812
surface contaminants, anal. by plasma chromatography-mass spectroscopy, and Raman microprobe technique 80−108773
surface monolayers on atm. water droplets, sources and effects 78−69412
surface treating of Fe, effects of triboelectric charging 78−60188
surfactant molecules reorientation on electrode surface, electrochem. kinetics 80−45522
surfactant-water liquid crystal phases, review 80−28913
sym-triazine, Landau mean field description, second-order phase transition, soft modes 80−108434
sym-trioxane, phase transition, polarised Raman spectra obs. 80−84742
synthesis on primitive Earth, volcanic processes 77−64434
tanane, crit. behaviour near ferroelec.-ferroelastic transition 78−52459
Tanane, dielec. and electrooptic meas. near ferroelec. transition 79−33587
Tanane, ferroelec. ferroelastic transition, X-ray and optical expts. 78−15110
Tanane, ferroelec. mol. cryst., strong piezoelec. coupling 80−75942
TANOL, free radical, spin flopping transition, temp. depend., mag. anisotropy energy 80−54890
TANOL, linear chain antiferromagnet, long-range order, magnetisation, PMR 78−23266
TANOL, linear chain-like organic free radical, EPR line widths 78−39404
D(+)-tartaric acid, absolute struct. factor determ. 77−65973
D-tartaric acid, cryst. struct., 35-295K, by X-ray diffr. 80−22369
dl-tartaric acid, radiation products, ESR-ENDOR OBS. 80−55682
tartaric acid, triboluminescence and cryst. fracture dynamics 80−50437
tartaric acid, troboluminescent intensity, fracture in air and liq. anhydrous diethylether 78−19582
tartaric acid and tartrates, inhibition of dendritic growth of Ag electrodeposits *(French)* 78−87894
tartaric acid salts, and deuterated forms, irrad.-crysts., primary reactions, EPR obs. 80−3370
tartrate, $Na[K_{1-x}(NH_4)_x].C_4H_4O_6.4H_2O$, dielec. relaxation 80−108152
tatrakis(ethyl isocyanide) platinum(II) tetracyanoplatinate(II), cryst. data, X-ray powder anal. 80−2003
TBAA, liq. cryst. cpds. synthesis and smectic B-smectic B transition 77−15562
TBAA, smectic B phase, deform. vibrs. of alkyl chains, Raman spectra obs. 77−39531
TBACA, chiral, ^{14}N NQR of smectic phases 78−59749
TBACA, chiral, smectic C* and H* phases, mol. orientational ordering, ^{14}N NQR study 80−75152
TBBA, achiral, ^{14}N NQR of smectic phases 78−59749
TBBA, biaxial liq. cryst., orientational order, ^{14}N NQR meas. 77−32288
TBBA, biaxial smectic phases, orientational order, neutron scatt. and NQR results 78−91225
TBBA, cryst. phase, struct. at 20°C, butyl side chains disorder *(French)* 77−58998
TBBA, cryst. phase, struct. at 20°C, comparison with smectic B *(French)* 77−58999
TBBA, dielec. const. in cryst. and smectic phases 79−78607

organic compounds continued
TBBA, liq. cryst., evidence for cybotactic cluster pretransition formation, X-ray diffr. meas. 78−10179
TBBA, liq. cryst., metastable phase, thermodynamic props., differential scanning calorimetry meas. 78−94985
TBBA, liq. cryst., orientational order in tilted smectic phases, high resolution neutron quasi-elastic scatt. 77−80413
TBBA, liq. cryst., smectic A-nematic transition, cybotactic cluster form., X-ray obs. 78−95138
TBBA, liq. cryst., smectic C layer thickness meas. by X-ray scatt. 78−94986
TBBA, low temp. phase, inelastic coherent neutron scatt. exam. 78−26429
TBBA, mesophase identification by X-ray diffr., review 80−100166
TBBA, nematic liq. crystal, self diffusion coeffs., NMR spin echo 77−31789
TBBA, new cryst. phase, calorimetric meas. 79−51254
TBBA, order parameters in nematic and smectic phases, X-ray diffr. meas. 79−94874
TBBA, phase transitions involving ordered biaxial phases, X-ray diffr. study 79−95136
TBBA, phonon dispersion curves in cryst. and smectic phases 79−86863
TBBA, self-diffusion and undulation modes, high resoln. neutron scatt. 77−11471
TBBA, smectic, freq. dispersion of proton Zeeman relax. time and quadrupole reson. of ^{14}N 77−62468
TBBA, smectic, proton ^{14}N nuclear double reson. 77−58947
TBBA, smectic, spin-lattice relax., self-diffusion, mol. rot. 78−35055
TBBA, smectic and cryst. phases, far IR absorpt., struct. and dynamical props. 77−84636
TBBA, smectic C to smectic A transition, crit. exponent, neutron diffr. obs. 78−95143
TBBA, smectic liq. cryst., crystalline at liq.-cryst. phases phonon modes, coherent neutron inelastic scatt. study *(French)* 79−51216
TBBA, smectic liq. cryst., polarised Raman spectra, 90-300K, 0-400 cm^{-1} 77−12383
TBBA, smectic phases, orientational order, ^{14}N NQR and double NMR obs. 78−94974
TBBA, smectic polymorphism *(French)* 77−35470
TBBA, smectic VI and H phases, orientational order, temp. depend. 79−46555
TBBA, smectic VI and H phases, orientational order 77−84648
TBBA, smectic-A, self-diffusion, neutron incoherent scatt. law 78−83726
TBBA, temp. depend. of deuteron NMR splittings in nematic and smectic phases 79−32898
TBBA, US absorpt. and dispersion at nematic-smectic-A transition 79−82287
TBBA liquid crystal, monoclinic cell parameters of solid, smectic and metastable phases, temp. dependence 80−70122
TBBA liquid crystal, self diffusion coeffs., neutron diffr. and NMR study 80−19689
TBBA mesophases, mol. orientational order 79−37619
TBBA/4-n-pentylphenyl-4-(4-cyanobenzoyloxy)benzoate, mixture, possibility of smectic A-smectic A transition 79−95132
TBBA/n-hexyl-4′-n-dodecyloxy-biphenyl-4-carboxylate, mixtures, orthogonal smectic B to tilted smectic B (smectic H) transition 79−94881
TBP-n-paraffin extractant for Th reactor fuel reprocessing, radiation dose 77−70315
TBP-n-paraffin extractant for Th reactor fuel reprocessing, degradation 77−70316
TBPA, liq. cryst., smectic F phase, X-ray diffr. obs. 80−44122
TCNB, electron donor-acceptor complex, triplet state phophoresc. kinetics, MIDP obs. 78−62839
TCNB, heat capacity, 10-300K 77−11702
TCNB complexes, hole mobility, photocurrent meas., 260-300K 78−60161
TCNB-HMB complex high density excitation effects on fluoresc. 79−1782
TCNB-MTHF EDA complex, sensitized biphotonic radical anion formation 77−40556
TCNB-pyrene 1:1 charge transfer complex, heat capacity, 10-300K 77−11702
TCND, IR and Raman spectra, vibr. anal. 79−36630
$TCNE^{-}$, anionic spin probe for ESR of amphiphilic liq. cryst. 78−75548
TCNE, electron donor-acceptor complexes, EPR *(German)* 78−55187
TCNE, hole drift mobility, temp. depend. and anisotropy, photocond. meas. 80−80314
TCNE, K salt, in nematic liq. crystal solvent, ion pairing, EPR spectra 78−73020
TCNE, lattice dynamics 79−28055
TCNE, Raman active fundamental vibrations, revised assignment 77−68049
TCNE, semiempirical CNDO calcs. of electronic struct. and absorpt. spectra 78−995
TCNE aromatic donor/acceptor complexes, reson. Raman excitation and absorpt. profiles, model theory 77−18982
TCNE electron donor/acceptor complexes, photoionic dissoc., photocurrents 77−14502
TCNE-benzene, charge transfer theory, Mulliken population, ab initio calc., multiconfiguration scheme 80−106392
TCNE-benzene, charge-transfer complex, change of C≡N and C=C band intensities 77−88448
TCNE-naphthalene π-π three mol. complexes, UV-visible spectra assoc. const., extinction coeff. determ. *(German)* 77−35464
TCNE-naphtheene π-π three mol. complexes absorpt. spectra, assoc. consts., extinction coeff.s *(German)* 77−35465
TCNE-paraxylene, charge-transfer complex, change of C≡N and C=C band intensities 77−88448
TCNE-stilbene complexes, and analogs, charge transfer energy calc. isomer prediction 78−21854
TCNE-substituted benzene complexes, isomers, stability, rel. to charge transfer band intensity 77−68051
TCNQ:Rb, 3:2 complex, cryst. struct. at 113K 79−99169
$TCNQ_2$-TEA, quasi 1-D cryst., interaction between electronic and vibr. states 77−52102
$TCNQ^{0}$, crysts., extraordinary exciton polaritons in refl. spectra, macroscopic dielec. theory 77−89715
$TCNQ^{-}$, ESR probe for phospholipid membrane polar head motion study *(French)* 80−45865
$TCNQ^{-}$, electron affinity, compound states 77−65530

organic compounds continued
$TCNQ^{x}$, (x=0, −1, −2), elec. dipole polarisability, π-electronic components, SCF calcs. *(Russian)* 78−84204
TCNQ, ab initio SCF LCAO band struct. calc. 80−70608
TCNQ, adsorption on metal oxide surface, strength and distrib. of electron donor sites 78−84055
TCNQ, and anions, PRDDO method using Slater orbital basis 79−764
TCNQ, anions, screened INDO model, appl. to photoelectron, optical, Raman spectra 79−765
TCNQ, charge transfer complexes, changes in valence electronic structure 80−7477
TCNQ, cryst., metallic refl., damping theory 77−16294
TCNQ, dimer gas model 78−87926
TCNQ, elastomeric complexes, doped with pure TCNQ, elec. conductivity 78−84220
TCNQ, elect. struct. determ., CNDO parametrisation and UPS data 77−1350
TCNQ, electron donor-acceptor complexes, EPR *(German)* 78−55187
TCNQ, electron mobilities from 210 to 350K using transverse photocond. meas. 79−19618
TCNQ, electron- and phonon-polaron effects in valence and cond. bands 77−76757
TCNQ, electron-mol. vib. coupling 77−15782
TCNQ, electronic struct., HAM/3 semiempirical calcs. 79−6866
TCNQ, enthalpy of sublimation and vapour press. meas. 80−92661
TCNQ, exciton surface polaritons at room temp. 79−47476
TCNQ, generalised Wigner lattices and band motion effects 80−24815
TCNQ, infinite stacks, all valence electron band struct. 78−39001
TCNQ, lattice softening mechanism 80−6481
TCNQ, lattice vibrs., temp. depend., NQR obs. 79−38402
TCNQ, metallic reflection band, vibronic struct. 78−19502
TCNQ, nonlinear 3rd-order elec. susceptibility calcs. 79−54786
TCNQ, optical IR antireson. absorption, characts. rel. to cryst. parameters 77−77183
TCNQ, Raman scatt. and charge transfer 77−69817
TCNQ, resonance Raman spectra 79−56787
TCNQ, salt, $(NMe_3H)(I)(TCNQ)$, semicond. 'metal-like' complex, optical props. 79−95761
TCNQ, salt, DBTTF-TCNQ, elec. resistivity and thermoelec. power meas. 80−20193
TCNQ, salt, $Me\phi_3As(TCNQ)_2$, nonOhmic elec. cond., tunnelling model and expt. 79−99558
TCNQ, semiempirical CNDO calcs. of electronic struct. and absorpt. spectra 78−995
TCNQ, single cryst., photocond., electron donor gas effects 77−20357
TCNQ, single crystal, exciton surface polaritons, attenuated total reflection spectra 79−91460
$TCNQ(perylene)_2$, cryst. struct. determ. 78−75651
$(TCNQ)_2$, dimeric interactions, MO calcs., applicability to crystal struct. 80−75215
$(TCNQ)_2$ MEM, crystal struct. of 1:2 complex, at −160°C 78−10031
$(TCNQ)_2TEA$, refl. spectra 77−90154
$(TCNQ)_5^{2-}(DBzPE)^{2+}$, cryst. struct., elec. cond. and thermoelec. power 77−72606
$(TCNQ)_5^{4-}(DEPA)_2^{4+}$, cryst. struct., elec. and mag. props. 77−72605
$(TCNQ)(TTF)_{1-x}$-$(TSeF)_x$, quasi 1-D metal, mag. susceptibility, temp. depend. 77−8267
TCNQ 1:3 radical salt, $[Pt(dipy)_2]^{2+}[TCNQ]_3^{2-}$, cryst. struct. 78−63741
TCNQ addition compounds, high-temp. cond. and impurity bridge struct. 77−15838
TCNQ alkali salt, spin-Peierls transition 80−29395
TCNQ alkali salts, charge transfer enhanced IR absorpt. spectra 77−28558
TCNQ alkaline salts, phase transitions, vibronic intensity enhanced IR spectra 78−23441
TCNQ and its salts, XPS meas. surface effects 78−11075
TCNQ anion, one-electron Hamiltonian method in SCF theory 78−9055
TCNQ anion radical charge transfer salts, semiconducting behaviour 79−11118
TCNQ anion radical salt, $[(C_6H_5)_3PCH_3]_{1-x}^{+}[(C_6H_5)_3AsCH_3]_x^{+}(TCNA)_2^{-}$, phase transition and phase diagram 77−76555
TCNQ anion radical salts, adsorpt. on Al_2O_3, EPR and electronic spectra 77−72776
TCNQ anion radical salts, phase transition $\alpha\gamma \rightarrow \beta\gamma$, volume change 78−26684
TCNQ anion radical salts, phase transitions, solid solns., thermodynamic props. 77−47571
TCNQ anion radical salts, solid solns. phase transition, heats of mixing 78−47519
TCNQ bipyridine salt, single cryst. cond. for symm. and asymm. donors 77−32003
TCNQ charge transfer complexes, elec. cond. 79−38058
TCNQ complex, 1,2-di (N-ethyl-4-pyridinium) ethylene $(TCNQ)_4$ elec. resist. and thermoelec. power meas. 80−107777
TCNQ complex, $(C_{13}H_{21}N_2S_2)^{+}(C_{12}H_4N_4)_2$, cryst. and mol. struct. 77−62514
TCNQ complex, Adn $TCNQ_2$, nuclear-spin-lattice relaxation 80−39886
TCNQ complex, dibenzotetrathiofulvalinium $(TCNQ)_2$, elec. resist. and thermoelec. power meas. 80−107777
TCNQ complex, ethyltriphenylphosphonium $(TCNQ)_2$, elec. resist. and thermoelec. power meas. 80−107777
TCNQ complex, [1,2-bis(1-benzyl-4-pyridinio)ethane]$^{24}(TCNQ)_5^{2-}$, cryst. struct. and elec. cond. 79−19236
TCNQ complex formed from cation (methyl-l-N-ethyl benzimidazolium)$^{+}$ conductivity transition 80−10954
TCNQ complex salts, mag. props., ESR meas. 79−56603
TCNQ complex salts, optical absorption spectra 79−15486
TCNQ complex salts, temp. depend. of elec. cond., CPA approach 77−8078
TCNQ complex salts, with pyridinium cations, cond. and structural studies 79−87087
TCNQ complex with 5-phenyl-[1-thiol]-3-selenol-2-thione, charge-transfer salt, cryst. and mol. struct. 80−33986
TCNQ complex with N-methyl-Z-ethylthiazoline, cryst. and mol. struct. 78−10034
TCNQ complex with o-phenanthroline, orientational disorder 77−72603
TCNQ complexes, disordered, thermodynamics of random exchange models 80−103826
TCNQ complexes, low temp. sp. ht. 77−51514

organic compounds continued
TCNQ complexes, Qn(TCNQ)$_2$, NMePh.TCNQ, and Li$^+$TCNQ$^-$, extrinsic and intrinsic mag. susceptibility 78−43556
TCNQ complexes with dipyranylidene and dithiadipyranylidene, high cond. investigs. and related props. 78−6368
TCNQ complexes with ferrocenes, charge transfer type, struct. and mag. props. 80−24439
TCNQ complexes with N-methyl derivatives of pyridine, cond. and thermoelec. power meas., band model anal. 80−10952
TCNQ complexes with pyridine, polarised IR refl. spectra, evidence for electron-vibr. coupling 79−47448
TCNQ compounds, electron-proton couplings, dimensionality of triplet excitons 78−91974
TCNQ compounds adsorbed on alumina, inelastic electron tunnelling spectroscopy 77−42367
TCNQ derivatives, intramol. charge transfer, electronic absorpt. spectra obs., electron density calcs. 77−65490
TCNQ derivatives, substituted, org. cond. with low-symmetric acceptors, cond. behaviour rel. to cryst. struct. 78−6365
TCNQ dimers, extended Huckel hamiltonian supermol. CNDOS calcs. 80−27953
TCNQ donor-acceptor complexes, refl. and absorpt. spectra 79−73965
TCNQ film, energy loss spectra of low energy electrons 78−19116
TCNQ intercalated 2H-NbSe$_2$, elec. resistivity temp. behaviour anomaly *(Russian)* 80−10953
TCNQ ion radical salt, DECA(TCNQ)$_2$, IR absorpt. spectra obs. of first-order transition 80−71397
TCNQ ion-radical polymeric salts prep. and props. *(Russian)* 78−76061
TCNQ ion-radical salts, strain sensitivity 79−65461
TCNQ ion-radical salts, struct. disorder 79−99885
TCNQ salt, 1,1′-diethyl-2,2′-cyanine-[TCNQ]$_2$, electric and mag. props. 79−42523
TCNQ salt, 1-ethyl-3′-methyl-2,2′-quinoselenacyanine-(TCNQ)$_2$, EPR linewidth, angular and temp. depend. 78−76313
TCNQ salt, 1-methyl-3′-ethyl-2,2′-quinoselenacyanine-[TCNQ]$_2$, two-dimens. ferromag., EPR 77−16148
TCNQ salt, 3,3′-diethyl-6,6′-dimethyl-2,2′-thiacyanine-(TCNQ)$_2$ EPR linewidth, angular and temp. depend. 78−76313
TCNQ salt, (1,2,-bis(di-n-alkyl-4-pyridinium) ethene)$^{2+}$ (TCNQ)$_x^{2-}$, cryst. struct. and elec. props. 79−56209
TCNQ salt, (1,3,-bis(di-n-alkyl-4-pyridinium) propane)$^{2+}$ (TCNQ)$_x^{2-}$, cryst. struct. and elec. props. 79−56209
TCNQ salt, (DEPE)$^{2+}$(TCNQ)$_4^{2-}$, elec. and mag. props. of two crystallographic form 77−28166
TCNQ salt, (DEPE)$^{2+}$(TCNQ)$_4^{2-}$, elec. props., semicond. and metallic phases 78−34826
TCNQ salt, (DEPE)$^{2+}$ (TCNQ)$_4^{2-}$, semicond. form., cryst. struct., X-ray diffr. meas. 77−4094
TCNQ salt, (Me1-NEtBz)$^+$(TCNQ)$_2^-$ 79−47087
TCNQ salt, (N(CH$_3$)$_3$H)(I)(TCNQ), elastic props., semicond. transitions 79−95072
TCNQ salt, (N(CH$_3$)$_3$H)(I)(TCNQ), proton spin-lattice and spin-spin relax. times 79−8065
TCNQ salt, (N-methylphenazinium)$_x$(phenazine)$_{1-x}$, 1 band filling, carrier mogility and disorder effects 80−24904
TCNQ salt, (NMe$_3$H)(I)(TCNQ), one-dimens. semicond. with metal-like cond. 80−24909
TCNQ salt, (NMP)$_{0.5}$(phenazine)$_{0.5}$ TCNQ, transport props. 80−24891
TCNQ salt, (NMP)$_x$(Phen)$_{1-x}$(TCNQ), band filling and disorder 78−87968
TCNQ salt, (NMP)$_x$(phen)$_{1-x}$(TCNQ), thermoelectric power temp. depend. 80−15548
TCNQ salt, (TMA$^+$)$_3$(I$_3^-$)(TCNQ$^-$)$_2$(TCNQ^0), struct., phys. props. and lattice distortion evidence 78−6305
TCNQ salt, (TSeF)$_x$(TTF)$_{1-x}$-TCNQ, struct., elec. and mag. props., review 80−20158
TCNQ salt, acridinium (TCNQ)$_2$ low temp. heat capacity, Debye temp. 80−2180
TCNQ salt, acridizinium, one-dimens. cond., permittivity 25 to 60 GHz, 4.2K 78−88248
TCNQ salt, Ag.TCNQ, cryst. struct. 80−70186
TCNQ salt, alkali transition metal, elec. cond. and phase transition 78−43370
TCNQ salt, bis(dipyridyl)platinum(II)-TCNQ, crystal struct. and EPR, TCNQ radical dimerisation 77−80490
TCNQ salt, Cs$_2$(TCNQ)$_3$, elec. cond. and elastic const., mol. bending *(Korean)* 78−23090
TCNQ salt, Cu-TCNQ thin film between Cu and Al electrodes, elec. switching and memory phenomena 79−65562
TCNQ salt, DECA (TCNQ)$_2$, struct., phys. props. and irreversible phase transition 78−6273
TCNQ salt, decamethylferrocenium, monomeric and dimeric, optical and EELS study 80−100660
TCNQ salt, dibenzo-TTF-TCNQCl$_2$, one-dimens. mag. semicond., mag. and elec. props. 80−88601
TCNQ salt, HF-TCNQ in acetonitrile, absorpt. spectra, 200-1200 nm 77−83617
TCNQ salt, HFTTF-TCNQ, phase transitions, calorimetry study 79−51253
TCNQ salt, HMTSeF-TCNQ, Hall effect, temp. and press. depend. 77−35929
TCNQ salt, HMTSF-TCNQ, lattice phase transitions and conduct. anomalies obs. 77−1226
TCNQ salt, HMTTF-TCNQ, electron-electron interactions, mag. susceptibility and optical reflectivity 77−81104
TCNQ salt, HMTTF-TCNQ, Madelung energy, intermol. charge transfer, 1-dimens. disorder 79−7572
TCNQ salt, HMTTF-TCNQ, metallic organic charge transfer complex, chemical prep. and phys. props. 78−2471
TCNQ salt, HMTTF-TCNQ, quasi-one-dimensional organic conductor, mag. susceptibility meas. 78−6508
TCNQ salt, HMTTF-TCNQ, sp. ht., 30 to 80K 80−24614
TCNQ salt, HMTTF-TCNQ, structure, metallic cond. and thermopower 77−8080
TCNQ salt, HMTTF-TCNQ, three-dimens. ordering, Ginzburg-Landau model for Peierls instability 80−20160
TCNQ salt, K$^+$TCNQ$^-$, cryst. struct. above and below 122°C transition 77−35541
TCNQ salt, K$^+$TCNQ$^-$, spin polarised band struct., effective Coulomb repulsion 77−15734

organic compounds continued
TCNQ salt, K$^+$TCNQ$^-$, temp. depend. of dynamic nucl. polarisation enhancement of protons 78−6601
TCNQ salt, K$^+$TCNQ$^-$ particles, light scatt., absorpt. spectra 79−24332
TCNQ salt, K-TCNQ, ^{14}N NQR temp. depend. rel. to Peierls transition 79−82892
TCNQ salt, K-TCNQ, cryst. struct. *(French)* 78−43006
TCNQ salt, K-TCNQ, energy gap, electron-phonon interaction, IR spectrum 78−15167
TCNQ salt, K-TCNQ, EPR linewidth, ang. and freq. depend. 80−80591
TCNQ salt, K-TCNQ, high and low temp. phases, dielec. const. 80−34844
TCNQ salt, K-TCNQ, single crystal, charge transfer band interpretation, refl. spectrum obs. 80−25353
TCNQ salt, K-TCNQ, spin-Peierls system, paramag. susceptibility, Heisenberg chains 79−38299
TCNQ salt, MeDABCO(TCNQ)$_2$, elec. cond. and IR and visible spectra meas. 79−42526
TCNQ salt, MeDABCO(TCNQ)$_2$, optical, elec., and mag. props. 80−65539
TCNQ salt, MEM(TCNQ)$_2$, dielec. const. obs., DC and microwave cond. obs. 80−59963
TCNQ salt, MEM(TCNQ)$_2$, phase transition electronic struct. interpretation 80−24781
TCNQ salt, MEM(TCNQ)$_2$, phase transitions, elec. cond., ESR, mag. susceptibility study 80−24981
TCNQ salt, Mn(TCNQ)$_2$, mag. props. 77−85558
TCNQ salt, MTPA (TCNQ)$_2$, IR refl., dielec. function and cond. 80−34924
TCNQ salt, N,N′-di(n-propyl)-4,4′-bipyridylium^{2+}(7,7,8,8,-TCNQ)$_4^{2-}$, cryst. struct., elec. props. 79−27971
TCNQ salt, N-methyl-N-ethyl-morpholinium-(TCNQ)$_2$, spin-Peierls transition 79−82803
TCNQ salt, n-methyl-n-ethylmorpholinium, unpaired electron states, IR refl. study 80−75491
TCNQ salt, N-n-butyl-quinolinium (TCNQ)$_2$, ESR spectrum fine struct. splitting 80−44904
TCNQ salt, N-propyl-quinolinium(TCNQ)$_2$, defect conc. depend. phase transition 80−44577
TCNQ salt, NH$_4$-TCNQ, crystal structure and phase transition 78−91330
TCNQ salt, NMeQn(TCNQ)$_2$, phase transition, role of acetonitrile solvent 78−60119
TCNQ salt., NMeQn(TCNQ)$_2$, role of solvent in phase transition, thermal anal. and transport props. 79−33312
TCNQ salt, NMP$_{0.63}$phenazine$_{0.37}$TCNQ, mag. susceptibility, 0.03-4.2K 80−25191
TCNQ salt, NMP-TCNQ, electronic struct., SCF calc., total energy polarisation effects 80−15469
TCNQ salt, NMP-TCNQ, realisation of disordered Hubbard model, dielec. props. 78−79917
TCNQ salt, NMP-TCNQ, X-ray diffuse scatt. rel. to charge transfer 77−80496
TCNQ salt, NPQn (TCNQ)$_2$, neutron irrad. induced defect concentration depend. phase transition 80−29449
TCNQ salt, polyvinylcarbazole-TCNQ complex, elec. cond. meas. 80−34456
TCNQ salt, pyridine (TCNQ)$_2$, phase transition at 80K investig. and interpret. 78−6530
TCNQ salt, pyridinium (TCNQ)$_2$, low temp. mag. phase transition, ESR study 80−25139
TCNQ salt, Qn(TCNQ)$_2$, decrease of electronic coherence length by impurities 79−69501
TCNQ salt, Qn(TCNQ)$_2$, defect depend. of dielec. permeability and cond. 79−78608
TCNQ salt, Qn(TCNQ)$_2$, defect depend. of dielec. permeability and conductivity 79−91340
TCNQ salt, Qn(TCNQ)$_2$, Heisenberg antiferromag. chain for low temp. thermometry and cooling, EPR expts. 79−63217
TCNQ salt, Qn(TCNQ)$_2$, non-Ohmic cond. 80−20169
TCNQ salt, Qn(TCNQ)$_2$, non-ohmic elec. cond. 79−4553
TCNQ salt, Qn(TCNQ)$_2$, nonlinear electric field depend. 79−78088
TCNQ salt, Qn(TCNQ)$_2$, nonlinear transport 79−87089
TCNQ salt, Qn(TCNQ)$_2$, one-dimens. spin glass with antiferromag. exchange, Knight shift meas. 80−25231
TCNQ salt, Qn(TCNQ)$_2$, organic transfer salt, impurity effects on cond. 77−76799
TCNQ salt, Qn(TCNQ)$_2$, phase transition, paramag. shifts and PMR line width *(Russian)* 77−43892
TCNQ salt, Qn(TCNQ)$_2$, temp. and freq. depend. of nucl. relax. rate 78−6594
TCNQ salt, Qn(TCNQ)$_2$, thermoelec. power and cond., large Coulomb repulsion model 80−24893
TCNQ salt, Qn (TCNQ)$_2$, configurational entropy, thermoelec. power meas. 80−34432
TCNQ salt, quinilinium, one-dimens. cond., permittivity 25 to 60 GHz, 4.2K 78−88248
TCNQ salt, quinolinium, electron spin location, elec., mag., and thermal props. 80−25189
TCNQ salt, quinolinium (TCNQ)$_2$, mag. chain double resonance study, deuteration 80−25250
TCNQ salt, quinolinium (TCNQ)$_2$, random-exchange Heisenberg antiferromag. chain, sp. ht., 0.07-5K 78−14976
TCNQ salt, quinolinium (TCNQ)$_2$, transport props. 80−24891
TCNQ salt, Rb$_2$TCNQ$_3$, cryst. struct. refinement 78−55859
TCNQ salt, Rb$^+$TCNQ$^-$, cryst. struct. of new form 77−24311
TCNQ salt, Rb-TCNQ, ^{14}N NQR, Zeeman perturbation study, charge transfer 78−39438
TCNQ salt, Rb-TCNQ, electronic spin-lattice relax. time 77−51939
TCNQ salt, TEA(TCNQ)$_2$, Hall effect and thermopower sign anomaly 79−56205
TCNQ salt, TEA (TCNQ)$_2$, anomalous conductivity, conductivity transitions 80−15508
TCNQ salt, tetramethylhexamethylenediammonium-TCNQ-iodine, elec. and mag. props., struct., specific heat 80−24898
TCNQ salt, TMPD-TCNQ , mag. excitation gap attributed to spin polarisation instability 78−31086
TCNQ salt, TMTSF-DMTCNQ, cond. and thermopower meas. 80−20165

organic compounds continued
TCNQ salt, TMTSF-DMTCNQ, mag. susceptibility meas. under press. 80−29521
TCNQ salt, TMTSF-DMTCNQ, metallic state at low temp. under pressure 79−91033
TCNQ salt, TMTSF-TCNQ, microwave cond. at 35 GHz 80−24963
TCNQ salt, TMTTF-TCNQ, mag. gaps, EPR meas. 77−8390
TCNQ salt, TSeF-TCNQ, anal. of harmonic microwave mixing 80−44635
TCNQ salt, TSeF-TCNQ, CDWs, X-ray study 79−28301
TCNQ salt, TSeF-TCNQ, doped with TTF-TCNQ, phase transitions 77−80732
TCNQ salt, TSeF-TCNQ, electrical conductivity, press. depend. 77−51729
TCNQ salt, TSeF-TCNQ, nonlinear transport in pinched one-dimensional CDW system 77−89754
TCNQ salt, TSeF-TCNQ, Peierls transition and CDW ordering, X-ray study 80−20101
TCNQ salt, TSeF-TCNQ, short-range ordering investigated by XDE 80−59652
TCNQ salt, $TTF_{1-x}TSeF_x$-TCNQ, mol. substitutional disorder 80−24438
TCNQ salt, [1,2-di(N-methyl-4-pyridinium)ethane]$^{2+}$(7,7,8,8-TCNQ)$_4^{2-}$, struct. and elec. cond. 77−80491
TCNQ salt, [1,3-di(N-pyridinium)propane]$^{2+}$(7,7,8,8,TCNQ)$_4^{2-}$, struct. and elec. cond. 77−80492
TCNQ salt, [1,4-di(N-quinolinium-methyl)benzene]$^{2+}$ $(TCNQ)_3^{2-}$, cryst. struct., elec. anisotropy 77−35542
TCNQ salt, $[Pt(NH_3)_4]^{2+}[(TCNQ)_2]^{2-}$ cryst. and mol. struct. and EPR props. 78−55860
TCNQ salt films, textured TCNQ and NMP-TCNQ, cond. and dielec. props. 77−51733
TCNQ salt in aqueous media, electrochem. behavior 80−6976
TCNQ salt QCTCNQ, strong Coulomb correlations 79−56203
TCNQ salt with MDCA cation, first order phase transition 79−73122
TCNQ salts, (N-methyl pyridine) $(TCNQ)_2$, struct. and cond., 280 to 340K 79−23955
TCNQ salts, aminopyridinium $(TCNQ)_2$, elec. and mag. props., 4.2 to 300K 80−24889
TCNQ salts, anomalous infra-red activity and the determination of electron-molecular vibration coupling constants 80−25389
TCNQ salts, bond lengths and charge transfer *(French)* 77−80493
TCNQ salts, charge transfer and cond. 80−20164
TCNQ salts, charge transfer and ionic bonding 77−39558
TCNQ salts, chem. trends and stabilisation of nearly one-dimens. state 78−10328
TCNQ salts, complex, optical absorption meas. 79−4824
TCNQ salts, complex, with aromatic donors, interchain coupling and disorder 78−6314
TCNQ salts, complex, with symmetric and asymmetric donors, transport and mag. props. 78−6315
TCNQ salts, conducting, Raman spectra, estimation of degree of charge transfer from vibrational frequencies 80−50344
TCNQ salts, $Cs_2(TCNQ)_3$, quasi-one-dimens., IR spectra, electron-vibr. interaction 78−88309
TCNQ salts, direct current conductivity and thermo-electric force, 4-400K *(Hungarian)* 79−56251
TCNQ salts, elec. and optical props. 79−73498
TCNQ salts, elec. cond. spectrum fine struct. 80−96884
TCNQ salts, electron arrangement in ground state, optical spectra interpretation 78−47715
TCNQ salts, electron localized and band motion, IR spectra 77−66487
TCNQ salts, electron tunnelling 78−47769
TCNQ salts, electron-vibrational interaction consts. 79−28054
TCNQ salts, ETPP $(TCNQ)_2$ and DEPE $(TCNQ)_4$, thermoelec. power 80−59966
TCNQ salts, hexamethylenetetraheterofulvalene donors in systematic mol. modifications 78−91680
TCNQ salts, ionene polycation-TCNQ salts, elec. cond. rel. to polycation struct. 80−34428
TCNQ salts, IR, X-ray electron spectra, tetrathiotetracene $(TCNQ)_2$ cond. investig. 77−44005
TCNQ salts, K(TCNQ), $Ba(TCNQ)_2$ and $Ca(TCNQ)_2$, electronic absorpt. spectra, vibronic struct., charge transfer bands 79−24331
TCNQ salts, lattice vibr. freezing, Kohn anomalies, lattice struct. 77−15401
TCNQ salts, $Li^+(TCNQ)^-$, $Cu^+(TCNQ)^-$ and $Cu^+(TCNQ)_2^-$, low temp. EPR of impurity reson. 77−85548
TCNQ salts, mag. props. 77−43869
TCNQ salts, microdomain model for struct. rel. to cond. 77−11902
TCNQ salts, $Mn(TCNQ)_2$ and hydrates, mag. and elec. props. 79−82767
TCNQ salts, model, 3D Coulomb coupling and charge ordering 78−60075
TCNQ salts, model for cond. 78−10426
TCNQ salts, modulated struct., dynamical processes, X-ray and neutron scatt. 79−95155
TCNQ salts, n-methylacridium $(TCNQ)_2$, 2,2′bipyridinium $(TCNQ)_2$ and $Qn(TCNQ)_2$, with asymmetric donors, mag. susceptibility, 0.035-4.2K 80−25190
TCNQ salts, NMR relax. time mag. field depend. *(Russian)* 79−61254
TCNQ salts, PMR, electron-proton couplings, local susceptibilities 79−82883
TCNQ salts, polymer composites, elec. cond. 80−20157
TCNQ salts, proton nucl. relax. meas. 80−20484
TCNQ salts, $Qn(TCNQ)_2$, $NMeAd(TCNQ)_2$, dielec. const. and cond. 78−79985
TCNQ salts, $Qn(TCNQ)_2$ and $Cs_2(TCNQ)_3$, surface magnetism obs. 78−6561
TCNQ salts, $Qn(TCNQ)_2$ and $Cs(TCNQ)_3$, surface magnetism 78−2703
TCNQ salts, $Qn(TCNQ)_2$ and N-propyl-$Qn(TCNQ)_2$, low temp. mag. susceptibility, neutron irrad. effects 80−60311
TCNQ salts, $Qn(TCNQ)_2$ and $NMeAd(TCNQ)_2$, dielec. const. and elec. cond. 78−60116
TCNQ salts, $Qn(TCNQ)_2$ impurity effects on electronic coherence length 79−73500
TCNQ salts, quasi-one-dimensional, Wigner cryst. model 78−47273
TCNQ salts, quasi-one-dimensional organic crystals, charge transfer, Raman scatt. *(German)* 79−28731
organic compounds continued
TCNQ salts, Rb^+TCNQ^-, and TMB^+TCNQ^-, triplet exciton dipolar splitting tensors rel. to mag. susceptibility 77−62839
TCNQ salts, simple, triplet exciton obs. by ESR 78−10373
TCNQ salts, sp. ht. meas., 0.2-300K, extended Hubbard model *(French)* 77−35710
TCNQ salts, spin density distribs., estimation from EPR fine struct. and cryst. data 79−11347
TCNQ salts, surface magnetism, magnetisation field curves meas. 77−59428
TCNQ salts, thermoelec. power, two-band model 79−4551
TCNQ salts, TSF-TCNQ, and HMTSF-TCNQ, low temp. fast neutron irradiation, elec. cond. meas. 80−59964
TCNQ salts, vibr. and electronic spectra 79−45704
TCNQ salts, Wigner crystal model 79−42008
TCNQ salts, with disorder, singularities in density of electronic states 77−8006
TCNQ salts 78−6356
TCNQ salts of 1:1 stoichiometry, kinetic models of form. 79−46596
TCNQ salts with alkali metals, intensities of IR absorpt., electronic transfer magnitude 78−6691
TCNQ salts with alkali metals, optical absorpt. spectra of small particles 78−19505
TCNQ salts with asymmetric donors, mag. susceptibility 78−60264
TCNQ salts with asymmetric donors, transport props. 78−60115
TCNQ salts with asymmetric donors, transport props. 79−23953
TCNQ salts with heterocyclic amines and hydroquinone form. via redox reaction 80−26013
TCNQ salts with NMP and Rb, elec. cond., temp. and press. depend. *(Japanese)* 78−43366
TCNQ solids, quasi-one and -two dimensional materials crystal growth *(Japanese)* 80−35073
TCNQ solt, $CS_2(TCNQ)_3$, cond. and thermopower meas., deep level acceptor model 79−42529
TCNQ-ϕ_4DTP, chemisorbed O_2 effects on mag. susceptibility 80−15679
TCNQ-bipyridinium salt, chain stabilisation, cond. enhancement 78−51978
TCNQ-DIP Φ_4, electronic diffusion coeffs. in chains, proton spin-lattice relax. and dynamic nucl. polarisation 80−25241
TCNQ-DTT, cryst. data 79−51094
TCNQ-HMTSeF, large Hall effect obs. below room temp. 78−6364
TCNQ-HMTSeF, nucl. spin relax. obs., diffusive character of response function and interchain coupling 78−10797
TCNQ-HMTSeF, polarised single cryst. reflectance obs. and one-dimens. behaviour interpret. 78−6690
TCNQ-HMTSeF, press. effects on mag. props., review 78−6505
TCNQ-HMTSeF, X-ray diffuse scatt., one-dimens. distortion in phonon spectrum and interpret. 78−10144
TCNQ-HMTSF, de Haas-Shubnikov oscills. 80−10956
TCNQ-HMTSF, irrad. effects on resist. 21K 78−60113
TCNQ-HMTTF, metallic state stabilisation at low temp. under press. 78−30911
TCNQ-HMTTF, struct. evidence of CDW 78−51912
TCNQ-K, dielectric function of 1-dimens. Hubbard model 79−60740
TCNQ-K, X-ray exam. of phase transitions 78−55933
TCNQ-M_2P charge transfer complex, triplet spin excitons, EPR spectra 78−80192
TCNQ-Na, X-ray exam. of phase transitions 78−55933
TCNQ-NMP, disordered, paramag. susceptibility 78−10645
TCNQ-NMP, elec. cond. temp. depend. 77−85203
TCNQ-NMP, incomplete charge transfer, NMR relax. and line-shift meas. 80−20485
TCNQ-NMP, metal-insulator transition theory based on generalised Hubbard model 78−18966
TCNQ-NMP, nucl. relax. and spin dynamics 78−52370
TCNQ-NMP, reduced Coulomb repulsion, intrachain and interchain polarisation 77−85162
TCNQ-NMP, transport props. 80−24891
TCNQ-NMP type crystals, low temp. behaviour of paramag. susceptibility *(Russian)* 77−85127
TCNQ-perylene, electronic absorpt. spectra, vibronic struct., charge transfer bands 79−24331
TCNQ-potassium, dynamic nucl. polarisation exam., temp. depend. 78−39447
TCNQ-pyrene complex, evaporated layers and single crysts., photocond. *(Russian)* 78−6416
TCNQ-Rb, X-ray exam. of phase transitions 78−55933
TCNQ-TMTSF, conducting salt, cryst. and mol. struct. 77−24307
TCNQ-TMTTF, conducting salt, cryst. and mol. struct. 77−24308
TCNQ-TMTTF, press. effects on mag. props., review 78−6505
TCNQ-TMTTF phases comparison with TTF-TCNQ, ESR 77−40116
TCNQ-TSeF:TCNQ-M, thermopower determ. 78−47772
TCNQ-TSeF, crit. behaviour at electronically driven struct., phase transition 77−80767
TCNQ-TSef, Drude optical edge, press. depend. 79−19882
TCNQ-TSeF, mag. suscept. meas. 78−56287
TCNQ-TSeF, model for phase transition and low-temp. phase 77−47734
TCNQ-TTF, chemisorbed O_2 effects on mag. susceptibility 80−15679
$TCNQF_4$, charge transfer complexes and salts, C(1s) and N(1s) XPS anal. of shake-up satellites 77−14492
TCOOB, smectic A and C liq. cryst., A-C phase transition, diffuse-cone model description 79−86674
TDOBAMBCC, chiral smectic C liq. cryst., dielec. consts., electroclinic effect 78−94980
TEA$(TCNQ)_2$, elec. cond. and thermoelec. power under hydrostatic press. 80−11024
TEA $(TCNQ)_2$, mixed electronic-vibr. states in far IR spectra, dielec. const. *(Russian)* 77−36249
technetium glucoheptonate, prep. using formamidine sulfinic acid 80−51252
teflon gas injected into shock layer flow, hypersonic flow past blunt body 80−74998
tellurium-thiourea compounds, Mossbauer investig. of ^{129}I, quadrupole interactions and bonding 77−48111
tellurophene(-d_4), cryst., struct., phonon spectrum, exciton splittings, assignments 77−81088
TEM, appl. to organic crystals 80−24327
teracene, photoionisation of triplet excitons 77−62837
terbium chelate solns., fluoresc. quenching by voltage appl. 79−87498
terbium ethyl sulphate, mag. and thermal props. 79−7971

organic compounds continued
p-terephthal-bis-aminocinnamate, smectic phases, orientational order, ^{14}N NQR and double NMR obs. 78−94974
terephthal-bis-n-alkylaniline, homologous series, prep. and mesomorphic props. 78−26436
terephthal-bis-p-p'-butylaniline, pretransitional anomaly, US obs. 78−75818
terephthalate liquid crystals, vibr. spectra, vol. struct. 78−18547
terephthalylidene-bis-4-n-alkylanilines, smectic F planes 78−42902
terephthalylidene-bis-(4-n-alkylanilines), smectic polymorphism, calorimetric study 80−88307
terephthalylidenebis-4-n-pentylaniline, smectic F phase, characterisation and struct. 79−86707
terephtylidene-bis-(4-nalkylanilines), smectic polymorphism, miscibility meas. 79−86678
ternary gas mixture, natural convection, naphthalene sublimation appl. 80−6511
ternary liquid mixtures, evaluation of US vel. 80−38201
ternary liquid mixtures, nonlinear effects with high amplitude US prop. 78−51613
terpenes, conc. meas. in Adirondack Mountains pine forest 78−32185
terpenes, IR absorption bands of α- and β-pinenes above forests 80−12539
terpenes, methyl groups internal rotation, ^{13}C spin lattice relaxation times and force field calcs. 80−74255
p-terphenyl:anthracene, impurity effects on positron lifetime spectrum 78−43954
p-terphenyl:pentacene, mol. mixed cryst., picosec. coherent transients obs. 79−46013
p-terphenyl:pentacene, optical coherence and resonance decay 77−24859
p-terphenyl, and PBD mixtures, tunable narrow bandwidth 2 MW lasers 79−41378
p-terphenyl, crit. slowing down at struct. phase transition, high resolution neutron spectroscopy 79−82329
p-terphenyl, cryst., DC photocond. in near UV, carrier generation 79−82644
p-terphenyl, cryst., double injection and electrolum. 80−97342
p-terphenyl, cryst., exciton phosphoresc. at 300K 80−108277
p-terphenyl, cryst., highly excited states decay, mag. field effects 78−10962
o-terphenyl, cryst. struct. determ. by neutron diffr. 79−42046
p-terphenyl, cyclic hydrocarbon admixtures, positronium lifetimes meas. 78−19595
p-terphenyl, cyclohexane soln., solute excited state form. kinetics in pulse radiolysis 79−79263
o-terphenyl, dipolar solutes, reorientational motions, dielectric relax. below glass transition 80−19706
p-terphenyl, dye laser, flashlamp pumped driven by Marx-bank generator 77−19311
p-terphenyl, far IR absorption spectra, 300-1.3K, phase transition obs. *(French)* 77−90140
terphenyl, hydrogenised, flow model in helical channel of solar receiver *(French)* 79−24910
o-terphenyl, liq. and glassy, dynamics of dissolved ferrocene, Mossbauer obs. 80−55000
terphenyl, liq. cryst., thermal diffusivity, Rayleigh scatt. obs. 78−94977
p-terphenyl, long range order at phase transition, neutron diffr. exam. 77−1228
p-terphenyl, lowest excited singlet states, polyexcited CI calc. 79−772
p-terphenyl, melting temp. and latent heat 79−55869
p-terphenyl, narrow bandwidth pulsed UV laser, 3350 to 3450 Å 80−38032
terphenyl, ortho-, para-, meta-, total neutron cross sections for subthermal energies 78−74779
p-terphenyl, phase transition, heat capacity meas. 79−46801
p-terphenyl, polycrystalline thin film, elec. cond., temp., thickness and elec. field depend. 79−65572
p-terphenyl, positronium form. at elevated temps. 77−89473
p-terphenyl, radiolysis, ion-pair clusters and excited-state yields 77−29024
p-terphenyl, Raman scatt., order-disorder phase transition 78−43841
p-terphenyl, Raman spectra, struct. transitions 79−19870
p-terphenyl, saturated vap. press., absorpt. and fluoresc. spectra 79−76442
p-terphenyl, single cryst., delayed fluoresc., mag. field depend., 130-300K 79−69879
p-terphenyl, substituted, dye laser and spectral characts., output power, conversion efficiency 80−23681
p-terphenyl, substrate for epitaxial crystn. of polyesters 79−61521
p-terphenyl, triplet exciton annihilation and triplet spin relax. 80−29792
terphenyl, two photon absorptivities, CNDO/S-CI calc. with second order time depend. perturbation eqns. 80−74122
p-terphenyl, vac. UV scintillators, characteristic props. at 253.7 nm 79−71525
p-terphenyl, valence electronic structure 79−72360
p-terphenyl, vap., electron energy loss spectra rel. to lasing 78−29947
p-terphenyl−pentacene, optical dephasing, optical mixing-detected ps photon echoes obs. 78−71155
p-terphenyl(d_{14}), Brillouin scatt. at room temp. 80−71433
p-terphenyl anion radicals, photoisomerisation, local heating effects 78−85179
p- terphenyl cryst., low lying single state 80−97320
p-terphenyl dye laser, tunable uv emission, KrF laser pumped 77−7117
p-terphenyl host, breakdown of anisotropic Lorentz approximation 78−5276
p-terphenyl in benzene, triplet state resonance Raman spectroscopy 79−6944
p-terphenyl in cyclohexane, 1 MW laser, conversion efficiency and tuning curve 77−58323
p-terphenyl polycrystalline layers, AC cond. 80−44746
p-terphenyl solns., mag. field effects on scintillation pulse shape, ion pair recomb. 77−16835
p-terphenyl vapour, spectral, fluoresc., photochem. and laser props. 80−106344
p-terphenyl-naphthalene derivs. mixed mol. cryst., positronium formation 78−91647
terphenylene mesophase, X-ray diffr. meas. 79−41946
2,2':6.2''-terpyridine, photoelectron spectra, SCF LCAO calcs. 78−33551
tert-butyl chloride, separation of collision-induced from intrinsic mol. depolaris. Rayleigh scatt., C-Cl bond optical anisotropy 78−27244

organic compounds continued
tert-butylchloride-d_9, extended diffusion with internal rot., NMR test 79−31549
tertiary alkylamines as sensitisers for charge injection from Se, and as charge carriers in n-dodecane 79−91116
tertiary amines, lasing action feasibility, excited state absorpt., two step photoionisation 80−23682
tertiary phosphine oxide+aliphatic alcohol, pπ-dπ conjugation, electronegativity and H-bond energy 78−82863
tertiarybutylisocyanide-borane, vibr., rot. consts., moment of inertia, microwave spectra obs. 80−32706
testosteron, dielectric props. under UV excitation 80−6912
testosterone, dielectric transient response following UV-irradiation 80−51166
tetra(trifluoromethyl) germanium, gas and liq., IR and Raman spectra, normal coord. anal. *(German)* 79−72315
1-(2,3,4,6-tetra-0-acetyl-β-D-glucopyranosyl)-2,3-(2R)-epoxypropane, molecular and cryst. struct. 78−25746
tetra-4-tert-butylphthalocyanine-H_2 mol. in solid tetradecane, luminesc. 77−18965
tetra-alkylammonium halide interionic potential models and far IR spectra 79−33689
tetra-alkylammonium halides, far IR spectra, interionic pot. energy 78−27217
tetra-alkylammonium salts, effect on props. of lipid bilayers of different surface charges 77−21489
tetra-ammine cadmium acetate:Cu, EPR dynamical effects 79−61204
tetra-chloroethylene, working fluid for Rankine cycle engine, waste heat recovery from ceramic tunnel kilns 79−52955
tetra-glycine, cyclic, mol. polaris. and diamag. suscept. calcs. 80−63858
tetra-isoamyl phosphonium bromide hydrate, clathrate, cryst. struct., X-ray study 80−64987
tetra-l-alanine, cyclic, mol. polaris. and diamag. suscept. calcs. 80−63858
tetra-n-butylammonium halide-$MnCl_2$ melts, density, elec. cond., and viscosity 80−24631
tetra-n-butylammonium halides in benzene, chloroform, CCl_4, far IR spectra, ion-ion, ion-mol. interactions 80−60562
tetra-n-butylammonium iodide $NiCl_2$ melts, densities and kinematic viscosities 79−77793
tetra-n-butylammonium picrate, soln. in benzene, field dissoc. effect on ion pairs 79−91061
tetra-n-pentylammonium salts, molten, thermodynamic props., cation struct. 79−55639
2,3,4,5-tetraacetoxymercurithiophene, dark-field imaging, computer simulation 80−100151
2,3,4,5-tetraacetoxymercurithiophene, dark-field TEM image simulation, rel. to S atom image 78−70229
tetraalkoxysilanes, prep. of SiO_2 films by activation pyrolysis 79−87583
tetraalkylammonium bromide, solid and liq., Raman spectra, longitudinal acoustic vibr. mode, mol. dimensions of ions 78−31183
tetraalkylammonium bromide soln., conductance and viscosity, temp. and concentration depend. 80−6531
tetraalkylammonium halides, mol. reorientation, spin lattice relax. time study 80−18875
tetraalkylammonium halides in methanol, struct., IR spectra 77−23500
tetraalkylammonium hydroxide intercalates with TaS_2, NbS_2, prep. and struct. 80−79752
tetraalkylammonium tetrahalometalates, opt. lifetimes rel. to thermal transitions 77−28608
tetraalkyllead in air, natural source 79−2367
tetraalkyltin compounds, heats of mixing meas. 78−15693
1,4,5,8-tetraazanaphthalene radical ion pairs, EPR spectra 79−50051
tetrabenzo-[a,cd,j,lm]perylene thin films, high photoresponse, O_2, N_2 and SF_6 effects 77−32036
tetrabenzo[a, cd, j, lm]perylene evaporated film, crystn., time depend. as function of purity 80−88449
tetrabiomethane, electronic struct., Xα SW calcs. 80−102447
tetrabrommethane, surface melting, transition from atomically smooth to rough struct. 77−76648
1,2,4,5-tetrabromobenzene, lattice vibrs., Raman and far IR spectra 78−76444
1,2,4,5-tetrabromobenzene, structural phase transition, Raman and IR spectra meas. *(French)* 77−66503
meso-1,2,3,4-tetrabromobutane, IR and Raman spectral studies 80−32722
1,1,2,2-tetrabromocyclopropane, IR and Raman spectra 79−41170
1,1,2,2-tetrabromoethane, dil. soln. in benzene, dielec. relax. study 80−29679
tetrabromoethane-EBBA, binary liq. cryst. system, two-phase premelting, NMR obs. *(Russian)* 78−30743
tetrabromoformaldazine, mol. struct., electron diffr. determ. 79−45858
tetrabromomethane, adsorption on Fe (100), AES, LEED, work function, and thermal desorption meas. 80−39422
tetrabromomethane, excimer laser photolysis, luminesc. from Br_2, Br, and C_2 79−39184
tetrabromomethane, fine struct. resolution in Raman-active fundamentals 79−42967
tetrabromomethane, in disordered phases, IR active mode Raman line shape, dipole-dipole interaction 80−9603
tetrabromomethane, liq. and plastic cryst., rot. Brownian motion, far IR absorpt. 77−36234
tetrabromomethane, monoclinic monocryst., polarised Raman spectra *(French)* 80−93302
tetrabromomethane, plastic phase, neutron diffr. obs. and theory 79−77533
tetrabromophthalic anhydride-hexamethylbenzene, long-lived emission of charge-transfer cryst. 79−33752
tetrabromophthalic anhydride-naphthalene, complex cryst., visible spectra, singlet-triplet absorpt. 79−19897
tetrabutoxytitanium, thermal decomposition in MgO-Al_2O_3-SiO_2 glass, effect on crystallisation 78−87627
tetrabutylammonium, selective uptake of ions into PMMA gel 78−35719
tetrabutylammonium bromide, aq. soln., thermal diffusion, heat of transport *(French)* 78−18808
tetrabutylammonium dicarbollyl cobaltate in nitrobenzene+MgU_2 in water system, electrolyte dropping electrode investig. 77−25279
tetrabutylammonium europium yttrium isothiocyanate, conc.-depend. electron-phonon coupling, and self-quenching 80−60657
tetrabutylammonium halides, solutions in organic solvents, IR spectra and struct. 79−38534
tetrabutylammonium hexatungstate, cryst. struct. *(German)* 78−63740

organic compounds continued
tetrabutylammonium iodide, alcoholic soln., repulsion phenomena in thin layers 80−107619
tetrabutylammonium iodide, in aq. proline soln., elec. conductance investigation 80−10692
tetrabutylammonium iodide/I solid/liquid electrolyte interface, impedance study 80−26031
tetrabutylammonium iron tetraiodide, structural and mag. props., ^{57}Fe and ^{129}I Mossbauer spectra 79−61282
tetrabutylammonium picrate, elec. cond. in nematic (smectic) 4-alkyloxy-4′-cyanobiphenyls, temp. (conc.) depends. *(German)* 78−55966
tetrabutylammonium tetrahalomanganate, phosphoresc. lifetimes in fused salts and solids 78−72573
tetrabutylammonium tetraphenylborate in nitrobenzene+LiCl in water systems, electrolyte dropping electrode investig. 77−25279
tetracene:pentacene, exciton migration, picosec. meas. 78−15207
tetracene:pentacene, pressure-induced phase transition, mag. field effect on guest fluoresc. 79−33083
tetracene:pentacene, thermally activated heterofission, fluoresc. 77−85787
tetracene, amorphous film, TSC meas., carrier traps 80−2496
tetracene, cryst., fluoresc. decay time, synchrotron radiation excitation 77−4675
tetracene, cryst., hole drift mobility, photoexcitation 77−1444
tetracene, cryst., prompt fluoresc., mag. field depend. 77−85788
tetracene, cryst., singlet exciton fission rate const. RYDMR spectra meas. 78−91619
tetracene, cryst., solid-state transitions, Raman spectra, prompt fluoresc. in mag. field 79−99865
tetracene, cryst., triplet exciton pair kinematics, diffusion model, prompt fluoresc. decay 78−79931
tetracene, cryst., triplet exciton pairs, EPR spectra 77−43906
tetracene, disordered, vapour deposited on glass substrate, fluoresc. and energy transfer 80−84761
tetracene, disordered solid layer, absorpt. spectra 80−93417
tetracene, double quantum external photoelec. effect 79−87564
tetracene, excimer luminesc. spectra, 4.2-300K 79−87478
tetracene, fluoresc. fading curve of lowest triplet state 79−36691
tetracene, fluoresc. time decay, exciton interaction depend. 77−8618
tetracene, fluorescence, effect of weak external electric field *(Russian)* 78−80416
tetracene, impurity in organic glass, hole burning fluoresc., struct. 79−31588
tetracene, in MIM struct., depletion layer, LF capacitance meas. 79−56328
tetracene, in p-terpheny. mixed cryst., low temp. optical phase relax. obs., mechanism 77−52112
tetracene, in p-terphenyl, polarisability calcs., from Stark meas., anisotropic Lorentz approx. breakdown 78−5276
tetracene, intramol. dynamics and energetics in isolated ultracold state 79−98144
tetracene, intrastate scrambling in large mol. bound level struct. 80−63696
tetracene, monocrystal, photoelectron emission, quantum yield spectral dependence, in near-threshold region *(Russian)* 79−69954
tetracene, noncryst., localised valence states in forbidden gap 78−72113
tetracene, optical obs. of charge transfer 78−35199
tetracene, organic insulator action spectra of photocurrent 80−34482
tetracene, photoluminescence spectra, 4.2-300K, phase transition and excitons 79−4847
tetracene, polycryst., SCL currents and trap distrib. 79−1603
tetracene, press.-induced phase transition, fluoresc. mag. field depend. 77−1728
tetracene, radical cation, EPR, acidic surface anisotropic rot. diffusion 78−27095
tetracene, single cryst., exciton interactions, ps laser pulse intensity depend. 77−63448
tetracene, singlet exciton fission and fluorescence, mag. field depend. 78−39026
tetracene, singlet exciton transitions, energies and oscillator strengths, boson theory with PPP wavefunctions 80−92820
tetracene, solid, electronic struct., comparative ESCA study of polyacenes 78−52631
tetracene, space-charged-limited photo-enhanced currents 79−82599
tetracene, spatial distrib. of electrolum. and recomb. process 79−19938
tetracene, theory of fission of singlet Frenkel exciton into two localised triplet excitons 79−23901
tetracene, thin cryst., electrolum. detection and determ. of spatial distrib. 79−19937
tetracene, trapping effects on emission-limited current flow 80−29413
tetracene, triplet exciton diffusion and double photon absorpt., delayed fluoresc. obs. 77−36287
tetracene, unrelaxed fluoresc., direct picosecond obs. 80−89046
tetracene, vibrational quasicontinuum threshold, spectrosc. criterion 80−52972
tetracene anion+tetracene cation, electron transfer reaction, singlet fission 78−11502
tetracene anion radicals, enthalpy of disproportionation, calorimetric determ. technique 79−96296
tetracene dianions in dimethyl ether, rotational diffusion meas. 80−65262
tetracene in alcoholic glasses, laser-induced hole burning mechanisms, zero-phonon fluoresc. 78−43912
tetracene in liquid crystal, temp. depend. of absorption and fluoresc. *(German)* 80−18887
tetracene molecules in Ar clusters, excited state intramol. dynamics, laser-induced fluoresc. spectra obs. 80−78674
tetracene radical cation EPR spectra, ion-pair effects 79−13742
tetracene single crystals, Davydov splitting, press. depend., phase transition obs. 78−27250
tetracene single crystals, exciton refl. spectra, 4.2 to 300K 79−47478
tetracene surface states, electric field effects, exciton-charge carrier interactions *(Russian)* 80−24989
tetracene-Kr(Xe), intramol. intersystem crossing in supersonic beam, external heavy atom effect 80−14167
tetracene/aq. electrolyte contact, illuminated, space charge behaviour 78−84290
1,1,4,4-tetrachloro-1,3-butadiene, reson. Raman intensities, mol. struct., excited states, vibr. anal. 77−65470

organic compounds continued
2,3,4,4-tetrachloro-1-keto-1,4-dihydronaphthalene, photochromic single cryst., triplet photochem. 79−39164
1,2,3,4-tetrachloro-7,8-diphenylcalicene, excited states, moments anal. of electro-optical spectra 79−22698
tetrachloro-p-benzoquineone, IR and Raman spectra of phase transition *(French)* 78−60445
tetrachloroaurates and tetrachloroiodates, ^{35}Cl NQR freqs., correl. with crystallographic data 79−33559
1,2,3,5-tetrachlorobenzene, chemical perturbation of cryst. structs., Raman phonon spectra 78−26559
α1,2,4,5-tetrachlorobenzene, cryst. struct. and lattice vib. freqs. 77−19939
tetrachlorobenzene, dimer triplet state line shape, small excitons 80−48041
1,2,4,5-tetrachlorobenzene, excited triplet state dimer, intermol. exchange integral, isotope effect 80−15826
1,2,4,5-tetrachlorobenzene, exciton migration and trapping, X-trap phosphoresc. 79−1780
1,2,4,5-tetrachlorobenzene, exciton states in crystals and dimers 80−70620
1,2,4,5-tetrachlorobenzene, impurity induced states, spin dephasing, spin coherence expts. 78−84498
tetrachlorobenzene, in durene, 1.6K, $S_1 \sim\!\!\rightarrow T_1$ relax. mechanism, Zeeman phosphoresc. and PMDR obs. 77−30912
1,2,4,5-tetrachlorobenzene, in durene host, phosphoresc., cross-relax. between spin levels 78−9186
1,2,4,5-tetrachlorobenzene, lattice dynamics, thermodynamic functions and phase transitions 78−67777
sym-tetrachlorobenzene, LF Raman bands and space symmetries 77−66504
1,2,4,5-tetrachlorobenzene, linear chain triplet excitons, electron spin-echo and ODMR 78−76357
1,2,4,5-tetrachlorobenzene, localised excitations thermal promotion to exciton band, impurity states effect 78−52539
1,2,4,5-tetrachlorobenzene, mol. cryst., coherent 1-dimens. exciton transport and impurity scatt. 78−14666
tetrachlorobenzene, mol. crystal, exciton band spin-orbit coupling 78−39025
1,2,4,5-tetrachlorobenzene, mol. solid, heat pulses, phonon-induced delocalisation of trapped excited triplet states 80−89053
1,2,4,5-tetrachlorobenzene, multiple-quantum spin-phonon interactions, acoustically-induced phosphoresc. obs. 77−40150
1,2,4,5-tetrachlorobenzene, proton spin relaxation by optically excited triplet states 79−19810
tetrachlorobenzene, pure and doped crysts., triplet exciton trapping, phosphoresc. spectra 77−85766
1,2,4,5-tetrachlorobenzene, structural phase transition, Raman and IR spectra *(French)* 77−66503
1,2,4,5-tetrachlorobenzene, triplet energy transfer in substitutionally disordered system 79−52000
1,2,4,5-tetrachlorobenzene, triplet exciton, ESR and optical absorption lines 80−96791
tetrachlorobenzene, triplet exciton spectral line shape, 2-45K 78−19498
1,2,4,5-tetrachlorobenzene, triplet excitons, ESR and ODMR 78−43681
1,2,4,5 tetrachlorobenzene, triplet excitons, high. mag. field, spin-lattice relax. study 80−20517
1,2,4,5-tetrachlorobenzene, triplet excitons, zero field ODMR 80−88891
1,2,4,5-tetrachlorobenzene, triplet state spin-lattice relax. in cryst. and matrix isolated mol. 79−11449
meso-1,2,3,4-tetrachlorobutane, IR and Raman spectral studies 80−32722
2,2,3,3-tetrachlorobutane, vibr. spectra, liq. and solid-state, conform. struct. 79−73936
tetrachlorocyclopropene, A_1 vibrs., laser Raman obs. 79−76437
tetrachlorodibenzo-p-dioxin determ. by low resolution gas chromatography-mass spectrometry 80−66893
tetrachloroethylene, cryst., IR spectra in polarised light, cryst. struct. 78−27223
tetrachloroethylene, liquid, twisting vibration, direct obs. via hyper-Raman effect 77−28559
tetrachloroethylene, Raman line intensities, modified CNDO/2/INDO calc. 78−25621
tetrachloroethylene, trimerisation, IR laser action and BCl_3 sensitiser effects 77−12809
tetrachloroethylene filled liq. core quartz fibres, transmission loss meas. at 3.39 μm 79−81532
tetrachloroethylene-benzene(toluene)(p-xylene)(carbon tetrachloride) binary mixtures, dielec. polarisations 79−56713
tetrachlorohydroquinone+p-chloranil, H atom abstraction by p-chloranil triplet 78−80720
tetrachloroisophthalonitrile, vapour press. by effusion method, solid phase eqn. of state 80−49350
tetrachloromethane, Auger emission anomalous spectra and yield, chemical species depend. 78−55152
tetrachloromethane, boiling, under increased gravitation, heat exchange mechanism, review 77−46895
tetrachloromethane, electronic characts. from electron scatt. meas. 79−59576
tetrachloromethane, fluid, collision induced light scatt. intensity 80−103955
tetrachloromethane, fluid vibr. spectra, repulsive force depend. line broadening *(Russian)* 80−47970
tetrachloromethane, He(II) photoelectron spectra, spectral intensity patterns 79−98152
tetrachloromethane, in atmosphere, interhemispheric gradients meas. 78−81289
tetrachloromethane, liq. struct. and dynamics 80−79669
tetrachloromethane, liq. struct. temp. depend., X-ray meas. 79−77478
tetrachloromethane, liqs., refractive index, pressure effect 80−71375
tetrachloromethane, separation of collision-induced from intrinsic mol. depolaris. Rayleigh scatt., C-Cl bond optical anisotropy 78−27244
tetrachloromethane, UV laser photolysis 80−66826
tetrachloromethane, UV photodissoc., mechanism and quantum yield 79−52723
tetrachloromethane+H_2, (oriented), total collision cross-sections, anisotropic pot. parameters calcs. 78−13568
tetrachloromethane+n-heptyl alcohol, measurements of US vel. and related parameters 80−38200
tetrachloromethane+Sn, crossed beam kinetics, SnCl recoil vel. spectra 79−1947

organic compounds continued
tetrachloromethane+Xe, excitation functions and rotational polarisation, chemiluminesc., crossed beam study 80−76491
tetrachloromethane in dil. soln., dynamic dipole induced interactions in absorption spectra 78−13553
tetrachloromethane isotopic liq., Rayleigh and Raman depolaris. components *(French)* 79−99895
tetrachloromethane-cyclohexane liq. mixtures, heat of transport, Dufour effect 80−44344
tetrachloromethane-cyclohexane system, interdiffusion, ternary diffusion eqn., radioactive tracer obs. 78−79792
tetrachloromethane-I_2 soln., $I_2(B^3\pi_0^+{}_u)$, ps excitation, ultrafast decay and spectrum 78−9184
1,2,3,4-tetrachloronaphthalene, intramol. heavy atom effect, PMDR obs. 79−13745
tetrachlorophthalic anhydride, IR and Raman spectra 79−50015
tetrachlorophthalic anhydride-hexamethylbenzene, long-lived emission of charge-transfer cryst. 79−33752
tetrachlorophthalic anhydride-naphthalene, complex cryst., visible spectra, singlet-triplet absorpt. 79−19897
tetrachlorophthalic anhydride-pentamethylbenzene, long-lived emission of charge-transfer cryst. 79−33752
N-d-tetrachlorophthalimide, IR and Raman spectra 79−50015
1,1,1,3-tetrachloropropane, Raman and IR obs. of rot. isomerism, entropy difference between vapour and liq. phase isomer *(Russian)* 79−31529
tetrachlorotetraiodofluorescein, rot. diffusion, fluoresc. spectra, solvent effects 77−75198
tetracosane melt, Brillouin spectroscopy obs. of struct., 65-250°C 79−55642
1,2,4,5-tetracyanobenzene, CT complex in micellar soln., fluoresc. and photolysis study 79−61911
tetracyanobenzene+methylated benzene, fluorescent exciplex form., electronic relax. 80−5573
s-tetracyanobenzene+p-xylene, photoassoc., exciplex form., excitation energy and isotope depend., vibr. effects 80−55634
1, 2, 4, 5-tetracyanobenzene and -d_2, IR and Raman spectra, vibr. anal. 79−36629
1,2,4,5-tetracyanobenzene complexes, electron donor-acceptor interaction, ionic photodissoc. yield 79−6975
tetracyanobenzene-naphthalene, Raman spectra, phase transition and isotopic substitution 78−80364
tetracyanoethylene, oriented adsorption on KCl, LEED-AES study 77−62737
tetracyanoethylene(d), charge-transfer complex, fluoresc. quantum field and decay time 78−42107
tetracyanoethylene anion in acetone-d_6, anion solvation, electron spin echo modulation 80−63676
tetracyanoethylene anion in methanol-$d_3(d_1)$, anion solvation, electron spin echo modulation 80−63676
tetracyanoethylene charge transfer complex, nonradiative decay of excited states, D isotope effect 79−31580
tetracyanoethylene in dimethylsulphoxide-d_6, anion solvation, electron spin echo modulation 80−63676
tetracyanoethylene molecule with high electronegativity on field polarisation, electron affinity determ. 79−27111
tetracyanoethylene-hexamethylbenzene, electron-donor/acceptor complex, reson. Raman scatt. 77−24831
tetracyanomethane, molecular vibration analysis 79−803
tetracyanomethane, multiple scatt. Xα calc. of electronic struct. 78−78626
2,2,6,6-tetracyanonaphthoquino dimethane, nonlinear 3rd-order elec. susceptibility calcs. 79−54786
tetracyanoplatinates, quasi 1d anion deficient, elec. and struct. props. 80−103683
tetracyanoquinodiamine, LCAO-Xα-SCF atoms in mols., theory and appl. 77−57869
^{131}I-tetracycline, prep. and stability 77−29204
tetracyclo[3.2.0.$0^{2,7}$.$0^{4,6}$]heptan-3-one, microwave spectrum and effect of cyclopropyl-carbonyl group interactions on dipole moment 78−9138
tetracyclo[4,2,2,$O^{2,5}$,$O^{5,7}$] decane-10-carboxylic acid, lactone substituted, molecular, crystal struct. 79−90640
tetradecafluoroheptene+Xe, high Rydberg state, ionis. 78−50620
tetradecane, wetting on solid substrates, disjoining pressure isotherms 78−51794
tetradecane, with tetra-4-tert-butylphthalocyanine impurity mols., luminesc. 77−18965
tetradecanoic acid monolayers, liq.-expanded/liq.-condensed phase changes press., effect of temp. diff. between liq. substrate and air 80−54476
p-n-tetradecyloxy benzoic acid, liq. cryst. phase transition, thermal studies 78−71843
tetraethoxysilane, thermal conductivity and density, −13.5 to +90°C 77−15637
tetraethylammonium, selective uptake of ions into PMMA gel 78−35719
di-(tetraethylammonium)tetrahalomanganate, mag. circular and linear dichroism obs. 80−29725
tetraethylammonium acetate tetrahydrate, stoichiometry and cryst. data 78−67702
tetraethylammonium bromide, adsorpt. at Hg/electrolyte interface from H_2O, D_2O solns. 79−83459
tetraethylammonium bromide, aq. soln., thermal diffusion, heat of transport *(French)* 78−18808
tetraethylammonium chloride tetrahydrate, stoichiometry and cryst. data 78−67702
tetraethylammonium fluoride hydrate, stoichiometry and cryst. data 78−67702
tetraethylammonium iodide-Ag_nI_{n+1}, ionic conductors, electrochem., props. 77−31808
tetraethylammonium iron tetraiodide, structural and mag. props., ^{57}Fe and ^{129}I Mossbauer spectra 79−61282
tetraethylammonium neptunium hexachloride, Mossbauer spectra and mag. susceptibility meas. 80−108140
tetraethylammonium sulphate monohydrate, stoichiometry and cryst. data 78−67702
tetraethylammonium triiodide, solvent effects on electronic transitions of I_3^- 77−27080
tetraethylene glycol dodecyl ether-H_2O, binary micellar solns. and emulsions, dielec. behaviour 80−44994
tetraethylene glycol dodecyl ether-H_2O-heptane, binary micellar solns. and emulsions, dielec. behaviour 80−44994
tetraethylene iridium chloride, ligand-ligand interactions; low freq. vibr. obs. 78−94255

organic compounds continued
tetraethylene iridium chloride dimer, ligand-ligand interactions, low freq. vibr. obs. 78−94255
tetrafluoremethane, compressed gas, apparatus for depolarisation ratio meas. of scatt. light 80−38527
tetrafluoro-1,3-dithioethane, ^{19}F chem. shift tensor multiple pulse NMR 77−77111
tetrafluoro-dibromo-ethylene-Ar-Xe mixture, experimental study of stimulated emission 79−98347
tetrafluoro-p-benzoquinone, mol. struct., gas phase electron diffr. obs. 80−58386
tetrafluorobenzene, cation, visible emission spectra of gas, Jahn-Teller effect 79−50034
tetrafluorobenzene, microwave spectra, dipole moment, centrifugal distortion consts. 77−75133
1,1,2,2-tetrafluorocyclobutane, ion-mol. reactions, reaction pathways, mass spectra 77−21368
1,1,2,2-tetrafluorocyclobutane, microwave spectrum, dipole moment, rot. and vibr. modes assignments 77−18914
tetrafluorodilhietane, IR photolysis, multiphoton dissoc. models 80−30253
1,1,2,2-tetrafluoroethane, anti- and gauche-rotamers, struct., spectra, electron diffr. 77−50439
1,1,1,2-tetrafluoroethane, mol. struct. studied by gas-phase electron diffr., vibr. amplitudes, bond angles and lengths calc. 80−95740
tetrafluoroethane, specific refractivity, interferometric meas. 80−95124
tetrafluoroethylene, electronic struct., CNDO/S2 calcs., photoelectron and UV absorpt. spectra 77−30783
tetrafluoroethylene, high temp. oxidation behind refl. shock waves 77−36743
tetrafluoroethylene, photolysis, CF_2, form., excitation by Hg 253.7 nm line, reson. fluoresc. spectra 80−63694
tetrafluoroethylene, Raman line intensities, modified CNDO/2/INDO calc. 78−25621
tetrafluoroethylene+Al_2O_3, AlF radical, form. in arc plasma, spectra 77−28989
tetrafluoroethylene+O, triplet difluoromethane spectra, phosphoresc. and triplet-triplet annihilation 78−53196
tetrafluoroethylene anion, EPR spectra in organic matrix 79−76453
tetrafluoroethylene radical anion, isotropic and anisotropic EPR spectra, conform. 78−13532
tetrafluoroethylene radical ion+tetrafluoroethylene, cycloaddition 78−13533
tetrafluoromethane, ^{18}F recoil labelling 79−52732
tetrafluoromethane, ^{19}F chem. shielding, depend. on internal coords. 78−5249
tetrafluoromethane, ^{19}F NMR, chem. shielding, intermol. interactions and rovibr. motion effects 78−9171
tetrafluoromethane, $\nu_2+\nu_4$ band, high resolution diode laser spectra 80−69138
tetrafluoromethane, ν_4 fundamental of three isotopic species 78−70835
tetrafluoromethane, atmospheric, ν_3 vibr.-rot. band identification in balloon-borne IR solar spectra 79−100894
tetrafluoromethane, Auger emission anomalous spectra and yield, chemical species depend. 78−55152
tetrafluoromethane, Auger transition energies, transition state approx. SCF Xα calc. 77−65426
tetrafluoromethane, binary collision-induced light scatt., rot. Raman scatt. 80−78660
tetrafluoromethane, binary collisions induced light scatt. 80−83428
tetrafluoromethane, bond length and chemical shielding, NMR lineshape anal. of multispin system 80−32741
tetrafluoromethane, bond order and Raman intensity, delta function eqn. 77−61693
tetrafluoromethane, collision induced rot. Raman scatt., polarisability effects 78−86874
tetrafluoromethane, collision-induced light scatt., spectral features 78−13493
tetrafluoromethane, collision-induced Rayleigh scatt. intensity calcs. 77−46569
tetrafluoromethane, collision-induced rot. spectrum 79−98101
tetrafluoromethane, collision-induced scatt., many-body correls. 80−87127
tetrafluoromethane, collision-induced scattering at a vibrational Raman frequency 78−62814
tetrafluoromethane, compressed fluid ang. momentum relax., NMR 78−19354
tetrafluoromethane, elastic and inelastic electron scatt. differential cross section, obs. and calc., struct., binding energy 80−28110
tetrafluoromethane, electron diffraction cross-section, finite scatt. geom. in mol. beam expt. 78−74803
tetrafluoromethane, electron impact dissoc., light emission from fragments 79−13826
tetrafluoromethane, electronic struct., Xα SW calcs 80−102447
tetrafluoromethane, gas, DID Rayleigh and Raman depolarised scatt., lattice-gas model 80−10356
tetrafluoromethane, gas, liq., collision-induced microwave absorpt. 77−42312
tetrafluoromethane, in disordered phases, IR active mode Raman line shape, dipole-dipole interaction 80−9603
tetrafluoromethane, intermolecular pot., lattice energy and heat of sublimation 80−38995
tetrafluoromethane, IR spectrum, Fermi reson. sequences, cubic pot. energy, anharmonicity consts. 77−10674
tetrafluoromethane, Kerr effect in gas, statistical theory 79−50842
tetrafluoromethane, Kr diffusion, 243.15K, density depend., size effect 78−75859
tetrafluoromethane, liq., mol. reorientation 80−106320
tetrafluoromethane, liq. pure vibr. Raman spectra 80−97262
tetrafluoromethane, M-X bond flexibility, by compliance scheme 80−37805
tetrafluoromethane, mol. consts. and mean vibr. amplitudes calcs. 80−106318
tetrafluoromethane, molecular charge density contours for cryst. struct. 78−38645
tetrafluoromethane, multipole moments, far IR spectrum determ., pot. function effects 77−50435
tetrafluoromethane, optically pumped laser, 11-17 μm 78−46581
tetrafluoromethane, photoabsorpt. cross-section, 175-770 Å 77−88462
tetrafluoromethane, photoions. cross section calc., for YMζ line, HF vs OPW method 77−42353

organic compounds continued
tetrafluoromethane, plasma etching of $Si_3N_4(SiO_2)$ in dry processing, active etchant species 80−79581
tetrafluoromethane, plasma oxidation in presence and absence of Si in tubular-alumina fast-flow reactor 79−96297
tetrafluoromethane, pot. consts., IR spectra 78−82808
tetrafluoromethane, RF discharge chemistry, added H_2 effect 80−33832
tetrafluoromethane, sign of rot. g-factor, mol. beam expt. 79−59600
tetrafluoromethane, specific refractivity, interferometric meas. 80−95124
tetrafluoromethane, spectral shape of collision-induced scatt. 78−37687
tetrafluoromethane, spherical top mol. vibr.-rot. spectrum with tunable diode laser 78−82734
tetrafluoromethane, US absorpt. for vibr. self-relax., 139-183K 78−63529
tetrafluoromethane, valence electron binding energies, molecular symmetry restrictions effect 80−63528
tetrafluoromethane, vap. press., triple pt. to 173K 80−6522
tetrafluoromethane, X-ray photoelectron spectral linewidth of F core, ab initio HF calc. 78−62841
tetrafluoromethane+Ar, differential scatt. cross-sections, intermol. pots. calcs. 79−89742
tetrafluoromethane+C react. in ionising radiation of nuclear reactor 77−63934
tetrafluoromethane+CO, vibr. relax. rates, energy transfer 80−37862
tetrafluoromethane+H_2, (oriented), total collision cross-sections, anisotropic pot. parameters calcs. 78−13568
tetrafluoromethane+H_2 collision-induced simultaneous transitions, IR spectra 77−50438
tetrafluoromethane+HCl, vibr.-rot. line broadening 77−27117
tetrafluoromethane+He gas mixture, collision induced for IR translational spectra 80−83353
tetrafluoromethane+I_2, D-state lifetime and UV laser action 77−14471
tetrafluoromethane+S_2, fluoresc. quenching and lifetimes of S_2 78−46386
tetrafluoromethane adsorbed on graphite, adsorption isotherms, crit. temps. *(French)* 80−34312
tetrafluoromethane gas, total dissociation, in reactive ion etching system, reactant supply 79−83349
tetrafluoromethane laser, pulsed, high repetition rate, average power limitations at 10.6 and 16 μm 80−58503
tetrafluoromethane molecule, laser spectrosc. and optical pumping from CO_2 laser 80−74202
tetrafluoromethane optically pumped laser, tuning and stabilisation 79−13985
tetrafluoromethane plasma, appl. to etching of Si 79−15832
tetrafluoromethane-H_2 glow discharge, plasma etching of Si and SiO_2 surfaces 79−98922
tetrafluoromethane-inert gas, compressed fluids, ang. momentum relax., NMR 78−19355
tetrafluoromethane-trifluoromethane-chlorotrifluoromethane, vapour-liq. equilib. compositions, calc. 80−19925
tetraglycine, aq. soln., density, viscosity and dielectric const., 0-60°C 78−47462
tetrahydro-2-methylfuran glass, γ-irrad., spin trapping of radicals by BNB, EPR obs. 78−10776
Δ^9-tetrahydrocannabinol, detect. by GC/MS selected ion monitoring 79−43643
tetrahydrofuran, aq. mixtures, miscibility, enthalpy of mixing, solvation *(German)* 78−18779
tetrahydrofuran, clathrate hydrate, struct. II, for IR spectra, 4-100K 79−13707
tetrahydrofuran, effective force constant corrections, in redundant mol. coords. 78−13634
tetrahydrofuran, optical spectra of solvated electrons, band resolution 79−78698
tetrahydrofuran, reversible intercalation in graphite-alkali metal lamellar cpds. 80−16211
tetrahydrofuran, sorpt. kinetics in polyarylates, struct. transform *(Russian)* 79−51432
tetrahydrofuran+OH, reaction rate const., in irrad. NO_x mixture 78−7171
tetrahydrofuran clathrate, reorientation, residence times, Debye-Waller factors, activation energy, neutron scatt. study 79−41989
tetrahydrofuran clathrate deuterate, rotational motion, quasi-elastic neutron scatt. study 79−51022
tetrahydrofuran-benzene, soln., excess thermodynamic props. and interactions, US vel. and density meas. 80−39288
tetrahydrofuran-d_8, clathrate hydrate, ^2H NMR lineshapes for anisotropic diffusion 79−78533
tetrahydrofuran-Rb solution, polarised photoelectron and loose ion pair (Rb^+, e) obs., optical-ESR study 80−85196
tetrahydrofuran-water-NaCl system, heat. of soln. meas. using Calvet microcalorimeter *(French)* 77−44504
1,2,3,4-tetrahydronaphthalene-H_2O, liq.-liq. phase equilib., crit. phenomena 78−18764
tetrahydrothiophene, microwave spectrum, centrifugal perturbation effects 77−3350
3,3,4,4-tetrahydrothiophene-1,1-dioxide, vap. press. by effusion method 78−26680
1,4,5,8-tetrahydroxyanthraquinone, selective excitation, luminescence of long-wavelength component of multiplet 79−3478
1,4,5,8-tetrahydroxyanthraquinone-d_0,-d_4, mol. vibr., IR spectra 77−467
tetraiodoethylene, cryst. and mol. struct. at 4K 77−59001
tetraiodoethylene, disorder, neutron powder diffr. data refinement 78−34501
tetrakis(thenoyltrifluoroacetonato)thorium(IV), X-ray cryst. struct. determ. 79−37689
tetrakis-carbamide scandium (III) trinitrate, electron density distrib. from X-ray diffr. data 79−94994
tetralin, diffusion in liq. polyethylene, gas chromatography determ. 78−2277
tetralin-polyisobutylene, binary liq. soln., surface cluster functions 78−67631
tetramethoxysilane, thermal conductivity and density, −13.5 to +90°C 77−15637
tetramethyl ammonium cobalt chloride, ferroelec., Curie temp. determ. 79−38485
tetramethyl ammonium silver iodide, superionic solid film, surface diffusion coeff. 80−92709
tetramethyl germanium, methyl reorient., lattice vibrs., neutron scatt. obs. 79−51016

organic compounds continued
tetramethyl germanium(-d_{12}), vibr. spectra, normal coord. calcs 79−22717
tetramethyl gruop VIa cation silicon hexafluorides, ^1H and ^{19}F nucl. spin lattice relax. 78−80234
tetramethyl lead(-d_{12}), vibr. spectra, normal coord. calcs. 79−22717
tetramethyl orthocarbonate, enthalpy of hydrolysis meas., microprocessor-controlled system 80−22361
2,2,6,6tetramethyl piperid-4-one N-oxide, aq. soln., ESR spin probe for H_2O struct. alteration 77−59460
tetramethyl pyrazine in durene, phosphorescent mols., quantum beats in triplet states 80−58312
tetramethyl silicon, methyl reorient., lattice vibrs., neutron scatt. obs. 79−51016
tetramethyl silicon+Na, rainbow scatt. at thermal energy, anisotropic pot. 78−29837
tetramethyl silicon(-d_{12}), vibr. spectra, normal coord. calcs. 79−22717
tetramethyl tin(-d_{12}), vibr. spectra, normal coord. calcs. 79−22717
tetramethyl-1,3-cyclobutanedithione-h_{12} and -d_{12}, visible spectra, $n\pi^*$ transitions obs., mol. vibr. 80−97297
2,2,6,6-tetramethyl-4-oxopiperidine-1-oxyl, aq. soln., nucl. spin-lattice relax. times, cross-correl. method 79−95679
2,2,5,5-tetramethyl-4-phenyl-3-imidazalin-3-oxide-l-oxyl, deform. electron density determ., X-ray diffr. 80−88135
tetramethyl-p-benzoquinone, mol. struct., gas phase electron diffr. obs. 80−58386
N,N,N′N′-tetramethyl-p-phenylenediamine, alkane soln., charge carrier generation, elec. field depend. 80−107846
2,3,5,6-tetramethyl-p-phenylenediamine, reson. Raman spectra 77−58009
N,N,N′,N′-tetramethyl-p-phenylenediamine, TMPD, glassy soln., photoionisation, recombination isothermal luminesc. *(French)* 77−16404
N,N,N′,N′-tetramethyl-p-phenylenediamine+2,6-diphenyl-1,4-benzoquinone, triplet exciplex quenching 79−79228
tetramethyl-p-phenylenediamine-methylcyclohexane, γ- and UV-irrad. solvent matrices at 77K, H^- fluoresc. 78−70779
N,N,N′,N′-tetramethyl-p-phenylenediamine-p-chloranil, soln., optical spectra, temp. and environment effects 79−54861
2,2,2,6-tetramethyl-piperidino-oxy, cryst. growth and polymorphism 80−96645
tetramethylaminelithium(0), $Li(CH_3NH_2)_4$, existence, conduction- and localised-electron spin reson. 80−66035
tetramethylaminoborane, B_3H_8 large-angle anisotropic motion, ^{11}B BMR, temp. depend. 77−90045
tetramethylammonium, selective uptake of ions into PMMA gel 78−35719
tetramethylammonium bromide, aq. soln., thermal diffusion, heat of transport *(French)* 78−18808
tetramethylammonium cadmium chloride, EPR of Mn^{2+} meas. 77−59452
tetramethylammonium cadmium trichloride:Mn^{2+}, EPR spectrum temp. depend. 78−19314
tetramethylammonium chlorate, order-disorder transitions, DTA and NQR meas. 77−66022
tetramethylammonium chloride in HCl, Cl^- solvation no., Raman spectra 79−96410
tetramethylammonium chloride solns., aq. and methanolic, Raman spectra 79−28750
tetramethylammonium cobalt tetrachloride, ferrielectricity, triple 60 Hz D-E hysteresis loops 80−71365
tetramethylammonium cobalt tetrachloride, Raman spectra near incommensurate phase transitions 80−76013
tetramethylammonium compound, $(TMA)_2C_2S_6.1/2CS_2$, IR spectra in 200 to 4000 cm^{-1} range *(French)* 79−33711
tetramethylammonium copper chloride, S=1/2 Heisenberg 1-dimens. ferromag., mag. props. 79−82766
tetramethylammonium halides, libration amplitudes, NMR second moment determ. 77−1603
tetramethylammonium halides, UV exciton absorpt. bands 78−72547
tetramethylammonium hexabromotellurate, far IR and Raman spectra and phase transitions 80−11376
tetramethylammonium hexachloroplatinate, order-disorder transitions due to weak CH-Cl hydrogen bonds 78−92060
tetramethylammonium hexachlorotellurate, IR and Raman spectra, lattice and internal modes, phase transition 78−6659
tetramethylammonium hexafluorophosphate, X-ray cryst. struct. determ., full-matrix least-squares refinement 80−92514
tetramethylammonium hydrogen bis-trichloracetate (−d_n), ^{35}Cl NQR study 80−66064
tetramethylammonium iodide, field emission mass spectrometry, emitter characts. and production 77−63980
tetramethylammonium iodide, in aq. proline soln., elec. conductance investigation 80−10692
tetramethylammonium ion, normal and perdeuterated, aqueous solution, Raman and IR spectra 78−82741
tetramethylammonium manganese(II) tribromide, cryst. struct. at 235 and 115K 78−63745
tetramethylammonium manganese chloride, energy migration rel. to impurity trap behaviour 77−55811
tetramethylammonium manganese trichloride, ESR meas., evidence for two paramag. species 79−61208
tetramethylammonium manganous chloride:Cu, impure Heisenberg chain paramagnet, EPR sidebands, intensity, linewidths 78−76300
tetramethylammonium mercury iodide, NQR spectra of ^{127}I and cryst. struct. 77−12230
tetramethylammonium neptunium hexachloride, Mossbauer spectra and mag. susceptibility meas. 80−108140
tetramethylammonium octahydrotriborate, NMR study of proton and B dynamics 80−93200
tetramethylammonium perfluorooctanoate-water, lamellar lyotropic liq. cryst., neutron diffr. struct. obs. 80−64888
tetramethylammonium salt of $[Me_2N(ICl)_2]^-$, cryst. struct., secondary and multi-centre bonding 78−63751
tetramethylammonium silicate, X-ray cryst. struct. determ. 79−94996
tetramethylammonium silver iodide superionic film, electrocodeposition, electrochem. cells 80−107478
tetramethylammonium tetrachlorocobaltate, ferroelec., effects of hydrostatic press. on successive phase transitions 79−47402
tetramethylammonium tetrachlorocobaltate, ferroelec., pressure-temp. phase diagrams 80−97205
tetramethylammonium tetrachlorocobaltate, ferroelectricity 78−76408

organic compounds continued
tetramethylammonium tetrachlorocuprate, incommensurate phase, neutron diffr. study 80−79935
tetramethylammonium tetrachlorocuprate crystal, incommensurate-ferroelastic (commensurate) phase transition obs. 80−75352
tetramethylammonium tetrachloroferrate, press. induced ferroelectricity, dielec. and DTA meas. 80−80722
tetramethylammonium tetrachlorozincate, ferroelec., effects of hydrostatic press. on successive phase transitions 79−47402
tetramethylammonium tetrachlorozincate, ferroelec., incommensurate-commensurate transition, neutron scatt. study 80−40073
tetramethylammonium tetrachlorozincate, ferroelec., pressure-temp. phase diagrams 80−97205
tetramethylammonium tetrachlorozincate, ferroelectricity 78−39513
tetramethylammonium tetrachlorozincate, incommensurate phase transition, US propag. meas. 79−91382
tetramethylammonium tetrachlorozincate, incommensurate phase study, ferroelectric-paraelectric phases *(French)* 80−88318
tetramethylammonium tetrachlorozincate, low temp. phases, superstruct., X-ray study 80−39065
tetramethylammonium tetrachlorozincate, X-ray study of incommensurate phase 80−71351
tetramethylammonium zinc tetrachloride, ^{13}C NMR and PMR study of incommensurate phase transition 80−34863
tetramethylammonium zinc tetrachloride, ferrielectricity, triple 60 Hz D-E hysteresis loops 80−71365
tetramethylammonium zinc tetrachloride, incommensurate phase transitions, ^{13}C NMR study 80−75968
tetramethylammonium zinc tetrachloride, Raman spectra near incommensurate phase transitions 80−76013
tetramethylbenzene: 2,3-dichloroquinoxaline, sublevel phosphoresc. spectra 78−70863
1,2,4,5-tetramethylbenzene, liq. and solid, vibr. dephasing, intermol. energy exchange mechanism 78−74737
2,2,3,3-tetramethylbutane, γ-irrad., EPR spectrum assignment 80−15800
2,2,3,3,-tetramethylbutane, CH stretching local mode anharmonicity, intramol. perturbation overtone spectra 79−18171
2,2,3,3-tetramethylbutane, pyrolysis, 699 to 735K and 3 to 19 torr 78−92478
2,2,3,3-tetramethylbutane, radiolysis, radical prods., EPR obs. 80−32747
tetramethylbutane in hexachlorobutadiene soln., local mode overtone bands 80−83444
tetramethylcarbon, force fields and vibr. mean amplitudes 77−30856
2,2,4,4-tetramethylcyclobutane-1,3-dione, Rydberg transitions, spectra, LCRO calcs. 77−34659
3,6-tetramethyldiamino-N-methylphthalimide soln., hot luminesc. and vibr. relax. 79−22752
3,6-tetramethyldiamino-N-methyphthalimide, in organic solvent, hot luminesc. 79−4842
tetramethyldiaminodiphenyl ketone, binder layer, photoinduced polarisation and voltage 80−75923
tetramethyldiaminodiphenylmethane, exciplex form. with anthracenes, form. kinetics and luminesc. props. 80−66792
3,3,4,4-tetramethyldiazetine, photoelectron spectra, ring size effects on azo group ionis. pots. 77−61793
tetramethyldioxetane, collisional dissoc. by supersonic Xe beam, chemiluminesc. 78−40029
tetramethyldioxetane, gas phase unimol. decomp. and chemiluminesc. initiated by TEA CO_2 laser 77−60068
tetramethyldioxetane, IR laser dissociation, chemilum. spectrum 79−5171
tetramethyldioxetane, multiphoton dissoc., collisional vibr. relax., rate eqns. model 80−63729
tetramethyldioxetane, multiphoton dissoc. time depend. 79−16020
tetramethyldioxetane, photolysis, unimolecular decay probed by picosec. spectroscopy 77−60083
tetramethyldiphosphine, UV photoelectron spectra trans/gauche isomer equilib. 79−31600
tetramethylethyl-cyclopentadienyl thorium trichloride, prep., NMR and IR spectra 79−76428
tetramethylethyl-cyclopentadienyl uranium trichloride, prep., NMR and IR spectra 79−76428
tetramethylethylene, adsorbed on silica, laser Raman spectra 77−3367
tetramethylethylene, electron energy loss spectra, 0-90°, 20-150 eV impact 79−68322
tetramethylethylene, photoelectron spectrosc., ang. depend. 80−9641
tetramethylgermanium, force field and vibr. mean amplitudes 77−30856
N,N,N′,N′-tetramethylparaphenylenediamine, recomb. fluoresc., elec. field quenching 78−92107
tetramethylphenylenediamine chlorate, EPR investig. of exchange interaction 77−40114
2,2,6,6-tetramethylpiperidine nitroxide radical-alcohol complexes, EPR, PMR, hyperfine coupling const. 79−65736
2,2,6,6-tetramethylpiperidine nitroxide radical.alcohol complex, NMR chem. shift 78−46366
1,1,3,5-tetramethylpiperidinium iodide, model cpd., struct., ^{13}NMR 77−565
tetramethylpyrazine, PMMA soln., fluoresc. and phosphoresc. quantum yield and lifetime, 20-120 kbar 79−54902
tetramethylpyrazine-d_{12}, in durene matrix, intersystem crossing of 859.5 MHz transition 79−27015
tetramethylpyrazine-d_{12}, photoexcited triplet state, in durene, phosphoresc., spin coherence and quantum beats 78−76517
tetramethylpyrazine-d_{12}, photoexcited triplet state, phosphoresc., quantum beats 77−71827
1,1,3,4-tetramethylpyrrolidinium iodide, model cpd., struct., ^{13}C NMR 77−565
tetramethylsilane, dielectric liquid, drift mobility and conduction band energy of excess electrons 77−4348
tetramethylsilane, field emission into liq., 275-334K 78−88406
tetramethylsilane, force fields and vibr. mean amplitudes 77−30856
tetramethylsilane, IR and visible spectral intensity data and the universal intensity concept 80−28066
tetramethylsilane, liq., electron drift vel. saturation, skeletal vibr. 80−34451
tetramethylsilane, liq., electron mobility up to crit. point 77−76809
tetramethylsilane, liq., O_2^- electron laser-photodetachment 79−64057
tetramethylsilane, liq., photocond., ionis. threshold 79−15191
tetramethylsilane, liq., self-diffusion coeff., temp. and density depend. 78−91461
organic compounds continued
tetramethylsilane, liquid, effect of nonelectronegative molecules on excess electron mobility 78−2534
tetramethylsilane, liquid, ground state energy of excess electrons 78−68976
tetramethylsilane, local mode combination bands and local mode mixing 80−27999
tetramethylsilane, phase rels. under press., DTA obs. 78−71850
tetramethylsilane, thermodynamic props. of polymorphic phases 77−84943
tetramethylsiloxane dicarbonxylic acid Langmuir films on Cu surface, surface EM wave absorpt. study 80−97359
tetramethyltetraphenyltrisiloxane film, DC-704, on Ge, Al and KRS-5, IR refl. spectra anal. 77−59630
tetramethyltetraphenyltrisiloxane-treated substrate, effect on metal film deposition props. 79−90917
tetramethyltetrathiofulvalene salts, complexes with anisotropic props. *(French)* 77−69307
tetramethyltin, dielectric liquid, drift mobility and conduction band energy of excess electrons 77−4348
tetramethylurea-d_0,-d_{12}, IR spectra, normal coord. anal. 78−978
tetranitrophenothiazine-5, molecular complex, elec. cond. *(Rumanian)* 79−73518
tetraoxane, NMR obs. of mol. motion, rel. to polymerisation temp. effects on polytetraoxane texture 77−84663
tetraoxane crystals, growth and perfection by evaporation of solns., X-ray topography 79−61510
1,3,6,8-tetraphenyl-pyrene, UV absorpt. spectra, SCF CI method 79−59479
tetraphenylarsonium, Raman and IR spectra of the dicyanoiodate (I) ion 80−60572
tetraphenylborate, appl. to titrimetic determinations using ion-selective electrodes 79−83530
tetraphenylboron sodium aq. soln., dielec. relaxation spectroscopy in microwave region, double-beam interferometry *(German)* 80−71309
tetraphenylchlorin-d_0, -d_1, lowest triplet state, intersystem crossing rates, temp. and isotope effects 80−48026
tetraphenylcobalt porphyrin, XPS, valence electron levels 78−82785
tetraphenylcopper porphyrin, XPS, valence electron levels 78−82785
tetraphenylcyclobutane, in hexamethylphosphoric triamide soln., pulse radiolysis, optical absorption decay obs. 79−16019
tetraphenyldithiadipyranylidene-iodine, synthesis and cond. props. 80−24910
tetraphenyldithiapyranylidene mixed valence polyiodides, crystalline struct. and optical props. 80−92516
tetraphenyldithiapyranylidene triiodides, elec. cond. and thermoelec. power 79−56207
tetraphenylnickel porphyrin, XPS, valence electron levels 78−82785
tetraphenylphosphonium, Raman and IR spectra of the dicyanoiodate (I) ion 80−60572
meso-tetraphenylporphine, NH H^+ tunnelling rate 80−97158
meso-tetraphenylporphine, potential parameters of H migration tunnel rates calcs. 80−5600
tetraphenylporphyrin, dispersion induced circular dichroism, determ, of mag. dipole allowed transitions 80−14163
tetraphenylporphyrin, free base in PVC matrix, excited state props., electrochromism obs. 80−37815
tetraphenylporphyrin, XPS, valence electron levels 78−82785
tetraphenylsilane, crystn. from chem. transport reaction 80−104439
tetraphenylzinc porphyrin, XPS, valence electron levels 78−82785
tetraphersylanonium-tetraphenylborate assumption for single ion thermodynamics in amphiprotic and dipolar-aprotic solvents 80−55675
tetrapotassium tetrakis(oxalato)zirconate (IV) pentahydrate, cryst. struct. determ. 78−63746
2,2′,2″,2′″-tetrapyridine, photoelectron spectra, SCF LCAO calcs. 78−33551
tetraselenafulvalene, monomer and dimer electronic struct. scattered wave calc. comparison with photoelectron spectra 78−50465
tetraselenatetracene, neutral, cation and conducting complex reson. Raman spectra, vibr. lines, charge transfer 79−4794
tetraselenatetracene bromide complex, optical props. 78−6680
tetraselenatetracene cation radical salts, cryst. struct. by X-ray anal., rel. to elec. props. 80−24436
tetraselenotetracence chloride, cryst. and mol. struct. 79−94992
tetraselenotetracene bromide, positive microwave dielectric const. 78−47771
tetraselenotetracene chloride, quasi 1-D metal *(Russian)* 77−59281
tetraselenotetracene iodides, struct. and physical props., DC electrical cond. and EPR linewidth meas. 80−103312
tetraselenotetracene thiocyanate complex, X-ray struct. anal. 80−2006
tetraselentetracene chloride, elec. cond. below 1K *(Russian)* 80−6820
tetrathiofulvalene, LCAO-Xα-SCF atoms in mols., theory and appl. 77−57869
tetrathiofulvalene, Raman spectra 77−24832
tetrathiofulvalene-based salts, isomorphous series systematic investig. of solid-state props. 77−55517
tetrathiotetracene, charge transfer state parameters, evaluation by mag. field effect *(Russian)* 80−10924
tetrathiotetracene iodide, positive microwave dielectric const. 78−47771
tetrathiotetracene iodine high-conductivity complex, TTT_2I_3, magnetoresist. *(Russian)* 77−39886
tetrathiotetracene salts, IR, X-ray electron spectra, tetrathiotetracene $(TCNQ)_2$ cond. investig. 77−44005
tetrazaporphin, coord. polymer with transition metal, one-dimens. conductor, band struct., EHT theory 79−90941
s-tetrazine, cooled supersonic jet, Van der Waals complex, isotope effects, fluoresc. obs. 78−55194
s-tetrazine, dimethyl-s-tetrazine, photodissoc., in hexane soln., Ar matrix, and mol. cryst. 78−73059
s-tetrazine, fluoresc. excitation spectra, 1K rot. struct. 78−1020
sym-tetrazine, gas phase separation of ^{13}C and ^{15}N isomers, CW dye laser 79−27097
sym-tetrazine, isotope selective mol. spectroscopy and isotopically pure mols. prod. with dye laser 80−11926
sym-tetrazine, isotopic isomers, spectroscopic obs. 80−53009
s-tetrazine, laser photodissociation, product vibr. excitation 78−88652
sym-tetrazine, mol., isotope spectra, from unseparated natural mixture, spectrosc. technique 79−31736
s-tetrazine, mol., pot. functions of bending modes 80−9753
s-tetrazine, pot. surface of low-freq. out-of-plane modes 78−62741

organic compounds continued
s-tetrazine, UV and vis. photodissoc., three-body half-collision dynamics 80−78664
s-tetrazine, vapour, reson. CARS spectrosc., radiationless relax. rate 80−78614
s-tetrazine, visible absorpt. band assignment, vibr. anal. 78−994
s-tetrazine(-d_1), and $^{15}N_2$-substituted, rot. consts., ground and $^1B_{3u}$ excited states geometries 78−82862
s-tetrazine in Ar matrix, laser induced isotope enrichment 77−88599
s-tetrazine in n-hexane, picosecond time-resolved fluoresc., vibr. relax. 80−48025
tetrazine-Ar, van der Waals bond, nonstatistical vibr. energy distrib., photochemical reaction effects 80−30255
s-tetrazine-benzene, mixed cryst., 2K, lifetime limited photochem. hole burning 78−9183
s-tetrazines, mol. crysts., laser-induced photochem., isotope separation and hole burning 78−85185
tetrazolium salt, catalytic reduction to formazan dye 79−39170
tetrebromomethane, thermal resistivity, heat capacity and phase diagram under pressure 80−65316
tetrodotoxin, interactions with quaternary lidocaine and Na channel gates in squid axons 79−83745
tetrohydrofuran-$HgBr_2$ complexes, IR and Raman vibr. spectra, inter- and intramol. forces 77−66489
tetrolyl fluoride, IR and Raman spectra 79−41171
1,3,5,7-tetroxocane, vibr. spectra and intermol. forces 77−36216
(TETTF)$(TCNQ)_2$, charge transfer complex, phys. props. and phase transition 78−64032
TETTF.$TCNQ_2$, cryst. struct. *(French)* 78−18625
TGFB, deuterated, single cryst. growth from soln. and props. 79−24422
TGFB, dispersion and temp. depend. of refr. index *(Russian)* 77−66472
TGFB, emission of free charge carriers in vacuum as symptom of pyroelec. props. 79−42908
TGFB, ferroelec. and paraelec. phases, X-ray diffr. 79−86776
TGFB, ferroelec. Curie point press. coeff. tensor 79−33635
TGFB, high press. influence on anomalous specific heat, tricritical point 80−25322
TGFB, IR and UV absorpt. spectra, temp. var. of fund. absorpt. edge 78−84604
TGFB, IR spectra and optical consts. *(French)* 79−95748
TGFB, optical props. in 5 to 22 eV region, reflectance spectra 79−33652
TGFB, refl. spectra 4-22 eV, optical consts. 79−4821
TGFB, refractive dispersion, absorpt. spectra characteristics 78−68469
TGS:α-alanine, electro-optic props. *(Russian)* 79−78654
TGS:α-alanine, piezoelectric props., ferroelec. phase existence *(Russian)* 79−47387
TGS:α-alanine, single crysts., dielec. spectrum in RF range *(Russian)* 80−66097
TGS:α-alanine, single crysts., pyro- and dielectric props. *(Russian)* 77−59520
TGS:($CuSO_4$), internal friction 80−44257
TGS: nitroaniline, dielec. and pyroelec. props. 80−75916
TGS:Cr^{3+}, EPR and spontaneous polarisation stabilisation during annealing 77−4610
TGS:Cr^{3+}, EPR obs. of ferroelectric monocrystals, fine struct. EHT-SCCC-MO calcs. 79−19769
TGS:Cr^{3+}, EPR obs. of fluctuations near phase transition 78−43820
TGS:Cr^{3+}, polarisation reversal and ageing mechanisms, EPR meas. 79−8044
TGS:Cr^{3+}(VO^{2+}), polarization reversal, static hysteresis loops, switching processes, EPR 78−43633
TGS:Cr single cryst., lattice defect influence on critical behaviour 80−25315
TGS:Fe^{3+}, crysts. and their aq. solns., ESR 80−39862
TGS:Fe^{3+}(Cu^{2+})(Mn^{2+})(Ni^{2+}), dynamical props. using slowly varying elec. fields, hysteresis *(Spanish)* 77−69785
TGS:Fe^{3+} and aq. solns., optical absorpt. spectra 79−82997
TGS:L-alanine, unirradiated, optical spectroscopy of scintillations 80−80863
TGS:nitroanilines, permittivity, elec. cond. and Curie temp. 80−25273
TGS:VO^{2+}, single cryst. H^2 ENDOR investig. 79−99791
TGS, γ-irrad., lattice defect effects on ferroelec. dispersion 79−51904
TGS, acoustic emission, threshold electric field 79−60874
TGS, admixed with nitroanilines or L-alanine, US vel. and absorpt., ferroelec. transition 77−32333
TGS, alignment on domains of nematic liq. cryst. 79−38506
TGS, autostabilised state, elec. second harmonic generation 80−103921
TGS, Barkhausen jump, elec. pulse shapes- 77−66465
TGS, Brillouin scatt. spectra, depolarisation field effect 78−15177
TGS, calorimetry, sp. ht., 0-80°C 78−15122
TGS, capacitive bolometer effect in paraelectric phase 77−57389
TGS, characts. of dispersion of permittivity near phase transition 79−28695
TGS, cleavage surface, electron microscopy using shadow decoration technique 77−7955
TGS, complex dielec. permitt. near Curie temp., ferroelec. polarisation mechanism interpretation 78−43808
TGS, conditions for electret state 78−43773
TGS, correlation between domain struct. and dielec. props. 79−42927
TGS, crit. behaviour, electrostrictive coupling role 80−71329
TGS, crit. behaviour of thermal expansion, neutron diffr. study 80−75371
TGS, crit. dynamics, NMR data compared with dielec. data 78−76415
TGS, critical behaviour in thermal expsn. coeff. and dielectric const. 79−91334
TGS, critical region in sp. ht. 79−28106
TGS, cryst., characteristic absorption edge shape 77−85712
TGS, cryst., vibr. bands, ferroelec. and paraelec. phase H bonds *(Russian)* 78−15172
TGS, cryst. struct. exam. after X-irradiation/field treatment 77−11531
TGS, cryst. struct. exam. at low radiation doses 77−11530
TGS, crystallisation by epitaxial germination *(French)* 77−21040
TGS, deuterated, Brillouin spectra and elastic consts., behaviour near T_c 78−15178
TGS, deuterated, dielectric props., ageing 77−16257
TGS, deuterated, ferroelec., dielec. nonlinearity 80−75959
TGS, deuterated, paraelec. phase, D atom positions 78−14334
TGS, deuterated, undoped and alanine-doped, growth by rotating disc method and elec. props. 79−47611
TGS, deuterated and undeuterated, pyroelectric, dielectric and thermal props., temp. depend. 78−43809

organic compounds continued
TGS, deuterised, growth in form of oriented blocks, domain struct. obs. 77−90266
TGS, dielec. behaviour near transition temp. 78−15127
TGS, dilatometric study, examination of logarithmic connection to classical Landau-type theory 78−6642
TGS, dispersion and temp. depend. of refractive index *(Russian)* 77−66472
TGS, domain boundaries, X-ray topographic study 78−48136
TGS, domain boundaries, X-ray topography 78−60409
TGS, domain growth shapes 78−27168
TGS, domain nucleation in AC elec. fields 80−34867
TGS, domain wall dynamics and small signal permitt., loss mechanism absence 78−43825
TGS, domain wall thickness determ. from longit. US wave propagation meas. 77−66463
TGS, effect of aniline in aqueous crystal growing soln. on physical props. 78−43810
TGS, effect of edge dislocations on shapes of moving domain boundary 80−20602
TGS, effect of Fe^{3+} admixture on phys. props. 80−76052
TGS, elastic and dielec. consts. from Brillouin scatt. 77−48180
TGS, elastic vs. polarisation energy near transition 78−15118
TGS, electrogyration during phase transitions 79−19859
TGS, electromech. coupling of surface acoustic waves near ferroelec. transition 78−19415
TGS, electrooptic switching anomalies 78−52473
TGS, electrostrictive and dielec. coeffs., neutron diffr. study 80−75943
TGS, emission of free charge carriers in vacuum as symptom of pyroelec. props. 79−42908
TGS, epitaxial growth method from soln., on Ag layer 77−32536
TGS, eqn. of state near ferroelec. Curie temp., including tunnel effect 77−12342
TGS, exponential switching by sidewise domain wall motion 80−29703
TGS, ferroelec., domain wall orientations and domain shapes 79−38508
TGS, ferroelec., elec. SHG in autostabilised state 77−85661
TGS, ferroelec., meas. of sp.ht. at constant elec. flux density by AC method 79−33098
TGS, ferroelec., negative ENDOR study of radiation damage 78−19373
TGS, ferroelec., phonon contributions to anomalous sp. ht. near phase transition temp. 77−52023
TGS, ferroelec., positron lifetime meas. during phase transitions 78−6644
TGS, ferroelec., repolarisation in SEM 79−15424
TGS, ferroelec., spontaneous polarisation, 2.2-20K 79−19849
TGS, ferroelec., temp. autostabilisation, impedance var. with DC bias 78−72467
TGS, ferroelec., thermal expansion 79−37855
TGS, ferroelec., vacuum cleaved, charge compensation 80−60510
TGS, ferroelec. activation field change 80−71358
TGS, ferroelec. cleavage surface microscopic struct. by electron microscopy 79−51403
TGS, ferroelec. cryst., complex permittivity at microwave freq. and high press. 80−2685
TGS, ferroelec. crystal, Barkhausen effect study 79−38507
TGS, ferroelec. Curie point press. coeff. tensor 79−33635
TGS, ferroelec. domain struct., polarisation obs. *(Chinese)* 80−20603
TGS, ferroelec. single crystal, low freq. nonlinear effects 80−84490
TGS, ferroelec. transition, electrooptical hysteresis and crit. behaviour of electrooptical props. 78−2817
TGS, ferroelec. transition, struct. changes, ^{13}C NMR obs. 78−60344
TGS, ferroelectric, domain pattern using pyroelectric effect 77−40196
TGS, ferroelectric crystal, non-linear pyroelec. effect in phase transition region 79−47393
TGS, ferroelectric domain exam., decoration with auramine 77−16268
TGS, ferroelectric hysteresis, dielectric and pyroelectric props. *(Chinese)* 80−88938
TGS, ferroelectric phase transition, high resolution NMR study 80−97214
TGS, ferroelectric transition, neutron diffr. obs. 80−25324
TGS, gamma irrad. effects on heat capacity, Curie temp., permittivity 78−67737
TGS, growth from solution containing aniline, dielec. and pyroelec. props. 78−6639
TGS, growth of large area, doped and undoped crysts. by rotating disc method 78−19652
TGS, interaction of γ-irrad., induced defect electron microscope expts. 79−10876
TGS, internal bias field, hysteresis loops *(Chinese)* 80−84705
TGS, internal field prod. in layer periodical domain struct. by X-ray irrad. 80−71359
TGS, investigation of switching characts. using cct. containing bipolar square pulse generator 80−62687
TGS, kinetics of domain formation during phase transition 80−66130
TGS, L-α-alanine disordered regions, dielec. prop. changes in transition region 80−108159
TGS, large scale inhomogeneity effect on ferroelectric transition *(Russian)* 78−76411
TGS, laser light scatt. spectroscopy 78−10156
TGS, layered domain struct. form., theory and expt. 77−52029
TGS, monocrystalline, ferroelectric, domain boundary dynamics contrib. to permittivity near Curie point *(Russian)* 79−73875
TGS, morphology of Au and AgCl films on complementary cleavage planes 79−15031
TGS, neutron diffraction enhancement near Curie point with DC field appl. *(Chinese)* 78−68462
TGS, nitroaniline admixture effect on thermal parameters 80−107580
TGS, on Ag film, saturated soln. evaporation, crystallisation by epitaxial nucleation *(French)* 77−35831
TGS, optical props. in 5 to 22 eV region, reflectance spectra 79−33652
TGS, orientation depend. of l-alanine incorporation 78−42938
TGS, paraelec. phase, elastic and thermoelastic consts. 77−47503
TGS, perfect and imperfect, sp. ht. and sound vel., crit. anomalies 80−71331
TGS, photoelastic const. behaviour new ferroelectric transition 78−19441
TGS, piezoelectric resonance spectra in 17 to 60 MHz range 77−16269
TGS, polarisation reversal, cryst. defects effect 78−27156
TGS, positron annihilation and ferroelectric transition 78−19594
TGS, proper and improper ferroelec., direct meas. of figure of merit 79−95711
TGS, proton and deutron NMR anal. of temp. depend. 80−33919

organic compounds continued
TGS, proton spin-lattice relax. time, temp. depend., near transition pt. 78−43668
TGS, pure and Cu doped, growth from soln., dislocation density 79−52096
TGS, pure and deuterated, domain wall thickness and surface energy 79−87408
TGS, pure and doped, thermal diffusivity, domain wall thickness determ. 79−42324
TGS, pure and Fe^{3+}-doped, thermal diffusivity, 25°C 79−90833
TGS, pure and nitroaniline-admixtured, longit. US wave propag., domain struct. effects 77−55322
TGS, pure and with lattice defects, elec. cond. 79−42538
TGS, pyroelec. effect in phase transition region *(Russian)* 79−87401
TGS, pyroelec. IR detectors, permanent polarisation due to X-rays, optimum non-ferroelec. behaviour 77−41684
TGS, pyroelec. signal, domain struct. determ. 77−43951
TGS, pyroelec. single cryst., elec. field meas., thermally stimulated charges 80−45012
TGS, pyroelectric coeff., 1.8-300K, dynamic method *(French)* 79−19844
TGS, pyroelectric coeff., polarising field effect 79−47391
TGS, pyroelectric figures of merit 77−59519
TGS, refl. spectra 4-22 eV, optical consts. 79−4821
TGS, refractive dispersion, absorpt. spectra characteristics 78−68469
TGS, SAW phase velocity in b-plane 77−85043
TGS, soln. growth of large single crystals, using cylindrical seeds 78−60556
TGS, sound group vel. vector direction, temp. depend. 78−67774
TGS, spin-lattice relax. meas. of ^{1}H, ^{13}C, and ^{15}N near ferroelec. transition 77−1646
TGS, spontaneous polarisation, low temp. meas. 80−75921
TGS, spontaneous polarisation and coercive field from 30 to 1000 Hz 77−66464
TGS, static and dynamic crit. behaviour of uniaxial ferroelectrics 78−35103
TGS, static crit. phenomena, lattice defect influence 80−71336
TGS, substrate for PbTE film, induced elec. inhomogeneity 77−15909
TGS, surface alignment of nematic liq. cryst. controlled by domain struct. 79−99068
TGS, surface pot. between ferroelec. domains 78−15132
TGS, switching induced electrolum. 79−38669
TGS, tan δ depend. upon sample thickness 77−59510
TGS, temp. behaviour of optical phonons near T_c, evidence of non-linear pseudospin-phonon interaction 77−7824
TGS, temp. depend. and effect of Cr and α-alanine impurities 78−91448
TGS, temp. depend. of spontaneous polarisation, microscopic mechanism, NMR expts. 77−81070
TGS, temp. depend. of spontaneous polarization near ferroelec. transition 79−33597
TGS, thermal expansion and dielec. const. near ferroelec. crit. temp. 77−40188
TGS, thermal expsn. coeffs. log. anomaly 79−28112
TGS, thermoluminesc. near Curie temp., effect of DC elec. field 79−33848
TGS, under electrostatic field, mechanism of enhancement of neutron diffr. *(Chinese)* 79−51907
TGS, US propag. and vel. rel. to growth defects 79−28049
TGS, US relax., just above T_c, velocity and attenuation coeffs. 77−35637
TGS, US vel. and absorpt. anisotropy and crit. anomalies, acousto-opt. obs. 78−95574
TGS, US vel. and absorpt. in ferroelec. transition region 77−66461
TGS, vacuum-cleaved cryst., charge compensation, ferroelec. field effect obs. 78−95556
TGS, with radiation defects, dielec. dispersion 79−42882
TGS, X-irrad., glycine radicals, geom. struct. by ENDOR and INDO calc. 79−24230
TGS, X-irrad., thermal diffusivity, cooling const. and heat transmission coeff. 79−86935
TGS(Se), optical phonons near T_c, IR refl. and Raman spectra 77−48136
TGS(Se), optical phonons near T_c, nonlinear pseudospin-phonon interaction 77−48137
TGS γ-ray irrad. cryst., heat capacity anomalies near phase transition *(Russian)* 80−49375
TGS $(-d_6)$, sp. ht. near ferroelec. phase transition 80−70420
TGS and deuterated cpd., ferroelec. US relax. time constant 80−84257
TGS biaxial crystal, Cherenkov radiation from 660 MeV protons 77−16416
TGS cleavage faces, ferroelec., oriented growth of Te 79−38509
TGS crystal, generation of second acoustic harmonics 78−18711
TGS crystals, influence of domain struct. on pyroelec. props. 78−31159
TGS crystals, thermal props., γ-radiation defects and inhomogeneity of domain deposition 79−46810
TGS crysts., effects of radiation induced defects on internal bias field 80−88941
TGS deuterated, X-irrad., negative ENDOR, collective motion 79−47357
TGS epitaxial thin film, IR absorption spectra *(French)* 78−35129
TGS family, change of order of phase transition under hydrostatic pressure 78−52452
TGS powder, complex dielectric const. temp. depend. 79−47379
TGS powders, dielec. dispersion 80−97180
TGS pyroelectric detector, compared with W-C point contact, appl. to temporal coherence meas. of HCN laser 80−31871
TGS substrate, ferroelec. field effect in Te films 79−42675
TGS substrate, for AgCl epitaxial growth, model system for orientation mechanism determ. during epitaxy 79−11022
TGS substrate, influence of polarisation reversal on elec. cond. of CdTe thin film 80−65720
TGS type crystal, phase transition model due to nonlinear reson. of lattice oscills. *(Russian)* 77−31746
TGS type ferroelectric, US absorpt. anomalies near T_c 77−16264
TGS vidicon tube, used with optical multichannel analyser as IR detector 78−86329
TGS X-irradiated, paramag. relax, spin-echo study 80−7168
TGS-d, single cryst. films, epitaxial growth method, IR transmission spectra *(French)* 78−72742
TGS-TGSe solid soln., phase transitions under hydrostatic press. 79−99840
organic compounds continued
TGS-TGSe solid solution, temp. depend. of fundamental reflection spectra meas. 77−16337
TGS-type crystals:Cr^{3+}, radiospectroscopic studies 79−15341
TGSe:Cu^{2+}, EPR ang. depend., coord. of Cu^{2+}, Cu-ligand bond obs. and ferroelec. transition anomaly 80−7156
TGSe:Cu^{2+}, EPR studies 80−7153
TGSe:D,L-α-alanine crysts. with large unipolarity, dielec., piezoelec., elastic props. and internal friction 79−33615
TGSe, acoustic and thermal anomaly correlation near ferroelec. transition 79−4775
TGSe, anomalous sound velocity near ferroelec. phase transition at high pressure 78−52456
TGSe, behaviour under press. near tricritical point 79−95716
TGSe, Brillouin scatt. spectra, depolarisation field effect 78−15177
TGSe, crit. behaviour, electrostrictive coupling role 80−71329
TGSe, cryst., US vel., crit anomaly and electromech. effects 79−55832
TGSe, deuterated, dielectric props., ageing 77−16257
TGSe, deuterated, NMR investig. of ferroelec. and press. induced transition mechanisms 77−16189
TGSe, deuterated, thermal and dielectric props. at high hydrostatic press. 80−34864
TGSe, deuterised, elec. field induced Merz double hysteresis loop obs. 78−31164
TGSe, dielectric const. near ferroelec. transition temp., effect of surface capacitance 78−56438
TGSe, domain growth shapes 78−27168
TGSe, domain-wall orientations and wall energies 78−23420
TGSe, emission of free charge carriers in vacuum as symptom of pyroelec. props. 79−42908
TGSe, ferroelec., dielec. nonlinearity 80−75959
TGSe, ferroelec., domain wall orientations and domain shapes 79−38508
TGSe, ferroelec., effect of gamma irradiation on dielec., piezoelec. and elastic props. 77−43943
TGSe, ferroelec., meas. of sp.ht. at constant elec. flux density by AC method 79−33098
TGSe, ferroelec. cryst., complex permittivity at microwave freq. and high press. 80−2685
TGSe, ferroelec. Curie point press. coeff. tensor 79−33635
TGSe, ferroelec. transition, electrooptical hysteresis and crit. behaviour of electrooptical props. 78−2817
TGSe, hydrostatic pressure and deuteration effects on order of phase transition 77−12334
TGSe, IR and UV absorpt. spectra, temp. var. of fund. absorpt. edge 78−84604
TGSe, IR trichroism, epitaxial prop. process 77−63475
TGSe, pyroelectric coeff., 1.8-300K, dynamic method *(French)* 79−19844
TGSe, Raman and far IR spectra, lattice vibrs. in para- and ferroelec. phases 77−77190
TGSe, refractive dispersion, absorpt. spectra characteristics 78−68469
TGSe, sp. ht. anomaly, AC calorimetric obs. 78−23414
TGSe, surface layers effect on coercive field, spontaneous polarisation, and dielec. const. 79−61321
TGSe, temp. behaviour of optical phonons near T_c, evidence of non-linear pseudospin-phonon interaction 77−7824
TGSe, US vel. and absorpt. anisotropy and crit. anomalies, acousto-opt. obs. 78−95574
TGSe, US vel. and absorpt. in ferroelec. transition region 77−66461
TGSe, US velocity and absorpt., 10 MHz, crit. anomalies 77−15504
TGSe-d, single cryst. films, epitaxial growth method, IR transmission spectra *(French)* 78−72742
TGSSe, autostabilised state, elec. second harmonic generation 80−103921
thallium acetate, aq. soln., $^{205}Tl^{+}$ NMR, dissolved O_2 on nuclear spin relax. rate 78−19356
thallium hexanoate, soliton conduction, elec. cond. field and temp. depend. anomaly *(Russian)* 80−103703
theobromine, electronic struct., UV photoelectron spectra, CNDO calc. 79−24949
theobromine, UV PES, constitutive subunits, methylatron effects 78−29798
$(theobromine)_2.H_2I_8$, cryst. struct. determ. using Patterson methods 79−46647
theophylline, electronic struct., UV photoelectron spectra, CNDO calc. 79−24949
theophylline, UV PES, constitutive subunits, methylatron effects 78−29798
thermodynamics at high-press., review 79−24500
2-thiaadamantane, plastic phase, transition and fusion thermodynamics, DSC meas. 78−75603
thiaalkanes pure crysts., thermal press. coeffs. and expansivity at 298.15K 80−49381
1,2,5-thiadiazole, liq., light scatt. from orientational and density fluctuations, hypersonic vel. 77−81110
1,2,5-thiadiazole, NQR coupling const., dipole moment of mol. 79−27010
1,2,4-thiadiazole, struct., double reson. modulation microwave spectra 77−14424
1,2,5-thiadiazole, substitution struct., mag. double reson. 79−27105
1,2,4-thiadiazolidine derivatives, isomers, negative ion mass spectrometry *(Japanese)* 78−5367
thiamine, fission fragment induced desorption, correlated events in TOF mass spectrometry 78−58089
thiamine, radiolysis, one electron redox pot. 79−53048
thiamine (vitamin B_{12}), aq. soln., radiation induced reactions 80−93779
thianaphthalene, plastic cryst., Rayleigh scatt. of Mossbauer radiation 78−27125
thianaphthene-H_2 mixtures, gas-liq. equilib. 79−65177
thianthrene, heat of sublimation, cryst. lattice and polarisation energy 79−32941
2-thiapyridone, dimer, vibr. Hamiltonian for IR spectra of H bonding 78−37620
thiapyrylium, photosensitisation of Lexan:triphenylamine 78−34856
thiazine dye-Fe photoelectrochem. cells for H_2 production, cell instabilities 80−16814
thiazole, ^{14}N NQR of mol., expt. and MO calc. 79−36667
thiazole, rot. Zeeman effect, localised susceptibilities 80−91600
thiazolidine, IR spectroscopy of mol. association *(French)* 79−50178
thiazolidine, mol., vibr. anal., IR and Raman spectra *(French)* 79−26964

organic compounds continued
thiazolidine, valence force field transferability *(French)* 79−10091
Δ-2 thiazoline and alkyl derivatives, IR and Raman vibr. spectra, conformation *(French)* 79−10104
-4 Δ-thiazoline-2 thione and N deutero homologue, force field determ. *(French)* 77−14407
1-(2-thiazolylazo)-2-naphthol, cryst. struct. 77−11536
thieno(3,2-b)thiophene, electronic and vibr. spectra, vapour phase and cryst. 77−34654
thiirane+O_3, autocatalytic reaction, stopped-flow study, reaction rate meas. 80−85152
thiirane+olefin+O_3+SO_2 80−83300
thiirene and deuteroderivatives, Fourier transform IR spectra using Ar matrix isolation, vibr. band assignments 80−14142
thiirene-d_0(-d_1)(-d_2), IR spectra, normal coordinate anal. 80−87107
thioacetaldehyde (-d_1), microwave spectrum, substitution struct. internal rot. barrier, dipole moment 77−6762
thioacetamide, IR spectra, amino group inversion transitions and pot. functions 80−43041
thioacetamides, CNDO calcs., internal rot., ionisation pots., photoelectron spectra 78−5143
thioacetic acid, −d_1, principle axis method anal. of microwave spectra 78−9139
thioamides, characteristic pattern in IR and Raman spectra 78−29818
p,p′-thiobenzophenones, (He I) photoelectron spectra, assigned by perturbational mol. orbital and CNDO/2 calcs. 78−46396
thiocarbocyanine dye, adsorpt. on AgBr photographic gelatin dispersion 78−32908
thiocarbonyl bromide, IR spectra, gas, liq. and matrix isolated, mol. force consts. *(German)* 79−36640
thiocarbonyl chlorofluoride, second excited singlet state emission spectroscopy, resonance fluorescence obs. 80−69158
thiocarbonyl halogen substituted cpds., geometric and electronic struct., LCAO-SCF calc. 79−89603
thiocyanate complexes at Ag electrode surface, Raman spectroscopic study 80−37813
thiocyanates, nonbonding and π-orbital interactions, photoelectron spectra 80−32774
p-thiocyanatoaniline, cryst. struct. 78−71717
thioether+Li^+_x pair pots., ab initio LCAO SCF MO calcs. 80−58184
thioether+Na^+ interaction, pair pots., ab initio SCF LCAO MO calc. 79−36721
thioformaldehyde, $\tilde{a}^3A_2$←$\tilde{X}^1A_1$ IR absorpt. spectra 80−83362
thioformaldehyde, and -d_2, $\tilde{A}^1A_2$-$\tilde{X}^1A_1$ visible electronic absorpt. spectra, vibr. anal. 79−45733
thioformaldehyde, double resonance Stark spectrosc., Doppler-free, using acousto-optic modulator 79−44935
thioformaldehyde, elec. dipole moment determ. using elec. field spectroscopy 78−70870
thioformaldehyde, electronic struct., dipole moments, mol. polarisability, force fields, ab initio calcs. 80−78531
thioformaldehyde, forbidden transitions, laser optoacoustic spectroscopic obs. 77−61756
thioformaldehyde, hyperfine interactions, mol. beam elec. reson. spectra 77−88445
thioformaldehyde, interstellar, 3 GHz absorpt. transition obs. 80−67837
thioformaldehyde-d_0, -d_2, A^1A_2-X^1A_1 vis. absorpt. system, rot. anal. 80−5559
thioformaldehyde-d_0,-d_2, far UV spectrum meas. 2200 to 1800 angstroms 78−25553
thioformamide(-d_2), photoelectron and absorption spectra, vibr. struct., excited state configs. 77−6847
thioformic acid, g-values, mag. susceptibility, quadrupole moments, rot. Zeeman effect, isomer effects 78−25520
thioformyl ion, theoretical study 78−37553
2-thiohydantoin-d_0, (-d_2), mol. vibr. and force field calcs. 78−62779
thioindigo, cis⇌trans isomerisation, nanosecond flash photolysis and steady state methods, triplet state 78−35648
thioindigo, in nonpolar solvent, photoisomerisation mechanism, fluoresc. obs. 77−63933
thioindigo, vibronic fluoresc. spectrum, vibr. struct. 77−54571
thioindigo adsorbed on Al_2O_3, photoisomerisation 80−89503
thioindigo dyes, triplet state config., laser flash absorpt. spectrosc. obs. 80−5557
thiolic antifoggants, chem. struct., adsorpt. on AgBr emulsions, ESCA investig. 78−32907
thiolic antifoggants sensitizing emulsions, latent image form. enhancement 79−17519
thiomethoxide anion, electron affinity, vibr. struct., photodetachment electron spectra 78−94282
thiomethoxyl anion, and deuterate, electron photodetachment, affinities, vibr. freq. and spin-orbit splitting 80−53063
thiomine-Fe solution, modified, photogalvanic effect 78−91722
thiones, N-H-S weak and medium strong H bonds, IR spectra 80−69132
thionine, photoredox system, chem. equilibria *(German)* 77−90630
thionine in sodium lauryl sulphate micellar solns., absorpt. spectra and fluoresc. yield, local dye conc. depend. 80−106343
thionine triplet+haloanilines, electron transfer reaction, radical yield meas. 80−3330
thionine-coated electrode for photogalvanic cells, electrochem. and XPS anal. 80−72071
thionine-Fe photoelectrochemical cell, performance 79−52691
thionine-monohaloaniline triplet exciplex, quenching position dependent heavy atom effect, intersystem crossing 78−53197
thiopen-2,5- dicarboxaldehyde, in lyotropic mesophase, mol. struct. and orientation 78−1004
thiophen, gas, X-ray photoelectron spectra, satellite struct. 78−5281
thiophen-2-carboxaldehyde, in lyotropic mesophase, mol. struct. and orientation 78−1004
thiophene, flash photolysis, new transient absorption spectrum, C_4H_3 radical, assignments 78−46354
thiophene, mag. circ. dichroism, vis. transitions 77−83628
thiophene, mean free path meas., US relax. 80−59585
thiophene, Penning election spectra and photoelection spectra, rel. intensities 80−95725
thiophene, photoelectron ang. distrib. from mol. 79−31596
thiophene, single cryst., UV spectrum, ab initio CI calcs. 79−19898
thiophene, US and hypersonic investigations of vibrational relaxation 80−33377
organic compounds continued
thiophene- or benzene-light alcohol binary system isobaric liquid-vapour equilibrium *(Spanish)* 79−77738
thiophenols, Hammett freq. factors, effects of non-monotonic ν(XH) function variations *(French)* 79−22690
[2,2](2,5)thiophenophane, through bond and through space interactions, UPS obs. 78−82786
thiophosgene, a^3A_2-X^1A_1, dye laser excitation spectra, 539 to 610 nm 78−42083
thiophosgene, B^1A_1-state, photophys., fluoresc. lifetime meas. 80−53033
thiophosgene, laser induced phosphoresc., triplet system 77−61783
thiophosgene, laser Raman spectra, vibr. anal., Cl isotope splitting 77−65486
thiophosgene, photolysis, $^1A_2$-state lifetime, fluoresc. 77−52653
thiophosgene, second excited singlet state emission spectroscopy, Franck-Condon anal. 80−69157
thiophosgene, triplet state, detected by electron energy-loss spectra 78−78808
thiophosgene, vibronic anal. of electronic transition, inversion doubling splittings obs. 80−83388
thiophosgene vapour, fluoresc. from S_2 single vibronic states, quantum yields and quenching 77−34675
thiophosphoryl compounds, bond ionisation energies, mol. struct. from UV photoelectron spectra 78−82782
l-thioproline single cryst., X-irrad., ESR and ENDOR study of radicals 80−45528
thiopyronine-sensitised photodynamic inactivation of RNA synthesis 77−29177
thiosemicarbazide, mol. cryst., transition moment directions 78−64351
thiosuccinimide-d_0,-d_1, normal coord. anal. calcs. 77−30844
thiourea, bond charges, comparison of exptl. and theoretical X-ray scatt. curves 78−55782
thiourea, Brillouin scatt., Debye relax. 79−87453
thiourea, commensurate-incommensurate phase transition, X-ray diffuse scatt. meas. *(French)* 79−19856
thiourea, cryst. with modulated struct., neutron scatt. obs. 79−95713
thiourea, deuterated, commensurate-incommensurate phase transition, inelastic neutron scatt. 79−28098
thiourea, dielec. const. and IR spectra in ferroelec. and antiferroelec. phases 79−33589
thiourea, effects of incorrect phases on difference density distribs. 78−55783
thiourea, expansion coeffs. in phase transition range 78−76407
thiourea, ferroelec., soft mode and Debye relax., IR reflection spectra 77−90111
thiourea, ferroelec. transitions into inhomogeneous modulated phase, Landau theory analysis 77−8527
thiourea, ferroelectric, Raman and IR study 80−71406
thiourea, ferroelectric transition, X-ray scatt. 79−47398
thiourea, ground and first excited triplet state configs., ab initio SCF calcs. 79−89597
thiourea, incommensurable phase transitions. thermodynamic pot. 80−79941
thiourea, incommensurate phase, soft modes, condensation of even-order harmonics 80−103313
thiourea, incommensurate phase transition, X-ray and neutron scatt. study 80−75963
thiourea, inhibition of acid dissolution of iron and steel 79−79181
thiourea, IR reflectivity study of ferroelec. and antiferroelec. phases, dielec. function model 79−33686
thiourea, lattice vibrs. in incommensurate phase 79−28056
thiourea, lock-in phase transform. 80−29698
thiourea, order-disorder transitions, soft modes 78−80361
thiourea, phase transitions accompanied by noncommensurate superstruct. form. 77−32336
thiourea, phonon modes near order-disorder transforms., hard-core modes due to pseudospin-phonon coupling 80−44285
thiourea, phonon modes near phase transitions, IR and Raman spectra 80−45084
thiourea, polycryst., mol. dynamics under hydrostatic press., NMR study 80−80619
thiourea, pyroelectric coeff., 1.8-300K, dynamic method *(French)* 79−19844
thiourea, Raman scattering spectra, soft mode frequency 79−24305
thiourea, Raman spectra of external frequencies 77−24840
thiourea, room temp. photoelastic consts., Brillouin scatt. obs. *(French)* 78−15182
thiourea, soft mode and Debye relaxations 78−80347
thiourea, struct., hydration, ab initio SCF calcs. 80−58142
thiourea, thermally stimulated depolarisation currents, peaks interpreted in terms of molecular relaxations 78−19407
thiourea adducts of SbF_3, cryst. struct. and IR spectra *(French)* 78−87643
thiourea and its derivatives, appl. to inhibition of Fe corrosion in acids 79−20262
thiourea crystal, ferroelec., i.r. reflection spectra meas., shift of soft mode obs. *(French)* 77−4635
thiourea dioxide crystals, use in prod. of harmonic-free X-ray beams 77−15284
thiourea effect on visual pigment responses to prolactin in trout 78−69065
thiourea monocrystals, γ-irrad. effects on dielec. props. 79−91391
thiourea SbF_3, cryst. struct., single cryst. X-ray diffr. study, influence of secondary binding *(French)* 79−32987
thiourea single cryst., γ-irrad. effect on elec. permittivity 78−64311
Thiourea-^{35}S, appl. to autoradiographic image intensification, quantitative anal. 80−90343
thiourea-cyclohexane inclusion compound, phase changes, molecular motion exam. 78−31116
thiourea-d_4-ferrocene inclusion cpd. mol. motion, PMR spectrum 80−84656
thioureas, alkyl and phenyl groups trisubstituted, conformation, steric and stacking interaction 80−95587
thioureas, inhibitive action for brass corrosion in acetic acid soln. 79−87759
thioureas, substituted, normal coord. anal. 79−98246
thioxanthene, chem. shift, ring-current and excess-charge effects, semi-empirical calc. 78−33523
thioxanthone, fluoresc. and internal conversion, rel. to proximity effects 80−91592
thirene, ab initio SCF calc., thermodynamic stability 78−25420

organic compounds continued
tholins, complex organic solids prod. from cosmically abundant mols., rel. to interstellar grains and gas 79−25695
thorium oxalate, natural, separation of ^{228}Ra 80−45600
thorium phthalocyanine, phase contrast characteristics in STEM 80−100153
thromboxane, evidence against prostaglandin hairpin conformation 80−3585
thulium ethyl sulphate, Van Vleck paramag., mag. reson. on uniaxial and uniform compression *(Russian)* 79−61243
thulium phthalocyanine, mol. image in high resolution electron microscopy, radiation damage effect 80−107203
thymidine, ^{11}C labelled, scintigraphy, in vivo distrib. in rabbits 79−5344
thymidine, electron adduct, spin density distrib., INDO calcs. 77−71754
thymidine, frozen aq. solns., final products of gamma radiolysis 78−77001
^{3}He-thymidine effects on circadian rhythms, mouse epithelial cell proliferation 77−21572
thymidine monophosphate, gamma irradiated, inorganic phosphate release, in presence and absence of O_2 80−67168
thymidine monophosphate aqeous solution, gamma irrad. effect on base damage, phosphate release 80−89806
thymidine-5-monophosphate, γ-irrad. aq. soln., spin-trapped radicals, liq. chromatography and EPR spectroscopy 78−53340
thymidine-t induced inhibition of cell-cycle progression in Pisum root meristems 77−56425
thymidylate, ^{11}C labelled, scintigraphy, in vivo distrib. in rabbits 79−5344
thymine, tautomers, polarisation, barriers and tunneling times calcs. 79−41114
thymine+muonium, radical form. in aq. soln., spin reson. obs. 78−74679
thymine aq., and N_2O solns., radiolysis products anal. 80−30257
thymine base damage release, DNA of γ-irrad. Tetrahymena pyriformis 80−72268
thymine damage in chromatin from heated cells after X-irrad., excision obs. 80−45980
thymine damage production and excision, mammalian cell DNA, high-LET irrad. obs. 80−72261
thymine film, polycryst., energy conversion processes, quantum yields, 4 to 10 eV 80−88589
thymine monoanions in soln., tautomer identification by laser Raman spectroscopy 80−14148
thyroxine, free, radioimmunoassay for quantitative meas. of serum conc. 80−94344
thyroxine, free, radioimmunoassay with prebound anti-T_4 microcapsules 80−46014
1,2,3-timethoxybenzene, weak electronic transition, solid, and in rigid glass, UV assignments 78−17681
tin 2,3-dihydroxybutanedioate, Sn(II) valency config., Mossbauer and X-ray electron determ. *(Russian)* 77−8483
tin dithiocarbamate complexes, IR, electronic and mass spectra, mag. susceptibility, cond. meas. 80−97270
tin oxalate, cryst. struct. rel. to those of $Na_2C_2O_4$, $Na_2Sn(C_2O_4)_2$ *(French)* 80−2004
tin oxalate, Sn(II), valency config., Mossbauer and X-ray electron determ. *(Russian)* 77−8483
TMBP.HCNB and TMBTP.HCNB complexes, elec. and mag. props. 78−6512
TMCC chain compounds, Raman spectra and struct. phase transitions 79−56794
$(TMCHDT)_2ClO_4$, organic conductor, struct. study *(French)* 80−88133
TMMC:Cu, dynamic props. using local-moment pair correl. functions 80−15728
TMMC:Cu, EPR lines, dynamic effect of low-symmetric spin distrib. 80−39854
TMMC:Cu, EPR linewidth freq. depend., spin dynamics 80−15794
TMMC:Cu, random one-dimens. Heisenberg antiferromag., spin fluctuations 79−61140
TMMC:Cu(Ni)(Cd), mag. and non-mag. impurity effects on suscept. and Neel temp. 77−66312
TMMC:M, impurity (M) effects on Neel temp. and low temp. mag. susceptibility 78−88113
TMMC, 1-D antiferromag., excitation linewidths, temp. depend. 77−20574
TMMC, 3d ordering, effect of mag. field, PMR meas. 77−4569
TMMC, antiferromag., nuclear spin-lattice relax. by solitons 80−97159
TMMC, antiferromag. coupling in linear chains, molecular orbital approach 78−52239
TMMC, antiferromag. reson. below 1K 78−39408
TMMC, antiferromagneric chain, 3-D ordering temp. controlled by solitons and defects, mag. field depend. 80−60275
TMMC, classical Heisenberg antiferromagnet, one-dimens., dynamic props., review 80−15737
TMMC, crossover transition, effects on susceptibility and EPR shift 80−71047
TMMC, Cu-substituted, spin dynamics, neutron scatt. cross section 80−60312
TMMC, effect of impurity spins on three-dimensional ordering 79−24159
TMMC, EPR lines in one-dimensional mag. systems, dynamic effect of low-symmetric spin distrib. 80−39853
TMMC, exchange-narrowed EPR linewidth, temp. depend. 78−52292
TMMC, field-suppression of spin fluctuations, NMR obs. 78−91971
TMMC, half-field EPR transitions in 1-D Heisenberg paramagnet 79−51843
TMMC, Heisenberg antiferromagnet, magnetism in one dimension, mag. behaviour 79−28495
TMMC, impurity doped, antiferromag. three-dimensional ordering, proton NMR meas. 79−78414
TMMC, linear antiferromag., 3D ordering and spin correlations, mag. field effect 78−19262
TMMC, linear antiferromag., energy gaps in spin-wave dispersion, neutron inelastic scatt. 79−91223
TMMC, linear antiferromag., mag. field effect on nucl. spin-lattice relax. time, 2 to 4.2K 79−61255
TMMC, linear antiferromag., mag. phase diagram, expt. and theoretical study 80−71038
TMMC, linear Heisenberg antiferromag., effect of mag. field on 3d ordering and spin correlations 78−68229
TMMC, linear Heisenberg antiferromagnet, EPR half-field transitions 80−15792
organic compounds continued
TMMC, low-dimensional system, obs. of sidebands on EPR lines 77−80993
TMMC, low-symmetry spin distrib. effect on EPR line 80−66018
TMMC, mag. heat capacity and Neel temp. in mag. field 79−61147
TMMC, Neel temp. in large mag. fields 77−89953
TMMC, neutron scatt. obs. of mag. behaviour 77−66254
TMMC, one dimens. antiferromag., neutron scatt. exam. of impurity effects 78−43598
TMMC, one dimens. Heisenberg system, shift of half-field EPR line 78−23325
TMMC, one dimensional antiferromagnet, EPR expts. 80−20454
TMMC, one-dimens. antiferromag., nonlinear dynamics 80−80521
TMMC, one-dimens. antiferromag., spin wave line widths, neutron scatt. study 79−51767
TMMC, one-dimens. Heisenberg magnet, EPR sidebands 78−88163
TMMC, one-dimens. magnet, local magnon modes 80−65829
TMMC, one-dimensional, EPR at HF and low temp. 78−80205
TMMC, one-dimensional antiferromag., solitons, neutron inelastic-scatt. meas. 80−44810
TMMC, one-dimensional Heisenberg antiferromag., relax. function 77−69474
TMMC, one-dimensional Heisenberg mag., EPR, spin diffusion of 4-spin correl. functions 77−4549
TMMC, one-dimensional mag., anomalous shift of EPR field 78−15010
TMMC, one-dimensional paramag., anomalous freq. depend. of EPR linewidth 80−15784
TMMC, one-dimensional paramag., half-field EPR transition 77−80995
TMMC, paramagnetic relax. rates, anisotropic diffusion model 77−69668
TMMC, quasi-1D antiferromag., mag. phase diagram 80−2573
TMMC, spin dynamic exam., effect of mag. field at low temp. 79−73733
TMMC, symmetry crossover in spin dynamics, proton spin lattice relax. calc. 77−40147
TMMC, XY-Ising crossover transition, quasi-elastic neutron scatt. obs. 80−44826
TMMC(-d) chain compounds, Raman spectra and struct. phase transitions 79−56794
TMMC linear chain antiferromag., optical absorption, magnon sideband intensities calc. 77−59569
TMMC one-dimens. antiferromagnet, effect of mag. field on correl. length 79−91244
TMMC phase behaviour, DTA using Ge-Ag thermocouple 79−65186
TMNB, and deuterated derivative, low temp. far IR spectra 79−24309
TMNB, ferromag. chains with easy-plane anisotropy, exchange const., anisotropy const. and g-value 77−80927
TMNB, linear S=1 ferromag., easy plane anisotropy, low-temp. mag. props. 78−23250
TMNC, ferromag. chains with easy-plane anisotropy, exchange const., anisotropy const. and g-value 77−80927
TMNC, linear S=1 ferromag., easy plane anisotropy, low-temp. mag. props. 78−23250
TMNC, phase transition, low temp. far IR spectra 79−24309
TMNC, quasi one dimensional planar ferromag., low temp. NMR study im mag. field 80−97157
TMP ester, viscosity and density determ. up to 150°C and 150000 psig 77−59940
$[TMPD^+]_2[Cu_xNi_{1-x}(mnt)_2]$, ESR obs. of triplet excitons and Cu(II) ions, mag. interactions 79−95633
TMPD, 2,2,4-trimethylpentane, fluoresc. quenching by elec. field, above photoionis. threshold 78−33539
TMPD, fluoresc. in nonpolar organic liqs. for excitation energies above and below photoionis. threshold 78−1018
TMPD, nonpolar photoionised soln., geminate pair quantum field, recombination fluoresc. elec. field quenching 79−20389
TMPD cation, fluoresc. quenching of hydrocarbons, diffusion effects 77−6823
$(TMTSF)_2AsF_6$, linear-chain conductor, semicond.-metal transition in small elec. field 80−103730
$(TMTSF)_2PF_6$, ESR g-factor, linewidth, spin susceptibility, metal-insulator transition 80−103887
$(TMTSF)_2PF_6$, linear-chain conductor, semicond.-metal transition in small elec. field 80−103730
$(TMTSF)_2PF_6$, one dimens. conductor, superconds., resist. meas. and mag. field effects *(French)* 80−44753
$(TMTSF)_2PF_6$, organic one-dimensional superconductor, transition temp. 80−44754
$(TMTSF)_2PF_6$, quasi-dimens. cond., diamagnetic AC susceptibility 80−103781
$(TMTSF)_2X$, ($X=PF_6^-$, AsF_6^-, SbF_6^-, BF_4^-, NO_3^-) highly conducting salts, props. 80−59969
TMTSF-DMTCNQ, cryst. and mol. struct. 78−63742
TMTSF-DMTCNQ, metallic state, transport props. 80−24974
TMTSF-DMTCNQ, metallic state at low temp. under press. *(French)* 79−82579
TMTSF-DMTCNQ, role of individual stacks in phase transition 79−73307
$(TMTTF)_2BF_4$, cryst. struct. *(French)* 78−26556
$(TMTTF)_2Br$, cryst. struct. *(French)* 78−34503
TMTTF fluoroborate, transmission spectra with electron-phonon coupling phenomenological model 79−19891
TMTTF salts, $(TMTTF)_2$-X, ($X=BF_4^-$, ClO_4^-, SCN^-, PF_6^-, Br^-), physical props. 79−47085
TMTTF-TCNQ, quasi one-dimens. conductor, diffusive hopping, theory 80−54677
TMTTF-TCNQ crystals grown from several organic solvents 80−25544
TNCQ complex, methyltriphenylphosphonium $(TCNQ)_2$, elec. resist. and thermoelec. power meas. 80−107777
TNF-carbazolyl compound charge transfer complexes, equilib. consts. 78−64877
2,6 p-TNS fluorescence probe bound to apomyoglobin, nsec decay 77−29091
TNT, creamed, dimensional stability, irreversible thermal expansion 79−73316
TNT, role of HNS in grain modification 79−100129
tobacco, density changes during burning as obs. by β-source attenuation 78−11792
tobacco mosaic virus, solutions, Rayleigh scatt., elec. induced variations, spectral width and intensity meas. 78−48187

organic compounds continued
α-tocopherol in phospholipid bilayers, struct., order parameters, liq. cryst. transition, entropy 79−83713
tolan, polarisability optical anisotropy 79−72441
tolan-mercury diphenyl, energy characts. determ. of mol. interaction and short range order parameters 79−14794
tolan-mercury diphenyl solid soln., anal. of diffusely scatt. intensity distrib. of X-rays 78−95048
tolanes, molecular conformational mobility study by optical probing method *(Russian)* 80−92459
tolualdehyde, dil. soln., dielectric relax., solid rotator phase 79−42890
toluence, hydrogenation catalysed by Pt implanted cryst. supports 79−20462
toluene, 91^{2+} ion fragmentation, ion kinetic energy spectrum peaks, collision gas sensitive 80−40679
toluene, asymmetric bending vibrs. 79−13696
toluene, $C_7H_8^+$ ion photodissociation on dye-laser irrad. 77−25286
toluene, coherent polarisation spectroscopy of Raman scatt. 78−13758
toluene, depolaris. Rayleigh scatt., optical anisotropy 78−27245
toluene, dielec. const. meas. using 3-terminal meas. cell 78−21170
toluene, dynamic polarization in radiation resistant materials 79−31283
toluene, electronic-vibr. spectra calcs., Franck-Condon and Herzberg-Teller approx. 80−37735
toluene, field ionis. to excited states 77−19002
toluene, film condensation inside pipes, heat transfer, general correlation 79−46312
toluene, fluoresc. quantum yield in soln., dipole-dipole interaction 78−25598
toluene, free convection heat transfer in tube at supercrit. press. 78−42518
toluene, gas, liq. and crit., cation mobility 80−48842
toluene, gaseous, critical and liquid, electron transport 80−64673
toluene, H at. abstraction by free radical, transition state charge development 79−83438
toluene, He ion stopping cross sections, ring struct., bond strain and Bragg rule deviations 79−98188
toluene, heat transfer to ascending (descending) streams, near-crit. press. 77−65742
toluene, in benzene soln., mol. motion, correl. functions 80−96431
toluene, in polar solvent, excess thermodynamic props., Rayleigh scatt. meas. 78−52523
toluene, linear electrooptic effect 77−16283
toluene, liq., Brownian reorientation barriers *(Russian)* 79−27901
toluene, liq., NMR spin-lattice and dielec. relax. 79−33604
toluene, liquid, high-speed schlieren studies of elec. breakdown 77−89332
toluene, luminesc. excitation spectra in rare gas matrices 78−66575
toluene, melting curve up to 9 kbar and down to LNT *(French)* 77−15551
toluene, microemulsion, dynamical and structural props., by chem. physics method 79−79308
toluene, mol., UV prereson. Raman scatt., interference effects 79−64008
toluene, mol., UV prereson. Raman scatt. intensity 79−64007
toluene, mol. geometry, electron diffraction obs. 78−9270
toluene, mol. struct., ab initio calcs. 80−106262
toluene, mol. struct., electron diffr. obs. 77−88559
toluene, molecule translational mobility in depolarised Raman spectra 80−14150
toluene, NMR spin energy transfer using zero mag. field, spin echoes 79−95675
toluene, nonlinear acoustic coeff. determ. *(French)* 77−1175
toluene, optoacoustic spectroscopy using cell with ultimate corrosion resistance 80−42269
toluene, PMMA soln. in toluene, diffusion, viscosity rel. to temp. *(German)* 79−42289
toluene, polystyrene solution, acoustic absorption and dynamic compressibility 77−55321
toluene, refr. index temp. depend., deviation from Lorentz-Lorenz formula 77−40200
toluene, relationships between thermal cond., dynamic viscosity and density, high state parameters 78−83861
toluene, scintillators activated by 1,3,5-triarylpyrazolins containing difluoromethylsulphonyl group *(Russian)* 77−52187
toluene, shock compression, dynamic high press. eqns. of state 80−6450
toluene, simultaneous meas. of NOE and T_1 79−42854
toluene, singlet-singlet electron transitions, modified CNDO-CI method exam. 78−25552
toluene, solid, solubility in liq. N_2 79−37843
toluene, tables of thermodynamic props. 77−24419
toluene, thermal cond., high-precision meas. by obs. technique 80−101792
toluene, thermal cond. meas. by transient hot wire method 77−30144
toluene, transition energies, oscill. strength, time-depend. Hartree-Fock model *(Spanish)* 77−6684
toluene, two-photon ionisation spectrum, of $^1L_b \leftarrow S_0$ transition 80−14180
toluene, vapour, thermal conductivity, 300-700K 78−38444
toluene, viscosity meas. at 353 to 463K and corresponding vapour press. 77−69107
toluene, visible absorpt. spectra, local mode overtone intensity of C-H stretching mode 79−81207
toluene+cyclohexane, energy transfer, pulse radiolysis obs. 80−16714
toluene+ethylbenzene (cyclohexane) (cyclooctane), binary liq., viscosity and excess free energy of mixing 78−51680
toluene+O_2, fluoresc. quenching kinetics 77−18964
toluene+$O(^3P)$, absolute reaction rate consts., 299-440K 79−70304
toluene+$O(^3P)$, reaction product identification by mass spectrometer 78−7185
toluene+OH, cross mol. expt., product anal., 300K 78−44353
toluene+OH, rate constant under simulated atmospheric conditions 80−50846
toluene+OH(D), vibrational and rotational energy effect 80−76497
toluene($-d_8$)-tetracyanoethylene, excited charge transfer state nonrad. decay, vibrs. role 78−82765
toluene cation in solid Ar, absorption and photodissociation spectra 80−69156
toluene derivatives, temp. coeff. of refr. index *(Japanese)* 77−28537
toluene in ethanol-d_0-d_1, dry electron scavenging efficiency, isotope effect on electron localisation 78−27784
toluene polymerisation in CC N_2 afterglow, chem. reactions rel. to plasma props 80−3346

organic compounds continued
bis p-toluene sulphonate diacetylene, low-temp. spectral line splitting 77−32397
toluene vapour, two-photon excitation spectrum under low resolution 79−41212
toluene-1-hexene(1-pentene), radiolysis at 77K, fluoresc., energy transfer processes 78−20037
toluene-9,10-diphenylanthracene, soln., electron beam pulse radiolysis, energy transfer 80−7808
toluene-benzene system vapour-liquid equilib. meas., automatic gas chromatographic anal. *(German)* 78−88667
toluene-brine microemulsion, liquid interfacial tension meas. from scatt. light intensity 80−20012
toluene-bromobenzene, perfect binary liquid mixtures on silica gel, adsorption thermodynamics 80−44428
toluene-chlorobenzene, benzene-toluene, perfect binary liquid mixtures on silica gel, adsorption thermodynamics 80−44428
toluene-d_0, -d_1, mol. reorientation and D nucl. relax. time, temp. depend. 78−39424
toluene-d_0,-d_8, polycryst., methyl torsion, Raman spectra 79−82970
toluene-d_5, liq., vibr.-vibr. near resonant energy transfer, Raman spectra 77−61836
toluene-d_8, soln., fluoresc. quantum yields, temp. and deuteration effects 77−3396
toluene-n-octane, vapour-liquid equilibrium, T-x meas. by semi-micro method 78−87782
toluene-nitrobenzene binary mixtures, with weak charge transfer interactions, thermodynamic props. 80−54360
toluene-sodium dodecyl sulphate-butanol 1-water mixture, interface light scatt., interface tension meas. 80−76039
toluene-sodium salicylate, singlet-singlet energy transfer in Manoxol OT-cyclohexane-water 80−9531
toluene-tetrachloroethylene binary mixtures, dielec. polarisations 79−56713
toluene-triethylamine mixture, US absorption, 7.56 MHz 77−39630
toluene-xylene, liq. mixtures, excess free vol., US vel. meas. 77−51294
toluene-xylene liquid mixtures, US absorpt., appl. of Bauer-Sette theory 79−77682
m-toluenediamine, single crysts., revealing dislocations by selective etch pit technique 77−11560
toluenes, substituted, average mol. polarisability, δ-function calcs. 77−551
toluenes, substituted, methyl torsion, internal rot., neutron inelastic scatt. 77−43160
m-toluidene+glycerol, coexistence curve, exactly solvable decorated lattice model predictions 78−95158
p-toluidine, cryst., low-freq. polarised Raman spectra 78−84574
p-toluidine, kinetics and morphology of lamellar-spiral growth hillocks 78−18566
p-toluidine, vibr. spectra, normal mode calcs. 77−65482
o-toluidine+carbon tetrachloride, binary liquid mixtures, excess free vol. calcs. 80−34202
o(m)-toluidine+o-chlorophenol, H-bonded mol. complex, microwave absorpt., dipole moment and relax. times 80−14134
m-toluidine+o-cresol, binary liquid mixtures, excess free vol. calcs. 80−34202
toluidinonaphthalenesulphonate, room temp. phosphoresc., isomer effects 79−61429
toluol, liq., thermal cond. coeffs. at high-press., 298-573K 79−73350
tolusafranine-EDTA, photoredox reaction, photopot. and photocurrent generation 77−81420
4-m-toluylene diamine, single crysts., conditions of growth and heat treatment influence in dislocation struct. 79−95020
m-toluylenediamine, quadratic optical susceptibility dispersion 79−18477
tolyl cation+alkyl nitrate, reactions and ion struct. 77−52619
tomato bushy stunt virus crystals, appl. of oscillation method to data collection 80−14961
TOPOT, 1,4-bi[2-(5-p-tolyloxazolyl)]benzene laser, bleaching of vapour 80−19027
TOPOT, fluoresc. spectrum light quenching factor wavelength depend. 80−18882
TOPOT, polarisation of spontaneous and stimulated radiation 79−31583
TOPOT vapour dye lasers, multiplate reflectors 80−83606
2-(2-tosylaminophenyl)-4H-3,1-benzoxazine-4-one, cryst. and mol. struct. 80−84167
toxin, penicillum roqueforti, struct. and absolute configuration 80−39064
TP-C-DMP, new bifluorophoric laser dye with intramolecular energy transfer, lasing characts. 78−74899
TP-CSC-DMP, bifluorophoric mol. ultrafast intramolecular energy transfer 78−74900
trace analysis 78−85255
trace elements analysis, in thick samples, photon excited X-ray fluoresc. 78−3423
trace organic pollutants in water, conc. and gas chromatographic determ. methods 79−52854
trans-butadiene, ionis. pot., π-π* energies, open shell many-body formalism calc. 77−46508
trans-butadiene, ionis. spectral intensity, valence electron binding energy depend. 78−90234
trans-dichloroethane, polycrystalline, effect of mag. field on quadrupole spin echo 77−12245
trans-hexatriene, 6.2 eV Rydberg state symmetry, multiphoton ionis. spectrum polaris. assignment 78−70759
trans-p-n-alkoxy-α-methyl p′-cyanophenyl cinnamates, liq. cryst. of strong positive dielec. anisotropy, static dielec. consts. meas. 78−2790
trans-propargyl amine, microwave spectra, dipole moments and struct., isotopic species 78−974
trans-stilbene, fluoresc. lifetimes, 77-295K 78−1029
transdecaline-cyclohexane mixture, percolation model of electron and hole mobility 80−29452
transition metal oxalate hydrates, powders, precipitation from aq. solns., cryst. numbers, sizes 77−44143
tri(trifluoromethyl) germanium halides, gas, liq. and solid, IR and Raman spectra, normal coord. anal. 79−72316
2,4,6-tri-(3,5-di-ter-butyl-4-hydroxybenzyl)-mesitylene, cryst. and mol. struct. 79−86783
tri-(trimethylsilylmethyl) tin monoiodide, molecular and cryst. struct. 79−65068
tri-i-propygermylamine, and isotopomers, IR and Raman spectra, normal coord. anal. *(German)* 80−32716

organic compounds continued
tri-n-butyl ammonium picrate+o-terphenyl, liquid systems, dielectric and dynamic Kerr-effect studies 80−60496
tri-n-butylammonium picrate, complex permitt. meas. by time-domain spectroscopy 77−49741
tri-n-propylamine, fluoresc. decay 80−91590
tri-n-propylamine, in CO_2 laser 79−22935
tri-n-propylamine, laser seed cpds., photoionisation and photoabsorpt. charcts. 78−13688
tri-n-propylamine, low ionis. pot. effect on vol. discharge with UV preionis. 80−44065
tri-n-propylamine doped CO_2 TEA laser, parametric meas. 80−78830
2,3,4,- tri-O-acetyl-1,6,-anhydro-β-D-mannopyranose, pulse Fourier transform proton mag. resonance equivalent to CW INDOR 77−32293
tri-O-ethylamylose-solvent complexes, cryst. struct., chain conforms. 79−65067
tri-p-tolylamine and its paramag. radical cation, disordered mol. solid, direct obs. of superexchange 80−39848
tri-p-tolylamine doped polycarbonate amorphous film, elec. and mag. props 80−49959
triacetoxymercuraurine, direct observation of Hg atoms in make-up of heteroorganic compounds 79−35898
triacetylene, UV spectra of mol. excited states 79−31540
n-triacosane, chain axis cryst., quasi-elastic neutron scatt., plastic phase transform 78−6023
trialkyl silanes, IR absorption vibration spectra, true parameters of isolated bands calc. *(Russian)* 77−83586
trialkylammonium, iodides, absorpt. and luminesc. spectra of self-localized excitons 80−97340
trialkylthioureas, N-H stretching vibrs. and conformation 80−95586
triallyl orthoformate, photoelectron spectra, ionisation pot. bands, conformation, SPINDO calc. 78−9194
triallylarsine, vibr. spectra 79−22696
triallylphospine, vibr. spectra 79−22696
triamantane, phase transistions, X-ray diffr. meas. 79−14930
triamantane, plastic and solid-solid transitions, Raman study 80−60590
triamino-trinitrobenzene, UV and shock-induced decomp. XPS obs. 79−31595
1,3,5-triaryl-2-pyrazolines, glass-forming props. 77−11677
1,3,5-triarylpyrazolins containing difluoromethylsulphonyl groups, scintillation activators for toluene and α-methylnaphthalene *(Russian)* 77−52187
triazastilbenes, photoelectron spectrosc. 80−106353
s-triazene, second order phase transition, mol. reorientation, ^{14}N NQR 78−48074
1,2,4-triazine, and methyl derivs., photoelectron spectra 77−30922
s-triazine, charge density anal. 78−38578
s-triazine, in nematic soln., ^{1}H NMR, struct. ^{1}H, ^{13}C, ^{15}N direct coupling meas. 77−50452
s-triazine, mol. cryst., low temp. mol. reorientation, phase transition, ^{14}N NQR 77−36150
s-triazine, molar Cotton-Mouton const., Kerr const., 298K, 633 nm 77−16286
sym-triazine, molecular reorientation in cryst., PMR determ. 79−73114
1,3,5-triazine, photoelectron ang. distrib. meas. 79−50082
s-triazine, Raman spectrum, lattice vibrs. 78−19465
s-triazine, sp.ht. 130-380K, melting enthalpy and solid-state transition 79−46812
s-triazine, structural phase change, lattice energy calc. 78−55945
s-triazine, structural phase change, sp. ht. meas. 78−55944
s-triazine, structural phase changes, X-ray diffraction and NQR reconciliation 79−46798
s-triazine, structural transitions, low temp. phase 78−55943
s-triazine, transverse elastic mode softening at structural phase transition 79−46777
s-triazine, triplet instability, RPA calculations 80−27938
s-triazine($-d_3$), gas phase IR band contours obs., computer simulation 77−6774
triazine dithiols, for thermal stabilisation of PVC *(Japanese)* 80−108386
triazinyl-stilbene compounds, lasing characts. 78−29948
triazinyl-stilbenes, sulphonated, laser dyes, CW operation in blue and violet spectral region 78−42334
1,2,3-triazole, nucl. quad. coupling in microwave spectrum 77−57987
bis-triazolopyridazines, conformation calcs. by mol. mechanics and CNDO/2 method 80−69079
bis-triazolyls, conformation calcs. by mol. mechanics and CNDO/2 method 80−69079
tribenzo [12] annulene, monovalent anion, MCD and absorpt. spectra 78−70859
sym-tribenzotridehydro [12] annulene, electronic spectra in Shpolskii type hydrocarbon matrices, electronic struct. and fluoresc. 78−66589
tribenzylmethylammonium sulphate, condensed adsorbed layer, effect on electrode reaction rate 80−93769
tribromobenzene, Raman spectra line intensities 79−65863
1,3,5-tribromobenzene mesophase, spiral-like, struct., PMR of dissolved mols. 78−1981
tribromoethanol UV storage films, HBr prod. and sensitivity optimisation *(German)* 79−14068
tribromofluoromethane, liq., ^{13}C and ^{19}F nucl. relax., ^{19}F-^{79}Br and ^{13}C-^{79}Br scalar coupling consts. 78−76330
tribromomethane, multiphoton dissoc., free radical prod. 79−61842
tribromomethane+POPOP, physical and chem. kinetics competition, fluoresc. quenching obs. 79−43567
tribromomethane-methane, mass spectra, vel. distrib. effects 77−54627
tribromomethane-propyl alcohol conc. fluctuation kinetics, holographic study *(Russian)* 78−19508
2,4,6-tribromophenol, Raman and IR spectra, hydrogen bonds 80−84735
1,3,5-tribromotrifluorobenzene in gaseous state, emission spectra 80−63648
tribromotrifluoroethane, IR and Raman spectra, normal coord. anal. *(German)* 80−32726
tributyl phosphate, fuel reprocessing solvent 77−65320
tricarbocyanine, laser dyes, flashlamp-pumped, photochemical stability 80−83604
tricarbocyanine dye passive Q-switch for Nd^{3+} lasers 79−10333
tricarbocyanine solns., photoisomerisation, fluoresc. and absorpt. spectra of photoisomer 78−85181
trichloracetonitrile, IR dispersion, complex refractive index and permittivity, time correl. function 80−45057

organic compounds continued
1,1,2-trichlorethane, soln. in acetone, US relax., solvent effects 79−99275
trichlorethylene, detect. in ambient air by gas chromatography 78−85739
1,3,5-trichloro,2,4,6-trifluorobenzene radical cation, $B^2A_2' \rightarrow X^2E''$ laser-induced fluoresc. spectra 80−14172
trichloro(methyl)germane, mol. struct. determ. by vap. phase electron diffr. 77−54621
1,1,1-trichloro-2,2-bis(p-chlorophenyl)ethane (DDT), in soils of Everglades National Park and adjacent agricultural areas 79−92098
1,1,2-trichloro-2,2-difluoroethane, vac. UV photodecomp. 80−66828
1,3,5-trichloro-2-bromobenzene, chemical perturbation of cryst. structs., Raman phonon spectra 78−26559
1,2,3-trichloro-5-bromobenzene, chemical perturbation of cryst. structs., Raman phonon spectra 78−26559
B-trichloro-m-carborane, cryst. electrophilic chlorination of 9, 10-dichloro-m-carborane, cryst. and mol. struct. from X-ray diffr., cryst. struct. 78−9268
2,4,6-trichloro-s-triazine, molar Cotton-Mouton const., Kerr const., 298K, 633 nm 77−16286
trichloroacetic aced, soln., vibr., IR spectra 80−63633
trichloroacetic acid, proton chem. shift tensor 79−24224
trichloroacetic acid, proton chemical shift tensor 78−13520
trichloroacetic acid, self association, IR spectra, book contrib. 78−21931
trichloroacetic acid molecular compounds, intramolecular configs., nucl. quadrupole double reson. obs. 80−34821
trichloroacetic acid-base H bonded complex, ^{35}Cl NQR meas. 78−25555
3,4,5-trichloroaniline, polymorphism, ^{35}Cl NQR 80−54163
trichloroanilines in solutions, IR absorpt. spectra 80−69136
1,3,5-trichlorobenzene, ^{35}Cl NQR, high press. behaviour 79−33560
1,3,5-trichlorobenzene, ^{35}Cl spin-lattice relaxation under press. 79−4738
1,2,3-trichlorobenzene, anisotropic reorientation, nucl. relax. in coupled spin systems 77−40145
sym-1,3,5-trichlorobenzene, cation, emission spectrum, Jahn-Teller effect 79−89681
1,2,3-trichlorobenzene, Fourier transform double resonance NMR 78−80249
1,2,4-trichlorobenzene, in KOH-2-propanol soln., chain dechlorination by γ-rays 78−56904
1,3,5-trichlorobenzene, lattice vibr., Raman spectra line intensities calc. 77−69825
1,2,3-trichlorobenzene, low freq. vibs. 77−32365
1,2,3-trichlorobenzene, oriented mols., ^{13}C satellites use in proton spectra, r_α-structure 80−18872
trichlorobenzene cation, selectively excited wavelength resolved emission spectra 80−87136
1,2,4-trichlorobenzene liq., mol. reorientation, translation and vibr. relax., Rayleigh and Raman spectra 80−95632
1,3,5-trichlorobenzene mesophase, spiral-like, struct., PMR of dissolved mols. 78−1981
1,3,5-trichlorobenzene radical cation, emission and photoelectron spectra, lifetimes meas. 78−86905
trichlorobenzene radical cation, gas and matrix isolated vibr. resolved electronic spectrum 79−68252
trichlorobenzene radical cation, symm. substituted, fluoresc. and emission spectra in Ne matrix 79−89702
trichloroethane, atm. conc. meas. in southern hemisphere 79−5602
trichloroethane, CH_3-stretching modes, Raman spectra reson. energy transfer obs. 78−48162
1,1,1-trichloroethane, detect. in ambient air by gas chromatography 78−85739
1,1,1-trichloroethane, in nonpolar solvents, permanent dipole moment determ. 77−43125
1,1,1-trichloroethane, optimised additive to improve Si thermal oxidation technology 79−29239
1,1,2-trichloroethane, phase diagram, 0-10 kbar 77−72679
1,1,2-trichloroethane, phase-modulated spin echoes, derivation of pure absorpt. spectra 80−22410
1,1,1-trichloroethane, polymorphism under high pressure *(French)* 80−96644
1,1,1-trichloroethane, Raman spectra, vibr. dephasing 79−59465
trichloroethane, separation of collision-induced from intrinsic mol. depolaris. Rayleigh scatt., C-Cl bond optical anisotropy 78−27244
1,1,1-trichloroethane, thermodynamic and structural studies of polymorphism 78−18571
trichloroethane, vibr. population lifetimes in liqs. anti-Stokes Raman scatt. 78−74665
trichloroethane+OH, reaction rate consts. and quenching kinetics, reson. fluoresc. obs. 79−72349
trichloroethane+$OH \rightarrow H_2O+CH_2CCl_3$, rate const. and tropospheric chem. 80−16658
trichloroethane + OH, 1,1,1- and 1,1,2-isomers, reaction kinetics 298-460K, lower atmos. chem. 80−16657
2,2,2-trichloroethanol($-d_2$), vibr. spectra and normal coord. anal. 79−72319
trichloroethylene, effect of addition on thermal oxidation of Si at 1200°C 78−27660
trichloroethylene, film condensation inside pipes, heat transfer, general correlation 79−46312
trichloroethylene, interaction with thermal-energy electrons, cyclotron reson. obs. 77−19097
1,1,2-trichloroethylene, liq., transport through barrier plastic 78−76921
trichloroethylene aqueous hetero-azeotrope mixture, condensation heat transfer coeff. *(German)* 80−33425
trichlorofluoreomethane, UV laser photolysis 80−66826
trichlorofluoromethane, 8-12 μm band model calcs. 80−43112
trichlorofluoromethane, 8-12 μm bands intensities, temp. depend. 80−43048
trichlorofluoromethane, ^{19}F spin-rot. tensors, appl. to liq.-phase rot. diffusion 80−43068
trichlorofluoromethane, ^{1}H and ^{19}F dynamic polarisation, Cl scalar coupling enhancement 78−66568
trichlorofluoromethane, atm. conc. meas. in southern hemisphere 79−5602
trichlorofluoromethane, conc. meas. in air over Europe 77−37351
trichlorofluoromethane, conc. meas. in stratosphere 78−32171
trichlorofluoromethane, dissoc. electron attachment, pot. curves calcs. 79−98231
trichlorofluoromethane, dissoc. into metastable fragments following electron impact excitation 78−37757

organic compounds continued
trichlorofluoromethane, electron impact dissoc., light emission from fragments 79−13826
trichlorofluoromethane, in atmosphere, interhemispheric gradients meas. 78−81289
trichlorofluoromethane, ion pair formation by photoionisation 79−89718
trichlorofluoromethane, IR multiple-photon laser-induced decomposition, Cl and Cl_2 form. 78−40066
trichlorofluoromethane, matrix radiolysis and photoionis. at 15K,IR spectrochem. anal. 78−76893
trichlorofluoromethane, rate const. for reaction with OH and tropospheric lifetime 77−64366
trichlorofluoromethane, threshold electron attachment cross-section 79−89708
trichlorofluoromethane, transport processes indicator in urban atmosphere 78−36264
trichlorofluoromethane, tropospheric lifetime 78−3920
trichlorofluoromethane, tropospheric lifetime 79−53497
trichlorofluoromethane, UV absorpt. cross sections temp. depend. stratospheric 77−64423
trichlorofluoromethane, UV photodissoc. cross-section, 223 and 296K 79−52729
trichlorofluoromethane, UV photoelectron spectra, vibr. fine struct. 78−9196
trichlorofluoromethane, vertical profile meas. in seawater *(German)* 78−3814
trichlorofluoromethane (F-11) in N Atlantic water columns, exploratory anal. 78−88847
trichlorofluoromethane anion, dissoc. electron attachment, pot. curves calcs. 79−98231
trichlorofluoromethane in stratosphere, height profile meas. at several latits. 80−72601
trichlorofluoromethane mols., electron scavenging studied by electron cyclotron reson. 79−50143
trichlorofluoromethane reaction rate with atmospheric-like ions 77−70723
trichloromethane, and -d_1, depol. Raman scatt. line shapes in liq., density effects 79−4796
trichloromethane, and -d_1, liq., vibr. relax., Raman spectra 78−19471
trichloromethane, chemisorption on Cu low-index and stepped surfaces, LEED, AES and UPS obs. 80−84391
trichloromethane, liq., radial pair distrib. function determ. 79−77476
trichloromethane, low-energy X-ray emission spectra, MO anal., ionis. pot., rel. to CCl_4 and CH_4 79−85975
trichloromethane, matrix isolation IR spectra, $^{35/37}Cl$ and $^{12/13}C$ isotope shifts 78−977
trichloromethane, mol. struct. factors, X-ray diffr. 77−76291
trichloromethane, separation of collision-induced from intrinsic mol. depolaris. Rayleigh scatt., C-Cl bond optical anisotropy 78−27244
trichloromethane, vibr. population lifetimes in liqs. anti-Stokes Raman scatt. 78−74665
trichloromethane+N, CN quartet state production, fluoresc. anal. 78−68888
trichloromethane(-d_1), electrooptical parameters and Raman intensities obs., bond polaris. calcs., vibr. force field 77−50441
trichloromethane glass:O_3, ^{17}O, NQR by proton double reson., broad reson. assignments 80−53014
trichloromethane in dil. soln., dynamic dipole induced interactions in absorption spectra 78−13553
trichloromethane in nematic liq. crystal, AX($^{13}CHCl_3$) nuclear relax., dipole-dipole interaction 77−54567
trichloromethane-d_0,-d_1, soln., far IR spectra, band shape and moment anal. 80−58252
trichloromethane-d_1, in nonpolar solvents, vibrational and rotational relax. 79−10182
trichloromethane-d, Raman band shapes, mol. oscill. bands *(German)* 80−69154
trichloromethoxysilane, normal vibr. and force field calc. 79−54994
trichloromethyl peroxynitrate, UV absorpt., spectra, photodissoc. lifetime meas. 80−83386
trichloronitromethane, visible and near UV spectra, 295K, photoabsorpt. cross-section 79−22720
trichloronitrosomethane, visible and near UV spectra, 295K, photoabsorpt. cross-section 79−22720
2,3,4-trichlorophenol, AX spin system, two-dimens. J-resolved NMR, spin decoupling 80−31823
2,4,6-trichlorophenol, Raman and IR spectra, hydrogen bonds 80−84735
trichlorophosphazenes, ^{35}Cl NQR spectra and reorientational motion of PCl_3 group 78−25567
trichlorophosphazo compound, $Cl_3P{:}NCCl(CF_3)_2$, nuclear quadrupole spin-lattice relax. 80−66062
trichlorophosphazoperfluoro-1,1-dimethylethane, cryst., ^{19}F NMR and mol. mobility, fluorination influence 80−34809
trichlorosilane liquid, Si-H stretching mode vibr. dephasing, Raman study 80−84736
1,3,5-trichlorotrifluorobenzene, IR and Raman vibr. spectra 77−3356
trichlorotrifluoroethane, diffusion in smectic A liq. cryst., NMR spin echo obs. 78−94975
trichlorotrifluoroethane, IR and Raman spectra, normal coord. anal. *(German)* 80−32726
trichlorotrimethyl benzene, disordered solid, vibr. state, itinerant oscill. model 79−73278
1,2,3,-trichlorotrimethylbenzene, disordered mol. solid, electrodynamic influences on dielec. absorption 80−40040
tricosane, single cryst., polarised Raman spectra 77−61888
tricresyl phosphate, in DMF, electrochem. reduction, automatic pH control appl. 77−63928
tricresyl phosphate in gasoline, P determ. by at. absorpt. spectrometry 78−31729
tricresyl phosphate treated AISI 52100 ball bearing steel, Auger anal. 79−52413
tricresyl phosphate-polystyrene solns., viscoelastic props., conc. depend. 80−76299
tricresylphosphate, appl. of spectroscopic methods for surface anal. in area of lubrication *(French)* 80−26095
tricresylphosphate, supercooled liq., LF region of scatt. line wing 79−65888
p-tricyanovinylphenyldicyanomethide ion, donor props., cyclic voltammetry and π-complex form. 80−88520
tricyclo(3.3.0.$0^{2,6}$)octane, liq., Raman spectrum, vibr. assignments 77−61753

organic compounds continued
tricyclobutadiobenzene, graph theory for axial symmetry molecules *(Chinese)* 79−36792
tricycloquinazoline, excited states, fluoresc., phosphoresc. 77−61789
n-tridecane, calorimetry at high state parameters 78−57953
triethanolamine, US relax., intermol. H bonds redistrib. 77−69050
triethyl methacryloxystannane, protection from biological overgrowths 78−18034
triethylacetic acid, high resolution ^1H and ^{13}C NMR spectra at liquid-solid phase transition 80−11281
triethylamine, fluoresc. decay 80−91590
triethylamine, gas (soln.), fluoresc. quenching by 'inert' perfluoromethylcyclohexane 78−46438
triethylamine, laser seed cpds., photoionisation and photoabsorpt. charcts. 78−13688
triethylamine, photoionisation for imaging Cherenkov detector using gas-filled MWPC 80−91400
triethylamine, Rayleigh line and acoustic spectra, fine struct. 77−39629
triethylamine-H_2O, crit. fluid, refr. index, α and Δ components 79−82940
triethylamine-H_2O, crit. phenomena, US vel. and absorpt. 78−91382
triethylamine-I_2, n-σ charge-tranfer complex, frozen soln., Mossbauer spectra obs. 80−91655
triethylamine-perfluoro-T-butanol, photoelectron and Rydberg bands, UV spectra study 80−18865
triethylamine-water, critical mixture, specific heat anomaly 79−42268
triethylamine-water, near crit. soln. pt., sp. ht. at const. press. and crit. conc., −1-22°C 78−38847
triethylamine-water critical mixtures, US absorpt. 79−28045
triethylamine/alcohol mixtures, theoretical evaluation of sound vels. and AB interactions 78−18706
triethylamine/phenol mixtures, theoretical evaluation of sound vels. and AB interactions 78−18706
triethylene, in polystyrene matrix, energy barriers, dielec. absorpt. meas. 78−70958
triethylene glycol, critical nuclei, meas. of number of mols. and surface tension from rate of nucleation 79−65293
triethylenediamine, aq. soln., stimulated Raman scatt., struct. enhancing solute 78−27222
triethylenediamine, multiphoton ionis. and two-photon fluoresc. excitation spectra 79−98164
triethylenediamine, plastic cryst., thermolum. curves 80−2876
triethylenediamine, Raman spectra study *(French)* 80−80768
triethylenediamine aq. soln., dielectric relaxation rate 79−78619
triethylenediamine cation radical, ESR 77−24745
triethylenediamine complexes, structural relationships *(French)* 80−54213
triethylsilylamine, and isotopomers, IR and Raman spectra, normal coord. anal. *(German)* 80−32716
trifluoracetic acid-water, molecular dynamics simulation of chemical reactions in solution 80−40673
trifluoraethanol solvent for poly[(R)-oxypropylene], effect on opt. rot. dispersion and vac. UV circular dichroism 80−40084
trifluoremethane-d_1, IR photolysis, kinetics of multiphoton dissoc., ^1H isotope separation 79−79276
1,1,1-trifluorethyl halides, internal rot. barriers and LF Raman spectra 77−65478
1,1,1-trifluoro-3-chloropropane, Raman and IR obs. of rot. isomerism, entropy difference between vapour and liq. phase isomer *(Russian)* 79−31529
trifluoroacetamide, single cryst., X-irrad., transient radical form., INDO and ESR calcs. 77−12814
trifluoroacetamide, X-irrad., CF_3...F radical ESR 78−73066
trifluoroacetates, methyl and ethyl, intramol. relax. at microwave freqs. 80−55020
trifluoroacetic acid, ab initio MO calcs. of geometry, torsional barriers 78−90313
trifluoroacetic acid, monomer and dimer, photoelectron spectrosc. 80−87172
trifluoroacetic acid, soln., polarisable H bonds, IR spectrosc. obs. 80−58408
trifluoroacetic acid, US absorpt. 77−15505
trifluoroacetic acid-acetic acid, equimolar mixture, US absorpt. 77−15505
1,1,1-trifluoroacetone, photochem. and photophysics, 330-250 nm, 0-1000 torr 78−17706
1,1,1-trifluoroacetone, triplet state trapped electron ICR spectrosc. 79−59373
α,β-β-trifluoroacetonitrile, liq.-liq. transition rel. to mol. motion, NMR study 80−70383
trifluoroacetophenone+dimethoxy benzene. in acetonitrile photoreaction, nuclear spin polarisation, criterion for triplet-Overhauser mechanism 80−69168
trifluoroacetyl fluoride, triplet state trapped electron ICR spectrosc. 79−59373
trifluoroacetyl iodide, UV photodissoc. into three fragments, expt. and trajectory calc. 79−70356
1,2,3-trifluorobenzene, ^{13}C, ^{19}F, and ^1H NMR spectral anal. 78−37659
trifluorobenzene, cation, visible emission spectra of gas, Jahn-Teller effect 79−50034
trifluorobenzene, equilib. config. and barriers, microwave spectra 80−95606
1,3,5-trifluorobenzene, IR rot.-vibr. band contours 79−76430
1,3,5- trifluorobenzene, liq., NMR spin-lattice and dielec. relax. 79−33604
1,2,4-trifluorobenzene, microwave spectrum, dipole moment and centrifugal distortion constants 78−37630
trifluorobenzene, symmetrical ^1H and ^{19}F NMR, cross relax. 79−38406
symtrifluorobenzene cation, Jahn-Teller effects, intermode interactions and intensity anomalies 80−78553
sym-trifluorobenzene cation, Jahn-Teller effects, quadrupole coupling 80−78554
trifluorobenzene cation, selectively excited wavelength resolved emission spectra 80−87136
trifluorobenzene cations, Jahn-Teller distortions, quadratic and mode mixing effects., distortion geometry determ. 80−91462
1,3,5-trifluorobenzene radical cation, laser induced fluoresc. spectra, vibronic anal., Jahn-Teller distortion 79−3470
trifluorobenzene radical cation, symm. substituted, fluoresc. and emission spectra in Ne matrix 79−89702

organic compounds continued
1,3,5-trifluorobenzene-d_0(-d_3), cation, emission spectrum, Jahn-Teller effects 79−89680
trifluorobromomethane, ^{19}F chem. shielding, temp. depend., FT NMR obs. 78−86888
trifluorobromomethane, multiphoton laser induced chemistry 79−91974
trifluorobronomethane, $CF_3{}^{79}Br$, precision IR spectra from IR-microwave double reson. 77−14428
trifluorochloromethane, ^{19}F chem. shielding, temp. depend., FT NMR obs. 78−86888
trifluorochloromethane, Raman and IR spectra, $^{35/37}$Cl isotope splitting and mol. constants *(German)* 77−83595
trifluorochloromethane+^{38}Cl, reactions due to ^{37}Cl(n,γ)^{38}Cl 77−86342
trifluorochloromethane mols., electron scavenging studied by electron cyclotron reson. 79−50143
trifluoroethane, chemistry of nuclear recoil ^{18}F atoms, high. press. study 77−86339
trifluoroethane, isolated CH stretching freqs. and bond props. 79−94104
trifluoroethane, MODR, rot. consts. 78−9177
1,1,2-trifluoroethane, mol. struct., gas phase electron diffraction, rotamer abundance 79−76514
trifluoroethane(-d_3), IR and Raman spectra, normal coord. anal. *(German)* 80−32726
trifluoroethanol, H-bonding investigated with supersonic mol. beam using photoionisation quadrupole mass spectrometer 80−102543
2,2,2-trifluoroethanol, multiphoton absorpt. and dissoc. 80−99530
2,2,2-trifluoroethanol(-d_2), vibr. spectra and normal coord. anal. 79−72319
trifluoroethene, dissociation from 2,2-dichloro-1,1,1-trifluoroethane, fluence threshold 79−64112
trifluoroethene-d_0,d_1, mol. struct., microwave and electron diffr. obs. 80−58384
β,β,β-trifluoroethyl radical in Ar matrix, EPR, F and H^+ hyperfine interaction and motional effects 77−14460
trifluoroformamide, electronically excited, vibr. relaxation, stochastic description 78−37715
trifluoroformamide, photodissoc., obs. of NO (v=1) 78−74712
trifluoroformamide, radiationless pathways, time-resolved fluoresc. obs. 78−66577
trifluoroformamide, thermal dissoc., shock wave study 79−34284
trifluoroiodomethane, double resonance Stark spectrosc., Doppler-free, using acousto-optic modulator 79−44935
trifluoroiodomethane, high press., selective isotope dissociation with pulsed CO_2 laser 79−72370
trifluoroiodomethane, highly excited, intermol. vibr. energy transfer, transient UV absorpt. spectra 80−106381
trifluoroiodomethane, IR multi-photon excited mols. 80−74207
trifluoroiodomethane, IR multiphoton dissoc. yields, new technique, non-linear pumping effects 79−100406
trifluoroiodomethane, isotopic sensitivity of IR laser photodissociation 80−7805
trifluoroiodomethane, K+trifluoroiodomethane→KI+trifluoromethane, molecular beam reactive scattering, angular distribution study 79−98198
trifluoroiodomethane, laser isotope separation by multiple photon IR excitation and subsequent UV dissoc. 79−18301
trifluoroiodomethane, laser microwave double reson. spectroscopy with CO_2 laser lines 80−87156
trifluoroiodomethane, laser photolysis, I* form., quenching obs. 77−3299
trifluoroiodomethane, liquefied gas solns. bound exciton model for Rydberg bands 78−31214
trifluoroiodomethane, molecular vibration energy stochastization in intense IR laser field by Raman spectroscopy *(Russian)* 80−14149
trifluoroiodomethane, multiphoton dissoc., isotopically selective 80−28113
trifluoroiodomethane, multiphoton IR excitation and dissoc. *(Russian)* 80−35562
trifluoroiodomethane, multiple IR photon excitation and dissoc., primary characts. 80−11909
trifluoroiodomethane, optically pumped laser, 11-17 μm 78−46581
trifluoroiodomethane, photolysis in I laser, chem. kinetics 80−48235
trifluoroiodomethane, pyrolysis in Ar:O_2 matrix, forming trifluoromethylperoxy radical 80−50845
trifluoroiodomethane, solns. with liq. Ar, Kr, Xe, CH_4 and CF_4, Rydberg band positions, temp. depends. 78−17686
trifluoroiodomethane, UV absorpt. spectrum broadening by laser-induced vibr. excitation 80−53050
trifluoroiodomethane, UV absorption induced by excitation of ν_1 vibrational mode 78−50552
trifluoroiodomethane, UV absorption profile modification with vibr. excitation, for I laser fusion ignition 78−58717
trifluoroiodomethane, vac. UV absorpt. cross section 80−91574
trifluoroiodomethane, vap. phase photolysis, UV irrad. 78−73070
trifluoroiodomethane, X→B Rydberg transition, Jahn-Teller coupling parameter, vibronic level calc. 78−50536
trifluoroiodomethane+F, IF product internal rot.-vibr. distribs., fluoresc. obs. 80−48078
trifluoroiodomethane+F reactions, product state analysis using laser-induced fluoresc. 80−11915
trifluoroiodomethane+K(Ba)→K(Ba)I+CF_3, products translational distrib., crossed beam reaction 78−31629
trifluoroiodomethane+O, I atom abstraction by O, mol. beam study 78−48638
trifluoroiodomethane+O, vel. distrib. and cross section, reactive scatt. 80−26011
trifluoroiodomethane cation, photodissoc. by quasi-continuum single IR photon absorption 80−61124
trifluoroiodomethane ion, dissociation, induced by collision with Kr atom, mass spectra *(Russian)* 77−88549
trifluoroiodomethane nuclear pumped lasers, electron impact cross section meas. 80−63985
trifluoroiodomethyl cation, IR photodissoc. 80−87188
trifluoromethane, ^{129}Xe chem. shift, chem. shielding 77−6707
trifluoromethane, ^{19}F chem. shielding, temp. depend., FT NMR obs. 78−86888
trifluoromethane, and -d_1, microwave spectra in ν_6=1 state, accidental degeneracy, mol. struct. 79−3436
trifluoromethane, D ultrahigh single-step enrichment by CO_2 laser photolysis 80−45527
trifluoromethane, dielectric const. near critical point 79−15394
organic compounds continued
trifluoromethane, dielectric constant effect on nuclear spin-spin coupling constants 79−72240
trifluoromethane, electron impact dissoc., light emission from fragments 79−13826
trifluoromethane, gas phase IR rot. velocity correl. functions *(French)* 78−62778
trifluoromethane, IR spectra, spectral bandshape and intensity of C-H chromophore 80−83355
trifluoromethane, photoionis. cross section calc., for YMζ line, HF vs OPW methods 77−42353
trifluoromethane, polar gas thermomagnetic torque meas. 77−42960
trifluoromethane, pure and mixtures, vibr. relax. times at 298K 77−525
trifluoromethane, PVT study by Burnett method 77−42949
trifluoromethane, quadratic CNDO force fields calcs., coord. effects 79−6877
trifluoromethane, RF discharge chemistry, added H_2 effect 80−33832
trifluoromethane, rot. isomerism, internal rot. splitting 78−94232
trifluoromethane, rot. transitions, self-broadening and self-shifting meas. 79−59426
trifluoromethane, US absorpt. for vibr. self-relax., 163-299K 78−63529
trifluoromethane plasma etching of SiO_2, optical spectroscopy appl. 80−87940
trifluoromethane-methane, liq.-liq. phase equilib., crit. phenomena 78−18764
trifluoromethanesulphonic acid, and salts, electrochem. characts. in nonaqueous solvents 80−89499
trifluoromethanesulphonic acid monohydrate, electrochemical props. and use as fuel cell 79−61969
trifluoromethoxide gas phase ion reactions with carboxylic acids, ion cyclotron reson. obs. of competitive solvation 79−79227
trifluoromethyl bromide, microwave spectra, mol. rot., isotopic variation in bond lengths, Stark meas., dipole moments determ. 80−74165
trifluoromethyl cation bombardment of Si, F desorption 79−70367
trifluoromethyl chloride, IR multiphoton dissociation, isotopic selectivity and yield, temp. effect 80−53069
trifluoromethyl cyanides and isocyanides, isomerisation, ab initio (STO-3G) geometry optimised calc. 78−46265
trifluoromethyl halides, matrix photoionis., IR spectra of $CF_3{}^+$, CF_2X^+ and CF_3X^+ cations 78−74710
trifluoromethyl halides, multiphoton dissoc. products, ^{13}C enrichment 79−18302
trifluoromethyl hydroperoxide(-d), CF_3 torsional vibrs., low freq. Raman spectra 80−91565
trifluoromethyl hypochlorite, vibr. spectra and normal coord. anal. 80−102517
trifluoromethyl hypofluorite, vibr. spectra and normal coord. anal. 80−102517
trifluoromethyl hypofluorite+Kr($^3P_2$), KrF* bound-free oscill. emission spectra calc. 80−7799
trifluoromethyl hypofluorite (hypochlorite), CF_3 torsional vibrs., low freq. Raman spectra 80−91565
trifluoromethyl iodide, ^{13}C isotope separation by selective multiphoton dissoc. 78−25734
trifluoromethyl iodide, ion-molecule reactions, amongst radiolysis products, reaction rates, mechanisms, mass spectra 79−5136
trifluoromethyl iodide, microwave spectra, mol. rot., isotopic variation in bond lengths, Stark meas., dipole moments determ. 80−74165
trifluoromethyl iodide+Ba, BaI vibr. states bimodal distrib. 78−27743
trifluoromethyl liquid crystals, effect of mol. struct. on mesomorphism 78−51414
trifluoromethyl peroxyfluoride (peroxychloride), CF_3 torsional vibrs., low freq. Raman spectra 80−91565
bis-trifluoromethyl phosphine iodide, stimulated emission, photodissoc. laser appls. 79−10295
trifluoromethyl sulphonyl chloride, mol. struct., electron diffr. obs. 79−7016
trifluoromethyl systems, in smectic liq. cryst. soln., Fourier transform ^{19}F NMR 77−79631
trifluoromethyl trifluoracetate, mol. image reconstruction by electron holography 79−68367
trifluoromethylhalide radical anions, formation, ESR and struct. 77−32809
trifluoromethylsulphonyl chloride, geom. struct., CNDO/2 calc., comparison with CH_3SO_2Cl 79−81295
5-trifluoromethyluracyl, electron beam damage assessed by EELS 80−89809
2,4,6-trifluoronitrobenzene, ^{19}F shielding anisotropies, nematic phase NMR 77−27090
trifluoronitrosomethane, visible and near UV spectra, 295K, photoabsorpt. cross-section 79−22720
3,3,3-trifluoropropene, struct. and vibr. spectra, IR, Raman polarisation study 80−18845
trifluorotrichloroethane, influence of porous coating of heating surface on rate of heat transfer on boiling *(Russian)* 79−10452
trifluorotriiodoethane, IR and Raman spectra, normal coord. anal. *(German)* 80−32726
triglycerides, diacid and triacid, IR spectra, diathesis (vibr. moieties) anal. 77−44525
triglycerides, serous, evolution in mice exposed to 2 to 10 GHz radiation *(French)* 77−64083
triglycine, aq. soln., density, viscosity and dielectric const., 0-60°C 78−47462
triglycine calcium bromide:Cu^{2+}, ESR studies 80−97136
triglycine fluoberyllate, deuterated, dislocation line defect X-ray topographic analysis 80−59465
triglycine fluoberyllate, pyroelectric, dielectric and thermal props., temp. depend. 78−43809
triglycine fluoroberyllate, ferroelec. transition, electrooptical hysteresis and crit. behaviour of electrooptical props. 78−2817
triglycine fluoroberyllate, solution growth of large single crystals, using cylindrical seeds 78−60556
triglycine fluoroberyllate, spin-lattice relax. meas. of ^{1}H, ^{13}C, and ^{15}N near ferroelec. transition 77−1646
triglycine fluoroberyllate, thermodynamic props. 78−15123
triglycine selenate, elastic moduli matrix, and temp. depend. of elastic moduli 79−46738
triglycine sulfate crystal, nematic liquid crystal behaviour on cleavage face 79−94899
triglycine sulphate: Cu^{2+}, cryst., struct., hyperfine coupling consts., ^{1}H ENDOR, isotope effects 77−71822

organic compounds continued
triglycine sulphate, deuterated, reticulated target for pyroelectric vidicon, IR imaging 80−77858
triglycine sulphate, ferroelec., decoration patterns on cleavage surface, domain obs. 80−97218
triglycine sulphate, ferroelec. coercive field as function of impressing rate of field 79−8108
triglycine sulphate, paraelec. phase, thermal expansion coeff. and dielec. constant 79−8100
triglycine sulphate-Ge contact, thermal resist. 77−4226
trihalomethanes, determ. in water, comparison of dynamic and static head space and solvent extraction techniques 79−92114
trihalonitromethanes, mol. dissoc. lifetime in atmosphere 79−22720
trihalonitrosomethane, mol. dissoc. lifetime in atmosphere 79−22720
trihydroxybenzophenone on wafer surface, trace analysis 78−3433
3,3′,5′-triiodothyronine plasma to tissue transport rate estimation from 3-compartment model 78−31792
trimesic acid, L-(or DL-) histidinium trimesate-$^1/_3$ acetone, X-ray cryst. struct. determ. 79−77586
2,4,6-trimethoxy-s-triazine, thermal isomerisation, nematic solvent effects 79−91944
1,3,5-trimethoxybenzene, solid, and in 77K glass, electronic absorption spectra interpretation 79−36659
1,1,1-trimethoxyethane, mol. struct., electron diffr., vibr. spectra 78−37765
trimethyl ammonium cobalt chloride dihydrate, antiferromag., ^{59}Co NMR 77−77124
trimethyl orthoacetate, enthalpy of hydrolysis meas. microprocessor-controlled system 80−22361
trimethyl orthoformate, photoelectron spectra, ionisation pot. bands, conformation SPINDO calc. 78−9194
trimethyl phosphate, ^{31}P normal Fourier transform spectra, line narrowing, selective population transfer induced 80−31827
2,4,6-trimethyl pyridine-aliphatic alcohols, molar excess enthalpies and vols. 79−42254
2,4,6-trimethyl pyridine-N-oxide, linear dichroism in liq. cryst. matrix, out-of-plane components 78−17701
trimethyl tin chloride, orientation of adsorbed mols. on graphite, recoilless gamma reson. 77−76663
2,2,5-trimethyl-1,3-dioxane-4,6-dione, cryst., X-irradiated, methyl group hindered rot. tunnelling, EPR, ENDOR, and ELDOR 79−68328
trimethyl-d_9-vinylsilane, IR and Raman spectra, struct., vibr. assignment, barriers to internal rot. calc. 80−87102
trimethylacetic acid, and complexes with acetone, correlation between chem. shift and charge for OH 77−18946
trimethylacetic acid, high resolution ^{1}H and ^{13}C NMR spectra at liquid-solid phase transition 80−11281
trimethylacetic acid, large ultra-pure single crysts., grown by modified Bridgman technique 77−55883
trimethylamine, adsorption on Mo (100), adsorbed O effect, LEED and AES obs. 80−39443
trimethylamine, and analogues, struc. struct. and vibr. force fields, electron diffr. and microwave spectra 77−54609
trimethylamine, collision induced fluoresc. enhancement and quenching, relax. processes 80−83412
trimethylamine, electronically excited isolated mol., relax. and intramol. processes 80−83411
trimethylamine, fluoresc. decay 80−91590
trimethylamine, laser seed cpds., photoionisation and photoabsorpt. charcts. 78−13688
trimethylamine, SCF calcs. including polaris. functions 80−87034
trimethylamine+BCl_3→$BCl_3N(CH_3)_3$, complex formation, reaction product isotopic composition change *(Russian)* 80−81316
trimethylamine+OH, rate const., 298-426K, Arrhenius expressions and activation energy 78−48619
trimethylamine-doped polymers, field-depend. UV photogeneration of holes, polymer composition depend. 78−76104
trimethylamine-water critical fluid, ratio of sound dispersion to attenuation 79−55826
trimethylaminegallane, microwave, IR and Raman spectra, struct., vibr. assignment 80−95600
trimethylamine.HCl coated piezoelec. quartz crysts. for HCl gas determ. in air 78−92532
trimethylamino borane, ^{11}B NMR 78−90190
trimethylammonium cadmium chloride, $(CH_3)_3NHCdCl_3$, struct. phase transitions 79−1502
trimethylammonium cadmium trichloride, struct. phase transitions, low-freq. Raman scatt. obs. 80−80783
trimethylammonium chloride, cation and CH_3 groups rot. diffusion, quasielastic neutron scatt. 77−27840
trimethylammonium chloride, cation and CH_3 groups rot. diffusion, quasielastic neutron scattering 77−27841
α-trimethylammonium chloride, disordered, lattice vibrs. Raman spectra 77−85699
trimethylammonium chloride and deuterated forms, cryst., inelastic neutron scatt. H bond vibr. obs. 77−7796
trimethylammonium chloride in HCl, Cl^- solvation no., Raman spectra 79−96410
trimethylammonium cobalt chloride, low-dimensional Ising-like system, nucl. spin-lattice relax. of protons meas. 77−85609
trimethylammonium cobalt trichloride:CU, bound impurity effect, heat capacity meas. 79−61146
trimethylammonium cobalt trichloride, mag. heat capacity and Neel temp. in mag. field 79−61147
trimethylammonium cobalt trichloride, metamagnet, AC susceptibility and exchange consts. 80−70961
trimethylammonium cobalt trichloride dihydrate, Ising-like system, nucl. spin-lattice relax. of ^{1}H and ^{35}Cl 80−29638
trimethylammonium copper chloride dihydrate, mag. props., evidence for lattice dimensionality 77−89967
trimethylammonium copper heptachloride, one-dimens. ferromag., mag. susceptibility, 2 to 300K 79−61077
trimethylammonium manganese bromide, mag., anisotropy, biquadratic exchange 78−14952
trimethylammonium manganese chloride dihydrate, optical absorpt. spectrum, 300K, 90K, cryst. field parameters 78−27253
trimethylammonium manganese heptachloride(-bromide), antiferromag. chain systems, high-field magnetisation meas. 79−61187
trimethylammonium manganese trichloride, Heisenberg antiferromag. chain, specific heat and EPR 80−65931

organic compounds continued
2,4,5-trimethylbenzaldehyde, durene host, dipole moments in lowest electronic states 77−18954
2,4,5-trimethylbenzaldehyde, in durene, cryst., photochem. and photophys. processes 77−60092
1,3,5-trimethylbenzene, rotational and vibrational energy effect 80−76497
1,2,4-trimethylbenzene, visible absorpt. spectra, local mode overtone intensity of C-H stretching mode 79−81207
trimethylbenzene+$O(^3P)$, reaction product identification by mass spectrometer 78−7185
1,3,5-trimethylbenzene+OH, cross mol. expt., product anal., 300K 78−44353
trimethylborane, vibr. spectra and force constants *(German)* 79−26981
N-trimethylborazine, triplet state, ICR trapped electron spectra obs. 79−6884
trimethylbromosilane, microwave spectra, struct., chemical bonding 80−95602
trimethylcarbinol complexes in soln., weakly H-bonded, IR bandshapes 80−106354
trimethylchlorosilane, chemisorption on goethite, IR spectra 80−7855
trimethylene, singlet state, rot. barrier origin, MINDO/2 calc. 79−81170
trimethylene biradical, rot. barrier of mol., INDO calc. 79−68192
trimethylene diradical, generalised Hartree-Fock natural orbital config. interaction approach 77−75062
trimethylene diradical, geometry optimisation by generalised Hartree-Fock 78−25427
trimethylene diradicals, geometry optimisation ab initio SCF CI calcs., energy gradient 79−85903
trimethylene oxide, ^{12}C NMR, coupling consts. 78−25570
trimethylene sulphide, ^{12}C NMR, coupling consts. 78−25570
trimethylene sulphoxide, microwave spectrum, mol. struct., methylene group, bends, tilts, twists 77−50431
trimethylene sulphoxide, ring puckering vibr., IR spectra obs. 80−32710
trimethylene trinitroamine, ^{14}N NQR *(Chinese)* 79−91310
trimethylenemethane, bisected singlet state, using general CI method 79−36539
trimethylenemethane, ground state triplet, HFS, EPR obs. 80−50188
trimethylethylene, electron energy loss spectra, 0-90°, 20-150 eV impact 79−68322
trimethylethylene, photoelectron spectrosc., ang. depend. 80−9641
2,2,4-trimethylpentane, field emission into liq., 275-334K 78−88406
2,2,4-trimethylpentane, liq., O_2^- electron laser-photodetachment 79−64057
2,2,4-trimethylpentane, liquid, ground state energy of excess electrons 78−68976
2,2,4-trimethylpentane, visible absorpt. spectra, local mode overtone intensity of C-H stretching mode 79−81207
2,2,4-trimethylpentane-chlorobenzene, soln., positronium formation inhibited by chlorobenzene 79−50170
trimethylphenylammonium benzoate, cryst., nitrobenzene anion radical impurity, EPR 77−1597
trimethylphosphate, plastic and hard crysts., liq., nucl. spin-lattice relax. mol. motion 78−48065
trimethylphosphine, chem. shift anisotropy, struct., liq. cryst. NMR 77−61768
trimethylphosphonium oxide (sulphide) (selenide), chem. shift anisotropy, struct., liq. cryst. NMR 77−61768
trimethylsilyl azide, vibr. spectra, normal mode assignment 78−86867
trimethylsilyl isocyanate, vibr. spectra, normal mode assignment 78−86867
trimethylsilyl isothiocyanate 78−86867
trimethylsilyl sulphide, UV spectra, assignments 78−46359
trimethylvinylsilane, IR and Raman spectra, struct., vibr. assignment, barriers to internal rot. calc. 80−87102
trimethyoxybenzenes, liq. and solid, IR and Raman spectra, vibr. assignments 78−58701
1,3,5-trinitro 1,3,5,-triazacyclohexane, shock-induced intramol. bond breaking, XPS and EPR study 80−76512
trinitrofluorene layer, diffraction effectiveness, registration of discrete holograms *(Russian)* 79−7100
trinitrofluorenone-polyvinylcarbazole, freq. depend. photocond. 77−8141
trinitromehtane, electron diffr. study of gas phase mol. struct., rot. isomerism 78−1080
trinitromethane, microwave and rot. spectra, effect of twist of NO_2 groups, rot. and centrifugal distortion const. determ. 80−95605
trinitrotoluene, shock-induced intramol. bond breaking, XPS and EPR study 80−76512
trioctadecanoate solution in toluene, diffusion through cellulose membrane nonstationary 79−52767
trioctylphosphine oxide chromatography for trans-Pu solvent extraction recovery and purification 80−93826
trioxane, $\nu_{19}(E)=\nu_{20}(E)=1$ state, rot. spectrum assignment, microwave obs. 80−58248
trioxane, D_2CO, HDCO, CW optically pumped laser action CW optically pumped laser action 77−88700
trioxane, in nitrobenzene soln., polymerisation, polyoxymethylene morphology 80−59403
S-trioxane, lattice vibrs. from Raman spectra 78−6672
trioxane, NMR proton relax., mol. rot., rel. to polymerisation 79−73843
trioxane, polymerisation, epitaxial crystn. of polyoxymethylene during 79−55676
s-trioxane, Raman spectra of single crystal, liquid and chloroform-d solution 79−94000
1,3,5-trioxane, vibr. spectra and intermol. forces 77−36216
trioxane $^{13}C(^{18}O)$ substituted, mol. consts. and rot. spectra 80−87096
trioxolane, methyl substituted, stability, pseudorotation, electronic effects in final ozonide 79−45654
trioxolanes, methyl substituted, stability, pseudorotation, electronic effects in primary ozonide 79−49961
trioxolanes, pseudorotation surface, mol. struct. and conform. 79−45653
triphenyl phosphonium ytterbium chloride, $Yb^{3+}(4f^{13})$ absorpt. spectrum, cryst. electric field splitting 77−73151
1,3,5-triphenyl pyrazolin, luminophore, luminesc. under action of atomic H *(Russian)* 79−8177
triphenyl-(triphenylgermanylperoxy)silane, cryst. and mol. struct. 80−39066
triphenylamine+2,6-diphenyl-1,4-benzoquinone, triplet exciplex quenching 79−79228

organic compounds continued
triphenylamine cation radical, condensed and vapour phase geometry, photoelectron spectra 79−31597
triphenylamine coated piezoelec. quartz crysts. for HCl gas determ. in air 78−92532
triphenylamine doped bisphenol-A-polycarbonate polymer, photoinjection of holes from amorphous Se 78−72191
triphenylamine in 3-methylpentane and ethanol glasses, γ-radiolysis, IR spectra, trapped electron 77−16842
triphenylamine polycryst. film, hole photogeneration 79−19617
triphenylamine-bisphenol-A-polycarbonate, binary solid soln., hole photogeneration, Onsager theory and expt. 78−39148
triphenylantimony, single crystal, irrad. by UV, diphenylantimony radical prod., ESR 78−31662
triphenylbenzene, cryst., nonlinear optical susceptibility and spontaneous polarisation 77−58372
triphenylbromophosphoranyl bromide, X-irradiation, phosphoranyl radicals ESR study 79−56611
triphenylcarbinol complexes in soln., weakly H-bonded, IR bandshapes 80−106354
triphenylene, excited state Faraday values mag. circular dichroism spectra and MO Cl calcs. 80−18877
triphenylene, excited state polarisabilities, electrochromism and pot. energy curves 79−7034
triphenylene, hexasubstituted, thermotropic mesophases 79−86681
triphenylene, in n-heptane cryst., 2-photon excitation spectrum 78−82760
triphenylene, in n-heptane cryst., polarised fluoresc. spectrum, mol. deformation 79−10135
triphenylene, in PMMA matrix, two-photon phosphoresc. spectra 77−42366
triphenylene, mono- and diamons, reson. spontaneous Raman spectra, vibronic interactions 79−3451
triphenylene, multiplet struct., insertion modes, Shpol'skii spectra 79−13752
triphenylene, trapped in n-heptane single cryst., ESR and orientation *(French)* 78−91928
triphenylene, triplet state, MIDP and T-S excitation spectrosc. 79−81233
triphenylene(-d_{12}), lowest $T_1[^3A_2'(\pi\pi^*)]$ state vibronic coupling 80−47955
triphenylene core, discotic mesophase potentiality, isobaric phase diagram method 79−86680
triphenylene derivatives, hexasubstituted, disc-like cpd., mol. conform. and arrangement, semiempirical calcs. 80−107048
triphenylene derivatives, liq. cryst. discotic phase form. *(French)* 78−91223
triphenylene esters, crystalline arrangement of disc like compounds 79−99175
triphenylene hexa-n-dodecanoate, mesomorphic polymorphism 79−41950
triphenylene hexaoctylbenzoate, carbonaceous mesophase and disc-like liquid crystals 80−79687
triphenylene in Shpolskii matrix, orientation, ESR and fluoresc. spectra 79−36688
triphenylene positive ion, MCD spectra, test of pairing theorem 79−31565
triphenylene-d_{12}, in ethanol soln., external heavy atom effect on triplet state, phosphorescence meas. 79−18231
2,4,6-triphenylheptane, depolaris. Rayleigh scatt., optical anisotropy 78−27245
triphenylmethane dye, S_1-lifetime determ. by two-photon fluoresc. 77−18966
triphenylmethane dye soln., electronic relax., viscosity-depend., using picosec. flash photolysis 80−66258
triphenylmethane dyes, IR and Raman vibr., spectra, vibr. anal., vibronic theory of Raman scatt. 77−68048
triphenylmethane dyes, Weigert effect, additional chroming effects 77−58406
triphenylmethyl, in triphenylamine, photon-echo decay, in lowest doublet-doublet electronic transition 77−79903
triphenylmethyl in triphenylamine, photon echo stimulated from optically induced nucl. spin polarisation 79−76460
triphenylmethyl-triphenylamine mixed cryst., optical coherence storage in spin states 80−58649
triphenylmethylphosphonium-TCNQ, paramag. echo from triplet excitons obs. 77−28130
triphenylphosphine compounds, $(C_6H_5)_3PM_xM'_{1-x}(CO)_5$, M,M'=Cr, Mo, W, mixed cryst., CO vibr. spectra, modal anal. 78−35128
triphenylphosphite, acoustically induced birefringence 80−93274
triphenylseleniumchloride, X-irrad. cryst., forming Ph_2SeCl, ESR study 79−39167
triphenyltin bromide, cryst. struct. determ. using Patterson and Fourier methods 79−42044
triplet exciton dynamics, kinetic model 78−67948
triplet methylene reactions, reaction rate const. determ. 77−36727
triplet molecule concentration after excitation by different forms of impulses 77−18809
triplet state quenching by ruthenocene 77−83630
tripropylamine, additive for CO_2 laser 78−13679
tripropylamine, CO_2 laser additive, amplification characts. *(Russian)* 78−25848
tripropylamine, in CO_2 laser gas mixture, photoionisation meas. 80−78829
tripropylamine admixtures, influence on optical characteristics of CO_2 laser 80−23669
triptycene, soln., correl. times from ^{13}C relax. 80−23438
triptycene hydrogenation products, ACC and TCC, cryst. data 80−100224
tris(2-cyanoethyl)phosphine selenide, X-ray cryst. data 79−94989
tris(2-cyanoethyl)phosphine sulphide, X-ray cryst. data 79−94989
tris(3-deutero-2,4-pentadionato)aluminium, in soln., deuteron spin-lattice relax. time, mol. rotational correl. time 78−84491
tris(bipyridine)ruthenium(II)dichloride, fluoresc. decay meas. by high repetition rate gated photon counting 80−86402
tris(dimethylamino)phosphorus, ^{15}N and ^{31}P NMR aligned in liq. cryst., geom. struct. 78−82751
tris(ethylenediamine)metal(III), H bonding *(French)* 80−87241
tris(hydroxymethyl)aminomethane, crystalline and plastic structs. phase transforms. studied by X-ray diffr. 80−84130
tris(hydroxymethyl)aminomethane, standard for soln. calorimetry, enthalpy of react. in HCl determ. 77−73462
organic compounds continued
tris(hydroxymethyl)methylamine buffer effect on acetylcholine responses in Aplysia neurons 77−64020
tris(hyroxymethyl)aminomethane, water solution calorimeter, determination of energy equivalent 78−23961
tris(trimethylstannyl)amine, gas phase electron diffraction 80−106401
tris (3-mercapto-1, 3-diphenyl-2-propen-1-onato) Co(III), multiple twinning 80−100250
tris (N,N'-diethyldithiocarbamate) iron II, high field Mossbauer study 79−54873
tris sarcosine calcium chloride:VO^{2+}, EPR and absorpt. spectra 78−60330
tris-butadienyl metal D_3 complex pairwise chiral discriminations, stereochem. basis, extended transition monopole model 78−74725
tris-sarcosine calcium bromide and chloride solid solns., Mn^{2+} doped, EPR linewidths and ferroelec. behaviour 79−24213
tris-sarcosine calcium chloride:Mn^{2+} ferroelec. dynamics, EPR and ENDOR study 80−75972
tris-sarcosine calcium chloride:Mn(Fe), influence of cryst. defects on ferroelec. transition, EPR 79−38466
tris-sarcosine calcium chloride, ferroelec., ferroelasticity and hypothetical hexagonal to orthorhombic phase transition 77−63377
tris-sarcosine calcium chloride, ferroelec., US attenuation and vel., elastic consts., and permitt. near Curie temp. 79−37761
tris-sarcosine calcium chloride, ferroelec. transition, order parameter 77−1204
tris-sarcosine calcium chloride, ferroelec. transitions, soft modes, Raman scatt. spectra obs. 80−80763
tris-sarcosine calcium chloride, phase transition, hydrostatic press. effect, dielec. const. meas. 80−71327
trisarcosine calcium chloride crystals, ferroelec., electrooptic and ferroelastic props. 80−34865
trishydrazyl radical in s-butylbenzene, slowly slowly tumbling triradicals EPR 80−32748
trissarcosine calcium chloride:Mn^{2+}, ferroelec., electron spin-lattice relax. 78−80208
trissarcosine calcium chloride, ferroelec. phase transition, Raman and Brillouin scatt. studies 80−71340
trissarcosine calcium chloride, ferroelec. transition, press. effect 80−84681
tristearin irreversible liq.-liq. phase transition, ^{13}C NMR meas. 78−26681
triterpenes, isolated from Japanese Cimicifuga plants, cryst. struct. determ. 78−34504
S-trithiane, lattice vibrs. from Raman spectra 78−6672
trithiane, NMR proton relax., mol. rot., rel. to polymerisation 79−73843
trithiane, Raman spectrum, press. effect on internal rot. angle 78−37642
1,3,5-trithiane, single cryst., photocond. meas. 77−11959
Triton X100-water-coumarine 1-rhodamine 6G, micellar dye soln., energy transfer 80−45581
n-tritriacontane, C-phase, mol. motion obs., incoherent quasielastic neutron scatt. 79−4260
n-tritriacontane, non periodic molecular motions, neutron scatt. study 79−51024
tRNA in soln., selected topics review, book contrib. 80−108839
2-tromopropane, tilt-effect and interference with rel. sign determination in weak irrad. expts. 80−32742
tropolone, π-π^* singlet state, H^+ tunnelling dynamics and equilib. geometry 80−102539
tropolone, in water and cyclohexane, electronic relax., absorption, excitation and fluoresc. spectra 78−66588
tropolone vibr. spectra and proton tunneling 80−28014
tropone, proton affinity, MINDO/3 results compared to ICR obs. 78−1103
troposphere, non-methane organic C budget 78−73462
truxene derivatives, temp. inverted nematic-columnar sequence in disc-like mesogens 80−88032
trypaflavine, on silica gel, luminesc. quenching, activator location effects 77−52172
trypaflavine solutions in polyvinyl alcohol matrix, spectrum-luminesc. characts. 79−13761
tryphoton, aqueous, one and two photon ionisation by Na laser harmonics 80−69193
trypsin, in suspension, radical form. and inactivation after Γ-irrad. 78−3564
trypsin inhibitor, conformation, distance geometry calcs. 77−50553
tryptamine:1-thyminylacetic acid (1:1), cryst. and mol. struct. determ. using MULTAN 79−73156
tryptamine, near ab initio and pseudopotential calcs. 77−71749
tryptophan, aq. alkaline soln., charge transfer, luminesc. obs., 77 and 300K 79−69876
tryptophan, aq. soln. charge transfer, luminesc. obs., 77 and 300K 79−69875
tryptophan, fluoresc. intensity increase due to deuteration 78−78739
tryptophan, Fourier transform PMR in aq. soln., ^1H exchange and relax. rates meas. method 78−15049
l-tryptophan, gas, UV photoelectron spectrum, photoionisation threshold 79−86004
L-tryptophan, in polar glass, UV and γ-prod. electrons geminate recombination, radical yield 77−9094
tryptophan, laser flash spectroscopy in presence of nitroxide radicals, protein-membrane interaction probing 79−87855
tryptophan, pH dependent fluoresc., quenching by histidine *(Russian)* 78−90209
tryptophan, photoionised, in γ-irrad. alkaline glass, electron traps, stimulated luminesc. 78−11536
DL-tryptophan, polycryst., amino group rot., reorientation, mol. struct., 77-555K, PMR obs. 78−35047
tryptophan, Raman line characterisation 79−26996
D-tryptophan, soln., excitation spectra rel. to recording wave length *(Russian)* 77−12438
tryptophan, stereoselective energy transfer induced by circularly polarised light 80−1010
tryptophan, triplet state, zero-field splittings, wavelength depend. 78−43680
tryptophan in Co Cl_2, γ- and UV-irrad. solvent matrices at 77K H^- fluoresc. 78−70779
tryptophan residue in horse liver alcohol dehydrogenase, room-temp. phosphoresc., temp. and enzymic complex form. effects 80−61512
tryptophan soln. containing histidine, fluoresc. rel. to soln. pH 80−2826
L-tryptophan-HCl radical form. after X-irrad. 78−64940

organic compounds continued
L-tryptophan.HCl, irradiated single crystals at 295K, EPR study 79−11900
tryptophanyls, singlet and triplet states, role in protein inactivation 79−57564
tryptophanyltryptophan, laser flash photolysis, photoionis. mechanism 77−90619
tryptophanyltyrosine, laser flash photolysis, photoionis. mechanism 77−90619
tryptophyl peptides, pulse radiolysis, hydrated electron reaction 78−48679
TSCC:Mn^{2+}, microscopic, mechanism of ferroelectric transition, EPR fine struct. tensor calc. 78−35104
TSCC ferroelastic monodomain crysts., dielec. behaviour 79−42888
$(TSeF)_x(TTF)_{1-x}(TCNQ)$, interstack hybridisation role in metal-insulator transition temp. determ. 78−6304
$(TSeF)_x(TTF)_{1-x}TCNQ$, struct., cond., phase transitions 78−47770
TSeF salts, mol. props., one-dimens. cond. salts form. 78−6363
TSeF-TCNQ, Ginzburg-Landau model for metal-insulator transition 78−6301
TSeF-TCNQ, Kohn anomaly of metallic state, X-ray diffuse scatt. meas. 80−19887
TSeF-TCNQ, nonlinear electronic transport, microwave harmonic mixing obs. 80−20168
TSeF-TCNQ, resist., crit. behaviour anisotropy 78−10430
TSeF-TCNQ, X-ray diffuse scatt., one-dimens. distortion in phonon spectrum and interpret. 78−10144
TSet, resonance Raman spectra 79−56787
$(TSeT)_2Cl$, high press. metallic phase *(Russian)* 78−95316
$(TSeT)_2Cl$, one-dimens. conductor, metallic phases 80−20159
$(TSeT)_2Cl$ complex, metal-semimetal transition, magnetoresist. and cond. *(Russian)* 79−38138
$(TSeT)_2Cl$ complex, phase transform. under press., cond. *(Russian)* 80−92674
TSeT-I_2, physical props., elec. cond. 80−24908
$TSeTBr_{0.5}$, phase transition, mag. props., thermal capacity and cond. *(Russian)* 79−99537
αTTF:Br, transport and mag. props., effect of doping 80−24934
$TTF_{0.4}TSeF_{0.6}$-TCNQ, $2k_F$ and $4k_F$ CDWs, X-ray study 80−65474
$TTF_{0.97}Se_{0.03}$-TCNQ, Peierls-superlattices and soft phonon anomalies, X-ray scatt. meas. 78−75795
$TTF_xTseF_{1-x}TCNQ$ solid soln., DC conductivity, struct. 78−10423
TTF^+, cryst., vibr. assignments, IR spectra 79−99869
$(TTF^+)_2$ dimer, cryst., vibr. assignments, IR spectra 79−99869
(TTF^+) radical cation, optical props. in mixed-valence and monovalent halide salts and solns. 79−61399
TTF, ab initio SCF LCAO band struct. calc. 80−70608
TTF, cryst., vibr. assignments, IR spectra 79−99869
TTF, enthalpy of sublimation and vapour press. meas. 80−92661
TTF, heat of sublimation, cryst. lattice and polarisation energy 79−32941
TTF, infinite stacks, all valence electron band struct. 78−39001
TTF, origin of Raman spectrum instability 79−15456
$TTF(Br)_{0.7}$, EPR temp. depend., metal-insulator transition 77−43863
$TTF(I)_{0.71}$, EPR temp. depend., metal-insulator transition 77−43863
$TTF(I)_{0.71}$, physical props., Fermi energy scaling of metal-insulator transition temp. 77−8081
TTF(MBDT) spin-Peierls transition, mag. exchange interactions, mag. props. 80−25138
$TTF(SCN)_{0.54}$, physical props., Fermi energy scaling of metal-insulator transition temp. 77−8081
$TTF(SCN)_{0.588}$, Peierls instability, strain coupled charge density waves, X-ray scatt. obs. 78−79949
$TTF(SeCN)_{0.54}$, physical props., Fermi energy scaling of metal-insulator transition temp. 77−8081
$(TTF)_{12}(SCN)_7$ charge-transfer salt, elec., mag. and optical props. 77−43575
$(TTF)_{12}(SeCN)_7$, charge-transfer salt, elec., mag. and optical props. 77−43575
$(TTF)_2$, dimeric interactions, MO calcs., applicability to crystal struct. 80−75215
$(TTF)_2(NiS_4C_4H_4)_3$, disordered solid soln. and struct. modulation obs. 79−94986
$(TTF)_7I_{5-x}$, incommensurate crystal phases symmetry, incommensurate basic struct., superspace group approach 80−79727
$(TTF)_7I_5$, superstruct. modulation, X-ray obs. 78−14333
$(TTF)Br_{0.74-0.79}$, lattice distortions 79−55733
$(TTF)Cl_x$, disorder transition, cond. decrease and commensurate charge density waves 80−70153
$(TTF)CuS_4C_4(CF_3)_4$, spin Peierls system, mag. field effects 80−7123
TTF and $(TTF)_7I_5$, Raman scatt. and charge transfer 77−69817
TTF and derived cpds., intramolecular vibrs. and vibronic effects, IR and Raman spectra 80−25387
TTF and TTN derivatives, quasi-one-dimens. cond., phys. and electronic props. 78−6366
TTF conducting salts, ESR of itinerant spins 77−66424
TTF crystals, polarised Raman spectra meas. 78−6681
TTF derivatives, smectic and nematic, for liq. cryst. device appl. 80−54124
TTF dimer, nonbonding intermolecular forces 80−83443
TTF film, energy loss spectra of low energy electrons 78−19116
TTF halides, charge transfer effect on internal modes, Raman scatt. 80−25392
TTF halides, spin-lattice relax. 78−88190
TTF salts, mixed valent, Raman spectra, formal charge rel. to Raman freq. 80−93317
TTF salts, PMR, electron-proton couplings, local susceptibilities 79−82883
TTF salts, quasi-one-dimensional organic crystals, charge transfer, Raman scatt. *(German)* 79−28731
TTF stacks, intermolecular energy and struct. from atom-atom potentials 80−79738
TTF-^{13}C, mol. struct. determ. from PMR in nematic solvents 77−88468
TTF-(2,5-diethyl)TCNQ, cryst. and mol. struct. temp. depend. 77−35531
TTF-bis-dithiolene metal complex compounds, donor-acceptor type, one-dimens. mag. variety and props. 77−66271
TTF-bisdithiolene metal complexes, spin Peierls transition 77−4523
TTF-$Br_{0.79}$, charge transfer and ionic bonding 77−39558
TTF-chloranil visual pressure or temperature indicator 80−87443
TTF-Cu bis-dithiolene, dimer, mol. displacements at 4.2K 80−10539

organic compounds continued
TTF-CuBDT, inter- and intra-chain exchange couplings, proton spin-lattice relax. time meas. 80−71220
$TTF\text{-}CuS_4C_4(CF_3)_4$, quasi-one-dimens. antiferromag., spin-lattice dimerisation, X-ray scatt. obs. 77−85464
$TTF\text{-}CuS_4C_4(CF_3)_4$, spin-Peierls system, high-field phase 80−39816
TTF-d_0, -d_4, IR and Raman spectra, vibr. assignments 78−23436
TTF-DETCNQ, heat capacity, elec. cond., cryst. struct., metal-insulator transition 77−8077
TTF-DETCNQ, metal-insulator transition, struct., elect. cond. and sp. ht. expts. 78−14662
TTF-halides, conductors with chain struct., lattice phonons and distortions, incommensurability transitions 80−24549
TTF-I_n, single cryst. optical props., polarised specular reflectance meas. 77−12400
TTF-SCN, quasi one-dimens. conductor, CDW phase transform., X-ray scatt. study 80−24594
TTF-TCNO, optical evidence for Coulomb interactions, review 78−6704
TTF-TCNQ:TCNQ-M, thermopower determ. 78−47772
TTF-TCNQ, 1:1 complex, atom-atom approx. and lattice energies 79−7568
TTF-TCNQ, $4k_F$ anomaly, density correlation of classical dimensional electron gas 77−80744
TTF-TCNQ, $4k_F$ anomaly, explanation 77−35875
TTF-TCNQ, 53 and 38K transitions, mag. and elec. props. meas., doping effect 77−66159
TTF-TCNQ, ^{13}C Knight shift and spin-lattice relax. meas., local susceptibility determ. 77−4571
TTF-TCNQ, ^{15}N, ^2H isotope labelled, IR, Raman spectra, mol. vibrs., electron-phonon interactions 77−69835
TTF-TCNQ, anal. of harmonic microwave mixing 80−44635
TTF-TCNQ, and related 1D conductors, temp. depend. microwave dielec. const. 77−31967
TTF-TCNQ, and related compounds, low temp. irrad. effects 80−24906
TTF-TCNQ, and related cpds., elastoresistivity by strain gauge technique 80−24892
TTF-TCNQ, and related cpds., lattice modulations, X-ray diffuse scatt. obs. 80−19787
TTF-TCNQ, and related cpds., partial charge transfer and CDW modulation 79−95349
TTF-TCNQ, and Se analogues, microwave conductivity meas. by coaxial resonator technique 77−4384
TTF-TCNQ, anharmonic effects of phonons with Kohn anomalies 77−1197
TTF-TCNQ, anharmonic effects on resistivity 78−84202
TTF-TCNQ, anharmonic props., temp. (press.) depend., rel. to naphthalene and anthracene 80−15200
TTF-TCNQ, anisotropic cond., X-ray effects 80−96855
TTF-TCNQ, antiferroelectric ordering of TCNQ ion elec. polarisation 80−20598
TTF-TCNQ, band struct., Fermi surface and density of states, LCAO calc. 78−60048
TTF-TCNQ, band struct., soft phonon instability 77−72821
TTF-TCNQ, CDW and phase transition exam. 78−6283
TTF-TCNQ, CDW instability, classical vs. crit. behaviour 78−39041
TTF-TCNQ, CDW transition with tripling of period along chains 80−96805
TTF-TCNQ, charge transfer, mode shift study, Raman scatt. *(German)* 79−28731
TTF-TCNQ, charge transfer change with press. 80−39564
TTF-TCNQ, charge transfer determ. from spectral line shift using Raman scatt. 80−25392
TTF-TCNQ, collective-mode conductivity in metallic phase 78−64031
TTF-TCNQ, commensurate ordering 77−7829
TTF-TCNQ, cond. and longitudinal sound attenuation above Peierls transition point 77−28168
TTF-TCNQ, cond. in phase transition region 80−24979
TTF-TCNQ, conductivity and dielec. permeability, freq. depend. 78−79984
TTF-TCNQ, conductivity model 79−51557
TTF-TCNQ, const. vol. resist., linear temp. depend. 78−51977
TTF-TCNQ, const. volume resistivity anomalous behaviour 80−103682
TTF-TCNQ, controlled defects effect on microwave cond. and dielec. function 80−24885
TTF-TCNQ, core exciton exam. by inelastic electron scatt. 77−4296
TTF-TCNQ, coupled Peierl's systems, model, phase transitions 77−69230
TTF-TCNQ, covalon conduction 78−10427
TTF-TCNQ, crit. behaviour at electronically driven struct. phase transition 77−80767
TTF-TCNQ, crit. behaviour near 53K phase transition, Ginzburg-Landau theory 79−33249
TTF-TCNQ, cryst. binding energy, enthalpy of form., calorimetric 77−52663
TTF-TCNQ, cryst. struct. and cond., rel. to lateral elastic interaction between chains 77−39827
TTF-TCNQ, crystal, Raman scattering 78−80356
TTF-TCNQ, DC Hall effect meas. 77−89753
TTF-TCNQ, delocalisation in organic molecular conductors 79−78086
TTF-TCNQ, deuterated, compressibility under hydrostatic press., neutron diffr. meas. 78−2197
TTF-TCNQ, deuterated, isotope effect on mag. susceptibility 80−25080
TTF-TCNQ, deuterated, phase transition exam. by elastic neutron scatt. 77−4194
TTF-TCNQ, dimeric interactions, MO calcs., applicability to crystal struct. 80−75215
TTF-TCNQ, dimers and trimers, Xα scattered wave calc. 78−10326
TTF-TCNQ, divergent mag. responses at $2k_F$ and structural phase transitions 80−20376
TTF-TCNQ, Drude optical edge, press. depend. 79−19882
TTF-TCNQ, dynamic nucl. polarisation exam., temp. depend. 78−39447
TTF-TCNQ, effect of benzene ring substitution on supercon. and metallic props. 80−20193
TTF-TCNQ, elastic neutron scatt. evidence for charge transfer change at high power 80−2163
TTF-TCNQ, elastic- and inelastic-neutron scatt. study 79−69208
TTF-TCNQ, elec. cond., role of librations 79−19580
TTF-TCNQ, elec. cond., SEM technique 80−86507
TTF-TCNQ, elec. cond. and spin susceptibility, press. and temp. depend. 80−24894
TTF-TCNQ, elec. resist., electron-phonon scatt. 80−92884

organic compounds continued
TTF-TCNQ, electron-electron interaction as source of metallic resist. 80−20162
TTF-TCNQ, electron-electron interaction strength, electron scatt. and spin-lattice relax. data 78−30878
TTF-TCNQ, electron-electron interactions in physics of one dimensional conductors 80−24895
TTF-TCNQ, electron-molecular distortion coupling near Peierls transition, IR spectra obs. 80−25390
TTF-TCNQ, electronic energy level shift, mag. susceptibility, anomalous temp. var. 79−4499
TTF-TCNQ, electronic props., connection between theory and expt. 79−19581
TTF-TCNQ, electronic props. and comparison with $(SN)_x$, review 78−6306
TTF-TCNQ, electronic spin-lattice relax. time 77−51939
TTF-TCNQ, electronic struct. near Fermi level, tunnelling spectra 77−85126
TTF-TCNQ, energy gaps, far IR photocond. meas. 77−32004
TTF-TCNQ, enhancement of mag. susceptibility by Coulomb correlations 77−77023
TTF-TCNQ, enthalpy of sublimation and vapour press. meas. 80−92661
TTF-TCNQ, exchange effects in plasmon dispersion 78−91628
TTF-TCNQ, fluctuation cond. and commensurability pinning 80−34429
TTF-TCNQ, Hall mobility using Faraday rot. method at 9.3 GHz 77−47801
TTF-TCNQ, high press. structural transitions, neutron scatt. study 80−96647
TTF-TCNQ, implications of amplitude solitons in incommensurate Peierls systems 80−92841
TTF-TCNQ, impurity effects on CDW fluctuations 80−44576
TTF-TCNQ, inelastic neutron scatt., Peierls transition exam. 78−10134
TTF-TCNQ, inelastic neutron scatt., re-examination 78−30721
TTF-TCNQ, interchain tunnelling effect on nucl. spin-lattice relax. time, interchain coupling of CDW 80−20163
TTF-TCNQ, interpretation of the $2k_F$ and $4k_F$ X-ray scatt. 77−63487
TTF-TCNQ, IR absorption peak theory 77−43991
TTF-TCNQ, IR reflectance in conducting phase 80−25388
TTF-TCNQ, irradiated, IR reflectance, optical and low-freq. transport comparison 79−51961
TTF-TCNQ, irradiated, libron and phonon equilibration, resistivity meas. 79−42530
TTF-TCNQ, isotope effect on Peierls transition temp. 78−43367
TTF-TCNQ, isotope effect on Peierls transition temp. 78−43369
TTF-TCNQ, Kohn anomaly, electron-mol. vibr. coupling 77−31734
TTF-TCNQ, Kohn anomaly, electron-phonon coupling, neutron scatt. 77−7812
TTF-TCNQ, Kohn anomaly and Peierls-type transition, X-ray obs. 78−14435
TTF-TCNQ, Landau free energy function, CDW-libron interaction, sp. ht. near phase transitions 80−19963
TTF-TCNQ, Landau theory of phase transitions 78−30914
TTF-TCNQ, Landau theory of phase transitions 80−92666
TTF-TCNQ, lattice distortion, displacive transform., Landau theory 77−31743
TTF-TCNQ, lattice distortion, displacive transform., Landau theory 77−84879
TTF-TCNQ, lattice phase transitions and cond. anomalies obs. 77−1226
TTF-TCNQ, linear CDW, melting of phase locking *(Japanese)* 77−43522
TTF-TCNQ, low temp. fast neutron irradiation, elec. cond. meas. 80−59964
TTF-TCNQ, low. temp. phase stochastic theory of nonlinear DC cond. 77−80768
TTF-TCNQ, low temp. phase transitions, elastic neutron scatt. obs. 78−14464
TTF-TCNQ, Madelung energy, electronic struct. *(Russian)* 78−6253
TTF-TCNQ, mag. suscept. meas. 78−56287
TTF-TCNQ, Matthiessen's rule, effective defect resistivity 80−6821
TTF-TCNQ, metallic cond., nonlinear amplitude-phase interaction 80−88490
TTF-TCNQ, metallic cond. press. depend., single particle phonon scatt. description 79−69503
TTF-TCNQ, metallic conductivity press. depend. thermal expansion effects 79−69502
TTF-TCNQ, metallic conductivity temp. depend. 78−6357
TTF-TCNQ, microscopic model for three low temp. phases 79−73303
TTF-TCNQ, microwave eddy currents and EPR 77−80996
TTF-TCNQ, mixed valency in organic crystals *(Japanese)* 79−78051
TTF-TCNQ, modulated phases in terms of four-and five-dimens. superspace groups 78−47310
TTF-TCNQ, mol. core excitons, high energy electron inelastic-scatt. spectra 77−69235
TTF-TCNQ, molecular coordination along stacking directions 79−47031
TTF-TCNQ, near commensurability, longit. cond. meas. and X-ray scatt. 79−78084
TTF-TCNQ, neutron and X-ray diffuse scatt., phase transitions, one-dimens. behaviour and interpret. 78−10381
TTF-TCNQ, neutron scattering 78−10133
TTF-TCNQ, new transition *(French)* 77−59263
TTF-TCNQ, non-linear elec. transport by pinned CDW 80−20172
TTF-TCNQ, non-ohmic conductivity, bion dissociation interpretation 79−63048
TTF-TCNQ, nonlinear electronic transport, microwave harmonic mixing obs. 80−20168
TTF-TCNQ, nonlinear transport at low temp. 77−8079
TTF-TCNQ, nonlinear transport in pinched one-dimensional CDW system 77−89754
TTF-TCNQ, nucl. spin relax. obs., diffusive character of response function and interchain coupling 78−10797
TTF-TCNQ, one-dimens. supercond. mechanism *(Chinese)* 79−47189
TTF-TCNQ, one-dimensional cond., review 78−60070
TTF-TCNQ, one-dimensional conductor, fluctuation conductivity in high press. phase 79−91034
TTF-TCNQ, one-dimensional conductor, Raman scatt. 78−80355
TTF-TCNQ, ordering types below 54K, perp. phase depend. 78−6300
TTF-TCNQ, organic metal, Van der Waals donor stacking 80−15037
TTF-TCNQ, origin of Raman spectrum instability 79−15456
TTF-TCNQ, Peierls instability and consequences 78−6303
TTF-TCNQ, Peierls insulator and antiferromagnetic mixed phase, mean field approx. 77−20626

organic compounds continued
TTF-TCNQ, Peierls transition, photocond. meas., absorption coeffs. above gap 78−72198
TTF-TCNQ, Peierls transition temp. and 0K energy gap, mean field theory calc. 80−24782
TTF-TCNQ, Peierls-superlattices and soft phonon anomalies, X-ray scatt. meas. 78−75795
TTF-TCNQ, periodic lattice distortions, charge density waves 79−82536
TTF-TCNQ, phase transition model, interchain coupling of CDW 77−76558
TTF-TCNQ, phase transitions, thermoelec. power meas. 79−65464
TTF-TCNQ, phase transitions and CDW state, controlled disorder effects 80−15507
TTF-TCNQ, phase transitions and CDW state, induced defect depend., transport and mag. studies 80−24980
TTF-TCNQ, phason and metal-insulator microdomain model, Young's modulus temp. depend. anal. 77−31964
TTF-TCNQ, phason instability at 49K phase transition 77−4303
TTF-TCNQ, phonon anomalies and superstructures, Peierls transition, X-ray diffuse scatt. obs. 77−27962
TTF-TCNQ, phonon dispersion and Kohn anomaly, inelastic neutron scatt. 77−1196
TTF-TCNQ, physical properties, reviews *(Japanese)* 80−24883
TTF-TCNQ, physical props., Fermi energy scaling of metal-insulator transition temp. 77−8081
TTF-TCNQ, pinned CDW in very far IR 80−25391
TTF-TCNQ, pinned charge density wave, far IR bolometric observations, damping 79−60735
TTF-TCNQ, plasmon spectrum, tight binding model 78−84158
TTF-TCNQ, positive microwave dielectric const. 78−47771
TTF-TCNQ, possible Lifshitz point, struct. transitions exam. 78−2423
TTF-TCNQ, press. effects on mag. props., review 78−6505
TTF-TCNQ, pure and irrad., nonlinear transport, ESR study, 1.2-4.2K 80−20167
TTF-TCNQ, pure and irrad. crystal, nonlinear transport at low temp. 79−4552
TTF-TCNQ, quasi one-dimensional low temp. mag. susceptibility 80−93069
TTF-TCNQ, Raman scatt. and charge transfer 77−69817
TTF-TCNQ, Raman spectra, formal charge rel. to Raman freq. 80−93317
TTF-TCNQ, reflectance meas. at press. to 70 kbar by micro-optic system 77−61133
TTF-TCNQ, resist., crit. behaviour anisotropy 78−10430
TTF-TCNQ, segregated stack stability 78−55831
TTF-TCNQ, short-range and long-range order of phason clusters 77−35874
TTF-TCNQ, single cryst., mag. susceptibility in phase transition region, two-gap model 78−6511
TTF-TCNQ, sound vel. in a a dand b directions, 0-300K 77−84851
TTF-TCNQ, sound vel. measurements using capacitive transducers 79−72775
TTF-TCNQ, sp. ht. meas., phase transition obs. at 46K 77−43326
TTF-TCNQ, spin susceptibility below 53K, compared with elec. cond. data 77−43865
TTF-TCNQ, spin waves, scatt. at $4k_F$, spin-Peierls fluctuations 78−72093
TTF-TCNQ, struct. phase transitions, coupled phasons model 78−83942
TTF-TCNQ, struct. rel. to quasi one-dimensional elec. props. 78−14716
TTF-TCNQ, surface magnetism 78−2703
TTF-TCNQ, surface magnetism obs. 78−6561
TTF-TCNQ, symmetry changes and phase transitions 78−6299
TTF-TCNQ, TCNQ and TTF bandwidths, extended Huckel and CNDO/2 calcs. 79−7771
TTF-TCNQ, temp. depend. of dynamic nucl. polarisation enhancement of protons 78−6601
TTF-TCNQ, temp. depend. of phonon frequencies at constant vol. 80−10616
TTF-TCNQ, theory of structural phase transitions 78−38831
TTF-TCNQ, thermal cond. above and below Peierls transition, electronic and lattice contribs. 79−95394
TTF-TCNQ, three dimensional ordering 77−59087
TTF-TCNQ, transport props. of dynamically disordered chains 78−72137
TTF-TCNQ, two-chain Fermi gas, response behaviour 80−2381
TTF-TCNQ, two-chain inverted band model 78−6313
TTF-TCNQ, vaporisation. mass spectroscopy 77−1224
TTF-TCNQ, X-ray, neutron scattering, low temp. modulated lattice, 3D modulated lattice 78−10033
TTF-TCNQ, X-ray exam. of $2k_F$ and $4k_F$ anomalies 78−10162
TTF-TCNQ, X-ray irrad., transverse cond. 80−6432
TTF-TCNQ, XPS, surface electronic struct. 78−52627
TTF-TCNQ, Young's modulus, temp. depend., rel. to transition points 77−15475
TTF-TCNQ , elec. props. in high temp. regime, effect of controlled disorder 78−30912
TTF-TCNQ analogues, TTTF-TCNQ and METTF-TCNQ, cryst. structs., X-ray anal. 80−19788
TTF-TCNQ and derivatives, 1.8 to 40K, three dimens. state, specific heats 80−44333
TTF-TCNQ and related compounds, cryst. struct., organisation, dimensionality, interchain disorder 80−19790
TTF-TCNQ and related cpds., elastoresistivity 79−23956
TTF-TCNQ and related cpds., magnetic props., press. effects 77−47981
TTF-TCNQ complex, trans-diethyl-dimethyl TTF-TCNQ, one-dimens. cond. 80−96853
TTF-TCNQ complex *(Japanese)* 77−1412
TTF-TCNQ complex salt press. dependence elec. cond. at low temps. *(Japanese)* 79−87090
TTF-TCNQ complexes, charge transfer, X-ray photoelectron spectra determ. 77−73210
TTF-TCNQ crystal, antiferroelec. ordering of electronic polarisation, simple model anal. 78−92028
TTF-TCNQ crystal, charge transfer, dipolar polaris. binding energy 77−80754
TTF-TCNQ crystals, X-ray topographic study of cryst. perfection 80−96525
TTF-TCNQ derivatives, transport props., reflectance spectra 78−91683
TTF-TCNQ electronic props., PMR 78−2763
TTF-TCNQ family, donor stack dominance of transport props. 80−20166

organic compounds continued
TTF-TCNQ film, energy loss spectra of low energy electrons 78−19116
TTF-TCNQ film, mag. field effects on IR spectra *(French)* 77−48260
TTF-TCNQ film on KBr, IR spectra in mag. field 77−16310
TTF-TCNQ low temp. mag. susceptibility, neutron irrad. effects 80−60311
TTF-TCNQ phase transition, press. depend., longitudinal lockin, stacking axis resistivity meas. 78−47520
TTF-TCNQ powder, phase transition at 49K 77−89539
TTF-TCNQ salts, self-consistent continued-fraction theory of cond. 79−69482
TTF-TCNQ series, cryst. struct., elec. cond., and EPR meas., steric factor effects 80−19789
TTF-TCNQ single crystal, nonlinear electronic transport, microwave harmonic mixing 78−91684
TTF-TCNQ type organic metals, study of interstack interactions 79−47089
TTF-TCNQ type salt, trimethylene-TTF-TCNQ, unsymmetric cation, phys. props. 78−76059
TTF-TCNQ-d_8, large single cryst. platelet growth by diffusion method 78−3010
TTF-TNCQ, mobility due to mol. optical phonon scatt. 77−85202
TTF.CuBDt, spin 1/2 Heisenberg chain, spin-Peierls transition 79−61135
TTFCuBDT, spin-Peierls transition in spin 1/2 Heisenberg chains, RPA calcs. 80−25150
$TTF.CuS_4C_4(CF_3)_4$, spin-Peierls system, nucl. spin-lattice relax. process 78−19361
$TTF.PtS_4C_4(CF_3)_4$, quasi-one-dimensional cpd., exchange, thermal and mag. study 78−68209
TTG-BDT(Cu), giant struct. distortion, high speed photography obs. 78−43121
TTSeF-2,5-dimethyl TCNQ, donor and acceptor stack stability against Peierls distortion 78−51979
$TTT_2^+.I_3^-$, cryst. and mol. struct. by X-ray study 79−51096
$TTT_2-(I_3)_{1+x}$, physical props., elec., mag. and optical meas. 80−24908
$TTT_2I_{1.5-x}Br_x$, chem. impurities and neutron irrad. induced defects, effects on DC cond. 80−49699
$TTT_2I_{3+\delta}$, thermoelec. power and metal-semicond. transition 80−34431
$TTT_2I_{3+\delta}$ complex, influence of press. on metal-dielectric phase transition *(Russian)* 80−92818
TTT_2I_3, charge transfer salt, Coulomb effects, Madelung energy calcs. 80−19747
TTT_2I_3, charge transfer salt, Coulomb effects 79−28308
TTT_2I_3, charge transfer salt, Coulomb effects 79−46599
TTT_2I_3, chem. impurities and neutron irrad. induced defects, effects on DC cond. 80−49699
TTT_2I_3, neutron irrad. induced defects and chemical impurity effects on DC cond. 80−39565
TTT_2I_3, organic metal, mag. susceptibility meas. 78−23241
TTT_2I_3, quasi one-dimens. organic metal, elec. cond. and thermoelec. power 80−24899
$TTT_2I_xBr_{3-x}$, charge transfer complex, optical and elec. props. 79−4554
TTT^+Br^-, cryst. and mol. struct., X-ray method 80−107202
TTT, donor-acceptor system, physico-chemical studies *(Hungarian)* 80−75554
TTT, neutral, cation and conducting complex reson. Raman spectra, vibr. lines, charge transfer 79−4794
TTT, resonance Raman spectra 79−56787
$(TTT)_2I_{3+\delta}$, struct., X-ray diffuse scatt. study 80−24437
$(TTT)_2I_{3+\delta}$, 1 dimens. conducting chains, supercond. fluctuations 78−39099
$(TTT)_2I_{3+x}$, three-dimensional organic chain conductors, one-dimensionalisation by impurities 78−91681
$(TTT)_2I_3$, metal-insulator phase transition, elec. cond. and mag. susceptibility meas. 78−14719
$(TTT)_2I_3$, optical, spin-reson., magnetoresist. study, nature of ground state 78−68023
$(TTT)_2I_3$ quasi-one-dimensional organic metal, effects of disorder on cond. and thermoelec. power 79−56206
TTT cation radical salts, cryst. struct. by X-ray anal., rel. to elec. props. 80−24436
TTT cation-radial salts, new class of quasi-one-dimens. org. cond. 78−6367
TTT salts, charge transfer salts, optical props. 79−61403
TTT salts, charge transfer salts, optical props. 79−73970
TTT salts, IR spectra, mixed-valence salts 80−40121
$TTT-(I_3)_{0.5}$, one-dimens. metal, mag. susceptibility, elec. resist., thermopower meas. 78−87967
$TTT-I_{1.6}$, dimensionality and disorder 77−66160
$TTT-I_c$, direct current conductivity and thermo-electric force, 4-400K *(Hungarian)* 79−56251
$TTT-I_n$, charge transfer salt, electronic spectra in soln. and solid state 78−2878
TTTF-TCNQ, crystal and molecular structure determination *(French)* 78−91329
$TTTI_xBr_{1.5-x}$, optical and transport props. 80−24911
TU-20 turbine oil, 4-methyl-2,6-ditertiarybutylphenol determ., using IR spectrophotometry *(Polish)* 80−13161
di-tungsten cyclopentadienyl tri-carbonyl, dual luminesc., ps pulse excitation 80−32754
twisted intramol. charge transfer states, dual fluoresc. 79−36683
tyramine, Gaussian wavefunctions, transcorrelated method 77−61678
tyrosine, photoionised, in γ-irrad. alkaline glass, electron traps, stimulated luminesc. 78−11536
tyrosine, polycryst., NMR, selection of nonprotonated C resonances 80−50201
tyrosine fluorescence at 345 nm in proteins lacking tryptophan 79−39360
ubiquinone-Fe complex, bacterial photosynthesis primary electron transfer processes, psec. dynamics 78−80841
ubisemiquinone interaction with Fe-S centre of succinic dehydrogenase of submitochondrial particles, EPR 78−69016
umbelliferone, excited state tautomeric forms, solvent polarity effects 79−59377
umbelliferone, excited states, in ethanol-water soln., absorption and emission spectra 79−13763
umbelliferones, 3-substituted, fluoresc. spectra, pH depend. 77−88492
n-undecane, calorimetry at high state parameters 78−57953
undecane, liquid, chain reorientation, Brownian dynamics simulation, comparison of models 80−49067
organic compounds continued
n-undecane, organic impurity molecular fluoresc., effect of heat pulses 78−88360
n-undecyl-p-azoxy-α-methylcinnamate, smectic C phase, domains, walls, and disclinations 79−86687
undecylazoxymethylcinnamate, crit. angular fluctuations above second order smectic-A to smectic-C transition 77−4190
undecylenate, mesogenic compounds, thermal stabilities, packing coeffs. and mol. packings 79−46558
N_3-undecyllumiflavin, high resolution fluoresc. and excitation spectroscopy, vibronic transitions obs. 80−78639
undissociated polar compounds, reverse osmosis transport processes at membranes *(German)* 78−95946
unsaturated hydrocarbons, dipole polarisabilities, STO-4G calcs. 80−83255
unsaturated P-containing peroxides, electron structure, stability and reactivity 80−14086
UPS of biological mols., ionisation energy, assignments and electron donation 78−77005
uracil, aq. soln., fast electron induced radical identification 79−24870
uracil, nucleic acid component, selective action by ps light pulses 80−72213
uracil, RNA component, review of props. 79−53035
uracil cryst., theory of IR spectra of H-bond 77−40223
uracil derivatives, effects of UV radiation, IR spectra obs. 78−27801
uracil derivatives, photosensitised induction by H-addition radicals in frozen aqueous soln. 78−20146
uracil film, far vacuum UV transmission spectrum 77−8671
uracil in aq. electrolyte, adsorpt. isotherm and solute activities from spreading pressure-surface charge data 78−14576
uracil in carbonaceous chondrites, Murchison, Murray and Orguiel meteorites 80−31261
uracil monoanions in soln., tautomer identification by laser Raman spectroscopy 80−14148
uranin in ethanol soln., and dye mixtures, excitation by Cu vapour laser 80−28230
uranine, intercombination conversion rate consts. from triplet quenching by 1,4-diphenylbutadiene 79−956
uranocene, reson. Raman spectra, anomalously polarised electronic band, energy level assignment 79−59451
uranyl acetate solns., radiocolloidal and pseudoradiocolloidal state 78−44390
uranyl acetates, cubic crysts., optical spectra fine struct. 77−1693
uranyl hexafluoroacetylacetonate tetrahydrofuran, IR laser photodissoc., O and U isotope selective 80−50868
uranyl phenanthraquinone radical ion complex, longitudinal spin-lattice relax. time determ. 80−108076
uranyl propionates, cubic crysts., optical spectra fine struct. 77−1693
urea, aqueous soln., mol. reorientation, Raman spectra 78−64354
urea, aqueous solutions, mol. associations, X-ray diffr. meas. 77−76290
urea, bond charges, comparison of exptl. and theoretical X-ray scatt. curves 78−55782
urea, bond electron density distrib., 123K, simple refinement 78−55857
urea, density distributions of bonding electrons 78−75616
urea, efficient phase-matched SHG over wide spectral region 77−83929
urea, electro-optical coeffs. meas., rel. to nonlinear optics calcs. 80−34889
urea, electrochem. removal, basis for a regenerative dialysis system 80−26417
urea, electron density distrib., multipolar expansion 80−96501
urea, fifth harmonic generation, high-efficiency high-power UV generation at 2128 Å 80−99793
urea, force field for planar vibrs., CNDO/Force MO calcs. 79−76416
urea, internal modes contrib. to Debye-Waller factors 79−73264
urea, low temp. phase transition, X-ray diffr. expts. 79−1501
urea, quantitative structural studies by means of the energy-dispersive method with X-rays from a storage ring 80−24314
urea, second and third order hyperpolarisabilities, SHG and four-wave mixing meas. 79−59759
urea, single cryst., optical SHG, refr. index, susceptibility 78−63152
urea, single crystal Compton profiles, H-bonding and dimer config. effects, calc. and meas. 78−80431
urea, thermally stimulated depolarisation currents, peaks interpreted in terms of molecular relaxations 78−19407
urea+acrylic acid (acrylamide), γ-irradiated reactions under high pressure *(Japanese)* 79−52707
urea adducts, crystn., geometry of urea-cation bonding 80−39061
urea antimony fluoride, X-ray cryst. struct. determ. *(French)* 80−44196
urea crystal, efficient phase-matched SHG and sum freq. mixing 80−14391
urea in NaI aq. soln., Raman scatt., mol. reorientation relax. time 79−8136
urea mixed and adsorption mixed crystals and epitaxial growth from solns., tracht and habit *(German)* 80−38973
urea molecule, bond-length corrections for external and internal vibrs. 80−106402
urea monocrystals from aq. soln., growth kinetics 79−99092
urea nitrate single cryst., elec. cond. anisotropy 78−79807
urea percutaneous electrophoresis 78−61237
urea-formaldehyde resins, appl. for radioactive waste solidification, technical evaluation 79−67875
urea-$Li^+(K^+)$, assoc. in aq. soln., potentiometric obs. 77−29005
urea-malonic acid, room-temperature ENDOR spectra obs. 80−106339
urea-n-paraffin adducts, order-disorder transition, thermal anal., X-ray diffr., and NMR 79−33084
urea-$NaNO_3(KNO_3)$ solid eutectic mixtures, Raman, IR spectra, line shifts, widths 77−55793
urea-oxalic acid (1:1), X-ray cryst. struct. determ. and thermal expansion 79−46645
urea-uranyl sulphate, $UO_2SO_4.2CO(NH_2)_2$, lattice parameters, space groups, X-ray crystallography 78−59798
urea-uranyl sulphate, $UO_2SO_4.3CO(NH_2)_2$, lattice parameters, space groups, X-ray crystallography 78−59798
ureas, alkyl and phenyl groups trisubstituted, conformation, steric and stacking interaction 80−95587
uric acid occurrence, growth morphology of $C_5H_4N_4O_3$ anhydrous monoclinic modification 80−84123
uridine, pulse Fourier transform proton mag. resonance, equivalent to CW INDOR 77−32293
uridine 5'-phosphate (Na salt), EPR study of PO_4^{2-} radical 79−57592

organic compounds continued
uridine 5'-phosphate (Na salt), NO_2 species in an irrad. single crystal, EPR obs. 80−40719
uridine monophosphate, excited state geometry distortion, normal modes reson. Raman intensity anal. 79−68236
uridine-5'-monophosphate gamma-irrad. solutions, short-lived radical detect. by spin-trapping method 77−21479
uridine-5'-phosphate.$2Na^+$ single crysts., radiation damage, ESR obs. 80−108964
5-uridylic acid, electron adduct, spin density distrib., INDO calcs. 77−71754
uro-porphyrin I octa-n-dodecyl ester, discotic phase 80−103240
uronic and other organic acids in Baltic and Black Sea sediments 78−49007
US relaxation of aqueous mixtures of methanol and ethanol *(French)* 80−6468
l-valine, cryst., electron damage, electron microscope study 78−22762
DL-α-valine in aq. soln., dielectric dispersion 78−20141
valine surface, heavy-ion induced desorption of organic cpds. 80−100739
valinomycin, appl. of three phase struct. invariant, in $P2_1$, probabilistic theory 79−51033
valinomycin, effect on phospholipid artificial membrane phase state and passive permeab. for Ca ions 78−80836
valinomycin monolayers, struct., area and compressibility determ. 78−44461
valinomycin-cholesterol (stearic acid) monolayers, struct., area and compressibility determ. 78−44461
valyl-h-tRNA synthetase of chick embryo brain, ^{60}Co γ-irrad. obs. 80−72222
vanadyl alkanoates, ^{51}V NMR, quadrupole splitting in nematic phases 79−28637
vanadyl bisacetylacetonate, frozen soln., proton ENDOR, ligand hyperfine tensors 79−99792
vanadyl bisacetylacetonate, polarised X-ray absorption and double refraction 80−50459
vanadyl carboxylates, EPR and mag. susceptibility, near one-dimens. antiferromagn. 77−63265
vanadyl mixed ligand complexes, mechanism of spin transfer to next neighbours ^{13}C and ^{31}P 78−86892
vanadyl octaethylporphyrin, radical cation EPR linewidth inversion, relax. theory 77−10693
vanadyl phthalocyamine dye solns., laser destruction, highly excited states participation 78−53231
vanadyl phthalocyanine, sublimed layer, IR absorption, vibr. assignments 78−55174
vanadyl phthalocyanine-copper phthalocyanine mixed crysts., α-β phase transform., heat of transform., DTA investig. *(German)* 78−30754
vanadyl porphyrins, anion radicals and dianions, reson. Raman spectra 77−471
vanadyl triisopropylate, chem. shifts, NMR line widths, temp. and solvent depend. 78−70853
vapour liquid critical pressures and volumes 79−99306
vapour sorption on PVC and polystyrene powders, glassy-state relaxation induction and meas. 80−44415
vapours, lasing characteristics 80−99716
vapours, light scatt., depolaris. factor meas. *(Russian)* 79−13780
versatic acid, extraction equilibria of Cu, Ni, Co and Mn 79−43620
versatic acid 10, solvent extraction of Pb (II) *(Japanese)* 79−4928
vibrational relaxation and dephasing, Raman spectra, review 80−88987
vincristine, combined effect US and cytotoxics on Zea mays root growth 77−5025
vinyl acetate, Fourier transform double resonance NMR 78−80249
vinyl acetate, He I and He II photoelectron spectra, CNDO/S calcs. 78−55201
vinyl acetate, model for exciton theory of excited states in poly-2,4-hexadiyn-1,6-diol bis(p-toluene sulphonate) 77−80733
vinyl acetate, monomer and polymer, Raman and IR spectra, liq. and solid 78−58700
vinyl acetate, oligomers, dielectric relax., end-group effects 78−92019
vinyl acetate, pulse Fourier transform proton mag. resonance, equivalent to CW INDOR 77−32293
vinyl alcohol, struct. from ab initio calcs. 78−29857
vinyl alcohol-d_0, -d_1, microwave spectrum, centrifugal distortion 77−71796
vinyl azide, microwave spectrum 77−57985
vinyl bromide, mol. struct., from gas-phase electron diffr. and microwave data 80−23571
vinyl bromide+Cl, rate consts., stratospheric temps., radiotracer meas. 77−48632
vinyl bromide maser, CO_2 laser pumped, stimulated emission at 45 freqs. 77−645
vinyl bromide-d_3, ^{13}CBr bond, coupling consts., correl. with C hybridisation s-character 80−34806
n-vinyl carbazole, radiation induced polymerization ESH study 80−7817
n-vinyl carbazole-acrylamide, post radiation induced polymerisation 80−7818
n-vinyl carbazole-acrylamide, radiation induced polymerization, monomer crystallinity effects 80−7819
vinyl cation, dissociative recomb. cross section determ., merged beam obs. 80−78715
vinyl chloride, air pollution monitoring, computer controlled CO_2 laser absorpt. system 80−89699
vinyl chloride, air pollution monitoring by CO_2 laser system 78−49182
vinyl chloride, intracavity IR absorpt. in CO_2 laser, enhanced sensitivity 78−78835
vinyl chloride, IR laser induced photoreactions, product identification 79−57257
vinyl chloride, IR multiphoton energy deposition and reaction yield, press. and intensity 78−95936
vinyl chloride, monitoring using Fourier IR technique 79−16106
vinyl chloride, multiple IR photon dissoc. 77−88510
vinyl chloride, polymerisation, two-phase model *(German)* 79−15996
vinyl chloride, trace determ. in water by direct injection GC/MS 78−35739
vinyl chloride, trace gas detection, using IR laser 79−43653
vinyl chloride+O_3 reaction, IR matrix and microwave spectroscopy 77−90587
vinyl chloride monomer sorption by PVC 79−4470
vinyl cyanide, electronically excited species production via collisionless, IR laser photolysis 79−57255
organic compounds continued
vinyl cyanide, IR multiphoton dissoc., CN internal energy distrib., time depend. 80−78638
vinyl cyanide, microwave spectra data tables 79−59445
vinyl cyanide+$C_2(a^3\Pi_u)$, laser-generated radical kinetics 79−100352
vinyl fluoride, geometries, props. and protonation, ab initio mol. orbital study 79−22588
vinyl fluoride, IR multiphoton dissoc., inert gas collision effects 79−16021
vinyl fluoride, vibr. excitation effects on ion-molecule reaction pathways, photoionisation mass spectra 77−16804
vinyl formate, rot. Zeeman study, g-factors, mag. susceptibility, quadrupole moments 78−50572
vinyl halides+OH, reaction rate consts., 299-426K 77−81389
vinyl isocyanate, and vinylcyano ether, geometry and conform., ab initio minimal STO-3G MO calcs. 80−23337
vinyl isocyanate, conformers, geometrical and electronic structures, microwave spectra 78−9142
vinyl isocyanate, microwave and photoelectron study of cis- and trans-forms 78−70819
vinyl mercaptan -d_0, -d_1, anti rotamer, conform., microwave spectrum 80−9592
vinyl mercaptan -d_0, -d_1, synrotamer, conform., microwave spectrum 80−5535
vinyl methyl ether, stopping cross section for 0.3 to 2.0 MeV He^+ ions 78−63537
vinyl methyl ether+$O(^3P)$, absolute rate consts. meas., 297-439K 78−7196
vinyl methyl ether+OH reaction rate consts., 299-427K 77−86301
vinyl monomers, radical polymerisation, const. elec. field effects *(German)* 78−61008
vinyl monomers, specific heat, calorimetric method based on ^{60}Co source *(Italian)* 77−72694
vinyl radical, MINDO/3-FORCES, geom. of heat of formation 78−66472
vinyl stearate multilayers, struct. determ. by electron diffraction 79−4469
vinyl sulphides, divalent S linking with multiple bonds, spectrosc. obs. *(Russian)* 78−21929
1-vinyl-o-carborane, orientationally disordered, γ-irrad. free radical defects, positron probe obs. 79−23647
vinylacetate-H_2O suspensions, particle size, surface tension, stabilizer conc. effects meas. *(German)* 79−24834
2-vinylanthracene, conform. conversion kinetics, fluoresc. 80−9631
N-vinylcarbazole, polymerisable monomer, structural chemistry, cryst. struct. determ. 77−4096
N-vinylcarbazole, polymerisation in presence of C black 79−20366
vinylchloride, mol. struct., gas-phase electron diffraction and microwave spectra, vibr. amplitudes 79−76421
vinylcyano ether, and vinyl isocyanate, geometry and conform., ab initio minimal STO-3G MO calcs. 80−23337
vinylcyclopropane, Raman study of rotational isomers 79−18194
vinylfluoride, gas phase electron diffr. and microwave spectra, rot. consts., struct., isotope shifts 79−31686
n-vinylformamide, torsional pot. barriers, ab initio and partition of energy methods 77−88588
vinylidene chloride, radn. induced emulsion polymerisation 79−74383
vinylidene chloride, trace gas detection, using IR laser 79−43653
vinyloxirane, Raman and IR vibr. spectra and conformations 80−83379
vinylsilanes, substituted, torsional pot. anal., from spectrosc. data 78−62787
vinylsilanetriol-d_0,(-d_3), soln., vibr., IR and Raman spectra 78−86854
violanthrene-A, electron escape depths and absorpt. coeffs. 78−23580
violanthrene-A film, amorphous and crystalline, carrier mobility differences 78−60125
violanthrone, free radical, EPR meas. 78−27094
viologen films, on transparent oxide electrodes, morphology, electro-optical obs. 80−100703
viologens electrochromic solutions, for display appl., oxidant impurities elimination 80−78922
virus solid, low density, yield stress model 78−88725
visual chromophores, two-photon absorptivities, SCF-PPP-CI calcs. 79−31631
visual pigment model systems, spectroscopy and photochem. 77−32871
visual pigments, slow flash photolysis using conventional spectrophotometer 78−68904
vitamin A, in DMF, electrochem. reduction, automatic pH control appl. 77−63928
vitamin A, visual chromophores, two-photon spectra, lowest excited state 78−64934
vitamin A deprivation rel. to behavioural threshold and rhodopsin content in rat 77−70463
vitamin B_{12b}:B_{12r}, cryst. growth, orientation, ESR obs. 79−34486
vitamin B_{12}, CARS near one-photon reson. 77−65466
vitamin B_{12}, circular dichroism and birefringence, polarisation modulation meas. 79−21803
vitamin B_{12}, electrochemical reduction of methylcobalamin and methylcobinamide, one electron intermediates 78−85286
vitamin B_{12} derivatives, vis. and UV reson. Raman spectra, rapid flow method 77−66796
vitamin B_{12} field-desorption mass spectrosc. 78−80821
vitamin B_6 fluorescence in cells 77−21496
vitamin C radioprotective effects obs. in Chinese hamster ovary cells 77−73546
vitamin D, role of free radicals in conversions and mechanisms of physiological action 77−70430
vitamin E distribution among tissues and subcellular fractions in sublethally irrad. mice 77−64098
vitamin K_3 effects on chlorophyll a fluoresc. duration in chloroplasts 77−25393
vitamin V_{12r}, monomeric O_2 adduct, struct., single cryst. ESR obs. 79−39351
vitamins, B group, γ-irrad. resist. 78−76890
volatile, in water, gas chromatography/mass spectroscopy anal. 79−12151
volatile compounds determ. in city air, gas chromatography techniques 78−12003
volatile trace organics, aqueous environmental samples, head space anal. 80−40763
water dodecane potassium oleate hexanol, micro emulsion, Rayleigh scatt., micellisation *(French)* 80−43055

organic compounds continued
in water supply in Cleveland, Ohio 79−16550
water toluene sodium dodecylsulfate butanol, micro emulsion, Rayleigh scatt., micellisation *(French)* 80−43055
water-cetyltrimethylammonium bromide-haxanol system, ^{13}C NMR, catalysis in micellar and liq. cryst. phases 79−61909
water-dioxan mixtures, positron annihilation, o-positronium pick-off quenching 79−24386
water-ethanol, vapour-liquid equilibrium, transpiration method meas. 79−99305
water-imidazole, H bond interrupted chain, cooperative effects, STO-3G ab initio calcs. 80−63535
water-methanol-(ethanol), vapour-liquid equilibrium, transpiration method meas. 79−99305
Wolffram's red salt, mixed valence, reson. Raman calcs. using vibronic coupling model 80−97249
Wurster's blue cation, fluoresc. quenching of hydrocarbons, diffusion effects 77−6823
Wurster's cation dimers, reson. Raman spectra 77−58009
xanthene, chem. shift, ring-current and excess-charge effects, semi-empirical calc. 78−33523
xanthene, dye solns., luminesc. spectra, conc. depend. effects 79−54885
xanthene dye, solute-solvent hydrogen bonding and temp. effects on internal conversion 77−3402
xanthene dye N-92+inert gas buffer, electron beam excited, fluoresc., energy transfer 78−25877
xanthene dye sensitisation of ZnO electrode, role of triplet states 78−76869
xanthene dyes, effect of pH on laser output power 77−38881
xanthene dyes, fluorescence efficiency of laser dyes 77−42531
xanthene dyes, hidden vibr. band determ. method, fluorescence and excitation spectra meas. 80−40158
xanthene dyes, internal heavy atom effect on radiative and non-radiative rate consts. 80−32765
xanthene dyes, phosphoresc. spectra of T_1 state in ethyl alcohol soln. 79−85981
xanthene dyes, phosphorescence and orbital nature of triplet state *(Russian)* 77−85797
xanthene dyes in n-alcohols (ethylene glycol) (glycerol), rot. relax., time-resolved fluoresc. depolaris. obs. 80−58300
Xanthene N-92 plasma, nanosecond excitation using photopreionisation-stabilised discharge scheme 79−98982
xanthene-acridine dye laser mixture, tuning props. 77−3579
xanthine, and biological methyl derivatives, electronic struct. from UV photoelectron spectra 79−24949
xanthine, planar autoassoc. energy 80−53086
xanthine oxidase (dehydrogenase), EPR, mag. spin-spin dipolar interaction 80−53026
xanthione, large zero-field splitting of lowest triplet state 80−58171
xanthione, solns., triplet state quenching by ground state xanthione 78−42180
xanthione in benzene, second excited singlet state, ps spectra 77−3399
xanthone, excited singlet state, fluoresc. quenching by metal ions, rate meas., mechanism 77−38685
xanthone, in n-pentane, heat pulse induced delayed phosphorescence 80−83404
xanthone, single cryst., polarised UV absorpt. spectra 78−19500
xanthone in host crysts., triplet state PMDR, phosphoresc. spectra, transition mechanisms 77−46585
xanthone in n-hexane, 77 and 4.2K, phosphoresc. spectra, triplet lifetime 78−21957
xanthone-biphenyl derivative donor-acceptor solns., triplet-triplet energy transfer under Shpolskii effect conditions 79−64031
xanthoporphinogen, IR electronic excitation spectra, CNDO/S calcs. *(German)* 77−79617
xanthrene, dye soln., transient dichroism, rot. diffusion anomalies 79−87414
XH_2 molecules 1:2 complexes, H-bonding fluctuation hypothesis, IR and Raman vibr. spectra 77−34632
XY_2 bent symmetrical molecules, Coriolis coupling consts., centrifugal distortion consts. 80−58236
p-xylene, ^{13}C chem. shielding tensors 78−60342
p-xylene, electronic-vibr. spectra calcs., Franck-Condon and Herzberg-Teller approx. 80−37735
o-xylene, in external transverse resonator, stimulated Rayleigh wing scatt. line, anomalous shift 78−13763
p-xylene, isotopically mixed cryst., phosphoresc. triplet state, ESR and MIDP obs. 77−58071
p-xylene, liq., heat capacity rel. to temp. 80−44335
xylene, liquid, interface with photoconductor, carrier injection 80−24970
p-xylene, melting surface, ablation in impingement region of water jet 80−14766
m-xylene, mol., UV prereson. Raman scatt., interference effects 79−64008
m-xylene, mol., UV prereson. Raman scatt. intensity 79−64007
p-xylene, mol. geom. struct. and ring distortion, gas-phase electron diffr. 79−59573
xylene, plasma polymerisation deposition and ESR of trapped free radicals 79−83455
p-xylene, plasma polymerised films on glass, as laser fusion targets, deposition method 78−60860
xylene, presence in TEA CO_2-laser, optimum operational conditions *(Bulgarian)* 78−33720
p-xylene, stimulated Raman scatt., intensity changes 78−13753
p-xylene, visible absorpt. spectra, local mode overtone intensity of C-H stretching mode 79−81207
o-xylene, volume effect in metastability of crystalline phases on cooling 79−77716
p-xylene+s-tetracyanobenzene, photoassoc., exciplex form., excitation energy and isotope depend., vibr. effects 80−55634
n-xylene dissociation, C precipitate with preferred orientation [100] *(Russian)* 80−45484
xylene liq. jets induced by electrostatic field, disintegration and convergence 79−81986
p-xylene-benzene liq. mixture, excess energy of vaporisation, US study 80−65209
xylene-carbon tetrachloride (toluene) liq. mixtures, excess free vol., US vel. meas. 77−51294
p-xylene-d_{10}, soln., fluoresc. quantum yields, temp. and deuteration effects 77−3396
organic compounds continued
p-xylene-sodium dodecyl sulphate-pentanol-water system, micellar solns. vs microemulsions 77−60131
p-xylene-tetrachloroethylene binary mixtures, dielec. polarisations 79−56713
xylenes, fluoresc. and triplet state quantum yields, biacetyl method 78−37671
xylenes, singlet excited states decay, substituent effects 77−75175
xylideneaniline-p′-benzonitri 80−44328
xylitol, X-irrad., 4.2K, electron traps, alkoxy hyperfine coupling, ENDOR obs. 80−50863
xylol, liq., thermal cond. coeffs. at high-press., 298-573K 79−73350
Yang's biradical, EPR, g- and D-tensors, electronic struct., deuteration and conformation effects 77−42343
yeast phenylalanine tRNA, macromolecular structures, struct. factor least squares refinement procedure 77−84573
yeast phosphoglycerate kinase crystals, rotation camera data, empirical method correction for absorpt. and decay effects 80−14962
yellow pigment, photoconducting, electric field-induced fluoresc. quenching 80−34967
ytterbium ethyl sulphate, crystal field effects on mag. and hyperfine props. of Yb^{3+} 80−97101
ytterbium etiophorphyrin, electronic energy transfer with porphines and metalloporphyrins, luminesc. 77−474
yttrium ethyl sulphate:Yb, spin refrigerator, proton polarisation 77−83435
yttrium ethylsulphate, rare earth doped, NMR of protons adjacent to impurity 77−85589
yttrium ytterbium tri(ethyl sulphate) nonahydrate, free proton polarisation 79−63833
zeaxanthin, aq. soln., aggregate, reson. Raman spectra, and IR spectra, exciton interactions 78−31770
zeaxanthin ([3R,3′R]-β,β-carotene-3-3′diol) as optical probe of membrane struct. 79−92124
zinc(II) metalloporphyrin, Z-ray photoelectron spectra satellites 80−5582
zinc bisdiethyldithiocarbamate:Cu^{2+}, exchange interaction of Cu^{2+}-Cu^{2+} pairs, spin-lattice relax. 78−48034
zinc chlorophyll b, triplet state population at 4.2K, magnetic field effects 77−30915
zinc complex, $Co_{1-x}Zn_x$hexa(pyridine-N-oxide)$(ClO_4)_2$, dilute cubic S=1/2 XY antiferromag., sp. ht. data 77−66358
zinc dialkyldithiophosphate surface film, prep. and nature 80−104300
zinc formate dihydrate, Co^{2+}-doped, EPR spectrum, g-factor anisotropy for A- and B-sites 77−77089
zinc glutarate complexes in aqueous soln., enthalpy and entropy meas. *(Italian)* 79−19378
2-zinc insulin, rhombohedral, cryst. struct. refinement, experience with fast Fourier least squares 78−92595
zinc malonate dihydrate, cryst. struct., X-ray refl. obs. 78−75652
zinc oxalate, crystal growth in silicate gel, X-ray diffr. and i.r. spectrum 77−4724
zinc oxalate, crystallisation kinetics, specific surface energy at cryst.-soln. interface 78−26471
zinc oxalate, effect of supersaturation on crystallisation kinetics, turbidimetry meas. 78−30569
zinc oxalate, isothermal crystallisation from soln. 80−108336
zinc phthalocyanine, resonant two hole bound state at 3p core threshold 80−60750
zinc porphin, ESR study of metastable triplet state, in n-octane matrix, 1.3K 79−72340
zinc porphin, in anthracene, triphenylene, n-octane, fluoresc. and optical absorpt. spectra 79−68240
zinc porphin, in n-alkane crystals. at 4.2K, Zeeman spectra for Jahn-Teller instability 78−27256
zinc porphin in n-octane, population hole-burning using triplet reservoir 79−87491
zinc porphin soln., mag. circular dichroism spectra, Jahn-Teller coupling 77−3391
zinc porphyrins, anion radicals and dianions, reson. Raman spectra 77−471
zinc pyrochlorophyllide in nematic liquid crystals, oriented photoexcited triplets, EPR study 80−84636
zinc stearate, additive to UO_2 green pellet fuel, effect on sintering 80−68908
zinc stearate lubricant, admixed, effect on Fe sintered compact, shrinkage and mech. props. 80−45402
zinc stearate lubricant effect on Fe powder compact, apparent density, mixing, and friction 80−45403
zinc tetraphenylporphin anion, IR spectra and vibr. anal. 79−54852
zinc-porphyrins, photodestruction in E. coli in presence of O_2 79−79601
zone refining *(Japanese)* 78−48312
Ag, adsorpt. of N,N-dimethyl aniline, adsorpt. on Ag colloids, surface enhanced Raman spectra obs. 80−97251
Ag complexes, Ag(II) porphyrins, picosec. flash photolysis, transient absorpt. 80−52976
Ag(II) protoporphyrin IX dimethyl ester, fluoresc. relax. after picosec. excitation 79−45751
Al complex of glycine, XPS study of glycine binding 79−41196
Al corrosion in chloroacetic acids, 2-mercaptobenzothiazole inhibitor effectivenes 79−57148
Al-stearic acid-Al, low-loss thin film capacitor 80−71317
aliphatic hydrocarbons in Antarctic marine sediments 79−92096
Ar-methane (iodomethane), mol. interactions, differential scatt. cross-sections meas. 79−89732
Ar-methyl chloride, mol. beam elec. reson. spectrosc. 80−23477
Ar-Xe-tetrachloromethane, self-sustained electrophotoionised discharge in compressed gas 80−38003
Ar-Xe-tetrachloromethane excimer discharge laser 79−13957
Ar+10% CH_4, Fano factor determ. from α-particle pulse height distribs. 79−76284
As_2S_3, temp.-independent mobilities, phonon-induced electron hopping 79−28347
Au deposition at high rates from organic plating baths *(French)* 80−66441
B^++CH_4, 200 keV, Auger spectra, single and double K-vacancy states 77−83706
BCl_3-$COCl_2$, impurity removal by laser irrad., IR spectra meas. 78−15686
BH_3-ethylene complex, semiorthogonalised orbitals, integral approx. scheme 80−83262

organic compounds continued
Ba_xI_y cyclodextrin, quasi-one-dimens. cpd., synthesis, elec. and mag. props. 80−2380
(BaTi) citrates, thermal decomp., thermal anal., IR and X-ray diffr. obs. 79−24735
Be^+ + methane, Be Auger spectra 77−57951
C chain molecules in interstellar clouds, form. schemes 80−26935
C chemistry of lunar soil samples from Luna 16 and 20 77−22122
$C-^+NH_3$ radical, exchangeable H^+ hyperfine coupling, ENDOR obs. 79−36669
C-C, C-H, vibr. amplitudes-internucl. distance relation validity, Badger's rule 77−68028
C-C bonds, single, double, triple, electron density distrib., X-ray diffr. data accuracy rel. to ab initio calcs. 79−89805
C-C σ bonds, mag. suscept., refined variational calc. 77−68136
$C-CH_2-C$ fragments, bond angles 77−14601
C-H, isolated IR stretching freqs., LeFevre bond parameter anal. 77−57965
C-H bond, acidity in organic mols. and anions, SCF MO calcs. 77−83497
C-H bonds, mag. suscept., vector pot. variational calc. 77−68137
C-H Raman stretching bands in soln., vibr. freqs. and linewidth 80−78622
C-H-O(-N) gas mixtures, high temp. emissivity, 4.8 μ region, shock waves 77−76027
C_5 hydrocarbons, in binary mixtures, phase equilibria *(German)* 79−37822
$C_{12}A_7H$, X-ray powder diffr. patterns *(Slovak)* 79−69099
C_3AH_6, X-ray powder diffr. patterns *(Slovak)* 79−69099
CBr_2 emission in solid Ar, laser excitation spectra and lifetimes 80−48034
CBrCl emission in solid Ar, laser excitation spectra and lifetimes 80−48034
CCN radical in solid Ar, emission and excitation spectra 78−70868
CCO radical, heat of form. calc., geometries excitation energies and vibr. freq. calc. using POL-CI wave functions 80−89512
CCl+alkynes, absolute reaction rate consts. 78−27728
CCl_2FO_2+NO(NO_2), reaction, photolysis obs. 79−74931
$CCl_2FO_2NO_2$, thermal dissoc., rel. to photodissoc. and stratospheric Cl budget 79−74931
CD, Λ-type doubling in excited rot. levels 77−57979
CD^+, $A^1\Pi$, rot.-vibr. population distrib. 80−23396
CD^+, in RF ion trap, laser induced fluoresc. spectrum, 0,0 vibr. band and rot. consts. 80−74189
CD_2, fusion ignition, focus expt., current sheath struct., fast particle beams 77−76206
CD_2, laser plasma, ion energy distrib. 78−30461
CD_2, laser produced plasma, X-ray photography using quartz analyser crystal 77−35403
CD_4^+, laser photodissoc. cross sections 78−66611
CD_4^+, rot. predissociation, observed by metastable peak struct. in translational spectra 78−25635
CF_2, absolute IR intensity of fundamental vibrs. 78−58743
CF_2 dimerisation reaction, UHF and MINDO/2′ calcs. 77−12793
CF_2, emission during vacuum ultraviolet photodissociation of CF_2Br_2 79−47955
CF_2, force fields using Redington method 77−18899
CF_2, in Ar matrix, conc. determ. by intensity calcs. 78−68941
CF_2, matrix-isolated, vibr. unrelaxed fluoresc., lattice mode coupling 77−14485
CF_2, photoproduct, vibr. distrib., fluoresc. meas. 77−88511
CF_2 radical, UV emission in microwave discharge, assignments 77−50461
CF_2, $X\ ^1A_1$ radical, form. in chlorofluoromethane collision-free multiphoton dissoc., translational energy meas. 78−92491
CF_3, absolute IR intensity of fundamental vibrs. 78−58743
CF_3, CF_3^-, and CF_3^+, optimised struct. and bonding, ab initio SCF MO calc. 80−23334
CF_3, in Ar matrix, conc. determ. by intensity calcs. 78−68941
CF_3 radical, dipole moment from beam mass spectrometric anal. 79−59596
CF_3^+ cations, IR spectra in Ar matrix 78−74710
CF_3+CH_4(H_2)(HCL), H abstraction, energies of activation calc. 78−31632
CF_4-He(Ne)(Ar)(N_2)(CO_2)(CH_4) mixtures, viscosity and diffusion coeffs. 77−89225
CF_4-SF_6(O_2) mixtures, viscosity and diffusion coeffs. 77−89225
$CF_2(^1B_1)$ energy distrib., from triplet-triplet $CF_2(^3B_1)$ annihilation and C_2F_4 vuv photolysis 80−50861
CF_2Br^+, CF_2Cl^+, IR spectra, matrix isolation study, C-F stretching fundamentals 78−37632
CF_3^+CO, core ionisaton phenomena, nonempirical LCAO MO SCF investig. 80−37906
CF_2Cl^+, and parent cations, IR spectra in matrix radiolysis and photoionis. of Freons 78−80767
$CF_2Cl_2^+$, CF_3Cl^+, IR spectra, in matrix radiolysis and photoionis. of Freons 78−80767
$CF_3NO \rightarrow CF_3NO$, photodissociation dynamics, two-photon laser-induced fluorescence study 80−43122
CF_3O^-, bonding, ab initio calcs. 77−50350
CF_2S, mol. consts., kinetic consts. method calcs. 80−58235
CF^2Se, mol. consts., kinetics consts. method calcs. 80−58235
CH A-X, B-X and C-X systems, rotational dependence of Franck-Condon factors 78−74701
CH, $A^2\Delta$ state, radiative lifetime 77−34698
CH, $B^2\Sigma^-$ state predissoc., calcs. and time resolved spectrosc. 80−23576
CH, CD, interstellar, Λ-doublet population inversion by collisions 80−22065
CH, CH_2 formation in interstellar dark clouds, grain surface reactions rel. to chemical and thermal equilib. 79−44593
CH, CH^+ lines in solar facula models, equivalent widths 79−66972
CH, CH^+ towards Cepheus OB2 association, interstellar lines obs. 80−22052
CH, chemiluminesc. in flowing afterglow of Ar+methane 78−64839
CH, collisionless form., rovibronic relax., reson. fluoresc. 78−68902
CH, evidence for predissociation in SiH from comparison of rot. level lifetimes of A states 79−3496
CH, far IR laser mag. reson. spectrum 79−3466
CH, force constants, local mode approx. 77−71791
CH in F- and G-type stars, bands oscillator strengths rel. to C abundances 77−91530
organic compounds continued
CH, in low pressure flame, laser-excited fluoresc. 78−90199
CH, interstellar, ground state inversion, collisional excitation 78−28503
CH, interstellar, maser emission obs. towards W49 region 77−87511
CH, interstellar, obs. in three bright rimmed mol. clouds 80−62238
CH, interstellar, obs. of weak lines below 3400 Å in ζ Persei 77−45509
CH, interstellar, rot. levels struct., excitation mechanisms 78−21908
CH, interstellar excitation temps. and abundance rel. to H_2CO 79−48883
CH, Λ-type doubling in excited rot. levels 77−57979
CH, one-centre integrals of semiempirical theories of valence, ab initio calcs. 80−102441
CH, photoionis. and photodissoc. near ionis. threshold, SCF MO CI and Steltjes imaging 78−58749
CH photospheric lines and $^{12}C/^{13}C$ atmospheric ratio determ. 77−5518
CH, prod. by multiphoton dissoc. of organic compounds 80−5586
CH, radiative lifetimes, electron-photon delayed coincidence meas. 78−50594
CH radical, SCF theory, multiconfig., direct orbital optimisation 80−87049
CH radical, sputtered, rotational and vibrational excitation 80−69224
CH radical, sputtered from acetone chemisorption layer on Si, rot. and vibr. population distrib. 78−64436
CH, search for RF emission in Comet West (1975n) 78−20735
CH^+, $A^1\Pi$, rot.-vibr. population distrib. 80−23396
CH^+, $a^3\Pi$ state, form. from C^++H_2, energy spectra 77−1918
CH^+, $a^3\Pi$-$b^3\Sigma^-$ transition moment, ab initio calcs. 80−87047
CH^+, CD^+, $A^1\Pi$-$X\ ^1\Sigma^+$ band system, spectroscopic consts. and radiative lifetimes 78−5237
CH^+, continuum electron wavefunction, electron capture width 78−78805
CH^+, electron correl. energies, Pade approximants and many-body perturbation theory 79−59366
CH^+, electron impact excitation, rot. transitions 79−41244
CH^+, excitation energies and transition moments in a second order polarization propagator approach 79−10051
CH^+, excitation energy and transition moment anal. of electronic transitions 78−25620
CH^+, excited states, pot. curves and transition moments determ. by ab initio CI methods 80−106286
CH^+, expt. oscillator strength 77−34693
CH^+ formation in hot gas behind interstellar shock fronts 78−61910
CH^+, ground state photodissoc. cross sections into $A^1\Pi$ state 78−82793
CH^+, in interstellar diffuse clouds, prod. by interstellar shock waves 80−56898
CH^+ in upper atmospher, obs. following trimethylaluminium high altitude release 79−48591
CH^+, interstellar, $^{12}CH^+/^{13}CH^+$ abundance ratio meas. 80−67809
CH^+, interstellar, upper limit towards τ Scorpii 78−4309
CH^+, PNO-CI and CEPA calcs. of electron correl. effects 77−34561
CH^+, photodissoc., $A^1\Pi$ state shape resonances 79−54924
CH^+ polar molecular ion, electron vibr.-rot. excitation *(Russian)* 80−1053
CH^+, predissociated levels obs. 80−37838
CH^+, sub-Doppler laser spectroscopy using fast ion beams 80−9655
CH^+ $X\ ^1\Sigma^+$, dissoc. recomb. rate coeff., rel. to interstellar mol. form. 78−56884
CH+O reaction, absolute rate const. 80−97690
CH+p-H_2(He), collisional pumping of Λ-doublet transitions, pot. energy surface 80−23516
CH^++H_2, reaction products translational energies 77−86298
CH_2 and CH_2^+, valence states, ab initio calcs. 79−6859
CH_2, CI calcs. using modified virtual orbitals 80−58163
CH_2, dimerisation reaction, UHF and MINDO/2′ calcs. 77−12793
CH_2, FSGO LCAO calc., bond angles 77−34557
CH_2, laser plasma, ion energy distrib. 78−30461
CH_2, line search in C star spectra 77−78786
CH_2 molecular beam source 80−37908
CH_2, photoprod. from ketene, singlet-triplet energy separation and rovibronic level obs. 80−11936
CH_2 radical, fluoresc. induced by laser 588.9-595.6 nm, (a^1A_1−X^3B_1) energy separation 78−42121
CH_2^-, photodetachment cross section, 0.5 to 3.0 eV photon energy *(German)* 77−65518
CH_2^+, $^4A_2$ states, large CI wavefunctions, non-adiabatic coupling matrix elements 80−37744
CH_2^+, $^4A_2(2,3)$ states, unimolecular decay, nonadiabatic interactions, transition probability as function of Massey parameter 80−35503
CH_2^+, ground state potential surface, analytic fit 77−50380
CH_2^+, radiative association, rate const. rel. to interstellar clouds 77−45512
CH_2^+, unimol. decay, nonadiabatic interaction, selection and propensity rules 78−23932
CH_2^+, Walsh's rules and small bond angle states 80−106255
CH_2+$H_2 \rightarrow CH_4$, MINDO/3-FORCES calc., acativation energy and enthalpy of reaction 78−66472
CH_2+$H_2 \rightarrow$methyl radical, SCF calc. involving orbital symm. forbidden reaction pathway 79−98004
CH_2^++D_2, reaction products translational energies 77−86298
CH_2^++H_2O, reaction rate consts., product distrib., ICR obs. 79−8428
CH_3 average internal excitation formed in F+$CH_3I(CF_3I)$, fluoresc. obs. 80−48078
CH_3, CH_2 and CH deformation vibration group frequencies and MO electron densities, interaction force const. 80−87101
CH_3, experimental determ. of the geometry and electron affinity 78−82860
CH_3^-, photodetachment cross section, 0.5 to 3.0 eV photon energy *(German)* 77−65518
CH_3^+ affinities of methylamine, ab initio SCF calculations 80−102443
CH_3^+ affinities of NH_3, ab initio SCF calculations 80−102443
CH_3^+, CD_3^+, collisional activation to form $C(H,D)_{0\text{-}3}^+$ products, energy transfer 77−44474
CH_3^+, CD_3^+, reactions with acetic acid methyl acetate, dimethyl ether and ethylene oxide 77−63901
CH_3^+ ion, radiative assoc. reactions in interstellar clouds 78−41021
CH_3-d_n, matrix isolation IR spectra, rot. and vibr. struct. 77−83589
CH_3+CH_4(H_2)(HCl), H abstraction, energies of activation calc. 78−31632
CH_3+$O_2 \rightarrow$OH+H_2CO, 368K, rate const. upper limit 80−7771
CH_3^++CH_4(NH_3)(H_2S), condensation reactions mechanism 80−25996

organic compounds continued
CH_3^++e, dissociative recomb. reaction in interstellar clouds, products, statistical theory 78−57604
CH_3^++small molecules, binary and ternary reactions at thermal energies, rate coeffs., product distribs. 78−44358
CH_3^++ethylene, transition state, ab initio calc. 78−48640
CH_4, in atm. CO-OH-CH_4 cycle, implications of anthropogenic CO emissions 77−49160
CH_4^+, CD_4^+, collisional activation to form $C(H,D)_{0-3}^+$ products, energy transfer 77−44474
CH_4^+, CD_4^+, rot. predissoc., metastable peaks 79−13774
$CH_4^+ \rightarrow CH_3^+$+H, MINDO/3-FORCES calc., activation energy and reaction enthalpy 78−66472
CH_4^+, laser photodissoc. cross sections 78−66611
CH_4^+, rot. predissociation, observed by metastable peak struct. in translational spectra 78−25635
CH_4-SF_6(CF_4) mixtures, viscosity and diffusion coeffs. 77−89225
CH_4+H^+(He^+)(O^+), 1 MeV dissociation, kinetic energy spectra 78−94302
CH_4^++CH_4(CH_2D_2), dissoc. charge transfer reactions, H and D atoms elimination 78−85141
CH_4^++$CH_4 \rightarrow CH_5^+$+CH_3, ion cylcotron resonance technique for absolute rate constants determ. 79−8462
$CH_{n_1}^+$, gaseous diffusion in He gas, ion mobility and longit. diffusion of Ar^+ and CH_x^+ *(French)* 79−94766
CH_n^++COS(H_2S)(formamide)(methanol)(methylamine), (n=Q-4), reactions at 300K 78−44357
CH_n^++NH_3, rate coeffs., ionised product distribs. 77−40522
C_2H, interstellar, distrib. in vicinity of young B-type stars *(Russian)* 80−105321
$C_2H_2^+$, dissociative recomb. cross section determ., merged beam obs. 80−78715
C_2H_2+$OH^- \rightleftharpoons C_2H^-$+$H_2O$, equilib. consts., ab initio SCF and CEPA calcs. 78−3361
C_2H_3 species formed in chemisorption of ethylene on Pt, vibr. anal. 80−61150
$C_2H_3^+$+HF, interaction, struct. and stability, ab initio calcs. 80−58347
$C_2H_7^+$, ab initio SCF, CI, CEPA-PNO struct. and energy calcs. 78−94197
C_4H_3, in flash photolysis of thiophene, transient absorption spectrum 78−46354
$C_4H_6^+$, fragmentation, kinetic energy release 77−77737
$C_5H_9^+$, highly vibr.-excited, intermol. pot. well depth estimation method 79−86034
C_6H_4 radical, force constants, local mode approx. 77−71791
C_6H_5 radical, force constants, local mode approx. 77−71791
$C_6H_6^+$, gas, laser-induced-fluoresc., rel. to photodissoc. and Jahn-Teller X and A states distortion 79−72345
CH($A^2\Delta$) radicals, electronically excited, lifetimes and quenching rate constants meas. 80−69188
CH_2CCH radical, electronic struct., geometry, INDO calcs. 77−14358
CH^+(CD^+), A-X luminesc., in near-thermal charge exchange, from He^++acetylene-d_0($-d_2$) 78−50632
$CH(CH_2)(CH_3)$, semiempirical electron impact ionis. cross-sections 78−1089
$CH_3(CH_3^+)(CH_3^-)$, HF, GVB and CI calcs. 77−75063
$CH_3C^{15}N$, rot. relax. time meas., self- and foreign-gas collisions, Stark-switched microwave, obs. 79−86048
CH_3CO^+, ground-state, two-config. SCF wavefunction 77−46481
CH_3CO^+, heat of form. from acetone cation+ketene proton transfer 77−90592
CH_3^+CO, core ionisaton phenomena, nonempirical LCAO MO SCF investig. 80−37906
CH_3CO', low lying states, struct., energetics, ab initio STO calcs. 77−61682
CHF dimerisation reaction, UHF and MINDO/2′ calcs. 77−12793
CHF radical, $\tilde{A}^1A''$-$\tilde{X}^1A'$ transition, laser induced fluoresc. 80−95660
CHF+$O(^3P) \rightarrow$HF+CO, product vibr. energy distrib. 79−61853
CH_2F, far IR laser mag. reson. spectrum 78−9174
$(CH_3)_4NAl_2Br_7$, ^{81}Br NQR and ^{27}Al NMR 78−6597
C_3H_5NH radical, valence shell ionis. pot. determ. 77−31014
$(CH_3)_3NHCoCl_3.2H_2O$, chain ferromag. two magnon bound state, nuclear spin-lattice relax. 78−88206
$C_6H_6NNHCSNH_2$ radical, prod. in X-irrad. 1-phenyl-3-thiosemicarbazide, ESR, ENDOR 77−36770
CH_3NN', low-lying states, struct., energetics, ab initio STO calcs. 77−61682
CHNO isomers, interconversion pot. energy surfaces, geometries, electronic structs. 78−35660
CH_3O_2, radical, form. and decay rates, UV absorpt. spectra 77−48631
$C_2H_5O^+$ and $C_2H_5S^+$, stability, proton affinity, ab initio SCF, CEPA PNO, MINDO/3 and MNDO calcs. 79−59357
CH_3OHF^-, IR photodissoc., fluence depend., saturation effects 80−78663
CH_3PF_4, nonrigid mol., tunnelling mechanisms, spectrosc. theory 80−78605
CH_2SiH_2, ab initio GO calc. 78−94187
$(CH_3)_3SnH$, radical initiated dissoc., Sn isotope separation *(Russian)* 79−59604
$(CH_3)_2X$ molecules, perturbational MO anal., methyl rot. barriers, fragmentation mode 77−88386
CH($X^2\Pi$), production by multiphoton dissociation, methylamine, rate constant, laser induced fluorescence and chemiluminescence study 79−98135
CH($X^2\Pi$) radical, prod., detect. and reactions 79−61842
$CH_2(a^1A_1$-$X^3B_1)$ energy separation 79−8443
$CH_2(b^1B_1)$, radiative lifetime from $b^1B_1 \rightarrow a^1A_1$ emission in electron irrad. methane 77−3476
CN, from IR photolysis of cyanomethane, photoluminesc. spectroscopy 77−73452
CN^-, electron propagator theory, mol. electron affinities calcs. 80−83521
CNC radical vibr. and electronic spectra, in VUV photolysis of matrix-isolated cyanomethane 78−85180
CO-alkane, liq. soln., vibration-rot. IR spectra, rot. diffusion 77−83584
CO-cycloalkane solns., CO IR vibr.-rot. spectra, solvent mol. struct. 77−83585
CO_2, Kerr consts., depolarisation ratios and hyperpolarisabilities meas. 78−25624
CO_2-CF_4-CH_4-SF_6, viscosity of multicomponent gas mixtures, prediction and meas. 77−31414

organic compounds continued
CO_2-propane system, radiolysis by fission fragments, CO form., G-values 77−48657
CO_2+propyl alcohols, collisional deactivation, of CO_2 (00^01), 303-514K 78−17759
COH^+, orbital contribs. to relax. energies accompanying core ionis., ΔSCF HF calcs. 78−82642
C^+(^2P)+CH_4 reaction, 0.1-10 eV, complex formation 77−9073
CSFCl, vibr. excited states, microwave spectra *(German)* 78−55167
$CSFCl_2$ vibr. spectrum, anharmonicity corrections *(German)* 79−41173
CSH_3^+ ions, structs. and relative energies 78−82861
CSiH, matrix Hartree-Fock calcs. 79−5874
CX_n radical, (X=H,D; n=1,2,3), thermodynamic function in ideal gas state 80−14871
^{13}C, CIDNP, obs. in reactions of organic and inorganic radicals during pulse radiolysis 80−63660
^{13}C NMR, chem. shift, effective excitation energy calcs. 77−14457
$^{13}C/^{12}C$ ratio analysis in organic materials by mass spectrometry *(Portuguese)* 80−7875
^{13}C-enriched mols., proton relax. and nuclear Overhauser effect from NMR meas. 77−68058
^{13}C-labelled organic radicals, ^{13}C- and proton-ENDOR in soln. 78−55190
^{13}CH, predicted Λ-doubling spectrum 77−30857
^{13}CH fragment, selective population transfer expts., density matrix formalism appl. to NMR spectroscopy 78−15059
^{14}C labelled, gaseous, anal., radioactivity meas. using piston type counter tube, automated 77−56281
^{14}C labelled compounds synthesis, technological aspects 78−76895
$CaSO_4$:Tm/polythene mixture, thermoluminesc. response to fast neutrons 80−5340
Cd etiochlorin complex, visible spectrum, intracomplex electron phototransfer, vibr. effects 79−72330
ClCF radical in solid Ar, emission and excitation spectra, vibr. anal. 78−9164
$ClCO_3NO_2$, synthesis by UV irrad. of Cl_2, NO_2, CO in air, decomp. kinetics 78−76880
ClFCS, second excited singlet state fluoresc., spectra 79−6957
ClFCS, second excited singlet state photophysics, laser excitation obs. 80−32758
ClH-dimethyl ether, vibr.-rot. IR spectra, quantum and classical mechanics 80−91561
Cl(^2P)+methane, absolute rate and temp. depend. 78−80731
$Cl_3PNCCl(CF_3)_2$, cryst., ^{35}Cl NQR obs. of molecular reorientations between unequal potential wells 80−54989
^{38}Cl+ethylene+HI(H_2S), thermal, mechanisms and rate consts., fluoroethane decomp. 77−86343
$Cl(3p^5(^2P_{1/2}))$+carbon tetrachloride (Cl_2)(He), VUV metastable state quenching, absolute rate const. 77−79641
Co complexes, EXAFS obs. 80−998
$CoCl_2$-LiCl-glycerin-water system, Co^{2+} ion coordination transition, spectral investig. 79−42953
Co(II) Schiff base complexes, structure and bonding, book contrib. 80−972
Co(II)-octaethylporphyrin, Mossbauer emission spectra 80−8020
Co[Ag(SeCN)$_2$]$_2$, and complexes, softness values and struct., IR spectra 79−59459
Cs perfluoro-octanoate, amphiphilic liq. cryst., ^{19}F multipulse NMR study 78−76328
CsBr-dioxane-H_2O solns., elec. cond. calcs., computer program, data anal. *(German)* 77−32806
Cu complex, 1,2-ethanediammonium tetrachlorocuprate, layered struct. mag. susceptibility 80−7094
Cu complexes, EXAFS obs. 80−998
Cu complexes, porphins, and deuterated derivatives, resonance Raman spectra 79−64010
Cu-ascorbic acid, physical development process (non-Ag) *(Russian)* 79−67413
Cu-etioporphyrin I, phosphoresc. polaris. of monomers and dimers 77−34685
Cu-phthalocyanine, electron escape depths and absorpt. coeffs. 78−23580
Cu(II) iminodiacetates in aqueous solution, gamma-ray radiolysis 80−35560
Cu(II) protoporphyrin IX dimethyl ester, fluoresc. relax. after picosec. excitation 79−45751
Cu(II)-nucleic acid base interaction, MO calcs. 79−10013
Cu(ethylenediamine)$_2^{2+}$, electron tunnelling probability as function of distance for chem. reactions 78−80759
DCO^+/HCO^+ abundance ratio in cool interstellar clouds 78−65673
DCl-cycloalkane solns., CO IR vibr.-rot. spectra, solvent mol. struct. 77−83585
DPM-4, electroviscous effect 79−69010
dimethyl sulphide, emission from open oceans 79−70805
Eu piperidinium salts, emission spectra, ligand field symmetries 79−61413
Eu^{3+} compounds, chloride, sulphate, nitrate, carbonate, oxalate and acetate, Mossbauer study 79−99801
F compounds, ground states, mol. parameters, MINDO calcs. 78−41955
F+benzene derivatives, deuterated, IR chemiluminesc. 80−102506
F+carbonyl compounds, HF IR chemiluminesc., vibr. and rot. energy disposal 77−86318
F+chlorobenzene$\rightarrow$fluorobenzene+Cl, statistical theory, phase space theory 79−74369
F+ethylene, intermediate complex reaction, vibr., translational distrib., pot. hypersurface calc. 77−52612
F+ethylene derivatives, deuterated, IR chemiluminesc. 80−102506
F+hydrocarbon (substituted methane)(inorganic hydride), HF IR chemiluminesc., H abstraction rel. rate consts. 77−86319
F+iodobistrifluoromethylphosphine, reaction mechanism and kinetics, ESR 77−86294
$FeCl_4^-$ in organic solvents, dilute, ESR linewidths *(German)* 80−11258
Fe_xI_y cyclodextrin, quasi-one-dimens. cpd., synthesis, elec. and mag. props. 80−2380
H-bonded complexes, OH stretching vibr. band, temp. effect 78−90158
H+bromotrifluoromethane, reaction rate consts., flash photolysis-reson. fluoresc. obs. 78−3327
H+$CH_4 \rightarrow H_2$+CH_3, transition state, UHF method in INDO approx, 79−43578
H+chlorotrifluoromethane, reaction kinetics, ESP obs. 77−21358
H+Cl_2(organic molecule), rate const., discharge flow-reson. fluoresc. meas. 78−7178

organic compounds continued
$H^- + CH_4 \rightleftharpoons CH_4 + H^-$ intrinsic reaction coord., ab initio SCF calc. method 77−48626
HC_2, ground state energy surface, ab initio SCF calc. 78−33446
HC_2 radical, electron affinity, ab initio SCF and CI calcs. 78−50468
HC_2^-, ground state energy surface, ab initio SCF calc. 78−33446
$HCC \rightarrow H + C{=}C$ dissoc., trajectory calcs., random vibr. excitation 80−45491
HCCN, a cyanocarbene, geom. struct., electron correl. effects 80−1077
HCCN, free radical, matrix isolation spectra and ab initio calcs. 78−46329
$HCHO.H^+ + H_2O(H_2S)(HCN)$(formaldehyde), proton transfer, rate and equilib. consts. 78−48636
H_2CN^+ isomers, role in interstellar HCN and HNC form. 78−81672
HCNH radical, valence shell ionis. pot. determ. 77−31014
H_2CNH_2 radical, valence shell ionis. pot. determ. 77−31014
$H_2CN^+H_2 \rightarrow HCN^+H + H_2$, ab initio GO SCF pot. energy surface, saddle point, reaction path 77−50379
H_3CNH_3 radical, valence shell ionis. pot. determ. 77−31014
HCO, microwave spectra, hyperfine struct. 77−75139
HCO, UV matrix isolation spectra, 14K, 210-260 nm, C-X transition 78−62819
HCO, vibr.-rot. transitions, IR laser mag. resonance 77−27098
HCO^+, orbital contribs. to relax. energies accompanying core ionis., ΔSCF HF calcs. 78−82642
$HCO + NO(O_2)$, reaction rate consts. 78−31617
H_2CO^+ ion, unimolecular decay paths of electronically excited species 79−3359
$H_3CO^+ + H_2S \rightleftarrows H_3S^+ + HCHO$, chemical equilib. consts., proton affinity of HCHO and H_2S 78−85189
$H_3CO^+ + HCN \rightleftarrows H_2CN^+ + HCHO$, chemical equilib. consts., proton affinity of HCHO and HCN 78−85189
HCOH, prediction, potential energy surface for ground state of formaldehyde 80−42967
HCO′, low lying states, struct., energetics, ab initio STO calcs. 77−61682
HCP, force fields and force consts. of electronically excited states 80−69116
HCS^+-CSH^+, struct. and stability, ab initio SCF calcs., CNDO calcs. 80−32608
H_3CS^+, struct. ab initio (4-31G) SCF calc. 79−68201
HF-fluoromethylene anion, in solid Ar, IR spectra, vibr. modes 79−68231
HNN′, low-lying states, struct., energetics, ab initio STO calcs. 77−61682
H_2O-ethanol-chloroform mixture, shear viscosity near plait point, non-linear effect 77−84960
H_2O-organic aerosol-n-heptane reverse-type micellar soln., neutron small-angle scatt. *(French)* 80−26059
HOBHA, thermotropic mesophase, DMR chain segments assignment 80−24356
HOCO and HOCO* formed by OH+CO, thermochem. props., ideal gas state 78−27805
$HPO_4^-(H_2PO_4)$ radicals + organic compounds, reaction rate consts. 78−15669
^{3}H-2-deoxyglucose, appl. to retinal neurones differential labelling 79−92447
He-benzene, van der Waals, complexes, $^1B_{2u}(\pi\pi^*)$-$^1A_{1g}(6_0^1)$ band, in supersonic jet, rot. anal. 79−31578
He-Ne-methane ring laser, power resonances 80−99761
He-Ne-methane ring laser, freq. synchronisation interval for oppositely directed waves 80−99762
He-O_2-acetylene flame atom cell, for at. spectrometry, characterisation 78−32876
$He_2(^3\Sigma_u) + Ne(Ar)(N_2)(CO)(C_2)(CH_4)$, excitation transfer reaction rates 78−5332
Hg emission rel. to Hg-sensitised UV photoreactions in abiogenetic organic synthesis on primitive Earth 77−37173
$Hg(6^3P_0)$+t-butylamine, attachment mechanism, kinetics, dimer emission, luminesc. spectra 77−73442
I_2-aromatic complexes, photodissociation, I-aromatic complex in soln. formation ps laser studies 80−40711
IBr-benzene in n-decane soln., IR line broadening by chemical exchange 80−87111
In-EDTA tracer, for groundwater flow investig., neutron activation anal. 78−11921
KC_{24}-tetrahydrofuran, physical props. *(French)* 78−26692
$K^+CF_3SeO_2^-$, IR and Raman spectra, normal coordinate anal. for $CF_3SeO_2^-$ anion 80−87122
LC-440, shear modulus and viscosity relax. near isotropic-nematic phase transition *(Russian)* 77−39543
Li salt of β-ketoaldehyde, configurations of anions in solutions studied by IR spectroscopy, H-bond form. 80−87117
Li soaps, n.C_{13}-n.C_{20}, phase transition temps. and enthalpies, DSC obs. 80−45544
Li-methylamine soln., metal-nonmetal transition, electron and nucl. spin-lattice relax. 79−87306
LiI complexes, ionic cond., electrochem. props. 77−60072
LiX-alcohol mixtures, (X=Cl, Br, ClO_4), OH(OD) vibr. bands in sat. solns. and crysts. 77−8564
lithium ammonium tartrate monohydrate ferroelastic phase transition *(Japanese)* 79−77747
Lu porphyrin complexes, luminesc. 77−18958
methane cation, Jahn-Teller distortion 80−48098
methane, solid, librational tunnelling and proton relax. temp. 80−38969
Mg porphyrins, additional ligands deuteration effect on luminesc. charcts. 79−99932
Mg-chlorin, electronic struct. props. and photosynthesis 80−16902
Mg-meso-tetraphenylporphine-coated glass electrode, in photogalvanovoltaic cell *(Chinese)* 80−40865
Mg-porphine, electronic struct. props. and photosynthesis 80−16902
MnII-ATP system, exchange mechanism, FT NMR and EPR obs. 79−22733
N bases, solutions in organic solvents, IR spectra and struct. 79−38534
N-containing cpds., ^{13}C chem. shift calcs. using approx. SCF perturbation theory 77−18945
N-containing heterocycles, nonlinear 3rd-order elec. susceptibility calcs. 79−54786
N-containing organic compounds, Raman spectra, systematic interpretation 79−26995

organic compounds continued
N+organic molecule, rate const., discharge flow-reson. fluoresc. meas. 78−7178
N_2:methane-d_4, liq., vibr. relax., Raman scatt. obs. 78−92061
N_2-chloromethane mixture, binary diffusivities, 25-110°c 79−23391
N_2-methane mixture, binary diffusivities, 25-110°c 79−23391
$(N(CH_3)_3H)_2SnF_6$, phase transition and temp. effects, Mossbauer and NMR spectra 78−88236
NCO^+, partial pot. energy surfaces, ab initio SCF CI calcs. 78−37554
NH_2+propylene, reaction kinetics, laser reson. absorpt. obs. 77−9096
NH_4 perfluoro-octanoate, amphiphilic liq. cryst., ^{19}F multipulse NMR study 78−76328
$NH_4^+CF_3SeO_2^-$, IR and Raman spectra, normal coordinate anal. for $CF_3SeO_2^-$ anion 80−87122
NH_2CO', low-lying states, struct., energetics, ab initio STO calcs. 77−61682
NO_2, vibr. excited, from nitroalkane photodissoc., fluoresc. obs. 78−37693
$NO_2 + ROO \rightarrow ROONO_2$, ($R = C_nH_{2n+1}$), Fourier transform IR spectroscopic meas. 78−53194
N_2O-acetylene flame, background compensation in differential atomic emission spectrometry *(French)* 78−7296
^{14}N, NQR in organic compounds, correl. anal. 77−12240
Na fluoresceine, soln., lasing kinetics calcs. *(Russian)* 79−13778
Na-fluorescein, glycerol-alcohol soln., luminesc. decay time, conc. depend. 80−34960
$Na_3Pr(C_4H_4O_5)_3.2NaClO_4.6H_2O$, single cryst., forbidden $A_1 \rightarrow A_1$ transition, mag. field induced intensification 80−50302
$Na_2S_2O_5$-picric acid-ethanol-H_2O etchant for high-strength dual-phase steel 80−100951
Ni complexes, Ni(II) porphyrins, picosec. flash photolysis, transient absorpt. 80−52976
Ni porphin, reson. Raman excitation profiles, simulation, vibronic coupling consts. 77−65471
$Ni(CN)_2$-dodecylamine, lamellar paraffinic system, phase transitions, wide-line NMR obs. *(French)* 80−44929
trans-$Ni(S_2N_2CH_3)_2$, IR and Raman spectra, normal coord. anal. 80−28019
O-containing compounds, dipole moments, NDDO calcs. 80−47894
O-containing compounds, LCAO-SCF calc. core binding and relax. energies, rel. to polymer surface oxidation 79−76344
O+acetaldehyde(propylene), rate const., discharge flow-reson. fluoresc. meas. 78−7178
O+acetylene reaction, kinetics, flash photolysis-reson. fluoresc. meas. 77−73439
O+chloroethylene reaction, kinetics, flash photolysis-reson. fluoresc. meas. 77−73439
O_3+ethylene, dioxirane form., decomp. products, mass spectrometric obs. 78−11504
O_3+ethylene, dioxirane form., identification by microwave spectra 78−15659
OH+dimethyl ether (vinyl methyl ether) reaction rate consts., 299-427K 77−86301
OH+ethylene, reaction rate consts., 229-425K 77−40535
OH+haloalkanes (haloalkenes), reaction kinetics in microwave discharge, reson. fluoresc. obs. 77−77744
OH+methane+M, absolute rate consts., 296K, flash-photolysis reson. absorpt. technique 77−86290
$O(^3P)$+1-butyne (2-butyne), CO pro dynamics, mechanisms 78−11510
$O(^3P)$+tetrafluoroethylene, time-resolved absorpt. spectra, triplet CF_2 formation 77−44472
$O(^3P)$+vinyl halides, reaction rate consts. 298-442K flash photolysis obs. 78−7195
PO_4^{2-} anion radicals + organic compounds, reaction rate consts. 78−15669
(1,10-phenanthroline-2-carbaldehyde phenylhydrazone) iron perchlorate, high spin to low spin transition, X-ray diffr. and Mossbauer obs. 79−38418
Pt complex, ethylenediamine dihalide, reson. Raman spectra, dissoc. energy 79−26990
Pt porphin in n-alkane single cryst. ^3E_u-$^1A_{1g}$ transition, Zeeman expts. at 4.2K 80−78645
Pt-Mn(III)-porphyrin electrode for possible wet solar cell 79−100529
Pt-nucleoside complexes, Raman spectra, vibr. anal. 77−65473
Pt(diethylenetriamine)(guanosine)$(ClO_4)_2$, crystal and molecular struct. 79−73157
Rb-tetrahydrofuran soln., photolysis, photoelectron emissive EPR signal, scavenger electron affinity reactivity 78−53224
$Rb^+CF_3SeO_2^-$, IR and Raman spectra, normal coordinate anal. for $CF_3SeO_2^-$ anion 80−87122
Ru bipyridine ion, electron transfer limiting efficiency and rate constant meas., step excitation method expt. 79−91929
Ru complex, Creutz-Taube ion, ground state, single crystal EPR obs. of mixed valence Ru dimer ion 80−34766
Ru complex, Ru(II)-polypyridine, excited charge transfer states, multiple emissions 79−3468
S determination methods 79−11869
SO_2-tetrachloromethane, solns., near critical point, ultrasound absorpt. obs. 80−65160
^{35}S-labelled, liquid-scintillation counting, automatic sample prep. 78−70688
Si compounds, free mol. chemical shift, binding energy and Auger spectra 80−32782
Si phthalocyanine, monomer and dimer, UV photoelectron spectra, valence level splitting 77−38695
Si substrate for PMMA electron sensitive layer, 400 Å linewidth electron beam lithography 80−65392
SiCH, matrix Hartree-Fock calcs. 79−5874
SiO_2-liquid heptane interface, adsorption of organic liqs., IR spectra obs. 79−57295
SnO_2-copper phthalocyanine-Ag systems, elec. and electroluminescent behaviour 80−80864
T determ. in org. cpds. by combustion with isotope exchange 79−57333
TaS_2(pyridine)$_{1/2}$ intercalated layered supercond., fluctuation induced diamag. and dimensionality 77−77006
TaS_2(pyridine)$_{1/2}$, superconducting intercalation complex, proton spin lattice relaxation time 78−80096
TaS_2(pyridine)$_{1/2}$, upper and lower critical fields, supercond. props. from Ginzburg-Landau theory 79−56456
^{99m}Tc-bleomycin selective labelling for tumour imaging 79−53228
Th porphyrin complexes, luminescence 77−18958

organic compounds continued
Th(AcAc)$_4$, 4f level XPS shake-up satellites, assignments 78−1023
Th(OAc)$_4$, 4f level XPS shake-up satellites, assignments 78−1023
Th(oxin)$_4$, 4f level XPS shake-up satellites, assignments 78−1023
$TiCl_4$.trimethylaluminium+ethylene, Zeigler-Natta reaction mechanism, restricted Hartree-Fock calcs. 77−73441
$U^+ + N_2(D_2)(CD_4)$, endothermic reactions, heat of formation 77−73444
$UO_2(DMSO)_5^{2+}$ in DMSO soln. kinetics of DMSO exchange by NMR method 79−81214
$UO_3.HCONH_2.0.5H_2O$, prep., cryst. struct. and charact 80−29010
UO_2(acac)DMSO, in DMSO soln. kinetics of DMSO exchange by NMR method 79−81214
VO-etioporphyrin I, phosphoresc. polaris. of monomers and dimers 77−34685
cis-vinylisocyanate, dipole moment from microwave spectra 79−98078
Y porphyrin complexes, luminesc. 77−18958
YC(H,D)$_3$ (Y=F, Cl, Br, I) mols., applicability of bidimensional approach to force field 77−68026
Zn corrosion in HCl and H_2SO_4, alkaloid inhibitor effectiveness 79−57146
Zn etioporphyrin, excited triplet states absolute rate consts., ODMR meas. 78−33533
Zn porphin, in triphenylene, single site fluoresc. and visible spectra, vibr. assignments 77−58031
Zn protoporphyrin, solns., anal. by fibre optic filter fluorometer 77−36813
Zn-porphin(-d_4,d_8,d_{12}), nonradiative transition probabilities, deuteration effects 79−3485
Zn-tetraphenylporphine/metal electrode, photocurrent generation mechanism 78−76868
Zr complex of glycine, XPS study of glycine binding 79−41196

organic insulating materials
see also insulating oils; paper; plastics; rubber; silicones; varnish; waxes
arc tracking, comparative tracking index 77−90528
butane liquid, high-field electronic conduction obs. 79−4587
carrier traps in polymeric insulating materials, investigation by X-ray induced thermally stimulated current and thermoluminescence methods 80−93240
corrosion influence of thermal destruction products on Cu, Ag and Au *(Ukrainian)* 77−52525
epoxy mica generator insulation, dielectric stress conc. influence on voltage endurance 78−15094
epoxy polymers, unfilled and filled effect of specimen size on elec. strength expt. 77−8505
epoxy resin, low temp. irradiation effects on mechanical props., use in superconducting magnets 78−60737
epoxy resin based composites, superconducting magnet insulators, gamma-ray radiation effects 80−24495
epoxy resin insulation of HV electrodes, effect on dielec. breakdown voltage of polymer sheets 80−60502
epoxy resins, phenomena and mechanisms of tree inception 80−29687
epoxy resins, VLF partial discharges meas. over freq. range 0.1 to 50 Hz 77−76227
ethylene propylene diene terpolymer, crosslinked, AC elec. breakdown studies 78−43787
ethylene propylene terpolymer, dose rate effect on degradation behaviour 79−99239
ethylene propylene/polyolefin blends, radiation cross linking 80−66801
films, electronics and communications engineering appls. *(German)* 78−44011
fluorinated-ethylene-propylene, secondary emission and elec. fields near dielectric-metal interface 79−38697
fusion reactor, TFTR outer poloidal field coil insulation and mould design 80−91261
fusion reactor coil insulation and winding techniques 79−31210
gamma radiation effects on dielect. parameters, expt. *(Hungarian)* 78−59836
gases, replacement for SF_6 80−59313
glass fibre reinforced epoxy resin composites, fatigue behaviour, influence of superposition of elec., mech. and environmental stresses 80−97590
glass-epoxy laminate, superconducting magnet insulators, gamma-ray radiation effects 80−24495
hexafluoropropylene-tetrafluoroethylene copolymer, surface component of vac. absorpt. and resorpt. currents, source of dielec. loss 80−70792
high molecular weight polyethylene for HV cables, characterisation using size exclusion chromatography 80−66897
hydrocarbon liquids, streamer breakdown in divergent field 80−25308
Large Coil Program, insulation system cryogenic elec. test 80−91263
liquid, bubble injection and elec. induced hydrostatic press. 77−81055
liquid, laser induced breakdown 77−81056
liquid conductivity and bulk charge determ. cell *(Russian)* 80−57328
liquid N_2 immersed, short-term insulating characts. of some polymeric materials 79−85145
liquids, high-field electric conduction, thermal activation energy, anal. 78−43399
liquids, purified, elec. breakdown meas. 78−84523
methacrylic polymers, multiple dielectric relaxations, investigation by thermally stimulated current and creep methods 80−93238
methane liquid, high-field electronic conduction obs. 79−4587
neopentane liquid, high-field electronic conduction obs. 79−4587
neutron irradiation effects on organic insulators at 5K for superconducting magnets 80−107336
nylon-6, ns breakdown voltage, polarity effect, mechanism 77−63367
n-octane, liquid, polarity effect on breakdown voltage, comment on hyperconjugation 77−76229
parylene, for chronically stable reproducible microelectrode insulation 77−40942
PET, ionic cond. current rel. to neutralisation at polymer-metal interface at elevated temps. 80−24664
plastics, extrusion props. prediction using capillary rheometer 79−90204
PMMA, and hydroxides, heat resistant, electrically insulating, production methods 79−38787
PMMA, immersion in high press. gaseous media, breakdown characts. for direct voltages with ripple 80−45009
PMMA, ns breakdown voltage polarity effect, mechanism 77−63367
PMMA, treeing effects on electric breakdown *(Korean)* 77−81053
polycarbonate, plastic insulation for cryogenic power cable, exam. of dielectric, tensile props. 80−25823
polycarbonate plate, impulse surface flashover in vacuum, effect of normal elec. stress 79−4199

organic insulating materials continued
polyester (Mylar), plastic insulation for cryogenic power cable, exam. of dielectric, tensile props. 80−25823
polyester thermoplastic, for electrical insulators 80−103685
polyethylene:NaCl, internal field strength, Raman spectra obs. 80−40061
polyethylene, cross-linked and low-density, pseudo spherulite structures and elec. discharges 78−42920
polyethylene, DC treeing breakdown with space charge formation, expt. 77−24789
polyethylene, elec. trees free radical ESR study 78−60393
polyethylene, electrical capacitance under high DC elec. field 80−54705
polyethylene, elongated low density film, TSC 79−47106
polyethylene, low density, water tree growth under DC voltage stress, expt. 77−77148
polyethylene, low temp. dielec. loss due to antioxidants 79−99822
polyethylene, microwave dielec. losses variation rel. to different sample treatments 80−25881
polyethylene, ns breakdown voltage, polarity effect, mechanism 77−63367
polyethylene, partial discharges degradation effects, expt. 77−7617
polyethylene, plastic insulation for cryogenic power cable, exam. of dielectric, tensile props. 80−25823
polyethylene, space charge injected from electrode at low temps., luminesc. obs. 80−25464
polyethylene, tree initiation by DC and impulse voltage appl., expt. 77−24790
polyethylene, tree initiation under impulse voltage, effect of needle electrode materials 77−73112
polyethylene, treeing at 77K, expt. 77−24792
polyethylene, treeing inception voltage, effect of blending and crosslinking 78−43788
polyethylene, VLF partial discharges meas. over freq. range 0.1 to 50 Hz 77−76227
polyethylene, voltage-induced charge transfer and its effects on tree initiation 80−25307
polyethylene cables carrying DC current, TSC and space charge effects *(French)* 80−40042
polyethylene film, elongated, elec. impulse breakdown strength temp. depend. 20 to 80°C 77−73113
polyethylene film, partial discharges energy content effect on breakdown *(German)* 77−81052
polyethylene terephthalate, insulating material, photoinjection 77−47849
polyethylene terephthalate polymer insulator, conduction and breakdown mechanism *(German)* 80−100469
polyethylenes, dielec. losses, for use in AC superconducting power transmission lines 80−25302
polyimide film, dielec. AC props., expt. 78−43783
polyimide film, thermally stimulated depolarization anal. 79−69766
polyimide films, transient current in time range 10^{-4} to 10 s at temps. 180 to 280°C 80−65729
polymer, amorphous, excess charges, band gap levels and elec. props. 78−23053
polymer, photoelectric effects and relation to cond. processes 77−43640
polymer electric strength rel. to permittivity, loss-angle, and volume resistivity 78−6631
polymer films, superconducting magnet insulators, gamma-ray radiation effects 80−24495
polymer irradiation by high energy electron beams, industrial applications 80−3210
polymer radiation resistance of cable insulating materials for nuclear power stations, expt. 78−59835
polymeric, cable insulation, radiation modification using electron beams 80−66848
polymeric dielectric materials exposed to partial discharges, degradation product anal. 79−4765
polymeric insulating materials, water treeing initiation and growth, effects on cable service life 80−84698
polymeric insulators, controlled current DC meas. 78−57982
polymers, book 80−7257
polymers, charge carrier species determ. using interfacial phenomena 80−24978
polymers, morphology and elec. props., correl., review 78−43786
polymers, space charge behaviour and luminescence at 77K 79−99947
polymers, streamer breakdown in divergent field 80−25308
polymers, surface component of vacuum absorpt. and resorpt. currents, surface charge accumulation 80−60063
polymers, surface component of vacuum absorpt. and resorpt. currents, origin and magnitude 80−70791
polymers, tree initiation mechanism 77−24791
polyolefin, cross-linked, insulation system for wire and cable for locomotives 80−66851
polyolefin, cross-linked, irradiation appl. to provide improved insulation props. to wires and cables 80−66850
polypropylene, plastic insulation for cryogenic power cable, exam. of dielectric, tensile props. 80−25823
polypropylene, stretching reduces electrical values *(German)* 79−43446
polypropylene film, dielectric relaxation, β-mode investigation 80−93239
polypropylene film, in MIM struct., electroforming 80−25019
polypropylene films, meas. of dielectric losses at cryogenic temps. 80−25301
polypropylene-polyurethane laminates, meas. of dielectric losses at cryogenic temps. 80−25301
polypyromellitimide film, elec. cond., 120-180°C 80−60124
polystyrene, ns breakdown voltage, polarity effect, mechanism 77−63367
polysulphone, elec. appl., dielec. props. meas. 77−55750
polysulphone, plastic insulation for cryogenic power cable, exam. of dielectric, tensile props. 80−25823
polythene, stretching reduces electrical values *(German)* 79−43446
PTFE, discharge at surface in liq. He 77−84558
PTFE, ns breakdown voltage, polarity effect, mechanism 77−63367
PVC, cross-linked, irradiation appl. to provide improved insulation props. to wires and cables 80−66850
PVC, ns breakdown voltage, polarity effect, mechanism 77−63367
PVC materials, cross-linkable, for wires and cable insulation 80−66849
rubber, temp. depend. of elec. resist. determ., expt. *(Croatian)* 77−74426
solid dielectrics, treeing 78−80285
solid insulating materials, dielectric properties at cryogenic temps. 80−90867
teflon, elec. resist., meas. technique *(French)* 78−77929

organic insulating materials continued
tetramethylsilane liquid, high-field electronic conduction obs. 79−4587
thermal lifetime prediction, thermal anal. appl. 79−15913
toluene, liquid, polarity effect on breakdown voltage, comment on hyperconjugation 77−76229
treeing and elec. breakdown, tutorial 78−84524
treeing in solid extruded electrical insulation, bibliography 77−24788
trifluorotrichloroethane, liq., as insulating material and coolant, dielectric strength, HVDC convertor appl. *(German)* 77−76218
Valox 752m thermoplastic, for electrical insulators 80−103685
wetting and discharge inception in atmosphere of fog *(Japanese)* 79−4201
XLPE, dose rate effect on degradation behaviour 79−99239
XLPE from HV cables, high-pressure liquid chromatography and differential scanning calorimetry 79−100466

organic molecule configurations
see also isomerism
2-naphtoxy α-substituted acetic acid, influence of chiral solute structure on helicity induced by nematic solvent *(French)* 77−68909
2,4,6-tri-(3,5-di-ter-butyl-4-hydroxybenzyl)-mesitylene, cryst. and mol. struct. 79−86783
N_1-aryl-N_2-alkyl thioureas herbicides, structure-activity relationships 79−62176
1,1′-Bis[phenylglyoxyloyl]-ferrocen, mol. and cryst. struct. *(German)* 80−10538
S,S′-dimethyldithiocarbonate, pot. for rot. about C(sp^2)-S bonds, electron diffr. obs. 80−23572
3,3,3-trifluoropropene, struct. and vibr. spectra, IR, Raman polarisation study 80−18845
acetaldehyde, first triplet state geometry, fragmentation into free radicals 80−47915
acetaldehyde, optimum geometry, force fields, CNDO/force method 77−46498
acetate crystal hydrates, bonding determ. from IR spectra 77−42321
acetate-ferrileghemoglobin, X-ray struct. anal., 3D refinement at resoln. of 2.0 Å 80−104554
acetic acid, chemisorbed on Cu(100), acetate species struct. obs. 79−98232
acetic acid, dimer, config and energy, ab initio MO SCF calc. 79−37657
acetic acid dimer, gas phase, H-bonded complex struct. from elec. dipole moment obs. 78−74791
acetic acid-pyridine, H-bonding, proton transfer, isolated system, solvent effect, MO calc. 80−55629
acetone-toluene-tetrachloromethane, mol. interaction and thermodynamic props. 80−71935
acetonitride-d_1, ^{2}H NMR spectra, vibr. and asymmetry corrections to quadrupole coupling consts. 80−74184
acetonitrile, liq., $CD_3C^{15}N$, neutron diffr. 77−11460
acetonitrile-toluene-benzene, mol. interaction and thermodynamic props. 80−71935
acetyl cyanide-d_1, microwave spectra, r_s, r_0-struct. 78−13491
acetyl halide-titanium tetrahalide adducts, coordination, IR and Raman spectra 78−42050
N-acetyl-D-alloisoleucine, ^{13}C NMR, soln. struct., dynamics, proton relaxation mechanisms 80−76708
acetylene, angular dependent photoelectron spectral meas. 80−28060
acetylene, chemisorbed on α-Fe, struct., bonding, dissoc., UPS obs., MO calcs. 78−84050
acetylene, chemisorbed on metal surfaces, geometric and electronic struct., UPS obs. and HF LCAO calc. 79−86988
acetylene, chemisorbed on W(100), geometry distortion 77−30919
acetylene, effective core potential calcs. 79−31437
acetylene, equilib. geometry rel. to polarisation functions, ab initio calcs. 77−83567
acetylene, excited state, photochem. and spectrosc. investig. 80−95553
acetylene, ground and triplet states, electronic and geom. struct. 78−94184
acetylene, mol. geometry basis set depend., geometry optimisation ab initio method 79−31382
cis-acetylene, triplet state, near IR electronic absorption spectrum, and form. 79−63997
acetylene, triplet states, electron impact energy-loss spectra 77−68128
acetylene chemisorbed on Cu, Ni, Pd and Pt surfaces, UV photoemission meas. and SCF-LCAO calc. appl. 79−19454
acetylene chemisorption on Rh (111), EELS, LEED and thermal desorption mass spectrometry 80−80057
acetylene dimer, ab initio HF calc. for 64 conforms. 80−23333
acetylene-d_0(-d_1)(-d_2) metastable state, mol. beam elec. deflection obs. 80−74137
acetylene-LiH, struct. and props., SCF ab initio calcs. 80−106250
acetylenic iron carbonyls, mass spectra *(Italian)* 79−18313
N-acetylglycine, X-irrad., stable radical electronic and mol. struct., ENDOR and ESR 80−80637
acrolein, mol., conformational anal., inapplicability of MINDO/3 79−94105
adamantane, orientation and deform. in nematic liq. cryst., PMR obs. 77−71815
alanine, unionised, ab initio equilib. structs. calcs. 79−68181
alarm pheronomes, activity rel. to mol. similarity, electron density function meas. 80−91413
alcohols, long chain conformations, ^{13}C pseudocontact shifts 79−13743
alcohols, modified CNDO calcs., conformations, binding energies 77−6682
alene, -d_2, -d_4, harmonic force field, ground state average struct. 77−61732
alicyclic ring cpds., vibr. spectra, conformational props., book contrib. 78−78702
aliphatic alcohols, conform., rot. isomerism calcs. *(German)* 78−50541
aliphatic ketones, freq.-topology-milieu relation, IR study, struct. and solvent effect *(French)* 80−95623
alkane dimer, PCILO calc. of geom. struct. and energy 79−63930
n-alkane gases, depolarised light scatt., internal field effects 79−76471
alkane glass, γ-irradiated, charge trapping, isotope and mol. struct. effects 79−5164
n-alkane mol. config. in melt and cyclohexane soln., small-angle neutron diffr. 78−55800
alkanes, liq., mol. struct., selective deuteration and IR vibr. spectra 80−96432
alkanes, liquid, press. induced changes in mol. conform. 78−9269

organic molecule configurations continued
alkanes, molecular topology, branching, distance matrix, information theoretic calcs. 78−25405
n-alkanes, single cryst., γ-irrad., ESR, energy deposition rel. to alkyl radical form. 77−16844
alkyl β-ketoacetals, cyclic, diamag. susceptibility, O at. contribution rel. to ring closure 77−14606
n-alkyl amines, long chain conformations, ^{13}C pseudocontact shifts 79−13743
alkyl benzenes, jet-cooled, intramol. vibr. relax., reson. fluoresc. and excitation obs. 80−14152
alkyl cyanobiphenyls, pretransitional behaviour, alkal chain length depend., light scatt. in isotropic phase 80−44301
alkyl fluorides, geometries, props. and protonation, ab initio mol. orbital study 79−22588
alkyl halides, conform. energy calcs., polar bonds and polarisability, polaris. model appl. 80−58188
4-alkyl-3-phenyl-3 4-dihydrocoumarins cis- and trans-, ^{13}C NMR spectra 80−43067
alkynoyl cations, struct., charge distrib., ab initio population anal. calcs. 80−58407
allyl radical, restricted SCF and MC SCF calc. of C_{2v} and C_s structs. 80−83289
amides, geometry from ab initio calcs. 80−23338
amidofluorosulphuric acid, and Hg salt, IR spectra *(French)* 80−18858
amines, modified CNDO calcs., conformations, binding energies 77−6682
amino acids, naturally occurring, helix-coil stability consts., random copolymer method determ. 78−94333
5-amino-1-hydrogen-1,2,4-triazole, cryst. and mol. struct., X-ray study 79−55735
2-amino-4-chlorophenol in solutions, IR absorpt. spectra 80−69135
2-amino-p-cresol in solutions, IR absorpt. spectra 80−69135
aminoacetaldehyde, conformation calcs. rel. to protein struct. and bonding 80−74273
p-aminobenzoic acid hydrochloride, X-ray cryst. struct. determ. 80−39063
aminobenzonitrile, para- and meta-, NQR linewidth, Zeeman effect, mol. config., H bonding, cryst. struct. 77−51986
2-aminoethanol(-d_2)(-d_3), microwave spectra, hydrogen bonding, rot. const. 77−6765
β-1′-aminofuranoside, mol. geometry, computer retrieval and anal. 78−83645
3-aminopropanol, and deuterated forms microwave spectrum, dipole moment, struct. 79−59441
aminopyrazine, far IR spectra, barrier to planarity, pot. function and energy levels 80−69137
2-aminopyrimidine(-d_1), amino inversion vibr., planarity, far IR obs. 79−31515
aniline, in p-xylene host cryst., phosphoresc. triplet state, ESR and MIDP obs. 80−66077
18-annulene, geometrical parameters, STO-3G ab initio calc. 80−52867
annulenes, graph theoretical polynomials 80−69048
anthanthrene, mol. imaging by high resolution electron microscopy 78−79600
anthracene, Raman intensities rel. to vibronic coupling and excited electron state geometries 77−27075
anthracenes, anthronyl substituted, solvent-assisted form. of luminesc. intramol. exciplexes 78−25589
anthraquinone in pentane solvent, sublevel phosphorescence spectra, molecular distortion 80−74190
L-arginine L-ascorbate, X-ray cryst. struct. determ. 80−35826
aromatic amides, intersystem crossing, mol. geom. effects 77−6828
aromatic compounds, mol. rearrangement in excited electronic state, fluoresc. with anomaiously large Stokes shift 79−85983
aromatic five-membered heterocyclic ring system, covalent radii determ. method 80−23332
aromatic hydrocarbons, kata-annellated, para band energy-topology empirical correlations *(German)* 79−13657
aromatic hydrocarbons, mol. struct. determ. from electronic spectra, oscill. strengths *(French)* 77−71888
aromatic hydrocarbons, struct., UV absorption band calc. *(French)* 77−18989
aromatic polyesters, with S atoms, configurational props. 80−74269
autonitryl, electronic struct. and geometry, open-shell SCF calcs. 79−18106
axial symmetry molecules, graph theory *(Chinese)* 79−49964
azacyclobutadienes, conjugated mols. electronic struct. and geometry, Hartree-Fock instability 80−69055
1-aziridineethanol, mol. spectrum and hydrogen bonding 78−70820
azo dyes, tautomerisation, structs., laser Raman spectra 77−38672
azulene, multiphoton ionisation, mass spectra 80−63717
azulene(-d_8), ultrafast $S_2 \rightarrow S_0$ internal conversion 79−3474
basketene, electron diffr. determ. of struct. 78−37764
benzaldehyde, and isomeric phthalaldehydes, dipole moments meas., config., ab initio MO calc. 80−58410
benzaldehyde, electronic spectra, Cl and F substitution effects 80−23456
benzaldehyde, nπ^* and pi pi* triplet states, props., SCF calcs. 77−6695
benzaldehyde, proton affinity, MINDO/3 results compared to ICR obs. 78−1103
benzene, monosubstituted, dipole moments, isomerisation and H bonding, INDO calcs. 77−54515
benzene, Raman scatt. cross sections 79−6945
benzene liquid multiphoton ionisation polarisation experiments, molecular symmetry 79−98162
benzene radical anion, ab initio MO calcs., struct. 79−18113
benzene rings, substituted, planar ring distortion, geom. constraints 78−18624
benzene-Br_2 complex, cryst., IR spectrum assignments, site symmetry, rel. to benzene 77−36217
benzene-d_1, ^{2}H NMR spectra, vibr. and asymmetry corrections to quadrupole coupling consts. 80−74184
benzenes, disubstituted, monosubstituted, effect of bonding electrons on molecular dimensions as determ. by X-rays 79−7595
benzenes, nitrohalide substituted, microwave absorpt., mol. struct. 78−75522
benzenoid aromatics, triplet zero field splitting parameters, ODMR obs., struct. effects 80−78636
benzenoid hydrocarbons, atom numerical code scheme for classification of chemical shifts 78−94205

organic molecule configurations continued
benzenoid-o-quinoidal systems, valence isomerisation, EHT calcs. 77−77757
benzil, ENDOR study of geom. struct. of lowest triplet state 79−89696
benzil, free radical adducts, organometallic group dynamic migration, EPR 77−58049
benzil X-trap, ODMR, near planarity in triplet state 77−32295
3,4-benzo-1,6-methano(10)-annulene, mol. geom. and gas phase thermodynamic props., minimisation scheme 78−78829
1,3-benzodioxole, far IR spectrum anal., pot. function 79−76427
1,3-benzodioxole, geometry, electronic absorpt. spectra 80−971
benzoic acid, struct. refinement at room temp. 80−96502
benzophenone-N,N-dimethylaniline, intramolecular exciplex systems, laser photolysis obs. 80−35550
p-benzoquinone, mixed crysts., PMDR and thermal modulation spectroscopy, electron-phonon interaction 77−32297
1,4-benzosemiquinone, monoprotonated radical, spin distrib., INDO calcs. 77−14357
benzyl fluoride, mol. struct., NMR and gas electron diffraction obs., ab initio and mol. mechanics calcs. 80−23574
benzyl mercury chloride, cryst. struct. and absorpt. calcs. 80−84166
benzyl radical, MINDO/3-FORCES, geom. of heat of formation 78−66472
benzyl radical trapped in X-irrad. potassium hydrogen bisphenylacetate, ENDOR 77−10695
benzyl-phosphonium radical, EPR spectra temp. depend., H-P coupling consts., conformation and rot. *(German)* 77−18950
benzyne, struct. and IR spectrum, MNDO calc. 79−31403
benzynes, geometry optimisation by generalised Hartree-Fock 78−25427
beryllocene, gas phase struct., ab initio LCAO SCF calc. 78−41942
1,1′-bianthryl derivatives, dimer optical activity, vibronic circ. dichroism, theoretical anal. 78−62821
biaryls, dimer optical activity, vibronic circ. dichroism, theoretical anal. 78−62821
bicyclic ring compounds, Raman circular intensity differential spectra obs., mol. struct. 80−87130
Δ^6-bicyclo(3,2,0)heptane, conformational mobility 80−99587
bicyclo(4,2,0)octane, cis and trans isomers, struct. mol. mechanics and electron diffr. 77−54608
bicyclo [4.4.0] dicane, cis and trans forms, mol. struct., electron diffr., mol. mechanics 78−50658
bicyclo[3.1.0]hex-2-ene, microwave spectra, rot. consts., ring struct. and config. 78−42041
bicyclo[3.1.0]hexane, zero-point average struct., microwave spectra and electron diffraction 78−25738
Δ^6-bicyclo[3.2.0]heptene, microwave spectrum and dipole moment 80−9591
1,1′-binaphthyl, conformational changes, picosec. dynamics 78−25625
1,1′-binaphthyl mononegative ion conformation 77−30774
binary complex, quinone-phenol radical pair EPR, geometry calc. 78−90101
biological carrier molecules, configuration rel. to active transport thermodynamics 77−9178
biologically active compounds, design using MOLY computer system 80−63852
biomolecule, non-centrosymmetry, optical second harmonic generation 80−72133
biomolecule conformational anal., solvent effects 80−3583
biomolecules, struct. and vibr. Raman spectra 77−52939
biomolecules, ZDO method for very large mols., low computer time 77−14356
biopolymer soln. heat capacity, conformational props. temp. depend. 80−8009
biphenyl, INDO geometry optimisation 78−74575
biphenyl in Ar matrix, mol. struct., IR spectra 77−30875
biphenylic bridged systems, appl. of Faraday rot. data to conform anal. 77−65495
2,2′-bipyrimidine, in nematic solvent, conformation, ab initio and PMR determ. 80−47869
bis(tetrathiotetracene)triiodide, struct., reson. Raman spectra 78−66556
bis(trimethylstannyl)-acetylene, mol. struct. determ. from gas phase electron diffr. 78−25740
bispyrrol-indigo, π-electronic struct., PPP-type calc. and config. anal. 78−21855
bovine trypsinogen, low-temp. study, effect on flexibility, temp. factor, mosaic spread, extinction and diffuse scattering 80−54214
bromoacetic acid, cryst., films, polarised IR spectra, struct. 78−72502
bromoacetonitrile, ground state microwave spectrum assignments, mol. struct., rot. consts., quadrupole coupling 77−6763
bromobenzene, in EBBA, ^{1}H NMR and NQR of D, geometric struct. 78−17689
bromochlorofluoromethane, Raman optical activity parameters, circular intensity differentials comput. 79−85950
bromocyclotriphosphazatrienes, ^{81}Br NQR, conformation investig. 80−63665
bromomethane, ab initio SCF MO calcs., ionis. pots., dipole moment, config., electronic props. 78−1104
bromomethyl oxirane, conformation, microwave spectrum in ranges 12.5-18 and 26.6-40 GHz 79−98076
2-bromophenoxaycetyl-4-propylbenzene, cryst. and mol. struct., X-ray anal. 79−60349
4-bromophenoxyacetyl-4-ethylbenzene, single crystal, X-ray struct. determ. 79−1426
N-bromosuccinimide lone-pair struct., photodetection spectra 78−37684
bromotrifluoromethane, mol. struct., electron diffr., microwave spectra, CNDO/2 calcs. 78−37766
butadiene, mol., conformational anal., inapplicability of MINDO/3 79−94105
butadiene, twisted zwitterionic excited states, SCF calcs. 80−58179
1,3-butadienes, methyl substituted, singlet-triplet transitions, energies, relative cross-sections, $He^+(H_2^+)$ impact spectra 78−86942
butane, adsorbed on graphite, struct. and dynamics, empirical interatomic pots. 79−99417
n-butane, vibr. shrinkages, mol. struct., electron diffr. obs. 77−50535
n-butane in liq. solvents, conformational structure 80−28115
2,3-butanedione, mol., conformational anal., inapplicability of MINDO/3 79−94105
t-butanol, melting point, structure function, H-bonded hydroxyl groups 79−99053
1-butene oxide, gas, microwave spectrum 79−13703
organic molecule configurations continued
cis-butene-1, microwave rot. spectrum, centrifugal distortion effects, rot. consts. 78−9137
t-butyl acetate, rot. isomerism, dielect. and Raman spectra 80−106328
butyl cation, H-elimination, energy partitioning, transition state geometry calc. using MINDO/3 80−104430
t-butyl cyanide-HF, hydrogen bonded heterodimer, spectroscopic consts. from IR and microwave spectra 80−43039
t-butyl formate, rot. isomerism, dielect. and Raman spectra 80−106328
t-butyl radical, VUV photoelectron spectrum, geometry, vibr. struct. and ionisation pots. 78−50577
t-butyl radicals, ab initio geometry calc., ^{13}C hyperfine coupling 77−10580
t-butylbenzene, α-substitution effect and radiative lifetime, solvent effects, rel. to ethylbenzene 79−98154
butylsilane-d_0,(−d_n), vibr. spectra, normal vibrs. and rot. isomerism 79−31523
3-butyn-1-ol, vibr. spectra, assignments, rot. isomerism 80−58257
cadmium formate, anhydrous, cryst. struct. 80−107195
capsular polysaccharide antigen, structure investig. by ^{13}C NMR 80−35828
carbamide phosphate, neutron diffr. 77−31652
carbenes, core ionised states, singlet and triplet state binding energy, struct. changes, LCAO-SCF calc. 79−97982
carbenes, heterosubstituted, singlet-triplet splitting depend. on heteroatom electronegativity and conform. 80−63553
carbocations, degenerate $(CH)_N^+$ type, permutation description *(German)* 79−45658
carbocyanine dye, orientation in erythrocyte membrane, microscopic fluorescence polarisation obs. 79−83694
carbon tetrachloride, and cryst. struct. 79−77559
carbon tetrachloride, clusters, collision induced polarisability, mol. frame distortion 80−32798
carbon tetrachloride, internucl. parameters meas. using total scatt. of fast electrons 80−32857
carbon tetrachloride, mol. characts. from fast low-angle scatt. 77−50537
carbon tetrafluoride, clusters, collision induced polarisability, mol. frame distortion 80−32798
carbonyl compounds, metastable triplet states, var. and perturbational calcs. 77−61680
carbonyl halogen substituted cpds., geometric and electronic struct., LCAO-SCF calc. 79−89603
carbonyl to oxacarbene rearrangement, conformation, ab initio SCF MO calcs. 77−32780
carotenoids related to visual chromophore, electronic struct., band shape model 78−20142
catechol borane, geometry, electronic absorpt. spectra 80−971
CBOOA, smectogenic, cryst. and mol. struct. determ. 78−2103
ceruloplasmin, human, calc. of rotation function for tetragonal. cryst. at 10 Å resoln. 80−108843
cetyltrimethylammonium bromide, aq. soln., mol. conform., laser Raman spectra 78−21934
chiral molecules, detection, identification by Cahn-Ingold-Prelog rules, computer program, for teaching 79−58499
chirality rel. to biological mols. origin and evolution *(Russian)* 77−52739
chloramine, HOCl, isoelectronic mols., vap. phase UV photoelectron spectra, struct. 78−66600
chloro(2,4-dithiobiuret)copper(I)-N,N-dimethylformamide, cryst. and mol. struct. 79−99170
chloro(ethyl)silanes and its C derivatives, Raman spectra, mol. vibr. and rot. isomerism 80−87134
1-chloro-2-methylbutane, conformer depend. C-Cl stretching vibrs., Raman optical activity spectrum simulation 80−14146
trans-3-endo-chloro-4-(phenylthio)-9,10-cis-endo-bis(methoxycarbonyl)tricyclo[4,2,2,$0^{2,5}$]dec-7-ene, cryst. and mol. struct. 79−90639
6-chloro-α-pyridine anthraquinone, cryst. and mol. struct., X-ray diffr. meas. 77−43206
chlorobenzene, gas phase electron diffr. struct. determ. 80−69251
chlorobenzene in EBBA, ^{1}H, D NMR and NQR, geometric struct. 78−17689
chlorobenzene-d_5, and isotopic forms, microwave spectrum, rot. consts. 78−58667
p-(N-chlorobenzylidene)-p-chloraniline, cryst., polymorphism, cryst. struct. rel. to mol. conform. 78−75611
trans-1,4-chlorobromocyclohexane, liquid, crystalline and amorphous state, conformation and vibr. spectra, IR obs. 80−60568
chloroethane, reson. multiphoton dissoc. 80−53077
2-chloroethyl radical, struct., ab initio calcs. 80−83252
trans-1,4-chloroiodocyclohexane, liquid, crystalline and amorphous state, conformation and vibr. spectra, IR obs. 80−60568
chloromethyl cyclopropane, microwave spectra, gauche conformation 79−36625
chloromethyl formate($-d_1,d_2,d_3$), gas, solid. and liq., IR spectra assignments and struct. 80−32715
chloromethyl oxirane, microwave spectra and conformations of cis and gauche-2 forms 80−5534
chloromethylethyl ether, GT isomer, microwave spectra and geom. config. 79−59444
p-chloronitrobenzene, struct. determ. by electron diffr., influence of NO_2 group on C-Cl bond 80−69251
2-chloropropane, conformation, vibr. spectrum, from simple harmonic force field 78−33494
N-chlorosuccinimide, lone-pair struct., photodetection spectra 78−37684
chlorotrifluoroethylene radical anions, EPR spectra and struct. 79−31558
chlorotrifluoromethane, mol. struct., electron diffr., microwave spectra, CNDO/2 calcs. 78−37766
cholesteric liquid crysts., light reflection by crysts. with tilted molecular struct. 80−29713
cholesterogens, non-sterol, odd-even effect in helix 80−19701
cholesterol benzoates, intermolecular interaction, influence on optical props. *(Russian)* 79−77516
cholesterol cinnamates, intermolecular interaction, influence on optical props. *(Russian)* 79−77516
cholesteryl acetate, cryst. struct. at 123K 79−46643
cholesteryl alkanoates, mol. packing coeffs. 79−82195
cholesteryl bromide, cryst. and mol. struct. 79−82194
cholesteryl chloride, cryst. and mol. struct. 79−82194

organic molecule configurations continued
cholesteryl ethyl carbonate, long periods in sol. state, X-ray diffr. study 80−96503
cholesteryl laurate, X-ray cryst. struct. determ. at 298K 79−37692
choline phosphate calcium chloride tetrahydrate, struct., conformation, metal coordination, model for membrane surface interactions 80−15085
cis-1-cholobutadiene-1,3, microwave spectrum, struct., nuclear quadrupole coupling, distortion const., thermodynamic functions calc. 80−99500
chromophores, semiempirical rules in circular dichroism, Cotton effect sign correl. with stereochem. 80−1006
chrysene, excited singlet and triplet state, CARS obs. 80−83374
cobalt(III) complexes, mixed glycylglycinate, synthesis and config. *(French)* 80−2005
cobalt (III) diacetylmonoxime, Schiff base cryst. and mol. struct. 79−94998
cobalt (III) diacetylmonoxime thiosemicarbazone, X-ray cryst. and mol. struct. 79−90641
cobalt (III) methylhydrazinedithiocarboxylate, cryst. and mol. struct. 79−94998
cobalt dimethyl glyoximate, molecular struct., cryst. structure 80−79769
collisional activation mass spectra 80−48106
computer applications in organic struct. chem. and mol. spectroscopy in USSR 78−88624
computer-assisted interpretation, using fluoresc. spectra 77−36805
conference, Crystal XII, Canberra, Australia (Jan.-Feb. 1980) 80−62388
conjugated hydrocarbons, conformational analysis and heats of form. by force field method 77−60105
conjugated molecules, conformation, electronic spectra, NDDO calcs. 79−85901
conjugated molecules, excited state, self-consistent HMO theory *(Japanese)* 77−42253
copper(II) methylphosphonate monohydrate, cryst. struct. *(French)* 79−99172
copper acetate mono-α-picoline, binuclear, cryst. and mol. struct. 79−99174
copper benzoate di-(γ-picoline)hydrate, structural study using heavy atom method *(French)* 79−69098
copper iminodiacetate dihydrate, X-ray cryst. struct. and molecular struct. determ. 79−19237
cordycepin, X-ray cryst. struct. determ. 80−107198
core ionisation and electronic redrganisations, LCAO MO SCF calcs. 79−18115
coronene, triplet mol. in n-heptane Shpol'skii sites, distortion and orientation meas. by MIDP 78−37668
coumaran, geometry, electronic absorpt. spectra 80−971
coumarin deriv. solns., mol. struct. effects on luminesc. and lasing charcts. *(Russian)* 77−83873
coumarin laser dyes, fluoresc. quantum yields and lifetimes, polar solvent effects 80−87054
CT complex, equilib. distances and stabilisation energy, PCILO calc. 78−41963
p-cyano-N,N-dimethylaniline in polar solvents, double fluorescence, theoretical model 80−58296
cyanoacetylene, microwave spectrum, mol. consts. 78−74647
9-cyanoanthracene excimer emission, in glassy and cryst. matrices 79−11445
6-cyanobenzquinuclidine, intramol. electron-transfer excited state 80−58295
cyanobiphenyls molecular conformational mobility study by optical probing method *(Russian)* 80−92459
cyanobutadiyne-d_0,d_1, microwave spectrum, substitution struct., dipole moment 77−3348
N-cyanoformimine, stability, identification by microwave spectroscopy 79−10095
N-cyanoformimine-d_2, struct., microwave transitions 80−973
cyanogen azide, electron-density maps of bent bonds 80−1084
2-cyanoguanidine, electron-density maps of bent bonds 80−1084
cyanomethane-HF, hydrogen bonded heterodimer, spectroscopic consts. from microwave spectrum 80−43038
cyanomethyl radical, electronic struct. and props. 79−49938
cyanuric acid, molecular charge distrib. refinement 79−55730
cyclic 3- and 4-membered ring cpds., saturated, ab initio struct. anal. 80−58192
cyclic 4-ring rotation-puckering, use of spherical coords. 80- 58193
cyclic ethers-HF H-bonded complexes, calorimetry, IR spectra and MO calcs. 79−52738
cyclic mol. struct., topological characterisation 80−74254
cyclic olefin, ($C_{20}H_{19}ClN_2O_8S$), stressed, cryst. and mol. struct. X-ray anal. 79−86784
cycloalkane, mol. ion struct., photodissoc., charge transfer, ICR obs. 79−45774
cyclobutadiene, π face bonding with CO, HCN, benzene 79−98180
cyclobutane, MS-Xα-MT study 80−52906
cyclobutane(-d_8), centrifugal distortion const. calc., rel. to struct. and mol. wt. 80−95580
cyclobutanol-d_0,-d_1, conformation, microwave spectrum 78−86852
cyclobutenedione derivatives, photoelectron spectra, 2p lone pair delocalisation 78−46392
cyclobutylmethylether, IR and Raman spectra, config. 79−31525
1,3-cycloheptadiene, microwave spectrum, conform. 79−98074
1,3-cycloheptadiene, Raman and IR spectra, normal coord. analysis, conform. 77−77203
cycloheptane, conformation maps 77−57900
cycloheptane, geom. struct. by electron diffr. 79−31682
cycloheptanone, vibr. spectra, pot. functions and conformers 77−83569
2-cycloheptene-1-one, microwave spectrum, dipole moment and mol. conform. 79−72303
cyclohexadepsipeptide, refinements of mol. and cryst. struct. 77−39576
cyclohexahydroxyisovaleryl, $C_{30}H_{48}O_{12}$, cryst. and mol. structs. 77−31653
cyclohexane, conform. equilib., CNDO/2 calcs. on six-membered rings 80−23336
cyclohexane, conformation, distance geometry calcs. 77−50553
cyclohexane, conformation maps 77−57900
cyclohexane derivatives, low melting nematic cpds., characterisation 79−10798
cyclohexane-d_{12}, Raman linewidth and molecular diameter meas. 80−69153
cyclohexanecarbonitrile, rot. consts., conformers, struct., microwave spectrum 77−42314
organic molecule configurations continued
cyclohexanol, struct. information from OH-stretching freqs., axial/equatorial hydroxyl ratio 79−72438
cyclohexene vapour, IR spectra anal. 80−63628
2-cyclohexene-1-one, planarity barrier, from LF Raman spectrum 79−54859
cyclohexyl halide-thiourea clathrate, conform., Raman spectra 77−77200
1,2,6-cyclononatriene, mol. struct. and conformation, gas phase electron diffr. 80−106400
1,2-cyclooctadiene, conformational energy surface, Boyd's iterative force field investig. 80−95737
cyclooctane-d_{14}, in oriented solvent, conformation, NMR determ. 77−61770
cyclooctanone, vibr., rot. spectra and conformations, pot. function 78−78707
cyclopentadienyl cation, geometry optimisation by generalised Hartree-Fock 78−25427
cyclopentadienyl radical, vibronic valence isomerisation, Jahn-Teller effect, D_{5h} symmetry 79−97986
bis-π-cyclopentadienyltitanium dichloride, struct. parameter refinement 78−87660
bis-π-cyclopentadienylzirconium dichloride, struct. parameter refinement 78−87660
cyclopentene, ring puckering, semi-empirical and ab initio calcs. 78−9065
cyclopentene-3,5-dione(-d_1) microwave spectrum assignments, rot. consts., dipole moment, config. 78−55168
cyclopentyl chloride, microwave spectrum, conformation, quadrupole coupling consts. 79−3434
cyclopentylamine, vibr. spectra and struct. 80−102516
cyclophosphazene-DNa complex, spectrofluorometric and spectrophotometrics investig. 80−95643
cyclopopane, conformations, rot. consts., microwave spectrum 79−98075
cyclopropane(-d_6), centrifugal distortion const. and thermodynamic functions calc. 80−95582
cyclopropyl chloride, ab initio SCF-MO calc., electronic and mol. struct. 78−25425
cyclopropylamine struct., microwave spectrum 79−10096
cytochrome c, PMR, eight-ring current model heme ring, conformation depend. shifts 80−74185
decanol, dynamic mol. struct. in cyclohexane-d_{12}, ^{13}C NMR 78−33519
deuteromethane, crystalline, X-ray powder diff. study 80−96500
1,2-di(N-piperidyl)ethane-bis-N-oxide tetrahydrate, synthesis, cryst. and mol. struct. obs. 79−32985
di(tert. butylperoxy)triphenylantimony, X-ray cryst. struct. determ. 80−92517
di thioformic acid, cis and trans isomers, rot. microwave spectra and config. 79−63989
di-2-pyridyl sulphide, mol. struct. gas phase electron diffr. obs. 79−81296
di-(4-n-alkyloxy) benzoic esters, of hydroquinone series, effect of polar substituents on electro optical props. 79−46569
2,4-di-p-bromophenyl pentane, polystyrene model mol., US relax., mol. dynamics 79−73258
3,5-di-tert-butyl-4-hydroxybenzylidenemalononitrile, excited-state proton transfer, cryst. and mol. struct. 78−84630
N,N′-diacetyl-1,2,1′,1′-tetrahydro-1,1′-diisoquinoline, cryst. and mol. struct. 78−2106
diacetylene, near UV band system, rot. and vibr. anal., rot. fine struct. 77−61761
N,N′-dialkyl dipyridinium cation radicals, struct., INDO calcs., EPR obs. 77−71821
dialkyl tartrates, Raman circular intensity differential spectra obs., mol. struct. 80−87130
diamino-quinone, π-electronic struct., PPP-type calc. and config. anal. 78−21855
α,ω-diarylperfluorpolienes, X-ray spectra, phase transition temp. depend., struct. and mesomorphic props. *(Russian)* 78−38621
diastereomeric compounds, nonrigid mols., in soln., conform. determ., NMR, lanthanide shift reagents 77−30887
2,7-diazanaphthalene, cryst. and mol. struct. 77−59002
diazines, cavity radius and mean polarisability 79−45862
1,5-diazo-3,7-dithiabicyclo (3,3,1) nonane, molecular and cryst. struct. 78−51528
dibenzylmercury, cryst. struct. and conformation determ. 79−42045
dibromoalkanes, energy partitioning in mass spectrometric displacement reactions 80−89471
1,3-dibromobutane, IR and Raman spectra, normal coord. anal., C-halogen stretch bands and conformers 79−31522
1,2-dibromoethane in various solvents, dipole moments, concs. of anti and gauche forms 79−27106
dicadmium dimethylammonium pentachloride dihydrate, X-ray cryst. struct. 79−77588
1-10-dicarba-closo-decarborane (10), mol. struct., vibr. and shrinkage corrections calc. from force field 80−95739
dichloro(dimethyl)germane, mol. struct. determ. by vap. phase electron diffr. 77−54621
2,3-dichloro-1,4-napthoquinone in EBBA, PMR obs., mol. struct., orientation and solute-solvent interactions 77−27806
p-dichlorobenzene, orientation and deform. in nematic liq. cryst., PMR obs. 77−71815
p-dichlorobenzene, triplet state symmetry, geometry, ODMR, ENDOR obs. 79−18214
1,3-dichlorobutane, IR and Raman spectra, normal coord. anal., C-halogen stretch bands and conformers 79−31522
1,1-dichlorocyclopropane, ab initio SCF-MO calc., electronic and mol. struct. 78−25425
dichlorodinitromethane, mol. struct., electron diffr. investig. 78−86950
1,2-dichloroethane, enclathrated, conform., reorientation, PMR line shape anal. 79−91300
3,6-dichloropyrazine, orientation and deform. in nematic liq. cryst. 77−71815
dicyanoketene, and isomeric forms, heat of form., ab initio STO-3G calcs. 80−58190
p,p- diethoxythiocarbonylthiomethylaniline, cryst. and mol. struct. 79−94990
3,3′-diethylthiatricarbocyanine iodide, cryst. and molecular struct. 78−26554
difluoroacetaldehyde, optimum geometry, force fields, CNDO/force methods 77−46498
1,1-difluoroethane, mol. struct., gas phase electron diffr. obs. 80−58385

organic molecule configurations continued
cis-1,2-difluoroethylene oxide, substituent and isotope effects, microwave assignments 78−78682
difluoromethylborane, microwave spectra and struct. obs. 80−43036
difluoromethylborane, nonrigid, symmetry group calcs. 80−106254
trans-1,4-dihalocyclohexanes, far IR spectra of high press., using diamond anvil cell 79−12874
2,3-dihydropyran vapour, IR spectra anal. 80−63628
dihydroquinoxalinediones, conjugated mols. electronic struct. and geometry, Hartree-Fock instability 80−69055
dihydroxycarbene, singlet and triplet state rot. pot. surfaces 80−32627
diimide, electron-density maps of bent bonds 80−1084
1,2-diiodotetrafluoroethane, Raman and far IR spectra, conformation 78−78715
diketomorpholine, cyclodepsipeptide, cryst. and mol. struct. 78−2104
diketopiperazine, cryst. and molecular struct. determ. 77−11534
1,4-dimethoxy-2,6-dimethylbenzene, methyl reorientations, NMR relax. and inelastic neutron scatt. obs. 79−61253
5,7-dimethoxyindane-1-one, cryst. and mol. struct. 80−100223
dimethyl cadmium, partially oriented in nematic EBBA, mol. geom., PMR obs. 77−71819
dimethyl ethyl amine, mol. struct. determ. by gas phase electron diffr. 80−95743
dimethyl mercury, indirect coupling constants, vibr. corrections 79−50050
dimethyl oxide, geometric struct. 79−13835
2-dimethylaminoethanol(-d_1), microwave spectrum, hydrogen bonding, rot. consts., struct., dipole moment 77−6764
dimethylboric anhydride, IR and Raman spectra, vibr. and struct. 78−25531
cis-3,4-dimethylcyclopentanone, conformational analysis, vib. spectra 77−75325
dimethyldichlorosilane, microwave spectrum, rot., centrifugal distortion and quadrupole coupling consts. 80−91547
dimethylether, equilib. struct., ab initio SCF calcs. 77−3265
dimethylsulphoxide, r_3-struct. calcs. 78−70770
dimethyltin halides complexes with dimethyl sulfoxide and dimethylformamide, cryst. and mol. struct. 79−42047
9,10-cis-endo-dimethyltricyclo[4,2,2,$0^{2,5}$]dec-7-ene, substituted, crystal and molecular struct. 79−86785
dinitrato[N,N′-propane-1,3-diylbis(salicylideneimine)]calcium(II), cryst. struct. anal. 79−99171
1,8-dinitronaphthalene, orthorhombic, X-ray obs., 22 and 97°C 78−6048
2,4-dinitrophenol, cryst. and mol. struct. 77−15394
1,4-dioxane, conform. equilib., CNDO/2 calcs. on six-membered rings 80−23336
p-,(m-)dioxane, conformation maps 77−57900
dipeptides, bend form., conformational space, statistical mech. anal. 77−68146
diphenyl-d_{10}: diphenyl, triplet state EPR and ENDOR, 1.9K, mol. struct. implications 79−94021
N,N′-diphenyl-m-phenylenediamine, crystal and mol. struct., X-ray diffr. 78−47312
N,N′-diphenyl-p-phenylenediamine, cryst. and mol. struct. 77−7706
N-(4-diphenylamino) phthalimide, X-ray cryst. struct. determ. 79−42048
9,10-diphenylanthracene, soln. grown, cryst. struct. by computational and X-ray study 79−37690
diphenylethers, 1st ionisation energy, substituent effects, photoelectron spectra 77−42354
diphenylethylene, UV spectra, quantum-mechanical investigation of isomerisation pathways 80−43065
diphenylhaloselenium radical trapped in single crysts., FSR, struct. 80−44919
diphenylmethylene, triplet state, ENDOR in $P2_1$ benzophenone, conformation and spin distrib. 77−483
diphenylpolyene molecules, excited electronic states, vibronic mixing, wave functions, method of fragments anal. 80−63615
diphenylsulphides, 1st ionisation energy, substituent effects, photoelectron spectra 77−42354
dipotassium uridine 5′-diphosphate trihydrate, X-ray cryst. struct. determ. 79−57569
disilylmethane, microwave spectrum, struct., dipole moment and internal rot. 79−13699
distamycin A, analog cryst. and molecular struct. 79−88051
dithioformic acid, pot. for rot. about C(sp^2)-S bonds, ab initio calc. 80−23572
DNA, possible conformations calcs. 80−76705
DNA compact form, tertiary struct., small angle X-ray scatt. 80−72129
EBBA, mol. and cryst. struct., X-ray diffr. study 80−88134
EBBA, NMR and Raman scatt. studies in nematic phase 80−100619
n-eicosane, single cryst., electron irrad., free radical pair form., ESR 77−4913
eigenvalues of graphs with twofold symmetry (molecular configuration) 79−72437
empirical potential model EPEN/2 for conform., intermol., solvation studies 79−50102
enniatin B, DLLLLL-stereoisomer, molecular and cryst. struct. 78−25745
epichlorohydrin, microwave spectra, gauche conformation 79−36626
epifluorohydrin, IR and Raman spectra and conformations 80−60576
ethane$^+$, stability and struct., Cl-SCF ab initio calc., Franck Condon anal. 77−54575
ethane, adsorbed on graphite, struct. and dynamics, empirical interatomic pots. 79−99417
ethane, effective core potential calcs. 79−31437
ethane, nuclear spin-spin coupling consts., vicinal proton-proton coupling calcs. 80−32737
ethane, valence electronic struct., model pot. in floating spherical GO formalism 78−74563
ethane gas, local mode overtone bands 80−83444
ethanedithiol, mol. vibr., conformational anal., Raman spectra 79−31534
10,10′-ethanediylidenedianthrone, fluoresc. efficiency, mol. geom. effects in two cryst. structs. 77−18953
ethanol, config. and vibr. heat capacities, H-bonds 79−99331
ethanol, conformational anal., barriers of internal rotation, electronic structure 79−63916
ethanol, conformational analysis and electronic structure 78−33429
ethenediol, σ conjugative interactions role in rot. isomerism 79−31443
ethenethiol, σ conjugative interactions role in rot. isomerism 79−31443
ethenol, σ conjugative interactions role in rot. isomerism 79−31443
ethers, modified CNDO calcs., conformations, binding energies 77−6682

organic molecule configurations continued
ethers, Raman spectra, interpretation 77−65483
ethinyltetrafluorophosphorane, mol. struct., electron diffr. obs. 79−50133
ethyl cyanoformate, conformers, dipole moments, rel. energies, microwave spectra 78−55164
ethyl methyl sulphide, low freq. vibr. spectra, methyl torsional pot. functions and internal rot. 80−5543
ethyl p-methoxybenzilidene aminocinnamate, dimer, mesogenic, intermol. interactions 79−46564
ethyl radical, geom. struct., Hartree-Fock calcs. 78−62722
ethyl-3-chloropropionate, liq., microwave absorption and relax. 78−60386
ethyl-furan-2-carboxylate, skeletal vibr. of IR spectra, conformational props., solvent polarity effect 80−87118
(N-ethyl-o-phenanthrolinium)(TCNQ), cryst. and mol. struct. *(French)* 77−15396
N-ethylacridone, cryst. and mol. struct. 80−33988
ethylbenzene, α-substitution effect and radiative lifetime, solvent effects, rel. to t-butylbenzene 79−98154
ethylbenzene, vapour, conform. and struct. obs. 80−69247
ethylcyclopropane, solid, liquid, vapour phase, IR and Raman vibr. spectra 80−84740
ethyldifluoroborane, microwave, Raman, IR spectra, conform., dipole moments, vibr. assignment 78−90155
ethylene, C atom pyramidalisation rel. to bonding, ab initio SCF calcs. 79−93936
ethylene, chemisorbed on α-Fe, struct., bonding, dissoc., UPS obs., MO calcs. 78−84050
ethylene, chemisorbed on metal surfaces, geometric and electronic struct., UPS obs. and HF LCAO calc. 79−86988
ethylene, chemisorbed on Rh (111), EELS, LEED and thermal desorption mass spectrometry 80−80057
ethylene, chemisorbed on W(100), geometry distortion 77−30919
ethylene, effective core potential calcs. 79−31437
ethylene, mol. geometry, ab initio calcs., basis set depend. 78−82636
ethylene, molecular geometry optimisation, variable metric method, internal geometry 80−95744
ethylene+Cl_2(Br_2) complex, intermolecular interaction and struct. SCF-MO-LCAO CNDO/2 calc. 78−58763
ethylene(-d_1,d_2), high-resolution UPS, mol. ion vibr. assignments, symmetry 79−27032
ethylene as singlet methylene dimer, nonempirical double zeta calculations, zwitterionic singlet excited states 80−83258
ethylene cation, state geometries, electronic vibr. coupling consts., HF calcs., comparison with Xalpha calcs. 80−27946
ethylene chemisorbed on Cu, Ni, Pd and Pt surfaces, UV photoemission meas. and SCF-LCAO calc. appl. 79−19454
ethylene dimer, IR spectra 79−36638
ethylene dimer, PCILO calc. of geom. struct. and energy 79−63930
ethylene glycol, conformational anal., photoelectron spect. 80−43107
ethylene glycol, IR spectra, ab initio calcs., vibr. anal., conformations of isotopic modifications 78−5210
ethylene oxide cation, existence of open isomer, ab initio calcs. 79−22593
ethylene ozonide, ab initio gradient and MC SCF calc., conformational anal. 80−83290
ethylene radical cation, electronic states assignments, ab initio SCF CI calcs. 77−10584
ethylene V state, ab initio study of spatial extension 80−27952
ethylene-LiH, struct. and props., SCF ab initio calcs. 80−106250
ethylenes, substituted, unstable twisted forms, excited states, DODS-NO CI calcs. 79−13643
ethylgermane, microwave, IR and Raman spectra, struct., internal rot., dipole moments 77−79605
ethyloxirane, solid, liquid, vapour phase, IR and Raman vibr. spectra 80−84740
ethynol, ab initio calc., energy levels and geom. struct. of C_2H_2O isomers 78−62716
ethynol, struct., isomerisation, ab initio SCF MO calcs. 78−41941
2-exo-acetoxy-7-anti-dinitrophenylthionorbornane, mol. and cryst. struct. 80−2007
Faraday effect measurement in pulsed mag. field 80−80758
Fc-fragment crystals, low-temp. study, effect on flexibility, temp. factor, mosaic spread, extinction and diffuse scattering 80−54214
ferrocene, metal to ring distance, ab initio MO SCF calcs. 80−47870
ferrocene, mol. struct., ordered phase, 130K *(French)* 79−51093
ferrocene, neutron diffr. study of cryst. struct. 79−55728
ferrocene, quantum mechanical delta-function potential study of atomic, bond and mol. polarisability 77−23571
ferrocene, triclinic, struct. anal. at 101, 123 and 148K 80−19785
1,1′-ferrocenedicarboxylic acid, triclinic, X-ray and neutron cryst. and mol. struct. determ. at 78 and 298K 80−29008
fluoranil-macrocyclic polyether mol. complexes, configs., IR and NMR obs. 78−33529
fluoresceindiacetate conversion to fluorescein, in living cells and in vitro, kinetics 77−56332
fluorinated hydrocarbons, mol. recognition and self-organisation, information storage appls. 78−82806
1-fluoro-2-propanol, conformational energies and rot. barrier, ab initio calc. 79−31390
fluorobenzene radical anion, ab initio MO calcs., struct. 79−18113
fluorobenzenes, negative ion states, comments and reply 80−32599
fluoroethanes, mol. liqs., dielectric solvent effects, quantum chem. calcs. 77−14375
fluoromethanes, optimum geometries, force fields, CNDO/force method 77−46498
fluoromethanes, vibr. spectra, force consts. and geom., SCF ab initio calcs. 78−62785
fluorometh.HF, H-bonded complex, ab initio calcs. *(French)* 80−52866
fluoronitrobenzene, equilib. config. and barriers, microwave spectra 80−95606
formaldazine, mol., conformational anal., inapplicability of MINDO/3 79−94105
formaldehyde, adiabatic CI pot. surface LCAO calc., gradient determ., mol. dynamics, equilib. geometry 80−48056
formaldehyde, rot. struct. of 3500 Å transition, large amplitude vibr. effect 79−93976
formaldehyde, semi-empirical excited state Morokuma's EHP calc., geometry and order of states 78−46256
formaldehyde, X^1A_1, a^3A'' and A^1A'' states, SCF and CI ab initio calcs. 79−36545
formaldehyde dimers, matrix isolated, struct., IR spectra 80−99504

organic molecule configurations continued
formaldehyde-d_2, reson. multiphoton dissoc. 80−53077
formamide, force consts. and dipole moment derivatives, ab initio MO calcs. 80−95521
formamide, low temp. electron density distrib. 78−34502
formamide, low-lying triplet states, relative energies and conformational preferences 77−3266
formamide, mol. geom., self-consistent MINDO calcs., torsion and relax. effects 77−42243
formate ion, hydration, ab initio LCMO calcs. 79−59342
formic acid, ^{16}C, ^{18}O, microwave spectra and centrifugal distortion consts. 80−83352
formic acid, conform. hypersurface determ. and analysis 80−1078
formic acid, dimer, config. and energy, ab initio MO SCF calc. 79−37657
formic acid, dimerisation energy, ab initio calcs., distortion energy effects 79−10022
formic acid, electron-density maps of bent bonds 80−1084
formic acid, fragmentation, fragment structs. and energies calcs. 80−74124
formic acid, H bonding, electronic struct., geometries, moments, dimerisation energies, charge distrib., pseudopotential calcs. 80−27942
formic acid dimer, gas phase, H-bonded complex struct. from elec. dipole moment obs. 78−74791
cis-formic acid geometry, force fields and fundamental vibr. freq., ab initio study 80−87040
formic acid-water polymers, gas phase, H-bonded complex struct. from elec. dipole moment obs. 78−74791
formyl chloride, equilib. geometries and one-electron props., ab initio calcs. 80−47878
formyl fluoride, and isotopic forms, mol. struct., from electron diffr. and microwave data 80−23570
formyl fluoride, equilib. geometries and one-electron props., ab initio calcs. 80−47878
formyl radical, electronic struct., dissoc. energy and pot. energy surface many body perturbation theory and couple cluster doubles calc. 80−23296
β-D-fructose, film, electron irrad., struct. changes, tunnelling spectra 77−10781
fulminic acid, semirigid bender Hamiltonian, rot.-vibr. level separations, config., bending pot. 79−41152
functional group discovery using central atoms concept 77−34537
geometry optimisation, Newton-Raphson method algorithm 77−10612
glyceraldehyde 3-phosphate dehydrogenase, EPR, saturation transfer EPR 79−98124
γ-glycine, cryst. struct. by neutron diffr. at 83K and 298K 80−35825
glycine, mol. conformation and struct., mm wave spectrum 79−3435
glycyl anion radical, in α-glycine cryst., struct., ESR obs. 78−33530
glyoxal, 4550Å bond system, rot. anal. mol. consts. and geometry 77−42330
glyoxal, mol., conformational anal., inapplicability of MINDO/3 79−94105
gramicidin A in biomembrane channel, IR spectroscopic obs. 80−16901
group IV hydrides, pseudopot. FSGO calc. 79−22591
guanine, ^{15}N and D substituted, in acid and base solutions, vibr. anal. 79−26994
gummosine, cryst. and mol. structs., and absolute config., X-ray expts. 78−79602
haematoporphyrine, complexed with chloranil and tryptophane, energy spectra, transition moments and intermolecular distances 80−72127
haemocyanin of Limulus polyphemus, quaternary struct. 80−85337
haemoglobin, sickling deer type III, macromol. struct. refinement by restrained least-squares and interactive graphics 80−28870
halides, aryl and aryl-alkyl 193 nm photodissoc., fragment translational energy distrib. 80−48048
1-halo-1-n-propylcyclohexanes, conform. equilib., and pot. barriers, IR spectra *(Russian)* 78−21928
2-haloethanols, gauche conformer stability, exchange interaction 79−18311
2-haloethyl ethers, relative conformational energies, Raman obs. 79−27002
halogermane radical anions, ESR spectra and struct. 80−87153
heaxadecane solvents of different mol. shapes, effect on DCl vib.-rot. spectra 77−34623
heparin, in soln., small angle X-ray scattering 80−14993
heptafulvene, microwave spectrum and dipole moment 77−14421
hexa-host inclusion compound, cryst. and mol. struct. 77−42436
n-hexadecane, pure liq. and solns., small angle neutron scatt., ang. depend. 79−1384
hexafluorobenzene, quadrupole moments, elec. field-gradient birefringence method 80−95746
hexafluorobenzene anion, EPR obs. of struct. 77−58048
hexafluorobenzene radical anion, ^{13}C hyperfine interaction, EPR obs. 80−83392
hexafluorocyclopropane, centrifugal distortion const. and thermodynamic functions calc. 80−95582
hexafluoropropene, mol. struct. by electron diffr. of gas phase 79−59572
hexafluoropropene, struct. and vibr. spectra, IR, Raman polarisation study 80−18845
hexamethylbenzene, quadrupole moments, elec. field-gradient birefringence method 80−95746
hexamethylbenzene in tetrachloromethane soln., local mode overtone bands 80−83444
P-hexamethylcyclotriborophosphanes, substituted, struct., vibr. spectra 77−65460
hexamethylenetetramine, orientation and deform. in nematic liq. cryst., PMR obs. 77−71815
hexamethylenetetramine in oriented mesophases, mol. distortion, PMR 77−6802
hexamethylethane, crystal structures and phase transitions, X-ray diffr. study 79−73158
n-hexatriacontane, pure liq. and solns., small angle neutron scatt., ang. depend. 79−1384
n-hexylamine.Gd(FOD)$_3$, flexible chain dynamics, NMR, steric effects calcs. 77−6800
histone H4 N-terminal oligopeptide struct., circular dichroism and IR spectroscopy 78−24025
histones H_2A and H_4, mixed solns., oligomer structs. 80−30648
HOAB, chain ordering model 80−24357
HOAB, cryst. and mol. struct. rel. to smectic C phase struct. 79−55732
organic molecule configurations continued
hyaluronic acid, Raman spectrum, primary and secondary structs. 79−59467
hydrazine-1,2-d_2, microwave spectra, mol. structural parameters 77−27056
hydrazoic acid, electron-density maps of bent bonds 80−1084
N-hydro-N′-methylphenaziniumyl cation in HMP-ClO_4, mol. config. 78−62938
hydrocarbon chains, stability of lyotropic phases 80−24359
hydrocarbon ions, mass spectra, H atom scrambling, delocalisation 80−58135
hydrocarbon liquid, residual energy and entropy, rel. to liq. and mol. structs. 78−71869
hydrocarbons, alternate conjugated, topological props. of HOMO-LUMO separations 80−69049
hydrocarbons, conformational anal., modified Urey-Bradley force field, gauche-H_2 interactions 77−6749
hydrocarbons, mol. geometry, CNDO/BW and MINDO/2 calcs. 79−41109
hydrocarbons, mol. graphs, eigenvalues 77−26996
hydrocarbons, mol. thermodynamics, information-theoretic aspects 78−13409
hydrocarbons, molecular packing anal. of alkyne structs., lattice energy minima 78−95011
hydrocarbons, saturated, modified CNDO calcs., conformations, binding energies 77−6682
hydrocarbons proximity and conform. effects, ^{13}C chem. shifts at γ position, INDO computations 77−50451
hydroxymethyl cation, geom. and electronic struct., ab initio SCF calc. 79−76331
hydroxymethylene radical cation stability, $CH_2O^{+\cdot}$ isomers, ab initio MO study 80−42965
2-hydroxytropone, in β-cyclodextrin complex, UV circ. dichroism spectrum assignments, complex struct. 78−46358
idolalkylamines, conformational varieties in cryst. 78−10030
imidazole, cryst. struct. at 103K by neutron diffr. 79−37691
1,3-indandione derivatives, higher-order harmonic generation, laser-induced nonlinear optical effects *(Russian)* 78−55412
indene, microwave spectrum, assignments, rot. consts. and config. 79−31510
indigo dyes, triplet state config., laser flash absorpt. spectrosc. obs. 80−5557
information content, thermodynamic props., electropy (bondtropy) theory 77−54500
2-iodoacetamide, mol. struct., electron diffr. obs. 80−63819
iodotrifluoromethane, mol. struct., electron diffr., microwave spectra, CNDO/2 calcs. 78−37766
ion struct. determ. from collisional activation spectrometry *(Japanese)* 79−76531
isocyanic acid, molecular structure and centrifugal distortion constants 80−47974
isocyanomethyl radical, electronic struct. and props. 79−49938
isopropyl radical, pot. energy surfaces, ab initio UHF calcs. 80−106258
isopropylamine-d_0,-d_1,-d_2, microwave spectra, struct., dipole moments and quadrupole coupling consts. 77−34613
isopropylcyclopropane, solid, liquid, vapour phase, IR and Raman vibr. spectra 80−84740
isorhodopsin chromophore conform. and orientation in frog disc membrane 78−64980
isothiocyanic acid, H^{15}NCS, HN^{13}CS and HNC^{34}S, ground state spect. constants and molecular struct. 80−47973
Kekule valence structures, correl. with conjugated circuits 79−89582
ketene, ab initio calc., energy levels and geom. struct. of C_2H_2O isomers 78−62716
ketones, saturated, MCD spectra, forbidden transitions generated by struct.-vibr. perturbations 77−50460
Kruszewski's rule, for stability of isomeric polycyclic conjugated cpds., proof 80−106249
lead triphenyl isocyanate, X-ray cryst. struct. determ. and refinement 79−51097
leghemoglobin, X-ray structural determ. at a resolution of 2.8 Å, electron density synthesis 79−42049
lepidopterene exciplex, luminesc. intramolecular anthracene-ethylene exciplex, mol. geometry-fluoresc. relationship 78−58728
lipid bilayer phase transition, semiphenomenological model 77−35670
lipids of myocardium mitochondria, composition and phase transitions rel. to depth of hypothermia, rats and dogs 78−53350
liquid crystal, theoretical foundations of chain ordering props. 80−38907
liquid crystal, thermotropic mesophase, DMR chain segments assignment 80−24356
liquid crystals, mol. conformation and orientational order, NMR studies, review 80−75151
liquid crystals, nematic and smectic mol. dynamical investigation 78−91252
liquid crystals, smectic-A phase, mol. model, steric effects 78−67646
maleic anhydride, struct., DRM microwave spectra, isotope shifts 78−21918
malondialdehyde, UV electronic absorpt. spectra, G_4 mol. symmetry group 77−6798
malonic acid, and α-alkyl derivatives, photoelectron spectra, lone-pair interactions 80−58315
manganese (II) D-gluconate hydrate, X-ray cryst. struct. determ. 79−77587
manganese carboxylate, dodecanuclear mixed-valence, prep., struct., and mag. props. 80−107196
matrine, X-ray cryst. and mol. struct. determ 79−94993
matrine N-oxide, X-ray mol. and cryst. struct. 79−94997
MBBA, NMR and Raman scatt. studies in nematic phase 80−100619
MBBA-d_8, mol. order and conformation, ^2D NMR line shape obs. 77−61771
MBPAA, nematogen, cryst. and mol. struct. 77−72604
melanostatin, correl. between X-ray struct. and conform. in soln. 77−48752
membrane-active complexon fragments, nonrigidity effects calcs. 80−91704
menthane ring compounds, Raman circular intensity differential spectra obs., mol. struct. 80−87130
mesophase pitch, magnetically-oriented, phys. props., mol. struct. 80−64885
N-methacryloil-ω-aminolauric acid cholesterol ester, liq. cryst. polymers, copolymers, structuring *(Russian)* 79−55665

organic molecule configurations continued
methane, and isotopic forms, anharmonic force field, equilib. struct. 79−76365
methane, clusters, collision induced polarisability, mol. frame distortion 80−32798
methane, effective core potential calcs. 79−31437
methane, elastic and inelastic electron scatt. differential cross section, obs. and calc., struct., binding energy 80−28110
methane, force consts., equilib. geom., Hartree-Fock and CEPA calcs. 78−70753
methane, liq., medium cluster model, vapour press. isotope effects, mol. orientation effect 77−72542
methane, mol. cations, struct., Jahn-Teller effect, MINDO/3 calcs. 80−74135
methane+O(^{3}P), barrier height and transition state geometry, POL-CI calc., H abstraction reaction 80−66782
methane cation, photodissoc., ab initio RHF and MRD CI calcs. 80−95695
methane derivatives, stabilisation of planar tetracoordinate C, substituent effects, RHF/STO-3G calcs. 77−6671
methane-d_2, rotation-vibration constants, C−H bond length 79−94055
α-methane-d_4, crystalline, X-ray powder diff. study 80−96500
methanesulphonyl chloride, geom. struct., CNDO/2 calc., comparison with CF_3SO_2Cl 79−81295
1,5-methano(10)-annulene, mol. geom. and gas phase thermodynamic props., minimisation scheme 78−78829
methanol, and $-d_{1,3,4}$, thermodynamic props. struct. and spectroscopic data 77−39396
methanol, and deuterates, dissoc. ionisation mechanisms, photoionisation mass spectra, ionic struct., interstellar formation 79−3503
methanol, C-O-H bending mode in α- and β-forms at 85K 77−8588
methanol, charged fragments, structure and stability 78−90085
methanol, conformational anal., barriers of internal rotation, electronic structure 79−63916
methanol, equilib. struct., general valence force field, ab initio calcs. 77−3265
methanol, field ionisation, geometry changes, INDO-SCF-MO calc. 77−38614
methanol, H bonding, electronic struct., geometries, moments, dimerisation energies, charge distrib., pseudopotential calcs. 80−27942
methanol, molecular geometry optimisation, variable metric method, internal geometry 80−95744
methanol, polymers, structs., binding energies, LCAO SCF MO calcs. 77−83498
methanol-water, assoc. mixture, rot. barrier solvent effect, CNDO/2 calc. 78−29861
methotrexate-dihydrofolate reductase complex form., conform., laser Raman obs. 80−104553
2-methoxacyclobutane, mol. struct., electron diffr. obs. 80−1065
p-methoxy-XY-p′-alkyl tolanes, mol. struct., packing coeffs., and thermal stability 78−95046
p-methoxybenzylidene-cyanoaniline, mol. and cryst. struct., X-ray diffr. study 80−88134
methoxydifluorophosphine-d_0 and -d_3, IR and Raman spectra, mol. vibr. and struct. obs. 80−87103
3-methoxynaphthalide, cryst. and mol. structure. 77−31654
methoxytrimethylsilane-d_0,($-d_3$) 78−86853
methyl anion, geometric struct., electron correlation effects, self-consistent electron pairs 78−22050
methyl beryllium hydride, equilib. geometries and electronic states, FSGO calcs. 79−10019
methyl chloride, ab initio SCF-MO calc., electronic and mol. struct. 78−25425
methyl chloride, charge distrib., substituents effect 80−905
methyl chloroformate, struct., microwave, Raman, far IR and NMR spectra 77−34614
methyl cyanides and isocyanides, isomerisation, ab initio (STO-3G) geometry optimised calc. 78−46265
1-methyl cyclohexanol, struct. information from OH-stretching freqs., axial/equatorial hydroxyl ratio 79−72438
methyl fluoride, charge distrib., substituents effect 80−905
methyl fluoroformate, isomer conformation, CNDO and ab initio STO calcs. 80−58151
methyl formate, microwave spectra, rot. consts., moments and struct., radio astronomy appl., review 80−17637
methyl formate($-d_1$,d_3,d_4), mol. vibr. spectrum, struct., beginning with PCILO calc. *(French)* 80−23401
methyl furan-2-carboxylate, skeletal vibr. of IR spectra, conformational props., solvent polarity effect 80−87118
methyl furan-2-thiolcarboxylate, skeletal vibr. of IR spectra, conformational props., solvent polarity effect 80−87118
methyl green-DNA binding, linear dichroism anal. 77−88479
methyl group, ^{13}C chemical shifts, H/H, H/Me and Me/Me interactions 80−95652
methyl group, conform. problems, correlation effects 79−97999
methyl ion, electrostatic force theory appl. to mol. geometry ab initio verification 79−98002
N-methyl m-fluoroaniline, conformational anal., microwave spectra obs. 80−58247
methyl meristotropate, mol. and cryst. struct. 78−95047
s-methyl nitrite, methyl group rot. barriers in cis and trans forms, ab initio calcs. 80−74111
methyl oxirane, centrifugal distortion consts. and struct. parameters calcs. 77−34616
methyl radical and anion, electron affinity determ., ab initio SCF and CI calcs. 78−5149
methyl salicylate, vapour phase, absorption and fluorescence spectra 79−81232
methyl selenocyanate, and isotopic forms, microwave spectrum 79−13705
methyl vinyl ether, microwave spectrum, quartic centrifugal distortion and rot. consts. 79−10099
methyl vinyl sulphide, syn-gauche equilib., force field and ab initio calcs., microwave and Raman spectra 80−23573
methyl-3-bromopropionate, liq., microwave absorption and relax. 78−60386
N′-methyl-N-β-D-xylosylurea 79−94995
N-methyl-p-fluoroaniline, struct. of $HNCH_3$ group 80−95741
N-methyl-piperidinium-acet-meta-chloro-anilide-iodide, crystallisation from water, X-ray exam. of cryst. struct., mol. config. *(German)* 79−51095
methylanilines, far IR spectra, pot. energy barriers 80−43043

organic molecule configurations continued
N-methylanilines, substituent effects on geometry, IR spectra obs. 79−10107
7-methylbicyclo[2.2.1]-hept-2-ene-5-one, config., microwave spectrosc. obs. 80−9593
methyldichlorosilane, Stark effect and microwave-microwave double reson., struct. *(German)* 80−47975
methylene, 2^1A_1 state, CI and multiconfiguration SCF calc. 79−10052
methylene, geometry, SCF and CI calcs., basis set effects 78−62715
methylene chloride, microwave spectra, rot. consts. and geometric struct. 79−63990
methylene fluoride, anharmonic pot. function and equilib. struct. 78−78774
methylene iodide, benzene soln., spin-lattice relax., struct., dynamics 77−1610
methylene ion, pot. energy surfaces of excited states, ab initio GTO SCF CI calcs. 78−58602
methylene manganese, electronic struct., equilib. geometry, ab initio SCF calcs. 77−71747
methylene peroxide, multiconfig. SCF CI calcs. 80−18803
methylene peroxide, struct., energy levels, ab. initio UHF and MRUHF NO CI calcs. 80−83287
methylene-bridged liquid crystals, homologous series, mol. struct. effects on mesomorphism 77−47347
4-methylene-cyclohexadiene-2,6-one-1, proton affinity, MINDO/3 results compared to ICR obs. 78−1103
4,4′-methylenebis(1,3,5-trimethyl-4-imidazolin-2-one), cryst. and mol. struct. 80−107201
3-methyleneoxetane, electron structure, orbital-O interaction, MO calcs., UV photoelectron spectra 80−28058
methylenimine, lowest excited state, singly excited config. interaction calcs. 79−59361
methylenimine, mol. struct., microwave spectra, isotope effects 77−61738
N-methylformamide intercalate, cryst. struct. determ. using film-scanned data 79−55729
1-methylindan, circular dichroism, rot. strengths, CNDO/S calc. 79−3452
6-methylmercaptopurine riboside, 4 MeV electron irrad., 77K radicals form., EPR obs. 78−39405
N-methylphthalimide in ethanol soln., gain and induced absorpt., struct. props. 77−24890
methylpropylether, trans-trans isomer, microwave spectra, struct., dipole moment and rot. barriers calcs. 80−83348
12-methylsulphonyl-1-phenylethanol, S-O interactions, conform. anal. 79−31418
methylzinc methoxide, tetrameric, X-ray cryst. struct. determ. 80−107197
molecular charge transfer complexes, mol. and cryst. struct. 78−62942
molecular crystals, optical diffr. patterns, comparison with X-ray scattering photographs 80−78783
molecular reactivities rel. to struct., Taft and Kirkwood-Westheimer eqns. 78−62738
molecules D_{6h}, D_{3h} and D_{3d}, appln. of Aliev-Watson maxima-minima criteria for quartic centrifugal distortion const. 80−87132
α-monochloroacetic acid, hydrogen-bond motifs 77−11529
β-monochloroacetic acid, hydrogen-bond motifs 77−15397
monochlorobenzene, partially oriented, r_α-struct., ^{13}C satellite PMR obs. 79−50048
monothioformic acid, pot. for rot. about C(sp^2)-S bonds, ab initio calc. 80−23572
mucochloric acid-d_0, -d_1, vibr. spectra, struct. 78−46326
myoglobin , oxyhaeme complex, single cryst., visible spectrum, electronic struct., coord. geometry 78−44456
N-methylhydroxylamine, microwave spectra, struct., moments, internal rot., HFS and rot. consts. 79−45708
naphthalene, fluoresc. and phosphoresc., singlet/triplet excimers conform. difference 77−14469
naphthalene, multiphoton ionisation, mass spectra 80−63717
naphthalene, Raman intensities rel. to vibronic coupling and excited electron state geometries 77−27075
naphthalene, thermal diffuse scattering, errors in X-ray diffr. intensities and atomic parameters 79−73155
naphthalene, triplet excimer conformation, σ-π interaction transitions 77−6701
naphthalene in EBBA, PMR obs., mol. struct., orientation and solute-solvent interactions 77−27806
1,4-naphthoquinone in EBBA, PMR obs., mol. struct., orientation and solute-solvent interactions 77−27806
naphtho[1,8-cd:4,5-c′d′]bis[1,2,6]thiadiazine, mol., electronic, cryst. struct. 80−64984
β-naphthylamine, cryst., amino group reorientation, PMR obs., 77-373K 79−82881
nematic liquid crystals, molecular structure and elastic consts. 79−77512
neopentane liq., local mode overtone bands 80−83444
nicotinamide adenine dinucleotide, and reduced form, pH induced modification, Raman spectra 80−85343
n-nitro-n′-methylbenzylidene-aniline, triclinic, cryst. and mol. struct. 77−43205
nitrocyclopropane, vibr. spectra struct. and bonding 80−102520
nitromethane, ab initio SCF MO calcs. of geom. and bond energies 79−31381
nitromethyl anion, ab initio SCF ab initio MO calcs. of geom. and bond energies 79−31381
nitromethyluracil reduction product of X-ray irrad., ENDOR and ESR 77−32816
nitronaphthylamines, ESCA and UV photoelectron spectra, assignments 78−50588
o-nitrophenol, cryst. and mol. struct., H bond distance 78−51523
4-nitrophenyl 4′-decyloxybenzoate, mol. struct. rel. to mesomorphic props. 77−89372
N-nitroso-dimethylamine-d_0, -d_3, -d_6, struct., microwave spectra 79−59446
nitrosomethane, microwave spectrum, structure, dipole moment and centrifugal distortion 78−66540
nitrosomethane, mol., spectra 600-720 nm, and geom. change on excitation 79−72329
nitrosomethane-d_3, electronic excitation, conformational changes obs. 79−98233
nitroxide groups in crystals, H bonds and short intermolecular contacts 80−63855
nitroxyl radicals, cyclic, conform. flexibility, EPR obs. 80−91581

organic molecule configurations continued
NMR study of molecular conform. in soln., use of La ion probe 77−60324
nonafluorobutane(-d_1), and halo-substituted forms, gas and liq., IR and Raman spectra, normal coord. anal. *(German)* 79−72318
nucleic acids bases, excited state dipole moments and geometries 80−95738
nucleoside conformations from NMR studies, review 78−76990
nucleotide conformations from NMR studies, review 78−76990
nucleotide sugar-phosphate region, γ-irradiated, deoxycytidine 5′-phosphate alkoxy radical EPR 79−5249
octamethylcyclotetrasilazane, gas, liq., cryst., CCl_4 soln. IR and Raman spectra, assignments, struct. *(French)* 78−29790
4′-n-octyl-4-cyanobiphenyl, chain ordering model 80−24357
olefins, minimum energy goemetry, torsion of double bond 77−71755
organic chemistry, textbook, undergraduate level 78−57711
organic compounds, low freq. anharmonic vibr., pot. function determ., Raman and IR spectra obs. 80−52997
organic dyes, fluoresc. spectra calcs., β-variation method *(German)* 80−69182
organic liquids, glasses and glassy crystals, entropy of struct. disorder, rel. to mol. struct. 79−65219
organic mass spectroscopy, techniques and appls. 79−43667
organo tin dichlorides, tetrahedral, dilute soln., dielec. and thermodynamic behaviour, microwave region 77−36170
organolithium cpds., ab initio SCF-MO calcs. of C-Li bond character 77−410
organonitrogen derivatives of Si, Ge and Sn, prep. and props. 78−60456
organosilane coupling agent interphase of glass-fibre reinforeced plastics, molecular organisation 80−44195
organotin compounds, mol. and cryst. struct., X-ray diffr., NMR and Mossbauer spectra meas. 77−47441
ovalene, isolated ultra cold mol., intermediate level structure of S_2 state 80−28048
oxa-bis(t-butylperoxytriphenyl-antimony); X-ray cryst. and mol. struct. determ. 79−60350
7-oxabicyclo (4.1.0) hept-3-ene, conformation, dipole moment, microwave spectrum 78−66539
oxalyl chloride (fluoride), centrifugal distortion consts. and thermodynamic functions, pot. energy calc. 79−22619
oxazole(-d_1), dipole moment, quadrupole coupling tensor, from microwave spectrum 78−55166
3- oxetanone, electron structure, orbital-O interaction, MO calcs., UV photoelectron spectra 80−28058
oxiranecarboxaldehyde, microwave spectrum, torsional excitation energy, partial struct., dipole moment 77−38655
oxiranylidene, struct., isomerisation, ab initio SCF MO calcs. 78−41941
oxirene, ab initio calc., energy levels and geom. struct. of C_2H_2O isomers 78−62716
PAA-d_8, mol. order and conformation, ^{2}D NMR line shape obs. 77−61771
palladium bis-β-diketonates, IR and Raman spectra 78−46327
palmitic acid-choleic acid complex, cryst. struct. and van der Waals energy 80−64983
papain models, active site α-helix and ion pair stability 80−74265
parabanic acid, charge density and cryst. struct. redeterm. by X-ray and neutron diffr. 79−46644
paramagnetic systems, multiple internal motions, nucl. spin dipolar relax. obs. 80−28037
pentachlorotoluenes, positional isomers, ^{13}C Fourier transform NMR spectrometry, struct. and compositional anal. 80−91576
pentamethinemerocyanine dye, electronic spectrum and struct., solvatochromism, microstructural model 77−61817
pentane isomers, vapour and liq., electron mobility 79−72984
pentaphenylantimony, Coulombic interactions in anomalous structure 77−24285
pentofuranosyl nucleosides, isomeric, ^{1}H NMR coupling consts., SCF FPT INDO approx. calc. 80−14156
peptide, NMR spectroscopy study 78−88694
peptide and glycopeptide research methods 80−51307
peptide architectural units, ab initio SCF MO calcs. 78−96004
peptides, bradykinin-potentiating, spatial structs. 80−95736
perchloro-3cyclopentenone, ^{35}Cl NQR Zeeman obs. 80−54981
perfluorocyclobutanone, IR and Raman spectra, vibr. anal. 77−38661
perfluoroneopentane, geom. struct. of mol., gas phase electron diffr. 78−78810
perhalonitrosomethanes, gas phase IR spectra, assignments, isomerism 80−28017
peroxy chain radicals, reactivity and struct., EPR spectra, trapped in PTFE 80−66783
phenanthrene, low freq. Raman spectra intensity temp. depend., phase transition, conformation change 77−36211
phenol, PMR in absence of intermol. proton exchange, long-range coupling and conformations 77−34660
phenol-cyclohexane (-ether), UV spectra, solvent effects, matrix rank anal., species determ. 79−22768
phenol-organic solvent mixtures, UV spectra, solvent effects 79−22769
phenols, ^{13}C and D substituted, microwave spectra, substitution struct. and absolute dipole moment 79−31511
phenyl cation, struct., ion-molecule reactions studied by trapped ion mass spectroscopy 80−102586
phenyl isocyanate, electronic absorpt. spectrum, vibr. struct., f-values, spectroscopic moment and config. 78−58715
phenyl-trimethine-merocyanine, X-ray diffr. exam. of cryst. and mol. struct. 80−6398
p-phenylene bis (p-substituted benzoates), cryst.-nematic transition, mol. struct. effects, DTA 78−47504
phenylnaphthalenes isomers, fluoresc. lifetime difference and mol. geometry 80−69176
phosphamides, carcinostatic, ^{14}N NQR, electron distrib. and bonding configs. 80−48018
1-phosphapropyne, microwave spectrum, vibration-rotation analysis, dipole moment, structural parameters 79−93989
phospholipid bilayers, struct. dynamics from deuterium spin-lattice relax. time meas. 79−79485
photosynthetic pigment, intersystem crossing 77−58057
phthalan, geometry, electronic absorpt. spectra 80−971
phthalozine, oriented in lyotropic mesophase, proton NMR spectra 79−82886
1,4-piperazine, conform. equilib., CNDO/2 calcs. on six-membered rings 80−23336
organic molecule configurations continued
piperazine-2,5-diones, and N-chloro derivatives, UV photoelectron spectra and geom. struct. 79−18235
1-piperidine carboxylic acids, intramol. H bonds, struct., IR spectra 77−14426
piperidine-$MnBr_2$ complexes, substituted, excitation spectra, ligand field theory 77−27103
polyacenes, electronic transition bands, Franck-Condon factors, PPP SCF MO/CI calc. 78−33430
polyacetylene, pristine and acceptor doped isomers, EPR, DC cond., evidence against solitons 80−15782
polyatomic mol. gas phase spectra, struct., review and tabulation 80−14136
polydimethylsiloxane end-linked chains, nonGaussian effects 80−65127
polyenes, symmetric, combinatorial enumeration of chemical isomers 80−28114
polyethylene, cryst., soln. grown, neutron scatt., mol. dimens. rel. to mol. wt. 79−41258
polyethylene, dielec. props. rel. to mol. struct. 80−29681
polyethylene, lightly crosslinked, processed under mol. orient., struct., props., review 80−38957
polyglucosan, soluble, single crystals from Acetobacter xylinum, internal structure resemblance to Cellulose Hydrate II *(Japanese)* 79−94121
polyglycine, total energy, conformational calc. using quantum mech. partitioning method 78−94189
polymethin cyanine dyes, vibronic energy relax., picosec. spectrosc. obs. 80−5526
polymethine dye laser, near IR, optimal molecular struct. and lasing characteristics 80−19026
polymethine dyes, mol. struct., lasing props. 79−3693
polymethylene chains, conformations, mag. field dependent biradical CIDNP 77−27097
polypeptides, total energy, conformational calc. using quantum mech. partitioning method 78−94189
polypyridines, photoelectron spectra, SCF LCAO calcs. 78−33551
polystyrene and model cpds., conformational struct. influence on normal modes of benzene ring, Raman study 80−14144
polysubstituted peri-condensed compounds, combinatorial enumeration of chemical isomers 80−28114
porphin, ground-state energies, force consts. and vibr. freqs., CNDO/2 calc. 79−18118
porphyrins, non-radiative deactivation of lower excited states, effect of mol. struct. 78−68987
potassium butyl xanthate, X-ray cryst. struct. determ. 80−33987
potassium formate, X-ray cryst. struct. determ. 80−107194
potassium hydroxymethanesulphonate, X-ray cryst. and mol. struct. determ. 79−32983
potassium p-chloranil, solvated with acetone, X-ray cryst. struct. determ. 80−39062
potassium palmitate-d_{31}, spin-lattice relax., chain position and temp. depends. 78−68405
promethazine picrate, cryst. data and molecular packing 79−94988
propane, adsorbed on graphite, struct. and dynamics, empirical interatomic pots. 79−99417
n-propanol, centrifugal distortion constants, OH-trans-trans and OH-trans-gauche conformers *(Russian)* 79−10089
n-propanol, preferred conformers, PCILO study 80−95542
β-propiolactone, electron structure, orbital-O interaction, MO calcs., UV photoelectron spectra 80−28058
propiolamide(-d_2, d_3), microwave spectrum, struct., dipole moment 78−78685
propiolyl chloride(-d), 357-333 nm absorpt. system 80−69161
propiolyl fluoride(-d), 290 nm absorpt. system 80−87142
propion-aldehyde ion, fragment/mol. ion current ratio, field ionis. mass spectrum, CNDO/BW calc. 77−65544
p-propoxysalicylidene-p′-butylaniline cryst. and mol. struct., intramolecular bonding 80−44197
n-propyl radical, and propane, struct., ab initio calc. 79−98006
n-propylhalides, gauche conformer stability, exchange interactions effects 79−13817
propylsilane-d_0(−d_n), vibr. spectra, normal vibrs. and rot. isomerism 79−31523
propynyl cation+propyne, reactant structure effects 80−89469
protein, NMR spectroscopy study 78−88694
protein architectural units, ab initio SCF MO calcs. 78−96004
proteins, model building procedure 80−51036
protocatechualdehyde, PMR, 77-427K, OH group rot., struct. 77−30886
PVC, reduced, dielec. props. rel. to mol. struct. 80−29681
pyrazine, excited and N_{1s} ionised states, ab initio calcs. broken orbital symm. 80−27931
pyrazine, in pyrazine-d_4, p-dioxane, X-trap, p-xylene, benzene(-d_6), cryst., MIDP, PMDR, low temp., assignments 77−36154
pyrazine, mol. struct. determ. from gas phase electron diffr., r_α struct. 78−25739
pyrazine, physisorbed on Ni (111), UV spectroscopic ellipsometry obs. 79−86997
pyrazine, reson. Raman and absorpt. spectra to $S_2(\pi,\pi^*)$ state, excited state geometry 79−76433
pyrazine (-d_4) vapour, single vibraonic level fluoresc. from n, π^* 80−37827
pyrazine absorbed on electrode, surface enhanced Raman spectra, symmetry and polarisability changes 80−50310
pyrazine-d_4, in p-dioxane, p-xylene, benzene, cryst., MIDP, PMDR, low temp., assignments 77−36154
pyrene, excimer fluoresc., struct. depend. in cryst. 77−75200
pyrenophanes, excimer fluoresc., struct. depend. in cryst. 77−75200
pyridine, and -d_1, microwave spectra, mol. struct., rot. consts. 78−25517
pyridine-3-aldehyde, partially oriented in nematic solvent, rot. isomerism and conformation, NMR obs. 77−71820
pyridine-acetic acid, H-bonding, proton transfer, isolated system, solvent effect, MO calc. 80−55629
pyridine-$MnBr_2$ complexes, substituted, excitation spectra, ligand field theory 77−27103
di-α-pyridyl hydroperchlorates, intramol. H bonds, steric conditions and polarisability obs. 80−53160
2-pyridyl phenyl sulphide, dipole moments, absorpt. spectra, meas. and calcs. 77−46574
2-pyridyl phenyl sulphone, dipole moments, absorpt. spectra, meas. and calcs. 77−46574
pyrimidine bases, water vapour effect on struct. and amorphous-cryst. transition 77−70408

organic molecule configurations continued
pyronine, reson. Raman scatt., normal and excited mol. struct. determ. 77−58024
pyrrole-acetonitrile, H-bonded complex, ab initio MO calcs. 80−102440
qauche NMR effect in ^{13}C, ^{19}F and ^{31}P chem. shifts and directly bonded coupling consts., bond angle effects 77−68056
quinazolines, enzyme inhibitory, structure-activity quantitative study 80−78540
quinoxaline^{+}, (singly protonated), struct. and kinetics of fluoresc. and phosphoresc. states 77−30906
quinoxaline, oriented in lyotropic mesophase, proton NMR spectra 79−82886
quinoxaline, triplet state symmetry, geometry, ODMR, ENDOR obs. 79−18214
quinuclidine struct. determ. by gas phase electron diffr. 80−95742
radialenes, graph theoretical polynomials 80−69048
retinal, all-trans, reson. Raman excitation profile 78−73137
9-cis retinal, visual pigment chromophore, twisting mechanism 80−58333
11-cis retinal visual pigment chromophore, twisting mechanism 80−58333
rhodamine 6G, orientated relax. times, streak camera meas. 80−14168
rhodamines, reson. Raman scatt., normal and excited mol. struct. determ. 77−58024
rhodamines in ethanol soln., gain and induced absorpt., struct. props. 77−24890
ribonuclease A, bovine, cryst. struct. determ. by X-ray and neutron diffr. 80−108841
ring current theories in NMR 80−53020
ring current theory 80−87240
saturated ring cpds., six- and seven-membered, conformation mapping 77−57900
saturated six and seven membered rings, conformation maps 79−3383
scandium octaethylporphyrin, μ-oxo bridged dimer, triplet states and geometrys, ODMR obs. 80−9625
scandium octaethylporphyrin, triplet states and geometrys, ODMR obs. 80−9625
Schiff's bases, nematic phase, relation between elasticity and mol. struct. 79−90711
Schiff base azo dyes in nematic liq. cryst. hosts, order parameters, optical density meas. 80−84055
second-row molecular orbital calcs., INDO calc. for Na to Cl 78−82643
1,2,5-selenadiazole, partially oriented in mesophase, r_z struct. PMR obs. 78−58719
selenoketene, formation, microwave spectrum, struct. determ. 78−25515
selenoketene, microwave spectra, 26.5-40 GHz, mol. config., bond angle and length 78−46322
L-serine-L-ascorbic acid, X-ray cryst. struct. determ. 80−35827
Shpolskii spectra, identification and struct. anal. of unknown compounds in organic mixture 79−87891
silver methanedisulphonate, cryst. struct. and information determ. 79−90633
simple molecules, conformation, electronic spectra, NDDO calcs. 79−85901
six-membered rings, conformation, nomenclature 80−78721
smectic liquid crystal, polymorphism, mol. struct. effects 77−47348
sodium dodecyl sulphate: Gd^{3+}, micellar system, chain folding, ^{13}C NMR obs. 80−61158
sodium dodecyl sulphate micelles-ω-(α-naphthyl) dodecanoic acid soln. fluoresc. decay obs. 80−61158
squaric acid, neutron diffr. mol. and crystal struct. determ. 78−26557
stereodiagrams, 3D coordinates of mol. structs. 80−64824
stereoisomer generation, specification and enumeration, config. symmetry group appl. 80−1079
sterically hindered molecule, torsional angle calc. 77−79553
stibabenzene, struct., microwave spectrum and nucl. quadrupole coupling consts. 78−70817
trans-stilbene dianion, photolysis, intermediate struct., time-resolved reson. Raman spectra obs. 79−52695
stramonin-B, X-ray cryst. struct. anal. 79−77589
streptomycin oxime selenate tetrahydrate, antibiotic, cryst. and mol. struct. 78−24028
structural elucidation, CHEMICS-F computer program system 79−18310
structure and conformation of dissolved mol. in liq. crystal, NMR 78−62829
structure determ. from spectral data by CHEMICS-F computer program 79−36794
succinic acid, partially deuterated, ^{1}H and ^{2}H distant ENDOR obs. of mol. struct. parameters 80−23445
TCNQ:Rb, 3:2 complex, cryst. struct. at 113K 79−99169
TCNQ, and anions, PRDDO method using Slater orbital basis 79−764
TCNQ complex, $(C_{13}H_{21}N_2S_2)^{+}(C_{12}H_4N_4)_2$, cryst. and mol. struct. 77−62514
TCNQ complex with 5-phenyl-[1-thiol]-3-selenol-2-thione, charge-transfer salt, cryst. and mol. struct. 80−33986
TCNQ complex with N-methyl-Z-ethylthiazoline, cryst. and mol. struct. 78−10034
TCNQ salt, $[Pt(NH_3)_4]^{2+}[(TCNQ)_2]^{2-}$ cryst. and mol. struct. and EPR props. 78−55860
TCNQ-TMTSF, conducting salt, cryst. and mol. struct. 77−24307
TCNQ-TMTTF, conducting salt, cryst. and mol. struct. 77−24308
teaching, mol. models based on Petri dishes 78−73817
o-terphenyl, cryst. struct. determ. by neutron diffr. 79−42046
1-(2,3,4,6-tetra-0-acetyl-β-D-glucopyranosyl)-2,3-(2R)-epoxypropane, molecular and cryst. struct. 78−25746
tetraalkylammonium bromide, solid and liq., Raman spectra, longitudinal acoustic vibr. mode, mol. dimensions of ions 78−31183
tetraalkylammonium halides in methanol, struct., IR spectra 77−23500
1,4,5,8-tetraazanaphthalene radical ion pairs, EPR spectra 79−50051
tetrabromoformaldazine, mol. struct., electron diffr. determ. 79−45858
2,2,3,3-tetrachlorobutane, vibr. spectra, liq. and solid-state, conform. struct. 79−73936
1,1,1,3-tetrachloropropane, Raman and IR obs. of rot. isomerism, entropy difference between vapour and liq. phase isomer *(Russian)* 79−31529
tetracyclo[4,2,2,$O^{2,5}$,$O^{3,7}$] decane-10-carboxylic acid, lactone substituted, molecular, crystal struct. 79−90640
tetrafluoro-p-benzoquinone, mol. struct., gas phase electron diffr. obs. 80−58386
1,1,2,2-tetrafluorocyclobutane, microwave spectrum, dipole moment, rot. and vibr. modes assignments 77−18914
organic molecule configurations continued
1,1,2,2-tetrafluoroethane, anti- and gauche-rotamers, struct., spectra, electron diffr. 77−50439
1,1,1,2-tetrafluoroethane, mol. struct. studied by gas-phase electron diffr., vibr. amplitudes, bond angles and lengths calc. 80−95740
tetrafluoroethylene radical anion, isotropic and anisotropic EPR spectra, conform. 78−13532
tetraiodoethylene, cryst. and mol. struct. at 4K 77−59001
tetrakis(trifluoromethyl)germane, gas phase electron diffr. struct., torsional force consts., CNDO/2 calc. 79−31687
tetrakis(trifluoropropynyl)-tin, mol. struct. determ. from gas phase electron diffr. 78−25741
2,2,5,5-tetramethyl-4-phenyl-3-imidazalin-3-oxide-l-oxyl, deform. electron density determ., X-ray diffr. 80−88135
tetramethylammonium silicate, X-ray cryst. struct. determ. 79−94996
tetramethylbutane in hexachlorobutadiene soln., local mode overtone bands 80−83444
3,3,4,4-tetramethyldiazetine, photoelectron spectra, ring size effects on azo group ionis. pots. 77−61793
tetramethylene bridged ferrocene derivatives, mol. struct., Mossbauer expt. 78−60372
1,1,3,5-tetramethylpiperidinium iodide, model cpd., struct., ^{13}NMR 77−565
1,1,3,4-tetramethylpyrrolidinium iodide, model cpd., struct., ^{13}C NMR 77−565
tetraselenotetracence chloride, cryst. and mol. struct. 79−94992
tetraselenotetracene thiocyanate complex, X-ray struct. anal. 80−2006
tetravinyltin, electron diffr. determ. of struct. 78−37763
s-tetrazine, fluoresc. excitation spectra, 1K rot. struct. 78−1020
s-tetrazine(-d_1), and $^{15}N_2$-substituted, rot. consts., ground and $^{1}B_{3u}$ excited states geometries 78−82862
TGS, X-irrad., glycine radicals, geom. struct. by ENDOR and INDO calc. 79−24230
1,2,4-thiadiazole, struct., double reson. modulation microwave spectra 77−14424
1,2,5-thiadiazole, substitution struct., mag. double reson. 79−27105
Δ-2 thiazoline and alkyl derivatives, IR and Raman vibr. spectra, conformation *(French)* 79−10104
2-thio alkyl (allyl, benzyl) pyrimidines, IR and Raman spectra anal., mol. vibr. and symmetry *(French)* 80−87123
thioacetaldehyde (-d_1), microwave spectrum, substitution struct. internal rot. barrier, dipole moment 77−6762
thiocarbonyl halogen substituted cpds., geometric and electronic struct., LCAO-SCF calc. 79−89603
thioformyl ion, theoretical study 78−37553
thioindigo dyes, triplet state config., laser flash absorpt. spectrosc. obs. 80−5557
thioketen, microwave spectrum, substitution structure and dipole moment 80−975
thiones, N-H-S weak and medium strong H bonds, IR spectra 80−69132
thiopen-2,5- dicarboxaldehyde, in lyotropic mesophase, mol. struct. and orientation 78−1004
thiophen-2-carboxaldehyde, in lyotropic mesophase, mol. struct. and orientation 78−1004
thiourea, ground and first excited triplet state configs., ab initio SCF calcs. 79−89597
thiourea, struct., hydration, ab initio SCF calcs. 80−58142
thioureas, alkyl and phenyl groups trisubstituted, conformation, steric and stacking interaction 80−95587
thromboxane, evidence against prostaglandin hairpin conformation 80−3585
thymopoietin active fragment in H_2O, soln. conformation by DNMR spectroscopy 80−89710
TMTSF-DMTCNQ, cryst. and mol. struct. 78−63742
tolanes, molecular conformational mobility study by optical probing method *(Russian)* 80−92459
toluene, mol. geometry, electron diffraction obs. 78−9270
toluene, mol. struct., electron diffr. obs. 77−88559
tolyl cation+alkyl nitrate, reactions and ion struct. 77−52619
2-(2-tosylaminophenyl)-4H-3,1-benzoxazine-4-one, cryst. and mol. struct. 80−84167
toxin, penicillum roqueforti, struct. and absolute configuration 80−39064
tri(trifluoromethyl) germanium halides, gas, liq. and solid, IR and Raman spectra, normal coord. anal. 79−72316
tri-(trimethylsilylmethyl) tin monoiodide, molecular and cryst. struct. 79−65068
trialkylthioureas, N-H stretching vibrs. and conformation 80−95586
triallyl orthoformate, photoelectron spectra, ionisation pot. bands, conformation, SPINDO calc. 78−9194
1,3,5-triaryl-2-pyrazolines, rel. to glass-forming props. 77−11677
s-triazine, in nematic soln., ^{1}H NMR, struct. ^{1}H, ^{13}C, ^{15}N direct coupling meas. 77−50452
bis-triazolopyridazines, conformation calcs. by mol. mechanics and CNDO/2 method 80−69079
bis-triazolyls, conformation calcs. by mol mechanics and CNDO/2 method 80−69079
trichloro(methyl)germane, mol. struct. determ. by vap. phase electron diffr. 77−54621
trichloroanilines in solutions, IR absorpt. spectra 80−69136
1,2,3-trichlorobenzene, oriented mols., ^{13}C satellites use in proton spectra, r_α-structure 80−18872
1,1,1-trifluoro-3-chloropropane, Raman and IR obs. of rot. isomerism, entropy difference between vapour and liq. phase isomer *(Russian)* 79−31529
trifluorobenzene, equilib. config. and barriers, microwave spectra 80−95606
1,3,5-trifluorobenzene, quadrupole moments, elec. field-gradient birefringence method 80−95746
trifluorobenzene cations, Jahn-Teller distortions, quadratic and mode mixing effects., distortion geometry determ. 80−91462
trifluorodimethylmercury, gas phase mol. struct., electron diffr. and microwave spectra obs. 80−78609
1,1,2-trifluoroethane, mol. struct., gas phase electron diffraction, rotamer abundance 79−76514
trifluoroethene-d_0,d_1, mol. struct., microwave and electron diffr. obs. 80−58384
trifluoromethane, and -d_1, microwave spectra in $\nu_6=1$ state, accidental degeneracy, mol. struct. 79−3436
trifluoromethyl cyanides and isocyanides, isomerisation, ab initio (STO-3G) geometry optimised calc. 78−46265

organic molecule configurations continued
trifluoromethylsulphonyl chloride, geom. struct., CNDO/2 calc., comparison with CH_3SO_2Cl 79−81295
triindenylcerium pyridinate, X-ray cryst. struct. determ. 79−32984
1,3,5-trimethoxybenzene, solid, and in 77K glass, electronic absorption spectra interpretation 79−36659
1,1,1-trimethoxyethane, mol. struct., electron diffr., vibr. spectra 78−37765
trimethyl orthoformate, photoelectron spectra, ionisation pot. bands, conformation SPINDO calc. 78−9194
trimethyl-d_9-vinylsilane, IR and Raman spectra, struct., vibr. assignment, barriers to internal rot. calc. 80−87102
trimethylamine, and analogues, struc. struct. and vibr. force fields, electron diffr. and microwave spectra 77−54609
trimethylaminegallane, microwave, IR and Raman spectra, struct., vibr. assignment 80−95600
1,3,5-trimethylbenzene, quadrupole moments, elec. field-gradient birefringence method 80−95746
trimethylbromosilane, microwave spectra, struct., chemical bonding 80−95602
trimethylene diradical, geometry optimisation by generalised Hartree-Fock 78−25427
trimethylene diradicals, geometry optimisation ab initio SCF CI calcs., energy gradient 79−85903
trimethylene sulphoxide, microwave spectrum, mol. struct., methylene group, bends, tilts, twists 77−50431
trimethylgermylisocyanate, IR and Raman spectra, struct. 78−37637
trimethylgermylisothiocyanate, IR and Raman spectra, struct. 78−37637
trimethylvinylsilane, IR and Raman spectra, struct., vibr. assignment, barriers to internal rot. calc. 80−87102
trioxane $^{13}C(^{18}O)$ substituted, mol. consts. and rot. spectra 80−87096
trioxolane, methyl substituted, stability, pseudorotation, electronic effects in final ozonide 79−45654
trioxolanes, methyl substituted, stability, pseudorotation, electronic effects in primary ozonide 79−49961
trioxolanes, pseudorotation surface, mol. struct. and conform. 79−45653
triphenyl-(triphenylgermanylperoxy)silane, cryst. and mol. struct. 80−39066
triphenylamine cation radical, condensed and vapour phase geometry, photoelectron spectra 79−31597
triphenylene, in n-heptane cryst., polarised fluoresc. spectrum, mol. deformation 79−10135
triphenylene derivatives, hexasubstituted, disc-like cpd., mol. conform. and arrangement, semiempirical calcs. 80−107048
triphenylmethane dye soln., electronic relax., viscosity-depend., using picosec. flash photolysis 80−66258
triphenyltin bromide, cryst. struct. determ. using Patterson and Fourier methods 79−42044
triptycene hydrogenation products, ACC and TCC, cryst. data 80−100224
tris(trimethylstannyl)amine, gas phase electron diffraction 80−106401
tris-butadienyl metal D_3 complex pairwise chiral discriminations, stereochem. basis, extended transition monopole model 78−74725
tropone, proton affinity, MINDO/3 results compared to ICR obs. 78−1103
trypsin inhibitor, conformation, distance geometry calcs. 77−50553
tryptamine:1-thyminylacetic acid (1:1), cryst. and mol. struct. determ. using MULTAN 79−73156
TTF-^{13}C, mol. struct. determ. from PMR in nematic solvents 77−88468
TTF-(2,5-diethyl)TCNQ, cryst. and mol. struct. temp. depend. 77−35531
TTF-TCNQ, molecular coordination along stacking directions 79−47031
$TTT_2^+.I_3^-$, cryst. and mol. struct. by X-ray study 79−51096
TTT^+Br^-, cryst. and mol. struct., X-ray method 80−107202
TTTF-TCNQ, crystal and molecular structure determination *(French)* 78−91329
unimolecular rearrangements, principle of least motion technique 77−36737
urea adducts, crystn., geometry of urea-cation bonding 80−39061
urea antimony fluoride, X-ray cryst. struct. determ. *(French)* 80−44196
ureas, alkyl and phenyl groups trisubstituted, conformation, steric and stacking interaction 80−95587
valence-nonbonded H atoms interaction and two-centre contrib. to total energy of mol. 80−32624
valinomycin conformation in a phospholipid bilayer, ^1H NMR obs. 80−40958
Van der Waals complex, PCILO calc. of dispersion energy and geom. conf. 79−63930
vinyl alcohol, struct. from ab initio calcs. 78−29857
vinyl bromide, mol. struct., from gas-phase electron diffr. and microwave data 80−23571
vinyl cyanide, microwave spectra data tables 79−59445
vinyl fluoride, geometries, props. and protonation, ab initio mol. orbital study 79−22588
vinyl isocyanate, and vinylcyano ether, geometry and conform., ab initio minimal STO-3G MO calcs. 80−23337
vinyl mercaptan -d_0, -d_1, anti rotamer, conform., microwave spectrum 80−9592
vinyl mercaptan -d_0, -d_1, synrotamer, conform., microwave spectrum 80−5535
vinyl radical, MINDO/3-FORCES, geom. of heat of formation 78−66472
vinylchloride, mol. struct., gas-phase electron diffraction and microwave spectra, vibr. amplitudes 79−76421
vinylcyano ether, and vinyl isocyanate, geometry and conform., ab initio minimal STO-3G MO calcs. 80−23337
vinylfluoride, gas phase electron diffr. and microwave spectra, rot. consts., struct., isotope shifts 79−31686
vinyloxirane, Raman and IR vibr. spectra and conformations 80−83379
vitamin V_{12r}, monomeric O_2 adduct, struct., single cryst. ESR obs. 79−39351
water-imidazole, H bond interrupted chain, cooperative effects, STO-3G ab initio calcs. 80−63535
xanthene dyes in n-alcohols (ethylene glycol) (glycerol), rot. relax., time-resolved fluoresc. depolaris. obs. 80−58300
xanthine, planar autoassoc. energy 80−53086
p-xylene, mol. geom. struct. and ring distortion, gas-phase electron diffr. 79−59573
Yang's biradical, EPR, g- and D-tensors, electronic struct., deuteration and conformation effects 77−42343
Ar-methyl chloride, mol. beam elec. reson. spectrosc. 80−23477

organic molecule configurations continued
CF_3, CF_3^-, and CF_3^+, optimised struct. and bonding, ab initio SCF MO calc. 80−23334
CF_3O^-, bonding, ab initio calcs. 77−50350
CH_2 and CH_2^+, valence states, ab initio calcs. 79−6859
CH_3, experimental determ. of the geometry and electron affinity 78−82860
$C_2H_3^+ + HF$, interaction, struct. and stability, ab initio calcs. 80−58347
$C_2H_7^+$, ab initio SCF, CI, CEPA-PNO struct. and energy calcs. 78−94197
CH_2CCH radical, electronic struct., geometry, INDO calcs. 77−14358
CH_3CO', low lying states, struct., energetics, ab initio STO calcs. 77−61682
CH_2F, far IR laser mag. reson. spectrum 78−9174
CH_3NN', low-lying states, struct., energetics, ab initio STO calcs. 77−61682
CHNO isomers, interconversion pot. energy surfaces, geometries, electronic structs. 78−35660
$C_2H_5O^+$ and $C_2H_5S^+$, stability, proton affinity, ab initio SCF, CEPA PNO, MINDO/3 and MNDO calcs. 79−59357
CSH_3^+ ions, structs. and relative energies 78−82861
Co II complexes, with tetradentate Schiff bases, synthesis, struct. and ESR obs. 80−80598
$Co[Ag(SeCN)_2]_2$, and complexes, softness values and struct., IR spectra 79−59459
CuH, UV absorpt. spectra 80−87143
N,N-dimethyloxamide, conform. anal., CNDO/2 energy optimisation, mol. props. 77−75328
F compounds, ground states, mol. parameters, MINDO calcs. 78−41955
α-D-glucose, struct. refinement, mol. conformation and H bonding 79−42043
H-bonded systems, MINDO/3 geom. optimis. calcs., heats of form. of monomer and dimer 79−31399
HCCN, a cyanocarbene, geom. struct., electron correl. effects 80−1077
HCCN, matrix isolation IR and UV spectra, vibr. anal., struct. 77−65457
H_2CN^+, isomers configurations rel. to role in interstellar HCN and HNC form. 78−81672
H_2COLi^+, geom. and electronic struct., ab initio SCF calc. 79−76331
HCO', low lying states, struct., energetics, ab initio STO calcs. 77−61682
HCS^+-CSH^+, struct. and stability, ab initio SCF calcs., CNDO calcs. 80−32608
H_3CS^+, struct. ab initio (4-31G) SCF calc. 79−68201
HNN', low-lying states, struct., energetics, ab initio STO calcs. 77−61682
HNOO, singlet and triplet diradicals, unrestricted 79−97975
K salt of β-ketoaldehyde, configurations of anions in solutions studied by IR spectroscopy, H-bond form. 80−87117
Li salt of β-ketoaldehyde, configurations of anions in solutions studied by IR spectroscopy, H-bond form. 80−87117
methane cation, Jahn-Teller distortion 80−48098
NCO^+, partial pot. energy surfaces, ab initio SCF CI calcs. 78−37554
NH_2CO', low-lying states, struct., energetics, ab initio STO calcs. 77−61682
Na salt of β-ketoaldehydes, configurations of anions in solutions studied by IR spectroscopy, H-bond form. 80−87117
$Na_4\ Fe(CN)_6.10H_2O$, single cryst., X-irradiated product ESR, 4.2K 77−48659
Ni complex, bis[3,4,-benzo-N-(S)-sec butylsalicilaldiminato] nickel (II), stereochemistry, De Voe theory 77−14600
Pd complex, 1,1,1-trifluoro-2,4-pentanedionate, struct., chem. ionisation mass spectra 78−61079
Pt complex, 1,1,1-trifluoro-2,4-pentanedionate, struct., chem. ionisation mass spectra 78−61079
Pt(diethylenetriamine)(guanosine)$(ClO_4)_2$, crystal and molecular struct. 79−73157
Ru complex, tris-1,1,1-trifluoro-2,4-pentanedionate, struct., chem. ionisation mass spectra 78−61079
$(TMCHDT)_2ClO_4$, organic conductor, struct. study *(French)* 80−88133
$\{Th[(CH_3)_5C_5]_2H(\mu\text{-}H)\}_2.C_6H_4CH_3$, molecular structure by neutron diffraction 79−89801
Tl(III) organocompounds, XPS study *(French)* 79−64047
B-trichloro-m-carborane, cryst. electrophilic chlorination of 9, 10-dichloro-m-carborane, cryst. and mol. struct. from X-ray diffr., cryst. struct. 78−9268

organic molecule electronic structure *see molecular electronic states*

organic semiconductor materials *see organic semiconductors*

organic semiconductors
2,4-hexadiyne-1,6 diol bis(p-toluene sulphonate) ester, demonstration of high mobility 80−20212
2,4-hexadiyne-1, 6-diol, bis(p-toluene sulphonate), dark-current meas. 80−15520
acceptor-donor-acceptor complex, Frenkel excitons and ionic excited states 80−92824
adenine film, polycryst., energy conversion processes, quantum yields, 4 to 10 eV 80−88589
aggregate organic photoconductor, composition prep., struct. and optical props. 79−24006
aggregate organic photoconductor, photoconduction props. 79−24007
anthracene:2-chloroanthracene, electrolum., voltage- and freq.-brightness characts., dopant conc. depend. 78−2916
anthracene: 1-chloroanthracene, electrolum. meas. 78−84659
anthracene:perylene crystal, trapping factors anisotropy 77−59291
anthracene:rhodamine, triplet exciton density, isotope substitution effect, in weak mag. field 77−90184
anthracene:tetracene, fluorescence decay with X-irrad., energy transfer by excitons 77−20915
anthracene:tetracene, singlet exciton fission, fluoresc. in mag. field 79−69877
anthracene:tetracene (pentacene), effect of elec. field on fluoresc. *(Russian)* 78−56521
anthracene, α-induced radical production beyond Bragg peak 79−24773
anthracene, and deuterate, electron drift mobility temp. depend., transient photocond. obs. 77−66164
anthracene, charge storage and trapping levels, TSC studies 80−6875
anthracene, charge-carrier generation by singlet-singlet collision-ionisation process, singlet photoionisation process 78−72195
anthracene, cryst., cyclotron reson. and carrier scatt. 77−76746

organic semiconductors continued
anthracene, cryst., photocurrent induced by detrapping of charge carriers trapped by radicals 79−82643
anthracene, cryst., radiation induced radicals, optical absorpt. bands, SCF-CI MO calc. 79−91463
anthracene, cryst., with electrolytic contacts, photocurrent anomalous behaviour, current-volt. characts. 77−39933
anthracene, cryst.-electrolyte system, pot. well, hole residence time 77−8190
anthracene, crystal-electrolyte interface, ionis. energy of uppermost cryst. mols. 78−27764
anthracene, dislocations effect on elec. props. 77−35947
anthracene, drift mobility expts., arrival-time detection 79−33308
anthracene, electron and hole generation under electron bombardment 79−73524
anthracene, electron bombardment, field and temp. depend. of carrier yield 77−8117
anthracene, electron irrad., creation and evolution of excited states, scintillation obs. 78−92128
anthracene, excess electron and excess hole cryst., band struct., drift and Hall mobilities, depend. on press. 79−60709
anthracene, field depend. of photocond. 79−99578
anthracene, fission of singlet excitons into triplet-exciton pairs 78−14672
anthracene, hole mobility mechanism interpretation of cyclotron reson. results 78−10438
anthracene, impurity effects on elec. cond. *(Russian)* 77−62930
anthracene, irradiated, optical absorption and EPR meas., low temps. 78−68538
anthracene, isotopically mixed cryst., exciton dynamics 80−29329
anthracene, laser excited single crystal, numerical anal. for TSC results *(Japanese)* 80−34464
anthracene, laser-induced photocond., excited charge carriers 77−28211
anthracene, luminesc. spectra, exciton-phonon interaction, triplet exciton bands 79−65387
anthracene, metastable triclinic phase 80−59452
anthracene, mol. cryst., elec. field independent electron drift mobility 79−51645
anthracene, monocryst., additional absorpt. spectrum at low temp. 78−92096
anthracene, O-O exciton absorption bands, thermomodulation study 78−39563
anthracene, off-diagonal electron mobility and lateral space charge drift 78−72192
anthracene, phonon-assisted mobility due to intermol. vibrs. 78−6383
anthracene, photo-oxidised, current oscills. due to recomb. instability in high field domain 77−4353
anthracene, photocond. spectrum induced by excitons *(Japanese)* 80−29440
anthracene, photoconduction *(German)* 79−78129
anthracene, photogeneration of charge carriers through two photon excitation 80−11033
anthracene, polarised reflection spectra, surface and vol. exciton coupling, vibronic states 78−72543
anthracene, prep. and growth of single cryst. 78−64463
anthracene, pure and doped, singlet exciton diffusion lengths, fluoresc. quenching by dye 78−43923
anthracene, single cryst., photocond. threshold, excitation spectrum 80−44639
anthracene, single cryst., X-ray radiation damage, delayed fluoresc. meas. *(Japanese)* 79−37736
anthracene, single cryst. triplet excitation form. 79−69437
anthracene, single cryst. with discrete shallow traps, computer simulation of TSC 79−99819
anthracene, single cryst. with photoinduced local centres, luminesc. 79−61433
anthracene, single crystal, contact charging and photoemission 79−47586
anthracene, single crystal, disperse photocurrent transients rel. to multiple trapping 79−99564
anthracene, single crystal, photoconductivity quantum yield, experimental validation of fund. theory 80−6909
anthracene, single crystals, TSC excited by Q-switched ruby laser 80−29417
anthracene, singlet exciton annihilation kinetics 79−19926
anthracene, singlet exciton fission, fluoresc. in mag. field 79−69877
anthracene, solid, electronic struct., comparative ESCA study of polyacenes 78−52631
anthracene, surface photovoltage 80−2419
anthracene, surface states and persistent internal polarisation via photocurrent transients 77−89825
anthracene, temp.-independent mobilities, phonon-induced electron hopping 79−28347
anthracene, thermally stimulated currents from shallow trapping centres *(Japanese)* 78−92015
anthracene, TSC meas. induced by Q-switched ruby laser 78−19087
anthracene, vibr. amplitude of mol. in condensed phase, five-parameter approx. 79−82295
anthracene crystal, resonance secondary emission, Raman scatt. in exciton absorpt. region *(Russian)* 80−40120
anthracene crystal, sensitised injection from surface oxidation products 78−76143
anthracene crystal, singlet-triplet exciton annihilation 78−31240
anthracene crystal, triplet exciton absorpt., high resolution photoconductivity spectroscopy 78−10504
anthracene crystals, α-particle induced scintillation, mag. field effects 80−40161
anthracene crystals, carrier trapping in deformed surface region 78−47806
anthracene crystals, orientationally disordered, exciton trap depths 80−88481
anthracene crystals, photocond. by polaritons 77−69373
anthracene crystals, resonance Raman spectra sensitivity to exciting light intensity *(Russian)* 78−52504
anthracene crystals, superficial trapping levels, pulsed photocurrent transients 78−76021
anthracene crystals, TSC, monomolecular glow peak 77−39869
anthracene crystals, TSC, monomolecular glow peak revealed by thermal cleaning 77−39870
anthracene crysts., Frenkel exciton dissoc. near charged defect 77−51669
anthracene crysts., nonlinear fluorescence quenching, recomb. of free excitons 80−7397

organic semiconductors continued
anthracene crysts., structural imperfections and delayed fluorescence 78−68551
anthracene derivative, Langmuir-Blodgett multilayer film, semiconducting props., optical and elec. meas. 80−11122
anthracene film, effect of struct. on luminesc. quenching *(Russian)* 80−7411
anthracene film, electroabsorption spectra obs. 80−50301
anthracene film, switching and memory phenomena 77−12031
anthracene Langmuir films, lightly substituted, AC and DC cond. 80−80425
anthracene single cryst., injection of holes, current-voltage characts. *(Russian)* 77−1433
anthracene single crystals, effect of γ-irrad. on photolum. *(Russian)* 80−2852
anthracene thin films, high field effects and switching, local centres importance 79−73548
anthracene with adsorbed rhodamine B, electron-hole pair in external elec. field 79−73558
anthracene-phenanthreen-TCNB, exciton transport obs. 80−65461
anthracene-pyromellitic dianhydride complex, optical and photoelectric props. *(Russian)* 80−15570
anthracene-tetracene amorphous films, host-guest energy transfer 78−60505
anthracene-tetracyanbenzene, charge transfer, magnetic resonant modulation of photoconductivity 78−64062
anthroquinone, temp. depend. and anisotropy of electron drift mobilities 78−19089
auramine crystal, photocond. and intermol. electron interaction, tight binding approx. 77−15765
azulene, drift mobility expts., arrival-time detection 79−33308
biopolymers, role in biochemical phenomena, book contrib. 80−12053
bipolymer, charge carriers origin and mobility, adsorbed water effects 79−92461
β-carotene, hole mobility meas. by transient photocond., Poole-Frenkel effect 77−11957
β-carotene glass, photoconductivity mechanism 79−28368
cetyl alcohol with dipoles, switching and negative resist. phenomenon, quantitative model 78−14769
cholesterol film with dipoles, switching and negative resist. phenomenon, quantitative model 78−14769
chromophore phospholipid Langmuir films, photoeffects 80−80409
chrysene, crystal-electrolyte interface, ionis. energy of uppermost cryst. mols. 78−27764
conference on organic conductors and semiconductors, Siofok, Hungary (Sept. 1976) 78−6284
copper phthalocyanide, cryst. struct. sensitivity of band struct. 79−42444
copper phthalocyanine, Al/copper phthalocyanine/Au cell, photoexcitation, doping, energy loss mechanisms 79−99573
copper phthalocyanine, imperfect cryst., elec. transport phenomena, charge carrier conc. 77−1421
copper phthalocyanine dye deposition on Si (111), low energy electron optically modulated transmission increase 79−78133
copper phthalocyanine film, electroconductivity, effect of adsorption 77−85356
copper phthalocyanine film, electron acceptor surface states due to O_2 adsorption 80−88586
copper phthalocyanine film, photoelectrochem. behaviour on SnO_2 electrodes 80−15626
copper phthalocyanine in MSM struct. with Schottky barrier 77−43740
copper phthalocyanine-iodine, amorphous cpd. prep. by I_2 diffusion in polycrysts., triplet EPR signals obs. *(Russian)* 80−66016
cupferron and complexes, amorphous, hopping cond., 0 to 150°C 79−60828
decamethylferrocene-bis(TCNQ), vac. UV photoemission 77−85883
2,6-N,N-diacetyldiaminopyridine elec. cond., γ dose and temp. (303-363K) effects 80−103696
2,6-N,N-dibenzoyldiaminopyridine elec. cond., γ dose and temp. (303-363K) effects 80−103696
9,10-dichloroanthracence, monoclinic, photocond. carrier mobility 80−39630
α-9,10-dichloroanthracene, crystal, hole mobility temp. depend. 78−26858
β-9,10 dichloroanthracene, hole mobility anisotropy and cryst. struct., transient photocond. 78−95310
1,1′-diethyl-2,2′-quinocyanine-$[TCNQ]_2$ anion radical salt single crystals, photovoltaic effect *(Japanese)* 78−2522
p-diiodobenzene, phase transition obs. using interferometry 78−34616
dimethyl stilbene chloride, organic semiconductor thin film on glass, voltampere charact. *(Rumanian)* 79−38196
2,3-dimethylnaphthalene, transient photocurrents, hole trapping *(German)* 77−59303
N,N′-diphenyl-p-phenylenediamine, current carrier traps, space-charge-limited currents 78−47799
durene, photoconductivity, charge carrier mobility 77−47852
dyes, cond. type, I-V characts. 78−6391
electrical conduction and polarisation phenomena at low fields 78−48113
electron energy states of solid, alternate mol. orbital method 79−65353
electron mobility, temp. independent, theory 79−69509
electronic structure of organic conductors and semiconductors 79−35496
film, Schrieffer effect 80−60118
films, relax. currents, polarisation and depolarisation currents obs. 80−49764
fluorenone derivatives as electron transport materials, electron affinity and electrochemistry, rel. to photocond. 79−38127
fuchsin in MSM structure, field depend. of electroabsorption spectra 77−40263
germanium phthalocyanine, elec. cond. temp. depend. 80−80271
hexamethyltriaminotriphenylcarbenium chloride, cryst. violet, photoconductive characts. 78−39163
indanthrone film, SCL conduction, trapping 77−15978
injected charge drift and localisation in amorphous and organic layers *(German)* 78−91794
iron phthalocyanine film, electroconductivity, effect of adsorption 77−85356
isostructural heterojunctions of organic materials 78−39194
Kapton, pyrolysed, cond. polymer, transport and mag. props. 80−96887
lead phthalocyanine:O_2, photocond., impurity-induced 79−47120
lead phthalocyanine:O_2(I), Schottky barrier effect on AC current response 80−75623

organic semiconductors continued
Lexan:triphenylamine, molecularly doped, hole transport by hopping 78−34831
Lexan:triphenylamine, photosensitisation using rhodamine B or thiapyrylium 78−34856
linear crystal, donor-acceptor complex, Frenkel excitons and ionic excited state mixing 79−99485
linear molecular crystal, mixing of Frenkel excitons and ionic excited states 77−15771
magnesium phthalocyanine, film, depletion layer studies, temp. depend. of LF capacitance 80−65617
molecular crystals, anomalous elec. field depend. of temp. independ. electron mobilities 79−42548
molecular crystals, electronic props. *(German)* 78−23089
naphthalene:1-hydrodynaphthyl, cryst., charge transfer optical transitions 77−44027
naphthalene:benzofuran, luminescence spectra and intensity, 1.6-77K 79−87477
naphthalene:indole, luminescence spectra and intensity, 1.6-77K 79−87477
naphthalene:thionaphthalene, luminescence spectra and intensity, 1.6-77K 79−87477
naphthalene, charge carrier drift mobility, semi empirical anal. 80−65553
naphthalene, crystal-electrolyte interface, ionis. energy of uppermost cryst. mols. 78−27764
naphthalene, crystalline, singlet exciton diffusion coeff. meas., fluorescence quenching anal. 78−67945
naphthalene, deep exponential distrib. of traps, long-time decay of surface pot. 79−47041
naphthalene, electron and hole off-diagonal mobility component determ. 80−65552
naphthalene, electron band hopping transition 78−39155
naphthalene, electron trapping, one-carrier TSC and SCL currents 80−70715
naphthalene, hole mobility, anomalous current transients 78−76091
naphthalene, mol. cryst., elec. field independent electron drift mobility 79−51645
naphthalene, pure and deuterated, band-hopping mobility transition 80−6833
naphthalene, temp.-independent mobilities, phonon-induced electron hopping 79−28347
naphthalene, vibr. amplitude of mol. in condensed phase, five-parameter approx. 79−82295
naphthalene crysts., nonlinear fluorescence quenching, recomb. of free excitons 80−7397
naphthoxazole derivatives, elec. cond., thermoelec. power, energy gap, absorpt. spectra 77−32053
neopentane:n-butane, electron mobility and electron-ion recombination rate const. 79−73557
nickel phthalocyanide, cryst. struct. sensitivity of band struct. 79−42444
nickel phthalocyanine, ohmic and space-charge-limited currents in vacuum ambient 77−20323
nickel phthalocyanine film, electron acceptor surface states due to O_2 adsorption 80−88586
9-nitroanthracene, semiconductive props., gas adsorpt. effect 79−65471
one-dimensional, resonant states, mag. excitations and impurities 80−24839
optical consts. by refl. and transmission, errors 77−16414
organometallic semiconductors, activation energy of elec. cond. rel. to press. 78−24811
p-terphenyl, positronium and thermal defects 80−24496
pentacene, evaporated film elec. cond. meas. for various temps., SCL 78−10584
pentacene, surface photovoltage 80−2419
pentacene layers, photogeneration, charge carrier transport *(Russian)* 78−56181
perylene, crystal-electrolyte interface, ionis. energy of uppermost cryst. mols. 78−27764
phenanthrene, crystal-electrolyte interface, ionis. energy of uppermost cryst. mols. 78−27764
phenothiazine derivatives, semicond. elec. props., optical spectra, and EPR 80−103693
photoelectrode processes and effects *(German)* 80−26145
phthalocyanine, metal-free, singlet-triplet fusion rel. to carrier photogeneration 77−36276
phthalocyanine, molecular crystals, electronic props. *(German)* 78−23089
phthalocyanine film, surface photovoltage, central ligand effect 79−78231
phthalocyanine films, metal-free, adsorbed o-chloranil effect on surface photovoltage 80−34485
phthalocyanine layers, metal-free, between Ag and Al electrodes, switching effects 80−65706
phthalocyanine metal free films, TSC, ferroelectric-semiconductor transition 80−66105
phthalocyanine thin films, transient photocond. obs. technique, freq. depend. 77−76860
phthalocyanine thin layers, metal-free, mobility and thermally stimulated polarisation meas. 79−73527
phthalocyanine-halogen complex, influence of halogen on elec. and optical props. *(Japanese)* 79−51586
phthalocyanine-metal interfaces, surface photovoltage 80−20308
γ-platinum phthalocyanine, energy band struct., carrier mobilities 77−72817
poly(p-phenylene), electronic struct., one-electron band theory 80−65450
poly-2-vinylpyridine-iodine, semicond. film, elec. cond., depend. on I conc. and temp. 79−73606
poly-α-naphthol, semicond., isothermal depolarisation currents, electron trap parameters 80−60492
poly-α-naphthol film, SCL currents obs. 77−47910
poly-N-epoxypropylcarbazole layers, optical and photoelec. props. 77−39896
poly-N-vinyl carbazole, and Br-substituted derivative, transient hole hopping transport, 150-500K 78−39108
poly-N-vinyl carbazole, containing carbazylium cation radicals, synthesis and semicond. props. 77−85224
poly-N-vinylcarbazole films, drift mobility of photocarriers, polymerisation method influence 77−76986
poly-N-vinylcarbazole thin amorphous film, hole drift mobility, mol. mass. depend. 80−75663

organic semiconductors continued
poly-N-vinylcarbazole-polycarbonate mixture, hole drift mobility and photosensitivity 77−85260
polyacene quinone radical polymers, elec. props. described by variable range hopping model 80−44588
polyacene quinone radical polymers, two-dimens. variable range hopping 79−51608
cis-polyacetylene:AsF_5, conductivity meas., non-Ohmic effects 80−96891
polyacetylene:AsF_5, heavily doped, transport props., evidence for metallic state 79−87121
polyacetylene:AsF_5, mag. susceptibility, Fermi surface density of states, semicond.-metal transition 79−95566
polyacetylene:AsF_5, thermal decomp. kinetics, elec. cond., ESCA and mass spectra 80−50830
polyacetylene:AsF_5, thermopower and transport props. 80−65611
polyacetylene:AsF_5(I), pure and doped, electronic excitations, momentum depend., EELS study 80−76121
polyacetylene:Br(Pd), ion implantation effect on elec. props. 80−65026
polyacetylene:I, semiconductor-metal transition, thermoelec. power meas. 79−56271
polyacetylene:SbF_5, elec. cond. meas. 80−60055
polyacetylene, and derivatives, thin polycryst. film, solar cell applic. 80−92899
polyacetylene, doped, fluctuation-induced tunnelling cond. in metallic regime 80−65516
polyacetylene, doping with AsF_5, mechanism, effect on elec. cond. and spectra 80−24473
polyacetylene, electronic struct., one-electron band theory 80−65450
cis-polyacetylene, electronic struct. 79−47012
polyacetylene, lightly doped, donor and acceptor states, IR absorpt. obs. 79−73979
polyacetylene, n- and p-type doping, and compensation, p-n junction formation 78−76070
polyacetylene, phototransport effects 80−44653
polyacetylene, pristine and acceptor doped isomers, EPR, DC cond., evidence against solitons 80−15782
polyacetylene, pure and doped, electronic props. from one-dimens., tight-binding LCAO-SCF-MO calcs. 79−56123
polyacetylene, pure and heavily doped, optical and IR studies, electronic struct. calcs. 80−7347
polyacetylene, semiconducting and metallic, thermoelec. props. 80−40884
cis-polyacetylene, static lattice calcs. for crysts. 80−10509
polyacetylene and derivatives, chemically doped, elec., chem. and phys. props. 80−24912
polyacetylene film, $(CH)_x$, synthesis, struct. and elec. props., doped materials, review 80−15623
polyacetylene film, heavily doped with AsF_5, conductivity and Hall effect meas. 79−28353
polyacetylene film, partially oriented, anisotropic elec. cond., quasi-one-dimens. behaviour of fully oriented doped material 80−11112
polyacetylene films, AsF_5 doped, photocond. and junction props. 80−70770
polyacetylene films, doping effect on elec. cond., chem. and optical props. 80−65572
polyacetylene films, doping investigation, insulator-metal transition, optical transmission meas. 80−103729
polyacetylene films, electrical properties *(Japanese)* 80−96888
polyacetylene films, pure and Br and I doped, Raman scatt. 79−47457
polyacetylene films, stretch-aligned, prep. and morphology 80−66471
polyacetylene photoelectrochemical solar cell, fabrication and efficiency 80−50954
polyacrylonitrile, pyrolyzed, surface layer, anal. of elec. cond. mechanism by impedance diagram *(Japanese)* 78−23148
polyaromatics, elec. cond. correl. with chem. struct. and synthesis, charge transfer complexes *(German)* 80−15514
polycarbonate: tri-p-tolylamine, chemical control of conductivity 80−59984
polycarbonate:tri-p-tolylamine amorphous film, elec. and mag. props 80−49959
polycarbonate, photoconductivity, UV-IR light, absorpt. and photoluminescence. spectra *(Japanese)* 78−34857
polydiacetylene, cryst., one-dimens. conjugated semicond., vibronic coupling, Fano interference effects 80−34939
polydiacetylene, photoconduction in multilayer structs. and single cryst. 78−80024
polydiacetylene bis-(toluenesulphonate), single cryst., charge carrier mobility and recomb. 77−8132
polydiacetylene polymer crystals, one dimensional conjugated, optical props. 77−43993
polydiacetylene-bis(toluenesulphonate), transient photocond. meas. 78−30951
polydiacetylene-toluenesulphonate, photocond. meas., 0.62-3.1 eV 80−70757
polydiacetylenes, band struct., ab initio cryst. orbital method, and transport props. calc. 78−26811
polydiacetylenes, photocond. action spectrum of single crysts., charge transport obs. 80−15557
polydifluoroacetylene, electronic struct., tight-binding LCAO-SCF-MO calcs., prep. 80−70591
polyene, mol. cryst., elec. cond. *(German)* 78−23089
polyene, one-dimensional chain, Raman scatt., one-phonon final states and many-body effects 80−34913
polyene chain, collective excitations and optical absorpt. 79−47019
polyenes, compensation temp. 80−39625
polyethylene, oxidised, charge carrier, transport phenomena 80−15515
polyethylene naphthalate, photoconductivity, UV-IR light, absorpt. and photoluminescence. spectra *(Japanese)* 78−34857
polyethylene terephthalate, photoconductivity, UV-IR light, absorpt. and photoluminescence. spectra *(Japanese)* 78−34857
polyfluoroacetylene, electronic struct., tight-binding LCAO-SCF-MO calcs., prep. 80−70591
polyglycine chain, electronic struct. and transport props., ab initio Hartree-Fock crystal orbital calc. 79−42448
polymer, conjugated, synthesis and elec. props., review 80−15513
polymer, in MSM struct., thermionic field emission from metal 79−1629
polymer, synthesis from Cu^{2+} chelate of PVA and iodine, optimum prep. conditions 79−91612
polymer p-n junction, rectification effects in dark and photocurrents 77−69407
polymeric conductors, struct. and phys. props., symposium, San Jose, USA (March 1979) 80−62379

organic semiconductors continued
polymethine semiconducting films, surface photovoltage 80−70857
polynaphthol film, trap depth and trapping cross section from TSC curves 79−51700
polyparaxylyrene, photoconductivity, UV-IR light, absorpt. and photoluminescence. spectra *(Japanese)* 78−34857
polypyrrole, electronic struct., one-electron band theory 80−65450
polyquinoline carboxylic acid film, effective electron mass determ. from IV characts. 77−85135
polystyrene, photoconductivity, UV-IR light, absorpt. and photoluminescence. spectra *(Japanese)* 78−34857
polyvinylcarbazole-trinitrofluorenone, organic photoconductor, photoinduced paramag. centres 80−25188
porphyrin films, methine bridge substituted, surface photovolt. depend. on fabrication method 80−60119
potassium acetylacetonate, polycryst., elec. cond., pyroelectricity, phase transition, UV spectrum 78−76392
pyrazoline-based carrier transport layers use in layered photocond. systems for electrophotography 77−69375
pyrene, crystal-electrolyte interface, ionis. energy of uppermost cryst. mols. 78−27764
pyrene, positronium and thermal defects 80−24496
p-quaterphenyl, polycryst. thin layer-metal sandwich, elec. cond. 80−34526
p-quaterphenyl layers, thermally induced switching 77−43673
p-quaterphenyl oriented layers, field depend. mobility 79−91169
refined AMO calcs. 79−36514
rhodamine B surface state hole traps, surface photovoltage meas. 80−39654
Schottky barriers, capacitance meas. 79−82659
silicon phthalocyanine, elec. cond. temp. depend. 80−80271
squarylium dye films, surface photovolt. 80−75594
stilbene, single cryst., free charges and excitons generated by electron pulses 78−63988
stilbene, single cryst. under pulsed electron excitation, spectral and elec. characts. 79−7838
TCNQ, salt, $(NMe_3H)(I)(TCNQ)$, semicond. 'metal-like' complex, optical props. 79−95761
TCNQ, salt, DBTTF-TCNQ, elec. resistivity and thermoelec. power meas. 80−20193
TCNQ, salt, $Me\phi_3As(TCNQ)_2$, nonOhmic elec. cond., tunnelling model and expt. 79−99558
$(TCNQ)_2$ benzacridinium, small bandgap semicond., cond. and thermoelec. power meas. 77−35946
TCNQ bipyridine salt, anisotropic semicond. state for symm. donor mols. 77−32003
TCNQ complexes, elec. resist. and thermoelec. power meas. 80−107777
TCNQ complexes with N-methyl derivatives of pyridine, cond. and thermoelec. power meas., band model anal. 80−10952
TCNQ salt, $(DEPE)(TCNQ)_4$, elec. props., semicond. behaviour obs., no stable metallic state 77−51772
TCNQ salt, (DEPE) $(TCNQ)_4$, semicond. phase, cryst. struct. 77−80497
TCNQ salt, $(N(CH_3)_3H)(I)(TCNQ)$, elastic props., semicond. transitions 79−95072
TCNQ salt, $(NMe_3H)(I)(TCNQ)$, one-dimens. semicond. with metal-like cond. 80−24909
TCNQ salt, $(NMP)_x(phen)_{1-x}(TCNQ)$, thermoelectric power temp. depend. 80−15548
TCNQ salt, $Cs_2(TCNQ)_3$, elec. cond. and elastic const., mol. bending *(Korean)* 78−23090
TCNQ salt, Cu-TCNQ thin film between Cu and Al electrodes, elec. switching and memory phenomena 79−65562
TCNQ salt, dibenzo-TTF-$TCNQCl_2$, one-dimens. mag. semicond., mag. and elec. props. 80−88601
TCNQ salt, K-TCNQ, EPR linewidth, ang. and freq. depend. 80−80591
TCNQ salt, K-TCNQ, high and low temp. phases, dielec. const. 80−34844
TCNQ salt, n-methyl-n-ethylmorpholinium, unpaired electron states, IR refl. study 80−75491
TCNQ salt, Rb-TCNQ-II, two carrier cond. 80−44625
TCNQ salt, TMPD-TCNQ, enthalpy of combustion, calorimetric meas. 77−52663
TCNQ salt in aqueous media, electrochem. behavior 80−6976
TCNQ salts, complex, with aromatic donors, interchain coupling and disorder 78−6314
TCNQ salts, complex, with symmetric and asymmetric donors, transport and mag. props. 78−6315
TCNQ salts, elec. cond. spectrum fine struct. 80−96884
TCNQ salts of ionene polymers containing triethylenediammonium or 4,4′-bipyridilium ring, chem. struct. correl. with cond. 79−91032
TCNQ salts organic semiconducting polymers, electron transfer mechanisms 79−42544
$TEA(TCNQ)_2$, elec. cond. and thermoelec. power under hydrostatic press. 80−11024
$TEA(TCNQ)_2$, linear chain semicond., phase phonons, intramol. electron-phonon coupling 77−32373
p-terphenyl, carrier generation and transport, temp. depend. around phase transition at 180K 78−47783
p-terphenyl, cryst., DC photocond. in near UV, carrier generation 79−82644
p-terphenyl, hopping cond. among localised states 80−70861
p-terphenyl film, polycryst., charge carrier transport and DC cond. 80−70858
p-terphenyl polycrystalline layers, AC cond. 80−44746
tetracene, amorphous film, TSC meas., carrier traps 80−2496
tetracene, excimer luminesc. spectra, 4.2-300K 79−87478
tetracene, film, depletion layer studies, temp. depend. of LF capacitance 80−65617
tetracene, hopping cond. among localised states 80−70861
tetracene, in Al/tetracene/nesatron cell, electroabsorption and electrorefl., interfacial elec. fields 79−65548
tetracene, layers, photogeneration, charge carrier transport *(Russian)* 78−56181
tetracene, noncryst., localised valence states in forbidden gap 78−72113
tetracene, polycryst. film, thermoelec. absorpt. spectroscopy 79−61451
tetracene, polycrystalline layer, carrier mobility and AC cond. 79−65569
tetracene, singlet exciton fission, kinematic theory 78−87913
tetracene, surface photovoltage 80−2419
tetracene surface states, electric field effects, exciton-charge carrier interactions *(Russian)* 80−24989

organic semiconductors continued
tetraselenotetracene, electronic structure, conductivity studied by ESCA 79−4889
tetraselenotetracene iodides, struct. and physical props., DC electrical cond. and EPR linewidth meas. 80−103312
tetrathionaphthalene, electronic structure, conductivity studied by ESCA 79−4889
tetrathiotetracene, dark cond., photocond. mechanisms, refined energy level spectrum *(Russian)* 78−52103
tetrathiotetracene, electronic structure, conductivity studied by ESCA 79−4889
thymine film, polycryst., energy conversion processes, quantum yields, 4 to 10 eV 80−88589
$(TMTSF)_2PF_6(AsF_6)$, linear-chain conductor, semicond.-metal transition in small elec. field 80−103730
αTTF:Br, transport and mag. props., effect of doping 80−24934
TTF-TCNQ, semicond., driven oscills. of carrier conc. 80−15551
TTF-TCNQ and derivatives, 1.8 to 40K, three dimens. state, specific heats 80−44333
TTT, dark cond. and photocond. effect of strong mag. field, at charge carrier injection *(Russian)* 79−69607
TTT, dark injection current, sign inversion of low mag. field *(Russian)* 79−73602
TTT film, hopping cond. AC and DC meas. and EPR 80−11111
TTT film, Schrieffer effect 80−60118
vibrational IR excitons, spectra *(Russian)* 78−15173
violanthrene-A film, amorphous and crystalline, carrier mobility differences 78−60125
vitamin A alcohol and acetate, compensation effect 79−51573
xerographic photoconductors, bimolecular recomb., reciprocity failure 80−49798
zinc phthalocyanine film, between Au or Ag layers, microstruct. characterisation by TEM method 78−95241
Co complex, 2,6-N,N-diacetyldiaminopyridine-Co(II) elec. cond., γ dose and temp. (303-363K) effects 80−103696
Co complex, 2,6-N,N-dibenzoyldiaminopyridine-Co(II) elec. cond., γ dose and temp. (303-363K) effects 80−103696
Cr-phthalocyanine-Cr sandwich, I-V and C-V characts. 80−60106
9,10-dichloroanthracene, mag. field effect on exciton processes and photodetrapping 77−4668
Ni complex, 2,6-N,N-diacetyldiaminopyridine-Ni(II) elec. cond., γ dose and temp. (303-363K) effects 80−103696
Ni complex, 2,6-N,N-dibenzoyldiaminopyridine-Ni(II) elec. cond., γ dose and temp. (303-363K) effects 80−103696
PF_5 dopant for polyacetylene 80−88171

organometallic compounds
amines, Raman and IR spectra, band intensity and assignment, force const. determ., vibr. props. *(German)* 80−87133
aminoarsines, NQR freq. of ^{14}N, ^{75}As, ^{35}Cl, N-As bonds 78−25566
aminoboranes, NQR freq. of ^{14}N, ^{75}As, ^{35}Cl, N-B bonds 78−25566
antimony ethyl derivative, Et_3Sb, IR and Raman spectra, rot. isomerism 79−41167
antireflection coatings derived from liquid precursors 80−5847
arsenic ethyl derivative, Et_3As, IR and Raman spectra, rot. isomerism 79−41167
benchrotrene, EHT method calcs., parametrisation, population anal. *(French)* 80−58157
benzenechromium tricarbonyl, sp. ht. and thermal expansion tensor meas. *(French)* 78−79788
benzenetricarbonylchromium, neutron inelastic scatt. spectrum and valence force field 80−48096
beryllocene, gas phase struct., ab initio LCAO SCF calc. 78−41942
bis(cyclopentadienyl)Ti(IV)chloride, reactions with oximes, IR spectra 78−92471
bis(trimethylstannyl)-acetylene, mol. struct. determ. from gas phase electron diffr. 78−25740
bistrifluoromethylmercury, scalar coupling between rare spins 80−66047
boranes, $OCH_3(B_9C_2H_{10})_2Co$ and $(C_2H_5)_2Co_2CB_9H_{10}$, cryst. struct. *(Czech)* 78−87649
n-butyl-lithium, intercalation with transition metal chalcogenophosphates, possible appl. in Li batteries 80−71446
calorimetry, standard for quantity-of-heat unit 79−17421
chemical analysis by secondary-electron capture negative-ion mass spectrometry 77−16892
chlormerodrin-203, radiochem. purity determ., electrophoretic method 77−56283
chromocene, heat capacity meas., phase transitions 78−38853
chromocene, mag. props., complete ligand field theory 78−31048
chromocene, mag. suscept., zero-field splitting, ligand field, 1-303K 77−89924
chromocene, solid, Raman transition assignments, mag. susceptibility, mag. moment 78−43861
cobaltocene, mag. props., complete ligand field theory 78−31048
copper organoacetylenides, photoconductivity sensitisation using dyes *(Russian)* 79−58824
cyclopentadienyl cobalt dicarbonyl, mol. stuct., gas phase electron diffr. obs. 79−31688
cyclopentadienyl Ho(III), cyclooctadienyl sandwich compound, mag. circular dichroism and absorption spectra, anal. 80−23449
cyclopentadienyl platinum (IV) complexes, ring rot. meas. using mech. spectroscopy 80−74259
cyclopentadienylhafniumdichloride, gaseous, far IR and Raman spectra 80−95624
bis-π-cyclopentadienyltitanium dichloride, struct. parameter refinement 78−87660
cyclopentadienyltitanium trichloride 80−95624
cyclopentadienyltitaniumdichloride, gaseous, far IR and Raman spectra 80−95624
bis-π-cyclopentadienylzirconium dichloride, struct. parameter refinement 78−87660
cyclopentadienylzirconiumdichloride, gaseous, far IR and Raman spectra 80−95624
decamethylferrocene, vac. UV photoemission 77−85883
decamethylferrocene-bis(TCNQ), vac. UV photoemission 77−85883
decomposition by reaction with photoelectron, appl. to metal film deposition 80−71599
1,1′-diacetylferrocene, ^{57}Fe Mossbauer effect, probe study of smectic liq. cryst. glass-supercooled transition and Debye temp. 80−54999
1,1′-diacetylferrocene, MBBA soln. nematic glass-supercooled nematic transition, Mossbauer temp. obs. 79−95687

organometallic compounds continued
dibenzene chromium, heat capacity meas., phase transitions 78−38853
dibenzenechromium, cryst. and soln., dynamic struct., NMR expts. 77−15328
dibenzenechromium-dibenzenevanadium, proton HFS data, ENDOR obs. 80−66073
dibenzenevanadium, substituted in Fe dicyclopentadiene and dibenzenechromium proton HFS data, ENDOR 80−66073
dibenzylchromium, EHT method calcs., parametrisation, population anal. *(French)* 80−58157
n-dibutyl(ethylene-1,2-dithiol)stannane, cryst. data 77−15400
dicyclopentadienyl Ti^{3+}-N_2 compound complexes, reson. Raman scatt. 80−99510
diethyl aluminium hydride, Al coating produced by thermal decomp. of alkyls on steel 78−15590
diethyl cadmium, core d-level high resolution photoelectron spectra, spin-orbit splitting 78−50579
diethyl tin dihalides, cryst. struct., secondary and multi-centre bonding 78−63751
diisobutyl aluminium, Al coating produced by thermal decomp. of alkyls on steel 78−15590
dimethyl aluminium hydride dimer, electron density distrib., electrostatic mol. pot. anal. 80−52885
dimethyl beryllium, equilib. geometries and electronic states, FSGO calcs. 79−10019
dimethyl cadmium, core d-level high resolution photoelectron spectra, spin-orbit splitting 78−50579
dimethyl cadmium, core level ligand field splitting, PES, model for covalent mols. 78−37681
dimethyl cadmium, partially oriented in nematic EBBA, mol. geom., PMR obs. 77−71819
dimethyl cadmium, photoelectron spectra, 4d spin-orbit splitting, crystal field and band-broadening effects, CNDO calcs. 78−76577
dimethyl di(trifluoromethyl) germanium, and perdeuterated analogues, vibr. spectra, normal coord. anals. *(German)* 80−5547
dimethyl mercury, ^{199}Hg nuclear shielding anisotropies rel. to isotropic chem. shifts 77−3384
dimethyl mercury, coupling consts., solvent depend., ^{1}H, ^{13}C and ^{199}NMR 78−76334
dimethyl mercury, high resolution photoelectron spectra, 5d orbital energy ordering reassignment 78−74700
trans-dimethyl organometallic moieties, nuclear elec. quadrupole moment from elec. field gradients 80−29371
dimethyl stannous chloride di(pyridine 1-oxide), ^{119}Sn Mossbauer spectra, elec. field gradient 80−15909
dimethyl tin difluoride, crystallographic phase transition, 70K, Mossbauer obs. 79−47366
dimethyl tin difluoride, solid, methyl reorient., low temp. phase transition, neutron scatt. obs. 79−27932
dimethyl tin diisothiocyanate, ^{119}Sn Mossbauer spectra, elec. field gradient 80−15909
dimethyl tin diisothiocyanate 79−7506
dimethyl zinc, core level ligand field splitting, PES, model for covalent mols. 78−37681
dimethyl zinc, core level photoelectron spectra, electric field gradient splittings 77−88494
dimethyl zinc, valence band and Zn 3d levels, electric field gradients 77−88495
dimethylmercury, mol. force field, generalised inverse method for calc. 78−25505
dimethyltin halides complexes with dimethyl sulfoxide and dimethylformamide, cryst. and mol. struct. 79−42047
diphenyl.2$SbCl_3$, Raman spectra 77−16291
diphenyl tin sulphide trimer, cryst. data 77−15400
diphenylantimony radical, EPR spectral parameters, nuclear quadrupole coupling 77−81010
diphenylmercury, cryst. struct. refinement 77−24310
diphenylmercury, mol. photoionisation, up to 13.5 eV, formation of $HgPh^{+}$ 78−25633
EHT method calcs., parametrisation, population anal. *(French)* 80−58157
enzyme, nucl. quadrupole interaction parameter related to structure-function 77−8472
ethyl-trimethylstannyl phosphines, $(C_2H_5)_{3-n}P\{Sn(CH_3)_3\}_n$, (n=0,1,2,3), (^{1}H, ^{13}C, ^{29}Si, ^{31}P, ^{119}Sn) NMR 80−32744
ethylgermane, microwave, IR and Raman spectra, struct., internal rot., dipole moments 77−79605
ethyllithium, ab initio SCF-MO calcs. of C-Li bond character 77−410
ethynyllithium, ab initio SCF-MO calcs. of C-Li bond character 77−410
ferricenium complex, Franck-Condon light scatt. transitions 77−57999
ferrocene, cryst., stable low-temp. phase 80−34185
ferrocene, cryst. and soln., dynamic struct., NMR expts. 77−15328
ferrocene, dynamics in liquid and glassy o-terphenyl, Mossbauer obs. 80−55000
ferrocene, EHT method calcs., parametrisation, population anal. *(French)* 80−58157
ferrocene, electronic and mag. struct., semiempirical MO cluster calcs. 78−62733
ferrocene, electronic struct., excited states, semiempirical PEEL MO calcs. 78−33431
ferrocene, metal to ring distance, ab initio MO SCF calcs. 80−47870
ferrocene, mol. struct., ordered phase, 130K *(French)* 79−51093
ferrocene, multiphoton dissoc. and ionisation by tuneable dye lasers 80−99524
ferrocene, multiphoton ionis. spectra, at. Fe transitions 80−106361
ferrocene, noncryst. state struct., Willis disorder model *(French)* 78−83732
ferrocene, ordered, disordered phases, structs. *(French)* 78−63749
ferrocene, orthorhombic low-temp. cryst. phase, characterisation 80−96507
ferrocene, proton irradiated, Mossbauer study of induced chemical changes 79−28656
ferrocene, quantum mechanical delta-function potential study of atomic, bond and mol. polarisability 77−23571
ferrocene, triclinic, struct. anal. at 101, 123 and 148K 80−19785
ferrocene, vac. UV photoemission 77−85883
ferrocene derivatives, mixed and averaged valence types, Mossbauer spectra 80−15906
ferrocene derivatives in smectic B phase liquid cryst. BBOA, ^{57}Fe Mossbauer study 78−27136

organometallic compounds continued
ferrocene films, plasma-polymerised, carrier trapping, elec. cond. meas., 300 to 525K 80−100543
ferrocene related compounds, $C_5R_5Fe(I)$-$C_6R'_6$ paramag. sandwiches, Mossbauer study 80−39982
fluoromethyl methyl mercury-d_0, -d_3, vibr. spectra, normal coord. anal. 79−50017
fluxional, solid state chem. exchange, ^{13}C NMR magic angle spinning 80−7775
group V organometallics, XPS spectra interpretation, pot. model 78−50587
hexa(trifluoromethyl) germanium, gas and liq., IR and Raman spectra, normal coord. anal. *(German)* 79−72315
hexamethyldialuminium, methyl group rotation and bonding, CW proton second moment and line shape studies 79−47346
hexaphenylene mercury, bright-field imaging of single heavy atoms in an electron microscope with superconducting lens system 80−10472
indium(I) cyclopentadienide, He I and He II photoelectron spectra 79−13767
intercalation compounds, metal guests in chalcogenide hosts, struct., review 79−46627
intermolecular interaction, Mossbauer spectra 80−15899
lead alkyls in polluted atmospheres, conc. obs. 80−85313
lead triphenyl isocyanate, X-ray cryst. struct. determ. and refinement 79−51097
liquids, vaporizer, for CVD appls. 77−77388
lithium acetylene, SCF MOGO calc. of electronic struct. 77−34556
lithium ethylene, SCF-MO calc., bonding and electronic struct. 77−38610
Menshutkin complexes, Raman spectra 77−16291
mercurochrom, fluoresc. polarisation, solvent effects 77−14470
metal alkyl compounds, excited metal atom prod. by UV multiphoton dissoc. 79−6974
nido-metalloborane, high -resolution ^{11}B NMR obs. of $[(B_{10}H_{12})_2Ni]^{2-}$ 79−31553
metallocenes, orbitally degenerate, EPR 78−86893
metallocenes, photoelectron spectra, band assignment 80−91604
metallomacrocytes, mixed valent, cofacial assembly, cond. polymeric material 80−70143
metalloprotein solns., use of Faraday magnetic balance 78−70170
methyl derivatives, simple, organometallic, spin-spin coupling between metal nucleus and protons 78−37656
methyl mercuric halides, ^{199}Hg nuclear shielding anisotropies rel. to isotropic chem. shifts 77−3384
methyl mercury halide electron impact dissoc., excited fragment emission 79−18296
methyl tri(trifluoromethyl) germanium, and perdeuterated analogues, vibr. spectra, normal coord. anals. *(German)* 80−5547
methylene manganese, electronic struct., equilib. geometry, ab initio SCF calcs. 77−71747
methyllithium, ab initio SCF-MO calcs. of C-Li bond character 77−410
methylmercuric halides, partially oriented, ^{1}H and ^{13}C NMR obs. 80−23437
methylmercury, determ. in fish, mol. activation anal. 79−24848
methylmercury halides+N_2, $A^3\Sigma_u^+$-state quenching obs. 80−108693
methylmercury nitrate, in nematic and lyotropic liq. crysts., r_α-struct. and anisotropy of Hg-C coupling const. 80−43071
methyltin compounds, separation and determ. in environmental samples 79−79416
molecules, chemically active sites calc. 79−52757
molybdenum compounds, low-valent, stoichiometric and catalytic reactions with azobenzene 77−86370
Mossbauer spectra of spin crossover 80−15903
naphthalene.2$SbCl_3$, Raman spectra 77−16291
neptunium cyclopentadienyl compounds, $(C_5H_5)_3NpX$, (X=F, Cl, Br, I, $(SO_4)_{1/2}$), mag. susceptibility 80−11152
nickel-benzene, second order two-spin cross-relax. 79−95632
nickelocene, multiphoton dissoc. and ionisation by tuneable dye lasers 80−99524
organo tin dichlorides, tetrahedral, dilute soln., dielec. and thermodynamic behaviour, microwave region 77−36170
organo tin polymers, glow discharge formed, interface composition and adhesion 79−82467
organo-tin polymer films, glow discharge prep., comp. determ. by XPS and AES 80−35109
organoindium cpds., ^{115}In nucl. quad. coupling consts., additive calcs. 77−50453
organolead compounds, aliphatic and aromatic, ^{13}C and ^{207}Pb NMR 79−95657
organolead cpds., quenching of carbonyl triplets in quinones, CIDEP and ESR obs. 80−95654
organosilane binding to TiO_2 electrode surface, effect on semicond. props. 79−96364
organosilicon binder, for prod. of spalling-resistant quartz glass based ceramic 80−40313
organosilicon ladder polymers, struct. and phys. props., book contrib. 79−65012
organotellurium compounds, thermally developable light sensitive systems 79−2850
organotin compounds, mol. and cryst. struct., X-ray diffr., NMR and Mossbauer spectra meas. 77−47441
organotin compounds, with remote substitutions, ^{119}Sn NMR constants 79−65748
organotin cpds., quenching of carbonyl triplets in quinones, CIDEP and ESR obs. 80−95654
pentaphenylantimony, Coulombic interactions in anomalous structure 77−24285
phenanthrene.2$SbCl_3$, Raman spectra 77−16291
bis-(phenylethinyl)-mercury, spin-orbit coupling, heavy atom and D isotope effects 79−59372
phosphines, substituted, γ-irrad. EPR spectra and struct. of free radicals 80−29623
bis cantena pol methylarsenide, energy gap depend. on As electron delocalization *(German)* 78−43296
bis-catena-poly(methylarsenic), one-dimensional homonuclear molecular systems, nature of energy gap 79−11063
polyborodiphenylsiloxane, binder for SiC and Si_3N_4 sintered bodies 77−40401
polyborodiphenylsiloxane, synthesis and thermal decomposition 77−40541

organometallic compounds continued
polycarbosilane+Fe-13 wt.% Cr alloy, powder metallurgy, characts. 77−85962
polyferrocene film, plasma polymerised, dielec. props., 40 kHz to 50 MHz, 30-400°C 78−52439
n-propyl(n-butyl) tin dichloride, prep. and Lewis acid charact. 77−90597
rare earth complexes, with organometallic bonding, formation and props., book contrib. 80−43204
ruthenocene, cryst. and soln., dynamic struct., NMR expts. 77−15328
ruthenocene, quenching of triplet state organic mols. 77−83630
sandwich complexes, mag. props., effective Hamiltonian method 80−37731
sodium tetraphenylborate soln., electrolyte, steady state electrochemiluminesc. 79−57250
sodium tetraphenylborate solns., stationary electrochemiluminesc. *(Russian)* 78−48243
tellurium (II) organometallic compounds, ^{125}Te, ^{13}C, ^{1}H NMR spectra, nucl. coupling, exchange processes 79−95658
tetra(trifluoromethyl) germanium, gas and liq., IR and Raman spectra, normal coord. anal. *(German)* 79−72315
tetraethyl lead, core d-level high resolution photoelectron spectra, spin-orbit splitting 78−50579
tetraethyl lead, core level photoelectron spectra, electric field gradient splittings 77−88494
tetraethyl tin, thermal conductivity and density, −13.5 to +90°C 77−15637
tetrakis(trifluoromethyl)germane, gas phase electron diffr. struct., torsional force consts., CNDO/2 calc. 79−31687
tetrakis(trifluoropropynyl)-tin, mol. struct. determ. from gas phase electron diffr. 78−25741
tetramethyl germanium, methyl reorient., lattice vibrs., neutron scatt. obs. 79−51016
tetramethyl silicon, methyl reorient., lattice vibrs., neutron scatt. obs. 79−51016
tetramethyl silicon+Na, rainbow scatt. at thermal energy, anisotropic pot. 78−29837
tetramethyl tin, methyl reorient., lattice vibrs., neutron scatt. obs. 79−51016
tetramethyl tin, rainbow scatt. at thermal energy, anisotropic pot. 78−29837
tetramethylene bridged ferrocene derivatives, mol. struct., Mossbauer expt. 78−60372
tetramethylgermanium, Zeeman spin-lattice relaxation rate maxima 80−84666
tetramethyllead, tunnel splitting, rot. pot., μeV neutron scatt. study 79−41993
tetramethyls, of IVA metals, pseudo-exact force consts., force fields 77−31022
tetramethyltin, adsorbed on graphite, nature of 2 D diffusion, Mossbauer meas. 80−84372
tetramethyltin, in liq. cryst., ^{1}H, ^{115}Sn, ^{117}Sn and ^{119}Sn NMR spin-spin relax. 78−91973
tetravinyltin, electron diffr. determ. of struct. 78−37763
thallium(I) cyclopentadienide, He I and He II photoelectron spectra 79−13767
thiophenechromium tricarbonyl, sp. ht. and thermal expansion tensor meas., order-disorder phase transform. obs. *(French)* 78−79788
tin tetrahedral molecular solids, ^{119}Sn Mossbauer and Raman spectra 78−15070
titanocene, alkyl-substituted ^{13}C and ^{1}H NMR, chemical shifts prediction 80−63671
transition metal hydride complexes, struct. geometry bonding, neutron diffr. studies 79−46641
tri(trifluoromethyl) germanium halides, gas, liq. and solid, IR and Raman spectra, normal coord. anal. 79−72316
tri-i-propygermylamine, and isotopomers, IR and Raman spectra, normal coord. anal. *(German)* 80−32716
tri-t-butylstannyl hydroxide, Mossbauer spectrum, tin coordination *(German)* 80−32716
tri-t-butylstannylamine, and isotopomers, IR and Raman spectra, normal coord. anal., Mossbauer spectrum *(German)* 80−32716
tributyltin sulphate, cryst. struct. 78−18632
triethyl aluminium, Al coating produced by thermal decomp. of alkyls on steel 78−15590
triethylsilylamine, and isotopomers, IR and Raman spectra, normal coord. anal. *(German)* 80−32716
trifluorodimethylmercury, gas phase mol. struct., electron diffr. and microwave spectra obs. 80−78609
trifluoromethyl trimethyl germanium (tin)(lead), and perdeuterated analogues, vibr. spectra, normal coord. anals. *(German)* 80−5547
triindenylcerium pyridinate, X-ray cryst. struct. determ. 79−32984
triisobutyl aluminium, Al coating produced by thermal decomp. of alkyls on steel 78−15590
trimethyl gallium, core level photoelectron spectra, electric field gradient splittings 77−88494
trimethyl indium, core d-level high resolution photoelectron spectra, spin-orbit splitting 78−50579
N-trimethyl stannyl phthalimide, cryst. struct. refinement and determ., Sn atom position 79−90638
trimethyl tin chloride adsorbed on grafoil, Mossbauer study 80−80643
trimethyl tin cyanide, ^{119}Sn Mossbauer spectra, elec. field gradient 80−15909
trimethyl-indium trimethyl phosphine adduct, cc InP VPE with new metallorganic compound 80−55278
trimethylaluminium release in upper atmosphere, CH^+ obs. 79−48591
trimethylantimony, use in VPE growth of $GaAs_{1-y}Sb_y$ 80−60788
trimethylantimony(V) dihalides, normal coord. anal., comparison of force fields 78−968
trimethylarsenic, use in VPE growth of $Ga_{1-x}In_xAs$ 80−60788
trimethylarsenic+trimethylgallium etherate, epitaxial deposition of GaAs 77−47689
trimethylgallium, product catalysed reaction with PH_3 or AsH_3, CVD mechanism for GaP or GaAs 77−48345
trimethylgermylisocyanate, IR and Raman spectra, struct. 78−37637
trimethylgermylisothiocyanate, IR and Raman spectra, struct. 78−37637
triphenyl telluronium pseudohalides, cryst. data 77−15399
triphenyl tin chloride adsorbed on grafoil, Mossbauer study 80−80643
triphenyl tin isocyanate, struct. determ. and refinement 78−67704
triphenylgermanium isocyanate, X-ray crystal struct. determ. and refinement 77−7708

organometallic compounds continued
triphenylstannyl radical, EPR in single cryst. matrix, ^{119}Sn hyperfine coupling tensors 78−23346
triscyclopentadienyl uranium chloride, ^{13}C NMR shifts, 160-320K 77−16190
vanadocene, order-disorder phase transition, sp. ht. and crystallographic study *(French)* 80−84131
vibrational spectra, book 77−38671
vinyllithium, ab initio SCF-MO calcs. of C-Li bond character 77−410
VPE using organometallics for III-V semiconductors *(French)* 79−33936
X-ray spectral study of electronic struct., organometallic compounds containing hydrocarbon π ligands 77−27088
zirconocene dichlorides, alkyl-substituted, ^{13}C and ^{1}H NMR, chemical shifts prediction 80−63671
Au organometallics, ESCA core binding energies 78−50586
$(C_6H_5)_3AsI_3$, solvent effects on electronic transitions of I_3^- 77−27080
$(C_2H_5)_2Fe^+$ complexes, vibrational electronic (Franck-Condon) Raman transitions 78−42070
CH_3MCl_3, (M=Ge, Si, Sn), polycryst., proton spin-lattice relax. times meas. 78−39430
Cu phthalocyanine, grain boundary struct., crystallographic planes 80−103366
Fe dicyclopentadienyl-dibenzenevanadium, coalescence temps., full proton HFS tensor, ENDOR obs. 80−66073
Fe organometallics, interaction of naked Fe atoms with small mols., Mossbauer study of bonding in products 80−43080
FeOCl/ferrocene (cobaltocene) intercalation cpds., X-ray diffr. obs. 79−65066
In compounds, photoelectron spectra, valence bands, ligand field broadening 77−63525
$Mn\text{-}C_2H_2$ and $Mn\text{-}C_2H_4$, π-bonded, pot. energy curves, SCF calc. 78−5136
$Ni(Ni)_2$-ethylene cluster complex, electronic struct. 78−82641
Np(IV)-tetracyclopentadienide complex, H^1-NMR studies, paramagnetic moments, temp. depend. 80−93186
Pb compounds, photoelectron spectra, valence bands, ligand field broadening 77−63525
Sb compounds, photoelectron spectra, valence bands, ligand field broadening 77−63525
Sn compounds, photoelectron spectra, valence bands, ligand field broadening 77−63525
Sn organometallic cpds., chem. shifts in ESCA and Mossbauer spectra *(French)* 77−28685
$\{Th[(CH_3)_5C_5]_2H(\mu\text{-}H)\}_2.C_6H_4CH_3$, molecular structure by neutron diffraction 79−89801
triethylarsenic+trimethylgallium etherate, epitaxial deposition of GaAs 77−47689

organs (artificial body) *see artificial organs*
origin of elements *see element origin*
origin of life *see evolution (biological)*
orthicons *see television camera tubes*
orthogonalised plane wave calculations *see OPW calculations*
orthosis *see orthotics*
orthotics
see also prosthetics
alignment, using visual presentation of centre of press. 77−56535
animal model selection haematological and biochemical comparison of species 77−56540
aorto-coronary saphenous bypass surgery, ^{201}Tl myocardial perfusion scintigrams 79−25068
appendages, manipulators and robotics prospects 78−53582
arm, thumb driving mechanism, arm orthotics finger tip mechanisms CO_2 powered *(Japanese)* 78−28126
artificially evoked movement plasticity improved by gradually modulated elec. stimulation 77−64153
assisted circulation apparatus cardiosynchronisation method, problems 78−7534
assisted circulation methods and apparatus, classification 77−81653
atrio-aortal left ventricular bypass, haemodynamics in calf *(German)* 78−88763
audible training aid for visually impaired infants, motion activated 80−36193
auxiliary blood circulation pump, electronic control circuit 77−78050
axial loading on static knee-ankle-foot orthosis, method and evaluation 77−48937
balloon pump counterpulsation, increasing operational safety 80−3869
Baylor left ventricular bypass pump, calf expts. 78−73295
Baylor left ventricular bypass pump, recent experience 78−44718
beacon guidance system for walking blind aid 80−81676
bifocal lens designs, marginal aberrations 78−48927
bilateral shoulder disarticulated children's jaw-controlled manipulator 78−53578
biomechanics, foundations and appls. *(French)* 80−89778
blind persons' aids, review 77−29227
blood assisted circulation apparatus and artificial heart, hydrodynamic test bench rigs 79−48372
blood circulation apparatus, improved electromechanical drive regulator 80−3871
blood circulation assist devices, antithrombotic polymeric materials 78−36052
blood circulation assist devices 77−78044
blood circulation pump unit redesign for sterilisation 77−48932
blood damage by artificial part-hearts and pumps, dwell minimisation model *(German)* 79−16345
blood oxygenation perfusion system for treatment of acute respiratory failure in infants 80−3866
blood pressure control, mechanical-chemical balloon implant 79−20712
blood pump, controlled high pressure, for heart support systems *(German)* 79−8580
blood pump, experiences with miniaturised press.-controlled servo *(German)* 78−88762
blood pump, pulsatile, in vitro eval. of erythrocyte bulk lysis 77−44840
blood pump, pulsatile, stabilisation of unsteady ball valve motion 78−44708
blood pump artificial heart valve *(German)* 78−81065
blood pump for completely implantable circulatory assist systems 78−44723
blood pump human fitting studies using computerised axial tomography scanning 78−40432

orthotics continued
blood pump implantations in animals, regulation mechanisms in circulation and fluid balance *(German)* 78−81064
blood pump pressure servovalve control, moving coil system *(German)* 78−24182
blood pump regulation electropneumatic servo operation *(German)* 79−8579
blood pumps, pneumatic, closed-loop control system 77−52930
bone, plate, variable-stiffness, absorbable 79−79691
bone fixation plate, laminated polymer-metal fabrication 79−79685
breathing gas supply regulator, for continuous positive airway pressure breathing *(German)* 79−2164
cardiac assist device pumping, effect on mech. props. of vascular walls 78−40429
cardiac assist devices, in-series, digital afterload phase angle controller 77−44843
cardiac assist devices, selection of prosthetic valves 78−44730
cardiac assist system, intrathoracic, self-sufficient instantaneous haemodynamic control 77−44842
cardiac assistance, in-series, by intra-aortic balloon pumping, haemodynamic responses, computer model 79−96711
cardiac in-series assistance using balloon pump, effects on left ventricular afterload/aortic power dissipation 78−3669
cardiac massage unit, pneumatic, effects under ventricular failure, dog expt. 77−78036
cardiac stimulator power supply battery selection 77−48931
cardiac-assist in-series devices, controller 78−81075
cardiopulmonary resuscitator, programmable, for evaluation of standards 80−72374
centrifugal blood pump for cardiac support 78−44709
circulation assist equipment, improved electromechanical drive response 79−100790
circulation augmentation, end-diastolic air compression boot 80−101291
circulation-assist, steady state anal. of press. and flow 80−17193
circulatory assist apparatus, stabilisation of gas vol. in pneumatic transmission unit 80−3863
circulatory assist device using blood pumping by mag. field 77−56518
circulatory assist equipment, trends in devel. and realisation 79−100789
communication device for mute paralytic 78−40420
communication/control systems for motor impaired people, standardisation 80−17198
conference, London, England (Mar. 1980) 80−94926
corneal lens, soft radius of curvature meas., using autostigmatic microscope 77−60198
counterpulsation assist pumping, optimum performance determ. under computer control 78−24181
counterpulsation operating mechanisms for assisted circulation 79−48371
dental crown restoration fixation, dynamic shear testing 78−36068
Dwyer cable, noninvasive telemetric determ. of anterior spinal fusion after corrective surgery 77−44851
earphone cushion, comparison between one-piece model 51 and conventional two-piece MS-41AR cushion 80−51123
electrical stimulation of organs and tissues in clinical medicine 78−35977
electrical stimulator for leg muscle stimulation during walking 79−48377
electrophrenic respiration, feedback control of tidal vol. *(Japanese)* 80−41316
electrophrenic respirator, implantable, Hg battery powered, design, features *(Japanese)* 78−3675
electrostimulating device for telemetric human movement correction 77−86656
electrostimulator for leg muscles to correct defective walking 78−36051
EMG activated spatial morse code general purpose communication device 80−30946
EMG control enhancement using predictor feedback technology 77−48952
engineering in medicine and biology, conf. Atlanta, USA (Oct. 1978) 79−39332
extracorporeal blood circulation apparatus, tabulated data 77−78045
extracorporeal circulation apparatus using thermoelec. heat regulating systems 80−3870
extracorporeal circulation equipment, automatic control 80−3865
extracorporeal circulation system, energy parameters of temp. stabilisation system 80−3867
femoral fracture brace, biomech. study of function during stance 80−97990
fractured bone fixing pins, stainless steel, strength, ultrasound effect 80−71710
functional electrical stimulation control using volitional EMG signal 78−57128
functional electrical stimulation of extremities 77−40926
functional electrical stimulation of motor activity, control, rehabilitation appl. 77−86708
functional electrical stimulation orthoses, gait parameter variability *(French)* 77−9302
functional electrical stimulators, multisite appls. extremity stimulation 77−48936
gait control, peroneal nerve stimulation sequence effect *(Croatian)* 78−44692
haemodialysis, single-needle, recirculation anal. 80−41320
hand, ORTHOMOT OM2M myoelec. control and driving system *(German)* 77−56517
hand opening by proportionally controlled electrical stimulator *(Croatian)* 78−44693
handicapped persons technical aids, R&D in Sweden *(Japanese)* 78−48934
heart assist blood pump, counterpulsation dynamics simulation 80−16996
hemiplegic upper extremities, feedback elec. stimulation trainer 78−44683
hip guidance articulations, principles and practice 80−3873
implantable stimulation electrode, standardisation problems 77−64151
implantable stimulators for studying functional adaptation in skeletal muscle of rabbit 77−86721
implanted diode stimulation, long-term viability 78−44716
in-series cardiac assist devices, expt. and theoretic observations 78−36063
insulin release, electronically controlled piezoelec. pump and valves 78−53565
intra-aortic balloon heart assist device fluidic drive system 78−53566
orthotics continued
intra-aortic balloon pump control, real-time microcomputer ECG recognition system 78−36067
intra-aortic balloon pump controller, within computerised evaluation system 77−56538
intra-aortic balloon pump simulator for dynamic demonstration and teaching 77−56537
intra-aortic balloon pumping, flow obs. and model expts. on blood damage 77−81664
intra-aortic balloon pumping apparatus trials 79−48368
intra-aortic balloon pumping efficacy evaluated by nonlinear cardiovascular system model 78−44732
intra-aortic balloon support, prognostic indices, rel. to left ventricular assist device use 77−56536
intra-aortic balloon timing, microprocessor control 78−44725
intracorporeal long-term blood pumps, design criteria and physiologic performance criteria 78−40430
knee locking, sensor-controlled external system, exptl. study 78−40406
left heart bypass, partial and subtotal systems compared 77−81660
left ventricle, auto-regulating, with 4 operational modes, evaluation in dogs 77−48942
left ventricular assist device, diaphragm-type, factors affecting pumping dynamics 78−44706
left ventricular assist device, implantable piezoelec. drive invertor improvement 78−15927
left ventricular assist device, intrathoracic, with biolised blood-contacting surfaces 78−7540
left ventricular assist device, mech. anal. of human neointimas developing on flocked surface 78−40431
left ventricular assist device, transapical 79−84021
left ventricular assist device and total artificial heart 79−84017
left ventricular assist device development and utilisation 77−25600
left ventricular assist device long-term expts., maintenance of efficient pump performance 78−44722
left ventricular assist device testing using calf model 78−73296
left ventricular assist device use, rel. to prognostic indices in intra-aortic balloon support 77−56536
left ventricular assist mech. pump effectiveness in acute myocardial failure model 78−44719
left ventricular bypass performance, influence of power waveform 78−40433
LeVeen shunt, patency testing technique 79−57763
lower extremities, adaptive control principle 78−48932
lower-limb orthoses, force-line visualisation system 80−17200
lung ventilator, development, engineering appraisal 78−3673
manipulator, powered, for spinal cord injury patient 77−25607
material characterisation by mech. impedance method 78−36066
microprocessor based 4 channel preprogrammable stimulator for paralysis treatment *(Slovenian)* 80−104809
micturition reflex elec. restoration, sequential stimulator 78−53567
mobility aid for blind people based on US sensing 80−56290
motorized shoe for submaximal assist 80−56289
multichannel implantable stimulator *(Slovenian)* 80−81773
muscle contraction strength control during elec. stimulation, using PWM and FM 77−40929
muscular dystrophy, Duchenne, patient dynamic long leg orthosis 79−96715
myoelectric processor and human operator dynamic error performance 79−96714
myofeedback control system, design 80−51296
nonimplantable electrostimulator advances for urinary incontinence correction 79−57817
ophthalmic lens distortion display 78−7338
orthodontic appliance, facial skeleton strain distrib. 80−67143
orthodontic appliance mechanical behaviour determ., computer-controlled device 78−44727
orthodontic appliance uniplanar force meas. system 78−31970
orthodontic appliances, 3-dimens. large displacement anal. 77−29228
orthopaedic engineering in Oxford 80−17187
orthotic-prosthetic and manipulator system uses of microprocessors *(Croatian)* 78−44694
Oxford external fracture fixator, anal. of fixation 80−17188
paralysed leg stimulation, programmed six-channel stimulator for walking *(Slovene)* 77−40923
paralysed upper extremities rehabilitation systems, control signals *(Slovenian)* 80−81772
parameter assessment based on telemetric heart rate monitoring, paediatric patient appl. 78−31974
paraplegic human leg orthosis, hydraulic power control system 78−53577
paraplegics' multitask exoskeleton computer control 78−53580
parathoracic ventricular assist device for use with nucl. or elec. actuation systems 77−48941
partially paralysed patients, medical rehabilitation designs 78−53579
perfusion and intraaortic balloon pumping system, Biopul's-3 78−7536
physically handicapped persons' apparatus, recent status of R&D *(Japanese)* 78−44703
physically handicapped persons' apparatus standardisation *(Japanese)* 78−44699
plaster casts, treatment of tibial fractures, biomech. study 79−74696
polymeric biomedical materials 79−83998
pulsatile blood pump, vortex diode used as outflow valve 78−44724
pulsatile blood pump development and characteristics 77−81659
quality health care and cost containment, conf., Washington, USA (Mar.-Apr. 1978) 79−39333
rehabilitation engineering *(Japanese)* 80−12304
respiration electrical stimulation, appls. and equipment 78−36054
respirator, fully automatic or patient controlled, for intensive care and respiration ward appl. 77−81641
respirator, narcosis, ergonometric design *(German)* 79−2163
respirator, optimal control of long-term forced ventilation of lungs 77−60296
respirator, servo control of end-tidal CO_2 in paralysed animals 79−39607
respirator based on jet-flow vortex-type components *(Russian)* 79−79683
respiratory ventilator model and design optimisation 79−20713
robots and manipulators, symposium, Warsaw (Sept., 1976) 78−53574
roller pump for pulsatile blood flow 78−44721
roller pumps, automatic safety shutdown 78−44720
scoliosis correction, by lateral surface elec. stimulation of muscles 78−44717

orthotics continued
SCRIBE, system to help the badly handicapped, using a microprocessor *(French)* 80−56282
sensory feedback, recommended electrocutaneous codes 78−44715
spectacle lens design, computation of unwanted sphere and cylinder in periphery 78−48928
speech synthesizer for severely handicapped children, portable 80−56154
splint making materials, comparative study 79−39606
standardisation of technical terms *(Japanese)* 78−44700
stimulator, implantable RF powered dual channel device for hip stabilisation 77−40930
stimulator encapsulation for implantation, biomaterials 78−40416
tetraplegics' jointed manipulator with joystick control 78−53581
tibial shaft internal fixation, biomech. study 78−20313
tooth-jaw system, mech. anal. 77−40703
transapical left ventricular bypass, prolonged use in sheep and man 78−40435
transapical left ventricular bypass with continuous blood filtration 77−48940
upper extremity orthosis, externally powered, actuator development *(Japanese)* 79−44059
urinary incontinence device for surgical implant 78−40419
ventilation feedback control in small infants after open-heart surgery 79−70710
ventilator patients, effect of body temp. humidification on thermal regulation 78−85295
ventilator-patient circuits, long-term monitoring using turbulent air flowmeter 77−64149
ventilator-patient coupling, effects of positive press. ventilation on cardiac output and pulmonary arterial flow 78−31852
ventricle type blood pump, blood damage 78−44707
voice controlled system for the disabled 79−5407
walking appliance for paraplegic adult, design 77−60299
walking appliances for paraplegics, misuse of technology 78−41132
weak speech amplification device with suppression of respiration noise 80−30929
wheelchair locomotion, power output requirements for manual operation 80−94416
wheelchair sent evaluation by time-lapse and quantitative thermography of skin after sitting 80−51205
Pt electrodes for elec. stimulation, exposed electrode area determ. 77−86704
Pt electrodes for elec. stimulation, max. surface redox limits estimation 77−86705

oscillations
see also circuit oscillations; electromagnetic oscillations; harmonic oscillators; harmonics; liquid oscillations; piezoelectric oscillations; plasma oscillations; resonance; stability; vibrations; waves
A-type stars, rot. and mixing rel. to vibr. instability and variability 77−87397
absorbing-scattering semitransparent planar layer, flat temp. waves 78−90683
accretion disks, optically thick, pulsational instability to axially symm. oscills. 80−82190
aeroautoelasticity, active control and suppression of flutter in aircraft *(Russian)* 78−67079
aerofoil, in transonic cascade, choking flutter 77−75885
aerofoil, oscillating, viscous incompressible flow, finite element anal. 80−38427
aerofoil in oscillating flow, vel. field, surface press. 78−75164
aerofoil in unsteady viscous flow, numerical soln. procedures 78−75165
airfoil, oscillating, exact soln. by integral eqn. 77−84270
airfoil vibration in transonic flow *(Russian)* 77−39308
analogue circuits, dual mechanical and dual electrical, mutual energies and reciprocity law *(German)* 77−53772
analytic signal in oscillation theory, review 79−5988
artificial satellite with gravitational attitude control, dynamics 77−25905
asteroid orbits in vicinity of 1:3 commensurability with Jupiter, semi-major access oscills. *(Russian)* 80−36486
atmosphere, five day oscill. in E.African low-level jet 78−53705
atmosphere, freely convecting, above water surface, oscills. natural freq. *(Russian)* 78−11964
atmosphere, theory of travelling planetary waves in stratosphere 80−105030
atmosphere boundary layer, auto-oscillation solns. of barotropic problem *(Russian)* 77−49106
atmospheric oscillations and Ruchhardt's experiment, theory, for teachers 79−71198
atom spin transition, nonadiabatic, in time-depend. mag. field 80−9576
autocatalytic reaction system, sustained oscills., deterministic and stochastic theories 78−95922
balloons, vertical oscills. of constant volume sphere 79−53545
bar, eccentrically tensioned, parametric excitation 78−34050
bar, stability against self-excited frictional oscillations *(German)* 77−54916
beam balance, oscill. meas. using laser interferometer, construction *(German)* 77−79090
beam of finite length joined to infinite plate, mechanical admittance 77−11080
beams, finite element soln. using element averaging technique 78−26079
beats, interference phenomenon demonstration 79−75307
Belousov-Zhabotinskii reaction, chaotic oscills. 79−5151
Belousov-Zhabotinskii reactions, periodic and nonperiodic behaviour for different flow rates 79−100380
bending vibrations in their plates, layer potential method of solution *(French)* 78−59336
betatron oscillations, obs. of reson. buildup via synchrotron radiation 77−65368
bifurcations of straight line oscills., rel. to Stormer and spring pendulum problems 78−71278
biharmonic action on oscillator *(Russian)* 78−12556
biochemical model, spatial differentiation 78−44476
biochemical multiple-loop negative feedback control networks, oscills., periodic metabolic systems 78−85285
black holes, rotating, reson. freqs. of free oscills. rel. to gravit. waves 80−105271
Bodewadt flow, spin-up, angular momentum adjustment 80−28511
boundary layer, transitional, oscills., stability waves, vortices 78−38287
boundary layer perturbations, three freq. wave resonance *(Russian)* 79−32538

oscillations continued
building structures, interaction with seismic Rayleigh surface waves 78−81109
BT Cancri (38 Cancri), δ Scuti star, multiple periods rel. to radial and nonradial pulsation periods 80−85948
cantilevered cylindrical shells, ovalling oscillations induced by cross-flow 79−86375
capsules, neutrally buoyant, in Lake Tahoe, oscills. damping 80−12438
cascade, with large-deflection oscills., unsteady aerofoil theory, numerical soln. *(Japanese)* 78−67211
cavitation gas bubble in compressible liquid, influence of inhomogeneous sound field on motion 80−6131
cell population auto-activation, math. model 78−77017
β Cephei stars, pulsation excitation mechanisms 77−87425
Cepheid stars with He enriched inhomogeneous outer layers, three mode reson. 80−101600
Cepheids, double-mode, period ratios from linear and nonlinear theory 78−40953
Cepheids, pulsation theory and multiperiodic variables 77−87429
ZZ Ceti white dwarfs, non-radial oscills. theory 80−82356
channel, straight (buckled), two-dimens. flow, stability anal. 78−59490
chaos source in distributed kinetic systems 79−47890
chemical, equilibrium reactions *(French)* 79−57205
chemical composition centre waves, periodic chaotic, Pade approximant scheme 78−80716
chemical oscillations, reaction systems with exactly evaluable limit cycles 79−66262
chemical reaction, oscillating, entrainment by periodic light pulses of variable freq. *(French)* 80−35551
chemical reactions, abstract 3-variable systems, toroidal oscills. 77−44462
chemical reactions, oscill., kinetic model based on catastrophe theory 79−43557
chemical reactions in closed illuminated system, oscills., runaway states 78−7188
chemically reacting system, temporal oscillations 77−25359
circular oscillator, Cartesian and polar wave functions connection, rel. to dynamical O(3) symmetry *(Russian)* 79−49073
circular rings, stability obs. *(Russian)* 79−76990
combustion, vibrational, parameters rel. to resonator impedance *(Russian)* 77−9082
compressible oscill. boundary layer, numerical anal. 77−89140
conducting cylinder motion in solenoid field, contactless elec. cond. meas. *(Russian)* 79−214
conductivity probe, oscillating, density and density gradient meas., hysteresis effect 78−32796
conservative, nonlinear oscillators, connection between dissipative and resonant types 79−58619
convectively neutral fluids, pure perturbation spectra 77−41292
corona discharge, positive, sound effects 80−28858
coupled, demonstration using permanent magnets 80−42015
coupled nonlinear oscillators, Brownian motion, thermalised solitons and nonlinear response 78−29053
cracks, circular, forced torsional oscillations at low frequencies 80−53703
cryogenic system, thermally driven acoustic oscillation, stability limit 80−8992
curvilinearly aeolotropic thin rubber tubes, forced oscillations soln. 78−9589
cylinder, hollow, linear viscoelastic, dynamical loading by internal press. 79−18793
cylinder, torsional oscills. due to flow *(Russian)* 78−67178
cylinders heaving in water, added mass, damping coeff. 77−58828
cylindrical resonator with coaxial ring flange, inherent oscillations *(Russian)* 78−34051
cylindrical shell, reinforced laminer, intrinsic oscill. 80−99957
cylindrical shell with cutout, dynamic behaviour 77−75735
cylindrical shell-filler system, natural and parametric vibrations, taking tangential interaction into account 78−67085
cylindrical shells, dynamic response to concentrated impulse loads 78−22259
cylindrical shells, natural and parametric oscills. rel. to atm. pressure *(Russian)* 78−67086
damped harmonic torsional oscill., period and logarithmic decrement meas. 77−30142
damped oscillator, exact Green's function 79−80467
damping, light, influence of eigenvalues *(German)* 80−31490
damping characts., apparatus for examining, based on amplitude-frequency relationship resonant trough 78−64803
Dedekind ellipsoids, fourth-harmonic oscills. in post-Newtonian approximation to general relativity 78−32734
degenerate stars, high-luminosity, with He burning near surface, pulsational props. 77−5519
diffusion processes, nonlinear, chemical and biochemical 77−73440
disc, high freq. torsional oscills., Reissner Sagocci problem 78−26082
disc galaxies, large-scale modes from stellar hydrodynamics eqns. 79−25706
disc in electrically conducting fluid, hydromagnetic flow due to torsional oscillations about non-zero mean 80−74992
dissipative and nonequilibrium media, pulse spreading 80−94961
distribution, meas. techniques *(Japanese)* 78−41300
drag reduction of an oscillating flat plate with an interface film 80−10268
driven oscillator motion with nondecreasing input vels., use in inertia actuated fuse 78−59293
dry-friction periodic relay system analysis *(Russian)* 79−10455
dynamic axisymmetrical elasticity problems soln. using factorised differential systems of second-order accuracy *(Russian)* 80−8796
dynamic linear dipolar elasticity eqns. soln., convergence to classical elastodynamic solns. 77−888
dynamic system, piecewise-linear non-linear, several degrees of freedom, forced oscillations 78−54173
dynamic system behaviour near exist. boundary for periodic motions *(Russian)* 77−84138
dynamical system, effect of spin on non-linear reson. motions 77−75839
dynamical system construction from pre-assigned family of solns. 80−39
dynamical systems, equilib. configurations and small oscillations 79−25832
dynamical systems with oscillating elements, optimal and free motions 77−72229
Earth, annual motion of excitation pole *(Russian)* 78−40461

oscillations continued
Earth, corrections to eigenfreqs. due to dynamic shear modulus 77−81800
Earth, elastic tides and natural oscills. with Coriolis force included 77−37122
Earth, elasticity inverse problem soln. using amplitude and natural freq. data 77−2119
Earth, free oscill. data inversion, eigenvalue problems, angular order spectra 79−8602
Earth, shell of uniform layers, asymptotic distrib. of torsional eigenfreqs. 78−92797
Earth, torsional eigenfreqs. of spherical shell, asymptotic distrib. 78−88800
Earth, viscoelastic, free oscillations attenuation theory 80−21652
Earth core, internal waves 77−91082
Earth deformation, mag. field effects 80−109085
Earth free modes excited by Indonesia earthquake, Aug. 19th 1977 obs. 80−61767
Earth free oscillation data inversion, asymptotic approach 79−92624
Earth free oscillations, rot. and elliptical splitting 79−88257
Earth free oscillations, unresolved split normal mode multiplets spectra 79−74845
Earth free oscillations from Colombian deep earthquake (1970, July 31), and source mechanism 79−16394
Earth normal mode oscillations, tensor spherical harmonics appl. to anisotropic Earth model 80−98296
Earth rotating model, normal modes excitation by earthquake fault 78−73312
Earth tides, forced oscills. theory assuming Earth as viscoelastic body 80−67333
Earth torsional eigenfrequencies, effects of density and shear vel. discontinuities on asymptotic overtone struct. 77−78111
Earth torsional normal modes eigenfreqs., asymptotic overtone struct., model study 77−78110
education, gravitational fields, brachistochrones and isochrones 77−87596
education, mechanical mutual inertia in spring coupled system, mutual inductance analogue 78−49590
education, non-isochronous small oscills. 78−36749
education, spring-mass oscillator, parametric instability 77−78921
education, sprung pendulum, anal. of nonlinear coupling 80−51987
elastic half space, torsional oscillations due to rigid annular disc 78−28958
elastic inhomogeneous medium, high freq. Reissner-Sogocci problem, exam. of stress singularity 78−83239
elastic-viscoelastic correspondence principle for harmonic oscills., alternative representation 77−65710
electric elastic dipole, in periodic struct., free oscills. 79−27145
elliptic cylinder unsteady aerodynamics and vortex induced oscillations, test results 78−94746
elliptical and sinusoidally curved bars, in-plane vibrations 78−18211
equations with slowly varying coefficients, approx. integration *(Italian)* 77−5627
excitable medium, auto-oscillatory, 1-dimens., stability complex regimes 78−15752
excitable medium diffusion discrete models and spatial patterns 78−93629
ferromagnetic thin film energy absorption by magnetisation vector forced oscillation *(Polish)* 77−80970
flexible filament in liquid flow, dynamics using Riemann's method *(Russian)* 77−68670
floating body, oscillations damping by liq., inertial effects *(Russian)* 78−22295
flow, turbulent boundary layer, separation region, imposed oscills. effect 78−75127
flow, turbulent boundary layer, unsteady, near separation, struct. features 78−75126
flow, unsteady, transitional and turbulent boundary layers, expt. and calc. methods *(French)* 78−75125
flow characteristics of conical diffuser, oscill. turbulence 77−51047
flow induced by a torsionally oscillating wavy cylinder 79−64772
flow oscillations in duct 77−35241
flow past an oscillating plate in a viscoelastic fluid 79−27670
flow-induced oscills., bifurcations and flutter, finite dimens. analysis 78−5682
fluidised bed, relax. autooscills., math. model 77−75975
forced, effect of Coulomb friction in mass on spring system *(Russian)* 78−67027
forced, lower bound on forcing amplitude for stability, third order nonliner system 80−52013
forced 2-D oscillations of rigid strip in smooth contact with elastic half space 77−50963
forced oscillations, averaging and chaotic motions 80−73166
forced oscillations, existence and numerical approx. 80−62466
forced oscillations experiment for students 80−17780
forced periodic oscillations of the simple pendulum 80−94951
forced van der Pol oscillator, frequency entrainment 78−57794
forced van der Pol oscillator, variational eqn. bifurcations 78−77681
free surface, simple fluid between torsionally, oscill. cylinders 77−57202
galaxies, global instability of polytropic gaseous discs with Toomre density distrib. 80−98725.
galaxies, radial oscill. modes of cool stellar discs 78−57628
galaxies, spheroidal, perturbations and stability of interstellar gas disc *(Russian)* 77−91616
galaxies discs, second-harmonic oscills. of Maclaurin spheroids in halos 79−8993
gas, in multicylinder fluid machinery manifolds, lumped parameter descriptions 80−19511
gas, in tube, pressurisation in liq. He storage vessel 80−57305
gas, oscills. in tubes at reson. freq., shock wave heating *(Russian)* 79−32570
gas, reson. oscills. in channel, local heat transfer coeffs. 78−1659
gas bubble oscills. in viscoelastic liq. 77−80202
gas bubble pulsations in viscoelastic polymeric liquids, assoc. dissipation effects 80−59079
gas bubbles, appl. of subharmonic threshold to damping meas. 77−31374
gas bubbles, effect of backscattered acoustic wave on bubble oscillation 79−1021
gas bubbles, thermal effects and damping mechanisms in forced radial oscills. 77−31375
gas column, onset of oscillation due to heat conduction field 78−14027
gas column, onset of oscillations due to heat conduction, limiting condition 78−14028
gas flow into duct, self-excited oscillations 80−33647
gas in closed tube, resonant oscills., Chester's eqn. soln. 77−3869
gas oscillations in pipe with nonlinear active load 77−89201
gas torus in liquid, natural modes of pulsation 80−58999
gas-liquid flow, in homogeneous channel, forced oscillations anal. 77−11250
gas-liquid flow in channel, forced oscills. charact., expt. 77−11251
gaseous rotating masses with mag. fields, stability and existence of bifurcation point 78−53924
GCFR core and core support struct., seismic model test 78−41869
giant stars, late type, nonlinear coupling between pulsation and convection 77−13356
gravity meters, quartz, main springs, oscills. freqs. rel. to microseisms effect on readings *(Russian)* 79−39967
gyroscope, unsteady oscillations reduction using inner gimbal-base elastic damping coupling *(Ukrainian)* 77−30143
gyrotron, freq. charact. determ. *(Russian)* 79−14241
H-shaped section cylinder in laminar and turbulent flows, aerodynamic charact. 80−106813
harmonic force acting on free mass, soln. of differential eqn., for teachers 78−28893
heart, long-term adaptation modelling, oscillatory phenomena *(Russian)* 78−40212
heat exchanger tube banks, crossflow induced vibr. 78−50245
heater, effect on boiling process 77−55355
heaving cylinders, added mass and damping coeffs. 79−3988
helical springs, numerical soln. of dynamic response 78−67026
high voltage transmission cables, oscillations, coupled rope model study *(German)* 79−90173
highly nonlinear oscillation equation, perturbation soln. 78−33938
hot wire in liquid, heat transfer, transverse oscills. effects, holographic interferometry 77−15013
hypoelastic solid, oscillatory shearing 79−88810
immobilised enzyme membrane oscillations and pH fronts 77−25387
impact bending, investig. by load-time oscillograms 77−63849
incompressible viscous oscill. flow past porous sucking vertical plate, convection 78−30283
inertia-buoyancy oscillations in hurricanes, excitation and relation to spiral bands 80−56538
infinite pendulum system, finite controllability 80−31494
internal friction test unit for threadlike crysts. 78−36997
internal resonance in forced vibration nonlinear two-degree-of-freedom system 77−62192
interstellar medium in stellar component gravitational field, oscillations *(Russian)* 80−41883
ionosphere, transitional oscillations rel. to geomag. disturbances 77−60515
ionosphere pressure oscillations, generation of atmospheric acoustic-gravity waves 78−77296
jet in resonance tube, thermodynamic charact. 77−89174
Josephson self-resonant modes analysis, using mechanical analogue model *(Chinese)* 80−34563
Jupiter, Red Spot 90 day oscill. rel. to position of Mercury 77−82158
Kolmogorov eqn., separation of variables, applied to oscill. Brownian motion 80−36945
Lagrangian-mean flow, exact theory of nonlinear waves 79−37331
laminar flow over shallow cavities, oscills. 77−89091
laminar to turbulent boundary layer transition, outer-stream turbulence effect 77−75881
laminated plates subjected to transverse dynamic loading, transient response 77−31245
large-scale spatial oscillations of a cavity in a sound field 78−94775
LF oscillation period meas., digital method 78−93676
Liapunov's periodic motions at heavy rigid body with fixed point *(Russian)* 80−22190
libration in systems of many degrees of freedom *(Russian)* 78−86141
Ligurian Sea, free oscill. correl. with meteorological perturbations 79−34826
limit cycles as invariant functions of Lie groups 79−35520
linear system, external parametric random perturbations, oscillations *(Russian)* 79−17207
linear systems with time delays, stability analysis 77−62198
liquid in complex cavity, appl. of finite difference method *(Russian)* 77−72227
liquid metal viscosity meas. by torsional oscillation method, crucible size effect 77−51139
Lissajous figures, mechanical system, for student demonstration 80−31459
RR Lyrae stars, pulsation theory and multiperiodic variables 77−87429
Mandel'shtam and nonlinear oscillations and wave theory, review 80−105515
many-dimensional oscillator problems, 'Arnold diffusion' instability 79−75334
mass-on-a-spring (autoparametric oscillations) 77−22403
massive stars, nonradial pulsational instability 77−56908
mathematical models, oscillation theory, for teachers 78−86087
matrix theory, for teachers 78−61986
measurement and analysis, elec. and optical sensing techniques, review *(French)* 77−2646
measurement of small mechanical oscillations or vibrations by laser beam 79−77032
mechanical oscillations amplifier 80−13069
mechanical oscillator, relativistic spin quadrupole gravitational effect *(Russian)* 80−68103
mechnical coupled-transmission lines 78−52
membrane, stability of nonlinear oscillations from Liapunov method 80−96212
1 Monocerotis, δ Scuti star, oscillation modes from photoelectric radial vels. and BVRI photometry 80−51787
Morse oscillator, classical motion, calcs. 78−73796
multilayered basements, harmonic oscills. anal. *(Ukrainian)* 77−68474
multiply connected thick plates, oscillations, elastic medium model anal. *(Ukrainian)* 79−94525
natural convective oscillatory flow from heated wire on axis of horizontal cylinder 77−72295
near resonant oscillating systems, integration in slow-fluctuation approx. 80−62483
nearly conservative systems *(Russian)* 78−62069

oscillations continued
neural net temporal oscillations, cortical neurons interactions model 80−3636
neutron star torsional oscills., period determ. 80−90464
neutron stars anisotropic models, stability against radial and nonradial pulsations 77−13378
non-linear, free vibration, numerical soln. 80−68034
non-linearly coupled harmonic oscillators, asymptotic approx. 77−23792
non-Newtonian fluid film flow along vertical oscillating plate *(German)* 78−59431
nonconservative elastic systems, stability under periodic effects *(Ukrainian)* 79−32309
nonlinear, for n^{th} order delay inequalities 78−89300
nonlinear, note on weighted mean square linearisation method 78−83303
nonlinear, ultraspherical polynomial approx. averaging method 77−84183
nonlinear, with slowly varying system parameters 79−37219
nonlinear differential equations for oscillatory systems, u-procedure applic. for asymptotic soln. *(Ukrainian)* 77−49561
nonlinear diffusion processes, slowly modulated oscillations 78−16758
nonlinear dynamic damper, subharmonic oscillation extinction 79−25835
nonlinear flexural oscillations of orthotropic shallow spherical shells 79−3939
nonlinear forced oscillations of rectangular plate *(Russian)* 78−55586
nonlinear Mathieu eqn., chaos and successive subharmonic bifurcations 79−63153
nonlinear mechanical systems of arbitrary order, stationary oscillations *(Russian)* 78−65765
nonlinear multidegree-of-freedom system, superdivision harmonic oscillations due to fourth order nonlinearity 77−57175
nonlinear oscillations, damping decrement 77−58581
nonlinear oscillations with parametric excitation, system with one degree of freedom *(Russian)* 77−89018
nonlinear oscillator problems, weighted mean square linearization method, comments 79−37220
nonlinear oscillator systems, primary resonances do not overlap 80−59176
nonlinear oscillators, necessary-sufficient condition for synchronisation 77−39
nonlinear oscillators, turning point approx. and appl. 80−67952
nonlinear oscillatory systems with delay, stability props. of differential eqn. solns. *(Russian)* 77−41475
nonlinear oscills. by Hamiltonian mechanics *(Russian)* 77−39215
nonlinear oscills. of round plate, difference eqn. approx., Lyapunov methods *(Russian)* 77−39259
nonlinear planar oscillators, stability of modes 80−74790
nonlinear resonances, asymptotic first approx. *(Russian)* 77−17808
nonlinear resonant oscillations of body containing liquid *(Russian)* 78−18222
nonlinear stochastic models of oscillator systems 79−80525
nonlinear system, delay effects *(German)* 77−53773
nonlinear system under impulsive periodic loading, steady-state response 77−46959
nonlinear system with slowly varying parameters, resonance 80−62463
nonlinear third order system with weak forcing function 78−30119
nonlinear two-degree-of-freedom system, internally resonanced, forced vibrs. 80−36838
nonlinear vibrating system, fourth order parametric resonance, influence of frictions 77−58620
nonlinear vibratory system, ultra-subharmonic oscillations analysis 77−50944
nonlinear x^{2p+2} damped oscillator, perturbation treatment 77−17807
normal modes of coupled nonlinear oscillators, stability 78−89330
novae, transition zone oscills. inception 77−87402
nuclear plant, seismic testing of structures and components using two axial shaking table 78−44300
nuclear power station, Caorso plant, dynamic tests and seismic records of RHR building 78−41872
nuclear power station response to aircraft impact 78−41875
ocean, current vel. and temp. oscills. with periods to inertial oscills. *(Russian)* 77−33088
ocean, normal Rossby modes of closed basin with topography 78−73385
ocean basins (connected), theory of natural oscills. 80−61806
oceanic thermocline, large-scale oscills. rel. to short-period internal gravity waves *(Russian)* 78−16024
oscillator with even non-linear damping 78−28938
oscillator with hysteresis, dynamic anal., Fokker-Planck eqn. *(French)* 77−50947
oscillators in convective biperiodic regime, velocity oscills. 80−53759
parabolic lens, mag. field limited, mech. strength and dynamic loading 79−18341
parametric excitation of combined resonant systems 77−2539
parametric instability, demonstration and discussion 80−57032
parametrically excited, combination resonance of coupled second order systems with nonlinear damping 80−86078
particle heavy spring system, oscills., Stieltjes integral calcs. 79−71180
peak harmonic response of locally non-linear systems 78−51109
pendulum oscillation optimal passive suppression *(Russian)* 79−10454
penny shaped crack in inhomogeneous medium high freq. torsional oscills., stress anal. 78−26086
periodic system induced oscillation and rotation analysis 77−37753
piezoceramic microwelding transducer component oscillation amplitudes 79−26046
pipe containing flowing fluid, forced oscillations *(Russian)* 80−38304
pipe mode characteristics determination, pipe flow conditions effects *(French)* 78−79246
pipelines with liquid, stability and oscillations 80−14612
plane two-dimensional motion in acoustic medium caused by kinematic excitation, Laplace transform study *(Russian)* 80−43503
plate, oscillating in fluid, with suction or intermediate film, conducting flow analysis 77−47098
plate, vertical, free convection boundary layers and heat transfer 80−59002
plate oscillation effect on horizontal free convection flow 77−75904
plate temp. oscillations, response of horizontal free convection boundary layer 78−59391
plates, pre-stressed, 3-D problems, basis systems of homogeneous solns. *(Ukrainian)* 80−10177
plates, solid anisotropic thick, homogeneous solns. of steady oscillations *(Ukrainian)* 78−90739
Poincare cycles of the linear chain of oscillators 80−4662
oscillations continued
polymer rod, longit. oscills., continuous viscoelastic spectra *(Russian)* 77−19546
postural equilibrium automatic meas. and real-time evaluation in man, instrumentation system 78−77127
profile, nonstationary transonic flow analysis by fractional step method *(French)* 77−51079
proton (antiproton) storage ring, incoherent motion damping by dissipative elements 80−5419
pulsating stars, modal selection theory rel. to double-mode Cepheids 80−82372
pulsational instability of accretion disks to axially symmetric oscillations 79−16938
pulsed photolysis of gas, radial oscills. in a cylindrical cell 78−56908
quantum anharmonic-oscillator energies using operator recursion mech. 77−22443
quasi-ideal pendulum, small amplitude oscills. 79−84897
quasi-linear nonautonomous systems, motion stability condition for periodic oscills. *(Russian)* 77−33855
radial and spheroidal oscills. of elastic sphere 79−44130
random oscills., RMS level estimation, fast method 77−70857
reactors, chem., relaxation oscills. 79−39120
rectangular prisms, galloping in smooth and in turbulent flow 77−75840
red giant variable stars, pulsation mechanisms rel. to multiple periods 77−87427
relativistic oscillatory motion, general, Einstein's field eqns. 80−73217
resonance, internal, of two damped oscillators 77−46905
resonance between weakly coupled oscillatory systems 79−40357
resonant oscills. in tube with jet inlet 78−59440
respiratory total resistance meas. in pre-school children using modification of forced oscill. technique 78−77129
retina of Limulus, spatially synchronised oscillatory response theory 78−73158
ribbed cylindrical shell with solid body, free oscill. 80−99956
rigid rotor in elastic ball bearings, free oscillations *(Russian)* 79−18773
rigid shaft in short journal bearings, aperiodic behaviour 78−46905
rigid shell, oscillatory flow through perforated surface, sound generation 79−18950
rocket engine oscills. due to burning instability *(Russian)* 77−14893
rod with limited excitation, parametric oscillations *(Russian)* 77−75832
rods, natural twist, influence on oscillations *(Russian)* 79−76996
rotating fluid, trapped oscillations, viscous effects, num. simulation 77−55015
rotating stars, non-radial oscills. rel. to cataclysic variables short-period light oscills. 78−32477
rotating stellar systems, two-dimensional, nonlinear nonradial oscills. stability 78−53992
rotational-oscillatory system with many degrees of freedom, resonant motions *(Russian)* 77−33859
rubber bands and filaments, length oscill. pulse generation, instabilities *(Russian)* 78−30227
sapphire monocrystal high-Q mechanical resonator *(Russian)* 77−75851
satellite, elastic, gravitationally oriented, spatial oscills. and stability of relative equilib. 78−4068
satellite eccentricity oscills., compensation with stabilizer 78−69643
δ Scuti stars, empirical period-luminosity-colour relations 79−25610
secondary flow in oscill. torus 77−15121
seismic oscillation sources, ground response and theoretical problems *(Russian)* 77−44938
self-gravitating fluids, definition of g-modes and p-modes 77−41291
self-gravitating fluids in perturbed configurations, perturbational-variation procedure for normal modes 78−32336
self-gravitating fluids normal modes, expansion of g- and p-modes of non-adiabatic fluid 78−32337
self-maintained oscillatory systems, possibilities of asynchronous resonances *(Ukrainian)* 78−89327
self-oscillating system, parametrically excitable, forms of movement, stability conditions *(Russian)* 78−16635
self-oscillating system analysis, accuracy of first approx. *(Russian)* 77−26134
self-oscillatory system with external heating 77−14888
shaft mounted in ball-bearing angular oscillations anal. *(Russian)* 78−75092
shell, cylindrical composite, with viscoelastic filler, parametric oscills., dynamic instability *(Russian)* 78−38221
shell, spherical, with rigid core, deform. under effect of plane press. wave *(Ukrainian)* 77−31239
shell, thin momental and momentless problems in oscillations theory *(Russian)* 78−22296
shell of revolution, resonant oscillation obs. by holographic interferometry *(Russian)* 78−22297
shell-fluid system, steady periodic motions appearance *(Ukrainian)* 77−31240
shells, highly stressed nonhomogeneous thick-walled cylindrical and spherical, radial oscillations 77−3768
shells, layered thick-walled cylindrical, large amplitude radial oscillations 77−72215
ship oscillation, wave-generated, numerical methods *(French)* 78−30216
short wave generation by cylinder oscillating at liquid interface 78−79331
sieving of fine powders by sonic oscillating air column *(Japanese)* 78−95712
sinusoidally oscillating cylinder in Newtonian fluid, mass transfer *(French)* 77−57287
soft spring, dynamic behaviour, mathematical anal. 78−12491
solar, surface oscillations and pulsations, rotation speeds 80−67676
solar atmosphere temperature minimum, five-minute oscills. obs. 79−62808
solar five-minute oscillations, horizontal energy flows struct. 80−62103
solar oscillation periods, correl. with cosmic ray short-term fluctuations periods 80−67483
solar oscillations, Fe I 5124 Å Doppler shift obs. 78−53905
solar oscillations, influence of Sun outer layers on detect. 79−5800
solar photosphere, search for long period modes 77−41370
solar surface oscillations, geophysical effects 79−8777
solid friction damping of mech. vibrs., math. model approach 77−42764
solotone effect and torsional eigenfreqs. of spherical shell 78−92798
solution of a highly non-linear oscillation equation, single particle analogue of field equations of chiral Lagrangian theories of pion interactions 80−62470

oscillations continued
space frame structure of variable cross-section rods, eigenfrequency determination 77−75831
spatial oscills. of gravit. oriented elastic satellite, nonlinear resonances 78−69644
spatial Xe oscillation time-optimal control in PWR 79−628
sphere suspended in fluid, vel. in sound wave 77−23800
spherical bubble in dilute polymer soln., natural freq. of oscill., theoretical study 77−24017
spherical bubble in finite vol. of liquid, natural freq., numerical calcs. 77−51106
spheroids, acoustomechanical characts. 77−34991
spheroids, harmonically oscillating, unsteady airload prediction, analytical soln. 78−51184
spindle unit on test stand, wheel failure 80−19277
spiral flow between coaxial cylinders, branching and stability loss 80−19406
springs, cylindrical helical, dynamic coupling of torsional and flexural strains 77−62202
stability of interaction between oscillator and tie in relative motion *(Polish)* 77−53789
stability of periodic motion and nonlinear oscillation theory *(Russian)* 78−86147
star, rotating, low-freq. gravity modes 79−16934
30 M⊙star, stability towards g^+ modes of high spherical harmonic values 77−9740
star in thermal imbalance, pulsational stabilities, comparison of methods 78−45316
stars, adiabatic non-radial oscillations with moderate or large l 80−56819
stars, adiabatic nonradial oscills., freq. splitting by slow differential rot. 80−105233
stars, equilib. struct. and oscill. of uniformly rotating mag. polytrope 77−87366
stars, junction conditions across perturbed contact discontinuities 80−94787
stars, local stability rel. to radial and nonradial dynamics 77−5521
stars, magnetic, stability with respect to high-order oscill. modes and convection 80−94781
stars, massive, in slow rot., vibr. instability and oscill. props. 77−5536
stars, neutrino damping of nonradial pulsations during gravit. collapse 77−56999
stars, nonradial oscillations, theories and obs., review 77−26003
stars, oscill. freqs. line broadening due to convective fluctuations 80−31293
stars, second harmonic oscills. of Jeans spheroids with toroidal mag. fields 78−45319
stars in thermal imbalance, vibr. stability coeff. energy methods 77−13320
stars in thermal imbalance, vibrational stability 78−40916
stationary response to random excitation, nonlinear damped oscillators 77−42769
steel sheet, irregular oscills. induced during internal friction meas. 77−32752
stellar atmosphere, free convection effects on oscillatory flow past infinite porous vertical limiting surface 79−92751
stellar atmospheres, hydromagnetic flow near oscillating porous limiting surface 78−12200
stellar collapsing core, neutrino dissipation rel. to differential rot. and oscills. damping 79−101166
stellar magnetic configurations linear oscills., unrestricted second-order tensor virial eqns. 79−44461
stellar models, tidally distorted, small oscills., Roche coordinates appl., second-order terms effect 79−44462
stellar motion, z-oscills. theory rel. to force field normal to galactic plane 80−46669
stellar pulsations, nonlinear coupling 80−62115
stochastic properties of complex nonlinear oscillation regimes 80−8919
stochastic systems, Bubnov-Galerkin method appl. *(Russian)* 77−49578
streaming, of vel. and temp., in oscill. boundary layers 78−83358
structural analysis, combined finite element-transfer matrix method 77−62201
structural system under multiple support excitation, seismic response anal. 78−53623
structure radiation of simple emitters, radiated sound power *(French)* 77−19471
structure vibrations, reduction by increase in damping factor *(French)* 77−19472
subharmonic in accelerometer with element with gas dynamic suspension *(Russian)* 79−88948
submerged hemispherical shells, dynamic response to earthquake motions 78−51110
Sun, 160 minute period, evidence 80−82324
Sun, active region McMath 15403, 5 minute oscills., SHF obs. 80−98639
Sun, evidence for long-period global oscills. 79−2539
Sun, free oscills., theoretical spectrum 79−5805
Sun, global oscills. energy transport, upper bound from photosphere radiative equilib. 78−32430
Sun, high-freq. oscills. rel. to upper photosphere spectral line shifts 80−85912
Sun, nonradial oscills. of 1968 nonstandard solar model 79−35218
Sun, obs. results and theories of oscills. 78−12182
Sun, oscill. periods of dirty models contaminated by surface accretion 79−44436
Sun, oscillations in solar diameter, obs. and techniques *(Danish)* 77−22153
Sun, oscills. in context of variable stars *(French)* 79−2540
Sun, oscills. period obs. rel. to internal struct. 80−105226
Sun, photosphere temp., luminosity vars. and global oscills. from C I 5380 Å line obs. 77−53487
Sun, pulsation with 2^h40^m period, possible magnetospheric origin 78−7961
Sun, soft X-ray flux, Skylab obs., temporal oscills. 78−53904
Sun, structure from global studies of 5-min. oscills. 80−26838
Sun 5-minute oscillations, C I 5380 Å line response, effects of granular convection 80−85910
Sun acoustical oscillations, period comp. 77−29756
Sun global oscillations, implications limb darkening function possible temporal vars. 80−67677
oscillations continued
sunspot chromosphere, radial vel. and brightness oscills. regimes *(Russian)* 80−51727
superfluorescence, oscill., quantum statistics 79−917
supermassive stars, general relativistic theory for radial pulsation freqs. 77−41376
supernovae, self-similar oscillations of gas *(Russian)* 79−17001
supersonic flow, self-induced oscills. 78−67215
supersonic jet, underexpanded, impinging on barrier, sound field 78−9495
surface-boiling flow in pipe, high-frequency pressure oscillations 77−35239
suspension of water, air and oil, dynamic behaviour under periodic perturbations *(Russian)* 77−19631
swinging spring with oscillating support, stability boundaries 77−68384
synchrotron, effects of induced voltage and forces of space charge on motion *(Bulgarian)* 80−47792
systems with hysteresis, linear, and quasilinear self-oscill. *(Russian)* 77−58590
teaching experiment, exploration apparatus for introductory phys. lab. 77−57121
thermokinetic, equilibrium reactions *(French)* 79−57205
thick walled sphere, nonsteady hydroelastic oscills. 78−18227
thin hyperelastic spherical shell, finite amplitude oscillations 78−93533
thin walled elements, unbound quasistatic random thermoelastic fields, oscillations 80−69673
three oscillators coupled by weak nonlinearity, response 77−68513
torsion of elastic layer, by annular die, Fredholm integral equation anal. 79−3969
torsion pendulum, automatically driven, for continuous meas. of amplitude and amplitude-independent damping 77−35099
torsion pendulum, with anelastic solids of discrete relaxation spectra, resonant system 80−69687
torsion pendulum with elastic wire element, free torsional vibr. anal. *(Spanish)* 79−68613
torsional, free and forced, methods of calc. *(Russian)* 77−35065
torsional decaying oscillations of sphere and plane, secondary flow effects 77−3808
torsional oscillation of inhomogeneous elastic half space *(Russian)* 77−19559
torsional oscillation test instrument with process computer control *(German)* 77−21344
torsional pendulum damping meas. system *(Polish)* 77−71314
transonic channel flows, two-dimensional, shock-wave motion 79−60005
transtropic thick plates, multiply-connected, forced oscills. *(Russian)* 77−39241
tropical middle atmosphere, observational evidence of semiannual oscillation 80−109216
tube array, whirling instability, phase relationships 78−51175
turbomachinery ring chamber, oscillatory behaviour of confined ring vortex 80−6075
two coupled systems, reduction of effective noise temp. *(Russian)* 77−75790
two-airfoil systems, with aerodynamic interference, flutter anal. 78−51181
two-level system, Rabi oscillations in partially coherent field 80−102688
unstable flow past cavities, shear layer oscill. freqs. 77−84228
unsteady turbulent boundary layer developing in oscillatory external flow *(French)* 77−72288
valve connected to pipe, acoustic oscills. from flow 78−59491
van der Pol oscillator, functionals over discontinuous sample paths 78−29052
variable parameters systems, variation of oscillation phase and amplitude *(Russian)* 78−81799
variably constricted beams, transversal oscillations and critical loads *(Italian)* 78−51113
viscoelastic rod, dynamical behaviour, effect of thermomechanical conjugation under forced longitudinal oscillations *(Ukrainian)* 78−67074
viscoelastic rod, forced longitudinal oscillations, thermomechanical coupling effect 80−19274
viscoelastic rod, standard linear body, free torsional ascills. 80−99940
viscoelastic rod analysis, using Boltzmann-Volterre memory theory, second-order approximate solution *(Russian)* 78−87278
viscoelastic-plastic torsion pendulum, prismatic *(Spanish)* 77−3733
viscous effects on perturbed spherical flows 77−51105
viscous fluid oscill. decrements in complex pipelines 78−5801
viscous liquids, US shear absorption, effect of pulse width 78−83878
vortex collapse, periodic oscills. *(Russian)* 77−58697
wedge oscillations in confined vesicle *(Russian)* 80−43651
white dwarfs, theoretical review of nonradial oscills. 77−87398
white dwarfs seismological theory for 1 $M_\odot$ model with crystalline core 80−17577
wind induced oscillations, domains of stability 80−64441
wing, in transonic flow, unsteady airloads and flow linearisation 80−19426
wristwatch balance period/oscill. amplitude meas., photoelec. method *(German)* 77−87755
Al-Ag, type-II superconductor, torque oscillations in mag. field *(Russian)* 80−103800
Fe-Si (3 wt.%), internal friction, instantaneous, depend. on phase of torsional oscills. *(Russian)* 80−71142
Fe-Si (3 wt.%), magnetisation variation during bending oscills., rel. to ΔE effect *(Russian)* 80−65983
H_2O_2 decomposition, IO_3^- catalysed, oscillatory Bray-Liebhafsky reaction 79−91931
He, thermoacoustic oscillations in nonuniformly heated tubes 80−33441
He transfer line, oscillation damper 80−37041
Ni, internal friction, instantaneous, depend. on phase of torsional oscills. *(Russian)* 80−71142

oscillator strengths
2^l-pole oscillator strength sum rule, hydrodynamic analogy to quantum mechanics 79−26873
acentric crystals, optical phonons, small oscillator strength meas. from frequency-angular polariton spectra 80−92629
acetic acid amides, polarisabilities and π-π^* transitions, dipole interaction calcs. 80−23411
acetone, solvent effects on oscillator integrated strength, IR absorpt. bands 78−84575
acetyl radical, absorpt. spectrum obtained by flash photolysis and kinetic spectroscopy 79−13731

oscillator strengths continued
alkali halide:Ga^+,In^+,Tl^+, cryst. field effect on spectral characts. 77−24880
alkali homonuclear dimers, quasi-static wing profiles of self-broadening reson. lines 80−48042
alkali isoelectronic series, transition probabilities, oscill. strengths, lifetimes, branching ratios 78−33470
alkali metal, oscillator strengths, nonlocal Simons pot. anal. 80−32795
alkali metal atom, Rydberg state emission oscill. strength minima 80−32662
alkali metal atom, Rydberg state Stark struct. 80−37754
alkali metal atom, transition oscillator strengths in discontinuous and continuous spectra, review 80−52937
alkali metal atoms, principal series, scaled Thomas-Fermi method 77−46549
alkali metal atoms, static polarisability, lower bounds, oscill. strength calcs. 77−75074
alkali metal hydride, variational time-dependent H-F calcs. in pseudopot. framework 77−10588
alkali-inert gas system, mol. band profiles of induced dipole transitions 78−42135
alkaline earth atoms, static polarisability, lower bounds, oscill. strength calcs. 77−75074
alkylbenzenes, electronic struct., photoelectron spectra rel. to semiempirical CNDO/S CI calcs. 79−54770
anthracene, singlet exciton transitions, energies and oscillator strengths, boson theory with PPP wavefunctions 80−92820
anthracene-pyrometallitic dianhydride cryst., refl. and absorpt. spectra of singlet charge transfer excitons 80−71442
aromatic hydrocarbons, mol. struct. determ. from electronic spectra, oscill. strengths *(French)* 77−71888
aromatic hydrocarbons, struct., UV absorption band calc. *(French)* 77−18989
astrophysical objects, general aspects 80−12656
atom, absolute value, collision broadened absorption linewidths method 77−10639
atom, force experienced in electrostatic field, Feynman-Hellmann theorem and oscillator strengths 80−65275
atom, inner shell, generalised oscill. strengths, with outer shell effects 78−50507
atom, inner shell, outer shell rearrangement effect 77−42418
atom, ns-electron ionis. transitions 78−5173
atom, rel. oscill. strengths determ. by combined absorption/emission meas., Ti appl. 80−37784
atom, Schumann region absorpt. spectrum, oscill. strengths, line profiles, collisional and autoionis. broadening 77−18818
atom, screened potential model, and energy levels 79−63896
atom-electric dipole radiation interaction, length vs. vel. form, gauge invariance 79−41142
atomic oscill. strength, gauge props. of HF and RPA approx. 78−950
atomic oscillator strength, meas. using stimulated electronic Raman scatt. polarisation flip method 79−31471
and atomic structure, book contrib. 77−26959
atomic system, oscillator strengths determ. with phase matching condition 77−10638
atomic vapour, f-value determ. method using stimulated electronic Raman scatt., appl. to Cs 78−82693
atoms, complex, oscill. strength distribs., Stieltjes imaging determ. 77−6731
atoms, excited state, oscillator strengths, core relax. effects calcs. 79−10050
atoms, ground and excited states, polarisability and scaling, oscillator strength, continuum spectrum contribution 80−27923
atoms, near threshold struct. in K-shell spectra, photoionisation or fast charged particle ionisation 80−87064
atoms, oscill. strength in presence of level crossings 80−99480
atoms, Pade approximant interpolation formulae calcs. 79−31466
atoms, singly excited states, oscillator strengths, ab initio calcs. 80−920
atoms, theory and calc., review 78−17616
azulene, Shpol'skii matrix, $S_2 \rightarrow S_1$ fluoresc., spectral anal. 77−18956
beam-foil lifetime measurement, cascading problem, ANDC method use and error limits 80−14249
beam-foil spectra oscillator strengths, neutral and ionised atoms, non-closed shell many electron theory 77−38612
beam-foil spectroscopy, appl. to oscill. strengths meas., for astrophysics 79−50168
benzaldehyde, $n\pi^*$ and pi pi^* triplet states, props., SCF calcs. 77−6695
benzene, $^1B_{1u}$ state, vibronic mag. rot. strengths and oscill. strengths, CNDO/S calcs. 77−34670
benzene, and deuterated forms local mode oscill. strengths 79−27039
benzene, electron impact-induced generalised oscill. strength, 400 eV, 500 eV, momentum change depend. 78−1088
benzene, extinction coeff. in 4.6-36 eV range 78−86877
benzene, liq., visible region absorpt. spectra, overtones meas. 80−78625
benzene, symmetry forbidden transitions in MCD and electronic spectra 77−65494
benzene+acetone, energy transfer cross-sections, generalised oscill. strength calcs. 79−10173
benzene($-d_6$) vapour, SVL fluoresc. lifetimes and quantum yields 77−10701
benzene-acetone donor-acceptor pair, energy transfer cross sections rel. to generalised oscill. strengths 78−46452
biacetyl in supersonic jet, emission spectra, energy-resolved decay times 79−81224
bounds on van der Waals coeffs., oscillator strength sum rules 80−27941
4-bromoisoquinoline, UV and IR spectra, f-values and ground state vibr. freqs. 78−58714
butadiene, oscillator and rotatory strengths, RPA in ab initio calc. 78−25617
trans-2-butene, twisted, oscillator and rotary strengths, ab initio calculations 77−65510
C III, excited states, transaction oscill. states and wavefunctions 79−59367
C IV, optical oscillator strength 80−47941
calculation from electron collision data, limit of zero momentum transfer 79−98155
chlorofluoromethanes, electron energy loss spectra, oscill. strengths 78−58846
chlorophyll-a, solns., vis. absorpt. spectra of monomer, dimer and oligomers 77−29101
CNDO-CI method, parameterisation role 77−46497
CNDO/S-CI method, convergence problems 77−46496
conjugated molecule, oscill. strengths calc. from dipole length and dipole vel. formalisms 78−78757
Coulomb approximation oscillator strengths and multipole radial integral calc. 79−63959
9-cyanoanthracene, cryst., polarised refl. spectra at 2K, 360-460 nm, dielec. function 79−91461
diamond, electric quadrupole sum rules rel. to optical consts. 79−38036
diatomic astrophysical molecules, review of spectroscopic information in visible and UV regions 77−88459
diatomic isovalent sequence, free-mol. electronic transition intensity consts., systematics 78−42137
diatomic molecules, excitation energies, oscillator strengths, many body approach, eqns. of motion method 80−47969
p-difluorobenzene, electron impact singlet-singlet transition generalised oscill. strength 78−66668
p-difluorobenzene+acetone, generalised oscill. strength, for reson. electronic energy transfer 78−66668
diphenylethylene, UV spectra, quantum-mechanical investigation of isomerisation pathways 80−43065
dipole properties and dispersion energies additivity, using atoms and small mol. models 80−53091
dispersion energy consts., dipole oscill. strength sums, refractivity, for Li, N, O, H_2, N_2, O_2, NH_3, H_2O, NO, N_2O 77−50492
DNA hypochromic effect, oscillator strength, perturbation theory calc. 79−96515
doubly ionised atoms, $3s^23p^N$-$3s3p^{N+1}$ transitions, oscill. strengths calcs. 77−83542
Drude oscillator model, atomic and molecular props. for different oscillator freq. 80−37846
dynamic multipole polarisability, dispersion forces and oscillator strengths, Coulomb approx. 80−63520
electric quadrupole oscillator strengths, adaptation of ACRZ program 78−90119
electron impact spectroscopy, low-energy aspects, book contrib. 80−14243
N-ethyl carbazole, CNDO/S spectrum calc. rel. to poly-n-vinylcarbazole solid state spectrum 79−89815
ethylene, electronic states, optical rot. dispersion, oscill. strength calcs. 78−9095
ethylene, excited states, continuum embedded, SCF-stabilisation approach 78−928
ethylene, self-consistent many-body theory, self-energy effect 79−63901
ethylene, twisted, oscillator and rotary strengths, ab initio calculations 77−65510
ethynyl radical, vertical electronic spectrum, CI calcs. 77−34656
excited states, oscill. strengths calcs., influence of wave function determ. method 80−99478
exciton resonances, interacting, dielec. theory 78−14673
excitonic molecule, two-photon excitation of first vibr. state, giant strength 79−7789
fast electron collision, K, L, M-shell generalised oscillator strengths and ionisation cross section, Hartree-Slater calc. 80−53141
first-row elements, dipole oscill. strength distribs., moment calcs. 77−6733
first-row elements, dipole oscillator-strength distribs. 78−58626
fluorobenzenes, UV spectra calc., oscill. strengths 79−18203
formaldehyde, electronic states, oscill. strengths calcs. 78−9095
formaldehyde, emission spectrum, forbidden $n\text{-}\pi^*$ transition, electronic-vibr. struct., CNDO/2 calcs. 77−58035
formaldehyde, Rydberg states, excitation energies, oscillator strengths ab initio GVB-CI calcs. 77−54518
formic acid amides, polarisabilities and $\pi\text{-}\pi^*$ transitions, dipole interaction calcs. 80−23411
glass, optical, refractive index, oscillator strength effect *(Japanese)* 77−28538
ground state atoms, Van der Waals coeffs., polarisabilities and oscill. strengths calcs. 79−93913
group IV homologous ions, oscillator strength trends 80−42991
heavy atoms, collective oscillations, of individual shell 79−45674
heavy ions, beam-foil decay curves for reson. transitions, simulation 80−9721
heterocycles, five membered ring, MCD spectra dnd π-electron approx. calcs. 79−812
homologous ions series, struct.-related trends in line strengths and Stark widths 80−105157
hook spectra, evaluation limitations 80−90905
hydrocarbons, conjugated, effect of semi-empirical parameters on simple RPA calcs. 79−10037
hydrocarbons, vibr. intensities, G sum rule appls. 80−32776
1-hydronaphthyl radical, in naphthalene single cryst., anisotropic oscill. strength 78−50591
inert gas, oscill. strength determ. from resonance radn. self-absorpt. 77−18847
interacting systems, oscillator strength sums, dynamic polarisabilities, one-term approximations 79−22782
interpolation formulae for ground state transitions for H to Al isoelectronic sequences 77−71778
ion-neutral atom, in foil, inner-shell processes, oscill. X-ray spectra excitation 77−54565
ionic crystals, oscillator strengths of defects, Smakula eqn. generalisation 80−108232
ions, two vacancies in K shell, 2 electron 1 photon, and hypersatellite transition probabilities 78−46294
isoelectronic sequences, regularities in f-value distribs. 77−38642
lanthanide(III) complexes, f-f transition intensities, general theory of solvent effect 80−18811
lanthanides in molten $LiNO_3$-KNO_3, transition probabilities in absorpt. and fluoresc. spectra 79−50085
lithium formate, optical phonons, small oscillator strength meas. from frequency-angular polariton spectra 80−92629
magnetooptical parameter sums, sum rule analogue 79−89697
many-electron systems, oscill. strengths, Bates-Damgaard approx. calcs. 77−3311
measurement using reson. Faraday effect in monochromatic light 80−23363
methane, ν_4 fundamental band strength, line-intensity meas. 79−22700
methane, ground state, dipole oscill. strength distrib., rel. to molar refractivity and dispersion energy 77−71835
methane, pseudospectral dipole oscillator strength distribs. 78−50503

oscillator strengths continued
methane, triple-dipole energy calc. using pseudo spectral theory 78−46418
methyl indoles, UV and IR absorpt. spectra, f-values and ground state vibr. freqs. 78−58716
3-methyl lumiflavin, in soln., absorpt. spectrum 80−58277
N-methylacetamide, vertical excitation energies, ab initio SCF CI calcs. 79−45647
methylammonium chloride, torsional motion, harmonic oscillator and free rotor bases calcs. 79−72232
methyoxy radical, electronic absorpt. spectra, visible, vibr. freqs., vibronic intensities and oscill. strengths 80−28025
molecular cryst., dipolar exciton band struct., optical model 77−15770
molecular crystal, surface exciton levels, radiation corrections 80−34962
molecular electron-donor-acceptor complexes, solvent effect on charge transfer absorpt., thermodynamic props. 77−83615
molecular gas, IR saturation characts. versus oscill. strength 78−78751
molecular glass, density of states for IR active internal modes of tetrahedral mols. 78−75788
molecular interactions, two-body van der Waals coeff., combination rules 80−78677
molecular system, oscillator strengths determ. with phase matching condition 77−10638
molecular transition energies, oscill. strengths, time-depend. HF model *(Spanish)* 77−6684
molecules, transition probability studies, review of recent advances 78−17655
monoclinic crystal, refl. spectra dispersion anal. 79−99877
$n\rightarrow\pi^*$ singlet-singlet transition probabilities 80−95689
naphthalene, LCAO SCF MO CI calcs., integral approx. scheme using semiorthogonalised orbitals 79−6873
naphthalene, oscill. strengths of π^*-π transits., absorption spectrum in rare-gas matrices 79−3454
naphthalene, singlet exciton transitions, energies and oscillator strengths, boson theory with PPP wavefunctions 80−92820
naphthalene-tetrabromophthalic anhydride, complex cryst., visible spectra, singlet-triplet absorpt. 79−19897
naphthalene-tetrachlorophthalic anhydride, complex cryst., visible spectra, singlet-triplet absorpt. 79−19897
neutral atom, excited state struct., electron correl., oscill. strengths, theory 79−6889
neutral atoms, $3s^23p^N$-$3s3p^{N+1}$ transitions, oscill. strengths calcs. 77−83542
nitroanilines electronic states, CNDO/s-CI correlative calcs. 78−58604
o-nitrophenol, solvent effects on oscillator integrated strength, IR absorpt. bands 78−84575
nonhydrogenic atoms, radial transition integrals, Coulomb approx. calcs. 79−45625
nonlinear polarisation resonances in a continuum, optical activity, spin-orbit interactions *(Russian)* 80−53391
one-electron ion+He(N)(Ar), sum-rule Born cross sections, excitation and ionis. contribs. 79−22812
one-term approximation to oscill. strength sums, calc. 79−45656
optical joint density of states, oscillator strength effects 77−11838
organic charge transfer complexes, refl. spectra, excitons 79−47477
particle stopping power meas., mean excitation energy from oscillator strength distrib. 80−9481
pentacene, singlet exciton transitions, energies and oscillator strengths, boson theory with PPP wavefunctions 80−92820
perturbation theory calcs. in length and rel. forms 79−72275
phenyl isocyanate, electronic absorpt. spectrum, vibr. struct., f-values, spectroscopic moment and config. 78−58715
photosynthetically relevant mols., electronic structural props. 80−16902
phthalazine, excited states, protonation influence, semiempirical CNDO/S CI calc. 79−76353
phytochrome chromophore, models, absorption wavelengths and oscillator strengths calc. 77−81469
plasma electron density, determ. by spectral line width, at. oscill. strength effects 77−51230
polar semiconductor, exciton, energies, oscillator strengths, and phonon side bands 80−44512
polar semiconductors, exciton-phonon interactions, optical absorpt. spectra, theory 80−49614
polarisation potential, quasiadiabatic, for elastic electron-atom scatt. 77−6929
polyatomic molecule, torsional motion, harmonic oscillator and free rotor bases calcs. 79−72232
polyatomic molecules, excitation energies, oscillator strengths, many body approach, eqns. of motion method 80−47969
polyelectron atom He-Xe, strength sum evaluation method 77−75229
polyenals related to visual chromophores, absorpt. spectra rel. to chain length 79−34494
polyenones related to visual chromophores, absorpt. spectra rel. to chain length 79−34494
polymer solution, conjugated, polymer two-photon dispersion, freq. depend., symmetry assignment and oscillator strengths 79−86094
porphin, MCD, LCAO MO SCR π-electron calcs., PPP approx. 78−9178
porphyrin a, MCD, LCAO MO SCR π-electron calcs., PPP approx. 78−9178
protoporphyrin, MCD, LCAO MO SCR π-electron calcs., PPP approx. 78−9178
quinoxaline, excited states, protonation influence, semiempirical CNDO/S CI calc. 79−76353
Raman effect in solids, interacting elementary excitations, review 78−43846
Raman scattering, continuum, time-depend. excitation profile 79−41175
rare earth ions, optical transitions, hypersensitivity to environment, mechanism 79−72255
rare earth metaphosphates, glasslike, spectral intensity, effect of number of 4f electrons 78−84602
relativistic effects in central field approximation, RELAC method and use 80−9520
relativistic effects introduction, ab initio methods 80−9519
relativistic electron-transition operators, matrix elements 78−82789
relativistic RPA calcs. for He(Be)(Mg)(Zn)(Ne) isoelectronic series 80−47925
resonant energy transfer cross section, form factor formalism, 1st Born approx. appraisal 77−65519
rhodamines, solutions, electronic absorption spectra and dimeric props. 77−88458
Rydberg INDO method, mol. Rydberg S←S and T←S transitions and oscill. strengths 78−17572
Rydberg-valence mixing, oscillator strengths 79−31492
screened potential model, for at. energy levels and oscill. strengths 79−36516
second-row elements, dipole oscill. strength distribs., moment calcs. 77−6733
second-row elements, dipole oscillator-strength distribs. 78−58626
semiconductor, bound exciton recombination, phonon replicas 79−38649
semiconductor, diamagnetic excitons, odd states, oscillator strengths and optical absorption line positions 79−11072
semiconductor, direct-gap, oscillator strengths for electron-hole complexes (A^0X) 77−35869
semiconductors, Auger and radiative recombination of acceptor bound excitons 79−47023
semiempirical, relativistic oscillator strengths including core polarisation for p-, s-, d-series 78−74609
singlet-triplet energy difference and singlet generalised oscillator strength, Lassettre-Dillon relation 80−63508
singly ionised atoms, $3s^23p^N$-$3s3p^{N+1}$ transitions, oscill. strengths calcs. 77−83542
singly-ionised atoms of Fe group, oscillator strengths for $3d^N4p\rightarrow3d^N4s$ dipole transitions 77−71780
solar and stellar element abundance, atomic and mol. f-values 78−20792
solids, liquids and mols., optical oscill. strengths and excitation energy 78−6648
solvated electrons, optical absorption spectra, temp. depend. moments, many-particle theory 79−72301
stilbene, single cryst. under pulsed electron excitation, $T_2\leftarrow T_1$ transition, oscillator strength 79−7838
tetracene, singlet exciton transitions, energies and oscillator strengths, boson theory with PPP wavefunctions 80−92820
Tokamak impurity problems, atomic and mol. struct. and collision data, review 80−43959
transfer of oscillator strength in regions of avoided crossings, two state approx. 78−25484
transition metal, atom, ion, solid, $M_{2,3}$ excitation spectra 78−91653
transition metals, 3d, M III excited states, radiative lifetimes, beam-foil obs. 77−30979
tropolone, in water and cyclohexane, electronic relax., absorption, excitation and fluoresc. spectra 78−66588
tunable laser interferometry, oscillator strength meas. 80−105697
two-electron systems, RPA eigenvalue eqns., excitation frequencies and oscillator strengths 78−17570
two-valence electron systems, valence, Rydberg and continuum orbitals 77−3259
Van der Waals coefficients, new bounds using oscill. strength sum rules 79−41219
velocity and length forms, QED 78−74615
water, low-density amorphous solid, OH stretching spectrum 79−11413
water, oscill. strengths of UV lines, rel. to abundance in interstellar clouds 78−90104
Wolf-Rayet stars, calc. of oscillator strengths of transitions for ion spectra C III, N IV, and O V *(Russian)* 78−57566
Ag film, granular, transmission and reflection spectra, validity of sum rule 80−97358
Ag, ionisation energies and oscill. strengths calcs. 80−5488
Ag isoelectronic series, excitation energies and oscillator strengths 79−54918
Ag, relativistic HF, core-polarisation model pot. 78−86818
Ag, semiempirical, relativistic oscillator strengths including core polarisation for p-, s-, d-series 78−74609
AgI isoelectronic series, oscill. strengths, relativistic HF calcs. 79−98034
β-AgI thin film, exciton spectrum 80−55216
Al, electron scatt., transitions, oscill. strengths, config. superposition calcs. 77−6732
Al I, $4s^2S_{1/2}$ reson. level, mean life 79−59400
Al II to Al VI, beam-foil obs. from 1100 to 1900 Å, lifetimes and oscillator strengths 80−14108
Al II to Al VI, beam-foil obs. from 300 to 2000 Å, mean lives and oscillator strengths 80−14109
Al IX to Al XI, beam-foil obs. of lifetimes and oscillator strengths, 300 to 1000 Å 80−14110
Al, laser produced plasma, X-ray spectroscopy 77−72502
Al, oscillator strengths and radiative lifetimes 79−54811
Al sequence, $4s^2S$-$4p^2P$ transition, f-values 78−78651
Al transitions, Stark broadening and oscillator strengths 78−29761
Al XII, He-like ion, oscillator strengths of transitions between low-lying S and P states 78−13470
$3Al_2S_3$:La_2S_3:Ho^{3+}, radiative and multiphonon relax. 79−33794
Ar, $2p^6$ shell, oscillator strength, photoionisation cross sections, electron shell alterations determ. *(Russian)* 80−58144
Ar, absorpt. spectra, field induced autoionisation near ionisation threshold 80−106301
Ar, and isoelectronic sequence, E1 transitions, relativistic oscill. strengths 78−949
Ar, electron impact ionis., single charge, inter-shell correl. 77−88567
Ar IV to Ar XII, beam-foil obs. of lifetimes and oscillator strengths, spectral identifications, 400-2000 Å *(French)* 80−9555
Ar IX, Ne I like reson. and Na I-like satellite lines, relativistic HF calc. and expt. 78−94210
Ar ions, spectral classification in θ-pinch plasma 79−6896
Ar line broadening by at. collisions, meas. of oscillator strength of ArI lines reson. *(French)* 78−5172
Ar, nonempirical calc. of X-ray K-absorpt. spectra 77−88465
Ar, optical oscillator strengths, 3p-ns and 3p-nd transitions, independ. particle model 78−86816
Ar, oscillator strengths, determ. from self-absorption of reson. radiation 79−89641
Ar plasma jet, weakly ionised reson. lines 77−75106
Ar, reson. transition oscill. strengths, rel. to electron impact 80−27985
Ar VIII, beam-foil lifetime meas. using ANDC anal. for reson. doublet 79−93964
Ar XV, wavefunctions and oscill. strengths, CI calcs. 80−23317
As I, rel. oscill. strengths, 193.8 and 197.3 nm lines 79−791
As, L-shell soft X-ray emission spectra, oscillator strengths 80−32651
As XXV, 2p-4d and 2p-4s transition arrays, wavelengths and oscillator strengths 80−47933
Au film, granular, transmission and reflection spectra, validity of sum rule 80−97358

oscillator strengths continued
Au I, relativistic oscill. strengths 77−14388
Au, relativistic HF, core-polarisation model pot. 78−86818
Au, semiempirical, relativistic oscillator strengths including core polarisation for p-, s-, d-series 78−74609
AuI isoelectronic series, oscill. strengths, relativistic HF calcs. 79−98034
B I, weighted oscillator strengths for elec. dipole and forbidden transitions, data tables 80−37779
B I and II, high spin and mixed states 77−61709
B II, oscill. strengths for $2s^2$, $2p^2$, $2s3s(^1S)$-$2s2p(^1P)$ transitions 77−46533
B III, optical oscillator strengths for excitations from $1s^22s(^2S)$ ground state 79−98044
B isoelectronic series, dipole oscill. strengths, multiconfigurational Hartree-Fock calcs. 77−83540
B, oscill. strength distribs., Stieltjes imaging determ. 77−6731
B-like ions, highly ionised, up to Fe XXII, Breit-Pauli approximation 78−53810
Ba, atom, electron impact step-wise excitation *(Russian)* 80−83497
Ba I, hook method, gf values of intercombination line, 7911.38 Å 78−66511
Ba I, oscillator strength meas. 78−74607
Ba+Kr, collision induced dipole transition, elec. quadrupole transition, oscillator strengths 79−41128
BaF_2, strain induced splitting and oscillator strength anisotropy of IR transverse optic phonon 80−92625
$BaO-M_xO_y-B_2O_3$ glass, UV absorpt., inherent absorpt. wavelength and oscill. strength, cation effects 78−80374
Be, and isoelectronic sequence, oscillator strengths, relativistic RPA calcs. 77−57929
Be, highly excited states, electronic struct., oscillator strengths and resons., HF calcs. 77−46506
Be I, weighted oscillator strengths for elec. dipole and forbidden transitions, data tables 80−37779
Be I isoelectronic sequence, radiative props. determ. by model-pot. method 78−70788
Be I isoelectronic series, $2p^2$-2s2p and 2s2p-$2s^2$ transitions, oscill. strengths, transition probabilities 77−46532
Be II, optical oscillator strengths for excitations from $1s^22s(^2S)$ ground state 79−98044
Be, ionisation energies and oscillator strengths, polarised frozen core approx. 79−36524
Be, isoelectronic sequence, relativistic transition probability calcs. 77−54533
Be isoelectronic sequence, mag. quadrupole transitions probabilities 78−37592
Be isoelectronic sequence, electron impact excitation 79−81286
Be isoelectronic sequence, highly ionised, beam-foil obs. of oscillator strengths for E1 transitions 80−14112
Be isoelectronic series, excited states, oscill. strengths calcs., influence of wave function determ. method 80−99478
Be isoelectronic series, transitions involving $2s3l^3L$ states, oscill. strengths 77−3308
Be, oscillator strengths, generalised RPA with exchange calcs. 79−98030
Be-like ions, oscill. strengths and transition probabilities, Breit-Pauli approx. calcs. 79−36570
BeF_2, aq. glass, 76K, solvated electron spectrum evolution, following ns radiolysis 78−88295
BeF_2:Eu^{3+} glass, luminesc. of Eu^{3+}, transition probabilities 80−80845
Bi, Dirac eqn. calc. 79−22620
Bi V, relativistic oscill. strengths 77−14388
Br, fluoresc. in Ar^*+Br_2 lamp 78−46466
Br, L-shell soft X-ray emission spectra, oscillator strengths 80−32651
BrVI(VII), reson. line oscill. strengths, beam-foil spectra 77−38630
C I, f-values of interstellar lines in ζ Puppis and ζ Ophiuchi 79−35332
C I, weighted oscillator strengths for elec. dipole and forbidden transitions, data tables 80−37779
C I transition probabilities and oscillator strengths, rel. to H I regions 77−49448
C III, atoms, static polarisability, lower bounds, oscill. strength calcs. 77−75074
C, optical oscillator strengths, independent particle model, excited state wave functions, LS coupling and Born approx. 80−32674
C, radiative lifetimes of visible and near IR transitions, solar abundance 78−50506
C, theoretical ionis. energies and oscill. strengths, excited s-, p- and d-levels 78−86823
C_2 vapour, Swan bands, oscillator strength 80−63712
C_3, Swings band system, absorpt. cross section, oscill. strength meas. 79−98116
CH in F- and G-type stars, bands oscillator strengths rel. to C abundances 77−91530
CH^+, expt. oscillator strength 77−34693
CH^+, photodissoc., $A^1\Pi$ state shape resonances 79−54924
CN in F- and G-type stars, bands oscillator strengths rel. to C and N abundances 77−91530
CO, electronic states, oscill. strengths calcs. 78−9095
CO, ground-state, absorpt. oscillator strengths for vibr. rot. transitions 78−62846
CO, high resolution lifetime meas., perturbation and collisional transfer correl. 78−78699
CO, oscill. strengths for shape resonances near K edges 77−75224
CO, photoabsorption, photoionisation cross section, separated channel static exchange Stieltjes-Tchebycheff calc. 79−3502
CO, X-ray K-absorpt. spectra, reson. obs., near fine struct. 80−37817
CO_2, electron impact, transitions, generalised oscill. strengths 78−94327
CO_2, photoionisation, partial oscill. strengths 79−6973
CO_2, valence shell ionic photofragmentation, oscill. strengths, EELS and electron-ion coincidence meas. 80−37879
Ca, quantum defect theory of oscill. strength density 79−81183
Ca, valence shell states, calc. 78−17611
Ca XVII, wavefunctions and oscill. strengths, CI calcs. 80−23317
Ca+inert gas, collision-induced dipole transitions assoc. with high-lying states 80−37866
CaF_2, strain induced splitting and oscillator strength anisotropy of IR transverse optic phonon 80−92625
$Cd(Ca)F_2$:Co^{2+}, Jahn-Teller split $^4A_{2g}\rightarrow{}^4T_{1g}(P)$ absorption band, elec. field effect 78−15202
$CdCr_2S_4$, ferromag. semicond., IR refl. spectra, phonon props. and dielec. function 80−66191
oscillator strengths continued
CdS(Se), single cryst., band parameters from optical exciton spectra 79−47021
Cl, 4s-$3p^5$ transitions 77−46537
Cl (IX-XV) allowed intra L-shell transitions, oscill. strengths and radiative lifetimes meas. 79−13676
Cl ions, multiply-charged, beam-foil obs. of allowed L-shell transitions 80−14113
Cl, kinetic spectroscopy in far vacuum UV, oscillator strengths of transitions 78−13457
Cl, photoionis. cross sections, RPA with exchange method generalisation 79−10077
Cl VIII, Ne I like reson. and Na I-like satellite lines, relativistic HF calc., beam-foil spectra 78−94210
Cl^-, far UV spectra in solns. 78−94208
Cl_2, inner shell excited states, X-ray absorpt. spectra, HF calcs. 80−78536
ClO, $A^2\Pi_i$-$X^2\Pi_i$ absorpt. cross-sections and oscill. strengths, f-values 77−38649
ClO, vibr.-rot. bands, intensity parameters 78−17722
Co I, excited levels lifetimes and absolute oscillator strengths 78−5178
Cr, atomic transition probabilities, oscill. strengths 78−74601
Cr I, discrepancies between theoretical and experimental oscillator strengths 77−83539
Cr I excited levels, lifetime meas., oscill. strengths 77−71777
Cr I in photospheric spectra, solar abundance and oscillator strengths 78−69757
Cr I lines, 200-541 nm, oscillator strengths determ. from hook-method and absorpt. meas. 77−79582
Cr II lines, A_{mn} transition probabilities 80−14099
Cr(II) lines, oscill. strengths in 2413-2718 Å wavelength range 80−106294
Cs, discrete level raising into far continuum, oscillator strength to shape reson. transfer 78−78624
Cs, hook spectra, evaluation limitations 80−90905
Cs inert gas, pot. energy curves, collision induced oscillator strengths 79−22659
Cs, oscill. strengths of principal series doublets 79−13671
Cs, oscillator strengths in principal series, Rozhdestvenskii hook obs. 80−37760
Cs, photoabsorption oscillator strengths, $17<n<\infty$ transitions, interpolation formula 80−9559
Cs, quadrupole lines, oscillator strengths, broadening 77−18846
Cs, Rydberg states, principal series doublets, intensity ratio anomalies 79−18148
Cs+He, interaction pot. and oscill. strength 80−91645
Cs_2, oscill. strengths 77−18846
CsI, isoelectronic series, oscill. strengths, relativistic HF calcs. 79−98035
$Cs(5D_{5/2,m=1/2})$+inert gas, dipole-induced transitions, pot. curves, oscillator strength 80−32816
Cu atoms, formula for cancellation disappearances 78−90124
Cu isoelectronic series, core polarisation influence on oscillator strengths 79−45672
Cu, isoelectronic series, oscillator strengths of reson. transitions 79−22666
Cu, isoelectronic series, semi-empirical oscillator strengths, lifetime, transition probability 80−32672
Cu, L-shell soft X-ray emission spectra, oscillator strengths 80−32651
Cu, relativistic HF, core-polarisation model pot. 78−86818
Cu, resonance lines, relative oscill. strengths, absorpt. spectra 78−42005
Cu sequence, ^2S-^2P transitions, oscill. strengths calc. 77−50406
Cu XXI, 2p-4d and 2p-4s transition arrays, wavelengths and oscillator strengths 80−47933
Cu^+, reson. transition, effect of correl. in $3d^n$ core, HF calcs. 80−47911
Cu-like ions, E1 transitions, wavelengths, oscillator strengths and transition probabilities, data tables 80−37780
CuBr(Cl)(I), polariton Raman spectra, oscillator strengths, temp. depend. 80−66197
CuCl, induced absorption due to exciton-biexciton transitions 78−15187
D_2, Lyman bands, Morse Franck-Condon factors and R-centroids 77−58088
Er, absolute oscill. strengths of spectral lines 79−85928
Er, spectral lines, relative oscill. strengths determ. 77−83657
EuO(S), ferromagnetic electronic structure, absorption, thermoreflection and thermotransmission spectra *(French)* 80−97300
EuP_5O_{14}, luminesc. of Eu^{3+}, transition probabilities 80−80845
F III, IV, beam-foil spectra, mean lives, 2150-3200 angstrom 78−55224
F, kinetic spectroscopy in far vacuum UV, oscillator strengths of transitions 78−13457
F V, F VI, transition probabilities calcs. 79−54792
F^-, photodetachment cross section, Stieltjes imaging method 78−55149
F_2, eqns. of motion method, transition energies, oscill. strengths, electron impact Born cross section 77−18983
FNO, electronic transitions, limited GSMO and ESMO CI calcs., oscillator strengths, spectra 78−70750
Fe complex, Fe (III) acetylacetonate, solvent effects on oscillator integrated strength, IR absorpt. bands 78−84575
Fe group second spectra, correction to absolute oscillator strengths 77−3310
Fe I, a^3F_{2-4} levels, relative oscillator strengths 80−63572
Fe I, excited levels lifetimes calcs. from oscillator strengths compared with measured values 79−36586
Fe I, gf-values rel. to metal-poor dwarf stars abundance anals. 79−92760
Fe I, precision oscillator strengths from levels a^5F_{1-5} and a^5D_{0-4}, comparison 79−36584
Fe I, relative oscillator strengths for transitions from $a^5D_{0,1,2}$ levels, precision meas. 77−438
Fe I oscillator strengths, comparison of calc. and meas. 77−3310
Fe I transition from levels a^5F_{1-5}, relative oscillator strengths precision meas. 79−36585
Fe I transitions from levels a^5D_{0-4}, relative oscillator strengths precision meas. 79−36583
Fe II, oscill. strengths, astrophys. appl. 79−59398
Fe II, oscillator strengths derived from solar spectrum, choice of solar model atmosphere 80−56791
Fe VI forbidden emission under nebular conditions 79−8970
Fe X (XI), energy levels and oscill. strengths, Slater radial integrals 77−79583
Fe XII and XIII, energy levels and oscillator strengths for XUV transitions 78−46277

oscillator strengths continued
Fe XIX and isoelectronic ions $2p^4$-$2p^3$3d transition array 77−42267
Fe XVIII and XIX $2s^22p^n$-$2s^22p^{n-1}$4d classification, for laser produced plasmas and solar spectra 77−42268
Fe XX and isoelectronic ions, $2p^3$-$2p^2$3d transition array 77−65434
Fe XXI and isoelectronic spectra $2p^2$-2p3d transition array 77−38632
Fe XXII, allowed transition CI wave functions, oscill. strengths and transition probabilities 80−32664
Fe XXII, coupling energy levels, oscillator strengths, electron collision energies 80−69068
Fe XXII, intercomb. transitions, oscill. strengths, transition probs., rel. to solar spectra 80−52935
Fe XXIII, wavefunctions and oscill. strengths, CI calcs. 80−23317
Fe XXIII and XXIV, reson. and intersystem transitions, oscill. strength, lifetime, beam-foil spectra 78−82685
Fe XXIV, oscillator strengths, electron impact excitation collision strengths, solar flare spectra appl. 80−32647
Fe XXV, He-like ion, oscillator strengths of transitions between low-lying S and P states 78−13470
Fe^+, gf values determ. in laboratory, for solar studies 80−42994
Fe-group, atoms and singly ionised, f-value meas., review 78−17617
FeVIII-XXVI energy level tables and Grotrian diagrams 80−74142
Ga I, relativistic HF calculations, $np^2P_{1/2,3/2}\rightarrow(n+1)^2S_{1/2}$ and $np^2P_{1/2,3/2}\rightarrow nd^2D_{3/2,5/2}$ transitions 79−89609
Ga, L-shell soft X-ray emission spectra, oscillator strengths 80−32651
Ga, oscillator strengths and radiative lifetimes 79−54811
Ga XXIII, 2p-4d and 2p-4s transition arrays, wavelengths and oscillator strengths 80−47933
GaAs:Cr, 0.84 eV no-phonon luminesc., fine struct. and origin 80−103980
$Ga_{1-x}In_xAs$, IR reflectivity, cluster effect on optical phonons 80−97259
$3Ga_2S_3.La_2S_3:Ho^{3+}$, radiative and multiphonon relax. 79−33794
GaSe, electron-phonon interaction and optical props. 80−34942
Gd^{3+} in solution, absorpt. spectrum intensity *(Russian)* 78−35169
Ge, electric quadrupole sum rules rel. to optical consts. 79−38036
Ge, group III acceptor impurities, oscillator strengths of dipole optical transitions 79−56823
Ge IV spectra, nonrelativistic oscillator strengths calc. 77−83538
Ge, sum rule for intraband optical absorpt. of shallow acceptor impurities 79−28793
Ge:B(Al)(Ga), shallow acceptor spectral line intensities 80−88517
H, 2s-3p transition, Glauber approx. 78−74613
H, oscillator strength, sums, one-term approx. 78−66509
H, oscillator strength sums, one term approx. 79−45656
H, photoionisation cross sections elec. field-induced oscills. 80−955
H plasma, thermal emission and Debye shielding 80−64692
H, pseudospectral dipole oscillator strength distribs. 78−50503
H, Stark and photoabsorption spectrum, density of oscillator strengths, atom c.f. semiconductor spectra 80−83318
H, transition probabilities and expectation values, in intense mag. field 79−10066
H, triple-dipole energy calcs. using pseudo spectral theory 78−46418
H^-, $^1P_0$-reson., DC Stark effect calcs. 78−42000
H^- vac. UV spectra, narrow reson. at 1129.5 Å, H-arc spectra 78−66490
H-Xe atom, strength sum S(2) evaluation method 77−75230
H^++He, 25-1000 keV, $1^1S\rightarrow n^1S$ excitation cross sections, Glauber approx. calc. 79−54959
H_2, D_2, photoionisation, body-frame Hund's case b description 78−94295
H_2, dipole oscill. strength distribs., sums 78−21975
H_2, electron impact excitation total cross sections, oscill. strengths, independent particle model calcs. 77−61856
H_2, Lyman bands, Morse Frank-Condon factors and R-centroids 77−58088
H_2, oscillator strength, $X\ ^1\Sigma_g^+$-$C^1\Pi_u$ transition, upper and lower bounds 77−83654
H_2, pseudospectral dipole oscillator strength distribs. 78−50503
H_2, triple-dipole energy calcs. using pseudo spectral theory 78−46418
H_2, quadrupole vibration-rotation transition probabilities 78−25512
H_3^+, struct. props., in mag. fields, var. calcs. 78−21843
HCN, electronic states, oscill. strengths calcs. 78−9095
HCl, $C^1\Pi$-$X^1\Sigma^+$ system, (0, 0) and (0, 1) bands, oscillator strength determ. and UV spectra 80−91570
HCl, nonempirical calc. of X-ray K-absorpt. spectra 77−88465
HD, Lyman bands, Morse Franck-Condon factors and R-centroids 77−58088
HF, nonempirical calc. of X-ray K-absorpt. spectra 77−88465
HNO^+_1, ab initio SCF and CI comparison of struct. and spectra, rel. to NOH^+ 77−26972
H_2O, dipole oscill. strength distribs., sums 78−21975
H_2O, dipole oscillator strengths, 10-60 eV, for photoabsorpt., photoionis. and fragmentation 78−42133
H_2O, electronic states, oscill. strengths calcs. 78−9095
H_2O, pseudospectral dipole oscillator strength distribs. 78−50503
H_2O, triple-dipole energy calcs. using pseudo-spectral theory 78−46418
H_2O_2, electronic states, optical rot. dispersion, oscill. strength calcs. 78−9095
H_2S, electronic struct., ab initio CI SCF calc., spectra assignments 77−10586
H_2S, valence shell binding energy spectrum, 8-34 eV, electron scatt. simulation of photoionis. 79−10213
He, elastic electron scatt. phaseshifts, 2s2p ^3P autoionisation, 1s2s $^3S\rightarrow$1sep ^3P triplet continuum photoionisation 79−31480
He, generalised oscill. strength, variational determ., extremum principle appls. 78−94213
He, isoelectronic sequence, E1 and E2 oscillator strengths, MCHF calcs. 80−106292
He isoelectronic series, dipole oscillator strength distrib. moments, systematics 78−86821
He like atoms, dipole transitions, transition integral cancellation 80−69052
He metastable state, two- and three-photon ionisation 80−91518
He, oscill. strength and first derivative, optical limit 77−3305
He, oscill. strength distribs., Stieltjes imaging determ. 77−6731
He, oscillator strength, sums, one-term approx. 78−66509
He, photoabsorption, modified RPA calcs. with exchange 78−13477
He, photoionisation, frozen-core HF perturbation theory, oscillator strength, dipole length and vel. calc. 78−78672
He, pseudospectral dipole oscillator strength distribs. 78−50503

oscillator strengths continued
He, RPA eigenvalue eqns., excitation frequencies and oscillator strengths 78−17570
He, tight bounds on multipole dispersion coefficient calcs. for interaction of atoms 80−83320
He, triple-dipole energy calcs. using pseudo-spectral theory 78−46418
He^-, highly excited states, electronic struct., oscillator strengths and resons., HF calcs. 77−46506
He-like atoms, n=2 states radiative transition rates, oscill. strengths, RRPA extension 77−34584
He-like atoms, oscillator strength calc., allowed np-n'd and nd-n'f transitions 79−31467
He-like ions, $2^3P_1^0$-1^1S_0 and $2^1P_1^0$-1^1S_0 freqs. and transition rates, relativistic calc. 79−68210
He-like ions, oscillator strengths of transitions between low-lying S and P states 78−13470
He+e, generalised differential oscillator strengths on impact ionisation 78−55239
^{4}He, soft-core radial wave function, photo-disintegration calculation 80−18209
Hf IV, $6s\ ^2S_{1/2}$-$6p\ ^2P^\circ_{1/2,3/2}$ transition, relativistic oscillator strengths, influence of core polarisation 80−58132
Hg II, relativistic oscill. strengths 77−14388
Hg II line oscillator strength determ. in Ap-type stars, diffusion model implications 80−72966
Hg vapour, absorpt. spectrum, 1849 Å line, self-broadening, interatomic interaction *(French)* 80−32661
p-HgTe, far IR reflectivity spectra, experimental and theoretical study of the dynamic dielectric function 78−92069
Ho I, Ho II, excited level lifetimes and oscillator strengths, visible spectra 80−63573
HoI, relative oscill. strengths 79−98038
$Ho(NO_3)_3$ solns., f-f transitions, intensity anal., correl. with cond. and US absorpt. 80−97292
I II, reson. lines, oscill. strengths determ. by absorption method 80−58214
I VI and I VII, beam-foil obs. of lifetimes, spectral assignments, 400 to 1300 Å 80−9556
I VII, beam-foil lifetime meas., cascading problem 80−14249
I_2, relativistic HF calcs., $np^2P_{1/2,3/2}\rightarrow(n+1)^2S_{1/2}$ and $np^2P_{1/2,3/2}\rightarrow nd^2D_{3/2,5/2}$ transitions 79−89609
In, oscillator strengths and radiative lifetimes 79−54811
$In_{1-x}Ga_xP$, quantitative characterisation of chemical disorder from wavelength-modulated no-phonon absorpt. 79−15482
InSe, spin orbit split off valence bands, exciton transitions, Hopfield's quasicubic model, visible absorpt. spectrum 80−50370
KCN_xCl_{1-x}, finite field local field catastrophe phenomena in spectra 80−92830
KCl, irradiated crystal, determ. of oscillator strength of V_3-centre *(Russian)* 78−92095
KCl:Eu^{2+}, optical absorpt. meas. for Eu^{2+} conc. determ. 79−51137
KCl:Tl^+, cryst., electron transfer, optical and thermal excitation 79−4833
KCl(Br)(I):Eu^{2+}, single cryst. optical absorpt. spectra 80−45117
$KD_{2x}H_{2(1-x)}PO_4$ crystals, $0<x<0.98$, light scatt. by polaritons 80−96802
KI, oscillator strengths of defects, Smakula eqn. generalisation 80−108232
$KMgF_3$:Fe^{2+}, Jahn-Teller quenched spin-orbit, splitting of $^5T_{2g}$ state 77−63442
K_2O-BaO-SiO_2 glass, rare earth ion activated, spectral intensity, effect of number of 4f electrons 78−84602
K(5S)Xe, K(5S)Kr, excimer, visible emission band, exptl. results relative to theory 78−82779
Kr, absorpt. spectra, field induced autoionisation near ionisation threshold 80−106301
Kr, DC glow discharge excited atoms, radial conc. distrib. obs. 78−67494
Kr, electron energy loss spectra, energy-depend. multichannel quantum defect theory anal. 77−61860
Kr I-VIII, beam foil mean life meas., f-values 77−30974
Kr II, calcs. of radiative lifetimes, absolute transition probabilities and oscillator strengths 77−50405
Kr VIII, beam-foil decay curves for reson. transitions simulation 80−9721
Kr VIII, beam-foil lifetime meas. using ANDC anal. for reson. doublet 79−93964
Kr VII(VIII), reson. line oscill. strengths, beam-foil spectra 77−38630
Kr XXXIII and Kr XXXIV, beam-foil obs. of transition wavelengths and oscillator strengths 80−14115
$(La_{1-x-y}Pr_xA_y)Cl_3$ (A=Ce, Gd, Y), satellite lines in optical absorpt. spectra, Zeeman effect 79−65912
Li atoms, photoexcitation and ionisation cross sections, Stieltjes-Tchebycheff procedure 78−17633
Li, core charge polarisation, HF calcs. 79−45627
Li, dipole oscill. strength sums, dipole-dipole and dipole-quadrupole van der Waals consts. 78−9127
Li, dipole oscill. strength distribs., sums 78−21975
Li, electron impact excitation, 15-190 eV, generalised oscill. strengths, differential cross sections 80−23556
Li, highly excited states, electronic struct., oscillator strengths and resons., HF calcs. 77−46506
Li I laser, 207 Å, oscillator strengths 80−83598
Li isoelectronic sequence, oscill. strengths 77−3309
Li isoelectronic sequence, Hartree-Fock wavefunctions *(French)* 77−34586
Li, isoelectronic sequence, radiative transition probabilities calcs. 77−83544
Li isoelectronic series, relativistic pseudopot. appl. in HF calcs. 80−27960
Li, optical oscill. strengths calcs. 80−91495
Li, pseudospectral dipole oscillator strength distribs. 78−50503
Li, quartet states, transition energies, oscill. strengths, CI calcs. 78−58597
Li, triple-dipole energy calcs. using pseudo-spectral theory 78−46418
Li-He, oscill. strength, for induced dipole transitions, pot. energy curves 77−75100
LiF:OH crystals, X-irradiated, H centres formation and annealing 80−54226
Lu III, $6s\ ^2S_{1/2}$-$6p\ ^2P^\circ_{1/2,3/2}$ transition, relativistic oscillator strengths, influence of core polarisation 80−58132

oscillator strengths continued
Mg, and isoelectronic sequence, relativistic effects on transition probabilities 77−54532
Mg, Hanle effect density depend., $3s4p\,^1P_1{}^0$ level, and oscill. strengths 79−72282
Mg I, $3\,^1P_1{}^0$ level reson. broadening and lifetime 77−57916
Mg I isoelectronic sequence, intercombination line oscillator strengths 80−23360
Mg IX, wavefunctions and oscill. strengths, CI calcs. 80−23317
Mg, intercombination line oscill. strength, including core-polaris. and relativistic effects 78−25475
Mg isoelectronic sequence, mag. quadrupole transitions probabilities 78−37592
Mg, isoelectronic series, oscill. strengths and excitation energy, RRPA calcs. 78−13471
Mg, photoabsorpt. and photoionisation, RPA with exchange calcs. 77−54543
Mg sequence, D-F transitions 79−54809
Mg VII, UV lines, theoretical intensity ratios 78−90108
Mg, valence shell states, calc. 78−17611
Mg XI, He-like ion, oscillator strengths of transitions between low-lying S and P states 78−13470
MgH, and MgD, $B'\,^2\Sigma^+$-$X\,^2\Sigma^+$ band system, ab initio CI calcs. 79−93970
MgH, X and $B'\,^2\Sigma^+$ and $A\,^2\Pi$ ab initio CI calc. 79−31415
MgH, X→A and X→B′ band systems, oscill. strengths and photodissoc. cross-sections 79−94045
^{24}MgH, IR rot.-vibr. bands, stellar atm. appls. 77−18918
Mn, atomic transition probabilities, oscill. strengths 78−74601
Mn^+, oscillator strengths, from level lifetimes and branching ratios 78−17619
Mo I, relative oscill. strengths in dissoc. $MoCl_5$ pulsed discharge 78−25479
Mo^{13+}, energy levels for transition probabilities, oscillator strengths, rad. lifetimes 78−17589
Mo^{30+}, VUV reson. lines, transition probabilities calcs. 78−41989
N, dipole oscill. strength distribs., sums 78−21975
N, far vac. UV spectra, oscillator strengths for 3s, 4s, 5s, 3d and 4d ^4P_J-$2p^3\,^4S_{3/2}{}^0$ 80−74178
N I, forbidden radiative transition probabilities rel. to NGC 7027 low-excitation emission 77−64823
N I, weighted oscillator strengths for elec. dipole and forbidden transitions, data tables 80−37779
N I resonance lines 79−5741
N I transition probabilities and absolute oscillator strengths, rel. to H I regions 77−49448
N II, electron impact excitation cross sections, rel. to solar corona abundance 80−58391
N II, optical oscill. strengths 79−98032
N III, electron impact excitation cross sections, generalised oscillator strengths, Born approx. 80−18928
N III, optical oscill. strengths meas. 79−98031
N IV, dipole lengths, dipole vels. and transition probabilities 79−35113
N IV, excited states, transaction oscill. states and wavefunctions 79−59367
N IV, transition probabilities calcs. 79−54792
N isoelectronic sequence ions, theoretical EUV oscillator strengths and electron scatt. data 80−51649
N, oscillator strength calc. for $^4S^0$ to ^4P sequences 78−25485
N, pseudospectral dipole oscillator strength distribs. 78−50503
N, radiative lifetimes of visible and near IR transitions, solar abundance 78−50506
N, triple-dipole energy calcs. using pseudo-spectral theory 78−46418
N V, optical oscillator strength 80−47941
N_2, 400 eV core-excited valence states, limited CI calc., transition energies and oscillator strengths 79−68196
N_2, B-state collisional transfer, press. effects, oscillator strengths, time resolved spectra 79−36744
N_2, continuum, energy loss cross sections for 300, 400 and 500 eV electrons 79−94090
N_2, dipole oscill. strength distribs., sums 78−21975
N_2, electron impact excitation total cross sections, oscill. strengths, independent particle model calcs. 77−61856
N_2, electron impact excitation, 12.5-14.2 eV energy-loss region 78−17811
N_2, N K-shell excitation, high-resolution electron energy loss spectra 80−53152
N_2, oscill. strengths for shape resonances near K edges 77−75224
N_2, oscill. strengths of $W^3\Delta_u$-$X^1\Sigma_g{}^+$ band system 79−59486
N_2, pseudospectral dipole oscillator strength distribs. 78−50503
N_2, triple-dipole energy calcs. using pseudo-spectral theory 78−46418
N_2 triplet-triplet transitions, Einstein-A coeffs., oscill. strengths, lifetimes, theory and experiment comparison 80−47876
N_2, X-ray K-absorpt. spectra, reson. obs., near fine struct. 80−37817
NH in F- and G-type stars, bands oscillator strengths rel. to N abundances 77−91530
$NH_2{}^+$, low lying states, ab initio MRD-CI pot. surface calcs. 79−89611
NH_3, dipole oscill. strengths for excitation, ionisation and fragmentation by 5-60 eV electrons 77−68129
NH_3, dipole oscill. strength distribs., sums 78−21975
NH_3, electron impact, 35 keV, Bethe surface and Compton profile 80−87235
NH_3, photoionisation branching ratios and partial oscill. strengths 78−5303
NH_3, pseudospectral dipole oscillator strength distribs. 78−50503
NH_3, tripledipole energy calcs. using pseudo-spectral theory 78−46418
N_3H_3 radical, lowest two electronic states 80−925
NO, dipole oscill. strength distribs., sums 78−21975
NO, γ band lines, collisional broadening coeff. and optical collision diameter 80−63714
NO, γ(0,0) band, collisional broadening parameters 80−63713
NO, N K-shell excitation, high-resolution electron energy loss spectra 80−53152
NO, pseudospectral dipole oscillator strength distribs. 78−50503
NO, triple-dipole energy calcs. using pseudo-spectral theory 78−46418
NO+N_2(CO_2)(CO)(CH_4)(Ar), NO γ(0,0) band, oscillator strength and line broadening 80−106356
N_2O, dipole oscill. strength distribs., sums 78−21975
N_2O, N K-shell excitation, high-resolution electron energy loss spectra 80−53152
N_2O, pseudospectral dipole oscillator strength distribs. 78−50503
oscillator strengths continued
N_2O, triple-dipole energy calcs. using pseudo-spectral theory 78−46418
N_2O, valence shell ionic photofragmentation, oscill. strengths, EELS and electron-ion coincidence meas. 80−37879
NO($A^2\Sigma^+$, v'=0,1,2) lifetimes, $A^2\Sigma^+$-$X^2\Pi$ transition moment, oscill. strengths, internucl. separation depend. 78−82787
NOH^+, ab initio SCF and CI comparison of struct. and spectra with HNO^+ 77−26972
Na, absolute photoabsorpt. cross section, 45-250 eV 77−88434
Na core polarisation effect on oscillator strengths and energy level locations 78−82688
Na, first reson. doublet, anomalous dispersion meas. 77−71891
Na, high resolution inelastic electron scatt. at zero angle, oscillator strengths 78−9255
Na isoelectronic sequence, electron impact excitation, transition probabilities, oscill. and collision strengths 78−25718
Na isoelectronic sequence, theoretical f-values 78−37593
Na isoelectronic sequence, hypervirial theorem, screening parameters and oscill. strengths 79−6882
Na isoelectronic series, oscill. strengths, effective orbital quantum no. method 80−9521
Na, measurement using reson. Faraday effect in monochromatic light 80−23363
Na, oscill. strengths, Bates-Damgaard approx. calcs. 77−3311
Na, photoabsorpt. and photoionisation, RPA with exchange calcs. 77−54543
Na V(VI)(VII), beam-foil spectra, extreme UV mean lifes and oscillator strengths 79−31456
Na-like ions, transition probabilities for reson. transitions 78−66494
Na_3, electronic struct., pot. energy surface, ab initio CI study 78−70996
NaCl:Eu, secondary Eu phase dissolution, EPR and optical absorpt. study 80−96655
NaCl:Eu^{2+}, optical absorpt. meas. for Eu^{2+} conc. determ. 79−51137
NaCl:Eu^{2+}, single cryst. optical absorpt. spectra 80−45117
$Na_2Nd_2Pb_6(PO_4)_6Cl_2$, high-Nd conc. laser material, oscillator strengths and laser effect 79−55140
$NaPO_3$:Eu^{3+} glass, luminesc. of Eu^{3+}, transition probabilities 80−80845
Na(4S)Xe, Na(4S)Kr, excimer, visible emission band, exptl. results relative to theory 78−82779
Nd complex, with ortho-phenanthroline and αα′-dipyridyl tris-trifluoroacetate, absorption spectra 79−98113
Ne, $2p^6(^1S_0)$ ground state electron impact excitation cross sections 80−23558
Ne (II-VI), 209-602 Å, mean lives and oscill. strengths beam-foil spectroscopy 77−79561
Ne, dipole dynamic polarisabilities and two-photon photoionisation cross section calc., R-matrix approach 80−102444
Ne I isoelectronic sequence, X-ray spectra, K X to Fe XVII 79−22641
Ne, isoelectronic sequence, excitation energy and oscillator strength, level crossing anomaly, relativistic RPA calc. 80−14077
Ne, nonempirical calc. of X-ray K-absorpt. spectra 77−88465
Ne, optical oscill. strengths calc. 79−6914
Ne, oscillator strengths, determ. from self-absorption of reson. radiation 79−89641
Ne, reson. transition oscill. strengths, rel. to electron impact 80−27985
Ne VII, excited states, transaction oscill. states and wavefunctions 79−59367
Ne VII, transition probabilities calcs. 79−54792
Ni I, UV lines, oscillator strengths from hook method and absorpt. meas. in furnace 80−83319
Ni I solar photosphere from oscillator strength obs. 80−98625
Ni II, near UV lines, wall-stabilized arc meas. 78−42003
Ni XII, XIII, XIV, XV, 3s-3p and 3p-3d transitions, oscillator strength and energy levels calcs. 80−83251
Ni XVIII solar XUV flare lines, oscillator strength meas. 79−5796
Ni XXVII, He-like ion, oscillator strengths of transitions between low-lying S and P states 78−13470
O, dipole oscill. strength distribs., sums 78−21975
O, dipole transition oscill. strengths, photoionis. cross section 78−9120
O I, oscillator strengths interstellar O abundance 78−16498
O I, weighted oscillator strengths for elec. dipole and forbidden transitions, data tables 80−37779
O I transition probabilities and oscillator strengths, rel. to H I regions 77−49448
O II, III, IV, beam-foil spectra, mean lives, 270-490 angstrom 78−55223
O III, electron impact excitation cross sections, independent particle model calcs. 80−63823
O III, optical oscillator strengths for astrophysically interesting lines 80−32660
O IV, electron-impact excitation cross sections 80−14236
O IV, optical oscillator strengths 79−98043
O IV bound states, oscillator strengths and photoionisation cross sections 80−106293
O isoelectronic sequence, optical oscillator strengths 80−63589
O, ns ^3S-$2p^4\,^3P_2$ transitions, for VUV, oscill. strengths 77−34580
O, pseudospectral dipole oscillator strength distribs. 78−50503
O, radiative lifetimes of visible and near IR transitions, solar abundance 78−50506
O, triple-dipole energy calcs. using pseudo-spectral theory 78−46418
O V, excited states, transaction oscill. states and wavefunctions 79−59367
O V, O VI, dipole lengths, dipole vels. and transition probabilities 79−35113
O V, transition probabilities calcs. 79−54792
O_2, dipole oscill. strength distribs., sums 78−21975
O_2, electron excitation total cross sections, oscill. strengths, independent particle model calcs. 77−61856
O_2, oscillator strengths and linewidths, Schumann-Runge bands 78−90186
O_2, photoabsorpt., photoionis, and photodissoc., dipole oscill. strengths in UV 79−76468
O_2, pseudospectral dipole oscillator strength distribs. 78−50503
O_2, Schumann-Runge band system, oscill. strengths and linewidths 79−98120
O_2, Schumann-Runge bands, predissoc. linewidths and oscill. strengths, vibr. level depend. 79−45735
O_2, Schumann-Runge continuum, oscill. strength and electron impact excitation 80−69121
O_2, spin-forbidden transition intensities, selective heavy atom effects 80−58240

oscillator strengths continued
O_2, triple-dipole energy calcs. using pseudo-spectral theory 78−46418
OH, (0,0) UV transitions, band oscill. strength 80−69162
OH, band oscill. strength, rot. excitation effects 80−23460
OH, continuum opacity oscillator strength rel. to solar atmosphere model 79−40162
OH^+, rot.-vibr. bands, line positions, oscill. strengths transition probabilities 80−67828
Pb Dirac eqn. calc. 79−22620
Pb IV, relativistic oscill. strengths 77−14388
PbI, $np^2 \rightarrow np(n+1)s$ transition array, relativistic oscill. strengths 79−31465
PbI_2, film, highly excited, oscillator strength of excitons, absorpt. and emission spectra 78−76001
PbI_2, visible exciton spectrum, exciton-phonon interactions, dielectric const. and oscill. strengths 80−25405
Pr complex, with ortho-phenanthroline and $\alpha\alpha'$-dipyridyl tris-trifluoroacetate, absorption spectra 79−98113
Pr^{3+}, anomalous hypersensitive $^3H_4 \rightarrow {}^3P_2$ transition 80−106296
Rb atom in Xe, collision-induced dipole transitions, absorpt. meas. 80−95718
Rb, first reson. line oscillator strength, phase matching condition determ. 77−10638
Rb, forbidden quadrupole lines, oscill. strengths meas. 77−50390
Rb, ionisation energies and oscill. strengths calcs. 80−5488
Rb, L-shell soft X-ray emission spectra, oscillator strengths 80−32651
Rb, oscillator strength ratios for principal series, relativistic and correlation effects 79−784
Rb, oscillator strengths of 5s-4d first forbidden lines 78−86824
Rb, principal series doublets, oscillator strengths 79−22656
RbCl:Eu^{2+}, optical absorpt. meas. for Eu^{2+} conc. determ. 79−51137
RbCl(Br):Eu^{2+}, single cryst. optical absorpt. spectra 80−45117
RbI isoelectronic series, oscill. strengths, relativistic HF calcs. 79−98035
S compounds, unstable, forbidden transitions, laser optoacoustic spectroscopic obs. 77−61756
S IV, P-, D-, S-states, oscillator strengths, transition strengths, CI calcs. 80−922
S V, VI, beam foil spectra, radiative lifetimes, oscillator strengths 77−30973
S XI, UV lines, theoretical intensity ratios 78−90108
S XIV, splitting and oscillator strengths for $2s^2S\text{-}2p^2P^0$ doublet 77−49348
S XV, He-like ion, oscillator strengths of transitions between low-lying S and P states 78−13470
S^{12+}, S^{13+}, in-shell dipole transitions, oscill. strengths, beam-foil spectra 77−71861
SF_6, laser isotope separation model 77−31016
SF_6, photoabsorption and ionic fragmentation, 5-63 eV, absolute oscill. strengths 79−72367
Sb I, ratio of oscillator strengths for 217.6 and 231.1 nm lines *(Russian)* 79−31457
Sc I, oscill. strength calc. 80−78571
$SeOCl_2$:Pr^{3+}(Nd^{3+})(Er^{3+}), $SbCl_5$ acidified, Racah and Judd-Ofelt parameters in laser liqs. 80−106516
Si (III), excitation thresholds and oscillator strength calc. using CI wavefunctions 80−91496
Si, glow discharge deposited, optical spectra, reflectance, dielectric function and oscillator strength 80−11492
Si II, transition probabilities between excited states, SCF treatment 78−82658
Si III, IV, beam foil spectra, radiative lifetimes, oscillator strengths 77−30973
Si IV, spectra, nonrelativistic oscillator strengths calc. 77−83538
Si IX, UV lines, theoretical intensity ratios 78−90108
Si isoelectronic sequence, CI calcs. of oscillator strengths, L-S framework 80−14089
Si, mass-anisotropy exciton splitting determ. 78−6685
Si XI, allowed transitions, radiative lifetimes and oscill. strengths meas. 78−78797
Si XI, wavefunctions and oscill. strengths, CI calcs. 80−23317
Si XII, allowed transitions, radiative lifetimes and oscill. strengths meas. 78−78797
Si^{n+}, foil excited, satellite lines in X-ray spectrum 79−85929
Si:Tl, optical absorption and photolum. of bound exciton 78−88359
SiH, A state new predissociations, improved dissoc. energy value from rot. level lifetimes 79−3496
SiH, SiH^+, line positions and oscill. strengths of rot.-vibr. bands, interstellar medium appl. 78−58644
SiH^+, oscillator strengths and dissoc. energy determ. from time resolved precision spectroscopy 80−58272
SiO, valence-excited bound states, spectroscopic consts., radiative lifetimes 77−6752
Sm complex, with ortho-phenanthroline and $\alpha\alpha'$-dipyridyl tris-trifluoroacetate, absorption spectra 79−98113
Sm, excited state lifetimes, oscillator strengths 77−83531
Sn, oscillator strengths and hyperfine splitting of $5^3D_1{}^0$ and $6^3P_2{}^0$ levels, line absorpt. meas. 80−18818
SnI, $np^2 \rightarrow np(n+1)s$ transition array, relativistic oscill. strengths 79−31465
SnO, $D^1\Pi\text{-}X^1\sigma$ transition, oscillatory strengths and Einstein coeffs. 79−41197
Sr I, oscill. strength calc. for resonance $^1S\text{-}^1P$ transition 78−90125
Sr I, oscillator strengths for certain transitions 79−18143
Sr, L-shell soft X-ray emission spectra, oscillator strengths 80−32651
SrF_2, strain induced splitting and oscillator strength anisotropy of IR transverse optic phonon 80−92625
Ta I and Ta II, oscill. strength determ. in 40 MHz inductively coupled plasma 79−48031
$TaSe_2$(2H), plasmon behaviour at charge density wave onset 80−10900
Te I, UV line rel. oscill. strengths and unexcited atom conc., AAS meas. *(Russian)* 78−31749
Th II, oscillator strengths calc. 80−27982
Ti I, hook and emission meas. 78−42002
Ti I, solar lines oscillator strengths and Sun Ti abundance 78−45306
Ti II, oscillator strengths from combined hook and emission expts. 80−87081
Ti, neutral, oscillator strengths for hook method meas., lines from $^3F_{2,3,4}$ levels 78−70790
Ti, reson. lines relative oscill. strengths, hook technique using wall-stabilised arc 78−13628
oscillator strengths continued
TiO, ($C^3\Delta\text{-}X^3\Delta$) system, radiative lifetimes, oscillator strengths, flame spectroscopy 78−42136
Tl, Dirac eqn. calc. 79−22620
Tl I, relativistic HF calcs., $np^2P_{1/2,3/2} \rightarrow (n+1)^2S_{1/2}$ and $np^2P_{1/2,3/2} \rightarrow nd^2D_{3/2,5/2}$ transitions 79−89609
Tl, ionisation limit and oscill. strength in VUV absorpt. spectra 80−74152
Tl, oscill. strengths, Bates-Damgaard approx. calcs. 77−3311
Tl, oscill. strengths, semiempirical relativistic one-electron central field, model pot. calcs. 80−78575
Tl, oscillator strengths and radiative lifetimes 79−54811
Tl, vacuum UV absorpt. spectra, at. consts. 77−57917
Tl_3AsS_4, optical phonons, Raman and refl. spectra 80−11400
Tm I, lifetimes of excited states, and oscill. strengths 79−3411
Tm, spectral line oscill. strengths determ. 77−3312
U II, oscillator strengths for calibration 77−42280
U III, in hexamethyl phosphoric triamide soln., absorption spectrum, intensities, oscill. strengths 78−74599
U, neutral atomic, oscill. strengths, 2289.8-2860.3K, 355.2-359.4 nm 79−10069
UI plasma, absolute emission coeff. 80−64693
V, atomic transition probabilities, oscill. strengths 78−74601
V III, absolute oscill. strengths determ. 78−82691
V VII, VIII, IX, X, 3s-3p and 3p-3d transitions, oscillator strength and energy levels calcs. 80−83251
VO_2, semicond. phase, optical spectrum, CNDO CI calc. 78−27258
W radiation from Tokamak-produced plasmas 78−9835
WI lines, relative oscill. strengths 79−63962
Xe, $5s^2$ shell, oscillator strength determ. *(Russian)* 80−58144
Xe, $5s^2$ subshell, discrete excitations, generalised oscill. strength calcs. 77−65441
Xe, electron energy loss spectra, energy-depend. multichannel quantum defect theory anal. 77−61860
Xe, intershell correlation, double electron ejection from outer shell 78−42019
Xe, s-p transitions, Stark consts. and oscill. strengths, shock tube meas. 80−18822
Xe, transition oscill. strengths, electron spectrometric obs. 77−10769
Xe VIII, beam-foil lifetime meas. using ANDC anal. for reson. doublet 79−93964
Xe VIII, beam-foil lifetime meas., cascading problem 80−14249
YAG:Er^{3+}(Ho^{3+})(Tm^{3+}), oscillator strengths of impurities, 5000 to 30000 cm^{-1} 79−4830
Y_2O_3, reflection spectra, oscillator strength determ. 79−8161
Yb II, 6s $^2S_{1/2}$-6p $^2P^o{}_{1/2,3/2}$ transition, relativistic oscillator strengths, influence of core polarisation 80−58132
Zn I isoelectronic series, resonance transitions 78−74616
Zn I isoelectronic series, $4s4p^1P$ lifetimes meas. 80−42998
Zn isoelectronic sequence, RRPA calcs. of oscillator strengths in resonance transitions 78−17612
Zn isoelectronic sequence, resonance oscill. strengths 79−3413
Zn, isoelectronic sequence, oscill. strength and MCHF wavefunctions, outer correl. 80−91505
Zn, isoelectronic series, oscillator strengths of reson. transitions 79−22666
Zn, L-shell soft X-ray emission spectra, oscillator strengths 80−32651
Zn, solar photosphere abundance, discrepancy with meteorite abundance 80−72897
Zn XXII, 2p-4d and 2p-4s transition arrays, wavelengths and oscillator strengths 80−47933
Zr II and III, oscillator strengths for certain transitions 79−18143
ZrF_4:Eu^{3+} glass, luminesc. of Eu^{3+}, transition probabilities 80−80845
ZrO, $B^3\Pi$ state radiative lifetimes, transition rates and oscillator strengths, reson. fluoresc. decay 80−28053

oscillators
see also Gunn oscillators; harmonic oscillators (circuits); microwave oscillators; parametric oscillators; radiofrequency oscillators; relaxation oscillators; tunnel diode oscillators; variable-frequency oscillators
10-50 MHz, superregenerative, spectrometer of nuclear quadrupole resonance for Cl compounds *(Slovak)* 77−18059
440 Hz standard A tone generator 78−46863
AC impedance meter, battery-operated, for contact resist. determ. before patient monitoring 78−81006
anharmonic, energy eigenvalues, partition function and specific heat calc. 79−55321
anharmonic electron oscill., radiation damping 77−50596
anharmonic oscillator, perturbed, applics. of scaling transformations 77−82384
anharmonic oscillator model for dispersive optical bistability 80−58623
anharmonic oscillators, single or quartic coupled, energy levels, Schrodinger eqn. 78−70014
auto-oscillator with improved freq. stability for string transducers, using ICs *(Russian)* 77−13741
autodyne, for low-temperature measurements up to 400 MHz 77−13755
autodyne spin detector, broadband, for NMR signal detection 77−74471
biological free running oscillator, phase transition curve due to perturbation 79−83737
biological rhythm phase response curve study, homotopy theory 79−8491
biological system, coherent mode excitations, bose condensation-like, Frohlich vibr. model, Boltzmann eqn. approach 79−39336
chain of coupled nonlinear oscillators, large amplitude motion, numerical study 79−25993
convective biperiodic regime, velocity oscills. 80−53759
coupled biological oscillators, describing function techniques 77−25361
coupled oscillators, nonlinear, with slow, nonexplicitly time-depend. evolution 80−52009
doubly tuned oscillator configuration, nonlinear mode interactions, freq. jump effects 80−77824
Duffing oscillator, statistical linearisation approx. method for nonlinear stochastic processes 77−17790
electrooptical oscillator, integrated cutoff modulation 80−48424
electrostatic electron oscillator design optimisation, ion source and vacuum gauge 78−74107
fibre optic relay with metallic pads heated by light 78−18038
first passage failure time under nonlinear damping 79−6053
Fitch oscillator operation in nanosec. electron accelerator 78−828
fixed-frequency laser beam scanning device 78−59135
flexural combination, effect on props., of geometry effect of piezoelectric ceramic platelets *(German)* 79−32168

oscillators continued
for quartz thermometer 78−81967
forced damped harmonic, meas. separation and half-width of components of doublets, high-Q systems 80−74590
four-variable oscillator, for hyperchaos 79−63151
Frohlich steady state model, asymptotic solns. 80−21435
fundamental mode, SAW resonators at 1.43 GHz appl. 80−87687
harmonic general time depend., quantal fluctuations and invariant operators 80−36898
HF generator for supplying quadrupole mass spectrometer *(Rumanian)* 77−29628
Hodgkin-Huxley, frequency entrainment, for modelling gastro-intestinal electrical activity 77−81489
hydraulic lines, wave phenomena, coupled vibrations in bending and branching lines 80−14778
IC Robinson oscillator, for NMR detection 77−74475
injection semiconductor laser oscillators, pumping via generator producing rectangular pulses 77−27299
integrated, SAW device using Si-SiO_2 struct. 78−83186
interdigital transducer and 1.1 GHz SAW oscillator, photolithographic contact printing *(Japanese)* 78−33981
internal friction meas. system using one-crystal composite oscillator 77−42789
ion cyclotron double resonance expts., oscillator coupling elimination 77−67530
ion cyclotron resonance marginal oscill. detector, rot. elec. monopole theory 78−41371
ion cyclotron resonance spectroscopy, sensitivity calibration of marginal oscillators 78−21177
Josephson oscillators, synchronisation props., single point junctions and chains 79−19703
Josephson transmission line oscillators, soliton solns. 79−87211
length meas., capacitive transducer method, precision, procedure and instruments *(German)* 79−26024
linear oscillator, vibrations, excitation by stationary random force *(Russian)* 80−27116
liquid two-dimensional itinerant oscillator model testing by molecular dynamics 79−32868
low frequency, 0.25-2.5 Hz generation, for student lab. demonstrations 78−24624
low-level gated, ion cyclotron resonance 80−86492
macroscopic oscillator motion parameter meas., quantum restrictions *(Russian)* 80−12943
maser, injection priming of pulsed molecular-beam maser oscillator 79−27226
mechanical networks and appls. 79−81615
monolithic SAW amplifier and periodic grating oscillator 79−50447
multidimensional infinite mechanical oscill. system, resonance and controllability 80−33444
non-linear oscillators, development of Kolmogorov spectrum 79−60140
nonferromagnetic film sheet resistance meas., eddy-current method 78−45658
nonlinear, stochastic instability 79−67150
nonlinear noisy sine wave oscillator, optimal control 80−27218
nonlinear oscillator, randomly excited, energy envelope approx. 79−14319
nonlinear oscillator and reflectors, periodic vibr. and impact characteristics 80−92089
nonlinear oscillator eqn., Poincare-Lindstedt solns. 78−30
nonlinear oscillators, limit cycle, chaotic response 80−148
nonlinear oscillators, normal modes, uncoupling and stability 80−27115
nonlinear oscillators, random excitation, response envelope statistics 79−6052
with nonlinear restoring forces, first passage failure probability calc. 78−42562
nonlinear stochastic, triangular wave, optimally controlled, Weiner process and Poisson process, numerical studies 80−52128
one-dimensional oscillator, matrix elements of position coord., upper and lower bounds 79−35578
parameter-dependent system, energy soln. method 80−8828
period variation due to nonlinear feedback 77−68382
polymer chain, of bistable oscillators, Brownian dynamics of transitions 78−86983
power flow between linearly coupled oscillators, statistical energy anal. 77−84022
pulse generator, HF oscillator with single coil transducer, for NMR spectrometer 79−2802
quantum magnetometer spin oscillator, phase error détection 77−74468
quartic oscillator, upper and lower bounds for matrix elements, numerical results 79−35578
quartz crystal oscillator checking against standard frequencies in LF/VLF ranges 77−74372
quasimonochromatic self-oscillations, phase self-stabilisation 80−18973
reference time interval reproduction device 78−77869
RF generator, for plasma dynamic stabilisation 77−24142
RF size effects meas., optimisation of marginal oscillator for 77−26377
rotating anharmonic oscillators in resonator, stimulated emission power 80−99689
SAW, development 77−34987
SAW, influence of acceleration *(French)* 79−32176
SAW, physical props. and communication signals processing applications and devices 80−38162
SAW, status and designs review 78−55542
SAW delay line and resonator oscillators for phase locking 78−59254
SAW delay line for UHF radio receiver 79−7272
SAW devices, appls. of amorphous magnetic-layers 80−28389
SAW oscillator frequency stability developments 78−59253
SAW oscillator with two acoustic paths 77−23846
SAW temperature independent oscillator *(Japanese)* 79−81613
segmented bidirectional amplifier SAW oscillator 78−1528
selective digital voltmeter, electronic control of tuning frequency 77−10052
self-oscillator harmonic synchronisation, self-vibr. freq. capture *(Russian)* 77−3507
self-oscillator harmonic synchronisation, transient processes *(Russian)* 77−3506
self-oscillator with soft limiting cycle, nonresonant action *(Russian)* 77−3505
semiconductor-compatible SAW devices 77−80044
solid-state oscillator with superconducting sapphire resonator, freq. stabilisation 79−12823
oscillators continued
spin oscillator action of transverse fields 78−49873
stochastic analysis of oscillators with nonlinear damping 79−41567
submillimeter wave heterodyne detection, with a laser LO 78−70183
superconducting resonators, high stability oscillators, appl. to fundamental physics, metrology 79−26034
time and freq. standards, design principles and characteristics 77−22533
time meas. system adjustment and calibration signal generator 78−57903
transient behaviour for two harmonic signals *(Russian)* 77−14895
tunable magnetoelastic surface wave oscillators, freq. control 79−32177
two-resonator CRM oscillator with external feedback 80−87362
U-path HF periodic grating oscillator 77−23847
US Diasonograph incorporating pulsed Doppler system 77−77955
US Doppler signal analyser, real-time, multichannel, blood vel. meas. appl. 77−73551
valence electrons, finite energy, f-sum rules 78−88276
valve oscillator, VHF, construction and transmissions line expts., for teachers 78−28894
van der Pol, coupled oscillators, for intestinal modelling 79−96530
waves in nonlinear media, Poincare normal form method 80−36875
Wien bridge, low-power, for low-temps. ~25 mK 78−93680
Wien bridge oscillator, critical phenomena simulation, threshold instabilities 77−1211
Wien bridge oscillator, for continuous recording of elec. resist. changes 77−53931
Wien-Robinson, digital temp. meter appl. *(German)* 78−29110
Zeeman multioscillator ring laser gyro, props. 79−72604
H, four dimensional oscillator, rot. invariance of coordinate transform., appln. to Stark problem 80−99436
VO_2 film, negative resist. region, applic. as oscillator element and transducer *(Russian)* 77−85359

oscillograms *see oscillographs*

oscillograph recorders *see oscillographs*

oscillographs
see also cathode-ray oscilloscopes
acousto-optic deflector for TV and oscillograph displays 77−39099
CRO photographic recording status 79−93247
DFS-8 spectrograph, attachment for oscillographic recording of line shapes 80−105721
differential cathode ray polarograph, exam., determination of Cd, Zn 78−56930
eight-channel, for recording one-shot processes 77−37872
electrical phenomena, production of analogue by recording electrical impulses on oscillograph 79−17515
electroglottograph application experience 77−78062
exploding wires expts., oscillograms processing with aid of microcomputer and main-frame computer *(Russian)* 80−28854
fast process recording, galvanometer construction 80−73346
fibre-optic CRT recording oscilloscope, characts. 77−37911
fracture toughness evaluation of steel using oscillograms 79−57169
hysteresis loops, oscillography using ferroprobe transducers 79−87785
light beam oscillographs, construction and performance *(German)* 79−93119
loop freq. response meas. using stroboscopic methods *(Polish)* 78−29102
measuring techniques, trends *(German)* 78−74020
photographic plate spectral line setting photoelectronic arrangement 78−78015
photographic recording device based on oscillographic delayed-coincidence method 77−38025
photographic recording using Polaroid camera *(Italian)* 78−78007
random process, distribution functions meas. 78−4607
rapid-scan spectrometer control unit 78−74067
reversible counter with digital indication geophysical meas. appl. *(Russian)* 77−41209
solid state oscilloscope using 10 LED bars 78−21113
steel, low strength, impact tests with oscillography, exam. of fracture toughness using new method 80−21215
steel 45G2, fracture resistance, from impact bending tests and oscillograms 80−61047
tensile test diagram remote recording device 78−7139
time-mark circuit with controlled delay 79−35703
transient store, fast response, description of appls. *(German)* 79−80607
TV camera system for digitising single shot oscillograms at sweep rate 0.1 ns/cm 77−406
universal 18-channel light-beam oscillograph H117/1 *(Russian)* 78−70105
wave process modelling, on oscillograph screen *(Russian)* 79−21558

oscilloscopes, cathode-ray *see cathode-ray oscilloscopes*

Oseen method *see flow*

osmium
see also nuclei with .....
atom, even config., parametric calcs. 78−82631
atomic vibr. and fermion behaviour of HCP metals 80−6474
catalyst, interaction of CO, NO and H_2, NH_4OCN formation 78−73082
correlation effect of crystal pot., RAPW calcs. 78−6265
diffusion in Si, diffusion parameters using photocapacitance and four-probe methods 79−51314
dispersed metal catalyst clusters, EXAFS obs. 79−91530
electrical resistivity, thermal diffusivity, and thermal cond., 290 to 3300K 79−11101
electrical resistivity and thermal diffusivity meas. 80−15495
electronic energy band struct. 80−107697
EPR, quadrupole interaction 78−48027
ESCA on in situ cleaned surface 79−83101
field ion microscope exam. *(German)* 77−36376
HCP, elec. field gradient 78−14698
impurity in Cu-Ni sulphidised alloys, behaviour during carbonylation *(Russian)* 80−40584
isotopic anomalies from different ore deposits, LAMMA determ. 80−61800
lattice parameters, densities and atomic vols., tabulation for Pt metals 79−65033
metallography 78−3289
Mossbauer meas., elec. field gradients at ^{186}Os nuclei 79−47373
sorption of O_2 and H_2 in H_2SO_4 soln. 79−61873
thermal EMF quantum oscills. *(Russian)* 80−88543
wear coefficients determ. using pin-on-cisc apparatus 80−76366

osmium continued
Be:Os, anomalous displacement of Os atoms from substitutional site 77−59039
$Cs_2ZrBr_6:Os^{4+}$, intraconfig. absorpt. and MCD spectra 80−80776
$Cs_2ZrCl_6:Os^{4+}$, intraconfig. absorpt. and MCD spectra 80−80776
$Cs_2ZrCl_6:Os^{4+}$, multiple state luminesc. 78−72584
$K_2PtCl_6:Os^{4+}$, multiple state luminesc. 78−72584
$K_2PtCl_6:Os^{4+}$, sharp line luminesc. band at 10K, vibr. assignment 78−95600
Os VIII, one-electron spectra energy levels and line lists 79−49953
Os^{2+}, Sternheimer valence shielding antishielding factor including exchange 77−85182
Os, A=189,190, absolute atomic masses 79−89228
^{186}Os and ^{187}Os neutron capture cross sections rel. to Re/Os cosmochronology 80−17485
$^{187}Os/^{186}Os$ in terrestrial samples, rel. to use of Os isotopes as petrogenetic and geological tracers 80−89989
^{88}Os, muonic resonance spectra, deduced isomer shifts and electric moments 80−18948
^{191}Os, K-shell internal conversion, $K\alpha_1$ hypersatellite line energies, intensities 77−18885
^{187}Re-^{187}Os systematics in meteorites, rel. to solar system early chronology and Galaxy age 80−41778
Si:Os, P, photoelec. props., depend. on P conc. 79−91099
Si:Os, photocapacitance meas. of impurity levels 77−55579
n-Si-Os Schottky contact barrier height meas. 80−65675
W:Os coated dispenser cathode, chemical and physical process obs. 79−28885

osmium alloys
see also osmium compounds
rare earth alloys, R_3Os, cryst. struct. 80−96475
rare earth alloys, R_3Os (R=La, Pr, Nd, Gd, Tb, Dy, Ho, Er, Y), cryst. struct. 80−96474
Co-Os, short-range order parameters, ordering energy on first coordination sphere *(Russian)* 79−69058
Cr-Os, Invar alloys, thermal expansion, plasticity *(Russian)* 79−55907
Cr-Os, magnetic transformations, triple point *(Russian)* 80−88747
Cr-Os, magnetic transition T-P-C diagram, triple points *(Russian)* 80−54895
Cr_2Os, σ phases, ordering, X-ray cryst. struct. determ. 80−107107
Fe-Os, antiferromag. ordering, hyperfine fields 80−15867
Fe-Os, CC hexagonal phase, ^{57}Fe Mossbauer study 79−91321
Fe-Os, mag. hyperfine interactions, Mossbauer effect meas. 77−66442
Mo-Os, recovery after deform. and annealing, destrengthening mechanism *(Russian)* 80−97546
Mo_3Os, effect of high energy neutron irradiation on supercond. transition temp. 77−36012
Nb-Os, alloying element influence on strength, ductility, surface and grain boundary energies *(Russian)* 79−74234
Nb-Os, dil., impurities effect on elec. resist. at 0.4 and 77.3K *(Russian)* 79−91196
Nb-Os, phase diagram exam. 77−21103
Nb_3Os, A-15 struct. ^{93}Nb NQR spectra 80−20496
Nb_3Os, X-ray $M_{IV,V}$ emission bands *(Russian)* 80−45170
Nb_3Os, XPS of valence electrons meas. 77−21003
Ni-Os, short-range order parameters, ordering energy on first coordination sphere *(Russian)* 79−69058
$NpOs_2$, band magnetism due to f-electrons, T_c 77−73039
$NpOs_2$, itinerant ferromagnet, sp. ht., 3-25K 77−63212
Os-Hf, dil., ^{178}Hf Mossbauer transition, electric quadrupole interaction 80−39928
Os-Re alloy, mag. suscept. of HCP transition metal alloys *(Russian)* 78−80138
$PuOs_2$, Laves phase cpds. thermodynamic props. 77−20092
η-$Pu_{19}Os$, cryst. struct. 78−42954
ζ-$Pu_{19}Os$, X-ray cryst. struct. determ. 79−99117
Re-Os nuclear chronometer, reliability, rel. to element rel. abundance 78−85919
Th-Os system, phase diagram and thermodynamic props. *(German)* 79−47958
V-Os system, equilib. phase fields, X-ray diffr., elec. resist., DTA, and EPMA meas. 79−47661
$V_3Ge_xOs_{1-x}$, low temp. props. 79−99652
$V_{50}O_{50}$, nuclear spin-lattice relax. time, electronic density of states 77−59354
$V_3Si_xOs_{1-x}$, supercond. transition temp. and paramag. susceptibility 79−28436
W-Os system films, condensation temp., conc., and phase comp. effect on struct. and props. *(Russian)* 80−24749
Y_3Os, cryst. struct. 80−96475
Zr-Os, $\alpha \rightleftarrows \beta$ transform. *(Russian)* 78−80540
Zr-Os quenched alloys, metastable phases *(Ukrainian)* 78−84804

osmium compounds
see also osmium alloys
borides, MOs_3B_2 (M=Lu, U), supercond. and mag. props. 80−97028
double oxides, elec. cond. 80−34438
$Os0_4$, multiphoton absorpt., inverse radiationless transitions detect. *(Russian)* 79−22753
$CO_2/^{192}OsO_4$ laser, absolute light oscill. freq., universal const. variation meas. possibilities *(Russian)* 80−5723
$H_2Os_3(CO)_{10}$, and $H_4Os_4(CO)_{12}$, polycryst., PMR chem. shift 79−95655
K_2OsCl_6, displacive phase transition, thermal expansion meas. 78−10188
K_2OsCl_6, single cryst. with H^+ interstitials, protonic cond. from dielec. meas. 80−107515
$La_3Os_2O_{10}$, cryst. struct., Os_2O_{10} clusters with metal-metal bonds 79−86753
O_5O_4 vapour staining, handling of semi-thin sections of GMA-Quetol 523 for light/electron microscopy 78−92766
$Os^{16,18}O_4$, pseudo-exact force consts. 77−31022
Os complexes, N-1-adamantylimido OsO_3, bis(N-tert-butylimido) OsO_2, cryst. struct., bonding, ligands π-donor capability 80−64969
OsB_2, possibility of semicond. props., rel. to atomic volume 77−69317
$OsBr_6^{2-}$, complex Raman tensors, irreducible tensor method, antisymmetric scatt. 78−37623
$(OsBr_6)^{2-}$, resonance spectra, vibrational and electronic Raman effects 79−47437
$Os(CO)_5$, chem. thermodynamics 78−18799
$Os_6(CO)_{18}$, electronic struct., metal cluster carbonyls mol. orbital description obs. 80−63879
OsF_6, ionis. energies, optical spectra, Dirac-Slater model 77−83488

osmium compounds continued
OsO_4 absorber for freq. stabilised CO_2 laser, output freq. reproducibility 78−50800
OsO_4, and isotopic forms, stretching fundamental, 961 cm^{-1}, high resolution spectroscopy 78−90162
OsO_4, CO_2 laser freq. stabilisation appl., expt. *(Russian)* 78−33747
OsO_4, HFS and fine struct., saturation spectroscopy obs. visible spectra 80−53008
OsO_4, IR laser dissociation isotope separation appl. 77−18993
OsO_4, IR vibr.-rot. spectrum, theoretical interpretation 77−6776
OsO_4, isotope selective dissociation by IR radiation pulses, luminesc. intensity 77−83665
OsO_4, isotope separation by dissociation in two-freq. IR laser field 78−25638
OsO_4, MS Xα calc., ionis. pots., energy levels, atomic spheres radii effect 77−18789
OsO_4, mol. orientation resonant optical detect. in gases, laser spectroscopy appl. 79−27742
OsO_4, mol. vibrs. and reaction pathways, min. energy coords. and compliance consts. 77−57966
OsO_4, multiphoton absorpt. under two CO_2 laser pulse excitation 78−86925
OsO_4, multiphoton dissociation by two freq. tunable CO_2 laser pulses 78−50606
OsO_4, multiple IR photon absorpt., rovibr. transitions 79−54926
OsO_4, multiple photon excitation by dissociation yield saturation 79−3505
OsO_4, spectroscopy using tunable high-press. CO_2 waveguide laser 80−43054
OsO_4, tunable diode laser spectrosc. obs. 78−82061
OsO_4, two IR pulse multiphoton absorpt. selective dissoc., obs. 78−82798
OsO_4^{2-}, valence level electron struct. by XPS 77−4712
OsO_3F_2, normal coordinate anal. in Urey-Bradley force field 79−49966
OsO_3F_2, OsO_4 matrix-isolated IR and Raman spectra 77−75166
$ROsB_4$, R=Y, Gd, Tb, Dy, Ho, Er, Tm, struct. and mag. props. 78−79584

osmosis
see also membranes
acrylonitrile methallylsulphonate copolymers in DMF, polyelectrolyte behaviour 79−66351
aerosols, atmospheric, water uptake and equilib. sizes at high relative humidities 78−61516
alkali halide, aq. soln., interionic forces and thermodynamics *(German)* 79−52688
alkaline earth halides, aq. solns., activity and osmotic coeffs. 78−53242
binary electrolytes, pair distrib., osmotic coeff. in conc. up to 1 mol/l 80−61148
biological intracellular energy transform., phys. aspects 77−86462
biological longitudinal transport, electroosmotic model 80−45870
biomolecule osmosis, educational model 77−26110
cameral liquid transport rel. to buoyancy control in chambered nautilus 80−89732
capillaries of different geometries, electrokinetic parameters 77−48650
cation-exchange membranes, electrochem. props. rel. to interfacial polarization during electrodialysis 79−16038
cellulose acetate, reverse osmosis membranes, ion mobility, diffusion coeff., elec. resist. obs. 80−45550
cellulose acetate butyrate, in soln., hydrodynamic behaviour 80−64876
cellulose acetate membrane, asymmetric, elec. and electroosmotic transport behaviour in dialysis-osmosis expts. 80−108745
cellulose acetate membrane, asymmetric, elec. and electroosmotic transport behaviour in hyperfiltration expts. 80−108746
cellulose acetate-g-polyacrylamide membranes, radiation grafted, appl. in water desalination by reverse osmosis 80−45548
cellulose diacetate membrane, diffusive permeability 80−104460
cellulose diacetate membranes, unilayer, transport phenomena, hydration and dialysis coeffs. 80−76556
charged membrane osmotic transport, generalised flux eqns. 78−24050
chloroplast membrane proton gradient and osmotic vol. determ. 78−28143
chromaffin granules, osmometer model for changes in buoyant density 77−90737
coal liquids characterisation, analytical use of dialysis 80−30334
colligative properties of simple solns. 77−21466
colloidal capillary-porous body, mass transfer parameters, adsorpt., osmotic moisture 78−11563
convective-diffusive transfer in cylindrical channel, soln. 77−7391
corneal environment, osmotic responses to contact lenses 80−12078
corneal hydration endothelial control theory 78−35841
desalination plant utilising reverse osmosis, and wind powered plant 80−61282
dialyser performance improvement by osmotic flow induction 77−48946
Donnan systems displaced from equilib., transient press. changes 77−52749
double layer diaphragm, electro-osmosis of different arrangements of layers, rel. to poles of current source 79−70373
drug delivery osmotic pump, design and operating principles 77−56544
education, chemical, osmotic and electrochemical equilibrium, principle of virtual work 77−33767
electro-osmosis, degree of coupling and efficiency of energy conversion 79−74416
electro-osmosis inversion point, Onsager coeff. transformation principles 79−74417
electro-osmotic enhancement of the neutral tracer transfer through a capillary membrane 78−3371
electrodialysis and its applications 80−55702
Electrokinetic measurements with submicron particles and pores by the resistive pulse technique 77−86384
electrolytes, binary solns., nonideality, thermodynamics 79−39155
electrolytes, osmotic coeffs., mean spherical approx. refined model 79−1965
electroosmosis as distinguished from electrophoresis 80−45514
electroosmotic flux eqn., nonlinear, second-order phenomenological coeff. 78−31687
electroosmotic permeability coefficient in charged membrane model 80−108749
electroosmotic pump for regulated release of medicaments *(German)* 78−7518

osmosis continued
electroosmotic transport, of nonaqueous media, in strong electric fields 77−29043
electroosmotic zeta potential meas. on single crysts. 77−60112
emulsion, osmotic compressibility, hard sphere fluid calcs. 77−9129
epithelia, pathways for hydraulically and osmotically-induced water flows 77−29112
epithelium, small intestine, asymm. behaviour under influence of osmotic press. 77−52747
epoxy resin, destruction by diffused water 78−48511
erythrocyte, human, dynamic osmotic haemolysis and ghost repair, resistive pulse spectra 79−62208
erythrocyte osmotic fragility curve, statistical synthesis 78−65070
erythrocytes, frozen human cells, conc. polarisation effect 78−3460
erythrocytes, human, effect of hydration on water content 77−16921
ethylene-vinylacetate-copolymers charact. by gel chromatography, viscometry, osmotic meas. *(German)* 78−14496
gallbladder epithelial cells, compartmental anal. of osmotically induced permeability changes 78−3455
glass fibre reinforced epoxy resin, destruction by diffused water 78−48511
glass fibre reinforced epoxy resin, destruction by freezing or boiling of phase separated water 78−48512
glassy polymer, solvent osmotic stresses, prediction of Case II transport kinetics 80−26049
haemoglobin, in salt soln., diffusion rel. to intermol. interactions, light scatt. investig. 77−44585
highly dispersed substances, electrosurface props. meas. 78−53249
intestinal epithelium, effect of Ca ions and pH on osmotic pot. 78−20156
ion transport model, intracellular osmoregulation mechanism 77−25400
ion-exchanger membranes, coarse-grained, oscillatory phenomena 79−34356
ionic solution, charged square well model, virial osmotic coeffs. 79−4217
latex, monodisperse, Kirkwood-Alder transition press. meas. 78−7239
lecithin bilayer force meas. and modification 77−56346
liver cell contacts and surface, effect of raised osmotic press. 77−56354
lung circulation, density dilution method appl. to obs. of fast osmotic fluid shifts 80−104781
macromolecular solution, semidilute, scaling law describing conc. depend. 79−70377
membrane-solution interface, phase jump of osmotic press., theory 79−11825
membranes, cellulose acetate, vector mass transport obs. and appl. 79−96360
membranes, reverse osmosis transport processes *(German)* 78−95946
microemulsions of micelles, interpretation of second virial coeff. of osmotic press. *(French)* 78−64891
molecular weight determ. by osmometry 77−88593
molecular weight determ. by vapour pressure osmometry 77−46658
muscle, smooth, effect of hyperosmolar soln. on elec. connections between cells 78−69027
muscle cell osmotic state and membrane permselectivity repeated microwave irrad. effects quantitation 80−56131
muscle fibres, skinned, swelling 77−73513
nephron functioning, diffusion and selective osmosis *(French)* 80−45864
neuronal adaptation to osmotic stress and facultative blood-brain barrier in marine osmoconformer 77−29127
oil-water microemulsions, osmotic press., micelle diameters, second virial coeff. *(French)* 78−20075
ordered colloidal dispersion, electrostatically stabilised, polydispersity and osmotic press. 79−74428
organic solute rejection by reverse osmosis, regular soln. theory appl. *(Japanese)* 80−101041
Osmo-Hydro power, salinity gradient energy conversion feasibility and system design 80−45721
Osmo-Hydro power systems, technical feasibility and economics of salinity power 80−40893
physiology, flow problem, one tube 80−89703
plant protoplast membrane, osmotically induced changes in elec. props. 78−27910
PMMA isotactic, syndiotactic stereocomplex formation in soln., composition, struct. 79−66292
poly(γ-benzyl-L-glutamate) solns., osmotic press. in isotropic and anisotropic phases 79−94886
poly-γ-methyl-L-glutamate, conformational props., viscosity, osmotic press. meas. 77−31032
polyelectrolyte in solution, variation of contrast, neutron forward scatt. calc. *(French)* 80−54104
polyelectrolyte solution, thermodynamic props. determ. from Donnon equil. obs. 80−7846
polyelectrolyte solutions, activity coeffs. and osmotic coeff., higher-order limiting laws 79−29387
polyethylene oxide, aq. salt soln., meas.-based thermodynamic quantities 78−75525
polyethylene wax characterisation by gel chromatography, osmotic meas. and scattered light meas. *(German)* 77−86420
polymer, non-ion-exchange type, electrolyte solubility *(Russian)* 80−54391
polymer membrane, transport of organic liqs., review 80−16720
polymer solution, osmotic pressure, correlation functions, in grand canonical formalism 80−100159
polymer solution, partially deuterated, osmotic compressibility from elastic neutron scatt., general formulation 79−90517
polymer solution, virial coefficients and osmotic press. 79−90751
polymer solutions, semi-dilute, field theoretic formalism 77−31575
polymers, water absorption, osmotic effects 80−65366
polymers in poor solvent, loop expansion of irreducible diagrams 80−100160
polyphenylquinoxaline-cellulose acetate, battery separator membrane, diffusion meas. 80−35574
polystyrene, conc. solns., diffusion and sedimentation, frictional coeff., crit. soln. temp. 79−95195
polystyrene, diethyl malonate soln., near-crit., osmotic compressibility, correlation length, scaled functions 80−11422
polystyrene in toluene, unstirred solns., transient diffusion through membrane 78−92508
polystyrene sulphonic acid, charged membrane, electroosmosis and streaming potential *(Japanese)* 78−31696
polystyrene-diethyl malonate system, osmotic compressibility and correlation range near crit. point 78−6694
porous cellulose acetate membranes for mixed uni-valent electrolytes in aqueous solns. reverse osmosis predictability 78−53250
Porphyra osmoregulation, struct. aspects 80−85370
Portland cement, a model describing the hydration process 78−23654
power generation appl., using aqueous saline solutions, technical and economic feasibility 79−52916
pressure-retarded, two-coeff. water transport eqn. 79−83509
proteoglycans, swelling pressures at the concs. found in cartilaginous tissues 80−67327
PTFE grafted membranes, struct.-properties relationships, bifunctionality *(French)* 80−61137
PVC soln., mol. wt. meas. by membrane osmometry 79−7045
red blood cells, equilib. shapes in osmotic swelling 80−85368
reinforced cellulose acetate membrane water and salt permeability, complementary direct osmosis test 79−96359
renal brushborder membrane vesicle, proline and glycine uptake 77−44614
renal medulla, osmotic equilibration by descending limbs of Henle's loop 77−40701
reverse, desalination plants using solar and wind powered pumps *(French)* 80−55807
reverse, hybrid, using ultrafiltration membranes, water treatment appl. 77−44507
reverse, membranes using sulphonated aromatic polysulphone obs., water treatment appl. 77−44508
reverse, using cellulose diacetate membranes, transport phenomena analysis, pressure effects on permeability characts. 79−96361
reverse osmosis, mechanisms, membranes, transport and appls. 79−29396
reverse osmosis salt rejection, membrane pore size 77−9122
reverse osmosis system, combined forced and free convection system 79−52750
reverse rejection of organic solutes from aqueous soln., cellulose acetate membrane *(Japanese)* 77−36790
reverse separations of inorganic ions in aqueous solns., free energy parameters 77−32831
reverse separations of ions and ion pairs in aqueous solns. free energy parameters 78−53251
sarcoplasmic reticulum vesicle permeability, light scatt. meas. 77−12889
silicate gardens, growth morphology, mechanisms 80−100765
silicic and aluminosilicic acids, effect of increased size of scattering centres in sols 78−53270
solar power plant, using semipermeable membrane and low-head reaction turbine 79−57418
solid disperse systems, electro-osmotic mass transfer, surface cond. influence *(Russian)* 80−76546
solutions, dilute, colligative props., kinetic derivation from elastic collision processes 78−91048
structural constitution and function *(German)* 79−5256
styrene-p-chlorostyrene triblock copolymers in dil. soln., conform. behaviour, temp. depend. 79−90519
subcellular particle pot. difference, chemiosmotic and chemielec. generation mechanism 77−52751
supraoptic neurons, rat hypothalamus, osmosensitivity obs. 80−104578
suspension of charged particles in ionic solutions, elec. cond. 80−7866
teaching, solvent tension, dilution explanations 78−73803
thermo-osmosis, phenomenological equations, fluxes and forces 77−5779
thermoosmosis, liq. in capillary pore media 79−41750
thermoosmotic concentration difference meas. for gaseous mixtures across membranes 79−83508
tissues, unperfused, osmotic behaviour 80−104574
transcapillary water movement resulting from non-oncotic osmotic forces 78−44548
trioctadecanoate solution in toluene, diffusion through cellulose membrane nonstationary 79−52767
4-vinylpyridine acrylonitrile copolymer membrane, reverse osmosis charact. *(Japanese)* 78−31694
vinylpyrrolidone-tert-butylphenyl methacrylate copolymers, prep., soln. props. 79−18854
water, thermoosmotic flow, filtration, in porous glasses 78−53248
water in single capillary, electrokinetic and rheological parameters 80−10220
wind powered brackish water purification by electrodialysis and reverse osmosis 80−35630
CaCl, aq., mean activity and osmotic coeffs., free energy, 298.15K, review 77−81411
$CaCl_2$, isopiestic studies of aqueous solns., 382 to 474K 79−24815
Co bi-univalent cpds., soln., activity coeffs., osmotic coeffs., water activity, Gibbs energy, molality depend. 80−51963
CsCl, CsCl+KCl mixtures, osmotic coeffs. at 298.15K 78−92509
CsCl+KCl mixtures, osmotic coeffs. at 298.15K 78−92509
Cu bi-univalent cpds., soln., activity and osmotic coeffs., H_2O activity, Gibbs energy, molality depend. 80−51964
$Dy(ClO_4)_3$, osmotic coeffs. 80−45556
$Er(ClO_4)_3$, osmotic coeffs. 80−45556
$FeCl_2$, soln., activity coeffs., osmotic coeffs., water activity, Gibbs energy, molality depend. 80−51963
$Gd(ClO_4)_3$, osmotic coeffs. 80−45556
$Gd(NO_3)_3$, osmotic coeffs. 80−45556
HCl/membrane/NaCl+HCl isotonic osmotic systems, inversion 79−52775
H_2O, thermoosmosis through cellulose acetate membranes 79−52768
^3He-^4He, superfluid, osmotic and mag. props., review *(French)* 80−10733
^3He-^4He mixture, liquid, differential osmotic press. meas. of conc. suscept. near lambda curve and tricritical point 79−73371
^3He-^4He mixture, osmotic pressure along phase separation curve 77−89613
^3He-^4He mixtures, osmotic response function near tricrit. point, meas. method 78−2331
^4He, superfluid, thermo-osmotic convection, at incipient lambda transition, above crit. press. 78−95199
$Ho(ClO_4)_3$, osmotic coeffs. 80−45556
KCl, isopiestic studies of aqueous solns., 382 to 474K 79−24815
$La(ClO_4)_3$, osmotic coeffs. 80−45556
$Lu(ClO_4)_3$, osmotic coeffs. 80−45556
$MgCl_2$, isopiestic studies of aqueous solns., 382 to 474K 79−24815
Mn bi-univalent cpds., soln., activity and osmotic coeffs., H_2O activity, Gibbs energy, molality depend. 80−51964
NaCl-KCl, aq. solns., isopiestic studies, 383 to 474K 80−21320

osmosis continued
Na_2SO_4-$CoSO_4$-H_2O, phase equilib., activities, Pitzer eqn. calcs. *(Russian)* 80−65190
$Nd(ClO_4)_3$, osmotic coeffs. 80−45556
$Nd(NO_3)_3$, osmotic coeffs. 80−45556
Ni bi-univalent cpds., soln., activity coeffs., osmotic coeffs., water activity, Gibbs energy, molality depend. 80−51963
O_2-ethylene mixture, thermo-osmosis, heat of transport 79−43628
Pb bi-univalent cpds., soln., activity and osmotic coeffs., H_2O activity, Gibbs energy, molality depend. 80−51964
$Pr(ClO_4)_3$, osmotic coeffs. 80−45556
$Sm(ClO_4)_3$, osmotic coeffs. 80−45556
$Sm(NO_3)_3$, osmotic coeffs. 80−45556
$Tm(ClO_4)_3$, osmotic coeffs. 80−45556
$Yb(ClO_4)_3$, osmotic coeffs. 80−45556

osmotic pressure *see osmosis*

otology *see ear*

ovens
see also domestic appliances; electric heating
atomic beam source, low-consumption, with recycling oven 78−5376
crystal ovens using temp. gradient-free change of state for quartz cryst. standard *(Polish)* 79−30481
induction heated, for laser induced fluorescence spectroscopy of U 78−21230
laser-heated miniature oven, for prop. of matrix isolation samples for Raman studies 78−45737
microwave, ceramic humidity sensors appl. 80−86325
microwave, Intern. Microwave Power Symposium, Minneapolis, Minn., USA May 1977 77−70492
pilot-lamp controller crystal oven stabilisation 78−54374
self-cleaning catalyst, 'SC ceramic coating' *(Japanese)* 80−55557
temperature-controlled, reliable, inexpensive oven for temp. stabilizing crystals 77−82503
temperature-controlled ovens, electronic controller using TTL cct. *(German)* 79−67304
zonal refinement, description of oven for material's with MP<700°C *(Spanish)* 78−44009

overcurrent protection
900 mW solar battery construction and characteristics *(German)* 80−12008
arc quenching system for transient and statistical flashover, fusion reactor systems 78−75455
chart recorder timer control, pen overload protection systems, at. absorpt. appl. 77−73481
diadynamic current therapy apparatus Tonus-1 78−7523
electro-medical measuring equipment, leakage current protective measures *(German)* 78−3629
fusion, TFTR, neutral beam sources overcurrent protection during spark down 80−102331
fusion reactor, neutral beam ion source, core snubber network design, fabrication and testing 80−102378
fusion reactor, TFTR, energy conversion and storage systems, fault detection and protection 80−95431
HV electron gun power supply protection 79−44989
neutral beam source 8 MW voltage series regulator, for fusion reactor 78−70631
pulsed electrical systems, circuit using ICs and constant-current measuring transformer 79−3263
superconducting magnet quench protection system for ISABELLE 77−83233
superconducting magnets, superconducting switch 80−9007
wire chamber powering, current-limiting technique 77−54424

Overhauser effect
see also nuclear Overhauser effect
CIDNP, triplet Overhauser mechanism 78−13531
dielectrics, solid, dipole electron-nucleus interaction, review 80−29649
polarised targets in high energy 79−68065
polyacetylene, dynamic nuclear polarisation of protons *(French)* 80−43217
solvent-paramagnetic solute system, nucl. spin-lattice relax. times, cross-correl. method 79−95679
spin system, X_3-{A} experiment 80−25251
trifluoroacetophenone+dimethoxy benzene. in acetonitrile photoreaction, nuclear spin polarisation, criterion for triplet-Overhauser mechanism 80−69168
p-CdTe, ESR optical detect., Overhauser shift, g-factor 78−80252
CdTe, optical detection of ESR 79−65770
Cr, hyperfine interactions on ^{111}Cd-probe nuclei, TDPAC meas. 80−75904
p-GaSb, CESR, optically detected, giant Overhauser shift 79−4722
Si, Overhauser effect in optically pumped compensated samples 79−73857
Si:P, EPR of interacting donor centres, Overhauser effect and ENDOR 77−77085

overhead line conductors
DC transmission conductors, corona discharge and elec. charge on water drops, obs. 79−82114
impulsive corona discharge around conductors, phys. aspects consideration *(French)* 80−92406
MV, cross section optimum choice/nomogram *(Bulgarian)* 77−60917
steel-Al bimetallic wire for overhead lines, manufacturing methods 80−16247

overhead line mechanical characteristics
see also oscillations; poles and towers
high voltage transmission cables, oscillations, coupled rope model study *(German)* 79−90173

overhead line sagging *see overhead line mechanical characteristics*

overhead lines
see also power overhead lines
galloping oscillations, effect of added mass 79−81777
HV lines, noise, publications review *(Czech)* 80−23827

overvoltage
air breakdown formative time lag rel. to gap geometry, pressure, and overvoltage 79−18994
anodic oxidation, open-cct. transient method for overpotential anal. 78−27776
discharge, axially symmetric, narrow, at high overvoltage, computer simulation 79−19101

overvoltage continued
electrocrystallisation, galvanostatic transients, crystn. overvoltage 78−76867
electrode processes possessing charge transfer mechanism, overvoltage theory, in book, for teachers 78−8204
electrode systems, nonequilib. polaris. states props. overvoltage theory, in book, for teachers 78−8205
electrodes, packed fluidised beds, kinetic behaviour for quinone electrochem. reduction 79−57235
indifferent salts, acid conc. aq. solns., H evolution at Hg electrode 78−53215
lightning and spark discharge leader-stroke velocity comparison 78−94947
oil electric strength for switching surges and long flash-over distances, expt. *(Czech)* 78−56427
overhead lines, impulsive corona discharges around conductors, phys. aspects consideration *(French)* 80−92406
photographic development rate, effect of developer ion charge 79−24753
spiral wire underwater explosion characteristics *(Russian)* 79−94809
superconducting magnet HV insulation problems 79−30512
theory, nonequilib. thermodynamics appls. 77−40550
wire, exploding, resistance increase phase, elec. characts., applications 77−55192
Ag/α-Ag_2S, interface, electrochemical transfer across phase boundaries 78−73046
Cu electrocrystallisation from $CuSO_4$ solns., current density/overvoltage curves *(Russian)* 79−8236
Cu electrocrystallisation from $CuSO_4$ solns., current density under stationary surface diffusion *(Russian)* 79−8237
Cu electrocrystallisation from $CuSO_4$ solns., expt. and slow surface diffusion theory *(Russian)* 79−11505
Ga, electrode, crystallite interfacial impurities, electrochem. effects, microprobe anal. 77−44569
Li_xCoO_2, cathode material for batteries of high energy density 80−101089
N_2 breakdown formative time lag rel. to gap geometry, pressure, and overvoltage 79−18994
N_2, plane overvoltage discharge 77−19780
O_2 breakdown formative time lag rel. to gap geometry, pressure, and overvoltage 79−18994
SF_6, partial discharge overvoltage dependence 77−76243
Ta, anodic oxidation, open-cct. transient method for overpotential anal. 78−27776
Ti anode, with RuO_2-TiO_2 active film, Cl overvoltage, γ-irrad. effects 79−16005

overvoltage protection
600 MW pulsed energy convertors for toroidal field coil, design philosophy 78−58496
analogue safety data link, for Princeton Large Torus control room 78−54938
contactless cct. in AC/DC transfer standard 77−18035
flashover voltage calc. of uniform-field gaps under steep-front impulse voltages *(Japanese)* 79−64932
fusion reactor, JET neutral injector overvoltage injection system 80−99398
gas-supply line which permits high voltage across its ends without breakdown 77−9998
inductive storage systems motor-generator sets, voltage protection scheme 78−55037
intensive care unit ECG protection against defibrillator pulse 77−25586
Jupiter Voyager electrostatic discharge protection 78−89042
long spark-gaps, breakdown voltage *(French)* 80−33828
power supply, three-phase system, computer aided cct. design 78−54959
sodar system tone-burst protector, cct. design, micrometeorological appl. 79−18641
spark gaps, electrode shape influence on SF_6 dielectric strength *(Czech)* 80−10444
spark gaps, SF_6, limiting sparkover voltage values determ. and dielectric strength testing in power equipment *(Czech)* 80−87962

oxidation
see also anodisation; combustion; corrosion; reduction (chemical)
abietic acid in polymer matrix, photosensitised oxidation, singlet O_2 diffusion *(Russian)* 79−52655
acetic acid, photocatalytic oxidation, photoacoustic spectroscopic obs. 79−16010
acrylic fibre, oxidative stabilisation, O_2 takeup and general model 79−38998
acrylic fibres, oxidative stabilisation, moisture sensitivity 80−16524
acrylic fibres, oxidative stabilisation dynamics 79−38999
actinides, oxidation potential 80−5495
actinides in aqueous solutions, oxidation state and complex formation *(French)* 77−26858
AES, effect of Coster-Kronig energy changes 78−56548
AES, in-situ obs. using galvanic cells 78−19615
AGR coolants, CO oxidation 77−54282
air pollution control, evaluation of catalysts for vapour phase oxidation of odorous organic compounds 79−70482
albumin, human serum, kinetics of eosin-sensitised photochemilum. of solns. 78−68991
alcohols, electrochem. oxidation, kinetic isotope effect *(German)* 78−15681
aliphatic short chain compounds, oxidation and degradation by hyperazeotropic nitric acid 78−37431
alkali silicate glasses, internal friction, influence of red/ox ratio of multivalent ions 78−31447
alloy, binary internal oxidation beneath external scales, onset criteria 79−5074
alloy, compositional changes due to removal of one constituent by surface reaction 77−8996
alloy, high temp. oxidation studies using $^{18}O(p,\alpha)^{15}N$, ^{18}O distrib. determ. 79−87912
alloy, high temperature, mechanical, thermal and corrosion props. 78−95763
alloy, high-temp., scale behaviour in carbonaceous gas atmos. 77−36693
alloy, HTR material, oxidation and carburization in He 80−108645
alloy, internally oxidised, orientational relationships of precip. oxide phase 77−4783
ALLOY 713LC, corrosion kinetics and products under low oxygen partial pressures *(German)* 79−87764
alloys, Auger spectra 78−14600

oxidation continued
alloys, binary, oxidation, solid solution scale formation, approx. calc. of O_2 activity profile 78−88577
alloys, binary, selective oxidation with quasiparabolic kinetics, fixed alloy-scale boundary soln. 78−72930
alloys, high-temp. oxidation resist. improvement by alloying additions 80−66702
alloys, ion implantation in tribology and corrosion science, overview 79−14830
alloys, oxidation mech., exam. using autoradiography 79−20326
alloys, oxidised, heat resistant, radiation emission props. depend. on oxidation conditions 77−43358
alloys, passivatable, role of oxide films in stress corrosion cracking initiation 80−50762
alloys for solar thermal power system 78−18071
α-amino acids, γ-irradiated, primary oxidation products, ESR and ENDOR 77−48754
p-aminophenol, oxidation in aq. soln., chem. equilib. of free radicals, review 79−43573
anisothermal, asymptotic charact. 79−61763
anisothermal, model for kinetics 78−44375
anodic, of ethyl alcohol and acetaldehyde, voltammetric meas. 79−57247
anodic, of Mn in solns. of Mn salts *(French)* 78−11520
anodic oxide film, exam. using SIMS and ellipsometry 79−61770
anthracene, in atmosphere, photooxidation on particulate matter 80−61487
anthracene, oxidation to anthraquinone, in fixed bed catalytic reactor with KS-14 catalyst *(Russian)* 79−66268
anthracene, spectral evidence for green incipient dimers after photo-oxidation and photodimerisation 78−15687
anthracene crystal, sensitised injection from surface oxidation products 78−76143
anthracene single crystals, hole trapping by photo-oxidation products, injection currents *(Russian)* 80−92904
aromatic compounds, oxidative bromination, chem. oscills. 80−3335
arsenides (Ti, V, Cr, Mn, Fe, Co, Ni, Cu, Zn, Ga, Ge), oxidation, hardness and electromechanical polishing response 80−71776
ascorbic acid, action with perhydroxyl radicals, radiolytic study 80−35523
atmosphere photooxidation reactions, rates, reactivity and mechanism for organic compounds reaction with OH radicals 80−72104
atmosphere S, homogeneous oxidation chemistry 78−49119
azides, in polymer matrices, photooxidation, rel. to crosslinking 80−66832
bacteriochlorophyll *b* and pheophytin pair redox potential obs. 79−39338
bacterioviridin, photochem. oxidation mechanism 77−25370
bacterioviridine photo-oxidation in monomer and aggregated states, free radical form., EPR 78−76994
basaltic magmas, O_2 fugacity, role of gas forming elements 78−77218
basalts, terrestrial, lunar and planetary, redox state 78−77217
benzene, deep oxidation on Al-Pt catalyst, kineti model depend. of reaction rate 77−90583
benzene+$O_2(^1\Sigma_u^-)$, photo-oxidation mechanism, optoacoustic determ. 77−12808
binary alloys, activity of most oxidizable element *(French)* 79−61868
binary alloys, diffusion-controlled growth of solid soln. scales 77−70232
bitumen, phys. props. and constitution, effect of air blowing 77−44384
blood, preserved, oxidative pot. 77−81771
bonding material of basic refractories, effect of SO_3, Na_2SO_4 and V_2O_5 79−83343
borides (Ti, V, Cr, Mn, Fe, Co, Ni), oxidation, hardness and electromechanical polishing response 80−71776
brass, α- and β-phase, oxidation, prompt. nucl. reactions and reson. alpha scatt. study 80−66690
brass, cold-worked, anal. by X-ray photoelectron spectroscopy 78−11423
brass coated steel wire, surface composition, oxidation, sulphidation, study by XPS 78−11423
butadiene, effect of redox initiation in emulsion polymerisation *(German)* 78−85158
n-butane-CO_2 mixture, oxidation under RF discharge conditions 78−15670
C W, staged flow of O_2 interaction process, secondary ion emission obs. 78−11386
carbide coating, oxidation protection 77−32704
carbides (Ti, V, Cr, Mn, Fe), oxidation, hardness and electromechanical polishing response 80−71776
carborundum, oxidation protection via phosphate impregnation 77−44374
β-carotene in PVC matrix, photo-oxidation *(French)* 79−34327
catalyst, polycryst., Auger spectra 78−14600
catalysts activity, determ. using interference oxide film 79−83501
catalytic oxidation of H_2 and D_2, matrix isolation and laser fluoresc. obs. of prods. 80−66865
chalcopyrite, aq. oxidation in hydrochloric acid 79−61764
chalcopyrite, electrooxidation in ACl, stoichiometry and reaction mechanism, Cu extraction appl. *(French)* 80−16231
chalcopyrite oxidation, in acidic chloride medium electrochem. study 78−95817
chlorophyll, electron transfer across octane-water interface 77−81474
chlorophyll, photooxidation, triplet state mechanism 78−27791
chlorophyll a, cation radical formation by pulse radiolysis, oxidation and demetalation rate consts. 80−61505
chlorophyll a, photo-oxidation by p-benzoquinone, nature of electron-excited state 78−76991
chlorophyll a, photo-oxidation obs. using pulse photoconductivity 79−79447
chlorophyll and analogues, role of O_2 in regeneration of photoreduced pigments in soln. 78−68980
chlorophyll excited stated, redox pots. 77−25372
chlorophyll photo-oxidation, role of singlet-excited and triplet states 80−51156
chlorophyll photo-oxidation, spectral detect. of exciplex in triplet state 77−25368
chlorophyll photo-oxidation by quinones, cation-radical yield 77−86442
chlorophyll photo-oxidation mechanism, effect of spectral composition of light 77−25369
chlorophyll pigments of photosynthetising organisms redox pots. rel. to evolutionary development 77−56337
chlorophyll-a radical cation lifetime in water-acetonitrile soln. 80−72136
chlorophyll-duroquinone photochemical interaction, photopot. 77−16903
chlorophylls a and b, photo-oxidation primary processes 79−79468
oxidation continued
chloroplast suspension, photoinduced changes in oxidation-reduction pot. rel. to photosystem II activity 77−25399
chloroplasts, EPR signal in response to illum. sequence of four flashes 78−7325
cholesterin ethers, dielec. absorption, heating/cooling and oxidation depth effects *(Russian)* 79−50984
Chromel alloy, influence of elastic strain on oxidisability *(Russian)* 79−70116
CO_2 ferrite, crystal structure, X-ray absorpt. spectra, chemical shifts 80−88118
coal, electrochemical oxidation for H_2 prod. 79−61962
coal ash characterisation with X-ray photoelectron spectroscopy 79−1977
cobalt phthalocyanine, electrochromism and oxidation 80−93768
conference on solid-vacuum interface, Amsterdam, Netherlands (June 78) 79−42342
copper molybdates, oxidation, reduction and thermal decomp. mechanisms 80−50847
CVD oxide, distributed fixed charge elimination using HCl 79−42661
cyclopentadiene-butyl vinyl ether copolymer, oxidative degradation *(Japanese)* 80−108714
cytochrome *a* interaction with mitochondrial matrix H^+ ions 79−43806
cytochrome C, immobilised, investigs. using magnetic micromixer attachment for SPECORD UV VIS spectrophotometer 80−56302
cytochrome c interaction with bilayer phospholipid membranes 78−69001
cytochrome c oxidase, coupled to proton pump in mitochondria 77−25406
cytochrome c oxidase, oxidised and reduced, X-ray absorpt., edges, using synchrotron radiation 78−48758
DBTTF halogen complexes, IR, UV spectra, EPR study 80−108215
defect theory and processes, review 80−2009
deformation effects in nuclear reactors and mech. structures 80−3211
diamond, powders, oxidised surfaces, thermal desorpt. spectra 78−47661
diamond, synthetic, oxidized in fused salts, etch features 80−97604
diamond powder, rapid oxidation development, kinetic model *(French)* 78−68917
diazo materials, system aspects of spectral sensitization 79−20434
dielectric films on semiconductor devices, review of deposition techniques 78−23611
diffusion laws in solids, phenomenological 80−39341
1,3-diphenylisobenzofuran, oxidation, dissoc. oxciplex relax., solute reencounter probabilities 79−34285
1,3-diphenylisobenzofuran, rubrene sensitised photooxidation, efficiency meas. 78−27792
1,3-diphenylisobenzofuran solns., rubrene sensitised photooxidation, S_1 excited state O_2 quenching 80−45529
dipotassium glucose-1-phosphate, X-irrad., ESR-ENDOR obs 80−60419
duroquinone, soln., electrochem. props. obs. *(French)* 79−66301
dynamic, in power units in hot industrial gas stream 78−35567
earth reentry exposure, simulated, effect on mech. props., oxidation of ThO_2 dispersion hardened alloys, Haynes 188 and Hastelloy X 79−5086
electrical resistance alloys *(Polish)* 79−79143
electrochemical, kinetics, modified double pulse technique, appls. 77−25280
electrochemical reactions, visible region internal refl. method investig. 77−60069
electrochemical surface reacts. driven by linear pot. sweep, sequential reactions, kinetics 77−25276
electrode surface, covalently bound molecules, redox reactions, steric effects 78−73077
electrode-redox system electron transfer reacts. time-depend. perturbation theory 78−61027
electrolyte, ionic mass transfer in narrow rectangular conduits 80−61105
electron cyclotron resonance plasma, for metal surface cleaning of Cu 79−47822
electroreflection exam., short range order in surface layers 78−6703
emulsions, reduction sensitised by dyes, redox potentials, quantitative correls. 79−34298
ethanol, chemisorpt. and oxidation on Cu(110) and Ag(110) catalysts 78−61044
ethylbenzene, oxidation, complex network calcs. 78−11497
Fe base alloy, with metallic coating, oxidation effects, wetting, adherence 78−7085
ferrite, hot pressing, charge:oxidizer ratio 77−48379
ferritic alloy DT02, oxidation behaviour in CO_2 or Ar with H_2O and H_2, 823-123K 80−3249
ferromagnetic metals, thermal oxidation rate determ. using nanowebermeters 80−61045
ferrous material fractured surface exam., oxide scale removal 78−95886
ferrous sulphamate radiolytic instability in nuclear process solns. 77−70314
flame propagation through stratified charge combustion channel, model 79−64795
formaldehyde, oxidation, appl. of sensitivity analysis, numerical Green's function procedure 79−100334
formamide oxidation at Pt alloy catalytic electrodes 79−57245
formyl radical, atmospheric oxidation, IR Fourier transform spectroscopic obs. 79−66785
fuel rod microstruct. changes associated with post-DNB operation during power-cooling-mismatch 78−21688
GaAs, Schottky barrier, effect of oxide composition on elec. behaviour, AES meas. 79−87141
GCFR advanced alloy cladding, oxidation behaviour in the environment 80−104350
Ge film, oxide layer elec. props. 77−76927
glass, ageing use, photothermal processing, sorptive and luminescence props. *(Polish)* 78−11250
glass, alkali silicate, oxidation reduction equilibria and optical absorption of Cu ions *(Japanese)* 77−12824
glass, Libyan Desert Glass, redox form. conditions, EPR obs. of as-received and irrad. samples 78−28228
glass, redox number 79−29392
glass fibre reinforced plastic greenhouse sheets, ageing behaviour, natural and artificial weathering *(German)* 80−81226
α-glycine, irradiated, oxidation prod. N-centred π radical ERR 77−14459
glycine-$AgNO_3$, single cryst., X-irrad., oxidation product form. 77−48660

oxidation continued
graphite, ATJS, tensile strength, oxidation effects up to 2500K 80−3209
graphite, Br_2 intercalation, oxidation and residual Br effects 79−43565
graphite, Fe-catalysed gasification, electron, microscopy 80−104358
graphite, from reactor, quantitative microanalysis by laser emission spectroscopy 80−81384
graphite, nucl. grade, neutron small angle scatt., thermal and radiolytic oxidation effect, porosity size distrib. 79−17977
graphite, oxidation, corrosion resistance, bend strength, assessment for rotary glass fibre making apparatus 78−64753
graphite, oxidation kinetics near 1000K 77−48616
graphite, oxidation resistance, effect of P cpds., metal impurities and struct. defects 77−81331
graphite, oxide coating protection effectiveness estimation 77−86198
graphite, trifluoromethanesulphonate intercalate, prep. by anodic oxidation 78−27439
graphite+O_2 reaction, standard Gibbs free energy change, electrochemical determ. 77−29041
graphite $AlCl_3$ intercalation compound, electrochem. characterisation method 80−55666
graphite catalytic gasification using Pt, Ir, Pt-Ir, small bimetallic particle identification by controlled atm. electron microscopy 79−83502
graphite crucibles, oxidation loss and wettability of inorganic fluxing materials *(Japanese)* 78−84755
graphite intercalation compounds, magnetic resonance determ. of oxidation state 78−35051
graphite monolayer on Ni (110) surface, oxidation mechanism 80−101037
graphite oxidation and coolant chemistry of CEGB gas-cooled reactors 80−42774
groundwater flow systems, oxidation-reduction sequences 79−84303
haeme proteins and metalloporphytins, redox chem. and oxygen binding 80−3573
halocarbon waxes, thermoxidative stability study, hybrid microcircuit appl. 79−100271
Hastelloy B-2, decomposition of metal oxide films under electron bombardment 78−19928
Hastelloy-X, Ni-Cr-Fe-Mo, cyclic oxidation resist. improvement by high temp. etching treatment 80−97627
heat exchanger materials, oxide protective layer formation meas. by hydrogen permeation 78−8895
heat shrinkage tubing, crack resistance *(Japanese)* 79−61709
heterogeneous oxidation catalysts, effects of Pb compounds 79−24817
high temperature metallic species, absorpt. and fluoresc., high temp. fast flow reactor technique 80−42231
HTGR, structural materials, effect of coolant impurities on mech. props. *(German)* 78−25297
HV electrode, Fe microsphere impact, charge reversal, oxidation effect 77−12042
hydrocarbon emissions from vegetation, oxidation as atmospheric CO and H_2 source 78−88881
hydrocarbons, gas phase oxidations and pyrolysis, wall-less reactor technique 80−45500
hydroquinone development, effect of oxidation products 79−24796
4-hydroxy-2,2,6,6-tetramethylpiperidine, radiation-induced oxidation to paramag. nitroxide free radicals 80−81341
hypotaurine oxidation to taurine by UV irradiation 79−96617
Iconel, oxide film quantitative anal. by XPS and rastered ion bombardment 77−40604
III-V semiconductor, oxide coatings by thermal and anodic oxidation 77−32706
III-V semiconductor anodic oxidation and applications 77−77598
III-V semiconductors, anodic oxidation *(Japanese)* 78−92385
III-V semiconductors, oxide film growth, optical props. *(German)* 78−34730
Incoloy 800, carburisation, oxidation and creep, review 79−47837
Incoloy 800, chem. behaviour and mech. performance in HTR He at high temps. 79−47842
Incoloy 800, clean and steam oxidised, T_2 permeation 80−88364
Incoloy 800, high temp. oxidation in low O_2 pressures, SEM obs. of oxide morphologies 79−47844
Incoloy 800, mechanisms of corrosion in He, oxidation kinetics 79−47843
Incoloy 800, oxidation resistance, alloy depletion effect 77−8989
Incoloy 800, steam oxidised, oxide coating anal. 80−89399
Incoloy 800, thin wall tubing, increase of oxidation as function of creep rate and rupture time 79−47774
Incoloy 800 Fe base heat resistant alloy oxidation 77−86231
Inconel 600, nuclear reactor boiler corrosion, XPS 80−66709
Inconel 600, nuclear reactor boiler corrosion, XPS 80−71816
Inconel 600, oxide layer, mechanical impedance meas. method 80−45444
Inconel 600, XPS exam. of initial growth of oxide films 79−20240
INCONEL 617, corrosion kinetics and products under low oxygen partial pressures *(German)* 79−87764
Inconel 750, volatilisation of oxides during oxidation at 1200°C 78−23873
Inconel 800, simulated, steam oxidation 80−76405
inositol, X-irrad., radical form. detection by ESR and ENDOR, oxidation process 78−27797
insulating film for semicond. devices, props., rel. to deposition conditions 78−23612
intertransition metal compounds, hardness and oxidation resist. 77−63773
ion implanted, F influence on oxidation-induced stacking faults 80−65011
ion techniques, conf., Manchester, England, (Apr. 1975) 77−8962
isopropanol, anodic oxidation *(Rumanian)* 78−19907
isopropylbenzene, IR spectra of oxidation products *(Rumanian)* 78−23838
Josephson junction, fabricated by RF plasma oxidation, IV characts. *(Japanese)* 80−84564
ketone chemiluminescence during disproportionation, nonradiative transition processes 79−87846
Kevlar 49, fibre, mech. props., environmental effects incl. sunlight, ionising rad. 77−36560
lake sediments, E_h meas. reliability conditions 79−48528
lanthanides, oxidation potential 80−5495
laser treatment of material influence of oxidising atmosphere *(Russian)* 78−23840
layer thickness measurement by kinetic method 77−24503
oxidation continued
lipid, peroxide photo-oxidation, increase in liposome proton permeab. 78−69024
lipid bilayers, effect of oxidation and hydrolysis on elastic props. 79−92165
lipid free radical oxidation, UV effect on lipid-protein complexes and membranes 77−36874
lipid free radical oxidation kinetics rel. to lipid composition, photoreceptor membrane 78−80872
lipid peroxide oxidation fluorescing products, effect of UV on formation 79−57585
lipid photoperoxidation in isolated chloroplasts, role of superoxide anion radicals and superoxide dismutase 78−77016
lipid systems, anti-oxidant action mechanism determ. by chemiluminesc. 77−56330
lipids, peroxide oxidation, sarcoplasmic reticulum membrane rearrangements 78−69025
lipids, peroxide oxidation in photoreceptor membrane, protein-lipid interactions 77−21522
lipids of bilayer membranes, coupled with NAD.H oxidation by atm.O 77−36875
liquid film, falling, O_2 adsorpt. with zero order react. in entrance region 80−64652
liver tissue, mouse, appearance of free radical centres on low temp. oxidation 78−69013
lodestones, oxidation rel. to microstruct. and mag. props. 78−16004
lubricants, ester-type, thin-film test for meas. of oxidation and evaporation 80−40626
lutetium diphthalocyanine, solid-state anion migration in anodic oxidation 80−60994
manometer reference free-piston oxidation process for trimming mass of weights 78−93715
Mars surface, constraints due to atmospheric chemical processes 77−5475
membrane damage caused by light irradiation of fluorescent concanavalin A 80−56123
metal, chemiluminescent oxidation using laser vaporisation, kinetics 79−100385
metal, coated, heat resistance assessment at varying temps. *(Russian)* 77−25189
metal, foil, surface temp. meas. during laser irradiation heating *(Russian)* 79−74030
metal, interference phenomena and integral emittance, during high temp. oxidation *(Russian)* 78−91458
metal, laser heating kinetics, influence of oxide film interf. effects 80−11841
metal, microcrack, generated in oxides during high temp. oxidation, detection by slight sulphidisation 77−8999
metal, nitridation and oxidation, comparison of behaviour at high temp. 79−74288
metal, O Auger peak studies 77−1769
metal, oxidation, Auger electron, X-ray fluoresc. spectroscopy appls. 77−44412
metal, oxidation, oxide thickness and oxide transfer in wear 77−16755
metal, oxidation, Rosenburg kinetic method applied to determ. of parabolic rate const. 78−64774
metal, oxidation kinetics, effects of control of scale structure 77−16751
metal, oxidation of high temp. material, lattice vacancy effect 77−70203
metal, oxide film growing by cation diffusion, stress generation 78−60865
metal, oxidisable, DC reactive sputtering, glow discharge mass spectrometry and X-ray diffr. 79−38701
metal, passivation termination, ESCA study 79−20267
metal, pure, multilayer scale form. and parabolic oxidation, different rate const. 78−64758
metal, pure, multilayer scale form. and parabolic oxidation, temp. and press. depend. of rate const. 78−64759
metal, pure, oxidation in mixed atmosphere, simultaneous oxide/sulphide form. 79−61788
metal, pure, vacancy injection during oxidation, reexamination of evidence 78−60864
metal, standard free enthalpy of oxidation meas. *(French)* 79−61867
metal, surface layer transform. and failure, kinetic charact., under dry friction 77−52506
metal, surface O_2 content anal. by reson. α-scatt. from ^{16}O 78−64778
metal atom oxidation lasers, book contrib. 77−10913
metal atom oxidation reactions, kinetics of chemilum. emitter form. and quenching 78−63107
metal film, evaporated, resistivity change on oxidation *(Japanese)* 79−11723
metal film and foil, surface IR wave propag. distance, imperfection and oxidation effects 77−28641
metal grinding in oxidising medium, electromechanical processes *(Russian)* 79−79149
metal hydride, oxide, nitride prod. in electron diffr. camera 77−65937
metal mirrors, for high-power appls., multithreshold damage analysis 77−88884
metal oxidation, secondary ion energy spectroscopy 80−71788
metal oxide thick film growth, fund. theory 80−89391
metal oxide ultrathin layers by reactive sputtering, controlled deposition and characterisation 79−78887
metal oxides, nonstoichiometric, work function and near-surface chem. diffusion 80−80034
metal powder mixture with decomposing oxide, growth kinetics of surface film during annealing 79−96216
metal surface, reactivity, review of electron spectra 77−62748
metal surface oxidation, refl. spectra obs. 78−39958
metal surface oxidation study, vacuum microbalance investigation 80−76552
metal target, gas breakdown near surface, pulsed CO_2 laser focusing effect 79−52051
metal target, irradiated by pulse-periodic CO_2 laser, absorpt. coeff., air breakdown effect 79−52052
metal wettability, using macroscopic theory of mol. forces *(Russian)* 77−66073
metal with dispersed oxide phase, charged particle theory 78−19925
metal-slag interface, interaction under diffusion conditions, impurity oxidation *(Russian)* 80−35390
metallic coatings, sputtering in inert atm. with uncooled cathode, X-ray diffr. obs. 78−3041

oxidation continued
metalloporphyrin, cation radical formation by pulse radiolysis, oxidation and demetalation rate consts. 80−61505
metals, in hostile environments, oxidation, in situ meas. method 78−44277
metals, influence of oxide films on photoemission *(Russian)* 77−81194
metals, ion implantation and backscattering anal. 77−8980
metals, oxidation mech., exam. using autoradiography 79−20326
metals, sintering, surface oxide layer effects, oxide dissolution process, anal. 80−11588
metals and alloys, gas corrosion, in composite atmospheres *(Polish)* 79−79142
metals and alloys, protective oxide layer stress accumulation and perturbation of parabolic kinetics 79−5076
metals heating kinetics in oxidising medium, exam. using CO_2 continuous laser emission *(Russian)* 79−57135
metals in gaseous oxidative medium, reaction diffusion theory 79−20463
methane, atmospheric circulation, destruction through photochemical oxidation *(German)* 79−84424
methane, oxidation, complex network calcs. 78−11497
methane, shock-tube oxidation, equilibrium and nonequilibrium radiation emission 78−27760
methane-CO_2 mixture, oxidation under RF discharge conditions 78−15670
methanol, oxidation to formaldehyde in fluidized bed, Fe-Mo/SiO_2 oxide catalyst 79−100440
methanol, to formaldehyde, effect of Al_2O_3 additives on catalytic activity of Cr_2O_3-Mo_2O_3 catalysts *(Russian)* 79−66346
methanol adsorbed on Ag (110) catalyst, oxidation 78−88556
methanol oxidation mechanisms at Pt electrodes in acid electrolytes in methanol-air fuel cells 80−45661
3-methoxybenzanthrone in ethanol, photoprotolytic reactions, spectra, rate consts. and lasing thresholds 80−43327
methyl viologen, chlorophyll a sensitised reduction in non-ionic micelles 79−1962
methylhydrazine, electrochem. oxidation on Au, appl. to gas monitoring 79−39248
migration of implanted species during annealing and oxidation, small angle Rutherford backscatt. obs. review 77−44108
mitochondria of bovine heart, EPR investigation of two forms of Fe-S centre N-2 78−69014
MNOS capacitors, retention and endurance characts., annealing and oxidation effects 79−74274
molten carbonate fuel cell, electrolyte comp. effect on electrode kinetics 80−101092
mordenite-hosted redox reactions 80−55939
MOS inverted-channel carrier scatt., effect of oxidation in Cl media 78−76156
MOS plasma-oxidised nitride structures, characts. 79−65552
MOS structure, effect of pre-oxidative chemical treatment on quality of active oxide 79−42647
MOS structures, Na^+ neutralisation characteristics of HCl oxides 78−10572
mutual alloying behaviour of the elements straddling the line Li-Mg-Cu-Au in the long periodic table 78−84769
N_2H_4, electrochem. oxidation on Au, appl. to gas monitoring 79−39248
NAD.H, by atm.O, coupled with peroxide oxidation of lipids in bilayers 77−36875
NAD.H, oxidative phosphorylation, role of respiratory chain 78−15795
NADH oxidation using pyrolytic C film electrode 78−92487
Nb-O, effect of O_2 on penetration of Li at 400°C 79−11719
Nichrome, volatilisation of oxides during oxidation at 1200°C 78−23873
NIMONIC 80A, corrosion kinetics and products under low oxygen partial pressures *(German)* 79−87764
Nimonic PE16, oxidation in Ar-H_2O-H_2 atmosphere 78−35584
nitromethyluracil, radiation-induced oxidation and reduction 77−32816
noble metal, interfacial corrosion in metal to ceramic reaction welding 78−53035
Nomex, fibre, mech. props., environmental effects, incl. sunlight and ionising rad. effs. 77−36560
nonequilibrium plasma chemical reaction kinetics 78−76863
nuclear reactor core meltdown, chemical reacts. between core melt and concrete 80−13588
nucleation and growth at surfaces, kinetic studies, review 78−72046
optical fibre preparation methods and performance factors 80−69557
optical image phase recording using sensitised photooxidation reactions 80−87350
organic compounds, evaluation of Cd_3O_4 catalysts for oxidation 77−37353
organic compounds, photocatalytic oxidation on Mars 78−85883
organic fluid charge carrier generation, role of molecular electroinduction effects *(Russian)* 79−96321
organic laser dyes, electrochemiluminescence, electrochem. oxidation, reduction 77−70304
organic molecules, catalytic effects on electrode reactions, review 80−61110
oxidation, water vapour and O_2 excitation effects, XPS obs. 79−100274
oxide film prod. by pulsed evap., capacitor prod. and characts. *(Russian)* 78−60584
oxide thickness measurements up to 120 Å on silicon and aluminium using the chemically shifted Auger spectra 78−23586
oxidising metal heating by periodically pulsed CO_2 laser 80−7445
oxiphenol, oxidation-reduction interaction with metal ions *(Russian)* 79−39138
PAN fibre, pre-oxidised, IR absorpt. 77−28561
PAN fibres, SO_2 treatment 79−52403
PBI fibre, mech. props., environmental effects, incl. sunlight and ionising rad. effs. 77−36560
Permalloy, magnetic head wear resistance and surface charact. against magnetic tape *(Japanese)* 80−35335
Permalloy, oxidised film, magnetic noise, low temp. depression *(Russian)* 79−99734
Permalloy corrosion resistance enhancement 79−79150
Permalloy film, oxidation, quartz cryst. microbalance, AES and XPS obs. 78−27676
Permalloy film oxidation, microbalance, AES, ESCA and sputter profiling 78−15600
Permalloy films, oxidation effects on atmospheric corrosion, AES, XPS and ion sputtering anal. 80−11829
pheophytin a, photo-oxidation primary processes 79−79468

oxidation continued
phospholipid auto-oxidation during conform. changes in rod outer segment membranes 77−21523
photochemical diode using p-n heterojunction or Schottky barrier immersed in electrolyte 77−66201
photoredox reactions of metal ions for photochemical solar energy conversion 77−86334
photosynthesis, effect of bivalent cations on photo-induced redox conversions of P700 78−77014
photosynthesis, interaction of paramag. probe I (12,3) with bean chloroplast membranes 78−77015
phthalocyanines, partially oxidised, highly conductive molecular solids 77−47800
picrate anion active transport through organic liq. membrane 78−11556
plasma oxidation in microwave discharge 80−76382
polyacetylene, doping with AsF_5, mechanism, effect on elec. cond. and spectra 80−24473
polyacetylene films, doping investigation, insulator-metal transition, optical transmission meas. 80−103729
1,4-polybutadiene, oxidation stabilisation by singlet O_2 quencher 4-(1-imidazolyl)-phenol 80−16677
polycarbonate, colour appearance during oxidation *(Russian)* 79−24643
polycarbonate, turning yellow during oxidation, kinetic regularities *(Russian)* 79−24644
polychlorotrifluoroethylene wax, thermoxidative stability study, hybrid microcircuit appl. 79−100271
polyethylene, cross linking by energy rich radiation, mech. and elec. props. *(German)* 78−20035
polyethylene, cross-linked, thermal oxidation stability, influence of Cu 80−30128
polyethylene, elec. cond. of high and low density samples, oxidation effects 80−107784
polyethylene, elec. props. and oxidation after electron beam irradiation and heat treatment 79−87092
polyethylene, high density, carrier trapping, X-ray induced TSC 80−11005
polyethylene, high density, thermolum. and its oxidation effects 77−77305
polyethylene, high density, trapped carriers, thermally stimulated currents, influence of oxidation 77−80792
polyethylene, high density corona charged, TSC, oxidation effect 78−26882
polyethylene, low density, increase in oxidation on flame treatment, XPES 79−66179
polyethylene, oxidation rel. to spherulitic crystn. *(Russian)* 78−71689
polyethylene, oxidised, low-temp. dielectric spectrum 79−61304
polyethylene, oxidised, origin of high temp. anomalous luminesc. 77−85812
polyethylene, oxidised, paraelectricity, dielec. relax. obs. 77−48123
polyethylene, oxidised and gamma-irradiated, carrier traps, thermally stimulated currents 78−19050
polyethylene, pulsed NMR obs., crystallinity effects 78−76342
polyethylene, thermally oxidised, low-temp. dielec. relax., dipolar tunnel states 78−2797
polyethylene, with various antioxidant, stabilized and TiO_2 pigment additions, photo-yellowing and oxidation 79−16015
polyethylene coating on galvanized steel, thermal oxidation affect on adhesion *(German)* 80−35419
polyethylene film, partial discharge degradation, effect of discharge products in air *(Japanese)* 77−69774
polyethylene single cryst., FT IR spectra, CH_2 rocking mode 78−2843
polyethylene stabilized with home-made antioxidants, thermal resistance *(Polish)* 79−52328
polyethylene with rutile pigment-antioxidant, photo-oxidation 77−63816
polyketo cpds., Mo complex formation, kinetics mechanism 77−77732
polymer, ESCA investigation of struct., reactivity and bonding, O_2 (inert gas) surface modification 78−3438
polymer, photo-oxidation 80−3380
polymer coatings for corrosion protection, electrochem. techniques for performance monitoring 80−3234
polymer film coating of Al particles *(Russian)* 77−86232
polymer melt, oxidative stability determ. technique 80−45412
polymer surface, LCAO-SCF calc. of core binding energies of O-containing organic mols. 79−76344
polyphenylene oxide, with and without impact resisting polystyrene, photo-oxidative ageing, Cu and Fe trace effects *(German)* 79−100191
polypropylene, oriented, thermooxidative degradation kinetics, durability, influence of mech. initiated processes *(Russian)* 79−24591
polypropylene, photooxidation, initiation process nature 77−52523
polypropylene on oxidised Cu, degradation, ion scatt. anal. 77−40463
polypyrrole films, electrochemical prep., chem. and phys. characterisation 80−70708
polystyrene, props. changes upon photooxidation 80−30123
polyvinylcarbazole, fluoresc., photooxide quenching, exciton migration effects 79−56830
porphyrin, reduced, photoregeneration mechanism in the presence of O_2 79−57582
positronium oxidation react. in aq. soln., positron hydration energy 78−61039
propane, Pt catalyst surface morphology and faceting obs. 77−52669
propene, catalytic oxidation, modification of V_2O_5(001) surface *(French)* 80−45557
propene soft oxidation, gas-solid catalytic reaction, kinetics, automatic meas. *(French)* 77−1912
propylene, oxidation on MgO:Mo catalyst, surface structs., IR absorpt spectra obs. 80−66868
protein-lipid model systems, chemiluminesc. on exposure to formalin 77−56329
PVA, photooxidation, kinetic eval. for carbonyl form. *(Japanese)* 79−39007
PVA carbonisation process and carbonised block props., high temp. resistant materials *(Russian)* 79−8268
PVC, thermooxidative degradation, crosslinking and chain scission 80−71912
PVC surfaces, natural and stabilised, composition, ageing, oxidation and weathering, ESCA obs. *(French)* 80−61139
pyrocarbon, oxidation behaviour at high temps. 80−55551
pyrocatechol, oxidation pots., correl. of V-I characts. and photographic developing power *(Russian)* 80−45534
pyrographite, elec. resist., during electrochem. insertion of H_2SO_4 *(French)* 80−2437

oxidation continued
quartz, single crysts., Ar and O_2 interaction at high temp., surface struct. changes *(German)* 80−96725
quinoline, photooxidation on rutile, ESR and effects of surface states 79−66352
rare earth aluminates, effects of roasting in reducing and oxidizing media on elec. props. 78−52736
rare earth metal films, reactions with O_2 and water, XPS obs. 77−31888
rare earth oxides, binary, struct. and props., book contrib. 80−45292
rare earth thiohafnates, thermal stability and oxidation products in air 79−83346
rare earths, purification, laser methods 80−16712
reactor fuel cladding failure under reactivity initiated accident conditions *(Japanese)* 79−30955
refractory metals, oxidation, high-temp., mechanism, review *(Polish)* 79−34184
Rene 41, Ni-Cr-Co-Mo-Ti-Al-Fe (18.96, 11.09, 9.65, 3.06, 1.59, 0.89 wt.%) formation of Cr_2O_3 monocrystals on heat treatment 79−52455
Rene 41, volatilisation of oxides during oxidation at 1200°C 78−23873
resistant alloys, metastable microcrystalline, appl. 80−84887
retinal, highly polar excited electronic states, electron transfer 78−48757
retinals, prod. and quenching of singlet oxidation 80−35840
reversible photoredox system, thionine type and I_2 type, chem. equilibria *(German)* 77−90630
rhodamine 69, soln., bleaching and laser props., detergent effects 79−59697
rhodamine 6G, aqueous soln., absorpt. spectra, ground and triplet state photoprotonation pH depend. 80−42961
rhodamine 6G in ethanol, photobleaching mechanism *(Russian)* 78−48680
rhodamine B, adsorption on ZnO single crystal, photooxidation, electrochem. meas. 78−31645
rhodamine B, soln., bleaching and laser props., detergent effects 79−59697
rhodamine dyes in soln., bleaching, electronic and vibr. absorpt. spectra, fluoresc. 80−42960
RNA synthesis in vitro, thiopyronine-sensitised photodynamic inactivation 77−29177
rubber, for prep. of diene oligomers with hydroxyl groups *(German)* 80−85175
rubrene, photooxidation, photoacoustic spectroscopic obs. 79−16010
rubrene film, photooxidation in solid, UPS obs. 79−52693
scale growth rate, rel. to comp., diffusivity and molar volume 77−36694
scale-resistant metallic materials, cyclic oxidation method for spalling and scale resist. determ. 77−77695
scales, cation distrib. calc. by approx. analytical method 77−48594
secondary ion yield calculations for oxidised metal surfaces, empirical formula 78−6821
sediments anoxic pore waters, effects of oxidation during sampling on silicate content 78−61394
semiconductor, detection of trace Na in furnace 77−4955
semiconductor, dopant impurity redistrib., Chen and Chen series method 79−1457
semiconductor, tetrahedrally coordinated, review of surface struct., chem. and spectroscopy 80−59764
semiconductor p-n junction, conversion of chem. energy into elec. power thermodynamic props. 79−11219
semiconductor-electrolyte interface, photoelectrochem. processes, hologram recording utilisation 77−88667
Sendust alloy, magnetic head wear resistance and surface characts. against mag. tape *(Japanese)* 80−35335
n-Si:B, ion implanted, rapid identification of faulted loops 79−19254
Si_3N_4-Ce_2O_3-SiO_2 materials: phase relations and strength 80−97465
Si, X-ray step scanning section topography, lattice imperfection characterisation, automatic Bragg angle control 79−60221
sialon, oxidation 77−56126
SiC (6H) thermal oxide layers, AES *(Japanese)* 79−96386
silane, prod. of SiO_2 films 78−3038
silicide coating, oxidation protection 77−32704
silicides, oxidation and hot corrosion resistance kinetics 80−25896
SIMS, solid surface investig. applications *(Rumanian)* 80−49510
sintered frictional material, environmental effects on props. 78−11338
smoke plumes SO_2 conversion *(Dutch)* 77−70825
smouldering discharge at O_3 liq. surface in N_2, thin solid pellicle formation of N_2O_5 80−38827
SO_2 diffusion-coupled oxidation in atmosphere 78−65371
soft magnetic mat. prep. by precip. of insulating film on Fe powder in polishing bath 78−23637
solid, improved calorimeter eqn. 79−66278
solid surfaces, surface processes, and solid/gas interactions 80−73125
solid-state redox reaction, electron tunnelling rate, transfer model 78−76844
space charge effects on steady-state transport in oxide films 80−11124
sphalerite, kinetic study on press. leaching 77−4893
sputtered refractory carbides, adhesion to metal substrates, improved 80−76481
stainless steel, austenitic, surface, interaction with O_2, and work function obs. 80−65364
stainless steel, Cr-depleted zones 77−8992
stainless steel substrate, effect on mechanochem. degradation of thin polymeric coatings 79−79134
steam oxidation of reactor fuel sheathing, strain effect 77−6525
steel, AGR boilers, gas side corrosion, breakaway oxidisation treatment 78−48558
steel, Al and Cr coated, structural transformations oxidation effect in Kh25N20S2 steel 79−57154
steel, alloy, carburisation, internal oxidation of excess carbides *(Russian)* 80−25903
steel, alloy, oxidation resistance at elevated temps., effect of various alloying additions 77−56134
steel, alloy cladding, oxidation behaviour in GCFR He environment 80−16594
steel, austenitic, Cr-Ni (18, 15 wt.%), oxidation resist., metallic alloying additions effect 79−52419
steel, austenitic and martensitic, corrosion under boiled conditions, Mossbauer spectroscopy study 79−47800
steel, austenitic stainless, Cr-Ni (20, 25 wt.%), Nb stabilized, oxidation behaviour in CO_2, surface ion implantation effect 80−71791
steel, austenitic stainless, current maxima in passivity range 79−66200
steel, austenitic stainless, fretting wear in air and CO_2 at elevated temps. 80−21119
oxidation continued
steel, austenitic stainless, high temp. oxidation, high temp., in low O_2 press., surface anal., impurity diffusion effects 77−56142
steel, austenitic stainless, metastable, Si effects, unlubricated adhesive wear, oxidation resistance, solid soln. hardening 77−59949
steel, austenitic stainless, oxidation and spalling resistance 80−30133
steel, austenitic stainless, oxidation of (100)-plane, LEED-AES obs. *(German)* 78−68841
steel, C, corrosion during cyclical exposure, to wet elemental S, and He atmosphere 78−92391
steel, C, hot plastic deform., vac. colour etching investigation 80−61036
steel, C, wear charact. of worn surface layer under lubrication *(Japanese)* 78−35526
steel, C-Mn, anisothermic oxidation 79−66195
steel, chromoaluminosiliconising with electroheating, for oxidation resistant coatings 79−52457
steel, combined saturation with C, N and O by chemicothermal, surface treatments, oxidation carburisation 78−95856
steel, continuously cast, segregation at halfway cracks 80−60869
steel, Cr, ferritic, oxide scale etching 79−70204
steel, Cr (9 wt.%), oxidation in CO_2, early stages study by AES 78−7080
steel, Cr-Mn, high temp. oxidation, sub-cinder layer formation, protective coating role *(Russian)* 80−93686
steel, Cr-Mn-C-Si (20, 14, 0.2, 0 to 3 wt.%), high-temp. oxidation *(Russian)* 80−25904
steel, Cr-Mo, crack decoration in oxides by electrodeposited metals *(German, English)* 79−70266
steel, Cr-Mo, oxidised, mechanism of crack decoration of oxides by electrodeposition 80−97560
steel, Cr-Mo (10-14, 2-6 wt.%), heat-resist., creep-rupture strengths 80−104271
steel, Cr-Mo (2.25, 1 wt.%), oxidation effect on hold time fatigue behaviour 80−30161
steel, Cr-Mo-V, fatigue crack growth rate and threshold under oxidising conditions 79−20272
steel, Cr-Mo-V low-alloy, mech. props. and stress relief cracking, effects of impurities and deoxidation practice 80−66599
steel, Cr-Si, oxidation resist. in high pressure CO_2, Si effect 80−66704
steel, disintegrated stream, simplified model of oxidation 77−73373
steel, eutectoid, activation energy of oxidation in wear 77−52507
steel, Fe_2O_3, transformation to Fe_3O_4 in oxide scales conversion kinetics 80−7561
steel, Fe-Cr-Al, sulphidation behaviour, 750°C, preoxidation effect *(French)* 78−15566
steel, heat-exchanger alloys for use in nuclear steam coal gasification plant 78−15589
steel, high and low C, wires, electroheated, thermal cycling and corrosion behaviour 80−61006
steel, high Mn, heat resistant, alloying additions, effect on mech. props. *(Korean)* 77−12631
steel, insulation layers of magnetic laminations meas., by X-ray and electron microscopy *(Polish)* 77−12743
steel, internal oxidation during carburizing and heat treating 79−24660
steel, low alloy, medium C, sliding interfaces, division of heat and surface temp. rel. to oxidative wear 78−64712
steel, low-alloy, hardened deoxidised, delayed failure, influence of internal adsorpt. of impurities 80−60974
steel, low-alloy, oxidation resist., N effect 80−66706
steel, magnetite film formation at metal scale interface, during cooling 78−88575
steel, medium C, 45, deposition of composite, wear resistant Ni-B-Cr coating 78−11420
steel, mild, hot shortness mechanism, surface enrichment of residual elements and oxidation *(Chinese)* 79−74230
steel, mild, N_2 on oxidation resistance 79−61786
steel, mild, nitrided, oxidation resist. 78−95846
steel, mild, oxidation of contaminated crevices exposed to CO_2 79−20243
steel, molten, deoxidised, reaction with oxidising gas bubbles 78−88438
steel, molten deoxidised, reaction with oxidising gas bubbles 78−84739
steel, Ni-Cr, oxide layer form., SIMS obs. 79−52464
steel, nitrided stainless, internal attack 77−36692
steel, oxidation reaction of Si and Mn during CO_2-O_2 arc welding 77−60116
steel, oxidation-reduction processes on surface during heating in vacuum *(Russian)* 78−11403
steel, oxide inclusions 78−23648
steel, pearlitic structural, austenite grains, growth rate during heating 80−100860
steel, railway, oxidation by Fe-Si-Ca-V complex alloy, nonmetallic inclusions *(Russian)* 80−93685
steel, rapid, ZrB_2 surface treated, resistance Co high temp. oxidation 79−66203
steel, rare earth additions, effect on physicomechanical props. 77−12639
steel, Si, commercial, O_2 diffusion coeff. determ. *(Slovak)* 79−39040
steel, Si, nonoriented elec. sheet, solute oxidation effect on mag. props. 79−83335
steel, Si-Al, non-oriented elec., internal oxidation and nitridation effects on mag. props. 79−83336
steel, sintered, oxidation in superheated steam, corrosion protection 79−39049
steel, spalling and scale resist. determ. by cyclic oxidation method 77−77695
steel, stainless, 316, oxidation behaviour in the environment, appl. to GCFR fuel claddings 80−104350
steel, stainless, austenitic, oxidation in CO_2, charged-particle nuclear techniques 80−61022
steel, stainless, boiling water reactor, corrosion and oxidation potentials monitoring 79−20252
steel, stainless, component metal oxidation, reflectance IR study 79−47811
steel, stainless, corrosion behaviour of composite materials in N_2O_4 oxidising atmospheres *(Russian)* 80−76421
steel, stainless, Cr-Ni (20, 25 wt.%), TiN dispersion effect on oxidation 79−20279
steel, stainless, Cr-Ni-Mo, surface, scraping, mech. (electrolytic) polishing, ion etching, effects on ESCA 78−53037
steel, stainless, deoxidation in melting with Si *(Korean)* 78−19947
steel, stainless, electrode material, annealing temp. cycle which improves emission props. 78−95858

oxidation continued
steel, stainless, emittance, oxidation and surface roughness effects 80−96673
steel, stainless, Fe-Cr-Al (15, 4 wt.%) Fecralloy, oxidation behaviour, Al and Y surface ion implantation effect 80−71790
steel, stainless, ferritic, 430 Zr, oxidation, forming and mech. props. 80−11680
steel, stainless, ferritic, alloyed with Y, high temp. scaling 79−47834
steel, stainless, ferritic, Fecralloy, with and without Y, oxidation in Ar-H_2O-H_2 atmosphere 78−35584
steel, stainless, gas liberation in vacuum, depend. on oxidation process *(Russian)* 80−25901
steel, stainless, heat treated, oxide comp. and corrosion susceptibility of grades 410 and 430, AES study 80−66692
steel, stainless, Kh18N10, oxidation in Ar-O_2 and N_2-O_2 mixtures *(Russian)* 79−52451
steel, stainless, Nb, oxidation in Ar-H_2O-H_2 atmosphere 78−35584
steel, stainless, oxidation, localised pit development, 1073-1173K 80−89414
steel, stainless, oxidation in melting *(Korean)* 78−19946
steel, stainless, oxidation in N_2O_4, 200-700°C, anal. using Fick's second law *(Russian)* 77−73377
steel, stainless, oxidation resistance, effect of C, Zr, Ti and Nb 80−35394
steel, stainless, passivation in H_2SO_4, oxidising agent effects 79−20246
steel, stainless, surface implantation of Y and Ce, effect on oxidation resistance at high temp. 77−8977
steel, stainless, Type 304, surface analysis by SXAPS *(Japanese)* 77−70231
steel, stainless 304, fine grained, sputter deposited, oxidation resistance 79−57150
steel, stainless 316 80−16606
steel, superheated-steam oxidation, exam. of catalyst influence 78−85030
steel, surface cleaning in glow discharge, ion bombardment effect *(Russian)* 78−95848
steel, type AISI 316, thermal passivation in controlled vacuum 80−76276
steel melting, oxidation processes in jet refining unit, activation anal. 79−87898
steel ShKh15, high C, wear tests in fuel oil, O_2 conc. effect in oil *(Russian)* 77−16694
steels, austenitic stainless, Cl and H_2S effect on oxidation resist. 80−45418
steels, oxidation of structural steels in gas-cooled reactors 80−45447
steels, tempered with different Ni contents, scaling behaviour obs. 80−71817
Stellite 6B, volatilisation of oxides during oxidation at 1200°C 78−23873
Stellite-6, XPS obs. of aqueous oxidation, surface comp. and gaseous oxidation effect 80−81238
styrene, effect of redox initiation in emulsion polymerisation *(German)* 78−85158
submarine pillow balsalts, mag. minerals oxidation rel. to geomag. palaeointensities determ. 80−3927
succinamic acid, X-irrad., primitive radn. damage, ESR, ENDOR 78−3352
sulphides (Fe, Co, Ni, Cu, Zn), oxidation, hardness and electromechanical polishing response 80−71776
surface, use of vacuum ultramicrobalance 79−71465
surface cracks, oxide wedging 79−5046
surface processes investigated by alpha-particle effect on electron work function 78−2547
surface structure, distribution of defects, LEED 80−44402
TCNQ salts with heterocyclic amines and hydroquinone form. via redox reaction 80−26013
tetracyanoplatinates, quasi 1d anion deficient, elec. and struct. props. 80−103683
tetraethylammonium iodide-Ag_nI_{n+1}, ionic conductors, electrochem., props. 77−31808
tetrafluoroethylene, high temp. oxidation behind refl. shock waves 77−36743
tetrafluoromethane, plasma oxidation in presence and absence of Si in tubular-alumina fast-flow reactor 79−96297
tetrahedral semiconductor/oxide interface, continuous random network and tight-binding models 77−89866
thiol, influence on mitochondria and submitochondrial particle phosphate transport 78−27913
Ti alloy type OTCh-1, oxidation initial stages in Ni-O_2 mixture *(Russian)* 79−74302
Ti-Ta system, high-temp. oxidation *(Russian)* 79−74301
tissue, animal, lyophilised, paramagnetic centres 80−30681
titanomagnetite deuteric oxidation, monodomain behaviour in multiphase material 77−60366
tolusafranine-EDTA, photoredox reaction, photopot. and photocurrent generation 77−81420
transition metal, group VIII, O_2 chemisorption, UPS 79−7752
transition metal, group VIII, O_2 chemisorption, UPS 79−7751
transition metal oxides, surface oxidation, study by AES 80−45175
transition metal silicides, refractory for ICs, review 80−100820
transition metal sulphides, ion bombardment damage, XPS obs. 80−97404
troposphere, nonurban, oxidation of NH_3, H_2S and methane 78−32183
turbulent reactive gas flows, two-dimens., nonequil. processes analysis 77−51129
TZM-Mo alloy, mech. props., effect of exposure to high temp. He containing O_2, room temp. study 80−93639
unsaturated fatty acids, free radical oxidation, mag. field effects 79−15992
urease shear inactivation, metal ion effect, rel. to shear deform. effects in enzyme catalysis 78−76982
Venus, oxidation state of atmosphere and crust from Pioneer Venus results 80−98586
Venus oxidation state, comparison with Earth 77−29680
water, photo-oxidation at $BaTiO_3$ electrodes 77−12000
water, photoassisted oxidation at TiO_2:Be electrodes 80−30502
water, photoelectrochemical oxidation, using TiO_2 electrode with dye sensitisation 79−91964
water, photooxidation at α-Fe_2O_3:TiO_2 electrodes 78−15684
water photo-oxidation in phospholipid bilayers containing chlorophyll a 77−16917
oxidation continued
water photo-oxidation in presence of porphyrins adsorbed on octane-water interface 78−64933
wear frictional heating and oxidational theory 80−44255
X-ray photoelectron O 1s lines 77−44121
XX Ge, anisotropic oxidation, ellipsometry meas. *(Russian)* 79−43451
zinc phthalocyanine, electrochromism and oxidation 80−93768
Zircaloy, hydriding reaction kinetics, oxidised specimens 78−26728
zircaloy, nuclear microprobe methods for investigating oxidative corrosion 80−71787
Zircaloy, steam oxidised, partitioning behaviour of O_2 78−68839
Zircaloy 2 and 4, oxidation kinetics appl. to loss of coolant accidents, data review 78−19958
Zircaloy cladding, enhanced steam oxidation by deformation under LWR LOCA 80−73917
Zircaloy corrosion in water reactors, comparison of uniform and nodular forms 79−47817
Zircaloy internal oxidation process, O diffusion during UO_2-Zircaloy interaction 79−10986
Zircaloy oxidation, improved evaluation model 80−32349
Zircaloy sheath tube, calc., computer appl. *(German)* 77−346
Zircaloy sheaths, oxidation rate calc. method 80−78394
Zircaloy-2, anodic oxidation kinetics, in 0.05M oxalic acid (aq. and alcoholic) 80−104331
Zircaloy-2, hot-pressed, influence of diffused C on structure and oxidation 80−61016
Zircaloy-2, mech. props. after exposure to I_2-methanol solutions, SEM study 80−93689
Zircaloy-2, oxidation, protective oxide layer stress accumulation and perturbation of parabolic kinetics 79−5076
Zircaloy-2, role of oxide plasticity in oxidation behaviour 77−36680
Zircaloy-2, TEM and SEM of anodically formed oxides 77−21313
Zircaloy-2 and associated oxide layers, thermal property meas. 77−8063
Zircaloy-2 anodic oxidation in 0.05 M Na_2SO_4 electrolyte 79−57144
Zircaloy-2 claddings, oxidation reaction kinetics in steam environment in temp. range 1273-1673K 80−35401
Zircaloy-4, accelerated corrosion in high temp., high press. steam, effect of heat treatment 78−44263
Zircaloy-4, anomalous oxide growth during transient temp. oxidation 80−50773
Zircaloy-4, oxidation at 900 and 1100°C in high pressure steam 79−66208
zircaloy-4, oxidation in high temp. steam atm. effect on cladding ductility 79−26515
Zircaloy-4, oxidation in steam, 900-1500°C, kinetics 80−3241
Zircaloy-4, oxidation in steam, 900-1500°C, O diffusion in oxide and α-phases 79−100288
Zircaloy-4, oxide coating effect on ductility 79−47819
Zircaloy-4, PWR tubes, ZrO_2 scales formed in steam, microstruct. 77−6524
Zircaloy-4 PWR cladding, effect of oxide coating on ductility 79−89381
Zirconium-4, oxidation reaction kinetics in unlimited steam environment 77−8988
α-Zr, crystalline anisotropy in α-phase, charact. by thin oxide film form. *(French)* 79−20269
Ag, adsorption of O_2^-, catalytic oxidation mechanism 78−61046
Ag alloy, wear resistance, internal oxide effect *(French)* 77−52503
Ag, chemisorption of O_2, isosteric heat of adsorption determ. 77−55453
Ag films, UV photostimulated oxidation, electron microscopic study *(Russian)* 78−95850
Ag foil, interface with liq., oxide props., refl. and scatt. light spectroscopy 80−60702
Ag surface, clean and oxidised, $M_{4,5}VV$ Auger spectra, anal. based on self-convolution of measured UPS 77−77332
Ag-Cd alloys, internally oxidised, thermal stability of CdO, exam. of particle coarsening 78−76789
Ag-Cd(-Ni), internally oxidised, oxide particle size control *(Japanese)* 80−89480
Ag-Ga (0.42 to 2.09 at.%), internal oxidation *(Japanese)* 77−63908
Ag-Ga solid soln., internally oxidised, hardness *(Japanese)* 78−60744
Ag-In-Sn, internal oxidation, precipitation behaviour of oxide *(Japanese)* 80−66515
Ag-In-Sn, internal oxidation, solute element and O_2 behaviour *(Japanese)* 80−89479
Ag-O-Cs surface, oxidation, role of Cs suboxides in low work function surface layers, XPS 80−76131
Ag-Te-O, partial pressure diagrams 77−36681
Ag-Zn, internally oxidized, elec. contact characts., alloying additions effect *(Japanese)* 80−88619
Ag-Zn (2 to 12 wt.%) containing several metals, internal oxidation *(Japanese)* 80−16570
Ag-Zn-Te(-Sn)(-In), internally oxidised, oxide particle size control *(Japanese)* 80−89480
AgBr, photographic emulsions, sensitivity, fog rel. to treatment in redox-buffered solns. 78−32906
AgCdO, powder metallurgy production, for switchgear in power engineering 80−104094
(Al,Ga)As DH laser degradation, facet oxide formation 79−86185
Al (111), bonding of O, electronic struct. calcs., rel. to UPS data 80−59801
Al (111), oxidation, initial stages, LEED anal. 80−80082
Al (111) and (100) surfaces, initial interaction with O_2, LEED and AES meas. 79−83383
Al (111) surface, ordered O overlayer associated with chemisorption state 78−47665
Al, adsorpt. of O_2 (NO), 80 to 290K, 10^{-6} to 10^{-2} Pa, XPS study 78−95657
Al, adsorption of O_2, AES, XPS, and LEED obs. 79−46938
Al alloy, anodic oxidation, direct coloured oxide layer *(Rumanian)* 78−23852
Al, anodic oxidation, effect of vacuum and heat treatment *(German)* 79−96225
Al anodic oxidation, in H_2SO_4, pH-values effect *(German)* 80−76419
Al, anodisation, barrier and porous layer regions of Al_2O_3, eqn. 79−5089
Al, anodised in phosphoric, sulphuric and tartaric acids, barrier layer growth study 77−8983
Al, chemisorption of O, O-Al and O-O bond lengths, surface extended X-ray absorpt. fine struct. 80−29267
Al, clean and oxidised surfaces, secondary electron spectrum, EELS and AES, comparison 80−55237

oxidation continued
Al clean films, O_2 interaction study using synchrotron-radiation-induced-photoemission 80−55709
Al coating, plasma sprayed on steel substrate, microstructural investigation and oxidation effects 78−11426
Al, creep behaviour, at high temp., influence of oxidation 80−97538
Al film, evaporated, in distilled water, ellipsometric obs. 77−48590
Al, film, initial oxidation, AES, work function and gravimetric meas. 78−7087
Al film, initial oxidation, electron energy loss spectra 78−7088
Al film, internal stress, effect of residual gas press. 77−66100
Al film, polycryst., chemisorpt. of O_2, synchrotron radiation photoemission expts., 70-150 eV 78−95228
Al film, room temp. oxidation, scanning HEED expts. 78−91567
Al, film and polished bulk specimens, initial stages of oxidation obs. using SIMS 80−81239
Al film on GaAs, plasma oxidation, AES and TEM 77−77621
Al films, anodisation rate and augmentation factor, oxidation in ammonium tartrate 79−79152
Al, foil, influence of O_2-pressure on oxidation rate, TEM study 80−104355
Al foil electrolytic perforation, surface film phase composition obs. *(Russian)* 80−61004
Al, IR refl. obs. of oxide film 78−35591
Al in $(NH_4)_2CO_3$ solutions, to form amorphous self-supporting vac.-tight Al_2O_3 films 80−16177
Al, in water, oxide growth rate and struct. 78−76783
Al, influence of oxide films on photoemission *(Russian)* 77−81194
Al, initial interaction of O with single cryst. faces, LEED, AES and work function study 80−84392
Al, initial oxidation, interatomic Auger transition spectroscopy 79−7746
Al, initial oxidation exam. by inter-atomic Auger yield spectroscopy 78−11419
Al magnetron sputtering target, oxidation in Ar/O_2 mixtures 80−55291
Al, meas. using quartz oscillator microbalance 77−70219
Al, multiple oxidation states, obs. by photoelectron spectra of core level shifts 77−8720
Al, negative corona 80−40593
Al, oxalic acid bath, pH and conc. effects on form. and dissolution of Al_2O_3 77−16754
Al, oxidation, direct obs. in TEM 79−61789
Al, oxidation, influence on deformation map 80−40599
Al, oxidation by exposure to O_2 and H_2O, soft XPS exam. 78−80683
Al oxidative vaporisation, thermochemical analysis 78−11447
Al, oxide covered, tensile deform. in high vac., particle and photon emission 78−39672
Al, oxide films, metal and O_2 transport, AES and inert marker, techniques 80−97641
Al oxidised surface, EXAFS in soft-X-ray region 79−37921
Al, pitting mechanism, obs. using Engell-Stolica potentiostatic method 80−25905
Al, single cryst., surface reson. and oxidation 78−72225
Al, sputtered excited Al particles, effect of O during ion bombardment on spectra 79−38703
Al surface, oxidation, synchrotron radiation photoelectron obs. 78−52634
Al, surface energy and adhesion props. 80−10774
Al surface hydrous, oxide film formation 78−15602
Al surfaces, interaction with O_2, work function changes and ellipsometric parameters 79−47831
Al, thermal desorption of oxide film, influence of grain boundaries and recrystn. 80−61023
Al-Al_3Ni, electrolytic prep. of Al_3Ni fibres, SEM and anodic polarisation 80−100817
Al-based coatings, for high temp. alloys, process development and props. 80−40614
Al-Cu (1 to 10 wt.%), vapour deposited films, ion scattering spectrometry characterisation 80−15386
Al-Fe-Ni alloy, oxidation in hot water, electron microscope obs. of initial stages 79−11718
Al-Li-Mg-Be alloys, phase composition of surface films, oxidation protection mechanism *(Russian)* 80−65417
Al-Mg, foil, oxidation in O_2 atm., TEM study 80−104356
Al-Mg, oxidation control study, electron opt. techniques eval. 80−85089
Al-Mg, oxidation induced stresses, dislocation network form., HVEM obs 80−14978
Al-Mg (1 to 14 wt.%), oxidation in air, O_2, CO_2 and flue gas 77−73374
Al-Mg (2.5wt.%) sheet, surface oxide state and weldability 80−59769
Al-Mg alloy, growth of AMgO film with high secondary electron emission 78−35590
Al-Mg alloys, 3004 and 5182, oxide films, IR refl. spectra characterisation 77−77644
Al-Mg-Li alloy, 01420, surface layer props. *(Russian)* 78−80674
Al-Mg-Si, oxide layer structure after heat treatment in air and vacuum 79−57013
Al-Mg(Zn), oxide layer structure after heat treatment in air and vacuum 79−57013
Al-oxidised Al-Pb tunnel junction, nature of oxide barrier for IETS 77−72922
Al-SiO_2 interface in MOS capacitors, conductivity effects of oxidation temperatures 80−100518
Al-Sn, Sn effect on electrochemical behaviour in acetate buffer 78−19927
Al-Zn-Mg, oxide layer structure after heat treatment in air and vacuum 79−57013
$Al+NO_3^-$, reactions between metal and aq. nitrate solns., XPS 77−12825
$Al+O_2$ reaction, surface chemiluminesc. study 80−55708
AlAs epilayers, MBE growth on GaAs, self-terminating thermal oxidation 78−92374
AlAs, oxidised, as multidielectric for GaAs MIS devices 79−65333
(AlGa)As DH laser degradation due to facet oxidation 78−42336
α-Al_2O_3, annealing, stable hardened subsurface layer form. 77−56128
Al_2O_3, plasmochemical synthesis, oxidised from metals, exam. of props. 80−2984
Al_2O_3, porous, anodic, growth, physical model 78−48662
Al_2O_3, porous, anodic, growth, ionic cond. 78−48663
α-Al_2O_3 protective scale, influence of Pt 77−16749
Al_2O_3 supermicrogrid preparation and props. use in electron microscopy, noise reduction 80−99010
Al_2O_3:Fe, pore form. during oxidative annealing, grain growth slowing 80−100856

oxidation continued
Al_2O_3-$MoSi_2$ for use as heating element, anti-oxidation and anti-erosion props. *(Japanese)* 79−95989
Al_2O_3-SiO_2 glass ceramic, surface streaks and blisters, UV fluoresc. study 80−84347
Al_2O_3-TiO_2 powder, plasma-prepared, morphology and phase constitution 80−100833
Al(100) oxidised surface structure anal., extented appearance potential fine struct. study. 80−75411
Al(111), oxide layer amorphous to cryst. surface transition, slow positron obs. 80−75417
Am cpds., prep. and stability of highest oxidation states in phosphoric acid. soln. 77−29029
Am(VI) formation in molten salts 77−29039
As(III) and As(V), redox stability in aq. soln. 80−61068
As_2S_3, amorphous film, light enhanced vaporisation, photolithographic process, photographic appls. 77−5949
As_2S_3, amorphous film, photooxidation, substrate depend. 78−64866
As_2S_3 films, kinetics of light-enhanced vaporisation rel. to photocond. 77−84919
Au films on Cu, oxidation exam. by ion scatt. spectra 79−79153
Au polycrystalline wire, internal oxidation of impurities 78−83842
Au^-, electrochemical generation, oxidation, standard pot., in liq. NH_3 79−100386
Au/Cu, double layer film *(Japanese)* 80−61010
Au-Co electrodeposits, Co hardened, high temp. film formation 79−91848
Au-Cu, oxidation kinetics of Cu out of Au soln. at 50-150°C 80−21171
Au-Cu alloy, internal oxidation, calorimetric meas. 79−43258
Au-GaAs Schottky barrier solar cells, effect of interfacial oxide layer on cell charact. 80−61365
Au-Mg alloy, internal oxidation, calorimetric meas. 79−43258
Au-Si film, elec. resist. decay and struct. change on exposure to air 77−72924
B-transition metal, amorphous thin film, crystallisation, TEM obs. 79−19483
B_4C, kinetics of high temp. oxidation in oxygen, chromatography method 77−21305
BN ceramic with organosilicon polymer additions, strength and oxidation resistance 80−20880
BN ceramics, sintered oxidation kinetics 79−96171
BN fibres, prep., struct., thermal, mech. and elec. props., appls., book contrib. 78−48360
BN-SiO_2 composites, sintered, oxidation kinetics 79−96171
(Ba,La)TiO_3, redox reactions, defect chemistry and elec. cond., thermogravimetric meas. 77−39580
Ba, oxidation, SXAPS 77−73189
BaB_6, thermionic emission, O_2 adsorption effects 77−8711
$BaB_{12}H_{12}.10H_2O$, struct. dehydration, intermediate phases and thermooxidative degradation 80−33951
BaF_2, formation and growth of oxidation centres result of O^{2-} diffusion 80−7706
BaF_2-UF_4-CeF_3 solid soln., surface degradation, complex admittance analysis 78−55980
$BaFe^{2+}{}_2Fe^{3+}{}_{16}O_{27}$, metal deficient, hexagonal with W struct., chemical instability 78−27662
BaO reversible oxidation energy storage system feasibility 79−83637
BaO-Al_2O_3-B_2O_3-V_2O_5 glass, spectra, oxidation-reduction behaviour, DC cond. 77−76814
BaO-B_2O_3-V_2O_5 glass, oxidation-reduction of V, thermodynamics 80−85169
$BaTeO_3$, oxidation, X-ray powder anal. *(French)* 80−15080
Ba_xVO_2, oxygen vanadium bronze, phase comp., heating in air 77−40417
Be, anodised, emissivity, in 400-1000K range on function of oxide layer struct. 77−35726
Be, implanted D and He, interaction and radiation enhanced oxidation 80−39120
Be powders, gas evolution during heating from 20-700°C 79−61796
Be, slowly oxidised, secondary electron yield changes, and AES characterisation 80−71524
Be-Si-Al-O-N ceramic, phase assemblages, relationships with props. 80−60848
(Bi, $Sb)_2Te_3$ solid soln., semiconductor film, oxidation, electrophysical props. 80−45407
Bi, charge transfer obs., from final state changes 77−51703
Bi film, oxidation kinetics and interfacial bonding using final states 77−56127
Bi, film, UPS, valence band, cond. band and 5d core states 77−20995
Bi film, vac. evaporated, thermally oxidised, struct. by electron diffr. and TEM obs. 80−6678
Bi, oxidation kinetics 80−25914
Bi, thin film, oxidation process rel. to X-ray diffraction *(Japanese)* 79−29273
Bi-Pb(Te)(Sn)(Tl)(In)(Sb), dilute, oxidation kinetics 80−25914
$Bi_2Mo_2O_9$, thermal decomp. rel. to catalytic oxidation 80−35520
Bi_2O_3, oxide film on polycrystalline Bi, exam. of oxide film growth rate using XPS *(German)* 79−11041
BiOI, synthesis, thermal decomposition in dry O_2 *(French)* 78−53205
C, activated, surface oxidised, adsorpt. of organic vapour rel. to paramag. props. 77−32238
C, amorphous, catalytic oxidation by Pd particles, TEM obs. 80−76555
C and low-alloy steel inherent austenitic grain size determ., exam. of methods used 78−85071
C blacks, surface polarity, surface activity, slurry pH, oxidation effects 78−68915
C, colloidal layers, sputtering, chem. etching in DC glow discharge 78−27667
C fibre, coated with pyrolytic SiC 78−60857
C fibre, thermal treatment temp. effect on struct. and props. 78−23743
C fibre coated with Si or ZrC, mech. props. 77−70197
C fibre composite, oxidation and mech. strength at intermediate temps. 77−81330
C fibre reinforced, C oxidation behaviour, rate-controlling steps 80−55550
C fibre reinforced C matrix composites, wear, oxidation contribution 79−52383
C fibres, oxidation, surface props. *(French)* 78−44238
C fibres, oxidation by NO_2, struct., props. modification 78−44237
C fibres, PAN-based, surface charact., active surface area, microporosity 78−35536

oxidation continued
C fibres, PAN-based type I, II and III, oxidation effect on skin, TEM study 79−77465
C fibres, SiC protective coatings *(Polish)* 79−52408
C fibres and C fibre reinforced epoxy phenol, oxidation, effect on props. 80−40574
C film, oxidation, IR spectroscopic study 79−96162
C impregnated oxide refractory melt, C oxidation 79−91828
C oxidation in flow conditions at 1000 to 6000K 78−11445
C oxidation kinetics, in Fe-C melts by CO_2 *(Russian)* 80−40680
C, oxidation kinetics on Ni (110), AES meas. 79−79291
C, phenolic resin-derived, oxidation, ht. treatment effects 78−56790
C, pyrolytic, oxidation resist. in liq. corrosive medium 77−90471
C refractories, alkali attack as catalyst for oxidation 80−40562
C, vitreous, tensile strength, oxidation effects up to 2500K 80−3209
C-C composite, oxidised, SEM study 77−52522
C_3+O_2—C_2*+CO+O, chemiluminesc., rate consts. 77−44466
$CN^-.H_2O$, redox processes, MINDO/3 calcs. 79−47895
CO, adsorbed on Pd (111) surface, catalytic oxidation, mol. beam investig. 78−88656
CO, adsorbed on Pt (111), oxidation process, reflection-absorpt. IR study 78−76468
CO, catalytic oxidation on Pt, CO_2 product vel. and ang. distribs. 78−20065
CO, catalytic oxidation reaction over Pd(111) surface, mechanism 78−40079
CO catalytic oxidation on spinel type ferrites, role of mag. exchange interactions 78−56916
CO, catalytic oxidation over NiO, activated complex struct., rate consts. 78−80786
CO, catalytic oxidation on ferrites, IR spectrosc. investig. 80−89524
CO, chemisorbed on metals, electronic struct., vibr. spectra, and chem. 79−42390
CO, electrochemical oxidation in fused alkali metal carbonates 80−72040
CO, on CoO, catalytic oxidation 80−71945
CO on Pd, catalytic oxidation and chemisorption 77−70339
CO on Pt, surface struct. effects on rate, data assessment 78−43251
CO, on Pt or Pd surface, oxidation kinetics 79−61903
CO, on Pt surface, oscillatory oxidation of CO 79−61905
CO, oscill. oxidation on Pt surface, kinetic model 77−4926
CO oscillatory oxidation over Pt, theory 80−85215
CO oscillatory oxidation over Pt, theory 80−85216
CO, over Ir, tracer studies on reaction path and kinetics of CO oxidation 80−7857
CO, over Pt, kinetics determ. using ^{13}C tracer 79−29400
CO oxidation by NO on Ir surface XPS and UPS 78−15702
CO, oxidation on Ir films, IR absorpt. spectroscopy 80−71398
CO, reaction with adsorbed O_2 on Pd, kinetic behaviour, AES obs. 77−90640
CO, reaction with O_2 chemisorbed on Pt, AES expts. 77−90639
CO, titration of pre-adsorbed O on Ir (111), XPS investigation 79−91994
$^{14}CO_2$, respiratory, determ. by $Ba^{14}CO_3$ decomposition in sample oxidiser 79−88153
CS_2, COS, atmospheric, oxidation as SO_2 sources 80−4085
CU, effect on polyethylene adhesion 79−74340
Ca, low temp. oxidation by water vapour 78−3256
Ca, oxidation, SXAPS 77−73189
Ca, study using solid-state galvanic cell *(Japanese)* 77−56151
$CaB_{12}H_{12}.10H_2O$, struct. dehydration, intermediate phases and thermooxidative degradation 80−33951
$CaCeAl_3O_7$, melilite struct., prep. and props. 80−93524
CaF_2:Mn^{3+}, fluorite, radiation and thermal redox processes 80−55678
CaF_2-UF_4CeF_3 solid soln., surface degradation, complex admittance analysis 78−55980
CaO-Cu concentrate pellet, fluidised bed roasting 77−4934
CaS, oxidation kinetics 79−52407
$CaTeO_3$, oxidation, X-ray powder anal. *(French)* 80−15080
$CaTiO_3$, protection against reduction during roasting in H_2 77−36426
Ca_xVO_2, oxygen vanadium bronze, phase comp., heating in air 77−40417
Cd (0001), LEED and AES obs. 79−87756
Cd, oxidation, chemisorption and oxide regimes, UPS and EELS study 80−81236
CdS, dry process formation from CdO and S *(Spanish)* 78−56607
CdS films, amorphous and polycrystalline, microinclusion distrib. of high resist. phase and residual cond. 80−7008
CdS+NaCl, roasting processes rel. to flux growth of phosphors 78−23590
Cd_xS, electrochemical characterisation and comp. modification at 25°C 77−25272
CdSe, oxidation by atmos. O_2 and SeO_2 vapour 77−52520
CdTe, Cl compensated detectors, polarisation suppression methods 77−61661
CdTe, clean and oxidised surfaces, O_2 sticking coeff., ionicity effects, XPS expts. 77−85887
CdTe, clean and oxidised surfaces, surface states, low-energy EELS study 80−11522
CdTe surface, sputter cleaning and dry oxidation, XPS and LEED study 80−108618
$CdUO_4$, phase transforms., anomalous oxidation state change 80−54369
Ce, ESCA and UPS meas., core levels 77−63542
Ce, oxidation agent for Fe-Armco, grain size and strength depend. on nonmetallic inclusions *(Russian)* 80−100894
Ce oxidised surface, comparative sputtered neutral mass spectrometry and SIMS studies 79−90856
Ce, photochemical separation from rare earth mixtures in aq. soln. 79−39165
Ce^{3+}, oxidation kinetics in X zeolite on O_2 adsorpt. 78−3373
Ce-Si-Al-O-N ceramic, phase assemblages, relationships with props. 80−60848
CeB_6, thermionic emission rel. to surface state 78−39654
$CeCo_{5-x}Cu_x$, $0 \leq x \leq$ internal oxidation kinetics, oxide struct., X-ray study 80−104329
$CeFeO_3$, enthalpy of formation determ. from heat of oxidation, calorimetric investig. 77−25300
$CeNbO_{4+x}$, oxidation-reduction reactions 78−39930
Ce_3NbO_x, $CeNbO_x$ and $CeNb_3O_x$, redox processes, elec. resist., phase anal., mag. suscept., thermogravimetric meas. 78−34482
oxidation continued
CeO_{2-x} ($0<x<0.3$), oxidation-reduction study, Cahn electrobalance appl. 77−79084
CeO_n, redox reactions, quasiisothermal thermogravimetric obs. 79−15980
$CeTaO_{4+x}$, oxidation-reduction reactions, phase equilibrium, thermogravimetry and magnetic susceptibility meas. 78−39930
CfO_x-O_2 system, for $1.50<O/Cf<1.72$, temp., press. and stoichiometry depends. 77−28009
Cl+formaldehyde, photolysis, Fourier transform IR studies, metastable species detection 80−81293
Co (0001), chemisorption of O_2, surface oxidation and CO oxidation 79−60631
Co alloys, dil., factors affecting high-temp. oxidation behaviour, alloying effects 77−77638
Co base alloys, cyclic oxidation, static and dynamic, high temp. alloys 78−88576
Co, clean surface, interaction with O_2 and air, XPS 77−16466
Co diffusing out of high current density plated Au, oxidation kinetics 78−92393
Co, kinetics, effect of Curie temp. 77−48592
Co, monolayer, oxidation, quasisimultaneous SIMS, AES, XPS 78−72919
Co, oxidation, use of SIMS for ^{18}O location 79−8394
Co, oxidation at Curie temp. 79−29279
Co, oxidation at high temp. 78−23877
Co, oxidation at high temps., parabolic rate const. determ. 78−64779
Co oxide surface layer, TOF atom probe anal. 78−64766
Co, polycryst. surface interaction with O_2, CO and CO_2 *(French)* 77−73219
Co, reaction, in Ar-SO_2 atmosphere, 500 to 900°C 78−39953
Co, ultrafine particles prepared by vacuum evap. on running oil substrate, mag. behaviour 79−28565
Co, XPS and UPS *(French)* 77−36362
Co, XPS obs. of epitaxial CoO form. 80−66396
Co^{2+} complex, ammoniated zeolite, oxygenated product form., electronic spectrosc. obs. 80−991
Co-$(Cr,Co)_7C_3$ eutectic, oxidation effect on toughness and strength 80−89404
Co-Al-Cr(Nb)(Ta), eutectic alloys, charact. by melting, oxidation resistance and composition 78−52768
Co-Cr, containing dispersion oxides formed by internal oxidation, oxidation behaviour 78−19922
Co-Cr, isothermal oxidation in 760 Torr O_2 at 1000°C 77−77639
Co-Cr (up to 25 wt.%), sulphidation and oxidation in Ar-SO_2, effects of increase in Cr content 80−11839
Co-Cr-Al, exam. of cyclic oxidation resistance at 1100 and 1200°C, comparison with Ni-Cr-Al system 78−88572
Co-Cr-Al, oxidation at 1000°C 77−59963
Co-Cr-Al-Y coating, Pt-modified, oxidation and hot corrosion resist. 78−11437
Co-Cr-Al-Y(Hf), high temp. oxidation 78−11432
Co-Cr-Mo (Zr)(Nb)(Ta), eutectic alloys, charact. by melting, oxidation resistance and composition 78−52768
Co-Cr-Ni alloy FSX 414, electrochemical corrosion meas. in molten sulphate 79−96178
Co-Cr-Si alloy hot corrosion and oxidation expts. for ionic conducting scale 78−11446
Co-Cr-Ta(Al) alloy, high temperature wear resistant coatings, CrO_2 hardened 79−24677
Co-Cr(VC)((Ti,V)C)-(Al), eutectic alloy, unidirectional solidification, oxidation and tensile tests 78−52790
Co-Fe(70 wt.%), diffusional scale growth at 1200°C 77−16748
Co-Gd-Mo films, sputtered, O effects on mag. props. during annealing 80−89374
Co-Mn (0 to 45 wt.%), high temp. oxidation 80−35371
Co-Mo oxidic precursory state, supported on SiO_2 and γ-Al_2O_3 hydrotreating catalysts 79−61898
Co-Ni (0.45 to 7.23 wt.%) theoretical analysis of cation distrib. in (Co, Ni)O scale 77−12747
Co-Ni alloy surfaces, oxidation, APS 79−87755
Co-Ni-Cr (20,20 wt.%), internal oxidation, improvement of mech. props. *(French)* 77−16521
Co-Ni-Cr-Al-Ta, S-57 alloy hot corrosion, cyclic oxidation, depth of attack determinations 80−11837
Co-Ni-Cr-W-Fe, HA-188 alloy, hot corrosion, cyclic oxidation, depth of attack determinations 80−11837
Co-Si-Nb(Zr), eutectic alloys, charact. by melting, oxidation resistance and composition 78−52768
Co-Sn alloy, electroplated, oxide films, XPS/AES expts. 79−15862
Co-superalloy, cast, high temperature fatigue behaviour 80−40485
Co-Ti, dilute, internal oxidation 77−31810
Co-VC (12 wt.%), directionally solidified eutectic, oxidation 80−11821
CoCrAl alloy, Al_2O_3 forming, oxidation resistance improvement by dispersed oxide addition 79−83379
CoCrAl-Hf, Hf effect on oxidation 78−44275
$Co_{0.5}Mg_{0.5}O$, sintered pellets, oxidation mechanism and kinetics, optical and SEM study 79−79137
$Co_{20}Ni_{80}$, oxidation study by Auger electron spectroscopy *(Ukrainian)* 80−7711
CoNiZn ferrites, Fe excess, complex permeab. var. with annealing temp. 77−89979
CoO, defect struct. and self-diffusion 78−63759
CoO, high temperature physico-chemical interactions with oxygen under pressure *(French)* 78−31549
CoO, sintered pellets, oxidation mechanism and kinetics, optical and SEM study 79−79137
Cr (100), adsorption of O_2 and initial oxidation at room temp. 80−20034
Cr (111) face LEED and RHEED meas. *(French)* 78−39955
Cr alloys, ESCA meas. of oxide layer 78−15584
Cr carbides, catalytic oxidation of H_2 80−104462
Cr, combined AES and threshold potential spectroscopy 78−11026
Cr, corrosion by O_2 containing H_2O and gaseous NaCl, volatile products 78−27674
Cr, corrosion in SO_2, 700-1000°C 80−97642
Cr electrolytic oxidation in SO_2 atmosphere, CrO_3 ionic defect effects *(Ukrainian)* 78−92504
Cr film, Cr_2O_3 percentage determ., film struct. and elec. props. 80−103607
Cr film, pattern generation by laser-induced oxidation 80−61009
Cr, in pure CO_2, AES 77−86224

oxidation continued
Cr, oxidation, Cr-O bonding, characterisation by high resolution AES *(French)* 79−100468
Cr oxidation, in air, CO_2 and H_2O vapour, kinetic peculiarities in formation of oxide films *(Russian)* 79−74303
Cr, oxidation, in hostile environment, in situ meas. method 78−44277
Cr, oxidation in TEM 77−48593
Cr, oxidation kinetics, 300 to 600°C, struct. and morphology of oxide film 77−59982
Cr, oxidation kinetics, 300 to 600°C, O_2 press. effects 77−59983
Cr oxidative vaporisation, thermochemical analysis 78−11447
Cr, oxide film form., combination anal. using ESCA, AES and SIMS 79−16092
Cr, pure, oxidation, electron microscope study *(Japanese)* 77−48577
Cr, rare earth impurities effect 80−66703
Cr, rel. to component of stainless steel 79−47811
Cr-$(Cr,Co)_7C_3$ eutectic, oxidation effect on toughness and strength 80−89404
Cr-AlN, dispersion strengthened, hardness and oxidation rate, 1000 to 1500°C *(Russian)* 78−15574
Cr-Fe alloy (up to 50%), hardness, oxidation and electronic constitution 80−30154
Cr-O system, initial oxidation, combination anal. using ESCA, AES and SIMS 78−72924
Cr-rare earth, dil., oxidation of Cr, effect of rare earth impurities 79−79160
Cr-Ti/MgO-NbC(TaC) dispersion-strengthened, high temp. wear and oxidation resist. 80−25877
Cr-Ti/NbC(TaC) dispersion-strengthened, high temp. wear and oxidation resist. 80−25877
Cr-Y_2O_3 dispersion hardened, oxidation and nitridation resistance, embrittlement 78−44267
CrC, plasma sprayed coating 78−68835
Cr_3C_2 fibre reinforced Ni-based composite, oxidation and creep, Y additions effect 80−66685
Cr_3C_2, on Cr, mechanism of high-temp. oxidation, 1050 to 1100°C *(Russian)* 79−20226
γ-γ'-Cr_3C_2-Y eutectic, Y addition effect on oxidation during thermal cycling 79−74310
CrMoV, surface coating to prevent oxidation during high temp. AE 80−16539
Cr_2O_3-Cr film, electrodeposited, optical degradation rel. to surface morphology, SEM and AES obs. 79−79401
$Cr_{1-x}Rh_xO_2$, new ferromag. material, high pressure oxidation prep. 79−43164
Cs, adsorbate-induced structs., UPS obs. 79−47828
Cu, (100), oxidation, electron spectroscopic study 78−64782
Cu, (100) single crystal surface 80−11846
Cu (100) surface, adsorption of O_2, angularly resolved UPS meas. 78−71956
Cu (100) surface, interaction with O_2, AES, EELS, LEED and work function studies 80−24731
Cu (111), growth modes of (111)Cu_2O, UHV-RHEED and TEM obs. 79−19481
Cu (111), misfit dislocations between Cu_2O and substrate, TEM obs. 78−14629
Cu (111), photoelectron angle resolved spectra, perpendicular momentum conservation oxidation induced breakdown 79−24412
Cu (111), reaction kinetics using precursor state model 79−65317
Cu, (111) single cryst. surface, laminar Cu_2O growth 78−72025
Cu (111) surface, misfit dislocations between Cu_2O and substrate, TEM obs. of annealing 79−82228
Cu (111) surface, room-temp. oxidation, press. effects 79−79283
Cu alloy, internally oxidised, FIM 77−20074
Cu alloys, H(D) permeation, in situ stable oxide barrier growth 78−75883
Cu and Cu-S, liquid, oxidation kinetics, by CO_2 77−28986
Cu, anodic oxidation, photoelectrochemical effects *(French)* 80−93701
Cu, commercial pure, creep-rupture props., vacuum, oxide film form. *(Japanese)* 78−72843
Cu, corrosionprotection by ion implantation of Al and Cr 80−71789
Cu, CuO monolayer form., SIMS 79−89038
Cu, diffusion/oxidation through Au, rate-controlling step 80−34240
Cu dilute alloys, compositional changes in oxide thin films, Auger electron microanalysis *(Japanese)* 77−21319
Cu dilute alloys, oxide, compositional changes *(Japanese)* 77−21319
Cu, EXAFS investigation 80−71808
Cu, electroless deposition, electrochemistry 79−61520
Cu, epitaxy in aqu. oxidation of (001) single crystal 80−11844
Cu film, on Au substrate, oxidation and interfacial behaviour, ion scatt. spectroscopy study 80−66691
Cu film, oxidised in ^{18}O, ion scatt. anal. 77−40463
Cu film, partially oxidised, oxide removal and O_2 desorption on vac. annealing 77−12738
Cu, film, partially oxidised, EXAFS studies on superficial regions 80−75474
Cu film, struct., oxidation, and exoelectron emission rel. to bulk samples *(Russian)* 79−37927
Cu, high purity, identification of imperfections by thermal resistivity meas. 80−59951
Cu, in CO_2, 800-1000°C 78−76784
Cu, liq., deoxidation rates by CO_2-CO gas mixture *(Japanese)* 80−89394
Cu, metal surface cleaning, by electron cyclotron resonance plasma of hydrogen 79−47822
Cu, nucleation and growth of oxidation zones during diffusional creep *(Russian)* 79−52431
Cu, oxidation, electron scattering study 79−83377
Cu, oxidation in controlled clean air and standard laboratory air, 50-150°C 79−70202
Cu, oxidation in controlled clean air and standard laboratory air at 50 to 150°C 79−79154
Cu, oxidation kinetics, influence of intermediate annealing treatment 80−89412
Cu, oxide identification by AES, EELS and UPS 80−60747
Cu polycrystals, oxidation, secondary ion energy spectra 80−71788
Cu, pure, form of double oxide layer 77−77637
Cu, resistometric study of anodic oxide films in neutral soln. 77−16739
Cu, tarnishing in humid atmosphere 79−70210
Cu, thermal oxidation, influence of ion implantation 78−64768
Cu, thin film, RMEED/SEM studies 80−100968

oxidation continued
Cu, two stage metastable and stable surface Cu_2O nucleation, 800-1000°C 77−70214
Cu, wire, residual resistivity reduction by internal oxidation 79−87747
Cu^+, in LiCl-KCl fused eutectic, diffusion and surface effects, chronopotentiometry *(French)* 78−11524
Cu-Al, dispersion hardening by internal oxidation 78−56649
Cu-Al, internally oxidised, structural, elec. and mech. characts. 78−60761
Cu-Al, surface segregation during adsorption and low pressure oxidation *(French)* 78−75932
Cu-Al (0.05 wt.%), dil. alloy, anisotropic oxidation, electron microprobe Auger spectroscopy 77−12748
Cu-Al alloys, internally oxidised, elec. resist. meas. 77−35753
Cu-Al solid soln., internally oxidised, mech. props. *(Japanese)* 77−52411
Cu-Al_2O_3 disperse phase alloy oxidation kinetics 77−48584
Cu-Al-Ti-Zr, internally oxidized, morphology of precipitates and dispersion hardening *(Russian)* 79−52217
Cu-Be, dynode surface, SEM and Auger microanalysis 80−100384
Cu-Be(Al)(Mg)(Ti), study of internal oxidation using central diffusion of X-rays *(French)* 79−37839
Cu-CaO concentrate pellet, oxidation kinetics 77−4894
Cu-containing films, room temp. 77−48572
Cu-Cr, formation of internal oxidation band 79−47820
Cu-Cu_xO film, numerical anal. of normal reflect. data 79−99457
Cu-Fe, dil., internally oxidised mag. and electrical prop. 77−12100
Cu-Fe (0.2 at.%), clustering, precipitation, and oxidation, 298 to 919K, Mossbauer study 80−7242
Cu-Fe (0.2 at.%), surface oxidation, Mossbauer obs. 80−55564
Cu-Ga, high dislocation density alloys and oxide precipitated struct., NMR, spin echo 80−39892
Cu-Ge-La, Cu+Misch metal, eutectic alloy, internally oxidised, mech props. *(Japanese)* 77−52411
Cu-Hg, dil., pool electrodes, passivation in alkaline soln. 79−70214
Cu-Mg, high temp. oxidation 79−43485
Cu-MgO, dispersion hardened alloys, prep. and props. 80−40291
Cu-Mn (3, 5, 10 at.%) alloys, surface segregation of Mn and oxide film form., AES study *(French)* 79−66065
Cu-Mn(Ti)(Sn)(Si), dil., oxide film form. in ammoniacal Cu(II) solns., AES obs. 80−45415
Cu-Ni, AES analysis of protective oxide film 79−39035
Cu-Ni, annealing effect on oxidation kinetics, reduction in vacancy level 80−50760
Cu-Ni, initial oxidation study by microprobe-AES method *(Japanese)* 79−15867
Cu-Ni, nucleation and growth of oxidation zones during diffusional creep *(Russian)* 79−52431
Cu-Ni (0.1 to 51 wt.%), oxidation, diffusion kinetics in porous inner layers 80−16546
Cu-Ni alloy, oxidised with NO, surface comp., AES obs. 77−20176
Cu-Ni film, (001), in situ oxidation, TEM obs. 78−23874
Cu-Si, high dislocation density alloys and oxide precipitated struct., NMR, spin echo 80−39892
Cu-Si (up to 4.75 wt.%), exam. of high temp. oxidation in low O_2 and pure CO_2 atmospheres, by thermogravimetry 78−88574
Cu-Ti, and Cu-Ti-Si(Fe), struct. and coalesc. of oxide particles during internal oxidation *(Russian)* 79−90781
Cu-Ti, internally oxidised, morphology, struct., particle precipitation singularities *(Russian)* 79−70067
Cu-Ti-Cr(Fe), internally oxidised, morphology, struct., particle precipitation singularities *(Russian)* 79−70067
$CuAl_2O_4$, pure and NiO promoted catalysts, surface oxidation state and comp., XPS study 80−76134
CuBe, Be distrib. in vicinity of oxidation boundary *(French)* 80−11984
$CuFeO_2$, oxidation, thermogravimetric obs. 77−86203
$CuFeS_2$, superficial degradation in air and water, XPS obs. *(French)* 80−89110
Cu_5FeS_4, bornite, AES investig. of surface struct., oxide layer form. 77−15669
Cu(I) complex, oxidation, fast reactions meas. by pulsed-flow instrument 80−66890
$Cu_xMo_6S_8$, prep. by topotactic electrode reactions, struct., supercond. 79−99158
CuO, plasmochemical synthesis, oxidised from metals, exam. of props. 80−2984
CuO-containing glass, Cu^+ diffusion and oxidation 80−79980
Cu_2O, prep. rel. to defect levels by TSC 77−66138
Cu_2S, $Cu_{1.8}S$, $\alpha \rightarrow \beta$ transition, thermographic investigation of heats, entropies and activation energies 80−88314
Cu_2S, molten, oxidation, exam. of product phase composition by X-ray anal. *(Russian)* 79−34166
Cu_2S, solid, oxidation mechanism, kinetic factors 78−85133
Cu_2Se, oxidation by atmos. O_2 and SeO_2 vapour 77−52520
Cu(100) surface, oxidation studied by angle-dispersive photoemission spectra 78−15585
Cu(111), bulk s orbital bands, sensitivity to oxidation, photoelectron spectra 79−47597
ErT_2, film, surface oxide form. and interfacial metal loss, AAS, XES 78−31733
EuS film, struct., elec. and opt. prop. changes during annealing in air 77−7983
EuS, thermal stability in air, 20-900°C 77−52519
(Fe, Mn)-V spinels, complex, oxidation, effect of Cr_2O_3, TiO_2, MgO additions 79−43453
Fe (001) surface, first monolayer at. struct. 78−34706
Fe, adsorption of O_2, oxidation 80−108730
Fe aerosol powders, oxidised, nucl. gamma reson. study *(Russian)* 79−1725
Fe, aerosoled ultrafine particles oxidation 80−21183
Fe and Fe-Cr alloys, friction behaviour in oxygen, development of wear-protective oxides and influence on sliding friction 80−30111
Fe, Armco, SCC in phosphate soln. 79−96184
Fe, atomised powder compacts for mag. cores, oxidation, compressibility, heat treatment *(Japanese)* 78−72752
Fe base alloys, cyclic oxidation, static and dynamic, high temp. alloys 78−88576
Fe base alloys, influence of ΔT (oxidising temp. minus cooling temp.) on oxide spallation 77−52551
Fe based sintered friction material, wear rate, depend. of phase struct. 79−15801

oxidation continued
Fe, cast, anodic polarisation in slag melt *(Russian)* 80−45513
Fe colloidal dispersion, mag. props., struct. and oxidation 80−34699
Fe, core and valence level photoemission studies of Fe oxides 78−15290
Fe, corrosion, oxidation, ion-, electron-beam techniques appl. 79−43700
Fe, corrosion and oxidation, new technique for simultaneous acquisition of Mossbauer spectra and microbalance data 78−44252
Fe, deoxidation of liq. by Al, Mossbauer meas. 80−20553
Fe, electrolytic, oxidation in melting *(Korean)* 78−19946
Fe, electron re-emission Mossbauer spectroscopy 77−16752
Fe, FIM obs. 80−89388
Fe film, chemisorption of O_2 and water vapour, XPS obs. 77−48587
Fe, in CO_2 at 1330°C 79−5077
Fe, in O_2 and CO_2 at 550°C, growth and struct. of oxide films 77−52549
Fe, in SO_2 atmospheres, study by means of ^{35}S radioisotope 77−52550
Fe, inital oxidation kinetics using proton-induced X-ray emission 80−35618
Fe, on O_2 adsorpt., XPS/UPS obs. 77−85074
Fe, oxidation, in hostile environment, in situ meas. method 78−44277
Fe, oxidation, scanning electron diffr. appl. 77−25178
Fe, oxidation and domain structure, electron microscope exam. *(Russian)* 79−1437
Fe, oxidation at 1100°C, thickness of oxide layers 77−77640
Fe, oxidation at 300°C 79−61792
Fe, oxidation at Curie temp. 79−29279
Fe, oxidation at elev. temp., scale/metal interface charact. 79−74286
Fe, oxidation in CO_2, early stage obs. by AES 78−48570
Fe, oxidation in NaCl soln., ferric oxide film form. 80−25898
Fe, oxidation in pure O_2 at 973 to 1173K, morphological study of oxide scale 78−15595
Fe, oxidation kinetics near Curie temp. 79−66218
Fe, oxide film thickness determ. by electron backscatt. Mossbauer spectroscopy 78−72933
Fe, oxide overlayer thickness determ. by ^{57}Fe conversion elec. Mossbauer spectroscopy 79−57142
Fe, oxide scale fracture on substrate deform. 78−11407
Fe, oxide sputter rates, AES and ellipsometry 78−72661
Fe oxide surface layer, TOF atom probe anal. 78−64766
Fe oxides, phase equilibrium and microstructure interpretation 80−60847
Fe, oxidised powder in prod. of soft mag. mat. 77−63813
Fe, passivity in aq. soln., correlation with mol. struct. 80−16541
Fe pellets, re-oxidation at high temp., growth of needle-like haematite crystals 80−35431
Fe, powder, oxidation magnetically soft material form., elec., mag. props. 77−8778
Fe powder, sponge and atomized types, steam oxidation, pore closure and surface hardness 80−45441
Fe powder compacts, surface oxidation influence on shrinkage anisotropy 80−50574
Fe, reaction with sodium disilicate glass, Mossbauer effect 78−11190
Fe, rel. to component of stainless steel 79−47811
Fe, secondary ion emission, effects of initial ion bombardment and oxidation 77−1777
Fe sheet, cyclic oxidation and reduction kinetics in O_2-H_2 atmosphere *(Korean)* 80−71906
Fe, sintered, steam oxidation effect on porosity 77−59997
Fe, sponge, oxidation kinetics by nuclear γ-resonance method *(Russian)* 80−40681
Fe ultrafine particles, Fe_3O_4/γ-Fe_2O_3 surface layers, Mossbauer expts. 79−8081
Fe, ultrafine particles prepared by vacuum evap. on running oil substrate, mag. behaviour 79−28565
Fe, under low O_2 partial press., wustite whisker form. obs. 79−77972
Fe^{3+} solute in MgO, oxidation reduction behaviour in defect model 79−99181
Fe-Al, electron-beam-induced surface oxidation, HVEM obs. 80−14978
Fe-Al (up to 7.2%), oxidation process 78−85022
Fe-Al oxide system, depth profile anal. by secondary ion mass spectra *(Japanese)* 78−7290
Fe-base fibres, extruded, heat treatment 78−35414
Fe-C, oxidation at 700°C, electron diffr. obs. 79−61790
Fe-C alloy, oxidation at 500°C cold work and annealing effects 78−44276
Fe-C-(P)(S), drops, oxidation kinetics in oxidizing slags 78−11153
Fe-Co (33 wt.%), oxidation and domain structure, electron microscope exam. *(Russian)* 79−1437
Fe-Co-Ni-Al-Nb (15-20, 14, 9, 0.1-5.5 at.%), Nb effect on magnetic props., lattice parameter *(Russian)* 77−55689
Fe-Cr, Auger electron and appearance pot. spectroscopic study of surfaces 80−11520
Fe-Cr, high temp. oxidation, internal stable nitride and oxide dispersion 79−39017
Fe-Cr, high-temp. oxidation, borate inhibitors 80−66705
Fe-Cr, microstructural study of oxidation, selective etching 78−44245
Fe-Cr, oxidation, in H_2/H_2O vapour mixtures, epitaxial oxide phase formation, effect on oxidation 78−88568
Fe-Cr, oxidation, in hostile environment, in situ meas. method 78−44277
Fe-Cr, surface and bulk alloys, oxidation at 300°C 79−61792
Fe-Cr, surface composition change caused by heating in high vacuum, XPS obs. 78−44254
Fe-Cr (13 wt.%)+polycarbosilane, powder metallurgy, charact. 77−85962
Fe-Cr (17.3 wt.%), oxidation at 1000°C, alloy grain growth effect 78−7075
Fe-Cr (20 wt.%), high temperature oxidation resistance, effect of rare earth and reactive element additions *(Japanese)* 79−20271
Fe-Cr (20 wt.%), role of rare earths and reactive elements in high-temp. oxidation 79−79178
Fe-Cr (20 wt.%) high temp. oxidation behaviour with small La additions (0 to 1.3 wt.%) *(Japanese)* 78−85039
Fe-Cr (24 wt.%), low temperature oxidation, kinetics, oxide morphology 80−11838
Fe-Cr (27.4 wt.%), oxidation, alloy depletion profiles resulting from preferential removal of less noble metals 79−11728
Fe-Cr (5, 10 and 20 wt.%), microcrack generation, healing of oxide scale 79−20280
Fe-Cr (5 to 40 wt.%), breakdown and healing of oxide scale during oxidation 77−63836
Fe-Cr (5 wt.%), friction and wear in controlled environments, oxide film effect 78−15546
oxidation continued
Fe-Cr (9 wt.%), oxidation studied using $C^{18}O_2$ and D_2O tracers 80−71784
Fe-Cr alloy, (100) and (110) surfaces, initial oxidation stages, simultaneous LEED and AES obs. 77−20175
Fe-Cr alloy, sputter etching oxide film, comp. profile, quantitative AES 80−81383
Fe-Cr alloys, corrosion, oxidation, combined ion-, electron-beam techniques appl. 79−43700
Fe-Cr alloys, $NaClO_3$ and NaCl effects on corrosion behaviour in hot NaOH soln. *(Japanese)* 80−35407
Fe-Cr-Al (14, up to 2 wt.%), Al effects on high temp. oxidations *(Japanese)* 79−15865
Fe-Cr-Al, Al addition effect on oxidation, 900 to 1200°C 79−66222
Fe-Cr-Al, Al effect on high temp. oxidation in wet O_2 79−66223
Fe-Cr-Al, blackness change in air, 1-8 micron, 1200°C, film props. depend. 77−66033
Fe-Cr-Al, elec. heating alloy, effect of rare earth additives on quality *(Chinese)* 78−84825
Fe-Cr-Al, electrical heating material, SEM obs. and surface analysis of oxide films formed at high temps. 77−16738
Fe-Cr-Al, HOS 875, oxidation, cyclic, role of thermal shock 80−97640
Fe-Cr-Al, scale and spalling resist. determ., appl. of cyclic oxidation method 77−77695
Fe-Cr-Al, scales, α-Al_2O_3, early stages development at high temp. 80−89413
Fe-Cr-Al (0.3 wt.%), oxidation behaviour at high temps. *(Japanese)* 80−35404
Fe-Cr-Al (14, 0.1 to 2 wt.%), oxidation at high temps. *(Japanese)* 78−60872
Fe-Cr-Al (7, 5 wt.%), expt. stainless alloys, phys. and mech. props. 80−97637
Fe-Cr-Al-Ce, Ce effect on high temp. oxidation 79−100301
Fe-Cr-Al-Ce, high temp. oxidation *(Japanese)* 78−11413
Fe-Cr-Al-Y, high temp. corrosion depend. on Y, oxidation, stress growth *(Russian)* 80−40588
Fe-Cr-Al-Y, influence of Y additions on oxide-scale adhesion 77−8993
Fe-Cr-Al-Y, oxidation resistance, heat treatment and Al^+ ion implantation 80−71785
Fe-Cr-Al-Y, scales, α-Al_2O_3, early stages development at high temp. 80−89413
Fe-Cr-Al-Y-C, GE-1541, volatilisation of oxides during oxidation at 1200°C 78−23873
Fe-Cr-Al(-Y), isothermal oxidation behaviour at 1200°C, SEM 80−50755
Fe-Cr-Al(-Y), thermal cycling influence on oxidation behaviour at 1200°C, SEM 80−50756
Fe-Cr-Al(-Y) alloys, oxide grain morphology and growth mechanism 80−3239
Fe-Cr-B, B inhibition of oxidation, AES study 79−61785
Fe-Cr-La(Y)-Al, La or Y with Al addition effect on high-temp. oxidation 79−100302
Fe-Cr-Mn alloys, Mn content effect on Cr distrib. in suboxide layers *(Russian)* 77−12732
Fe-Cr-Mn-C, high temp. oxidation, X-ray and weight gain meas. *(Russian)* 78−15571
Fe-Cr-Mo-C, X-ray investigation after friction and oxidation 78−52997
Fe-Cr-Ni, austenitic, oxidation behaviour on addition of Si 77−12740
Fe-Cr-Ni, foil, in situ oxidation in HVEM 80−104354
Fe-Cr-Ni alloys, oxidation-sulphidation in gas mixture, parabolic kinetics, thermochem. diagram 78−72932
Fe-Cr-Ni based alloys, surface oxides at high temps., backscattering Raman spectroscopy 80−93291
Fe-Cr-Si, oxidation resist. in high pressure CO_2, Si effect 80−66704
Fe-Cr-Ta, eutectic alloy, exam. of eutectic temp., composition, and oxidation resistance 78−52767
Fe-Cr-Ti (18, 0.1-0.9 wt.%), high temp. oxidation *(Japanese)* 80−71806
Fe-Cr-Ti-TiO_2 (13, 2.5, 2 wt.%), dispersion hardened, ferritic alloy DT02, oxidation, 823 to 1123K 79−61803
Fe-Cr-Y, Y addition effect on high temp. oxidation resistance *(Japanese)* 79−70223
Fe-Cr-(C), oxidation, grain size and growth effects *(Japanese)* 77−48583
Fe-Cr(Ni) surface alloys, corrosion resistant, formation by ion implantation 79−28009
Fe-Cu (2 wt.%), furnace cooled, ageing and steam oxidation 78−23744
Fe-Cu (4.54 wt.%) alloy, scaling behaviour, 700-1000°C, 1 atm. O_2 80−93679
Fe-Cu (75 ppm), internal oxidation, local struct. determ. by EXAFS 80−25916
Fe-Fe_2O_3-$NaFeO_2$, study of Na-containing wustite region *(French)* 77−73264
Fe-Fe_2O_3-SiO_2-Si melt, interacting system, oxidation products *(Russian)* 78−19728
Fe-Hl (Si) (Ti) (V), molten, gaseous O_2 absorption 80−11836
Fe-Ni, ferro-nickel oxidation, appl. of mag., thermomag. methods *(French)* 79−20318
Fe-Ni, oxidation, Mossbauer spectroscopy, metallography, SEM and X-ray diffr. anal. 78−15577
Fe-Ni (19 wt.%) alloy, oxidation in CO_2, 700 to 1000°C, kinetics study 78−72931
Fe-Ni (50 wt.%), surface comp. and oxide film thickness after various surface treatments, AES study 80−66693
Fe-Ni (9.21 wt.%), oxidation in CO_2 at 700-1000°C 78−44265
Fe-Ni-Al, oxidation in O_2 at 600 to 800°C 79−83376
Fe-Ni-Cr, austenitic with dispersed phases, oxidation 80−16540
Fe-Ni-Cr, oxide film form., combination anal. using ESCA, AES and SIMS 79−16092
Fe-Ni-Cr (30.6, 21.3 wt.%), Alloy 800, high temp. oxidation at low O_2 press., SEM, AES and electron probe microanal. study 80−93688
Fe-Ni-Cr (44, 17 wt.%), nuclear microprobe methods for investigating oxidative corrosion 80−71787
Fe-Ni-Cr alloy, oxide layer struct. and comp., compar. study by secondary ion emission and electron microprobe *(French)* 77−56286
Fe-Ni-Cr base alloy, oxidation and hot corrosion *(Chinese)* 80−21149
Fe-Ni-Cr melts, O solubility *(Russian)* 80−15250
Fe-Ni-Cr-Al-Y, oxidation mechanism, Y addition effect on kinetics and oxide adherence 80−97623
Fe-Ni-Cr-Mn-Al-Ti Incoloy 800, exam. of scale morphology, alloying element distrib. after oxidation 78−80677

oxidation continued
Fe-Ni-Cr-Si, superalloy, Cr and Si effect on mech. props. and microstruct. *(Chinese)* 79−100207
Fe-Ni-Cr-Si (35, 18, 2 wt.%), heating element wire, failure and oxidation 79−83378
Fe-Ni-Cr-Y, oxidation at 800 to 1300°C, Y addition effects, comparison with Ni-Cr-Y alloy *(French)* 79−43481
Fe-Ni-Cr-Y, Y addition effect on selective oxidation/diffusion phenomena relationship *(French)* 80−108623
Fe-O system, initial oxidation, combination anal. using ESCA, AES and SIMS 78−72924
Fe-O-V melts, phase equilib. *(Russian)* 80−16273
Fe-rare earth, amorphous thin film, crystallisation, TEM obs. 79−19483
Fe-Si (3.25 wt.%), mag. props., influence of struct. and chemical composition of surface oxide layer 78−2700
Fe-Si protective oxide film form. 80−11818
Fe-Si-Al, high temp. oxidation resist., comp. depend. 77−12739
Fe-Si-Al, surface oxide layer struct., AES study 80−89396
Fe-Si-Al (2.8-3.4, 0-0.86 wt.%) oxidation, annealing 80−89395
Fe-Si-B, surface tension, density, and oxidation kinetics 80−20028
Fe-Si-M, eutectic alloy, M = Ti, Zr, V, Nb, oxidation resist. 78−52767
Fe-Si-Mn (3, 0.004 to 0.1 wt.%), Mn effect on oxidation in H_2O-H_2 atmos. 78−31560
Fe-Si(Al), oxide layer form. during annealing, AES in-depth anal. *(German)* 80−16576
$Fe+H_2O$, clean surface oxidation and passivation by H_2O vap., XPS 77−81424
$FeAl_{2-x}Cr_xO_4$, spinel, elec. cond. behaviour during oxidation 79−19593
γ-$(Fe_{1/3}Al_{2/3-x}Cr_x)_2O_3$, lacunar spinels, elec. cond. behaviour during oxidation 79−19593
$(Fe_{1-y}^{3+}Al_y^{3+})_2O_3^{2-}$, γ to α transform. elec. cond. study, oxidation initial stage kinetics, lacunar spinel form. 78−92384
Fe_3C, catalytic oxidation of H_2 80−104462
$Fe(CN)_6^{4-}-Fe(CN)_6^{3-}$, redox reactions, mass transfer at vibr. spheres 80−57220
$Fe(CN)_6^{4-} \rightleftharpoons Fe(CN)_6^{3-}$, redox pot. in nonaqueous-water mixtures 79−52654
$Fe(CO_5)$ adsorbed on graphite, oxidation to Fe_2O_3, Mossbauer spectra 80−60474
$Fe^{2+}Cr_x^{3+}Al_{2-x}^{3+}O_4^{2-}$, finely divided, oxidation kinetics 80−50848
$FeCr_2O_4$, $FeAl_2O_4$, solid solns. and oxidation products (lunar spinels), IR spectra 77−81099
$(Fe_{1-y}^{3+}Cr_y^{3+})_2O_3^{2-}$, γ to α transform. elec. cond. study, oxidation initial stage kinetics, lacunar spinel form. 78−92384
$(Fe^{2+}Fe_{2-x}^{3+}M_x^{3+})O_4^{2-}$ ($M^{3+}=Al^{3+}$, Cr^{3+}), oxidation to γ lacunar spinels, rate law vs. O_2 press. 80−50849
$Fe_{2-x}M_xO_4$, M=Al,Cr, time dependence of oxidation, elec. cond. obs. *(French)* 77−66710
(FeNi)PB amorphous wires, surface oxidation and annealing influence on induced anisotropy 80−100957
$FeO \rightarrow Fe_3O_4$, in-situ AES using galvanic cells 78−19615
$Fe_{1-x}O$, surface struct., XPS study 80−20759
Fe_2O_3, plasmochemical synthesis, oxidised from metals, exam. of props. 80−2984
α-Fe_2O_3, reduction to active magnetite and direct air oxidation to α-Fe_3O_4 *(German)* 78−7060
Fe_3O_4, effect of Al ion on formation and structure *(Japanese)* 77−59727
Fe_3O_4, magnetite, oxidation kinetics, influence of cryst. size 78−79778
Fe_3O_4, magnetite, oxidation rate anomaly at Curie temp. 79−96298
Fe_3O_4, magnetite, oxidation mechanism during roasting of nodules *(Russian)* 80−40567
Fe_3O_4 powder, oxidation to γ-Fe_2O_3, coercivity changes 80−44864
Fe_3O_4, substituted magnetite, oxidation kinetics 77−1889
Fe_xO_y, adsorption of H_2O, oxidation and reduction effects on adsorption 78−43237
Fe_xO_y films, electron microscopy and energy-loss spectroscopy 80−80137
$Fe_{1-x}Pd_x$ film, air-exposed, comp. profiles by AES, ESCA and ion sputtering 78−95245
$Fe_{1-x}Pd_x$ film, vac. deposited, oxidation and corrosion, AES, XPS and STEM obs. 79−100286
FeS_2, oxidation, Mossbauer spectroscopic and magnetokinetic studies, 400-500°C 80−44880
FeS_2, pyrite, magnetokinetics of oxidation, appl. to mag. separation from coal 77−12161
FeS_2, superficial degradation in air and water, XPS obs. *(French)* 80−89110
$FeSO_4$ aq. soln., oxidation by high-energy electrons 79−52700
$FeSO_4$ oxidation by SO_2-O_2-H_2SO_4 soln. 80−61083
$Fe_{2-x}SiO_4$, fayalite, oxidation kinetics and growth of Fe_2O_3 whiskers 78−84113
Ga-As-O, equilib. phase diagram, GaAs oxidation 80−104130
GaAlAs oxide, plasma grown, anal. by combined ion beam techniques 79−7760
$Ga_{0.64}Al_{0.36}As$, plasma grown oxide, phys. and elec. props. 78−48550
$Ga_xAl_{1-x}As$, Schottky barrier, effect of oxide composition on elec. behaviour, AES meas. 79−87141
$Ga_{1-x}Al_xSb$, surface oxidation, Raman spectra, residual Sb layers 80−71419
GaAs (110), 3d core level binding energy, multiple bonds 78−35543
GaAs (110), 3d core level binding energy, single bonds 78−35544
GaAs (110), adsorption of O_2, oxide form., XPS/UPS study 80−49497
GaAs (110), chemisorbed O_2, extrinsic surface states 78−91535
GaAs (110), coadsorption of Cs and O_2, initial oxidation, soft XPS obs. 80−10793
GaAs (110), electronic states and initial steps in oxidation 78−91534
GaAs (110), initial oxidation, XPS and AES study 80−11542
GaAs (110), O chemisorption, surface EXAFS meas. 80−50460
GaAs (110), optical technique, detection of external reflectivity change on oxidation 80−6939
GaAs (110), order-disorder interaction with O_2, LEED anal. 80−75445
GaAs (110), reconstruction and oxidation initial stages, ab initio calc. 80−49473
GaAs (110), with ultrathin Al and Cs overlayers, O_2 adsorption, comparative studies 80−50740
GaAs (110) cleaved surface, oxidation, XPS exam. 78−31551
GaAs (110) surface, chemisorption of O_2, electronic struct. theory, oxidation, electron spectra interpretation 79−42376
GaAs (110) surface, O_2 interaction, order-disorder effects, LEED, UPS anal. 80−6634
GaAs, (110) surface, oxidation, photoemission spectra obs. 77−16460

oxidation continued
GaAs (110) surface, oxidation model 77−32703
GaAs (110) surface oxidation process, XPS study 79−15585
GaAs (110) surfaces, ordered and disordered, O_2 adsorption, XPS meas. 80−49498
GaAs, adsorption enhancement by electron beam excitation of gas mols. 78−43238
GaAs, adsorption of O_2, adsorption states and Ga depletion, UPS, AES, and thermal desorption meas. 79−46952
GaAs, anodic native oxides for MOS devices, quality assessment 79−61767
GaAs, anodic oxidation 77−16710
GaAs, anodic oxidation and MOS devices 77−80845
GaAs, anodic oxidation in nonaqueous electrolyte and MOS charact. 79−38183
GaAs, anodic oxidation in O plasma 79−66188
GaAs, anodic oxidation under dark and illuminated conditions, behaviour of cell voltage 77−16826
GaAs anodic oxide, quantitative chem. depth profiles 77−72799
GaAs anodic oxide chem. depth profiles, neutron activation analysis and Auger spectroscopy 77−77619
n-GaAs, anodic oxide film, exam. using SIMS and ellipsometry 79−61770
GaAs, anodic oxide film comp. profile anal., radioactive tracer technique 77−59956
GaAs anodic oxide films, optical studies using rot. light-pipe reflectometer 80−76096
GaAs, anodic oxide for device application, crystallisation dynamics 79−66190
GaAs anodic oxide formation, galvanostatic obs. 77−77620
GaAs, anodisation in HF O_2 plasma, oxide film form. mechanism and kinetics *(Japanese)* 80−93667
GaAs, chemisorption and oxidation states of (110) surfaces 79−24049
GaAs, chemisorption of O_2, effect of surface index and atomic disorder AES, LEED and optical ellipsometry 79−60638
GaAs, clean and oxidised surfaces, O_2 sticking coeff., ionicity effects, XPS expts. 77−85887
GaAs cleaved (110) face, interaction with O_2, influence of cleavage defects, AES study 80−66684
GaAs conducting MIS structures and metal-semicond. structures, effects of ultrathin oxides 79−1626
GaAs, device compatible anodic oxidation technique 78−44236
GaAs, dislocation-free, point defects and rad. damage 80−88141
n-GaAs, electrodes in acetonitrile soln., photoassisted oxidation, development of under-potential 79−70341
GaAs film, plasma oxidation and oxide props. 78−95825
GaAs film plasma oxidation process 77−77614
GaAs, heavily oxidised photoemission escape depth for electrons, energy depend. 77−69969
GaAs hydrothermal oxidation kinetics, exam. 80−40566
GaAs interface with anodic and thermal oxides, comparison of AES and ESCA 78−95980
GaAs, low temp. plasma oxidation and MIS struct. charact. 78−31546
n-GaAs MIS structs., native oxide, effect on interface props. and removal by sputter etching 79−11228
GaAs, microscopy with an ellipsometric arrangement 80−17998
GaAs, native oxide encapsulation, surface effects, RHEED 77−1883
GaAs, native oxide growth under MBE conditions 79−77943
GaAs, nitridation, following oxidation, surface and contact props. of GaN produced 77−20436
GaAs, oxidation, initial process and oxide/semicond. interface formation 80−50739
GaAs, oxidation, water vapour and O_2 excitation effects, XPS obs. 79−100274
GaAs, oxidation in multipole plasma, MOS elec. props. 80−44737
GaAs oxidation saturation and MOS diode equivalent cct. 78−47875
GaAs, oxide, grown in O plasma, phys. and elec. props. 79−66189
GaAs oxide, passivated layers, quantitative in-depth profile, AES-SIMS thermal, anodic and plasma oxidations 78−84087
GaAs oxide, thermal and anodic, in-depth profiles, XPS expts. 78−84086
GaAs oxide film, plasma-grown, analysis using Rutherford backscatt. and ion-induced X-rays 77−43438
GaAs oxide film form., ion implantation effects 80−100266
GaAs, oxide film growth, thermal oxidation, optical obs., model 77−56120
GaAs oxide film growth in As_2O_3 vapour, As incorporation 79−77928
GaAs, oxide film influence on adsorption and electrophys. props. 79−42369
GaAs oxide growth kinetics and physical props. 79−77937
GaAs, oxide layers prepared by anodic, thermal and plasma oxidation, in-depth profiles and annealing effects 79−61768
GaAs oxides, appl. of selective chemical reaction concept for controlling props. 79−47790
GaAs oxides, plasma-grown, in situ meas. and anal. with spectroscopic ellipsometry 80−76386
GaAs oxidised surface, detection of excess crystalline As by Raman scatt. 78−19453
GaAs, photolum. intensity degradation caused by excitation-enhanced oxidation 78−15205
GaAs, plasma oxidation, semiquantitative chemical depth profiles, Auger spectroscopy and neutron activation anal. 78−53284
GaAs, plasma-grown oxides, in situ anal. using spectroscopic ellipsometer 79−79138
GaAs, plasma-grown oxides, physical props., Auger and IR spectral anal. 79−91821
GaAs, polycryst., wet and dry oxides, comparative study by AES, SIMS and XPS 80−80116
GaAs, selective plasma oxidation, interface props. 80−100933
GaAs, shallow-homojunction solar cell by MBE, conversion efficiency 80−30476
GaAs solar cell, polycryst., grain boundary passivation by oxidation, AES, SIMS and XPS obs. 80−81467
GaAs solar cell fabrication, using AMOS tech., single and polycrystalline cells 78−39935
GaAs, substrate for epitaxial growth, backscatt. anal. of surface prep. and anodic oxidation 77−25175
GaAs surface, growth of anodic Al_2O_3 and composite oxides 79−83344
GaAs, thermal oxidation, 450 to 760°C, Rutherford back scattering obs. 78−76780

oxidation continued
GaAs thermal oxidation rate and activation energy obs., 470° to 830°C *(Japanese)* 77−52517
GaAs, thermal oxidation in wet and dry atm., 470-830°C 77−86204
GaAs, thermal oxidation in As_2O_3 vapour 78−56792
GaAs, thermal oxide film growth and characterisation 80−11808
GaAs thermally oxidised surface, in-depth comp. profile, Auger analysis 77−89621
GaAs, thermally oxidised, TEM obs. 78−72036
GaAs thin film polycrystalline Schottky barrier solar cells, grain boundary chemistry 80−94067
GaAs, UPS, 5-450 eV, surface states, oxidation behaviour 77−66579
GaAs, vapour phase equilibria of As_2O_3 79−66181
GaAs, XPS study of native oxides on surface 80−16141
GaAs:Cs, oxidation process, UPS obs. 80−50511
GaAs-anodic oxide interfaces, struct. and chem. props., Raman scatt. obs. 79−47168
GaAs-anodic oxide MOS struct., interface state band 79−60930
GaAs-GaAs oxide interface layer characterisation by spectroscopic ellipsometry 80−50738
GaAs-native oxide interface, Raman scatt. expts. 77−85709
GaAs-oxide interface, physical struct. 79−60644
GaAs-oxide interfaces, local atomic and electronic struct., high resolution XPS 80−49927
GaAs-plasma grown oxide interface, new resonant ellipsometric technique for characterisation 79−40606
n-$GaAs_{0.6}P_{0.4}$, anodic oxide film, exam. using SIMS and ellipsometry 79−61770
$GaAs_{0.6}P_{0.4}$, anodic oxide, electronic props. 79−61771
$GaAs_{1-x}P_x$, thermal oxides, elemental composition and C-V charcts. 79−61772
GaAs(110), surface and interface states, effects of chemisorption, oxidation and passivation 77−85284
GaAs(111), O bonding, thermodesorption and ESCA meas. 77−86206
GaP (110), initial oxidation, XPS and AES study 80−11542
GaP (110) surface oxidation process, XPS study 79−15585
GaP, anodic oxidation and MOS devices 77−80845
GaP, anodic oxide film comp. profile anal., radioactive tracer technique 77−59956
GaP, O_2 adsorpt. monitoring by Auger spectroscopy, electron beam effects 77−72777
GaP, O_2 adsorpt. monitoring by Auger spectroscopy, electron beam effects 78−6218
GaP, substoichiometric native oxide layers, $^4He^+$ backscatt. obs. 77−77610
GaP, surface cleaning by oxidation and heating, characterisation for electron emitter appl. 78−35548
GaP, XPS exam. of thermally grown oxide film 78−31552
GaP:Cs-O simultaneous adsorption, oxidation interface chemical struct. 80−103584
GaSb (110), initial stages, photoemission study 80−16529
GaSb, chemisorption and oxidation states of (110) surfaces 79−24049
GaSb oxidised surface, detection of excess crystalline Sb by Raman scatt. 78−19453
GaSb, UPS, 5-450 eV, surface states, oxidation behaviour 77−66579
Gd oxidised surface, comparative sputtered neutral mass spectrometry and SIMS studies 79−90856
Gd-Co, amorphous films, mag. props. ferromag. reson. meas., 20-520°C *(Russian)* 80−97144
Gd-Co-Mo amorphous film, MCD, oxide surface layer effect 77−90132
GdFe(Co), amorphous film, XPS meas. 79−87295
Ge dissolution by oxidation and solvation, hole injection effect 80−26051
Ge film, elec. resist., long term stability rel. to ambient atmosphere changes 78−2597
Ge gas phase reactions with oxidisers, visible chem. laser development 79−948
Ge, oxidation of clean cleaved (111) surfaces, EELS and AES 80−3230
Ge, photoemission spectroscopy of surface states and oxidation 77−55863
Ge, second-phase inclusions after O_2 treatment, electron microscope obs. 77−43238
Ge, single cryst., anisotropic oxidation, ellipsometric obs. 77−70194
Ge:O, Cu, amorphous thin film, impurity effects on struct. 80−107054
Ge-$Na_2S_2O_3$ interface anodic oxidation electron transfer 79−56304
$GeCl_4$ hydrolysis and oxidation kinetics for graded-index fibre vapour phase axial deposition 80−48477
GeO, population inversion of electronic levels by oxidation, visible emission 78−13697
GeO, produced in Ge+N_2O reaction, kinetics of chemilum. emitter form. and quenching 78−63107
GeTe, oxidation kinetics 77−44380
GeTe, partial pressure diagram 79−83183
Ge(111)2×1, oxide layer, surface states detect optical reflectivity obs. 80−50368
Ge(3^3P_0)+O_2(Cl_2)(COS)(N_2O)(NO_2)(NO+Ar) oxidation reacts., gas phase, kinetics 78−92468
H production from coal using steam-Fe process, development status 80−55942
H_2 electrochemical oxidation in fused alkali metal carbonates 80−72040
H_2, production by solar energy, homogeneous photoredox system 80−3387
H_2, reaction kinetics calc. using thermodynamic model *(German)* 79−5130
H_2 selective oxidation in air streams before CO anal. 77−63978
H_2+N_2O, HO radical form. on Pt surface, laser-induced fluoresc. obs. 80−108738
H_3AsO_4, reduction with aqu. SO_2 77−4901
H_2O, photooxidation by α-Fe_2O_3 electrodes 78−76886
H_2S oxidation by active C, electrochem. model *(German)* 78−35717
Hf, corrosion in buffer soln., revealed by impedance and potential meas. 79−96182
Hf electrode, surface oxide film, impedance and pot. behaviour 80−61001
Hf, microstructural study *(French)* 80−45436
Hf oxidation in flow conditions at 1000 to 6000K 78−11445
Hf-Fe alloys, oxidation 79−52460
Hf-Fe(Co)(Ni)(Cu), alloys, oxidation of intermetallic phases 79−100298
HfB_2, oxidation in O_2 atmosphere, exam. 80−11814
HfO_2:M^{n+}, M=Ce, Pr, Tb, Eu impurity valence transitions 77−51694
$Hg_{0.8}Cd_{0.2}Te$ surface, sputter cleaning and dry oxidation, XPS and LEED study 80−108618

oxidation continued
$Hg_{1-x}Cd_xTe$, anodic oxide films, formation and props. 80−3212
HgTe surface, sputter cleaning and dry oxidation, XPS and LEED study 80−108618
I^- in aq. soln., anthracene sulphonate sensitised photooxidation via singlet $^1O_2$ 77−32812
In, chemisorption of O_2, XPS and static SIM spectral study 80−80055
In film, oxidation, XPS excited by Zr Mζ radiation 80−40236
In film, RF plasma oxidised, surface analysis using ESCA 80−50742
In, optimal reactive sputtering conditions for prep. of conductive, transparent oxide films 79−95295
In-In_xO_y-Pb tunnel-junction barriers, evidence for chemical annealing effects 79−42701
InAs anodic oxide films prep. and props. 80−55553
InAs, oxidised surface, detection of excess crystalline As by Raman scatt. 78−19453
InAs, thermal oxidation, growth rate and chem. comp., temp. depend. 80−108619
InGaAsP, anodic oxidation, refractive indices 80−97601
In_2O_3:Sn, film, HF sputtered, cond., Hall mobility, oxidation, charge carrier density 78−72287
InP (110), initial stages, photoemission study 80−16529
InP, chemisorption and oxidation states of (110) surfaces 79−24049
InP hydrothermal oxidation kinetics, exam. 80−40566
InP interface with anodic and thermal oxides, comparison of AES and ESCA 78−95980
InP, ion implanted, anodic oxidation and elec. carrier conc. profiles 79−70185
InP, thermal oxidation, growth rate and comp. of oxide 80−55555
InSb (110), initial oxidation, XPS and AES study 80−11542
InSb (110) surface oxidation process, XPS study 79−15585
InSb, charact. and phys. props., review *(Japanese)* 80−39576
InSb, optical constants and oxidation with various surface treatment *(Russian)* 80−88955
InSb, oxidation, water vapour and O_2 excitation effects, XPS obs. 79−100274
InSb, oxidised surface, photocond. meas. *(Russian)* 77−43664
InSb oxidised surface, detection of excess crystalline Sb by Raman scatt. 78−19453
InSb, Raman scattering study of unoxidised Sb in anodic oxide films 80−88985
InSb, single crystal, chem. and ion etching, surface changes *(French)* 80−108614
InSb, surface analysis, X-ray photoelectron spectra, surface oxidation-etchant correlation 78−56029
InSb(111) surface, oxidation props., LEED and surface cond. meas. 78−15559
In_2SnO_3 film, effect of ambient atmosphere during annealing, elec. props. 80−97510
$In_{2-x}Sn_xO_{3-y}$-insulator-poly-Si solar cells, photovoltaic conversion parameters 80−101093
Ir (111), oxidation, combined LEED/UPS obs. 78−19955
Ir (111) surface, kinetics of CO oxidation reaction, appl. of XPS 77−31886
Ir, evaporation/oxidation kinetics 77−36691
Ir oxidation and vaporisation of the volatile oxides, gravimetric exam. comparision with losses due to vacuum annealing *(Russian)* 79−57136
Ir, thin film, electrographic investigation of interaction with atmospheric O_2 *(Russian)* 77−25196
IrO_x, electrochromic, oxidation state changes and struct. 80−100950
Ir(111), chemisorption of O_2, LEED-Auger expts. 77−20191
Ir(111), O_2 chemisorption, XPS obs. 77−20190
K, adsorbate-induced structs., UPS obs. 79−47828
K, oxidation at low pressure, 77 and 295K 78−76792
K surface, clean and O_2-exposed, X-ray and UV photoelectron spectra 78−52636
$K_{1+x}Fe_yGa_{11-y}O_{17}$, electron hopping and excitation at room temp., ^{51}Fe Mossbauer spectra 80−25257
$K_{0.3}MoO_3$, thermochemistry 77−77801
β-K_2O-Al_2O_3, synthesis 77−81238
$K_{0.27}WO_{(3+y)}$, struct. analysis 77−11510
K_xWO_3 bronze, oxidation to $K_2O(WO_3)_n$, struct. changes 78−68925
$K_xWO_{(3+y)}$, direct imaging of ordering 77−11511
LaB_6 (001) surface, struct., initial oxidation, XPS, UPS, LEED, AES, work function meas. 79−99403
LaB_6 (210) surface, work function, struct. and chemisorpt. stability, XPS, UPS and LEED 80−65344
LaB_6, clean and oxidised (100) surface, LEED, AES, work function, evaporation meas. 78−71989
LaB_6, high temp. interaction with 0_2, AES and mass desorption expts. 80−7698
LaB_6, thermionic emission rel. to surface state 78−39654
LaB_6(001) surface, struct. and initial oxidation, UPS, XPS and work functions meas. 77−86195
$LaCrO_3$, vaporization in oxidizing atmos. 80−24579
$LaMnO_3$, O_2 environment, phase stability and nonstoichiometric behaviour, 1200°C 78−43134
LaO, chemiluminescence due to bimolecular oxidation of La metal 77−29011
La_2O_3-Cr_2O_3 mixtures and $LaCrO_3$ *(French)* 77−52524
Li (100), O adsorption, cluster models, ab initio HF LCAO theory 78−71978
Li, chemisorption of O_2, KVV Auger spectrum of oxidised Li 77−55454
$LiFe_5O_8$, spinel, transients in two point DC electronic cond. due to surface oxidation 79−60877
LiNa ferrite, effect of sintering temp. on oxidation kinetics, conductivity meas. 77−21298
LiOH, anodic oxidation of Cu amalgam at room temp. 79−61865
Mg (0001) face, incipient oxidation, EELS and LEED studies 80−81237
Mg, adsorption of O_2, at 100 and 300K, XPS, UPS and X-ray AES meas. 78−18901
Mg alloy, H_2 evolution during isothermal treatment in vacuum *(Russian)* 77−77625
Mg clean films, O_2 interaction study using synchrotron-radiation-induced-photoemission 80−55709
Mg film, polycryst., chemisorpt. of O_2, synchrotron radiation photoemission expts., 70-150 eV 78−95228
Mg, influence of oxide films on photoemission *(Russian)* 77−81194
Mg, vacancy loop behaviour on high-temp. oxidation, X-ray topography 77−76414

oxidation continued
Mg-Si-Al-O-N ceramic, phase assemblages, relationships with props. 80−60848
$Mg+O_2$⇌$MgO+O$, shock-tube study of evap. and oxidation kinetics 80−16651
$MgB_{12}H_{12}.10H_2O$, struct. dehydration, intermediate phases and thermooxidative degradation 80−33951
MgO, plasmochemical synthesis, oxidised from metals, exam. of props. 80−2984
MgO, thermal decomposition oxidising properties 79−100339
MgO:Fe, Fe^{2+} oxidation and Fe^{3+} reduction kinetics, EPR obs. 79−70399
MgO:Fe cryst., oxidised, optical absorpt. spectra at low temps. 77−63436
MgO:Li, enhancement of elec. cond. by oxidation 80−44600
MgO:Li, oxidation and reduction up to 1700K, defect prod. 79−39013
MgO:Mn^{2+}(Fe^{2+})(Cr^{2+}), redox behaviour of ions, ESR and X-ray diffr. 78−52341
MgO-C in melts, corrosion resist., rel to oxidation, porosity, content 80−40578
Mg_2SiO_4, forsterite, decorated dislocations 80−54245
Mn-Zn ferrite, oxidation-reduction equilib. and struct. defects 77−20189
Mn-Zn ferrite powder, spray dried calcination 77−12558
$MnO-P_2O_6$ system, formation of manganese phosphates 77−90331
MnO_2, oxidation under UV irradiation rel. to Viking gas exchange reaction on Mars 80−72831
Mo 77−70227
Mo (110), oxidation exam. of LEED 78−92402
Mo (110), oxidation of adsorbed C, electron diffr., contact pot. difference, and AES obs. *(Russian)* 79−52430
Mo, coadsorption of CO_2 and O_2, AES and SIMS obs. 79−46928
Mo complex, dithiocarbamate, model for molybdoenzymes, thermochem. meas. 77−86365
Mo complex, $MoOCl_3L_2$ (L=Ph_3PO or $(Me_2N)_3PO$), O transfer reactions and molybdoenzymes 77−86306
Mo complexes, oxo- and sulphido-bridged, binuclear, in aprotic media, electrochem. and redox mechanisms 77−86324
Mo, corrosion by O_2 containing H_2O and gaseous NaCl, volatile products 78−27674
Mo, discontinuous film, room temp. oxidation rate consts., resist. meas. 77−32723
Mo, electron field emission energy distrib. from surface oxide clusters 77−63548
Mo film, CVD, passivating against IR reflectance losses caused by oxidation 79−3758
Mo film, carbonisation and oxidation, electron diffr. exam. *(Russian)* 77−44399
Mo foil electrolytic perforation, surface film phase composition obs. *(Russian)* 80−61004
Mo, mech. props., effect of exposure to high temp. He containing O_2, room temp. study 80−93639
Mo, monolayer, oxidation, quasisimultaneous SIMS, AES, XPS 78−72919
Mo, oxidation, IR emission spectrosc. obs. 78−68942
Mo oxidation in flow conditions at 1000 to 6000K 78−11445
Mo, oxidation kinetics, Mossbauer study 80−40005
Mo oxides, low-grade, soda roasting study *(Korean)* 80−93508
Mo, rel. to component of stainless steel 79−47811
Mo single cryst., effect of high elec. fields, 1000-1200K, field emission and TEM obs. 77−90258
Mo, staged flow of O_2 interaction process, secondary ion emission obs. 78−11386
Mo, substitution and redox reactions in oxidation states III to VI, role in enzymes 77−86364
Mo, surface oxide softening in single crystals 78−95860
Mo-O system, initial oxidation, combination anal. using ESCA, AES and SIMS 78−72924
Mo-W 77−70227
Mo-Zr, nucleation conditions, effect on formation of oxide phase during internal oxidation *(Russian)* 80−81064
Mo-Zr-C (0.12, 0.002 wt.%), prep. of diffusion metal coating on alloy, oxidation rates *(Russian)* 78−56816
Mo-ZrC, internal oxidation, struct. formation law, microstruct. examination 78−84836
Mo_2B_5-based alloys, mech. props., rel. to appl. as electrodes in electrospark machining 80−21174
MoO_3, fluidised bed roasting, operating variables effect 77−4933
MoO_x, AES expts., chem. shift and beam effects 79−15566
MoS_2 solid lubricant, antifriction and elec. props. depend. on oxidation temp., dopant influence 80−108584
$MoSi_2$, effect of Al on oxidation behaviour *(German)* 78−31587
$MoSi_2$, oxidation behaviour, Ge additions effect *(German)* 80−71782
$MoSi_2$ oxide film, dielec. props. and growth kinetics 80−81215
$MoSi_2$, SiO_2 coating effect on oxidation, AES study *(German)* 79−74298
$MoSi_2$ sputtered films, protective layer form. on oxidation, Auger anal. and backscatt. meas. 79−15029
$MoSi_2/TiGe_2$ mixed crystals, direct obs. of surface oxide form. *(German)* 77−12721
$MoSi_2$-$TiSi_2$, high-temp. oxidation 79−83341
N_2, in atmosphere, relativistic electron beam stimulation by collective effects *(Russian)* 77−77763
N_2, in intense electron beam maintained glow discharge 79−32841
NH_3 oxidation leaching of chalcopyrite, surface deposit effects 77−48643
NH_3 oxidation leaching of chalcopyrite, reaction kinetics 77−52639
NH_3, photooxidation mechanism, computer simulation 77−32810
NH_3, Pt catalyst surface morphology and faceting obs. 77−52669
NH_3, rel. to amino acid photodegradation in presence of TiO_2 78−11531
NO, oxidation by electron beam irrad., appl. to exhaust gas treatment 78−80765
NO, oxidation in O_2 matrix, IR spectra of products 78−23936
Na (110), Na_2O (111) surface comp., LEED obs. 77−72761
Na droplet, preignition oxidation process, rel. to LMFBR accident 79−30996
$Na_4Fe(CN)_6.10H_2O$, single cryst., X-irradiated product ESR, 4.2K 77−48659
Na_3AlF_6 film, evaporated, electron bombard. effect on secondary electron emission, Auger peak shifts 80−2903
$Na_x^+(H_2O)_y[CrS_2]^{x-}$, form. and reactions 79−91961
$NaMo_6O_{17}$, thermochemistry 77−77801

oxidation continued
Na_2O particles, effect on optical props. of Na vapour 80−1736
Na_2O-B_2O_3:Au glasses, Au solubility, oxidation state and opt. absorpt. 80−44321
Na_2O-CaO-SiO_2 glass, redox phenomena evaluation in melting-fining process, SO_2 evolution 80−84900
Na_2O-SiO_2(-CaO) glass, molten, metal ion diffusion and redox behaviour, electrochemical studies 80−81332
NaRhY zeolite, Rh complexes with CO and methyl iodide ligands, spectrosc. obs. 80−85159
Na_xWO_3 bronze, oxidation state of W, oxidation by air exposure 77−8719
Nb alloys, cold worked, chemicothermal strengthening, internal oxidation 80−35229
Nb and alloys, Mo-Si protective coating against oxidation *(Russian)* 79−39029
Nb, ESCA obs. *(French)* 77−36361
Nb films, oxidation, XPS study 80−80944
Nb, heterogeneous reaction kinetics, microcalorimetric and thermogravimetric curve comparison 77−21359
Nb, interaction with O_2, AES and low-energy SIMS meas. 79−47832
Nb, magnetic surface barrier breakdown by O diffusion, permeability meas. 79−56601
Nb metal, high temp. and low O_2 pressure, ESCA study *(French)* 77−25179
Nb, O enrichment of surface layers, supercond. penetration depth and resist. meas. 78−19180
Nb oxidation in H_2 atmospheres, TEM exam. of precipitated phase morphology and struct. 78−76790
Nb, oxidation in imperfect vac., solute O_2 level change and ductility loss 79−52452
Nb, oxidation kinetics, abnormal, at high temp. 79−29289
Nb, oxidation mechanism, 673 to 823K 80−108644
Nb, oxide growth and oxide coatings, XPS and AES studies 80−50765
Nb, pure, reaction with gas residual in vacuum, physicomech. props. effect 80−16587
Nb, staged flow of O_2 interaction process, secondary ion emission obs. 78−11386
Nb superconducting cavities, AES depth profile meas. on oxide layer 77−8984
Nb surface, clean and oxidised, electronic struct., UPS meas. 78−95682
Nb, surface oxide softening, anisotropy 78−60716
Nb-alloys, reaction with gas residual in vacuum, physicomech. props. effect 80−16587
δ-Nb-N, plates and powder, oxidation *(French)* 79−66184
Nb-Nb_2O_5-Pb(In) Josephson junctions, props. of Nb_2O_5 thermally grown tunnel barriers 80−100568
Nb-NbO_x-Pb Josephson tunnel junctions, fabrication using FR glow discharge oxidation 80−34559
Nb-NbO_x-Pb superconductive tunnel junctions, oxide tunnelling barriers, ESCA characterisation 80−65745
Nb-NbO_x-PbIn window type junctions, critical Josephson current depend. on magnetic field 79−65607
Nb-Ti alloys, ESCA obs. *(French)* 77−36361
Nb-V oxidation in air, rate determining process *(Russian)* 80−21170
Nb-V-Cr, Nb-V, and Nb-Cr, oxidation resist., Cr and V effects *(Russian)* 80−40585
Nb-W-Mo-Zr (5, 2, 1 wt.%), surface-layer struct. and mech. props., effect of O_2 diffusion saturation 79−5087
Nb-Zr (1 wt.%), internal oxidation state of O_2, dispersion hardening by diffusion alloying, X-ray diffr. and internal friction *(Russian)* 79−70102
Nb-Zr-Ti alloys, scale formation 77−44229
$Nb+O_2$, high temp. interaction kinetics and mechanism 79−100432
$NbBe_{12}$, by diffusion saturation in vacuum, resistance to heat 78−44259
$4NbO_{0.76}$ thin film, FCC cell struct. investigation 80−92796
$NbSe_2$ solid lubricant, antifriction and elec. props. depend. on oxidation temp., dopant influence 80−108584
Ni (001) surface, Ar ion bombarded, enhancement of oxidation, AES study 80−97644
Ni (001) surface, initial oxidation, RHEED and X-ray emission meas. 77−31885
Ni (100), initial oxidation process, angle-resolved AES and LEED obs. 79−52463
Ni (100), initial oxidation, electron energy loss spectra, LEED, AES, and work function meas. 79−61795
Ni (100) face, O-Ni system vibrs. rel. to struct. during oxidation 77−66089
Ni (110), chemisorption of O_2 and initial oxidation, AES, EELS, and work function meas. 80−54523
Ni (110), initial stage kinetics, RHEED and X-ray emission 78−15588
Ni (110), interaction with O_2, electron energy loss spectra and AES obs. 79−47826
Ni (110), struct. anal. during O_2 adsorption, low energy ion scatt. meas. 79−82424
Ni, (110) and (111) surfaces, oxidation exam. at room temp. by combined SIMS-AES/LEED method 79−20241
Ni (110) surface, partially oxidised, decomposition of formic acid-d, flash desorption meas. 77−85066
Ni, adsorption of O_2, oxidation 80−108730
Ni alloy, oxidation resistance at elevated temps., effect of various alloying additions 77−56134
Ni alloy, oxide film isolation and obs. method 77−52563
Ni alloys, dil., factors affecting high-temp. oxidation behaviour, alloying effects 77−77638
Ni alloys, heat resistant EI437B and EI929, surface condition, air stream effect 80−76409
Ni amalgam, anodic polarisation in alkaline soln. 80−11823
Ni, and Ni alloys, rolling and oxidation, effect on magnetostriction and texture 77−36671
Ni, anodic oxidation in 1N H_2SO_4 soln. 79−91849
Ni, anodically oxidised, 100 keV proton channelling investig. of oxide layer struct. 77−84820
Ni base alloys, cyclic oxidation, static and dynamic, high temp. alloys 78−88576
Ni base alloys, hot corrosion in coal conversion system atmos. 79−96200
Ni base alloys, IN-702, IN-601, TD-Ni-Cr-Al, B-1900+Hf, oxidation, cyclic, role of thermal shock 80−97640
Ni base alloys, influence of ΔT (oxidising temp. minus cooling temp.) on oxide spallation 77−52551

oxidation continued
Ni base alloys, oxidation reaction investigation by X-ray diffr. and fluorescence *(German)* 79−57345
Ni based alloys, hot hardness and oxidation resistance meas. 78−31588
Ni based superalloys 713C and Mar-M200, Si effect on oxidation, hot corrosion and mech. behaviour 78−39950
Ni, chemisorption and oxide nucleation stages, low-energy SIMS and AES obs. 79−43083
Ni, corrosion in SO_2, high temp. 79−20281
Ni, corrosion rates in SO_2-O_2-SO_3 atmospheres under simultaneous sulfidation-oxidation 79−79162
Ni, elec. cond. of scale 77−48568
Ni, electrodeposited, oxidation 78−64756
Ni, electroless plating, oxidation kinetics 78−95847
Ni, electron beam influence, disappearance potential spectroscopy obs. 77−1766
Ni film, interaction with O_2, AES, EELS, work function, and gravimetric meas. 80−75433
Ni film, struct., oxidation, and exoelectron emission rel. to bulk samples *(Russian)* 79−37927
Ni, foil, oxidation to produced NiO for elec. cond. meas. at 1000°C 78−10451
Ni foil electrolytic perforation, surface film phase composition obs. *(Russian)* 80−61004
Ni, galvanic oxidation in borate buffer soln. 80−100948
Ni, inner layer of high temp. oxide scale, metallographic obs. 80−3240
Ni, oxidation, diffusion enthalpy and entropy 78−7084
Ni, oxidation, high temp., effect of C on cavity form., SEM study 80−97638
Ni, oxidation, role of grain growth 77−81337
Ni, oxidation at Curie temp. 79−29279
Ni, oxidation in air, 50-150°C, film growth obs. using AES and contact resist. 80−3242
Ni, oxidation kinetics, influence of intermediate annealing treatment 80−89412
Ni, oxidation kinetics near Curie temperature 78−88578
Ni, oxidation rate transition, at Curie temp. 78−27685
Ni, oxidation study by X-ray photoelectron spectroscopy 79−61787
Ni, oxidation transport processes using tracers in growing NiO scales 80−25913
Ni, oxide covered, tensile deform. in high vac., particle and photon emission 78−39672
Ni, oxide films, metal and O_2 transport, AES and inert marker, techniques 80−97641
Ni oxide surface layer, TOF atom probe anal. 78−64766
Ni, oxidised surface, oxidising conditions effect on thermally stimulated exoelectron emission *(Japanese)* 80−89127
Ni, passive surface, anodic process kinetics 79−15861
Ni, quenched vacancies, effect of oxidation *(French)* 78−27686
Ni, rel. to component of stainless steel 79−47811
Ni, S penetration of NiO scales 78−64776
Ni, self-diffusion in NiO, 700-1400°C, rel. to oxidation mechanism 78−27681
Ni, simultaneous sulfidation-oxidation at 603°C in Ar-SO_2 atmospheres 79−8389
Ni, staged flow of O_2 interaction process, secondary ion emission obs. 78−11386
Ni sulphide surface, oxidation studied by AES 79−83505
Ni surface, (110), O_2 adsorption, LEED and ion scatt. study 80−84386
Ni surface, oxidation, structural changes, low energy ion scatt. study 80−35423
Ni surface, polycryst., interaction with O_2, SIMS and flash filament meas. 79−47829
Ni surface with adsorbed S, oxidation studied by AES 79−83505
Ni, surfaces (100), (110), and (111), interaction with O_2, 295 and 485K, photoemission obs. 77−72784
Ni, tarnishing in air, 23-200°C, relative humidities from ambient to 95% 78−19940
Ni thin films, annealing and oxidation effects in stress, Michelson interferometer meas. 77−2650
Ni, ultrafine particles prepared by vacuum evap. on running oil substrate, mag. behaviour 79−28565
Ni-Al, (2 and 6 wt.%), oxidation, α-Al_2O_3 growth, microstruct., precip. 80−108626
Ni-Al, CC Ni-Al (42 at.%), Al_2O_3 growth, morphology and spalling model 78−53030
Ni-Al, dil., oxidation mech. at 800 to 1200°C 77−90483
Ni-Al (0.5 wt.%), microstruct. formation during internal oxidation, effect of additional microalloying *(Russian)* 77−80650
Ni-Al spraying powders, alumina and aluminide formation 80−25920
Ni-Al-Cr_3C_2, eutectic, directionally solidified, high-temp. oxidation 80−50775
Ni-Al-Cr_3Cr_2, eutectic alloy, directionally solidified, oxidation resistance, influence of Y 80−89409
Ni-Al-Mn alloy system, oxidation resist. 79−24661
Ni-Al-Ti, eutectic alloy charact. by melting temp., composition and oxidation resistance 78−52771
Ni-Al-Ti protective coating, on Ni-Al alloy IN 100, Ti content influence, oxidation behaviour *(French)* 78−3258
Ni-Au alloy, oxidation in air, 50-150°C, film growth obs. using AES and contact resist. 80−3242
Ni-based alloys, binary, ternary, complex, TiC additions, effects 78−92305
Ni-based superalloys, corrosion by O_2 containing H_2O and gaseous NaCl, volatile products 78−27674
Ni-based superalloys, mechanical integrities of surface oxides, oxidation 78−95844
Ni-based superalloys, mechanical integrities of surface scales, contaminant corrosion 78−95845
Ni-Co, oxide scales, cation distrib. calc. by approx. analytical method 77−48594
Ni-Co-Cr-Al-Y, plasma-arc-sprayed, metallurgical characts. and oxidation behaviour 80−40618
Ni-Cr, austenitic alloy, oxidation mechanism, adhesion of Cr_2O_3 scale *(Polish)* 79−79143
Ni-Cr, oxide layer struct. and comp., compar. study by secondary ion emission and electron micrprobe *(French)* 77−56286
Ni-Cr (20 wt.%), Al and Ti containing, oxidation, effect of dispersal oxides 77−44404
Ni-Cr (20 wt.%), oxidation, 800 to 1300°C, effect of volume and intergranular diffusion *(French)* 77−86228

oxidation continued
Ni-Cr (20 wt.%), oxidation, O_2 press. effects *(Japanese)* 78−15578
Ni-Cr (20 wt.%), oxidation in humid air, 800 to 1250°C *(French)* 79−79165
Ni-Cr (27.4 and 40.2 wt.%), compositional changes, in underlying alloy produced by oxidation 79−8395
Ni-Cr (44 to 50 wt.%), oxidation 79−43483
Ni-Cr (70 wt.%), oxidation behaviour, 1073-1473K 80−89416
Ni-Cr austenitic alloy, oxidation mechanism, intergranular diffusion effect *(French)* 80−81229
Ni-Cr/Au films, interdiffusion processes and oxidation phenomena 80−59735
Ni-Cr-Al, oxidation, NaCl vapour effects on microstruct. 78−44274
Ni-Cr-Al, oxidation at 850°C in air containing HCl gas 79−8396
Ni-Cr-Al, resist. to cyclic oxidation at 1100 and 1200°C 77−77641
Ni-Cr-Al (15, 5 wt.%), oxide dispersion strengthened, effect of dispersoids on oxidation 78−80679
Ni-Cr-Al (20, 4 wt.%), tensile stress effect on high temp. oxidation *(Japanese)* 80−89393
Ni-Cr-Al alloy, Al_2O_3 adherence, improvement by addition of Pt and Rh 77−8995
Ni-Cr-Al-ThO_2, hot corrosion, cyclic oxidation depth of attack determinations 80−11837
Ni-Cr-Ce, Ce effect on oxidation 79−43484
Ni-Cr-Co alloy IN738, electrochemical corrosion meas. in molten sulphate 79−96178
Ni-Cr-Co-Mo-Al, IN-67 alloy, hot corrosion, cyclic oxidation, depth of attack determinations 80−11837
Ni-Cr-Co-(Fe), oxidation 77−21320
Ni-Cr-Fe, high temp. corrosion and creep in carburizing and oxidising atmos. 79−11727
Ni-Cr-M alloys, M = minor alloying addition Y, La, Ce, Sm, Th, U, Zr, V, corrosion rates 77−16750
Ni-Cr-Nb-Al eutectic alloys, sulphidation/oxidation at high temps., corrosion mechanism 78−72934
Ni-Cr-Si (10, 1.8 wt.%), Zr, Hf, La or Sm alloying additions effect on oxidation resist. 77−63831
Ni-Cr-Si alloy system, oxidation resist. 79−24661
Ni-Cr-Ti(Nb)(Zr), eutectic alloy charact. by melting temp., composition and oxidation resistance 78−52771
Ni-Cr-W, oxidation behaviour in air at 1000-1250°C 80−89407
Ni-Cr-W (20, 3 wt.%), high temp. creep, atmospheric effect on anomalous behaviour 78−80617
Ni-Cr-Y, oxidation at 800 to 1300°C, Y addition effects, comparison with Fe-Ni-Cr-Y alloy *(French)* 79−43481
Ni-Cr-Y, Y addition effect on intergranular and volumetric diffusion, oxidation reduction *(French)* 79−83382
Ni-Cr(-Fe), blackness change in air, 1-8 micron, 1200°C, film props. depend. 77−66033
Ni-Cr(-W) alloys, heat-resistant, integrated hemispherical degree of blackness, specific elec. resist., oxidised surfaces 79−86912
Ni-Cr(Mo), oxidation effect on magnetic props. *(Russian)* 78−23868
Ni-Cr(20 wt.%), oxidation at elevated temps., struct. effects *(French)* 77−59994
Ni-Cr(20 wt.%), oxidation in pure O_2, 800 to 1200°C, secondary ion emission exam. of oxide film *(French)* 77−59995
Ni-Fe, (100) surface, O interaction, LEED and XPS studies 79−82437
Ni-Fe, adsorption of O_2, oxidation 80−108730
Ni-Fe (2 wt.%) oxidation, 800 to 1000°C 77−36686
Ni-Fe alloy, oxidation, diffusion enthalpy and entropy 78−7084
Ni-Fe reed contact, Au-plated, submicron Auger spectroscopy exam. 79−15027
γ-Ni-γ'-Ni_3Al-TaC fibre reinforced eutectic, oxidation protection 77−40475
Ni-Nb (5, 10 at.%), initial oxidation process at high temps., appl. of high energy ion backscattering anal. for O oxidation *(Japanese)* 79−24651
Ni-Nb alloys, oxidation at high temp., high energy ion backscattering anal. *(Japanese)* 80−35405
Ni-Nb_2O_5, fibrous composite, aligned in situ growth by preferential internal oxidation 78−6879
Ni-O system, initial oxidation, combination anal. using ESCA, AES and SIMS 78−72924
Ni-O system, oxidized polycryst. Ni films, H_2 reduction, AES 77−12472
Ni-Si-B powder, oxidation at 850°C, SEM, ESCA, and elec. cond. meas. 80−7717
Ni-Si-Mn(Al) alloy systems, oxidation resist. 79−24661
Ni-SiC, electrodeposited, oxidation 78−64756
Ni-Sn alloys, passive film, AES obs. 77−48575
Ni-ThO_2, oxidation, cyclic, role of thermal shock 80−97640
Ni-Ti (1.6, 7.64 wt.%), monophase high temp. scaling, metallography study 80−21159
Ni-V dil., behaviour at 1200°C 77−77636
NiAl, compositional depend. of oxidation rates 79−8393
β-NiAl, oxidation, α-Al_2O_3 growth and microstruct. 80−108627
NiAl, oxidation, effect of gaseous NaCl 78−95853
β-NiAl, oxide films, metal and O_2 transport, AES and inert marker, techniques 80−97641
Ni_3Al-Ni_3Nb, eutectic, temp. and thermal cycling influence on oxidation 80−45417
Ni_3Al-Ni_3Nb directional eutectic, oxidation and interaction with protective coatings *(Russian)* 77−52526
Ni_3Al-Ni_3Nb eutectic, directionally solidified, high-temp. oxidation mechanism 80−16544
Ni(Cr)/Ni_3Al-Ni_3Nb directional eutectic, oxidation and interaction with protective coatings *(Russian)* 77−52526
Ni_4Mo alloy, high temp. oxidation, oxide layer growth, struct., mech. behaviour 78−44269
Ni_3Nb intermetallic compound, oxidation kinetics in 500-1000°C range *(Russian)* 77−56144
NiO films, on Ni (100) electrodes, oxide defect sites role in breakdown 79−43587
NiO, nonstoichiometric, near-surface and bulk chem. diffusion 80−80035
NiO, plasmochemical synthesis, oxidised from metals, exam. of props. 80−2984
NiO, powder pressed disc, oxidising conditions effect on thermally stimulated exoelectron emission *(Japanese)* 80−89127
NiO, single cryst. cleavage plane, oxidising conditions effect on thermally stimulated exoelectron emission *(Japanese)* 80−89127
$Ni_{1-x}S$, oxidation, TG/DTA/MS obs. 78−31745
Ni_3S_2, oxidation 79−83354
NiTa, exam. of oxidation 79−96221

oxidation continued
NiZnCo ferrite, excess Fe type, saturation magnetostriction meas., oxidation effects 79−82852
Ni(100), oxidation, UPS obs. 80−6648
Ni(100) oxidised surface structure anal., extented appearance potential fine struct. study. 80−75411
$Np^{4+/3+}$ in fused salts, redox and chem. props. 77−29038
Np(V)/Np(IV) catalytic redox reactions, kinetics and mechanisms 77−29006
Np(VII) formation in molten salts 77−29039
O-containing anions of d-elements forming hydration-active phases, electron structs. and props. 79−42005
$O+Cl_2(CS_2)$, reactive scatt., O atoms seeded in Ne supersonic nozzle beam 78−48637
O_2+Be(Mg)(Ca)(Sr)(Ba), reaction kinetics in diffusion flame 77−90579
O_3 oxidation of Br, Cl and organic C in seawater 79−16518
OH+alkanes (alkenes), photooxidation, 305K, absolute and rel. rate consts. 77−16782
^{18}O tracer used to study growth mechanism of oxide scale 77−8964
P, amorphous, stability in air, XPS study, comparison with cryst. polymorphs 80−25517
P, amorphous, XPS anal. of stability, form. of oxidised layer *(German)* 79−11496
P_4, vap., oxidation, chemiluminesc., reduced press. system 77−32795
$P_4+H_2O(D_2O)$, vapour, chemiluminesc., transient emitting species 77−1926
Pb (100) and (110) surfaces, oxidation and sulphidation, LEED and XPS obs. 78−20070
Pb electrode, porous, in H_2SO_4 solutions, expt. 79−100514
Pb film, oxide form. on (111) surface, orthorhombic PbO 77−63835
Pb film, oxidised (111) surfaCe, electron microscope anal. of oxides 78−23878
Pb overlayers, on Cu substrate, oxidation, AES and XPS obs. 79−47833
Pb, passivation in H_2SO_4 soln. 78−76871
Pb porous electrode oxidation in H_2SO_4, potential step expts. 79−96438
Pb superconducting tunnel barrier, oxidation in humidity-controlled O_2 regulated atm. 78−19187
Pb surface, oxidation, XPS and SIMS study 79−15873
Pb/Au/Pb, Josephson junction, oxide formation process, ellipsomesric meas. *(Japanese)* 80−11561
Pb-In and Pb-In/Au, Josephson junction, oxide formation process, ellipsomesric meas. *(Japanese)* 80−11561
Pb-In(-Au) base electrode film Josephson junctions, tunnel barrier oxide struct. 80−65750
Pb-Sb molten alloys, oxidation and drossing *(German)* 79−74313
Pb-Te-O, thermal stability 78−44104
$Pb_3Fe_2WO_9$, perovskite ferroelec., characts. of dielec. polarisation, influence of oxidation and reduction 77−8496
PbInAu film, RF plasma oxidised, surface analysis using ESCA 80−50742
PbO-Si-O, general features of reaction 79−11819
PbO_2, corrosion in HBF_4, redox mediator effects 77−90480
$4PbO.PbSO_4$, oxidation to PbO_2 in positive plate of Pb-acid battery 79−70336
PbS, oxidation, $PbSO_4$ distrib. in products *(Polish)* 80−25883
PbS, superficial degradation in air and water, XPS obs. *(French)* 80−89110
PbS(Se)(Te), chemisorption of O_2, room temp., UPS and XPS obs. 78−91529
PbSe surface, clean and O_2-exposed, XPS (UPS) obs., electronic struct. 78−52637
$Pb_{0.8}Sn_{0.2}Te$ surfaces, oxidation in air and thermal desorption, XPS and LEED meas. 79−47830
$Pb_{1-x}Sn_xTe$ anodic oxide film form. conditions, IR absorpt. spectra 80−11494
$Pb_{1-x}Sn_xTe$, MBE, O_2 uptake, AES, XPS and UPS expts. 78−95227
$Pb_xSn_{1-x}Te$, thin film, appl. of Mossbauer method 80−45410
PbTe surfaces, oxidation in air and thermal desorption, XPS and LEED meas. 79−47830
PdH_x layer, galvanostatic desorption of hydrogen, quantitative theory 80−40694
Ph, Josephson junction, oxide formation process, ellipsomesric meas. *(Japanese)* 80−11561
$PrO_{1.714}$, oxidation, kinetic study 80−108707
Pt, adsorption of H_2 and CO on (110) clean and oxidised surfaces 77−28078
Pt, adsorption of O_2, surface struct. depend., LEED, AES, and electron energy loss spectra 79−46934
Pt anode, oxide film growth in H_2SO_4 solns., temp. study 80−71802
Pt, boiling water reactor, corrosion and oxidation potentials monitoring 79−20252
Pt electrodes, polymeric surface film form. by electrooxidation of phenolic cpds., ellipsometric study 80−104450
Pt, hydrocarbon reactions catalysed by surfaces with variable kink concs., surface O_2 effects 80−35576
Pt oxidative vaporisation, thermochemical analysis 78−11447
Pt, polycryst. wire, multilayer surface oxidation 78−88579
Pt, preanodised or passivated, DTA, Pt-O system 77−16733
Pt resistance thermometer, oxidation problems 80−52206
Pt resistance thermometers, effect of Pt oxidation 80−101794
Pt, single cryst., Auger spectra 78−14600
Pt, surface, (111), O_2 interactions, UPS, EELS and thermal desorption study 80−100409
Pt surface, electrochem. oxidation and reduction, XPS obs. 78−95653
Pt, surfaces, oxidation by electrosorpt., of H_2, effect of soluble prods. *(German)* 80−55717
Pt, XPS spectra study 80−3254
Pt-Al, development, growth and adhesion of Al_2O_3 77−8994
Pt-Al (22 wt.%), elec. props. of growing alumina scales 79−20282
Pt-Pb fibre, CO adsorption and oxidation, AES and ESCA obs. 79−52469
Pt-Rh alloys, surface behaviour on heating in air, XPS and SIMS *(French)* 77−40327
PtO, electrochemically formed, anisotropy of optical constants, reflection spectroscopy and Kramers-Kronig analysis 77−32456
$Pt_{90}Rh_{10}$/Pt thermocouple, Inconel sheathed, MgO-insulated, decalibrations during 1200°C use, ion microprobe obs. 78−57957
Pu, in Irish Sea, oxidation state 79−16516
Pu loaded on TBP, reduction stripping, reactor appl. 77−6548
Pu, oxidation, binding energies, Auger and X-ray photoelectron spectra study 80−76550

oxidation continued
Pu radioactive waste, oxidation by radiation, effect on migration rate 80−13714
$Pu^{4+/3+}$ in fused salts, redox and chem. props. 77−29038
Pu-Ga (3.3 at.%) alloy, in air, 250-400°C 77−44401
PuO_{2-x}, O_2 chem. diff., dilatometry and thermogravimetry study *(French)* 79−73339
Pu(VII) formation in molten salts 77−29039
Rb, adsorbate-induced structs., UPS obs. 79−47828
Re, LEED patterns during oxidation on different stepped surfaces 79−65323
Re, oxide formation and surface rearrangement, field ion microscope obs. 77−28936
Re-O_2, surface interactions and catalysis, 77 to 773K 79−79286
Rh (111), interaction with O_2, thermal desorption spectra, AES and LEED obs. 79−51428
Rh, catalytic oxidation of CO on polycrystalline sample 79−79294
Rh, film, annealing effect on struct., TEM, electron diffr. study 78−76682
Ru ($10\bar{1}0$) surface, oxide form., thermal desorption and ESCA obs. 79−82442
Ru complex, (2,2′-bipyridyl)$_3$ruthenium^{2+}, excited-state redox processes, electron transfer theory 79−39126
Ru electrodes, reversibility and growth behaviour of surface oxide films 79−20263
Ru, oxidation resistance in Ar and air 77−25201
Ru surface, clean, oxidation, atom probe anal. of oxide films 79−47797
Ru surface, clean, oxidation, FIM study 79−47796
Ru, thin film, electrographic investigation of interaction with atmospheric O_2 *(Russian)* 77−25196
RuP_2, oxidation resistance in Ar and air 77−25201
S compounds homogeneous oxidation in atmosphere 78−96258
SO_2, adsorption and oxidation on atmospheric particles 78−96287
SO_2, aerosol-catalysed oxidation, expt. under atm. conditions 79−1941
SO_2, atmospheric, photochem. oxidation 79−70873
SO_2 conversion to SO_4^{2-}, meas. during manned balloon flight 79−83658
SO_2, gas, photooxidation, cloud chamber obs. 79−1961
SO_2, homogeneous oxidation mechanism in troposphere 78−96257
SO_2, in coal-fired power plant plumes 77−87065
SO_2, in moist atm., aerosol growth kinetics 78−96255
SO_2, oxidation by O_2 and O_3 in aq. soln., kinetics, rel. to atm. rate processes 79−20905
SO_2 oxidation by O_3 in cloud droplets, HSO_3^- aerosols form. 78−44894
SO_2 oxidation chemiluminesc., appl. to atm. chem. *(German)* 79−52670
SO_2 oxidation in clouds and rain, O_2, O_3 and H_2O_2 role 79−84351
SO_2, oxidation in moist O_2-N_2 mixture by electron irrad., appl. to exhaust gas treatment 78−80766
SO_2 oxidation in stored rainwater samples, rel. to Mn content 79−84352
SO_2, oxidation on surface of fly ash particles under low relative humidity conditions 79−62160
SO_2 oxidation rate, CO effect, smog chamber expt. 79−74925
SO_2 oxidation to sulphates in dispersing plumes 77−70806
SO_2, oxidation via OH radical, rel. to atm. fate of HSO_x radicals 79−62559
SO_2, photooxidation, aerosol evolution, rel. to air pollution 78−81392
SO_2, photooxidation, gas phase, in cloud chamber 79−47951
SO_2, photooxidation in gas phase, nucleation appls. 79−83479
SO_2, precursor effects on oxidation, rel. to air pollution 79−1960
SO_2 to sulphate conversion processes in atmosphere 77−37389
SO_2+OH, role for stratospheric HSO_3 layer, reaction rate consts. 78−32202
$SO_3^-+BrO_3^-$, fast oxidation in acid medium, laser Raman multichannel spectroscopy 78−27754
^{125}Sb, in HCl solns., valency states investig., radioanal. tracer preparation, stability 77−63943
Sc, oxidation by O_2 and H_2O, XPS obs. 79−47827
$Sc+O_2(NO_2)(N_2O)(O_3)$, oxidation, single collision chemiluminesc. 77−25267
Se film on brass, ESCA interface study 78−43269
n-Si (100), O_2 partial press. depend. of fixed surface state charge due to thermal oxidation 79−70179
Si (100), oxidation induced stacking fault retrogrowth, O_2 press. depend. 78−64747
n-Si (100), oxidation-induced stacking faults, O_2 partial press. depend. 78−39922
Si (111), adsorpt. of O and stimulated oxidation by electron bombardment, AES 78−14599
Si (111), electronic states and initial steps in oxidation 78−91534
Si (111), intermediate oxidation state, core photoelectron absorpt. vs. chemical shifts 80−81220
Si, (111), struct. depend. oxidation, high resolution photoemission yield spectroscopy 77−1305
Si, (111) surface, EXAFS of oxidation stage, O-Si bond length 79−95876
Si, (111) surface, oxide formation, AES and EELS meas. 80−3232
Si (111) surface, oxidised, energy depend. of photoelectron attenuation length 78−52643
Si, adsorption of O_2, early stages, AES, LEED, and XPS obs. 79−46937
Si, ambient effect of O precipitation, self interstitial mechanisms, IR spectra, TEM study 80−66510
Si, amorphous, hydrogenated, work function and Auger spectroscopy of initial oxidation 78−76132
Si, and Si:H, amorphous, sputter deposited, O_2 incorporation during and after fabrication 80−49541
Si and Si:H amorphous films, porosity and oxidation of evap., sputtered and plasma-deposited films 80−10838
Si, annealing, impurity film form., energy loss anal. 77−31916
Si, anodic oxidation, high electronic current density 80−89386
Si, anodic oxidation at constant voltage, mechanism 79−70184
Si, anodic oxidation for abrading thin layers from wafers *(German)* 77−25176
Si based MOS device irradiation with γ-rays, minority carrier generation, CV characts. 80−88637
Si, bonding states of adsorbed O_2, photoemission obs. 78−92170
Si, CC HCl oxide growth, ellipsometric meas. 78−7073
Si, CCD processing, elimination of stacking faults 78−10065
Si, chemical staining due to suboxide form. 78−35540
Si, chemically etched, model of structural transforms. during thermal oxidation 78−79557
Si, Cl incorporation in O_2-HCl ambients 78−11378
Si, clean SiO_2 film prep., use of poly-Si oxidation tubes 78−39924

oxidation continued
Si, crystal, dislocation slip bands formation due to pores, nondestructive monitoring 79−55749
Si Czochralski wafer oxidation-induced stacking faults correl. with bulk defects 77−76428
Si, Czochralski wafers, oxidation induced stacking fault sources 77−7737
Si Czochralski wafers, thermally oxidized, stacking fault distrib., O conc. depend. 80−2042
Si Czochralski wave, oxid. induced stacking fault, oxygen content influence 78−10062
Si, defect form. during high press. low temp. steam oxidation 79−29238
Si, defect struct. of vitreous SiO_2 films, role of defect struct. in growth 80−65403
Si defects in surface due to oxidation, exam. using double crystal back reflection topography *(German)* 79−51098
Si, diffusion of P, oxidation effects 79−51309
Si, dislocation generation, influence of film stress and thermal oxidation 79−23609
Si, dislocation generation in local oxidation 80−107245
Si, doped oxide film formation mechanism, X-ray spectral anal. 79−87008
Si double polycrystalline VLSI devices, low temp. differential oxidation 80−16521
Si dry pressure-oxidation for low-temp. IC processing 78−7068
Si, early oxidation stages, AES study *(French)* 79−8379
Si, effect of chlorinated ambients 79−100278
Si, epitaxial stacking faults, nucleation sites 77−20201
Si epitaxial stacking fault nucleation site identification, annihilation, and suppression 77−76705
Si epitaxy and oxidation, first-order process models 78−72049
Si, F-enhanced plasma growth of native layers, Auger profiles 80−93662
Si film, low press. CVD prep., struct., elec. and optical props. 80−70548
Si film, porous, form. and oxidation by anodic reaction 79−28966
Si film removal using anodic oxidation, determination of active impurity distrib. 80−40583
Si, float zone, process-induced effects on carrier lifetime and defects 80−81216
Si, form. of carbonaceous layer during high dose ion implantation, removal by cleaning, annealing and oxidation 79−70374
Si, growth and thermal evaporation kinetics of oxide film on Si surface 78−3246
Si, growth kinetics of low-temperature SiO_2 films by oxidation of SiH_4 77−8763
Si, HCl oxidation conditions for stacking fault nuclei gettering and undesirable etching 78−68830
Si, high press. techniques, review 79−100279
Si, high quality oxidation *(Chinese)* 79−52401
n-Si, high resistivity wafer, oxide layer anodically grown, improved homogeneity 79−24642
Si, high-press. pyrogenic oxidation in the production environment 78−35547
Si high-pressure oxidation process *(Japanese)* 79−29249
Si, impurity redistribution during single oxidation step, computer program calc. 80−2060
Si, in HCl/O_2 ambients, phase separation and Na passivation in thermal oxides 80−3219
Si, in $HCl-O_2$ gas mixture, mobile Na ion passivation 79−70187
Si, in high press. O_2, residual stress, chemical etch rate, refr. index and density meas. 80−71768
Si, initial oxidation rate 79−91817
p-Si inversion-channel photoelectric cell characteristic *(Russian)* 80−49941
Si, ion implanted, dopant depend. of oxidation rate 80−89384
Si, ion implanted, interstitial generation and loop form. during annealing in oxidising medium 80−107225
Si, ion-implanted, thermally oxidised, Rutherford backscatt. analysis 78−19910
Si, laser annealing for improved stacked-struct. oxide quality 80−65386
Si, lattice strains induced by localized oxidation, high temp. real-time X-ray topographic studies 80−108489
Si, light reflection, effect of repeated oxidation 79−52402
Si, microwave O^+ plasma, magnetoactive, for oxidation of Si 80−38831
Si, microwave oxidation, negative role of fast electrons 78−64744
Si, n- and p-type (100) wafers, oxidation induced stacking faults 77−32699
Si, Ne ion implanted, oxidation expanded defects, effect on MOS parameters 78−19152
Si, O, F, B isotopes in profiling of oxide films by quantitative SIMS 77−9147
Si, oxidation, AES photoelectron spectra exam. of early stages 79−74272
Si oxidation, dopant redistrib., Cs^+ SIMS anal. appl. 79−39265
Si, oxidation, in dry O_2 and H_2O ambients, initial oxidation regime obs. 79−29240
Si, oxidation, oxidation-induced lattice defects, review *(Japanese)* 78−39931
Si, oxidation, thermal growth kinetics, SiO_2 profile meas. 78−88551
Si, oxidation at 1000°C, Na contamination and furnace cleaning procedures 77−59955
Si, oxidation comparison with O_2 adsorption, SIMS 78−15273
Si oxidation in flow conditions at 1000 to 6000K 78−11445
Si oxidation in $HCl-O_2$ atms., Si etching and SiO_2 bubble form. 77−63823
Si, oxidation in high-press. steam, 800 to 1000°C, rate consts. 77−48565
Si oxidation in O_2-H_2-HCl mixture, kinetics, SiO_2 film props. 80−40569
Si, oxidation in presence of Cl and Cl cpds. 78−53009
Si, oxidation induced by ion or electron bombardment, AES-SIMS study 80−108606
Si, oxidation induced stacking fault growth, role of point defects 78−10061
Si, oxidation induced stacking faults, wafer orientation and ion implantation effects 78−10063
Si oxidation mechanism and kinetics 78−95833
Si, oxidation of dry O_2, revised model 78−92373
Si oxidation rate constants and role of H_2O 78−7072
Si, oxidation stacking faults and microdefects, growth behaviour during high temp. annealing 78−72901
Si, oxidation stacking faults, shrinkage and growth, bulk O_2 effects 80−96546
Si, oxidation with trichloroethylene additive to eliminate oxidation induced stacking faults 80−39118

oxidation continued
Si, oxidation without stacking fault form. 78−7062
Si, oxidation-induced Frank sessile dislocation loops, struct. change 80−75228
Si, oxidation-induced stacking faults, refl. X-ray topography 77−84767
Si, oxidation-induced stacking fault form., by high press. steam oxidation 78−83830
Si, oxidation-induced stacking faults, control by Cl implantation 79−46682
Si, oxidation-induced stacking faults, nucleation mechanism 80−15122
Si, oxidation-induced stacking faults, influence of annealing ambient on shrinkage kinetics 80−29035
Si, oxidation-induced stacking faults, distinction between clean and decorated faults by etching 80−79818
Si oxidative vaporisation, thermochemical analysis 78−11447
Si oxide, photoresist residual film, ellipsometric characterisation 77−48266
Si, oxide film struct. determ. by electron diffr. 79−15050
Si, oxide formation in microwave discharge 79−52406
Si, oxide growth, ambient water vapour trace effects 77−77618
Si, oxide growth kinetics for SiO_2 films in low O_2 partial press. *(Japanese)* 78−27665
Si, oxide layer form. by O^+ ion implantation, Rutherford backscatt. and IR transmission obs. 79−51141
Si, oxide layer formation on O_2^- ion implantation, phase comp. 77−90470
Si, oxide scale microstruct. of oxidised single cryst. 80−108613
Si, oxidised, angular-dependent X-ray photoemission at low X-ray incidence angles 77−32492
Si, oxidised in trichloroethylene-O_2, Cl incorporation and elec. props. 79−91827
Si, oxidised on one side, elastically flexed, dynamic X-ray scatt. *(Russian)* 77−43115
Si, oxidised surface, irregular growths of $B(OH)_3$ 78−39926
n-Si, passivation, photoactivation kinetics in conc. alkali, ellipsometric investig. 77−1885
Si, phase comp. of SiO_x, electron spectroscopy obs. 78−60042
Si, photoemission spectroscopy of surface states and oxidation 77−55863
Si, planar technology, insulating thin film preparation and props. 78−10589
Si, polycryst., morphological aspects 80−76388
Si, polycrystalline, electrode shape effects on oxide conduction 80−96890
Si, polycrystalline, thermal oxide anomalous stress 80−93661
Si, polycrystalline multilayer support struct., control of deform. in dielec. isolated substrates 80−107681
Si, Schottky diode ageing, influence of metal electrode O diffusion coeffs. 79−99620
Si selective anodic oxidation in O_2 plasma 80−108610
Si, selective oxidation in high press. steam, using Si_3N_4 mask 79−38997
Si, single cryst., Auger spectra 78−14600
Si, solubility and transport behaviour of water, dissolution 80−93801
Si, stacking fault annihilation by impurity diffusion 77−19968
Si, stacking fault form. model during oxidation and ageing, defect clustering 77−24322
Si, stacking fault formation, elimination by preoxidation annealing in $N_2/HCl/O_2$ mixtures 78−88550
Si, stacking fault generation and annihilation 77−76419
Si, stacking fault growth, oxidation-induced, HCl and interstitial effects 80−49241
Si, stacking-fault nuclei gettering by trichloroethylene oxidation 77−43226
Si, steam oxidation, low temp., high press., oxide growth kinetics and props. 80−16523
Si, steam oxidation at any elevation, improved theoretical predictions 79−20230
Si, stress in thermal SiO_2 during growth 79−91812
Si, struct. and comp. of oxides grown in HCl/O_2 ambients 79−42404
Si substrate for Pb, Sb, and Bi silicate films, form. kinetics and props. 80−35358
Si, substrates, review of defects 77−39597
Si, superthin SiO_2 film production 77−76690
Si, surface, (111) 2×1, cleaved, O_2 adsorption, low-energy electron loss spectra 79−15840
Si surface, oxide overlayer, angular-depend. XPS exam. 77−55864
Si surface, thermal oxidation induced defects, origin and growth *(Chinese)* 80−66681
Si, surface layer defects, influence of multiple oxidation *(Russian)* 78−47650
Si, surface oxidation, after Ar^+ bombardment *(Russian)* 79−15028
Si, surface oxidation, in wet O_2 environment 80−3410
Si, surface prep. prior to thermal oxidation, chem. struct. of Si-SiO_2 interface 78−27654
Si surfaces etched in CF_4 or CF_4-O_2 plasma, morphology 80−93671
Si, TEM and EELS identification of oxide precipitates 80−100723
Si, thermal growth mechanisms of vitreous oxide layers 80−93675
Si, thermal oxidation, ^{18}O study 79−52400
Si, thermal oxidation, high resolution Rutherford backscatt., implanted ions analysis 79−87911
Si, thermal oxidation, in O_2/N_2 mixture, kinetics, 950-1100°C 77−86202
Si, thermal oxidation, in O_2-HCl mixture, Cl incorporation in SiO_2 films 79−70186
Si, thermal oxidation, in presence of oxides of group III metals 77−12722
Si, thermal oxidation, mechanism of appearance of surface roughness and surface defects 77−7956
Si, thermal oxidation, role of H_2O, ellipsometry expts. 78−27656
Si, thermal oxidation, role and effects of Cl 80−108622
Si, thermal oxidation, SiO_2 amorphous film form., struct., mechanism 77−12725
Si, thermal oxidation at 1200°C, effects of trichloroethylene addition 78−27660
Si, thermal oxidation in Cl-H-O ambient, gas phase comp. considerations 77−48562
Si, thermal oxidation in O_2-H_2O and O_2-Cl_2 mixtures 78−44239
Si, thermal oxidation in O_2-trichloroethylene mixture, 900, 1000 and 1100°C 80−3221
Si, thermal oxidation in wet O_2/trichloroethylene mixtures at 1200°C 80−16522
Si, thermal oxidation kinetics in O_2/HCl mixture, rate consts. 77−59953
Si thermal oxidation kinetics in O_2/HCl mixtures 77−77617

oxidation continued
Si, thermal oxidation kinetics in pyrogenic water and HCl-H_2O mixture 78−64748
Si, thermal oxidation kinetics, steady-state transport anal. 80−71773
Si, thermal oxidation kinetics, theoretical perspective 80−76387
Si, thermal oxidation technology, improved using 1,1,1-trichloroethane as optimised additive 79−29239
Si, thermal oxides prepared in O_2-HCl and H_2O-HCl ambients, Cl conc. profiles using SIMS 79−65110
Si, thermally oxidized, chemical shift meas. by ESCA *(Japanese)* 79−61761
Si, thinly oxidised wafer reflectance at normal incidence, calc. 79−78641
Si, trichloroethylene and HCl grown oxides compared 77−76988
Si, tunnelable film form. using vap. O_2 source at liq. N_2 temp. 78−76774
Si, use of new high press. steam apparatus 77−63818
Si wafer, automatic meas. system for resist. profiles 80−39574
Si wafer, contaminated, Au redistrib. during oxide growth 77−4121
Si wafer, Czochralski grown, interstitial O gettering 77−86196
Si wafer, Czochralski grown, precipitation during high temp. oxidation 78−11381
Si wafer, oxidation induced stacking faults, surface vs. bulk nucleation 77−62545
Si wafer, stacking faults, preoxidation gettering by reverse side P diffusion-induced misfit dislocations 80−60988
Si, wafer, suppression of oxidation stacking fault generation by preannealing in N_2 atm. 78−30648
Si wafer, thermally oxidised, stress and strain meas. *(Russian)* 78−11375
Si wafer, trichloroethane oxidation, effect on SiO_2 and Si props. 79−70193
Si wafers, n- and p-type (100), oxidation-induced stacking faults 77−39599
Si, work function and Auger spectroscopy of initial oxidation 78−76132
Si, X-ray photoelectron spectra 77−18971
Si:As, implanted As redistrib. during annealing in oxidising ambient, carrier distrib. meas. 79−19275
Si:As, thermal oxidation in wet ambient from 650°C to 850°C 79−61758
Si:As implanted emitters, oxidizing drive-in ambient deleterious effect 80−2044
Si:As(B), heavy-doping effects and impurity segregation during high-press. oxidation 80−65014
Si:As(P), oxidation-enhanced diffusion of impurities 79−46840
Si:B, diffusion of B atoms and growth kinetics of oxidation induced stacking faults, correlation 79−37720
Si:B, heavily implanted wafers, secondary defect generation suppression by HCl oxidation 78−10069
Si:B, implanted, oxidation-induced precipitate defects, TEM 78−31556
Si:B, implanted, oxidation-induced stacking faults, EBIC and TEM expts. 78−39923
Si:B, ion implanted, structure defects formation and behaviour under annealing in various ambients 80−65033
Si:B, lateral effect of oxidation on B diffusion 80−29217
Si:B, near intrinsic ⟨100⟩ and ⟨111⟩ samples, inert and oxidising ambients, diffusion, segregation 78−75882
Si:B, redistrib. of B during thermal oxidation, numerical and analytical calcs. 80−49259
Si:B redistribution after oxidation, integro-differential eqn. 77−76453
Si:B(P), single crysts., oxidation investigations, 780°-1150°C 79−5068
Si:N, ion implanted, oxidation characts. 80−89385
Si:P, B diffusivity, versus Si oxidation rate 77−15436
Si:P, heavily doped, thermal oxidation 78−56793
Si:P, ion-implanted, carrier conc. reduction caused by wet O_2 oxidation 80−10565
Si:P, polycrystalline, thermal oxidation in wet O_2 78−92376
Si:P, polycrystalline laser recrystallised film on Si substrate, cryst. struct., thermal oxidation 80−65391
Si:P, secondary defect generation suppression and diffusivity restraint by HCl oxidation 79−70191
Si:P film, CVD polycrystalline, low press. and atmos. press., oxidation 80−3214
Si:P(As)(B)-SiO_2 interface oxidation kinetics, high doping levels, experiment 80−11828
Si:Pb oxides, thermal oxidation, kinetics and mechanism 77−36673
Si:Sb, ion implanted, Sb diffusion during oxidation, snow-plough effect 80−88366
Si/SiO_2 interface, transition region thickness, determ. by He^+ backscatt. 77−62762
Si-Al electrical steel, surface oxidation during annealing 78−68838
Si-Al-O-N, oxidation mechanisms 80−40570
Si-Al(Ti)C, sintered, exam. of props. 80−25644
Si-B, exam. of two stage diffusion of B, under a gas phase oxide film 79−95044
Si-B based CVD coating for gas turbine blading, props. 80−40615
Si-B system, liq., surface tension, density, and oxidation kinetics, 1410-1700°C 80−20011
Si-based coatings, for high temp. alloys, process development and props. 80−40614
Si-containing films, formed by reaction of Si with organic compounds of N, struct. investigation 79−87009
p-Si-Mn contact, barrier height, oxidation effects 80−34510
Si-SiC chemical interaction in rarefied O_2 under pulsed action of concentrated solar radiation 80−71930
Si-SiO_2, bonding at (111) interface, stoichiometry and kinetics, synchrotron radiation photoemission spectroscopy 80−24744
Si-SiO_2, ESR centres, interface states and oxide fixed charge 80−2474
Si-SiO_2, impurity redistrib. during oxidation, numerical soln. including interfacial fluxes 80−25888
Si-SiO_2, influence of oxidation conditions on elec. props. of ultrathin SiO_2 layers 78−39226
Si-SiO_2, interface, reconstructing states 80−49925
Si-SiO_2, interface defect states obs. by constant capacitance DLTS 80−49924
Si-SiO_2, thermally oxidised, origin of fixed charge, Si diffusion in transition region 77−20381
Si-SiO_2 bonding layer, EPR exam. 78−15022
Si-SiO_2 interface, Auger-sputter profiling obs. of P pileup 78−95240
Si-SiO_2 interface, backscattering-channelling study 80−34320
Si-SiO_2 interface, chem. struct. of transitional region 78−95824

oxidation continued
Si-SiO_2 interface, effect of oxidation time and temp. using AES 80−35359
Si-SiO_2 interface, electronic struct. calc. 80−100531
Si-SiO_2 interface, ion implantation induced interface states, effect of oxidation and N_2 annealing 77−39949
Si-SiO_2 interface, oxidation stacking faults, growth rel. to self-diffusion 80−49239
Si-SiO_2 interface, thermally grown, surface pot. inhomogeneities after stress ageing 80−92993
Si-SiO_2 interface, thermally grown oxide, spectroscopic ellipsometric anal. 80−107659
Si-SiO_2 interface in MOS solar cells, operational characts. and struct. 80−93901
Si-SiO_2 interface layer characterisation by spectroscopic ellipsometry 80−50738
Si-SiO_2 interface oxidation kinetics, high doping levels, theory 80−11827
Si-SiO_2 interface state density, dependence on thermal oxidation process variables 80−15607
Si-SiO_2 interface struct., transient region 77−85115
Si-SiO_2 interfaces, local atomic and electronic struct., high resolution XPS 80−49927
Si-SiO_2 interfacial region, nature of fixed oxide charge 78−56047
Si-SiO_2 interfacial regions obs., by XPS, ultrathin oxide films 79−15039
Si-SiO_2 interfacial region on TCE/O_2 and CCl_4/O_2 oxidised Si, struct. and comp. 80−50741
Si-SiO_2 system, structural defect formation rel. to thermal oxidation kinetics *(Russian)* 78−43478
Si-undoped poly Si interface, in oxidation process, defects generation 80−40571
SiAlON, oxidation 77−56130
SiAlON, pressureless sintered, decrease in oxidation resistance with increase in Y_2O_3 content 79−66029
SiAlON system, β′, 15 R phases, oxidation resist. *(French)* 78−72899
SiAs, deterioration in air, product identification 77−36675
SiC, chem. stability, mech. and thermal props. rel. to appls. 80−21103
SiC, controlled nucleation thermochemical deposition, charact. and props. 80−108355
SiC, high-temp. oxidation in glow discharge oxygen plasma, oxide scale struct. 77−25174
SiC, hot pressed, oxidation *(German)* 79−96161
SiC, oxidation and corrosion behaviour, formation of protective SiO_2 coatings *(German)* 80−25885
SiC, oxidation and hot corrosion resistance kinetics 80−25896
β-SiC, oxidation in CO-CO_2 mixture *(German)* 78−23844
SiC, oxide scale microstruct. of oxidised single cryst. 80−108613
SiC, pyrolitic coating for nuclear fuel particles 77−79465
SiC, reactions with oxidising atms. 80−11812
SiC, resist. to oxidation and corrosion at high temps. *(German)* 80−35357
SiC single crysts., polytypism obs. by high temp. oxidation expts. 78−59797
β-SiC, submicron powder, prep. by siliconization of C black, props. *(Japanese)* 79−66192
SiC, thermal oxide layers, AES depth-profiling anal. 79−43454
SiC-SiO_2 interface, Auger anal. 78−95375
$SiCl_4$ hydrolysis and oxidation kinetics for graded-index fibre vapour phase axial deposition 80−48477
$SiCl_4$, oxidation kinetics 78−92380
$SiCl_4+O_2$ in modified CVD process for optical fibre prod., reaction IR spectra 78−80472
SiH_4, low temp. oxidation, film growth rates, IR absorption spectra 80−15399
SiH_4, props. of film obtained by oxidising in HF gas discharge plasma 77−11804
Si_3N_4, effect of Al on oxidation behaviour *(German)* 78−31587
Si_3N_4 film, thermal oxidation rate and masking effect against Si oxidation 78−64749
Si_3N_4 films, struct. and oxidation characts. 80−54545
Si_3N_4, hot pressed, rate controlling process in oxidation 78−27659
Si_3N_4, impure, oxidation, phase equilibria 79−70045
Si_3N_4 layers produced by ion implantation, oxidation inhibition and etching 80−103374
Si_3N_4, oxidation, 1300 to 1500°C 77−8966
β- Si_3N_4, oxidation 77−56130
Si_3N_4, oxidation and hot corrosion resistance kinetics 80−25896
Si_3N_4, oxidised, with Y_2O_3 densification aid, temp. and compositional stability of $Y_6Si_6O_{21}$ 78−27664
Si_3N_4, oxidised ceramic, O_2 depth profiling using ^4He backscatt. 77−89463
Si_3N_4, pyrolytically-deposited, engng. significance 79−38746
Si_3N_4, reaction bonded, creep, internal oxidation effects 78−56701
Si_3N_4, reaction bonded, Na assisted oxidation, exam. 78−56795
Si_3N_4, reaction sintered, time depend. strength degradation 79−29235
Si_3N_4, reaction-bonded, added oxides effect on strength after oxidation 79−39012
Si_3N_4, reaction-bonded, gaseous boundary layer influence on oxidation at 1400°C 79−24638
Si_3N_4, reaction-bonded, internal oxidation processes role in high-temp. mech. props. 79−38915
Si_3N_4, reaction-bonded, Na ion assisted oxidation, 800 to 1300°C 79−39011
Si_3N_4, reaction-sintered, effect of oxidation on thermal diffusivity 79−86933
Si_3N_4, synthesis and props. of shapes 79−47650
Si_3N_4, thin sheets, reaction sintered, exam. of oxidation in damp air 78−48552
Si_3N_4, Zr-based hot pressing aids effect on oxidation resist. 77−8971
Si_3N_4:C film struct., oxidation, defects 79−51455
Si_3N_4/ZrO_2, hot-pressed, compressive surface stresses developed by oxidation induced phase change 80−60992
Si_3N_4-CeO_2, surface stress development during oxidation 80−50736
Si_3N_4-CeO_2 additive, hot-pressing and oxidation behaviour 80−71618
Si_3N_4-MgO, compressive creep, oxidation induced compositional change 80−50676
Si_3N_4-MgO, hot pressed, oxidation kinetics 79−29243
Si_3N_4-SiO_2-MgO, phase relations and interrelation with mech. strength, and oxidation 78−48386
Si_3N_4-Y_2O_3, hot-pressed, oxidation kinetics 80−16520
Si_3N_4-Y_2O_3 ceramic, thermal degradation, C impurity effect 80−50708

oxidation continued
Si_2N_2O, sintered with MgO or BeO additives, effect on oxidation *(French)* 79−20233
SiO_2 film, CVD on GaAs using tetraethoxysilane oxidation 78−60582
SiO_2 film, effect of oxidation on dielec. strength 77−16249
SiO_2 film deposition by SiH_4 oxidation, kinetics and physicochemical model 79−42419
SiO_2 film on Si, negative bias instability 78−91773
SiO_2 films, DC plasma Si anodisation, dielectric const., O_2 pressure influence 80−70564
SiO_2 films, on Si, role of H_2 79−69376
SiO_2 films, produced by thermal oxidation of Si, control of oxide defects 77−20477
SiO_2 films, vac. thermal evaporation, parameter stabilisation 80−87571
SiO_2 grown anodically over Si, optical and electrophys. props. 77−72934
SiO_2 in MOS structure, Cl conc. effect on negative bias instability 77−59332
SiO_2 layer used for MOSFETs, electron trapping behaviour 80−92981
SiO_2 layers, crystallisation, structural props. rel. to annealing 78−34724
SiO_2 on Si, chem. stability of films produced by catalytic oxidation 77−86353
SiO_2, thermally grown films, thicknesses 30-600 Å, defect density meas. 80−84412
SiO_2, thin film, prep. from low-temp. oxidation of tetraisopropoxysilane, dielec. props. 77−8759
SiO_2 vitreous film on Si, defect struct. comparison with crystalline SiO_2 and Si-O bond nature 80−54557
SiO_2:B, B segregation during dry, nearly dry and wet O_2 oxidation 79−66178
SiO_2-MgO-CaO-Al_2O_3:Ce,Fe, redox equilib., expt. 80−85171
SiO_2-Si interface, Cs doped, distrib. of impurity and oxide depth 78−6395
SiO_x ultrathin oxide on Si, struct. obs. by high-resolution electron microscopy 80−103592
$Si_lO_mN_p$, CVD from SiH_4-CO_2-NH_3-H_2 system, physicochem. props. 78−38978
SiP, deterioration in air, product identification 77−36675
Si(111), ion-bombard., O_2 adsorption, SIMS study 80−70522
Si(111), water vap. and O_2 interactions, EELS 78−14571
Si(111)2×1, oxide layer, surface states detec., optical reflectivity obs. 80−50368
$SmCo_5$, powder, exam. of protective preps. of organic media against oxidation 79−96220
$SmCo_5$ spheres, exam. of sintering in vacuum and Ar atmospheres 78−84738
Sn, (100) surface, clean and O_2 exposed, slow positron studies, positronium formation 80−93429
Sn, anodic behaviour in neutral phosphate soln. 79−96187
Sn, clean and oxidised, Auger spectra expt., fine structure anal. 80−29831
Sn, electron inelsatic MFP from photoionisation cross sections and ang. var. studies 77−66572
Sn gas phase reactions with oxidisers, visible chem. laser development 79−948
Sn, metallic thin film, oxidation mechanism, depth selective Mossbauer spectroscopy method 78−35549
Sn mixed oxide film formation and meas. 77−77622
Sn, oxidation, exam. by ESCA 78−72920
Sn, oxidation kinetics, in high-temp. fast flow reactor, chemiluminesc. titration meas. 77−48623
Sn-Ni equiatomic electrodeposited alloy, surface comp. 78−47649
Sn-O system, amorphous, characterisation by appl. of Mossbauer effect 79−61283
Sn-SnO_4-Sn junctions, oxide growth, tunnelling characts. 79−47173
Sn-SnO_x-Sn tunnelling junctions, fabrication by modified RF plasma oxidation method 80−103787
Sn+N_2O, oxidation chemiluminesc., quenching kinetics 79−52672
SnO, population inversion of electronic levels by oxidation, visible emission 78−13697
SnO, produced in Sn+$N_2O(O_2)(O)$ reactions, kinetics of chemilum. emitter form. and quenching 78−63107
SnO_2, two-step deposition process using DC sputtering and oxidation, and characterisation 78−95691
$Sn_{1-x}Pb_xSe(Te)$ films, rel. to annealing temp. and time, Mossbauer spectra, X-ray and microstruct. obs. 80−104311
$Sn_{1-x}Pb_xSe(Te)$ thin films, resistance to oxidation, Mossbauer study 80−39986
$SnS(Se)(Te)(S_2)(Se_2)$, oxidation, thermal decomp., Mossbauer spectra 79−11713
SnTe, film, heat treatment in air, effect on struct., props. 79−11037
SnTe, mechanochem. and thermal oxidation comparison, Mossbauer obs. 80−104310
SnTe surfaces, oxidation in air and thermal desorption, XPS and LEED meas. 79−47830
$Sn(4^3P_0)+O_2(Cl_2)(COS)(N_2O)(NO_2)(NO+Ar)$ oxidation reacts., gas phase, kinetics 78−92468
Sr, oxidation, SXAPS 77−73189
$SrB_{12}H_{12}.10H_2O$, struct. dehydration, intermediate phases and thermooxidative degradation 80−33951
SrF_2-UF_4-CeF_3 solid soln., surface degradation, complex admittance analysis 78−55980
$SrTiO_3$ surface, oxidation and reduction by D_2O, $H_2{}^{18}O$, D_2, isotope exchange study 80−104461
Sr_xVO_2, oxygen vanadium bronze, phase comp., heating in air 77−40417
T, kinetics of oxidation in water vapour, comparison with Ti-6Al-4V 77−21321
T, metal and alloys, mechanical props., electrochemistry, oxidation and corrosion resist., conference, Nantes, France (Nov. 1978) 80−41932
T removal from air streams of reactors by catalytic oxidation and water adsorption 77−50292
$TABe_{12}$, by diffusion saturation in vacuum, resistance to heat 78−44259
Ta film, optical const. var. with struct., ellipsometric meas. 77−63478
Ta film, oxidation in ambient conditions, resist. and ellipsometric meas. 79−34209
Ta film on GaAs, form. of Ta_2O_5 after oxidation 79−61769
Ta foil, electron bombardment effects on surface composition, Auger spectroscopy, electron desorption measurements 79−77874
Ta, formation of Ta_2O_5 on GaAs, interface props. 80−49935
Ta, nonstationary heating and oxidation in low temp. plasma flow, heat and charge transfer obs. *(Russian)* 80−104341

oxidation continued
Ta on Nb duplex layers, cation-transport processes during anodic oxidation, Rutherford backscatt. and nucl. microanal. 79−20264
Ta, oxidation comparison with O_2 adsorption, SIMS 78−15273
Ta, oxidation in O_2-N_2 and O_2-inert gas mixtures 78−3255
Ta, sputtered layer, thermal oxidation, reaction kinetics 78−39959
Ta-8W-2Hf wt.% (t-111) alloy, dissolution kinetics of small amounts oxygen, internal oxide disp. reactions, annealing 77−16612
TaC surface, effect of C oxidation on work function, 1250-2000K, AES 79−24054
TaC-Ni(-W) alloys, oxidation resistance 77−60000
TaN, sputtered thin films, cross-sectional composition by SIMS, elec. resist. calcs. 79−77953
Ta_2N, and TaN_x, films, thermal oxidation and resist. 80−60125
Ta_2N, sputtered layer, thermal oxidation, reaction kinetics 78−39959
TaO_n, combined SIMS, AES and XPS investigation 79−33199
$2Ta_2O_3$ thin film, FCC cell struct. investigation 80−92796
Ta_2O_5, reactive DC sputtering deposited films with magnetron-plasmatron, mechanical elec., optical props. 80−25566
Ta_xO_y on Ta, anodic film, electrochem. reactions by tunnel current 77−81340
$TaSi_2$ films, on polycrystalline Si, oxidation characts. 80−97602
Te, film, AES, LEED, XPS, energy loss spectra studies oxidation effects 78−73086
Te film, stability in moist air, rel. to information storage capability, atmospheric corrosion model 80−71774
Th (111), struct., Debye temp., and oxidation, LEED and AES obs. 77−89625
Th, O_2 adsorpt., and oxidation, electron-induced luminesc. expts. 78−38946
$(Ti,Cr)B_2$, sintering kinetics and props. 80−100811
Ti, 300-1250°C, TiO_2 films X-ray diffr. 79−11730
Ti (0001) surface, oxidation, LEED and AES meas. 77−31851
Ti alloy, high temp., NaCl-induced accelerated oxidation 77−21322
Ti alloy, mechanical props. at high temp., effect of Pt ion plating 79−29156
Ti alloy, $TA6V_4$, oxidation mechanism determ. at high temp. *(French)* 77−21312
Ti alloys, AT3 and AT6, tensile props. prolonged oxidation effects 78−85050
Ti alloys, oxidation resist, 400 to 800°C 80−50768
Ti, anodic film structure, intensiostatically formed, pH and current density influence, TEM study *(French)* 79−66217
Ti, antifriction props. 77−90467
Ti, clean and oxidised surfaces, refl., 2-25 eV 80−55123
Ti, conference, Rennes, France (Nov. 1976) 78−23857
Ti, corrosion by O_2 containing H_2O and gaseous NaCl, volatile products 78−27674
Ti, crevice corrosion in NaCl soln., 100 to 250°C *(Japanese)* 78−72927
α-Ti, diffusion of O_2, 700 to 950°C, lattice parameter and microhardness meas. *(French)* 79−86929
Ti, ESCA and UPS meas., core levels 77−63542
Ti, ESCA obs. *(French)* 77−36361
Ti, exam. of oxidation kinetics, and oxide film structure 78−56822
Ti film, chemisorption of O_2 and CO, quartz cryst. microbalance obs. of O/Ti and CO/Ti atom ratios 79−4475
Ti film, effect of surface and bulk oxidation on charact. electron energy loss spectra *(French)* 78−39641
Ti film, electrochemical oxidation, AES, XPS and electrochem. characterisation 78−7086
Ti, film electrode, oxidation, electrochem. and surface analytical characterisation 79−39034
Ti foil electrolytic perforation, surface film phase composition obs. *(Russian)* 80−61004
Ti, for thin oxide film, optical consts. determ. by ellipsometric method *(Russian)* 77−81164
Ti, heat- mass- and charge-transfer in high temp. oxidation 79−83369
Ti, hydriding, surface condition and environment influence 80−35380
Ti, in Ar-O plasma, effect of oxidation on reactive sputtering rate 77−24955
Ti, interaction with O_2, resist. and work function changes obs. 80−45431
Ti, ion implantation, comparison with thermal oxidation of Zr 77−8976
Ti, monolayer, oxidation, quasisimultaneous SIMS, AES, XPS 78−72919
α-Ti, O_2 diffusion from oxide surface layer, chem. anal. by nucl. reaction *(French)* 79−7710
Ti oxidation, high temp., exam. and comparative study with Ti-Cu, Ti-Ni oxidation *(French)* 79−20285
Ti, oxidation, linear, O diffusion coeff. depend. on rutile layer struct. *(French)* 80−104328
Ti, oxidation behaviour in high temp. steam after heat treatments *(Japanese)* 78−48565
Ti, oxidation behaviour under pure O_2 atmos., temp. range 600-800°C 80−89415
Ti, oxidation by water vapour *(French)* 78−76787
Ti oxidation in air, scanning electron microscope meas. 79−61794
Ti, oxidation in monolayer range, SIMS, AES and XPS meas. 77−86215
α-Ti, oxidation in O_2 atmosphere, role of oxide layer and mechanism of oxidation *(French)* 78−23859
Ti, oxidation kinetics in water vapour-Ar ambient mixtures 77−90498
Ti, oxidation under hydrothermal cond. to produce brookite *(Japanese)* 80−35433
Ti, oxide film form. during thermal treatment, morphological and struct. study *(French)* 80−50766
Ti, oxide layer form. in acid soln., electrochem. and optical props. 78−48560
Ti, oxide layer growth by dry oxidation at 25°C, ESCA obs. *(French)* 80−45434
Ti, passive surface, anodic process kinetics 79−15861
Ti, sintered, fatigue strength, oxidation effect 79−96137
Ti, XPS exam. *(French)* 78−23858
Ti-6Al-4V, kinetics of oxidation in water vapour, comparison with pure Ti 77−21321
Ti-Al alloy thin film, anodic voltage-time dependence obs. *(Polish)* 80−55574
Ti-Al-Sn-Zr, Ti-680, O contamination under high temp. *(Chinese)* 80−66688
Ti-Al-Sn-Zr-Mo-Si (6, 2, 4, 2, 0.1 wt.%), effect of elevated temperature and environment on fatigue crack growth 80−40486
Ti-Al-V, oxidation by water vapour *(French)* 78−76787

oxidation continued
Ti-Al-V (6, 4 wt.%), high temp. cyclic oxidation, AE monitoring 79−83413
Ti-Al-V (6, 4 wt.%) effect of high temp. oxidation on eddy current conductivity 78−76770
Ti-Al-Zr, TA6Zr5D, oxidation at high temp. *(French)* 78−23860
Ti-coated C steel, effect of heat treatment on struct. and props. 77−56159
Ti-Cu (Ni), oxidation, high temp., comparative study with Ti *(French)* 79−20285
Ti-Cu thin films, oxidation kinetics in air at 100 to 300°C, meas. 80−40590
Ti-Fe(Co)(Ni)(Cu) alloys, oxidation of intermetallic phases 79−100298
Ti-Nb (4.32 wt%), high temp. oxidation kinetics under 1 bar pressure, 1255-1471K 80−89410
Ti-Nb system, high-temp. oxidation *(Russian)* 79−74301
Ti-Ni, passive surface, anodic process kinetics 79−15861
Ti-O system, nonstoichiometry between Ti_3O_5 and TiO_2 comps. at high temps. 77−15594
Ti-Pd, crevice corrosion in NaCl soln., 100 to 250°C *(Japanese)* 78−72927
Ti-Ta (4.37 wt%), oxidation kinetics, 1258-1473K, and at pressure of 0.013, 0.133 and 1.0 bar 80−89411
$Ti+O_2$ reaction, surface chemiluminesc. study 80−55708
Ti_3Al, Cu, Fe, Mo (1 at.%) additions, oxidation resistance, 700 to 800 degrees C 77−12744
$Ti_3Al(Sn)$, oxidation *(Russian)* 78−19939
TiB_2, electric arc melting prep. and oxidation props. 80−20860
TiB_2-$TiSi_2$ composites, high-temp. oxidation, scale comp. 78−155€1
TiC, oxidation at various O_2 pressures 79−96172
TiC reactively sputtered coatings on Ni-Cr-Mo-Ti (19,11,3 wt.%), adherence, XPES and wear study 80−25565
TiC sputtered coatings on Ti-Al-V (6,4 wt.%), adherence, XPES and wear study 80−25565
TiC-Fe-Cr powder mixture, exam. of milling condition effects 80−16237
TiC_xO_y, oxidation mechanism 77−86200
TiH_x film electrode, oxidation, electrochem. and surface analytical characterisation 79−39034
TiN, from high-temp. reaction of NH_3 and $TiCl_4$, physicochem. props. 80−55334
TiN, synthesised in SHF discharge plasma, exam. of props. *(Russian)* 80−7524
$TiN_{0.91}$ plates, oxidation kinetics *(French)* 78−85199
TiN_x, oxidation in oxygen, of plates 79−61766
TiN_x, oxidation mechanism 80−25912
TiO 77−90472
TiO_2 brookite synthesis from Ti in NaF or Ti compounds, form. mechanism *(Japanese)* 80−93529
TiO_2, chemisorption of O_2 and H_2O, electron stimulated desorption, AES and charact. loss spectra 78−22963
n-TiO_2 electrode, photo-oxidation of acetate and iodide 80−81331
n-TiO_2 electrode in $AlCl_3$-NaCl melt, electrochem. and photoelec. props. 80−81328
TiO_2, metal-TiO_2-Si structure, I-V characteristics, deposition, post-deposition oxidation effects 78−80063
TiO_2, plasmochemical synthesis, oxidised from metals, exam. of props. 80−2984
TiO_2, reactive DC sputtering deposited films with magnetron-plasmatron, mechanical elec., optical props. 80−25566
TiO_2, reactive- and chemical-sputter deposition from Ti and TiC target 79−100051
TiO_2-Sb_2O_3 system, phase comp. of roasted coprecipitates 78−23651
Tl_2TeO_3, $Tl_2Te_3O_7$, $Tl_2Te_2O_5$, Tl_2TeO_6, Tl_6TeO_{12}, synthesis, thermal stability, crystallographic data *(French)* 78−51518
(U,Pu)C, controlled oxidation for head-end step reprocessing 80−5308
$(U,Pu)O_2$ (30 wt.%), oxidation behaviour 79−66210
$(U,Pu)O_2$, oxidation rates 80−37557
U, AES and loss spectra, changes on oxidation 77−20965
U, foil and powder, oxidation kinetics in CO_2, 375 to 602°C 77−50240
U, oxidation in air and CO_2, Al content effect 77−50236
U-Nb (4.5 wt.%), correlation between oxidation and stress corrosion cracking 79−20253
UO_2, ionisation potential, cohesive, electronic and redox props. 79−47916
UO_2, irradiated, T loss during oxidative processing in air 79−97831
UO_2, non-stoichiometric, oxidation reactions and dopants 79−42087
UO_2, oxidation effects in CANDU spent fuel storage canister 77−6539
UO_2, oxidation rates 80−37557
UO_2 pellet surfaces, β-$UO_{2.33}$ formation in air at 229 to 275°C, X-ray diffr. study 80−35362
UO_2, polycrystalline, oxidation in air at room temp. 77−23206
U_3O_8, radioiodine release in O_2 and inert gas atm., chem. identities 77−57712
U_3O_8, oxidation rates 80−37557
$U_{0.75}Pu_{0.25}O_{2-x}$, variation in O_2 potential with simulated burnup 78−70597
USb, UPS and XPS, surface oxidation 80−7465
V alloys, strengthening in internal oxidation *(Japanese)* 78−11493
V foil, air-oxidised, reversible switching, mechanism determ. 79−28387
V, oxidation during energetic particle irrad., influence of reactive gases on sputtering and secondary ion emission 78−72656
V, oxidation in low press. O_2 at high temp. *(Japanese)* 80−71807
V, oxidised in air during laser irradiation, switching effect *(Russian)* 80−24977
V surface interaction with O_2, H_2, H_2+O_2 and H_2O, SIMS, EID 77−62753
V, to form VO_2, ionic cond. 79−51299
V-Mn-O system, phase comp. during oxide prep. 78−27447
V-Nb-Mo(Cr), corrosion in liquid Na, O_2 effects 77−8987
V-Si, strengthening by internal oxidation 80−55424
V-Ti (20wt.%), corrosion in liquid Na, O_2 effects 77−8987
V-Zr, strengthening by internal oxidation 80−55424
$V+O_2(NO_2)$, oxidation, VO chemiluminesc. 77−9077
V_2O_5 and lower oxides, defect structures and related props., review 80−59454
V_2O_5 and lower oxides, electronic, optical, structural and surface props., review 80−88120
$V_6O_{13}+O_2=3V_2O_5$, reaction enthalpy, entropy, from O_2 vapour press. above V_2O_{5-x} 79−16029
$(V_2O_5)_{0.93}(MoO_3)_{0.07}$ solid soln., struct. transform. in oxidizing and reducing gas atm. 79−23740

oxidation continued
W (100), chemisorpt. of O_2, LEED, electron energy loss, desorption and work function obs. 77−55451
W (100), oxide layer prep., electron stimulated desorption of O^+ from WO_3 79−23840
W, anodic oxidation, effect of electrostriction, ellipsometry meas. 78−92394
W, chemisorption of O_2, initial oxidation, reaction probability 78−15700
W, clean and oxidised, mol. binding states of SiO 79−7750
W, contact interaction between oxide film and graphite, interference effect *(Russian)* 79−11721
W fibre reinforced Ni composite, study at high temp. in O_2 and combustion gases 77−48567
W film, carbonisation and oxidation, electron diffr. exam. *(Russian)* 77−44399
W foil, electron bombardment effects on surface composition, Auger spectroscopy, electron desorption measurements 79−77874
W, oxidation, WO_3 amorphous anodic film growth in acidic soln. 80−81232
W, oxidation during energetic particle irrad., influence of reactive gases on sputtering and secondary ion emission 78−72656
W oxidation in flow conditions at 1000 to 6000K 78−11445
W, oxidation mechanism, 773 to 973K 80−108644
W, surface oxide softening in single crystals 78−95860
W surface wetting by liquid Cu depend. on preliminary surface treatment *(Russian)* 80−35388
W, thermal and anodic oxidation, production of WO_3 layer semiconductor electrode 80−35544
W-Al_2O_3 cermet films, oxide evaporation deposited on Mo, Ti, Al_2O_3 substrates, struct., props. 80−25581
W-Cu-(Ti)(Zr), exam. of mech. props. as function of temp., composition, and oxidation props. 80−16472
W-O system, surface elect. cond. of oxides in equilib. with gas phase 79−61791
W-O-Br system, appl. of mass transfer model of halogen doped incandescent lamps 77−32832
W_2B_5-based alloys, mech. props., rel. to appl. as electrodes in electrospark machining 80−21174
WC, plasma sprayed coating 78−68835
WC-Co, composition and oxidation resistance of coatings deposited by thermal diffusion, using TiB_2 *(Bulgarian)* 80−45430
WC-Co, phase comp. and oxidation resist. of coatings deposited by thermal diffusion using TiB_2 80−21173
W_2C, oriented struct. transform. to W, FEM and TEM obs. 80−30124
WO_2, nonstoichiometric, surface oxidation, XPS meas. 77−48307
WS_2 solid lubricant, antifriction and elec. props. depend. on oxidation temp., dopant influence 80−108584
WSi_2 film, FET gate electrode, oxidation mechanism, SiO_2 overlayer formation 78−76773
WSi_2, sputtered, props. for MOS IC appl. 80−70831
WSi_2 sputtered film on Si and SiO_2 substrate, thermal oxidation kinetics 80−3208
WSi_2, steam-oxidized, Auger sputter profiling studies 80−107663
Y-Si-Al-O-N ceramic, phase assemblages, relationships with props. 80−60848
$Y+O_2(NO_2)(N_2O)(O_3)$, oxidation, single collision chemiluminesc. 77−25267
$YCrO_3$-Cr (40 wt.%) cermet, effect of Cr preoxidation on props. 79−87603
YIG:Ca, epilayer, reversible oxidation, ferromag. reson. 78−76781
YIG:Ca, oxidising effects of high temp. annealing in reducing atmosphere 80−66696
(Zn,Cd)S:Cu,Al, luminesc. efficiency deterioration due to surface oxidation by $(NH_4)_2Cr_2O_7$ thermal decomp. 80−29810
Zn (0001), oxide film growth, at. and electronic struct. 78−15587
Zn (0001) surface, interaction with water, UPS meas. 78−76585
Zn, interaction with O_2, evolution of O-derived struct., UPS study 79−100296
Zn, $L_{2,3}M_{4,5}M_{4,5}$ Auger spectra, solid state and oxidation effects 77−63501
Zn, MVV Auger spectra, line shape relax. energies 77−73195
Zn, oxidation kinetics in O_2-CO_2-SO_2 gas mixture rel. to elec. cond. of ZnO 80−34448
Zn surface oxidation, 78-493K, kinetics 78−64886
Zn, surface oxidation, Auger spectrosc. obs. 80−97388
Zn-salt, molten system, separation of Hf and Zr 80−11884
Zn-Te-O, partial pressure diagrams 77−36681
$ZnFe_2O_4$-Fe_3O_4 solid solns., form. of α-Fe_2O_3 during oxidation 80−25889
ZnO $10\bar{1}0$ surface, reaction of O_2, AES, LEED, EPR, desorpt., surface cond. and work function expts. 78−95950
ZnO electrode, role of triplet states in xanthene dye sensitisation 78−76869
ZnO film, surface react. of adsorbed O_2, adsorpt. logarithmic law 79−42392
ZnO, plasmochemical synthesis, oxidised from metals, exam. of props. 80−2984
ZnS evaporated film, refl. loss on UV irrad., ZnO form. 80−99813
ZnS, oxidation in fluidised bed 77−4929
ZnS, superficial degradation in air and water, XPS obs. *(French)* 80−89110
ZnS:Ag, luminesc. efficiency deterioration due to surface oxidation by $(NH_4)_2Cr_2O_7$ thermal decomp. 80−29810
ZnS(Se)(Te), clean and oxidised surfaces, O_2 sticking coeff., ionicity effects, XPS expts. 77−85887
ZnSe, oxidation by atmos. O_2 and SeO_2 vapour 77−52520
ZnSe pulses and single crystals, oxidation in air 77−12724
ZnSe(Te), clean and oxidised surfaces, surface states, low-energy EELS study 80−11522
ZnSe(100) surface, anomalous oxidation props. 78−15558
ZnTe (110) and (111) surfaces, O_2 adsorption, electron energy loss and Auger spectra 79−47568
ZnTe clean and adsorbed O_2 (110) surfaces, UV photoemission spectra *(Japanese)* 80−93456
$ZnTeO_3$, oxidation, X-ray powder anal. *(French)* 80−15080
Zr alloys with Fe, Cu, Cr, Nb role of oxide plasticity in oxidation behaviour 77−36680
Zr, anodic oxidation, ionic incorporation 79−57160
Zr anodic oxidation in 0.05 M Na_2SO_4 electrolyte 79−57144
Zr, breakaway oxidation at 573K, SEM study 79−74305
Zr, breakaway oxidation kinetics at 623K, SEM study 80−97633

oxidation continued
Zr, heat- mass- and charge-transfer in high temp. oxidation 79−83369
Zr, integral emittance, during high temp. heating and oxidation *(Russian)* 80−39327
Zr, ion implantation, comparison with thermal oxidation of Ti 77−8976
Zr, ion-implanted polycryst., thermal oxidation 80−71786
Zr, microstructure exam. by electron microscopy, oxide film appl. 79−70243
Zr oxidation in flow conditions at 1000 to 6000K 78−11445
α-Zr, oxidation in O_2-N_2 atmospheres 80−104353
Zr, oxide film texture determ., corrosion in air and water vapour 77−56163
Zr-Fe(Co)(Ni)(Cu), alloys, oxidation of intermetallic phases 79−100298
Zr-Hf (2.2 wt.%), high temp. oxidation in flowing O_2, 873-1173K 80−93687
Zr-Hf (2.2 wt.%), oxidation kinetics in flowing CO_2, 873 to 1173K 80−16596
Zr-Hf (2.2 wt.%), oxidation kinetics in flowing CO_2 at high temp. 80−47575
Zr-Nb (2.25 wt.%), oxidation kinetics in flowing CO_2, 873 to 1173K 80−16596
Zr-Nb (2.5 wt.%), cold worked, in reactor oxidation of crevices and cracks 78−23865
Zr-Nb (2.5 wt.%), high temp. oxidation in flowing O_2, 873-1173K 80−93687
Zr-Nb (2.5 wt.%), oxidation kinetics appl. to loss of coolant accidents, data review 78−19958
Zr-Nb (2.5 wt.%) alloys, microstruct investigation by electron microscopy using oxide films 79−70243
Zr-Nb (2.5 wt.%) neutron effects on oxidation kinetics 78−690
Zr-Nb-Sn (3.0, 1.0 wt.%), oxidation kinetics in flowing CO_2, 873 to 1173K 80−16596
Zr-Nb-Sn (3.0, 1.0 wt.%), high temp. oxidation in flowing O_2, 873-1173K 80−93687
Zr-Nb-Sn(3 wt.%, 1 wt.%) 80−47575
Zr-Nb(2.5 wt.%), oxidation kinetics in flowing CO_2 at high temp. 80−47575
Zr-Nb(2.5 wt.%) alloy, effect of pre-irradiation on oxidation 78−88580
Zr-Ni, surface layer, segregation of ferromag. Ni, magnetooptic investigation 80−2256
Zr-Ni-H_x(x=2.8 to 3), surface layer, segregation of ferromag. Ni, magnetooptic investigation 80−2256
Zr-Sn, oxide film texture determ., corrosion in air and water vapour 77−56163
Zr-Sn, Zircaloy-2 and 4, high temp. oxidation in steam 78−80676
Zr-Ti, oxide film texture determ., corrosion in air and water vapour 77−56163
Zr_3Al, ordered, oxidation, weight gain and metallography 80−89398
ZrB_2, electric arc melting prep. and oxidation props. 80−20860
ZrB_2, oxidation in O_2 atmosphere, exam. 80−11814
ZrB_2, prod., oxidation rate, corrosion resistance 77−52274
ZrB_2-SiC-C(-V)(-Nb), refractory cermet, hot pressing and oxidation resist. 80−3231
ZrB_2-TiB_2 solid solns., prod., oxidation rate corrosion resist. 77−52274
Zr(C,N), coating on Zr substrate, oxidation by water vap., kinetics, 0.2-20 torr, 500-600°C *(French)* 78−44266
ZrC_xN_{1-x} coating, on Zr, oxidation kinetics, 450-600°C 50-400 Torr O_2 press. *(French)* 77−25171
ZrN coating, on Zr, oxidation kinetics, 550-700°C, 50-500 Torr O_2 press. *(French)* 77−25170
ZrN, coating on Zr substrate, oxidation by water vap., kinetics, 0.2-20 torr, 550-700°C *(French)* 78−44266
ZrO_2 coatings, prod. by low-temp. oxidation, props. 78−23856
ZrO_2 films on Zr alloys, model of stress distrib. 79−49694
ZrO_2-CeO_2, semiconducting ceramics, electronic conductivity and oxido-reduction *(French)* 78−26919
ZrO_2-Y_2O_3-Nd_2O_3, high-temp. thermophys. props. 78−26663
$ZrSi/ZrSi_2$ coating on Ar, exam. of oxidation behaviour by O_2, H_2O *(French)* 79−20284

oxide coated cathodes
see also thermionic electron emission
arc-cathode emitting sites, effect of Cu-oxide thickness, obs. 77−55190
cathode emission theory using semiconductor theory, Ebers-Moll eqn. *(German)* 78−95646
electrical conductivity of coating, temp. and porosity effects 78−11062
electron velocity and energy variance in elec. field 78−88402
elementary discharge of the electric arc at slightly oxidated cathode *(Polish)* 80−19663
emission local nonuniformities, electron energy distribution, film conduct. 77−20978
ionisation gauges, heated cathodes, emission characteristics, selection *(German)* 80−236
joule heating in emitting sites on various nonrefractory arc cathodes 80−100106
magnetically deflected arcs, forward and retrograde motion, cathode oxide film effects 78−87576
oxide-cathode emission anal. by semiconductor theory *(German)* 78−88401
rare earth oxide, work function, influence of surface and bulk effects 78−11065
steel, mild, cathode arc craters, oxide thickness effects meas. *(German)* 78−38558
steel, mild, phosphate pickled, behaviour during deep electrolytical water enrichment, T meas. 80−93764
steel, stainless, cathode arc craters, oxide thickness effects meas. *(German)* 78−38558
Al, cold, vapour deposited, for He-Ne lasers, performance improvement by Cu addition 80−5748
$BaCO_3$-$SrCO_3$-$CaCO_3$, phase inhomogeneity effects on oxide cathode props. 78−52614
BaO, epitaxial, on Ir, low energy electron spectra, electron affinity, conduction band edge position 78−14790
BaO, on W cathode, struct. transforms., LEED obs. 78−11061
BaO-Ba coated cathode, role of surface donor centres 78−11063
(BaSrCa)O, cathodes, thermionic emission characts., X-ray struct. obs. 78−48270
(BaSr)O on Ni, oxide thickness depend. of emission 77−48299
Cu, arc cathode, erosion rates, SEM expts. 77−55185
Cu arc cathode with 100 nm thick oxide film, energy balance components 77−39481

oxide coated cathodes continued
Cu cathode with oxide film, emitting site lifetimes and current densities, meas. 77−27761
Cu cold cathode arc craters, oxide thickness effects meas. *(German)* 78−38558
In_2O_3 additions, effect on emissive props. 77−48298
Ni, Medicus matrix cathode, surface characts. 80−66378
$SrCO_3$, $NiCO_3$ impurity effect on dissoc. 78−27425

oxygen
see also nuclei with .....
^{16}O conc. profiles anal., using (d,p) and (d,α) reactions with mag. spectrom. 79−5215
$\delta^{18}O$, variations in snow on Devon Island ice cap, NWT, Canada 80−4050
absorbed layer on W, $Ar^+(Ar^{+,m})(Ar^2su+)$ impact, electron emission obs. 80−60740
absorption by liquid Co, Fe and Ni 78−51686
absorption in molten Cu, kinetics, influence of surface tension-driven flow effect 78−6199
abundance in B-type stars in associations and general field 80−67702
abundance in galaxies 80−8686
abundance in H II regions 80−46680
accelerated atom+O_2, chemiionisation, crossed beam obs. 77−9085
accumulation, in Au-Si contacts, determ. by SIMS, nuclear reaction and Rutherford backscatt. anal. 79−4482
acetylene+O_2 detonation products, enhancement of CO laser gain measurements 78−33729
activation analysis by photonuclear reaction *(Japanese)* 78−76945
activity in liquid Pb and Sb from electrochem. meas. 80−55695
activity meas. in liquid Na, development of electrolytic probes 80−18550
adatom coverage on Nb surface as function of adsorption sputtering and diffusion rates 79−69354
addition to polycrystalline V, effect on strength, ductility, 4.2 to 3-400K 77−36529
adlayer effect on CO and H_2 adsorption and desorption on Fe(100) 80−71573
adsorbed, on Ag, EPR of O_2^-, rate of angular reorientation 78−72413
adsorbed, on Cu (001), core-level XPS, azimuthal anisotropy 79−19969
adsorbed c(2×2) on Cu (001), surface geometry determ. by deep-core-level XPS 80−40224
adsorbed gas, on glassy AsSe, surface cond., photocond. 78−80038
adsorbed half monolayer on W (100), surface reconstruction, struct. props. 80−44421
adsorbed layer, on W(100) and W(110), electron stimulated desorption 79−33181
adsorbed layer on Au, thermomag. effect, ferromag. props. *(Russian)* 78−64256
adsorbed layer on Cu(100), electronic props., UPS, XPS and Auger spectra 77−66088
adsorbed layer on Cu (100), ejection by ion bombard. 79−42373
adsorbed layer on graphite film, mag. susceptibility 78−43241
adsorbed layer on Ni, sputtering 77−36335
adsorbed layer on Ni {100}, crystallographic effects in low energy ion scatt., local ion-atom neutralisation 80−84377
adsorbed layer on Ni (001), angle-resolved UPS 77−40333
adsorbed layer on Ni (111) surface, bonding geometry and electronic struct. 79−77909
adsorbed layer on Si (111) surface, ion scatt. obs. 80−59810
adsorbed layer on stainless steel, low energy ion scatt. *(Japanese)* 77−1774
adsorbed layer on W (110), island size determ., response function and substrate struct., LEED meas. 79−42414
adsorbed layers, on Vycor and Grafoil substrates, mag. susceptibility as probe of restricted geometry 79−51436
adsorbed layers on graphite, heat capacity meas. 80−49511
adsorbed monolayer on Cu surface, UV-visible polarised modulation spectra obs. 78−72619
adsorbed monolayers, antiferromag. struct. obs. by neutron diffr. 77−66257
adsorbed on α-cyclodextrin surface, effects on positron annihilation 79−65952
adsorbed on Ag (110), interaction with ethylene, LEED and AES obs. 80−89520
adsorbed on Al, ang. depend. on plasma loss features in XPS 78−43987
adsorbed on Al (100), Xα-scatt. wave cluster approach 80−49851
adsorbed on Al (111), band dispersion and symmetry, photoelectron spectrosc. obs. 79−61490
adsorbed on Al (111) surface, surface struct., LEED and SEXAFS data 80−92782
adsorbed on Be, secondary ion emission, coverage dependence 80−35043
adsorbed on Be, secondary-ion emission energy depend. 80−50502
adsorbed on CdS, EPR of O radicals, temp. depend. 80−80612
adsorbed on clean metal surfaces, sputtering effects, combined analytical techniques 80−35047
adsorbed on Cu, ion-bombarded, ejected particle ang. distrib. 78−95643
adsorbed on Cu (001), Ar^+ bombarded, particle ejection, ang. depend. 80−50489
adsorbed on Cu (100), ion bombard., ejected atom energy distrib., classical trajectory calc. 79−100011
adsorbed on Cu (110), low-energy ion bombardment investigation 80−34302
adsorbed on Fe surface, effect on chem. reaction kinetics 80−55572
adsorbed on GaAs surface, EPR spectrum HFS 77−40118
adsorbed on graphite, props. calc. 80−103568
adsorbed on Ir (111), titration by CO, XPS investigation 79−91994
adsorbed on metal-sapphire interface, effect on shear strength 80−49485
adsorbed on Nb, effect on polarised Balmer radiation from scatt. H^{2+} 80−99569
adsorbed on Ni, sputtering by low energy ions 77−62758
adsorbed on Ni (001) surface, angle-resolved UV photoemission calc. 77−24927
adsorbed on Ni (100), electron ejection by metastable He atom impact 79−8217
adsorbed on Ni (100), electron stimulated desorption ion energy distrib. and surface struct. 78−75940
adsorbed on Ni (100), overlayer electronic struct. 79−47144
adsorbed on Ni (100), RHEED study 79−77912
adsorbed on Ni (110) and Ir (110), surface struct. anal. using hybridisation model 80−44423
adsorbed on Ni (111), order-disorder transition 79−82447

oxygen continued
adsorbed on Ni (111) surface, Raman spectra 79−28769
adsorbed on Ni surface, location of adsorbed atoms, surface channelling meas. 80−84373
adsorbed on PbSe, XPS and UPS obs., lattice diffusion and sticking coeff. 78−52637
adsorbed on Pd (111) surface, UPS and thermal desorpt. characts. 80−54754
adsorbed on porous Vycor glass, props. characteristic of amorphous antiferromag. obs. 78−10665
adsorbed on Pt, isotopic exchange and thermal desorption *(French)* 78−43249
adsorbed on Pt, reaction with H_2 80−49514
adsorbed on Pt, stability and struct. of high Miller index forces in vacuum and with adsorbed C and O 77−76651
adsorbed on Pt (111), chemisorbed and oxide states, low energy ion scatt. obs. 80−65372
adsorbed on Pt wire, Ne(Kr) accommodation coeff. meas., 400-1400K 77−63948
adsorbed on Re, Na ionisation, field reversal and surface ionisation expts. 77−90232
adsorbed on Ru (001), characteristic slow electron energy loss meas. 79−47562
adsorbed on Si (111) surface, electron energy loss spectroscopy 78−2374
adsorbed on Si (111) surface, UHV cleaved, electronic transitions 78−39183
adsorbed on Si surface, light sensitive electron loss meas. 79−24396
adsorbed on SiO_2 supported W, EPR evidence for surface mobility of O_2^- 78−84046
adsorbed on stepped W (100) surface, electron stimulated desorption ion ang. distribs. 80−20035
adsorbed on Ta, effect on kinetics of H_2 absorption, 77-700K 79−95169
adsorbed on W, coverage degree meas. by ion induced secondary electron emission 80−55251
adsorbed on W, surface diffusion, secondary electron emission study 80−76117
adsorbed on W(100), polycryst. W, and V, electron stimulated desorption of O^+ ions 79−99428
adsorbed on W (100), ion scatt. spectroscopy 77−73205
adsorbed on W (110), three-adatom non-pairwise interaction, Monte Carlo simulations 79−82466
adsorption, and desorption on stepped W surface 77−47675
adsorption, by noble metal film, modulated surface-plasmon reson. in situ meas. 77−77311
adsorption, effect on ion bombard. induced photon and secondary ion emission 77−90231
adsorption, ion-induced, on Cu (110) 80−54510
adsorption, jointly with Cs, on Mo (110) and (111) faces, and emission props. 78−2364
adsorption, on Ag, dielec. perm., plasma surface vibr., modulation spectroscopy 77−48198
adsorption, on Al, 80 to 290K, 10^{-6} to 10^{-2} Pa, XPS study 78−95657
adsorption, on CdS:Li film, effect on photocond. 78−34854
adsorption, on CdS, AES study *(Japanese)* 78−88008
adsorption, on Cu_5FeS_4, bornite, effect on surface struct. by AES 77−15669
adsorption, on Cu (100) single crystal surface, oxidation 80−11846
adsorption, on graphite, mag. phase transition, theory 78−38811
adsorption, on LaB_6 (100), LEED, AES, work function meas. 78−71989
adsorption, on metal, effect on sputtering-induced photon and ion emission 77−28674
adsorption, on MgO, $(O_2^-)_s$ form., thermal activation, reducing gas effects, EPR 77−9119
adsorption, on Nb, electron-stimulated desorption study 79−11017
adsorption, on Ni, photoemission intensities from core states 78−95654
adsorption, on Pt(110) surface, Ar^+ bombardment effects on reactivity 80−89099
adsorption, on Si (111), and stimulated oxidation by electronic bombardment, AES 78−14599
adsorption, on W, electron stimulated desorpt. study, 300K, kinetics, order-disorder transition 78−71985
adsorption, on W, order-disorder transition, theory 78−38811
adsorption, on WO_n, struct., rel. to catalysis 78−51826
adsorption and catalytic reactions with H_2 and CO on Pt 80−81362
adsorption and condensation on Al (111) at 30K, UPS obs. 79−60635
adsorption and desorpt. on Pt(110), thermal desorpt. LEED/AES obs. 77−72788
adsorption and dissociation on graphite, CNDO/2 calcs. 79−28206
adsorption and field-desorption on GaAs and GaP surfaces, FEM studies 80−34304
adsorption and incorporation on Cu(100) 78−56042
adsorption and migration on graphite, CNDO/2 calcs. 79−28205
adsorption and reaction with CO on IR (110), transient study 80−30284
adsorption by Fe, oxide formation, XPS/UPS obs. 77−85074
adsorption isotherm, determ. of porous texture of solids 79−77897
adsorption of Cs+O on GaAs (111) epitaxial film, ellipsometric study 80−29282
adsorption of Cu ($\bar{1}10$), low energy Ne^+ ion scatt. meas. 79−51431
adsorption of mol. O_2 species on Ag (110) surface 80−103578
adsorption of Pd (111), LEED, photoelectron spectra and thermal desorpt. expts. 77−69180
adsorption of Rh (111), thermal adsorption spectra, AES, and LEED obs. 79−51428
adsorption of SnO_2 ESR of adsorbed O species *(Japanese)* 78−10750
adsorption of ZnO film, logarithmic law 79−42392
adsorption on (111) surface, possible ordered struct. 80−44412
adsorption on Ag, isosteric heat of adsorption determ. 77−55453
adsorption on Ag, surface species identification by XPS, high press. 79−28191
adsorption on Ag(111) and polycrystalline surfaces, LEED, AES and energy loss spectra 80−34310
adsorption on Ag (110) and interaction with CO, ellipsometry-LEED expts. 78−91542
adsorption on Ag (111) ordered and damaged surfaces, CO interaction 78−14583
adsorption on Al, AES, XPS, and LEED obs. 79−46938
adsorption on Al, interatomic Auger transition spectroscopy 80−11521
adsorption on Al, intrinsic and extrinsic plasmon coupling, XPS of adsorbed atoms core states 78−10278
adsorption on Al, relation between energy-band and cluster model 78−52048

oxygen continued
adsorption on and interaction with Ni film, AES, EELS, work function, and gravimetric meas. 80−75433
adsorption on Au, Auger spectra 78−87879
adsorption on $BaTiO_3$, effect on work function and spontaneous polarisation *(Russian)* 78−6211
adsorption on $BaTiO_3$, mechanism calc. 78−63927
adsorption on CdS, effects on surface pot. *(Russian)* 77−47686
adsorption on clean annealed Mg surface, exoelectron emission 78−39671
adsorption on clean InSb (110), AES, LEED, RHEED and field effect meas. 80−49501
adsorption on cleaved Si (111) 2×1 surface, electron energy loss spectra 79−15840
adsorption on Co (0001), XPS and UPS study 79−74050
adsorption on Cr, Cu and Ni, effect on secondary negative ion emission *(Russian)* 79−28881
adsorption on Cr(111), photoemission exam. 79−19976
adsorption on Cr (100) and initial oxidation at room temp. 80−20034
adsorption on Cr (111) face, LEED and RHEED meas. *(French)* 78−39955
adsorption on Cs monolayer on Cu(111), dilution of electron gas, plasmon energy losses 79−47036
adsorption on Cs-covered GaAs (110) 80−10793
adsorption on Cu, surface struct., O_2 press.-temp. diagram *(Japanese)* 78−79884
adsorption on Cu(001) surface, deep core level XPS anisotropy 78−72690
adsorption on Cu (001) surface, effect on surface barrier, LEED study 80−84378
adsorption on Cu (100), ang. resolved AES and LEED 78−18908
adsorption on Cu (100) surface, angularly resolved UPS meas. 78−71956
adsorption on Cu (100) surface, EELS study 80−2260
adsorption on Cu (100) surface, LEED study 80−100408
adsorption on Cu (100) surface, reaction with CO 80−103583
adsorption on Cu (110), adsorbed layer reaction with CO, ellipsometry, AES, LEED study 80−6635
adsorption on Cu (110) and surface reaction with CO 80−15373
adsorption on Cu (111), surface band energy shift, angle-resolved UPS study 80−40228
adsorption on Cu (111) from 23°C to 400°C, AES, LEED and ellipsometric meas. 79−65317
adsorption on Cu (210) surface, LEED and AES meas. 78−71998
adsorption on Cu films, study of gravimetric uptake and work function 79−33179
adsorption on Cu vicinal surfaces, LEED study 80−103575
adsorption on $ErFe_2$ surface, effect studied by spin polarised photoemission 80−29854
adsorption on Fe, oxidation 80−108730
adsorption on Fe(100), adsorbate coverage determ. by LEED, AES and XPS 80−103566
adsorption on Fe (110), UPS and LEED/Auger meas. 77−72773
adsorption on Fe surface, core-level photoemission and LEED methods appl. 79−15003
adsorption on GaAs, adsorption states and Ga depletion, UPS, AES, and thermal desorption meas. 79−46952
adsorption on GaAs, photoemission expts., exciton effects 77−85055
adsorption on GaAs(Pt), surface electronic struct. (surface chem.) using synchrotron radiation 78−53254
adsorption on GaAs(Sb) and InP, surface chemistry and electronic struct., photoemission meas. using synchrotron radiation 77−20985
adsorption on GaAs (110), effect on surface electronic struct., photoemission expt. 78−43453
adsorption on GaAs (110), oxide form., XPS/UPS study 80−49497
adsorption on GaAs (110), surface photovolt. spectroscopy 80−49499
adsorption on GaAs (110) ordered and disordered surfaces, XPS meas. 80−49498
adsorption on GaAs (110) surfaces, elec. props. *(French)* 78−34690
adsorption on GaAs surface, work function and photovoltage meas. 77−1446
adsorption on GaP, monitoring by AES, electron beam effects 77−72777
adsorption on GaP, monitoring by AES, electron beam effects 78−6218
adsorption on Gd-Co, Gd-Fe amorphous films, effect on perpendicular anisotropy 80−34713
adsorption on Ge, degree of freedom of rot. and translational motion of O particles 79−23842
adsorption on Ge(111), electron-beam enhanced reaction, AES meas. 77−4256
adsorption on Ge 79−65325
adsorption on Ge (111), photoemission yield spectroscopy of electronic surface states, sticking coeff. 79−91122
adsorption on graphite, graphical determ. of entropy of adsorpt. *(French)* 77−11790
adsorption on graphite, partially localised, partially mobile monolayer films, adsorption isotherms 80−107646
adsorption on In, AES study 79−82451
adsorption on InP (110), low coverage, SIMS study 80−49500
adsorption on Ir, effect on Ir work function 77−66094
adsorption on Ir, field emission energy distrib. spectra 80−25535
adsorption on Ir, work function changes by continuous meas. method 79−33328
adsorption on Ir(110), structure of c(2×2)O overlayer 79−19463
adsorption on Ir (110), LEED obs. 79−77880
adsorption on Ir (110) surface 78−38961
adsorption on Ir and surface reaction with H_2, thermal desorption and FEM obs. 79−52774
adsorption on LaB_6, using retarding potential method in axial magnetic field 79−80719
adsorption on LaB_6 (100) surface, UPS and LEED study 80−49519
adsorption on lamellar halide, bidimensional condensation *(French)* 78−75941
adsorption on Li (100), cluster models, ab initio HF LCAO theory 78−71978
adsorption on MgO during α-irrad., thermostimulated surface cond. obs. 80−34499
adsorption on MgO powder, 77 to 150K, mol. motion anal. 78−84051
adsorption on MgO-CoO, EPR, volumetric investig. 80−10782
adsorption on Mo, effect on refl. of metastable He atoms 79−11493
adsorption on Mo, low energy SIMS and electron induced desorpt. exam. 77−76667

oxygen continued
adsorption on Mo, metastable He de-excitation spectroscopy and UPS study 80−34314
adsorption on Mo (100), AES, LEED, work function, and desorption meas. 80−6654
adsorption on MoS_2, LEED, Auger and work function meas. 78−71994
adsorption on Nb, continuous meas. of surface pot. variations using mirror electron microscope 77−47680
adsorption on Nb (110), variation in work function, retarding field and thermionic emission meas. *(French)* 79−78823
adsorption on Nb and W (100) planes, LEED-AES obs. 77−69186
adsorption on $NbSe_2$, 200-300K 78−26767
adsorption on Ni, electronic struct. and UPS 78−15281
adsorption on Ni, oxidation 80−108730
adsorption on Ni(110) surface, LEED and ion scatt. study 80−84386
adsorption on Ni(Al)(Mg), internal and external sources of electrons 77−44097
adsorption on Ni {100}, low energy ion scatt. study 80−39420
adsorption on Ni (100), combined XPS/LEED/SIMS exam. 79−83075
adsorption on Ni (100), effects on secondary electron spectra 80−50480
adsorption on Ni (100) and reduction of surface oxide by H_2 80−108741
adsorption on Ni (100) surface, surface phonons 78−2359
adsorption on Ni (110), coverage effects on surface relax., medium energy ion scatt. obs. 79−28181
adsorption on Ni (110), obs. by electron microscopy, AES and LEED *(French)* 77−62732
adsorption on Ni (111), LEED and low-energy ion scatt. investigation 79−65324
adsorption on Ni and Ag electrodes in KOH soln. 79−61871
adsorption on Ni-Fe, oxidation 80−108730
adsorption on Ni-Fe (100), LEED and XPS 79−82437
adsorption on PbS (100) surface, electronic struct., UPS study 80−54756
adsorption on PbTe (111), UPS and XPS exam. 78−71962
adsorption on Pd(100) surface, obs. of O^- and O^+ during electron bombardment 79−95883
adsorption on Pd(111), mutual interactions, transient product formation with CO 78−87871
adsorption on Pd (111), UPS and thermal desorption spectra meas. 79−78833
adsorption on Pd film, reciprocal titration with H_2, film surface area determ. 77−1318
adsorption on plasma-treated SiO_2, reactivity, EPR obs. 79−51418
adsorption on polar ZnO surfaces, cond., EELS study 80−71525
adsorption on polycryst. Co, XPS and UPS *(French)* 77−36362
adsorption on polycryst. Mg at 100 and 300K, XPS, UPS, XAES 78−18906
adsorption on polycrystalline Mg, at 100 and 300K, XPS, UPS and X-ray AES meas. 78−18901
adsorption on polycrystalline Ti at room temp., UPS and XPS 77−89645
adsorption on Pt, AES, LEED and thermal desorption spectroscopy exam. 78−79891
adsorption on Pt, anal. by low energy ion scatt. *(French)* 77−59663
adsorption on Pt, surface composition, AES and temp. programmed desorption meas. 80−34313
adsorption on Pt, surface struct. depend., LEED, AES, and electron energy loss spectra 79−46934
adsorption on Pt, surface struct. effects on rate, data assessment 78−43251
adsorption on Pt, thermal desorpt. spectra 78−14607
adsorption on Pt, UV photoemission spectra 78−14608
adsorption on Pt(S)-[9(111)×(111)] face, flash desorption LEED and AES obs. 77−69182
adsorption on Pt (111), cooxidation, AES *(German)* 78−14619
adsorption on Pt (111), kinetics of interaction with H_2 77−55461
adsorption on Pt (111) and Pt(S)-12(111)×(111) surfaces, thermal desorption, AES, XPS, and LEED study 80−70534
adsorption on Pt (111) surface, UPS, EELS and thermal desorption study 80−100409
adsorption on Re, effect of struct. defects, steps and kinks 80−29269
adsorption on Re(0001), XPS, UPS and temp. programmed desorption 80−71574
adsorption on Re vicinal faces, mirror electron microscopy, LEED and AES obs. 79−65323
adsorption on reconstructed GaAs (100) surfaces, ang. resolved photoemission from surface states 80−16143
adsorption on Rh (111), AES, LEED, and thermal desorption mass spectra meas. 79−77900
adsorption on Ru ($10\bar{1}0$), oxide form., thermal desorption and ESCA obs. 79−82442
adsorption on Ru ($11\bar{2}0$), ellipsometry-LEED study 80−103570
adsorption on SbSI, effect on work function and spontaneous polarisation *(Russian)* 78−6211
adsorption on Sc and Lu surfaces, effect on reflection EELS 80−20742
adsorption on Si, surface charging during illumination, effect of various surface treatments 79−51651
adsorption on Si, UPS, new adsorption state 78−34702
adsorption on Si(111) electronic density of states changes, AES obs. 79−65528
adsorption on Si (111)7×7, reflectometric study 79−99600
adsorption on Si (111), electron energy loss spectra exam. 77−39736
adsorption on Si (111) surface, atomic steps and residual gas effects 80−54517
adsorption on Si and Ta, comparison with oxidation, SIMS 78−15273
adsorption on SiO_2, effect on EPR spectra of surface defects 80−7163
adsorption on SiO_2 gel, EPR *(Russian)* 79−52776
adsorption on SiO_2 rel. to EPR relax. time *(German)* 79−95645
adsorption on SnO_2, desorpt., ESR and cond. meas 80−10790
adsorption on SnO_2 gas sensor, effect on cond. 78−76067
adsorption on $SrTiO_3$ surface, electron energy-loss spectra obs. 80−89521
adsorption on steel in ultra-high vacuum system at room temp. 77−20188
adsorption on stepped Pt (111) surface 78−71992
adsorption on Ta, FEM obs. of work function changes 78−26771
adsorption on Ta auto-cathode, effect on emission and surface diffusion *(Russian)* 79−77892
adsorption on Th, and oxidation, electron-induced luminesc. expts. 78−38946
oxygen continued
adsorption on Ti, SIMS expts. using 500 eV primary Ar^+ ions 77−72785
adsorption on TiO_2 surface, heat cleaning, O_2^- radical form., EPR 77−35806
adsorption on U and Th, XPS study 80−7473
adsorption on vacuum-deposited Ta film photoelec. props. 78−15298
adsorption on W, Auger signal comparison using differential and integral Auger spectra 78−76561
adsorption on W, surface reflectance spectroscopy on low index planes 78−71965
adsorption on W(100), AES, desorption, LEED and work function obs. 77−1317
adsorption on W(100), effect on NVV Auger spectra, comp. to band struct. calcs. 78−72643
adsorption on W(100) surface, adsorbate density determ. 77−1320
adsorption on W(111), angle resolved electron stimulated desorption, LEED and AES 80−6645
adsorption on W (100), surface struct. and thermally stimulated reaction 77−55451
adsorption on W (100) and (110) surfaces, chemical effects in N_7 VV Auger spectra 77−32474
adsorption on W (100) with ordered C overlayer, UPS meas. 79−77907
adsorption on W (110), adatom interaction energies, Monte Carlo calc. 78−71948
adsorption on W (110), electron impact and thermal desorption at high temp. 78−30821
adsorption on W (110), mobility, 300 to 800K, field emission current meas. 79−33187
adsorption on W (110)(112) and Mo (110), work function and thermal stability 80−44427
adsorption on W (111), AES, LEED and electron stimulated desorption obs. 79−46935
adsorption on X-irrad. TiO_2, EPR meas. 78−80211
adsorption on ZnO (0001) surface, AES and refl. electron energy loss spectra 79−46927
adsorption on ZnO powder, light irrad. effects *(Japanese)* 78−95230
adsorption on ZnO surface, electron energy loss spectra meas. 78−14601
adsorption on ZnTe (110) and (111) surfaces, electron energy loss and Auger spectra 79−47568
adsorption on Zr, dissoc. and diffusion 80−80085
adsorption onto Al film 77−24486
adsorption onto Ge:Na (111) surface, work function, surface cond. changes investig. 78−79875
adsorption rate, on Ge (111) clean surface 80−59779
adsorption with La on W, work function changes *(Russian)* 77−35816
adsorption with Na on Ag (110) surface, LEED, thermal desorption and AES meas. 77−31883
adsorption-desorption kinetics on Si and Ge surfaces 77−47684
aerosol particles, size-fractionated, C, N and O determ. by particle elastic scatt. anal. 78−81466
afterglow quenching, in adsorbate phosphor-silica gel system 77−77275
alkali halide: O^{2-}, photoluminesc. spectra, phonon using struct. *(Russian)* 78−2912
alkali halide:O_2^-, frozen soln., impurity luminesc., zero-phonon lines interpretation 79−87488
alkali halide aq. solns. with O^{2-} anion impurities, luminescence spectra regularities *(Russian)* 77−69876
alkali metal:H(0), impurity investigation using residual resist. and optical absorpt. meas. 79−95816
alkali metal chloride crystal, F centre energy level shift and splitting in O^- field 80−70640
alkali metals, liquid, O_2 pot. and O_2 distrib. coeffs. between alkali and struct. metals 80−65231
Allende meteorite, O isotope anomalies 77−78724
ambient effect of precipitation in Si, self interstitial mechanisms, IR spectra, TEM study 80−66510
analysers, instrumentation and operation 78−69237
analysis, direct readout instrument 77−40606
annealing furnace O_2 gettering by NiSi or Pd_2Si 79−100160
anomalously heavy isotope, mass spectrometric search 79−81290
antiprotonic atoms of light nuclei and isotopes, p̄-n strong interaction effects 78−29867
aromatic hydrocarbons, oxygen quenching of triplet states, charge-transfer interactions 77−23516
arterial PO_2 continuous meas. 80−56240
arterial pO_2 intravascular monitoring using catheter-tip polarographic electrode *(German)* 78−85408
arteriovenous O_2 difference, noninvasive meas. method *(German)* 78−85441
artery avascular region transport analysis 77−40691
atmosphere, conc. enhancement near fires, convection-diffusion coupling model 77−7481
atmosphere, O_2 content rel. to O_3 evolution and variability over geological time 79−96788
atmosphere, O_2 level rel. to O_3 content evolution 80−98400
atmosphere, oxidation of metal selenides 77−52520
atmosphere, Phanerozoic O budget, S isotope variations in marine sulphate evaporites 77−73810
in atmosphere, photodissoc. in stratosphere and mesosphere through solar UV radiation absorpt. 80−109248
atmospheric, rot. Raman and elastic scatt. for temp. profiles 77−9515
atmospheric absorption line parameters, AFGL, compilation update 79−21013
atom, 1304 angstrom absolute emission cross section from $CO(CO_2)$ UV photodissoc. 80−32652
atom, 2^3P_2-2^3P_1 fine struct. splitting by laser mag. resonance 79−98010
atom, 2-photon excitation, cross-section calcs. 78−58641
atom, ($^1D_2$) state, quenching, rel. to O_2 $b^1\Sigma_g^+$ prod. and deactivation 80−76493
atom, (^3P_J) state, direct obs. from O_3 photolysis at 248 nm 80−101028
atom, ab initio effective valence shell Hamiltonian for neutral and ionic valence states 80−74117
atom, and 1st row ats., Compton profiles, momentum distribs., correlation effects 77−88429
atom, associative ionisation, merging beams experiment 80−63789
atom, autoionis., radiative emission, competition in excited state decay 77−75109
atom, beam-foil excited ^4P state, delayed coincidence Auger electron lifetime meas. 80−14117

oxygen continued
atom, beam-foil populations, charge state distribs., independent electron model 77−19035
atom, chemisorption on Cu, cluster theory 80−29264
atom, chemisorption on Ni, cluster theory 80−29264
atom, CNDO/S nucl. screening const. calcs. 78−86787
atom, dipole oscill. strength distribs., sums 78−21975
atom, dipole properties and dispersion energies additivity, using atoms and small mol. models 80−53091
atom, dipole transition oscill. strengths, photoionis. cross section 78−9120
atom, distrib. in lower thermosphere assuming tidal effects, one dimens. nonstationary diffusion-photochemical model 80−4160
atom, electron affinity, for two electrons, from alkali and alkaline earth oxides cohesive energies 78−25736
atom, electron affinity, modified variational approx. 78−66679
atom, electron and proton interaction cross sections 77−50538
atom, electron attachment, low energy electron elastic scatt., review of theory 77−68111
atom, electron impact excitation, close coupling expsn. 77−83740
atom, electron impact ionis., 7-1000 eV, cross-section 78−86956
atom, electron impact ionis., triple differential cross sections 79−10207
atom, electron impact ionis. cross-section, accuracy of fast at. beam method 79−81283
atom, electron impact ionisation, differential and total cross-sections 80−18935
atom, electron scatt. and photoionis., correlation effects 78−58842
atom, electron scatt. Bethe-Goldstone and pseudostate approx. 77−68112
atom, electrons effective collision freq. calc. 79−3567
atom, excitation cross section, Born approximation 77−10772
atom, far IR laser mag. reson. 78−37576
atom, fine struct. excitation by H impact 77−42384
atom, ground and excited state, laser-induced photolysis of ozone reactions 80−11928
atom, ground and excited states, atomic polarisability calc. 77−83756
atom, ground state energy, HF calc., second-order correction 78−86784
atom, ground state static polarisability and hyperpolarisability, numerical SCF method 79−36567
atom, in beam-foil system, X-ray ang. distrib. spin rot. 77−23545
atom, in upper atmosphere, electron impact cross-section 78−28398
atom, in upper atmosphere, electron impact yield spectra 78−28401
atom, intermediate coupling props., relativistic average of config. wavefunctions applicability 78−17574
atom, ionis. cross-section, accuracy of crossed at. beam method 79−81284
atom, isoelectronic sequences, energy spectra inc. relativistic corrections 78−924
atom, Kα spectrum, intensity of high energy peak as function of oxide layer thickness 80−936
atom, K-shell ionis., double and single, cross section meas. by ion bombardment 78−50629
atom, low-energy electrons elastic scatt. cross sections 78−42213
atom, low-energy electrons integral scatt. cross section 78−69556
atom, many electron autoionisation states, perturbation theory Z-expansion, numerical results 80−52863
atom, metastable ^{3}S-state, optical pumping 80−32678
atom, min. basis of Slater-transform-Preuss functions 79−59343
atom, model pots., STO calcs. 77−408
atom, ns ^3S-2p^4 $^3P_2$ transitions, far VUV, oscill. strengths 77−34580
atom, photoelectron ang. distrib. anal. branching ratios determ. 78−5181
atom, photoelectron ang. distrib. meas. 77−61721
atom, photoionisation absolute cross section 78−94218
atom, photoionisation cross sections and ang. distribs., outer p subshell 80−9572
atom, photoionisation cross sections and asymmetry parameters, SCF Xα scatt. wave calcs. 80−63542
atom, photoionisation cross-section calc., 304 and 584 Å 80−43015
atom, polarisation functions for Gaussian basis sets 78−5126
atom, pseudopotential calculations, parameter fitting scheme appls. 78−41928
atom, pseudospectral dipole oscillator strength distribs. 78−50503
atom, radiative lifetimes of visible and near IR transitions, solar abundance 78−50506
atom, SCF electron-gas local-spin-density model including correlation 80−9488
atom, spectra in Ar inductively coupled plasma 80−91473
atom, triple-dipole energy calc. using pseudo spectral theory 78−46418
atom, two-photon absorpt., auroral transition relax. obs. *(Japanese)* 80−47954
atom+1-alkyne, CO prod., vibr. population distrib., rate consts., laser reson. absorpt. technique 80−40676
atom and molecule, photoionis. and photoabsorpt. cross sections for aeronomic calcs., data tables 80−41599
atom in methane-air flame, reactions, radical overshoot 79−34308
atom in molecule, K-shell fluoresc. yield, statistical scaling 80−78644
atom or ion, sputtered from SiO_2 and oxidised Al surfaces, light emission 80−58199
atom photoionisation, electron impact calcs. using R-matrix and linear algebraic methods 79−59579
atom production and removal in DC glow discharge 79−77432
atom X-ray spectra, mass absorpt. coeffs. in ultrasoft region, spectral depend. 77−10622
atomic beam cooled micrwoave discharge source 78−5373
atomic O_2 supersonic nozzle beam source development 80−58016
atomic polarisability, effective potential approximation method 77−88587
atomic source with improved long term stability for chemiluminescence reaction, mol. dissoc. and recombination 80−93758
atoms, form. and recomb. in U-tube downstream from DC discharge 78−67333
atoms, in silicates, XPS quantitative anal. *(Japanese)* 77−48710
atoms, reactions with MgO and zeolite, EPR anal. via ultrahigh vacuum/flow system 78−7232
atoms and molecules, dispersion energy consts., dipole oscill. strength, refractivity 77−50492
attachment cooling, press. depend. 80−91663
Auger spectra, KLL O line, intensity ratios in different cpds. 79−87531
aurora, near IR O emission lines obs. 77−53272
aurora, O_2 ($^1\Delta_g$) emission, vibr. excitation process 80−82125
aurora, O I (989 Å) and O I (1027 Å) emissions 78−28367
auroral O, O_2 emission, rocket meas. and anal. 78−57380

oxygen continued
backscattering anal. appl. of ^{16}O ions *(Japanese)* 79−28871
bacterial luminescence excitation by singlet O_2 79−39340
bare nucleus+He, electron capture to excited states, X-ray cross-sections 77−71814
barley seeds, minimum γ-exposure and O_2 concs. to produce post irrad. O_2 damage enhancement 80−30779
benzene+O_2($^1\Sigma_u^-$), photo-oxidation mechanism, optoacoustic determ. 77−12808
benzene+O(^{3}P), reaction product identification by mass spectrometer 78−7185
binding to Fe-, Co-substituted myoglobins, comparisons, thermodynamic investig. 80−67030
biological tissue diffusion and reaction, Michaelis-Menten kinetic model 78−31793
biomolecular transport proteins and metabolism 79−24946
blood, O_2 diffusion, analysis of carrier facilitated transport is heterogeneous media 77−39360
blood, O_2 saturation meas. in nonhaemolized sample, by laser light *(German)* 77−44735
blood, saturation in haemoglobin, metrological problems 77−90952
blood, shear-induced augmentatin of O_2 transfer 80−94274
blood, steady state diffusion in red blood cell and model suspensions 77−40644
blood concentration measurement using P electrodes 79−20725
blood gas catheter, fast-responding, flow-independent, for O_2 meas. 80−101277
blood gas catheters, flow-dependent, in vivo calibration 79−16330
blood level in artery and vein, quantitative continuous meas. 78−40363
blood level measurement, optical continuous noninvasive method 77−2068
blood monitoring, intraarterial vs. transcutaneous monitoring in newborn infants 80−56266
blood O_2 affinity variability, automated meas. method 79−39544
blood O_2 monitoring, combined system for transcutaneous and intravascular determ. of partial press. 80−56241
blood O_2 partial pressure meas. with membrane covered probe, signal non-linearity 79−53264
blood O_2 saturation measurement, analogue electronic calculator 77−81614
blood oxygenation in complex coiled silicone rubber tubes 77−60304
blood oxygenator, stationary membrane type, O_2 and CO_2 diffusion process 77−78046
blood pO_2 meas. polarographic technique 79−100782
blowing of Martin bath, smelting dust phase comp. determ. 77−52705
boiling, press. effect on internal charact., bubble growth 77−15568
boiling point and triple point, realisation rel. to IPTS 77−105
boiling point and triple point, rel. to IPTS 77−104
bonding to Ni (100) surface 78−79889
bonding to Tokamak walls, XPS studies 80−80942
brain O_2 tension dynamics 77−36965
brain pO_2 dynamics in cerebral angiography, rel. to contrast agent neurotoxicity 78−35954
breakdown formative time lag rel. to gap geometry, pressure, and overvoltage 79−18994
breakdown potential 6.2 MHz elec. field, perpendicular mag. field, 350 G, 500 G, 0.5-8 torr 77−35422
breathing, on-line uptake meas., analogue approach 78−28134
broad beam ion source used for sputtering and etching 80−69002
bubbles, rising in water, dissolution mass transfer coeffs. 79−41737
BWR, H_2 and O_2 monitoring in containment and off-gas systems 80−32414
BWR, O_2 monitoring and control 78−25309
$c^4\Sigma_u^-$ state predissoc. calcs. 79−50095
C C O I, 5577 Å emission, plasma column dynamic and reaction processes in meteor wakes 77−82176
capacitative discharge, high-freq. gas overheating suppression 80−38856
catalytic surface activity, $LaNi_5$ surface segregation *(German)* 80−51008
cellular irradiation, repair and prolonged hypoxia 79−74721
cellular O_2 enhancement ratio, hypothesis test and microdosimetric implications 80−26212
cerebral regional O_2 distrib. model during continuous inhalation of $^{15}O_2$, $C^{15}O$ and $C^{15}O_2$ 78−65108
chemisorbed c(2×2)O on Ni (100), photoemission angle-of-incidence depend. 77−32502
chemisorbed in TTF-TCNQ and ϕ_4DTP-TCNQ, effect on mag. susceptibility 80−15679
chemisorbed on Ag film, reflectance and elec. resist. changes 80−11495
chemisorbed on Al (100), photoemission ang. depend., MO cluster model calc. 78−76576
chemisorbed on CdS, electron beam desorption, AES meas. 79−77921
chemisorbed on Cu, molecular cluster ejection on ion bombardment, model 79−87543
chemisorbed on Cu(001), Ar^+ bombardment, angle resolved SIMS, surface struct. 79−77913
chemisorbed on GaAS (110), extrinsic surface states 78−91535
chemisorbed on Hg, Ag, Pb, Ga, Fe, Pt, effect on surface props. 78−60187
chemisorbed on Ir, electron states, electron field emission 78−84704
chemisorbed on $MgCr_2O_4$, mobility of O_2 mols. 77−51595
chemisorbed on Ni, influence on surface vibrs. 80−84361
chemisorbed on Ni, ion bombard., particle ejection, SIMS obs. 79−78810
chemisorbed on Ni (001), dynamical calc. of angle-resolved UV photoemission 77−85890
chemisorbed on Ni (001) surface, angle resolved photoemission from chemisorption induced states 77−85898
chemisorbed on Ni (001) surface, electronic struct. and overlayer struct. theory 79−28391
chemisorbed on Ni (100), rapid LEED intensity meas. 80−44420
chemisorbed on Pd and Pt, catalytic activity, SCF-Xα-SW calcs. 78−15711
chemisorbed on Pt surface, reaction with CO, transient kinetics obs. 78−7229
chemisorbed on Si (111), electronic struct. tight-binding calc., XPS and UPS meas. 80−49845
chemisorbed on Si (111) surface, electron states by AES 80−54747
chemisorbed on W (110), island form. and condensation 80−49517
chemisorbed on W (110), order-disorder transform., theory compared with LEED data 79−7748

oxygen continued
chemisorbed overlayer on Al (111), angle-resolved photoemission, band struct. 80−40229
chemisorption, and coadsorpt. with Cl_2 on Ag (331) 78−34711
chemisorption, effects on LaB_6 (210) surface, XPS, UPS and LEED 80−65344
chemisorption, on Al, orbital resons., Xα cluster model calcs. 77−72774
chemisorption, on Al(111), SCF X_α scatt. wave MO calc. 79−42374
chemisorption, on Au(Pt) electrode, volume of adsorbed species, temp. and press. effects 78−84060
chemisorption, on Cu(110), enhancement during Ne^+ bombard. 80−65070
chemisorption, on GaAS(110) surface 79−95466
chemisorption, on graphite, CO-NDO calcs. 78−75937
chemisorption, on graphite, influence of Fe as impurity 80−96732
chemisorption, on metal films, active sites, chemiluminesc. and vacuum microbalance obs. 78−22950
chemisorption, on Ru (001) surface, high resolution electron scatt. spectra 79−11013
chemisorption, on Ru catalyst, EXAFS obs. 78−15708
chemisorption, on Si (III) surface, appl. of UPS ultra high vacuum apparatus *(Japanese)* 80−37125
chemisorption, on stepped Ru (~001) cryst., 300K, LEED and AES obs. 80−11947
chemisorption, on transition metals, chemisorpt. energy trends 80−107631
chemisorption, on W(100) and Mo(100), low-energy SIMS, ion yields depend. on surface chem. and primary ion energy 78−73105
chemisorption, on W(110) surface, adatom-adatom interaction energies determ. 78−67904
chemisorption, on W(110) surface, phase transitions, coverage effects 78−79879
chemisorption and photodesorption on ZnO, conductivity effect 78−43441
chemisorption bonding on Ni (001), c(2×2)O, self-consistent electronic struct. 79−78146
chemisorption by Nb-O solid soln. at low press., segregation equilib. *(French)* 77−24483
chemisorption in non-polar cpd. semicond. surfaces, π-bonding contrib. 80−6631
chemisorption of Cr, Mo and W, SXAPS obs. 79−52048
chemisorption of TiO_2 and $SrTiO_3$, phase investig. by UPS 78−72684
chemisorption on β-carotene, use as vacuum gauge *(Czech)* 77−139
chemisorption on Ag and Cu, surface-plasmon modulated reson. 79−83045
chemisorption on Ag film, modulated surface plasmon reson. method 79−82439
chemisorption on Ag-Pd alloy, correl. of heat of adsorpt. data with AES expt. results 78−34684
chemisorption on Al, (111) and (100) faces, AES and work function obs. 77−35822
chemisorption on Al, photon and electron emission as indicators of intermediate states 80−39439
chemisorption on Al, site determ. by LEED 80−39421
chemisorption on Al, unoccupied extrinsic surface resonances and site struct. determ. by soft X-ray absorpt. 79−73403
chemisorption on Al(111) surface, ordered overlayer obs. 78−47665
chemisorption on Al (100), mol. orbital cluster calc. 78−14582
chemisorption on Al (100), overlayer electronic struct. 77−85058
chemisorption on Al (111), electronic struct. calcs. rel. to UPS data 80−59801
chemisorption on Al (111), O-Al and O-O bond lengths, surface extended X-ray absorpt. fine struct. 80−29267
chemisorption on Al (111), ordered overlayer, angular resolved photoemission 79−82462
chemisorption on and initial oxidation of Nb (110) and (750) 80−44408
chemisorption on Au, catalytic effect of Ca, AES study 79−15021
chemisorption on Au (111) surface, AES investig. 77−55446
chemisorption on austenitic stainless steel surface, electron spectroscopy, Auger spectra and work function obs. 80−65364
chemisorption on Bi (0001), LEED, AES and electron loss meas. 79−77908
chemisorption on CaO:Bi surface, positive ion emission determ. 80−92785
chemisorption on CaO and MgO, adsorboluminescence from surface F-centres 80−20723
chemisorption on CdS evap. film, kinetics, effect on elec. cond. 78−6464
chemisorption on cellulose char, kinetics 80−96730
chemisorption on Co, LEED anal. of Co{001}c(2×2)-O struct. 78−91546
chemisorption on Co (0001), surface oxidation and CO oxidation 79−60631
chemisorption on Cu(100) surface, angle-resolved UPS study 80−84384
chemisorption on Cu (001), Cu3d-O2p interaction study by angular-resolved photoemission using synchrotron radiation 80−84836
chemisorption on Cu low-index and stepped surfaces, LEED, AES and UPS obs. 80−84391
chemisorption on d-band perovskites, concepts of surface states, book contrib. 80−107651
chemisorption on Fe (100), molecular orbital theory of bonding 77−85059
chemisorption on Fe and Ni films, surface demagnetisation, ferromagnetic reson. study 80−80616
chemisorption on Fe film, XPS obs. 77−48587
chemisorption on GaAs, effect of surface index and atomic disorder AES, LEED and optical ellipsometry 79−60638
chemisorption on GaAs, electronic struct., photoemission meas. 77−20385
chemisorption on GaAs (110), ab initio theory 80−75612
chemisorption on GaAs (110), bonding sites 78−38938
chemisorption on GaAs (110), effect on surface and interface states 77−85284
chemisorption on GaAs (110), surface EXAFS meas. 80−50460
chemisorption on GaAs (110) surface, electronic struct. theory, oxidation, electron spectra interpretation 79−42376
chemisorption on GaP (110), initial steps, electronic surface states 80−49844
chemisorption on Ge (111), surface-molecule model 79−90885
chemisorption on Ge (111) and (100), CNDO calc. 77−55464
chemisorption on group VIII transition metals, UPS 79−7751
chemisorption on group VIII transition metals, UPS 79−7752

oxygen continued
chemisorption on Ir, photoemission, multiplets 77−15694
chemisorption on Ir(111), LEED-Auger expts. 77−20191
chemisorption on Ir(111), XPS obs. 77−20190
chemisorption on Ir (110), AES, LEED, thermal desorption mass spectra, and contact pot. difference meas. 79−77901
chemisorption on Ir (110), sorption and dissoc. kinetics 79−33186
chemisorption on Ir (111) surface, dynamics 77−59211
chemisorption on LaB_6, time of flight atom-probe FIM study 80−6652
chemisorption on Li, KVV Auger spectrum of oxidised Li 77−55454
chemisorption on Mg (0001) face, incipient oxidation, EELS and LEED studies 80−81237
chemisorption on MgO and desorption, light emission phenomena 78−38949
chemisorption on Mo (100), Cs submonolayers effect on electron stimulated desorption of O^- 79−86991
chemisorption on narrow d-band metals, semiempirical theory 78−75927
chemisorption on Ni, orbital energy spectrum of chemisorbed electrons 78−2542
chemisorption on Ni, Pt and W (001) surface, localised orbital approach 78−14587
chemisorption on Ni(100), struct. and energy levels calc. 77−47663
chemisorption on Ni (001), electronic struct., KKR model calcs. 78−56200
chemisorption on Ni (001), MSXα total energy calcs. with non-muffin-tin corrections 77−72795
chemisorption on Ni (100), (110) and (111), photoemission obs. of oxidation process 77−72784
chemisorption on Ni (100), geometry of overlayers 78−2373
chemisorption on Ni (100), molecular cluster theory 77−1309
chemisorption on Ni (100), SIMS and XPS 79−15019
chemisorption on Ni (100), surface vibrs., electron energy loss spectra 79−33173
chemisorption on Ni (110), 2D lattice gas model 79−69357
chemisorption on Ni (110), initial stage kinetics, RHEED and X-ray emission 78−15588
chemisorption on Ni (110), LEED 77−24470
chemisorption on Ni (110) and initial oxidation, AES, EELS, and work function meas. 80−54523
chemisorption on Ni (111), adlayer phases and binding sites 80−80069
chemisorption on Ni and Pt (001), localised orbital approach 77−69166
chemisorption on PAN-based C fibres, surface charact. 78−35536
chemisorption on PbS, PbSe, and PbTe, room temp., UPS and XPS obs. 78−91529
chemisorption on Pd(111) surface, mol. beam scatt. expts. 78−79878
chemisorption on polycryst. Ti, secondary electron yield spectrum obs. 78−38933
chemisorption on polycryst. Ti surface, secondary electron yield obs. 78−71971
chemisorption on Pt, LEED, AES obs. of surface struct. and states 77−1300
chemisorption on Pt, Pt-Au and Ni (100) surfaces, interaction with H_2 77−51600
chemisorption on Pt, thermomag. effect, temp. depend. *(Russian)* 78−60034
chemisorption on Pt 6(111)×(100), UPS studies 80−76151
chemisorption on Pt (100), (1×1) and (5×20) configs. 77−51599
chemisorption on Pt (111), XPS, UPS, EELS, and work function meas. 80−76139
chemisorption on reduced and stoichiometric $SrTiO_3$(111), UPS and XPS studies, illum. effects 80−71572
chemisorption on Rh (111), catalytic reaction between adsorbed O_2 and gaseous H_2 79−83503
chemisorption on Rh (111) and (100) surfaces, LEED, AES and thermal desorption meas. 78−38951
chemisorption on Ru (001), uptake meas., thermal desorpt. spectroscopy and AES 80−108739
chemisorption on Ru (101), interaction with CO 77−73471
chemisorption on Si, AES and photoelectron spectra exam. of early stages of oxidation 79−74272
chemisorption on Si (111), electronic states and initial steps in oxidation 78−91534
chemisorption on Si (111), low-energy electron loss spectroscopy obs. 77−1303
chemisorption on Si and Ge, XPS investigation 77−69170
chemisorption on Sn, AES and EELS study 79−46917
chemisorption on Sn, appl. of electron energy loss struct. in Auger anal. 79−47559
chemisorption on SnO_2, elec. cond. and EPR meas. correlation 80−84369
chemisorption on Th (111), LEED and AES obs. 77−89625
chemisorption on Ti (0001), valence band struct., XPS and UPS study 80−35062
chemisorption on Ti film, changes in work function 77−59221
chemisorption on Ti film, quartz cryst. microbalance obs. of O/Ti ratio 79−4475
chemisorption on TiC (001) surface, change in work function 80−29461
chemisorption on TiO_2, electron stimulated desorption, AES and charact. loss spectra 78−22963
chemisorption on TiO_2 (100), electron spectroscopy, evidence for Ti^{3+} photogeneration 78−38940
chemisorption on transition metals 78−2378
chemisorption on W, atom interactions, Monte Carlo simulation 77−52667
chemisorption on W, initial oxidation, reaction probability 78−15700
chemisorption on W, island form., adatom interactions 79−46922
chemisorption on W, SIMS hysteresis effect 77−72771
chemisorption on W(100), SIMS spectrum 78−34712
chemisorption on W(110), absolute coverage and work function meas. 100 and 300K 78−71986
chemisorption on W(110), island dissolution phase transition 77−80698
chemisorption on W(110) surface, effects on dielec. function, refl. spectra 80−75616
chemisorption on W (110), displacement reconstruction model 79−46949
chemisorption on W (110), Monte Carlo modelling of phase changes 78−71969
chemisorption on W (110) surface, low temp. precursor state 77−11794
chemisorption on ZnO powder, surface cond. 77−11980
chemisorption on ZnO prismatic surfaces 77−31899
chemisorption on ZnS after illumination and in presence of CO and O_2 78−87877

oxygen continued
chemisorption props. and catalytic activities of Pt surfaces with variable kink concs. 80−35576
chemisorption Rh (755), (331), desorpt. temp. and decomp. charact. 79−65318
chemisorption with CO on Pt surfaces, SCF-Xα cluster calcs. 80−65365
chemisporption on Mo (100) surface, electron energy loss spectra meas. 77−16440
chloropentafluoroethane-O_2, multiphoton dissoc., ^{13} enrichment factor, CO_2 laser wavelength and fluence depend. 80−58331
circulation in human organism, model *(Russian)* 79−2093
co-adsorption with Cu on W{100} surface 78−38950
coadsorbed with Cs and Cu (100), influence on work function of Cs 79−15014
coadsorbed with Cs on W (100), high photoemission efficiency 77−55862
coadsorption, with Cs, on W(110) surface 77−89656
coadsorption of K and O_2 on Ge (111) rel. to work function 78−79874
coadsorption with CO_2 and Mo, AES and SIMS obs. 79−46928
coadsorption with CO_2 on MgO surface, ESR 78−6572
coadsorption with CO on Ru (001), uptake and flash desorption meas. 80−39450
coadsorption with Cs on Mo (110), electron emission props. and thermal stability 80−66878
coadsorption with ethylene on Re *(French)* 78−85194
coadsorption with H_2 on Rh (111) below 140K 80−29276
coadsorption with K on Fe (110), XPS, UPS, AES, and LEED study 80−80084
coadsorption with N_2, on W {100}, AES obs. 77−35821
coadsorption with Na, on Ag (110), XPS and UPS obs. 77−69183
coadsorption with Xe on W (110) and (100), work function and thermal desorption meas. 80−39448
coadsorption with Zr on W(100) 80−6653
coal, 14 MeV neutron activation analysis ^{16}O and ^{14}N 77−86430
coal and coal derivatives, 14 MeV neutron generator in analysis of ^{16}O 77−86431
coating, on Al thin film, effect on supercond. 80−7026
codeposited with S on (111) surface, AES and photoelectron spectra 78−71957
codeposition with Cs on W (110), Cs_2O form. 80−44425
coherent anti-Stokes Raman scattering in hollow dielec. waveguides 77−50721
combustion products, appl. in CO_2 gasdynamic laser 79−27240
Comet Kohoutek (1973 XII), C and O spectra and prod. rates 77−49331
concentration, thermomagnetic gas analyser type MN5130 appl. *(Russian)* 77−44558
concentration determ., based on contact potential meas. *(Czech)* 79−70386
concentration in metals and semiconds., neutron activation anal. standardised determ. technique 79−100478
concentration in prebiological atmosphere, photochem. model 79−84486
concentration in tissue, meas. by pulse-mode conduction method 78−7551
contact charge transfer interactions at 10K between oxygen and aromatic mols. 77−46637
contact lens, hard gas-permeable type, O_2 tension underneath 78−3473
contaminated Ni surface, coadsorption of Sn, AES study 80−88437
contamination of ion irrad. Th surface, AES obs. 78−71775
content determ. by ceramic probes, manufacture of props. 77−54308
cornea O_2 flux, meas. when covered by soft contact lens 79−34705
corneal O_2 flux when covered by a soft contact lens, humans 79−34549
corona discharge, $^1\Sigma_g^+$ state lifetime obs., using spectroscopic analysis *(French)* 77−24230
corona discharge, force exerted on electrode 77−19803
critical index test, measurement and appl. 79−79337
crystal, α-phase, exciton, exciton-magnon, and biexciton absorpt. at 1.5K 80−84750
crystal, isotopically mixed, IR absorption spectra (7000-15000 cm^{-1}) at 1.5K *(Russian)* 77−32362
crystalline, polyexciton light absorpt. *(Russian)* 78−27251
cyclotron resonant laser induced breakdown obs. 77−39499
cystic fibrosis, mitochondrial Ca uptake and O_2 consumption 79−43839
deficiency in Elefsis Bay, Greece 79−84299
density of saturated liq. and vapour, pressure-density temp. meas. 79−55802
density of solid in equilib. with vapour 78−93656
depletion in Hamilton Harbour on Lake Ontario 79−16554
deposition in a mesh-packed cold trap 80−22905
desorption, electron stimulated, of O^+ and O^- from W 79−90875
desorption, electron stimulated, of O^+ and O^- ions from Mo (100) 79−82444
desorption, electron stimulated, of O^+ from WO_3 (100) and (111) layers, LEED obs. 79−23840
desorption, electron stimulated, on W (100) surface, hysteresis and ion yield minimum 77−59218
desorption, electron-stimulated, from W (100) and Ta (110) 78−2363
desorption, from Fe, surface anal., XPS appl. 79−24875
desorption, from Ir (111) textured surface, of O^+, electron stimulated 300-1085K *(Russian)* 77−47672
desorption, photon-stimulated, angle-resolved, of O^+ from W (111) 80−88434
desorption, thermal, from metal oxides, expt. technique *(French)* 78−64884
desorption by electron impact from W (110), isotope effects 77−76658
desorption from CdS and CdSe films, heating depend. 80−24737
desorption from CdSe induced by laser radiation *(Russian)* 77−55462
desorption from diamond powder oxidised surfaces 78−47661
desorption from metals by light ion bombardment, cross sections 78−95096
desorption from Nb in a vacuum, thermodynamic props. calcs. *(Russian)* 80−54501
desorption from stainless steel, during laser irrad., etching, AES study 80−66338
desorption from Ta in a vacuum, thermodynamic props. calcs. *(Russian)* 80−54501
desorption from W(011), bonding and kinetics 77−62746
desorption from W(100), photon and electron stimulated 80−100397
desorption from W (100), electron desorption cross sections 79−46944
desorption from W and Re, electron-induced *(French)* 77−85853
oxygen continued
desorption of O^+ and O, W surface, electron stimulated, cross-section temp. depend. 77−31908
determination, by solid electrolyte sensor with internal reference 78−20092
determination, in BN, heat treatment temp. depend., neutron activation anal. obs. 80−16356
determination, in flue gas of 200 MW plant, trial operation *(Czech)* 80−89562
determination, in H_2O after photolysis, gas chromotography 78−61089
determination, in liquid Na, electrochem. meter 78−58337
determination, in metals, neutron activation anal., sensitivity 78−15742
determination, in minerals, anal. of C and O_2, ZAF correction procedure *(French)* 80−11983
determination, in nonferrous metals by nucl. reaction method, surface treatment effects 78−11596
determination, in $O_2(CO)(CO_2)$ glow discharges, by mass spectrometry *(Russian)* 78−87512
determination, in steel, using Rutherford backscatt. and (α,p) reaction anal. 79−5216
determination, in Ta film on Corning glass, nondestructive method *(German)* 78−43272
determination by ^{3}He activation anal. in Si_3N_4 films on Si wafers 80−71981
determination by alpha-induced X-ray spectrometry 78−53275
determination in blood or gas by polarographic sensor 79−62412
determination in Zn dust by 14 MeV neutron activation anal. *(Japanese)* 80−11977
determination of distrib. in metals using nuclear microprobe, ^{16}O(d,p)^{17}O react. 77−36846
diamond:O, substitutional impurities 79−87056
diamond surface interaction with gases and metals 77−72758
diatomic mols., internal partition functions for O_2, N_2, NO and their ions, max. summation indices 80−27995
diffusion, facilitated, in muscle tissues 80−56327
diffusion, facilitated by haemoglobin and myoglobin 77−48747
diffusion and dissolution effects on optical props. of metal in radiative heating, appl. to Ti 79−65884
diffusion and trapping in refractory metal alloys 79−77816
diffusion coefficient in α and β Zr alloys, 675-1800°C 77−62680
diffusion coefficient in liqs. determ. by ESR line widths 78−91929
diffusion during UO_2-Zircaloy interaction 79−10986
diffusion in α-Ti, 700 to 950°C *(French)* 79−86929
diffusion in α-Ti, atomic jumping model 80−44366
diffusion in α-Ti oxidised at high temp. *(French)* 79−7710
diffusion in α-Zr, 290 to 1500°C 77−76613
diffusion in α-Zr and Zircaloy-4, ^{18}O tracer 78−51737
diffusion in β-Zircaloy 78−6181
diffusion in abietic acid under photosensitised oxidation *(Russian)* 79−52655
diffusion in blood plasma, effect of plasma constituents 79−92460
diffusion in Cu, temp. depend., 650-1020°C *(Russian)* 77−84996
diffusion in GeO_2, gamma-ray induced 79−99358
diffusion in group V refractory metals, statistical calculations on Arrhenius lines 80−59722
diffusion in LiF, high-temp. 77−84988
diffusion in liq. GaIn, thermodynamic activity and solubility 78−38860
diffusion in liquid Fe and Ni *(Russian)* 77−55369
diffusion in liquid Sb, activity coeff. 80−65267
diffusion in Nb, internal friction meas. 77−89586
diffusion in Si, determ. from optical absorpt. 79−69294
diffusion in Ta, internal friction meas. 78−75888
diffusion in V, least squares computer technique 78−38881
diffusion in water, laser interferometric study 77−76584
diffusion in YIG:Ca, d defect conc. depend. 78−67857
diffusion profiles in surface layer of superconducting Nb 79−24101
diffusion rate in Au thin layers 80−100359
diffusion with absorption, cubic spline appl. to moving boundary problem 79−75475
diffusivity and solubility in liq. metals, electrochem. obs. using solid oxide electrolytes 80−59669
diffusivity in liq. Cu-Pb alloys 78−51713
diffusivity in liquid Ni and Fe, EMF meas. 78−14494
diffusivity in Nb, exam. 78−51741
diffusivity in TiO_2(-Cr_2O_3) rutile, Cr_2O_3 effects, depth profile meas. by SIMS 80−24651
p-dimethylaminoacetophenone, ps reversible isomerisation kinetics, O_2 quenching obs. 79−5133
diploid yeast, O_2 effect in killing by photon irrads. of different energies 80−36018
discharge, conditions, self-consistent electron energy distrib. functions calc. 80−38746
discharge, HF, prod. of cold plasma rich in metastable species *(French)* 78−14238
discharge, nonequilib. vibr. population, dissoc. rate, role of ats. and dissoc. 79−64933
discharge, RF, moderate press., O production kinetics 79−64934
discharge, RF capacitively coupled low press., spatial and temporal emission spectroscopy 79−27847
discharge plasma, metastable states role, two-step ionisation, electron densities and transition pts. 80−44019
disordered overlayer on W (001), effect on electron spin polarisation in LEED 79−60632
dissociation by field-accelerated electrons, macroscopic props., rel. to dry air 80−61118
dissociation rates, nonequilib., vibr. populations in elec. discharges 78−46427
dissociation relaxation behind regular reflected and stationary oblique shocks 78−85159
dissociative adsorption on W, energy accommodation and reactivity 77−86352
dissolved, in Nb, effect on channelling study of $^4He^+$ irradiation 79−82270
dissolved gas mass transfer through tubular membrane 77−35225
dissolved in Fe-Ni liq. alloys, thermodynamic props., electrochem. meas. 80−30244
dissolved in water, effect on $^{205}Tl^+$ nucl. spin relax. rates 78−19356
dissolved O_2 in rivers, reliability parameter in probabilistic programming models 80−26179
dissolved O_2 in water, pollution indices, automatic analyser *(Japanese)* 80−35812

oxygen continued
distribution function in interplanetary corotating energetic particle streams 79−70938
DNA inactivation by γ-rays in vitro, O_2 effect in presence of metalloporphyrins 79−92303
dye solution, amplified spontaneous emission, effect of O_2 80−95885
Earth atmosphere, O_3 and O_2 photolysis, translationally hot $O(^3P)$ energy distrib. 80−21811
Earth atmosphere O deficit consequences *(German)* 77−70799
effect of graphite-$FeCl_3$ intercalation compound formation *(German)* 79−52634
electrocatalytic O_2 evolution on reactively sputtered electrochromic IrO films 80−26125
electrochemical adsorption on Au film electrode, elec. resist. obs. *(French)* 79−29372
electrochemical fugacity meas. rel. to geothermometry 77−2256
electrochemical measurement transducers, actual distribution of errors 80−45605
electrochemical O_2 meter calibration in 10^{-7} bar range 78−80812
electron backscattering coeffs., 100 eV to 5 keV 80−9750
electron binding in N_2 plasma, mechanism 79−55452
electron irrad. effect on electrolum., defects form. and quenching obs. 80−55194
electron lateral diffusion to mobility ratio 80−6203
electron stimulated desorption from W (100) and (110), threshold behaviour 77−47678
electron stimulated desorption from W (110) stepped surface, atomic steps and defects influence 80−80091
electrons, field-accelerated, in dry air and pure O_2, macroscopic props. comparison *(French)* 80−59161
electrotransport behaviour in Sc 77−11738
electrotransport in La 80−24674
element abundance charts, construction method for tropical Atlantic *(Russian)* 77−60485
elementary excitations, effect of mag. anisotropy *(Russian)* 78−76317
enhancement of sputtered ion yields from Ar^+ ion bombarded Si, Cu 79−38705
EPR in gas and adsorbed on Si 77−69176
EPR spectra of γ-O_2 *(Russian)* 78−6565
ethylene-O_2-N_2-Al particle mixture, two-phase detonation and combustion *(French)* 80−61097
Europa, O cloud rel. to UV emissions 79−5775
evolution, H_2O electrolysis, nucleate boiling, vapour bubble behaviour, heat and mass diffusion 80−67013
evolution on Teflon bonded $NiCo_2O_4$ porous electrodes 80−30247
evolution reaction kinetics on $NiLa_2O_4$ electrochem. electrodes 80−30430
exam. of whether interstitial O can cause internal friction in Ti 78−48537
exchange between $AsO_2(OH_2)^-$ and water in $NaAsO_2$ aq. solns. 78−92459
excimer fluoresc. induced by singlet O_2 organic molecule in polymer matrices 77−6832
exosphere O atoms, polar corona atom distrib. 80−82120
filtered neutron beam of 2.35 MeV 80−27848
flame, Na-seeded H_2-O_2-Ar, population inversion, two-photon laser excitation 79−34307
flame gas, electron-neutral energy exchange in AC field 77−42519
flow regulator, solid-state, high-temperature 80−57301
free surface and grain boundary chemistry in Fe alloys 80−75410
fuel cell electrocatalytic O_2 reduction mechanism with metal chelate coating 78−23951
fuel cell electrodes, galvanostatic switching curve shapes 80−66965
GaAs:O, growth, O_2 solubility determ. rel. to temp. 78−34624
n-GaAs:O, press. depend. of deep level associated with O, transient capacitance meas. 78−64000
Galaxy, O enrichment determ. from planetary nebulae O/H ratios 80−105328
gamma-photon activation technique for O trace levels determ. 79−87910
gas, μ, ρ and T-surfaces, global behaviour, rel. to catastrophe theory 78−26226
gas, electron and negative ion swarms 80−28595
gas, electron mobility to lateral diffusion coeff. ratio 80−43836
gas, eqn. of state, second virial coeffs., intermol. pot. at low temp. 79−46416
gas, heat-flow birefringence 77−84395
gas, influence on field emission of glassy C tips 80−11543
gas, magnetically enhanced thermal convection 79−50802
gas, magnetothermal convection in nonuniform mag. field 78−1746
gas, photoabsorption cross-section, 55-350 Å 78−46364
gas, pulsed electron beam propag., self-focusing polyatomic additives effects 77−68164
gas, pure rotational CARS obs. 80−99511
gas, thermal cond., mag. field effects 78−34255
gas, vibr. Raman spectrum, anomalous behaviour near crit. point 78−55179
gas, viscosity rel. to ionis., skin friction of wetted oscill. disc 78−34252
gas, weakly ionised, electron transport coeffs., Boltzmann eqn. anal. *(Japanese)* 80−59183
gas and liq., shear viscosity coeff., 75-300K, up to 34 MPa 78−34253
gas breakdown, cross-field, in coaxial cylinder geometry 79−82029
gas breakdown threshold using laser radiation 79−1283
gas discharge development, relative motion between gas and electrode, theory 78−63616
gas refractive index meas., 150 GHz to 6 THz 77−5892
gas-discharge plasma, interactions with Si surface 78−83840
gaseous and dissolved oxygen analysis, direct readout instrument 77−40606
glow discharge, DC, particle concs. calc. 80−1859
glow discharge, electron collision rates and distrib. functions 79−10631
glow discharge, low press. and current, theory 78−87560
glow discharge, O atom conc. determ. by mass spectrometry *(Russian)* 78−87512
glow discharge, polymer surface modification, ESCA obs. 78−3438
glow discharge, positive column contraction characts. 79−90483
glow discharge atomic radial distribution obs. 78−67501
haemoglobin-O_2 equilibrium curve, instrument for determ. based on membrane diffusion 80−81761
haemoglobin-O_2 equilibrium curve determ., semipermeable membrane transport model 79−92418
haemorrhagic shock, effect of anemia on O_2 transport 80−67330
oxygen continued
haemorrhagic shock, effect of increased blood-O_2 affinity on O_2 transport 80−67331
half-monolayer on W (100), surface reconstruction kinetics 80−65375
heart, minimal O_2 consumption and optimal contractility, theoretical approach 79−74694
hexafluorobenzene-O_2, soln., NMR for translational O_2 diffusion 79−65749
hypoxia, sinusoidal, cerebral blood flow dynamic characts. in goat 79−100652
implantation in LiF:Mg, Ti, luminesc. increase 78−64412
implanted in Si, lattice location of ^{16}O by α-particle backscatt. method 78−10080
impurities effect on epitaxial regrowth of amorphous Si 80−84401
impurities in Cu, effect on drawability and mech. props. 79−83272
impurities in GaAs epitaxial layer, quantitative anal. of O by SIMS 79−5233
impurity at glass-metal seal interface, composition and conc. determ. by AES 80−76587
impurity determ. by atm. press. ionisation mass spectrometer anal. technique 77−56263
impurity determination in group VA metals, from internal friction meas. 79−39246
impurity gas, role in H_2 embrittlement of steel 77−59904
impurity in amorphous Ge film, depth profiling by SIMS 80−39480
impurity in CaF_2 crystals, influence on elec. cond. 80−2431
impurity in CC CO_2-gas dynamic laser, combustion-type, effect of residual CO on performance 79−68378
impurity in d-transition metals, integration with large-angle grain boundaries 80−39148
impurity in liquid Fe, influence on short-range order struct. *(Russian)* 80−38901
impurity in Nb, distrib. determ. by neutron activation anal. *(Russian)* 80−70243
impurity in Si, equilib. of dissolved C and O with CO in ambient atm. 80−1949
impurity in W and Mo, struct., mech. props. and purification 79−52277
impurity in ZnS single crystals, determ. by fast neutron activation anal. 80−15142
impurity in Zr-Cu, Nb-Ni and Ti-Ni amorphous alloys, effect 80−75168
impurity luminescence centres in alkali halide solns., EPR *(Russian)* 79−15339
incorporation in Ni HCP and amorphous RF sputtered films, ESCA obs. 80−10832
inert gas+O^{n+}, (n=4 to 7) small impact parameter collisions, dynamic screening model 77−50525
inhalation automatic control for patients with respiratory failure 80−17181
initial interaction with Al single cryst. faces, LEED, AES and work function study 80−84392
initial reaction probability with Ba getter film, AES obs. 80−61153
interaction with Pd (111) surface, EELS, AES and LEED obs. 79−86985
intercalation reaction with TaS_2 (2H), reaction rates, X-ray diffr. expts. 77−12828
interstellar abundance toward ζ Ophiuchi 79−44583
interstellar O edge detectability and possible interp. 77−60811
interstellar O edge in X-ray spectrum of Crab Nebula 79−67079
interstitial diffusion in Cu, Nb, and Ta, sink/barrier phenomena 79−60553
interstitial in Fe, magnetic aftereffect 78−91903
interstitial in V, neutron diffr. determ. of site 77−19944
interstitials, in transition metals, electronic structure 79−1583
interstitials, Si Czochralski wafer, rel. to oxid. induced stacking faults 78−10062
intravascular O_2 continuous monitoring, electrochem. sensor 80−56238
intravascular O_2 measurement, current-to-voltage convertor 79−34684
intravascular O_2 saturation continuous meas. using fibre optic catheter *(German)* 78−85411
intravascular O_2 sensors, Monopolar, in vitro evaluations 79−34683
intravascular PO_2 probe routine appl., practical experience 80−56239
ion, channelling through Si and Ag, radiative electron capture 79−77658
ion, in Fe(Ni)(Co), transient mag. field discontinuity 80−24515
ion beam, heavy element ionisation cross-section ratio determ., X-ray method 77−6920
ion implantation in Ge, influence on crystal struct., electroreflection method 77−84783
ion impurity in linear Z-pinch He plasma, outer 2s-shell electron excitation emission 78−22113
ion-implantation in SOS, gettering effect, Hall and Rutherford backscattering meas. 79−65103
ion-surface impact, X-ray prod., 5 MeV/amu, projectile X-ray prod. by 5 MeV/amu deuterons (oxygen ions), projectile Z depend. depend. 80−42982
ionisation states of energetic C and O emitted by the Sun 77−49249
ionosphere D-region, O conc. vars. during polar cap absorpt. 77−37481
ionosphere upward flowing energetic O^+ ions latit., diurnal and altitudinal distribs. 78−49199
ions, beam-foil excitation, relative initial populations, lifetime curves 80−14210
ions, beam-foil spectra 80−42977
ions, energy loss in tissue-equivalent gas for elastic nuclear collisions 78−86759
ions, ionisation equilib. and radiative energy loss rates in low-density plasmas 78−87430
ions, Li-like Auger contribs. to electron impact ionisation 80−87231
ions in Earth's upper atmosphere, coupled time-dependent diffusion eqns. 80−109285
ions in Jupiter magnetosphere, plasma cloud injection from IO 80−90358
isoelectronic sequence, optical oscillator strengths 80−63589
isoelectronic sequence, two photon transition probabilities 79−22680
isoelectronic sequence, X-ray spectra 80−87071
isotope abundance in Luna 16 and 20 soil 77−22120
isotope abundances in lunar samples 77−60676
isotope analysis, parallel changes in species diversity and palaeotemp., Lower Miocene 79−39866
isotope comp. and origin of high $^{87}Sr/^{86}Sr$ andesites 79−34817
isotope comp. of water in Sea of Azov 77−49083
isotope composition of Matanuska Glacier, Alaska, rel. to basal zone origin 79−79884

oxygen continued
isotope composition of plutonic granitic rocks 78−65221
isotope doping technique for use during hydrothermal cryst. growth, appl. to quartz 77−28706
isotope enrichment, photochemical, from methanolic UO_2F_2 soln. 79−36786
isotope exchange between feldspar and water, effect of fluid press. 78−57204
isotope fractionation in decarbonation metamorphism, Mottled Zone Event 78−65307
isotope geochemistry of cherts from South Africa 79−34820
isotope geochemistry of deep sea cherts 77−5182
isotope partitioning among minerals in igneous and metamorphic rocks 77−86870
isotope ratio, mass spectrometric anal. double inlet system with viscous gas flow 77−18131
isotope record, marine, in Pleistocene coral, Barbados, West Indies 79−66675
isotope record in coral growth rate (1944-74) 79−62524
isotope records rel. to global freshening of upper ocean layer during deglaciation 78−53658
isotope separation, supersonic molecular beam technique using RF spectroscopy, mag. reson. 80−47725
isotope thermometry for sulphate-water reaction in geothermal systems 78−69383
isotopes, lung perfusion determination using O isotopes and dilution principle *(German)* 78−85327
isotopes, origin and abundance ratios evolution 78−93201
isotopes in dissolved sulphate and water from hot springs and drill holes, reservoir temp. indicators 78−69382
isotopes in silica minerals in Monterey Shale 77−64267
isotopic anomalies in meteorites 77−87354
isotopic composition determ. using RMO-4S omegatron mass spectrometer 78−5368
isotopic composition of Canadian Shield surface crystalline rocks 79−62496
isotopic composition of minerals in ureilitic meteorite Kenna 77−41367
Jupiter's upper atmosphere, Galilean satellites as source 79−40128
KERMA values, consistent set for H, C, N, and O for neutrons from 10 to 80 MeV 80−68967
labelled molecular O_2 formation by ^{15}O recoils from $^{16}O(n,2n)^{15}O$ 78−3359
lactate dehydrogenase, O_2 effect in radiolysis obs. 80−72223
Lamb shift, fine structure, $1s3s\,^3S$-$1s3p\,^3P$ transition 79−89637
laser, auroral and transauroral transitions, high energy storage 77−10897
laser, photolytic, expts. for fusion research 78−63101
laser, possible high energy laser at 1.27 μm 79−13950
late-type supergiants, C, N and O abundances for G AND K Ib stars 78−24509
lead phthalocyanine:O_2, photocond., impurity-induced 79−47120
lead phthalocyanine:O_2(I), Schottky barrier effect on AC current response 80−75623
left ventricle time-varying capacitance model, driving energy and cardiac O_2 consumption *(Japanese)* 80−21486
liberation from electrolytic Ni during vacuum heating, Mossbauer spectra *(Russian)* 80−35594
liquid, Brillouin scatt. obs., US vel. and absorpt. 80−45085
liquid, EPR temp. depend. *(Russian)* 78−31103
liquid, estimation of solubility of solidified substances by Preston-Prausnitz method 80−39285
liquid, exchange interaction, EPR absorpt. line shape anal. 80−71158
liquid, Faraday effect anomalous dispersion 79−99856
liquid, fast neutron filter effect of antiresonance of 2.37 MeV beam prod. 77−79494
liquid, for efficient IR AC Kerr switches 80−19078
liquid, investigations on heat transfer during pool boiling 79−60494
liquid, modified droplet model, mean droplet interaction below T_c 80−70363
liquid, mol. correl. functions, effective pair pot. evaluation 80−10476
liquid, photoluminesc., dimer effects 78−31233
liquid, pool boiling in inhomogeneous mag. field 77−31766
liquid, possible active media in high-power Raman lasers 80−19028
liquid, principle of corresponding states for viscosity 77−84959
liquid, pure vibr. Raman spectra 80−97262
liquid, Raman Q branch temp. depend., interferometric obs. 77−43987
liquid, spontaneous Raman scatt., vibr. dephasing, review 77−28568
liquid, stimulated Raman scatt., vibr.-translational relax. rate, schlieren technique meas. 80−9955
liquid, thermodynamic perturbation theory, equilib. props. 79−64976
liquid, US absorpt., bulk viscosity and relaxation 77−35639
liquid, vibr. dephasing calc., diatom anharmonicity 78−94959
liquid, vibr. energy relax., 53-96K 79−77477
liquid, viscosity, density depend., theory 77−20105
liquid structure, thermal neutron diffraction 79−46542
low energy electron drift velocity at 293K 80−103101
low-pressure discharge, plasma atomic species, mass spectrometric obs. 78−67502
lower atmosphere, energetic O atoms distrib. functions 77−41127
lung, duck, O_2 and CO_2 exchange and cardiopulmonary control interaction model 80−3600
lung, intrapulmonary haematocrit maldistrib., effect on O_2, CO_2, inert gas exchange 80−8033
lung tissue simulation, O_2 exchange in silicon rubber capillaries 79−44060
LWR fuel-cladding gap, Cs-U-Zr-H-I-O system, chemical thermodynamics 78−82440
magnetosheath bursts obs. by Imp 8, 1974, February 16, evidence for escaping terrestrial O^+ 79−29937
man's transport system, functional state, math. model 80−104548
marine oil pollution, retardation of O_2 exchange with atmos. 80−109175
marine sediments in coastal area, depth penetration of O_2 80−104952
Martin bath, blowing with oxygen, smelting dust phase comp. determ. 77−52705
mass identified ions in O, N, CO and CO_2, transport properties, obs. and calc. 79−50837
medicine, blood O_2 anal. and O_2 conc. meas., for teaching 78−49622
mesosphere, O_2 density profiles from solar H Lyman-α radiation extinction meas. 78−44947
in metal-poor stars, O abundances from O I IR triplet 80−36610
oxygen continued
metastable and O_3 production in electron-beam-controlled high-pressure discharge 78−71607
methane:O_2, crystal field, O_2 catalysis of spin-species conversion 77−51706
methane+$O^+{}_4(O_2{}^+)$, products, rate consts., rel. to stratosphere 77−9040
^{13}C-methane-d_1:O, annealed, spin conversion and proton 2nd moment time-depends. 80−11283
methane-O_2, solid mixture, electron diffraction study *(Russian)* 78−83953
methane-O_2 aquamechanical foam, propag. characts. of detonation waves 78−31713
methane-O_2 mixture, laser initiated combustion 80−55661
methane-O_2-N_2 mixtures, prediction of propagating laminar flames 79−52663
methane-O_2-N_2 premixed flat flame, ruby laser-induced gas breakdown thresholds 79−1951
methanol-O_2 flame, combustion and ionisation 79−20357
methyl radical+O_2 (NO), mass spectra, absence of reaction in combustion system 78−53195
m-methyl-p-cyanodimethylaniline, ps reversible isomerisation kinetics, O_2 quenching obs. 79−5133
micelle forming detergent solutions, fluoresc. quenching by O_2, dynamic parameters and solubility characts. 79−83513
microanalysis in dislocation-free Czochralski-grown Si crysts. *(German)* 78−26592
microcirculation O_2 distrib. during and after arteriolar occlusion 78−44529
microwave absorpt. at 60 GHz, for atmos. remote sensing 80−77172
microwave absorption, spectral line press. broadening theory 77−30864
microwave absorption meas. by Fabry-Perot spectrometer 77−46558
microwave spectrum, expt. v. theory 77−37298
molecular, $A'^3\Delta_u$ state, inversion, presence in nightglow and discharges 80−63616
molecular, glow discharge, positive column analysis, oxygen 79−55577
molecular, quenching of luminescence by porphyrins and metalloporphyrins 79−50058
molecular cluster formation, in rarefied nozzle flowfield 80−5639
molecular dissociation in discharge plasma 79−100356
molecular dissociation relax. behind oblique shocks 77−548
molecular dissociative recombination, repulsive term, states of products 77−65537
molecular dynamics, allotropy, solid-state phase transitions effects, Raman spectra *(French)* 77−42372
molecular electron attachment in non-self-maintained discharge, plasma decay obs. 80−43844
molecular gas, K-shell photoabsorption coeffs., 500-600 eV 80−9617
molecular metastable states, obs. in electron-beam controlled discharge *(French)* 77−30880
molecular photodissoc., $O(^1D \rightarrow {}^3P)$ and $O_2(b^1\Sigma_g{}^+ \rightarrow X^3\Sigma_g{}^-)$ energy transfer 79−11810
molecular photodissoc. ionis., 16-41 eV 77−18995
molecular photodissociation on MgO surface, $O_3{}^-$ form. 79−100431
molecule, 0-10 eV photoelectron spectra obs., new differential retarding field analyser characts. 77−41735
molecule, 2,0 band, highly forbidden optical transitions using intracavity laser spectroscopy 77−42331
molecule, 7 to 10 eV electron energy loss spectra, Rydberg states excitations 77−27193
molecule, $^1\Delta_g$ singlet state, spectrosc. obs. in dye-sensitised fluorocarbon solns. 80−85178
molecule, $^1\Delta$ states, corrections to effective orbital g-factor 79−7036
molecule, $^3\Pi_g$ diabatic Rydberg states, ab initio CI calcs. 80−95554
molecule, $(0,0)b^1\Sigma_g{}^+$-$X^3\Sigma_g{}^-$ band, press.-induced line shift 79−98160
molecule, (0-0) atmospheric band, laboratory discharge lamp source 80−4148
molecule, $a^1\Delta_g$ and $b^1\Delta_g{}^+$ state, MCSCF wavefunctions 78−37561
molecule, ab initio CI STO calc., photoelectron spectra 78−74585
molecule, absorpt. 177.5 to 178.3 nm, appl. of vac. UV 6 m monochromator 78−37969
molecule, anharmonicity const., Raman meas. 77−34637
molecule, $b^1\Sigma_{g+}{}^+$ state excitation by 0.75-6 eV electrons 78−86958
molecule, $b'^1\Sigma_g{}^+$-$X^3\Sigma_g{}^-$ electronic transition, absorpt. coeffs. and transition moments 80−43061
molecule, bonding, spin density functional theory 78−17558
molecule, $C^3\Delta_u$−$a^1\Delta_g$ band system, vibr. anal. 80−5556
molecule, computer controlled CARS spectra of Q branches 78−62241
molecule, dipole oscill. strength distribs., sums 78−21975
molecule, dipole properties and dispersion energies additivity, using atoms and small mol. models 80−53091
molecule, dissoc. in shock tubes, induction and transient times 77−12794
molecule, dissoc. induction times, high-temp., exact simple model numerical calcs. 78−9230
molecule, dissociation, weak bias and anharmonicity effects 78−82661
molecule, dissociation energy, determ. by laser photofragment spectroscopy 78−70957
molecule, dissociative attachment coeff. calc. 77−19100
molecule, dissociative electron attachment 77−42431
molecule, distrib. in lower thermosphere assuming tidal effects, one dimens. nonstationary diffusion-photochemical model 80−4160
molecule, double curve crossing model, predissoc. linewidths and level shifts 77−75070
molecule, effect of spin orbit interaction on magnetic dipole transition intensity *(Russian)* 79−6948
molecule, effective spin-spin parameter, ab initio calc. 78−9067
molecule, electron attachment threshold photoelectron spectra, vibr. excitation 80−83422
molecule, electron coincidence spectrosc., valence electron momentum distrib. and binding energies 80−102583
molecule, electron diffraction parameters, spectrosc. calc. 78−70932
molecule, electron impact, energy loss spectra, electronic transitions obs. 78−17805
molecule, electron impact excitation, energy transfer, source of $O(^1S)$ in aurora 79−48598
molecule, electron impact excitation, high vibr. levels of ground state, decay of reson. states 77−88581
molecule, electron impact excitation, optically allowed transitions from ground state 79−10216
molecule, electron impact excitation, optically forbidden transitions from ground state 79−10217

oxygen continued
molecule, electron impact excitation total cross sections, oscill. strengths, independent particle model calcs. 77−61856
molecule, electron impact ionis., mean energy expended per ion pair 78−74777
molecule, electron impact ionisation, in RF ion source, effective cross-sections 78−22034
molecule, electron impact vibr. excitation, direct and stepwise, rate coeffs. 80−5630
molecule, electronic electron impact excitation, rot.-electronic coupling 78−9265
molecule, electronic states calc. using five-parameter pot. function *(Russian)* 77−3270
molecule, electronic struct., self-consistent pseudopot. calc. 80−9508
molecule, equilib. geometry, orbital energies, ab initio rel. to pseudopot. calcs. 78−82613
molecule, Franck-Condon factors, semiempirical three-parameter pot. functions 77−18986
molecule, from γ-irradiated $NaClO_3$, reson. Raman scatt., excitation profile, polarisation meas. and decay kinetics 77−14437
molecule, ground state, ab initio pot. curve calcs. 77−83510
molecule, ground state MNDO calcs. 78−911
molecule, harmonic oscillator model in predissoc., level widths, shifts and curve crossing 78−90239
molecule, Hertzberg II bands, Venus night airglow excitation 77−41340
molecule, I and I′ resonance series, vibr. level populations in autoionisation, photoelectron spectra, bond length determ. 80−91612
molecule, in β-quinol clathrate, guest-host interaction, mag. reson. spectra 78−76346
molecule, in liq. inert gas, electron attachment, elec. field effects 77−31009
molecule, in upper atmosphere, electron impact cross-section 78−28398
molecule, in upper atmosphere, electron impact yield spectra 78−28401
molecule, in zeolitic matrix, IR active fundamentals obs. 77−71800
molecule, interactions with slow electrons 79−45848
molecule, internal partition function calc. 78−55159
molecule, ionisation, photodissoc. of positive and negative ions, mass spectrometric obs. 78−13559
molecule, ionisation pots. and excitation energies, correl calcs. 77−26986
molecule, K-shell, excitation and ionisation, vibr. struct., electron energy loss spectra obs. 80−18943
molecule, laser photochemistry 79−43604
molecule, light polarisability parameters, Raman scatt. ang. meas. 80−37814
molecule, liq. and gas, induced absorpt. spectral moment, mol. calcs. 80−63737
molecule, low energy elastic and inelastic electron scatt., rot. transitions, close coupling calc. 80−78706
molecule, low energy electron impact dissociative ionis., O^{2+} form. and energy distrib. 80−5626
molecule, low-energy electrons elastic scatt. cross sections 78−42213
molecule, mag. dipole transitions, line positions and strengths from stratospheric emission spectra 80−78604
molecule, master eqn. theory, dissoc. rate consts. 77−77742
molecule, metastable, laser-induced photolysis of ozone reactions 80−11928
molecule, metastable, sensitisation of $SO(^1\Delta_g, {}^1\Sigma_g{}^+)$ chemiluminescence 80−26016
molecule, metastable level electron impact excitation, resonances *(Russian)* 80−43198
molecule, metastable state mol. ion form. by electron impact 77−14594
molecule, microwave absorpt. coeff. 77−64378
molecule, microwave spectrum, press. broadening 80−23412
molecule, MSXα calc., partial wave expansion, binding energy and orbital energy 80−37738
molecule, multiconfig. Hartree-Fock calcs. convergency 80−47901
molecule, multipole moments, far IR spectrum determ., pot. function effects 77−50435
molecule, nonlinear optical polarisability meas. 79−54991
molecule, O_2, $(b^1\Sigma_g{}^+\text{-}X^3\Sigma_g{}^-)$ system in auroras, vibr. development 77−2293
molecule, photoabsorpt. cross section, 10 to 50 nm 77−61797
molecule, photoabsorpt. cross-section, 50-340 Å, as sum of empirical at. cross-sections 78−58718
molecule, photoabsorpt. cross-section, photoionis. continuum 77−68029
molecule, photoabsorption and photionisation, UV region meas. 78−42087
molecule, photodissoc., $O(^1D)$ production quantum yields, 1160-1770 Å 78−33557
molecule, photoelectron ang. distrib., photon energy depend. , 16-25 eV 80−53046
molecule, photoelectron ang. distrib. asymmetry parameter for 30.4 nm photons 79−98151
molecule, photoelectron asymmetry parameters 80−95684
molecule, photoelectron spectroscopy using supersonic mol. beam source 79−68264
molecule, photoexcitation and photoionisation cross sections, HF Gaussian method 80−53064
molecule, photoionisation, angular distribution of photoelectrons 78−90235
molecule, photoionisation, partial channel cross-sections calcs. 80−53061
molecule, photoionisation cross section and asymmetry parameters calc. in UV region using static pot. 80−95692
molecule, photoionisation cross sections, 100-800 Å 78−5302
molecule, polarisability tensor anisotropy, Raman spectra differential scatt. cross section 80−18860
molecule, pseudospectral dipole oscillator strength distribs. 78−50503
molecule, Q-branches, high resolution pulsed CARS 78−17676
molecule, quenching of afterglow, quenching var., activator penetration to region inaccessible to quencher 80−64813
molecule, Raman spectra of fundamental vibr. band, rot. consts. 78−21932
molecule, reaction with radiation induced free radicals in DNA or polynucleotides 78−48759
molecule, relaxation by IR and microwave coherent transients 80−28092
molecule, reson. cross-sections, predissoc. and preassoc., isotope effects 78−58750
molecule, RH-GTO-MCSCF calc., 1s photoelectron spectra, multiplet intensity ratio 78−5134
molecule, rot. Raman spectra fine struct., press. broadening *(French)* 79−94003
oxygen continued
molecule, rot. struct. in Zeeman effect 79−50078
molecule, Rydberg states, $^3\Sigma_g{}^-$, $^3\Sigma_u{}^+$, $^3\Pi_g$, $^1\Pi_g$, $^1\Sigma_g{}^+$ symm., ab initio CI study 80−99460
molecule, Schumann-Runge band system, oscill. strengths and linewidths 79−98120
molecule, Schumann-Runge bands, predissoc. linewidths and oscill. strengths, vibr. level depend. 79−45735
molecule, Schumann-Runge continuum, oscill. strength and electron impact excitation 80−69121
molecule, Schumann-Runge system, electronic transition probabilities 80−78603
molecule, singlet, energy transfer in quenching, kinetics 77−68072
molecule, singlet, energy transfer in quenching, statistical theory of vibr. energy distrib. 77−68073
molecule, singlet energy transfer in quenching, vibr. excited mols. 77−71828
molecule, singlet state, form., quenching and reactions, review 77−29002
molecule, singlet state radiative lifetime, perturbation-variation calc. 77−14496
molecule, singlet states, quenching by $O_2(N_2)$, shock tube study 80−23511
molecule, singlet-state luminesc. in energy transfer from dissolved pigments 79−54886
molecule, singlet-triplet transitions, external theory at. selective effect 79−98159
molecule, soft X-ray photoionisation cross-sections, 6 to 22 Å 77−14499
molecule, spin-forbidden transition intensities, selective heavy atom effects 80−58240
molecule, structural second virial coeff., intermol. pot. and mag. scatt. 80−78678
molecule, symmetry adapted wave function generation using group theoretical projection operators 80−102428
molecule, thermal decomposition, vibr.-rot. state depletion, Monte Carlo calc. 80−35506
molecule, thermal electron attachment with various compounds present, microwave cavity-radiolysis 77−42422
molecule, three-body electron attachment in pure and He discharge 80−24245
molecule, triple-dipole energy calc. using pseudo spectral theory 78−46418
molecule, UHF description of ground and lowest singlet states 78−90056
molecule, vacuum UV molecular photoabsorpt. cross-section meas. 80−37096
molecule, valence states, ab initio config. interaction calcs. 78−25448
molecule, vibr. excited, form. in charge transfer reactions 77−3455
molecule, vibrational relaxation and dissoc. behind a shock front, absorpt. spectroscopy *(Russian)* 77−88536
molecule, X-ray and electron scatt., first Born approx. calcs. 77−61867
molecule, zeolite matrix isolated, induced IR spectra 78−46333
molecule + $H^+(He^+)(O^+)$, dissoc. ionisation, kinetic energy spectra 78−25684
molecule 80−58165
molecule electron impact dissociation rel. to O_3 generation in air-fed ozonisers 80−3323
molecule electron impact excitation, indirect mechanism for $O(^1S)$ prod. in aurora 79−48597
molecule reduction flow probe for cerebrospinal fluid 79−100777
molecule transport to artery walls, in arteries with longit. ridges 77−44702
molecule trapped in $KBrO_4$ cryst., detection by ESR spectra 78−84474
molecules, $b^1\Sigma_g{}^+$ state prod. and deactivation following $O(^1D_2)$ quenching 80−76493
molecules, Lennard-Jones 12:6 parameters calc. from viscosity data 77−46612
monitoring instruments, trace oxygen measurement 80−52181
monolayer, 1/4, on Ir (110) unreconstructed surface, LEED study 79−14990
monolayer, adsorbed on graphite, phase diagram 79−73401
monolayer, adsorbed on Ni (100), surface EXAFS, secondary electron yield meas. 79−47544
monolayers, on graphite, mag. α-phase and α-β-phase transition 80−70530
muonium depolarisation in fine SiO_2 powder vac. interstices 78−42250
naphthalene-O_2 in polystyrene fluff, oxciplex emission 77−23515
Nb-O, effect of O_2 on penetration of Li at 400°C 79−11719
nebulae, N and O abundances 78−8093
negative ion mobility in O_2 and N_2, temp. depend. 79−14513
neutron activation anal. of O in non-ferrous metals 79−24865
neutron kerma factors for H, C, N, O and tissue, 20-70 MeV 77−73584
nightglow at 762 nm, rocket-borne photometry 77−13128
nonthermal O plasma stationary states 78−63544
Norrish type II reaction biradicals + O_2, diffusion controlled rate const. 77−90617
$(np)^4$ $^1S_0$-level photoionisation via autoionising levels 79−76398
nuclei in molecules, isotope shifts calcs. 78−86917
nucleosynthesis in supernova remnant in NGC 4449, spectrophotometric evidence 80−56895
O_2, CO_2 and heat transport in the placenta, construct. and usefulness of models 80−3604
O_2 in Precambrian atmosphere, elements in sedimentary rocks 77−5272
O^+ + Ar, electron emission, double differential cross sections, Auger spectra 79−45684
O + tetrafluoroethylene, triplet difluoromethane spectra, phosphoresc. and triplet-triplet annihilation 78−53196
O(1s), XPS energies from oxidised metal surfaces and powders 77−16457
ocean, dissolved O_2 distrib., numerical simulation 79−53367
ocean utilisation rate meas. by $^3H/^3He$ dating, appl. to Sargasso Sea 77−56654
OER for π^- irradiation of Chinese hamster cells 79−88126
OH masers, interstellar, obs. near Orion population stars 80−67716
order-disorder interaction with GaAs (110), LEED anal. 80−75445
Orion Nebula, Ne, S and O abundances from fine-struct. lines obs. 80−4410
in Orion Nebula peripheral regions, O/H ratio and O ionisation 80−36686
α Orionis (Betelgeuse), C and O underabundances from UV flux 77−22231
overlayer, (2×2), on Ir (111) surface, LEED study 80−2264

oxygen continued
overlayer, c(2×2), on Ni (100), angle-resolved photoemission study 79−33903
overlayer on W(110) surface, structure refinements, via reliability factors for surface crystallography 77−59193
overlayer structure on Ni (001), theory of electronic struct. 79−65319
oxidation of H_2S by active C, electrochem. model *(German)* 78−35717
oxidation of Ti, XPS exam. *(French)* 78−23858
oximeter, noninvasive tissue reflectance, development and evaluation 79−20703
oximeter for spectrophotometric monitoring of arterial O_2 saturation in the fingertip 80−41161
oxyacetylene, critically-initiated detonation waves, quasi-steady regime 78−90930
Pacific Oean, surface distrib., and min. conc. depths 77−25696
paramagnetic molecule, trapped in Al-insulator-Au tunnel junction conductance peaks produced by Kondo scatt. 78−95387
partial pressure control of V_2O_5 type liq. semicond. elec. props. *(Russian)* 78−72142
partial pressure determ. in biological fluids, electrochem. cell 78−85420
partial pressure measurement with thin-layer polarographic probe, intracortical appl. *(German)* 78−85410
patient consumption, monitoring instrumentation using replenishment technique 79−39547
patient consumption continuous measurement, under N_2O anaesthesia during surgery 77−81640
permeability in CaO stabilised ZrO_2 79−10980
permeability in hard elastic polypropylene films, extension effects 80−40412
permeability in polymer membranes, determ. with Zircon gas analyser 79−39195
permeability through ethylene-vinyl alcohol copolymer *(Japanese)* 78−31702
petroleum-acetylene-O_2 combustion products, seeded, elec. cond., for MHD power plant 78−34256
phase equilibria near 298K, Raman spectral study of solid and fluid 80−19937
photon and electron stimulated desorption energy and angular distributions from W {001} 80−96734
photosensitised luminescence of singlet $^1O_2$ in soln. 77−70309
photosmog inhibitors, O atom reaction rate constants 79−12185
pionic, Auger electron emission *(Russian)* 80−69271
pionic atom, isotope effects, 1s state energy shift and line broadening for ^{16}O-^{18}O pair *(German)* 80−48107
planetary nebulae, O III/O II abundance ratios rel. to central stars temps. 79−2565
planetary nebulae in Magellanic Clouds, He, N and O abundances, effects of excitation class 80−109519
plasma, 10000-13000K, VUV continuum radiation 78−91152
plasma, calc. profiles of emission rates for VUV oxygen lines in Thor Tokamak 78−83536
plasma, carbon tetrafluoride+4% O_2, Si etch rate uniformity 80−40568
plasma, charge exchange in collisions of multi-charged ions *(Russian)* 79−98859
plasma, electron beam energy branching, discrete energy loss method 80−48905
plasma, electron energy distrib. function, electron sink and plasma resist. effect *(Russian)* 80−106987
plasma, quasistationary, non-LTE props. calcs. *(German)* 77−58844
plasma, surface treatment of polyester fabric, effect on surface struct., props. 78−95831
plasma, UV continuum spectra, mol. recomb. of ground state atoms 78−91078
plasma electron energy distribution obs. 78−63595
plasma electron-impact ionis. rate coeffs. obs., Li-like N and O 79−41878
plasma etching characts., effect of dark space in RF glow discharge, photoresist ashing characts. 79−15830
plasma impurities, neutral-beam-injected, in 2XIIB mag. mirror 79−37547
plasma impurity, flux on wall of DITE Tokamak 80−28688
plasma impurity, high-temp. ionis. equilib. and radiative cooling 78−42712
plasma impurity, Microtor Tokamak, trapping and removal in low-temp. H plasma 78−22541
plasma impurity, radiation loss effects on Tokamak expts. 78−22465
plasma impurity, radiation losses 77−19678
plasma impurity in N_2 RF capacitative discharge, effect on heating 80−59312
plasma impurity radiation, metastable transitions in Tokamak, modified coronal model 78−26255
plasma injection, in TFR Tokamak current plateau, effect on Mo impurity 78−22565
pneumocytes, isolated type II, effects of high O_2 exposure on bioenergetics 80−30685
poisoning of LaB_6 cathodes in vac. systems, thermionic emission decay 78−27364
polymer degradation products, chem. anal. by UV photoelectron spectroscopy 78−53300
in Population II stars, abundance rel. to age determ. 77−56912
potential in equilibrium with impure high temp. inert gases 80−104135
precipitation in dislocation-free Si, IR and TEM obs. 80−29173
precipitation in Si, 1000°C TEM, IR absorpt. and X-ray studies 80−34194
precipitation in Si, 650°C, IR absorpt. and X-ray diffr. 80−76258
precipitation in Si by homogeneous nucleation 77−11695
precursor adsorption on Sn, activation energy for chemisorption 78−71950
premixed H_2-O_2-N_2 laminar flames, temp. profile, comparison of spectroscopic meas. 80−42227
primitive ionosphere O content rel. to thermal struct. 78−40754
probe measurements in semi-killed and rimmed steels 77−21050
prod. and props. in liq. Ar and N_2, by N_2O photodissociation 80−43063
production from H_2O using solar energy, eval. of a hybrid process 80−104519
production from water using solar energy, one-step effusional process 78−15672
propane-O_2 aquamechanical foam, propag. characts. of detonation waves 78−31713
propane-O_2 mixture, combustion to detonation transition, stochastic aspects 79−100381
oxygen continued
propane-O_2-air flame, temp. meas. by laser Raman spectroscopy 77−5833
pulmonary contusion and flail chest, effects on perfusion and O_2 exchange 80−67119
pulmonary gas exchange model, effect of ventilation-perfusion, diffusion-perfusion ratios *(French)* 79−8516
quenching of dye fluorescence for surface flow visualisation 80−79422
quenching of rubrene S_1 excited state in 1,3-diphenylisobenzofuran soln. photooxidation 80−45529
radiation belts, energetic O ions charge states theory 78−77427
radiobiological effect, molecular and cellular basis 80−26211
rare earth-transition metal alloy thin films vapour deposition, influence of gaseous phase on mag. props. *(Polish)* 80−39820
reactions with La_2O_3-Cr_2O_3 mixtures and $LaCrO_3$ *(French)* 77−52524
reactive sputtering of Sn cathode, ion formation *(Japanese)* 80−50494
recombining atomic plasmas, population inversion 80−32679
red blood cell shape, optimality, O_2 diffusion approach 80−30693
red giant stars, meridional circulation and CNO anomalies 79−48786
reduction of Pt low index surface, struct. sensitivity 79−70343
removal from Fe, by dry H_2 method *(Japanese)* 78−11234
respiration, rat brain mitochondria, mechanism of oxidative phosphorylation 79−53068
retinal damage by visible light, role of singlet O 78−15858
rivers, O_2 and pH fluctuations, math. model 78−92866
rubrene, excited singlets, O quenching, singlet O formation 78−27792
seawater, conc. in POLYMODE area (Sargasso Sea) rel. to eddy dynamics 80−85685
seawater, isotopic cycle of oceanic phosphate 77−5232
seawater concentration, rel. to Al, control by biological activity 78−61437
self-diffusion coeff. in single crystal Al_2O_3 78−30792
self-diffusion in feldspars, ion microprobe determ. 78−69325
self-diffusion in SiO_2 and GeO_2 glasses, theory 79−95214
sensors, solid electrolyte, noncatalytic electrodes 80−76573
Si:O, ion implantation, SiO_2 layer form., crystallisation, structural props. rel. to annealing 78−34724
silent discharge, numerical simulation 78−63629
simultaneous interactions with Cl_2 on Ta under low press. and high temp. 80−71938
single state quenching by Ni complexes 79−94028
singlet O_2 photoluminescence in solns. of chlorophylls and pheophytins 78−80831
skeletal muscle, canine, blood flow and O_2 uptake obs. in acute anaemia 80−45930
solar emission lines, Draper's 'discovery' and subsequent debate 77−37706
solar flares, O I 1355.6 Å and C I 1355.8 Å lines obs. 80−90381
solar O abundance, influence of diffusion 80−4318
solar photosphere, O I 7774.177 Å line asymmetry rel. to O isotope abundance 77−17530
solar quiet corona, X-ray spectrum of highly ionised O and N 78−45297
solid, α-β transition, mag. susceptibility *(Russian)* 80−6592
solid, α-phase, UV absorption at 1.3K, $^1\Sigma_u^- \leftarrow {}^3\Sigma_g^-$ transition *(Russian)* 77−48186
solid, β-γ transition as ref. temp. for IPTS 77−103
solid, β-phase, mag. excitations spectrum *(Russian)* 80−7101
solid, β-phase, possible mag. struct. *(Russian)* 79−56500
solid, antiferromagnetic, internal sublattice fields, nucl. heat capacity meas. of ^{17}O 79−95597
solid, energy loss of 0.5 to 2 MeV ^4He ions, from backscattering meas. 79−4346
solid, lattice dynamics 79−95095
solid, mag. susceptibility, temp. depend. as function of press. and mag. field, α-β transition obs. 77−47991
solid, magnetic props. theory for Heisenberg system *(Russian)* 80−54900
solid, struct. elementary excitation spectrum and thermodynamic props. *(Russian)* 79−55696
solid, transformation charact. and orientation relations 80−33917
solid α-phase, quasi 2D antiferromag., magnon and libron excitation spectra *(Russian)* 77−36067
solid γ-phase and liq., mol.-dynamic study of struct., dynamics 80−96467
solid film, optical and structural props. 78−56052
solid film spectroscopy, using Lummer-Gehrcke interferometer 77−5898
solid-solid transition discovery, international practical temp. scale precision appl. 78−87786
solubility and activity in liq. In and Cu-In 77−43331
solubility and activity in liquid Ga and Ga-Cu 77−59122
solubility and activity in liquid Ge and Ge-Cu 78−44109
solubility in Fe-Si melts *(Russian)* 80−15252
solubility in liq. U and composition of lower phase boundary of UO_2 at 1950K 80−49366
solubility in liquid Nb, exam. using thermodynamic anal. *(Russian)* 79−55889
solubility in molten Na_2SO_4 and Na_2CO_3 79−69251
solubility in Nb, steady state *(German)* 78−38851
solubility in Nb, temp. depend. 79−99326
solubility in plasticized PVC *(Polish)* 79−69252
solubility in solid Cu 77−69089
solubility in Ti-Al-Kh18 steel, thermodynamical anal. *(Russian)* 80−92676
solubility parameters, calc. from eqn. of state 77−11660
sorption, on ZrC, effect on work function, thermionic emission and thermal desorption obs. 79−56285
sorption by cobalt phthalocyanine film, AES obs. 78−91531
sorption on metal film work function 78−19125
sorption on Os cryst. in H_2SO_4 soln. 79−61873
sorption on polar ZnO surfaces, EELS 78−64434
sorption on Si(111), EELS 78−14571
sputtering of ice, MeV ions, erosion rate 78−48268
steel, C, friction faces, S, O content, secondary ion-ion emission obs. 80−55545
steel, O content determ. by fast neutron radiation *(Hungarian)* 78−92586
steel, stainless, stress corrosion susceptibility in high purity water, O_2 and temp. effects 80−61002
sticking coefficient, on cpd. semicond. (111) surfaces, ionicity effects, XPS expts. 77−85887
sticking coefficients on W (110) and (100) planes 79−82464

oxygen continued
submonolayer-covered Ni (111), surface phonons obs. by EELS 80−39403
superconducting junction electron tunnelling, effect of dissolved O^{2-} 78−80100
superheated liquid, spontaneous boiling and life-time, press. variation *(Russian)* 78−22839
supersonic beam production using microwave discharge source 79−80720
supersonic molecular beam source, simple calibration method 80−82845
surface diffusion on (110) W single crystal plane, constant pot. difference meas. 77−39921
surface diffusion on W (110), coverage-distance plots, diffusion coeff. 77−62755
surface interaction, with polycryst. Ni, SIMS and flash desorption obs. 78−76568
surface interaction on polycryst. CO, XPS, UPS *(French)* 77−73219
surface interaction with Cu (100), AES, EELS, LEED and work function studies 80−24731
technology and conservation in metallurgical extraction 78−7169
terrestrial atmosphere, O_2 and O_3 early history 79−84487
thermal conductivity, 400 to 1500K, vibr. internal energy calc. 79−18986
thermal conductivity, calcs. 79−37434
thermal conductivity, simple relation, 1000-3000K 77−24048
thermal conductivity, vibr. energy diffusion coeff., 400-1600K 77−27644
thermochemical prod. by H_2O decomposition using solar energy 80−40919
thermodynamic dissolution in Fe-Ni-Mn melt *(Russian)* 78−27473
thermomagnetic effect, interaction with Au or Pt surface *(Russian)* 77−11302
thermosphere, 0, 0_2 density profiles meas. between 90 and 220 km altitude 78−77383
thermosphere, annual var. from Aeros Nims data 80−12578
thermosphere, atomic oxygen content, 100-160 km, new spectral method 80−41578
thermosphere, O_2 concs. and absorpt. cross sections from EUV occultation profiles 78−28356
thermosphere, O conc. at 400 km altitude, incoherent scatter obs., model construction *(French)* 78−12030
thermosphere, O global distrib., dynamical effects 79−74996
thermosphere O, composition seasonal-latitudinal tidal struct. and mass density 80−101467
thermosphere O and O_2 densities, photochemical deviations from diffusive equilib. 77−37470
thermotransport and thermopower in α-Hf 78−76055
thermotransport in Ta base alloy 79−95216
three-body electron attachment, Boltzmann eqn. method 79−855
tissue composition measurement by fast neutron activation 77−64131
tissue mass transport and regulation, microelectrode and math. modelling study 78−44534
tissue O_2 electrode design criteria and perform. characts., recessed cathode 79−39543
tissue O_2 uptake continuous meas., high-sensitivity device 78−20324
tissue tension, skeletal muscle of rabbit, short-range FM telemetry 77−86722
tissue tension measurement in rabbits, using galvanic electrode 77−13040
Tokamak plasma reaction dynamics, corona model, spectroscopic diagnostics *(German)* 79−60103
toluene+O_2, fluoresc. quenching kinetics 77−18964
toluene+$O(^3P)$, reaction product identification by mass spectrometer 78−7185
transcutaneous O_2 and skin blood flow, laser system for simultaneous meas. 80−26321
transition metal-O bond energy in O_2 glow discharge, mass spectrometry obs. 80−64808
transport, during fatigue crack growth in Al-Zn-Mg alloy 78−52981
transport, during fatigue crack growth in Ti 78−52981
transport, exam. in fatigue crack growth in Ni-Cr 78−52981
transport during fatigue crack growth in Al-Cu alloy 78−52981
transport phenomena correlations, in non crystalline silica 78−47581
Trichel corona, negative ions 78−30503
trimethylbenzene+$O(^3P)$, reaction product identification by mass spectrometer 78−7185
triple point, determination at low temp. *(Japanese)* 80−31749
triple point temp. determ. by calorimetry 79−12806
tumour X-radiation response after prior exposure to reduced O_2 environment 79−88127
in tunable dye lasers, quenching effect 79−72564
upper atmosphere, O+O radiative assoc. rel. to nightglow near IR continuum 77−78551
upper atmosphere atom density, rel. to airglow intensity *(Chinese)* 80−90269
vapour, fluorescence quenching of pyrene 78−5266
vapour pressure, effect of high mag. fields 78−38825
vapour pressure meas., 90 to 154.6K, eqn. 77−27993
ventilation of ocean in Lower Palaeozoic, black shale origins 78−61436
Venus nightglow spectrum, $O_2(C^3\Delta_u$ to $a^1\Delta_g)$ 79−16856
Venus spectrum, $^1\Delta g \rightarrow {}^3\Sigma g^-$ band, prod. mechanisms 80−82251
vertical distrib. in Atlantic and Mediterranean near Gibraltar *(Russian)* 78−16058
viscosity and diffusion coeffs. 77−89225
viscosity coeffs., modified hard-sphere calcs. 77−11295
void swelling in neutron irradiated V, O_2 effect 78−6106
water thermolysis, solar furnace, thermodynamic analysis 79−83625
X-ray emission spectra from organic compounds 77−28653
X-ray transitions for F and O ions moving in Ne, Ar, Kr gases and C foils and slabs 77−69020
Zircaloy fuel cladding, O embrittlement obs. 78−89947
Zircaloy-4, elastic props., O additions effect 80−66565
Zircaloy-O_2 phase diagram 80−3003
0 I, 63 μm emission and quenching cross section in thermosphere and ionosphere 79−16732
0_2+hydroxymethyl radical, rate coefficient meas. by laser magnetic resonance flow tube method 80−66767
0_2+OCS, gas, EPR of rot. transitions, T_1 press. depend. 80−9621
$^{18}0$, abundance in Kirin meteorite shower *(Chinese)* 79−16900
ALN, O_2 effects on sintering 77−77451
adsorpt. on supported Ag surface, catalytic oxidation mechanism 78−61046
oxygen continued
adsorption on W (110), LEED, AES and thermal desorption meas. 78−38957
Ag:O wires, effects of O on internal friction and rigidity modulus 78−3160
Al, sputtered excited Al particles, effect of O during ion bombardment on spectra 79−38703
Al, thin film, K X-ray production due to ^{16}O ions, 0.25-2.25 MeV/amu 79−69906
Al:O, perforated supercond. film, RF resist. in mag. field, pinning force const. 79−56471
Al:O supercond. film, RF complex impedance meas., dynamic pinning 80−84573
Al-O (100), extended appearance potential fine struct. anal., LEED study 80−50467
AlAs-GaAs stripe heterojunction laser, O^+ implantation effect on threshold characts. 79−41383
$Al_{0.5}Ga_{0.5}As$:O insulator layers on GaAs, meas. of MIS capacitors 78−95371
$Al_{0.5}Ga_{0.5}As$:O surface layer, on GaAs p-n junction, surface recomb. current reduction 80−49878
$Al_{0.5}Ga_{0.5}As$:O-GaAs:Zn, p-n junction, reduction of surface recomb. current 79−69585
$Al_xGa_{1-x}As$:O, appl. as insulating layer in MIS struct. 78−64115
$Al_xGa_{1-x}As$:O-n-GaAs heterojunction for MIS device, capacitance voltage meas. 79−87157
AlN:O, deep impurity states, orbital spectra, CNDO/2 calcs. 78−6319
AlN:O, influence of O on luminesc. excitation spectrum in interband transition range 77−8644
AlN:O, thermolum. mechanism, 80-420K 79−78761
AlN:O, UV spectra of deep impurity centres, radiative recombination 79−87490
Ar:O_2, long wave UV luminesc. *(Russian)* 78−88347
Ar:O_2 (6%) cryst., vibr. Raman spectra 80−60558
Ar/O_2 plasma treatment of SiO_2 surface, reactivity modification 78−64890
Ar-O_2, diffusion, search for Senftleben-Beenakker effect 77−15155
Ar-O_2 liquid mixture, dielectric polarisation and permittivity *(Russian)* 77−90095
Ar-O_2 mixture, adsorption on CsI, test of eqns. for gas mixture adsorption on heterogeneous surface 78−60030
$Ar+O^+(^4\Sigma^-)$, differential elastic cross sections, 2-20 eV, interatomic pot. 77−6885
Ar^++$(N_2)(H_2)(O_2)$, charge exchange reaction rates 77−86295
Ar^++$H_2(O_2)(CO_2)$, reactions in flow-drift tube, rate consts. 78−15664
Ar^++O_2, charge transfer cross sections 77−34751
Ar^++O_2, charge transfer mech., implication of inner-shell level mixing 77−61852
Ar^{2+}+$O_2(CO_2)(C_2H_2)$, reactions in flow-drift tube, rate consts. 78−15664
$Ar^+(Ar^{2+})+O_2$, reaction rate consts. 78−48613
$Ar(4s^3P_{2,0})+O$, specific channel rate construction 77−46627
As_2Se_3, glassy, Cu, Ag and O impurities influence on electronic energy spectrum and mol. vibr. spectrum 77−90181
As_2Se_3, glassy, influence of oxygen added in As_2O_3 and SeO_2 forms on phys. props. 77−76314
Au-Cu-O surface, quantitative Auger analysis using relative sensitivity factors 78−7295
Au-Ni-O surface, quantitative Auger analysis using relative sensitivity factors 78−7295
Au-O bond energy glow discharge, mass spectrometry obs. 80−64808
Ba+O_2 flame, chemilum. from three-body recombination reactions 77−77759
Br+O_2(NO), quencher paramagnetism, deactivation rate const., spin-orbit relax. study 80−21263
Br_2+O_2, reaction with W surface, rate of reaction meas., gas flow experiment 78−92510
in C polymer chars 78−11551
C-H-O(-N) gas mixtures, high temp. emissivity, 4.8 μ region, shock waves 77−76027
C+O^+ ion-molecule reaction, 15 eV energy O^+ production system 80−84817
C_2+O_2, $C_2(X^1\Sigma_g^+)$ and $C_2(a^3\Pi_u)$ intersystem crossing and free radical kinetics 80−95668
$C_3+O_2 \rightarrow C_2^*+CO+O$, chemiluminesc., rate consts. 77−44466
CH+O reaction, absolute rate const. 80−97690
$CH_4+H^+(He^+)(O^+)$, 1 MeV dissociation, kinetic energy spectra 78−94302
CNO anomalies in spectra of OB stars 77−29835
CO, vaporisation temp. and press., state eqn. *(French)* 77−43323
CO-He-O_2 gas discharge laser plasma, positive ion generation mechanism *(Russian)* 79−99005
CO-He-O_2-H_2O laser discharge, stability, influence of recombination and ion chem. 78−17915
CO-He(-O_2), glow discharge ion cluster in positive column, ion mass spectra diagnostics 80−38752
CO-O_2 liq., polarised vibr. Raman scatt. lineshapes 78−27199
CO-O_2 liq. mixture, enhancement of nonlinear optical processes with double-pass tight-focusing geometry 79−18472
CO-O_2 liq. mixture, IR four wave sum and difference freq. generation 78−33771
CO-O_2 liquid, IR third harmonic generation 77−88849
CO-O_2-He low-press. laser discharge, increased power and efficiency 78−17914
CO-O_2-SF_6, liquid, phase matched IR third harmonic generation 78−42384
CO-$O_2(Ar)(N_2)$ dil. liq. solns., resonant IR third harmonic generation 77−31116
CO+$NO(O_2)(D_2)$, (v=1) relax., temp. depend. 78−17760
CO+O, vibr. deactivation 78−94305
CO+O+M$\rightarrow CO_2$+M, time-resolved and flame-band emissions in shock tube expts. 77−36729
CO_2-N_2-He-O_2 discharge mixture, three body electron attachment to O_2 80−64779
CO_2-N_2-O_2 mixtures, thermalisation under reson. excitation by laser radiation *(Russian)* 78−26231
CO_2-O_2, negative ion form., photodissoc., mass spectrometric obs. 78−13558
CO_2-O_2-H_2O, mixture, mol. negative ions, photodissoc. and photodetachment cross section 77−27129

oxygen continued
CO_2-O_2-H_2O, photodissoc. and photodetachment of negative ions 80−14182
$CO_2+O_2(N_2)$(air), bending mode vibr. deactivation rate, 1500-350K, shock tube meas. 77−38714
$CO_2^-+O_2$, nanosec. pulse radiolysis, react. rate const. meas. 77−16843
$CO_2(01^10)+N_2(CO)(O_2)$, collisional deactivation rate const., 160-375K, photoacoustic obs. 79−10179
$C(^3P)+O_2(^3\Sigma_g^-)\rightarrow CO(^3\Sigma^+)+O(^1D)$, pot. energy surface, vibr. population inversion, classical dynamics 77−52630
$CS+O\rightarrow CO+S$, shock tube reaction, chemiluminescence and lasing 77−16824
CS_2-O_2 flame, rate of population of CO vibr. levels, CO emission intensity 78−7186
CS_2-O_2 pulsed chemical laser and pulsed CO TE laser, comparative study 79−31876
CS_2+O_2, vibr. relax., effect of atomic O 79−66300
$CS_3+N_2O+O_2$ combustion, CO laser performance characts. *(Russian)* 78−55348
$Ca+O_2$ reaction, chemiluminesc. absolute cross sections, photon yields and CaO dissoc. energy 80−97697
CaF_2 laser window surface O_2 detection by X-ray photoelectron spectroscopy 79−14056
CaF_2:O, absorpt., ionic cond., and thermal depolarisation 79−14960
CaF_2:O, absorption, ionic cond. and thermal depolarisation 78−14502
CaF_2:O_2^-, OH^-, ion incorporation by reaction with surrounding atm. 80−55143
CaF_2:O_2^-, struct. and dynamics, EPR and ENDOR obs. 79−33562
CaF_2:O^-, Jahn-Teller distortion, electronic struct., MS Xα calc. 78−23057
CaF_2:O^{2-}, CaF_2:Na^+, O^{2-} and CaF_2:Y^{3+},O^{2-}, thermal depolarisation obs. of defect clusters 80−71299
CaF_2:O^{2-} lattice, effect on thermal/elec. props. 77−76599
CaF_2:Pb,O, UV absorption, impurity centres 78−68534
$Ca_2LaFe_3O_{8+x}$, influence of O_2 partial pressure on nature of point defects, characterisation by elec. cond. meas. *(French)* 79−42055
$^{44}Ca+O_2(O_3)$, reaction products identification by IR spectra in N_2 matrix 78−9151
CdS:Li, O film, chemical bath deposited, photocond. and optical props., O trap level 80−2426
CdS-O_2, photoactivated O desorption 80−100391
CdSe-O_2, photoactivated O desorption 80−100391
Ce-S-O equilibrium in molten Fe *(Chinese)* 80−104423
Cl+He(C)(O)(Ne), K-shell ionising collisions, average L-shell ionisation probability, K_α spectra 79−72408
$ClO+O\rightarrow Cl+O_2$, reaction kinetics, 220 to 426K, at. fluoresc. obs. 77−21380
$ClONO_2+O(^3P)$, fast flow reaction, rate const. 77−12777
$ClONO_2+O(^3P)$, rate consts., flash photolysis-reson. fluoresc. obs. 77−77796
Cs-O adsorbed films on Si (100), oxide formation, ionisation loss spectra, AES 79−69365
Cs-O_2, desorption from W, activation energy 80−103562
$Cs+O_2$, reaction kinetics, time-resolved meas. 77−90588
CsBr:O_2^-, Stokes' losses on cryst. vibrs. in luminesc. spectra of mol. centres *(Russian)* 77−55827
CsBr:O_2^- centres, luminesc., polarisation temp. depend. 78−87943
Cu, surface tension cct. cavities under Cu^+ ion irradiation, O_2 and He effects *(French)* 77−35611
Cu-Ge-O, phase diagram and thermodynamics, electrochem. study 80−50617
Cu-O-polymer complex on polystyrene formation 78−92372
Cu-SiO_2 alloy, fracture at elevated temp. 78−39896
$D_2^++O(^3P)\rightarrow OD^++D$, reaction dynamics, cross-section at. quadrupole moment effects 78−3324
Eu-W-O, reaction system, thermodynamics, mass spectrometric obs. 77−77748
$Eu+O_2$, reaction cross-section, energy depend. 77−9054
$F+O_2+M\rightarrow FO_2+M$, flash photolysis IR chemiluminesc., rate const. 78−3311
Fe, cast, air-atomized powder, effect of particle size on C and O contents 78−15340
Fe, single cryst., segregation behaviour of S, O and P at (100) surface 80−100841
α-Fe:O, valency effect of interstitials 80−65502
Fe:O,N, bonding of Al, growth of intermediate phases, effect of O and N impurities 78−27680
Fe:Yb,^{18}O, interaction between implants 77−27921
Fe:Yb,O, interaction between impurities, perturbed ang. correlation meas. 77−1628
Fe^{3+}-O^{2-}, overlap and covalency contrib. to zero field splitting, LCAO-MO calc. 80−24850
$Fe+O_2$, cyclic complex form., matrix isolated IR spectra assignments 77−88449
FeGd:O film, amorphous, O_2 contamination effects on mag. props. 78−64231
GaAs, C, O, Si impurities 78−59832
GaAs, O^+ implantation, energy levels, photoluminesc. 80−24838
GaAs thin film, effect of O on thin film compositions obtained by secondary ion emission 80−26079
GaAs: O_2, impurity levels charact. using dark capacitance and photocapacitance transient techniques 80−59920
GaAs:0, effect of displacement upon impurity levels, psuedopotential calc. 77−39803
GaAs:C,O, impurity conc. determ. in LEC grown cryst. 77−39612
GaAs:Cr, O, effect of O in photoluminesc. meas. 80−29799
GaAs:Cr,O, semi-insulating, photocond. anal. of levels 80−20243
GaAs:Cr,O semi-insulating monocrystal development and four-level model 80−88191
GaAs:Fe(Ni) O_2 effects on opt. props. 77−16350
GaAs:O, annealing effects, optical absorpt. and I-V charact. 80−29037
GaAs:O, deep impurity levels, AC photocond. meas. 78−19082
GaAs:O, deep level, Franck-Condon shift, photocond. and Hall effect study 80−70642
GaAs:O, deep traps, photocapacitance meas., complementary transition energy threshold determ. 79−19550
GaAs:O, defect states, IR absorption spectra meas. 77−4666
GaAs:O, electrolum., photolum., negative differential resist. rel. to recomb. processes 80−66304
GaAs:O, electronic struct., multiple-scatt. Xα mol. cluster model 80−15445
oxygen continued
GaAs:O, evidence for metastable state of O centre, Schottky barrier photocapacitance meas. *(French)* 78−10556
GaAs:O, Fe, temp. depend. of ionisation energies of O and Fe levels, electroabsorption meas. 78−47736
GaAs:O, field depend. of radiative recomb. 80−20700
GaAs:O, high-resist., extrinsic photocond. meas. 77−85255
GaAs:O, implantation, effect on LPE growth and elec. props. 80−24477
GaAs:O, impurity photocond. in high elec. field, 90K 78−19095
GaAs:O, junction barrier depletion region, capture from free-carrier tails 80−70802
GaAs:O, LPE layers, O effect on defects and elec. props. 77−76683
GaAs:O, mechanism of thermal quenching of luminesc. and photocurrent stimulation 77−55821
GaAs:O, optical characterisation of deep O implants 77−55294
GaAs:O, oxygen-compensated single GaAs cryst., photoelec. memory 79−11184
GaAs:O, photocapacitance quenching effect 78−91727
GaAs:O, photocapacitance of deep levels obs. 79−38021
GaAs:O, photocond., electron traps, level-broadening, 90 to 150K 78−60158
n-GaAs:O, photocond. associated with deep level at 0.4 eV 80−44640
GaAs:O, relax. semicond., Dember effect meas. 79−28372
GaAs:O, semi-insulating, excitation temp. effect on TSC 80−70717
GaAs:O, slow domains, origin 78−60132
n-GaAs:O carrier removal profiles meas. 78−56154
GaAs:O epitaxial film, impurity states, photocapacitance spectra 80−65625
n-GaAs:O film, influence of O on elec. props. 79−11252
GaAs:O p-ν-n structs., injection current and negative photocond., saturation mechanism 80−92967
GaAs-O_2 system, electron beam induced adsorption, ion beam effects 77−11778
GaF+O matrix reaction, OGaF IR spectrum 79−11787
GaP, deep O^- state, model impurity calc. 80−6780
GaP:0 effect of displacement upon impurity levels, pseudopotential calc. 77−39803
GaP:Cs-O simultaneous adsorption, oxidation interface chemical struct. 80−103584
n-GaP:N,O,S,C end, dielec. const. from S-C donor acceptor pair spectra 79−65788
GaP:N,O epitaxial struct., luminesc. study of degradation during heat treatment 80−45139
GaP:O, donor centre struct. and conduction band nonparabolicity 78−14695
GaP:O, EPR investig. of deep donor centre, delocalisation 77−28428
GaP:O, impurity concentration determ. by donor-acceptor luminescence 78−6090
GaP:O, multicharged state of O, TSC and photoinduced currents 79−7808
GaP:O, optical transitions via deep levels, phonon interaction 78−87939
GaP:O, optical transitions via deep levels, cross section temp. depend. 78−87940
GaP:O, photoionisation of deep impurity levels 80−34386
GaP:O, spectral depend. of O photoneutralisation cross-section near threshold 79−1788
GaP:O, wave functions and optical cross sections associated with deep centres 78−34801
GaP:O^-, two electron state, electron capture 78−39054
GaP:O^-, two-electron O^- state evidence, ODMR, IR emission, phonon replicas 80−15828
GaP:Zn, O, influence of impurity-absorbed illumination on luminesc. 80−93395
GaP:Zn, O LED, neutron irrad. effects on capacitance, I-V and electrolum. charact. 77−66543
GaP:Zn,O, Auger coeff. from luminesc. decay and Hall effect 77−48226
GaP:Zn,O, Auger coeff. from luminesc. efficiency and Hall effect 77−48227
GaP:Zn,O, bulk electrolum. degradation in LEDs 77−81156
GaP:Zn,O, degradation of bulk luminesc. induced by laser excitation 77−1715
GaP:Zn,O, kinetics of X-ray luminesc. 78−10984
GaP:Zn,O, photodiodes, high temp. emission spectra *(Russian)* 77−66545
GaP:Zn,O, red LED, deep-level changes associated with degradation 77−1472
GaP:Zn,O LED, 76K electrolum, spectrum, γ-irrad, and forward bias effects 79−78756
Ge, amorphous and crystn. films, contamination behaviour, XPS examin. 79−1815
n-Ge:Bi,O, plastically deformed, dislocation scatt. anisotropy, effect of state of O in Cottrell atm. 78−19028
Ge:Li,O, EPR and piezospectroscopy 80−25338
Ge:Li-O, donor complex EPR and photoelectron piezoelectric spectra, dynamic tunnelling 79−1711
Ge:O, Cu, amorphous thin film, impurity effects on struct. 80−107054
n-Ge:O, Czochralski growth, O content rel. to props., IR, Li precipitation determs. 77−15445
Ge:O, elec. props., O donor levels determ. 77−8123
Ge:O, elec. props., O interaction with point defects 79−11081
Ge:O, IR absorpt. at low temp. *(Chinese)* 80−108228
Ge:O, intrinsic γ detector, deep level defect connection with O content *(Russian)* 78−43331
Ge:O, shallow defects, PTIS meas. 80−24971
Ge:O, slow thermal relax. of cond. rel. to donor complexes 80−70704
Ge:O amorphous film, ion-implanted, absorpt. edge and elec. props. 77−39970
Ge:O ion implanted, O localisation determ. 79−95040
Ge:O(Si), effect of impurities on mech. strength in brittle fracture region 79−87682
Ge-O, removal from a-Ge in pre-crystallisation annealing 78−9957
H-O electrochemical matrix-type cells, transport effects study 80−26027
$H+B^{q+}(C^{q+})(N^{q+})(O^{q+})$, $(2\leq q\leq 4, 5)$, cross sections at keV energies 80−78705
$H+H^+(Arq^+)(Kr^{q+})(B^{q+})(C^{q+})(N^{q+})(O^{q+})$ charge transfer and impact ionis. cross sections calcs. 77−88555
$H+O_2$, charge prod. cross sections and differential scatt. calcs. 78−94313
$H+O_2$, excitation of Hα and Lα emissions, rel. to aurora 79−68309
$H+O_2$ system, production of $O_2(^1\Sigma_g^+)$ 77−63918
$H+O_2+Ar$, HO_2 free radical prod., rate const. calc. 80−101026

oxygen continued
$H+O^{2+}$, ionization model for NGC 7027 planetary nebula 78−36671
$H+O^{8+}\rightarrow H^{+}+O^{7+}$*, during neutral beam injection into Tokamak 77−58899
H^{+}+He(Ar)(Kr)(O_2)(H_2)(N_2), 2.2-8.2 keV, H(n=3) form., absolute cross sections 77−34755
$H^{+}+O_2^{-}$, nanosec. pulse radiolysis, rate consts. meas. 77−16843
H_2-F_2-O_2, chem. laser mixture, multiatm., spontaneous explosions 78−73044
H_2-O_2 gas mixture in chem. equilib., elemental diffusional separation in nonisothermal flow 79−55429
H_2-O_2 mixture, explosion limits as stochastic phenomenon 77−21387
H_2-O_2 reaction boundary layer, numerical anal. *(German)* 77−35253
H_2-O_2 seeded system for MHD generator, elec. cond. 80−76642
H_2-O_2 system with N_2, O_2 diluents, detonation wave instabilities 78−5762
H_2-O_2-Ar flame, excitation profiles of Na D-doublet 77−88436
H_2-O_2-N_2 flame, photochem. reactions involving Na*, laser saturated conditions 78−80762
H_2-O_2-N_2 flames, diffusion coeff. meas. for CO, Br, I and Tl 78−51272
H_2+O_2, adsorbed on Pt particles supported on SiO_2 gel, low press. reaction 77−52668
H_2+O_2, combustion, kinetic modeling and sensitivity anal. 80−89490
H_2+O_2 fuel, equilib. compositions, 1000 to 6000K *(Ukrainian)* 79−50571
H_2+O_2 on polycryst. Ni surface, SIMS and thermal desorption meas. 80−40742
H_2+O_2+CO, 500°C, rate consts. involving OH and HO_2 radicals 78−35646
$H_2+O\rightarrow OH+H$, vibr. energy effects, classical trajectory calcs. 77−63904
HCN compact CW laser, output increased by He, Ar, air and O_2 buffer gases 79−10293
HCO+NO(O_2), reaction rate consts. 78−31617
HCl+O^{-}(O_2^{-})(NO_2^{-})(CO_3^{-})(CO_4^{-}), rate consts. at 300K 78−76829
$HCl+O(^1D_2)\rightarrow OH+Cl$, correl. diagram 77−16798
$HCl(\nu=1,2)+O(^3P_g)$, reaction and deactivation, laser-induced fluoresc. obs. 78−35669
HF with interstitial O, quantitative TEM obs. of small agglomerates 80−107227
$HF+O_2(a^1\Delta_g)$, E-V energy transfer 77−30960
H_2S+O_2, press. broadening of spectral linewidth, calcs. 77−30932
He-Co_2(O_2) volume discharge, electron recombination and attachment 77−19799
He-O mixture, RF discharge, mass spectroscopy, floating double probe meas. 80−84016
He-O_2, diffusion, search for Senftleben-Beenakker effect 77−15155
He-O_2 corona discharge CV characteristics 78−91168
He-O_2 DC discharge, electron distrib. function 80−92407
He-O_2 diffusion coeff., two-bulb meas. 77−11299
He-O_2-acetylene flame atom cell, for at. spectrometry, characterisation 78−32876
He+B^{3+}(C^{4+})(N^{5+})(O^{6+}), electron transfer 78−13598
He+H_2 (O_2), rot. cross-section, exponential distorted wave and effective Hamiltonian 78−37709
He+N_2(O_2)(HCl), Pennin ionis. electron spectra, new differential retarding field analyser characts. 77−41735
He+O_2, vibr. energy transfer, exact classical and quantal calcs. 77−19014
$He^{+}+O_2$, (N_2), charge transfer reactions, product ion distribs. 77−73445
^{4}He stopping cross sections, 1-8.5 MeV 78−58558
α-Hf, electrotransport of O impurities *(German)* 78−87826
$I+I+O_2\rightarrow I_2+O_2$, photolysis, rate const. obs., mechanism 77−63883
$I+O_2$, chemical generation of population inversion between spin-orbit states of I 78−17767
$I_2+O_2\rightarrow IO$, flash photolysis reaction mechanism 77−32813
In:O surface, impurity precipitation and resolution at melting point 78−14553
$In_{1-x}Al_xP$:Zn,O, radiative recombination at isoelectronic centres 79−52027
$In_{1-x}Ga_xP$:Zn,O, radiative recombination at isoelectronic centres 79−52027
InMb:O, influence of O and lattice disorder on Kondo resist. 79−38061
InP: C, O, impurity conc. determ. in LEC grown cryst. 77−39612
$K+O_2\rightarrow K^{+}+O_2^{-}$, electron transfer kinematics 77−6903
KBr(Cl)(I):O_2^{-} centres, luminesc., polarisation temp. depend. 78−87943
KCl:O_2^{-}, Stokes' losses on cryst. vibrs. in luminesc. spectra of mol. centres *(Russian)* 77−55827
KCl:Pb^{2+}, role of O impurity in 420 nm emission 77−40279
KOH-O_2-N_2O-t-butane pulse radiolysis, kinetics of transient O compound form. meas. from Cherenkov emission 77−70321
$KZnF_3$:(Fe^{3+}-O^{2-}), overlap and covalency contrib. to zero field splitting, LCAO-MO calc. 80−24850
Kr:O, laser, electron beam excitation 77−711
Kr-O_2, high press. mixtures, gain profile near 5577 Å 77−68204
$Kr^{+}+O_2$, charge transfer mech., implication of inner-shell level mixing 77−61852
Li/O_2, surface complex form. obs. using photoelectron spectra 79−69359
LiF:O, impurity effect on elec. cond. 79−7709
Mn^{2+}-O^{2-}, overlap and covalency contrib. to zero field splitting, LCAO-MO calc. 80−24850
Mo, cast state, interaction nature between C, O_2 and N_2 *(Russian)* 79−70114
N-O mixtures, positive glow corona in quasi-uniform fields 80−100104
$N^{+}+O_2$, branching ratio kinetic energy depend. 80−97703
N_2-Ar-O_2, liq. vap. equilib. prediction using cubic eqn. of state 78−18737
N_2-Ar-O_2 system, vapour-liq. equilib. 80−54358
N_2-O_2, electron impact dissoc. ionisation, N^{-} form., mass spectra 77−75320
N_2-O_2, liquid, high resolution CW CARS spectra 80−63635
N_2-O_2, vap.-low. equilib., mag. field effect 78−91429
N_2-O_2 gas mixture, weakly ionised, electron transport coeffs. anal. *(Japanese)* 80−59184
N_2-O_2 gas mixtures, elec. breakdown voltage, 113-293K 79−1363
N_2-O_2 mixture, impulse breakdown processes at low press. 80−44021
N_2-O_2 mixture, moist, electron beam irrad., SO_2 oxidation, appl. to exhaust gas treatment 78−80766
N_2-O_2 mixture, NO synthesis, reactions of vibr. excited N_2 in nonequilib. plasmachem. system 77−86310

oxygen continued
N_2-O_2 mixture transient discharges, RF techniques 80−70067
N_2-O_2 nonselfsustaining discharge plasma, current establishment/relax. processes, rel. to CO_2 laser *(Russian)* 79−99011
N_2-O_2-Ar saturated air vapour mixture, film, mixed condensation, comparison with water vapour 77−11780
N_2+Ar^{+}, reaction kinetics, mass spectrometer with selective introduction drift tube *(French)* 79−11839
N_2+O_2, binary diffusion coeff. pressure depend. meas. 80−43826
N_2+O_2 collinear collision, quantum-mech. model 77−30955
N_2+O_2 electron beam irrad., rel. to exhaust gas treatment 78−80765
$N_2^{+}+O$ reaction, in ionosphere, rate coeff. determ. 77−53288
$N_2^{+}+O_2$(H_2)(He), ($A^2\Pi_u$) Meinel band deactivation cross sections above thermal energies 78−66635
N_3+O, NO chemilum. obs. in NaN_3 thermal decomp. N_3 form. 79−100351
$N_4^{+}+O_2$, reaction rate determ. 78−60985
$NH+O_2$ energy transfer rate const., time-resolved fluoresc. rise 79−83489
NH_3+NH_3(He)(Ar)(N_2)(O_2), ν_2 state vibr. relax., laser induced vibr. fluoresc. obs. 79−18269
NH_3+O_2, flash photolysis, NH_2+HO_2 rate const. 79−47943
NO+O, chemiluminesc., rate const., optical comparison method meas. 77−90603
NO_2+O^{-}(O_2^{-}), charge exchange excited NO_2^{-} formation 77−75236
$N_2O_5+O_2^{+}=NO_2^{+}+NO_3+O_2$, rate const. 78−56879
$N(^4S)+O_2(^3\Sigma_g^{-})\rightarrow NO(^3\pi_u)+O(^3P)$ doublet surface minimum energy path calcs. 78−7194
Na:O, evaluation of V wire equilibration method, for determining O content 78−79626
$Na+O_2$, total elastic cross sections meas. 77−30954
NaCl crystals with dipole O colour centres, radiation colouring and holographic recording 80−48187
NaCl:O, hologram recording, colloidal type centre transformation *(Russian)* 80−55147
NaCl:O, photographic recording in far-UV, colour-centre formation 79−23035
NaCl:O_2^{-}, excitation and absorpt. spectra at 2K, O_2^{-} excited state field 79−56843
Na(3^2P)+O_2(SO_2), near-threshold ionis. of Na* 77−88544
Nb:O, $^4He^{+}$ irrad.-induced lattice site change 79−99252
Nb:O, interstitial O impurities, diffuse neutron scatt. 78−83809
Nb:O, muon diffusion and trapping 79−56685
Nb:O, type II supercond., radiation-induced flux pinning 78−80106
Nb-O, lattice location measurements of O, using $^3H/^{16}O$ and $^1H/^{18}O$ prompt nucl. reactions, ion irrad. effects 79−86813
Nb+O_2, high temp. interaction kinetics and mechanism 79−100432
Ne:O_2, long wave UV luminesc. *(Russian)* 78−88347
Ne-O_2, DC glow discharge, Ne I spectral line intensities 78−74610
Ne+O^{8+} K-shell ionisation cross-sections, Glauber approx. calcs. 77−46629
Ne^{+}+O, K-shell excitation cross sections, variable screening model 77−42387
Ni (001)/CO(O) system, adsorbate geometries determ. from final state scattering in X-ray photoemission 80−54488
Ni-Cu, liq., activity meas. of O_2 by EMF method *(Japanese)* 80−54408
Ni-Nb (5, 10 at.%), initial oxidation process at high temps., appl. of high energy ion backscattering anal. for O oxidation *(Japanese)* 79−24651
Ni+H^{+}($^4He^{2+}$)(O)(Li), K-shell ionis., impact parameter depend. 77−83707
O 2.53 mm line, Zeeman splitting rel. to geomagnetic field vars. 80−77124
O (^1D), collisional quenching by inert gas atoms 78−66648
O (^1D) 6300Å photoelectron induced predawn enhancement, altitude profiles 77−17290
O (^1D) production in upper atm. by O_2^{+} dissociative recomb. 77−41251
O (^1D)+O_2(N_2)(CO_2)(O_3)(H_2O), 100-350K, reaction rate consts. 77−21355
O ($^1S_0$)$\rightarrow$O($^1D_2$), nightglow 5577 Å intensity latit. var. calc. 77−37474
O (^1S) production in lower thermosphere, comparison of Chapman and Barth mechanisms 77−33235
O (^1S)+N_2O, quenching rate const. determ. 77−10626
O (^3P)+CH_3CN(CF_3CN), reaction mechanisms and kinetics 77−36728
O (^3P)+H_2S(D_2S), reaction rate, flash photolysis-reson. fluoresc. obs. 77−4918
O (^3P)+inert gas atom, absolute total cross sections, 0.6-2.0 km sec^{-1}, model pots. 77−19010
O (^3P)+n-butane (NO(M=Ar)), reaction rate constants using flash photolysis-NO_2 chemiluminesc, method 77−44458
O (^3P)+tetrafluoroethylene, time-resolved absorpt. spectra, triplet CF_2 formation 77−44472
O (O^{+}) (O^{2+}), Rayleigh and Compton X-ray scatt. cross sections in plasma 80−43884
O (2^1D_2)+Cl_2, reaction kinetics, vac. UV at. spectra 77−21365
O (2^3P,2^1D)+N_2O(CO_2), diabatic correlations 77−25256
O, adsorbed on metals, ion impact desorption, adsorption energy depend. 80−39442
O and O^{+}, one-electron capture cross sections in alkali metal vapours 79−59553
O atmosphere spectral emission at 557.7 nm, 100 km altitude 80−61933
O concentration in mesosphere, inference from from positive ion comp. data 80−8405
O depth profiling in solids using ^{16}O(d,p) 79−5212
O, electron impact, collision freq. in ionospheric F-region 79−53641
O I, 3s′ $^3D^0$ and 3d $^3D^0$ levels excitation and radiative decay 79−80064
O I, 63 μm emission spectrometric meas. in thermosphere 78−81474
O I, anal. of chromospheric spectrum in α Bootis (Arcturus) 77−56923
O I, interstellar, fine struct. levels population ratios 79−35351
O I, lifetimes of 2s2p $^3P^0$ state 77−27027
O I, new absorpt. lines 79−26923
O I, nightglow spectra correl. to atmos. Na density 80−41585
O I, O II, permitted lines excitation cross-sections, rel. to auroral emissions 78−37745
O I, oscillator strengths interstellar O abundance 78−16498
O I, photoionis. cross section 79−13685
O I, resonance line broadening in low press. He discharge lamps 78−9123
O I, weighted oscillator strengths for elec. dipole and forbidden transitions, data tables 80−37779
O I 1304 Å, airglow emissions from cometary inner comas 78−45282

oxygen continued
O I 1304 Å atmospheric emission, nadir intensity/column prod. rate ratio rel. to airglow 77−45213
O I 5577 and 6300 Å emissions in dayside cleft aurora 77−2294
O I 5577 Å, airglow in upper atmosphere, semi-annual vars. 78−28360
O I 5577 Å airglow wave vars. and meteor zone wind speed 79−62637
O I 5577 Å and 6300 Å, laboratory discharge lamp source for lines of known width 80−4148
O I 5577 Å and 6300 Å forbidden emissions during aurora, line profile vars. 78−45081
O I 5577 Å auroral emission, calc. from electron flux meas., comparison with obs. 77−9592
O I 5577 Å emission of meteors, vel. dependence 78−20758
O I 5577 Å forbidden line in meteor trains, emission mechanism 78−49395
O I 5577 Å forbidden line rel. to O_2 and OH band atmospheric spectra 78−61639
O I 5577 Å forbidden line and O_2 7620 Å band auroral excitation 78−88964
O I 5577 Å line depend. on E_s-layer 77−67006
O I 5577 Å line nightglow, intensity var., related to solar tides *(Russian)* 80−12585
O I 5577 Å lower thermosphere emissions, vars. rel. to thermal tides 77−78550
O I 5577 Å meteoric forbidden line collisional quenching 77−17448
O I 5577 Å nightglow, correl. with OH and Na D-line emissions 79−80067
O I 5577 Å nightglow, meas. via two-channel rocket photometer 78−45078
O I 5577 Å nightglow line profiles, thermospheric temp. vars. determ. 77−9584
O I 5577 Å nightglow obs., evidence for vertical transport latit. var. near mesopause 79−70903
O I 557.7 nm forbidden line emission structure in airglow 79−35027
O I 557.7 nm nightglow in central polar cap 77−33238
O I 5588 Å green line airglow emission rel. to HF wintertime absorption in D-region 79−58148
O I 630 nm airglow profile, daytime thermospheric temps., wind vels. and emission intensities 79−58144
O I 630 nm nightglow line profiles, thermospheric temps. and winds 79−58143
O I 630 nm predawn airglow, excitation by conjugate photoelectrons 78−49196
O I 6300 Å airglow, anal. of consistency of ground-based obs. with satellite results 80−98496
O I 6300 Å airglow, interferometer meas. rel. to global model of exospheric temp. 77−53265
O I 6300 Å airglow rel. to O atoms creation and destruction 79−8735
O I 6300 Å emission in twilight airglow, thermospheric temperature depend. 77−45215
O I 6300 Å forbidden line high resolution obs. in dayglow 77−41252
O I 6300 Å forbidden line nightglow, ground-based meas. contamination by OH emissions 78−4020
O I 6300 Å in type A aurora rays, emission intensification 80−4163
O I 6300 Å line, ground meas. for exospheric temp. determ. 77−67003
O I 6300 Å line correl. with electron content in nighttime F-region 77−67007
O I 6300 Å line meas. of $O(^1D)$ quenching coeff. by molecular collision, optical meas. 79−2419
O I 6300 Å nightglow, first obs. in Guinea 79−58146
O I 6300 Å pre-dawn emission and super-thermal ions from conjugate points 77−9589
O I 7773 Å triplet obs. in late-type giant stars 79−35250
O I 7774 Å line in O6 to G2 stars, equivalent widths and narrow-band photometry 80−8621
O I 7774 Å multiplet obs. of nightglow over Arecibo during magnetic storm 80−72663
O I 7990 Å and 11287 Å branching ratios, astron. appl. 79−41134
O I 7990 Å branching ratio, lab. study, rel. to airglow and auroral emissions 79−775
O I 8446 Å emission excitation mechanism, visible and IR obs. of Seyfert 1 galaxies 80−85991
O I airglow emission rate, midlatitude maximum characts. obs. 79−84561
O I auroral emissions, ground-based photometric meas. 78−77387
O I dayglow red emission at 630 nm in Mars atmosphere 80−62063
O I EUV and far UV emissions obs. in tropical ionosphere 77−2297
O I emission resonance triplet lines form. in solar spectrum 78−24504
O I forbidden 6300 Å airglow at mag. equator, rel. to vertical E×B plasma drift vel. 80−36435
O I forbidden lines in nightglow, historical review 79−5699
O I green line (5577 Å) in nightglow 79−48596
O I green line airglow, obs. during Winter Anomaly Campaign (1957/76) 78−45075
O I ionospheric red line luminesc. amplification by radiowave anomalous absorpt. *(Russian)* 79−29925
O I lines in A-type stars, non-LTE anal. 77−41378
O I nightglow, 557.7 nm line excitation 79−75008
O I transition probabilities and oscillator strengths, rel. to H I regions 77−49448
O II, III, IV, beam-foil spectra, mean lives, 270-490 angstrom 78−55223
O II, O III, Stark, broadening estimates 77−18841
O II, relative intensities and lifetimes in nebulae, conventional radiation theory 80−109513
O II 537 and 581 Å lines contrib. in He I 584 Å dayglow meas. 77−41253
O II 7319-7330 Å dayglow, meas. and theory 77−37475
O II 7320-7330 Å emissions meas. at twilight 78−88962
O II and III, mean lifetimes of astrophysically important excited levels 77−46528
O II dielectronic recombination through the forbidden levels, in low density and T_e highly ionised plasma 80−43850
O II forbidden lines as determinant of reddening and electron density, astron. appl. 79−30114
O III, 88.35 μ forbidden line obs. in Orion Nebula 77−5557
O III, electron impact excitation of semi-forbidden transitions 80−48092
O III, electron impact excitation cross sections, independent particle model calcs. 80−63823
O III, forbidden lines in quasars and active galaxies, theory 78−93408
O III, m-representation approach to atomic structure 79−45645
O III, optical oscillator strengths for astrophysically interesting lines 80−32660
O III, production by Auger effect, astrophysical appls. 78−20633
O III, Z 80−43972
O III 1666 Å line used in electron density determ. for quiet Sun and polar coronal holes 79−21245
O III 5007 Å forbidden line profiles from M16 H II region 79−8976
O III 5007 Å forbidden line splitting, NGC 7293 (Helix Nebula) obs. 79−25694
O III 51.8 μ forbidden emission line obs. of Orion Nebula 78−65510
O III forbidden line in Seyfert galaxy NGC 1068, high-resolution profile 80−46665
O III forbidden lines in Seyfert galaxy Markarian 335, intensities rel. to gas props. *(Russian)* 79−101204
O III forbidden lines in Omega Nebula (W38, M17, NGC 6618), IR spectra obs. 80−90495
O III+e, low energy reson. struct., distorted wave approx. 77−75307
O IV, electron-impact excitation cross sections 80−14236
O IV, intersystem multiplet as density indicator for solar plasmas 80−31264
O IV, low lying levels, excitation equilib. 79−12401
O IV, optical oscillator strengths 79−98043
O IV 1402.5 Å semi-forbidden line, identification with 1400 Å emission feature in quasi-stellar objects 80−12825
O IV bound states, oscillator strengths and photoionisation cross sections 80−106293
O IV solar intersystem line obs. in EUV, electron density at 10^5K 78−53903
O IV(VI), circular polarisation of light emitted in beam-foil collisions, cascade free lifetimes 78−55228
O $I(^3P)$ in lower thermosphere, nighttime conc. obs., using new rocket borne instrument 80−105066
O in atmosphere, effects on abundance of nearby supernova 80−94584
O in lower ionosphere, conc. determ. by fluoresc. technique 80−36434
O, in thermosphere, 63 μm radiation field and influence on H temp. 79−80066
O, in upper atmosphere, concs. rel. to F-region electron density parameters 77−91346
O in Venus upper atmosphere, consequences of exosphere temp. day-to-night var. 79−35164
O, inelastic electron scatt., 100-500 eV, $^3P \rightarrow {}^3S^0$ oscill. strength 79−81282
O ion, A=16, 18, +atom collisions, K-X-ray production 77−23554
O ion, range calc., number of primary atoms created in diatomic target *(French)* 79−1473
O ion+Au, L-shell X-ray production and subshell ionisation cross sections meas. 80−91637
O ion+inert gas, small impact parameter scatt., charge distrib. 77−30989
O ions+B(C), 10-40 MeV, soft X-ray spectra 77−75089
O isotope fractionation in alkali halide H_2O and D_2O solns. 78−22629
O isotope stratigraphy and Late Pleistocene coral terraces in Barbados 77−78182
O, O_2 distribution in lower thermosphere 80−4159
O remote sensing in mesosphere and lower thermosphere, two-photon lidar technique 79−39869
$\delta^{18}O$ scales, proportional vars., interlaboratory comparison 78−69326
O silent discharge, excited species reactions, O_3 form., discharge channel characts., numerical simulation 80−38813
O, spectral line shape in upper atm. following dissociative excitation 80−105097
O V, $2s^2S_0$-$2s2p^3P_1{}^\circ$ intercombination line wavelength determ. 80−102470
O V, $2s3p\ ^3P_1$-$2s^2\ ^1S_0$ intercombination line transition probabilities 80−18823
O V, EI transition probabilities, lifetimes, CI calc. 80−83321
O V, electron collisional excitation, R-matrix calc. 77−58169
O V, electron impact excitation cross sections, Coulomb-Born approx. 77−75302
O V, electron impact excitation, resons. converging to n=3 thresholds 79−50136
O V, electron-impact excitation calcs. 79−81286
O V, excited states, transaction oscill. states and wavefunctions 79−59367
O V, independent particle pots. comparison 80−52846
O V, intercombination lines, transition probabilities determ. 79−89645
O V, O VI, dipole lengths, dipole vels. and transition probabilities 79−35113
O V, solar emission line ratios interpretation 78−28598
O V, transition probabilities calcs. 79−54792
O V,VI plasma impurity UV emission, poloidal asymmetry obs., grad B drift 78−26331
O VI, $2s^2S$-$2p^2P$ reson. lines, wavelength determ. 80−102470
O VI, electron ionisation cross sections of excited atoms and ions 80−43186
O VI, in plasma, ion electron collisional radiative recomb. coeffs., bottleneck calc. 80−53942
O VI, interstellar, absorpt. lines statistical anal. rel. to coronal gas in Galaxy 78−36653
O VI, ionis. rate meas. in theta-pinch plasma, VUV obs. 78−26254
O VI absorption in interstellar cloud surfaces 79−97049
O VI gas in solar corona, circumstellar or interstellar origin 78−57528
O VI in OB-type stars stellar winds, P Cygni line profiles obs. 80−8630
O VI interstellar survey, UV spectra of OB stars 78−36679
O VII, beam foil lifetimes in 10-100 ps range 77−23471
O VII, electron impact collision rates, reinterpretation of solar emission line ratios 80−98624
O VII, electron impact excitation cross section calcs. using nonrelativistic Coulomb-Born approx. 77−42414
O VII, emission line obs. in diffuse soft X-rays from Hercules N_H minimum region 79−25759
O VII, ground-state electron impact excitation strengths, close-coupling calcs. 80−23561
O VII, laser produced plasma, satellite spectra 78−5165
O VII and VIII, beam foil excited, alignment effects 77−34605
O VII electron impact excitation, reson. effects 79−41243
O VII line intensity ratios depend. on temp. and ionization balance 79−16903
O VII line ratio for solar flare, X-ray obs., electron density determ. 80−82326

oxygen continued
O VIII, and isoelectronic series, in laser-produced plasma, Balmer fine struct. (broadening) 80−48860
O VIII 18.97 Å resonance line emission detect. in Puppis A supernova remnant 77−45535
O VIII emission line detect. from M87 in Virgo cluster 80−26977
O^- ($^2P^0$), attachment energies, ab initio calc. 77−30768
O^- and O_2^- ion swarm in O_2, reactions and transport, Monte Carlo calc. 78−59539
O^-, electron impact detachment, cross-section, 10-1000 eV 79−31702
O^-, electron impact detachment cross sections 79−89787
O^-, form. from O_2 adsorbed on reduced Mo_2O_3-Al_2O_3 catalysts 78−85197
O^-, free-free absorpt., multichannel theory 77−18816
O^-, in silicates, XPS quantitative anal. *(Japanese)* 77−48710
O^-, interstellar, ionisation and interstellar medium heating by photoelectrons 78−36666
O^-, photodetachment, fine struct. transitions, photoelectron spectra 78−55151
O^-, photodissoc. and photodetachment in $O_2/CH_4/H_2O$ mixtures, 3500-8600 Å 79−45776
O^-, spectra in pure O arc plasma, 2000-9000 Å, 9000K 79−32750
O^-, Xα method predicting unstable state 78−82640
$O^{+,4+}$, electron impact calcs. using R-matrix and linear algebraic methods 79−59579
O^+ (^2P) ionisation freq. determ. using satellite airglow and neutral comp. data 77−5384
O^+, absolute electron impact ionisation cross section 80−83496
O^+ and O_2^+, beam-foil excitation, optical radiation obs. 80−9724
O^+, appearance potential by anal. of field-dispersed ions 78−85234
O^+ atmospheric daily vars. at mid-latitudes at sunspot max. 79−58167
O^+, beam-foil excitation, absolute Auger yield meas. 80−14203
O^+, beam-foil excitation; absolute Auger yield meas. 79−45685
O^+, beam-tilted C foil interactions, charge-state distrib., photon emission, 100-400 keV 79−22814
O^+, distrib. in auroral arc 77−2292
O^+, electron impact excitation, ionisation, rel. to auroral spectral intensities 79−84563
O^+, excited state, oscillator strengths, core relax. effects calcs. 79−10050
O^+, expt. results on W-values for heavy particles 79−7000
O^+, from exploding fast mol. ions, Auger spectra 80−32781
O^+, implantation in Cu along channelling directions, stopping power 77−69021
O^+, in Earth's magnetotail obs. 77−33284
O^+, in ionosphere mid-latit. F_1-layer, mean diurnal var. 79−96856
O^+ in Jupiter inner magnetosphere, forbidden emission detect. 80−51687
O^+, in magnetotail lobe plasma, evidence from double-peaked ion spectra 78−32299
O^+-isolated GaAs-GaAlAs DH laser compared with SiO_2 isolation 80−74382
O^+, O_2^+, stratospheric chemistry, reaction rate coeffs. and product distribs. 78−81305
O^+, O^{2+}, electron impact ionisation cross section in hollow beam trap 78−25717
O^+ reactions with N_2O, O_2, and NO, nonthermal rate coeffs. in ionosphere 78−57375
O^+, reson. line regularities in plasma Stark widths and shifts 80−43881
O^+ transequatorial breeze rel. to equatorial daytime topside ionosphere 79−84584
O^{++} in thermosphere, photochemistry 77−45226
^{16}O, diffusion profile determ. in natural feldspars by ion analyser *(French)* 77−55400
^{16}O, enrichments in carbonaceous chondrite minerals, rel. to distrib. of pre-solar component 77−37582
$^{16}O^+$, stopping power in Au at 50-500 eV 77−76478
^{17}O enrichment by formaldehyde photopredissociation using Ne II ion laser 77−19112
^{17}O, in red giant stars, nucleosynthesis 77−26005
^{18}O concs. and rel. discharges in Negro and Solimoes rivers in Amazon 77−5268
^{18}O, diffusion profile determ. in natural feldspars by ion analyser *(French)* 77−55400
^{18}O, in belemnite rostra, effects of post-depositional alteration on palaeotemps. determ. 77−29455
^{18}O, self-diffusion in ThO_2, isotope exchange meas. 77−11725
^{18}O tracer diffusion coeff. determ. in Ti_nO_{2n-1}, continuous mass spectrometry 77−20124
^{18}O tracer used to study growth mechanism of oxide scale 77−8964
^{18}O variations in deep sea dissolved O 77−5231
$^{18}O^+$ ion implantation in channelling directions in Al, Ni, Cu single crystals, expt. conditions and range profile obs. 80−65022
$^{18}O^+$ ion implantation in channelling directions of Al, Cu and Ni single crystals, stopping power determ. 80−65078
O^{2-}, ion, in crysts., X-ray scattering factors using Xα method 79−7521
O^{2-} ion transport in δ-phase Bi_2O_3 thermoelectric cell 80−92713
O^{2-} low partial press., thermogalvanic meas. using O^{2-} ion conductors 80−73389
O^{2-}, parameters for analytical radial orbitals, total and binding energies 77−6668
O^{2-} polarisability rel. to ferroelec. phase transitions 80−71326
$O^{2+,3+,4+,5+}$ induced K-shell X-ray production cross sections, S to Br, 7 to 24 MeV 77−61850
O^{2+}, collision strengths, radiative transition probabilities, solar atm. appl. 79−86069
O^{2+} collisions with O_2 and N_2, reaction rates 79−16726
O^{2+} ions in disturbed ionosphere 79−62647
O^{2+} reactions with atoms or molecules of ionospheric importance, lab. meas. 80−26004
O^{2+}, terrestrial origin, discovery in outer magnetosphere 78−32295
O^{4+}, electron impact ionisation, close coupling calcs. 80−106293
O^{4+}, resonant-scatt. contributions to excitation rates 80−58393
O^{4+} to Be isoelectronic series, transition values and energies, transition-operator method 77−30826
O^{5+}, 1s3s3p $^4p^0$ state, Hartree-Fock function, third-order energy 78−37569
O^{5+}, electron impact, inner shell excitation cross-sections 79−59580
O^{5+}, fine struct. and lifetimes, doubly excited quartet system 78−78827
O^{5+}, ionisation cross-section, excitation autoionisation effects 79−45850

oxygen continued
O^{5+}, O^{6+}, production and acceleration in cyclotron *(Japanese)* 78−5084
O^{5+}, spectra, 7-32 nm, doubly excited quartet system 78−62757
O^{6+}, electron impact excitation, cross-sections, modified Oppenheimer approx. 78−82843
O^{6+} enriched plasma in driving piston of solar flare-generated shock wave 80−72740
O^{6+}, line emissions from He-like ions, electron params., ion diffusion in Tokamak plasmas 79−4114
O^{6+}, solar wind spectrum, ion frequencies and velocities *(German)* 80−51636
O^{6+} to O, photoionis. cross sections, from ground states, Hartree-Slater model 77−57947
O^{7+}, resonant coherent excitation of channeled ions 79−51178
O^{7+}, solar wind spectrum, ion frequencies and velocities *(German)* 80−51636
O^{n-} (n=0 to 2), core binding energy shifts, ΔSCF calcs. 80−95558
O^{n+}, electron inner shell excitation/ionis. cross sections 77−23564
O^{n+} ions, role in solar wind interactions with lunar surface grains 80−62050
O^{n+}, n=1 to 4, gas and foil-excited, 2-18 MeV, projectile Auger spectra 79−59414
O^{q+}, electron loss, forward peak oscill. struct. 78−78796
O/C ratio in massive stars, core convection effects 80−17579
O/H abundance ratio determ. in Galaxy from H II regions radio obs. 80−36692
O^+/electron density ratio in 140-200 km height range of atmosphere 80−105102
O^+/n_e, ionospheric ratio at 170 km for specific heliogeophysical conditions 79−12332
$^{17}O/^{18}O$, ratio in red giants after main-sequence mixing 77−33475
$^{18}O/^{16}O$ for rocks in Tertiary igneous complex of Skye 77−33012
O-Ar pot. parameters, from CO in Ar matrix, empirical evaluation 80−48057
O-like ions, Fe to Zn, intercombination lines, lab. obs. 77−3289
O-like ions, spectral line intensity, density depend., plasma diagnostic appls. 78−83617
O-orbital interaction 3-methyleneoxetane, struct., MO calcs., UV photoelectron spectra obs. 80−28058
O-orbital interaction in 3-oxetanone, struct., MO calcs., UV photoelectron spectra obs. 80−28058
O-orbital interaction in β-propiolactone, struct., MO calcs., UV photoelectron spectra obs. 80−28058
O-treated polystyrene, interaction with vapour-deposited Cr and Ni atoms 80−3407
O^+-O, in F-region, experimental estimate of reson. charge transfer cross-section 77−45231
O+acetaldehyde(propylene), rate const., discharge flow-reson. fluoresc. meas. 78−7178
O+acetylene reaction, kinetics, flash photolysis-reson. fluoresc. meas. 77−73439
O+AlCl(AlF), matrix reactions, OAlCl and OAlF IR spectra *(German)* 79−11785
O+Al(Sn), inner-shell multiple ionisation systematics, X-ray obs. 80−63790
O+Ar(Kr)(Xe), magnetically selected O(^3P) state scatt. 80−99543
O+benzene(-d), phenol radical prod., crossed mol. beam investig. 80−71902
O+biradical, from γ-methyl valerophenone photolysis, lifetime and quantum yield meas. 77−60086
O+BrO→Br+O_2, reaction rate constant, 200-360K 78−73024
O+CN→N+CO, flash photolysis, absorption spectrosc. obs. 79−66289
O+CO, adsorbed on Ir (111), Langmuir-Hinshelwood reaction mechanism 79−29408
O+CO_2^+, in Mars thermosphere, effects of energetically produced O_2^+ on ion temps. 79−96945
O+CS_2→CS+SO, vibrational distribution of CS, laser-induced fluorescence meas. 80−71895
O+CS_2→OCS+S, branching ratio meas. 79−52656
O+CS→CO+S, rate const. temp. depend., ESR-mass spectrometer obs. 78−20013
O+C(N), K-shell excitation, Auger electron spectrosc. obs. 80−9715
O+chloroethylene reaction, kinetics, flash photolysis-reson. fluoresc. meas. 77−73439
O+Cl_2, reactive scatt. in supersonic at. beam 79−36754
O+Cl_2 (CS_2), reactive scatt., O atoms seeded in Ne supersonic nozzle beam 78−48637
O+Cl_2O, reaction rate const. 79−20344
O+$Cl_2(CS_2)$, reactive scatt. of beams, vel. distribs. 77−73443
O+$ClONO_2$, in stratosphere, rate constants 77−33134
O+ClO→Cl+O_2, rate consts. calc., 220-1000K 79−79233
O+ClO→O_2+Cl, rate const. meas. 77−60059
O+Cs_2, reactive scatt. in supersonic at. beam 79−36753
O+dimethylamine, reactive routes, identification 79−39129
O+ethylene, (OCS), reaction dynamics, IR laser excitation effects 79−66288
O+ethylene, OH chemiluminesc., mechanism, rate const., mathematical model calcs. 78−48655
O+fluoromethane, reactions, selective vibr. excitation effects 78−35643
O+formaldehyde, absolute rate consts., discharge flow and flash photolysis reson. fluoresc. meas. 80−55648
O+formaldehyde, reaction, absolute rate coeffs., 250-500K 79−100349
O+H_2, classical trajectory calcs., ab initio surface, singlet state, rate consts. 80−66786
O+H_2, pot. energy surfaces and reaction rates, ab initio calcs. 80−63531
O+H_2, trajectory calcs., fitted ab initio pot. energy surface 79−74358
O+$H_2O(NH_3)$, rot. excitation, classical Monte Carlo calcs. 77−34727
O+H_2O(methane/halomethane), direct reaction in flow system 80−3333
O+H_2O→OH+OH, energy partitioning 80−101009
O+H_2S, ^3P-state, absolute reaction rate, flash photolysis reson. fluoresc. obs. 79−66283
O+H_2S, matrix reactions, IR spectra of products, chemiluminesc. 77−60057
O+H_2SO_4, atmosphere chemistry, collisional reaction probabilities 80−90168
O+H_2(HCl), relax. and chem. reaction, time resolved IR fluoresc. and mass spectrometry obs. 80−69177
O+H_2→OH+H, pot. surface, HF calc. 80−16669

oxygen continued
$O+H_2 \rightarrow OH+H$, product state distrib., laser photolysis-laser induced fluoresc. determ. 79−83446
$O+H_2 \rightarrow OH+H$, rot. energy distrib. of $OH(X^2\Pi,v=0)$ 79−87829
$O+H^+$, electron capture cross sections 78−62912
$O+H^+$, in upper atm., rel. to H^+ loss during solar cycle 78−93021
$O+H^+(He^+)$, double K-shell ionis., projectile Z depend. 78−25680
$O+H^+(He^{2+})$, K-shell Auger electrons ang. distrib. 79−89756
O+HCl, vibr. excited, laser enhanced reaction rate, OH vibr. distrib. obs. 78−95912
$O+HO_2 \rightarrow HO+O_2$, rate coeff. meas. by laser mag. reson., atm. chem. appl. 77−52614
$O+I_2(CS_2)(OCS)$, crossed-beam investigation of translational energy 79−5145
O+inert gas, ^1S-^1D collision-induced transitions 78−33588
$O+Li^+(Cs^+)(Au^+)$, cross-section, closure-Born approx. 78−66630
O+methane, H abstraction, rate consts. calcs. 78−95921
O+methane, photochem. reaction, high temp., rate coeff. meas. 80−16699
O+methane→OH+methyl reaction, photolytically initiated, high temp. kinetics meas. technique 80−61085
O+methyl radical, infrared chemiluminescence obs. 80−61080
O+N, endoergic chemiionisation, semiclassical theory 79−98208
$O+N_2$, excitation and deactivation at above-thermal energies 80−43171
$O+N_2$, intermolecular pots. from Thomas-Fermi-Dirac functional 77−19009
$O+N_2$, quenching of $O(^1D)$ state, at 300K, semiclassical study 79−45823
$O+N_2^+(O^+)(O^{2+})$, rate coeffs. in thermosphere, AE satellite meas. 79−48594
$O+N_2^+ \rightarrow NO^+ + N$, aeronomical determ. of rate coeff. 79−75000
$O+N_2O_5$, rate const., 220K, 300K, discharge-flow method 78−44352
$O+N_2(^1\Sigma_g^+)$, energy transfer, classical trajectory model *(Spanish)* 79−89745
$O+N^{2+}$, collision, correl. diagram calcs. 80−23504
$O+NF_2$, electronically-excited free radical reactions 80−97707
O+NO, chemiluminescenc., absolute rate const., O_3 effect 80−45507
O+NO, in Ar matrix, chemiluminesc. 78−35688
O+NO, vibr. relaxation of NO, laser induced IR fluoresc. study 80−9626
O+NO binary reaction, crossed beams, NO_2 chemiluminesc. 78−64843
O+NO+M, rate const., 217-500K 79−52626
$O+NO+M \rightarrow NO_2+M$, (M=He, Ne, Ar, Kr), 217-500K, absolute rate consts. 77−16787
$O+N(^2D)$, associative ionisation 80−4161
$O+N(^2D)$, endoergic assoc. ionisation, merged beam obs. 79−100348
O+NaO, nightglow, excitation and abundance of Na 80−98497
O+nitroethane (nitromethane), H atom abstraction in discharge flow system 78−35671
O+O, K-shell excitation, Auger electron spectrosc. obs. 80−9714
$O+O_2$, quenching of $O(^1S)$ state, rate coeff. 80−41581
$O+O_2 \rightarrow O_3$, Hartley band during formation, metastable states, vibr. excitation and relax. 80−55632
$O+O_3$ collisionally induced relax. processes and vibr. energy transfer 80−53107
$O+O_3$ reaction, vibr. enhancement 80−30215
O+OCS (ethylene), reaction dynamics, IR laser excitation, vibr. effects 77−12788
O+OH, direct rate meas. 80−30217
O+OH, reaction rates 77−52610
$O+O \rightarrow O_2$, chemiluminesc. matrix reaction, diffusion controlled, 8-20K 78−61013
O+olefin, reactions, relative rate consts., N_2O photolysis obs. 79−83472
O+saturated hydrocarbon, chem. reaction dynamics. OH prod. investig. 80−101016
O+saturated hydrocarbon, reaction dynamics, model pot. surfaces, quasi-classical trajectory calcs. 80−97696
O+saturated hydrocarbon→OH+alkyl radical, reaction dynamics, mol. beam-laser induced fluoresc. obs. 80−97695
$O+Se \rightarrow SeO$, chemiluminescent reaction, $B^3\Sigma \rightarrow X^3\Sigma$ band emission 79−79254
O+transition metal clean surface, 10^{-3} to 10^{-10} mbar, 77 to 370K, reactions 78−64889
O+trifluoroiodomethane, I atom abstraction by O, mol. beam study 78−48638
O+trifluoroiodomethane, vel. distrib. and cross section, reactive scatt. 80−26011
$O^-+CO(Mg)(N_2)$, electron detachment cross-sections, 20-150 keV 78−25690
$O^-+CO \rightarrow CO_2^+ + e^-$, vibr. chemiluminesc. 78−3340
$O^-+D_2 \rightarrow OD^- + D$, crossed beam studies product ang. and energy distrib. 78−53203
$O^-+H_2(He)(CO_2)(Ar)(Li)(Na)(Mg)$, negative ion stripping, at. beam form. 77−6926
O^-+N_2, electron detachment, collision with vibr. excited mols. 79−54961
$O^-+N_2 \rightarrow N_2O+e$, rate studies 78−40036
$O^-+Ne(Ar)(Kr)$, 0.2-1 keV, elastic and inelastic reduced differential cross-sections 80−32829
O^-+O_2, electron detachment, collision with vibr. excited mols. 79−54961
$O^-+O_2 \rightarrow O_2^- + O$, cross sections, 0-100 eV *(German)* 77−32785
$O^-+O_2 \rightarrow O_2^- + O$, cross section kinetic energy depend., rate consts. meas. and Monte Carlo calcs. 80−78701
$O^-+SF_6 \rightarrow SF_5+F+O$, electron affinity of SF_5 radical 80−45495
O^++Al, Al K-vacancy cross sections, 0.15 to 91 MeV, recoil effects and mechanisms 77−19033
O^++alkali metal, charge exchange, negative ion form. 79−50128
O^++atmospheric gases, thermal energy reaction rates 78−92443
O^++CO_2, in Mars thermosphere, effects of energetically produced O_2^+ on ion temps. 79−96945
O^++CO(NO), dissociative ionis. 79−10188
O^++Ca, 30 MeV K-shell double ionis., K$\alpha\alpha$ and K$\alpha\beta$ obs. 77−57918
O^++H, cold dense H plasma, charge exchange, impurity losses, Monte Carlo simulation 78−34260
O^++H, in upper atm., rel. to H^+ loss during solar cycle 78−93021
O^++H_2, H^+ prod., from H_2^+ dissoc. states or H_2^{2+} 78−20015
O^++H_2, linear approach, pot. energy surface for H_2O^+ 80−47922
O^++H_2O, 50 to 250 keV, OH radical form. 78−56890
$O^++H_2(N_2)$, reactant ion electronic states, effect on charge transfer cross sections 80−63809

oxygen continued
$O^++H(H_2)$, 0.1-13 keV electron capture cross-sections meas. 79−36761
O^++hydrocarbons, chemiluminescent reactions 79−96299
O^++inert gas, potential energy curves from elastic scatt. cross sections 80−23502
O^++Kr, charge exchange cross-sections *(German)* 77−10753
O^++N_2, atom transfer, reaction rates and cross-section determ. 77−60052
O^++N_2, charge exchange collision, rate coeff. and ionosphere implications 80−87224
O^++N_2, luminescent charge transfer, metastable and ground state ions 78−42202
O^++N_2, reaction rate coeff. in ionosphere 77−87167
$O^++N_2(H_2)$ 79−3561
$O^++N_2(O_2)$, reaction rates, 300-900K 79−8434
$O^++N_2(O)$, rate coeffs. in thermosphere, AE satellite meas. 79−48594
$O^++N_2 \rightarrow N+NO^+$ react., mechanism, ab initio SCF calcs. 78−60996
$O^++NH_3(H_2O)(Ne)$ symmetric collisions, double K-shell ionisation, two-electron-one-photon transitions 77−19067
O^++NO, charge transfer, reaction rates and cross-section determ. 77−60052
O^++Ne, pot. energy curves, nonadiabatic coupling matrix elements 80−53110
O^++O_2, charge exchange collision, rate coeff. and ionosphere implications 80−87224
O^++O_2, dissoc. ionisation, kinetic energy spectra 78−25684
O^++O_2, excited ion reactions, charge transfer coeffs. at thermal energy 80−95721
O^++O_2, ion speed distribution effects in flow-drift tubes 77−56219
$O^++O_2(N_2)(NO)$, ion speed distribution effects in flow-drift tubes 77−56219
O^++Th, charge transfer cross-section, 1-500 eV 78−82835
O^++U, charge transfer cross-section, 1-500 eV 78−82835
$^{17}O+^{16}O$, fractionation by chemical equilib. 80−89513
$^{18}O+^{16}O$, fractionation by chemical equilib. 80−89513
O^{2+}+Al(Si)(S)(Cl), chem. environment effect on Kα satellites intensity 77−54527
O^{2+}+B(F), K Auger electron spectra 79−89758
O^{2+}+H, charge transfer process, astrophys. plasmas appl. charge transfer process, astrophys. plasmas appl. 79−59550
$O^{2+}+H_2$, charge transfer rate coeff. and astrophysical appls. 80−56701
$O^{2+}+H^+$, ^3P_J fine structure transitions 80−37864
O^{2+}+He, electron transfer cross-section, <100 eV 78−66654
O^{2+}+inert gas, electron transfer meas., 60-200 keV 80−83480
$O^{3,4,5+}+H_2$ single and double electron capture cross sections, (0.3-1.2) 10^8 cm s^{-1} 77−34756
$O^{4,5,6,7+}$+Ne(Ar)(Kr)(Xe), 10-30 MeV, charge exchange 77−34757
O^4+Ar, intense low energy autoionisation lines 79−31674
O^{5+}+Ag(Pd)(Sn), L-shell X-ray prod. cross-section determ. 77−6913
O^{5+}+Ti, ratio of single K-shell ionisation cross section to double K-shell ionisation cross section 80−53119
O^{7+}+H, excitation distrib. following electron capture 79−36763
O^{8+}+Ar, bound- and continuum-state electron capture in gas, strong correlations 80−9730
O^{8+}+H, electron capture into n, l levels, 100 keV/amu 79−22826
O^{8+}+H, electron removal, charge transfer and impact ionisation cross-section 79−76504
O^{8+}+H(1s), charge transfer, 0.025-200 keV/amu 79−22823
O^{8+}+H(1s)(He($1s^2$)), electron capture into n,l excited states 80−23543
O^{8+}+He, electron capture and impact-ionis. cross sections, Monte Carlo calcs. 79−27083
O^{8+}+Ne, double K-shell electron capture, theory 79−68315
O^n+H_2, single electron capture cross-section 79−59560
O^{n+}+Al, X-ray prod. and electron transfer cross-section 79−45790
O^{n+}+C, 4 to 40 MeV, beam-foil K-shell X-ray prod. cross sections 78−33461
O^{n+}+gas targets, 50 keV, multiple scatt., target at.+energetic ion spatial correlation influence 79−27062
O^{n+}+H, charge transfer cross sections, oscillatory behaviour in low-energy collisions 80−63806
O^{n+}+H, electron capture cross-sections, He- and Li-like ions 79−59559
O^{n+}+H, single electron capture cross-section 79−59560
$O^{n+}+H_2$, electron capture cross-sections, He- and Li-like ions 79−59559
O^{n+}+N, charge exchange contribution to K-vacancy production 80−102553
O^{q+}+Ar, continuum electron capture and loss, 1.6-2.8 MeV/A 78−46443
O^{q+}+Ar, continuum electron capture, projectile vel. and Z depend. 78−55222
$O^{q+}+H(H_2)$, q=1-5, single electron capture cross sections 78−55233
O^{q+}+He(Ar)(Ne), electron capture to continuum states, forward ejected electron spectra 79−45831
O^{x+}+He, electron capture, K X-ray emission ang. distrib. 77−57919
O_2, $^3\Pi_u$ states, large CI wavefunctions, non-adiabatic coupling matrix elements 80−37744
O_2, $^3\Sigma_u^- - ^3\Sigma_u^+$ spin-orbit mixing in Schumann-Runge predissoc. 77−6875
O_2 0.762 μ band absorption coeff. in atmosphere *(Russian)* 78−28315
O_2 1.27 μ A-band intensity in lower atmosphere *(Japanese)* 78−61486
O_2 1.27 μm airglow, middle latit. meas. rel. to mesospheric O_3 concs. 80−72606
O_2 1.27 μm airglow emission, zenith angle dependence 77−45216
O_2 1.27μ emission, auroral enhancement 78−81485
O_2 5 mm absorption bands, long distance meas. of cloudy atm. by radiometry 80−90196
O_2 7594 Å telluric A-band on objective prism spectra of stars, radial vel. meas. appl. *(Japanese)* 78−89083
O_2 7619 Å band in aurora, rocket obs. 77−25813
O_2 ($^1\Delta$), atmospheric, collisional emission rel. to new diffuse bands in twilight 80−72662
O_2 ($^1\Sigma_g^+$)+H_2, collisional relax. temp. depend. 77−32783
O_2 (0,0) 7619 Å emission band, altitude distrib. from rocket obs. of nightglow 77−29530
O_2, (0,1)$b^1\Sigma_g^+ - X^3\Sigma_g^-$ band, integral absorption coeff. 78−20512
O_2 ($b^1\Sigma^+g$)+$O_2(X^3\Sigma)$, quenching rate coeff. meas., density depend. 77−38721
O_2 A band differential absorpt. lidar meas., using ruby lidar and stimulated Raman scatt. 79−39904
O_2, $A^3\Sigma_u^+$, $C^3\Delta_u$ and $C^1\Sigma_u^-$ states in van der Waals solids, electronic spectra, dynamics 78−1000

oxygen continued
O_2 A-band in nightglow 79−48596
O_2, adsorbed on SiO films, infrared spectra exam. 79−45725
O_2, adsorption on reduced Mo_2O_3-Al_3O_3 catalyst, O^- form. 78−85197
O_2 ambient gas, computer expts. on ionic rcombination, coeff., binary recombination 78−22028
O_2 analyser, OTOX 90, operation, and multipoint monitoring 80−55736
O_2 and [O I] nightglow intensity var. 77−73899
O_2 and WO_2 adsorption on W (110) 80−34317
α-O_2, antiferromagnetic polycrystal, splitting of exciton absorpt. lines in mag. field *(Russian)* 80−103943
O_2, atm. density seasonal vars. near 100 km altitude 78−12034
O_2, atmos. spectra at 100 km altitude, (0-1) band 80−61933
O_2 atmospheric band system in nightglow, rocket meas. *(Japanese)* 80−94631
O_2, atmospheric electric quadrupole transitions detection in A band 80−85746
O_2, atmospheric system in aurora 77−13144
O_2, CI calc. of ground and $^3\Sigma_u^-$ excited states 79−81158
O_2, canonical exchange energy modulation parameters, MTXα calc. 79−97997
O_2, chemisorption on Cu, cluster theory 80−29264
O_2, chemisorption on Ni, cluster theory 80−29264
O_2 concentration in primitive prebiological atmosphere 78−73514
O_2 concnetrations, effect on radiation survival of cell spheroids 80−76792
O_2 consumption of mouse, effects of microwaves and environmental temp. 80−51161
O_2, core photoelectron line shape, localisation role 79−59512
O_2 covered metals, secondary ion yield, quantitative determ. *(German)* 79−48003
α-O_2, cryst., exciton effects, spectra *(Russian)* 79−47481
γ-O_2, cryst., vibr. Raman spectra 80−60558
β-O_2 crystal, thermodynamics of mol. libration motion *(Russian)* 80−70328
α-O_2 crystals, absorpt. line polarisation biexciton existence *(Russian)* 80−108242
α-O_2 crystals, absorption line biexciton polarisation *(Russian)* 80−89028
α-O_2 crystals, spin ordering effect on light absorpt. *(Russian)* 80−89029
O_2 dayglow and O_3 abundance latit. var. on Mars 79−53750
O_2 density in thermosphere, solar flux var. 80−72659
O_2, density in upper atm., UV extinction meas. 79−2406
O_2 diffusion distance and necrosis development in multicell spheroids 80−81570
O_2 diffusion into mammalian cells following ultrahigh dose rate irrad. 80−30694
O_2 discharge, O_3 production 80−38780
O_2 dissolved in Ar, mol. orientation, Raman spectrosc. obs. 80−52994
O_2 dissolved in physiological saline, movement in mag. field 79−57678
O_2, electron attachment kinetics in flames 80−3349
O_2 electron capture rate from geminate ion recombination fluoresc. data 80−74245
O_2, electronic spectra, parity nonconservation effects *(Russian)* 78−13488
O_2, fluoresc. efficiencies of electrons, 4900-10500 Å wavelength range 77−61870
O_2 formation rate on pulsed illumination of plant cells 79−57606
O_2, Franck-Condon factors, rot. quantum number effect 79−31613
O_2 fugacity of basaltic magmas, role of gas forming elements 78−77218
O_2, gas, intermol. pot. for spectra, acoustic absorpt., rot. relax., etc. 79−68224
O_2, gas, temp. meas., vibr. Raman intensity, 500-2000K 79−37436
O_2 gas RF breakdown in longit. mag. field, diffusion theory validity 77−39491
O_2 glow discharges, current modulated, O atom production and removal rates 79−90477
O_2 Herzberg nightglow bands, emission rates 77−70901
O_2, high energy pulsed laser feasibility at 1.27 μm, O_3 photolysis 78−63117
O_2, IR nightglow bands excitation mechanism, reaction rate consts. 78−65448
O_2, impurity control in EBR-II sodium systems 79−93696
O_2, impurity in alkali halides, reorientation, linear dichroism *(Russian)* 80−45127
O_2, in auroral upper atmosphere, vibr. excitation rel. to IR emissions 77−33247
O_2 in chloroform and carbon tetrachloride solns., sensitized luminesc. 80−32762
O_2 in D-region, positive ion chemical scheme for electron density and comp. 79−40007
O_2 in early Precambrian atmosphere, photodissociation rather than photosynthesis 78−81409
O_2 in liquid Xe, electron capture 80−102402
O_2, in mesosphere, densities meas. from atmospheric absorpt. of solar Lyman α radiation 77−87010
O_2 in mesosphere, seasonal vars. in 70-90 km altitude range 79−100994
O_2, in meteor wakes, ion-molecule reactions rel. to red afterglow 78−36536
O_2 in neutral atmosphere, seasonal vars. rel. to E-region ionisation 79−12331
O_2 in Venus atmos., O_2, Ar, CO abundances, error of Pioneer Venus chromatography obs. 80−105189
O_2, ionisation by electron bombard., empirical and semi-empirical calcs. 79−36784
O_2 isotopes, $^{17}O_2$, $^{16}O^{17}O$, $^{17}O^{18}O$, pure rot. Raman spectra, bond lengths 78−42071
O_2, isotopically enriched, prep. and storage under press. 79−29620
O_2, laser excited, quenching by CO_2, H_2O and I_2 80−99515
O_2, lifetimes and reactivity in aq. micellar system 78−46398
O_2, metastable emission bands 79−64015
O_2, microwave absorpt. at high-press., 9, 23 and 60 GHz 78−13490
O_2, molecular fluid, Rayleigh and Raman light scatt. props., orientational and collision induced effects 80−63644
O_2, multiconfig. HF procedure, 2nd- and approx. 2nd-order, convergency 79−93907
O_2, multiphoton ionisation, electron energy spectra 77−6865
O_2, negative point-plane corona, electrical characts. 78−71567
O_2 nightglow, Herzberg bands excitation 79−75008
oxygen continued
O_2, nightglow spectral intensity changes correl. with NaD spectra 80−61932
O_2, nonempirical calc. for molecules in electric field 78−25459
O_2, oscillator strengths and linewidths, Schumann-Runge bands 78−90186
O_2 partial pressure, transcutaneous meas. 79−83965
O_2 partial pressure and bioelectric potential simultaneous meas. in living tissue *(German)* 78−85453
O_2 partial pressure meas. in cat cerebral cortex 79−83826
O_2, photoabsorpt., photoionis, and photodissoc., dipole oscill. strengths in UV 79−76468
O_2 photoabsorption cross section near Lα line, temp. depend., aeronomy appl. 77−64499
O_2, photodissoc. and spectral absorpt. in stratosphere and mesosphere 80−51497
O_2 photofragment, produced by O_3 photolysis at 266 nm 80−50865
O_2, predissoc. of $B'^3\Sigma_u^-$ state, Rydberg-valence crossing model 80−1032
O_2, pressure broadening of HNO_3 linewidth, 200 and 300K 78−46399
O_2 profiles in E.Mediterranean Sea, meas. 80−17298
O_2 quenching by porphyrin singlet and triplet states 79−92141
O_2, rate of entry into myoglobin 79−8471
O_2, rotational collision number, diffusion coeffs. 79−1281
O_2, rotational Raman intensities and polarisability anisotropy change meas. with internuclear distance 80−63641
O_2, Schumann-Runge band system in sunspots UV spectrum 80−12735
O_2, Schumann-Runge bands, atmospheric absorpt. model 79−96823
O_2 sensing, operation of Pt microelectrodes 79−84043
O_2 sensitisation of CHO cells at ultrahigh dose rates 80−36000
O_2 singlet in natural waters 77−56659
O_2 singlet in solns., luminesc. duration following pulsed laser excitation 80−76070
O_2, singlet product. detect. by EPR 79−66597
O_2, singlet state lifetime in D_2O soln., decay of micellar system 78−46301
O_2, spectral line shape, Fourier representation of Voigt profile 78−90223
O_2 supply to porous implants in bone analysis 79−70707
O_2 thermal and wind-induced var., AE-D thermospheric meas. 79−53592
O_2, thermospheric densities, calc. and meas. values comparison 78−28357
O_2, thermospheric density indirect determ. from AE-C satellite meas. 78−12032
O_2, total scatt. cross sections for intermediate-energy positrons 80−91692
O_2, total Xα energy, LCAO calc., rel. to local density models 80−32607
O_2 transmural transport to retina, mathematical model 79−34583
O_2 triple point cells, comparison 78−73996
O_2, UV absorpt. into $^3\Pi_u$ state, calc., atmos. opacity 80−12582
O_2, UV nightglow emission meas. 80−41590
O_2, vac. UV absorpt. spectra of excited states 78−82749
O_2, vac. UV photodissoc., kinetic energy and ang. distribs. of fragments 77−30938
O_2, X-ray K emission spectra, band interpretation and satellites 77−88464
O_2, Zeeman effect, g-factors 79−3492
O_2 zone in Black Sea, boundary determ. rel. to water mass dynamics *(Russian)* 80−12435
O_2^-, $A^2\Pi_u$ state pot. energy curve, MCSCF calcs. 80−63565
O_2^-, ab initio pot. curves of $X^2\Pi_g$, $A^2\Pi_u$, $a^4\Sigma_u^-$, $^2\Sigma_u^-$ states 78−66483
O_2^- anions impurity luminescence spectra in alkali halide solid solns., Stokes law for crystalline vibr. *(Ukrainian)* 79−43012
O_2^-, electron transfer reactions, singlet O_2 form. and quenching 77−29002
O_2^-, form. on reduced MoO_3-TiO_2 surface 77−90590
O_2^-, generation in CdS aq. dispersion by photolysis, spin trapping detect. 78−11538
O_2^-, in aq. solns. of alkali halides, spectral props. *(Russian)* 78−6766
O_2^-, in ionosphere, effects on EM wave propag. 79−8762
O_2^-, in nonpolar liqs., laser photodetachment, elec. cond. obs. 79−64057
O_2^-, in silicates, XPS quantitative anal. *(Japanese)* 77−48710
O_2^- ion, form. by O_2 adsorpt. on CaO 80−61155
O_2^- molecular ion in alkali halide crysts., peculiarities of luminesc. spectra 77−52174
O_2^-, photodissoc. and photodetachment in $O_2/CH_4/H_2O$ mixtures, 3500-8600 Å 79−45776
O_2^- species adsorbed on Ce-X zeolites, identification by ESR 77−27096
O_2^+, $^4\Pi$ states, spin-spin coupling consts., ab initio calc. 79−97981
O_2^+, 1NG bands spectral synthesis, for auroral obs. anal. 77−2296
O_2^+, $A^2\Pi_u \rightarrow X^2\pi_g$ and $b^4\Sigma_g^- \rightarrow a^4\Pi_u$ emissions by photoionis. of O_2 79−94041
O_2^+, ab initio CI STO calc. 78−74585
O_2^+, absorpt. linewidth of predissociated levels, lifetimes 79−36711
O_2^+, $b^4\Sigma_g^-$ state, laser-induced predissoc. in ion beam 78−70886
O_2^+, $b^4\Sigma_g^-$-$a^4\Pi_u$ band, rot. lines, rel. intensities, theoretical and exptl. results 78−13505
O_2^+, CI calc. of ground and $^3\Sigma_u^-$ excited states 79−81158
O_2^+ cluster ions, photodissoc. cross sections meas., 3500-8600 Å 79−24763
O_2^+ dissociative recomb., $O(^1D)$ prod. in upper atm. 77−41251
O_2^+, dissociative recombination rates 77−86295
O_2^+, electron impact, rate coeff. in thermosphere, AE satellite meas. 79−48594
O_2^+, electron impact dissoc. recomb., pot. energy curves calcs. 80−53150
O_2^+, electron impact dissociative recombination, ion-beam expt. 79−54981
O_2^+, electron impact excitation, ionisation, rel. to auroral spectral intensities 79−84563
O_2^+, $f^4\Pi_g$ state, quasi-bound levels, predissociation, band rot. anal., photofragment kinetic energy anal. 80−63650
O_2^+, first negative system, high-resolution photofragment spectroscopy 80−47971
O_2^+, fragmentation ang. distrib., energy disposal, branching, photoelectron-photoion coincidence spectra 79−68263
O_2^+, Franck-Condon factors calc. using Rydberg-Klein-Rees pot. 78−70878
O_2^+, $He_2^+ + O_2$ charge exchange laser 78−50759
O_2^+, high mag. field spectroscopy 79−72445
O_2^+, IR spectra, rot. anal. of $b\,^4\Sigma_g^- a^4\pi_u$ first negative band 78−5219
O_2^+, in ionosphere mid-latit. F_1-layer, mean diurnal var. 79−96856

oxygen continued
O_2^+, in winter anomalous D-region over Sardinia (40°N), prod. rates 80−21871
O_2^+, ion transport in electrical discharge 78−87435
O_2^+, laser-induced photodissoc. spectrum 79−68280
O_2^+, laser-induced predissoc. spectrum, rot. anal. 77−71839
O_2^+, lateral diffusion in O_2, mass spectra meas. 78−91055
O_2^+, mobility in CO_2, obs. using injected-ion drift tube mass spectrometer 78−1784
O_2^+, mobility in CO_2 80−43834
O_2^+, photodissoc. by visible light, predissociation 78−66612
O_2^+, photoelectron spectra, vibronic transition ionisation energies, ground state mol. consts. 79−89710
O_2^+, photofragment spectroscopy using fast ion beams 80−9755
O_2^+, predissociated $b^4\Sigma_g^-$ state, high resolution laser spectroscopy in fast ion beam 80−9656
O_2^+, predissociation of $b^4\Sigma_g^-$, $c^4\Sigma_u^-$ states, threshold photoelectron-photoion coincidence 78−42144
O_2^+, quartet states, predissoc. photofragment spectroscopy 78−82794
O_2^+, radiative lifetimes and UV spectra, $b^4\Sigma_g$-$a^4\Pi_u$, $A^2\Pi_u$-$X^2\Pi_g$ transitions 78−17724
O_2^+ recombination rate in ionosphere 77−25830
O_2^+, rotational analysis of $A^2\Pi_u$-$X^2\Pi_g$ band system of $(^{16}O\ ^{18}O)^+$ 78−58678
O_2^+, second negative ($A^2\Pi_u$-$X^2\Pi_g$) band system, rot. anal. 77−18911
O_2^+, second negative bands excitation cross-sections, rel. to auroral emissions 78−37745
O_2^+, spectroscopic consts., remeas. 77−58197
O_2^+, sub-Doppler laser spectroscopy using fast ion beams 80−9655
O_2^+, symmetric charge transfer reactions, selected states, photo-ion, electron coincidence 78−73028
O_2^+, vibr. energy levels, dissoc. energy, photoelectron spectra 77−83651
O_2^+, vibr. intensity distribs. for electronic states prod. by photoionis. 78−25614
O_2^+, $X^2\Pi_g$ photoelectron spectra, vibr. intensity, Franck-Condon factors 77−42352
$^1O_2$, singlet, role in anthracene sulphonate sensitized photooxidation of I^- in aq. soln 77−32812
$^{18}O_2$, Raman spectrum and mol. parameter 77−46565
O_2^{2+}, auroral ionosphere spectral emission process 80−41577
$O_2^{\cdot-}$, superoxide radical role in lipid photoperoxidation in isolated chloroplasts 78−77016
O_2-^{85}Kr-Xe, liquefaction, retention of ^{85}Kr from fission exhaust gases, separation technique *(German)* 80−27753
O_2-Ar, gas, thermal cond., mag. field effects 78−34255
O_2-Ar, thermal dissoc. of dilute mols., vibr. bias mechanism 79−61854
O_2-Ar mixtures, positronium form. and quenching, orthopositronium quenching cross section determ. 80−74261
O_2-Ar system, low temp. liquid-vapour equilib. 78−83927
O_2-CO coadsorbed complexes evolving from Ag surface, mass analysed thermal desorption spectra 77−60121
O_2-CO_2 (ethylene)(neopentane), thermal electron attachment meas., microwave cond., pulse radiolysis 80−28592
O_2-CO_2 mixture, temp. dependence of molecular vibr. relaxation freq. from 300 to 675K 80−74238
O_2-CO_2-H_2O, gas mixture, photodetachment and photodissoc., mass spectra meas. 77−500
O_2-CO-SF_6, efficient CO_2 laser radiation 3rd harmonic generation, for fusion ignition 78−59087
O_2-CS_2 mixture, stimulated emission of CO behind overdriven detonation wave front *(Russian)* 77−23668
O_2-ethylene mixture, thermo-osmosis, heat of transport 79−43628
O_2-exposed K surface, X-ray and UV photoelectron spectra 78−52636
O_2-H_2 mixture, temp. dependence of molecular vibr. relaxation freq. from 300 to 675K 80−74238
O_2-H_2 plasma, electrical conductivity tensor in mag. field *(Russian)* 80−87864
O_2-H_2-Ar flame, atm. press., Na(3^2P) lifetime obs. 79−39149
O_2-He, binary diffusion coeffs., press. depend., 300 and 323K, Thorne's eqn. 80−1724
O_2-He, thermal cond. Senftleben effect meas. 79−18985
O_2-He afterglow, $O_2(C^1\Sigma_u^-, C^3\Delta_u, A^3\Sigma_u^+)$ generation from at. recomb. fluoresc. obs. 79−31576
O_2-He mixture, temp. dependence of molecular vibr. relaxation freq. from 300 to 675K 80−74238
O_2-He(N_2)(CO_2), O_2 electron attachment coeff. meas., O_2 partial press. depend. *(German)* 79−13821
O_2-He(SF_6), breathing, effect on respiratory mechanics 78−27992
O_2-I_2 100 W transverse-flow chem. laser 79−41374
O_2-N_2, gas mixtures, mass transfer, mag. field effects 78−63535
O_2-N_2 mixture, attachment cooling, press. depend. 80−91663
O_2-N_2 plasma mixture decay, effective recombination coeffs. *(Russian)* 77−47144
O_2-N_2(H_2), gas mixture, mag. field effect on thermal conductivity 78−59533
O_2-NO-acetylene, combustion products, 1400-2600K, minimisation of NO, computer model 78−85161
O_2-propane system with Ar, N_2 diluents, detonation wave instabilities 78−5762
O_2-SF_6, cryogenic liq., SF_6 mol. motions, IR and Raman spectra 79−69823
O_2-sseded Ar plasma supersonic free jet expansion flow, population density measurements *(Japanese)* 80−96351
O_2^+-N_2, temp.-dependent ion mobilities 79−86553
O_2+ N_2^+, electron capture and ion loss cross-section, 2.4-24.3 keV 80−58373
O_2+Al^+, reaction cross sections 77−29000
O_2+Al→AlO+O, product. rot., vibr., translational energy, AlO fluoresc. 78−23928
O_2+Ar, binary diffusion coeff. pressure depend. meas. 80−43826
O_2+Ar, molecular fluid mixtures, equilibrium props. 80−64867
O_2+Ar, shock-heated, collision induced dissoc. 79−34290
O_2+Ar^++→O_2^++Ar, thermal energy charge transfer, energy disposal determ. 79−64099
O_2+Ar^+(Kr^+)(Xe^+), near-resonant charge transfer, 4-45 keV 77−27176
O_2+Ar*, ion pair form. explained by charge transfer model 80−99546
O_2+Ar(O_2), collision induced UV absorpt. in Herzberg continuum, dimer form. 77−30883
O_2+B, chemiluminesc. metal oxide formation 80−35509
O_2+B, chemiluminesc. reaction, vibr. state distrib. 79−20354
oxygen continued
O_2+B, gas phase rate consts., 300K, at. absorption obs. 79−83445
O_2+Ba crossed beam kinetics, BaO recoil velocity spectra 80−76500
O_2+Be(Mg)(Ca)(Sr)(Ba), reaction kinetics in diffusion flame 77−90579
O_2+Br^-, total electron detachment cross sections for energies around threshold 80−99550
O_2+bromomethyne radical, absolute reaction rate parameters 77−1909
O_2+butyl radical, reaction rate consts. meas. 80−45490
O_2+C_2, IR laser photolysis of polyat. mols. photochem. appls. 80−66835
O_2+C_2O, absolute reaction rate consts. meas. by laser induced fluoresc. 80−93738
O_2+$C_2(a^3\Pi_u)$, reaction rate consts. and quenching, multiphoton UV photolysis, fluoresc. obs. 79−74355
O_2+C_3, reaction kinetics, laser induced fluoresc. obs. of allene photolysis 80−66820
O_2+C^+*, charge transfer cross-sections, 0.7-2.4 keV, $C^+(^2P)$ and $C^+(^4P)$ 78−58806
O_2+CF_4 plasma, loading effect and temp. depend. of etch rate of Si, SiO_2 and Si_3N_4 79−34167
O_2+CH_3→OH+H_2CO, 368K, rate const. upper limit 80−7771
O_2+CN(*v*) react., prod. energy distribs. meas., CO vibr. level population *(German)* 78−76833
O_2+CO, surface reaction of chemisorbed layers on Ru(001) 79−46924
O_2+CO, vibr. deactivation of CO, 80-300K, laser fluoresc. study 78−25661
O_2+CO isotope exchange reactions on Re 77−70338
O_2+CO_2, Senftleben-Beenakker effect, saturation field, Kohler-Raum theory and obs. 80−28596
O_2+C(2^1S_0) 80−74241
O_2+Ca, CaO form., product states obs. 78−92450
O_2+Ca, reaction, electronic branching, statistical and dynamical influences 78−92451
O_2+Cl^-, total electron detachment cross sections for energies around threshold 80−99550
O_2+Cl^+, reactions at room temp. 80−93749
O_2+Cs, collisional ionisation, energy spectra of forward and backward directed positive and negative ions 80−87200
O_2+Cs(K), mol. target internal motion 80−78697
O_2+dimethylamino radical, reaction rate constants, FTIR obs. 80−16652
O_2+F^-(Cl^-)(Br^-)(I^-), 0.2-100 eV, reaction differential cross sections energy depend. meas., exoergicity 77−63902
O_2+fluoromethane, laser induced translational-vibr. energy conversion obs. 79−72396
O_2+fluoromethane, vibr. energy equilibration, IR laser fluoresc. 79−846
O_2+fluoromethylene, vibr. energy distrib., lasing action 78−48644
O_2+Ge(Si), reaction rate consts. at 350K 78−53186
O_2+H, 20-500 eV, ion pair and free electron production, integral cross sections 78−46437
O_2+H, collisional coherent excitation, meas. of Lyman α-photons 80−99552
O_2+H, singlet state O_2 form., reaction mechanism, mass spectrometric obs. 78−53204
O_2+H_2, on Pd (111), mol. beam relax. and isotopic exchange meas. 80−35575
O_2+H_2O^+, rate constants determ. as function of relative kinetic energy 80−81292
O_2+H_2O+SO_2, condensation nuclei form., ion polarity and age depend. 79−39220
O_2+$H_2(D_2)(N_2O)$, Wassiljewa coeffs., thermal conds., 50 and 100°C 79−37437
O_2+H^+, charge transfer to H(n=2), mixed parity elec.-dipole oscillations 79−31678
O_2+H^+, energy transfer, dissoc., cross section calcs. 77−50522
O_2+H^+, energy transfer, vibronic excitation, emission spectra 78−66578
O_2+H^+, K-shell capture cross-section, Auger effect 78−33602
O_2+HBr, rate consts. for vibr. energy transfer meas. using laser. induced fluorescence technique 80−87206
O_2+HCl, HCl linewidth, impact parameter calcs. 79−89714
O_2+HCl, HCl ν_0-ν_1 band perturbations, linewidth and shifts calcs., IR spectra obs. *(French)* 80−58251
O_2+HF, HF(v=3) relax. and rate consts. 80−61069
O_2+HF, vibr. relax. laser fluoresc. obs. 77−14484
O_2+HF, vibr. relax. laser induced fluoresc. obs. 79−64037
O_2+H(F), quantum reactive scatt. theory, 3-dimens. 80−55637
O_2+H(He), vibr. state distrib., charge exchange 150-2400 eV 78−42195
O_2+H→OH+O, combustion, quasiclassical trajectory calcs. 78−53201
O_2+H→OH+O, kinetic study, pot. energy surface of HO_2, MO theory 79−74353
O_2+He, anisotropic intermol. pots., crossed beam expts. 79−31639
O_2+He, binary gas mixture, mutual diffusion press. depend. 77−24047
O_2+He, long lived collision complexes, exact classical and quantum mech. calcs. 78−33576
O_2+He, Penning ionisation of target mol., for He(2^3S) 79−41228
O_2+He^+, 0.7-2 MeV, charge-changing collisions, electron capture 80−58372
O_2+He^+, charge transfer product state distribs., time of flight obs. 80−87223
O_2+He^+, metastable O^+* ion production 79−91933
O_2+He^+, thermal energy charge transfer, O^+ product ion obs. 79−64100
O_2+He^+(2s), metastable ion electron capture, loss and de-excitation 77−6904
O_2+He^{2+} 78−82837
O_2+He*(2^3S), (2^1S), ion pair form., ion beam neutralisation reionisation spectroscopy 80−53120
O_2+heavy inert gas, small clusters, beam cluster intensity and collision cross section 77−38711
O_2+HgBr, vibr. relax., rate coeffs., fluoresc. obs. 80−63697
O_2+Hg(6^3P), photosensitised reaction, excited intermediates, energy transfer detect. 78−73030
O_2+hydrated electron, rate const., Arrhenius parameters 78−20041
O_2+I, near-resonant electronic energy transfer, surface-hopping model 79−86030
O_2+inert gas, dissoc. induced by collision, rot. energy depend. 79−100341
O_2+inert gas, reactant decomp., rot.-vibr. energy transfer, relax. analytic soln. 80−55650
O_2+inert gas, state-to-state rates from press.-broadened linewidths, data reduction method 78−46430

oxygen continued
O_2+inert gas atom, absolute total elastic cross sections 78−9220
O_2+K, collisional ionisation, energy spectra of forward and backward directed positive and negative ions 80−87200
O_2+Kr^{2+}, charge transfer reactions, rate coeffs. and product-ion distributions meas. 80−104431
O_2+Kr^{2+}(Xe^{2+})(C^{2+}), charge transfer reaction rate consts. 80−7779
O_2+La(Y)(Sc), crossed beam chemiluminescence reaction, spectral simulation, hyperthermal energy meas. 78−80732
O_2+Li^+, vibr. excitation cross sections, 100-1200 eV 79−27077
O_2+Li(Na)(K), excited atom quenching, semi-empirical model 78−1065
O_2+methane H abstraction, rate consts. calcs. 78−95921
O_2+methyl cation, ternary assoc. reaction, rate coeffs., 100-300K 79−61845
O_2+Mg($^1P_1$) metastable atom, afterflow quenching rate consts. 77−6720
O_2+muonium, aq. soln., reaction rate const., spin-conversion 79−100422
O_2+N_2, collinear collisions, anharmonicity effects, vibr. excitation 79−31656
O_2+N_2, collision induced UV absorpt., Herzberg continuum, dimer form. 78−9167
O_2+N_2, ionis. at low energy 78−58791
O_2+N_2, molecular fluid mixtures, equilibrium props. 80−64867
O_2+N_2, N_2 fixation, catalytic processes in non-equilibrium plasma chemical reactors *(French)* 80−89484
O_2+N_2, O_2 absorption in Herzberg region, N_2-induced, temp. effect 78−87429
O_2+N_2, vibr. transitions, semiclassical theory 78−66633
O_2+N_2 plasma jet, NO synthesis, chem. kinetics anal., model 80−38728
O_2+N_2^+, collisional dissoc. cross-section, 2.4-24.3 keV 80−58373
O_2+N_2+NO, mixtures with nonthermal vibr. excitation of mol. N_2, formula for calc. equilib. const. 80−76545
O_2+N^+, charge exchange, 1-3 keV, N^+(^3P) and (^1D) states 79−36760
O_2+N^+, electron capture and ion-loss cross-section, 2.4-24.3 keV 80−58373
O_2+N^+, NO^+($a^3\Sigma^+$) ion prod. 80−7784
O_2+N^+(N_3^+), drift tube mass spectra, rate coeffs., prod. distrib. 77−77746
O_2+N^+(O^+)(C^+), rate coeffs. meas. at 300 and 100K in flowing afterglow 79−20346
O_2+NO^+, reaction rate consts. meas. 80−7782
O_2+N(^2D) as source of O(^1D) atoms in aurorae 79−35028
O_2+Na*(3^2P), electronic to vibr.-rot. energy transfer, differential cross sections 77−38715
O_2+Na(K)(Cs), negative ion pair form., total cross sections 79−3550
O_2+Na(Li), semiempirical pot. surfaces, dynamical considerations 79−11766
O_2+Na($3p^2P_{3/2}$), electronic energy quenching dynamics, crossed beam expt. 80−9683
O_2+Ne^+, thermal energy, reaction rate coeffs. and product distrib. 79−29333
O_2+Ne^+→O^++O+Ne, thermal energy charge transfer, energy disposal determ. 79−64099
O_2+Ne^{2+}, charge transfer reactions, rate coeffs. and product-ion distributions meas. 80−104431
O_2+Ne^{m+}(N^{n+}), K-shell vacancy prod. cross-section, charge state depend. 78−17751
O_2+negative ion, electron-loss cross sections 80−37877
O_2+Ni, complex form. in NiCa-Y zeolite, EPR, UV obs. 77−63949
O_2+O, quenching of O(^1S) state, rate coeff. 80−41581
O_2+O_2(H_2), vibr. energy transfer, collinear and 3-dimens. rate consts. 80−48065
O_2+O_2(N_2), IR spectral absorpt. induced by press. in atmos. *(Russian)* 80−56600
O_2+O_2(N_2)(H_2O)(Ar)(He), 118750 GHz transition, press. broadening 77−75136
O_2+O_3, collisional deactivation of laser excited O_2($^1\Delta_g$), addition effects and pathways 78−25673
O_2+O^+, charge exchange collision, rate coeff. and ionosphere implications 80−87224
O_2+O^+(^4S)(^2D), charge transfer reactions, cross-sections meas. 78−92462
O_2+O^{n+}(Xe^{n+})(Pb^{n+}), 50 keV, multiple scatt., target at.+energetic ion spatial correlation influence 79−27062
O_2+OH, OH(ν=1) relax., time resolved spectra 80−74240
O_2+OH, rot. inelastic collision, microwave spectra 79−45806
O_2+OH^+(H_2O^+), reaction, ICR obs. 79−8429
O_2+OH($A^2\Sigma^+$), quenching rates and fluoresc. efficiency, rel. to atmosphere 80−14199
O_2+O(^1S), collisional interaction products, reson. fluoresc. obs. 78−46423
O_2+S^{q+}, (q=6-16), K X-ray prod., charge-state depend. 80−106391
O_2+SO_2=SO+O_2, gas phase reaction, rate coeffs. meas. 80−97704
O_2+S→SO_2, chemiluminesc. matrix reaction, diffusion controlled, 8-20K 78−61013
O_2+Sc(Y), nascent product state distribs., laser fluoresc. detect. 78−7187
O_2+Sc(Y), oxidation, single collision chemiluminesc. 77−25267
O_2+Si*, collisional quenching, reson. line absorpt. expt. 78−46297
O_2+U, chemi-ionisation reaction involving laser excited atoms *(Japanese)* 79−13830
O_2+U^+(UO^+), reaction cross-sections, ion beam apparatus study 80−97691
O_2+X^{n+}, (X=Ar,Kr,Xe,U), Auger emission line shape after dissoc. 78−86838
O_2+Xe^{2+}, charge transfer from ground and metastable states 79−31677
O_2^-+H_2O_2, Haber-Weiss reaction kinetics, chain mechanism 79−83444
O_2^-+N_2, electron detachment, collision with vibr. excited mols. 79−54961
O_2^-+O_2, electron detachment, collision with vibr. excited mols. 79−54961
O_2^-+O_2, endoergic reactions, energy depend. of cross section meas. 77−12792
O_2^++atmospheric gases, thermal energy reaction rates 78−92443
O_2^++H_2O, 50 to 250 keV, OH radical form. 78−56890
O_2^++methane, reaction rate const. kinetic energy depend., 300K, 0.125-0.450 torr 78−76850
O_2^++NO→NO_2^++O, photoionis. mass spectra, photoionis. efficiency 77−40537
O_2^++N→NO^++O, rate constant rel. to atm. ion chem. 77−41245
O_2^++O_2, three-body ion-neutral assoc. reactions, saturation 79−39134

oxygen continued
O_2^++Xe→Xe^++O_2, Xe^++O_2→O_2^++Xe, charge transfer, photoionisation mass spectra 77−16793
$(O_2)_2$ formation, rot.-vibr. symmetry correlation, building-up principle from mol. fragments 78−76849
$(O_2)_2$, struct., energy transfer, high resolution electronic spectra 78−25550
$(O_2)_2$, struct., vibr. relax., local modes, isotope effects 78−25669
$(O_2)_2$, van der Waals mol., WKB vibr. eigenvalues 78−33498
O_3-O_2 mixture, significant struct. theory appl. to phase separation 77−51503
O_3+Br→BrO+O_2, reaction rate constant, 200-360K 78−73024
O_3+inert gas, rot. energy transfer, centrifugal sudden approx. 80−27933
O_3+O^-(OH^-)(S^-)(SH^-), associative detachment, rate coeffs. 78−3325
O_3+Tb^{3+}(Dy^{3+}), in H_2SO_4 soln., electrochemiluminesc. emitters quenching by electrolysis products 79−1794
O_4 molecule, equilib. struct., vibr. freqs., SCF closed shell calcs. 80−74101
O_4 molecule, SCF-CI calcs. 80−78517
O_4^-, photodissoc. and photodetachment in O_2/CH_4/H_2O mixtures, 3500-8600 Å 79−45776
O_4^+, form., in O_3 photoionisation, mass spectra 77−50477
O_4^+, photodissoc. cross sections meas., 3500-8600 Å 79−24763
O_5^+, form., in O_3 photoionisation, mass spectra 77−50477
O_5^+, produced by collisional dissoc. method, mass spectrometric study, dissoc. energies determ. 80−95707
O_5^{2-}, hypothetical, mol. self-consistent study, possible prep. method *(French)* 80−91717
O_6^+, produced by collisional dissoc. method, mass spectrometric study, dissoc. energies determ. 80−95707
O(^1D, ^3P) isoelectronic series, Sternheimer valence shielding and anti-shielding factors 80−18807
O^+(^2D) in thermosphere, quenching by electrons 80−94630
O^+(^2D) metastable ions, charge exchange with O_2 in thermosphere 79−58141
O^+(^2D) quenching by O in thermosphere, Atmospheric Explorer data 78−28355
O(^1D), chemical reactions of stratospheric importance, temp. depend. 79−53494
O(^1D), energy transfer contrib. to heating of low nighttime ionosphere 79−44288
O(^1D), excited states prod. by O_2 photodissoc., quantum yield 78−33557
O(^1D) formation, in O_3 near UV photolysis 78−15689
O(^1D) formation by O_3 photolysis, tropospheric meas. 78−73536
O(^1D), photoprod. rate determ., tropospheric solar UV flux meas. 79−12197
O(^1D), quantum yields from O_3 photolysis as function of temp. (230-320K) and wavelength (295-320 nm) 78−56903
O(^1D) quantum yields from laser flash photolysis of O_3 in fall-off region 80−45524
O(^1D) quenching in Earth atmosphere, translationally hot O(^3P) energy distrib. 80−21811
O(^1D), rel. quantum yield in O_3 photolysis in 250-300 nm region 79−20383
O^+(^2D)+N_2, charge exchange rate coefficient, effect of N_2^+ recomb. on aeronomic determ. 78−88954
O^+(^2D)+N_2, thermal rate coeff., products and branching ratios in ionosphere 80−82117
O^+(^2D)+N_2 charge exchange, rate coeff. temp. depend. 80−77179
O(^1D)+Ar(Kr)(Xe), inelastic collisions, spin-orbit coupling 80−5605
O(^1D)+CO, deactivation rate consts. temp. depend., 113-333K 78−88629
O(^1D)+chlorofluoromethane, stratospheric chem. reactions 79−53499
O(^1D)+H_2O, rate coeff., atm. OH prod. 79−58009
O(^1D)+H_2(HCl)(NH_3)(N_2O)(methane), rate consts., temp. depend. 78−27747
O(^1D)+haloalkanes, deactivation reactions, absolute rate consts. determ. 79−11783
O(^1D)+N_2, electronic quenching resons., collinear collision, quantum mech. calcs. 77−60050
O(^1D)+O_3, UV photolysis, O(^3P) prod., rate consts. determ. 80−55636
O(^1D)+Xe(Kr)(Ar), deactivation rate consts., 110-330K 78−88628
O($^1D_2$)+CO($^1\Sigma^+$), collisional quenching, energy transfer processes 80−23501
O($^1D_2$)+NH_3→OH(v,N)+NH_2, bimodal OH rot. distrib. obs. and energy disposal 80−76501
O_2($^1\Delta$) content determ. in chemical generator gaseous effluents, ratiometric system 78−76970
O_2($^1\Delta_g$), 650-1650K reaction in combined discharge flow/shock tube study 79−89618
O_2($^1\Delta_g$) airglow, emission height profile meas. during winter anomaly event 78−45077
O_2 $^1\Delta_g$, singlet and triplet precursors of photosensitised addition to organic acceptor 79−52714
O_2($^1\Delta_g$)+HNO, excitation in NO+C_2H_4 system 79−52674
O_2($^1\Delta_g$)+I($^2P_{3/2}$), possible electronic transition chem. laser 78−63116
O_2($^1\Delta_g$)+O_2, deactivation rate const. meas. 78−5262
O_2($^1\Delta_g$)+O_3, UV photolysis, O(^3P) prod., rate consts. determ. 80−55636
OH+NO(NO_2)(O_2), OH(ν=1) relax., time resolved spectra 80−74240
OI 5577 Å line, ground obs. 77−70900
$^{16}O^{16}O$, Raman spectra, direct determ. of rotation-vibration coupling coeff. 77−38675
$^{18}O^{18}O$, Raman spectra, direct determ. of rotation-vibration coupling coeff. α_{e_v} 77−38675
O^+(O^{8+})+He, p-state alignment, X-ray emission polaris. obs. 79−50123
O^-(O_2^-), optimum pot. model used to generate numerical pot., energies and electron affinities determ. 80−99534
O(^3P,^1D)+H_2($^1\Sigma_g^+$)→H_2O, potential energy surfaces, extended basis first-order CI study 80−7776
O^+(^2P), atmospheric, ionisation freq. vars. during solar cycle 21 from airglow meas. 80−77195
O(^3P) atom yield in radiolysis of water by $^2H^+$ and $^4He^{2+}$ 80−35556
O(^3P) prod. by O_3 photolysis, quantum yield determ. 80−78568
O(^3P), translationally hot, in Earth atmosphere, energy distrib. function 80−21811
O(^3P)+1-butyne (2-butyne), CO pro dynamics, mechanisms 78−11510
O(^3P)+2-methyl-2-butene, reaction rate consts. meas. 78−61001
O(^3P)+alkenes, absolute reaction rate consts., 298-439K, photolysis-chemiluminesc. determ. 77−77747

oxygen continued
$O(^1P)$+allene (butadiene)(vinyl methyl ether), absolute rate consts. meas., 297-439K 78−7196
$O(^3P)$+amines, rate consts. temp. depend., 298-440K 78−48616
$O(^3P)$+benzene (toluene), absolute reaction rate consts., 299-440K 79−70304
$O(^3P)+C_3O_2 \rightarrow 3CO$, reaction dynamics and monoxide vibr. distrib., laser reson. absorpt. method 78−68882
$O(^3P)$+CHF→HF+CO, product vibr. energy distrib. 79−61853
$O(^3P)$+CN(v) react., prod. energy distribs. meas., CO vibr. level population *(German)* 78−76833
$O(^3P)+CO(X^1\Sigma^+)$, vibr. deactivation and atom exchange, rate. consts., Monte Carlo anal. 77−48627
$O(^3P)+CS_2 \rightarrow CS+SO$, reaction rate enhancement, triat. mol. symmetric vs. asymmetric stretch excitation 79−91927
$O(^3P)+ClONO_2$, photolytic gas phase kinetics at 245K 79−52719
$O(^3P)$+dimethyl disulphide, absolute reaction rate const. determ. 80−89472
$O(^3P)$+dimethyl sulphide, fast flow reson. fluoresc. obs. of absolute rate consts. 80−61077
$O(^3P)+H_2$, reaction rate constants, Monte Carlo quasi-classical trajectory calculations 79−74366
$O(^3P)+H_2 \rightarrow OH+H$, potential energy surface, theory 80−45492
$O(^3P)$+HCl, reaction rate const. temp. depend., stratospheric implications 78−31616
$O(^3P)$+HCl(HBr)(HI), rate consts. temp. depend. 79−52627
$O(^3P)$+mercaptans, reaction rate consts., O_2 effect 79−52630
$O(^3P)$+methane, barrier height and transition state geometry, POL-CI calc., H abstraction reaction 80−66782
$O(^3P)+O_3$, bimolecular reaction rate coeff. reactant vibr. excitation depend., reson. fluoresc. obs. 78−76837
$O(^3P)$+vinyl halides, reaction rate consts. 298-442K flash photolysis obs. 78−7195
$O(^1S)$, absolute quantum yield meas. by XeO luminesc. in CO_2, N_2O photolysis 80−35561
$O(^1S)$ airglow, lab. prod. rate coeff. meas. 79−53604
$O(^1S)$, auroral production sources determ. from rocket and satellite meas. 80−26662
$O(^1S)$ formation in upper atmosphere, comparison of Chapman's and Barth's mechanisms 79−62636
$O(^1S)$ in upper atmosphere, auroral prod. and loss processes from artificial expt. 79−66855
$O(^1S)$ production indirect mechanism in aurora 79−48597
$O(^1S)$ source in aurora, energy transfer from excited N_2 and O_2 79−48598
$O(^1S)$ yield from O_3 photodissoc. at 1700-2000 Å 80−97714
$O(^3S)$ impact on Cu-Be-O surface, secondary electron yield 78−58797
$O(^5S)$ metastable state, radiative lifetime determ. 78−74614
$O^+(^4S)+N_2(X^1\Sigma_g^+) \rightarrow NO^+(X^1\Sigma^+)+N(^4S)$, MCSCF potential energy surface for collinear $^4\Sigma$ pathway 80−63540
$O(^1S)+CO_2(H_2O)(NO)(N_2O)$, product channels 78−46422
$O(^1S)+O_2$, collisional interaction products, reson. fluoresc. obs. 78−46423
$O(^5S)$+inert gas, de-excitation cross sections 80−53118
$O(^5S)$+Ne(Ar)(Kr)(Xe), total cross sections 78−42188
$O(^5S)+O_2 \rightarrow O(^3S)+O_2$, reson. radiation 80−53122
$O(^5S_2)$ metastable state g_J factor, TOF at. beam mag. reson. obs., rel. to $He(^3S)$ 79−3593
$O^+(^4S)(^2D)+Ar(H_2)(N_2)(O_2)(CO)(NO)(CO_2)$, charge transfer reactions, cross-sections meas. 78−92462
$O_2(^1\Sigma)$ airglow, gravity waves interaction theory 79−29918
$O_2(^3\Sigma^-)$, geometry optimisation, using bond function augmented basis sets 78−905
$O_2(^1\Sigma_g)$, 650-1650K reaction in combined discharge flow/shock tube study 79−89618
$O_2(^1\Sigma_g^+ \rightarrow {}^3\Sigma_g^-)$, in O-COS-$O_2(^1\Delta_g)/O_2$ system, chemiluminescence 80−66806
$O_2(^3\Sigma_g^+)$, charge density, X-ray scatt. factors, gas phase electron diffr. 78−930
O_2(0-1) 8645 Å atmospheric band, ground obs. 77−70900
O_2(0-1) 8645 Å band rel. to OH and forbidden O I atmospheric spectra 78−61639
^{15}O, absorbed dose comparison rel. to γ-ray emitters 79−70647
^{15}O activity decay determ. of cerebral perfusion rate after photon activation 80−26341
^{15}O production for nuclear medicine use 80−30889
^{15}O radioisotope preparation at variable energy cyclotron of Frederic Joliot Hospital Service *(French)* 77−65361
^{15}O, serial positron imaging, assess. of pulmonary embolism resolution rates 80−3789
^{16}O, $^{18}O_2$, vac. UV absorpt. spectra, band intensities and designations 78−5245
^{16}O, chemisorbed on W (100), isotope effects obs. by SIMS 79−5234
^{16}O ions, mag. hyperfine interactions, PAC meas. 80−95734
^{16}O isotopic anomalies in solar system, local proton irradiation model 78−93128
^{16}O, low conc. depth profiling using $^{16}O(d,\alpha)$, α-particle energy anal. 79−5214
^{16}O, precision absolute thin film standard reference targets for nuclear reaction microanal. 79−2880
$^{16}O^{8+}$+Au K-shell ionis., δ-ray emission 77−79557
$^{16}O^{x+}$+Al, energy-loss straggling, charge exchange effects 78−58799
^{17}O, ^1H, ^2H in muscle water, study of spin-lattice and spin-spin relax. times 80−21443
^{17}O, NQR at natural isotope abundance, double reson. new techniques, review 80−53013
^{17}O, naturally abundant, nuclear quadrupole resonance spectrum for fine struct. detection 80−75881
^{17}O nuclear quadrupole double resonance spectroscopy, line shapes and examples 80−31820
^{17}O, precision absolute thin film standard reference targets for nuclear reaction microanal. 79−2881
$^{17}O/^{16}O$, $^{18}O/^{16}O$ in Chainpur meteorite, meas., rel. to D conc. in early Solar system 80−36518
$^{17}O/^{16}O$ abundances in interstellar clouds 77−87528
$^{17}O/^{18}O$ ratio in Allende meteorite inclusion HAL, possible member of FUN family 80−105211
$^{17}O_2^-$, adsorbed on alkaline earth oxides, electron transfer, EPR obs. 78−76296
^{18}O, chemisorbed on W (100) isotope effects obs. by SIMS 79−5234
oxygen continued
^{18}O composition of metamorphosed chert and Fe formation from W.Greenland 78−81155
^{18}O concentration in Amazon Basin water, evidence for recycling 80−81955
^{18}O fractionation in calcite-depositing spring, chemical vars. and calcite precipitation 79−44202
^{18}O in equatorial Pacific core, glacial time scales and climate 80−21817
^{18}O in estuaries 80−26532
^{18}O in natural waters, appl. to tracing of air and water pollution *(Italian)* 77−53078
^{18}O in quartz silt, resistance to isotopic exchange when buried and weathered 79−39709
^{18}O ions, radial dose, LET and energy per ion pair in N_2 and tissue-equivalent gas 78−7452
^{18}O isotope shift in ^{13}C NMR, struct. depend. 80−69165
^{18}O, palaeoclimatic features, based on stable isotope compositions, Lake Biwa, central Japan 79−12230
^{18}O, precision absolute thin film standard reference targets for nuclear reaction microanal. 79−2881
^{18}O record for past 150000 years in N.Pacific sediments, palaeoclimate marine-continental correl. 79−80008
$^{18}O/^{16}O$, groundwater seepage, control Kentucky karst 80−8370
$^{18}O/^{16}O$, in SiO_2 from diatoms, 20000 yr record in deep-sea sediments 78−32247
$^{18}O/^{16}O$ geochemistry, of potassic igneous rocks from Roccamonfina volcano, Roman comagmatic region, Italy, 80−41420
$^{18}O/^{16}O$ in Archaen clastic metasediments, rel. to use as petrogenetic indicator for Archaean gneisses 78−20410
$^{18}O/^{16}O$ in cellulose, lignin and whole wood from tree rings, climatic appls. 78−24355
$^{18}O/^{16}O$ in DSDP Leg 37 rocks, ratios and geochemistry 77−91072
$^{18}O/^{16}O$ of river runoff on US east coast 79−100879
$^{18}O/^{16}O$ ratio analysis in carbonates by mass spectrometry *(Portuguese)* 80−7875
$^{18}O/^{16}O$ ratio in precipitation, correl. with temp. and altitude 80−77067
$^{18}O/^{16}O$ ratio in waters from El Tatio geothermal field, N.Chile 79−16525
$^{18}O/^{16}O$ ratio of dissolved O during FLEX 76 in North Sea 78−73404
$^{18}O/^{16}O$ ratios in granites from British Late Caledonian 80−36276
$^{18}O/^{16}O$ ratios of rocks from Canadian Precambrian Shield, N.W.Ontario 77−78130
$^{18}O/^{16}O$ stratigraphy of deep sea sediments rel. to Eemian interglacial 79−29770
$^{18}O/^{16}O$ trends, Middle Pliocene climate change in W.Mediterranean 80−26605
$^{18}O/^{16}O$ variations in deep sea carbonate shells from East Pacific Rise hydrothermal field 80−109173
$^{18}O/^{17}O$, abundance, ratio in hot CNO nucleosynthesis 77−78767
$^{18}O_2$, Herzberg transition I in absorpt. spectrum 79−72313
^{18}O-D relationship for atmospheric precip., global climatic interpretation 80−17331
$^{18}O^{16}O$, in atmosphere, photodissociation as source of atmospheric O_3 80−94559
$^{18}O+D_2{}^{16}O$ exchange reacts., water adsorpt. on Pt surfaces investig. 77−80695
O^*+H_2S, chemiluminesc. matrix reaction, diffusion controlled, 8-20K, $O(^3P)$ 78−61013
$O^*+H_2 \rightarrow OH^*+H$, rate const. and vibr. energy distrib. in OH*, for $O(^3P)$ 78−60998
$O^{+*}+O_2$, metastable ion reactions, rate consts. and ion mobility at 300K 80−95722
O_2^*, vibrationally excited, study by variable temp. photoelectron spectroscopy 78−21972
O_2^{-*}, vibr. excited, lifetime obs. 77−42422
$O_2^*+O_3$, UV photolysis, $O(^3P)$ prod., rate const. determ. 80−55636
$O(1D)$, in Comet Bennett (1970 II), brightness profiles 79−35192
$O(2^1D_2)$, prod. by O_3 photolysis, collisional deactivation 79−20384
$O(2^1D_2)+N_2(O_2)(N_2O)(CO_2)(H_2O)$(methane), collisional deactivation meas., 295K, rel. to atmospheric processes 80−16663
$O(3p^3P)$, population and depopulation of $O(3P^3P)$ in supersonic freejet of O_2-seeded Ar plasma 80−42958
$O(3p^5P)$, population and depopulation in supersonic freejet of O_2-seeded Ar plasma 80−42958
$O(3p^3P)+H_2O$, radiation quenching in pulse radiolytically excited water vap. 79−89738
$^{17,18}O$, from formaldehyde, ion laser induced isotope separation 77−61871
$O_{2-3}^-.H_2O$, photodissoc. and photodetachment in $O_2/CH_4/H_2O$ mixtures, 3500-8600 Å 79−45776
$O_2^+.O_2$, reactions with CO_2, O_3 and methane rel. to stratospheric ion chemistry 79−2343
$O_2^+.O_3$, reactions with H_2O and methane rel. to stratospheric ion chemistry 79−2343
$O_2^+(a^4\Pi_u)$+methane, 0.04-1.2 eV, reaction rate consts. 79−47911
$O_2(b^3\Sigma_g^-, v'=4, N', F')$ predissociation fragments, ang. distribs., separation energies 80−5588
$O_2^+(b^4\Sigma_g^-)$ predissociation, branching ratio determ. 80−14181
$O_2(b^1\Sigma_g^+)$ quenching by $O(^3P)$ and O_3, rate coeffs. 79−70309
$O_2(b^1\Sigma_g^+)$, temp. dependent quenching, photochemical study by H_2-VUV laser 80−63702
$O_2(c^1\Sigma_u^-)$, in Ar(Kr)(Ar-Kr) matrices, multiphonon vibr. relax. time-resolved emission obs. 80−18861
O^+ in magnetosphere ring current, rel. to hiss generation by magnetosonic waves 77−82085
Pb:O, thin film, microstruct. and thermal stress, doping effects 80−88458
$Pb+O(O_2)$, PbO chemiluminesc. spectra 77−9087
Pd melting point, effect of surrounding O_2 80−27299
Pt electrode O_2 reduction kinetics in conc. H_3PO_4, H_2SO_4 and $HClO_4$ 78−23952
Pu-O system, partial molar enthalpy of solution of O 77−47578
RbBr:O_2^- centres, luminesc. polarisation temp. depend. 78−87943
Re-O_2, surface interactions and catalysis, 77 to 773K 79−79286
Re-O-Cl system, gas-transition metal interaction, kinetic model *(French)* 80−108740
$S+O_2 \rightarrow SO_2(a^3B_1)$, in Ar:OCS:$O_2$ matrix thermoluminescence of SO_2 77−48647
$S^++O_2 \rightarrow SO^++O+0.26$ eV, rate consts. kinetic energy depend., drift tube meas. 80−7778

oxygen continued
SO_2-$^{18}O_2$ mixtures, IR laser pumped, intermol. vibr. energy transfer dynamics obs. 80−87207
$SO_2+O_2(O_3)$, in aq. soln., kinetics, rel. to atm. rate processes 79−20905
$Sb(5^4S_{3/2})+NO(O_2)$, rate consts., time-resolved reson. fluoresc. meas. 78−27732
$Sc+O_2 \rightarrow ScO+O$, chemiluminescence, $A^2\Delta X^2\Sigma^+$ transition 77−1927
Se:O, amorphous, O impurity addition rel. to elec. cond. 79−38067
Se:O, amorphous, photocond. spectrum impurity effect 77−76862
Se:O(Cl)(K) amorphous, elec. cond. increase on impurity addition 77−11920
n-Si (100), O_2 partial press. depend. of fixed surface state charge due to thermal oxidation 79−70179
Si, Czochralski crystals, O microsegregation, swirl defect distrib., growth rate depend. meas. 80−39295
Si, Czochralski grown, inhomogeneous O precip. and stacking fault form. 79−14820
Si Czochralski grown, O distrib. meas. 77−11580
Si, dislocation free, C and O impurity clouds, heat treatment influence on light scatt. 80−6427
Si, O content determ. by spectral analysis, phonon absorpt. effects *(Russian)* 77−48177
Si resistivity and carrier mobility effects of dissolved interstitital O_2 77−76824
Si thin film, effect of O on thin film compositions obtained by secondary ion emission 80−26079
Si wafer O interstitial IR absorption spectrometry, multiple reflection correction 80−55131
Si:0, electrical activity due to heat treatment, Hall effect meas. 80−15543
Si:Al(Ga), O_2 diffusion, conc. profile meas. 80−79990
Si:Au, O, film, amorphous, elec. cond. meas. 80−80423
Si:C(O), photoluminescence spectra, radiation damage investig. 77−28620
Si:H,F,O amorphous, plasma deposited, comp. and optical props. 80−50441
Si:Ni,O, interaction of Ni with O, influence of heat treatment, IR absorption meas. 77−4667
Si:O, 9 μm absorpt. band attributed to dissolved O, from expts. on quartz particles 79−19914
Si:O, A centre, theoretical study 80−75521
Si:O, amorphous, sputtered, influence of O and deposition conditions 80−54693
Si:O, annealed, minority carrier lifetime 79−23985
Si:O, annealed, precipitates, dislocation and stacking fault loops, TEM characterisation 77−4111
Si:O, annealing behaviour of O donor, conc. reductions via resistivity meas. 79−51129
Si:O, C, impurity conc. profiles and process-induced defects 78−6094
Si:O, CVD layer, RHEED study of surface crystallinity, annealing effect on structure 79−69371
Si:O, carrier lifetime depth distrib. due to Ar ion implantation 80−70232
Si:O, carrier recomb. processes, role of vacancy-O complexes 80−65592
n- Si:O, charge carrier scattering on neutral centres 80−49762
Si:O, comparision of depth profiling techniques 80−29048
Si:O, crit. stress of dislocation movement, determ. new method 77−80503
Si:O, cryst., annealed, struct. defects 78−75673
Si:O, cryst., donor form. during annealing, elec. resist. study 80−49653
Si:O, Czochralski crystal, oxygen striation and thermally induced microdefects 80−100275
Si:O, Czochralski grown crystal, O precip., nucleation behaviour and dislocation loop form. *(Japanese)* 80−59664
Si:O, dislocation-free, Si-O complexes, heat treatment effects 77−62557
Si:O, EPR spectra of heat treatment centres 78−48039
Si:O, effect of interstitial O on elec. props. 77−76846
Si:O, electrial and infrared spectroscopic investigations 80−34389
Si:O, electron irrad., multivacancy-O complexes, EPR expt., correl. with IR absorpt. data 77−28443
Si:O, evaporated amorphous film, effect of O_2 on props., ESR spectra 80−11265
Si:O, heat treated, excess carrier recomb. rate, defect levels 80−75579
Si:O, high temp. annealing effect on impurities 78−38745
Si:O, IR absorpt. at low temp. *(Chinese)* 80−108228
Si:O, IR absorpt. spectra of Si:O complexes 78−19520
Si:O, implant redistribution, annealing effects, SIMS meas. 80−96561
Si:O, implanted O location, channelling effect meas. 78−26593
Si:O, impurity conc. profiles, scanning IR absorpt. using semicond. laser 80−50376
Si:O, incorporation of O during pulsed-laser irrad. 80−96557
Si:O, interstitial Si atom formation by light ion bombardment 78−47406
Si:O, ion implanted, nature of defect reverse annealing 80−88875
Si:O, ion-implanted between 2 and 20 MeV, range and range straggling 80−44241
Si:O, kinetics of donor formation, under heat treatment in 450-900°C range 80−75523
Si:O, mechanism of O precipitation and stacking fault formation 77−76427
Si:O, O rich polycryst. film, carrier transport 78−80076
Si:O, semi-insulating polycryst. film, cond. through localised and extended states 77−28268
Si:O, specific resist. rel. to annealing, Si-O complex form., O_2 distrib. *(German)* 77−72863
Si:O, striated impurity distrib. calc. in melt-grown crystals 80−24488
Si:O, Xe, ion implanted, Xe retention, Rutherford backscatt., comparison with SiO_2+Xe 79−4320
Si:O,H amorphous, plasma-deposited, electronic and struct. props. 80−50391
Si:O film, near IR absorption, O impurity states 78−88333
Si:O film, near IR reflectivity at high temps. 78−56532
Si:O film, thermally deposited, semi-insulating, crystallographic study 78−75954
Si:O polycrystalline layers in Si p-n junction, charge transport and passivation 79−38206
Si:O wafer, annealed, surface- and inner-microdefects, TEM obs. 80−54236
Si:O wafer, dislocation pinning effect of O atoms 77−89437
Si:O wafers, impurity meas. by Fourier transform IR spectra 80−89030
Si:O wafers, impurity meas. by Fourier transform IR spectra at low temp. 80−89031
oxygen continued
$Si:O_2^+$, in-depth distrib., Cs^+ SIMS anal. appl. 79−39265
Si:P(As), conc. profiles of P (or As) and recoiled O atoms after ion implantation into SiO_2-Si, SIMS obs. 79−51138
Si:P(O) p^+-n-n^+ solar cells, comparison rel. to resistance to 1.5 MeV electron irrad., majority carrier trapping 80−94087
Si-Au Schottky diodes, role of O in formation mechanics 79−42639
Si-O bonds, cryst. chem. at high press., rel. to Earth mantle mineralogy 79−48470
Si-O system, modern view 78−10045
$Si+H_2(O_2)(He)(SiCl_4)$, $3p^2(^1D_2)$ state behaviour, at. absorpt. spectra 78−29846
SiC, thin film, effect of O on thin film compositions obtained by secondary ion emission 80−26079
n-SiC:N, O, cathodolum. spectra meas. 78−19573
$SiCl_4+O_2$ in modified CVD process for optical fibre prod., reaction IR spectra 78−80472
$a\text{-}Si_{1-x}H_x$, oxygenated thin film, sputtered, elec. cond. and optical props. 79−15239
SiO, role of O in phonon conductivity 79−42326
$Si(3p^2(^1S_0))+He(SiCl_4)(O_2)(N_2O)$, attenuation of reson. radiation, time-resolved kinetic obs. 78−5329
Si:O, effect of displacement upon impurity levels, pseudopotential calc. 77−39803
$Sn+O_2$, crossed mol. beam kinetics, SnO time of flight recoil vel. spectra 78−68883
$Sn+O_2(NO_2)$, chemiluminescence and photon yields 77−29012
SnS(Te):O, impurity assoc. with Fe microtraces, Mossbauer effect meas. 77−20763
$SrCl_2$, O_2^- pair centre EPR spectrum 77−24742
$SrCl_2:O_2^-$, perturbed O_2^- molecule ion, EPR results 77−20682
T 80−41588
Ta, evidence for slow strain-rate embrittlement due to O_2, SEM study 79−79109
Ta film, determ. of thickness and O, N content 78−80824
Ta-O, steady state O_2 solubility *(German)* 80−44322
Tb-Fe: O film, amorphous, microstruct. and mag. props. 79−91273
Ti:O, channelled ions, flux peaking study using protons, H_2^+ and H_3^+ ions 79−1450
α-Ti-O system, exam. of static strain ageing 78−76675
Ti-O system, O/Ti<1, high-temp. thermodynamics using Tian-Calvet microcalorimetry 78−85190
$Ti(^3F)+N_2O(O_2)(NO_2)$, chemiluminesc., TiO dissoc. mechanisms, confirmation of $D^\circ_0(TiO)$ 77−40534
$(U,Pu)O_2$ fuels, O distrib. during irradiation, calc. using CODIF program 78−70604
$(U,Pu)O_2$, irradiated fuel, O_2 pot. meas. using galvanic cell 79−49689
$U+O_2$, assoc. ionisation, electron energy distrib. 78−35656
$U+O_2$, laser excited atoms, chemical reactions 77−90594
UC:O, sample prep. method importance in O determ. *(Japanese)* 80−23100
V, anomalous slip, suppression by O interstitials 77−28875
V:O, lattice location study, of 0, 1 MeV deuteron channelling 79−10846
V:O, neutron irrad., void form., 673-1073K 80−29066
V:O, purification and plastic props. 80−25810
$V+O_2(NO_2)$, oxidation, VO chemiluminesc. 77−9077
V_2O_{5-x}, O_2 equilib. press. as measure of O_2 binding energy in oxide system 79−16030
V_2O_{5-x}, O_2 equilib. press. above oxide system, thermodynamic props. 79−16029
W, cast state, interaction nature between C, O_2 and N_2 *(Russian)* 79−70114
W-O-F system, gas phase, comp. and chem. transport reactions in discharge lamp *(German)* 77−32826
$Y+O_2 \rightarrow YO+O$, $A^2\Delta\text{-}X^2\Sigma^+$ transition 77−1927
$Yb+O_2 \rightarrow YbO+O$, crossed mol. beam expt. 77−44468
Zn surface, O_2 interaction, chemisorpt. and oxidation 78−64886
ZnO:Cu, O, Fe(Co)(Ni) photocond., electron escape probabilities and trap depths 77−32041
ZnS:Cu, O(Fe,Co,Ni) photoconductors, killer impurities effect on electron escape probabilities and trap depths 77−4392
ZnS:Cu,O, photocurrent spectral distrib., Fe, Co and Ni impurity effects 77−8135
ZnS-O, single cryst., fast neutron irrad., optical props. 78−27331
ZnTe:Li, O, Hagemark theory, O modification isoelectronic trap 80−75517
ZnTe:O, deep centres, photocapacitance detection 79−95362
ZnTe:O, electronic and optical parameters of O related centre 77−24534
ZnTe:O, Ne or Al implantation, electronic and optical parameters of O-related centre 78−6399
ZnTe:O,Zn, dual ion implantation, luminesc. spectra obs. 78−87697
α-Zr, internal friction and O_2 pair diffusion 77−16634
Zr-O-N system, struct. and plastic deform. *(Russian)* 78−80588

oxygen compounds
allene+OH, absolute rate consts. 78−23927
bridged complexes, vibr. and electronic props., reson. Raman spectra appl. 80−52996
chemisorbed oxygen surface complexes on C, thermal desorpt. analysis 78−56032
chlorine oxides in MOS structs., high-temp. annealing in N *(Russian)* 77−89858
crystal chemistry of inorganic compounds with P 79−1406
ESCA chemical shift, indirect evaluation of Coulombic contribution to ionis. pots. for nonbonding electrons 78−92572
ESCA shifts and effective charges 80−78648
fluoride-oxide slags, elec. cond., Al and Si addition agents influence *(Russian)* 80−39572
hydroxide ions, desorption from GaAs single cryst., activation energies and lifetimes meas. 78−20072
interstellar cloud gas phase chemistry 80−105319
interstellar OH, 1720 MHz transition survey, comparisons with 1612, 1665, and 1667 MHz obs. 77−45586
metal oxides, Auger quantitative anal. 78−73104
metal oxides, chemical dissoc. under pressure as alternative to metallisation, feasibility study *(Russian)* 78−48553
molecule, ground state MNDO calcs. 78−911
OH, interstellar, abundance and column density in post-shock gas 80−56911
OH, interstellar, obs. of weak lines below 3400 Å in ζ Persei 77−45509

oxygen compounds continued
OH, interstellar, VLBI synthesis obs. and struct. of maser source W3(OH) 80−105368
OH main lines, IR pumping in Mira variable stars and OH-IR sources 80−46632
OH maser luminosity and expansion velocity gradient in Mira envelopes 79−71043
OH near galactic plane, 18 cm lines survey 79−75265
OH-ion distribution in high-silica optical fibre preforms 79−14121
organic, dipole moments, NDDO calcs. 80−47894
oxide, X-ray photoelectron O 1s lines 77−44121
oxide compounds, binary, solid-phase reactions of form., direction of diffusion 79−43179
oxide crystals, rutile-type, interionic pots., cohesive energy, bulk modulus, calc. 80−79741
oxide glasses, multivariant system of oxides and partial props. prediction from V-phenomenon 78−79540
oxide ions, desorption from GaAs single cryst., activation energies and lifetimes meas. 78−20072
oxide systems, exam. of techniques used to determine phase diagrams and equilibria, and effects on equilibria 79−8415
oxides, ABO_4 type, high press. phase transforms. and struct. types, cryst. chem. aspects 80−79940
oxides, binary, variable electronegativity of oxygen, relevance to molten fluorides 78−5157
oxides, brittle materials, swelling, blistering, p, d and He ion irrads. porosity effects 77−35603
oxides, chem. formulae, advances in preparative chem. 79−47915
oxides, dislocation climb model 80−100230
oxides, excited states of F-centres 78−64006
oxides, interaction between point defects and dislocations, cryst. plasticity 80−15149
oxides, liquid, surface tension calc. *(Russian)* 80−15335
oxides, low expansion, common structural features 78−83981
oxides, muonic X-ray spectra, empirical intensity correls. 78−90326
oxides, non-porous, powder geometric surface meas., chemical planimetric method *(German)* 79−88915
oxides, nonstoichiometry influence on plasticity *(German)* 79−24592
oxides, plastic deform., TEM obs. *(French)* 77−44304
oxides, point defects diffusion coeffs. calc. *(Japanese)* 80−15302
oxides, spinel struct., impurity ion pairs, local struct. charcts. 78−2146
oxides, stoichiometry meas. and control 78−51694
oxides, struct. and props. 79−27964
oxides, surface microphases investigation by X-ray electron spectral anal. 79−51269
oxides ang. distrib. of muon decay electrons of mesic O *(Russian)* 78−48105
oxides of third-row elements, Auger LVV transitions, X-ray photoelectrons and emission spectra 78−21978
oxides with perovskite struct., neutron diffr., ferri- and ferromag. props. 78−52214
oxidic ceramics, electron and ion conductivity, instrument for meas. up to 2000°C 79−96247
perovskites, nonstoichiometric, ordering of oxygen vacancies, model *(French)* 77−68963
β-Al_2O_3-OH_3^+, proton dynamics neutron scatt. study 80−59408
Ar:OCS, liq., dissoc. studies 80−78716
Ar:OCS, O(^{1}S) and S(^{1}S) photodissociative prod., photoluminesc. excitation spectra, exciton energy transfer 80−89508
C-O-H-N-Si-Ar, computer calculations of heterogeneous equilib. 79−66044
$C_2H_2+OH^-\rightleftharpoons C_2H^-+H_2O$, equilib. consts., ab initio SCF and CEPA calcs. 78−3361
$COCl_2$, microwave spectra, 24-154 GHz, rot. and centrifugal distortion consts. 78−46324
COS, asymmetry parameter, angle resolved photoelectron spectra, multiple scatt. method 80−63708
COS, atmospheric, oxidation as SO_2 source 80−4085
COS, dissoc. photoionisation, mass spectrometric obs. 79−72366
COS, high resolution UV photoelectron spectra 80−91603
COS in atmosphere, biomass burning as source 80−26586
COS^+, photoionis. reson. study of ($^2\Pi$) and ($^2\Sigma^+$) states, vibr. freqs., ionis. pot. 78−29821
$COS+Cl^+$, reactions at room temp. 80−93749
COS+He(Ne)(Ar), Penning ionis., electron spectra, vibr. transfer 77−14555
COS+OH, reaction rate consts., 299-430K 78−35653
Ca-S-O system, sulphide-sulphate equil., solid state EMF obs. 79−83492
CaF_2:O_2^-, OH^-, ion incorporation by reaction with surrounding atm. 80−55143
CaO:OH^-, room temp. IR spectra, heat treatment and electron irrad. effects 79−51992
Cl+OH*→HCl*+O, reaction dynamics, vibr. excited reagent and product 77−81392
$ClONO_2$+OH, reaction kinetics 77−86303
Fe-Ti oxide minerals from Asama volcano, Japan, in 1973 eruption 77−17065
GaP-anodic oxide devices, optoelectronic device, processing appl. 78−84304
HO, average tropospheric concs. in northern and southern hemispheres 78−32140
HO+CO→H+CO_2, 700 and 100 torr, 25°C, FT-IR anal. 77−25247
HO+isobutane→H_2O+iso-(or t-)C_4H_9, 700 and 100 torr, 25°C, FT-IR anal. 77−25247
HOCl, photolysis product of Cl_2-O_3-H_2 dil. mixtures, absolute integrated IR band intensities 80−26033
He+OCS, emission spectra in He afterglow 80−87139
Hf-O, phase props. 77−40415
KCl:Na^+, OH^-, IR absorpt. spectra, Na^+ ions rel. to OH^- stretching vibr. 79−47442
KCl:OH, absorpt. in high-transparency region 80−89037
KCl:OH, low temp. spectrophotometry, impurity absorpt. band *(Russian)* 79−40635
KCl:OH^- type dipole-phonon system, superradiative phase transition *(Russian)* 78−71806
KCl:OH^- type paraelec. systems, phonon superradiant phase transition *(Russian)* 79−69206
KI:OH^-, paraelec. reson. at 1.5 and 4.2K from 12 to 150 GHz 79−38512
$KTaO_3$:OH^-(OD^-)(OT^-), IR spectra, spectrosc. consts. 80−100671

oxygen compounds continued
Kr:OCS, O(^{1}S) and S(^{1}S) photodissociative prod., photoluminesc. excitation spectra, exciton energy transfer 80−89508
LiF:OH crystals, X-irradiated, H centres formation and annealing 80−54226
LiF:OH^-, IR spectra 80−20676
LiF-OH, γ-irrad., colour centre lasing at 0.84-1.13 μ at 300K 80−5739
MgO:OH^-, room temp. IR spectra, heat treatment and electron irrad. effects 79−51992
Mn-S-O system, sulphide-sulphate equil., solid state EMF obs. 79−83492
MnF_2:OH^-, thermal cond., temp. depend., role of reson. scatt. of phonons by OH^- defects 78−38889
MnF_2:OH^-, thermal cond., role of phonon scatt. by OH^- defects 78−38890
$N_2O_4\rightleftharpoons 2NO_2\rightleftharpoons 2NO+O_2$, working fluid for power-producing thermodynamic cycles 80−13536
NaCl:OH^-, additively coloured, form. and decay of defect clusters and elec. double layers, Au decoration obs. 79−10850
NaCl:OH^-, UV and IR absorpt. spectra, colour centres transformation 79−28791
Nb-O solid solutions, desorpt. of oxides *(French)* 78−14610
O-bearing gases, K X-ray yields induced by proton bombardment 79−45736
O+$I_2(CS_2)$(OCS), crossed-beam investigation of translational energy 79−5145
O+OCS (ethylene), reaction dynamics, IR laser excitation, vibr. effects 77−12788
O_2 $^1\Delta_g$, produced in HF low-press. plasma, use in organic cmpd. synthesis 80−61099
O_3+H_2S(OCS), SO chemiluminesc. in Ar matrix 79−5146
OAlCl and OAlF, IR matrix spectra, vibr. freqs. *(German)* 79−11785
$O_2^+AsF_6^-$, thermal decomposition, Raman spectra study, free radical mechanism 80−55652
OBF, band strengths, shock tube IR spectrosc. meas. 80−106358
$OCBr_2$, IR spectra in Ar matrix, force consts. *(German)* 79−36641
OCN^-, linear mol., Compton profile bond additivity, HF calc. 79−68268
OCS, 5.3 μm vibr.-rot. bands, rot. consts., spin-flip Raman laser obs. 77−34631
OCS, atmospheric concs. in S.W. and E.United States 78−20466
OCS, collisional excitation of interstellar molecule 78−81664
OCS, collisional rot.-line widths and shifts, microwave region 78−25619
OCS, detect. of new interstellar transitions 77−60808
OCS, dipole moment, laser microwave double reson.-Stark effect meas. 78−55191
OCS, electron elastic scatt., 0 to 100 eV 80−23547
OCS, electron impact dissoc., CS heat of form. determ. 78−73074
OCS, electron impact excitation of low-lying electronic states 79−10215
OCS, electron impact excitation and ionisation 80−63837
OCS, electron scatt., absolute total cross-section meas. 78−74774
OCS, fundamental vibr. bands in liq. phase 79−54856
OCS, gas, EPR of rot. transitions, T_1 press. depend. 80−9621
OCS, high-intensity laser photolysis at 157 nm, S(^1S) prod., photoionisation, and loss, laser appl. 80−21306
OCS, IR spectra, diode laser calibration 80−83363
OCS, IR spectra using spin-flip Raman laser, combination band near 1890 cm^{-1} 78−37640
OCS, IR spectral moments and mean squared torques, rare gas effects 78−62944
OCS, IR spectroscopy 79−98088
OCS in Ar matrix, photolysis, S_2 and S_3 absorpt. spectra 79−5149
OCS in Ar soln., IR spectra, solvent shifts, vibr. band assignment and anharmonic force consts. 80−9607
OCS, in atmosphere, contrib. to stratospheric aerosols and climate 80−41524
OCS, interstellar, in $^1\Sigma$ state, collisional excitation by H_2 80−109508
OCS interstellar transition in Orion, shock chemistry 79−21391
OCS laser, for 16 μm range, review *(Rumanian)* 80−87408
OCS laser, two-quantum excitation, photolysis, energy transfer, for fusion expts. 78−59003
OCS, laser Stark spectra, 9.5 micron, band origins, dipole moments 77−18969
OCS, lattice dynamics and phonon sidebands of vibr. excitons calc. 77−20028
OCS, M-resolved rot. Stark levels, four-level microwave-microwave double reson., collision induced 77−10696
OCS, MM wave spectrum, centrifugal distortion const. 77−34618
OCS, MODOR in ν_2=1 state, nondipolar collision-induced transitions 77−6812
OCS, microwave absorpt. coeff. 77−64378
OCS, microwave rot. absorpt. lines, press. broadened width and shift 77−61807
OCS, microwave rot. lines, self-broadening 78−58668
OCS, microwave rot. transitions, phase shift effect, collisional effects 79−98073
OCS, microwave spectrum, width and shift parameters 77−18985
OCS, microwave spectra, rot. Q-band *(Polish)* 78−29866
OCS, microwave spectral lineshape of J 1→2 line 79−68225
OCS, microwave spectra, Ku-band Fourier transform spectrometer appl. 80−68265
OCS, microwave-microwave double resonance 80−53029
OCS, millimeter wave rot. spectra, isotope shifts, freqs. and mol. consts. 80−78611
OCS mixtures, rot. energy collisional transfer, M-depend., microwave double reson. 78−46435
OCS, mol. consts. of ν_2 levels 77−14429
OCS, mol. photodissoc., 142-170 nm, quantum yield of S(^{1}S) 79−83477
OCS, mol. quadrupole moments, mag. shielding and spin-rot. tensors 79−22609
OCS, motion, regular and irregular spectra, theory 80−9590
OCS, multiphoton dissociation by IR laser 79−36710
OCS, multiphoton i.r. absorption, optoacoustic detection 77−507
OCS, ν_3 band absolute wavenumbers *(French)* 79−98099
OCS, optically pumped roto-vibr. mol. laser, rate eqn. model 78−37874
OCS, optically pumped roto-vibr. mol. laser, low temp. operation and performance 79−50315
OCS, optically pumped CW subMM cmission lines 80−95876
OCS photodissociation, S(^{1}S) prod. and props. in liq. Ar and N_2 80−43064
OCS photolytic laser, for fusion reasearch 78−59002

oxygen compounds continued
OCS, polar gas thermomagnetic torque meas. 77−42960
OCS, pressure-broadened linewidths in microwave region, temp. depend. 77−34694
OCS, pure and seeded beams, rot. cooling, electric reson. meas. 79−13795
OCS, r_m struct. determ. from rot. consts. 78−42236
OCS, relaxation by IR and microwave coherent transients 80−28092
OCS, rot. relax. cross section, beam maser meas. 79−31654
OCS, rot.-vibr. levels and semiclassical energy levels 80−37804
OCS, roto-vibr. mol. laser, low-temp. performance 80−9871
OCS, seeded beam, rot. cooling 79−18266
OCS, self-broadening linewidth parameters 79−18268
OCS, semiclassical energy levels calc., vibr. freqs. 78−46315
OCS, spectroscopic reference freqs. in 9.5 μm band, heterodyne freq. meas. 80−18850
OCS, stratosphere content, solar spectra meas. by 12 km attitude aircraft 80−41486
OCS, T_2 relax. meas. using budge-type superhet. microwave spectrometer 80−91551
OCS, third order coupling coeffs. for two phonon absorpt. 80−10621
OCS, two photon and vibr. depend. photolytic prod. of S(^{1}S) atoms 79−13775
OCS, UV photolysis producing S(3^1D_2) 79−79274
OCS, VUV photolysis in Ar matrix, thermoluminescence 77−52659
OCS, vibr. energy transfer map 80−99560
OCS, vibr. excitation and stimulated emission, CO_2 laser pulse pumping 77−23662
OCS, vibr.-rot. bands of Raman spectra 78−29173
OCS^+, photodissociation cross section, UV and visible spectral obs. 80−28077
$^{16}O^{12}C^{34}S$ and $^{16}O^{13}C^{34}S$, IR spectra, v_3 band anal. 80−95620
OCS-CO-N_2, liq. mixture, vibr. energy relax. and exchange, laser induced fluoresc. obs. 78−70905
OCS-N_2-SF_6 mixture laser, OCS photodissociation, electron dipole forbidden transition, absorpt. spectra 79−68389
OCS+benzene, microwave line width and quadrupole moments, perturbation theory 80−69190
OCS+benzene (S_1), V-V reson. energy, transfer, microscopic reversibility, level degeneracies role 79−86045
OCS+bromomethane, microwave spectral line width, dipole-dipole interaction calc. 78−74648
OCS+CO_2, collisional line broadening of microwave spectra, semiclassical theory 78−29776
OCS+CO_2(H_2)(N_2)(OCS), collisional line broadening of microwave spectra, semiclassical theory, calcs. 78−25516
OCS+H_2, rot. excitation, classical and quantum calcs. 78−1059
OCS+H_2, rot. excitation, infinite order sudden approx. 78−74740
OCS+H_2, scattering cross-sections, factorisation and fitting, IOS approx. 78−33575
OCS+H_2(CO_2) (fluoromethane), rot. relax. parameters, microwave spectra linewidth parameters 80−28009
OCS+H_2(j=0) 79−76492
OCS+H→HS+CO, absolute rate parameters, flash photolysis reson. fluoresc. 78−3312
OCS+He, translational-vibrational energy transfer, quantum dynamical study 80−63746
OCS+He^+, dissoc. charge-transfer, $CS^+(B^2\Sigma^+$-$A^2\Pi_i)$ emission prod., Morse pot. Franck-Condon factors calc., vibr. anal. 80−99539
OCS+He(Ar), rot. lines, collisional broadening 79−18267
OCS+He(Ne)(Ar)(Kr)(H_2)(O_2)(CO_2), gas, EPR of rot. transitions, T_1 press. depend. 80−9621
OCS+methanol (H_2)(He), collisional rot. energy transfer, microwave-microwave double reson. obs. 77−19016
OCS+N_2* 80−48063
OCS+nonpolar perturber, J1-2 line broadening 77−6848
OCS+nonpolar perturbation, J=1→2 microwave line press. broadening 80−9644
OCS+O, reaction dynamics, IR laser excitation effects 79−66288
OCS+O_3, double-quantum vib. energy transfer 77−6897
OCS+OCS, rot. transition, interpolation scheme 79−22776
OCS+OCS(He)(Ar), rot. spectral line shift and widths, collision induced phase shifts 77−75222
OCS+OH, flash photolysis reson. fluoresc. rate consts. determ., global S cycle 78−95914
OCS+OH, lower atmosphere chem. 80−61870
OCS+S, electronically excited atom, reson. fluoresc. 80−99476
OCS+S→S_2+CO, reaction kinetics of S(3^1D_2) reactions 79−79274
OCS+Si(Ge), SiS and GeS multiple collision chemiluminesc., intercombination systems 80−45505
OCSe, flash photolysis, Se(4^1D_2) direct obs. 78−25461
OCSe, isotopic species, microwave and IR spectra 77−38658
OCSe, laser photolysis using ArF laser, Se(^{1}S) quantum yield rel. to OCSe vibr. excitation 79−83478
OCSe, laser photolysis using ArF laser, Se*+OCSe and Se_2*+OCSe quenching rates 79−86050
OCSe photolysis, laser action from Se($^1S_0$) 79−31889
OCSe, photolysis, Se(^{1}S) prod., quenching of high concs. 79−6904
OCSe photolysis producing Se, using high efficiency ArF laser source 80−33032
OCSe, quantum yields for Se, $^1S_0$, $^1D_2$, and $^3P_{0,1,2}$ atoms determ. in photolysis, lifetime and quenching rate meas. 80−97741
OCl_2^+, radical cation, struct. and electronic props., ab initio RHF SCF MO calc. 80−52883
OClNO, form. in matrix reaction, IR absorpt. obs., photoisomerisation 78−15667
OD, $^2\Pi_{3/2}$ state EPR spectra 78−21949
OD, A-X system, relative transition probabilities 77−6860
OD, $A^2\Sigma^+\rightarrow X^2\Pi_i$ radiation after dissociative excitation of D_2O 78−46455
OD laser, pure rot. lasing intensity, pumping by collision induced energy transfer 78−74897
OD, quenching of rare earth ion luminesc. in tellurite glasses *(Russian)* 79−28839
OD radical, in $NiSiF_6.6D_2O$, optical absorption spectrum, 300 and 80K 79−73966
OD, reson. cross-sections, predissoc. and preassoc., isotope effects 78−58750
OD, spectra, A-X system Einstein coeffs. 79−36703
OF_2, core electron binding energies, XPS spectra 77−3417
oxygen compounds continued
OF_2, photoelectron spectra, ionisation energies, ab initio many-body Green's function calc. 79−89709
O_2F radicals, preparation, EPR spectra rel. to phase, temp. 77−51954
$O_2F+Cl+O_2$, ClF*($B^3\pi_o+$) prods., B-X emission spectrum 79−57216
$O_2F+N\rightarrow N_2$(NF), lasing potential of excited fluorides 78−63106
O_2F(Cl)(Br) radicals, matrix IR spectra, bonding 78−90160
$OGaF_3$, matrix IR spectrum, vibrs. and force consts. 79−11787
OH, $^2\Pi$ states, $^2\Delta$ states, $^2\Pi$ ground state, g-factor, Zeeman effect 79−98149
OH, 13.4 GHz absorpt. line width *(French)* 77−61801
OH 1612 MHz emission from M-type supergiants, search in southern objects 78−69792
OH 1612 MHz survey at high declinations 80−4452
OH 1667 MHz line absorption detection in Comet Kohler (1977m) 78−4152
OH 18 cm line obs. of young stellar clusters 79−25655
OH 1.6 GHz maser emission from W3(OH), 49N and 51, spatial distrib. 78−93355
OH ($A\ ^2\Sigma^+$) radical, predissoc. investig., shock-radiational recombination method 77−1924
OH, ($A^2\Sigma^+\rightarrow X^2\pi$) fluoresc. prod. by H_2O photodissoc., cross sections 78−25604
OH, ($A^2\Sigma^+$), abnormal rot. following H_2O photodissoc., semiclassical calcs. 78−40069
OH ($A^2\Sigma^+$)+H_2(N_2)(Ar), collisionally induced population change rates, laser-induced fluoresc. obs. 78−5326
OH, (0,0) UV transitions, band oscill. strength 80−69162
OH (6-2) and (8-3) nightglow bands, rotational temps. and intensities 79−58147
OH (7,2) Meinel 6861 Å emission band, altitude distrib. from rocket obs. of nightglow 77−29530
OH (8, 3), nightglow spectra correl. to atmos. Na density 80−41585
OH (8-3) Meinel band in nightglow 79−48596
OH, A-X system, rot. transition probabilities 80−43027
OH, $A^2\Sigma$ state, predissoc. rates, high freq. deflection meas. 78−62864
OH $A^2\Sigma^+$ state, laser excited, vibr. energy transfer, flame thermometry appls. 80−58349
OH, $A^2\Sigma^+$ state, predissociation and tunnelling 78−29823
OH, $A^2\Sigma^+$ state, predissociation, tunnelling 78−29824
OH, $A^2\Sigma^+{}_{1/2}$ state, g-factor meas. by quantum beat obs. 79−18176
OH, $A^2\Sigma^+$-$X^2\Pi_i$ system, vibrational and rotational levels, transition probability determ. 80−43034
OH, $A^2\Sigma^+\rightarrow X^2\Pi_i$ radiation after dissociative excitation of H_2O 78−46455
OH A→X intensity measurement, Tesla discharge temp. diagnostic method 79−64939
OH adsorbed on Ni, energy depend. of vibr. excitation, electron energy loss spectra 79−28201
OH airglow, spectrum rel. to atmosphere warming at 90 km during 1976-77 winter *(Russian)* 79−88518
OH, airglow in upper atmosphere, semi-annual vars. 78−28360
OH and trace gases, laser induced fluorescence system for aircraft appl. 80−36425
OH astronomical maser sources OH 231.8+4.2, CY Canis Majoris, M1−92, UHF obs. 80−90550
OH, atm. conc. meas. by laser fluoresc., O_3 dissoc. interference 77−49110
OH, atmospheric, vibr. excited states, time and altitude vars. 80−41589
OH, band oscill. strength, rot. excitation effects 80−23460
OH celestial masers physics, review 79−21455
OH, chemiluminesc., form. from O+ethylene, mechanism, rate const., mathematical model calcs. 78−48655
OH, collisionless form., rovibronic relax., reson. fluoresc. 78−68902
OH column densities in stratosphere from far IR rotational lines 80−36367
OH conc. in troposphere, rel. to halocarbons, SF_6 and N_2O concs. 77−45069
OH, conc. meas. in atm. boundary layer by monitoring CO oxidation 79−58012
OH conc. meas. in flat methane-air flames 80−16687
OH concentration in flame, local and instantaneous meas. by laser induced fluoresc. obs. *(French)* 79−15999
OH concentration profile in methane-air flames 80−35534
OH, correlation between chem. shift and charge in organic cpds. 77−18946
OH, determ. in flames, spectrosc. method 77−32853
OH, diffusion in nonuniform chemically reactive atmosphere, three-dimensional time depend. modelling 79−66846
OH, Dunham pot. energy coeffs. 78−41979
OH emission, photometric obs. to find mesosphere neutral temp. 80−82121
OH emission and absorption in H II region *(Russian)* 80−36733
OH emission as recorder of internal gravity waves near mesopause 78−12031
OH emission from Comet Meier (1978f) at 1665 and 1667 MHz 78−61800
OH emission from early-type stars with large IR excess 79−71035
OH emission from IR stars and planetary nebulae, survey 79−48787
OH emission from Mira variables, high-sensitivity search 78−89203
OH emission obs. of Lynds 134 dark nebula 80−22062
OH, emissivity calc. 78−90675
OH, exact hyperfine struct. and Einstein A-coefficients, astrophys. appl. 77−83762
OH, excitation and band rot. temp. of plasma jet light source 77−44555
OH, excitation in interstellar clouds 78−65669
OH, excited free radicals, form. by ion-mol. reactions 78−56890
OH excited states, satellite lines anomalies 77−42315
OH, fluoresc. lidar instrument for stratospheric temp. and press. determ. 79−80033
OH formation in H_2-NO flame, OH collisional broadening parameter, curve of growth method 80−53052
OH formation in interstellar dark clouds, grain surface reactions rel. to chemical and thermal equilib. 79−44593
OH, free radical, vibr.-rot. level population determ., including unresolved doublet struct. *(Russian)* 77−68033
OH, fundamental vibr. band, mag. rot. spectrosc. obs. 80−86446
OH, high resolution emission spectrum in oxyacetylene flame, mol. vibr.-rot. consts. 77−3409
OH, IR vibr.-rot. overtone bands in Mira variable R Leonis 78−36574

oxygen compounds continued
OH impurities in GeO_2-P_2O_5-SiO_2 glass fibre made by modified CVD process 80−50560
OH, in atm. CO-OH-CH_4 cycle, implications of anthropogenic CO emissions 77−49160
OH in direction of T Tauri stars, radio obs. 79−25662
OH in flames, laser excitation dynamics 80−74201
OH, in fused SiO_2, interactions, IR and Raman spectra 78−80383
OH, in inert gas matrix, H-bonding and charge transfer, fluoresc. 78−25602
OH, in interstellar diffuse clouds, column densities rel. to temps. determ. 78−93385
OH, in lower atm., vibr. energy distrib. 77−25735
OH in mol. cloud in NGC 2264 80−94847
OH in southern globular clusters, maser emission upper limits 80−22047
OH in upper atmosphere, emission spectrum meas. rel. to internal gravity waves *(Russian)* 78−16224
OH in vitreous silica, effects on viscosity 78−64580
OH, internal state distrib., crossed mol. beam H+NO_2 reaction, laser-induced fluoresc. 77−4905
OH, interstellar, $^{16}OH/^{18}OH$ abundance ratio obs. in three H II regions 78−54024
OH, interstellar, absorpt. in Cassiopeia A direction 78−45381
OH, interstellar, absorpt. line meas. towards galactic H II region (G48.6+0.0) 78−85996
OH, interstellar, excitation towards dust clouds 78−4318
OH, interstellar, ground state Λ double maser emission as result of overlapping far IR transitions 77−45533
OH, interstellar, new main line maser obs. with probable Zeeman pattern 80−56908
OH, interstellar, obs. in mol. cloud near (RCW 36) 78−69862
OH, interstellar, radio lines absorpt. obs. in galactic radio sources 78−54068
OH, interstellar, rot. excitation by H_2 rel. to maser emission 80−62232
OH, interstellar, search for 18 cm absorpt. lines in high latit. H I clouds 80−67841
OH, interstellar, towards galactic centre, absorbing clouds struct. determ. using regularisation method 80−17505
OH, interstellar, type IIc radio emission sources in (W33) *(Russian)* 80−62247
OH, interstellar emission sources, 13 GHz OH features obs. 77−33619
OH, interstellar maser lines intensity vars. due to induced Compton scatt. 78−4319
OH interstellar maser source, OH 205.1-14.1, 1667 MHz emission monitoring 77−64819
OH, interstellar masers, radial vel. struct. 77−33617
OH interstellar masers, 18 cm lines pumping by H+OH collisions 79−48892
OH, interstellar masers assoc. with compact H II regions, model 78−81666
OH, isotope effects, Zeeman effect, far IR laser mag-reson. spectra obs. 80−63674
OH, J=9/2 Λ-doublet line detect. in W3(OH) 78−65670
OH laser, pure rot. lasing intensity, pumping by collision induced energy transfer 78−74897
OH, laser absorption spectrum, scanning technique, appl. to atmospheric monitoring 78−17664
OH, laser induced fluorescence, preferential population of π^+ component of Λ doublet in H+NO_2→OH+NO 78−31620
OH, laser induced fluoresc. spectrosc. for flame temperature meas. 80−90839
OH local concentration in flame, direct meas. from single laser pulse induced fluoresc. 79−39229
OH, Λ-doublet splitting calc. rel. to predicted radioastronomical freqs. accuracy 79−48666
OH, Λ-doublet transitions induced by ion collisions 78−9222
OH, main line emission outbursts in spectrum of U Orionis 79−101158
OH main line maser in interstellar cloud, pumping mechanism 80−67824
OH main line masers in compact H II regions, magnetic field and inversion mechanism 79−48884
OH maser, OH removal by magnetic heating 79−98328
OH, maser emission from OH/IR sources 78−16432
OH, maser emission from stellar sources, bright IR star monitoring at 2.7 μm 78−16433
OH maser emission from W3 (OH), Zeeman effect 78−93377
OH maser emission from late-type stars, catalogue of objects 79−70965
OH maser in IRC+10420, new feature spatial struct. 79−48946
OH maser in pulsating Mira type variables atm., IR line overlap pumping mechanism 80−72764
OH maser lines from long-period variable stars, struct. and saturation 78−93264
OH maser obs. at 1612 MHz of IRC+10420 supergiant star 79−44471
OH maser pumping efficiency of Mira variable stars 80−82379
OH maser sources, accurate position meas. 80−46646
OH maser sources, interstellar, radiative transport effects on inversion 80−17681
OH maser sources near galactic centre, systematic search at 1612 MHz 79−35415
OH masers, type I, interstellar, positions, polarisation, nearby H_2O masers, radio and IR props. 79−25671
OH Meinel bands, in airglow, rot. temp., radiative lifetime 78−61643
OH Meinel bands in nightglow, rocket meas. *(Japanese)* 80−94631
OH Meinel bands intensity distrib. in airglow, OH* quenching mechanisms 78−65447
OH Meinel bands intensity var. in nightglow at Poona, rel. to O_3 conc. 79−5698
OH, methane-air flame, conc., temp. and rot. temp., laser absorption spectroscopy 78−76862
OH, microwave absorpt. coeff. 77−64378
OH, microwave maser emission obs. from VY Canis Majoris 78−53949
OH, microwave spectral line breadth in NH_3, H_2O, NO_2, SO_2, O_2, H_2, He, N_2, chloromethane 79−45806
OH, mol. beam electric reson., hyperfine Λ-doubling transitions 79−36628
OH molecules, detection of monopoles by nonlinear effects in interstellar masers 77−91609
OH, multipredissoc. of $A^2\Sigma^+$ state, multichannel scatt. theory 79−94046
OH, near IR airglow emission, Spacelab image intensifying TV obs. 77−21966
oxygen compounds continued
OH nightglow, correl. with Na D-line and O I 5577 Å emissions 79−80067
OH, nightglow emission diurnal and seasonal vars., correl. with O I 5577 Å 77−64506
OH, nightglow emissions, rot. temp. calc. 77−64507
OH, nightglow emissions, equilib. nature of rot. temp. 77−64508
OH, nonthermal main lines in interstellar dust clouds and OH abundance 80−36683
OH, OD, interstellar, Λ-doublet population inversion by collisions 80−22065
OH, optimum mol. consts. and term values, $X^2\Pi$ and $A^2\Sigma^+$ states, vibr.-rot. and microwave freqs. 80−95577
OH, potential u.v. laser, proton beam excited Ar-H_2O mixture 77−662
OH, prod. by photolysis, Λ-doublets, population, rot. states, hyperfine struct., microwave spectra 80−32694
OH, product state distrib. in O+H_2 reaction, laser photolysis-laser induced fluoresc. meas. 79−83446
OH production, O^++hydrocarbon chemiluminescent reactions 79−96299
OH, Pt catalytic oxidation of H_2 and D_2, matrix isolation and laser fluoresc. obs. of prods. 80−66865
OH, quenching of rare earth ion luminesc. in tellurite glasses *(Russian)* 79−28839
OH, radiative lifetimes of $A^2\Sigma$ state and A-X Einstein coeffs. 79−36703
OH, radical, atmospheric reactivity with organic compounds 79−61860
OH, radical, far IR laser mag. reson. spectra, fine struct. transition 79−76454
OH radical, gas phase EPR, rot. states electronic struct. and Zeeman parameters 78−86896
OH radical, in Earth's atmosphere, pure rot. lines 79−92593
OH radical, matrix-isolated, from H_2 oxidation on Pt, laser diagnostics 80−5572
OH radical, reactions with ester vapours, reaction rate consts. determ. at 292K 78−27729
OH radical calculated densities in troposphere and stratosphere, uncertainties 79−53426
OH radical concentration in methane-O_2-N_2 flames, hook method meas. 77−77762
OH radical concentration in troposphere, determ. via atmospheric ^{14}CO meas. *(German)* 80−8419
OH radical in premixed laminar methane-air flame, fluoresc. meas. of rot. temp. 79−80622
OH radical in upper atmosphere, meas. using lidar from Space Shuttle 80−51590
OH radical lifetime in comets at 1 AU 80−46488
OH, radical $v=1^2\Pi_{3/2}$ state, microwave spectrum 79−26972
OH radical participation in terminal muon spur for muonium prod. 79−57271
OH radicals, microwave spectra data tables 78−50542
OH radicals in glow discharge, rot. levels distrib., temp. meas. 78−47169
OH radicals vibrationally excited in stratosphere, instantaneous rate model 77−5273
OH, reson. cross-sections, predissoc. and preassoc., isotope effects 78−58750
OH, rot. transitions broadened by press., laser mag. reson. study 79−94020
OH rotational temp. determ., successive approx. 80−23389
OH, search in interstellar diffuse clouds, Copernicus UV obs. 79−40233
OH, Simon-Parr-Finlan potential appls. 80−18785
OH, solar, continuum opacity contrib. to atmospheric model 79−40162
OH sources in CRL objects and late-type stars, 18 cm obs. 79−35427
OH spectroscopy using freq.-doubled dye laser radiation *(Dutch)* 79−50039
OH, spin-extended Hartree-Fock ab initio calculations for small radicals 78−70746
OH, spontaneous vibr.-rot. Raman scatt. from $X^2\Pi$ state 79−36646
OH, stratospheric chemistry rel. to HF/HCl ratio 79−16568
OH, submicron airglow bands correl. studies during Spacelab simulation 79−25381
OH, subthermally excited, shocked clouds in IC 443 SNR 79−35349
OH type I maser source G 109.7+2.2 near Herbig-Haro object *(Russian)* 80−17684
OH, UV light absorpt. at 3080 Å, for Gibbs free energy of mol. 79−100425
OH, upper atmosphere emissions, 80-100 km altitude 78−93025
OH, vibr. excitation by H_2O photodissoc. 77−75242
OH, vibr. ground-state, MFS, rot. spectra and electronic band anal. 78−5206
OH, vibr.-rot. system in aurora 77−13144
OH, vibrationally excited, high-resolution hyperfine Λ-doubling spectrum 78−90153
OH, weak interstellar masers detect. in H_2O masers direction 77−33618
OH, $X^2\Pi$ state, microwave spectrum calcs. 77−30858
OH, Zeeman effect, relativistic corrections 77−83646
OH^-, and OD^-, photodissoc. and photodetachment in $O_2/CH_4/H_2O$ mixtures, 3500-8600 Å 79−45776
OH^- and rare earth doped solid 80−7398
OH^-, electron distrib. in LiOH 78−75973
OH^- excitation, cause of laser Raman fluoresc. background at oxide surfaces 78−10875
OH^- impurity in $BaTiO_3$, IR spectra meas. 80−20679
OH^- impurity in quartz, electron irrad. effect on IR absorpt. 79−99913
OH^-, mobility in polyester, from ionic injection current at strong diffusion 80−2210
OH^-, proton affinity, integral Hellmann-Feynman theorem 78−70767
OH^- vibr. dipole field and ion-pair processes with rare earth ions 79−38624
OH^+, $^3\Pi_i$ state, lifetime, delayed coincidence meas. 78−70874
OH^+, fine struct. in $X^3\Sigma^-$ and $A^3\pi$ states, GTO and STO calcs. 77−6679
OH^+ fragment obs. from H_2O threshold PES 80−78647
OH^+ ion beam, Coulomb explosion in thin C foil, charge state depend. 79−31649
OH^+, PNO-CI and CEPA calcs. of electron correl. effects 77−34561
OH^+, rot.-vibr. bands, line positions, oscill. strengths transition probabilities 80−67828
OH^+, Simon-Parr-Finlan potential appls. 80−18785
OH-CH rotationally inelastic collisions, maser action 79−94068
OH-HF, H-bonded complex, ab initio calcs. *(French)* 80−52866
OH+2-methyl-2-butene, reaction rate consts. meas. 78−61001

oxygen compounds continued
OH+acetylene (CO), reaction rate consts. meas. 78−35663
OH+alkanes (alkenes), photooxidation, 305K, absolute and rel. rate consts. 77−16782
OH+alkene, absolute rate consts., 297K 79−100353
OH+Ar, colisional relax., laser mag. reson. study of press. broadening 79−94020
OH+Ar, pure rot. collisionally pumped laser, vibr.-rot. transfer 77−42523
OH+Br_2, hydroxyl radicals reactive scatt. 80−85172
OH+CO, HOCO and HOCO* form., thermochem. props. 78−27805
OH+CO, reaction mechanism, HOCO radical stability 77−73436
OH+CO, reaction rate consts. at 296K, press. effect 77−73435
OH+$COS(CS_2)$(dimethyl thioether), reaction rate consts., 299-430K 78−35653
OH+CO(+isobutane), reaction rate consts., press. depend. 78−35654
OH+CO(trichloroethane), reaction rate consts. and quenching kinetics, reson. fluoresc. obs. 79−72349
OH+$ClONO_2$, in stratosphere, rate constants 77−33134
OH+$ClO(Cl_2)(Cl_2O)$, rate const. at 298K, rel. to stratospheric O_3 depletion 79−87831
OH+$Co(NH_3)_5Br^{2+}$, polyelectrolyte catalysis, high pressure effect 80−55657
OH+dimethyl ether (vinyl methyl ether) reaction rate consts., 299-427K 77−86301
OH+dimethyl sulphide, flash photolysis reson. fluoresc. rate consts. determ., pollution aspects 78−95913
OH+dimethylamine, rate const., 298-426K, Arrhenius expressions and activation energy 78−48619
OH+ethylamine, rate const., 298-426K, Arrhenius expressions and activation energy 78−48619
OH+ethylene, reaction rate consts., 229-425K 77−40535
OH+ethylene (and halogenated derivatives), reaction rate consts. 77−21356
OH+formaldehyde (acetaldehyde), rate consts., 299-426K, UV flash photolysis, reson. fluoresc. obs. 78−68873
OH+gaseous S compounds, lower atmos. chem. 80−61870
OH+H, interstellar, role in OH 18 cm maser lines pumping 79−48892
OH+H_2, pot. energy surface, barrier heights and transition state geometry, POL-CI calc. 80−55649
OH+H_2O, OH linewidth rot. depend. on UV transitions 80−91606
OH+H_2O_2, reaction rate const., 298K, flash photolysis-reson. fluoresc. obs. 79−57215
OH+$H_2O(NO_2)(CH_3Cl)(N_2)(H_2)$(He), mean collision cross sections from microwave spectroscopy 80−1046
OH+H_2SO_4, collisional reaction probabilities atmospheric chem. 80−90168
OH+$H_2\rightarrow H_2O$+H, rate constant, ab initio calc. 80−45478
OH+$H_2\rightarrow H_2O$+H, reaction product vibr. distribs, quasiclassical trajectory, calcs. 80−85162
OH+HBr→H_2O+Br, absolute rate const., 249-416K 79−70303
OH+HCN, reaction rate, press. depend. 78−85135
OH+$HNO_2\rightarrow H_2O+NO_2$ react. kinetics, at high temps. behind shock waves 77−44477
OH+$HO_2\rightarrow H_2O+O_2$, rate const. meas. *(German)* 79−52629
OH+$HO_2\rightarrow H_2O+O_2$ gas flow reaction, upper bound and probable value of rate const. 79−24730
OH+H(H_2), rot. excitation in interstellar medium 78−4306
OH+H→$H_2O+h\nu$, radiative association reaction for mol. synthesis in interstellar clouds 80−90509
OH+haloalkanes (haloalkenes), reaction kinetics in microwave discharge, reson. fluoresc. obs. 77−77744
OH+halocarbons rate consts., appl. to tropospheric degradation 79−52622
OH+halomethane(haloethane), reaction rate consts., reson. fluoresc. meas. in discharge-flow system 79−72350
OH+He, colisional relax., laser mag. reson. study of press. broadening 79−94020
OH+He, O_2, N_2, H_2, NO_2, H_2O, NH_3, SO_2, chloromethane, rot. inelastic collision, microwave spectra 79−45806
OH+methane+M, absolute rate consts., 296K, flash-photolysis reson. absorpt. technique 77−86290
OH+n-propyl acetate (sec-butyl acetate) (tetrahydrofuran) (peroxyacetyl nitrate), raction rate consts., in irrad. NO_x mixture 78−7171
OH+NO radical-molecule reactions, relax. and rate consts. 80−11918
OH+NO_2, colisional relax., laser mag. reson. study of press. broadening 79−94020
OH+NO_2+M→HNO_3+M, reaction kinetics, temp. and press. depend. 79−66284
OH+NO_2+M→HNO_3+M, rate constant under simulated atmospheric conditions 80−50846
OH+N(O), direct rate meas. 80−30217
OH+$O_3\rightarrow HO_2+O_2$, reaction rate const., 238-357K 79−47902
OH+$OCS(CS_2)$, flash photolysis reson. fluoresc. rate consts. determ., global S cycle 78−95914
OH+$OCS(CS_2)$, lower atmosphere chem. 80−61870
OH+OH→H_2O+O, rate meas. by UV absorpt., 1200 to 1800K 78−35642
OH+organic compounds photooxidation reactions in atmosphere, rates, reactivity and mechanism 80−72104
OH+p-H_2(He), collisional pumping of Λ-doublet transitions, pot. energy surface 80−23516
OH+RH→H_2O+R, radical substitution reaction 80−81321
OH+SO_2, role for stratospheric HSO_3 layer, reaction rate consts. 78−32202
OH+toluene, rate constant under simulated atmospheric conditions 80−50846
OH+toluene (1,3,5-trimethylbenzene), rotational and vibrational energy effect 80−76497
OH+trans-2-butene, reaction products, O_2 and NO_2 effects obs. 80−85156
OH+trichloroethane, 1,1,1- and 1,1,2-isomers, reaction kinetics, 298-460K, lower atmos. chem. 80−16657
OH+trichloroethane→$H_2O+CH_2CCl_3$, rate const. and tropospheric chem. 80−16658
OH+trimethylamine, rate const., 298-426K, Arrhenius expressions and activation energy 78−48619
OH+vinyl halides, reaction rate consts., 299-426K 77−81389
$OH^-+CO_2\rightarrow HCO_3^-$ react., MO-LCAO-SCF calcs., energy barrier 78−76846
$OH^-+C(N_2)$, electron stripping and breakup, proton spectra 77−83685

oxygen compounds continued
OH^-+inert gas, collision-induced dissociation 78−29834
OH^-+methoxybenzene (o-cresol), gas phase reaction, 299-435 K, kinetics and mechanism 78−11515
OH^-+O_3, associative detachment, rate coeffs. 78−3325
OH^++diatomic (polyatomic) molecule, reaction, ICR obs. 79−8429
OH^++NH_3, bimolecular reactions, product. distrib., rate consts. 78−11513
OH^-+CH_3SH, $OH^-+CH_3NH_2$, reaction rate consts., 299-426K 77−40525
$OH^-+CO(N_2O)$, rate consts. 77−16781
OH^-+O, OH^-+CO, reaction rates, mechanism, flow discharge chemilum. obs. 77−52610
$^{18}OH+CO_2(CO)$, evidence for at. exchange 79−47910
OH_2^+, and OH_3^+, fast mols., dissoc. in thin C foils, Doppler broadening obs. 78−22019
$(OH)_2^{2-}$, electrostatic mol. pot. curves, proton transfer and bridging pot., CNDO/2 calc. 79−94054
OH_3^+, bond polarisability and force constants 80−69260
OH_4^+, stability, ab initio calcs. 77−30775
OH_n, ab initio LCAO SCF calcs. of ionisation pot., electron, proton, H and hydride affinities 77−88387
OH_n, LCAO-MO-SCF with Gaussian polarisation functions, energetic effect of p-, d-, and f-functions 78−41944
$OH(A^2\Sigma^+\rightarrow X^2\Pi_i)$ yields from H_2O photodissoc. 80−71927
$OH(A^2\Sigma^+)$ form. during H_2O photodissoc., luminesc. spectrum 79−57270
$OH(A^2\Sigma^+)$, form. from $H_2O+Kr(^3P_1)$, internal energy distrib. 79−10183
$OH(A^2\Sigma^+)$, production by multiphoton dissociation, methylamine, rate constant, laser induced fluorescence and chemiluminescence study 79−98135
$OH(A^2\Sigma^+)+N_2(O_2)(H_2O)$(air), quenching rates and fluoresc. efficiency, rel. to atmosphere 80−14199
$OH(A^2\Sigma_{1/2}^+)$, and OD, hyperfine struct. determ. by freq.-doubled dye laser radiation 79−72333
$OH(C^2\Sigma^+)$, prod. by water radiolysis, time-resolved emission, quenching rate consts. 79−10138
$O_2^+H_2O$, produced by collisional dissoc. method, mass spectrometric study, dissoc. energies determ. 80−95707
OH(OD), $A^2\Sigma^+$ state, vibrational energy transfer in collisions, rot. resolved fluoresc. 78−74742
OH(OD), spin-rot. consts., Van Vleck approx., ab initio calcs. 77−34610
$OH^+(OD^+)$, $A^3\Pi_i\rightarrow X^3\Sigma^-$ emission branching ratios, r-centroid depend. 77−6830
$OH(^2\Pi_{3/2}, v=1)$, population inversion of Λ doublets in microwave spectrum 80−974
$OH(^2\Pi)$, rot and translational temps. in gas discharge 78−5243
$OH(^2\Pi)$+H, rel. to interstellar OH maser action 79−101186
$OHX^2\Pi$ radical, ground and vibr.-excited ($v\leq 6$) levels, microwave spectrum 79−63985
$OH(X^2\pi)$ nightglow emissions, theory and meas. in (9-3) band 78−88960
OH(8-3) 7274 Å band rel. to O_2 and forbidden O I atmospheric spectra 78−61639
OH.+N_2O reaction, rate const. meas., N_2O atmospheric residence time appl. 77−21352
$OH(v=0, 1)+H_2(v=1)$, rate consts., 298K 79−11768
OH(v,N) bimodal rot. distrib. from $O(^1D_2)+NH_3$ 80−76501
ON+azomethane, rate const. meas. 80−7771
ONBr, (3×3) order systems, force const. calcs. using isotopic freqs., parametric method 78−21907
$ON^{81}Br$, anharmonic force field from IR and microwave data 78−82809
ONCN, IR spectra isotope shifts and ab initio calc. for harmonic force field 79−13715
ONCl, (3×3), order systems, force const. calcs. using isotopic freqs., parametric method 78−21907
ONCl, vibr. freq., anharmonic ab initio/empirical pot. energy functions 80−99457
$ON^{35}Cl$, anharmonic force field from IR and microwave data 78−82809
ONF, (3×3) order systems, force const. calcs. using isotopic freqs., parametric method 78−21907
ONF, geom. and electronic struct., ab initio calcs. 79−76342
ONF, J transitions, rot. Zeeman effect 80−63707
ONF, vertical electronic spectrum, CI and SCF calcs. 77−75123
ONF_3, vibr. anal. using Green function 77−57962
ONI, IR matrix isolated spectra, force consts. 79−10111
$OPBr_3$, mol. struct., electron diffr. and spectroscopic vibr. amplitude 80−58387
OPCl radical, absorpt. spectra, PO (β and B′-X) systems, vibr, numbering 77−75173
OPF_3, forbidden transitions, mol. beam elec. reson. obs. using avoided crossings 78−29775
OPF_3, mol. beam elec. reson. spectrum, mol. props. 79−94011
$^{16}OPF_3$, microwave centrifugal distortion moment spectrum 78−78684
OSC, N_2O, submillimetre rot. lines, press. shifts 80−23463
$O_2(SO_2)^-$, photodestruction 80−63722
$OSiF_2$ prod. from SiO+F_2 matrix reactions, IR spectra and force consts. calcs. *(German)* 80−97718
^{17}O, isotropic hyperfine coupling consts. in small radicals 80−52894
O_4* van der Waals complex, radiative lifetime, dimole intensity press. depend. 78−58741
Pb-Cr-O system, equil. relationships, stability limits 77−59765
PuO, nuclear oxide fuel anal., coulometry, emission anal., chromatography, X-ray anal. 80−18420
QCS, static polarisability, ab initio SCF wave functions 80−74106
S-O-C, equilibrium 550 to 1100°C 79−38807
Si_5-Al-O-N_7, hot pressed, exam. of fracture mechanisms 78−72879
SiO_2:OH^-, vitreous, elec. dipolar echoes 78−52430
SiO_2:OH^- glass, relax. times of mol. OH^- ions at very low temps., elec. dipolar echoes 79−78616
UO, nuclear oxide fuel anal., coulometry, emission anal., chromatography, X-ray anal. 80−18420
Zn-Ti-Fe-O, spinel solid solns. 77−48409

ozone
$^1A_1$ ground state, dipole moment function, ab initio SCF and CI calcs. 80−32628
absorption coefficients for backscatter UV expt. 80−46254
air, negative corona current O_3 density depend., 46-87 kPa 80−1852
air composition at Barrow, Alaska, wind direction depend. 80−85704

ozone continued
air pollutant eddy correlation flux meas. by fast response sensor 78−45009
air pollutants three-dimens. distrib. in Los Angeles basin 78−61542
air pollution, Jerusalem and Tel-Aviv at nighttime 80−89689
air pollution in NE.USA, ozone source study 80−41482
aircraft ambient and cabin air O_3 conc. simultaneous determ. 80−90198
Antarctica, surface O_3 meas., annual variations 77−9465
atmophere, columnar meas. by aircraft-borne UV spectrophotometer 78−73522
atmosphere, 9.6 μm band radiance calc., excitation processes 78−36350
atmosphere, ^{7}Be distrib. within E.United States high press. systems rel. to stratospheric O_3 contrib. 80−4072
atmosphere, absorpt. by natural surfaces 77−45139
atmosphere, altitude profiles during Aladdin 74 program above Wallops Island 78−57247
atmosphere, anthropogenic effects on UV radiation and climate 78−28289
atmosphere, Chapman mechanism, appl. of sensitivity analysis, numerical Green's function procedure 79−100334
atmosphere, chemistry and O_3 vars., depletion 80−104534
atmosphere, conc. and distrib. from absorption spectrum in UHF region *(Russian)* 79−100897
atmosphere, conc. meas. at ground level at unpolluted maritime site 78−3951
atmosphere, conc. meas. by Dobson spectrophotometer in Seychelles 77−17250
atmosphere, conc. meas. on aircraft flight 79−58010
atmosphere, conc. rel. to visibility reduction in Midwest 78−61507
atmosphere, daytime and nighttime distrib., ground-based mm wavelength obs. 78−57256
atmosphere, daytime O_3 layer, photographic obs. from Skylab 77−60505
atmosphere, depletion theories, rel. to atm. nuclear tests 79−70848
atmosphere, distribution vars. rel. to urban heat island circulation in St. Louis 80−51488
atmosphere, Dobson meas. of total content, aerosol extinction effects 79−84431
atmosphere, effects of energetic particle precip. on O_3 catalytic removal 80−109213
atmosphere, effects on turbidity 77−78420
atmosphere, elevated levels from natural sources 79−62552
atmosphere, global monthly vars. correl. with solar activity 78−85664
atmosphere, ground level conc., rel. to regional transport of pollutants 78−44990
atmosphere, high conc. in rural surface layer correl. with high press. systems 78−24325
atmosphere, inhomogeneous 9.6 μm O_3 band heating, new approx. method 78−88918
atmosphere, interaction with airborne particles 78−81342
atmosphere, ion cycle importance in O_3 destruction 78−53697
atmosphere, IR heterodyne absorpt. spectrum 77−91267
atmosphere, IR heterodyne spectroscopy 77−45160
atmosphere, IR transmissivity 78−11998
atmosphere, long-term vars. global distrib. during 1957-75 period 79−84429
atmosphere, maintenance of zonal mean O_3 distrib. in N.Hemisphere 80−109220
atmosphere, meas., calibration using UV photometer 78−69505
atmosphere, mechanisms for transport in lower atm., general circulation model 80−109196
atmosphere, monitoring with airborne laser absorpt. spectrometer 77−91303
atmosphere, monitoring with IR heterodyne radiometer 78−16216
atmosphere, monitors calibration, modification of KI method for improved stoichiometry 79−88037
atmosphere, nighttime conc. from OH nightglow obs. 79−5698
atmosphere, nighttime equatorial density determ. from UV stellar occultation obs. 77−53259
atmosphere, nocturnal maxima, vertical mixing of remnant daytime boundary layer 79−5547
atmosphere, O_3 budget, zonal mean circulation model and linearized photochem. 77−70780
atmosphere, O_3 conc. meas. at high latit. during twilight 77−41128
atmosphere, O_3 content evolution 80−98400
atmosphere, O_3 depletion, supersonic gas sampling error 77−33193
atmosphere, O_3 depletion as result of nearby supernova 80−94584
atmosphere, O_3 fluxes from zonal mean circulation model *(Russian)* 78−36224
atmosphere, O_3 photochem. prod., W.Europe, rel. to meteorology 77−78292
atmosphere, O_3 profile rel. to solar mag. activity 78−65373
atmosphere, O_3 reduction effects on sunburn dosage 77−37285
atmosphere, O_3 rel. to wavelength depend. of optical mass *(Russian)* 77−2239
atmosphere, O_3 transport, mesoscale lake breeze and synoptic-scale aspects 77−2232
atmosphere, obs. for 1976 July-September period *(French, Flemish)* 77−70752
atmosphere, obs. for 1976 October-December period *(French, Flemish)* 77−70753
atmosphere, over Middle East in summer, vars. rel. to general circulation *(Russian)* 77−53156
atmosphere, perturbed, O_3 cones. rel. to thermal struct. and relaxation rates 80−8408
atmosphere, photochem. O_2, nocturnal depletion at rural site 79−57527
atmosphere, photochem. smog enhancement by N,N′-diethylhydroxylamine in polluted ambient air 77−91262
atmosphere, photochemical-diffusive model, chlorocarbon industry impact on O_3 layer 78−40648
in atmosphere, photodissoc. in stratosphere and mesosphere through solar UV radiation absorpt. 80−109248
atmosphere, photostationary state assumption in NO, NO_2, O_3 system 79−88391
atmosphere, pollution effects on O_3 layer, numerical modelling 80−40943
atmosphere, possible role in ice form. in clouds *(Russian)* 77−29367
atmosphere, prod. through $^{18}O^{16}O$ photodissoc. 80−94559
atmosphere, profile meas. by airborne dual-channel IR heterodyne radiometer 78−57369
atmosphere, reduction due to industrial fixed N fertilizers 77−78383
ozone continued
atmosphere, remote meas. in IR absorpt. bands, information content estimation *(Russian)* 78−88883
atmosphere, review of O_3 concs. over Australia 80−109223
atmosphere, seasonal and interannual vars., Nimbus 4 BUV expt. 80−41506
atmosphere, sounding correction procedures and implications 78−20486
atmosphere, soundings at Uccle, Belgium, 1976, April, May, June *(French)* 77−64407
in atmosphere, sources and transport in NE. United States 79−92110
atmosphere, total amount and vertical distrib. periodic vars. 77−78336
atmosphere, total amount at Belsk, Poland, harmonic anal. 78−92883
atmosphere, total content, backscatter UV and ground-based meas. comparison 79−84430
atmosphere, total content and mixing ratios obs., (1976 January 5 to March 31) *(French, Flemish)* 77−33174
atmosphere, total content determ. by UV spectroradiometry 79−53401
atmosphere, total content determ. from total optical depth spectral var., solar radiometer meas. 77−53235
atmosphere, total content determ. using remote spectroscopy 78−65437
atmosphere, total content estimation from UV radiance meas., aerosol effects 79−8662
atmosphere, total content meas. using four-filter photometer 78−61597
atmosphere, total content trends, from daily Dobson data 78−92915
atmosphere, total O_3 meas., evaluation of electrochem. conc. cell sonde 79−70860
atmosphere, total O_3 vars. rel. to general circulation 79−44233
atmosphere, transport from stratosphere to troposphere 78−7687
atmosphere, twilight obs. from Atmosphere Explorer 5 78−28261
atmosphere, Uccle, Belgium, 1977, Jan.-Mar. 77−86998
atmosphere, Uccle, Belgium, O_3 meas., 1973, Jul.-Sept. *(French, Flemish)* 77−17204
atmosphere, Uccle, Belgium, O_3 meas., 1973, Oct.-Dec. *(French, Flemish)* 77−17205
atmosphere, Umkehr vertical profile errors caused by presence of stratospheric aerosols 79−70849
atmosphere, vertical distrib. from airborne backscatt. UV expt., error anal. 78−92985
atmosphere, vertical distrib. in boundary layer 77−49102
atmosphere, vertical distrib. meas. (1977, April 1 to June 29) *(French, Flemish)* 78−11966
atmosphere, vertical distrib. over Aspendale, Australia, climatology 78−20475
atmosphere, vertical profile calc. from umkehr obs. 78−81328
atmosphere, vertical profile correl. with thermodynamic parameters *(Russian)* 77−73804
atmosphere, worldwide total O_3 trends 77−33138
atmosphere composition at 95 km altitude from Na enhancement region obs. 80−101466
atmosphere conc., fast oscills. in 3140 and 3690 Å obs. 77−53161
atmosphere concs. and meteorology in 1975 in Tel-Aviv 79−12172
atmosphere content during March-April 1976 stratospheric warming 80−12494
atmosphere content rel. to 80−26607
atmosphere content rel. to solar activity 80−41488
atmosphere meas. with Dobson spectrophotometer, aerosol effects 77−45186
atmosphere O_3, conc. determ. by Chappuis-band absorpt. 80−77063
atmosphere O_3, evolution and variability over geological time 79−96788
atmosphere O_3, obs. of flux by transient eddies in 0 to 30 km height range 80−109224
atmosphere O_3, observations for 1978 January 4 to March 31 period *(French, Flemish)* 79−5561
atmosphere O_3 conc. at ground-level, Oslo, Norway, summer 1977 obs. 80−81965
atmosphere O_3 concentrations meas., UV photometric standards interagency comparison 79−35000
atmosphere O_3 layer and evolution of life 80−104883
atmosphere O_3 photodissoc., annual var. of effects of diffuse solar radiation 80−109210
atmosphere O_3 production transport and distribution, numerical simulations with global general circulation model 80−56544
atmosphere O_3 total content, determ. using satellite meas. 80−77027
atmosphere over Uccle, Belgium, 1978 April-June obs. of O_3 concs. 79−53429
atmosphere ozone content, July-Sept. 1978, Belgium 80−12484
atmosphere total content, Dobson spectrophotometer meas. errors 80−72644
atmosphere total content using Dobson spectrophotometer, pollution and absorb. mol. errors 80−72643
atmosphere total O_3, comparison of simultaneous IRIS, BUV and ground based meas. 78−81291
atmosphere total O_3 content, 1964-75, season and latitude depend. 80−41534
atmosphere total O_3 content, natural fluctuations 79−29819
atmosphere total O_3 determination, large particle light scatt. coeffs. approximation 80−82091
atmospheric, depletion resulting from nitrogen oxides pollution *(Russian)* 78−16154
atmospheric, estimates from Dobson direct Sun meas., temp. variations and scatt. effects 77−45049
atmospheric, long term effect of nitrogen oxides produced by thermonuclear explosion 79−84345
atmospheric absorption line parameters, AFGL, compilation update 79−21013
atmospheric composition, air over N.Germany coast, obs. 80−26584
atmospheric composition, ground level monitoring apparatus, chemiluminescence reaction with ethylene 78−96310
atmospheric conc. meas. by differential absorpt. CO_2 laser radar 79−96829
atmospheric content from aircraft-borne spectrophotometry *(Russian)* 79−34903
atmospheric content variation meas. *(Dutch)* 79−70838
atmospheric density from STRATCOM VII-A meas. 79−58079
atmospheric distribution, moving high pressure system, E.United States 79−83664
atmospheric measurement, using CW CO_2 lasers, long path differential absorption 78−32256
atmospheric O_3 heating, induced antisymmetric tidal modes at equinox 79−35024

ozone continued
atmospheric O_3 obs. and atm. physics research at Belsk, Poland *(Polish)* 77−21825
atmospheric O_3 vertical distrib., shortened version of Umkehr ob. method 80−8430
atmospheric oxidation rel. to SO_2 reaction with O_3 in water 78−16083
atmospheric pollution monitoring by lidar systems 78−53765
atmospheric profile, from photodissoc. wave obs. 78−79407
atmospheric reductions rel. to N_2O life cycle 78−16140
atmospheric seasonal var. from rocket-borne UV obs. 77−29402
atmospheric total field, statistical anal. *(French)* 79−84358
atmospheric total O_3 determ., particulate scattering approx. 77−21864
atmospheric vars. rel. to 11-yr. solar cycle 79−12189
atmospheric vertical profile rel. to UV backscattering 78−7762
Australia, total O_3 trends rel. to lower stratosphere circulation 77−21866
Belgian obs. (1977 Oct.-Dec.) *(French, Flemish)* 78−92903
calibration methods, accuracy 78−69506
calibration standards, generated by gas phase titrations 78−69507
catalysis and O_3 destruction in stratosphere 79−34879
concentration in lower stratosphere, far IR spectroscopy, quantitative anal. 79−39790
concentration in water, chemiluminescent meas. method 77−60159
corona discharge, $^1\Sigma_g^+$ state lifetime obs., using spectroscopic analysis *(French)* 77−24230
cyclic, stability, ab initio GVB-POL-CI calcs. 78−915
decomposition flame, flat, laminar, vel., struct. 78−51256
depletion in troposphere and stratosphere by halomethanes 80−16866
detection over snow surfaces 79−12281
determination, in atmosphere, intercalibration of monitors 78−69529
dissociation interference in atmospheric OH conc. meas. by laser fluoresc. 77−49110
Dobson total content meas., atmospheric aerosol effects 80−12463
Earth atmosphere, O_3 and O_2 photolysis, translationally hot $O(^3P)$ energy distrib. 80−21811
emission meas. network, Baden-Wurtemberg *(German)* 79−52977
SE.England, 1976 summer O_3 concs. 77−91240
field ionisation at Ir surface 78−35273
filter instrument total O_3 accuracy, bandwidth effect 78−16181
fluorocarbon ozone problem, evaluation of current knowledge *(German)* 79−96826
fluorocarbon-ozone theory, atm. modelling, diurnal steady state calc. 79−88390
form. in silent discharge, excited species reactions, discharge channel characts., numerical simulation 80−38813
formation and control strategy options for Sydney, precursor distrib. 80−16859
formation by heated corona wires of electrostatic precipitator 80−47081
formation dynamics in cities 80−31112
formation rel. to power plant emissions over Lake Michigan 79−74575
gas, UV absorpt. spectrum, Hartley continuum, IR laser induced changes 80−95639
gas discharge, yield, rel. to discharge field strength and gas pressure 79−19116
generation in air-fed ozonisers 80−3323
generation in pure O_2 or dry air by field-accel. electrons *(French)* 80−59161
global distribution, effects of pollutants, book contrib. 77−29429
global vertical distrib. 78−73475
health physics aspects of 20- to 40-MeV LINAC operations 79−45482
high oxidant days in Melbourne, atmospheric characts. 79−70484
hydrofluorocarbon monitoring using telluric absorption line *(German)* 78−49133
infrared spectra, vibr.-rot. bands 79−64001
insolation absorption and thermal excitation of atmospheric tides 79−34890
ionosphere D-region, O_3 conc. vars. during polar cap absorpt. 77−37481
IR absorption spectrum using CO_2 TEA laser injection locked, tunable single longitudinal mode operation 80−33018
IR cooling calcs., simple strategies for inclusion of Voigt effects 79−94768
IR high resolution spectroscopy of ν_3 band, rel. to atm. O_3 monitoring 79−63993
jet stream and associated O_3 enhancement *(Russian)* 80−94568
line and band strengths in IR spectra, variational calcs. 80−87112
line parameter data, 10 μm and 4.8 μm regions 80−61895
line position and intensities of $2\nu_3$, $\nu_1+\nu_3$ bands 80−87181
long-range transport across mid-W. and E. United States 78−16147
lower stratosphere content, Nimbus 4 remote sensing method 80−77154
lung function effects, tracer study 77−25552
Mars, O_3 global distrib. 77−78710
Mars atmosphere, O_3 layer and two aerosol layers detect. by Mars 5 spacecraft UV obs. 78−49357
Mars atmosphere, seasonal var. of O_3 density 79−70984
mesophere O_3, obs. of shadow on D-region in ionosphere VLF guide over Atlantic Ocean 79−58161
mesosphere, IR nonthermal emissions from O_3, Spacelab obs. 77−21906
mesosphere, lower, O_3 abundance from backscattered solar radiances 78−69414
mesosphere, lower, O_3 number density profile 80−41579
mesosphere, meas. from ground-based mm wave obs., comment 78−11967
mesosphere, O_3 concs. meas. from 1.27 μm O_2 airglow at middle latit. 80−72606
mesosphere, O_3 meas. from ground-based millimetre wave obs. 77−29381
mesosphere O_3, response to changes in UV solar flux 77−33167
metastable cyclic ozone predictions 77−46511
microwave and IR spectra, ν_2 state, $(\nu_3+\nu_2)-\nu_2$ band, 10 micron lines 78−82718
molecular, mol. beam Stark, Zeeman effects, polarisability, moments, mag. susceptibility anisotropy 77−79649
molecule, (010) and (020) states, 14 μm diode laser spectra, assignments 79−98079
molecule, ab initio projected unrestricted Hartree-Fock calcs. 78−58582
molecule, ab initio UHF and UHF-natural orbital CI studies 80−102452
molecule, ab initio VB wave functions, π-electrons 78−70748
molecule, analytical potentials from spectroscopic data, vibr., bond length, dissoc. 77−10613
molecule, anharmonic force field and isotopic relation 77−58198
ozone continued
molecule, approximate spin extended HF calcs., singlet and triplet states 78−78621
molecule, chemical analysis by acoustic emission following laser irradiation *(Russian)* 77−21451
molecule, CI calc., ground and excited states, energy locations, transition probabilities 78−74584
molecule, combination bands $(\nu_1+\nu_2)$ and $(\nu_2+\nu_3)$, anal. 78−9150
molecule, conformation, ab initio HFS method calc. 79−36526
molecule, core electron binding energies, XPS, Xα scatt. wave calcs. 77−75332
molecule, dissoc. in O_2+O, MNDO semi-empirical SCF MO calc. 77−44465
molecule, excited state geometries and energies, ab initio pot. energy surfaces 78−5151
molecule, Hartley band during formation, metastable states, vibr. excitation and relax. 80−55632
molecule, Huggins bands, vibr. anal. 78−42085
molecule, inertia defects and dipole moments by kinetic consts. method 80−928
molecule, IR and microwave spectra, ν_3 vibr.-rot. band 77−38663
molecule, IR spectroscopy 79−98088
molecule, laser flash photolysis, $O(^1D)$ quantum yield 78−20033
molecule, localised natural orbitals 77−83482
molecule, microwave absorpt. coeff. 77−64378
molecule, mol. beam electric resonance, electric and mag. props. determ. 77−27055
molecule, multiphoton dissoc. dynamics, classical model 80−11904
molecule, multiphoton dissociation by IR laser 79−36710
molecule, open and closed forms, bond angle and length, MC SCF and MC CI calcs. 78−78831
molecule, open and closed forms, energy separation 77−83511
molecule, open-shell SCF secular eqn., iterative algorithm soln. 80−52868
molecule, photodissoc. cross section, vibr. excitation effects obs. 80−95696
molecule, photoelectron spectra, HAM/3 MO calcs. 78−13414
molecule, photoelectron spectrum, vibr. struct., ionos. pot. 77−75217
molecule, photolysis, laser flash, $O(^1D)$ quantum yields in fall-off region 80−45524
molecule, pot. energy surface analytical function, atmospheric reactions 78−7174
molecule, radiative electron attachment spectra, vibr. stretching, electron affinity, theory 77−54617
molecule, sextic centrifugal distortion constants 77−57972
molecule, sextic centrifugal distortion consts. calc. 79−59430
molecule, unoccupied orbitals, excitation energy, electron affinity, HAM/3 MO calcs. 78−13415
molecule, UV absorpt. spectra, IR laser induced changes 80−83385
molecule, UV absorption bands, new vib. quantum no. assignments, based on isotope effect 79−94008
molecule, vibr. and rot. variational calc., isotope shifts 77−57967
molecule, vibr. energy anal., form. by recomb. 77−75119
molecule, wave function calc. rel. to energy separation, cyclic and open isomers 79−93929
molecule$+O_3$, reaction rate const., rel. to atmospheric processes 80−85155
molecule in soln., IR spectra, nonlinear absorpt. 79−98100
molecule isotope effects, complete quartic force field calc., algorithm 80−37736
monitoring, calibration reference instrument calibration 78−73524
natural rubber vulcanisates, creep under tension, O_3 effects 78−92302
nighttime concentration (15-68 km), Nimbus 6 obs. comparison with OAO-3 obs. 80−105016
oxidation of Br, Cl and organic C in seawater 79−16518
ozonograms, Oct.-Dec. 1978, Uccle, Belgium *(French, Flemish)* 80−21797
ozonosphere and N_2O pollution from fertilisers 80−36370
ozonosphere reactions affected by CO_2 stratosphere cooling 80−36369
palaeoatmosphere, O_3 conc. effect on surface temp. 79−96807
palaeoatmosphere O_3 content rel. to biological evolution 77−78425
partial pressure profile minimum at 38 mb level 79−79941
photochemical generation, sources, air sampling programme 79−66430
photochemical pollution during summer 1976 in Greater London 79−16648
photochemical tropospheric O_3 transport, effect on pollution at rural site 80−61481
photochemistry and dynamics of the ozone layer of atmosphere 79−5590
photodissoc., $O(^1S)$ yield at 1700-2000 Å 80−97714
photodissociation, effects of radiation scattered by aerosols 79−2371
photodissociation rate under ozonosphere conditions 80−40722
photoionisation, O_4^+ and O_5 form., mass spectra 77−50477
photolysis, high energy pulsed O_2 laser feasibility at 1.27 μm 78−63117
photolysis, laser-induced, reactions of $O(^3P)$, $O(^1D)$ and $O_2(^1\Delta)$ 80−11928
photolysis, near UV, temp. depend. of $O(^1D)$ formation 78−15689
photolysis, $O(2^1D_2)$ prod. and deactivation 79−20384
photolysis, $O(^1D)$ quantum yield 79−53492
photolysis, $O(^1D)$ quantum yields as function of temp. (230-320K) and wavelength (295-320 nm) 78−56903
photolysis, $O(^3P)$ quantum yield at 266 nm 80−78568
photolysis, primary products electronic and vibr. state distrib. 80−50865
photolysis, rel. quantum yield of $O(^1D)$, in 250-300 nm region 79−20383
photolysis by sunlight, rate constants at ground level 80−61836
pollution, St. Louis urban plume, form. and transport of secondary air pollutants 77−5316
pollution in British Isles from plant damage obs. 79−21008
production by dissoc. of O_2 or air 80−61118
production in homogeneous O_2 discharge 80−38780
production in unipolar HF discharge 80−1855
profile in tropical stratosphere, BUV meas. 78−49091
propylene ozonide formation in gas phase ozone+cis-2-butene+formaldehyde, reaction mechanism 77−33132
PTFE, ozone-induced chemiluminescence 77−55839
quenching of orthopositronium by O_3, meas. by two-photon coincidence rate difference technique 80−74262
reference methods, international comparative programme 79−88038
San Francisco air basin, biogenic emission related to high ozone levels 79−83676
sea breeze affecting surface level conc., Wallops Island, Virginia 80−51473

ozone continued
Siemen's type ozonizer, count rate emission with time of exposure to discharge 79−64936
smouldering discharge at O_3 liq. surface in N_2, thin solid pellicle formation of N_2O_5 80−38827
solar cycle assocs., O_3 and temp. trends 79−84443
solar MUV photometer, rocket borne, stratospheric ozone concentration measurement 80−52292
spectrophotometric determ. of total O_3 using interference filters 78−16180
spectroscopy at submillmetre-waves at NPL 77−18111
stratosphere, 10 μ absorption line obs. with IR heterodyne spectrometer 78−61494
stratosphere, absorption effects on NO_2 at latitude 45°S at midsummer, ground based meas. 79−96784
stratosphere, at. Cl and ClO radical in situ obs., rel. to O_3 depletion 78−36241
stratosphere, calc. of O_3 layer depletion by chlorofluorocarbons using two-dimensional model 80−109221
stratosphere, changes in chemical balance 78−92933
stratosphere, chemistry of ozone depletion 77−91256
stratosphere, chlorofluorocarbon effects, O_3 photochemistry 77−41160
stratosphere, CO_2 and O_3, two-dimens. model calc. 79−62564
stratosphere, CO_2-O_3 coupling in Cl free atm., photochemical-radiative column model 80−85723
stratosphere, conc. meas. at sunrise and sunset *(French)* 79−48535
stratosphere, creation and destruction, probability distribs. 78−20496
stratosphere, density meas. using lidar, feasibility 77−60493
stratosphere, depletion by chlorofluoromethanes, contradiction of theory 78−49099
stratosphere, depletion by chlorofluoromethanes, two-dimens. time-depend. model 78−24341
stratosphere, distrib. and circulation in meridional plane *(French)* 77−49100
stratosphere, effect of increased N fixation 78−28288
stratosphere, effects of CO_2 increase, photochem. and radiative transfer model 78−65370
stratosphere, effects of O_3 78−16123
stratosphere, environment monitoring system, benefit assessment 78−73507
stratosphere, fluorocarbon hazard to O_3 layer, assessment 79−79963
stratosphere, formation and destruction, book contrib. 77−37339
stratosphere, highly excited metastable O_3 rel. to photochemistry and heat balance 79−44225
stratosphere, impact of methyl chloroform 78−53722
stratosphere, influence of 1972 August 4 solar proton event 78−7732
stratosphere, influences on and effects of changes in O_3 layer *(French)* 77−5271
stratosphere, instantaneous global O_3 balance including observed NO_2 80−109211
stratosphere, laser photochemistry of O_3 and distant spectroscopy *(Russian)* 78−28314
stratosphere, laser spectroscopy relevant to stratospheric photochemistry 78−88951
stratosphere, laser-radar obs. using excimer lasers 80−17410
stratosphere, latitude-dependent depletion due to supersonic transports, model predictions 77−45051
stratosphere, lower, NO and O_3 concs. geographical vars. 78−73438
stratosphere, meas. with ozonometer using chemiluminescent reaction of ozone and olefins *(French)* 79−48574
stratosphere, model, temp. feedback effect on O_3 conc. 78−28277
stratosphere, monitoring, satellite benefit assessment 77−78613
stratosphere, natural depletion mechanism, energetic radiation belt electron precip. 77−41134
stratosphere, net vertical flux, implication for troposphere O_3 budget 80−101402
stratosphere, NO_x catalytic O_3 destruction, sensitivity to rate coeffs. 77−37472
stratosphere, NO and O_3 meas., mixing ratio 78−44915
stratosphere, NO photolysis rel. to effects of chlorofluorocarbon pollution 77−29399
stratosphere, numerical model of effect of N oxides on O_3 77−53269
stratosphere, O_3, effect of CH_4, HCl and ClO 77−87032
stratosphere, O_3 and aerosol monitoring using orbiting photodetectors 77−78445
stratosphere, O_3 and Aitken nuclei conc. correl. over Americas 77−49141
stratosphere, O_3 and temps., satellite obs. for 1970-71 period 77−9466
stratosphere, O_3 behaviour and thermal structure during S. Hemisphere spring 80−105014
stratosphere, O_3 column density effect on radiative-photochemical relaxation 79−16592
stratosphere, O_3 destruction by fluorocarbons 77−9459
stratosphere, O_3 destruction by NO_x catalysis, comment 77−73812
stratosphere, O_3 distrib. in winter polar low region 77−78371
stratosphere, O_3 diurnal var. and scattering rel. to Cl concs. 78−7710
stratosphere, O_3 global distrib. Ogo obs. 77−73809
stratosphere, O_3 heterogeneous decomposition, lab. study 79−70850
stratosphere, O_3 layer depletion by nearby supernova explosion 78−32499
stratosphere, O_3 perturbation by N fertilisers, independent variables anal. 77−53134
stratosphere, O_3 reduction due to pollution, system-theoretic model 77−73848
stratosphere, O_3 response to nuclear bomb tests 77−81966
stratosphere, O_3 vertical distrib. in upper layers, satellite and surface-based obs. 78−40620
stratosphere, O_3 vertical profile determ. by lidar sounding from ground 78−11972
stratosphere, obs. in N.hemisphere for three seasons 78−81288
stratosphere, perturbing influences, 1955-75 catalogue 80−41502
stratosphere, photochemistry interpretations 79−74943
stratosphere, reassessment of O_3 models 79−5553
stratosphere, reduction by natural NO_x and man-made pollution, model 77−60461
stratosphere, rel. to fluorocarbons world prod. and release 78−3919
stratosphere, rel. to N_2O emission from soils during nitrification of fertilizer N 78−57313
stratosphere, seasonal conc. vars., Umkehr and Nimbus 4 BUV obs. 79−100911
stratosphere, temp. and O_3 vars. (1958 to 1977) 80−109222
ozone continued
stratosphere, temperature/O_3/water vapour trends in N. temperate latitudes 79−53474
stratosphere, thermal response to 0_3 fluctuations 79−39797
stratosphere, thermal struct. and trace constituents, effects of solar UV variability 78−61492
stratosphere, thermal structure and total O_3 obs., Nimbus 4 Iris expt. 77−21839
stratosphere, total content vars. correl. with ionospheric f_0F_2 vars. 78−45098
stratosphere, tropical O_3 spatial variations, influence of meridional transport and planetary waves 78−20463
stratosphere, two-dimens. model of behaviour *(French)* 78−49104
stratosphere, vertical distrib., during polar front passage over Uccle 80−94582
stratosphere and troposphere content, circumpolar airliner flight obs. 80−51475
stratosphere composition, effect of chlorofluoromethan photolysis 80−109197
stratosphere composition, implications of OH+trichloroethane reactions 80−16657
stratosphere concentration var. during total solar eclipse 80−105017
stratosphere content at mid-latitude, simultaneous N and S hemisphere obs. 80−77052
stratosphere O_3-CO_2 coupling, photochemical radiative column model with Cl chemistry 80−85724
stratosphere to troposphere O_3 transport, Project Dustorm, tropopause folding 78−32177
stratospheric, spacecraft solar extinction data inversion 79−74961
stratospheric, spectroscopy with CO_2 waveguide laser 77−13117
stratospheric chemistry, implications for environmental hazards 77−17267
stratospheric concs., increased CO_2 effect 78−57250
stratospheric far IR emission, balloon-borne obs. 79−34896
stratospheric ion chemistry, O_3 reactions with $O_2^+.O_2$ 79−2343
stratospheric O_3 affecting ground-level oxidant concs. at Santa Rosa 78−16112
stratospheric O_3 decreased sensitivity to Cl perturbations 79−12190
stratospheric O_3 stability and depletion scares 77−70722
stratospheric ozone levels, solar activity, cosmic rays effects 77−53362
summer, O_3 rel. to winter rain in San Francisco Bay Area 79−12224
surface concentration forecasts for polluted areas, Model Output Statistics appl. 80−12035
Sydney airshed, O_3-precursor relationships 79−34880
terrestrial atmosphere, O_2 and O_3 early history 79−84487
thunderstorm production of O_3 and N oxides 77−37300
transport by planetary waves, mechanistic model of stratosphere 80−8402
transport in St. Louis area 79−16650
trichloromethane glass:O_3, ^{17}O, NQR by proton double reson., broad reson. assignments 80−53014
tropographere O_3 production rate, implications of NO meas. in equatorial Pacific region 79−100893
tropopause, O_3 vertical and horizontal fluxes, GASP data 78−7720
troposphere, background mean. conc., balloon obs. 78−32189
troposphere, differential absorption lidar meas. 80−12554
troposphere, kinetic photochem. downwind over water from urban areas 78−28278
troposphere, meas. in rural areas 78−32179
troposphere, meas. using microprocessor controlled lidar 79−58137
troposphere, meridional distrib. and seasonal vars. 77−60453
troposphere, mesoscale anal. of O_3 meas. in Boston metropolitan area 78−32178
troposphere, O_3 budget, one-dimens. photochem. model 78−32180
troposphere, O_3 distrib., evidence for higher background values, comment 79−39801
troposphere, O_3 distrib. and origin 78−85663
troposphere, O_3 distribs. meas. with airborne laser absorpt. spectrometer 79−2344
troposphere, O_3 mixing ratio meas. rel. to stratospheric-tropospheric exchange at polar latits. in summer 80−72599
troposphere, O_3 photochemical prod. and influence on climate 80−36365
troposphere, O_3 photochemistry 77−81968
troposphere, O_3 transport and photochemistry 77−53137
troposphere, O_3 vars. from Gasp meas. 79−100905
troposphere, radiation attenuation, aureole around UV source at finite distance 78−77320
troposphere, review of first near surface meas. at Hohenpeissenberg *(German)* 78−65369
troposphere, stratospheric source for O_3 overabundances over Pacific Ocean during Gametag, August 1977 80−72600
troposphere, surface conc. rel. to general weather situation 80−101397
troposphere, variations along meridional band 78−32190
troposphere and stratosphere, effects of NO_x emissions of high-altitude aircraft 78−32176
troposphere O_3, evidence for significant in situ photochemical source 80−72619
troposphere O_3, long-range transport 78−61514
Uccle, Belgium, 1977 July-Sept. obs. *(French, Flemish)* 78−40618
upper atmosphere, O_2 and O_3 concs. from $O_2(^1\Delta_g)$ airglow height profile meas. 78−45077
upper atmosphere, O_3 and Cl densities from OAO 3 stellar occultation meas. 77−9580
UV absorption, use as tracer for qualitative and quantitative flow visualisation 79−72972
UV emitting lamps, method for estimation of O_3 concs. in vicinity 80−81765
UV photofragment spectroscopy 79−10122
UV photometer for atmospheric ozone monitors calibration 78−77960
variations in Auckland, comparison between city and urban regions 80−17350
vertical and horizontal distrib. covering Kanagawa Prefecture, Japan, meas. *(Japanese)* 77−70768
vinyl chloride+O_3 reaction, IR matrix and microwave spectroscopy 77−90587
Ar-O_3 Van der Waals complex, struct. and props., RF and microwave obs. 80−32704
$Br+O_3 \rightarrow BrO+O_2$, rate consts., mass spectrometric obs. 77−63897
$^{44}Ca+O_2(O_3)$, reaction products identification by IR spectra in N_2 matrix 78−9151
$Cl+O_3 \rightarrow ClO+O_2$, rate consts. meas. 77−60059

ozone continued
Cl_2-O_3 system photochemistry rel. to stratospheric composition 77−16849
Cl_2-O_3-H_2 dilute mixtures, photolysis products, Fourier Transform IR kinetic obs. 80−26033
$D+O_3+CO_2$ mixture supersonic jet, gain meas. for CO_2 laser 79−89902
$F+O_3$ reaction, $FO(X^2\Pi_i)$ radical VUV photoelectron spectra 80−104455
$H+O_3 \rightarrow HO_2+O(^3P)$, reson. fluoresc. obs. 79−70317
$H+O_3 \rightarrow HO_2+O(^3P)$, yields 80−71900
HNO_2+O_3 reaction kinetics under stratospheric conditions 78−11499
$HO_2+O_3 \rightarrow OH+2O_2$, rate coeff., effects on stratospheric O_3 78−96275
on Mg, chemisorptive luminescence systems for surface reaction obs. 78−7236
$Mg+O_3$, matrix reaction, IR spectra, isotope shifts and blue matrix shift 78−80736
NO+O, O_3 effect, chemiluminesc., absolute rate const. 80−45507
$NO+O_3$*, laser excitation effects, fluoresc. meas. 77−21372
$NO+O_3(001) \rightarrow NO_2(^2B_{1,2})+O_2$, laser enhanced reaction, temp. depend. 77−81397
$NO+O_3 \rightarrow NO_2+O_2$, rate const., 203-361K, fast flow method 77−33143
NO_x aircraft emission effects on atmos. O_3 column increase 78−11979
$NO(NO_2)+O_3$ reactions in power plant plumes 78−3923
$Na+O_3 \rightarrow NaO^*+O_2$, in upper atm., rel. to Na I nightglow intensity vars. 79−70905
$NaClO_3$:O_3^-, form. by γ-irrad., reson. Raman scatt., temp. depend. 78−92062
$O+O_3$ reaction, vibr. enhancement 80−30215
O_2+O_3, collisional deactivation of laser excited $O_2(^1\Delta_g)$, addition effects and pathways 78−25673
O_3, and isotopic substitutions, rot. spectra calcs. 77−38659
O_3 photolysis at 248 nm, $O(^3P_J)$ direct obs. 80−101028
O_3, unimolecular reactions, rate theory 79−74348
O_3^-, $(O_3^-.H_2O)$, photodetachment and photodissoc. cross-sections meas. 79−98170
O_3^-, form. on MgO surface, irrad. effects 79−100431
O_3^-, photodissoc, cross section 79−832
O_3^-, photodissoc. and photodetachment in $O_2/CH_4/H_2O$ mixtures, 3500-8600 Å 79−45776
O_3^-, photoelectron, photodetachment and photodestruction spectra 79−64042
O_3-Ar(CO), photorecombination laser, shock wave triggered, waveguide mode optical gain 80−5730
O_3-ClO_2 mixtures, photolysis quantum yields, atmos. chem. 79−52724
O_3-O_2 mixture, significant struct. theory appl. to phase separation 77−51503
O_3+Al, AlO chemilum., perturbations and vibr. population anomalies obs., mechanism 77−63917
$O_3+Al \rightarrow AlO+O_2$, chemiluminesc., $A^2\pi$-$X^2\Sigma^+$ transition obs. 78−31639
O_3+B, chemiluminesc. metal oxide formation 80−35509
O_3+CO, O_3+OCS, double-quantum vib. energy transfer 77−6897
$O_3+Cl(^2P_{3/2})$, reaction kinetics, temp. depend., reson. fluoresc. obs. 77−4903
O_3+D+CO_2, mixing in supersonic streams to produce CO_2 chem. laser 77−676
O_3+ethylene, dioxirane form., decomp. products, mass spectrometric obs. 78−11504
O_3+ethylene, dioxirane form., identification by microwave spectra 78−15659
$O_3+Fe(CO)_5$, modulated chemiluminesc. by CO addition 80−40692
O_3+H, absolute reaction rate const., 219-360K 78−80734
O_3+H, reaction mechanism studied using photoionisation mass spectrometer, form. of $O_2(a'\Delta g)$ 80−85168
O_3+H_2S(OCS), SO chemiluminesc. in Ar matrix 79−5146
O_3+HCl, nonreactive vibr. relax. rate of O_3 (001), 173-419K 79−3545
O_3+HI, HOI formation, matrix reaction, IR spectra, isotope shifts and band assignments 78−80737
O_3+HNO_2, rate consts. determ. with diode laser 79−70310
O_3+HO_2, reaction kinetics, laser mag. reson. obs. 80−102528
O_3+He(Ar)(Xe), collisional energy transfer in unimol. reaction, classical trajectory calcs. 78−62882
O_3+He(D_2)(H_2), vibr. relax. rate consts. 80−74231
O_3+NO, chemilum. reaction, NO_2 light amplification *(Russian)* 77−88717
O_3+NO, fs-states and rot. states, effect on reactivity 80−89473
O_3+NO, IR laser enhanced reaction rate, vibr. excitation 77−1911
O_3+NO, laser enhanced reaction, fluoresc. obs. 79−66285
O_3+NO reaction in turbulent jet 77−62310
$O_3+NO(v=1)$, IR laser enhanced reactions 79−66286
$O_3+NO \rightarrow NO_2^*+O_2$, kinetic energy and internal state depend. 79−66287
$O_3+NO \rightarrow NO_2^*$, mol. beam chemiluminesc., kinetic and internal energy depend. 78−31638
$O_3+NO \rightarrow NO_2^* + O_2 \rightarrow NO_2+h\nu+O_2$, chemiluminesc., translational and rot. energy effects 80−30218
$O_3+N(^4S)$, rate const. at 298K, upper limit determ. 79−74360
$O_3+Ni(CO)_4$, modulated chemiluminesc. by CO addition 80−40692
O_3+O, collisionally induced relax. processes and vibr. energy transfer 80−53107
$O_3+O_2(^1\Delta_g)(O_2^*)$, UV photolysis, $O(^3P)$ prod., rate consts. determ. 80−55636
$O_3+O^-(OH^-)(S^-)(SH^-)$, associative detachment, rate coeffs. 78−3325
$O_3+OH \rightarrow HO_2+O_2$, reaction rate const., 238-357K 79−47902
$O_3+O(^1D)$, UV photolysis, $O(^3P)$ prod., rate consts. determ. 80−55636
O_3+p-H_2(n-H_2), vibr. relax. quenching rate consts. meas. 79−13792
O_3+Sc(Y), oxidation, single collision chemiluminesc. 77−25267
O_3+thiirane, autocatalytic reaction, stopped-flow study, reaction rate meas. 80−85152
O_3+thiirane+olefin+SO_2, excited neutral metastable SO_2 form. mass spectrometric study 80−83300
O_3+U(Th), assoc. ionis. cross sections, in crossed beams, mass spectra obs. 78−94317
O_3+Zn(Cd), matrix reactions, IR, Raman and visible spectra in Ar and N_2 matrices 80−87110
$O_3^- + CO_2 \rightleftharpoons CO_3^- + O_2$, rate const., 200-600K in flowing afterglow 78−7193
O_3^-+molecule reactions, thermochemistry, electron affinity and rate consts. 78−40040
$O_3^- + X \rightarrow O^- + O_2 + X$, X=He, Ar, CO_2, long-lived excited (or isomeric) state of O_3^- 78−5318
ozone continued
$O(^1D)+O_2(N_2)(CO_2)(O_3)(H_2O)$, 100-350K, reaction rate consts. 77−21355
O_3H^+, isomeric structs. ab initio MO calcs. 80−83270
$O(^3P)+O_3^+$, bimolecular reaction rate coeff. reactant vibr. excitation depend., reson. fluoresc. obs. 78−76837
$O_3(001)$+NO, laser enhanced reaction, temp. depend., reactive and non-reactive channels 78−48642
$O_3(001)$+NO, laser-enhanced reaction, rates, temp. depend. 78−48675
$^{16}O_3$ and ^{18}O isotopic species, rot. spectra 18 to 382 GHz, force and Coriolis coupling consts. 77−75137
$O_3^-.H_2O$ and $O_3^-.2H_2O$, photodissoc, and photodetachment 79−833
Pb+O_3, PbO chemiluminesc. spectra 77−9087
Pb+O_3 reactions, chemiluminesc. 79−52673
SF_6+NO+O_3, laser sensitised reaction, time-resolved NO_2* emission obs. 78−20017
SO_2 oxidation by O_3 in cloud droplets, HSO_3^- aerosols form. 78−44894
$SO_2+O_2(O_3)$, in aq. soln., kinetics, rel. to atm. rate processes 79−20905

ozonosphere
atmosphere total O_3 content, monthly averages correls. with solar activity vars. 79−16571
aviation effects 79−16657
catalysis and O_3 destruction 79−34879
chemical balance changes 78−92933
chemistry and O_3 vars. depletion 80−104534
chlorofluorocarbon residence times in stratosphere, two-dimens. model 80−45834
chlorofluorocarbons and ozone depletion in the lower atmosphere 79−53498
chlorofluoromethane effects *(German)* 79−20959
chlorofluoromethane induced O_3 depletion, atmos. chem. theory 80−51477
chlorofluoromethane photolysis in stratosphere, effect on O_3 conc. 80−109197
chlorofluoromethanes effect on O_3 layer rel. to stratosphere natural structure 79−84436
chlorofluromethane + $O(^1D)$, stratospheric chem. reactions 79−53499
composition of middle atm., in situ meas. 80−17339
density profile, determ. from outgoing thermal radiation 78−92945
depletion of O_3 and trace chemicals in atmosphere *(German)* 79−96492
depletion of ozone layer by supersonic flight, rel. effects of latitude and altitude 77−64360
dichlorodifluoromethane, UV photodissoc. cross-section, 223 and 296K 79−52729
Dobson meas. of total O_3 content, aerosol extinction effects 79−84431
electron scavenging by halomethanes 79−50143
environment monitoring system for O_3 and aerosols 78−73507
fluorocarbon hazard to O_3 layer, assessment 79−79963
fluorocarbon-ozone theory, atm. modelling, diurnal steady state calc. 79−88390
formaldehyde, chem. of stratosphere, UV absorpt. spectra implications 80−109209
gravity waves, density response of O_3 layer 78−81290
halocarbon depletion of O_3 layer, climate effects 80−98436
halocarbons, hydrocarbons and SF_6, global distrib., sources and sinks, rel. to 0_3 depletion 80−4088
hydrofluorocarbon monitoring using telluric absorption line *(German)* 78−49133
ion cycle importance in O_3 destruction 78−53697
laser radar obs. using XeCl excimer laser 79−16681
laser-radar obs. using excimer lasers 80−17410
meridional migration of O_3 *(Russian)* 77−73816
natural depletion mechanism, energetic radiation belt electron precip. 77−41134
ozonograms, July-Sept. 1978, Belgium 80−12484
ozonograms, Oct.-Dec. 1978, Uccle, Belgium *(French, Flemish)* 80−21797
ozonometer, using chemiluminescent reaction of ozone and olefins *(French)* 79−48574
partial pressure profile minimum at 38 mb level 79−79941
perturbation by N fertilisers, independent variables anal. 78−73505
perturbing influences, 1955-75 catalogue 80−41502
photochemistry, review 79−74943
photochemistry and dynamics 79−5590
photochemistry model, O_3 calcs. uncertainty 79−16567
planetary waves, mechanistic model of O_3 transport 80−8402
remote measurement in IR absorpt. bands, information content estimation *(Russian)* 78−88883
remote sensing of lower stratosphere from Nimbus 4, O_3 content 80−77154
remote sensing of O_3 and temp. by satellite IR limb scanning method 80−105086
season and latitude depend. of total O_3 content, 1964-75 period 80−41534
seasonal composition variation at high-latitude 80−77051
solar activity affecting total O_3 content of atmos. 80−41488
solar activity fluctuations, reln. to variation in O_3 conc. and layer temp. 80−31110
solar cycle assocs., O_3 and temp. trends 79−84443
solar cycle-O_3 relationships 80−17342
solar eclipse effect on NO_2 and O_3 conc. and atm. temp. 80−105017
solar proton event of 1972 August, effects 79−35227
solar radiation models, atmospheric ozone estimation 79−70875
SSTs, nitrogen fertiliser and stratospheric ozone 79−21007
stratosphere, chemical studies using Concorde aircraft, air sampling equipment 79−80058
stratosphere and troposphere, vertical distrib. during polar front passage 80−94582
stratosphere O_3, simultaneous effects of CO_2 and chlorofluoromethanes on column density 79−74940
stratosphere O_3 density perturbations, photochemical-radiative damping rel. to instability 78−81286
stratosphere O_3 depletion thermal effects at 85°N latit., airborne particles influence 78−81279
stratospheric warming, March-April 1976, tropical O_3 content, 35-60 km altitude 80−12494
tetrachloromethane, UV photodissoc., mechanism and quantum yield 79−52723
total content, Dobson spectrophotometer meas. errors 80−72644
total content determ. using remote spectroscopy 78−65437

ozonosphere continued
total content measurement, using Dobson spectrophotometer 80−72643
trichlorofluoromethane, UV photodissoc. cross-section, 223 and 296K 79−52729
volcanic eruptions effects on O_3 79−84437
Br chemistry of stratosphere and O_3 depletion 80−98391
CO_2 and stratospheric O_3, two-dimens. model calc. 79−62564
CO_2 cooling of atmos. affecting O_3 content of stratosphere 80−36369
CO_2 increase effects on stratospheric O_3, photochem. and radiative transfer model 78−65370
CO_2-O_3 coupling, photochem. radiative column model with Cl chem. 80−85724
CO_2-O_3 coupling in Cl free atm., photochemical-radiative column model 80−85723
Cl effects on O_3 layer, zonally averaged two-dimens. model 79−84435
ClO_2-O_3 mixtures, photolysis quantum yields, atmos. chem. 79−52724
$ClONO_2+O(^3P)$, photolytic gas phase kinetics at 245K 79−52719
HO_2+ClO, reaction product distrib. 80−72586
HO_2+NO reaction rate constant effects on O_3 perturbations, model of stratosphere 78−73474
HOCl involvement 80−26033
N oxides produced by thermonuclear explosions, effect on O_3 79−84345
NO_x from SST and subsonic aircraft emission, potential O_3 column increase 78−11979
N_2O from fertilisers and O_3 content of stratosphere, latitudinal effects 80−36370
O_3 content effects on troposphere radiative energy balance 80−51466
O_3, densities in stratosphere and mesosphere rel. to radiative equilib. temps. 78−81280
O_3 density reductions, zonally averaged circulation response 79−53461
O_3 depletion by chlorofluoromethanes, contradiction of theory 78−49099
O_3 depletion chemistry 79−70872
O_3 depletion prediction, effect of temp. coupling 78−57246
O_3 depletion theories, rel. to atm. nuclear tests 79−70848
O_3 destruction, chemical-kinetic criteria of effect of substances of natural and anthropogenic origin *(Russian)* 78−53699
O_3 destruction by Cl, prospects of HOCl as atmospheric Cl reservoir 79−12207
O_3, high resolution spectroscopy of ν_3 band, rel. to atm. O_3 monitoring 79−63993
O_3, nighttime concentration (15-68 km), Nimbus 6 obs. comparison with OAO-3 obs. 80−105016
O_3, partial press. profile over Uccle, Belgium, April-June 1979 obs. *(French, Flemish)* 80−98385
O_3, partial pressure profile over Uccle, Belgium, 1979 obs. *(French, Flemish)* 80−94571
O_3 photolysis, $O(^1D)$ quantum yields as function of temp. (230-320K) and wavelength (295-320 nm) 78−56903
O_3 reduction estimates, effects of water vapour changes 78−73444
O_3 seasonal var. from rocket-borne UV obs. 77−29402
O_3, stratosphere content at mid-latitude, simultaneous N and S hemisphere obs. 80−77052
O_3, stratospheric determ. at ground level using $^7Be/O_3$ ratios 79−58011
O_3, UV photodissoc. rate, expt. and theory 80−40722
O_3, Umkehr vertical profile errors caused by presence of stratospheric aerosols 79−70849
O_3 vars. correl. with cloudiness vars. rel. to UV radiation protection 78−73456
$O_3+OH \rightarrow HO_2+O_2$, reaction rate const., 238-357K 79−47902
OH^+ trichloroethane reaction rel. to O_3 content 80−16657
$OH+ClO(Cl_2)(Cl_2O)$, rate const. at 298K, rel. to stratospheric O_3 depletion 79−87831
$^{18}O^{16}O$, photodissociation as source of atmospheric O_3 80−94559

P invariance
1.87 GeV/c^2 states, evidence for parity nonconservation in decays 77−10245
$1/2^+$, baryons, vector mesonic decay, charm changing mode, SU(4) and SU(8) 80−47283
θ-vacua energy depend., P and T conservation in the presence of instantons 78−89628
ρ-exchange isovector parity-violating potential 79−93525
atom, contact interactions, parity-violating and parity-conserving, new evaluation techniques 79−26872
atom, heavy, parity non-conserving E1 matrix elements, many body calcs. 80−47924
atom, metastable, sensitivity and level crossing role in parity nonconservation meas. 80−43005
atom, parity violation due to radiative corrections 78−78108
atom, search for parity nonconservation 79−36593
atom parity breaking, implications for unification of weak and EM interactions 77−57479
atomic, review of laser appl. to precision meas. 78−42246
atomic parity conservation, left-right symm. unified theoreies 78−70306
atomic processes, parity violation 77−22657
atomic spectroscopy, search for parity-violating weak interaction of electrons with nuclei 79−36571
atomic transitions, obs. of parity nonconservation effects 77−13889
atomic transitions, search for parity nonconservation 79−36574
atomic transitions, weak interaction effects, review 77−13890
atoms, and ions, parity nonconservation effects 79−10086
atoms, heavy, parity non-conservation, relativistic many-body perturbation theory 78−923
atoms, Hiller-Sucher-Feinberg identity, generalisation, accuracy for approx. wavefunctions 80−63512
atoms, many-electron, relativistic theory of P violation 80−91042
atoms, parity violation effects 77−71457
atoms, parity violation in neutral-weak current interactions, meas. method 79−45670
atoms, photoionisation cross sections, electron correl. reson. struct., relax. effects many body perturbation calcs. 80−47852
atoms, weak electron-nucleon interactions, testing Laporte's rule, review 78−37564
axion properties, strong T and P conservation enforcement 79−67481
baryon nonleptonic decay, light-like reduction formula and derivation of PC and PV Lee-Sugawara relation 80−32032
baryon nonleptonic weak decay, parity violating amplitudes 78−45917
black holes, rotating, parity nonconservation 79−12491
bound states from instantons 78−78087
bremsstrahlung, parity nonconservation due to neutral currents 77−6076
broken supersymmetry theories, parity conservation 77−41785

P invariance continued
broken symmetries at high temperature 80−42357
charge-monopole composites, Poincare invariance and parity violation 77−2762
charmed baryon decays, nonleptonic, parity-violating, single-quark and two-quark transitions 80−68453
charmed baryon decays, weak hadronic, SU(3) dynamical scheme 80−68454
charmed baryon hadronic decays, parity violation in SU(8) 79−89077
charmed baryons, $\Delta C=\Delta S=1$ nonleptonic decays, amplitude relations 79−54339
charmed baryons, parity violating and conserving decays, $(1/2^+ \rightarrow 3/2^+ + 0^-/1^-)$ in Abe, Fujii and Sato model 79−97623
charmed-baryon nonleptonic decays, parity-violating amplitudes 78−62398
chiral symmetry spontaneous breaking, using vacuum stability condition 79−35986
classical V-A theory and non-conservation of the dynamical parity 79−54014
coherent parity-violation experiments with neutron beams 79−59073
colour gauge theory of strong interactions, P and T invariance 78−37153
Compton amplitude, parity violating part 77−2840
cosmological ν sea, EM wave propagation, torsionic background 80−77283
CP symmetry spontaneous breaking in nonstationary isotropic metric 79−89079
diatomic mol. parity breaking in rot. levels *(Russian)* 79−2954
Dirac equation, two-component first-order equations for the quantum-relativistic electron 79−17649
dynamically broken-gauge theories, P and T violation in QCD 80−9093
dyonium model, space reflection operator and boson fermion puzzle 79−36118
elastic electron scatt. and atom parity nonconservation caused by nuclear parity violation 80−27427
electron anapole moment, static parity violating coupling to EM field, unified gauge theory 80−68390
electron-hadron interactions, P-invariance, lepton, quark anapolar moments with pol. e *(Russian)* 80−52518
elementary particle properties from atomic phys. expts., weak neutral currents 77−34578
EM interactions, connection with absence of magnetic monopoles 77−6044
EM interactions, gauge formulation, $SU_\tau(2)$ internal symmetry and P- and CP-violation *(Russian)* 80−42368
EM systems, parity and time inversion symmetries 77−45721
EM systems, parity and time inversion symmetries 79−67169
experimental progress, few-body aspects 77−22665
extended relativity, T-violation and new particle 80−37182
fermion Reggeization without parity doubling, Reggeized absorpt. 78−54622
fermion scattering from parity violating potential 77−79245
ferroelectrics, P- and T-nonconserving interactions, macroscopic effects 78−84532
fission, spatial parity nonconservation *(Russian)* 78−25170
flavour changing weak radiative decays, short and long distance effects 80−73712
forbidden M_1 transitions, parity violation, stray static elec. fields 80−87078
fundamental physics with reactor neutrons and neutrinos [conf. ILL, Grenoble, France (Oct. 1977)] 79−59112
G-parity nonconservation, ev ang. correlation for allowed beta-decay 78−17151
gauge model with spontaneous P-violation, anal. of spontaneous CP violation 77−38113
gauge theories, manifest L-R symmetry, strong P and T noninvariances and neutron electron dipole moment 79−63372
gauge theory, implications of absence of parity nonconservation in atomic physics 77−41758
gauge theory, P-symmetric, $\mu \rightarrow e\gamma$ rate 77−49941
geometry of spacetime founded on spacelike metric 79−63102
gluon exchange diagrams, effect on parity violating weak interactions 79−97565
hadron resonance decay, intermediate vector boson and high energy weak interaction detect. 79−22012
hadron-hadron large p_T collision, weak interaction effects 78−21462
heavy atom, parity nonconservation, weak interaction *(Russian)* 79−45182
heavy atoms, P-odd effects, weak interaction eqn., SU(2) theory, four fermion theory *(Russian)* 78−93820
Higgs bosons, effects on experimental observables, and fermion mass scale 80−32061
Higgs exchange in guage models with right-handed charged currents P and CP invariance 78−12824
Higgs-boson exchange P and CP violation, Weinberg model 78−8575
historical introduction, weak interactions, book 78−78133
hyperon weak EM decays, 27th Hamiltonian component contribution 79−22101
inclusive lepton pair prod., P violation, quark-parton model in Weinberg-Salam theory, QCD 80−37217
internal conversion and parity nonconservation in nuclei 78−50125
ion, multiply charged, two-electron, parity nonconservation in spectra 79−10087
ions, multiply charged, highly excited states, parity nonconservation effects 80−52898
left-right symmetric $SU(2)_L \times SU(2)_R \times U(1)$ gauge theory, atomic P violation 78−74144
left-right symmetric SU(N) gauge models, parity violation in atoms 79−21966
left-right symmetry, spontaneous breakdown, parity violation, leptonic right handed, currents 78−21351
lepton-hadron scatt., polarised beam and target, review and survey of expts. and theoretical implications 79−67560
lepton-nucleus elastic scatt. with $0^+ \rightarrow 0^-$ nuclear transition, P nonconservation *(Russian)* 77−61402
lepton-nucleus scattering, bremsstrahlung and neutral currents 80−32268
magnetic monopoles, PT-invariant theory of massive dually charged particles, Dirac-like eqn. 80−52429
manifest left-right symm., parity nonconservation via spontaneous breakdown, expt. consequences 77−57465
massive particles with any spin. consistent eqns., Klein-Gordon divisor, review 80−73577

P invariance continued
molecular electronic spectra, parity nonconservation effects *(Russian)* 78−13488
molecules, parity-violating effects of weak interactions 80−52455
multielectron atom, parity nonconservation *(Russian)* 79−45033
muonic atom, heavy, polarisation mechanism of parity nonconservation, weak neutral interaction effect *(Russian)* 77−79712
muonic atoms, parity violating neutral current effects, E1-E2 interference 79−41254
Nd scattering, parity non-conserving effects, predictions 79−93448
neutral current, P-violation in nuclear transitions 79−13243
neutral current expts., left-right symmetry for $SU_L(2)\times SU_R(2)\times U(1)$ gauge group 78−21375
neutral current interactions in $SU(2)_L\times SU(2)_R\times U(1)$ gauge models, natural parity conservation, gauge bosons 79−321
neutral current P-violation, gauge flavours, Weinberg model testing 77−61240
neutral current phenomena, gauge model of parity nonconservation 79−17656
neutral currents, P-violating in L-R symmetric gauge model 77−82698
neutral currents, $SU(2)_L\times SU(2)_R\times U(1)\times U(1)$ 79−6308
neutral transitions, vector-like weak currents, parity violation *(Russian)* 78−24995
neutrino fluxes from rotating black holes and thermal radiation, parity violating effects 80−22034
neutron's gravitational interaction, expt. evidence for parity violation 79−58617
neutron optical activity in helicoidal antiferromagnetic materials 78−74419
neutron reactions, expt. determination of parity violation 79−59048
neutron scatt. from parity violating pot. 78−25167
neutron scattering theory, parity violating interaction 78−25166
(non)conservation of isospin, parity, charge conjugation, and time reversal invariance in intermediate energy phys. 79−80772
non-leptonic parity violating decays in SU(8) 77−26523
non-leptonic weak interactions, book contrib. 78−78163
nonleptonic decays of ordinary and charmed hadrons, vector-like model 78−41545
nonleptonic weak interaction, SU(4) symmetry struct., parity violating Hamiltonian 80−52456
nuclear β-decay, parity nonconservation, coupling constants, intermediate boson mass ratio 79−9516
nuclear effects, parity violating, low energy anal., NN scatt. parametrisation 78−66218
nuclear force, parity violating, unified treatment 80−47400
nuclear parity violating effects in vector-like quark models 77−61249
nuclear weak and EM interactions, P-violation in e-nucleus scatt. 77−71479
nuclei, parity non-conservation review 80−32207
odd proton nuclei, parity nonconserving effects, phenomenological proton-nucleus weak interaction 79−40853
optical isomer crystal, energy difference due to parity nonconservation *(Russian)* 80−106405
oriented nuclei, β-γ ang. correl., G-parity nonconservation 78−54723
P and T violating electromagnetic interaction of the quark in the instanton field 80−52430
parity non-conservation effect in atoms and molecules 80−68395
parity non-conserving processes, weak interaction theory, review 78−50002
parity nonconservation, discovery and nondiscovery, history 80−370
parity nonconservation in heavy atoms and weak magnetism in neutral currents *(Russian)* 80−82932
parity nonconserving nuclear interactions and weak neutral currents, review 77−41936
parity violating asymmetries in polarized electron scattering from p, d, e 80−9111
parity violating internucleon potential due to vector meson exchange, asymptotically free theories 77−10210
parity violating neutral currents, radiative corrections, Weinberg-Salam and left-right symmetric models 80−52451
parity violating neutral currents in two-photon and autoionisation atomic transitions 80−32034
parity violating nuclear forces, neutral current effects 77−30497
parity violating reactions, fundamental phys. expts. with reactor neutrons and neutrinos, summary 79−67543
parity violating terms in nuclear EM operators and struct. effects 79−6482
parity violation and the masslessness of the neutrino 79−85258
parity violation effects in neutron scattering and capture 80−105808
parity violation in atoms, $SU(2)\times U(1)$ models, higher-order corrections 78−45807
parity violation in He and Cs atomic electrons and e-e interaction effects 79−54788
parity violation in nuclear processes with polarised neutrons 79−59008
parity-violating vector-meson-exchange internucleon potential, weak nuclear processes, modified factorisation approach 77−30418
pion form factor, ω and ϕ effects G-parity violation 79−35963
pion photoproduction, weak interaction induced parity violating assymetries 79−71758
polarised lepton-hadron scattering, lepton and quark anapole moments *(Russian)* 79−17730
potential model, Dirac eqn. with linear confining pot., symmetric model, conserved parity 79−364
probability current and boundary conditions for wave functions of parity violating interactions 77−71459
PT asymmetry and four-fold EM degeneracy lifting, appl. to ring laser mode splitting 80−23606
quantum field theory, relativistic, discrete symmetries 80−68387
quark fragmentation in P conserving jet production reactions, spin observables 79−71658
quark model, weak interactions, quark masses, spontaneous violation of parity 77−6054
quark-lepton correspondence in neutral current interactions 80−27450
quarks and leptons, fermion physics in terms of $SU(2)\times SU(1)$ gauge theory 78−74197
Reggeization of elementary fermions in arbitrary renormalizable gauge theories 80−68367
relativistic classical nonlinear field theory, PCT violation 77−65081
relativistic QFT, spontaneous symmetry violations 80−52411
rotation of plane of polarisation close to reson., nonconservation of parity effects 79−41129

P invariance continued
S-matrix theory of overlapping resonances, constraints imposed by analyticity and unitarity 77−22656
selections from 1977 Comments on Modern Physics, book 79−30181
Sodium ammonium tartrate, L- and D-mol. energy difference, parity violation 78−25744
stellar collapse, parity nonconservation 79−92789
strong P and T noninvariance, natural suppression in $SU(2)_L\times SU(2)_R\times U(1)_{L+R}$ gauge model 79−9303
strong P and T noninvariances in a superweak theory 78−82123
$SU(2)_L\times SU(2)_R\times U(1)_L\times U(1)_R$ gauge models, parity violation in SLAC neutral current expt. 79−9305
$SU(2)_L\times SU(2)_R\times U(1)$ gauge models, neutral currents, P-violation 79−54293
$SU(2)_L\times SU(2)_R\times U(1)$ gauge models, parity violating effective interaction 79−9304
$SU(2)_L\times SU(2)_R\times U(1)$ gauge symm., Higgs particles, parity conservation 78−70305
$SU(2)_L\times SU(2)_R\times U(1)$ gauge theory, left-right symm., neutral current struct. 78−41420
$SU(2)_L\otimes SU(2)_R\otimes U(1)$ weak model, ν mass and spontaneous P nonconservation 80−62884
$SU(2)_L$ x $SU(2)_R$ x U(1) gauge models, neutral current sector, natural parity conservation 79−9324
SU(2), unification of isospin and hypercharge, electroweak interactions of leptons 80−27439
$SU(2)\times SU(2)\times U(1)$ supersymmetric gauge model, atomic parity violation and neutral current predictions *(Russian)* 79−54294
$SU(2)\times U(1)$, P and T invariance violation suppression, quark mixing angles 79−54278
$SU(2)\times U(1)\times U(1)$ gauge models, neutral current struct., parity nonconservation 79−292
$SU(2)\times U(1)$ gauge model and parity violation in atoms 78−4775
$SU(2)\times U(1)$ unified gauge theories, implications of parity violating obs. on heavy atoms 77−46006
$SU(2)\times U(1)$ vectorlike model: new leptons, quarks, and the axion question 79−40711
$SU(2)\otimes U(1)\otimes U'(1)$, anal. in neutral current interactions, parity nonconservation in ed scatt. 79−17731
$SU(2)\otimes U(1)\otimes U(1)$ gauge model without parity violation in heavy atoms 78−82097
SU(6) unified gauge group, parity violation in atoms 78−54626
thermal radiation, parity violating currents 79−17633
TP inversion in quantum gravity 79−58613
two-electron atoms, autoionisable states decay, parity violation effects 79−72231
two-electron ions, autoionisable states decay, parity violation effects 79−72231
two-level system, hyperfine struct. transitions, weak interaction meas. *(Russian)* 80−58196
unified model for atomic parity violation and neutral currents in gauge theories 80−4912
unified parity-conserving interactions based on SU_4 77−74629
unified theory of EM and weak interactions 80−82928
unstable particles in electric field, physical meaning of Zel'dovich dipole moment 79−36594
V_3(W) gauge theory, spontaneous symm. breaking, parity violation in atomic physics 77−71476
vector mesons, neutral, P-odd effects in decay *(Russian)* 78−54628
vectorlike theory of weak interactions 77−67613
vectorlike theory with parity violating neutral current and natural symmetry 77−13909
violation search in highly forbidden mag. transition in Cs atom 78−82709
weak electron-nucleus interaction, parity violation, mol. evidence *(Russian)* 77−30793
weak interaction between nuclear particles, parity violation, review 77−6295
weak interaction models explaining null parity violation in Bi, tests on other weak interactions 79−2974
weak interaction theory, review 78−4822
weak interaction theory review, nature of parity violation 78−78131
weak interactions, optical experiments as a means of verification 79−6313
weak interactions, renormalisable model on gauge group $SU(2)_L\times SU(2)_R\times U(1)$ 78−12855
weak interactions of quark fields, quark masses, spontaneous parity violation 77−34115
weak interactions vectorlike model with six quarks, gauge theory, $SU(2)\times U(1)$, νN appl. 77−57480
weak neutral currents, parity non-conservation in e-N, μ-N forces 77−57484
weak-EM interference, neutral currents, P-violation, in polarised e-scatt. and e^+e^- interactions 79−63404
Weinberg model, NN parity-violating π-exchange pot. 77−65133
Weinberg model, spontaneous CP violation 77−26480
Weinberg-Salam model, flavour symmetry breaking and isovector parity-violating potentials 79−80780
X-ray atomic spectra, parity violating effects from electron nucleus weak currents *(Russian)* 79−22642
y anomaly in $SU(2)\times U(1)$ vector like model, with parity violating neutral current 79−13013
D meson parity violating nonleptonic decays, vector meson dominance model 80−78058
e d polarised elastic scatt., parity violation 79−36085
e^-+nucleus parity violating neutral current interaction, gauge theory predictions, radiative corrections 78−86436
eD, 19.4 to 22.2 GeV, unpolarised target, parity violation in inelastic scatt. of polarised electrons 79−63482
ed, polarized scatt., parity violation Weinberg-Salam model without parton model 79−40787
ed deep inelastic scatt., p-violating asymmetries, neutral current couplings, sea quark contrib. 79−97630
ed deep inelastic scatt., parity nonconservation 79−75776
ed deep inelastic scatt. at 19.4 GeV, polarised electrons, search for P violation 77−34156
ed→e′+X, polarised e, parity non-conservation in inelastic scatt. 78−89719
ed→e′+X, polarised electrons, asymmetric inelastic scatt., effect of odd-parity components of deuteron 79−89166

P invariance continued
ed elastic scatt., P-odd effects due to neutral weak currents, cross sections *(Russian)* 80−13312
ed elastic scatt., recoil d vector polarisation, p-violation 79−398
ed scatt., P-violation calc. in weak interaction theory 80−42469
$e^+d \rightarrow e^+np$, polarised, parity violating asymmetry 80−78080
e^-e^- neutral weak currents in atoms and ions, parity nonconservation *(Russian)* 77−46037
e^+e^-, weak corrections to three-jet angular distributions 80−22629
$e^+e^- \rightarrow F\bar{F}$, with polarised particles, weak asymmetries, unified gauge theory anal. 78−8636
e^+e^- inclusive hadron prod., polarisation and p nonconservation asymmetries, π, $K^{\pm}$, $D^{\pm}$ prod. 80−78084
$e^+e^- \rightarrow L^+L^-$, longitudinally polarized beams collisions, energy depend. of parity asymm. 77−38154
$e^+e^- \rightarrow \mu^+(\tau^+)\mu^-(\tau^-)$, neutral current couplings, lepton polarisation, p violation in SU(2)×U(1) model 80−4975
$e^+e^- \rightarrow \tau^+\tau^-$, parity violating effects measurement 79−36057
$e^+e^- \rightarrow \tau^+\tau^- \rightarrow$cascade π and ρ, parity violation from weak and EM interaction interference *(Chinese)* 79−49504
eN, pion production, vector-like theories *(Russian)* 78−37221
eN deep inelastic scattering asymmetries, gauge theory predictions 79−22104
eN elastic scatt., pol. e, nucleon form factors, P violating symmetry, Weinberg-Salam calcs. 80−68461
eN elastic scatt. in nuclei, P violating asymmetry due to weak neutral currents 80−73713
eN interactions, parity nonconservation, $SU(2)_L \times SU(2)_R \times U(1)$ gauge model anal., Z boson decay widths 80−47302
eN scatt., polarised e, testing unified gauge theories prediction 79−17732
eN weak interactions, indications given by optical activity of heavy metal vapours *(Russian)* 77−10618
$e^-N \rightarrow e^-\Delta(3/2, 3/2)$, P-odd asymmetry, P nonconserving neutral current interaction 80−57611
$e^-N \rightarrow e^-X$, parity violating asymmetry, constraint on right-handed electron weak charge 79−17734
ep, high Q^2, QCD corrections to parity-violating asymmetries 80−22618
ep deep inelastic scatt., p-violating asymmetries, neutral current couplings, sea quark contrib. 79−97630
ep deep inelastic scatt., parity violation and neutral currents 80−22559
$ep \rightarrow e'+X$, polarised e, parity non-conservation in inelastic scatt. 78−89719
eq parity violating neutral current couplings, model independent anal. 79−17737
η, neutral weak current effect on decay mode Weinberg-Salam model, P-violation contrib. 78−86450
F parity violating nonleptonic decays, vector meson dominance model 80−78058
$\gamma+N \rightarrow N+\pi$, spatial parity nonconservation in π-meson photoproduction *(Russian)* 77−61301
$\gamma N \rightarrow l^+l^-X$, pol. γ, neutral current effect, Weinberg Salam model calcs., p violation 80−5000
$\gamma N \rightarrow l^+l^-X$, polarisation effects on P-violating asymmetry in Weinberg-Salam model 80−32055
$\gamma N \rightarrow N\pi$, P-odd effects, weak interaction *(Russian)* 78−54638
$\gamma N \rightarrow N\pi$, P-odd multipole amplitude, dispersion relations *(Russian)* 79−93435
$\gamma p \rightarrow$ lepton pair, P violating asymmetry 80−105901
$\gamma p \rightarrow p\pi^0$, quantum chromodynamics and P-odd effects *(Russian)* 79−89172
m, polarised, false effects in decay triple correlation, time-parity violation search *(Russian)* 78−78180
μ decay correlations and lifetime meas. 80−77996
$\bar{\mu}N$, deep inelastic cross sections, search for P-nonconservation *(Russian)* 77−245
(n,n), forward scatt. amp., parity violation 79−67482
nd scattering, 14.4 MeV, parity nonconserving asymm. 78−21449
NN interactions, parity violating, review of ab initio calc. problems 78−62327
NN low energy scatt., parity violating observables 78−50045
NN P-violating interaction in Bars-Halpern-Yoshimura gauge model 77−22758
NN parity nonconserving pot., evidence for enhanced $\Delta S=0$, $\Delta T=2$ weak interaction in nuclei 77−18419
NN scatt. formalism 78−21463
$NN\pi$ amplitudes, parity violating, QCD calc. in Weinberg-Salam model and SU(4) flavour symmetry breaking 79−67520
$NN\pi$ coupling, parity violating, quark, model calc. in Weinberg Salam model 79−35987
$NN\rho$ couplings, parity-violating, QCD and MIT bag model, $1/2^-$ resonance contribs., $SU(6)_w$ symmetry 80−57540
np capture, parity violation in nucl. anal. 77−46165
$np \rightarrow d\gamma$, parity nonconservation effects due to $\rho^{\pm} \rightarrow \pi^{\pm}\gamma$, short dist. contrib. to γ circular polarisation 77−41855
$np \rightarrow d\gamma$, parity-nonconserving nucl. force 77−10333
$np \rightarrow d\gamma$ radiative capture, relativistic effects, parity violation, Weinberg-Salam model *(Russian)* 80−32120
$np \rightarrow \gamma d$, gamma polarisation due to weak parity violating effects 77−41851
$N\pi$ amplitude in unified gauge invariant models 77−6070
ν interactions, parity violations in neutral currents 77−13910
ν_μ, $\bar{\nu}_\mu$ interactions, $pion^0$ prod., P violation 77−65151
$\bar{\nu}+N$ inelastic scatt., neutral current evidence for parity nonconservation 77−2815
p-d scatt. at 15 MeV, parity conservation 77−30445
p-H_2O 6 GeV/c scatt. with polarised protons, helicity-depend. and P-violation 77−30403
p-p scatt. at 15 MeV, parity conservation 77−30445
pN, dilepton production by pol. protons, parity violating, asymmetry, Weinberg-Salam calcs. 80−42488
pN scatt., 6 GeV/c, polarised beam, P-violation, longit. asymmetry meas. 79−63500
pp, 45 MeV, longitudinally pol. p, parity nonconservation in anal. powers 80−57626
pp, polarised p, W prod. estimates for hadron jet decay detection, parity violating asymmetries 79−40821
pp elastic scatt., 6 GeV/c, polarisation anal. 78−41568
pp inelastic scatt. in $\Delta(1232)$ prod. region, parity violation 78−62435
pp interactions, polarised beam, P violating asymmetries and estimates of W prod. 79−63538
P invariance continued
$pp \rightarrow$jet+X, P-violating weak effects in high transverse momentum collisions, QCD anal. 79−63559
$p\bar{p} \rightarrow \mu^+\mu^-X$, parity violating effects in dilepton production using polarized targets 79−67613
$pp \rightarrow N\Delta$, parity violation in Weinberg model 78−8701
$pp \rightarrow \pi^+X$, P-violating weak effects in high transverse momentum collisions, QCD anal. 79−63559
pp scatt., <300 MeV P-odd asymmetry for pol. ρ *(Russian)* 80−102063
pp scattering, 15 MeV, polarised beam P-violation, longit. asymmetry meas. 79−63499
pp scattering, parity violation at 50 MeV *(German)* 80−68471
pp scattering, parity violation meas. at 45 MeV 80−78092
pp,$\bar{p}$p, polarised and unpolarised, jet cross sections vector boson signals, QCD-weak interference 80−5026
π^0, neutral weak current effect on decay mode Weinberg-Salam model, P-violation contrib. 78−86450
πN, strength of parity violation in vector meson dominance 79−71653
πN coupling, parity violating, weak and EM interaction model anal. 79−67599
πN elast. scatt., parity-violating scatt. amplitude calc. using soft-pion techniques 79−75787
$\pi^+n \rightarrow p\pi^0$, quantum chromodynamics and P-odd effects *(Russian)* 79−89172
πp radiative scattering, calc. of polarisation asymmetries using Lagrangian isobar model 79−89184
$\pi^-p \rightarrow \delta^-p$, near production threshold, nonobs. of $\delta^- \rightarrow \pi^+\pi^-\pi^-$ enhancement 79−13113
ψ' decay, Higgs bosons, five-quark model, P and T nonconservation 77−74686
ρ^0-electroproduction, parity violating effects 80−9178
$\Sigma^0 \rightarrow \Lambda e^+e^-$, parity violating effects, standard and pure vector Weinberg Salam model 79−36075
$\Sigma^0 \rightarrow \Lambda e^+e^-$, parity violation 78−25045
$\Sigma^0 \rightarrow \Lambda\gamma$, weak effects, small P violating E1 component in M1 EM decay 79−89160
$\Sigma^+ \rightarrow p\gamma$, $1/2^-$ resonance poles to parity-violating amplitude, two-quark weak transitions 80−78062
Bi, atomic, parity nonconservation effect *(Russian)* 80−77985
Bi, atomic, parity violation in M1 transition 79−85927
Bi, electron config. mixing and parity nonconservation 78−13439
Bi, neutral current-induced parity nonconserving optical rot., Dirac-HF calcs. 80−47948
Bi, parity non-conservation effect 80−68395
Bi, parity non-conserving optical rot., Weinberg-Salam relativistic central field theory vs. obs. 78−953
Bi, parity nonconservation, light polarisation plane deflection by components of ultrafine splitting *(Russian)* 78−46456
Bi, parity nonconserving optical rot. upper limit, obs. vs. Weinberg-Salam theory 78−952
Bi, search for parity nonconservation 79−36593
Bi, vapour, optical activity, Faraday effect, parity nonconservation, mag. transitions *(Russian)* 80−55070
Bi, vapour, optical rot., parity nonconservation 80−23353
Bi, vapour, optical rot., parity nonconservation expts. 80−23354
Bi, vapour, parity violation in optical activity 79−26938
Bi weak charge, SU(2)×U(1) model anal. 79−26281
Bi_2, vap. phase Faraday effect, P-invariance in M1 transitions, calc. 78−82805
^{209}Bi coherent scattering of polarised thermal neutrons, parity violating effects 78−29461
^{209}Bi, P violating eN pot., determ. of effects by optical rotation meas. 79−26277
^{209}Bi, transitions, parity nonconservation due to neutral weak currents 77−13913
^{209}Bi(n,n), direct scatt., polarised thermal neutrons, empirical parity-violating potentials and neutron optical activity 79−59074
Cs, forbidden M1 transitions, parity nonconserving effects 78−21844
D, parity violation as consequence of isoscalar axial-vector current 79−93316
H, parity mixing, relativistic neutral current interactions and nonrelativistic pots. 79−26908
H, parity violation of consequence of isoscalar axial-vector current 79−93316
H parity violations, fundamental struct. of weak current, unified gauge theories 78−12849
H simultaneous mag./elec. microwave resonance transition, parity nonconservation, Weinberg-Salam theory test 77−54066
H, two-photon transitions, parity nonconservation effects *(Russian)* 78−21892
H^- photofragments angular distribution, parity favoured electric dipole transitions 80−58330
H- and He-like ions, effects impeding obs. of parity nonconservation *(Russian)* 77−75078
H_2 ortho-para transition as means of observing weak interaction parity nonconservation *(Russian)* 80−900
^{1}H+d, polarised projectile, parity nonconservation in low energy scatt. 78−66271
^{1}H(n,γ), polarised neutrons, calc. of P-violating asymmetry 77−18565
^{1}H(n,γ), thermal, photon circular polarisation in parity violating capture 77−6375
^{1}H(n,γ), thermal calc. of γ-circular polarisation, p-nonconservation effects 77−18564
^{1}H(n,γ)^{2}H, relativistic invariant approach, parity violation 79−3147
^{2}H photodisintegration and electrodisintegration, weak interaction and P nonconservation 78−89849
^{2}H+p, polarised projectile, parity nonconservation in low energy scatt. 78−66271
^{2}H+p, polarised projectile, parity nonconservation in low energy scatt. 78−70522
^{2}H(e,e'), 19.4 GeV, polarized electrons, parity violation 79−13286
^{A}H, A=1, 2, nuclear electric dipole moments from P nonconserving atomic transitions 80−57681
He parity-violating elec. dipole transitions 80−69094
He photofragments angular distribution, parity favoured electric dipole transitions 80−58330
He+p, A=3,4, polarised projectile, parity nonconservation in low energy scatt. 78−66271
He+p, A=3,4, polarised projectile, parity nonconservation in low energy scatt. 78−70522

P invariance continued
^{3}He-B, superfluid, macroscopic parity nonconservation due to neutral currents 77−80671
H(n,γ), parity violation study, high-rate counting circuitry for γ-rays 78−62527
NH_3 inverse level doubling mol., space and combined parity nonconservation *(Russian)* 80−52879
O_2, electronic spectra, parity nonconservation effects *(Russian)* 78−13488
Pu^{239}, product separation asymmetry in fission by slow polarised neutrons *(Russian)* 80−106088
SiS, electronic spectra, parity nonconservation effects *(Russian)* 78−13488
$^{117}Sn(n,\gamma)^{118}Sn$, parity violation obs. 78−8820
Tl, $6^2P_{1/2}$-$7^2P_{1/2}$ M1 transition, parity violation detection in neutral weak interaction 77−30819
Tl, $6^2P_{1/2}$-$7^2P_{1/2}$ transition, parity nonconservation obs. 79−31446
Tl, parity non-conservation effect 80−68395
TlF, P- and T-violating interactions in hyperfine struct., mol. beam reson. expt. 80−53019
^{205}Tl, transitions, parity nonconservation due to neutral weak currents 77−13913
U^{233}, product separation asymmetry in fission by slow polarised neutrons *(Russian)* 80−106088
^{233}U fission by polarised neutrons, P odd asymmetry of emitted fragments *(Russian)* 80−18354

p-n heterojunctions
abrupt junction, energy band lineup 78−10541
$Al_{1-x}Ga_xAs$-GaAs heterophotoconvertors, HV, investigations 80−101097
amorphous/crystalline heterojunction, energy-band diagram construction 77−55602
Anderson theory, proposal for new approach 80−6961
avalanche breakdown sensitivity of multiplication layer *(Russian)* 78−34888
carrier behaviour in p-n junctions at high current densities 80−6968
chalcogenide glass-GaAs(InP) p-n junction, fabrication, characterization, switching 80−49892
characteristics, impact on field of semiconductors *(Polish)* 80−39664
composite barrier, thermally assisted tunnelling 78−19136
differential admittance theory in the presence of surface electron states 80−96981
dipole barrier role, many-electron interaction 78−23151
discontinuities predicted from bulk band structs. 77−20409
effective band edges, due to quantum and grading effects 80−20305
electronic structure calcs. 79−1613
energy band profile and interface states calcs. 79−78162
epitaxial heterostructure superlattice, construction of bound states in continuum 77−32076
forward-biased, charge accumulation 80−107902
GaAlAs-GaAs heterostruct. solar cells, Al, P, Zn incorporation by LPE *(French)* 79−24899
GaAs-$Ga_{1-x}Al_xAs$, ultrathin layer heterostruct., pseudopot. calcs. 78−95343
gain-guiding double-heterostructure laser transverse carrier diffusion effects 79−55139
heterojunction, thin, energy band diagram 77−43712
II-IV p-n amorphous heterojunction, phenomenological model 80−54769
II-VI, photovoltaic props. 77−55600
II-VI cpd. applic. in solar cells, mats. characterisation 77−77377
II-VI heterojunctions, photovoltaic effects and solar efficiency 78−52076
II-VI semiconductors, photovoltaic cell appl., recent results 78−39206
III-V compound heterojunctions, recomb. vel., appl. to $Al_xGa_{1-x}As$-$GaAs_{1-y}Sb_y$ solar cells *(Korean)* 80−54771
III-V heterojunctions, misfit dislocation banding, stress-induced birefr. 77−28542
III-V multilayer structs., contact resistance profiling method 78−56213
III-V quaternary-binary heterojunction, X-ray characterisation of defects 78−95239
III-V semiconductor heterostructures, growth and dissolution kinetics by LPE 80−49543
III-V semiconductors, defect formation, appl. in optical electronics, review 78−23160
III-V semiconductors, p-n heterostructures, epitaxial growth techniques, appl. to optoelectronics, review 80−54770
III-V semiconductors, radiative recomb. and related phenomena, conference, Prague, Czechoslovakia (Sept. 1979) 80−51940
III-V semiconductors for optoelectronic appls., review 78−30975
interface boundary position effect on interface states 78−47855
interface electronic struct., book contrib. 79−42619
interface spacing effect on interface states in heterojunctions between monatomic semicond. 79−95478
interface state electrostatic effects on carrier transport 79−78160
interface state parameters from differential admittance 77−15944
interface states, two-band-narrow gap approximation 79−24059
interface states in one-dimensional models of deformed heterojunctions 78−64100
intervalley junction is homogeneously doped semiconductor, phenomenological model 77−4433
IR detection, metal layer between two dissimilar semiconductors 77−74501
isostructural heterojunctions of organic materials 78−39194
LCAO theory of band-edge discontinuities 77−89840
LED, DH, output power and response time, thickness depend. 79−95479
misfit dislocation density in double and triple layer heterojunction devices 78−51850
MOS structure with buried layer, characterisation 79−33355
multilayer epitaxial heterostructures, use of two-photon absorption in study 79−8185
multilayer semiconductor structure, current noise 80−20302
multilayered structures, impact ionisation 80−88621
multipass heterostructures, external quantum efficiency of luminesc. 77−20419
p^+-n(n^+-p) heterojunction, optical absorpt. coeff. and minority-carrier diffusion length, differential photocurrent method of meas. 80−96896
p-n heterojunction solar cell, general formulation of current-voltage charcts. 80−80361
photochemical diode using p-n heterojunction or Schottky barrier immersed in electrolyte 77−66201
photovoltaic convertor, heterojunction phenomena and interfacial defects, review 79−74523

p-n heterojunctions continued
photovoltaic effect, solar energy convertor theory with p-n junction 78−72201
photovoltaic heterojunctions, growth and charact. 77−39931
polyacetylene, pure and doped, metal; and semicond.-semicond. junctions 79−95474
polymer system, rectification effects in dark and photocurrents 77−69407
review of semicond. heterostructures, elec. and optical phenomena, discrete devices 78−72250
Schottky layers, homogeneous avalanche breakdown instability mechanism, microplasma form. 78−72262
semiconductors with position-dependent band gap and electron affinity, current densities 77−85210
solar cell, interface state and energy barriers effect on efficiency 78−43464
solar cell model, design and evaluation 80−93964
solar cells, cryst. and polycryst. band structure and photocurrent collection 80−21402
solar cells, heterojunction thin films, survey or semi-conductor combinations 80−50974
solar cells, polycrystalline and tandem, for high efficiencies, using compound semiconductors 80−72052
solar cells, semiconductors, direct gap 79−92075
solar cells appl., props. obs. by electron beam induced currents 80−3518
superinjection in structs. with separate p-n and heterojunctions 80−50427
superlattice doping, electronic states, elec. props. 79−95480
ternary semiconductors, use in thin film heterojunction and homojunction photovoltaic devices 78−39208
thin film heterostructure, energy spectrum study 80−70787
thin film heterostructures, optical transition selection rules 80−66319
Thomas-Fermi dielectric function calcs. of anaytic charge distrib. 79−78161
transient response of DH devices approx. techniques 78−68078
zincblende semiconductors, lattice-mismatched, orientation depend. of energy band lineups 78−95344
(Al,Ga)As/GaAs, LPE grown heterostructures, X-ray diffr. exam. of interfacial elastic strains 78−72019
Al-amorphous Ge-nSi, photoelectric props. 80−70822
Al-Ga-As heterostruct. with confined current flow, fabrication 78−68081
Al-Ga-As heterostructure formation by LPE 77−32517
AlAs-GaAs, binary heterostruct. LED, external quantum yield *(Russian)* 77−8661
AlAs-GaAs (100) interface, tight binding calc. of electronic struct. 78−95342
AlAs-GaAs (110) interface, self-consistent calc. of interface states and electronic struct. 78−52066
AlAs-GaAs abrupt (110) interface, electronic struct. 78−95339
AlAs-GaAs film heterojunction, VPE growth and charcts. 78−6439
AlAs-GaAs heterojunctions, on graphite substrate, props., solar cell appls. 78−91760
AlAs-GaAs multipass heterostructure, spectral and ang. charact. of luminesc. 77−20418
AlAs-GaAs multipass heterostructures, external quantum efficiency of luminesc. 77−20419
AlAs-GaAs stripe heterojunction laser, O^+ implantation effect on threshold charcts. 79−41383
AlAs-GaAs:Ge double heterojunctions, efficiency of radiative recombination 77−77286
Al_xGa_{1-x}-GaP structure, LPE, double heterostruct. light modulator appl. 79−28963
AlGaAs DH, temp. depend. of intensities and times of radiative transitions 79−38660
AlGaAs electroluminescent heterostructures, LPE, appl. to LED fabrication 80−55308
AlGaAs, heteroepitaxial waveguides for image transmission *(Russian)* 77−11037
AlGaAs, heteroepitaxial waveguides, far radiation field charcts. *(Russian)* 77−11038
AlGaAs heterojunctions, nonradiative recomb. vel. estimate from edge luminesc. props. 80−65668
AlGaAs heterojunction photocell with luminesc. wavelength converter 80−108800
AlGaAs-GaAs, minority carrier lifetime, photon recycling effect *(Japanese)* 79−42556
AlGaAs-GaAs cascade solar-cell structure, fabrication and characteristics 79−43758
AlGaAs-GaAs heterostructures, luminescent charcts., efficiency and radiative lifetime conc. depend. 80−55151
(AlGa)As-GaAs solar cells, theoretical perform. of multi-layer grid patterns 80−55846
$Al_{0.35}Ga_{0.65}As$-GaAs N-p heterojunction diodes, current suppression by cond. band discontinuity 80−80362
$Al_{0.5}Ga_{0.5}As$-GaAs heterojunction phototransistors, growth by metalorganic vapour deposition 79−67380
$Al_{0.5}Ga_{0.5}As$-GaAs minimum heterojunction width determ. by sputter Auger techniques, interface broadening 79−69586
$Al_xGa_{1-x}As$, DH, defect generation in active regions at high optical excitation rates 79−23845
$Al_xGa_{1-x}As$ DH, origin of $n \simeq 2$ injection current, photolum. expts. 78−14799
$Al_xGa_{1-x}As$ DH p-n junction, surface recomb. effects on current, luminesc. expts. 78−72246
p-$Al_xGa_{1-x}As$, DH under optical orientation conditions, diffusion of spin labelled electrons 77−8189
$Al_xGa_{1-x}As$ epitaxial diode, neutron and γ-irrad. effects on cathodolum. in SEM 79−11473
$Al_xGa_{1-x}As$ epitaxial layers on GaAs, struct. study by scanning Auger electron microscopy 80−80110
$Al_xGa_{1-x}As$, graded band-gap heterostruct., photo-EMF 79−24072
$Al_xGa_{1-x}As$, Γ-X intervalley junctions 77−4433
$Al_xGa_{1-x}As$ heterojunction laser diode, technology and spectral charcts. 77−38885
$Al_xGa_{1-x}As$ heterojunction LED, fabrication by negative profiling of substrate and charcts. 78−56523
$Al_xGa_{1-x}As$ high-resistivity film, in n-i-n heterojunction, LPE growth 77−44179
$Al_xGa_{1-x}As$ layer, LPE, graded bond gap solar cell, composition profile, Rutherford backscatt. 78−76612

p-n heterojunctions continued
$Al_xGa_{1-x}As$ p-n junction, photolum. and current, interface recomb. effects 78−95346
$Al_xGa_{1-x}As$, p-n junction solar cells, effect of interface recombination on photoluminescence and current 80−93893
$Al_xGa_{1-x}As$, waveguide heterostruct. epitaxial growth with gradual composition change 79−42416
$Al_xGa_{1-x}As$-GaAs, Auger depth profiling 77−89657
$Al_xGa_{1-x}As$-GaAs, epitaxial heterostructure, influence of defects on diffusive distrib. of group I impurities 78−43045
$Al_xGa_{1-x}As$-GaAs, MBE, diffusion across interface, optical annealing expts. 78−2305
$Al_xGa_{1-x}As$-GaAs, p-n heterojunction laser, low temp. operation 80−1204
$Al_xGa_{1-x}As$-GaAs, p-n heterostruct. laser, tunnel injection and phonon-assisted recomb. 80−5733
$Al_xGa_{1-x}As$-GaAs DH photodetector, optical power conversion at 8500 Å and I-V characts. 77−87833
$Al_xGa_{1-x}As$-GaAs heterostructure, effect of photon recycling on diffusion length and internal quantum efficiency 77−39929
$Al_xGa_{1-x}As$-GaAs heterostructure photoluminesc., origin of large dark spots 77−85763
$Al_xGa_{1-x}As$-GaAs heterostructures, nonradiative large dark spots exam. 78−23149
$Al_xGa_{1-x}As$-GaAs heterojunction photodiodes, high-efficiency fast-response 78−52073
$Al_xGa_{1-x}As$-GaAs heterostructures, MO-CVD, phonon assisted recomb. and stimulated emission 80−1205
$Al_xGa_{1-x}As$-GaAs heterostructure, quantum-well, hot electrons and phonons 80−84505
$Al_xGa_{1-x}As$-GaAs heterostruct., varizonal, parameter determ. by photoluminescence method *(Russian)* 80−108291
$Al_xGa_{1-x}As$-GaAs LED design and characterisation for fibre-optic communications 78−46796
$Al_xGa_{1-x}As$-GaAs multilayer heterostructures, optical birefringence 78−64422
$Al_xGa_{1-x}As$-GaAs quantum-well heterostruct., exciton in recomb. 80−103990
$Al_xGa_{1-x}As$-$GaAs_{1-y}Sb_y$ solar cells, appl. of recomb. vel. at III-V cpd. heterojunctions *(Korean)* 80−54771
p-$Al_xGa_{1-x}As$-n-GaAs solar cells, optical characts. study 77−24609
AlGaAsSb LPE growth, lattice-matched to GaSb, characterisation 80−60794
AlGaAsSb, photodiode, lattice-matched to GaSb 79−71527
$Al_xGa_{1-y}As_{1-x}Sb_x$ heterostructure, electroluminesc., appl. to LED's 77−8663
$Al_yGa_{1-y}As_{1-x}Sb_x$-$Ga_{1-z}Sb_z$ buried heterojunction electroabsorption modulation 78−55439
$Al_xGa_{1-x}AsZn$-GaAs solar cells by LPE, open circuit voltage, fill factor 80−101108
AlGaSb, growth and characts. for 1.0-1.8 μm heterojunction devices 78−6870
AlGaSbAs heterostructures and LED's luminesc. props. in 1-2 micron band 78−10988
As-Te-Ge/n-Si, film on cryst., heterojunction, elec. and photovolt. props. 80−100514
As_2Te_3-GaAs, amorphous-monocrystalline heterojunctions, space charge limited conduction 78−64099
Au-$Al_{0.5}Ga_{0.5}As$ -GaAs heterojunction Schottky-barrier solar cells, barrier height enhancement 80−85284
Au-AlGaAs-GaAs heterojunction Schottky barrier solar cells, barrier height enhancement 80−94071
BP-Si, VPE growth of BP, device appls. 78−56585
BP-Si junctions epitaxial growth and device appls. 78−48333
$CdGeAs_2$-$ZnGeAs_2$, and $CdGeAs_2$-$GdGeP_2$, material distrib., possibility of heterostructure *(Russian)* 78−30979
n-$CdGeP_2$-p-$CdGeAs_2$ heterojunction photocells, polarisation-sensitive 80−11075
n-$CdIn_2S_4$/p-$CuInSe_2$ heterostructure, form. and photovolt. meas. 80−10831
CdS, for thin film and ceramic solar energy convertors 80−93870
CdS heterojunction solar cells by CVD method 80−45685
CdS sprayed thin films for CdS-Cu_2S heterojunction solar cells 79−61988
CdS/Cu_2S heterojunction solar cells, optimal material props. theory and experimental verification 80−45686
CdS/Cu_2S heterojunction solar cells diffusion length determ. using minority carrier SEM 80−61359
CdS/Cu_2S solar cell fabrication, performance rel. to Cu_2S mats. props. 77−77426
CdS/Cu_2S thin film heterojunctions, photocapacitance meas. of solar cell parameters 80−93897
n-CdS/n-InP/p-InP heteroface solar cell with ultrathin window layer, computer anal. 80−97788
n-CdS/p-$ZnIn_2Se_4$ thin film solar cell, photovoltaic props. 80−89628
CdS-CdTe p-n junction screen printed thin film solar cells 80−72055
CdS-CdTe solar cells fabrication, thin film *(Japanese)* 79−87992
CdS-CdTe-Te, effect of low cond. CdTe interlayer on charact. 80−44721
CdS-Cu_2S, thin film heterojunction, dark I-V characts. and heat treatment 79−56294
CdS-Cu_2S heterojunction, influence of surface recomb. on photoelec. props. 77−43711
CdS-Cu_2S heterojunction, slow relax. of photocurrent 78−26943
CdS-Cu_2S heterojunction, energy-band struct., capacitance-voltage characts., illumination effects 80−96982
CdS-Cu_2S junctions, carrier trap density, deep level defects 80−107801
CdS-Cu_2S single cryst. heterojunction, trap depths in depletion region 78−52064
CdS-Cu_2S solar cells, microstructural study of heterojunction materials 80−93978
CdS-Cu_xS heterojunctions produced by RF sputtering, for thin film solar cells 79−100053
CdS-Cu_xS solar cell, prep. and characts. *(Croatian)* 80−93876
CdS-CuI film heterojunction photocells, prep., photoelec. props. 78−80044
CdS-$CuInSe_2$, solar cell, grain boundary effects on performance 79−83603
CdS-GaAs, junction current transmission mechanism *(Russian)* 77−39924
CdS-GaAs, prep. by CdS CVD and etching 78−52062

p-n heterojunctions continued
CdS-Ge, grown by chemical transport, props., 77−4422
CdS-InP n-p heterodiodes, junction props. using injection electroluminescence 79−82667
CdS-InP(CdTe)(GaAs)(Ge), solar cell heterojunctions, CVD fabrication, photovoltaic response 80−93878
CdS-PbS, photoresistive props. 80−6970
CdS-PbTe and CdS-Te, electron irrad. effect on electrophys. props., prep. conditions depend. 79−28421
CdS-Te, effect of low cond. CdTe interlayer on charact. 80−44721
CdS-Te-Ge heterojunction, prep. photosensitivity, and negative cond., 77K *(German)* 77−20413
CdSb heterojunction, formation by laser irradiation, photoelec. meas. *(Russian)* 77−76915
CdSe, for thin film and ceramic solar energy convertors 80−93870
CdSe-Ge (111) heterojunctions, epitaxial, azimuthal rotation 78−84085
CdSe-Sb_2Se_3 heterojunction, photoelec. props. 80−70816
$CdSiAs_2$ chalcopyrite photovoltaic material 79−74526
$CdSnAs_2$-InP, n-p heterojunction, elec. props., electroluminesc., band struct. 80−75632
$CdSnAs_2$-$ZnSnAs_2$, and $CdSnAs_2$-$CdSnP_2$, material distrib., possibility of heterostructure *(Russian)* 78−30979
CdTe/$Hg_{1-x}Cd_xTe$ multilayers, LPE growth 80−80104
CdTe-CdS, closed-tube vapour growth 80−55302
CdTe-CdS, photovoltaic energy conversion, solar efficiency 77−43700
CdTe-CdS heterojunctions, growth by closed-tube chem. transport, elec. props. 80−60070
CdTe-CdS heterojunction, photocapacitance and photocond. 80−96978
CdTe-CdS p-n film heterojunction, photoelectric props. 79−39298
CdTe-CdS p-n heterojunction, coordinate sensitive photoelements, longitudinal photovoltage 79−95440
CdTe-CdS photocell, photocurrent and max. efficiency calc. 79−39295
CdTe-CdS thin film p-n solar cells, spectral response temp. depend. 80−93871
CdTe-Ge heterojunction, photoelec. props., sensitivity in near IR region *(Russian)* 77−69405
CdTe-Si heterojunctions, epitaxy and electrical props. *(Japanese)* 77−32074
(CdZn)S-Cu_2S solar cell, film form. and characts. 78−68080
$Cd_{1-x}Zn_xS/Cu_2S$ thin film heterojunction solar cells, operational charact. 80−45687
$Cd_{1-x}Zn_xS$-p-GaAs, electrical and photovolt. props. 80−29466
$Cd_{1-x}Zn_xS$-PbS heterojunctions prepared by spray pyrolysis 79−60917
$Cd_xZn_{1-z}S$-Cu_2S, heterojunction interface double layer, dislocation field, charge compensation 79−7855
P-Cu_{2-x}-n-CdS, heterojunction, energy band diagram 79−24070
$CuGa_{0.5}In_{0.5}Se_2/Zn_{0.29}Cd_{0.71}S$ heterojunction solar cell, preparation and props. 80−101110
$CuGaS_2$-ZnS heterojunction, for LED appl., prep. and characterisation 79−1831
$CuInSe_2$-CdS, photovoltaic effect, rel. to optimum conditions for solar cell fabrication 77−51810
Cu_2O/Si, solar cell applic. 79−7914
Cu_2S/CdS solar cells, thin film, sputtered 79−43774
Cu_2S-CdS, elec. and photoelec. characts., effect of etching of CdS 78−80048
Cu_2S-CdS, photovoltaic junction, prep. by chemical deposition 79−66019
Cu_2S-CdS, role of deep levels in controlling photovoltaic props. 80−92941
Cu_2S-CdS, solar cell, photocurrent, spectral depend. 79−7853
Cu_2S-CdS film junction formation by dry-barrier process 78−64109
Cu_2S-CdS heterojunction characteristics and CdS polarity *(Japanese)* 78−23154
Cu_2S-CdS heterojunction model 78−39205
Cu_2S-CdS heterojunctions, electron trap characterisation by capacitance transient meas. 79−78163
Cu_2S-CdS heterojunction diodes, barrier model estimated from photovoltage and cathodoluminesc. spectra 79−78165
Cu_2S-CdS heterojunction solar cell, interface recomb. vel. determ. by capacitance/collection efficiency variation 80−50959
Cu_2S-CdS heterojunction solar cells, carrier transport, nonmonotonic band profiles 80−61361
Cu_2S-CdS heterojunction interface, depth distribution profiles, Auger spectra 80−88622
Cu_2S-CdS heterophotocells based on CdS films of stoichiometric composition, elec. and photoelec. props. 80−93873
Cu_2S-CdS p-i-n structure diode, photoelec. characts. 78−2557
Cu_2S-CdS photocell, thin film structure, props., manufacture 77−51806
Cu_2S-CdS solar cell fabrication by magnetron reactive sputtering deposition 80−61363
Cu_2S-CdS solar cells, interface recombination phenomena and tunnel effect 80−66978
Cu_2S-CdS solar cells, thin film fabrication processes and conduction mechanism, review 79−74522
Cu_2S-CdS thin film heterojunctions, base doping effect on elec. and photoelec. props. 78−80043
Cu_2S-CdS thin film planar junction devices, quantitative photon loss anal. 80−61362
Cu_2S-Zn_xCd_{1-x}, heterojunction, composition meas. near interface using aqueous ion-exchange 80−29465
Cu_2S-$Zn_xCd_{1-x}S$ heterojunction, improved model of electro-optic behaviour 80−94023
$Cu_{2-x}S$, single cryst., as p-component of heterojunction, props. 77−39926
$Cu_{2-x}S$/CdS heterostructures, heat treated, capacitance voltage meas. anal. 80−20292
$Cu_{2-x}S$-CdS, chem. formed heterojunction, photosensitivity characts. of $Cu_{2-x}S$ 78−72199
$Cu_{2-x}S$-CdS, copper sulphide growth features during formation *(Russian)* 80−107898
$Cu_{2-x}S$-CdS, solns. cell, photo-emf, depend. on degree of doping of CdS 79−52934
$Cu_{2-x}S$-CdS heterojunction, current flow characts. and energy band struct. 77−43709
$Cu_{2-x}S$-CdS heterojunction V-I characteristic and max. photovoltage, long-term changes *(Russian)* 78−43468
$Cu_{2-x}S$-CdS heterojunctions, nature of longwave photo EMF 78−84284
$Cu_{2-x}S$-CdS junction, low temp. growth, AES obs. 79−28924
$Cu_{2-x}S$-CdS p-n heterojunction solar cells, props., Burstein-Moss effects 80−21404

p-n heterojunctions continued
$Cu_{2-x}S$-CdS p-n heterojunction, optical energy convertor, struct. and recomb. props. 80−72065
$Cu_{2-x}S$-CdS solar cells, fabrication and features *(Korean)* 79−60916
Cu_xS-CdS, electron diffr. obs. of phases of Cu_xS on CdS substrate 78−51847
Cu_xS-CdS, reactively sputtered, solar cell applic. 79−11256
Cu_xS-CdS heterojunction solar cells spectral distrib. and photocapacitance 80−55864
Cu_xS-CdS solar cell, minority carrier diffusion length, SEM determ. 77−72911
Cu_xS-CdS solar cell, p-n junction shape and struct. 77−55599
Cu_xS-CdS solar cell junction formation and open-circuit voltage 79−61986
Cu_xS-CdS solar cells, SEM parameter meas. for space charge region recombination 80−16808
Cu_xS-CdS solar cells, SCL current 80−76634
Cu_2S(Se)-CdS(Se) p-n heterophotoelements of optronic converters, props. on X-irrad. of scintillator 80−34505
Cu_2Se-$AgInSe_2$ heterojunction, photodetection props. 78−39195
$Cu_{2-x}Se$, single cryst., as p-component of heterojunction, props. 77−39926
p-Cu_2Sn-n-ZnS heterojunction, I-V characts., photocond. and electrolum. 78−72251
$Cu_{2-x}Te$, single cryst., p-component of heterojunction, props. 77−39926
$Cu_{2-x}Te$-CdSe, elec. and opt. props. *(Korean)* 77−51811
(Ga, Al, As) heterostructures and compounds, electronic props., empirical pseudopot. calc. 80−80366
Ga-GaAs heterojunctions, electronic struct., tight-binding and pseudopot. models 79−42633
Ga-In-As-Sb quaternary system, phase equilib. and heterojunctions 79−34016
GaAlAs based, integrated optics appl., technology advancements and heterostructure types *(Slovak)* 80−33226
(GaAl)As, LPE, GaAs dissolution kinetic in undersaturated isothermal solns. in Ga-Al-As system 80−80106
GaAlAs light intensity modulators using p-n junctions 80−99871
GaAlAs p-n heterostructures, current-flow mechanisms, luminesc. spectra 80−20298
GaAlAs/GaAs solar cells, efficiency optimisation at high and low current levels *(French)* 80−61348
GaAlAs-GaAs, laser fabrication, using horizontal and vertical LPE furnaces 77−42538
(GaAl)As-GaAs concentrator solar cells, series resistance effects 79−57427
GaAlAs-GaAs double heterostructure, interfacial recomb. velocity, photolum. meas. 78−68075
GaAlAs-GaAs heterojunction prep., Zn conc. effect in epitaxial layer, high-power IR emission *(Spanish)* 77−39932
GaAlAs-GaAs heterojunction solar cells, high temp. props. 25 to 300°C 80−94035
$Ga_{0.5}Al_{0.5}As$-GaAs, DH, interfacial recomb., photolum. time decay meas. 78−95347
$Ga_{0.9}Al_{0.1}As$, nucleation morphologies on $Ga_{0.65}Al_{0.35}As$ surfaces grown by LPE 78−15323
$Ga_{1-x}Al_xAs$ based layer structures, optimum growth conditions, comp. and struct. perfection 80−104069
$Ga_{1-x}Al_xAs$ heterostructure, LPE prep., growth and dissolution kinetics, thermodynamic and kinetic models 80−75456
$Ga_{1-x}Al_xAs$, p^+-n-n^+ heterostructure, distrib. of injected carriers, forward V-I characts. *(Russian)* 80−6973
$Ga_{1-x}Al_xAs$:Si, linear-gradient, barrier capacitance 77−43705
$Ga_{1-x}Al_xAs$/GaAs heterostructure solar cell design for space usage 79−96450
$Ga_{1-x}Al_xAs$-$Ga_{1-y}Al_yAs$, minority carrier lifetime, elec. charcts. and electrolum. meas. 78−2554
$Ga_{1-x}Al_xAs$-GaAs heterojunctions grown by metallorganic CVD 80−15599
$Ga_{1-x}Al_xAs$-GaAs p-n and p-p-n heterojunction solar cells, high efficiency, prep., eval. and characters *(Japanese)* 80−61342
$Ga_{1-x}Al_xAs$-GaAs p-n structures, variable-gap front layer, photoelec. props. 79−7884
$Ga_{1-x}Al_xAs$-GaAs solar cell, deep level obs. 77−89834
$Ga_{1-x}Al_xAs$-GaAs:Si, momentum distrib. of valence electrons, positron annihilation meas. 79−51530
$Ga_{1-x}Al_xAs$-GaAs-GaAs, p-p-n junctions, variable gap solar photocell with coordinate depend. band gap gradient 79−11213
$Ga_{1-x}Al_xAs_{1-y}P_y$-GaAs, light-induced misfit dislocation motion, photoluminesc. and X-ray diffr. meas. 79−11200
$Ga_{1-x}Al_xAs_{1-y}P_y$ epitaxial layer heterojunction, nonradiative recombination at misfit dislocations 80−96901
$Ga_{1-x}Al_xAs_{1-y}P_y$-GaAs quaternary heterojunction strains and IR laser diode performance 78−9385
GaAlAsSb-GaSb p-n heterojunction CCD; charge transfer, charge exchange 80−65658
$Ga_{1-x}Al_xSb$ p-n structure, variable-gap, elec., photoelec. and electrolum. props. 77−11996
$Ga_{1-x}Al_xSb$ p-n structure, variable-gap, electroluminescence 78−52582
GaAs integrated multijunction photodetector with high output voltage 79−6178
GaAs, lightly doped, p-n structure, parameters of nonequilib. carriers, transient photoeffect method 79−11143
GaAs n-p solar cells, theoretical perform. of multi-layer grid patterns 80−55846
GaAs, solar cell, thin film, prep. by Peeled Film Technology 79−29472
GaAs solar cell structs., photoluminesc. props. 80−50958
GaAs:Si, heteroface solar cells, diffusion lengths 78−47849
GaAs:Zn-$Al_{0.5}Ga_{0.5}As$ p-n junction, surface layer effect on surface recombination current 79−69585
GaAs/$Al_xGa_{1-x}As$ heterostruct., anomalous elec. and optical characts. 80−2865
GaAs/III-V solid soln. heterostructure composition profile by photoemission microanalysis 80−44717
GaAs-$Al_{0.4}Ga_{0.6}As$, p-n heterojunction, quantum confinement and compositional grading effects on band struct. 79−87151
GaAs-$Al_xGa_{1-x}As$, coupled-waveguide optical modulator, high freq. modulation 77−75678
GaAs-$Al_xGa_{1-x}As$, MBE grown, photocollection efficiency and interface charges 79−11199
GaAs-$Al_xGa_{1-x}As$, negative differential resist., real-space electron transfer 80−6958

p-n heterojunctions continued
GaAs-$Al_xGa_{1-x}As$, heterojunction and superlattice, magnetophonon reson., polaron mass 80−44715
GaAs-$Al_xGa_{1-x}As$ double heterojunctions, dark-line defects and recomb. centres, scanning photocurrent microscopy 79−35822
GaAs-$Al_xGa_{1-x}As$ heterostructure superlattice, construction of bound states in continuum 77−32076
GaAs-$Al_xGa_{1-x}As$ heterojunction, avalanche phototransistors, detectivity and noise 78−2558
GaAs-$Al_xGa_{1-x}As$ heterostruct., photon recycling, diffusion length and lifetime determ. 79−47499
GaAs-$Al_xGa_{1-x}As$ heterojunctions, LPE grown, 2D electron gas obs. 79−99606
GaAs-$Al_xGa_{1-x}As$ heterojunction interface, two-dimensional hole gas obs., Shubnikov-de Haas meas. 80−80357
GaAs-$Al_xGa_{1-x}As$ heterostructures, real-space electron transfer by thermionic emission, analytical model 80−100512
GaAs-$Al_xGa_{1-x}As$ LPE heterojunction, interface states 78−19128
GaAs-$Al_xGa_{1-x}As$ optical modulator for coupled-waveguides 78−71235
GaAs-$Al_xGa_{1-x}As$ superlattice, electronic props. 80−11080
GaAs-$Al_xGa_{1-x}As_x$, heterojunction photodiode, electric and photoelectric characts. 77−55604
GaAs-$Al_xGa_{1-x}As$-GaP photocathodes, minority carrier diffusion length determ. by photoluminesc. 80−103992
GaAs-AlAs, formation by VPE growth of n-AlAs on GaAs 77−1814
GaAs-AlAs, heterolight diodes, mesoconstruction, output *(Russian)* 77−12441
GaAs-AlAs, heterostructure, effects of cation order on energy bands 80−11081
GaAs-AlAs, large area, vapour phase epitaxially grown, elec. characterisation 77−11990
GaAs-AlAs and related monolayer heterostructures, pseudopot. calc. 78−60198
GaAs-AlAs heterojunction, recombination currents 78−14806
GaAs-AlGaAs DH layers, tapered growth by wipingless LPE 77−66594
GaAs-AlGaAs heterojunction superlattices, electron mobilities 80−29473
GaAs-AlGaAs heterojunction superlattices, obs. of intersubband excitations in multilayer two dimensional electron gas 80−29753
GaAs-AlGaAs heterostructure thyristors, operation and elec. characts. 79−7891
GaAs-AlGaAs solar cells *(Rumanian)* 80−93877
GaAs-AlGaAs superlattices, inelastic light scatt. by two-dimens. electron gas 80−93360
GaAs-AlGaAs:Si heterojunction interface, two-dimens. electron gas, Hall effect and cyclotron reson. meas. 79−65530
GaAs-$Ga_{1-x}Al_xAs$, DH, improved LPE growth method 77−4746
GaAs-$Ga_{1-x}Al_xAs$ DH lasers, electron beam induced current microscopy 80−95899
GaAs-$Ga_{1-x}Al_xAs$ heterostruct. superlattice, props. in high mag. fields 79−73570
GaAs-$Ga_{1-x}Al_xAs$ heterostructures, quantum size effect in superlattices, electronic props. 80−29471
GaAs-$Ga_{1-x}Al_xAs$ multilayer struct., growth over preferentially etched channels, MBE 77−40388
GaAs-$Ga_{1-x}Al_xAs$ superlattices, resonance enhanced Umklapp Raman process 78−39547
GaAs-$Ga_{1-x}Al_xAs$ variable gap p-n junction, variable gap and photo EMFs 80−15596
GaAs-$Ga_{1-x}Al_xGaAs$ heterostructure, electron tunnelling theory 78−47861
GaAs-$Ga_{1-x}In_xAs$ heterojunction, thermally assisted tunnelling 78−19136
GaAs-$Ga_{2.2}Al_{0.8}As$:Be, LPE, diffusion of Be into GaAs substrate 80−103517
GaAs-$Ga_xAl_{1-x}As$, Cu doped, spatial distrib. of nonradiative defects, STEM imaging spectroscopic technique 77−89438
GaAs-$Ga_xAl_{1-x}As$ DH laser material crystal cathodoluminescence, SEM analysis 80−97349
GaAs-$Ga_xAl_{1-x}As$ heterostructure, depend. of efficiency of radiative transitions on composition 78−2909
GaAs-$Ga_xAl_{1-x}As$ superlattice, photoconductor with high sensitivity and reduced dark current appl. 79−7881
GaAs-$Ga_xIn_{1-x}P$ heterostructure, elastic stresses and substrate/epitaxial film mismatch, X-ray diffr. method 80−92794
GaAs-GaAlAs, GaAs preferential etching, using O_2 and CCl_2F_2 mixture 79−8373
GaAs-GaAlAs, growth by metal-alkyl-hydride process 78−15313
GaAs-GaAlAs, superlattice, subband related anisotropy in negative magnetoresistivity 80−11082
GaAs-GaAlAs (100) abrupt interface, carrier transmission and refl. coeffs. 79−69588
GaAs-GaAlAs (100) interfaces, carrier transport coeffs., tight binding calc. 80−49889
GaAs-GaAlAs DH LEDs, with thin active layer, Burrus type, internal interference in emission spectrum 78−27325
GaAs-GaAlAs DH LED, transient current trap spectroscopy 78−80049
GaAs-GaAlAs double heterostruct., self-absorpt. effects on radiative lifetime 77−39928
GaAs-GaAlAs LPE layers, DH material, TEM obs. of crystal defects 78−6241
GaAs-GaAlAs multilayer struct., Hall mobility enhancement 80−100511
GaAs-GaAlAs superlattices, metalorganic VPE growth, in sites ellipsometry monitoring 80−70547
GaAs-GaAlAs wafers, defects and degradation, transmission cathodolum. evaluation 80−65395
n-GaAs-GaAs:Cr. semiinsulating, low freq. current pulses 77−8176
GaAs-GaInAs structure, dislocation struct., TEM anal., appl. as IR LED 80−70206
GaAs-GaP heterostructure, radiative recomb. under influence of mech. stresses 80−66291
GaAs-GaP(InSe), electronic processes *(Russian)* 79−56312
GaAs-GaSe n-p heterojunction, elec. props., interface states 80−65670
GaAs-Ge, electronic struct., self-consistent calc. 77−24611
GaAs-Ge, heterostructure, zincblende-on-diamond type systems, MBE growth, (110) orientation as preferred orientation 80−80099
GaAs-Ge heterojunction, band discontinuities, angle-resolved UPS obs. 79−7878
GaAs-$Ge_{1-x}(GaAs)_X$ n-p heterojunctions, hydrostatic press. effect on elect. and photoelectric props. 80−20304
GaAs-InP heterojunction laser output wavelength control 80−74384
GaAs-InSe p-n junctions, 'optical' contacts, elec. props. 78−56222

p-n heterojunctions continued
GaAs-n-$Al_xGa_{1-x}As$ heterojunctions, selectively doped, FET 80−80364
p'-GaAs-n-(Ga,In)As heterostructure, thermally assisted tunnelling currents 77−20412
GaAs-Si heterojunction, IR quenching of photocapacitance 80−92968
GaAs-ZnS, struct., multibeam electron microscopy obs. 79−11031
GaAs-ZnSe (110) interface, electronic struct., self-consistent calc. 79−95486
GaAs-ZnSe heterojunction, elec. and photoelec. props. *(Russian)* 77−32070
$Ga_{1-x}As(Al,In)_x$, heterojunction solar cells, optimum bandgap, computer anal. 79−43767
$GaAs_{1-x}P_x$ heterostructure, LPE prep., growth and dissolution kinetics, thermodynamic and kinetic models 80−75456
$GaAs_{1-x}P_x$-GaP heterostructure, photomodulation spectroscopic exam. 77−40257
$GaAs_{1-x}Sb_x$, narrow-gap film on wide-gap GaAs, energy gap grading, optical transmission meas. 77−20943
p-$(GaAs)_x(ZnSe)_{1-x}$-nn^+-GaAs, avalanche heterojunctions, inverse branch of volt ampere characts. *(Russian)* 80−6974
$Ga_yIn_{1-y}As_xP_{1-x}$-InP heterostructure, lattice matching and cryst. perfection 78−6437
$Ga_xIn_{1-x}As$ p-n junction, growth and electrolum. spectra 77−20420
$Ga_xIn_{1-x}As$-InP heterostructure, growth by MBE 79−8251
$Ga_{1-x}In_xAs_{1-y}P_y$-InP DH lasers, 1000-hour CW operation 78−1265
$Ga_xIn_{1-x}As_yP_{1-y}$/GaAs structure, LPE growth and lattice consts. matching conditions 80−59822
GaInPAs heterostructures and LED's, luminescent props. in 1-2 micron band 78−10988
$Ga_{1-x}In_xSb$-$Ga_{1-y}In_ySb$, heterojunction parameters 80−50550
$Ga_xIn_{1-x}Sb$ p-n junction photodiode fabrication, sensitivity as 1 to 2.5 μm detectors *(Japanese)* 80−52311
GaP-GaAlP, heterojunction cold cathode 79−69965
GaP-GaAs, amorphous film/crystal junction, optical and elec. props. 79−99611
GaP-Si, heteroepitaxial growth, electronic and optical props. 80−104075
GaP-Si, heterostructure, zincblende-on-diamond type systems, MBE growth, (110) orientation as preferred orientation 80−80099
GaP-Si heterojunction solar cell, computer simulation 79−74529
GaP-ZnSe heterojunction, elec. and photoelec. props. *(Russian)* 77−32070
$(GaP)_x(ZnSe)_{1-x}$/GaP, epitaxial heterostructures, chem. microinhomogeneity 77−80831
GaSb-$Ga_{1-x}In_xSb$, electrolum. spectra and elec. props. 77−12444
$GaSb_{1-x}As_x$-$In_{1-x}Ga_xAs$ heterojunction, prep. by MBE, transport props. 77−80827
p-GaSb−n-$Ga_{1-x}Al_xSb$, photodiode, LPE, spectral response, quantum efficiency 78−47850
GaSe-InSe, electronic processes *(Russian)* 79−56312
GaSe-InSe, heterostructure fabrication using laser radiation 79−73580
GaSe-SnO_2 heterojunction, elec. props. and electrolum. spectra 77−59328
Ga_xSe_{1-x}-SnO_2 heterostruct., amorphous, photovoltaic effect 78−14803
GaSe(Te)-SnO_2 spray heterojunction, electro-optical props. 78−64102
GdS-InP, prep. by CdS CVD and etching 78−52062
Ge/GaAs (110) heterojunction, valence band discontinuity in XPS spectra, precise determ. 80−84834
Ge-Al (Sb) amorphous film junction, I-V and C-V characts. 77−85307
Ge-GaAs, (100) interface, electronic struct. calc. 80−49861
Ge-GaAs, electrostatic dipole shifts contrib. to valence band discontinuities 79−51657
Ge-GaAs, heterojunction, electronic structure 79−73572
Ge-GaAs, p-n heterojunctions, surface electron states 79−73578
Ge-GaAs, p-nn^+ junction, I-V characts., inverse branch, effect of dislocation defects *(Russian)* 79−15217
Ge-GaAs (100) interface, electronic struct., scattering-theoretic approach 78−95340
Ge-GaAs (110), heterojunction chemistry, photoemission expts. 78−95244
Ge-GaAs (110) interface, self-consistent calc. of interface states and electronic struct. 78−52066
Ge-GaAs abrupt (110) interface, electronic struct. 78−95339
Ge-GaAs abrupt interface, electronic struct., self-consistent wave mechanical calcs. 77−89837
Ge-GaAs abrupt interface, orientation depend. of interface dipole energies, XPS expts. 78−39196
Ge-GaAs heterojunction, elec. and recomb. props., interface defect effects 80−80365
Ge-GaAs heterojunction, interface geometry, model 80−49879
Ge-GaAs heterojunctions, electronic struct. 78−19138
Ge-GaAs heterojunctions, effect of γ-radiation on current-voltage charact. *(Russian)* 80−2459
Ge-GaAs interface, electronic struct. of Ge overlayers on (100) GaAs 80−49880
Ge-GaAs interface, XPS obs. of electronic struct. 78−95341
Ge-GaAs p-n heterojunction, current fluctuations 79−11209
Ge-GaAs p-n junction, microparameters determ. 79−11216
Ge-GaAs structure, electronic struct., ang.-resolved photoemission obs. 80−49881
Ge-GaAs superlattice and interface, electronic struct. 78−52065
p^+-Ge-n-GaAs abrupt heterojunction, reverse currents *(Russian)* 78−10542
p-Ge-nn^+-Si, heterojunction, γ-radiation effect on forward I-V characteristics *(Russian)* 78−72255
$Ge-Pb_{1-x}Sn_xTe$, amorphous/crystalline heterojunction, rectification props., IR detector appl. *(Japanese)* 78−60197
Ge-Si, UHV-produced epitaxial structs., electrophys. props. 78−3060
Ge-Si(GaAs) heterodiodes, interfacial structural defects effect on avalanche breakdown 79−42644
Ge-Te-Se/Si amorphous film-cryst. heterojunction, electron-beam-induced current 79−24060
Ge-ZnSe, (100) interface, electronic struct. calc. 80−49861
Ge-ZnSe, effect of interfacial condition on optoelectronic props. 79−24061
Ge-ZnSe abrupt (110) interface, electronic struct. 78−95339
Ge-ZnSe heterojunction, change in interfacial microstruct. on high temp. annealing 77−28242
Ge-ZnSe heterojunction, elec. and photoelec. props. *(Russian)* 77−32070
$Ge_{20}Te_2Se_{80-x}Si$, amorphous-cryst. heterojunctions 79−65546

p-n heterojunctions continued
HgCdTe, 0.1 eV photodetector performance background dependence 77−32038
HgCdTe, 0.1 eV photodetector performance 77−32039
HgCdTe-CdTe photodiode, 1.33 μm, grown by LPE, phys. props. 80−107892
$HgCr_2Se_4$-$CdIn_2S_4$, prep. and photovoltaic prop. 78−34892
$HgCr_2Se_4$-$CdIn_2S_4$ heterojunction, prep. and photovoltaic prop. *(Japanese)* 78−34889
HgSe/CdSe lattice-matched heterostructs. as Schottky barriers, CVD epitaxial growth and elec. props. 80−49877
HgSe-Se, photo-field model, rel. to anomalous photocond. in Se:Hg 77−43658
n-$(In,Sn)O_x$-p-InP solar cell, growth, efficiency 77−72910
InAs, on GaAs, heteroepitaxial layers, compositional profile, AES 77−20212
InAs-$Al_xGa_{1-x}Sb$ heterojunctions, elec. and photoelec. props. 79−11206
InAs-GaSb (110), electronic states, Green's function technique, tight binding approx. 80−49855
InAs-GaSb heterojunction, photoelec. props. 77−28245
InAs-GaSb heterostruct. superlattice, props. in high mag. fields 79−73570
InAsSb/GaSb broad-spectral-band IR detector, backside-illum. heterostructure approach 80−73450
$InAs_{1-x}Sb_x$-InAs stepwise-graded struct., steady-state LPE, etching, investig. 77−21042
InGaAs-GaSbAs periodic structures, with controlled emission 79−7880
InGaAs-InP heterojunction detector for 1.0-1.7 μm wavelength range 78−49895
p-$In_{0.53}Ga_{0.47}As$:Zn on InP, elec. and optical props. 80−75662
$In_{0.53}Ga_{0.47}As$-InP heterostructure, LPE growth 80−11582
$In_{1-x}Ga_xAs$-$GaSb_{1-y}As_y$, new heterostruct. characts. 78−72247
$In_{1-x}Ga_xAs$-$GaSb_{1-y}As_y$ superfine heterostruct., MBE 78−95348
$In_{1-x}Ga_xAs$-$GaSb_{1-y}As_y$ superlattice, with nonlinear energy-wave and energy-momentum relationships 79−7871
InGaAsP DH, luminesc., quantum efficiency determ. 80−108273
InGaAsP heterojunction cathode, transferred electron photoemission 78−48272
InGaAsP LPE heterostructs., interface grading, Auger depth profile 80−103585
InGaAsP, lattice-matched, LPE growth on (100) InP, heterojunction photodiodes fabricated 78−64483
InGaAsP/InP DH, vapour phase growth by dual-growth-chamber method 80−50559
InGaAsP-InP, anomalous luminesc., near heterojunction interface 79−65932
InGaAsP-InP, LPE grown, impurity effect on surface morphology 80−29291
InGaAsP-InP DH lasers, temp. dependence of threshold and elect. characts. 80−99725
InGaAsP-InP heterojunction, LPE, lattice mismatch, Auger depth profile 79−87005
InGaAsP-InP high-gain heterojunction phototransistor 80−103745
InGaAsP-InP lattice-matched heterojunction, LPE growth and characterisation 77−21041
$In_xGa_{1-x}As_xP_{1-x}$-InP photodetectors, construction and performance 78−65966
InGaAsSb, LPE growth, and appl. in GaSb/AlGaAsSb/InGaAsSb/AlGaAsSb/GaSb DH 80−16205
$In_{0.5}Ga_{0.5}P$-GaAs, interfacial recomb. vel. determ. 77−51809
$In_{1-y}Ga_yP$-GaAs, VPE, energy band gap and lattice parameter, lattice mismatch effects 78−95345
$In_{1-x}Ga_xP_{1-z}As_z$, DH, diode and laser performance, limitations of direct-indirect transition 77−39927
$In_{1-x}Ga_xP_{1-z}As_z$ well in InP, tunnel injection into confined particle states 78−19130
$In_{1-x}Ga_xP_{1-z}As_z$-$GaAs_{1-x}P_x$:N, N_x and N_Γ bound states, electroluminesc. meas. 77−11870
$In_{1-x}Ga_xP_{1-z}As_z$-InP, LPE heterojunctions, lattice matching and dislocations 78−23150
In_2O_3:Sn-Si, current mechanisms and barrier height 80−11083
n-In_2O_3/p-InP solar cell, photovolt. effects 80−12014
In_2O_3-Si highly photosensitive diodes, and their appl. 78−23152
In_2O_3-Si(Ge)(GaAs)(InP) heterostructure solar cells, photovoltaic and rectifying props., electron affinity determ. 79−1618
In_2O_3-SnO_2 film on Si, heterojunction, photovoltaic effect, sunlight induced 77−1470
In_2O_3-SnO_2/InP junction, ion probe analysis of chemical nature 79−73411
In_2O_3-SnO_2-InP solar cell junctions, efficiency, InP surface props. 80−85288
In_2O_3-SnO_2-Si heterojunctions, elec. and photovoltaic characts. 78−52070
$InP/In_{1-x}Ga_xAs_yP_{1-y}$ heterostruct., optically induced degradation 79−86791
$InP/In_xGa_{1-x}As_yP_{1-y}$ interfaces, sputter-profiled, depth resolution degradation by cone form. 80−80094
InP/InGaAs heterojunction phototransistor, high-sensitivity 80−100505
InP/InGaAsP avalanche photodiodes, with guard ring structure 80−100506
InP-CdS, InP planar reactive deposition on CdS, heterostruct. formation and elec. evaluation 78−72738
InP-CdS, integrated optics appl., prep. and props. *(Slovak)* 80−33225
InP-CdS heterojunction, injection electrolum. 78−23153
InP-CdS solar cell, fabrication and power conversion efficiency 77−1813
InP-$CdSnP_2$, integrated optics appl., prep. and props. *(Slovak)* 80−33225
$InP-Ga_xIn_{1-x}As_{1-y}P_y$ heterojunctions, energy band diagram 77−16400
InP-GaInPAs DH lasers, misplaced p-n junctions due to Zn contamination 78−87051
$InP-In_{1-x}Ga_xP_{1-z}As_z$ quantum-well LPE heterostructure lasers, band filling and gain, quaternary DH behaviour 79−22955
$InP-In_xGa_{1-x}As_yP_{1-y}$ photodiode, characts. 78−14800
InP-InGaAs, integrated optics appl., prep. and props. *(Slovak)* 80−33225
InP-InGaAsP, integrated optics appl., prep. and props. *(Slovak)* 80−33225
InP-InGaAsP p-n junction avalanche photodiodes, surface passivation techniques 80−100508
InSe based heterojunctions, props. 79−11210
InSe solar cells, photovoltaic conversion efficiency 80−61356

p-n heterojunctions continued
In_2Se-InSe p-n junctions, 'optical' contacts, elec. props. 78−56222
In_xSe_{1-x}-SnO_2 heterostructure, anomalous temp. depend. obs. on photovoltage 78−56209
$(In_{1-x}Sn_x)_2O_2$-Si-N solar cell efficiency and elec. props. 80−35676
$In_{2-x}Sn_xO_{3-y}$-CdTe(InP) photovoltaic heterojunctions, surface and interface studies, efficiency 80−45691
$In_{2-x}Sn_xO_{3-y}$-$Ga_xIn_{1-x}P$(-InP_yAs_{1-y}) heterojunction solar cells, chemistry and prep. 80−94073
$In_{2-x}Sn_xO_{3-y}$-n-Si, electron deposited solar cell, photovoltaic props. 79−96446
InTe-InSe p-n junctions, 'optical' contacts, elec. props. 78−56222
NiO:Li_2O-ZnO, contact resist., effect of water vapour 80−34506
$Pb_{1-x}Hg_xS$-Si heterojunctions, elect. props. 80−100513
PbS heterojunctions nonideal, photoelec. props. and elec. charact. 79−15215
PbS-Ge heterojunction, influence of conduction band discontinuity on lux-ampere charact. 78−39200
PbS-Si, photosensitive p-n heterojunction, energy band diagram 79−95489
PbS-Si charact. and operation, IR detector appls. 78−52075
PbS-Si heterojunction, struct. and comp. 80−54530
PbS-Si heterojunction, chem. struct., AES anal. 80−76115
PbS-Si heterojunction, related optical and IR detector props. 80−77866
PbS-Si heterojunction, space charge capacitance, PbSn film thickness depend. 80−88630
PbS-Si heterojunction detector, direct injection readout 80−4765
PbS-Si p-n heterojunctions, AC admittance meas. 80−96979
PbSe-CdSe, elec. props. 77−1478
$Pb_{1-x}Sn_xSe(Te)$ epitaxial layers, growth, phase diagram, p-n junctions, optical, elec. props. 78−44029
PbSnTe detector and preamplifier modules for heterodyne detection of CO_2 laser radiation 78−32875
PbSnTe-PbTe heterostructs., effect of electrical grounding on electron irrad. 78−60194
$Pb_{0.8}Sn_{0.2}Te$-PbTe p-n heterojunction, prep., elec. and photoelec. props. 79−51664
$Pb_{1-x}Sn_xTe$ LPE grown heterostructures, dislocation etch pitch, interfaces 80−2023
$Pb_{1-x}Sn_xTe$ p-n heterostructure, VPE, struct. and electrophysical characts. 78−10547
$Pb_{1-x}Sn_xTe$-$Pb_{1-y}Sn_yTe$, p-n heterojunction, prep. and props. 79−51662
$Pb_{1-x}Sn_xTe$-PbTe, amorphous/crystalline heterojunction, rectification props., IR detector appl. *(Japanese)* 78−60197
$Pb_{1-x}Sn_xTe$-PbTe, interface recombination velocity reduction with decreasing lattice parameter mismatch 79−98370
$Pb_{1-x}Sn_xTe$-PbTe, Sn diffusion and elec. effects of dislocations, elec. and metallurgical expts. 77−89839
$Pb_{1-x}Sn_xTe$-PbTe heterostructures, MBE produced on mica and $LiNbO_3$, elec. props. study 80−88629
$Pb_xSn_{1-x}Te$-PbTe, epitaxial, elec. props. and photoresponse 78−56225
PbTe surfaces, Te coating, struct. and junction charact. 80−50743
PbTe:Bi-PbSmTe-PbTe, epitaxial laser struct., growth, p-n junction position and lasing region 79−89908
PbTe-CdTe fabrication and characterisation *(German)* 80−89151
n-PbTe-p-$Pb_{1-x}Sn_xTe$, heterojunctions, heavily doped, current-flow mechanisms 80−96974
PbTe-$Pb_{0.82}Sn_{0.18}Te$, p-n heterojunctions, electrical and photoelectrical properties 78−39193
PbTe-$Pb_{1-x}Sn_xTe$ n-p^+ heterojunction photodetector, hot wall evaporation technique 80−65673
Se-Ag_2Se, electrically controlled negative differential conductance mechanism 80−44720
Se-Ag_2Se, heterojunction with memory, transient switching characteristics 80−44718
Si crystalline-amorphous p-n junction, DC sputtering growth, photocond. and photovoltaic effects 79−33337
n-Si epitaxial layers on oppositely conducting substrates, two layer Hall coeff. meas. technique 80−80297
Si, heteroepitaxial film, minority carrier lifetime from I-U data 77−85264
a-Si ITO/p-i-n solar cells 80−101113
Si, n^+-p-p^+ structure with two-sided photosensitivity for terrestrial applications, structure and fabrication technology requirements 80−101096
Si, n-p-n heterojunction transistor 80−6959
Si/Si-Ge junction, elec. and photoelec. props. 78−10545
Si-A_2S_3 isotype crystalline-amorphous heterojunction, electrophys., props. 79−24063
Si-As_2S_3 heterojunctions, hole transport obs. in vitreous As_2S_3 80−49727
Si-CdS, detector for integrated optics appl. *(Czech)* 80−33227
Si-CdS heterojunction memory diodes, switching process 78−80046
Si-CdS p-n heterojunction photodetector fabrication and charact. 78−52068
Si-CdSe vacuum deposition, photovoltaic effects *(Korean)* 77−28243
Si-GaAs heterojunction photothyristor, spectral charact. 78−10546
Si-GaP, heterojunction, photosensitivity spectrum, charact. 79−24071
Si-GaSe n-p heterojunction, elec. charact., interface states 80−70812
p-Si-$In_{2-x}Sn_xO_{3-y}$ solar cells, thermal degradation mechanisms 80−55841
n-Si-In_2O_3:Sn, solar cell characterisation *(French)* 79−39306
Si-SiC, photovoltaic effect of sheet Si dip-coated on graphite substrate 80−29442
Si-SiC p-n and n-n heterojunctions, prep. by ion implantation, tunnelling cond. 77−43710
Si-SnO_2, prep., elec. and optical props., expt. *(Korean)* 77−4427
Si-SnO_2 highly photosensitive diodes, and their appl. 78−23152
Si-V_2O_5 p-n heterostructure, photocond. *(Russian)* 79−42622
p^+-$Si_{1-x}Ge_x$-nSi junction diodes, lattice misfit effects on I-V charact. 80−70804
Si_xGe_{1-x}-GaAs, heterojunction, elec. and recomb. props., interface defect effects 80−80365
Si_xGe_{1-x}-GaAs, p-nn$^+$ junction, I-V charact., inverse branch, effect of dislocation defects *(Russian)* 79−15217
Si_xGe_{1-x}-Si(GaAs) heterodiodes, interfacial structural defects effect on avalanche breakdown 79−42644
SnO_2/n-Si spray-deposited solar cells 80−12007
SnO_2/n^+-pSi heterojunction solar cells, fabrication by paint-on-diffusant method 80−94048
SnO_2/V_2O_5-P_2O_5/Si heterojunction, static optoelectronic charact. 79−87146

p-n heterojunctions continued
SnO_2-GaAs heterojunctions, elec. and optical props., photovoltaic appls. 77−43714
SnO_2-GaSe heterojunction photocell, fine struct. of photo-EMF spectra 80−6967
SnO_2-GaTe(GaSe)(InSe) heterojunctions, photoelec. props. 80−96945
SnO_2-InP heterojunctions, elec. and photovoltaic charact. 80−75628
SnO_2-polySi solar cells, fabrication, grain size effects on device parameters 80−94045
SnO_2-Si, elec. and photoelec. props. 77−1477
SnO_2-Si, heterojunction solar cells, anomalous photocurrent 80−3515
SnO_2-Si heterojunctions, elec. and photovoltaic props. 80−26141
SnO_2-Si solar cells, electron-beam-deposited, fabrication, angle-of-incidence effects 79−52931
SnO_2-Si solar cells, electron-beam deposited, struct., photovolt. props. 80−50956
SnO_2-SiO_2-n-Si heterojunction, cheap solar elements for ground-based appls. 80−40860
$SrTiO_3$-Si, photoresponse 78−72254
Zn_3As_2-$(Cd_xZn_{1-x})_3As_2$, LPE 78−35324
$Zn_{0.1}Cd_{0.9}S$-CdTe p-n junction, prep. by spray pyrolysis, photovoltaic props. 78−60196
$Zn_xCd_{1-x}S$ film, prep. and use as heterojunction optical energy converters 79−95488
$Zn_xCd_{1-x}S$/GaAs heterojunction solar cells, meas. of minority carrier diffusion length 80−26158
$Zn_xCd_{1-x}S$-Cu_2S heterojunction solar cells, props., comp. meas. of interfacial region 80−81472
$Zn_xCd_{1-x}S$-Cu_yS solar cell, fabrication, elec. charact. 77−8208
$Zn_{1-x}Cd_xTe$, LPE growth process, elec. props. 77−7981
ZnO-CdTe heterojunctions and ZnO films preparation using spray pyrolysis 80−96985
ZnO-Cu_2O heterojunction solar cells, prop. by RF sputtering 80−93945
ZnO-Si p-n diode monolithic storage correlator 78−18119
ZnS, zinc blende-wurtzite-zinc blende, optical quenching of photocond. *(Russian)* 77−28240
ZnS-BiOCl, electroluminesc. heterojunction phys. props. 77−66198
ZnS-$CuGaS_2$ heterodiodes, LPE, emission spectra 79−33335
ZnS-Ge(GaAs), n-p, epitaxial, elec. props. *(Russian)* 78−88023
ZnSe, high conductivity films appl. to p.n. heterojunctions 78−68100
ZnSe-BiOCl, electroluminesc. heterojunction phys. props. 77−66198
ZnSe-CdTe heterojunction, radiative recomb., electrolum. obs. 77−32445
ZnSe-CdTl, epitaxial film, cond. transition, laser switched memory *(Russian)* 77−8182
ZnSe-GaAs, LF noise, I-V and C-V charact., illumination effects *(Russian)* 77−66200
ZnSe-GaAs narrow junction lasers 80−43334
ZnSe-GaAs thin film DE electroluminescent cell with 20 V threshold voltage 78−76141
ZnSe-Ge(GaAs) epitaxial heterostructs., growth and struct. 78−43257
ZnSe-Si heterojunctions, IR quenching of photocapacitance 80−92968
ZnSe-ZnTe amorphous thin-film p-n heterojunction, fabrication and characts. 79−47154
ZnSe-ZnTe heterojunction, prep. and props. 79−95483
n-ZnSe−p-GaAs heterojunction high-detectivity threshold photodetectors 79−6181
$ZnSnAs_2$, LPE in open tube system, on GaAs (InAs) substrates, heterojunction fabrication 78−92206
ZnTe-CdS(Se)(S_xSe_{1-x}), prep. and electrolum. charact. 77−24610
ZnTe-CdSe heterojunction, radiative recomb., electrolum. obs. 77−32445
ZnTe-CdSe single cryst. film heterojunctions, prep. and props. 79−19652
p-ZnTe-n-GaN, electroluminescent hetero-junctions, memory effect, I-V charact. *(Russian)* 77−40289
ZnTe-ZnSe(CdSe), LPE growth, elec., photoelec. and luminesc. meas. 77−4745

p-n homojunctions
avalanche multiplication factor and reverse current 77−11991
back surface field semiconductor junction, temp. depend. of open circuit photovoltage 80−15593
barrier capacitance of p-n junction in region of strong ferroelec. instability 79−11218
breakdown voltage for onesided abrupt junctions, anal. *(German)* 78−56210
capacitance, differential, epitaxial layer carrier conc. profile obs. 77−12036
capacitance transient spectroscopy, book contrib. 78−10548
conversion of chem. energy into elec. power in semicond. p-n junction, thermodynamic props. 79−11219
deep centre activation energy determ. by capacitance method 79−11215
deep-level centre discrimination from capacitance versus time transients 78−10395
diamond, ion implanted, p-i-n structure, double injection of carriers 79−11214
diamond, synthetic, p-n junction prod. and doping, I-V charact. 77−15943
diffusion length and surface recomb. vel. determ., light excitation 78−91725
diode, electron-beam annealing of ion-implantation damage 79−77622
education, forbidden energy gap meas. in Si and Ge p-n junctions 80−57027
formation in doped semiconductors by laser radiation *(Russian)* 77−15947
high-low junction contact at low temp., appl. to extrinsic Si detectors 77−39925
highly doped, behaviour of buried O_2 implanted layers 80−59499
hyperabrupt junction, C-V index, junction parameters depend. 80−49876
III-V multilayer structs., contact resistance profiling method 78−56213
III-V semiconductor, avalanche breakdown voltage for p-n junction, calc. 78−88020
impurity centre mobility at room temp. *(Russian)* 78−34891
injection characteristics in strong elec. fields 77−76913
integrated tandem solar cell performance 80−3521
ion implanted junction elec. props. correl. with n^+ region microstructure 77−76916
IV-VI compounds, dielec. props., elec. meas. 78−15119
MOS structure, with reverse biased p-n junction, impulse current behaviour *(German)* 79−82675
n^+-n-p high-low-emitter junction solar cell, open-circuit voltage in conc. sunlight 80−50957

p-n homojunctions continued
n^+-p-p^+-Si structure, low temp. electron irradiation of p-region 77−84801
p^+-i-n^+ double-injection struct., regional approx. 78−14805
p^+-n diode under forward bias, effects of radiation-induced deep levels on admittance 78−23157
p^+-n-$^+$ structure made of direct gap semiconductor, lightly doped n-type region conductance modulation 79−42634
p^+n-n^+ structures with strong carrier accumulation, current-voltage charcts. theory 79−42626
p-n junction photovoltaic diode, appl. as IR detector 78−86330
p-n-n^+ junctions, epitaxial planar, two-dimensional anal. of breakdown 78−80045
p-n-n^+ structures, Zn doped Si, use as light sensitive devices 77−8178
p-n-n^+ structures containing deep traps, double injection currents 80−15592
passivation by Si:O polycrystalline layers, charge transport 79−38206
photoelectric convertors, p-n mesa structure for investigating optical and energy charcts. of solar and radiant energy concentrators 80−97783
photovoltaic effect, solar energy convertor theory with p-n junction 78−72201
planar, capacitance calc. 78−30978
polyacetylene, doped, p-n junction, elec. props., review *(Japanese)* 80−29410
polyacetylene, n- and p-type doping, and compensation, p-n junction formation 78−76070
reduction doping using zone recrystn. with temp. gradient, two-layer struct. with p-n junction creation 80−104062
reliability, imperfections in Si crystals, effect on microplasma formation 77−8177
Schottky layers, homogeneous avalanche breakdown instability mechanism, microplasma form. 78−72262
secondary breakdown plasmon mechanism 78−95352
semiconductor, deep impurities, exptl. techniques *(Japanese)* 80−15476
semiconductor induced current obs., stroboscopy appl. 77−19855
semiconductors, amorphous, doped, electronic props. 80−80283
Si:Au, step junction, mathematical model *(Rumanian)* 79−87148
Si p^+pn^+ junction, diffusion of transition elements, anomalous behaviour 80−29044
n^+-Si-Al ohmic contacts, metallisation structs. for very shallow n^+/p junctions 80−60084
solar cell, direct gap, theoretical limit efficiency 80−97795
solar cell, polycryst., grain boundary influence on recomb. 80−93913
solar cell arrays, Si, fixed-base, flat panels, possible developments for more competitive power production 80−72050
solar cell fabrication, laser-induced p-n junction formation 80−93880
solar cells, CdTe, shallow homojunctions, characteristics and surface resistance influences 80−45690
solar cells, power conversion efficiency monitoring 80−50989
solar cells, Si_xGe_{1-x} diffused p-n junction, electric and photoelectric props. 80−101095
solar homojunction photovoltaic cells, conversion efficiency, maximum theoretical efficiency as a function of temp. 80−81469
surface avalanched p-n junctions, localised charge injection and trapping 77−76907
surface microfield thickness modulation of photolytic polymer film 78−10561
ternary semiconductors, use in thin film heterojunction and homojunction photovoltaic devices 78−39208
thermally associated field emission near precipitates 78−14801
thermometer, using single quad op amp 77−45839
thermomigration of molten metal wires, p-n junction fabrication 78−67870
Thomas-Fermi dielectric function calcs. of analytic charge distrib. 79−78161
varactor diode with multilayer p-n junctions, computer simulation, charcts. 79−42625
variable-gap, recomb. currents 80−20303
voltage transients, defect centres emission rates and density profile 78−10467
n-Si, deep levels in p-n junctions or Schottky barriers determ., hybrid method 79−24067
AlGaAs p-n diodes, I-V charcts., tunnelling 80−100510
$Al_xGa_{1-x}As$, hot carrier recomb., overheating luminesc. 78−92122
$Al_xGa_{1-x}As$ variable gap junction, photosensitivity 78−39204
$Al_xGa_{1-x}Sb$:Zn, impurity diffusion, p-n junction depth 80−24678
AlSb Schottky barrier solar cells, characteristics and efficiency of Czochralski-grown crystals 80−61366
Au-n-Si-p-Si structure with wavelength depend. photocurrent sign, photodetector 79−12849
BN glass transfer process 80−107459
Bi_2Te_3, thermoelectric p-n junction, pulse refrigeration 78−23156
$CdGeAs_2$, p-n junction form. by heat treatment, photosensitivity 77−28247
(CdHg)Te, ion implanted graded gap photodiodes 78−39192
$Cd_{0.24}Hg_{0.76}Te$, mag. quantum oscills. in photovoltaic effect 79−19619
n-$Cd_xHg_{1-x}Te$, action of laser pulses, elec. charcts. 79−11212
$Cd_xHg_{1-x}Te$, epitaxial layer p-n junction, current-voltage characteristics of photovoltaic detectors, 1 to 15 μm 80−86407
$Cd_xHg_{1-x}Te$, graded gap epitaxial layers, elec. and photoelec. props. 77−85362
$Cd_xHg_{1-x}Te$ inhomogeneous p-n junctions, elec. props. at high hydrostatic press. *(Russian)* 77−80835
$Cd_xHg_{1-x}Te$ photodiode, IR responsivity and detectivity 78−19139
$Cd_xHg_{1-x}Te$, tunnelling effect in p-n junctions 80−75630
$Cd_xHg_{1-x}Te$, variable-gap struct., additional p-n junction in epitaxial film, photosensitivity 77−24588
CdS-Al_2O_3-Al diodes fabricated by MBE, junction charcts. 79−65550
CdS_xTe_{1-x}, surface layer conductivity type inversion by ruby laser radiation *(Russian)* 77−15948
CdSb:Al, p-n junction formation by laser emission, photoelectric effects *(Russian)* 80−70815
CdSb:Al(In)(Ga)(Te), p-n junction formation by laser radiation 80−96983
CdTe, film, anomalous-photovoltage, current-voltage charcts., representation of chain of junctions 79−69549
CdTe, growth by photostimulated VPE, electrophys. props. 77−40390
CdTe homojunctions from VPE growth, solar cell appl. *(French)* 77−43453
CdTe, short-circuited, estimation of surface recomb. rates, electron-probe meas. 77−43713

p-n homojunctions continued
CdTe:Ag, with microscopic p-n junction, photopolarisation in anomalous photovoltage 79−11175
CdTe:As^{2+}, photovol. props. of p-n junction prod. by ion implantation 78−43038
$CuInS_2$ film homojunction solar cell, fabrication, performance 77−80832
$CuInS_2$, p-n junction photovoltaic props. and detectors 79−99574
$CuInSe_2$, photovoltaic props. and p-n junction form. 77−69371
$Ga_{1-x}Al_xAs$ p-i-n structure photoelectric props. 78−95353
$Ga_{1-x}Al_xAs$ p-n structure, charge-storage diode, variable-gap 80−11076
$Ga_{1-x}Al_xAs$:Si, doping in LPE, elec. and luminesc. props. *(Czech)* 78−47851
$Ga_{1-x}Al_xAs$:Si p-n junction, reemission effects 78−15230
p-$Ga_{1-x}Al_xAs$-n-$Ga_{1-y}Al_yAs$, graded band gap, solar cells, theoretical efficiency *(French)* 77−62987
$Ga_{1-x}Al_xSb$ p-n homojunction LPE and photovoltaic effect obs. *(French)* 78−64108
$Ga_{1-x}Al_xSb$ variable-gap p-n struct., selective photoelec. effect 77−76912
$Ga_{1-x}Al_xSb$ variable-gap p-n structures, wide-band photoelec. effect 79−42635
GaAs amorphous film/GaAs crystal junction, optical and elec. props. 79−99611
GaAs, as pressure/temp. transducers *(Polish)* 77−67424
GaAs, conductance oscillations in a two-dimensional impurity band 79−95477
GaAs, coupled-waveguide optical modulator, high freq. modulation 77−75678
GaAs, deep level profile anal., double correlation technique 77−80830
GaAs, deep levels obs. 77−89834
GaAs, direct biased, temp. depend. of low freq. voltage fluctuations 79−56298
GaAs, elec. breakdown mechanism 79−87147
GaAs, electroepitaxy and thermal LPE growth, elec. charcts. 80−2290
GaAs, electron irrad. induced defect levels, hydrostatic press. effect 80−92858
GaAs epilayers and p-n junctions, anisotropic phonon generation 79−37784
GaAs, evaluation of Be doping of p-type region 77−51397
GaAs forward-biased diode structures, numerical anal. based on direct gap semicond. 79−65542
GaAs, grown by current-controlled LPE, elec. charcts. 78−6436
GaAs, HV, current induced by electron probe in space charge region 79−24065
GaAs homoepitaxial interface, thermal degradation 77−11988
GaAs homojunction LED, mechanical stress induced degradation 80−2860
GaAs homojunction solar cells, large-grained, passivation method to improve open-circuit voltage 80−94070
GaAs, implanted p-n junction form. using laser pulse annealing 77−15946
GaAs, lightly doped, p-n junctions, forward branches of current-voltage charcts. 79−7890
GaAs, low-field study of p^+nn^+ or p^+pn^+ structs. on forward direction 80−60072
GaAs, n^+-n-n^+ and n^+-p^--n^+ structs., ballistic electron motion at room temp. 80−80360
GaAs n^+-p^--n^+ ballistic structure 80−80359
GaAs n-p solar cells, potential for high efficiencies concentrator applications 79−100534
GaAs negative electron affinity cold cathode 79−87558
GaAs, nonradiative capture, direct obs. of phonons 78−30976
GaAs optical modulator for coupled-waveguides 78−71235
GaAs p^+-n^0 junction, photocurrent, hole diffusion length in lightly doped n-type region 77−28246
GaAs, p^+-n^0-n^+ struct., control of modulation of base resist. 79−91133
GaAs p^+-n-n^+ diode, ns modulation of 10.6 μm radiation by elec. injection 77−34937
GaAs p^+-p(i)-n^+ structures, S-shaped I/V characteristics based on laminated semicond. cryst. structures *(Russian)* 79−42628
GaAs, p-n junction, Zn^+ implanted, residual radiation defect influence on charcts. *(Russian)* 78−84287
GaAs p-n junction formation, laser assisted, TEM and elec. props. 79−69138
GaAs p-n junction pressure transducer characteristics *(Polish)* 77−89832
GaAs, periodic doping structure, nipi superlattices, HBE growth and charcts. 79−95484
GaAs, piezotunnel current *(Russian)* 77−47890
GaAs, planar diffusion of Sn from doped SiO_2 films, for planar junction fabrication 79−69289
GaAs planar junctions, Be ion implantation, fabrication and charcts. 78−88022
GaAs planar p-n junction fabrication by Be ion implantation 78−43470
GaAs, reverse-biased, current-controlled negative resist., switching investig. 77−69410
GaAs, shallow homojunction solar cell, resist. to 1 MeV electron radiation 80−50953
GaAs, shallow-homojunction solar cell by MBE, conversion efficiency 80−30476
GaAs shallow-homojunction solar cells on single crystal GaAs and Ge substrates, CVD fabrication and conversion efficiency 80−61364
GaAs shallow-homojunction solar cells, electron radiation effects 80−97798
GaAs, short-circuited, estimation of surface recomb. rates, electron-probe meas. 77−43713
GaAs solar cells, photoreactance of p-n junction diodes 80−81464
GaAs solar cells on Ge substrates, thin film shallow homojunction struct., quantum efficiencies 80−35677
GaAs, surface recomb. current reduction with $Al_{0.5}Ga_{0.5}As$:O surface layer 80−49878
GaAs, surface recomb. velocity, determ. from SEM expts. on p-n junctions 77−55601
GaAs:Cd, effect of As vapour press. on etch pit density and junction depth 78−26937
GaAs:Fe, p-π-ν-n struct., photoelec. props. 80−107862
GaAs:Fe p^+-n junction minority carrier trap meas. by photo-excited DLTS 80−96816
GaAs:Fe reverse biased π-ν-n struct., switching effect 80−88628
GaAs:Ge p-n junctions by mol. beam epitaxy 79−56289

p-n homojunctions continued
GaAs:O p-ν-n structs., injection current and negative photocond., saturation mechanism 80−92967
GaAs:Se, and undoped sample, annealed, surface cond. change, n-p double layer 78−64095
GaAs:Si, electrolum. power, injection current and temp. depend. *(Russian)* 77−16401
GaAs:Si, LED, effect of struct., defects on quantum efficiency 79−11211
GaAs:Si defect density before and after Zn diffusion, SEM and TEM obs. 80−96529
GaAs:Si LED p-n structures, speed *(Russian)* 79−43044
GaAs:Si p-n junction LED, electroluminesc. efficiency 80−71491
GaAs:Si p-n light-emitting structs., soln. of general minority carrier transport eqn. 80−15597
GaAs:Si p-n structs., effect of growing conditions on distrib. of recomb. parameters 80−39668
GaAs:Si p-n structure, radiative recombination region 78−52071
p-GaAs:Zn, Mn, degenerate, tunnel p-n junction and semicond.-metal struct., I-V characts. 78−72252
$GaAs_{0.6}P_{0.4}$, deep level profile anal., double correlation technique 77−80830
$GaAs_{1-x}Sb_x$ photodiode structures, current-voltage characts., photo-EMF spectra 80−29472
$Ga_{0.47}In_{0.53}As$, band-to-band tunnelling current 80−107895
$Ga_{1-x}In_xAs$ epitaxial layer growth by organometallic pyrolysis, homojunction LED prep. 80−76194
GaP, electron beam excited carrier avalanche multiplication 79−69587
GaP, electron traps around dislocations in p-n junction and metal-semicond. structs. 80−34388
GaP, epitaxial struct., cathodolum. in SEM 78−10991
GaP, LPE, cathodo- and electrolum., residual impurity and struct. defect effects 78−19570
GaP lamps, green emitting deep level photocapacitance spectra 77−69409
GaP, light emitting diode structure, effect of neutron irradiation on cathodoluminesc. 79−28843
GaP, n-type, Zn diffusion, p-n junction depth 77−89841
GaP negative electron affinity cold cathodes, vidicon appls. 78−19133
GaP, p^+-n diode junction, admittance meas. and carrier traps 78−91757
GaP, p-i-n LED, I-V characts., electrolum., and photocond. meas. 77−20930
GaP p-n junction, capacitance-freq. dispersion and electroluminescence efficiency 78−64101
GaP:Cu p^+-n junction, deep level parameters, TSC meas., rel. to photocurrent techniques 78−72249
GaP:N p-n structure yellow light emitting source 77−69412
GaP:N VPE layers, thermal emission energies, trapping, and carrier lifetimes, deep level capacitance spectroscopy 79−42487
GaP:N(N,O) epitaxial struct., luminesc. study of degradation during heat treatment 80−45139
GaP:Si p-n struct., on n-$Ga_{1-x}Al_xP$ and n-GaP substrates, electrolum. spectra 79−24368
GaP:Zn, growth, I-V characts., electroluminesc. *(Korean)* 78−52653
GaP:Zn,O, electron irrad. effect on electrolum., defects form. and quenching obs. 80−55194
GaP:Zn,O, epitaxial p-n junction, IR electroluminesc. exam. *(Russian)* 78−35207
GaSb, as pressure/temp. transducers *(Polish)* 77−67424
GaSb p-n junction pressure transducer characteristics *(Polish)* 77−89832
GaSb, photolum., electrolum. meas. in p-n junction, temp. influence 78−72594
GaSb:Sn, p-n junction, electroluminesc. and photoluminesc. 80−66306
Ge, amorphous, doping, Schottky barrier and p-n junction form. by RF sputtering 77−8187
Ge, current filament form., fluctuations and thermal noise 77−69411
Ge diode, influence of mechanical stresses on effective carrier diffusion length in base region 77−35987
Ge, epitaxial-diffusion p-n junction, inductive props. in secondary breakdown 80−15598
Ge graded p-n junction, volume EMF of hot carriers 77−47895
Ge high-grade, temp. gradient zone melting in production 77−4747
Ge, hot photocarrier and hot electron effects 78−30980
Ge, IR radiation modulation, light absorption by injected current carriers *(Russian)* 80−10013
Ge, injection characteristics in strong elec. fields 77−76913
Ge, low-field study of p^+nn^+ or p^+pn^+ structs. on forward direction 80−60072
Ge p^+-ν-n^+ structures, charge transport under impurity freezeout conditions 80−92965
Ge p^+-ν-n^+ structures, large-scale trap characts. 80−92966
Ge, p-i-n struct., Li ion drift thermal profile 77−51813
p-Ge, p-n junction with hot carriers in charge accumulation regime, influence of light on operation 79−51661
Ge, p-n junction with hot carriers, current-voltage characts. 79−91135
Ge p-n junctions, impurity photoelec. effect 79−56300
Ge p-n junctions with hot carriers, current amplification, elec. domain form. 80−6966
Ge, photo-EMF generation in saturation region 80−75635
Ge, radiative electromagnetic effect, alpha-particle irrad., Hall effect, photoelectromagnetic effect 78−10434
Ge, voltage-current curve for microplasma breakdown, at. size difference effect 78−2550
Ge:Au, p-n junction, injection amplification of photocurrent 79−51663
Ge:B, ion implantation and depletion at low temps., radiation and DC characts. 79−60392
Ge:Li, Cu p-n junctions, current stimulated LiCu complex formation, photocurrents 80−107897
n-Ge:Ni p^+-n-n^+ structs., double-injection current-voltage characts. 80−60074
n-Ge:Sb, deep levels obs., freq. depend. of capacitance 77−4315
Ge-Si alloy, Sb-diffused, TSC 80−20289
HgCdTe epitaxial material, ion implantation, junction form. 80−100260
HgCdTe Schottky barrier diode and n-p diffused junction IR detectors, comparison 80−9039
$Hg_{1-x}Cd_xTe$ photodiodes, implanted n^+-p, improved performance using insulated field plates 80−52309
InAs, impact ionisation and Auger recomb. 77−20329
InAs p-n junction, carrier multiplication and ionisation coefficients 77−8188

p-n homojunctions continued
n-InAs:Cd, photosensitivity spectra depend. on mag. field 79−91137
InAs:S(Mg), ion implanted, photocond., photo-EMF, and optical absorpt. spectra 80−70763
$InAs_{1-x}Sb_x$ p-n junctions, avalanche multiplication 80−6965
InGaAs p-n junction, carrier multiplication and ionisation coefficients 77−8188
$In_{0.53}Ga_{0.47}As$ p-i-n photodiode-FET photoreceiver for 1.0 to 1.7 μm wavelength optical fibre communications systems 80−58794
$In_xGa_{1-x}As$, MBE grown, electrolum. meas. 78−84328
$In_xGa_{1-x}As$:Si, p-n junction form. in LPE layers, In content effect on inversion temp. 77−4266
$In_xGa_{1-x}As$:Si p-n structs., electrolum. spectra, 77 to 300K 80−93408
InGaAsP avalanche photodiodes, breakdown mechanism, donor conc. effect 80−70710
$In_{1-x}Ga_xAs_xP_{1-y}$, p-n junction diodes, fabrication by Be ion implantation 79−47156
$In_{1-x}Ga_xAs_yP_{1-y}$:Be, ion implantation, hole conc. and mobility, junction depth 79−46685
In_2O_3-SnO_2-CdTe:P, p-n homojunction solar cell, elec., photovoltaic props., photoluminescence 80−81463
InP n^+-p-p^+ homojunction solar cells, high efficiency, LPE layer growth, photolithographic fabrication 80−93929
InP p^+-n abrupt junctions, ionisation coeffs., photomultiplication meas. 80−65655
InP, p-i-ν diode, Franz-Keldysh effect 77−55790
InP p-n junction, grain boundary etching 80−96541
InP p-n junction diodes, fabrication by Be ion implantation 79−47156
n-InP, p-n junction form. by Be ion implantation 80−29474
InP photodiodes, dark current and breakdown characts. 80−70806
InP, planar Zn diffusion process for p-n junction formation 78−43040
InP:Be, ion implantation, hole conc. and mobility, junction depth 79−46685
InP:Cd, p^+-p^--n^- junction form. by diffusion doping 80−84504
InP:Cd(Zn), avalanche photodiode characts., impurity diffusion effects 80−70709
InP:Fe, deep levels 79−56166
InSb, ion bombard. and defect annealing, n- and p-type cond. layer prod. 78−26606
InSb, minority carrier injection in mag. field, recomb. radiation obs. 80−11078
InSb n^+-p junctions, photocurrent spectrum near long wavelength edge of fundamental absorption band 80−100483
InSb p-n junctions, diffused, avalanche multiplication and impact ionisation 80−15595
InSb planar p-n junction fabrication by Be ion implantation, CCD chip appls. 77−89833
InSb, reverse biased diode, negative resist. 78−19129
InSb:Se p-n tunnel diodes, influence of doping on characts. 79−73575
InSb:Zn p-n junctions, ion implantation and diffusion spreading, elec. and photoelec. props. 79−73573
In_2Se with p-n junctions produced by laser radiation, photoelec. characts. *(Russian)* 78−56226
$MgSiP_2$, elec. props. and diode struct. exam. 79−51665
n^+-n-pGe avalanche photodiode, noise factors, internal quantum efficiency 80−70803
$Pb_{1-x}Ge_xTe$, capacitance meas., dielec. const., ferroelec. nature of phase transition 78−88269
$Pb_{1-x}Ge_xTe$, ferroelec. constants, C-V and C-T characts. of abrupt p-n junctions 80−25323
$Pb_{1-x}Ge_xTe$, ferroelectric phase transition effect on forbidden band width 80−24794
$Pb_{1-x}Ge_xTe$, p-n junctions, elec. characts., effect of ferroelec. phase transition 79−33338
$Pb_{0.97}Hg_{0.03}Te$ photovoltaic detector produced by Sb^+ ion implantation 80−82821
$Pb_{1-x}Mn_xTe$, photovoltaic effect, p-n junction, energy gap determ. 80−92931
$PbS_{1-x}Se_x$ (X=0.18) homojunction injection lasers, near-field emission 80−95896
PbS_xSe_{1-x} film, prep. by co-evaporation method, p-n junction diodes fabricated, props. meas. *(Japanese)* 78−64477
$PbSe_{1-x}Te_x$, p-n junction, inversion of conduction level 78−47856
$Pb_{1-x}Sn_xSe(Te)$ epitaxial layers, growth, phase diagram, p-n junctions, optical, elec. props. 78−44029
$Pb_{0.83}Sn_{0.17}Te$, carrier tunnelling through potential barrier in p-n junctions *(Russian)* 78−52074
PbSnTe(Se) Schottky barrier diode and n-p diffused junction IR detectors, comparison 80−9039
PbTe, epitaxial film on fluorphlogopite, effects of annealing in Te vapour 77−80709
PbTe, minority carrier lifetime, step pulse recovery 77−11995
Se diode surface states determ. by conductance and capacitance 77−85318
Se:Ta, electrophysical meas. rel. to control of conductivity type 77−24323
Si, advanced material for space solar cell 80−94007
Si alpha-particle effects, photoelec. parameters determ. *(Russian)* 77−31702
Si, amorphous, doping, Schottky barrier and p-n junction form. by RF sputtering 77−8187
Si, amorphous, elec. props., ion implantation effects 80−79828
Si, amorphous, luminesc. of diode structures 77−8656
Si, amorphous, p-n junction devices, barrier profile effect on elec. props. 80−49890
Si, amorphous, preparation by SiH_4 decomposition *(Czech)* 77−63560
Si, amorphous, Schottky barrier and p-n junction props. 79−28407
Si, amorphous, solar cells, barrier props. determ. by differential I-V characts. meas. 80−94053
Si, amorphous, substitutional doping, electronic props. 77−1418
Si, amorphous and crystalline, hydrogenation and dehydrogenation, monitoring via elec. characts. of p-n junction 78−51677
Si, amorphous films, ion implanted, elec. and photocond. props. 80−49717
Si amorphous p-n junctions, high current, characts. 80−70807
Si, As-diffused ion implantation effects on leakage current 77−62555
Si, As-doped, effect of elec. and struct. parameters on avalanche breakdown localisation 77−11926
Si, as-grown Czochralski crystal, multiple p-n junction structure obtained by heat treatment, appl. to solar cells 80−101099

p-n homojunctions continued
Si, B implanted, enhanced annealing behaviour, p-n junction formation 77−43233
Si beam epitaxy for epitaxial film growth and p-n junction formation in high vacuum 80−16187
Si breakdown voltage drift, walk-out phenomenon, model 77−80834
Si, charact. linearisation for temp. meas. 77−53904
Si, charge carrier recomb. at dislocations, combined SEM and TEM study 80−15105
Si, compressed by shock wave, rectifying props. 77−4429
Si, DC charact. at avalanche breakdown including selfheating 79−42629
Si, deep centres, majority carrier thermal capture cross section, TSC meas. 78−10468
Si depletion layer, recombination theory 77−80828
Si, detector for integrated optics appl. *(Czech)* 80−33227
Si, dielectric props., freq. depend. of capacitance and conductance 78−43469
Si diffused horizontal homojunction solar cells, effects of junction depth and impurity conc. 80−55877
Si diffused n-P^+ junction miniature for electron meas. 77−30718
Si, diffused p-n junction, computer calcs. of photoresponse using Gummel-de-Mari algorithm 78−56221
Si, diffusion of Ga through SiO_2 layer, junction depth 78−51574
Si, diffusion of Na, retarding action of radiation defects 77−1140
Si diode, impurity profiles, scanning electron microprobe anal. 80−79832
Si, dislocation images, comparison of SEM and scanning optical obs. 79−51112
Si, dislocation study by high voltage electron microscopy and SEM 79−82217
Si, dopant conc. diffusion length and lifetime variations, SEM obs. 79−82604
Si, EMF appearance under action of thermal field pulses with high temp. gradients 79−56252
Si, electrolytic anodic oxidation method of decoration 80−60069
Si, electron beam scan annealed, deep levels 80−65481
Si, electron probe determ. of pn-junction depth *(German)* 78−2552
Si, ellipsometric method of temp. meas. rel. to secondary breakdown *(Russian)* 80−11074
Si, epitaxial film, struct. defects, effects on planar diffused p-n junction elec. props. *(Russian)* 78−60195
Si epitaxial p-i-n photoconvertor characteristic deterioration at high illumination 78−89536
Si epitaxial photoconvertors, props. 77−51807
Si epitaxial structures, junction layer width and impurity conc. estimates *(Russian)* 80−49893
Si heavily doped shallow-emitter p-n junction solar cells, diodes and transistors, Auger recombination 79−96445
p-Si, high-resistivity, TSC and photo-EMF in p-n junction, deep levels 77−72913
n-Si high-temp. vacuum etching, p-n junction photodetectivity 78−95355
Si, high-voltage, elec. props. by optical scanning 80−6969
Si, high-voltage, microplasma charact. 77−11997
Si, ion implantation with Li^+, charact. for thin film solar cell use *(Korean)* 77−51812
Si ion implanted p-n junction, cryst. damage influence on elec. props. 78−56219
Si ion-controlled diodes, acid-base exposure effects, Si-SiO_2 interface state density 80−96984
Si, ion-implanted, lapping and staining techniques, junction depth determ. 80−29468
Si junction diode, diffused, with deep level traps, negative capacitance 80−96976
Si junctions, made by ruby laser pulses *(Polish)* 78−84286
Si, laser annealed, elec. props. 79−69609
Si, laser assisted doping, ohmic contacts and p-n junction form. 78−79621
Si, magnetodiode, effect of mag. field on current-voltage charact. at low temp. 79−91134
Si, mesoplasma formation, light-emitting properties of secondary breakdown region *(Russian)* 79−91131
Si, microplasma charact., temp. depend. 77−4430
Si, microplasma instability, effect of space-charge field of mobile carriers 78−19140
Si multilayer structure dopant distrib. and minority carrier diffusion length, SEM obs. *(Russian)* 78−10543
Si n^+pp^+ solar cells, back illuminated, internal quantum efficiency 79−34435
Si n^+-p diffused diode, optical lifetime meas. in heavily doped diffused regions 77−80829
Si, n^+-p diode, γ-radiation defects, annealing and recomb. props. 80−65045
Si n^+-p junction, microplasma sites, SEM and TEM characterisation 77−43702
Si, n^+-p junction, surface peripheral leakage currents 78−26939
Si n^+-p junction solar cells, electron irrad., DLTS spectra and defect effects 80−93999
Si n^+-p solar cell, forward and reverse bias tunnelling 80−85274
Si, n^+p junction, spin dependent recombination *(French)* 78−80047
Si n-p junction vertical solar cells, Al-plated, photovoltaic effect variation with impurity conc. 79−100522
Si, negative resist. permanently induced in reverse-biased junctions 78−56214
p-Si, neutron irrad. effects, admittance meas. of n^+-p diode 78−51587
Si p^+-i-n^+ diodes, double-injection switching, effect of surface recomb. 78−88025
Si, p^+-n abrupt junction, carrier drift vel. effect on meas. ionisation coeffs. 79−69516
Si p^+-n contaminated junction, precip.-induced and generation-recomb. currents 78−2555
Si, p^+-n diode, neutron irrad., defect levels, G-T and C-T curves obs. 77−62986
Si p^+-n high efficiency solar cell, B diffusion process 77−85302
Si p^+-n junction, defect free, very shallow, photovoltaic effect rel. to solar cell appl. 79−15218
Si, p^+-n junction, irrad. with α-particles, defect form 80−24509
Si, p^+-n junction diodes, flow fluence S implanted unequal defect densities, dynathermal obs. 80−20293
Si, p^+-n-n^+ high efficiency back surface field solar cells, design and fabrication 78−84283
p-n homojunctions continued
Si p^+nn^+ reverse-bias struct. with confined space-charge region, field profile 79−73581
Si $p^+\pi pn\nu n^+$ structure form. by epitaxial growth 77−76906
Si p-i-n structure, ESR of conduction electrons 80−93179
Si p-n diode, 1/f noise calc., free carrier mobility interpretation 80−54774
Si p-n homoepitaxial junctions, elec. and struct. charact. 80−6662
Si p-n junction, avalanche multiplication of electron beam generated carriers 77−80833
Si, p-n junction, current-voltage charact., misfit dislocations, high press. effects 80−65671
Si p-n junction, negative annealing of γ-radiation defects 77−43246
Si p-n junction, reverse bias high voltage, secondary surface breakdown 80−70813
Si p-n junction depletion layer, electron beam damage inhibition 80−70817
Si p-n junction diodes, emitter and base lifetimes determ. 77−43701
Si p-n junction diodes and solar cells, minority carrier diffusion length 80−107894
Si p-n junction formation, laser assisted, TEM and elec. props. 79−69138
Si p-n junction I-V reln. calc. 77−43704
Si p-n junction in surface region obtained by evaporation in UHV 78−39198
Si p-n junction local temp. meas. using pulsed SEM, induced-current mode 80−54775
Si, p-n junction photodiode growth by ionised-cluster beam deposition, sensitivity 77−32527
Si p-n junction pressure transducer characteristics *(Polish)* 77−89832
Si p-n junction radiation detector behaviour in temp.-compensated cct. 78−33389
Si p-n junction solar cells, photon degradation effects 79−92078
Si p-n junction solar cells, importance of surface recombination and energy-bandgap narrowing 79−100520
Si, p-n junction struct., electron-irrad., surface defect distrib., deep-level transient spectroscopy 79−1459
Si p-n junctions, avalanche breakdown anisotropy 80−70811
Si, p-n junctions, current-voltage relation 79−42632
Si p-n junctions, electron emission from depletion layers 80−100509
Si, p-n junctions, neutron transmutation doping, breakdown process 80−15600
Si p-n junctions, spin depend. surface recomb., electron irradiation effect 80−88627
Si, p-n junctions, voltage-current charact., fast neutron irrad. effects *(Russian)* 80−65659
Si p-n step junctions, temp. depend. of capacitance 79−15210
Si, p-n-n^+ structure, external resistance effect on current-mode second breakdown 78−56216
Si, passivation by amorphous Si:H layer 79−47155
Si, passivation by slightly conductive chalcogenide film 78−2556
Si, photocell, ionized cluster beam deposition and epitaxy, cell charact. 77−77416
Si photocell, with field-induced p-n junction, inversion layer solar convertor 77−15906
Si, photodiode, semiconductor junctions, dark currents *(Russian)* 77−24612
Si planar semiconductor junctions, disruptive voltage calc., ionisation coeff. *(Rumanian)* 80−103746
Si, polycryst. p-n junction solar cells, grain-boundary and intragrain recombination currents 80−81442
Si, polycryst. rods, p-n junction appls. and transport props. 79−99612
Si, polycryst.-single cryst. p^+-n and n^+-p junctions, elec. charact. 80−11077
Si, polycrystalline, p-n junctions, solar cell appls. 78−56220
Si polycrystalline p-n junction deposition 78−10549
Si polycrystalline thin-film solar cells 79−57426
Si, prep. using laser pulse processing 79−69920
Si, radiation defects due to 30 MeV proton irrad. 78−71776
Si radiation detector DC cct., transient processes 77−70556
Si, reverse bias V-I charact., presence of acceptor states around Fermi level of amorphous Si 78−2445
Si, reverse biased, carrier conc. profiles, C-V charact. 77−32097
Si reverse-biased p-n junction DC characteristics interpretation *(Polish)* 78−91761
Si, sensor for high intensity solar flux mapping 78−40720
Si, shallow p-n junction, energy loss and escape depth of hot electrons 79−78159
Si, small signal equivalent circuit, finite carrier multiplication 80−65664
Si, solar cell, forward bias capacitance and current meas. for lifetime and band narrowing detn. 79−7892
Si solar cell array with concentration, design and development 80−45700
Si solar cell design and fabrication for concentrated light 79−61995
Si solar cells, junction formation techniques using spray-on polymer dopants, cost effective, high throughput 80−94014
Si solar cells, n^+-p, Li-counterdoped, radiation damage 80−94000
Si solar cells, photoreactance of p-n junction diodes 80−81464
Si solar cells, polycrystalline n^+/p, computer model of spectral response and photocurrent 80−55853
Si solar cells, polycrystalline p-n junctions, recombination currents, physical models 80−93892
Si solar cells, radiation damage annealing mechanisms and low temp. annealing 80−94003
Si solar cells, realisation by laser induced diffusion of deposited Sb 80−93998
Si solar cells, single-crystal, HV, multijunction, parameters and characteristics 80−89615
Si solar cells, solid source diffusion process for fabrication 80−93994
Si, subnanosec. current drops in delayed breakdown 80−75633
Si, subnanosec. current drops in delayed breakdown 80−75634
Si surface layers, impurities, elec. and photoelec. props. 80−2298
Si surface-controlling functions for ZnO/Si monolithic SAW convolver 77−88988
Si, technology and physics, review 80−34353
Si, thermal diffusion of Li, photostimulated using concentrated solar rays 77−51544
Si, thin sheet, Sb impurity profile eval. in p-n diffusion junction by anodisation and resist. meas. 79−46695
Si, through oxide As implantation, Ar implantation gettering 78−14802
Si, unified approach to breakdown phenomena 79−42630

p-n homojunctions continued
Si vacuum deposited polycryst. films, p-n junctions investigation 77−28249
Si vacuum sublimated thin film structure impurity distrib. 78−95354
Si wafer, migration of fine molten Al rich wires, vertical p-n function fabrication 78−68077
Si, with hot carriers, amplification 78−39203
Si with oxide surface, Ga diffusion into solid, doping profile 79−77621
Si:Al, P-diffused, recomb. centres, thermally stimulated capacitance meas. 77−72834
Si:Al p-n lamellar structures, processing by molten Al rich wire thermomigration 78−10068
Si:As, electron irradiated, majority carrier trap prod., effect of O_2 enhanced annealing 77−1151
Si:As, p-n junction form. by laser annealing, space charge region, effects on reverse current 80−54772
Si:As, shallow junctions by high-dose implants 80−96694
Si:As ion implanted shallow junction 80−70228
Si:Au, p^+-n junction, quantitative study of Au atoms by TSC method 80−2458
Si:Au diodes, diffused, influence of gamma irradiation, Au levels monitored 77−66199
Si:Au forward-biased, space charge recombination current variation *(Rumanian)* 78−19131
Si:Au n^+p diodes, deep level transient spectroscopy, system effects and data anal. 79−99501
Si:Au p^+-i-n^+ diode, double injection switching, effect of trapped space charge 77−1473
Si:Au p^+-n junction, small area, acceptor level conc., determ. from TSC curves 80−75631
Si:Au(Pt), heavily doped, gradual p^+-n junctions, trap levels *(French)* 80−34392
Si:B, N-implanted junction capacitance meas., appl. of dynamic lateral photovoltaic effect 77−85304
Si:B, p-n junction form. by B deposition and laser-induced diffusion 78−87690
Si:B,P, double implanted layer, n-p-n struct., single pulse laser annealing 80−49247
Si:B(BF_2), p^+-n junction form., ion implantation damage, leakage current 77−24334
Si:B(P), diffusion induced imperfections, laser annealing, rel. to junction characts. 78−75678
Si:B(P)(As), impurity diffusion from implanted layer, influence of radiation damage 77−76621
Si:Fe(Au)(Pt)(Ag)(Ti), photoionisation cross-sections and energy levels 79−87060
Si:H, amorphous, HV photovoltaic cells, design parameters 80−101105
Si:H, amorphous, in p^+-i-n^+ struct., hole diffusion length meas. 80−44712
Si:H, amorphous, p^+-i-n^+ struct. solar cells, material parameters and deposition condition optimisation study for higher efficiencies 80−45676
Si:H, amorphous, solar-cells, charge collection and spectral response 80−85275
Si:H, amorphous and crystalline, hydrogenation and dehydrogenation, luminesc. spectra 80−11477
a-Si:H film, glow discharge deposited, H profiles, doping level 80−84202
Si:In, doping conc., meas. by Hall, C-V and junction breakdown methods 79−14824
Si:Ir S-type diodes, characts. 78−56224
Si:K, ion implanted, influence of doping and annealing on carriers 78−38742
Si:Ni p^+n and n^+p diodes, thermally stimulated capacitance obs. of Ni acceptor levels 78−19137
Si:P dislocation p-n junctions, capacitive props. 80−20300
p-Si:P p-n junctions, dislocations investig. rel. to P diffusion, SEM, X-ray topography techniques 77−76433
n-Si:Pd Schottky diodes photocapacitance meas., photon and carrier capture cross sections 80−20309
Si:Pt, deep level, exam. by thermally stimulated current and capacitance techniques 79−1579
Si:Re diode, photocapacitance and induced photocapacitance spectra 77−4404
Si:Rh, p^+-n-n^+, n^+-n-n^+, p^+-n-p^+, structs., S- and N-type I-V characts. 77−43706
Si:S p^+-n junction, optical props., photocurrent meas. 77−4425
Si:Sb, in solar cell struct., heavily doped, dopant striation, SEM 79−39312
Si:Sb vacuum deposited coating, p-n junction, pulsed electron beam annealing doping, diffusion 80−75480
Si:V p-n junctions, thermal emission rates and capture cross sections of majority carriers at V centres 80−96980
Si:Zn, P^+-n-n^+ struct., deep doubly ionized centres, impedance calc. 79−11202
Si:Zn, p-n-n^+ and p-n-p struct., reson. characts. of impedance near excitation threshold of recomb. waves 80−20301
Si:Zn p-n junctions, I-V characts. using exact DC circuit model 79−95476
Si-Ge solid solns., p-n junctions, photoelec. props. obs. 77−1471
Si-poly Si; epitaxial crystal growth, recombination currents 77−76904
Si(:Au), gamma-induced trapping levels 79−87059
SiC (6H), blue-emitting diodes by CVD 80−97439
SiC, α-β heterojunctions, spectral characts. *(Russian)* 77−63467
SiC p-n junction, electroluminesc. 80−97343
SiC p-n junction, epitaxial, grown by sublimation, elec. and struct. props. *(Chinese)* 80−60067
SiC p-n junction photodetector, spectral characts. 77−41685
SiC p-n junctions, current-voltage characts. 80−60073
SiC p-n junctions, electrolum. spectra and kinetics 80−66305
SiC reverse biased p-n junctions, prebreakdown violet luminesc. 80−7420
SiC, vapour grown, elec. breakdown field 78−19135
B-SiC:Al, ion implanted, elec. props. and luminesc. meas. 77−12443
SiC:Al^+ p-n junctions, elec. props., defect effects 80−15594
β-SiC:B, diffused structures, current-voltage characts. 78−47865
SiC:B, LED with new low-temp. alloy 79−73582
β-SiC:B p-n junction, IR electroluminesc. spectrum 77−44067
SiC:silumin, LED, highly stable *(Russian)* 77−8183
$ZnGeP_2$ p-n homodiode, polarisation photosensitivity and photopleochroism spectra 80−107866
ZnO, varistor action, homojunction breakdown mechanism 78−60193

p-n homojunctions continued
ZnSe:Cu, I ceramic, injection electroluminesc. of p-n microjunctions 80−40163
ZrO_2-Y_2O_3 (10 mole%), electron transport, elec. induced p-n junction 77−43597

p-n junctions
see also p-n heterojunctions; p-n homojunctions
1/f noise, expt. and analytical dependences *(Russian)* 79−19648
1/f noise in barrier layers 79−82666
abrupt, forward-biased, transition region behaviour anal. 77−76909
abrupt, space-charge layer capacitance, approximation eqns. 77−35989
amorphous semiconductors, barrier controlled charge carrier transport in structures *(German)* 79−47162
asymmetric junctions, revised model 79−99607
avalanche breakdown voltage and differential resistance *(Russian)* 78−47858
avalanche multiplication 78−84289
avalanching, temp. dependences 78−14808
background dopant density calc. fron C-V meas. 78−26936
bevelled p-n junction in Si power device, elec. field in controlled region and blocking capabilities determ. 77−1474
bevelled shallow junctions, spreading resistance data correction 80−80358
boundary conditions 80−20295
boundary layer theory 77−24613
Bourgoin mechanism, method for determ. 77−43534
capacitance, temp.-depend., by space-charge methods 78−91758
capacitance meas., appl. of dynamic lateral photovoltaic effect 77−85304
capacitance meas., using bridge circuit with analogue multiplication *(Bulgarian)* 78−57977
capacitance transients, appl. to deep level impurities spectrometry 77−51816
convertors, photoelectric, optical methods for checking parameters of semiconductor doped layer 80−93869
deep impurity concentration profile in diffused junction, capacitance meas. 78−26945
deep impurity levels, spectroscopic determination by compensation method 80−108229
deep level profile anal. by double deep level transient spectrosocpy 77−20378
deep level properties measurement, capacitance spectrometer *(German)* 80−15471
defect and impurity centre detection, junction capacitance and current techniques 78−10550
defects, SEM 79−23507
degenerate junctions with position-dependent band struct., density-voltage relations 79−87150
depletion layer, determ. of doping levels using nondestructive IR emission meas. 78−95338
depletion layer capacitance in abrupt junction, theory 78−52067
diffused, concentration profile of deep-level impurity by capacitance method 77−55299
diffused, space-charge recombination current 80−88623
diffused, transition capacitance calc. methods, comparison *(Rumanian)* 80−88625
diffusion layer, method for determining dopant and defect distribs. using polishing agent 79−37727
diode, cut-off freq. 77−39923
diode, normal modes for material parameter determ. 77−4426
diodes, Schottky vs. p-n, for various appls., charge carrier speed *(Dutch)* 80−65662
direct conversion of chemical energy into elec. energy 78−39201
directly biased, current-voltage charact. effect of generation-recombination *(Rumanian)* 78−2553
dislocation effects in semicond. devices 79−82221
dislocation electric barrier appl. in devices 79−82551
dislocations, TEM/SEM observations comparing diffr., elec. and luminesc. contrast 78−38714
doping profile, arbitrary, determ. in p-n junctions 78−88021
double injection into p^+-π-n^+ structures 79−42627
double injection p-i-n structures in magnetic field 80−107899
double-injection negative differential resist. problem, surface recomb. effects 78−88024
dynamic base capacitance and time const. 78−68076
electric field maximum formulation for abrupt p-n junction with one side heavily doped 80−75629
electrical parameters, optical derivative meas. 80−2455
electrical parameters determ. by electron probe method 79−9259
electrically active stacking faults 79−78191
electron-hole pairing, collective modes, current states 77−39838
electron-phonon scatt. 80−24997
excess currents 78−56223
Fletcher's boundary conditions 79−73571
Fletcher boundary condition, inconsistencies in original form 79−38153
forced current pinching in p-n-p-n structure due to action of base current 79−95487
Gaussian graded p-n junction under high forward bias, depletion region width calc. 79−47157
generation recombination current, noise reduction, SRH centres in space charge layer 77−76905
heat pulse technique for bonding thermoelectric modules contacts 80−107904
heavily doped device, collection efficiency and surface recomb. vel. modulation 80−20291
high-low junction, heavy doping effects on minority carrier reflecting props. 79−42623
high-power large-area inhomogeneous, I-V characts. theory 78−47859
hot carrier, as a contact with negative differential capacitance and conductance 79−69590
hot carrier junctions, current-voltage characts., effect of space charge defects 80−25001
hot carrier-voltaic effect, electron emitter and light detector appls. 77−76861
hot-carrier, instability of EMF 78−26941
HV, current induced by electron probe in space charge region 79−24065
hyperabrupt with exponentially retrograded n-region, C-V index calc. 78−47860
IC phototransistor static characteristics, effect of insulating p-n junction *(Russian)* 78−52069
impurity detection by admittance-freq. dispersion 77−43536

p-n junctions continued
impurity ions, overcharging, effect on movement in p-n junction *(Russian)* 80−11079
impurity profile meas., two-freq. method 79−23633
impurity profiles within shallow p-n junction, differential spreading resist. data 77−7755
inhomogeneous, theory of LF noise 78−2559
inhomogeneous semiconductor structure with p-n junction, nonlinear current-voltage characts. 77−11929
injected carriers, detection in operating junction devices, IR emission obs. 79−38151
junction termination extension technique for increasing avalanche breakdown voltage and controlling surface elec. fields 78−47866
laterally illuminated, spectral response calc. 77−8180
layer system, theory of Hall effect 79−69589
linearly graded, linearly graded, characterisation 80−6962
low-frequency noise 78−6419
luminescence due to photoinduced injection 78−10939
magnetic injection of minority carriers 80−107900
majority carrier flow model, diffusion effects in equilib. field distrib. 77−51808
majority carrier flow model, props. of forward conducting diode 77−35986
microplasma position determ. method in high-voltage junctions 77−20407
microwave reflection *(Russian)* 79−95481
minority carrier charge accumulation effects on semicond. diode parameters *(Russian)* 79−73569
minority carrier diffusion length determ., using angle-lapped p-n junctions 79−42631
minority carrier diffusion length determ. near p-n junction, SEM appl. *(French)* 78−43466
minority carrier diffusion length meas. by short-circuit current ratio 80−31849
minority carrier diffusion lengths meas. using SEM 79−60848
minority carrier lifetime-meas. technique using SEM-electron beam induced current 80−59999
minority carrier surface recombination velocity, lifetime, AM electron beam determ. 79−87145
minority carrier transport parameters determ. using electron microscope 80−65665
MOS structures with external p-n junction, linear gate volt., impulse-current behaviour *(German)* 79−56319
MOS-structure, with adjoining reversed biased p-n junction, charge pumping current and reverse current *(German)* 80−88636
multilayer p-n systems, nonstationary photoelectric effect *(Russian)* 77−76908
multilayer structure with p-n junctions, excess cond. relax. 78−39199
n^+-p junction, injection properties *(Russian)* 78−23159
n^+-p spherical junction, strong impact ionisation 78−39202
narrow band gap semiconductor multilayers with p-n junctions, relaxation and photocurrent analysis 79−7883
noise diagnostics *(Czech)* 78−10544
nonequilibrium processes in open systems, fluctuation dissipation relations, p-n junction appl. *(Russian)* 79−58668
nonlinear small signal distortion, numerical anal. 77−11989
n.p.i structure, current-voltage characts calc. and anal. 77−20415
one-sided abrupt junctions, distinction between avalanche and tunnelling breakdown 78−56211
p^+-π-n^+ structure with low cond. region, double injection, IU characts. of single-level semicond. 79−56296
p^+-n, n^+-p solar cell structures on polycrystalline material, performance 80−89640
p^+-n junction diffusion capacitance calc., discrepancy problems 80−60068
p^+-n junction shallow, surface recomb. effect on props. 79−82664
P^+-P-N^+ junctions, thermocapacitive behaviour *(Spanish)* 80−2457
p^+np^+ diode below reach through, current voltage characteristics 79−56292
p-i-n diode, influence of high temp. processes on props. of high resistivity region 77−35988
p-i-n structure, forward biased, with band to band Auger recombination, numerical simulation 79−7879
p-n junctions, microplasma noise, stochastic model, breakdown voltage of microplasma 78−47854
p-n-p-I-M structure, tunnel cathode thyristor, theory of switching effect 77−39930
p-n-p-n structures, turn-on at high voltages and high currents 77−1475
photoconverter, bilateral sensitivity, n^+-p-p^+ structure, volt-ampere characts. under illumination 80−40855
photodiode, switching process and plasma effects, theory 80−65667
photodiode terminology 80−70800
photoeffect, quantity effective diffusion length *(Russian)* 78−56212
photoeffect obs. with flying light spot 79−28401
photoelectromagnetic effect, current research status, review 79−69559
photomagnetic current generated by front illum. 79−51666
planar, junction breakdown walkout exam. 78−60199
planar, nondestructive determ. of depth by SEM 78−19132
planar junction, oxide thickness and breakdown voltage relationship 79−99608
potential step meas. by SIMS 80−34503
pulsed radiation effects on elec. cond. and EMF relax. 77−89842
quantum statistical theory in thermal equilibrium 78−39197
quasiequilibrium equations 78−47853
recombination phenomena as function of temp. and applied voltage *(Polish)* 80−53294
relaxation semiconductor, theory of carrier transport in p^+-ν junction 79−60914
reverse biased, fluctuations of returning carriers current 79−38152
reverse biased, TEM, defocused images, stationary field approx. 78−67628
reversed biased, with inhomogeneous impurity distrib., space-charge layer 78−30982
Schottky gate n-p structure, depletion layer, pot. fluctuations 80−88512
secondary breakdown calc., effect of thermally generated carriers 77−43703
SEM, diffusion length meas. of minority carriers, accel. voltage of primary electrons effect *(Czech)* 78−34844
SEM, EBIC mode, stroboscopic principle and resolution enhancement 80−100515
SEM examination, modified REhMP-2 system 78−58095
p-n junctions continued
semiconductor diode, with overcompensated semicond., deep centres, isothermal relax. of current 78−52072
semiconductor junction device, quasi-equilib. assumption 79−91130
semiconductor junction device quasi-equilib. assumption, quasi-Fermi level approach 79−91128
semiconductor junction device quasi-equilib. assumption, quasi-Fermi level calcs. 79−91129
semiconductor layers, thin, theory of lifetime meas. with SEM, transient anal. 80−88573
semiconductors, deep level carrier trapping and emission, transient spectroscopy, book contribution 80−80216
short circuit, SEM investigation 80−6957
small signal equivalent circuit, finite carrier multiplication 80−65664
solar cell, front surface field effect, spectral response, theory 80−76633
solar cell, photoinjected carrier lifetime meas. by reverse voltage pulse response 80−45664
solar cell, photovoltaic effects in p-n junctions, Schottky barriers, review *(Czech)* 77−24583
solar cell, two-stage, fraction of radiation usefully converted, power prod. efficiency 80−30477
solar cell response to concentrated sunlight and partial illum. 79−61996
solar cells, minority carrier lifetime meas. from photo-induced open-cct. voltage decay 79−87990
solar cells, polycryst., recomb. at grain boundaries, effect on photoresponse 80−108796
solid state physics rel. to solar cells, review 80−49601
solid-state electronics, introductory theory, book 80−22160
space charge region impurity centre parameters, thermally stimulated current 77−85237
structure during preparation, X-ray topography visualisation *(Russian)* 78−26386
surface channel tunnel junctions, subband spectroscopy 78−64104
surface depletion and inversion, arbitrary doping profile, theory 80−107912
surface flicker noise at high injection level 77−47892
surface recombination, effect on excess charge carrier distrib. and on base current 77−39866
TEM image interpretation, p-n junction with one-sided step model internal field topography 79−82129
TEM image interpretation 79−51659
temperature effect of forward current switching transients 77−62988
temperature measurement using several junctions *(Polish)* 80−13075
thermal second breakdown prediction test 79−82668
thermally assisted field emission near precipitates 78−14809
thermophotoelectric effects in junction with hot carriers 79−73576
thinned, TEM image interpretation 77−20414
three-frequency parameter systems, equivalent conductivities, partially opened p-n junctions *(Russian)* 80−24998
transition region anal. using quasi-equilibrium assumptions 80−6963
TSC, impurity centre parameter determ. 78−47857
tunnel junction, photoinduced transitions, theory 80−65669
tunnel junctions, phototransitions accompanied by impurity scatt. 80−107901
tunnelling and negative resistance phenomena, book 78−26947
US wave effect on effective current relaxation time in base 77−4434
variable-gap, current-voltage and spectral characts. 79−7885
variable-gap p-n-p structure, impedance 77−43707
volt-farad characts. meas. with semiautomatic installation 77−41643
voltage-current characts., fast neutron irrad. effects *(Russian)* 80−65659
voltampere characteristics expression, for uniformly distributed impurities *(Russian)* 78−23158
X-ray diffraction by semicond. with p-n junctions, photoelec. EMF produced *(Russian)* 79−8225
CdTe-based, photoeffect quantum efficiency depend. on photon energy *(Russian)* 79−78168
GaAs:Cr, carrier transport in p^+-ν junction based on relaxation semiconductors 79−65543
Ge surface with p-n junction, photovoltaic effect under conditions of surface recomb. of H atoms 77−66185
$Pb_{0.82}Sn_{0.18}Te$, layers on mica substrate, Hall constant peculiarities 80−75588
Si p-n junctions, secondary breakdown, pre-mesoplasma state expsn. *(Russian)* 79−56723
Si:In, p-n junction, spin-dependent recomb. at dislocations, revealed at reverse current 79−24062
ZnO-on-Si SAW convolver development 77−27430

P-V-T relations *see equations of state*

pacemakers
see also patient treatment
60 Hz field and current effects on implanted cardiac pacemakers 78−88769
aortic shear stress reduction by cardiac pacing 78−40239
arrhythmia treatment by temporary cardiac pacing 77−81648
arrhythmia treatment with permanent cardiac pacing 77−81674
asynchronous cardiostimulators, increasing interference immunity 80−3868
atrial electrode placement, transmediastinal retrocardiac and transvenous endocardial methods 77−81685
atrial fixation permanent transvenous corkscrew electrode 77−81751
atrial tracking pacer, artificial conduction system 77−25608
atrial-triggered cardiac pacing method and long-term results 77−81690
atrioventricular conduction disturbances with permanent pacemakers 77−81672
atrioventricular sequential demand pacemaker, R-wave sensing methods *(Japanese)* 79−5406
automated test system developments 80−30944
automatic threshold following pacemaker concept and application 77−81671
autoregulating pacemaker responsive to metabolic requirements 77−81726
base rate follow-up reliability for long-term pacing 77−81694
batteries, neutron radiography investigation of electrolyte, USA National Bureau of Standards 80−56179
battery characteristic meas. microcalorimeter 80−30936
battery internal loss characterisation calorimeter 80−30934
battery longevity estimation using statistical methods 78−57131
battery microcalorimetric testing 80−30933
battery self-discharge process assessment by microcalorimetry 80−30935

pacemakers continued
biogalvanic and biofuel cells, animal expts. 77−81657
biogalvanic implanted pacemaker performance 77−81732
bipolar sensing for demand pacing, effect of interelectrode distance 78−40418
bladder pacemaker, implantable induction device *(Japanese)* 78−31971
body potentials and currents from ELF elec. fields and household appliances, pacemaker interference 78−88770
brain, energy optimisation, epileptic seizure control appl. 77−52934
cardiac, isotopic power supplies appl. *(Spanish)* 78−15922
cardiac pacemaker, high-reliability hybrid IC procurement 80−30942
cardiac pacemaker electrode threshold current and optimal design *(Japanese)* 78−53569
cardiac pacemaker function control, value of patient participation 77−81716
cardiac pacemaker long-life battery test results 77−81735
cardiac pacemaker principles, specifications and testing, review 78−69258
cardiac pacemaker reliability technology workshop, Gaithersburg, USA (Oct. 1977) 80−27038
cardiac pacemaker responses to power frequency signals 78−88771
cardiac pacemaker RF susceptibility tests 78−48935
cardiac pacemaker semiconductor component reliability trends 80−30943
cardiac pacemaker treatment principles and experience 80−8213
cardiac pacemakers and batteries, microcalorimetric study 78−57130
cardiac pacing, symposium, Tokyo, Japan (Mar., 1976) 77−81666
cardiac pacing as diagnostic tool 77−81629
cardiac stimulator for evaluation of mech. and elec. responses 79−44058
cardiostimulator, implanted, contactless rhythm indicator 79−39602
Chagas' cardiomyopathy treatment with implantable pacemakers 77−81681
CMOS R wave inhibited threshold adaptive pacemaker 77−25610
computer-controlled stimulator for ventricular myocardial function analysis 77−60267
coronary bypass surgery, left ventricular function and myocardial metabolism evaluation by atrial pacing 77−81646
coronary care unit emergency cardiac pacing experience 77−81651
coronary heart disease, demand pacing hazards 77−81668
demand pacemaker, with adjustable-pulse-width, clinical experience 77−81697
demand pacemaker, with variable-pulse-width, clinical experience 77−81696
demand pacemaker interference sensing functions 78−57123
demand pacemaker leads, time and freq. domain comparison of unipolar and bipolar electrograms 78−44726
demand pacemaker standard test signal proposal 77−81721
demand pacemakers, false sensing 77−81708
development progress 78−3646
Devices, output characts. 77−90963
diode, implanted, cardiac pacing of dogs, long-term viability 78−44716
Dutch development of medical physics *(Dutch)* 80−3877
electrocardiostimulator parameter tester 77−21658
electrode effects on pacing thresholds 78−36071
electrode electrochemical structure and possible improvements 77−81745
electrode geometry rel. to pacing threshold and R-wave sensing 77−25611
electrode insertion via cephalic vein, thrombosis obs. 77−81714
electrode leads, transvenous, anchoring measures 79−84008
electrode longevity analysis 77−81750
electrode material evaluation 77−81742
electrode orientation, simulation of vol. conductor effects on cardiac dipole 78−28108
electrode stimulating and sensing characteristics 77−81743
electrogram, filtering characteristics of pacemaker electrodes 77−81744
electrostatic discharge sensitivity grouping 80−30941
EM interference by diathermy, simulation models 79−84007
endocardial balloon-tipped pacing catheter 77−81752
endocardial electrode, low-threshold 77−81748
endocardial electrode lead and pacemaker failure, actuarial analysis 80−30945
endocardial electrode sensing characts. for optimal pacemaker system design 78−36072
endocardial electrogram and pacemaker sensing 77−81720
endocardial screw electrode stability enhancement 77−81746
energy sources, clinical use 77−81731
epicardial electrode implantation 77−81703
fibrillation threshold for intracardiac catheter, vs. current flow duration and electrode area 77−37101
fixed-rate pacemaker competition hazards 77−81706
follow-up network and computer-assisted pacemaker centre 77−81691
function analyser, automatic, for pacemaker patient surveillance 78−3679
function check by patient self-monitoring system 77−81718
galvanic coupled interference effects due to electronic sensor switches and electrostatic discharges 77−81753
IC advantages and disadvantages 77−81725
impedance determination in man from resist. meas. 78−40417
implantable, for increasing heart rate 78−7533
implantable cardiac pacemakers, non-polarizable stimulating electrode development 79−92428
implantable heart pacemakers, review *(German)* 79−100787
implantable lead performance evaluation, status report 78−57135
implantation, therapy/measuring combined unit *(German)* 78−7519
implantation site breast cancer development 77−81713
implantation surgery, intracardiac ECG derivation during electrocoagulation 78−40397
implanted, automatic parameter assessment system 78−11778
implanted cardiac pacemaker experience and trends 77−81701
implanted cardiac pacemaker function analyser 77−81717
implanted cardiostimulator pulse recording 77−78041
implanted electrodes, signal source impedance 80−56275
implanted pacemaker patient long-term surveillance unit 77−81722
implanted pacemaker patients, physical fitness evaluation 77−81702
impulse and pulse rate self-monitor 77−81719
induction pacemaker with 100 kHz transmission during pulse intervals 77−81728
interference due to amateur radio installations, cars, domestic appliances 79−25155
interference simulation by models 78−81069
interference test signal generator, operation and cct. *(Spanish)* 78−20315

pacemakers continued
intermittent runaway malfunction 77−81712
intractable tachyarrhythmia treatment with pacemaker and β-receptor blocking agents 77−81675
ischaemic heart disease studied by cardiac pacing 77−81628
lead failure type discrimination 78−53570
lead fluid penetration detection by capacitance meas. 77−81749
lead wire fracture 78−57134
leak testing methods for cardiac pacemakers 78−57133
malfunction diagnosis, ECG before and after thoracic wall stimulation 77−81707
medical electronics, new forms and techniques 80−3856
microcalorimeter for nondestructive anal. of pacemakers and pacemaker batteries 79−57813
microprocessor based pacemaker tracking system, hardware considerations 78−36070
microprocessor-controlled dual-channel stimulator 80−56279
microwave interference effects on implanted pacemakers 79−92421
monitoring by telephone 77−52903
muocardial infarction ECG diagnosis in patients with transvenous ventricular pacemakers 77−81624
myocardial and endocardial screw-in electrode expts. 77−81747
myocardial infarction, antiarrhythmic drug and hyperkalaemia effects on ventricular electrogram 77−81667
myocardial infarction diagnosis in endocardially paced patients 77−81625
myocardial pacing threshold determ. with external RF transmitter 77−81730
myopotentials and endocardial potentials causing pacemaker malfunction 77−81723
NDT by holographic interferometry and optical correl. 80−40659
oesophageal pacing in infants, conductive rubber electrode 77−81741
ohmic electrode-tissue contact resistance and voltage applied to myocardium, meas. method 80−67284
pacemaker, batteries, characterisation of internal power losses by calorimetry 78−92747
pacemaker computerised data management systems 77−81698
pacemaker impulse and pulse rate self-monitor 77−81719
pacemakers, survival of heart block patients 77−81686
pacing threshold and sensed signals, influence of electrode positions 77−81729
paroxysmal supraventricular tachycardia management by scanning pacemaker system 77−81676
paroxysmal supraventricular tachycardia termination by overdrive pacing 77−81649
patient and medical education journal 77−81700
patient follow-up using telephone-telemetry system 77−90957
patient simulator 80−41322
performance testing automation using microcomputer *(German)* 78−81068
permanent pacing, analysis of 536 patients 77−81688
permanent right ventricular pacing, right bundle branch block patterns 77−81704
pervenous atrial sensing and pacing 77−81684
power source, Li-I hermetically-sealed cells, long life expectancy 80−40850
power source development 78−15917
power sources, comparison of Hg_2O_3-Zn and Li based systems 77−52920
power supplies, biogalvanic, biofuel cells, implant in dogs, exp. results 77−52935
prognostic determinants of late survival of patients 77−81693
programmable pacemaker with digital memory *(Chinese)* 80−36192
protein detection in implanted cardiac pacemaker epoxy housing 79−25156
pulse duration measurement, thousandfold pulse duration convertor for automatic pen recorders 77−56521
pulse generator design, manufacture and performance documentation for reliability 77−81715
pulse generator replacement and other problems 77−81705
pulse generator replacement indicator 77−81692
R-wave detection with intramyocardial electrodes 78−44713
radioisotope-powered cardiac pacemaker 77−81734
radiotherapy machine ionising radiation and EM interf. effects on cardiac pacemakers 79−62406
rate-dependent left bundle branch block patients, atrial pacing expts. 79−44019
reliability prediction, appls. and pitfalls 78−57132
reliability technology conf., Gaithersburg, USA, (Jul. '76) 78−57129
resistance and facilitation gradient demonstration in cardiac pacing 77−81669
respiration linked cardiac pacemaker system 80−26416
response to ventricular pacing 77−81525
selection criteria with different Li batteries *(German)* 78−3670
senile dementia patients, unrecognised intermittent bradycardias, rel. to cardiac pacing 77−81644
sensitivity testing, sine squared waveform generator 77−25612
sick sinus syndrome, cardiac pacing problems 77−81680
sick sinus syndrome applications of cardiac pacing 77−81679
sinoatrial bradycardia treatment by transvenous atrial synchronised pacing 77−81683
sinus node function electrophysiology rel. to long-term cardiac pacing 77−81673
sinus node response to premature atrial stimulation, microelectrode analysis 77−81630
stimulation threshold, time var. 77−25609
stimulation threshold noninvasive meas., long-term follow-up 77−81711
supraventricular tachycardia, diagnosis and management, instrumentation and therapeutic techniques, review 79−39598
surveillance by telephone photoanalysis 77−81699
survey of 2243 pacemaker implantations in 1228 patients 77−81689
survey of clinical results over 10 years 77−81687
systemic lupus erythematosus treatment with permanent pacemakers 77−81682
T-wave inversion obs. 79−44063
tachycardia termination system, microcomputer-based 80−56280
tachycardia treatment by implanted pacemaker 77−81677
ten years operational life using LiI battery, design *(German)* 79−12031
testing in vivo, computerised system 80−94412
therapy, importance of R-vector direction 79−44049
thick film resistor trimming for pacemakers 78−31977

pacemakers continued
time constant variations with normal and malfunctioning electrodes 77−81724
transthoracic intramyocardial pacing wire for emergencies 78−69254
unipolar demand pacemaker myopotential inhibition prevention 77−81709
unipolar endocardial long-term pacing, stimulation threshold behaviour 77−81710
unipolar stimulation system with bipolar sensing 79−70705
vector cardiograph for pacemaker pulse display 80−41325
vector cardiographic assessment system for automated testing of implanted pacemakers, PDP 11/40 computer, disc storage 78−11771
ventricular arrhythmias and depolariation effect of simultaneous biventricular pacing 77−81642
ventricular muscle excitation threshold current rel. to electrode area, volume effect 77−81670
ventricular programmed pulse generator, testing by waveform generator and cardiac simulator 79−16351
ventricular synchronous demand cardiac pacemaker advances 78−77152
ventricular tachycardia termination by rapid ventricular pacing bursts 77−81678
Al anode, implanted in heart-blocked dog, AC impedance and corrosion investig. 77−60297
Hg-Zn rechargeable, free from EM interference 77−40925
Li battery long use cardiac pacemaker choice, technical considerations *(German)* 78−88765
Li pacemaker battery similarities and differences 77−81737
Li powered pacemaker status and performance 77−81740
Li-$AgCrO_4$ pacemaker cell construction 77−81739
Li-I cell solid state, cardiac pacemaker power source, testing 79−66584
Li-I_2 batteries for cardiac pacemakers, capacity rating system 80−97773
Li-I_2 pacemaker battery electrolyte exam. by neutron radiography 80−30940
Li-I_2 pacemaker cell end-of-life characteristic approximation 80−30937
Li-I_2 power cell accelerated discharge test for battery longevity model 80−30938
Li-$SOCl_2$ battery for implantable cardiac pacemakers 80−30939
LiI hybrid IC pacemaker, reliability, experience 77−81736
LiI powered pacemaker types evaluated 77−81738
NiCd rechargeable cardiac pacemaker system clinical experience 77−81727
^{147}Pm fuelled betavoltaic pacemaker system status 77−81733
^{238}Pu for cardiac pacemakers, radioactive controls *(French)* 77−44752
^{238}Pu fuelled cardiac pacemaker, evaluation *(French)* 77−44833
^{238}Pu isotopic pacemakers, 2 to 4 years' follow-up 77−81695
^{238}Pu, sources for cardiac pacemakers, manufacture and safety tests *(French)* 77−44751
Ti as anode and container passivation and muscle twitch 77−40934
Ti as anode and container 79−44052

packaging
see also encapsulation; modules
biological fluid mixing and bottling unit improvement 78−61291
buried-heterostructure laser packaging for wideband optical transmission systems 78−74920
electronic components, H_2O content determ., plasma chromatograph-mass spectrometer applic. 78−86379
fibre optic packaging concept, interconnection system 79−90026
IR detector system limitations 78−77988
leak detection by He mass spectrometer *(French)* 77−37901
multifuel fluidised bed combustion packaged boiler to supply 10000 lb/h saturated steam at 100 psig 80−108779
offshore seismic exploration streamer cable connector design and programming 77−25803
optical fibre fabrication, attenuation, packaging and interconnection properties 77−27373
optical fibre packaging in loose fitting tubes of orientated polymer 78−1338
optical fibres, loose tube packaging, buckling obs. 78−25962
optical fibres, packaged, tensile performance 79−55212
package, potential source of corrosion 79−70230
polyimide thin film vacuum deposition 78−39695
radioactive materials, package design, construction and testing for safe transportation 80−63412
radioactive materials, safe transportation, using type A, exempt and LSA packages 80−63401
SAW 300 MHz resonator oscillator close-in phase noise rel. to vibration 79−55289
Schottky-barrier diode, for submillimetre heterodyne detection 77−37983
semiconductor packages, hermetically sealed, calibration and anal. of moisture by gas mass spectrometry 80−90928
solar cells, for space appl., coverglass development 79−48133
solar cells and arrays, wraparound contact, status and space appl. 79−48132
temperature-stabilised enclosure for 54 standard cells 77−5872
tobacco shreds, determ. of filling capacity, friction effects *(Japanese)* 78−7167
weights and measures, conference, Washington (1978) 80−27260
Al_2O_3 moisture sensor for sealed hybrid packages 77−87754
H spacecraft maser, operating development model 79−54105
PbSe IR detector, pollution detection and control appl. 78−24378
Si detectors, packaging approaches, review 77−10108

packing *see packaging*

paging *see virtual storage*

pair algebra *see algebra*

pair annihilation, electron *see electron-positron interactions*

pair breaking, Cooper *see Cooper pairs*

pair production, electron *see electron pair production*

pairing, Cooper *see Cooper pairs*

pairs, electron *see electron pairs*

palaeomagnetism
Abitibi greenstone belt, palaeomag., Archean apparent polar wander curve construction 77−70596
AC demagnetisation apparatus, design characts. 78−85733
Adelaide Geosyncline, Australia, Late Precambrian palaeomagnetism 80−101325
Afar depression, palaeomagnetism of lavas from axial zone 77−37126
S.Africa, kimberlites, palaeomagnetic obs. and tectonic implications 80−109093
palaeomagnetism continued
African palaeomagnetic pole, determ. from Cambrian forms. in Morocco *(French)* 77−37125
N.African shield palaeomagnetic situation at end of Pan-African Orogeny *(French)* 80−85579
Alaska, tectonic implications of palaeomag. data 77−32998
Alcaparrosa Formation (Upper Ordovician), Argentina, palaeomagnetism and K-Ar age 78−96135
S.Alps, Late Mesozoic pelagic limestone, megatectonic obs. from palaeomagnetism obs. 80−109095
S.Alps, western region, palaeomag. and rock magnetic props. of Permian volcanics 80−89948
Amadeus Basin, Central Australia, palaeomag. directions rel. to Precambrian-Cambrian boundary problem 79−29697
N.America, palaeopoles and palaeolatits, displaced terrains 80−12367
N.America, unconventional Proterozoic palaeomag. polar wander path and advantages 79−66619
N.American pole wandering, evidence from Montana Early Eocene intrusions 80−104868
ancient geomagnetic field intensity, early research 77−37131
ancient magnetic field intensity determ. by nonthermal method 77−52980
ancient oceanic lithosphere, mag. props. as alteration indicators, Othris ophiolite example 80−8297
Antarctic igneous rocks, palaeomag. and K-Ar age 80−12332
E.Antarctica, Mesozoic lava flows in Dronning Maud Land 80−30984
Antarctica, palaeomag. results and test for oroclinal bending 78−73311
N.Appalachian-Caledonides and Acadian Orogeny, palaeomagnetic results 77−9390
Appalachians, Newark Trend igneous rocks, palaeomagnetism 80−51320
apparent polar wander path for Mexico, tectonic implications 79−25191
Archaean rocks from Superior Geotraverse, regional palaeomagnetism 80−30980
Archaean Shelley Lake granite, ^{40}Ar-^{39}Ar dating of magnetizations 80−30982
archaeological ceramics, Peru, geomag. variations over last 2000 yrs. 80−94455
archaeomagnetic data compared with analytical representation of geomag. field for last 2000 years 78−73305
archaeomagnetic field determ. and secular var. in Caucasus 78−73309
archaeomagnetic field magnitude, rapid changes 79−74830
archaeomagnetic polaeointensity study of Hohokam potsherds from Snaketown, Arizona 78−44769
archaeomagnetic polarity excursion, aboriginal fireplaces, thermoluminescent dating 77−21679
Argentina, El Salto-Almafuerte lava flows 78−85471
Arizona, palaeomag. poles and polarity zonation from Cambrian and Devonian strata 78−28156
central Arizona, reversal chronology from volcanic sequence rel. to ocean floor polarity record 80−72419
Arkansas, St. Joe Limestone, Early Carboniferous 80−21628
Armorican Massif, France, Late Devonian to Early Carboniferous palaeomag. poles rel. to tectonics 79−84100
Arran dykes of British Tertiary igneous province, palaeomagnetism and ages 78−73306
ash-flow tuffs, microanalytical recognition of TRM components 80−72497
Asia, evidence for large Cainozoic crustal shortening from palaeomag. data 78−57189
N.Atlantic, geomag. field Late Tertiary secular var. 80−109094
E.Equatorial Atlantic, magnetic anomalies, Jurassic spreading and reversals 77−64253
Atlantic Jurassic red sediments from DSDP leg 11, remanent magnetisation 77−81787
N.Atlantic Ocean, mag. anomalies rel. to struct. of S.E.Greenland continental margin 77−33014
S.Atlantic Ocean, plate kinematic implications of mag. anomalies and equatorial fracture zone trends 78−85527
S.Atlantic Ocean opening, prior and post continental movements from palaeomag. data 77−21744
peri-Atlantic Precambrian 79−5451
Mid Atlantic Ridge, palaeomag. studies, direct test of Vine-Matthews hypothesis 79−34734
SE.Australia, Lake Devonian palaeomagnetic field, Lochiel Formation and Catombal Group 78−28163
Australia, palaeomag. pole positions for Mesozoic 78−20356
Australian Mesozoic palaeomag. pole position 77−2098
Australian Mesozoic revised palaeomag. data rel. to Gondwanaland breakup 77−52984
Austria, palaeomag. data from Northern Calcareous Alps, tectonic implications 79−53307
averaging out of secular variations, theory 80−61755
Bakersfield, California, study at nuclear power plant site 78−40487
basalt flows from Absaroke Mountains, Wyoming, palaeomag. study 77−86765
basalts, from Egypt, palaeopole position determ. 79−25188
basalts, Lower Silesian, K-Ar ages, Tertiary polarity events 78−53614
basalts, mag. grains nature and implications for palaeomag. 79−84243
beach ridges in S.Australia, palaeomag. chronology rel. to Milankovitch theory of ice ages 80−98307
Beaufort Sea sediment cores, NRM, geomag. excursion record 78−20349
Belchertown pluton, W. central Massachusetts, palaeomag. evidence for tectonic rot. 77−44919
Bingham distrib. function in palaeomagnetic studies 80−72649
Black Sea, mag. anomalies and palaeopoles rel. to mantle material intrusion age *(Russian)* 78−85473
Blue Mountains, Oregon, Jurassic plutons tectonic rot., palaeomagnetic obs. 80−109099
book, palaeomagnetism and plate tectonics 80−36789
Boothia Uplift, Canada 79−57846
Borrowdale Volcanic Group, English Lake District, palaeomag. results 77−32984
Borzsony Mountains, Hungary, Miocene rocks palaeomag. 78−32011
Botwood Group and Mount Peyton Batholith, Newfoundland, orogenic history 80−3917
British Columbia, geotectonics of Cretaceous and Eocene plutons, palaeomag. fold test 77−91090
British Columbia, north-central, northward displacement during late Cretaceous/early Tertiary 80−76955

palaeomagnetism continued
British geomagnetic master curve 10000-0 yr B.P. for dating European sediments 79−70740
Brunhes epoch palaeosecular var. studies in volcanic province, Germany 79−25198
Butte mining district, Montana, palaeomagnetism, rock magnetism and aspects of structural deform. 80−101326
Cainozoic field inversions, W.Turkmenian data 79−44098
Cainozoic results, 1927-75 catalogue 77−52978
N.Calcareous Alps, Permo-Triassic red sandstone 80−56358
Caledonian palaeomagnetism, tectonic implications 79−88244
N.California, Medicine Lake Highland lavas, inclination anomalies 79−34735
Cambrian red beds, Cartaret, Normandy, palaeomagnetic obs. 80−109088
Cambrian rocks, Bohemian Massif, palaeomag. stability tests 79−39649
Cambrian volcanites in Quebec Appalachians 79−62429
Cambro-Ordovician redbeds, Armorican Massif, France and Channel Islands, palaeomag. 80−21617
Campbell Plateau and Lord Howe Rise, plate tectonics of SE.Gondwanaland 80−17244
Canary Island palaeomagnetism, and continental margin evolution 80−56363
Canary Islands, palaeomagnetism and early magmatic history 80−72431
Capraia, Italy, volcanic rocks 79−16418
Carboniferous Andacollo series (Argentina), palaeomagnetism, K-Ar dating and hydrothermal overprinting age 79−29698
Cayman Trough, rock and palaeomagnetic evidence for spreading centre 79−84215
Chamita Formation stratotype (Mio-Pliocene) of northcentral New Mexico, mag. polarity stratigraphy 77−78087
Chile, Camaraca Formation of Middle Jurassic, palaeomag. and plate rotation 80−85586
China, Quarternary magnetic stratigraphy *(Chinese)* 80−56359
Clear Lake, California, absence of Mono Lake geomagnetic excursion in sediment palaeomagnetic record 78−11801
conference, Amsterdam, Netherlands (Sep. 1976) 78−28164
Connemara Antiform, tectonic evolution from palaeomag. data 78−36093
continental blocks, palaeomagnetism rel. to drift since Devonian 78−11864
continental plates pre-Tertiary velocities from palaeomag. data 80−21848
continential shelf sediment core, anomalous declination due to slumping 80−76964
converging remagnetization circles for separation of superimposed remanences 78−28348
Coronation Geosyncline, palaeomag. poles rel. to arrangement of continents in middle Proterozoic 79−84101
Coronation Geosyncline and Middle Proterozoic continental arrangement 80−94456
Corsica, rotation rel. to palaeomag. data, comment 77−64251
Cretaceous and Eocene mag. pole positions, Turkish tuffs 80−31020
Cretaceous magntic stratigraphy from Cismon section, N.Italy 79−44086
Cretaceous Nubian Sandstone, Egypt, palaeomag. poles 78−85479
Cretaceous pelagic carbonate rocks, mag. stratigraphy obs. review 80−104876
Cretaceous pelagic limestone, Sicily, dual mag. polarity meas. in single bed 79−53306
Cretaceous Pirgua Subgroup (Argentina), palaeomag. rel. to age of opening of S Atlantic 77−90998
Cretaceous section of Chilean Andes, palaeomag. and K-Ar age 80−85585
Cretaceous-Tertiary boundary sediments, Red Deer Valley, magnetostratigraphy, biostratigraphy and geochronology 79−57888
Cretaceous-Tertiary extinctions, geomag. field effects 78−32013
data analysis, angle in Fisher distrib. that will be exceeded by given probability 80−51325
data analysis, Fisher's precision parameter 80−51326
data analysis, modes of directional data 80−56352
data analysis by least squares line and plane method 80−109259
data smoothing, objective method, comments 79−34975
data smoothing, objective method 78−28159
Deccan traps age from palaeomag. studies 77−48992
deep sea sediments, palaeomag. study using thin sections 77−78099
Denchai Basalt, N.Thailand, paleomagnetism, age and geochemistry 80−41421
Devonian Catskill red beds, evidence for tectonic motion 79−2183
Devonian John O'Groats Sandstone, N. Scotland, superimposed magnetisations resolution 79−92481
Devonian lacustrine sediments, from Caithness, Scotland, palaeomag. and mineralogy 78−28170
Devonian Onondaga limestone (New York), palaeomagnetism re-examination 80−3928
diabase dykes, Late Mesozoic, from S.Spitsbergen, thermomag. props. 79−92528
dike burial depth estimation by mag. palaeogeobarometric method 80−98220
dioritic dykes, from Egypt, palaeopole position determ. 79−25188
directional data sets, shape 79−39881
directions and pole positions, pole nos. 15/1 to 15/232 78−28160
DSDP abyssal igneous cores, remanent mag. inclinations, postemplacement tectonic effects 78−28161
DSDP sediments, palaeomagnetism, phase shifting of mag. anomalies and W.Philippine Basin rots. 77−86764
Duffer Formation, Pilbara craton, Australia, 3.5 Ga old mag. field 80−104872
Duncansby volcanic neck, NE.Scotland, palaeomag., K/Ar ages, tectonic implications 78−61369
Early Cretaceous magnetic stratigraphy, Italian Umbrian carbonate rocks 80−36229
early Northern Hemisphere glaciation, ^{18}O isotope and palaeomagnetic evidence 78−7752
Early Palaeozoic rocks from Australia 80−89959
Early Permian Ingelside Formation, N.Colorado, palaeopole position 79−29704
Early Tertiary lava flows from Greenland rel. to Baffin Bay-Labrador Sea evolution 77−17020
Early Triassic field reversal 77−60353

palaeomagnetism continued
Earth's orbital eccentricity correl. with palaeoclimate and palaeomagnetism 77−78093
Earth contraction and palaeomagnetic data, comments 79−34739
Earth radius expansion, effect on palaeomagnetic data 80−56422
Egypt, field strength in Egyptian adobe bricks (3000-0BC) 80−104862
Elberton pluton, Georgia, USA, palaeomag. of granite 80−72423
SW.Ethiopia, magnetostratigraphy of Shungura and Usno Formations 78−85470
central Europe, geomag. reversals 79−39652
evolution of life, mechanism for influence of geomag. field 77−90977
ferromagnetics, remanence rel. to palaeomagnetic studies 77−33062
field intensity determ. by remagnetisation in alternating field 77−9535
field intensity determ. from integral TRM characts. 78−73310
field intensity meas. on ancient fired clays, weathering model 78−61328
field intensity variations during last 2500 years in Abkhazia 78−44762
field palaeointensity, meas. from DSDP Leg 37 samples 77−90996
field reversal time scale back to 13 Myr BP 79−44085
field reversals, nature of transition periods 79−8598
field reversals, results from mag. prehistory of mountain rocks *(Russian)* 77−44917
field strengths, determ. from sediments baked by lava flows, Chaine des Puys, France 79−44100
Fishnish dykes, Mull, Scotland 78−61320
NW.France, Eocambrian-Cambrian palaeomag. of Armorican Massif 80−72414
genetic and physiological process control by magnetic methods *(Russian)* 79−2088
geodynamics and palaeomagnetism 79−79737
geomagnetic excursions and palaeomag. record 77−86779
geomagnetic field palaeointensity, determ. at heated rock contact by stepwise remagnetisation method 80−21619
geomagnetic polarity time scale, revised, for interval 0 to 5 m.y. BP 79−57851
geomagnetic polarity transitions, in two oriented sediment cores from NW.Pacific Ocean 79−88243
geomagnetic reversals, rel. to stratospheric aeronomy 78−32215
Gondwana Palaeozoic apparent polar wander path 78−36094
Gondwanaland, east-west fit from palaeomagnetic data 80−61792
Gondwanaland reconstruction 77−66903
Gothenburg Magnetic Excursion and Flip 78−40488
Gran Canaria/Tenerife mag. discordance rel. to NW.African continental margin form. 78−85478
granites, lower Proterozoic, from W.Kenya, palaeomag. study, polar wander 79−84099
W.Greenland, crustal uplift 78−15954
Greenland, Gardar Igneous Province, dyke swarm palaeomagnetic poles 77−73639
E.Greenland, Skaergaard intrusion studies 79−44090
Grenville Belt magnetisation age, Rb-Sr and palaeomag. evidence from Swedish dolerites 77−81839
Grenville orogeny, palaeomag., Rb-Sr ages from dolerites, Canada and Greenland 79−34772
Grenville palaeomagnetism, implications of Frontenac Axis dikes $^{40}Ar/^{39}Ar$ dating 79−62466
Grenville Province, palaeomag. and tectonics 78−88794
Grenville series of Ontario, palaeomag. rel. to Ar isotope dating 80−98232
Grenvillian palaeopoles, calibration by $^{40}Ar/^{39}Ar$ dating 79−20778
Hadrynian Polar Track discovery rel. to Grenville problem 77−48991
Harp Lake Complex and associated rocks, Labrador, palaeomagnetism 77−90997
Hawaiian lava flows, geomagnetic palaeointensities and Pacific nondipole low 78−61324
high-latitude palaeomagnetic poles, reasons for deficiency 78−65181
Himalayan basic volcanic formation, palaeomagnetic study 80−51328
E.Hindukush, Pakistan, Upper Devonian palaeomagnetic data 79−44087
Hispaniola, Cretaceous and Tertiary rocks palaeomag. study 79−44103
Holocene lake sediments, N.Poland, palaeomag. 80−21616
Holocene lake sediments, N.Poland, palaeomag. records anal. rel. to short period secular geomag. vars. 80−98221
Huronian polar wander and Thessalon volcanics palaeomag. 79−5444
SW.Iceland, geomag. excursion in late-glacial basalt outcrop 80−85587
N.Iceland, lava succession, K-Ar dating, geological and palaeomagnetic obs. 80−109096
Iceland, magnetostratigraphy 77−66885
Iceland, palaeointensity meas. on postglacial lavas 80−89952
SW Iceland, stratigraphy and palaeomagnetism of Esja, Eyrarfjall and Akrafjall mountains 80−89950
Icelandic palaeomagnetic data, appl. to offset dipole and zonal nondipole geomag. field models 79−57852
igneous rock bodies, in situ mag. meas. 79−84521
igneous rocks, thermoremanent magnetization 77−91113
igneous rocks from Jamaica, Late Cretaceous and Miocene, palaeomag. rel. to tectonics 78−20352
inclination data analysis by statistical method 80−109101
India, northward motion since Late Cretaceous, palaeolatitudes 78−28209
Indian apparent polar wandering rel. to India-Asia collision 80−26452
Indian Ocean, deep-sea sedimentation, lithologic and palaeomag. study 79−20810
intensity and direction from long grain deposition orientation method 80−77148
intensity determination of rock sample, reliability test 80−61917
intensity in Athens, 2000 BC to AD 400 79−44099
intensity variation, over last 10000 years, archaeomagnetic record 80−36237
intensity variation recorded in Brunhes epoch deep sea sediment core 77−32995
IRM of Yellowstone Group comparison with DRM of Pearlette ash beds 80−21624
Israel, Mesozoic palaeomag. results and inferences for microplate struct. in Lebanon 80−61760
Jacobsville Formation, apparent polar path for N.America in Precambrian 78−53616
Jalisco, Mexico, palaeomagnetism of Tertiary igneous rocks 78−11799
Japan, Permian greenstones, geological significance 80−21629
Jersey, Gt.Britain, volcanics and dykes remanent magnetisation 80−46125
Jotnian dolerites of central-E.Sweden 79−34738
Jurassic field polarity from Colorado and Wyoming rock 80−104875

palaeomagnetism continued
Jurassic rock in N.Armenia, palaeomagnetic directions rel. to remanent magnetisation 80−104870
Kenya, palaeomag. results from Narosura and Magadi volcanics 79−79740
Ketilidian metamorphic rocks, SW Greenland, palaeomagnetism and apparent polar movements, 1850 to 1600 Myr 77−13059
Keweenawan diabase dikes from N.Michigan 80−51321
Keweenawan palaeomag. reversals at Mamainse Point, Ontario, fault repetition or three reversals 79−92477
kimberlites, Precambrian and Cretaceous, in S.Africa, remanent magnetisation 78−96134
kimberlites, South Africa, palaeomag. determ. of emplacement temp. 77−78180
Komyoike volcanic ash horizon sediments in Osaka Group 79−70742
Koobi Fora Formation, Kenya, palaeomagnetic stratigraphy 77−29250
Korostenian pluton gabbro-anorthosite rocks, NRM origin and palaeomag. pole position *(Russian)* 79−8599
La Tinta Formation, Argentina, Late Precambrian, palaeomagnetism obs. 80−104860
Labrador Trough, Quebec, magnetization chronology 77−52972
Ladakh Intrusives, NW.Himalaya rel. to two-stage collision model 79−88241
Lake Michigan sediment cores, palaeomag. records of geomag. secular var. 77−60347
Lake Mungo palaeomagnetic excursion, geomag. source models and their implications 77−86771
Lake Tahoe, California-Nevada, sediments, palaeomag. and sedimentological studies 80−41371
Lake Vuokonjarvi, Finland, palaeomagnetic secular variation 78−32004
Lake Vuokonjarvi, Finland, sediments, time series alignment by new statistical approach 79−92623
Laschamp geomagnetic polarity reversal, K-Ar and $^{40}Ar/^{39}Ar$ age 78−81105
Laschamp magnetic reversal *(French)* 79−48401
Laschamp palaeomagnetic excursion age reconsidered 79−44091
Late Brunhes polarity episodes, palaeomagnetism and radiochemical age estimates 78−11797
Late Cretaceous polarity sequence, Scaglia Rossa limestone, Italy, rock and palaeomag. studies 78−11803
Late Devonian palaeomagnetic pole for Mulga Downs Group, Western NSW 78−15959
Late Ordovician Juniata Formation, palaeomag., remag. hypothesis 78−36096
Late Pleistocene and Holocene dry lake deposits, Mexico, palaeomag. record 80−21618
Late Tertiary field reversal, palaeomag. record in Tatoosh intrusion 78−48962
Late Tertiary Verde Formation, Arizona, magnetostratigraphy 78−65179
lava flows, W.Iceland, Upper Miocene and Pliocene mag. secular var. 77−56575
lava flows of Mt. Etna, partial self-reversal and NRM 80−46126
Lewisian foreland, NW.Scotland, central zone palaeomag. rel. to tectonics 80−26443
limestones, Upper Jurassic, from Southern Germany, mag. props. 79−25197
limestones from Gargano Peninsula, Italy 78−11804
Loch Lomond, Scotland, palynology, palaeomag. and ^{14}C dating of Flandrian marine and freshwater sediments 78−81234
Lower and Middle Cambrian sedimentary rocks, Desert Range, Nevada, palaeomag. rel. to polar wander 80−21620
Lower Ordovician rocks of NW.Argentina, paleomag. and K-Ar age 80−89938
Lower Palaeozoic polar wander for Europe 80−46125
Lower Silesia, Tertiary volcanic rocks 80−98219
magnetic polarity time scale, implications of ages of E.Greenland Tertiary basalts 77−5153
magnetite and Fe, grain-size thresholds, palaeointensity determ. appl. 77−37188
magnetite particle size effect on palaeointensity determ. 77−37186
magnetometers, RF-driven SQUID, rock magnetism and palaeomag. appls. 77−45201
magnitude and direction of palaeomag. field during polarity transition, new technique 77−37429
magnitude of palaeomag. field, nonthermal nondetrital method using Sun-dried bricks 77−45176
magnitude of palaeomag. field during polarity transition, evidence for strong intermediate state 77−44911
Maikop series in Crimean-Caucasus region, palaeomagnetic obs. 80−89941
N.Maine, USA, Devonian rocks and W. limit of Avalon microcontinent 80−41373
Makapansgat Formation (South Africa), palaeomag. results and age 77−25637
marine magnetic anomalies, Atlantic Ocean, palaeomag. field anomalous behaviour 79−29699
marine ophiolite complexes, evidence for past magnetism 80−109092
marine sediments, mag. stratigraphy using susceptibility meas. 79−84520
marine short-wavelength mag. anomalies coherence, effect of random crustal magnetisation 80−36225
Matuyama epoch, short geomag. episodes meas. 79−66616
Maubisse Formation, East Timor, palaeomag., tectonic implications 78−3716
Mehadia Basin, Rumania, Permian red sediments *(Rumanian)* 79−57855
Melanesia Basin deep-sea sediments, palaeomag., polarity reversals 78−36102
Mesozoic formations in N.Mexico, palaeomag. study, comments 78−57164
Mesozoic igneous rocks from N.Brazil and S.Atlantic opening time 79−44089
Mesozoic plutons, Coast Complex, British Columbia, palaeomag. pole positions 78−20350
Mesozoic Serra Geral basaltic lava flows, S Brazil, palaeomag. anal. 77−21674
meta-igneous rocks from Labrador Trough 77−78100
metamorphic rocks thermal remagnetisation and palaeointensity record 77−37132
meteorite impact site, Slate Islands, Canada, shock remanent magnetisation 80−30986
N.Mexico Mesozoic formations, palaeomag. pole positions 77−2099

palaeomagnetism continued
Michigan Basin borehole, palaeomag, results from igneous and sedimentary rocks 79−39636
Michikamau Intrusion, Labrador, palaeomag. pole position and age 77−5130
Middle Jurassic magnetic polarity, from Summerville and Curtis Formations, Utah 78−65180
Middle Ordovician volcanic rocks from Quebec, palaeomagnetism 78−15965
Middle Silurian Rose Hill Formation, Central Appalachians, Palaeomag., remag. problems 78−36097
Miocene-Pliocene lava sequence at Bassastadaa, E.Iceland 77−17046
Moenkopi formation, SE.Utah, USA, magnetostratigraphy 80−72422
Mongolia, past geomag. field vars. from archaeomag. investigation 77−48997
Mongolia, Soviet Central Asia and Caucasus, ancient geomag. field parameters 77−91002
Mono Lake geomagnetic excursion 79−48397
Monteregian intrusives, Quebec, palaeomagnetic polarity pattern 80−26438
Morocco, volcanic rock palaeomagnetism and K-Ar dating *(French)* 80−51322
Morro Rock-Islay Hill igneous complex, palaeomag., rel. to crustal block rot. in California 79−84106
Mull lava succession palaeomag. study rel. to Eurasian Plate motion 77−48995
multiphase magnetizations, recognition and separation techniques 78−28349
Munster Basin, NW.Germany, upper Cretaceous limestones palaeomagnetism 80−89949
Nain anorthosite (Labrador), palaeomagnetic results and tectonic implications 78−77178
neogene eruptive rocks from Calimani-Gurghiu-Harghita mountains, Rumania, natural remanent magnetisation 77−25640
Neogene-Quaternary volcanogenic formations, Dzhavakhet highland, palaeomag. 79−74834
New Brunswick rock units, palaeomagnetism rel. to N.America Lower Palaeozoic tectonics 79−100809
W.Newfoundland, palaeomag. evidence against rotation hypothesis 77−37129
Nexo sandstone from Bornholm Is., Denmark 78−85472
nondipole field intensity and direction changes during polarity transition 77−37134
nondipole moments, long term, in last 130 my. 80−104873
North America Early Carboniferous palaeomag. field rel. to N. Appalachians tectonics 80−8249
N.Norway, palaeomagnetic evidence for movement on Trollfjord-Komagelv Fault 78−40535
Notre Dame Bay lamprophyre dikes, Newfoundland rel. to Atlantic opening 80−26440
NRM in deep sea sediments, time series anal. 79−29757
oceanic basalts from DSDP Leg 37, palaeointensity studies 77−37133
oceanic crust mag. props., DSDP Leg 34 results from Nazca plate 77−17024
Odaka, Japan, Late Pleistocene sediments, reversed magnetozone 78−40486
Olby-Laschamp geomag. polarity event, age 79−12067
Ordovician lamprophyres Taylor Valley, Antarctica, palaeomag. pole position 78−32010
N.E.Pacific and Alaska, plate tectonics and palaeomagnetism 77−91092
Pacific Ocean sediments, ^{10}Be dating compared with palaeomagnetic ages 78−32058
Pacific plate, Neogene motion relative to mantle and Earth spin axis 79−44167
Paganzo Group (Argentina), red beds palaeomagnetism and correl. of Upper Palaeozoic-Lower Mesozoic rocks 77−90999
palaeocene pole for N.America from central Montana alkalic intrusions 80−104869
palaeocontinental maps for Early Phanerozoic and Proterozoic 79−44150
palaeointensities determ. from submarine pillow basalts, effects of seafloor weathering 80−3927
palaeointensity and thermoluminescence measurements on Cretan kilns from 1300 to 2000 BC 80−36232
palaeointensity determ. by continuous thermal cycling technique 77−37425
palaeointensity determ. using anhysteretic remanent magnetisation 77−37430
palaeointensity determ. using anhysteretic remanent magnetisation 77−37431
palaeointensity determ. using archaeological samples from Bulgaria 77−37136
palaeointensity determination, ARM correction method 79−34968
palaeointensity meas., comparison of anhysteretic remanence and thermoremanence in magnetite 77−5191
palaeointensity meas. of baked sediments, weathering effects 77−37135
palaeointensity measurement, conf., Grenoble, France (Aug. 1975) 77−37130
palaeointensity measurement, sediment particle size var. rel. to DRM/ARM ratio 78−32067
palaeointensity methods using AF demagnetisation and anhysteretic remanence, reliability 78−77352
palaeointensity vars. rel. to Earth orbital eccentricity fluctuations, mechanism, discussion 79−88466
Palaeozoic and Mesozoic palaeomag. poles for Morocco 78−32012
Palaeozoic anorthosite of Arden Pluton, Appalachian Piedmont, Delaware, USA 80−61752
Palaeozoic igneous rocks, Welsh Borderlands, palaeomag. survey rel. tectonic rot. of Britain 78−48961
Paleocene pole in N.America from Gringo Gulch volcanic rock obs. 80−109091
Pearson Formation (Great Slave Supergroup, NWT), palaeomagnetism and Coronation loop 78−77179
NW Peninsular Malaysia, palaeomag. evidence from Ordovician and Silurian rocks 80−89936
Pennsylvania, Lower Ordovician geomagnetic pole 79−88242
Permian geomagnetic field configuration, rel. to reconstruction of Pangaea 77−56577
Permo-Triassic dolerites, Guyana, rel. to palaeomag. synthesis problems 78−57163
Phanerozoic palaeomagnetic restructurings, chronological distribution curves 79−53302

palaeomagnetism continued
phanerozoic polar wander curve for India 80−51328
Late Pleistocene geomagnetic var. and ^{14}C time scale changes 79−62433
Pleistocene magnetic stratigraphy of New England tills 79−70744
Pliensbachian limestones at Bakonycsernye (Hungary), resonance and mag. reversal pattern 80−90074
Pliocene Centerville Beach section (N.California), palaeomag. stratigraphy 77−60346
Pliocene-Quaternary deposits in Ukrainian SSR, model of regional magnetostratigraphic scale *(Russian)* 77−44916
polar paths, graphical approach rel. to palaeomag. cycles and global tectonics 79−66618
polarities from cyclothermic sediments in Carboniferous Appalachian Basin, USA 79−70743
polarity sequences to best lithostratigraphic correlations, central Australia 79−84112
pole positions, displacement rate curves 77−91005
pole positions and palaeomag. directions, pole numbers (16/1 to 16/296) 80−72415
pole positions and palaeomag. directions (pole numbers 14/1 to 14/574) 77−48993
Precambrian Fe formations in Labrador Trough 77−52968
Precambrian Gardar lavas, S.Greenland, mag. stratigraphy and mag.-petrologic props. 77−40973
Precambrian geodynamics, palaeomagnetic data for Africa, Australia and N.America 77−66889
Precambrian geologic history 77−2131
Precambrian polar wandering rel. to plate tectonics 80−31024
Precambrian rocks, Lake Superior, separation of superimposed remanences 78−28348
Late Precambrian rocks of Midland Craton of England and Wales, palaeomag. study 79−66617
Precambrian schist belt, Karnataka, India, remanent magnetisation direction from aeromag. anomaly inversion 79−44094
Proterozoic Belt Supergroup in Montana and Idaho, palaeopoles and polarity zonation 80−72420
Pyramid Lake, Nevada clay record rel. to geomagnetic excursions 80−101321
quartz-magnetite rocks, Karimnagar, India, palaeomag. poles 79−84103
Quaternary data from British Columbia, spectral anal., rel. to geomag. secular var. 78−11806
Quaternary profiles, SW.Slovakia, palaeomag. study *(Russian)* 79−39654
Recent tidal-flat sediments, post-depositional remanent magnetization 80−101320
red beds, Moenkope Formation, Arizona magnetisation acquisition 80−72421
red beds, secondary magnetizations significance and utilization 78−28165
Red Sea Hills, Egypt, Late Precambrian and Early Palaeozoic rock, polar wander obs. 80−109100
remanence direction from converging remag. circles, least-squares method 77−45182
reversal transition widths and fast spreading centres 77−17022
reversals, transitional field configs. 78−65182
Reydarfjordur area, E.Iceland, dyke magnetisation and upper crustal struct. 77−78139
Rio Dell Formation, California, new results 79−70741
Roccamonfina Volcano, geochronology and palaeomag. *(Italian)* 77−49036
rock samples, removal of rot. remanent mag. acquired during alternating field demag. 77−60474
rocks and roof tiles, palaeointensity determ. by single heating method 77−37427
Rose Hill Formation, USA, Middle Silurian pole position 80−56353
Rubjerg low-inclination excursion from Middle Weichselian marine clay 79−39640
San Juan volcanic field, S.Colorado, palaeomagnetic poles 78−32002
San Vincenzo, Tuscany, study of Pliocene rhyolite 80−56357
Sardinia, late Palaeozoic volcanics multivectorial mag., partial remag. and tectonic rot. 78−48960
Scandinavian Caledonides, gabbro complex palaeomag., plate rot. or polar shift theories 80−21615
Scottish Devonian volcanic rocks, palaeomag. and palaeointensity studies 79−29707
Seal Group rocks, Quebec, magnetisation study 80−3918
Searles Valley, California, lacustrine sediment core chronology 80−89955
secular variation, recent, in lake sediments from New Guinea Highlands 79−12069
secular variation periods, spectral anal. of archaeomagnetic data 80−41372
secular variations during last 250000 years, results from rapidly deposited sediments 77−32983
secular vars. recorded in Loch Lomond sediments 79−44088
sedimentary and igneous rocks, palaeointensity determ. by AF remag. 77−37432
sedimentary and igneous very old rocks, palaeointensity determ. problems 77−37428
sedimentary rocks, Hornsund region, Spitsbergen, palaeomag. pole positions 79−66607
sediments, from Nova Scotia, stratigraphic position of carboniferous mag. horizon marker *(French)* 77−78088
sediments, late Precambrian and lower Palaeozoic, from W.Africa, palaeomag. poles 78−65178
sediments anomalous magnetic fabric which records apparent geomag. field excursion 78−81152
sediments magnetization, depositional and postdepositional processes 77−86869
Shabogamo gabbro, New Quebec and Labrador *(French)* 79−84092
shock-diminished remanence at Charlevoix impact structure, Quebec 80−26441
Sicily, Mesozoic continental margin, palaeomagnetism and deformation 80−61761
Sila nappes (Calabria), palaeomag. evidence for non-Apenninic origin 80−56369
silicic volcanics, Jurassic, from Nevada, thermochemical remanent magnetisation age rel. to palaeomagnetism 80−98310
Silurian continental distributions, palaeogeography climatology and biogeography 77−66888
palaeomagnetism continued
Silurian-Devonian rocks of NW.Argentina, paleomag. and K-Ar age 80−89938
Siwalik Group, Dhok Pathan, Potwar Plateau, Pakistan, mag. polarity stratigraphy and age 79−29725
Skye lavas, NW.Scotland, remanent mag. struct. 78−28167
sounding, inverse mag. problem numerical soln. *(Russian)* 79−34747
Spokane Formation, Montana, Late Hadrynian and Helikian pole positions 77−44907
St-Urbain and other Grenville palaeopoles 80−26442
stalagmite deposits, palaeomagnetism 79−84107
stratigraphy of Meadowcliffe Till, late Pleistocene excursion evidence 79−70745
Sudbury dykes, Grenville Front region, palaeomag., petrochem., K-Ar ages 78−7633
Sudbury irruptive, depth of burial from remanent magnetisation 77−44942
Suiko seamount, Emperor seamount chain, palaeomagnetism meas. 78−57162
Sulawesi, Indonesia, palaeomag. data rel. to palaeogeographic reconstructions 78−61330
Sulawesi (E Indonesia) western arc, palaeomag. studies and fission-track dating rel. to tectonic history 80−89957
Superior Geotraverse symposium (Toronto, 1978 October 23-26) 80−27029
S.W.Sweden, Permian multiple intrusion dykes in Bohuslan, mag. studies 80−36228
Swedish Ordovician limestones, mag. directions 78−28169
Swedish rapakivi suite, palaeomag. study rel. to Proterozoic tectonics of Baltic Shield 80−56346
tectonic rotation and structural tilt in palaeomagnetic studies 80−109097
tectonomagnetism and tectonoelectricity, symposium (Japan, 1975, September 5) 77−2084
temperature-dependent magnetic cleaning 77−41204
E.Tennessee, palaeomag. results from Ordovician Moccasin, Bays and Chapman Ridge Forms. 79−57854
Tertiary basalts with low Curie temps., palaeomag. data reliability 78−28166
Tertiary rocks, Faeroe Islands, remagnetization 78−28168
Tertiary volcanic rocks, N. Bavaria, palaeomag. and rock mag. meas. 77−64203
Tertiary volcanics from Sardinia 80−56343
Tertiary volcanics of Sardinia 80−46127
Thanet gabbro complex, Ontario, mag. overprinting 79−25187
thermoremanent magnetisation intensity, cooling rate effect in single domain magnetite 80−109139
Thetford Mines ophiolites, Quebec, palaeomagnetism 80−61757
Thunder Bay Late Quaternary sediments, palaeomagnetic record from remanent mag. meas. 80−17230
Tibetan Plateau underthrust by India, palaeomagnetic constraints 80−56449
W.Tien Shan, crustal movements from geology of palaeomagnetic data 77−9392
till on Lake Huron E coast, mag., physical and lithologic props. and age 77−33057
time-averaged field anomalies, rel. to lower mantle 78−11808
Timor and Australia relative positions in Upper Permian 77−29244
Transdanubian Central Mountains, palaeomag. pole position, tectonic implications 78−48970
Triassic Chugwater redbeds, Wyoming, palaeomag. pole positions 77−81796
Triassic Hound Island Volcanics, Alaska, crustal movement from palaeomagnetic obs. 80−89945
Triassic Nikolai Greenstone, Alaska, palaeomag. 78−36166
W.Turkmaniya, Gauss/Matuyama epoch boundary, geomagnetic field inversion 78−15957
NW Ukrainian Shield, palaeomagnetism of rocks of sulphide mineralisation zones *(Russian)* 79−96758
Ukrainian Shield dyke complex, palaeopoles and Precambrian field *(Russian)* 77−32988
Umbria, Italy, palaeomagnetism and tectonics 78−96129
Umfraville gabbro, Ontario, 1180 Ma Grenvillian stock palaeomagnetism 78−92777
Umfraville Gabbro, Ontario, palaeomag. study and K-Ar age 80−12330
unit vectors, time series interpolation 79−92625
Upper Cretaceous kimberlite in South Africa 77−29245
Upper Cretaceous palaeomagnetic stratigraphy at Moria (Umbrian Apennines), verification of Gubbio section 78−96132
Upper Cretaceous Plutonian, in Maritsa neointrusive zone, palaeomag. stability 77−37124
Upper Jurassic limestones, S.Germany, palaeomag. pole position 77−64204
upper Keweenawan sediments, virtual geomag. pole position determ. 77−78089
Upper Palaeozoic-Lower Mesozoic red beds and igneous rocks, Argentina, palaeomag. 79−84098
Upper Pliocene deposits, W Turkmenia, NRM origin and palaeomag. 79−25192
Upper Precambrian sedimentary rocks, Desert Range, Nevada, palaeomag. rel. to polar wander 80−21621
Upper Proterozoic apparent polar wander, analogous loops from Laurentia, Fennoscandia and Africa 80−56360
Varanger peninsula, Norway, Late Precambrian dolerite dykes 80−30989
varved sediments from W.New England, palaeomagnetic recorder var. 79−70738
varved sediments from W.New England, secular var. 79−70739
Ventura, California, high rates of vertical crustal movements 77−56614
volcanic rocks, from Colli Euganei and Monti Lessini, Italy, palaeomag. rel. to tectonics 79−66613
volcanic rocks, from Colli Euganei and Monti Lessini, Italy, palaeomag. rel. to tectonics 79−66614
volcanic rocks, palaeointensity determ. by modified Thellier method 77−37426
volcanic rocks from Mt. Etna, stress effects on magnetic props. 77−37192
volcanic rocks in Lesser Antilles island arc, palaeomagnetic survey and age determ. 80−8265
Voltzia sandstone from Vosges Massif, Lower Triassic *(French)* 77−81786

palaeomagnetism continued
S.Wales, Lower Cambrian Caerfai Bay Shales, diagenetic magnetisation 80−36227
Wascana Creek Ash, Canada, characterisation, source, fission track age, palaeomag., stratigraphy 77−66913
Watkins seamount, Pacific Ocean, Cretaceous origin, palaeomagnetic obs. 80−104874
weak dipole field epochs, nondipole components effect on auroral zone config. 80−105098
Wilberns Formation, Texas, palaeomag. and Lake Cambrian field for North America 77−17025
Wrangellia, displaced terrane from Vancouver Island to S.Central Alaska 78−36165
Yellowstone and Jackson Lakes, mag. props. and secular var. in sediment cores 78−48968
Yellowstone Group, palaeomag. of welded tuffs 78−48967
Yellowstone Lake, seismic refl. and refr. surveys and palaeomag. study 78−49049
Yellowstone volcanic plateau, conf., USA (1974) 78−49004
Yoldia Clay sequence from Denmark, 14-40000 yr B.P., geomag. variations 80−94454
Zijderveld vector diagrams, use in multicomponent palaeomag. studies 80−17420

palladium
see also nuclei with .....
abundance in stone and Fe meteorites, mass spectroscopy 80−8601
adsorbed CO on (210) surface, inclined bonding config., electron stimulated desorption and LEED obs. 80−39430
adsorbed layer, surface diffusion on W, anisotropy effects due to substrate struct. 79−99422
adsorbed layer, surface diffusion on W, spreading behaviour 79−99421
adsorbed layer on W (110) surface, growth, struct., stability, desorption 80−59794
adsorbed layer on W FEM tips, conc. determ. by nucl. microanal. *(French)* 80−29860
adsorbed on Ag (001), electronic states calc. 78−6318
adsorbed on Si, effect on surface electronic props. *(Russian)* 79−91124
adsorbed on W (110), long range interatomic interactions with coadsorbed Re, W 80−59789
adsorption, of CO, on (111) surface, catalytic oxidation, mol. beam investig. 78−88656
adsorption, of CO(NO) on SiO_2-supported surface, IR spectrosc. obs. 80−92780
adsorption and diffusion on W surface, effect on self-diffusion, field emission expts. 78−38945
adsorption energies on W calc. 79−51464
adsorption of CO, AES obs. 77−35818
adsorption of CO, effect of interactions on chemisorption bond 77−51598
adsorption of CO, geometrical struct., LEED and high-resolution EELS study 80−20037
adsorption of CO, UPS of CO on Pd clusters, binding energy, d-electron emission particle size depend. 79−4888
adsorption of CO on polycryst., SIMS 78−14585
adsorption of H_2 on ribbon, thermal desorption and work function meas. 80−70538
adsorption of NH_3, NH_x and N, decomposition of NH_3 and hydrogenation of N, AES 77−1315
adsorption of NO on surface (111), LEED, UPS, and thermal desorpt. expts. 77−69179
adsorption of O_2 and NO on surface (111) LEED, photoelectron spectra and thermal desorpt. expts. 77−69180
adsorption of Xe on (110) surface, anomalous 5p photoemission 80−7471
adsorption of Xe on Pd(110) surface AES, UPS, LEED, work function, flash desorption 80−6633
annealed, cold worked, H_2 diffusion effect on mech. props. *(Japanese)* 78−10222
atom, ionisation cross sections for L_1 and L_2 subshells by 250-500 keV protons *(Russian)* 77−6918
atom, $K\beta_3/K\beta_1$ and $K\beta_2/K\beta_1$ relative intensities 77−75088
atom, $K\beta/K\alpha$ rel. intensity obs. 80−32665
atom, K-shell ionis. by electron impact, cross-sections, 300-600 keV 78−29853
atom, K-shell X-ray spectra, $K\beta_2/K\beta_1$ determ. 77−23456
atom, $L\alpha$ X-ray spectra, $_{40}Zr$ to $_{48}Cd$, linewidths 79−41131
atom, XPS and XES, dynamical effects 80−52924
atomic N-shell vanacy state widths, X-ray photoelectron, Auger spectra 77−18875
Auger peaks, $M_{45}N_{45}N_{45}$ transition, influence of surface environment 80−7447
automotive exhaust gas catalysts, radiometric determ. of Pt and Pd attrition 78−31740
automotive exhaust gas catalysts 79−100433
band model, mag. susceptibility of exchange-enhanced paramagnet 78−2644
black, form. from neutron, α-irrad. PdO, adsorpt. props. 77−11796
catalyst, on glass, used in electroless deposition, proton backscattering anal. 80−16749
catalyst, Z-contrast, in STEM 79−46530
catalyst for oxidant impurities elimination, in viologens electrochromic solutions 80−78922
catalyst hollow cone dark field microscopy on γ-alumina substrates 78−61049
catalyst on Al_2O_3, surface atomic composition by AES 77−86377
catalyst on tetrazolium salt, formation of formazan dye 79−39170
catalytic oxidation of amorphous C by Pd particles, TEM obs. 80−76555
cathode, porous, for implantable hybrid cells, recent improvements 77−40933
cathodic polarisation in alakaline earth metal salt solns., surface changes 79−61869
CESR, expts. using transmission technique 78−91954
CESR obs., g-factor and susceptibility enhancement factor 79−65734
chemisorbed benzene on (100) surface, angle-resolved photoemission symm. anal., polarisation depend. and lateral interactions 79−91568
chemisorption, of acetylene, substrate effects on bonding, electronic spectrum 78−63933
chemisorption and catalytic oxidation of CO 77−70339

palladium continued
chemisorption and decomp. reactions of O containing organic mols., UPS 77−63953
chemisorption bonding of H on surface (111), UPS obs. 77−76671
chemisorption of Cl_2 on (111) face, LEED, AES, thermal desorption, and work function meas. 80−75444
chemisorption of CO, N_2, NO, semiempirical calcs. 78−14611
chemisorption of CO, Penning ionisation electron spectroscopy, metastable He impact, electron energy distrib. 79−52060
chemisorption of H, bond nature 80−34297
chemisorption of H, bonding, photoemission spectra, SCF electronic struct. 79−33320
chemisorption of H, embedded cluster model 80−39427
chemisorption of H, model, comparison with UPS data 79−46932
chemisorption of $He(CO)(O_2)$, mol. beam scatt. expts. 78−79878
chemisorption of N_2-containing gases at high-press., XPS 77−20990
chemisorption of O_2 and CO, catalytic activity, SCF-Xα-SW calcs. 78−15711
clean surface (111), electronic struct. using LCAO band model 79−65531
cluster, calculated structural stability 78−95268
cluster, catalytic, XPS obs. of electronic struct. 77−77345
clusters, adsorption/desorption of CO, AES and thermal desorption meas. 80−75436
clusters, density of states profiles, Hartree-Fock-Slater model 77−31930
clusters, electronic struct. and mag. props., MO calc. 77−20219
clusters, size, geometric effects, catalysis implications 78−73131
clusters, valence band and core binding energies, UPS meas. 79−38721
coated Si wafers, interference effects on irrad. with laser beam 80−66333
coating, electron beam deposition and ion plating 77−44166
coating, H-permeable, on V, Nb and Ta foils, Auger and secondary ion mass spectroscopy 79−52467
coating, on stainless steel, interdiffusion at reactor wall temps., Rutherford backscatt. obs. 80−39361
cohesive properties 79−94952
Compton profiles, comparison with band struct. calcs. 78−84675
concentration determ. by gamma-ray absorption from $^{119}Sn^m$ 80−108123
confined geometry, p-wave supercond. or itinerant ferromag. 80−11129
core level binding energies 80−71564
crystallite morphology, surface struct., electron microscopy obs. 80−29257
dielectric screening and phonon frequencies using isotropic noninteracting s-d-band model 79−19343
diffusion coefficients calc. for H and D *(Russian)* 78−91483
diffusion in Au, 700-1000°C *(Russian)* 78−91484
diffusion in Au grain boundaries, determ. using AES data 77−11742
diffusion of H_2, induced elec. pot. investig. *(French)* 77−43379
diffusion of $H_2(D_2)$, quantum rate theory for symmetric double well pot. 78−55970
diffusion of H, book contrib. 79−82390
diffusion of H, model 79−73338
diffusion of H, next-neighbour jumps of H in quasi-elastic neutron scattering 78−91487
diffusion of H(D), role of tunnelling, reson./nonreson. approaches 80−59718
diffusion of H and trapping 80−70447
diffusivity of H_2, 496 to 946°C 79−77815
dilute alloys, electronic struct. calc. using KKR method 80−15438
discovery and elemental nature, Wollaston/Chenevix controversy 79−30185
double beam photoemission study of electronic struct. 79−83098
elastic consts. 4 to 300K 80−6455
electrical resistance and H solubility at high press. *(Russian)* 79−91018
electrical resistivity, and supercond. transition temp., electron-phonon contrib. 78−80085
electrical resistivity, temp. depend. data 80−51967
electrical resistivity due to interstitial H (D) 80−96848
electrocatalysts, reversible poisoning by CO, air pollution detection appl. 77−37363
electrode, evaporation rate from cathode spot in vac. arcs. 80−49024
electrode, reliable bonding to Bi-Te thermoelements, radioisotope thermoelectric generator for biomedical appl. 79−52952
electrodeposited layers, props., deposition parameters influence *(German)* 80−20808
electrodeposition, on to $Al_xGa_{1-x}Sb$ solid soln. 80−93505
electrodeposition on B single crystals to form ohmic contacts 77−44177
electrodes for electrolytic H prod., reaction kinetics 80−30434
electrodes in H_2O/D_2O electrolysis, H/D isotopes separation factors 79−50149
electron-phonon coupling and supercond. transition temp. 79−56360
electron-phonon interaction, expt. test of rigid muffin tin approximation 79−65364
electron-phonon parameters and supercond. p-state pairing 80−25041
electronic band struct. and photoemission 80−97410
electronic band structure, comparative study of electric and mag. props. 78−95259
electronic density of states, recursion method 79−90937
electronic struct. determ. by relativistic APW method, rel. to UV spectroscopy 77−4289
electronic structre, Compton scatt., soft X-ray emission and X-ray photoelectron spectra 79−77999
electronic structure, effects of press. and alloying with Ru, Rh, Ag, and Rh+Ag 78−91581
electronic structure, self-consistent mixed-basis approach 79−69394
electronic structure from annihilation quanta ang. distribs. 77−66107
electronically driven phonon anomalies and phase transforms. 78−63834
energy dispersions for valence and conduction bands 79−38719
epitaxial, on (111) Au, periodic arrays of misfit dislocations, electron diffr. 78−51857
epitaxial film on Au, misfit dislocation nucleation and growth 77−1338
epitaxial growth, cluster mobilities, in-situ electron microscopes obs. 80−15407
epitaxial growth on (001)W and (001)Mo 79−99450
epitaxial growth on MoS_2, epitaxial orientation variation *(French)* 78−43256
epitaxial layer on alkali halide, particle orientation and struct. 78−84108
Fermi radii, Fermi velocities and many body enhancement 79−65363
Fermi surface, extremal cross section, press. derivative, determ. by de Haas-van Alphen meas. 79−11055

palladium continued
Fermi surface, stress depend., oscillatory magnetostriction and de Haas-van Alphen torque obs. 78−91602
Fermi surface volume depend. 79−65365
field evaporation, search for high ionic charges 78−35269
film, adsorption of H_2 or O_2, reciprocal titration of gases, film surface area determ. 77−1318
film, band struct., appl. of extended rigorous cellular method 78−52055
film, catalytic activity on effect of Ag interdiffusion in Ag_2S film reduction 78−14519
film, contact reaction with amorphous Si 79−23846
film, discontinuous, on rocksalt, elec. cond., H_2 absorpt. effects 77−47905
film, elec. resist. 80−93013
film, electrical resist., influence of hydrogenation 77−85348
film, electrolytic deposition on semicond. substrates 77−77425
film, evaporated, hydrocarbon chemisorptions, IR refl. study 79−69343
film, growth on amorphous C, electronic props., UPS and XPS obs. 79−82476
film, high dose Si^+ ion implantation, silicide phases, backscatter spectra 80−19820
film, laser induced reactions with Si 79−70365
film, laser-induced reaction with Si, surface struct. obs. 79−19471
film, on Melinex, resistance-strain behaviour, island struct. effects 77−55621
film, on Si, ion-induced intermixing 80−15420
film, on Si substrate, Pd-Si layer form. by laser irrad. 79−99438
film, on ZnO, struct., elec. props., AES, UPS study 78−76168
film, optical absorption meas. using synchrotron radiation, 20-250 eK 77−12457
film, quantum size effect, field emission study 80−70849
film, two-dimens. nucleus form. on Ag (111), UHV electron microscope obs. 80−10760
film, vacuum deposited, ethylene adsorption and reactivity with adsorbed H, surface pot. meas. 79−86995
film, work function changes due to adsorbed H_2, surface and interface dipoles 80−96972
film and foil, surface IR wave propag. distance 77−28641
film growth on graphite and amorphous C, electronic struct. by photoemission and Auger obs. 79−77947
film on Si, ion implanted, inert-gas-bubble form., TEM and Rutherford backscatt. anal. 79−90682
film on Si, Xe ion beam induced form. of PdSi 80−10800
film on Si substrate, laser irrad., cellular struct. and silicide form. 80−10710
film on W (110), field ion microscope exam. 78−34731
film presence effect on PdGe dissoc. 79−47892
film with defects, field-induced resist. min. 80−11050
films, evaporated, resist and thermoelec. power, annealing effects 80−39684
fine particles, prep. by gas evaporation technique, crystal habit 77−52239
fission product, corrosion of SiC coating of HTGR coated particle fuels 80−102237
float zone purification, residual resistivity ratio 78−44008
foil, traversed by $H^+(He^+)$, energy loss and straggling meas. 78−95100
g tensor of d holes near X point in Brillouin zone 79−23890
generalised susceptibilities and phonon anomalies, band struct. calcs. 79−90953
growth on MoS_2, reorientation of small particles 78−84103
high field de Haas van Alphen spectroscopy 79−73425
hydride, proton diffusion mechanism, NMR determ. 77−90060
interaction with Ni_xS_y *(Russian)* 79−52758
interatomic pair potential, phonon spectra 80−33927
interatomic potentials from experimental phonon spectra 78−75621
ion plated onto Nb and Ta, prep., H_2 absorption and desorption rate *(Japanese)* 80−108358
irradiated film, supercond. 79−78249
isoelectronic sequence, UV spectra (60-600 Å), resonance line identifications 78−33455
isotopes, cumulative yields from U and Pu neutron induced fission 79−576
isotopic comp. and at. wt., using solid source mass spectrometry 79−864
K-edge photoabsorption spectra, linear APW calc. 78−43960
Kambalda (W.Australia) komatiite sequence, Au, Pd, Ir and Ag in interflow sedimentary rocks 79−20830
Knight shift calcs. 79−56620
Kohn anomalies and phonon dispersion, model including exchange-correl. corrections 78−59886
Lande g-tensor for d-holes 79−61221
lattice atom displacements near end of implanted μ^+ tracks 78−55890
lattice dynamics, local frequency spectrum, mean thermal displacement of H 80−59604
lattice dynamics, non-central forces and normal modes 79−99278
lattice dynamics, phonon dispersion curves, θ-T curves 78−26642
lattice parameters, densities and atomic vols., tabulation for Pt metals 79−65033
lattice parameters at low temps. 78−26496
lattice vibrs. and Debye temp. calc. 77−15516
layer, adsorption and absorption of H_2, kinetic analysis of models 77−47679
layers, H-transparaent, coating of metals using spot welding technique 79−47816
liquid, electrical resist. calc. using muffin-tin pots. 77−69287
liquid, energy bands and electronic density of states, resistivity 78−34755
liquid, mag. susceptibility 78−95415
liquid, multiple scatt. calcs. of resist. 78−76039
liquid, Percus-Yevick equation, perturbation theory calcs. 78−75515
liquid, thermal volume expansion, MP to BP 79−90802
liquid and solid, thermophysical props. 78−75808
localised vacancies produced by thermal neutron capture recoil 78−26598
in mafic and ultramafic rocks from Mid-Atlantic Ridge, Pd, Ir, and Au contents 77−91073
magnetic form factor, field-induced magnetisation density and electronic struct. 77−4496
magnetic form factors, neutron diffr. study 79−47234
magnetic ground state props., simple one-electron theory 77−63063
magnetic properties in para-process region *(Russian)* 78−2672
magnetic susceptibility temp. depend. 78−60265
mechanical props., effect of H diffusion 79−65138
melting point determ., effect of surrounding O_2 80−27299
membrane, D beam interaction, permeability 77−51538
membrane, gaseous H quasiequilib. processes, 100-500°C, 10^{-4}-10^{-2} torr 77−29047
membrane, H atom interaction, superpermeability 80−81365
membrane, H penetrability reduction by C coating *(Russian)* 77−77808
membrane, sorption of H_2, adhesion and penetration probabilities, extreme values 80−101040
membrane, superpermeability, of atomised H_2, under different gas and membrane boundary conditions 79−71469
membrane for diffusion-cell for separation H_2 containing mixtures, solar furnace appl. 80−92245
metallic, positive muon Knight shift 80−71280
Mossbauer effect on ^{119}Sn and ^{197}Au meas. 78−15080
Mossbauer resonance, electric field gradient 79−19823
Mossbauer spectra, 2nd-order Doppler shift, 1-100K 79−91317
motion of H and D, thermodynamic data 79−65254
muon$^+$ Knight shift, cond. electron polarisation 77−66450
muon depolarisation, hyperfine anomaly 77−28503
muonic X-rays, circular polarisation, atomic capture process 78−25758
nuclear acoustic resonance from 4-200K 80−25247
optical properties, 0.1 to 6 eV 78−92092
overlayers, on Nb, form. of Pd (111) surface states and reson. d-levels, photoemission obs. 80−50523
pair potentials calc., appl. to point defect props. 80−19798
particle array, on amorphous SiO_2 substrate, model catalyst, electron microscopy and UPS expts. 79−4899
particles, chemisorpt. of CO, ultra high vacuum technique 78−71960
particles on UHV-cleaved mica substrate, obs. using scanning Auger microscopy 80−80149
permeation, of $H_2(D_2)$, isotopic effect *(Russian)* 78−75881
phase transformation, $\alpha \rightleftarrows \beta$, influence on mech. props. *(Russian)* 78−68681
phonon density determ. and heat capacity *(Russian)* 77−24415
phonon density of states determ. from thermodynamic functions 80−96616
phonon dispersion, simplified Frielek model 78−79683
phonon dispersion calcs. on basis of Fielek model 79−19335
phonon dispersion curves in highest-symmetric directions 79−51219
phonon dispersion using non-central force model 78−91392
phonon linewidths, inelastic neutron scatt. meas. 79−95100
phonon linewidths and electronic mass enhancement, electron-phonon contrib. 79−95099
phonon mediated interaction for triplet pouring 79−23911
photoemission, angle-resolved, from clean surface 78−15294
photoemission at 21.2 and 16.8 eV, ang. resolved 77−63543
photoemission spectra, valence band and core level satellite due to excitation of d electron 80−97408
plasma oscillations, Fermi level position effect on excitation energies for band transitions 79−99493
polyacetylene-Pd, ion implantation effect on elec. props. 80−65026
positron lifetime spectra, influence of adsorbed H 80−25480
powder, sponge, sintering shrinkage kinetics 80−29900
proton-induced L-shell ionisation cross-sections 80−100707
radiance temperature at 653 nm, at melting point 79−90805
reaction and bonding with MgO or quartz, below MP of starting materials, obs. in TEM 77−21419
reactive trapping of energetic 18 keV deuterons 78−10096
recovery and use of noble metals from radioactive waste 80−99242
scattering, adsorption, and absorpt. of H_2 and D_2 on (111) surface, mol. beam study 80−29277
sd hybridisation, paramagnetic Curie temp. and susceptibility *(Russian)* 80−103808
secondary electron emission, discrete levels in energy distrib. 79−87535
semiconductor pulse diodes, application of Pd for reducing recovery time of reverse current *(Russian)* 79−99226
silicide formation due to laser and electron beam annealing 80−84849
size effect in metallic sandwiches 79−73604
solubility, of S, 600-1000°C, H_2-H_2S gas phase composition depend. *(French)* 78−87791
solubility of $H_2(D_2)$, isotope effect model 77−66026
solubility of H, lattice defects influence, extended core model 80−88326
sorption of H_2, piezoelectric quartz microbalance meas. 79−60626
specific volume meas., for ruby R_1 fluoresc. press. gauge calibration, 0.06-1 Mbar 78−70150
spectrophotometric methods of determination, review 78−61115
spin fluctuation model interpretation of mag. susceptibility 80−80477
spin-density functional theory of temp. depend. spin susceptibility 79−56497
spin-orbit projected d density-of-states 78−38999
sputtering coating in oil-contamination free vacuum for SEM 79−12784
stopping power nucl., in ferromag. Gd, transient mag. field 78−34555
strained, anisotropic electron scatt. in elec. resist. 78−91656
substrate, Ag film growth, interface cpd. form., AES study *(French)* 80−80131
substrate for Ag epitaxial growth, influence on film growth modes *(French)* 80−84408
superconducting transition temperature, ab initio calc. 80−25036
superconductivity, search for, at very low temps. 78−91799
superconductivity in disordered film after He^+ irrad. 79−11261
surface, (100), $(\sqrt{2}\times\sqrt{2})$R45°, S layer, adsorbate induced surface reson. obs. in photoemission 80−7470
surface, (100), adsorption of Xe and CO, lateral interactions, effect on work function, UPS, and IR spectra 79−77904
surface, (110), adsorbed Xe, anomalous 5p photoemission 80−100750
surface, (110), adsorption of S, characterised by LEED *(French)* 80−88422
surface, (111), adsorbed CO, Penning ionisation by metastable He beam, theory 80−60735
surface, (111), adsorbed O_2, UPS and thermal desorpt. characts. 80−54754
surface, (111), adsorption of O_2, UPS and thermal desorption spectra meas. 79−78833
surface, (111), desorption, of H, preexponential factors 79−46918
surface, (111) chemisorbed acetylene, complex form., UPS spectra 77−12826
surface, adsorbed CO, photoelectron spectra, 40-180 eV, adsorbate sensitivity enhancement 78−80453

palladium continued
surface, ang. distrib. of electrons photoemitted from benzene mols. 77−69968
surface, chemisorbed O, reaction with CO, AES obs. 77−90640
surface, chemisorption of CO, IR spectroscopic evidence for localised site adsorption 78−47669
surface, CO chemisorpt., mol. cluster calc. 80−100407
surface, CO chemisorption, SIMS, XPS study 80−84382
surface, coverage and desorption of CO flash desorption spectrum 80−49493
surface, fast D_2 desorpt. mechanism, time-of-flight spectra 80−84379
surface, H_2^+ and $^3He^+$ ion bombardment, H^+ and He^+ yields at elastic scatt. energy 78−88394
surface, kinetics of CO oxidation 79−61903
surface, Pd black, adsorbed H_2 vibr. spectrum assignments, inelastic neutron scatt. obs. 78−71942
surface, segregated S state, AES, EELS, UPS and XPS study 80−93452
surface (001), adsorpt. of CO, LEED, electron energy loss spectra study, surface struct. effect on weak chemisorpt. bonding 78−71987
surface (100), chemisorption of CO, adsorbate band formation, UPS expts. compared with calcs. 79−77916
surface (100), CO monolayers, electronic states, tight-binding method appl. 80−49564
surface (100), with CO adlayer, band formation, calcs. and photoemission expts. 79−95463
surface (111), adsorpt. of CO and O_2, mutual interactions, transient product formation 78−87871
surface (111), angular-resolved UPS meas. 79−95902
surface (111), clean and CO covered, metastable He impact, electron emission, energy and ang. distrib. 80−60744
surface (111), electronic states calc. and adsorbate-induced photoemission struct. interpretation 78−60179
surface (111), H_2+O_2 reaction, mol. beam relax. and isotopic exchange meas. 80−35575
surface (111), H_2 adsorption, UPS obs. 77−1786
surface (111), interaction with O_2 79−86985
surface (111), mechanism of CO catalytic oxidation reaction 78−40079
surface (111)(110), H adsorption, inert model 80−50889
surface chemical reactions using MOS structure 77−73470
surface phenomena, electron microscopy 80−103556
thermomodulation spectra of high-energy interband transitions 80−108226
thin film, temp. coeff. of resist. meas. 80−107930
thin film on Si substrate, epitaxial silicide growth, LEED and AES study 80−103590
thin surface overlayer, H uptake rate enhancement of bulk Nb(Ta) 79−82345
transport props. 40 mK-6K 78−51968
triplet pairing, spin fluctuation and phonon contribution 79−7929
triplet pairing, spin fluctuation contrib. 78−10711
ultrafine particles, size effect on vibr. sp. ht. 78−10153
UV irradiated electroless selective plating, improvement 80−84848
vacuum deposition on C film, UPS, Pd valence band width 78−88403
vapour growth of small particles on Al_2O_3 substrate 78−75958
vibrational spectrum modification relation with 55K heat capacity anomaly in PdH_x 77−51516
VPE film growth on Au(111), interface struct. 79−95297
wear coefficients determ. using pin-on-cisc apparatus 80−76366
wire, H_2 sorption, heat of adsorpt., sticking probabilities 78−43240
X-ray emission L-spectra, influence of temp., liq. N_2 temps. *(Russian)* 80−80907
X-ray reflection intensities, charact. temps. 78−18731
XPS, electron level binding, energy determ., and spectrometer calibration method 77−16458
XPS, electronic struct. 80−7464
XPS line intensity ratios for outer electron shells 79−100018
Ag-Pd, investigation of mechanical props. and recrystallization process, for use as wire-spring relay contact material 79−52278
AgBr:Pd, EPR of Pd^+ ions 78−27087
AgBr:Pd(II), photolysis-induced trapping behaviour, EPR study 80−54949
AgCl:Pd^+, ESR spectra, superhyperfine struct. lines 77−12197
AgCl:Pd^+, ESR spectrum, quasistatic Jahn-Teller effect 80−71170
AgCl:Pd^{2+}, EPR, role of vacancies in impurity based trapping 77−28439
Al-Al oxide-Pd tunnel junctions, exposed to H_2, inelastic electron tunnelling spectra 80−20327
Al-Al_2O_3-Pd diodes, resonant tunnelling via localized inpurity states 79−28416
$Al_xGa_{1-x}Sb$-Pd contacts, struct., preparation elec. props. 80−65684
$Al_xGa_{1-x}Sb$-Pd contacts, band gap depend. of barrier height 80−65685
Au/Pd, bicrysts., in situ relax. of interphase interfaces 80−39455
Au-Pd-Au sandwich, obs. of strongly enhanced mag. susceptibility 80−93076
$CaCO_3$-Pd, catalyst for H gettering of dimerised phenyl propargyl ether 77−18001
$CaCO_3$-Pd catalyst, hydrogenation rates of solid alkynes, H gettering 77−44510
CaS:Bi^{3+}, Pd^{2+}, phosphor, electroluminesc., brightness and mechanism 77−48248
CaS:Pd phosphor, thermally stimulated elec. cond., kinetics, 300-413K 78−76088
CaS:Pd phosphors, trap and luminescent centre location, photo-, thermo- and electroluminescence studies 80−71482
GaAs-Pd junction, contact reactions 79−56308
Ge:Pd and pure, photoelectric props., surface states *(Russian)* 80−60043
Ge-Au-Pd trilayer film, interdiffusion obs., on annealing 78−2308
Ge-Au-Pd trilayered film, annealing, interdiffusion 78−22902
H isotope separation by desorption, isotopic conc. depend. 79−71979
H phase hardened, recrystallisation study 80−60883
KF:Pd^{2+}, pure and doped, two-step photoionisation, laser-active F_2^+ centre form. 79−963
MgO-Pd metal-ceramic reaction, micro/macro obs. 80−66467
Pd cluster-H, electronic struct. calc., H-metal bonding 77−89823
Pd complex, L-alanyl-L-serine, PMR, EPR and absorpt. spectra 78−46367
Pd, electrospark coating on alloys, corrosion resist. increase *(Russian)* 78−27669
α-Pd, H_2 diffusion by galvanostatic charging 78−84001

palladium continued
Pd, H(D) interstitial interactions rel. to diffusion and ordering transition 80−34249
Pd:^{111}Cd, radiation damage in DPAD expts., quad. interaction 77−27917
Pd:H, elastic props. of dilute solid solutions 78−75706
Pd:H, electron density of states of interstitial H 77−47766
Pd:H, energy and electron density of states 78−51929
Pd:H, energy of interstitial H 77−47765
Pd/Al thin film couples, thermal reactions 80−59830
Pd/Al_2O_3, adsorption of CO, IR study 80−108193
Pd/Al_2O_3 catalyst, contact poison 2-methylthiophene damage reduction by neutron irrad. *(Russian)* 79−20467
Pd/Ge film on GaAs substrate, sintering, AES, Schottky barrier energy 79−69581
Pd/Ni/Cr layered catalyst for H_2-O_2 recombination in BWR coolant 80−18504
Pd/Si, Schottky-barrier type devices, chemical and polarisation characteristics, comparative study 79−78173
Pd/Si interface, chem. and struct. props. during silicide form., AES and TEM obs. 80−49430
Pd/W (110), metastable 2D condensations, epitaxy, growth modes, exp. techniques, book contrib. 80−49558
Pd-Al metallisation on Si, Cr thin film used as barrier to interaction of Pd_2Si with Al 77−43724
Pd-amorphous Si thin film interaction, metal rich Pd-silicide formation 80−2284
Pd-D, crystallite size effects, simultaneous sorption and X-ray study 80−65737
Pd-GaSb surface barrier struct., elec. and photoelec. props. 78−56229
Pd-Ge planar interface, first phase to nucleate 77−62764
Pd-H, dil. α-phase, influence of deform. on low-temp. sp. ht. 77−31783
Pd-H, dil. soln., partial molar props., temp. depend. 78−68910
Pd-H, elec. resist., temp. depend., H conc. var. *(Russian)* 77−39819
Pd-H, incoherent phase transition, lattice gas model 80−29171
Pd-H, interstitial position of H from entropy of soln. 77−65989
Pd-H, optical phonons in supercond. 77−63021
Pd-H alloy, 50K transition, internal friction, LF torsion pendulum meas. 77−15490
Pd-H alloy, 50K transition, sp. ht. and thermal relax. meas., diffusion effects 77−15596
Pd-H alloys, thermal expansion, low and room temp., Gruneisen parameters 77−63026
Pd-H like compounds, supercond. T_c increase by optical phonons 77−1509
Pd-H system, anharmonicity effects on superconducting transition temp. 79−33380
Pd-H system, α and $\alpha+\beta$ phases, annealed and deformed, anelastic effects 80−66567
Pd-H system, controlled H phase-induced strain hardening *(Russian)* 79−1878
Pd-H system, effect of α-β phase change on β-phase solubility of H 77−89544
Pd-H system, energy and electron density of states, improvements to theory 80−70636
Pd-H system, energy band struct., magnetic susceptibility meas. 78−18953
Pd-H system, instability and superconductivity 78−39248
Pd-H system, lattice parameter increase meas. by X-ray diffr. *(German)* 77−62560
Pd-H system, magnetisation, type I and type II supercond. behaviour, homogeneity effects 77−28291
Pd-H system, many-body contrib. to XPS line asymm. 77−66575
Pd-H system, phase diagram and thermodynamic properties calcs. 80−66480
Pd-H system, review of props., book contrib. 80−24605
Pd-H system, solvus hysteresis 80−71659
Pd-H system, thermodynamic aspects of atomic vibr. 78−59913
Pd-H system, XPS line shape asymmetry, role of electron screening 77−21001
Pd-H sytem, electronic struct. of H, mol. cluster and pseudojellium models 80−24832
Pd-H_2, dilute soln., high temp. thermodynamics, partial molar props. 77−15597
Pd-H(D), isotope effects in supercond. properties 78−6471
Pd-H(D), superconducting transition temp., conc. depend. and inverse isotope effects 77−80864
Pd-H(D), vibr. modes Raman study 77−85713
Pd-KCl composite, far IR absorption 78−56466
Pd-Ni bilayers, on single cryst. Si, vacuum annealing, silicide form. 79−51444
Pd-Pt bilayers, on single cryst. Si, vacuum annealing, silicide form. 79−51444
Pd-Si, interface modification by ion implantation 80−70475
Pd-Si (111) interface, microscopic Pd_2Si form., UPS obs. 80−24743
Pd-Si film struct., silicide form. He^+ back scatt. and X-ray diffr. obs. 79−51442
Pd-Si Schottky barrier chemical sensor, for H_2 detect. 78−44646
Pd-SiO_2 interface, H induced interfacial polarisation, internal photoemission meas. 77−1490
Pd-SiO_2 interface, work function changes due to adsorbed H_2, surface and interface dipoles 80−96972
Pd-TiO_2 Schottky barrier, work function depend. on adsorbed species 80−54782
Pd-ZnO Schottky-barrier diode, H_2 sensitivity 80−11085
Pd+H^+(O^{5+}), L-shell X-ray prod. cross-section 77−6913
Pd+SiC, high temp. chem. reactions, products obs. by X-ray diffr. 78−17312
Pd_2, ab initio relativistic core pot. studies of metal-metal bonding 80−106257
Pd_9, and Pd_{19} clusters, Hartree-Fock-Slater model calcs. 77−72899
α-$PdD_{0.007}$, lattice location and thermal props. determ. of D by ^{3}He channelling 78−38747
PdH_x film, elec. resist. meas. 78−31011
β-PdH_x, muon depolarisation rate 77−32312
PdH_x-Gd, EPR of Gd^{3+} in temp. range 1.6 to 30K 77−43882
PdO-Pd miniature pH electrode description and use 80−89886
^{103}Pd inhalation studies, derivation of X-ray counting efficiencies for lung Pu 78−85391
^{103}Pd, lung burdens of low-energy photon-emitters, interlaboratory comparison of meas. techniques 79−20671

palladium continued
^{105}Pd muonic X-rays, nuclear charge parameters, quadrupole moments 78−29377
^{106}Pd, KLM- and KLN-Auger transitions 77−18884
Si:Pd, deep levels, conc., activation energies, thermal emission rate 79−51524
Si:Pd, doping, low temp. radiation induced impurity diffusion 77−15439
Si:Pd, energy levels obs. 77−35890
Si:Pd, Schottky diode, capacitance characts., acceptor levels 77−43697
n-Si:Pd, surface, photocond. and photo-emf spectra 79−73544
Si:Pd, surface doped with metal impurities, water adhesion energy *(Russian)* 77−89620
n-Si:Pd Schottky diodes photocapacitance meas., photon and carrier capture cross sections 80−20309
Si/Pd system, solid phase epitaxial growth control by C ion implantation 80−75466
n-Si-Pd diodes, chemical reduction process for fabrication 80−60082
Si-Pd-Si structure, epitaxial growth, backscattering and transmission electron microscopy studies of layered structures 80−80123
Si-Pd-Ti, silicide form. in evaporated films 80−80006
T solubility isotherms, at low equilib. press. 79−14935
Ti:Pd, ion implanted, corrosion behaviour and Rutherford backscatt. anal. 80−71792
Ti-Pd-Au metallisation, patterning by plasma etching of Ti 78−27677

palladium alloys
see also palladium compounds
Ag-Pd, surface comp. changes under ion bombardment, AES study 80−55250
controllable hydrogen phase naklep, hardening and phase-strengthening 80−16323
electronic band structure, comparative study of electric and mag. props. 78−95259
hardness, elec. cond., photo emission, and mag. props. *(Norwegian)* 79−32909
neutron activation determ. of microcomponents Pt, Pd, Ir, Rh, in noble metal alloys *(Russian)* 77−32858
Pd_3Fe, ferromag. spin wave meas., inelastic scattering of polarised neutrons 78−2665
phase transformation, $\alpha \rightleftarrows \beta$, influence on mech. props. *(Russian)* 78−68681
rare earth alloys RPd_2X_2 (X=Si,Ge), cryst. struct. 80−1964
rare earth palladinides, R_3Pd_4, mag. props. 77−47980
spin glass-ferromag. alloys, high-field magnetisation 79−33488
Ag-Au-Pd, liquidus and solidus surfaces 78−60649
Ag-Pd, composition modulated foils, layer struct. and mech. props. 79−95300
Ag-Pd, dil., elec. field gradients due to Pd near neighbour configs., TDPAC obs. 78−19391
Ag-Pd, dil., elec. field gradient, conc. and temp. effects 78−68416
Ag-Pd, dil., electric field gradient temp. depend., TDPAC meas. 78−39451
Ag-Pd, dil., electric field gradient meas. by TDPAC method 78−39452
Ag-Pd, dil., TDPAC exam. of radiation damage 78−39464
Ag-Pd, dil., virtual bound states, transport props. obs. 80−70667
Ag-Pd, surface comp., AES expts., correl. with O_2 heat of chemisorpt. data 78−34684
Ag-Pd, thermoelectric force meas., test of virtual bound d-state model 77−32001
Ag-Pd (20 at.%)/Pb, thin film reaction kinetics, X-ray diffr. expts. 77−89594
Ag-Pd alloys, inert gas ion bombardment, dynamic surface composition changes, AES obs. 80−60745
Ag-Pd film, thermal treatment and comp. depend. of resist., 273 to 700K *(French)* 77−76963
Ag-Pd film, valence band spectra, XPS meas. 78−52618
Ag-Pd system, low temp. resist., 1.5 to 40K 77−62887
Ag-Pd system, surface segregation 79−69330
Ag-Pd-Cu, contact-spring props., fatigue and spring limit *(Japanese)* 79−29117
Ag-Pd-Cu alloys, contact-spring props. and age hardening 78−88473
Ag-Pd-Cu-Au dental alloy, age-hardening characts. 79−87646
Ag-Pd-Ni, corrosion in marine atm., potentiometric technique, appls. 79−24693
AgPd alloys with Mn and Fe impurities mag. susceptibility 79−73677
AgPd, dil. alloys, electronic states, virtual bound states model test *(French)* 77−62809
Al-Pd, composite, paramagnetic resonance and electron-positron annihilation *(Russian)* 79−87314
Al-Pd, preferred sputtering on surface, mass difference and chemical bonding difference effects, AES obs. 79−83078
Al-Pd, rapid quenching, struct. and decomp. 80−76244
Al-Pd, rapidly solidified, new ordered phase, electron microscope obs. 79−11645
Al-Pd (6 at.%), metastable Al_2Pd phase formed by rapid quenching, electron diffr. obs. 79−51054
Al-Pd eutectic, microstruct. morphology 80−3018
Al-Pd film, preferred sputtering on surface, mass and bonding difference effects, AES obs. 79−87552
Al-Pd_2Si contacts on Si, elec. and structural characterisation 77−43695
Au/AuPd, bicrysts., in situ relax. of interphase interfaces 80−39455
Au-Cu-Ag-Pd (35.4, 17.8, 9.7 at.%), dental alloy, age-hardenable, TEM obs. 77−21156
Au-Mn-Pd, ferro- to non-magnetic transform. 77−12117
Au-Pd, bicryst. thin film couples, interphase interfaces, TEM 80−70540
Au-Pd, biological specimen prep. for SEM 79−5421
Au-Pd, dil., Friedel d-reson. scatt. and elec. resists. 80−44566
Au-Pd, dil., virtual bound states, transport props. obs. 80−70667
Au-Pd, disordered, shaft range order diffuse scatt., electron diffr., interpretation 77−84596
Au-Pd, elect. resistivity, temp. depend. between 1.6 and 4.2K *(German)* 79−28337
Au-Pd, He(I) photoelectron spectra, 5d band 79−33892
Au-Pd, surface comp. changes under ion bombardment, AES study 80−55250
Au-Pd, surface composition determ. 79−69328
Au-Pd (1(50) wt.%), quenched, vacancy annihilation and short-range order formation, elec. resist. 80−108487
Au-Pd alloy, on rock salt, epitaxial growth and struct. 77−20211
Au-Pd alloy, surface comp., polishing, cleaning and Ar sputtering effects 77−72763

palladium alloys continued
Au-Pd coating for radioactive source backing, spontaneous resistance variations 77−54386
Au-Pd dil. alloys, electronic states, virtual bound states model *(French)* 77−62809
Au-Pd-Pt-Ag, composition-property diagrams, mathematical models for diagrams *(Russian)* 79−11554
Au-Pd-Zn system, quasibinary section phases investig. 77−12596
Au-Pt-Pd-Ag-Cu, commercial dental alloy, age-hardening characts. 80−89235
Au(Pd)-Zn, martensitic transformation, Hall coeff., specific elec. resistivity and X-ray powder diffraction 78−72774
$(Au_{1-x}Pd_x)Ga_2$, supercond. transition temp. and crit. field 79−38232
$Au_{50-x}Pd_xZn_{50}$, ($0 \leq x \leq 15.02$) β'-phase, Hall effect and elec. cond. 80−107768
BaPd, gaseous, dissoc. energies, obs. and calc. values 78−58864
$BaPdSn_3$, prep. and crystal structure *(German)* 80−84138
$CePd_3$, dil., local mag. moments, neutron scatt. study 79−61058
$CePd_3$ fluctuating-valence compound, anomalous far IR absorption 80−66210
$CePd_3$, intermediate valence system, mag. neutron scatt. cross-section meas. 77−20552
$CePd_3$, magnetic neutron scatt. cross-section and linewidth, temp. depend. 77−63080
$CePd_3$, mixed valence cpd., theory of inelastic mag. neutron scatt. 79−15284
$CePd_3$, mixed-valence, 3d and 4d core levels, XPS study 80−89111
$CePd_3$, neutron scatt., spontaneous relax. of 4f magnetisation, interconfig. fluctuations 77−77025
$CePd_3$, susceptibility, sp. ht. and magnetisation 79−28512
$CePd_3$, tunnelling anomalies due to intermediate valence phenomenon 77−62873
$CePd_3$, unstable valence system, model for thermodynamics props. 77−69487
$CePd_3$-Er, dil., low field mag. susceptibility, electro-nuclear effects 80−60189
$CePd_3$-Er(Gd)(Yb), dil., EPR spectra 80−25201
$CePd_3$-Gd, EPR of Gd^{3+} impurities in host with interconfig. fluctuations 78−56377
$CePd_3$-Gd, ultralow interaction temp. and cryst. field effects for Gd impurities 79−61100
$CePd_3$-MPd_3 mixed valent systems, nonlinear conc. depend. of resist. 80−65528
$CePd_{3-x}Rh_x$, resistance behaviour and intermediate valence effects 79−78068
$CeRh_{3-x}Pd_x$, electronic and cryst. struct. comparison, catalytic behaviour 78−84398
$CeRh_{3-x}Pd_x$, lattice spacing and mag. suscept., effect of prep. and hydrogenation 77−58976
$CeRh_{3-x}Pd_x$, powdered alloys, catalytic behaviour correlation with electronic struct., lattice struct. and surface comp. 79−82181
Co-Pd, transfer phenomena and association with electronic struct. *(Russian)* 79−91017
Co-Pd alloys, 0-70 at.% Pd, conc. depend. of anomalous Hall field and resistivity *(Russian)* 78−14713
CoPd, single crysts., domain struct., temp. and field depend. 80−71085
Co_3Pd epitaxial films, multiray dynamic theory of diffr. contrast to explain defects nature 79−64962
Co_3Pd film, ordered, stacking fault obs. by TEM and interpret. using many-beam theory 80−107680
$Co_xPd_{80-x}Si_{20}$, amorphous, low field susceptibility near transition temp. 77−66359
$Co_xPd_{80-x}Si_{20}$, amorphous, structural and mag. heterogeneities 80−80484
Cr-Pd dilute alloys, itinerant antiferromag., neutron diffr. meas. 77−77032
$Cr_xPd_{82-x}Ge_{18}$, amorphous, RF sputtered, elec. resist. and magnetoresist., Kondo type behaviour 78−76066
$Cr_xPd_{82-x}Ge_{18}$ amorphous alloys, magnetoresist., mag. susceptibility, magnetisation 78−80148
Cu-Pd, (100) and (110) surfaces, LEED patterns 77−85031
Cu-Pd, composition modulated foils, layer struct. and mech. props. 79−95300
Cu-Pd, dil, perturbed angular correlation exam. of Pd impurity, ^{111}Cd probe 79−78588
Cu-Pd, dil., screening charge density round $\Delta Z = -1$ impurities, vacancies, NQR study 80−103897
Cu-Pd, disordered, antiphase domain boundaries, high resolution electron microscopy obs. 79−95030
Cu-Pd, disordered, shaft range order diffuse scatt., electron diffr., reinterpretation 77−84596
Cu-Pd, Fermi surface comp. depend. by positron annihilation ang. correl. 77−76727
Cu-Pd, mag. susceptibility and electronic struct. of ordering *(Russian)* 80−11161
Cu-Pd, microconductors, cast, struct. and physical props. exam 78−44232
Cu-Pd, surface comp. changes under ion bombardment, AES study 80−55250
Cu-Pd, surface struct. from LEED and AES meas. 79−77882
Cu-Pd, surface structures, LEED obs. 80−10761
Cu-Pd (4 at.%), anneal hardening mechanism 80−60879
Cu-Pd alloy, pressure effect on β-phase transition by elec. resist. meas. 79−15660
Cu-Pd alloy, singularities of physical props. and ordering *(Russian)* 78−76643
Cu-Pd dil. alloys, electronic states, virtual bound states model test *(French)* 77−62809
Cu-Pd foil, composition-modulated, elastic modulus enhancement 77−52382
Cu_3Au-Cu_3Pd, quasibinary system, order-disorder transform., superlattice form. 80−2159
Cu_2AuPd, struct., TEM and electron diffr. meas. 78−38666
Cu_2MnAl-Pd_2 MnAl mixed Heusler alloys, mag. props. 80−60269
CuPd, chemical shift effects and origin of Pd 3d core level satellite 80−104039
Cu_3Pd, electron irrad. in electron microscope, radn. ordering 79−86818
Cu_3Pd, periodic antiphase boundaries, electron microscopy study *(French)* 80−59481
$Cu_{83}Pd_{17}$, Cu^+ (Au^+) ion-bombarded, displacement cascades and disordered zones, TEM studies 80−15167

palladium alloys continued
$Cu_{1-x}Pd_xMnSb$, mag. phase transition 80−60268
$Cu_{0.5}Pd_{0.5}Ti_2$, solubility of H_2, decomp. reacts. 79−65197
Dy_5Pd_2, mag. props. 77−20547
$Er_5Ce_{1-5}Pd_3$, cryst. field spectra, neutron scatt. study 80−50047
$ErPd_3$, specific heat at low temp. 80−20413
Er_5Pd_2, mag. props. 77−20547
EuPd, mech. of H absorption, Mossbauer, mag. and X-ray diffr. meas. 78−38846
$EuPd_2$, elec. field gradient, spin echo NMR meas. 80−20509
$EuPd_2$, indirect exchange, spin echo NMR meas. 80−15822
Fe-Cr-Pd, electrospark coating on alloys, corrosion resist. increase *(Russian)* 78−27669
Fe-Cr-Pd, Pd alloying effects on passivation 80−35373
Fe-Pd, anomalous elec. cond. near mag. phase transition point, α to γ phase transition 80−15722
Fe-Pd, diffusion coeffs. of ^{59}Fe and ^{103}Pd meas. *(French)* 77−15617
Fe-Pd, FCC, ferromag., spin wave stiffness constant 78−91851
Fe-Pd, mag. moment, comp. depend. *(Russian)* 78−47280
Fe-Pd, magnetic after-effect of H isotopes 80−75817
Fe-Pd, magnetic struct. changes assoc. with crystallite thickness increase *(Russian)* 77−80913
Fe-Pd, residual resist., s-d hybridisation effect 80−39559
Fe-Pd (1-2 wt.%), solution of ^{119}Sn, study by Mossbauer spectroscopy 80−75888
Fe-Pd (31.2 wt.%), thermoelastic FCC-FCT martensitic transformation 80−104156
Fe-Pd (47 at.%) alloy, powders and powder compacts, mag. props. rel. to heat treatment *(Russian)* 79−15816
Fe-Pd (50 at.%), ordering under load, nuclear gamma reson. obs. *(Russian)* 78−92258
Fe-Pd (50 at.%), structural changes during ordering *(Russian)* 77−77471
Fe-Pd alloy, mag. struct. determ., neutron scatt., Mossbauer and mag. meas. *(Russian)* 78−2648
Fe-Pd alloy, uniaxial ferromag., anisotropic component of localised mag. field, Mossbauer meas. *(Russian)* 79−15382
Fe-Pd alloys, spin density radial distrib. determ. 79−73685
Fe-Pd crystalline alloy, positive large linear magnetostriction 80−25173
Fe-Pd film, depth profiles, sputter etching obs. 79−83079
Fe-Pd Invar, low temp. FCT phase obs. 80−93538
Fe-Pd Invar alloy, Young's modulus, magnetostriction, Curie temp. 80−65988
Fe-Pd Invar alloys, elec. and mag. props. and thermal expansion 80−75732
Fe-Pd-Pt alloy powders, coercive force and specific remanence *(Russian)* 79−47302
FePd epitaxial film, vacuum-deposited, for thermomag. recording, mag. and magneto-optical props. *(Russian)* 78−60319
$FePd_{1-x}Pt_x$, permanent magnet, coercive force increased by Pt 79−24157
$Fe_{1-x}Pd_x$ film, air-exposed, comp. profiles by AES, ESCA and ion sputtering 78−95245
$Fe_{1-x}Pd_x$ film, UHV deposited, effects of applied stress on B-H loops 78−64239
$Fe_{1-x}Pd_x$ film, vac. deposited, oxidation and corrosion, AES, XPS and STEM obs. 79−100286
$Fe_{1-x}Pd_x$ films, vacuum deposited, mag. and corrosion props. 79−56574
Fe_3Pd, quenched, or annealed exam. of magnetostriction, galvano- and thermomagnetic props. *(Russian)* 79−19757
$Fe_{50}Pd_{50}$, order-disorder transition, Mossbauer study 80−71268
$Fe(Pd_{1-x}Au_x)_3$, mag. struct. ferro-antiferromagnetism coexistence *(Russian)* 79−82759
$Fe(Pd_{1-x}Au_x)_3$ ordering alloys, mag. props., 4.2 to 500K *(Russian)* 79−47301
$Fe_{25}Pd_{50}Au_{25}$, atomic ordering influence on mag. props. and elec. resistance *(Russian)* 80−7551
$Fe_{34}Pd_{46}P_{20}$, amorphous, sp. ht. and resist. near ferromag. phase transition 78−56333
$Fe_xPd_{80-x}Si_{20}$, amorphous, structural and mag. heterogeneities 80−80484
$Fe_xPd_{80-x}Si_{20}$, low field susceptibility near transition temp. 77−66359
$Fe_xPd_{82-x}Si_{18}$, amorphous, magnetisation, magnetoresist., spin glass and ferromag. phases 80−34697
$Fe_xPd_{82-x}Si_{18}$ metallic glass, long range interaction and spin wave interactions 80−65949
$Fe_xPd_{82-x}Si_{18}$ metallic glass, mag. transitions, weak ferromagnetism 80−100583
Gd-Pd, amorphous, mag. and elec. props. 80−80499
Gd-Pd, amorphous, mag. props. and ferromag. reson. 80−75862
Gd-Pd, amorphous alloy, mag. coupling 78−88108
$Gd_xLa_{1-x}Pd_3$, EPR of Gd, g-factor and thermal broadening, temp. and comp. depend. 77−48048
$Gd_xPd_{82-x}Si_{18}$ amorphous alloys, mag. susceptibility, 4.2-300K 77−66248
H_2/D_2 solubility ratios in Pd alloys, meas. 79−99325
Ho_5Pd_2, mag. props. 77−20547
$La_{1-x}Ce_xPd_3$, resistance behaviour and intermediate valence effects 79−78068
$LaPd_3$, heat capacity at low temps. 79−28547
Li-Pd, phase diagram and mag. props. 77−90321
Li-Pd (60 to 75 at.%), phase diagram and cryst. struct. of $LiPd_2$ phase *(German)* 79−51055
Li_yPdH_x, production and cryst. props. *(German)* 77−43176
Mg_6Pd structure types alternative description of cryst. struct. 79−7577
γ-Mn-Pd, antiferromag. defect neutron scatt. study 79−47252
Mn-Pd, atomic and mag. order, neutron diffr. exam. 79−73697
γ- Mn-Pd, magnetic struct. for compositions near onset of antiferromag. ordering 77−63111
Mn-Pd (10 at.%), antiferromag. defect scatt., neutron polarisation anal. 78−2652
$Mn_xPd_{82-x}Ge_{18}$ amorphous alloys, elec. resistivity and magnetoresistivity 79−51543
$Mn_xPd_{82-x}Ged_{18}$, amorphous alloys, mag. props. 78−91906
Nb-Pd, impurity diffusion and vacancy-impurity binding energy 80−15307
Nb-Pd constitution diagram, metallographic and X-ray diffr. anal. 80−89204
$NdPd_3$, crystalline elec. field parameters 77−20278
Ni-Cu alloy, surface comp. and catalysis 80−54489
Ni-Fe-Pd thin films, mag., surface and corrosion props. 80−34707

palladium alloys continued
Ni-Pd, anodic behaviour, potentiodynamic current density and impedance potential meas. *(German)* 80−25925
Ni-Pd, directional order anisotropy energy induced by neutron irradiation, temp. depend. 77−66294
Ni-Pd, disordered, local environment effects, neutron scatt. expts. 78−68172
Ni-Pd, FCC disordered polycryst. alloy, magnetisation, band ferromag. 78−80180
Ni-Pd, ferromag., influence of local ordering on spin wave stiffness const. 77−89937
Ni-Pd, ferromag., press. effect on Curie temp. 79−51781
Ni-Pd, high mag. field effects, mag. isotherms near Curie point, exchange splitting energies 80−60272
Ni-Pd, itinerant electron ferromagnet, magnetovolume effects 80−60397
Ni-Pd, mag. moment distrib., one-mag.-species model calc. 80−65788
Ni-Pd, mag. props., average and local density of states, CPA calc. 77−59242
Ni-Pd, renormalisation of spin wave stiffness 79−51764
Ni-Pd (1 at.%), surface comp. and surface segregation, AES obs. 79−51404
Ni-Pd alloy, magnetostriction and mag. anisotropy meas. 79−4713
Ni-Pd surfaces, electrochem. passive film form. and comp. determ. by SEM, SIMS, XPS 80−39401
Ni-Pd-Ge, phase relationships and struct. 77−36451
Ni-Pd-H, film, struct. and phases formed, when Ni, Pd are sputtered in H 80−29289
Ni-Pd-Mn, ternary FCC solid soln., saturation magnetisation and Curie temp., medical appl. *(Japanese)* 79−61114
Ni-Pd-Mn ternary alloys, mag. characts., use for thermoseed 80−107995
Ni-Pd-P, metallic glass, amorphous and electronic structs., NMR Knight shifts and linewidths meas. 78−68400
Ni-Pd-P, metallic glass, electronic structure, pulsed NMR study 80−75869
Ni-Pd-P amorphous alloys, tensile deform. 77−32646
Ni-Pd-Si, amorphous, low-field mag. susceptibility meas., 4.2-580K 79−61057
Ni-Pd-Si, phase composition, isothermal section at 800°C *(German)* 77−16544
NiCoPd, anodic dissolution, SFE effect *(German)* 80−25924
$Ni_{0.98}Pd_{0.02}$, dil. ferromag., nucl. mag. relax. meas. 77−16198
$(Ni_{0.5}Pd_{0.5})_{82}P_{18}$ amorphous alloy, liquid-quenched, crystn. kinetics, effect of thermal history 80−100175
$(Ni_{0.5}Pd_{0.5})_{82}P_{18}$ amorphous alloy, liquid-quenched, crystn. kinetics, nucleation 80−100176
$(Ni_5Pd_5)_{82}P_{18}$, amorphous alloy, crystallisation 77−89382
$(Ni_5Pd_5)_{82}P_{18}$ amorphous alloy, glass transition temp. 77−84909
$NpPd_{3-x}Rh_x$, Mossbauer spectra, hyperfine interactions and mag. ordering 77−20783
$PD_{0.75}Ni_{0.25}$, spin wave excitations, neutron inelastic scatt. meas. 77−47983
Pb-Ni-Si, metallic glass, electron irrad., positron annihilation radiation, angular correlation study 78−84678
Pb-Pd, diffusion of Au, de-enhancement by Pd impurities 80−19990
Pb-Pd, liq. alloy activity by effusion method *(German)* 79−29023
Pb-Pd equilibrium diagram, Pb-rich region 77−48398
$Pb_2MnSb_{0.99}Sn_{0.01}$, ^{119}Sn Mossbauer study, compositional and heat treatment effects 79−42875
Pd alloy membrane pump, for thermonuclear fusion devices 78−89980
Pd alloy-H system, α-β phase transformations, hysteresis of press., elec. resistance, review 80−60859
Pd alloy-H system, review of props., book contrib. 80−24605
Pd based 3d metal alloys, mag. phase diagram calc. 78−80144
Pd Ni, effect of hydrogenation on thermopower 80−39562
Pd-Ag, dilute, low temp. sp. ht. and mag. susceptibility 77−62650
Pd-Ag, disordered, extension of Taylor's theory of lattice vibr. 79−4387
Pd-Ag, elec. resist. meas., 300-900K 77−47792
Pd-Ag, Fermi energy influence on soln. behaviour of H, B and C *(German)* 80−44323
Pd-Ag, H-H interaction in dil. solns. 78−71862
Pd-Ag, influence of adsorbed H on positron lifetime spectra 80−25480
Pd-Ag, ion bombarded, surface segregation, XPES obs. 79−77885
Pd-Ag, surface segregation, Auger studies 78−87849
Pd-Ag, thermal conductivity, data anal. and synthesis 78−95284
Pd-Ag, thin layer, deposited on glass or Si substrate, X-ray microanalysis *(French)* 80−50902
Pd-Ag (25 at.%) H_2 permeability and solubility, comparison with other Pd solid soln. alloys 79−23738
Pd-Ag alloy, asymmetry of XPS of shell electrons *(Russian)* 78−76579
Pd-Ag alloys, elec. resist. meas., density of states and Debye temp. 77−76715
Pd-Ag alloys, epitaxial growth and surface characterisation 78−14638
Pd-Ag alloys, photoelectron spectra of core electrons 79−100021
Pd-Ag electrical contacts in H_2S atmospheres, formation of contaminating layers *(German)* 80−71811
Pd-Ag electrical resistivity, thermo-EMF and thermal diffusivity at high temps. *(Russian)* 80−6808
Pd-Ag microwires, electrical resistance, influence of gaseous environment in heat treatment *(Russian)* 80−20146
Pd-Ag thin-walled tubes, for thermal diffusion apparatus H diffuser 80−100358
Pd-Ag-Au, lattice parameters and thermal expansion coeffs., X-ray diffr. meas. 79−99121
Pd-Ag-Au, temp. effect on lattice parameters and thermal expansion 78−51473
Pd-Ag-Cu (35,25 at.%), determ. of ageing transformations by resist. meas., metallography, TEM and X-ray diffr. 79−4967
Pd-Ag-D system, instability and superconductivity 78−39248
Pd-Ag-Fe, (0.5, 1.0, 2 at.% Fe), elec. resist. reduction near ferromag. and spin glass ordering 77−69299
Pd-Ag-H, alloys, 25-50% Ag, thermodynamic props., 555-700K 79−65216
Pd-Ag-H, band struct. and supercond. props., APW calc. 79−56354
Pd-Ag-H(D), elastic energy dissipation peak 80−60905
Pd-Ag-Si alloys, amorphous, crystn. kinetics, DSC meas. 80−1933
Pd-Ag(Au)(Cu) film on $BaTiO_3$ dielectric ceramic substrate, interaction between film and substrate during sintering 79−33958
Pd-Ag(Cd)(In)(H), electronic struct. from annihilation quanta ang. distribs. 77−66107
Pd-Ag(Cu) systems, positron annihilation, absorbed H_2 effect *(Russian)* 79−91528

palladium alloys continued
Pd-Ag(V), H mobility and solubility, appearance pot. spectra obs. 80−55231
Pd-Al, transition metal group VIII aluminide, NMR near equiatomic composition *(Russian)* 80−20479
Pd-Al alloys, Fermi level position rel. to mixing behaviour, Al activity, thermodynamic props. *(German)* 78−75835
Pd-Al appl. of quasichem. method of cluster components *(Russian)* 77−80623
Pd-Au, electronegativity and core electron binding energy shifts of Au 77−15346
Pd-Au, low temp. thermoelectric power 79−47084
Pd-Au, thermal conductivity, data anal. and synthesis 78−95284
Pd-Au:$H_2(D_2)$, thermodynamic props. at 555 and 700K, vibr. freqs. and excess entropies 80−29186
Pd-Au-Ag ternary system, isoparametric curves and Wegard's law plots 79−47657
Pd-Au-Si, amorphous films, RF sputter deposition, composition and thermal behaviour 80−55292
Pd-Au-Si, influence of struct. on elec. resist. of glass forming alloys 80−65518
Pd-Ba (1.5 wt.%), thermionic emitter, Auger spectrum fine struct. 78−2954
Pd-Ba alloy emitter, thermionic emission props. and Auger spectrum 78−11066
Pd-C, dil., C segregation to single cryst. surfaces 80−39301
Pd-C (graphite), adhesion and wettability of graphite *(Russian)* 80−20008
Pd-C solid solution, dechannelling of α-particles by C atoms *(French)* 79−7643
Pd-Cd eutectic, unidirectionally solidified, tensile and compressive props. 78−27567
Pd-Ce (5.75 at.%), H_2 permeability and solubility, comparison with other Pd solid soln. alloys 79−23738
Pd-Ce alloy, SRO determ. 77−7738
Pd-Co, dil., breakdown of ferromag. order, magnetoresist. obs. 80−71046
Pd-Co, dil., giant moment and Kondo-like coupling, nuclear orientation meas. 77−32160
Pd-Co, dil., Mossbauer emission spectra, fast relaxation regime, ^{57}Co hyperfine field 78−60362
Pd-Co, dil., relax. of oriented ^{57}Co nuclei, Mossbauer meas. using ^{3}He-^{4}He refrigerator 78−24909
Pd-Co, dilute, extraordinary Hall effect meas., 2-250K 80−34420
Pd-Co, dilute, nuclear orientation expt., Co impurity in singlet Kondo state 77−63296
Pd-Co, dilute alloy, ferromag. ordering, depend. on Co impurity at low temp. 79−61055
Pd-Co, Mossbauer effect under press. for ^{119}Sn impurity atoms and hyperfine mag. field model *(Russian)* 77−55742
Pd-Co, normal Hall effect *(Russian)* 80−103676
Pd-Co, pressure effect on Curie point, Debye temp. in ferromag. state *(Russian)* 77−32194
Pd-Co, very dil., Mossbauer emission spectra of ^{57}Co, relax. effects 80−29656
Pd-Co (0.1-45.7 at.%), thermo EMF at 4.2-300K *(Russian)* 80−92881
Pd-Co-P amorphous alloy, mag. an elec. props. 77−40043
Pd-Co(Ni), dil. local orbital moment evidence 77−20299
Pd-Cr, dil., appearance of mag. order for Cr impurities in exchange enhanced hosts 79−4690
Pd-Cr, dil., elec. resist., 7.4 to 300K, anomalous temp. depend. associated with cond. electron scatt. 79−73491
Pd-Cr, dil., temp. dependent scatt. 80−59973
Pd-Cr (11-18 at.%), resistivity comparison with canonical spin glass system 78−10432
Pd-Cr spin glass, magnetisation and magnetoresist. meas. 79−69680
Pd-Cu, H solubility enthalpy and entropy, effect on elec. cond. 77−35699
Pd-Cu, influence of adsorbed H on positron lifetime spectra 80−25480
Pd-Cu, T diffusion, effect on freq. factor and activation energy 78−63880
Pd-Cu, thermal conductivity, data anal. and synthesis 78−95284
Pd-Cu alloy, asymmetry of XPS of shell electrons *(Russian)* 78−76579
Pd-Cu alloys, epitaxial growth and surface characterisation 78−14638
Pd-Cu compound, KKR electronic struct. 80−59864
Pd-Cu-Ga, cold work and annealing-induced hardening, X-ray diffr. anal. and metallographic exam. *(Russian)* 79−38844
Pd-Cu-H(D) dilute alloy soln., thermodynamic props. at high-temp. 79−99334
Pd-Cu-Si, glass form., crit. cooling rate 80−75169
Pd-Cu-Si, laser melting and splat quenching to form foils for TEM obs. 80−29986
Pd-Cu-Si, metallic glass, miscibility limits, computer study 79−65198
Pd-Cu-Si glass, cold drawn, serrated plastic flow, optical and SEM study 79−79052
Pd-Cu-Si metallic glass, energy loss spectra and Auger spectra 78−23563
Pd-Cu(Ag)(Au) alloys-H solid solutions, superconducting transition temp. behaviour *(Russian)* 80−70879
Pd-D, band struct. and supercond. props., APW calc. 79−56354
Pd-D, mag. susceptibility 6 to 150K 79−38300
Pd-D alloys, phonon dispersion relation meas., elastic constants and Debye temp. 78−26639
Pd-Er, dilute alloy, EPR spectrum, effect of fine and hyperfine interactions 78−19323
Pd-Er, dynamic Jahn-Teller effect of Er^{3+} 79−73478
Pd-Er, fine struct. of Er^{3+}, dynamic Jahn-Teller effect of electronic Γ_8 quartet 77−35895
Pd-Fe, del. alloy, Mossbauer obs., 0.018-300K 77−69740
Pd-Fe, dil., anisotropy of neutron polarisation near ferromag. phase transition 77−32234
Pd-Fe, dil., anomalous lattice parameters and H_2 solubilities 79−33091
Pd-Fe, dil., ferromag. and spin-glass states, cond. electron polarisation studied by positive muons 77−28397
Pd-Fe, dil., plastically deformed, positron annihilation study of recovery of crystal, imperfections *(German)* 77−85835
Pd-Fe, dil., spin polarisation effect on hyperfine interactions, anal. of Mossbauer meas. *(Russian)* 79−47055
Pd-Fe, dil., transport props. at low temp. 0.05 to 5K 79−38046
Pd-Fe, dil. alloy, conduction electron polarisation at 0.1K, μ^+SR 77−20784
Pd-Fe, dilute, muon$^+$ Knight shift, cond. electron polarisation 77−66450
palladium alloys continued
Pd-Fe, disordered FCC, exchange stiffness consts., temp. depend. of magnetisation 77−69528
Pd-Fe, highly dil., mag. behaviour, 0.06-300K, Mossbauer expt. 78−43711
Pd-Fe, hydrogenated and unhydrogenated, EPR and demagnetisation field 77−32250
Pd-Fe, magnetic anisotropy near Curie point, quasi domain struct. *(Russian)* 80−65867
Pd-Fe, magnetoresist., rel. to dil. ferromag. model 78−30907
Pd-Fe, molecular field distribution function in disordered Ising model *(Russian)* 80−54859
Pd-Fe, Mossbauer effect under press. for ^{119}Sn impurity atoms and hyperfine mag. field model *(Russian)* 77−55742
Pd-Fe, Mossbauer spectra, scatt. and transmission geometries, differences in crit. behaviour near T_c 78−76367
Pd-Fe, NMR of ^{27}Al meas. 77−12215
Pd-Fe, normal Hall effect, temp. and conc. depend. *(Russian)* 77−80763
Pd-Fe, normal Hall effect *(Russian)* 80−103676
Pd-Fe, onset of ferromagnetism 78−23270
Pd-Fe, Pd-Fe-H and Pd-Fe-D, Mossbauer effect, internal hyperfine field temp. depend. 77−12283
Pd-Fe, resist. min. 80−11050
Pd-Fe, scatt. and transmission Mossbauer spectra near Curie temp. 80−15864
Pd-Fe, very dil., Mossbauer emission spectra, relax. effects 80−66084
Pd-Fe, very dilute, very low temp., spin glass-like behaviour 79−99708
Pd-Fe (0.54-8.0 at.%), thermo EMF at 4.2-300K *(Russian)* 80−92881
Pd-Fe (1 wt.%), alloy component surface conc. changes kinetics under vac. sputtering and volatilisation *(Russian)* 79−60608
Pd-Fe (25-55 at.%) ^{57}Fe effective field and mag. struct., Mossbauer and magnetisation expts. *(Russian)* 77−90085
Pd-Fe alloy, IR absorpt. charcts., 0.9 to 19 μm, mag. order effect 78−84577
Pd-Fe alloys, H_2 absorption and mag. behaviour 78−35012
Pd-Fe disordered alloy, Landau model for mag. props. 77−66276
Pd-Fe type dil. ferromag. alloys, spin wave propag. *(Russian)* 77−12110
Pd-Fe-H, elec. resistivity, 4.2 to 300K *(Russian)* 79−7814
Pd-Fe-H alloy, Mossbauer line shift with H conc. *(Russian)* 77−40165
Pd-Fe-Mn, differential susceptibility, spin glass and ferromag. transition 79−61169
Pd-Fe-Mn, dil. alloy, high press. study 80−34600
Pd-Fe-Mn, ferromag. and spin-glass props; comment 80−2591
Pd-Fe-Mn, ferromagnet-spin glass, thermal expansion forced, magnetostriction and magnetisation under high press. 80−65255
Pd-Fe-Mn, ferromagnetic-spin glass transition 78−39339
Pd-Fe-Mn alloy, spin glass-ferromagnetic systems, differential susceptibility 78−88131
Pd-Fe(Co)(Ni), dilute ferromagnets, press. effect on Curie temp. 80−65873
Pd-Fe(Co)(Ni) dilute alloys, ferromag., magnetoresist. 78−91665
Pd-Fe(Mn), dil., depend. of neutron small-angle scatt. intensities on appl. mag. field and temp. 79−11291
Pd-Gd, dil., EPR, 35 and 9 GHz, very dil. limit 78−15019
Pd-Gd (1 at.%), lattice distortion around impurities determ. by polarised neutron method 79−1372
Pd-Ge, metallic glass, theoretical studies on structural models 79−37633
Pd-Ge glass, short range order obs. for $Pd_{80}Ge_{20}$ and $Pd_{78}Ge_{22}$, EXAFS expts. 78−55815
Pd-Ge metallic glass, appl. of EXAFS methods for struct. determ. 79−37624
Pd-H, 50K transition, internal friction, LF torsion pendulum meas. 77−15490
Pd-H, band struct. and supercond. props., APW calc. 79−56354
Pd-H, degree of positron localisation on components 77−85833
Pd-H, dil., electronic states, de Haas Haas-van Alphen effect meas. 77−47718
Pd-H, dil. α-phase, influence of deform. on low-temp. sp. ht. 77−31783
Pd-H, elastic interaction and phase transition, book contrib. 79−83178
Pd-H, elec. resist., temp. depend., H conc. var. *(Russian)* 77−39819
Pd-H, electronic states from de Haas-van Alphen measurements 79−7777
Pd-H, H phase hardened, recrystallisation study 80−60883
Pd-H, in high press. H conditions, published results anal., atomic ratio calcs. 79−69254
Pd-H, interstitial position of H from entropy of soln. 77−65989
Pd-H, lattice strains, book contrib. 79−82202
Pd-H, low temp. transport props., heterogeneous-mixture model 80−24871
Pd-H, mag. susceptibility 6 to 150K 79−38300
Pd-H, mech. props., influence of dissolved H_2 *(Russian)* 80−81109
Pd-H, nature of the 50K anomaly, residual resist. 79−7818
Pd-H, optical phonons in supercond. 77−63021
Pd-H, solid soln., excess entropies, variation of H solubility with pressure 79−46846
Pd-H, supercond. and phonon softening in unstable systems 79−65587
Pd-H alloy, 50K transition, sp. ht. and thermal relax. meas., diffusion effects 77−15596
Pd-H alloys, in situ electron microscope obs. of precipitation 79−61589
Pd-H alloys, low temp. lattice parameter meas., β and mixed ($\alpha+\beta$) phases study 78−26496
Pd-H alloys, thermal expansion, low and room temp., Gruneisen parameters 77−63026
Pd-H dilute alloy, de Haas-van Alphen oscill. freq., absolute amplitude, Dingle temp. 80−49575
Pd-H dilute alloy, impurity elec. struct. 80−103643
Pd-H like compounds, supercond. T_c increase by optical phonons 77−1509
Pd-H system, anharmonicity effects on superconducting transition temp. 79−33380
Pd-H system, α and $\alpha+\beta$ phases, annealed and deformed, anelastic effects 80−66567
Pd-H system, α-β phase transformations, hysteresis of press., elec. resistance, review 80−60859
Pd-H system, cluster calc. of electronic struct. of interstitial H 78−43326
Pd-H system, effect of α-β phase change on β-phase solubility of H 77−89544

palladium alloys continued
Pd-H system, energy and electron density of states, improvements to theory 80−70636
Pd-H system, enthalpy and entropy changes for non-stoichiometric hydride formation 79−52741
Pd-H system, instability and superconductivity 78−39248
Pd-H system, lattice parameter increase meas. by X-ray diffr. *(German)* 77−62560
Pd-H system, magnetisation, type I and type II supercond. behaviour, homogeneity effects 77−28291
Pd-H system, many-body contrib. to XPS line asymm. 77−66575
Pd-H system, phase diagram determ. using Gd^{3+} EPR 79−87608
Pd-H system, positron localisation *(Russian)* 77−66555
Pd-H system, thermodynamic aspects of atomic vibr. 78−59913
Pd-H system, thermodynamic props., 245-352°C, up to 34 atm. 79−23749
Pd-H system containing d impurities, chem. binding energies of point defects 80−107214
Pd-H thin film system, phase diagrams using quartz crystal thickness monitor 80−7537
Pd-H_2, dilute soln., high temp. thermodynamics, partial molar props. 77−15597
Pd-H_x, model possibilities for the 50K transition 79−8299
Pd-H-Fe, Mossbauer effect, hyperfine field, effect of changing spin susceptibility 77−20494
Pd-H-Gd, dil., ESR exam. of low temp. region of phase diagram, and electronic props. 80−29930
Pd-H(D), isotope effect, theory 78−91806
Pd-H(D), isotope effects in supercond. properties 78−6471
Pd-H(D), superconducting transition temp., conc. depend. and inverse isotope effects 77−80864
Pd-H(D), superconductivity and electron-phonon interaction 80−49975
Pd-H(D), thermal expansion and lattice anharmonicity 9 to 270K 80−39241
Pd-H(D) alloy, low temp. ordering 79−14654
Pd-H(D) system, normal state phonon resist. and supercond. tunnelling density of states 79−56402
Pd-H(D) system, superconductivity and phonon softening 79−73626
Pd-In alloys, thermodynamic props., 800 to 1000°C 79−20454
Pd-Mn, alloy with mixed types of order, uniform mag. phase diagram 79−78368
Pd-Mn, Curie temp. and magnetisation, vol. depend. 80−34629
Pd-Mn, dil., mag. moment distrib., polarised neutron diffuse scatt. meas. 77−80914
Pd-Mn, dil., mag. ordering, sp. ht. calc. by Monte Carlo method 77−77030
Pd-Mn, dil. alloy, giant moment at very low temp. 78−88094
Pd-Mn, dil. alloy, very temp. magnetisation 80−34692
Pd-Mn, dilute, nuclear orientation expt., Mn impurity giant moment 77−63296
Pd-Mn, dilute, paramag. diffuse neutron scatt. 77−63094
Pd-Mn, ESR meas., evidences of bottlenecked relax. for Mn^{2+} ion 78−72401
Pd-Mn, ferromagnetism to spin glass behaviour transition 80−71062
Pd-Mn, NMR of ^{27}Al meas. 77−12215
Pd-Mn, spin freezing in spin glass phase, susceptibility meas., sp. ht. analysis 77−69582
Pd-Mn, spin glass, low temp. spin dynamics, numerical studies 79−78385
Pd-Mn, spin glass-ferromag. alloys, high-field magnetisation 79−33488
Pd-Mn (1-10 wt.%), mag. ordering, influence on resistivity 80−75557
Pd-Mn (10 at.%), spin glass, inelastic neutron scatt. exam. 79−61170
Pd-Mn alloy, spin glass, neutron scatt. 78−68265
Pd-Mn system, superstructure, electron diffr. and X-ray powder diffr. study 79−94958
Pd-Mn(Fe), mag. ordering phenomena, neutron scatt. obs. 80−44812
Pd-Mo, dilute, low temp. sp. ht. and mag. susceptibility 77−62650
Pd-Nb, dilute, low temp. sp. ht. and mag. susceptibility 77−62650
Pd-Ni, Auger sensitivity factors 78−43964
Pd-Ni, dil., ferromagnetism, local moments, susceptibility, magnetisation and Curie temp. *(Russian)* 78−88115
Pd-Ni, dil., resist. min. 80−11050
Pd-Ni, dil., Zeeman splitting of cond. electrons 77−11884
Pd-Ni, dil. paramag. alloy, local moments, rel. to nearly mag. impurities in nonmag. host 78−2647
Pd-Ni, disordered alloy, onset of ferromagnetism, effect of press. 79−61111
Pd-Ni, local susceptibilities, ^{61}Ni Mossbauer spectroscopy 78−95536
Pd-Ni, magnetovolume effects near crit. conc. for ferromag. 79−56591
Pd-Ni, NMR of ^{27}Al meas. 77−12215
Pd-Ni, nearly ferromag., quasiparticle picture for de Haas-van Alphen effect 78−91592
Pd-Ni, neutron radiation stimulated diffusion, electrical resistivity exam. *(Russian)* 79−14959
Pd-Ni, normal Hall effect *(Russian)* 80−103676
Pd-Ni, onset of ferromagnetism 78−23270
Pd-Ni, spin fluctuation alloy, thermopower peak diffusion origin 80−88542
Pd-Ni, surface comp. and catalysis, AES and thermal desorption meas. 79−46898
Pd-Ni, thermal expansion and magnetostriction meas. near crit. conc. for ferromagnetism 80−65881
Pd-Ni, thermopower and crit. conc., spin fluctuation system 78−30909
Pd-Ni (15-90 at.%), thermo EMF at 4.2-300K *(Russian)* 80−92881
Pd-Ni alloy, dil., magnetothermopower meas. 79−78079
Pd-Ni alloy, paramag. giant moments 78−56291
Pd-Ni alloys, kinetic props., transverse magnetoresistance *(Russian)* 77−76790
Pd-Ni alloys, kinetic props., anomalous Hall coefficient *(Russian)* 77−76791
Pd-Ni alloys, onset of ferromag. 79−56533
Pd-Ni disordered alloy, Landau model for mag. props. 77−66276
Pd-Ni-H, hydride formation in high press. range 80−65235
Pd-Ni-H alloys, hydrogenation under high press., superconducting crit. temp. 78−88058
Pd-Ni-H alloys hydrogenised under high press., supercond. crit. temp. 77−51834
Pd-Ni-P, amorphous, elec. resistivity negative temp. coeff., CAP calcs. 79−42515
Pd-Ni-P, metallic glass, viscous flow, alloying effect 78−79793
Pd-Ni-P metallic glass, energy loss spectra and Auger spectra 78−23563

palladium alloys continued
Pd-Ni-Si amorphous alloys, crystn. process during isothermal ageing 80−89275
Pd-Ni(Co)(Cr), liquid alloys, enthalpy of form. *(Russian)* 77−56244
Pd-Ni(Si), melt, struct. and physical-chemical props., thermodynamic props. *(Russian)* 78−18536
Pd-noble metal solid solns., with dissolved H, thermodynamic props. 80−108402
Pd-Pb-Bi supercond. alloy, X-ray, microscopic, thermographic anal. *(Russian)* 77−32106
Pd-Pt, adsorption, of CO(NO), on SiO_2-supported surface, IR spectrosc. obs. 80−92780
Pd-Pt, and other substitutional alloys with large mass disorder, phonon modes 78−95122
Pd-Pt, elect. resistivity, temp. depend. between 1.6 and 4.2K *(German)* 79−28337
Pd-Pt, local environment and mag. props. effect of disorders 77−63085
Pd-Pt, low temp. magnetoresistance up to 60 kG 78−91668
Pd-Pt, mag. props., average and local density of states, CPA calc. 77−59242
Pd-Pt, resonant modes, rel. to CPA predictions 78−75757
Pd-Pt, T diffusion, effect on freq. factor and activation energy 78−63880
Pd-Pt alloys, soln. of H_3, partial thermodynamic parameters determ. 77−66027
Pd-Pt surface, adsorbed Xe, 5p photoemission, local surface struct. influence 80−2920
Pd-Pt-Au alloys for low-temp. precision resistors 79−69490
Pd-Pt-H(D), elastic energy dissipation peak 80−60905
Pd-refractory metal/Si interactions, phase separation 80−65303
Pd-Rh, dil., hyperfine anomaly between bound negative muon and Rh nucleus 79−56707
Pd-Rh, dilute, low temp. sp. ht. and mag. susceptibility 77−62650
Pd-Rh, disordered, Hubbard model for electron correl. and spin susceptibility 77−76762
Pd-Rh, disordered, vol. paramagnetostriction calc. 77−80985
Pd-Rh alloys, soln. of H_2, partial thermodynamic parameters determ. 77−66027
Pd-Rh-Ag, mag. susceptibility, pressure effect up to 4000 atms. 77−16142
Pd-Rh-Ag, magnetic susceptibility press. depend., d-band deform. and exchange var. 77−47967
Pd-Rh-H, band struct. and supercond. props., APW calc. 79−56354
Pd-Rh-H and Pd-Ni-H, hydride formation in high press. range 80−65235
Pd-Ru, dilute, low temp. sp. ht. and mag. susceptibility 77−62650
Pd-Ru, electron transport props., 50 mK-4.2K 78−14707
Pd-Ru-W(V)(Ti), elec. resist. and thermal cond. *(Russian)* 78−19017
Pd-Sb film, rhombohedral phase, cryst. struct. electron diffr. determ. 80−39008
Pd-Se, thin layers, phase identification and struct., electron diffr. 77−51615
Pd-Si, amorphous, compositional study on short-range struct. 80−84095
Pd-Si, amorphous, neutron irradiated, small angle X-ray scatt. study 79−14850
Pd-Si, amorphous, struct., crystn. and Hall effect meas. 80−75178
Pd-Si, amorphous, US velocity, freq. and temp. depend. 78−63812
Pd-Si, amorphous alloys, elastic props. and temp. coeff. of delay time, appl. to US delay lines *(Japanese)* 79−96069
Pd-Si, amorphous metallic, sound propag. at low temps. 77−72656
Pd-Si, amorphous metallic glass, with defined local coordination, struct. model 80−84092
Pd-Si, amorphous $Pd_{0.8}Si_{0.2}$, struct. anal. by dense random packing model 79−51003
Pd-Si, amorphous viscoelastic behaviour *(Japanese)* 77−86110
Pd-Si, glassy, phonon transport below 100K 78−14422
Pd-Si, liq., mag. susceptibility 78−95415
Pd-Si, metallic glass, phonon propagation at low temp. 78−87756
Pd-Si, metallic glass, theoretical studies on structural models 79−37633
Pd-Si, metallic glasses, XPS and UPS studies 79−74062
Pd-Si, struct. obs. by X-ray diffr., low temp. annealing and deform. effects 79−56995
Pd-Si alloys, metallic glass, structural model 79−14690
Pd-Si amorphous, internal friction and shear modulus 77−25085
Pd-Si amorphous alloy, heat treated, low temp. lattice sp. ht. 80−75368
Pd-Si amorphous alloy, neutron irradiation effects *(Japanese)* 77−84806
Pd-Si amorphous alloy, positron annihilation exam. of crystallisation 79−43061
Pd-Si amorphous alloys, anal. of crystallisation kinetics 79−32912
Pd-Si amorphous films, RF and DC sputter deposition, composition and thermal behaviour 80−55292
Pd-Si glass, thermal cond., 01.-30K 77−20286
Pd-Si glasses, changes in density of states with alloys comp., UPS obs. 80−50531
Pd-Si layers, form. by laser irrad. of Pd film on Si substrate 79−99438
Pd-Si melts, appl. of quasichem. method of cluster components *(Russian)* 77−80623
Pd-Si metallic glass, high-resolution electron microscopy 80−84097
Pd-Si-Cu metallic glass tips, appl. as electron field emission source 79−8229
Pd-Si-Fe amorphous alloy, Mossbauer spectra, struct. and bonding 80−7224
Pd-Si-H(D) alloys, superconductivity in solid solution and amorphous phase regions, isotope effect 79−56347
Pd-Si-Sb, amorphous, phase separation and crystallisation 79−51002
Pd-Si-Sb, mostly crystalline, rapidly quenched, mech. props. 79−61610
Pd-Si(-Cu), amorphous, Hall effect meas. and electronic struct. 80−75551
Pd-Si(-Cu) amorphous ribbons, low temp. sp. ht., density of states trends 80−79957
Pd-Si(−Cu), glassy, liq. and cryst., mag. and elec. props. 77−66249
Pd-Sn-Cd, non-unique stress/strain rate relations during superplastic flow 77−28855
Pd-Te liquid alloys, thermodynamic activities *(German)* 79−29022
Pd-Th, thermodynamic stability 79−55903
Pd-Ti, hydrogenation, lattice spacings, microhardness and mag. susceptibility meas. 79−77557
Pd-Ti, Matthiessen's rule breakdown 77−15823
Pd-Ti liquid alloy, mass spectrometric study of high temp. thermodynamic stability 78−15369

palladium alloys continued
Pd-transition metal, dil., itinerant versus localised magnetism 78−64188
Pd-V, alloy and bilayer, silicide form. solid phase reaction with Si 80−6568
Pd-W, elect. resist., mag. susceptibility, Hall coeffs., in plastically deformed state and after annealing *(Russian)* 79−66174
Pd-W, substrate temp. influence on shallow contact formation on Si 80−96963
Pd-W (20 wt.%), permeability, diffusion, and solubility of H_2, elec. resist., heat treatment effects *(Russian)* 79−51307
Pd-W/Si, contact reactions, backscattering, X-ray diffr. meas. 80−20040
Pd-Y (8 at.%), H_2 permeability and solubility, comparison with other Pd solid soln. alloys 79−23738
Pd-Zn, γ-phase region, X-ray and electron diffr. obs. 79−61562
Pd-Zn, $L1_0$ type intermetallic phase, X-ray diffr. study of lattic compression 80−49182
Pd-Zn system, phase characterisation *(German)* 78−60654
Pd-Zn system, struct. stability of B2 and $L1_0$ phases 78−26495
Pd-Zr, metallic glasses, valence band struct. investigation 80−11533
Pd-Zr alloy, activity coeff. rel. to electronic props. *(German)* 77−20084
PdAg (4.7 at.%), effect of alloying on activation energy of H_2 diffusion 80−107571
PdAg, dil., disordered, virtual bound states, reson. model pot. theory 79−23934
PdAg surface, CO chemisorption, SIMS, XPS study 80−84382
PdAg wire, H_2 sorption, heat of adsorpt., sticking probabilities 78−43240
$Pd_{0.9}Ag_{0.1}$, H and D motion, thermodynamic data 79−65254
$Pd_{0.96}Ag_{0.04}$, phonon dispersion curves at 296K 80−24546
$Pd_{1-x}Ag_{1-x}$-Au, dil., electron density at Au, Mossbauer reson. 78−39473
$Pd_{70}Ag_{30}$, force-const. disorder system, obs. of reson.-like phonon mode 79−90745
Pd_cAg_{1-c}, possibility of superconductivity 80−10862
PdAgFe, ferromag., Curie temp. depend. on susceptibility, non-mean field theory 80−44829
$(PdAg_{0.2})H_2$, molar heat capacity, 2-6K, absence of supercond. transition 77−1516
$Pd_{1-x}Ag_xH_c$, superconducting transition temp. conc. var. 77−8221
$Pd_{1-x}Ag_xH_n$, positron annihilation examination of electronic structure *(German)* 77−69931
$Pd_{1-y}Ag_yH_x$, electronic struct. and supercond., APW calc. 79−95318
$Pd_{1-y}Ag_yH_x$, superconducting transition temp., APW band struct. calcs. 78−95393
$Pd_{0.91}Ag_{0.045}Rh_{0.045}H_x$, supercond. transition temp. rel. to optical phonon spectrum 79−56355
$Pd_{78}Ag_4Si_{18}$, amorphous, crystallisation kinetics 77−35487
$Pd_{82-x}Ag_xSi_{18}$, amorphous, roller-quenching conditions determ. 77−21051
PdAl-Fe(Ni), phase diagrams, eutectic points and solubility *(Russian)* 80−40333
$PdAl_x$ hydrides, supercond. transition temp. 79−47188
Pd_2AlCu-PdAl system, interactions and solid-state transforms *(Russian)* 80−16272
$PdAl_xH_y$ films, ion implantation prop., supercond. crit. temp. 79−87182
PdAl.r, cryst. struct. determ. 77−84700
Pd_xAs, cryst. struct. and cryst. binding *(German)* 78−42958
PdAu (4.7 at.%), effect of alloying on activation energy of H_2 diffusion 80−107571
PdAu, dil., disordered, virtual bound states, reson. model pot. theory 79−23934
$(Pd_{1-x}Au_x)_{0.99}Co_{0.01}$, mag. hyperfine interaction for impurity Co atoms *(Russian)* 80−7078
$(Pd_{0.8}Au_{0.2})D_{0.04}$, lattice location of D, ion channelling obs. 78−67708
$(Pd_{0.8}Au_{0.2})D_{0.04}$, thermal vibr. temp. depend., ion channelling exam. 78−47457
$Pd_{1-x}Au_xH_c$, search for superconductivity 77−8221
$(Pd_{80}Au_7Si_{13})/Fe_{30}$, compositionally modulated amorphous film, diffusion, struct. relax. 80−103518
PdB_xH_c, superconducting transition temp. conc. var. 77−8221
PdBi, rhombic, cryst. struct. determ. *(German)* 79−77556
Pd_5Bi_2, cryst. struct. *(German)* 79−51053
γ-Pd_8Cd_{43}, X-ray cryst. struct. determ. 80−54172
PdCo, dil., ferromag., nucl. mag. relax. 78−6590
PdCo, effect of hydrogenation on thermopower 80−39562
PdCo, extraordinary Hall effect 78−76053
$(Pd_{0.996}Co_{0.004})_{1-x}Mn_x$ alloys, ferromag. and spin glass transition, NMR 79−65761
$Pd_{1-y}Cr_yH_x$, resistive Kondo behaviour as function of Cr and H conc. 80−59971
$Pd_{1-x}Cu_xH_c$, superconducting transition temp. conc. var. 77−8221
$Pd_{0.775}Cu_{0.06}Si_{0.165}$ alloys, glassy and crystallised, low-temp. specific heat 79−60516
$Pd_{0.775}Cu_{0.06}Si_{0.165}$ glass, optical props. in energy range 0.67 to 5.6 eV 80−34872
$Pd_{0.775}Cu_{0.06}Si_{0.165}$, undercooled metallic melt, viscous behaviour 77−66037
$Pd_{68.5}Cu_{15}Si_{16.5}$ glass, elec. resist., struct. and mag. props. 79−65423
$Pd_{77.5}Cu_6Si_{16.5}$, cold drawn wires, surface markings, fracture stresses 79−56997
$Pd_{77.5}Cu_6Si_{16.5}$, heat of crystn. and viscous behaviour 80−75166
$Pd_{77.5}Cu_6Si_{16.5}$ metallic glass, diffusion of Au 78−55983
$Pd_{77.5}Cu_6Si_{16.5}$, metallic glass, composition, mech. props., simulation 80−49117
$Pd_{77.5}Cu_6Si_{16.5}$ metallic glass wire, cold drawing 80−50650
$Pd_{77.5}Cu_6Si_{16.5}$, ternary miscibility gap, simulation, dispersed phase composite form. 80−54379
$Pd_{77.5}Cu_{6.0}Si_{16.5}$ metallic glass, glass transition temp., cooling rate depend. 80−75181
$Pd_{77.6}Cu_6Si_{16.5}$, metallic glass, viscosity meas. from rates of thermal transformations 78−26713
$Pd_{781}Cu_{55}Si_{164}$ glass, erosion craters produced by spark machining, scanning microscopy obs. 78−44268
$Pd_{781}Cu_{55}Si_{164}$, liquid quenched metallic glass, wear resistance 79−66079
α-$PdD_{0.007}$, lattice location and thermal props. determ. of D by ^3He channelling 78−38747
$PdD_{0.63}$, inelastic neutron scatt. line shapes, Pd-D, D-D force consts. 78−47481
$PdD_{0.73}$, (1, 1/2, 0)-superlattice reflection splitting near 50K, neutron diffr. studies 80−70168
PdD_{1-x}, deuteron density modulation of D atoms 79−99101

palladium alloys continued
PdD_x, superconducting, molar sp. ht., γ-coeff. and Debye temp., 2 to 12K 77−1517
PdFe (4.7 at.%), effect of alloying on activation energy of H_2 diffusion 80−107571
PdFe alloy, magnetoresistance meas. below 295K 79−78070
PdFe, extraordinary Hall effect 78−76053
$Pd_{0.5}Fe_{0.5}$, disordered, spin wave dispersion relation, neutron inelastic scatt. 79−61090
$Pd_{0.98}Fe_{0.01}$ $Gd_{0.01}$, Pd-Gd exchange const., neutron diffuse scatt. meas. 80−71002
Pd_3Fe, ferromag., spin wave spectrum 77−69515
Pd_3Fe foil, $L1_2$ superstructure, antiphase boundary orientation and energy 80−39112
Pd_3Fe, hyperfine interactions during atomic ordering, Mossbauer obs. *(Russian)* 78−56630
Pd_3Fe, itinerant ferromagnet, neutron inelastic scatt. 79−7970
Pd_3Fe, spin wave dispersion relation at 4.2K, neutron inelastic scatt. meas. 77−63157
Pd_3Fe, spin wave dispersion, neutron inelastic scatt. meas. 78−14943
Pd_3Fe, X-ray and electron microscope obs. of antiphase domains and superdislocations *(Russian)* 77−86017
$(Pd_{0.67}Fe_{0.33})_{1-x}Au_x$, ordering effects on mag. props. *(Russian)* 78−47942
$Pd_{50}Fe_{37.5}Co_{12.5}$, elec. resist., cond. electron scatt. and heterogeneities of spin system *(Russian)* 79−56189
$PdFe_{1-x}Cr_x$ ordering alloys, elec. resist., temp. depend. *(Russian)* 80−24866
$Pd_{0.98}Fe_{0.01}Gd_{0.01}$, ferromag., Pd-Gd exchange const. and Pd polarisation, neutron scatt. meas. 80−25122
$(Pd_{0.9965}Fe_{0.0035})Mn_{0.05}$, ferromag. and spin-glass props. 80−2590
$(Pd_{0.9965}Fe_{0.0035})_{1-x}Mn_x$, mag. behaviour at Fe sites, Mossbauer effect meas. 80−66085
PdFeRh, ferromag., Curie temp. depend. on susceptibility, non-mean field theory 80−44829
$Pd_{70}Fe_{10}Si_{20}$ alloy, amorphous to cryst. transition, 350 to 450°C, Mossbauer spectra 78−59758
$Pd_{55}Ga_{45}$, ordered BCC phases at high temp. 79−32948
$Pd_{0.95}Gd_{0.05}$, mag. transition temp. determ., magnetisation data 77−12123
PdGe, dissociation in presence of Pd film 79−47892
PdGe, Pd_2Ge, growth kinetics and structure on Ge substrate 79−11514
Pd_2Ge, PdGe, growth kinetics on single cryst. and evaporated Ge 78−22985
$Pd_{21}Ge_8$, cryst. struct. *(German)* 78−18586
Pd_5Ge, cryst. struct. and cryst. binding *(German)* 78−42958
PdH, electronic struct. and proton spin-lattice relax. calc. 78−67937
PdH, electronic struct. and supercond., APW calc. 79−95318
$PdH_{0.72}$, Compton profile, electronic struct. *(German)* 78−92140
PdH_x (α′)$Fe_{0.003}$ 79−61054
PdH_x, diffusion of H, influence on nucl. spin-spin relax. time *(Russian)* 77−51977
PdH_x film, elec. resist. meas. 78−31011
PdH_x film, elec. resist., comp. depend. 79−1631
β-PdH_x, muon depolarisation rate 77−32312
PdH_x, optical phonon spectra, inelastic neutron scatt. study 79−42186
PdH_x, PdD_x, ordering, resistivity, annealing and neutron diffr. obs. 79−34030
PdH_x, upper crit. field determ. 78−47919
PdH_x, x=0.915 to 0.996, thermoelec. power, 10 to 170K, rel. to optical phonon spectra 79−56201
PdH_x, x≃1, type I supercond. props. 79−56448
PdH_x-Au, dil., electron density at Au, Mossbauer reson. 78−39473
PdH_x-Fe, dil., Kondo system, local moment hyperfine studies, Mossbauer expt. 80−39908
PdH_x-Gd, EPR of Gd^{3+} in temp. range 1.6 to 30K 77−43882
$Pd_{1-x}H_x$ (x=0.59, 0.65), magnetic susceptibility meas. in temp. range 4.2 to 300K 78−18953
Pd_xH-^{54}Mn, dil., nucl. orientation of ^{54}Mn 77−12257
PdH(D), stoichiometric, ^1H and ^2D NMR, rel. to supercond. T_c 78−72430
PdH(D), supercond., isotopic vol. effect 77−1511
PdH(D), superconducting props., effect of hybridisation, band struct. determ. 79−69628
$PdH_x(D_x)$ films, electron-phonon coupling, elec. cond. obs. 80−50011
$PdH_xFe_{0.003}$, Kondo system, local moments, hyperfine fields, Mossbauer study 80−80478
PdHg-Rh, dil., quadrupole interaction of ^{100}Rh 79−99520
β′-PdIn, electrical resistance, mag. susceptibility and IR freq. dispersion *(Russian)* 80−107759
PdIn, refractive index, reflectivity and band struct., APW calcs. 80−40139
$PdIn_xH_y$ films, ion implantation prop., supercond. crit. temp. 79−87182
$Pd(M_nCo)$, giant moments, Mossbauer study of ^{57}Fe 80−44969
$(Pd_{1-y}M_y)_{100-x}Fe_x$, M=Ag, Rh, exchange-enhanced alloys, mag. ordering 79−61050
PdMn, extraordinary Hall effect 78−76053
PdMn, giant moment-spin glass high field magnetisation, exchange parameter, saturation moment estimation 79−61143
Pd_3Mn, disordered, mag. correls., neutron scatt. study 80−50105
$Pd_{1-y}Mn_yH_x$ alloy, spin glass, transition temp., susceptibility and EPR meas. 80−65930
$Pd_2MnIn_{1-y}Sb_y$, Heusler alloy, mag. order obs. 80−29528
$Pd_2MnIn_{1-x}Sb_x(Sn_x)$, Heusler alloy, Mossbauer effect exam., mag. coupling 79−69755
$Pd_2MnIn_{1-x}Sb_x(Sn_x)$, Heusler alloy, Mossbauer effect exam., hyperfine interactions in ferromag. phase 79−69756
$Pd_2MnIn_{1-x}Sn$, and $Pd_2MnIn_{1-y}Sb$, Heusler alloys, mag. order, disorder effects 80−88723
$Pd_2MnIn_{1-x}Sn_x$-Cd, dil., Heusler alloy, hyperfine mag. field on Cd, TDPAC obs. 79−8075
$Pd_2MnIn(Sn)(Sb)$, Cd impurities, hyperfine field meas. 78−15074
$Pd_2MnIn_{1-x}Sn_1-_x$, mag. order exam. 77−40036
$Pd_2Mn_{1-x}Nb_xSn$, Heusler alloy, NMR and mag. coupling 78−43676
PdMnSb, Heusler alloy, hyperfine fields of 5sp shell impurities substituting Sb, Mossbauer spectra 78−80261
PdMnSb, hyperfine field at ^{125}Te, Mossbauer expts., compared with Jena-Geldart model 78−43707
PdMnSb, Pd_2MnSb, Heusler alloys, ^{129}I mag. hyperfine struct., Mossbauer meas. 79−33580

palladium alloys continued
Pd_2MnSb and PdMnSb, Heusler alloy, hyperfine field at ^{111}Cd, TDPAC meas. 78−43705
Pd_2MnSb, ferromag. Heusler alloy, mechanical and heat treatment effects 79−78582
Pd_2MnSb, Heusler alloy, hyperfine fields of 5sp shell impurities substituting Sb, Mossbauer spectra 78−80261
Pd_2MnSb, mag. hyperfine field of ^{129}I, Mossbauer spectra 78−43706
Pd_2MnSb:^{119}Sn, ferromag., mag. hyperfine structure, Mossbauer obs. 77−32309
$Pd_{2-x}MnSb$, struct., appl. as improved neutron polariser 80−60199
$Pd_2MnSb_{1-x}Sn_x$, Mossbauer meas. of ^{119}Sn mag. hyperfine struct. 77−12258
Pd_2MnSn alloy, ionic spin distribution and RKKY interactions 78−27028
Pd_2MnSn, ferromag. Heusler alloy, electronic struct., spin polarisations, theory 80−54598
Pd_2MnSn, Heusler alloy, interaction between local mag. moments 77−1540
Pd_2MnSn, Heusler alloy, mag. interactions and cond. electron polarisation, spin echo NMR meas. 77−77125
Pd_2MnSn, Heusler alloy, NMR and mag. coupling 78−43676
$Pd_2Mn_{0.95}Sn_{1.05}$, hyperfine mag. fields, Mossbauer spectra 80−15870
$Pd_2Mn_{0.98}Sn_1In_{0.02}$, Heusler alloy, hyperfine fields at sp elements, spin echo NMR meas. 78−84496
$Pd_2MnSn_{1-x}Sb_x$, Heusler alloy, Mossbauer effect exam., hyperfine interactions in ferromag. phase 79−69756
$Pd_2MnSn_{1-x}Sb_x$, mag. order exam. 77−40036
$Pd_2MnSn_{1-x}Sb_x$, Mossbauer spectra, mag. hyperfine field 80−15868
$Pd_2Mn_xV_{1-x}Sn$, Heusler alloy, structural disorder, Mossbauer study 80−80650
PdNb, dilute, NMR obs. of ^{93}Nb 80−71203
PdNi, extraordinary Hall effect 78−76053
$Pd_{48}Ni_{32}P_{20}$, metallic glass, viscosity meas. from rates of thermal transformations 78−26713
$(Pd_{99}Ni)_{1-x}Pt_x$, spin-fluctuation thermopower 79−60802
$Pd_{60}Ni_{20}Si_{20}$, amorphous, struct., high resolution electron microscopy 80−1969
PdNi(4.7 at.%), effect of alloying on activation energy of H_2 diffusion 80−107571
$PdPb_2$-Rh, dil., quadrupole interaction of ^{100}Rh 79−99520
Pd_3Pb, Ll_2 ordered alloy, positive temp. depend. on strength, phase destabilization 80−81203
Pd_2PbBi, and Pd_4PbBi_3, cryst. struct. *(German)* 79−94963
PdPb.r, crystal structure *(German)* 80−96472
$Pd_{13}Pb_9$.r, cryst. struct., X-ray study 80−103293
$Pd_{1-x}Pr_x$ (x=0.02 and 0.03), dil. alloy, min. resist. around 20K 79−19583
$(Pd_xPt_{1-x})_3Fe$ atomically ordered alloy, thermoelectric power, carrier energy spin shift, mag. props. 80−29394
$(Pd_xPt_{1-x})_3Fe$, magnetisation intensity and coercive force, antiferro- to ferromag. transition *(Russian)* 77−48008
$Pd_{0.9}Rh_{0.1}$, lattice dynamics, inelastic neutron scatt. meas. at 296K 80−29135
$Pd_{0.95}Rh_{0.05}$, exchange-enhanced, phonon dispersion relations exam. 77−84868
$Pd_{95}Rh_5$, low-temp. spin-fluctuation resist., effect of pot. scatt., effect of Ni addition 77−15840
$(Pd_{95}Rh_5)Co$, exchange enhanced system, AC susceptibility meas. 77−16096
$Pd_{1-y}Rh_yH_x$, electronic struct. and supercond., APW calc. 79−95318
$(Pd_{95}Rh_5)_1H_x$, elec. resistivity studies 80−59957
PdRu (4.7 at.%), effect of alloying on activation energy of H_2 diffusion 80−107571
$Pd_{81}S_{19}$ and $Pd_{84}Si_{16}$, metallic glasses, optical refl. spectra and optical consts. 79−87464
PdSb, de Haas-van Alphen effect, Fermi surface 79−7773
PdSb, XPS, electronic struct. 80−7464
PdSb-Rh, dil., quadrupole interaction of ^{100}Rh 79−99520
$Pd_{20}Sb_7$, cryst. struct. determ. *(German)* 77−19905
$Pd_{75}Sb_{25}$, ordered BCC phases at high temp. 79−32948
Pd_7Se_4, cryst. struct. determ. *(German)* 78−75628
PdSi alloys, amorphous thermal behaviour and crystallisation kinetics 78−26446
PdSi, amorphous, crystn. kinetics 79−99078
PdSi, amorphous, structural relaxation enhancement following stress reduction 80−3118
PdSi films, on Si, stress obs. 80−80145
PdSi, formation by Xe ion beam bombard. of Pd film on Si substrate 80−10800
PdSi-Si interfaces, chemical state, AES expts. 78−91767
a-$Pd_{0.8}Si_{0.2}$ alloy, struct. factor determ. rel. to short-range correlations 77−1060
$Pd_{0.8}Si_{0.2}$, amorphous, He^{2+} ion irradiation effect on structure 79−42120
$Pd_{0.8}Si_{0.2}$, amorphous ribbon, struct. factor anisotropy, pulsed neutron diffr. study 78−87619
$Pd_{0.8}Si_{0.2}$, liquid and amorphous states, short-range order comparison 77−1069
$Pd_{0.81}Si_{0.19}$, amorphous, partial densities of states, XPS, UPS and AES meas. 79−95315
Pd_2Si, Cs ion-bombarded, surface Cs concs., AES meas. 79−83073
Pd_2Si, epitaxial film on Si, ^4He ion channelling meas. and RHEED anal. 80−10834
Pd_2Si film on Si, metallic, resist. and Hall mobility meas. 78−47886
Pd_2Si film on Si, substrate temp. effect on microstruct., TEM obs. 78−14621
Pd_2Si films, on Si, stress obs. 80−80145
Pd_2Si films on Si, lattice imaging obs. of structural details 80−103604
Pd_2Si, form. in Si-Pd-Ti evaporated films 80−80006
Pd_2Si, formation at Pd-Si (111) interface, UPS obs. 80−24743
Pd_2Si formation from Pd-Si sample, obs. by ^{31}Si tracer and Rutherford backscatt. methods 79−4431
Pd_2Si layer, on Si, ion implantation damage, channelling obs. 78−30676
Pd_2Si layer 79−4489
Pd_2Si, on Si substrate, thermally induced Si accumulation, AES study 80−24718
Pd_2Si, Schottky barrier, resistivity, elec. characts., barrier heights, solar cell use 78−14825
Pd_2Si, solid-phase epitaxy in Si (100)/Pd_2Si/Si (amorphous) system, radioactive tracer obs. 77−89663

palladium alloys continued
Pd_2Si-Si, substrate ion implantation, channelled, through metal silicide film 80−70231
Pd_2Si-Si Schottky barrier diode grown by solid phase epitaxy 77−80837
Pd_2Si-Si:As(Sb), implanted dopant redistrib. after silicide form., appl. to ohmic contacts 79−37729
$Pd_{80}Si_{20}$, amorphous, electronic struct. calc. 79−87032
$Pd_{80}Si_{20}$, amorphous, elec. resist. and magnetoresist. 80−49693
$Pd_{80}Si_{20}$, amorphous, structural changes by neutron irradiation, X-ray scatt. meas. 78−6104
$Pd_{80}Si_{20}$, amorphous, struct. factor temp. depend., X-ray diffr. study *(Japanese)* 79−51005
$Pd_{80}Si_{20}$, amorphous, structural changes with neutron irrad., X-ray scatt. obs. 80−33898
$Pd_{80}Si_{20}$, amorphous alloy crystn., high press. effect 78−95001
$Pd_{80}Si_{20}$, amorphous alloy, partial struct. functions, X-ray, electron and neutron diff. studies *(Japanese)* 80−88050
$Pd_{80}Si_{20}$ amorphous alloy, skip deform. and crit. shear stress, using tensile testing machine 80−89321
$Pd_{80}Si_{20}$, glass, deform. localisation, plastic instabilities and fracture 80−89320
$Pd_{80}Si_{20}$ glass, struct. simulation 78−38624
$Pd_{80}Si_{20}$ metallic glass, struct. relax., X-ray expts. 79−1400
$Pd_{80}Si_{20}$ metallic glass, vibrational spectrum, inelastic neutron scatt. meas. 79−60465
$Pd_{80}Si_{20}$ metallic glass, high-resolution XPS study, electronic state struct. 80−29846
$Pd_{80}Si_{20}$, metallic glass, composition, mech. props., simulation 80−49117
$Pd_{80}Si_{20}$ metallic glass, inelastic deform., free energy spectra 80−71699
$Pd_{80}Si_{20}$ metallic glass, tensile deform., shear band form., high-speed cinematographic obs. 80−89322
$Pd_{80}Si_{20}$, plastic flow, fracture, slanted necking and elongation at high temps. 79−57057
$Pd_{80}Si_{20}$, shear band form. 78−68756
$Pd_{80}Si_{20}$, vapour quenched amorphous alloy, atomic arrangements 80−100173
$Pd_{82}Si_{18}$ glassy, long term creep tests, isoconfigurational viscosity rel. to annealing treatment 79−66122
$Pd_{82}Si_{18}$, stress/strain rate depend. of homogeneous flow 80−71687
$Pd_{82.5}Si_{17.5}$, amorphous and liq. alloys, struct., X-ray diffr. 77−24275
$(Pd_{86}Si_{15})_{61}/(Fe_{85}B_{15})_{39}$, compositionally modulated amorphous film, diffusion, struct. relax. 80−103518
PdSiCu, amorphous, US attenuation and vel. studies 80−19881
PdSiCu, amorphous, US attenuation and vel. studies at low temps. 80−88278
$Pd_{0.775}Si_{0.165}Cu_{0.06}$, glassy alloy, resist. minimum associated with mag. impurities 79−56187
$Pd_{0.775}Si_{0.165}Cu_{0.06}$, metallic glass, intensity-depend. US attenuation at low temps. 78−79671
$Pd_{0.775}Si_{0.165}Cu_{0.06}$, metallic glass, 0.01-10K, relax of tunnelling systems by conduction electrons, US expts. 79−14889
$Pd_{0.78}Si_{0.16}Cu_{0.06}$, phonon propagation below 1K 78−71824
$Pd_{1-x-y}Si_xCu_y$, glassy, low temp. specific heat 78−83969
$Pd_{18}Si_{14}Cu_6$, glass, changes in density of states with alloys comp. UPS obs. 80−50531
$Pd_{77}Si_{17}Cu_6$, amorphous, struct. changes due to cold rolling and low temp. annealing 79−66072
$Pd_{77.5}Si_{16.5}Cu_6$ amorphous, indentation recovery, defect struct. produced by deformation 79−43275
$Pd_{80}Si_{17}Cu_3$, glass, changes in density of states with alloys comp., UPS obs. 80−50531
$Pd_{100-x-y}Si_xFe_y$, amorphous, ^{57}Fe Mossbauer spectra, X-ray diffr., ageing behaviour 79−28651
$Pd_{80-x}Si_{20}Fe_x$, amorphous, low x, hyperfine interactions and mag. ordering temp. 79−15303
$Pd_{0.97}Sm_{0.03}$ dil. alloy, assist. meas. 79−19583
$Pd_{0.99}Sn_{0.01}$, lattice dynamics of ^{119}Sn impurities, Mossbauer meas. 77−76507
Pd_xSn_y (x=0.95, y=0.05; x=3, y=1), Mossbauer spectra, high press. effects, force consts. 80−84669
PdTe-Rh, dil, quadrupole interaction of ^{100}Rh 79−99520
$PdTe_2$, bandstructure, Fermi surface, LMTO method 78−6264
$Pd_{20}Te_7$, cryst. struct. determ. *(German)* 77−19905
$Pd_{75}Te_{25}$, ordered BCC phases at high temp. 79−32948
Pd_9Te_4, cryst. struct. and binding *(German)* 78−51471
$Pd_xTh_{1-x}Pu$, magnetism of actinide impurity 77−51883
$PdTi_2$, solubility of H_2, decomp. reacts. 79−65197
Pd_4Ti, Ll_2 ordered alloy, positive temp. depend. on strength, phase destabilization 80−81203
$Pd_{0.97}Tm_{0.03}$, dil. alloy, elec. resist. meas. 79−19583
$Pd_{82-x}V_xSi_{18}$, amorphous, effect of structural relax. on elec. resist. 79−56186
$Pd_{82-x}V_xSi_{18}$, metallic glasses, effect of press. on elec. resist. 80−6805
$Pd_{1-x}W_x$, calc. of short-range order parameters from X-ray scatt. data *(Russian)* 80−75367
PdZr, amorphous, supercond., US props. 80−44765
PdZr, photoemission study 80−104046
$Pd_{30}Zr_{70}$, amorphous alloys, supercond. transition temp., press. depend. 80−84524
$Pd_{35}Zr_{65}$, mag. susceptibility meas. 80−75740
$PrPd_3$, crystalline elec. field parameters 77−20278
$PrPd_3$, heat capacity at low temps. 79−28547
Pt-Pd, surface comp. and catalysis, AES and thermal desorption meas. 79−46898
Pt-Pd alloy, surface composition determ. by AES 78−79869
Pt-Pd melts, surface tension and density *(Russian)* 80−39388
Pt-Pd system, sorption of H_2 during cathodic charging, deflection technique meas. 79−51427
Pt-Sn alloys, thermodynamic props. *(German)* 78−52769
$Pt_{37.5}Pd_{12.5}Co_{50}$, elec. resist., cond. electron scatt. and heterogeneities of spin system *(Russian)* 79−56189
$Pt_{12.5}Pd_{37.5}Fe_{50}$, elec. resist., cond. electron scatt. and heterogeneities of spin system *(Russian)* 79−56189
Rh-Pd, mag. moment of Ni, Co, Fe, Mn and Cr impurities 78−95416
Rh-Pd-Co, dil., local moment formation 78−43562
Rh-Pd-Co(Fe), dil., local environment and mag. props. 78−64187
Sc-Pd, electronic struct., susceptibility, sp. ht. and Knight shift meas. 77−43485
ScPd, electronic struct., NMR relax. times meas. 79−51871
ScPd, UPS exam. 78−48276

palladium alloys continued
Si-Pd, (LMM) Auger electron emission by keV Ar^+ bombardment 79−95880
Si-Pd, preferred sputtering on surface, mass difference and chemical bonding difference effects, AES obs. 79−83078
Si-Pd film, preferred sputtering on surface, mass and bonding difference effects, AES obs. 79−87552
n-Si-Pd_2Si contact, interface struct. and Schottky barrier height, correl. obs. using TEM 80−100504
Si-$Pd_{80}Si_{20}$, amorphous, Pd_2Si layer form., shallow contact 80−103586
$Sm_{10}Pd_{21}$, X-ray cryst. struct. anal. 79−99118
$SrPdSn_3$, prep. and crystal structure *(German)* 80−84138
Ta-Pd system, phase diagram exam. of composition by X-ray diffr., electron microprobe anal., and metallography 78−76632
$TbPd_3$, specific heat at low temp. 80−20413
Tb_5Pd_2, mag. props. 77−20547
Ti-Pd, crevice corrosion in NaCl soln., 100 to 250°C *(Japanese)* 78−72927
Ti-Pd, dil., ion implanted, corrosion rate and electrochemical props. 79−43467
Ti-Pd, eutectoid decomposition 79−24491
Ti-Pd (0.15 wt.%), IMI-260, strain rate effect on mech. behaviour 80−3153
Ti-Pd-Cu-Ni-Au metallisation systems, in 85°C 78% RH SO_2 contaminated environment, performance 79−74304
$TiPd_3$, valence band struct., X-ray emission spectra *(Russian)* 77−40304
Tm_5Pd, mag. props. 77−20547
UPd_3, anomalous behaviour in low temp. props. 79−28108
UPd_3, crystalline elec. field studies using neutron inelastic scatt. at NRCN 80−10931
UPd_3, crystalline electric field levels of U, neutron scatt. exam. 78−60267
UPd_3, U^{4+} mag. form factor meas. by inelastic neutron scatt. 78−52221
UPd_4, localised cryst. field states, neutron inelastic scatt. obs. 78−14697
UPd_2Si_2, magnetic phase transition, neutron diffr. meas. 79−47284
V-Pd, dil. alloys, surface segreg. 78−18883
V_3Pd, nuclear spin-lattice relax. time, electronic density of states 77−59354
W-Cr-Pd, Pd effects on diffusion 77−24445
YPd_3, rare earth impurities, magnetostriction 79−4714
YPd_3-Gd, ultralow interaction temp. and cryst. field effects for Gd impurities 79−61100
Y_3Pd, cryst. struct. 80−96474
Y_3Pd_2, structure determ., rhombohedral Er_3Ni_2 type 77−80443
Y_5Pd_2, mag. props. 77−20547
$Y_{1-x}Tb_xPd_3$, magnetisation, magnetostriction, and inelastic neutron spectra 80−65998
YbPd-YbAg system, valency state, Yb behaviour *(French)* 80−45277
Zr-Pd, heat treated, mech. props. and struct. 78−80571
Zr-Pd, metallic glasses, electronic props. and supercond. 79−73486
$ZrPd_2$, valence band struct., X-ray emission spectra *(Russian)* 77−40304
$Zr_{0.7}Pd_{0.3}$, amorphous supercond., sp. ht. and thermal cond., 0.1-10K 78−26991
$Zr_{70}Pd_{30}$ amorphous alloys, struct. factors and radial distrib. functions 80−84096
$ZrRh_{3-x}Pd_x$, electronic and cryst. struct. comparison 78−84398
$ZrRh_{3-x}Pd_x$, powdered alloys, catalytic behaviour correlation with electronic struct., lattice struct. and surface comp. 79−82181

palladium compounds
see also palladium alloys
double oxides, elec. cond. 80−34438
electronic absorpt. spectra, band assignments 78−50553
ethylenediammonium palladium chloride, struct. and mag. props., vibr. spectra 79−10842
gelatin-Pd II complex formation, circular dichroism and absorpt. spectra meas. 79−61881
hydride, Compton profiles 79−8206
layer, galvanostatic desorption of hydrogen, quantitative theory 80−40694
linear mixed valence compounds, lattice modes obs. 79−46763
linear mixed valence compounds, longit. modes 78−95119
mixed valence-mixed metal compounds, ionic crystals, longitudinal lattice modes, Raman spectroscopy 80−40099
palladium porphin, Zeeman expt. on phosphoresc. triplet and quartet states 79−33786
palladium-octaethylporphyrin, gas phase delayed fluoresc. and phosphoresc., triplet excimer formation 80−18884
porphin, in n-alkane, $S_1 \leftarrow S_0$ absorpt. spectrum, vibronic coupling and avoided crossing, field splitting 78−84613
porphin, in n-alkane crystal, Zeeman and crystal field effects, absorpt. vibr. anal. 80−7372
porphin, in n-octane cryst., lowest triplet state, ESR-optical detect. 77−58050
porphin, optically detected EPR and Zeeman meas. 79−19809
Cr-Pd_2Si-Si, $CrSi_2$ form. kinetics 77−24492
$CrSi_2$ formation on Pd_2Si and PtSi, radioactive Si tracer obs. 78−60578
$Fe_xPd_{82-x}Si_{18}$ metallic glass, mag. phase diagram, weak ferromagnet-spin glass transition 80−54893
Ni-Pd-H, film, struct. and phases formed, when Ni, Pd are sputtered in H 80−29289
$PaCl_2$, thin films, reduction to Pd by Ne^+ ion irrad., 2 MeV He^+ ion backscatt. anal. 79−4493
β-Pb hydride, electron diffr. investigation 79−65062
Pd and Pt mixed valance complex, $[Pd(ethylenediamine)_2Pt(ethylenediamine)_2Cl_2](ClO_4)_4$, Raman spectra 80−84734
Pd complex, 1,1,1-trifluoro-2,4-pentanedionate, struct., chem. ionisation mass spectra 78−61079
Pd complex, 1,2-benzoquinonedioximates, refl. spectra, 0.5-2.5 eV, Young's modulus and internal friction 78−39562
Pd complex, 1-(2-thiazolylazo)-2-naphtholato Pd (II), cryst. struct. 77−11536
Pd complex, bis(N-allylsalicylaldiminato)-palladium(II) cryst. and mol. struct. 79−32972
Pd complex, dichlorobis(N-methylimidazole)palladium(II), cis and trans, cryst. data 79−51078
Pd complex, dimethylglyoxymate film, prep. and physical props. 79−90923
Pd, complex, linear chain type, synthesis 78−6047

palladium compounds continued
Pd complex, linear ionic mixed valence cpd., IR and resonance Raman spectra rel. to lattice modes 80−25393
Pd complex, Pd (II) diamine, ^{13}C NMR *(Japanese)* 79−6952
Pd complex, $Pd^{II}Pt^{IV}(CNCH_3)_6(PF_6)_2$, vibr. spectra, M-M bonds. *(French)* 80−47997
Pd complex, $Pd(C_{18}H_{25}O_3)_2$, synthesis and props., possible mesomorphism 78−18749
Pd complex, S_4N_4 with $PdCl_2$, mass and IR spectra, config. 78−13494
Pd complex, tetrabenzo tetra-azacyclohexadecine, I_2 oxidation product, synthesis and characterization 79−47900
Pd complex, tetrakis(N-methylimidazole)palladium(II), crystal data for the tetrachloropalladate 79−51077
Pd complex, tetrakis(imidazole)palladium(II), crystal data for the chloride 79−51077
Pd complex di-μ-chloro-bis(2-methyl-allyl-3-norboryl)palladium, cryst. data 78−34484
Pd mixed valence complexes, quasi-one-dimens., elec. props. at ultrahigh press. 78−2470
Pd-D, crystallite size effects, simultaneous sorption and X-ray study 80−65237
Pd-D-H, equilib. H/D separation factors 80−59668
Pd-H, degree of positron localisation on components 77−85833
Pd-H, Mossbauer study of local environment of substitutional Co and Fe impurities 80−60475
Pd-H system, XPS line shape asymmetry, role of electron screening 77−21001
Pd-H-Gd, dil., ESR exam. of low temp. region of phase diagram, and electronic props. 80−29930
Pd-H(D), elastic energy dissipation peak 80−60905
Pd-H(D) system, superconductivity and phonon softening 79−73626
Pd-S mixtures, binding of phases, two-correl. model 77−80438
Pd-S system, phase diagram and cryst. struct. of $Pd_{16}S_7$ *(German)* 77−11516
Pd-Se mixtures, binding of phases, two-correl. model 77−80438
Pd-Si, amorphous thin films, laser irrad., metastable phases 80−96622
Pd-Te mixtures, binding of phases, two-correl. model 77−80438
Pd^{2+}-L-Cl^-, model fragment (L=Cl^-, F^-, OH^-, H_2O, NH_3) bond strengths, EHT calcs. 77−23434
$Pd_{0.7}$, D spin-lattice relaxation time, D quadrupole coupling, D atom diffusion 79−73844
$PdAl_2Cl_8$, Raman resonance spectra of vapour 78−94251
Pd_2B, and other Pd_xB_y cpds., cryst. chem. 80−19769
Pd_2B, cryst. struct., X-ray diffr. study 80−54204
$PdBr_4^{2-}$, Raman scatt., interference effects 77−68047
$PdBr_n(H_2O)_{4-n}^{2-n}$, electronic absorpt. spectra, band assignments 78−50553
$Pd(CO)_4$, ab initio LCAO MO SCF results invalidate pseudopot. calc. 77−6675
$Pd(CO)_4$, valence orbital energies, pseudopot. calcs. 78−37546
$Pd(CO_4)_4$, valence mol. orbital energy, nonempirical pseudopot. 79−22592
$PdCl_2$, diffusion coeff. in graphite 79−42310
$PdCl_4^{2-}(Br_4^-)$, mean vibr. amplitudes and force field, Muller approx. 77−10659
$PdCl_2(Br_2)(I_2)$, prep. using chem. transport via gas complexes *(German)* 79−15599
PdD, electron-phonon mass enhancement factor and supercond. crit. temp. 79−87184
PdD, isotope effect on transition temp. 79−73615
γ-PdD, struct. determ. by neutron diffr. 79−7593
$PdD_{0.63}$, inelastic neutron scatt. line shapes, Pd-D, D-D force consts. 78−47481
$PdD_{0.63}$, phonon lineshapes Debye-Waller factors, 80K, inelastic neutron scatt. study 79−42187
$PdD_{0.64}$, neutron scatt. exam. of 50K transition 78−55942
$PdD_{0.73}$, (1, 1/2, 0)-superlattice reflection splitting near 50K, neutron diffr. studies 80−70168
PdD_{1-x}, deuteron density modulation of D atoms 79−99101
β-PdD_x, (1, 1/2, 0) superlattice reflection, neutron diffr. exam. 79−65038
PdD_x, model of instabilities 78−75619
PdD_x, optical phonon spectra, supercond. tunnelling meas. 79−19701
PdD_x, supercond. transition temp., isotope effect *(Russian)* 80−88665
β-PdDx (x=0.710, 0.742, 0.754, 0.780), structural changes in temp. region of 50K anomaly 80−100131
PdF_2 flourite-type form, mag. props., structure studies *(French)* 80−34187
PdF_2, high press. modification, cryst. and mag. props. 80−38988
Pd_2F_6, evidence of an electronic transition under high press. *(French)* 79−42596
PdGdH, diagram of state elec. props., indirect exchange interaction, EPR study *(Russian)* 80−50179
Pd_2Ge and PdGe film formation on Ge 77−69197
PdH, ab initio relativistic core pot. studies of metal-H bonding 80−106257
PdH, electron-phonon mass enhancement factor and supercond. crit. temp. 79−87184
PdH, electronic struct., heat of formation, single particle lifetimes, Dingle temp. meas. 78−51923
PdH, electronic struct. and proton spin-lattice relax. calc. 78−67937
PdH, electronic struct. and supercond., APW calc. 79−95318
PdH, isotope effect in supercond. *(Russian)* 77−89892
PdH, role of optic phonons in superconductivity 78−39251
PdH, stoichiometric, electronic density of states, recursion method 79−90937
PdH, supercond., book contrib. 80−25037
PdH, supercond., simple scaling theory of isotope effect 78−14878
PdH, supercond. state, nucl. mag. relax. rate *(Rumanian)* 78−60247
PdH, superconducting transition critical temperature, BCS theory, phonon spectra *(Spanish)* 80−84535
$PdH_{0.65}$ film, thermoreflectance spectra 78−56463
β-$PdH_{0.66}$, elastic consts. 4 to 300K, Debye temp. 80−6455
$PdH_{0.72}$, Compton profiles, comparison with band struct. calcs. 78−84675
$PdH_{0.72}$, Compton profile, electronic struct. *(German)* 78−92140
$PdH_{0.73}$, 50K transition, γ-ray and neutron diffr. study 79−14932
$PdH_{0.76}$, ^1H spin-lattice relax. meas. 78−43672
$PdH_{0.97}$:Fe(Cr), supercond. transition temp. depression, coexistent mag. behaviour 80−49976

palladium compounds continued
$PdH_{1.18}$, $PdH_{1.20}$, prep., cryst. struct., chem. comp. determ. by thermal decomp. 80−34334
PdH_2 internally-charged electrode stability rel. to charging current density 79−57251
PdH_x 55K heat capacity anomaly, relation with vibrational spectrum modification of Pd 77−51516
PdH_x, CPA calculations of density of states 79−23882
β-PdH_x diffusion of H, high resolution neutron scatt. meas. 79−60551
PdH_x, diffusion of H atoms, quasielastic neutron scatt. obs., book contrib. 79−82383
PdH_x electronic band struct., comparative study of electric and mag. props. 78−95259
PdH_x, electronic props., H alloying effects, book contrib. 79−82522
PdH_x, electronic states calc. 79−7769
α-PdH_x, electronic states and Fermi surface props. 80−29310
PdH_x film, elec. resist., comp. depend. 79−1631
PdH_x foils, supercond. props. 77−32114
α-PdH_x, H-motions, conc., temp., momentum transfer, annealing depend., neutron scatt., study 79−42197
α-PdH_x, impurity motion, neutron scatt. obs. 80−24682
PdH_x, incoherent phase transition, lattice gas model 80−29171
PdH_x, inelastic neutron scattering meas. of optical vibr. freq. distribs. 80−59605
PdH_x, local, soft modes, superconductivity thermal neutron inelastic scatt. *(Chinese)* 80−70331
α-PdH_x, local mode intensity var. with conc., temp., direction and annealing 77−11653
PdH_x, model of instabilities 78−75619
β-PdH_x, Mossbauer fraction, diffusion induced reduction 80−108131
α-PdH_x, next-neighbour jumps of H in quasi-elastic neutron scattering 78−91487
PdH_x, optical phonon spectra by supercond. tunnelling meas. 79−19701
PdH_x, optical phonon spectra, inelastic neutron scatt. study 79−42186
PdH_x, positron localisation *(Russian)* 77−66555
PdH_x, preparation by low temp. electrolysis *(French)* 79−78910
PdH_x, supercond. below 1.5K *(Russian)* 79−91178
PdH_x, supercond. transition temp., isotope effect *(Russian)* 80−88665
PdH_x, superconducting transition temp., inverse isotope effect, Einstein model 80−65734
PdH_x:Co(Fe), diffusion and interstitial site occupancy, Mossbauer spectra 80−20555
PdH(D), energy loss spectra and Auger spectra 78−23563
PdH(D), stoichiometric, ^1H and ^2D NMR, rel. to supercond. T_c 78−72430
PdH(D), supercond., isotopic vol. effect 77−1511
PdH(D), superconducting, electronic spin density, isotope effects 78−39262
PdH(D), superconducting props., effect of hybridisation, band struct. determ. 79−69628
$PdH_x(D_x)$, acoustic and optic phonons, neutron diffr. obs., book contrib. 79−82296
$PdH_x(D_x)$, band struct., supercond. props., APW calcs. and neutron scatt. 78−43511
$PdH_x(D_x)$, nonstoichiometric, phonon spectra calc., Born-von Karman treatment 77−11650
$PdH_x(D_x)$, optical mode phonons, nonadiabaticity 78−55916
$PdH_x(D_x)$, superconducting transition temp., 0.2K to 4K 79−99651
PdI_2, removal of I from fission reactor fuel solns. 77−42164
Pd(II)-Gly-Tyr complexes, aq. soln., PMR obs., conform. 77−50450
$Pd_{1-x}M_xSe_2$ (M=Ru,Co,Ni), high pressure phase transformation studies, lattice constants and densities 79−65187
PdO, electronic struct., XPS and UPS study 80−35061
PdO, free energy of form. using impedance dispersion analysis 80−108728
PdO, neutron, α-particle irrad., black form., adsorpt. props. 77−11796
PdO, optical props., 0.5-5.4 eV 79−56813
PdO, semiconductivity and stability, optical props. 78−43497
PdO-Pd miniature pH electrode description and use 80−89886
PdP_3, cryst. struct. determ. *(German)* 77−89414
$Pd_3P_{0.8}$, pure and deuterated, cryst. struct., neutron diffr. study 80−84152
Pd_3P_{1-x}, nonstoichiometric, $H_2(D_2)$ solubility 80−59662
$Pd(PF_3)_4$, force fields mean obs. amplitude calcs. 77−54552
$Pd(PO_3)_2$, synthesis and struct. 79−90623
$Pd_{1-x}Rh_xTe_2$, high-press. phase transform. obs. 77−15584
PdS, electronic struct. from X-ray emission spectra 77−28661
PdS_2, polymorphism at 75 kbars, 400-1350°C 79−82173
$Pd(S_3N)_2$, IR and Raman spectra, normal coord. anal. 80−28019
PdSb, electronic struct., optical transitions, Fermi surface 78−51885
PdSb, optical props., 0.5-5 eV 78−39522
$PdSe_2$, polymorphism at 75 kbars, 400-1350°C 79−82173
Pd_2Si epitaxial islands on Si (001) substrate 80−96748
Pd_2Si, form. by laser irrad. of Pd film on Si substrate, Rutherford backscatt. obs. 79−42317
Pd_2Si, form. from solid phase reaction between Si and Pd-V 80−6568
Pd_2Si formation on Si with Pd-W alloys, effect of substrate temp. 80−96963
Pd_2Si-Si heterostructure growth by solid-phase epitaxy from Si (111)-Pd-Si (amorphous) 77−51617
Pd_4Si and Pd_2Si, amorphous, crystallisation by energy beam annealing 79−69012
$PdTe_2$, polymorphism at 75 kbars, 400-1350°C 79−82173
Pd_3Te_2, struct. and binding *(German)* 77−43192
PdX_4^{n-}, X=Cl, Br, n=1, 2, force consts., bond polarizability 78−5201
SnO_2-VO_x-PdO ceramic, switching and oscill. phenomena 78−6417

p.a.m. *see pulse amplitude modulation*

paper
see also paper industry
albumen paper, manufacture and use 79−35515
capacitor, dielec. loss, effect of simultaneous application of AC and DC voltages, freq. and temp. depend. 78−15091
charge decay and resistance parameters correlation determ. 80−70795
conductive paper transducer output signal fluidity reduction 77−57318
contact-resistance transducers using electrically conductive paper 77−13747
elastic moduli, in-plane, depend. on basis weight *(Japanese)* 77−77523
elastic properties, inhomogeneity with reference to basis wt. depend. of elastic moduli *(Japanese)* 80−2110

paper continued
fibre orientation, automation of real-time optical meas. of small structures 79−85115
fracture behaviour, paper sheets and single fibres, SEM investigation 79−34149
gravure and embossed papers, printability prediction by time series anal. 80−15345
impact force vs. displacement curves, expt. determ. 78−83344
laminated, decorative, deform. and internal stresses 79−61671
laser inexpensive detector, use of yellow and white bond paper 80−78880
laser pulse, position determ. using ordinary paper 80−33046
machine-made paper orthotropic US plate wave theory and expt. 79−68460
mechanical strength anisotropy, NDT determ., using radiowave method 80−25969
membrane sound generation by impulsive tension 78−90581
MG kraft paper, meas. of shear modulus and damping in a torsion pendulum 79−4989
modulus of brittleness, crit. tensile span 78−92318
non-impregnated, non-destructive breakdowns 80−55035
photographic paper, resin-coated and polyethylene 80−86474
polyethylene resin coated paper formulation for photography 80−4794
printing ink transfer analysis 79−17516
rubber, friction against paper and polymer film surfaces, microroughness effect 80−71763
surface characterisation and printability criteria, stochastic approach 78−18878
veiling reflections and reflected glare from glossy paper, lighting conditions for visual comfort 80−76733
wear of steel due to paper 79−15812
C black loaded, low temp. resist. charcts., for resist. thermometry 77−74404
TiO_2 paper filler, quantitative determination, using radioisotope X-ray fluorescence anal. 78−56935

paper industry
instrumentation and control automation, conf., Brussels, Belgium (1976) 77−27638
kraft mill effluents control in Finland 79−52988
kraft process black pulping liquor, alkali and sulphidity meas. using computer 77−29085
mills equipment noise reduction, means 77−7256
mineral content on-line meas. and control 77−29086
paper fibre suspension properties, u.s. appl. 77−27447
photographic pulp quality control using He-Ne laser scanning system *(German)* 80−3272
pulp mill stack plume meas., LANDSAT satellite imagery photoprints appl. 78−88905
waste waters of paper manufacture, radiative purification, polymer prod. *(Russian)* 78−61035
wood chip refiner, steam flow anal. 79−50787
wood chippings, neutron technique for moisture meas. *(German)* 80−105661

paraelectric materials *see dielectric materials*

paraelectric resonance
broadening mechanism in tunnelling systems 79−28701
ferroelectric, ion-ion interaction due to soft phonon modes 79−99838
ferroelectric, paraelectric reson. of H-bonds and related phenomena 77−28531
induction and echo form. under strong inhomogeneous broadening conditions 80−108168
nonstationary tunnelling state paraelectric resonance, weak photon coupling *(Russian)* 80−34869
orbital doublet, paraelec. reson. in presence of Jahn-Teller interaction 78−15137
single-pulse excitation of paraelectric induction and echo signals 80−80732
KBr:Li, paraelectric reson. meas. 77−36190
KCl:CN^-, paraelectric reson. study, tunnelling parameters and elec. dipole moment 80−25326
KCl:Li, 9.4 GHz pulse paraelec. reson. at zero elec. field 77−81076
KCl:Li_+ microwave modulation by paraelec. reson. *(Russian)* 77−20809
KCl:Li^+, single-pulse excitation of paraelectric induction and echo signals 80−80732
KI:OH^-, paraelec. reson. at 1.5 and 4.2K from 12 to 150 GHz 79−38512

parallel processing
acoustic image reconstruction in parallel processing analog electronic systems, secondary images 79−81638
algorithms and data structs. for array processing 80−83530
array processor AP 120B simulating relativistic electron beams 79−26789
arrhythmia analysis, dual-processor computer 79−66569
blood cell differential counter, ADC 500, pattern recognition based image processing system 78−73282
coherent optical pattern recognition using normalized invariant moments 80−99653
coherent-optics image recognition using contour transparencies *(Russian)* 77−58260
computers, appls. in University research 79−54114
electro-optic crystal, holographically recorded data pages, digital processing 77−42511
high concurrency data bus using arrays of optical emitters and detectors 79−76805
holographic index memory system *(Russian)* 77−58259
holographic numerical optical processor configurations 80−48194
image processing, digital, parallel logic device and half-adder circuit 80−10027
image processing using parallel array processors 77−38816
liquid crystal electro-optical modulators for two-dimensional data processing 78−79141
magnetic field parallel computation array-processor structure 79−41277
medical image structural analysis, fast feature extraction *(German)* 79−5393
micro-optoelectronic parallel processors *(Russian)* 78−46517
noncoherent optical memory multichannel data searching *(Russian)* 77−58261
noncoherent optical processing, two-pupil hybrid systems 78−74858
nuclear fusion plasma simulation with parallel pipeline programming 79−68947
optical, importance of redundancy 80−95831

parallel processing continued
optical fibre channels, pulse skew model 77−68279
optical fibre laser plate for optical parallel processing 79−76695
optical techniques for matrix multiplication 77−71936
parallel preprocessing, nucl. data acquisition system 78−46247
pattern recognition, hybrid parallel optical and serial digital processing systems 80−99657
reflected-beam laser anemometry using photon correlator 80−106861
remote sensing multichannel data sets, integrated optical comparator 80−64213
residue-based optical processor 80−48169
sensory information processing, parallel and sequential *(French)* 77−12873
signal processing research programme of United States Air Force 80−48171
space shuttle reentry, unsteady nonequilib. chemically reactive flow, parallel computation 78−47065
speech signal processing in real-time 79−64436
tomography, thorax 3D reconstruction, ultra-high speed, parallel processing computers appl. 79−48338
visual and nervous systems simulation, straight line recognition algorithm 79−34562

paralleled resonator filters *see band-pass filters*

paramagnetic-antiferromagnetic transitions
see also Neel temperature
amorphous ferromagnet, spin-glass and ferromagnetic behaviour induced by random uniaxial anisotropy 78−39338
antiferromagnet, dil. paired, bond dilution problem, CPA theory 79−78389
antiferromagnet, transversely anisotropic, spin-wave theory of paramag. phase boundary 77−69552
band theory of antiferromagnetism, crit. exponents *(Russian)* 78−2646
bicritical point, spin dynamics in uniaxial antiferromag. 77−16090
1,3-bisdiphenylene-2-(p-chlorophenyl)-allyl, antiferromag. resonance, antiferromag. phase transition 78−6579
calcium copper acetate hexahydrate, $CaCu(CH_3COO)_4.6H_2O$ and $CaCu(CD_3COO)_4.6H_2O$, susceptibility meas. 78−2680
classical mag. moment system, antiferromag. phase transition, secular dipole interactions 80−80551
copper benzoate, low-dimensional Heisenberg antiferromag., high field magnetisation 80−80558
copper tetraamine sulphate, two-dimensional Heisenberg antiferromag., high field magnetisation 80−80558
critical dynamics above crit. temp., dipolar coupling 78−52286
exchange interaction, kinetic, in narrow S-band 77−55655
graphite, neutron-irrad., sp.ht., 0.4-4.5K, rel. to localised spin transition 77−28389
Heisenberg model, quasi-one-dimens., reaction field approx. and dipolar interaction 77−36088
Hubbard model, CPA treatment, two sublattice alloy analogy method 78−19208
Hubbard model, low temp. phase transitions 78−72359
Hubbard model, neutral, strong-coupling props. 77−24667
intermediate valence, mag. susceptibility and mag. instabilities 80−39532
Ising model, dipolar antiferromag., phase transition at negative absolute temp., Monte Carlo procedure *(Russian)* 78−43594
Ising model, triangular, mag. field depend. transition temp. 77−8323
magnetic material, fluctuational breakdown of metastable states at phase transitions *(Russian)* 78−52245
magnetically ordered metals, possible first order phase transformation 79−95589
manganese acetate, crit. slowing down, 180-350 MHz 77−16083
metals, magnetic, Seebeck coefficient anomaly near spin ordering temp. 77−20302
metamagnetic transitions, theory 77−16076
press. or stress induced, neutron scatt. obs. 80−65880
1,3-propanediammonium tetrachloromanganate(II) mag. props. 4.2-220K 77−20567
rare earth alloys, magnetic and electronic phase transitions 79−87254
rare earth alloys, RFe_4Al_8, mag. props., Mossbauer spectra, ordering effects 77−63179
rare earth heavy binary alloys, press. effect on mag. props. *(Japanese)* 77−43835
rare earth vanadites, mag. ordering, susceptibility meas., 60-300K 77−32190
rare-earth germanides, R_5Ge_3, thermal expansion, phase transition effects 80−70433
s-f model with electron-hole reson., antiferromag. behaviour and phonon spectrum 78−47992
semiconductor, magnetic phase transitions in impurity band *(Russian)* 80−50097
site Ising model, spin glass phase, transition temps. 79−95592
static properties of spin systems with truncated secular dipolar coupling 78−88130
steel, austenitic, 0Kh14AG12M, temp. depend. of mech. props. and kinetics of phase transforms. *(Russian)* 78−92297
steel, austenitic, Mn-Cr-C(20, 4, 0.5 wt.%), intrinsic stacking fault energy, temperature variation 77−31679
steel, austenitic, quenched state, influence of austenite stability on impact strength *(Russian)* 80−81146
TCNQ salt, pyridine $(TCNQ)_2$, phase transition at 80K investig. and interpret. 78−6530
TMMC, linear antiferromag., 3D ordering and spin correlations, mag. field effect 78−19262
transition metal oxides, sulphides, and selenides, Mott transition electronic and mag. phase diagrams 78−51894
trimethylammonium manganese trichloride, Heisenberg antiferromag. chain, specific heat and EPR 80−65931
uniaxial antiferromagnets in transverse mag. field, quantum theory, spin configuration 79−69647
vector models with $n \geq 4$, renormalisation group analysis 77−66340
AuMn, mag. struct., phase transition, and magnon spectrum, random anisotropy effects 80−88722
$B_2O_3.Fe_2O_3.2CoO$, mag. props. up to 1200K transitions and magnetisation curves 77−36069
$B_2O_3.Fe_2O_3.2MgO$, mag. props. up to 1200K transitions and magnetisation curves 77−36069
$B_2O_3.Fe_2O_3.nMO$, (n=2 or 4, M=Mg, Co, Ni, Cu), mag. props., transitions 80−75763

paramagnetic-antiferromagnetic transitions continued
$BaMnF_4$, mag. and structural phase transitions, neutron scatt. obs. 79−87259
$BaNiF_4$, obs. of anomalous pyroelec. behaviour due to cooperative mag. singularity 77−59517
$BiFeO_3$, ferroelec., antiferromag., cryst. and mag. struct., neutron diffr. study 80−65786
$Bi_2Fe_4O_9$, mag. struct., neutron diffr., transition 78−52217
$Bi_2Fe_4O_9$, mag. struct., neutron diffr. meas. 78−91844
C, soft, low temp. sp. ht. anomalies, spin-spin interactions 79−15307
C, soft, sp. ht., 0.4-4.5K, rel. to localised spin transition 77−28389
Ce-La, mag. ordering, sp. ht., susceptibility and resist. 78−68238
$CeAl_2$, Anderson lattice system, thermal expansion meas. 1.5 to 10K 79−37860
$CeAl_2$, mag. anisotropy, transition, crystal field splitting 78−52243
$CeAl_2$, mag. ordering, neutron diffr. meas. 78−6518
CeP(As), single crystals, low temp. thermal, electrical and mag. props. meas. 78−27051
CeSb, antiferromag., first-order transitions, mag. phase diagram 80−60252
Co complex, Co(II)(1,2,4-triazole)$_2$(NCS)$_2$ quasi two-dimens. canted S=1/2 antiferromag. 80−70976
$CoBr_2.6[(D_2O)_{0.48}(H_2O)_{0.52}]$, antiferromag. ordering, quasi-elastic neutron scatt. study 79−61068
$CoCl_2$, antiferromag., phase diagram, heat capacity meas. 80−93126
$CoCl_2.2H_2O$, Ising antiferromag., high field transverse magnetisation meas. 80−93143
CoF_2, antiferromag. crit. props., neutron scatt. obs. 80−88749
$Co_{1-x}Zn_xF_2$, antiferromag. crit. props., neutron scatt. obs. 80−88749
$Co(urea)_2Cl_2.2H_2O$, two-dimens. mag. props., cryst. struct., specific heat 80−75777
Cr, antiferromagnetic transition, first order, crit. neutron scatt. obs. 79−33480
Cr, crystal structure below Neel temp., X-ray diffr. study 78−83772
Cr, mag. struct., phase transition, and magnon spectrum, random anisotropy effects 80−88722
Cr, magnetic phase transition at Neel temp. 78−2681
Cr, single Q-state, antiferromag. phase, rel. to band struct. 77−15759
Cr-Co, phase transformations and magnetostriction *(Russian)* 80−103869
Cr-Co (4 wt.%) alloy, antiferromag. transitions effect on opt. props. 77−12371
Cr-Fe, antiferromag. phase boundary, neutron diffr. meas. 78−95437
Cr-Fe (0.8-8 at.%) alloy, mag. phase transforms, sp. ht. obs. *(Russian)* 77−80941
Cr-Fe-V, dil., V effect on para- to incommensurate and commensurate transitions 78−68260
Cr-Mn, order of mag. transitions in antiferromag. alloys 79−4677
Cr-Mn (0.5 at.%) alloy, mag. phase transforms, sp. ht. obs. *(Russian)* 77−80941
Cr-Mn alloys, elec. resist. near T_N 77−69313
Cr-Re, phase transformations and magnetostriction *(Russian)* 80−103869
Cr-Sb alloy, dil., mag. phase diagram, elec. resist. and thermal expansion obs. 79−1669
Cr-Si-V, (2, 0.1 at.%), paramag. to commensurate spin density wave transition 80−65875
Cr-Si-V, dil., V effect on para- to incommensurate and commensurate transitions 78−68260
CrAs, antiferromag.-paramag. transition up to 5 kbar 79−87256
CrAs, high press. paramag. antiferromag. transitions, elec. props., band model development *(Russian)* 80−60277
CrAs, mag. transition under press., volume striction mechanism 77−24696
$CrAs_{0.42}Sb_{0.58}$, mag. and struct. transitions under press., elec. resist. meas. 78−27038
Cr_2BeO_4, magnetoferroelectricity, weak pyroelectric effect 79−42914
Cr_2O_3, mag. phase boundaries near bicrit. and Neel points 78−34980
Cr_2O_3, magnetic susceptibility, near Neel temp. 79−56509
Cr_2O_3, magnetostriction anomalies near mag. field induced transitions 77−66315
Cr_2O_3, paramagnetic-antiferromag. transition temp. increase in mag. field 77−12121
Cr_2O_3, US wave vel. near mag. transition 78−84263
Cr_2O_3:Ga_2O_3 EPR, antiferromagnetic coupling energy temp. depend. *(German)* 78−10766
$CrSb_2$, heat capacity and thermodynamic props., mag. transition, enthalpy of decomposition 78−43591
$Cs_2FeCl_5.H_2O$, cryst. struct., superconducting susceptometer mag. meas. 79−73717
$CsMnF_3$, mag. struct., phase transition, and magnon spectrum, random anisotropy effects 80−88722
$CsMnF_3$, specific heat, crossover from Heisenberg to XY like behaviour 77−85461
$CsNiBr_3$, nearly one-dimensional antiferromag., thermal and mag. props. meas. 77−77041
$CsNiF_3$, quasi-one-dimens. Heisenberg system, reaction field approx. and dipolar interaction 77−36088
$CuBr_2$, NQR freqs. temp. depend., paramag.-antiferromag. transition 79−42867
$CuCl_2.2H_2O$, antiferromag. to paramag. transition, high field magnetisation meas. 78−64204
$CuCl_2.2H_2O$, effect of press. on mag. phase transition, NMR meas. 78−19253
$CuCl_2.2H_2O$, group theoretical anal. of second order phase transitions 79−91239
$Cu_4NiSi_2S_7$, X-ray cryst. struct. determ., mag. props. 80−107172
$CuSO_4.5H_2O$, $CuSeO_4.5H_2O$ and $CuBeF_4.5H_2O$, mag. ordering in external field, NMR obs. 77−66350
Dy, magnetic transitions and internal friction temp. depend. *(Russian)* 78−39317
Dy, magnetocaloric effect and mag. phase transitions, 80 to 300K 80−60279
Dy, resistivity anomalies at mag. transitions, sp.ht. 80−39785
Dy, US attenuation maxima in mag. field 77−16140
Dy-Sm alloys, elec. resist. singularities and mag. transitions *(Russian)* 79−47075
Dy-Y paramagnetic-antiferromagnetic transition temp., depend. on Dy conc. 79−69673
DyAG, cubic antiferromagnet, multiaxis phase transitions 79−78377
DyAG, tricritical crossover exponent 77−4239

paramagnetic-antiferromagnetic transitions continued
$Dy_3Al_5O_{12}$, antiferromag., optical birefringence in fields along [111] meas. 77−28540
$Dy_{1.2}Mo_6S_8$, low temp. heat capacity anomaly rel. to antiferromag. transition in supercond. state 80−25044
$DyPO_4$, mag. transitions under hydrostatic press., neutron diffr. study 80−71030
$DyPO_4$, susceptibility near mag. phase boundaries 78−52258
Er-Tb, elasticity modulus, ΔE-effect, internal friction, magnetic transformations *(Russian)* 79−91723
$ErFeO_3$, weak ferromag., high freq. props. in ordering region of spin system, antiferromag. reson. study *(Russian)* 80−2644
Eu, mag. and struct. transitions, X-ray K-line shift, 77-1000K *(Russian)* 77−4518
$EuSO_4$, sp. ht. and susceptibility meas. 78−14977
Eu_2Sb_3, cryst. struct., elec. and mag. props. 80−33958
EuSe(Te), phase transition spectroscopy 77−63426
EuTe, field depend. correl. function theory of Raman scatt. near antiferromag.-paramag. transition 78−68490
Fe (III)M (II)$F_5.7H_2O$, M=Fe, Co, Ni, Zn, antiferromagnetism 77−59395
Fe complex, Fe(1,2,4-triazole)$_2$(NCS)$_2$, quasi-2-dimens. S=$^1/_2$ antiferromag., mag. props., hidden canting 80−107986
Fe, film, FCC, antiferromag. ordering, Mossbauer expts. 77−85508
Fe-Cr-Ni alloy, Kh18N10, rel. to thermal expansion, 4.2-290K *(Russian)* 78−47537
Fe-Mn (14.1 wt.%), G14, α-martensite formation in mag. field 79−91648
Fe-Mn mag. contributions to γ⟷ε phase transformations 80−25694
Fe_2As, antiferromagnet, Mossbauer spectra determ. 77−8480
$FeBO_3$, magnetisation near crit. temp., up to 3 kbar hydrostatic press., scaling theory 77−8316
$FeBr_2$, hyperfine interaction, ^{57}Fe Mossbauer expts., mag. transition obs. 78−43720
$FeBr_2$ metamagnet, unusual phase diagram, theory 80−93119
$FeCl_2$, metamagnet, optical determ. of thermodynamic phase diagram 78−60285
$FeCl_2$, mixed antiferromag.-paramag. state, light scatt. in mag. field 77−40069
$Fe_{1-x}Cl_2$:Cd_x, randomly disordered, tricrit. behaviour, light scatt. 78−68255
$Fe_{1-x}Co_xGe_2$ solid solns., mag. susceptibilities, multiple stages in mag. transitions, effective mag. moment 77−8286
FeF_2, dielectric properties, IR spectra, lattice dynamics *(French)* 80−76026
FeI_2, hyperfine interaction, ^{57}Fe Mossbauer expts., mag. transition obs. 78−43720
$FeMo_2S_4$, Mossbauer spectra, 79-300K, Neel pt. determ. 78−60360
FeP, mag. suscept., resistivity and thermal expansion meas. 78−2661
$Fe_{1-x}Rh_x$, press. effects on mag. phase transition, resist. meas. 77−4516
Gd-Tb, elasticity modulus, ΔE-effect, internal friction, magnetic transformations *(Russian)* 79−91723
$GdAlO_3$, ^{155}Gd excited states, determ. of nuclear parameters using Mossbauer effect 79−28646
$GdAlO_3$, spin-flop bicritical line obs. 77−66306
$GdCrO_3$, EPR linewidth, Neel point to 700K 80−39849
$Gd_{1.2}Mo_6S_8$, low temp. heat capacity anomaly rel. to antiferromag. transition in supercond. state 80−25044
$GdVO_4$, ^{155}Gd excited states, determ. of nuclear parameters using Mossbauer effect 79−28646
$GdVO_4$, antiferromag., US attenuation at 9 GHz 77−24728
GeSe, antiferromagnetic behaviour, res. to negative magnetoresistance effect 79−73719
^{3}He, BCC, four-spin interaction effects on ordering processes 77−39721
^{3}He, solid, mag. susceptibility near ordering temp., pulsed NMR meas. 78−18869
$Hg_{1-x}Mn_xS(Se)$ solid solution, magnetic props. 79−51758
$Hg_{1-x}Mn_xTe$, EPR investigation of ordering effects 79−47330
$HoVO_3$, at. and mag. struct., neutron diffr. meas. 79−24142
$HoVO_4$, below 1K, nuclear orientation study of Van Vleck enhanced nuclear antiferromagnet 80−88899
$K_2FeCl_5(H_2O)$, phase diagram, antiferromag., paramag. and spin flop phases 80−44831
K_2FeO_4, antiferromag., critical fluctuations obs. using Mossbauer spectroscopy 80−39955
K_2FeO_4, crit. slowing down of spin fluctuations, Mossbauer spectra and relax. theory 80−65882
K_2IrCl_6, thermal expansion meas. near antiferromag. transition 77−20610
$KMnF_3$, EPR antiferromag. reson. linewidths near Neel point, exchange interactions *(Russian)* 77−8386
$KMnF_3$, Mossbauer effect in ^{57}Fe, struct. and mag. transition investig. 77−20779
$KMnF_3$, phonon scatt., thermal cond. meas. 77−7916
$KMn_{1-x}Ni_xF_3$, antiferromag. crit. props., neutron scatt. obs. 80−88749
K_2ReCl_6, thermal expansion meas. near antiferromag. transition 77−20610
$LaVO_3$, successive phase transitions, X-ray anal. 80−108437
Mn-Cu, mag. and cryst. struct., neutron and X-ray diffr. meas. *(Russian)* 78−22694
Mn-Cu alloy, volume effect, paramagnetic-antiferromagnetic and structural transition, lattice consts. 80−39007
Mn-Ni, single cryst. or polycryst., elastic anomalies at antiferromag. transition 78−14972
Mn-Ni-Ti(Zr), non-ferromagnetic Elinvar-type alloys 79−24566
Mn-Ni-V(Nb)(Ta), nonferromagnetic Elivar type, mech. props. meas. 77−48473
$MnAs_{1-x}P_x$, high spin-low spin transition 77−20591
γ-MnAu, antiferromag., phase diagram, X-ray diffr. and Young's modulus meas. 80−71024
$MnCl_2.2H_2O$, magnetisation and mag. resonance 79−11349
α-$MnCl_2.4H_2O$, crossover from divergent to non-divergent nature of paramag. transition 79−73735
MnF_2, reson. NMR near phase transition 78−76265
Mn_3Ga, formation of DO_{22} superstruct. and para-antiferromag. transition 79−19737
Mn_3GaN, sp. ht., 6 to 350K, mag. and crystallographic phase transitions 80−71060
$Mn_2N_{0.86}$, cryst. and mag. struct. at low temps. *(French)* 77−73003
$Mn_xNi_{1-x}Cl_2.nH_2O$, antiferromag., sp. ht. meas. 79−91226
MnO, antiferromag. reson. linewidth below and above T_N 77−40133
paramagnetic-antiferromagnetic transitions continued
MnO, antiferromagnetic-paramagnetic phase transiton at high press. 80−39778
MnO, elastic props. singularities near phase transition 77−16093
MnO, first order, transition, elastic consts. meas. 77−66316
MnO, linear optical anisotropy meas. at antiferromag. transition 77−36205
MnS, thermal cond., temp. depend., paramag.-antiferromag. transition effects 80−65321
MnS_2, first order antiferromag. phase transition 77−8317
$MnSO_4$, mag. struct. and phase transitions, neutron diff. study 80−60208
$MnSe_2$, pyrite struct., mag. suscept. and thermal expansion 77−32176
MnSi, crit. transverse US attenuation, spin fluctuations 78−48022
MnSi, mag. phase diagram, crit. US attenuation 77−12122
MnTe, magnetic resonance at high hydrostatic pressure 78−76247
MnTe, resistivity anomalies at mag. transitions, sp.ht. 80−39785
$Mn_cZn_{1-c}F_2$, crit. neutron scatt. near percolation threshold 78−2693
Mn_3ZnN, sp. ht., 6 to 350K, mag. and crystallographic phase transitions 80−71060
$NaMnCl_3$, mag. props., 2-25K, antiferromag.-paramag. transition *(Russian)* 78−88125
Na_xVS_2, intercalation cpd., mag. phase transitions 77−69558
$Na_xVS_2(Se_2)$, mag. and elec. props. rel. to struct. transitions 78−91848
Na_xVSe_2, intercalation cpd., mag. and structural phase transitions 77−69558
Nd-La, mag. ordering, sp. ht., susceptibility and resist. 78−68238
Ni complex, $Ni(C_5H_5NO)_6(ClO_4)$ field-induced mag. phase transition obs. 77−36072
Ni complex, tris(ethylenediamine)nickel(II) nitrate, mag. props. from susceptibility and sp. ht. meas., 0.3-3.0K 78−91877
$NiCl_2.6H_2O$, antiferromag., phase diagram, low temp. canted paramag. boundary, bicritical point 79−47282
$(Ni_{1-x}Fe_x)S$, solid solns., electronic props., X-ray, thermal and Mossbauer study 79−78376
$Ni_{1-x}Li_xO$, $0.01 \leq x \leq 0.08$, mag. susceptibility in region 80 to 800K *(Russian)* 78−2664
$NiNb_2O_6$, antiferromag., principle mag. susceptibility and field induced magnetisation meas. 77−20589
$NiNb_2O_6$, magnetisation and susceptibility, antiferro-paramag. transition, expt. and theory 77−43822
NiO, linear birefringence in S-domains near antiferromag. phase transition 80−60261
NiO, magnetic susceptibility, near Neel temp. 79−56509
NiO, multidomain mat., opt. anisotropy meas. at T_N 77−16279
$Ni_{1-x}Rh_xS$, nonvolume effect of Rh substitution on paramag. metal-antiferromag. nonmetal transition 79−28277
NiS, antiferromag., press. effect on metal-nonmetal transition 77−69229
$Ni_{1-x}S$, and $Ni_{1-x}S_{1-y}O_y(Se_y)$, mag. state in metal-semicond. transition region, neutrnon diffr. obs. *(Russian)* 77−89926
$NiS_{2-x}Se_x$, elec. resistivity temp. depend., pressure depend. 78−10690
NiS_yTe_{1-y}, mag. susceptibility, correl. with metal-insulator transition data 79−24145
O_2, monolayer, adsorbed on graphite, first-order and continuous transitions 79−73401
O_2, solid, susceptibility, temp. depend. as function of press. and mag. field, α-β transition obs. 77−47991
PrSb, magnetic to nonmagnetic transition, press. or stress induced, neutron scatt. obs. 80−65880
PrSb, pressure-induced antiferromag., neutron scatt. study 80−39750
$Rb_2FeCl_5.H_2O$, cryst. struct., superconducting susceptometer mag. meas. 79−73717
$RbMnF_3$ universal relations among crit. amplitude, calc. up to order ϵ^2 for systems with continuous symm. 77−17936
$RbNiFeF_6$, pyrochlore, Mossbauer spectra in paramag. and mag. ordered states 77−52003
Sm, mag. and struct. transitions, X-ray K-line shift, 77-1000K *(Russian)* 77−4518
$SrEu_2Fe_2O_7$, ferrite, Mossbauer effect study of hyperfine interactions, spin reorientation 78−19383
$SrTb_2Fe_2O_7$, ferrite, Mossbauer effect study of hyperfine interactions, spin reorientation 78−19383
$TbBe_{13}$, magnetic structure at low temps., antiferromagnetic, neutron diffraction study *(French)* 80−39743
TbD_2, mag. struct., neutron diffr. study 77−85421
$TbFeO_3$, R-Fe exchange, Van Vleck interaction *(Russian)* 79−61105
Tb_5Ge_4, mag. struct. and mag. transitions, neutron diffr. expts. 78−43564
$Tb_{1.2}Mo_6S_8$, low temp. heat capacity anomaly rel. to antiferromag. transition in supercond. state 80−25044
TbP (As)(Sb)(Bi), mag. transitions, quadrupolar interaction effects 80−80512
TbP, mag. excitations above antiferromag. ordering temp., inelastic neutron scatt. obs. 80−50112
TbP, neutron scatt. study above paramagnetic-antiferromagnetic transition temp. 80−11159
$TbPO_4$, anomalous magnetostriction at low temp. 78−84470
$(Ti_{1-x}V_x)_2O_3$ spin glass, mag. props., metallic antiferromagnetism 79−82791
Tm, lattice dynamics, thermal expansion, spt. ht., mag. contrib. 79−37778
$UAs_2(Sb_2)$, heat capacities, antiferromag.-paramag. transitions 78−76253
U_2C_3, elec. resist., 4 to 1900K, mag. transition at 54K 80−59953
UN, cubic antiferromag., anisotropic critical neutron scatt. behaviour 79−61112
UN, photoelectron spectra study, core and valence levels, antiferromag. transition effects 80−66394
UO_2, cross over, discontinuous to continuous phase transition in external mag. field 78−43592
UO_2, crystalline elec. field studies using neutron inelastic scatt. at NRCN 80−10931
UO_2, symmetry changes 77−20597
$(V_{1-x}Cr_x)_2O_3$, thermal props., rel. to phase transition 77−35709
VI_2, MCD spectra, interpretation rel. to mag. struct. 80−66222
VN-CrN systems, solid solns., mag. props. 77−12086
V_2O_{3+x}, $0 \leq x \leq 0.08$, mag. and elec. props. 80−49833
V_2O_{3+x}, nonstoichiometric compositions, mag. transition exam. by Mossbauer effect 77−28385
V_2O_{3+x}, nonstoichiometric, microscopic mag. props., NMR and inelastic-spin-flip neutron scatt. 79−38323

paramagnetic-antiferromagnetic transitions continued
V_3O_5, spin order, one-dimensional, Neel transition 80−39799
V_nO_{2n-1} Magneli phases, elec. and mag. props. 79−37990
$V_2O_{3-x}F_x$ ($0 \leq x < 0.3$), preparation and physical props. 78−76619
$(V_{1-x}Ti_x)_2O_3$, solid solution, phase transition exam. 77−15590
$YCrO_3$, EPR linewidth, Neel point to 700K 80−39849

paramagnetic Curie temperature *see Curie temperature*

paramagnetic-ferromagnetic transitions *see ferromagnetic-paramagnetic transitions*

paramagnetic properties of substances
see also paramagnetic resonance; paramagnetism
actinide systems, nearly magnetic, thermoelectric power determ. 78−56133
alkali metal-transition metal double molybdates, susceptibility, 90-800K, moments *(French)* 80−39734
alkali metals, paramag. and electronic susceptibility calc. 78−52205
alkaline earth transition metal ternary and quaternary oxides, ATO_3, $ATi_{1-x}T_xO_3$, and $AZr_{1-x}T_xO_3$, prep., mag. props. and struct. 79−15277
alkaline earth-ReO_6, ordered or perovskite type struct., magnetic and elec. props. 79−65053
amorphous semiconductor, localised gap states, variable range hopping, susceptibility and EPR 77−72866
anthracene crystals, α-particle induced scintillation, mag. field effects 80−40161
axial crystal system, paramag. susceptibility 79−42730
beryllides, magnetic susceptibility meas., Faraday method 77−47969
binary alloys, disordered, electron-electron correl, T-matrix approx. 79−78026
bis(p-toluene sulphonate) diacetylene polymer, EPR, thermal history and temp. effects 78−52352
bis(p-toluene sulphonate) diacetylene polymer, spin conc., g-values of single cryst. from EPR study 78−48037
bis(triethylbenzylammonium)tetrachlorocuprate(II), mag. anisotropy, susceptibility, EPR of Cu^{2+} 78−52344
bis(trimethylbenzylammonium)tetrachlorocuprate(II), mag. anisotropy, susceptibility, EPR of Cu^{2+} 78−52344
borate glass: Ni, absorption spectra, mag. props., coordination behaviour *(German)* 80−40147
bubble garnet film, non-implanted, surface mag. struct. 80−84628
calcium copper acetate hexahydrate, and deuterated cpd., tunnelling reson. effects in nonreson. spin-lattice relax. 79−86726
catalysis of ortho-para H_2 conversion, mag. field effects, theory 78−61050
chromocene, mag. props., complete ligand field theory 78−31048
closed shell system, paramagnetism, harmonic oscill. model 77−58194
coal, mag. susceptibility and Mossbauer meas. 80−60464
cobaltocene, mag. props., complete ligand field theory 78−31048
copper formate anhydrate, cryst. struct. and mag. props. 80−79768
copper quaternary thiospinels, mag. and elec. props. *(French)* 80−65771
coronene, triplet state, photomagnetism 80−97125
$CuBr_2$, finite Heisenberg chain effects, temp. depend. 79−47230
cyclic polyphenylacetylene, thermally excited paramag. props. 77−88614
$DBTTF(BF_4)_{0.8}$, new conducting compound, synthesis, elec. and mag. props. 79−28341
deoxymyoglobin, single cryst., paramag. anisotropy meas. 77−21469
di(propylammonium) copper tetrachloride, mag. suscept. meas. 77−63131
di-(2,2,6,6-tetramethyl-4-piperidinyl-1-oxyl) suberate, nitroxide radical polarised neutron study in paramag. phase 79−47231
di-(2,2,6,6-tetramethyl-4-piperidinyl-1-oxyl)-suberate, spin densities, polarised neutron diffr. meas. 80−50037
diacetylene polymer, EPR exam. of partially crystalline polymer extracts 78−39400
dialkylammonium copper chloride, two-dimens. ferromag., energy transport by paramag. magnons 77−80909
dibenzenechromium-dibenzenevanadium, proton HFS data, ENDOR obs. 80−66073
diethylammonium copper tetrachloride, antiferromag. mode excitation in EPR spectra 78−56373
5,10-dihydro-5,10-diethylphenozinium-iodide, average struct. and props. 79−90636
dilute alloy, paramag. Curie temp., exchange field 77−47970
electron gas, paramag. and diamag. susceptibilities, density depend., ring diagram contrib. 79−95571
Elinvar, Curie point, magnetisation and susceptibility, heat treatment effects *(Russian)* 78−47973
ethylenediammonium metal chlorides, $(NH_3CH_2CH_2NH_3)MCl_4$, M=Ni,Pd,Cu,Cd,Mn, struct. and mag. props., vibr. spectra 79−10842
f^n-electron system, paramag. principal susceptibilities, calcs. using ang. overlap model 77−32158
ferrocene related compounds, $C_5R_5Fe(I)\text{-}C_6R'_6$ paramag. sandwiches, Mossbauer study 80−39982
ferrous alloy, FCC, anomalous thermal expansion in paramagnetic temp. range 77−35724
ferrous formate dihydrate, paramagnetic specific heat, decoration iteration transformation anal. 80−70938
ferrous nitrosylhaemoglobin, NO binding, spin distrib., orbital model and mag. props. 80−81534
garnets, ferro- and paramag., gyromag. ratio determ. by magneto-optical method *(Russian)* 77−32356
glass, Faraday effect in pulsed megagauss field 77−69804
glass, magnetic susceptibility measurement, torsional reson. technique 80−82796
graphite intercalation compounds with alkali metals and halogens, physical props. 78−31050
graphite intercalation compounds with K and tetrahydrofuran *(French)* 78−26692
graphite intercalation cpds., mag. susceptibility, tight-binding model 80−44796
graphite intercalation cpds. with alkali metal, interlayer screening and mag. susceptibility 80−44794
graphite-alkali metal intercalation cpds., large anisotropy and stage depend. 80−44795
graphite-K inclusion compounds, paramagnetism after treatment by π or n donors *(French)* 78−10749
graphite-nitrate residue compounds, phys. props. 78−10199
graphite-UF_6 intercalation compounds, NMR exam. 78−39416
guanidinium vanadium sulphate hexahydrate, singlet ground state system, low temp. mag. props. 80−44843

paramagnetic properties of substances continued
haemoglobin, deoxygenated, vibronic coupling effect on paramagnetisms 77−57899
holmium ethylsulphate, pseudomagnetic moment of ^{165}Ho and spin-lattice relax. times 77−63306
impurities, in Cr and Cr alloys, effects on Neel temp. 79−4678
impurities, in itinerant electron antiferromagnet, effects on Neel temp. 79−4678
intermediate valence compounds, sum rules and inelastic neutron scatt. 79−61037
Invar, deformed, magnetism and temp. depend. of effective field on ^{57}Fe *(Russian)* 79−24234
iron(II)-A-zeolites, reduction, mag. and Mossbauer study 80−71115
lanthanide complexes, paramag., and shift reagents, NMR, book contrib. 80−53023
localised spin fluctuations, Knight shift obs., for α-Mn 80−60181
lymphocytes, living and dead, mag. props. and mag. sedimentation 80−35925
manganese acetate tetrahydrate, paramag. susceptibility, spin trimer model 80−97055
matrix isolated species, MCD spectrosc. appls. 78−46378
metal, CESR linewidth and g-shift in presence of spin-orbit perturbation, spin-phonon scatt. 77−63285
metal, orbital magnetic and spin paramag. susceptibilities, effect of strain 77−16137
metal borides, $MM_4'B_4$ (M=Y,R; M'=Os,Ir), mag. meas., Curie Weiss behaviour 80−20375
metal film, electronic density of states, sp. ht. and spin susceptibility 77−15730
metal particles, thermodynamics and paramag. props. of electrons 78−31051
metals, crit. transverse US attenuation, spin fluctuations 78−48022
metals, electric properties calc., book 79−28274
metals, HCP struct., anisotropy of paramagnetostriction 77−32231
metals, inelastic neutron scatt. cross-section, effect of cryst. field 79−65642
metals, neutron mag. form factors, magnetisation densities, APW wavefunction calcs. 79−47243
metals, polarised neutron studies of the field induced magnetisation 80−25084
$MgAl_{2-x}Fe_xO_4$ solid solution system, solid state properties study 80−93094
molecular complexes, nucl. spin-lattice relax., electron spin density matrix theory 78−13521
N-alkylated phenazine type radicals, mag. props. 79−73671
$Na_2V_2Ti_6O_{16}$, characterisation and mag. props., 90-800K, $Na_xTi_4O_8$ bronze isotypes *(French)* 80−39735
narrow-band with strong Coulomb correlations, electron sp. ht. *(Russian)* 80−103487
neodymium ethyl sulphate, electronic spectra Stark pattern, crystal elec. field and mag. props. 77−12084
neptunium cyclopentadienyl compounds, $(C_5H_5)_3NpX$, (X=F, Cl, Br, I, $(SO_4)_{1/2}$), mag. susceptibility 80−11152
neutron polarisation, crit. scatt. above Curie pt. 78−43565
niobates, mixed metal, Eu oxidation state, mag. props., Mossbauer study 80−66080
NMP-TCNQ, low temp. specific heat 78−52297
NMP-TCNQ, magnetic susceptibility and chem. pot. of two-site Hubbard Hamiltonian 77−47963
one-dimensional conductor, Curie const. discontinuity explained as paramag. domain tip alignment 77−16035
organic paramagnetic systems, multiple internal motions, nucl. spin dipolar relax. obs. 80−28037
oxyhaemoglobin, mag. susceptibility of frozen aq. soln., 25 to 250K 78−6507
paramagnetic liquid, mag. field effect on depolarised light scatt. *(Russian)* 80−108221
particles, quantum size effect obs. by CESR and NMR 77−20700
phosphate glass: Ni, absorption spectra, mag. props., coordination behaviour *(German)* 80−40147
pnictides, cubic Van Vleck compounds, paramag. fluctuations, ESR or NMR relax. 77−66420
polarised neutrons in condensed matter [conference, Zaborow, Poland (Sept. 1979)] 80−22136
polyacetylene:AsF_5, mag. susceptibility, Fermi surface density of states, semicond.-metal transition 79−95566
polyparaphenylene:SbF_5, pure and doped, metallic, absence of Pauli paramagnetism, mag. susceptibility meas. and ESR obs. 80−97060
rare earth alloys, amorphous, with random anisotropy axes, spin excitations in paramag. phase 80−80476
rare earth alloys, R_3Pt_4, R=Nd, Gd, Tb, Dy, Ho, Er, Tm, mag. props., 4.2 to 160K 79−78343
rare earth alloys, RCu_x, mag. props., 4.2 to 200K 79−87233
rare earth binary insulating compounds, exchange interactions, paramag. susceptibility expts. 80−60177
rare earth chromates (lanthanide series), paramag. state, crystalline elec. field calcs. 78−39074
rare earth cobalt intermetallics, RCo_2, elastic moduli, 4.2-300K 78−52332
rare earth compounds, mag. dynamics of singlet-triplet system in paramag. phase 79−91203
rare earth compounds, paramagnetic, Faraday and Cotton-Mouton effects for acoustic phonons 78−52476
rare earth compounds, phenomenological study of supercond. 78−43512
rare earth cpds., with cryst. field splitting mag. inelastic neutron scatt. cross-section 77−55659
rare earth dodecaborides, mag. susceptibility temp. depend., 90-1200K 80−20374
rare earth dodecaborides, nature of magnetism *(Russian)* 78−31049
rare earth double nitrate, Van Vleck temp. independent suscept. 78−43555
rare earth heavy binary alloys, press. effect on mag. props. *(Japanese)* 77−43835
rare earth hydrides, magnetic props., book contrib. 79−82754
rare earth intermetallic, RCu_4Ag, mag. props. and cryst. struct. 77−20562
rare earth intermetallic compounds with Cu_3Au structure, crystal field splitting 80−54663
rare earth intermetallics, cubic, third-order mag. susceptibility, quadrupolar effects 79−99674

paramagnetic properties of substances continued
rare earth intermetallics, RAl_2, exchange modification of cond. bands 79−82568
rare earth intermetallics, RAu_3 (R=Gd, Tb, Dy, Ho, Er, Tm), mag. props. *(German)* 79−51761
rare earth intermetallics, RMg_2, cryst. and mag. props., ordering 78−68185
rare earth intermetallics, $RNiSi_3$, susceptibility, 80-1200K *(Russian)* 77−66281
rare earth iron silicides, $R_2Fe_4Si_9$ and $RFeSi_3$, cryst. struct. and mag. suscept., temp. depend. *(Russian)* 78−34957
rare earth manganites, catalytic activity correlated with paramag. Weiss constant 80−71941
rare earth metal compounds, high temp. paramagnetic-supercond. phase transitions, mag. cell symm. *(Russian)* 79−78255
rare earth metals, paramag., c_{11}, c_{33}, mag. field depend. 77−16143
rare earth metasilicates, $R_2(SiO_3)_3$, mag. susceptibility, temp. depend., 77-800K 80−20372
rare earth molybdates, cryst. growth, cryst. chem., and phys. props., book contrib. 80−44194
rare earth molybdates, mag. susceptibility meas. 79−69650
rare earth molybdenum selenides, supercond., mag. props., 0.7 to 295K 77−32113
rare earth orthotitanites, unusual mag. props., role of mag. moments 78−84400
rare earth oxides, binary, struct. and props., book contrib. 80−45292
rare earth pnictides, mag. props. 78−72325
rare earth selenides of yttrium subgroup, susceptibility and moments *(Ukrainian)* 77−32153
rare earth sesquioxides, exchange interactions, paramag. susceptibility expts. 80−60177
rare earth strontium vanadates, $R_{1-x}Sr_xVO_{3-0.1x}$, elec. cond. and mag. susceptibility, temp. depend., 77-300K 77−47816
rare earth titanotantalates, mag. susceptibility, temp. depend., 78-293K 77−36050
rare earth tungstates, mag. susceptibility determ. 77−4495
rare earth vanadites, mag. ordering, susceptibility meas., 60-300K 77−32190
rare earth-copper intermetallic cpds., RCu_2, metamag., mag. props. 79−87243
rare earth-gold intermetallics, RAu_2, mag. props., 4.2-300K 79−7972
rare earth-iron, RFe_2, Laves phase intermetallics, ordered and paramagnetic phases, mean field exchange consts. 80−50084
rare earth-transition metal hydrides, magnetic props., book contrib. 79−82754
rare earth-transition metal intermetallics, struct. and props. review 78−10668
rare-earth magnets, low-frequency modes 78−88087
rare-earth-Pd alloy, mag. props. 77−20547
ruthenates, $ACu_3Ru_4O_{12}$, A=Na,Ca,Sr,Cd,La,Pr,Nd, synthesis, cryst. struct., mag. and elec. props. *(French)* 80−107151
solution, rel. to magnetochem. separation 77−20628
spin cross-relaxation, temp. depend. of transition probability 80−25184
steel, austenitic stainless, magnetic susceptibility and magnetisation, low temp. 80−25102
steel, Cr-Ni-Mo-V, magnetic induction, struct. dependence *(Czech)* 80−50141
steel, spring alloy, microstruct. and props. at low temps. 77−44286
substitutional alloys of intermediate valence systems, static mag. susceptibility con. and temp. depend. 80−84586
tantalates, mixed metal, Eu oxidation state, mag. props., Mossbauer study 80−66080
$(TCNQ)_5^{4-}(DEPA)_2^{4+}$, cryst. struct., elec. and mag. props. 77−72605
TCNQ complex salts, mag. props., ESR meas. 79−56603
TCNQ complexes, Qn$(TCNQ)_2$, NMePh.TCNQ, and Li^+TCNQ^-, mag. susceptibility and sp. ht. 78−43556
TCNQ complexes with dipyranylidene and dithiadipyranylidene, high cond. investigs. and related props. 78−6368
TCNQ complexes with ferrocenes, charge transfer type, struct. and mag. props. 80−24439
TCNQ salt, $(DEPE)^{2+}(TCNQ)_4^{2-}$, elec. and mag. props. of two crystallographic form 77−28166
TCNQ salt, $(TMA^+)_3(I_3^-)(TCNQ^-)_2(TCNQ^0)$, struct., phys. props. and lattice distortion evidence 78−6305
TCNQ salt, DECA $(TCNQ)_2$, struct., phys. props. and irreversible phase transition 78−6273
TCNQ salt, HMTTF-TCNQ, metallic organic charge transfer complex, chemical prep. and phys. props. 78−2471
TCNQ salt, K-TCNQ, spin-Peierls system, paramag. susceptibility, Heisenberg chains 79−38299
TCNQ salt, tetramethylhexamethylenediammonium-TCNQ-iodine, elec. and mag. props., struct., specific heat 80−24898
TCNQ salt, TMTSF-DMTCNQ, mag. susceptibility meas. under press. 80−29521
TCNQ salt with MDCA cation, first order phase transition 79−73122
TCNQ salts, complex, with symmetric and asymmetric donors, transport and mag. props. 78−6315
TCNQ salts, sp. ht. meas., 0.2-300K, extended Hubbard model *(French)* 77−35710
TCNQ-K, dielectric function of 1-dimens. Hubbard model 79−60740
TCNQ-NMP, disordered, paramag. susceptibility 78−10645
TCNQ-NMP type crystals, density of states, rel. to low temp. paramag. susceptibility *(Russian)* 77−85127
tetrabutylammonium iron tetraiodide, structural and mag. props., ^{57}Fe and ^{129}I Mossbauer spectra 79−61282
tetraethylammonium iron tetraiodide, structural and mag. props., ^{57}Fe and ^{129}I Mossbauer spectra 79−61282
tetraethylammonium neptunium hexachloride, Mossbauer spectra and mag. susceptibility meas. 80−108140
2,2,5,5-tetramethyl-4-phenyl-3-imidazalin-3-oxide-l-oxyl, deform. electron density determ., X-ray diffr. 80−88135
tetramethylammonium manganese trichloride, ESR meas., evidence for two paramag. species 79−61208
tetramethylammonium manganous chloride:Cu, impure Heisenberg chain paramagnet, EPR sidebands, intensity, linewidths 78−76300
tetramethylammonium neptunium hexachloride, Mossbauer spectra and mag. susceptibility meas. 80−108140
tetrathiofulvalene-based salts, isomorphous series systematic investig. of solid-state props. 77−55517
tetrathiotetracenenickel bis(ethylene-1,2-dithiolene), one-dimens. cond., preparation and props. 77−85201

paramagnetic properties of substances continued
(TETTF)$(TCNQ)_2$, charge transfer complex, phys. props. and phase transition 78−64032
thulium ethyl sulphate, Van Vleck paramag., mag. reson. on uniaxial and uniform compression *(Russian)* 79−61243
TMBP.HCNB and TMBTP.HCNB complexes, elec. and mag. props. 78−6512
TMMC:Cu(Ni)(Cd), mag. and non-mag. impurity effects on suscept. and Neel temp. 77−66312
TMMC, half-field EPR transitions in 1-D Heisenberg paramagnet 79−51843
TMMC, one-dimensional paramag., anomalous freq. depend. of EPR linewidth 80−15784
transition metal, band model, mag. susceptibility of exchange-enhanced paramagnet 78−2644
transition metal, surface density of states, continued fraction method 77−20388
transition metal borides, cryst. struct., prep. methods, chem., elec., mag. props., appls., book contrib. 78−47307
transition metal borides, narrow band types, electronic density of states, many-electron Hubbard model calcs. 80−20064
transition metal chalcogenides, struct. and mag. props., book contrib. 77−43808
3d-transition metal complexes, low spin-high spin paramag. transition, Ising model calc. 80−93073
transition metal complexes, mag. exchange in $s=1/2$ systems 78−43553
transition metal diiodides, (V, Cr, Mn, Fe, Co, Ni, Cd), Mossbauer spectrum, electronic and mag. props. 77−32302
d-transition metal hydride, mag. suscept. and quasirigid model *(Russian)* 78−26805
transition metal intermetallic cpds., H absorption and mag. props. 80−60224
transition metal ions in amorphous cpds., crystal field theory and mag. props. 78−72318
transition metal pyrites, mag. and elec. props., review *(Japanese)* 78−47941
transition metals, 4d and 5d, susceptibility max. and grand Fermi-liq. effect 77−63082
transition metals, electronic structure and ordering of sp defects 78−91639
transition metals, energy of cohesion calc., Hubbard Hamiltonian with exchange interaction 77−69261
transition metals, paramagnetic state, itinerant electron model 80−65769
transition metals, paramagnetic susceptibility, phonon instability, mixed localised-collective electron states 80−103811
transition metals, photoemission spectra, core-level satellite struct. 80−29855
transition metals, role of electron correlation 77−72974
transition metals and alloys, 3d, Hall effect, electron scatt. processes 80−34419
3d-transition-metal dichalcogenides, mag. props. rel. to Hubbard model 79−78373
trimethylammonium manganese bromide, mag., anisotropy, biquadratic exchange 78−14952
triscyclopentadienyl uranium chloride, ^{13}C NMR shifts, 160-320K 77−16190
$TSeTBr_{0.5}$, phase transition, mag. props., thermal capacity and cond. *(Russian)* 79−99537
TTF salts, physical props., Fermi energy scaling of metal-insulator transition temp. 77−8081
TTF-TCNQ, phase transitions and CDW state, controlled disorder effects 80−15507
TTF-TCNQ, single cryst., mag. susceptibility in phase transition region, two-gap model 78−6511
$TTT_2-(I_3)_{1+x}$, physical props., elec., mag. and optical meas. 80−24908
vanadyl carboxylates, EPR and mag. susceptibility, near one-dimens. antiferromagn. 77−63265
W-dichalcogenide, valence band nature, elec. and mag. props 78−39014
Ag, conduction electron spin transmission 77−69693
Ag-based alloys, α-phase, mag. susceptibility correl. with lattice parameter 78−68154
Al, nuclear paramagnetism used for calibration of SQUID magnetometer 79−67358
Al-Cu-Fe alloys, solid and liquid, exam. of constitution and mag. props. *(German)* 78−52206
Al-Zn, liq., physical props. study by electrodiffusion method *(Czech)* 77−84956
$Al_2O_3:V^{3+}$, magnetocaloric effect in high magnetic fields 80−25140
$Al_2O_3-Fe_2O_3:Cr^{3+}$, dil. paramag. system, Cr^{3+} conc., effect on cross relax. 79−15387
$Al_2O_3-Fe_2O_3(:Cr^{3+})$ paramag. system, cross relax. temp. and mag. field effects on Mossbauer spectra 79−33576
$(Al_2O_3-Fe_2O_3):Cr^{3+}$, (0.04 mol.% Fe_2O_3), paramag., cross relax., annealing temp. effect from Mossbauer meas. 80−44983
AmB_2 (B=Al, Co, Rh, Ru), mag. props. of Laves phases 77−27851
As, amorphous, thermally generated paramagnetism 79−19720
As_xSe_{100-x} glasses, temp. depend. of mag. susceptibility and EPR 77−63073
Au, conduction electron spin transmission 77−69693
Au-Fe, dil., local mag. moments, neutron scatt. study 79−61058
Au-Ni, magnetisation and sp. ht., ferromag., paramag. and crit.-conc. regions 79−38330
Au_4V, effect of structural changes on phys. props. 78−31400
BH, $^1\Sigma^+$ ground state, mag. susceptibility, paramag. contrib., large config. interaction wave function calcs. 80−47899
BH, susceptibility and mag. screening calcs. 77−57861
$BaCuO_2$, prep. and props. *(French)* 77−43201
$Ba_3Fe_{2-x}Lu_xUO_9$, crystallographic and mag. props. *(French)* 77−15380
$BaFe_4Ti_2O_{11}$, R-type hexaferrite, spin struct. and mag. props. 78−52216
$Ba_xLa_{1-x}CoO_3$, x=0 to 0.5, structural, elec. and mag. props., Zener double exchange and Goodenough's model 79−65663
$BaO-Fe_2O_3$ system, splat cooled phases struct., magnetisation and susceptibility 300-1100K *(French)* 77−48017
$Ba_3Re_2O_9$, cryst. struct., mag. and semicond. props. 79−10836
$BaTiO_3$, magnetochemical exam. of phase transition, mag. suscept. meas. 78−88265
$BaX_{1/3}Ru_{2/3}O_3$ (X=Ca, Cd, Mg, Sr), crystal struct., mag. susceptibility and exchange integrals *(French)* 77−16037
$Ba_2Zn_2Fe_{12}O_{22}$, model for low mag. moment, magnetisation meas., 5-1375K 78−2655
$Be_5(Fe_{1-x}Mn_x)$, mag. and calorimetric props. 77−63083

paramagnetic properties of substances continued

$Be_{1-x}Mn_x$, Be-rich, NMR and paramag. susceptibility 80−71206
Bi-MnBi eutectic composites, microstructure and mag. props., annealing effect 79−82827
$BiCoO_3$, paramagnetism, negative Curie temp. 79−64956
$Bi_2Fe_4O_9$, mag. struct., neutron diffr. meas. 78−91844
Bi_2O_3-ZnO(CdO), elec. cond., dielec. const., mag. susceptibility meas., effect of melting transition 77−7849
C, amorphous, anomalous low temp. mag. and thermal props. 78−10647
C, anthracene char, density fluctuations effect on physical properties 78−51420
C chars, thermally activated paramagnetism, mag. susceptibility meas. 80−75709
C, evaporated, paramag. and diamag. susceptibility meas., 77 to 1400K 77−28362
C powder magnetisation thermometry for very low temps. 79−63219
$CaCo_2(PO_4)_2$, reflection spectrum and mag. susceptibility meas. 77−59586
$CaCrF_5$, one-dimens. magnetism *(French)* 79−73670
CaF_2:Tm^{2+}, spin density parameters at ^{19}F nuclei 78−68001
$CaFeF_5$, one-dimens. magnetism *(French)* 79−73670
$CaFeO_3$, preparation, cryst. struct., mag. and elec. props. 78−44066
$(Ca_{1-x}Mg_x)RuO_3$, mag. props. 78−27027
$Ca(OH)_2$, mag. ordering of proton spins 79−73746
Cd, magnetic susceptibility, temp. depend., electron-phonon interaction effects 79−61046
$CdCr_2S_4$, EPR line profiles in paramag. and ferromag. phases 79−28602
$CdCr_2S_{4-\gamma}$, spinel, anomalies in paramag. susceptibility, Curie pt. *(Russian)* 77−80910
CdF_2:Cu, paramagnetic centre coordination, g-tensor orientation by anisotropy of ^{19}F ENDOR 80−54993
$Cd_{1-x}Ga_xCr_2S_3$, spinel, anomalies in paramag. susceptibility, Curie pt. *(Russian)* 77−80910
$CdGe_{1-x}M_xAs_2$ (M=Si,Sn,Pb), amorphous struct., mag. susceptibility 78−22651
$CdGe_{1-x}Sn_xAs_2$, amorphous, radial distrib. anal. and mag. susceptibility meas. 77−43152
$Cd_{1-x}In_xCr_2Se_4$, electric, photoelectric and mag. props., metal-semicond. transition *(Russian)* 80−54738
CdInGaS$_4$:Er^{3+}, cryst. field parameters, thermal and mag. props. calc. 77−20540
$CdIn_2S_4$:Er^{3+}, cryst. field parameters, thermal and mag. props. calc. 77−20540
$Cd_{1-x}Mg_x$, magnetic susceptibility anisotropy, press. effects, electronic phase transitions *(Russian)* 80−54869
CdMnTe, semimagnetic semiconductor, band structure, optical properties 79−95331
$CdPS_3$, layered, organometallic intercalates, X-ray diffr., optical absorpt. and mag. props. 80−45103
CdS, magnetic susceptibility, grinding-induced states 79−61040
CdSe, magnetic susceptibility, grinding-induced states 79−61040
CdTe, mag. susceptibility at 20-1400°C 77−12085
CdTe:Mn^{2+}, exciton refl. spectra and mag. susceptibility 80−66253
$CdTm_2Se_4$, mag. susceptibility meas. 4.2 to 300K cryst. field approx. 77−66246
γ-Ce, field induced mag. form factor 78−68151
Ce, inelastic neutron scatt. cross-section, effect of cryst. field 79−65642
Ce, liq., 4f electron susceptibility temp. depend. 80−20378
β-Ce, susceptibility meas., 2-300K 77−4320
Ce-Co-Si system, mag. props. in 77-300K range *(Russian)* 78−56290
Ce-Fe-Si system, mag. props. in 77-300K range *(Russian)* 78−56290
Ce-Ni-Si system, mag. props. in 77-300K range *(Russian)* 78−56290
Ce-Pt, paramag. suscept. 79−61047
$CeAl_2$, dynamic Jahn-Teller effect, neutron energy loss obs. 79−78060
$CeAl_2$, mode softening due to magnetoelastic interaction, elastic consts. meas. 1.5 to 280K 77−32233
$Ce_{30}Au_{20}$, amorphous, cryst. field effects and mag. interactions, magnetisation and transport props. meas. 78−68191
CeB_6, mag. and electronic props. 80−71048
CeB_6, magnetostriction, US absorpt. and thermal expansion 80−66004
$CeBe_{13}$, intermediate valence state, XPS, resist. and susceptibility study 80−71565
$CeCo_3$, and ternary hydride, mag. props. 80−108007
$Ce(Cu,Ni)_2$, pseudobinary phases, struct. and mag. props. rel. to Ce valence 78−6032
$CeCu_4$ Knight shifts and mag. susceptibility 79−95656
$CeCu_5$, Knight shift and mag. susceptibilities 79−95656
$CeCu_2Si_2$, local mag. moments, neutron scatt. study 79−61058
$CeCu_2Si_2$, strong Pauli paramagnetism, superconductivity obs. 80−29499
$Ce_xEu_{1-x}B_6$, mag. susceptibility, 80-1000K 79−73674
$Ce(In, Sn)_3$, mag. susceptibility, temp. depend., intermediate valence 80−65779
$CeIn_3$, Kondo effect, mag. suscept. exam. 77−8270
$CeIn_{3-x}Sn_x$, conduction electrons role in valency fluctuations 78−47741
$Ce_{1-x}La_xAl_2$, extraordinary Hall effects, 4.2-300K, cryst. field interaction 78−79980
$(Ce_xLa_{1-x})Al_2$, inelastic neutron scatt. cross-section, effect of cryst. field 79−65642
$Ce_xLa_{1-x}F_3$, paramag. mixed crystal, scattering of optical phonons by rare earth ions 78−68518
$(Ce_xLa_{1-x})_2Mg_3(NO_3)_{12}.24H_2O$, mag. susceptibility meas., AC method meas., appl. as thermometer in mK region 77−17999
$(Ce_xLa_{1-x})_2Mg_3(NO_3)_{12}.24H_2O$, adiabatic demagnetisation temp., mag. entropy *(Russian)* 80−65892
$Ce_x(La_yY_{1-y})_{1-x}Al_2$, local mag. moments, neutron scatt. study 79−61058
$Ce_2Mg_3(NO_3)_{12}$, AC mag. susceptibility, mag. field depend., 1-4K 79−56516
$CeNi_2$-$CePt_2$ system, structural and mag. studies on valence behaviour of Ce 80−103809
$CeNi_3$, and ternary hydride, mag. props. 80−108007
CeP(As), single crystals, low temp. thermal, electrical and mag. props. meas. 78−27051
$CePd_3$, dil., local mag. moments, neutron scatt. study 79−61058
$CePd_3$, magnetic neutron scatt. cross-section and linewidth, temp. depend. 77−63080
$CePt_3$, ^{195}Pt NMR and susceptibility meas. 77−63299
$CePt_5$, mag. susceptibility, 4.2 to 295K *(German)* 79−47233
CeSb, mag. phase diagram and mag. struct., neutron diffr. determ. 77−63182
$CeSn_3$, low temp. mag. behaviour, press. induced valence change 77−63078
$CeSn_3$, polarised neutron study of induced magnetisation 80−34594
$Ce_{0.74}Th_{0.26}$, mixed valence alloy, spin dynamics 78−10708
$Ce_2(WO_4)_3$, mag. susceptibility, paramag. Curie temp., 300-900K 79−82753
CeX (X=P, As, Sb, Bi), neutron inelastic scatt. expts. 80−19674
Cm, antiferromag. state, paramag. suscept. meas., electronic struct. *(Czech)* 78−80133
Co complex, $Co(C_3H_4N_2)_6(NO_3)_2$ and $Co(C_{11}H_{12}ON_2)_6(ClO_4)_2$, paramag., hyperfine sp. ht. 77−55683
Co complex, Co(III) five coordinate, paramagnetic behaviour 79−15276
Co complexes, Co(III) mixed complexes, orbital angular momentum reduction, ^{59}Co NMR chemical shift 80−58137
Co, diffusion of Mn, 860-1246°C, mag. transform. effects 77−24427
Co, FCC, self-diffusion and isotope effect, influence of mag. order-disorder transition 80−29205
Co, small-angle crit. neutron scatt. 78−31087
Co-Al alloys, deformed, mag. props., positron annihilation *(Russian)* 77−85416
Co-Al system, nucl. spin relaxation exam. 79−19798
Co-based Heusler alloys, Co_2TAl, (T=Ti, Zr, Hf), paramag. state NMR and susceptibility meas. 79−65643
Co-Mn (10.24 at.%), Mn diffusion, 903-1148°C 77−24427
Co-Mn (5.22 at.%), Mn diffusion, 868-1200°C, mag. transform. effects 77−24427
Co-Ni (5 to 95 at.%), paramag. props., 800-1800°C *(Russian)* 77−55660
Co-V, solid and liq., mag. susceptibility and electronic struct. 80−39738
$CoBr_2$, paramag. and antiferromag., Raman scatt. from electronic excitations and phonons 79−69826
$Co(C_5H_5NO)_6(ClO_4)_2$ $[(BF_4)_2]$, X-Y antiferromagnet, Neel temp., spin correlation functions 80−60345
$CoCO_3$, LF exciton and Raman spectra, one-magnon and two-magnon scatt. 80−93333
$CoCl_2.6H_2O$, paramag., PMR 78−91962
$Co_{1-x}Cu_xCr_2S_4$, paramag. susceptibility 80−20373
$(Co_xFe_{1-x})_5Ge_3$, Mossbauer investig. of hyperfine field at Fe nuclei 77−20776
$(Co_{1-x}Fe_x)_2Y$, substitutional Fe atoms effect on mag. and elec. props., paramagnon scatt. 77−36054
$CoGa_{2-x}Fe_xO_4$, x=0.1−0.4, mag. susceptibility temp. depend. *(Russian)* 80−70957
$(Co_{1-x}M_x)B$, M=Mn or Fe, paramag., spin echo NMR spectra, ferromag. transition, spin-lattice relax. 80−29645
$(Co_{1-x}Mn_x)_2B$, $0\leq x\leq 1$, magnetisation, lattice consts., press. depend. of Curie temp. 80−7137
CoO, paramag. shifts of ^{19}F at O 78−43719
CoS_2, microscopic mag. props., NMR meas. 79−91306
$CoS_{2-x}Se_x$, conc. and temp. effects on metamagnetic transition 80−15716
$Co(S,Se_{1-x})_2$, $(0\leq x\leq 1)$, mag. props. and elec. resist. 79−65657
CoSb, at. struct. and mag. susceptibility 77−39561
$CoSe_2$, bulk mag. susceptibility, anomalous temp. depend., NMR and X-ray diffr. meas 79−87229
$CoSe_2$, hyperfine parameters and quadrupole splitting determ., ^{57}Fe Mossbauer spectra 77−77131
$CoSe_2$, paramag. metal, sp. ht., Mossbauer effect, absence of ordering 77−16036
$CoSe_2$, temp. induced local mag. moments, ^{59}Co NMR 79−65747
Co_2SnO_4, $CoMg(Zn)SnO_4$ and $Co_{2-x}Mg_2TiO_4$, magnetic props., short-range ordering 77−32155
$Co_2(Ti,Mn)Sn$, Heusler alloy, mag. meas. 79−47261
$CoTi_{1-x}Al_x$, mag. and electronic props., ferromag. and paramag. state 80−65814
Co_2TiAl, ^{59}Co NMR, above and below Curie temp. 78−2760
$Co_2Ti(Y)(Zr)(Nb)$, Laves phase, elec. resist. rel. to mag. props. 77−59282
$Co_cZn_{1-c}F_2$, Raman scatt. from Zeeman split levels 77−66243
$Co_{2-y}Zn_yTiO_4$, spinel series, exchange integrals, mag. struct. and coercive force, magnetisation meas. 77−69507
Cr, band structure and Fermi suface of paramag. solid *(Russian)* 79−65375
Cr, δ- and BCC, fine particles, mag. props. 78−52314
Cr, Hartree band struct., Fermi surface, nesting wave vector 80−49583
Cr, paramag., mag. form factors, neutron diffr. study 79−47234
Cr, spin density wave, CDW and strain wave, effect of spin polarisation of reservoir and imperfect nesting 78−56284
Cr, transverse magnetoresist. meas. in antiferro- and paramag. states, 15 to 80°C 77−85197
Cr-Co-V alloys, dil., elec. resist. min. 80−54680
Cr-Fe, low conc. alloys, coexistence of itinerant antiferromagnetism with paramagnetism 78−84386
Cr-Ge system, XPS, X-ray and neutron diffr. and mag. meas. to study chem. bonding and electronic struct. 80−60749
Cr-Ni(V), dil., mag. susceptibility, 77 to 400K *(Russian)* 80−50066
Cr-V-Fe alloy, resistivity minimum, press. effect 79−38043
$CrBr_3$, reflectance and thermoreflectance spectra in paramag. and ferromag. phases 79−56770
$Cr_{0.5}NbSe_2$, cryst. struct., metallic cond., mag. and phys. props. *(French)* 80−33956
$CrPS_4$, phys. props. and Li intercalates 79−19788
$CrPr_2Se_4$, synthesis, single crystal growth, mag. and elec. props. 79−78857
$CrSe_2$, layered, phys. and elec. props. 80−44594
$Cr_{1-x}V_xCo$, localised mag. moment of Co impurity 78−27014
$Cr_{1-x}V_xCo$, mag. state of Co impurity, NMR exam. 78−27100
Cs fluid, metallic and nonmetallic, mag. props. 80−44799
$CsCdBr_3$:Cr^{3+}(Cr^+), EPR of impurities, charge compensation, X-ray effects 80−60407
Cs_2CoCl_4, paramag. mag. exchange rel. to low temp. mag. characts. 77−55669
$Cs_2KTmBr_6(Cl_6)(F_6)$, Cs_2NaTmF_6 and Cs_2RbTmF_6, mag. behaviour 2.9 to 251.3K, cryst. field levels, ang. overlap model *(German)* 80−29520
Cs_2KYbF_6, mag. behaviour, 3.5-251.3K *(German)* 80−50041
$CsMgCl_3(Br_3)$:Cr^{3+}(Cr^+), EPR of impurities, charge compensation, X-ray effects 80−60407
$CsMnBr_3.2H_2O$, pseudo-one-dimensional mag. system, low-temp. sp. ht. 77−85471
$CsMnCl_3$, electron resonance linewidth anisotropy 79−28588

paramagnetic properties of substances continued
$CsMnCl_3.2H_2O$, pseudo-one-dimensional mag. system, low-temp. sp. ht. 77−85471
Cs_2NaYCl_6:^{249}Cf, mag. susceptibility of Cf^{3+} in octahedral site 77−12089
$Cs_2NaYbBr_6$, mag. behaviour, 3.5-251.3K *(German)* 80−50041
$Cs_2NaYbCl_6$, electronic struct., paramag. susceptibility and electronic Raman spectrum, cryst. field parameters *(German)* 77−63072
Cs_2NaYbF_6, mag. behaviour, 3.5-251.3K *(German)* 80−50041
$CsNiCl_3$, nuclear spin-lattice relax., temp. depend., anisotropic effects 78−64293
$CsNiCl_3(F_3)$, one-dimensional anisotropic paramag., nucl. relax. rate and spin dynamics 77−69723
$CsNiF_3$, longit. paramag. susceptibility, reaction field approx. 80−97059
$CsNiF_3$, one-dimens. anisotropic paramagnet, EPR meas. 79−73799
Cs_2NpCl_6, Mossbauer spectra and mag. susceptibility meas. 80−108140
Cs_2RbYbF_6, mag. behaviour, 3.5-251.3K *(German)* 80−50041
$CsTmO_2$, mag. props. of normal-temp. form, 2.9-251.3K *(German)* 79−91205
Cu complex, bis-(salicyladoximato) Cu(II), ENDOR multiplet HFS, energy level non-crossing 79−72341
Cu complexes with amino acids, static mag. susceptibility and effective mag. moment 77−12082
Cu, conduction electron spin transmission 77−69693
Cu triazole complexes, finite Heisenberg chain effects, temp. depend. 79−47230
Cu-Al-Co liquid alloys, constant Co-content of 5 wt.%, mag. props. *(German)* 80−88720
Cu-Al-Fe, dil. liq. alloy, localised mag. state interactions *(German)* 77−1539
Cu-based alloys, α-phase, mag. susceptibility correl. with lattice parameter 78−68154
Cu-Fe, dil., local mag. moments, neutron scatt. study 79−61058
Cu-Fe, dilute, low temp. heat capacity in mag. field, superparamagnetism 80−39804
Cu-Mn, dil., local mag. moments, neutron scatt. study 79−61058
Cu-Mn-Al, mag. props. and atomic ordering 79−24139
Cu-Ni dil. paramagnetic alloys, sp. elec. resist., effect of Ni clusters *(German)* 78−95293
$CuAl_{1-x}Fe_xS_2$ system, delocalisation of d-electrons, mag., elec. and optical obs. 78−34804
$CuBeF_4.5H_2O$, NMR, interactions between paramag. ion system and antiferromag. linear chains 77−63295
$CuCl_2$, anhydrous paramagnetic phase, mag. susceptibility depend. on temp. 79−7965
$CuCl_2$, finite Heisenberg chain effects, temp. depend. 79−47230
$CuCr_2S_{4-\gamma}$, spinel, anomalies in paramag. susceptibility, Curie pt. *(Russian)* 77−80910
CuF_2, ^{63}Cu NQR meas. 80−50219
Cu_cNi_{1-c}, solutions of KKR-CPA equations for paramagnetic alloys 78−95256
Cu_cNi_{1-c}, Fermi surface of concentrated paramag. alloys 78−95257
Cu_xNi_{1-x}, paramag., electronic struct., atomic sphere approx. to KKR-CPA 79−19502
Cu_2O-CuO-MoO_3, subsolidus phase diagram, mag. props. 80−50615
$(Cu_2O)_{1-x}U_{1.4}M_{4.6}O_{18}$, M=Mo, W, $0 \leq x \leq 0.4$, crystallographic identification, paramag. props. *(French)* 79−46633
$Cu_{2-x}Se$, nonstoichiometric, diamag. and paramag. props., susceptibility meas. 80−70936
$CuSeO_4$, S=$^1/_2$ Heisenberg antiferromag. linear chain, proton spin-lattice relax., rel. to paramag. state 78−39433
CuV_2S_4, preparation, cryst. struct. and physical props. *(French)* 79−55714
Dy, Curie-Weiss law anisotropy, paramag. susceptibility meas. 80−15686
Dy, elastic consts. in paramag. temp. range, magnetoelastic contrib. 77−4538
Dy, mag. anisotropy and susceptibility 77−69539
Dy, parasusceptibility meas., 4.2-130K, spin wave anal. 79−95583
Dy, US attenuation in mag. field 77−40104
Dy-Sm alloys, elec. resist. singularities and mag. transitions *(Russian)* 79−47075
Dy-Y, paramag. susceptibility in basal plane and hexagonal axis 77−20548
$DyAu_6$, mag. props. temp. depend. *(French)* 77−51879
$Dy_3Ga_5O_{12}$, crystal field effect on paramag. props. of Dy^{3+} ion 80−50040
DyH_2, mag. and crystal field props. from ^{161}Dy Mossbauer studies 79−95692
DyH_3, mag. and crystal field props. from ^{161}Dy Mossbauer studies 79−95692
DySb, quadrupole interactions above T_N 79−78304
Dy_2Se_3, mag. susceptibility 77−40032
Er, paramagnetic and antiferromagnetic states, optical absorption *(Russian)* 78−56497
Er, US attenuation, longitudinal, in mag. ordered region and at phase transitions 77−28422
Er, US attenuation in mag. field, temp. and field depend. 79−91279
$Er_3Au_3Sb_4$, mag. suscept. meas., 4 to 300K 79−51742
$Er(C_2O_4)(C_2O_4H).3H_2O$, single cryst., mag. susceptibility, 1.5-20K, g-factors 77−77094
$ErFe_2Ge_2$, magnetisation, 4.2-273K 77−8310
ErGa garnet, crystal field theory of Er^{3+} ion behaviour 77−8259
$Er_{1-x}Ho_xRh_4B_4$, re-entrant supercond. and mag. ordering 78−60240
$ErNi_5$, cryst. field parameters in ferromag., paramag. states, susceptibility meas. 77−63139
Er_2O_3, mag. susceptibility, elec. cond. and dielectric const., hopping cond. 77−12083
$ErRh_4B_4$, superconductivity destruction at onset of long-range mag. order 77−76994
Er_2Se_3, mag. susceptibility 77−40032
Er_2Te_3, magnetic susceptibility meas., cryst. field interpretation 80−11156
$ErVO_3$, produced by $Er_2O_3+VO_2$ high-press. reaction, cryst. struct. and mag. props. meas. 80−19773
$ErVO_4$, phonon resistivity mag. field depend. in paramag. phase 80−2226
Eu chalcogenide, spin-disorder Raman scatt., mag. phase depend., theory 78−10887
Eu chalcogenides, heavily doped mag. semiconductors, effect of carriers statistics on indirect exchange 77−69280
Eu chalcogenides, magnetic semiconductor, light scatt. exam. 79−61372

paramagnetic properties of substances continued
Eu chalcogenides, optical orientation of 4f electrons, transverse and logit. pumping 77−69799
Eu chalcogenides, paramag., spin-disorder-induced Raman scatt. 78−19474
Eu, mag. and struct. transitions, X-ray K-line shift, 77-1000K *(Russian)* 77−4518
Eu, saturation of polarisation paramagnetism *(Russian)* 79−47232
Eu-Cd compounds, Mossbauer effect, mag. props. and lattice consts. 77−36164
Eu^{2+}-ionic compounds, magnetic interaction potential 78−10682
$EuB_{6-x}C_x$, magnetic and elec. props. 78−91842
$EuCl_2$, $EuCl_2$-$EuCl_3$, $EuCl_2$.HCl, mag. props., 77-292K 78−52197
Eu_2IrH_5, prep., cryst. struct., mag. and elec. props. 80−88117
$Eu_2Mg_3(NO_3)_{12}.24H_2O$, Zeeman effect in absorpt. spectrum 77−63402
EuO, Eu doped, temp. depend. of carrier conc. and mag. susceptibility 77−69483
EuO, magnetostriction, spin-spin correl. function, above T_c 77−4541
EuO, paramag. phase, cond. due to electron jumps 79−69544
EuO:Eu, paramag. triplet state, mag. susceptibility 77−72820
EuO:La, metallic, photothreshold, correl. and exchange energy of electron gas 77−62852
EuO(S), effect of pressure on energy gaps 78−19239
EuS, exchange magnetostriction in paramagnetic phase 79−78492
$Eu_2(SO_4)_3.8H_2O$, mag. props., thermal var., cryst. field reduced matrix elements 77−51875
EuSe, mag. phase depend. Raman scatt. 78−10886
EuSe, mag. phase stability, theory 77−63183
EuSe, optical absorption exam., electron phonon interactions 78−10923
$Eu_xSr_{1-x}M_4O_{11}$, M=Nb, Ta, electrophys. and mag. props. 77−89760
$Eu_xSr_{1-x}S$, paramag. susceptibility, expt. and comparison with high temp. series expansion 80−60176
$EuTi_{1.5}W_{0.5}O_6$, Stark sublevels in mag. suscept. and luminesc. 77−51876
Eu_2VO_4, prep. and props. 77−15379
$Eu_2(WO_4)_3$, mag. susceptibility, paramag. Curie temp., 300-900K 79−82753
EuX(X=0,S,Se) 80−20635
EuX(X=0,S,Se), spin-disorder-induced Raman scatt. from phonons, theory 80−20636
Fe complex, $[Fe(S_2C_2O_2)_2X]^{2-}$, (X=Cl,Br,I), Mossbauer effect, EPR, mag. susceptibility 79−11366
Fe complex, Fe (II) pseudo-tetragonal high-spin cpds., paramag. susceptibility amd Mossbauer quadrupole splitting 78−26834
Fe complex, Fe(5-methylpyrazole)$_4X_2$, X=Cl, Br, I, mag. susceptibility, mag. saturation; Mossbauer and ligand field spectra, single model interpretation 78−23064
Fe complex, Fe(pyrazole)$_4X_2$, X=Cl, Br, I, mag. susceptibility, mag. saturation; Mossbauer and ligand field spectra, single model interpretation 78−23064
Fe complex, perchlorato(meso-tetraphenylporphinato) iron (III), mag. props., Mossbauer study 79−99802
Fe complex, tetraphenylporphynate iron III bromide, mag. props., zero-field splitting 80−34584
Fe, crit. fluctuations, Mossbauer obs. 78−43724
Fe, density of states, photoemission expts. above and below T_c, rel. to magnetism model 77−20536
Fe dicyclopentadienyl-dibenzenevanadium, coalescence temps., full proton HFS tensor, ENDOR obs. 80−66073
Fe, magnetic moments, local short range order, high temp. effects 80−65902
Fe, molten, mag. neutron scatt. at small momentum transfer caused by spin fluctuations 77−47968
Fe, molten, mag. small-angle scatt., persistent spin fluctuations 79−11288
Fe, Mossbauer energy shift near Curie temp. 78−52388
Fe, neutron critical scatt., above T_c, polaris. asymmetry 78−34994
Fe, paramagnetic, orbital magnetic susceptibility calc. 80−7075
Fe, paramagnetic mag. entropy 77−63081
Fe-Al, paramag. props., T_c to 1500K 78−68153
Fe-Al-Si alloy, order-disorder transform. exam. by Mossbauer spectroscopy 77−63334
Fe-alloy, FCC, Invar, thermally excited electron transitions 79−56559
Fe-B, amorphous paramag. alloys, hyperfine field distrib., Mossbauer study 80−39958
Fe-C melt, mag. susceptibility and short range order, 900-1800°C 78−84382
Fe-Mn(0 to 80 wt.%), paramagnetic susceptibility by Faraday method, band model interpretation *(Russian)* 77−20545
Fe-Ni, thermal expansion, ferromagnetic-paramagnetic transition *(Russian)* 80−54412
Fe-Ni, thermodynamic props., anomalous 80−39313
Fe-Ni Invar alloys, thermodynamic props. 79−56560
Fe-Ni ordered phase in meteorites, Mossbauer studies 80−41776
Fe-Ni-P-B, amorphous paramag. alloys, hyperfine field distrib., Mossbauer study 80−39958
Fe-Ni-Si-B, amorphous paramag. alloys, hyperfine field distrib., Mossbauer study 80−39958
Fe-Ni(Co), solid and liq., paramag. susceptibility and electron struct., 800-1800°C *(Russian)* 80−25081
Fe-Pt, Invar alloy, paramag. susceptibility 80−70940
Fe-Rh, mag. phase transitions, triple point 79−1672
Fe-Rh alloy, nonmag. and mag., band theory 79−37973
Fe-Si amorphous film, struct. and crystallisation, Mossbauer study 80−11300
Fe-Si(Ge)(Al), solid and liq. paramag. props. *(Russian)* 77−66247
Fe-Ti, magnetism and H_2 storage 80−70941
Fe-Y(Th)(Zr), amorphous, charge transfer and mag. props., ^{57}Fe Mossbauer spectra 79−19719
$Fe_{0.25}$-Cu-Al, liquid, transition from Curie-like susceptibility to enhanced Pauli paramagnetism 79−24132
Fe_2 magnetism, randomised exchange field theory 80−39733
$Fe_{0.7}Al_{0.3}$, local environment effects and magnetic clustering 78−10658
Fe_3Al, super-lattice, band theory 77−15758
FeAs, Mossbauer spectra of paramag. and ferromag. states, helimagnetic spin ordering 80−7197
$FeBO_3$-MBO_3 solid soln., (M=Mn, Cr, Al, Ga, In), synthesis, crystal chem. and mag. props. 78−31058
$FeBr_2$, dynamic Jahn-Teller system, Raman scatt. from electronic excitations and phonons 78−56474
FeC_x ($x \leq 0.05$), splat-quenched, struct., elec. and mag. props. 77−21187

paramagnetic properties of substances continued
$FeCO_3$:Mn^{2+}, far IR host and impurity excitations, antiferromag. and paramag. temp. ranges 77−52140
$FeCl_2$, dynamic Jahn-Teller system, Raman scatt. from electronic excitations and phonons 78−56474
$FeCl_2$, reorientation of mag. moments under mech. stresses at 0K 80−93153
$FeCl_2.4H_2O$, pressure effects on hyperfine interaction in single crysts. in mag. field 77−16211
$FeCoCrO_4$, Mossbauer study, cation distrib. and Neel temp. determ. 79−33571
$FeCoF_5.2H_2O$, ferrimag. props., suscept. and transitions, 3-296K 79−87240
$Fe_{2-x}Cr_xP_{1-y}As_y$ mag. props., Mossbauer obs. 77−40156
$Fe_5(Fe_{1-y}Co_y)$, mag. and calorimetric props. 77−63083
$Fe_{1-x}Mn_xCl_2$, low-lying electronic excitations in antiferromag. and paramag. phases Raman scatt. study 80−71414
$FeMo_2S_4$, Mossbauer spectra, 79-300K, Neel pt. determ. 78−60360
$(Fe_{0.5}Ni_{0.5})$-Co, solid and liq., paramag. susceptibility and electron struct., 800-1800°C *(Russian)* 80−25081
$Fe_{0.7}Ni_{0.3}$, Invar alloy, bulk moduli, pressure effect on lattice spacing 79−55805
$(Fe_{0.5}Ni_{0.5})_{1-x}Co_x$, solid and liq., susceptibility, 1000-1800°C *(Russian)* 77−16040
$Fe_{0.5}(Ni_xMn_{1-x})_{0.5}$, elec. resist., anomalies in temp. depend. 79−23942
$Fe_{0.5}(Ni_xMn_{1-x})_{0.5}$, FCC, anomalies in sp. ht. and thermal expansion in paramag. temp. range 79−19739
$(Fe_{1-x}Ni_x)_2P$, mag. props. 78−23248
$Fe_{2-x}Ni_xP_{1-y}As_y$, mag. props. Mossbauer obs. 77−40156
$(Fe_xNi_{100-x})_{80}P_{10}B_{10}$, amorphous, elec. resist., 2 to 300K, composition depend. 80−44562
$Fe_xNi_{80-x}P_{14}B_6$ (x=0, 20, 40, 60, 80), metallic glass, low temp. sp. ht. 80−2588
$FeNi_2S_4$, violarite, mag. and elec. props., struct. determ. 77−43633
$(Fe_{1-x}Ni_x)_{77}Si_{10}B_{13}$ amorphous alloy system, saturation mag. moment, Curie temp., mag. susceptibility 80−39753
$Fe_{1-x}O$, wustite, cryst. dynamics, mag. excitations, neutron scatt. study *(French)* 79−51740
FeOOH:Cl(F), quadrupole interaction, Mossbauer spectra 80−15895
$20Fe_2O_3.80[3B_2O_3.(1-x)PbO.xGeO_2]$ glass, phys. props. 80−49119
FeS_2 (marcasite), temp. depend. mag. susceptibility 80−20391
FeS_2, mag. susceptibility press. depend., bandstruct. calcs. 78−19212
FeS_2, natural single cryst., mag. susceptibility, 4.2-620K 77−40031
$FeSO_4$, α- and β-forms, magnetic interactions, neutron inelastic scatt. study 80−107980
$FeSO_4.n\ H_2O$ (n=1,4,5,7), Fe^{2+} ion mag. interaction with crystallisation water protons, proton NMR obs. 80−60447
$Fe_{1+x}Sb$, hyperfine interactions of ^{57}Fe, room temp. Mossbauer meas. 79−47374
$Fe_{1+x}Sb$-CoSb solid soln., mag. props., Mossbauer spectra, solubility limits, and lattice consts. *(Russian)* 77−59394
$Fe_{1+x}Sb$-NiSb solid soln., mag. props., Mossbauer spectra, solubility limits, and lattice consts. *(Russian)* 77−59394
$Fe(Sb_{1-x}Te_x)_3$ system cpds., prep., cryst. struct., elec. and mag. characteris. 80−108349
Fe_3Se_4, mag. props., 4.2-600K 78−43570
Fe_3Se_4, thermal expansion, compressibility, magnetisation, susceptibility and magnetostriction 77−66318
$FeSn(OH)_6$, mag. props. 78−43574
$Fe_{3-x}Ti_xO_4$, Mossbauer spectra in paramag. phase 80−39943
$(Fe_{1-x}V_x)_3Ge$, magnetic and X-ray studies 80−1966
$Fe_xV_{1-x}O_2$, mag. props. and Mossbauer spectra meas., exchange-coupled Fe^{3+} clusters at lower temp. 78−31136
θ-$Fe_xV_2O_5$, spin glass and paramag. props., susceptibility, EPR and Mossbauer studies 80−75782
$Fe_xV_2O_5$, spin glass transition range, cluster blocking distrib. function 80−80548
Ga, magnetic susceptibility near melting point 80−60186
$Ga_{1-x}Co_x$, cluster spin glass system, host and impurity NMR studies 79−65745
GaP:rare earth, magnetic susceptibility, impurity states 79−61044
GaP-based III-V solid solns., bonding and energy gap, mag. meas. 78−18580
GaS-YbS system, phase diagram, reacts., thermal, mag. and elec. meas. 79−11578
Gd clusters in faujasite type zeolites, mag. suscept. temp. depend. 78−14925
Gd, ferromag., magneto-optical reson., optical consts. determ. 78−6657
Gd, optical consts. polarimetric meas., mag. ordering effects 78−15184
Gd, temp. variation of absolute thermoelec. power 77−11900
Gd^{3+} Gd-ionic compounds, magnetic interaction potential 78−10682
Gd-Mn alloy, mag. props. and effect of H_2 absorpt. 78−19250
$Gd_{1-x}Ca_xAl_2$, mag. props. and phase relations 80−107991
$Gd_2Co_6Al_{11}$, NMR and mag. susceptibility 79−15367
$GdCoO_3$, spin state of Co^{3+} ion, X-ray photoemission line broadening 79−82751
$Gd_2Cu_6Al_{11}$, NMR and mag. susceptibility 79−15367
$GdFeB_4$, mag. susceptibility meas., paramag. Curie-Weiss behaviour 79−61041
$Gd(Fe_xCo_{1-x})_2$, paramag. behaviour, itineracy 78−39289
$GdFeO_3$ orthoferrite, rare earth-Fe interactions 79−56525
$Gd_xLa_{1-x}Zn$, magnetisation and paramag. suscept. 78−88101
$Gd_{1-x}M_x$, M=Ni, Fe, Co, CPA calcs., mean mag. moments 77−72997
$GdMn_2$-$GdAl_2$ intermetallics, mag. props., 80-650K 78−60282
$Gd_2Ni_{17-x}Al_x$, mag. behaviour in paramagnetic region 79−73675
Gd_2NiTiO_6, mag. study, paramag. behaviour *(French)* 79−46629
c-Gd_2O_3, electrical cond., dielectric const. mag. susceptibility, polymorphic transition 77−59505
Gd_2Se_3, mag. susceptibility 77−40032
$GdVO_4$:Ho^{3+}, optically excited doublet splitting in magnetically ordered state 78−19238
$Gd_2(WO_4)_3$, mag. susceptibility, paramag. Curie temp., 300-900K 79−82753
$(Gd_xY_{1-x})Fe_2$, high temp. mag. behaviour 77−1538
Ge-Se-Fe films, metallic and semicond., amorphous, mag. and elec. props. 78−52319
$H_{1.6}MoO_3$, electronic props., mag. susceptibility and spectra 80−80266
^3He, BCC, NMR multiple echoes, soln. of eqn. of motion of magnetisation 79−86961
^3He, BCC solid, nucl. mag. order and paramag. susceptibility 80−59757

paramagnetic properties of substances continued
^3He in Grafoil, ultralow temp. NMR mag. susceptibility, surface magnetisation and transition 78−79843
^3He, solid, melting, formal treatment of low temp. props. 79−69315
^3He solid, paramag., low-temp. diffusive transport for polarons and defectons 78−43174
^3He, solid, strongly magnetised, low-temp. melting props. 77−11765
^3He, solid BCC, four spin exchange, susceptibility behaviour below 10 mK 78−10253
$Hf(Fe_{1-x}Co_x)_2$, mag. props., Mossbauer spectra and magnetisation meas. 80−39948
$HfSe_{2-x}Te_x$ and $HfTe_{2-x}$, elec. resist. and mag. suscept. studies 80−44599
HfV_2, elec. resist. and mag. suscept., anomalous temp. depend. 79−69491
$HgCr_2S_4$, cooling efficiency near 60Kas mag. refrigerant 80−71034
$HgCr_2Se_4$, initial mag. permeab., 77 to 300K, domain wall motion and damped ferromag. reson. 79−28562
HgMnTe, semimagnetic semiconductor, band structure, transport phenomena 79−95331
$Hg_{1-x}Mn_xTe$, mag. susceptibility, 2.3-300K 77−63074
$Hg_{1-x}Mn_xTe$, mag. susceptibility, 2.4 to 300K 80−20379
HgTe, Γ_8 symm. acceptor centre hole mag. props. *(Russian)* 80−88733
Ho, elastic consts. in paramag. temp. range, magnetoelastic contrib. 77−4538
Ho, magnetoelastic coupling in paramag. region 77−80984
Ho-Au, dil., hyperfine interaction of Ho^{3+}, nuclear orientation expts. 78−43717
$HoAl_2$, magnetoelastic effects on elastic consts., 4.2-280K 78−72385
$Ho_3Au_3Sb_4$, mag. suscept. meas., 4 to 300K 79−51742
$HoCo_2$, paramag. and ordered phases, Pauli type Co susceptibility, polarised neutron diffr. obs. 77−63077
$HoCoO_3$, spin state of Co^{3+} ion, X-ray photoemission line broadening 79−82751
$HoCrO_3$, Ho^{3+} mag. form factor meas. by inelastic neutron scatt. 78−52221
$HoFeO_3$ orthoferrite, rare earth-Fe interactions 79−56525
HoIG, mag. permeability, Faraday rotation expts. 77−16287
$Ho(Ir_xRh_{1-x})_4B_4$ pseudoternary system, supercond. and mag. ordering 80−70876
$HoNi_5$, ferromag., magnetisation and paramag. susceptibility 80−25082
Ho_2Se_3, mag. susceptibility 77−40032
$HoVO_4$, RF susceptibility below 1K, mag. sp. ht. 80−84585
$Ho_xY_{1-x}Sb$, mag. props. 80−34634
In, two stage nuclear demagnetization experiments 79−65644
InR_2 (R-Y, Nd, Sm, Gd, Tb, Dy, Ho, Er, Tm), mag. props., 4.2 to 270K 79−56512
Ir ternary and quaternary oxides, prep., cryst. struct., and mag. props. 79−14771
K, Pauli susceptibility and Knight shift meas., electron wave functions 80−44937
K, spin susceptibility and volume dependence 79−95569
$KCoF_3$, mag. suscept. and Neel temp. determ. 77−77044
$KCoF_3$, single crystal, mag. susceptibility, ^{19}F NMR and static measurements 79−11301
$K_2Cr_2V_6O_{16}$, Hollandite type compound, synthesis, struct. and magnetic props. 79−11543
$K_2CuCl_4.2H_2O$, paramag. single cryst., PMR temp. depend., hyperfine const. and exchange interaction *(Korean)* 80−29630
$KCuF_3$, ^{63}Cu NQR meas. 80−50219
K_2CuF_4, spin relax., crit. behaviour, high freq. susceptibility meas. 80−65936
K_2IrCl_6, mag. susceptibility in ordered and paramag. phases 79−73759
$KM_{nx}Mg_{1-x}F_3$, randomly diluted Heisenberg paramag. nucl. relax. 80−60444
$KMgF_3$:Ni^{2+}, acoustic Faraday and Cotton-Mouton effects, theory 80−65987
$KMg_{1-x}Mn_xF_3$, disordered paramagnet, ^{19}F NMR study 80−71216
$KMnF_3$, Faraday effect mechanism in paramag. phase 80−60552
$KMnF_3$, temp. depend. of NMR linewidth of ^{19}F in paramag. region 78−60346
K_2MnF_4, low-dimensional system, obs. of sidebands on EPR lines 77−80993
K_2O-Al_2O_3-B_2O_3:Fe_2O_3, glasses, liq.-liq. phase separation, Fe^{3+} ions rel. to mag., optical props. 77−15322
La, FCC, NMR 4.2 to 296K, mag. susceptibility and sp. ht. 80−15813
La-Gd-Au alloys, amorphous, high Gd content, bulk mag. props. 77−59426
LaAg, band calcs., rel. to mag. and electronic props. and martensitic transform. 77−8014
$LaCO_{1-x}M_xO_3$, M=Mg, Ti, cryst. struct., elec. and mag. props. 79−86748
$La_xCa_{1-x}RuO_3$, metallic, mag., electronic and structural props., ^{99}Ru Mossbauer spectroscopy 77−48107
$LaCoO_3$, Mott isolator, paramag. props., calc. 80−93071
LaMg, Pauli paramagnet, mag. susceptibility, nonlinear band behaviour 80−75706
$(La_{0.5}Na_{0.5})RuO_3$, mag. props. 78−27027
La_3NbO_7, weberite-type, elec., mag. and opt. props. 77−85212
$LaNi_5$ hydrides, 4.2K paramag. susceptibility 80−70934
$LaNi_5$, magnetism and H_2 storage 80−70941
$LaNi_5$, Pauli paramagnet, adsorption of H, proton and ^{139}La NMR 79−78535
$LaNi_{1-x}Co_xO_3$, mag. props. 77−85411
$LaNi_{1-x}Fe_xO_3$, mag. props., 7 to 300K 79−4648
$LaNi_{1-x}Mn_xO_3$, ^{55}Mn NMR study, magnetisation meas., ferromag. and Pauli paramag. components 80−7191
$La_{0.71}Pb_{0.29}MnO_3$, metal-semicond. transition at Curie point, transport props. obs. 79−73554
$(La_{1-x}Pr_x)_3Tl$, comp. depend. of paramag. susceptibility, simple phenomenological model 77−16041
$LaPt_3$, ^{195}Pt NMR and susceptibility meas. 77−63299
$La_xSr_{1-x}RuO_3$, metallic, mag. electronic and structural props., ^{99}Ru Mossbauer spectroscopy 77−48107
$La_{1-x}Tb_xAg(Sn_3)(Al_2)$, paramag. anisotropy of Tb^{3+} in cubic cryst. field 80−15687
$La_{1-x}Tb_xAl_2$, competing paramag. anisotropy from cryst. field and indirect quadrupolar coupling 80−60180
Li, 3.7-294K, mass susceptibility *(German)* 78−68156
Li, Pauli susceptibility meas. by CESR transmission 79−61217
Li, spin susceptibility and volume dependence 79−95569

paramagnetic properties of substances continued
Li-MG alloy, BCC, electron exchange-induced paramag. enhancement *(Russian)* 77−51878
Li-Pd, phase diagram and mag. props. 77−90321
Li-transition metal dioxide intercalation compounds, mag. props., decomposition effects 80−25075
$Li_2Gd_4(MoO_4)_7$, ferroelec. and paramag. props. 78−39517
$Li_xMn_{1-x}Se$, anomalies obs. in mag. and elec. props. 77−69509
$(Li_2O)_{1-x}U_{1.4}W_{4.6}O_{18}$, $0 \leq x \leq 0.4$, crystallographic identification, paramag. props. *(French)* 79−46633
$LiRF_4$, (R=Tb, Dy, Ho, Er, Yb), paramag. phase props., basal plane anisotropy and cryst. field parameters 77−69486
$Li_{2.6}Ti_xO_4$, superconducting, upper critical field, paramag. limiting effects 77−8251
$LiTmF_4$, ^{169}Tm NMR spectrum, hyperfine field parameters, and cryst. field calcs. 77−12213
$LiTmF_4$, local mag. field at ^{19}F rel. to paramag. susceptibility, NMR meas. *(Russian)* 77−81023
$LiTmF_4$, spin density parameters at ^{19}F nuclei 78−68001
$LiTmF_4$, strongly isotropic Van Vleck paramag., nucl. spin interaction *(Russian)* 80−34792
$LiTmF_4$, Van Vleck paramag., mag. reson. on uniaxial and uniform compression *(Russian)* 79−61243
$LiTmF_4$ Van Vleck paramagnet, electron and nuclear spin-lattice relaxation of Er^{3+} ions 79−95643
$LiTmF_4$, van-Vleck paramagnet, giant magnetostriction *(Russian)* 80−103872
$LiY_{1-x}Er_xF_4$, phase relationships and melting, mag. characterisation 77−39665
$LiYF_4:Tm^{3+}$, cryst. field parameters, appls. 77−20277
$Li[Mn_2]O_4$ spinels, crystallographic, electronic and mag. props. *(German)* 79−60324
Lu-Mn alloy, mag. props. and effect of H_2 absorpt. 78−19250
Lu-rare earth, dil., cryst. fields 78−80127
Lu-rare field, dil. alloy, cryst. field parameter determ. 78−10650
$LuCo_2$, paramag., field induced mag. density localisation 77−72999
$LuRh_4B_4$, superconducting and normal state props. 79−73632
Mg-Eu, dil. alloy, mag. suscept. meas. 77−89925
MgEu, dil. alloy, cold worked, valence transform. of Eu due to defect association, mag. suscept. and Mossbauer meas. 77−51404
Mg_2Ni, magnetism and H_2 storage 80−70941
$MgO:Cr^{2+}$, spin-phonon coupling, inelastic neutron scatt. obs. 79−60441
$MgO:Fe^{2+}$, lifetime of coupled spin-phonon excitations 77−69053
$MgO:Mn^{2+}$, clustering of mag. ions, study method 80−11155
$MgSO_4.xH_2O$, mag. susceptibility, polaris. paramag., water of crystallisation effect 78−31047
$MgVO_3$, high-pressure modification, struct. and mag. props. 79−23727
α-Mn, NMR and susceptibility max., paramag. phase 78−56386
δ-Mn, paramag., antiferromag. and ferromag., magnetic moment calcs. 80−60223
β-Mn, spin fluctuations effect on sp. ht. 79−82788
Mn ternary carbides, Mn_3MC, M=metal, mag. props. 77−63116
Mn ternary nitrides, Mn_3MN, M=metal, mag. props. 77−63116
Mn^{2+} compounds, strongly exchange coupled, solid and liq. states, EPR and NMR, 300-1450K 77−73077
Mn-V(Cr)(Fe)(Co)(Ni), spin fluctuations effect on sp. ht. 79−82788
$MnCl_2.2H_2O$, ordered, paramag. phases, optical absorpt. spectra, V-lines, Zeeman effects 78−6698
$MnCl_2.2H_2O$, paramag. phase, external mag. field depend. of $^4T_{2g}$(II) Kramer doublets of Mn^{2+} 78−6700
α-$MnCl_2.4H_2O$, crossover from divergent to non-divergent nature of paramag. transition 79−73735
$MnCl_2.4H_2O$, single cryst., mag. phases, obs. by ^{54}Mn nucl. polarisation 77−81031
MnF_2, uniaxial antiferromag. anisotropy in paramag. susceptibility, cluster variation theory 78−52200
$MnGd_2S_4$, mag., struct. and Mossbauer effect study 78−51507
$Mn_xMg_{1-x}S$, mag. props. 77−66244
$Mn_{0.25}NbS_2$, mag. anomaly rel. to struct. disordering 78−43557
MnO, elastic props. singularities near phase transition 77−16093
MnO, multidomain single cryst. and monodomain cryst., crit. and elastic behaviour, T_N to 300K 77−66407
MnO, negative muon spin rot., paramag. shift 79−56706
MnO, paramag., μ^- spin rotation at O site 77−20785
MnO, paramag., neutron scatt., spin-wave-like excitations, obs. 78−68146
MnO, paramagnetic, positive muon longit. spin relax., temp. depend. 78−80268
MnO, positive muon spin relax. 79−56669
α-$MnSeO_4$, magnetic interactions, neutron inelastic scatt. study 80−107980
MnSi, μ^+ probe, itinerant electrons spin fluctuations 79−56671
MnSi, μ^+ spin-lattice relax rate, paramag. phase, near T_c, temp. depend. 79−19825
MnSi, weak itinerant magnetic compound, paramagnetic response function, polarised neutron scattering 80−107982
Mn_3SnN, perovskite type struct., mag. props., neutron and Mossbauer meas. 77−32159
Mo ternary chalcogenides, supercond., compared with band struct. calcs. 78−51871
Mo X-ray electron spectra, paramag. susceptibility, depend. on plastic deform. for single crystals 77−28683
Mo-dichalcogenide, valence band nature, elec. and mag. props. 78−39014
$MoCl_5$-MoF_5 system, magnetochem. and IR study of phase struct. 77−85710
MoO_2, cryst., neutron diffr., mag. props. 77−16038
$Mo_{1-x}Re_xCo$, mag. state of Co impurity, NMR exam. 78−27100
$MoRh_2O_6$, crystn. and cryst. struct., paramag. and elec. cond. props. *(French)* 77−80480
NH_4CoF_3, susceptibility and magnetisation meas. 77−85432
$(NH_4)_2IrCl_6$, mag. susceptibility in ordered and paramag. phases 79−73759
$(NH_4)_2Ni(SeO_4)_2.6H_2O:Mn^{2+}$, EPR spectra, spin quenching 78−2732
NI_3Al, structural order and homogeneity, X-ray, mag. susceptibility and Mossbauer meas. 77−63663
Na, Pauli susceptibility meas. by CESR transmission 79−61217
Na, spin susceptibility and volume dependence 79−95569
NaA neolyte, Hg cluster transition to paramagnetic state due to mag. field *(Russian)* 80−60183

paramagnetic properties of substances continued
$NaCeS_2$, mag. susceptibility, 3.7 to 297K, extended mol. field model 79−87227
$Na_2Co_2Ti_6O_{14}F_2$, characterisation and mag. props., 90-800K, $Na_xTi_4O_8$ bronze isotypes *(French)* 80−39735
$Na_2Cr_2Ti_6O_{16}$, characterisation and mag. props., 90-800K, $Na_xTi_4O_8$ bronze isotypes *(French)* 80−39735
$Na_2FeTi_6O_{16}$, characterisation and mag. props., 90-800K, $Na_xTi_4O_8$ bronze isotypes *(French)* 80−39735
$Na_3M_2^{3+}Li_3F_{12}$ garnets, M=Al,Cr,Fe, synthesis from aq. soln., props. 77−44184
$Na_2Ni_2Ti_6O_{14}F_2$, characterisation and mag. props., 90-800K, $Na_xTi_4O_8$ bronze isotypes *(French)* 80−39735
$NaUO_3$, anomaly in mag. susceptibility-temp. curves 77−32152
Nb, paramag., mag. form factors, neutron diffr. study 79−47234
Nb-Mo alloy, electronic density of states, temp. depend. of elec. resist. and mag. susceptibility 77−11891
Nb-S system, phase relations at high temp., elec. and mag. props. 80−29932
Nb-Ta (54 at.%) cylinder, superconducting mag. and resistive behaviour 77−8252
Nb_2Al, $NbAl_3$, supercond. and mag. props. 77−47922
Nb_3Al based ternary solid solns., supercond. transition temp., paramag. susceptibility and lattice parameters meas. *(Russian)* 77−43766
Nb_3Al, superconductivity, crit. temp., paramag. susceptibility comp. depend. *(Russian)* 77−66219
$Nb_xCr_{1-x}O_2$, cryst. prep. and struct., mag. props. 78−52198
NbH_x, proton Knight shift and mag-suscept., high resolution meas. 77−55716
$Nb_{50}Ni_{50-x}Fe_x$, magnetically dil. glass, 3d moments, mag. susceptibility and magnetisation meas. 79−95574
$NbSe_3$, mag. susceptibility, CDW effect 80−88716
$NdAg_x$, low temp. mag. meas. 80−107989
$Nd_{21}Ag_{79}$, amorphous, mag. props. 80−60182
$NdCl_3$, adiabatic susceptibility meas., interaction tensors for Nd^{3+} ions 77−69485
$Nd_xEu_{1-x}B_6$ solid solution, mag. susceptibility, lattice parameters, Weiss temp. 80−29535
NdF_3, mag. props. between 2 and 4.2K *(French)* 79−61039
Nd_3NbO_7, weberite-type, elec., mag. and opt. props. 77−85212
Nd_2O_3, A-type, optical absorpt. spectrum and paramag. susceptibility 79−56811
$Nd_2Ti_2O_7$, Nd_2TiO_5, paramag. props., mag. susceptibility meas. 1.6 to 70K 78−10649
$NdVO_3$-$CaVO_3$ solid solns., mag. props. rel. to cryst. struct. 78−43571
$NdVO_4$, elastic modes in applied mag. field 79−60423
$NdVO_4$, magnetoelastic interactions, finite strain and rot. effects, elastic consts. 79−87303
$Nd_2(WO_4)_3$, elec. transport and mag. props. meas. 77−24668
$Nd_2(WO_4)_3$, mag. susceptibility, paramag. Curie temp., 300-900K 79−82753
$Nd_xY_{1-x}Zn$ system, solid soln., mag. susceptibility, 77 to 600K *(Russian)* 80−65776
Ni, anomalous resistivity near Curie temp., band theoretical calc. 78−56127
Ni, atomic layers, Pauli paramagnetism to band ferromagnetism transition thickness depend. 78−72377
Ni complex, hexamethylphosphorotriamide Ni (II), paramagnetic, pulsed NMR, substitution reaction *(French)* 78−10793
Ni complex, tris(ethylenediamine)nickel(II) nitrate, mag. props. from susceptibility and sp. ht. meas., 0.3-3.0K 78−91877
Ni, density of states, photoemission expts. above and below T_c, rel. to magnetism model 77−20536
Ni, effective exchange parameter, q-depend, intra-atomic interaction 79−4542
Ni, mag. form factors in Stoner-like model 80−97061
Ni, muon spin rot. Knight shift, 637 to 906K 80−75908
Ni, paramag., generalised Wannier functions to fit MAPW band struct. 79−19509
Ni, paramag., model calc. of dynamical spin susceptibility 77−69489
Ni, paramag., μ^- relax. 77−24776
Ni, paramag. region, Fe and Co impurity effects on susceptibility, Faraday obs. *(Russian)* 80−88731
Ni, photoemission near Curie temp. 79−78841
Ni, temp. depend. of spin susceptibility 79−4651
Ni, thermal expansion, 300-1000K, and power law consts. near Curie temp. 78−38858
Ni-Al-Fe(Co), electrical and mag. anomalies due to substitutional atoms 77−15839
Ni-Co, solid and liq., paramag. susceptibility and electron struct., 800-1800°C *(Russian)* 80−25081
Ni-Cr, dil. alloy paramag., μ^- relax. 77−24776
Ni-Cr alloys, low temp. transform. mechanism, electrophys. props. obs. *(Russian)* 77−59777
Ni-Cu, Ni-rich, temp. depend. resist. 80−10943
Ni-Cu alloy, sp. ht. in mag. field, 1.2-15K 78−68262
Ni-Fe solid soln., precip. hardened, paramag.-ferromag. transition on ageing 78−52255
Ni-Pd alloys, mag. props., average and local density of states, CPA calc. 77−59242
Ni-Pt alloy, spin susceptibility, temp. variation, band model calc. 77−28365
Ni-Pt alloys, thermal expansion, mag. contribs. 77−43355
Ni-rare earth intermetallics, RNi_3, amorphous alloys, mag. and transport props. 79−42513
Ni-Rh alloys, disordered, vol. paramagnetostriction calc. 77−80985
Ni-Ti, Ni-rich, temp. depend. resist. 80−10943
Ni-V, solid and liq., mag. susceptibility and electronic struct. 80−39738
Ni-V(Nb)(Ta)(Si)(Ge), dil., mag. props. at elevated temps. 77−63089
$Ni_x Cu_{1-x}$ paramag., coherent pot. approx. for nonoverlapping muffin tin potentials 78−2451
Ni_3Al, Mossbauer experiments on homogeneity 78−48395
Ni_3Al, thermal expansion, mag. contribs. 77−43355
$NiBr_2.6H_2O$, antiferromag. ordering and paramag. behaviour 78−14941
$(Ni_{1-c}Co_c)_{0.78}P_{0.14}B_{0.08}$, amorphous, mag. props., local environment model 77−12119
NiF_2, thermal expansion and magnetostriction, 55K to room temp. 80−80586
Ni_3Ga, strongly enhanced itinerant paramag., theory of anomalies in field depend. of magnetisation 77−69488

paramagnetic properties of substances continued
$NiI_2.6H_2O$, disordered linear chain mag., ESR, mag. susceptibility and NMR meas. 77−20688
$Ni(NH_3)_6X_2$, (X^-=Cl^-, BF_4, ClO_4^-) spin dynamics at struct. phase transition 79−15309
NiO, paramag. shifts of ^{19}F at O 78−43719
$Ni(Rh_{1-x}Cr_x)_2S_4$, ferromag. spinel system with metallic conduction 79−56513
$Ni_{1-x}S$, and $Ni_{1-x}S_{1-y}O_y(Se_y)$, mag. state in metal-semicond. transition region, neutrnon diffr. obs. *(Russian)* 77−89926
$NiS_2O_3.6H_2O$, cryst. data and mag. susceptibility 77−76368
$NiS_{2-x}Se_x$, sp. ht. and elec. resist. in metallic regime 77−69589
NiS_yTe_{1-y}, mag. susceptibility, correl. with metal-insulator transition data 79−24145
NiSb, at. struct. and mag. susceptibility 77−39561
$NiSe_2$, hyperfine parameters and quadrupole splitting determ., ^{57}Fe Mossbauer spectra 77−77131
$NiSe_2$, paramag. props., NMR, mag. susceptibility 80−60175
$Ni_2(Ti,Mn)Sn$, Heusler alloy, mag. meas. 79−47261
Ni_xZr_{1-x} metallic glass, crystallisation kinetics, elec. resist. and mag. susceptibility meas. 80−103659
^{61}Ni, paramag. solid and liq. phases, nucl. spin relax. and Knight shift 78−76327
Np(IV)-tetracyclopentadienide complex, H^1-NMR studies, paramagnetic moments, temp. depend. 80−93186
$NpRu_2$, spin fluctuation cpd., sp. ht., 3-25K 77−63212
P-Se system glasses, magnetochem. investig. 77−51325
$PaSb_2$ and Pa_3Sb_4, cryst. structs., mag. susceptibility *(French)* 79−65641
Pb-Te, molten mag. susceptibility, conc. and temp. depend. 78−80121
PbSe, electron gas magnetisation, energy band parameters determ., use of Faraday effect 80−45047
PbSe, Faraday effect and electron gas magnetisation, Kane two band model calcs. *(Russian)* 80−34899
$Pb_{1-x}Sn_xTe$, Faraday effect and electron gas magnetisation, Kane two band model calcs. *(Russian)* 80−34899
$Pb_{1-x}Sn_xTe$: Mn, Mn mag. and elec. active states, mag. impurity behaviour 80−44627
PbTe:In, mag. susceptibility, temp. depend., 4.2 to 200K 80−65773
Pd, band model, mag. susceptibility of exchange-enhanced paramagnet 78−2644
Pd, electronic struct., field-induced magnetisation density and mag. form factor 77−4496
Pd, high field de Haas van Alphen spectroscopy 79−73425
Pd, mag. suscept. temp. depend. 78−60265
Pd, magnetic properties in para-process region *(Russian)* 78−2672
Pd, paramag., mag. form factors, neutron diffr. study 79−47234
Pd, sd hybridisation, paramagnetic Curie temp. and susceptibility *(Russian)* 80−103808
Pd, spin fluctuation model interpretation of mag. susceptibility 80−80477
Pd-Co, dil., Mossbauer emission spectra, fast relaxation regime, ^{57}Co hyperfine field 78−60362
Pd-Co, dilute, extraordinary Hall effect meas., 2-250K 80−34420
Pd-Fe, del. alloy, Mossbauer obs., 0.018-300K 77−69740
Pd-Fe(Mn), dil., depend. of neutron small-angle scatt. intensities on appl. mag. field and temp. 79−11291
Pd-Ni, local susceptibilities, ^{61}Ni Mossbauer spectroscopy 78−95536
Pd-Ni alloy, paramag. giant moments 78−56291
Pd-Pt alloys, mag. props., average and local density of states, CPA calc. 77−59242
Pd-Rh alloys, disordered, vol. paramagnetostriction calc. 77−80985
Pd-Rh-Ag, magnetic susceptibility press. depend., d-band deform. and exchange var. 77−47967
Pd-Si(−Cu), glassy, liq. and cryst., mag. and elec. props. 77−66249
$(Pd_{0.67}Fe_{0.33})_{1-x}Au_x$, ordering effects on mag. props. *(Russian)* 78−47942
$PdH_xFe_{0.003}$, Kondo system, local moments, hyperfine fields, Mossbauer study 80−80478
$(Pd_{1-y}M_y)_{100-x}Fe_x$, M=Ag, Rh, exchange-enhanced alloys, mag. ordering 79−61050
$Pd_2MnIn_{1-x}Sb_x(Sn_x)$, Heusler alloy, Mossbauer effect exam., mag. coupling 79−69755
$(Pd_{99}Ni)_{1-x}Pt_x$, spin-fluctuation thermopower 79−60802
$Pd_{95}Rh_5$, low-temp. spin-fluctuation resist., effect of pot. scatt., effect of Ni addition 77−15840
$Pd_{80}Si_{20}$, amorphous, elec. resist. and magnetoresist. 80−49693
Pr $(NO_3)_3.6H_20$, Van Vleck paramag., Orbach processes and nucl. relax. 77−8439
Pr, central peaks and soft modes, quasi-elastic mag. scatt. obs. 77−66377
Pr compounds, Van Vleck paramagnets, mag. props., anisotropy from NMR anal. 80−54862
Pr intermetallic compounds, singlet ground state magnetism, hyperfine enhnaced nuclear cooling *(Japanese)* 79−51744
Pr, mag. excitation line shape, calc. compared with expt. 77−69482
Pr-Nd (5 at.%), paramag. excitation spectrum, CPA calc. 80−50043
Pr-rare earth dilute alloy, low field magnetic props. 78−84443
$PrAg_x$, low temp. mag. meas. 80−107989
$Pr_{21}Ag_{79}$, $Pr_{50}Ag_{50}$, and $Pr_{10}Lu_{40}Ag_{50}$, amorphous, mag. props. 80−60182
$PrAl_{2-x}Ag_x$, cryst. field and exchange interactions 77−63076
$PrAlO_3$, tetragonal, mag. props. 77−90052
PrAs(Bi)(P)(Sb):Gd, EPR relax. of impurity in Van Vleck paramag., host ion fluctuation spectra 77−48049
$PrAu_{3.6}$, ordering temps. and effective moments 78−60283
$PrBe_{13}$, hyperfine enhanced nuclear mag. cooling 79−63216
$PrBe_{13}$, nuclear demagnetisation, prod. of μK temps. 77−17987
$Pr_{1-x}Ca_xAl_2$, mag. props. and phase relations 80−107991
$PrCo_2$, strongly exchange-enhanced paramagnetism, susceptibility 80−60179
$PrCu_4$ and $PrCu_5$, Knight shift, mag. susceptibilities 79−95570
PrF_3, Pr^{3+} mag. form factor meas. by inelastic neutron scatt. 78−52221
PrF_3, van Vleck paramagnetic, nuclear acoustic resonance of ^{141}Pr using US *(Russian)* 79−78539
$PrIn_3$, two stage nuclear demagnetization experiments 79−65644
$PrIn_3$:Gd, EPR relax. of impurity in Van Vleck paramag., host ion fluctuation spectra 77−48049
$PrIn_3$:Gd, indirect nuclear exchange interactions, ESR-linewidth meas., sp. ht. determ. 80−103825

paramagnetic properties of substances continued
PrN, compressibility, mag. susceptibility and NMR freq. shift meas. 77−85595
$PrNi_5$, crystal-field effects, comparison of calcs. with expts. 79−87071
$PrNi_5$, LF dynamics and ^{141}Pr thermal relax., coupling parameter and RKKY exchange mechanism 80−103812
$PrNi_5$, metallic Van Vleck paramag., nucl. interactions, NMR meas. 80−44953
$PrNi_5$, nucl. demagnetization, end temps., nucl. entropy 79−19718
$PrNi_5$, two stage nuclear demagnetization experiments 79−65644
PrP(Sb)(Bi), singlet ground state paramag. system, microwave resist. meas. 77−20353
$PrPt_3$, ^{195}Pt NMR and susceptibility meas. 77−63299
$Pr(ReO_4)_3.4H_2O$, Van Vleck paramag., Orbach processes and nucl. relax. 77−8439
PrS, hydrostatic press. depend. of mag. suscept. 78−80122
$Pr_2(SO_4)_3.8H_20$, Van Vleck paramag., Orbach processes and nucl. relax. 77−8439
PrSb, compressibility and NMR freq. shift 77−85595
Pr_3Te_4, rotational invariance and magnetoelastic phenomena 77−48027
$Pr_2(WO_4)_3$, mag. susceptibility, paramag. Curie temp., 300-900K 79−82753
pt, band model, mag. susceptibility of exchange-enhanced paramagnet 78−2644
Pt, generalised susceptibilities and phonon anomalies, band struct. calcs. 79−90953
Pt, high field de Haas van Alphen spectroscopy 79−73425
Pt, induced magnetic form factor, 73 kOe at 78K 79−33454
Pt, spin fluctuation model interpretation of mag. susceptibility 80−80477
Pt, spin-density functional theory of temp. depend. spin susceptibility 79−56497
Pt-Fe alloys, supported, mag. prop. meas. in H_2 and O_2, 77 to 700K 79−91257
Pt-Ni alloys, disordered, vol. paramagnetostriction calc. 77−80985
$PuTe_3$, magnetis. meas., $NpSe_3$, Np_3Se_5 and $NpTe_3$, magnetis. meas. 77−20542
$ROsB_4$, R=Y, Gd, Tb, Dy, Ho, Er, Tm, struct. and mag. props. 78−79584
$RRuB_4$, R=Y, Cd, Tb, Dy, Ho, Er, Tm, struct. and mag. props. 78−79584
$RbCrI_3$, radiocrystallographic and mag. study *(French)* 79−46632
$Rb_2CuBr_4.2H_2O$, dynamic props. in paramag. state, spin-lattice relax. time meas. 80−71214
$Rb_2CuCl_4.2H_2O$, and isomorphs fine struct. on NMR lines due to indirect nuclear spin-spin coupling 79−61244
$RbCuF_3$, ^{63}Cu NQR meas. 80−50219
$RbMnCl_3$, high-pressure cubic phase, mag. props. 79−47260
α-$RbMnCl_3.2H_2O$, pseudo-one-dimensional mag. system, low-temp. sp. ht. 77−85471
$RbMnF_3$, Faraday effect mechanism in paramag. phase 80−60552
$RbMnF_3$, Heisenberg antiferromagnet, paramag. region, NMR, spin pair correl. 78−15032
$RbMnF_3$, two-spin Raman scatt. at high temp. 77−40225
Ru ternary and quaternary oxides, prep., cryst. struct. and mag. props. 79−14771
$(SN)_x$, temp.-depend. of elec. resist. and mag. susceptibility, density of states determ. 77−51877
Sc, paramag., mag. form factors, neutron diffr. study 79−47234
Sc, spin susceptibility, exchange correlation enhancement 77−85167
Sc, susceptibility, temp. depend., theoretical explanation 78−47944
Sc-Dy(Er)(Tb), dil. alloy, high field magnetisation 78−56292
Sc-rare earth, dil. alloy, cryst. field parameter determ. 78−10650
Sc_3In, itinerant electron ferromag., NMR and relax. 78−6586
ScSi, paramag. susceptibility 80−50035
Si, electron-hole drops, nonequilib. paramagnetism 80−6749
Si, liq., mag. susceptibility and diamag.-paramag. transition at melting pt. 78−95415
Si, muon depolarisation, diamag. and paramag. states obs. *(Russian)* 79−87370
Si:B, heavily doped, paramagnetic props., anomalous hole spin susceptibility *(Russian)* 80−54861
Si:Cr^+ EPR spectra and spin state population inversion with unpolarised optical lighting *(Russian)* 80−44909
Sm, mag. and struct. transitions, X-ray K-line shift, 77-1000K *(Russian)* 77−4518
Sm-Eu alloy, dil., mag. and elec. hyperfine interac., TDPAD obs., paramag. behaviour, exchange integral 80−103908
SmAs, low temp. props. 79−28528
$SmAu_6$, mag. props. temp. depend. *(French)* 77−51879
SmBi, low temp. props. 79−28528
$SmCl_2$, mag. props., 77-292K 78−52197
$Sm_{1-x}Gd_xS$ (x=0.15 to 0.18), magnetic susceptibility meas., phase transition 77−63071
$Sm_6Mn_{23-x}Fe_x$, magnetic behaviour, temp. and comp. depend. 80−93090
SmP, low temp. props. 79−28528
SmS, mag. susceptibility in semicond. phase, in homogeneity region 79−28502
Sm_3S_4, mag. susceptibility meas., valence state of Sm 80−15684
Sm_3S_4, magnetic susceptibility and valence fluctuations 77−8266
SmSb, low temp. props. 79−28528
$SmTi_{1.5}W_{0.5}O_6$, Stark sublevels in mag. suscept. and luminesc. 77−51876
$Sm_2(WO_4)_3$, mag. susceptibility, paramag. Curie temp., 300-900K 79−82753
Sn, single crystal cylinder, threshold current of paramagnetic effect *(Russian)* 79−87194
Sn, superconductor, paramagnetic effect fine struct. apparent mag. permeability *(Russian)* 79−95550
Sn_3As_2, and Sn_4As_3, mag. susceptibility components 78−43551
$Sr_2Fe_xRu_{1-x}O_4$ solid soln., Mossbauer spectrosc. study 80−50235
$SrLaCoO_4$, struct. and mag. props., electronic struct. of trivalent Co *(French)* 79−86760
Sr_2MNBO_6, (M=Ti, Zr, Nb), perovskite struct., synthesis, lattice constants and elec. props. 77−21369
$SrO.R_{1-x}Sr_xVO_{3-0.1x}$, R=Nd, Eu, Gd, solid solns., elec. and mag. props. 77−89819
$SrRFeO_4$, (R=La,Pr,Nd), Mossbauer spectra, spin reorientation 80−15880
$Sr_2(SbCo)O_6$, spin state of Co^{3+} ion, X-ray photoemission line broadening 79−82751

paramagnetic properties of substances continued
ΓMMC, low-dimensional system, obs. of sidebands on EPR lines 77−80993
Ta-W alloy, electronic density of states, temp. depend. of elec. resist. and mag. susceptibility 77−11891
TaH_x, proton Knight shift and mag. suscept., high resolution meas. 77−55716
Tb, elastic consts. in paramag. temp. range, magnetoelastic contrib. 77−4538
Tb, small particles, disappearance of mag. order., mag. susceptibility and magnetisation meas. 77−16117
Tb-Ho alloy, anomalous thermal expansion, up to 273K 79−7967
Tb-Y-Zn, magnetic props. conc. and temp. depend. *(Russian)* 77−47989
$TbAg_{1-x}Zn_x$ solid solns., mag. props. *(Russian)* 77−77049
$TbAu_6$, mag. props. temp. depend. *(French)* 77−51879
$Tb_3Au_3Sb_4$, mag. suscept. meas., 4 to 300K 79−51742
$TbCrO_4$, mag. susceptibility and magnetis. meas., 1.7-1000K, Curie pt. positron 77−66266
$TbFeO_3$, mag. phase transitions, Van Vleck interaction and R-Fe exchange *(Russian)* 79−61105
$TbNi_5$, ferromag., magnetisation and paramag. susceptibility 80−25082
TbP, mag. excitations above antiferromag. ordering temp., inelastic neutron scatt. obs. 80−50112
TbP, neutron scatt. study above paramagnetic-antiferromagnetic transition temp. 80−11159
$TbPO_4$, zircon struct., cryst. field analysis 80−80232
$Tb_cY_{1-c}Sb$, elec. resist., cryst. field and exchange interaction contribs. 80−39556
Tc, paramagnetic form factor, polarised neutron diffr. study 80−39745
Te, liq., mag. susceptibility, temp. depend. 78−47943
Te, liquid, localized impurity states, paramag. susceptibilities 78−64185
Th-Dy, dil., type I superconductor, paramag. Dy moment relax., Mossbauer spectra study 80−65755
Th-Mn alloy, mag. props. and effect of H_2 absorpt. 78−19250
Th_7Co_3, effect of absorbed H_2 on mag. behaviour 80−60184
$Th_{1-x}Fe_x$ amorphous alloys, mag. props. and Mossbauer spectra 79−91326
Th_7Fe_3, Mossbauer spectra, mag. props. 80−15852
Th_7Ni_3, effect of absorbed H_2 on mag. behaviour 80−60184
Ti, paramag., mag. form factors, neutron diffr. study 79−47234
Ti-Cu alloys, mag. susceptibility meas., paramagnetic susceptibility meas. Curie temp. and mag. moments calc. *(Russian)* 78−34956
Ti-Nb-Zr-Fe, supercond. and paramag. props., effect of Fe additions *(Russian)* 80−65730
TiC, mag. suscept. rel. to temp. in homogeneity region 78−34953
$TiCl_3$, layer compound, theoretical study of phase transition, paramag. susceptibility calc. 79−10945
$Ti_{0.5}NbSe_2$, cryst. struct., metallic cond., mag. and phys. props. *(French)* 80−33956
Ti_5O_9, phase transitions, elec. cond., mag. susceptibility, sp. ht., EPR and struct. aspects 78−10526
$(Ti_{1-x}V_x)_2O_3$, $O<x<0.1$, magnetisation and mag. moments 80−65772
$(Ti_{1-x}V_x)_2O_3$, single crystal, anisotropic susceptibility 79−87228
Tl-Te, liq. alloys, mag. susceptibility rel. to elec. cond. and density of states 77−51880
$TlCoCl_3$, paramag., spin density, NMR study 78−88200
$TlCoF_3$ paramagnetic, nonmagnetic atomic nuclei spin density, NMR study 80−29633
$Tl_2Cr_2O_7$, $Tl_2Mn_2O_7$, pyrochlore type, synthesis and physical props. 80−33963
$TlMnCl_3$, paramag., spin density, NMR study 78−88200
$TlNiCl_3$, paramag., spin density, NMR study 78−88200
Tl_xSe_{1-x}, liquid semiconductor, diamagnetism and paramagnetism, dangling bond paramag. centres, mag. susceptibility obs. 80−44797
$Tl_xV_6S_8$, prep., struct., props. 77−19935
Tm, magnetisation, uniaxial anisotropy, mean field model 78−2660
Tm pnictides, van Vleck paramag., relax., host exchange parameters 78−2735
Tm-Zn, paramagnetism, mag. excitations, exchanges interactions 80−88718
$Tm_3Au_3Sb_3$, mag. suscept. meas., 4 to 300K 79−51742
TmCd, parastriction, magnetoelastic and quadrupolar exchange coeffs. 79−19758
TmCd quadrupolar ordering and magnetic interactions 79−73676
$TmCo_2$, paramag. and ordered phases, Pauli type, Co susceptibility, polarised neutron diffr. obs. 77−63077
TmN(P)(As)(Sb), singlet ground state paramag. system, microwave resist. meas. 77−20353
Tm_2O_3, susceptibility, 4.2-270K 77−12081
TmSb, rotational invariance and magnetoelastic phenomena 77−48027
TmSe, intermediate valence cpd., susceptibility, single-ion approach 80−70935
TmSe, mixed valence cpd., thermal, mag., and transport props. 79−61074
TmSe, paramag. intermediate valence cpd., single ion approach to susceptibility 79−61042
Tm_2Se_3, mag. susceptibility meas. 4.2 to 300K cryst. field approx. 77−66246
Tm_3Se_4, mag. susceptibility 77−40032
TmZn, parastriction, magnetoelastic and quadrupolar exchange coeffs. 79−19758
$TmZn_2$, Mossbauer effect meas. in antiferromag. and paramag. states 80−71265
U complex, cyclopentadienyl-U-halides, paramag., U IV ligand interaction, mag. susceptibilities, 1-300K *(German)* 79−15279
U complex, $U(acac)_4$, cryst. fields, mag. susceptibility, chem. shift *(French)* 78−84179
U monopnictides, mag. props. 78−43554
U-Ga system cpds., elec. resist., paramag. susceptibility magnetis., temp. depend., mag. struct. 77−20559
U-Pt, paramag. suscept. 79−61047
U_3As_4, mag. struct., mag. refls. in paramag. state 77−20559
UCo_2, mag. props., ferromag. transition *(Russian)* 78−68148
$U(Co_xNi_{1-x})_2$, cryst. struct. and mag. props. at 4.2K 80−54175
$UF_4(Cl_4)(Br_4)(I_4)$, paramag., U IV ligand interaction, mag. susceptibilities, 1-300K *(German)* 79−15279
UGa_2, cryst. struct., mag. and magnetoelastic props. *(Russian)* 79−38364
UGe_3, magnetisation density, neutron scatt. meas. 80−50038
UH_3, magnetic props., book contrib. 79−82754
paramagnetic properties of substances continued
UMn_2, mag. props., ferromag. transition *(Russian)* 78−68148
UMn_2-UCo_2, mag. props., ferromag. transition *(Russian)* 78−68148
UMn_2-UFe_2, mag. props., ferromag. transition *(Russian)* 78−68148
UN, single crystal, mag. props. 77−77042
$U(OH)_2SO_4$, antiprismatic crystal field, paramag. susceptibility, 4.2 to 300K 79−1655
$U(OH)_2SO_4$, mag. susceptibility, heat capacity anomalies at 21K 80−11151
$U_6O_4(OH)_4(SO_4)_6$, antiprismatic crystal field, paramag. susceptibility, 4.2 to 300K 79−1655
UOX_2 (X=Cl, Br, I) crystal struct., IR spectra, and mag. meas. *(French)* 79−60331
U_3P_4, Knight shift, paramag. susceptibility 77−66430
UPd_3, crystalline elec. field studies using neutron inelastic scatt. at NRCN 80−10931
UPd_3, U^{4+} mag. form factor meas. by inelastic neutron scatt. 78−52221
URh_3, magnetisation density 78−52203
$U(SO)_2.4H_2O$, antiprismatic crystal field, paramag. susceptibility, 4.2 to 300K 79−1655
U_3Si, crystalline elec. field studies using neutron inelastic scatt. at NRCN 80−10931
$USiO_4$, cryst. field parameters, paramag. susceptibility, 2-500K 77−55658
USn_3, crystalline elec. field studies using neutron inelastic scatt. at NRCN 80−10931
$(U_xTh_{1-x})S$, metallic, 5f virtual bound states, elec. resist. and mag. susceptibility meas. 77−28363
$(U_xTh_{1-x})Se$, metallic, 5f virtual bound states, elec. resist. and mag. susceptibility meas. 77−28363
U_3X_4, (X=P, As, Sb, Bi), molecular field approx. study of mag. ordering, Curie temp., paramagnetic susceptibility 79−78410
V, dynamic susceptibility, model pot. theory 80−75710
V, energy bands, calcs. using LCGO method 78−91608
V fine particles, appearance of mag. moment 78−68152
V hyperfine particles, appearance of mag. moments, mag. susceptibility meas. 77−36097
V hyperfine particles, surface magnetisation, explanation of expt. work 78−23303
V, magnetic moment near surface, one-electron band model 79−82747
V, orbital magnetic susceptibility calc. 80−7075
V, paramag., mag. form factors, neutron diffr. study 79−47234
V, small particles, crystal structure, magnetic and superconducting props. 80−97121
V-Cr alloy, electronic density of states, temp. depend. of elec. resist. and mag. susceptibility 77−11891
V-Mn-Cr, disordered BCC state, mag. phase diagram, mag. and elec. props. 77−63185
V-Pt, sp. ht. and mag. meas. in ordered and disordered phases 80−70422
V-Zr-Nb alloy, rel. between density of states and martensitic and superconducting phase transition temps. 78−10594
$(V_{1-x}Cr_x)_3Si$, mag. susceptibility, 4.2 to 320K, density of states model 80−7035
VF_2, nearly one-dimensional, paramag. susceptibility 79−15278
$V_{1-x}Fe_x$, low temp. sp. ht. and mag. props. 80−2548
$V_{1-x}Fe_xH_n$, low temp. sp. ht. and mag. props. 80−2548
$V_{1-x}Fe_xO_{2-x}F_x$, mag. susceptibility *(German)* 79−78305
$V_{1-x}Ga_xO_2$, M1→T phase transition, X-ray and mag. meas. 77−11692
VH_x, proton Knight shift and mag-suscept., high resolution meas. 77−55716
V_xMo_{1-x} solid soln., mag. susceptibility 79−91208
$V_{0.5}NbSe_2$, cryst. struct., metallic cond., mag. and phys. props. *(French)* 80−33956
VO_2, metallic, magnetisation distribution and band structure 78−76223
VO_2:Ga(Al)(Fe), phase transforms., influence of nonstoichiometry 77−85274
V_2O_3, high-temp. transition domain, small angle diffuse neutron-scatt., 400-600K 77−69231
V_2O_5-V_2O_4-$BaZnO_2$ glass, V ion states, mag. and elec. props. 80−88556
V_3O_5, high-temp. phase transition, resistivity, valence photoelectron spectra 80−49357
V_3O_5, mag. anisotropy 77−85441
V_3O_7, microscopic mag. props., NMR 80−7177
$V_{1-x}Re_xO_2$ ($0\leq x\leq 0.15$), insulator-metal transition, DTA, X-ray, mag. and elec. meas. 78−10353
V_3S_4, and V_5S_8, itinerant antiferromag. spin fluctuations, NMR studies 80−93198
V_5S_8, paramag. cryst., struct. factors using polarised neutron diffr. 80−15691
VSe_2, metallic behaviour obs., anomalous elec. and mag. props., temp. effects 77−15819
$VSe_{2-x}S_x$ ($0<x<2$) solid solutions, characterisation 80−88730
V_3Si based ternary solid soln., supercond. T_c and paramag. susceptibility *(Russian)* 77−59348
V_3Si, electronic props. calc. 79−7780
V_3Si, exam. of superconductivity and props. 79−1649
V_3Si, magnetic susceptibility, density of states model for lattice transformation in A-15 compounds 80−65219
V_3Si, temp. depend. of mag. susceptibility *(Russian)* 77−36053
$V_3Si_xOs_{1-x}$, supercond. transition temp. and paramag. susceptibility 79−28436
VTe, mag. and elec. transport props. 80−92897
Y, paramag., mag. form factors, neutron diffr. study 79−47234
Y-Mn alloy, mag. props. and effect of H_2 absorpt. 78−19250
Y-Mn(-Co) alloys, amorphous, paramag. props. and Hall effect 79−73692
Y-Ni amorphous alloy, spontaneous magnetisation, Curie temp. and paramag. susceptibility 78−68189
Y-rare earth, dil., cryst. fields 78−80127
Y-rare earth, dil. alloy, cryst. field parameter determ. 78−10650
YAG:Er^{3+}, crystal field theory calcs. 77−8259
$Y_{1-x}Co_x$, CPA calcs., mean mag. moments 77−72997
$YCoO_3$, spin state of Co^{3+} ion, X-ray photoemission line broadening 79−82751
$Y_2Cr_2O_7$, $Y_2Mn_2O_7$, pyrochlore type, synthesis and physical props. 80−33963
$Y_xEr_{1-x}Al_2$, paramag. anisotropy 80−39737
$Y(Fe_cAl_{1-c})_2$, mag. props. 79−38308
$Y(Fe_xCO_{1-x})_2$ model, Co, mean mag. moment composition depend.; reciprocal susceptibility, thermal var. 78−47945

paramagnetic properties of substances continued
$YFe_2(Co_2)(Ni_2)$, density of states, mag. props. 79−90936
$Y_6(Fe_{1-x}Mn_x)_{23}$, struct. and mag. props. 80−25083
YFe_2O_4, Mossbauer spectra of ^{57}Fe in antiferromag. and paramag. states 80−15834
$(Y_{1-x}Gd_x)Co_2$, spin echo NMR of mag. states 80−7190
YIG: Si single crysts., mag. props. 80−107981
YMg, Pauli paramagnet, mag. susceptibility, nonlinear band behaviour 80−75706
YMn_2, lattice consts. and mag. props. before and after H_2 absorption 77−36061
YNi_3, loss of ferromagnetism after H_2 absorpt., Pauli paramag. props. 80−34588
Y_5Pd_2, mag. props. 77−20547
$YVO_4:Nd^{3+}$, zircon struct., cryst. field analysis 80−80232
$YVO_4:Tm^{3+}$, cryst. field parameters, appls. 77−20277
Yb intermetallic compounds, mag. susceptibility, 1.4 to 1060K, investig. of Yb valency 77−20543
$YbAl_2$ and $YbAl_3$, intermediate valency cpds., paramag. susceptibility, 1.4 to 1060K 77−63079
YbB_{12}, mag. props., cryst. struct., valence of Yb *(Russian)* 78−60263
YbB_4, mag. props. *(French)* 77−20566
YbCuAl, intermediate valency cpds., paramag. susceptibility, 1.4 to 1060K 77−63079
YbCuAl, mixed valence behaviour, mag. props. 78−68150
$YbCu_2Si_2$, local mag. moments, neutron scatt. study 79−61058
$YbGa_2$, intermediate valency cpd., paramag. susceptibility, 1.4 to 1060K 77−63079
YbIG, mag. permeability, Faraday rotation expts. 77−16287
$YbInAu_2$, intermediate valence cpd., mag. susceptibility expts., 4.2-280K 78−39288
$YbNi_2Ge_2$, intermediate valence cpd., mag. susceptibility expts., 4.2-280K 78−39288
$YbOsB_4$, mag. susceptibility meas., paramag. Curie-Weiss behaviour 79−61041
$YbRuB_4$, mag. susceptibility meas., paramag. Curie-Weiss behaviour 79−61041
$YbS_{1.387}$, magnetic and thermal props. 80−34586
Yb_xSy, synthesis and mag. props. 78−23242
$ZnCr_2Se_4$:Mn, paramagnetic, giant cubic anisotropy 80−7073
$ZnIn_2S_4:Er^{3+}$, cryst. field parameters, thermal and mag. props. calc. 77−20540
ZnTi ferrites, electron exchange between Fe^{2+} and Fe^{3+}, paramag., Mossbauer spectra and susceptibility meas. 77−63327
Zr, magnetic form factor, field-induced, polarised neutron scatt. meas. 80−50044
Zr-Co-Ga alloy, mag. susceptibility in phases of structural type Th_6Mn_{23} *(Russian)* 79−24130
Zr-Cu-Ga alloy, mag. susceptibility in phases of structural type Th_6Mn_{23} *(Russian)* 79−24130
Zr-Ni-Ga alloy, mag. susceptibility in phases of structural type Th_6Mn_{23} *(Russian)* 79−24130
ZrC-NbN, mag. susceptibility, zone struct., conc. and temp. depends. 77−8788
$Zr_{40}Cu_{50}Fe_{10}$, magnetically dil. glass, 3d moments, mag. susceptibility and magnetisation meas. 79−95574
$Zr_{40}Cu_{60-x}Fe_x$, electronic and mag. props. 77−8271
$Zr_{40}Cu_{60-x}Gd_x$, magnetically dil. glass, 4f moments, mag. susceptibility and magnetisation meas. 79−95575
$Zr_{40}Cu_{50}Mn_{10}$, magnetically dil. glass, 3d moments, mag. susceptibility and magnetisation meas. 79−95574
$Zr_{40}Cu_{60-x}Tb_x$, magnetically dil. glass, 4f moments, mag. susceptibility and magnetisation meas. 79−95575
ZrN-NbC solid solns., mag. susceptibility and elec. resist. in 300-1300K range 77−24670
$Zr_{0.5}Nb_{0.5}C_xN_{1-x}$, mag. susceptibility, zone struct., conc. and temp. depends. 77−8788
$Zr_{1-x}Nb_xZn_2$, microscopic mag. props., NMR investigation 80−15807
$ZrSiO_4$:Er(Yb), anisotropic mag. susceptibility meas. 77−43806
ZrV_2, elec. resist. and mag. suscept., anomalous temp. depend. 79−69491
ZrV_2, Knight shift vs. susceptibility plot 80−75712
$ZrZn_2$, itinerant electron ferromag., nucl. spin-lattice relax. time meas. 77−63308

paramagnetic resonance
see also acoustic paramagnetic resonance; CESR; CIDEP; electron spin-lattice relaxation; ENDOR; EPR line breadth; paramagnetic resonance of colour centres; paramagnetic resonance of free radicals; paramagnetic resonance of ions and impurities; spin echo (EPR); spin-spin relaxation
acridine dyes in methanol-water glasses, EPR spectra of triplet state 79−18212
adamantine ceramic, structural, thermophysical and electrophysical props. 80−6918
alcohols, long chain conformations, ^{13}C pseudocontact shifts 79−13743
alkali metal, HMPA frozen soln., Wannier-Mott impurity ground state, EPR 77−8054
alkali metal vapour O-O transition resonance line obs. *(Russian)* 78−57999
alkali oxide-Al_2O_3-SiO_2 glass, EPR 78−91930
alkaline ice, trapped electrons, photostimulated decay, time-depend. rate const. 79−52692
n-alkyl amines, long chain conformations, ^{13}C pseudocontact shifts 79−13743
alternating magnetic field meas. using EPR 80−52277
amino acids and their complexes, corrected G-values 79−20516
amorphous and liquid semiconductors, conference, Cambridge, MA, USA (Aug. 1979) 80−41933
amorphous insulators, defects, EPR characterisation 79−38379
amorphous semiconductors, DC and AC cond., high field effects, magnetoresist., EPR, carrier transport, review *(Japanese)* 77−35943
amorphous semiconductor, localised gap states, variable range hopping, susceptibility and EPR 77−72866
amorphous semiconductors, optically induced metastable paramag. state, optical absorpt. and ESR meas. 77−40113
analytical accuracy improvement 79−52827
analytical chemistry appls., conf., Denver, CO, USA (Aug. 1979) 80−90598
animal tissues in vitro, 13 to 43K, Fe-S proteins in mitochondria 77−16919

paramagnetic resonance continued
anisotropic fluid, diffusion, EPR spin exchange and nuclear spin relax., theory 80−34753
anisotropic rotational diffusion studied by passage saturation transfer EPR 80−60403
anthracene: tetracene cryst., triplet-state EPR for isolated mol. orientation 78−26583
anthracene-d_{10}-s-tetracyanobenzene, rotational mode coupling in phase transition 78−71827
anthracene-phenanthrene-tetracyanobenzene, CT-cryst., mini-excitons and lattice dynamics, ESR, optical and Raman spectra 80−60406
anthracene-TCNB charge transfer crystal, orientational phase transition, EPR, Raman spectroscopy exam. 78−26817
anthracene-tetracyanobenzene, charge transfer complex, phase transitions, deuteration effect, mag. reson., spectral and thermal meas. 79−4412
anthracene-tetracyanobenzene charge-transfer complex, EPR of triplet excitons, phase transitions 77−28425
anthracene-tetracyanobenzene cryst., triplet excitons, zero-field EPR splitting temp. depend. 78−10748
anthracene-tetracyanobenzene crysts., deuteration effect on phase transition, triplet state EPR study 80−50163
antiferromagnet, short range order effects on EPR frequencies 77−69669
L(+)arabinose, irradiated single crystals, electron trapping, ESR obs. 78−88646
arabinose, X-irradiated single crystal, intermol. electron trapping, hyperfine ESR pattern 79−39166
aromatic molecular crystals, optical nuclear polarization, appl. to EPR and ODMR 79−19804
aromatic molecules, phosphoresc. triplet spins phase coherence, ESR 79−31559
atomic reactions with solid surfaces, via ultrahigh vacuum/flow system 78−7232
azaphenanthrenes, lowest triplet state zero field splitting parameters calcs. 80−83391
bacteria, photosynthetic, triplet-state EPR spin polaris., intramol. model 78−44469
benzenes, lowest triplet states, instability rel. to environmental effects 77−57893
biacetyl, triplet kinetics, EPR fine struct., ODMR 77−71824
biomembrane drug tolerance, spin label study of ethanol effects 77−66799
biomolecules, Fe-containing, appl. of spectroscopy 79−24956
bis(p-toluene sulphonate) diacetylene polymer, EPR, thermal history and temp. effects 78−52352
bis(p-toluene sulphonate) diacetylene polymer, spin conc., g-values of single cryst. from EPR study 78−48037
blue proteins, activation of electron transfer reactions 78−44446
book, principles of magnetic reson. 78−80189
bounded medium, nonlinear parametric reson., limit cycle solns. 80−19071
bovine bone, degraded, ESR study 79−39432
cancer, appls. of EPR and NMR, review 78−69173
carbene in polydiacetylene, zero field splitting parameter 78−27075
carbohydrate compounds, X-irrad., trapped electrons, ESR and ENDOR obs. 80−93161
cavity loading effect on analytical ESR spectroscopy 78−7253
cavity matching device for use at low temps. 78−54420
chalcogenide glass, mech. for electron-hole recomb., induced ESR 78−72196
chalcogenide glasses, optical versus transport processes. 80−84449
charge transfer complexes, doped, excited cryst., fine and hyperfine struct., ESR 77−12188
Chichibabin's hydrocarbon, ESR spectra, electron exchange integral 78−50562
chlorophyll, photosynthesis mechanism, upconversion, EPR and O_2 evolution data anal. 78−35811
chlorophyll photochemical activity, rel. to microviscosity of detergent micelles 77−21478
chlorophylls, triplet state ESR, fine struct. and rate consts. determ. 78−25574
chlorophylls, triplet state ESR, fine structs. and rate consts. determ. 78−25575
chlorophylls, zero field triplet spin sublevel ordering, magnetophotoselection obs. 77−42342
chloroplast EPR signal props., effect of ferricyanide, dark adaption, ageing 79−57607
chloroplast fragments, paramagnetic centres and photochemical reactions 79−53061
chloroplasts, spin glass type structs., mag. anisotropy obs. 79−79490
chloroplasts and subchloroplast particles, optical absorpt. at 700 nm and EPR spectra 77−25394
cholestanyl benzoate, liq. cryst., orientational order, EPR study 78−75540
cholesteryl benzoate liq. cryst., orientational order, EPR study 78−75540
chromophores, model for simulation of EPR spectra, in partially oriented membrane multilayers 78−86894
coaxial microwave cavity for improved EPR sensitivity with loss solvents 80−62705
coke, preparation for ESR exam. 77−90517
computation of EPR and ST-EPR spectra, perturbation approx. extension for overmodulation 78−82754
computer analysis, absorption curve, spin concentration, numerical double integration, computer subtraction *(German)* 77−37954
condensed matter, Summer School, Pula, Yugoslavia (Sept., 1976) 78−76293
copper acetate monohydrate, ESR in resonant cavity, meas. of Cotton-Mouton-Voigt effect *(French)* 78−89514
coronene, in n-heptane, Shpol'skii effect multiplets, struct. obs. by ESR and X-ray diffr. 77−62513
Cotton-Mouton-Voigt effect in reson. cavity *(French)* 79−47324
cryostat for low temperature X-irradiation and electron paramagnetic resonance 80−86321
crystal field theory, finite symmetry adaptation in spectroscopy 80−43032
crystal orienting device for ESR studies 77−82581
cupric mixed ligand complexes, mechanism of spin transfer to next neighbours ^{13}C and ^{31}P 78−86892
cyanine dyes in methanol-water glasses, EPR spectra of triplet state 79−18212
cyclic A_{2n}-systems, trans induction effect in NMR and ESR spectra 78−29799

paramagnetic resonance continued
cyclopentanone, excited triplet state, intramolecular tunnelling, optically detected electron spin coherence 77−61774
dating method, appl. to archaeological materials from Greek Petralona cave 79−26094
dating method with digital ESR 80−86542
dating of minerals by EPR method 80−36415
dating using ESR *(Japanese)* 79−48437
Dewars for EPR expts., containing liq. N_2, bumping elimination 79−40600
di-tert-butyl nitroxide, N hyperfine coupling const., solvent effect, model 79−54870
diacetylene polymer, EPR exam. of partially crystalline polymer extracts 78−39400
diacetylene-d_2, excited quintet states during photopolymerisation, ESR obs. 80−84635
diamond, high temp. ion implantation EPR meas. 79−23623
diamond, low-temp. electron-irrad., EPR 77−59045
diamond, natural type IB, thermal conductivity anomaly, defects obs. 77−85003
diamond, paramag. centres, ESR spectra 77−36132
diamond, paramagnetic N centres spatial distrib., EPR imaging method 79−65732
diamond, type IIa, electron irradiated, annealed to high temps., EPR spectrum 77−90034
diamond powders, EPR of defect centres 77−66423
diamonds, natural, irradiated with electrons and neutrons, paramag. centres with S=5/2 79−47334
diamonds synthesised in metal-carbon medium by static and dynamic methods, EPR spectra 77−90015
diatomic molecule, rel. to theory of high-precision Zeeman effect 77−14486
dielectric materials, EPR study *(Japanese)* 77−85550
differential EPR susceptance unit, USSR primary standard 77−30190
digital block for electronic sweep of mag. field 77−26371
digital calibration device for mag. field, appl. to EPR spectroscopy *(French)* 77−152
digital data acquisition using microprocessor 80−17975
digitised EPR system, appln. to saturation transfer 80−77825
directional field dependence of ESR and relaxation 78−91931
disordered system, spin diffusion 77−8392
DNA conformation, influence of intermol. interactions 80−16900
p-ndodocyloxy benzylidene p-azophenyl aniline, smectic phases, mol. order, EPR study 80−79693
drug tolerance, spin label study of ethanol effects 77−66799
dulcitol, X-irradiated single crystal, intermol. electron trapping, hyperfine ESR pattern 79−39166
dyed Ag halide powders and emulsions, light induced ESR signals 79−24211
dynamic magnetoresonance effects in solids 80−20447
eigenvalues and eigenvectors, error anal. 79−51840
electric field modulated, appl. to study of ferroelectrics 80−75841
EPR multipurpose cavities, 1.6-1300K appl. 78−8430
EPR of triplet excitons, model Hamiltonian, Kubo-Tomita approximation 77−24734
EPR spectroscopy data handling and processing method *(German)* 77−53968
erythocyte membranes, complement proteins interaction, ESR 79−100584
erythrocyte membrane protein alterations in Huntington's disease 77−56347
ESR spectrometers with crossed resonators in K-X range 77−87798
ESR/ENDOR spectrometer sensitivity enhancement using microwave amplifiers 78−82014
ferredoxin, soluble, investigation of 2 forms from pea leaves 80−45851
ferric haeme protein, anal. of low-spin ESR spectra 77−60185
ferromagnetic alloys, hyperfine field rel. to paramag. reson. of shift 77−24537
flint artefacts, ancient heat treatment identification by ESR spectroscopy 79−12831
fluorene:acridine, EPR of excited triplet state complex 79−19767
fluorene:phenazine, excimer form. transient EPR phenomena, wide-band detect. 77−13793
formaldehyde+Br reactions, rate consts. by EPR 80−93736
formaldehyde+F reactions, rate consts. by EPR 80−93736
fossil dating by ESR technique 80−95209
free radical reactivity rel. to paramag. centre unpaired electron density 77−52633
free radicals, high resolution spectroscopy *(Japanese)* 79−79355
g-factor and spin concentration, EPR standard, Picein 80 cement 79−80658
gases, electron cyclotron resonance absorpt. signals 78−51278
generalised spin Hamiltonian, reduction in no. of consts. by unitary transform. 77−43867
glass fragments discrimination, window, container glasses, forensic science appl. 79−11841
glasses, elec., mag., and optical props., conference, Troy, NY, USA (Aug. 1979) 80−105417
glasses, ESR, review 80−108049
glassy semiconductors, neutron irradiated, paramag. centres 79−82872
glauconite group minerals, Norwegian-Greenland basin, age determ. by EPR and Mossbauer spectra 80−26467
globular protein rotatory mobility meas. by spin probe method, soln. viscosity 77−16902
glyceraldehyde 3-phosphate dehydrogenase, EPR, saturation transfer EPR 79−98124
graphite, EPR, effect of motional averaging, anisotropy, skin effect rel. to heat treatment and neutron irradiation *(French)* 80−34752
graphite, neutron-irradiated, EPR, rel. to electronic struct. *(Japanese)* 78−19326
graphite, polycryst., reactor-grade, neutron irradiated, crystal structure recovery obs. *(Japanese)* 77−43254
graphite intercalation compounds with K and tetrahydrofuran *(French)* 78−26692
graphite-K inclusion compounds, paramagnetism after treatment by π or n donors *(French)* 78−10749
haemoglobin g-value change obs. *(Japanese)* 77−90724
haloanilines, T_1-states, EPR and zero-field ODMR obs. 78−58725
haloanisoles, T_1-states, EPR and zero-field ODMR obs. 78−58725
halobenzonitriles, T_1-states, EPR and zero-field ODMR obs. 78−58725
paramagnetic resonance continued
heart tissue and mitochondria, bovine, heterogeneity of N-2 Fe-S centres 77−86461
Heisenberg magnet, pseudo-one-dimens., EPR freq. temp. depend. 77−32241
Heisenberg magnets, pure and pseudo-one-dimens. temp. depend. of EPR freqs. 78−6563
heme-proteins, general spin Hamiltonian for determ. of ligand nucl. Zeeman and hyperfine interactions 77−85617
hexacyanobenzene-naphthalene, charge transfer triplet states, electron distrib., ESR 77−3388
high-temperature molecules, matrix isolation spectra, review 78−46340
high-temperature studies using CO_2 laser-heated EPR spectrometer 80−68233
HOAB, smectic C liquid crystal, spin label probe obs. 77−19867
hydrocarbons, γ-radiolysis in glassy and polycryst. states, EPR spectra 77−52658
insulators, mag., interference effects in NMR line shape 77−8435
intensity operator and its use in exact analysis of EPR line intensities 80−20448
intermediate conducting solid, microwave eddy currents and EPR 77−80996
intermolecular mechanics, T_1 and T_2, by microwave meas., zero- and non-zero field 79−45738
interstellar molecules, matrix isolation spectra, review 78−46340
Jahn-Teller effect, intermediate, in orbital triplet, effect on EPR 80−34756
Ka-band EPR/ENDOR spectrometer, modified, obs. of electron spin echoes at 35 GHz 80−13113
Kapton, pyrolysed, cond. polymer, transport and mag. props. 80−96887
kinetic equations for solid paramagnet in alternating longitudinal field 78−2725
lipid bilayers, spin probes EPR partitioning between lipid and aq. phases 79−79455
lipid planar multibilayers, spin label study of nystatin and amphotericin B action 77−29108
liquid crystals, nematic and smectic, EPR and NMR relax., first-rank tensor component effects 78−14275
liquid nitrogen bubbling problem in ESR 78−263
liquid solutions, dilute, electron paramag. relax. theory 77−80998
literature review July 1975 to July 1977, applications to chemical systems 78−82753
liver and hepatoma samples, γ-irradiated, spectral anal. 79−92289
liver tissue and transplantable hepatoma, EPR spectrum and paramag. centre conc. 77−86459
low symmetry effects, theory *(Russian)* 79−61202
low temperature spectra, inexpensive quick-freeze technique 80−9012
lowest triplet state zero field splitting parameters calcs. 80−83391
magnetic alloys, dil., relaxational paramag. absorpt. of RF power *(Russian)* 79−65645
magnetic field modulator, EPR radiospectrometer having discrete set of modulation frequencies 80−52285
magnetic field operator 80−108051
magnetic system, 1D, effect of low-symmetric spin distrib. 79−78505
magneto-microwave effects, rel. to EPR 77−55853
magneto-microwave effects, rel. to ESR, review 77−69667
magneto-optical effect, influence of ESR saturation, allowance for dipole-dipole reservoir of electron spins 79−15442
magneto-optical effects, magnetic resonance saturation in paramagnetic system with quadrupole splitting 80−60404
maize mutation distinguishment by EPR 79−57580
MBBA, nematic liq. cryst., mol. order and motion, EPR study 77−76298
MBBA liquid crystal, premelting detected by spin probes, effect of spin probe size 79−46563
MBBA-EBBA eutectic mixture, vitrified orientation of Cr(III) acetyl acetonate in liquid cryst. 77−16152
measurement using SQUID magnetometer system 79−75560
mechanical detection of EPR dispersion signals 79−30520
membrane, spin probe distrib. between water and membrane in different conditions 77−21491
membrane fluidity of fatty acid auxotroph, EPR study 79−70574
membrane organisation using D-NMR and spin label EPR as probes 77−44600
membrane surfaces, antibody association kinetics with spin-label haptens 80−66787
metalloproteins, recent EPR studies 78−64936
metals, ESR of localised moments 80−71153
methane, H abstraction by thermal H, 10-30K, ESR evidence 78−76839
methanol dehydrogenase, enzyme, electron spin echo, 35 GHz 80−13113
methanol glass solvated electrons, EPR, ^1H spin flip satellites, geometrical model 80−7146
methoxy-benzylidene-alkyl-cinnamates, smectic mesophase, ESR of spin probes, nonunique ordering 77−47344
methyl groups correlated quantum rotation effects 77−18948
N-methyl-N-nitrosourea, electronic interactions with DNA, ESR obs. and INDO calcs. 80−94154
mica, EPR spectra using mag. field and US strain modulation 77−69688
microemulsions, struct. aspects, using dielec. relax. and spin label techniques 80−26199
microwave cavity for high hydrostatic pressures 78−89518
minerals, nonsilicate, review 78−39384
molecular crystals, spectroscopy, bibliography for 1976 78−72585
molecular fragmentary composition, determ. by IR, EPR and US mag. reson. spectra *(Russian)* 78−13624
molecular motion dynamics in crystal influence on spectral parameters of NQR, NMR and EPR 80−20486
molecular motion effect, averaging for quantum finite motion with large amplitude 77−58046
molecular vibration, IR spectra 79−98084
molecules, high temp., appl. of ESR isolation technique 80−57399
molecules or clusters, interpretation of data from Mossbauer, ESR, susceptibility, optical and XPS meas. 80−37825
molten salts, IR, Raman, EPR and NMR spectroscopy, review *(French)* 79−69832
montmorillonite group minerals, Norwegian-Greenland basin, age determ. by EPR and Mossbauer spectra 80−26467
morphine, spin-labelled, EPR study of synaptosome opiate receptor 77−9215

paramagnetic resonance continued
multilevel system, low-freq. dipole moment in reson. amplitude modulated signal 78−72394
myosin conformational conversions, using acetate and acetamide spin labels 77−52733
nanosecond time-resolved EPR in pulse radiolysis via spin echo method 80−43075
naphthalene: anthracene, cryst., triplet-state EPR for isolated mol. orientation 78−26583
naphthalene-tetracyanobenzene, charge transfer complex, phase transitions, deuteration effect, mag. reson., spectral and thermal meas. 79−4412
naphthalene-tetracyanobenzene, doped cryst., EPR of triplet state for mol. reorientation 79−38368
nematic liq. crystal spin-relaxation, composite Markov process, rot. reorientation and director fluctuations 77−62471
nematic liquid crystal, spinning in tilted mag. field, lag angle 78−38615
nitrocomplexes, planar dynamic Jahn-Teller effects 77−15804
NMR-ESR spectroscopy, miniature magnetic assembly, teaching 80−105467
nonlinear effects in parallel static and harmonic mag. fields 77−59449
nuclear magnetic shielding constant, calc. by extended Huckel method with expansion by Gaussian functions 77−79634
one dimensional, with anisotropic interaction, high freq. props. *(Russian)* 77−80902
one-dimensional magnetic system, high-temp. dynamics 79−4716
orbital doublet with weak Jahn-Teller interaction, ESR spectra 77−28427
order parameter fluctuation spectrum, central peaks near ferroelectric phase transitions, review 79−19851
organic charge-transfer salts, comparison of ESR spectra 80−50164
organic compounds, irradiated single crystals, electron trapping, ESR obs. 78−88646
organic compounds, structural energy characteristics, rotational isomerism, mol. motion *(Russian)* 79−56602
organic molecular crystals, intermolecular interactions, spectroscopic studies, review 80−103958
oxide semiconducting glass, structural energy characteristics, rotational isomerism, mol. motion *(Russian)* 79−56602
oxovanadium carboxylates, near one-dimensional antiferromagnetism, thermal and mag. props. calc. 77−20602
oxyhaemoglobin, spin labelled, rot. correl. times, saturation transfer EPR 77−8387
packed cell sample prep. 78−28145
paramagnetic centre inhomogeneous distrib. meas. by EPR 79−93184
paramagnetic crystal resonator dynamics, low temp. anomalies *(Russian)* 80−7147
paramagnets, low-dimens., EPR spectra 80−71154
pentamethylbenzene-TCNB, charge transfer triplet states, electron distrib., ESR 77−3388
peptide-metal complexes, EPR, models of natural systems 78−64937
phenanthrene, lowest triplet state zero field splitting parameters calcs. 80−83391
phenanthrene-PMDA, spin polarization of charge-transfer excitons, EPR meas. 79−19766
phenanthrene-pyromellitic acid dianhydride, single cryst., EPR, delocalised and localised charge transfer excitons 77−85545
p-phenylphenol in stretched polyvinyl alcohol film, phosphorescent triplet states, ESR spectra obs. 80−83393
pheophytins, lowest triplet state, zero field splitting consts., decay rate consts., EPR determ. 78−27896
phonon avalanche due to nonequilib. dipole reservoir, theory 79−99751
phosphatidylcholine membranes, interaction of colchicine, spin-label study 77−86455
photographic emulsion, nature of paramag. centres causing singlet EPR signal *(Russian)* 77−36112
photosynthesis, appl. of ESR, review 79−92450
photosynthetic redox conversions, electron transport 79−92179
photosynthetic systems of higher plants, electron transport, P700 redox conversions 77−21494
photosynthetic systems of higher plants, electron transport, P700 redox conversions 77−21495
picene, EPR in p-terphenyl cryst., triplet state 79−36668
point defects in crystals, book 77−47442
polyacetylene, pristine and acceptor doped isomers, EPR, DC cond., evidence against solitons 80−15782
polyacetylene, thin film, ESR study, effects of O_2, NO and halogens 80−25186
cis-polyacetylene film, unpaired electrons, isomerisation, EPR obs. 80−60405
polyacetylene films, pure and doped, cond., ESR 79−82859
polyarylenealkyls, colour, EPR, electron density delocalisation degree determ. *(Russian)* 80−7152
polycaprolactam, pure and TiO_3 filled, radiation effects *(Bulgarian)* 79−33015
polycarbonate, colour appearance during oxidation *(Russian)* 79−24643
polycarbonate films, effect of UV and visible mono- and polychromatic radiation, stability *(Russian)* 79−57268
polyconjugate system, interrelation between physicochem. props. and microstruct. 78−55816
polycrystalline system, additional absorpt., in axially symmetric ESR spectra 77−16151
polycrystalline system, conditions for additional absorpt. peaks 77−43866
polyethylene, radiation effects on EPR and differential thermal anal. *(Bulgarian)* 79−46698
polyethylene oxide, dilute solns., mol. motion, EPR and NMR investigations 79−94863
polyhedral A_{2n}-systems, trans induction effect in NMR and ESR spectra 78−29799
polyhydroxy compounds, X-irrad., trapped electrons, ESR and ENDOR obs. 80−93161
polymers, structural energy characteristics, rotational isomerism, mol. motion *(Russian)* 79−56602
polyparaphenylene:SbF_5, pure and doped, metallic, absence of Pauli paramagnetism, mag. susceptibility meas. and ESR obs. 80−97060
polyphenylacetylene, crystallizable, DC cond., annealing and defect effects 77−62923
polypropylene, electret, trapped injected electrons, EPR obs. 78−27093
polypropylene fibres, γ-irrad., microstruct. changes in glassy-high elastic state transition *(Rumanian)* 80−49347
polyvinylcarbazole-trinitrofluorenone, organic photoconductor, photoinduced paramag. centres 80−25188
paramagnetic resonance continued
porphyrin, triplet-state EPR spin polaris., intramol. model for photosynthetic bacteria 78−44469
porphyrins in liquid crystal, oriented photoexcited triplets, EPR study 80−84636
protein-lipid interaction effect on struct. of artificial vesicular membranes 77−25385
proteins, EPR absorption of tissue constituents, colour correlation, using mouse liver 77−90727
pyrene, crystalline, EPR spectrum of triplet excitons 78−27076
pyrene-tetracyanobenzene, charge transfer complex, phase transitions, deuteration effect, mag. reson., spectral and thermal meas. 79−4412
quadrupole interaction for nucl. spin=3/2 systems 78−48027
quantitative, precision using Cu (II) bound to ion exchange resins 77−56261
quartz:Cu(Ag), paramagnetic centre formation after α-irradiation *(French)* 77−69690
α-quartz, hydrogenic trapped hole species, EPR studies 80−44915
quartz, muonium EPR transitions by muon-spin rot. 80−29668
quartz glass, boron-containing, struct. investig. using ESR spectra 77−7673
quick access sample system for low temp. K-band ESR and ENDOR 80−57352
quinones, triplet quenching by organometal cpds., time resolved CIDEP and ESR obs. 80−95654
radiation emissions due to saturation of magnetic resonance 78−39386
'reduced' spectra calc. 80−23444
relaxation processes, influence on microwave signal detection 77−66413
relaxation processes *(Chinese)* 79−87307
review of magnetic resonance, book contrib. 80−11242
rhodamine dyes, methanol-water solns., triplet state EPR spectra, aggregation, mol. orientation 77−48031
rhodamine dyes in methanol-water glasses, EPR spectra of triplet state 79−18212
rhodopsin, presence of two closely arranged SH groups in mol. 78−53323
rhodopsin, solubilised, photoinduced conform. changes, spin-label method 77−81496
rotation of US plane of polarisation under ESR saturation conditions 80−29123
rotational diffusion, passage saturation transfer EPR 77−8387
ruby, magnetisation precessing, optically induced, near level anticrossing points in $^4A_2$ 77−36111
sample tube, gas-permeable 78−260
sandwich compounds, orbitally degenerate, EPR 78−86893
saturation spectrum, effect of strong microwave field 80−15785
saturation transfer data, tape library 79−51841
saturation transfer EPR spectroscopy, source modulation, mol. reorientation effects 78−41339
semiconductor, combined resonance, basic mechanisms 79−61229
semiconductor and semimetal powders, EPR, effect of mag. field depend. of elec. parameters 79−99749
semiconductors, ferromag. and nonmag., paramag. waves travelling near the paramag. resonance freq. 78−88168
semiconductors, recombination processes, review 79−38088
semiquinone Q_{10}, EPR signal with unusual relax. parameters 77−56338
serum albumin, bovine, binding of spin-labelled stearic acid 79−96506
signal recording method, without field modulation 77−34009
signal recording unit at modulation freq. of magnetic field 79−21795
significance plots use in spectra interpret. 80−22409
silicates, ESR, review 78−88166
simple cell for chem. analysis of lossy samples 77−90664
simulation of ESR spectra by FFT 79−19763
single crystal ESR spectrum simulation, Fortran IV computer program 77−59447
size-quantised films, sound amplification under ESR conditions 80−70322
slotted tube resonator pulsed ESR and ODMR expts. 80−86360
soap system, C_{18} mono-cis-unsaturated, lyotropic liq. cryst., X-ray diffr. and EPR meas., Monte Carlo simulation 78−94981
solid, thermally stimulated processes 78−10828
solutions, bibliography of 1975-76 literature 80−51979
solutions, EPR, review 78−88165
solvated electron, ESR, time profile meas. and anal. 77−5878
spectral simulation program, appl. to NO spin labels 78−78730
spectral simulation via finite elements, variational method and stochastic-Liouville eqn. 79−85157
spectrometer, 2 mm band EPR, with re-entrant resonator 78−86311
spectrometer, conversion to 1 MHz field modulation 77−49759
spectrometer calibration by EPR spectra recording 78−89513
spectrometer with klystron freq. control and ICs 79−21796
spectroscopy, spectra collection and anal. using KRS-4200 minicomputer *(German)* 78−57998
spectroscopy in strong elec. fields at 77 and 4.2K 78−86310
spin diffusion at low temp. in conc. solid paramagnet *(Russian)* 77−32240
spin glass, EPR frequency and mag. transverse susceptibility with remanent magnetisation *(French)* 80−7145
spin glasses, spin dynamics, EPR, NMR, muon precession, Mossbauer, and neutron scatt. results 79−65689
spin Hamiltonian, perturbation treatment, M=0 electronic state, HFS of triplet state EPR 80−25185
spin Hamiltonian consts., computation from EPR single cryst. data 77−90013
spin Hamiltonian diagonalisation, theory and appls. of generalised operator transforms 77−4546
spin system saturation characts., acoustic wave excitation *(Russian)* 80−66013
spin system with weak exchange couplings, temp. depend. 78−64258
spin-Hamiltonian parameter from EPR, data by least-squares fitting 77−1585
standard samples, g-factor meas. technique 77−26370
strong electric fields, method for appl. in EPR at low temp. 79−21792
superheterodyne UHF spectrometer for temp. 0.04-4.2K 78−257
superionic conductors, mag. reson., book contrib. 80−25240
superlattice, EPR line dip taking into account spin correl. via phonon field *(Russian)* 77−69671
symmetry adaptation, operator equivalence, mag. reson., operator equivalent formalism *(French)* 78−84374
symmetry adaptation and operator equivalents *(French)* 78−91924

paramagnetic resonance continued
TCNQ, salt, $Me\phi_3As(TCNQ)_2$, nonOhmic elec. cond., tunnelling model and expt. 79−99558
$(TCNQ)(TTF)_{1-x}$-$(TSeF)_x$, quasi 1-D metal, mag. susceptibility, temp. depend. 77−8267
TCNQ complex salts, mag. props., ESR meas. 79−56603
TCNQ complexes with dipyranylidene and dithiadipyranylidene, high cond. investigs. and related props. 78−6368
TCNQ salt, $(TMA^+)_3(I_3^-)(TCNQ^-)_2(TCNQ^0)$, struct., phys. props. and lattice distortion evidence 78−6305
TCNQ salt, bis(dipyridyl)platinum(II)-TCNQ, crystal struct. and EPR, TCNQ radical dimerisation 77−80490
TCNQ salt, N-n-butyl-quinolinium $(TCNQ)_2$, ESR spectrum fine struct. splitting 80−44904
TCNQ salt, pyridine $(TCNQ)_2$, phase transition at 80K investig. and interpret. 78−6530
TCNQ salt, quinolinium, electron spin location, elec., mag., and thermal props. 80−25189
TCNQ salt, Rb-TCNQ, electronic spin-lattice relax. time 77−51939
TCNQ salt, tetramethylhexamethylenediammonium-TCNQ-iodine, elec. and mag. props., struct., specific heat 80−24898
TCNQ salt, TMTTF-TCNQ, mag. gaps, EPR meas. 77−8390
TCNQ salts, aminopyridinium $(TCNQ)_2$, elec. and mag. props., 4.2 to 300K 80−24889
TCNQ salts, simple, triplet exciton obs. by ESR 78−10373
TCNQ-M_2P charge transfer complex, triplet spin excitons, EPR spectra 78−80192
TCNQ-TMTTF phases comparison with TTF-TCNQ 77−40116
techniques, developments 78−74045
temperature variator coupling to EPR radiospectrometer 78−58003
1,2,4,5-tetrachlorobenzene, triplet excitons, ESR and ODMR 78−43681
tetramer clusters, ESR spectra, spin Hamiltonian analysis 77−28429
N,N,N′,N′-tetramethyl-p-phenylenediamine-p-chloranil, soln., optical spectra, temp. and environment effects 79−54861
theoretical chemistry, NMR, ESR and NQR, review 77−18943
time resolved EPR spectroscopy, stopped flow EPR apparatus for biological appl. 80−36206
time resolved ESR, time profile meas. and anal. 77−5878
time-resolved spectra, field modulation effect 78−78731
TMMC, one-dimensional Heisenberg mag., EPR, spin diffusion of 4-spin correl. functions 77−4549
TMMC, one-dimensional paramag., half-field EPR transition 77−80995
TMMC, paramagnetic relax. rates, anisotropic diffusion model 77−69668
transient EPR phenomena, wide-band detect. method 77−13793
transmission EPR spectrometer, appl. of tunable waveguide refl. maser. 78−5443
trapped electrons, ESR and ENDOR obs. 80−93161
1,3,5-trinitro 1,3,5,-triazacyclohexane, shock-induced intramol. bond breaking, XPS and EPR study 80−76512
trinitrotoluene, shock-induced intramol. bond breaking, XPS and EPR study 80−76512
trinuclear clusters with half-integral spins, theory, inc. anisotropy effect in antisymmetric exchange 77−8391
triphenylamine in 3-methylpentane and ethanol glasses, γ-radiolysis, IR spectra, trapped electron 77−16842
triplet oriented mols. in solid matrix, slow mol. motion, ESR spectra 77−90014
triplet states in photosystem I of spinach chloroplasts and subchloroplast particles 80−85344
$TTF(Br)_{0.7}$, EPR temp. depend., metal-insulator transition 77−43863
$TTF(I)_{0.71}$, EPR temp. depend., metal-insulator transition 77−43863
TTF(MBDT) spin-Peierls transition, mag. exchange interactions, mag. props. 80−25138
$(TTF)_{12}(SCN)_7$ and $(TTF)_{12}(SeCN)_7$, charge-transfer salts, elec., mag. and optical props. 77−43575
TTF salts, physical props., Fermi energy scaling of metal-insulator transition temp. 77−8081
TTF-bisdithiolene metal complexes, spin Peierls transition 77−4523
TTF-TCNQ, 53 and 38K transitions, mag. and elec. props. meas., doping effect 77−66159
TTF-TCNQ, electronic spin-lattice relax. time 77−51939
TTF-TCNQ, microwave eddy currents and EPR 77−80996
TTF-TCNQ, pure and irrad. crystal, nonlinear transport at low temp. 79−4552
TTF-TCNQ, spin susceptibility below 53K, compared with elec. cond. data 77−43865
TTF-TCNQ complex, trans-diethyl-dimethyl TTF-TCNQ, one-dimens. cond. 80−96853
TTF-TCNQ series, cryst. struct., elec. cond., and EPR meas., steric factor effects 80−19789
$TTT_{1.2}NiS_4C_4H_4$, quasi-one-dimensional cond., cryst., mag. and elec. props. 78−10424
$(TTT)_2I_3$, optical, spin-reson., magnetoresist. study, nature of ground state 78−68023
two radiation source spectrometer, signal decrease, beat phenomena *(French)* 78−41338
two-dimensional electron gas, reson. excitations, using IR spectroscopy, review 79−60889
two-way ESR cavity for magnetic- and electric-dipole transitions 79−17459
vanadium hexacarbonyl, EPR in frozen glasses, optical spectra in soln., solid, assoc., bonding 77−6807
vanadyl carboxylates, EPR and mag. susceptibility, near one-dimens. antiferromagn. 77−63265
vanadyl mixed ligand complexes, mechanism of spin transfer to next neighbours ^{13}C and ^{31}P 78−86892
vibrationally excited diatomic radicals 77−18949
X-band ESR spectrometer, microwave kit for conversion to K-band operation 78−21192
X-Y model, mag. reson. calc. *(Russian)* 77−80992
p-xylene, isotopically mixed cryst., phosphoresc. triplet state, ESR and MIDP obs. 77−58071
xylene plasma-polymerised film, ESR 79−99750
zinc pyrochlorophyllide in nematic liquid crystals, oriented photoexcited triplets, EPR study 80−84636
AgBr emulsion grains, adsorbed dyes, light-induced ESR spectra 80−88862
AgM (M=Mg, Ca, Sr, Ba, Zn, Hg) intermetallic mols., Ar matrix isolated, ESR investig. 79−811
Al_2O_3, neutron irrad., EPR spectra, F^+-centres 77−4558

paramagnetic resonance continued
$Al(OH)_3$, coprecipitated with $Cr(OH)_3$ gel, mag. and optical studies, calcination 79−47995
AlSb (110), surface struct., EPR meas. and elastic energy minimisation calcs. 79−51405
As, amorphous, electron irrad.-induced paramag. centres, 77K 78−88187
As_2S_3, glassy, photoinduced defects, EPR and absorpt. spectra 80−59398
$As_2S_3(Se_3)$, X-ray induced paramag. states and luminesc. 78−95520
As_2Se_3, amorphous, electron irrad.-induced paramag. centres, 77K 78−88187
As_2Se_3, glass, density of optically induced localised paramagnetic states 78−52354
As_xSe_{100-x} glasses, temp. depend. of mag. susceptibility and EPR 77−63073
As_2Te_3, amorphous, defect and impurity states, hopping cond. obs., EPR meas. 80−54650
B-C, B-C-Ti, B-C-Cr, paramagnetic centre struct. and defect form. 80−66034
$BaWO_4$ crystals, X-irradiated, EPR, TSC and thermoluminescence spectra meas. 79−1791
Br matrix isolation ESR 80−106336
C, activated, surface oxidised, adsorpt. of organic vapour rel. to paramag. props. 77−32238
C, amorphous, diamond-like 3-fold coord. 80−50323
C, amorphous film, spin resonance, IR spectra, microhardness 80−71157
C fibres, from mesophase pitch, resist. magnetoresist., EPR and mech. props. rel to struct. 79−78116
C, soft and hard, sp. ht. anomalies and spin-spin interactions, review 79−69261
C_3O_2 polymer, preparation, spectra rel. to polymerisation temp. electron spin resonance 77−32239
CS+O→CO+S, rate const. temp. depend., ESR-mass spectrometer obs. 78−20013
$Cd(ClO_3)_2$, irrad., bleaching and annealing expts., EPR and optical absorpt. 79−91476
$Cd(ClO_3)_2$ irradiated single crystal, ESR and annealing, trapped defect centre 80−55141
CdO-ZnO-Al_2O_3-Fe_2O_3-SiO_2 system glass, ESR spectra 79−65711
CdTe and CdTe:Cl, grown by travelling heater method, EPR defect charact. 77−40125
$Ce_2Mg_2(NO_3)_{12}.24H_2O$, EPR line, saturation rel. to Mandel'shtam-Brillouin scatt. by hot phonons 77−52110
Co/γ-Al_2O_3 catalyst, ESCA and EPR meas. after hydrodesulphurization reaction *(French)* 79−52755
CoMo/γ-Al_2O_3 catalyst, ESCA and EPR meas. after hydrodesulphurization reaction *(French)* 79−52755
Cr complexes with glycilglycine, structure, optical, e.p.r. and mag. investig. 77−1103
CrH(CrD), molecular vibration, IR spectra electron spin resonance, 4K 79−98084
$Cr(OH)_3$, coprecipitated with $Al(OH)_3$ gel, mag. and optical studies, calcination 79−47995
Cs^-, in tetrahydrofuran soln., transient photoelectron nutation 79−3418
CsI, pure and Na(Tl)-doped, luminesc. from bound excitons, UV absorpt. and EPR 77−77282
$CsMnCl_3.2H_2O$, paramagnetic relax. rates, anisotropic diffusion model 77−69668
$CsMnF_3$, solid and molten paramag. high-temp. e.p.r. linewidth meas. 77−4548
Cu complex, bis(N-methylsalicylaldimine) copper (II), Jahn-Teller effect in EPR 77−80994
Cu complexes with glycine, in aqueous soln., EPR meas. 77−36115
D, stabilised in low temp. frozen aqueous acidic solns., two-proton forbidden transitions 78−27804
D_2O, ice cryst., electron traps, electron irrad. effects, EPR 77−1939
F+iodobistrifluoromethylphosphine, reaction mechanism and kinetics, ESR 77−86294
GaAs (100) surface struct. determ. by LEED, UPS, and EPR 80−49475
GaAs (110), surface struct., EPR meas. and elastic energy minimisation calcs. 79−51405
GaP (110), surface struct., EPR meas. and elastic energy minimisation calcs. 79−51405
GaP (110), wave functions and surface struct., EPR expts. 78−91519
GaP:Zn, isolated Ga vacancy due to electron irrad., EPR study 78−95519
GdAs(Sb)(Bi), antiferomag., EPR meas., Neel temp. determ. 77−32242
GdS(Se), antiferromag., EPR meas., Neel temp. determ. 77−32242
Ge, amorphous, EPR expts. 78−88167
Ge, amorphous film, annealing, effect on localised states 79−4535
Ge amorphous film, effects of alloying chalcogen atoms 80−49670
Ge film, amorphous, influence of deposition parameters on e.p.r. 77−1586
Ge, neutron irradiated, positron annihilation, ESR and resist. meas. 80−15160
Ge powder, diamag., strong mag. particle form., mag. props., EPR *(Russian)* 80−54863
n-Ge:P, electric dipole excitation of spin resonance 77−4551
n-Ge:Sb, neutron-irradiated, paramag. defects, analysis of EPR spectra 77−55703
Ge-P-S glass system, EPR of intrinsic and Mn^{2+} impurity centres 80−88870
Ge-S, amorphous, photocond., photo-induced ESR, optical edge shift 80−49809
Ge-S, Ge-S-Ag, amorphous prop. and origin of paramagnetic defects 79−10801
Ge-S amorphous film, defect states, ESR 80−49670
Ge-S film, amorphous, photo-induced ESR and optical absorption edge shift 78−88374
Ge-S glass, melt-quenched photoinduced ESR, annealing behaviour and glass comp. depend. 80−71156
Ge-S glasses, EPR study 78−43644
Ge-S-Ag glasses, bulk and film, EPR study 78−43644
Ge-Si amorphous film, ferromagnetic interaction between spins 78−2710
GeO_2, gamma-ray induced O diffusion, ESR measurement 79−99358
GeO_2, hexagonal and glassy, X and γ-irrad., thermolum. and paramag. centres 77−63472
GeO_2:Al, Ga, EPR, transferred hyperfine interactions of impurity-related trapped hole centres 77−85568
$Ge_{42}S_{58}$, amorphous, bulk and film forms, elec. props. and ESR study 80−103691

paramagnetic resonance continued
$GeSe_2$, amorphous film, photocond., photo-induced ESR, optical edge shift 80−49809
$Ge_{1-x}Se_x$ film, EPR, elec. and optical props. meas. 78−48038
H, gas at low-density, transitions between hyperfine levels, 4.2-77K 79−50053
H+chlorotrifluoromethane, reaction kinetics, ESP obs. 77−21358
H+HCl, reaction kinetics, ESR and mass spectrometric obs. 77−21357
HI, H abstraction by thermal H, 10-30K, ESR evidence 78−76839
H_2SO_4 glass, γ-irrad., trapped H ESR, vol. relax. effects 79−52703
$Hg_{1-x}Mn_xTe$, microwave helicon propag. and helicon excited EPR 77−43637
^{199}Hg optically oriented atom interaction with cell wall paramag. centres 80−37762
I_2 atomic ESR spectra, broadening by He, O_2 and HI 79−68205
^{127}I atoms in Xe matrices, ESR spectrum 80−1005
n-InAs, transverse magnetoresistance oscill. in weak mag. field 79−91086
InSb (110) surface struct. determ. by LEED, UPS, and EPR 80−49475
InSb, electron spin relaxation 80−25187
n-InSb, transverse magnetoresistance oscill. in weak mag. field 79−91086
KBr:V, covalency effects EPR meas. 77−85557
$KMnF_3$, solid and molten paramag., high-temp. e.p.r. linewidth meas. 77−4548
K_2MnF_4, EPR g-shift and anisotropic mag. susceptibility 77−85546
K_2MnF_4, low-dimensional system, obs. of sidebands on EPR lines 77−80993
KN_3, ESR undergraduate expt. 80−105471
K_2O-TeO_2 glass, radiational EPR centres, struct. model *(Russian)* 77−28426
$K_2Pt(CN)_4Br_{0.3}.xH_2O$, one-dimensional cond., effects of dehydration on mag. props. 77−85549
KUO_3, EPR and mag. susceptibility, temp. depend. 79−33451
$La_{3-x}Gd_xIn$, mag. impurity ordering and superconductivity, EPR exam. *(Russian)* 77−8400
Li-methylamine soln., metal-nonmetal transition, electron and nucl. spin-lattice relax. 79−87306
Li_2O-LiCl-B_2O_3 system, fast Li^+ ion vitreous superconductors, EPR study *(French)* 80−11269
Li_2O-TeO_2 glass, radiational EPR centres, struct. model *(Russian)* 77−28426
$LiUO_3$, EPR and mag. susceptibility, temp. depend. 79−33451
MnF, MnF_2, EPR, in inert gas matrices, high spin mag. parameters, level diagrams 78−66565
MnF_2 in Ar matr-x, X-band ESR spectra, extra line assignment 79−81218
MnF_2, solid and molten paramag., high-temp. EPR linewidth meas. 77−4548
MnH_2 in Ar matr-x, X-band ESR spectra, extra line assignment 79−81218
MnH(MnD), $^7\Sigma$-state, mol. parameters, ESR and optical spectrosc. 78−94264
$MnH_2(MnD_2)$, $^6A_1$ state, mol. parameters, ESR and optical spectrosc. 78−94264
MnO, ESR spectra, matrix isolated at 4K 78−33531
MnO_2, ESR spectra, matrix isolated at 4K 78−33531
MnO_3, ESR spectra, matrix isolated at 4K 78−33531
MnO_4, ESR spectra, matrix isolated at 4K 78−33531
MnSi, itinerant electron helical mag., ESR 77−59446
Mo complexes, mononuclear, EPR ligand superhyperfine interactions, implications for enzymes 77−86372
Mo-containing enzymes, investigation using EPR 77−86373
MoO_3, rel. to H_2 reduction *(French)* 77−36365
$MoSCl_3$, prep. and characterisation 77−59705
N_2 matrix multiple trapping sites of N 78−56367
$(NH_4)_2BeF_4$, γ-irrad. cryst., F_2^- ions, ESR meas. 80−34770
NH_4NO_3, shock-induced intramol. bond breaking, XPS and EPR study 80−76512
NO, adsorbed on MgO, dimer form., heat of dissoc., EPR obs. 78−82755
NO_2, EPR, mag. dipole transitions, Zeeman parameters 78−17697
NO_{x_s} Stark effect investig., using two-way EPR cavity system 80−90872
$NO(^2\Pi_{3/2}, J=3/2)$ at X-band, high resolution EPR spectra 78−37661
Na_3, EPR spectrum, Ar matrix, bonding models 77−14462
NaCl, Mn^{2+}-□ reorientation, ESR elec. field effect meas. 79−8050
$NaClO_3$, X-irrad., thermal stability of radiation damage products 79−34324
Na_2O-TeO_2 glass, radiational EPR centres, struct. model *(Russian)* 77−28426
Na_2O-TiO_2-SiO_2 glass, IR refl., Raman and EPR spectra, struct. *(Russian)* 78−2860
$NbSCl_3$, prep. and characterisation 77−59705
O_2, gas, intermol. pot. for spectra, acoustic absorpt., rot. relax., etc. 79−68224
O_2, in gas and adsorbed on Si 77−69176
O_2 liquid, EPR temp. depend. *(Russian)* 78−31103
OCS, gas, EPR of rot. transitions, T_1 press. depend. 80−9621
OCS+He(Ne)(Ar)(Kr)(H_s)(0_2)(CO_2), gas, EPR of rot. transitions, T_1 press. depend. 80−9621
$PbFe_{2/3}W_{1/3}O_3$-$BaTiO_3$ system ferroelec., antiferromag., ESR and dielec. props. meas. 77−40172
$Pb_{1-x}Sn_xTe$, correlation between elec. props. and crystalline environment 77−80773
$Pb_{1-x}Sn_xTe$ solid solutions, EPR at Te vacancies *(Russian)* 77−48050
$Pb_{1-x}Sn_xTe$ solid solution, electron scatt. by charged Te vacancies 77−69328
PbTe, far IR spin flip reson. 79−82979
Pd, influence of K depend. of g tensor on cond. spin reson. signal from d holes 79−23890
α-quartz:Ge,Ag^+, Ag-compensated Ge centre, EPR meas. 77−77098
Rb^-, in tetrahydrofuran soln., transient photoelectron nutation 79−3418
Rb-tetrahydrofuran soln., photolysis, photoelectron emissive EPR signal, scavenger electron affinity reactivity 78−53224
RbBr:V, covalency effects, EPR meas. 77−85557
$RbMnF_3$, solid and molten paramag., high-temp. EPR linewidth meas. 77−4548
$RbUO_3$, EPR and mag. susceptibility, temp. depend. 79−33451
$(SN)_x$, polymerisation, EPR obs. 79−73800
ScF_2, ESR spectra of radical in Ar matrix, 12K, hyperfine splitting 79−98122

paramagnetic resonance continued
Se, amorphous, electron irrad.-induced paramag. centres, 77K 78−88187
Se, glassy, localised electronic states, photoluminesc. and ESR studies 80−65501
Se, glassy, pure and K-doped, photolum. and optically induced ESR 80−50398
SeO, $X^3\Sigma^-$ state mol. parameters, Zeeman and EPR spectra 79−6966
Si (111), low-pressure-baked, EPR study 79−82860
Si, amorphisation by bombardment with O ions, electron diffr. and EPR meas. 78−10098
Si, amorphisation by ion implantation energy depend. 77−7769
Si, amorphisation by ion implantation, ESR meas. 77−11578
Si, amorphised by ion implantation, EPR obs. of mag. ordering 79−24186
Si, amorphous, doped, optically induced ESR, correl. effects 77−40115
Si, amorphous, EPR and spin-dependent effects 80−80592
Si, amorphous, EPR expts. 78−88167
Si, amorphous, glow discharge produced, defect creation, high optical excitation 80−97327
Si, amorphous, large vacancy cluster annealing by ion bombard, EPR investig. 77−68965
Si, amorphous, spin depend. recomb., luminesc. and light induced ESR 80−50393
Si, amorphous, structural defects EPR 80−25208
Si, amorphous, UHV evaporated, annealing behaviour of spin density 80−93163
Si amorphous film, dangling bond ESR, light-induced quenching 80−50162
Si, amorphous film, ESR, cond. secular change on annealing *(Japanese)* 79−15238
Si, amorphous film, effect of gas exposure on EPR signal 78−84475
Si, amorphous film, RF plasma deposition from $SiCl_4$-H_2, characterisation 80−66435
Si, amorphous film, RF-sputtered, influence of O_2 and deposition conditions, elec. cond., IR absorpt. and ESR 80−2949
Si amorphous film, saturation meas. on ESR signals 79−33535
Si, amorphous films, hopping conduction, dangling bond generation by high temp. annealing 80−60115
Si, amorphous films, RF sputtering prep. at high Ar press., props. obs. 80−80418
Si, amorphous ultrahigh vacuum evaporated films, ESR obs., deposition effects 79−33534
Si, annealed, neutron-irradiated, EPR centre (S=1), charact. 80−71177
Si, annealing of vacancy clusters produced by ion bombardment 77−89485
Si, dangling bonds, EPR, localised states and unpaired electrons on microcrack surfaces 78−52351
Si, defects detect. by EPR superheterodyne spectrometer 77−43885
Si, deformed, photo-EPR of dislocations 80−11267
Si, dislocation energy spectrum, appl. of EPR and elec. meas. 79−82547
Si, dislocations, EPR meas. 79−82871
Si, EPR and spin-lattice relax. of dislocation spin chains *(Russian)* 79−91291
Si, EPR of radiation damage due to complete stopping of 30 MeV protons 77−65994
Si, EPR of thermally induced defect 77−81005
Si, ESR in neutron transmutation doped samples 80−20462
Si, electron irrad., multivacancy-O complexes, EPR expt., correl. with IR absorpt. data 77−28443
Si, electron irradiated, EPR of C-O divacancy complex 77−69691
Si, energy depend. of amorphisation by ion implantation 78−2175
Si, ferromagnetism induced by ion irrad., e.p.r. investig. *(Russian)* 77−1595
Si films, polycryst., annealing of paramag. vacancy-type defects, EPR obs. 79−10848
Si, heat treated, spin-depend. recomb. at dislocations 79−47122
Si, heavily irrad., ESR obs. of annealing charact. 78−10771
Si implanted layers, interaction of defects and impurities stimulated by induced ionisation, ESR 80−11270
Si, ion-implanted, cryst. to amorphous transform., ESR expts. and composite model 78−59825
Si, ion-implanted layers, radiation defect prod., EPR obs. 78−87696
Si, laser annealed, EPR and cyclotron resonance 80−34773
Si, mechanically damaged surfaces, EPR meas., role of microcracks 79−42836
Si, neutron irrad., EPR, ⟨100⟩ split di-interstitial, positive charge state 77−20698
Si, paramagnetic defects produced by electron irrad., EPR 79−19779
Si, plastically deformed, EPR spectra of point defects., temp. depend. 77−90033
Si, spin dependent effects, theory 78−23342
Si, spin dependent recomb. at dislocations, EPR and photocond. 79−38095
Si, spin dependent recombination and photoconductive resonance 78−43439
Si surface interacting with adsorbed gases, paramag. props., EPR study 80−34772
Si, vacuum-crushed surface, adsorption of H_2 and Cl_2, EPR meas. 79−46957
Si:As, implanted through SiO_2 films, elec. props., defect struct. 80−54264
Si:B, heat treatment centres changes, EPR obs. 80−29601
Si:B:P, dislocated crystals, EPR spectra, estimation of dangling bond conc. 78−10400
Si:B(P), deformed, EPR fine struct. spectrum of dislocation 77−66422
Si:Ge,Sn, role of interelectronic correl. in paramag. props. of impurity-vacancy complex 77−62858
Si:H, amorphous, defect creation and H evolution 80−50392
Si:H, amorphous, exodiffusion of H, EPR expts. 80−49102
Si:H, amorphous, light-induced ESR and photoluminesc., dangling bonds with positive correl. energy 80−50161
Si:H, amorphous films, plasma-deposited, defect states, IR, ESR, and refractive index meas. 79−65944
Si:H amorphous films, ESR, optical gap and elec. cond. meas. 80−75842
Si:H film, amorphous, bombarded, defects, luminesc. and ESR meas. 80−34977
Si:H(D), amorphous films, CVD, post-hydrogenation 80−54552
Si:P, distrib. of implanted impurity after laser annealing, e.s.r. and neutron activation analysis 77−4122

paramagnetic resonance continued
Si:P, EPR line shift, 0.56 to 4.2K, investig. of interacting donor clusters 77−77084
Si:P, metallic, heat treatment effects, EPR and photoluminesc. 77−77262
Si:P, optically induced divacancy reorientation, EPR spectra 78−80216
Si-Au, amorphous, linewidth var. with temp. and comp. 77−48033
Si-H, amorphous, plasma-deposited, H evolution and defect creation 80−44914
Si-H amorphous, defect model, light-induced ESR obs. 79−69721
Si-SiO_2 bonding layer, EPR exam. 78−15022
Si-SiO_2 interface, light induced reson. centres, photocond. reson., EPR obs. 80−50184
Si_xAs_{1-x}:H, amorphous system, struct. and defects, Raman and EPR meas. 80−49103
α-SiC (6H), paramag. N impurity levels, IR absorpt. and ESR expts. 77−59598
$Si_{1-x}Ge_x$ amorphous, ESR centres, effect of annealing 77−55701
SiO amorphous thin film capacitor, EPR, elec. cond. 78−68358
SiO-B_2O_3 composite dielec. films, EPR, dangling bonds and dielec. loss 80−11246
SiO_2 film, on Si, radiation damage structures, EPR obs. 78−95097
SiO_2, RF sputtered, stoichiometry and atomic defects obs. 79−60647
SiO_2, vitreous, grown from vapour, gamma ray irradiated, ESR and thermoluminescence exam. 78−88189
SiO_2, vitreous, heat treatment effect on viscosity and struct. 80−19714
$Si0_2$ film, RF sputtered, stoichiometry and atomic defects obs. 79−90904
$SrCl_2$, O_2^- pair centre EPR spectrum 77−24742
$SrTiO_3$:Fe, photochromic Fe^{3+} in non-cubic local fields, EPR spectra of $S=^3/_2$ centre obs. 77−40127
TCNQ salts, mag. props. 77−43869
TMMC, low-dimensional system, obs. of sidebands on EPR lines 77−80993
TMMC, one-dimensional mag., anomalous shift of EPR field 78−15010
TTF-TCNQ, pure and irrad., nonlinear transport, ESR study, 1.2-4.2K 80−20167
$TaSCl_3$, prep. and characterisation 77−59705
$TiF_2(TiF_3)$, ESR spectra in rare-gas matrices at 4K 77−88474
TiO_2 powder, radiation induced defects 77−62562
TiO_2, slightly vacuum-reduced, {312} planar defects, correl. with EPR defect centres 78−22736
Ti_2O_3, cryst. growth by chem. transport and tri-arc methods, and characterisation 78−3003
UCl_5, ESR, g-factor 77−43864
UO_2, U_2O_5, U_3O_8 and UO_3, bonding and valence obs. 77−28696
V_2O_5 EPR of O vacancy 78−72406
V_2O_5, hydrated amorphous, EPR, struct. and electron mobility *(French)* 77−15319
V_2O_5-P_2O_5 glass, EPR investig., samples with varying V^{4+} content and cond. 77−8389
$WSCl_3$, prep. and characterisation 77−59705
XeCl, in Ar, ESR spectrum at 4.2K 77−18947
$ZnCrFeO_4$, ferrite spinel, unsupported and SiO_2 supported, structural and catalytic studies 80−44191
ZnO 10$\bar{1}$0 surface, reaction of O_2, AES, LEED, EPR, desorpt., surface cond. and work function expts. 78−95950
ZnO, EPR spectra, g∼1.96 signal intensity var. 77−63264
ZnO, electron irrad., vacancies and interstitials, EPR meas. 79−14803
ZnTe (110) surface struct. determ. by LEED, UPS, and EPR 80−49475

paramagnetic resonance of colour centres
inc. other defects involving initial vacancy or interstitial formation
alkali fluorides, ESR study of interstitial atomic H centres 79−56609
alkali halide, dynamics of nonrelaxed and self-trapped holes *(Russian)* 80−80607
alkali halides:Ga^+, Jahn-Teller effect, EPR study 78−43690
alkali halides, ^{14}N impurities, molecular point defects, EPR isotropic hyperfine triplets 80−2636
alkali halides, EPR in relaxed excited state of F-centres, detection via saturated optical pumping 78−6606
alkali halides, F-centres, ESR in different states of relaxed configuration 80−108067
alkali halides, self-trapped holes, ESR *(Japanese)* 79−73811
alkali halides, spin lattice relax. and g-shift 80−15799
alkali metal halide crystals, g-tensor anal. of S^- and Se^- centres, ESR 80−84650
alkali metal halides, F_2^- mag. reson. absorpt. spectrum 77−73079
alkaline earth fluoride, EPR of triplet state of self-trapped excitons 78−43684
alkaline earth molybdates, luminesc. centres, EPR meas. *(Russian)* 77−28442
alkaline earth orthosilicates, gamma-irrad., ESR spectra 79−51853
alkaline earth tungstates, luminesc. centres, EPR meas. *(Russian)* 77−28442
aluminophosphate glasses, multicomponent, γ-irrad., EPR study 79−91290
apatites with Ca deficiency, H atom stabilisation 78−23340
borate glass, containing Ag_2O, ESR obs. of electron trap centres 77−20697
chars, heat treatment, EPR rel. to temp., A-centers 78−43639
chars, heat treatment, EPR rel. to temp., spin centres 78−48036
chloroplast photosystem II photoinduced EPR centres 79−39372
conference on optical techniques in mag. reson. spectroscopy, Dublin, Ireland (Aug. 1977). 78−43683
diamond: Sb, ion implanted, defect study using optical absorpt. and EPR 80−24480
diamond, electron irrad. induced ESR centres 77−84798
diamond, plastically deformed, EPR of two N atom centre 78−72408
diamond, type-IIa, electron irrad., EPR spectrum 80−25210
discussed, IIa, electron irradiated, at 80K, interstitial-impurity complexes 78−76310
F centre, EPR in relaxed excited state, via mag. circular polarisation of emission 79−24232
F- and F_A-centres, EPR and spatial extn. of relaxed excited state 79−73812
F-centres, relaxed excited state, spin polarisation, saturated optical pumping 79−15522
fluorochloroapatite, synthetic, defect struct. and colour centres obs. *(Russian)* 78−30612
glass, colour centre form. by UV irrad., afterglow, thermolum. and EPR obs. 78−10047

paramagnetic resonance of colour centres continued
glass, Libyan Desert Glass, redox form. conditions, EPR obs. of as-received and irrad. samples 78−28228
glass-ceramics, transparent, microstruct. and props. 78−59960
high-pressure cell for meas. at hydrostatic pressures to 60 kilobars 78−54418
II-VI compounds, electron energy radiation damage threshold meas., EPR and luminesc. 77−84799
ionic crystal defects, mag. reson. studies 80−108066
ionic halide crystals, mol. model for V_k centre 77−85567
metal colloids in ionic cryst., preparation, optical, mag. resonance, elec. props. 80−59459
nonmetallic crystals, ENDOR of impurity centres 80−25249
oxides, excited states of F-centres 78−64006
polypropylene, gamma-irradiated, active centres recombination kinetics, ESR study *(Rumanian)* 79−19778
porous glass, irradiated, accumulation and decay of paramagnetic centres *(Russian)* 77−85570
α-quartz:Ag, Ag atom paramagnetic centre, $A_{Ag\text{-}Si}$ 78−76308
α-quartz, CNDO/2 calcs., electronic props. of perfect cluster, EPR parameters of O^- vacancy 80−107701
α-quartz, EPR of E'_4-centre 79−73810
quartz, rose, charge transfer mechanism for origin of colour, EPR and optical expts. 78−52537
quartz, synthetic, Al centres conc. and anomalous pleochroism depend. on crystn. parameters 80−107311
quartz, synthetic, deuterisation, EPR and IR absorpt. characterisation 80−92721
quartz, synthetic, electron beam irrad., defect form., annealing and migration effects, ESR obs. 80−50180
quartz, synthetic, electron beam irrad.-induced interstitial ion mobility, ESR centres and IR spectra meas. 80−39153
α-quartz, synthetic, growth, defects induced by seed orientation 80−96454
α-quartz, uncompensated Ti^{3+} centre, annealed, X-irrad. 79−65731
α-quartz, X-irrad., paramag. Ag_2^+/AlO_4 centre, EPR obs. 79−28612
quartz fibre, ESR and IR obs. of microinhomogeneities 77−8401
radiation damage tetragonal R2 centre, optical and EPR spectra 78−2888
silicate glass, dangling bond states 80−24846
sodium metaphosphate glasses, γ-irrad., ESR 78−23339
spinel transparent glass ceramics, colour centre form. due to alkali metal vapour and X-ray irradiation 79−87316
trialkylammonium, iodides, absorpt. and luminesc. spectra of self-localized excitons 80−97340
Zeeman interaction, relativistic corrections and very small g-shifts, contrib. to EPR 78−72393
zircon, natural and synthetic crysts. Hf and Tb activated, capture centres and luminescence mechanism *(Russian)* 77−28626
α-quartz:Ge, Ge^{3+} centres, dynamic interchange, EPR obs. 79−19776
Ag halide, EPR of triplet state of self-trapped excitons 78−43684
Ag halides self-trapped holes, ESR *(Japanese)* 79−73811
AgBr:Ni^{2+}, low-temp. EPR 77−77091
AgBr:Pd(II), photolysis-induced trapping behaviour, EPR study 80−54949
$AgBr_{1-x}Cl_x$, ESR of self-trapped holes, Jahn-Teller and reorientation effects 78−27092
$AgBr_{1-x}Cl_x$, mixed cryst., formation of self-trapped holes 78−39399
$AgBr_{1-x}Cl_x$, self-trapped holes, ESR meas. 77−36131
$AgBr_{1-x}Cl_x$, self-trapped holes, Jahn-Teller and reorientation effects in ESR 78−64273
AgCl, paramagnetic S-centres, saturation props., ESR meas. 80−50181
AgCl:Ni^{2+}, low-temp. EPR 77−77091
Al_2O_3, γ-irrad., hole centres, luminesc. and EPR obs. 77−32256
β-Al_2O_3-$K_2O(Na_2O)(H_3O^+)$, ESR of paramag. defects in cond. planes 80−29617
β-Al_2O_3-Na_2O, colour centre ESR by localised tunnelling states 80−108073
β-Al_2O_3-Na_2O, EPR and optical absorpt. studies of X-ray produced defects 78−95517
β-Al_2O_3-Na_2O, tunnelling states, electron spin relax. 79−78518
β-Al_2O_3-Na_2O, X-ray induced defects, EPR and ENDOR study 80−60456
$AlPO_4$, synthetic berlinite, electron irrad. effects, ESR, ENDOR, optical spectral study 80−80608
As, amorphous, thermally generated paramagnetism 79−19720
As_2S_3, glassy, X-ray induced paramag. colour centres 78−19327
As_2Se_3, glassy, X-ray induced paramag. colour centres 78−19327
B-C system, struct. of paramag. centres 80−20460
B_2O_3-Li_2O-LiCl glass, X-irradiated, EPR of Cl_2^- centres *(French)* 79−47333
$[(100\text{-}x)B_2O_3.xLi_2O]_{98}.2CdO$, glass, X-ray irrad., EPR study of Cd^+ centres *(French)* 78−43638
$BaBr_2$:K^+, X-irradiated, perturbed F-centre, EPR and optical absorption 77−68966
$BaCl_2(Br_2)$, F-centre localisation, absorpt. spectra calc. and EPR spectra analysis 77−48203
BaF_2, mag. hyperfine const. and lattice distortion of V_k-centre 77−62864
BaF_2:Cd^{2+}, X-irrad., ESR of Cd^+ centres 77−59459
BaO-Al_2O_3-B_2O_3:Ce^{3+} glass, EPR spectra, before and after X-irrad. 78−19320
BaO-Al_2O_3-B_2O_3:Ag, X-ray irrad., atomic centre interactions, EPR spectra 80−25207
$BaSO_4$, X-ray irrad., electron and holes traps, g-factors, ESR obs. 80−50183
$BaT:O_3$:Mn, ferroelec. domain stabilisation by bulk ordering of defects 79−42925
$BaTiO_3$, H_2-reduced, elec. cond. mechanism, EPR, resist. and Seebeck coeff. meas. 80−10976
$BaWO_4$:Mo, P, thermoluminesc. traps, EPR meas. 77−90032
BeO, ceramic and single cryst., EPR-ENDOR study of [Li]° centre 77−85569
CSI:Na cryst., V_K-Na^0 centre pairs, tunnelling recomb. 78−91952
Ca fluorapatites, carbonated, B-type, EPR of F^+-centre after X-irrad. *(French)* 80−108065
$CaCO_3$:Li, CO_3^{3-}-Li^+ centre, irradiated synthetic single crystal, bond angle and wave function 77−81006
$CaCO_3$:Li, synthetic calcite, $(CO_3Li)^{2-}$-Li^+ defect after X-irrad., EPR study 80−75852
CaF_2, doped, colour centre form. by UV irrad., afterglow, thermolum. and EPR obs. 78−10047

paramagnetic resonance of colour centres continued
CaF_2, low symmetry U^{5+} centres 78−76307
CaF_2, mag. hyperfine const. and lattice distortion of V_k-centre 77−62864
$CaF_2:Cd^{2+}$, X-irrad., ESR of Cd^+ centres 77−59459
$CaF_2:Dy^{3+}$, EPR of colour centres, spin-spin interaction of pair of Dy^{3+} ions *(Russian)* 79−69751
CaF_2:Ni, X-irradiated, optical and EPR meas. 80−108235
CaF_2:U, γ-irrad., EPR and luminesc. studies of U^{5+} and U^{6+} centres 79−51854
$CaF_2:U$, U^{5+} centres, nonoctahedral symmetry 80−11266
$CaF_2:U^{3+}$, Na^+, EPR, orthorhombic U^{3+} centre 77−77100
$CaF_2:U^{5+}$, single cryst., EPR 78−19325
$CaF_2:U^{5+}$, trigonal centres, hyperfine parameters, EPR 78−43643
$CaF_2:U^{5+}$, trigonal EPR spectrum 78−15021
$CaFPO_3$, colour centre form., X-ray and electron bombardment *(Russian)* 77−19948
$CaMoO_4$, scheelite struct., intrinsic hole centres, EPR study 78−64274
CaO, $^3T_{1u}$ of F-centre, EPR, unaxial stress effects 78−48040
CaO, $^3T_{1u}$ state of F-centre, ODMR spectra 78−43685
CaO, $^3T_{1u}$ state of F-centre, paramag. relax. optical detect. 78−43687
CaO, additively coloured powder, F+ centre, 295K *(Russian)* 80−84649
CaO, doped, thermal stability of hole centres and hole recombination luminescence *(Russian)* 78−72614
CaO, F_A(Mo) centre, spin coherence zero-field double reson. 78−43689
CaO, F-centre, selective excitation, detection of EPR 78−43688
CaO, F-centres, $^3T_{1u}$ relaxed excited state, uniaxial stress effect and spin-lattice coupling 78−72405
CaO, F-centres, laser selective excitation and double reson. in Jahn-Teller systems 78−19379
CaO, line broadening of EPR and zero phonon lines of F centres 78−43686
CaO, undoped and Cl-, F- or Al-doped, X-ray and UV luminesc., electron-hole recombination processes *(Russian)* 78−76528
CaO:F(Cl)(Al), phosphon, luminesc., electron-hole recombination processes 79−65919
$Ca(OH)_2$, V-centres, EPR obs. 77−48051
$Ca_3(PO_4)_2$-$CaCl_2$:F^-, EPR of electron excess centres 78−10772
CaS, additively coloured powder, F+ centre, 295K *(Russian)* 80−84649
CaS, polycryst., point defects, EPR obs. 79−61214
$CaSO_4$, γ-irradiated, ESR and bleaching studies of radical ion centres 80−2637
$CaSO_4$ with rare-earth and Y dopants, ESR, thermolum. correlation studies following gamma irradiation 77−59628
$CaWO_4$, scheelite struct., intrinsic hole centres, EPR study 78−64274
$CaWO_4$:Mo, P, thermoluminesc. traps, EPR meas. 77−90032
$Cd_xCa_{1-x}MoO_4$, intrinsic hole centres EPR study, thermoluminescence and thermal decay 79−99957
CdS, electron and hole trapped centres, EPR, photoluminescence, photoconductivity study 80−108071
CsBr, F-centres, EPR in relaxed excited state, detection via saturated optical pumping 78−6606
CsBr, F-centres, relaxed excited state, ESR, detected via optical pumping 78−43693
CsBr, luminesc., mag. circ. polaris., self-trapped excitons, EPR 79−33805
CsBr, second relaxed excited state of F-centre, optically detected EPR 79−87335
CsBr:Tl^+, ESR of [X_2^-] centres 79−33533
CsBr(Cl), spin-lattice relax. of F-centres, magneto-optical meas. 77−43884
CsCl, F-centres, EPR in relaxed excited state, detection via saturated optical pumping 78−6606
CsCl, F-centres, relaxed excited state, ESR, detected via optical pumping 78−43693
CsCl:Tl^+, ESR of [X_2^-] centres 79−33533
CsCl(Br)(I), F-centre ESR in relaxed excited state, isotropic superhyperfine interaction consts. 79−65733
CsI, determ. of centres producing 300 nm emission band 78−75998
CsI:Na, X-ray irradiated, optical and ESR studies in IR absorption band 80−80828
CsI(Br)(Cl):Tl, [X_2^-] centre dynamic props. 79−65730
$CuGaS_2$, coloration, pure and Fe doped, EPR and optical absorpt. obs. 78−88336
EuO nonstoichiometric film, ESR spectra and exchange interaction 80−93176
GaP:Fe(Cr), photo-ESR of annealed crysts. 80−15795
Ge-S, glass, ESR, model of paramag. defects 79−78517
GeO_2, radiation damaged, paramag. point defects, F-centres, ESR, absorpt. spectra 78−80213
$GeO_2:Sc^{3+}(Y^{3+})(In^{3+})$, trapped-hole centres, ESR meas. 79−77597
$Ge_{100-x}S_x(Se_x)(Te_x)$, amorphous film, effect of alloying chalcogen atom on elec. cond., optical transmission and ESR 79−78101
Ge_xSe_{1-x}, amorphous, excitation spectra of photolum. fatigue and creation of paramag. centres 80−50402
Ge_xSe_{1-x} glasses, defect states, photoluminesc. and ESR obs. 79−61418
HfO_2, stabilised, low temp. induced centres, ESR meas. 78−72409
KBr, cation defects creation mechanism 80−75224
KBr, F-centre spin-lattice relax., theory and MCD meas., phonon-modulated HFS 77−43883
KBr, S centres, luminesc. and photochemistry *(German)* 77−44055
KBr, with Frenkel cation defects, EPR and thermolum. of V_F, V_2-centres 78−10769
KBr:Ag, formation of electron centres and self-localised holes, ESR exam. 78−91947
KBr:Li(Na), F_A centres, optical detection of ESR 79−99793
KBr:NO_2, X-irrad., paramag. and nonparamag. hole centres 77−16176
KBr:Na, U-centres, HFS and g-factor, EPR spectra 80−39869
KBr(Cl), F_A(Li)-centre spin-lattice relax. at 4.2K 78−91950
KBr(Cl):Eu, Z_2-centre investig. by EPR and optical absorpt. 77−16177
KCN, relax. times of F-centres meas. at 83K phase transition 77−59458
KCN:HCN^-, structural props. using ESR 80−25205
KCl, F centre, EPR in relaxed excited state, via mag. circular polarisation of emission 79−24232
KCl, F-center pairs, light excitation, mag. field and resonance effects on absorption bands 78−92094
KCl, S centres, luminesc. and photochemistry *(German)* 77−44055
KCl, with Frenkel cation defects, EPR and thermolum. of V_F, V_2-centres 78−10769
paramagnetic resonance of colour centres continued
KCl, Z_2 centres in triplet state, EPR study 80−108068
KCl:Ag, Br, EPR spectra of $Ag^0(Br_I)$ paramag. centres *(French)* 79−11346
KCl:Ag, formation of Ag atoms and self-localised holes by illumination, EPR meas. 78−31108
KCl:Ag(Tl), formation of electron centres and self-localised holes, ESR exam. 78−91947
KCl:Br^-(I^-), interstitial atomic H centres, formation kinetics and struct. MO calc. and EPR studies 80−75854
KCl:Ca, Z_2-centres, optical absorpt. and ESR spectra 79−91480
KCl:Cd, EPR of anisotropic Cd_F^+ centres, similarity to Z-centres 77−77101
KCl:Cu, EPR, optical absorpt. and luminesc. investig. of anisotropic Cu_F^0 centres 77−20893
KCl:Eu, additively coloured, ESR obs. of $^{2+}$ complex 77−16170
KCl:Eu, OH^-, EPR meas. on Eu^{2+} complex 78−10773
KCl:Ga(In), ESR of impurity centres, impurity optical absorpt. bands 80−29618
KCl:Ga(Tl,Pb), X-irradiated, EPR spectra 79−28613
KCl:H, dichroic H- and U-centres by polarised bleaching of interstitial H, ESR study 80−29766
KCl:H, ENDOR and ESR study of anion sites 80−108118
KCl:H, migration and stabilisation of H atoms, ESR and thermolum. study 79−1430
KCl:$K_4Os^{II}(CN)_6$, electron irrad., EPR, ligand hyperfine struct. 78−60335
KCl:Li,H optical and EPR exam. of H centre, $(LiH)^+$ absorpt. spectra 79−99920
KCl:Li^+, restricted interstitial motion of $H_A(Li^+)$ centre, ESR and uniaxial stress expts. 77−48053
KCl:Na, F_B centres, optical detection of ESR 79−99793
KCl:Na,Br, EPR of interstitial and diinterstitial $BrCl_2^{2-}$ centres 77−81007
KCl:Na(Ag), UV irrad. anionic H and D atoms, ESR and optical absorpt. expts. 79−99187
KCl:Sn^{2+}, EPR exam. of struct. and prod. of $Sn^-(5p^3,4S)$ defects 79−61215
KCl:$SnCl_2$, Sn^+ centres, polarised luminesc. and EPR 79−65076
KCl:$SnCl_2$, X-ray irrad., polarised luminesc. and EPR study of Sn^{3+} centres 80−39868
KCl:Sr, triplet state of F_2-centres, ESR spectra 80−29616
KCl:Tl, ESR of trapped electron and hole centres 79−78516
KCl:Yb, Z_2-centres, optical absorpt. and ESR spectra 79−91481
KCl-Mg, X-irrad. and F-bleached, optical and ESR spectra 77−48052
KCl(Br), second relaxed excited state of F-centre, optically detected EPR 79−87335
$KClO_4$, X-irrad. induced paramag. defects, ESR study 80−24493
KF:U, X- and γ-irrad., EPR of U^{5+} centre charge compensation mechanism 77−90030
KH_2PO_4:KH_2AsO_4, X-irrad., EPR 77−32257
$KMgF_3$, F-centre ENDOR study 80−108117
$KMgF_3$, struct. of H-centre, low-temp. EPR meas. 77−12202
$KMg_3[AlSi_3O_{10}].F_2$ with excess Al, synthetic fluorphlogopite, radiation-induced paramag. O^- centres 80−60417
Li disilicate glass, radiation induced centres, EPR exam. 78−35033
LiCl, neutron irradiated, EPR exam. 78−76309
LiCl:Cd, EPR of anisotropic Cd_F^+ centres, similarity to Z-centres 77−77101
LiF, V_t centre (F_3^{2-}) identification, ESR spectrum anal. 80−7164
LiF:Mg, X-irrad., colour centres, ESR and UV asborpt. meas. 80−108069
LiF:Mg(Ag), electron spin-lattice relax. of V_k-centre 78−95518
LiF:OH, neutron irrad., interstitial H-centres, ESR obs. 80−93175
LiF:U, X- and γ-irrad., EPR of U^{5+} centre, charge compensation mechanism 77−90030
LiF:U, X-ray and γ-ray irrad., EPR of U^{5+} centres 79−91295
LiF:U_3O_8, X- and γ-irrad., U^{5+} luminesc. molecular centres, optical and ESR expts. 77−48224
LiH, defect form. at low temp., EPR, thermolum. and TSC study 80−107222
LiH, formation and annihilation of Li colloids and H bubbles 80−107228
Li_3N, defect struct., quartet state paramag. centres, EPR meas. 79−42837
Li_3N, superionic conductor, cryst. growth and struct., phys. props., book contrib. 79−42308
$LiNbO_3$, pure, two-photon photorefractive recording 78−31220
$LiNbO_3$, two-photon and X-ray induced Nb^{4+} and O^- small polarons, ESR and optical absorpt. 78−76306
$LiNbO_3$, X-ray photovoltaic effect and its correl. with ESR 79−82639
Li_2O, neutron irradiated, ESR of F^+, O^-, H^0 and colloidal Li centres 78−2737
Li_2O pellets, sintered, neutron irradiated, ESR study 80−92566
$LiYF_4$, electron-irrad. induced defects, optical and EPR study, impurity effects 80−66238
MgF_2, EPR of electron irrad. induced F interstitial H- and H_A-centres 77−77099
MgF_2, gamma- or neutron irradiated, ESR meas. on hole centres 77−12201
MgO, doped, thermal stability of hole centres and hole recombination luminescence *(Russian)* 78−72614
MgO, radiation induced O interstitials, EPR meas. 78−55866
MgO:Al(Li)(F)(Sn), hole processes in photostimulated luminesc., electron emission, X-ray irrad., ESR relaxation 79−69889
MgO:Fe^{3+}, Mn^{2+}, X-irrad. induced anion Frenkel defects, stabilisation by Fe^{3+}, optical and ESR obs. 77−68969
MgO:Ga, γ-irradiated, EPR and optical studies 79−73809
MgO:Li, $[Li]^0$ defect, high temp. and ionisation induced effects 78−34509
MgO:Li, thermally generated $[Li]^0$ defects, valence compensation 79−77598
MgO:Sn(Al), ESR of colour centres-destruction temp. 78−10998
MoO_3 amorphous films, EPR of Mo^{5+} centres 80−34771
MoO_3, EPR investig. of defect centres 77−59457
$NaAl_3(PO_4)_2(OH)_4$, EPR of at. H caused by X-rays 79−28614
NaBr(Cl), spin-lattice relax. of F-centres, magneto-optical meas. 77−43884
NaCl, migration of nonrelaxed holes, self-trapping, ESR and luminesc. obs. *(Russian)* 80−66033

paramagnetic resonance of colour centres continued
NaCl, second relaxed excited state of F-centre, optically detected EPR 79−87335
NaCl:$(Mn^{2+}$-□$)_{Fanion}$, F^- assoc. complex, ionic thermocurrent and EPR 79−8086
NaCl:Ag, formation of Ag atoms and self-localised holes by illumination, EPR meas. 78−31108
NaCl:Ag, formation of electron centres and self-localised holes, ESR exam. 78−91947
NaCl:Cd, EPR of anisotropic $Cd_F{}^+$ centres, similarity to Z-centres 77−77101
NaCl:Cu^+, X-irrad., anisotropic Cu centre anal. 79−78714
NaCl:Ga(In), ESR of impurity centres, impurity optical absorpt. bands 80−29618
NaCl:Ga(Tl,Pb), EPR spectra 79−28613
NaCl:Li, U-centres, HFS consts., g-factor, EPR spectra 80−39869
NaCl:$Mn^{2+}(Zn^{2+})(Sn^{2+})$, electrolytically coloured, CESR 77−16174
NaCl:V^{2+}, X-irrad. and unirrad., EPR of isolated V^{2+} ions 79−15347
NaCl:Zn^+, X-irrad., EPR and optical absorpt. 78−43642
NaCl(Br), X-ray or UV irradiated, cation defects creation mechanism 80−75224
NaF:K^+, γ-irradiated, H_A(K) centres, EPR obs. 77−69689
NaF:U, X- and γ-irrad., EPR of U^{5+} centre, charge compensation mechanism 77−90030
$NaLa(MoO_4)_2$, luminesc. centres, EPR meas. *(Russian)* 77−28442
NaN_3, UV irradiated, F-centre ESR 77−28444
Na_2O-SiO_2:CuO glass, gamma-irradiated, EPR and optical spectra 80−103885
$Na_5P_3O_{10}$, γ-irrad., $PO_3{}^{2-}$ EPR obs. 78−27091
$NaReO_4$, EPR spectra of paramag. centres and free radicals 80−108072
PbO-SiO_2 and Na_2O-PbO-SiO_2 system glasses, radiative paramag. and optical absorpt. centres 77−8402
PbS film, appearance of EPR centres in initial form. stage *(Russian)* 77−63283
RbBr(Cl) F centre, EPR in relaxed excited state, via mag. circular polarisation of emission 79−24232
$RbCaF_3$, V_K centres, lattice distortion in tetragonal phase, EPR meas. 77−20699
RbCl, F-centre ESR in relaxed excited state, isotropic superhyperfine interaction consts. 79−65733
RbCl:$Br^-(I^-)$, interstitial atomic H centres, formation kinetics and struct. MO calc. and EPR studies 80−75854
RbCl:Na, U-centres, HFS consts., g-factors, EPR spectra 80−39869
RbCl(Br), cation defects creation mechanism 80−75224
^{85,87}RbCl isotope enriched cryst., optical registration of EPR F-centres *(Russian)* 80−103886
Si, amorphisation due to heavy ion irradiation, ESR meas. 77−11606
Si, amorphous layer prod. by ion implantation, diffusion broadening, ESR study 80−92552
Si, divacancies orientation induced by IR light, EPR spectra 80−25209
Si, EPR of radiation defects, temp. depend. 78−15023
Si, electron irrad., two-vacancy defect EPR 80−29619
Si, electron irradiated, O-vacancy pair, EPR of optical absorption 77−16173
Si, interstitials and lattice vacancies 78−10038
Si:Ar(Ne)(O)(N), ion-implanted, defect reverse annealing, 550-650°C 80−88875
Si:C, electron irrad., C interstitial, photo EPR 77−16175
Si:H, amorphous, defect states, luminesc. and ESR obs. 80−76075
Si:O, EPR spectra of heat treatment centres 78−48039
Si:P, heavily doped, EPR spectra of electron irradiation induced defects 77−81008
Si:P, polycryst. films, elec. props., EPR, defect states, doping effects 80−75660
Si-SiO_2, ESR centres, interface states and oxide fixed charge 80−2474
Si-SiO_2 interface, electrically active paramag. centres detect., photocond. reson. obs. 80−50185
Si-SiO_2 interface, surface states and elec. defects obs. using ESR 78−23169
n-SiC, thermal defects, ESR study 80−88876
SiO, doped, thermal stability of hole centres and hole recombination luminescence *(Russian)* 78−72614
SiO_2, dangling bond states 80−24846
SiO_2, disperse, EPR, O_2 vacancy relax. rel. to substrate struct., gas adsorpt. *(German)* 79−95645
SiO_2, fused, γ-irrad., O-associated trapped-hole centres, optical absorpt. and ESR spectra obs. 79−65729
SiO_2, g-tensor and ^{29}Si hyperfine tensors of E_1'-centre for model of O^- vacancy, EPR parameters 79−19777
SiO_2, g-tensor of interstitial O and broken Si-O bond, MO model calc. 79−78520
SiO_2, glass, ^{29}Si hyperfine struct. of E′ centre, microwave saturation props. 80−7165
SiO_2, glass, irrad., EPR of Al E_1′ centres 80−11268
SiO_2 glass, low press. plasma treatment, paramag. defect form. *(German)* 78−23341
SiO_2, noncryst., radiation-induced defect centres, ESR spectra and struct. 78−23343
SiO_2 surface, Ar plasma-treated, O_2 adsorption reactivity, EPR obs. 79−51418
SiO_2, vitreous, low temp. thermal props. and intrinsic defects 80−29057
SiO_2, vitreous, neutron irrad., luminescence nature and ESR signals correl. 79−43038
SiO_2, vitreous, paramag. centres associated with bonding defects 80−80609
SiO_2:Ag, fused, crystalline, ESR 78−10954
SiO_2-K_2O-CeO_2-Sb_2O_3, polychromatic glass, Sb^{4+} centre, EPR obs. 79−87317
SiO_2-Na_2O-CeO_2-Sb_2O_3, polychromatic glass, Sb^{4+} centre, EPR obs. 79−87317
SiO_{2-x} system, model for paramagnetic E′-centre 78−35034
SiO_x, amorphous, ESR and hopping cond., He^+ irrad. effects 79−61213
$SrCl_2$:S, S_2^- and S_3^- mol. paramag. centres, investigation using EPR, Raman and optical spectroscopy 79−51855
SrF_2, mag. hyperfine const. and lattice distortion of V_k-centre 77−62864
SrF_2:Cd^{++}, X-irrad., ESR of Cd^+ centres 77−59459
SrO, hydrogenated, EPR and ENDOR meas. of γ-irradiated cryst. 77−8403
SrO, trapped hole defects, ENDOR and EPR spectra of V-centres 77−32255
SrO:D, γ-irrad., V_{OD} defects, EPR and ENDOR 78−27116

paramagnetic resonance of colour centres continued
$SrSO_4$, celestite, colouring mechanisms 79−82998
SrO, x-irradiated, intrinsic V^- and V^0 centres, ESR exam. 77−40126
TiO_2, X-irrad., adsorpt. of O_2, EPR meas. 78−80211
TiO_2:Ga^{3+}, EPR spectra of trapped hole centre 78−80214
WO_3 films, ESR study after colouring by H_2 injection and after bleaching in air 80−39867
WO_3, single cryst. and amorphous film, ESR of defects 78−10770
α-$W_xV_2O_5$, paramag. defect study by ESR 80−103881
YAG, transient colour centres caused by UV radiation 77−84744
Y_2O_3, formation and changes in point defects, EPR, optical transitions and thermolum. spectra 78−2118
Y_2O_3:Zr^{3+}, F-centre charge state, ESR and thermally stimulated luminesc. obs. 80−60418
ZnO:Li, electron irrad., F^+ centre, photosensitivity of e.p.r. spectrum 77−1594
ZnS, electron irrad., ESR 79−91293
ZnS:Pb, blue luminesc., photoexcited EPR spectrum 80−108070
ZnSe:Mn^{2+} Schottky barrier diodes, spin depend. cond. and photovoltage, donor reson. deep centre studies 79−91141
ZrO_2 $1.6H_2O$, anion defect formation and annealing during thermal decomp. in vacuum 77−51366
ZrO_2, stabilised, low temp. induced centres, ESR meas. 78−72409
$ZrSiO_4$, natural, radiation defect centre, EPR obs. 80−75853
$ZrSiO_4$, X-irrad., trapping and emission centres, OH^- ion contribution 80−80876

paramagnetic resonance of conduction electrons *see CESR*

paramagnetic resonance of free radicals
acenaphthene single crystals, radicals produced by γ irrad., room temp. EPR study 78−84483
acetate radical CIDEP, appl. of ns time-resolved EPR in pulse radiolysis 80−43075
N-acetyl-DL-valine, monocrystal, γ-induced free radicals at 77K 79−24774
N-acetyl-DL-valine, single cryst., paramag. centre form. by UV photolysis, room temp. 77−21480
N-acetyl-L-cysteine, X-irrad., ^{33}S nucl. coupling and nature of free radicals 77−52743
acetylacetonate, in nematic liq. cryst., EPR singularities in partially ordered matrix 77−77103
N-acetyle DL-methionine, γ-irradiated, radical cation EPR, ^{33}S hyperfine coupling 77−40559
N-acetylglucosamide, substrate-inhibitor of lysozyme, localisation of unpaired electrons 78−68992
N-acetylglycine, X-irrad., stable radical electronic and mol. struct., ENDOR and ESR 80−80637
acid amide+H_2O_2, aq. solns., photolysis, EPR study of spin-trapped radicals formed during photolysis 78−68996
acridine C-radical, polarised absorpt. and ESR spectra, dichroism and HF-CI calc. 78−50563
acyloxy radical ion, in irrad. Rochelle salt, decarboxylation, pulse radiolysis and EPR obs. 78−70854
adamantane, γ-irrad., free radicals EPR and ENDOR 80−69170
agriculture applications 80−56298
L-alanine:Cr^{3+}, X-irrad., thermoluminesc., ESR, UV photobleaching 77−9104
L-α-alanine, cryst., cationic radicals, EPR 78−11537
β-alanine, cryst., X-irrad. producting radicals, ESR and ENDOR 79−56612
alcohols, glassy, diffusion of radical-ion pairs, spatial distrib., electron spin echo obs. 80−29622
aliphatic alcohols-2,2,6,6-tetramethylpiperidine nitroxide radical complexes, EPR, PMR, hyperfine coupling consts. 79−65736
aliphatic amino acids, N-acetyl substituted, photolytic production of methyl radicals 79−96622
alkali borate and silicate glasses, γ-irrad., paramag. SO_3^- radicals 79−42838
alkanes, electron localisation and solvation, radical ion theory 78−87936
n-alkanes, single cryst., γ-irrad., ESR, energy deposition rel. to alkyl radical form. 77−16844
alkoxy free radicals, produced by X-irrad. of hydroxy containing cpds., characterisation by ESR and ENDOR 78−95938
alkoxy radical, trapped in nucleosides or nucleotides, EPR, INDO calcs. 77−90623
N-alkyl free radicals, ESR study, conformational anal. of N-alkyl group 78−62831
alumina, adsorption of electron acceptors, ESR and electronic spectra 77−48681
aluminosilicate glasses, Cr_2O_3, TiO_2 and Nb_2O_5 containing, paramagnetic defect formation, ESR study during crystn. 79−65739
amides, substituted, aqueous solns., UV-irradiated, EPR and spin-trapping studies 79−16154
amino acid, in polycryst., γ-irrad. induced radical pair form., 77K, EPR obs. 78−85292
α-amino acids, γ-irradiated, primary oxidation products, ESR and ENDOR 77−48754
amino acids, aq. solns. EPR of spin-trapped radicals, hydrated electron reactions 78−27796
amino acids, X-irradiated, determ. of radical yields 79−34491
amino radical adsorbed on zeolite, extra coupling with ^{23}Na 77−7963
4-amino-2,2,6,6-tetramethylpiperidine-N-oxyl and deuterated derivatives, mag. resonance study 80−63686
α-aminoisobutyric acid, cryst., γ-irrad., cation radicals, ESR obs., SCF-MO-INDO calcs. 78−11537
ammonium acetate, irrad. crysts., freq. swept ELDOR obs. at 77K, resolution of spin packets 79−95686
amobarbital, radiation-prod. free radicals in pyrimidines 77−25374
dAMP.dTMP costacking complexes, γ-irrad., charge migration, computer-assisted EPR 77−86446
animals cells, effect of lyophilisation on free radical states 77−25391
anisotropic media, line broadening of ESR spectra of spin probes 77−12203
anthracene, α-induced radical production beyond Bragg peak 79−24773
anthracene, γ-irrad., radical pairs EPR detection 78−31664
anthracene, irradiated, optical absorption and EPR meas., low temps. 78−68538
anthracene, radiation-induced radicals, EPR and optical absorpt. obs. 77−12816
anthracene, radical cation, EPR, acidic surface anisotropic rot. diffusion 78−27095

paramagnetic resonance of free radicals continued
anthronyl radicals, ESR, temp. depend. phenyl twist angles 79−18210
aromatic hydrocarbons, melting behavior and role of free radicals and molecular site in producing mesophase pitch 79−90523
aromatic polycrystals, γ-irrad., radical pair form., EPR meas. 78−80757
aromatics in stretched PVA films, ESR of phosphorescent triplet state 77−30908
L-asparagine.H_2O, X-irrad. at room temp., ESR and ENDOR 77−40131
atmospheric free radicals, meas. by matrix isolation EPR 78−46374
atmospheric radical conc. meas. 78−73535
atomic parameters, He to Bi, Hermann-Skillman wavefunction calc. 78−91956
ATPase, Ca^{2+}-depend., struct. rearrangements during function 80−81527
9-aza-bicyclo (3,3,1)nonan-3-one-9-oxyl, dimerisation, ESR, NO radical pair exchange 78−19330
bacteria, photosynthesis, primary electron acceptor, EPR, ENDOR investigs. 78−77004
bacteriochlorophyll radicals, role in primary charge separation of Rhodopseudomonas viridis 80−63688
bacteriopheophytin b radicals, role in primary charge separation of Rhodopseudomonas viridis 80−63688
bacteriorhodopsin photoconversion products, EPR and low temp. spectrophotometry 78−15769
bacterioviridin, photochem. oxidation mechanism 77−25370
bacterioviridine photo-oxidation in monomer and aggregated states, free radical form., EPR 78−76994
barium formate, γ-irrad., ESR of free radicals 79−65737
benzene, γ-irrad., radical pairs EPR detection 78−31664
benzene, γ-radiolysis, phenyl radical intermediate, spin trapping, EPR 78−7218
benzene, plasma polymerisation in glow discharge, thin film IR and free radical EPR obs. 80−2964
benzophenone in isopropanol, submicrosecond time resolved EPR, lser photolysis, CIDEP polarisation mech. 78−80764
1,4-benzosemiquinone, monoprotonated radical, spin distrib., INDO calcs. 77−14357
p-benzosemiquinone monoprotonated radical, submicrosecond time resolved EPR, lser photolysis, CIDEP polarisation mech. 78−80764
2,1,3-benzothiadiazole, EPR of phosphorescent state 77−8405
benzyl-phosphonium radical, EPR spectra temp. depend., H-P coupling consts., conformation and rot. *(German)* 77−18950
binary complex, quinone-phenol radical pair EPR, geometry calc. 78−90101
biological tissue, Dy^{3+} as free-radical relax. agent in biological tissues 78−81090
biomolecular EPR and saturation transfer EPR spectra at high microwave field intensities 79−34488
biomolecules, conformation and struct., ESR, NMR and optical meas. 80−26201
biphenyl gluterate diacetylene, monomer, single cryst., stable and metastable UV photoexcited states, EPR obs. 79−78522
biphenyl single crysts., γ-ray induced radicals, EPR and optical absorpt. studies 80−44921
biradical metal chelates, rot. motion in polar solvents, rel. to ESR lineshape 80−27994
1,2-bis(p-tolysulphonyloxymethylen)-l-buten-3-inylen, ESR of X-irrad. cryst., 77K 79−11806
1,3-bisdiphenylene-2-phenyl allyl benzene complex, free radical, EPR, antiferromag. long range ordering 79−47335
bisgalvinoxyl biradical, cryst., spin-spin dipolar and exchange interactions, EPR 78−52356
borate glass, ESR of SeO_2^- and SeO_3^- radicals 79−65740
5-bromodeoxyuridine, single cryst., X-irrad. at 77K, C_5-centred deoxyribose radical 78−20032
α-bromofluoro alkyl pi-radical, signs of hyperfine and quadrupole couplings, ESR determ. 80−97141
N-bromosuccinimide, X-irrad., ESR study of Br and σ* radical 80−66037
cis-butene, ozonolysis, radical form., matrix ESR spectrosc. 80−16653
cadmium formate, γ-irrad., ESR of free radicals 79−65737
calcium tartrate tetrahydrate, X-ray irrad. single cryst., result of C-H bond splitting 77−63936
carboxylic esters, γ-irrad. glass, trapped radical photolysis, ESR 78−85178
cavern, dating with ESR and thermolum. *(Japanese)* 77−44955
CBOOA:nitroxide, liq. cryst. phase transition study by electron spin relax. *(French)* 79−55874
cells, ^{125}IUdR-labelled and X-irrad., 4.2K and above 80−72211
cetyltrimethylammonium bromide, micelles, solubilised nitroxide spin probes, ESR 78−21950
α-chloro radical in X-irradiated 5-chlorodeoxyuridine single crysts., ESR, ENDOR 77−4916
α-chloroacetamide, alkoxy radical form., effect, of α-hydroxyacetamide, ESR study 80−80610
chloroacetamide, X-irrad., ESR of CH_2ClCO radical 78−76382
5-chlorodeoxyuridine, single cryst., X-irrad. at 77K, C_5-centred deoxyribose radical 78−20032
chlorophyll photo-oxidation by quinones, cation-radical yield 77−86442
chloroplast, bean, effect of salts on form of EPR II signal 78−64952
chlorotrifluoroethylene radical anions, EPR spectra and struct. 79−31558
CIDEP, examples of S-$T_{\pm 1}$ polarisation 78−86891
citric acid, single cryst., X-irrad., EPR and ENDOR, 4.2K radical identification 79−65764
ClF_6, EPR of matrix, isolated radical 79−85977
computation, fast, EPR (ST-EPR) spectra, master supermatrix eqn. soln. 78−62213
computation, fast, of EPR and saturation transfer EPR, perturbation approach 78−62212
computer analysis, conc. determ. and resolution of multiple-component spectra 78−259
condensed media, electron localisation and solvation, radical ion theory 78−87936
conjugated, solvent effect in π-approx. calcs. of electronic transitions and spin densities 77−38623
copper porphyrins, mag. susceptibility and EPR, sample grinding effects 80−60420
coronene trimer radical cation, spin densities in CH_3Cl_2-CH_3NO_2 solvent mixture, −100°C 80−5565

paramagnetic resonance of free radicals continued
cotton fibre grown from γ-irrad. seed, struct. and conform., using spin labels 77−81539
18-crown-6 complexed sodium-2, 6-di-+-butyl-p-benzosemiquinone ion pairs, soln. ESR spectra, temp. and conc. depend. 80−63675
18-crown-6 complexed sodium-duroquinone ion pairs, soln. ESR spectra, temp. and conc. depend. 80−63675
cyclic monocarboxylic acid radicals, ring inversion barriers, EPR 80−53025
cyclic polyphenylacetylene, thermally excited paramag. props. 77−88614
1,1-cyclobutanedicarboxylic acid, X- and γ-irrad. cryst., EI-EPR overlapping spectra resolution 77−16179
cyclodextrin, trapped electrons in cryst. matrices, ESR, optical absorption spectra 78−80768
cyclohexane, neutron irradiation, radical distribution, ESR study *(Japanese)* 80−44920
cyclohexane, plastic-phase, NO-doped, heterogeneous solid soln., mag. reson. evidence 78−34449
L-cysteine HCl, free radical formation by two photon absorpt. at 3371 Å 77−32815
cytidine-5′-monophosphate, γ-irrad. aq. soln., spin-trapped radicals, liq. chromatography and EPR spectroscopy 78−53340
3′-cytidylic acid, X-irrad., stable radical in ribose moiety, compared with cytidine 77−25375
cytochrome c oxidase, struct. of cytochrome a_3-Cu_{a3} couple, NO binding studies 80−67039
cytosine derivatives, photosensitised induction by H-addition radicals in frozen aqueous soln. 78−20146
cytosine monohydrate, single cryst., γ-irrad., ion radical recomb. 78−15776
cytosine monohydrate single cryst., X-irrad., OH addition radical and decay product 77−86447
cytosine.H_2O crystals, radical form. by X-irrad. at 77 and 300K 77−12886
DBTTF halogen complexes, IR, UV spectra, EPR study 80−108215
deoxycytidene 5′-phosphate-H_2O, cryst., X-irrad., ESR and ENDOR obs. 79−34330
deoxycytidine 5′-phosphate, H_2O, X-irrad., 3αH radial. form., ENDOR, ESR 77−73453
deoxyribonucleoprotein, gamma-ray protein damage 78−53338
deuterated nitroxide radical probe, synthesis and appls. *(French)* 78−76314
di-t-butyl nitroxide, in benzene, solvent-solute interactions, ESR, DNP 78−17698
di-tert-butylazodicarboxylate, photochem. generated alkali cationic triple ions, ESR 78−80758
diacetylene, low temp. photochemical polymenisation, decay kinetics, ESR spectra obs. 80−100616
diacetylene, single cryst., EPR of low-temp. photoproducts, photopolymerisation 78−85175
diacetylenes, solid state photopolymerisation, reaction products, electron spin resonance anal. 80−81338
N,N′-dialkyl dipyridinium cation radicals, struct., INDO calcs., EPR obs. 77−71821
dibenzoyl peroxide, UV irrad., radical pairs EPR 79−73813
5,5′-diethylbarbituric acid, EPR and INDO-MO study of radical formation after irrad. 80−93774
dihalogenated benzene derivatives, 77K, gamma radialysis radical pair formation, EPR 79−29334
5,10-dihydro-5,10-diethylphenozinium-iodide, average struct. and props. 79−90636
dihydro-6-methyl uracil single cryst., electron and UV irrad. 77−29100
5,6-dihydro-6-methyluracil, X-ray irrad., free radical form; ESR spectra obs. 80−50189
dihydropyrimidine bases in aq. soln., spin-trapped OH radical reactions 79−88053
dihydrouracil, EPR study of light- and temp.-induced free radical conversions 80−35824
4,6-dihydroxypyrimidine, aq. soln., reaction with OH, short-lived radicals, ESR 80−101031
α-diketone radical anions, spin-lattice relax. in soln. 79−22735
dimethyl sulfone, X-irrad. cryst., ESR spectrum 78−3351
dimethyldithiocarbamate, in lyotropic liq. cryst., EPR singularities in partially ordered matrix 77−77103
2,4-dimethylpentane, glasses, γ-irrad., trapped electron yields, mol. struct. and temp. effects 77−40561
dimethylseleniumchloride, formed by X-irrad. of Ph_3SeCl cryst., ESR study 79−39167
1,3-dimethyluracil, non-hydrogen bonding crystal, radical formation 80−35552
dipeptides, aliphatic, EPR studies of direct photolysis 78−48678
dipeptides, reactions with hydrated electrons, spin-trapping studies 79−16124
diphenylantimony radical, EPR spectral parameters, nuclear quadrupole coupling 77−81010
diphenylhaloselenium radical trapped in single crysts., FSR, struct. 80−44919
diphenylselenone crystals, gamma irradiation, ESR study of trapped phenylselenonyl radical 80−44917
dipotassium glucose-1-phosphate, X-irrad., ESR-ENDOR obs 80−60419
disordered matrix, effect of quadrupole coupling on electron spin echo modulation patterns 77−85571
DNA, free radical induction due to proflavine and light treatment, influence of DNA struct. 79−100573
DNA and constituents, gamma-irrad. at 77K, effect of visible light 77−52744
DNA costacking nucleotides, γ-irrad., charge-migration phenomena, EPR obs. 80−36015
DNA films, γ-irrad., rel. to X-ray induced luminesc. and optical absorpt. 77−5033
doublet states, energy weighted maximum overlap model 78−76315
DPPH, dil., saturated spin system, spin decoupling effect and variation of dipolar energy reservoir temp. 80−88877
DPPH, exchange integral determ. by ESR in weak Zeeman fields 78−2740
DPPH, polycryst., forbidden EPR transition 78−48044
duro-semiquinone monoprotonated radical, submicrosecond time resolved EPR, lser photolysis, CIDEP polarisation mech. 78−80764
dyes for tunable lasers, intersystem crossing rates and saturation parameters in triplet state 77−36280

paramagnetic resonance of free radicals continued
EBBA: nitroxide, mol. reorientation in nematic and isotropic phases, EPR study *(French)* 79−91297
EBBA, macroscopic and microscopic orientations, EPR of nitroxide probe *(French)* 78−75546
EBRA, nematic, EPR investig. 80−108077
n-eicosane, single cryst., electron irrad., free radical pair form., ESR 77−4913
electron spin echo spectra, instantaneous and conventional spectral diffusion 79−15355
electron spin echo theory, in nonviscous soln. 77−3386
epoxy resin, nitroxide spin label doped, EPR study 79−78523
erythrocyte membrane struct. changes due to cAMP, spin-probe study 78−31779
erythrocyte membrane-haemoglobin interaction, γ-ray effects, EPR 78−7402
erythrocyte membranes, ESR study of abnormalities in Duchenne muscular dystrophy 78−96111
ethane, X-irradiated, 4.2K, pairwise radical trapping mechanism, EPR obs. 79−100412
ethanol glasses containing anion radicals of fluorene and isologs, γ-irrad., optical absorpt. and EPR obs. after photobleaching 77−44491
ethanol-d_0, -d_1, -d_5, γ-irrad., trapped electron spin-lattice relax. 77−60089
ethyl radical, $^{13}C_\alpha$ and H^+ hyperfine interactions, EPR spectra, vibr. anal. 80−23443
ethyl radical proton exchange reaction with ethylene matrix, indirect ESR obs. 80−16700
ethylene, ozonolysis, radical form., matrix ESR spectrosc. 80−16653
ethylene glycol-water glass, γ-irrad., temp. depend. photobleaching of trapped electrons 79−66320
fast reaction kinetics meas. by ESR of free radicals 80−21286
fatty acids, unsaturated, containing peroxide oxidation products, free radicals formed on UV irrad. 80−51165
fluorene: pyrene-d_{10}, triplet state energy transfer, EPR 79−15354
fluorene ketone polycryst., radical pair formation, 77K, EPR study 79−56610
food components, irrad., ESR obs. of transient free radicals 79−52699
free radicals, spectroscopy, review, book contrib. 77−38653
furil, photochem. generated alkali cationic triple ions, ESR 78−80758
galvinoxyl radical in phenol matrix, ESR spectra 80−54950
glasses, aqueous soln., stabilising excess electrons, DTA at cryogenic temps. 78−76889
glassy organic matrices, electron spin-lattice relax. of radiation-produced Ag atoms, temp. depend., tunnelling relax. 79−34331
glutaric acid, γ-irrad. single crysts., free radical EPR obs. at 77K 80−81340
glycine, cryst., cationic radicals, EPR 78−11537
α-glycine, irradiated, oxidation prod. N-centred π radical ERR 77−14459
glycine-$AgNO_3$, single cryst., X-irrad., oxidation product form. 77−48660
glycine-d_2 crystal, X-irrad., H-D exchange reactions 77−16837
glycine-d_3, pulse radiolysis, primary reaction product optical and EPR spectra 79−79265
glycyl anion radical, in α-glycine cryst., struct., ESR obs. 78−33530
glyoxal-photoreduction-product-radicals, kinetics and intramol. dynamics 77−32808
dGMP γ-irrad. in frozen soln., free radical form., computer EPR spectra anal. 78−31774
halide dioxide radical form., H_2O_2 decomposition of halide-coated surface, EPR obs. 80−7851
halogermane radical anions, ESR spectra and struct. 80−87153
hexachlorobenzene, γ-irrad., ESR spectrum 79−65735
hexafluoride radicals, prep. and EPR spectra comparison, hyperfine splitting 78−68381
hexafluorobenzene anion, EPR obs. of struct. 77−58048
hexafluorobenzene anion-radicals in squalane, ESR spectrum optical detection 80−95655
hexafluorobenzene radical anion, ^{13}C hyperfine interaction, EPR obs. 80−83392
n-hexyl 4′-n-decyloxybiphenyl-4-carboxylate, smectic C phase, tilt angle using electron reson. spectroscopy 80−33886
hydrocarbons, glasses, γ-irrad., trapped electron yields, mol. struct. and temp. effects 77−40561
1-hydronaphthyl radical, in naphthalene single cryst., anisotropic oscill. strength 78−50591
4-hydroxy-2,2,6,6-tetramethylpiperidine, radiation-induced oxidation to paramag. nitroxide free radicals 80−81341
hydroxymethyl radical, isotropic hyperfine coupling consts., temp. depend., nuclear vibrs. 78−35039
hydroxymethyl radicals, adsorption on A-type zeolites, electron spin echo obs. 78−21947
3-hydroxyxanthine, monocrystals, UV-induced nitroxide radical and pair species 79−24775
hyperfine struct., EPR cepstra method determ. 80−102531
ice, aqua-acid, UV-radiation illuminated, nuclear-electron effects of atomic protium and deuterium *(Russian)* 79−20388
ice, pure and acidic, electron irrad., ESR of H atoms, motional narrowing and spin polarisation 77−20706
ice, X-irradiated, EPR spectra, obs. of thermally reversible radical, g-value 79−5144
ice matrices, polycryst., electron spin-lattice relax. of radiation-produced Ag atoms, temp. depend., tunnelling relax. 79−34331
imidazole, X-irrad., H exchange study 80−40718
imidazoles, reaction with photochemically generated α-hydroxyalkyl radicals, EPR study 80−35558
4-(1-imidazolyl)-phenol, ESR spectra 80−16677
inositol, X-irrad., deuteration effects, ENDROR and ESR meas. 78−73067
inositol, X-irrad., radical form. detection by ESR and ENDOR, oxidation process 78−27797
intracellular membrane microviscosity, rat liver and hepatoma 27 80−30675
intramolecular cation migration in alkali ion pairs, freezing out by crown ether addition 77−58047
invertase, S-containing glycoprotein, gamma-irrad., secondary radical reactions, EPR 77−9175
iodonium cyclic compound, ESR signal *(Chinese)* 78−15025
β-iodophenylacetylene radical, PhC_2I^-, from γ-irrad. morpholine β-iodophenylacetylene complex, EPR obs. 77−52652

paramagnetic resonance of free radicals continued
isobacteriochlorins, π cation radicals, implications for NO_2^-, SO_2^- reductases 80−63684
Krebs II ascites cells, subcellular localisation and paramag. props. of observed signals 80−108952
with large hyperfine interaction, analysis 77−20707
leaf $P700^+$ reaction centre reduction in higher plants 78−64954
Lexan polycarbonate, thermolum. radiation-induced EPR of free radicals and track etchability 79−76295
lipid-protein interaction in membrane bound Na^+, K^+-ATPase, spin label anal. 79−11902
lithium acetate dihydrate, γ-irradiated single crystal, $CH_3...CO_2$ pairs, e.s.r. 77−9100
liver tissue, mouse, appearance of free radical centres on low temp. oxidation 78−69013
liver tissue and transplantable hepatoma, EPR spectrum and paramag. centre conc. 77−86459
lysozyme, electron acceptor props. in photosensitized electron transfer, EPR study 79−79469
lysozyme macroradicals, ultraslow diffusion in an aq. matrix 79−92119
magnesium formate, γ-irrad., ESR of free radicals 79−65737
malonic acid, electron spin echo exam. of mutual flip flop electron spin reversals involving forbidden transitions 79−24216
mammary tumours, paramagnetic changes during development in rat 79−39425
mannose, γ-irrad., EPR spectra 79−73814
MBBA, nematic, flexibility gradient of fatty acid spin labels, EPR study 80−71181
6-mercaptopurine, electron beam irrad., free radical formation at 77K 79−5165
mesophase pitch, magnetically-oriented, phys. props., mol. struct. 80−64885
methane, X-irradiated, 4.2K, pairwise radical trapping mechanism, EPR obs. 79−100412
methanol dehydrogenase, enzyme powder, ESR and ENDOR, 9 and 35 GHz 79−70524
1-methyl cytosine: 5-fluorouracil X-irrad. at 300K 78−64941
methyl radical, isotropic hyperfine coupling consts., temp. depend., nuclear vibrs. 78−35039
methyl radical decay in methanol glass, accumulation and dark decay kinetics 79−74352
methyl radical in glassy organic matrices, electron spin-lattice relax. 78−76312
methyl radical in sodium acetate, EPR spectra, anisotropic hyperfine interaction, rot. tunnelling 80−34775
2-methyl tetrahydrofuran radical formation on liq. phase γ-radiolysis 77−60080
4-methyl-2,6-ditertiarybutylphenol, tunnelling methyl groups, EPR 79−4723
4-methyl-2,6-t-butylphenol, γ-irrad., electron-methyl group spin-spin interaction 77−85572
1-and 2-methyl-anthrasemiquinone radicals, EPR 'reduced' spectra 80−23444
α-methyl-D-glucopyranoside, X-irrad., ESR and ENDOR study of free radicals 80−45526
α-methyl-D-glucopyranoside, X-irrad. cryst., radical form., EPR-ENDOR study 79−56613
6-methyl-mercaptopurine, cryst., light sensitive free radical EPR after electron irrad. 80−7167
methylene, zero-field splitting, absolute sign, EPR determ. 77−10692
methylene-d_0, -d_2, in Xe matrix, EPR, temp. depend. 78−5255
6-methylmercaptopurine riboside, 4 MeV electron irrad., 77K radicals form., EPR obs. 78−39405
6-methylmercaptopurine riboside, S-substituted nucleoside, ESR and ENDOR obs. 77−36766
micelle solns., aq., pulse radiolysis, CIDEP in time-resolved EPR 77−30891
microwave EPR self-induced transparency in free radical powder, waveguide propag. 77−24747
MINDO/3 unrestricted open-shell calcs. 77−23429
mitochondria phosphorylation and respiration 78−31784
monoalkylbenzenides, anion radicals, EPR, temp. depend., vibronic interaction, proton HFS 77−34666
muscle proteins, rot. motions, saturation transfer EPR obs. 80−94151
N-acetyl-L-leucine, single crysts., X-ray induced free radicals 80−45525
naphthalene, γ-irrad., radical pairs EPR detection 78−31664
$(naphthalene)^-$ $(naphthalene)^+$ radical pairs, ESR absorption, optical detection 80−7166
nematic liquid crystal, ESR of symmetrical three-spin systems, slow motional spectra 77−36135
nematic mesophase orientation, spinning in weak mag. field, radical probe 77−68913
nerve rhythmic excitation conduction, investigation of free-radical processes, frog 79−70543
nitrobenzene, adsorbed radicals, oxide surface chem., ESR 77−21417
nitrobenzene, anion radical, in benzoate crysts., EPR and X-ray diffr. obs. 77−1597
nitromethyluracil, radiation-induced oxidation and reduction 77−32816
nitrosodisulphonate ion salt dimerisation, ESR of dimers in triplet state *(French)* 77−12791
nitrosofluorene-lipid adducts, mutagenicity, ESR spectra investig. 80−91583
nitrosylhaemoglobin, electron spin distrib. 80−83528
nitroxide free radical mag. interaction with lanthanides or Cu^{2+} in liqs., ESR 78−68380
nitroxide free radicals, neutral, EPR spectra, localised solvent-radical adducts 79−96290
nitroxide radical, long range Y-P hyperfine coupling, ESR spectra obs. 80−75858
nitroxide radicals, q- and A-tensor components, rot. mobility 2 mm EPR spectrosc. determ. 80−102530
nitroxide spin labels in rigid-lattice limit, EPR and ST-EPR spectra, rapid computer simulation 79−93189
nitroxide spin probes, unresolved hyperfine broadening convection in EPR, linewidth and Heisenberg spin exchange freq. determ. 80−71180
nitroxy radical probe study of struct. characts. of membrane preps. of Na, K-ATPase 78−64930
nitroxyl radical, slow anisotropic tumbling in ESR spectra 77−28448
nitroxyl radical rotation in liquids, ESR, dielec. relax. 77−28447
nitroxyl radical spin probe investigation of adsorpt. of non-paramag. compounds on proteins 78−65153

paramagnetic resonance of free radicals continued
nitroxyl radicals, cyclic, conform. flexibility, EPR obs. 80−91581
nitroxyl radicals, UHF saturation effects use for slow jumplike rot. obs. 79−28617
2-norbornyl radical, photolysis prod. and EPR, hyperfine splitting 77−56237
nucleotide sugar-phosphate region, γ-irradiated, deoxycytidine 5′-phosphate alkoxy radical EPR 79−5249
o-phosphorylethanolamine, ESR of phosphite radicals in X-irradiated single crystals 79−51857
octane radical cations in γ-irrad. pentane matrices, ESR 77−36765
organic crysts., γ-irrad., positron lifetime rel. to free radical conc. 78−72635
organic doublet radicals in nematic and smectic liq. crysts., ENDOR obs. 80−91585
organic radicals, EPR spectra, line intensity ratios, saturation 78−90192
organic single crystals, EPR spectra simulation 77−1598
oxaxine-1, laser dye, electrochem. reduction, EPR spectra 77−70304
oxide surfaces, electron donor sites and acid-base props., adsorbed radical ESR 77−21417
paraaminophenol and paraphenylenediamine analogue molecular complex, free radicals of developers, EPR obs. *(Russian)* 80−7814
PEBAB, nematic, EPR investig. 80−108077
peptide aqueous solution, EPR of spin-trapped radicals, OH radical reactions 78−68993
peptides and derivatives, mol. electron acceptor groups 80−30637
perdeuterio-N-1-oxyl-2,2,6,6-tetramethyl-4-piperidinyl maleimide, spin label, biological EPR 80−32746
peroxy chain radicals, reactivity and struct., EPR spectra, trapped in PTFE 80−66783
peroxylamine disulphonate, EPR lineshape, dispersion vs. absorpt. plots, modulation broadening and instrumental distortion 80−58290
perylene, anthracene, radical cation, EPR, acidic surface anisotropic rot. diffusion 78−27095
(perylene)$_3$TCNQ, prep. and spectra, electron-mol. vib. coupling 77−16290
PET fibre, irrad., radical yields 79−96343
Phase V, nematic, transient response to redirected mag. field, EPR study 80−33879
phenothiazine derivatives, semicond. elec. props., optical spectra, and EPR 80−103693
4-phenyl-3-thiosemicarbazide, single cryst., X-irrad., EPR, ENDOR, radical identification 79−31560
L-phenylalanine.HCl, X-ray induced radical form. 78−48755
9-phenylanthronyl radical, ESR, temp. depend. phenyl twist angle 79−18210
phosphatidyl choline, oxidised, free radical formation on UV irrad. 80−76790
phosphines, substituted, γ-irrad. EPR spectra and struct. of free radicals 80−29623
phosphonatomethylene radical, EPR spectra and rot. barrier height, comparison CNDO calcs. 79−74409
phosphoranyl radicals, Ph_3PBr, trapped in X-irradiated triphenyliminophosphonium bromide, ESR study 79−56611
phosphoranyl radicals obs. in ESR spectra of triphenylphosphine sulphide in deuterated methanol 80−84651
photolytic generation of transient radicals for EPR spectroscopy 80−11271
photosynthesis, effect of bivalent cations on photo-induced redox conversions of P700 78−77014
photosynthesis, electron spin polarisation and mechanism of electron transfer in photosystem I 78−40122
photosynthesis, interaction of paramag. probe I (12,3) with bean chloroplast membranes 78−77015
photosynthetic electron transfer by radical pair mechanism, electron spin polarisation 79−34471
photosynthetic electron transport in higher plants, adaptation rel. to light intensity 78−64953
photosynthetic reaction centre chromophore organisation, high-resolution magnetophotoselection 80−97880
piperdinyloxy 2,2,6,6-tetramethyl radical, recrystallised samples, EPR study 80−100615
PMMA, EPR of NO radicals, rot. mobility 79−33539
PMMA, mol. motions in benzene soln., ^{13}C NMR and EPR 79−78551
PMMA, neutron irradiation, radical distribution, ESR study *(Japanese)* 80−44920
PMMA, radical form. in explosive loading, electron spin reson. obs. 80−63678
PMMA bone cement, feasibility study 80−94318
PMMA in benzene solution, ultrasonic irradiation, polymer chain scissions obs. by ESR spectra and spin-trapping techniques 80−84653
polar glass, UV and γ-prod. electrons geminate recombination, radical yield 77−9094
poly-4-vinyl-pyridine in ethanol, spin label obs. of local density of monomer units and mol. dynamics 80−44099
polybutadiene, carbon black-filled, ESR 77−90036
polycarbonate, irrad., electron spin-lattice relax. at low temp. 78−68382
polydextran, γ-irrad. frozen gel, electron trapping, EPR and optical obs. 78−20030
polyester fibres, plasma surface treatment, ESR detect. of free radicals 79−15824
polyethylene, γ-irrad., alkyl radicals ESR and hindered oscill. 78−85182
polyethylene, elec. trees free radical ESR study 78−60393
polyethylene, EPR of NO radicals, rot. mobility 79−33539
polyethylene, irrad., trapping regions, allyl radical distrib. 78−91957
polyethylene, low-density, γ-irrad., spin trapping reaction 80−39873
polyethylene, neutron irradiation, radical distribution, ESR study *(Japanese)* 80−44920
polyethylene films, plasma surface treatment, ESR detect. of free radicals 79−15824
polyethylene oxide, solid-state relaxation, spin labelling technique 78−9963
polyethylene terephthalate, radiation grafting 79−96342
polyisobutylene, EPR, correlation with glass transition 79−11348
polymer, spatially cross-linked, spin-lattice relax. time meas. of free radicals 78−19331
polymer glass transition T_g rel. to ESR parameter T_{50G}, mol. interpretation 78−67817
polymer research, ESR spectroscopy, book 78−91958
polymer track detector, form. of heavy ion latent tracks 78−17522
polymers, in situ EPR tensile testing apparatus 78−85086

paramagnetic resonance of free radicals continued
polymethacrylamide copolymer, soluble, mobility of spin label bonded to chain end 80−63873
polypropylene, electron bombarded, radical formation, piezoelectric and pyroelectric effects, ESR study 80−7169
polypropylene, electron bombarded electret, trapped charges ESR study 80−7170
polypropylene, EPR of NO radicals, rot. mobility 79−33539
polypropylene, oriented, microcracks diagnostics by paramag. probe method 80−66736
polypropylene, stability under radiation sterilisation 77−60245
polypropylene fibres, EPR during glass transition, γ-irrad. 79−8445
polypropylene films, plasma surface treatment, ESR detect. of free radicals 79−15824
polypropylene-lignin system, X-ray diff., EPR exam. of interaction 78−68668
polystyrene, EPR of NO radicals, rot. mobility 79−33539
polystyrene, plasma polymerised, free radicals, O_2 effects, EPR study 80−71179
polystyrene, plasma polymerised, free radicals, transient elec. current, EPR, heat treatment 80−71178
polystyrene in benzene solution, ultrasonic irradiation, polymer chain scissions obs. by ESR spectra and spin-trapping techniques 80−84653
polyvinyl alcohol, γ-irrad., ESR of trapped free radicals 78−85183
polyvinylacetate in benzene solution ultrasonic irradiation, polymer chain scissions obs. by ESR spectra and spin-trapping techniques 80−84653
porphyrexide solutions, EPR meas., isotropic hyperfine coupling constants and g-factor determ. 77−81009
porphyrins, metal-free, EPR, sample grinding effects 80−60420
potassium hydrogen malonate, γ-irrad. cryst., ESR and ENDOR of trapped radical 79−78524
protein, radical limiting conc. on UV irrad. at 77K, effect of luminesc. quenchers 80−30662
protein aggregates exposed to UV radiation, limiting conc. of paramag. centres 78−24029
protein rotational motions, large-scale, detection by EPR and fluorescence 79−16120
protein-peroxide radicals, ^{17}O-labelled 80−85345
proteins, UV irrad., paramag. centre accumulation, kinetic eqn. 77−21476
PTFE, peroxy radical labelled, temp. dependent rots., EPR obs. 80−28125
purine, powder, γ-irrad., dose-response curves 78−7215
PVC, EPR of NO radicals, rot. mobility 79−33539
pyrene, single cryst., γ-irradiated, EPR and optical absorption meas. 78−72412
pyrene single crystals, γ-irradiated, free radical form. ESR spectra 78−72410
pyrene solutions, radical ion pairs, pulse radiolysis, time resolved EPR spectra meas. by ODMR of fluoresc. 80−83395
pyridine cation radical in trichlorofluoromethane matrix, gamma irrad., EPR and optical obs. 80−23442
pyrimidine H-addition radicals in single crystals, long range proton hyperfine coupling, EPR and INDO 77−54568
pyrimidines, substituted, UV irrad. in aq. solns. 78−40115
pyrrole, free radicals produced by X-irrad. and decay of tritium atom, EPR study 78−48676
quartz , fused and γ-irrad. 79−99770
quasi-one dimensional organic systems, ESR 78−52358
radical cation EPR spectra, ion-pair effects 79−13742
radical ion pair formation, ESR spectroscopic obs. 78−73038
radical pair with axial symmetry, EPR parameters and linewidth components 78−6573
radical pairs, electron spin motion, diamag.-paramag. exchange, mag. field effect 79−98123
radical species, tube electrode generation, laminar flow through EPR cavity, decomp., convection 77−24746
re-entrant nematic phase, orientational order, electron reson. study 80−103242
rhamnose, single cryst., X-irrad. at 4.2K, trapped electrons and electron traps characts. 79−78037
saturation effect rel. to quantitative analysis in biology 77−48963
semiquinones in protic solvents, saturation behaviour, ESR 77−6808
simulated spectra, compensation for integerisation errors 79−33537
slow molecular motion, stable-radical spectra calcs. 80−25212
sodium decanoate-n-decanol-water system, lamellar G-phase, orientational-order, EPR investigation 80−24355
solutions, spin exchange and broadening 78−52357
spin labels, appl. to study of assoc. of adenosine, AMP, ADP and ATP 78−81086
spin labels and biomembranes, review 78−69265
spin motion including hopping, semiclassical description 78−58724
cis-stilbene radical anion, ESR, proton coupling const. 78−21948
styrene, plasma polymerisation in glow discharge, thin film IR and free radical EPR obs. 80−2964
styrene, polymerisation, photoinitiation by aliphatic azo cpds., EPR obs. 78−80746
submitochondrial particle succinic dehydrogenase, interaction of ubisemiquinone with Fe-S centre, EPR 78−69016
succinamic acid, X-irrad., primitive radn. damage, ESR, ENDOR 78−3352
sucrose, single cryst., X-irrad. at 4.2K, trapped electrons and electron traps characts. 79−78037
TANOL, linear chain-like organic free radical, EPR line widths 78−39404
dl-tartaric acid, radiation products, ESR-ENDOR OBS. 80−55682
tartaric acid salts, and deuterated forms, irrad.-crysts., primary reactions, EPR obs. 80−3370
$TCNE^-$, anionic spin probe for ESR of amphiphilic liq. cryst. 78−75548
$TCNQ^-$, ESR probe for phospholipid membrane polar head motion study *(French)* 80−45865
TCNQ salt, 1,1′-diethyl-2,2′-cyanine-$[TCNQ]_2$, electric and mag. props. 79−42523
TCNQ salt, HMTTF-TCNQ, metallic organic charge transfer complex, chemical prep. and phys. props. 78−2471
TCNQ salts, spin density distribs., estimation from EPR fine struct. and cryst. data 79−11347
teflon, γ-irrad., rel. to positron liftimes 78−76550
1,4,5,8-tetraazanaphthalene radical ion pairs, EPR spectra 79−50051

paramagnetic resonance of free radicals continued
tetracene, radical cation, EPR, acidic surface anisotropic rot. diffusion 78−27095
2,3,4,4-tetrachloro-1-keto-1,4-dihydronaphthalene, photochromic single cryst., triplet photochem. 79−39164
tetrafluoroethylene anion, EPR spectra in organic matrix 79−76453
tetrafluoroethylene radical anion, isotropic and anisotropic EPR spectra, conform. 78−13532
tetrafluoroethylene radical ion+tetrafluoroethylene, cycloaddition 78−13533
tetrahydro-2-methylfuran glass, γ-irrad., spin trapping of radicals by BNB, EPR obs. 78−10776
2,2,6,6tetramethyl piperid-4-one N-oxide, aq. soln., ESR spin probe for H_2O struct. alteration 77−59460
2,2,3,3-tetramethylbutane, γ-irrad., EPR spectrum assignment 80−15800
2,2,3,3-tetramethylbutane, radiolysis, radical prods., EPR obs. 80−32747
tetraselenotetracene iodides, struct. and physical props., DC electrical cond. and EPR linewidth meas. 80−103312
tetrathiofulvalene-based salts, isomorphous series systematic investig. of solid-state props. 77−55517
TGS, X-irrad., thermal diffusivity, cooling const. and heat transmission coeff. 79−86935
TGS X-irradiated, paramag. relax, spin-echo study 80−7168
l-thioproline single cryst., X-irrad., ESR and ENDOR study of radicals 80−45528
thymidine-5-monophosphate, γ-irrad. aq. soln., spin-trapped radicals, liq. chromatography and EPR spectroscopy 78−53340
thymine, γ-irradiated, EPR study of post-radiolysis growth of spin-trapped radicals 79−16155
tissue, animal, lyophilised, paramagnetic centres 80−30681
transient radicals, EPR time profiles, CIDEP, electron spin-echo method 79−6953
transition metal, paramagnetic-NO· radical interactions, EPR spectra rel. to dipolar interactions 79−95647
triethylenediamine cation radical, ESR 77−24745
trifluoroacetamide, single cryst., X-irrad., transient radical form., INDO and ESR calcs. 77−12814
trifluoroacetamide, X-irrad., CF_3...F radical ESR 78−73066
β,β,β-trifluoroethyl radical in Ar matrix, EPR, F and H^+ hyperfine interaction and motional effects 77−14460
trifluoromethylhalide radical anions, formation, ESR and struct. 77−32809
2,2,5-trimethyl-1,3-dioxane-4,6-dione, cryst., X-irradiated, methyl group hindered rot. tunnelling, EPR, ENDOR, and ELDOR 79−68328
trimethylenemethane, ground state triplet, HFS, EPR obs. 80−50188
triphenylantimony, single crystal, irrad. by UV, diphenylantimony radical prod., ESR 78−31662
triphenylmethyl-^{13}C phosphonium chloride, Ph_3P^+-$^{13}CH_2$· EPR, reorientation and hyperfine coupling tensor 78−6574
triphenylstannyl radical, EPR in single cryst. matrix, ^{119}Sn hyperfine coupling tensors 78−23346
triradical spin probe, EPR of nematic liq. crystal struct. and mol. dynamics 78−63670
trypsin, in suspension, radical form. and inactivation after ∫-irrad. 78−3564
L-tryptophan-HCl radical form. after X-irrad. 78−64940
L-tryptophan.HCl, irradiated single crystals at 295K 79−11900
TTT_2-$(I_3)_{1+x}$, physical props., elec., mag. and optical meas. 80−24908
tumour and normal tissue of γ-irradiated mice, EPR spectra comparison 79−53193
unordered solids, EPR spin lattice relax., dipole induced contrib. 78−80193
uracil, aq. soln., fast electron induced radical identification 79−24870
uracil derivatives, photosensitised induction by H-addition radicals in frozen aqueous soln. 78−20146
uranyl phenanthraquinone radical ion complex, longitudinal spin-lattice relax. time determ. 80−108076
uridine 5'-phosphate (Na salt), NO_2 species in an irrad. single crystal 80−40719
uridine-5'-monophosphate gamma-irrad. solutions, short-lived radical detect. by spin-trapping method 77−21479
uridine-5'-phosphate.2Na^+ single crysts., radiation damage 80−108964
n-vinyl carbazole, radiation induced polymerization ESH study 80−7817
vinylidene chloride copolymer, stretched free radical form., meas. using indirect scavenger method 79−61923
violanthrone, free radical, EPR meas. 78−27094
vitamin D, role of free radicals in conversions and mechanisms of physiological action 77−70430
water, solvent, structure, ESR spin probe obs. 77−59460
water-acid ices, UV irrad., EPR of H and D, nucl. electron effects 79−83488
xylene, plasma polymerised, EPR of trapped free radicals 79−83455
Yang's biradical, EPR, g- and D-tensors, electronic struct., deuteration and conformation effects 77−42343
Ag, adsorbed O_2 layer, EPR of O_2^-, rate of angular reorientation 78−72413
Ag, adsorption of O_2^-, catalytic oxidation mechanism 78−61046
Ag halide dyed powders and emulsions, nature of light induced ESR signal 79−2852
$AgClO_3$, γ-irrad., ESR of O_3^-, ClO_2 and $(ClO_2$-$Cl)^-$ paramag. centres 77−9102
AlH^+ radical cation, EPR matrix isolation obs., hyperfine components calcs. 80−14158
Al_2O_3, adsorpt. of TCNQ anion radical salts, EPR and electronic spectra 77−72776
AsF_5 intercalation with graphite and benzenoid systems, EPR, NMR and X-ray diffr. obs. 80−19775
AsF_5^-, form. from AsF_6^- by radiolysis, ESR spectrum 77−16845
BF_3^-, radical, struct., EPR spectrum 77−8406
BH^+, spin-extended Hartree-Fock ab initio calculations for small radicals 78−70746
$BaGeF_6$, Group IV hexafluoride anion radical γ-irrad., EPR spectra 78−72411
$BaPbF_6$, Group IV hexafluoride anion radical γ-irrad., EPR spectra 78−72411
BeH, spin-extended Hartree-Fock ab initio calculations for small radicals 78−70746
BeO-P_2O_5-$RO(R_2O)$ (R=Li,Na,K,Mg,Ca,Sr,Ba) glasses, gamma irrad., cation modifier effect on radiation centre formation 80−40720
BiF_6^{2-}, prod. in gamma irrad. $CsAsF_6$:BiF_6^-, EPR 78−19329
BrF_6, EPR of matrix, isolated radical 79−85977
paramagnetic resonance of free radicals continued
BrF_6, EPR spectra, 'NMR' transitions, mol. symmetry 77−46580
C, activated, interaction with H_2, EPR spectra, alteration of paramag. props. 77−63957
C, pyrolysis mechanism, electron microscopy, DTA, IR, ESR obs. 78−56593
$C_5H_6NNHCSNH_2$ radical, prod. in X-irrad. 1-phenyl-3-thiosemicarbazide, ESR, ENDOR 77−36770
CO_2-O_2^- radical, on MgO surface, ESR spectrum, mobility effects 80−43076
CdF, mol., ESR spectra in inert gas matrix 79−76455
CdO-Al_2O_3-P_2O_5 glass, γ-irrad., EPR study 80−84639
CdS, aq. dispersion, O_2^- generation by photolysis, spin trapping detect. 78−11538
CdS, EPR of adsorbed oxygen radicals, temp. depend. 80−80612
CdS powder, surface O_2 adsorption, ESR studies 79−65738
2-chlorothiophene, σ* anion radical, prod., ESR spectrum assignment 78−11539
ClF_6, EPR spectra, mol. symmetry, INDO calcs. 77−46580
Co complex, triazene-1-oxide complexes, EPR spectra in frozen nematic liq. cryst. glass 80−88871
$CsAsF_6$, γ-irrad., EPR spectra, hyperfine interactions and g-value determ. 77−81416
$CsSbF_6$, γ-irrad., EPR spectra, hyperfine interactions and g-value determ. 77−81416
Cu complex, triazene-1-oxide complexes, EPR spectra in frozen nematic liq. cryst. glass 80−88871
Cu complex (acetylacetonate), in vitreous liq. cryst. matrix, ang. depend. of EPR spectrum 78−9175
Cu complexes, spin-labelled, EPR, electron-electron coupling 79−51858
$Fe(NO)_3CO$ radical, form. by $Fe(CO)_5$ photolysis in NO soln., EPR spectrum 80−53024
HO_2 radical, EPR spectrum, ground state parameters 78−90193
H_2O^- in γ-irrad. Y-type zeolite, alternative EPR triplet assignment to NO_3^{2-} 78−11534
H_2O^-, trapped in γ-irrad., Y-type zeolites, ESR obs. 77−9099
H_2SO_4, frozen soln., EPR of trapped H-atoms produced by UV and X-irrad. 80−3369
H_2SO_4:Fe^{2+}, frozen soln., photo- and radiation-produced H-atoms obs. 79−39162
$KClO_4$, ClO_3^- detection by EPR of ClO_3 radicals created by X-irrad. 78−76311
$KClO_4$, X-irrad., ESR spectra of O_3^- and ClO_3 exchange-coupled to O_2 78−64856
K_2CrO_4, ice, γ-irrad., electron trap depth, ESR 79−66317
KD_2PO_4, X-irradiated, hysteresis effects obs. by ESR 80−103928
$K_2Fe(CN)_6$ ice, γ-irrad., electron trap depth, ESR 79−66317
KH_2AsO_4, γ-irradiated, free radicals, EPR and ENDOR study of consequences of ferroelec. transition *(French)* 80−93209
$K(H_{1-x}D_x)_2PO_4$, single cryst., 77K, γ-radiation damage centres, and EPR obs. 78−68379
KH_2PO_4, X-irradiated, hysteresis effects obs. by ESR 80−103928
KH_2PO_4:AsO_4^{4-}, ESR_3 paraelectric phase, proton dynamics 77−81011
KH_2PO_4:AsO_4^{4-}-(SeO_4^{3-}), ferroelec., low freq. fluctuations, isotope effects, EPR, ENDOR, ESCA 77−73118
KH_2PO_4:$NH_4H_2PO_4$, EPR of arsenic and phosphorus oxyradicals 77−77102
$KHSO_4$:SO_3^-, X-irradiated, ESR saturation 78−80220
K_2O-Al_2O_3-B_2O_3-SiO_2, glass, ESR exam. of paramagnetic centres formed during mech. destruction by grinding 78−88188
KPF_6, γ-irrad., trapped free radicals EPR obs. 80−63683
KPF_6, temp. depend. hyperfine interactions of trapped pyramidal radicals 80−44918
K_2SO_4:$(NH_4)SO_4$, X-irrad., EPR of NH_3^+ 80−11272
K_2SeO_4, symmetry determ. of commensurate and incommensurate phases by EPR of γ-irrad. crysts. 79−78525
K_2SnF_6, Group IV hexafluoride anion radical γ-irrad., EPR spectra 78−72411
^{84}KrF in polycrystalline KrF_2 ESR spectra, struct. and dynamic parameters of radical sites determ. 80−84652
$^{83}Kr_2F$ radical, in UV-irrad. Kr/CF_3OF, 10K, ^{83}Kr hyperfine EPR spectrum, struct. 78−42101
LiH^+, spin-extended Hartree-Fock ab initio calculations for small radicals 78−70746
Li_2O-Al_2O_3-P_2O_5:Cd^+ glass, γ-irrad., EPR study 80−84639
Li_2O-P_2O_5:Cd^+ glass, γ-irrad., EPR study 80−84639
MgO, coadsorpt. of CO_2 and O_2, UV irrad., ESR of radicals 78−6572
MgO surface, mobile $(CO_2$-$O_2)^-$ radical, ESR spectrum 80−43076
$MgTiO_3$, ESR study of Fe^{3+} 80−50173
Mg_2TiO_4:Cu(Ni), ESR of Cu^{2+} and Ni^{3+} 80−97131
Mo-Al_2O_3 based hydrosulphurisation catalyst, used, ESR of SO_2^- and Mo^{5+} 77−70342
$(NH_4)_2$ $Zn(SO_4)_2.6H_2O$:VO^{2+}, γ-irradiated NH_3^+ ESR, N hyperfine coupling tensor 79−69722
$(NH_4)_2BeF_4$, γ-irrad., trapped H atoms, ferroelec. transition, EPR meas. 79−4724
NH_4ClO_4, γ-irrad., trapping and motion of NH_3^+ radical in cryst. lattice 79−33538
NH_4ClO_4, γ-irrad., motions of trapped NH_3^+ radical, ESR study 79−95648
NH_4ClO_4, γ-irrad. single cryst., NH_3^+ EPR obs., g-tensor hyperfine splitting 78−2739
$((NH_4)_{1-x}Cs_x)_2SO_4$ mixed cryst., EPR of NH_3^+ and SeO_3^- radicals 80−50190
$(NH_4)_2HPO_4$:KH_2AsO_4, EPR of arsenic and phosphorus oxyradicals 77−77102
$NH_4H_2PO_4$:AsO_4^{4-}-(SeO_4^{3-}), antiferroelec., low freq. fluctuations, isotope effects, EPR, ENDOR, ESCA 77−73118
$((NH_4)_{1-x}Rb_x)_2SO_4$ mixed cryst., EPR of NH_3^+ and SeO_3^- radicals 80−50190
$(NH_4)_2SO_4$, irrad., −50°C transition, librational mode softening, paramag. NH_3^+ probe obs. 77−20037
$(NH_4)_2SO_4$, of NH_3^+ and SeO_3^- radicals, ferroelec. transition obs. 77−16180
$(NH_4)_2SO_4$:SeO_3^-, γ-irrad., hyperfine interaction, ferroelec. transition effects, EPR expt. 78−15024
NO, EPR line shape in solvating mixtures 78−33532
NO radical, EPR (ST-EPR) spectra, fast computation, master supermatrix eqn. soln. 78−62213
NO radicals, slow rot., modulated EPR spectra 79−38382
NO radicals as spin labels in biophysics 77−44860

paramagnetic resonance of free radicals continued
NO spin label, EPR (ST-EPR) spectra, fast computation perturbation approach 78−62212
NO radicals, saturation transfer EPR effects anal. using hole-burning concept 79−94022
NO_2, radical, ENDOR and ESR obs. ^{14}N hyperfine coupling tensor 77−50455
NO_2 radicals adsorbed on silica gel, averaging-out of ESR spectrum 77−60119
NO_3^{2-}, ENDOR and ESR obs., ^{14}N hyperfine coupling and g-tensors 77−50455
NO_3^{2-}, in γ-irrad. Y-type zeolite, EPR triplet assignment, instead of H_2O^- 78−11534
NO_x biradicals, conform., spin probe appls. 78−86895
$Na_4Fe(CN)_6.10H_2O$, single cryst., X-irradiated product ESR, 4.2K 77−48659
$NaClO_4$, aq. glass, formation of trapped H-atoms and electrons on X-irrad. 80−35559
$NaClO_4$, frozen soln., EPR of trapped H-atoms produced by UV and X-irrad. 80−3369
$NaClO_4:Fe^{2+}$, frozen soln., photo- and radiation-produced H-atoms obs. 79−39162
$Na_2HPO_4.7H_2O:KH_2AsO_4$, EPR of arsenic and phosphorus oxyradicals 77−77102
$NaNO_3$, γ-irrad., electron trap depth, ESR 79−66317
Na_2O-Al_2O_3-B_2O_3-SiO_2, glass, ESR exam. of paramagnetic centres formed during mech. destruction by grinding 78−88188
Na_2O-B_2O_3:Se, EPR, γ-ray effects *(Russian)* 78−31109
NaOH, frozen soln., EPR of trapped H-atoms produced by UV and X-irrad. 80−3369
NaOH ice, γ-irrad, ESR and absorpt. spectra of trapped electrons 79−66318
NaOH ice, γ-irrad., electron trap depth, ESR 79−66317
$NaReO_4$, EPR spectra of paramag. centres and free radicals 80−108072
O_2, singlet product. detect. by EPR 79−66597
OD, $^2\Pi_{3/2}$ state EPR spectra 78−21949
O_2F radicals, preparation, EPR spectra rel. to phase, temp. 77−51954
OH radical, gas phase EPR, rot. states electronic struct. and Zeeman parameters 78−86896
OH, spin-extended Hartree-Fock ab initio calculations for small radicals 78−70746
PO_4^{2-} radical in crystal of uridine 5'-phosphate (Na salt) 79−57592
l-proline monohydrate single cryst., X-irrad., ESR and ENDOR study of radicals 80−45528
RbH_2PO_4, X-irradiated, hysteresis effects obs. by ESR 80−103928
S_3^-, stabilized on MgO surface, CNDO calcs. of g-tensors and hyperfine coupling consts. 77−83625
SF_5, anisotropic ESR spectrum in γ-irrad. SF_6 77−21400
SF_3BF_4:SF_3, cryst., γ-irrad., radical form., EPR 78−91955
SO_2^+ radical-ion formation 77−25285
ScF_2, ESR spectra of radical in Ar matrix, 12K, hyperfine splitting 79−98122
o-semiquinone, radicals, intra- and intermolecular H^+ transfer, ESR 77−16840
Si biradical, six-coordinate, mol. mobility two-spin probe investig. 80−102529
$SiCl_4^-$, ESR of radical in adamantane matrix, γ-irrad. of $SiCl_4$ in adamantane matrix 79−27011
SiF_3Cl^-, radical anion struct. and ESR spectrum 78−25571
$SiF_4Cl_{4-n}^-$ in γ-irradiated solid solution of tetramethysiline, EPR spectra obs. 80−80611
$SiF_3Cl^-(Br^-)(I^-)$ in γ-irradiated solid solution of tetramethysiline, EPR spectra obs. 80−80611
SiH_3 radical, in Ar(Kr)(N_2) matrix, anisotropic ESR spectroscopic parameters 80−63687
SiH_3X^-, X=Cl, Br, I, and isotopic forms, EPR spectra, mol. struct. 79−94023
SiO_2, fused, irrad., O_2^- radical defect centres, ESR obs. 79−61222
SiO_2, surface characterisation by free radical spin labels 77−90701
TiO_2, adsorpt. of O_2, vacuum heat cleaned, O_2^- radical form., EPR 77−35806
TiO_2 treated with quinoline, photooxidation and effect of surface states, ESR obs. 79−66352
V complexes, ^{51}V quadrupole coupling tensors form EPR meas. 80−88866
^{136}XeF in polycrystalline XeF_2 or XeF_4, ESR spectra, struct. and dynamic parameters of radical sites determ. 80−84652
ZnF, mol., ESR spectra in inert gas matrix 79−76455
ZnO-B_2O_3, glass, ESR exam. of paramagnetic centres formed during mech. destruction by grinding 78−88188

paramagnetic resonance of ions and impurities
see also paramagnetic resonance of iron group ions and impurities; paramagnetic resonance of palladium and platinum group ions and impurities; paramagnetic resonance of rare earth ions and impurities
actinide elements, expt. techniques, electronic and nuclear props. 78−52337
alkali halide:Hg, EPR and optical props. 78−91933
alkali metal-hexamethylphosphoramide, low temp. glass, EPR of solvated K, Cs and Rb 78−91927
alkaline earth oxides, electron transfer between adsorbed O_2^- ions, EPR obs. 78−76296
alkaline earth-uranium mixed oxides, EPR spectra 78−27090
angular variation, calc. using Feynman's theorem 80−54940
aniline, in p-xylene host cryst., phosphoresc. triplet state, ESR and MIDP obs. 80−66077
arenediazonium salts, photolysis, quantum efficiencies, reactive intermediaries, EPR 78−64860
aryl cations, triplet state, multiple site splitting, ESR obs. 80−97126
asymmetry of profile of mag. reson. line 78−91934
bottlenecked EPR, singly, doubly, multiply bottlenecked systems 78−27078
chalcogenide semiconductor amorphous film comp. monitoring by EPR 77−51940
charge transfer band identification by EPR conversion-rate meas. 78−76297
chlorophyll solutions, photopotential rel. to EPR signal 79−53045
chloroplasts, response to illum. sequence of four flashes 78−7325
clustering of mag. ions, study method 80−11155
collective excitations, contrib. to mag. relax. 77−12190
coordination compounds, EPR of doped mag. centres 78−64259

paramagnetic resonance of ions and impurities continued
cubic crystal field, small distortions, EPR transitions for ions with S=3/2 77−51941
d^1 ion in cryst., orbital singlet EPR parameters 78−10751
decacyclene anion, photoexcited quartet state, transient EPR 80−78635
defect pairs, dielec. relax. meas. using electric-field-modulated EPR of paramagnetic ion probe 78−23392
density matrix formalism for coupled dynamical systems 78−95522
diamagnetic perovskites, AMF_3, Fe^{3+}-O^{2-} pair EPR probe for struct. phase changes 77−36113
diamond:Sb, implanted, radiation damage and annealing study 80−100263
diamond, ESR studies, review 78−95521
diamond, exchange interaction of N paramag. centres, spin density delocalisation 80−39847
diamond, natural, dislocation-N_2 impurity interaction, photoconductivity spectra, resistivity and EPR 79−91097
diamond, natural, polycryst., distinctive features of struct. 79−92530
diamond, partial dissoc. of N aggregates by high press.-high temp. treatment, EPR meas. 78−43904
diamond, synthetic, N impurity effect on strength characts. and thermal stability 80−11726
diamonds, natural, N3 centre, EPR obs. 79−51842
dielectric crystal, APR and phonon spectroscopy to study paramagnetic ions 80−84634
dilute paramagnet, mag. reson. linewidth due to two-particle interaction 77−90012
diphenyl-d_{10}: diphenyl, triplet state EPR and ENDOR, 1.9K, mol. struct. implications 79−94021
dipolar splitting of spin pair in presence of avalanche phonons 79−61203
disordered solids, nonresonant paramagnetic absorption, quantum theory 79−69712
dynamic Jahn-Teller effect in ESR spectra, Green's functions calcs. 80−84643
electron spin-lattice relaxation, review 77−69672
exchange interaction caused by elementary excitations in solids, temp. depends. 80−25193
fast relaxing centres, in paramag. cryst., spin-lattice relax. *(Russian)* 79−15340
ferroelectric, H-bonded, soft and central modes, mag. reson., review 78−15108
ferroelectric, ion-ion interaction due to soft phonon modes 79−99838
fluorene:pyrene-d_{10}, single cryst., host-guest triplet pairs, mag. field effect 80−60649
fluorene:pyrene-d_{10} cryst., magnetic resonance absorpt. of host-guest triplet paired centres 80−34750
gapless superconductors, localised mag. moments, EPR *(Russian)* 78−34920
gas-solid interface, EPR centres induced by microwave gas plasma 78−80215
graphite lamellar cpds. with Li, K, Rb, HNO_3 and SO_3, EPR studies 80−44902
HMPA:alkali metal, density of states in band gap, EPR and optical correlations 79−61201
HOAB, smectic, C-phase, magnetic instabilities studied by electron spin resonance spectroscopy 79−82147
hyperfine structure, low symmetry effects, calc. 80−50165
hyperfine structure of EPR of heteropairs with strong exchange coupling 78−72395
impurity centre interaction with external elec. field 77−89727
inert gas:H, quasifree electron energy, inference from ESR studies 79−69459
interdoublet EPR spectrum ang. depend. for ions with arbitrary electron and nuclear spins in strong axial cryst. field 80−93164
ionic crystals incorporating S-state ions, expt. exam. 79−28326
ions in $^6S_{5/2}$ ground state, ESR line with 3.33 isotropic g-factor 80−15787
ions with S=3/2 and S=5/2, effective g values from EPR 79−42825
Jahn-Teller effect in EPR spectra, multistate theory for ^2E orbital states 78−56369
lineshape distortion in weak magnetic fields with zero-field splitting 77−48034
local electric field, impurity centre dipole transitions *(Russian)* 78−34811
magnesium porphin, ESR study of metastable triplet state, in n-octane matrix, 1.3K 79−72340
magnetically dilute crystal, with strong spin-spin interaction, EPR conc. depend. 79−42826
metal:magnetic ion, book 77−48037
metal oxide surface, strength and distrib. of electron donor sites, ESR meas. 78−84055
metals, non-S-state impurities, coupled ESR 79−47326
methyl cyanide-water (methanol), Ag^+ ion solvation, γ-irrad., ESR obs. 80−97726
naphthalene, triplet pairs in naphthalene-d_8, ESR, nonreson. 78−64257
nonlinear susceptibility of magnetically dil. paramag. insulators, in parallel mag. fields 77−59450
paramagnetic centres, quadrupole relaxation transitions due to carrier exchange scattering 79−73803
phenazine: azulene, EPR, azulene triplet state 78−35024
p-phenylphenolate ion in stretched polyvinyl alcohol film, phosphorescent triplet states, ESR spectra obs. 80−83393
trans-polyacetylene, and AsF_5 doped, EPR 79−42835
polystyrene, mol. wt., distrib. rel. to glass transition temp., ESR spin-probe investig. 79−8041
powder technique appls. *(Spanish)* 77−48036
powders, spectral simulation and anal. 78−80194
quadrupole effects in $S=^1/_2$, $I=^3/_2$ system 79−42827
quartz, alpha particle induced radiation defects, EPR and thermoluminescence study 80−20461
α-quartz, dynamic interchange among three states of P, EPR obs. 80−66010
α-quartz, EPR of Al-Ag centres 78−88186
quintet transition, exact axial reson. fields calc., rel. to powder spectra 80−2622
S-state ions, intensity spin operator for forbidden lines derived 77−1587
smectic liquid crystalline solvents, ESR obs. of anisotropic ordering, spin relax. and slow tumbling 79−95629
spin Hamiltonian parameters for paramagnetic ions in tetragonal symmetry, optimal computation 77−4550
spin-glass, dirty, paramag. reson. 80−11264

paramagnetic resonance of ions and impurities continued
spin-Hamiltonian parameters, fast computational method 77−73072
spin-phonon interaction shift of EPR line 79−65712
spontaneous coherent state transition, susceptibility singularities 77−40119
superconductors, type I, spectroscopy using mag. impurity relax. of Josephson junction-Fiske modes 77−80880
superhyperfine structures, paramagnetic impurity, ligand nuclei interaction, calcs. 78−80195
symmetry, effects of low site symmetry, review 80−71159
TCNE, electron donor-acceptor complexes, EPR *(German)* 78−55187
TCNE, K salt, in nematic liq. crystal solvent, ion pairing, EPR spectra 78−73020
TCNQ, electron donor-acceptor complexes, EPR *(German)* 78−55187
TCNQ salts, $Li^+(TCNQ)^-$, $Cu^+(TCNQ)^-$ and $Cu^+(TCNQ)_2^-$, low temp. EPR of impurity reson. 77−85548
teaching, introductory student expt. 78−41119
thermal splitting of reson. freq. for ions interacting with reson. RF field 78−10753
transition metal ion complexes, mag. g-tensors, spin-orbit coupling 78−10752
transition metal systems, ESR studies, polarised absorption, ligand field model, group theory applications 80−43077
transition probability determ., approx. methods 79−78506
triphenylene, trapped in n-heptane single cryst., ESR and orientation *(French)* 78−91928
triphenylene in Shpolskii matrix, orientation, ESR and fluoresc. spectra 79−36688
two-dimensional antiferromagnets, diffusion-controlled mode coupling, EPR linewidth 79−51844
type II superconductor, EPR of paramagnetic impurities and conduction electrons *(Russian)* 79−1641
unordered solids, EPR spin lattice relax., dipole induced contrib. 78−80193
vibronically coupled systems, cluster model 79−19540
Zeeman interaction, relativistic corrections and very small g-shifts, contrib. to EPR 78−72393
zinc porphin, ESR study of metastable triplet state, in n-octane matrix, 1.3K 79−72340
zircon, natural and synthetic crysts. Hf and Tb activated, capture centres and luminescence mechanism *(Russian)* 77−28626
$AgBr_{1-x}Cl_x$, Jahn-Teller type self-trapping of holes 79−65709
$AgBr_{1-x}Cl_x:Cu^{2+}$, EPR of $(AgBr_6)^{4-}$, Jahn-Teller effect 79−91294
AgCl(Br), multivalent impurities 79−19556
$AgClO_3$, ClO_2 spin Hamiltonian 78−60326
$AgClO_3$, γ-irrad., ESR of O_3^-, ClO_2 and $(ClO_2\text{-}Cl)^-$ paramag. centres 77−9102
AlN:O, UV spectra of deep impurity centres, radiative recombination 79−87490
Al_2O_3-Na_2O, β and β″ phases, stability, cond., paramag. impurity effects obs. 77−84976
^{40}Ar:^{41}K, matrix isolation model system 78−45722
As_2S_3:B glass, impurity effect on photoluminesc. and optically induced EPR 79−65918
As_2Se_3, amorphous, defect states, exptl. study. 80−54645
As_2Se_3 glasses, impurity effect on photoluminesc. and optically induced EPR 79−65918
As_2Se_3:Tl, hole transport, photoluminesc. and photoinduced ESR 79−8183
β-B:C, rhombohedral, EPR meas. partly resolved absorpt. spectra 80−20449
Be_2SiO_4:P, EPR and ENDOR 78−76295
BiI_3, doped, IR photolum. and EPR spectra 78−19558
CaF_2:O_2^-, struct. and dynamics, EPR and ENDOR obs. 79−33562
CaF_2:U, charge conversion of U^{3+}, ESR spectra 80−7150
CaF_2:U single crystal, Czochralski-Kyropoulos grown, U ion localization 79−91580
CaF_2:U^{3+}, anomalous magnetooptic props., optical detection of ESR and cross-relax. resonances 80−93287
CaF_2:U^{3+}, cubic site substituent, EPR spectra obs. 78−72392
CaF_2:U^{4+}, EPR hyperfine struct. 80−15781
CaF_2:U^{5+}, rhombic centre EPR spectrum, heat treatment effects 78−72407
CaO, formation of surface O_2^- ion by O_2 adsorpt., EPR 80−61155
CaO:Li, thermally quenched, generation of Li^0 centres 80−50382
CaO:Mg^+, EPR exam., hyperfine const. determ. 77−8388
$Ca_{10}(PO_4)_6F_2$:NO_2^{2-} apatite, ESR, struct. of ions *(French)* 78−43640
CaS, atomic and mol. centres of O, ESR and luminesc. methods *(Russian)* 80−84764
CaSe:Pb, luminesc. and EPR props. of Pb centres 80−55168
CaSe:Sn^{3+}, EPR study of octahedral Sn^{3+} centres, 4 to 290K *(Russian)* 80−84637
CdO-Al_2O_3-P_2O_5 glass, γ-irrad., EPR study 80−84639
CdS, donors, EPR and spin-lattice relax., Faraday rot. meas. 80−54939
Cl_2^-, in ion pairs with metals, ESR, in AR matrix, V-centre theory 77−16172
CsBr, gamma irrad., EPR of Br_2^- ions 79−51838
CsBr solution, EPR of O_2^- luminesc. centres, 4.2K *(Russian)* 79−15339
CsCl solution, EPR of O_2^- luminesc. centres, 4.2K *(Russian)* 79−15339
CsO_2, low temp. phases, mag. order, EPR and antiferromag. reson. 79−95630
Cs_2ZrCl_6:Np^{4+}, EPR obs. 79−33526
Cs_2ZrCl_6:Np^{4+}, EPR data interpretation for octahedral Γ_8 state in cubic cryst. field 80−2634
Cs_2ZrCl_6:Np^{4+}, EPR of np^4 ground state 80−44903
$CuGaS_2$, ESR assessment of S diffusion behaviour on annealing 78−35036
Cu(ethylenediamine)$_2^{2+}$, electron tunnelling probability as function of distance for chem. reactions 78−80759
D+HCl→DCl+H, rate consts., EPR 77−9059
GaAs, adsorbed O_2^- EPR spectrum, HFS 77−40118
GaP, electron irrad., EPR of antisite-impurity defect 80−25211
GaP:O, EPR investig. of deep donor centre, delocalisation 77−28428
Ge:Li,O, EPR and piezospectroscopy 80−25338
Ge:Li-O, donor complex EPR and photoelectron piezoelectric spectra, dynamic tunnelling 79−1711
GeO_2:Al, tetragonal, $[Al]^0$ centre, nuclear Zeeman and quadrupole effects 78−35035

paramagnetic resonance of ions and impurities continued
H, trapped in inert gas matrix, anisotropic hyperfine interactions 79−65728
He, liquid, EPR of negative ions field emitted into sample 77−47636
^{3}He, liq., negative ion obs. 79−60582
^{3}He, liquid, EPR of negative ions, antiferromagnetic transition possibility *(Russian)* 80−15322
(K,Na) ($AlSi_3O_8$), feldspar, N^{2-} ESR spectrum parameters *(Ukrainian)* 79−38366
KBr solution, EPR of O_2^- luminesc. centres, 4.2K *(Russian)* 79−15339
$KBrO_4$, UV- and X-irrad., ESR spectra of trapped O_2 78−84474
KCl solution, EPR of O_2^- luminesc. centres, 4.2K *(Russian)* 79−15339
KCl:Ag, formation of Ag atoms and self-localised holes by illumination, EPR meas. 78−31108
KCl:Hg^+, X-irradiated, ESR meas. 77−1588
KCl:Sn^{2+}, EPR exam. of struct. and prod. of $Sn^-(5p^3,4S)$ defects 79−61215
KCl:$SnCl_2$, electronic struct. of Sn^+ centres, model for ESR spectra interpretation 77−43530
$K_2Cr_2O_7$ single crystals, X-irrad., EPR spectra 80−2638
KD_2PO_4:Tl^{2+}, EPR of ferroelec. and paraelec. phases 80−66012
$KD_3(SeO_3)_2$, ferroelastic transition, EPR 80−7148
KF:U^{5+} EPR of U^{5+} centre meas. 77−20684
KH_2AsO_4-KH_2PO_4, AsO_4^{4-} centre, EPR central peak dynamics 79−33523
$KH_2PO_4^-$ (KDP) type crystals, irradiated or doped, behaviour of ESR probes 77−48035
KH_2PO_4:SeO_4^{3-}, slowing down of fluctuations near T_c, EPR obs. 78−60403
KH_2PO_4:Tl^{2+}, EPR of ferroelec. and paraelec. phases 80−66012
$KH_3(SeO_3)_2$, ferroelastic transition under uniaxial press., EPR study 80−59562
KI:S_2^-, spin-lattice relax. rate, 1.5 to 2.2K 77−20686
KO_2, low temp. phases, mag. order, EPR and antiferromag. reson. 79−95630
KPO_3-Fe_2O_3 glasses, γ-irrad., ESR 80−50182
β-K_2SO_4:Tl^{2+}, ESR spectra theory 78−23323
Li_3AsO_4:CrO_4^{3-}, EPR, 4.2K, cryst. field parameters 79−28586
LiBr solution, EPR of O_2^- luminesc. centres, 4.2K *(Russian)* 79−15339
LiCl solution, EPR of O_2^- luminesc. centres, 4.2K *(Russian)* 79−15339
LiF:U, X-ray and γ-ray irrad., EPR of U^{5+} centres 79−91295
LiH, effect of surface hydrolysis to LiOH on IR absorption, X-ray luminesc. and EPR spectra 80−60660
LiO_2-Al_2O_3-SiO_2-TiO_2:Sn^{3+}, ESR and X-ray phase anal. 79−99752
Li_2O-Al_2O_3-SiO_2:Cd^+, glass, ESR study 80−103879
Li_2O-Al_2O_3-SiO_2(P_2O_5):Cd^+ glasses, γ-irrad., EPR study 80−84639
Li_2O-P_2O_5:Cd^+ glass, γ-irrad., EPR study 80−84639
Li_3PO_4:CrO_4^{3-}, EPR, 4.2K, cryst. field parameters 79−28586
Li_3VO_4:CrO_4^{3-}, EPR, 4.2K, cryst. field parameters 79−28586
$LuPO_4$:Pb^{3+}, EPR, hyperfine interactions 80−108050
MgO, O_2 adsorption, $(O_2^-)_s$ form., thermal activation, reducing gas effects, EPR 77−9119
MgO:Al, and nominally pure single crystal, thermally stimulated luminesc. rel. to temp., and EPR *(Russian)* 80−84789
MgO-CoO, high surface area, O_2 adsorpt., EPR, volumetric investigs. 80−10782
$Mo_6O_{19}^{3-}$, in Mo/SiO_2 supported catalyst system, EPR, UV-visible spectra 79−99764
$NH_4Al(SO_4)_2.12H_2O$, CrO_4^{3-} centres, EPR and optical absorption spectra 79−91475
$NH_4H_2AsO_4$-$NH_4H_2PO_4$, EPR spectra of central peak fluctuations 78−91932
$NH_4H_2AsO_4$-$NH_4H_2PO_4$, AsO_4^{4-} centre, EPR central peak dynamics 79−33523
$(NH_4)_2SO_4$, ESR study of NH_3^+ radicals 79−38367
$(NH_4)_2SO_4$, ferroelec. transition, EPR study 79−38472
$(NH_4)_2SO_4$:Cd^+, ferroelec. transition, soft mode contrib., EPR obs. 78−72469
$(NH_4)_2SO_4$-K_2SO_4 mixed crystal, ESR study of NH_3^+ radicals 79−38367
NO_2 on Cu, ultrahigh vacuum ESR studies 80−97729
$Na_8(Al_6Si_6O_{24})Cl_2$, sodalite, photochromism, ESR and optical spectra obs. 77−32407
NaCaX zeolite, ion migration and $Ni(CO)_n^+$ form., EPR obs. 79−33522
NaCl:Ag, formation of Ag atoms and self-localised holes by illumination, EPR meas. 78−31108
NaCl:Hg^+, X-irradiated, ESR meas. 77−1588
$NaClO_3$, γ-irradiated, ESR of trapped O_3^- 79−29381
NaF:U^{3+}, U isotope abundance determ. by EPR hyperfine struct. 79−91296
NaN_3, X-irrad., EPR of N_2^- 77−66421
Na_2O-Al_2O_3-SiO_2-TiO_2-NiO glass, paramagnetic centres form. during crystn., ESR study 79−65710
$Na_3Sc_2P_3O_{12}$, fast-ion conductor, struct. phase transition 80−88362
β-$Na_xV_2O_5$, EPR evidence of Na clustering 78−43630
γ-O_2, EPR spectra *(Russian)* 78−6565
O_2^- species adsorbed on Ce-X zeolites, identification by ESR 77−27096
α-$PVW_{17}O_{40}^{5-}$, α$_2$-$P_2VW_{17}O_{12}^{8-}$, aq. soln., hydrodynamic radii from ESR line width 79−78504
PbF_2, gamma-ray and neutron irrad. at low temps., EPR of Pb^{3+} ions 77−63262
$PbWO_4$, EPR of radiation induced MoO_4^{3-} centres 78−80217
α-quartz:P, X- and γ-irradiated, EPR studies of phosphoric ion 77−63263
Rb-tetrahydrofuran solution, polarised photoelectron and loose ion pair (Rb^+, e) obs., optical-ESR study 80−85196
$RbCdF_3$, Fe^{3+}-O^{2-} pair EPR probe for struct. phase changes 77−36113
RbO_2, low temp. phases, mag. order, EPR and antiferromag. reson. 79−95630
Si, (111) surface, low press. baked, dominant interactions and average distances between paramag. centres 80−15783
Si, amorphous film, plasma-deposited, photoluminesc. and EPR meas. 79−4864
n-Si, EPR linewidth, Orbach relax. process, conc. depend. 80−44901
Si, EPR of quenched-in defects 80−29620
Si, ion implanted, spin density effect on laser annealing 80−11517
Si, ion-implanted polycrystalline film, defect build-up efficiency 80−2054

paramagnetic resonance of ions and impurities continued
Si, neutron-transmutation doped, annealing behaviour, EPR obs. 79−86804
Si, vacancies and interstitials 80−29015
Si:Al, recomb. enhanced migration of interstitial Al 79−82201
Si:Ar(Ne)(O)(N), ion-implanted, defect reverse annealing, 550-650°C 80−88875
Si:As(P), Orbach spin-lattice relax. rate, uniaxial stress depend. 78−72391
Si:B, ESR at zero and small external stress, interpreted in spin Hamiltonians 78−43641
Si:B, ESR at zero and small external stress, elastic strengths for point defects 79−19764
Si:H, electron states 80−29355
Si:Li, EPR in mechanically affected sampler 78−39385
Si:Li, nonrandom strain, EPR of thermally excited donors 78−43629
Si:N, laser-annealed, Jahn-Teller distorted donor, EPR meas. 80−84642
Si:O, amorphous, sputtered, influence of O and deposition conditions 80−54693
Si:O, evaporated amorphous film, effect of O_2 on props., ESR spectra 80−11265
Si:P, amorphous, CVD, defect compensation, ESR meas. 80−54644
Si:P, heavily doped, 100 GHz ESR of impurity band 79−95631
Si:P, heavily doped, paramagnetic spin susceptibility 79−78306
Si:P, neutron transmutation doped, EPR obs. of annealing behaviour 79−1453
Si:P, neutron transmutation doped, EPR, electron trapping 79−73179
Si:P^+, Zeeman energy transfer at surface layer 80−11247
Si-SiO_2, ion implantation through SiO_2 film, recoil implantation of O, EPR study 80−88180
$Si_{100-x}Al_x$, RF sputtered, amorphous, props. 80−34754
SiO_2 film, on GaP substrate, N ion implantation, optical refl. and EPR meas. 80−84197
SiO_2 gel, adsorption curves of O_2, EPR *(Russian)* 79−52776
SiO_2, vitreous, irradiated, EPR exam. of H_2 hyperfine spectra 79−28611
SiO_2:Al, vitreous state, EPR of Al defects 78−91951
SnO_2, ESR of adsorbed O species *(Japanese)* 78−10750
SnO_2, O chemisorption, elec. cond. and EPR meas. correlation 80−84369
SnO_2 surface, interactions with O_2, H_2O and H_2, desorpt., ESR and cond. meas 80−10790
$SrCl_2:O_2^-$, perturbed O_2^- molecule ion, EPR results 77−20682
SrO, EPR of molecular ions 77−90031
$SrTiO_3$, structural phase transition, intrinsic and extrinsic central peak properties 80−34168
$ThO_2:U^{4+}$, spin-lattice relax. time calc., nearest neighbour point charge model 77−16146
UCl_5, mag. susceptibility, ESR and g-value, crystal field model anal. 79−91292
$VW_5O_{19}^{4-}$, aq. soln., hydrodynamic radii from ESR line width 79−78504
W surface, SiO_2 supported, adsorbed O_2, EPR evidence for surface mobility of O_2^- 78−84046
$YPO_4:Pb^{3+}$, EPR, hyperfine interactions 80−108050
YbF($^2\Sigma^+$), matrix isolated ESR spectra 78−86890
Zn-astrakhanite single crysts., EPR spectra of ion radicals SO_4^-, PO_4^{2-} and SeO_4^{3-} 79−51845
$ZnFeO_4$, ferrite spinel, structural and catalytic studies 80−44191
ZnO, chemisorpt. of water, cond. and ESR meas. 79−56072
ZnO powder, effect of dry grinding in EPR and catalytic activity *(Japanese)* 80−84640

paramagnetic resonance of iron group ions and impurities
agriculture applications 80−56298
L-alanine:Cr^{3+}, X-irrad., thermoluminesc., ESR, UV photobleaching 77−9104
L-alanine:Cu(II), EPR and ligand-ENDOR measurements 80−44907
alaninium copper tetrahalides, exchange, mag. anisotropy, and spin diffusion contribs. to EPR linewidth 80−80597
alkali bromide (chloride):V^{2+}, electron spin transfer 78−87949
alkali halide: Mn^{2+}, powder EPR *(Spanish)* 77−48036
alkali silicate glass, CuO doped, ESR spectra of Cu^+, quadrupole effects 78−64265
alkali silicate glasses, behaviour of VO^{2+} as spectroscopic probe 79−78510
alkali trihydrogen selenite: Mn^{2+} single crystal, EPR 78−72396
alum:Cr^{3+}(Fe^{3+}), forbidden EPR transitions, theory 78−31106
alumina based ceramics containing Mn and Ti compounds, sintering and paramag. props. 77−21069
aluminoborate glass, Fe and Cr ion interaction, mag. and spectral props. 80−103883
amethyst, Fe^{3+} diffusion, associated phenomena 77−36269
ammonium oxalate monohydrate: Mn^{2+}, ESR, 77-345K 79−19768
ammonium oxalate monohydrate:Mn^{2+}, model for defect formation, EPR 80−103880
biomolecules, radiation damage studies using aqueous LiCl glass as neutral matrix 79−96632
bis(diethylammonium) copper tetrachloride, mag. susceptibility, EPR spectra 78−68193
bis(triethylbenzylammonium)tetrachlorocuprate(II), mag. anisotropy, susceptibility, EPR of Cu^{2+} 78−52344
bis(trimethylbenzylammonium)tetrachlorocuprate(II), mag. anisotropy, susceptibility, EPR of Cu^{2+} 78−52344
blood plasma total Fe-binding capacity meas. by EPR 77−17003
boracite, single cryst. prep. and phys. props. 80−100763
borate glass:Cu^{2+}, EPR spectra 77−8394
borate glass:Fe^{3+}, EPR spectra 77−8394
borate glass:Mn^{2+}, EPR spectra 77−8394
borate glass, ESR study of effect of glass composition on symmetry of Cr complexes 80−88052
borosilicate glass, Fe and Cr ion interaction, mag. and spectral props. 80−103883
cadmium acetate trihydrate, hyperfine forbidden ESR lines of Mn^{2+}, spin Hamiltonian calc. *(French)* 77−28431
cadmium maleate dihydrate:Cu^{2+}, EPR at 77 and 303K 79−33530
calcium cadmium acetate hexahydrate, Mn^{2+} doped, EPR 79−65715
CdS:N, Mn, ion implanted, anomalous enhancement of EPR signal of Mn^{2+} 78−27080
ceramic 22KhS, glass phase, valence state of Ti and Mn ions, ESR determ. 77−43871

paramagnetic resonance of iron group ions and impurities continued
chalcogenide amorphous semiconductors, ESR studies of doped Mn, review *(Japanese)* 77−90019
chloroplast, EPR signal II and Mn-water splitting, factors influencing stability 78−24038
chloroplasts, EPR investigation of state of Mn^{2+} 78−69008
chloroplasts in pulsed illumination, light-dependent reactions of Mn^{2+} and $P700^+$ 79−53062
Cl Mn II complex with protein, EPR spectra and zero field splitting interaction 78−35793
cobalt formate dihydrate, ordered state, paramag. cross relax. *(Japanese)* 77−43873
copper benzoate, EPR sidebands 79−78508
copper benzoate trihydrate, half-field EPR, 1.5-300K 78−60333
copper diethyldithiocarbamate single crystal, EPR exchange coupled pairs, low temp. hyperfine anomaly 77−90021
copper dipyridine dichloride, dynamic shift of the ESR field 80−2630
copper phthalocyanine, polycrystalline, forbidden ESR transition 79−95638
copper phthalocyanine-iodine, amorphous cpd. prep. by I_2 diffusion in polycrysts., triplet EPR signals obs. *(Russian)* 80−66016
copper porphine, Xα multiple scatt. calcs., EPR and electronic spectra 78−13426
copper tetraphenyl porphyrins, mag. diluted, EPR meas. 78−39391
corundum, defect cryst. struct. study 80−103316
cytochrome P-450$_{cam}$, Fe^{3+} zero-field splitting, Orbach relax. rates 77−21483
cytochrome P-450, anomalous T^7 temp. depend. of Raman spin-lattice relax. 77−21482
di(ethylene diamine H_2)$_2$ zince hexachloride, single crystals, EPR parameters for Mn^{2+} 79−56607
di(methylamino) zinc tetrachloride, single crystals, EPR parameters for Mn^{2+} 79−56607
diacetylene, single cryst., photopolymerisation, intermediate states, struct. changes 80−30235
diamagnetic lattice, EPR parameters of V^{4+}, cryst. field effects 78−64263
diamond, spin-spin interaction of N_2 and Ni centres, temp. effects 78−88177
dicarboxylic acids, low-energy electron irrad., ESR obs. 79−95646
diethylammonium copper tetrachloride, antiferromag. mode excitation in EPR spectra 78−56373
diethylammonium manganese chloride, Heisenberg magnet, spin diffusion, EPR study 80−66019
diethylammonium manganese chloride, planar Heisenberg magnet, spin diffusion, EPR study 80−15793
diethylammonium manganese chloride, T_1 and T_2 meas. by LODESR 78−15064
diethylammonium-manganese chloride, spin diffusion, quasi-two-dimensional Heisenberg paramagnet 78−88129
diglycine barium chloride monohydrate:Cu^{2+}, optical absorpt. and EPR, lattice sites, hybridisation 77−43872
dimethyl ammonium copper manganese tetrachloride, EPR study *(German)* 80−54941
dimethylammonium copper manganese chloride, two-dimens. mixed magnet, EPR 80−66030
dimethylammonium manganese tetrachloride, antiferromag. and spin-flop resonance obs., 70 to 100 GHz 80−71190
exchange-coupled pairs of paramag. ions, second-order corrections to spin Hamiltonian formalism 78−68133
ferredoxin, from Clostridium pasteurianum, Mossbauer effect, ESR, and mag. susceptibility meas. 80−40961
ferredoxin, from Halobacterium, Mossbauer and EPR spectrum 78−76998
ferredoxin synthetic analogues, $[Fe_4S_4(SR)_4]^{3-}$ clusters, Mossbauer effect, EPR, and mag. props. 80−41057
ferredoxin-like centres, membrane bound, in photosystem I of blue-green algae, Mossbauer and EPR study 80−40974
ferric haemoglobin, EPR studies before and after irradiation 79−29503
ferric haemoglobin chains, crystalline state disorder and hyperfine component line widths 79−34482
ferric haemoglobin single crystals, contribs. to EPR line width 79−34484
ferroelectrics, isostructural, pressure measurement from ESR 79−38375
ferrous tetrakis thiophenolate, powder, far IR mag. reson., zero field splitting 77−81000
fluorite type crystal, Ti^{2+} doped, electronic struct. and EPR of Ti^{2+} 78−76034
garnet:Fe^{3+}, spin Hamiltonian parameters, g-factors, temp. depend. EPR obs. 77−48038
garnet:Mn^{2+}, spin Hamiltonian parameters, g-factors, temp. depend. EPR obs. 77−48038
garnets, mag. props. of V^{4+} ion, effect of covalency 78−64010
glass:Fe^{3+}, EPR line shape, H to g transforms. 77−12193
glass:Fe, thermally detected EPR meas. 77−63273
glass:Mn^{2+}, EPR, low-field hyperfine struct. 78−95513
glass, Libyan Desert Glass, redox form. conditions, EPR obs. of as-received and irrad. samples 78−28228
glass, phase separated, EPR rel. to struct., elec. and opt. props. 78−23333
glass formation by meteorite impact, EPR study 80−85659
graphite intercalation compounds, $C_{13}CrO_3$ and $Cr_{27}CrO_2Cl_2$, Cr oxidation state determ. 78−35051
guanadinium zinc sulphate:Cu^{2+}, EPR of Cu^{2+} at tetrahedrally coordinated Zn^{2+} sites 78−39388
guanidine aluminium sulphate hexahydrate:Cr^{3+}, ESR spectra fine struct. 80−93169
guanidine aluminium sulphate hexahydrate type ferroelectrics, ESR of Fe^{3+} exchange pairs 77−90022
guanidinium aluminium sulphate hexahydrate:Cr^{3+}, EPR, 295.5, 78.45, 1.61K, zero field splitting 78−68359
guanidinium aluminium sulphate hexahydrate:Cr, temp. depend. of zero field splitting parameter in EPR spectra 77−69679
guanidinium aluminium sulphate hexahydrate:Fe^{3+}, EPR spectra, angular var. calc. 80−54940
guanidinium aluminium sulphate hexahydrate:Mn^{2+}, NMR 78−91939
guanidinium aluminium sulphate hexahydrate, ESR of V^{3+}, 21.5 GHz, 4.2K 78−91942
guanidinium vanadium sulphate hexahydrate, susceptibility meas. spin-lattice relax. effects 77−66279
haemoglobin, human, EPR spectrum, g-value during oxygenation-deoxygenation reaction 78−53333

paramagnetic resonance of iron group ions and impurities continued
hexa-urea aluminium complex: VO^{2+}, cryst., one-dimens. interactions, EPR 77−73074
hexaurea aluminium perchlorate:VO^{2+}, single cryst. ESR 77−16158
high spin d^5 system, isotropic g-tensor 78−10757
high-potential Fe protein of Chromatium vinosum, low-lying excited state 78−3448
human serum Cu, EPR spectrum obs. 80−91582
II-VI semiconductor, Cr^{2+}-doped, Jahn-Teller interaction energy calc. 78−2455
(iron, chromium) carboxylates, heteronuclear trimer exchange clusters, ESR spectra 80−80603
iron porphin in triphenylene, ESR 78−60329
iron porphyrin chlorides, X-ray, EPR and mag. susceptibility obs., intermol. exchange interaction 78−10765
iron tetraphenylporphyrin chloride, electron spin pairs, low and ultralow temps. 77−77092
lead acetate trihydrate:Mn^{2+}, ESR, elec. cond. 80−93165
lithium potassium tartrate monohydrate: Mn^{2+}, isomorphism with lithium ammonium tartrate monohydrate, EPR obs. 80−29607
magnesium hexahydrate $H_2EDTA:VO^{2+}$, single cryst., ESR spectra and spin Hamiltonian parameters 80−75845
manganese acetate tetrahydrate, single cryst., ESR spectra, temp. depend. 77−43877
manganese copper formate dihydrate, conc. depend. of EPR linewidth 79−38376
manganese stearate, literally two-dimensional magnet, mag. ordering, EPR 79−28597
manganese stearate, two-dimensional mag. struct. 80−108040
manganese stearate monolayer, two-dimensional mag., prep. and characterisation 78−31097
metal:magnetic ion, book 77−48037
metallo-octaethyl porphyrins, I oxidation products, metallic cond., EPR and reson. Raman spectra 80−29610
methylammonium aluminium sulphate dodecahydrate, single crysts., high-order EPR transitions of Cr^{3+} 80−108052
methylammonium aluminiumselenate:Cr^{3+}, EPR and linewidth anomaly 77−12191
methylammonium chromium alum, single cryst., Cr^{3+} EPR, g-factor, hyperfine splitting 78−2729
methylammoniumgallium sulphate:Cr^{3+}, EPR and linewidth anomaly 77−12191
mica, Fe^{3+} localisation determ. by EPR *(French)* 77−43196
mitochondria of bovine heart, EPR investigation of two forms of Fe-S centre N-2 78−69014
monopyrazine zinc sulphate trihydrate:Cu^{2+}, ESR meas. 78−84478
met-myoglobin:Cu^{2+}, single cryst., EPR, conform. changes 77−73505
nickel acetate tetrahydrate:Mn^{2+}, EPR spectra, angular var. calc. 80−54940
nitroxide free radical mag. interaction with lanthanides or Cu^{2+} in liqs., ESR 78−68380
nitroxide free radical spin label EPR spectra, determ. of rot. correl. time and HFS coupling 80−74260
p-n-octyloxy benzylidene-p-toluidine, mol. order, EPR VAAC probe 80−70114
oxide glasses, γ-irrad., CuO effects on EPR 80−84645
oxide glasses, charact. by magnetic resonance and optical absorption of metallic probe ions *(Japanese)* 79−95640
peptide-Cu II interaction, EPR and optical absorpt. 78−27881
phosphate glasses:Cu^{2+}, EPR, optical spectra 78−72399
phosphate glasses:V^{4+}, EPR, optical spectra 78−72399
phosphate glasses, ESR of VO^{2+} ions 80−100610
polyvinyl acetate:Cu, and undoped, thermally stimulated currents exam. 78−35083
polyvinyl alcohol film containing Cu^{2+} complexes, photoconductivity 80−107849
potassium oxalate, EPR of Mn^{2+} and VO^{2+} 80−39858
1,3-propanediammonium $MnCl_4$, 2-dimens. antiferromagnet, with dipolar broadening, spin diffusion, EPR obs. 79−38371
1-3-propanediammonium-$CuCl_4$, ferromag., antisymmetric and anisotropic exchange, EPR linewidth 78−10761
quanidinium aluminium sulphate hexahydrate:Fe^{3+}, EPR, zero-field splitting 77−8395
α-quartz:^{57}Fe, anomalous hyperfine splitting 80−103650
α-quartz:Cu^{2+}, γ-irradiated, stabilisation of impurity atoms 79−8047
quartz:Fe^{3+}, EPR for phase transform., reduced signal above 670K 77−90016
resin:Cu^{2+}, interaction with ligands, EPR meas. 78−10756
resin:VO^{2+}, interaction with ligands, EPR meas. 78−10756
review of 1974 literature 80−11253
Rochelle salt, VO^{2+}-doped, EPR study 80−34762
ruby:Cr^{3+}, ESR saturation, dynamical mag. susceptibility increase in zero mag. field 77−40122
ruby:Cr, relaxation behaviour, EPR study, environmental effects 80−66021
ruby:Ni, cross relaxation 78−39389
ruby, Cr^{3+} ESR transition influence on ^{27}Al, distant ENDOR and dynamic nucl. polarisation 80−2664
ruby, distant nuclei ESR and ENDOR experiments, dipole-dipole reservoir importance 80−71241
ruby, effect of relax. processes on microwave signal detection 77−66413
ruby, elec. field induced double quantum transitions 80−80595
ruby, EPR intensity standard, description and use 79−54164
ruby, EPR method of predicting cryst. characts., laser appl. 79−11345
ruby, EPR spectrum, temp. depend., cryst. field parameters determ. 78−15016
ruby, ESR and NMR correl. line broadening effect assoc. with external mag. field inhomogeneities 80−50227
ruby, high mag. field spin-lattice relaxation rate of Cr^{3+} 78−52340
ruby, resonant cross-relaxation to Jahn-Teller Cr^{4+} ion 79−65723
ruby, spin-strain coupling tensor meas. US modulated EPR obs. 80−50170
ruby, two-photon spectroscopy of reson. three-level spin system, reson. shift 79−82864
ruby rod, EPR study, comparison of Verneuil and Czochralski grown crystals 78−91945
ruby rods, quality control, EPR method 79−14047
S=1, singlet ground state systems, mag. props. 80−11157
scheelites, zero-field splitting of Mn^{2+} ions 80−75531
serum transferrin bound Fe^{3+} during rat lymphosarcoma development 77−77878

paramagnetic resonance of iron group ions and impurities continued
silica gel, Mn^{2+} adsorption rel. to H_2O adsorpt., EPR study 79−5180
silicate glass, $NiFe_2O_4$ precipitation process, ESR study, effective g value, transition temp. 80−25194
sodium iron fluorophosphate glasses, EPR and Mossbauer resonance study 80−39968
sodium oxalate:Cu^{2+}, anhydrous spin Hamiltonian and bonding parameters and orbital-reduction factors 80−60408
solid, review of 1973 literature 77−69675
stalactites, chem. decomp., ESR obs. 80−15788
strontium acetate hemihydrate:Cu^{2+}, EPR of cryst. 78−19312
strontium acetate hemihydrate:$Mn^{2+}(Cu^{2+})$, EPR, spin Hamiltonian anal. and unit cell symmetry 80−29603
strontium formate:Mn^{2+}, cryst., e.p.r., spin Hamiltonians 77−4552
strontium formate dihydrate, EPR and optical absorption spectra of VO^{2+} ion 77−40112
submitochondrial particle succinic dehydrogenase, interaction of ubisemiquinone with Fe-S centre, EPR 78−69016
sulphides, mag. interactions of Fe group ions 79−99753
TCNQ salt, $Mn(TCNQ)_2$, mag. props. 77−85558
TCNQ salts, $Mn(TCNQ)_2$ and hydrates, mag. and elec. props. 79−82767
tetra-ammine cadmium acetate:Cu, EPR dynamical effects 79−61204
tetramethylammonium cadmium chloride, EPR of Mn^{2+} meas. 77−59452
tetramethylammonium cadmium trichloride:Mn^{2+}, EPR spectrum temp. depend. 78−19314
tetramethylammonium manganese trichloride, ESR meas., evidence for two paramag. species 79−61208
tetramethylammonium manganous chloride:Cu, impure Heisenberg chain paramagnet, EPR sidebands, intensity, linewidths 78−76300
tetrathiotetracenenickel bis(ethylene-1,2-dithiolene), one-dimens. cond., preparation and props. 77−85201
TGFB:Cr^{3+}, polarisation reversal and ageing mechanisms, EPR meas. 79−8044
TGS:Cr^{3+}, EPR and spontaneous polarisation stabilisation during annealing 77−4610
TGS:Cr^{3+}, EPR obs. of ferroelectric monocrystals, fine struct. EHT-SCCC-MO calcs. 79−19769
TGS:Cr^{3+}, EPR obs. of fluctuations near phase transition 78−43820
TGS:$Cr^{3+}(VO^{2+})$, polarization reversal, static hysteresis loops, switching processes 78−43633
TGS:Fe^{3+}, crysts. and their aq. solns., ESR 80−39862
TGS-type crystals:Cr^{3+}, radiospectroscopic studies, elec. field effects on EPR, EM EPR 79−15341
TGSe:Cu^{2+}, EPR ang. depend., coord. of Cu^{2+}, Cu-ligand bond obs. and ferroelec. transition anomaly 80−7156
TMMC:Cu, EPR lines, dynamic effect of low-symmetric spin distrib. 80−39854
TMMC:Cu, EPR linewidth freq. depend., spin dynamics 80−15794
TMMC, crossover transition, effects on susceptibility and EPR shift 80−71047
TMMC, EPR lines in one-dimensional mag. systems, dynamic effect of low-symmetric spin distrib. 80−39853
TMMC, exchange-narrowed EPR linewidth, temp. depend. 78−52292
TMMC, linear Heisenberg antiferromagnet, EPR half-field transitions 80−15792
TMMC, low-symmetry spin distrib. effect on EPR line 80−66018
TMMC, one dimens. Heisenberg system, shift of half-field EPR line 78−23325
TMMC, one dimensional antiferromagnet, EPR expts. 80−20454
TMMC, one-dimensional, EPR at HF and low temp. 78−80205
$[TMPD^+]_2[Cu_xNi_{1-x}(mnt)_2]$, ESR obs. of triplet excitons and Cu(II) ions, mag. interactions 79−95633
transition metal ions in solids 80−51968
transition metal-V_O pair centers, microscopic struct. 79−60354
triglycine calcium bromide:Cu^{2+}, ESR studies 80−97136
trimethylammonium manganese trichloride, Heisenberg antiferromag. chain, specific heat and EPR 80−65931
tris sarcosine calcium chloride:VO^{2+}, EPR and absorpt. spectra 78−60330
tris-sarcosine calcium bromide and chloride solid solns., Mn^{2+} doped, EPR linewidths and ferroelec. behaviour 79−24213
tris-sarcosine calcium chloride:Mn^{2+} ferroelec. dynamics, EPR and ENDOR study 80−75972
tris-sarcosine calcium chloride:Mn(Fe), influence of cryst. defects on ferroelec. transition, EPR 79−38466
trissarcosine calcium chloride:Mn^{2+}, ferroelec., electron spin-lattice relax. 78−80208
TSCC:Mn^{2+}, microscopic, mechanism of ferroelectric transition, EPR fine struct. tensor calc. 78−35104
Tutton salt:Mn^{2+}, EPR, 298K, spin-Hamiltonian parameters, cryst. fields 78−27086
Tutton salts:Mn^{2+}, EPR, 300K 79−51848
valency assessment, appl. to ceramics and glass industries *(German)* 80−34757
vitamin B_{12b}:B_{12r}, cryst. growth, orientation, ESR obs. 79−34486
vitamin V_{12r}, monomeric O_2 adduct, struct., single cryst. ESR obs. 79−39351
water:Cu(II) adsorbed on silica surface, freezing props. of water 77−4555
zeolite surface, bonding of Cu^{2+}, Cr^{3+}, Co^{2+} ions EPR, optical spectroscopy investig. *(German)* 79−95266
zinc bisdiethyldithiocarbamate:Cu^{2+}, exchange interaction of Cu^{2+}-Cu^{2+} pairs, spin-lattice relax. 78−48034
zinc formate dihydrate, Co^{2+}-doped, EPR spectrum, g-factor anisotropy for A- and B-sites 77−77089
$24BaO.V_2O_5.25P_2O_5$, ESR and absorpt. spectra, V(IV) ions conc. 78−64266
$24CaO.V_2O_5.25P_2O_5$, ESR and absorpt. spectra, V(IV) ions conc. 78−64266
$3d^5$-ions, variation of hyperfine splitting consts. with interatomic distance 80−97133
$\{Cu(NH_3)_4\}^{2+}$ complex, superhyperfine interaction 79−91284
Ag halide, photochromic glasses, optical properties, effect of Cu ions 80−93364
Ag halide photochromic glass:Cu^{2+}, characterisation of Cu ions 78−5530
Ag halide:Cu^{2+} photochromic glasses, darkening mechanisms, from flash photolysis and EPR studies 77−16156
Ag-Mn, dil., spin glass, AC susceptibility 79−33490

paramagnetic resonance of iron group ions and impurities continued
Ag-Mn, dilute spin glass, AC susceptibility and ESR meas. 79−7968
AgBr:Ni^{2+}, low-temp. EPR 77−77091
AgCl:Ni, double quantum EPR transition, superhyperfine struct. 80−7154
AgCl:Ni^{2+}, low-temp. EPR 77−77091
$AgGaS_2$, optical quality, grown from melt, EPR characterisation 78−64260
$AgGaS_2$:Fe, EPR of Fe-associated defect 80−60412
Al complex, Al urea$_6(ClO_4)_3$:Cr^{3+} structural phase transition, ESR meas. 77−20681
Al-Co(Ni), composite, paramagnetic resonance and electron-positron annihilation *(Russian)* 79−87314
$Al_2Be_3Si_6O_{18}$:Cu^{2+}, synthetic beryl, ESR, optical spectra and X-ray diffr. meas. 77−16166
$Al_xGa_{1-x}As$:Mn epitaxial layers, Mn-O association, EPR meas. 77−69677
α-Al_2O_3:Co,H, Co and proton ENDOR, IR and optical spectra charge compensator nature and defect struct. 80−44956
Al_2O_3:Cr, electron irrad. induced cond., TSC and EPR study 80−80277
Al_2O_3:Cr_2O_3, saturation effects by double-quantum transitions 78−80197
Al_2O_3:Cr^{2+}, Jahn-Teller study, EPR data anal. 78−84172
Al_2O_3:Cr^{3+}, inhomogeneous spin system, time evolution towards saturated state 80−88869
Al_2O_3:Cr^{3+}, new method for spin-lattice relax. time, inhomogeneously broadened ESR lines 79−15343
Al_2O_3:Cr^{3+}, standard reference material for EPR 79−12757
Al_2O_3:Mn^{2+}, EPR meas., comparison with theory of EPR of S-state ions 77−1587
α-Al_2O_3:Mn^{2+}, intensity of forbidden $\Delta m=2$ EPR lines of S-state ions with axial cryst. environments 77−77090
Al_2O_3:Ni^{3+}, effect of uniaxial stress on EPR spectra 79−82862
Al_2O_3:Ni^{3+}, Jahn-Teller effect for Ni^{3+} 79−82564
Al_2O_3:Ni(Cr), thermally detected EPR of Ni^{3+}, Cr^{2+}, Cr^{3+} and Cr^{4+} ions 77−63273
Al_2O_3:V, valency changes of V ions, γ irradiation, thermal cond. optical absorption and EPR meas. 77−80541
β-Al_2O_3-Ag_2O:Cu^{2+}, EPR of Cu^{2+} ions in conduction plane 77−69678
β-Al_2O_3-Na_2O:Cu^{2+}, EPR of Cu^{2+} ions in conduction plane 77−69678
β-Al_2O_3-Na_2O:Mn^{2+}, EPR of Mn^{2+} 78−6569
β-Al_2O_3-Na_2O:Mn^{2+}, ESR exam. 78−19313
Al_2O_3-SiO_2-MO-Fe_2O_3 glass, M=Ca, Mg, Ba, Sr, UV and EPR absorpt. spectra 80−89018
β-Al_2O_3-Tl_2O:Cu^{2+}, EPR of Cu^{2+} ions in conduction plane 77−69678
$Al(OH)_3$, based ceramics containing Mn and Ti compounds, sintering and paramag. props. 77−21069
$Al(OH)_3$:Fe^{3+}, thermal decomposition, EPR obs. 78−40047
β-Al_2O_3.Na_2O:Cu, EPR, localisation of Cu^{2+} and linewidth effect 78−39395
$AlPO_4$, synthetic berlinite, electron irrad. effects, ESR, ENDOR, optical spectral study 80−80608
$AlPO_4$:Fe^{3+}, EPR, α-β phase transition 77−90016
Al_2SiO_5, EPR of Fe^{3+} at V-band and the pair spectra 78−80204
Al_2SiO_5:Fe^{3+} appl. of sensitive EPR spectrometer to zero field splitting determ. *(Russian)* 77−57372
As_2S_3:Fe glass, photolum. and ESR, Fe impurities as non-radiative recomb. centres 80−29788
$(As_{0.4}S_{0.6})_{100-x}Cu_x$, glassy, struct. and elec. cond. study 80−59399
As_2Se_3, and As_4Se_5Ge glasses, struct. changes, Mn^{2+} EPR expts. 78−79534
As_2Se_3, effect of Cu and I, investigated by Mn^{2+} EPR spectra 77−73075
As_2Se_3:Mn^{2+} film, reversible photostructural change, ESR obs. 77−32411
As_xSe_{100-x}:Mn^{2+}, $0\leq x\leq 70$, composition depend. and struct. 77−24736
As_xTe_{100-x}:Mn^{2+}, $40\leq x\leq 70$, composition depend. and struct. 77−24736
$As_4Te_5Ge(Si)$ glass, struct. changes, Mn^{2+} EPR expts. 78−79534
$(As_2Te_3)_{1-x}Mn_x$, defect and impurity states, EPR meas. 80−54650
Au-Fe solid soln. alloys, reson. and relax. effects 79−82865
α-B, rhombohedral, magnetic props. and ESR spectra 80−20452
$BaBr_2.2H_2O$:VO^{2+}, EPR meas. 77−16145
$BaCl_2.2H_2O$:VO^{2+}, EPR meas. 77−16145
$Ba_2Cu(OH)_6$, EPR, g-values 79−19770
$Ba_3Fe_2BO_9$ (B=Ke, Te, W), siegnette magnets with hexagonal barium titanate structure 78−76397
$BaMgF_4$:Mn^{2+} ferroelec., EPR and ENDOR study, cryst. field tensor 80−71162
$BaMnF_4$, ESR linewidth and reson. field for Mn^{2+}, 25 to 300K, spin diffusion 77−69681
$BaMo_4$, M=Mo,W, EPR spectrum, temp. depend. of zero field splitting 79−15346
BaO:Mn^{2+}, impurity pot. well shape calcs. 78−87950
BaO-Al_2O_3-B_2O_3-V_2O_5 glass, spectra, oxidation-reduction behaviour, DC cond. 77−76814
BaO-B_2O_3-SiO_2:Ti^{3+}, Ti^{4+}, glass EPR spectra, variation of g-factor with temp. 79−99757
BaO-B_2O_3-V_2O_5 glasses, polaron hopping cond., optical absorpt. and ESR spectra 79−23966
BaO-B_2O_3-V_2O_5 glass, oxidation-reduction of V, thermodynamics 80−85169
BaO-B_2O_3-V_2O_5(Fe_2O_3)(Cu_2O), glass, resist. and activation energy, reduced valency 77−51749
BaO-V_2O_5-CuO, P_2O_5-V_2O_5-CaO-CuO glasses, EPR, Cu impurity effect on elec. props. 79−51849
BaO-V_2O_5-CuO semiconducting glasses, impurity effects, elec. resist. and EPR study 80−103692
$Ba_5(PO_4)_3Cl$ with substituted CrO_4^{3-}, ESR study 80−2629
BaT:O_3:Mn, ferroelec. domain stabilisation by bulk ordering of defects 79−42925
$BaTiO_3$, antireson. in EPR spectra of Fe^{3+} ions *(Russian)* 80−11257
$BaTiO_3$:Cu, Cu ion as electron trap, rel. to Curie temp., Γ_{15} phonon freezing 80−25318
$BaTiO_3$:Fe^{3+}, local position of Fe^{3+} in ferroelec. phases, EPR study 80−25196
$BaTiO_3$:Fe^{3+}, local position determ. by EPR 80−108057
BaV_2O_6:Cr, EPR spectra temp. depend., paramagnetic ion point symm. 80−71166
$BaVS_3$, exam. of ferromagnetic, antiferromagnetic behaviour, depending on stoichiometry 78−52233
$Be_3Al_2Si_6O_{18}$:Cr^{3+}, EPR spectra, exchange-coupled pairs 79−28596

paramagnetic resonance of iron group ions and impurities continued
$Bi_{12}GeO_{20}$:Cr^{3+}, level distrib. of Cr^{3+} ion, spectroscopic parameters, spin Hamiltonian, EPR spectrum 78−48030
BiI_3:Cr^{3+}, ESR, spin-lattice relax., temp. depend. 78−88178
BiI_3:Mn^{2+}, ESR, spin-lattice relax., temp. depend. 78−88178
$BiTaO_4$, X-ray and ESR study of phase changes 78−72476
β'-$Cu_xV_2O_5$, mag. and spectroscopic study, semiconductor to metal transition 80−2628
$C(NH_2)_3Al(SO_4)_26H_2O$:Cr^{3+}, isotope effect, zero field splitting, vibr. coupling temp. depend. 78−6570
$CaCO_3$, Akiyoshi stalactite, thermoluminescence and ESR dating comparison 78−88807
$CaCO_3$:Mn, calcite, EPR and ENDOR absorpt. spectra of divalent Mn in single cryst. 79−47328
$CaCO_3$:Mn^{2+}, calcite, on axis half-field forbidden lines, numerical prediction 77−16161
$CaCo_2$, aragonite, EPR of Mn^{2+} impurities, orthorhombic spin-Hamiltonian parameters 80−2631
CaF_2: Ni crystals, X-irradiated, EPR study of Ni^+ and Ni^{3+} 80−75849
CaF_2:Mn, EPR and optical absorpt. spectra 80−93171
CaF_2:Ni, X-irradiated, optical and EPR meas. 80−108235
$Ca_3Fe_2Ge_3O_{12}$ garnet, light absorpt. spectral study 80−93322
$CaMO_4$:Mn^{2+}, M=Mo,W, EPR spectrum, temp. depend. of zero field splitting 79−15346
$Ca_2Mn_3O_8$, mag. props. 79−78339
$Ca_2Mn_3O_8$, mag. props. and EPR 79−91215
$CaMoO_4$:Fe^{3+}, single crystals, structure and kinetics, EPR meas. 79−99760
CaO:Cr^{2+}, APR spectra 79−87313
CaO:Mn^{2+}, impurity pot. well shape calcs. 78−87950
CaO:V^{3+} orbital triplet, intermediate Jahn-Teller effect, APR 80−34758
CaO-Fe_2O_3-B_2O_3 glasses, phys. props. rel. to struct. and comp. 78−23331
CaO-MnO system, solid soln. form. and analysis 80−28996
CaO-P_2O_5 glass, pulsed EPR study of Cu 78−84479
$Ca(OD)_2$:Cu^{2+}, ESR, secondary spectra 78−88174
$Ca(OH)_2$:Ni^{2+} single cryst., X-irrad., Ni^+ EPR, g-factors and point-charge model 80−2626
$Ca_3(PO_4)_2$:Cu^{2+}, ESR, high press. struct. transition 80−97134
$Ca_5(PO_4)_3F$: Cr^{5+}, spin-lattice relax. time and Debye temp., EPR obs. 79−28601
$Ca_5(PO_4)_3F$:Cr^{5+}, ESR, polymorphic transform., spin Hamiltonians 77−36117
CaS:Cr^{3+}(Cr^+), EPR *(Russian)* 78−91946
CaV_2O_6:Cr, EPR spectra temp. depend., paramagnetic ion point symm. 80−71166
$CaWO_4$:Fe^{3+}, EPR, spin Hamiltonian parameters from anal. of Kramers' doublets 79−28595
$CaWO_4$:Mn^{2+}, polycryst., EPR spectra calc. using Bir's method, compared with expt. 79−1707
$CaWO_4$:Mn^{5+}, new EPR center *(Russian)* 79−1709
Cd complex, dichlorobis (pyrazole) cadmium:Cu(II), ESR, compressed tetragonal symmetry 78−6568
Cd complexes, dithiocyanato(diethylenetriamine) Cd(II) and dithiocyanato(pentamethyldiethylenetriamine) Cd(II), Cu^{2+} doped, ESR 80−108059
$CdBr_2$:Co, spectroscopic studies of interactions 80−29769
$CdBr_2$:Co^{2+}, ground state g-value, EPR meas. 77−16159
$CdBr_2$:Mn^{2+}, layered, pressure effect of ESR on axial field const. of spin Hamiltonian *(Russian)* 77−32254
$CdCl_2$:Co, spectroscopic studies of interactions 80−29769
$CdCl_2$:Co^{2+}, ground state g-value, EPR meas. 77−16159
$CdCl_2$:Mn^{2+}, e.s.r. spectra meas. 77−4554
$Cd(ClO_4)_2.6H_2O$ and $Cd(ClO_4)_2.6D_2O$, single crystals, EPR study of phase transitions 80−66025
$Cd(ClO_4)_2.6H_2O$:Mn^{2+}, phase transition, EPR of Mn^{2+} meas. 79−56604
$CdCr_2S_4$, EPR line profiles in paramag. and ferromag. phases 79−28602
$CdCr_2S_4$, single crysts., EPR linewidth near Curie point, temp. and susceptibility depend. 77−63272
$CdCr_2S_4(Se_4)$, EPR linewidth, 100-300K, spin-lattice relax. 77−51942
$CdCr_2Se_4$, Crit. relax. processes, mag. reson. expts. 80−60425
$CdCr_2Se_4$:Cu(Ag), ferromag. reson. and ESR line widths 80−60413
$CdCr_2Se_4(S_4)$, ESR line intensity near Curie point 78−64269
CdF_2:Cr^{2+}, orthorhombic Jahn-Teller distortion 78−19007
CdI_2:M^{2+}, M=V, Mn, Co, EPR 78−68362
$Cd_{1-x}In_xCr_2S_4$, ferromagnetic spinel, Cr^{3+} exchange interaction mechanism, Cr^{2+} relaxation, EPR line width depend. 79−69715
$Cd_{1-x}In_xCr_2S_{4-x}P_x$, ferromagnetic spinel, Cr^{3+} exchange interaction mechanism, Cr^{2+} relaxation, EPR line width depend. 79−69715
$CdIn_2S_4$:CQ^{2+}, site symmetry, spectral meas. 79−78729
$CdIn_2S_4$:Cr^{3+}, ESR and ENDOR 77−20692
$Cd_2Mn_3O_8$, mag. props. 79−78339
$Cd_2Mn_3O_8$, mag. props. and EPR 79−91215
$Cd_{1-x}Mn_xTe$, EPR, mag. crit. point 80−39851
$CdMoO_4$:Mn^{2+}, EPR spectrum, temp. depend. of zero field splitting 79−15346
$Cd(NH_3)_6(BF_4)_2$:Ni^{2+}, EPR of $[Ni(NH_3)_6]^{2+}$, temp. depend. at phase transition 77−20685
$Cd(NH_3)_4Cl_2$:Cu, EPR dynamical effects 79−61204
$Cd(NH_4)_2(SeO_4)_2.6H_2O$:$Mn^{2+}$, EPR of Mn^{2+}, spin-Hamiltonian parameters 79−33528
$Cd(NO_3)_2.4H_2O$:Mn^{2+} single cryst., low symm. effects in EPR 77−90020
$Cd_2Nb_2O_7$, Mn^{2+} ESR, hyperfine interaction const., ferroelectric domain orientation 80−54943
CdS:Mn, vacuum deposited film, Mn migration, EPR and X-ray study 80−65411
CdS:Mn gamma-irradiated ESR meas. 79−11342
CdS:Mn^+, cryst., X-band ESR 78−2730
CdS:Mn^{2+}, spin-lattice relax. ang. depend. 79−73807
CdS:Mn^{2+}, temp. depend. of rate of spin-lattice relax. 79−42832
$CdSiP_2$:Fe, EPR and optical absorpt. of Fe^+, Fe^{2+}, Fe^{3+} and Fe^{4+} on tetragonal sites 77−8397
CdTe:Cr, impurity photoionisation transitions, EPR meas. 80−39857
CdY_2S_4:Fe (Mn), superhyperfine interaction of Mn and Fe, ESR spectra 77−63271
Cl_2O_3:Ni^{3+}, EPR spectra anal. using dynamic Jahn-Teller model 79−82863
Co complex, $CoCl_2$(indazole)$_2$, linear chain ferromagnetism 79−56519
Co complex, $CoCl_2$(pyrazole)$_2$, linear chain ferromagnetism 79−56519

paramagnetic resonance of iron group ions and impurities continued
Co complex, Co(II)(1,2,4-triazole)$_2$(NCS)$_2$ quasi two-dimens. canted S=1/2 antiferromag. 80−70976
Co complex, cobalt pyridine chloride, EPR, effective g-values 79−42825
Co complexes, 1,2-bis(diphenylphosphino)-ethane in-plane ligand ^{31}P hyperfine interaction, ESR obs. 77−77087
Co complexes, Co II tetraphenylporphyrins, constraint, ESR and optical detect. 80−83394
Co II complexes, with tetradentate Schiff bases, synthesis, struct. and ESR obs. 80−80598
Co salts:M^{2+}, M=Mn,VO, spin-lattice relax. time meas., 180-380K 78−64268
Co Schiff base complex, N,N′-ethylene-bis (salicylideniminato)-Co II pyridine doped in Znsalenpy crystal, ENDOR, EPR studies 80−34819
$CoCl_2 6H_2O$, g-tensor and exchange parameters, mag. reson. studies 79−87324
$CoCl_2.2NC_5H_5$, 1-dimens. Ising ferromag., charact. EPR modes 79−91287
$CoCl_2.6H_2O$, antiferromag., spin flop and paramag. resons. at very low temp. 77−66426
$CoK_2(SO_4)_2.6H_2O:Mn^{2+}$, EPR spectra, spin-Hamiltonian anal. 77−77088
$CoK_2(SO_4)_2.6H_2O:VO^{2+}$, ESR, ion orientations 78−48029
$CoK_2(SeO_4)_2.6H_2O:Mn^{2+}$, Tutton salt, EPR exam. of cryst. field parameters 78−39394
$Co_xMg_{1-x}O$, solid solution, EPR of Co^{2+} *(Russian)* 80−11251
CoO-ZnO-MgO ternary systems, solid solns., struct. charact. 80−60629
CoS_2, itinerant ferromagnet, ferromag. reson. and EPR meas. 80−66044
$CoSO_4.7H_2O:Mn^{2+}$, host spin-lattice relax. narrowing in single cryst. 78−27079
$CoSiF_6.6H_2O:Co^{2+}$, spin Hamiltonians and pair interactions 77−36119
$Co_xZn_{1-x}Rh_2O_4$, mag. props., EPR spectra, antiferromag. order 80−75736
Cr complex, dimer di-μ-diphenylphosphinatoacetylacetonatochromium(III), EPR of exchange coupled Cr^{3+} pairs 78−88172
Cr complex, influence of anisotropy of spin-Hamiltonian parameters on EPR spectra *(Russian)* 77−28432
Cr^{3+}, in alums, ENDOR, resolution enhancement through multiple quantum transitions 78−19374
Cr-tissue complex detection 77−9310
CrN, antiferromagnetic EPR spectra, binding energy, isotropic exchange and ordering *(German)* 80−80604
CrO_n, mag. and optical obs., prep. by calcination of $CrCl_3$ 79−24736
Cr_2O_3, EPR linewidth, near Neel temp. 78−23327
$Cr_2O_3:Ga_2O_3$ EPR, antiferromagnetic coupling energy temp. depend. *(German)* 78−10766
$(1-x)Cr_2O_3$-xαFe_2O_3, influence of Fe^{3+} on phase transition *(Russian)* 79−28522
$(1-x)Cr_2O_3$-xαFe_2O_3, mag. phase diagram, EPR method *(Russian)* 79−28521
CrTe, mag. ordering under high-press., ferromag. transition, ESR and neutron diffr. *(French)* 78−31053
$CsAl(SO_4)_2.12H_2O:Cr^{3+}$, ESR spectra 78−91944
$CsCaCl_3:Co(Mn)$, EPR, 4.2 to 450K, ferroelec. transition 80−60414
$CsCdBr_3:Cr^{3+}(Cr^{+})$, EPR of impurities, charge compensation, X-ray effects 80−60407
$CsCdCl_3:Co^{2+}$, ground-state g-value, EPR meas. 77−16159
$CsCl:Cr^{3+}$, ESR of Cr^{3+} centres, room temp. 78−91943
$Cs_2HfCl_6:Mn^{2+}$, ESR of mol. jumps, zero-field splitting tensor 77−51944
$CsMgCl:Cr^{3+},Mo^{3+}$, Cr^{3+}-Mo^{3+} exchange coupled pair, EPR study 79−42830
$CsMgCl_3:Mn^{2+}$, EPR spectrum temp. depend. 78−19314
$CsMgCl_3(Br_3):Cr^{3+}(Cr^{+})$, EPR of impurities, charge compensation, X-ray effects 80−60407
$CsMn_{1-x}Co_xCl_3.2H_2O$, impure Heisenberg linear chain, EPR meas. 78−43634
$CsSrCl_3:Mn^{2+}(Gd^{3+})$, structural transitions, EPR meas. 78−34619
$CsZnCl_4:Cu^{2+}$, electron spin echo, 35 GHz 80−13113
$Cs_2ZnCl_4:Cu^{2+}$, single cryst. and powdered single cryst., EPR, linear elec. field effect 80−11250
$Cs_2ZrCl_6:Mn^{2+}$, ESR of mol. jumps, zero-field splitting tensor 77−51944
$(Cu,Zn)Cs_2(SO_4)_26(H,D)_2O$, thermal contact between nucl. Zeeman and electron dipole-dipole interaction system 77−90065
$(Cu,Zn)Cs_2(SO_4)_2.6(H,D)_2O$, proton spin-lattice relax. exam., rel. to EPR 77−90064
Cu complex, bis-(2,2′-bipyridyl) thiourea copper II perchlorate, single cryst., ESR 79−38373
Cu complex, bis-acetylacetonatocopper II, in stretched PVA film, ESR 79−51847
Cu complex, bis-salycylal-1,2-ethylenediiminatocopper II, in stretched PVA film, ESR 79−51847
Cu complex, bis(N,N-diethyl-N′-benzoylthioureato)Cu(II), ESR 77−8393
Cu complex, bis(1,1-diisobutyl-3-benzoyl-selenoureato)Cu(II), single cryst. ESR, ^{77}Se hyperfine struct., bonding 77−77086
Cu complex, catena-μ-isothiocyanato-(N′-pyridylmethylene-N″-salicyloylhydrazinato-NN′O) copper (II), EPR and visible spectra 80−5566
Cu complex, copper (II) [2,5-diphenyloxazole]$_2$ $(ClO_4)_2.4H_2O$, ESR studies 80−88867
Cu complex, Cu-glycine in water, EPR spectral parameters, temp. depend. 80−2623
Cu complex, Cu(II) impurity in α-glycine crysts., ligand ENDOR spectra 79−65765
Cu complex, Cu(II)-L-asparagin complexes, ESR spectra, mag. and bonding parameters 78−23326
Cu complex, $Cu(ONC_5H_5)_6X_2$, X=ClO_4, BF_4, cooperative Jahn-Teller ordering and mag. struct., EPR meas. 79−60505
Cu complex, $Cu(en)_3Cl_2.0.75$ en, X-ray and ESR data, Jahn-Teller distortions 78−80206
Cu complex, di-μ-thiocyanato bis[di-(2-aminoethyl)amine] dicopper II diperchlorate, ESR 79−38374
Cu complex, diaquobis(2,3-dihydroxy-2-methyl propanato) copper(II), cryst., EPR, room-temp. 79−82861
Cu complex, glycylglycinatocopper trihydrate, mol. g values, EPR meas. *(French)* 77−43874
Cu complex, halocuprates, ferromagnetic insulator, two-dimens. Heisenberg layers, mag. susceptibility 80−50068

paramagnetic resonance of iron group ions and impurities continued
Cu complex, hexakis pyridine-N-oxide cuprate ion, pure and Zn doped, EPR, Jahn-Teller effect 78−10754
Cu complex, L-alanyl-L-serine, PMR, EPR and absorpt. spectra 78−46367
Cu complex, N,N′-tetramethylene bis-(2-pyridinaldimine) thiourea copper II perchlorate, single cryst., ESR 79−38373
Cu complex, polyacrylic acid-polyethyleneimine-Cu(II), struct. *(Russian)* 79−55018
Cu complex, polyvinylimidazole.Cu(II) complex, ESR studies on dimer form. between copper ions 80−100613
Cu complex, Schiff-base, ESR and optical absorpt. in soln. and powder 79−65892
Cu complex, substituted Cu(II) acetates, exchange interactions, EPR, struct. 79−42829
Cu complex, with acetylene, Ar matrix-isolated EPR obs., bonding 78−50564
Cu complex with adenine, powder, physical properties obs. *(Japanese)* 77−43878
Cu complex with L-phenylalanine amino acid, ESR spectra and magnetic susceptibility measurement 80−34761
Cu complexes, of polyamines, ESR in soln., coordination around Cu(II) ions 78−5254
Cu complexes, spin coupled ion pair, singlet-triplet splitting 77−85552
Cu complexes, spin-labelled, EPR, electron-electron coupling 79−51858
Cu complexes, with L-glutamic acid and DL-aspartic acid, EPR, bonding and hyperfine linewidth 78−25572
Cu complexes, with tridentate Schiff bases, exchange interactions, EPR, mag. susceptibility 78−23324
Cu complexes with dipeptides, EPR spectra of high pH aq. solns. 77−32248
Cu II complex, bis(pyrrolidonecarbodithioato) copper II, ESR, solvent effects 78−1008
Cu II complexes, 5-coord., ESR, optical absorpt., solvent effects 78−5253
Cu II complexes, 5-coord., ESR and optical absorpt. spectra 79−64020
Cu oxalate complex with aliphatic amines, X-band ESR line width 77−20687
Cu^{2+} complex, in water-ethanol soln., struct., EPR 78−50565
Cu^{2+} complexes, ground state wave functions, g-factor anisotropy, lattice structs. 77−24536
Cu^{2+}, dopant, ground state wavefunctions and Δg 78−64012
Cu^{2+} ion, ground state wavefunctions and ESR parameters 80−88868
Cu^{2+} ions, ground state wave functions, cryst. field effect, ESR data anal. 78−23060
Cu-Fe, dil., transmission ESR meas. 2 to 40K 78−68364
Cu-Mn, exchange-coupled localised moments, Korringa relaxation rate 80−75851
Cu-Mn, zero field ESR in spin glass state 80−66017
Cu-Mn spin glass, spin freezing and exchange narrowing of mag. reson. 80−60411
Cu^{2+}-imidazole complex, electron spin echo, nuclear modulation effect 79−18211
CuCl, pressure depend. of structural, chemical, elec. and mag. props. 80−96596
$CuCl_2$-$2H_2O$, mag. g-tensors for ion complexes, spin-orbit coupling 78−10752
$Cu_2Cl_8^{4-}$, in Co (III), Cu (II) complex, single cryst. EPR 77−16157
$CuCl_2.2H_2O$, nearly one dimensional mag. system, EPR line shape 79−99759
$CuCl_2.2H_2O$, submillimetre ESR meas. using pulsed high mag. field 80−44905
$CuCl_2.2H_2O$, X-band ESR magneto-microwave effects 77−28434
$CuCr_2O_4$ and $CuCrO_4$, IR spectrometry and EPR study *(French)* 79−47452
$CuCr_2Se_4$, Crit. relax. processes, mag. reson. expts. 80−60425
$CuCr_2Se_4$, mag. reson. and valence state of Cu and Cr ions 80−60413
$CuF_2.2H_2O$ powder, EPR and Cotton-Mouton Voigt effect in Q-band *(French)* 79−8045
$CuF_2.2H_2O$, X-band ESR powder spectrum and related magneto-microwave effects 79−24214
$CuGaS_2$, coloration, pure and Fe doped, EPR and optical absorpt. obs. 78−88336
Cu(II) complex, 2,2′,2″-triaminotriethylamine, EPR and optical absorpt. obs. 80−108055
Cu(II) complex, hexamethyltriaminotriethylamine, EPR and optical absorpt. obs. 80−108055
Cu(II) complex with poly(vinyl pyrrolidone), polyacrylamide and poly(vinyl alcohol), ESR study 79−61199
Cu(II)-DL-proline complex, ESR, magnetic susceptibility and optical absorption 80−93167
$CuInSe_2$, melt-grown, EPR characts. 78−35030
$Cu_xMg_{1-x}Al_2O_4$, spinel solid solns., solid-state and surface props. 77−66415
$Cu_{75}Mn_{25}$, spin glass, EPR line breadth, exchange-narrowed 79−15345
$Cu(NH_3)_n(ClO_4)_2$, (n=4 or 5), EPR parameters and dilatometry 80−39850
$Cu(NH_3)_4SO_4.H_2O$, EPR around Neel temp. 78−39390
$Cu(NH_3)_4SO_4.H_2O$, submillimetre ESR meas. using pulsed high mag. field 80−44905
$Cu(NH_4SO_4)_2.6H_2O$, X-band ESR magneto-microwave effects 77−28434
$Cu(NO_3)_2$, frozen aq. soln., phase transitions, struct., ESR 77−16154
Cu_2O, photomemory effect, EPR expts. 78−52353
α-$Cu_xV_2O_5$, EPR and mag. susceptibility meas. 80−2627
$Cu_xZn_{1-x}ZrF_6.6H_2O$, distortions of nearest Jahn-Teller $[Cu(H_2O)_6]^{2+}$ centres 78−68000
dibarium cobalt formate tetrahydrate Cu^{2+} doped, EPR of Cu-Co interactions 78−60334
Fe complex, $[Fe(S_2C_2O_2)_2X]^{2-}$, (X=Cl,Br,I), Mossbauer effect, EPR, mag. susceptibility 79−11366
Fe complex, ferrous pseudo-tetrahedral compounds, paramag. relax., Mossbauer spectra 80−15869
Fe complex, tris-(4-morpholinecarbodithioate-S,S′)Fe(III), and dichloromethane solvate, Mossbauer and EPR spectra, spin 3/2 state 78−9169
Fe III, high-spin, in cancer 78−53466
Fe particles in glass-like C matrix, identification and props. 80−11229
Fe, phosphites, polycryst. EPR and Mossbauer spectra 78−76369
Fe, spin 3/2, in strong crystal field, axial and rhombic symmetry, EPR parameters 79−28591

paramagnetic resonance of iron group ions and impurities continued
Fe^{3+}, zero-field splittings, correl. with axial site distortions, superposition model 80−93168
$FeBr_2$:Mn^{2+}, antiferromag., impurity spin reson. 77−43876
$FeCl_4^-$ in organic solvents, dilute, ESR linewidths *(German)* 80−11258
$FeCr_2S_{4-x}Se_x$ chalcospinels, ESR spectrum and paramag. susceptibility 80−15789
$FeCs_2(SO_4)_2.6H_2O$:VO^{2+}, EPR, spin Hamiltonian parameters 79−19771
$Fe_{0.5}Cu_{0.5}Cr_2S_4$, ESR spectra, elec. and mag. props., Curie temp. 80−97137
Fe(III) Laeme complex, EPR g-value anal. 80−30657
$FeK_2(SO_4)_2.6H_2O$:Mn^{2+}, EPR spectra, spin-Hamiltonian anal. 77−77088
$Fe_{1-x}M_xCl_2$, disordered, Mn spin excitations by microwave absorption at high freqs. 80−34759
$Fe(N_3)_5^{2-}$, paramag. relax. in trigonal bipyramidal environment, Mossbauer spectra 80−15871
$Fe(NH_4)_2(SO_4)_2.6H_2O$, Fe^{3+} EPR, tetragonal cryst. field 77−51946
$Fe_{32}Ni_{36}Cr_{14}P_{12}B_6$, Metglas 2826A, EPR at 20 GHz 80−75848
Fe_2O_3 ultrafine particles in PTFE matrix, EPR and Mossbauer study 80−100625
$20Fe_2O_3.80[3B_2O_3.(1-x)PbO.xGeO_2]$ glass, phys. props. 80−49119
$FeSiF_6.6H_2O$, powder, far IR mag. reson., zero field splitting 77−81000
$FeSiF_6.6H_2O$, submillimetre EPR and zero field spectra, spin Hamiltonian 80−29604
$FeSiF_6.6H_2O$:Mn^{2+}, EPR line positions and intensities, spin Hamiltonian 79−65714
θ-$Fe_xV_2O_5$, spin glass and paramag. props., susceptibility, EPR and Mossbauer studies 80−75782
$FeZrF_6$, phase transition at 212.3K, Mossbauer, EPR study, quadrupole splitting, Jahn-Teller effect *(German)* 78−68430
Ga complex, $Gaurea_6(ClO_4)_3$:Cr^{3+} structural phase transition, ESR meas. 77−20681
GaAs:$^{56}Fe(^{57}Fe)$, paramag. centres, identification from ESR and ENDOR spectra 80−80600
GaAs:Co^{2+}, EPR expts., γ-factor determ. 78−76301
GaAs:$Co^{2+}(Ni^{3+})$, mag. and optical props. 78−10763
GaAs:Cr, Cr^+ and Cr^{2+} centres, thermal treatment effects, EPR 80−65492
GaAs:Cr, EPR, annealing and IR excitation effect on Cr^+ signal, Cr content by colorimetry 77−69680
GaAs:Cr, effect of light on EPR centres 78−10767
GaAs:Cr, hole traps, ESR studies 80−75843
GaAs:Cr, optical charging of paramag. centres, effect of potential relief 77−20694
GaAs:Cr, optically induced transient EPR phenomena 80−50168
GaAs:Cr, photoionisation transition $Cr^{3+} \rightarrow Cr^{2+}$, EPR studies 80−60638
GaAs:Cr, semi-insulating, defect chemistry, EPR study 79−99754
GaAs:Cr, semi-insulating, Cr charge states conc., EPR determ. 80−20450
GaAs:Cr^{2+}, effect of uniaxial stress and temp. variation on Cr^{2+} centre, EPR expts. 79−95636
GaAs:$Cr^{2+}(3d^4)$, Jahn-Teller distortion, photoinduced charge conversion, EPR 78−10758
GaAs:$Cr^{3+}(3d^3)$, 5K, evidence for strong Jahn-Teller effects 77−43875
p-GaAs:Fe, ESR line width, temp. depend., 4.2-330K 77−12195
GaAs:Fe_3 exchange-coupled pairs, ESR 79−11343
GaAs:Fe^{3+}, energy spectrum of deep centres, ESR spectrum 77−90023
GaAs:Mn, Mn-O association, EPR meas. 77−69677
GaAs:$Ni^{3+}(Co^{2+})(Fe^+)$, EPR assessment of $3d^7$ transition metal impurity state 78−48031
$GaBO_3$:Fe^{3+}, ESR spectra, lattice parameters 80−93170
$Ga_xIn_{1-x}P$:Mn, ESR of Mn 79−11341
GaP:$^{56}Fe(^{57}Fe)(^{53}Cr)$, paramag. centres, identification from ESR and ENDOR spectra 80−80600
GaP:Cr, diffusion parameters and solubility and influence on elec. and optical props. 79−73343
GaP:Cr, ESR of doubly ionised Cr acceptor and IR luminesc. 78−56374
p-GaP:Cr, hole traps, ESR studies 80−75843
GaP:Fe, double electron trap state, ESR identification 77−36124
GaP:Fe, heat treated, EPR spectra, struct. defects 80−7158
GaP:Fe, photo-EPR study $Fe(3d^6)$ centres and deep electron traps 80−44910
GaP:Fe^{3+}, deep impurity states investig. 77−15794
GaP:Fe^{3+} ESR spectrum, elec. field, uniaxial compression influence 80−103882
GaP:Fe(Cr), photo-ESR of annealed crysts. 80−15795
GaP:Ni, optical and EPR study of two-electron-trap state 79−73806
GaP:Ni(Fe), multivalence impurities, EPR and optical absorpt. meas. 80−75844
GaP:V, ESR exam. 79−11344
GaP-$Ni^{3+}(Co^{2+})(Fe^+)$, EPR assessment of $3d^7$ transition metal impurity state 78−48031
GaSe:Mn, ESR spectra, influence of temp. and antiferromag. inclusions 79−99763
$Ga_xV_{1-x}O_2$, resistivity, EPR, enthalpy and entropy meas., rel. to semicond.-metal transition 78−88004
$GdAl_2$-$GdCo_2$ system, EPR and mag. props. 79−33478
$Gd(Co_xNi_{1-x})_2$, EPR exam. 79−28600
$GdCrO_3$, EPR linewidth, Neel point to 700K 80−39849
$GdNi_x$, (x=3, 3.5, 8.5), ferrimag., mag. reson. above and below Curie temp. 80−97148
$Gd(Rh_{1-x}Fe_x)_2$, $x \leq 0.15$, magnetisation and EPR studies 80−34767
Ge:Mn, amorphous, EPR meas. 77−85559
Ge-P-S glass system, EPR of intrinsic and Mn^{2+} impurity centres 80−88870
Ge-Se-Fe phase system, amorphous films, mag. and elec. props. 79−51695
GeO:Cr, dielectric thin film, transmission and EPR spectra 77−69676
GeO_2:Mn^{2+}, EPR, struct. of vitreous and crystn. states 77−48039
GeO_2:V^{4+}, crystal field splitting from ESR and optical absorpt. results 79−47063
$Ge_{25}S_{75}$:Mn, bond struct. and character in Ge-S system, EPR obs. 80−66014
$Ge_{40}S_{60}$, $Ge_{25}S_{75}$ glasses, Mn^{2+} EPR spectra investigation 79−11340
$Ge_{40}S_{60}$ glass, Cu doped, EPR study 79−65713
$Ge_{40}S_{60}$:Mn (Ag)(Cu), bond struct. and character in Ge-S system, EPR obs. 80−66014
$Ge_{42}S_{58}$ glass, Cu(Ag)(I) impurity effect on e.p.r., dangling bonds 77−4553
$(Ge_{1/3}Se_{2/3})_{100-x}Ni_x$, ESR, rel. to elec. cond. 80−7155
$(Ge_{0.32}Se_{0.32}Te_{0.32}As_{0.4})_{100-x}Ni_x$, ESR, rel. to elec. cond. 80−7155
GeTe, degenerate semiconductor, EPR experiments on Mn^{2+} 79−11339
H_2SO_4:Fe^{2+}, frozen aq. soln., photolysis, H form., distrib. and diffusion 78−20044
$(HfO_2)_{0.9}(Y_2O_3)_{0.1}$:$Cu^{2+}$, ESR at room temp., spin Hamiltonian parameter determ. 77−16167
$HgCr_{2-x}Al_xSe_4$ and $HgCr_{2-x}Ga_xSe_4$, temp. depend. of ESR linewidth, 105-300K 80−71161
$HgCr_2Se_4$, ESR line intensity near Curie point 78−64269
$HgCr_2Se_{4-x}S_x$, EPR linewidth, 100-300K, spin-lattice relax. 77−51942
$Hg_{1-x}Mn_xTe$, EPR investigation of ordering effects 79−47330
$Hg_{1-x}Mn_xTe$, helicon-excited ESR 79−95437
$Hg_{1-x}Mn_xTe(S)(Se)$, EPR of Mn^{2+}, order-disorder transitions 80−50176
HgSe:Mn^{2+}, temp. depend. of EPR of ^6S state ions 80−80593
$InBO_3$:Fe^{3+}, ESR spectra, lattice parameters 80−93170
InP:Fe, Fe acceptor charge states, photolum., absorpt. and ESR meas. 77−36123
InP:Fe_3 influence of covalence on EPR spectra 78−26827
InP:Fe^{3+} (Cr^{2+}), symm., spin Hamiltonian parameters 78−10759
InP:$Ni^{3+}(Co^{2+})(Fe^+)$, EPR assessment of $3d^7$ transition metal impurity state 78−48031
$KAl(SO_4)_2.12H_2O$:Cr^{3+}, ESR high-order transitions 79−11338
$K_2C_2O_4.H_2O$:Cu^{2+}, ESR and isomorphism of Cu^{2+} 77−32252
K_4CdCl_6:Co^{2+}, ground-state g-value, EPR meas. 77−16159
$KCdF_3$:Cr^{3+}, EPR, successive phase transitions 79−65717
KCl:$Fe(CN)_6^{4-}$, electron irrad., Mossbauer and ESR study 80−7238
KCl:V^{2+}, EPR spectrum temp. depend., crystal field theory 77−16163
KCl:V^{2+}, EPR spectra above 300K 80−34765
KCl:V^{2+}, spin-lattice relaxation 78−91941
KCr alum, relaxation behaviour, EPR study, environmental effects 80−66021
$KCr_xAl_{1-x}(SO_4)_2.12H_2O$, EPR of single crystals, zero-field splitting of Cr^{3+} 80−66015
$K_2Cr_5F_{17}$, monocrystal, cryst. field and mag. props., EPR and optical absorpt. spectra 79−19773
$KCr(SO_4)_2.12H_2O$, phase transition associated fluctuations, Cr^{3+} EPR obs. 77−32247
$KCr(SO_4)_2.12H_2O$, ESR, spin-lattice relax., ambient gas atm. thermal cond. effect 79−8046
$K_2Cu_cZn_{1-c}F_4$, EPR, spin correlation decay rate 79−19772
KD_2AsO_4, Cr^{5+} EPR, line shape and elec. field effect 79−11336
KD_2PO_4:Fe^{3+}, ESR, anomalous temp. depend. of D tensor 79−61205
KH_2AsO_4, KD_2AsO_4, slow dynamics from Cr^{5+} EPR 78−15126
KH_2AsO_4:Cr^{3+}, ferroelec. phase transition, EPR intensity and linewidth meas. 79−4721
KH_2PO_4, KD_2PO_4, slow dynamics from Cr^{5+} EPR 78−15126
KH_2PO_4:Fe^{3+}, ESR, anomalous temp. depend. of D tensor 79−61205
KH_2PO_4:VO^{2+}, EPR spectra, Hamiltonian parameters, ferroelec. transition 78−39387
$KH_3(SeO_3)_2$:Cr^{3+}, EPR, ferroelectric phase transition 79−65716
$KH_3(SeO_3)_2$:Cr^{3+}, ferroelastic material, EPR, 77-300K 78−60331
$KH_3(SeO_3)_2$:VO^{2+}, electron spin reson. obs. 78−80196
$KMgF_3$, spin Hamiltonian parameters for Fe^{3+} ions, superposition model anal. 80−108053
$KMgF_3$:Cr^{3+}, EPR spectrum, effect of external elec. field 78−68368
$KMgF_3$:Cr^{3+}, trigonal centres, EPR lines, pseudo-Stark splitting 78−68367
$KMgF_3$:Fe_3 EPR temp. depend. 78−80202
$KMgF_3$:Fe^{2+}, anomalous acoustic relax. absorpt. and APR 80−88864
$KMgF_3$:Fe^{2+}, super hyperfine struct., Zeeman splitting and dynamic Jahn-Teller effect 77−85555
$KMgF_3$:Fe^{2+}, transferred hyperfine interactions, EPR exam. 78−31105
$KMgF_3$:Fe^{3+}, superposition-model anal. of second- and fourth-order spin Hamiltonian parameters, EPR study 79−87311
$KMgF_3$:Ni^{2+}, EPR meas., g-factor, spin-orbit coupling const. and mag. moment determ. 77−80999
$KMgF_3$:Ti^{3+}, ESR and ENDOR spectra 77−40121
K_2MnF_4, 2-dimens. antiferromagnet, with dipolar broadening, spin diffusion, EPR obs. 79−38371
K_2MnF_4, two dimens. Heisenberg system, shift of half-field EPR line 78−23325
K_2MnF_4, two-dimens. antiferromag., diffusion-controlled mode coupling, EPR linewidth 79−51844
$K_3Mn_2F_7$, crit. EPR line broadening near Neel temp. 80−71165
$K_2Mn_xM_{1-x}F_4$, (M=Mg,Zn,Cd), 2-dimens. antiferromag., sidebands on EPR lines 78−56370
$K_2Mn_cMg_{1-c}F_4$, EPR spectra 78−76298
$K_2Mn_cMg_{1-c}F_4$, impurities effect on EPR spectra 79−91283
$K_2Mn_xMg_{1-x}F_4$, two-dimensional antiferromag., ESR meas. 77−36121
$KNbO_3$:Fe, orthorhombic, EPR of Fe^{3+} 80−39861
K_2O-B_2O_3:Cu II, glass, O basicity, ESR study 78−80199
K_2O-B_2O_3:Mn^{2+} glass, fine struct. parameter distribs., EPR meas. 80−11256
K_2O-BaO-B_2O_3 glasses, ESR detection of immiscibility rel. to Cu II ions 80−20916
K_2O-CaO-B_2O_3:$CuII_1$ immiscibility, ESR detect. 78−80200
K_2O-MgO-B_2O_3:Cu^{2+}, micro-inhomogeneities, EPR and Raman study 80−84080
$K_2PbCu(NO_2)_6$, uniaxial stress, EPR meas. 80−20455
K_2SO_4:MnO_4^{2-}, electronic struct. by ESR 80−44906
K_2SO_4-$ZnSO_4$:Cu II, glass, O basicity, ESR study 78−80199
$KTa_{1-x}Nb_xO_3$:Fe^{3+} ($0 \leq x \leq 0.16$), octahedral pot., local cryst. field, EPR meas. *(French)* 79−11337
$KTaO_3$, ferroelec., local field determ., phase transition study by EPR 79−38471
$KTaO_3$:Fe^{3+}, EPR, elec. field effect, local fields *(Russian)* 79−8048
$KTaO_3$:Fe^{3+} local phase transition, EPR line temp. broadening *(Russian)* 80−54944
$KTaO_3$:Ti^{3+}, EPR meas. 78−35028
$K_6(V_2,Mo_{10})VO_{40}.13H_2O$, X-ray cryst. struct., electron spin resonance spectrum 80−88096
KVO_3:Cr^{3+}, study of ESR spectra 80−80601
$KZnF_3$, spin Hamiltonian parameters for Fe^{3+} ions, superposition model anal. 80−108053
$KZnF_3$:Cr^{3+}, ESR spectra of tetragonal Cr^{3+} centres, in external elec. field, 77K 77−24738
$KZnF_3$:V^{2+}, calc. of t_{2g} antibonding mol. orbital in $|VF_6|^4$, rel. to ESR 80−50174
$K_2Zn(ZrF_6)_2.6H_2O$, EPR of Cu^{2+}, temp. depend. 78−80201

paramagnetic resonance of iron group ions and impurities continued
$K_2Zn(ZrF_6)_2.6H_2O:CO^{2+}$, anisotropic exchange interactions between Co^{2+} ions, ESR spectra 79−95637
$LaMg(NO_3):Ni^{2+}$, pressure depend. of zero-field splitting of two mag. centres *(Russian)* 77−32249
$LaMg(NO_3)_2:Cu^{2+}$, spin-lattice recovery rate 78−10760
$La_2Mg_3(NO_3)_{12}.24D_2O:Mn^{2+}$, ESR spectra and non-diagonal cryst. field paremters 77−55705
$La_2Mg_3(NO_3)_{12}.24H_2O:Mn^{2+}$, ESR spectra and non-diagonal cryst. field parameters 77−55705
$La_2Mg_3(NO_3)_{12}.24H_2O:Mn^{2+}$, linear electric field effect on ground state splitting, EPR 78−80198
$La_2Mg_3(NO_3)_{12}.24H_2O:Co^{2+}$, Ce^{3+}, relax. and ESR in magnetically cooled systems 78−88225
$La_2O_3:Mn^{2+}$, position and intensity of forbidden hyperfine lines, ESR spectra 79−19775
$(La_2O_3)_{1-x}$-$(CeO_2)_x$:Mn, valence state of Mn, effect of annealing in H_2 atm., ESR obs. *(French)* 80−71164
$(La_2O_3)_{0.95}(CeO_2)_{0.05}:Mn^{2+}$, X-band EPR study 80−60409
$La_2Zn_3(NO_3)_{12}.24H_2O:Mn^{2+}$, pair spectra and mag. props. of Mn^{2+} 77−8396
$La_2Zn_3(NO_3)_{12}.24H_2O:CO^{2+}$, Mn^{2+}, Ni^{2+}, mag. exchange interactions, EPR 77−36118
Li aluminosilicate glasses, containing Cu and halogen impurities, ESR spectra 80−66027
$LiAlSiO_4$:Cu, β-eucryptite solid electrolyte, Cu^{2+} EPR obs. of ion exchange props. 80−108056
$LiBaF_3:Cr^{3+}(Mn^{2+})(Fe^{3+})(Co^{2+})(Ti^{3+})$, EPR, spin Hamiltonian parameters 79−65718
$LiCl:Ni^{2+}$, EPR meas. of Ni^{2+} vacancy dipoles 79−28594
$LiCrO_2$, EPR of Cr^{3+} ion, g-factor and effective mag. moment 77−73073
$LiCrX_2$, X=S, Se, EPR meas., g-factors, effective mag. moments, and dipolar shifts 79−8043
LiF:Mg,Ti, defect states, ESR and ionic cond. study 80−108058
LiF:Ti, EPR exam., superhyperfine interactions 78−31107
LiF:U, Mn, EPR of Mn^{4+} centre, g-values and hyperfine struct. 77−12192
$LiGa_5O_8:Cr^{3+}$, antisymmetric exchange interaction, EPR study 79−47331
$LiH_3(SeO_3)_2:VO^{2+}$, ferroelectric, 298K, EPR 79−51846
α-$LiIO_3:Cr^{3+}(Fe^{3+})$, zero-field splitting const. calc. 77−51709
α-$LiIO_3:Cr^{3+}(Fe^{3+})$, hyperfine interactions, RF discrete saturation of EPR lines 78−48032
α-$LiIO_3:Cr^{3+}(Mn^{2+})(Fe^{3+})$ and radn. induced defects, EPR spectra *(German)* 78−84480
α-$LiIO_3:Fe^{3+}$, local environment and superhyperfine interactions by RF discrete saturation 77−85554
$Li_2Mn_xTi_{1-x}O_3$, EPR exam. of antiferromag. props. 78−15015
$LiNbO_3$, photorefractive sensitivity, dependence on impurity Fe^{2+}/Fe^{3+} ratio, EPR and APR data 79−73893
$LiNbO_3:Cu^{2+}$, EPR and optical spectra 80−20453
$LiNbO_3$:Fe, characts. for holographic storage appls. 77−23630
$LiNbO_3$:Fe, optical damage, Fe ion conc., EPR and optical spectra evaluation 79−42933
$LiNbO_3$:Fe(Cu), photorefractive centres, optical absorption, EPR and Mossbauer spectra meas. 77−32403
Li_2O-Al_2O_3-P_2-$O_5:V^{4+}$, glass exam. of ESR spectrum of V^{4+}, optical spectra, and structure 78−88180
Li_2O-$B_2O_3:Mn^{2+}$ glass, fine struct. parameter distribs., EPR meas. 80−11256
Li_2O-TiO_2-Al_2O_3-SiO_2 glass, γ-irrad., struct. position of Ti, EPR study 80−84644
$LiSO_4.H_2O:Cr^{3+}$, single cryst., EPR and optical absorpt. spectra 80−39855
$LiVO_3:Cr^{3+}$, study of ESR spectra 80−80601
$LuBO_3:Fe^{3+}$, ESR spectra, lattice parameters 80−93170
Mg complex, $Mg(H_2O)_6H_2$(EDTA), Cu^{2} doped EPR and ground state wavefunction of Cu^{2+} 79−56605
Mg-Mn, dil., mag. props., EPR meas. 79−73804
$MgAlO_4:Cr^{3+}$, exchange parameters of Cr^{3+} pairs, optical and EPR meas. 77−69282
$MgCl_2:Co$, spectroscopic studies of interactions 80−29769
$MgCl_2:Co^{2+}$, ground-state g-value, EPR meas. 77−16159
$Mg(ClO_4)_2.6H_2O:Mn^{2+}$, cryst., EPR 78−91935
$MgCs_2(SeO_4)_2.6H_2O$, EPR, crystal field and hexahydrate distortion 78−91938
$MgCs_2(SeO_4)_2.6H_2O:Mn^{2+}$, EPR spectrum 78−64261
$MgF_2:Fe^{2+}$, γ-irrad., F-centres, Fe^{2+} ion hole traps, absorpt. and EPR meas. 79−7598
$Mg(H_2O)_6SiF_6:Mn^{2+}$, phase transition effects in EPR spectrum 79−42831
$MgIn_2S_4$:Co(Cr), EPR powder spectra 80−25197
$MgK_2(SO_4)_2.6H_2O:Mn^{2+}$, EPR spectra spin-Hamiltonian anal. 77−77088
$MgK_2(SeO_4)_2.6H_2O:Mn^{2+}$, EPR, crystal field and hexahydrate distortion 78−91938
Mg_6MnO_8, EPR in magnesium-manganese spinel *(Russian)* 78−91936
$Mg(NH_4)_2(SeO_4)_2.6H_2O:Mn^{2+}$, EPR spectra 80−100608
MgO, EPR of Mn^{2+} diffusion 78−91477
MgO, Fe^{2+} and Fe^{3+} conc. and valency, optical density, EPR and MCD obs. 77−89462
MgO:Co ions, impurity distrib. from EPR 77−51401
$MgO:Co^{2+}$, ESR linewidths of Co^{2+} 80−80596
$MgO:Co^{2+}$, strain modulated ESR, extensional and flexural modes 78−68365
$MgO:Co^{2+}$, strain modulated ESR, extensional and flexural modes 78−68366
MgO:Cr, Co, optical and ESR studies 80−50175
MgO:Cr, high resolution far IR spectroscopy of lower energy levels of Cr^{2+} 80−80822
$MgO:Cr^{2+}$, APR spectra 79−87313
$MgO:Cr^{2+}$, APR under applied stress 80−88865
$MgO:Cr^{2+}$, dynamic Jahn-Teller effect, APR obs. 77−20693
$MgO:Cr^{3+}$, axial centres, EPR and fluoresc. meas. 78−2731
$MgO:Cr^{3+}$, cubic centre, high resolution ESR, superhyperfine interaction 77−16162
$MgO:Cr^{3+}$, EPR obs., S=2 spin state D-tensor components 77−28433
$MgO:Cr^{3+}$, EPR spectra obtained at room temp. and 1200°C 80−68233
$MgO:Cr^{3+}$, single cryst., ESR linewidth 80−29605
$MgO:Cr^{3+}$, strain modulated ESR 78−88175

paramagnetic resonance of iron group ions and impurities continued
$MgO:Cr^{3+}$ (Mn^{2+}) spin Hamiltonian parameters, lattice expansion and vibr. effects 80−24851
$MgO:F_c^{3+}$ forbidden $\Delta m_s=2$ transitions in EPR spectrum 78−64267
MgO:Fe, Fe^{2+} oxidation and Fe^{3+} reduction kinetics, EPR obs. 79−70399
$MgO:Fe^{2+}$, microwave acoustic relaxation losses 78−43635
$MgO:Fe^{2+}$, phonon-induced transition interf. in EPR and IR spectra, ion-lattice coupling 77−51945
$MgO:Fe^{3+}$, clustering, EPR meas. 78−56372
$MgO:Fe^{3+}$, EPR of Fe^{3+} in orthorhombic symmetry sites 77−20689
$MgO:Fe^{3+}$, EPR spectra obtained at room temp. and 1200°C 80−68233
$MgO:Fe^{3+}$, spin-lattice relax. 77−90037
$MgO:Fe^{3+}$ single cryst., exchange energy 80−96834
MgO:Li, Fe(Cr), valence compensation of thermally generated $[Li]^0$ defects, EPR and ENDOR 79−77598
$MgO:Mn^{2+}$, clustering of mag. ions, study method 80−11155
$MgO:Mn^{2+}$ EPR, X-band freq., powder pattern for cubic symm. anal. *(Spanish)* 78−43636
$MgO:Mn^{2+}$ polycrysts. with varying impurity concentration *(Russian)* 77−28438
$MgO:Mn^{2+}(Fe^{2+})(Cr^{2+})$, redox behaviour of ions, ESR and X-ray diffr. 78−52341
$MgO:Mn^{2+}(Fe^{3+})$, EPR, 94-600K, temp. depend. of cubic spin Hamiltonian parameter 78−60332
$MgO:Ni^{2+}$, elastic interaction of mag. centres, EPR line width meas. 78−19315
MgO:transition metal, single cryst., grown with modified plasma torch furnace *(Japanese)* 79−95923
MgO-Al_2O_3-SiO_2 system glasses and glass ceramics, EPR obs. of transition elements, crystn. effects 78−23332
MgO-Al_2O_3-SiO_2-NiO glass, gamma ray irradiated, exam. of ESR spectrum of Ni(I) 79−4719
MgO-FeO-P_2O_5 system, glass, ESR spectra, heat treatment conditions effect 79−65722
MgO-Mn^{2+}, Q band ESR spectrum, spin Hamiltonian calcs. *(French)* 78−64262
MgO-NiO, solid soln. formation, initial stage obs. 77−81243
MgO-TiO_2-Al_2O_3-SiO_2 glass, γ-irrad., struct. position of Ti, EPR study 80−84644
MgO-V_2O_5 system, heat treated, EPR meas. *(Russian)* 77−90025
$Mg(OH_2)_6(NO_3)_2:Mn^{2+}$, EPR spectra, crystal field symm. and strength 77−69674
$Mg(PO_3)_2:Mn^{2+}$, EPR, computer simulation compared with expt. *(French)* 79−95635
$MgRb_2(SeO_4)_2.6H_2O:Mn^{2+}$, EPR spectra 80−100608
$MgSO_4.7H_2O:(Cu[H_2O]_6)^{2+}$, EPR and optical spectra anal. 79−38377
$MgSeO_4.6H_2O:Mn^{2+}$, EPR obs., rel. to Mn crystallographic sites 78−79628
$MgSiF_6.6H_2O:Co^{27}$, spin Hamiltonians and pair interactions 77−36119
$MgSiF_6.6H_2O:Ni^{2+}$, EPR meas., low temp. phases 77−63269
$MgTe:Cr^{+}$, cryst. growth and EPR 78−39393
$MgTe_2$:Mn, pyrite phase, strong axial cryst. field of Mn^{2+}, EPR meas. 78−27081
$MgTiF_6.6H_2O:Ni^{2+}$, EPR meas., low temp. phases 77−63269
$MgTiO_3:Fe^{3+}(Mn^{3+})$, EPR spectra 79−91285
$Mg_2V_2O_7$, elec. props. and EPR meas. 79−11114
$MgWO_4:Fe^{3+}$, effect of electric field on ESR of Fe^{3+} ions 78−88176
Mn complexes in solution, hyperfine linewidth 78−91937
Mn^{+}, in soln., EPR relax. probe 78−31104
Mn^{2+} doped EPR powder samples, hyperfine line intensities and axial cryst. field 79−78511
Mn^{2+} EPR spectra in glasses with $g_{ef}=4.29$ computer simulation 80−34764
Mn^{2+}, in polycrysts., EPR spectra calc. using Bir's method 79−1707
Mn^{2+}, in polycrysts. of low symmetry, computer simulation *(French)* 79−95635
Mn^{2+}, powder pattern analysis in cubic crystalline fields 79−47327
Mn^{2+} salt soln., ESR expt. using balanced resonator 77−53966
Mn^{2+}, zero-field splittings, correl. with axial site distortions, superposition model 80−93168
Mn^{2+}-Cu^{2+} coupled pair, ESR spectrum, strong isotropic exchange model 80−29606
$Mn_3Al_2Si_3O_{12}$, amorphous, spin-glass, insulating, Mn^{2+} mag. reson. 80−65918
$MnCl_2$-KCl system, molten, EPR spectra, linewidth study 78−88173
MnF_2, local mag. ordering above Neel point, EPR *(German)* 77−36125
MnF_2, molten, superexchange, EPR linewidth 79−19774
MnII-ATP system, exchange mechanism, FT NMR and EPR obs. 79−22733
$Mn_xMg_{1-x}O$, solid solution EPR, mag. interactions *(Russian)* 80−44908
MnO, EPR spectra of ceramic and epitaxial monocrystalline thin film samples *(Russian)* 80−11252
$MnO:Mn^{2+}$, EPR, antiparallel spin coupling above Neel point, antiferromagnetic clusters *(German)* 77−16168
γ-MnOOH, antiferromag., prep. and mag. props., EPR meas. 79−87310
xMnO.(100−x)[$19TeO_2$.PbO] glasses, EPR studies of Mn^{2+} ion distribution 80−71167
MnSe, thermal hysteresis, ESR spectra 79−99758
Mo complex, halogenoxomolybdenum (V), cryst. and electronic struct., reactivity 77−76369
Mo complex, influence of anisotropy of spin-Hamiltonian parameters on EPR spectra *(Russian)* 77−28432
Mo complexes with poly(iminoethylene)-dithiocarbamate polymer, synthesis and spectra 77−77189
Mo cpds, chemistry and uses, conf., Oxford, Eng., Sep (1976) 77−77749
$(Mo_xV_{1-x})_2O_5$, mag. and spectroscopic investigation 80−25206
ND_4Br, phase states and transition, from ESR of Cu^{2+} 79−99762
$ND_4Br:Cu^{2+}$, pseudo-Jahn-Teller effect manifestation in ESR spectrum 80−71168
$ND_4Cl:Cu^{2+}$, high-press. EPR, order-disorder transitions 78−19310
$(ND_4)_2Zn(SO_4)_2.6D_2O:Cu^{2+}$, EPR exam. 77−24735
$(NH_4)_2$ $Zn(SO_4)_2.6H_2O:VO^{2+}$, γ-irradiated NH_3^+ ESR, N hyperfine coupling tensor 79−69722
$(NH_3$-$(CH_2)_2$-$NH_3)Cd_{1-x}Mn_xCl_4$, Mn^{2+} single ions, clusters and layers, ESR study 79−78507
$NH_4Al(SO_4)_2.12H_2O:Cr^{3+}$, zero-field fluctuations in Cr^{3+} near phase transition 77−28435
$NH_4Br:Cu^{2+}$, ESR and absorpt. spectra, 300-1500 nm 78−60492

paramagnetic resonance of iron group ions and impurities continued
$(NH_4)_2Cd_5Fe_3Al(SO_4)_{12}.18H_2O$, EPR above ferrimag. transition 78−10762
$NH_4Cl:Cr^{3+}$, ESR of Cr^{3+} centres, room temp. 78−91943
$NH_4Cl:Ni^{2+}$, EPR spectrum, spin Hamiltonian, zero-field splitting effects 80−97135
$(NH_4)_2Co(SO_4)_2.6H_2O$, sbumillimeter ESR meas., SH^3 term of effective spin Hamiltonian 78−64264
$(NH_4)_2Co(SO_4)_2.6H_2O$, submillimetre ESR meas. using pulsed high mag. field 80−44905
$(NH_4)_2Co(SeO_4)_2.6H_2O:Mn^{2+}$, EPR 77−90017
$(NH_4)_2CuCl_4.2H_2O$, submillimetre ESR meas. using pulsed high mag. field 80−44905
$NH_4H_2AsO_4:Cr^{5+}$, fast and slow dynamic reorientation 78−80306
$NH_4H_2AsO_4:Cr^{5+}$, antiferroelec. phase transition, EPR intensity and linewidth meas. 79−4721
$(NH_4)H_2PO_4:Cr^{3+}$, EPR exam. above and below T_c 78−68363
$NH_4H_2PO_4:VO^{2+}$, EPR of VO^{2+} ions in antiferroelec. cryst. 79−47329
$NH_4HSO_4:VO^{2+}$, ferroelastic, inernal strains, ferroelec. transitions, EPR 79−47400
$(NH_4)_2InCl_5:Fe^{3+}$ EPR, site g-tensor, spin Hamiltonian factors 77−63270
$(NH_4)_6MnMo_9O_{32}.8H_2O$, mag. susceptibility, rel. to EPR, zero field splitting parameter 77−36122
$(NH_4)_2Ni(SeO_4)_2.6H_2O:Mn^{2+}$, EPR spectra, spin quenching 78−2732
$(NH_4)_xRb_{1-x}Al(SO_4)_2.12H_2O:Cr^{3+}$ EPR study, effect of monovalent ions on trigonal distortion 80−11255
$(NH_4)_2SO_4:Cr^{5+}$, EPR study of ferroelec. phase transition 78−64337
$(NH_4)_2SO_4:Cu^{2+}$, ESR parameters, effect of pH of mother soln., trapping sites 80−15791
$(NH_4)_2SO_4:Cu^{2+}$, ferroelec., ESR, Cu^{2+} in trigonal bipyramidal coord. 78−23330
$(NH_4)_2SO_4:Cu^{2+}$, ferroelec. transition, ESR study 79−91286
$(NH_4)_2SO_4:VO^{2+}$, EPR spectrum, temp depend. 110-300K 80−11249
$(NH_4)_2SO_4:VO^{2+}$, ferrielectric phase transition, two-sublattice model, EPR of polar VO^{2+} probes 78−48127
$(NH_4)_2SO_4.Al_2(SO_4)_3.24H_2O:Cr^{3+}$, and deuterated derivative, structural transition studied by EPR 77−85553
$(NH_4)_2SeO_4:Mn^{2+}$, single cryst., EPR and phase transition 79−73805
$(NH_4)_2SeO_4:VO^{2+}$, EPR spectrum 79−61207
$(NH_4)_xTl_{1-x}Al(SO_4)_2.12H_2O:Cr^{3+}$, zero field splitting, g-values, EPR spectra obs. 80−50169
Na-Fe fluorophosphate glass, EPR and Mossbauer resonance study 80−15838
Na_2-B_2O_3 glass, pulsed EPR study of Cu 78−84479
NaBr:V, covalency effects, EPR and optical spectra 77−85557
NaCl, Mn^{2+}-□ reorientation, ESR elec. field effect meas. 79−8050
$NaCl:Ca^{2+},Mn^{2+}$, EPR of Mn^{2+}, effect of Ca^{2+} on Mn^{2+} vacancy dipole decay 78−56371
$NaCl:Cu^{+}$, X-irrad., anisotropic Cu centre anal. 79−78714
$NaCl:Cu^{+}$, X-irrad., thermoluminesc. centre, EPR anal. 79−43045
$NaCl:Cu^{+}$, X-irrad. at room temp., ESR of Cu^{2+} centres 78−52343
$NaCl:Cu^{++}$, EPR spectra anal. spin-Hamiltonian parameters determ. *(Spanish)* 77−69673
$NaCl:Eu^{2+}(Mn^{2+})$, ESR and elec. field effects 77−28441
$NaCl:Mn^{++}$, Mg^{++}, doubly doped, ionic thermocurrent study of linear dimer 80−79977
$NaCl:Mn^{2+}$, CN^{-}, EPR spectrum rel. to Mn^{2+}-vacancy-CN^{-} complex 80−54942
$NaCl:Mn^{2+}$, dimer detection, EPR and ITC expts. 78−59833
$NaCl:Mn^{2+}$, X-irrad., thermoluminesc. and EPR 79−61444
$NaCl:Mn^{2+}$, X-ray irradiated, thermolum. and EPR 77−81161
$NaCl:V^{2+}$, EPR and optical absorpt. spectrum temp. depend., crystal field theory 77−16163
$NaCl:V^{2+}$, EPR spectra above 300K 80−34765
$NaCl:V^{2+}$, spin-lattice relaxation 78−91941
$NaCl:V^{2+}$, X-irrad. and unirrad., EPR of isolated V^{2+} ions 79−15347
$NaCl:V^{2+}(Mn^{2+})$, X-irrad. effects on divalent metal aggregates, EPR meas. 79−82263
NaF: Mn^{2+}, VUV absorpt. spectrum and EPR 80−55142
$Na_2HAsO_4.7H_2O:Cu^{2+}$, ESR, Cu lattice location 78−52342
$NaHSO_4:Mn^{2+}$, EPR 79−24215
$NaH_3(SeO_3)_2:Cr^{3+}$, deuterated, phase transitions, EPR 77−48135
$NaH_3(SeO_3)_2:VO^{2+}$, ESR spectra 79−4718
$NaNO_2:Mn^{2+}$, ferroelectric phase metastable struct., EPR obs. 78−60328
$NaNO_2:Mn^{2+}$, zero-field splitting, ferroelec. soft-mode contrib., phase transition, EPR obs. 79−15344
$NaNbO_3$, ferroelec., local field determ., phase transition study by EPR 79−38471
$NaNbO_3:Mn^{2+}$, ferroelec., memory effect, ESR meas. 79−28696
$NaNbO_3:Mn^{2+}$, T_2 phase, EPR spectra 78−88179
$NaNbO_3:Mn^{2+}$, temp. depend., −269-750°C, fine splitting 77−51948
Na_2O-$3SiO_2$:Fe^{2+}, Fe^{3+} glasses, Mossbauer and ESR spectra and internal friction 80−100865
Na_2O-B_2O_3:Cu^{2+}, glasses, ESR and optical absorpt. 80−34760
Na_2O-B_2O_3:Cu^{2+}, Mn^{2+} glasses, Cu^{2+}-Mn^{2+} interaction studied by ESR 80−93166
Na_2O-B_2O_3:Mn^{2+} glass, fine struct. parameter distribs., EPR meas. 80−11256
Na_2O-Fe_2O_3-SiO_2 glass and crystals, leucite type, Mossbauer ESR study of Fe^{3+} distrib. 79−65774
Na_2O-MgO-B_2O_3:Cu^{2+}, micro-inhomogeneities, EPR and Raman study 80−84080
Na_2O-P_2O_5:Cu II, glass, O basicity, ESR study 78−80199
Na_2O-SiO_2 glass, pulsed EPR study of Cu 78−84479
Na_2O-SiO_2:Cu^{2+} glass ESR and optical absorption 79−77526
Na_2O-SiO_2:CuO glass, gamma-irradiated, EPR and optical spectra 80−103885
Na_2O-TiO_2-Al_2O_3-SiO_2 glass, γ-irrad., struct. position of Ti, EPR study 80−84644
$5Na_2O.Fe_2O_3.8SiO_2$, glass crystallisation study by Fe^{3+} EPR and Mossbauer spectra 80−64904
$Na_2O.11Al_2O_3$, Cr, impurity ion struct., ESR study 80−80605
$Na_2S:Mn^{2+}$, polycrystalline, EPR and luminesc. of Mn^{2+} 78−27082
$Na_2S:Mn^{2+}$, single crystal, EPR expts. and interpretation 79−1708
$NaVO_3:Cr^{5+}$, study of ESR spectra 80−80601
$Na_xV_2O_5$ β-phase single cryst., phase transitions EPR meas. 78−95514
$Na_2Zn(SO_4)_2.4H_2O:VO^{2+}$, EPR spectra at X-band, spin-Hamiltonian parameters 79−56606
$Na_2Zn(SO_4)_2.4H_2O$:Ni, X-irrad., unit cell site doublets obs. 78−76501

paramagnetic resonance of iron group ions and impurities continued
$Na_20.3B_2O_3.xFe_2O_3$, borate glass, Fe^{3+} spin state and distrib. meas. 80−39966
$Nd_3Mg_3(NO_3)_{12}.24H_2O:Mn^{2+}$, EPR spectra, spin Hamiltonian anal. 79−33527
$Nd_2Zn_3(NO_3)_{12}.24H_2O$, EPR of Mn^{2+}, Gd^{3+} doped single crystal 79−24212
Ni complex, (1,4,5,8,9,12,13,16-octamethyltetradbenzporphinato nickel)$^{+\gamma}$ $(I_3^{-})_\gamma$, atomic limit of Hubbard model and polarons 80−39860
Ni complex, $Ni(NH_3)_6(ClO_4)_2$, high-press. phase, EPR meas. 78−38842
Ni complex, Ni(5-methylpyrazole)$_4X_2$, (X=Cl, Br, I), mag. props., EPR, ligand field calcs. 77−62880
Ni complex, $Ni(detc)_2$, spin-lattice relax. of Cu^{2+} 77−59453
Ni complexes, with CO, O_2 and NO ligands, in NiCa-Y zeolite, EPR, UV obs. 77−63949
Ni complexes hexamethylamine nickel halides, Ni^{2+} EPR in high pulsed mag. field, zero field splitting parameters 80−71160
Ni^{2+} aqueous complex, EPR, PMR and spin-spin relax. 79−69713
$Ni(BF_4)_2.6H_2O$, EPR, cryst. field symmetry 79−28593
$Ni(BrO_3)_2.6H_2O$, low temp. EPR meas. 77−81001
$Ni(ClO_4)_2.6H_2O$, EPR and IR spectra, 98-298K, phase transition at 224K 78−84477
$NiI_2.6H_2O$, disordered linear chain mag., ESR, mag. susceptibility and NMR meas. 77−20688
$Ni_xMg_{1-x}O$, EPR in magnetoconcentrated solid solution *(Russian)* 80−39856
$Ni(NH_3)_6(ClO_4)_2$, EPR determ. of phase transition temp., line shape anal. 77−20063
$Ni(NH_3)_6I_2$, EPR of Ni^{2+} ion near structural phase transformation 80−11248
$Ni(NH_4)_2(SO_4)_2.6H_2O$, Mn^{2+} doped, EPR study 80−34763
NiO-MgO, ESR and refl. spectra, Ni^{2+} distrib. 79−33745
$Ni(OH_2)_6(NO_3)_2:Mn^{2+}$, EPR spectra, crystal field symm. and strength 77−69674
$NiPtCl_6.6H_2O$, singlet-ground-state magnets, ESR at low temps. 80−97132
$NiSO_4.7H_2O$, Mn^{2+} doped, EPR study 80−34763
$NiSiF_6$, dilute, single-spin cross-relax. calcs. 80−97129
$NiSiF_6.6H_2O$, EPR line shape, Tanaka-Kondo method 80−29602
$NiSiF_6.6H_2O$, ESR spectra at low temperatures and high pressures 78−52339
$NiSiF_6.6H_2O$, non-Kramers system, spin-lattice relaxation at strong fields 80−100612
$NiSiF_6.6H_2O$, single cryst., EPR, 77-300K, Debye temp. 77−85551
$NiSnCl_6.6H_2O$, singlet-ground-state magnets, ESR at low temps. 80−97132
$NiSnCl_6.6H_2O$, ESR line shift at very low temps. 78−56375
$Ni_2(ClO_4)_2.6H_2O:Mn^{2+}$, EPR obs. of high temp. phase transition 79−28598
P_2O_5-WO_3:CuO glass, EPR, Cu impurity effect on elec. props. 79−51849
Pb ceramic glaze, Cu^{2+} doped, Pb^{2+} release 80−49101
Pb glazes, Cu^{2+} doped, alkaline substitution, crystal field modifications, EPR study 79−95634
$PbF_2:Fe^{3+}$, F^{-} motion, ESR study 80−66023
$PbF_2:Mn^{2+}$, superionic, cryst. field fluctuation dynamics, EPR 78−23328
$Pb_5Ge_3O_{11}$, ESR of Fe^{3+} ions 79−95639
$PbI_2:M^{2+}$, M=V, Mn, Co, EPR 78−68362
$PbMo_4$, M=Mo,W, EPR spectrum, temp. depend. of zero field splitting 79−15346
$PbMoO_4:Fe^{3+}$, effective g-factors, Fe^{3+} sites 77−51947
$PbMoO_4:Fe^{3+}$, single crystals, structure and kinetics, EPR meas. 79−99760
PbO-B_2O_3:Cu^{2+}, glasses, ESR and optical absorpt. 80−34760
PbO-SiO_2 glass, EPR of Cu^{2+}, V^{4+}, and Mn^{2+} 78−39392
PbO-SiO_2 glasses, high temp. ESR of Fe(III) 80−60410
$(PbO.2B_2O_3)_{1-x}(Fe_2O_3)_x$ glass, mag. resonance studies 79−78509
$PbO.3B_2O_3$:Fe_2O_3, EPR of Fe^{3+} ions 78−72400
$Pb_3(PO_4)_2:Mn^{2+}$, EPR study around ferroelastic transition point of $Pb_3(PO_4)_2$ 78−76303
Pd-Fe alloys, hydrogenated and unhydrogenated, EPR and demagnetisation field 77−32250
Pd-Mn, ESR meas., evidences of bottlenecked relax. for Mn^{2+} ion 78−72401
$Pd_{1-y}Mn_yH_x$ alloy, spin glass, transition temp., susceptibility and EPR meas. 80−65930
$Pr_2Mg_3(NO_3)_{12}.24H_2O:Mn^{2+}$, X-band EPR 77−66418
$Pr_2Zn_3(NO_3)_{12}.24H_2O:Mn^{2+}$ 78−64270
$Pt(NH_3)_4CuCl_4$, ferromag., antisymmetric and anisotropic exchange, EPR linewidth 78−10761
$RbAl(SO_4)_2.12H_2O:Cr^{3+}$, high order EPR transitions 79−22736
$RbCdF_3:Cr^{3+}$, EPR meas. of phase transition 79−61206
RbCl:Cu, X-irrad., ESR of noncentral Cu^0 atoms, 20-180K 77−24739
$RbCl:Mn^{2+}$, spin-Hamiltonian parameters anal., superposition model applicability 79−28592
$RbCl:V^{2+}$, EPR spectrum temp. depend., crystal field theory 77−16163
$RbCl+V^{2+}$, spin-lattice relaxation 78−91941
$Rb_2Cu(SO_4)_2.6H_2O$, single cryst., fine struct., mag. dipole coupling, EPR obs. 78−68360
$RbH_3(SeO_3)_2$: VO^{2+}, EPR spectra, spin Hamiltonian parameters 80−100609
$RbIn(MoO_4)_2:Fe^{3+}$ monocrystals, EPR spectrum in the phase transition neighbourhood 80−2624
$RbMgF_3:Mn^{2+}$, spin Hamiltonian, HFS and Mn^{2+} site occupation, struct. implications *(French)* 80−50167
$RbMnF_3:Fe^{2+}(Co^{2+})$, high-temperature EPR linewidth, impurity fast relax. effects 77−85556
$RbMn_{1-x}Mg_xCl_3$, dilute pair antiferromag., mag. susceptibility and ESR meas. 79−78338
$Rb_2Mn_xMg_{1-x}F_4$, spin dynamics near percolation threshold, EPR study 80−39859
$Rb_2PbCu(NO_2)_6$, uniaxial stress, EPR meas. 80−20455
$RbVO_3:Cr^{5+}$, study of ESR spectra 80−80601
$SbTaO_4$, X-ray and ESR study of phase changes 78−72476
$ScBO_3:Fe^{3+}$, ESR spectra, lattice parameters 80−93170
Si, irrad. with Cr^{+}, form. and annihilation, of defects, ESR investigation 79−90707
Si, Jahn-Teller Mn^0 centre ESR spectrum, depend. on axial press. 80−44911
Si:Cr, spin-lattice relax. of Jahn-Teller Cr^0 centre *(Russian)* 78−72402

paramagnetic resonance of iron group ions and impurities continued
Si:Cr^0(Mn^+), spin-lattice relax. of Jahn-Teller centres, coexistence of minima with different symmetries 80−80602
Si:Cr^+ EPR spectra and spin state population inversion with unpolarised optical lighting *(Russian)* 80−44909
Si:Fe, anisotropic broadening of linewidth in EPR spectra of Fe^0 77−66417
Si:Fe, cryst. field under stress, C_{11} and C_{44} meas. 77−12194
Si:Fe, EPR and neutron activation anal. of thermal defects 78−91355
Si:Fe, interstitial form., Au dopant effect 80−29611
Si:Fe, solubility study by EPR and neutron activation anal. 80−75361
Si:Fe group ion, energy spectrum of deep centres, ESR spectrum 77−90023
Si:Fe^0, solid soln. decomp., Fe deposition on dislocations 77−51943
Si:Fe^0, spin relax. rate ang. depend. for pulsed saturation of inhomogeneously broadened ESR line 79−65721
Si:Fe^0 interstitial localisation, EPR spectrum 79−1582
Si:Fe(Cr), EPR line intensity and widths, temp. depend. 79−28604
Si:Mn, amorphous, EPR meas. 77−85559
Si:Mn(Fe)(Ni) amorphous films, ESR and elec. cond. 80−50171
SiO_2 surface, bonding of Cu^{2+}, Cr^{3+}, Co^{2+} ions, EPR, optical spectroscopy investig. *(German)* 79−95266
$Sm_2Mg_3(NO_3)_{12}.24H_2O:Mn^{2+}$, EPR spectra, 77-298K 79−15342
SnTe:Mn, EPR as probe of phase transitions 80−15790
$(SnTe)_{1-x}(MnTe)_x$, ESR, effect of Mn ion conc. on line width and area 78−35026
$Sr_{0.5}Ba_{0.5}Nb_2O_6$:Fe, ceramic, additive effects on ferroelec. and pyroelec. props., EPR 77−16256
SrCl:Mn^{2+}, shape of potential well, calc. 78−87951
$SrCl_2$:Fe^{3+}, EPR spectra of Fe^{3+}($^6S_{5/2}$), 4-100K 78−95512
$SrCl_2$:Mn^{2+}(Co^{2+}), cubic impurity EPR spectra, elec. field effect, mechanism 78−68361
$Sr_2Cu(OH)_6$, EPR, g-values 79−19770
$SrMo_4$, M=Mo,W, EPR spectrum, temp. depend. of zero field splitting 79−15346
SrO:Co_2 noncentral and interstitial ion complexes, ESR obs. 80−71169
SrO:Co^{2+}, EPR, optical, MCD absorpt. spectra 78−43692
SrO:Cu^{2+}, ESR spectrum averaging due to motion near paramagnetic centres 77−24737
SrO:Cu^{2+}, phonon-induced tunnel hopping, ESR obs. 79−69714
SrO:Mn^{2+}, impurity pot. well shape calcs. 78−87950
SrO:Mn^{2+}, spin Hamiltonian parameters 77−20691
SrO:Ni, EPR of Ni^+, two-stage increase in symmetry, reorientation of cryst. field axes 78−27085
SrO:Ni^+, noncentral Jahn-Teller ion, energy minimum localisation, ESR study 80−25198
SrO:Ni^{2+}, EPR line splitting rel. to Jahn-Teller coupling and soft localised mode 80−66022
SrO_2:Fe^{2+}(Fe^{3+}), EPR spectra, evidence for off-centre displacement of Fe^{2+} 78−72398
$Sr_5(PO_4)_3Cl$:CrO_4^{3-}, EPR, cryst. field parameters 79−87309
$SrTiO_3$, EPR meas., Hamiltonians with quartic anharmonicities 78−27083
$SrTiO_3$, EPR of Fe^{3+}-V_O centre, above T_c 80−39870
$SrTiO_3$, flame fusion growth, dislocation density, lattice const. and EPR spectra 78−11099
$SrTiO_3$, stressed, trigonal-to-tetragonal transition, EPR data, realisation of 3-state Potts model 77−28525
$SrTiO_3$:Cr^{3+}, nonlinear Jahn-Teller coupling, local dynamics, near struct. transition 80−2625
$SrTiO_3$:Cr^{5+} Jahn-Teller system, EPR, electric field effects 79−28599
$SrTiO_3$:Fe, EPR of Fe^{3+}-rhombic, Fe^{2+}-V_O and Fe^{1+}-V_O complexes 78−76302
$SrTiO_3$:Fe^{3+}, displacive struct. transition, order-disorder behaviour, phonon softening, EPR obs. 79−23695
$SrTiO_3$:Fe^{3+}, order-disorder and central peak behaviour, EPR study 80−75970
$SrTiO_3$:Mn^{n+}, reduced, EPR of Mn centres 78−35029
$SrTiO_3$:Ni, photochromism, optical absorption spectra and EPR meas. 77−1708
$SrTiO_3$:V, Jahn-Teller impurity, V^{4+} EPR 80−29608
T:O_2:Cr(Mo), anatase single cryst., ESR of Cr^{5+} and Mo^{5+} ions 79−28603
TGSe:Cu^{2+}, EPR studies 80−7153
Ti^{4+}, valence transition in fluorphlogopite, ESR and optical absorption data 77−16155
Ti-molten glass system, interactions and wetting, EPR anal. 78−14542
TiO_2, Mn^{3+} ion electron spin-lattice relaxation 80−108054
TiO_2, polycryst., paramag. centres, illumination effects, ESR 77−48041
TiO_2:Fe, rutile, ESR meas. 80−54945
TiO_2:Fe^{3+}, microwave second harmonic generation and freq. conversion 80−50166
TiO_2:Fe^{3+}, rutile, temp. depend. of spin Hamiltonian parameters, ESR meas. 77−32251
TiO_2:Fe^{3+}, uniaxial stress method for determ. of spin-lattice coeff. for Fe^{3+} 77−90018
TiO_2:Fe^{3+}, appl. of sensitive EPR spectrometer to zero field splitting determ. *(Russian)* 77−57372
TiO_2:Mn, ESR spectrum anal. *(French)* 78−19309
TiO_2:Mn^{2+}(Mn^{4+}), anatase single cryst., ESR spectra at 77K, 300K 78−10764
TiO_2:Mn^{4+}(Cr^{3+}), rutile, temp. depend. of EPR 78−76299
TiO_2:V, localisation and migration of V^+ ions, ESR and ESCA study *(French)* 79−33529
TiO_2:V(Cr)(Mn)(Fe), impurity levels, photocurrent and ESR meas. 80−29346
TiO_2-Al_2O_3-P_2O_5 glass, ESR of Ti^{3+}, exam. 78−88181
Ti_4O_7 and $(Ti_{1-x}V_x)_4O_7$, metal-insulator transitions, EPR, elec. and mag. props. 80−2336
Ti_5O_9, phase transitions, elec. cond., mag. susceptibility, sp. ht., EPR and struct. aspects 78−10526
$Tm_3Ga_5O_{12}$:Cr^{3+}, Val Vleck paramagnet, EPR g-shifts and linewidths, tamp. depend. 77−66419
V complex, vanadyl ion-pyridyliminonitroxide radical mag. interactions, ESR 77−83623
V^{4+}, cryst. field effect on ESR parameters 77−36116
V^{4+}, doped in single crysts. bonding character and g-factor interpretation 77−55704
V^{4+} in glasses, numerical optimisation of ESR spectra 79−38370
V^{4+} ion complexes in diamagnetic crystals, ground state wavefunctions, hyperfine interaction parameters, EPR meas. 78−19311

paramagnetic resonance of iron group ions and impurities continued
$V_{1-x}Al_xO_{2\pm y}$, mag. and struct. props. meas. 78−2658
VO^{2+} EPR in solids, review 80−11254
VO^{2+} ion impurities, in hydrated crysts., EPR obs. 80−97130
VO^{2+} spin probes, slowly tumbling, in nematic liq. crysts., EPR 79−50985
V_2O_5, amorphous, hydration and fibrous texture, EPR study *(French)* 79−24826
V_2O_5 amorphous films, CVD prep., structural charcts. 80−49114
V_2O_5 and lower oxides, defect structures and related props. 80−59454
V_2O_5 and lower oxides, electronic, optical, structural and surface props., review 80−88120
V_2O_5 bronze catalysts, α- and β-phase, rel. to decomp. mechanism determ. for isopropanol 78−11553
V_2O_5, reduction in butyllithium, ESR study 80−100611
V_2O_5:Fe^{3+}, 5-300K, spin Hamiltonian parameter determ. 77−81002
V_2O_5-CuO-BaO glass, unpaired electron localisation, ESR study 80−66026
V_2O_5-P_2O_5 glass, splat-cooled, EPR of V^{4+}, polaron hopping and carrier localisation 77−28436
V_2O_5-P_2O_5-MO system glasses, (M=Ba,Ca,Cu and Mg), phase separation, crystn. and EPR spectra 77−76321
V_2O_5-TeO_2 glasses, ESR spectra 78−10755
V_2O_5-water, EPR of VO_{aq}^{2+} formed by solar light photoreduction, electrolysis appl. 78−11540
V_3O_7, ESR spectra of V^{4+} ions 77−28437
mV_2O_5.(100-m)P_2O_5, (m=100-2), V(IV) complexes conc., absorpt. and ESR spectra 78−64266
α-$W_xV_2O_5$, paramag. defect study by ESR 80−103881
YAG crystals, EPR spectra of V^{2+} ions, ion energy levels 80−7157
YAG:Fe^{3+}(Cr^{3+}), ESR absorption spectra, line broadening 78−91940
YAG:V_2O_5, CaO, V^{4+} ion impurity spectral anal. 79−78719
$YCrO_3$, EPR linewidth, Neel point to 700K 80−39849
$Y_3Ga_5O_{12}$-$Y_3Fe_5O_{12}$ garnets, EPR spectra of ferric ions 77−66414
Y_2O_3:Fe^{3+}, EPR obs. of non-cubic phase 78−19316
zinc formatedihydrate: Co, spin lattice relax. of Co^{2+} ions 80−75847
Zn complexes, $Zn(detc)_2$ and $Zn(desc)_2$, spin-lattice relax. of Cu^{2+} 77−59453
Zn II complex, hexaimidazole-zinc(II) dichloride tetrahydrate:Cr(III), D-tensor orientation, charge-compensation vacancies 80−50172
Zn-Cl boracite, reinterpretation of EPR expt. on Cu^{2+} rel. to struct. 79−38372
$ZnAl_2S_4$:Fe(Mn), superhyperfine interaction of Fe and Mn ESR spectra 77−63271
$Zn(BF_4)_2.6H_2O$:Ni, phase transition study, EPR of diluted Ni^{2+}, 98-298K 80−75846
$Zn(BrO_3)_2.6H_2O:Cu^{2+}$, Jahn-Teller system, EPR and spin-lattice relax. 78−10760
$ZnCr_2Se_4$, EPR linewidth, 100-300K, spin-lattice relax. 77−51942
$ZnCs_2(SO_4)_2.6H_2O:VO^{2+}$, single cryst., X-band EPR meas. 77−90024
$Zn_{1-x}Cu_xGeF_6.6H_2O$, depression of dynamic Jahn-Teller effect 77−16164
$ZnGa_2O_4$:Cr^{3+}, weak exchange interaction determ., ESR study 80−93107
$ZnGa_2O_4$:Fe^{3+}(Mn^{2+}), EPR, spin Hamiltonian parameters 80−25195
$ZnGeF_6.6H_2O$:Mn (II), phase transition, ESR meas. 77−62636
$ZnK_2(SO_4)_2.6H_2O:Mn^{2+}$, EPR spectra, spin-Hamiltonian anal. 77−77088
$(Zn(NH_3)_4)(ClO_4)_2$:Mn, EPR study of Mn^{2+} detection of structural transition 79−87308
$Zn(NH_4)_2(SeO_4)_2.6H_2O:Mn^{2+}$, EPR spectra 80−100608
ZnO:Co ions, impurity distrib. from EPR 77−51401
ZnO:Cu,H, motional effects in EPR spectra 78−80207
ZnO:Cu^{2+}, electronic struct., optical absorpt. and ESR 79−87312
ZnO-Al_2O_3-SiO_2, transparent glass-ceramics, EPR obs. of glass crystallisation 78−80507
ZnO-B_2O_3:Cu^{2+}, glasses, ESR and optical absorpt. 80−34760
$ZnRb_2(SeO_4)_2.6H_2O:Mn^{2+}$, EPR spectra 80−100608
ZnS:Co^{2+}, EPR and spin-lattice relax. of Co^{2+} centres *(Russian)* 79−1706
ZnS:Co^{2+}, spin-lattice relax., phonon heating effect *(Russian)* 78−19317
ZnS:Cr^{2+}, Jahn-Teller interaction energy calc. 78−2455
ZnS:Fe, luminesc. and ESR investigations 80−2822
ZnS:Fe^{3+}, spin-lattice relax., expt. evidence for optical phonons 80−20451
ZnS:Mn^{2+}, cubic, EPR, ENDOR 77−77093
ZnS:Mn^{2+}, spin-lattice coupling coeffs. of Mn^{2+} ions in stacking faults 77−20690
ZnS:Mn^{2+}, spin-lattice relax. time, continuous saturation expts., spin diffusion 77−36120
ZnS:Mn^{2+}, spin-lattice relaxation, EPR, optical phonons 80−39852
ZnS-Mn^{2+}, microregions disorientation degree anal. by birefringence, ESR and decoration methods 79−60389
$ZnSO_4.7H_2O:Mn^{2+}$, compared with isomorphous cryst.. 77−16165
$ZnSO_4.7H_2O:VO^{2+}$, single cryst., struct., EPR 78−15014
ZnS(Se)(Te):Cu^{2+}, absence of EPR spectra due to strong spin-lattice coupling of Kramers doublets 77−85181
ZnSe, single crysts., opt. band gap and Mn^{2+} EPR, effects of prep. conditions 77−47730
ZnSe:Ga,As, characts. of simultaneous incorporation, by Mn^{2+} ESR and X-ray fluoresc. anal. 80−34017
ZnSe:Mn, single crysts., associated pt. defects, EPR method 77−48040
ZnSe:Mn^{2+}, refined spin Hamiltonian parameters *(French)* 77−63268
ZnSe:Mn^{2+} Schottky barrier diodes, spin depend. cond. and photovoltage, donor reson. deep centre studies 79−91141
ZnSe:Ti^{2+}, EPR meas. 80−80594
$ZnSeO_4.6H_2O:Cu^{2+}$, crystal struct. orientational degeneracy removal scheme, space groups, ESR spectra 78−47267
$ZnSiF_6$:Cu^{2+}, spin-spin interactions of impurity pairs *(Russian)* 78−72397
$ZnSiF_6.6H_2O:Mn^{2+}$, ESR spectrum, effect of uniaxial compression 80−29609
$ZnSiF_6.6H_O$:Co^{2+}, spin Hamiltonians and pair interactions 77−36119
$ZnSiF_6.6H_2O$, spin-phonon interaction between Ni^{2+} ions, phonon bottleneck effects, splitting parameters *(Russian)* 80−15796
$ZnSiF_6.6H_2O$:Co, influence of hydrostatic press. on Co^{2+} EPR spectrum 78−27084
$ZnSiF_6.6H_2O:Ni^{2+}$, EPR 77−59451
$ZnSiF_6.6H_2O:Ni^{2+}$, cryst. field, uniaxial compression method *(Russian)* 78−35027

paramagnetic resonance of iron group ions and impurities continued
$ZnSiF_6.6H_2O:Ni^{2+}$, spin-lattice relax. at press. up to 6.5 kbar 78−48033
$ZnSiF_6.6H_2O:V^{2+}$, paramagnetic impurity ion spin multiplet initial splitting parameter, immediate environments distortion influence on sign 79−65720
$ZnSiF_6.6H_2O:V^{2+}$, spin-lattice relax. at normal and high press. 80−2632
$ZnWO_4:V^{4+}$, suitability of $VOWO_4.3H_2O$ as paramag. impurity 77−48670
ZrO_2-CaO:Mn^{2+}, EPR spectra, impurity substitution behaviour in various phases 77−16160
$(ZrO_2)_{0.9}(Y_2O_3)_{0.1}$:Cr, Mn, stabilised single crystal, EPR of Mn^{2+} and Cr^{3+} obs. 80−66024
$(ZrO_2)_{0.9}(Y_2O_3)_{0.1}$:Ti, γ-irrad., ESR of trigonal centres, attributed to Ti^{3+} at cation sites 77−24740
$(ZrO_2)_{0.9}(Y_2O_3)_{0.1}:VO^{2+}$, ESR of V^{4+} at room temp., spin Hamiltonian parameter determ. 77−16167

paramagnetic resonance of palladium and platinum group ions and impurities
alkali halide:Ag film, EPR and optical exam. of Ag impurity centres 77−85562
ice:Ag, solvation in ice matrix, ESR and irrad. at 4.2 and 77K 79−8444
perovskite, Re containing, new seignettomagnets and ferroelectrics 78−19425
phosphate-tungstate semicond. glass, W (V) complex, EPR and electronic spectra interpretation 77−69682
α-quartz:Ag^{2+}, γ-irradiated, stabilisation of impurity atoms 79−8047
quartz:Ag glasses, EPR of atomic Ag centres 79−15349
α-quartz, X-irrad., paramag. Ag_2^+/AlO_4 centre, EPR obs. 79−28612
S=1, singlet ground state systems, mag. props. 80−11157
solid, review of 1973 literature 77−69675
TCNQ salt, $[Pt(NH_3)_4]^{2+}[(TCNQ)_2]^{2-}$ cryst. and mol. struct. and EPR props. 78−55860
transition metal ions in solids 80−51968
Ag solvation in ice matrix, electron spin echo modulation 78−39396
AgBr:Pd, EPR of Pd^+ ions 78−27087
AgBr(Cl):$Ru^{3+,2+}$, dopant vacancy config., EPR 79−91288
AgCl:Pd^+, ESR spectra, superhyperfine struct. lines 77−12197
AgCl:Pd^+, ESR spectrum, quasistatic Jahn-Teller effect 80−71170
AgCl:Pd^{2+}, EPR, role of vacancies in impurity based trapping 77−28439
AgCl:Pt^{2+}(Pt^{4+}), single crystal EPR, substitution effects on photochemistry 79−15348
Ag(I) ions, in methyl cyanide, electron loss and capture, ESR spectra 79−33531
$AgNO_3$-KF in ice matrix, γ-irrad., Ag at., form., solution, ESR 77−59454
Al-Ru(Rh)(Pd)(Ir), composite, paramagnetic resonance and electron-positron annihilation *(Russian)* 79−87314
$Al_2O_3:Mo^{3+}$, zero field splitting study by ESR 80−7159
β-Al_2O_3-Na_2O_3:Ag^{2+}, EPR measurements 78−95515
Au, quadrupole interaction 78−48027
BaO-P_2O_5:Mo^{5+} glass, EPR spectra, computer simulation 80−88872
$Ba(PO_3)_2$-WO_3, electron-absorpt. spectra and structure of W centres 80−88873
Bi molybdates on SiO_2, rel. to surface processes *(French)* 78−64271
$CaMoO_4:Mo^{5+}$, g-factor, ground state, line broadening, EPR obs. 80−39863
CaO:Ag^{2+}, EPR spectrum, static, quasistatic and quasidynamic Jahn-Teller effect 77−85561
CaO:Ir, quadrupole interactions and static Jahn-Teller effect in EPR spectra 77−72842
CaV_2O_6:W^{6+},Mo^{5+}, g-factors and hyperfine coupling parameters of V^{4+} 77−12196
$CdBr_2$:Ag^{2+}, strong Jahn-Teller coupling, EPR 79−28605
$CdCl_2$:Ag^{2+}, strong Jahn-Teller coupling, EPR 79−28605
CsMgCl:Cr^{3+},Mo^{3+}, Cr^{3+}-Mo^{3+} exchange coupled pair, EPR study 79−42830
$GE_{40}S_{60}$-Ag glass, EPR exam. 78−23334
$Ge_{40}S_{60}$:Mn (Ag)(Cu), bond struct. and character in Ge-S system, EPR obs. 80−66014
$Ge_{42}S_{58}$ glass, Cu(Ag)(I) impurity effect on e.p.r., dangling bonds 77−4553
$H_{1.6}MoO_3$, electronic props., mag. susceptibility and spectra 80−80266
Ir, quadrupole interaction 78−48027
KBr:Ag, formation of electron centres and self-localised holes, ESR exam. 78−91947
KCl:Ag(Tl), formation of electron centres and self-localised holes, ESR exam. 78−91947
KCl:Au, EPR and optical absorpt. 78−39397
$KCl:K_4Os^{II}(CN)_6$, electron irrad., EPR, ligand hyperfine struct. 78−60335
LiD:Rh, EPR spectra of Rh centres, UV-irrad. cryst. 79−65724
LiH:Rh, EPR spectra of Rh centres, UV-irrad. cryst. 79−65724
LiH(D):Rh, EPR of axial impurity complex 77−40123
LuAl garnet:Mo^{3+}, single crysts., EPR *(Russian)* 77−63267
MgO:Ag^{2+}, EPR spectrum, static, quasistatic and quasidynamic Jahn-Teller effect 77−85561
MgO:Ir^{2+}, quadrupole interactions and static Jahn-Teller effect in EPR spectra 77−72842
MgO:Ir^{2+}, superhyperfine struct. of ^{25}Mg in EPR spectra of Ir^{2+} 77−69683
MgO:Pt^{3+}, Jahn-Teller effect in EPR spectrum 80−7160
MgO:Rh^{2+}, EPR of Jahn-Teller ions, ^{17}O superhyperfine structure 77−32253
Mo ion incorporation into TiO_2 matrix, ESR, UV, and ESCA spectral anal. 79−43670
Mo-Al_2O_3 based hydrosulphurisation catalyst, used, ESR of SO_2^- and Mo^{5+} 77−70342
MoO_3:Li, elec., catalytic props. 78−60122
MoO_3:Re, ESR and optical absorption obs. 77−36127
MoS_2, prep. and mag. props. *(French)* 80−93072
$NH_4Al(SO_4)_2.12H_2O:Mo^{3+}$, EPR, X-band, ion position and spin-Hamiltonian parameters 77−48042
$NH_4Cl:[MoOCl_5]^{2-}$, single cryst., struct. investigations 77−66524
NaCl:Ag, formation of electron centres and self-localised holes, ESR exam. 78−91947
NaCl:Au, EPR and optical absorpt. 78−39397
$NaCl:K_3IrCl_6$ electron irrad., ligand field anal., EPR obs. 80−29612
Na_2O-Al_2O_3-B_2O_3-SiO_2:Ag, photochromic glass, EPR of Ag^0 and Ag_2^+ centres 77−24741

paramagnetic resonance of palladium and platinum group ions and impuriti continued
$Na_2Zn(SO_4)_2.4H_2O:Ag^{2+}$, EPR, Ag^{2+} dimeric struct., hyperfine and fine struct. tensors 77−51949
Nb complexes, ^{93}Nb quadrupole coupling tensors form EPR meas. 80−88866
Nb_2O_5, B-form single crysts., ESR of Mo^{5+} and W^{5+}, site symmetry 80−54946
Os, quadrupole interaction 78−48027
P_2O_5-MoO_3 glasses, EPR study 79−82866
P_2O_5-MoO_3-CaO glasses, EPR study 79−82866
$Pb(WO_4)_{1-x}(MoO_4)_x$ mixed crystals, X-irrad., EPR and thermoluminesc. 79−15352
Pd complex, L-alanyl-L-serine, PMR, EPR and absorpt. spectra 78−46367
RbCl:Au, EPR and optical absorpt. 78−39397
$ReNCl_4^-$, EPR in $Ph_4As[RuNCl_4]$, hyperfine splitting and spin Hamiltonians 78−64272
Ru complex, Creutz-Taube ion, ground state, single crystal EPR obs. of mixed valence Ru dimer ion 80−34766
Si:Au, EPR spectrum, strong nucl. quadrupole effect 80−93172
SiO_2:Ag, cryst. and glassy, X-ray induced EPR and luminesc. centre 80−65043
$SnO_2:Mo^{5+}$, hyperfine and superhyperfine interactions, EPR 77−8398
$SnO_2:W^{5+}$, EPR parameters, g hyperfine and superhyperfine tensors 77−85560
$Sr_{2y}Eu_{2-2y}NbO_4$, synthesis and props. 77−52265
SrO:Ag^{2+}, EPR spectrum, static, quasistatic and quasidynamic Jahn-Teller effect 77−85561
TiO_2:Cr(Mo), anatase single cryst., ESR of Cr^{5+} and Mo^{5+} ions 79−28603
$TiO_2:Mo^{5+}$, interstitial EPR, g-tensor and hyperfine tensor 80−84647
$TiO_2:Ru^{4+}$, rutile, EPR and cryst. field const. 80−60415
WO_3 electron density map of W^{5+} polarons, EPR and optical absorpt. obs. 80−44912
WO_3, light induced W^{5+} ESR 77−36126
WO_3, single cryst. and amorphous film, ESR of defects 78−10770
$Y_2O_3:Zr^{3+}$, ESR spectrum 79−69716
ZnS(Se)(Te):Ag^{2+}, absence of EPR spectra due to strong spin-lattice coupling of Kramers doublets 77−85181

paramagnetic resonance of rare earth ions and impurities
anisotropic exchange Hamiltonian, for rare earth in nonmag. host 77−20696
crystal field splitting, parametrisation of temperature dependence, applic. to axial ^8S state ions 78−91652
cubic metal:Gd, influence of cryst. field on EPR 78−52346
exchange induced broadening in low lying crystalline field system 80−108062
fluorites, natural colour centres and associated rare earth ions 79−61408
ions, optically excited states, EPR, ENDOR 78−43637
$KZnF_3$:Er excitation of 650 GHz phonons in spin-lattice relax. 78−27089
lanthanide and actinide ions, review of 1974 literature 80−11253
lanthanum ethyl sulphate.$9D_2O:^{160}Gd^{3+}$, EPR transition energies at low mag. fields 77−12198
lanthanum ethyl sulphate:Gd^{3+}, EPR lineshape distortion in weak fields with zero-field splitting 77−48034
lanthanum ethyl sulphate:Gd^{3+}, spin Hamiltonian, higher-order spin terms 77−48044
lanthanum ethyl sulphate:Gd^{3+}, X-band EPR, near room temp., spin Hamiltonian parameters 77−63275
lanthanum ethyl sulphate nonahydrate: Tb^{3+}, ESR spectrum, spin lattice relax., effect of hydrostatic compression 78−88185
lanthanum nicotinate dihydrate:Nd^{3+} cryst., H coords., EPR and ENDOR determ. 77−59005
metal:magnetic ion, book 77−48037
metallic monopnictides:Gd, coupling between 4f electrons and conduction electrons, EPR linewidth 78−52347
metallic rare earths, conference, St. Pierre-de-Chartreuse, France (Sept. 1978) 80−12844
metallic Van Vleck pnictide, ESR of non S-state ions 77−43881
nitroxide free radical mag. interaction with lanthanides or Cu^{2+} in liqs., ESR 78−68380
$Pb_5Ge_3O_{11}:Gd^{3+}$, ESR spectra, electric-field effect and reversible permittivity 80−29614
perovskite:Er^{3+}, ESR spectrum, higher order Zeeman effects 79−99766
pnictides, cubic Van Vleck compounds, paramag. fluctuations, ESR or NMR relax. 77−66420
praseodymium ethylsulphate:Sm, one-dimens. X-Y system, spin dynamics, electron spin echo meas. 80−66031
rare earth alloys, dil., ESR linewidth of rare-earth ions 78−68373
rare earth complexes, formation and props., book contrib. 80−43204
rare earth compounds, cryst. field effects on EPR and NMR *(Japanese)* 77−43879
rare earth compounds, cryst. field effects on EPR and NMR *(Japanese)* 77−43880
rare earth compounds, cryst. field effects on EPR and NMR 79−4736
rare earth ethyl sulphate:Gd^{3+}, host lattice effects on EPR spectra 77−69684
rare earth ethyl sulphate nonahydrate:Gd^{3+}, high-precision EPR of cryst. 79−69717
rare earth ethyl sulphate nonahydrates:Gd^{3+}, $g_\parallel$, EPR obs. 78−35031
rare earth intermetallics, AB_2, (A=Y, La, Ce, Lu; B=Ir, Rh) 77−85564
rare earth intermetallics, RAl_2, exchange modification of cond. bands 79−82568
rare earth intermetallics, RAl_2-Gd(Er)(Dy)(Nd), dil., (R=La, Yb, Lu), EPR and mag. susceptibility 80−15797
rare earth ions in solids 80−51968
rare earth mag. conc. cubic Laves phase cpds., ESR 80−71174
rare earth pseudobinary intermetallic compounds, ESR studies 80−108064
rare earth sulphate:Gd^{3+}, hydrated, EPR spectra, host lattice effects 78−95516
rare earth systems, NMR, EPR, and Mossbauer effect, book contribs. 80−39883
rare earth trichloride hexahydrate:Gd^{3+}, EPR meas. 78−15017
rare earth trichloride hexahydratee Gd^{3+} EPR, linear point charge model predictions 80−25200

paramagnetic resonance of rare earth ions and impurities continued
rare earth trichloride hexahydrates, Tb to Yb, EPR of Gd^{3+}, spin Hamiltonian parameters 77−36128
rare earth trinitrate hexahydrate:Gd^{3+}, EPR, spectral parameters 79−4720
rare earth-nonmagnetic metal intermetallic cpds., struct. and props., review 79−95377
scheelite:Er^{3+}, ESR spectrum, higher order Zeeman effects 79−99766
silicate glass:Eu, redox equilibria, EPR meas. 78−26447
singlet ground states, low freq. modes 78−68131
solid, review of 1973 literature 77−69675
thulium ethyl sulphate, Van Vleck paramag., mag. reson. on uniaxial and uniform compression *(Russian)* 79−61243
transition metal intermetallics ESR of Nd^{3+} and Gd^{3+} 79−87315
Ag:Er(Dy), orbit-lattice coupling, nonuniform strain effects 78−88182
Ag-Dy, dil., EPR linewidth anisotropy and mag. field depend., internal stress effects 79−33532
Ag-Dy, dil., thin films, ESR spectra, stress effects 80−39866
Ag-Er, dil., reflection EPR residual linewidth 77−81004
Ag-Er film, stress-induced g-anisotropy, EPR of Er 77−85566
$Ag_{83.3}Nd_{16.7}$ amorphous alloy, EPR of Nd^{3+} 79−65727
Al:Er(Dy), orbit-lattice coupling, nonuniform strain effects 78−88182
Al-Er alloy, dil., TESR and direct EPR expts. 77−20704
β-Al_2O_3:Gd^{3+}, EPR, ion site occupancy 77−81003
Au-Er, dil., cold-worked, EPR expts. 80−39864
Au-Er, dil., EPR at 100 mK to 1K 80−66028
Au-Er film, stress-induced g-shift, ESR meas. on Er 77−51951
Au-Gd, dil., crystal-field splitting of localised Gd^{3+} moments, ESR obs. 79−82869
Au-Yb, dil., EPR at 100 mK to 1K 80−66028
Au-Yb thin films, ESR spectra, strain effects 80−71172
$BaCl_2$:Gd^{3+}(Eu^{2+}), electrostatic versus superposition model 78−23337
BaF_2, spectral diffusion, coherent effects in ESR of Gd^{3+} 79−51852
BaF_2:Ce^{3+}, EPR of low-symmetry sites 79−47332
BaF_2:Eu^{2+}, spin-lattice coeffs., meas. using uniaxial stress method 77−36129
BaF_2:Gd^{3+}, dielectric relax. and EPR line broadening 79−56608
BaF_2:Gd^{3+}, high-order EPR transitions of Gd^{3+} centre 78−23335
BaF_2:Gd^{3+}, spin-lattice coeffs., EPR study 80−66032
BaF_2:Gd^{3+}-m^+ complex, cryst. field parameters 78−10768
BaF_2:Tm^{2+}, EPR, optical recording in weak mag. field 78−68376
BaF_2:Tm^{2+}, EPR meas. of Tm^{2+} ion pair interactions 79−95641
BaF_2:U^{3+}, single crystal, superhyperfine interaction of tetragonal centres 79−42834
$BaTbO_3$, perowskite struct., Tb^{4+} EPR obs., cryst. field parameters determ. *(Italian)* 78−52350
$BaWO_4$:Er^{3+}, spin-lattice and spin-spin relax. times, electron spin echo obs. 79−28609
BaY_2F_8:Nd^{3+}(Ho^{3+})(Er^{3+})(Yb^{3+}), ESR spectra and spin-lattice relax. 80−11263
$CaAl_4O_7$:Gd^{3+}, symm. effects 77−36130
CaF_2:Ce^{3+}, Kapitza limited spin-bath relax., paramag. Faraday effect meas. at liq. He temp. 79−95642
CaF_2:Dy^{3+}, cubic sites, Γ_7 state energy 77−1590
CaF_2:Dy^{3+}, Γ_8 quartets, orbit-lattice interaction, e.p.r. under stress 77−1591
CaF_2:Dy^{3+}, spin-lattice interaction in Γ_8 quartets, models tested for EPR data 78−23336
CaF_2:Er, hydrogenated and deuterated, optical and EPR spectra 79−61209
CaF_2:Er^{3+}, fluorite, defect equilibria cluster control 79−99231
CaF_2:Eu, oxidation and reduction of Eu, EPR and optical studies 80−25199
CaF_2:Eu^{2+} single cryst., temp. depend. of second-order spin-lattice coeffs. 77−90029
CaF_2:Gd^{3+}, cubic, strain effects on EPR by UMER method 77−1592
CaF_2:Gd^{3+}, effect of strain on cryst. field, EPR longitudinal and shear strain parameters 77−90027
CaF_2:Gd^{3+}, Eu^{2+}, natural, EPR study of impurity centres 78−19318
CaF_2:Gd^{3+}, S-state splitting, investigation by ESR and ENDOR at high pressure 78−52345
CaF_2:Gd^{3+}-M^+, (M=Li, Na, K, Rb, Cs, Ag), electric field effect expts., EPR line breadths, lattice distortions 78−80210
CaF_2:Gd^{3+}-m^+ complex, cryst. field parameters 78−10768
CaF_2:Pr^{2+}, EPR data interpretation for octahedral Γ_8 state in cubic cryst. field 80−2634
CaF_2:PrF_3, EPR of cubic Pr^{3+} 79−28607
CaF_2:rare earth ion, elec. dipole-dipole interaction, ionic thermocurrent and EPR study 80−108060
CaF_2:Tb, EPR in new photoexcited centre 78−19319
CaF_2:Tm^{2+}, EPR, optical recording in weak mag. field 78−68376
CaF_2:Tm^{2+}, EPR meas. of Tm^{2+} ion pair interactions 79−95641
CaF_2:Tm^{2+}, ultra-low nuclear spin temp., low field behaviour, EPR study 80−100614
$CaMoO_4$:Er^{3+}, phase relax., EPR spin echo expts. 79−99767
$CaMoO_4$:Er^{3+}, phase relax. time rel. to g-factor anisotropy, electron spin echo obs. 80−29615
CaO, Eu, Eu^{2+} to Eu^{3+} charge transformation *(Russian)* 78−72403
$Ca_5(PO_4)_3F$:Nd^{3+}, selective site laser spectroscopy and ESR studies 79−19909
$Ca_5(PO_4)_3F$:Nd^{3+} site symmetries, EPR and spectral obs. 78−6571
$Ca_5(PO_4)_3F$:Yb^{3+}(Nd^{3+}), spin-lattice relax. times meas., Raman processes 77−51953
CaS:Eu, Eu^{2+} to Eu^{3+} charge transformation *(Russian)* 78−72403
$CaSO_4$, with rare earth and Y dopants, ESR, thermolum. correlation studies following gamma irradiation 77−59628
$CaWO_4$, Yb^{3+}, Nd^{3+} phase relaxation electron spin echo spectra 80−29613
$CaWO_4$:Er^{3+}, phase relaxation, spin echo meas. 78−68375
$CaWO_4$:Gd, site occupation 79−28608
$CaWO_4$:Tb^{3+}(Tb^{4+}), new EPR centres *(Russian)* 79−1709
$CaWO_4$:Yb^{3+}(Nd^{3+}), phase relax. time rel. to g-factor anisotropy, electron spin echo obs. 80−29615
$CdBr_2$:Eu^{2+}, layered, temp. depend. of consts. in ESR Hamiltonian, 16-300K *(Russian)* 77−32254
CdF_2:Eu^{2+}, EPR spectra, hydrostatic press. and temp. effects 80−84648
CdF_2:Eu(Gd)(Nd), semicond., symmetry of optical centres, optical and elec. props. 77−59592
CdF_2:Gd^{3+}, hydrostatic press. and temp. effects on EPR spectrum 78−76304

paramagnetic resonance of rare earth ions and impurities continued
CdF_2:Gd^{3+}, investigation of superhyperfine struct. in EPR spectra 79−51851
$3CdSO_4.8H_2O$:Gd^{3+}, EPR, spin Hamiltonian 79−42833
α-Ce, ESR of Gd, Dy and Er impurities 78−39398
Ce^{3+}, in Van Vleck paramagnets, EPR meas. 77−12199
Ce^{3+}, local symmetry in frozen aq. solns., EPR and linear electric field effect 77−16169
CeM_2:Nd^{3+}, M=Ru, Rh, Ir, ESR investigation 79−78514
$Ce_2Mg_3(NO_3)_{12}.24H_2O$, EPR detection at mK temps. using SQUID magnetometer 79−63290
$Ce_2Mg_3(NO_3)_{12}.24H_2O$, EPR of Ce^{3+} appl. of SQUID detection system 79−75560
CeP_5O_{14}:Gd^{3+}, EPR and emission spectra *(French)* 77−69686
$CePd_3$-Er(Gd)(Yb), dil., EPR spectra 80−25201
$CePd_3$-Gd, EPR of Gd^{3+} impurities in host with interconfig. fluctuations 78−56377
$CePt_2$, ESR of Er^{3+} 79−87315
$CeRu_2$, type II supercond., ESR of Nd^{3+} meas. 79−28444
$Ce_2(SO_4)_3.8H_2O$:Gd^{3+}, single cryst., EPR study, spin Hamiltonians 80−80606
$Ce_{1-x}Sc_xPd_3$, intermediate valence of Ce, susceptibility, lattice const., ESR meas. 80−103648
$CsCdBr_3$:Gd^{3+}, EPR of coupled pairs of Gd^{3+} ions 78−19322
$CsCdBr_3$:Gd^{3+}, EPR spectra of mag. coupled Gd^{3+} ions 78−35032
$CsMgCl_3(Br_3)$:Gd^{3+}, EPR spectra of mag. coupled Gd^{3+} ions 78−35032
Cs_2NaRCl_6:Er^{3+}(Gd^{3+}), R=lanthanide, EPR parameters and interpret. 77−59456
Cs_2NaYCl_6:Yb^{3+} electron spin-lattice relax. 77−63274
$CsSrCl_3$:Mn^{2+}(Gd^{3+}), structural transitions, EPR meas. 78−34619
Cu:Dy^{3+}, g-factor, hyperfine struct. 77−48046
Dy^{3+}, free-radical relax. agent in biological tissues 78−81090
Dy^{3+}, in Van Vleck paramagnets, EPR meas. 77−12199
Er^{3+}, local symmetry in frozen aq. solns., EPR and local electric field effect 77−16169
$Er_xLa_{1-x}Be_{13}$, mag. sp. ht. and ESR, cryst. field interactions 80−60290
$Er(PO_3)_3$ glass, Faraday resonance effect in pulsed mag. field, optical freq. EPR *(Russian)* 80−2734
Eu, metal, g-shift determ. 77−48045
$EuAl_2S_4$, mag. susceptibility and EPR meas. 80−71173
$EuAsO_4$:Gd, dynamical interactions, EPR meas. 80−7162
EuB_6, pure single crystals, magnetic and electric props. 80−11260
EuB_6, single and bulk polycryst., EPR, temp. and freq. depend. 79−28606
$EuBe_{13}$:Gd, Van Vleck paramagnet, exchange parameters determ. 77−4557
$EuCl_2$, $EuCl_2$-$EuCl_3$, $EuCl_2$.HCl, mag. props., 77-292K 78−52197
$EuCl_3.6H_2O$:Gd^{3+}, EPR spectrum, g-tensor and zero-field splitting 77−55706
$EuGa_2S_4(Se_4)$, mag. susceptibility and EPR meas. 80−71173
$Eu_xLa_{1-x}Al_2$, cryst. fields and exchange parameters, ESR meas. 80−71175
$Eu_xLa_{1-x}Al_2$, dil. EPR, cryst. fields and effective exchange interaction 80−66029
EuO, zero-wave vector kinetic coefficient near T_c 79−73714
$Eu_{1-x}Sm_xO$, ferromag. semiconductor with elevated Curie temp. 77−51903
$Eu_{1-x}Sm_xS$, ESR, exchange interaction, susceptibility, elec. cond., thermoelectric power 80−93174
$EuVO_4$:Gd, dynamical interactions, EPR meas. 80−7162
$Eu_{1-x}Yb_xO(S)$, solid soln., ferromag. semicond., increase of exchange interaction 78−88109
Gd, EPR linewidth and spin-spin relax. near T_c 78−68369
Gd, EPR near Curie temp. 78−19321
Gd in CsCl type alloys, exchange between localised 4f and cond. electrons 77−63279
Gd, in polycrystalline cubic metallic cpds., cryst. field effects 77−77096
Gd magnetically conc. cubic Laves phase cpds., ESR 80−71174
Gd, metal, g-shift determ. 77−48045
Gd^{3+} impurity ions, EPR spectra, linewidth narrowing due to spin-lattice relax. of lanthanide Kramers host ions 80−108061
Gd^{3+} in $R_2(SO_4)_3.8H_2O$, (R=Pr, Nd, Sm, Eu, Yb and Y), EPR 80−20458
Gd^{3+}, in Van Vleck paramagnets, EPR meas. 77−12199
Gd-Al, amorphous film, microwave mag. reson. 78−91948
Gd-Al, amorphous film, microwave mag. reson. 78−92060
$Gd_{0.37}Al_{0.63}$ sputtered film, amorphous, conc. spin glass, microwave reson. spectrum obs. 78−15018
$Gd_{37}Al_{63}$ amorphous film, spin glass, microwave mag. resonance, freq. dependence 80−39798
$Gd_xCe_yLa_{1-x-y}Be_{13}$, high electron lattice relax., Gd EPR meas. 78−2736
$Gd(Co_xIr_{1-x})_2$, C15 Laves phase struct., g shift, linewidth, Fermi level movement interpretation 79−61210
$Gd_{1-x}Dy_xAl_2$, EPR bottleneck, Dy substitution effect 77−63281
$Gd_{0.5}Dy_yY_{0.5-y}Ir_2$, effect of dil. Dy substitution on Gd ESR 79−82868
$Gd_xLa_{1-x}Al_2$, cryst. fields and exchange parameters, ESR meas. 80−71175
$Gd_xLa_{1-x}Be_{13}$, $0.001 \leq x \leq 1$, EPR, indirect exchange, bottleneck effect 77−16171
$Gd_xLa_{1-x}Be_{13}$, high electron lattice relax., Gd EPR meas. 78−2736
$Gd_xLa_{1-x}Pd_3$, EPR of Gd, g-factor and thermal broadening, temp. and comp. depend. 77−48048
$Gd_xLa_{1-x}Pd_3$, ESR linewidths, g-shifts, effective electron interaction, spin-lattice relax., spin-flip scatt. 78−68372
$Gd_xMo_6Se_8$, Gd^{3+} ESR meas., 1.4-290K 78−88184
$GdNi_x$, (x=3, 3.5, 8.5), ferrimag., mag. reson. above and below Curie temp. 80−97148
$Gd_2Ni_{17-x}Al_x$, EPR of Gd^{3+} ions 80−97139
$Gd(Rh_{1-x}Fe_x)_2$, $x \leq 0.15$, magnetisation and EPR studies 80−34767
$Gd_xY_{1-x}Ir_2$, ESR meas., bottleneck and relax. rates 79−38369
$HoVO_4$:Gd, indirect superhyperfine interaction, EPR line width meas. 80−2633
$KCdF_3$:Gd^{3+}, EPR, spin Hamiltonian parameters 79−65725
KCl:Eu, additively coloured, ESR obs. of $^{2+}$ complex 77−16170
KCl:Eu, OH^-, EPR meas. on Eu^{2+} complex 78−10773
KCl(Br):Eu, Eu^{2+} ESR meas. 78−80209
KF+Eu^{2+}, cryst., hyperfine splitting, EPR 78−2733
$K_2M(SO_4)_2.6H_2O$:Gd^{3+}, M=Co, Ni, EPR, low-symmetry effects 77−48043

paramagnetic resonance of rare earth ions and impurities continued
$KMgF_3:Er^{3+}$, Orbach-Aminor paramag. relax. processes, phonon bottleneck 79−28610
$KMgF_3:Yb^{3+}$, cryst. field parameters, optical, EPR spectra, spin-lattice relax. time 77−51950
$KSc(MoO_4)_2:Gd^{3+}$, hyperfine struct. of ESR spectrum 77−8399
$KTaO_3:Gd^{3+}$, influence of external elec. field on EPR 78−15020
$KZnF_3:Gd^{3+}$, EPR, spin Hamiltonian parameters 79−65725
$KZnF_3:Yb^{3+}$, cryst. field parameters, optical, EPR spectra, spin-lattice relax. time 77−51950
La-Er, superconducting, EPR for localised Er mag. moments *(Russian)* 77−47931
La-Eu(Gd), EPR investig. of local moment, correl. with supercond. props. 77−63282
La-Gd, exchange-coupled localised moments, Korringa relaxation rate 80−75851
$LaAl_2$, cryst. field splitting and spin-spin interaction of Eu^{2+} and Gd^{3+}, ESR meas. 78−68370
$LaAl_2:Gd^{3+}(Eu^{2+})$, cryst. field parameters, relax. rates 78−84482
$LaBe_{13}$:Er, ESR, appl. of exchange induced broadening in low lying crystalline field system 80−108062
$LaBe_{13}$:Er, ESR spectra, Er spin-spin exchange broadening 78−23338
$LaBe_{13}$:Er(Dy)(Gd), ESR, crystalline field single ion effects 78−84481
$LaBe_{13}$-Er(Dy), dil., ESR, crystalline elec. field splitting, exchange parameters 78−52348
$LaCl_3:Gd^{3+}$, EPR spectra, linear-electric-field effect 79−73808
$LaCl_3:Nd^{3+}$, coherent interactions of Kramers doublet system with microwaves in zero static mag. field 77−73078
$LaCl_3:Pr^{3+}$, coherent transients by optical phase switching 80−95962
$La_xEu_{1-x}B_6$, EPR linewidth conc. depend., $Sr_xEu_{1-x}B_6$ comparison, exchange interaction in EuB_6 80−20457
$LaF_3:Nd^{3+}$, spin echo envelope modulation exam. 79−61212
LaH_x, x=2.3 to 2.98, EPR investigation 79−78513
$LaM_2:Nd^{3+}$, M=Ru, Rh, Ir, Pt, ESR investigation 79−78514
LaM_2-Gd, M=transition metal, correl. between g-shift and stability, EPR study 80−88874
$La_2Mg_3(NO_3)_{12}.24H_2O:Ce^{3+}$, electron spin-lattice relax. under uniform compression 77−90028
La_2MoO_6, paramag. resonance and struct. 80−84162
$LaNbO_4:Tb^{3+}(Ho^{3+})$, EPR and spin-lattice relax., Stark levels *(Russian)* 77−85563
$LaNi_5$:Gd, exchange induced g-shift, H_2 uptake effect 77−4556
$LaNi_5$-Gd, dil., ESR spectra, fine struct. and random stresses 80−25203
$LaRh_2$, ESR of Yb^{3+} 79−87315
$LaRh_2:Nd^{3+}$ cubic metallic host, spin-lattice relaxation, ESR obs. 79−1710
$LaRu_2$, type II supercond., ESR of Nd^{3+} meas. 79−28444
$La_2(SO_4)_3.9H_2O:Gd^{3+}$, single cryst., EPR study, spin Hamiltonians 80−80606
$La_{3-x}V_xS_4:Gd^{3+}$ localised moment-conduction electron interact., ESR obs. 78−88183
$La_{3-x}\square_xS_4:Gd^{3+}$, indirect mag. interaction *(Dutch)* 77−63277
$La_{3-x}\square_xS_4:Gd^{3+}$, localised moment-cond. electron interactions, EPR data interpretation 77−63280
$LiErF_4$, EPR studies, lowest levels of rare-earth ions, submillimetre freq. 80−39865
$LiHoF_4$, dipolar-coupled Ising ferromag., submillimetre ferromag. and paramag. reson. 77−69697
$LiHoF_4$, EPR studies, lowest levels of rare-earth ions, submillimetre freq. 80−39865
$LiTbF_4$, dipolar-coupled Ising ferromag., submillimetre ferromag. and paramag. reson. 77−69697
$LiTbF_4$, EPR studies, lowest levels of rare-earth ions, submillimetre freq. 80−39865
$LiTmF_4$, Van Vleck paramag., mag. reson. on uniaxial and uniform compression *(Russian)* 79−61243
$LiTmF_4$ Van Vleck paramagnet, electron and nuclear spin-lattice relaxation of Er^{3+} ions 79−95643
$LiTmF_4$:rare earth, EPR spectra, elec. field effects, cryst. field interactions 80−71176
$LiYF_4$, ESR spectra of non Kramers ions, elec. field influence 80−103884
$LiYF_4:Dy^{3+}(Yb^{3+})(Er^{3+})$, ESR, nonlinear effect of elec. field 80−2635
$LiYF_4$:rare earth, EPR spectra, elec. field effects, cryst. field interactions 80−71176
$LuBe_{13}$:Er(Dy)(Gd), ESR, crystalline field single ion effects 78−84481
$LuBe_{13}$-Er, dil., ESR, crystalline elec. field splitting, exchange parameters 78−52348
$LuIr_2$-Nd^{3+}, dil., ESR, hyperfine crysts. of $^{143,145}Nd$, g-factor, crystalline field splitting 78−52349
$LuPO_4:Gd^{3+}$, zircon struct. EPR investig., rel. to radiation resistance 80−97138
$LuPO_4$:Sc, Gd^{3+} EPR spectrum, satellite resonances 78−2734
$LuRh_2$-Nd^{3+}, dil., ESR, hyperfine crysts. of $^{143,145}Nd$, g-factor, crystalline field splitting 78−52349
MgO:Er^{3+}, Γ_8 quartets, orbit-lattice interaction, e.p.r. under stress 77−1591
MgO:Er^{3+}, spin-lattice interaction in Γ_8 quartets, models tested for EPR data 78−23336
MgO:R, single cryst., grown with modified plasma torch furnace *(Japanese)* 79−95923
NaCl:Eu, secondary Eu phase dissolution, EPR and optical absorpt. study 80−96655
NaCl:Eu^{2+}, reorient. of Eu^{2+}-vacancy complexes, ESR method using elec. field effect 79−99768
NaCl:$Eu^{2+}(Mn^{2+})$, ESR and elec. field effects 77−28441
NaCl(Br);Eu, Eu^{2+} ESR meas. 78−80209
NaF+Eu^{2+}, cryst., hyperfine splitting, EPR 78−2733
$Na_2S:Gd^{3+}$, EPR and ENDOR meas., spin-stress Hamiltonian 77−63278
$Na_2S:Gd^{3+}$ crystal field splitting, parametrisation of temperature dependence 78−91652
$Na_3Sc_2V_3O_{12}:Yb^{3+}$, EPR of Yb^{3+} in octahedral sites 80−54948
Nd complex, Nd^{3+}:ATP, electron spin echo decay envelope anal. 79−54871
Nd^{3+}, local symmetry in frozen aq. solns., EPR and linear electric field effect 77−16169
$NdCl_3.6H_2O:Gd^{3+}$, EPR spectra, angular var. calc. 80−54940
$Nd_3Mg_3(NO_3)_{12}.24H_2O:Gd^{3+}$, EPR spectra, spin Hamiltonian anal. 79−33527

paramagnetic resonance of rare earth ions and impurities continued
$Nd_2(SO_4)_3.8H_2O:Gd^{3+}$, EPR, zero field splittings, spin-Hamiltonian parameters 78−91949
$Nd_2Zn_3(NO_3)_{12}.24H_2O$, EPR of Mn^{2+}, Gd^{3+} doped single crystal 79−24212
β-PbF_2, spectral diffusion, coherent effects in ESR of Gd^{3+} 79−51852
$PbF_2:Gd^{3+}$, EPR and ENDOR of Gd^{3+} at cubic sites 80−7161
$PbF_2:Tb^{3+}$, ESR spectrum of ions in cryst. field of cubic symmetry 79−38378
$PbFCl:Gd^{3+}(Eu^{2+})$, crystal field splitting, parametrisation of temperature dependence 78−91652
$Pb_5Gd_3O_{11}$, trigonal Gd^{3+} centre structure 79−69720
$Pb_5Ge_3O_{11}$, spectral diffusion, coherent effects in ESR of Gd^{3+} 79−51852
$Pb_5Ge_3O_{11}:Gd^{3+}$, discrete saturation of ESR, due to superhyperfine interaction 77−28440
$Pb_5Ge_3O_{11}:Gd^{3+}$, displacive phase transition, S ion spin Hamiltonian parameter dependence on order parameter 80−70356
$Pb_5Ge_3O_{11}:Gd^{3+}$, EPR hyperfine struct. 79−82867
$Pb_5Ge_3O_{11}:Gd^{3+}$, ferroelec. transition, temp. depend., EPR study 80−66127
$PbMo_6S_8$:Gd, EPR meas. *(French)* 80−54947
$PbMo_6S_8:Gd^{3+}$, powder EPR spectra, cryst. field, supercond. energy gap 80−34769
$Pb_3(PO_4)_2:Gd^{3+}$, EPR near ferroelastic transition point 79−15350
$Pb_3(PO_4)_2:Gd^{3+}(Eu^{2+})$, EPR spectra of α- and β-phases 80−11261
Pd-Er, dilute alloy, EPR spectrum, effect of fine and hyperfine interactions 78−19323
Pd-Er, fine struct. of Er^{3+}, dynamic Jahn-Teller effect of electronic Γ_8 quartet 77−35895
Pd-Gd, dil., 35 and 9 GHz, very dil. limit 78−15019
Pd-H system, phase diagram determ. using Gd^{3+} EPR 79−87608
Pd-H-Gd, dil., ESR exam. of low temp. region of phase diagram, and electronic props. 80−29930
PdGdH, diagram of state elec. props., indirect exchange interaction, EPR study *(Russian)* 80−50179
PdH_x-Gd, EPR of Gd^{3+} in temp. range 1.6 to 30K 77−43882
PrAs(Bi)(P)(Sb):Gd, EPR relax. of impurity in Van Vleck paramag., host ion fluctuation spectra 77−48049
$PrBe_{13}$:Gd, Van Vleck paramagnet, exchange parameters determ. 77−4557
$PrIn_3$:Gd, EPR relax. of impurity in Van Vleck paramag., host ion fluctuation spectra 77−48049
$PrIn_3$:Gd, indirect nuclear exchange interactions, ESR-linewidth meas., sp. ht. determ. 80−103825
$Pr_2Mg_3(NO_3)_{12}.24H_2O:Gd^{3+}$, EPR X-band, fine struct., low field lines 79−15351
$PrNi_5$-Gd, dil., single crystal, ESR study 80−75850
$PrNi_{5-x}Gd_x$, nucl. cooling agent, relax. and exchange, EPR and NMR study 80−25237
$Pr_2O_3:Gd^{3+}$, EPR, zero-field splitting 79−51850
PrSb (Bi):Gd, Gd ESR, Gd-Pr exchange, conduction electron effects 79−69719
PrSb:Gd, ESR study, relaxation narrowing 79−99765
PrX:Dy^{3+}, (X=P,As,Sb), singlet-ground-state paramagnets, EPR meas. 77−20695
$Pr_2Zn_3(NO_3)_{12}.24H_2O:Gd^{3+}$ 78−64270
RbCaF$_3$:Gd, shift of first order transition under hydrostatic press. EPR of Gd^{3+} meas. 80−59649
RbCaF$_3$:Gd_2O_3, Gd^{3+}-O^{2-} pair, EPR study of displacive transform. *(French)* 78−27088
RbCaF$_3$:Gd^{3+}, O_h^1-D_{4h}^{18} struct. transition, ESR obs. 80−50178
RbCaF$_3$:Gd^{3+}, struct. phase transition, EPR study 80−71171
RbCaF$_3$:Gd^{3+}, uniaxially stressed, transcrit. behaviour, EPR obs. 79−33086
RbCdF$_3$:Gd^{3+}, EPR 79−91289
RbCdF$_3$:Gd^{3+}, O_h^1-D_{4h}^1 struct. transition, ESR obs. 80−50178
RbCdF$_3$:Gd^{3+}, struct. phase transition, EPR study 80−71171
RbCl:Eu, γ-irrad., thermoluminesc., EPR meas. 78−84670
RbCl:Eu^{2+}, EPR of $^{153}Eu^{2+}$ and $^{151}Eu^{2+}$ 80−11259
RbCl:Eu^{2+}, tetragonal sites, spin Hamiltonian parameters, EPR and UV absorpt. spectra obs. 80−50177
RbCl(Br):Eu, Eu^{2+} ESR meas. 78−80209
RbF+Eu^{2+}, cryst., hyperfine splitting, EPR 78−2733
$RbIn(MoO_4)_2:Gd^{3+}$, hyperfine struct. of ESR spectrum 77−8399
$RbIn(WO_4):Gd^{3+}$ hyperfine struct. in ESR spectrum 77−8399
$RbSc(MoO_4)_2:Gd^{3+}$, hyperfine struct. in ESR spectrum 77−8399
$RbSc(WO_4)_2:Gd^{3+}$, hyperfine struct. of ESR spectrum 77−8399
$ScAl_2$-Er(Dy)(Nd), dil., EPR and mag. susceptibility 80−15797
$ScAl_2$-Gd, dil., EPR, comparison with YAl_2, $LaAl_2$, $LuAl_2$ 77−63276
$Sc_{0.995}Gd_{0.005}H_{1.9}$, low temp. anomaly, Gd^{3+} EPR linewidth and X-ray meas. 77−69687
$ScH_{1.9}$:Pt, Gd, effect of Pt on Gd^{3+} ESR lineshape 78−68371
ScH_x:Er, ESP determ. of proton locations 80−34768
ScH_x:Er, ESR evidence of octahedral site occupation 79−78512
ScH_x:Er, proton distrib. and site energies, ESR meas. 80−59509
$ScPO_4:Gd^{3+}$, zircon struct. EPR investig., rel. to radiation resistance 80−97138
SmB_6, mixed valence cpd., EPR and heat capacity obs., metal-semicond. behaviour 80−20456
$SmB_6:Gd^{3+}(Eu^{2+})$, mixed valence compound, ESR g-shifts and linewidths 78−48035
$SmCl_3.6H_2O:Gd^{3+}$, X-ray band EPR lines, exact anal. using intensity operator 80−20448
SmS:Eu, excited-state exchange interactions, EPR meas. 78−68374
Sm_3S_4:Eu, excited-state exchange interactions, EPR meas. 78−68374
$Sm_2(SO_4)_3.8H_2O:Gd^{3+}$, cryst., EPR 77−59455
$Sm_2(SO_4)_3.8H_2O:Gd^{3+}$, EPR, zero field splittings, spin-Hamiltonian parameters 78−91949
SmSe:Eu, excited-state exchange interactions, EPR meas. 78−68374
$Sm_2Zn_3(NO_3)_{12}.24H_2O:Gd^{3+}$, EPR X-band, fine struct., low field lines 79−15351
$SnMo_6S_8$:Gd, EPR meas. *(French)* 80−54947
$SnMo_6S_8:Gd^{3+}$, powder EPR spectra, cryst. field, supercond. energy gap 80−34769
$SrCl_2:Gd^{3+}$, small dielec. particles, cryst. field size effects 80−44913
$SrCl_2:Gd^{3+}$-m^+ complex, cryst. field parameters 78−10768
$SrCl_2.6H_2O:Gd^{3+}$, evaporation technique prep. of $SrCl_2:Gd^{3+}$, H_2O content, EPR powder spectrum obs. 80−60416
$Sr_xEu_{1-x}B_6$, EPR linewidth conc. depend., $La_xEu_{1-x}B_6$ comparison, exchange interaction in EuB_6 80−20457

paramagnetic resonance of rare earth ions and impurities continued
$Sr_{2x}Eu_{2-2x}NbO_4$, synthesis and props. 77−52265
SrF_2, spectral diffusion, coherent effects in ESR of Gd^{3+} 79−51852
$SrF_2:Ce^{3+}$, EPR of low-symmetry sites 79−47332
$SrF_2:Eu^{2+}$, superfine struct. in EPR obs. 77−1593
$SrF_2:Gd$, hydrogenated, IR and EPR spectra 77−69865
$SrF_2:Gd^{3+}$, dielectric relax. and EPR line broadening 79−56608
$SrF_2:Gd^{3+}$, dipole strengths and conc. effects influenced by dipole-dipole interactions 79−69718
$SrF_2:Gd^{3+}$, high-order EPR transitions of Gd^{3+} centre 78−23335
$SrF_2:Gd^{3+}$, $Na^+(Kr^+)(Rb^+)(Ag^+)$, EPR of orthorhombic Gd^{3+}-univalent metal ion complexes 80−11262
$SrF_2:Gd^{3+}$, orientation kinetics of Gd^{3+}-F^- dipole complexes 77−51952
$SrF_2:Gd^{3+}$, spin-lattice relax. of Gd^{3+}, EPR line shifts meas. 78−72404
SrF_2:rare earth ion, elec. dipole-dipole interaction, ionic thermocurrent and EPR study 80−108060
$SrF_2:Tm^{2+}$, EPR, optical recording in weak mag. field 78−68376
$SrF_2:Tm^{2+}$, EPR meas. of Tm^{2+} ion pair interactions 79−95641
$SrTbO_3$, EPR study of perovskite struct. 77−69685
$SrWO_4:Er^{3+}$, spin-lattice and spin-spin relax. times, electron spin echo obs. 79−28609
$TbFeO_3$, ortho-ferrite, electron spin relax. time temp. depend. 77−90026
$ThBe_{13}$:Er(Dy)(Gd), ESR, crystalline field single ion effects 78−84481
$ThH_2:Er^{3+}$, EPR of Er localised electron mag. states, Kondo effect 80−25202
$Th_4H_{15}:Er^{3+}$, EPR of Er localised electron mag. states, Kondo effect 80−25202
$ThOS:Gd^{3+}$, EPR study, g-factor and cryst. field parameters 80−25204
$ThRu_2$, type II supercond., ESR of Nd^{3+} meas. 79−28444
$ThRu_2:Nd^{3+}$, supercond. state, ESR investigation 79−78514
Tm pnictides, van Vleck paramag., relax., host exchange parameters 78−2735
$Tm_3Al_5O_{12}:Yb^{3+}$, g-shift meas., EPR 78−56376
$TmAsO_4$:Gd, cooperative Jahn-Teller system, dipolar and random strain effects 77−40124
$TmBe_{13}$:Gd, Van Vleck paramagnet, exchange parameters determ. 77−4557
$Tm_3Ga_5O_{12}:Gd^{3+}(Yb^{3+})$, Van Vleck paramagnet, EPR g-shifts and line-widths, temp. depend. 77−66419
$TmPO_4:Gd^{3+}$, EPR spectrum and Jahn-Teller induced nonuniform dynamic strains 77−85565
TmS(Se)(Te):Gd^{3+}, EPR studies of valence states of Tm 77−77095
TmSb, Gd ESR, Gd-Pr exchange, conduction electron effects 79−69719
$TmVO_4:Gd^{3+}$, EPR linewidth temp. var., random strains due to Jahn-Teller effect 77−12200
$TmX:Dy^{3+}$, (X=P,As), singlet-ground-state paramagnetics, EPR meas. 77−20695
UBe_{13}:Gd, Van Vleck paramagnet, exchange parameters determ. 77−4557
$YAG:Gd^{3+}$, EPR absorpt. spectrum 78−76305
YAl_2-Er, dil., EPR, $Er^{3+}\Gamma_8$ ground state 80−15798
YAl_2-Er(Dy)(Nd), dil., EPR and mag. susceptibility 80−15797
$YAlG:Gd^{3+}$ ESR absorption spectra, line broadening 78−91940
$Y(C_2O_4)(C_2O_4H).3H_2O:Er^{3+}$, 4.2K, paramag. ordering 77−77094
YCl_3:($^{145}Nd^{3+}$/$^{145}Nd^{3+}$), EPR and ENDOR spectra 79−78515
YH_x:Er, proton distrib. and site energies, ESR meas. 80−59509
$YLiF_4$:rare earth, spin-lattice relax. and nuclear polarisation *(Russian)* 79−8049
$YM_2:Nd^{3+}$, M=Rh, Ir, Pt, ESR investigation 79−78514
YM_2-Gd, M=transition metal, correl. between g-shift and stability, EPR study 80−88874
$Y(OH)_3:Tb^{3+}$, spin-lattice relax. at high gap energies using pulsed tunable dye laser 77−48047
$YPO_4:Gd^{3+}$, zircon struct. EPR investig., rel. to radiation resistance 80−97138
$Y_2SiO_5:Ce^{3+}(Nd^{3+})(Er^{3+})(Yb^{3+})$, EPR and spin-lattice relax. 80−108063
Yb^{3+}, local symmetry in frozen aq. solns., EPR and local electric field effect 77−16169
$YbBe_{13}$, mag. props. and EPR meas. 80−11175
$YbCl_3.6H_2O$, paramag. relax., Mossbauer spectra 80−20536
$YbCl_3.6H_2O:Gd^{3+}$, EPR, temp. depend., spin-lattice relax. time 80−93173
YbH(YbD), and isotopic forms, optical and EPR matrix isolated spectra, HFS, bonding 77−83613
$ZnS:Yb^{3+}(Nd^{3+})$, spin-lattice relax. times meas. 78−19324
ZnS-Eu^{2+}, microregions disorientation degree anal. by birefringence, ESR and decoration methods 79−60389

ıramagnetism
see also paramagnetic properties of substances
anisotropic, effect of bond dilution on dynamics at high temp. 78−39343
anisotropic binary paramagnet, uniform susceptibility, critical behaviour 77−59384
anisotropic paramagnet, site- and bond-diluted, spin dynamics at high temp. 79−61117
anisotropic paramagnet, spin dynamics, exchange-bond dilution effects 80−88763
anisotropic paramagnet, statistical mechanics using second order Green's function theory 80−25074
anisotropic paramagnet with exchange-bond dilution, sixth freq. moments 80−44789
anisotropic paramagnets, spin dynamics 77−69481
anisotropic paramagnets, temp. depend. single ion excitation 79−33445
Bethe lattice, random ordered phase, statistical theory 77−85457
binary paramagnetic mixtures, phase separations, tetracritical phenomena 79−65638
classical paramagnet, static and dynamic response functions 79−47227
classical paramagnet, wavelength-depend. fluctuations in mag. field 80−7069
closed-shell many-electron systems 77−20539
clustering of mag. ions, study method 80−11155
collectivised electrons and localised spins, thermodynamic props. 77−8257
critical dynamics of paramagnets with dipolar couplings 78−52286
crystal, magnetisation change by light pulse 80−70932
crystal field parameters computation using Ewald method lattice sums 79−91003
Curie Weiss law for ferroelectric solid soln., perovskite struct., review *(Russian)* 77−48134

paramagnetism continued
dielectric crystal, APR and phonon spectroscopy to study paramagnetic ions 80−84634
dielectric function of 1-dimens. Hubbard model 79−60740
dilute system under bottleneck conditions, kinetics 77−77029
diluted Heisenberg magnet, spin diffusion const., conc. depend. 78−88089
diluted Ising and Heisenberg systems with competing interactions, mag. ordering, appl. to $Eu_xSr_{1-x}S$ 80−65914
dipolar interaction, reduction by off-resonance phonon avalanche 77−63260
disordered system, spin diffusion 77−8392
double exchange mechanism theory 77−24689
dynamical correlated-effective-field approximation 79−24122
effective field models in magnetism, unifying theory 77−32136
elastic modes in applied mag. field 79−60423
electron, nonrelativistic, and Euclidean massless Dirac particles, paramagnetism 79−63396
electron gas, mag. susceptibility, RPA calc. 78−43559
electron gas, spin polarised, exchange and correl. energy 77−85163
electron gas, two dimensional, mag. props. 78−56095
electron gas, two-dimensional, polarised, correl. energy, para- and ferro-mag. states 77−47757
electron gas in ultraquantum limit of strong mag. field, mag. moment *(Russian)* 77−28361
electron liquid with any spin polarisation, correlation energy, local exchange-correlation pot. 79−65399
electron spin density functional gradient expansion, local approx. calcs. 80−44792
electron state density for narrow-band model with Coulomb interaction 80−10852
electronic props. of atoms and mols., orbital mag. moments, paramagnetic currents 77−46476
erythrocyte high gradient magnetic separation 78−53585
ESR line shift, phonon relax. influence 78−88171
exchange enhanced alloy, double d-band model appl. to mag. suscept. 77−66238
f^n-electron system, paramag. principal susceptibilities, calcs. using ang. overlap model 77−32158
Fermi liquid, with Coulomb interactions, susceptibility temp. var. 77−40017
ferromagnet, magnetic moment fluctuations and sp. ht. near crit. point 77−28388
ferromagnetic impurity conc. determ. from Curie-Weiss law deviations *(Russian)* 77−47965
free electron paramagnets, muonic and hydrogenic Knight shifts 78−43759
gas in radiation field, magnetisation 78−78667
Heisenberg, paramagnetic with bond dilution, freq. moments of spin correlation function 79−15272
Heisenberg antiferromagnet at high temp., two-spin Raman scatt. 77−40225
Heisenberg model, correlation functions long time behaviour 77−89919
Heisenberg model, high temp., dynamical 4-spin 2-time correl. functions 77−40026
Heisenberg model, quasi-one-dimens., reaction field approx. and dipolar interaction 77−36088
Heisenberg model, randomly diluted, high temp. series expansion 78−56280
Heisenberg model, sixth frequency function of relaxation shape function 78−39348
Heisenberg paramagnet, 2-spin dynamic autocorrels. and energy diffusion 77−47959
Heisenberg paramagnet, dil., uniaxial anisotropy, frequency moments of spin correlation function 78−84377
Heisenberg paramagnet, dil. isotropic, freq. moments of spin-correlation function 78−31037
Heisenberg paramagnet, electronic spin dynamics, NMR 78−76266
Heisenberg paramagnet, exchange bond dilution, freq. moments of spin correl. function 80−50030
Heisenberg paramagnet, relax. and response functions 77−51867
Heisenberg paramagnet, site- and bond-diluted, correl. function and susceptibility 77−51869
Heisenberg paramagnet, two-spin Raman scatt. 77−85715
Heisenberg paramagnets, low freq. props., nonlinear Langevin eqn. 78−31038
Heisenberg-biquadratic and Blume-Emery-Griffiths interactions dipolar and quadrupolar susceptibility 78−76257
Heisenberg-biquadratic and Blume-Emery-Griffiths interactions dipolar and quadrupolar susceptibility 78−76258
Hubbard chain, strong coupling, electron dynamics 78−39342
Hubbard Hamiltonian, coupled spin and charge fields 77−32147
Hubbard model, doubly degenerate, functional integral approach 79−99711
Hubbard model, local moments 78−95414
Hubbard model, Mott metal-insulator transition, ten-fold spin-orbital degeneracy 78−52285
impurities, influence on saturation of NQR lines 80−20491
impurities in metal, nonlinear elec. resist., due to scatt. effect 77−15826
induced moment paramagnet, singlet ground state, mag. fluctuations 77−4482
insulating solid, nonmagnetic, anisotropic mag. effect 78−6509
insulator-to-metal transition for half-filled Hubbard band in paramagnetic state 80−92817
intermediate valence compounds, mag. susceptibility and sp. ht., mean-field theory of periodic Anderson model 78−47937
intracellular water, effect of paramag. impurities on proton spin-lattice relax. 80−51134
Ising model, constant-coupling approx., successive phase transitions 80−97108
Ising model in transverse field 77−8260
Ising model with competing interactions, critical properties and exact results 80−93129
Ising model with transverse field in paramagnet 78−68138
Ising paramagnet, impure, influence of spatial short range order 78−43542
Ising paramagnet, transverse, spectral density approach 77−80897
Ising site model, random mixtures, Monte Carlo simulation 78−73936
Ising spin glass, d-dimensional, frustration effect and dilution problems 80−108018
Ising transverse paramagnet, Dyson eqn. 79−82736

paramagnetism continued
Ising-like, spin-1/2 system, paramagnet, formalism at very low temps. 79−4647
isotope separation, supersonic molecular beam technique using RF spectroscopy, mag. reson. 80−47725
itinerant electron paramagnets, coupled charge and spin fields 77−72991
itinerant electron paramagnets, spin wave like modes 77−63067
itinerant ferromagnet, sloppy spin waves above T_c 77−72979
itinerant paramagnets, strongly enhanced, theory of anomalies in field depend. of magnetisation 77−69488
Kapitza conductance, mag., paramag. substances in contact with superfluid ^{3}He 77−4235
Kondo alloy, mag. interactions 77−59385
liquid, depolarized light scatt. in mag. field 80−80759
liquid metal, phys. chem., conf., Konigstein, Germany (Mar. 1976) 77−1059
localised site cluster expansion, interacting paramagnetic sites, spin symmetry projection 79−7951
low-dimensional dense paramagnets, magnetic resonance spectra 79−47322
low-dimensional paramagnet, NMR lineshape 78−23356
low-dimensional paramagnets, EPR spectra 80−71154
magnetic cooling of class of model paramagnets 77−36076
magnetic form factor meas. by inelastic neutron scatt. 78−52221
magnetic susceptibility determination, paramagnetic matrix with ferromagnetic inclusions 79−97407
magnetically soft cylinders, micromagnetics of curling configurations 79−82826
magnetisation of paramagnet with noninteracting mag. moments *(Russian)* 78−47938
magneto-microwave effects, rel. to EPR 77−55853
metal, band struct. contribs. to shear consts., deform. pot. formalism and Stoner model 79−91280
metal, electron-phonon interaction, magnetism influence 77−73040
metal, logarithmic terms of susceptibility 78−80126
metal, narrow band electron system, temp.-induced local mag. moment 78−76221
metal, Pauli susceptibility enhancement for strong electron correl., Gutzwiller theory 77−43527
metal, polarised neutron inelastic and quasi-elastic scattering 80−50045
metal with nonmag. impurities, spin-flip scatt. 77−4497
metals, electronic struct. and magnetism, review 80−70573
metals, EM excitation of sound, Mossbauer study *(Russian)* 79−99794
metals, magnetic suscept., optical data determ. of individual contributions 77−12088
metals, nonphonon mechanism of supercond. and static screening *(Russian)* 79−78258
metals, temp. depend. of susceptibility, microscopic Fermi liq. theory 77−28364
mixed valence state, electronic structure 79−11092
mixed-spin paramagnet, dynamics 80−60173
Mori continued fraction in paramagnets, approxs. 77−20529
Mott insulator susceptibility 79−78302
Mott magnetic semiconductor, freq. depend. elec. cond. 77−11907
multimode linear chain, strong spin-phonon interaction 78−51623
muon spin relaxation, paramag. state (μ^+e^-) in Si and Te at high temp. 79−56676
narrow-band s-d magnetic materials, ground state and thermodynamic parameters, cond. electron density depend. 78−47934
nearly-one-dimensional paramagnet, self-consistent diffusion coeff. 77−80997
NMR lineshape exchange narrowing, for Heisenberg paramag. 77−69717
NMR linewidth, paramagnetic contribs. calcs. 80−58286
NMR paramagnetic material effect on chem. shift and relax. times, mol. struct. effect 78−46373
non-Kramers paramagnetic ions, induced nuclear spin-lattice relax. calc. at low temps. 77−8442
nuclear relaxation, effect of heating of electron spins in conc. paramagnets 77−8438
nuclear spin-lattice relax. caused by paramag. impurities, statistical approach 77−48081
one-dimensional electron system, with attractive interaction in mag. field, paramag. transition 80−7072
one-dimensional magnetic system, high-temp. dynamics 79−4716
one-region light scattering from antiferromag. in spin flop and paramag. regions 79−33677
particle stream trajectories near ferromag. fibre 79−86128
partly disordered magnetic structures 77−51908
plasma, penetration of external RF mag. field 80−6225
polarisation analysis of diffuse neutron scattering from magnetic systems 80−25098
polarisation and magnetisation of electronic matter 80−75929
polarized neutron diffractoin in high magnetic fields, for complicated paramagnets 79−73684
quadrupolar exchange effects on spin dynamics of high-temp. paramagnets 79−61038
quantum mechanical theories of magnetism, review of properties and explanations 78−76215
random binary Ising system with transverse field, Curie temp., paramagnetic susceptibility 80−65938
random Hubbard alloys, paramag. susceptibility singularities, derived from Fermi liquid approach 78−43547
random Ising bond interactions, paramag. phase, thermodynamic props. 77−20523
random Ising model with transverse field term 79−56545
relativistic paramagnetism, statistical mechanics in strong mag. field 80−17865
rutile structure Heisenberg paramagnets, two-spin light scatt. 78−80336
S=1, singlet ground state systems, mag. props. 80−11157
semiconductor, double exchange and small-polaron hopping 79−19591
semiconductor, heavily doped paramag., linear response functions and magnetoresist. 77−51770
semiconductor, paramagnetism switching off in strong electric field *(Russian)* 78−80124
singlet ground state system, line shape of mag. excitations, diagrammatic expansion calc. 77−69482
singlet-triplet paramagnet, collective excitations 77−72995
singlet-triplet system in paramag. phase, low-freq. response 80−60172
sphere, strongly magnetised, interaction with weakly magnetised particles carried by fluid flow 80−69320
spin excitation spectrum in mag. fields of arbitrary direction 77−24662
spin glasses, dilute, at zero temperature, low concentration series expansion 80−93131
spin glasses, phase transition, mag. susceptibility, specific heat, Ising model calcs. *(Russian)* 80−34671
spin system, paramagnetic, two-level open system, kinetic theory of resonance and relaxation 80−88859
spin systems, conservation of ang. momentum and thermal mixing *(French)* 78−6562
spin waves, classical approach 80−29519
spin waves in systems with weak exchange fields 79−4664
spin-wave spectrum, of systems without long-range mag. order 79−33450
superconducting alloy containing paramag. impurities, Raman scatt. of light 79−73634
superconducting crystals without symm. centres, paramag. susceptibility 77−15994
superconducting film, Pauli paramagnetism and Fermi surface topology changes under press. 78−2612
superconducting sandwiches, proximity effect, in high fields, effects of Pauli spin paramagnetism 77−85394
surface, ortho to para H_2 conversion 79−34362
three-dimensional crystal, with strong spin-phonon interaction, domain wall quantum mechanics 78−51622
transition metal, 3d, paramag., energy band calcs. 78−91608
transition metal, 3d and 4d, local density theory, mech. and mag. props. evaluation 78−91630
transition metal, dislocation magnetism *(Russian)* 78−39379
transition metal, Hall coeff., force correlation function method 79−91028
transition metal, magnetic moment near surface, one-electron band model 79−82747
transition metals, conf., Toronto, Canada (Aug. 1977) 78−91577
triple dynamic magnetisation fluctuation correl. and feasibility of polarised neutron exam. near T_c *(Russian)* 78−88133
two-sublattice biquadratic systems, phase transitions 79−99710
type II superconductor, giant-vortex state, temp. depend. 80−7051
type II superconductors, thermodynamics near $H_{c2}(T)$ and scaling law 79−60968
uniaxial Heisenberg antiferromagnet, phase diagrams 80−15730
Van Vleck compounds, LF dynamics, NMR linewidth, RKKY exchange mechanism role 80−103812
vapours and condensing materials, apparatus for susceptibility meas., 300-1600K *(Russian)* 79−93178
velocity of sound, temp. depend. modification due to spin-phonon interaction, phonon relax. 78−19303
wavevector-dependent spin susceptibility, variational principle 78−91586
X-Y magnets, two-dimens., with annealed non-mag. impurities 79−78391
X-Y model, two-dimensional, disordered, finite susceptibility phase 79−61031
Cu complex, $Cu(H_2O)_6^{2+}$, ligand hyperfine interactions, orbital angular momentum contrib. 80−96833
LiHLiH array, Mott transition mag. analog, Hamiltonian for paramagnetic-diamagnetic transition 79−95565

parameter estimation
adaptive control and parameter identification, applic. to nuclear reactor systems 80−22970
animal carcinogenicity expts. low-dose-rate data extrapolation 77−56327
aquifer parameters, invariant imbedding and identification 79−57992
artificial heart, atrial charact. estimation using analogue simulation 77−44846
astronomy, parameter estimation via appl. of likelihood ratio 79−44374
beam on elastic foundation with large deflections, and built in at both ends 79−27520
bilinear system Volterra-kernel estimation 79−26512
biological membrane, electrically excited, nonlinear dynamic models for simulation 80−94178
biological models, reliability range 79−96500
biological signal conditioning for system identification 77−44578
biological stochastic compartmental models 78−40109
biological two compartment model, computer expt. study 77−70402
blood glucose regulation, optimal inputs 78−64920
blood pressure control system dynamic behaviour identification 79−2097
BWR power plant, direct cycle, low sensitivity optimal controller study 78−8947
Calvin photosynthesis cycle parameter identification 79−92186
cardiovascular, nonlinear filter statistical parameters optimal choice 79−5308
cardiovascular system, identification and parameter estimation 80−35947
catchment model design, optimisation technique 79−5536
cell kinetic parameters estimation from flow microfluorometry 78−73143
chemical reaction kinetic models, parameter estimates, correl. reduction 79−39121
clonal survival curves with cellular recovery, parameter fitting 77−56352
cloud chamber adaptive closed-loop expansion control system 79−93889
confidence density method for parameter estimation, appl. to charged particle mass *(Chinese)* 78−81811
cooled gas transport by pipelines, temp. and pressure distrib. determ. 79−23326
coronary haemodynamics, using elec. analogue 77−37092
coupled-core nuclear reactor, distributed parameters identification, pseudorandom perturbation and correlation anal. 80−86966
diffusion neuron model 77−40654
diffusion nonlinear parameter identification by hybrid computation 77−53766
distribution function parameters determ. in real time, instrument description 80−202
EEG power spectra, using Gaussian functions 77−21635
EEG segments classification, autoregressive models usefulness 78−80989
enzymic kinetics, rate constants estimation 79−70505
estuarine dynamics, mass balance eqn., longitudinal dispersion function estimation 77−37262
estuarine P model synthesis for Jamaica Bay, NY 77−21777
exchange parameters in compartmental models, identification, biomedical appls. *(French)* 80−42044
field problem inference-finite element model 78−81923
fission reactor, via recursive nonlinear estimators 77−14253
flood event real-time predictors, stochastic model 80−67383
flood wave propagation in Lake Maggiore, recursive method 79−8650

parameter estimation continued
forward-looking IR sensor image segmentation by maximum likelihood parameter estimation 80−99662
geophysical interference fields separation, statistical algorithms *(German)* 77−29462
geophysical objects parameters, interval estimation via identification methods 77−82024
geopotential fields interpretation, statistical algorithms *(German)* 77−29461
heart disease, haemodynamical parameters optimal control 79−53182
heart left ventricle model, global search algorithms *(French)* 78−3529
HWR dynamics modelling for digital control system design 79−9829
hydrological system, state space modelling and identification 79−79908
instrument resolution power, influence on estimation of basic method spatial struct. parameters 79−52543
IR calibrator, continuous-temp., for temp. measurement using IR scanner, analytical eqns. 79−75530
kinematic parameter estimation for transport of pollutants in overland flow 79−52971
laser designation system spot motion model identification 79−94277
left ventricle and systemic vascular bed model 77−21548
likelihood method for plastic thermal properties identification 77−26297
limb function discrimination performance using EMG parameter identification 80−8220
limnological ecosystem modelling, real-time estimation methods appl. 79−5541
linear parameter estimation, for chem. anal. 79−24843
linear predictive coded speech digitisers, background noise spectral subtraction 80−96140
liver disease computer-aided diagnosis using nonlinear stochastic modelling technique 78−36024
lung, nonlinear mathematical model, parameter tracking adaptive algorithm 77−60227
lungs, artificially ventilated, mechanical properties monitoring 77−21642
marine boundary layer microwave sensing, estimation techniques 79−74993
maximum entropy spectral estimation of frequency and arrival angle 80−96129
MHD generators, Window-Frame, with nonuniform velocity and conductivity in transverse plane, electric effects, anal. 79−68960
minicomputerized automatic radiocardiogram analysis *(Japanese)* 79−29614
Monte Carlo computations, multi-parameter, adaptive estimation procedures 80−105572
multidimensional measuring block, parameter tolerance estimation *(Polish)* 78−29079
multimodal probability density functions fitting, FORTRAN program 77−37748
multivariate air pollution models, computationally economical identification technique 79−57545
mutlicompartment analysis, direct estimation of parameters, appl. to drug conc. 77−44580
myocardial regional blood flow from dynamic anal. of ^{201}Tl 79−70627
neurotransmitter release statistics: moment estimates for inhomogeneous Bernoulli trials 79−62228
noninvasive radiocardiographic data, for left ventricular ejection and valvular regurgitant fraction determ. 78−48886
nonstatistical parameter estimation adaptive algorithms 80−91995
nuclear power plant identification methods 77−88219
nuclear power station model validation and automatic control 77−88261
nuclear reactor systems, appl. of stable adaptive schemes 80−13635
nuclear reactor theory, transfer function by parameter estimation *(German)* 77−74905
nuclear reactors, process monitoring and parameter estimation, multivariate signal analysis algorithms 80−47585
ocean-bottom subsurface layered media, spatial parameter estimation 80−77134
oculomotor system parameter identification, strabismus appl. 78−3478
one dimensional distributed parameter system parameter and state estimation, heat conduction experimental result *(Japanese)* 80−83727
optical image, potential accuracy anal. 77−88648
optokinetic reflex, mathematical model 80−41008
orientation of long particles in a uniform electric field *(Russian)* 79−72451
partially polarised waves, polarimetry, accuracy 77−46666
photo-copiers, organic photoconductors, charge acceptance calc. 78−80020
physiological systems, accuracy anal. 78−31762
physiology, martingale model for estimation in nonlinear stochastic systems 77−77865
pollution modelling, numerical estimation of unknown parameters *(Japanese)* 80−89702
process dynamics investigation using time-varying models 77−41099
protein-ligand binding parameters estimation from continuous ultrafiltration results 77−12878
pulmonary and recirculation parameter identifiability following sequential bolus inputs of ^{133}Xe 78−44605
pulmonary arterial circulation process nonlinearity model 77−12944
pulmonary blood flow estimation, Ljung's algorithm sensitivity 80−56107
pulmonary function analysis, parameter estimation, lumped-parameter model 77−44815
pulmonary parameter identification adaptive analogue tracker 77−48911
pure harmonic tide in canal, eqns. of motion quadratic resistance term linearisation 78−69369
PWR, sensor response monitoring, time series modelling 79−26659
radiocardiogram parameter identification *(Slovene)* 78−44586
rainfall, Delhi, recursive prediction model 79−79998
random pulse train processing by linear filter *(Russian)* 78−46518
random threshold element networks with absolute refractory period 77−29143
reactor malfunction detection by Dynamic Data System methodology 79−622
respiratory mechanical behaviour lumped parameter models evaluation using simplex algorithm 80−89783
respiratory system, human, modelling and parameter estimation 80−12169
respiratory system, human, modelling and parameter identification 79−39444
risks of maximum likelihood estimators of parameters of Ito-like process 77−49576
parameter estimation continued
river, dissolved oxygen and biochemical oxygen demand, random signal anal. applic. 77−45047
seismometer digital automatic amplitude controller with preliminary smoothing, parameter selection *(Russian)* 79−74985
solar thermal systems long-term performance predictions using closed-form solutions 80−30556
speech processing, parameter estimation of noisy all-pole process using pole-zero modelling 79−64419
surface roughness estimation by the laser-section method *(German)* 79−49198
survival curve fitting with theoretical models, goodness-of-fit tests 79−79606
systemic arterial bed, quantitative evaluation by parameter estimation of a simple model 80−56094
thermal conductivity equation, nonlinear physical parameter determ. 79−23196
time series, conference, Nottingham, England (Mar. 1977) 80−82580
tissue parameter identification by digital processing of real-time US clinical cardiac data 80−51191
two-scale meter, max. likelihood method, probability density function 77−61047
undirected Earth satellite, estimate of attitude precision 77−64593
valvular regurgitant fraction meas. by radionuclide angiocardiography, iterative estimation 79−34668
vascular beds, optimum modelling using indicator-dilution measurements 77−40686
ventilation inhomogeneity identification using minicomputer data processing 77−44816
ventricular function computer simulation, development of model and parameter estimation 78−53439
visual processor, human colour-vision discrimination, statistical-communications approach 79−5288
voice controlled system for the disabled 79−5407
water pollution dynamic models synthesis, finite-difference method 77−81950
water pollution model, Streeter-Phelps type 79−5539
water quality modelling, Kalman filter theory and practice 78−45058
water resource system, time variable, recursive estimation techniques appls. 79−5538
wind velocity estimation via optical signal processing 77−41107
X-ray source position determ., parameter estimation method 78−61748
O_2 diffusion and reaction in biological tissue, Michaelis-Menten kinetic model 78−31793

parameter identification *see parameter estimation*

parametric amplifiers
see also acoustic parametric amplifiers; microwave parametric amplifiers; optical parametric amplifiers
beam-plasma parametric amplifier, nonlinear hydrodynamic amplifier 79−23462
energy relations for bandlimited signals in gyromagnetic media *(German)* 80−91725
Josephson junction parametric inductance fluctuations, upconvertor 80−25052
liquid nitrogen level control, sensing diode and Norton amplifier 78−29121
magnetostatic waves, semicond.-dielec.-YIG-metal system, amplification of surface and bulk waves 77−1582
radiometer, using a cryogenically cooled two-channel paramp for 47 GHz 77−37982
semiconductors, theory of parametric amplification 77−69382
Very Large Array multiband low-noise receivers 77−41299
X-ray laser, parametric non-threshold amplification *(Russian)* 77−79902

parametric devices
see also acoustic parametric devices; microwave parametric devices; optical parametric devices
betatron, electron beam rapid extraction by parametric reson., analogue computer anal. 77−18731
certain ineffective parametric interactions 80−43396
radiators, high-power, operating characts. 78−94469
superconducting accelerometer using Nb-on-sapphire RF resonator 79−49210

parametric oscillators
see also acoustic parametric oscillators; microwave parametric oscillators; optical parametric oscillators
external-noise-driven, multiplicative stochastic processes in statistical physics appl. 80−22289
magnetic field detector using second harmonic oscillation 79−54161
mass-on-a-spring (autoparametric oscillator) 77−22403
nonlinear dielectric resonators, parametric interaction of EM oscillation *(Russian)* 78−13767
phase transition, noise induced, in parametric oscillator 79−58665

parametric up-convertors *see parametric devices*

parametric varactor diodes *see varactors*

parametrons *see parametric oscillators*

parcel post *see postal services*

Pariser-Parr-Pople calculations *see PPP calculations*

parity
see also baryon spin and parity; lepton spin and parity; meson spin and parity; nuclear spin and parity; P invariance
atomic processes, parity violation 77−22657
atoms, handedness and parity non-conservation 78−29757
chiral molecule, optical activity as mixed parity phenomenon 79−86011
collision model for spectral line shapes, explicit parity considerations 77−58110
D_{4h} symmetry, even and odd parity orbital combination Clebsch-Gordan coefficients 78−45514
gyroscope weight reduction in left turning due to spontaneous symmetry breaking *(Japanese)* 80−98798
heavy atom, parity violation in forbidden mag. transitions, chiral absorpt. of polarized light and circular dichroism in crossed DC fields 80−23370
heavy atoms, parity nonconservation, weak electron-electron interaction *(Russian)* 78−55132
Kekule structure classification, partity concept evaluation 77−88366
L-amino acids, weak neutral currents and biological stereoselection 80−26196

parity continued
left-right symmetric $SU(2)_L \times SU(2)_R \times U(1)$ theory, atomic parity, e^+e^- collisions asymm. at PETRA, PEP energies 78−12820
minimum uncertainty states representation of parity operator 78−86191
mirror image molecules, parity non-conserving energy difference 79−76366
muonic atoms, long range parity violating interaction from γ-Z^0 conversion 80−48108
neutral current expts., left-right symmetry for $SU_L(2) \times SU_R(2) \times U(1)$ gauge group 78−21375
neutral currents, vectorlike model, parity violation 78−4823
nonleptonic weak interactions, irregular G_u-parity term, hadronic currents 77−2770
nuclear levels with anomalous parity, excitation by nucleons, rel. to models of nucleon-nucleon amplitudes *(Russian)* 77−79383
orbital angular momentum and parity 80−77564
$Q\bar{Q}$ systems, new flavours, internal parity and the quark line rule 79−13034
quark fragmentation products parity-odd correls., longit. polarisation 78−433
radiative corrections to parity violation in atoms in $SU(3) \times U(1)$ gauge theory 78−62402
relativistic two-particle forces 78−73847
stars, relativistic collapsing, radiation, linearized even-parity EM and gravit. radiation 79−75228
$SU(2)_L \times SU(2)_R \times U(1)$ based L-R symmetric gauge theory, spontaneous breakdown of parity 79−75681
unstable particles in elec. field 78−562
weak interaction, parity violation, correl. with biomolecules optical asymm. 78−69000
Wigner function, parity operator expectation value appls. 77−45732
$\gamma^*N \rightarrow \psi N$, gluon momentum, spin, parity and coupling 80−42395
$\tilde{p}$, parity determ. from ang. momentum anal. 78−4889
$\tilde{p}$ parity determ. in $\tilde{p}p \rightarrow \pi^- \pi^+$ asymmetry 77−2860
$\tilde{p}p \rightarrow \Delta^{++}\Delta^{++}$, 3.6-12 GeV/c, cross sections and decay, parity exchange contribs. from quark model 79−13146
$\tilde{p}p \rightarrow \pi^+\pi^-$, polarised target, charge parity determ. 77−57567
pp scatt., natural and unnatural parity exchanges, exact separation, A, exchange 79−13144
π condensation and tensor binding, parity and isospin 78−33139
t 79−17722
Bi, outer electron shielding, parity non-conserving optical rot. 79−18153
Bi parity non-conserving optical rotation search 77−10642
H, atom, parity mixing 78−32999
H, parity mixing of atomic states, spin-depend. weak interaction coupling const. 78−8572
He, $(2p^2)^3P$ state, electron impact excitation, parity unfavoured transition 80−91680
SI odd parity levels, configuration interaction effects 79−72246
Tl, parity nonconserving effects in $6^2P_{1/2}$-$7^2P_{1/2}$ transition 78−13458

parking control *see traffic control*

parsers *see grammars*

partial differential equations
see also boundary value problems; wave equations
$-\Delta+V$, self adjoint for $0 \leq V \leq \infty$ 77−64925
$\varepsilon \text{grad}^2 u = \delta u/\delta y$, $0 < \varepsilon \ll 1$, over rectangle, asymptotic soln., MHD appl. 77−9863
acoustic wave, linear, in perfect fluid at rest *(French)* 78−55488
acoustic wave propagation in isotropic viscous weakly compressible medium, eqn. limits problem *(French)* 80−8808
active parts electrodynamic equations general solutions using orthotropic modelling *(Russian)* 80−99601
advection-diffusion, finite element method soln. 78−92880
anisotropic media, natural oscills., partial differential eqn. system 80−57091
anisotropic solid fluid flow with free or artesian surface analysis, finite element method soln. 78−92872
approximate solution using patched variational principles, appl. to elliptic and mixed elliptic and hyperbolic problems 77−89144
atmospheric transport problems, contaminant movement, Galerkin finite element method 80−74902
axial radiation reception from point source within axially symmetric medium 77−64948
axially symmetric form of biharmonic eqn., elec. analogue technique for approx. soln. 77−27502
axially symmetric Helmholtz eqn., fundamental solution 78−77722
Bachlund problem, Lie algebra bundles *(French)* 80−18085
Backlund problem for the equation $\partial^2 z/\partial x^1 \partial x^2 = f(z)$ 79−2597
Backlund transform. for nonlinear partial differential-difference eqns. 78−16625
Backlund transformation in language of jet bundles *(French)* 78−28913
Backlund transformations as nonlinear Dirac eqns. or Cauchy Riemann eqns. 78−49965
Backlund transformations in several variables, differential geometric anal. 80−86073
beam, buckled, forced oscillations, global bifurcations and chaos 79−27580
beam, pretwisted, slender, coupled torsional and longitudinal vibr. 79−18770
beam, rotating slender, bending vibrs., Galekin method anal. 80−1465
Belousov-Zhabotruskii reaction, existence of solitary travelling wave solns. 80−35525
Beltrami-Michell and Beltrami-Michell type eqns. in static and dynamic elasticity 77−53782
Benjamin-Ono eqn., props. 79−63050
Benjamin-Ono equation, meromorphic solns. 79−62998
bifurcation of stable stationary solns. from symmetric modes 78−57752
biharmonic potentials, inverse problem *(German)* 77−9862
black holes, construction of metric and vector pot. perturbations 80−8647
blast waves, spherical, time-depend. energy deposition 78−9655
blood flow in artery, math. model 78−31831
blood pulsative flow digital simulation, finite element method soln. 78−92670
boundary element methods, direct and indirect, formal equivalence 78−81814
boundary layer, thermal, singular parabolic partial differential eqns., impulsive motion appl. 78−38326
boundary layer extraction through a system of slots of finite width *(Russian)* 79−27692

partial differential equations continued
boundary layer flow singular nonlinear differential eqns. 78−63413
boundary layer similarity problems, unified approach 79−10543
boundary value problem for linear partial differential eqns., approx. soln. *(Russian)* 77−57170
bounded water bodies finite amplitude waves, dynamics study 78−77273
Boussinesq equation, group theoretical approach 80−82914
brain O_2 transport, nonlinear Monte Carlo simulation, hybrid computer implementation 78−40131
bubbly, two-phase mixtures, numerical anal. of press. transients by explicit-implicit method 78−34185
buckled states of spherical shell under uniform external pressure, asymptotic methods and Newton's method 80−43635
building two-dimensional heat load, finite element method solution 78−71336
capillary wave form. on gravity water waves, model eqn., surface tension, viscosity 78−83421
catalyst deactivation, nonlinear partial differential eqns. 79−39123
Cauchy problem, classical mechanics of diffusion and Schrodinger eqn. 78−28985
Cauchy problem for Laplace's eqn., solution approximation 77−78966
Cauchy problem for nonstationary surface waves of perfect fluid *(French)* 79−27653
Cauchy problem for nonstationary surface waves of perfect liquid *(French)* 79−27652
chemical kinetics models, partial and differential eqn. parameters, estimation using Galerkin's method 79−66258
chemical network, nonlinear pattern as transform. group symmetries 78−27878
chemical system far from equilibrium, bifurcation and stability 77−73461
Cholesky factorisation method for mixed boundary conditions and discontinuous material prop. problems 79−81715
circular loop induced eddy current distrib. and loss calc. 80−9771
clamped circular membranes dynamic anal. *(Japanese)* 79−35541
classical unidimensional model of fluid motion, Burgers eqn., absence of turbulence 78−87328
coherent optical feedback analogue computer for partial differential eqns. with inhomogeneous terms 79−76870
coherent waves in nonlinear medium, nonresonant interaction, eqns. system development and examples *(Czech)* 80−24149
complex potential eqns., all solns. to nonlinear system 80−46795
complex potential equations, special relativity, and complexified Minkowski space-time 80−52018
composite wall, constant props., transient heat cond. problem *(French)* 78−87229
computational methods, book 78−81820
condensation method for acceleration of convergence of solns. 77−67253
conducting media, eddy current phenomena, neglect of displacement current 79−13868
conference, Bethlehem, PA, USA (June 1979) 80−86039
confined solutions of multidimensional inversion equations 78−77678
conical flow of non-Newtonian elastic power law fluid with injection/suction, similarity solns. 79−14439
conjugate gradient method for singular capacitance matrix equations., algorithm 78−36791
conservation equation, numerical soln. by variational approach, mass transfer problem appl. *(French)* 80−19317
conservation laws for the classical Maxwell-Dirac and Klein-Gordon-Dirac equations 79−49066
conservation theorems, group theoretical nature 77−64919
constants of motion and separable solns. in classical mechanics, group theoretical aspects 79−75332
continuum mechanics, partial differential eqn. system integration 79−30233
convection, forced, turbulent, in square cavity, shear effect 79−1180
convection, natural, transient and steady-state numerical solns. 80−10119
convection along plate, MHD boundary layer eqns. soln. 77−11276
convection-diffusion, finite element method soln. 78−90889
convective difference schemes and Hermite interpolation 77−68368
corotational stretch theories, higher order, nonlinear finite element anal. appls. 79−32245
coupled fields in solid mechanics 77−68391
coupled nonlinear evolution eqns., infinite sequence of conservation laws 77−57156
curved domains, geodesic finite-difference method, simulation of tidal motion on sphere 80−109153
cylinder, circ., elastic, axial eigenfunctions orthogonality 78−51080
dam porous media unsteady flow calculation, combined finite element/characteristics methods soln. 78−91012
deep fast trapping dielectric, SCL current injection 80−6862
deflagration waves, heterogeneous, flame model for gas phase, partial differential eqn. 80−85177
demagnetising field, calc. by FFT 79−38355
difference analogues to nonlinear partial differential eqns., reducible to linear eqns. 79−25831
diffusion, two-way, separation of variables, decaying and growing eigenfunctions 80−62594
diffusion equation, linear, separation of variables *(Russian)* 77−13712
diffusion equation, nonlinear, invariance props., Lie-Backlund groups 80−62596
diffusion equation, separation of variables, covariant and symm. props. *(Russian)* 77−26135
diffusion equations, geometric approach, equivalent set of differential forms 78−54321
diffusion in media with double diffusivity, discrete random walk model 80−92702
diffusion of immiscible fluids in porous media 79−90329
diffusion processes satisfying Ventcel's boundary conditions, existence *(French)* 77−71182
diffusion reaction nonlinear eqns., secondary bifurcation 77−9860
diffusion with chemical reaction, probabilistic interpretation 78−35645
diffusion-convection, finite element method soln. 78−90888
diffusion-convection eqn. anal. with explicit difference methods 78−62165
diffusional boundary value problems, approx. analytical soln. 78−36947
Dirichlet problem, Fourier transform technique for boundary condition of infinitely long strip 77−45679
Dirichlet problem, response function method for fast soln. of Laplace eqn. 78−86119

partial differential equations continued
Dirichlet problem for semilinear eqn. $\Delta^k u = f$ on a disc, approx. techniques 79−40377
Dirichlet problem for semilinear eqn. $\Delta^k u = f$ on a disc, series soln. 79−40376
Dirichlet-type time like boundary, discontinuous condition *(French)* 77−49559
discrete kinetic theory, maths. and numerical aspects, Couette flow appls. 80−19413
discrete ordinate neutrons transport, weighted-residual method soln. 79−6725
dispersive nonlinear waves, conservation laws group theoretic aspects 77−30016
dispersive wave equation, spatial discretisation effect on steady state and transient solns. 77−30014
dissipative operators for infinite classical systems and equilibrium 80−12982
domain monotonicity of first eigenvalue of boundary value problem 77−5638
double sine-Gordon equation, perturbation theory 79−75403
drift diffusion unipolar conduction between parallel plate electrodes, closed form steady state solutions 80−91720
drying, heat and mass transfer, optimal control 78−67006
dual variational principles 78−77676
dynamic axisymmetrical elasticity problems soln. using factorised differential systems of second-order accuracy *(Russian)* 80−8796
dynamical system construction from pre-assigned family of solns. 80−39
dynamical systems with extremely heterogeneous inertia props., Lagrangian eqns. of motion analysis 77−53775
education, Schrodinger eqn. for free particle, wave packet spreading in coord. representation 80−17736
eikonal eqn., underlying geom. struct. 77−60957
elastic material, non-linear, thermodynamic theory, considering thermal vel. waves 77−62189
elastic porous media, transient compressible liq. flow, linearisation of nonlinear partial differential eqn. 78−63490
elastic quadrilateral plates 79−46201
elastic-viscoplastic proportional combined twist and stretch of circular bar of rate sensitive material 80−23912
elasticity equations transformation 79−2630
elasto-plastic stress and strain in cracked bars under torsion and shear, finite element method solution 79−68654
elastostatics, error estimates of finite element approx. 80−8793
electric machine end zone magnetic field calc. using approx. analytic method 80−106416
electrochemical flux equations, solns. with variable diffusion coeff. and transference number 78−48666
electrochemical machining, approx. method for solving problems 78−44241
electrodynamic aspects of electrophotography *(Japanese)* 80−13170
electrodynamics, nonlinear, energy density convexity and hyperbolicity of partial differential eqns. *(French)* 80−62491
electron scatt. theory, eqn. of mixed type 77−67388
electron-hole avalanches with constant ionization coefficients 79−91054
elliptic, grid generation, automatic mesh-point clustering 80−31487
elliptic, local mesh refinement with finite elements 79−9091
elliptic, soln. of interface problems by homogenisation 77−22387
elliptic, soln. of interface problems by homogenisation 77−22388
elliptic 2nd order problems, soln. using global element methods 80−46805
elliptic boundary problems, reduction to elliptic systems of pseudodifferential eqns. *(Russian)* 79−12573
elliptic boundary value problem, second order, hybrid finite element methods, Dirichlet problem 78−73835
elliptic equations, second order, three dimens. boundary-value problems solns. *(Russian)* 77−60904
elliptic equations and systems, free-boundary problem solution method 80−69941
elliptic interior layer problem asymptotic soln. 78−12535
elliptic operator, perturbation algebra 77−17774
elliptic operators, Cauchy problem uniqueness *(French)* 77−17773
elliptic partial differential eqns., numerical methods evaluated 78−65756
elliptic partial differential equations, nonlinear, approx. soln. by mesh refinement and local inversion 77−26160
elliptic PDE with discontinuous coeff., finite difference soln. 78−89347
elliptic problems with singularities, finite element approx. 78−41140
elliptic sine-cosine eqn., solitonlike solns. using harmonic functions 78−57741
elliptic systems and numerical transforms. 78−65780
elliptic type equations, num. soln. of mixed boundary-value problem *(Russian)* 77−67243
elliptic-hyperbolic eqns. finite element soln. 77−33851
elliptic-hyperbolic sine eqn. in 2+1 dimens. space-time 77−49567
EM field problem with a non-linear condition 79−18326
EM fields analysis, stationary, by Trefftz's method, using quasiharmonic polynomials *(German)* 79−27128
equation, numerical integration using time level schemes 79−2609
equilibrium of plasma in Tokamak machine 79−19080
Euler equation, analyticity of 3 dimens. periodic solns. *(French)* 77−5628
Euler-Lagrange differential in fibred manifolds 78−45469
Euler-Lagrange hyperbolic systems of second order, relativistic strings 78−54209
evaluation equations, nonlinear, canonical transforms. 77−87643
evolution eqns. with infinitely many symmetries 77−60902
evolution equations, connection to P-type differential eqns. 80−57078
extended Graetz problem, approx. soln. by orthogonal collocation 77−89118
extrapolation methods 78−36810
extremum principles for linear initial and mixed boundary value problems of math. phys. 78−49637
Feller eqn., generalised, boundary condition solns. 78−62167
fields solution, Monte Carlo approach using transmission line matrix, random walks appl. 79−53991
filtration theory problem soln. *(Russian)* 80−74970
finite element anal., preservation of conservation props. of anal. 78−16628
finite element anal. of nonlinear partial differential eqns., appl. to estuarine flow *(Japanese)* 78−8233
finite element moving boundary computation with an adaptive mesh 79−35536

partial differential equations continued
finite elements homework exercise 77−26157
first boundary value problem for singularly perturbed semilinear parabolic eqns. 77−67221
first-order, energy description of propagation of monochromatic radiation along multimodal fibre 80−38116
flame, laminar premixed, two-dimens. elliptic partial differential eqns. soln. 79−94738
flat plate solar collector thermal behaviour model and performance parameters 79−62045
flawed elastoplastic structure, method of lines applied to crack problem 79−46259
flow, in two-dimens. channel, turbulent, with separation 80−19356
flow, laminar or turbulent boundary layers, fourth-order numerical method 79−1174
flow, turbulent, incompressible, numerical prediction 79−1171
flow between rotating discs, finite element anal. using exponentially weighted basis functions 78−16655
flow density function approximation, compressible, subsonic *(Hungarian)* 79−14421
flow on two-dimensional torus, first order quasilinear partial differential eqns. *(French)* 78−89345
flow-induced oscillations, bifurcation to divergence and flutter, infinite dimensional anal. 78−89336
fluid bidimensional flow past symmetric profile 77−60942
fluid discontinuities, subgrid resolution in tracking methods 80−105506
fluid dynamics, finite element method 77−80135
fluid dynamics, initial boundary-value problems for partial differential equations 79−30256
fluid flow, finite difference methods 79−9117
fluid saturated porous elastic solid, equil. soln. 77−65683
fluid-structure coupling problem soln. using boundary-integral eqn. method 77−54920
Fock-Leontovich method, appl. to radiowave propagation 79−36816
Fokker-Planck, numerical solutn. 80−18622
forced vibrations, nonlinear systems, appl. to Duffing eqn. 77−60925
Fourier analysis of difference schemes for Laplace eqn. in rot. symm. system 78−77677
fourth order, mixed finite element method 77−33848
free boundary problems with radiation boundary conditions 79−71386
free surface flow digital simulation, finite element method soln. 78−90819
free vibrational analysis of frame structures 79−32329
frictionless tidal channel behaviour digital simulation, finite element and finite difference methods solution 78−92876
fusion reactors, high-energy water-cooled heat sink and 25 MW power tube 79−49838
Galerkin methods, interior penalty procedures 77−33847
gas dynamics, numerical investigation by net-characteristic method 80−19420
gas flow in catalytic convertor, numerical soln. 78−67281
gas mixture, binary, condensation in boundary layer flow, numerical method 79−1236
Gel'fand-Levitan kernel for 3-D Schrodinger eqn. 80−36892
general stochastic differential eqn., existence, unicity of soln. *(French)* 78−36800
generalised axisymmetric Poisson eqn., separable cases, Green-Dirichlet problem in circle 77−22383
generalised biharmonic eqn., appl. to hydrodynamic stability using homogeneous boundary conditions 78−90834
generalized symmetries of nonlinear partial differential equations, Lie derivatives 80−4886
Green's function discontinuities across characteristic surfaces of field eqns. 79−93279
Green's function for surface physics, partial differential eigenvalue eqn. 80−6929
Green's function methods for linear second order systems 79−12578
ground water flow calc., boundary element method soln. 78−94634
groundwater discrete kernel generator model, finite element method soln. 78−92873
groundwater flow analysis, finite element method soln. 78−92875
groundwater flow digital simulation, finite element method soln. 78−93018
Hamilton-Jacobi eqn., generating function soln. for shocks in fields *(French)* 77−9890
Hamilton-Jacobi method generalised, for nonholonomic systems, appl. to classical mechanics 77−71207
Hamilton-Jacobi theory, differential geometrical methods 78−45471
heat cond. eqn., random generalised solns. 77−84103
heat cond. in moving anisotropic rectangular slab, generalised Jacobi transform appl. 78−30149
heat conduction, finite element formulation in general orthogonal curvilinear coords. 77−14882
heat conduction, H-function of two variables applic. 79−94450
heat conduction, nonstationary, nonlinear inverse problem, soln. uniqueness *(Russian)* 78−22245
heat conduction, Sommerfeld problem generalisation for one-dimens. ring 80−5908
heat conduction, steady-state, soln. using heat balance integral method 77−14880
heat conduction, unidimensional, inverse Cauchy problem solution, coeff. identification *(German)* 80−33419
heat conduction eqn., Crank-Nicolson noise control 77−75769
heat conduction eqn., hyperbolic, exact soln. for variable relax. propag. 78−79184
heat conduction eqn., inverse, boundary conditions recovery, using Cauchy soln. and regularising algorithms 78−26016
heat conduction eqns., analytic solns. 78−63264
heat conduction equation, hyperbolic, integral variational principle *(Russian)* 78−83213
heat conduction equation, unsteady, numerical soln. charcts. at early times 78−79185
heat conduction in finite rectangular plate, superposition of boundary conditions in temp. distrib. eval. 77−14883
heat conduction in random medium, method of time ordered cumulants 78−54320
heat conductivity, two-dimensional inverse problems solution *(German)* 80−1404
heat diffusion process, parabolic boundary-value control problem, numerical treatment 77−847
heat eqn., solvability of boundary value problem *(Ukrainian)* 77−67204

partial differential equations continued
heat eqn. Cauchy problem, numerical procedure 77−5644
heat eqn. with u.s.c. obstacle, soln. existence *(French)* 79−26001
heat equation solution regularity for non-rectangular plane domain *(French)* 77−67199
Heisenberg spin chain, operator equation, nonlinear differential form, auxiliary constraint 80−65762
Helmholtz eqn., exterior Robin problem 79−35528
Helmholtz eqn. soln. for interactions between particles of arbitrary shape 79−100453
Helmholtz equations, accurate approx. to solns. *(Russian)* 77−57171
higher order parabolic differential eqn., probabilistic soln. from heat eqn., with Brownian motion 79−97322
Hill equation, simplified stability criterion, applications 78−36820
Hodgkin-Huxley nerve cond. eqns., bifurcation of periodic solns. 79−5269
homogeneous viscoelastic mixtures, speed of sound 80−33272
human movements, computer modelling 77−21544
Huygens principle for equations dissociating into factors 80−31581
hybrid system heat conduction solution 78−5745
hydrodynamic calculations for container pipeline systems with non-Newtonian liquids 80−106817
hydrodynamic numerical modelling of tidal basins, Lagoon of Venice appl. 79−34832
hydrodynamic type, lowering of order of system of eqns. 79−17234
hydrology, leaky aquifer, approx. differential eqn. 78−81242
hyperbolic, analogue/hybrid soln. 80−36336
hyperbolic, governing nonlinear vibr. systems in resonance 77−39242
hyperbolic, leap frog scheme 79−2616
hyperbolic, soln. for peristaltic flow in elastic tubes *(German)* 79−37396
hyperbolic balance laws in continuum physics 80−4525
hyperbolic conservation laws, Glimm scheme for solving, deterministic version 78−20972
hyperbolic differential eqn., charact. initial value problems, interval-analytic soln., iterative procedure *(German)* 78−8234
hyperbolic eqns. in one space dimens., finite-difference approx., method of lines 77−2525
hyperbolic eqns. soln. by method of lines 77−5648
hyperbolic heat eqn., equilibrium soln., asymptotic stability 78−13887
hyperbolic in oceanographic circulation, numerical solutn. 80−21864
hyperbolic mixed problems, leading wavefront propagation 78−36836
hyperbolic orbits, differential eqns. for non-angular elements *(Russian)* 78−16284
hyperbolic partial differential equations linear system, numerical soln., boundary methods accuracy 77−67245
hyperbolic quasi-linear well-posed second order systems, appl. to nonlinear elastodynamics and general relativity 77−53743
hyperbolic system, first order, supplementary conservation law 79−9077
hyperbolic system, simple wave growth, charact. shock instability, fluid appl. *(French)* 77−68623
hyperbolic systems, high-order methods, dynamic problems 80−68033
hypergeometric functions, partial differential matrix eqns. 77−37730
hyperparabolic linear eqn., covariant props. and symm. *(Russian)* 77−26136
hypersonic viscous shock layer equations, num. soln. scheme 79−90280
impurities dispersion in river, model *(Dutch)* 79−88011
incompletely parabolic problems in fluid dynamics 79−44749
incompressible flows in three dimensions, finite-difference methods 80−33554
incompressible liquid oscills. in variable cross section viscoelastic tube due to pulsating press. 80−31519
inhomogeneous heat eqn., uniqueness and representation theorems 79−71383
inhomogeneous thermal conduction equations 78−70074
initial boundary value problem for three dimensional heat equation, Rothe's line method *(German)* 78−30147
integrable evolution eqn. struct. 80−105492
integration, appl. of semi-implicit Runge-Kutta methods 78−12542
intensive air flow round thin and sharp axially symmetric bodies *(Russian)* 79−37330
invariance groups for class of countable systems of first-order partial differential eqns. 78−49635
inverse scatt., generalised problem prolongation structs., soliton solns. 77−3833
inverse scattering method, commutator representation of Painleve type ordinary differential eqns. 80−68052
ionosphere incoherent scatter data, analytic partial derivatives for least-squares fitting 78−73581
Jaulent-Miodek family of nonlinear evolution eqns., Hamiltonian formulation 80−31511
jets, confined, flow pattern and turbulence quantities prediction *(Japanese)* 79−18923
KdV equation, perturbative expansion and initial value problem 80−62487
Keplerian orbit calc., partial differentiations of vis-viva and Lambert equations 78−7864
kidney counter current mass transport spatially discrete models 79−39442
Klein Gordon, nonlinear generalisations, exact solns. 79−35569
Klein-Gordon equation, for Kelvin-Helmholtz instability of fluid layers, nonlinear wave packets 79−46289
Kolmogorov direct equation, solution, Galerkin measures *(Russian)* 80−46981
Kolmogorov eqn., separation of variables, applied to oscill. Brownian motion 80−36945
Kolmogorov eqn., separation of variables *(Russian)* 77−78970
Kolmogorov eqn., separation of variables 80−36835
Korteweg de Vries equation, Pade approximants, soliton solns. 80−42071
Korteweg-de Vries, statistical theory of nonlinear dispersive waves 78−16662
Korteweg-de Vries eqn., higher order, prolongation struct., Lie algebra, soliton solns. 78−8249
Korteweg-de Vries equation, algebraic soliton 77−9858
Korteweg-de Vries generalised eqn., pseudopotentials and inverse scatt. problems 77−87627
Korteweg-de Vries-Burgers equation, time evolution, stability, of shock soln. 77−37743
lakes or bays landslide wave generation simulation, Galerkin finite element method soln. 78−92879

partial differential equations continued
laminar boundary layer flow, three-dimens., soln. using method of integral relations 77−58645
laminar to turbulent boundary layer shear flow, three-dimens., stability eqns. 78−38284
Laplace's equation, numerical soln. by integral eqn. method without Green's function 79−12564
Laplace eqn., appl. of integral eqn. method, heat conduction through layered media 77−68366
Laplace eqn., half plane representations and harmonic continuation 77−22391
Laplace equation, inhomogeneous anisotropic media, finite difference operators 77−46670
Laplace operator on spherical domain, fundamental eigenvalue numerical determ. 77−87628
large algebraic eqn. systems, direct and iterative solns. 79−41274
leaky aquifer analysis, finite element method soln. 78−93017
least squares approx. for partial differential eqns. of mixed type, indefinite problems 78−36807
Lie algebras, finite and infinite, physics and deformation theory 77−33831
lifting-line theory, alternative treatment as perturbation problem 79−27663
linear, canonical forms of some completely integrable systems 77−67214
linear, inversionlike integral eqn. in multidimensional case 78−62054
linear degenerative parabolic, first boundary problem *(Russian)* 77−22374
linear elliptic and parabolic partial differential eqns. with boundary singularities, numerical soln. 78−41142
linear elliptic PDE, numerical soln. 79−97187
linear elliptical eqns., appl. of direct variational method to mixed boundary-value problems 77−67252
linear hyperbolic initial boundary value problems, hydraulic system appl. *(German)* 79−9115
linear hyperbolic partial differential equation, reciprocity rels. 77−37732
linear parabolic for dam groundwater flow calculation, finite element Galerkin method soln. 78−89320
linear partial differential eqns. describing transport phenomena, soln. technique 80−13004
linear system, multidimensional inversion formalism as compatibility condition 79−84961
linear system with constant coeffs., Cauchy problem 77−67215
linear system with multiple characteristics, Cauchy problem *(French)* 77−5629
linear time dependent partial differential eqns., solns. by Laplace transform and FFT 78−57763
linearized evolution eqns., integration 78−32657
liquefied natural gas, nonsteady-state flow calculations in horizontal pipeline systems 80−106838
liquid-liquid extraction column online control by modal control techniques 78−54865
magnetic field analysis by separation of variables *(Polish)* 78−90338
magnetic field calc., saturable, by finite element method, using scalar magnetic potential 77−38773
magnetic field computation, by Schwarz-Christoffel mapping function numerical integration *(German)* 79−89826
magnetic field diffusion, on nonuniform Lagrangian mesh, exact energy conversion 78−91080
magnetic field problems, numerical techniques 80−32878
magneto-elastodynamics, boundary-value problems 79−49046
magnetoionic plasma, hyperbolic eqn. system, inverse problem 78−75354
magnetostatic equations, axially symmetrical, solution by difference methods 77−50585
magnetotelluric analysis, soln. of electrometry inverse problem via variational method *(Russian)* 77−44915
many-body problems, special solns. of partial differential eqns., poles and zeros motions 78−41226
Maxwell, AC magnetic field analysis, using finite element method, Tokamak device appl. 79−50191
Maxwell's equations as one quaternion eqn., appl. to wave propag., for teaching 78−54133
Maxwell equation integration in laminar media 80−68059
mean molar functions, calc. using partial differential eqns. 79−21685
membrane and plate vibrations, functionals method for lateral vibr. freqs. determ. *(Japanese)* 80−12918
meromorphic solutions of nonlinear partial differential equations and many-particle completely integrable systems 80−31523
metal, axisymmetric drawing simulation, numerical method development 78−30206
metals, heating by concentrated energy sources, simple analytical expressions *(Russian)* 80−38215
Method of Lines, for time depend. eqns., compared to finite difference methods 78−79291
MHD, transient phenomena, simultaneous solns. to coupled gasdynamic-EM equations of motion 80−6157
MHD liquid nonstationary two-dimens. flow, rot. mag. field, differential eqns. *(Russian)* 78−5814
MHD nonviscous flow equations, steady plane, plane radial, and vortex flow 79−32697
micropolar fluid with stretch, convection, appl. to Earth mantle 78−51202
Miura transformation of Kaup and Mikhailov eqns. 80−57103
modified dissipativity for a non-linear evolution equation arising in turbulence 79−94594
molecule, diamagnetic, NMR shielding tensor and mag. susceptibility tensor, current density calc., appl. to H_2 *(German)* 79−76445
moving boundary problems, weak soln. 80−179
multi-dimensional two-phase flow finite difference solutn. 80−18564
multicompartment diffusion and reaction modeling system applied to transmitter-mediated photoreception 79−70547
multidimensional nonlinear, integration by inverse scatt. problem method 77−60905
multigroup diffusion eqns., soln. methods *(Czech)* 77−38312
N-dimensional Thomas-Fermi equation 77−37725
Navier-Stokes eqns. and Hausdorff measure 77−75870
Navier-Stokes in fixed bed reactor radial flow, Runge-Kutta method soln. 79−10546
nerve conduction eqn. periodic travelling wave solns. stability 79−16194
nerve conduction in squid axon, Hodgkin-Huxley equations, large amplitude periodic solns. 78−20166
nerve impulse eqn., periodic solns. 77−66812

partial differential equations continued
neural populations, simplified model eqns. and envelope eqns. 78−31798
neutron dynamical diffraction, gravitational and mag. field effects 80−59345
non-equilibrium laminar boundary-layer, of dissociating air 77−952
non-linear transport equations: Properties deduced through transformation groups 80−4680
non-Newtonian pulsatile laminar pipe flows, multiviscous approx. 77−3871
non-Noether invariant origin, relation to Euler eqn. transformation props. 80−31493
nondivergent elliptic equations boundary value problems, bifurcation of solns., critical point index *(Russian)* 77−57159
nonholonomic Chetaev systems, Lagrange eqns. derivation from modified Pontryagin maximum principle 78−12557
nonhomogeneous medium, backwards heat eqn. soln. approx., partial differential eqn. 80−53611
nonisothermal heat transfer equations, hyperbolic, derivation from variational principle *(Russian)* 79−68543
nonlinear, appls. 80−4510
nonlinear, Cauchy problem, existence and uniqueness of smooth global soln. *(French)* 78−93513
nonlinear, elastic stability theory *(Russian)* 79−9128
nonlinear, evolution equations soln. using spectral transform method 78−57745
nonlinear, Galerkin method error analysis 77−78986
nonlinear, interactions between short and long waves 77−67299
nonlinear, inversion eqn. method generalised to matrix case 78−8223
nonlinear, nonstationary motion in one-dimens. continuous medium, partial analytic solns. *(Russian)* 78−73859
nonlinear, partial spectral expansions 79−32193
nonlinear, relativistic electron field theory 77−2779
nonlinear, Runge-Kutta method appl. to fluid flow problem 77−42796
nonlinear, special multi-soliton solns. 80−105763
nonlinear acoustics, asymptotic solns. of model eqns. 79−76905
nonlinear differential eqn. soln. by discrete least squares 78−45474
nonlinear diffusion eqns., evolution of stable profile 79−17363
nonlinear diffusion equation, stable profile evolution 80−82731
nonlinear dispersive equation, weak solns. 77−74194
nonlinear eqns., linear correspondents 78−20949
nonlinear evolution eqns., conserved densities 79−71256
nonlinear evolution eqns., prolongation structs. in two-dimens. 77−36
nonlinear evolution eqns., solitons on moving space curves 77−74254
nonlinear evolution eqns., soln. by inverse spectral transforms 77−57228
nonlinear evolution equation with linearly x-depend. coeffs., spectral transform, single soliton soln. 78−57746
nonlinear evolution of three-wave interactions in inhomogeneous medium 77−74272
nonlinear excitations by numerical determination 79−71372
nonlinear hyperbolic eqn., approx. periodic soln. 77−17778
nonlinear hyperbolic eqn., special classes of solns. *(German)* 79−21526
nonlinear isotropic medium, symmetric spherical wave propagation eqns., permissible transform. *(Russian)* 78−87292
nonlinear lattice, wave propagation 77−13707
nonlinear multiphase wave interactions, instabilities and solitary envelope soln. 77−9888
nonlinear parabolic eqn. in noncylindrical domain, existence of weak solns. 77−67208
nonlinear parabolic eqns., automatic technique for solving coupled vector systems, geophys. appl. 77−41468
nonlinear partial differential eqns. 79−39123
nonlinear partial differential equations soln., using inversionlike integral eqns. generalisation 78−86117
nonlinear plasma three-wave damped interaction 77−979
nonlinear plate and shell theory problems soln. 77−53784
nonlinear reaction-diffusion eqns., large time behaviour of solns. 79−12741
nonlinear reaction-diffusion models for interacting populations 78−65886
nonlinear Schrodinger eqn. inverse scatt. problem, prolongation structs. 77−33890
nonlinear Schrodinger equation, existence, uniqueness and regularity *(French)* 77−67202
nonlinear singular diffusion eqn., perturbation soln. 79−71387
nonlinear singular perturb. problems, asymptotic equiv. 77−9875
nonlinear transformations for partial differential eqns. 80−42043
nonlinear wave and spinor eqns., causal solns. by regularisation 77−33872
nonlinear wave propagation, hyperbolic partial differential eqns. and mathematical models 78−77729
nonlinear waves in dissipative or dispersive media 78−49672
nonlinearly viscoelastic bodies one dimensional dynamic stability 79−32282
nonmagnetic conductors, three-dimensional eddy current calc. *(French)* 80−14270
nonsteady filtration of two immiscible liquids alternative to kdV-Burgers eqn. 80−6019
Norset methods for implicit time integration 77−82376
nuclear reactor fluid dynamics, prospects for accurate computer simulation 77−79422
nuclear reactor nodal fluxes determination using approx. analytical method 77−65261
numerical generation of boundary fitted curvilinear coord. systems on fields containing 2-D bodies, TOMCAT code 77−64941
numerical method, fast, iterative, implicit, for solving multidimensional partial differential eqns. 78−93519
numerical methods for flows through porous media. II 80−69914
numerical solns., new techniques reduce work involved 79−75326
ocean waves generation, propagation and dissipation spectral simulation model 80−31060
operator, spectral anal., unified approach 78−73827
optical processor, confocal feedback system for partial differential eqn. analogue soln. 80−102630
optimum control theory, Hamilton-Jacobi theorem, canonical transforms 78−20962
oscillators, nonlinear stochastic, triangular wave, optimally controlled, Weiner process and Poisson process, numerical studies 80−52128
overhead line corona discharge calc., iterative method soln. 79−4204
overland flow equations soln., comparison of finite element methods 79−12152
packed bed, optimal control of heat and mass transfer *(Ukrainian)* 79−32655

partial differential equations continued
Painleve nonlinear ordinary differential eqns. and nonlinear partial differential eqns., corrections 79−5966
Painleve transcendents, linearisation 77−49568
parabolic, atmospheric flow over two-dimensional obstruction description *(Italian)* 79−20956
parabolic, reduction by Galerkin, collocation, and method of lines 78−77693
parabolic, sensitivity anal., appl. to reaction and diffusion processes 79−49178
parabolic, TEDDY2 program package using ADI method 79−2613
parabolic, with M-matrices, iterative processes comparison, w.r.t. rate of convergence *(German)* 80−1405
parabolic capacity and heat equation with irregular obstacle *(French)* 79−26002
parabolic eqn. boundary value problems, differential, difference method *(Russian)* 79−58534
parabolic nonlinear eqns., control to meet finitely many terminal conditions 77−5647
parabolic nonlinear partial differential equation, numerical soln. using asymm. finite difference eqns. 77−33845
parabolic partial differential eqns., finite difference methods, comparison of accuracy 79−72796
parabolic partial differential eqns., finite element methods 79−72797
parabolic partial differential equations, operator compact implicit soln. methods 78−89348
parabolic problem exact control finite element collocation method 77−26156
partial-wave Schrodinger differential and integral eqns., comparison of numerical solns. 78−16671
particle diffusion across mag. fields, stable profile for nonlinear diffusion eqns. 78−22456
partition of energy for uniformly propagating systems 77−67303
periodic helical flow in pipe, linear stability, Hermitian forms and eigenvalue bounds 79−37401
phase change region, cond. and natural convection, numerical method 79−41563
pin-ended rod under parameter excitation dynamic response anal., solutions 77−74199
plane eikonal eqns., class of complete integrals 77−49562
planetary boundary layer equations soln. using sensitivity analysis 77−54957
plasma, inhomogeneous diffusion eqn., analytical solns. 77−55129
plasma decay under constant voltage *(Russian)* 80−106988
plasma high temp. transport process, numerical soln. 80−19559
plasma MHD eqns., linear and non-linear calc. 77−27705
plasma wave propagation, method of strained coords. 79−4127
plate, eigenvalue problem, bidimensional approximation *(French)* 80−33445
plate, rectangular, with clamped/simply supported edge conditions, free-vibr. anal. 78−59340
plates, thin rectangular elastic, bending, finite difference anal. 79−46181
Poincare invariant differential equations for particles of arbitrary spin 79−30689
Poisson, MOST structure modelling, using hybrid computer *(Slovak)* 80−75643
Poisson's, numerical solution using curvilinear finite differences 78−28923
Poisson's equation for isolated source distribs., computer soln. using finite mesh, Green's function 78−35
Poisson's equation integration for complex system with arbitrary geometry 77−47705
Poisson brackets, on extension 79−63080
Poisson eqn. on surface of sphere, shooting method for finite-difference soln. 77−2527
Poisson eqn. soln. by successive overrelaxation technique, optimisation hazard 78−81813
Poisson eqn. with RHS$=f(z)/\{1+[b(z).r]^2\}^{3/2}$ 77−9859
Poisson equation over complex domain, finite difference method, Neumann boundary conditions 78−79189
Poisson equation solver for potential and press. fields on staggered grid with obstacles 77−54959
Poisson-Boltzman equation linearization, in classical mean space charge model for solvation 78−76841
pole expansions of nonlinear partial differential eqns., corresponding many body problems 77−82372
polymer foil, electron irradiated, charge dynamics, computer simulation 79−82915
polytropic star, equilib. poloidal mag. field, finite difference-finite expansion method, Fortran program 77−13322
porous media eqn., strong soln. existence and uniqueness *(French)* 78−62084
porous media one-dimensional unsteady drainage digital simulation, finite element method soln. 78−91011
predictive relativistic mechanics, partial differential eqns. on accel., integration 79−44716
prismatic bar torsional rigidity estimation inequalities 79−88808
prolongation struct. of nonlinear eqns. of self-induced transparency 79−44752
prolongation structure for a nonlinear equation with explicit space dependence 80−82664
pseudo-Lie algebra, local solvability of nonlinear sequences 79−5965
pulsed DC glow discharge, cataphoresis eqns. 78−67506
for pump pipeline pressure surges, calc. by method of characteristics *(Spanish)* 79−23364
pure harmonic tide in canal, eqns. of motion quadratic resistance term linearisation 78−69369
quasi-linear initial value problems, variational formulation 77−13579
quasilinear parabolic, numerical methods comparison 77−2523
quasilinear parabolic system, chemical reaction study 80−7759
quasilinear partial differential equations, separability 78−65784
quasisteady primitive equations with associated upper boundary conditions, appl. to large scale atmospheric flow 79−62563
radiation problem simplified boundary elements 78−86226
radiative transfer, moment method anal. *(Russian)* 78−59284
rarefied binary gas mixture, two-dimens. channel flow, separation phenomena, num. soln. 77−58740
reaction-diffusion eqns., axi-symmetric time periodic solns. 78−81930
reaction-diffusion eqns., stability of solns. 78−16759
reaction-diffusion system, instability of stationary solns. *(French)* 78−20055

partial differential equations continued
reactor neutron field analogue simulation, one-group diffusion approximation and finite difference methods solution *(Russian)* 78−74416
rectilinear oscillations of a rigid spheroid in an elastic medium 79−71253
relativistic fluids, partial differential eqns., hodograph transformations 77−955
relativistic string moving in uniform static external field, 2-D space-time surface 80−57087
relativistic wave eqn., criterion for reducibility 77−57439
renal medulla solute cycling model soln. by Laplace transforms 77−40694
respiration model analytical soln. 79−48282
Reynold's equation, free boundary problem in hydrodynamic lubrication including surface tension 80−19542
river/atmosphere time dependent, single dimensional heat exchange, appl. *(Bulgarian)* 78−57221
rocket propellants, thermodynamic evolution, extension of Huff's method 78−75054
rotational transonic flow and inviscid potential computation by quasi-natural numerical methods 79−64666
Saint Venant, four point implicit numerical method soln. 79−10582
Saint-Venant principle in 2-D, for second order linear elliptic eqns. 77−26177
scattering theory, propagation of singularities for the transmission problem and application to the inverse problem of scattering *(French)* 80−94994
Schlesinger systems, isomonodromy deformation, integrable Hamiltonian systems 80−22229
Schrodinger invariant generalised heat eqns., similarity methods and trivial solns. 78−62164
Schrodinger nonlinear eqns., Cauchy problem soln. blowing up 78−8220
Schrodinger operations with L_{loc}^{p} pots., closure 77−45718
Schrodinger time dependent eqn., initial value problem, fund. soln. 79−25902
Schrodinger type partial differential equations, principal fundamental soln. using integral eqn. approach 78−81806
Schrodinger-Hartree nonlinear eqns., soln. asymptotic behaviour 77−37728
second order, undirect boundary problem on finite interval *(Russian)* 77−22375
second order linear partial differential eqns. of math. phys., integration by separation of variables *(Italian)* 78−81798
second order symm. tensors in compact Riemannian manifold, compatibility and orthogonal decomp. 77−57161
second-order, soln. for dynamics of elastic anisotropic media *(Russian)* 77−23878
second-order eqns., boundary points regularity *(Russian)* 77−9960
sedimentology, Rayleigh-Ritz method soln. 78−92878
seismic surface waves dispersion curves, partial derivatives calc. *(Russian)* 79−34764
semiconductor charge flow, attenuation-free upwind difference formula 77−28241
shear deformations, generalised, for isotropic incompressible hyperelastic materials 78−94599
shells, cylindrical homogeneous, nonlinear partial differential eqn. system, soln. existence and uniqueness 79−71249
shells of revolution, computer program for linear and geometrically nonlinear static analysis, ISTRAN/SR *(Japanese)* 80−64500
shells of revolution, variable thickness, stress state determ. 80−38275
shock structure, numerical, nonlinear corrections for difference schemes in conservation form 80−36878
shock tube flows, unsteady non-equilibrium, discretisation of boundary layer terms 80−14742
shock wave diffraction, by compression corner, regular reflection 77−58730
simple fluid, Coleman-Noll eqn., appl. hereditary partial differential eqn. 77−35454
simulation of quasilinear parabolic equations, by networks of FETs 77−50854
sine-Gordon, N-soliton constructon, domain walls appl. 78−19198
sine-Gordon eqn., Goursat and Cauchy problems 78−77682
sine-Gordon eqn., separability 78−65784
Sine-Gordon eqn. in 3-D, diffusion theory *(French)* 77−61174
sine-Gordon eqn. separable solutions in terms of Painleve transcendent 80−52037
sine-Gordon eqn. with perturbative term, synchronised solitons 77−57204
sine-Gordon equation, difference analogue 78−20976
sine-Gordon equation, intrinsic geometry 80−86553
sine-Gordon equation, one dimens., group of invariance, dimens. anal. method 78−54528
sine-Gordon equation, separability, variable transforms 80−57102
singular perturbation of an Exterior Dirichlet problem 79−12613
singular perturbations for initial value problems, hyperbolic nonlinear partial differential eqns. 78−58111
singularly perturbed nonlinear boundary value problems with turning points 79−5971
slowly varying nonstationary flow, solution by method of characteristics with fixed net *(German)* 79−5515
small amplitude plane waves in quasilinear dissipative medium *(French)* 79−25866
smoke-motion, numerical anal. by finite-element method *(Japanese)* 80−69910
solar regenerator of hygroscopic solutions, for air dehumidification 79−57464
solitary wave solns. of classical nonlinear field eqns., for teaching 80−17756
soliton eqns., Lie group framework 78−24635
soliton solns. of infinite component wave eqns. 77−26180
soliton solns. of nonlinear partial differential eqns. 77−82368
solitons and SL(2,R) 78−57748
solitons geometrical interpretation, rigid body motion along helical space curves 78−24684
space shuttle reentry, unsteady nonequilib. chemically reactive flow, parallel computation 78−47065
spectral resolution of boundary value problems in half space for partial differential matrix operators 79−25825
Spencer-Lewis eqn., orders of scatt. soln. 79−85098
spray drying, of highly viscous conc. solns., heat and mass transport *(Russian)* 78−83230
partial differential equations continued
stability of systems of coupled partial differential eqns. with random excitation 77−72218
steady plane magnetohydrodynamic flows with orthogonal magnetic and velocity fields 79−27697
steady-state laminar flow in turbulence amplifier, numerical integration *(Bulgarian)* 80−106779
Stefan one-phase quasilinear problem *(Ukrainian)* 78−65884
Stefan problems, two-dimensional, approx. of integro-differential eqn. 77−80050
stimulated and Cherenkov radiations, differential eqns. with respect to coupling constants, S-matrix 79−50278
stimulated electron radiation due to wiggled magnetic field 80−58451
Stokes-Beltrami equations, generalised, solns. derivation 77−41457
straight line method for loaded hollow cylinder calcs. *(Russian)* 78−26027
stratified turbulent flow digital simulation, finite element method soln. 78−90964
stress analysis of elliptic paraboloid shells, generalised computer program 78−59294
string vibrations, linear and nonlinear, physical discretisation 78−45480
structural analysis, nonlinear theory of shells 79−30230
SU(2) gauge field theory, nonlinear scalar field eqn., spherical symmetric exact solns. *(Chinese)* 80−62886
SU(3) wave equations and soln. 77−9850
successive over-relaxation procedure, optimum accelerating factors 79−92928
supersonic flow, steady two- and three-dimensional, shock discontinuities detection method 77−58736
supersonic laminar viscous flow, numerical soln., separation 80−24062
supersonic plane flow past a curved wedge, quasi-linear hyperbolic systems *(French)* 80−10261
surface field calc., floating random walk method 79−41273
surface loads, reciprocating dynamic stresses produced in elastic half space 78−9562
symmetry and separation of variables, book 78−36798
systems, appl. to Lie pseudogroups, book 79−25823
Szebehely equation for potential of prescribed family of orbits, solns. 78−40808
Szebehely equation in celestial mechanics, modification 78−24447
teaching, appls. to environmental problems 77−13523
tetrachloromethane-cyclohexane liq. mixtures, heat of transport, Dufour effect 80−44344
thermal conductivity infinite and finite integral transforms solution 77−75773
thermal desorption model analysis *(German)* 78−63940
third-order constants of motion in quantum mechanics 79−6002
throughflow between rotating and stationary disk calc., using Goertler series, finite difference method appl. *(Japanese)* 80−6064
time dependent heat condution solution 80−106707
time varying systems, stability anal. 78−37
time-varying, numerical solns. 78−45463
Tokamak transport eqns., nonlinear partial differentials, soln. technique 80−19556
tornado-like boundary layer flow, two-eqn. simulation 77−35151
transfer theory, numerical soln. by direct reduction method 80−22309
transformation group techniques appl. to nonlinear fluid and plasma eqns. *(French)* 80−77623
transformation groups for resolution of partial differential eqns., appl. to gravity, quantum mech. and heat transfer *(French)* 79−49099
transient and unconfined groundwater flow analysis, finite element method soln. 78−92871
transient combined heat cond. and convection problem, finite difference method solution 79−81869
transient field initial-boundary value problems, hybrid simulation 77−41469
transient temperature distribution in the reactor vessel wall after cooling system failure 79−54473
transonic flow fast implicit procedure 80−19430
transonic potential flow, finite element method solutn. 80−24045
tsunami long wave propagation analysis, finite element method soln. 78−92849
tsunami wave propagation analysis, finite element method soln. 78−92848
turbulence, isotropic two-dimensional, energy dissipation, correl. relationships and Taylor length scale 80−19334
turbulence models, Reynolds stress 77−68575
turbulent boundary layer, Hassid-Poreh energy model anal., inc. accel. and surface heat transfer step change 78−51158
turbulent boundary layers, three-dimens., around ship hulls, exact integral method of soln. *(Japanese)* 77−54985
turbulent flow in passage central region *(German)* 77−23939
TV-optical analogue computer soln. 79−76869
two dimensional recirculating flow, finite difference grid for non-rectangular flow fields 79−14374
two-dimensional crystal boundary, oscill. propag. 78−63924
two-dimensional flow with singularities formulation, finite element method soln. 78−90822
two-dimensional Gauss-Markov field, pinned Karhunen-Loeve transform 77−83827
two-dimensional hydrodynamics and water quality digital simulation, finite element method soln. 78−92877
two-dimensional infiltration in unsaturated soils, nonlinear diffusion eqn. numerical soln. 80−69918
two-dimensional wave propagation, method of characteristics 78−73863
uniqueness of Dirichlet, Neumann and mixed boundary value problems for Laplace's and Poisson's equations for a rectangle 79−9076
unsaturated porous media flow analysis, finite element method soln. 78−92869
unsaturated soil simultaneous heat and moisture transport analysis, finite element method soln. 78−92868
unsteady flow in open channels, num. analysis method, teaching aid paper 77−29972
variational principles for system of scalar eqns. 79−30255
velocity distribution, in abruptly expanding circular duct 77−65798
vibrating isotropic beams, Timoshenko's correction for shear 77−72226
vibration analysis of two-layered beam, with unconstrained viscoelastic layer damping *(Japanese)* 80−5968
vibrations transverse, of isotropic circular plate with parabolically varying density 77−42767

partial differential equations continued
viscoelastic circular membrane, nonlinear, large axisymmetric deform. under its own weight 80−64380
viscoelastic fluid flow, eqns. of state and motion, direct numerical soln. 79−60021
viscous laminar jet flow in slipstream calculation *(Russian)* 79−77209
Voigt function, partial differential equations, for stellar atm. line profile calcs. 78−28507
Voigt functions analysis, appl. to astrophys. spectral line profiles and neutron cross sections 80−22879
vortex wakes, implicit finite-difference procedure 78−14018
vorticity of free stream adjusting to flat plate, Laplace eqn. soln. 78−59406
water pollution prediction, finite element method appl. 78−93019
water wave caustic region, nonlinear theory 77−11211
water waves, in nonhomogeneous incompressible fluid, nonlinear differential eqns. 78−55657
water-cooled water-moderated reactor cooling system faults, hybrid simulation *(Russian)* 78−5008
wave eqn. in space-time and Lie theory, Lorentz group 77−26179
wave eqn. with nonlinear dissipative term, asymptotic stability of bounded or almost periodic soln. 77−67295
wave eqns. in space-time, Lie theory and semisubgroup coords. 77−33873
wave equations, asymptotic solns. using methods of averaging and two-timing 78−59
wave front set of soln. of simple initial boundary value problem with glancing rays 77−41458
wave propagation in randomly inhomogeneous media, quasi-optical parabolic approx., validity analysis 80−106422
wave quadratic path solns. for initial-value problem 77−67298
wave supporting system, lossless, distributed parameters from boundary meas. 78−16658
weakly disturbed unharmonic operator, spectral function *(Russian)* 77−22378
weather forecasting nonlinear evolutionary problems, finite element methods appl. 80−21865
well flow analysis, finite element method solution 78−92870
whale biothermal mathematical model 80−12059
wind-driven lake circulation models, boundary conditions 80−85688
zeros of polynomial satisfying second order linear partial differential equation 80−12889
^{3}He, superfluid B phase, soliton-like spin waves 80−44385

partial discharges
amplitude spectra, acquisition and automatic processing system *(Italian)* 79−93108
artificial voids, partial discharges, electro-optical obs. 78−87558
bubbles behaviour in electrically stressed liquid obs. 80−71313
charge density distribution along positive streamer on dielectric surface 78−87536
creep discharge at dielectric surface, charge transported rel. to no. of photons emitted 77−80383
current and voltage instrument transformers, MV, constructional principles and production technology *(Hungarian)* 80−100118
data acquisition, on-line computerised system for meas. in insulation structures 77−5863
DC, repetition rate, cavity surface cond. depend. 77−11421
dielectric stimulated arcs in lighting-arrestor connectors, substantial lowering of breakdown voltage 79−99013
dielectrics, inhomogeneous, breakdown model 80−50268
epoxy mica generator insulation, dielectric stress conc. influence on voltage endurance 78−15094
epoxy resin, partial discharge initiation phase, effects of field strength, temp. and internal mech. stresses *(German)* 78−72461
epoxy resins, VLF meas. over freq. range 0.1 to 50 Hz 77−76227
epoxy treeing breakdown, slit model 80−15970
ice and ice-silica compound system, electrical breakdown at cryogenic temps. 80−45007
insulating solid, elec. strength and degradation 78−83631
in insulation, dielectric internal discharge, apparent charge evaluation *(Polish)* 80−19659
liquid dielectric gassing rate and discharge energy loss meas. 80−15965
liquid hydrocarbons, electric breakdown, light emission investigation 80−93241
liquid N_2 immersed polymeric materials, short-term insulating characts. 79−85145
long-time tests, automatic data acquisition and computation *(German)* 79−71432
mechanisms, of single-avalanche, Townsend and channel discharges *(Polish)* 80−79609
PMMA, ageing characts., sub-atm. pressure partial discharge obs. 80−1867
polyethylene, artificial voids, partial discharge charact. *(German)* 78−92023
polyethylene, DC partial discharge and current 78−43790
polyethylene, degradation effects, expt. 77−7617
polyethylene, electrical tree growth anal. using simultaneous meas. of light intensity and partial discharges 80−45008
polyethylene, VLF meas. over freq. range 0.1 to 50 Hz 77−76227
polyethylene film, partial discharge degradation, effect of discharge products in air *(Japanese)* 77−69774
polyethylene thin film, partial discharges energy content effect on breakdown *(German)* 77−81052
polymer film, partial discharges, HNO_3 absorption, expt. *(German)* 77−77147
polymeric dielectric materials, degradation product anal. 79−4765
polymeric insulating materials, simulation and meas. *(German)* 77−77146
power transformers, electromagnetic testing of partial discharges for failure and breakdown prevention *(Russian)* 80−97743
secondary electron emission due to negative corona discharges 78−67592
spectra meas. by multichannel amplitude analyser system *(Italian)* 80−33847
N_2, liq., insulation breakdown characts. of composite insulation cryogenic temps. 78−1920
SF_6, determ. of inception voltage from field distrib. of electrode arrangement *(German)* 79−94829
SF_6, disintegration product meas. *(Czech)* 78−67450
SF_6, overvoltage dependence 77−76243

particle accelerator accessories
see also storage rings
5 MeV electron accelerator modulator charging system 79−13563
8UD Pelletron tandem accelerator, fast neutron time-of-flight spectrometer facility 79−85856
40 kV neutral beam injector, modified duoPIGatron ion source 79−68117
250 kV water Blumlein, off-resonance transformer charging 79−13564
500 MeV synchrotron ring magnet power supply 79−18068
accelerator ion beam position monitor 79−89040
angular distribution meas. of recoil prods. of high-energy nuclear reactions, geometry calcs. 77−6596
anode foil changing system for heavy-current field-emission electron accelerator 78−9005
automatic radioisotope production devices adapted to a medical cyclotron 80−12260
autoresonant, computer system data acquisition and processing 80−99433
beam buncher improvement at Univ. of Manitoba cyclotron 77−88308
beam scanner design for cyclotron facility 80−99365
beam steering unit for cyclotron beam guiding system 78−21799
beam toroid for 750 keV polarised proton beam monitoring at ZGS 79−68072
BEAMSCOPE, device for meas. of emittances and betatron amplitude distribs. 79−72145
betatron bremsstrahlung field shaping apparatus for teletherapy 78−57062
betatron electromagnet pulsed power supply 78−82546
booster accelerator for separated-sector cyclotron at Holifield heavy ion facility 77−83199
cascade cyclotron magnet 77−83193
ceramic vac. chamber, bunched beam EM field penetration 77−83368
CERN, 50 MeV proton linac injector, performance 79−67972
CERN ISR, 50 MHz transverse feedback system 77−83319
CERN ISR, phase displacement accel. of high intensity stacks 77−83254
CERN ISR clearing current monitoring system 77−83249
CERN OMEGA spectrom., slow proton trigger 78−17467
CERN Omega spectrum., data monitoring system 77−18768
CERN PS booster, reliability and maintenance anal. 77−83281
CERN SPS, target stations and beam dumps 77−83385
CESR injection linac, electron beam modulator, design, performance 77−83374
Chalk River superconducting cyclotron project, injection system design 79−54615
chopper buncher system for tandem Van de Graaff 80−13989
Cockcroft Walton 860 keV preaccelerator for SIN high current injector cyclotron 79−67975
collective accelerator magnetic field meas. apparatus 79−31354
conference on particle accelerator engineering and technology, San Francisco, USA (Mar. 79) 79−67979
coupled-cavity structures in high duty factor accelerator, operational experience 79−67992
CPS at CERN, pulse to pulse modulation, extraction modes, beam intensity 77−83277
CRYEBIS ion sources for Saturne synchrotron *(French)* 80−63432
cryogenic equipment for point defects in solids research *(French)* 77−132
cryogenic pump for long continuous running *(French)* 78−32829
current accumulator at low energy for high-energy proton rings 77−83329
cyclotron, emittance measuring instrumentation, program for phase ellipse area *(German)* 78−58512
cyclotron beam phase probe, isochronism studies at IUCF 79−54720
cyclotron cryopumps, selection criteria 79−54670
cyclotron extraction efficiency improvement through central region studies 79−54719
cyclotron ion source gas feed system 79−81112
deflecting magnet for external beam of 150 keV accelerator, influence of magnetic fringing field 78−46195
deflecting septum magnet for cyclic accelerator 78−78525
detector systems for LEP 79−97952
dose field monitoring by independent detectors in cassette 77−81578
duoplasmatron ion source in KEK-PS 77−83390
eight-magnet spin precession snakes, survey for new configurations 80−91352
electron 2 MeV injector for pulsed betatron 78−824
electron beam spectrum monitor using synchrotron light 79−72146
electron collimation system for use with electron cones of Varian Clinac 18 accelerator 78−11725
electron diodes, relativistic, low impedance, behaviour in converging mag. gradient 77−370
electron gun system, pulsed, for use with superconducting accelerator and free-electron laser 80−68989
electron guns, high-current, laminar beam formation for linear accelerators 78−74516
electron injection system into collective accelerator model compressor 77−14277
electron injector in HV terminal, control and protection system 80−27836
electron linear accelerator, dose monitoring system 78−92710
electron linear accelerator prebuncher design calcs. 79−54624
electron polarised source, injection gun for Stanford linear accelerator 79−76242
electrostatic accelerator, large stripper foil mounting method 78−29664
electrostatic inflector and extractor for cyclic accelerators, HV expts. 78−50421
electrostatic wire septums, leakage field 80−5423
EN-tandem, foil stripper *(German)* 79−36437
energy doubler quenches, pressure development 79−76200
energy Doubler refrigeration system 79−72013
Enge split-pole spectrograph, limits on differential hysteresis and accuracy of proton beam energy calib. 78−55082
extractor for 10 kV D^+ injection 79−45468
fast cyclotron beam emittance measuring device 79−54712
fast electrostatic chopper of low power consumption 79−31284
Fermilab, aperture meas., beam obstruction location 77−83384
Fermilab 500 GeV main accelerator RF cavity 128 MHz mode damper 77−83299
Fermilab booster, transverse instabilities suppression, fast feedback system 77−83298

particle accelerator accessories continued
Fermilab booster accelerator, mag. system modification, increased energy 77−83222
Fermilab booster beam, longitudinal dipole oscills., effects, damping 77−83259
Fermilab booster bunches, linac bunch struct. during adiabatic capture and accel. 77−83261
Fermilab Booster Ring, 30 to 53 MHz super cavities for 10-GeV acceleration 79−68058
Fermilab Booster synchrotron, broadrange beam signal limiter 79−72082
Fermilab booster synchrotron, transverse instability damping electronics 77−83318
Fermilab booster tunes, control system 77−83382
Fermilab capacitor tree 77−83242
Fermilab Central He liquefier, characts. of main components 79−67991
Fermilab control system, computerized network of distributed processors 77−83302
Fermilab energy doubler, at Fermilab, supercond. dipole magnet technology 77−26901
Fermilab main ring power supply, minicomputers control system 77−83303
Fermilab master slave servo-manipulator, control system 77−83309
Fermilab neutrino focusing horn, pulse stretching in high current power supplies 77−83367
Fermilab phase controlled pulsed power supplies, characts. of inversion operation 77−83223
Fermilab Tevatron He liquefier power supply 79−68044
floating deck modulators for high voltage protection of ion beam accelerators 78−66392
FN tandem accelerator, telemetry component tests 77−83156
FN-7 tandem, matching of heavy-ion direct extraction Penning source 78−13357
foil strippers, remote control system 78−29670
GANIL separated sector cyclotron, injector design 79−54613
gas discharge ion source for on line EM mass separator at heavy ion accelerator 78−17456
gas discharge ion source for on-line EM mass separator at heavy ion accelerator 78−17457
gas target, differentially pumped and recirculating 79−13570
goniometer for nuclear reaction cross section and channelling expts. 78−21801
Harwell linac II total scatt. spectrometer, calibration using Ni diffr. data 78−86725
heavy ion 1.5 megavolt preaccelerator, high intensity, ion beam fusion appl. 79−67970
heavy ion and He dosimetry and instrumentation 79−20675
heavy ion facility, target production 80−23213
heavy ion linear accelerator, Munich, 50 kW transmitter, power stage design 77−83175
heavy ion postaccelerator section using independently phased spiral resonators 77−83148
heavy ion separation velocity selector 77−88324
heavy ion stripping in dilute gases and C foils, data anal., semiempirical formulas 78−33354
heavy-ion beam buncher for ion pulsing into tandem accelerator 79−31280
heavy-ion beam intensity enhancement using support gas in ion source 77−34490
heavy-ion booster, Stony Brook project 77−83125
heavy-ion cyclotron at Chalk River, extraction system, design 77−83266
helium refrigeration system and cryogenic system for superconducting Switchyard magnets at Fermilab 79−67990
HICONEX 834 sputter source, negative ion test injector of Munich MP tandem 78−13363
high current DC injector for accelerator breeding systems, future developments 79−93846
injection in proton synchrotrons intensity and energy spread 77−83131
injection method at zero gradient synchrotron 77−83133
injection methods in Fermilab booster synchrotron 77−83132
injector, with field emission cathode for betatron 78−5064
injector for deuteron linac 79−67969
ion beam position location and profile measuring system *(Croatian)* 77−75025
ion beam scanning device for rapid meas. of emittance and brightness 78−58522
ion pump, design, to accelerator specifications 79−63256
ionisation chamber, noninteractive beam position and size monitor for heavy ions 79−72149
ionisation profilometer for dynamic measurement of radial dimensions of electron beam in betatron *(Russian)* 78−13359
IPCR separated sector cyclotron, injection 79−54614
ISABELLE closed orbit correction system 77−83336
ISOCELE high-current on line separator development 77−26922
isochronous cyclotron mag. field automatic meas. system 78−82547
ISOLDE-2 on-line isotope separator at CERN 600 MeV synchrocyclotrons 77−23330
isotope separation on-line system employing cooled and NaCl loaded He-jet methods 77−14288
ISR RF cavities, beam load compensation, feedback system 77−83294
IUCF control system 79−54702
JULIC cyclotron, beam phase detection with fixed intermediate frequency system 79−54711
Karlsruhe isochronous cyclotron, trim coil design 79−54654
KEK, beam position monitor system, design, operation 77−83306
KEK booster to main ring beam transfer system, construction operation 77−83264
KEK main ring, dipole magnets field meas., B-clock system 77−83308
KEK preinjector, recent progress 77−83123
KEK proton synchrotron, synchronous beam transfer from booster to main ring 77−83263
KEK proton synchrotron vacuum system design and construct. 77−83225
Kiev isochronous cyclotron, diagnostics of beam phase characteristics 79−54718
klystron self excited oscillator with short time delay microwave pulse 77−6578
Lamb shift polarised ion source with spin filter proton acceleration, operating performance 78−33348
LAMPF Alvarez sections, high-power low-freq. klystron as drive 77−83174

particle accelerator accessories continued
LAMPF linac, Monitor remote-handling system, status, improvements and accomplishments 79−71997
LAMPF particle separator 77−83388
LAMPF primary beam line protection system 79−72014
large multiwire proportional chambers for experiment NA3 at the CERN SPS 80−102388
laser monochromator for relativistic proton beam 78−90010
laser polarimeter for e^+e^- beam polarisation meas. in storage ring 80−14019
Leuven isotope separator on-line at CYCLONE cyclotron 78−70682
linear accelerator, pulse amplifier with digital gain control 80−68977
linear accelerator beam profile scanner 80−101267
linear accelerator emittance meas. unit for 100% duty factor Linac injector beams 77−38490
linear accelerator pulse amplitude instability meas. apparatus 78−82537
linear accelerators, plasma waveguides appl. as accelerating structures 80−9438
liquid He cryopump for 1 MV accelerator, cryogenic supply and boil-off removal 79−72011
low cost 500 kV Mercury preaccelerator, for heavy ions 79−76155
magnetic field quality requirements for PEP 77−83205
magnetic undulator in electron synchrotron motion and radiation of relativistic electrons *(Russian)* 78−62997
Mainz 300 MeV linear accelerator, energy loss system of electron scatt. facility 78−58524
Manitoba Univ. cyclotron, 20 to 50 MeV H^-, injection system, status report on upgrading 79−54646
mass separator facility on-line to UNILAC heavy ion accelerator 77−14299
mass separators, on-line, progress in targets and ion sources 77−14300
microprocessor applications in upgrading accelerator controls 77−83173
microtron booster resonator in HF path 78−830
microtron voltage control system using thyristor convertors 77−14280
MIMAS, low energy accumulator-injector for SATURNE, project description 79−71985
minicomputer data acquisition system for Princeton cyclotron facility 78−90048
mirror system, wideband, for electron ring diagnostics 78−78518
model magnet for superconducting cyclotron at Milan 77−83194
MP tandem at Munich, variable circular beam apertures 78−33324
MP-Tandem at Munich, light link coupled current monitor 78−33311
multi-cavity prebunching systems 77−83119
multichannel nanosecond pulse generator for cyclotron stroboscopic system 79−68168
multiple rabbit, pneumatic multi-target transfer system, design, operation 77−54385
Munich heavy ion postaccelerator 79−22500
muon flux measuring system for neutrino spectrum reconstruction at IHEP accelerator 78−21817
MWPC instrumentation for CERN SPS secondary beams 78−46206
negative heavy ion beam production by charge exchange in metal vapour, EN tandem accelerator accessory 78−33346
neutron shutter for cyclotron facility 78−21794
neutron time of flight facility with mag. beam swinger, time, energy resolutions 77−57796
Nevis proton synchrocyclotron extraction system, design, operation 77−83265
NIMROD 70 MeV injector, 665 keV pre-injector 77−38435
NUMATRON project, high energy heavy ion facility, design, performance 78−62665
ondulator as EM radiation source in synchrotron orbit 79−72174
open sector injector cyclotron, for SIN 600 MeV ring accelerator, design of RF system 79−54685
optical reflector for energy extraction for electron synchrotron 80−78467
Orsay MP tandem, zero degree detection system 78−13353
Osaka RCNP 230 cm cyclotron, recent development and proposal for new ring accelerator 79−54632
OSIRIS on-line mass separator, study of short lived fission products 77−23352
Pakhra synchrotron, split microtron injector, design and characts. 77−83136
passive filter for annular electromagnet of synchrotron 78−5074
PEP at SLAC, high efficiency high power UHF klystron, performance 77−83296
PEP injection line, sensitivity to perturbations 79−72096
PEP magnet power supply systems 77−83216
PETRA storage ring, intensity monitor, design, operation and performance characts. 79−72081
PETRA storage ring control system, control console for man machine communication 79−72084
phase space cooling for $p\bar{p}$ colliders at CERN and Fermilab 80−99360
photon position monitors for CHESS synchrotron source, using split photoelectron detectors and ionisation chamber 80−91336
PIA, positron intensity accumulator for PETRA injection 79−71984
PIGMI, 250 kV proton injector system 79−45467
pion conversion target for Saclay electron linear accelerator 77−54384
polarised electron gun at SLAC, operating experience 77−83396
polarised proton target, using high homogeneous field supercond. magnet for Argonne ZGS 77−26911
power source, pulsed power conversion with inductive storage, fusion appl. 78−13340
precision gated current integrator and live time meter system 79−9973
Princeton Cyclotron data acquisition system 80−102415
proton beam heavy ion source, injector for cyclotrons, feasibility study 79−54730
proton beam heavy ion source, possible use as cyclotron injector 79−45496
proton linac, non-destructive bunch length monitor 77−376
proton radiography beam line establishment at Fermi National Accelerator Laboratory 78−65121
proton recoil polarimeter for zero gradient synchrotron 77−38511
proton storage ring, neutral beam injection, LASL 79−76156
proton synchrotron, 12 GeV, beam size meas. by fast rotary scraper 79−72078
proton synchrotron, beam position monitor for ΔR feedback on RF system 79−72079
proton synchrotron, multiturn injection efficiency increase 77−83129
proton synchrotron slow extraction beam parameter monitoring and control system in CAMAC standard online with ES 1010 computer 78−29674

particle accelerator accessories continued
PS booster at CERN, longit. active damping system electronics, tracking band pass filters 77−83297
pulse magnetometer output amp., for accurate meas. of synchrocyclotron mag. fields 79−2793
pulse transformer design for pulse forming transmission line charging appls. 80−63419
pulsed electron accelerator current density distrib. multichannel recorder 78−58520
pulsed electron gun systems, 1 ns pulse width 79−67977
pulsed septum magnet for extraction from Fermilab booster synchrotron 77−83219
quadrupole gradient-length product meas. device 79−76232
racetrack magnets, press.-impregnated, training behaviour 77−22585
RF charged-particle separator power recovery, for synchrotron 78−66440
RF deflector, HV, reduction of cyclotron beam repetition rates 77−57789
RF ion source, modified extraction geometry 78−33349
RF quadrupole accelerating struct. research at Los Alamos 79−71988
RF quadrupole beam dynamics 79−71986
RF structures for static accelerator upgrading 79−45477
RF superconducting resonators for booster linac 79−54623
rotating target wheel with thin targets for heavy ion beams of high current densities 79−76241
Saturne II, beam liner computerised control system, organisation, function, hardware 77−83400
Saturne II, secondary emission detector system for beam profile monitoring 77−83402
Saturne II at Saclay, RF system 77−83301
scanning microprobe, digitally controlled for p and heavy ions 79−13571
scattering chamber, rotatable lid, vacuum sealed, with semicond. detector arrays, INS cyclotron accessory 77−6599
scintillation hodoscope counter for beam meas. in CERN SPS 79−36472
secondary emission multiwire chamber for GANIL cyclotron beam tuning 79−54733
Serpukhov proton synchrotron ion-getter pumps, operation evaluation 77−83347
shaping of highly stable flat top in excitation current pulse of electromagnet in Sirius synchrotron 78−5075
SIN 590 MeV ring cyclotron, recent and future developments 79−54642
SLAC, beam containment electronics operational experience 77−83466
SLAC, control and monitoring system, use of microprocessors, cost 77−83177
SLAC, microwave beam position monitors 77−38488
SLAC, microwave developments, beam-test results 77−83405
SOLIS, surface ionisation integrated target-ion source 77−14303
space charge limited harmonic beam interceptor, increased cyclotron beam intensity 77−381
SPEAR transport line toroids, intensity monitors calib. system 77−88295
spiral resonator for bunching picosecond heavy-ion pulses 77−83122
spiral resonators, for Heidelberg heavy-ion postaccelerator 79−13558
split ring resonator for superconducting heavy ion booster 77−83126
SPS, CERN, extraction modes anal. 77−83255
SPS beam instrumentation, closed orbit correction 77−83305
SPS computer control system, operational experience 77−83292
sputter ion source, low prod. of stable N^- ions, design implications for tandem for sensitive C anal. 78−33350
Stanford superconducting heavy ion linac, reentrant cavities 77−83124
stochastic betatron cooling, slot type pick-up and kicker 78−33332
stripper foils, energy straggling of heavy ion beams at tandem energies, C foil appl. 78−33353
stripper foils for electrostatic accelerator, new mounting method 78−33355
superconducting bending magnets, large aperture design for Brookhaven AGS 77−26910
superconducting cavity multipactoring suppression in accelerator appls. 77−83121
superconducting dipole magnet construction, from Nb_3Sn filaments 77−28758
superconducting dipole magnets, ESCAR, gas cooled Cu leads 79−67995
superconducting heavy ion cyclotron, Chalk River, movable steel trim rods, orbit dynamics 77−83267
superconducting magnet, for energy saver doubler project, testing and field meas. 77−26899
superconducting magnet system, ESCAR, mid-term report 77−26902
superconducting Pb resonators, polishing procedure for high surface electric fields 77−83197
superconducting quadrupole magnet construction for CERN ISR 77−10507
superconducting RF separator at CERN 79−81113
superconducting solenoid, Basque project 77−23325
superconducting solenoids, large dia., mag. spectrometers for colliding beam accelerators 77−26919
synchrocyclotron, in-line mass spectrometer, electrostatic filter 80−86490
synchrotron miniature pulse deflector construction 78−82545
synchrotron secondary emission chamber, stability tests in high flux photon beams 79−72077
tandem, for heavy ions, pulsing system 78−33323
tandem accelerators, MV heavy ion injection 78−13356
tanked tube for open air accelerators 80−99356
targets for storage rings, molecular beam apparatus 77−6586
Tevatron Central Helium Liquefier, Fermilab, process control system 79−72012
TOF pulsed neutron diffraction of liquids using electron linac, CCl_4 appl. 78−18504
Tonus 2M accelerator, high-voltage pulse generator of stored energy 135Kj 78−5067
transformer, 3 MV, for PFL pulse charging 79−76173
TRIUMF 100 μA beam, achievement and control 79−54699
TRIUMF cyclotron, meas. and corrections to beam props. 79−54710
UNILAC, He-jet transport system for short-lived nuclei 79−13569
Unilac beam diagnostic system 77−38489
UNISOR integrated target-ion source 77−14302
vacuum feedthrough, bakeable, with 22 pins, for monitor system of proton synchrotron 78−21798
vacuum gauge design 78−17546
Van de Graaff, 10 MV, digital data telemetry system 77−83155
Van de Graaff terminal for VICKSI 77−83127
velocity spectrometer for 10 meV to 10 keV atoms 77−3210

particle accelerator accessories continued
vibrating wire beam profile monitor for electrostatic accelerator with high stability 80−99368
VICKSI beam line instrumentation and control system 77−83401
VICKSI cyclotron, RF system, design, operation 77−83300
wall current beam position monitor with improved low frequency response 79−72150
wall current monitor for KEK proton accelerator 79−72080
Wideroe-based heavy ion preaccelerator for the SuperHILAC 79−71987
wiggler, helical wiggler and free electron laser *(Japanese)* 80−37658
wiggler magnets, control of low-energy characteristics, appl. to CERN LSR 77−6585
zero gradient synchrotron, resonance extraction slow spill control system 77−83256
ZGS, 30″ bubble chamber 80−91304
ZGS, Effective Mass Spectrometer 80−91310
ZGS, superconducting magnet bubble chambers, history 80−91368
ZGS 500 MeV booster synchrotron, data acquisition and control, sequential logic and minicomputer 77−83304
ZGS beam transport for transverse and longitudinally polarised protons 78−55074
ZGS booster, intensity and position meas. systems 77−83307
ZGS streamer chamber and kaon physics 80−91308
e^+e^- storage ring, parallel coupled RF cavity struct. 77−83295
C foils, stripping of heavy ions with energy 0.4-0.9 MeV/A, straggling, foil behaviour 78−33351
C stripper foil, lifetime meas. 80−23216
C stripper foil preparation, under heavy ion bombardment 80−18717
C, stripper foil prepared by cracking hydrocarbon vapour in glow discharge 79−31286
C stripper foils, ethylene cracking in glow discharge, irradiation lifetimes 80−23207
C stripper foils, lifetime enhancement by slackening technique 80−23186
C stripper foils for heavy ions, preparation method 79−22516
C, stripper foils under 4.8 MeV Ar^{++} ion bombardment, shrinkage, rupture, lifetime 78−33352
Cs sputter ion source, survey of negative ions for use with tandem accelerator 77−83412
H^- injection linac, Fermilab, operation and uses 79−71989
H^- ion direct extraction source 77−83393
H^- multiturn charge exchange injection system for Fermilab Booster accelerator 79−67971
H^- short bunches shaper at entrance of linear accelerator 79−700
H^- source development at ANL 77−83394
He-jet transport system for nuclear reaction prods. using heavy ion accelerator ALICE *(French)* 77−3202
Li negative polarised ion beam source at Heidelberg EN-Tandem 78−33356
Na vapour charge exchange cell development 77−83395
Nb, microwave cavity of muffin-tin type, for accelerator use 77−26905
Nb TM_{010} superconducting RF cavities for high energy storage rings, 700 MHz meas. 79−68059
^{32}S 96 MeV heavy ion ps pulses, rebunching of MP Tandem pulses by spiral resonator 78−33357

particle accelerators
see also beam handling equipment; beam handling techniques; cyclotrons; electron accelerators; electron ring accelerators; electrostatic accelerators; linear accelerators; proton accelerators; synchrotrons
1 MV accelerator struct. for cluster injector 77−83128
ANL HVEM-TANDEM accelerator facilities 80−101896
application of small accelerators in research and industry, conference, Denton, TX, USA (Nov. 1978) 79−45470
applications of small accelerators conf., Texas (Oct. 1976) 77−67912
astrophysical acceleration of particles 78−81537
atomic physics expts. on small accelerators 77−68141
automatic klystron power supply system transient behaviour theory *(German)* 78−5077
beam induced e.m. fields, coupling impedance struct. above tube cutoff frequency 77−375
bending magnet for energy doubler, prototype test 77−83366
betatron oscillation, short-cut method for soln. *(Chinese)* 77−34489
betatron oscillations, frequency shift in nonlinear mag. fields 78−1137
bi-periodic accelerator structure *(Chinese)* 79−59286
breeder reactor 77−83065
bunch lengthening due to potential well distortion from cylindrical cavities with beam ports 77−83375
bunched proton and electron beams, longitudinal instability theory 77−83208
calibration using $^{27}Al(p,n)$ threshold energy 79−36241
cancer therapy, particle accelerator appl., current status 79−74783
cavity instabilities, improvement by mutual coupling *(Slovene)* 78−29663
ceramic accelerator tube of improved construction 78−827
CERN, 25 years of physics, review 80−82626
charge transfer cross sections in high-flux, low-energy accelerators 79−30609
charged particle motion in alternating elec. fields, scaling conditions 80−63903
charged particle motion in mag. field, acceleration and focusing 78−1142
circular, transverse coupling impedance meas., 79−36446
circular beam tube, longitudinal coupling impedance of step discontinuities 79−72115
cluster ion accelerators, ioniser 77−74551
collective acceleration with ionisation front accelerator 77−83169
collective ion accel. in travelling virtual cathode 77−83166
collective ion accel. program at Maryland, electron ring and linear beam methods 77−83168
collective ion acceleration, effect of high ν/γ electron beams 77−6579
collective ion acceleration by relativistic electron beam 77−88291
collective ion electrostatic accel. in evacuated drift tube geometry 77−83170
collective methods of particle acceleration, conf., USSR Acad. of Science, (June 1977) 79−18062
colliding beam arrangement using laser linac, feasibility study, laser accelerator problems 78−78521
computer model, system anal. of accelerators for inertial fusion 77−83474
conference, accel. engineering and technology, Chicago (March, 1977) 77−83184

particle accelerators continued
conference, general congress, Societe Francaise de Physique, Toulouse, France (June 1979) 80−77536
conference, theoretical aspects of beam behaviour, Erice, Sicily (1976) 78−78878
conference on particle accelerator engineering and technology, San Francisco, USA (Mar. 79) 79−67979
conical accelerator, plasma cluster vel. calc., snow-plough and erosive models *(Russian)* 80−27839
cryostat mass production 79−68045
crystal accelerator, radiative energy loss 80−23611
cyclic, Coulomb shift of betatron freqs., stability of coherent oscills. of circulating bunch 77−46436
cyclic accelerators, beam interaction with the accelerating system 78−78524
data acquisition system designing for accelerator development facility 77−57307
decommissioning, radioactive waste management 80−18720
decommissioning, re-utilisation potential of components 79−72029
dense plasma, coaxial acceleration and plasmochemistry *(Russian)* 78−92482
depolarisation during acceleration and storage of polarised protons and deuterons 78−58519
design, influence of stochastic character of Hamiltonian solutions 78−93606
diagnostics using laser beam 80−95497
dual-ion accelerator, appl. to simulation of radiation damage to fusion reactor materials 78−13325
effluent monitoring programme design and organisation principles 79−13548
electron accelerators, pulsed power technology for fusion expts. 78−50321
electron gun, coaxial, electron flux formation in strong mag. field *(Russian)* 79−98998
EM wave shock accel., relativistic charged particles 77−54661
EPICS pion channel at LAMPF, performance 77−10500
fast blowup of particle bunches, theory 77−30681
Fermilab energy doubler, supercond. magnets, mag. field meas. 79−31258
Fermilab energy doubler magnets, support design and cryostat system 79−31257
flux control, charge exchange method *(Russian)* 78−70662
fusion oriented, power flow studies 78−50320
fusion reactor microexplosion ignition 79−18030
gas discharge, variable density, for high speed charged particle prod. 78−51381
heavy ion, appl. to pellet fusion reactors 79−678
heavy ion+atom collisions, accelerators and X-ray emission spectra *(Norwegian)* 78−22013
heavy ion accelerator facilities in Europe, review 80−42880
heavy ion accelerator VICKSI, status 77−83152
heavy ion facility for radiation therapy 77−86588
heavy-ion accelerator projects, review 77−83137
heavy-ion beam inertial-confinement fusion, commercial power generation 79−6762
heavy-ion collective acceleration in electron rings, 'Pustarex' expt. 77−83285
heavy-ion fusion preaccelerator, 1.5 MeV, fibre-optic remote control system 80−73993
heavy-ion low energy accelerators 77−14654
high current particle beam prod. by low pressure spark discharges, accelerator 79−31247
high energy accelerators, superconducting dipole magnets with high field uniformity, development and investigation *(Russian)* 80−5416
high energy accelerators and interactions of elementary particles *(German)* 79−97642
high power accelerators for spallation breeders of fissile materials *(Japanese)* 79−26517
high-energy physics, particles and interactions 80−77944
historical review, impact on scientific culture 80−868
IHEP accelerator storage complex USSR, design 77−83338
induction accelerator charact. meas. instrument 78−5073
industrial uses, role in national economy of USSR 77−23314
inhomogeneous waveguide system, self-consistent beam dynamics 78−9009
intense pulsed ion beam accelerators, review 77−71707
ion, applications outside nuclear physics *(Polish)* 79−40641
ion, atomic collision processes rel. to vacuum system, review 80−54290
ion, EM isotope separation and sources 77−14276
ion, small-size direct-action 80−23184
ion acceleration, collective field propagation using slow wave struct. 77−83286
ion acceleration in quasi-static field of electron beam 77−71915
ion accelerator systems for ion implantation research 80−32540
ion accelerators and their use for controlled thermonuclear reactions, review *(German)* 79−67933
ion accelerators pulsed power, for inertially confined fusion *(Russian)* 77−67915
ion beam accelerators, high voltage protection, using floating deck modulators 78−66392
ion beam intensity measurement, noninterceptive method *(German)* 77−387
ion beam production and manipulation, general considerations 79−93256
ion beam sources, for sputtering technology, review 78−72719
ion extractor for large area plasma source 77−84466
ion source, accelerator system computer solns. 77−88309
ion source, design, for milling appl. 78−70222
ISX-B neutral beam injector expt. on prototype beam line 80−74039
klystron development, UHF, 600 kW, stability and durability improvement *(German)* 80−106211
laer beam acceleration of particles along cryst. channel axis 77−30677
laser accelerator, phase-adjusted focusing 80−63434
laser radiation-surface launching of macroscopic particles 80−6290
lasers and accelerators 79−72015
Lawrence Livermore Laboratory accelerator safety program 77−83118
leakage measurements, medical appls. 80−89839
Leningrad Institute of Nuclear Physics synchrocyclotron, neutron source 80−87003
magnet systems, piggy back power supplies advantages 77−83365
magnetic field azimuthal variations, two-dimens. approx. calcs. 77−26908
particle accelerators continued
magnetic field configuration recovery, in interpolar gap 78−5070
magnets, differentiated-effect shims for medium field levels and saturation 77−6595
medical, international standards 80−51272
meson facilities, higher energies 77−54380
modern atomic and nuclear physics (book) 80−11
multidetector technique readings, interpetation for dose equivalent determ. 79−49875
multiple charged and polyatomic ions, use in implantation accelerator 77−54017
multiple superconducting energy doubler accelerator magnets, series operation 77−83214
multiply-charged and polyatomic ions, use in implantation accelerator 77−74554
multipurpose *(Japanese)* 80−87000
Munich MP tandem, HICONEX 834 sputter source, negative ion test injector 78−13363
National Synchrotron Light Source, distributed computerised control system 79−72086
negative ions from accelerated hydrogen clusters, fusion ignition appl. 80−13883
neutral atomic beam source, power supply system 78−66393
neutron sources, review and development, neutron production processes, particle accelerator appl. *(Dutch)* 79−81108
next generation, possibility of multinational sponsorship 80−47791
next generation of accelerators 79−72122
nonidentical resonators with narrow coupling slits, dispersion and field distrib. characts. 79−41047
nonlinear crystal, optical acceleration of charged particles by 'rectified' light 80−23610
nuclear structure, conf. 78−50059
nuclei and particles, introductory text book 78−78234
nucleosynthesis explosions, accelerator expts. and theory 77−71110
NUMATRON project, high energy heavy ion facility, design, performance 78−62665
Numatron project, high-energy heavy-ion accelerator *(Japanese)* 79−26791
Numatron project *(Japanese)* 77−83342
operating principles and construction, review *(French)* 79−45486
paint coatings in radiation fields of reactors and accelerators, and after contamination by radionuclides 77−75006
Pelletron, He^- ion source for injector 78−5085
PEP magnet power supply systems 77−83216
phase free AC accleration, proof of second order effect 77−6984
polarised beams, acceleration and storage 78−58518
polarised high energy particle production in cyclic accel. and storage rings, possibilities 79−63843
polarised proton beams, higher energy, conf., Ann Arbor, MI, USA, Oct. 1977 78−58514
potential and field produced by elllptical beam in confocal elliptic vac. chamber 77−83798
pulse forming network 34 kA rapid cycling supply for driving injection magnets 79−67974
pulsed accelerator for neutron travel time meas. *(German)* 78−17475
pulsed neutron sources by accelerators, appl. to neutron scatt. *(Japanese)* 77−383
Pulselac accelerator high-intensity current source of carbon ions, design 79−89512
radiation control for health and safety act 1968, manufacturers' responsibilities 77−83114
radiation exposure, proper design of cooling and ventilation systems 80−5350
radiation generated by charged beam near plane flanged waveguide 79−13880
radiation protection, state registration and inspection programmes 77−83117
radiation shielding, sanitary-safety zone, cost optimization of structural design 78−17443
radioactive nuclei acceleration at ORNL 77−10502
radiobiological studies in space and at ground-based accelerators 80−41266
radioisotope direct detection using accelerators 80−63468
radiological safety in design and operation, American National Standard 79−89511
radionuclide migration in groundwater from accelerator earth shields 79−48194
review of 30 years work by Nuclear Reactions Lab. Dubna, USSR 79−36204
review of new developments *(Czech)* 77−42196
RF common anode high power amp., particle accelerator appl. 79−68051
Sandia particle beam fusion accelerator facilities 80−37592
SEPAC for ionosphere and magnetosphere studies from Space Shuttle/Spacelab 77−73925
shielding problems *(Japanese)* 80−99343
Siberian Snake configuration, efficient configuration 79−63849
spiral resonators for heavy-ion accel., meas. at high field levels 77−10503
steel, mag. anisotropy, magnetostatic fields, numerical simulation 77−27220
superconducting accelerator magnets, magnetization effects on field shape 79−31253
superconducting coil for beam transport dipole magnet 79−31256
superconducting dipole magnets, stress and strain distrib. 79−31250
superconducting dipole ultra stable window frame magnet 77−83235
superconducting dipoles SPD-3 and SPD-3′, testing 77−26904
superconducting high energy beam line dipole-magnetostatics, design 77−83363
superconducting magnet stability problem at accelerators under high-energy particle irradiation, review *(Russian)* 80−68972
superconducting magnetic energy storage applic. 78−25360
superconducting magnets, pulsed and DC types, appl. *(German)* 78−21834
superconducting magnets, relationship between supercond. and high energy phys. 79−33441
superconducting split ring resonator as accel. struct. for ^{16}O and ^{32}S beams 77−6577
synchronous slow space-charge wave accelerator 78−17448
synchrotron radiation, spectral chart of radiation from circular accelerator 78−46498

particle accelerators continued
synchrotron radiation, spectroscopic applications, properties, characteristics as radiation source *(Norwegian)* 80−63420
synchrotron radiation, techniques and appls., book 80−5668
synchrotron radiation source, book contrib. 80−5421
TFTR neutral beam source, power supply system 78−66394
theory, rel. to fundamental consts. 77−22345
thermal particle motion effect on autoresonance acceleration process *(Russian)* 80−69007
Tokamak plasma confinement devices, use of accelerator technology 77−84527
toroidal resonator excitation by uniformly moving charge 80−18726
Torus accelerator, transport of high current relativistic electron beams in large vols. *(Russian)* 78−82544
transfer maps for linear and nonlinear beam elements 79−72107
TRIUMF meson factory, basic and applied research 78−21792
Very Big Accelerator complex, worldwide cooperation, discussion 77−83339
waveguide, self-reson. charged particle motion in EM wave with varying propag. vel. 77−75399
X-ray laser, tunable, using high energy accelerator beam of one-electron atoms 79−86154
d acceleration in CERN PS and ISR 77−83283
D ion accelerator, intense neutron source, design and operation 79−49883
D^-, prod. of 100 keV beam, transport, accel. and diagnostics 77−83440
H^- cluster ion beam high power injector 80−13889
He unit requirements, for superconductive energy appl. in USA 78−89999
Nb, RF superconductivity, appl. to particle acceleration, overview 79−31244
$SmCo_5$ material for accelerator permanent magnets 79−6776

particle backscattering
see also electron energy loss spectra
γ-ray single backscatt. 77−88323
absolute Rutherford backscatt. yields, accuracy 79−47572
aerosols, backscattered fraction in two-stream approxs. 77−45150
AES, backscattering factor, Monte Carlo method calc. 80−7449
AES, quantitative, backscatt. effects, review 80−81398
AES, quantitative, Monte Carlo calc. 80−84813
air electron backscattering coeffs., 100 eV to 5 keV 80−9750
alpha-particle backscattering, microanal. appls. 77−25324
amorphous and polycryst. surfaces, anomalous yield enhancement, for 180° He^+ scatt. 79−100008
amorphous layer thickness meas. by electron back scattering method 80−100721
anodic oxide superficial layer, X-ray emission spectrometry and ion backscattering *(French)* 80−49482
atomic transport and conc. profiles 80−59723
Auger scanning microscopy, backscattered electron lateral resolution effects 78−15262
backscattering spectrometry and related analytical techniques 80−50505
beam profile monitor using Rutherford backscatt., emittance and luminosity meas. 79−45497
beam profiling by backscattering from thin wires 79−59289
beta-ray backscatt. from thick targets 80−32567
beta-ray surface imaging using extended beta-ray sources 78−48588
Boltzmann equation, appl., electron transmission, secondary electron emission *(French)* 80−20740
bone mineral concentration estimation by beta-ray backscatt. *(German)* 78−69179
carbonaceous insulating films, RF diode sputtering growth, IR absorpt. and Rutherford backscatt. meas. 79−99458
chalcogenide glass film, drift and thermal diffusion of Au electrodes, α-particle backscatt. meas. 79−4434
chalcogenide glass thin film, thermal diffusion of Au electrode layer, α-particle backscatt. obs. 78−10228
channelling, charged particles in single crystal, physical principles, uses and future trends *(Russian)* 79−82269
channelling backscattering use for radiation damage studies, review *(Japanese)* 77−72640
channelling in surface, charged particle reflection, two-wave approx. 78−6822
channelling of fast electrons, temp. depend. of anomalous Rutherford scatt. *(Russian)* 78−83857
coating, thin, on bulk materials, electron backscatt. w.r.t. thickness determ. *(German)* 77−10146
coating chemical characterisation by surface and near-surface sensitive techniques 79−15053
coating thickness meas., beta backscatter method, meas. uncertainty prediction 77−56206
coherent X-ray generation from CO_2 laser backscattered relativistic electron beam 80−53252
coincidence measurements between scattered particles and X-rays to obtain high depth and mass resolution 80−54278
complex materials, charged particle anal., range effect corrections, geological material appl. 77−48738
concrete, density meas. by back-scattered gamma radiation 77−36699
conference on ion beam anal., Washington, USA (June-July 1977) 79−5194
depth profiling of H, He isotopes, elastic scatt. technique 77−24327
depth profiling of light elements in materials with high-energy ion beams 77−59036
depth profiling techniques for thin film interdiffusion and interfacial reactions, book contrib. 79−1564
diamond:Sb, implanted, radiation damage and annealing study 80−100263
diamond:Sb, ion implanted under channelling conditions, depth profile, distribution tail 80−2057
diamond, natural, high conc. of implanted Si ions, He backscatt. and IR absorption 77−89466
dilute alloy, electron scatt. by impurity cluster, lattice distortion and backscatt. effects 77−20306
dilute alloy, quantitative Auger anal., correction factors for atomic density, escape depth and backscattering 79−69927
disorder distribution extraction, semiempirical method of applying dechannelling correction 78−22781
dose depend. in laser annealing 78−91354
dose enhancement due to backscatt. secondary electrons at interface 77−2058

particle backscattering continued
doubly-ionised beams, nucl. backscatt. anal. of energy and ion impurities 77−75017
electron, backscatt. by solids 80−2906
electron, backscattering image, materials investigations uses 77−60015
electron, in field emission gun SEM 80−100142
electron, transport equation theory, SEM and EPMA appl. 80−57439
electron backscatt. coeff., 10 to 120 keV 78−63788
electron backscattering, X-ray prod., transport eqn. soln. 79−38698
electron backscattering from solids and double layers 77−20972
electron backscattering in Si surface-barrier detector 78−55095
electron channeling pattern, large angle, generation and appl. 80−100296
electron detector, multi-purpose 80−102404
electron gas, 1-D, 2-D Coulomb gas, and 2-D epitaxial monolayer problems, family of mappings 80−34346
electron imaging, in scanning Auger microprobe, tailored modulation techniques appl. 80−68305
electron probe analysis, spatial distrib. of electrons in homogeneous, isotropic target 79−43687
electron probe microanalysis, quantitative, 4-40 keV, electron backscatt. coeff. meas. 80−35608
electron probe penetration and energy loss characts. in solid target, diffusion model 80−96585
electron scattering, in the scanning electron microscope 79−21880
electron scattering in solids, high energy, Monte Carlo calcs. 80−96422
electron transmission and backscatt. in solid layers, energy loss, 10 to 30 keV 77−59653
electrons, estimation of backscattering factor for low atomic number elements and their alloys 78−72649
EM analyser control, automatic registration of the back-scattered ions 80−18042
emerald, artificial single crystal, distrib. of Cr^{3+} impurity 80−59505
energy reflection by backscatt. and sputtering, total yields and ang. distrib. 80−89101
EPMA, stopping power and backscatt. factors, rel. to atomic number correction 78−20118
EPMA correction procedure, Monte Carlo derivation of surface ionisation function 78−20119
film, backscattering spectrum edge determ., theory, and expt. for Ag on Si 77−8702
film reactions, $^{16}O^{2+}$ effect elimination in backscatt. 78−23575
film thickness determination in electron microscopy, electron backscatt. method 77−47703
films, metal-semicond. and metal metal studies in ultra high vacuum scatt. chamber 79−2780
fluoride film, contamination by 1 MeV proton bombardment, backscatt. obs. 77−11811
foil, electron backscatt., eikonal approx. 77−48289
gamma photon number albedo meas. 79−36490
gamma-ray, survey of principal research 77−65340
gamma-ray backscattering coefficients, Monte Carlo calcs. 77−61171
gamma-ray backscattering from various barriers, characts. and spectral ang. distribs. 77−61621
gamma-ray sky-shine spectra, ^{60}Co source 77−65341
gas flow detector, back-scatter-type, conversion electron Mossbauer spectrometry 80−37680
graphite, pyrolytic, behaviour of implanted D and He 78−95071
heavy ions, low energy total backscattering 80−71535
high resolution Rutherford backscatt. techniques, appl. to near surface anal. 79−5207
hybrid pulse pile-up rejection system, Rutherford backscatt. appl. 79−2884
Inconel 625, plasma nitriding, hardness meas., Rutherford backscatt. surface anal. 80−45442
ion, light, total backscattering from solid target in keV range 77−1772
ion, material characterisation technique 79−96407
ion, MeV spectrom., electron and ion currents rel. to accurate current integration 79−47571
ion anal. of shallow surface layers 77−77338
ion backscattering analysis standards 79−2883
ion backscattering and implantation, H and He ions, computer simulation, comparison of MARLOWE and TRIM codes 80−66350
ion backscattering channelling surface peak calc. 79−8219
ion backscattering under planar channelling conditions, ion-atom pot. and stopping power 80−24519
ion beam impurity anal. 78−70223
ion beam material characterisation, conf., Aleria, Corsica (Sept. 1976) 79−96403
ion beam monitoring using thin self-supporting reference foils 80−50911
ion beam surface crystallography, channelling and blocking effects, double alignment backscattering 80−65350
ion beams, use in material analysis by nuclear reactions and scatt. and ion-induced X-rays 77−4968
ion implantation, range parameters, nucl. stopping power, ion backscatt. determ. 80−88232
ion implantation, research at Central Physical Research Institute in Hungary *(Hungarian)* 77−51395
ion implantation depth profiles, influence of straggling using backscatt. and nucl. reacts. 78−47401
ion neutralisation at surfaces 78−35237
ion scattering from solid surfaces, single scatt. and ion neutralization *(Japanese)* 80−50500
ion-impact spectrometer, 2-100 keV, for ion-solid interaction studies 79−49338
ionosphere, electron scatt. from artificially injected electron beams 77−21983
ions backscattered from solid surfaces, radiative electron capture 78−11057
light atoms in crystal lattices, position determ. by α-particle channelling and backscatt. 79−65113
low energy ion backscattering, struct. anal. 78−15271
low energy ion scattering for composition and struct. anal. of outer surface 79−4458
magnetic shield, particle scatt. props. 79−21791
marker studies of silicide formation, Si self-diffusion, and Si epitaxy by ^{31}Si tracer and Rutherford backscatt. methods 79−4431
material analysis technique using 2 MeV $^4He^+$ ions *(Chinese)* 80−35590
metal, electron-impurity scattering, lattice distortion effects, phase shifts, calc. 80−96860

particle backscattering continued
metal, impurity depth conc. profiles using Rutherford backscatt. 79−52448
metal, irrad., self-interstitial type defects, combined single-double alignment channelling backscatt. 78−34561
metal surface finish meas., backscattered electron intensity *(Japanese)* 79−4465
metal target preparation for stopping power meas. of channelled ions in low energy region 80−63431
metal-semiconductor interactions, low temp. cpds. form., backscatt. and X-ray obs. 79−28217
metal-Si system, ion implanted, inert-gas-bubble form., TEM and Rutherford backscatt. anal. 79−90682
metallic thin films, electron backscattering, empirical study 80−108310
metallic thin films, Everhart theory extension of backscattered electron energy spectra 80−108309
metals, analysis of H ratios and profiling using nucl. techniques and Rutherford backscatt. 80−61202
metals, electron penetration and energy transfer in solid metal targets, film bulk method 78−2963
metals, Z dependence of thick target β-ray backscattering 80−76118
microcrystal orientation, SEM determ. using electron back-scatt. patterns 77−76268
monolayer overgrowth obs. in Auger electron spectra 77−85081
Monte Carlo analysis of backscattering and sputtering in vacuum systems 80−235
noble gas ions, low energy, from single cryst. surface, computer simulation of ang. depend. 79−19961
noise distorted backscatt. spectra, deconvolution of high energy edge 79−56903
nozzle erosion, ion implantation effects, ion beam anal. 79−48011
nuclear microprobe anal. of stable isotope tracers spatial distrib. 80−50909
optical emission from low-energy particle-surface collisions 77−36300
parallel-plate sputtering system deposition rate model 79−87579
peak energy and target thickness in backscatt. data 78−70719
phase diagrams, ion beam determination of phase boundaries, exam. of techniques 79−8418
phosphosilicate glasses, P content determ. by Rutherford backscatt., PIXE, and activation anal. *(Hungarian)* 80−85233
photon, spectra of gamma rays backscattered by infinite air (skyshine) 80−101436
photon backscattered ang. distrib. for oblique incidence *(Rumanian)* 80−47456
planar channelling, oscill. behaviour of backscatt. spectra from small depths 80−6447
plasma containment vessels, backscatt. and sputtering from pocket and finned structs. 79−14558
plasmon excitation by large-angle scatt. electrons, density effect and plasmon bremsstrahlung 78−47718
polycrystalline solid, electron backscatt. energy distrib. spectrometer *(German)* 79−95882
polystyrene, gamma photon backscattering, energy dependence *(Rumanian)* 79−76316
polythene, Z dependence of thick target β-ray backscattering 80−76118
porous and microporous materials, pore size meas. using reson. ion beam backscatt. 79−2747
protons, 5 to 8 MeV, appl. of scatt. spectrometry to special anal. problems 79−5210
radiation device, layer thickness measurement by backscattered radiation 80−47829
radiotherapy megavoltage depth-dose value corrections due to reduced backscatt. thickness 77−48871
random backscatt. yields from crystals, rot. sample technique, appl. to β-alumina 79−5208
random solid, light ion backscattering energy spectra calcs. 78−72655
randomly stepped surface, He backscattering 78−11055
rare earth metal silicide thin film formation on (100), (111)Si substrates, backscattering study 80−70542
Rutherford, ang. depend. of MeV H^+ backscatt. yield in glancing geometry, uniformity of near surface layers obs. 79−4874
Rutherford, hybrid pulse pile-up rejection system 77−54468
Rutherford, improved depth resolution of chanelling meas. by tilted detector 79−5209
Rutherford 180° backscatt. anomaly in solid, Monte Carlo simulation 80−45189
Rutherford backscatt. standard for ion beam expts. 80−50496
Rutherford backscattering, review of technique and applications 79−43082
Rutherford backscattering, small angle high resolution, ion implantation appls., review 77−44108
Rutherford backscattering, surface comp. and struct. *(French)* 78−43976
Rutherford backscattering analysis, automatic ang. distrib. measuring system 77−20975
Rutherford backscattering and LEED for surface struct. 79−82419
Rutherford backscattering in solids, meas. of relative stopping powers of light ions 79−4348
Rutherford backscattering meas. at MeV energies, screening corrections 80−88204
Rutherford backscattering microanalysis, precision absolute thin film standard reference targets 79−2882
Rutherford backscattering spectra, double peak pulse pileup distortions 79−1805
Rutherford backscattering spectrometry, signal overlap subtraction, surface struct. studies 80−50486
Rutherford scattering cross section correction 80−66369
Rutherford spectra anal 80−50497
Rutherford spectrometry, comparison of depth profiling techniques of O in Si 80−29048
sample contamination, by sputtering, during ion implantation 80−54274
scanning Auger electron microscope, calc. of effects of backscattered electrons on spatial resolution 80−81412
scanning Auger microscopy, effect of backscatt. electrons on resolution 79−2898
scanning Auger microscopy, effects of backscattering on resolution 80−104021
SEM, backscattered, using CdS layer scintillator, reflected SEM proposal 78−21291
SEM, backscattered electron image, review 78−21304
particle backscattering continued
SEM, backscattered electrons, contrast mechanisms and detectability limits 78−21305
SEM, electron scattering influence on detection of fine topographic detail 78−21290
SEM, emission area of back scattered electrons 77−27795
SEM, energy filtering, backscattered electrons *(French)* 77−74558
SEM, magnetic contrast, type-2, isolation by lock-in technique 80−13184
SEM specimen-electron interactions 80−68317
SEM with movable Faraday cup, illuminator and backscatt. diode detectors for planar diode characterisation 78−21292
semiconductor, ion-implanted, post annealing meas. using Rutherford backscatt. and channelling 79−69121
semiconductor film, heteroepitaxial, on insulating substrates, characterisation, book contrib. 79−82497
p-Si:P, random and aligned implants, damage form. and annealing, Rutherford backscatt. exam. 78−47454
solid, He ion backscatt., charge state distribs., target temp. depend. 79−95887
solid, Monte Carlo simulation of energy distrib. of transmitted or backscatt. keV electrons 78−43057
solid surface, backscattering of H, D, and He, positive charge fractions 80−66375
solid surface, H^- ion backscatt. due to proton bombardment 80−99554
solid surfaces, ion and neutral scatt., backscatt. energy spectra anal. by TOF technique 79−5236
solid target, anomalous enhancement of 180° backscatt. yields for light ions 80−45188
solid-electron interaction, Monte-Carlo simulation, appl. to electron probe microanal. 77−12853
solidified gases, energy loss of ^4He ions from backscattering meas. 79−4346
solids, backscattering coeff. meas. of 15 to 60 keV electrons at various angles of incidence 80−80919
solids surface finish, backscattered electron intensity meas. *(Japanese)* 77−66081
spatial electron beam-matter interaction, model calcs. for Cu *(German)* 80−84815
sputtered alloys and compounds, surface layer composition changes 77−73200
sputtered layer on metal collector, thickness distrib. meas. by electron backscatt. 78−18927
sputtering process study on Au, Al, Si targets, Rutherford backscatt. technique 77−8703
steel, stainless, retention and re-emission of 0.125-1 keV D^+ ions 80−66349
steel, stainless, spatial distribution of limiter material and impurities on the first wall of TFR 400 79−651
steel, stainless, with Pd coating, interdiffusion at reactor wall temps., Rutherford backscatt. obs. 80−39361
steel surface, O and N profiles determ. by Rutherford backscatt. anal. 79−5216
stopping powers determ. from backscattered ions spectra 79−97959
straggling meas. anal. by the backscatt. technique 79−4355
surface, composition analysis, by ion beams *(French)* 79−8467
surface analysis, atomic beam scatt., SIMS, and vibr. spectra, book contrib. 79−42357
surface analysis, quantitative, by collision spectroscopy of backscatt. medium energy ions 77−8704
surface and thin film analysis by high-energy ion beams 77−40320
surface backscattering yields, effects of correlated lattice vibrs. 79−69942
surface chemical analysis, low energy ISS compared with SIMS 78−64908
surface roughness meter using backscattered electron intensity *(Japanese)* 79−93131
surface topology usin Rutherford backscattering 80−47015
surfaces and thin films, combined ion, electron and X-ray beams for anal. and struct. determ. 77−86412
tailored low Z impurity distribs. in solids, proton backscatt. evaluation of distrib. 79−5199
thick target, energy spectrum of backscattered particles, multiple scatt. and ion effective charge deviation effect 77−81192
thin crystal foil, large angle electron scattering by dependent Bloch wave model 79−99257
thin film, thickness determ., by electron backscattering 80−101904
thin films, thickness determination, using backscattered electrons as tool 79−21704
thin layer thickness determ. from backscatt. ion spectrum 79−24399
total backscattering coefficient for thick absorbers, segment model calc. 77−72642
ultrahigh vacuum system, for channelling backscattering experiments *(Japanese)* 79−26061
universal β-backscatter thickness gauge calibration method 77−32747
V-Be diffusion couple, ion backscatt. anal. 77−35752
X-ray signal backscattered from semi-infinite reflector, quantitative analysis of intensity controlling factors 77−54371
β, total backscattering coefficient for thick absorbers, segment model calc. 77−72642
Ag, electron backscatt. by bulk target, theoretical model *(French)* 80−60722
Ag, energy reflection coefficient for 5 to 10 keV He ions 78−95639
Ag film, on Si, backscatt. spectrum edge determ., theory and expt. 77−8702
Ag, stopping power for 0.3 to 2.0 MeV ^4He ions 79−60415
Ag-Al polycryst. thin-film couples, interaction process 79−51443
Ag-Cu couple, grain boundary diffusion of Ag through Cu film, Rutherford backscattering obs. 80−34252
Al, beta-ray backscattering variation with target thickness, self-absorpt. coeff., Z depend. 79−78801
Al, defect structures depend. on Ca and Ga implanted species 80−59494
Al, determ. of optimum depth resolution for Rutherford backscatt. anal. using ^4He 79−14840
Al, electron backscatt. by bulk target, theoretical model *(French)* 80−60722
Al, electron backscatter fractions, exptl. determ. 80−18617
Al, electron transmission, secondary electron emission, appl. of Boltzmann equation *(French)* 80−20740
Al, fission fragment backscatt. 80−16138

particle backscattering continued
Al, gamma photon backscattering, energy dependence *(Rumanian)* 79−76316
Al, heavy ion ranges, 120 keV Pb ions backscatt. obs. 80−19855
Al, heavy ion ranges, He^+ backscatt. obs. 78−63796
Al, implanted Xe behaviour during anodic oxidation 80−71800
Al, ion-implanted, dechannelling by dislocations, backscatt. expts. 79−7642
Al, obliquely incident 15-25 MeV electrons, total backscatt. coeff. 77−63508
Al, primary electron backscatter yield using material model parameters 80−39184
Al, proton energy straggling in ion backscatt. expt. 79−37750
Al, stopping power and energy straggling meas., Li ion backscatt. anal. 79−3328
Al supercond. film, granular O content and oxide barrier thickness, Rutherford backscatt. 79−15250
Al surface, ^4He backscatt., Rutherford scatt. cross section correction test 80−66369
Al surface bombardment by fast H^+ 80−66376
Al, surface exfoliation and blistering induced by He ion bombard. in energy range 10-80 keV 80−39173
Al, surface roughness effects on the energy dispersion of backscattered protons 79−24403
Al, surface roughness meas. using Rutherford backscattering of protons 79−51400
Al, thick anodised films, O conc. determ. using non Coulomb H ion backscatt. 80−55753
Al:Sb(Zn), ion implanted electron beam annealing, ion backscatt. and TEM meas. 80−59500
Al-Ag, dil., radiation damage by channelled and random He^+ ion beams 79−46719
Al-Cu, surface enrichment of Cu due to Xe sputtering, AES and He ion backscatt. meas. 77−4250
Al-Cu film, galvanostatic formation anodic oxide, Rutherford backscattering and depth profiling 78−92395
Al-Cu film bilayers, growth kinetics of θ phase, He^+ backscatt. and X-ray exam. 78−84105
Al-Ge (0.1 wt.%), channelling meas. of Al interstitial atom trapping by Ge atoms 80−59537
Al-silicide-Si systems with $CoSi_2$, $Pt_xNi_{1-x}Si$, and $MoSi_2$ as silicide, diffusion, compound form., and microstructure 80−34253
Al-Xe film, ion implanted radiation enchanced Xe outdiffusion, Rutherford backscatt. 77−76609
$Al_xGa_{1-x}As$ layer, LPE, graded bond gap solar cell, composition profile, Rutherford backscatt. 78−76612
Al_2O_3 film, RF sputtered by planar magnetron, phys. props. 77−43448
Al_2O_3, O conc. determ. using non Coulomb H ion backscatt. 80−55753
Al_2O_3, stopping power and energy straggling meas., Li ion backscatt. anal. 79−3328
Au, α-particle Rutherford spectra anal. 80−50497
Au, backscatt. of H and He ions, fraction reflected 80−60741
Au, discontinuous film, degradation under MeV heavy ion bombard., Rutherford scatt. and TEM obs. 79−24397
Au electrode, diffusion into polymer film, particle backscatt. anal. 79−77821
Au, electroplated, thickness meas. by beta-ray backscattering *(Slovene)* 78−6860
Au, energy reflection coefficient for 5 to 10 keV He ions 78−95639
Au film, integrated condensation coeff. on NaCl cleavage faces, Rutherford ion backscatt. obs. 80−59827
Au film, interface reaction with n-type $Ga_{0.7}Al_{0.3}As$ and GaAs 80−39482
Au film, surface roughness effects on the energy dispersion of backscattered protons 79−24403
Au films, thickness meas. standards for Rutherford backscatt. 79−40529
Au, fission fragment backscatt. 80−16138
Au, H and He atom backscattering, ang. and energy distribs. 80−76123
Au, irrad., self-interstitial type defects, combined single-double alignment channelling backscatt. 78−34561
Au, precision stopping cross section meas. for ^4He, 0.5 to 2.1 MeV 79−4353
Au, primary electron backscatter yield using material model parameters 80−39184
Au, stopping cross sections of protons, 350 to 650 keV, backscatt. technique 79−4352
Au, stopping power for 0.3 to 2.0 MeV ^4He ions 79−60415
Au, stopping powers and backscatt. charge fractions for 20-150 keV H^+ and He^+ 80−42907
Au surface, ^4He backscatt., Rutherford scatt. cross section correction test 80−66369
Au, surface, energy spectra of charge state fractions of backscattered H and D 77−8705
Au surface, high energy ion backscatt., computer simulation *(German)* 77−59664
Au/Ni(Ni-P), interdiffusion, backscatt. study 80−79991
Au/Pt/Cr films, diffusion of Si, depth anal., optical and Rutherford backscatt. meas. 79−10981
Au/Sn evaporated film, interdiffusion, X-ray diffr. and ion backscatt. obs. 79−33121
Au-As, system interactions due to heat treatment, backscattering anal. 79−91719
Au-Sb, system interactions due to heat treatment, backscattering anal. 79−91719
Au-Si contacts, O depth distrib. determ., backscatt. anal., 1 MeV $^4He^+$ ions 79−4482
Au-Sn film, evaporated, interdiffusion and phase formation, in situ He ion backscattering meas. 78−22901
AuCu-Al thin film bilayer system, phase formation, backscattering spectra 80−96728
Be alloy, dil. metastable, produced by ion implantation, lattice location of impurities 79−51132
Be and Be alloys, low temp. solubility of Cu, ion backscatt. analysis 77−62646
Be, blisters due to He irrad., proton backscatt. study 80−75273
Be, implanted D and He, interaction and radiation enhanced oxidation 80−39120
Be, lattice location results for implanted impurities, Rutherford backscatt./channelling technique 79−4329
Be, oscillatory channelled $^4He^+$ ion scatt. yield 78−52610
Be, proton energy straggling in ion backscatt. expt. 79−37750

particle backscattering continued
Be, surface hardening by B ion implantation, Rutherford backscatt. obs. 80−16604
Be-Al-Fe, phase equilibria and diffusion using high energy ion beams 77−16542
C, determ. of optimum depth resolution for Rutherford backscatt. anal. using ^4He 79−14840
C film, backscattered electron intensities, ang. depend 77−40317
C, low energy electron backscattering, 0.5-10 keV 77−52206
C, proton energy straggling in ion backscatt. expt. 79−37750
C, proton straggling determ., using 0.47 and 1.73 MeV 79−4356
C, reflection of H, D and He ions 78−95640
C with Au and Al implants, Rutherford backscatt. standard 80−50496
CaF_2 film, ionic migration study by Rutherford scatt., defects, secondary emission *(French)* 78−55982
CaF_2, overlaid with Au and CaF_2 films, channelling meas. 78−67762
CdS, clean surface, AES and LEED exam. 80−10762
CdTe, surface characterisation by high resolution Rutherford backscatt. 80−25511
CdTe surfaces, SIMS, Rutherford scatt. and ellipsometry 79−56046
Co, effect on surface roughness on backscattering spectra 80−47016
Co-Si film system, diffusion marker expts. 78−79824
Co-Si film system, interaction kinetics 78−79823
Cr film, vacuum-evaporated, with A-15 struct., prep. and characterisation 77−62768
Cr-Pt thin film couple, diffusion, new Cr-Pt phases obs. 79−42319
Cr-rare earth, dil., oxidation of Cr, effect of rare earth impurities 79−79160
Cr_2O_3, fine struct. in elastic-electron-yield spectra at transition-metal core energies 79−69938
Cs, backscatt. of H and He ions, fraction reflected 80−60741
Cu, 4-30 keV H_1^+, H_2^+, H_3^+ impact, excited H backscatt., O_2 effect 78−15268
Cu, beta-ray backscattering variation with target thickness, self-absorpt. coeff., Z depend. 79−78801
Cu, blisters due to He irrad., proton backscatt. study 80−75273
Cu, determ. of optimum depth resolution for Rutherford backscatt. anal. using ^4He 79−14840
Cu, electron backscatt. by bulk target, theoretical model *(French)* 80−60722
Cu, electron backscatter fractions, exptl. determ. 80−18617
Cu, energy reflection coefficient for 5 to 10 keV He ions 78−95639
Cu, fine struct. in elastic-electron-yield spectra at transition-metal core energies 79−69938
Cu, fission fragment backscatt. 80−16138
Cu, in Hg plasma, sputtered atom angular distrib., mass effects 79−87538
Cu, obliquely incident 15-25 MeV electrons, total backscatt. coeff. 77−63508
Cu, polycryst., back sputtering of 100 to 500 eV Ne ions, computer simulation 78−60537
Cu, self ion irrad., determ. of the nature of defect clusters by Rutherford backscatt. of He ions 79−4342
Cu single crystals Au ion implanted, pulsed electron beam irrad. 80−65019
Cu surface, ^4He backscatt., Rutherford scatt. cross section correction test 80−66369
Cu surface, conditions for total refl. of low-energy atoms 79−19958
Cu, surface morphology influence on sputtered yield angular distribution 80−65338
Cu, thermal displacement of surface atoms, elastic backscatt. of He atomic beam *(French)* 77−4709
Cu, thin film, sputtering yields due to Ar^+ milling, He^+ Rutherford backscattering and AES obs. 79−65969
CuI, film, prep. on NaCl by reactive sputtering, struct. and composition investigation 79−90900
$CuInS_2$ films, RF sputtered, growth and props. 80−80124
$CuInS_2$ thin films, growth, struct., and elec. props. 79−38729
$CuInSe_2$ amorphous thin film, flash evaporation, struct., stoichiometry 80−89150
Fe, diffusion and solid solubility of Sb, 773-873K, ion backscatt. anal., rel. to intergranular embrittlement 78−71880
Fe, gamma photon backscattering, energy dependence *(Rumanian)* 79−76316
Fe, oxide film thickness determ. by electron backscatt. Mossbauer spectroscopy 78−72933
Fe:Bi, impurity site distrib., channelling and nucl. orientation obs. 77−15447
Fe-Ti-Sb-C alloys, Sb trapping effect on temper embrittlement, ion beam study 78−92312
FeF_3 film, elec. cond. mechanisms 79−99649
^{57}Fe backscatt. electron Mossbauer spectroscopy 80−29661
GaAlAs oxide, plasma grown, anal. by combined ion beam techniques 79−7760
$Ga_{0.64}Al_{0.36}As$, plasma grown oxide, phys. and elec. props. 78−48550
GaAs, 40 keV N^+ implantation, disorder profiles meas. by Rutherford backscatt. and channelling 80−54270
GaAs, amorphous layers, ion-implanted, low-temp. epitaxial regrowth 80−92790
GaAs, disorder distrib. extraction, semiempirical method of applying dechannelling correction 78−22781
GaAs, ion beam induced annealing effects 80−59530
GaAs, ion implanted, laser induced damage and recrystallisation by freq.-doubled Nd:YAG laser 79−73197
GaAs, ion implanted, laser induced recrystn. and damage, ion backscatt. and Raman scatt. obs. 80−49248
GaAs, ion implanted, laser annealing 80−107296
GaAs, ion-implanted, laser pulse annealing of amorphous surface layer, TEM 80−55436
GaAs, laser annealed, Ga precipitation, Rutherford backscattering and TEM study 79−79127
GaAs oxide film, plasma-grown, analysis using Rutherford backscatt. and ion-induced X-rays 77−43438
GaAs, stoichiometry meas. by 15 MeV He^{2+} backscattering 79−99330
GaAs, substrate for epitaxial growth, backscatt. anal. of surface prep. and anodic oxidation 77−25175
GaAs, surface characterisation by high resolution Rutherford backscatt. 80−25511
GaAs, surface chem. changes on annealing, α-particle Rutherford scattering and channelling study 79−73383

particle backscattering continued
GaAs, X-ray and Rutherford backscatt. yields from channelled $^4He^+$ ions 79−46730
GaAs:P^+, defect form. on P^+ implantation at various temp., He^+ backscatt. obs. 78−59828
GaAs:Sn thermal diffusion from spin-on SnO_2/SiO_2 source 80−96691
GaAs:Te, ion implanted, laser annealing 79−73192
GaAs:Te, ion implanted, surface crystallinity and stoichiometry of laser annealed samples 79−73198
GaAs:Zn, implanted, furnace annealed, electrical, Rutherford backscattering and TEM meas. 80−100272
GaAs:Zn, implanted, laser annealing, elect., Rutherford backscattering and SEM meas. 80−100273
$Ga_xIn_{1-x}P$ MBE layers, comp., Rutherford scatt. and X-ray diffr. meas. 80−75457
p-$Ga_xIn_{1-x}PyAs_{1-y}$/Au-Zn, specific contact resist. 80−84509
GaP, disorder distrib. extraction, semiempirical method of applying dechannelling correction 78−22781
GaP, substoichiometric native oxide layers, $^4He^+$ backscatt. obs. 77−77610
GaP:Sn(Sb), lattice location of implanted atoms, ion backscatt. and ion-induced X-ray obs. 77−84785
GaSb, elastic scatt. of He^+ ions by atomic chains, screening 80−2915
Gd, stopping power and energy straggling of $^4He^+$ ions in vacuum-evaporated films 80−88231
Gd-Co amorphous film, DC or RF sputtered, mag. props., He^+-backscatt. investig. 77−20650
Ge, amorphous, scatt. of 2 MeV He^+ 77−69954
Ge amorphous evaporated film, to metal contact resist. diffusion and microstruct. 77−89880
Ge, amorphous layer, comparison of laser and electron beam pulsed annealing, $^4He^+$ backscattering spectrometry 79−69374
Ge, backscattered energy spectra, charged particles energy losses 79−83086
Ge, channelling of H^+ and He ions, backscatt. particles ang. distrib. 79−51174
Ge, energy loss spectra of C^{2+} ions 80−65114
Ge epitaxial film, ion implantation and electron beam anneal effects on carrier conc. 80−75255
Ge, mol. and atomic ion damage, Rutherford backscatt./channelling meas. 77−59056
Ge, proton energy loss, 0.1-1.0 MeV 80−42909
Ge, solid-phase epitaxial growth through PdGe layers, channelling and backscatt. obs. 77−85936
Ge-Au-Ni(Pt)(Pd) trilayered films, annealing, interdiffusion 78−22902
H, backscatt. from Au, charge fraction ang. depend. 80−71540
H^+, reflection, from metal surface, atomic excitation calcs. 79−87541
H^+, reflection from stainless steel and Nb 77−36336
He, backscatt. from Au, charge fraction ang. depend. 80−71540
He ion, meas. of range of heavy ions implanted in solids 77−14322
He ions, electrostatic anal., electronic reduction of charge state energy doublets 80−27870
He^+, isotope effects in elastic surface scatt. on sol. and liq. Ga 80−71536
He^+, reflection, from metal surface, atomic excitation calcs. 79−87541
^4He, 2 MeV, influence of polycrystalline film target texture on backscatt. particle yield 79−4875
^4He, ion, backscattering anal. 79−96408
^4He stopping power, 0.15 to 1 MeV, backscatt. determ. 80−88233
$HfAl_3$, anomalous growth in thin films, AES, TEM and He backscatt. meas. 77−43462
Hg surface, ^4He backscatt., Rutherford scatt. cross section correction test 80−66369
$Hg_{1-x}Cd_xTe$, implanted with Hg, Al, damage and lattice location study 80−103381
InAs-GaSb superlattices, crystallography, Rutherford backscatt. and channelling obs. 80−49533
InP film, electron-beam annealed, surface conduction 80−84500
$IrSi_x$, formation, Ir films on Si, He ion backscatt. X-ray diffr. study 79−82471
LiF, alkali ion implantation, migration, segregation, effect on optical props. 80−100269
LiH+Te exothermic solid-state reaction, ion backscatt. obs. 78−20064
Li_2O, Ar^+ implantation, depth distrib. by proton backscatt. 78−51577
Li_2O, C atom conc. profile determ. by proton backscattering 78−10079
Li_2O-Al_2O_3-SiO_2 glass, crystn. aggregation and migration of ion-implanted Ag 77−55240
Mg film, deposition using low-energy ion beam, Rutherford backscatt. and SEM anal. 77−59700
Mg film, deposition using low-energy ion beam, Rutherford backscatt. and SEM anal. 77−70004
MgO coated detector for SEM backscatter to secondary electron conversion 80−68332
MgO, planar channelling of He ions along (100), (110) and (111) directions 79−28023
Mn, stopping power of 0.5-2.0 MeV ^4He ions, elastic backscatt. meas. 78−87730
Mn-Sb two layer film, cpd. formation kinetics, ion backscatt., X-ray diffr. and mag. meas. 77−72801
Mo, 4-30 keV H_1^+, H_2^+, H_3^+ impact, excited H backscatt., O_2 effect 78−15268
Mo, electron backscatter fractions 78−87717
Mo film, on Si, silicide formation obs. 78−43261
Mo, in Hg plasma, sputtered atom angular distrib., mass effects 79−87538
Mo, proton energy loss, 0.1-1.0 MeV 80−42909
Mo, reflection of H, D and He ions 78−95640
Mo single crystals, ion implanted, energy dependent channelling and backscatt. anal., $^4He^+$ ions, 1 to 2.8 MeV 79−4360
Mo surface, H^- production by low energy H atom bombardment 79−100006
Mo surfaces, backscatt. of excited H atoms in the presence of oxygen 79−3388
Mo:H(He), depth profiles of implanted atoms, proton backscatter meas. 79−51136
Mo-W bilayer films on Si substrates, silicides formation, marker expt., Rutherford backscatt. obs. 79−99376
MoS_2, clean surface, AES and LEED exam. 80−10762
MoS_x RF reactively sputtered film, struct. and comp. 78−60038
$MoSi_2$ sputtered films, protective layer form. on oxidation, Auger anal. and backscatt. meas. 79−15029

particle backscattering continued
N ion backscatt., appl. to metal impurities anal. in Tokamak plasma 79−4182
N_2, electron backscattering coeffs., 100 eV to 5 keV 80−9750
^{14}N ions emerging from solids, equil. charge state distribs. meas. 77−65388
Nb, 14 MeV neutron sputtering, ion microprobe, SEM, He^+ backscatt. anal. 77−36317
Nb, (001) surface, low energy H^+ and He^{++} ion refl., computer simulation 80−11524
Nb, blisters due to He irrad., proton backscatt. study 80−75273
Nb, channelling study of $^4He^+$ irradiation damage, effect of dissolved O_2 79−82270
Nb, channelling study of $^4He^+$ irradiation damage, effect of irradiation temp. 79−82271
Nb film on Si, Ar ion bombard., $NbSi_2$ form. 80−10709
Nb, He depth profile meas. by nuclear reaction methods 79−14839
Nb, lattice location measurements of O using $^3He/^{16}O$ and $^1H/^{18}O$ prompt nucl. reactions, ion irrad. effects 79−86813
Nb thin films on Si substrate, intermixing, ion induced silicide formation 80−34101
Nb-Ti films, ion beam sputtered, study by ^4He backscattering and nucl. reaction microanal. 79−42400
NbO, ion channelling, 1 MeV deuterons 79−60416
Ne^+, isotope effects in elastic surface scatt. on sol. and liq. Ga 80−71536
^{20}Ne ions emerging from solids, equil. charge state distribs. meas. 77−65388
Ni, (110), surface relaxation and composition, medium energy ion scatt. spectra 78−63916
Ni (110) surface, ion impact desorption of O_2 by ion scatt. 77−35805
Ni, (111) surface, scatt. of mol. and atomic H ions 79−69943
Ni, CO adsorption, mol. orientation, ion scatt. 78−71949
Ni, charge states of 1.5 to 15 keV backscatt. He and Ne ions 79−4882
Ni, energy loss spectra of C^{2+} ions 80−65114
Ni film, amorphous layer covered, target prep. for channelled ion stopping power meas. 80−63431
Ni film, inelastic electron scattering 78−92155
Ni, He depth profile meas. by nuclear reaction methods 79−14839
Ni, implanted with Dy, annealing study by Rutherford backscatt., TEM, and total current spectroscopy 79−4343
Ni, ion-implanted and virgin, laser irrad. effect, Rutherford backscatt. and channelling obs. 80−108306
Ni, Li ion scatt., expt. and computer simulation 77−63511
Ni, reflection of H, D and He ions 78−95640
Ni, small angle backscattering of H_2, D_2, He and Ne from single and polycrystalline surfaces 79−24404
Ni, stopping power of 0.5-2.0 MeV ^4He ions, elastic backscatt. meas. 78−87730
Ni surface, (110), O_2 adsorption, LEED and ion scatt. study 80−84386
Ni surface, mech. for reflection of protons at kilovolt energies 79−8215
Ni target, surface layer anal. medium energy ion backscatt. expts., solid state detector 79−4456
Ni:Bi, impurity site distrib., channelling and nucl. orientation obs. 77−15447
Ni/Pt double layers on Si substrate, silicide formation 78−84010
Ni-Cr film, vac. deposition, elec. props. and comp. struct. 79−77966
Ni-In, ion-implanted, impurity defect interaction and diffusion, Rutherford backscatter and TDPAC expts. 80−34039
Ni-Nb alloys, oxidation at high temp., high energy ion backscattering anal. *(Japanese)* 80−35405
Ni-Pt silicide Schottky diodes, current-voltage characts. and comp. profiles 80−84508
Ni-Si:As(Sb), implanted dopant redistrib. after silicide form., appl. to ohmic contacts 79−37729
Ni-Ta(Sn)(Er)(La) ion implanted surface alloys, solid solubility and radiation-induced disorder, backscatt. obs. 79−46692
$NiCr_2O_4$, cooperative Jahn-Teller phase transition, channelling obs. 78−38839
$NiCr_2O_4$ single crystal, appl. of particle channelling to the study of a cooperative Jahn-Teller phase transition 79−4413
NiF_2 film preparation and characterisation 80−59815
NiO, fine struct. in elastic-electron-yield spectra at transition-metal core energies 79−69938
NiO-Al_2O_3 reaction at film-substrate interface, Rutherford backscatt. obs. 80−59733
$NiSi_2$, epitaxial film on Si, ^4He ion channelling meas. and RHEED anal. 80−10834
$NiSi_2$ epitaxial film on (111) Si substrate, interfacial order, backscatter, channelling study 80−65390
O_2, electron backscattering coeffs., 100 eV to 5 keV 80−9750
^{16}O backscatt. appl. *(Japanese)* 79−28871
$PaCl_2$, thin films, reduction to Pd by Ne^+ ion irrad., 2 MeV He^+ ion backscatt. anal. 79−4493
Pb, beta-ray backscattering variation with target thickness, self-absorpt. coeff., Z depend. 79−78801
Pb film, deposition using low-energy ion beam, Rutherford backscatt. and TEM anal. 77−59699
Pb film, deposition using low-energy ion beam, Rutherford backscatt. and TEM anal. 77−70003
Pb, gamma photon backscattering, energy dependence *(Rumanian)* 79−76316
Pb, obliquely incident 15-25 MeV electrons, total backscatt. coeff. 77−63508
β-PbF_2 film, ionic migration study by Rutherford scatt., defects, secondary emission *(French)* 78−55982
PbO-SiO_2 binary glasses, Pb depth profiles after acid etching, α-particle backscatt. 79−79343
PbO-SiO_2 glass, corrosion in acid, conc. profile meas. 78−92379
PbO-SiO_2 reduced glass, electron backscattering 77−85855
PbS, clean surface, AES and LEED exam. 80−10762
PbS film, vac. deposited, optical and phys. props. 80−2315
$PbTiO_3$, single cryst., He^+ backscatt. shoulder spectra struct., domain struct. 80−35048
$PbTiO_3$ single crystal, channelling of He^+ ions, polarisation effects 79−99258
Pd, catalyst on glass, used in electroless deposition, proton backscattering anal. 80−16749
Pd film, high dose Si^+ ion implantation, silicide phases, backscatter spectra 80−19820
Pd, film form. on Si surface by ion beam plating 77−90284

particle backscattering continued
Pd film on Si, Xe ion beam induced form. of PdSi 80−10800
Pd-amorphous Si thin film interaction, metal rich Pd-silicide formation 80−2284
Pd-Si, amorphous thin films, laser irrad., metastable phases 80−96622
Pd-Si:As(Sb), implanted dopant redistrib. after silicide form., appl. to ohmic contacts 79−37729
Pd-V, alloy and bilayer, silicide form. solid phase reaction with Si 80−6568
Pd_2Si, epitaxial film on Si, ^4He ion channelling meas. and RHEED anal. 80−10834
Pd_2Si, form. by laser irrad. of Pd film on Si substrate, Rutherford backscatt. obs. 79−42317
Pt (100), CO or C_2N_2 adsorpt. induced backscatt. enhancement 77−90227
Pt (100) (5×20) and (1×1) surfaces, stability and reactivity, adsorption of H 80−75434
Pt, (100) surface, phase transition and relax. by MeV ion backscatt. and channelling 79−86970
Pt (111) and (100), surface struct. anal. by MeV ion backscatt. and channelling 78−71916
Pt (111) surface, backscattering, channelling spectra, H adsorption, surface relaxation 80−71552
Pt coated razor blades, surface roughness effects on the energy dispersion of backscattered protons 79−24403
Pt films, high-purity, sputtered onto Si, PtSi and Pt_2Si form. 77−76676
Pt-Si, amorphous thin films, laser irrad., metastable phases 80−96622
Pt-Si:As(Sb), implanted dopant redistrib. after silicide form., appl. to ohmic contacts 79−37729
PtSi, 10-160 keV Ar ion sputtering, Rutherford backscatt. obs. 79−15574
PtSi, epitaxial film, cryst. perfection and thermal stability, channelling and backscatt. meas. 79−99255
PtSi, epitaxial film on Si, ^4He ion channelling meas. and RHEED anal. 80−10834
PtSi, growth under protective layers on Pt covered Si substrates, X-ray diffr. and Rutherford backscattering anal. 78−22965
PtSi surface, and interface with Si, impurity effects 80−80037
PtSi thin film structures, preferential sputtering meas. Rutherford backscatt. 79−43087
Pt_2Si, and PtSi, growth rate for form. by Pt film deposition under ultrahigh vac. and controlled impurity atm. 80−65388
Si, 40 keV N^+ implantation, disorder profiles meas. by Rutherford backscatt. and channelling 80−54270
Si (100), H adsorption, MeV ion scatt. study 80−80071
Si (100), P implanted, dechannelling by edge dislocations, obs. by backscatt. spectrometry and TEM 79−4308
Si (100), self-ion implanted, laser annealing, channelling and TEM meas. 80−24466
Si (110) surface peak anal. by 100-350 keV protons 80−55247
Si, (111) surface, low energy H^+ and He^{++} ion refl., computer simulation 80−11524
Si, (111) surface, proton dechannelling under channelling, blocking and double alignment conditions 80−88235
Si, amorphous, epitaxial regrowth by pulsed laser beam 78−91554
Si, amorphous, H isotope backscattering, trapping, and depth profiles, model 79−99233
Si, amorphous, heavy ion ranges, He^+ backscatt. obs. 78−63796
Si, amorphous, substrate orientation effect on regrowth by laser pulses, channeling, backscatter 80−84409
Si, amorphous films, characterisation by Rutherford backscatt. spectrometry 80−50498
Si, amorphous layer, comparison of laser and electron beam pulsed annealing, $^4He^+$ backscattering spectrometry 79−69374
Si amorphous layers, on Si substrates, deposited and ion-implanted, laser-annealing behaviour 79−69373
Si, and Si:H, amorphous, sputter deposited, O_2 incorporation during and after fabrication 80−49541
Si, anodic oxidation, mobile ion identification, Rutherford backscatt. analysis 77−44381
Si, Ar(Xe) ion bombarded, sputtering yield energy and fluence depend. 79−78805
Si, channelled-ion implantation of group III and group IV ions 78−75682
Si, channelling of H^+ and He ions, backscatt. particles ang. distrib. 79−51174
Si, channelling surface peak rel. to thin film anal. 78−43966
Si, damage profile after H_3^+-ion irradiation, proton backscatt. exam 79−60410
Si, dechannelling by twins, ^4He backscatt. spectra 78−18691
Si, disorder distrib. extraction, semiempirical method of applying dechannelling correction 78−22781
Si, displacement of group III, IV, V, and VI impurities in Si by He^+ and H^+ analysing beam 79−4330
Si, EFG ribbon, characterisation by ion beam tech. 80−79833
Si, epitaxial layers, cryst. quality improvement by ion implantation, backscatt. and TEM obs. 79−42397
Si epitaxial layers, dechannelling by stacking faults, channelling effect technique using He^+ and D^+ ion backscatt. 79−4361
Si film, CVD or evaporated, covered with Al layer, solid-phase crystn. obs. 77−85100
Si films, RF sputtered, Ar conc. as function of operation frequency and discharge pressure 80−65393
Si, gettering by ion damage, minority carrier lifetime and backscatt. study 80−100286
Si, heavy ion induced disorder in surface and at shallow depths 80−59535
Si, heavy ion ranges, 120 keV Pb ions backscatt. obs. 80−19855
Si heavy ion surface barrier detector, plasma delay times, electron backscattered from fission fragment or alpha particle 80−58095
Si, high dose Pb^+ and Cs^+ distribs., determ. using low angle Rutherford He ion backscatt. 79−4327
Si, high-dose implantation damage, reflectivity, Rutherford backscatt. and TEM obs. 77−7743
Si, implanted ^{16}O, lattice location of ^{16}O by α-particle backscatt. method 78−10080
Si, implanted annealed layers, amorphised structure formation mechanism and crystallographic nature 80−29091
Si, implanted Bi distrib., planar oscills. effects, low angle He^+ backscatt. obs. 78−34534
Si, impurities displacement by H^+ or He^+ irrad. 79−86824
particle backscattering continued
Si, impurity solubility limit after laser induced melting, Rutherford backscatt. spectrum 80−107426
Si, ion bombardment, anomalous surface damage from channelling-backscatt. meas. 80−84222
Si, ion implantation, high dose, solid phase epitaxial regrowth 80−103380
Si, ion implantation and pulsed laser annealing of group III and group V dopants, supersat. alloy form. 80−54267
Si, ion implantation of noble gases, high fluence retention 79−23627
Si, ion implantation-induced damage after Ar and P implantation, defect density and distrib. *(German)* 77−24337
Si, ion implanted, damage profiles, Rutherford backscattering 80−100733
Si ion implanted, doping profile meas. by He^+ backscattering spectra 79−60390
Si, ion implanted, laser annealed, elec. props. and annealing kinetics 79−69508
Si, ion implanted, radiation defect production at different temps. 80−103398
Si, ion implanted, spin density effect on laser annealing 80−11517
Si ion implanted layers, pulsed electron beam annealing, TEM and particle backscatt. meas. 79−69134
Si, ion irradiated, room temp., depth distrib. of disorder 79−37745
Si, ion-implantation damage, annealing using pulsed-electron-beam 79−55768
Si, ion-implanted, thermally oxidised, Rutherford backscatt. analysis 78−19910
Si, ion-implanted layers, epitaxial regrowth by laser beam and flash annealing 80−100420
Si, laser pulse induced amorphous to cryst. transition, thickness depend. 78−47678
Si layers, ion implanted, pulsed electron beam annealing, He^+ backscatt. and TEM study 79−51152
Si layers, solid phase epitaxial growth, crystalline qualities, ^4He backscatt. and TEM exam. 78−10306
Si layers amorphized by molecular ions, laser annealing 80−103379
Si on sapphire, gettering effect by O implantation, Hall and Rutherford backscattering meas. 79−65103
Si, oxide layer form. by O^+ ion implantation, Rutherford backscatt. and IR transmission obs. 79−51141
Si, postimplantation damage profiles, backscatt. meas. 78−47402
Si, proton damage, depth profile anal. by channelling 78−43054
Si, proton energy loss, 0.1-1.0 MeV 80−42909
Si, proton energy straggling in ion backscatt. expt. 79−37750
Si, proton random and aligned stopping powers, 80 to 300 keV, backscatt. meas. 77−27931
Si, self-implanted, ⟨100⟩ and ⟨111⟩, crystallised layers by laser annealing, struct. 78−47644
Si single crystal surface, ang. variations of backscatt. yield with 20 keV proton bombardment 79−4879
Si, small-angle backscatt. of 350 keV protons at grazing incidence 79−83085
Si, solid-phase-epitaxial, deposited above 380°C, defects obs. 78−63942
Si, sputter cleaning using Ar^+ ions, TEM and ion backscatt. investig. of damage 77−48558
Si substrate, silicide formation with large bilayers of Pd-Pt, Pd-Ni and Pt-Ni 79−51444
Si surface, ion bombardment enhanced mixing of Ag layers, Rutherford backscatt. meas. 80−65034
Si, surface, sputter etched, damage, contamination, ion backscatt. obs. 79−33167
Si surface electron beam deposited silicide formation using scanning CW laser beam 80−66862
Si, surface radiation damage cross sections, influence of distortions 80−6442
Si, thermal oxidation, high resolution Rutherford backscatt., implanted ions analysis 79−87911
Si thin crystal, electron backscatt. in electron microscope 78−75510
Si wafers, B predeposited, anal. by combined ion beam techniques and X-ray microanal. 79−5238
Si wafers, channelling dips for K and L X-ray prod., PIXE and Rutherford backscatt. anal. 79−4363
Si: As(Pb), high-dose ion implanted and annealed, implant redistribution 80−107309
Si:Ar, ion implant gettering of MOS capacitors using linear voltage ramp and N^+ backscattering 79−95502
Si:As, high-dose implanted, irrad. time and subsequent heat treatment effects on laser annealing 80−29041
Si:As, implanted, spatially varied activation during regrowth of amorphous layers, sheet resist. and backscatt. obs. 78−71749
Si:As, implanted, thermal diffusion of As 80−39352
Si:As, ion-implanted, CW IR laser annealing 80−34022
Si:As, ion-implanted, channelling anal. of CW Ar laser annealing 79−73186
Si:As, ion-implanted, laser recrystallisation by freq.-doubled Nd:YAG laser 79−77613
Si:As sputter rate meas. SIMS combination with Rutherford backscatter 80−21334
Si:As wafers, laser annealing, Rutherford backscatt., optical, and TEM obs. 79−1445
Si:As(Sb), implanted, pulsed ruby-laser annealing, Rutherford backscatt., TEM and ion channelling study 79−86805
Si:As(Sb), ion implant lattice location after pulsed ruby laser annealing 79−73204
Si:As(Sb), ion-implanted, thermally assisted Xe-flash annealing, Rutherford backscatt. meas. 79−10881
Si:As(Sb), ion-implanted, CO_2 laser annealing 79−73183
Si:Au Ar ion implant gettering obs. by MOS and Rutherford backscatt. techniques 80−39119
Si:B, self-interstitials location by Rutherford backscatt. of channelled ions 80−2101
Si:B diffusion at Si-SiO_2 interface, Auger spectra, Rutherford backscattering 80−70471
Si:B ion implantation, large-angle proton scatt., anal. using Promiss protonograph 80−19823
Si:B standards, ion implanted, absolute Rutherford backscatt. yields, accuracy 79−47572
Si:B(P)(As)(Cu)(Fe), dopant profile changes induced by laser irrad. using SIM and backscatt. meas. 79−69148

particle backscattering continued
Si:B(P)(As)(Sb), ion implanted, redistrib. of dopants by pulsed laser annealing 79−7620
Si:B(P)(As)(Sb)(Cu)(Fe), ion implanted, doping profile, pulsed laser annealing effects 80−88197
Si:C, disorder profiles by proton backscattering, proton bombardment annealing 78−47449
Si:Cu(Au), recoil implantation from thin surface films, backscatt. obs. 78−63783
Si:D, ion implanted, struct. of impurity centre 79−7623
Si:F, amorphous, thermal stability, comparison with Si:D 80−49542
Si:Fe(Cu)(Pt), implant redistrib. and enhanced solubility following laser irrad. 79−69129
n-Si:Ga laser doped, segregation, Rutherford backscattering 80−103483
Si:Ga(As), laser-doped, impurity distrib., Rutherford backscatt. and channelling anal. 80−59507
Si:Ga(Sb), epitaxial film, doping efficiency *(Japanese)* 79−73201
Si:Ge, regrowth behaviour from backscatt. and channelling meas. 80−2300
Si:N, ion implantation, refractive index, IR spectra, ion range and straggling meas. 80−34020
Si:Ne(Ar)(Kr), ion implantation damage, annealing, comparative study 79−10867
Si:O, Xe, ion implanted, Xe retention, Rutherford backscatt., comparison with SiO_2+Xe 79−4320
Si:P, Au gettering, depth profile anal. 78−91346
Si:P, diffusion-doped laser irradiation effects, electrical reactivation of P 80−39124
Si:P, implanted, two-stage laser annealing of lattice disorder 79−1452
Si:P, incoherent light flash annealing, elec. props., backscattering spectra 80−97504
Si:P, ion implanted, subsurface damage, TEM and channelled Rutherford backscatt. study 80−107337
Si:Pb, He^+ Rutherford backscatt. and TEM exam., implant species effect on recrystn. 78−47452
Si:Pb, ion-implanted and annealed, dose depend. of residual lattice disorder 77−43228
Si:Pb, lattice location of dopant and amorphous zones, by Rutherford backscatt. 77−68990
Si:Pb, low-solid solubility ion-implanted, pulsed and continuous laser annealing and furnace annealing comparison 79−73184
Si:Pb implanted layers, recrystn. on annealing, backscatt. and TEM obs. 77−51421
Si:Pt, depth depend. of atomic mixing by ion beams 80−29837
Si:Sb, high dose implanted, orientation dependent annealing effects 78−18665
Si:Sb, ion implanted, annealed, dislocation generation, channelling and Rutherford backscatt. meas. 80−88158
Si:Sb, ion implanted, annealing, Sb behaviour above solid solubility, Rutherford backscatt. meas. 80−88200
Si:Sb, ion implanted, Sb diffusion during oxidation, snow-plough effect 80−88366
Si:Sb, laser doping, evaporation loss and diffusion of Sb, under pulsed laser irrad. 80−59508
Si:Sb, low energy ion implantation, profile determ. 80−88176
Si:Sb wafers, laser annealing, Rutherford backscatt., optical, and TEM obs. 79−1445
Si:Sb(Ga)(Bi)(In), dopant solubility limit, laser irrad. effects 80−84295
Si/Pd system, solid phase epitaxial growth control by C ion implantation 80−75466
Si/Pd-W, contact reactions, backscattering, X-ray diffr. meas. 80−20040
Si/SiO_2 interface, transition region thickness, determ. by He^+ backscatt. 77−62762
Si-Al solid-phase epitaxial growth, substrate effects, SIMS and backscatt. spectra 79−42421
Si-As(Sb) temp. depend. of irradiation-induced displacement of impurities, backscattering meas. 78−26605
Si-Au system, ion implanted induced giant gettering, annealing effects 80−88221
Si-Au-Si, Auger line intensity, contrib. of backscattered electrons 79−65962
Si-$CoSi_2$Si, double heteroepitaxy, solid phase and MBE 80−104063
Si-Cr interfaces, metallurgical and electrical props. 80−60081
Si-epitaxial film, ionised-cluster-beam deposited, cryst. and elec. characts. 80−70553
Si-H, amorphous, H three-dimens. distrib., ion-induced AES and Rutherford backscattering 80−44132
Si-H (up to 15 at.%), amorphous, ion implanted, laser annealing obs. 79−69133
Si-metal interface, silicide formation, interface marker technique obs. 80−59734
Si-N film, passivation layer, density comp., and ref. index, Lorentz-Lorenz correl. 78−39697
Si-Ni(Pd)(Pt) film struct., silicide form. He^+ back scatt. and X-ray diffr. obs. 79−51442
Si-Pd_2Si-Si, Pd-silicide transport phenomena obs., MeV $^4He^+$ backscatt. spectrometry anal. 79−4491
Si-Pd-Si structure, epitaxial growth, backscattering and transmission electron microscopy studies of layered structures 80−80123
Si-Pd-Ti, silicide form. in evaporated films 80−80006
Si-SiO_2 interface, backscattering-channelling study 80−34320
Si-SiO_2 interface, MeV backscatt. channelling meas. of Si monolayers 79−11020
Si+Ga^+ ion implantation at high current density, lattice disorder, proton backscattering 80−34085
Si_xB_{1-x} films, anal. of H ratios and profiling using nucl. techniques and Rutherford backscatt. 80−61202
SiC, on Si and metal silicides, formation characteristics and mechanism, by ion backscattering techniques 79−60653
SiC:H amorphous reactively sputtered film, H content effect on film props. 80−75459
Si_xC_{1-x}:H reactive sputtering deposition, compositional and structural props. 79−99077
SiC(6H), ion-implanted, laser-induced recrystallization and defects 80−44221
Si_3N_4 layers, RF plasma deposition and props. 79−43155
Si_3N_4, oxidised ceramic, O_2 depth profiling using ^4He backscatt. 77−89463
Si_3N_4, reaction bonded, creep, internal oxidation effects 78−56701
SiO_2, amorphous anodic layer on Si, MeV light ion multiple through-scatt., backscatt. obs. 79−86828

particle backscattering continued
SiO_2, As diffusion , O_2 effects 78−43180
SiO_2 covered Si surface, scattering of keV H and He ions and neutrals 78−95638
SiO_2 film, grown on Si surface, in O_2-HCl mixture, Cl incorporation, Rutherford backscatt. meas. 79−70186
SiO_2 film, on Si, range distrib. of implanted As, He^+ backscatt. obs. 77−39611
SiO_2, RF sputtered, stoichiometry and atomic defects obs. 79−60647
SiO_2:Xe, ion implanted, Xe retention, Rutherford backscatt., comparison with Si-O, Xe 79−4320
SiO_x, metal layer interdiffusion Rutherford backscatt. 77−85000
SiO_x thin films on Si, anal. by backscattering techniques 79−96385
Si_xO_{1-x} films, anal. of H ratios and profiling using nucl. techniques and Rutherford backscatt. 80−61202
Si⟨111⟩/Al/Si, growth kinetics of ⟨111⟩ Si through Al layer by solid phase epitaxy 79−28236
Sn, beta-ray backscattering variation with target thickness, self-absorpt. coeff., Z depend. 79−78801
SnNi electroplate, anal. by SIMS, ion scatt. spectrometry, and Rutherford backscatt. 78−95979
Ta film, determ. of thickness and O, N content 78−80824
β-Ta film, Ta^{n+} transport number during anodic oxidation 79−39036
Ta on Nb duplex layers, cation-transport processes during anodic oxidation, Rutherford backscatt. and nucl. microanal. 79−20264
Ta_2O_5, ion-bombarded cryst., structural and compositional changes 79−46724
Ta_2O_5, XPS, low energy ion backscatt. spectra 78−72660
Ta_2O_5-TiO_2, anodic film, Rutherford backscatt., capacitance 77−16734
TeO_2 thin films, dielec. props. rel. to fabrication conditions 80−97199
Ti, energy loss spectra of C^{2+} ions 80−65114
Ti film, solid state reaction with Si or SiO_2 substrates, backscatt. anal. 80−34257
Ti, reflection of H, D and He ions 78−95640
Ti, stopping power of 0.5-2.0 MeV ^4He ions, elastic backscatt. meas. 78−87730
Ti-W films, bias-sputtered, quantitative anal. 80−80114
TiC film, CVD, on WC, diffusion processes, ion beam anal. 80−49424
TiO_2 layer form. by anodic oxidation, characterisation using ^4He backscatt. *(French)* 80−45433
$TiSi_2$, TiSi, Ti_5Si_3, formed by solid state reaction of Ti film on Si, backscattering anal., of layer structure 79−69377
Tll laser window films, stoichiometry, Rutherford backscatt. study 80−59831
U, in Hg plasma, sputtered atom angular distrib., mass effects 79−87538
UO_2 epitaxial films, epitaxial, channelling studies 79−49683
V single crystals, ion implanted, energy dependent channelling and backscatt. anal., $^4He^+$ ions, 1 to 2.8 MeV 79−4360
V thin film-amorphous Si interface, V silicide formation, backscattering diffraction meas. 80−2285
W, (001) surface, reconstruction and reordering by H adsorption, MeV ion scatt. studies 79−82443
W (001) surface structure by MeV ion backscattering, channelling 80−6605
W (100) single crystal, surface studies by MeV He scatt. 79−4455
W, (100) surface, scatt. of mol. and atomic H ions 79−69943
W (110), ionisation of hyperthermal Na atoms, temp. depend. 80−50504
W, backscattered energy spectra, charged particles energy losses 79−83086
W, CO adsorption, mol. orientation, ion scatt. 78−71949
W, channelling of H^+ and He ions, backscatt. particles ang. distrib. 79−51174
W crystal, backscatt. energy spectra, channelling particles energy loss determ. 78−2181
W, electron backscatter fractions 78−87717
W, H^+ and He^+ ion backscattering, reflection coeff. 79−43081
W, in Hg plasma, sputtered atom angular distrib., mass effects 79−87538
W, proton bombard., radiation damage, proton backscatt. obs. *(Russian)* 79−46720
W, reflection of H, D and He ions 78−95640
W single crysts., surface scatt. by MeV He ions 77−69952
WO_3 amoprhous film, sublimed under different conditions, elec. transport props. 80−7015
Wo_3, H^+ and He^+ ion backscattering reflection coeff. 79−43081
$(Y,Sm,Lu,Cu)_3(Fe,Ge)_5O_{12}$, ion implanted, hard bubble suppression 80−11238
YFe_2, amorphous, surface ferromag. layer, spin wave reson. Rutherford backscatt., and magnetisation meas. 79−73819
Zn, stopping power of 0.5-2.0 MeV ^4He ions, elastic backscatt. meas. 78−87730
$Zn_xCd_{1-x}S$ solid soln. films, reactive cosputtering, struct., comp. and opt. absorpt. edge *(French)* 78−6237
ZnS, clean surface, AES and LEED exam. 80−10762
ZnS, RF sputtered film, stoichiometry, chem. comp. 78−34727
$ZnSiP_2$, effect of crystal growth method, on physical props., effect of doping on physical props. *(German)* 79−52094
Zr-Au (0.3 and 0.2 wt.%), irradiated, backscattering meas. of Zr self-interstitial atom trapping by Au 77−69014
Zu, reflection of H, D and He ions 78−95640

particle beam diagnostics
14 UD Pelletron accelerator terminal, ion optics, high energy acceleration tube 78−33321
accelerator diagnostics using laser beam 80−95497
accelerator linear, intense electron beam transient radial motion 80−9434
acoustic signature of proton beams in fluid media 79−59317
AGS, microprocessor based beam loss monitor system 79−72070
AGS slow extracted beam, size meas. 80−37672
Alma Ata isochronous cyclotron, beam diagnostics, mag. field stabilising and resonator freq. control 79−54633
Arnold diffusion, numerical studies in Nekhoroshev region 80−37668
Arnold diffusion in near-integrable Hamiltonian systems with three degrees of freedom 80−37665
beam analysis tomography, current density and transverse/longit. emittance reconstruction 79−49336
beam optical components, anal. of misalignment effects 78−13355
beam position monitor for use with pulsed charge particle beams 79−59288

particle beam diagnostics continued
beam position monitor using a single cavity 79−72155
beam profile low matter secondary emission monitor 78−70665
beam profile monitor, determ. of intensity and polarisation profiles 79−76251
beam profile monitor using Rutherford backscatt., emittance and luminosity meas. 79−45497
beam profiles in uniform elec. field, including space charge effects 80−106222
beam profiling by backscattering from thin wires 79−59289
beam response information from longitudinal and transverse excitation 79−72151
beam scanner design for cyclotron facility 80−99365
beam spot measurements and beam divergence 400 keV electron accelerator 80−877
beam toroid for 750 keV polarised proton beam monitoring at ZGS 79−68072
BEAMSCOPE, device for meas. of emittances and betatron amplitude distribs. 79−72145
betatron, circulating electron current meas., ionisation method *(Russian)* 78−5069
betatron, orbit expansion and beam extraction, simulation 80−91353
bunched beam, coherent transverse instability induced by kicker magnet 80−58015
bunched beams, transport, second order aberrations 80−52801
CERN ISR, on-line Q meas. during phase displacement acceleration 79−72076
charged particle beam, short pulse detect. by reverse-current method 79−63856
charged particle beam homogeneity testing with surface barrier detector 78−25365
charged particle beam position detectors, dielectric use 79−26794
charged particle motion in mag. quadrupole element, linear transform. coeff. 80−78470
closed orbit distortions, stability of large synchrotron 79−76186
coherent radiation from electrons in transverse periodic fields 80−78748
coherent transverse bunch oscill. damping, in PETRA 79−72142
collective transverse beam instabilities, damper description, CERN SPS 79−72143
collective-effect electron acceleration 80−14016
colliding ring solenoidal detector magnetic system design and fabrication 79−31298
conductance for the gas flow of an accelerating tube 80−102359
conference, storage ring beam-beam interactions and nonlinear dynamics, Upton, NY, USA (March 1979) 80−36758
crossed-field energy analyser, stigmatic, focusing and dispersing props. 78−74832
current density meas. method for electron acceleration 80−102366
cyclotron, emittance measuring instrumentation, program for phase ellipse area *(German)* 78−58512
cyclotron beam emittance measurements with a dispersion-matched magnetic spectrograph 79−54732
cyclotron beam phase probe, isochronism studies at IUCF 79−54720
cyclotron beam transit phase automatic meas. 78−832
cyclotrons and beam lines, beam diagnostic techniques, review 79−54731
detector assembly for the Fermilab Energy Doubler 79−72156
detector systems for LEP 79−97952
deuteron beam estimation of density distrib. 80−68992
diagnostic instrumentation, recent improvements 79−72153
direct energy conversion optimisation with charged particle parabolic trajectories 80−37585
double cylindrical electrostatic sector as an ion energy analyzer 80−23208
Dynamitron 4 MV accelerator, energy calibration of analysing magnet 79−54736
Dynamitron tandem, energy calibration of heavy ion beam analysing magnet 79−59287
electron accelerator, electron current density distribution, approx. formula *(Japanese)* 80−14032
electron beam, pulsed high-intensity, self-focusing in low press. gas 80−32899
electron beam, relativistic, diocotron instability 80−27853
electron beam charge monitor, single pulse toroidal coil type 78−78036
electron beam current monitor using secondary emission detection 78−78033
electron beam diagnostics in the Fermilab electron cooling experiment 79−72147
electron beam spectrum monitor using synchrotron light 79−72146
electron cloud confinement, radial and longitudinal distrib. determ. 80−14928
electron relativistic beam in synchrotron, ang. spread of vel. using undulator radiation electron 80−14021
electron ring optical diagnostics using synchrotron radiation and light scattering meas. 80−5405
electrons in synchrotron, beam lifetime increase using pulsed mag. field 79−3265
electrostatic accelerators, beam transmission problems during design, operation, upgrading 78−33320
elliptical beam inside non-confocal elliptic vacuum chamber, potential 80−47799
emittance variations following guidance by quadrupole lens *(French)* 78−29679
energy spectrum monitoring in low-energy electron accelerators 80−68994
energy spread, cancellation by current loading 78−9007
EUT (Eindhoven) cyclotron, multi-input phase measuring system 79−54689
fast cyclotron beam emittance measuring device 79−54712
fast ion beam ($Z \leq 18$), semi-empirical determ. of charge states *(French)* 79−45867
Fermilab electron cooling expt., proton beam diagnostics 79−68005
fringing field effects in a cylindrical condenser 80−52821
fusion reactor, beam-profile fast scan monitor 78−54941
fusion reactor, DITE-II, neutral beam ion source particle beam identification 80−99397
fusion reactor, neutral beam injection reionisation power losses in duct, model 80−99385
fusion reactor, PLT, neutral beam duct reionisation losses, obs. and power loss model 80−99383
fusion reactor 120 keV neutral beam, calorimetric and optical beam diagnostics 78−54933

particle beam diagnostics continued
fusion reactor neutral beam injector, beam line studies 78−54969
generalised coordinate variation on crossing cyclotron gap *(French)* 80−37657
heavy-ion accelerator, dimensions of electron ring meas. by synchrotron radiation 80−42877
high current beam, bunching, autoacceleration in slow wave system 80−52805
high current ion beams, longitudinal bunching motion 79−68067
high intensity beam profile monitors for the LAMPF primary beam lines 79−72154
high resolution spectrometer facility at LAMPF, beam line 78−62674
high-current beam in focused channel, beam stability analysis 79−63325
HMI (Berlin) cyclotron, multi-input phase measuring system 79−54689
IHEP neutrino beam energy spectra reconstruction *(Russian)* 79−68119
intense ion beams in periodic channels, fluid and Vlasov stability 79−76225
invariant tori and cantori, variational principles 80−37666
ion beam, overneutralisation, by electrons in mag. field 79−10256
ion beam alignment and energy meas. analyser 79−6781
ion beam deceleration across mag. fields, expt. 80−99384
ion beam diagnostics by means of electron saturated plane Langmuir probe 79−94144
ion beam energy meas. of Van de Graaff accelerator using generating voltmeter 78−58508
ion beam impurity anal. by backscatt. meas. 78−70223
ion beam profile imaging by Ti tritide collector 78−78032
ion beam scanning device for rapid meas. of emittance and brightness 78−58522
ion temperatre diagnostic system design and operation at Princeton 78−54942
ionisation chamber, noninteractive beam position and size monitor for heavy ions 79−72149
ionisation profilometer for dynamic measurement of radial dimensions of electron beam in betatron *(Russian)* 78−13359
ISABELLE, bunched beams, instability threshold 80−37652
ISABELLE, linear and nonlinear beam-beam effects 80−37656
ISABELLE, nonlinear beam-beam interaction, computer model 80−37654
IUCF 200 MeV cyclotron, isochronisation studies 79−72087
JULIC cyclotron, beam phase detection with fixed intermediate frequency system 79−54711
K X-ray fluorescent multi-strip probe for accelerator beam studies 80−102362
KAM surfaces computed from the Henon-Heiles Hamiltonian 80−37664
Karlsruhe cyclotron, computerised diagnostics, control and extended beam optimization 79−54709
Kiev isochronous cyclotron, diagnostics of beam phase characteristics 79−54718
LAMPF, time resolved beam energy meas. 79−71995
LAMPF linac, Monitor remote-handling system, status, improvements and accomplishments 79−71997
LAMPF linear accelerator muon beam charact., surface and cloud beam polarisation 79−71994
linear accelerators, resonator sensor for the parameter of charged-particle beams 80−68991
liquid H chamber Lyudmila, electronic apparatus for expanded diagnostic system 80−23265
longitudinal beam behaviour, in KEK booster 79−76184
magnetic analyser for compact cyclotron 78−66439
magnetic analysis of charged particles, α-, β- and mass spectrometers *(Russian)* 80−87011
magnetic electron spectrometers and their in-beam use, review 79−68128
magnetomodulation device for current meas. of charged particle beam, 100 μA-300 mA 80−68993
MeV cluster ion beam diagnostics by calorimetry and time of flight spectra 80−13882
molecular beam, discharge characteristics from multichannel nozzle *(French)* 79−30603
molecular beam, modulated, detect. by electron bombard. detect. 79−2885
multichannel nanosecond pulse generator for cyclotron stroboscopic system 79−68168
Munich MP tandem, beam optical components, anal. of misalignment effects 78−13355
MWPC for beam definition in precision total cross section meas. 79−3268
nanosecond beam dynamics in linear electron accelerator 80−86996
NBS positron annihilation in flight facility, positron beam calibration 79−31306
neutral beam dynamics, paraxial approximation, single particle motion across magnetic fields 78−29890
neutral injection beam power monitor system for fusion reactor 78−54944
neutrino beam, monitoring systems, at the Protvino Institute of High-energy physics 79−9929
neutron filtered beams, 2 keV, 24 keV, 144 keV, calibration and use 79−9937
neutron rich fission fragments, excited state spin assignment, various methods 80−78506
normalized detector of beam transverse oscillations 79−93854
optical diagnostics of high-power neutral beam 79−17556
Orsay 200 MeV proton synchrocyclotron, beam optics and beam monitoring in beam lines 79−54636
particle dynamics computer modelling, alternating phase focusing LINAC *(Russian)* 80−23234
PETRA storage ring, intensity monitor, design, operation and performance charact. 79−72081
photon beam charact. of 20 MV accelerator for radiation therapy appls. 80−26430
PIA, positron intensity accumulator for PETRA injection 79−71984
planar channelling effects for relativistic protons and π^- mesons, deflection effects 79−77656
PLT, neutral beam test stand, data acquisition system 78−62622
polarimeter designs for high energy p and d beams, polarised beam spin anal. 78−58516
polarised atomic H beam intensities, effect of dissociator nozzle cooling 78−16895
polarised heavy ion beams, polarisation monitors 80−27910
profile monitor using holed sampling disc 78−54498

particle beam diagnostics continued
propagation of highly directed high perveance ion beams across mag. fields 79−49888
proton beam burst width and phase drift at the Indiana University cyclotron facility 79−76216
proton beam calib., limits on differential hysteresis in Enge split-pole spectrograph 78−55082
proton beam energy spread determ. from $^{12}C(p,p)$ excitation function at 14.232 MeV 78−70669
proton beam position monitor, based on detection of wall currents 79−58675
proton polarisation meas. for $^{12}C(p,p)$ at 40-75 MeV 80−52840
proton synchrotron, 12 GeV, beam size meas. by fast rotary scraper 79−72078
proton synchrotron, beam position monitor for ΔR feedback on RF system 79−72079
proton synchrotron slow extraction beam parameter monitoring and control system in CAMAC standard online with ES 1010 computer 78−29674
pulsed charged beams, phase meas. and control 78−58523
pulsed electron accelerator current density distrib. multichannel recorder 78−58520
pulsed electron beams, measurement of current density distrib. and energy spectrum 80−63426
pulseline driven neutralised linear ion accelerators, longit. instabilities 80−78459
quadrupole gradient-length product meas. device 79−76232
relativistic beam contraction in necked mag. field 80−9436
relativistic electron trajectories in self consistent field *(Russian)* 80−63435
resonant oscillations driven by a nonlinear forcing term 80−78473
RF field induced by a charged beam in a multigap resonator 80−52804
RF ion beam choppers, ion motion *(Chinese)* 80−99371
RF quadrupole beam dynamics 79−71986
scanning microprobe, digitally controlled for p and heavy ions 79−13571
scintillation hodoscope counter for beam meas. in CERN SPS 79−36472
second coordinate measurement in drift chamber using charge division method 80−27856
secondary beam profile monitor based on MWPC 79−6783
secondary electron imaging system for a nuclear microprobe 79−26799
secondary emission multiwire chamber for GANIL cyclotron beam tuning 79−54733
self-focused, relativistic, filamentation instability 80−74289
SIN, πE3 channel, cloud and surface muon studies 80−74055
SIN πE3 channel, pion prod. meas. 80−74056
space charge in beam transport 79−30610
SPEAR I, beam-beam limit simulation 80−37655
stable and unstable beam motions, mathematical statements 80−37663
stochastic cooling of particle beams, review 80−37675
storage rings, beam-beam interaction, radical diffusion simulation 80−37653
storage rings, beam-beam interactions, perturbation method solns. 80−37667
Texas A&M polarised proton beam meas. 80−102360
transition energy variation with momentum aperture in CERN ISR 79−76194
transverse beam instability in a resonator section, multimode approx. 80−52803
transverse coherent instability anal., in KEK booster 79−76183
TRIUMF cyclotron, meas. and corrections to beam props. 79−54710
TRIUMF stopped π-μ channel 80−102364
variable pion energies from a moderated fixed energy pion beam 80−78476
vibrating wire beam profile monitor for electrostatic accelerator with high stability 80−99368
wall current beam position monitor with improved low frequency response 79−72150
wall current monitor for KEK proton accelerator 79−72080
X-ray diagnostics on collective heavy ion electron ring accelerators 80−102358
π^- discrimination and absolute counting for nucl. capture at rest expts. 80−5432
Cs, ground state spins, moments, charge radii by laser spectroscopy 80−78147
He beam, magnetic spectrom. meas. using automatic tracking NMR system 80−27869
MgO scintillator prep. for viewing accelerator beam spots 79−6803
P ions, charge distrib., 72-123 MeV 80−27849
Rb, ground state spins, moments, charge radii by laser spectroscopy 80−78147

particle beams
see also atomic beams; beam handling techniques; electron beams; ion beams; molecular beams; particle beam diagnostics; particle optics
beam direct conversion for fusion injection at energies above 100 keV 78−13330
beam direct conversion for fusion reactor appl. 78−13329
betatron oscillation, short-cut method for soln. *(Chinese)* 77−34489
bunch lengthening due to potential well distortion from cylindrical cavities with beam ports 77−83375
bunching in cyclic focusing channel 80−23229
channel for high-current beam transportation, design parameters 79−59291
charged 2-dim. beams, invariance of order of focusing 79−94140
charged particle beam, collisional interaction with H target of arbitrary ionisation level 78−93095
charged particles, plane-symmetric finite-emittance beams, combined effect of space-charge and external fields 77−23605
charged sphere, particle emission into mag. field 80−69304
charged-particle beam, axisymmetric, focusing in hyperbolic electrostatic field 78−50688
charged-particle beam, current density distrib. calcs. 77−27238
coasting particle beam, RF fields due to Schottky noise 77−88632
coherent interaction between waves and particle streams 80−58452
collective acceleration methods based on high-current relativistic electron beams 79−18063
colliding-beam studies of atomic collision processes 79−31742
conference, theoretical aspects of beam behaviour, Erice, Sicily (1976) 78−78878
convergence conditions for particle in cell method *(Russian)* 79−76567

particle beams continued
CPS at CERN, pulse to pulse modulation, extraction modes, beam intensity 77−83277
cyclotron resonance, causing instability normal to beam *(Russian)* 79−13883
cylindrical beam of constant density, self-consistent description 80−78754
delayed coincidence techniques with accelerator beams, anal., optimisation rules 78−78598
dipole particles in axisymmetric electrostatic and magnetostatic fields, meridional trajectories 80−78750
effusive beam source, heterogeneous reaction type, chem. equilib. 80−52362
electron beam interaction with target, integral eqns. *(Ukrainian)* 80−32549
electrostatic energy analyzer with an approximately homogeneous field 80−78753
ellipsoidal charged particle bunch, self-consistent motion, approx. soln. 79−13881
energy loss of charged particles, review 79−95060
excited state populations, preparation, measurement and control, review 79−30607
extraction element design for long pulse multi-megawatt neutral beam 80−102373
fast particle beam differential scatt. instrument 78−86381
fluence and dose perturbations due to thin inhomogeneities 78−69219
fluence and dose perturbations due to thin inhomogeneities 78−69220
flux, single-component, generalised, like-charge particles, calc. methods 78−78877
focused 24 keV filtered neutron beam 80−63436
fusion, reactor, MFTF, neutral beam accel power supply protection 80−102380
fusion, TFTR, neutral beam sources overcurrent protection during spark down 80−102331
fusion reactor, Doublet III, neutral beam injector system, instrumentation and control 80−99322
fusion reactor, Doublet III, neutral beam interlock system using IR detector 80−106228
fusion reactor, field reversed mirror neutral beam startup, hybrid plasma code simulation 80−99313
fusion reactor, Heliotron E, neutral beam injector ion source power supply 80−99333
fusion reactor, ISX-B, neutral beam system 80−99388
fusion reactor, JET neutral injector overvoltage injection system 80−99398
fusion reactor, JIPP T-II, neutral beam injection system, design and expt. test 80−106226
fusion reactor, JT-60, prototype neutral beam injector unit 80−106225
fusion reactor, MFTF, neutral beam source development 80−102368
fusion reactor, MFTF, sustaining neutral beam power supply, shunt preconditioner, IBM-ASTAP anal. 80−102332
fusion reactor, neutral beam injector mag. cusp plasma source, design and fabrication 80−99377
fusion reactor, PDX, 6 MW Neutral Beam Project, overview 80−106223
fusion reactor, PDX, neutral beam elec. power system, ion source supply upgrade 80−102330
fusion reactor, PDX neutral beam injector, ion accel. structural anal. 80−102375
fusion reactor, PDX neutral beam injector development 80−99375
fusion reactor, PLT, neutral beam injection, power input and plasma temp. reconciliation 80−106224
fusion reactor, rectangular plasma generator, advanced ion source for ion injectors 80−99376
fusion reactor, TFTR, neutral beam injector prototype, construction and performance 80−99390
fusion reactor, TFTR, neutral beam injector test facility construction 80−102336
fusion reactor, TMX, injector system mech. design and installation 80−99393
fusion reactor, TMX, neutral beam control systems 80−99323
fusion reactor, TMX, neutral beam system startup 80−99306
fusion reactor, Wendelstein VII-A, neutral beam injectors, performance 80−99389
fusion reactor neutral beam injection, 120 keV, ion source 80−91357
fusion reactor neutral beam injection, 24 MW 400 keV H beam 80−91356
fusion reactor neutral beam source, 40 kV for TMX, engineering design 80−91358
fusion reactor PDX, ORNL prototype neutral beam injection system, ion source development 80−99391
fusion reactors, TFTR neutral beam support system 80−102376
fusion reactors, Wendelstein VII and ASDEX, neutral beam injectors, HV power supply system, thyristor control 80−99332
general purpose 1 GeV/c separated beam at Argonne ZGS, operation and design 77−10516
gravitoelectric antennas, direction sensitive, using uniformly moving charged particle beam 79−9164
Hadamard beam spectroscopy, computer simulation 79−93254
Hamburg isochronous cyclotron, influence of phase or time struct. of internal beam on extraction conditions *(German)* 78−94155
high-current relativistic beam, bunching, 2-dimens. finite size particle model 78−9310
high-power neutral beam, spectral resolution by optical diagnostics 80−33819
hyperfine interactions on charge particle beams, review of experimental methods *(Russian)* 79−13884
hyperon beam physics, review, book contrib. 80−68503
intense particle beams, production and handling 79−76117
ISR, CERN, overlap knock-out effects 77−83251
ISR at CERN, high luminosity operation, 26 GeV/c proton beams, loss rates, background control 77−83276
JXFR, neutral beam injection system, gas-beam interaction secondary particles 80−106227
kaon intense low-momentum beam at Argonne ZGS, design and operation 77−10515
LAMPF stopped muon channel 79−68115
light particles, model, three-particle scatt. rates, disconnected T matrix singularity 78−32726
light particles, three particle scatt. rates, double scatt., T-matrix singularities 78−32727

particle beams continued
magnetic interaction of moving current with thin conducting plate 77−19151
magnetomodulation device for current meas. of charged particle beam, 100 μA-300 mA 80−68993
metal neutral beams, low energy (0.1 to 10 eV) prod. by laser vaporisation of metals 80−77910
Migma-type solutions of the Vlasov equation in cylindrical coordinates 79−81082
molecular beam parameters meas. in presence of residual gas 79−27727
monochromatic and polarised photon beam at Frascati 80−23239
multiple scatt. of particle beams, axial mag. field effect 78−70712
muon beam channel, 40 GeV/c, Serpukhov, lens, guide reflector, filter 77−18729
muon channel, axisymmetric high flux 79−54727
muon low momentum surface beam for LAMPF 78−70672
neutral, efficient, high-power, high-energy, for reference mirror fusion reactor 79−49836
neutral beam, 120 keV, for fusion reactor, calorimetric and optical diagnostics 78−54933
neutral beam, continuously operating, convectively cooled ion accelerator, mech. design and fabrication 80−102374
neutral beam diagnostics of ion temp., Princeton large torus 78−54942
neutral beam generation, negative ion revolving multiple beam instabilities *(French)* 80−47798
neutral beam injection system power supply, 80 to 150 kV, development program 78−13367
neutral beam injection systems for plasma heating, beam intensity distribs. 77−34055
neutral beam injector, continuous operation, water cooled U-tube extraction grid 80−99392
neutral beam injectors for mirror reactors, arc snubbers 78−13333
neutral beam line upgrade for laser initiated target expt. 78−13334
neutral beam module, 80 keV 78−54917
neutral beam module component design and development for fusion reactor 80−91270
neutral beam source, cryopumping and mag. shielding, fabrication and operating cost 80−106229
neutral beam source manufacturing at Lawrence Livermore Laboratory 80−102377
neutral beam system for TFTR Tokamak 78−13331
neutral injection beam power monitor system for fusion reactor 78−54944
neutral injector modular cryopumping system 80−105656
neutrino, beam channel characts., Protvino Inst. 78−37474
neutrino beam, monitoring systems, at the Protvino Institute of High-energy physics 79−9929
neutrino focusing system, pulsed power supply 79−9974
neutron, non-monochromatic, spin flipper with prolonged working area 80−37673
neutron beam experiments *(Japanese)* 80−27684
neutron beams of the Leningrad Institute of Nuclear Physics synchrocyclotron 80−87003
neutron filtered beams, 2 keV, 24 keV, 144 keV, calibration and use 79−9937
neutron production by neutral beam sources, shielding design criteria for fusion program 80−99387
neutron radiotherapy facility at Fermilab 77−86590
nuclear polarised beams, review of appl. 79−45243
nuclear polarization, recent advances in technique 79−30822
PDX neutral beam injector, multi-aperture ion accel. electrodes thermal anal. 80−102371
periplasmatron ion source for intense neutral beam 80−99380
phase space imaging of charged particle beam by frictional forces 78−17850
phase space meas. at 2 MHz particle rate 77−54383
plasma science, conference, Monterey, CA, USA (May 1978) 79−37442
polarised beams, acceleration and storage 78−58518
polystyrene latex sphere beams, secondary electron emission 77−24914
positron beam, produced in electron-positron plasma by relativistic electron beam 79−19053
positron beam, relativistic, collimation in single cryst. 79−23669
potential and field produced by elllptical beam in confocal elliptic vac. chamber 77−83798
proton, LWR fuel enrichment 79−13497
proton, nuclear fuel enrichment 79−13498
proton beam burst width and phase drift at the Indiana University cyclotron facility 79−76216
proton beam calib., limits on differential hysteresis in Enge split-pole spectrograph 78−55082
proton beam energy spread determ. from $^{12}C(p,p)$ excitation function at 14.232 MeV 78−70669
proton intense beam production, ~1 MeV, pinched electron-beam diode 77−10521
radiation generated by charged beam near plane flanged waveguide 79−13880
relativistic, in medium, energy meas. by spontaneous γ-radiation emission *(Russian)* 78−29891
relativistic, injected into strong mag. field, cross-section limiting 80−5427
relativistic beam contraction in necked mag. field 80−9436
relativistic channelled particle beam, induced radn., tunable laser prod. 79−18391
relativistic charged beams, radiation cooling by channelling 77−72641
relativistic collimated particle beam ave. particle energy meas., difference method 80−14049
relativistic self-pinched beam, radial expansion with distrib. energy, anal. 80−19609
resonator, transient process, excited by beam 79−81347
secondary particle beams from accelerators, average momentum and comp. meas. 77−65382
sectioned Faraday system for time meas. of current-density distrib. over cross section 77−46455
SIN meson factory, facilities and expts. 78−13360
single-mode oscillations in slow-wave structure, max. beam current 78−71024
slow positron form. in MgO-coated moderators 80−62796
small spherical particles, focusing by axisymmetric mag. fields 80−78755
space charge in beam transport 79−30610
spatial distribution, poles of spherical harmonic 77−13575
particle beams continued
sputtered particles, vel. meas. by Doppler-shift laser spectrometer 80−62638
stored beam energy loss to vacuum components, particle bunch simulation meas. at PETRA 77−83258
synchrotron, beam parameter diagnostics via IR undulator emission *(Russian)* 78−836
thermal neutron beam, Soller slit collimators 77−45916
thermal neutron polarisation anal. experiments, corrections for instrument component inefficiencies and sample multiple scatt. 78−29725
TRIUMF neutron beam, monoenergetic polarised, 200 to 500 MeV 79−13573
turbulent stream, charge density vol. distrib. *(Russian)* 80−74288
ultra cold neutron production, by Bragg reflection from moving crystal, Monte Carlo simulation 79−701
ultrarelativistic beam anlaysis assuming classical ideal-gas statistics, algorithm 78−63003
uncharged spherical particle stream, longitudinal focusing by elec. fields in vac. 79−64165
vaporisation, partial wave propag., influence of rapid particle fluxes *(Russian)* 79−38696
d beam monitoring using $^{63}Cu(d,p)$ and (d,p2n) reacts. 79−36249
ψ particles and charm, 1975 and 1976 expts. *(Czech)* 79−26288
beam prod. from isotopically enriched sputter targets 80−23221
^{48}Ca, beam prod. from isotopically enriched sputter targets 80−23221
H isotopes, techniques for uniform charged particle generation, fusion reactor fuel 78−86682
H molecular ions beams, appl. to prompt nucl. react. anal. 79−36452

particle counters *see counters*

particle counting
counting of microscopic particles in disperse systems (aerosols, colloids etc.)
aerosol, photoelectric analyser, theoretical anal. of optical detector 79−67455
aerosol particle size meas., optical particle counter calibration by Doppler shift spectrometry 80−68173
aerosols, dispersity analysis, automatic photoelec. analyser for size range 0.3-40 μm 80−57251
air pollution appl. 79−70502
airborne, quantitative measurement by laser beam *(Japanese)* 77−29426
dust meter, EIP-9M, with optical and inductive-charge transducers 79−17595
intensity correl. spectroscopy, spherical particle continuous distrib. meas. 78−21228
Knollenberg light scattering counters, response to doublet latex aerosols 80−37152
laser applications in particulate analysis, multiple ratio single particle counter 78−35732
laser microphotometry with laminar hydrodynamic focusing 77−37965
leucocytes, differential counts, comparison between light and electron microscopic results 79−5429
liquid system monitoring for particulate contamination 77−28956
liquid-borne solids monitoring, optical instrument general principles 79−37424
metallic sample, specific activity determ., by mathematical modelling *(Rumanian)* 79−63881
optical electronic device for particle counting and vol. determ. in suspensions 78−57894
optical particle counters, field comparison 79−12279
optical-digital training method for particle counting by size 77−71305
particulate velocity and density meas., using microwave Doppler effect 77−27628
radioactive tracer detection techniques, flow problems appl. *(Japanese)* 78−96320
Royco aerosol particle counter 225, data processing system and modified system props. 80−37005
simulation unit for counter circuitry testing 78−81002
single particle trajectories, through ionising regions 79−6218
smoke detector design and smoke props. 79−63331
submicrometre particle detector and size analyzer 79−75672
unstable systems, repeated measurements effects, homogeneous chamber and general case 77−41563
unstable systems, repeated measurements effects, primary decay law in spark chamber 77−41562
unstable systems, repeated measurements effects, theory 77−22517

particle detectors
see also bubble chambers; ionisation chambers; particle track visualisation; position sensitive particle detectors; streamer chambers
1-hit, dose-response functions 77−65407
$4\pi\beta$-γ coincidence method for radioactive source standardisation *(Rumanian)* 77−46472
ΔE-E sample particle ddentification with wide dynamic range 80−14058
accelerated detectors, thermal like behaviour, quantum noise 79−139
acoustic detection of high-energy particles in water 79−59307
acoustic detector for beta and gamma radiation *(German)* 79−63876
acoustic detectors, technique for >10 TeV air shower expts. 79−62691
activation detector ave. cross sections in ^{252}Cf benchmark field 78−82598
activation detectors for meas. parameters of slow neutron field in channel of VVR-M-type reactor 79−31325
air showers for 10^4 to 10^6 particles, lateral distrib. of EM component, detection 80−17459
alpha survey instrument, portable 79−22535
analogue detection device for mol. beam scatt. expts. and vel. anal. 78−33635
analogue signal fast acquisition, for large particle detectors, CYCL-OP 78−17534
angular distribution meas. of recoil prods. of high-energy nuclear reactions, geometry calcs. 77−6596
automatic power control of IRT-M reactor using in-core detector system 77−50264
average solid angle subtended by right circular cylinder from distrib. sources, Monte Carlo calc. 77−67950
averaging within field of view, effects on recording equipment 78−53098
backscattered electron detector, forensic appls. 80−68319
backscattered electron detector, solid state, operating at TV scan rates in scanning electron microscope 79−18089
baseline restorer, deterioration of S/N *(French)* 77−3237

particle detectors continued
beam handling and detection system matching for optimum resolution in nucl. physics 79−45504
beam-position pickup, for relativistic electron beams 77−65392
black holes and particle detectors 78−12287
bolometer, fast superconducting instrument for molecular beams 78−86383
breakdown counter for fission fragments 77−38563
calorimeter, energy calibration of liq. Ar detector for EM showers 78−37497
calorimeter for high energy photons 79−36469
calorimeter for ion implanter neutral beam component meas. 79−30605
calorimeters, for meas. of ions, X-rays and scattered radiation in laser-fusion expts. 78−16800
CAMAC hodoscopic recording system, coding and reading data unit 78−13397
cellulose acetate solid state track detectors, catalytic oxidation sensitization *(Chinese)* 80−102399
cellulose acetate solid state track detectors, swelling sensitisation *(Chinese)* 80−99422
cellulose nitrate SSNTD, energy resolution enhancement for alpha particle detection 80−91392
Ceratron multiplier, for plasma diagnostics on charge-exchanged fast atoms, local counting efficiency 77−51233
CERN polarised d target, apparatus for two-body scatt. expts. 79−31287
CERN proton synchrotron, electron ring addition proposal, possible detection system 78−55062
channel detectors, operation and charact. *(Czech)* 77−18747
channel electron multiplier role in picosecond resolution time vacuum tubes 77−54429
channel multiplier made of phosphate glass 77−34522
channel plate electron multiplier, gain, detection dynamics *(French)* 78−46229
channel plate electron multipliers, direct detection of minimum ionising charged particles 77−54447
channel plate electron multipliers, single electron detection and timing 80−9458
charge sensitive high resolution amplifier 77−88352
charged particle beam position detectors, dielectric use 79−26794
charged particle spectrometer telescope 80−42895
charged particles, identification from nuclear reactions *(Rumanian)* 78−58564
cholesteric liquid crystal non-ionising radiation monitor, response charact. 79−2818
colliding ring solenoidal detector magnetic system design and fabrication 79−31298
combinatorial logic trigger system 77−54465
conference, nuclear power systems, San Francisco, CA, USA (Oct. 1979) 80−56994
contamination detectors assessment, w.r.t. German 1977 protective measures *(German)* 78−86693
continuous radiogauges with digital meas. system, dynamic charact. 79−59311
controllable secondary electron emission method for particle detection 77−30711
converted backscattered electron detection 80−68318
cosmic ray apparatus, transition radiation detector system for high energy hadron interactions research 77−61651
cosmic ray detection, acoustic radiation by charged atomic particles in liquids, theoretical anal. 79−89526
cosmic ray for high energy interactions above 10 TeV, summary 79−62706
cosmic ray muons and neutrinos, deep underwater detectors 80−8546
cosmic ray telescope, solid state, detection system for heavy ions, element and isotope separation 80−67563
counter telescope for neutron induced charged particle reactions, finite geom. correction 77−57815
current pulse counter for fission fragments 77−38564
cylindrical detector efficiency for off-axis point sources 79−49902
cylindrical particle analyser, fringing field 78−94165
data processing, high speed, histogram and tape writing 80−58101
dead time meas. of individual detecting system 80−9470
dead time of ionising radiation detectors, exptl. determ. 79−26826
deep water muon and neutrino detector appl. *(Russian)* 78−55109
diamond, radiation detector for light and charged particles 78−49900
diamond detectors, transport props 85 to 700K 79−45542
dielectric particle detector under pulsed power supply 80−74086
digital data logger, microprocessor-based, for radiation detectors 79−26848
digital radiation monitoring, plant-wide systems, design alternatives 79−41082
digitiser system, large scale, analogue convertors 77−54427
dosimetry diodes, irrad. by γ-rays and fast neutrons, lattice defect annealing *(Czech)* 79−45570
drift chamber two-dimens., with thin printed-circuit tape delay line 77−54422
drift chambers, flat helical delay lines for position readout along anode wire 77−54426
dust meter, EIP-9M, with optical and inductive-charge transducers 79−17595
EAS research, primary cosmic ray energy $>10^{17}$ eV, equipment system parameters, capabilities 77−64569
electron capture detector for liquid chromatography 79−16091
electron counting frequency meters with integrated electronics components *(Russian)* 79−72205
electron multipliers with discrete and continuous dynodes, detection of 5-50% keV electrons *(German)* 79−97946
electronics in nuclear science and technology 80−9347
energy analyser for charged particle energy and angle meas. in ultrahigh vacuum 78−86750
Faraday cup detector and digitizer for routine monitoring of ion emission from laser-driven implosions 80−57268
fast neutron detector (long counter) absolute calibration by associated activity technique 79−6801
field ionisation device for neutral particles, appl. to He^+ pulse height defect in Si 77−50330
finite geometry effects in scatt. expts., numerical integration method 78−82596
finite opening geometry effect on directional flux distrib. meas. 77−17362
fissile resistors, appl. to intense neutron flux pulse meas. 79−31326
flight chamber, fast large area zero time detector 77−18743
focusing ion detector and mass filter for use with time-of-flight vel. distrib. measurements 80−4819
Gaussian peak best fit, simple algorithm *(Italian)* 78−58538
Geiger counter circuit simple and inexpensive 79−63866
graphite calorimeter, multisection, for energy distrib. in high current relativistic electron beam 77−46456
gravitational emission detectors, optimum quantum meas. *(Russian)* 78−45556
gridless retarding potential analyser for use in very-low-energy charged particle detection 77−5343
hadron calorimeters, resolution determ. 77−30717
hadron-hadron hard collisions, calorimeter trigger, Ochs-Stodolsky scaling law derivation, parton model 79−17775
heavy ion transmission detector, TOF appl. 78−46208
heavy ions, experimental methods, targets and detectors, book 79−31242
heavy-ion reactions, ΔE-E particle identifier system 79−746
high energy phys. instrumentation, future needs, detector props. 78−33377
high energy physics detectors−limits to growth 79−89537
historical perspective of early detectors and counters 79−72189
hodoscopic detector registration systems, data coding/reading block 78−78602
hybrid pulse pile-up rejection system, appl. to Rutherford backscatt. 77−54468
in-core neutron detector using magnetically focused electrons 79−45564
inert gas mixtures, high-pressure discharges in nonuniform elec. fields. 78−74545
International Sun-Earth Explorers 1 and 2, medium energy particles expt. 78−85811
ion beam detection with VELU-6 channel multiplier 77−74555
ion beams, position location and profile measuring system for ion accelerators *(Croatian)* 77−75025
ion counting, operation of mass-depend. channel electron multiplier 78−5375
ion detector, Daly-type, plasma ion energy meas. 78−22570
ion detector, electro-optical, for spark source mass spectrometry 80−42246
ion detector *(Chinese)* 80−78496
ion sensor, low-energy, for space meas. with reduced photosensitivity 78−53764
ionisation detector for pulsed gas valve mol. beam source 78−66690
jet bias effect due to small detector size 79−22562
large mass detector for high energy neutrino interactions in Fe 78−29706
light integration boxes, painting technique 77−65403
liquid Ar calorimeters, props. of EM and hadronic showers 79−45599
LMFBR failed-fuel detection using gaseous fission-product detectors 79−97856
Lohengrin mass separator, techniques for fission product mass and charge distribs. *(German, English)* 78−16891
low background cold cathode ion source for molecular beam detect. 78−54506
low-background detection system for neutron reaction expts. 77−54395
magnetic analyser system, high resolution 78−66451
magnetised Fe-scintillator sandwich total absorption calorimeter, performance at 15-140 GeV 78−55103
Mariner-Jupiter-Saturn low energy charged particle expt. 77−70971
MARK J detector at DESY 80−95282
mean number of charged particles, method for determ. using low-efficiency detectors 77−42221
metal-nitride-oxide-semiconductor transistor as a radiation dosimeter detector 79−22486
microchannel plate detectors 79−72200
microchannel plate technology and applications 79−23075
microchannel plates, elec. props. during and after high-temp. vacuum bakeout 79−97935
microchannel plates, high gain, performance characteristics 78−37526
microfoil conversion electron detector for Mossbauer spectroscopy 78−70698
microprocessor-controlled data acquisition system for temporal/angular correl. between β- and γ-ray emission *(Spanish)* 80−106238
mirror field ion-electron convertor, particle trajectories, IBM 360/91 computer calcs. 77−6626
modular calorimeter system for hadron detection in high energy physics 79−41070
molecular beam detector, state-resolved, using laser and optical fibres 79−54999
Mott electron spin polarisation analyser, capable of inline meas. 79−17560
multi-needle detector with cathodic focusing *(French)* 80−102391
multichannel plate, detectors, operation, struct., performance charact. 78−12758
multiple detector data acquisition system, microcomputer based 78−90049
multivariate discrete information analyser, particle recording appl. 78−78601
natural quartz SSNTD, etching charact. 80−91401
neutral particle detection, channel electron multiplier characteristics 78−58554
neutral particles, detect. and energy anal., review 78−82590
neutron detection, using Dy_2O_3 activation detectors 80−887
neutron detectors for in-core flux monitoring 80−5297
neutron detectors in high-energy X-ray beams, photoneutron prod. 78−94174
neutron flux density meas., self-powered detector using current transducer *(Czech)* 77−50328
neutron instrument calibration checks, neutron source calibration at NBS 77−38540
neutron precision long counters, calibration for use with filtered neutron beams *(German)* 78−58529
neutron radiography by solid state nuclear track detectors 80−97671
neutron recoil proton counter, $^1H(n,n)$ 180° cross sections 79−36240
neutron spherical survey meter response 80−18679
ngutron detector for determ. of transuranic element comp. of nuclear fuel cladding hulls 80−63471
normalized detector of beam transverse oscillations 79−93854
nuclear accident dosimetry system, Czechoslovakia 80−57978

particle detectors continued
nuclear failed fuel element detection by delayed neutrons using solid state track-etch technique 80−5249
nuclear fuel nondestructive assay instruments, in-line evaluation 79−85589
nuclear radiation detection lab., desk top calculators 80−36821
nuclear track detector, appl. as neutron dosimeter, reponse to standard neutron sources 80−5342
on-line radiation monitoring at fuel reprocessing plant 79−85731
online filtering 79−89574
open microchannel multiplier secondary electron multiplication efficiency and nonlinearity 77−79513
optical gas-discharge chamber, spectrometric characts. in pulsed proportional amplification regime 79−97942
optical particle counter, portable, using He-Ne laser, for particles with 0.06 to 10 μm diameter 79−75674
optimum design of expts. on exponential absorpt., statistical errors anal. 78−885
particle multiplier gain factors for singly charged alkali ions 77−30215
passive personnel portal detectors for nuclear materials diversion protection using gamma-ray and neutron detectors 80−78389
peak detector circuits, use with single-particle detectors and multichannel analysers 80−37707
photicon, 2D array imaging detector for visible light, review of imaging characts. 79−45554
plasma-acoustic method of detecting large specific energy yields, principle 78−9037
plastic track detectors, method of producing thin sheets of proton-sensitive CR-39 80−35155
pocket calculator as counting cct. and display *(German)* 77−14314
polarization sensitive detectors, review 79−72207
polymer films as ultrasoft X-ray counter windows *(Chinese)* 78−82083
portal monitors for detecting and safeguarding special nuclear materials 80−63406
position readout by charge division, large two-dimens. detectors 77−54421
position sensitive 2-D detector for blocking expts., electronics and computer interface *(German)* 77−38551
position sensitive detection, courting pulse stacking method 77−10556
position sensitive detector for heavy ions in keV range 77−10548
position sensitive parallel plate avalanche detector for heavy-ion X-ray coincidence meas. 77−30719
programmable combinatorial logic trigger system for high energy particle physics expts. 77−38589
programmable command and data acquisition equipment *(French)* 77−54464
proton detection, helical channel electron multiplier, characts. *(Russian)* 79−3324
proton spectrometer/polarimeter for photoreactions below 1 GeV 80−18751
protons detect. efficiency of resist. strip mag. electron multiplier particle-counting system 77−10552
pulsed charged-particle beam, acoustic detector 77−30727
pulses time positions, meas. methods review 77−65410
PWR neutron flux detectors, reliability tests *(French)* 80−32403
quark, stable, detection using cyclotron mass spectrometer *(Czech)* 78−86375
quark detection using Nb balls *(Czech)* 79−26850
radiochemical solar neutrino detectors using (ν,e$^-$) reaction, (p,n) background from cosmic ray muons 77−61650
radiometric system design, mathematical modelling of relevant physical processes *(Rumanian)* 79−59313
radionuclide calorimeter for liquid He range 4.2 to 8K 79−18093
radionuclides in reactor circuits, continuous meas. techniques *(French)* 79−97857
random summing in multi-detector counting system meas. radionuclide mixtures 80−36097
recoil spectrometer for 5 GeV pion-He interactions 78−90011
relativistic charged particles, energy fluctuations of transition radiation 78−62681
review of methods of detection and appl. of electronics and computer technology 80−106235
review of the evolution and use ot nuclear detectors and systems 79−72188
secondary emission detector system for beam profile monitoring 77−83402
sectioned Faraday system for time meas. of current-density distrib. over beam cross section 77−46455
segmented calorimeter, high energy performance, Monte Carlo simulation 80−58029
self-powered detectors for incore monitoring 79−45367
self-powered neutron and gamma-ray detectors, review 79−45558
self-powered neutron detectors for incore meas., comparative performance 79−45369
self-powered neutron flux detectors, Pt, V and Co, response in mockup Bruce reactor core 78−58391
self-powered threshold gamma-ray detector, appl. for estimation of reactor kinetic parameters 79−59306
semiconductor, with alternating bias, formation of signal 79−13608
semiconductor charged-particle detector manufacture 79−93886
semiconductor particle detector utilizing impact ionisation, resolution 77−6639
SIMS detector sensitivity improvement 79−26172
solid dielectric detectors with breakdown phenomena and their applications in radioprotection 80−91388
solid state ionisation current comparator 77−23383
solid state nuclear track detectors, reactor neutron fluence meas. using Au and In foils 80−69035
solid state nuclear track detectors, review 80−37696
solid state track detectors in solutions of actinides, α track registration 80−63486
solid-state, glow technique for heavy ion induced nuclear react. investigs. *(German)* 77−14321
solid-state integrated cct. micro-detectors for high energy experiments 77−30705
solid-state track recorder applications in U.S. nuclear reactor energy programs 80−95506
space instrumentation for charged particles meas., review *(Russian)* 77−17368
Spanish reactor monitoring instrumentation *(Spanish)* 77−38420
SPS beam instrumentation, closed orbit correction 77−83305

particle detectors continued
SSNTD, AA 80−95500
SSNTD, alpha sensitive plastic detectors for Rn gas conc. meas. 80−94617
SSNTD, alpha sensitive plastic films for Rn gas conc. meas. 80−94618
SSNTD, appl. to meas. reaction parameters for Pu(n,f) reactions 80−91201
SSNTD, appl. to the search for superheavy elements 80−91200
SSNTD, automatic scanning techniques 80−91387
SSNTD, cellulose nitrate, for high energy neutron spectrometry 80−91394
SSNTD, development and appls., [conf. Nilore, Rawalpindi, Pakistan March 1979] 80−90608
SSNTD, development of etched nuclear tracks 80−91384
SSNTD, effect of etching conditions on energy resolution of phosphate glass and polycarbonate detectors 80−91390
SSNTD, electrochemical etching studies of the CR-39 plastic 80−91391
SSNTD, nuclear track research activities at GSI 80−95501
SSNTD, review of appls. in fission physics 80−91396
SSNTD, track registration and development efficiency 80−91385
SSNTD, track registration and development efficiency 80−91386
SSNTD, visualization of latent damage trails etching, decoration and observation techniques, review 80−91382
SSNTD for detection of heavy cosmic rays aboard Cosmos-936 80−94663
SSNTD for exam. of heavy ion reactions, multiprong events due to multiple sequential fission 80−91199
SSNTD for fast neutron meas. 80−91393
SSNTD to detect environmental α-emitters from natural sources 80−91292
SSNTD using mica muscovite for high neutron fluence meas. 80−91395
STV 4 counting set, features *(Croatian)* 78−78590
submicrometre particle detector and size analyzer 79−75672
superconducting double multivibrator used as near- and medium-infrared radiation detector *(German)* 80−90892
superconducting magnet system for time projection chamber at PEP 79−31320
superconducting microbridges, basic props. and appls. 77−26400
superheated supercond. colloid as a total absorption detector preliminary calcs. 78−78579
superheated superconducting colloid shower detector, rel. electron detection 0.1 to 6.0 GeV 80−91398
superheated superconducting detectors, magnetic field dependence 80−27893
superheated superconducting suspension as transition radiation detector, electron meas. 77−6628
survey assay meter developments at BNL for nuclear materials safeguarding appls. 80−69038
synchronization of time measurements at widely spaced locations, VLF radio signals and standard TV transmissions 80−63487
systems for intermediate energies 77−18750
thin Pb-Ar calorimeter, hadronic and EM cascade discrimination 77−65401
Time Projection Chamber expt., large high-current density superconducting solenoid 79−54219
time zero detector using isochronous transport of secondary electrons 77−30700
track density, device for determ. in solid-state particle detector 79−85859
track structure theory in radiobiology and radiation detection 78−50446
tracking chamber based on semiconductor detectors *(Russian)* 78−872
transition radiation detector, unconventional, data for X-rays, pions and protons 77−88341
two coil pickup, for meas. of electron beam parameters in adherer during compression 77−65393
ultra-sensitive particle identification systems based upon electrostatic accelerators, review 79−72182
ultrarelativistic charged particles traversing stable liquids, acoustic emission, particle detection possibility 77−61653
vacuum emission detector sensitivity to γ-rays 77−54462
visual ion beam images, on insulator surfaces, by the coincident interaction of a rastered electron beam 79−3622
wide-angle electron detector 79−21144
X-ray imaging, conf., Reston, USA (Apr. 1977) 78−45762
X-rays in solid state devices, algorithm for energy deposition at Au-Si (polyethylene) interfaces 77−28648
zero degree detection system at Orsay MP tandem 78−13353
α particle meas. in coincidence with X and γ rays 79−26851
ψ particles and charm, 1975 and 1976 expts. *(Czech)* 79−26288
Ag activation detector, determ. of neutron yield from pulsed neutron sources 79−31332
Al granular superconducting bolometer as mol. beam detector 80−73524
Al-NbTi solenoid magnet for high energy particle detector, conductor and cryostat design 79−31319
BF_3 detector ageing, depend. of temporal distrib. function 79−63872
CdS, luminesc. from heavy ion tracks 78−88365
CdTe detectors, nonlinear response 79−93878
CdTe metal-semicond.-metal detectors, degradation characts. due to e and γ irradiation 79−45543
Cu as activation detector for thermal neutron meas. 80−52814
Ge detectors used for high resolution gas ray spectroscopy 79−6804
Ge p^+-n-n^+ and p^+-i-n^+ structures, inhomogeneous, influence of longitudinal mag. field 77−1479
H atoms, detect. efficiency of resist. strip mag. electron multiplier particle-counting system 77−10552
H atoms in metastable 2s state, detector suitable for time-of-flight studies 77−3492
H_2O, acoustic rad. from ionising particles 78−71793
^3H monitors, calibration technique *(Czech)* 80−74075
Li transition radiators for electron identification at CERN ISR 77−30704
MgO dielectric detector characteristics 80−27898
Nb, point contact Josephson junctions, thermally recyclable, as low-noise mixers 78−62224
Pb/liq. Ar shower counter systems of SPEAR Mark II detector 78−37495
Pt self-powered detector, neutron sensitivity calc. 78−37449
Pt self-powered detectors, neutron/gamma sensitivity 78−78557
Pt-self-powered neutron detector, temp. and radiation tests 79−81132
Rh-self-powered neutron detector, temp. and radiation tests 79−81132
Si detector, self-windowed, packaging approaches, review 77−10108

particle detectors continued
Si diode heavy ion detector, all epitaxial, fabrication and performance 77−54414
Si ΔE.E counter telescope, particle identification limits *(Japanese)* 79−81133
Si, ion ion-doped, effects of 5.5 MeV α particle irradiation 77−65397
Si photovoltaic cell appl., for electron and proton radiation detection *(Czech)* 77−18748
p-Si surface barrier particle detectors 77−50326
Si surface-barrier detector, He ion pulse-height defect <30 keV 77−10546
Si thin detector, ionisation energy loss of relativistic electrons 78−55117
Si:Au use in weakly absorbed nucl. radiation detectors 77−67947
Si:Li detector, influence of distrib. of drift temp. on props. 77−3234
Si(Li) detector, cooling system with liq. N_2 *(Rumanian)* 79−85867
Si(Li) detector for energy dispersive analysis *(French)* 77−26445
$ThBr_4$, new inorganic scintillators for nuclear particle detection, review of props. 79−45549
$ThCl_4$, new inorganic scintillators for nuclear particle detection, review of props. 79−45549
U liquid Ar calorimeter, response to high energy protons, calc. 78−46224
ZnP glass heavy-ion track detectors 3 to 120 MeV 80−91389

particle focusing *see focusing; particle optics*

particle lenses, electrostatic *see electrostatic lenses*

particle lenses, magnetic *see magnetic lenses*

particle optics
see also aberrations; beam handling techniques; electrodynamics; electron optics; ion optics; particle beam diagnostics
accelerator, laser focusing, phase-adjusted 80−63434
accelerators, method of transfer maps for linear and nonlinear beam elements 79−72107
adiabatic magnetic trap, small axial perturbation due to displaced solenoid *(Russian)* 78−21800
arbitrary regular flows, theory of generalised single-component fluxes 78−71023
atomic beam, focused with laser beam, Na beam and dipole forces 79−7066
atomic beam deflection, by reson. standing EM wave 79−26959
axisymmetric high flux secondary particle channel 79−45502
beam depolarisation in magnetic field 78−33336
beam line magnet misalignment effects 77−30688
beam matching problems, improved analytic starting points 79−72163
beam multiple scatt. displacement by parallel mag. field 79−81110
beam optical components, anal. of misalignment effects 78−13355
beam trajectories through einzel lens for linear accelerator ion source *(Japanese)* 80−18718
beam-beam interactions in e-p storage rings 78−78889
betatron oscillations, frequency shift in nonlinear mag. fields 78−1137
bipotential lens, with axial pot. function $\Phi(\mu)=V \exp(K_0 \arccos \mu)$ 77−23606
bunch lengthening and microwave instability 77−83370
bunch lengthening due to potential well distortion from cylindrical cavities with beam ports 77−83375
bunched beam stability in storage ring, matched line interaction 78−50424
bunched beams, transport, second order aberrations 80−52801
bunched beams, transverse instabilities 78−78886
bunches with local elliptic energy distribs. 79−76565
CERN 50 MeV linac, beam emittance meas. in matching 77−38479
CERN 50 MeV linac, beam optics 77−38477
channel for high-current beam transportation, design parameters 79−59291
charged particle beam dynamics, moment method 78−33655
charged particle beam focusing, collimation and deflection 80−48132
charged particle beam interaction with monochromatic radiation in inhomogeneous medium *(Russian)* 77−31114
charged particle motion in alternating elec. fields, scaling conditions 80−63903
charged particle motion in mag. field, acceleration and focusing 78−1142
charged-particle beam, axisymmetric, focusing in hyperbolic electrostatic field 78−50688
chromatic corrections for large storage rings 79−72106
coasting beams, transverse instabilities 78−78885
coded aperture imaging of gamma-ray sources, class of near perfect coded apertures 78−40300
cold neutrons, diffraction by ruled gratings 79−94139
conference, theoretical aspects of beam behaviour, Erice, Sicily (1976) 78−78878
cylindrical diode for charged particle beam generation and focusing 77−67532
cylindrical lens systems, for neutral dipoles, using electrostatic or mag. fields 77−54663
differential spectroscopy of charged particle beams, cylindrical mirror 77−50600
dipole particle dyanmics, integrable problems 80−18980
electron bunch energy losses, along circular waveguide with periodically perturbed wall 79−76564
electronic collimation of neutrons using Ge(Li) detector, for (n,n′γ) cross section meas. 77−6591
electrostatic 77−50601
electrostatic coaxial lens, soln. techniques 80−69307
electrostatic mirror, approx. cylindrical field, focal line correction 77−50599
electrostatic mirror, second order focusing space charge effects 77−50598
electrostatic transaxial lens, curved charged particle beam focusing, image coords. and aberrations 78−46503
elliptical beam inside non-confocal elliptic vacuum chamber, potential 80−47799
emittance variations following guidance by quadrupole lens *(French)* 78−29679
fast neutron therapy system using cyclotron beam, beam optics and shielding 79−57756
Fermilab, 100 GeV beam storage, improved chromaticity control 79−76187
Gabor lenses, configurations and beam optical performance 79−68070
heavy ion, alternating phase focusing in linac 77−38476
high resolution spectrometer facility at LAMPF, beam line 78−62674

particle optics continued
high-current beam in focused channel, beam stability analysis 79−63325
high-power neutral beam, spectral resolution by optical diagnostics 80−33819
image formation with ultracold-neutron waves 80−78752
intense ion beam, production and focusing from self-pinched relativistic electron beam 77−24206
intense relativistic electron beam focusing with large aspect ratio diodes 77−23610
ion beams for pellet fusion, focusing and prod. 77−83353
ISR, longitudinal bunch dilution due to RF noise 77−83260
ISR at CERN, longitudinal instabilities of bunched beams, microwave instabilities 77−83270
Landau damping 78−78887
linac injection system beam dynamics, computer simulation 80−13989
linear accelerator incompatibility theorem, stability and focusing 77−3195
linear accelerator simulation, code PARMILA, longitudinal tuning of LAMPF 77−83159
linear proton accelerator, parameter errors, theory 77−30678
magnetic lenses monitored, multichannel analogue device 77−23604
magnetic optical achromat, second order, design 79−72161
mass-separator beam, quadrupolar focusing lens system 80−47801
mega-ampere ion beam production and focusing using self-pinched electron flow 77−24205
micro-Fresnel zone plates for coded X-ray imaging of laser produced plasmas 78−42814
multipole magnetic field, orbit-compression 78−17853
Munich MP tandem beam optical components, anal. of misalignment effects 78−13355
muon single and multiple scatt. in continuous media with focusing mag. field 77−24328
neutral beam injectors, multi-aperture extraction systems 80−42301
neutral beam line for plasma heating, stray particle loss near deflection magnet 80−47794
neutral particle optics, slab method calcs. 79−76566
neutrinos, beam focusing system, Protvino Inst. 78−37477
neutron holography, using Fresnel zone plate encoding 80−48131
neutron interferometer and fundamental expts. 79−45000
neutron optical props. of multilayer systems 79−55044
neutron optics, gravitational effects and applicability of Fermat's principle *(Russian)* 79−13376
neutron perfect crystal interferometer, coherent scatt. length meas. 79−46517
neutron spin echo, matrix anal. 78−86715
neutrons, imaging and focusing by zone plate 80−106433
neutrons, ultracold, zone mirrors for high resolution image form. 78−87003
non-conservative description of evolution in physics *(French)* 79−97328
nonrelativistic particle trajectory, analogy with optical ray trajectory 77−14657
Orsay 200 MeV proton synchrocyclotron, beam optics and beam monitoring in beam lines 79−54636
parasitic mode losses in cylindrical cavities with beam ports, SPEAR II and PEP vac. chambers 77−83271
particles in cylindrically symmetric mag. fields, least squares track fitting method 78−58896
phase space imaging of charged particle beam by frictional forces 78−17850
plasma-optical focusing of Hall-current accelerator beam 77−7605
potential and field produced by elllptical beam in confocal elliptic vac. chamber 77−83798
prism, cone-shaped, combined elec./mag. fields, relativistic particle optics 78−50690
prism, wedge-shaped, combined elec./mag. fields, relativistic particle optics 78−50689
proton beam for neutrino experiments, focusing, pulsed power supply 79−9974
quadrupole lens, aberration coeff. from rectangular model *(French)* 77−68161
quadrupole lens spatial field determ. 78−55292
quadrupole lenses with sector magnets, nonzero emittance beam focusing conditions 80−23612
quadrupole mass spectrometers, charged particle selection 77−5961
radiative damping effect for ultrarelativistic channelled particles 78−67758
relativistic beam focusing by nonuniform plane EM waves *(Russian)* 77−6988
relativistic particle ring, coherent oscillations, Vlasov eqn. 78−55060
retarding electrostatic prism, with increased transmission 78−71022
ring-type state selector and space focuser for mols. with positive induced dipole moment, appl. to mol. beam maser 78−54503
Runge-Kutta method for track fitting in mag. field 79−31782
separated sector cyclotrons, chromatic correlations at injection and ejection 79−72110
shaping electrodes for circular, conical beam, exact anal. 77−19155
SIN high resolution pion channel and spectrometer 79−22517
single-beam collective phenomena, longit. instabilities 78−78884
single-particle dynamics, Hamiltonian formulation 78−78881
single-particle dynamics, linear machine imperfections 78−78882
single-particle dynamics, linear machine lattices 78−78880
single-particle dynamics, linear theory of perfect machines 78−78879
single-particle dynamics, RF accel. 78−78883
SLAC 3 km accelerator, single bunch beam loading 77−83160
spherical electrostatic spectrum., props. of Keplerian orbits in inverse-square field 79−13581
SSC, energy spread without flat-topping 79−54698
statistical phenomena, theory 78−78888
storage rings, linear and nonlinear orbit motion 79−72109
superconducting magnets, aperture limitation due to coil block errors 77−386
synchrobetatron oscillation driving mechanism 79−72108
telescope electrostatic system with removable spherical aberrations 77−6989
telescope electrostatic system with removable spherical aberrations 77−6990
thermal neutron filter, Si single cryst. 79−45512
Tohoku Univ. 680 model cyclotron facility, emittance meas. and energy resolution 79−54638
transition energy variation with momentum aperture in CERN ISR 79−76194

particle optics continued
transverse coherent instability anal., in KEK booster 79−76183
two-dimensional electrostatic field construction for energy analysis 80−9796
Cu-Ge neutron monochromator 78−71643
Fe/Ge multilayer neutron polarizing monochromator 79−45513
Li cylindrical lens for high energy particle focusing, aberrations 77−14649

particle range *see energy loss of particles*

particle scattering *see collision processes; energy loss of particles; particle backscattering; potential scattering; radiation effects; transport processes*

particle separators
BNL short separators, modernisation and improvement 79−22525
cascade particle analyser for aerosol size distrib. and mass conc. 79−71583
dust sampler, CIP type, for personal use, particle separation 78−81469
electric breakdown in DC electrostatic separator for high energy physics 77−26921
electrostatic separator with built in HV generators 78−29693
EM mass separator at heavy ion accelerator, gas discharge ion source 78−17456
EM on-line mass separator at heavy-ion accelerator, gas discharge ion source 78−17457
fast reaction product separation, approaches, facilities 77−23358
ferrographic particle separation technique for wear analysis 79−70395
fission products, short lived, light, beta decay energies using online mass separator 78−8783
heavy ion separation velocity selector 77−88324
heavy-ion energy-mass spectrograph 77−87869
HV deflection condenser operated under high vac. conditions 80−27861
identification spectrometer for measurements of charged reaction products 79−36463
ISIS 1, full aperture, multiparticle identification 79−76258
LISOL on-line mass separator, decay of light In isotopes 77−23361
magnetic filter for separating aerosol particles from airflow 77−4945
multistep avalanche chamber, detection of far UV photons, Cherenkov light imaging 79−93871
MWPC with cathode read-out for separation of EM and hadronic showers 79−3273
neutral particles, detect. and energy anal., review 78−82590
neutron velocity selector, high resolution, applic. to materials research *(German)* 80−47803
on-line isotope separators 77−23337
OSTIS, on-line mass separator for thermically ionisable fission products 79−714
proportional counter, search for heavy particle with single positive charge *(Chinese)* 78−876
proportional counters, relativistic charged particle identification by ionisation energy loss with delta ray suppression 79−85863
pulse shape discriminator for n,γ separation, appl. to TOF spectroscopy 79−6786
scintillator Pb-acrylic shower detector, meas. of electron and pion cascades 79−81124
SIRIUS, on-line mass separator at Strasbourg reactor 79−22527
solar wind spectrometer, ion frequencies and velocities *(German)* 80−51636
superconducting RF particle separator, negative 16 to 37 GeV beam, results 78−89589
superconducting resonators, RF contact 77−26923
superconducting RF particle separator, 300 W 1.8K refrigerator for 77−18770
superconducting RF particle separator, large scale He II cryostat design 77−30742
superconducting RF separator for CERN 77−26948
superconducting RF separator for CERN 79−81113
velocity analysers response function, Auger electron spectrometry appl. 77−14298
velocity filter SHIP, a separator of unslowed heavy ion fusion products 79−49893
velocity filter SHIP, efficiency for unslowed evaporation residues 80−23244
Pb-plexipop calorimeter module viewed by wavelength shifter bars 79−81127

particle size
abyssal sediments, effect of particle size var. on DRM/ARM ratio 78−32067
AC test dust, particle size distrib. for filter media testing 78−53060
acoustic particle agglomeration due to hydrodynamic collision between monodisperse aerosols 80−26191
aerosol, atmospheric, at S.Pole, size distrib. and concs. obs. 80−41484
aerosol, atmospheric, large particles in convective storm environment 80−41512
aerosol, coagulation and condensation, dynamic behaviour 77−25312
aerosol, photochem. prod. of submicron particles of very narrow size distrib. 79−29491
aerosol, polydisperse, growth in adiabatic condensation nuclei counter, finite expansion time 79−79306
aerosol, stratospheric, in S hemisphere, meas. by impactor and in situ single-particle detect. 78−73437
aerosol formation, growth, general dynamic eqn., H_2SO_4/H_2O aerosol simulation appl. 79−47990
aerosol granulometric distrib. rel. to atmospheric pollution influences 77−37341
aerosol growth by condensation, general dynamic eqn., exact solns. 79−39218
aerosol growth in urban plume, obs. 77−37390
aerosol monitoring and control, using size distrib. 79−57534
aerosol optical extinction coefficients, practical upper limits 79−72486
aerosol over Milwaukee, theoretical and meas. size distrib. 80−7970
aerosol particle content study at cloud edges and in clear atmosphere *(Russian)* 80−21794
aerosol particle growth and size distrib., humidity effects, effects on visibility 77−25321
aerosol particle size distrib., dynamic behaviour, coagulation, condensation, nucleation and removal 78−35726
aerosol particle size distrib. meas. in stratosphere 80−51578
aerosol particle-small ion combination coeffs., size depend. 77−25320
aerosol particles attached to falling snow crysts., size distrib. 80−17362
aerosol size distrib. approx. determ. method 77−45188

particle size continued
aerosol size distribs. from inversion of spectral optical depth meas. 79−80020
aerosol size distribution by inverting spectral turbidity data 80−95796
aerosol size distribution retrieval, simulated aureole data inversion in presence of multiple scatt. 79−74957
aerosol size spectrum determ. in turbulent medium using coherent Doppler meas. 79−96841
aerosols, atmospheric, size spectra from inversion of optical scatt. and spectral extinction 79−62578
aerosols, in moist atmosphere, equilib, sizes and size spectra *(Russian)* 79−12194
aerosols, single particle dia. and aerodynamic relaxation time anal. 77−80205
aerosols, size distrib., effect of dispersed concentration 77−60128
aerosols, size distrib. characterisation, modified beta density function 78−69432
aerosols, urban, in Nagoya area, size distrib. and Si and Al concs. 80−26581
aerosols from coal-fired power plants, minor and trace elements emissions and particle size distribs. 79−92108
aerosols from South American continent, S and trace elements concs. rel. to size distrib. 78−57245
aerosols from urban and desert regions in Israel, size distrib. 80−41503
aerosols with Junge size distrib., IR extinction 80−51537
agglomeration, computer simulation *(Japanese)* 78−95706
agglomeration, Monte Carlo simulation *(Japanese)* 78−95707
aggregates, influence of particle size ratio on continuity 78−39712
agitated dispersion, breakage and coalescence processes, obs., data reduction 77−90645
air-water fogs, particle polydispersity rel. to audible sound propag. 78−1473
Aitken particles, atmospheric, dyanmics *(German)* 79−53413
p-alkylbenzenesulphonate mixed micelles, dimens. determ., small angle X-ray scatt. *(French)* 77−29053
alloy, dispersion hardened, work hardening due to Orowan loops, temp. depend. *(Japanese)* 80−66534
alluvial channels bed material, particle size rel. to gradient, discharge and braiding 79−20869
amethyst, Fe^{3+} diffusion, associated phenomena 77−36269
anisylidenebenzidine, particle size distrib. function, electrooptical diffusion method for determ. 80−8956
applications of integral equations in particle-size statistics 78−62050
atmosphere, particle size distrib. determ. by spectral phase functions 77−5281
atmosphere aerosol, diffuse atmospheric scatt. corrections to solar radiometry 79−80015
atmosphere aerosol, particle size distrib. statistical characts. rel. to light attenuation coeffs. *(Russian)* 78−53702
atmosphere pollution aerosol, particle size spectra rel. to cloud modification effects 80−56571
atmosphere turbulence and scattering particles, sizes rel. to EM pulse scatt. and diffusion 79−66775
atmospheric aerosol, Ankara, trace elements and size distribs. determ. by thermal neutron activation anal. 78−81377
atmospheric aerosol, N.England 77−70812
atmospheric aerosol, particle size, opt. and geom. determs. *(German)* 77−91259
atmospheric aerosol constituents, absorpt. coeff. rel. to imaginary refr. index 79−74956
atmospheric aerosols, IR extinction rel. to mass conc. 79−84473
atmospheric aerosols, particle size distribs. evolution via Brownian coagulation, num. simulation 80−41513
atmospheric aerosols, S assessment along urban freeway, proton induced X-ray emission anal. 77−60172
atmospheric background aerosol, elemental conc. and particle size distribs., PIXE anal. 77−49139
atmospheric dust, imaginary refr. index rel. to particle size 78−7763
atmospheric extinction and absorpt., effects of particulate complex refr. index and size distribs. 79−29849
atmospheric extinction coefficients for multimodal particle size distrib. 78−24370
atmospheric particulate trace elements, conc. and size distrib. 79−79937
atmospheric precipitation, particle-size depend. of optical array precip. probe response 80−51577
azo pigments, dispersions in flow system, nucleation and growth kinetics meas. 77−63967
basalts, mag. grains nature and implications for palaeomag. 79−84243
bend erosion, particle size effect 78−11346
benzo(a)pyrene, distrib. with respect to particle size in submicron atm. aerosols 79−74563
bituminous coal emulsification by ultrasonics 79−47997
bituminous surfaces, review of aggregate selection critera for improved wear and skid resist. 80−7689
bone, mechanical properties rel. to density and mineral phase orientation and particle size 80−16989
borosilicate glass, birefringent, X-ray small-angle scatt. study 80−103937
butyl rubber ethylene propylene ternary copolymer mixture, permeability, diffusion of gases and solvents 79−95217
calcium strontium propionate, compressed powder, dielectric props., particle size effects 77−59503
η Carinae, silicate grains size distrib. in Homunculus Nebula 80−4382
η Carinae and Carina Nebula, interstellar grains size rel. to polarimetric study 79−67043
cellulose, comparison of conclusions from small-angle X-ray scattering and electron microscope obs. 79−86717
ceramic, ultrafine powder, prod. by cryochemical, freeze drying, spray drying or soln. techniques 80−55336
ceramic compact, morphological investigations significance 79−33988
ceramic powder synthesis from laser-heated gas phase reactants 80−93525
chalk, grain size determ., sample preparation methods 79−24694
chondrules, from Bjurbole and Chainpur meteorites, size and shape 77−29734
circumstellar dust around Mira variables, supersonic mass flow and grain size 79−35270
cloud condensation nuclei, size distribs. effects on cloud droplet sizes 77−87006
cloud droplet growth, collisional problem in turbulent environment 77−5293

particle size continued
cloud droplet spectra, effect of nuclei spectra 77−64364
cloud droplets, hygroscopicity and surface tension effects in size distrib. *(Russian)* 77−33142
cloud droplets, interception collection efficiencies 78−3381
cloud droplets, size distrib. models, and visible and IR volume extinction coeffs. 77−25750
clouds, drop size spectra modification by urban pollution aerosol, physical demonstration 80−56571
clouds, particle size distrib. from spaceborne line spectrum imagery, theory 79−5613
coal liquefaction, particle size distrib. as function degree of coal conversion 80−35626
coal-dust aerosol, radiation-absorbing coeff., effect of spectral comp. of radiation and particle size 77−23859
coarsening, time depend. of average particle size 80−79994
coherent precipitates, particle size distrib. influence on extra-resist. 80−49689
colloid, electrooptical diffusion method for determ. 80−8956
colloid freeze-fracture, for electron microscopy 78−337
colloid particle separation by potential barrier chromatography 77−73474
colloidal dispersion, particle size distrib. change kinetics, statistical approach 78−7241
colloids, concentrated, appl. of modern concepts in liquid state theory 80−40750
colloids, rigid, size distributions, transient electric birefringence 80−85223
colloids, structure determ. by neutron diffr. and small angle scatt. 80−40748
cometary coma, dust grains sizes and comp. rel. to IR continuum interpretation 78−7923
component particle size analyser, using X-ray fluorescence *(Japanese)* 78−15615
concrete, fresh, behaviour under a vibr. action, large particle segregation *(Japanese)* 80−88329
condensation nuclei counter, particle size depend. 79−20476
conductive filler-polymer composite conductivity theory *(Japanese)* 78−11351
copper phthalocyanine, size distribs., transient elec. birefr. 80−85223
coronene, distrib. with respect to particle size in submicron atm. aerosols 79−74563
cosmic dust, grain size spectrum from protostar circumstellar shell 77−13327
Coulter counter technique, new method to follow cryst. growth rate in precipitating systems 79−52100
critical size for comminution by compression 78−52709
crystallisation, spontaneous, diffusion kinetics *(German)* 77−51334
crystallite with screw dislocation, determination of particle size and distortion 80−15098
crystallites, with step displacement, particle sizes and distortion determ., by means of X-rays *(German)* 80−14960
dendritic particle characterisation of automatic methods 80−25590
dental stones, effect of particle size on hardness and scratch resistance 79−79077
diamond, suspension, particle size distrib. function electrooptical diffusion method for determ. 80−8956
diamond, synthetic micropowder, degree of charging of polished Ti and Fe surfaces 78−60880
diamond, ultradisperse, ESR, particle size and lattice microdistortions 80−97140
diamond coatings, for increased wear resist. 80−76371
dicalcium lead propionate, effect of particle size on dielec. behaviour 79−38429
dicalcium strontium propionate, effect of particle size on dielec. behaviour 79−38429
dickite, unusual crystal habit, structural disorder 80−59445
diffusion sampling method for ambient aerosol size discrimination with chemical comp. determ. 77−37349
dilute binary alloy monocrystal, thermodynamics of growth, model *(French)* 78−87635
disperse system, spectral transparency approx. by Legendre polynomials, distrib. density of particle size 80−95800
disperse system coagulation, growth kinetics and soln. of microparticles *(Russian)* 77−32836
disperse system of oblate particles, turbidity 79−72496
disperse systems, turbidity spectrum, wave exponent, spherical particle size depend. 78−46514
dispersed particles in matrix, coarsening 80−30288
dispersion coarsening, computer simulations 80−30289
dispersive particle sizes, from scattering and polarization meas. *(Russian)* 79−34950
distribution, appl. of four-parameter distrib. model 78−85213
distribution, continuity eqn. 80−55406
distribution, determ. by rot. disc with turbulent boundary layer 78−22333
distribution characterisation by AE 78−62179
distribution curve quantitative evaluation, Fortran program *(Czech)* 78−80795
drop size in nozzle flow of moist water vapour 77−42904
droplet distribution in liquid breakup by atomiser 77−11246
dust grains, atmospheric, mean radius rel. to transparency meas. on Maidanak mountain *(Russian)* 80−72627
dust sampling system collection effeciency rel. to particle density and size 77−37456
dusty IR Test-1 lidar obs., transmission meas. 80−99625
elastico-viscous liquid, atomisation, drop size rel. to elasticity 77−35220
Electrokinetic measurements with submicron particles and pores by the resistive pulse technique 77−86384
electrophotographic developer, size distrib., particle charge and toner-carrier force *(German)* 80−73493
electroplated diamond-composite abrasion-resistant coatings 79−61737
elutriator, inclined tubular, for spherical particles, collection efficiency 79−90354
epoxy resin/particle composites, particle size effect in thermal expansion, filler effects on T_g 80−84305
ethylene, obtained from gas cylinder, particle size distrib. 80−55723
extraction replica evaluation, Ashby-Ebeling model analysis *(Czech)* 80−49062
Fe-N system, fine particles growth, prep. by reactive gas evaporation technique, lattice consts. and habit study 79−56919
particle size continued
feed size, ball mill grinding, rate constant determination *(Japanese)* 78−95828
feed size, ball mill grinding, wet, dry, rate constant determination *(Japanese)* 78−95827
ferritin particle visibility in SEM with field emission gun 79−25174
ferromagnetic particles, in mag. liqs. for energy conversion devices, size rel. to stability 77−29051
ferromagnetic sol, relaxation of mag. birefr. and dichroism 79−57301
fine particle clusters, mass distrib. and growth process, expt. 80−26937
fine particle profile, ruggedness and texture specification by fractal dimension 79−40535
fine particles aggregation, mechanism and rate at uniform shear field 80−101046
fine particles melting, model, surface phonon softening effect 79−99297
fine powders, electrogravitation classification by particle mass 79−61531
flotation of fine particles, effects of size and charge 77−16865
flotation of small particles, capture by bubble, theory 80−11959
fluid-particle separation, chainlike form. of particle deposits 77−77813
fluidised bed reactor discrete cut particle size distributions, calc. 80−14812
fluidised beds, liq., particle mixing and classification 79−90330
fluidised beds, three-phase, heat transfer 79−60056
fog droplets, size distrib. models, and visible and IR volume extinction coeffs. 77−25750
Fourier analysis of particle shape *(Japanese)* 79−88506
gas-solid suspensions flowing in steel and insulating coated pipes, electrification 77−77811
glass, Gaussian size distrib. of rigid particles, AE anal. 78−62181
glass sphere mixture, polydisperse system, AE anal. 78−62180
glass-ceramics, transparent, microstruct. and props. 78−59960
granular material, rel. to erosion by airflow, expt. and theory 77−942
granular materials, packing parameters, calc. from particle size anal. results 80−19294
graphite, suspension, particle size distrib. function electrooptical diffusion method for determ. 80−8956
graphite, suspensions, particle shape influence on light absorpt. in mag. field 80−60549
graphite-diamond equilibrium, thermodynamic stability 79−65184
gravel river, grain size var. statistics 79−5513
haemoperfusion through fixed-bed adsorber 78−31976
haze droplets in warm fogs, sizes and effects on visibility 79−100951
hexadecyltrimethyl-ammonium bromide, micelle form. in aq. soln., laser light scatt. 78−27825
hexamethylcyclotrisilazane film, plasma-polymerised, TEM study 80−44456
highly dispersed systems, phase size effect 80−6488
hydrocarbon vapour, spontaneous condensation in submerged turbulent jet 79−64721
hygroscopic particle size, air humidity depend., applic. to lung dynamics 77−90841
ice crystal size from droplet accretion growth 79−79933
ice crystal sizes for halo production 79−96798
ice particle/water droplet discrimination with an optical ice particle counter 79−100973
impact cratering on solid body by microparticles, viscous effects 79−66255
interface-controlled to diffusion-controlled coarsening kinetics, particle size distrib. 80−7579
interparticle percolation, lateral and axial diffusion coeffs., shear cell appl. 79−61666
interparticle percolation, statistical mech. anal. 79−96281
interplanetary dust between 1 and 5 AU, conflicting Pioneer 10 and 11 data 79−44410
interplanetary dust particles size distrib., new results from zodiacal light obs. *(German)* 79−80268
interstellar, UV scatt. props. and size distrib. 80−26932
interstellar charged dust grains, radii rel. to motion in interplanetary space 80−4300
interstellar dust, effects of grain collisions in turbulent gas on initial size distrib. 80−77470
interstellar dust grains, size rel. to temp. fluctuations 80−26938
interstellar dust in Merope nebula, UV phase function and grain size 78−32553
interstellar grain size, polarimetric obs. of four deviating stars 80−12792
interstellar grain size distrib. 79−21388
interstellar grain size versus colour excess ratios 79−17040
interstellar grains, mean size near stars with peculiar interstellar polarisations 77−53659
interstellar grains, shape and size rel. to near IR linear polarisation wavelength depend. 80−51833
interstellar grains, size for accretion by chemically peculiar A-type stars 79−67017
interstellar grains in NGC 2264, size rel. to polarisation in (Walker No.67) 78−12223
interstellar particle size distribution from linear polarisation calcs. 80−12787
interstellar porous graphite grains, radii rel. to 2200 Å extinction hump 80−62228
interstellar reflection nebulae, dust comp. and particle size from simplified models 78−96526
interstellar solid particles in contracting clouds, turbulence rel. to particles growth and size differentiation 80−62251
IR dispersion crystal-crystal filters, effect of particle size, layer thickness and vol. conc. on transmission *(Russian)* 77−27369
irradiated spheres, absorption centre distribution refractive index and size parameter dependence 79−50221
jets produced by shaped explosive charges, particle size distribution in breakup 80−23957
Jupiter atmosphere aerosol, particle size and conc. from 0.6 to 1.1 μ spectrophotometry 80−46468
kaolin grog particles, shape and density 80−97450
latex, laser spectrometer for submicronic aerosols, photoelec. determ. of conc. acid dispersity 79−54244
latex, monodisperse particle size determ., spectroscopic method 77−29055
CW Leonis (IRC+10216), IR C star, circumstellar dust size var. rel. to intrinsic polarisation 80−67730
Lindmann's melting law and the size dependence of melting temperature 78−59929

particle size continued
liquid particles, aerosol and hydrosol, separation by size in thermal fields 80−101044
LMFBR mixed-oxide fuel aggregates, dynamic shape factors 79−67853
logarithmic distribution functions for particle size 79−24838
lunar regolith particles, size distrib. rel. to Rosin's law 78−45248
lunar soil, particle size distrib. at Luna 16 and Luna 20 landing sites 77−53437
magnetic grain size, control on magnetic susceptibility anisotropy var. in deep-sea sediments 79−66680
magnetic minerals in basaltic dyke, grain size rel. to mag. props. 77−49062
magnetic particle inspection oxides, evaluation 80−40657
magnetities and titanomagnetites, in igneous rocks, grain size rel. to TRM 78−65270
marine atmosphere particulate matter, organic C conc. and particle size distrib. 78−32139
marine sediment particles, surface organic layer containing U and Th, thickness meas. 78−40592
Mars 1971 dust cloud particles, mean radii 79−84704
Mars soil, particle size from IR spectra and terrestrial analogues optical props. 78−85879
mass transport kinetics in sheared particulate beds, Markov chains appl. 79−60057
mathematical modelling of growth of spherical metallic particles during photographic development process *(Russian)* 80−50871
Maxwell Garnett theory, validity range 78−68507
metal crystallites of supported catalysts, size distrib. from wide-angle X-ray meas. *(German)* 77−84566
metal powder production, interactions between N_2 jets and liq. Pb and Sn streams 79−43170
metal powder suspension in air, spontaneous ignition temperature *(Russian)* 78−47027
metal submicron particle heating in hot gas, plasma metallurgy 80−81092
metallic, surface tension depend. on size, vaporisation time *(Russian)* 80−34290
metallic fine particles, melting and size depend. on melting temp. 79−73294
metallic powder, spark erosion prep. 78−27452
metals, particle size depend. of melting temp., thermodynamic theory 77−89523
meteorite chondrules, mass distrib. and Rosin and Weibull statistical functions 79−35201
meteoroid albedo and size distrib. in 0.3-4.8 AU range 78−36539
meteoroids from Periodic Comet d'Arrest, particle size distrib. and albedo 78−53876
microemulsion structural changes, light scatt. obs. 78−56920
mixed salt aerosols, phase transform. and droplet growth in moist atmosphere 79−52783
molecule embedded in dielec. spheroid, Raman and fluoresc. scatt. 80−99507
mortar bars, aggregate particle size influence as expansion caused by alkali-SiO_2 reaction 80−66762
multicomponent medium, heat radiation attenuation factor calc. model 79−94472
near IR diffuse reflectance analysis anomalies 80−86383
Nimonic, IN100, γ' precipitates, casting conditions effect on morphology 80−7548
noctilucent clouds, particle sizes rel. to available mesospheric H_2O vapour 78−57248
novae dusty circumstellar envelopes, size and development of particles *(French)* 77−56940
nucleation in clouds, minimum particle size 78−44939
oil shale retort dispersion, effect of particle size distrib. and flow nonuniformities 80−28560
oil-fired burners, particle size distrib. characterisation using Beta distrib. 78−81384
olivine, dynamic recrystallisation rel. to applicability limits of grain size geopiezometer 78−85715
optical transient method for particle sizes, mobilities, charges and particle substrate interaction forces 79−50218
organic pollutants, particle size distribs. in urban, rural and seashore aerosols 80−55958
Ostwald ripening, effect of precipitate vol. fraction 80−40356
oxide reactor fuel pellets, ammonium polyuranate precipitation, continuous, particle size distrib. and agglomeration control 79−93804
parallel cylinders radial size distrib. 79−100450
particle deposition, onto rot. disc, convective diffusion, external force field 78−40081
particle-filled polyurethane resin, tensile strength, particle size effect 77−73305
particles, ferromagnetic colloids in toluene, small-angle X-ray scatt., interparticle correlations 79−11831
particulate materials, cohesionless, mixing and segregation, microscopic mechanisms 79−37848
particulate materials, cohesionless, mixing and segregation, failure zone form. 79−42261
particulate materials, quantitative three-dimens. characters. using polished sections and computer-controlled SEM system 77−2714
Periodic Comet Encke dust, large grains in short supply 78−85908
phosphate fertilizer, specific activity of U and Th rel. to particle size 80−106244
platelet estimation in whole blood by electronic particle size anal. 78−28104
plume opacity related to particle mass concentration and size distribution 79−74566
polydisperse, vapour-liquid mixtures, acoustic velocity, damping decrement 80−66881
polydisperse dilute suspensions, of rod-like particles, anisotropy of electric polarisability 80−85224
polydisperse hard-disc systems, equations of state, particle size effects 78−73947
polydisperse hard-sphere systems, equations of state, particle size effects 78−73947
polydisperse suspension, two-parameter size distribs. eval. using photon correl. data 79−92011
polydisperse system, particle-size distrib. functions, determ. from SAS data by indirect transformation method 80−38860
polydisperse system, rotatory diffusion const., electro- optic decay curve, size distrib. 78−20079
particle size continued
polydisperse-particle-size-distribution function determined from intensity profile of angularly scattered light: comments 80−87311
polyethylene/ethylene vinyl acetate copolymer mixture, rel. between hypermol. struct. and stability *(German)* 80−64929
polyhedral particles, adhesion forces in liq. medium 79−70380
polymer crystal in suspension, light scatt. in streaming system, dimens. characterization 79−69852
polymer lattices, particle size control 79−38785
polymer soln. US atomisation efficiency and particle size distrib. rel. to supply volume rate 79−68468
polymer/metal powder compacts, cond. threshold, particle size ratio effect 80−80337
polymers and elastomers, cryogenic grinding technique 77−32555
polystyrene, high impact, particle size distrib. in discrete phase 77−56257
polystyrene, high-impact, improved Coulter counter method for particle size distrib. meas. 77−56258
polystyrene aerosols, monodisperse, depend. of attachment rate of ^{220}Rn and ^{222}Rn decay products 80−41256
polystyrene lattice, emulsions-polymerised, particle size determ. by soap titration 80−40753
polystyrene/polyethylene blend, particle dimension as function of melt viscosity added graft copolymer conc. 77−52279
polyvinyl alcohol, in water-ethanol mixture, processes of structure formation 80−10482
polyvinyl alcohol/vinyl acetate copolymer, in water-ethanol mixture, processes of structure formation 80−10482
powder, effect on thermal conductivity *(Japanese)* 78−6191
powder, mixing/segregation behaviour, 2 powders of different density, quantit. anal. 78−84733
powder, moist, granulation on vibrated chute *(Japanese)* 78−95710
powder, particle size analysis by chord method 77−4890
powder, ultra fine, surface roughness effect on formation by rotating friction mill *(Japanese)* 78−95709
powdered mixture, compaction, optimum porosity and particle sizes 77−85971
powders, air fluidisation, bubbling behaviour, rel. to particle size 77−31362
powders, particle nonequiaxiality effect on size distrib. meas. in pulse conductometric anal. 80−20833
powders and sintered bodies, particle size distributions from chord and area distributions *(German, English)* 80−35126
precipitation particles in frontal clouds 79−88437
PVC dispersion, rheology, particle size effects 79−92007
quartz, grinding and surface treatment by ball mill in cetyl alcohol *(Japanese)* 80−25890
radioactive particulates in gaseous effluents at nuclear fuel reprocessing facility 79−9848
raindrop size distrib. in hilly region of N.Wales 77−29390
raindrop size distrib. shapes 79−20949
random packing of spheres, computer simulation 80−77705
remote sensing, distributions, Rayleigh-Gans-Born approx. 79−27174
river sediments, transport mode depend. on particle size rel. to Martian outflow channels erosion 80−98363
salt nuclei, size rel. to critical supersaturation 78−44940
Saturn, ring particle composition and size distrib. from radar obs. 78−36501
Saturn A-ring, azimuthal brightness var. and particles size 78−32391
Saturn C-ring, particle size from IR brightness and eclipse cooling obs. 80−56763
Saturn ring particles, sizes from 3.71 cm wavelength interferometric obs. 79−96962
scattering particle dimension determination, by direct Fourier cosine transformation of expt. SAXS data 80−79624
scavenging, in-cloud, rel. to aerosol particle size, mechanisms 78−16108
sediments of Ismailia Canal, behaviour of radioisotopes in laboratory-scale aquatic ecosystem 78−3831
sediments of Vema Channel, transport of Antarctic Bottom Water during last ice age 77−21798
SEM characterisation, collection, handling and mounting of particles 79−21867
separation, high-resolution, by sedimentation field-flow fractionation 77−73473
sepiolite, electric polarisability, anisotropy, length depend. of ionic contrib. 80−85224
sepiolite, size distributions, transient electric birefringence 80−85223
sieving of fine powders by sonic oscillating air column *(Japanese)* 78−95712
silica gel, pore struct., effect of washing with aq. solns. containing Mg^{2+}, Ca^{2+} ions 79−52786
sodium dodecyl sulfate, micelle form. in aq. soln., laser light scatt. 78−27825
solid dielectric bridged vacuum gap microparticle collection and analysis 78−5964
south-east Baltic Sea silt granulometric and mineral composition *(Russian)* 79−96755
specific turbidity, fine structure of the Mie scattering, resonant structures of a_n and a_b 78−58913
spherical particle in free-fall, time-to-complete-dissolution prediction 80−15245
spheroids, particle size-shape distribs., stochastic model and practical guide 78−62055
spheroids in atmosphere and ocean, scattering rel. to size distrib. determ. *(Russian)* 78−36279
St. Louis aerosol, variation of elemental composition with particle size 77−49137
stearic acid, laser spectrometer for submicronic aerosols, photoelec. determ. of conc. acid dispersity 79−54244
steel, austenitic stainless, NbC precipitate particle size distrib., TEM study of grain to grain variations 79−29066
steel, C, wire, drawing effect on spheroidization *(Korean)* 77−66656
steel, Cr-Ni-Mo-Cu, ε phase particle precipitation from martensite, local internal stress relaxation *(Russian)* 79−78969
steel, high-speed, atomised powders and sintered blanks, particle size effects 77−44188
steel, high-strength low alloy, Nb(CN) precipitation and coarsening during hot compression 80−97514
steel, hypoeutectoid, C22, recrystn., influence of carbides distrib., mech. props. meas. *(German)* 79−38850

particle size continued
steel, ShKh15, carbide particle size and pearlite grain size changes during deform. and hot working *(Russian)* 78−6946
steel, sorbitic, yield point rel. to average carbide particle size *(Russian)* 78−6967
steel, stainless, creep ductility, intergranular particle size and spacing effect 80−40461
steel, stainless, creep ductility, sigmal phase influence 80−55478
steel, stainless, type 304 welded, low temp. sensitisation, nucleation of CR carbide nuclei along grain boundaries TEM, SEM study 79−38851
stratiform clouds particles, meas. of local mean radii and concs. *(Russian)* 77−53158
stratosphere aerosol, size meas. during 1974-1975 aerosol event 77−45084
stratosphere aerosol size distrib., lidar obs. at 0.6943 μm and 1.06 μm 77−41120
strengthening phase particle distrib., quantitative analysis 78−15629
styrene-H_2O suspensions, particle size, surface tension, stabilizer conc. effects meas. *(German)* 79−24834
submicron particle, size distrib. in colloidal suspension FODA 78−61057
superalloy, hot consolidation of rapidly solidified powders, review 79−33965
superparamagnetism, Mossbauer effect study of relaxation of magnetisation vector 78−19402
supported metal catalysts, particle growth, models 77−8830
supported metal catalysts, particle growth, obs. of Pt on alumina 77−8831
suspension, filtration in porous membranes, pore and particle size distribs. correl. *(Japanese)* 80−3418
suspension, in nonpolar dispersion media, particle size and number conc. meas. 80−9082
suspension, of ideally polarisable spherical particles, low-frequency dielectric dispersion 79−61912
suspensions, appl. of Gibbs-Thomson eqns. to particles of dissociative and associative substances 77−4944
suspensions, creeping flow, hindered settling, particle shape effect 80−14797
suspensions, degree of agglomeration assessment 77−70343
thermostimulated luminesc., mech. milling effects *(Russian)* 78−76537
thin dust layers, particle size effects automatic correction, computer appls. in spectrometry 79−83539
Titan atmospheric aerosol, size distrib. rel. to optical depth and replacement rate 79−96964
toner dispersions, positively charged, electrokinetic props., electrostatic image development 79−80713
toughened polystyrene, polystyrene-Kraton G blend, charact. by SEM 79−14697
transition metal clusters, particle size rel. to bulk metallic props. 80−44490
transition metal oxalate hydrates, powders, precipitation from aq. solns., cryst. numbers, sizes 77−44143
troposphere, particle size distrib. skewness and mode radius relationships 77−45121
troposphere aerosols having soil-derived component, commonalities in measured size distribs. 77−60454
turbulent flocculation, mathematical model *(Japanese)* 80−79389
two phase alloy hardening by second phase particle coalescence 80−7591
two-phase unpolymerised system, particle size, surface tension, stabilizer conc. effects meas. *(German)* 79−24834
ultrafine particles, production using cryopump *(Japanese)* 80−52252
uniform and nonuniform smoothly varying water stream, erosional capacity, rel. to particle size of granular bed material 77−84316
urban aserosol comp. and mass, particle size depend., rel. to visibility level 77−91258
urban-suburban air pollutant transport, chemical and physical transformations 77−37399
Venus cloud particles, sizes from Pioneer Venus nephelometer expt. 79−48716
Venus clouds, particle size distrib. meas. 79−48717
vinylacetate-H_2O suspensions, particle size, surface tension, stabilizer conc. effects meas. *(German)* 79−24834
volcanic ash particles, influence of shape on atmospheric settling vel. 79−84364
water drop breakup, catastrophic, free flight meas. of particle sizes 77−31361
water droplets size distrib. in cloud bases 78−73458
water drops in stratosphere, size distrib. rel. to sulphate aerosol growth by condensation *(Russian)* 80−94566
wire conductors, explosion, investigation of resulting particles *(Russian)* 79−37558
X-ray diffr. line profile analysis, on-line computer routine 78−79498
X-ray diffraction lines, use of approx. methods for Fourier series coeffs., particle size calc. *(French)* 77−31549
X-ray line-shape anal., simplifications using Fourier series, appl. to Mo film on Si 79−82123
YIG, hot spraying to give fine, free flowing, sinterable powder 80−20865
Ag, ellipsoidal small particle assembly absorption spectra, optical model *(Russian)* 78−60483
Ag, fine particles prep. by vacuum evap. onto running oil substrate 79−28925
Ag particles, light scatt. spectra, size and shape effects 77−44015
Ag powder, ultrafine, sintering, coalescence growth stage 80−89174
Ag ultrafine particles, effect of truncation of size distrib. 80−49562
Ag-Cd(-Ni), internally oxidised, oxide particle size control *(Japanese)* 80−89480
Ag-Sn (6(8.2)(11) wt.%), splat-quenched, X-ray line broadening 80−40397
Ag-Zn-Te(-Sn)(-In), internally oxidised, oxide particle size control *(Japanese)* 80−89480
AgBr emulsion, model system, Ostwald ripening obs. 77−2707
AgCdO, powder metallurgy production, for switchgear in power engineering 80−104094
AgI aerosol, particle radius depend. of ice-forming activity, verification of theory 80−101406
AgI aerosol particle size, struct. rel. to ice forming activity 80−61164
AgI aerosol particles, influence of particle size on cryst. struct., electron diffr. study 79−16048
AgI, aerosols, ice nucleation at different supercooled fog temps. *(Russian)* 77−27983
AgI aerosols, particle size influence on cryst. struct. 80−2000
particle size continued
Al alloy melts, centrifugally atomised, granule size distribution 79−100080
Al-Ge alloy, Ge particle size, determ. by small- and wide-angle X-ray scatt. 78−19966
Al-Si (1.2 wt.%), dispersion hardened, work hardening due to Orowan loops, temp. depend. *(Japanese)* 80−66534
Al-Si crystals, work hardened, softening and creep rates on annealing 80−11663
Al_2O_3, molten particles, complex refractive index *(Russian)* 77−55766
Al_2O_3 ultrafine gel particle form. from NH_3-$AlCl_3$ solution 80−93807
Al_2O_3-TiC sinter products, grain size meas. by combination etching process 79−74331
Al_2O_3-TiO_2 powder, plasma-prepared, morphology and phase constitution 80−100833
$Al_2O_3(H_2O)_n$, uniform colloidal dispersion, prep. by chem. reactions in aerosols 80−97735
Au black optical props. rel. to structural composition, appl. to solar absorption 79−83630
Au black solar absorber, struct. comp. and optical props. 78−27339
Au black solar absorbing film, particulate nature 77−39003
Au crystallites, formation in flowing Ar system, density, size distrib. and size dispersion 78−88415
Au, fine particles, gas evaporation technique for prep., X-ray diffr. study 80−75327
Au, fine particles, gas evaporation technique of prep., X-ray diffr. study, charact. temp. 80−75328
Au particles, light scatt. spectra, size and shape effects 77−44015
Au powder, ultrafine, sintering, coalescence growth stage 80−89174
Au, small particles, in polyester matrix, optical scattering spectra 79−73961
B-B_4C, hot pressed, particle size distrib. 79−79018
BN, high pressure synthesis, exam. of relationship between synthesis condition, and crystal shape, size *(Japanese)* 79−20018
$BaSO_2$, suspension, light scatt., optical anisotropy determ. by polarisation ratio 79−1772
$BaTiO_3$, powder compacts, sintered, physical and chem. inhomogeneities 79−87594
Bi, evaporated film, nuclei size distrib. 77−11802
Bi_2Te_3-Sb_2Te_3, solid solns. 78−60899
n-$Bi_2Te_{2.88}Se_{0.12}$, extrusion deformed, powder dispersion degree influence on thermal and elec. props. *(Russian)* 80−39366
C aerosol visibility vs. particle size distrib. 78−88911
C black, graphitised, chromatographic columns, efficiency rel. to particle size 78−92536
C black aerosol, coagulation, kinetics, particle size distrib. 79−39209
C, gas adsorpt. rate depend. on granule size and gas flow velocity 78−56033
C sphere aerosol, black smoke opacity, calc. variation with particle size and refr. index 79−72488
$CaCO_3$ aerosols, coagulation rate meas. 79−96374
β-Ca_2SiO_2, reaction kinetics with CO_2 and water vapour 80−76484
Ca_3SiO_2, reaction kinetics with CO_2 and water vapour 80−76484
Cd films, struct. and props., X-ray diffr. spectra anal. 80−80119
$Cd(OH)_2 \rightarrow CdO$, decomp. reaction, crystallite fragmentation, critical sizes and shapes 78−23635
CdS smoke particle growth, prep. by evaporation in inert gases 77−24938
Co single domain particles, randomly oriented easy axes and particle size distrib., coercivity 80−71119
$CoFe_2O_4$ ultrafine particles, prep. and mag. props. 80−71116
Cr, fine particle solar absorber, effective medium theory 80−21396
Cr-Co-Fe, chromindur alloy, field heat treatment, and mag. props. 80−35354
Cr-Cr_2O_3, black chrome films, surface microstruct. rel. to optical props. in solar absorbers 79−52036
Cr-Cr_2O_3, black chrome solar selective absorber, microstruct. 79−56875
CrO_2, synthesis and morphology 79−24481
$Cr_2O_3.SH_2O$, heat-treated, narrow particle size distrib., surface props. 78−85210
Cu complex, bis-(alkylammonium) Cu(11)tetrachloride, perovskite, face struct. and growth rate 78−87634
Cu crystals, two-phase, recrystn. retardation, particle size, spacing effects 80−89242
Cu particles, light scatt. spectra, size and shape effects 77−44015
β-Cu phthalocyanine electrophotographic props. rel. to particle size *(Japanese)* 80−13171
Cu powder, electrodeposition prep. conditions, statistical anal. 80−20828
Cu powder compacts sintering, depend. of neck form. on particle size and sintering temp. 79−28988
Cu wire, tough-pitch, cupping fracture, Cu_2O particle size effect 80−66668
Cu-Ni-Fe alloys superparamag. early stages of decomp. *(Russian)* 78−6890
Cu-SiO_2, low-temp. recovery creep, Orowan loop accumulation 80−81126
Cu-SiO_2 (0.0052 vol. fraction), work hardened, low temp. softening, particle size effects 77−52342
Fe, atomised powder, props. 80−25600
Fe, carbonyl powder, particle size distrib. anal. by microscopy with statistical anal. of results 78−19691
Fe, cast, air-atomized powder, effect of particle size on C and O contents 78−15340
Fe, cast, atomised powders, particle size effect on purification in US pickling 79−28985
Fe, oxidised powder in prod. of soft mag. mat. 77−63813
Fe powder, atomised, effect on props. of pressed and sintered material 80−11601
Fe, powder, atomised, processing props., particle size distrib. effect, with and without Zn stearate additions 79−100077
Fe-C-Si, spheroidization 77−66665
Fe-Ni-C, atomized, O/C ratio effect, particle size on annealing kinetics, physicotechnological props. 80−20832
Fe-Si (3 wt.%), grain growth inhibition by MnS spherical particles with size distrib. 80−35218
Fe-Si (3wt.%), grain-oriented, secondary recryst., grain growth inhibition 80−89245
$Fe^{2+}Cr_x^{3+}Al_{2-x}^{3+}O_4^{2-}$, finely divided, oxidation kinetics 80−50848
γ-Fe_2O_3, clean and SiO_2 coated, reduction temp. influence on coercivities, coercivity factors and rheological props. 79−69698

particle size continued
γ-Fe_2O_3, prep. from thermal decomp. of $[Fe_3(HCOO)_6(OH)_2]HCOO.4H_2O$ and characterisation 78−80741
γ-Fe_2O_3, small particles, vacancy sintering 77−65975
Fe_3O_4, effect of Al ion on formation and structure *(Japanese)* 77−59727
Fe_3O_4 ferrofluid suspension, mag. props., stability 79−87293
Fe_3O_4, magnetite, anhysteretic remanence and thermoremanence susceptibility, particle size depend. 77−5191
Fe_3O_4 powder, oxidation to γ-Fe_2O_3, coercivity changes 80−44864
α-FeO_2H, asymmetric line shapes of Mossbauer spectra *(Chinese)* 80−103902
α-FeOOH ultrafine particle NGR spectra, size distrib. and surface effects 80−11299
FeS_2, oxidation, Mossbauer spectroscopic and magnetokinetic studies, 400-500°C 80−44880
Ge particles, homogeneously nucleated, production and props. 77−56252
GeO_2, amorphous, obtained by hydrolysis of $GeCl_4$, exam. of props. 79−95956
H_2, cluster beam source, cryopumping 79−63258
H_2SO_4 aerosol growth, kinetic model 77−37340
^2H-^3H fuel pellet electrostatic injection *(Japanese)* 80−78434
Ho particles, effect of size on paramag. Curie temp. 78−60317
In_2O_3 smoke particles prepared by gas evap., morphology and coalescence growth 80−97738
^{115}In aerosol generation technique for atm. tracer obs. 80−26190
$KAl(SO_4)_2.12H_2O$, secondary nucleation, origin, nuclei size distrib. 79−94933
KCl, additively coloured, colloid size distrib., replica microscopy, absorpt. spectra 77−47449
KCl, growth, supersaturation rel. to cryst. charcts. 79−52101
KCl:TlCl, lattice defects, X-ray line profile obs. 80−24455
K_2O-Al_2O_3-SiO_2 system, crystallisation of glasses in primary phase field of leucite 78−67658
Li-Na ferrite powders, props. rel. to Fe_2O_3 chem., thermal, mech. historical 79−11539
$LiAlO_2$, fine particle size, heat treatment synthesis, molten carbonate fuel cell appl. 80−21395
LiF compact, particle size rel. to pore charcts. 78−60631
Mg films, struct. and props., X-ray diffr. spectra anal. 80−80119
MgF, polycryst., quartz particle impacts no. effect on erosion in elastic-plastic response regime 80−81209
MgO brick, particle-size distrib. depend. of texture and struct. *(Japanese)* 78−84753
MgO, effect of Cl^- and F^- ions on calcination and sintering *(Japanese)* 78−95719
MgO powders, hot pressing, mechanisms 80−40300
MgO, single cryst., order hardening by large precipitated vol. fraction of spinel particles 80−3085
MgO, smoke particles, size distrib. 80−104471
$Mg(OH)_2$, and calcination product, relations between particle size, shape and surface area 78−48355
MnZn ferrite powder prep., wet method 80−89180
Mo film, sputtered on Si, annealing effect on uniform and nonuniform strains 79−82504
Mo_2C powders, prop. from vapour phase reaction of $MoCl_4$-methane-H_2 system 79−100068
MoO_3 smoke particles prepared by gas evap., morphology and coalescence growth 80−97738
NH_4Cl, cryst. nucleation, growth rates from organic media, outline meas. technique 79−38730
NH_4Cl, submicron particles, density, morphology 80−61166
Na smoke particles, nucleation and growth, light scatt. study 80−35580
NaCl aqueous aerosols, fixation and microscopic sizing 80−16734
NaCl monodisperse aerosol, dry size depend. of critical supersaturation for droplets nucleation 80−82003
$NaNO_2$ powder, surface layer effects on dielec. props. 77−1631
Ni, fine particles, prep. by vacuum evaporation, crystal habits 78−88437
Ni powders, stereological appl. in study of compacting process, elec. and mech. props. *(French)* 80−40286
Ni sulphide ores from Kambalda, W.Australia, sulphide grain sizes and fabrics 78−77229
Ni wire plasma sputtering with W particles, coagulation, struct. and particle size *(Russian)* 80−40260
Ni-Co-Al alloys, continuous precip., SEM, TEM, X-ray diffr. study 80−89220
Ni-SiO_2 supported catalysts, particle size, H_2 chemisorption, Mossbauer study 80−7219
Ni-ZrO_2, electron-beam-evaporated condensate, cold deform. and annealing effects on microstruct. 80−16331
$NiCl_2$ aqueous solutions, autocorrelation spectroscopy 77−36796
$Ni(NH_4)_2(SO_4)_2.10H_2O$, precipitation, supersaturation, cryst. size distrib. changes 77−72573
NiO samples, colour difference, X-ray line broadening study 80−100206
NiO-Al_2O_3 powders, coprecipitated particle-size distrib. meas. 78−39726
PVC-Cu, particulate composite, mech. props. effect of particle size 78−95799
Pb from motor exhausts on motorways 79−12248
Pb powder size and shape distribution via image anal. 80−16221
$PbCrO_4$, cryst. growth kinetics and particle size in precipitating K_2CrO_4-$Pb(NO_3)_2$ mixed soln. 78−26472
$Pb_5Ge_3O_{11}$, dielec. behaviour, 60 Hz-100 kHz, particle size effects 79−33638
PbS, colloidal, light scatt. and electron microscopy 78−3379
Pb(Zr, Ti)O_3 cast tape, densification by pressing for piezoelec. devices 79−87595
Pd cluster, UPS of CO on Pd clusters, binding energy, d-electron emission particle size depend. 79−4888
Pt, small particles, contraction and relax. of interatomic distances using EXAFS 79−47546
PtO_2, finely divided, reduction 77−90643
Pu distribution in Ohio soils, local and stratospheric sources 78−16015
$^{239}PuO_2$, fragmentation of respirable particles in water by alpha decay 77−56487
$^{239}PuO_2$, in vivo solubility in rat lung 78−28093
$^{239}PuO_2$, size charcts., Rocky Flats soil, autoradiographic technique 78−96102
Rn, concentration of ^{222}Rn, ^{220}Rn and decay products in room air, exhalation, ventilation and deposition effects 78−73261
S aerosols, in atm., phys. props. 78−96285
S containing aerosols, physical charcts. 78−96284

particle size continued
p-$Sb_{1.48}Bi_{0.52}Te_3$, extrusion deformed, powder dispersion degree influence on thermal and elec. props. *(Russian)* 80−39366
Se, amorphous, vac. deposition on polymer substrates, use of temp. gradient vac. coating device 80−35099
Se, amorphous, vac. deposited on polymeric substrates, with dynamic coating device 80−100792
Se spheres embedded in polymer matrix, electrophotographic film, optical props. 78−83055
Si_3N_4, hot pressing, starting powder requirements, review 79−33987
Si_3N_4, reaction-bonded, theoretical model of manufacture, effect of ambient reaction temp. and compact size 80−108379
SiO_2 colloidal sol, particle size distrib., small-angle X-ray scatt. obs. 77−44516
SiO_2 particulates dispersed in CVD reactor, size distrib., semi-in situ obs. by light scatt. 78−27406
SiO_2:Al_2O_3, ultrafine and ultrapure powder prep., SEM study 79−70025
$Sm_{1-u}Ce_u(Co_{1-x-y-w}Fe_xCu_yCr_w)_z$, permanent mag., improved mech. props. 79−87593
SnO_2 powders, specific area, granulation and sintering *(Polish)* 79−52146
steel, Nb, deform., recrystn. and precip. interaction 80−97515
Ta powder, cathodic electrodeposit, effect of electrolyte composition and process parameters, on particle size distribution 80−16233
ThO_2, particle size of crystallites in soln. by line-broadening meas. 78−18488
Ti, sheets, porous, production and props. 78−60602
TiC, micropowder, degree of charging of polished Ti and Fe surfaces 78−60880
TiO_2, particle size, effects of coagulation struct. of Ti^{4+} hydroxide 78−52732
TiO_2 particles in suspension, light scatt. phenomena and abs. *(German)* 77−10835
TiO_2-ZrO_2, submicron powders, vapour phase production from $TiCl_4$-$ZrCl_4$-O_2 system 80−40301
U, specific α radioactivity meas. rel. to size using aerosol centrifuge 79−76255
UO_2, condensed vapour following core disruptive accident, particle-size distribs. using first-generation model 78−13295
V, small particles, crystal structure, magnetic and superconducting props. 80−97121
W, monocryst. particles and whiskers, reduction of vap. deposited WO_3 by TEM 77−52249
W powder, hydrostatic pressing 78−11161
W powders, influence of geometrical props. on compaction *(Russian)* 80−20818
W, sintered, porous struct. rel. to powder props. 79−61540
W/Cu powders, liq. phase sintering, particle rearrangement 80−45253
WC, powder prod. by vapour phase reaction in WCl_6-CH_4-H_2 system 78−60626
WC, sinterability of ultrafine powders obtained by CVD method 80−108378
WC-Co powder, prep. by direct carburisation of WO_3 in presence of Co_3O_4 80−50573
WO_3 smoke particles prepared by gas evap., morphology and coalescence growth 80−97738
WO_x, powders, coarseness meas. using powder surface reflectance 79−96246
WSe_2, lubricant, prep. by self-propagating high-temp. synthesis, technological charcts. 78−35338
Y_2O_2S:Eu phosphor, particles of different sizes, prep. by flux method 77−44140
Zn-rich paint, Zn particle size effects in mild steel protection 78−95840
ZnO powder, effect of dry grinding in EPR and catalytic activity *(Japanese)* 80−84640
ZrO_2 crystalline particles, TEM and electron diffr. meas. 77−21350

particle size measurement
abrasive particle shape control and quantitative eval. apparatus 78−4586
aerodynamic particle size calibration of optical particle counters 77−5879
aerosol, ambient sulphate particles size discrimination and chemical comp. by diffusion sampling 78−69528
aerosol, automatic method of determ. Stokes size of particles 79−93096
aerosol, Knollenberg light scattering counters, response charcts. 79−66369
aerosol, light-scatt. method for unknown refractive index 78−95957
aerosol, photoelectric analyser, theoretical anal. of optical detector 79−67455
aerosol, photoelectric analyser pickup, optical method of forming counting vel. 79−93270
aerosol, single droplet, size and mass meas. using electrodynamic balance 80−89535
aerosol, size distrib., laser Doppler velocimeter meas. 77−35273
aerosol, size distrib. determ. from mobility distrib. of charged fraction 78−61065
aerosol beam instruments, nozzle inlet design 80−6183
aerosol dispersed comp. analyser, small-size instrument design 77−17257
aerosol dispersion analysis by Kvant optoelectronic classifier 78−12739
aerosol droplet size and conc., simple transmittance meas. 77−9511
aerosol particle dimensions, equipment for transmitting dispersed compositions and measuring charcts. 79−70384
aerosol particle mass and charge determ. by one electron differentials 79−66368
aerosol particle size distribution errors of ratio-type single-particle counters 77−21898
aerosol particle size evaluation, response function optimisation of light scatt. instruments 79−50214
aerosol particle size meas. by microcomputer-modified elec. analyser 80−40756
aerosol particle size measuring device, using spectral transparency and small angle scatt. methods 80−95069
aerosol particle sizing, AC/DC quotient method 77−37462
aerosol particle sizing by laser beam Mie scatt., computer program 77−37457
aerosol particle sizing by laser Doppler dynamic relaxation time meas. 77−21897
aerosol particle sizing by optical scattering counters 77−21896
aerosol particle time-of-flight spectrometry 77−37451
aerosol particle-size classification by opposing jets, secondary effects 79−70383

particle size measurement continued
aerosol particle-small ion combination coeff. and size, simultaneous meas. 77−25320
aerosol particles, for medical use, inhalation technique development *(Slovak)* 79−74750
aerosol particles sizing, influence of chemical struct. 78−81471
aerosol size distribution, meas. by combined light scatt. and centrifugation 77−10083
aerosol size distribution by means of laser-induced fluoresc. 77−40576
aerosol sizing using slotted virtual impactor 78−57350
aerosol spectrometer, microcomputer-modified 79−39329
aerosol spectrometer using two-pulse Fraunhofer holography, fibrous particle motion anal. 80−58476
aerosol ultrafine particle size meas., diffusion battery anal. 79−92010
aerosols, Aitken range size distrib. meas. in N.Atlantic 80−98404
aerosols, atm., limitation on electrical measures 78−69431
aerosols, atm., physical charact. 78−69430
aerosols, atm., size distrib. meas. with particle Doppler shift spectrometer 78−69515
aerosols, atmospheric, at Mauna Loa Obs., Hawaii 77−78333
aerosols, atmospheric, sampling by in situ and standard methods 79−66840
aerosols, atmospheric, size distrib. and turbidity meas. over St. Louis, Project METROMEX 79−16670
aerosols, dispersity analysis, automatic photoelec. analyser for size range 0.3-40 μm 80−57251
aerosols, electronic cascade impaction method for particle size distribution meas. 80−72652
aerosols, fractionator for large-scale sampling 77−9140
aerosols, granulometric spectrum, in slightly polluted marine atm. 78−44893
aerosols, liquid and solid, size distrib. meas. by Doppler shift spectroscopy 78−33674
aerosols, monodisperse, 0.1-0.4 μm, size meas. by polarisation ratio of 90° scatt. light 80−40754
aerosols, optical particle counter calibration by Doppler shift spectrometry 80−68173
aerosols, parallel plate electrostatic classifier 80−95070
aerosols, size distrib. meas. by impactors, data inversion via nonlinear programming 77−2258
aerosols, size distribs. sampling errors rel. to Mie optical cross-sections calcs. 77−2243
aerosols, size meas. by optical methods, review 80−40746
aggregates, solid, aerosols, dynamic shape factors meas. appls. 80−61165
air pollution detector, condensation nucleus counter 80−55967
airborne, inertial sizing using laser velocimeter method 80−53901
airborne, particle sizing, 0.05 to 5.0 μm, using laser instrument 78−61624
airborne particulate matter, size distrib. of organic pollutants 79−57553
alumina powder, particle size analysis, using centrifugal sedimentation *(German)* 78−57890
anemometer signals, visibility charact., particle sizing appl. 77−42482
apparatus for sizes down to 5 μm 80−77753
asbestos fibres, particulate analysis, aspects of specimen prep. and a limitations of precision by SEM and TEM 79−17574
atmosphere, particulate matter props., remote and in situ meas. 78−61501
atmospheric aerosol size distribution determ., optical attenuation meas. *(Chinese)* 80−72570
atmospheric aerosols, size distrib. of water-soluble and insoluble particles 78−36218
atmospheric aerosols microphysical parameters from complex optical meas. *(Russian)* 77−13123
atmospheric environmental research, appl. of lasers *(German)* 80−97849
atmospheric haze and fog vertical struct., effects on visible and IR extinction 79−58086
atmospheric precipitation size distrib., small-particle response of optical array probe 80−51577
atmospheric sulphate aerosol, individual submicron particles size meas. 78−69527
automation of real-time optical meas. of small structures 79−85115
bimodal systems, particle size distrib. meas., forward scatt. techniques 79−21699
biological cell size meas. by static light scatt. Fourier transform 80−81793
biological sound scatterers in water, acoustic size measurement 80−38199
blood, stored, microaggregation direct meas., effects of micro-filtration *(German)* 79−2168
breakage distribution, in batch grinding, mathematical model determination 78−92416
bronze, spheroidal, equivalent sphere diameter calc., Saltykov method 78−31362
butyl rubber dispersion, electron-microscopic investigation 78−53268
di-butylphthalate, critical nuclei, meas. of number of mols. and surface tension from rate of nucleation 79−65293
cascade impaction instrument using quartz crystal microbalance sensing elements, for real-time meas. 78−65904
cascade particle analyser for aerosol size distrib. and mass conc. 79−71583
cavitation nuclei in liquid flows, size distrib. determ. technique 77−68716
cell distributions topographical size analysis, TOGA interactive program *(German)* 77−40951
cell membrane particles diameter meas. via picture processing 79−84065
ceramic powders, electron microscope determination of particulate sizes *(German)* 78−57891
chalk, grain size determ., sample preparation methods 79−24694
chemical analysis of atmospheric dust *(Dutch)* 79−16713
chondrules, from Bjurbole and Chainpur meteorites, size and mass distrib. 78−65556
chondrules, near-spherical, from Allegan meteorite, size and shape meas. 78−65555
circular, complete histogram determ., diffraction spectrum anal. 79−86130
city plume aerosol size distrib. and turbidity meas. 77−37408
coherent radiation scattering, calc. of diameter distrib. function of long hollow cylinders 77−70569
colloid, hydrodynamic chromatography technique 77−44530
colloid fractionation and size analysis using flow field-flow fractionation 78−61062
particle size measurement continued
colloid of submicron particles, ultrasonically induced birefringence technique 80−30290
colloid size distrib., photon correl. spectroscopy, methods of cumulants, histogram and Laplace transform 79−58801
colloidal dispersion, spherical particle, optical turbidity and refr., particle size and relative refr. index meas. 79−92012
colloidal particles, hydrodynamic chromatography, mathematical modelling 77−1951
combustion aerosols, particle size distrib., health hazards 78−81394
computer-aided anal. of optical counting data 78−77842
condensation nuclei, counter with inherent size resolution capability 78−81470
conductometric method, for particles in disperse systems 79−35664
contaminant particle microanalytical methods 80−86397
continuum source particle beam properties, comput. modelling 80−26062
Coulter counter method, improved technique for particle size distrib. meas. in high-impact polystyrene 77−56258
Coulter counter technique, errors in meas. of particle size distrib. in high-impact polystyrene 77−56257
crystal nucleation growth rates, on-line meas., data reduction technique 79−38730
crystallites in soln. by line-broadening meas. 78−18488
Debye-Scherrer line profile determ. of particle size and distortion moments *(German)* 78−62182
dense particulate system, particle size meas. device based on scatt. light 78−45006
dichroic colloidal particles, size distrib. determ. by electro-optical method 79−6087
dielectric spheres, resonances in radiation press., dielec. surface wave obs., and size meas. 77−58256
diethylene, critical nuclei, meas. of number of mols. and surface tension from rate of nucleation 79−65293
diffusion battery, screen type, theory 80−95208
digital control of laser beam expt. 78−70098
dioctylphthalate, monodisperse aerosol, automatic method of determ. Stokes size of particles 79−93096
diphenyl methane, critical nuclei, meas. of number of mols. and surface tension from rate of nucleation 79−65293
disperse particles, determ. of spectrum of diameters from scattering of light 80−61169
disperse system, parameters determ. from turbidity spectrum, allowance for nonspherical particles 78−55302
dispersed system, simultaneous determ. of refr. index and particle size from scattered radiation charact. 80−27335
dispersion, liq.-liq., new drop size distrib. mass. technique 80−3419
dispersions, particle size and velocity distribution, in flowing media, meas. methods *(German)* 78−34213
distribution, spectral transparency method, improvements 80−86254
distribution determ. methods for particles <10μm, review *(German)* 78−60894
distribution meas., online stroboscopic microscope apparatus 80−101783
distribution measurement apparatus, rel. time 79−17390
distribution parameters, estimation using forward scatt. techniques 80−36974
drop size distribution airborne meas. for drops >60 μm diameter 78−45008
drop size in dense fuel sprays, in-line holography meas. 78−37827
drop size measurement methods, review 80−17916
droplet size and falling velocity meas. using laser Doppler velocimeter 80−68185
droplet size distribution, reduced function, determ. from local meas. 77−68717
droplets, large, laser anemometry, size and velocity meas. equipment 78−86238
droplets produced by pneumatic nebulisers, size meas. method 80−71992
dust, airborne, Raman laser microprobe analysis appl. 80−57390
dust, destruction degree, determ. in mech. screening 80−66882
effective sampling volume increase of particle size spectrometer, computational technique 79−70863
electron beam particulate analysis of air samples 80−40785
electron interference method for particle shape determ. in films, inner pot. determ. and external field determ. *(Russian)* 78−29209
electron microscopy, scanning, high voltage computerised particulate charact. 79−48036
electron trajectory simulation in solids, Monte Carlo method, particle size anal. 79−43693
electrooptical diffusion method, determ. colloidal particle size distrib. function 80−8956
EM wave scattering to find shape of dielectric particles 79−67250
emulsion polymerisation, particle size calc., applicability of Gardon's eqns. 78−92479
environmental samples, X-ray fluoresc. anal., particle size correction method 78−48705
EPIQUANT, automatic structure analyser 80−85116
error contour charts rel. to particle sizing by forward-scattered lobe methods 77−79752
errors in measuring the dimensions of drops by holographic methods 79−67252
ethylene glycol, critical nuclei, meas. of number of mols. and surface tension from rate of nucleation 79−65293
ferritin, iron core particle size distrib., Mossbauer determ. 78−92696
ferrofluid, magnetically induced polarisation, particle size determ. 77−73130
filtration efficiency, comparing particle-size distribution, in feed stream to filtrate 78−92417
fine particle granulometric analysis, sieve and pulse methods *(German)* 80−22502
fine particle profile, ruggedness and texture specification by fractal dimension 79−40535
fine particulate emissions from coal-fired power plant, size distrib. 77−45135
flow device to measure γ radioactivity uptake and size of microparticles 77−5074
flowing aerosol, particle size distrib. *(German)* 78−20076
Fourier plane signal processing for real-time meas., using Fraunhofer diffr. pattern 79−76621
glacial till landforms, fabric anal. 77−44989
glycerin nonadecane, critical nuclei, meas. of number of mols. and surface tension from rate of nucleation 79−65293

particle size measurement continued
growing bubbles on heated plate, meas. using computerised image anal. system 80−22322
Gulf of Mexico, particle size distrib. of suspended matter in deep water 78−36177
hailstone size determ. from dents in cold-rolled Al sheet 79−39890
hazes, information provision on particle size distrib. of brightness and polarisation phase functions *(Russian)* 78−44998
holograms, in-line absorption, improved microimages 79−36857
holographic disdrometry for disperse system particle size determ. 79−7104
holographic droplet image analysis by TV camera and table calculator via IEC-Bus 78−36337
holographic meas. for fine particles *(Japanese)* 78−95873
holographic methods appls. 79−13924
holographic particle sizing high-resolution system 79−81392
holographically recorded particle field meas., Fraunhofer plane analysis 80−73306
HTGR nuclear fuel microspheres, automatic particle size analyser 79−12921
hydrometeors in clouds, size, conc. and struct. meas. 77−41218
hydrometer particle size analysis calc. method 79−62590
image dissector for size and position of statically suspended particles 80−26616
imaging system, real time Doppler, colour TV display of particle size or density 77−62038
irregular shape particles, from acoustic emissions 79−61825
Knollenberg light scattering counters, response to doublet latex aerosols 80−37152
laser applications in particulate analysis, multiple ratio single particle counter 78−35732
laser diffraction appl., particle and droplet size distributions meas. 80−17925
laser Doppler particle meas. system, using nonsinusoidal forced vibr. and bispectral analysis 78−41285
laser Doppler velocimeter for particle size and density simultaneous determ. 80−98880
laser Doppler velocimetry technique *(Japanese)* 78−24913
laser flowthrough microphotometer, double-beam technique, internal calibrated 79−17391
laser fringe anemometers, light scatt. aspects, particle size meas. appl. 78−83020
laser interferometry, fringe visibility in crossed beams 77−71292
laser light scattering spectroscopy method and apparatus, averaged size and polydispersivity index meas. 80−77754
laser particle size analyser, size estimated from diffraction pattern 79−6091
laser particle size analyser, using diffraction of light by particles 79−6090
laser photography appl. 78−81946
laser radiation effects on particle properties, radiation pressure effect on particle motion *(German)* 80−102755
laser scattering, log-normal size distrib. 79−6079
laser technique for simultaneous particle size and velocity meas. 78−70096
laser ultramicroscope for rapid measurement 79−44902
laser velocimeter, particle size meas., using forced vibr. synchronised detection, and power spectral anal. 78−36977
laser-Doppler technique, local size and vel. probability distrib., two-phase suspension flow 78−59517
latex particles, size determ. by combined filtration and turbidimetry method 79−79313
light extinction-sedimentation inversion technique, size distrib. meas. of artificial fogs 78−37042
light scattered intensity-ratio technique, forward lobe, diffr. theory errors 78−71031
light scattering analyser, for particle size analysis 79−6088
light scattering extrema for fast precise size distribs. determ. 78−54421
light single particle scattering, asphericity effects 79−7069
lipid vesicle suspensions, particle size distrib. determ. by photon correl. spectroscopy 77−86711
liquid-borne solids monitoring, optical instrument general principles 79−37424
low angle X-ray diffr., pore or particle size distrib. calc. 77−39512
lunar soil, particle size distrib. anal., Rosin's law 77−78682
magnified dark-field image holographic recording 77−19214
marine aerosols, organic and inorganic Cl gas concs. and particulate Cl size distrib. 78−32187
maximum midsection area, determ. for large coarse particles by photoelec. method 79−70240
mean size calculation simplification 80−90814
metal powder, particle size distribution determ. appl. of pulse conductivity 77−10157
meteoric matter, evaporated, mass spectrum of particles formed in condensation 79−71005
micellar dimensions determ., small angle X-ray scatt. *(French)* 77−29053
micropowder, cyclic classification, using variable electric field, device design 80−36982
microscopy, quantitative, appl. of statistical methods, review 79−17484
Mie theory calculations, particle sizing appl. 80−14282
monoparticulate film method *(Japanese)* 78−95874
multiphase flow optical fibre sensors, appls. *(German)* 78−26215
nonspherical particles size distrib. from scatt. meas., Mie theory 78−58909
on-line measurement techniques, instruments *(German)* 78−60895
optical array probes evaluation for cloud particle size distrib. meas. 77−41220
optical electronic device for particle counting and vol. determ. in suspensions 78−57894
optical particle counter, portable, using He-Ne laser, for particles with 0.06 to 10 μm diameter 79−75674
optical single-particle-size spectrometer calibration and testing, monofilament fibres as substitute particles 80−58819
optical-digital training method for particle counting by size 77−71305
photometer, differential light scatt., for rapid analysis of particles in flow, appl. to biological cells 80−77834
photon correlation spectroscopy, appl. to particle size distrib. meas. 79−67456
Pioneer Venus Sounder Probe Particle Size Spectrometer 80−67510
particle size measurement continued
Polirit, optical polisher powder, particle size distrib., dispersion analysis 77−9141
polycyclic aromatic hydrocarbons, in particles from coke oven, size distrib., health hazards 78−36268
polydisperse discs, particle size distrib., transient elec. birefr. data, two-parameter distrib. functions 78−40083
polydisperse ellipsoids, particle size distrib., transient elec. birefr. data, two-parameter distrib. functions 78−40084
polydisperse particle size distrib. function, angularly scatt. light intensity profile meas. 80−13040
polydisperse particle size distrib. function determ. from angularly scatt. light intensity profile 80−98879
polydisperse particles, fractional anal. by ring method *(Russian)* 78−71035
polydispersion size distrib. function, light scatt. determ. 77−10834
polyethylene terephthalate, joint prosthesis fragment dispersal meas. *(German)* 79−8566
polyethylene-polypropylene blend, size distribution determ. of spherical occlusions from photomicrographs *(Czech)* 80−89539
polymeric particles obtained by suspension polymerisation, particle size distrib. eval. using Coulter Counter data 80−76564
polystyrene latex, particle size determ. by electron microscopy 79−21698
polystyrene latex particle size by electron microscopy and light scattering 79−66365
powder, determ. from acoustic emissions 77−53861
powder, grain size determination by transient low press. air transmission 78−32965
powder, nonequiaxed orientation effect on pulse amplitude in pulse conductometric particle size anal. 79−100070
powder, particle size distrib. meas. by spectral transparency method 78−49876
powder and particle characterisation, survey of instruments and methods 78−11474
powder and sintered material particles, dimension and shape evaluation by SEM 80−40278
powder crystallite size determ. using SEM *(German)* 78−47218
powder particle size distrib. anal., photoelectric device 77−74379
powder particles in fluid, size distrib. anal. by light blockage principle 79−6089
powders, air-jet sifter for determining granulometric composition 79−75671
powders, grain size determ. by sedimentation, automatic recording system 78−60897
power plant plume, submicron particle size distribs. determ. 79−57526
precipitate, weak-beam contrast calculation for spherical coherent precipitates *(French)* 77−35450
precipitation processes, study by particle site anal. 80−50883
pulse height analyser for Coulter counter particle size distribs. display 79−70716
PVC latex size determ. by TEM, vertical shadowing technique 77−53857
rapid response, online methods, instruments, continuous industrial processes appl. 78−89429
reactor coated fuel particles, automatic size anal. 77−79460
red blood cell sizing, evaluation of automated Electrozone Celloscope in haemolysis study 78−40455
remote sensing, analytical inversions, angular (spectral) scatt. in diffr. approx. 78−73509
remote sensing, analytical inversions, multispectral extinctions in anomalous diffr. approx. 78−73508
remote sensing of size distribs., anomalous diffraction approx. solns. 80−17386
resistive-pulse particle-sizing instrument 79−12919
ring gap sizer, characterisation of particle shape in sieve range 78−84732
Royco aerosol particle counter 225, data processing system and modified system props. 80−37005
rubber powders, finely dispersed, sedimentometric anal. 80−66883
Saguenay fjord, distrib. of size spectra of suspended particles *(French)* 79−92543
scattering from naturally occurring aerosols, rel. to particle size statistics, 3.8 μ meas. 78−49136
section diameter method for nonspherical objects 77−41567
sedimentation particle track photography, semiautomatic device for photograph analysis 77−44515
sediments, polymodal, of river-lake system, interpretation 79−25273
sieves, automatic, for particle size analysis 80−52380
simulated microbes, suspension, size determ., teaching expts. 79−71178
simultaneous determination of diameters of velocity of moving solid particles with image sensor *(Japanese)* 78−95872
size measurement, using Fraunhofer diffraction 79−171
Skylab contaminant particulate environment, coronagraphic technique 77−78633
slurry conc. and particle size determ., on-line light backscattering method, fibre optic appl. 79−58674
smoke particle size and conc. meas., three-wavelength light transmission technique 79−79438
soil 81e p=sp 79−66836
solid rocket propellant combustion, holographic recording 78−82935
spatial struct. parameters estimation using extraction replicas *(Czech)* 79−35668
spectra attenuation data appl. considering light dispersion *(Russian)* 79−34981
spectrometer, Doppler shift, for research and calibration 80−4827
spectrometry using low power gas lasers 77−78485
sphere population overall mean caliper diameter estimation 79−70719
spherical particle velocity and size meas., crossed-beam light scatt. interferometry 80−47011
stack dust monitor based on particle counting and sizing 79−83683
stack effluent of coal-fired power plant, comp. and size distrib. of particulate material 77−45136
statistical reliability of distribs. 77−53858
stereology, estimation of linear functionals of size distributions 77−61056
strengthening phase particle distrib., quantitative analysis 78−15629
Streptococcus mutans 10449, size determ. by laser light scatt. 80−109062
structurometer, diffraction, annular method of recording scatt. indicatrix 79−54165
submicrometre particle detector and size analyzer 79−75672

particle size measurement continued
submicron particle size distrib. in colloidal suspension, FODA 78−61057
submicron particulates size determ. by sideway light scattering method 80−98883
submicronic aerosol laser spectrometer for photoelectric determ. of conc. and dispersity 79−54244
suspended particle size distrib. shape stability in Baltic sea 79−79876
suspended particles, fast moving, size and vel. meas. 77−42935
suspension, in nonpolar dispersion media, particle size and number conc. meas. 80−9082
suspension, particle size and concentration, determ. by light backscatter technique 78−85214
suspensions, colloidal, radiometric method for particulate processes characterisation, theory 80−45578
suspensions, colloidal, radiometric method for particulate processes characterisation, expt. 80−45579
techniques for different branches of physics 80−1113
technology, IR applications 80−86431
transmission holography limitations in particle analysis 77−19213
triethylene glycol, critical nuclei, meas. of number of mols. and surface tension from rate of nucleation 79−65293
two-phase flow, optical particle sizing counter for in situ meas. 79−75489
two-phase flow, optical particle sizing counter for in situ meas. 79−75490
two-phase flow, time-of-flight laser anemometer 77−39383
ultrafine particles in gas, information on size, surface props. from photoelectron emission 78−68598
virtual impactor for particle classif. and generation of test aerosols with narrow size distribs. 80−30626
virus size measurement using optical microscope, Virometer design 78−61296
water droplets in mists, clouds, size, density distrib. meas., laser remote sensing technique *(Japanese)* 78−49175
water-petroleum emulsions, mean particle diameter and conc. determ. by light scatt. 80−89538
wear debris anal., quantitative methods 78−64912
wind tunnel particle and droplet field holography 79−76642
wind tunnel water droplet size distrib. interferometer 79−80673
X-ray absorption anal., particle size effects 77−16882
X-ray absorption method using ^{55}Fe source combined with sedimentation cell 79−75491
X-ray scattering, small-angle, for distrib. functions determ., calc. methods 77−16420
Zircaloy-4, microstrain and particle size meas. by Warren-Averbach method 80−55420
AgI pyrotechnic nucleant charact., use in Florida Area Cumulus Expt. 79−100919
$BaTiO_3$ powder, dispersion effect on meas. in electrical sensing zone particle size counter 79−17383
Bi_2Te_3-Sb_2Te_3 solid solns., powders, particle shapes determ., device 78−60899
CdS, monodisperse particles form. from soln., light scatt. theory use in size estimation 80−76560
Cu, equivalent sphere diameter calc., Saltykov method 78−31362
H_2SO_4 aerosol particle size measured by impaction method 80−31134
H_2SO_4-H_2O droplets in atmosphere, equilib. size and comp., quick estimation method 79−66767
Li particle size distrib. meas. by SEM 80−101775
Na salt crystals in aqueous slurries, particle size distrib. determ. 79−61918
Na vapour, particle size meas. using anemometer 80−13195
NaCl, single cubic particles, suspended in laser beam, optical size determ. 78−33673
Pb powder, automatic image analysis for charact. of size and shape distrib. 78−11473
Pd, catalyst hollow cone dark field microscopy on γ-alumina substrates 78−61049
PtI_4, aerosol, X-ray fluoresc. anal., particle size correction method 78−48705
PuO_2, particle size meas. in UO_2-PuO tablets, image analysis by LEITZ-TAS with process computer 80−68773
S aerosols charact. in Florida, PIXE anal. 79−21030
SO_4^{2-} aerosols size depend. on relative humidity 79−20906
SO_4^{2-}, airborne particles, size meas. and chem. comp. by diffusion sampling 78−45007
SO_4^{2-} containing aerosols, dynamics, review 78−96286
SO_4^{2-}, individual submicron size particles detect. method 78−95973

particle sources
see also ion sources; neutron sources; radioactive sources
angular distribution meas. of recoil prods. of high-energy nuclear reactions, geometry calcs. 77−6596
atomic beam source, employing radiant heating 78−330
atomic beam source, three-stage oven design 77−42443
cluster beam generation of strong flux intensity using a slit nozzle *(Japanese)* 80−52361
DC Fano effect polarised electron source appl. to electron-atom scatt. 78−66689
deuterons, ANL ZGSynchrotron, high energy polarised deuteron beams 79−72054
electron, accuracy of electron brightness meas. by 2-limiter method, calc. 79−6234
electron, HV glow discharge as plasma electron source, charact. 80−44031
electron and ion beam generation at high power, review 80−13988
electron beam, high-current, compression in gas, on current pulse trailing edge 78−12789
electron beam generator at 100 GW 77−2711
electron beam production, μs, high-current, device design and charact. 77−82642
electron beam production, hollow cathode discharge as electron beam generator 80−44039
electron beams, spin-polarised, features, appls. 79−17559
electron diode accelerator, electron beam power increase by inductive accumulator 78−33339
electron gun, portable containing source, monochromator, counters, for particle detector calibration 78−78539
electron gun system, pulsed, for use with superconducting accelerator and free-electron laser 80−68989

particle sources continued
electron gun use of glow discharge lamp for Auger spectroscopy 77−31027
electron high dosage source for residual resistance specimens and irradiation expts. *(German)* 78−21274
electron polarised source, injection gun for Stanford linear accelerator 79−76242
electron source, high intensity polarised, illum. of GaAs with polarised light 77−38520
electron source, multiplier-assisted discharge, new type of cold cathode 79−55591
electron sources for high resolution AES in SEM 77−25330
electron spectroscopy, target sources, centrifuge method of prep. 80−74060
electron to positron conversion efficiency, 20 to 70 MeV 77−23335
electron-photon beams from proton accelerators, EM interaction investigation *(Russian)* 80−106214
electrons, polarised field emitters, regulator for annealing 78−86384
electrons, pulsed plasma source 77−46439
electrons, subpicosecond pulse generation and meas. 78−65996
electrons from Cu points, explosive emission 77−18144
field emission electron gun, off-axis electron holography 80−101905
field emission source, micro Auger anal. 80−104020
fusion reactor, TFTR, neutral beam source, arc current modulator design 80−102379
heavy current electron beams prod., survey 78−33337
high flux muon channel incorporating a high quality spectrometer field 79−72136
high-flux beam source of He, Ne and Ar metastable atoms 80−58416
high-voltage subnanosecond electron beam generator 78−4733
intense relativistic electron beam, $\nu/\gamma \sim 1$ diode characteristics 77−15249
isochronous two stage ring cyclotron kaon factory 79−54728
kaon, KEK synchrotron low energy kaon beam line charact. 79−72053
labelled α particles, miniature source 78−5080
LAMPF linear accelerator muon beam charact., surface and cloud beam polarisation 79−71994
LAMPF stopped muon channel 79−68115
laser beam source of polarised photons for photoprod. bubble chamber expts. 77−38521
Los Alamos Meson Physics Facility proton irradiation port 79−9935
low energy positron beams, spin polarisation 80−9442
microparticle accelerator and charged particle source description 78−41373
molecular structure and dynamics by pulsed mol. beams 80−102563
muon beam channel, 40 GeV/c, Serpukhov, lens, guide reflector, filter 77−18729
neutral beam, charged particle separation by space target blowup 78−9018
neutral beam, pulsed, arc (arc filament) power supplies, for fusion reactor 78−70637
neutral beam accelerator electrodes, spark discharge protection, for fusion reactor 78−62609
neutral beam filament supply, 15 V 10^3 A, programmable, regulated, for fusion reactor 78−70630
neutral beam high-voltage test stand, for fusion reactor 78−70632
neutral beam injector, decel voltage effect 78−9015
neutral beam power supply, 40 kV, 25 ms, for fusion reactor 78−62610
neutral beam power supply, series switch/regulator system, 40 kV, 80 A, 10 ms, for fusion reactor 78−66366
neutral beam power system, for Princeton TFTR fusion reactor 78−70639
neutral beam source 8 MW voltage series regulator, for fusion reactor 78−70631
neutral beam system for Princeton Large Torus 78−9019
neutral beams for reference mirror fusion reactor, efficient, high-power, high-energy 79−49836
neutral fast atoms, mol. beam sampling of hollow-cathode discharge plasma 77−68865
neutral injection power supply system, for Princeton large torus fusion reactor 78−70638
neutral-beam injection system for CTR, plasma source design 77−24105
neutrino, beam channel charact., Protvino Inst. 78−37474
neutrino beam focusing system, Protvino Inst. 78−37477
neutrino source at LAMPF, calibration from stopped π^+ decays in Cu beam dump 79−45503
nuclear polarised beams, review of appl. 79−45243
photon, electron and positron prod. from primary proton beams, Monte Carlo calcs. 80−32555
photon polarised monochromatic beam prod., Ladon project at Frascati 77−83437
pion conversion target for Saclay electron linear accelerator 77−54384
plasma electron source with high brightness, emitter and beam parameters 80−106218
polarised electron beams, production methods and current status of polarisation meas. 79−63836
polarised electron source PEGGY at SLAC 77−38519
polarised positron, electron production by colliding photon beams in storage ring 80−5426
positron, Au moderator surface preparation for increased yield 80−61011
positron apparatus for surface studies 80−86500
positron beam generation at low energy 80−5422
positron energy spectra and ang. distrib., 0.2-2 GeV electron conversion on W targets 78−86713
proton polarised source, H resonant ionisation by laser radiation 78−78541
pulse-power particle beam sources as fusion drivers, review 79−18066
pulsed gas valve as 10 μs mol. beam source 78−66690
pulsed polarised electron source with high repetition rate 77−10517
pulsed proton source, Penning type, beam parameters 80−87001
radioisotopes, production, for medical use, at TRIUMF 80−72325
relativistic electron beam deposition, field-enhanced, bremsstrahlung prod. 78−29677
relativistic electron beam diode, medium current 77−46443
SIN high resolution pion channel and spectrometer 79−22517
synchrotron orbital radiation, wiggler, helical wiggler and free electron laser *(Japanese)* 80−37658
trajectory of electron in electron beam source for vaporisation *(Russian)* 78−33657
X-ray high intensity sub.-kV calib. facility using Cockroft-Walton proton accelerator 77−71714

particle sources continued
X-ray low energy sources for detector calibration 77−75016
p̄ prod. in W+p, 25 GeV, flux optimisation using hadron cascade calcs. 77−83411
π production by electron linear accelerators, appls. *(Japanese)* 78−78533
F atom source using thermal decomposition of KrF_2 in duralumin reaction vessel 79−24724
GaAs spin-polarized electron source 80−69000
H, arc-heated high-intensity source 77−3493
H beam, microwave discharge source, extended cavity design 79−67427
H, cooled microwave discharge source 78−5373
H, D, polarised atoms, cryogenic source 78−5079
H_2, cluster beam source, cryopumping 79−63258
^{22}Na, glass positron source, preparation 80−102367
O, cooled microwave discharge source 78−5373
^{48}V positron source prep. for annihilation radiation lineshapes, positron lifetimes meas. 80−876

particle spectrometers
see also alpha-particle spectrometers; beta-ray spectrometers; electron spectrometers; gamma-ray spectrometers; neutron spectrometers; X-ray spectrometers
2-arm arrangement for investigating (γ,pπ⁻) reaction on nuclei 79−711
220 MeV/c superconducting π spectrometer for tissue irradiation 79−34667
1024-channel particle spectrometer power supply 79−68169
ΔE×E counter telescope, improved mass resolution 77−54458
ACCMOR collaboration spectrometer and expts. *(Dutch)* 77−46454
AES and characteristic energy loss spectra, apparatus design 78−27354
amplitude dependent count rate losses in pulsed optical feedback preamplifiers 80−91366
Amsterdam 500 MeV high duty factor electron scatt. facility, status report 80−23191
analyzing voltage instability in modulation method of measuring solar wind 80−67565
atomic beam magnetic resonance system for on-line hyperfine struct. meas. in short lived nuclides 78−25379
atomic beam spectrometer using a LiF analyzer crystal, for surface studies in UHV 78−71651
avalanche parallel plate detector, appl. to photofission expts. 79−76263
avalanche spherical fission detector with intrinsic α-discrimination 79−97945
beam analyser for electrons and protons 78−37482
beam handling and detection system matching for optimum resolution in nucl. physics 79−45504
Brookhaven multiparticle spectrometer drift chamber system 80−58044
Buechner magnet-position sensitive counter system for unslowed fission fragment spectroscopy 77−23360
Buechner magnet/PSD system, mass spectrom. of unslowed fission products, feasibility 78−29702
calibration by electron capture reactions 80−63445
calibration of optical particle counter 80−68173
calorimeter, segmented, hadron shower struct. meas. 79−63870
Cerenkov, total-absorption, characts. investigated with gamma-quantum, electron and positron beams 80−23242
CERN OMEGA spectrom., slow proton trigger 78−17467
CERN Omega spectrum., data monitoring system 77−18768
charged particle energy analyser, ang. focusing with cylindrical electrostatic field 78−78896
compact time-zero detector for heavy ions 79−76260
comparison apparatus for bunch excited fields and energy loss meas. 79−72164
continuous angular scanning meas. system 79−6787
conversion electron spectrometer, in-beam use 78−55086
cosmic ray spectrometer, for study of 6 to 50 MeV electrons 78−45235
cosmic ray variation spectrograph, data reliability ensurance 79−84610
cosmic-ray stations global network, appl. as spectrographic instrument set 79−12404
Crystal Ball data acquisition system 79−89531
cylindrical electrostatic analyser, design procedure 79−13885
Darmstadt linear accelerator, detector system and performance of elec. scatt. system 78−70680
Darmstadt linear accelerator electron scatt. facility, beam transport and spectrom. 78−70679
Darmstadt linear accelerator electron scatt. facility, data processing 78−70681
data anal., off-line, 168/E microprocessor 80−58102
differential Cherenkov counters with achromatic ring focus, hadron beam mass identification, CEDAR project 78−37522
double-arm, use as proton recoil polarimeter for zero gradient synchrotron 77−38511
double-focusing electron spectrometer, new effective transmission determ. from focalization props. 78−17463
drift chamber for multitrack particle identification 79−3276
electron, double-stage retarding field type, expt. 77−82649
electron, double-stage retarding field type, theory 77−82648
electron, for surface analysis, design, book contrib. 77−61169
electron, pulse shape anal. in fosfich detector 77−65387
electron, spherical electrostatic, for Mossbauer spectroscopy 78−25378
electron, superheated superconducting suspension as transition radiation detector 77−6628
electron, transmission props. of cylindrical mirror analyser viewed in energy-angle space 78−15745
electron, with double focusing, adjustment with nonuniform mag. field 77−6606
electron spectrometers, energy calibration 78−24888
electronic device for reduction of charge state energy doublets in electrostatic anal. of backscatt. He ions 80−27870
electrostatic analyser, double parallel-plate, for energy anal. of scattered and sputtered particles 79−80716
electrostatic analyser with oblique cut plates, focusing props. 77−54667
electrostatic analyser with parabolic electrodes, particle energy distribution after traversing spectrometer 80−99000
electrostatic analyser with parallel plates for ion energy selection 78−83610
electrostatic cylindrical mirror analysers, response functions 78−1146
electrostatic deflector for energy-loss spectrometers 79−9939
electrostatic electron energy analysers, cylindrical mirror appls., review 78−21265
electrostatic electron spectrometer, relativistic effects in calibration, toroidal analyser 78−29211
electrostatic electron spectrometer, relativistic effects in calibration, parallel plate and cylindrical mirror analysers 78−29212
electrostatic photoelectron spectrometer, analyser brightness determ. 77−25331
electrostatic spectrometer design, energy loss and UV spectroscopy *(French)* 77−82651
energy analyser for charged particle energy and angle meas. in ultrahigh vacuum 78−86750
energy analyser for neutral H, D, He and Ne atoms, 200 eV-10 keV range 77−83763
energy analyser/electron microscope combination, microanal. accuracy improvement 78−15737
Enge split-pole spectrograph, limits on differential hysteresis and accuracy of proton beam energy calib. 78−55082
Enge split-pole spectrom., solid angle increase without loss of resolution 77−30696
Erlangen double scatt. spectrom., sliding seal chamber 79−22526
Fermilab single arm spectrometer, MWPC system 78−82585
focal plane, large hybrid detectors, electric field uniformity improvements 80−37684
focal plane detector for both light and heavy ions 79−18077
focusing properties of a broad-range sector spectrometer with a 1/r-magnetic field 80−102383
gamma dosimeter testing, effect of air scattered radiation 79−6774
gamma ray shower detector of low press. flash tubes 78−70697
gamma-ray spectrometers; calc. of radioactivity induced during spaceflight 80−102382
glass track detectors, NaO_2-SiO_2, phosphate, quartz glasses, nculear phys. spectrometric appls., track diameter 78−17466
gridless retarding potential analyser for use in very-low-energy charged particle detection 77−5343
heavy ion deep inelastic processes fragments, element identification in ΔE-E telescope, computerised method 77−57839
heavy ion detection in low-press. noble-gas scintillation counter 77−83446
heavy ion electrostatic analyser control system *(French)* 77−42211
Heidelberg Q3D mag. spectrograph, 1.4 m ΔE-E position sensitive detector 79−45566
hemispherical collector for low-energy charged particle flux anal. 77−46449
high resolution Auger photoelectron spectrometer 77−48704
high resolution spectrometer facility at LAMPF, beam line 78−62674
high-resolution nuclear spectrograph magnet developments 79−31317
high-speed amplitude spectrometry, overlapping pulse elimination 78−78544
HISS computer facility 79−89559
hodoscope Cherenkov spectrometer, particle identification 77−88343
hodoscope containing scintillation counters, and small FEU-87 photomultipliers, charged particle meas. 78−78562
hodoscopes for high intensity muon beam, high-rate photomultiplier-base and precise timing calibration 79−22544
identification spectrometer for measurements of charged reaction products 79−36463
ion, energy analyser for surface scatt. studies 77−36333
ion analyser enhancement based on MI-1305 mass spectrometer 80−105745
ion identification with detector telescopes 79−72180
ion scattering spectrometer for surface studies 80−98995
ionisation calorimeter, separation of hadrons and EM particles 77−79523
ionisation chamber, ^{235}U fission products detection 79−93872
ionisation chamber, fission fragment atomic number identification 80−27863
ionisation chamber, multiplate, with intrinsic background reduction, response to photofission 80−37685
ionisation chambers, liquid, Fano factor limitations on energy resolution 78−37502
ionisation pulse spectrometer for microdosimetry, interpretation of instrument lines 77−73595
ionisation spectrometer with gas Cherenkov counter, appl. to cosmic ray studies 80−94662
LAMPF π^0 spectrometer 79−85508
large aperture, beam monitoring tech., MWPC construction, data acquisition system 80−102381
large solid angle spectrometers for colliding beam facilities, design, operation 79−719
Lass spectrom., performance of PWC cluster logic trigger 79−76262
leading-edge spectrometer for current signals from semiconductor detectors 77−6607
Leuven isotope separator on-line at CYCLONE cyclotron 78−70682
light nuclei, micron spectrometer for meas. with energy resolution of 1 MeV for 400 MeV/c momentum 78−13368
linear multiplexer, 14-channel, resolution, efficiency, nuclear spectroscopy appl. 78−33400
liquid scintillation spectrometry sample pre-processing 78−21816
low-background detection system for neutron reaction expts. 77−54395
magnetic, of Van de Graaff tandem, for heavy ion induced reaction study *(French)* 79−707
magnetic large acceptance spectrom. using wire chambers 78−46207
magnetic large aperture spectrometer for the study of multibody photoproduction in the incident energy range 1-5 GeV 79−715
magnetic mapping system for particle spectrometers at Fermilab 77−10513
magnetic quadrupole and solenoidal spectrometers, optical props. and experimental techniques 79−68127
magnetic spectrograph, fast resolution optimization 79−6792
magnetic spectrograph 79−54740
magnetic spectrograph for very heavy ions 79−31315
magnetic spectrographs, use in nucl. reaction studies, review *(Rumanian)* 80−87012
magnetic spectrographs for nuclear reaction studies, resolving power, kinematic broadening 79−68126
magnetic spectrom., MWPC as counter hodoscope for fast majority discrimination 78−33392
magnetic spectrom. with position- and cutting angle-sensitive detectors, ang. distrib. reconstruction 78−70687
magnetic spectrometer, reconstitution of heavy ion trajectories 78−70684

particle spectrometers continued
magnetic spectrometer, SPES II, use with multiwire props. counters of three-body nuclear reaction study *(French)* 79−708
magnetic spectrometer SPES I, for use with Saturne synchrotron *(French)* 79−709
magnetic spectrometers, approx. and ideal design, appl. to STEM 78−8475
magnetic spectrometers, cosmic ray muons multiple scatt. 80−4215
magnetic spectrometers, for heavy ion reactions, book contrib. 79−31314
magnetic spectrometers, momentum determ. using non diagonal weight matrix 79−59296
magnetic spectrometers data acquisition and anal. 79−89530
MAS-1 multichannel amplitude selector, for short-lived nuclei decay meas. 77−75029
MEA, magnetic detector at Adone 78−33367
microchannel plate based detector for a heavy ion beam spectrometer 80−58018
microfoil conversion electron detector for Mossbauer spectroscopy 78−70698
mini-orange spectrometers, wedge shaped $SmCo_5$ magnets 78−58531
momentum of particle moving in axially symm. mag. field 78−21806
multichannel charge-exchange energy analyser with high time resolution, plasma energy spectrum 79−41882
multigap proportional wire chamber system for multiparticle spectrometer 79−3271
multiparameter gas-scintillation counter for heavy charged particles 80−58051
multiple plate total absorpt. ionisation spectrom. based on compressed X-e 79−36476
multiple species ion energy analyser for laser-induced plasma expts. 78−55750
multistep avalanche chamber, new family of fast high rate particle detectors 79−49904
multiwire and drift chambers for the Omicron spectrometer 79−3277
muon, fast mass depend. trigger design based on ECL integrated ccts. 79−97954
MWPC, cylindrical, soft X-ray detection in $p\bar{p}$ spectroscopy 79−3279
MWPC, lateral distrib. of cathode charge 79−36470
MWPC appl. as focal plane detection system for mag. spectrograph 79−3295
MWPC appl. in multiparticle spectrometer, description and performance 79−3275
MWPC appl. in recoil spectrometer 79−3274
MWPC in synchrotron beam spectrometer, performance under very high fluxes 79−3272
MWPC instrumentation for CERN SPS secondary beams 78−46206
neutral particle detector and spectrometer for plasma diagnostics 79−23455
neutral particle spectrometer for measuring ion temperatures *(Chinese)* 79−37553
neutral-particle analyzer system, multichannel, for anal. of charge-exchange flux from magnetically-confined plasma 80−4804
neutron beam charged particle spectrometers, appl. of drift chambers 79−3278
neutron capture gamma and electron spectroscopy, instruments and techniques 80−37695
nuclear reaction-emitted charged particle mag. spectrograph, multi-ang. 80−5429
nuclear spectrometry, 4k, using 2k ADC with two biased amplifiers 78−46234
nuclear spectrometry, detector signal and noise parallel meas. 77−61667
Omega spectrometer, CERN, modular trigger basic techniques 80−58104
particle identification systems including magnetic analysis, review 79−72181
photoelectron, variable angle, for meas. electrons photoejected by rare gas reson. light 78−1110
photoelectron spectrometer, design for teaching lab. 78−86078
photoelectron spectrometer construction 78−27874
photovoltaic cells as fission product detectors 79−93873
$pion^0$ spectrometer at LAMPF 77−10524
pion non-dispersive low energy spectrom. 80−14038
pion spectrom. for meas. electro- and photo-pion spectra in high background environment 80−27868
pion spectrometer, 180° scatt. facility at SIN using modified SIN standard magnet 79−712
plane source-detector spectrometric system calc. 78−50428
plasma-ion analyser for H conc. in metals using pulsed laser and thin film scintillation detector 78−15746
plastic ball multi-detector large angle spectrometer for Belavac 80−58028
portable spectrometrical unit NZG 201 *(Czech)* 79−22538
position sensitive proportional counters as focal plane detectors 79−68159
position sensitive proportional detector system for focal planes of multigap mag. spectrograph 77−54454
positron annihilation investigation apparatus, review 80−23240
positron lifetime spectrometer for distance meas. with coincident gamma-ray 79−12765
positron spectrometer, low-background, many cryst. scintillation triple $\beta\gamma\gamma$ coincidence 77−54446
preamplifier, universal low-noise spectrometric design 77−14315
Princeton Cyclotron data acquisition system 80−102415
projected proton method for heavy ion energy meas., device for 3-6 MeV beams *(French)* 78−82567
proton spectra, high energy, emerging from 680 MeV synchrocyclotron shielding 78−17530
QDD type mag. spectrometer, high resolution and large solid angle 78−78552
radioactivity meas., fly-ash radioactivity meas., environmental protection *(Polish)* 77−14318
readout system for MWPC of focusing spectrometer 79−3280
recoil and fast particle spectrometers for 5 GeV $\pi+{}^4He$ study 78−82569
recoil spectrometer for 5 GeV pion-He interactions 78−90011
retarding field spectrometer for Auger spectroscopy, secondary electron emission effects 78−23564
scattering chamber, for ^3He energy spectra meas. in thin films microchem. anal. 79−1975
scintillation counter, thin film detector for heavy ion identification 79−13596
scintillation spectrometer stabilisation using LED reference light source 80−91365
scintillation spectrometric path, switch shaper 77−6641
secondary ions, mass and energy spectrometer 77−13814
semiconductor detectors, spectroscopy and applied phys. appls. 78−46218
semiconductor mosaic type, amplification-conversion tract meas./monitoring automation 78−78547
semiconductor thin window detectors for interplanetary particles, Compton-Getting effect complications 78−49269
sequential/parallel track selector, 1 μs hardware pre-analyser for CERN Omicron spectrometer 80−91364
shower spectrometer with combined radiator 77−23351
SIN π-channel and spectrometer, technical aspects of pion scatt. facility 79−13574
SIN high resolution pion channel and spectrometer 79−22517
SIN pion spectrom., status 77−14297
solid state nuclear track detectors, cellulose nitrate, for high energy neutron spectrometry 80−91394
solid-state detector spectrometer system, energy resolution, electronic aspects 78−46231
spark chamber gas monitor, used in Rutherford multiparticle spectrometer 79−3318
SPEAR Mark II shower counter system 80−58031
spectrometer magnets, field parametrisation 79−880
SPES I, at Saturne I, five years of expts. *(French)* 79−3262
spherical electrostatic. props. of Keplerian orbits in inverse-square field 79−13581
spin polarisation detector, experimental exam., using Hg+e scatt. 78−32927
square meter position sensitive parallel plate detector for heavy ions 79−93879
stabilization of spectrometric channel with automatic reference peak search 79−26803
stabilized differential discriminator with automatic threshold control 79−26841
strong focusing magnetic analyzer for charged particle recording up to 700 MeV/c 79−68123
superconducting flux exclusion tube for mag. field shielding in particle spectrometers 79−13578
superconducting magnet system (ANDROMEDA) for particle detection in medium energy physics 79−13582
superconducting quadrupole collector with large solid angle for heavy-ion expts. at high-energy 77−34506
superconducting solenoids, large dia., mag. spectrometers for colliding beam accelerators 77−26919
superconducting spectrometer for p polarisation meas. in high energy elastic scatt. 77−30439
surface barrier detector, pulse height defects, heavy-ion detection 78−55093
surface barrier detector, pulse height response to mass and energy separated fission fragments 77−57812
surface barrier particle spectrometer, testing by precise light pulser 77−79508
tandem surface analysers 78−33371
tapped delay line focal plane detectors for mag. spectrometers 79−68161
temperature-controlled, for surface barrier detectors study 77−83443
threshold photoelectron spectrometer, and applic. 77−14491
transition-radiation detector and shower detector combination for galactic electron meas. 77−57844
ultra-sensitive particle identification systems based upon electrostatic accelerators, review 79−72182
UPS, high resolution, fast pumping for study of transients and unstable species 77−83764
Vekton-1 double arm spectrom. for $\bar{\rho}^-$ meson photoproduction 78−33362
velocity spectrometer for 10 meV to 10 keV atoms 77−3210
XPS, prediction model for ang. distrib. intensity and lineshape 77−41734
XPS spectrometer, consistent calibration method, rel. to Pd Fermi level 77−16458
zero time detector for heavy ion spectroscopy 78−33368
zoom lens quadrupole magnets for Colorado Univ. energy-loss spectrograph 77−83410
e-γ coincidence spectrometer 77−23390
K^+ decays, branching ratio meas. by mag. spectrometer with streamer chambers 77−18275
ν detector based on combined operation of streamer chamber and Converse hodoscopic tubes 80−63455
Au-Si detectors, pulse height defect meas. for 2 to 400 MeV/nucleon ions 78−86733
Ge diode detector telescope for particle spectroscopy, design and performance 78−13384
He beam, magnetic spectrom. meas. using automatic tracking NMR system 80−27869
$^4He(\gamma,\pi^0)$, reaction cross section meas. equipment 78−29694
Si detectors, automatic anal. of complex charged particle spectra 78−33370
Si surface barrier detector, fission fragment pulse height defect 79−76292
Si surface-barrier detectors, characts. in Xe ion beam 78−78571
^{90}Sr bremsstrahlung radiation meas. for well logging using Ge spectrometer 80−94619
$ThBr_4$, inorganic scintillator, use in nucl. and accelerated particle detection 78−58540
W scintillator ionisation spectrometer, meas. of cascades initiated by 5 to 300 GeV hadrons 77−34526
Xe filled proportional scintillation detector for charged particles 80−32572

particle track visualisation
see also bubble chambers; cloud chambers; nuclear track emulsions; scintillation chambers; spark chambers; streamer chambers
air showers for 10^4 to 10^6 particles, lateral distrib. of EM component, detection 80−17459
alpha particle revelation characteristics, and heating of cellulose nitrate plastics 79−49910
alpha particles in diacel plastic track detector, track-diameter meas. 79−49911
alpha-recoil tracks in archaeological ceramic dating 78−70237

particle track visualisation continued
apatite, influence of crystallographic struct. on annealing of fission fragment tracks 77−38577
apatite, mean etchable fission track length, high fission track densities determ. 77−82041
automated method for fission-fragment track density determ. in solid state track detection using MAGMO-1 system 80−42891
borosilicate optical waveguide glass, B content determ. using nuclear track counting 80−95969
bronzite, influence of crystallographic struct. on annealing of fission fragment tracks 77−38577
cellulose acetate, bulk and track etch rate studies 79−31338
cellulose acetate, solid state track detector, sensitisation technique *(Chinese)* 79−22558
cellulose acetate track detector, sensitisation by swelling *(Chinese)* 79−18085
cellulose diacetate as solid state heavy ion track detector 78−17523
cellulose nitrate, ^{6}Li enriched, neutron detection props. 80−52828
cellulose nitrate, energy loss critical rate for charged particles 80−74082
cellulose nitrate, etching behaviour, nuclear track detector 78−17485
cellulose nitrate, He (A=3, 4) energy spectroscopy 78−13377
cellulose nitrate, neutron induced recoil particle tracks, automatic spark counting 78−17492
cellulose nitrate, nuclear track detectors, etch induction time, particle identification parameter 78−17486
cellulose nitrate, proton, H_2^+ mol. ion, and heavy ion irrad., track prod., etching obs. 78−86757
cellulose nitrate, sensitivity to α-particle registration 78−17498
cellulose nitrate, track detector direct dosimetry in fast neutron beams 78−20277
cellulose nitrate α-particle detector for Rn short lived daughters, results and calibration *(Czech)* 78−62663
cellulose nitrate (CN) detectors, effect of pre-irrad. thermal treatment on track revealing props. 78−94168
cellulose nitrate CA8015, calibration for fast neutron dosimetry 79−49907
cellulose nitrate detector, track formation confirmation for ^{7}Li from $^{10}B(n,\alpha)^{7}Li$ 79−36465
cellulose nitrate film, ion track density, quantitative assessment using Fourier transform techniques 79−86610
cellulose nitrate film, neutron dosimeter 78−20280
cellulose nitrate layer, α-particle autoradiography 78−17499
cellulose nitrate LR115, neutron personnel dosimetry at high energy accelerators 78−20284
cellulose nitrate plastic detector, charge resolution improvement for cosmic ray particles 79−84671
cellulose nitrate plastic detector, spallation products from energetic neutrons 78−17198
cellulose nitrate plastics, determ. of B in complex matrices from ^{4}He and ^{7}Li tracks 79−18080
cellulose nitrate solid state nucl. track detector, gamma dose meas. 78−73247
cellulose nitrate track detector, simultaneous determ. of p and α particle ang. distribs., (d,α) and (d,p) reactions 79−737
cellulose nitrate track detectors, bulk etch rate studies 79−36482
cellulose nitrate track detectors, detect. of efficiency and range meas. of alphas and protons 78−17524
cellulose proton track visualisation detectors *(French)* 80−74080
cellulose triacetate, IR spectroscopy appl. to charged part. dose meas. 78−94145
charged particle track analysis of sandstone-type U ore 80−91405
chlorite, fission track annealing and age determ. 78−36307
coral, alpha emitter analysis by solid-state track detect., Bikini lagoon 78−53661
cosmic ray, magnetic monopole candidate, reassessment of 1975 Lexan and emulsion meas. 79−3333
cosmic ray particle identification from tracketch rates in minerals 79−16788
CR-39 plastic, electrochemical etching, dosimetry appl. 80−52824
CR-39 polymeric nuclear track detector, props. and appls. 78−94170
CR-39 thermoset plastic nuclear track recorder, etching in hot NaOH 78−74535
crystals, track form., minimal energy loss rel. to thermal cond. 78−17525
dating techniques, effects of thermal annealing on track etching rate of sphene, $CaTiSiO_5$ 78−65435
density distribution of fission traces, meas. by tracer's method in dielectrics, fuel meas. appl. *(Rumanian)* 78−90033
Dhajala meteorite shower atmospheric fragmentation and ablation based on cosmic ray track obs. 77−82188
diacel plastic track detector, threshold energy for alpha-particles 79−59312
diacel solid state track detector, characts. for α-particle detect. 79−750
dielectric track detectors, neutron dosimetry appl. *(Czech)* 78−66425
dielectric track detectors, studies with Van de Graaff tandem *(French)* 79−4339
diffusion of $^{241}Am^{3+}$ ions in ion-exchange membrane, autoradiographic method 78−35721
digital picture analysis, book 77−17962
drift chamber, bidimensional 77−30703
drift chambers in high-energy gamma-ray telescope 80−41726
electrochemical track etching in plastic foils 78−17521
electron track reconstruction in small volume self shunted streamer chamber 77−57821
energy resolution enhancement for alpha particle detection 80−91392
etched, statistical distribs. using computer image anal. 80−83235
ethylene-tetrafluoroethylene copolymer, chem. etching of fission tracks 80−896
fast neutron induced tracks in plastics, comparison using electrochem. etching 80−23154
feldspar, crystalline track detector, etching characts. anisotropy 77−46465
feldspar crystals, natural, anisotropy of track registration 78−25397
filmless chambers in high energy physics, review *(Russian)* 77−67938
fision track method, physical state of fissionable material 78−41899
fission fragment track registration in crysts., development efficiencies, etchant (etching conditions) depend. 78−66454
fission track annealing characts. in crystals 79−26863
fission track dating, geom. factor for external detectors 77−82040
fission track etching and annealing anal., muscovite, dating appl. 78−32036

particle track visualisation continued
fission track registration technique for U conc. determ. in water samples 80−12565
fission track spark counting method for neutron monitoring 80−58080
fission track-etch-cum-γ-spectrometry method for absolute fission yield meas. 80−27859
fission tracks, anisotropic track etching in olivine crystals using WN solution 79−26836
fission tracks, quantitative assessment of geometry factors 79−26860
fission tracks in thick crystals, length distribs. 79−26858
flash chambers as 'active' detectors and a special processor for fast decision making 79−26832
flash chambers of polypropylene sheets, digital readout 79−26833
fluoroplastics, heavy charged particle detectors 79−26821
gamma camera, 3-D particle track chamber using Compton interactions 77−86622
gas discharge converters of X-ray pictures with Ne filling, memory time 79−26827
geological anal., rocks, minerals, nuclear track technique, B, Li, U, Th mapping 78−20553
glass, etching rate temp. and conc. depend. 77−10533
glass detections, thermometry 80−37031
glass detectors, appl. to α-particle and fission fragment ranges in air 79−45597
glass track detectors, NaO_2-SiO_2, phosphate, quartz glasses, nculear phys. spectrometric appls., track diameter 78−17466
glass track detectors, review 77−23370
glasses, effect of pre-irradiation and condition on etching 80−37702
glasses, effect of temp. on etching 79−76290
heavy ion physics, expt. methods for radiation detection and meas., review *(Russian)* 79−49900
heavy ion track lengths in solid dielectric track detectors 79−59319
heavy particle high-energy beam calib. with plastic track detectors 77−79525
high pressure proportional counters operating in pure hydrogen 79−3296
holographic camera, 2 laser techniques *(Russian)* 78−25827
holographic gas discharge chamber 77−10551
image processing in high-energy physics 77−18769
ionising particle beam interactions with liquids, acoustic effect, laser beam simulations 80−23262
isotropic detectors, etched-track kinetics 77−79512
Kodak CA 80-15 plastic detector, fast neutron radiography for extended objects 78−20267
Kodak LR 115 cellulose nitrate films, fast neutron dosimetry 78−20279
Kodak LR 115 dielec. track detect., applicability as α-particle detector *(Czech)* 79−8711
Lexan, bulk and track etch rate studies 79−31338
Lexan foil, and nuclear emulsion sandwich stacks, obs. of cosmic rays with $Z \geq 34$ 78−20597
Lexan polycarbonate, thermolum. radiation-induced EPR of free radicals and track etchability 79−76295
lexan polycarbonate track detector, for U estimation in zircon *(French)* 77−64445
Lexan polycarbonate track detector direct dosimetry in fast neutron beams 78−20277
Lexan track detector, appl. to ultra heavy comsic ray nuclei 78−20596
Lexan track detectors, cosmic ray element abundances from Ni-Kr 78−20598
light ion track fields, automatic rapid anal. by stylus 79−31336
long lived tracks, interpretation as new hadrons or background 77−23391
LR115 cellulose nitrate detector system for personal dosimetry near high energy accelerators 80−58081
LR115 red celluiose nitrate personnel neutron rem dosimeter, design 80−52826
LR-115 plastic track detector, etching behaviour 80−99423
Makrofol KG in KOH solution, bulk etching rate, light ion tracks 77−67942
Makrofol polycarbonate, electrochemical etching of neutron induced tracks, appl. to dosimetry 78−20282
Makrofol solid state track detector, automatic fission track counting, video-electronic image analyzing system 78−17494
Makrofol solid-state track recorder for fission rate meas. of $^{235}U/^{238}U$ 78−13396
Makrofol-E polycarbonate detectors, liq. N_2 enhancement of α-particle tracks 77−67946
Markrofol, fission fragment tracks and track distribs., rapid counting with multichannel spark counter 78−58549
mass identification scale depend. on different track form. models 78−17515
metaphosphate glasses, heavy ions, fission fragments energy determ. 78−17487
mica, bulk and track etch rate studies 79−31338
mica, obs. of fision tracks, meas. of sputterng yields 77−88340
minerals, fission fragment range and closing temp. for track retention 80−41566
minerals, thermal annealing of ion tracks 78−20604
multi-detector electrochemical etching and automatic scanning system 79−26837
multifragment decay reactions induced by heavy ions, mica track detector study 78−17234
multiuser particle track photograph meas. computer programs *(Russian)* 77−38591
multiwire drift chambers for the CERN intersecting storage rings 79−3301
muscovite mica, crystalline track detector, etching characts. anisotropy 77−46465
neutrino interactions in vertical emulsion target of hybrid apparatus 80−5126
neutron dose meas. with B-doped cellulose nitrate film 79−31321
neutron dosimetry with solid state nuclear track detectors, brief review 78−33299
neutron dual response albedo neutron personnel dosimeter 79−93885
neutron fluence meas. using mica muscovite as track detector 80−106237
neutron fluence meas. with solid state track detectors, international intercomparison 78−20283
neutron personal dosimeter based on track detector 77−70551
neutron personal dosimetry system, ^{237}Np neutron induced tracks in polycarbonate 78−31908

particle track visualisation continued
neutron personnel dosimetry in criticality accidents, fast neutron dosimetry system 79−85817
neutron response of solid state nuclear track detector 80−27876
neutron spectrometry in range 0.4 eV to 10 MeV 77−42210
non etching polymers, fluorescent and dyed tracks, state of art 80−47825
nonfilm TV method of high-speed process coords. meas., review 78−5093
nuclear emulsions, track struct. and particle identification 80−91383
nuclear failed fuel element detection by delayed neutrons using solid state track-etch technique 80−5249
nuclear particle track detectors, trends and developments *(Hungarian)* 80−18755
nuclear track detector, appl. as neutron dosimeter, reponse to standard neutron sources 80−5342
olivine from Marjalahti meteorite, cosmic ray tracks 78−36414
optical gas-discharge chambers in mode of pulsed proportional amplification 79−726
phosphate glass, for fission fragment energy meas. 77−67932
photographic tracking method, association with laser fringe anemometry 80−38512
plastic, etching rate temp. and conc. depend. 77−10533
plastic, rare fission track recording by matching method 78−33383
plastic detector, fragmentation and isotope meas. on Ne and Ar of 280 MeV/nucleon 77−38561
plastic detector, primary damage and secondary electron damage in heavy ion tracks 78−17514
plastic detector technique in fast neutron radiography 79−76299
plastic detectors, appl. to α-particle and fission fragment ranges in air 79−45597
plastic detectors, calib., heavy cosmic ray charge distrib. 78−17500
plastic detectors, effects of HV Tesla coil and spark gap discharges 78−86742
plastic detectors, electrochemical etching of neutron induced tracks using HV 50 Hz supply 78−86738
plastic detectors, isotope resolution 77−79511
plastic detectors, meas. of high-linear-energy transfer particles on Apollo, Skylab and ASTP space missions 77−41272
plastic film detectors for light and heavy element fission studies 79−72193
plastic flash chambers, particle identification 79−59301
plastic foils, automatic spark counting of α-tracks 77−79524
plastic foils, HV AC power supply for electrochemical etching apparatus 77−10541
plastic foils for neutron dosimeters, electrochem. etching prep. techniques 79−76298
plastic solid state nuclear track detector, large γ dose meas. 77−38559
plastic solid state nuclear track detectors, Rn and Th dosimetry 78−20556
plastic solid state nuclear track detectors, sensitivity and struct. variation 79−49912
plastic track detector, heavy ion tracks, automatic meas. device 78−17495
plastic track detector CR-39, detection of relativistic cosmic ray Fe group nuclei 79−80154
plastic track detectors, background holes and reduction methods *(Japanese)* 77−71721
plastic track detectors, efficiency enhancement by UV radiation 77−88350
plastic track detectors, processing 77−38560
plastic track detectors, Rn dosimetry 78−33298
plastic track detectors, treatment and application 77−46459
polycarbonate film, fission track etching charact., UV and ageing effects 79−76296
polycarbonate foil, α-particle track prod., electrochemical etching 80−52825
polycarbonate foil, neutron induced recoil particle tracks, automatic spark counting 78−17492
polycarbonate foil electrochemical etching for dosimetry, bulk etching rate evaluation 78−78506
polycarbonate foils, detection of low energy ^{4}He, ^{12}C, ^{14}N, ^{16}O ions, etching props. 78−13391
polycarbonate thin film, determ. of fission barrier in region Z=82, N=126, using electron linear accelerators 78−55104
polycarbonate track detector, electrochemically etched, meas. of low neutron fluences 80−32577
polyester foil neutron track detection, dosimeter appl. 80−5439
polyethylene terephthalate film, degree of crystallinity effect on particle tracks *(French)* 77−46471
polyethylene-terephthalate track detector, electrochemically etched, meas. of low neutron fluences 80−32577
polymer, form. of heavy ion latent tracks 78−17522
polymer, graft-and-dye method 78−17520
polymer dielectric nuclear track detector, particle stopping power depend. on preirrad. annealing 79−72185
polymer track detectors, high energy neutron detection 79−26861
polymeric detector particle track diameter rel. to etching time *(French)* 80−9463
polyvinylidene fluoride, chem. etching of fission tracks, growth of fine holes, TEM, SEM study 79−76297
position sensitive detectors of high spatial resolution 79−76276
proton-sensitive CR-39 for plastic track detectors, method of producing thin sheets 80−35155
quartz, grains, fission track dating, Oklo uranium ore deposit 78−20555
quartz, natural crystals, fission fragment track development anisotropy 77−1149
quartz, track retaining props. for high temp. in-core neutron fluence meas. 77−75032
radiography of extended biological and medical objects using fast neutrons *(German)* 78−15880
random path detection, Gaussian noise hypotheses testing 78−58551
reactor core gamma dosimetry, solid state nucl. track detector appl. 80−95466
rem-dose measurement of mixed p-n radiation using solid state detectors of fission fragments 80−36137
sediment age determination, ^{210}Pb, cellulose nitrate sheet 78−20554
semi-automatic meas. instrum. register for camera photograph reduction 78−78575
short lived particles, detection efficiency evaluation method 80−102390
silica aerogel Cherenkov detector development 80−58037
single surface electrochemical etching of charged particle tracks, simple set-up 79−76283
soda lime glass track registration, HF etching conditions effect 80−52815
soda-lime glass track detector etching in NH_4HF_2, NaOH and KOH aq. solns. 79−26816
solid dielectric detectors with breakdown phenomena and their applications in radioprotection 80−91388
solid state detectors, past and future uses, review 78−17484
solid state nuclear track detectors, ^{222}Rn and ^{220}Rn meas. 78−25396
solid state nuclear track detectors, conf., Neuherberg/Munich, (Oct. 1976) 78−17513
solid state nuclear track detectors, fast neutron dosimetry 78−20278
solid state nuclear track detectors, real time automatic evaluation with on-line television system 78−17496
solid state nuclear track detectors, review 80−37696
solid state track detector, actinide fission cross section meas., fragment ang. distrib. 79−76300
solid state track detector, thickness meas. by interferometric method 78−86735
solid state track detector, video electronic measuring system 78−17493
solid state track detectors, glass and plastic laser diffr. appl. to determ. of etched track parameters 80−95499
solid state track detectors, meas. of absolute fission rates/source neutron in Fe assembly 78−58559
solid state track detectors, track forming, stabilisation and development processes 78−17516
solid state track detectors, use in neutron dosimetry, verification of possibilities *(Czech)* 78−82574
solid state track recorders in nuclear medicine 79−26830
solid track detectors for fission fragments, efficiency 77−71726
solid-state nuclear track detectors, development and use for reactor phys. expts. 78−41886
solid-state track detectors, electron microscopy of etch pits 80−99424
solid-state track detectors, international α-particle registration intercomparison 78−17497
solid-state track detectors for mass of temp. of neutron gas 78−66455
sonic location spark counter system for mag. spectrometers 79−68162
spark counting of α-radiograms recorded on LR-115 strippable cellulose nitrate film 79−26859
spontaneous fission low background detection system 79−36475
SSNTD, automatic scanning techniques 80−91387
SSNTD, development and appls., [conf. Nilore, Rawalpindi, Pakistan March 1979] 80−90608
SSNTD, development of etched nuclear tracks 80−91384
SSNTD, effect of etching conditions on energy resolution of phosphate glass and polycarbonate detectors 80−91390
SSNTD, electrochemical etching studies of the CR-39 plastic 80−91391
SSNTD, review of appls. in fission physics 80−91396
SSNTD, track registration and development efficiency 80−91385
SSNTD, track registration and development efficiency 80−91386
SSNTD, visualization of latent damage trails etching, decoration and observation techniques, review 80−91382
SSNTD for fast neutron meas. 80−91393
superheated drop detector 79−72201
superheavy primary cosmic ray nuclei, obs. with solid-state track detectors and X-ray films *(Japanese)* 78−61688
target trajectory detection in multi-target environment, pattern recognition approach 79−26865
thermal neutron radiography facility on IRT-2000 reactor 78−17286
thin dielectric track detector as particle discriminator, α dosimetry appl. 78−17511
time expansion chamber, relativistic rise meas. by cluster counting method 80−58030
tourmaline, fission track etching and annealing, thermal retention 77−82042
track chamber slide processing, calibration programming problems *(Russian)* 80−73305
track data in plastics, rapid anal. using interactive programming and graphic displays 78−66456
track etch detectors, neutron energy depend. and threshold energy 80−61703
track etch imaging, model of directional effects 77−18739
track formation model, etch pit parameters, light nuclei, calc. 78−13390
track radiography of heavy-ion induced sputtering 80−91404
track sensitive target expts., automatic film meas. 78−55105
TRIGA core, gamma dose meas. by plastic detectors 80−9381
trigger processor for mag. detector 78−46244
TV camera system for digitising single shot oscillograms at sweep rate 0.1 ns/cm 77−406
vidicon systems, time digitiser in CAMAC format 80−14062
X-ray anal. of microcrystallite nucleation and detection threshold 80−890
π^- beams, direct track detector dosimetry 78−20281
AgCl, defects induced by energetic ion implantation 78−17518
AgCl single cryst. foil, photographic elementary process 78−17519
AgCl track detector prep. and props. 78−17517
B_i neutron irradiated, quantitive anal. using cellulose nitrate solid state track detectors 78−56937
Bi, mapping using ^{210}Po α-particle tracks 78−20129
$CaF_2.3Ca(PO_4)_2$, apatite, fission damage detection, absorpt. spectra 78−84617
^{252}Cf fission fragment tracks in quartz glass, electron microscope obs. 78−17526
dielectric track registering media, possible new sputtering mechanism 77−392
Fe peak isotopic resolution, Lexan detectors from Apollo 17 mission 77−56801
$Gd_3Ga_5O_{12}$, Ca, Zr and Mg substituted artificial garnets, track registration props. 78−62679
^{237}Np damage track detectors, effects of subthreshold fission on neutron dose meas. 78−33375
^{237}Np dosimeter and spark counting system, for routine personnel monitoring 78−89984
^{237}Np fission, appl. as neutron dosimeter for personnel 79−13539
^{239}Pu alpha particle tracks on polycarbonate foils 79−76310
Rn, moisture insensitive monitoring using solid detectors 79−31228
^{222}Rn, meas. of concs. in Earth using nuclear track technique 79−53574
Si-electrolyte interface, incident radiation image form. *(Russian)* 77−7199

particle track visualisation continued
U anal. of natural waters by fission tracks 78−82587
U in rock samples, meas. by track registration in plastic detectors 78−23533
U plastic calorimeter, response to low GeV protons 79−93882
U+^{136}Xe, 1080 MeV, reaction mechanisms obs. with mica detectors 77−79399
U+^{84}Kr, 800 MeV, reaction mechanisms obs. with mica detectors 77−79399
U(^{3}He, f), 530 MeV, cross section meas. by glass solid state track detectors 78−13179
U_3O_8, ^{235}U enriched aerosol, characterisation by solid state track recorders 78−17538
^{235}U content in enriched samples, fission track registration technique, solid state detectors 77−56291
^{235}U foil, sputtered, energy spectrum, fission track technique using time of flight spectrometer 78−68593
^{235}U-fission track micromapping, exam. of U mobilisation processes in Precombrian sediments 80−98477
^{235}U(n,f), thermal, determ. of high temp. diffusion of U in refractory metals 77−89587
^{238}U, determ. of time since arrival in matrix existing at time of discovery in Pakistan 79−34822
^{238}U(n,f), 1.8-16.8 MeV, fission fragment energy spectra using glass sandwich detectors 78−82399
Xe, liq., ionising particle detector, signal amplification by optical pumping 79−54746
ZnP glass heavy-ion track detectors 3 to 120 MeV 80−91389

particle tracks
see also energy loss of particles
alpha particles in mica, prompt process and post effect 78−43053
apatite, fission track retention as functions of heating time during isothermal expts. 80−36420
Bjurbole chondrite, origin of fission fragment tracks in whitlockite 78−81595
bubble chamber, CERN HPD, finite spot size in ionisation meas. 80−27892
bubble chamber track extraction using single vidicon tube 78−82580
bubble chamber track following, predictor-corrector technique 78−90044
bubble chamber tracks, automatic meas. 78−25399
bubble chamber tracks, semi-automatic bubble matching method 77−67941
CERN 2m HBC, automatic meas. of 12 GeV/c $\bar{p}p$ interactions 79−36471
charged particle track evaluation, distance distrib. and intratrack dose 80−26368
charged particle track reconstruction, fitting procedures, multiple scatt. effects *(German)* 78−74091
corona counter, determ. of U content in solid waste mats. by α-detection *(Russian)* 80−27904
cosmic ray induced fission of heavy nuclides, influence on apparent ^{238}U fission track ages 79−40047
cosmic ray nuclei in nuclear emulsion, appl. of energy loss params. on mass determ. 78−94175
cosmic ray tracks in Barwell meteorite, preatmospheric size determ. 78−53893
cosmic ray tracks in meteorites, mass ablation estimation 78−53894
cosmic rays, Be to Mg, test of Katz's track formation theory in nuclear emulsion 79−54754
delta-ray model of track effects, applicability to physical, chemical and biological systems 77−65407
detection and measurement of very short flight paths in nuclear emulsions 80−102389
drift chambers, track reconstruction decay electron trajectory meas., MSR at CERN 78−82593
electron interactions, low-energy, single and twin biological targets 80−12195
electron track end effects in water 80−11932
element 114, search in galena using EM isotope separator and fission track detectors 77−27203
emulsion nuclei, 28 GeV proton interactions *(Korean)* 80−18299
fission fragment tracks and track distribs., rapid counting with multichannel spark counter 78−58549
fission track annealing and dating of vermiculite 80−81885
fission track annealing characteristics of epidote, appls. to geochronology, geol. 78−94038
fission track annealing characts. in crystals 79−26863
fission track annealing of sphene, fission track age-temp. relationship 80−98316
fission track data reports standardisation 80−31436
fission track dating and annealing of Indian apatite and zircon 79−57891
fission track dating and estimation of U in garnets 78−94039
fission track dating method, standard error estimation 80−36419
fission track dating of biotite pegmatite in Calicut area Fe ore 77−13066
fission track dating of Himalayan muscovites, Nepal, and U conc. estimation 78−40524
fission track dating of pumice from KBS Tuff, East Rudolf, Kenya 77−5159
fission track dating technique 80−36417
fission track retention as function of heating time during isothermal expts. 80−36420
fission track retention in minerals, closing temp. rel. to dating 77−64268
fission track spark counter, correction for track-hole densities in aluminised mylar film 77−3231
fission tracks in thick crystals, length distribs. 79−26858
fission/alpha tracking counting for deep sea cores sedimentation rates determ. 78−61392
galactic cosmic ray composition determ. from tracks in lunar and meteoritic feldspars 78−20603
gamma-particle multiplicity distrib. moments meas., statistical method 77−30712
geological samples, f/α particle track anal. for U, Th and isotropic disequilibria 78−7799
heavy ion track reconstruction program 79−31348
heavy ion track width in nucl. emulsion, Katz's theory 80−32578
heavy ion tracks, separation from background by pulsed electric field 78−17491
heavy ion tracks in plastic detectors, automatic meas. device 78−17495

particle tracks continued
heavy-ion tracks in lunar and analogous crystals, etchable ranges 77−30734
heavy-particle track structure rel. to radical physical distrib. and chemical effects 80−11933
insulating crystals, track formation and minimal energy loss *(German)* 77−18757
inverse momentum, error estimation using Wind's quintic spline method 79−22563
ionisation data from SAMM, max. likelihood anal. 77−67940
iterative tracking for momentum determ. 78−70723
lunar fines, effect of annealing temp. on etching by adsorbed water 77−60632
lunar samples, charged particle track anal., thermoluminesc. and microcratering studies 77−60665
magnetic spectrometers, momentum determ. using non diagonal weight matrix 79−59296
meteorites, Estherville, Nakhala and Odessa, fission track records 79−35209
in meteorites, rare gases and fossil particle tracks in Kenna ureilite 77−41366
meteoritic hypersthene, fresh and fossil tracks, rel. to Fe abundance in cosmic ray flux 77−41276
mica, fissionable element impurities, nature and distrib., fission track method 78−44436
mineral fission fragment track annealing characteristics for geochronology 79−100827
multiplane hodoscope, D/A system for charged particle track analysis 77−14325
muscovite, fission track etching and annealing anal., dating appl. 78−32036
MWPC, missing data reconstruction in principal component anal. 78−17537
MWPC, programmable track selector 79−3316
nuclear tracks, etched, statistical distrib. of quadratic holes on planar surface, computer simulation 80−37705
particles in cylindrically symmetric mag. fields, least squares track fitting method 78−58896
photodensitometry of tracks of highly ionizing particles in the cosmic rays 79−22551
point to line data reduction, computer links and hardware processor test 79−45613
Runge-Kutta method for track fitting in mag. field 79−31782
search statistics, Monte Carlo study of random scatt. problem 78−58561
signal-processing procedure for inter-image identification of particle tracks in bubble chambers 78−70727
single atom detection 80−9475
soil, fissionable element impurities, nature and distrib., fission track method 78−44436
solid state track detectors in solutions of actinides, α track registration 80−63486
spark chamber, Ar filled low-pressure, short pulses, spark track structure 77−3230
spark chamber track shifts, causes 77−6618
spark counting of α-radiograms recorded on LR-115 strippable cellulose nitrate film 79−26859
St. Severin meteorite, flux of low energy particles in solar system 77−82096
structure analysis advantages over classical microdosimetry 80−26284
superheavy nuclei, spontaneous fission, natural 78−13172
tissuelike medium α trajectory heavy secondary ion ejection 80−9466
tissuelike medium α trajectory production of δ-rays 80−9465
track density, device for determ. in solid-state particle detector 79−85859
Track Etch techniques for Li determ. in brain tissue 80−98133
track shape of normally incident particles, use of microtome cuts in SSNT detectors 79−26862
Ar, nuclear emulsion track width by photometric meas. 78−94167
Au ion tracklengths in mica 78−38767
CdS, luminesc. from heavy ion tracks 78−88365
I ion tracklengths in mica 78−38767
Kr solid, particle track obs. in condensed matter, by emission method *(Russian)* 77−57824
^{8}Li, produced by K^- interactions with emulsion nuclei 78−17244
N nuclei, track in Ilford G-5 emulsion, track with meas. 78−17488
Ne, nuclear emulsion track width by photometric meas. 78−94167
Ne nuclei, track in Ilford G-5 emulsion, track width meas. 78−17488
Si detector, α-particle dense track charge losses 77−3233
U prospecting using microdistrib. anal. of Siwalik vertebrate fossils by nuclear Track Etch tech. 80−98489

particle velocity analysis
see also energy loss of particles; ion mobility; mass spectrometers; particle spectrometers
aerosol size spectrum determ. in turbulent medium using coherent Doppler meas. 79−96841
aerosol spectrometer using two-pulse Fraunhofer holography, fibrous particle motion anal. 80−58476
DC vacuum arc emitted particle flux 78−75470
holographic meas. for fine particles *(Japanese)* 78−95873
laser radiation effects on particle properties, radiation pressure effect on particle motion *(German)* 80−102755
molecular and atomic beams, vel., intensity and particle density, using mass spectrometer 79−67428
molecular beam reactions, transient complex form., product mol. translational energy distrib., theory 77−90602
molecular beam sampling of hollow-cathode discharge plasma, fast neutral source 77−68865
Mollenstedt velocity analyser for medium energy electrons, 500 eV to 3 keV 79−80721
shock-loaded solids, wave profile measurement 79−94564
simultaneous determination of diameters of velocity of moving solid particles with image sensor *(Japanese)* 78−95872
single particle trajectories, through ionising regions 79−6218
thermal neutron monochromators, Monte-Carlo simulation of mechanical velocity selectors 78−24886
wind tunnel particle and droplet field holography 79−76642
π^-p interactions at 40 GeV/c, cluster field features *(Russian)* 79−9421
CO flame rise vel. meas. by particle track method 80−89489
Cs atomic beam tube velocity distributions 77−37856

particle velocity analysis continued
Cs beam frequency standard drift and noise performance rel. to velocity distributions 78−57912
Li+Cl_2(Br_2)(ICl), product mag. deflection slotted disc velocity analysis 77−16806
Na atoms, 10 meV-10 keV, velocity spectrom. 77−3210

particles, elementary *see elementary particles*

parton model
$\Delta S=0$ weak hadron neutral current, quark parton model, νN and e^+e^- interactions 78−12859
η_9 prod. cross section ratio in quark parton model *(Korean)* 80−27466
νN deep inelastic scatt., scaling behaviour, quark-parton model, book contrib. 78−78171
additive quark parton model, hadronic fragmentation distribs. 78−8711
asymptotic freedom, quark-parton model 77−82675
asymptotic freedom and parton model appl. to leptonic processes 80−4959
asymptotic freedom beyond leading order, importance and use, parton model 79−71721
asymptotically free parton model, cf. massive muon pair prod. 78−8605
asymptotically free parton model, massive μ pair prod. in hadron-hadron collisions 77−13936
asymptotically free parton model, struct. function transverse momentum behaviour, SU(3) gauge model 80−27469
asymptotically-free parton model, $W^{\pm}$, Z^0, μ-pair prod. 78−12865
b-quarks, possible obs. in $\bar{\nu}$ interactions, nonleptonic decays and vector Ψ_h hadronic prod. 78−8613
baryon structure functions, dynamic relationship to baryonium trajectories 79−40763
baryonic and electric charge distribs. in multiparticle prod., quark-parton model 77−79285
baryons and mesons, parton distribs. consistent with naive quark model and QCD 80−62937
Bjorken and Feynman scaling violation, connection, wee parton region 77−18229
branching process study from parton distrib. evolution eqn., jet processes 79−89111
broken SU(6) parton model, spin depend struct. functions, deep inelastic lepton+nucleon appl. 78−428
canonical scaling in hadronic high-p_T processes, parton Fermi motion 78−45977
charged current ν and $\bar{\nu}$ interactions, hadron prod. at high energy, quark parton model 79−36058
charged spin-1 gluons, integer charged quarks, e- and ν- prod. 77−49894
charm production, mass scales, in deep inelastic processes, parton model, generalised VDM 77−13930
charmed particle weak semileptonic decays, free parton model 79−75766
charmonium model anal. 77−71490
charmonium potential models, testing Q^2 duality 79−45082
clustered, π^0 large p_T inclusive prod. in pp and πp interactions 77−67688
compound quarks, gluons and parton confinement 79−22017
conference, lepton-hadron physics, Karlsruhe, Germany (Sep. 1978) 80−73098
conference on high energy phys. with polarised beam and target, Argonne, USA (Oct. 1978) 79−63526
constituent interchange model, cross section normalisation, large transverse momentum 77−71486
covariant harmonic oscills., two bound quarks 77−34117
covariant model for N form factors, Drell-Yan-West relations 77−6086
covariant parton model, jets, quark confinement large p_T and leptonic inclusive processes 77−30317
covariant parton model, pattern of scaling violation, openings of new channels 77−41815
cumulative hadron production off nuclei, parton recombination model 79−71773
cut vertex formalism, parton model interpretation 80−86566
deep inelastic hadron electroproduction, charge retention, quark-parton and jet models 79−45090
deep inelastic hadron leptoproduction on nuclei, inclusive hadron final states 78−54741
deep inelastic hadronic final states, sum rules, quark parton model 77−87981
deep inelastic scatt., covariant parton model, Feynman integrals of perturbation theory 78−82221
deep inelastic scatt., field theoretical description, QCD, quark-parton, and light cone algebra *(Russian)* 80−42388
deep inelastic scatt., naive quark model 77−61251
deep inelastic scatt., quark-parton model 77−79270
deep inelastic scatt. and lepton pair prod., covariant parton model approach to scaling 78−21431
deep inelastic scatt. test of model, $e^+p\rightarrow e^+\gamma X/e^-p\rightarrow e^-\gamma X$ 77−41846
deep inelastic structure functions and the quark parton model 80−4992
deep-inelastic leptoproduction off nucleons, struct. function model in asymptotically free gauge models 79−40786
deep-inelastic neutral-current cross-sections 78−66074
deuteron, relativistic space-time description and short distance effects 77−2795
dilepton charge production cross section for ν and $\bar{\nu}$, parton model 80−62966
dilepton prod. during hadronic collision space-time evolution, quark-parton model 79−2980
dilepton production in hadronic collisions, review 79−49547
dimensional counting and Landshoff, multihadron reactions at large transverse momentum 78−33092
dimuon enhancement at 9.5 GeV, vector meson family with hidden 'beauty' *(Russian)* 78−33030
direct γ prod., large p_T, high energy hadron collisions 77−71547
distribution functions in hadrons, quark cascade model decay distrib. functions 79−36033
double-logarithmic quark and form factors and the evolution of parton jets 80−68421
Drel-Yan model, failure for J/Ψ prod. in NN conditions 79−89106
Drell-Yan conjecture in asymptotically free theories 79−17689
Drell-Yan process, heavy lepton pair prod., non-scaling parton model 77−13928
Drell-Yan process higher order corrections, QCD and parton model sum rules 80−95251
Drell-Yan processes, intrinsic transverse momentum, nongauge theories 80−82950

parton model continued
Drell-Yan trigger, hadronic prod. of dilepton pairs and muons 78−37182
dual parton model, hadron form factor 77−67619
dual topological unitarization, correspondence with quark-parton model and QCD 79−93361
EM probes of nucleons, photo- and electro-excitation, quark model anal. of nucleon struct. 79−49520
energy inclusive meas., parton model and scaling laws 77−74733
extended quark model, large p_T hadron prod. 78−29342
fast hadrons at low $p_\perp$, parton model, quark recombination, pp scatt. appl. 78−54618
Fermi-motion, canonical scaling of partons in hadronic high p_T processes 78−29314
Feynman's parton phenomenon, covariant forms of uncertainty relations 79−9137
field theoretic, large transverse momentum partons and massive μ pair prod. 77−30326
form factors, structure functions and charge radii for hadrons *(Russian)* 79−93381
forward hard scattering in hadron-hadron collisions in the energy region $\sim 10^{14}$ eV 80−86773
fragmentation functions beyond leading order in QCD 80−13282
fragmentation functions for pion electroproduction, parton-quark model consistency 77−79254
fragmentation functions of partons, Q^2 depend., lowest order QCD calcs. 78−62359
fragmentation in high-energy collisions, information about constituent partons 77−71533
gauge model of weak and electromag. interactions, polarised lepton scatt. 78−45901
generalised quark parton model, deep inelastic scatt., Drell Yan process 78−62373
generalized quark-parton model study of σ_L/σ_T and large k_T 78−29306
hadron, fragmentation from heavy quark partons 78−8603
hadron+hadron, jet production, large transverse momentum 80−42503
hadron+hadron$\rightarrow\gamma\gamma$X, scaling and quark mass dependence, quark parton model 80−73749
hadron+hadron inclusive cross section of symmetric hadron pairs produced, hard scatt., parton model and QCD 80−63052
hadron+nucleus interactions, Fermilab energies, inclusive rapidity distribs., parton-cascade model 78−37252
hadron bags, interactions under strict quark-line rule 78−41495
hadron calorimeter expts., asymptotic power laws, QCD and parton model predictions 80−57560
hadron collisions, theory and phenomenology of lepton pair production, review 78−82159
hadron distribs. in reactions with very heavy quarks 78−41486
hadron distributions in quark jets, pion and proton form factors 79−54317
hadron EM interactions, review 80−412
hadron final states in deep inelastic processes 77−34128
hadron high energy struct. models *(Hungarian)* 80−4924
hadron inclusive prod. cross sections at large P_T A-depend., quark-parton model *(Russian)* 80−86771
hadron inelastic scatt., secondary hadron multiplicity distribution, Regge like parton model *(Russian)* 80−78100
hadron interactions, dilepton ang. distrib. 78−21395
hadron interactions, neutral heavy lepton detection probability 78−8612
hadron jets, rapid parton and hadron distribution 80−86693
hadron microstructure, de Sitter microuniverse, relativistic Hooke group and nonrelativistic quark model 80−27480
hadron parton struct. and diffraction scatt. for soft processes 79−344
hadron total cross sections in quark parton model 78−45859
hadron-hadron collisions, hard and soft processes in small p_T inclusive reactions 78−41599
hadron-hadron hard collisions, calorimeter trigger, Ochs-Stodolsky scaling law derivation, parton model 79−17775
hadron-hadron interactions, lepton pair prod. 78−66138
hadron-hadron interactions, particle ratios and lepton prod. at large p_T 77−67620
hadron-hadron large p_T collision, weak interaction effects 78−21462
hadron-lepton deep inelastic scatt., review, book contrib. 80−47260
hadron-nuclei collisions, statistical mechanism of multiparticle prod. 77−46155
hadron-nucleus collisions, transverse momentum distrib. of secondary hadrons *(Russian)* 78−29444
hadron-nucleus high energy reactions, multiple prod., parton-hadron cascade model *(Russian)* 78−17066
hadron-nucleus inelastic collisions, multiplicities, ang. distrib., hydrodynamic and parton models *(Russian)* 77−250
hadronic μ-pair prod., hadron mass corrections and parton transverse momentum 79−36034
hadronic correlations at large transverse momenta, parton model 77−18228
hadronic events, inelastic, non-diffractive, charge correlations in jets, quantum number effects 80−86764
hadronic large p_T phenomena, effect of parton transverse momenta, QCD Born terms 79−30716
hadronic massive lepton pair prod., theory review, Drell-Yan model 78−89752
hadronic polarization in neutrino scattering, helicity struct. of weak neutral current 78−74245
hadronic structure using parton anal. of deep inelastic scattering and rel. processes 79−80803
hadrons, parton distribs. calc. 78−421
hard processes, large rapidity separation of baryonic number, partons, and dual topology 80−95255
hard processes, parton model and QCD, review 80−47258
hard QCD processes, relations through mass singularity universality 79−22054
hard scattering models, large transverse particle prod., cross section constraints from opposite side rapidity distribs. 78−29360
heavy meson inclusive semileptonic decays, lifetime estimates, quark-parton model difficulties 80−86704
heavy quark system prod. in QCD, duality predictions 79−13074
high energy collisions, cumulative particle prod., parton recombination and quark-parton models 80−82956
high energy interactions, quark role, appl. of quark parton model 79−30715
high energy low P_T hadronic reactions, Pomeron contrib., parton fragmentation framework 80−73688

parton model continued
high energy neutrino interactions, quark parton model anal. 79−30730
high p_T jet pairs, parton-parton scattering and π quark struct. functions 80−47248
high p_T processes, parton transverse momentum effects, QCD description 79−17774
high transverse momentum collisions, phenomenological description, pp, pn inclusive interactions 77−57574
high transverse momentum processes, quark-parton model anal. 78−82163
hydrodynamic theory of high energy interactions *(German)* 80−406
impulse approximation in QCD, partons p_t distrib., appl. to deep inelastic electron scatt. 78−62368
inclusive γ production in pp collisions, quark parton model 79−429
inclusive ν deep inelastic scatt. in SKAT bubble chamber, 2-30 GeV 78−62390
inclusive electroproduction of hadrons, virtual photon prod., quark fragmentation region 78−54634
inclusive high energy particle-nucleus interactions, A depend. of multiplicity, cross section, rapidity, momenta distrib. 77−79291
inclusive interactions of fast hadrons with nuclei, parton hard scatt. *(Russian)* 78−45985
inclusive lepton pair prod., P violation, quark-parton model in Weinberg-Salam theory, QCD 80−37217
inclusive leptoproductions, scaling violation, colour-octet model effect 79−13077
inclusive processes with large momenta, quark-parton model *(Russian)* 77−71538
intermediate vector boson, hadron-hadron collisions, Weinberg-Salam model 80−9186
internuclear cascades and multiple prod. of nuclei *(Russian)* 77−6330
intrinsic transverse parton momentum, struct. function determination 79−75722
jet quantum number, identification model 80−42423
jet quantum number identification event by event, original parton and gluon jets 80−52466
jet structure in high p_T events, importance of parton transverse momentum 78−432
jet-mass effects and high-p_T jet production 80−52473
jets, loading particles, in large transverse momentum events, quantum number effects 79−89198
jets in hadron collisions 78−54612
jets of quarks and gluons, leading logarithmic approx., parton interpretation 80−68433
kinematical scale breaking in high p_T interactions, parton fragmentation function 80−367
kinematical scale breaking in high P_T interactions 79−13064
large momentum transfer interactions, review 79−17686
large $p_\perp$ reactions, parton transverse momentum effect 78−33035
large p_T hadron prod. off nuclei, QCD parton model, nucleus as gluon filter 79−89110
large p_T processes, parton transverse momentum 79−13040
large p_t processes, parton-parton cross sections constraints from angular correls. 77−71540
large p_T processes, two particle distrib. and associated multiplicity 77−82782
large p_T production off nuclei, parton tubes, coherent tube model 78−21392
large p_T proton production, parton models 79−40743
large transverse hadron prod. in pionisation region, covariant parton model *(Russian)* 77−34131
large transverse momentum and large mass production in hadronic interactions review of theoretical models 79−89115
large transverse momentum processes, parton model, logarithmic corrections to Bjorken scaling 77−71483
lectures given at CERN School of Physics (6-19 June 1976) 77−61173
lepton+hadron, deep inelastic scatt., quark-parton model with logarithmic scaling violation 80−78071
lepton+nucleon producing polarised baryon+anything, polarisation transfer, parton model test 77−82746
lepton pair prod., thermal parton model 79−13075
lepton pair prod. struct. functions, QCD improved quark-parton model 80−73671
lepton pair production in hadronic collisions, parton model and scaling approach 78−82150
lepton scatt. off protons and deuterons nonscaling behaviour 78−8642
lepton-hadron generalised scaling variable in parton model 77−10259
lepton-nucleon deep inelastic scatt., modification of Kuti-Weisskopf parton model *(Russian)* 78−17027
lepton-nucleon scatt., deep inelastic, final state polarisation 78−458
light-cone field-theory and the parton model, book contrib. 78−82220
mass corrections to scaling in deep inelastic processes 77−13929
mass scale effects 78−25017
mass scale effects in parton model 78−21389
mass singularities factorisation for polarised parton legs in low order QCD perturbation theory 79−40737
massive μ pair prod. in hadronic collisions, ang. distrib, quark-partons+gluons model 77−82706
massive lepton pair hadroproduction, QCD and parton model anal. 80−42421
master equation for parton distributions 79−80792
meson structure function in covariant parton model context 80−78020
MIT bag model, parton dynamics 78−74204
MIT bag model cavity approx., parton distribs., Bjorken scaling 78−89664
Monte Carlo quark-parton model for multiparticle and low mass dimuon prod. 79−30697
multiparticle prod. charge distribs. and fluctuations, Monte Carlo quark-parton model 79−93363
multiparticle prod. in quark-parton model, Monte Carlo method 78−41607
multiparticle prod. long range correls. and parton model 77−82712
multiparticle reactions on deuterons, multiperipheral parton model anal. to rescatt. 79−22154
multiperipheral parton model, deep inelastic processes 80−82961
multiperipheral parton model, Reggeisation and dual unitarisation 80−37249
multiple formation process, parton model and statistical equilib., parton fluctuations *(Russian)* 79−13062
multiple prod. on ^{2}H, rescattering anal. 77−87945
naive model, concept and appl. 80−73675
naive quark parton model, x-depend. of parton transverse momentum 79−2976
neutrino reactions, theoretical anal., review 78−82202
nonhomogeneous string model 78−12884
nonscaling parton model, large p_T processes in hadron collisions 79−352
nonscaling parton models, physical struct. 78−4832
nuclear collisions, hadron prod. in quark-parton model 78−12868
nucleon charge radii 80−91064
nucleon chiral substructire 77−41787
nucleon production in quark parton model, e^+e^-, ep and large $p_\perp$ reactions 78−21391
nucleon structure function in rest frame, quark-parton model 77−87942
nucleon-nucleus unstable hadron coherent prod., cross section errors from parton model 79−22253
optical group Opt(3,1) and its subgroups 78−77759
parity violating effects in dilepton production using polarized targets 79−67613
parton confinement: A different perspective 78−86437
parton distrib. in rel. to transverse impulse in quantum chromodynamics *(Russian)* 79−63433
parton distribution functions, Q^2 depend., QCD parameterisation 80−82937
parton transverse momentum distrib., scaling violation mechanism 78−89661
Pati-Salam model, higher order parton transition effects in deep inelastic scatt. 80−78008
perturbative QCD, gluon bremsstrahlung by confined sources 79−45067
perturbative QCD, parton primordial transverse momentum 79−40728
philosphical similarities in ancient Greek, Hindu and Chinese thought, for teaching 78−54143
photoprod. of charged intermediate vector bosons 78−45855
polarised deep inelastic scatt., parton transverse momenta role, struct. function, QCD evolution 80−78034
polarised protons, parton distrib. functions, SLAC polarised ep data anal. 77−82747
pomeron with $\alpha(0)>1$ *(Russian)* 78−74235
proton, parton structure and charge distrib. in multiparticle production 77−6088
proton struct. function determ. from Lorentz deformed wave function 79−13070
pseudoscalar mesons, EM mass shifts, quark-parton model, SU_3 quark triplet 80−42459
Q^2 dependence of parton distribs. using asymptotically free gauge theories 78−33034
Q^2 dependence of parton transverse momenta and deep-inelastic scattering, structure functions 79−40741
Q^2 dependence of quark and gluon fragmentation functions in a parton picture based on QCD 79−9336
Q^2 dependent parton distribution function on QCD 78−93857
QCD, factorisation and the parton model 78−93848
QCD, impulse approx. and scaling phenomena 79−22043
QCD, in 2-dimens., bound states and asymptotic limits 79−71716
QCD, inclusion of parton transverse momentum 79−26290
QCD, inclusive distributions in extended leading logarithms 79−13066
QCD, long range parton correlations at large Q^2 *(Russian)* 80−68428
QCD, particle transversal momenta, parton distribs. in hadrons *(Russian)* 79−93370
QCD, parton and dimuon intrinsic transverse momenta 79−13038
QCD, parton and gluon distribs. 78−16981
QCD, parton cross sections, infrared and mass singularity regularisation 80−32075
QCD, parton distrib. function, transverse momenta, axial gauge ladder model 80−27467
QCD, parton jet and shower model 80−86663
QCD, parton transverse mass distrib. 78−8587
QCD, parton transverse momentum distribution 78−29301
QCD, scale breaking for quark and gluon distribs., diagrammatic anal. 79−71706
QCD, struct. functions, perturbation theory *(Russian)* 78−8595
QCD effects, parton transverse momenta, large-p_T hadron prod. 78−66083
QCD extended leading logarithm approx. for inclusive distribs. and lepton pair prod. 80−379
QCD in 2-D quark confinement and parton model 79−17670
QCD interactions, perturbation theory and the parton model 79−58927
QCD jets, algorithm for parton spectra 78−89680
QCD jets, multiparton distribs. 79−13065
QCD multijet model, universal quark-jet fragmentation in soft hadronic reactions 80−13285
QCD prediction for ang. distrib. of dileptons in hadron collisions 79−26300
QCD predictions, parton and gluon transverse momenta for large p_T particle prod. 79−40723
quantum number distribs. and fluctuations in multiparticle prod., quark-parton model 78−82249
quark and parton phys., introduction, book 79−85276
quark charge below colour threshold, rigorous theorems and parton model 79−85266
quark confinement, analyticity of parton model, QCD_2 calc. 78−41484
quark fragmentation functions in inclusive hadron muoproduction 79−67565
quark fragmentation functions in Monte Carlo quark parton model of e^+e^- annihilation 79−80791
quark masses and structure functions 80−22585
quark parton distribs. for deep inelastic scatt., calc. from 1-D Dirac box 78−45845
quark parton model, review 79−93368
quark parton model with large parton k_T 80−42412
quark recombination model, vector meson prod., effect on $\pi^\pm$ and $K^\pm$ fragments from proton 78−82160
quark-gluon-parton model, constituent quarks as clusters 77−30318
quark-parton, charge transfer in multiparticle prod. 77−57490
quark-parton cascades in nuclei and secondary hadron spectra from hadron-nucleus collisions *(Russian)* 80−57623
quark-parton distributions model, large transverse momentum hadrons, logarithmic scale breaking 78−16989
quark-parton fragmentation, support from data on μ^+p inclusive hadron distribs. 77−61296
quark-parton model, direct test in e^+e^- annihilation 79−75728

parton model continued
quark-parton model, Large-p_T correlations in scale-breaking model 77−82704
quark-parton model, leading proton-large p_T particle and proton-lepton pair correlations 79−353
quark-parton model, strong interactions of quarks, weak interaction *(Russian)* 77−82710
quark-parton model, three photon struct. function of proton, inelastic electron scatt. data 77−46022
quark-parton model, with scaling violations, large p_T processes anal. 78−45927
quark-parton model description of neutrino data, particle prod. in $\bar{\nu}$N and νN interactions 77−18270
quark-parton model predictions of $e^+e^-\rightarrow\gamma+$hadrons, sum rules, charge asymm. 77−10219
quark-parton model results for $\sigma(e^+e^-\rightarrow\text{hadrons})/\sigma(e^+e^-\rightarrow\mu^+\mu^-)$, asymptotic freedom predictions leading to paradox 77−49988
quark-parton model with charm for dimuon prod. in high energy νN and $\bar{\nu}$N interactions 77−57520
quark-partons, phase transition to baryons rel. to possibility of stable quark stars 77−45471
Regge formalism, quark fragmentation functions for inclusive hadron production 80−68462
Regge theory extension to supercritical case 77−79250
Reggeon field theory, meson trajectories, Markoffian approach 79−45037
Reggeon parton structure, from lepton-Reggeon scatt. data 77−6095
relativistic hadron, parton distrib. and Regge field theory parameters *(Russian)* 80−62931
relativistic oscillator formalism for hadron struct. and props. 80−9144
relativity, general, zitterbewegung, atoms with point particles 80−57147
in renormalisable field theory, anomalous dimension 77−22682
review of theoretical development, comparison with expt. data 77−57498
scale breaking parton model for electron and neutrino deep inelastic scatt. 78−66122
scaling violation mechanisms, electroprod. as quark sea effects *(Russian)* 79−9344
scaling violations, parton model anal. 78−62406
scattering, deep inelastic, energy flow and energy correlations, perturbative QCD, infrared safety 80−27465
Schrodinger handbag model 78−427
single particle inclusive distrib. at large p_T in parton models 77−79286
soft gluon resummation formulae for hard parton processes in QCD 80−105842
soft hadron-nucleus collisions, two chain parton model description 80−82944
soft hadronic processes, quark-parton model test for inclusive cross sections 79−17776
static bags, parton distrib. divergence 79−54313
Sterman-Weinberg formula for quark jets and gluon jets, leading log version, master equation 80−22552
stochastic-field multieikonal theory, high-energy hadron dynamics 78−8634
structure function relations, lepton pair processes at large transverse momenta 78−82214
structure function scaling between proton and neutron 78−16988
structure functions, nonsinglet, parton distributions, QCD parametrisation, leading and next-to-leading order corrections 80−68456
structure functions of mesons in quark-parton model, appl. to hadron prod. in e^+e^- annihilation 78−41482
SU(3)×U(1) model, heavy lepton prod. and decay signature 78−45900
SU(6) parton model, lepton prod. with large transverse momenta in hadron-hadron collisions 78−89673
SU(N) scalar QCD in two dimens., and the parton model 78−93856
sum rules, corrections in asymptotically free field theories 77−38092
supercritical pomeron, parton model interpretation, appl. to scatt. off nuclei 78−41497
target-mass effects in hadronic lepton-pair production, hadronic mass corrections to Drell-Yan formulae 79−89139
total cross section rise, parton mechanism *(Russian)* 78−41505
totally inclusive leptoprod., scaling anal., target mass corrections in QCD parton model 80−102052
transverse momenta, parton, influence on large p_T spectra 78−21380
transverse momenta of sea and valence partons, scaling violation effect 78−41483
transverse momentum cutoff, electroprod. data 77−10215
transverse momentum depend. on longitudinal momentum 78−25016
transverse momentum measurement for parton model differentiation 79−13076
transverse momentum of partons 77−49908
transverse momentum of partons determ. 77−67615
transverse momentum of partons inside hadrons 77−57489
trimuon prod. in ν and $\bar{\nu}$ interactions, EM μ-pair contrib. 78−66107
twist selection rule, mass zero representation partons 80−78027
two particle inelastic scatt., mass divergences, QCD and parton model 79−22049
two-hadrons inclusive reactions and correl., large p_T, scale-violating quark model 78−74292
two-stage model, parton distribs. and Q^2 depend. 78−66078
unified theories with spontaneously broken colour symmetry, QCD scalar parton effects 79−80783
valence quark-parton transverse momentum distrib. 78−12862
vector meson inclusive prod. cross section in hadron-nucleon collisions, parton transversal motion *(Russian)* 79−67617
vector meson production in pp interactions, constituent-interchange model 80−22579
virtual photon-nucleon scatt. anal. for spin 1/2 parton in covariant parton model 80−4966
weak and EM phenomenology, gauge theoretical prospective, charm and flavour conservation 80−4916
Wilson operator formalism, generalised parton model equivalence 78−93855
Yang-Mills theory without gauge fixing, perturbation Feynman rule 80−57462
d inelastic screening, form factor at $t\neq0$ 80−91070
eD, 19.4 to 22.2 GeV, unpolarised target, parity violation in inelastic scatt. of polarised electrons 79−63482
ed, deep inelastic scatt., quark-parton model with logarithmic scaling violation 80−78071
ed, $K^{\pm}/\pi^{\pm}$ ratio and symmetry props. of quark- parton model, fragmentation functions 78−93888
ed deep inelastic scatt. cross sections, quark-parton model with broken scaling *(Russian)* 80−32109
e^+e^- annihilation, parton model, finite energy results 78−419
e^+e^- 80−63010
$e^+e^-\rightarrow$ hadrons, scaling and quark struct. 80−425
e^+e^- annihilation, hadron multiplicity distribution, Regge like parton model *(Russian)* 80−78100
e^+e^- annihilation, hadron/muon pair prod. ratio, nonasymptotic contribution to quark-parton model 77−34169
e^+e^- annihilation, heavy quark fragmentation and parton transverse momentum 78−82150
e^+e^- annihilation, inclusive pion spectra, parton fragmentation model 77−18305
e^+e^- annihilation, opposite side quantum number correlations 80−105863
e^+e^- annihilation and quark fragmentation functions, Monte Carlo quark-parton model 79−22119
$e^+e^-\rightarrow\Delta X$, polarisation effects in nonperturbative parton model, scaling 80−105912
$e^+e^-\rightarrow\gamma+$hadrons, high energy, lepton radiation and γ struct. functions, quark parton model 80−32113
$e^+e^-\rightarrow h^{\pm}X$, violation Bjorken scaling, momentum fluctuation, range of timelike photon 79−3033
$e^+e^-\rightarrow hX$, naive parton model failure in quark-gluon theory 77−67618
$e^+e^-\rightarrow$hadrons, 13-31.6 GeV, gluon bremsstrahlung evidence, seagull effect, one sided jet broadening 80−430
$e^+e^-\rightarrow$hadrons, parton model and QCD 80−105860
$e^+e^-\rightarrow pX$, weak neutral current, polarisation effects, asymm. parameters *(Russian)* 78−459
$e^+e^-\rightarrow VX$, parton model, polarisation effects *(Russian)* 80−63002
eN deep inelastic scatt., parton model anal. 78−62405
ep, deep inelastic scatt., quark-parton model with logarithmic scaling violation 80−78071
ep, deep inelastic scatt. cross sections, quark-parton model with broken scaling *(Russian)* 80−32109
ep, deep inelastic scattering, scaling deviations, parton model anal. 79−58966
ep, high Q^2, QCD corrections to parity-violating asymmetries 80−22618
ep, $K^{\pm}/\pi^{\pm}$ ratio and symmetry props. of quark- parton model, fragmentation functions 78−93888
ep deep inelastic scatt., light-cone expansions 77−54077
ep deep inelastic scatt., renormalisation group anal., parton model connections 79−40784
ep deep inelastic scatt. in $\omega=1$ region, field theory and parton model anal. *(Russian)* 78−78190
ep deep inelastic scattering, rest frame quark-parton model of proton, scaling 78−70374
ep→e+hadron+x, parton picture from QFT, structure function scaling behaviour 79−402
ep→$W^+(Z^0)$+X, inclusive cross sections, quark-parton model calcs. 79−71755
$e^{\pm}p\rightarrow e^{\pm}\gamma+X$, deep-inelastic bremsstrahlung, quark charges, colour gluon mass 78−74216
eq parity violating neutral current couplings, model independent anal. 79−17737
$\gamma+$hadron→lepton pair, perturbative QCD, twist-2 photon operator, parton subprocesses 80−73716
$\gamma^*\gamma^*\rightarrow2$ jets in e^+e^-, parton model QCD corrections for doubly deep processes 80−73758
γp→γp, 2 to 6 GeV, differential cross section meas., parton model anal. of energy depend. 79−63485
γp→γp, expt. cross section energy dependence agreement with parton model 78−37214
γp→hX, SU(3)×SU(3) invariant interaction of quarks, large p_T, gluon bremsstrahlung 78−33072
γp→$W^+(Z^0)$+X, inclusive cross sections, quark-parton model calcs. 79−71755
$\gamma q\rightarrow\pi q'$ inclusive pion production in γN and e^-N collisions, quark-parton model *(Russian)* 80−78073
$hN\rightarrow\gamma(\mu^+\mu^-)+$jet+hadrons, gluonic jets, prod. mechanism *(Russian)* 79−58986
l(l̄)N, P-odd asymmetries in deep inelastic scatt. of polarised l and l̄ *(Russian)* 79−49527
$l^{\pm}N$, deep inelastic scatt., EM corrections to hadronic and neutral currents, systematic effects *(Russian)* 79−49526
lp→l'hX, azimuthal depend., parton model calc. 78−93887
μ pair prod., parton model, transverse momentum distrib. determ. 77−71484
μ pair production in hadron-hadron collisions, gluon effects, QCD predictions 78−78148
μ pair transverse momentum distrib., hard interaction mechanism of constituents 77−65139
μd, 147 GeV, inclusive hadron jet behaviour, hadron spectra, quark-parton anal. 79−71757
$\mu N\rightarrow3\mu N$, EM contribution cross section, using radiative quark-parton model 79−40788
μN deep inelastic scatt., asymm., quark proton model evaluation, gauge theories test 78−62408
μN inelastic scattering, dimuon events mech., parton fragmentation 77−10260
$\mu N\rightarrow\mu X$, broken colour gauge theory of integer charge quarks 80−13313
μp, 147 GeV, inclusive hadron jet behaviour, hadron spectra, quark-parton anal. 79−71757
μp, deep inelastic scattering, scaling deviations, parton model anal. 79−58966
μp, semi-inclusive, ang. correl. tests of QCD 79−17735
μp charged current interactions, hadron production, quark-parton model comparison 79−40769
μp semi-inclusive scattering, hadronic fragmentation initiated by pointlike probes 79−49551
n charge radius and quark-parton model, deep inelastic e-N struct. functions 77−71488
N form factors, parton separation determ. 78−33026
NN large angle elastic scatt., spin correlation asymmetries, partons and coloured quarks 79−63411
ν and $\bar{\nu}$ 'new physics' data, vectorlike quark-parton model anal. 79−9359
ν and $\bar{\nu}$ charged-current reactions, Bjorken scaling violations 78−74246
ν deep inelastic scatt., parton anomalous statistics *(Russian)* 78−29331

parton model continued
ν interactions, trimuon prod., EM muon-pair contrib., scaling parton model 78−66106
$\nu(\bar{\nu})$ high-energy interactions, dimuon distrib. anal., quark-parton model 78−33056
$\nu(\bar{\nu})$ interactions, charm model of weak interactions, parton model anal. 77−6106
$\nu(\bar{\nu})$N neutral current interaction, charm prod. in quark parton model 77−61246
$\nu(\bar{\nu})$N scattering, modified GIM model, scaling violations, naive parton model 78−21414
$\nu(\bar{\nu})$N→$\nu(\bar{\nu})\gamma$X, hadron neutral current, parton model *(Russian)* 78−45910
$\nu(\bar{\nu})$n→$\mu^-(\mu^+)$pX, semi-inclusive ν-scatt. and π-struct. functions 79−80819
$\nu(\bar{\nu})$p semi-inclusive scattering, hadronic fragmentation initiated by pointlike probes 79−49551
$\nu(\bar{\nu})$p→$\mu^-(\mu^+)\Delta^{++}$X, semi-inclusive ν-scatt. and π-struct. functions 79−80819
$\nu_\mu(\bar{\nu}_\mu)$N, charm meson prod. and decay, lepton inclusive distrib., c-quark fragmentation function *(Russian)* 80−52493
$\nu_\mu(\bar{\nu}_\mu)$N, multi muon events, associative charm generation mechanism, D, $\bar{D}$ mesons *(Russian)* 79−89145
$\nu_\mu(\bar{\nu}_\mu)$N, prod. of hadrons with new quantum numbers, quark parton model *(Russian)* 77−82735
$\nu_\mu(\bar{\nu}_\mu)$N→$\mu^-(\mu^+)$X, struct. functions meas., quark-parton model anal. 79−58951
$\nu_\mu(\bar{\nu}_\mu)$N→$\mu(\bar{\mu})$+hadrons, phenomenology, parton model, expt. data, dimuon events *(Russian)* 77−49943
νN, charm and strangeness production, role of gluons 79−13104
νN, deep-inelastic, electromagnetic radiative corrections 80−22602
νN interactions, dimuon prod., quark-parton model, threshold effects of charm prod. 77−46041
νN→$\mu^-\mu^-\mu^+$X, internal Drell-Yan mechanism, parton model approach 78−89656
νN→μ+charmed baryon, SU(4) breaking effects, quark parton model 79−40792
νN or $\bar{\nu}$N, deep inelastic scatt., quark-parton model with logarithmic scaling violation 80−78071
νN scatt. with charge exchange, quark-parton model and QCD description *(German)* 79−26324
νN single- and di-muon prod., colour excitation, weak interaction model anal. 78−45906
νN→X, determ. of all neutral-current coupling constants from inclusive cross sections alone 79−13106
ν_lN deep inelastic scatt., radiative correction inaccuracies, quark-parton and Weinberg-Salam theories *(Russian)* 79−93403
ν_μN→μ^-X, 2 to 30 GeV, charact. of deep inelastic processes *(Russian)* 79−80821
ν_μN→μ^-+hadrons, restraint on weak four-fermion interaction constants, quark-parton model *(Russian)* 77−6110
$\bar{\nu}$p charged current interactions, quark fragmentation, quark-parton model test 80−68444
ω, photoproduction at high energy, parton model, γ hadronic props. 78−74266
ω backward prod., baryon exchange dip and parton effects 78−17030
p, degenerate parton gas model, quark-lepton identification 80−68416
p production, compared to π, large transverse momentum, rearrangement of hard scattered partons 80−62934
p-nucleus interactions, 20 to 200 GeV/c, parton model anal. *(Russian)* 78−46065
p+nucleus→μ^++μ^-+anything, 400 GeV, high-mass dimuon continuum 78−37344
pN dilepton prod. quark-parton distribs., Drell-Yan model 79−17752
pN interactions, muon pair prod. and new parton radiative processes 79−17766
pN→$\mu^+\mu^-$X, determ. of parton sea 78−29304
$\bar{p}$p, 5.7 GeV/c, parton-cluster model, hadron struct. and non-diffractive collision impact parameters struct. 80−27454
pp, 62 GeV/c, multiparticle prod. mech., e^+e^- comparison in parton model 80−78103
pp, 70 GeV, $\pi^\pm$, $K^\pm$, p, $\bar{p}$ prod. cross sections, QCD-parton model anal. *(Russian)* 80−63044
pp, massive lepton pair prod., pion exchange model anal., quark parton interpretation *(Russian)* 80−82993
pp, p$\bar{p}$ inclusive interactions, lepton pair prod. and Drell-Yan mechanism 78−8718
p$\bar{p}$, $\pi^\pm$ inclusive spectra, comparison with Monte Carlo quark-parton model 79−30755
pp, transverse momentum fluctuations and high p_T processes in QCD 79−36014
pp, unitary impact-parameter model for multicluster prod. 78−33091
$\bar{p}$p annihilation, asymptotic props., parton model, kaon prod. *(Russian)* 78−466
pp collisions, Monte Carlo approach to multiparticle prod. in a quark-parton model 79−13171
pp elastic, differential and total cross sections, proton model, gluon-gluon annihilation 80−91114
pp elastic, inelastic, and inclusive interactions, spin effects, polarisation 77−30434
pp fragmentation at high energies, quark constituents 77−34185
$\bar{p}$p→γ, Z^0+X, charge asymmetry, QCD-parton model study 79−93349
pp interaction, quark-antiquark recomb. in fragmentation region 77−67690
pp→jet+X, P-violating weak effects in high transverse momentum collisions, QCD anal. 79−63559
pp→jets, 400 GeV, p_T plots, Monte Carlo and parton model predictions 78−89747
pp→l^+l^-X, massive lepton pair prod., quark-gluon-parton model, scaling 79−428
pp→l^+l^-X, parton density scale violations and quark-gluon correction to Drell Yan formalism 79−63560
pp→l^+l^-x, QCD corrections to Drell-Yan formula 80−22578
pp large inelastic diffraction in the quark-glue model, gluon distrib. in parton model 79−89138
pp large transverse momentum interactions, quark cascade model anal. 79−36101
pp→$\mu^+\mu^-$X, dimuon prod. using polarised beam, Drell-Yan parton model anal. 79−58981
pp→$\mu^+\mu^-$X, polarised p, polarisation direction, structure functions and Drell-Yan parton model test 79−63544
parton model continued
pp→$\mu^+\mu^-$+anything, Drell-Yan formalism 78−78229
pp($\bar{p}$)→$\mu^+\mu^-$X hadronic fragmentation initiated by pointlike probes 79−49551
$\bar{p}$p→p$\pi^\pm$X, 8.9 GeV/c, comparison with leptoprod., quark-parton model anal. 79−63512
pp→π^0X, parton model, polarised proton, large p_T π^0 prod. asymm. 78−12936
pp→π^0+X, π^0 prod. at large p_T 77−46090
pp→π^+X, P-violating weak effects in high transverse momentum collisions, QCD anal. 79−63559
pp→π+X, high p_T jet prod., QCD perturbation theory 79−89209
$\bar{p}$p soft annihilation, parton description in three chain model 80−83009
p$\bar{p}$→$W^\pm$X, front back asymmetry in QCD and Weinberg-Salam model 79−97579
p$\bar{p}$→Z+anything, front-back asymmetry differential cross section, $W^\pm$ prod. 79−6352
ϕ, photoproduction at high energy, parton model, γ hadronic props. 78−74266
π EM form factor asymptotics in QCD perturbation theory, partonic interpretation *(Russian)* 80−62984
π inclusive electroproduction, quark-parton model comparison with expt. data 78−37218
π^0 electroproduction, test of quark parton model 78−8672
π^+ structure from two jet events, parton scatt. anal. of π^+p and pp 79−49491
πN dilepton prod. quark-parton distribs., Drell-Yan model 79−17752
π^-N, 16, 22 GeV, dimuon prod. parton intrinsic transverse momentum, QCD perturbation 80−63037
πp, massive lepton pair prod., pion exchange model anal., quark parton interpretation *(Russian)* 80−82993
π^-p→$\mu^+\mu^-$+hadrons, π^-p→hadrons, quark-parton model 78−74222
π^+p→K^+X, π struct. function from low p_T hadron prod. 79−45123
$\pi^\pm$p, 150 GeV/c, multiparticle prod., quark parton model anal. 79−30756
$\pi^\pm$p, 2-9 GeV/c, large angle elastic scatt. cross sections, parton and bootstrap model test 78−78209
$\pi^\pm$p elastic scatt., 1.9-9.5 GeV, test of parton and statistical bootstrap models 78−89728
q$\bar{q}$→g$\mu^+\mu^-$, large q_T muon pairs ang. distribs. in perturbative QCD 79−85275
q$\bar{q}$ recombination model with resonance prod. 79−75740
ρ, photoproduction at high energy, parton model, γ hadronic props. 78−74266
Υ(9.46), prod. in e^+e^- interaction at DORIS, quark parton model agreement 79−93443
Υ(9.5) hadronic prod., parton distrib. and QCD 78−78142
Υ'(10.02), prod. in e^+e^- interaction at DORIS, quark parton model agreement 79−93443
W searches with hadron beams, parton model anal. 80−91046
γp→π^0p, 2 to 6 GeV, differential cross section meas., parton model anal. of energy depend. 79−63485

Paschen-Back effect *see Zeeman effect*

passenger traffic *see traffic*

passivation
Al, electrodes, use of soluble corrosion inhibitors to suppress electrode dissolution 78−88565
alloys, passivatable, role of oxide films in stress corrosion cracking initiation 80−50762
anodic oxide superficial layer, X-ray emission spectrometry and ion backscattering *(French)* 80−49482
deposition processes for passivation films, advances, review 78−23620
dissolution controlled cracking mechanism, repassivation effects 78−64772
glass, molten, reactions with conducting materials 80−85186
glass surfaces, corrosion, passivation and anal. 78−60854
glassy passivation films on Si substrates, appl. of silicates to flaw detection 77−39745
III-V semiconductor, KCl protective coating, LEED and Auger spectroscopy 77−89628
III-V semiconductors, anodic oxidation *(Japanese)* 78−92385
Incoloy 600 and 800, surface film in hot conc. NaOH, XPS study 80−11824
insulating coatings on Si, dissolution and corrosion in high temp. water and moisture 77−48564
metal, corrosion pit initiation and growth, salt film form. 80−16563
metal, ion implantation, surface treatment 77−8982
metal AC anodic dissolution rate, effect of H^+ evolution *(Russian)* 80−16693
metal foils, naturally passivated, ESCA, sputter etching 77−70218
metal surface, newly generated, occurrence of salt films during repassivation 79−15860
metals, electrocrystallisation and passivation kinetics, multiple stationary states and dissipative structs. theory *(French)* 80−7804
metals, passivation, using in situ polymerisation by microwave plasma discharge 78−64762
metals, precipitate films, ion selectivity effects on passivation and corrosion 80−35377
MOS structure with phosphosilicate glass layer, flat-band voltage, effect of growth conditions 80−107913
organic films, electronics and communications engineering appls. *(German)* 78−44011
oxide films, passivating, transient growth kinetics 80−93672
Permalloy corrosion resistance enhancement 79−79150
phosphosilicate glass, CVD, P conc. meas. 77−80533
phosphosilicate glass flow mechanism, and appl. in MOS devices 77−77393
phosphosilicate glass passivation layer P content, SEM analysis and interpretation 78−35759
phosphosilicate glass protective film for ICs, X-ray fluoresc. technique for rapid P determ. 77−40612
RBMK reactors, startup and shutdown, H_2O_2 and Fe compounds behaviour investigation 79−9822
review, passivity, in metals and alloys 80−50750
SEM, effect of passivation on obs. of voltage contrast 79−21856
semiconductor-insulator structure, charge transport in insulators 77−20452
solar cells, MIS, inversion layer 80−101098
solar cells, polycryst., influence of grain boundaries electronic structure on diode characts. 80−94068

passivation continued
stainless steel passivating film, comp., AES obs. 77−48571
steel, austenitic stainless, anodic polarization, Cr content effect 80−35382
steel, austenitic stainless, corrosion in hot conc. caustic soda, NaCl addition effects *(Japanese)* 77−8990
steel, austenitic stainless, corrosion resistance in passive state, cold work effects *(Czech)* 77−59987
steel, austenitic stainless, current maxima in passivity range 79−66200
steel, austenitic stainless, electrochemical behaviour in Ringer's soln., composition effects, SCC 77−90485
steel, austenitic stainless, Mo-bearing, ellipsometric meas. of passive films, optical constants *(Japanese)* 78−85041
steel, austenitic stainless, repassivation kinetics study in Ct media 80−97614
steel, C, corrosion and self protection in hot saline soln. 79−1925
steel, ferritic, Mo addition effect on corrosion resistance, X-ray photoelectron study 79−74285
steel, ferritic stainless, effect of Cl ions on passive layers 80−59766
steel, ferritic stainless (26 wt.% Cr) passivation, cathodic reduction and AES anal. 77−90500
steel, Fr-Cr-Al, sulphidation behaviour, 750°C, preoxidation effect *(French)* 78−15566
steel, galvanised, prepassivation, chem. nature of film and corrosion resist. *(French)* 79−43480
steel, galvanised strip, passivation treatment 80−61146
steel, low alloy, influence of accelerated weathering on corrosion 80−55565
steel, low-alloy, feasibility of electrochem. corrosion protection 79−70220
steel, mild, anodic polarisation behaviour in hot alkaline sulphide solns. 80−100949
steel, mild, corrosion and passivation in benzoate solutions 79−79180
steel, mild, surface oxide effect on acid corrosion inhibition 78−11384
steel, Ni-Cr, anodic dissoln. in NaCl solns. at high current densities *(Russian)* 80−76396
steel, passivation by sulphochromic soln. *(French)* 78−23869
steel, stainless, 18-8, impedance diagram in passive and transpassive state in Na_2SO_4 soln. *(Japanese)* 77−21318
steel, stainless, Cr, Mo effects on passivation AES and electrochemical anal. 79−74292
steel, stainless, depth profiling of passive film by quantitative AES 78−19611
steel, stainless, ferritic, corrosion in formic acid at 70°C, effect of Mo additions 78−35551
steel, stainless, ferritic, passivity in 1N HCl, X-ray photo-electron spectroscopic study 80−11817
steel, stainless, long-term corrosion stability rel. to use in joint endoprostheses 78−36059
steel, stainless, metallic element depth distribution, in passivation layer, luminescent discharge spectrometry exam. *(French)* 78−31585
steel, stainless, passivation in H_2SO_4, oxidising agent effects 79−20246
steel, stainless, passive layers, X-ray photoelectron spectroscopy analysis 77−32715
steel, stainless, passive state breakdown, and repassivation 79−39031
steel, stainless, repassivation ability in 3% NaCl at 80°C, stress effect, testing device *(French)* 77−77693
steel, stainless, type 304, corrosion fatigue and stress corrosion cracking, in boiling NaOH 80−7719
steel, stainless 18-8, ellipsometric meas. of optical const. and thickness of passive film 77−21326
steel, stainless 304, stress corrosion, high temp. electrochemical studies 80−30146
steel, stainless 304, stress crack initiation in chloride soln., role of corrosion pits *(Japanese)* 78−92397
steel, stainless and plain C, brazed joints used in thermal power plants, corrosion resistance 79−43492
steel, stainless type 304, anodically polarised, Cl^- ion effect on passive film 80−97621
steel, type AISI 316, thermal passivation in controlled vacuum 80−76276
steel sheet, Zn and Al-Zn coated, chromate passivation protection against wet-storage stain 78−95854
steels, stainless, passive state, electron spectroscopy anal. 80−59765
surface science, rel. to energy development and technology 78−88553
surface strength in friction, structural and energy conditions *(Russian)* 77−56111
surfactant adsorption on metal surface, effect on electrochem. reaction kinetics 80−40703
tinplate, passivation treatment 80−61146
TJS single-mode junction-up laser passivated with Si_3N_4 film, life tests 80−19045
Ag, in 0.1 M Na_2SO_4, passive (Ag_2O, AgO and Ag_2SO_4) films properties obs. *(Japanese)* 79−8399
Al, anodic attack in chloride medium, passivation *(French)* 79−96224
Al brass condenser tubes, XPS study of protective layers 80−35383
Al, cathodic polarization 80−21153
Al, corrosion resistant pure metal, passivity and pitting in chloride solutions 78−44258
Al pitting corrosion in Cl solns., electrochemical exam. 79−20248
Al, pitting mechanism, obs. using Engell-Stolica potentiostatic method 80−25905
Al-brass tubes, passivation treatment for atmospheric corrosion protection during storage and transport 80−85079
Al-Si_3N_4-Si struct., surface energy bands under step function illumination 80−49840
Al-Zn-Mg-Cu, alloy 7075-T6, corrosion in halide solutions, exam. of anion dependency 78−60867
Al_2O_3, anodic, passified, inhibition of reaction with water 80−89390
Al_2O_3, film, CVD on Si, chem., phys. and elec. props. 77−12543
Al_2O_3 film, RF sputtered by planar magnetron, phys. props., appl. as dielec. passivation layer 77−43448
Al_2O_3 films for Si devices, surface and bulk elec. conduction obs. 77−43761
Cd, high purity, passivity breakdown 80−100947
Ce, gettering of H, mass spectrometry and microgravimetry study, rel. to HTGR gas purification 80−73374
Co, passivation, film form., stability and breakdown 78−19937
Co, passivation films in neutral and alkalescent borate soln., modulation spectroscopic anal. *(Japanese)* 80−108628
CoB and Co_2B, electrochem. behaviour in H_2SO_4 79−39030

passivation continued
Cr, corrosion resistant pure metal, passivity and pitting in chloride solutions 78−44258
Cr, passivation, film form., stability and breakdown 78−19937
Cu anode, passivating behaviour and illum. effects in alkaline soln. 80−104449
Cu, corrosion inhibitive films formed by corrosion determination of thickness by X-ray photoelectron spectra 79−15845
Cu, passivation using protective glassy layers at 500°C 80−3246
Cu, protective glassy layers at 500°C 78−76785
Cu-Hg, dil., pool electrodes, passivation in alkaline soln. 79−70214
Cu-Ni alloys 706 and 715, corrosion in flowing sea water, dissolved sulfide effect 80−35379
Fe and Fe alloys, passive films studied using AES combined with ion sputtering technique 80−35378
Fe and oxides, passivity, electrochem. exam. *(Japanese)* 78−39946
Fe, anodic behaviour, in acidic solns. of liq. NH_3 78−27671
Fe, anodic behaviour in 1M H_2SO_4, influence of straining 80−97612
Fe, Armco, SCC in phosphate soln. 79−96184
Fe, corrosion and passivation in presence of halide ions in aq. solns. 80−50758
Fe, corrosion and passivation in LiCl soln., peripheral velocity effect 80−61000
Fe, dissolution and passivation, effect of phosphate and chromate corrosion inhibitors 80−21152
Fe, dissolution and passivation kinetics in solns. containing O 80−76547
Fe dissolution kinetics, and passivation depend. on temp. and ionic strength 80−97626
Fe, in H_2HO_4, model for anodic dissolution 80−35545
Fe, inhibition in Na_2SO_4 soln. containing aliphatic acids, electrochemical and ellipsometric study 79−74309
Fe, mechanism of action of weak acids and their salts on passivation by O_2 80−50886
Fe, oxide and benzoic acid film exam. by X-ray photoemission spectroscopy 78−88561
Fe, passivated, Fe_3O_4-Fe_2O_3 thin film, electron diffr. study *(German, English)* 80−89418
Fe, passivation, film form., stability and breakdown 78−19937
Fe, passive, interfacial impedance *(Japanese)* 77−48581
Fe, passive, semicond. model for oxide film 80−2493
Fe passive film AC electroreflectance and impedance obs. 78−7093
Fe, passive film form. in phosphate soln., intensity-following ellipsometry study 80−104345
Fe, passive films and phosphate layers, sputtering rate evaluation in glow discharge lamp 80−45443
Fe, passivity in aq. soln., correlation with mol. struct. 80−16541
Fe, passivity in aqueous soln., correlation with molecular struct., electrostatic hypothesis 79−91831
Fe powder, passivating oxide layer comp. 78−31558
Fe, pure, Auger anal. of passive films in neutral aqu. soln. 80−16605
Fe, pure, corrosion behaviour, effect of Ta ion implantation 78−31559
Fe, pure, surface oxide effect on acid corrosion inhibition 78−11384
Fe pyrophoric powders, stabilising layer form. during passivation, saturation moment meas. 80−44865
Fe, semicond. props. of anodic film 77−36003
Fe surface, nitride layer formation, activated surface, passivation 80−16577
Fe-Cr, grain-boundary segregation of carbon, electrochemical study 79−100147
Fe-Cr, passivity in H_2SO_4, XPS study 78−44256
Fe-Cr (25wt.%) alloy, surface comp. rel. to passivation phenomena *(French)* 79−43479
Fe-Cr (5 to 30 wt.%), transpassive behaviour in acidic sulphate soln. 78−15565
Fe-Cr alloys, feasibility of electrochem. corrosion protection 79−70220
Fe-Cr alloys, in acid and neutral solns., thickness and optical constants of passive and transpassive films 80−66698
Fe-Cr alloys, $NaClO_3$ and NaCl effects on corrosion behaviour in hot NaOH soln. *(Japanese)* 80−35407
Fe-Cr alloys, passivation films, modulation spectroscopy study 80−3244
Fe-Cr-Ni, corrosion behaviour in hot conc. NaOH soln. *(Japanese)* 80−85082
Fe-Cr-Ni (25, 20 wt.%), single crystal, stress corrosion cracking 78−35553
Fe-Cr-Pd, Pd alloying effects on passivation 80−35373
Fe-Cr(-Mo), passivated single crystal, selective dissolution and surface enrichment 80−16543
Fe-Mo (0 to 6 wt.%), in chloride solns., role of Mo as localised corrosion inhibitor 79−20255
Fe-Mo (5 wt.%), Auger anal. of passive films in neutral aqu. soln. 80−16605
Fe-Mo alloys, pitting 80−16549
Fe-Mo-P-C, amorphous, XPS study of passivity 79−96185
Fe-Ni martensite, TEM of passivity layer 77−36689
Fe-Ni-Cr coating, electrodeposited, exam. of passivity 78−80655
Fe-Ni-Cr-P-B amorphous alloy, localized corrosion 80−16559
Fe+H_2O, clean surface oxidation and passivation by H_2O vap., XPS 77−81424
$Ga_{0.64}Al_{0.36}As$, plasma grown oxide, phys. and elec. props. 78−48550
$Ga_{1-x}Al_xAs$ junction-up TJS laser electron injection efficiency improvement 80−48300
$Ga_xAl_{1-x}P$ high-temp. solar cell with 0.3 eV band gap 80−21400
GaAs anodic oxide, refr. index meas., Sellmeier eqn. 77−12454
GaAs anodisation, ellipsometric study *(Japanese)* 80−97610
GaAs, film, selective anodisation, grain boundary edge passivation 79−11711
GaAs homojunction solar cells, large-grained, passivation method to improve open-circuit voltage 80−94070
GaAs MESFET, possible use of anodic Al_2O_3 for passivation, elec. props. of GaAs-Al_2O_3 interface 80−49934
GaAs MIS structs., nitride-based passivation for reduced surface state density 80−16537
GaAs oxide, passivated layers, quantitative in-depth profile, AES-SIMS thermal, anodic and plasma oxidations 78−84087
GaAs p-n junction, surface recomb. current reduction with $Al_{0.5}Ga_{0.5}As$:O surface layer 80−49878
GaAs passivated and unpassivated surfaces, heat treatment effects 79−73383
GaAs Schottky barrier solar cells with grain boundary edge passivation 79−83592

passivation continued
GaAs solar cell, polycryst., grain boundary passivation by oxidation, AES, SIMS and XPS obs. 80−81467
GaAs, surface, electron struct. and Fermi level pinning by O_2 and metals 80−11066
GaAs surface passivation by GaO_xN_y films and multilayer systems 80−11809
GaAs, surface passivation using composite Al_2O_3 and native oxide, MIS characts. 80−93004
GaAs, surface passivation using Si_3N_4, interface characts. 80−93005
GaAs, surface passivation using GaO_xN_y based multiple insulating layers 80−93006
GaAs thin film polycrystalline solar cells, props. and prep. 80−81437
GaAs thin film polycrystalline Schottky barrier solar cells, grain boundary chemistry 80−94067
GaAs thin film polycrystalline solar cells, grain boundary edge passivated 80−94069
GaAs(110), surface and interface states, effects of chemisorption, oxidation and passivation 77−85284
GaSb, surface, electron struct. and Fermi level pinning by O_2 and metals 80−11066
$Gd_2(MoO_4)_3$, passivation of c surface against attack by HF by inert ion beam irradiation 78−35545
$Gd_2(MoO_4)_3$, surface passivation by He ion irrad., domain struct. obs. 78−84544
Ge film, elec. resist., long term stability rel. to ambient atmosphere changes 78−2597
InP, surface, electron struct. and Fermi level pinning by O_2 and metals 80−11066
InP, surface passivation using composite Al_2O_3 and native oxide, MIS characts. 80−93004
InP-InGaAsP p-n junction avalanche photodiodes, surface passivation techniques 80−100508
$In_{2-x}Sn_xO_{3-y}$-poly Si SIS solar cells 80−97787
Li, corrosion in alkaline soln. 77−73367
Li electrode, passivation layer, in $LiClO_4$-propylene carbonate solution, composition *(French)* 80−11899
Mo, electrochemical behaviour in alcoholic KOH soln. 79−87762
Mo electrolytic dissolution at high anodic potentials, surface quality *(Russian)* 79−39025
Mo film, CVD, passivating against IR reflectance losses caused by oxidation 79−3758
Mo fine tip cathode, field emission stability, rel. to passivation 80−100760
Mo_2C, corrosion and electrochem. props. in aq. H_2SO_4, HCl, HNO_3 and KOH solns. 80−11813
Nb, corrosion resistant pure metal, passivity and pitting in chloride solutions 78−44258
Ni (100) and(110) surface, effect of depassivation on state of activation 79−61777
Ni alloys, anodic charact. meas. by AC impedance method *(Japanese)* 79−70224
Ni, anodic oxidation kinetics, electrochem. props. 79−15861
Ni, anodic passive film form. in NaOH soln., refl. and ellipsometric study 80−104447
Ni, corrosion and passivation in phosphate soln., pH depend., ellipsometric study 80−104448
Ni, dissolution and passivation in acid medium, effect of S in solid solution *(French)* 78−64771
Ni, dissolution and passivation, role of adsorbed S 79−66340
Ni, dissolution and passivation in acid environment, effect of P *(French)* 80−45440
Ni electrodeposition cathode polarisation, influence of unsaturated sulphates *(Russian)* 79−91963
Ni electrodeposition from alkaline citrate electrolytes, Ni/electrolyte interaction *(Russian)* 79−11796
Ni, passivation, film form., stability and breakdown 78−19937
Ni passivation, S influence study by Auger and electron spectroscopy 80−65347
Ni, passive film, XPS study 79−100469
Ni-Cr, anodic dissoln. in NaCl solns. at high current densities *(Russian)* 80−76396
Ni-Cr-Co-Mo, long-term corrosion stability rel. to use in joint endoprostheses 78−36059
Ni-Pd, anodic behaviour, potentiodynamic current density and impedance potential meas. *(German)* 80−25925
Ni-S, dissolution and passivation, role of adsorbed S 79−66340
Ni-Sn alloys, oxidation, AES obs. 77−48575
P_2O_5-SiO_2 glass film, thickness and IR spectrum changes on heat treatment in H_2 80−70549
Pb, aq. corrosion film, IR and Raman spectroscopy 80−55567
Pb, passivation in H_2SO_4 soln. 78−76871
PbO_2, plate of Pb-acid battery, thermopassivation 80−3507
$Pb_{1-x}Sn_xTe$ IR detector, leakage currents, surface passivation by Te layer 77−20402
PbTe, electrochemical surface reactions 80−76389
PbTe surfaces, Te coating, struct. and junction characts. 80−50743
Pt electrode, in Na_2SO_4-NaCl melt, polarisation meas., reactions 78−68898
Pt, preanodised or passivated, DTA, Pt-O system 77−16733
RuO_2 anodic coating on Ti, struct., electrochem. props. *(French)* 79−83385
Si p-n junction, passivation by slightly conductive chalcogenide film 78−2556
Si p-n junction, passivation by amorphous Si:H layer 79−47155
n-Si, passivation, photoactivation kinetics in conc. alkali, ellipsometric investig. 77−1885
p-Si, photopassivation kinetics in alkali soln., spectral depend. 77−1886
Si, point defects, H passivation 80−75515
Si, polycrystalline, passivation of grain boundaries 79−56158
Si solar cells, surface passivation by SnO_x films, effect on cell transport props. and short circuit current 80−61360
Si, thermal oxidation kinetics in O_2/HCl mixture, rate consts. 77−59953
Si:O, evaporated amorphous film, effect of O_2 on props., ESR spectra 80−11265
Si:O, polycrystalline layer on Si p-n junction, charge transport and passivation 79−38206
Si-N, passivation layer, density comp., and ref. index, Lorentz-Lorenz correl. 78−39697
Si-N films, reactive plasma deposited for MOS-LSI passivation 78−56584

passivation continued
Si-$NaNO_3$ aq. soln., anodic polarisation of semicond. electrode 77−11999
Si-SiO_2 interface charge effects and related props. 78−10575
SiN_x films, plasma enhanced CVD, props., meas. and interpretations 80−80987
SiN_x films plasma deposition, process and props. 80−80986
Si_3N_4 amorphous film deposition by high rate DC reactive sputtering, passivation appl. 80−100784
Si_3N_4 CVD for thin film passive components fabrication for high temp. instrumentation 80−40266
Si_3N_4 film, high temp. annealing effect on struct. and comp. 77−15714
Si_3N_4 film, plasma-activated *(Japanese)* 80−85073
Si_3N_4 film formation by $^{14}N_2^+$ ion implantation into Si 79−99455
Si_3N_4 films for Si devices, surface and bulk elec. conduction obs. 77−43761
Si_3N_4, low temp. deposition using microwave-excited active N_2 78−84718
Si_3N_4 off-stoichiometric plasma-deposited layer, AES evaluation of comp. 78−26781
Si_3N_4 planar plasma deposition system, productivity increase for semiconductor device manufacture 80−40269
Si_3N_4:H, amorphous, ion induced H transfer from N to Si, band passivation, elec. props. 78−47439
SiO_2 layers, deposition by plasma decomp. in planar reactor 78−88430
SiO_2 MOS structure, Cl role in passivation 79−91150
SiO_2 thin films, mobile Na ion passivation in HCl oxides 79−70187
SiO_2-PSG-Si_3N_4 composite layer, on Si, crack occurrence, PSG film thickness and comp. effects 77−72806
SiO_x, grown in HCl/O_2 ambients, phase separation and Na passivation 80−3219
SiO_x, SIPOS, O determ. using differential thickness meas. 79−28228
Si_2Te_3, passivated single cryst., elec. conductivity 78−95299
Sn, anodic behaviour in neutral phosphate soln. 79−96187
Sn electrodes, potentiostatic polarisation in NaOH soln., XPS 77−90608
Sn mixed oxide film formation and meas. 77−77622
Sn plate, lacquer adhesions of passivation films, adhesion, ESCA exam. of constitution and effects 80−40776
Sn plate, passivated by cathodic dichromate treatment, nature of Cr 77−56139
Sn-Ni, electroplated, passive layer, ESCA study 78−23867
Sn-plate passivation films, TEM struct. obs. 80−45416
Ta, corrosion resistant pure metal, passivity and pitting in chloride solutions 78−44258
Ti anode, Pt-Ir coated, corrosion and passivation behaviour in Cu electrowinning appl. 80−55573
Ti, anodic behaviour, steady-state, in conc. HCl 80−45515
Ti, anodic oxidation kinetics, electrochem. props. 79−15861
Ti, corrosion resistant pure metal, passivity and pitting in chloride solutions 78−44258
Ti, gettering of H, mass spectrometry and microgravimetry study, rel. to HTGR gas purification 80−73374
Ti in acidic chloride solns., anodic dissolution and passivation 80−35541
Ti, passive oxide layer form. in H_2SO_4, ageing with and without photoexcitation *(French)* 80−45432
Ti, repassivation and pitting corrosion 80−30143
α-Ti sheet, texture dependent stress corrosion cracking in Br_2-methanol soln. 80−71803
Ti-Al-V, long-term corrosion stability rel. to use in joint endoprostheses 78−36059
Ti-Al-V (6, 4 wt.%), repassivation and pitting corrosion 80−30143
Ti-Ni, anodic oxidation kinetics, electrochem. props. 79−15861
W fine tip cathode, field emission stability, rel. to passivation 80−100760
Zn alloys, anodic corrosion in seawater 77−77628
Zn, by polythioglycolate 79−70217
Zn, passive film formation in borate buffer polarisation curves, from Mossbauer studies 79−61778
Zr, corrosion resistant pure metal, passivity and pitting in chloride solutions 78−44258
Zr, gettering of H, mass spectrometry and microgravimetry study, rel. to HTGR gas purification 80−73374

passive attenuators *see attenuators*

passive circuits *see passive networks*

passive filters
220 MHz acoustic bulk wave resonator and filter realisation 78−59245
400 MHz SAW timing filter for optical fibre transmission 79−50415
acoustic filters with open end, finite element prediction of transmission characts. 80−33349
adaptive, based on SAW monolithic storage correlator 78−87208
bandpass filters, technique, construction, appl. *(German)* 79−50544
ceramic SAW filter development and applications 79−23156
elastic surface waves propag., characts. for SAW filters, book contrib. 80−1378
electrode-withdrawal weighted SAW filters, suboptimization 79−27471
laser pulse autocorrelation by optical processing of Fabry-Perot spectrograms 80−58465
magnetostatic wave transversal filters, status report 80−28394
matched filters, using optical delay line provide encoding or decoding structures 78−74983
plasma line filter bank and high-speed correlator appl. to plasma line meas. at Chatanika 80−98507
programmable transversal filtering using baseband compatible SAW processors 79−98548
radiometric flaw-detector, performance evaluation and parameter choice for smoothing filter 79−15945
SAW, appls. in TV systems *(Italian)* 79−81642
SAW, band-pass, transversal, principle, design and performance 78−38147
SAW, bulk waves anal. 79−7259
SAW, compensation technique using multistrip couplers 77−75750
SAW, design and expt. results *(Czech)* 80−19201
SAW, developments for high frequencies 78−51010
SAW, fundamentals of design, interdigital transducer circuit model, book contrib. 79−50520
SAW, L-band low loss filter 80−74673
SAW, mathematical design model *(French)* 77−68331
SAW, method for accurately adjusting the centre freq. 79−32155
SAW, narrow band transversal types and interdigital transducers, review 80−28395

passive filters continued
SAW, physical props. and communication signals processing applications and devices 80−38162
SAW, signal sorting, identification in communications receivers, military appl. 79−18615
SAW, synthesis, limitations of phys. model in terms of number of fingers and material consts. 80−28399
SAW, UHF, using unidirectional interdigital transducers 79−32170
SAW, with three-transducer configuration 80−74610
SAW, Y-Z $LiNbO_3$, filamentary defects visualisation at wafer inspection stage 80−75315
SAW, Y-Z $LiNbO_3$ filamentary defects, acoustic effects 80−75314
SAW bandpass, two-port model 77−62117
SAW bandpass filter design, use of charge distribution model 80−74678
SAW bandpass filters, TV receiver appls. 78−51008
SAW Butterworth contiguous filters, design, fabrication and testing, 248.8 to 401.2 MHz 79−68493
SAW chirp, spectrum analyser appl. *(Japanese)* 80−79065
SAW chirp filter FFT processor 78−87209
SAW chirp filters based Fourier transformation processors 79−7270
SAW compensated filter used in wide spread MSK waveform generator 80−74670
SAW components review for signal processing equipment *(French)* 78−51013
SAW delay line, for GHz SAW oscillators, fabrication and performance 79−14185
SAW delay line filters, wideband, low insertion loss, VHF band 80−28398
SAW filter appls. in consumer electronics, review 80−74675
SAW filter design, low-sidelobe cascaded 80−74679
SAW filter design and implementation, book contrib. 80−1394
SAW filter design applied to group-delay equaliser in TV rebroadcast transmitters 80−74676
SAW filter design for TV, CATV and radar appls. 80−53579
SAW filter design using linear programming technique 79−32154
SAW filter design using optimisation technique 80−74671
SAW filter design with diffraction compensation 80−74672
SAW filter interdigital transducers, manufacturing inaccuracies influence on transmission characts. 79−10434
SAW filter technological advances 78−46862
SAW filters, design, construction, appl., book 80−1393
SAW filters, electrode-withdrawal weighted method for reducing side-lobes 80−5875
SAW filters, low insertion loss, using multiphased unidirectional transducers 80−28397
SAW filters, low insertion loss *(Japanese)* 79−72772
SAW filters, narrow pass-band, for transmission system appls. 79−50517
SAW filters, props. and appls. *(Japanese)* 79−18644
SAW filters, resonator, scattering analysis and design 79−68492
SAW filters with asymmetric amplitude-freq. response, synthesis *(Russian)* 79−68521
SAW GHz quartz transversal filters, fabrication limits and characteristics 80−43562
SAW grating-resonator filter, behaviour of unidirectional transducers 80−5877
SAW IDT filter with thre inclined tapered transducers 79−81637
SAW interdigital transducer, inverse phase, suppression of direct transmission in resonator filters *(Chinese)* 78−79181
SAW metallic gratings, equivalent circuit of step discontinuity, rel. to SAW devices 80−33389
SAW miniature filters, introduction 79−55282
SAW narrow pass band, transmission systems appl. *(Japanese)* 78−90602
SAW narrow pass band frequency stability study *(Japanese)* 78−90603
SAW reflective-array-compression filters, nonsynchronous scatt. loss 78−71246
SAW resonator filters, improved temp. stability using multiple coupling paths 80−19175
SAW resonator filters 79−55283
SAW resonator filters using tapered gratings 78−87224
SAW resonator for radio receiver 79−7271
SAW resonators using interdigital transducers, narrow band filters appl. *(Japanese)* 79−27478
SAW thin film filters *(Japanese)* 77−73116
SAW transversal, interdigital transducer models for accurate design implementation 80−28396
SAW transversal filters, status report 80−28394
SAW transversal filters, synthesis using interdigital transducer models 80−5897
SAW TV IF filter, temp. stable ZnO/Pyrex glass substrate 80−43566
shallow bulk acoustic wave delay line filters, narrowband and wideband implementations 80−28400
surface skimming bulk wave bandpass filters using Y-rotated quartz 80−74583
switchable SAW filter banks at UHF 79−41533
synchronous filter for signal shape reconstruction from derivative 77−37870
synchrotron, passive filter for annular electromagnet 78−5074
unidirectional transducers, group type, tuning method 79−68535
$LiNbO_3$ 400 MHz saw filters 79−23158
$LiNbO_3$ UHF SAW filters using group-type unidirectional interdigital transducers 78−59252
$PbTiO_3$-$PbZrO_3$-$In(Li_{3/5}W_{2/5})O_3$, piezoelec. ceramic characteris. for surface wave filters 78−95215
Si voltage stabilisers, power diodes, stabilisation precision measuring ccts. 77−53940
ZnO thin film SAW filters 79−23157

passive networks
see also passive filters
notch circuit for pulsed-off fusion power compression fields 77−23266
testing, microcomputer controlled admittance bridge 77−18037

patents *see industrial property*

patient care
anaesthesiology, characts. of elec. currents 80−46093
arrhythmia monitoring systems evaluation criteria 78−11765
baby incubator design for Ghanian manufacture and use 77−40900
bioelectronics symposium, Ahmedabad, India, (Dec 1975) 77−40808
breathing ratemeter for neonatal intensive care 80−41311
burn wound covering based on AN-DMAEMA, design and evaluation 78−44676

patient care continued
cancer, appls. of EPR and NMR, review 78−69173
cancer management, potential impact of particle radiation therapy 79−20620
cardiac output estimation from aortic pressure curves, simulation model 79−53177
cardiac surgical patient postoperative computerised meas., analysis, and treatment 78−36044
cardiovascular emergency clinical assessment, use of ECG telemetry 78−44677
catheter, conductive, reduced risk of cardiac fibrillation 78−35972
clinical engineering and health care in nonaffluent underdeveloped nations 78−80991
computed tomography, cost of technically improved diagnostic images 80−17084
computerised intensive care, postoperative management of cardiac surgical patients 77−40918
coronary care unit emergency cardiac pacing experience 77−81651
coronary care unit interactive ECG monitoring 78−7481
coronary intensive care unit, computerised monitoring system 77−21656
critical care fluid balance monitoring 79−25151
critical care unit instrumentation care and servicing, book 78−69231
ECG electrical shock hazards, reduction using opto-electronic appls. 79−44016
ECG telemetry system Telecare *(Spanish)* 77−9296
ECG three-dimensional recording technique 80−41274
echolocating blind mobility aid, interpretation of stereophonic output 80−108989
electrical safety in crit. care areas using isolated patient environment 77−40914
electronic communications systems and biomedical equipment, maintenance programme 79−5385
electronic meas. application areas 78−57094
haemodynamic data processing in intensive care unit *(French)* 77−40903
health care expansion aided by integrated electronics 78−11751
heart rate control device, appl. for cardiac rehabilitation 79−83995
implanted pacemaker parameter assessment system 78−11778
incubator, portable, with radiant heating system and fine O_2 control 77−56511
incubators, portable, improvements 78−81055
instrumentation for ill new born infants 77−32963
intensive care, instrumentation and control, conf., London, England (May 1979) 79−70702
intensive care instrumentation, book 77−17006
intensive care instrumentation 78−53559
intensive care unit, use and acceptance of automated monitoring systems 78−81057
intensive care unit ECG protection against defibrillator pulse 77−25586
intensive care unit/coronary care unit safety 78−69252
intensive care ventilator, microcomputer-controlled 80−51292
lung ventilation device for newborns, especially during incubation 79−100786
mechanical patient handling devices, problems, requirements 78−3667
mechanical respirator, ventilation failure detector cct. *(Spanish)* 77−52913
medical computing symposium, Toulouse (1977) 78−36003
microprocessor-based tilting bed for blood pressure control 80−26412
microwave and temperature effects on the murine ocular lens in-vitro 80−89798
mobile incubator transport for premature and newborn babies *(German)* 79−16336
myocardial imaging with time-modulated coded aperture, results with ^{201}Tl 79−92372
neonatal intensive care unit, surveillance aid *(French)* 77−44831
neonatological care, intensive therapeutical and monitoring system 79−100785
neurological intensive care facility requirements 79−92420
Northern Ontario interhospital telemedicine satellite link 77−56495
nuclear power reactor emergency medical assistance programmes 78−53532
obstetric computer system for intensive care of mother and foetus during labour *(German)* 80−3857
optometry, future of public and community health 80−12084
percutaneous elec. stimulation of nervous system for pain relief 78−3668
postoperative cardiac surgical patient care, automation of meas. and interventions 78−20310
postural training using visual presentation of centre of press. 77−56535
preoperative preparation for hypothermia, intercellular oedema due to reduced membrane efficiency 77−29225
prosthetic power supply requirements for disabled, survey 78−15929
pulmonary thromboembolism treatment and prophylaxis by percutaneous caval filter 77−48925
quality health care and cost containment, conf., Washington, USA (Mar.-Apr. 1978) 79−39333
radiation accident casualties, organisation and planning of medical aid *(French)* 78−53528
radiation accident casualty, organisational forms of medical care in German Democratic Republic 78−53529
rehabilitation medicine, potential research areas for biomedical engineering 77−40913
respirator, fully automatic or patient controlled, for intensive care and respiration ward appl. 77−81641
respirator based on jet-flow vortex-type components *(Russian)* 79−79683
respiratory assistance, mouldable infant face mask 77−52914
respiratory support system, portable, for vehicular patient transport 77−52917
rural area primary health care delivery, telecommunication aspects 78−57122
rural health care delivery system model 78−44633
rural telemedicine system planning, analysis 79−74785
safety design, probabilistic approach by appl. of Markov chains to n-element environments 77−37106
stress distribution meas. of patient sitting immobile, instrumented wheelchair 77−90930
switched audiovisual communications system, Picturephone, hospital appl. 79−74786
telecommunication technology in health service provision 79−74784
tissue breakdown prevention, material design criteria 78−31964

patient care continued
tissue stress state intensity measurement, infrared imaging, thermistors, pressure sore prevention appl. 77−48923
trauma indices 77−25588
trauma prognostic indices 77−25589
vascular laboratory instrum. management using computer 78−7460
vision research laboratory, clinically oriented, tasks and goals 80−12083
wheelchair cushion effect on skin temperature, heat flux, and relative humidity 79−83707
X-ray equipment selection for intensive care unit 79−92346
O_2 inhalation automatic control for patients with respiratory failure 80−17181
O_2-CO_2 transport real-time and interactive control in mechanically ventilated patients in ICU 79−62404

patient diagnosis
see also biomedical ultrasonics; electrocardiography; electroencephalography; medical diagnostic computing; radiography; radioisotope scanning and imaging; scanning radiography
2D images, 3D enhancement scheme 80−101255
abdominal and pelvic diagnosis, US and computed tomography evaluation 78−61228
abdominal diagnosis, combined, complementary appl. of echoscopy, echotomography and echography 80−21507
abdominal diseases diagnosis by computerised tomography 78−88739
abdominal fluid accumulation meas. using electric impedance 77−48912
abdominal foetal ECG and VCG recording/processing systems 78−31947
abdominal ultrasonography, clinical appl. 80−30826
acoustic diagnostic technique for prosthetic fixation evaluation 80−21510
acoustic holographic in medicine and biology, state of art and future 80−67175
acoustic holography appls. 77−81545
acoustic microscopy, tissue characterisation 77−64123
acoustic microscopy of excised tissue 80−17041
acupuncture diagnostic system *(French)* 79−62397
adenocarcinoma cell clump feature extraction methods in automated uterine cancer cytology *(Japanese)* 80−72362
amblyopia, interocular comparison of eye movements while reading 78−53393
amblyopia, speedy evoked pt. methods for vision assessment 80−61661
ametropia determination with laser refractor 78−35907
amniotic fluid, human proton relax. times in low field range, appl. to nucl. magnetography *(French)* 78−3574
aneurysm detection using bioacoustic signal processing techniques 78−28120
aneurysm detection using one-bit correl. 80−17175
angiocinedensitometry, blood flow values in iliac artery, conscious humans 79−25022
angiographic information visualisation correl. with measured system MTFs 78−73230
angiographic pelvis-leg programming, using test injection to determine contrast medium flow time 77−70523
angiography, effects of asymm. focal spots 77−21617
angiography, standardised general and cerebral under automatic exposure control 78−24121
angiography, validity of computer simulation of blood vessel imaging 78−3594
angiography, visual perception limits 78−85313
angiography visual perception limits 78−73231
Angioskop multidirectional examination unit for advanced radiographic examinations 78−28039
angiotomography in the diagnosis of intracranial tumours 79−48333
annular array design and logarithmic processing 79−34615
aortic stiffness noninvasive determ. methodology, echocardiographic recording 79−83875
apexcardiogram, math. model of endogenous thoracic forces 78−31849
arrhythmia and conduction disturbance diagnosis from His bundle electrogram 79−44032
arrhythmia detection by RR-interval comparison *(Bulgarian)* 78−15919
arterial diagnosis, appl. of impedance plethysmography 77−56508
arterial insufficiency, clinical appl. of elec. impedance meas. 79−83878
arterial insufficiency detect. and quantification using impedance plethysmograph 78−31957
arterial stenoses, fluid mechanics 80−35948
arterial US scanner, colour coded differential velocity display 79−34617
atrial electrical activity evaluation, external method 79−44030
atrial electrogram monitoring for diagnosis of complex cardiac dysrhythmias 79−39567
atrial pacing stress test quantification, normal, abnormal values, coronary artery disease in man 78−85449
atrial septal defect assessment by echocardiography 79−70600
atrioventricular block natural history and diagnosis 77−81626
atrioventricular block prod. by ligation of septal arteries, His bundle electrogram, dog 77−81631
audiological diagnosis, use of click-evoked elec. brainstem responses 79−92237
audiological diagnosis, use of click-evoked elec. brainstem responses 80−104689
audiometers, principles, appls. and commercial models 78−44669
audiometric impedance meas. instrumentation 77−78005
audiometric tests, automatic operation using a programmable system, hardware *(Italian)* 77−5006
audiometry using cortical evoked response, use of portable programmable tape recorder 77−60279
audiosonology, noninvasive diagnostic possibilities of phonocephalography and phonomyelography 78−48920
auditory brain stem responses in patients with acoustic neuromas 79−92235
auscultation, portable clinical electronic device for simultaneous multiple auscultation 77−56507
auscultation instruments, evaluation of acoustic props. 77−81601
automated patient testing 80−46088
axial tomography, computerised, abdominal area appl. 77−44782
bacterial diagnostic machine and cybernetics *(French)* 77−9162
ballistocardiograms, statistical pattern recognition 80−26408
bibliography of diagnostic uses of US in medicine and biology 79−96641
bibliography of diagnostic uses of US in medicine and biology 80−62407
binocular oculomotor problems, phoria, vergence and fixation disparity 78−35835

patient diagnosis continued
biofeedback controlled parameter determ. circuits, Medicor diagnostic bag 79−100775
biofeedback diagnosis system, physiological parameter meas. considering psychic effects 79−100774
biological tissue samples, normal and diseased, elemental comp., PIXE anal. 79−5364
biomaterials for diagnostic instruments, ionising radiation processing 77−70542
biomedical electronics developments 77−13017
biomedical image acquisition and processing system design and implementation 77−37086
biomedical image processing fundamentals 79−25144
biomedical system control sensors 79−48380
biomedical US, bibliography 79−34619
bleeding disease diagnosis by US meas. of blood coagulation time 79−83870
blood cell anal., weighted chi-squared test 80−30925
blood cell electrophoretic mobility study, semi-automatic system 80−3851
blood cell high-speed analysis, computer software system 78−44671
blood cell smear pathology differentiation by optical transform method 78−69248
blood fat emboli detection by Doppler US flow meter digital signal processing 77−25525
blood flow echography using Doppler techniques *(French)* 80−26303
blood gas and acid-base calculations, electronic data computing 79−25139
blood indicator dye microconcentration meas. instrument 79−39565
blood stream meas., use of US probes and Doppler technique *(German)* 79−2113
blood velocity meas., US Doppler velocimetry, experimental appls. *(French)* 79−34610
blood viscosity-temperature relationship, human plasma and serum 79−20564
body surface potential distribution map recording and processing 78−57116
bone acoustic emission diagnosis, soft tissue effects 79−48362
bone biopsies, undecalcified human bone prep. for electron microscopic investigation 78−20332
bone disease, US surface wave vel. rel. to mech. props. 77−32937
bone diseases, pot. use of stimulated positron emission in detect. and monitoring 80−81712
bone elemental analysis by prompt γ-ray spectra due to ^{252}Cf neutron irrad. 80−17065
bone fracture healing, sonic diagnosis 77−21580
bone in vivo properties determ., effect of soft tissue on wave propag. and vibr. tests 78−3660
bone mineral concentration estimation by beta-ray backscatt. *(German)* 78−69179
bone stress wave detection using piezoelec. effect, non-invasive technique 78−31948
brachial plexus neuropathies of the upper trunk, EMG F-wave electrodiagnostic confirmation 79−74779
Bragg diffraction scanner for ultrasonic tissue characterisation in vivo 77−77949
Bragg imaging in the reflection mode and designs for improved optics 80−17040
brain, clinical efficacy and cost anal. of cranial computed tomography and radionuclide brain scan 77−77974
brain, complementary role of computerised axial transmission tomography and radionuclide imaging 77−77975
brain, human, neural generator localisation underlying auditory evoked mag. fields 80−104703
brain impedance scanner principles and exptl. results 79−57804
brain stem electric response audiometry and middle ear effusion 80−56151
brain stem transmission time and auditory nerve response 80−45917
breast cancer connective tissue content correl. with US attenuation 80−45997
breast cancer screening by thermography, progress and prospects 77−48915
breast carcinoma detect. by US Doppler signals 80−8110
breast carcinoma imaging with line scanning NMR technique 79−48314
breast disease, importance and limitations of thermography in diagnosis and treatment *(French)* 78−7419
breast echography, possibilities, results and indications *(French)* 78−7408
breast examination by radiography, thermography and US, reviews *(French)* 78−7472
breast examination methods including radiography, thermography and cytology, review 78−3656
breast malignant tumour, freq. depend. US attenuation, fast Fourier transform technique 80−45996
breast pathology, liq. cryst. thermography *(French)* 78−7420
breast radiography, foreign body diagnosis *(French)* 78−7432
breast radiography with Mammomat, skin exposure and absorbed dose 78−73245
breast thermography, use of liq. cryst. sheets 80−41166
breast thermography vein-finding algorithm 78−40393
breast tissue characterisation in vivo by US TOF computed tomography 80−51186
breast tumour detection by US Doppler blood-flow signals 80−46001
breath volume and time components, computer aided meas. using magnetometers 79−16332
broadband US tomography 80−26311
bulk element lack, assess. by neutron activation anal. using anthropomorphic phantom 79−39497
cancer, appls. of EPR and NMR, review 78−69173
cancer, microscopic cell images classification by feature extraction 79−88225
cancer, microwave techniques for diagnosis 80−26320
cancer cell image segmentation using multispectral information 79−88224
cancer detection and therapy, stochastic anal. and control of physiological systems 77−90713
cancer detection by microwave thermography 78−24172
cancer detection by NMR, behaviour of different nuclear probes 79−62326
cancer detection by NMR in living animal 77−44736
cancer detection by optical meas. of cell-surface changes 79−79703

patient diagnosis continued
cancer prescreening, automated cell image analysing system *(German)* 79−83892
cancer thermographic diagnosis enhancement by US irradiation 79−79614
canine teeth localisation using X-ray equipment STATUS X 77−90881
cardiac acoustic model for computer-aided surface acceleration mapping 78−35791
cardiac arrhythmia, cerebral echo-pulsation curves and plethysmograms comparison 78−7413
cardiac arrhythmia, pill electrode, computerised system 79−39566
cardiac arrhythmia classification using R-R interval and difference histograms 77−40843
cardiac arrhythmias diagnosis, online real-time pattern recognition *(Italian)* 78−85439
cardiac biopotential distribution laws rel. to functional state 78−65142
cardiac catheterisation, automated processing and storage system 79−70694
cardiac catheterisation computer system 79−70695
cardiac catheterization laboratory sensitometric system application and clinical evaluation 78−20263
cardiac contraction kinetics recording method 79−12025
cardiac diagnosis, analysis of signals from pulsating arteries 77−48831
cardiac disorders mean electrical axis tracing on CRT, electronic technique, teaching aid 77−13022
cardiac energy density function encompassing elastic and contractile props. 79−62279
cardiac function, reliability of noninvasive methods for meas. during exercise 79−16231
cardiac pacing as diagnostic tool 77−81629
cardiac response sensitivity to time relationship between vibr. and cardiac cycles 77−56407
cardiac sound and vibration recording, electro-optical sensor 77−21648
cardiograms, image processing, cardiac function meas. *(Japanese)* 80−94354
cardiology, appl. of US in echography and bioecholocation, progress and prospects 80−21509
cardiology, pulsed Doppler velocimetry, clinical appls. 80−46003
cardiology, US real time system for simultaneous image displays 80−41148
cardiotocography, Partecust equipment, effect of technical recording conditions 77−44783
cardiovascular diagnosis, digital full range Doppler vel. flowmeter 78−88731
cardiovascular dynamics instrumentation evolution (1940-80) 79−83983
carotid angiography, eye shield 78−44615
carotid arterial disease evaluation using noninvasive photoplethysmography 78−40390
carotid arteriography real-time US imaging system 78−24108
carotid artery disease, blood velocity analysis during pulsed Doopler US imaging 77−29189
carotid artery disease, US detection techniques 79−11989
carotid artery occlusive disease detection, by supraorbital photoplethysmography 77−40731
carotid bifurcation scanner, differential velocity display with colour coding 77−21588
carotid bifurcation tomographic scanner, US Doppler colour coded vel. display 77−25529
carotid obstruction detect. by supraorbital opacity pulses 80−51200
carotid-vertebral circulation exam. by variable range-gated directional Doppler technique 77−29188
carpal tunnel syndrome, palmar conduction time of median and ulnar nerves 80−12075
cartilage generated noise, computer-aided acoustical correl. 78−40391
cell analysis, feature extraction for medical image analysis, cervical cancer early recognition *(German)* 79−5393
cell classification multistage systems, stochastic models 78−77143
cell type recognition by multiangle laser beam scattering flow system 77−21595
cellular identification of free cells by light microscopy and SEM 78−53589
cerebral angiography, brain O_2 tension response, using animal model 77−52872
cerebral angiography, cortical pO_2 and K^+ dynamics rel. to contrast agent neurotoxicity 78−35954
cerebral angiography, evaluation of Contrac injector 78−40293
cerebral angiography in stereoscopic magnification *(Japanese)* 77−73574
cerebral angiography routine enlargement system, Poly Diagnost N 77−86602
cerebral blood flow estimation in newborn infant, noninvasive technique 77−90949
cerebral palsied children, film projection system for eye movement monitoring 79−16329
cerebral regional blood flow meas. by ^{133}Xe inhalation, anal. method comparison 78−44604
cerebral vascular disease, experience with radionuclide imaging and computed tomography 77−77977
cervical cancer automatic cytoscreening, atypical cells classification 78−73289
cervical cancer detection, comparison of coherent optical transform processing systems 78−48922
cervical cytological sample screening, coherent optical processing, via Fourier transforms 78−36006
cervical cytological sample screening, coherent optical processing via Fourier transforms 78−36007
cervical cytological sample screening, coherent optical processing via Fourier transforms 78−36008
cervical smear screening with coherent optical processing 77−21653
chest photofluorograms, recognition of vessel shadows for automated meas. and classification 77−81566
chest radiograph optoelectronic processing for pulmonary venous hypertension detect. 79−74754
chest radiograph texture anal. model 78−40323
chest radiographs, algorithms for finding rib cage 77−44804
chest radiography, comparison of 350 kV and 120 kV techniques 78−73238
chest radiography screening for employees in nuclear industry 80−26342
chest tomography by gamma camera and external gamma source 78−61250
chest X-ray automated screening, texture anal. of lung fields 80−41228

patient diagnosis continued
chest X-ray images computer-aided anal. 78−40400
chest X-ray rib extraction algorithm for pneumoconiosis detect. 78−31904
cholangiography, intravenous, child obs. 79−62333
chromosome banding pattern technique, human, automatic classifying system 79−84062
chromosome classification system, banding technique 80−67320
chromosome classifying system based on banding technique 79−84060
chromosome-classification system based on banding technique 80−36199
chronic liver disease, ultrasonic detect. method 79−48295
chronic obstructive pulmonary disease detection, airway resistance model 79−96603
chronic splenic enlargement diagnosis by digital A-scan analysis 77−64110
cine-radiography in peripheral arteriography 78−24123
circulatory clinical model matching techniques 79−53176
circulatory diseases, absolute blood velocity meas., US Doppler method *(Japanese)* 79−43974
clinical applications of US techniques 79−79619
clinical laboratory technology, new developments, diagnostic immunology and microbiology 78−81037
clinical microwave focusing thermography 80−3771
clinical paediatric gait biotelemetry 78−3652
clinical perimetry, glossary of basic information *(Italian)* 79−39413
clinician and computer ECG diagnostic accuracy 78−7494
clonus, simplistic model rel. to diagnosis and therapy 77−48786
coal miner spirograms, feature selection appl. 78−40387
cold urticaria diagnosis and treatment assessment, stable low temp. source 78−61276
colonic diverticular disease population survey, patient X-ray dose 78−61259
Compton scatter imaging of transverse sections, corrections for multiple scatt. and attenuations 77−40742
computed axial tomography and nuclear medicine, scatter reduction 79−5368
computed tomography, electron density and at. no. determ. 77−81553
computed tomography, spectral artefact correction and determ. of electron density and at. no. 80−51231
computed tomography of liver, comparison with nucl. medicine scans 80−17109
computed tomography of liver and biliary tract 80−17108
computed tomography of thorax and abdomen, clinical study 80−17107
computer tomography, radionuclide imaging and ultrasonography in hepatic mass lesions 79−88211
computer-aided diagnosis of medical images, conf., Coronado, USA, (Nov. 1976) 77−78018
computer-aided tomography and US, conf., Haifa, Israel, (Aug. 78) 80−27035
computer-based instrument using SK.2 cylindrical coordinator *(Russian)* 80−76856
computer-processed ECG trends, conference, Amsterdam (1976) 78−7477
computerised axial tomography, for teaching 78−49619
computerised breast thermographic interpreter, comparison with human interpretation 77−81547
computerised fluoroscopy for non-invasive cardiovascular imaging 80−17121
computerised tomographic head unit, Siretom 2000, operation 78−28037
computerised tomographic scanner acceptance testing 77−73569
computerised tomographic scanner development for head and neck diagnosis *(Japanese)* 78−61277
computerised tomographic scanner image quality evaluation phantom 77−73573
computerised tomographic scanning, engineering status 77−73571
computerised tomographic scanning, reprocessing X-ray transmission data 77−73565
computerised tomography, body organ moulded picture representation 78−35951
computerised tomography, data processing of dual-energy scans 78−69215
computerised tomography, dynamic spatial reconstructor, high temporal resolution scanner 80−51235
computerised tomography, radiation protection requirements for patients and accompanying parent 77−70524
computerised tomography, rapid image reconstruction and examination speed of Somatom 78−92693
computerised tomography, reconstruction noise rel. to detectability 78−69213
computerised tomography, reconstruction simulation, no. of rays versus no. of views 78−69214
computerised tomography, Siretom 2000 initial clinical experience 78−28038
computerised tomography, Somatom fast whole body tomograph with direct image reproduction 78−28036
computerised tomography, X-ray, Rotate/Rotate type whole body scanner using direct magnification 80−21565
computerised tomography, X-ray photography appl. 78−44588
computerised tomography 77−48859
computerised tomography appl., X-ray, axial *(Spanish)* 79−20698
computerised tomography body scanners, comparison of translate-rotate, pure rotary types 78−69211
computerised tomography dosimetry, exposure meas. techniques 78−69212
computerised tomography equipment, for intracranial diagnosis 78−31884
computerised tomography image processing and evaluation using PDP-10 computer 78−44587
computerised tomography in pulmonary nodule diagnosis 80−17110
computerised tomography in urological diagnosis, possibilities and limitations *(German)* 78−85369
computerised tomography performance phantom optimisation 78−48892
computerised tomography scanner commissioning 77−73570
computerised tomography scanner resolution, geometrical limitations 78−73237
computerised tomography scanners, image noise and smoothing 78−85368
computerised tomography spectral artifact correction 78−35953
computerised tomography using video techniques 77−73568
computerised tomography with diverging X-ray beam, reconstruction algorithm 77−70535

patient diagnosis continued
computerised tomosynthesis serioscopy, and coded scan tomography, reconstruction 78−35920
computerised transverse axial tomography of brain, contrast 77−86608
computerised X-ray tomography, principles *(German)* 78−3601
computerised X-ray tomography, selective I imaging using K-edge energies 78−24131
computerized tomography with X-ray beams *(German)* 78−53480
contact lens wearer diagnostic testing 80−12312
coronary arteriography, current techniques and equipment 78−35940
coronary artery disease, abnormal left ventricular contraction pattern cineangiography 79−83930
coronary artery disease, early detect. by nonlinear anal. of ECG 80−26410
coronary artery disease, preclinical, detect. in male subjects using the omnigram 80−81767
coronary artery disease, serial VCG and ventriculogram sensitivity to infarct size 79−44044
coronary artery disease detection by exercise electrocardiograpy, measurements optimisation 78−11756
coronary heart disease screening, direct-writing ECG recorder ST segment distortion assessment *(German)* 77−90945
coronary lesions of left anterior descending artery, exercise ECG diagnosis 79−70692
Coulter electrical sizing principle, appl. to new multiparameter system 80−89911
craniofacial anomaly assessment, computerised versus conventional tomography 78−73239
critically ill patient monitoring by integrated computer systems 78−35998
CRT display documentation by photographic techniques 79−21827
cystic fibrosis, sweat Na meas. by elec. field, math. anal. of skin elec. field 77−73553
cystic fibrosis diagnosis by in situ sweat Na concentration meas. using elec. field 77−73554
cytogenetics, applications of photomicrography 80−21577
cytogenetics, automatic system 77−78021
cytological preparation evaluation, optical preliminary data reduction *(German)* 79−5392
cytological preparation image processing, filter construction *(German)* 78−36026
cytological preparations, optical real-time filtering *(German)* 78−36025
cytology, digital picture analysis 77−21650
cytology, quantitative optical microscope 77−60273
cytomorphological contour classification for mass cancer screening 79−79682
deafness, acoustic impedance of middle ear measurement 77−25460
deep venous thrombosis detection by plethysmography 77−40884
Delta Scan, computerised transverse tomographic equipment, entire body appl. 77−44781
demyelinating diseases, visual evoked response as a diagnostic tool 79−20538
dental drill with noise, vibr. radiointerference reduction 78−85450
dental radiography, phantom meas. of absorbed doses 77−81576
dental radiological safety, pilot survey 79−43993
dental X-ray tubes, improvements 78−65129
dermatology, photobiologic phenomena 78−35909
diazotype radiographic duplicating system as diagnostic aid 80−8137
dichotic listening as diagnostic tool, computerised dichotic tape generation 78−92740
differential energy absorpt. X-ray cassette, radiographic image contrast enhancement 78−20264
discography, diagnosis of posterior annulus fibrosus in the lumbar spine 79−53213
dynamic boundary surface detect. algorithm, appl. to X-ray tomography 77−78019
dynamic cardiac imagery, gross and segmental motion analysis 79−25093
dynamic clinical examinations under load, technical demands 77−81617
dynamically focused US diagnostic phased array 78−61232
dyslexia, detect. by computerised brain mapping 80−36185
ear impedance, interactions among tympanometric variables 78−27964
ear impedance, tympanometric asymmetry 78−27963
ECG, arrhythmia detection and classification, statistical approach 77−21644
ECG, automatic mass exams, computing device 77−81600
ECG, classification in terms of spectral characts. 80−56264
ECG, digital storage and analogue distortion 78−44674
ECG, exercise, automatic meas. of ST-segment response 78−77140
ECG, His bundle activity noninvasive recording 77−13023
ECG, microprocessor signal averaging for recording μV activity from cond. system of heart 77−44820
ECG, models solving direct and inverse problems, systems approach 78−28121
ECG analysis, microprocessor based system 78−73287
ECG analysis by remote computer, data terminal with voice indication, general practitioner use 77−81613
ECG analysis system oriented toward polarcardiology 78−85447
ECG body surface potential map estimation, limited lead selection 78−57111
ECG body surface potential mapping, improved diagnostic technique 80−26409
ECG body surface potential mapping, quantitative descriptors 77−44807
ECG computerised acquisition, compression, and retrieval 78−36019
ECG microcomputer-based evaluation system, improving diagnostic capabilities 78−88761
ECG P-wave recognition, using adaptive correlating filter *(Japanese)* 78−28119
ECG real-time contour anal. program using microprocessor system 78−73288
ECG recording system simplification *(Russian)* 78−40379
ECG signal shape parameter automatic meas. *(Russian)* 79−25134
ECG signals, diagnostical functions, effect of random noise *(Croatian)* 80−98169
ECG skin artifact reduction by skin puncture method 78−44672
ECG surface mapping recordings registered at rest and during exercise, diagnostic value 78−81044
ECG surface potential map reconstruction from limited no. of leads 78−57117
ECG transmission, 3-lead, over telephone network, central computer analysis appl. 77−86698
patient diagnosis continued
ECG U-wave correlation with repolarisation of Purkinje system 78−28122
ECG-VCG multivariate classification by linear regression, influence of populations 77−44789
ECG/VCG, rhythm diagnosis using statistical signal anal., identification of transient rhythms 78−77142
ECG/VCG rhythm diagnosis using statistical signal anal., identification of persistent rhythms 78−77141
echocardiogram, M-mode, automatic computer anal. *(Japanese)* 80−72274
echocardiogram Fourier analysis 78−28028
echocardiogram processing, microprocessor-based system 77−40726
echocardiographic, graphic representation of 2-dimens. structs. in motion 79−70597
echocardiographic tracking system, microprocessor-controlled 80−67169
echocardiography, 2D, transducer beam profile effects on tissue aperture detection 78−73185
echocardiography, safe method for acquiring morphological and functional data *(German)* 79−16261
echocardiography, US, picture processing of 2-dimens. data 77−77958
echocardiography appl. of pattern recognition 78−35898
echocardiology, book 77−64103
echocardiophone, CW swept freq. US echo location system 77−70514
echoencephalography, US pulsatile, prototype instrument and trial obs. *(Russian)* 80−17174
echoencephalography applied to brain stem tumours 77−70515
echographic diagnosis of lesions of the abdominal aorta and lymph nodes 80−17033
echography, real time, contrib. to diagnosis and management of palpable breast lumps 80−17027
echopyelographic visualisation of pacemaker induced contractility in calyceal structs. of human kidney 78−48850
echosonography, real-time, computer controlled bidirectional phasing 79−12023
echotomographic system, ultrafast, using optical processing of US signals 77−52855
EEG, children, 24 hr, 4 channel recording using miniature tape recorder and computer anal. 79−34697
EEG, computer display system, for brain lesion localisation *(Japanese)* 77−5100
EEG, detect. of intermittent transient patterns of brain elec. activity of unknown waveshape 78−31958
EEG, focal slow waves localisation 80−94406
EEG, magnetoencephalogram, current dipole model, central nervous system disease diagnosis applications 79−48238
EEG, multivariate pattern recognition technique, cerebral abnormality localisation 79−16327
EEG, simple computer-generated dot-density topogram 80−94407
EEG analysis methods and activation techniques *(Croatian)* 78−44666
EEG automated anal. as prognostic indicator in stroke 77−86699
EEG automatic analysis using adaptive segmentation of EEG records 77−25581
EEG data compression via computer-generated evoked response to sensory stimuli 78−36016
EEG discriminant function classification from renal patients, methods 78−28115
EEG features extraction by adaptive segmentation 77−44794
EEG montage standardisation, math. logic design 77−86685
EEG multichannel radiotelemetry for epileptogenic focus localisation 78−3653
EEG nonstationary point automatic detect. *(French)* 78−57112
EEG physiological data teletransmission system 77−86687
EEG signals with changing spectra, anal. using Kalman estimator 78−24167
EEG standard montages recommendation 77−86686
EEG technique, in diagnosis of subacute sclerosing panencephalitis 78−20301
effectiveness of clinical diagnostic methods, decision probability calc. *(Hungarian)* 78−65146
elastometer probe system for localised in vivo compliance meas. 78−31960
electric impedance computerised tomography, a new imaging technique 79−66500
electric impedance meas. using 4-terminal instrumentation system for oedema detect. 78−48853
electrical conductivity distributions imaging, systems limitation 80−89901
electrical diagnostic stimulator with insulated sources of power *(German)* 79−16324
electrical stimulation of organs and tissues in clinical medicine 78−35977
electro oculography, computerised diagnostic system 80−21566
electro-oculogram light-induced amplification, quantification in clinical practice 77−90771
electro-oculographic activity, computerised meas. during sleep 79−74781
electro-oculographic response, diagnostic tool for principal ocular disorders *(Italian)* 79−5391
electro-oculographic response interocular comparison, unpredictability of residual long-term effects 78−53392
electro-oculography, on-line system for quantitative study of ocular kinetics 79−34699
electro-optics appl., 1980 development trends 80−85464
electrobronchogram fringe effects 77−25542
electrocardiograms computer anal. 78−48917
electrocardiographs, portable, Phillips Cardiopan 531, clinical/electronic evaluation 78−11757
electrocardiological diagnostic efficiency improvement by cardiovascular system model dynamic optimisation 79−39569
electromechanical system for diagnosis of spinal abnormalities 78−73286
electromedical diagnosis and therapy techniques *(German)* 79−100687
electromyography, computerised, software support in clinical dentistry 79−74780
electromyography, diagnostic applications 77−44784
electron microscopic diagnosis using clinical pathology liver and kidney samples, computer assisted 80−85485
electron microscopy, wide-field, appls. in biology and medicine 77−56553
electronic diagnostic apparatus, input earth isolation 77−48905
electronic hygrometer, low inertia, no resistance to gas flow, diagnostics appls. *(French)* 77−70564

patient diagnosis continued
electronic linear-scanning US diagnostic equipment, high resolution 80−30813
electronic radiography, computerised, for early detect. of vacular disease 80−41226
electronics 1979 development trends, w.r.t Czechoslovak biomedical instrumentation *(Czech)* 79−70689
electrooculographic system for detect. of oculomotor abornormalities in neurological disorders 80−108888
electrophoretic mobility test, diagnosis of malignant tumours 79−79680
electroradiographic image laser readout 80−41225
electroradiography, image quality, charge transport random fluctuations influence 78−66015
electroradiography, phys. fundamentals *(German)* 78−73228
electroretinogram, photopic, freq. response characts. meas. with synchronous detect. 77−48796
electroretinogram signals computer anal. 79−8559
electrostatic X-ray imaging, book contrib. 80−36112
elementary particles from 1 GeV range accelerators, medicine appl. *(German)* 80−41210
EM methods for medical diagnosis, review 80−36063
EM strip transmission line energy coupler, for medical diagnostic appls. 80−17045
EMG, single pots., anal. by means of multivariate methods 80−98170
EMG, surface, digital simulation, spectral anal. 78−80863
EMG envelope spectral anal., Parkinson's disease diagnosis and treatment appl. 79−5390
EMG F response, radicular injury evaluation 80−3852
EMG of Vastus medialis for graded isometric torque tensions, power spectrum distrib. 78−44673
EMG potential sensing electrodes, types, selection criteria 77−90953
EMG quantitative analysis instrument 78−81041
EMI brain scanner, collimation effects on performance characts. 78−53484
EMI computerised tomography brain scanner, patient dose 78−28080
emission computed tomography, appls. of nuclear medicine, review, review *(Japanese)* 79−70610
endoscope for holographic diagnosis and laser therapy *(German)* 79−96645
endoscopic miniature camera with fibre-optic faceplate 80−77896
endoscopic retrograde cholangio-pancreaticography 77−73559
endoscopic roentgenography appliance users' experience 77−25544
endoscopy, rel. to double-contrast radiography in upper gastrointestinal tract haemorrhage 80−98063
engineering in medicine and biology, conf. Atlanta, USA (Oct. 1978) 79−39332
epilepsy diagnostics, EEG trace coding *(French)* 80−67277
epilepsy of late onset, visual and computer-assisted assessment 80−12294
epithelial tissue pattern recognition 79−25145
esophagogastroscope, flexible fibre optic instrument, experience of use of 79−34622
evaluation of diagnostic tests 80−17180
evoked potentials steady state, recording and appls., review 78−35823
evoked responses, peripheral versus foveal, multiple sclerosis early diagnosis appl. 80−67276
excised breast tumour US attenuation meas., 6 to 10 MHz 79−48311
exercise ECG automated anal., clinical experience 78−81050
exercise ECG computer-assisted anal., implementation and clinical anal. 78−81051
expected outcome loss for medical diagnosis and treatments evaluation 77−25587
eye, computer assisted examination, Refractor III system 79−29650
eye, human, holographic diagnosis 80−12209
eye, ophthalmological instrument design and construction 78−15918
eye continuous movement monitoring, proportional-integral adaptive system *(German)* 79−16320
eye fundus photographs, automatic assembly using blood vessel structure 79−83991
eye socket, X-ray computerised tomography for medical diagnosis *(German)* 79−100727
eye testing using screen image divider 78−57114
FET transducer, H^+, Ca^{++} and K^+-sensitive, features 78−28117
fibre optics in medicine, diagnostic and therapeutic appls. 79−39466
fluorescence bronchoscope for lung tumour localisation 77−60277
fluorescence bronchoscopy for localisation of small lung tumours, fibre optic system 77−86580
fluorescent microscopical technique in diagnostic microbiology 78−20339
fluorescent X-ray intensifying screen efficiency determ., standard method 78−69198
fluorography with image intensifier, apparatus for mass stomach survey *(Japanese)* 77−73575
fluoroscopic image recording using multiformat camera 80−51234
fluoroscopic installations, diagnostic X-ray survey procedures, automatic brightness controlled units 77−25560
fluoroscopic installations with undertable X-ray tubes, survey form and techniques 77−73597
fluoroscopic spot film system image quality evaluation and optimisation 78−69205
fluoroscopic system, alignment checking device 77−86604
fluoroscopy, absolute efficiency of (ZnCd)S:Ag phosphor 78−73203
fluoroscopy, automatic brightness control operating protocols and effect on image quality 80−17120
fluoroscopy, kVp variable, with automatic brightness stabilisation, X-ray tube pot. var. 78−69202
foetal development and placental function during pregnancy, US diagnosis and chem. anal. 78−35897
foetal heart and uterus diagnostic monitoring and functional mechanics 78−36009
foetus ECG appl. *(Spanish)* 78−11759
FONAR scans of cancer patients 79−62327
foreign-body detector for intraoperative localisation of stones in biliary tract 78−3657
functional residual capacity meas. in neonates with endotracheal tubes 78−53556
gait analysis, for daily orthopaedic practice, 2-D cinephotography, 6 component force measurement 77−48908
gait classification, multiple EMG signals pattern recognition 77−44795
gait evaluation technique for normal and abnormal subjects 78−11682
gall-bladder kinetics, real-time US study method 79−100682
gallbladder images obtained by radiographic magnification technique 78−69186
patient diagnosis continued
gamma cameras, field procedure for qualitative assessment 78−85444
gamma-ray imaging stochastic distributed filtering approach 77−13026
gastro-enterological X-ray diagnosis 77−86599
gastrointestinal pressure measurement using electronic transducer system 77−86695
gastrointestinal tract exam., automatic radiographic system and HT generator *(Japanese)* 79−88167
gated regional spirometry (GRS) 79−25097
glaucoma, early diagnosis by meas. of internal eye pressure 79−25140
glaucoma, optic disc changes meas. using retinal stereophotogrammetry 80−3757
glaucoma diagnosis and therapy, importance of tonometry 78−40383
glaucoma diagnosis by digital processing of optic nerve head images 78−81043
glomerular filtration rate, limitations of single sample tracer method 79−16271
grey-scale US images, local diagnoses and artefacts identification *(German)* 77−86571
gynaecologic specimens analysed with flowmicrofluorometer, pattern classification 78−73290
gyroscopic X-ray television apparatus for clinical studies 78−15883
haemangiomata betatherapy, diagnostic value of thermography *(French)* 79−5356
haematofluorometer, for testing Pb poisoning 78−53554
haematopoietic malignancy diagnosis, significance of SEM 80−85529
hand pathology, role of thermography 80−8120
hand tremor differential diagnosis, display system using data compression 77−86697
health care expansion aided by integrated electronics 78−11751
hearing, Staggered Spondaic Word Test, lead and lag effects 77−5008
hearing defect diagnosis using electro-cochleographic methods *(Dutch)* 80−3855
hearing disorders, EEG freq. following pots., masking and clinical studies 79−70553
hearing loss, electronic aids needing no patient feedback 78−11760
hearing loss, from acoustic reflex thresholds, comparison of three methods 78−3511
hearing loss, functional and nonfunctional, using auditory reaction times 77−56385
hearing loss, LF, simultaneous recording of brain stem and freq.-following responses 78−11665
heart attack early diagnosis appl. of statistical pattern recognition, results 78−40388
heart attacks, appl. of pattern recognition 77−25584
heart block computer detect. by correl. of surface and endocardiac ECG 80−94410
heart congenital defect evaluation from dynamic tracer meas. 78−40378
heart damage quantification, computer graphic technique 79−29654
heart diagnosis, using two dimensional real-time sector scanning facilities 80−81672
heart electrical generator integral characts. in normal humans 78−69244
heart monitor capable of supplying diagnostic information 79−83891
heart monitoring system for rhythm diagnosis of ECG 78−40392
heart rate monitor cct., construction 80−30920
heart volume determination by angiography, X-ray magnification estimation 78−73197
heavy ion radiography 80−17122
hemianopia, new mirror design for detect. 80−108992
hepatic disease, differentiation of bile ducts, blood vessels with pulsed Doppler system 79−34618
hepatic metastases detect. by grey-scale US scanning 78−73179
herpes simplex virus radiometric detect. 78−65117
high technology medical equipment, Angioscan, Cardiac Output Computer, Medishield Analyser, Tomographic Scanner 80−36171
histological data quantitative anal. using optical-mark-recognition computer cards 77−81612
histology appl. of interactive pattern recognition system PEEP/DECIDE/GRAPH 78−73291
histopathological information obtained from US tissue signatures and microscopy of biopsy samples 80−51195
holographic display of medical images 77−29193
holographically stored X-ray images, grey-tone reproduction 78−65120
holography in biology and medicine 79−8528
hormonal short time series, state-plane anal. 77−44800
human retinal blood flow meas. by laser Doppler velocimeter 79−79623
hydrocephalus, role of computed cranial tomography and radionuclide cisternography 77−77978
hyperaldosteronism screening test with rectal potential difference probe *(German)* 79−16323
hypertension classification using non-parametric technique 77−21558
image amplifiers, high performance for clinical use *(Japanese)* 77−73579
image analysis structural methods 77−86564
image display, medically significant features 77−78020
image formation, perception and measurement, conference, Leeds, England (Mar. 1976) 77−86561
image intensification in medical and industrial radiology *(French)* 77−30223
image intensifier fluorography, low-dose studies of infant hip dysplasia 79−48343
image intensifier fluorography with fast exposure technique 78−31900
image intensifier tomography in exam. of larynx 78−40312
image intensifier with 14 inch input field, clinical experience 78−31899
image processing and pattern recognition, activities in Japan, survey 79−62400
image processing in diagnostic radiology 80−81690
image quality vs. MTF, vision model 77−86487
image reconstruction from incomplete projections, iterative ρ-filter method 77−25582
imaging, conf., San Diego, USA, (Aug 1978) 80−17025
imaging, electronics developments 80−51285
imaging overview 80−98082
imaging system evaluation using contrast-detail-dose anal. 80−98108
imaging systems, characterisation and meas. of noise 77−86562
imaging systems, image quality assessments 77−90890
imaging systems, non-silver halide, recent developments and pot. 80−41223
imaging techniques, book 80−12861
imaging techniques, developments, review 80−26324
imaging techniques, receiver operating charact. curve anal. 78−65144

patient diagnosis continued
imaging techniques and instruments 79−96635
immunofluorescence diagnosis using AR laser *(German)* 79−5335
impedance camera for spatially specific meas. of thorax 78−53464
impedance plethysmography, origin of impedance changes measured in the human calf 80−56269
in-vivo activation analysis, diagnostic technique 80−56210
indicator dilution method, Stewart-Hamilton eqns. 79−16334
inflammatory joint disease assessment by quantitative thermography 78−31881
intestinal motility study by computerised anal. of sounds and EMG wall pots. *(German)* 78−31944
intra-atrial conduction block vectorcardiogram diagnosis 79−44036
intracardiac blood flow measurement, noninvasive ultrasonic technique 77−86569
intracardiac shunt noninvasive quantitation using cardiovascular sound complexes 78−48918
intracerebral spontaneous haematoma diagnosis and prognosis by computed tomography 78−73195
intracranial mass lesion detection, computerised cranial tomography and radionuclide imaging 77−77976
intrahisian block detection, endocavitary exploration classification 77−81623
intraocular pressure measurement, for glaucoma, comparison of Schiotz standard tonometer and applanation tonometer 78−48915
intraocular tumour diagnosis, Si(Li) detector probe with RFT radiation meas. unit *(German, English)* 78−20265
intraoperative coronary arteriography for graft patency prediction 79−92343
intraoperative use of X-ray TV chain with video recorder 79−92334
intraoperative X-ray diagnosis, exposure reduction by magnetic disc store 79−92345
intravenous angiography, digital video subtraction system 80−98089
ionization phenomena, appls. in medical diagnosis and treatment, review 80−67240
ionography, closed-system, image transfer to outside chamber, for diagnostic radiology 77−9242
ionography, edge contrast, effect of Mylar foil thickness 79−8532
ionography, high-press. gas, amplification and resolution degradation 77−70532
ionography, optimisation of design parameters 78−31888
ionography, powder cloud development technique 77−56462
ionography on thick dielectric sheets 79−57759
ionography sealed chamber system, optically projected X-ray charge images 78−4748
IR imaging of superficial vasculature using Vidicon camera with Si target 77−21592
IR pattern recognition for breast cancer screening 77−21652
IR photography, principles and appls., book 78−82068
IR thermography appl. aspects 78−61279
ischaemic and infarctive ECG simulation during ventricular activation and recovery 78−36018
ischaemic heart disease, conventional and orthogonal-lead ECG comparison by coronary angiogram discriminance analysis 79−44043
Japanese developments 78−24164
joint inflammation, radioisotope X-ray fluoresc. technique obs. 80−56184
kidney, intra-operative X-ray diagnostics in detection and localization of residual concretions 80−41202
knee analyser for mediolateral stability determ. 78−7475
knee arthrograph for study of stiffness 79−12022
knee joint impact response, comparison of normal and osteoarthritic joints 78−31848
laboratory test interpretation using computer 79−74770
laryngeal films, ultra high speed, automated anal. 78−36023
laryngeal pathology detection by glottal area/volume-velocity comparison 77−77920
laser applications, in USSR 77−73555
laser applications *(German)* 78−73192
laser applications in medicine *(German)* 77−9235
laser fibre optic bronchoscope for optical fluoresc. localisation of early lung cancer 78−48921
laser fluorescence bronchoscope for occult lung tumor localisation 80−30832
laser irradiation of fluid-suspended cell flow 77−21594
laser medicine development trends 80−51198
laser probe in biomedical research 77−9298
latency time meter LT-1, nerve conduction velocity measurement, locomoter organ disorder diagnosis appl. 77−40853
latent cardiac arrhythmia detection, His bundle electrogram and long-term ECG methods 79−44033
left ventricular aneurysm, triaxicardiometric criteria 79−39586
left ventricular cineangiograms, computing appl. for numerical information, wall movement obs. 77−90891
left ventricular flow pattern index of pumping efficiency 79−96601
left ventricular hypertrophy with bundle branch block, ECG/VCG and echocardiogram correlation 79−44035
left ventricular localised wall motion abnormality assessment, usefulness of quantitative parameters 80−89848
leg electrical impedance freq. characts. *(Japanese)* 80−56252
lesion contrast and photon count density rel. to D-log E curve 78−69195
leukaemia, acute, subclassification by automated morphological anal. 77−81620
leukaemia, rel. to blood U conc., meas. method using thermal neutron induced fission 80−21532
lingual tactile sensory system, automated instrumentation for research 80−8205
liver, comparison of radionuclide imaging, computer tomography and grey-scale US 77−52864
liver, comparison of scintigraphy, US and computerised tomography scanning 80−17105
liver fat content determ. by photon scatt. technique 78−24124
liver metastases diagnosis, conf., Brussels, Belgium (Nov.-Dec. 78) 80−82568
locomotor disorders of human skeletal muscle using tension development rate 77−40880
lumbar spine curvature in sagittal plane, meas. and modelling 79−96607
lung, small airway disease, possible diagnosis by pulmonary resistance meas. 80−30744
lung cancer detection by Kr laser fibre-optic bronchoscope *(German)* 79−12024
patient diagnosis continued
lung densitometer, 3-dimens., for oedema studies, using CdTe detectors 77−44749
lung emptying patterns, multiple breath N_2 washout data 78−92666
lung gas analysis using redox gas sensors *(German)* 78−85440
lung isopressure-flow-volume curves, electronic device for automatic recording 78−40382
lung obstructive disease, phase lags between chest wall motion and pulmonary airflow 77−40876
lung tissue characterisation by US, instrumentation, model and results, book 78−44575
lung volume determination, interactive graphics 77−77985
lymphocyte sensitisation meas., electrophoretic mobility test improvements 79−25138
macroradiographic X-ray diagnostic table *(Japanese)* 79−88166
maculopathy, Friedmann quantitative analyser for study of posterior pole disease *(Italian)* 80−17172
magnification mammography evaluation 80−17124
magnification skeletal radiography, imaging parameters and clinical relevance 78−69185
malignant melanomas, value of IR thermography 80−36062
mammarian growths in transilluminated breast, spatial filtering image enhancement 78−40288
mammary thermography classification by statistical filtering of spatial freqs. *(French)* 79−20610
mammogram densitometric distinction between cancer and fibrocystic lesions 77−25551
mammogram inspection by computer 79−57757
mammographic image quality comparison phantom 78−85357
mammographic image quality improvement by scattered radiation grids 79−92332
mammographic imaging, historical review in terms of image quality and reduced radiation dose 80−41229
mammographic imaging, new modalities, comparison of techniques 79−48335
mammographic screen-film system image props., laboratory and clinical evaluations 79−29616
mammographic screen-film systems, comparison of laboratory and clinical evaluations 78−69187
mammographic screen-film systems, laboratory and clinical evaluations of image props. 78−85365
mammography, backscatt. factors, var. with field diameter and half-value layer 78−3593
mammography, comparison of film and xerography methods in early diagnosis *(German)* 78−35946
mammography, detective quantum efficiency anal. of electrostatic imaging and screen-film imaging 80−41232
mammography, effective modelling of diagnostic examinations 78−85366
mammography, method for reducing radiation exposure and improving image quality 78−31901
mammography, optimum radiographic image conditions 77−90879
mammography, picture quality test *(German)* 78−20270
mammography, reduced dose, anal. of significance of scatt. radiation 79−62346
mammography, survey of patient skin dose, New Zealand 77−90901
mammography, use of phosphor X-ray screens, speed and resolution 77−90883
mammography, utility of modelling 78−69188
mammography film/screen combination, reciprocity law failure 78−65103
mammography modalities, advantages and limitations *(French)* 78−7430
mammography reliability for early breast cancer detection 80−8127
mammography techniques comparison, in vitro studies of breast microcalcification detectability 80−41230
mammography with magnification and grids: detail visibility and dose measurements 80−41231
mammography X-ray beam filtration 78−69207
mammography X-ray exposure meas., Baldwin-Farmer chamber response 78−28040
mandibular movements diagnosis, system for meas. and processing *(Japanese)* 80−101249
mass investigation locomotor and nervous system disorder, digital dynamometer DE 1 description 77−40854
mass spectrometry and metabolite profiling in study of human diseases 80−51289
maxillary lesion evaluation by bone-conducted vowel spectral estimation *(Japanese)* 79−5395
median nerve lesion localisation, usefulness of F-wave conduction time, post mastectomy patient 80−56267
medical physics conf., Atlanta, USA (July-Aug. 1979) 79−83858
medical X-ray diagnostics, NDT impetus, novel techniques *(German)* 78−7146
Medicor diagnostic bag assembly for out-of-hospital use 78−36014
metabolite mapping by ^{31}P NMR in whole animals, diagnosis appl. 80−36211
MICRO-VIDEOMAT, use in light microscopic liver diagnosis 77−78013
microchannel plate X-ray image intensifier, image resolution 78−35937
microprocessor based interactive radiographic image display 79−25092
microwave apexcardiography 79−74737
microwave appls. in diagnosis and pulmonary disease monitoring 80−85460
microwave attenuation measurement in human torso, 1.8-2.7 GHz 77−70517
microwave radiometry in detect. of breast cancer 78−40384
microwave scanner for soft tissue tumour detect. 80−17054
microwave system, dual mode, to enhance early detect. of cancer 80−89823
microwave thermography: principles, methods and clinical applications 79−100691
microwave thermography, appl. in cancer diagnosis *(Spanish)* 80−67195
microwave thermography, for breast cancer detection 79−29655
microwave thermography and local heating by same system, clinical applications 79−100695
microwaves appl., bio-clutter interference effects 79−11992
mm-wave thermography, application to breast cancer 79−100693
mobile X-ray unit, Mobil XR 78−24122
montages, in common clinical use, review 77−81599
motor nerve conduction vel. and evoked pots. in peripheral nerve lesion localisation 78−31802

patient diagnosis continued
motor nerve conduction velocity measurement, neuromuscular disorder diagnosis using semiautomatic meter 77−48909
motor neuron lesions, EMG positive sharp waves and fibrillation potentials 77−60194
motor unit potential recording using monopolar and bipolar leads 77−81615
MTF of X-ray tube focus rel. to current *(Japanese)* 77−70545
multiparameter clinical diagnostic miniature transducers, colloquium, London, England (May 1979) 79−100776
multiple sclerosis, evoked somatosensory response effects, expt. 77−44628
multiple sclerosis diagnosis using cerebral evoked response and optokinetics 80−36183
muocardial infarction ECG diagnosis in patients with transvenous ventricular pacemakers 77−81624
muscular dystrophy, Duchenne, erythrocyte membrane abnormalities monitored by EPR 78−96111
mutual impedivity spectrometry 80−17046
myocardial infarction diagnosis in endocardially paced patients 77−81625
myocardial infarction diagnostic data anal. database 79−70693
myocardial performance index from left ventricular area ratios 77−56465
myocardium, detect. of viable muscle in dysfunctional regions of left ventricle 77−37093
myoscope MG 23, two channel, ocular muscle measurement, myasthenia gravis diagnosis appl. 77−37085
neonatal jaundice detection, serum bilirubin conc. rel. to skin reflectance 79−92328
nervous system disease diagnosis using control characts. in manual control system 79−83990
neural diseases, quantitative EOG and CT obs. 80−36070
neurofunction laboratory, clinical trials appl. 79−96541
neurological, by sleep EEG 77−60271
neuromuscular disorders, motor unit action potential duration meas. by surface electrode EMG 78−81039
neuroradiography by NMR imaging 80−51197
Neuroscope, for multiprojectional isocentric fluoroscopy and angiography 78−40292
neurosurgical intraoperative X-ray equipment use 79−92344
neutron radiography of extended objects *(German)* 78−15880
NMR, field focusing method, visualisation of tumour in live animal 77−32950
NMR, field-focusing, formation of chemical scans in man 78−85354
NMR, human whole-body line-scan imaging 79−5334
NMR, radiographic thin-section image of human wrist 78−24112
NMR for biological and medical imaging 78−69172
NMR image recovery under nonuniform magnetic fields 78−40282
NMR imaging, and biomedical appls. 80−46006
NMR imaging, book contrib. 80−36064
NMR imaging, conf., London, England (Nov. 1978) 79−83876
NMR imaging, display of cross-sectional anatomy 78−44579
NMR imaging, improvement by low temp. SQUID detect., towards mol. kinetic meas. 80−104723
NMR imaging, multiple sensitive point method 80−81679
NMR imaging, multiple sensitive point technique 79−11993
NMR imaging, physiological effect threshold for RF and mag. fields 79−66484
NMR imaging, review *(Japanese)* 80−94312
NMR imaging, RF mag. field penetration, phase shift and power dissipation 78−73189
NMR imaging, three-dimens., using selective excitation 78−21190
NMR imaging application 77−73552
NMR imaging by multisensitive point method, appl. to ~10 cm biological systems 77−86581
NMR imaging of living organisms *(Polish)* 78−77098
NMR in cancer, FONAR scan of live human abdomen 80−8122
NMR limb blood flowmeter, clinical appls. 80−17178
NMR relaxation detect. of tumours, spectrum anal. of multiple components data 78−48851
NMR spin density imaging using line shaped mag. field 78−73190
NMR technique 80−8121
NMR zeugmatographic imaging, gradient control device using microprocessor 80−89822
NMR zeugmatographic imaging of heart and lungs 80−17053
non-invasive technology assessment, multiple endpoints 80−17179
noninvasive diagnostic technology, history and necessity 78−36029
noninvasive techniques, electronic equipment development in India 79−96698
nonprobabilistic measures of information with biological applications *(French)* 77−9160
nuclear magnetography in weak field *(French)* 77−52858
nuclear medicine, ^{123}I prod. in nucl. reactor 77−2051
nuclear medicine, hazards to personnel, protection problems 77−81587
nuclear medicine, Janus III, computer system for acquisition, processing of diagnostic units data 78−80948
nuclear medicine, radiochem. quality control of short-lived radiopharmaceuticals 77−52876
nuclear medicine diagnostics, for teaching 78−49618
nuclear medicine instrumentation trends 78−44594
nuclear medicine procedures, radiation dose to embryo due to radiopharmaceuticals 77−5083
nuclear scattering radiography using 500 to 1000 MeV protons 77−9244
nystagmus analysis, microprocessor based instrum. 77−44799
ocular foreign body detect. using computerised tomography 78−3577
ocular fundus reflectometry 78−48861
ocular motility test in strabismus and amblyopia evaluation, computer administration and analysis via PAL8 program 78−48784
ocular photography, accessory fill-in flash for the Nikon photo-slit lamp 80−36056
ocular pulse measurement, electronic/US system for carotid occlusion diagnosis 77−37081
ocular tonometry through sonic excitation and laser Doppler velocimetry 80−56152
oculoplethysmography for noninvasive detect. of extracranial carotid occlusive disease 79−83985
oncology, computer appl. *(Swedish)* 77−44763
one-sided cardiac failure differentiation by planimetric electrokymography 79−43990
ophthalmological diagnosis, US contact stabilisation method 77−25523
patient diagnosis continued
ophthalmological instrument manufacture, development trends 78−48903
ophthalmological tissue differentiation, digitisation of HF US signals 78−80935
ophthalmology, holography appl. 78−7342
ophthalmology and physics, review 79−53084
ophthalmology diagnosis, computer assisted 78−92739
opthalmology, appl. of picosecond optical range gating 77−81549
optical instrumentation in medicine, conf., San Diego, California (1976) 77−44829
optical instruments for medicine and biology 80−21517
optical monofibres for medical practice, appls. *(French)* 79−39462
orbicularis oculi reflex, diagnostic significance of reflex amplitude 79−34540
orthopaedic surgery, role on intraoperative X-ray diagnostics 79−92341
osteoporosis early detection by Compton gamma-ray spectroscopy 78−11729
pacemaker malfunction diagnosis, ECG before and after thoracic wall stimulation 77−81707
paediatric pneumogram patterns 80−3749
paediatric radiology, image intensifier fluorography 80−41201
paediatric radiology, the Diagnost 73 P, universal diagnostic system 79−48334
paediatric urography, tomography with short exposure times 79−48336
paediatric X-ray examination equipment assessment, point system 77−21603
pancreas carcinoma, grey-scale US characts. 79−53198
pancreas computerised tomography experience 79−88210
pancreatic disease, short circuit current rat jejunum bioassay 80−8204
pancreatic lesion visualisation and documentation by diagnostic US 78−11708
pap smear inspection, segmentation approach 80−8124
para-nasal sinus tomography with conventional and rare-earth screens, eye dose 77−37055
pathological conditions detection, neurological signal processing techniques appl. 79−83993
pathological gait assessment, foot force meas. device 79−20701
pathological knee joint cartilage damage, electroacoustic evaluation 79−20702
pattern classification of patients with essential hypertension 77−25583
percussion, chest-wall motion and assoc. tactile sensation 78−81040
percutaneous transhepatic cholangiography and endoscopic retrograde cholangiopancreaticography 79−92333
perimeter localising, for visual field study and retinal tear location 78−85442
petit mal epilepsy, portable detect. device 79−83984
phased-array US scanners, coarse phase quantisation effects 79−57739
phonoangiography for noninvasive detect. of extracranial carotid occlusive disease 79−83985
phonocardiogram classification, linear prediction analysis appl. *(Japanese)* 78−36010
phonocardiogram detection algorithm using spectral tracking 80−41151
phonocardiogram pattern classification using linear prediction analysis 77−90950
phonocardiogram quantitative anal. for murmur detect. 80−56270
phonocardiograph modulator design trends 78−24171
phonocephalography, passive noninvasive technique, normal tracing 77−81618
photogrammetric system, cancer diagnosis appl., cytographs automatic analysis *(Russian)* 78−24161
photoplethysmography, audio-visual heart monitor based on light transmission through skin 79−53206
physiological fluid, human, identification in situ by proton relax. *(French)* 79−48316
plethysmograph, automatic venous occlusion device 80−17176
pleural liquids in weak fields, PMR relaxation times, medical diagnosis appl. *(French)* 78−73187
PMR fast scan imaging 77−21591
PMR imaging, in vivo study of human fore-arm and hand 79−20605
PMR medical imaging, mice and phantom expts. rel. to cancer detection 77−86584
pneumoconiosis, suspicious, recognition with aid of pulmonary function meas. 80−21567
pneumoconiosis of coal-workers, optical-digital system for pattern recognition 78−40389
pneumoconiosis opacities in chest X-rays, improved detection algorithm 78−73242
pneumothorax diagnosis in deep-sea divers, using Sonicaid portable instrument 78−85351
polygraph for simultaneous recording of diagnostic parameters 78−36011
polyneuropathy, variability in nerve cond., vel. determ. 77−60274
polysomnographic recording techniques, sleep disorder diagnosis 79−34696
portable diagnostic bag model, operational experiences 77−5105
portable laboratory bag, for regional and district doctors 77−5104
portable system, principle and appl. 77−5103
posterior myocardial infarction, right ventricular hypertrophy, and normal variation differentiation 79−44045
posterodiaphragmatic myocardial infarction diagnosis, Frank lead Y reliability 79−44038
posture and spinal disease documentation by moire topography *(German)* 79−16264
proptosis diagnosis, contrib. of echography 78−28023
prostate, intra-rectal US imaging, equipment for 79−48296
prostate US sectional pictures, pattern recognition for tumour diagnosis 80−51194
proton (heavy ion) radiography in medical diagnosis 79−57753
proton imaging for medical applications 80−98129
proton radiography beam line establishment at Fermi National Accelerator Laboratory 78−65121
psychophysical laboratory unit organisation and meas. system for persons with impaired locomotor system *(Croatian)* 78−44667
pulmonary diseases, using microwave reflection/transmission meas. method 78−28031
pulmonary dysfunction detection using sound transmission 77−37031
pulmonary fibrosing disease diagnosis, histological section SEM and energy-dispersive X-ray microanalysis 80−72314
pulmonary function testing, continuous distribution of specific ventilation from N_2 washout 78−92665
pulmonary function testing, training course features 78−24169

patient diagnosis continued
pulmonary oedema, quantitative diagnosis from chest X-rays using computer controlled optical system 77−77981
pulmonary oedema detect. by quantitative elec. impedance plethysmography 78−31951
pulmonary oedema diagnosis by a surgically noninvasive microwave technique 80−61659
pulmonary testing equipment, training and application techniques 78−24170
pulse/phono pick-up appls. in ambulant cardiological practice 78−40377
pupilometry, instrumentation for stimulating and monitoring human pupil 78−48911
quality health care and cost containment, conf., Washington, USA (Mar.-Apr. 1978) 79−39333
radiation exposure of Italian population in 1974, genetically significant dose 77−66850
radiation induced Fe metabolism disturbance, by migration of ^{59}Fe as citrate 77−32942
radiogram, stomach contour extraction *(Japanese)* 78−53482
radiograph diazotype duplicating system with appl. as diagnostic aid 78−69249
radiograph digital tomogrpahic restoration 78−40322
radiograph quality control programme, economic analysis 78−73236
radiographic, table, remote-controlled, clinical experiences 79−43987
radiographic $CaWO_4$ intensifying screen, meas. of X-ray induced light photons emitted 80−41218
radiographic contrast improvement using fore-and-aft rotating aperture wheel device 80−41227
radiographic decision making and phys. image props. 78−69189
radiographic dose reduction 80−98087
radiographic equipment acceptance testing, systems approach 78−69203
radiographic equipment servicing by hospital-based group 78−69247
radiographic film/screen combinations and patient exposure, Nationwide Survey of X-ray Trends 78−73233
radiographic image anal., computer aided 78−61256
radiographic image analysis 77−21624
radiographic image formation, perceptual eval. of phys. parameters, computer-simulated images 80−41222
radiographic image quality comparison for different screen/film combinations by subjective judgments 78−73229
radiographic image texture anal. using pattern recognition 77−21643
radiographic images, texture analysis and EPQ 79−34643
radiographic imaging, 3-dimens. 80−85486
radiographic imaging, digital video acquisition system for extraction of subvisual information 78−69208
radiographic intensifying screen equivalent blur 78−69197
radiographic intensifying screen information content and contrast, comparison of rare earth with $CaWO_4$ 78−73232
radiographic intensifying screens, sensitivity to scattered radiation 77−77970
radiographic miniaturisation, X-ray image and optically coupled radiographic intensifiers, comparison 77−81560
radiographic mottle, screen sharpness quantum noise depend. 78−20261
radiographic observer performance meas. and characterisation, free response approach 78−69200
radiographic phototimers, acceptance testing and performance monitoring 77−5071
radiographic pictures, digital encoding, redundancy reduction 77−40850
radiographic proximity X-ray image intensifier tube 78−69206
radiographic quality, tube potential, and patient dose 79−62349
radiographic screen-film system comparisons, fluoresc. X-ray source 78−24132
radiographic screen-film system evaluation, intensity vs. time scale sensitometry 80−41219
radiographic screen-film system evaluation, sensitometric method 80−41220
radiographic screen-film systems, quantum fluctuations 79−58857
radiographic techniques, X-ray studies of the digestive tract 78−92694
radiographic tomography, comparative survey of multi-directional units 78−61242
radiographic video system psychophysical evaluation 79−74751
radiographic viewbox information capacity, viewbox improvements 79−74746
radiographic X-ray image intensifier video system, design characts. 78−69209
radiographic X-ray image intensifier video system, psychophys. evaluation rel. to system measures 78−73234
radiographic X-ray tube current, effect of electron evaporation 78−69204
radiography, anal. of making, reading and reporting films, rel. to equipment design 80−17123
radiography, appl. and limitations of the use of X-rays 79−79643
radiography, automatic computerised transverse axial tomographic scanner system 77−12985
radiography, autoradiographic image intensification 78−61255
radiography, backscatter X-ray technique 80−98096
radiography, characterisation of X-ray focal spot imaging props. 77−21596
radiography, computed, contrast-detail-dose evaluation 80−41221
radiography, computed, low-dose X-ray imaging system 80−98092
radiography, computed tomographic reconstruction noise, effect on detectability 78−40296
radiography, computed tomography 77−25549
radiography, computerised tomographic scanning, general principles, review 77−16973
radiography, computerised tomographic X-ray imaging *(Japanese)* 77−66845
radiography, computerised tomography, correction for spectral artifacts in cross-sectional reconstruction 77−21621
radiography, computerised tomography, data acquisition and reconstruction algorithm 77−77979
radiography, computerised tomography, equipment operation 77−86617
radiography, computerised tomography, max. likelihood reconstruction of random objects from noisy objects 77−37089
radiography, computerised tomography, present state and technical perspective, review *(French)* 77−16974
radiography, computerised tomography, scanning time and picture quality improvements 77−25550
radiography, computerised tomography, two-component spectral analysis 77−25548

patient diagnosis continued
radiography, computerised tomography using EMI general purpose scanner 77−5060
radiography, convolution reconstruction technique for divergent beams 77−12987
radiography, cost-effectiveness considerations in evaluation of new technology 78−69192
radiography, detection of bars and discs in quantum noise [radiography] 80−41042
radiography, detector sensitivity and image conversion improvement 77−25546
radiography, diagnostic isocon imaging system 77−40760
radiography, electrophotographic imaging using high purity Al_2O_3 78−35936
radiography, energy absorbed in $CaWO_4$ X-ray intensifying screens 77−70537
radiography, equipment needs for radiology department, math. model 78−65107
radiography, exposure and working procedure with paediatric chest stand 79−48337
radiography, exposure meas., energy depend. of correction factors for Victoreen 570 Condenser R-meters 78−3597
radiography, exposure meas. during exams. using phototiming techniques, attenuation phantoms 77−40766
radiography, falling load technique, performance evaluation 78−69201
radiography, fan beam computerised tomography, scatter effects 77−5097
radiography, field characts. of geometric unsharpness due to X-ray tube focal spot 77−21616
radiography, flashing tomosynthesis 80−67243
radiography, focal spot meas. for quality control, using random object distrib. 77−2047
radiography, held radiograph technique and radiation protection 78−73199
radiography, high-resolution low light level video systems 77−40759
radiography, holographic 3-D synthesis of X-ray pictures 80−67245
radiography, holographic methods of 3-D representation from no. of plane images 80−67244
radiography, image information content and patient exposure 78−35935
radiography, image quality and patient exposure 78−28060
radiography, image recording system choice 78−69180
radiography, impact of EMI scanning on meningioma diagnosis 77−5061
radiography, information storage requirements 80−98086
radiography, Keithley diagnostic ion chambers, energy depend. of correction factors 78−53507
radiography, low dose, intensified minification camera 78−20262
radiography, medical diagnostic decision making and image quality 78−28059
radiography, micro-dose system 80−51233
radiography, MTF determ. from edge response function, single step calc. 78−35938
radiography, noise equivalent parameters 78−28058
radiography, panoramic tomograph users' experience in exam. of teeth and jaws 77−21605
radiography, patient exposure 80−46066
radiography, photon path visualisation by Monte Carlo simulation 77−66848
radiography, principles of design of assemblies 78−57065
radiography, problems anal. 78−31903
radiography, processor control using preexposed control strips and visual comparative densitometry 78−69210
radiography, quadratic optimisation for image reconstruction 77−16981
radiography, quality assurance meas. for diagnostic X-ray systems 77−40763
radiography, quantitative meas. for estimating patient dose *(German)* 78−57073
radiography, Radon inversion formula for diverging X-rays 77−37088
radiography, rare earth oxysulphide intensifying screens, resolution and dose 77−21597
radiography, relative props. of tomography, K-edge imaging and K-edge tomography 77−70538
radiography, resolution, falling load principle, focal spot performance 77−2045
radiography, sampling tomography multi-sectional reconstruction method using computer *(Japanese)* 78−31896
radiography, sensitometry of X-ray and fluorographic films 77−48858
radiography, Siemens star X-ray image artifacts computer simulation 77−21615
radiography, solns. for film and data handling in large diagnostic departments 78−40294
radiography, star test pattern image interpretation 77−21614
radiography, straight-line tomography, linearising mechanisms 78−35934
radiography, subtraction, wax phantom simulating flat tumour with diffuse edges for film evaluation 77−70536
radiography, systems approach to scale of equipment 78−57064
radiography, test phantom for meas. of phys. parameters *(German)* 78−57068
radiography, three-dimens. image reconstruction, direct Fourier transform techniques 77−12986
radiography, tomographic image quality evaluation 77−86607
radiography, total unsharpness analysis 78−11730
radiography, transaxial scanning X-ray tomography, coronal or sagittal plane reconstruction 77−77986
radiography, transaxial tomography, quantum-statistical limitations 77−12990
radiography, unsharpness additivity 77−52871
radiography, US Nationwide Evaluation of X-ray Trends and state radiation meas. 77−40779
radiography, use and abuse of MTF concept 77−86623
radiography, working places incorporating Medicor equipment 78−35942
radiography, X-ray, antiscatter grid exptl. evaluation method 78−53485
radiography, X-ray beam photon energy distrib. 77−70530
radiography, X-ray photographic method for determ. of stable I in tissue 77−70540
radiography, X-ray spectra determ., high intensity 80−41217
radiography, X-ray spectroscopy by Compton-scatter method 77−2044
radiography, X-ray tomography, review 77−5073
radiography applications of holography 80−67242
radiography equipment, idealised, for routine chest exams., specifications and requirements 80−46034
radiography grid for elimination of scatter, zig-zag design 78−3598

patient diagnosis continued
radiography instrument calibration, energy depend. of correction factors for Victoreen 666 Survey System 78−3596
radiography localisation of intracavity Rn applicators with Diagnost C 79−48331
radiography of breast, recent techniques *(French)* 77−81564
radiography screen-film combination selection 80−46047
radiography transaxial tomography, analogue reconstruction methods 77−12998
radiography using fast neutrons 77−25554
radiography with fan-beam scanners, circular artefacts reduction 78−35924
radioimmunoassay, hypergeometric theory of competitive binding 77−77980
radioimmunoassay as aid to diagnosis, review *(French)* 80−21522
radioisotope production in cyclotron for diagnostic medical research appls. *(French)* 78−48895
radiologic decision making and physical image props. 78−85367
radiological-endoscopic combined setups for gastrointestinal organ exam., experience 77−90947
radiology, diagnostic, analytical stereo system 80−67231
radiology, introduction to computer systems 79−34663
radiology, mean active bone marrow dose to USA adult population 78−85382
radiology, review of past and future techniques 77−12984
radiology facilities, quality assurance programme, proposed recommendation 78−73235
radiology with electro-optical imaging 77−21651
radionuclide appls. in medicine, props. and use in radiopharmaceuticals and organ imaging 78−61241
radionuclide cumulative dose calcs., graphical representation 77−66852
radiopathology, clinical problems in diagnosis and treatment of radiation damage *(French)* 78−48845
radiopharmaceutical diagnosis, absorbed dose derivation techniques 79−12006
radiopharmaceuticals, cyclotron prod. for nuclear medicine appls. 77−44753
radiopharmaceuticals in diagnosis, patient dose 78−35967
radiosaturation diagnostic methods *(Slovenian)* 80−30863
radiotelemetry pill for biomedical meas. of ionising radiation using HgI_2 detector 78−40318
raylography, acoustic medium characterisation and imaging, non-biological model expt. 77−25528
raylography, freq. domain deconvolution technique for pulse echo ultrasonography 77−25527
real time data compression, realisation techniques *(Italian)* 79−5389
receiver operating characteristic and diagnostic benefit determ., visual detect. performance in medicine 77−86563
Refractor III system, computer-assisted eye examination 79−34698
renal arteriography, magnification selective obs. 79−53209
renal diagnosis by blood circulation angiocinedensitometry *(German)* 79−2127
renal insufficiency assessment by EEG quantification 77−73609
respiration, two-stage ladder network model for detect. of small airway disease 78−31846
respiratory flow integrator with improved stability 79−16331
respiratory system forced perturbation, traditional model 79−83815
respirometer, improved vane, flow rate measurement *(German)* 77−40826
retinal function, laser interference fringes meas. *(German)* 77−12910
retinal nerve fibre atrophy development computer evaluation 77−40856
retinal resolving power meas. by laser interferometry 80−36066
rheumatology, quantitative IR tele-thermography *(German)* 78−92684
right bundle branch block, cardiac and noncardiac patient vectorcardiograms 79−43853
right bundle branch block aetiology, morphological and clinical aspects diagnosis 79−43852
right ventricular wall thickness meas. by echocardiography, comparison with necropsy 78−40277
roentgen densitometer for detect. of congenital heart defects, patient dose 77−9239
roentgenocardiograph with photoelectronic sensors, calibration device 78−57061
roentgenogram foreshortening for biological vol. reprod., compound hologram method 79−57748
roentgenokymographic image formation, rel. to optimal grid slit width 78−57058
saphenous nerve normal sensory cond. in man 78−61162
schizophrenia, event-related auditory evoked pots. 80−85405
sensitometry in medical imaging applied in diagnosis and therapy 78−69193
sensors for diagnostic instruments, classification scheme 79−53267
serial quantitative EEG 80−61728
signal analysis applied to medical imaging 80−17038
single-transducer coupler for diagnostic pulsed Doppler or pulse-echo US instrumentation 78−61236
sinus node function electrophysiology rel. to long-term cardiac pacing 77−81673
sinus node response to premature atrial stimulation, microelectrode analysis 77−81630
sinus rhythm, diagnosis by IBM ECG anal. program *(Japanese)* 80−67278
skeletal demineralisation osteopathy, quantitative diagnosis, review *(German)* 80−30872
skeletal muscle disease, Fourier optical evaluation of histopathologic findings 77−37091
skin lesion Mn, Cu and Zn conc. meas. by neutron activation 80−17063
skull, acoustic losses and vel. meas., rel. to diagnostic imaging 78−69159
skull axial tomography, modified technique 77−86600
slope descriptor computation, time and frequency domain comparison 78−57115
somatosensory evoked potentials, review of acquisition and anal. 80−101281
Sono Diagnost R multi-element scanner, use for upper abdomen US diagnostics 80−17028
SonoChromascope, US B-scan image acquisition, display and recording 80−30818
sonography, diagnosis of tumours, comparison with other methods *(German)* 79−34614
Soviet requirements, X-ray diagnosis, radiotherapy, short lived isotopes in diagnosis, review 77−37032
patient diagnosis continued
speech, voice quality registration 77−21539
speech development disorders, by acoustic anal. of speech 77−5014
sphygmomanometry, automatic indirect methods, equipment, for blood press. meas. 77−81616
spin warp NMR imaging and appls. to human whole-body imaging 80−101250
spine, evoked elec. response surface recording 78−36028
spiral tomography, optimum blurring 78−69181
spirometric data, automatic classification 79−57803
SQUID appl., iron overloaded liver non-invasive diagnosis 80−101244
stability of human stance, meas. using vectorstabilograph 80−41275
stabilograms, influence of platform geometry 78−81038
stereopsis clinical test 80−61566
stereoradiology, single monitor systems using PLZT electro-optic shutters 77−60247
stereovision techniques *(Japanese)* 80−67279
stethophonendoscopes, design and production 80−104686
stomach double-contrast exam. using Orbiskop 78−73200
stroke disability assessment by tracking task performance meas. 77−60280
subtraction radiography, characts. and limitations of photographic films 77−2046
superficial vein imaging by infrared television 77−81546
superior vena caval pathway obstruction diagnosis following Mustard's operation, transcutaneous Doppler US 79−70596
supraventricular tachycardia, diagnosis and management, instrumentation and therapeutic techniques, review 79−39598
synchronised diagnostic and treament techniques 80−61727
synovial fluid analysis by ferrography 80−101242
systolic time interval meas. microprocessor system for heart malfunction detect 79−79681
teaching clinical experiences, computer simulated patients 79−17162
telemedicine technology development 77−21649
television fluoroscopy, for X-ray diagnostics, persistence 79−8558
temperature gradients in low-flow vessels, appl. to blood temp. distrib. 78−27990
thermal burns, multispectral colour photographic anal. 78−3648
thermal imaging, fast response system with 50 element detector 78−18064
Thermo-Acoustic Sensing Technique for noninvasive tissue analysis 77−64117
thermogram computer analysis, in breast cancer diagnosis *(Japanese)* 77−5099
thermogram enhancement by tissue-condition correction 79−39460
thermographic diagnosis, high resolution dynamic method, detector system 80−41167
thermographic imaging, breast screening 77−86585
thermographic meas., three-dimensional signal detection, expt. 78−3662
thermographic observability of tumours with microwave heating 78−73193
thermographic turnover detect., microwave enhancement with swept-freq. illum. 78−73194
thermography, cm and mm wave, tumour detect. survey 79−100690
thermography, dual-channel ratio thermograph counteracting skin emissivity errors 77−40892
thermography, eval. of distortion 80−3750
thermography, mm-wave, head and neck diseases, preliminary findings 79−100694
thermography, quantitation 78−31946
thermography, skin temp. meas. appl. 78−61280
thermography applications, heat transfer, equipment and techniques 77−44737
thermography in clinical diagnosis and monitoring 78−57113
thermography of breast, automated diagnosis of abnormality using minicomputer 77−21593
thermography of breast, feature extraction for mass screening 77−60237
thermography with radiometrically calibrated imagery 77−40893
thoracic sound characterisation by time series anal. using canine model 78−31959
thoracic X-ray image comparison automation *(Japanese)* 79−29615
Thoramat automatic thoracic radiography unit experience 80−12212
thrombophlebitis diagnosis, reliability of Doppler and impedance techniques 78−77144
thrombophlebitis patients, venographic, impedance and Doppler US findings 78−48919
thrombosis detection by US, plethysmography and phlebography 78−7435
thyroid diseases, differentiation, linear discriminant analysis application 79−53275
thyroid diseases, scope of different methods of exam. *(German)* 80−89840
thyroid fluorescent scanning system of concentric source-detector design 77−40738
tissue acoustic parameter characterisation by induced transient thermal gradient 77−64116
tissue characterisation by US frequency-dependent attenuation and scatt. 77−66832
tissue characteristion, static and moving, high spatial resolution US meas. techniques 80−51187
tissue parameter identification by digital processing of real-time US clinical cardiac data 80−51191
tissue structures characterisation, method of obtaining an acoustic impedance profile 80−67171
TOMAX autostereoscopic display, three-dimens. viewing of tomographic data 78−85446
tomodensitometry, image quality 78−44589
tomograph information characteristics 77−25541
tomographic system error propagation, hybrid anal. 78−40327
tomography, computerised, operating principles, image construction, appls. 78−28047
tomography, computerised, principles and development 78−31945
tomography, linear, optimum spread functions 77−66846
tomography, proton beams computed reconstruction 78−48870
tomography equipment for intracranial diagnosis, Japan 77−53877
tomography images, display processing, digital enhancement 78−48875
total cardiac monitoring integrated microcomputer/minicomputer system 78−35997
tracer diagnosis, displays in nucl. medicine 78−85443
transaxial scanning X-ray tomography, oblique viewing plane reconstruction 78−77114

patient diagnosis continued
transaxial X-ray tomography reconstruction using convolution methods, digital simulation *(Japanese)* 78−35931
transkull transmission of axisymm. focused US beams, 0.5 to 1 MHz 80−51184
transrectal echographical ultrasound system, prostate, seminal vesicles and bladder exam. 80−41153
transvenous xeroarteriography, peripheral blood vessel angiography *(German)* 79−2126
traumatised patient diagnostic radiology requirements 80−8128
triaxial vector accelerometry for quantifying tremor and ataxia 78−28116
tumour detection by US Doppler blood-flow signals 78−3571
tumour location, temp. distrib. model for warm-blooded animal body surface 78−64943
tumour microwave heating for thermographic detection enhancement 79−2124
TV installation for projection of high-resolution X-ray images *(German)* 79−57751
tympanic membrane vibration study, phase sensitive holographic technique *(German)* 78−3513
tympanic membrane vibrs. in human temporal bones, double pulsed holographic anal. 78−40289
tympanometry in neonates 80−3651
ultrasonographic diagnosis of pancreatic diseases 78−7416
ultrasonography of the kidney in 1979 *(French)* 80−56149
ultrasonotomogram of small tissue area, image magnification and smoothing 77−86572
ultrasonotomography with electronic sector scanning, cardiac diagnosis appl., features 77−66829
ultrasound image coding, mammograms appl. 77−81544
upper airways in newborn and infants, X-ray physiological exam. using Orbiskop 80−8130
ureteral catheterisation manometry and urodynamics *(Slovene)* 78−44668
urinary bladder interferometry, holography of bladder deforms. in vitro, rabbit expt. 80−67201
urinary bladder interferometry, tumour and lesion detect. by holography 80−67202
urinary flow rate meas. device 77−48906
urodynamic combination EMG and functional X-ray exam. technique 80−8131
urology, universal room using Uro Diagnost 78−31902
US, 1977 state of art and developments 78−48847
US, 2-dimens. colour display of spectral information 77−21584
US, appls., principles and equipment, review 78−11709
US, Bragg-diffraction imaging 79−64463
US, dynamic focusing improvement, using analogue-switch phase shifters 77−52856
US, human abdominal tissue phantom 80−51152
US, linear-filter model for signal transmission process 80−17026
US, newer clinical imaging appls. 80−30825
US, principles, instrumentation and appls. 78−44571
US, reconstruction of tissue refr. index and attenuation distrib. 77−64113
US, review of future developments and applications 79−79615
US, signal processing 80−36049
US, tissue simulators 80−51153
US, transmission tomography by reconstruction compared with pulse-echo imaging, tissue-equiv. test objects 80−51154
US, Vidoson 735, real time scanner for sonography 78−28024
US 2-dimensional scanning of excised brain, normal anatomy 77−77950
US A-scan quantitative analysis of normal and cirrhotic livers 77−64109
US abdominal scanners survey, clinician's viewpoint 79−66582
US appl., bibliography 78−7417
US appl. to urology *(Hungarian)* 78−35900
US applications, review 79−92308
US applications in obstetrics and gynecology, safety and pot. hazards, review 80−67170
US arrays for real-time diagnostics, image quality *(German)* 80−61656
US attenuation and velocity meas. by direct and phase-contrast imaging 77−64114
US attenuation and velocity meas. by time delay spectrometry 77−64111
US attenuation coefficient slope for soft tissue, parametric estimation 77−21582
US attenuation rel. to myocardial injury, correl. with enzymatic indices 77−21581
US B-mode scans, speckle reduction 78−22233
US B-scan appearance of gas in biliary tree 78−80930
US B-scan complementary use with radionuclide imaging 77−37043
US B-scanning in medicine, book 78−73180
US backscattering from human tissue, model 77−40715
US camera for patient diagnosis *(French)* 77−37028
US cardiology, electronic sector-scanning cross-sectional echocardiograph, model SSH-10A 79−57732
US cardiotomography, cardiovascular system diagnosis appl. *(German)* 77−77944
US computed tomography of breast, progress 80−51196
US damage of DNA in lymphocyte cells 80−67148
US delay technique using phased array imaging system 80−30810
US diagnosis, basic principles 80−17037
US diagnosis, F mode images for any diagnostic plane utilising microcomputer and light pen 80−41147
US diagnosis in medicine and biology, bibliography 78−69166
US diagnosis principles and tissue characteristic impedances 79−83861
US diagnosis review 79−92307
US diagnostic equipment, operation principles and constructional features, advantages *(German)* 79−100684
US diagnostic equipment, portable radiation-force balance 78−69163
US diagnostic equipment, US power and intensities produced 78−69162
US diagnostic equipment development *(Japanese)* 78−44572
US diagnostic equipment progress in Japan 79−25053
US diagnostic instrument performance evaluation, work of USA AAPM and AIUM 78−69170
US diagnostic techniques, basic principles *(Dutch)* 80−3744
US diagnostic uses, bibliography 79−62322
US Diasonograph incorporating pulsed Doppler system 77−77955
US diffraction scanner for in vivo tissue characterisation 78−61226
US digital imaging with microprocessor manipulation 78−96082
US digital moving target indicator system for diagnostic use 78−11710

patient diagnosis continued
US digitiser/processor for extraction of clinical parameters from Doppler-shift waveforms 80−36042
US display system, using colour TV, tissue disease diagnosis appl. 79−29576
US Doppler systems, development in Brazil 79−39455
US dynamic imaging, high resolution 80−17042
US echo probes, flexible, and prospects for use in oncology 80−56147
US echoaortocardiography, Kymo-two-dimensional, aortic root diagnosis appl. 78−24110
US echocardiographic system, two-and three-dimensional, computerised, atrial septal defect detection appl. 78−20237
US echoes from kidney, computer anal. 78−35901
US echography *(French)* 80−26305
US echoscopic meas., random error sources *(Croatian)* 78−44569
US echotomography for intrahepatic vessel and duct structure diagnosis 77−90868
US effects, review 79−66498
US electronic techniques, present appls. and future developments *(German)* 79−100683
US equipment quality control, tissue phantom *(German)* 78−3567
US grey scale display on storage oscilloscope system 78−3569
US grey scale scanner dynamic range testing 78−69169
US grey scale sonoarterographic imaging 77−25532
US holographic visualisation *(Slovak)* 79−41527
US image feature enhancement via digital processing 78−73183
US image processing, appl. to film recorded images 77−25531
US image reconstruction processing limitations 78−73184
US images corrected for refr. and attenuation, comparison of high resolution methods 80−30817
US imaging, clinical information, comparison of two types in detect. of focal intrahepatic lesions 77−64100
US imaging, digital scan convertors 79−66581
US imaging, overview of principles and instrumentation 79−66579
US imaging, prospects and limitations 80−98040
US imaging, single-transducer technology, state of art review 77−843
US imaging, use of fibre optic recorder 77−5057
US imaging and holography, devices, medical uses *(French)* 77−827
US imaging equipment, quality control problems 78−69171
US imaging of neoplasms 80−17032
US imaging over view, appls. and future trends 80−48536
US imaging system, 3rd generation development, high resolution, 3-D 77−86575
US imaging systems, high-resolution, real-time 78−69160
US imaging systems, methods and terminology 79−66580
US imaging techniques, theory and advantages 78−92682
US imaging techniques *(French)* 80−26304
US imaging techniques and appls. 78−49620
US impedance profiling, analytical and physical model 77−64121
US impediography, deconvolution and processing procedures and corrections 77−64122
US impediography, quantitative characterisation of lesions in vivo 80−17039
US in medical diagnosis, principles and methods 79−74733
US in medicine and biology, review 77−66830
US instrumentation standardisation, physician's need 78−69168
US liver sector scans, echoes across diaphragm 78−69165
US multiple freq. array for improved diagnostic imaging 79−14170
US multiple section tomogram simultaneous display equipment 78−61227
US ophthalmological diagnostics and therapy *(Croatian)* 78−44570
US pulse echo and Doppler diagnosis, technical and physical aspects *(Croatian)* 78−44568
US pulse-echo diagnostic equipment performance meas. methods 77−77957
US pulse-echo equipment, tissue equiv. test objects for routine performance checks 78−73182
US Pulse-echo transducer standardization 78−73181
US real time scanner, performance meas. 77−29191
US real-time diagnostic system 80−30819
US real-time image computerised anal. 79−70598
US real-time scanner with pulsed Doppler and T-M facilities, obstetrical appls. 80−67172
US reconstructive tomography 78−92681
US reflected amplitude from simulated vessel walls 77−25534
US renal diagnosis, clinical results 78−28027
US resolution improvement techniques and C-mode scan 79−25052
US scattering by human tissue, theoretical models 78−7411
US scattering in soft tissue characterisation 77−21586
US signals, physiological measurements and numerical analysis 77−86577
US signals in diffuse liver disease, computer anal. 80−67173
US synthetic aperture imaging resolution 77−25530
US system, real-time, for dynamic and still images, wireless echovision 78−65101
US system for internal organs imaging 79−5332
US techniques, experiences in private practice 78−92680
US time-of-flight tomography, computerised, breast pathology appl. 78−24107
US time-position mode scanning in obstetrics, heart model practice aid 78−24111
US tissue analysis, comprehensive system 80−51189
US tissue analysis, two-beam thermo-acoustic sensing technique 77−40716
US tissue characterisation, challenges and opportunities 77−64105
US tissue characterisation, conf., Gaithersburg, USA (Jun. 1977) 80−41940
US tissue characterisation, pattern recognition approach 78−73186
US tissue characterisation by scattering 77−64107
US tissue characteristics, swept freq. meas. of US attenuation and vel. 78−40278
US tomography, refr. index and attenuation images rel. to breast tissue types 80−17036
US tomography, review 78−31876
US tomography, signal processing for improved directivity 77−44729
US tomography for umbilical cord complications diagnosis 77−90867
US transducer, high resolution, with toroidal acoustic lens 77−65656
US transducer 2-D array technology, state of art review 77−844
US transmission tomography by reconstruction, imaging soft tissue through bone 77−70512
US use in medicine and biology 80−4481

patient diagnosis continued
US vascular imaging, Doppler method, improvement 78−24106
uterine cancer cells automatic classification via cellular differentiation 79−88226
uterine cytology, automated, adenocarcinoma recognition 79−88227
vascular disease, Doppler US system 77−29190
vector magnetocardiography, practical lead system 77−44698
vectorcardiogram, computer treated, discrimination between normals, LBBB with and LBBB without myocardial infarction 78−85448
vectorcardiogram and ECG correlation with angiocardiographic left ventricular mass 79−44027
vectorcardiogram and ECG correlation with coronary arteriorgram and left ventriculogram 79−44041
vectorcardiogram automatic anal., computer system 78−20302
vectorcardiogram computer interpretation method, prototype system 77−90954
vectorcardiography display and rate analysis,, minicomputer system 78−92738
venous occlusion plethysmography for the detection of venous thrombosis 80−56268
ventilation inhomogeneity identification using minicomputer data processing 77−44816
ventricular septal defect, prediction by non-invasive examination using interactive terminals 78−31954
ventricular wall dynamics and obs. on blood flow 78−80896
vestibular nystagmus, computer anal. of irregularities indicating central vestibular disorders 78−81036
video photography in computed tomography and US imaging, film selection 80−41224
viral infections diagnosis, contrib. of electron microscopy *(Italian)* 80−109024
virometer, real time virus detect. and identification in biological fluids 78−7555
vision, acuity rel. to illum., contrast and distance in partially sighted 78−53398
vision, time-varying response anomalies 80−16935
vision defects, remote subjective refractor employing continuously variable sphere-cylinder corrections 77−1992
visual concomitancy testing, new method 80−94305
visual contrast sensitivity function rapid meas. 78−56975
visual electrophysiological examinations of flying personnel 79−11929
visual evoked cortical potentials, transient response, techniques review 78−35844
visual evoked potential registration methods *(German)* 78−48916
visual evoked potentials, monocular, recording under binocular conditions 78−81035
visual evoked potentials, usefulness in multiple sclerosis diagnosis *(Italian)* 79−34555
visual evoked potentials in neurological disorders 79−24981
visual evoked potentials rel. to pattern reversal stimulus frequency *(German)* 79−16322
visual evoked response meas. using versatile pattern-reversal stimulator 80−17177
visualisation by nuclear medicine cross-modality techniques 79−79612
visually evoked elec. and mag. response simultaneous recording 78−53558
vocal diseases, spectrographic speech anal. *(Japanese)* 80−85455
walking pattern, EMG and temporal data telemetering 78−3638
white blood cells classification and feature extraction 78−3655
whole-body counter, 4 π, at Hamburg, performance parameters 77−16975
X-ray, film-screen characteristics effects on threshold detectability of small low-contrast objects 78−53487
X-ray, film-screen characteristics effects on threshold detectability of small low-contrast objects 78−53488
X-ray appls., equipment development trends *(German)* 80−3751
X-ray area exposure product monitor, DQ-20 *(Japanese)* 77−73578
X-ray beam characteristic time vars. meas. using solid state devices 80−46048
X-ray computed tomography, principles, reconstruction, equipment and dose 78−53481
X-ray departments, General Hospitals, planning standards 78−92741
X-ray diagnosis of digestive tract, dose to patient and radiologist *(German)* 78−28086
X-ray diagnostic department dimensioning problems in university hospitals 77−90946
X-ray diagnostic sets with automatic exposure relays, switching delays 77−48903
X-ray diagnostic system compatible with DHEW standards 78−7445
X-ray diagnostic table, computer controlled, multidirectional, CASSETTELESS spotfilm device *(Japanese)* 78−61278
X-ray equipment power supply design 77−21608
X-ray examinations, effects, risks and protection, review 78−3591
X-ray fibre-optic coupled image intensifier, large area contrast 77−70534
X-ray film charact., heuristic model 77−195
X-ray films sensitive to green light, reciprocity law failure 78−69199
X-ray fluorescence for static or dynamic organ studies *(French)* 77−37033
X-ray fluoroscopy, acute radiation injury caused by faulty use during cardiac procedures 77−9272
X-ray high potential generator, PD150L, standardisation of exposure factors *(Japanese)* 77−73577
X-ray high tension unit, HD150G-40 *(Japanese)* 77−73576
X-ray image analysis, design and construction of microdensitometer computer interface 77−44821
X-ray image intensifiers, quantum noise meas. 80−46033
X-ray image quality, MTF anal. of influencing factors *(Japanese)* 77−73580
X-ray image quality evaluation, visual and objective methods 77−25543
X-ray image transmission system response rel. to X-ray diagnosis 78−35941
X-ray images, electronic recording 80−62815
X-ray imaging, coded aperture, flashing tomosynthesis 77−40848
X-ray imaging using holography or electronics, tomosynthesis 77−40847
X-ray intensifier TV picture transfer 77−5077
X-ray intensifier viewing system, CCTV 77−9251
X-ray isodose curves in water phantom, for radiography machine 78−15892
X-ray microbeam scan system with interactive display terminal *(Japanese)* 77−81563

patient diagnosis continued
X-ray microchannel plate image intensifier, noise charact. 78−53483
X-ray picture examination TV equipment 77−21607
X-ray picture source coding for compact storage or fast transmission 78−40310
X-ray picture transmission over voice grade telephone channels 78−44607
X-ray quality and output determ. by TLD 77−60241
X-ray scanners, picture reconstruction 77−40849
X-ray scanning system, fast 3D, using limited tilting angle 77−73556
X-ray scatter data for diagnostic radiology 79−8533
X-ray screen-film processing sensitometry standard developed by ANSI 78−69196
X-ray systems for 3-D imaging, MTF 77−40851
X-ray tomogram reconstruction by holographic methods 80−67246
X-ray tomography by image reconstruction *(French)* 77−37037
X-ray transmission computerised tomography, review 77−48860
X-ray transverse tomography with incoherent optical reconstruction 78−28052
X-ray tube, grid control type, diagnostic, quality improvements 78−11733
X-ray tube focus, MTF rel. to current *(Japanese)* 77−70545
X-ray tube kVp indirect determ. using digital readout device 78−53486
X-ray tube performance characteristic rel. to radiologic image quality 80−17125
X-ray tube voltage error effects on image quality of roentgenograms 78−57060
X-ray TV, high-resolution system and video recorder 78−24120
X-ray TV display system, transmission charact. *(German)* 79−53215
X-rays, gonadal doses to 78070 patients 78−53503
X-rays, prenatal exam. freq. and radiation risks in Japan 77−5070
X-rays, pulsed and continuous, motion picture filming of moving objects 78−57057
xeromammography, technique and advantages *(French)* 78−7431
xeromammography exposure timing 78−40291
xeroradiographic image accuracy rel. to X-ray dose 77−77966
xeroradiography, for teaching 78−45449
xeroradiography, high kV techniques and optimal filtration 77−21598
xeroradiography, physical theory and photon noise obs. 77−5072
zeugmatography, state of the art 78−74043
Ca kinetics, use of ^{48}Ca stable tracer analysed by proton activation 77−21622
^{19}F NMR imaging for biomedical application 78−20240
^{123}I, prod. and use in nucl. medicine diagnosis *(German)* 78−28061
O_2 monitoring, intraarterial vs. transcutaneous monitoring in newborn infants 80−56266
^{31}P NMR of the perfused heart 80−77534
^{133}Xe trapping and re-use system for nucl. medicine 78−28051
^{133}Xe washout curve discriminant analysis for lower extremity vascular impairment 78−35949

patient monitoring
see also electrocardiography; electroencephalography
acoustic method for monitoring healing of human long bones 80−21511
ambulatory activity monitor with solid-state digital memory 77−52894
ambulatory arrhythmia monitoring, automated family classification 79−66566
ambulatory ECG computer anal., YALECG 79−70661
ambulatory ECG monitoring problems 78−11763
ambulatory noninvasive monitoring of physiological data, recording systolic time intervals 79−66574
amputee monitoring system for rehabilitation programmes, assessment 80−17167
anaesthesia level control system by EEG analysis 79−83974
anaesthesia stage indicator, signal divider 80−3858
antischistosomal drug screening in vitro by multichannel US activity monitor 79−20604
aortic ejection click and first heart sound description 80−30827
Argus ECG monitoring system reappraisal 78−7479
arrhythmia ambulatory anal. in real-time with minicomputer 80−85523
arrhythmia analysis, using modified ECG system *(Hungarian)* 78−35981
arrhythmia detection, edit and recall system, microprocessor-based 80−89891
arrhythmia detection program comparison data bank 78−15921
arrhythmia detection using a low-power, CMOS processor 78−73276
arrhythmia detection with a multi-microprocessor system for distributed and parallel processing 80−85524
arrhythmia identification and verification by 3-channel eval. of long-term ECG records 80−85518
arrhythmia incidence and cardiac freq., ECG recording during athletes' sleep 79−43860
arrhythmia monitoring, ARGUS/RT microcomputer system 78−81014
arrhythmia monitoring, multimorphology computerised system 79−70676
arrhythmia monitoring, single scan algorithm for QRS-detect. and feature extraction 80−85520
arrhythmia monitoring systems evaluation criteria 78−11765
arrhythmia monitoring using interactive computer system, clinical evaluation 78−81028
arrhythmia quantification, template matching algorithm evaluation 80−85519
arterial blood pressure, indirect noninvasive automatic meas. device 77−44771
arterial blood pressure noninvasive monitoring by US imaging and phono cuff-sphygmomanometry 80−36180
arterial blood pressure preprocessor 79−83979
arterial elasticity determ. and transcutaneous continuous pressure monitoring analysis 79−53179
arterial PO_2 continuous meas. 80−56240
arterial pO_2 intravascular monitoring using catheter-tip polarographic electrode *(German)* 78−85408
arterial pressure automatic indirect monitor 80−56231
arterial systolic blood pressure monitoring, circulation model 77−60224
arterial tonometer, microprocessor based 78−31955
arterial wall movement monitoring by microwave Doppler radar 79−96647
artificial arms, muscle- and externally-powered, comparative frequency of use *(German)* 79−12030
artificial blood circulation system, thermoelectric heat exchanger control unit 79−25149
artificial heart operation and monitoring system *(German)* 79−8583

patient monitoring continued
artificial kidney, wearable, monitoring instrumentation 77−64154
atrial electrogram monitoring for diagnosis of complex cardiac dysrhythmias 79−39567
atrioventricular block, ventricular overdrive test evaluation 77−81632
basal body temperature continuous monitoring in humans by radio telemetry 77−78015
beat-to-beat stroke volume estimation from pulmonary arterial pressure contour 79−53178
bioelectric process mag. recording, FM freq. convertor 78−7469
bioimpedance monitor 77−40845
biotelemetry, conf., Garmisch-Partenkirchen, W.Germany (May, June 1978) 79−43980
biotelemetry, conf., Pacific Grove, Calif., USA, May 1976 77−86653
birth monitoring by cardiotocography, interference effect by infusion pumps *(German)* 78−85416
blood, mean arterial pressure, noninvasive automatic determ. 79−57796
blood, pressure monitoring systems simulator 79−83963
blood gas analysis in vivo using gas chromatography 78−40355
blood gas continuous monitoring, current trends 80−56237
blood gases in artery and vein, quantitative continuous meas. of pO_2, pCO_2 78−40363
blood glucose monitoring technique for appl. in artificial endocrine pancreas 78−36062
blood glucose sensor for implantable artificial β-cell 79−83973
blood pO_2 meas. polarographic technique 79−100782
blood pressure ambulatory recordings, minicomputer processing 80−89887
blood pressure automatic monitoring, long-term, minicomputer system 80−101276
blood pressure control in hypertensive crisis, closed loop control of sodium nitroprusside infusion 78−44688
blood pressure direct measurement for intensive care and operations, computerised correction system 78−44635
blood pressure in brachial artery, monitoring by modified phonosphygmomanometry procedure 77−2065
blood pressure long-term recordings, fast data reduction, hybrid system 80−41278
blood pressure monitor, semiautomatic, using electronic sphygmomanometer 78−20300
blood pressure monitor, systolic-diastolic, using display stabilising circuit 78−40364
blood pressure monitor/conditioner, noninvasive cuff device 77−73605
blood temperature monitoring during extracorporeal circulation, noncontact transducer 80−85513
blood temperature monitoring transducer, during extracorporeal circulation 78−44639
blood volume change monitoring in menstruation, vaginal photoplethysmographic transducer 78−92733
body motion computer-aided tracking using CCD image sensor 78−61269
bone, fracture healing and disease, in vivo determ. of dynamic mech. props. 77−40906
bone diseases, pot. use of stimulated positron emission in detect. and monitoring 80−81712
brain retraction pressure monitoring, meas. system for surgical procedures 80−21563
breast disease, importance and limitations of thermography in diagnosis and treatment *(French)* 78−7419
calibrator for ECG/respiration monitor 80−98159
canopy ventilation monitor for quantitative meas. of ventilation during sleep 80−104792
cardiac activity continuous monitoring on commercial pilots using portable cassette recorder 77−86659
cardiac arrhythmia detect. and classification by computer using atrial electrogram 77−40867
cardiac arrhythmia detection systems, automatic, analogue trigger device P, QRS waves 77−86696
cardiac arrhythmia monitor, solid state delay unit 79−25126
cardiac arrhythmia monitoring, Aztec replacement by correl. for VPB detect. 79−62388
cardiac arrhythmia monitoring, joint interval histogram and correlation coeff. scatter diagram techniques 77−25572
cardiac arrhythmia monitors, review 78−69233
cardiac arrhythmia simulation device 78−44636
cardiac arrhythmias, computerised quantitative evaluation of cardiac arrhythmias 78−85435
cardiac arrhythmias detection and diagnosis, distributed microprocessor system 79−25142
cardiac automatic ambulatory rhythm monitoring 78−85431
cardiac dysrhythmia anal., automated systems, review of difficulties 80−17164
cardiac left ventricle function, nucl. medicine equilib. meas. 79−62357
cardiac output and shunt calc. from dye dilution curves using automated catheterisation system 78−81023
cardiac output automatic determ. by indicator dilution in computerised monitoring system 78−81022
cardiac output computerised monitoring by transthoracic admittance plethysmography *(Japanese)* 77−86693
cardiac output estimation from aortic pressure curves, simulation model 79−53177
cardiac output meas. by US transoesophageal probe 79−92315
cardiac output on-line determ. by thermodilution in coronary care unit 78−81021
cardiac pacemaker function control, value of patient participation 77−81716
cardiac probe, microprocessor-based, for gated equilib. and beat-by-beat left ventricle function 79−62396
cardiac R-R interval prediction models, comparison of 79−39549
cardiac sound frequency shifting stethoscope 79−29647
cardiac surgery, data acquisition and processing during operation by multiplexer *(German)* 78−92743
Cardiac Surveillance Unit experience with Argus ECG monitoring system 78−11762
cardiocirculatory computer-aided monitoring after open-heart surgery, appl. to adrenaline effects meas. 78−81059
cardiogram cart under microcomputer control 78−31942
cardiopulmonary function automated testing system 79−70673
cardiopulmonary monitoring in respiratory intensive care unit 78−20306
cardiopulmonary monitoring of high-risk infants using microprocessor-controlled memory 78−31962
patient monitoring continued
cardiopulmonary noninvasive noncontacting monitor using coherent microwave interferometer 78−40290
cardiotachometer histogram indicator, prototype 80−41268
cardiotachygram, anal. of recurring beat sequences *(German)* 78−88753
cardiotocograph for foetal heart-rate monitoring *(German)* 77−86566
cardiovascular computerised monitoring in medical intensive care unit 78−20304
cardiovascular monitoring, single freq. RF powered implantable multichannel telemetry system 77−52897
cardiovascular monitoring in the coronary care unit 78−20308
cardiovascular response to dynamic/static exercise, four-channel radiotelemetry 78−3633
cerebral activity monitor, using biofeedback rhythms inducing cct. *(Spanish)* 80−72359
cerebral blood flow automated analyser for ^{133}Xe studies 77−86597
cerebral magnetic field meas. and personnel selection 79−2026
cerebral palsied children, film projection system for eye movement monitoring 79−16329
cerebral regional blood flow, computerised monitoring system for stroke patients 79−79626
cerebrospinal fluid pressure meas. by passive telemetry, improved instrument 78−31927
cervical dilation during labour, continuous meas. with US device 77−86574
clinical paediatric gait biotelemetry 78−3652
clinical seizure, long term time-lapse video monitoring system, synchronised with EEG 79−39461
computer-aided monitoring of critically ill patients, signal interference problems *(German)* 78−3628
computer-based instrument using SK.2 cylindrical coordinator *(Russian)* 80−76856
computerised ECG monitoring, state of art 78−11766
computerised ECG monitoring system, features *(Swedish)* 79−44005
computerised ECG ventricualr arrhythmia monitor, performance standards and trends 78−7478
computerised intensive care, postoperative management of cardiac surgical patients 77−40918
computerised medical systems, automatic diagnosis systems 77−40841
continuous monitoring by ion-sensitive FET *(Spanish)* 79−83986
contourograph using ICs for quasi-periodic and nonidentical physiological signals 77−44791
corneal scattering, contact lens wear, border-enhancement spread, subjective monitoring method 79−29641
coronary artery bypass graft patient recovery trajectory classification algorithm 80−94411
coronary care unit equipment failure finding and prediction 78−44648
coronary care unit interactive ECG monitoring 78−7481
coronary intensive care unit, computerised monitoring system 77−21656
critical care fluid balance monitoring 79−25151
critically ill patient monitoring by integrated computer systems 78−35998
data reduction, consolidation, characterisation and expression of physiological signals in time domain 77−44767
deep tissue temp. monitoring by ultraminiature thermistors 80−3761
defibrillator, miniaturised implantable, automatic, heart monitoring appl. 77−81645
digital data store for radio monitoring of patients *(German)* 78−80998
digital pulse counter for cardiovascular monitoring 78−35978
dose from CT scan, meas. using pencil shaped ionisation chamber 79−20683
ECG, 24 hr, automatic analysis on minicomputer-based system 80−89889
ECG, ambulatory, computer processing system 80−89897
ECG, ambulatory arrhythmia quantification by correl. technique 78−81020
ECG, Argus algorithm development 79−70680
ECG, automated Holter anal., shape oriented system 79−70662
ECG, automatic analysis of 24 hr recordings, optimum ECG morphology and quality 79−70664
ECG, computerised Holter tape processing systems for drug testing, validation technique 78−81017
ECG, Frank xyz signal interpretation by unmodified 12-lead computer system 80−94400
ECG, Holter recording anal. using Argus/2H 79−70679
ECG, Holter recording processing, computer system 78−81015
ECG, Holter recordings, low cost arrhythmia analyser, GRETA 80−94403
ECG, Holter tape dual-channel anal. system, ARGUS/2H 78−81016
ECG, Holter tape high speed digital anal. with full editing capability 80−89896
ECG, interactive analysis techniques with Random Access Mass Storage ECG Analysis System 78−81034
ECG, long-term, efficient data compression and arrhythmia detect. 79−70678
ECG, long-term, flexible data presentation in DCG processing 79−70681
ECG, long-term continuous recorder *(Japanese)* 77−66871
ECG, long-term recording on mag. tape 80−56243
ECG, long-term recordings, rapid computer analysis system Argus/H 78−36002
ECG, microprocessor based ambulatory monitor 77−48918
ECG, monitoring abnormal QRS events, sequential improvements in on-line algorithm 78−81026
ECG, multiform ventricular complex identification, 2-dimens. clustering technique 79−66570
ECG, precision requirements for computer anal. 77−81607
ECG, premature ventricular beats detect. scheme 79−70657
ECG, premature ventricular contraction detection in heart beats 77−78022
ECG, QRS detector/delineator devel. and eval. 80−89892
ECG, random access mass storage anal., RAMSES, for quantitative anal. of long-term ECGs 79−70663
ECG, time correct. and two channel recording in 24 hour anal. 79−70658
ECG, two-electrode recording 78−28107
ECG 22 78−81027
ECG 24 hr recording, anal. using operator-controlled computer system 80−89888
ECG ambulatory monitoring, adaptive algorithm for noise rejection 79−66571

patient monitoring continued
ECG ambulatory monitoring, detect. algorithm for multiform premature ventricular contractions 79−66572
ECG arrhythmia analysis, dual-processor computer 79−66569
ECG arrhythmia classification in context, extension of single-beat algorithm 78−85426
ECG arrhythmias high speed pattern recognition 78−36004
ECG automated monitoring, new electrode system 80−89898
ECG continuous processing in accelerated time, pattern recognition program 78−92725
ECG frequency-domain analysis 80−85521
ECG Holter analysis, appls. of Dyna-Gram IIIB system 78−81019
ECG in ambulatory clinical practice 77−81627
ECG long term monitoring, automatic detect. of cardiac arrhythmias 80−3850
ECG long-term monitoring, with contourographic signal representation *(German)* 78−92714
ECG monitor, non-fade, battery-powered, emergency/surgery appl. 78−7528
eCG monitor interference from patient call systems 79−74776
ECG monitoring, R-R interval prediction models compared 78−35996
ECG monitoring by contour comparison, QRS triggering with real-time correlator *(German)* 78−92715
ECG monitoring in ambulatory patients 78−20309
ECG real-time telephone transmission usefulness and reliability 78−57108
ECG recorder, with statistical pulse train interval digital analyser *(German)* 77−78007
ECG signal parameter trend anal. 78−15920
ECG slow wave real-time anal., hardware implementation of selective Bouilland transform. 80−56233
ECG telemetry apparatus, PLL demodulator appl. *(German)* 78−57097
ECG telephone transmission, pacemaker, cardiac arrhythmias monitoring 77−52903
ECG three-dimensional recording technique 80−41274
EEG, automatic nocturnal sleep sampling 78−31916
EEG, automatic recognition of inter-ictal epileptic activity in prolonged recordings 80−3838
EEG, cable telemetry computer seizure monitoring system 77−5090
EEG, computerised statistical monitoring 77−40917
EEG, peak-detection algorithm for anal. 79−74772
EEG, source derivation or spatial filtering technique 77−44785
EEG, source derivations, clinico-diagnostic experience 77−44786
EEG 24-hour recording using 4-channel cassette recorder for epileptic patient 78−3639
EEG automatic classification, Kullbeck Leibler nearest neighbour approach 79−83975
EEG automatic K-complex detect. in sleep 78−53557
EEG automatic sleep staging detectors 78−53551
EEG biotelemetry, multielectrode, for remote monitoring and stimulation of ambulatory subject 79−5386
EEG brain function monitoring, microcomputer based system 77−73611
EEG digital recording system for epileptic event observation 78−3641
EEG epileptic transient detect., pattern recognition techniques 78−53542
EEG multichannel radiotelemetry for epileptogenic focus localisation 78−3653
EEG seizure-monitoring, cable telemetry system 78−3640
EEG sphenoidal electrode assembly for long-term monitoring of ictal or interictal EEG 77−48907
EEG TDM telemetry unit for fifteen scalp electrodes 77−40822
EEG telemetering, FM/PWM, multichannel, from unrestrained psychiatric patients 78−3636
EEG telemetry, including PWM multichannel system 78−31914
EEG telemetry time-multiplex unit, ambulatory patients 79−44007
EEG waveform detection by microprocessor 77−73610
electric admittance blood flow monitor, clinical evaluation 80−81759
electrical interference monitor and virtual earth, electrophysiological signal degradation reduction 79−57800
electro-oculographic activity, computerised meas. during sleep 79−74781
electrocardiodynamic continuous monitoring method 80−8195
electrocardioscopes, appl. and designs 80−41304
electrographic, skin-electrode processes obs. 77−40828
electromanometric system frequency response visualisation device 77−48890
electromedical equipment, computer controlled systems *(German)* 79−62421
electron beam treatment planning, patient specific data acquisition 79−100731
electronics 1979 development trends, w.r.t Czechoslovak biomedical instrumentation *(Czech)* 79−70689
electrosurgical hazard monitor 79−83882
EMG muscle activity of spastic gait monitoring, wideband telemetry system 77−90924
eneuresis alarm system, programmable op. amp., CMOS logic, Min. of Health Perf. Spec. 79−39600
enuresis alarm for mentally sub-normal children, low-cost and portable 79−53266
epidural intracranial press. monitoring with press.-sensitive on-off type switch sensor 78−44626
epidural pressure telemetering, implantable LC cct. transducer 77−32962
esophageal accelerometers, use in monitoring cardiovascular system 80−26403
exercise ECG anal. using microcomputer 79−70683
exercise ECG examination, telemetry, two channel storage cardioscope and multitrack video tape recorder appl. 77−70561
exercise rehabilitation of cardiac defect patients, QRS complex affinity assay 79−43854
exercise stress testing with continuous noninvasive cardiac monitoring 78−36000
extrasystole monitor using FIFO 80−72360
eye, internal pressure meas., early diagnosis of glaucoma 79−25140
eye continuous movement monitoring, proportional-integral adaptive system *(German)* 79−16320
eye movement, signal detect. via phase-locked sampling in mag. search coil 79−25124
eye-movement monitors, compensation for distortion 80−56244
fever alarm device using telemetry 80−21556
fibre optic probe for neonatal oximetry and dye curves 79−70603
fluid management records system 79−25150
patient monitoring continued
foetal breathing monitor for humans in utero, US pulsed Doppler instrument 78−69164
foetal breathing movement electronic anal., phase-lock-loop principles appl. 79−2152
foetal breathing movement meas. using US echographic time-distance recorder 78−24109
foetal ECG adaptive real-time noninvasive extraction using near-orthogonal functions 78−28110
foetal ECG and heart rate radiotelemetry monitoring 78−3651
foetal ECG detection, real-time system using near-orthogonal basis functions 77−21638
foetal heart and uterus diagnostic monitoring and functional mechanics 78−36009
foetal heart rate on-line data management during labour, prediction of one-minute Apgar scores 78−44655
foetal heart rate recording, interference due to infusion pump *(German)* 78−85414
foetal heart rate variability anal. using spectral anal. 78−28111
foetal heart rate variability monitoring by digital filtering 79−48353
foetal heartbeat semiautomatic monitor for nontechnical operators 77−56501
foetal movement monitors, detecting asymm. abdomen shape changes and wall impulses 77−52904
foetal valve movement, automated detect. using Doppler US 77−40727
foetal weight estimation using US B scanning method 78−3573
gait quality indication by temporal asymmetry 80−98164
glioblastoma tumour volume monitoring, autopsy rel. to computerised tomography meas. 80−21526
haemodialysis by extra corporeal ultrafiltration method, parameter estimation of vascular bed 79−84015
haemodynamic parameters monitoring by SOLO, an interactive minicomputer based bedside monitor 80−26392
haemofiltration control system *(German)* 79−5403
hand pathology, role of thermography 80−8120
health care and instrumentation, Indian scene 77−40813
health care expansion aided by integrated electronics 78−11751
heart beat counter, versatile digital SAMI 80−85510
heart beat counting, digital socially acceptable monitoring instrument 78−40367
heart beat disturbances anal. using LF direct meas. cct. *(German)* 79−96671
heart beat frequency monitoring circuit *(Bulgarian)* 77−78006
heart condition monitoring during bath therapy using immersed electrodes 78−3665
heart frequency monitor in microprocessor technology *(German)* 78−92718
heart monitor, using IR transducer, design and construction 79−83891
heart monitoring system for rhythm diagnosis of ECG 78−40392
heart rate analyser for long-term continuous ECG recordings *(German)* 78−3649
heart rate on-line statistical anal., using special-purpose computer 78−35984
heart-beat monitoring circuit with missed beat alarm 77−56500
heart-rate store, PLL circuit, portable *(German)* 78−65139
heart-rate variability measurement, clinical and neural cardiovascular research appl. 77−81610
high technology medical equipment, Angioscan, Cardiac Output Computer, Medishield Analyser, Tomographic Scanner 80−36171
Holter ECG high-speed anal. 79−66568
Holter tape processing, 60× computer system 79−66567
HP 5600A patient monitoring system 79−25152
human sleep EEG, spindle pattern recognition by real time anal. *(Japanese)* 80−89903
hyperthermia cancer treatment procedure, monitoring instrumentation 79−96716
idiopathic scoliosis, adolescent, monitoring with Moire fringe photography 80−17047
impedance cardio-telemeter *(Japanese)* 77−44790
impedance meter, AC, battery-operated, for contact resist. determ. before patient monitoring 78−81006
implantable accelerometer for cardiac performance telemetering 77−86670
implantable electronic pancreas and blood glucose monitor 78−88767
implanted pacemaker patient long-term surveillance unit 77−81722
indoor telemetry for ambulatory patients, 100 MHz tuned loop receiving antennas 77−90925
industrial health service automated ECG analysis results 79−39563
infant heart rate determ., clinical evaluation of miniature dry surface electrode 77−56505
initial QRS vector displacement in healthy young adults 79−43856
intensive care, 15-channel analogue selector 77−40898
intensive care, instrumentation and control, conf., London, England (May 1979) 79−70702
intensive care, O_2 conc., blood O_2, fluid balance, ocular microtremor, for teaching 78−49622
intensive care in paediatrics *(German)* 78−88754
intensive care instrumentation 78−53559
intensive care unit, use and acceptance of automated monitoring systems 78−81057
intensive care unit ECG protection against defibrillator pulse 77−25586
intensive monitoring computer system, SOLO, one-patient multiparameter bedside monitor 78−81053
intra-auricular P wave monitor, experience, performance evaluation 78−11764
intra-uterine pressure data, on-line computerised quantification 78−85424
intracranial pressure, remote meas. by passive reson. cct. detector *(French)* 77−37074
intracranial pressure and temp. two-channel telemetry system 77−81619
intracranial pressure monitoring by passive radiosonde 79−57798
intracranial pressure monitoring in neurotraumatology 80−17156
intracranial pressure noninvasive monitor for infants, fontogram 78−40373
intracranial pressure telemetering, in vivo and in vitro, with capacitance transducer 78−7457
intracranial pressure telemetric meas. *(German)* 78−85403
intracranial pressure telemetric monitoring system 79−74736
intracranial pressure/temp. telemetering, implantable two-channel system 78−3637
intraocular pressure, telemetry monitoring 78−3632

patient monitoring continued
intraoperative X-ray diagnosis, exposure reduction by magnetic disc store 79−92345
intrauterine pressure measurement during labour, limitations 77−56504
intravascular O_2 continuous monitoring, electrochem. sensor 80−56238
intravascular O_2 saturation continuous meas. using fibre optic catheter *(German)* 78−85411
intravascular PO_2 probe routine appl., practical experience 80−56239
IR noninvasive monitoring of cerebral and myocardial O_2 sufficiency and circulatory parameters 78−44583
IR recording retinoscope for accommodation monitoring 80−36055
IR telemetry system for surgical patient monitoring 80−30836
ischaemic episode, computerised continuous beat by beat anal. and rational plots 79−62394
ischaemic heart disease studied by cardiac pacing 77−81628
joint angle of limbs in two-dimensional movement, linear RF transducer appl. 77−90938
joint wear in humans, ferrography appl. 79−34694
knee ligament damage monitoring by acoustic emission, canine model 80−41149
knee-joint forces, routine clinical assessment method 79−83831
laboratory test interpretation using computer 79−74770
labour, Montevideo units computation algorithms 77−40896
labour meter with tape recorder for ambulatory patients *(German)* 78−85413
labour ward information and monitoring system *(German)* 78−88750
late pregnancy toxaemia, ongoing medical surveillance system 77−81602
limb blood flow automated monitoring system using venous occlusion admittance plethysmography 78−31937
locomotion evaluation equipment, computerised, clinical practice appl. 77−86676
lung function meas. system, mobile, computer aided *(German)* 78−3630
lungs, artificially ventilated, mechanical properties monitoring 77−21642
medical electronics, new forms and techniques 80−3856
micro-computer based system for the management of the critically ill 79−25153
microcomputer based cart, self-diagnosing 78−31943
microcomputer-based pulmonary wedge pressure measurements 80−26391
microcomputers for bedside monitoring of patients *(German)* 78−88751
microwave appls. in diagnosis and pulmonary disease monitoring 80−85460
microwave respiration monitor 79−96646
miniature pH-sensitive polymer membrane electrode 79−100781
mobile incubator transport for premature and newborn babies *(German)* 79−16336
Monitor DKS4T-01 system, surveillance of severely ill patients 79−34679
monitor using Walsh transform on standard microprocessor 80−26399
motion 3-dimens. monitoring by optoelectronic means, calibration and meas. 78−31913
motion three-dimensional monitoring by optoelectronic means, calibration 77−86658
movement-activated recording monitor for motor activity 77−25565
muco-ciliary transport monitoring method using ^{99m}TcS colloid, bronchiectatic patient appl. 80−30840
multi-microprocessor system *(German)* 78−88752
multichannel audio monitor for detecting electrical signals, neurophysiological expt. appl. 79−20694
multiple pregnancies, problems in US monitoring 80−41145
muscle potential, for electroconvulsive therapy 77−40899
muscular effort monitoring, prototype instrument 77−5092
myocardial ischaemia and necrosis monitoring in acute myocardial infarction 80−85525
myocardial pacing threshold determ. with external RF transmitter 77−81730
myocardial perfusion index calculator for prediction of subendocardial ischaemia in cardiac surgery 77−40915
neonatal intensive care unit, surveillance aid *(French)* 77−44831
neonate cardiorespiratory monitoring, automatic system with microprocessor 80−94399
neonatological care, intensive therapeutical and monitoring system 79−100785
neurological function tracking-task instrument, portable, features 77−86678
neurological intensive care facility requirements 79−92420
neurology monitoring system for stroke patients 80−26394
neuromuscular block, sweep frequency technique, conscious, unconscious patient appl. 77−52910
neuromuscular blockade monitoring device, twitch box 78−77132
neurosurgical intensive care, non-invasive monitoring techniques 80−81757
neurosurgical patient monitoring computer system 79−88206
obstetric computer-aided monitoring system *(German)* 80−41300
obstetrics, computer appls. to foetal monitoring 77−77999
obstetrics, microprocessor based system for studying kinematics of labour 77−44769
obstetrics, microprocessor data acquisition and preprocessing with minicomputer signal processing 77−44775
oedematous tissue quantification by elec. impedance meas. 78−44630
oesophageal accelerometer evaluation for cardiac function noninvasive meas. 79−92458
oesophageal multiprobe for temp., ECG and heart and lung sound meas. 78−77146
operating room monitoring, developing crisis 78−40401
operating theatre patient monitoring problems and trends 79−92422
oral force monitoring, piezoelectric transducer, with thin bite element 77−48888
orthotics parameter assessment based on telemetric heart rate monitoring, paediatric patient appl. 78−31974
oximeter calibration, humans exposed to centrifugation 78−92734
oximeter for spectrophotometric monitoring of arterial O_2 saturation in the fingertip 80−41161
oxyhaemoglobin dissociation curve direct obs. in man in vivo, computer investigation 78−85433
pacemaker base rate follow-up reliability for long-term pacing 77−81694
pacemaker function check by patient self-monitoring system 77−81718
pacemaker impulse and pulse rate self-monitor 77−81719
pacemaker patient surveillance by automatic pacemaker function analyser 78−3679
pacemaker surveillance by telephone photoanalysis 77−81699
patient monitoring continued
pacemaker tracking system based on microprocessor, hardware considerations 78−36070
Parkinson tremor, long-term recording and evaluation 77−21639
perfusion blood temp. monitoring, zero-heat-flow transducer 80−8201
perinatel radio telemetry 80−104722
pH determination, improved Sb-Sb_2O_3 electrodes 79−53270
photoplethysmography, audio-visual heart monitor based on light transmission through skin 79−53206
physiologic profiling, automated, in acute ill patients 80−30914
physiological signal on-line anal., multiple microprocessor system 80−26389
platelet aggregation studies using TEXAC whole picture analysis 79−25133
position monitoring during radiation treatment using transmitted X-ray beam 77−40894
postoperative cardiac surgical patient care, automation of meas. and interventions 78−20310
pressure monitoring device design infection control considerations 77−21641
pressure transducer, implantable 77−73606
pressure transducer performance, effect of zero offset changes 80−56255
pulmonary artery blood press. anal. algorithm 78−40376
pulmonary conductance, elastic recoil, computerized meas. 79−16317
pulmonary diseases, using microwave reflection/transmission meas. method 78−28031
pulmonary gas exchange data online acquisition system 78−28100
pulmophonography, propag. of sound waves in acoustic ducts of lungs 77−12981
pulse rate meter for heart monitoring 78−31915
pulse rate monitor, digital, IR absorpt. detect. 80−26322
pupilometry, instrumentation for stimulating and monitoring human pupil 78−48911
quality health care and cost containment, conf., Washington, USA (Mar.-Apr. 1978) 79−39333
radio pressure pills for back stress monitoring 77−73604
rapid eye movement automatic detect. system and normative data 79−74771
renal transplantation, photon absorptiometry of bone 77−48854
respiration, indirect monitoring, ballistocardiography 77−29222
respiration, microwave Michelson interferometer 79−8557
respiration monitor for children using belly-belt electronic sensor 77−56512
respiration monitor for premature infants, non-contacting device using air-transmitted US 77−52915
respiration rate automatic meas. device *(German)* 79−2146
respiratory data management subsystem 79−83980
respiratory gas analyser utilising glow discharge selective spectral emission, microprocessor based 79−100772
respiratory gas monitoring instrument using microprocessor *(Japanese)* 80−72358
respiratory monitors, instrumentation and maintenance, review 78−69236
respiratory patterns in premature infants, computerised apnoea monitor 77−81635
respiratory rate monitor using microphone pickup 79−79617
respiratory sounds, sensing by laser interferometer 77−90872
review of nucl. medicine 1977 78−85459
rheocardiography, 4-electrode, in computer-aided cardiac output determ. 80−61718
ROM based ECG monitor 80−26401
sample/long term hold digital circuit 77−40803
scintillation probe detector in assessment of cardiovascular disease 80−3800
scoliosis correction using Dwyer cable, noninvasive telemetric determ. of anterior spinal fusion 77−44851
second-generation ECG monitoring system development 78−7480
sick sinus syndrome 24-hour Holter ECG monitoring 79−39562
single-epoch somatosensory evoked vertex potential, time window for electro-ocular monitoring 79−96535
sinus node autonomic control in man, quantitative assessment 79−70684
sleep depth determ. by cluster anal. of heart rate data 78−44659
sleep EEG ambulatory monitoring and anal. 78−44650
sleep research, microprocessor appl. 79−96693
SOLO monitor, microcomputer bedside monitor 80−94404
spike-wave EEG patterns, quantification method clinical evaluation 78−11754
spinal cord, injured, monitoring of residual function with sensory evoked pots. 80−81747
SQUID gradiometer, second-derivative, magnetocardiogram meas. 80−104696
static charge sensitive bed, method for recording body movements during sleep 80−3840
supraventricular arrhythmia rapid anal. from long-term oesophageal recordings, drug assessment 80−89904
surgery, 4-channel telemetry system 78−31961
surgery, central venous-, pulmonary artery end-diastolic- and pulmonary capillary wedge-pressure meas. 77−90955
surgery, inexpensive general purpose computer 78−36045
surgery, microprocessor-based patient monitoring system 78−44681
systalic blood pressure monitor, type SCS-501 *(Japanese)* 77−70565
systolic time interval processing system, STIPS 78−81029
systolic time intervals from surgical patients, continuous real-time computation and display 77−37098
telemetric human movement correction using computer and electrostimulating device 77−86656
telemetry, conf., Sapporo, Japan (June 1980) 80−90604
telemetry, low power PAM/FM system for ventricular press. and cardiac dimension meas. 78−44747
telemetry device, chronically implanted, controlled transcutaneous powering 80−98152
telemetry system, implantable, single-freq., for monitoring body temp., blood pressure and ECG 77−86688
telemetry system, seven-channel fully integrated, features 78−3634
telephone-telemetry system for routine check-up of pacemaker patients 77−90957
temperature, deep body thermometer testing and modelling 77−40816
temperature, using temp. depend. of US vel. in tissue 78−40281
temperature distribution, using temp. depend. of US vel. 80−45994
temperature measurement, μA radiotelemetry transmitter 79−16356
temperature monitoring system using implantable thick film telemeter 77−40825

patient monitoring continued
thermography in clinical diagnosis and monitoring 78−57113
thermometer, electronic digital, for long-term patient monitoring 80−90849
tissue pressure, continuous monitoring instrument 79−100762
total cardiac monitoring integrated microcomputer/minicomputer system 78−35997
transcutaneous pO_2 measurement in computer-assisted monitoring of infants 78−85432
transient cardiac arrhythmia detection, 24-hour ECG recording 79−44020
transthoracic impedance curve processing, patient-computer interface 79−34686
trauma indices 77−25588
trauma prognostic indices 77−25589
two way scanning method for total body in vivo neutron activation anal. 78−92697
tympanic contactless membrane thermometer 79−34692
Unibed patient monitoring system based on microcomputer and LSI technology 78−20305
urine glucose analyser with audible output 77−52909
US applications, review 79−92308
US monitor for fetus cardiac pre-ejection period continuous meas. 79−74732
US telemetry for monitoring heart/respiration rate and body/skin temp. of scuba divers 77−90929
uterine activity monitoring, internal and external methods 78−35973
uterine contraction waveform online digital processing system 78−15916
uterus activity recording from abdominal EMG *(German)* 78−92712
vascular interface system for automation of haemodynamic monitoring and therapy 78−81054
vectorcardiogram, genetically determined variation study, computerised procedure 77−25579
ventilation automatic control, pulmonary model 77−21556
ventilation feedback control in small infants after open-heart surgery 79−70710
ventilator-patient circuits, long-term monitoring using turbulent air flowmeter 77−64149
ventilatory monitoring in operating room, current techniques and future requirements 78−20307
ventricular arrhythmia model 80−89893
ventricular arrhythmia on-line study, computer system 78−81060
ventricular arrhythmia quantification, minicomputer system 79−70677
ventricular ectopic activity, semiautomated data reduction 79−66573
ventricular ectopic beat detect. in rapid Holter scanners, prematurity and height as criteria 79−66575
ventricular fibrillation alerting device 77−78024
ventricular fibrillation detect. by computer 79−70675
ventricular fibrillation recognition using ECG power spectrum 78−81032
ventricular function monitor, ambulatory, CdTe detector, cardiac ejection fraction meas. 80−61680
ventricular pressure and ECG continuous monitoring during angina attacks, computer anal. 78−85436
video biofeedback for alpha monitoring of brain activity 78−20299
visual behaviour monitoring system, EMG triggered photographic technique 78−31919
visual electrophysiological examinations of flying personnel 79−11929
visual evoked human-scalp EEG data monitoring, processing and displaying system 77−90936
walking pattern, EMG and temporal data telemetering 78−3638
weight, continual in-bed monitoring 78−48910
wrist actigraphic measures of sleep and rhythms 79−16315
^{131}I treated patients, monitoring of I excretions and used materials 80−89873
K level in blood meas. using catheter-tip selective electrode 77−90935
K^+, in vivo continuous monitoring using ISFET probes 80−85512
O_2 consumption, monitoring instrumentation using replenishment technique 79−39547
O_2 consumption of surgical patients under N_2O anaesthesia 77−81640
O_2, intraarterial vs. transcutaneous monitoring in newborn infants 80−56266
O_2 monitoring, combined system for transcutaneous and intravascular determ. of partial press. 80−56241
O_2-CO_2 transport real-time and interactive control in mechanically ventilated patients in ICU 79−62404

patient treatment
see also biomedical ultrasonics; radiation therapy; surgery
actinides, inhaled, research at Nat. Radiological Protection Board, chelation and bronchopulmonary lavage 77−48879
acupuncture, search for elec. located skin stimulation points 79−43976
acupuncture, transient impedance between stimulation points 79−43977
acupuncture points Li-4 and Li-12 Laplace plane analysis of transient impedance 77−81772
acute myocardial infarction, electrophysiological aspects 79−43858
aerosol, from nebulizer, droplet size distrib., evaporation effect 78−24084
air compressor used in system for treatment of decubitus ulcers, noise reduction 80−48513
alcoholics, drinking consummatory response measuring device for automated aversion therapy 77−56510
amblyopia, ocular rivalry suppression, effect of 9 Hz flashing light 79−34566
antagonistic muscles, functional elec. stimulation optimisation, math. modelling, joint motion 80−61730
antitumor drug dosage schedule, cell cycle kinetics approach 77−86700
aortic valve replacement, computerised simultaneous press./vol. anal. before and after 80−85531
aphasia treatment session recording, momentary and interval sampling 79−96704
arrhythmia treatment by temporary cardiac pacing 77−81648
arrhythmia treatment with permanent cardiac pacing 77−81674
asthma-preventive cromolyn Na inhaler fluid mechanics 79−79587
auditory training apparatus, individual for persons suffering from severe hearing loss 79−39590
biofeedback, physiological responses control appl. *(Japanese)* 77−44830
biofeedback, psychotherapy applic. *(Dutch)* 77−37100
biofeedback control of skin potential level 80−21572
biofeedback therapy technique and application *(German)* 79−16341
biofeedback thermometer, low-cost research-oriented, with digital readout 79−29673

patient treatment continued
biofeedback training, control of prosthetic knee 79−34700
biofeedback training device for speech therapy, portable, microprocessor-based 80−104808
biomaterials for therapeutic instruments, ionising radiation processing 77−70542
biomedical electronics developments 77−13017
blood, filter evaluation 78−69250
blood cell suspensions, deep-freezing improvements by thermal history automatic detect *(German)* 79−88215
blood heating/cooling, heat exchanger thermal design, equipment and blood props. considerations, appls. 78−92744
blood oxygenation perfusion system for treatment of acute respiratory failure in infants 80−3866
blood pressure control in hypertensive crisis, closed loop control of sodium nitroprusside infusion 78−44688
blood toxic metabolites, dynamics of depend. sorption by C sorbents 77−70487
bone fracture, evaluation of finite element and exptl. models of internal fixation plates 77−48934
bone healing, effects of elec. stimulation on exptl. model for non-union, dog 77−60287
bone healing, elec. stimulation of growth, treatment of non-union and delayed fractures 80−17044
bone healing, elec. stimulation of growth in treatment of non-union, review 80−17043
bone healing, use of anodised Ta electrode, meas. of electrochem. reactions 78−95931
bone healing augmentation by electric currents and fields 80−8116
bone healing electrostimulation, clinical aspects 79−83879
bone healing enhancement by elec. stimuli, effect of stimulation modality 77−40907
bone healing in humans, appl. of pulsed mag. field to stimulation 78−28029
bone marrow transplant patients, clean room and laminar air flow room microbiology 80−26411
bone pyrogenic infection treatment by non-invasive EM technique 78−48854
bone remodelling, effect of internal fixation plate 77−48935
bone remodelling beneath internal fixation plates of varying stiffness, parametric study 80−16990
bone stimulation, EM fields in capacitative and inductive devices 78−40283
bone stimulation devices, anal. of sinusoidal EM fields 80−108990
bone strength, rel. to mineral supplemental diet in young rabbits 77−36986
brain lesion induction thermocoagulation, Ni-Pd-Mn alloy as thermoseed implant *(Japanese)* 79−61114
brain pacemaker energy optimisation, epileptic seizure control appl. 77−52934
brain tumour destruction by 8 MHz implanted metal powder eddy currents *(German)* 79−16337
bronchopulmonary lavage 78−15910
burn patient closed loop fluid resuscitation using microprocessor 78−36046
burn wound dressing, silicone rubber with radiation-grafted methacrylate 79−29657
burns, therapeutic effects of cooling 79−29663
cancer detection and therapy, stochastic anal. and control of physiological systems 77−90713
cancer treatment by hyperthermia *(French)* 80−17024
cardiac arrhythmias management, automated feedback control of drug therapy 80−41307
cardiac assistance, performance criteria for optimisation 79−74782
cardiac electrodes, safe voltage limits 79−16344
cardiac massage unit, pneumatic, effects under ventricular failure, dog expt. 77−78036
cardiac pacemaker treatment principles and experience 80−8213
cardiac pacing, signal source impedance of implanted electrodes 80−56275
cardiac response sensitivity to time relationship between vibr. and cardiac cycles 77−56407
cardiac resuscitator, automatic, emergency treatment of cardiac arrest 79−88147
cardiopulmonary bypass, portable, appl. to emergency instrumentation 78−44679
cavernous tuberculosis, local drug injection device 78−7520
cerebellum chronic stimulation and EEG, the utility of artifact 79−96643
cerebral palsied children, film projection system for eye movement monitoring 79−16329
Chagas' cardiomyopathy treatment with implantable pacemakers 77−81681
chelation therapy, DTPA treatment schedules for ^{239}Pu decorporation from simulated wounds 77−64137
chelation therapy for transuranic elements using Ca-DTPA and desferrioxamine B, rats 77−44758
chelation therapy with inhaled Ca-DTPA, effect on long-term $Pu(NO_3)_4$ effects 77−66861
chemotherapy with 5-fluorouracil, distrib. of ^{18}F labelled tracer in tumour-bearing mice and rats 78−48878
chromatic maculae of the skin, pulsed ruby lasers appl. *(German)* 78−24177
clonus, simplistic model rel. to diagnosis and therapy 77−48786
cold urticaria diagnosis and treatment assessment, stable low temp. source 78−61276
conference on cardiac defibrillation and cardiopulmonary resuscitation, Lafayette, USA (Sept. 1979) 80−67929
coordination therapy electronic aid using pattern recognition methodology 80−56276
corneal curvature alteration by elec. heating, rabbit expt. 77−40665
counterpulsation, external, computer anal. using nonlinear math. model of cardiovascular system 77−2069
cryogenic treatment device for (sub)atrophic rhinitis and pharyngitis 77−78028
cryomedicine, development trends *(German)* 77−25590
DC therapeutic transistorised apparatus *(Bulgarian)* 78−24175
deaf people, computer generated speech training patterns 80−51290
defibrillating trapezoidal waveforms, haemodynamic responses 80−72370
defibrillation, anal. and simulation of ECG recovery 77−40910
defibrillation, multiple-shock, effect of shock separation time 78−57053

patient treatment continued
defibrillation, myocardial damage, induction by open-chest low energy countershock, rabbit expts. 80−72150
defibrillation, myocardial damage rel. to high-energy elec. current 78−57051
defibrillation, performance characteristics of three commercial instruments in transthoracic ventricular defibrillation of animals 78−57048
defibrillation, thoracic impedance of humans, meas. using automatic recording device on defibrillator 78−61239
defibrillation, transchest, strength-duration curves for trapezoidal waveforms of various tilts, dogs and ponies 78−57054
defibrillation, transchest damped sine wave shocks producing cardiac damage 78−57052
defibrillation, transchest ventricular, comparative efficacy of damped sine wave and square wave in dogs and ponies 78−57055
defibrillation, transthoracic, square-wave, experience in dog and calf 78−57050
defibrillation, transthoracic chest resist. of 100 kg calves defibrillated with rectangular pulses 78−36047
defibrillation, transthoracic ventricular, in adults, success rate rel. to energy used 78−57049
defibrillation conference, Lafayette, USA, (Sept. 1977) 78−57047
defibrillator electrode gel testing, meas. of impedance to transthoracic DC discharge 78−57056
defibrillator ground-loop current elec. skin burn computer simulation 77−78039
defibrillators for emergency medical use, improvements and clinical studies needed 78−44678
dental drill with noise, vibr. radiointerference reduction 78−85450
dental instrument noise studies, canine evoked response audiometry system 77−29226
dental sealant application by laser 78−48868
dental unit US 10/100 78−36040
dentistry, preventive, laser processes 78−7530
diabetes, portable precision pumping system for insulin infusion 79−25148
diabetes mellitus, devices for control of continuous insulin infusion 80−17184
diabetes mellitus, public policy toward evaluation of control devices 80−17185
diadynamic current therapy, portable apparatus 79−57809
diadynamic current therapy apparatus Tonus-1 78−7523
diafiltration, with capillary membranes *(German)* 77−48921
diafiltration process, technical aspects *(German)* 77−48920
dialysis, ultrafiltration, meas. and control using differential flowmeter 77−21657
disabled children's therapeutic aid using myoelectric feedback 78−36048
drug administration, DC micromotor controlling feed rates in syringe pumps 78−48923
drug controlled administration, by implantable electro-osmotic valve 78−40399
drug release supports using reconstituted collagen, mech. prop. consideration 78−3666
drug screening using US intravascular mural thrombi formation technique 78−24091
drug-carrying microspheres, intravascular mag. guidance 78−73188
DTPA therapy, Pu body burden estimation from urine data 78−73259
education, human body, live, thermodynamics of cooling for treatment purposes 80−73128
EEG alpha-detection system, feedback stimulation and data analysis system 79−29642
EEG biofeedback conditioning, signal detection methodologies 79−29656
EEG feedback training, techniques and clinical appls. 78−36043
electrical brain stimulation for the control of chronic pain 78−77097
electrical stimulation, paralysed extremities, basis, technology and role 79−34620
electrical stimulation and callus *(Japanese)* 80−12204
electrical stimulation of organs and tissues in clinical medicine 78−35977
electrical stimulation of paralysed muscle, actuator of locomotor system *(Slovenian)* 80−81771
electro-optics appl., 1980 development trends 80−85464
electro-surgical dispersive electrode sites, temp. distrib. meas. 79−96519
electrochemical healing similarities between animals and plants 79−92316
electrocoagulation, monoactive, controlled destruction and temp. distribs. 80−94176
electroconvulsive, muscle potential monitor 77−40899
electroconvulsive therapy, servo-controlled volt. machine 78−77148
electroconvulsive therapy pulse instrument 78−53562
electrode-induced bone growth, function of implanted cathodes 80−41312
electrodialysis machine, hydraulic losses due to cracks *(Russian)* 77−32964
electromedical diagnosis and therapy techniques *(German)* 79−100687
electromedical equipment, computer controlled systems *(German)* 79−62421
electronics 1979 development trends, w.r.t Czechoslovak biomedical instrumentation *(Czech)* 79−70689
electroosmotic pump for regulated release of medicaments *(German)* 78−7518
electrophrenic respiration, feedback control of tidal vol. *(Japanese)* 80−41316
electrostimulation, external, solid-state therapeutical equipment *(Spanish)* 77−78038
electrostimulation, method and clinical use 79−83877
electrostimulator, portable, for transcutaneous analgesia 78−36032
electrostimulator for leg muscles to correct defective walking 78−36051
electrostimulator for muscles, Stimul-1 78−36035
electrostimulator for percutaneous nerve stimulation, chronic pain treatment *(German)* 79−16342
EMG assisted relaxation training with hyperkinetic children 80−21571
EMG biofeedback device 79−96706
EMG biofeedback in hemiplegic patient treatment, comparison of actual and simulated treatment 80−104806
EMG biofeedback in relaxation training 77−81636
EMG biofeedback training in low back pain treatment 80−21570
EMG envelope spectral anal., Parkinson's disease diagnosis and treatment appl. 79−5390
EMG feedback therapy after stroke, efficacy obs. 80−30927
patient treatment continued
endoscopic coagulation of mucous membrane lesions using HF elec. current *(German)* 78−80945
endosteal implants, alveolar bone growth enhancement by elec. stimulation, dog expts. 80−26413
epidural neurostimulation, percutaneous, histological reaction, short and long term study results 80−67285
epileptic seizures, operant conditioning of central nervous system activity 79−83881
epileptics, EEG feedback training 79−70696
exercise rehabilitation of cardiac defect patients, QRS complex affinity assay 79−43854
exercise therapy, walking simulator 80−81770
expected outcome loss for medical diagnosis and treatments evaluation 77−25587
external counterpulsation, optimal phase shift determ. model 79−29557
extraction wound non-invasive treatment by EM stimulation, dog expt. 80−17049
extremities wound management, controlled environment treatment 79−74787
eye, abnormal movements control method using audio feedback 80−41156
facial palsy, electromyographic biofeedback program 79−34701
femoral shaft fractures, early weight-bearing treatment using cast-brace, biomechanics 80−16985
fine muscular control rehabilitation using ramp threshold feedback 79−83996
forearm crutch with built-in load indicator, walking retraining after fractures *(German)* 79−8563
fracture fixation, oblique, mechs. using finite element model 77−52922
Fuchs's endothelial dystrophy, optometric management 79−83994
functional electrical stimulation for paraplegic patients *(Croatian)* 80−109058
functional electrical stimulation of the upper limb, joint moment charting 80−41310
functional rehabilitation, myophone appl. *(Spanish)* 78−48924
gait analysis, for daily orthopaedic practice, 2-D cinephotography, 6 component force measurement 77−48908
gait correction in paretic patients, multichannel functional electrostimulator design 79−57810
gait measuring system for treatment evaluation, microprocessor controlled 80−61731
gastrointestinal tract electrostimulator, Endoton-1 78−36033
glaucoma diagnosis and therapy, importance of tonometry 78−40383
gynaecological cancer care, Ne-He laser appl. *(German)* 78−24176
haemodialysers, hollow fibre type, haemofiltration and thrombus formation effects 78−3672
haemodialysis, PIXE meas. of trace element transport 80−36102
haemodialysis technique with dialysate regeneration by absorpt. and ion exchange *(German)* 77−48919
haemodialysis treatment model for metabolic waste conc. dynamics and cerebrospinal fluid pressure 77−60305
haemofiltration, appls. and limitations in clinical use *(German)* 80−21568
haemofiltration as alternative to conventional chronic dialysis *(German)* 80−21569
haemofiltration treatment, chronically intermittent, principles and results *(German)* 79−5404
haemoperfusion, large agarose beads, prep., props. and appls. 79−16349
haemoperfusion, using activated C cloth 77−37105
haemoperfusion device comparative evaluations 78−44690
heart block, survival of patients treated with implanted pacemakers 77−81686
heart pacemakers, review *(German)* 79−100787
heart rate and sinus arrhythmia obs. during health-resort treatment 79−43855
heart temporary artificial elec. stimulation 80−56272
hemiplegic upper extremities, feedback elec. stimulation trainer 78−44683
herniorrhaphy, mech. and struct. props. of prosthetic reinforcing materials 79−74789
hybrid neural stimulator for chronic expts. 78−28124
hydroelastic wave oscillator for treatment of human body tubular diseases *(Chinese)* 79−39588
hydrogel pilocarpine release rate control by plasma polymerisation 77−60284
hypertension treatment, elgctrosleep apparatus with rotating polarisation current 77−21655
hyperthermia, digital readout of feedback control temp. 79−70697
hyperthermia, dynamic temp. distribs. in normal and neoplastic tissues during diathermy 78−31776
hyperthermia, local, theoretical and expt. study, nonperfused phantom *(French)* 80−104559
hyperthermia, localised, in the patient, clinical requirements 80−98173
hyperthermia, localised, thermometry considerations, review 78−53561
hyperthermia phantom for point by point temp. mapping 79−70698
hyperthermia techniques in cancer management, clinical appls. 78−44682
hyperthermia therapy, temperature distrib. in human body 77−16911
hypothermia, local, Gipospast-1, thermoelec. apparatus 80−104807
inhalation apparatus, technique of continuous and intermittent working 78−36038
insulin delivery to diabetics, by computer controlled pulsed insulin infusion 77−37099
intensive care instrumentation 78−53559
intra-aortic balloon pumping apparatus trials 79−48368
intractable tachyarrhythmia treatment with pacemaker and β-receptor blocking agents 77−81675
intravenous antiarrhythmic drug infusion, automated delivery 78−81058
ionization phenomena, appls. in medical diagnosis and treatment, review 80−67240
iontophoresis device for safe elec. administration of ionised drugs 78−31965
jet injector, compressor operation mode 78−7524
keratoplasty, fluoresc. angiography of vascularised cornea using camera slit lamp 78−48855
kidney stone destruction by US shock wave focusing 77−32946
kidney stone non-contact destruction by shock waves *(German)* 78−7517
laryngeal dynamics, effects of Teflon injection 79−70560
laser application in medical and biological fields 77−77961

patient treatment continued
laser applications, book 78−48857
laser applications, in USSR 77−73555
laser applications *(German)* 78−73192
laser applications in medicine and biology, bibliography, 1963-74 77−25539
laser medicine development trends 80−51198
leg lengthening, tension/stretch ratio, method and clinical results *(German)* 78−36031
leg-load alarm system for partial-weight-bearing walking exercise *(Japanese)* 79−29658
LF interference current therapeutic apparatus *(Bulgarian)* 80−26314
lidocaine infusion regimes, computer assisted planning, clinical studies 77−40919
lung lavage for removal of inhaled radioactive particles, review 78−3618
magnetotherapeutic apparatus and application statistics *(German)* 79−16340
malignant tumours of head and neck, therapy eval. by ^{67}Ga scanning 77−37046
Marat, Jean Paul, medical use of electricity, historical note 80−17781
mechanical ventilation of infants, airway flow patterns 79−57685
mechanically ventilated patients' anatomic deadspace meas. by N_2 washout 79−96694
medical computing symposium, Toulouse (1977) 78−36003
medical physics conf., Atlanta, USA (July-Aug. 1979) 79−83858
MF current therapy, Nemec's interference maximum location *(German)* 79−16339
microwave diathermy equipment and power indicator 77−40901
microwave diathermy with surface cooling, elevated temps. induced in human leg 80−61638
multiple sclerosis, functional stimulation of spinal cord 79−20606
muscle fatigue resistance rel. to elec. induced exercise 77−37103
muscle transfer function online evaluation by impulse response transformation, rehabilitation test appl. 79−57637
muscular dystrophy, Duchenne, patient dynamic long leg orthosis 79−96715
myocardial infarction, antiarrhythmic drug and hyperkalaemia effects on ventricular electrogram 77−81667
myocardial threshold, pharmacological influence determ. 77−81643
neonatological care, intensive therapeutical and monitoring system 79−100785
neoplasia, apparatus for hyperthermia induction 79−44048
nerve stimulation apparatus and electrodes 78−36034
nervous system, electrical stimulation, laboratory research *(Norwegian)* 78−77096
nervous system electrostimulation, stainless steel electrode corrosion control 78−7464
nervous tissue damage parameters secondary to elec. stimulation 78−44491
neurological disorders, closed EEG feedback system 79−34703
neuromuscular disorders, biofeedback therapy, conscious control of motor neurons 79−34702
neuromuscular motor structures, programmed multichannel electrostimulation apparatus 77−25585
neuromuscular system electrical stimulator using biopotential amplifier 79−48315
nitroglycerine paste, efficacy evaluation using Hg strain gauge plethysmography 77−40905
oesophageal pacing in infants, conductive rubber electrode 77−81741
oncology, computer appl. *(Swedish)* 77−44763
oncology, role of radionuclides, review 77−9248
ophthalmological instrument manufacture, development trends 78−48903
oral sensori-motor disorder treatment appliances 78−36030
orthodontic adhesive joints, adherend topography effects 77−52916
orthodontic direct bonding systems, stress anal. 77−56513
osteosynthesis, compression, optimum plate prebending measurement methods *(German)* 77−40895
osteosynthesis, holographic interferometry appl. 79−88213
oxygenator, silicone rubber, tubular membrane, efficiency increase method 77−48930
pacemaker therapy, importance of R-vector direction 79−44049
pacing, meas. of ohmic electrode-tissue contact resistance and voltage applied to myocardium 80−67284
pain control by neural augmentation implant, electrophysiological approach 79−29660
pain control in man, medial thalamic permanent electrodes, electrophysiological and clinical study 80−67282
paralysed leg stimulation, programmed six-channel stimulator for walking *(Slovene)* 77−40923
paralysis, electric field control electrode for stimulation of peripheral nerve 80−21515
paralysis treatment, microprocessor based stimulator *(Slovenian)* 80−104809
parametric biostimulation, mag. field calcs. 80−36054
paraplegic patient muscles, provision of functional use by elec. stimulation, review 80−101289
parodontosis treatment portable vacuum apparatus 79−39593
paroxysmal supraventricular tachycardia management by scanning pacemaker system 77−81676
paroxysmal supraventricular tachycardia termination by overdrive pacing 77−81649
partial weight-bearing walk, limb load alarm system 79−29661
partially paralysed patients, medical rehabilitation designs 78−53579
percutaneous elec. stimulation of nervous system for pain relief 78−3668
percutaneous electrode system development 77−5106
petit mal epilepsy treatment, unobtrusive wearable device 77−25592
photographic appls. in medical treatment and litigation 80−36189
phototherapy of neonatal icterus, comparison of blue-light lamps 78−44582
plasma filtration from whole blood, effect of various parameters 78−48826
posthaemorrhage blood volume control model for intravenous fluid therapy 77−40697
psoriasis treatment, detect. of 8-methoxypsoralen in ocular lens 78−15937
psychosomatic and rheumatic complaints, magnetiser for generation of 2.5-5.8 Hz magnetic field, construction 78−15878
psychosomatic clinic audio-visual communication system 79−83997
pulmonary thromboembolism treatment and prophylaxis by percutaneous caval filter 77−48925
patient treatment continued
Pyran copolymer containing 5-fluorouracil, synthesis and antitumor props. 79−91613
quality health care and cost containment, conf., Washington, USA (Mar.-Apr. 1978) 79−39333
radiology, review of past and future techniques 77−12984
radiopathology, clinical problems in diagnosis and treatment of radiation damage *(French)* 78−48845
renal dialysis, improved patient management by computer simulation 79−70703
renal support using microorganisms 77−48950
respiration, human, managment of artificially ventilated patients 79−70576
respiration electrical stimulation, appls. and equipment 78−36054
respiratory therapy, automatic ventilator with digital electronic control 77−40897
retinal-image movement rel. to eye rotation, contact lens/spectacle system for correction 79−53281
scholiosis treatment, Electro-Spinal instrumentation 78−48925
scoliosis, electrospinal stimulation treatment 77−40908
scoliosis, electrospinal stimulation treatment 77−40909
scoliosis correction, by lateral surface elec. stimulation of muscles 78−44717
senile dementia patients, unrecognised intermittent bradycardias, rel. to cardiac pacing 77−81644
sick sinus syndrome, cardiac pacing problems 77−81680
sick sinus syndrome applications of cardiac pacing 77−81679
silicone membrane progesterone release rate control by plasma polymerisation 77−60285
sinoatrial bradycardia treatment by transvenous atrial synchronised pacing 77−81683
skeletal muscle const.-vel. contractions by sequential stimulation of muscle efferents 80−41309
skin mechanics, effects of some clinical treatments 79−100644
sorbent haemoperfusion systems, characterisation of solute removal 78−44689
speech synthesis, portable equipment *(French)* 80−51291
speech therapy, solid state delayed auditory feedback system 77−13028
speech trainers, with visual display system, systematic use for hard of hearing children *(Japanese)* 79−39596
speech trainers using visual display system, for hard of hearing children *(Japanese)* 79−39595
speech training aid, SIRENE, computerized 79−70701
speech training aid system tri-normalized speech processor 79−70700
spinal cord, electro stimulation for demyelinating and degenerative diseases 79−79621
spinal cord electrical stimulation, 2D finite element anal. 80−98054
spinal injury, μP controlled stimulation of paralysed muscle, exp. study, positive control, dynamic movement appl. 79−83883
spinal-cord stimulation in multiple sclerosis, electronic aspects 80−41313
spine, Carshalton halo-pelvic traction apparatus, design improvements 79−39594
stereodynamic interferential current, new electrotherapeutic technique 80−85458
stereodynamic interferential current therapy, fundamentals and initial results 80−85459
stimulation electrode, implantable standardisation problems 77−64151
stomatology, needle holder for intraosseous infusion 80−3859
subliminal communication for behaviour therapy and education, audiovisual technique 78−73293
supraventricular arrhythmia rapid anal. from long-term oesophageal recordings, drug assessment 80−89904
synchronised diagnostic and treament techniques 80−61727
synovial joints, rheology of synovial fluid, synthetic lubricants for degenerate joints 79−11955
systemic lupus erythematosus treatment with permanent pacemakers 77−81682
tachycardia suppression by programmed premature stimulation 77−81650
tachycardia treatment by implanted pacemaker 77−81677
telemedicine, development of medical treatment system for first deep sea mining ship 78−77147
tibial fracture fixation, forces in screws 77−60300
tibial fractures, treatment with plaster casts, biomech. study 79−74696
tibial shaft internal fixation, biomech. study 78−20313
tissue parametric stimulation by inductive transducer and US phased array 79−92320
tissue regeneration by electric potentials 80−41308
tongue movement observation using dynamic palatography 78−44687
tongue movement study using dynamic palatography 77−29160
tooth hard tissue operations, BN-1 apparatus for sonic anaesthesia 78−85350
transcutaneous electrical neurostimulation serial/parallel interface system 79−92321
tumour heating, calc. of intratumour temp. in superficial tumour 77−32876
tumour registry system using computer for follow-up treatment eval. and oncology teaching 77−44805
upper extremity rehabilitation, Bioconverter 79−48364
urethral closing muscle functional electrical stimulation effects 77−60286
urinary calculi in vitro destruction by laser-induced stress waves 78−77100
US therapy appls., review 79−92308
uterine contraction promotion and bleeding suppression cryocoagulator 79−39591
vaccine atomiser for liquid aerosol immunisation 77−81638
vaccine production, use of ^{60}Co-γ-irradiation, polymerisation conditions 78−40320
vascular bed modelling, optimal dialysis appl. 80−30758
vascular interface system for automation of haemodynamic monitoring and therapy 78−81054
vascular occlusion, selective, evaluation of silicone rubber mixtures 77−37104
venous infusion drop-rate calibrator 79−96705
ventricular arrhythmias and depolariation effect of simultaneous biventricular pacing 77−81642
ventricular defibrillation, transthoracic 100 kg calf, truncated and untruncated exponential stimuli 80−41306
ventricular defibrillation with myocardial electrodes in the dog, calf pony, and pig 80−72369

patient treatment continued
ventricular fibrillation and defibrillation 80−81769
ventricular tachycardia termination by rapid ventricular pacing bursts 77−81678
verbal communication aid for nonvocal patients 79−57816
vibrotactile speech training deaf aid, frequency analysis system 77−29214
vision, vertical fixation disparity, correction by horizontal prism 80−67281
visual deprivation studies rel. to therapy of strabismus, amblyopia and learning disorders 80−12081
visual therapy at home for constant esotropia with anomalous correspondence 80−8207
vocal pitch exercising apparatus, deaf children 79−25001
weight control through behavioural engineering using videotape biofeedback and subliminal communication 77−78040
whole-body hyperthermia, core body temp. regulation by oesophageal temp. feedback 80−72371
whole-body hyperthermia with oesophageal temp. feedback control 79−92423
wound healing promotion by UV burners, rat expts. 79−62310
wound treatment by RF EM radiation, rabbit expts. 80−61639
wound-healing, laser-stimulated, clinical and expt. results of action mechanism 77−9299
^{241}Am removal, Ca-DTPA vs. Zn-DTPA in beagles 77−73599
$^{252}CfCl_3$, metabolism in rat and effect of in vivo DTPA chelation therapy 78−85387
^{242}Cm removal, Ca-DTPA vs. ZnDTPA as chelate, in rat 77−64141
O_2 therapy equipment improvements 78−36039
^{210}Po intake through damaged skin and efficiency of methods preventing absorpt. 77−25561
^{239}Pu removal after inhalation of aerosol, bronchopulmonary lavage and chelation therapy 77−9270

pattern classification *see pattern recognition*

pattern recognition
see also character recognition; computerised pattern recognition; speech recognition
acoustic imaging signal processing, review 79−64403
acoustic sounding of atmosphere, pattern recognition studies 78−65416
adhesive bond strength classifier algorithm 79−91906
adhesive bond US inspection, aspects of model anal. and pattern recognition 78−31611
air pollution control appls. 79−70480
archaeology, trace element neutron activation analysis, pattern recognition techniques 77−40588
astronomical data reduction problem, appl. 80−8554
atmopsheric precipitation probability forecasts, nonparametric technique based on pattern recognition algorithm 78−44946
atom+diatom trajectories, collinear, pattern recognition appl. to $H_2+F(I)$, $He+H_2^+$ 80−45481
atomic spectra, classification, pattern recognition method, H model appls. 78−41982
atomic spectra, classification, pattern recognition method, appl. to Cm energy levels 78−41983
ballistocardiograms, statistical pattern recognition 80−26408
binary image statistical modelling, enhancement and recognition *(Russian)* 80−63929
biological cells in flow system, paraxial anal. of light scatt. 79−11907
biological pattern recognition, rotational matched spatial filter 80−76866
biological shape pattern recognition, average similarities of Fourier spectra 80−104818
biological specimen recognition with partially matched spatial filter 80−46113
biomedical, activities in Japan, survey 79−62400
biomedical Doppler US diagnostic technique of carotid artery disease, objective feature extraction 80−72273
biomedical signal modelling and recognition, system identification approach 80−51286
blood cell neutrophil automated classification, feature selection 78−73281
brain electrical potentials, approaches 80−109051
C-CD transversal filter anal. 78−71052
cardiac arrhythmia classification using R-R interval and difference histograms 77−40843
cardiac noise, automatic segment anal. *(German)* 78−88759
cardiogram arrhythmia detection and classification, statistical approach 77−21644
cell classification multistage systems, stochastic models 78−77143
cellular image segmentation using multispectral information 79−88224
cervical cancer automatic cytoscreening, atypical cells classification 78−73289
cervical cancer detection, comparison of coherent optical transform processing systems 78−48922
chemical, low-resolution mass spectra, super modified simplex evaluation 79−52795
chest radiograph texture anal. model 78−40323
chest X-ray automated screening, texture anal. of lung fields 80−41228
chromosome analysis, problems and progress in automation 80−94436
chromosome classification system, banding technique 80−67320
chromosome classifying system based on banding technique 79−84060
chromosome density profiles, description and classification 79−43830
classification problems of discrete and stationary stochastic signals 79−63002
cloud classification techniques, comparative study 78−7809
clouds, classification from visible and IR SMS-1 data 78−77309
coal miner spirograms, feature selection appl. 78−40387
coherent optical correlation techniques, review 80−43277
coherent optical pattern recognition using normalized invariant moments 80−99653
coherent optical processor for vehicle tracking and identification using laser diode light sources 80−37957
coherent optical processor with interference contrast microscope input 80−43281
coherent-optics image recognition by hybrid series-parallel processing *(Russian)* 77−58265
coherent-optics image recognition using contour transparencies *(Russian)* 77−58260
component shape monitoring, tolerance field image production *(Russian)* 79−94154

pattern recognition continued
component tolerance control, two-dimensional shadow image mapping filters *(Russian)* 79−94155
conference, Paris, France (June/July 1978) 79−59864
context-dependent automatic image screening system 80−95820
coordination therapy electronic aid using pattern recognition methodology 80−56276
correlator with matched filtering using band-limited illumination 80−69531
crime prevention measures, fingerprints, voice prints and identikit presentations *(Italian)* 79−100465
crops, Landsat data, pattern recognition, temporal trend analysis 78−65440
curved object shape description and recognition methodology 79−55077
cytological cell feature extraction using optical moments 80−98206
cytometry, fast flow-through, pattern recognition by light scatter meas. 79−88228
cytomorphological contour classification for mass cancer screening 79−79682
data management and analysis systems for hydrogeochemical reconnaissance 78−20520
data reading system, magneto-optical props. of magnetic thin film *(Russian)* 77−1572
diamond, identification from reflection pattern photographs 78−54481
diatom recognition and counting, matched-filter and statistical method 80−101304
digital processing aerial images, conf., Huntsville, Alabama, USA (May 1979) 80−48165
dimensionality reduction by linear regression with preselected cluster centres 80−106479
distortion error introduced by signal digitisation 77−27256
dot pattern locally parallel structure computation 78−65012
dot pattern perception process simulation 77−21532
dynamic clustering and strong patterns recognition, automatic classification appl. 78−28322
earthquake prediction, pattern recognition as a method of data analysis 80−4157
ECG, isopotential surface map data reduction 79−39557
ECG, QRS detection accuracy rel. to anal. of HF components 80−17158
ECG analysis program testing 79−25146
ECG prototype waveforms generation by piecewise correlational averaging 80−109053
ECG waveform automatic processing using syntactic methods 79−44006
ECG-VCG multivariate classification by linear regression, influence of populations 77−44789
echo cardiography appl. of classification methods 78−35898
edge detection, numerical, optical and hybrid methods compared 80−102662
EEG automatic analysis using adaptive segmentation of EEG records 77−25581
EEG automatic classification, decision rules comparison 80−109054
EEG automatic classification, Kullback-Leibler nearest neighbour rules 80−46079
EEG automatic classification, parametric ARMA time series models 77−90944
EEG automatic sleep staging detectors 78−53551
EEG features extraction by adaptive segmentation 77−44794
EEG patterns during cognitive tasks, methodology and complex behaviours anal. 80−61531
EEG segments classification, autoregressive models usefulness 78−80989
EEG signals hierarchical modelling 80−109052
EEG syntactic anal. method 79−96697
electronic feature extractor for action potential parameters 79−84047
EMG in moving finger muscle, pattern recognition by linear prediction 79−8555
environmental pollution regional distribution, pattern model for prediction 79−57501
epilepsy diagnostics, EEG trace coding *(French)* 80−67277
extratropical cyclones, real-time wind meas. by Doppler radar, colour display system 78−61594
eyeglass lipreading aid system 77−25602
fast image recognition by generalised harmonic analysis *(Russian)* 80−63930
feature enhancement using noncoherent optical processing 80−99651
feedback systems for analogue and digital optical image processing 80−102650
fingerprint identification, matched filtering on basis of thick holograms 77−79781
fission reactor surveillance appls. *(French)* 80−37477
form recognition, scale invariant, in man and machines 78−40176
forward-looking IR sensor image segmentation by maximum likelihood parameter estimation 80−99662
fracture, recognition from stereo photographs 78−54140
functional diff. between central vision, peripherial vision *(Japanese)* 79−29533
gamma spectra, accelerated fitting and nuclide identification by graphical and associative memory methods 79−9945
gamma-ray spectra identification, pattern recognition theory appl. 77−67931
gastric X-ray image, multi-contour detection by organising before identification 79−88177
gastric X-ray image using Ba, feature point extraction method 80−101259
generalised matched filters for coherent optical pattern recognition 80−99654
geological lineaments, human perception from remote imagery, model 79−2400
gynaecologic specimens analysed with flowmicrofluorometer, pattern classification 78−73290
hand radiographs, congenital abnormalities classification 80−30870
hearing, nonlinear systems theory appl. 78−40195
heart attack early diagnosis appl. of statistical pattern recognition, results 78−40388
heart radiographic images, automatic extraction of location of surgically implanted markers 79−88175
holographic pattern recognition for 'simple' objects 80−53230
holographic phase distributions, linear and nonlinear, determ. using electro-optical system 78−58954
holographic scanner for bar code reader 78−42309
holographic scanners for UPC symbols 78−42308

pattern recognition continued
human gait classification, multiple EMG signals pattern recognition 77−44795
human perception visual form interaction prediction 77−5003
hybrid image processing technique 78−58942
hybrid optical-digital processor for invariant moment computation 80−102646
hybrid parallel optical and serial digital processing systems 80−99657
hydrology, feature prediction model 79−5527
image analysis, opto-manual semiautomatic quantitative system 77−56551
image analysis via general theory of moments, Zernike polynomials 80−102629
image intensifier tube for optical image processing 80−99825
image registration and differencing by coherent optical pattern recognition 80−99648
image representation using genetic geometrical functions 80−5702
image understanding systems, seminar, San Diego, CA, USA (Aug. 79) 80−94918
incoherent optical correlation operations 80−99650
integrated optics coherent correlator for real-time signal processing 80−79007
IR signature classification system 80−86430
IR spectra, computer-assisted interpretation, pattern recognition and artificial intelligence methods 78−15732
land use mapping using radar imagery 77−73886
LANDSAT multispectral images clustering scheme 78−32241
LANDSAT-1 radiance data, Lake Superior internal standing wave pattern obs. 78−96244
landscape multispectral data, Karhunen-Loove analysis 80−48164
laser diode lensless MSF holographic optical element correlator, optical pattern recognition 80−102663
laser rangefinder and 3D object recognition algorithm 80−96016
layered relaxation network for object detection 80−99659
leucocyte classification by parametric and nonparametric analysis 77−78016
leukocytes automatic anal., nuclear texture parameters appl. 78−77136
LWR fuel rod mechanical performance predictor, SPEAR code 79−93730
mass spectra, computer-aided classif., pattern recognition techniques, decision-tree approach 80−40774
mass spectra, mol. substructures identification and retrieval, K-nearest neighbour methods 78−20084
mass spectra classification via pattern recognition 78−48722
matched filtering improvements for coherent optical pattern recognition 80−78786
matched filters for optical signal and pattern recognition 80−48392
meteorological data, functional dependency recognition *(Russian)* 78−40609
meteorological field analysis and forecasting pattern-recogniton theory methods appl. 80−98421
meteorological satellite data, IR, automatic segmentation and classification 79−5638
microbiology appl. investigation 78−81084
micrometeorology applic. using regression model 77−37404
microscopic cell images classification by feature extraction 79−88225
microscopic image anal. system, cell cycle, cancerous blood and bone marrow cells appls. 79−88223
mosaic IR image differencing for track assembly 80−86420
movement processing in the visual system model 79−66473
moving object imagery using large aperture telescope arrays 80−53225
multiclass, multivariant technique 80−87320
multifunctional prosthetic hand portable control system 78−57127
multilevel syntax analysis for geological data compression 79−48569
multisensor image pattern recognition, statistical and deterministic aspects 80−99647
multispectral images, region extraction and classification by entropy index 79−58130
multivariate autoregressive feature extraction and the recognition of multichannel waveforms 79−39878
music, MACSIM neural network 78−7373
natural and synthesized speech differences, pattern recognition approach 79−64430
neocognitron, self-organising neural network model, pattern recognition mechanism unaffected by shift in position 80−76745
neural feature detectors, coding model 79−74626
neural multiunit signals, educable waveform recognition system for sorting unit discharges 80−51312
neural net properties rel. to image processing algorithm 80−40993
neural nets, SYSTEMA approach to cerebral structure *(French)* 77−9164
neural signals, non-stationary, pattern trajectory anal. 78−36082
neuron model as universal element of self-learning network 77−44621
neuronal nets, randomly connected layered, pattern separation considerations 77−44644
neuronal waveforms, optimal recognition 80−56003
neutron transport, state-space splitting in Monte Carlo calcs. 77−65264
NMR substituent parameters, pattern recognition interpretation 80−58284
nonlinear, adaptive spatial filter for image classification *(Russian)* 78−42292
nuclear facility, optimisation of radiation detector position and number 78−55043
nuclear reactor behaviour unattended surveillance system 78−29621
nuclear reactor noise analysis by multivariate statistical system 77−14228
nuclear reactor normal and abnormal behaviour nonparametric recognition 79−81044
nuclear reactor surveillance, pattern recognition techniques appl. 80−63351
numerical coeffs. of series expansions, computation through pattern recognition 77−71199
numerical holography application 78−33692
object fixation and spontaneous pattern preferences in Drosophila melanogaster 79−43903
object recognition from incomplete spectra, simple algorithm 78−87023
obsfetrics, microprocessor based system for studying kinematics of labour 77−44769
ocean surface pattern morphogenesis and catastrophe theory 77−5217
oil bearing beds in inhomogeneous geological sections, recognition methods *(Russian)* 78−28337
pattern recognition continued
olfactory pattern recognition modelling by adaptive spatial filter 78−24080
one-dimensional projection recording and processing *(Russian)* 78−42291
optical, by diffraction pattern sampling 80−99643
optical, by thermoplastic complex filter 80−99656
optical, coherent systems 79−64182
optical, deformation invariant, space variant, book contrib. 79−76619
optical, discriminant hypersurface prod. by average filters 80−99649
optical, matched spatial filter synthesis, parameter optimisation 77−71925
optical, Mellin transform method 78−63021
optical, seminar, San Diego, CA, USA (Aug. 1979) 80−98759
optical, using adaptive holographic matched spatial filter 77−7011
optical coding method, scene analysis 78−82924
optical coherent correlator operation in image segment identification, aerial photograph anal. 80−102654
optical correlation, coordinate transform. preprocessing 77−61921
optical correlation, precision of detail recognition *(German)* 78−9340
optical correlation degradation sources 77−71924
optical correlation with holographic Vander Lugt filters, wavelength tuning compensation 77−79765
optical correlator, spatially coherent white light 79−3642
optical correlator, using real time chromatic filtering and extended white light source *(French)* 79−3641
optical image charact. processing methods 77−625
optical information storage, seminar, Washington, USA (Apr. 1979) 80−41942
optical Mellin transform using computer generated hologram 77−10850
optical modulator, space-time, based on $Bi_{12}GeO_{20}$ and $Bi_{12}SiO_{20}$ monocrystals *(Russian)* 77−1652
optical moments from diffr. pattern 77−19184
optical multiple-invariant space-variant processors 78−42279
optical pattern recognition, bipolar incoherent, by carrier encoding 79−50230
optical scene matching methods 80−48167
optical space-variant pattern recognition, using polar camera 78−66767
optical technique using Mellin transform for nonvertical imagery 77−75427
optical transforms for pattern recognition, positional, rotational and scale invariant 77−10854
organic compounds classification, IR and Raman spectra anal. using pattern recognition 77−75158
overlapping-cell clustering algorithm, biomedical appls. 80−30926
pap smear inspection, segmentation approach 80−8124
patients with essential hypertension 77−25583
pattern recognition, mathematical programming techniques 78−92523
peak identification in spectral analysis program 80−37706
perceptual analysers underlying visual texture discrimination 78−53412
perceptual analysers underlying visual texture discrimination 78−85310
periodic-pattern-defects omnidirectional-spatial-filter optical detection system 80−69333
perpendicular line intersection, detection method 80−69330
phonocardiogram automatic classification, linear predictive anal. processing *(Japanese)* 80−36036
phonocardiogram classification, linear prediction analysis appl. *(Japanese)* 78−36010
phonocardiogram pattern classification using linear prediction analysis 77−90950
photodiode array integration with optical power spectral analysis 80−99645
photoelastic fringe pattern analyzer, computer aided 80−38359
planar object photometric charact. recognition *(German)* 79−17463
pneumoconiosis opacities in chest X-rays, improved detection algorithm 78−73242
post-operative human gait, EMG mes. 79−34599
prediction model of air pollution adapted to pattern of daily fluctuation 79−57539
prosthetic arm decentralised control hierarchical approach 77−40924
protamine, electron microscopic recognition rel. to radiation exposure 79−62175
psychological aspects *(Japanese)* 80−97919
radiography, medical diagnostic decision making and image quality 78−28059
real-time recognition of microscopic phase objects 79−7085
remote sensing, design and pot. of decision tree classifier 77−56745
remote sensing, error probability estimation without ground truth and known a priori probabilities 77−56746
remote sensing, max. likelihood estimation of signature transformation algorithm 77−78497
remote sensing of natural resources, use of photographic imagery 77−64454
renogram curves, quantitative evaluation and imaging of functions 79−39495
repetitive image visibility, two-dimensional Fourier spectrum description 77−58282
respiratory system model, identification via mathematical pattern recognition 79−2096
riverine and coastal effluents, remote sensing of thermal alterations and circulation patterns 79−57524
robust feature matching through maximal cliques 80−99671
rotating wedge spatial filter, pattern recognition of biological speciemens (algae) 78−33837
satellite imagery interpretation and geological lineament reproducibility 77−53250
scalar fields structure, two dimensional, vision appls. 79−100594
scanning optical sensor signal peak extraction and multiframe correlation methods 79−81380
scene content measurement from aerial images, appl. to building complex scene 80−78788
scene matching with feature detection 80−48166
scene principal vector analysis by multiple spatial filtering 80−48179
scintigrams, investig. and appl. of pattern recognition technique 78−61252
sedimentary sea bottoms, machine classification 79−92626
seismic discrimination improvement for nuclear explosions and earthquakes using pattern recognition 78−40694
seismic events feature extraction and processing 78−81428
seismic signals, preprocessing of signals prior to input to pattern recognition scheme 79−62631

pattern recognition continued
seismology, location of strong earthquakes using information processing 77−73856
serial section alignment by serial filtering 79−20723
shape descriptors, Fourier-Walsh, radiographic image processing appls. 80−8153
side scan sonar data, adaptive sample set construction 80−43554
sky image coherent-optical processor for moving object location 78−78944
sleep EEG automatic K-complex detector 78−53557
sonar, A-scan data for object pattern classification 78−66980
sonar target recognition expt. 79−64389
sonoprobe survey, automatic recognition of submarine sediments *(Japanese)* 79−39985
space variant optical correlators, accuracy and space bandwidth 78−17864
space-variant optical pattern recognition by coordinate transformations 78−78945
spatial, by spectral feature classification and coherent optical correlation 80−99644
spatial light modulator, using KD_2PO_4 and Se photoconductor, optical processing appl. 80−9988
spectral/spatial classifier development for Earth observational data 78−73555
spectrochemical analysis, four level classification 79−52796
star patterns using CCD star sensors , real time spacecraft attitude determination appl. 78−96380
steel, austenitic stainless, pipe welds, US inspection pattern recognition reflector classification feasibility study 80−16615
stereophotogrammetry, automatic, using structural pattern recognition techniques 78−61632
steroids, mass spectra, computer-aided interpretation by pattern recognition, preprocessing effects 78−15733
styrenes, 4-substituted, NMR substituent parameters, pattern recognition interpretation 80−58284
submarine sediments, automatic recognition by sonoprobe survey, acoustic reflection pattern model *(Japanese)* 80−85776
sunspot group development, pattern recognition methods appl. *(Russian)* 77−64722
surface patterns in theoretical geography 78−57156
target trajectory detection in multi-target environment 79−26865
textural resolution, human, limits investigation 77−12928
texture analysis by hybrid optical/digital system 80−78787
theory and application, book 78−64927
three dimensional object recognition using multiple hologram *(French)* 77−46705
three-layer random neural net with inhibitory connections, pattern separability 78−44498
thyroid diseases, differentiation, linear discriminant analysis application 79−53275
trace element analysis, pattern recognition techniques 77−40588
tunable spatial filtering with a Fabry-Perot etalon 80−58668
turbulent channel flow, meas. of vorticity and turbulence prod., pattern recognition method 78−26194
Universal Products Code supermarket scanners, pattern optimisation 78−42297
US data processing, coherent, in health care systems, possibilities 79−66499
US tissue characterisation approach 78−73186
US-optical correlator for spatial freq. meas. 80−95995
uterine cancer cells automatic classification via cellular differentiation 79−88226
uterine cytology, automated, adenocarcinoma recognition 79−88227
ventricle, left, contour extraction from radioisotope angiocardiograms, and wall motion classification 79−88180
ventricular ectopic beat detect. in rapid Holter scanners, prematurity and height as criteria 79−66575
vibrotactile pattern perception extraordinary observers 77−64065
vision, assignment of invariant features and feature-relations 77−25445
vision, functional mechanisms in humans 80−81609
vision, human, pattern detection and recognition, review 77−73527
vision, human recognition system with thinking, model 80−76744
visual pattern matching, human performance, spatial freq. anal. model 78−40177
visual pattern recognition, models *(Japanese)* 80−97920
visual pattern recognition, transformation and relational-struct. models, random-dot pattern tests 79−53130
visual perception time integration, tactile mode comparison 79−53143
visual prosthesis design, human factors and electrophysiological considerations 78−53583
visual search complexity estimation, for objects against nonuniform backgrounds 80−67086
visual system, sensitivity variations, contrast resolution and eye movements 79−53088
visual system, systems analysis using detection expts. 77−36929
visual systems, fly, response properties 80−41021
visual word recognition, global attributes, contrib. of word length 77−9202
visually evoked potentials, classification for visual stimuli discrimiuation 79−92414
voltammetry, interpretation of severely overlapped data, expt. 78−7255
voltammetry, interpretation of severely overlapped data, theory 78−7254
water usage regions in Lithuania, multi-image classification *(Russian)* 78−16069
wavelength-multiplexed matched spatial filters 79−76603
weather contour maps classification problems 79−79999
weather forecast verification, pattern recognition techniques appl. 78−11958
weather forecasting, adaptive learning network approach 78−40643
white blood cells classification and feature extraction 78−3655
wind velocity estimation via optical signal processing 77−41107
X-ray diffr. scanning oscill. film 77−84582
^{13}C NMR data analysis 77−48059
$H_2+F(I)$, collinear trajectories, pattern recognition 80−45481
$He+H_2^+$, collinear trajectories, pattern recognition 80−45481
KD_2PO_4 photo-spatial light modulator, optical data processing 80−102839

Patterson diagrams *see crystallography; X-ray crystallography calculation methods*

p.c.m. *see pulse-code modulation*

p.c.m. links *see pulse-code modulation links*

PD control *see two-term control*

peaking circuits *see differentiating circuits*

Peierls instability
A15 compounds, high-temp. superconductors, martensitic transform., microscopic theory based on 3-dimens. band struct. 78−19752
antiferromagnetic chain, Peierls distortion energy, exact limit, renormalisation calc. 79−4643
antiferromagnetic Heisenberg chain, first order spin-Peierls transition 78−34986
antiferromagnetic Hubbard chain, interband absorpt., Peierls dimerisation, excitonic effects 80−25072
CDW phase transition, 1-D electron-phonon system, thermodynamic props. 78−14682
chain conductors, CDW ordering 78−79731
condensed Peierls phase, non-linear modes 78−56087
correlation length of Peierls distortion 78−87934
coulomb electron interaction and Peierls instability near the period doubling *(Russian)* 80−34343
$(DBTTF)_{2.67}.SnCl_6$, Peierls transition, fluctuations effect *(Russian)* 79−60809
degenerate semiconductor, Peierls instability in field of strong EM wave 79−15106
dimerized interrupted strand model, optical absorption 77−16271
disordered one-dimensional system, electron density of states and Peierls transition *(Russian)* 80−29304
electrical conductivity transition, fermion-boson system 79−60806
electron charge ordering, Peierls distortion, quasi one-dimensional spinless fermion model 79−87050
electron-electron interaction effect on Peierls struct. transition *(Russian)* 80−70629
electron-phonon interactions, structural phase transitions *(Japanese)* 79−4384
electron-phonon quasi-one-dimensional system, fluctuations anal. 77−89703
electron-phonon system with deform. interaction in mag. field, phase transition *(Russian)* 77−35873
electron-spin coupling, relative importance 79−28280
electronic and spin Peierls transition, gap eqns. 80−24801
electronic density of states, disorder and single electron spectrum, in linear chain *(Russian)* 78−56060
Fermi system, quasi-one-dimensional, electronic density of states *(Russian)* 80−6755
ferromagnetic, Peierls condition and no. of ground states 78−80150
Frohlich model, one-dimens., CDW stability, electron-phonon coupling 80−65452
Heisenberg and Hubbard models, spin-Peierls transition, theory 78−68242
Heisenberg antiferromagnetic alternating spin 1/2 chains, susceptibility calcs., spin-Peierls transition 79−78394
hexagonal lattice, mag. subband struct. of electrons 79−95307
HMTSF-TCNQ, metallic state at He temps., elec. props. and band struct. 79−65462
HMTTF-TCNQ chain, three dimensional ordering Ginzburg-Landau model 78−95152
impurities effect on Peierls transition 79−33237
incommensurate 1-D Peierls system, flucutation conductivity 78−91817
incommensurate Peierls-Frohlich system, fluctuation cond., Green's function calc. 80−24886
inhomogeneous state 78−67943
interchain bandwidth effect at low temp. 78−10352
Ising chain, with next-nearest neighbour interactions, mag. responses to spin-Peierls transition 80−71054
lattice models of screw dislocation high velocity motion, lattice model effects 79−77600
layered materials, struct. changes rel. to CDW, TEM, electron diffr., dichalcogenides appl. 80−39042
linear chain crysts. containing impurities, Peierls instability and supercond. *(Chinese)* 79−51486
linear conductor, CDWs and impurity effects 80−59967
linear conductor, dynamical aspects of fluctuations 79−33715
linear Ising-Heisenberg ferromagnet, spectrum of elementary excitations 79−61091
magnetic field dependence of the spin-Peierls transition 78−80170
magnetic order coexistence with charge density waves 80−97096
mean-field theory of Peierls and spin-Peierls instabilities−commensurability, harmonics and dimerized-state pinning 80−108014
metal, one-dimens., electron interaction effect on Peierls instability *(Russian)* 79−51490
metal, quasi one dimensional, Peierls instability criterion *(Russian)* 77−89516
metal-dielectric transition with lattice distortion, two-band model 77−8023
metallic ultrathin filaments, dielectric and superconducting fluctuations, Peierls transition *(Russian)* 80−65742
nearly free electron model with nonlinear screening 77−4304
NMP-TCNQ, Peierls insulator and antiferromagnetic mixed phase, mean field approx. 77−20626
nonequilibrium Peierls state 79−33235
one-dimensional classical and quantum chains, spin-Peierls transition theory 77−66375
one-dimensional conductivity, with arbitrary bandfilling, Peierls instability 80−59968
one-dimensional conductor, incommensurate Frohlich model, displacement correl. of classical ions 78−6291
one-dimensional conductor, lattice distortion, Kolmogorov Arnold Moser theorems, appl. to struct. problems in condensed matter 80−59878
one-dimensional conductor, lattice stability, phonon dispersion, Kohn anomaly 80−96603
one-dimensional conductor, mean-field model, fixed total current, CDW soln. 77−47748
one-dimensional conductors, conductivity peaks, Peierls transitions *(Russian)* 80−49700
one-dimensional conductors, incommensurate CDW 80−20174
one-dimensional conductors, libron effects on electron spectrum, theory 80−96854
one-dimensional conductors, Peierls instability, dynamics, structural energy, pseudopot. calc. 80−54676
one-dimensional conductors, Peierls transition temp. and 0K energy gap, mean field theory calc. 80−24782

Peierls instability continued
one-dimensional electron system, generalised susceptibilities in mag. field *(Russian)* 77−80750
one-dimensional electron-phonon system, dynamics, Frohlich model 77−15781
one-dimensional Hubbard model, antiferromag. and Peierls instability 78−23233
one-dimensional metal, displacement correlation of classical ions in incommensurate Frohlich model 77−39641
one-dimensional metal, phonon drag and sliding CDW 80−20173
one-dimensional metallic systems, theory of structural phase transitions 78−38830
one-dimensional metals, incommensurate sliding CDW 80−20156
one-dimensional metals, Peierls and CDW transition *(Chinese)* 79−51502
one-dimensional metals and charge density wave effects in these materials, review 79−78085
one-dimensional Peierls-Frolich state, impurity pinning of charge density wave 78−6298
one-dimensional system, cond. and longitudinal sound attenuation above Peierls transition point 77−28168
one-dimensional system, Frohlich cond. and superstruct. pinning *(Russian)* 77−55518
one-dimensional system, spill-over Peierls regime due to electron-electron interaction 79−33251
one-dimensional system, supercond. order and CDW coexistence, Peierls instability *(Russian)* 77−69445
organic linear chain cpds., diffuse $4k_F$ refls., small intramolecular Coulomb interaction 80−34376
organic materials metallic state at He temps. 79−65462
orientational metal-insulator phase transitions in quadrupolar strands with itinerant electrons 80−15455
Peierls one dimensional model, exact solution, electron spectra, static lattice deformation *(Russian)* 80−70609
Peierls systems with dil. impurities, microscopic theory of pinning effect 77−15837
Peierls-Frohlich condensate, attracting solitons and discontinuous lock-in transition 80−92840
Peierls-Frohlich dielectric, metallic screening, with pinning to impurities at finite temps. *(Russian)* 79−56208
Peierls-Frohlich state, electron excitation *(Russian)* 79−23909
Peierls-Frohlich state on many-phonon-coupling model, dynamical props. 78−47773
Peierls-Hubbard model, antiferromagnetism and lattice distortion 77−55656
Peierls-Hubbard model, quasione dimens., antiferromagnetism and Peierls distortion 78−67931
phase transition in BCC hard sphere lattice gas with second neighbour exclusions 80−160
phase transitions and reflection positivity, Peierl contour probabilities, long range lattice models 78−89398
bis cantena pol methylarsenide, energy gap depend. on As electron delocalization *(German)* 78−43296
polyacetylene, lightly doped, charged π-phase kinks 79−56163
polyacetylene, metallic, mixed Peierls phase, Hartree-Fock calcs. 80−70689
polyacetylene conductivity mechanism, Peierls phase one dimensional cond. *(Russian)* 80−88546
polyenes, long chain, electronic struct. in Peierls-PPP model 80−84423
proximity effect at low temp. for Peierls system 79−73643
pseudo-one-dimensional system, Ginzburg-Landau theory of phase transitions 77−15529
quasi one-dimensional conductor, Peierls-Frohlich correl. 79−60810
quasi one-dimensional metal, crit. temp. for phase transition *(Russian)* 79−78253
quasi one-dimensional spin lattice coupled system, collective modes 80−24896
quasi one-dimensional system, Peierls-Frohlich state, cond., Umklapp processes *(Russian)* 79−38059
quasi-one dimensional conductor, high temperature structural instability 77−8032
quasi-one dimensional metal, Peierls instability in field of strong EM wave 79−15106
quasi-one-dimens. system, Peierls insulator and antiferromagnetic mixed phase 77−20626
quasi-one-dimensional conductor, chiral charge density waves form. 78−6302
quasi-one-dimensional conductor, high temp. struct. instability, tight-binding approx. and fluctuation model 78−6292
quasi-one-dimensional conductor, Peierls instability and superconductivity, possibility of coexistence 78−31028
quasi-one-dimensional conductors, alloys, Peiels distortion 80−59965
quasi-one-dimensional conductors, order in coupled metallic chains problem 78−6358
quasi-one-dimensional conductors, review 78−60070
quasi-one-dimensional electron-lattice system, three dimensional CDW ordering temp. 78−23037
quasi-one-dimensional organic metals, electron spin relax., temp. depend., Peierls fluctuations, EPR meas. 79−73802
quasi-one-dimensional system, Frohlich cond. in fluctuation region 78−84203
quasi-one-dimensional systems, charge distrib. and lattice distortion 78−6317
quasi-one-dimensional systems, Peierls transition, possible pairing of spatially separated electrons and holes 79−15085
quasi-one-dimensional systems, spin-lattice Peierls instabilities, static and dynamic aspects 80−71052
quasi-one-dimensional systems, three-dimens. ordering in system of weakly coupled chains 78−6295
quasione dimensional compound, commensurability effect 78−72095
quasione dimensional crystal, phonon spectrum change due to struct. transition 78−67789
quasione dimensional crystals, effect of band filling on features of struct. transition 78−2424
quasione dimensional structures, collective excitation of CDW 78−18981
self consistent solution continuity between commensurate and incommensurate phases, numerical solution 77−28117
self consistent solution continuity between commensurate and incommensurate phases 77−31945
spin-Peierls phase diagrams, obs. and models 80−60330
spin-Peierls transition, dynamic struct. factor 78−14964

Peierls instability continued
spin-Peierls transition, first-order, theory 77−20605
spin-Peierls transition, mag. field effects 80−39796
spin-Peierls transition in mag. field, phonon freq., Heisenberg model calcs. 80−25151
spin-Peierls transition in magnetic field 78−84441
spinless fermion systems, Coulomb repulsion, bond alternation, Peierls distortion, HF approx. 80−44524
statical charge waves and lattice distortion, theory 77−72828
structural Peierls transition in quasi-one-dimensional systems with anisotropic electronic and elastic properties 79−7671
superconductivity and martensitic transform. in A15 compounds 77−8226
$(TCNQ)(TTF)_{1-x}$-$(TSeF)_x$, quasi 1-D metal, mag. susceptibility, temp. depend. 77−8267
TCNQ alkali salt, spin-Peierls transition 80−29395
TCNQ salt, $(TMA^+)_3(I_3^-)(TCNQ^-)_2(TCNQ^0)$, struct., phys. props. and lattice distortion evidence 78−6305
TCNQ salt, dibenzo-TTF-$TCNQCl_2$, one-dimens. mag. semicond., mag. and elec. props. 80−88601
TCNQ salt, HMTTF-TCNQ, quasi-one-dimensional organic conductor, mag. susceptibility meas. 78−6508
TCNQ salt, HMTTF-TCNQ, structure, metallic cond. and thermopower 77−8080
TCNQ salt, HMTTF-TCNQ, three-dimens. ordering, Ginzburg-Landau model for Peierls instability 80−20160
TCNQ salt, K-TCNQ, ^{14}N NQR temp. depend. rel. to Peierls transition 79−82892
TCNQ salt, K-TCNQ, spin-Peierls system, paramag. susceptibility, Heisenberg chains 79−38299
TCNQ salt, $MEM(TCNQ)_2$, phase transition electronic struct. interpretation 80−24781
TCNQ salt, N-methyl-N-ethyl-morpholinium-$(TCNQ)_2$, spin-Peierls transition 79−82803
TCNQ salt, NH_4-TCNQ, crystal structure and phase transition 78−91330
TCNQ salt, pyridinium $(TCNQ)_2$, low temp. mag. phase transition, ESR study 80−25139
TCNQ salt, $Qn(TCNQ)_2$, thermoelec. power and cond., large Coulomb repulsion model 80−24893
TCNQ salt, TSeF-TCNQ, doped with TTF-TCNQ, phase transitions 77−80732
TCNQ salt, TSeF-TCNQ, electrical conductivity, press. depend. 77−51729
TCNQ salt, TSeF-TCNQ, Peierls transition and CDW ordering, X-ray study 80−20101
TCNQ salts, simple, triplet exciton obs. by ESR 78−10373
TCNQ-HMTSeF, X-ray diffuse scatt., one-dimens. distortion in phonon spectrum and interpret. 78−10144
TCNQ-K, X-ray exam. of phase transitions 78−55933
TCNQ-Na, X-ray exam. of phase transitions 78−55933
TCNQ-Rb, X-ray exam. of phase transitions 78−55933
TCNQ-TSeF, model for phase transition and low-temp. phase 77−47734
tight-binding model, non half-filled, Peierls transition props. in commensurate phase 77−31933
TMTSF-DMTCNQ, metallic state, transport props. 80−24974
TMTTF-TCNQ, quasi one-dimens. conductor, diffusive hopping, theory 80−54677
transition in quantizing mag. field, possibility 80−103441
transition metal, 2H layer compound, theory of superstructures 79−99291
$(TSeF)_x(TTF)_{1-x}(TCNQ)$, interstack hybridisation role in metal-insulator transition temp. determ. 78−6304
TSeF-TCNQ, resist., crit. behaviour anisotropy 78−10430
TSeF-TCNQ, X-ray diffuse scatt., one-dimens. distortion in phonon spectrum and interpret. 78−10144
$TTF_{0.97}Se_{0.03}$-TCNQ, Peierls-superlattices and soft phonon anomalies, X-ray scatt. meas. 78−75795
TTF(MBDT) spin-Peierls transition, mag. exchange interactions, mag. props. 80−25138
$TTF(SCN)_{0.588}$, Peierls instability, strain coupled charge density waves, X-ray scatt. obs. 78−79949
$(TTF)CuS_4C_4(CF_3)_4$, spin Peierls system, mag. field effects 80−7123
TTF-BDT(M), BDT=$S_4C_4(CF_3)_4$, M=Cu, Au, spin-Peierls transition, sp. ht. meas. 77−28401
TTF-bisdithiolene metal complexes, spin Peierls transition 77−4523
TTF-Cu bis-dithiolene, dimer, mol. displacements at 4.2K 80−10539
TTF-TCNQ, $4k_F$ anomaly, explanation 77−35875
TTF-TCNQ, 53 and 38K transitions, mag. and elec. props. meas., doping effect 77−66159
TTF-TCNQ, band struct., soft phonon instability 77−72821
TTF-TCNQ, charge transfer change with press. 80−39564
TTF-TCNQ, coupled Peierl's systems, model, phase transitions 77−69230
TTF-TCNQ, elec. cond., role of librations 79−19580
TTF-TCNQ, electron-molecular distortion coupling near Peierls transition, IR spectra obs. 80−25390
TTF-TCNQ, electronic props. and comparison with $(SN)_x$, review 78−6306
TTF-TCNQ, interpretation of the $2k_F$ and $4k_F$ X-ray scatt. 77−63487
TTF-TCNQ, isotope effect on Peierls transition temp. 78−43367
TTF-TCNQ, isotope effect on Peierls transition temp. 78−43369
TTF-TCNQ, Kohn anomaly and Peierls-type transition, X-ray obs. 78−14435
TTF-TCNQ, lattice distortion, displacive transform., Landau theory 77−31743
TTF-TCNQ, lattice distortion, displacive transform., Landau theory 77−84879
TTF-TCNQ, low temp. phase transitions, elastic neutron scatt. obs. 78−14464
TTF-TCNQ, neutron and X-ray diffuse scatt., phase transitions, one-dimens. behaviour and interpret. 78−10381
TTF-TCNQ, ordering types below 54K, perp. phase depend. 78−6300
TTF-TCNQ, Peierls instability and consequences 78−6303
TTF-TCNQ, Peierls insulator and antiferromagnetic mixed phase, mean field approx. 77−20626
TTF-TCNQ, Peierls transition, photocond. meas., absorption coeffs. above gap 78−72198
TTF-TCNQ, Peierls-superlattices and soft phonon anomalies, X-ray scatt. meas. 78−75795

Peierls instability continued
TTF-TCNQ, phonon anomalies and superstructures, Peierls transition, X-ray diffuse scatt. obs. 77−27962
TTF-TCNQ, phonon dispersion curve meas., Peierls transition exam. 78−10134
TTF-TCNQ, physical properties, reviews *(Japanese)* 80−24883
TTF-TCNQ, resist., crit. behaviour anisotropy 78−10430
TTF-TCNQ, single cryst., mag. susceptibility in phase transition region, two-gap model 78−6511
TTF-TCNQ, spin waves, scatt. at $4k_F$, spin-Peierls fluctuations 78−72093
TTF-TCNQ, symmetry changes and phase transitions 78−6299
TTF-TCNQ, thermal cond. above and below Peierls transition, electronic and lattice contribs. 79−95394
TTF-TCNQ, three dimensional ordering 77−59087
TTF-TCNQ, X-ray, neutron scattering, low temp. modulated lattice, 3D modulated lattice 78−10033
TTF-TCNQ complex *(Japanese)* 77−1412
TTF-TCNQ salts, self-consistent continued-fraction theory of cond. 79−69482
TTF.CuBDt, spin 1/2 Heisenberg chain, spin-Peierls transition 79−61135
TTFCuBDT, spin-Peierls transition in spin 1/2 Heisenberg chains, RPA calcs. 80−25150
TTG-BDT(Cu), giant struct. distortion, high speed photography obs. 78−43121
TTSeF-2,5-dimethyl TCNQ, donor and acceptor stack stability against Peierls distortion 78−51979
TTT_2-$(I_3)_{1+x}$, physical props., elec., mag. and optical meas. 80−24908
two level commensurability in one-dimensional Peierls system *(Russian)* 80−70688
two-band system, coexistence of dielec. and supercond. ordering 80−10853
two-band systems, BCS pairing and Peierls distortion compatibility 78−88068
Umklapp processes effect on dynamics of Peierls-Frohlich state *(Russian)* 77−47752
X-Y quasi-one-dimens. system anisotropic, spin-Peierls phase transition, tricritical point 80−25142
$Co_{0.83}[Pt(C_2O_4)_2].6H_2O$, quasi-one-dimens. conductor, Peierls distortion and superlattice, X-ray study 80−29397
Ga ultrathin metallic filaments, appearance of dielec. instability, coexistence with supercond. 80−103784
Hg ultrathin metallic filaments, appearance of dielec. instability, coexistence with supercond. 80−103784
In ultrathin metallic filaments, appearance of dielec. instability, coexistence with supercond. 80−103784
$K_{1.75}Pt(CN)_4$. $1.5H_2O$, quasi 1D metals, electric conductivity meas., semiconductor-metal transition 79−99538
$K_2Pt(CN)_4Br_{0.3}3H_2O$ incommensurate linear conductors correlation length in 77−80745
$K_2Pt(CN)_4Br_{0.3}3.2H_2O$, linear conductor, dynamical aspects of fluctuations 79−33715
$K_2Pt(CN)_4Br_{0.3}\times3H_2O$, struct., neutron determ., Peierls distortion 79−46640
$K_2Pt(CN)_4Br_{0.3}.3H_2O$, one-dimensional cond., phys. props. *(Japanese)* 78−30916
$K_2Pt(CN)_4Br_{0.3}.3H_2O$, Krogmann salt, non-empirical localised orbital cal. of electronic struct. 78−91636
$K_2Pt(CN)_4Br_{0.3}.3.2H_2O$, deuterated, coupling of charge density wave and water mode 77−4646
$K_2Pt(CN)_4Br_{0.3}.xH_2O$, dynamical props. near Peierls instability, neutron scatt. 78−14436
$K_{1.75}Pt(CN)_4\times1.5H_2O$, struct., neutron determ., Peierls distortion 79−46640
$K_{1.75}Pt(CN)_4.1.5H_2O$, Raman scatt. and luminesc. studies 80−25394
$K_{1.81}Pt(C_2O_4)_2.2H_2O$, evidence for a Peierls Frohlich state 78−76060
$K_{1.75}[Pt(CN)_4]1.5H_2O$, elec. cond. studies, Peierls transition 80−24901
$(NH_4)_2[Pt(CN)_4]Cl_{0.42}.3H_2O$ quasi one dimensional conductor, physical props., cond. freq. depend. 79−95393
NbS_3, Peierls distortion, chain polytypism and dislocation coupling 78−79589
$NbS_3(Se_3)$, Peierls distortion, electron diffr. obs. 80−39503
$NbSe_3$, CDW form., direct electron diffr. 78−30877
$NbSe_3$, electronic props. variation with struct. 79−42438
PbTe, CDW in strong mag. fields, Peierls-type transition 80−34362
Pt chain compounds, one dimens. conductors, Fermi wavevector determ., X-ray scatt. obs. 80−44187
Pt complex, $(C(NH_2)_3)_2Pt(CN)_4Br_{0.23}.H_2O$, pseudo-one-dimens. cpd., solitary wave excitations, and cryst. struct. 78−6307
Pt complex, $Mg_{0.82}Pt(C_2O_4)_2.xH_2O$, X-ray diffuse scatt., 1-D Peierls-Kohn anomaly and struct. transforms. 78−14680
$Rb_{1.75}Pt(CN)_4$. $1.5H_2O$, quasi 1D metals, electric conductivity meas., semiconductor-metal transition 79−99538
$(SN)_x$, electronic props. and comparison with TTF-TCNQ, review 78−6306
Sn ultrathin metallic filaments, appearance of dielec. instability, coexistence with supercond. 80−103784
TTF-TCNQ , elec. props. in high temp. regime, effect of controlled disorder 78−30912
TaS_2, Peierls transit transition 77−66119
TaS_3, electron diffr. evidence for one-dimens. Peierls distortion 78−10024
TaS_3, monoclinic form, cryst. struct. determ., Peierls type transition obs. *(French)* 80−88109
TaS_3, one-dimensional compound, phase anal., X-ray and elec. meas. 79−51086
TaS_3, Peierls superstruct., low temp. X-ray diffr. obs. 78−59793
TaS_3, Peierls transition *(Japanese)* 78−30880
TaS_3, press. depend. of metal-semicond. transition 79−47016
TaS_3, transport props. 80−20175
$TaSe_3$, electronic props. variation with struct. 79−42438
VO_2, discontinuous metal insulator and spin dimerisation transition, Hubbard model 78−51893
V_3Si, A15 compound, microscopic model of supercond. and martensitic transform. 77−8226
$ZrSe_3$, electronic props, variation with struct. 79−42438

Peltier effect
anisotropic thermoelement used as heat pump, transverse Peltier effect 78−39098

Peltier effect continued
capacitive dew-point sensor 78−81421
cooler for Si/Li spectrometer *(Czech)* 78−49947
cooling efficiency of arbitrarily shaped thermoelec. element 78−67010
Czochralski growth system, time-depend. cryst.-melt interface shape 77−24280
degenerate semiconductors, longitudinal thermo-EMF in quantising mag. field, scatt. mechanism *(Russian)* 80−24960
education, Joule heating, Peltier and Seebeck effects, Cu-Constantan thermocouple expt. 79−9056
III-V semiconductors, electroliquid epitaxy, role of electrotransport 79−56095
inhomogeneous sandwich structure, electrogradient EMF, V-I charact. *(Russian)* 78−47852
irreversible phenomena in homogeneous materials, and single and double bimetallic junctions *(French)* 78−95291
LPE, Peltier-induced, in semiconductor films, composition control 78−48343
LPE, Peltier-induced, in semiconductor films 78−48342
metal-semiconductor thermoelectric coolers, effects of contact resist. and dopant conc. 80−81481
multicomponent systems, rel. to electroepitaxy, theoretical model 80−65396
nonequilibrium conducting media, boundary conditions *(Russian)* 79−91127
novel Peltier junctions, fast transient response 78−21141
semiconductor, appls. *(French)* 77−62908
semiconductor, crystn. in constant electric field, thermoelectric parameters 77−44146
semiconductor refrigerating thermojunctions with radial flow of current 79−2766
solar-powered solid-state heat transfer device based on photovolt. and Peltier effects 80−217
temperature compensating element, in $LiTaO_3$ optical modulator 77−42611
thermal conductivity meas. of gases and liqs. using Peltier effect 78−45615
thermocouple, thermometers, voltage generation, calibration 80−57295
thermocouples, thermoelectric effects, reversibility, theory 77−59280
thermoelectric discs, coaxial, radial current flow, heat transport 79−2767
thermoelectric energy conversion, heat losses compensation due to thermal cond. through Peltier heat 80−107773
transient behaviour of thermoelectric coolers with high current pulse and finite cold junction 80−27290
$Bi\text{-}Bi_{0.5}Sb_{1.5}Te$ system, stratified medium with artificial anisotropy, transverse cooling effect 79−28364
Cu-Fe wire, low-temperature measurements, undergraduate lab. project 78−54119
GaAs, liquid-phase electroepitaxial growth kinetics, Peltier effect and solute electromigration 79−42401
GaAs, Peltier induced growth kinetics of LPE 78−64485
GaAs, Peltier LPE, absence of electromigration of As and Al 77−81230
GaAs:Sn, dopant segregation during liq. phase electroepitaxy 80−54384
GaAs-GaAlAs DH CW laser, growth by Peltier effect induced LPE 77−48357
GaAs-GaAlAs heterostructures, LPE growth *(Polish)* 78−6861
Ge, molten zone movement under influence of Peltier effect 78−44007
HgI_2 thin sections with Peltier-cooled preamplification for X-ray spectrosc. 80−324
In-InP interface, current-controlled LPE growth, Peltier cooling 77−8770
InSb, periodically doped cryst. prod. by Peltier effect, helicon diagnostics *(German)* 77−48338
P-Si, highly doped, thermoelec. coeffs. meas. at semicond. solid-metallic liq. interface 77−39887
$Si_{1-x}B_x$:H, amorphous films, thermopower and cond. for mixed band and broad tail state cond. 80−49786
VO_2 needles, switching, rel. to voltage oscills. 79−15199

PEM effect *see photoelectromagnetic effects*

Pendellosung fringes *see X-ray crystallography*

pendulums
see also time measurement
adiabatic invariant motion, charged particle in space periodic wave, variable length pendulum *(Russian)* 79−2623
ball and spring, elliptical motion 80−82613
ballistic, momentum meas. of laser-produced plasma 78−83611
biased roulette, mathematical pendulum, limit distrib. of stopping angles 78−81821
bipedal locomotion, inverted pendulums stabilisation algorithm *(Japanese)* 80−81630
Collette torsion pendulum, limits of applicability to internal friction meas. 79−14359
compound, teaching appls. 78−12474
computer simulation of motion, undergraduate teaching aid *(German)* 77−67166
computer-aided laboratory exercise 80−67985
controlled solar tracking system and concentrator 79−62122
coupled inverted pendulums, stabilising control *(Japanese)* 79−35545
damping characteristics meas., digital, using amplitude-time convertor *(Czech)* 77−71310
double with varying length, probabilistic characteristics of solns. *(Polish)* 80−8781
double-pendulum vibration oscillator or seismograph 78−16200
dynamic torsion-effusion pendulum, video obs. 77−61077
education, ballistics pendulum 77−78914
education, classical mechanics, Hamilton's principle, variational formulation approx. solns., simple pendulum 77−33774
education, handing chain natural freqs. 77−78913
education, large amplitude pendulum expt. 77−45638
education, pendulum with oscill. support, square wave model 78−49597
education, simple pendulum, flexible cord mass effects, eqn. of motion perturbation expansion 77−82341
education, sprung pendulum, anal. of nonlinear coupling 80−51987
experimental design and statistical analysis of data, measurement of period of simple pendulum 80−42017
forced periodic oscillations of the simple pendulum 80−94951
Foucault pendulum, 10 m long charact. *(Korean)* 79−21541
Foucault pendulum, continuously operating, corridor teaching demonstration 78−54137
Foucault pendulum, continuously operating 80−73151

pendulums continued
Foucault pendulum, improved characts. for student demonstration 78−54138
Foucault pendulum model, for Earth rotation 79−58472
Foucault pendulums, long and short, precessional periods 78−73794
g determination, student expt., linear least squares data anal. 78−45450
gravitational constant expt. determ. using pendulum with two degrees of freedom 77−67371
gyropendulum, aperiodic single rotor 80−14561
gyropendulum system nonperturbability, motion in Newtonian gravitational field *(Russian)* 79−80422
history, theory of pendular motion, pre-Galilean era 79−37
horizontal pendulum tiltmeters, recording device 78−40679
impact machines, energy meas. using optical system 80−69746
in orbiting spaceship, equilibrium and stability 79−44667
internal friction measurement in solid metal via inverted torsion pendulum *(French)* 79−18847
internal friction test unit for threadlike crysts. 78−36997
inverted, design and stabilisation control *(Japanese)* 80−73167
Knudsen torsion-effusion pendulum method, computer-automated acquisition system, for measurement of vapour pressures at high temps. 79−49214
Lagrangian equations of motion analysis for systems with extremely heterogeneous inertia props. 77−53775
LF oscillations driven by HF force 79−53970
libration in systems of many degrees of freedom *(Russian)* 78−86141
Liebscher method of gravit. constant determ., theoretical analysis *(German)* 77−29465
linearised spring pendulum system, stability anal. 77−64945
low temp. torsion pendulum, magnetic shielding for ether drift expt. 79−88988
magnetic system stability *(Ukrainian)* 79−75329
many-dimensional oscillator problems, 'Arnold diffusion' instability 79−75334
mass-on-a-spring (autoparametric oscillator) 77−22403
massive cord, oscill. freq. calcs. 78−54121
mechanical analogue of Josephson junction *(Japanese)* 77−72948
multiple pendulum mirrors for telescope mirror testing 80−102792
optimal control and dynamics 77−72229
optimal starting with velocity limit and integral quality criterion *(Russian)* 79−23198
oscillation optimal passive suppression *(Russian)* 79−10454
parametric spring pendulum, recurrence effects 79−5938
pendulum, spherical weakly damped and weakly nonlinear, damped oscillations 79−63023
pendulum-gyroscopic platform stabilised in inertial space, autonomous determ. of coords. *(Ukrainian)* 78−65760
period variation due to nonlinear feedback 77−68382
physical pendula, reconstructed 19th century expt. 80−82612
point of suspension displacement vel., optimum high speed control *(Russian)* 79−80424
precessing spherical pendulum, nonreentrant orbits demonstration 79−5937
quantum, representation of canonical relns. 80−42084
quantum pendulum under periodic perturbation, stochastic behaviour 80−8834
quantum pendulums, classical, semiclassical and quantum aspects, teaching 80−101679
quasi-ideal pendulum, small amplitude oscills. 79−84897
random interactions anal. using computer *(Russian)* 80−73313
ring of torsion coupled overdamped pendulums, nucleation theory of overdamped soliton motion 80−12899
rolling pendulum bob, conservation of energy and partitioning of kinetic energy 79−62956
rotating pendulums, example of arbitrarily slow irreversibility 78−70083
seismometer using gyroscope for vertical seismic motion meas. *(Japanese)* 79−96842
semiautomated torsion pendulum for high temp. damping studies 77−11153
simple, large-amplitude, Fourier anal., for teaching 80−17767
simple, with uniformly shortening string length, behaviour 80−27111
simple pendulum, length definition, student expt. 77−57131
slightly perturbed, bounce resonance and Kolmogorov entropy 80−57199
solid friction damping of mech. vibrs., math. model approach 77−42764
spherical compound pendulum, natural freqs. 77−67265
spherical pendulum in fluid flow, transverse vibrations *(Russian)* 77−87644
string-coupled, normal mode anal., for teachers 79−21494
swinging spring with oscillating support, stability boundaries 77−68384
torsion, eqns. of motion for Ke, inverted and Collete types 77−89019
torsion, momentum meas. of laser-produced plasma 78−83611
torsion pendulum, automatically driven, for continuous meas. of amplitude and amplitude-independent damping 77−35099
torsion pendulum for damping capacity meas. and related phenomena 77−77687
torsion pendulum of 3 components for measurement of Snoek damping in sheet specimens 79−63010
torsion pendulum oscillations recording equipment for internal friction meas. 78−36998
torsion pendulum with elastic wire element, free torsional vibr. anal. *(Spanish)* 79−68613
torsion pendulum with modified inertia system, nylon-6 viscoelastic props. meas. *(Spanish)* 77−31264
torsion pendulums, Collette anal. 80−22349
torsional, for internal friction meas. up to 200 Hz, automated control 78−22308
torsional, oscillation damping meas. system *(Polish)* 77−71314
torsional pendulum, for rigidity modulus meas. 79−84894
torsional pendulum for internal friction meas. as function of freq. 78−13980
Trieste horizontal pendulum obs. of 1976 Friuli earthquake precursors 78−24216
triple coupled pendulum, analogy with coupled stationary states 78−16598
viscoelastic rod, standard linear body, free torsional ascills. 80−99940
viscoelastic-plastic torsion, prismatic, oscills. *(Spanish)* 77−3733

penetration depth (superconductivity)
antiferromagnetic superconductor, surface impedance 79−82709
automatic measurement by 8 bit microprocessor device *(French)* 79−28440

penetration depth continued
bimetallic loop, thermoelec. flux generation 79−65596
collective oscillations and electric field penetration, review 80−88678
composite superconductor, power increase at current close to crit. current, expt. meas. 77−28314
cylinder of rectangular cross section, 2-D current and field distrib. 78−72303
EM coherence length in supercond. with mag. impurities 79−42696
frequency dependence of penetration depth of elec. field *(Russian)* 80−34548
granular superconductors, coherence transition, structural disorder effects 80−88657
hard superconductor, flux trapping, penetration depth determ. 80−100572
interferometric meas. technique 78−72306
intermediate state, domain struct. near penetration field 77−16009
Josephson, junction of finite width, vortex penetration *(Russian)* 77−12065
junction, electron tunnelling, effect of dissolved O^{2-} 78−80100
junction, superconductor-normal metal-supercond., impurities in normal metal layer, pair penetration depth determ. 80−29508
layered superconductor, mag. field penetration 77−80872
longitudinal electric field in superconductors and oscillations 80−15664
magnetic flux structures in superconductors, book 79−91199
magnetic impurities, EM penetration depth 77−66225
metal foils, sensitive detection of superconductivity by change in penetration depth of electromag. fields 79−56372
nonequilibrium elec. field, temp. depend. *(Russian)* 78−23202
point contacts, three-dimens. assembly, crit. currents and penetration depth 80−84560
scattering model for DC Josephson effect, penetration depth 80−54838
strong-coupling superconductor, EM props. 77−24634
strong-coupling superconductors, press. coeffs. of critical field, Ginzburg-Landau parameter, penetration depth 80−54833
superconducting contacts, critical currents, density, penetration depth 80−25059
superconducting round wire, flux distribution and hysteresis loss 80−34570
superconducting thin hollow cylinder, mag. field penetration, Ginzburg-Landau calcs. *(Russian)* 80−75674
superconductor resistive state, coherence length, penetration depth 80−97030
superconductor with mag. impurities, elec. field distrib. 78−88070
superconductor with mag. impurities, longit. elec. field penetration *(Russian)* 79−19694
superheating field for finite κ calc. 77−12060
thin cylinder in transverse mag. field, metastable supercond., Ginzburg-Landau eqns. 79−60961
type 1 superconductor, first stage magnetisation and metastable migration field in slab 80−15655
type I and II superconductors, energy gap and penetration depth *(Chinese)* 79−51718
type I and II superconductors, penetration depth and influence of effective phonon spectrum on T_c *(Chinese)* 79−51705
type I and II superconductors, T_c and penetration depth *(Chinese)* 79−51706
type II superconductors, flux-line cutting 80−7055
uniaxial ferromagnetic superconductor, mag. domain struct. and mag. field penetration depth 79−65583
Al-Al_2O_3, supercond. granular film, mag. penetration depth, depend. on normal state resist. and temp. 79−56378
Al-formvar superconductive junction, Ginzburg's generalised jellium model 80−15663
In film, metastable states supercond. parameters 78−47903
In, supercond. penetration depth field depend. meas. 77−4464
In-Bi, dil., supercond. penetration depth field depend. meas. 77−4464
In-Bi, single spheres, supercond. props. 79−73617
La particles, supercond. props. *(Russian)* 80−7018
Nb and Nb_3Sn, inhomogeneity detection by penetration depth meas., proximity theory 77−28288
Nb film sputtered onto Cu substrate, microstruct. and supercond. props. 77−85370
Nb films, penetration depth measured with Nb-NbO_x-PbIn Josephson junctions 79−42691
Nb films, supercond. props. and electronic density of states *(Russian)* 79−28439
Nb, flux pinning by proton irradiation damage 77−47947
Nb, O enrichment of surface layers, penetration depth and resist. meas. 78−19180
Nb, plastically deformed, flux density gradients and pinning forces, Faraday effect obs. 79−61010
Nb tunnel junction, temp. dependent props., 2-9L 77−24642
Nb-NbO_x-Pb junction, static charact. of tunnelling cryotrons 79−28480
Nb-NbO_x-PbIn window type junctions, critical Josephson current depend. on magnetic field 79−65607
Nb-Ta bimetallic loop, thermoelec. flux effects due to penetration depth changes 77−24636
Nb_3Sn, delayed flux entry and surface barriers, tunnelling obs. 77−59355
Nb_3Sn, fast neutron irradiation, effect on critical current density 78−19197
Nb_3Sn, vapour deposited, supercond., surface resist. and penetration depth 79−33392
NbTi wire, supercond., magnetisation rel. to field orient. 78−52151
Pb, absolute surface reactance and penetration depth 78−68109
Pb, penetration field and magnetisation curve, lattice defect effects 77−28292
Pb, supercond., surface bound state, microwave surface impedance 77−12059
Pb:Au(In)(Bi), type II film, penetration depth meas. 77−28285
Pb-In-Au film, interferometric meas. technique 78−72306
Pb-Sn bimetallic loop, thermoelec. flux effects due to penetration depth changes 77−24636
PbIn films, penetration depth measured with Nb-NbO_x-PbIn Josephson junctions 79−42691
PdH_x, $x \simeq 1$, type I supercond. props. 79−56448
Sn film, crit. mag. fields, temp. depend., penetration depth thickness depend. 80−70908
Sn, superconducting loops, thermally generated mag. flux 79−56452
Sn, thin layers, EM field penetration, depend. on temp. in mixed and intermediate states 79−65598

penetration depth continued
Sn thin strips, nonequilibrium resistive state, penetration depth meas. 79−56377
Ta film sputtered onto Cu substrate, microstruct. and supercond. props. 77−85370
$Ta_{70}Nb_{30}$, Abrikosov vortex formation kinetics *(Russian)* 80−93055
V-VO_x-Pb Josephson tunnel junction, crit. currents exam. 78−23209

Penning ionisation
alkali metal +He(s^3S), Penning ionisation by slow collisions 77−50512
anode sheath, crossed field low press. discharge in magnetron and Penning cell 77−11432
anthracene surface, Ar impact, Penning ionisation electron spectra and photoelectron spectra 80−66352
atom+atom collision, Penning and assoc. ionisation, complex. pot. and electron spectrum 78−94310
atom+metastable atom collisions, ionis. processes 78−62907
atomic collisional ionisation, Penning ionisation, laser induced, two step optical collisional perturbation sequence 80−63778
atomic metastable states, props., energy transfer mechanisms, exptl. techniques 80−27921
beam-plasma interaction fast processes in gas and Penning discharges 79−64879
cathode sheath, RF impedance study 80−106935
collision processes, review *(Japanese)* 79−64092
collisional ionisation, Penning and associative ionisation produced by laser field 80−63802
collisional ionisation in intense laser field, quasimol. state reson., quantum mechanical anal. 78−33589
diatomic systems, mol. orbital correl. diagrams calcs. 77−50521
discharge, hot plasma devices, ion heating mechanism *(Rumanian)* 78−59710
discharge, HV, ionis. average freq. in anode sheath 80−44012
discharge, study of hot plasma obtained *(Rumanian)* 79−7504
duopigatron gas discharge ion source, perform. characts. 78−54505
electron angular distrib., Born-Oppenheimer approx., probability amplitude 78−25677
electron spectroscopy investig. of Penning ionisation processes 80−58364
electron spectroscopy of CO-covered Pd surface with metastable He impact 79−52060
electronic and at. collisions, conf., Kyoto, Japan (Aug.-Sept. 1979) 80−57011
excitation transfer and Penning ionisation, unified treatment 78−25672
excited atom thermal energy collisions, electron spectrometric studies 80−63788
excited atoms, merging-beams experiments 80−63789
gas-discharge chamber for uniform thickness film manufacture 77−44153
heavy particle collisions, electron spectroscopy 77−42397
heterocyclic aromatic molecules, Penning election spectra and photoelection spectra, rel. intensities 80−95725
hydrocarbons, unsaturated, Penning electron and photoelectron spectra, relative intensities comparison 79−81237
inert gas+diatomic (triatomic) mol., Penning ionis. process from electron spectroscopy 77−14555
ion excited state lifetimes meas. using orientation transfer in Penning collisions *(French)* 78−50621
ion source, Penning discharge type, HF instabilities 80−43997
kinetic reactions, pulsed afterglow technique obs. in Ar-II plasma 80−48854
laser-assisted excitive Penning ionisation 79−41232
magnetron ion source, Penning phenomena effects on Hg ionisation in plasma 79−18069
molecular metastable states, props., energy transfer mechanisms, exptl. techniques 80−27921
negative ion high current beams, source plasma parameters determ. 77−83376
organic compounds liq., new ionis. method using Penning effect and chem. ionis. *(Japanese)* 79−93255
Penning source for H^- and $^2H^-$ ions 77−83415
plasma, low-temp., with nonequilibrium ionisation, review 80−96343
polarization phenomena in electronic and atomic collisions, review 80−83501
positron detection, using Penning trap 78−21812
proportional counters, inert gas mixtures, Penning ionisation effect on resolution 77−26936
radiative, photoionis. cross section depend. of continuum radiation 77−19034
surface-plasma Penning source, intense H^- beam production, ion-optical characts. 79−13892
tripropylamine admixtures, influence on optical characteristics of CO_2 laser 80−23669
Ag, population mechanism, highly-excited states, hollow cathode discharge *(Russian)* 78−63610
Ar, collision processes, photoionisation mass spectra obs. 79−31479
Ar+He, Penning ionis., ejected electrons energy and ang. distrib. 79−81266
Ar+He, Penning ionis. of Ar, He in (2^3S) state 79−41228
Ar+He*, angular distrib. of Penning electrons 79−89763
Ar+He* Penning ionisation, semiclassical descretisation procedure 78−90275
Ar+He*($1s2s,^3S$), coupled channel calcs. of chemi-ionisation 77−27166
Ar+He*($1s2s,^3S$), Penning ionis., multichannel calcs. 80−53111
Ar+N_2, pulsed microwave discharge, early afterglow and radiative transitions, Penning ionisation 78−9874
Ar*+$Fe(CO)_5$, chemiionisation and chemiluminescence reactions, Penning ionisation and fluoresc. obs. 80−97689
Au, Auger spectra, $N_{4,5}N_{6,7}N_{6,7}$ and $N_{4,5}N_{6,7}O_{4,5}$ 80−89094
CO adsorbed on Pd (111), metastable He impact, electron emission, energy and ang. distrib. 80−60744
CO+He*, Penning ionisation of CO adsorbed on Pd, theory 80−60735
CO_2 doped TEA laser, Penning ionisation 79−3678
CO_2 laser, TEA, with seed gas, Penning ionisation 78−5449
CO_2 laser self-sutained discharge, effect of low-ionisation-potential additives 78−71616
CO_2+He, Penning ionisation of target mol., for He(2^3S) 79−41228
$CO_2(CS_2)(COS)$, Penning ionisation and photoelectron spectra 77−83653
CS+He, Penning ionisation, $CS^+(B^2\Sigma^+ \rightarrow A^2\Pi_i)$ fluoresc., flowing afterglow 80−14197

Penning ionisation continued
CS_2+Ar*, Penning ionisation and dissoc. fluoresc, collisional energy depend. 78−33584
Cd+He, Penning ionisation cross section of target atom, for He(2^3S_1) 80−63777
Cs-He afterglow, spectral emission from excited Cs ions, 380-750 nm 79−82116
Cu, population mechanism, highly-excited states, hollow cathode discharge *(Russian)* 78−63610
Cu vapour laser, electron temp. meas. using a microwave radiometer 77−7072
D+He(2^1S)(2^3S), associative and Penning ionisation, autoionisation, calcs. 78−25674
D_2O, Penning ionis. electron spectra 77−42392
H+He (2^3S), pot. energy surfaces and autoionisation lifetimes calcs. 77−34740
H+He(2^1S)(2^3S), associative and Penning ionisation, autoionisation, calcs. 78−25674
H+He($2^3S,2^1S$), Penning ions. 79−64089
H+Ne*, Penning ionisation, electron energy spectrum 79−72406
H_2 hot-iron plasma, ion temp. and electron density depend. studied by laser light scatt. and emission spectroscopy 80−96342
H_2+ He (metastable), Penning ionisation *(French)* 80−1060
H_2+He*, Penning ionisation, singlet interaction pot. anomalous struct. 77−75274
H_2+He(2^3S), Penning ionisation, quantum mech. scatt. calcs. rigid rotor approx. 77−34741
H_2+He(2^3S), pot. energy surfaces and autoionisation lifetimes calcs. 77−34740
HBr+He(2^3S), Penning ionis. electron spectra, 584å photoelectron spectra 77−79687
HCl+He(2^3S), Penning ionis. electron spectra, 584å photoelectron spectra 77−79687
HF+He(2^3S), Penning ionis. electron spectra, 584å photoelectron spectra 77−79687
HI+He(2^3S), Penning ionis. electron spectra, 584å photoelectron spectra 77−79687
H_2O, Penning ionis. electron spectra 77−42392
H_2S, Penning ionis. electron spectra 77−42392
H_2S, Penning ionisation and photoelectron spectra 77−83653
^2H, polarised beam in Penning discharge 77−3203
H(1^2S)+He(2^1S), Penning ionisation, semiclassical and Born total cross-sections 78−33586
He, 2^3S_1 metastable state, interactions, optical pumping investig. 80−23377
He (2^3P)+Ca(Sr), collisional quenching of metastable states, excitation transfer cross sections 78−66653
He^+, Auger deexcitation spectrosc., impact on Ni(100) with adsorbed K^+ 79−100010
He-Cd, afterglow, Cd^+ excited state prod. by Penning and charge exchange reactions 77−15252
He-Cd, hollow cathode discharge tube, 4416 Å transition and excitation mechanism for Cd ion lines, Penning ionisation 79−46505
He-Cd mixture, Penning ionis. and nonreson. charge exchange in afterglow 79−72414
He-N_2, de excitation rate consts., energy transfer, pulse radiolysis obs. 80−30303
He+Ar(Kr)(Xe), 2^1S and 2^3S assoc. and Penning ionisation cross sections vel. depend. 79−3551
He+CS_2, metastable atoms, energy transfer processes 80−83466
He+group II metal atoms, gas discharge plasma, Penning ionisation, cross section anal. 80−33735
He+H, associative and Penning ionis. cross-sections, pot. energy curve study 79−87836
He+He, metastable atoms, collisional ionisation cross-sections 78−70911
He+$N_2(O_2)$(HCl), Penning ionis. electron spectra, new differential retarding field analyser characts. 77−41735
He+OCS, emission spectra in He afterglow 80−87139
He^++atom, metastable state deexcitation, 2S- and 2P-state mixing and Penning ionisation 77−42394
$He^+(He_2^+)+N_2(CO)(CO_2)(H_2S)$, charge transfer Penning ionis. 78−17784
He*-Ne*, Penning ionisation of metastable He* 80−83472
He*+Ar, Penning ionisation, laser modified collisional effects in electron energy spectrum 78−90278
He*+D, Penning and assoc. ionis. with metastable He, 0.01 to 10 eV beams 79−27074
He*+H(H_2)(Ar), metastable state, ionis. processes 78−62907
He*+Ne*→He+Ne^++e, Penning ionisation, merging beams obs. 78−33585
He*(^3S)+Ar+ħω→He+$Ar^+(^2P)+e^-$, intense laser radiation assisted collisional ionis. 79−76497
He*(1s2s,^3S)+Ar, Penning ionis., discrete-continuum states coupling 79−10193
He*(2^1P)+Ar→He+Ar^++e^-, anisotropic interaction potential, impact parameter method 77−68102
He*(2^3S)+F, Penning ionisation and excitation transfer, unified treatment 78−25672
He(2^3S, 2^1S)+Ba(Y)(Ce), Penning process, double ionisation 77−3439
He(2^3S) collisions, elastic scatt., Penning ionisation, polarisations *(Russian)* 78−70922
He(2^1S)+Ar, optical interaction pots. from differential cross sections 77−30956
He(2^3S)+$H_2O(H_2S)$, energy transfer processes, reaction products, UV and visible obs. in flowing afterglow 78−85138
He(2^3S)+H(D), Penning and assoc. ionis. cross sections, vel. depend. 79−22815
He(2^3S_1)+Ca(Sr)(Ba), coherent $^2P_{3/2}$ levels excitation by Penning ionis., Hanle effect 80−5520
He(2^3S_1)+Na(K)(Rb)(Cs), Penning ionis. in stationary afterglow 78−42184
He(2^3S and 2^1S)+$H_2(D_2)$, Penning, rearrangement and total ionis. cross sections, vel. depend. 79−22816
He($2s^3S_1$)+Sr, alignment of ions in Penning collisions, polarised emission obs. 80−23533
Hg+He, excitation of $Hg^+(7^2P_{1/2}, 7^2P_{3/2})$ in afterglow, rate consts. *(Russian)* 78−29848
Ir, Auger spectra, $N_{4,5}N_{6,7}N_{6,7}$ and $N_{4,5}N_{6,7}O_{4,5}$ 80−89094
Kr afterglow plasma, electron energy distrib. funtion 80−38748
Kr*+Ar*, metastables, chemi-ionis,, merging beams. 0.01-10 eV 80−14198

Penning ionisation continued
LiF(Cl)(Br) film, electron emission under metastable He and Ne atom impact 80−20747
$^6Li^*+^7Li^*$, laser-induced Penning and associative ionis., $^{13}Li_2^+$ enrichment 78−58796
N_2+He, Penning ionisation of target mol., for He(2^3S) 79−41228
N_2+He*, Penning ionisation, ejected electron spectra obs. 80−48074
N_2+He($2^{1,3}$S,$2^{1,3}$P); effective cross section of N_2^+ $B\Sigma_u^+$ state 77−79688
NO+He, Penning ionisation of target mol., for He(2^3S) 79−41228
N_2O+He, in afterglow, N_2O^+ optical emission obs. 79−68251
N_2O+He, Penning ionisation of target mol., for He(2^3S) 79−41228
$N_2O(NO_2)$, Penning ionisation and photoelectron spectra 77−83653
Na+Ar*, Penning, associative and total ionis. cross sections 77−79683
Na+Na, crossed-beam collision, laser-induced Penning and assoc. ionisation, struct. obs. 80−83476
NaF(Cl) film, electron emission under metastable He and Ne atom impact 80−20747
Ne, hollow cathode discharge, role of Penning ionisation of minor species 79−86633
Ne-Xe-HCl, transient optical absorpt. meas. for XeCl laser 79−55115
Ne+CS_2, metastable atoms, energy transfer processes 80−83466
Ne^++Zn, charge exchange and Penning ionisation in pulsed discharge afterglow 79−7007
Ne*+Ar*, Penning ionisation studied by merging-beams technique 80−91646
Ne*+$Fe(CO)_5$, chemiionisation and chemiluminescence reactions, Penning ionisation and fluoresc. obs. 80−97689
Ne*+H_2O, pot. energy surfaces, MO and CI calcs., Penning ionisation electron spectra 80−106376
Ne*+Kr, Penning and associative ionisation 77−6910
Ne*+Xe, chemiionis. in metastable state collisions 79−68306
O_2+He, Penning ionisation of target mol., for He(2^3S) 79−41228
Pb-He discharge, excitation process, Pb^+ emission lines 78−66803
Pt, Auger spectra, $N_{4,5}N_{6,7}N_{6,7}$ and $N_{4,5}N_{6,7}O_{4,5}$ 80−89094
SO_2, Penning ionis. electron spectra 77−42392
SO_2, Penning ionisation and photoelectron spectra 77−83653
SO_2+He(2^3S), Penning ionisation, mol. ion fluores., vibr. and bending freqs. 77−50507
$Sn^+(5s5p^2)^4P_{1/2}$ level, lifetime and Lande g-factor *(French)* 80−52938
XeF laser, electron beam excitation, kinetics scheme 78−78999
$Xe^+(^2P)$+Ca(Sr), collisional quenching of metastable states, excitation transfer cross sections 78−66653
Zn^+-He, positive column laser discharge, upper and lower state densities, Penning collision 80−32964
Zn+He, Penning ionisation cross section of target atom, for He(2^3S_1) 80−63777

penny-shaped cracks
branching criterion, invalidity of proof based on energy balance arguments 80−33536
brittle solid materials, critical values and strength relations *(Russian)* 78−18703
composite systems, cracked, finite element microscopic stress anal. 78−34083
compression wave diffraction by penny-shaped crack in presence of mag. field 79−47318
crack initiation in elastic/plastic indentation fields, model 78−5668
crack scattering in polycrystalline media 78−75089
cylinder, stress-intensity factor for penny-shaped crack 78−30237
cylinder, weakened by penny-shaped cracks, thermoelastic stresses 80−10191
cylinder elongation, containing periodically located disk-shaped cracks 79−90186
cylinder with oblate spheroidal cavity or internal penny shaped crack under tension, stresses 80−69736
double cantilever penny-shaped crack propagation specimen, simple model 79−64588
Dugdale crack, dynamic effects in propagation, Hankel and Laplace transform methods 80−87741
elastic cylinder bonded to elastic surrounding material 80−19285
elastic fracture mechanics, boundary integral eqn. anal. 80−14622
elastic layer containing penny shaped crack, bonded to dissimilar half-spaces 77−58603
elastic solid, deformed, incompressible, penny-shaped crack problem 80−92085
elastic space, infinite micropolar, exact soln. 77−62205
elastic waves, multiple scattering by elastic ellipsoidal inclusions, self-consistent approach 78−63372
elastodynamic response of a penny-shaped crack in a cylinder of finite radius 79−37240
elastodynamic stress field and bifurcation, running crack 77−14969
finite orthotropic cylinder with penny-shaped crack, transient response under torsion 80−48640
glass plate, physically or chemically tempered, contact fracture resist., model 78−19895
graphite, pyrolytic, ion bombard., flaking, stress fields around penny-shaped cracks 78−52946
hydraulically fractured cracks in hot dry rocks 79−62491
infinite transversely isotropic solid, stress intensity factor 80−69738
infinite transversely isotropic solid containing penny shaped crack, stress intensity factor *(French)* 80−43663
interface penny-shaped crack, Fredholm integral eqn. soln. 78−90784
longitudinal wave interactions at interface of two bonded dissimilar elastic solids 80−33532
mirror/flaw-size relations, residual contact stresses effect 80−107363
multiaxial fracture, general approach to statistical anal. penny cracks distribs. 78−90785
non-homogeneous elastic medium, sudden twisting of penny shaped flow 78−87302
nonhomogeneous medium under shear, elasticity theory 78−86166
polycarbonate, crack instability under impulse loads, dynamic fracture toughness 77−48518
porous media, liquid saturated, disc-like crack development by hydraulic rupture *(Russian)* 80−19286
post-yield fracture mechanics to penny-shaped and semicircular cracks 77−54925
rocks, growth rate of crack in hydraulic fracturing 77−29289
rocks, hydraulic fracturing, penny-shaped crack growth rate 77−17084
soft ferromagnetic elastic solid, magnetoelastic interaction with penny shaped crack in const. mag. field 79−18829
steel, mild, microstructure effect on cleavage fracture stress 79−8358
steel, stainless, ferritic, high CR penny shaped central bursting defect in cold drawing 79−20071
stress analysis of penny shaped crack in inhomogeneous medium, high freq. torsional oscills. 78−26086
stress intensity factor for crack in sphere embedded in infinite medium 79−27585
thermal conductivity of solids, crack effects 79−10993
thermal stresses, elastic sphere embedded in infinite elastic space 80−64460
thick plate under torsion, transient elasto-dynamic response 80−5993
torsional oscillations at low frequencies 80−53703
torsional wave diffraction by penny shaped crack, in axial mag. field 79−24206
transverse tension, stresses, micropolar elasticity 80−64459
transversely isotropic composite with penny shaped crack, stress intensity, crack energy 79−98660
transversely isotropic cylinder, thermal stresses for penny-shaped crack 77−89070
transversely isotropic solid, penny shaped crack, stress anal. 80−92083
twisting, in a finite elastic cylinder 78−67110
two bonded elastic solids interface, penny shaped crack, torsional wave interaction 80−64484
US flaw detection, diffraction of normal modes by a compliant disk 80−87603
viscoelastic medium, infinite, stress field anal. 77−31254
weakening of an elastic solid by a periodic array of penny-shaped cracks 79−68658
Al_2O_3 rods, quenched, exam. of contact induced strength degradation 78−76731

pentary algebra *see algebra*

pentodes
No entries

perception (hearing) *see hearing*

performance index
see also control systems; reliability; sensitivity
aquifer permeability and storage identification by artificial recharge hybrid simulation 77−45043
left ventricular flow pattern index of pumping efficiency 79−96601
neutron flux optimum control during nuclear station load following 79−9761
PWR steam supply control system optimisation 78−50251

periodic system of elements
see also elements (chemical)
alloy systematics, rel. to the long periodic table 79−37649
diatomic molecules, internuclear separation 79−45859
diatomic molecules, periodic table, spectrophysical props. 79−45621
ionisation potential, periodic regularities, relativistic corrections calcs. 79−49950
Mendeleev law student laboratory exercise 77−26112
rare earth compound properties, periodicity at atom props. 80−96586
structure of periodic table, screened Coulomb pot. theory 77−75035
subclassification of lanthanides and actinides 77−26109
subshell filling order, method for determining 77−26111
zero-point energy of electrons and phonons 78−78603

peripheral equipment (computers) *see computer peripheral equipment*

peripheral models
see also multiperipheral models
2N interaction, light front field theory treatment, using $\phi^2\phi_0$ theory 79−67579
ρ-exchange isovector parity-violating potential 79−93525
baryonium Regge trajectories exchange in medium and high energy scatt., expt. evidence 78−50022
boson, Green function, rainbow approach of scalar model *(Russian)* 80−68436
deuteron wave functions, relativistic, π-NN coupling 80−22595
dual absorptive model with peripheral pomeron, energy depend. of dip in pp elastic scatt. 77−79281
eikonal expansion, scalar meson exchange 78−29278
exchange degeneracy breaking, hadronic selection rules 80−37248
exchange degeneracy evidence, Kp and πp total cross sections anal. 77−82796
exchange-degeneracy breaking, connection with multiquark states, dual approach 79−93387
hadron photoproduction nondiffractive processes, review, book contrib. 80−47313
hamiltonian for the nonrelativistic two-fermion bound state 80−13273
heavy meson exchange effect on $^1D_2$ and $^3F_3$ N-N partial waves, dibaryon resonances 80−105874
hyperon+nucleon interactions, one boson exchange pot. approach, multichannel Schrodinger eqn. soln. 77−57556
meson exchange, relativistic corrections, book contrib. 80−475
meson exchange currents, conservation principles, symmetries, book contrib. 80−473
meson exchange currents, inelastic EM form factors of the deuteron 79−93418
meson theory of nuclear vector and axial vecotr exchange currents, review, book contrib. 80−474
meson-baryon processes peripheral scattering dominance, possible interpretation 77−18241
multiparticle inclusive prod., cluster sequential decays, scaling violations 77−49934
multiperipheral parton model, Reggeisation and dual unitarisation 80−37249
multiple direct exchange in Yang Mills theory, high energy behaviour of Feynman diagrams sum 77−34088
multiplicity distribs., c.f. data. *(Russian)* 77−38149
multiquark states and the breaking of exchange degeneracy, dual approach 79−45061
neutral meson condensation, one boson exchange model 79−13235
nuclear vertex form factor in peripheral model, (p,d) (d,p) cross-sections *(Russian)* 77−82889
nucleon-nucleon scattering, phase shift anals., pp at 1-500 MeV, pn at 0-425 MeV 77−54115
nucleonic form factor, pion exchange, model 80−22608
one boson exchange model, OZI rule, nucleon-nucleon-boson coupling 80−32066
one photon exchange pot. in configuration space from Bethe-Salpeter eqn. 79−67527

peripheral models continued
one-boson-exchange-potential model of baryon-baryon scatt. 80−13295
one-pion-exchange model description of elastic pd scatt. and (p,Nd) reacts. 79−80834
parameter free model of p̄, D, ψ inclusive prod. 77−10293
Paris nucleon-nucleon potential, book contrib. 79−97665
parity-violating vector-meson-exchange internucleon potential, weak nuclear processes, modified factorisation approach 77−30418
phenomenological analysis of single pion photoproduction in the first resonance region 78−89721
photoprod. of heavy hadrons, peripheral and VMD models 78−33074
pion exchange at high energies, review 80−95259
reggeized one pion exchange model of nucleon charge exchange in inclusive reactions *(Russian)* 77−2888
relativistic effects on the two-nucleon and nuclear matter systems 79−89261
relativistic N-N one-boson-exchange potentials with asymptotic power-law energy dependence 78−82293
s-channel resonance model based on peripheral resonances, exotic peaks 80−91069
scattering theory, divergent perturbation and partial wave expansions, summation methods 79−67485
soft hadron-nucleus reactions at high energies, theoretical model 79−17870
strange quarks, Regge exchange building, K^-p data anal. 79−2995
strong exchange degeneracy analysed in Kp and πp reactions, pomeron behaviour 78−41515
tachyon exchange in two-body interactions 80−82960
two nuclear polynomial solitary wave exchange pots. 78−58202
two-body reacts., large angle behaviour 78−442
d, elastic form factor calcs. with Bethe-Salpeter eqn. 79−67554
d charge form factors, π-contrib., unity of relativistic corrections and meson exchange currents 79−67553
d electrodisintegration, Δ resonance admixtures in NN problem, OBE model 78−70373
D^+ decay, Cabibbo suppression, strong 20-plet dominance and W exchange 80−42453
DD̄, DD̄*, D*D̄*, charm molecules, dynamical model, light meson exchange 80−57572
ed→ed, nucleon forces, meson exchange current effects, impulse approx., review 80−57603
$e^+e^-\to l^+l^-$ via many-vector boson exchange, cross sections from unified models 80−22597
ep→e′nX, π exchange, π EM struct. functions calcs. 78−70375
γN→ωΔ, pion exchange mechanism anal. 77−82750
γp, low energy scatt., one-particle exchange model 80−22617
γp elastic scatt., one-particle-exchange model 78−457
γp low energy scatt., one particle exchange model 78−33070
γp→πΔ(1236), 744 to 1044 MeV, momentum spectra, differential cross sections *(Japanese)* 78−17032
$\gamma p\to\rho^-\Delta^{++}$, 9.7 GeV, pion exchange mechanism anal. 77−82750
$\gamma p\to\rho^+ n$, 9.7 pion exchange, mechanism anal. 77−82750
γπ, hadron photoprod. and saturation of sum rules *(Russian)* 79−49529
J/ψ meson photoproduction on nucleon *(Russian)* 77−38180
KN finite energy sum rules, Regge pole models, exchange amplitudes 78−470
$K^\pm N$ charge exchange reaction, tensor exchange amplitudes 79−63522
$K^\pm N\to K^+ +X$, double hypercharge kaon exchange *(Russian)* 78−29368
$K^-p\to K^-p\pi^+\pi^-$, 14 GeV/c, peripherally prod. π, possible preequilibrium π evaporation 79−80850
$K^-p\to K^{*-}\pi^+ n$, doubly peripheral exchange model 77−13980
$K^\pm p\to(K\pi)^\pm p$, 10 GeV/c, amplitude and natural parity exchange anal. 78−50053
$\mu^- d\to nn\nu_\mu$, meson exchange currents effect on Λ_d and Λ_q transition rates 79−85256
N diffr. dissoc., slope-mass correl. pion-exchange amplitude anal. 77−87959
nd break-up, quasi-free scattering, peripherical nature 78−89726
nd scattering, 14.4 MeV, parity nonconserving asymm. 78−21449
NΔ system, theoretical investigation of bound states and resonances 79−75749
NN, total cross sections, medium energy dynamics, OPE three-body theory 78−25064
NN̄ and πNN̄, ππNN̄ bound states from N̄N potentials 80−62951
NN dynamics at medium energies, elastic and inelastic scatt., unitary model 80−63101
NN dynamics at medium energies, phase parameters, one pion exchange model 80−63102
NN elastic scatt. with one boson exchange, Bethe-Salpeter eqn. 80−42485
NN forward scatt., two and three pion cut contribs., nucleon exchange model 80−63103
NN generalised one-boson-exchange pot. meson field theory 78−66096
NN I=1 scattering with one boson exchange, Bethe Salpeter eqn. 77−57455
NN interaction,, neutral scalar, pseudoscalar and neutral vector boson radiative corrections, explicit formulae 78−70372
NN interaction, field theoretical approach with stress on OBE pot. *(German)* 78−78203
NN̄ interaction, low energy, meson exchange forces, one boson exchange potential, dual quark models 78−62444
NN interaction, meson field theory, one-boson-exchange model 78−66216
NN interactions, one-boson exchange approach 77−22759
NN low-energy pot., Regge-pole theory 78−45889
NN→NN(NN̄π), isobar and peripheral model anal., and unified theory 79−80841
NN→NNπ, anal. via nonrelativistic field theory with HBE 79−85317
NN→NNπ, effect of π-baryon from factors on ang. depend. of cross sections 79−85318
NN→NNπ, isovector exchange, comparison with πN elastic scatt. 78−37189
NN̄ narrow meson resonances near threshold, theoretical approaches 80−9157
NN nonrelativistic 1-boson exchange potentials based on generalised meson field theory 78−70459
NN potentials, based on meson exchange, discussion and appl. to nuclear matter 79−80815
NN̄ potentials for bound and scattering states 80−47323
peripheral models continued
NN potentials from Regge pole model, one boson exchange, coupling consts., masses 78−70346
NN scatt., small angle, appl. of eikonal vector meson exchange theory 78 17052
nn scattering, ∼100 eV, ang. distrib., very light pseudoscalar boson exchange 78−62454
NN scattering, attractive retarded effect of one boson exchange pot. 77 2859
NN scattering, role of non-iterative diagrams 79−67576
NN scattering in nonAbelian gauge theory, π-, ρ-, and ω-exchange, scalar Pade approx. 79−67573
NN̄ spectrum in pot. models, meson exchange forces 80−9156
NN systems, resonances due to annihilation, baryonium states, many channel N/D method 78−66143
$np\to d(\pi\pi)^0$, 800 MeV, d momentum spectrum meas., two nucleon exchange model 78−70384
np→dγ, photon circular polarisation, relativistic one nucleon exchange model 78−70390
$np\to p\Delta_{33}^0$, 1.39 to 1.90 GeV/c, corrections to one pion exchange amplitudes 78−41560
np→pn, 5-25 GeV/c, charge exchange scatt., πNN vertex function, one pion exchange 80−37291
np thermal radiative capture, cross section calc. including meson exchange 79−67583
$\bar\nu_e d\to np\bar\nu_e$, axial meson exchange currents 79−85255
pd, backward elastic scatt., one nucleon exchange mechanism in light front dynamics *(Russian)* 79−40799
pd, backward elastic scatt. in Δ-reson. region, and OPE formfactor *(Russian)* 79−54353
pn, inelastic charge exchange, quark interchange 80−86759
$pn\to p_{slow}+x$, 195 GeV/c, triple Regge model anal., dominant π exchange 78−54657
pn scattering, 50, 325 MeV, phase shift anals., single energy and energy depend solns. 77−54116
pp, $^1D_2$ state, multichannel N/D formalism 79−63506
pp, bremsstrahlung, field theoretic calc., treatment of OBE external emission processes 78−62451
pp, inelastic charge exchange, quark interchange 80−86759
p̄p, low, energy scatt., one-boson exchange pot. model 77−74705
pp, massive lepton pair prod., pion exchange model anal., quark parton interpretation *(Russian)* 80−82993
$\bar pp\to\pi^+2\pi^-$, 5.7 GeV/c, transverse momenta correls., peripheral phase space explanation 77−2857
$pp\to(\pi^+ n)p$, π energy and transverse momentum distrib., DHD model with nucleon exchange *(Russian)* 80−13327
pp bremsstrahlung, Δ isobar excitation and radiative decay 79−67586
$pp\to d\pi^+$, ang. distribs., sensitivity to nuclear wavefunctions 79−85314
$pp\to d\rho^+$, N and N* exchanges 77−22804
$pp\to\delta^{++}(1236)$, Δ^0, 100 GeV/c, one-meson-exchange mechanism anal. 78−8712
$\bar pp\to\Delta^{--}(1236)X$, 22.4 GeV/c, inclusive and semiinclusive cross sections, one pion exchange contrib. 79−49548
p̄p→n̄n, 5-25 GeV/c, charge exchange scatt., πNN vertex function, one pion exchange 80−37291
$pp\to pn\pi^+$, two nucleon mechanism for pion production 79−85286
$pp\to pp\pi^0$, 800 MeV, Δ^+ prod., π and ρ exchange 79−85316
$pp\to\pi^0 X$, large p_T processes, pion exchange model anal. *(Russian)* 80−27527
$pp\to\pi^+ d$, interaction anal. by neutron exchange Born terms, ΔN states, diproton resonances 79−93391
$pp\to\pi^+ pn$, 1 GeV/c, momentum spectra ang. depend., one-particle-exchange model comparison *(Russian)* 77−10276
pp→ψX 70 GeV to ISR energies, pion exchange model anal. *(Russian)* 79−40823
pp reaction, exchange current corrections π and ρ exchange 80−26733
pp scatt., <300 MeV P-odd asymmetry for pol. ρ *(Russian)* 80−102063
pp scatt., intermediate energy, polarised p, three body model 79−67590
pp scattering amplitudes, 6 GeV, phase shift anal. 80−37290
π exchange contrib. to isoscalar current and mag. moment operators 77−67636
π photoproduction ≤450 MeV, one-particle exchange model 79−13135
π photoproduction in first resonance region, one particle exchange model 78−4864
$\pi^- d\to nn$, mechanism, cross-sections, EM form factors 79−89181
$\pi^- d\to\rho^0\pi^- d$, 9 Gev exchange Deck model anal. 80−47322
$\pi^+ d$, 15 GeV, high-mass even-g states, broad dipion states beyond g(1680) 80−68487
$\pi^+ d\to pp$, meson exchange currents, effects on pion absorption 79−85287
πN charge exchange scatt. saturation, trajectory props. *(Russian)* 79−89186
πN elastic scatt., backward polarisation as peripherality measure 77−2862
πN low energy scattering, one particle exchange model, spin 3/2 particle 78−4873
πN P-wave interaction, effect of non-condensed pions in nuclear medium 79−13237
$\pi N\to\pi(N\pi)$ diffraction dissociation, role of nucleon exchange 77−38192
$\pi N\to\pi\pi N$, isobar formalism, one-pion-exchange partial-wave cross sections 77−87957
πN scatt., spin flip dynamics and inclusive processes *(Russian)* 78−41589
$\pi^- n\to pX^{--}$, 21, 205 and 360 GeV/c, reggeised one-pion-exchange 80−57649
$\pi^- n\to\rho^0\pi^- n$, 9 GeV exchange Deck model anal. 80−47322
$\pi^+ n\to p_{slow}+x$, 195 GeV/c, triple Regge model anal., dominant π exchange 78−54657
$\pi^\pm n$ backward elastic scatt. 20-40 GeV, Regge theory description, angular distrib., radiative corrections 78−62461
πNN form factor, Δ(1236) contrib., calc. 80−22609
πNN form factors, influence on two nucleon data, one particle exchange 78−70369
πNN(πNΔ)(πΔΔ) vertices, study of the finite range struct. 79−85370
πp, massive lepton pair prod., pion exchange model anal., quark parton interpretation *(Russian)* 80−82993
πp→ψX, 70 GeV to ISR energies, pion exchange model anal. *(Russian)* 79−40823
$\pi^- p\to(\bar pn)p$, 12 GeV/c, peripheral p̄n prod. and decay ang. distribs. 78−33096

peripheral models continued
$\pi^-p \rightarrow (\pi^+\pi^-)n$, 17.2 GeV/c, role of A_1 exchange, Regge pole exchange 77−61325
$\pi^-p \rightarrow \Delta^{++}(1232)$, 15 GeV/c, multiplicity distrib. determ. 78−45982
$\pi^-p \rightarrow K_1^0K_1^0n$, 40 GeV/c *(Russian)* 77−261
$\pi^-p \rightarrow \bar{p}pn$, 10 and 16 GeV/c, anal. of $\bar{p}p$ and $\bar{p}n$ pairs 79−75788
$\pi^-p \rightarrow \pi^0X$, large p_T processes, pion exchange model anal. *(Russian)* 80−27527
$\pi^-p \rightarrow \pi^+\pi^-n$, $\pi\pi$ scatt. phases near threshold, pseudoperipheral approx. *(Russian)* 79−71763
π^+p, elastic scatt. 50 to 200 GeV peripheral Pomeron explanation 79−40803
$\pi^+p \rightarrow (\rho^0,\omega)\Delta^{++}(1238)$, q_L=7.1 GeV/c, role of new exchanges *(Russian)* 79−54355
$\pi^+p \rightarrow \Delta^{++}(1236)$, Δ^0, 100 GeV/c, one-meson-exchange mechanism anal. 78−8712
$\pi^+p \rightarrow \pi^+p\pi^0$, p diffractive dissociation, ρ^+ prod., one-pion-exchange model 78−21451
ψ meson photoprod., direct peripheral mechanism *(Russian)* 77−46056
A(p,Nd)B quasifree scatt. at backward angles, one-pion-exchange model description 79−80834
$\gamma N \rightarrow \eta\pi^{\pm}$, 9.7 GeV, one-pion-exchange model 78−25054
^{2}H, EM props. in relativistic one boson exchange model 79−67678
^{3}He, nuclear charge form factor, two-boson exchange charge density π, ρ, ω exchanges 80−63073
N*(1236) propagator, momentum depend. in N*-excitation current 80−27559
$pp \rightarrow pn\pi$, exclusive pion prod. OPE and VME amplitudes 79−85336

peripheral processors *see satellite computers*

peripheral speed *see velocity*

peristaltic flow
asymptotic method for peristaltic transport 80−87805
bio-fluid peristaltic transport, peripheral layer viscosity effects 80−61600
biological flow, efficiency 77−2018
blood in vessel with actively deforming wall, numerical simulation of movement 80−72205
deformable valved tube, viscous fluid flow in presence of gravity 77−25500
elastic tubes, theoretical model *(German)* 79−37396
incompressible flow in elastic pipes *(German)* 79−81982
nematode oesophagus pumping mechanism 78−69121
Newtonian fluid containing rigid particles, peristaltic pumping at low Reynolds number 79−10604
non-Newtonian flow in oscillating pipe, peristaltic and Poiseuille flow phenomena 78−63463
non-Newtonian fluid, long wavelength peristaltic transport, stream function and pressure field solns. 80−74922
nonlinear, Navier-Stokes eqns., soln. by implicit finite difference method using orthogonal curvilinear coords. 77−39346
nonlinear peristaltic flow, calc. and expt. 78−9718
pumping by a lateral bending wave 80−53862
transport, in arbitrary cross-section tube, asymptotic theory 78−91014
transport due to finite amplitude bending and contraction waves 79−50800
unsteady flow in contracting or expanding pipe 77−86523
valveless elastic tube, pumping effect, model *(German)* 78−59493
viscoplastic liq. in slot channel, peristaltic flow 78−5770

Permalloy
alloyed with refractory metal borides, mech. props., rel. to appl. as electrodes in electrospark machining 80−21174
barrier film, worm-like motion of domain boundaries *(Russian)* 78−39375
bubble domain interaction with infinite unsaturated sheet, statics 77−66397
coated garnet films, bubble statics, dynamics *(Japanese)* 78−52326
coated Sm-YIG garnet, planar domain walls associated with bubbles 77−85520
coercivity and conventional and unconventional compositions, development trends *(Slovak)* 79−4694
conductor crossing effect on bubble propagation margins 80−29588
corrosion resistance and mag. props., effect of Cr addition 77−86219
corrosion resistance enhancement 79−79150
demagnetisation eigenfunctions anal. of linear transverse magnetisation in long, thin stripes 80−34687
domain struct., influence of planar anisotropy 79−78472
domain structure observation technique, bubble propagation circuits 78−84464
FCC, mag. anisotropy induced by cold rolling 80−11188
ferro-fluid particle formation on permalloy overlay bar surface, calc. and anal. 78−68329
ferromagnetic noise eval. 79−2799
film, Bloch wall motion obs. *(German)* 77−16133
film, break-cross-tie domain walls, thickness depend. 78−43619
film, coating on Gd-Co(-Au) amorphous ferrimag. film 79−1695
film, coercive force associated with domain boundary displacement *(Russian)* 80−50151
film, coercivity control 80−15764
film, corrosion induced defects, scanning Auger microscopy 77−40464
film, corrosion kinetics, mass and resist. change techniques, comparison 78−27675
film, cylindrical, magnetisation in crossed steady/alternating fields, easy axis dispersion influence 79−8024
film, domain nucleation using low intensity US 80−34731
film, domain struct., nonuniform rotation of magnetisation *(Russian)* 79−47313
film, domain wall mass and energy, wall vel. depend. calc. 80−2614
film, domain walls, magnetisation components distrib. 79−87298
film, domain walls streaming *(Russian)* 79−82842
film, double layer, wall splitting effect 77−85530
film, electrodeposited, for cylindrical magnetometer sensor 77−82576
film, electrodeposition with zero magnetostriction composition, technological control 79−33955
film, Fe-overcoated, optical and magneto-optical charact., mag. preps. 79−82956
film, galvanomag. rotation charact., under uniaxial stress 78−84466
film, hysteresis loop meas. using magnetooptical system 79−69707
film, implanted with C ions, HCP struct. formation, electron diffr. study *(Russian)* 79−82469
film, in weak field, pulse mag. reversal mechanism *(Russian)* 77−80976

Permalloy continued
film, M-H curve meas., magneto-optical instrument *(Japanese)* 77−37953
film, mag. microstruct. obs. in nonlinear ripple magnetis. case *(Russian)* 80−65971
film, magnetic leakage fields above stripe domains 77−77077
film, magnetoconductivity modulation by substrate electrostriction 79−60908
film, magnetoresistive determ. of anisotropy energy and its strain depend. 79−56575
film, mobility of Bloch lines 77−28421
film, movement of circular Bloch line in cross-tie wall 78−31099
film, multi- and single-layer, reson. curves subjected to tangential mag. reversals *(Russian)* 80−50195
film, obliquely deposited, mag. anisotropy, annealing and deposition parameter effects *(Russian)* 77−80971
film, on quartz, two-layer disc, bending reson. vibrs. *(Russian)* 77−24797
film, oscillatory metallic field effect and surface magnetoelasticity 79−56282
film, oxidation, quartz cryst. microbalance, AES and XPS obs. 78−27676
film, oxidation effects on atmospheric corrosion, AES, XPS and ion sputtering anal. 80−11829
film, perpendicular anisotropy, structural and thermal stresses *(Russian)* 79−4708
film, quasistatic and pulsed mag. reversals of Neel domain walls *(Russian)* 78−39374
film, sputtered, bevelling by chemical etching, for this film mag. header 78−92375
film, stray fields arising during pulse reversal 77−80980
film, streaming of domain walls *(Russian)* 78−72380
film, stripe domain struct., distrib. of magnetisation *(Russian)* 77−66396
film, submicroscopical magnetisation structs. induced by fields normal to film plane 79−1697
film, two-layer, Permalloy-Cu(Al), mag. anisotropy, grain boundary diffusion *(Russian)* 80−71122
film, two-layer, with magnetostatic coupling, creep of domain boundaries *(Russian)* 77−43857
film, velocity of motion of nonequilibrium walls of edge domains *(Russian)* 79−1694
film, with band domain struct., pulse mag. reversals *(Russian)* 79−38361
film, with small surface anisotropy, ferromag. reson. 77−69701
film break-cross-tie wall energy 80−88842
film corrosion characterisation by crystal oscillator microbalance and resistance meas. 78−7101
film demagnetising field and magnetisation curve determ. 77−73059
film magnetometer, mag. props. and LF noise 78−48005
film oxidation, microbalance, AES, ESCA and sputter profiling 78−15600
film preparation by RF sputtering 78−3044
film strip, unidirectional domain wall propag. with in-plane magnetisation 80−71134
film strip, wall curvature calc. with in-plane magnetisation 78−2717
films, domain propelling tunnel, domain struct. displacement *(Russian)* 79−99736
films, Faraday rotation effect dispersion 80−40092
films, induced mag. anisotropy, temp. depend. *(Russian)* 79−42757
films, RF sputtered on Au, coercivity 80−80575
films, thickness depend. of Bloch line mobility 79−24204
garnet films, Permalloy-coated, bubble properties 78−2715
hardening additions effect on mag. props. *(German)* 79−28566
hysteresis loops, reference materials charact. obs., temperature effect 80−80563
I-bar elements, magnetostatic effects, unifying overview of domain and continuum results 80−44853
isopermalloy, permeability stability calc. rel. to texture *(Chinese)* 80−65959
Kerr magneto-optical effect meas., domain wall location determ., Kerr effect probe 78−68328
magnetic anisotropy of Permalloy film, temp. depend. *(Russian)* 77−51901
magnetic bubble state stability in rot. field 78−68317
magnetic developments in technologically important materials, review 79−33509
magnetic domains, cylindrical, static performance in inhomogeneous external field *(German)* 77−63226
magnetic head wear resistance and surface charact. against mag. tape *(Japanese)* 80−35335
magnetic properties, influence of grain struct. and non-mag. particles *(German)* 77−16112
magnetic properties and structure, environment effect during annealing, 50NP and 79NM alloys 80−60366
magnetisation improvement through solid state refining 78−91893
magnetisation reversal, fast, forced by external RF mag. field, Mossbauer obs. 78−52311
magnetoresistive mag. field and current sensor 77−10048
magnetoresistive magnetic, field sensor, performance calc. 80−57342
multi-layer flat ring Permalloy-SiO cond., with circular anisotropy, mag. props. *(Russian)* 77−8366
narrow stripes, permeability 77−89987
Neel wall transitions into cross-tie walls 79−95619
order-disorder transform. and magnetic props. obs., by neutron diffraction method *(Slovak)* 79−4963
overlay bars, bubble stray field effect on domain wall struct., interference contrast technique 79−78457
oxidised film, magnetic noise, low temp. depression *(Russian)* 79−99734
Permalloy, pressing velocity effect on quality of compacts 80−20834
Permalloy-Co film, domain walls, magnetisation ripple *(Russian)* 79−47314
Permalloy-Mn film, diffusion aftereffect causing mag. state change *(Russian)* 80−103860
Permalloy-Rh, film, influence of Rh on corrosion resist. and mag. props. 80−3235
Permalloy-SiO_2-Schott glass, bubble propagation struct. 80−34719
platelet, transmission reson. meas. 77−20710
platelets, FMR mode positions, spin pinning 77−4562
powder metallurgical production and props. of Permalloy 51N 78−60603

Permalloy continued
powders, electric pulse shaping and sintering 80−25605
proton radiation effects, Mossbauer obs. 80−40008
proximity transducer based on magnetoresistance effect 78−57929
RF sputtered films, O effects in mag. and elec. props. 80−100603
RF sputtered films, struct.-sensitive mag. props. 80−34705
solid boriding for mag. head appl., wear resist. and microhardness 80−21172
sputtered film, structuring rel. to laser sputtering method *(Russian)* 77−59689
Supermalloy, 24 GHz ferromagnetic antiresonance transmission 77−51957
Supermalloy, 9, 24 and 38 GHz ferromagnetic reson. absorpt., line shapes 77−51958
supermalloy, domain wall pinning rel. to coercive force 77−1561
supermalloy, foil, microwave transmission, parallel RF and mag. fields 77−59462
T bar, domain wall study employing ferrofluid, rel. to magneto-optical Kerr effect meas. 80−60360
T-shaped and I-shaped elements with cylindrical mag. domains, magnetisation distrib. 77−77074
thermoelastic stresses and magnetostriction effects during light recording *(Russian)* 79−97465
thermomagnetic recording, resolving power of films with band domain struct. *(Russian)* 80−75769
thin film cores, domain wall motion and flux patterns, Kerr magneto-optic effect obs. 80−34721
thin-film head pole struct., domain configurations, SEM obs. 80−65975
type I bars, hysteretic props., Bitter soln. obs. and Kerr effect meas. 79−78439
wear by magnetic tape, Auger spectroscopy exam. *(Japanese)* 78−39916
Cu-Permalloy, interafce, ferromagnetic and cond. spin reson. mode coupling 79−78521
Fe-Ni, electrodeposition, mag. props. *(French)* 78−64488
$(Fe_{0.2}Ni_{0.8})_{1-y}(SiO)_y$, Permalloy material, magnetisation, temp. and impurity atom conc. depend., band model calcs. *(Russian)* 80−93088
$(Fe_yNi_{1-y})_{1-x}(SiO)_x$, dielec. effect on magnetisation and Faraday rot. *(Russian)* 78−39298
Mo-Permalloy, galvanomag. props. 77−39822
Mo-permalloy, magnetic permeability and order form. kinetics under annealing, conc. depend. 77−8356
Ti-Permalloy films, interdiffusion, Auger anal. and X-ray diffr. obs., degradation of mag. props. 80−34251
Ti-Permalloy thin film diffusion couples, low temp. interdiffusion interdiffusion 78−71889

permanent magnet motors
plastic magnet appl., anisotropic, based on moulding ferromagnetic powder material with plastics *(Japanese)* 80−60829
thermomagnetic motor, dynamic characts. and stable operation *(Japanese)* 80−16840

permanent magnets
active permanent magnet suspensions, scientific instruments appls. 78−24829
Alnico 5, thermal treatment in mag. field, mag. props. 78−91905
Alnico 8, permanent magnetic alloy, topography of precipitate phase *(Chinese)* 80−66512
Alnico 8 permanent magnet, magnetic props. rel. with crystallographic texture 78−95483
Alnico type YuNDK25DA alloy permanent magnets, thermal mag. hysteresis 80−75818
bar magnet field, analogue simulation by electrostatic field, boundary conditions 77−61892
chromindur, phase separation, Mossbauer obs. 78−88116
coil and permanent magnet combination for large dia. ion source 80−74066
columnar structure production, for medical electronic instruments 79−54157
composite, magnetostatic and exchange interaction 77−69536
cylindrical rare-earth magnet repulsion dynamic characteristics *(Japanese)* 79−22878
defectoscopy of permanent magnets, using electromagnetic method 78−39998
development and appls. 80−27320
dynamic vibration absorber, consisting of three permanent magnets 78−9614
elastic, made from composite material, parameter anal. *(Russian)* 78−29132
EM transducer with periodic permanent magnets, horizontally polarised shear elastic wave excitation 79−76932
energy relations in hard and soft mag. materials 77−8353
Fe-Cr-Co-Si-Mo, plastic deform. influence on structure and mag. props. *(Russian)* 79−70176
ferrite/steel composite bar magnet, large size, for mobile appls. 78−93740
ferrites, forming 78−64495
flux stability enhancement, by thermomechanical treatments, inertial guidance systems appl. 80−50144
focusing quadrupoles for linear proton accelerators 77−23320
focusing system, complex shaped pole pieces, induction distrib. anal. *(Russian)* 77−83786
gap field with conical poles clad with soft mag. materials, anal. *(Russian)* 79−41266
high-coercivity, magnetisation characteristic linearity determ. using flux controlling technique *(Russian)* 80−100597
interaction force calc. between permanent and ferromagnetic material *(Russian)* 77−26347
intermetallic compounds development, 20-years research results 77−7843
interpolar space uniform region conformal mapping *(Russian)* 77−53960
ion beam transport equipment for low energy divergent H_2 beam 80−69001
ion linacs, permanent magnet quadrupoles, development 77−38494
linear accelerators, permanent quadrupole magnets 77−38498
magnetic developments in technologically important materials, review 79−33509
magnetic soft and hard materials, garnets, magnetic properties and applications, structural props. 80−65760
magnetic texture form. in double pole gap of electromagnet 77−89985
magnetisation, iterative calc. method 77−83777

permanent magnets continued
Magnico alloy, with Si, Nb, Ti and La, low-temp. thermomag. treatment 77−63812
Magnico alloy, with Si, Nb, Ti effect of Ub on mag. props. and grindability 77−63811
materials, technology, development *(Polish)* 77−89973
materials, trends in development 78−91895
in measuring instruments with partially closed mag. ccts., meas. errors *(Russian)* 77−67480
metallic magnets investigation, present state *(Polish)* 80−107987
micromagnetism, theory 78−52301
mischmetal-based magnets, $MM_{1-x}Sm_xCo_5$, demagnetisation, temp. depend., 175 to 425K 79−78440
mischmetal-cobalt alloy, $MMCo_5$, polished, domain wall grooving, optical microscopy and SEM obs. 77−8334
model magnet, for reson. spectrometer, reproducibility of fields, field heights and magnetisation props. of materials *(German)* 78−24832
multipole, oriented rare earth cobalt materials 80−37925
oscillations, coupled, demonstration using permanent magnets 80−42015
permalloy, cylindrical domain static performance in inhomogeneous external field *(German)* 77−63226
plane periodic system, mag field, energy and interaction force distrib. 78−46483
plane permanent magnet system field distrib. model *(Russian)* 80−28133
plastic, anisotropic, based on moulding ferromagnetic powder material with plastics *(Japanese)* 80−60829
pull force magnitude, ferrite particle struct. effect 80−31815
pulse magnetisation monitoring by pulse magnetometer 77−45871
radial field polariser for magnetising a moving liquid 78−250
radial pulse magnetisation, magnetising and testing fixtures 77−8354
rare earth, physics and technology 80−20433
rare earth alloys, RCo_5, sintered magnets, texture determ. 79−100085
rare earth cobalt intermetallics, Cu or Ni-substituted, narrow Bloch walls, magnetisation, 4.2K 77−8333
rare earth cobalt intermetallics, RCo_2, elastic moduli, 4.2-300K 78−52332
rare earth intermetallics, magnetocryst. anisotropy 77−8299
rare earth iron intermetallics, R_2Fe_{17} and $R_2Fe_{17-x}Ni_x(Co_x)$, mag. anisotropy and hyperfine interactions 77−8298
rare earth magnetically hard materials, review 77−73051
rare earth transition metal intermetallic permanent magnets, props. and technology, book contrib. 79−65696
rare earth-$(Co_{1-x}Ni_x)_5$, single cryst., mag. props., mag. reversal 77−85489
rare earth-Co, 2-17 comp., mag. props. 77−8348
rare earth-Co, generation mechanism of high coercive force *(Japanese)* 79−100269
rare earth-Co, processing and props., review *(Japanese)* 77−73049
rare earth-Co alloys, microstruct., TEM obs., magnetisation 78−91901
rare earth-Co alloys, powdered, fine grinding in gastight attrition mill 79−33967
rare earth-Co alloys, R_2Co_{17}, substituted, mag. props. 77−89947
rare earth-Co permanent magnet EM acoustic transducer design 77−19508
rare earth-cobalt intermetallics, production and props. 78−52309
rare-earth-Co, development, properties, manufacture and appl. 77−8331
repelling force system, with cylindrical rare-earth magnets, dynamic characts., forced vibrations of one-degree-of-freedom system *(Japanese)* 80−4744
restoration factor spread calc., manufacturing error anal. *(Russian)* 77−12152
review of theory, materials, fabrication and applications 79−42801
ring core flux-gate thickness transducer 79−67280
SI units in design calcs. 79−30406
single crystal permanent magnet, industrial technology and equipment for manufacturing process 80−35075
sintered permanent magnets, development history, magnetic and physical props., appl. 80−29901
temperature dependences meas., automated apparatus for −150 to 300°C range 80−31809
testing, automatic digital apparatus with incompletely closed mag. system 79−9226
testing, instruments, classification *(Russian)* 77−67479
testing parameters selection, meas. errors determ. 80−52280
Ticonal with Sm, magnetic props., phase transform. after thermomagnetic treatment 78−3155
two-domain analysis of field producing bodies using fictitious poles 78−33649
U-shaped, field construction using ferrofluid birefringence *(Russian)* 77−65553
US ellipsometer design and performance 79−57196
τ-Al-Mn-C, permanent magnetism and microstruct. 80−75811
Al-Mn-Fe(Co)(Ni)(Cu), permanent magnetic materials, grain struct. effect *(Rumanian)* 79−73773
$BaO-SiO_2-Fe_2O_3$ permanent mag. ceramics, exam. of phase diagram, using X-ray analysis, optical microscopy, electron probe anal., and thermal analysis *(German)* 79−29012
Ca ferrite magnets, anisotropic, BaO substitution effect on mag. props. *(Japanese)* 79−99697
$(CaO.nFe_2O_3)_{100-x}(La_2O_3)_x$ ferrite, permanent mag. material, mag. props. and preparation 79−83148
Ce-Co-Cu-Fe-Ti, sintered magnet, prep. and mag. props. 77−73043
Ce-Sm-Co-Fe-Cu alloy, permanent magnet props. 79−8013
$CeCo_5$ characteristics and appl. *(German)* 77−80966
$CeCo_5$, magnetisation and coercive strength 77−55688
$CeCo_{5+x}$, Cu and Fe modified, coercive force *(Czech)* 79−42805
$CeMM_{0.8}Sm_{0.2}Co_5$, (MM=mischmetal), thermal props. *(German)* 77−8359
(Co, Cu, Fe)$_5$Ce, sintered permanent magnets, magnetic charact. 78−60608
(Co,Cu,Fe)$_5$Ce, sintered, mag. props. 78−68302
Co permanent magnet material savings *(German)* 80−103851
Co-Cu-Fe-Ce, mag. characteristics of sintered permanent magnets 78−60312
Co-Cu-Fe-Ce alloys, sintered permanent magnets, mag. characts. 77−43855
Co-Fe-Ti (12,6 wt.%), semihard permanent magnet, magnetic precipitation hardening 78−52830
Co-mischmetall system, phase relations, microstruct., mag. props. 80−104118

permanent magnets continued
Co-mishmetal-rare earth alloys for high energy permanent magnets, manufacture technology *(Polish)* 80−35132
Co-Mn, permanent magnetic materials 78−8426
Co-rare earth, grain alignment, metallographic method using eutectoid transform. of Co_5R 77−9003
Co-rare earth magnets testing method for mag. parameters 79−49260
Co-Sm, grain alignment determ., metallographic method using eutectoid transform. of Co_5Sm 77−9003
Co-Sm magnets, H_2 atm. sintering effect on mag. props. 77−85504
Co-Sm-Gd(Ho) magnets, prep. and characterisation 77−8351
Co-W(Mo) magnetic alloys for high temp. appl. 77−85503
Co_xMM, (MM+mischmetal), coercive force, effect of preparation conditions 78−95467
Co_5Sm, coercive field temp. depend. 77−8358
Co_5Sm crystals, microstruct., homogeneous precip. and nucleation 80−104160
Co_5Sm sintered magnet, effect of surface conditions on mag. props. 79−28556
Cr-Co-Fe, chromindur alloy, field heat treatment, and mag. props. 80−35354
Cr-Co-Fe cold formable mag. alloys for use in telephone receiver 79−52227
Cr-Co-Fe permanent magnet anisotropic alloys, plastic deform., ageing, particle alignment temp. 80−35254
Cu-Ni-Fe, magnetic properties, heat treatment and compressive stress effects 80−60367
Cu-Ni-Fe, permanent magnet, temp. effect 80−34701
Dy_2Co_{17}, domain wall behaviour, TEM expts. 77−4524
Er_2Co_{17}, magnetisation, magnetocryst. anisotropy and magnetostriction 77−8303
$Er_3Co_{17-x}Fe_x(Mn_y)(Ni_x)$, saturation magnetisation, Curie temp., easy direction, and anisotropy field 77−8304
Fe-Co-Ti-Al alloy type YuNDK magnets, metallographic method of distinguishing cracks 80−85096
Fe-Cr-Co, mag. props. of ductile permanent ductile alloys *(Chinese)* 79−19746
Fe-Cr-Co, permanent magnet, temp. effect 80−34701
Fe-Cr-Co, phase diagram, miscibility gap 77−89984
Fe-Cr-Co (31 wt.%, 23 wt.%), microstruct. and mag. props., ageing and thermomag. treatment effects 78−76769
Fe-Cr-Co alloy, Mossbauer exam. of spinodal decomposition 77−69742
Fe-Cr-Co alloys, (5-9 wt.% Co), obtained by slow cooling under mag. field, permanent magnet props. 80−75797
Fe-Cr-Co alloys, permanent magnets, magnetic props. and heat treatment *(Russian)* 79−91809
Fe-Cr-Co ductile magnet, with high $(BH)_{max}$, processing, mag. props., and microstruct. 77−8957
Fe-Cr-Co ductile magnet alloys, phase diagram and mag. props., V or V+Ti addition effects 77−8959
Fe-Cr-Co system, miscibility gap, microstruct., and mag. props. obs. 80−76228
Fe-Cr-Co-Mo, microstruct., hardness, mag. props., influence of isothermal tempering and heat treatment 79−79129
Fe-Cr-Co-Mo high energy permanent magnets, mag. props. 80−97119
Fe-Cr-Co-V-(Ti) hard magnets, V and V-Ti effects on mag. and mech. props. 79−91810
Fe-Ni-Al alloys, phase diagram, miscibility gap, DTA meas. 78−92237
Fe-Ni-Al-Co-Cu alloy, sintered single-crystal mag. prod., props. 77−66709
Fe-Pd (47 at.%) alloy, powders and powder compacts, mag. props. rel. to heat treatment *(Russian)* 79−15816
$FePd_{1-x}Pt_x$, permanent magnet, coercive force increased by Pt 79−24157
$Gd_{2+x}Co_{17-x}$, magnetocryst. anisotropy, stoichiometry and temp. effects 77−8296
Ho_2Co_{17}, magnetisation, magnetocryst. anisotropy and magnetostriction 77−8303
Mn-Al alloys, defect structure, mag. props. TEM obs. 78−91902
Mn-Al-C, mag. props., machinability 77−85505
Mn-Al-C (70, 29.5 wt.%) alloy, Almax anisotropic mag. props. *(Japanese)* 80−60371
Mn-Al-C alloy appl., anisotropic, properties and production *(German)* 79−8309
Mn-Al-C anisotropic permanent mag., cryst. orientation and form., X-ray diffr. anal. 79−82778
$Mn_{55}Al_{45}$ alloy, permanent mag. props., depend. on particle size 78−91899
$NdCo_5$, spin reorientation, magnetisation and torque curves, 77-925K 77−4532
$Nd(Co_{1-x}Cu_x)_5$, coercive force temp. depend. 79−82823
$Nd_xPr_ySm_zCo_5$ permanent magnets, coercive force, low-temp. annealing influence *(Russian)* 80−39812
$Nd_2Y_{1-x}Co_5$, saturation magnetisation and anisotropy, 4.2K-T_c 77−85427
$Pr(Co_{1-x}Cu_x)_5$, coercive force temp. depend. 79−82823
$Pr_2(Co_{1-x}Fe_x)_{17}$, hard direction magnetisation, 5-300K, and anisotropy field 77−12114
$Pr_{0.75}Sm_{0.25}Co_5$ magnets, struct. and props. sintering temp. depend. *(Russian)* 79−82819
$Pr_xSm_{1-x}Co_5$, magnetisation and magnetocryst. anisotropy 78−68215
Sm-Co, permanent mag., O ion impact, 5.5 keV, secondary Co ion emission, magnetisation depend. *(Russian)* 78−2967
Sm-Co alloy magnets, operational control of residual induction, maximum mag. energy 79−15324
Sm-Co base ternary alloy, mag. props. and cryst. struct. 77−8352
Sm-Co-Cu, with Sm_2Co_{17} struct., aged, TEM high coercivity material, TEM obs. of microstruct. 77−77073
Sm-Co-Cu permanent magnets, phase diagram 77−21106
Sm-Co-Cu-Fe, single phase 2-17 sample, hard mag. props. 77−8349
Sm-Co-Cu-Fe-Ti magnets, comp. and sintering effects on coercivity 79−15326
Sm-Co-Cu-Fe-Zr magnet, production and mag. props. 77−40085
Sm-Hf-Co alloy, rare-earth electron transfer 77−40028
Sm-Pr-Co, added Fe_2Sn, demagnetisation curves, X-ray obs. 78−91900
Sm(-Pr)-Co, sintered, cryst. phases *(Russian)* 80−39004
$SmCO_5$ based permanent magnets, props. and cryst. orientation *(Russian)* 80−20431
$SmCO_5$ magnets, sintering time effect on props. 79−95977
$Sm_{1-u}Ce_u(Co_{1-x-y-w}Fe_xCu_yCr_w)_z$, permanent mag., improved mech. props. 79−87593

permanent magnets continued
$Sm_2(Co, Cu, Fe, M)_{17}$, M=Nb, V, Ta, Zr, effect of M on mag. props. 77−89978
$Sm(Co,Cu)_5$, eutectoid transform. 77−8799
$Sm(Co,Cu)_z$, precip.-hardened, mag. and metallographic props. 77−8339
$SmCo_5$, and related alloys, nucleation and pinning at 360° domain walls 77−73042
$SmCo_5$, and $SmCo_{3.5}Cu_{1.5}$, anisotropy and coercivity, Kerr effect, magnetisation and aftereffect expts. 77−8300
$SmCo_5$ based permanent magnets with low reversible temp. coeff. 79−51814
$SmCo_5$ based ternary and quaternary permanent mag. materials with low reversible temp. coeffs. 79−82822
$SmCo_5$, Bloch wall energy determ. *(German)* 78−19271
$SmCo_5$, Cu-modified, magnetisation reversal mechanism 77−8350
$SmCo_5$, free suspension in const. mag. field with aid of pyrolytic graphite 80−101807
$SmCo_5$, intrinsic coercivity losses, temp. depend. 78−95468
$SmCo_5$ isotropic plasma sprayed magnet, high coercivity 78−68295
$SmCo_5$, mag. properties in low temp. range, obs. *(Russian)* 77−73050
$SmCo_5$, mag. props., effect of phase and struct. transforms. during liq.-phase sintering 79−100086
$SmCo_5$ magnet, in recording rot. field magnetostrictometer 78−12733
$SmCo_5$ magnetic alloys, pressed, sintering rel. to mag. props., cryst. struct. 78−60600
$SmCo_5$, magnetic fastening for piezoelectric accelerometer 79−77035
$SmCo_5$, magnetisation and demagnetisation, heating effects 79−38357
$SmCo_5$ magnets for mini-orange spectrom. 78−58531
$SmCo_5$ material for accelerator permanent magnets 79−6776
$SmCo_5$, nucleation of reversed domains at Co_7Sm_2 precips. 80−75791
$SmCo_5$ permanent magnet, liq. phase sintered, hysteresis loops, ageing, temp. depend. *(Chinese)* 77−51921
$SmCo_5$, permanent magnet stability, during long-term ageing *(Chinese)* 80−55428
$SmCo_5$ permanent magnets for accelerators 79−31273
$SmCo_5$ permanent magnets, crystal texture effects on props. 80−100600
$SmCo_5$, polished, domain wall grooving, optical microscopy and SEM obs. 77−8334
$SmCo_5$, powder, exam. of protective preps. of organic media against oxidation 79−96220
$SmCo_5$ powder alloy, densification by cold working 77−4753
$SmCo_5$, radial pulse magnetisation, magnetising and testing fixtures 77−8354
$SmCo_5$, remanence and energy product, X-ray method of planar orientation 77−8342
$SmCo_5$, single cryst. and liq. phase sintered, magnetostriction, field depend. 77−63245
$SmCo_5$, single-cryst. and liq. phase sintered, elastic stiffness consts., US velocity obs. 77−73066
$SmCo_5$, sintered, hard mag. material, magnetisation behaviour 80−75805
$SmCo_5$, sintered, mag. after-effect, expt. and model 80−75816
$SmCo_5$, sintered, mag. props., 4.2-300K, fields up to 100 kOe 77−8341
$SmCo_5$, sintered, mag. props. *(German)* 77−43852
$SmCo_5$, sintered, orientation of particle easy axes, statistical model 77−8305
$SmCo_5$ sintered alloy based, magnetic properties *(Russian)* 78−72369
$SmCo_5$, sintered alloy permanent magnets, temp. depend. of domain struct. *(Russian)* 77−66380
$SmCo_5$ sintered magnets, periodic struct. and coercive force *(Russian)* 79−28554
$SmCo_5$ sintered magnets, eutectoid decomp. 80−89219
$SmCo_5$, sintered permanent magnet manufacture 80−20838
$SmCo_5$, specific heat and kinetic props. at elevated temp. *(Russian)* 79−28530
$SmCo_{5+x}$, Cu and Fe modified, coercive force, demagnetization curves *(Czech)* 79−42805
$SmCo_x$-Fe composite permanent magnet material, mag. props. 77−40089
$SmCo_{3.5}Cu_{1.5}$, single cryst., domain wall motion and domain form. 78−39359
$Sm(Co_{0.81}Cu_{0.15}Fe_{0.04})_{6.9}$ and $Sm(Co_{0.84}Cu_{0.16})_{6.9}$ powders, mag. props. *(Russian)* 80−20434
$Sm(Co_{0.86-x}Cu_{0.14}Fe_x)_7$, permanent magnet, sintering and heat treatment effects 80−39817
$Sm_2(Co_{1-x}Fe_x)_{17}$, magnetocryst. anisotropy, Tb, Mn or Cr substituent effects 77−8297
$Sm(CoFeCuMn)_7$, coercive force and anisotropy temp. depend. 78−68297
$Sm_2(Co_{1-x}M_x)_{17}$, bulk magnetisation and magnetocryst. anisotropy, interpretation 77−40055
$Sm_2(Co_{1-x}M_x)_{17}$, magnetocryst. anisotropy 77−40054
$Sm_2Co_{17-x}Ni_x$, effect of Ni on mag. props. 78−68296
$Sm_2Cu_{1.6}Zr_{0.16}Fe_{3.3}Co_{12}$, enhancement of mag. props. 79−82825
$Sm_xDy_{1-x}Co_5$, temp. compensated magnetic material, mag. and struct. characterisation 78−68177
$Sm_xEr_{1-x}Co_5$, temp. compensated magnetic material, mag. and struct. characterisation 78−68177
$Sm_{2-x}Gd_xCo_{17-y}Mn_y$, saturation magnetisation and anisotropy field temp. depend., suitability for microwave/millimetre wave TWT 79−82824
Sm_2M_{17}, sintered magnet, hard mag. props. optimisation 77−8340
$Sm_{1-w}MM_w(Co_{1-x-y}Cu_xFe)_z$, (MM-mischmetal), mag. meas. and metallographic exam. 77−56119
$Sm_{1-x}Nd_xCo_5$ alloys, magnetisation, magnetocrystalline anisotropy, 4.2 to 280K 78−91863
$SmNi_4M$, M=Fe, Cu, Al, intrinsic mag. hardness 77−85506
Sm_2O_7, sintered, coercive force and constitution, annealing temp. depend. *(Russian)* 80−88786
$Sm_{0.5}Pr_{0.5}Co_5$, sintered alloy permanent magnets, temp. depend. of domain struct. *(Russian)* 77−66380
$Sm_{0.5}Pr_{0.5}Co_5$ sintered magnets, periodic struct. and coercive force *(Russian)* 79−28554
$Sm_xTb_{1-x}Co_5$, temp. compensated magnetic material, mag. and struct. characterisation 78−68177
$Sm_{0.91}Zr_{0.09}(Co_{0.68}Cu_{0.10}Fe_{0.22})_{6.7}$, alloy permanent magnet, coercive force *(Russian)* 80−65966
$SnCo_5$, magnetisation and cohesive strength 77−55688
$SrFe_{12}O_{19}$, mag. props., effect of Sr dissolution by milling in water 77−25000
$SrO\text{-}SiO_2\text{-}Fe_2O_3$, permanent mag. ceramics, exam. of phase diagram, using X-ray analysis, optical microscopy, electron probe anal., and thermal analysis *(German)* 79−29012

permanent magnets continued
Tb_2Co_{17}, magnetisation, magnetocryst. anisotropy and magnetostriction 77−8303
YCo_5, substituted, magnetocryst. anisotropy, different contribs. of two Co sites 77−8301
$Y_2Co_{17-x}Ni_x$, effect of Ni or mag. props. 78−68296
$Y_{0.25}Nd_{0.75}Co_5$, basal plane anisotropy 77−8295

permeability
acrylonitrile-dimethylaminoethyl methacrylate membrane, as burn wound covering 78−44676
acrylonitrile-methylacrylate-acrylamide latexes graft copolymerised onto PVA,for haemodialysis membranes *(Japanese)* 80−12297
acrylonitrile-vinylacetate(styrene) copolymer films, gas permeation, chem. struct. effects *(Japanese)* 78−31691
adsorbed monolayers, permeation and evaporation resistance, attractive forces effects 78−67892
air-blood barrier, rel. to inhaled aerosol retention and transport 77−25630
albumin flux, differential permeability of endothelial and epithelial barriers, sheep expts. 80−81553
alkali germanate glasses, He permeability, diffusivity and solubility 79−51308
alkaline earth silicate glasses, morphology effects on props. 80−49118
alluvial aquifers, permeability determ. from resistivity meas. *(Italian)* 77−53079
anisotropic porous media, degrees of anisotropy of fluid flow and diffusion (elec. conduction) 77−51109
articular cartilage, asymptotic theory for thin layers with appl. to knee joint 78−44537
bilayer membranes, permeation of water mols. meas. using fluoresc. quantum yield solvent-isotope effect 79−34710
biological membrane, permeability *(French)* 79−16175
biological membranes, mol. transport, quantum mech. theory 79−8489
biomembranes, potential, rel. to surface pot., ionic permeab. 80−35853
blood vessel wall ion permeability 77−32934
blood-brain barrier, reversal of microwave-induced permeability 80−61641
brain vascular permeability, effect of π^- irradiation in neonatal rats 80−26275
butadiene nitrile rubber, air permeability, subject to high press. 78−27823
butyl rubber ethylene propylene ternary copolymer mixture, permeability, diffusion of gases and solvents 79−95217
capillary mass transfer of porous solids based on pore distrib. curves 77−7443
capillary permeability determ. from multiple indicator data, effects of finite red cell permeab. 78−44483
capillary permeability evaluation from multiple indicator data, effects of red cell and tissue exchange 80−101193
carrier-mediated extraction, development 80−66870
cartilage deformation and interstitial fluid flow, nonlinear interaction 77−32931
cell, membrane permeability, review 78−15813
cell water permeability during freezing and thawing, cryomicroscope multiple nonlinear regression analysis 79−92197
cellophane membrane, polarised, electret transport props., permeability coeff. 80−7860
cellulose acetate film, diffusion and permeation of gases 79−55934
cellulose acetate freeze-dried membrane, gas permeation rates 79−79295
cellulose acetate membrane, asymmetric, elec. and electroosmotic transport behaviour in dialysis-osmosis expts. 80−108745
cellulose acetate membrane water permeab. at low press., nature of flow 77−73467
cellulose acetate membrane water permeab. at low press., temp. var. 77−73466
cellulose diacetate membrane, diffusive permeability 80−104460
cellulose diacetate membranes, press. depend. of permeabilities *(French)* 79−52756
cellulose diacetate membranes, unilayer, transport phenomena, hydration and dialysis coeffs. 80−76556
cellulose membrane, methanol(formamide)-water soln. permeabilities 78−11557
cerebrovascular permeability, quantitative method for meas. of alterations 80−61748
cheese cloth filled cellulose acetate film, diffusion and permeation of gases 79−55934
cholinergic channel without const. field, permeab., phase-boundary pot. and conductance 77−60191
clay mineral dispersion and swelling, effect on soil hydraulic cond. 78−53668
composite membrane, anion exchanger-urease, coupling of transport and enzymic reaction 79−83510
compressible flow in permeable capillaries under deform., press. loss model 78−26141
consolidating semi-space, axisymmetric punch problem with mixed boundary, permeability conditions 78−51087
contact lens, hard gas-permeable type, O_2 tension underneath 78−3473
corrosion protective coatings, organic, performance evaluation of adhesion and permeability 78−64764
crosslinked collagen membranes, transport props., physical props. effects 78−77028
diffusion, through permeable barriers, applied to NMR with pulsed field grad. 78−91986
directional time-lag asymmetry in media with position-dependent sorption and diffusion props. 78−3372
Earth crust, permeability rel. to transport phenomena in hydrothermal systems 78−36206
electrolytes, solid oxide, elec. props., study methods *(French)* 80−22386
epithelial membrane conductance rel. to extracellular shunting, rabbit salivary duct 77−77881
epithelium intercellular contacts, small intestine, permeab. and mech. props. regulation by Ca ions 77−81482
epithelium membrane permeability, effect of intracellular Na conc. 77−32882
erythrocyte membrane hydraulic cond. determ. 79−34528
erythrocyte membrane permeability, sheep, O_2 effects with X-ray and neutron irrad. 77−5039
erythrocyte membrane water permeability defect in human epilepsy, NMR 77−29122
ethylene-vinyl alcohol copolymer, O_2 permeability *(Japanese)* 78−31702
ethylene-vinyl alcohol copolymer membranes for haemodialysis, prep. conditions and props. *(Japanese)* 80−12299
ethylene-vinyl alcohol laminated copolymer film, O_2 permeability *(Japanese)* 79−24824
ferrites, microwave, dielectric constants and permeability *(Chinese)* 80−66096
film permeability meas. using β-emitting vapours 77−56173
fixed swarm of permeable spheres, appl. of self-consistent model 78−67260
floc, settling velocity, rel. to permeability 79−43636
free air flows with perforated walls, permeability laws study *(French)* 79−10607
gallbladder epithelial cells, compartmental anal. of osmotically induced permeability changes 78−3455
gas diffusion in porous bodies with press. changes 77−62662
gas mixture separation by membranes *(Japanese)* 78−48691
gas permselective membranes, irrad. effects on permeation and separation performances 78−29591
gas separation by permeation, calc. methods and parametric anal. 78−80784
gas separation by permeation, permeate press. drop effect 78−80785
gas-solid barrier permeability, absorption dissoc. anomalous temp. depend. 77−7977
gases through solids, nondissoc. and dissoc. permeation 78−34645
gel, heterogeneous two-phase, permeability 80−76563
gelatin layer, dry, aqueous soln. penetration 80−85221
glass sintered powder porous bodies, liq. penetration mechanism *(Japanese)* 80−53853
glomerular permeability in foetal rabbit 80−85372
gramicidin A channel cation permeation interactions and anion binding 78−53370
granite, deformation and permeability of crushed samples 77−21763
graphite, CO_2 permeability meas. up to 41 bars 80−29176
graphite, reactor-grade, permeability, effect of neutron irradiation 79−71900
ground water, Cl^- content, appl. to Miocene aquifer isopermeability map 78−81256
haemodialyser membranes, permeability of Cuprophane and polyacrylonitrile *(Japanese)* 77−66873
haemodialysis membranes, for disposable dialysers, comparison of cuprophane and cellophane 77−78049
haemodialysis membranes, permeability and rejection coeffs. 80−26207
hailstones, permeability meas. rel. to foreign material derivation 78−96260
Hastelloy X, H permeability using permeation method *(Japanese)* 78−51740
Haynes alloy 188, H_2 permeability 77−46399
heat exchanger materials, oxide protective layer formation meas. by hydrogen permeation 78−8895
heat transfer from porous sphere in low Reynolds number flow 78−59482
heated porous body, impregnation with viscous liquid 80−79392
Hele-Shaw cell, permeability determ., geothermal modelling appl. 78−59466
HTGR fuel particles, inert gas intrusion as charact. procedure for pyrocarbon coatings 79−54512
HTGR fuel particles, influence of pyrocarbon props. on as-produced gas permeability of coatings 79−54511
hydraulic charact. of liqs. flowing through porous metal fibre mats., permeability laws 78−67848
hydrogel of high water content as a material for the soft contact lens *(Japanese)* 80−12300
hydromagnetic squeeze film between porous circular disks with velocity slip 80−74997
Incoloy 800, clean and steam oxidised, T_2 permeation 80−88364
Incoloy 903, H_2 permeation and diffusion 78−26730
Incoloy-800, meas. of H and D permeation for reactor safety anal. 79−77822
Inconel 718, H_2 permeation and diffusion 78−26730
intercellular contact high permeab. 78−48773
interparticle percolation, statistical mech. anal. 79−96281
ion flow through membrane, effect of chem. reaction on time depend., binding of mobile ion 78−95954
jointed granite in situ, elastic and transport props. 77−66909
kaolinite membranes, anion permeation 80−11952
limiting relative law of heat and mass transfer and friction, permeability parameter effect 80−23999
lipid bilayer, flat, permeab. in presence of vesicles of sarcoplasmic reticulum 77−21490
lipid bilayer membrane permeability modification by drugs 78−69026
lipid bilayer membranes, steady-state permeability behaviours induced by cyanine dyes 80−85357
liquids, permeability inlet press. effect *(German)* 79−100438
lung alveolar membrane, dog, role of bulk fluid flow in protein permeability 77−52814
lung vascular permeability after microemboli, effect of platelet depletion, sheep obs. 80−97972
magnesite artifacts, roasted, props., filler porosity effect 80−104099
mammal cell junction, permeability of cell-to-cell membrane channel 80−51061
mannitol, aq. solns., stirred, transient diffusion through glass membranes, thermodynamics 78−92507
maternal-placental blood flow model with vel.-depend. permeability 78−40224
membrane, gas flow diffusion eqn. soln. 78−56918
membrane, solid, superpermeability, gas evacuation 79−74422
membrane permeabilities, dynamic, meas. under non-equilib. conditions, appls. 80−46107
membrane selectivity, influence of particle/pore size ratio 80−11946
membrane vesicle, light scatt. meas. 77−12889
membranes, artificial, permeab. to pluridisperse soln. of ^{125}I-polyvinylpyrrolidone 77−12890
membranes, composite, relaxation time, network thermodynamics formalism 78−68926
membranes, linear laminated media, permeation, sorpt. 79−1966
membranes for ion exchange, ion and water transport eqns. 78−68930
membranes transport phenomena analysis, cellulose diacetate, for reverse osmosis, pressure effects 79−96361
metal fibre materials, permeable, porous struct. parameters 79−100083

permeability continued
metal gauze reinforced porous permeable mats. with prearranged struct., prep. 78−68652
metal powders, vacuum treatment, method of calc. evacuation time and permeability 80−20827
metal-H system, permeation technique for electron transport studies 77−7904
metal-H system, permeation technique for electrotransport studies 77−7903
metallic membrane, of H isotopes, apparatus for meas. *(Russian)* 77−70248
metallic membrane interface, mass transfer 80−81366
metals, deformed, apparatus for determining gas penetration 77−86240
microporous graphite compact, anomalous diffusion of N_2, time-lag and transient-state kinetic analysis 78−34655
migration in Na_2O-Al_2O_3-SiO_2 glass 77−7902
mitochondrial membrane monovalent Tl^+ ion transport 78−31787
mitochondrial permeability, transport and energy-coupling processes, effect of fatty acids and acyl-CoA 77−21498
molecular seive, permeability rel. to Br_2 mols., laser-induced changes *(Russian)* 79−91999
molecular sieves, adsorpt. of atmospheric gases, comparison of 13X and 4A at low temp., press. *(German)* 80−88423
monolayer permeation and evaporation resistance, hard disc fluid model 78−34678
muscle, skeletal, permeab. of stretched membrane rel. to EMF *(Japanese)* 77−36886
muscle cell osmotic state and membrane permselectivity repeated microwave irrad. effects quantitation 80−56131
muscle membrane, insect, permeation of Mn, Cd, Zn and Be through Ca channels 77−56357
myotonia and Ca permeab., math. model 78−11620
nerve ionic permeability of K, Na and Cl, regulation by fixed charges and pH, crayfish 77−66809
nexus, evidence for fixed charge, permeability, obs. 80−94193
Nichrome/steel, porous metal-thread sheet materials, filteration, permeability and strength props. *(Russian)* 79−78915
nuclear reactor, HTR, hydrogen and tritium permeation through He heated tube walls 77−50250
nylon 12 membranes, permeation characts. *(Japanese)* 78−31692
oolitic calcarenites, Ste. Genevieve Limestone (Mississippian), permeability est. techniques *(French)* 79−34801
oxide coating, pore size distrib. and permeability 79−24641
Pd membrane, H_2-D_2 isotope separation 80−68959
pentaerythritol, aq. solns., stirred, transient diffusion through glass membranes, thermodynamics 78−92507
percolation, universal critical amplitude ratios 80−101765
percolation probability for lattices of bonds and sites 77−63956
percolation problem for lattices of bonds, sites, perforation points, graphical technique 77−63954
percolation problem for lattices of bonds, sites, perforation points, graphical technique 77−63955
permeable polymer mol. in soln., intrinsic viscosity and friction coeff. 78−30353
phospholipid artificial membrane phase state and passive permeab. for Ca ions, effect of valinomycin 78−80836
phospholipid bilayer melting transition, thermodynamic fluctuations, ion permeability, statistical mechanics model 78−73140
photographic developer, permeation into a gelatin layer, potentiometric exam. *(Russian)* 80−73500
plugs, porous, in He II space cooling systems, characts. 78−49842
PMMA, water swollen membrane, permeability *(Japanese)* 78−31704
Poiseuille formula determ. for viscous flow through cylindrical tube *(Dutch)* 78−51238
Polimal 109, polymer resin laminate, density porosity, water vapour diffusion sorption and permeation *(Polish)* 80−59665
poly(2-hydroxyethyl methacrylate), membrane, solute transport 79−43630
poly(tetrahydropyran-2, 6-diyliminocarbonyl), permeability to H_2O liq. and vap. *(Japanese)* 79−70376
poly(vinyl alcohol)-acrylonitrile copolymer membrane, water permeability increase *(Japanese)* 79−70375
poly-n-hexyl L-glutanate, sorption and permeation mechanism 80−26048
polyacrylamide gel structure inhomogeneity from permeability and viscoelasticity 77−89384
polyamide 6 and 12 films, permeability to H_2O vap. *(Russian)* 78−53255
polycarbonate diflone, air permeability, subject to high press. 78−27823
polycarbonate membrane, porous, gas permeability *(Japanese)* 78−31698
polycarbonate porous membrane, pore size effect on gas permeability *(Japanese)* 78−31699
polydimethylsiloxane membrane, permeability of triethylamine vapour *(Japanese)* 78−31697
polyethylene films, fibres, radiation initiated graft polymerisation of acrylonitrile, initiation rate rel. to props. *(Russian)* 80−7531
polyethylene membrane, permeation of hydrocarbons 80−30281
polyethylene terephthalate CO_2 permeability above and below glass transition 79−73340
polymer, air permeability subject to high press., testing apparatus 78−27823
polymer, glassy, gas sorption and transport, review 80−15360
polymer, high, gas permeability meas. techniques 80−14854
polymer films, permeation, diffusional time lags determ. 80−65272
polymer films, vapour permeability determ., gravimetric test method 79−39066
polymer membrane gas permeation, pore size distrib. *(Japanese)* 78−79372
polymer membranes, O_2 permeability, determ. with Zircon gas analyser 79−39195
polymer membranes, use of McInnes glass electrode for determ. of CO_2 diffusion coeffs. 78−20067
polymer powder coatings, water permeability eval. by radioactive tracers *(Czech)* 78−11362
polymer rod, fluid-permeable, longit. stability during creep 79−57066
polymeric membrane, porous, gas permeability *(Japanese)* 79−24825
polymers, crosslinked, specific characts. *(German)* 78−75585
polymers, diffusion coeffs. of gases, sorption, permeation investigs., review 78−67868
polypropylene, isotactic, air permeability, subject to high press. 78−27823
permeability continued
polypropylene films, hard elastic, gas permeability, extension effects 80−40412
polystyrene in toluene, unstirred solns., transient diffusion through membrane 78−92508
polytetrahydropyran 2,6 diyliminocarbonyl hydrophilic membrane, water permeation and solute rejection 79−74419
polyvinyl fluoride, glass transitions, Ar permeability and diffusion obs. 79−32919
polyvinylidene fluoride, glass transitions, Ar permeability and diffusion obs. 79−32919
polyvinylidene fluoride and poly-1-vinyl-3-methylimidazolium iodide interpolymer ultrafiltration membranes 79−15639
polyvinylidene fluoride film, chem. etching of fission tracks, hole growth study by gas flow meas. 79−76297
polyvinyltrimethylsilane, diffusion, sorption, solubility, permeation of hydrocarbons, Xe *(Russian)* 80−6564
porous deep drawn conical shells 80−11728
porous materials, hydrodynamic calculations, porous struct. parameters, theory 79−98797
porous media, permeability calc. from Navier-Stokes eqns. 77−27593
porous medium, foaming, liquid and gas relative permeabilities 80−33669
powder, grain size determination by transient low press. air transmission 78−32965
PTFE, Ne, Ar, Xe and He diffusion and solubility 80−6561
PVA, hollow fibre membrane for industrial scale dialyser *(Japanese)* 78−31693
PVC, chlorinated, fibres, radiation initiated graft polymerisation of acrylonitrile, initiation rate rel. to props. *(Russian)* 80−7531
PVC, plasticized, permeability *(Polish)* 79−52771
PVC, sintered powder, permeability and porous struct. 77−63620
PVC film, permeability to H_2O vap. *(Russian)* 78−53255
PVC-poly-ε-caprolactone blends, gas permeation and compatibility 79−4433
pyrocarbon, low temp., isotropic, permeability study *(French)* 79−7549
pyrocarbon cladding, gas permeability *(French)* 77−14234
pyrocarbon coating, effect on Pu redistrib. in HTGR fuel 78−29578
pyrocarbon coating, isotropic, gas permeability, neutron irradiation effect *(French)* 80−63260
pyrocarbon coating, isotropic, gas permeability meas. *(French)* 80−63259
pyrocarbon coating permeability effect on U redistrib. in HTGR fuel 77−40460
pyrocarbon coatings, mass spectrom. determ. of fission gas permeabilities 78−12785
radioactive rare gas separation, using cell with two membranse of differing permeability 78−29590
red cell, human, increased passive permeability below 12°C 80−94185
reinforced cellulose acetate membrane water and salt permeability, complementary direct osmosis test 79−96359
renal medulla, osmotic equilibration by descending limbs of Henle's loop 77−40701
rock permeability changes due to stress 79−16452
rock specimen, meas. of flowing water average pore vel. 79−5473
rocks, of water, shear thinning and shear thickening polymer additives 80−72100
rocks, permeability from resistivity and pore shape 77−86866
rocks, permeability of whole and fractured porous specimens with confining pressure 79−53342
rocks, permeability rel. to transport phenomena in hydrothermal systems 78−36205
salivary gland cell junction, Ca^{2+} produces graded changes in membrane channel permeab. 77−64016
sand, resin-coated, curing effects on physicomech. props. *(Korean)* 78−60855
Sanicro 31, T_2 permeation 80−88364
sarcolemmal permeability changes during early myocardial anoxia 80−85371
skin, human, permeation of scopolamine in vitro 77−21487
soil hydraulic conductivity, numerical calc. from suction press.-moisture retention relation *(German)* 79−2297
soils, hillside, N.Yorkshire, England, pedological features affecting permeability 77−45021
solid electrolyte dielectric permeability, phase transition to superionic state *(Russian)* 80−49403
sonic flow simulation, permeability law study *(French)* 79−32567
spectrin-actin monolayer, adsorbed at Hg-H_2O interface, ionic permeability 80−12064
steel, bimetal, alloy with austenitic stainless, H permeability 80−107572
steel, H_2 permeability in inhibited H_2SO_4 corrosion, stress level effects *(Russian)* 77−52530
steel, martensitic, quenched, strength variation rel. to H behaviour 77−59924
steel, mild, and cold-rolled, diffusion, permeation, and accumulation of H_2 *(Japanese)* 77−39692
steel, porous, permeability, deform. effects 79−100229
steel, SAE 1045, permeation meas. of H trapping, rel. to cryst. microstruct. 80−84328
steel, stainless, D transport through membranes at low driving press. and 15 keV D bombardment 78−34552
steel, stainless, permeation by $^2H(^3H)$ in fusion reactor, oxide film inlfuence 80−34241
steel, stainless, T permeability and ultralow press. 79−19402
steel, stainless 310, permeation and diffusion of H and D, 472 to 779K 79−55937
steel, stainless types 321-SS and 430-SS, alumina coated, H_2 permeation 80−34244
sucrose, aq. solns., stirred, transient diffusion through glass membranes, thermodynamics 78−92507
tight junction disruption and recovery after sublethal γ-irrad. 80−36027
unsteady state meas. method 80−53895
vapour permeability mechanism of porous bodies 77−58782
vapour-gas phase, heat and mass transfer during evaporation of fluid 77−55354
vascular walls, physical theory of permeability rel. to atherogenesis, mech. effects 80−16908
villous membrane, permeability coeff. of wall 79−16177
N-vinylpyrrolidone-methyl methacrylate copolymer water swollen membrane, permeability *(Japanese)* 78−31704

permeability continued
viscous flow, slow, through rigid porous medium, macroscopic fied eqns. 79−94711
water self-diffusion in porous membranes, ionic solns., struct., props. 79−52765
Westerly granite, permeability changes during water flow at 100-400°C 78−40546
wettability dependent permeability in porous media 79−98795
Al, reaction with H_2, influence of surface reactions on rate *(Russian)* 80−66863
Al_2O_3, permeability and solubility of H_2, 1200-1450°C 80−39351
Al_2O_3 sintered tubes, H_2 permeability 80−24675
Co-Mo alloy electrodeposits, codeposited impurities rel. to H_2 permeation, props. 79−19493
D beam, interaction with Pd membrane 77−51538
Fe, annealed, Hz permeation, 230 to 300K *(Japanese)* 78−84004
Fe, annealed and cold-rolled, diffusion, permeation and accumulation of H_2 *(Japanese)* 77−39692
Fe, Armco, membrane, superpermeability to D 79−24830
Fe, effect of anion and organic corrosion inhibitors on H_2 penetration rate 80−100938
Fe fibre porous material, props. 79−98798
Fe, H_2 permeation, rel. to embrittlement, organic inhibitors, surface treatment 80−108635
Fe, membranes, effect of electrodeposited metals on H permeation, proposed catalytic mechanism 78−53252
Fe ore pellet, meas. of gas permeability of individual pellets 78−80711
Fe, permeability, solubility and diffusion of H and D, 9 to 73°C 77−76560
Fe, permeation by H in fusion reactor 80−34242
Fe, pure, of H and D at 10 to 60°C 78−75887
Fe, to H_2, influence of microstruct. changes induced by cold working *(Russian)* 77−20182
Fe-Co alloy, diffusion of H_2, diffusion coefficient and permeability *(Russian)* 78−79819
Fe-V alloy, H permeability, 300-700°C *(Russian)* 77−15627
H_2, change of diffusivity with order-disorder transformations in Ni_3Fe, Ni_3Pt and Ni_3Mn 80−59729
H_2 in liquid Na reactor coolant, effect of O_2 80−614
H_2 permeability in steel Kh18N10T, effect of surface treatment *(Russian)* 79−15853
H_2 permeation reduction using Pd foil in liquid metal *(Japanese)* 80−68770
H_2, permeation through metal barrier, adsorpt. processes 78−63879
H_2, through Pd membrane, diffusion-cell for separation H_2 containing mixtures, solar furnace appl. 80−92245
He, in glasses and Stycasts *(Japanese)* 79−7715
K^+ permeability of E. coli, membrane lipid role in radiation damage 78−48834
K^+ permeability of mitochondrial and artificial bilayer membranes 78−53365
Kr-N_2(He) gas mixtures, separation by silicone rubber, cellulose acetate membranes 77−36791
Mo, gas permeability (H, He, Ar) through monocrystalline and polycrystalline specimens *(Russian)* 79−60554
Mo, porous, permeability, deform. effects 79−100229
N_2, permeation through metal barrier, adsorpt. processes 78−63879
Na permeability inactivation in squid giant nerve fibres, review of exptl. work 78−73154
Na_2O-CaO-SiO_2 glass microbubbles, permeation eccentricities of He, Ne and D-T 78−47598
$2Na_2O$-CaO-$XSiO_2$ glass, He mobility, interconnectivity, miscibility limits, effect of morphology 78−67864
Nb, membrane, H permeation *(Japanese)* 80−100363
Ne, permeability in laser fusion glass microbubbles 77−35367
Ni, H permeability using permeation method *(Japanese)* 78−51740
Ni, of D thermal ats., anomalously high transmission, 20 to 520°C *(Russian)* 77−72752
Ni, of H, D and T 79−77823
Ni, permeability and diffusivity of hydrogen *(Japanese)* 78−66345
Ni-Mn, permeability, diffusion and solubility of H 80−107573
Ni-Mo alloy electrodeposits, codeposited impurities rel. to H_2 permeation, props. 79−19493
Pb, of $H_2(D_2)$, isotopic effect *(Russian)* 78−75881
Pd and Pd alloys, influence of $\alpha \rightleftarrows \beta$ phase transform. on physicomechanical props. and H_2 permeability *(Russian)* 78−68681
Pd membrane, H atom interaction, superpermeability 80−81365
Pd membrane, H penetrability reduction by C coating *(Russian)* 77−77808
Pd, membrane, superpermeability, of atomised H_2, under different gas and membrane boundary conditions 79−71469
Pd-Ag (25 at.%) H_2 permeability and solubility, comparison with other Pd solid soln. alloys 79−23738
Pd-Ce (5.75 at.%), H_2 permeability and solubility, comparison with other Pd solid soln. alloys 79−23738
Pd-W (20 wt.%), permeability, diffusion, and solubility of H_2, elec. resist., heat treatment effects *(Russian)* 79−51307
Pd-Y (8 at.%), H_2 permeability and solubility, comparison with other Pd solid soln. alloys 79−23738
SO_2 and nitrogen oxide automatic monitors, laboratory and field calibration *(French)* 77−37455
SiC, permeability and solubility of H_2, 1200-1450°C 80−39351
SiO_2, fused, He solubility and diffusion above transform. range 80−79965
T permeation through steam generator alloys 80−34250
ThO_2 microspheres, coated, coating permeability meas. 80−95343
Ti 78−60602
Ti, permeation of H plasma reduced by layer of interstitially built ϵ-Ti_2N 80−16566
Ti, through Croloy steel for LMFBR steam generator 80−68775
UO_2-UC microspheres, coated, coating permeability meas. 80−95343
V, H_2 permeability, surface impurity layer effect 77−24440
ZrC, solubility, diffusion and permeation of Cs 78−51684
ZrO_2, CaO stabilised, exam. of O_2 permeability and p-type electronic cond. 79−10980
ZrO_2, CaO stabilized, O_2 permeability at low O_2 partial press. 79−47980
ZrO_2, plasma deposited, porosity, gas permeability and dielectric strength 79−52125
ZrO_2, plasma sprayed coatings, elec. cond. and gas permeability 79−82478

permeability (magnetic) *see magnetic permeability*

permeability measurement (magnetic) *see magnetic permeability measurement*

permittivity
see also electric strength
abietic acid glass, determ. from TSC curves 77−55744
acetamides, N-methyl-, N,N-dimethyl-, in organic solns., dielec. const., dipole moments, monomer-dimer equilib. 80−40031
acetic acid, dil. soln., dielectric polaris., linear correlation factor 78−6624
acetylacetone, H bonding, dielec. dispersion obs. 77−63356
acrylonitrile, dielectric constant effect on nuclear spin-spin coupling constants, INDO approx. 79−72240
aerosol, polydispersity, unipolar charging, charging mobility analysis 78−61059
aerosol, unipolar diffusion charging, particle dielectric constant and ion mobility effects 78−61058
albumin, bovine serum, hydrated, dielectric props. at 9.9 GHz 78−15758
albumin, human serum, elec. cond. and dielec. const., 1 to 15 MHz 78−53315
alcohol, dielec. const., hindered mol. rot. influence 78−43767
alcohol binary mixtures, nonlinear dielec. effects, shift in assoc. equilib. 77−73108
alcohols, aliphatic, permitt., dielec. relax., time-domain multiple refl. meas. 77−57350
alkali halide, dielec. const., press. depend. from Szigeti relations 79−19828
alkali halide, dielectric constant and polarisability strain derivatives 77−90088
alkali halide, electric-dipole ordering of tunnelling impurity centres 80−2215
alkali halide, exchange charge polarisation, dielectric const., Dick and Overhauser model 78−55832
alkali halide, static dielectric const. temp. depend. 78−43770
alkali halide crystal, permittivity and polarisation behind shock wave front 77−52013
alkali halide crystals, high freq. dielectric const. press. derivative model calcs., electronic polarisation 80−7255
alkali halides, dielectric constant, Clausius-Mossotti and Mott-Littleton theories 79−82910
alkali halides, electronic and static dielec. consts., strain derivative theory 79−95701
alkali halides, electronic dielec. const., evaluation of second order strain derivatives 78−2792
alkali halides, F-centre photoionisation, semicontinuum model 79−99509
alkali halides, Mott-Littleton dielectric theory 78−80274
alkali halides, off to on centre defect transitions under hydrostatic press. 78−15199
alkali halides, static dielectric behaviour, vol. depend., many-body interactions effects 78−2786
alkali hydrides, bulk props. prediction from molecular behaviour 78−51468
alkali metal compounds, $ASbO_3$.1/6AF, dielec. spectroscopy study, 100 Hz to 10 MHz, 238 to 417K *(German)* 80−108144
alkali metal halides, Born repulsive parameters and dielectric behaviour 77−72579
alkali metal-rare earth oxides, $MLnO_2$, Ln=Y or Gd, synthesis and physicochem. props. 77−48216
alkaline earth chalcogenides, static dielec. const. 78−84513
alkaline-earth fluorides, electronic and static dielec. consts., strain derivative theory 79−95701
n-alkanes, dielec. permittivity and pvT data 80−44996
n-alkanols, complex. permitt. meas. by time-domain spectroscopy 77−49741
alklai halide, optic mode Gruneisen parameters and strain derivatives, Born-Mayer and Sziegti model 78−55929
p-alkoxybenzal-p′-ethoxyaniline, even-odd effect and chain config. 79−50989
L-p-alkoxybenzylidene p′-amino 2 methylbutyl cinnamate chiral smectic liq. cryst., dielec. and ferroelec. props. 79−91394
alkyl trichloroacetates, solns., intramol. rot., permittivity and dielectric loss, microwave meas. 78−31145
4′-n-alkyl-4-cyanobiphenyls, dielec. dispersion 78−2798
4-n-alkyl-4-cyanobiphenyls, liq. cryst. of strong positive dielec. anisotropy, static dielec. consts. meas. 78−2790
aluminium methylammonium selenate alum, effect of hydrostatic pressure on dielec. props., near transition pt. 79−56712
alums, dielec. behaviour and ferroelectricity 79−38431
aminobenzotrifluoride, benzene soln., permittivity and dielec. loss 78−64320
aminopyridines, in 1,4-dioxane soln., dielec. consts., losses and relax. 78−64319
ammonium hydrogen oxalate hemihydrate, low temp. dielec. and thermal props. 77−28510
ammonium Rochelle salt, thermodynamics of ferroelec. transition 80−84702
amorphous dielectrics, dielectric anomalies at very low temps., acoustic anomalies analogy 78−31146
amorphous materials, dielec. and US dispersion at low temps. freq. and temp. depend. 79−95092
aniline, in benzene, polar dielectric system, RF cond. and dipole moment 78−2788
anilines, substituted, in benzene soln., dielectric relax. time, dipole moment 80−50259
anilines, substituted, in nonpolar solvent, dielec. relax. obs. 80−55022
anisotropic artificial dielectrics, dispersion props, investigation, electrodynamic method 80−88903
anisotropic bodies properties interpretation, using inverse tensor property *(Rumanian)* 77−55743
anisotropic crystals, in which dielec. tensor has components with different signs, opt. props. 79−42931
anisotropic dielectric model, macroscopic Clausius-Mossetti eqn., extended Frohlich formula 77−36168
anisotropic inhomogeneous medium, elastic light scatt., orientation characterization 80−83553
anisotropic medium, inhomogeneity, orientation characterization by elastic light scatt. 80−83552
anisotropic semiconductors, light reflection in interband transition freq. *(Russian)* 80−88945
Arctic drift ice, microwave dielec. const. and absorpt. coeff. anisotropy 78−49037

permittivity continued
aromatic hydrocarbon crysts., effective mol. polarisability 77−88590
aryl esters, cyano-substituted, liq. cryst. props. 77−27822
associated liquid, dielec. props. calc. 77−81045
associated solutions, H bonding and anomalous saturation 78−52426
azoxy compound, liquid cryst. mixture, nematic, elec., optical and viscoelastic props. 79−55803
azoxybenzenes, nematic, refr. index, birefringence, internal field 78−34427
benzene, dielec. const. meas. using 3-terminal meas. cell 78−21170
benzene sulphonyl hydrazine, in nonpolar solvent, thermodynamics of dipolar relax. 79−91347
benzil, phase transition study be simultaneous Raman-scatt. and domain-struct. investigations 79−60504
benzil, structural transition model, cryst. symm. spontaneous strain components 80−2161
benzonitrile, hexane and CCl_4 solns., nonlinear dielec. effect 79−78602
benzonitrile-isooctane mixture, dielec. const. near consolute point, temp. and freq. depend. meas. 80−71292
benzothiazole, dielec. loss, relax. and const. in liq. and soln. 79−91346
benzoylacetone, dil. soln. in benzene, dielectric behaviour 79−42886
benzoylacetone, H bonding, dielec. dispersion obs. 77−63356
benzoylacetones, p-substituted, dil. soln. in benzene, dielectric behaviour 79−42886
benzyl cyanides, α-substituted, in dil. soln., dielec. absorpt. obs., enthalpy of activation 80−55019
binary crystals, press. depend. and theories of electronic dielec. const. 77−24780
binary dielectric mixture relative permittivity formulae compared 80−15939
binary liquid mixture, critical conc. determ. from dielectric const. meas. 77−20788
binary liquid mixtures near crit. pt., nonlinear dielectric effect 78−23384
biological substances, tabulation for freq. range 10 kHz to 10 GHz 80−108143
1,6-bis(2,4-dinitrophenoxy)-2,4-hexadiyne, obs. of apparent ferroelec. transition 80−66121
bis[catena-poly(methylarsenic)], LF dielec. response 79−56719
bone, bovine cortical, dielec. relax. 77−40964
bone, human cortical, US properties and microtexture 80−51144
Born model, electrostriction rel. to dielec. and thermoelastic props. 80−71322
borosilicate glass, new dielec. props. at 5 mK 77−63354
brain tissue, dog, dielectric props. between 0.01 and 10 GHz 80−16915
bromal, in benzene soln., dielec. relax., loss, and dipole moment 80−2692
4-bromo-m-thiocresol, liq., dielectric relax. mechanisms 79−42891
bromobenzene, nonlinear dielectric effect temp. depend. 79−82908
bromobenzene solutions, influence of strong elec. field on dielec. permeability 77−90086
4-bromobiphenyl, dielectric const., mol. reorientation in solid 78−72448
bromoform, solid, phase transform., dielec. dispersion and differential scanning calorimetric obs. 80−24582
m-bromophenylbenzoyloxybenzoate, nematic phase, freq. depend. of dielec. props. *(French)* 79−91337
butane diol, asymm. dielectric dispersion, 1-25000 MHz 78−15092
2,3-butanediol, dielectric dispersion 78−72455
1,4-butanediol, low freq. dielectric dispersion, charge carrier hopping anal. 78−43772
1-butanol, permitt., dielec. time domain spectroscopy, total transmission method study 80−27323
t-butyl acetate, rot. isomerism, dielect. and Raman spectra 80−106328
t-butyl alcohol, self-assoc., linear and nonlinear dielec. effects obs. 80−60484
tert-butyl alcohol in nonpolar solvents, liq. struct. from dielectric studies 80−38894
t-butyl formate, rot. isomerism, dielect. and Raman spectra 80−106328
calcium strontium propionate, compressed powder, dielectric props., particle size effects 77−59503
o-carborane, dielectric permittivity meas. *(French)* 79−71480
carnauba wax, polarised, simultaneous variation of dielec. const. and discharge current, room temp. to beyond melting point 80−11314
β-carotene, hole mobility, photocond. and dielec. const. meas. 77−11957
casein-methylglyoxal complex, electronic props. 77−52736
castor oil dielectric fluid, microwave propag., permittivity effect, demonstration 80−105468
CBOOA, liq. cryst. of strong positive dielec. anisotropy, static dielec. consts. meas. 78−2790
cellulose fibre, moist, dielec. props. 78−76380
celsian, with CaF_2 and ZnO additives, props. obs. *(Bulgarian)* 80−50579
ceramics, granular, electrophysical props. depend. on porosity, temp., solid-phase props. 77−69764
ceramics, TiO_2 based, variation of dielectric constant and resistivity with temp. 80−2683
ceramics, transparent ferroelectric, composition selection for appl. in light modulators *(Russian)* 80−91869
cermet film granular media, dielectric function theory, permittivity, percolation transport props. 80−88498
cetyliodide, cryst. phase transitions, mol. dynamics, spectroscopic and dielectric meas *(Russian)* 79−51965
chiral smectic C, ferroelec. props., dielec. meas. 78−52463
chiral smectic liquid cryst., ferroelectric, flexoelectric effects, dielectric const. 80−33877
chitin, in lobster shell and apodeme, piezoelec. rel. to remodelling 78−64929
chloral, dielec. consts. and dielec. losses meas. 77−20795
chloral, in benzene, permittivity, dielectric loss, 36 GHz 77−32323
chloral, liq., permittivity, dielec. loss, up to 60 GHz 78−60384
chloranil pellets, thermally stimulated discharge current and dielectric studies 80−93236
4-chloro-3-nitrobenzotrifluoride-benzene (carbon tetrachloride) dilute soln., dielec. relax. time, dipole moment, microwave obs. 78−35084
4-chloro-3-nitrotoluene-benzene (carbon tetrachloride) dilute soln., dielec. relax. time, dipole moment, microwave obs. 78−35084
4-chloro-α-toluothiol, liq., dielectric relax. mechanisms 79−42891
chlorobenzene, in CCl_4 soln., quadratic changes in elec. permittivity, intermol. interactions 77−73107
chlorobenzene, nonlinear dielectric effect temp. depend. 79−87372
chlorobenzene-cis-decalin, mixtures, dielec. const. and loss tangent in liq. and solid phases 80−100628
chlorobenzotrifluoride, benzene soln., permittivity and dielec. loss 78−64320
chloroform, CNDO approx. 79−72240
o-chloronitrobenzene-benzene (carbon tetrachloride) dilute soln., dielec. relax. time, dipole moment, microwave obs. 78−35084
chloroplasts, photoinduced dielectric const. shift *(French)* 78−61147
cholesteric liquid crystal mixture, with positive dielectric anisotropy influence of external fields *(Rumanian)* 78−59751
cholesterin ethers, dielec. absorption, heating/cooling and oxidation depth effects *(Russian)* 79−50984
cholesteryl laurate-cholesteryl caprylate (75 wt.%), polymorphic behaviour, optical, elec. and dielec. meas. 80−65208
cholesteryl linoleate, dielec. props., phase transitions rel. to temp. 79−33592
CL Al_2O_3, film, dielec. const. and resist., thickness depend. 78−39502
Clausius-Mossotti problem for cubic arrays of spheres 78−52422
coal dispersions, solvent refined, elec. props., surface characts. 80−80333
colloidal particles, interaction force, calc. of electronic component 79−11829
complex, corresponding to Havriliak-Negami function, Stieltjes inversion application *(Spanish)* 79−61291
complex, normalised, for Williams-Watts type of dielec. relax., num. table 80−7287
complex dielectric, humidity, temp., density, freq. and granulometric composition effects on elec. characts. *(Russian)* 79−42881
composite material, complex dielectric const., bounds 80−108170
composite material, dielec. const., charact. geometric function, rigorous upper and lower bounds 79−38438
composite material, dielectric const., microscopic geometry calcs. 78−76375
composite material, two-component, complex dielectric constant, exactly solvable microscopic geometries and rigorous bounds 80−75918
composite medium, effective bulk dielec. const., analytical props. 78−56414
composite medium, with regular struct., dielec. props. 80−20576
conductive liquid Kerr constant meas. 78−88279
conjugate interfaces: interfaces between transparent media of the same reflection coefficient for the parallel polarization at the same angle of incidence 80−87299
continuum dielectric approx. relax., Poisson-Boltzmann thermodynamics 77−36762
cooperative Raman scattering, effect of phase self-modulation of light 80−91855
copper formate tetrahydrate, antiferroelec., dielec. anisotropy 78−43768
copper formate tetrahydrate, dielec. anisotropy and dimer theory 79−38427
copper formate tetrahydrate, dielec. props. under hydrostatic press. 77−20789
copper formate tetrahydrate, stress effect on antiferroelec. phase transition, dielec. meas. 79−38498
Corning 7070 glass, relative permittivity at 3 GHz 79−33591
corundum ceramic, high-temp. treatment, powder medium effect on microstruct., comp., strength and dielec. props. 79−33984
critical binary mixtures, dielec. props., droplet model 79−69762
cryogenic gases and liquids, dielectric breakdown 80−40051
crystal under hydrostatic press., electronic polarisability and ion size var. 78−26487
cubic array of identical spheres, dielec. const. calc. 80−25271
cubic arrays of spheres in dielectric matrix, permittivity 78−56415
cubic lattice modelling for permittivity and conductivity 77−16236
cubic lattice of polarisable spheres, dielectric constant 80−60483
cupric formate tetrahydrate, dielec. props. under hydrostatic press. 77−12343
cupric formate tetrahydrate, pressure effect on dielectric props. *(Japanese)* 79−65787
4-cyano-4′-octylbiphenyl, dielec. props., 1 Hz-1 GHz, in smectic, nematic and liq. phases *(French)* 77−40168
4-cyano-4′-octylbiphenyl, dielectric relax. anal. in nematic and smectic phases 80−108153
p-cyano-p′-pentylbiphenyl/p-pentylbenzoic acid, mixture, induced smectic phase, dielec. props. 80−6498
cyanobiphenyl nematic homologous series, Kerr consts., relax. times, refr. index, dielectric const. 79−19863
cyanobiphenyls, nematic, diaelec. consots. and diamag. anisotropies 80−7253
cyanobiphenyls, physical props., appl. to Kerr cells 79−19142
t-cyanobutane, dielectric relaxation study, complex permittivity 80−80688
cyanocyclohexylcyclohexanes, nematic, diaelec. consots. and diamag. anisotropies 80−7253
2-p-cyanophenylazo-S-akloxypyridines, synthesis, phase transition temps., and dielec. props. 79−86876
m-cyanophenylbenzoyloxybenzoates, nematic phase, freq. depend. of dielec. props. *(French)* 79−91337
cyanophenylcyclohexanes, nematic, diaelec. consots. and diamag. anisotropies 80−7253
cyclohexane, dielec. const. meas. using 3-terminal meas. cell 78−21170
cytochrome-c, hydrated, dielectric props. at 9.9 GHz 78−15758
data presentation and interpretation 78−76376
n-decylammonium cadmium chloride, perovskite-type layer cmpd. n-decylammonium chain dynamics 79−99313
p-n-decyloxybenzoic acid p-n-hexyloxyphenyl ester, dielec. permittivity in nematic and smectic phases 79−32899
defective dielectrics, EM heating with time depend. param., WKB calcs. 80−71367
dense dipolar hard sphere fluid, integral eqn. theory 77−76278
DH stripe lasers, field model, effective permitt., complex permitt. profile 79−7128
DHAB, nematic, ordering change due to external DC elec. field, permittivity obs. 78−94990
di-n-butyl phthalate, complex. permitt. meas. by time-domain spectrosopy 77−49741
dialkyl carbonates, liq., US, microwave dielect. relaxation 79−56717
diatomic crystal, photoelasticity, exchange charge polaris. effect 77−81046
dibenzoyl methane, H bonding, dielec. dispersion obs. 77−63356
4,4′-dibromobiphenyl, dielectric const., mol. reorientation in solid 78−72448
dicalcium barium propionate, press. induced ferroelectricity, dielectric meas. 79−51920

permeability continued
viscous flow, slow, through rigid porous medium, macroscopic fied eqns. 79−94711
water self-diffusion in porous membranes, ionic solns., struct., props. 79−52765
Westerly granite, permeability changes during water flow at 100-400°C 78−40546
wettability dependent permeability in porous media 79−98795
Al, reaction with H_2, influence of surface reactions on rate *(Russian)* 80−66863
Al_2O_3, permeability and solubility of H_2, 1200-1450°C 80−39351
Al_2O_3 sintered tubes, H_2 permeability 80−24675
Co-Mo alloy electrodeposits, codeposited impurities rel. to H_2 permeation, props. 79−19493
D beam, interaction with Pd membrane 77−51538
Fe, annealed, Hz permeation, 230 to 300K *(Japanese)* 78−84004
Fe, annealed and cold-rolled, diffusion, permeation and accumulation of H_2 *(Japanese)* 77−39692
Fe, Armco, membrane, superpermeability to D 79−24830
Fe, effect of anion and organic corrosion inhibitors on H_2 penetration rate 80−100938
Fe fibre porous material, props. 79−98798
Fe, H_2 permeation, rel. to embrittlement, organic inhibitors, surface treatment 80−108635
Fe, membranes, effect of electrodeposited metals on H permeation, proposed catalytic mechanism 78−53252
Fe ore pellet, meas. of gas permeability of individual pellets 78−80711
Fe, permeability, solubility and diffusion of H and D, 9 to 73°C 77−76560
Fe, permeation by H in fusion reactor 80−34242
Fe, pure, of H and D at 10 to 60°C 78−75887
Fe, to H_2, influence of microstruct. changes induced by cold working *(Russian)* 77−20182
Fe-Co alloy, diffusion of H_2, diffusion coefficient and permeability *(Russian)* 78−79819
Fe-V alloy, H permeability, 300-700°C *(Russian)* 77−15627
H_2, change of diffusivity with order-disorder transformations in Ni_3Fe, Ni_3Pt and Ni_3Mn 80−59729
H_2 in liquid Na reactor coolant, effect of O_2 80−614
H_2 permeability in steel Kh18N10T, effect of surface treatment *(Russian)* 79−15853
H_2 permeation reduction using Pd foil in liquid metal *(Japanese)* 80−68770
H_2, permeation through metal barrier, adsorpt. processes 78−63879
H_2, through Pd membrane, diffusion-cell for separation H_2 containing mixtures, solar furnace appl. 80−92245
He, in glasses and Stycasts *(Japanese)* 79−7715
K^+ permeability of E. coli, membrane lipid role in radiation damage 78−48834
K^+ permeability of mitochondrial and artificial bilayer membranes 78−53365
Kr-N_2(He) gas mixtures, separation by silicone rubber, cellulose acetate membranes 77−36791
Mo, gas permeability (H, He, Ar) through monocrystalline and polycrystalline specimens *(Russian)* 79−60554
Mo, porous, permeability, deform. effects 79−100229
N_2, permeation through metal barrier, adsorpt. processes 78−63879
Na permeability inactivation in squid giant nerve fibres, review of exptl. work 78−73154
Na_2O-CaO-SiO_2 glass microbubbles, permeation eccentricities of He, Ne and D-T 78−47598
$2Na_2O$-CaO-$XSiO_2$ glass, He mobility, interconnectivity, miscibility limits, effect of morphology 78−67864
Nb, membrane, H permeation *(Japanese)* 80−100363
Ne, permeability in laser fusion glass microbubbles 77−35367
Ni, H permeability using permeation method *(Japanese)* 78−51740
Ni, of D thermal ats., anomalously high transmission, 20 to 520°C *(Russian)* 77−72752
Ni, of H, D and T 79−77823
Ni, permeability and diffusivity of hydrogen *(Japanese)* 78−66345
Ni-Mn, permeability, diffusion and solubility of H 80−107573
Ni-Mo alloy electrodeposits, codeposited impurities rel. to H_2 permeation, props. 79−19493
Pb, of $H_2(D_2)$, isotopic effect *(Russian)* 78−75881
Pd and Pd alloys, influence of $\alpha \rightleftarrows \beta$ phase transform. on physicomechanical props. and H_2 permeability *(Russian)* 78−68681
Pd membrane, H atom interaction, superpermeability 80−81365
Pd membrane, H penetrability reduction by C coating *(Russian)* 77−77808
Pd, membrane, superpermeability, of atomised H_2, under different gas and membrane boundary conditions 79−71469
Pd-Ag (25 at.%) H_2 permeability and solubility, comparison with other Pd solid soln. alloys 79−23738
Pd-Ce (5.75 at.%), H_2 permeability and solubility, comparison with other Pd solid soln. alloys 79−23738
Pd-W (20 wt.%), permeability, diffusion, and solubility of H_2, elec. resist., heat treatment effects *(Russian)* 79−51307
Pd-Y (8 at.%), H_2 permeability and solubility, comparison with other Pd solid soln. alloys 79−23738
SO_2 and nitrogen oxide automatic monitors, laboratory and field calibration *(French)* 77−37455
SiC, permeability and solubility of H_2, 1200-1450°C 80−39351
SiO_2, fused, He solubility and diffusion above transform. range 80−79965
T permeation through steam generator alloys 80−34250
ThO_2 microspheres, coated, coating permeability meas. 80−95343
Ti 78−60602
Ti, permeation of H plasma reduced by layer of interstitially built ϵ-Ti_2N 80−16566
Ti, through Croloy steel for LMFBR steam generator 80−68775
UO_2-UC microspheres, coated, coating permeability meas. 80−95343
V, H_2 permeability, surface impurity layer effect 77−24440
ZrC, solubility, diffusion and permeation of Cs 78−51684
ZrO_2, CaO stabilised, exam. of O_2 permeability and p-type electronic cond. 79−10980
ZrO_2, CaO stabilized, O_2 permeability at low O_2 partial press. 79−47980
ZrO_2, plasma deposited, porosity, gas permeability and dielectric strength 79−52125
ZrO_2, plasma sprayed coatings, elec. cond. and gas permeability 79−82478

permeability (magnetic) *see magnetic permeability*

permeability measurement (magnetic) *see magnetic permeability measurement*

permittivity
see also electric strength
abietic acid glass, determ. from TSC curves 77−55744
acetamides, N-methyl-, N,N-dimethyl-, in organic solns., dielec. const., dipole moments, monomer-dimer equilib. 80−40031
acetic acid, dil. soln., dielectric polaris., linear correlation factor 78−6624
acetylacetone, H bonding, dielec. dispersion obs. 77−63356
acrylonitrile, dielectric constant effect on nuclear spin-spin coupling constants, INDO approx. 79−72240
aerosol, polydispersity, unipolar charging, charging mobility analysis 78−61059
aerosol, unipolar diffusion charging, particle dielectric constant and ion mobility effects 78−61058
albumin, bovine serum, hydrated, dielectric props. at 9.9 GHz 78−15758
albumin, human serum, elec. cond. and dielec. const., 1 to 15 MHz 78−53315
alcohol, dielec. const., hindered mol. rot. influence 78−43767
alcohol binary mixtures, nonlinear dielec. effects, shift in assoc. equilib. 77−73108
alcohols, aliphatic, permitt., dielec. relax., time-domain multiple refl. meas. 77−57350
alkali halide, dielec. const., press. depend. from Szigeti relations 79−19828
alkali halide, dielectric constant and polarisability strain derivatives 77−90088
alkali halide, electric-dipole ordering of tunnelling impurity centres 80−2215
alkali halide, exchange charge polarisation, dielectric const., Dick and Overhauser model 78−55832
alkali halide, static dielectric const. temp. depend. 78−43770
alkali halide crystal, permittivity and polarisation behind shock wave front 77−52013
alkali halide crystals, high freq. dielectric const. press. derivative model calcs., electronic polarisation 80−7255
alkali halides, dielectric constant, Clausius-Mossotti and Mott-Littleton theories 79−82910
alkali halides, electronic and static dielec. consts., strain derivative theory 79−95701
alkali halides, electronic dielec. const., evaluation of second order strain derivatives 78−2792
alkali halides, F-centre photoionisation, semicontinuum model 79−99509
alkali halides, Mott-Littleton dielectric theory 78−80274
alkali halides, off to on centre defect transitions under hydrostatic press. 78−15199
alkali halides, static dielectric behaviour, vol. depend., many-body interactions effects 78−2786
alkali hydrides, bulk props. prediction from molecular behaviour 78−51468
alkali metal compounds, $ASbO_3$.1/6AF, dielec. spectroscopy study, 100 Hz to 10 MHz, 238 to 417K *(German)* 80−108144
alkali metal halides, Born repulsive parameters and dielectric behaviour 77−72579
alkali metal-rare earth oxides, $MLnO_2$, Ln=Y or Gd, synthesis and physicochem. props. 77−48216
alkaline earth chalcogenides, static dielec. const. 78−84513
alkaline-earth fluorides, electronic and static dielec. consts., strain derivative theory 79−95701
n-alkanes, dielec. permittivity and pvT data 80−44996
n-alkanols, complex. permitt. meas. by time-domain spectroscopy 77−49741
alklai halide, optic mode Gruneisen parameters and strain derivatives, Born-Mayer and Sziegti model 78−55929
p-alkoxybenzal-p′-ethoxyaniline, even-odd effect and chain config. 79−50989
L-p-alkoxybenzylidene p′-amino 2 methylbutyl cinnamate chiral smectic liq. cryst., dielec. and ferroelec. props. 79−91394
alkyl trichloroacetates, solns., intramol. rot., permittivity and dielectric loss, microwave meas. 78−31145
4′-n-alkyl-4-cyanobiphenyls, dielec. dispersion 78−2798
4-n-alkyl-4-cyanobiphenyls, liq. cryst. of strong positive dielec. anisotropy, static dielec. consts. meas. 78−2790
aluminium methylammonium selenate alum, effect of hydrostatic pressure on dielec. props., near transition pt. 79−56712
alums, dielec. behaviour and ferroelectricity 79−38431
aminobenzotrifluoride, benzene soln., permittivity and dielec. loss 78−64320
aminopyridines, in 1,4-dioxane soln., dielec. consts., losses and relax. 78−64319
ammonium hydrogen oxalate hemihydrate, low temp. dielec. and thermal props. 77−28510
ammonium Rochelle salt, thermodynamics of ferroelec. transition 80−84702
amorphous dielectrics, dielectric anomalies at very low temps., acoustic anomalies analogy 78−31146
amorphous materials, dielec. and US dispersion at low temps. freq. and temp. depend. 79−95092
aniline, in benzene, polar dielectric system, RF cond. and dipole moment 78−2788
anilines, substituted, in benzene soln., dielectric relax. time, dipole moment 80−50259
anilines, substituted, in nonpolar solvent, dielec. relax. obs. 80−55022
anisotropic artificial dielectrics, dispersion props, investigation, electrodynamic method 80−88903
anisotropic bodies properties interpretation, using inverse tensor property *(Rumanian)* 77−55743
anisotropic crystals, in which dielec. tensor has components with different signs, opt. props. 79−42931
anisotropic dielectric model, macroscopic Clausius-Mossetti eqn., extended Frohlich formula 77−36168
anisotropic inhomogeneous medium, elastic light scatt., orientation characterization 80−83553
anisotropic medium, inhomogeneity, orientation characterization by elastic light scatt. 80−83552
anisotropic semiconductors, light reflection in interband transition freq. *(Russian)* 80−88945
Arctic drift ice, microwave dielec. const. and absorpt. coeff. anisotropy 78−49037

permittivity continued
aromatic hydrocarbon crysts., effective mol. polarisability 77−88590
aryl esters, cyano-substituted, liq. cryst. props. 77−27822
associated liquid, dielec. props. calc. 77−81045
associated solutions, H bonding and anomalous saturation 78−52426
azoxy compound, liquid cryst. mixture, nematic, elec., optical and viscoelastic props. 79−55803
azoxybenzenes, nematic, refr. index, birefringence, internal field 78−34427
benzene, dielec. const. meas. using 3-terminal meas. cell 78−21170
benzene sulphonyl hydrazine, in nonpolar solvent, thermodynamics of dipolar relax. 79−91347
benzil, phase transition study be simultaneous Raman-scatt. and domain-struct. investigations 79−60504
benzil, structural transition model, cryst. symm. spontaneous strain components 80−2161
benzonitrile, hexane and CCL_4 solns., nonlinear dielec. effect 79−78602
benzonitrile-isooctane mixture, dielec. const. near consolute point, temp. and freq. depend. meas. 80−71292
benzothiazole, dielec. loss, relax. and const. in liq. and soln. 79−91346
benzoylacetone, dil. soln. in benzene, dielectric behaviour 79−42886
benzoylacetone, H bonding, dielec. dispersion obs. 77−63356
benzoylacetones, p-substituted, dil. soln. in benzene, dielectric behaviour 79−42886
benzyl cyanides, α-substituted, in dil. soln., dielec. absorpt. obs., enthalpy of activation 80−55019
binary crystals, press. depend. and theories of electronic dielec. const. 77−24780
binary dielectric mixture relative permittivity formulae compared 80−15939
binary liquid mixture, critical conc. determ. from dielectric const. meas. 77−20788
binary liquid mixtures near crit. pt., nonlinear dielectric effect 78−23384
biological substances, tabulation for freq. range 10 kHz to 10 GHz 80−108143
1,6-bis(2,4-dinitrophenoxy)-2,4-hexadiyne, obs. of apparent ferroelec. transition 80−66121
bis[catena-poly(methylarsenic)], LF dielec. response 79−56719
bone, bovine cortical, dielec. relax. 77−40964
bone, human cortical, US properties and microtexture 80−51144
Born model, electrostriction rel. to dielec. and thermoelastic props. 80−71322
borosilicate glass, new dielec. props. at 5 mK 77−63354
brain tissue, dog, dielectric props. between 0.01 and 10 GHz 80−16915
bromal, in benzene soln., dielec. relax., loss, and dipole moment 80−2692
4-bromo-m-thiocresol, liq., dielectric relax. mechanisms 79−42891
bromobenzene, nonlinear dielectric effect temp. depend. 79−82908
bromobenzene solutions, influence of strong elec. field on dielec. permeability 77−90086
4-bromobiphenyl, dielectric const., mol. reorientation in solid 78−72448
bromoform, solid, phase transform., dielec. dispersion and differential scanning calorimetric obs. 80−24582
m-bromophenylbenzoyloxybenzoate, nematic phase, freq. depend. of dielec. props. *(French)* 79−91337
butane diol, asymm. dielectric dispersion, 1-25000 MHz 78−15092
2,3-butanediol, dielectric dispersion 78−72455
1,4-butanediol, low freq. dielectric dispersion, charge carrier hopping anal. 78−43772
1-butanol, permitt., dielec. time domain spectroscopy, total transmission method study 80−27323
t-butyl acetate, rot. isomerism, dielect. and Raman spectra 80−106328
t-butyl alcohol, self-assoc., linear and nonlinear dielec. effects obs. 80−60484
tert-butyl alcohol in nonpolar solvents, liq. struct. from dielectric studies 80−38894
t-butyl formate, rot. isomerism, dielect. and Raman spectra 80−106328
calcium strontium propionate, compressed powder, dielectric props., particle size effects 77−59503
o-carborane, dielectric permittivity meas. *(French)* 79−71480
carnauba wax, polarised, simultaneous variation of dielec. const. and discharge current, room temp. to beyond melting point 80−11314
β-carotene, hole mobility, photocond. and dielec. const. meas. 77−11957
casein-methylglyoxal complex, electronic props. 77−52736
castor oil dielectric fluid, microwave propag., permittivity effect, demonstration 80−105468
CBOOA, liq. cryst. of strong positive dielec. anisotropy, static dielec. consts. meas. 78−2790
cellulose fibre, moist, dielec. props. 78−76380
celsian, with CaF_2 and ZnO additives, props. obs. *(Bulgarian)* 80−50579
ceramics, granular, electrophysical props. depend. on porosity, temp., solid-phase props. 77−69764
ceramics, TiO_2 based, variation of dielectric constant and resistivity with temp. 80−2683
ceramics, transparent ferroelectric, composition selection for appl. in light modulators *(Russian)* 80−91869
cermet film granular media, dielectric function theory, permittivity, percolation transport props. 80−88498
cetyliodide, cryst. phase transitions, mol. dynamics, spectroscopic and dielectric meas *(Russian)* 79−51965
chiral smectic C, ferroelec. props., dielec. meas. 78−52463
chiral smectic liquid cryst., ferroelectric, flexoelectric effects, dielectric const. 80−33877
chitin, in lobster shell and apodeme, piezoelec. rel. to remodelling 78−64929
chloral, dielec. consts. and dielec. losses meas. 77−20795
chloral, in benzene, permittivity, dielectric loss, 36 GHz 77−32323
chloral, liq., permittivity, dielec. loss, up to 60 GHz 78−60384
chloranil pellets, thermally stimulated discharge current and dielectric studies 80−93236
4-chloro-3-nitrobenzotrifluoride-benzene (carbon tetrachloride) dilute soln., dielec. relax. time, dipole moment, microwave obs. 78−35084
4-chloro-3-nitrotoluene-benzene (carbon tetrachloride) dilute soln., dielec. relax. time, dipole moment, microwave obs. 78−35084
4-chloro-α-toluothiol, liq., dielectric relax. mechanisms 79−42891
chlorobenzene, in CCl_4 soln., quadratic changes in elec. permittivity, intermol. interactions 77−73107
chlorobenzene, nonlinear dielectric effect temp. depend. 79−87372
chlorobenzene-cis-decalin, mixtures, dielec. const. and loss tangent in liq. and solid phases 80−100628
chlorobenzotrifluoride, benzene soln., permittivity and dielec. loss 78−64320
chloroform, CNDO approx. 79−72240
o-chloronitrobenzene-benzene (carbon tetrachloride) dilute soln., dielec. relax. time, dipole moment, microwave obs. 78−35084
chloroplasts, photoinduced dielectric const. shift *(French)* 78−61147
cholesteric liquid crystal mixture, with positive dielectric anisotropy influence of external fields *(Rumanian)* 78−59751
cholesterin ethers, dielec. absorption, heating/cooling and oxidation depth effects *(Russian)* 79−50984
cholesteryl laurate-cholesteryl caprylate (75 wt.%), polymorphic behaviour, optical, elec. and dielec. meas. 80−65208
cholesteryl linoleate, dielec. props., phase transitions rel. to temp. 79−33592
CL Al_2O_3, film, dielec. const. and resist., thickness depend. 78−39502
Clausius-Mossotti problem for cubic arrays of spheres 78−52422
coal dispersions, solvent refined, elec. props., surface characts. 80−80333
colloidal particles, interaction force, calc. of electronic component 79−11829
complex, corresponding to Havriliak-Negami function, Stieltjes inversion application *(Spanish)* 79−61291
complex, normalised, for Williams-Watts type of dielec. relax., num. table 80−7287
complex dielectric, humidity, temp., density, freq. and granulometric composition effects on elec. characts. *(Russian)* 79−42881
composite material, complex dielectric const., bounds 80−108170
composite material, dielec. const., charact. geometric function, rigorous upper and lower bounds 79−38438
composite material, dielectric const., microscopic geometry calcs. 78−76375
composite material, two-component, complex dielectric constant, exactly solvable microscopic geometries and rigorous bounds 80−75918
composite medium, effective bulk dielec. const., analytical props. 78−56414
composite medium, with regular struct., dielec. props. 80−20576
conductive liquid Kerr constant meas. 78−88279
conjugate interfaces: interfaces between transparent media of the same reflection coefficient for the parallel polarization at the same angle of incidence 80−87299
continuum dielectric approx. relax., Poisson-Boltzmann thermodynamics 77−36762
cooperative Raman scattering, effect of phase self-modulation of light 80−91855
copper formate tetrahydrate, antiferroelec., dielec. anisotropy 78−43768
copper formate tetrahydrate, dielec. anisotropy and dimer theory 79−38427
copper formate tetrahydrate, dielec. props. under hydrostatic press. 77−20789
copper formate tetrahydrate, stress effect on antiferroelec. phase transition, dielec. meas. 79−38498
Corning 7070 glass, relative permittivity at 3 GHz 79−33591
corundum ceramic, high-temp. treatment, powder medium effect on microstruct., comp., strength and dielec. props. 79−33984
critical binary mixtures, dielec. props., droplet model 79−69762
cryogenic gases and liquids, dielectric breakdown 80−40051
crystal under hydrostatic press., electronic polarisability and ion size var. 78−26487
cubic array of identical spheres, dielec. const. calc. 80−25271
cubic arrays of spheres in dielectric matrix, permittivity 78−56415
cubic lattice modelling for permittivity and conductivity 77−16236
cubic lattice of polarisable spheres, dielectric constant 80−60483
cupric formate tetrahydrate, dielec. props. under hydrostatic press. 77−12343
cupric formate tetrahydrate, pressure effect on dielectric props. *(Japanese)* 79−65787
4-cyano-4′-octylbiphenyl, dielec. props., 1 Hz-1 GHz, in smectic, nematic and liq. phases *(French)* 77−40168
4-cyano-4′-octylbiphenyl, dielectric relax. anal. in nematic and smectic phases 80−108153
p-cyano-p′-pentylbiphenyl/p-pentylbenzoic acid, mixture, induced smectic phase, dielec. props. 80−6498
cyanobiphenyl nematic homologous series, Kerr consts., relax. times, refr. index, dielectric const. 79−19863
cyanobiphenyls, nematic, diaelec. consots. and diamag. anisotropies 80−7253
cyanobiphenyls, physical props., appl. to Kerr cells 79−19142
t-cyanobutane, dielectric relaxation study, complex permittivity 80−80688
cyanocyclohexylcyclohexanes, nematic, diaelec. consots. and diamag. anisotropies 80−7253
2-p-cyanophenylazo-S-akloxypyridines, synthesis, phase transition temps., and dielec. props. 79−86876
m-cyanophenylbenzoyloxybenzoates, nematic phase, freq. depend. of dielec. props. *(French)* 79−91337
cyanophenylcyclohexanes, nematic, diaelec. consots. and diamag. anisotropies 80−7253
cyclohexane, dielec. const. meas. using 3-terminal meas. cell 78−21170
cytochrome-c, hydrated, dielectric props. at 9.9 GHz 78−15758
data presentation and interpretation 78−76376
n-decylammonium cadmium chloride, perovskite-type layer cmpd. n-decylammonium chain dynamics 79−99313
p-n-decyloxybenzoic acid p-n-hexyloxyphenyl ester, dielec. permittivity in nematic and smectic phases 79−32899
defective dielectrics, EM heating with time depend. param., WKB calcs. 80−71367
dense dipolar hard sphere fluid, integral eqn. theory 77−76278
DH stripe lasers, field model, effective permitt., complex permitt. profile 79−7128
DHAB, nematic, ordering change due to external DC elec. field, permittivity obs. 78−94990
di-n-butyl phthalate, complex. permitt. meas. by time-domain spectrosopy 77−49741
dialkyl carbonates, liq., US, microwave dielect. relaxation 79−56717
diatomic crystal, photoelasticity, exchange charge polaris. effect 77−81046
dibenzoyl methane, H bonding, dielec. dispersion obs. 77−63356
4,4′-dibromobiphenyl, dielectric const., mol. reorientation in solid 78−72448
dicalcium barium propionate, press. induced ferroelectricity, dielectric meas. 79−51920

permittivity continued
metals, energy gap determ. by optical methods *(Russian)* 78−30867
metals, lattice dynamics model *(Hungarian)* 77−27952
methane+N_2(Ar), compressed-liquid dielectric const., derived excess vol. 79−11377
methanol, 10 MHz-70 GHz, 10-40°C, Debye dispersion 78−43769
methanol, alcoholic electrolytic solutions, Dielectric constants 79−99813
methanol, dielectric const. in mag. field 79−78606
methanol, in carbon tetrachloride, permitt. meas. by time-domain spectroscopy 77−43926
methanol-ethanol mixture, dielectric const. composition depend. rel. to struct. effects 79−11378
methyl iodide, liq., mol. reorientation, dielec. and viscosity meas. 80−100157
methyl methacrylate, oligomers, dielectric relax., end-group effects 78−92019
methyl trichloroacetate, soln., dielectric props. and relax. mechanisms at microwave freqs. 78−15089
methyl-3-bromopropionate, liq., microwave absorption and relax. 78−60386
methyl-4-chlorobutyrate, liq., microwave absorption and relax. 78−60386
methylammonium aluminium sulphate dodecahydrate, ferro to paraelectric transition, low freq. dielectric behaviour 79−4770
methylammonium chromium selenate, lattice consts. and ferroelec. props. 79−33641
methylammonium chromium selenate dodecahydrate crystals, dielectric relaxation 80−40043
methylammonium gallium selenate, lattice consts. and ferroelec. props. 79−33641
methylammonium gallium sulphate dodecahydrate, dielec. relax. meas. 79−28677
3-methylthiomethylpropionate, liq., dielec. relax. and permittivity 80−15948
microscopically inhomogeneous material, theory of optical and microwave props. 77−77161
microwave conductivity measurement by eddy current loss method, effect of permittivity 78−24817
mixed salt solution approximating seawater composition, dielec. and radiation characts. 80−97184
mixture of dipolar hard spheres, dielec. props. 80−24335
moistened disperse and porous materials 79−95304
molecular crystals, polariton spectra and lattice dynamics 80−49313
molecular fluid, dielec. const. and equilib. props., interaction site cluster theory 77−84614
molecular fluid, optical props., intermol. forces effects, theory, appls. 77−28535
molecular gas orientation by reson. radiation, optical detect., laser spectroscopy appl. 79−27742
molecular liquid, of polarisable and deformable mols., theory 79−99043
multiphase material, average bulk props. calc., bounds 77−16237
muscle and nerve fibre electric field resolution for EMG analysis 79−57627
naphthalene, single crystal, anomaly in permittivity due to thermodielectric space charge 80−7258
naphthalenes, substituted, dielec. relax. and permittivity in pure liqs. 78−64318
naphthalenes, substituted, dielectric relax. in solns. 78−2795
natural clay permafrost, elec. props. 77−44967
negative, existence in stable steady state 77−43937
negative currents caused by injection-controlled polarization 79−28675
nematic liq. crystal, dielectric anisotropy, IR spectra, effect of AC elec. field 78−64355
nematic liquid crystal mixtures, dielec. permittivity dispersion 80−88921
nematic liquid crystal transducers, exam. of light absorption behaviour 79−40560
nematic liquid crystals, molecular mechanisms of dielec. polarisation and relaxation 80−34846
nematic liquid crystals, multicomponnet mixtures, dielec. props. 80−38909
nematic liquid crystals, temp. dependent props., twisted nematic displays 79−32901
nematic liquid crysts., dielec. polarisation and relax., mol. mechanisms 80−29673
nematic liquid crysts. of mols. containing nitrile groups, dipole moments determ. 77−19872
nematic-isotropic mixture, dielec. props., phase diagram 78−52424
nitrobenzene, dielectric const. in mag. field 79−78606
nitrobenzene, polarised, simultaneous variation of dielec. const. and discharge current, room temp. to beyond melting point 80−11314
nitrobenzene, solns., elec. permittivity near crit. point 78−76372
nitrobenzene-hexane, soln., dielec. permitt. in two phase region 80−2682
nitrobenzene-hexane critical solutions, crit. exponent determ. by nonlinear dielec. method 79−87373
nitrobenzene-hexane mixtures, nonlinear dielec. effect beyond critical pt. 79−99816
nitrobenzotrifluoride, benzene soln., permittivity and dielec. loss 78−64320
nitroethane, crit. soln. in cyclohexane, nonlinear dielectric effect 78−27152
nitroethane, cyclohexane and benzene solns., nonlinear dielec. effect 79−78602
nitroethane-cyclohexane, pretransitional effects above phase transition temp., nonlinear dielectric meas. 79−15390
nitromethane, shock-induced elec. polarisation *(French)* 79−11381
4-nitrophenyl 4-octyloxybenzoate, smectic-A and nematic phases, dielectric meas. 79−23516
p-nitrophenyl p-n octyloxy benzoate, liquid crystal, elec. cond. and dielectric constant, in solid phase 79−61293
nitrotoluene-pentane, pretransitional effects above phase transition temp., nonlinear dielectric meas. 79−15390
o-nitrotoluene-saturated hydrocarbon soln., critical exponent, permittivity meas. 78−22858
NLC, high frequency electrohydrodynamic instability, permittivity, elec. cond. *(Russian)* 80−49099
NOBAMBC, chiral smectic phases, pyroelectric and dielec. props. 79−91380
non-stoichiometric solids, correl. between dielectric const. and defect struct. 77−85638
nonlinear media classification for nonstationary electrodynamics 79−21567
nonlinear rigid polar molecular fluid, dielec. const. 78−72451
permittivity continued
nonlocal electrostatic 78−82879
nonpolar fluid, permittivity, comparison of Wertheim and Clausius Mossotti derivations, density depend. 77−77137
nonpolar fluid, permittivity, Kerr const., in terms of at.-at. correlation functions 77−36200
nonpolar fluid dielectric constant, comparison of formulae 77−20787
nonstoichiometry and dielectric props. 78−43135
nonuniform systems, effective conductivity from percolation and conduction theory 80−62597
Nylon 7-7 and 11, dielectric const. and dielectric relax. 80−25294
1-octanol, dielec. consts., solvent struct., effect of H bonding solutes, chain length 77−48674
1-octanol-H-bonding solute system, chain assoc., dipole correl. theory, dielec. const. anal 77−48675
1-octanol-nonhydroxylic solvent complexes, H bonding, assoc. consts., elec. dipole moments, dielec. consts. 77−48672
octyl-cyano-biphenyl, smectic-A and nematic phases, dielectric meas. 79−23516
p-n octyloxy benzylidine-p-toludine, liquid crystal, elec. cond. and dielectric constant, in solid phase 79−61293
n-p-octyloxybenzylidene-p-toluidine, dielectric behaviour in nematic mesophase at RF 80−34842
4-n-octyloxyphenyl 4-n-pentyloxybenzoate, permittivity, microwave dielectric relaxation 80−80671
OHMBBA, nematic, dielectric behaviour at RF 79−7548
oil shale from Piceance Creek Basin, Colorado, microwave radiation method 80−12378
oil shales, review of thermophysical properties 79−100479
one-dimensional conductor, broken strand model for dielec. const. and elec. cond. 79−87088
one-dimensional conductors, disordered, elec. props., coherence length, impurity effects 80−24903
one-dimensional strongly disordered conductor, localisation of electrons *(Russian)* 79−78046
opaque region, piezobirefringence anal. 80−60541
optical properties, temp. depend., transport eqn. 78−23421
optical waveguide, parabolic index with random dielectric constant gradient, Gaussian beam propag. 80−58698
organic liquids in UHF region, meas. *(Japanese)* 79−8085
organic liquids with branched chain, dielectric const. temp. coefficient *(Japanese)* 78−35079
organic rigid molecules solns. and mixtures, dielectric relax., const. and loss factor, microwave region 77−55747
orthovanadates, centrosymmetric exhibiting cooperative Jahn-Teller effect, dielec. props. 79−28694
p-alkoxybenzylidene-p′-amino-2-chloropropyl-cinnamate, chiral smectic, dielec. props. 80−96441
PAA, refractive index, dielec. const., mag. susceptibility, orientational ordering *(Dutch)* 80−33884
parathymol, negative uniaxial cryst., linear and nonlinear optical and dielec. props. 77−75602
partially ionised plasma, theory of dielectric constant 80−59173
particles, randomly oriented, generalised theory of average dielectric const. 79−28667
parylene polymers, synthesis, elec., phys., corrosion props. *(German)* 78−64521
patient electrical conductivity and permittivity imaging, computing tomography technique 80−98055
$Pb_5Ge_3O_{11}$:Gd^{3+}, ESR spectra, electric-field effect and reversible permittivity 80−29614
PBLG in dioxan, freq. and shear-rate depend. of relative permitt. 77−8489
PBLG solns., dielec. meas., using pseudorandom noise dielectric spectrometer 78−15084
pentachloronitrobenzene crystal, anomalous microwave permittivity, IR absorption and Raman spectra *(Japanese)* 78−15169
pentane-o-nitrotoluene critical solution, nonlinear dielectric effect 78−55952
p-pentoxy-benzylidene-alkylaniline series, smectic phases, dielec. anisotropy 80−55010
pentylcyanobiphenyl, nematic, elastic and dielec. props. from capacitance-voltage curve 79−32894
percolation threshold of heterogeneous system 79−42889
permafrost active layer, in situ meas. of dielectric const. 77−64333
phenol I and II, permittivity and molar polarisation at pressures between 140-2000 bar 77−77136
phenol-urethane composition based, properties and production methods *(German)* 79−56951
phenolic Mannich bases, dielec. relax. study 80−97196
phenyl 4(4-alkylphenyl)cyclohexanecarboxylates, mesomorphism and dielec. props. 77−27810
phenyl 4-alkylbiphenyl-4′-carboxylates, mesomorphism and dielec. props. 77−27810
phenyl 5-alkoxypicolinates, synthesis, phase transition temps., and dielec. props. 79−86876
phenyl 6-alkoxynicotinates, synthesis, phase transition temps., and dielec. props. 79−86876
phenylcyclohexanes, nematic, low melting liq. crysts. with positive dielec. anisotropy, phys. props. 77−43148
3-phenylpropanol-hexane, nonlinear dielectric effect, critical exponent 80−93227
phenylpyrimidines, liq. crysts., synthesis and phys. props. 78−1995
phonon-magnon interactions, dielectric function, theoretical anal. 78−80275
phospholipid bilayer, ion permeabiligy rel. to dielec. const. 80−81364
photoelasticity, nonlinear, in impure crystals, theory 80−108179
physiological sample, fusion progression during rapid freezing for electron microscopy 80−3884
piezoceramic complex composites near morphotropic phase boundary, dielec. and electromech. anomalies *(German)* 77−20800
piezoelectric hexagonal crystals., elastic wave propag. *(Russian)* 77−69777
planar double layers, Derjaguin force formula 80−107890
plasma, collisional, mixed mode operation, cross-focusing 80−83945
plasma, moving weakly nonsteady, plasma wave propag. 80−106918
plasma, radiative, with anisotropic permittivity, developing wavefronts 80−43896
plastic crystal, with steric hindrance, dielectric const. 77−24779
plastics, anisotropic reinforced, stress-strain state, theoretical principles of nonvisible exam. 78−68745